Aqueous nonelectrolyte solutions. Part XVI. Formula of deuterium sulfide D-hydrate and its dissociation thermodynamic functions

Colin W. Clarke and David N. Glew

Abstract: A method has been devised to approximate both the hydrate formula number *n* and the standard thermodynamic functions for hydrate dissociation from the temperature change of the hydrate former fugacity along a univariant three-phase (hl_1g) equilibrium line. Thermodynamic equations are derived, their validity discussed, and an iterative method for their solution is described. The univariant (hl_1g) equilibrium dissociation of deuterium sulfide D-hydrate ($D_2S{\cdot}nD_2O$ phase h) into gaseous deuterium sulfide (g) and liquid deuterium oxide (l_1) has been treated to give approximate formulae and dissociation constants at 58 temperatures from 2.798 to 30.666°C. Dissociation equilibrium constants $Kp(h{\rightarrow}l_1g)$ have been represented as a function of temperature by a four-parameter equation which yields both values and standard errors (*i*) for $\Delta H^{ot}(h{\rightarrow}l_1g)$ and $\Delta Cp^{ot}(h{\rightarrow}l_1g)$ the standard enthalpy and heat capacity changes for D-hydrate dissociation and (*ii*) for $n = r$ the approximate formula number of the D-hydrate at each experimental temperature. The formula $D_2S{\cdot}6.115D_2O$ with standard error $0.018D_2O$ is found for deuterium sulfide D-hydrate at lower quadruple point $Q(hs_1l_1g)$ 3.392°C; an approximate formula $D_2S{\cdot}5.840D_2O$ with SE $0.019D_2O$ is found at upper quadruple point $Q(hs_1l_2g)$ 30.770°C.

Key words: clathrate D-hydrate of deuterium sulfide, deuterium sulfide D-hydrate, formula of deuterium sulfide D-hydrate, thermodynamics of clathrate hydrate dissociation, dissociation equilibrium constant of deuterium sulfide D-hydrate, standard enthalpy, and heat capacity changes for dissociation of deuterium sulfide D-hydrate.

Résumé : En faisant appel à la variation en fonction de la fugacité du produit formant un hydrate en fonction de la température le long d'une ligne d'équilibre à trois phases (hl_1g) univariables, on a développé une méthode permettant déterminer de façon approximative la nombre, *n*, d'hydrates dans une formule ainsi que les fonctions thermodynamiques associées à la dissociation de cet hydrate. On en a déduit les équations thermodynamiques, on discute de leur validité et on décrit une méthode itérative pour leur solution. On a traité la dissociation en équilibre univariable (hl_1g) entre l'hydrate-D du sulfure de deutérium ($D_2S{\cdot}nD_2O$, phase h) et le sulfure de deutérium gazeux (g) et l'oxyde de deutérium liquide (l_1) pour en tirer les valeurs approximatives des formules ainsi que des constantes de dissociation à 58 températures entre 2,798 et 30,666°C. Les constantes d'équilibre de dissociation, $Kp(h{\rightarrow}l_1g)$, en fonction de la température peuvent être représentées à l'aide d'une équation à quatre paramètres qui permet d'en extraire, pour chaque température expérimentale, les valeurs ainsi que les erreurs standards (*i*) pour $\Delta H^{ot}(h{\rightarrow}l_1g)$ et $\Delta Cp^{ot}(h{\rightarrow}l_1g)$, les changements d'enthalpie et de capacité calorifique standards accompagnant la dissociation de l'hydrate-D ainsi que (*ii*) la valeur approximative du nombre de formule pour $n = r$. Pour le point quadruple inférieur à 3,392°C, $Q(hs_1l_1g)$, de l'hydrate-D du sulfure de deutérium, on a trouvé une formule $D_2S{\cdot}6{,}115D_2O$ avec une erreur standard de $0{,}018D_2O$ alors que pour le point quadruple supérieur à 30,770°C, $Q(hl_1l_2g)$, on a trouvé une formule $D_2S{\cdot}5{,}840D_2O$ avec une erreur standard de $0{,}019D_2O$.

Mots clés : clathrate, hydrate-D du sulfure de deutérium, formule, thermodynamique, constante de dissociation, enthalpie standard, changement de capacité calorifique.

[Traduit par la Rédaction]

Introduction

As part of our continuing study (1–4) of the thermodynamic properties of aqueous nonelectrolyte solutions and of their clathrate hydrate solid solutions, it became of interest in 1963 to compare the thermodynamic properties of nonelectrolyte solutions in deuterium oxide with their clathrate D-hydrate solid solutions. At that time the properties of aqueous hydrogen sulfide solutions (5, 6) and of the hydrogen sulfide gas hydrate (7–11) were well known, but the properties of deuterium sulfide solutions in deuterium oxide and of the deuterium sulfide D-hydrate had not been reported in the literature.

The volumetric properties of deuterium sulfide and its solubility in deuterium oxide were reported earlier (12, 13). Additional equilibrium measurements on the two-component

Accepted October 14, 1999.

C.W. Clarke and D.N. Glew.[1] Exploratory Research Laboratory, Dow Chemical Canada Inc., Sarnia, ON N7T 7M1, Canada.

[1]Author to whom correspondence may be addressed at 536 Highbury Park, Sarnia, ON N7V 2J9, Canada. Telephone: (519) 337-3136.

© 2000 NRC Canada

deuterium oxide (c_1) – deuterium sulfide (c_2) system up to 33.003°C were reported recently (14). In that work proper representation of the deuterium sulfide D-hydrate dissociation pressure $P(hl_1g)$ between 2.798 and 30.666°C required a seven-parameter equation, which requirement was primarily responsible for our development (15) of a general method for evaluation of thermodynamic functions from equilibrium constants.

In this report we develop a classical thermodynamic treatment for the dissociation with temperature of a deuterium sulfide D-hydrate of variable composition along its univariant (hl_1g) three-phase equilibrium line. It is shown that when the D-hydrate formula number n is known at the temperature of the lower quadruple point $Q(hs_1l_1g)$, approximate values of $n = r$ at higher temperatures may be estimated with good accuracy and small error up to the upper quadruple point $Q(hl_1l_2g)$.

In this work we evaluate further the (hl_1g) measurements, recently reported in Tables 2 and 5 of ref. 14: the results are presented in Tables 1 and 2. Regression equations are evaluated using the method of weighted least squares, and a predicted estimate is qualified with standard error, written SE.

Derivation of the thermodynamic equations

Dissociation equilibrium of deuterium sulfide D-hydrate into deuterium sulfide gas and deuterium oxide liquid

Consider the three-phase (hl_1g) equilibrium of solid deuterium sulfide D-hydrate (h) with gaseous deuterium sulfide (g) and liquid deuterium oxide (l_1) formally represented by the equation

[1] $D_2S{\cdot}nD_2O\ (h) \leftrightarrows D_2S\ (g) + nD_2O\ (l_1)$

$G_2^h\ nG_1^h \qquad G_2^g \qquad nG_1^{l1}$

$a_2^h\ a_1^h \qquad f_2 \qquad a_1^{l1}$

which defines the transfer of 1 mol (gram molar mass) of deuterium sulfide from the D-hydrate into the gas phase, with equilibrium molar Gibbs' energies G_2^h, nG_1^h, G_2^g, and nG_1^{l1}, equilibrium activities a_2^h, a_1^h, f_2, and a_1^{l1}, and dissociation equilibrium constant defined by

[2] $Kp(h{\rightarrow}l_1g) = f_2{\cdot}(1/a_2^h){\cdot}\ (a_1^{l1}/a_1^h)^n$

where the formula number n varies with temperature. The molar Gibbs' energies and activities are defined in eqs. [3]–[6]:

[3] $G_2^h = G_2^{oh} + RT \ln a_2^h = G_2^{oh}$

[4] $G_1^h = G_1^{oh} + RT \ln a_1^h = G_1^{oh} + [P(hl_1g) - 0.10](V^h/46)$

[5] $G_2^g = G_2^{og} + RT \ln f_2$

[6a] $G_1^{l1} = G_1^{ol1} + RT \ln a_1^{l1}$

[6b] $G_1^{l1} = G_1^{ol1} + RT \ln x_1^{l1} + [P(hl_1g) - 0.10]V_1^{l1}$

G_2^{oh} is the standard molar Gibbs' energy of deuterium sulfide encaged within the D-hydrate lattice at 0.10 MPa pressure with activity a_2^h defined as unity. The effect of pressure on G_2^h for the encaged hydrate-former is included within V^h in eq. [4]. G_1^{oh} and G_1^{ol1} are the standard molar Gibbs' energies of deuterium oxide in the D-hydrate lattice and in pure l_1 at 0.10 MPa pressure. G_2^{og} is the standard molar Gibbs' energy of gaseous deuterium sulfide at 1.0 MPa fugacity.

The deuterium sulfide D-hydrate molar volume V^h for a unit cell containing $46/n$ mol D_2S and 46 mol D_2O is taken to be invariant 1.0458 dm^3, assuming the same cubic Structure I lattice and 1.202 nm spacing reported for hydrogen sulfide hydrate (11, 16). The molar volume of the deuterium sulfide encaged within the D-hydrate lattice is already included within the unit-cell volume. The molar volume V_1^{l1} of our deuterium oxide sample (17) at 0.10 MPa is evaluated from the work of Kell (18).

For dissociation reaction [1] at equilibrium, at constant T and total pressure $P(hl_1g)$, the molar Gibbs' energy change, denoted $\Delta G(h{\rightarrow}l_1g)$, is zero and is given by

[7] $\Delta G(h{\rightarrow}l_1g) = 0 = G_2^g + nG_1^{l1} - G_2^h - nG_1^h$

Substitution of eqs.[3]–[6] into eq.[7] yields the basic relations

[8] $-\Delta G°(h{\rightarrow}l_1g) = -(G_2^{og} + nG_1^{ol1} - G_2^{oh} - nG_1^{oh})$

[8a] $= RT \ln Kp(h{\rightarrow}l_1g)$

[8b] $= RT \ln f_2 + nRT \ln a_1^{l1} - nRT \ln a_1^h$

[8c] $= RT \ln f_2 + nRT \ln x_1^{l1} + n[P(hl_1g) - 0.10][V_1^{l1} - (V^h/46)]$

connecting $\Delta G°(h{\rightarrow}l_1g)$, the standard molar Gibbs' energy change for reaction [1], with the dissociation equilibrium constant, the equilibrium phase activities and the volumetric properties of the phases. Rearrangement of eq. [8] and division by RT gives

[9] $\ln Kp(h{\rightarrow}l_1g) = \ln f_2 + n \ln x_1^{l1} + n[P(hl_1g) - 0.10][V_1^{l1} - (V^h/46)]/RT$

which defines $\ln Kp(h{\rightarrow}l_1g)$, the equilibrium constant for D-hydrate dissociation at temperature T K, in terms of the deuterium sulfide fugacity f_2 with corrections (*i*) for the deuterium oxide mole fraction of phase l_1 and (*ii*) for the effect of pressure on the phases h and l_1. To evaluate these corrections n must be known.

Dissociation equilibrium of deuterium sulfide D-hydrate into deuterium sulfide gas and D-ice

Consider the three-phase (hs_1g) equilibrium formally represented by

[10] $D_2S{\cdot}nD_2O\ (h) \leftrightarrows D_2S\ (g) + nD_2O\ (s_1)$

$G_2^h\ nG_1^h \qquad G_2^g \qquad nG_1^{s1}$

$a_2^h\ a_1^h \qquad f_2 \qquad a_1^{s1}$

at constant T and total pressure $P(hs_1g)$ for dissociation of deuterium sulfide D-hydrate into deuterium sulfide gas (g) and solid D-ice (s_1). Using a treatment similar to that following eq. [1], we define the dissociation equilibrium constant

[11] $Kp(h{\rightarrow}s_1g) = f_2{\cdot}(1/a_2^h){\cdot}(a_1^{s1}/a_1^h)^n$

© 2000 NRC Canada

Table 1. Equilibrium constants for dissociation of deuterium sulfide D-hydrate.

			$Kp(h \rightarrow l_1 g)$			
Temperature (°C)	Gauge	$w^{1/2}$	Observed (MPa)	Calculated (MPa)	Difference (%)	Error on calculated *Kp* (%)
30.770[a]	—	—	—	1.5731	—	0.022
30.666	500	0.195	1.5608	1.5587	0.133	0.022
30.462	500	0.4	1.5316	1.5305	0.073	0.021
29.940	500	0.4	1.4620	1.4610	0.070	0.018
29.883	500	0.4	1.4550	1.4536	0.100	0.018
29.375	500	0.4	1.3897	1.3891	0.044	0.016
28.945	500	0.4	1.3363	1.3366	–0.023	0.014
28.932	500	0.4	1.3347	1.3351	–0.027	0.014
28.378	500	0.4	1.2701	1.2704	–0.021	0.013
27.967	500	0.4	1.2241	1.2242	–0.006	0.012
27.967	500	0.169	1.2232	1.2242	–0.083	0.012
27.957	500	0.4	1.2227	1.2231	–0.034	0.012
26.985	500	0.192	1.1198	1.1205	–0.070	0.011
26.869	200	0.5	1.1084	1.1089	–0.045	0.011
26.845	200	0.5	1.1058	1.1065	–0.063	0.011
25.873	200	0.5	1.0128	1.0133	–0.041	0.011
25.853	500	0.115	1.0103	1.0114	–0.115	0.011
25.000	500	0.4	0.9354	0.9359	–0.056	0.011
24.879	200	0.5	0.9252	0.9256	–0.043	0.011
24.862	500	0.088	0.9228	0.9242	–0.156	0.011
23.997	200	0.5	0.8538	0.8540	–0.033	0.012
23.003	200	0.5	0.7795	0.7796	–0.018	0.012
21.961	200	0.5	0.7084	0.7083	0.012	0.012
20.980	200	0.5	0.6469	0.6469	0.010	0.012
19.971	200	0.5	0.5892	0.5890	0.030	0.012
18.981	200	0.5	0.5372	0.5370	0.029	0.012
17.972	200	0.5	0.4888	0.4886	0.032	0.012
16.972	200	0.5	0.4448	0.4447	0.024	0.012
15.968	200	0.5	0.4046	0.4044	0.032	0.011
14.987	200	0.409	0.3687	0.3684	0.073	0.011
13.963	200	0.331	0.3344	0.3341	0.064	0.011
13.383	200	0.294	0.3163	0.3161	0.065	0.012
12.975	200	0.271	0.3042	0.3039	0.080	0.012
12.381	200	0.240	0.2873	0.2871	0.089	0.012
11.980	200	0.221	0.2764	0.2762	0.078	0.012
11.379	200	0.122	0.2609	0.2606	0.126	0.012
10.983	200	0.085	0.2512	0.2508	0.173	0.012
9.977	200	0.078	0.2278	0.2274	0.184	0.012
9.144	200	0.054	0.2099	0.2096	0.155	0.012
7.998	200	0.04	0.18758	0.18731	0.142	0.011
7.997	200	0.04	0.18765	0.18730	0.191	0.011
7.961	16	1	0.18667	0.18663	0.018	0.011
6.993	200	0.04	0.16990	0.16964	0.153	0.010
6.974	16	1	0.16928	0.16932	–0.027	0.010
5.936	200	0.04	0.15307	0.15276	0.203	0.008
5.895	16	1	0.15207	0.15213	–0.040	0.008
5.068	200	0.04	0.14034	0.14009	0.175	0.007
5.014	16	1	0.13926	0.13934	–0.060	0.007
4.032	200	0.04	0.12649	0.12630	0.148	0.005
3.987	16	1	0.12572	0.12573	–0.011	0.005
3.485	16	1	0.11952	0.11953	–0.016	0.006
3.392[b]	16	1	0.11842	0.11842	–0.000	0.006
3.383	16	1	0.11832	0.11831	0.002	0.006
3.284	16	1	0.11715	0.11714	0.004	0.006
3.190	16	1	0.11605	0.11604	0.011	0.006
3.097	16	1	0.11497	0.11496	0.015	0.007

© 2000 NRC Canada

Table 1 (*concluded*).

			$Kp(h \rightarrow l_1g)$			
Temperature (°C)	Gauge	$w^{1/2}$	Observed (MPa)	Calculated (MPa)	Difference (%)	Error on calculated *Kp* (%)
2.998	16	1	0.11384	0.11381	0.021	0.007
2.895	16	1	0.11266	0.11264	0.016	0.007
2.798	16	1	0.11157	0.11154	0.024	0.007

[a]Upper quadruple point.
[b]Lower quadruple point.

Table 2. Standard enthalpy and heat capacity changes for dissociation and the formula of deuterium sulfide D-hydrate.

Temperature (°C)	$\Delta H^{ot}(h \rightarrow l_1g)$ (J/mol)		$\Delta Cp^{ot}(h \rightarrow l_1g)$ (J $mol^{-1}deg^{-1}$)		*r*	SE
30.770[a]	68304	51	174	8	5.840	0.019
30.666	68286	51	174	8	5.840	0.019
30.462	68250	49	174	8	5.841	0.019
29.940	68160	45	173	7	5.844	0.019
29.883	68150	45	173	7	5.844	0.019
29.375	68062	41	172	7	5.847	0.018
28.945	67989	38	172	7	5.849	0.018
28.932	67986	38	172	7	5.849	0.018
28.378	67891	35	171	7	5.852	0.018
27.967	67821	32	170	6	5.854	0.018
27.967	67821	32	170	6	5.854	0.018
27.957	67820	32	170	6	5.854	0.018
26.985	67655	27	169	6	5.860	0.018
26.869	67635	26	169	6	5.860	0.018
26.845	67631	26	169	6	5.860	0.018
25.873	67468	21	168	5	5.866	0.017
25.853	67464	21	168	5	5.866	0.017
25.000	67322	17	166	5	5.872	0.017
24.879	67302	17	166	5	5.873	0.017
24.862	67299	17	166	5	5.873	0.017
23.997	67156	14	165	4	5.879	0.017
23.003	66992	11	164	4	5.886	0.017
21.961	66822	10	162	4	5.894	0.017
20.980	66663	10	161	3	5.901	0.017
19.971	66501	10	160	3	5.910	0.017
18.981	66344	11	159	2	5.919	0.017
17.972	66184	12	157	2	5.928	0.017
16.972	66028	12	156	1	5.937	0.017
15.968	65872	13	155	1	5.948	0.017
14.987	65721	12	153	1	5.958	0.017
13.963	65565	12	152	1	5.969	0.017
13.383	65476	12	151	2	5.976	0.017
12.975	65415	11	151	2	5.980	0.017
12.381	65326	11	150	2	5.987	0.017
11.980	65266	10	149	2	5.992	0.017
11.379	65176	9	149	2	5.999	0.017
10.983	65117	9	148	3	6.004	0.017
9.977	64969	8	147	3	6.017	0.017
9.144	64847	8	146	3	6.028	0.017
7.998	64681	9	144	4	6.044	0.017
7.997	64681	9	144	4	6.044	0.017
7.961	64676	9	144	4	6.045	0.017
6.993	64537	12	143	4	6.059	0.017
6.974	64534	12	143	4	6.059	0.017
5.936	64386	16	142	5	6.074	0.017
5.895	64381	16	141	5	6.075	0.017
5.068	64264	19	140	5	6.088	0.017

© 2000 NRC Canada

Table 2 (*concluded*).

Temperature (°C)	$\Delta H^{ot}(h\rightarrow l_1g)$ (J/mol)		$\Delta Cp^{ot}(h\rightarrow l_1g)$ (J mol^{-1}deg^{-1})		r	SE
5.014	64256	20	140	5	6.089	0.017
4.032	64119	25	139	6	6.104	0.018
3.987	64113	25	139	6	6.105	0.018
3.485	64043	28	138	6	6.113	0.018
3.392[b]	64031	28	138	6	6.115	0.018
3.383	64029	28	138	6	6.115	0.018
3.284	64016	29	138	6	6.117	0.018
3.190	64003	30	138	6	6.118	0.018
3.097	63990	30	138	6	6.120	0.018
2.998	63976	31	138	6	6.121	0.018
2.895	63962	31	138	6	6.123	0.018
2.798	63949	32	137	6	6.125	0.018

[a]Upper quadruple point.

[b]Lower quadruple point.

for the transfer of 1 mol of deuterium sulfide from the D-hydrate into the gas phase together with the collapse of the D-hydrate lattice nD$_2$O (h) to form nD$_2$O (s$_1$) of D-ice. The equilibrium molar Gibbs' energy of D-ice is defined by

$$[12]\quad G_1^{s1} = G_1^{os1} + RT \ln a_1^{s1} = G_1^{os1} + [P(hs_1g) - 0.10]V_1^{s1}$$

in which a_1^{s1} is its equilibrium activity, V_1^{s1} its molar volume, and G_1^{os1} its standard molar Gibbs' energy at 0.10 MPa pressure.

Similarly following eq. [8], we obtain

$$[13]\quad -\Delta G°(h\rightarrow s_1g) = -(G_2^{og} + nG_1^{os1} - G_2^{oh} - nG_1^{oh})$$

$$[13a]\quad = RT \ln Kp(h\rightarrow s_1g)$$

$$[13b]\quad = RT \ln f_2 + nRT \ln a_1^{s1} - nRT \ln a_1^{h}$$

$$[13c]\quad = RT \ln f_2 + n[P(hs_1g) - 0.l0][V_l^{s1} - (V^h/46)]$$

connecting $\Delta G°(h\rightarrow s_1g)$, the standard change of molar Gibbs' energy for reaction [10], with the dissociation equilibrium constant, the equilibrium phase activities and the volumetric properties of the phases. Rearrangement of eq. [13] and division by RT gives

$$[14]\quad \ln Kp(h\rightarrow s_1g) = \ln f_2 + n[P(hs_1g) - 0.10][V_1^{s1} - (V^h/46)]/RT$$

which defines ln $Kp(h\rightarrow s_1g)$, the equilibrium constant for D-hydrate dissociation at temperature T K into D-ice, in terms of the deuterium sulfide fugacity f_2 with corrections for the effect of pressure on the solid phases h and s$_1$. To evaluate these corrections n must be known.

Results and discussion

Standard enthalpy change for dissociation of deuterium sulfide D-hydrate into deuterium sulfide gas and D-ice

Because we have no measurements for the temperature dependence of $P(hs_1g)$ for the deuterium sulfide D-hydrate equilibrium with D-ice, a method has been devised to evaluate the missing data as a small perturbation on the equilibrium $P(hs_1g)$ measurements for hydrogen sulfide hydrate with ice by Scheffer and Meyer (9).

Six experimental studies of the (hs_1g) equilibrium, namely, (*i*) hydrogen sulfide hydrate with ice from –26 to –l°C (9), (*ii*) bromochlorodifluoromethane hydrate with ice from –20 to –0.3°C (2), (*iii*) two cyclopropane hydrates with ice from –36 to –9°C and from –15 to –l°C (19), and (*iv*) two cyclopropane D-hydrates with D-ice from –63 to –10°C and from –30 to 0°C (20), all show that the derived standard dissociation enthalpy changes, $\Delta H^{ot}(h\rightarrow s_1g)$, are sensibly temperature invariant, with the standard heat capacity changes $\Delta Cp^{ot}(h\rightarrow s_1g)$ equal to zero within experimental error. This zero standard heat capacity change value is assumed for the similar equilibrium of deuterium sulfide D-hydrate with D-ice.

Comparison of the cyclopropane hydrates (19) with their D-hydrates (20) shows that values for the standard dissociation enthalpy change $\Delta H^{ot}(h\rightarrow s_1g)$ are slightly larger for the D-hydrates: for the Structure I D-hydrate the difference is 1.0% with SE 0.5%, for Structure II the difference is 0.2% with SE 1.2%, relative to the hydrates.

The measurements of hydrogen sulfide hydrate with ice (9) down to –21°C have been reevaluated using eq. [14] with n = 6.1, the hydrogen sulfide fugacity f_2 from the Redlich–Kwong equation of state (12, 13, 21, 22), and the molar volumes of hydrate (11, 16) and of ice V_1^{s1} (23). The standard dissociation enthalpy change $\Delta H^{ot}(h\rightarrow s_1g)$ is found to be 25 416 with SE 52 J/mol of hydrogen sulfide, with $\Delta Cp^{ot}(h\rightarrow s_1g)$ insignificantly different from zero. This value of the standard enthalpy change is slightly less than the 25 500 J/mol found by Scheffer and Meyer (9) using partial pressures.

The environmental similarity of aqueous solutes in water at low temperature with hydrate formers within their hydrate water polyhedra has been discussed in ref. 3, where in Table III of that work, similar values have been shown for the enthalpy change $\Delta H_2°(l_1\rightarrow g)$ for solute escape from aqueous solution and for $\Delta H°(h\rightarrow s_1g)$ for hydrate-former solute escape from clathrate hydrate solid solutions. Using that model (3), the enthalpy difference between dissociation of D$_2$S D-hydrate to D-ice and dissociation of H$_2$S hydrate to ice is taken as equal to the molar enthalpy difference for D$_2$S evolution from deuterium oxide solution minus that for H$_2$S

© 2000 NRC Canada

evolution from aqueous solution. Using the solubilities (13), the difference of molar enthalpies for D_2S and H_2S evolution from their solutions is 310 with SE 92 J/mol at the freezing points 3.82 and 0.0°C, respectively, and is 326 with SE 96 J/mol at the quadruple points 3.392 and –0.4°C.

The standard enthalpy difference of $\Delta H^{oq}(h \rightarrow s_1g)$ for the Structure I cyclopropane D-hydrate to D-ice minus that for the Structure I cyclopropane hydrate to ice at their quadruple points (19, 20) is 310 with SE 150 J/mol, in good agreement with the two enthalpy differences from the solubilities.

The mean of the three enthalpy differences, 315 with SE 94 J/mol, is added to the standard enthalpy change for hydrogen sulfide hydrate dissociation to ice, 25 416 with SE 52 J/mol, to give the standard enthalpy change for dissociation of deuterium sulfide D-hydrate to D-ice $\Delta H^{oq}(h \rightarrow s_1g)$, 25 732 with SE 108 J/mol, at 3.392°C.

Formula of deuterium sulfide D-hydrate at lower quadruple point $Q(hs_1l_1g)$

The formula of deuterium sulfide D-hydrate is evaluated by the method of Scheffer and Meyer (9) who first derived the thermochemical identity eq. [15] for n

$$[15] \quad \Delta H^{oq}(\, h \rightarrow l_1g) - \Delta H^{oq}\,(h \rightarrow s_1g) = n\, \Delta H^{oq}(s_1 \rightarrow l_1)$$

which is exact at the quadruple point $Q(hs_1l_1g)$, with the equilibrium standard enthalpy changes denoted by superscript q. Substitution into eq. [15], of 64 031 with SE 28 J/mol D_2S for ΔH^{oq} $(h \rightarrow l_1g)$, of 25 732 with SE 108 J/mol D_2S for $\Delta H^{oq}(h \rightarrow s_1g)$, and of 6263 with SE 13 J/mol D_2O for $\Delta H^{oq}(s_1 \rightarrow l_1)$ evaluated from Long and Kemp (24), yields n = 6.115 with SE 0.018 for the deuterium sulfide D-hydrate formula at 3.392°C.

Using this method, which they had developed for the purpose, Scheffer and Meyer (9) determined n = 6.06 for the formula of hydrogen sulfide hydrate at the quadruple point –0.4°C: later reevaluation (10) of the same data (9), using only the four most accurate (hl_1g) measurements, confirmed n = 6.06 with error 0.13.

The formula $D_2S{\cdot}6.115D_2O$ of deuterium sulfide D-hydrate at its quadruple point $Q(hs_1l_1g)$ is significantly larger by three standard errors than the $H_2S{\cdot}6.06H_2O$ found for hydrogen sulfide hydrate at its quadruple point (9, 10). Our formula is well within the error range $H_2S{\cdot}6.19H_2O$ and $H_2S{\cdot}5.93H_2O$ indicated for the hydrate by Korvezee and Scheffer (10).

Formula of deuterium sulfide D-hydrate at temperatures different from the lower quadruple point

We now extend eq. [15], valid at $Q(hs_1l_1g)$, for more general use at temperature t°C to evaluate an approximate formula number, defined as r, using the thermochemical identity [16]

$$[16] \quad \Delta H^{ot}(h \rightarrow l_1g) - \Delta H^{ot}(h \rightarrow s_1g) = r\, \Delta H^{ot}(s_1 \rightarrow l_1)$$

in which superscript t in eq. [16] has replaced q in eq. [15]. Values of $\Delta H^{ot}(h \rightarrow s_1g)$ and ΔH^{ot} $(s_1 \rightarrow l_1)$ at temperature t are equal to their values at the quadruple point plus the integral of their heat capacities from the quadruple point.

The first term in eq. [16] is from measurements of this work. Assumption 1 is that the second term $\Delta H^{ot}(h \rightarrow s_1g)$ is temperature invariant (2, 9, 19, 20) and is 25 732 with SE 108 J/mol D_2S, the same as $\Delta H^{oq}(h \rightarrow s_1g)$ in eq. [15]. Assumption 2 is that the final term in eq. [16] is the standard molar enthalpy change for fusion of D-ice D_2O (s_1) into liquid D_2O (l_1) at t°C. This can be evaluated using the Taylor's series expansion

$$\begin{aligned}[17] \quad \Delta H^{ot}(s_1 \rightarrow l_1) &= \Delta H^{oo}(s_1 \rightarrow l_1) \\ &+ \Delta Cp^{oo}(s_1 \rightarrow l_1){\cdot}(t - 3.82) \\ &+ d\Delta Cp^{oo}(s_1 \rightarrow l_1)/dt{\cdot}(1/2){\cdot}(t - 3.82)^2 \\ &+ d^2\Delta Cp^{oo}(s_1 \rightarrow l_1)/dt^2{\cdot}(1/6){\cdot}(t - 3.82)^3\end{aligned}$$

about the normal freezing point 3.82°C, with $\Delta H^{oo}(s_1 \rightarrow l_1)$ = 6280 J/mol (24). The standard molar heat capacity change and its temperature derivatives for fusion are evaluated at 3.82°C using (*i*) the heat capacities of D-ice between –74 and –2.6°C by Long and Kemp (24) and (*ii*) the tabulated heat capacities of liquid deuterium oxide between 20 and 100°C (25).

Method for evaluation of formula number r and dissociation equilibrium constant of deuterium sulfide D-hydrate

The phase rule requires that the equilibrium deuterium oxide – deuterium sulfide, two-component, three-phase, (hl_1g) system is univariant and that the intensive properties of each of the equilibrium phases are continuous functions of temperature along the (hl_1g) equilibrium line. In particular, the equilibrium hydrate composition and its component D_2O/D_2S mole ratio n are continuous functions of temperature only.

A method is now presented to evaluate the approximate formula number r for the D-hydrate $D_2S{\cdot}rD_2O$ and its dissociation equilibrium constant $Kp(h \rightarrow l_1g)$ at each experimental temperature on the univariant (hl_1g) equilibrium line, from 2.798°C just below the lower quadruple point $Q(hs_1l_1g)$ up to 30.666°C just below the upper quadruple point $Q(hl_1l_2g)$.

The convergence of the method to a stable solution depends on the temperature continuity of the intensive properties of the three equilibrium phases, in particular, that the approximate hydrate formula number r is a continuous function of temperature. Initially we assume that $n = r = 6.0$ in eq. [9] for all measurements, giving a first approximation for the logarithm of the equilibrium constant, abbreviated to ln Kp(lst). The ln Kp(lst) values are fitted as a proper function of temperature (15) by the method of weighted least squares (26) to yield the best thermodynamic equation of the form

$$[18] \quad \ln Kp(h \rightarrow l_1g) = b0 + b1{\cdot}u1 + b2{\cdot}u2 + b3{\cdot}u3$$

which is mathematically equivalent to

$$[18a] \quad \ln Kp(h \rightarrow l_1g) = A + B/T + C \ln T + DT$$

and contains the maximum number of significant parameters. These measurements require three temperature variables ($u1$, $u2$, $u3$) with $x = (T - 298.16)/298.15$, and define (15) the four thermodynamic function parameters ($b0$, $b1$, $b2$, $b3$) and their errors at 298.15 K. Derived from ($b1$, $b2$, $b3$) of eq. [18], the first approximation standard enthalpy changes $\Delta H^{ot}(h \rightarrow l_1g)$, abbreviated to ΔH(1st), for each

© 2000 NRC Canada

measurement at its temperature t are substituted into eq. [16], to give a first approximation formula number r(lst).

The values of r(1st) are substituted for n in eq. [9] for each measurement to provide a second approximation for the logarithm of the equilibrium constant ln Kp(2nd); the ln Kp(2nd) values are refitted by eq. [18], thence to obtain second approximation ΔH(2nd) values; these are substituted for $\Delta H^{ot}(h \rightarrow l_1g)$ in eq. [16] to give r(2nd) values which are recycled for n in eq. [9], and so on. Iterations for 35 cycles give converged values of Kp(h→l_1g) and r which are presented in Tables 1 and 2.

Equilibrium constant for dissociation of deuterium sulfide D-hydrate

Table 1 lists 58 determinations between 30.666 and 2.798°C of the equilibrium constant, $Kp(h \rightarrow l_1g)$ MPa, for dissociation of deuterium sulfide D-hydrate to deuterium sulfide gas and liquid deuterium oxide according to eq. [1] with $n = r$. Quadruple point temperatures are noted. The first row presents estimates extrapolated at 30.770°C, $Q(hl_1l_2g)$. Standard thermodynamic function changes refer to dissociation of one mole of $D_2S \cdot rD_2O$ (h) at 0.10 MPa pressure to form one mole of D_2S (g) at 1.0 MPa fugacity together with r mole of pure D_2O (l_1) at 0.10 MPa pressure.

The second column of Table 1 denotes the pressure gauge used (14), data marked 500, 200, and 16 used the 500, 200, and 16 psi (1 psi = 6.895 kPa) gauges, respectively. The third column gives the square root of the weights used to combine data from the various pressure gauges into a properly weighted least-squares regression of the logarithm of $Kp(h \rightarrow l_1g)$ as a function of temperature.

The fourth column lists $Kp(h \rightarrow l_1g)$ observed, the fifth gives $Kp(h \rightarrow l_1g)$ calculated from the converged best eq. [18]. The percentage differences between observed and calculated equilibrium constants, shown in the sixth column, give an overall SE of 0. 020% for a single determination of unit weight with 54 degrees of freedom. The seventh column shows the percentage error on the equilibrium constant estimated from the weighted regression model eq. [18].

Weights used in this work are derived from those used earlier for the representation of ln $P(hl_1g)$ as a function of temperature (14). However, here more measurements are assigned lower weights to reduce possible bias and to enable smoother transitions between the measurement ranges of the three pressure gauges. The 14 measurements at low pressure using the 16 psi gauge are by far the most accurate and these are assigned unit weight. In the region of overlap of the 16 psi gauge by the 200 psi gauge, the low weights, $w^{1/2} = 0.04$, are assigned to the low-pressure measurements using the 200 psi gauge in order to reduce possible bias of the regression equation by these less accurate measurements. At higher pressures the 13 measurements using the 200 psi gauge are assigned weights, $w^{1/2} = 0.5$, the same as in ref. 14. In the region of overlap of the 200 psi gauge by the 500 psi gauge, lower weights are assigned to the conflicting measurements using the 500 psi gauge. At high pressures the 10 measurements using the 500 psi gauge are assigned weights, $w^{1/2} = 0.4$, the same as in ref. 14. The five measurements using the 500 psi gauge with the lower weights, $w^{1/2} = 0.088$, 0.115, 0.192, 0.169, and 0.195 all showed differences of $Kp(h \rightarrow l_1g)$ of greater than five standard errors: the weights assigned are the inverse of the differences in standard errors, namely the inverse of the differences of 11.4, 8.7, 5.2, 5.9, and 5.1 standard errors, respectively.

The 14 residuals from measurements using the 16 psi gauge indicate a SE of 0.025%, the 13 residuals with weight, $w^{1/2} = 0.5$, from the 200 psi gauge indicate a SE of 0.036%, and the 10 residuals with weight, $w^{1/2} = 0.4$, from the 500 psi gauge indicate a SE of 0.054%. Comparison of these SE estimates for $Kp(h \rightarrow l_1g)$ with the gauge accuracies for pressure measurement (12) shows that (*i*) the data at low pressure are properly represented with SE 0.025% and a 0.020% accuracy of 16 psi gauge calibration, (*ii*) the data at intermediate pressure with SE 0.036% are comparable with the 0.030% accuracy of 200 psi gauge calibration, and (*iii*) the high-pressure data with SE 0.054% are about twice as variable as the 0.030% accuracy of 500 psi gauge calibration. These SE estimates from the four-parameter model are approximately double those indicated by the seven-parameter model for the D-hydrate pressures in ref. 14.

The four parameters of the converged eq. [18] with their (SE) are $b0 = -0.0662\ 35$ (0.000 11), $b1 = 27.1578$ (0.0070), $b2 = 20.0170$ (0.60), $b3 = 23.4281$ (9.0). We note that the deuterium sulfide D-hydrate equilibrium constants properly define three enthalpy parameters $b1–b3$ at 25°C, that these parameters are all positive with no alternation of sign, and that the value of the least significant parameter $b3$ could arise by pure chance at a probability level of about 1.3%.

By contrast, eq. [18] with four parameters is totally inadequate to represent the weighted ln $P(hl_1g)$ measurements as an accurate function of temperature, where the lack of fit indicates an eight-times enhanced SE of 0.16% for a point of unit weight, compared with SE 0.020% for the similarly weighted ln $Kp(h \rightarrow l_1g)$.

Approximate formula number r for deuterium sulfide D-hydrate

Table 2 presents estimates and SEs for the standard enthalpy change $\Delta H^{ot}(h \rightarrow l_1g)$, the standard heat capacity change $\Delta Cp^{ot}(h \rightarrow l_1g)$, and the approximate formula number $n = r$ for dissociation of deuterium sulfide D-hydrate according to eq. [1]. We note that the results listed in Tables 1 and 2 are biased estimates, except for those given at the lower quadruple point $Q(hs_1l_1g)$ 3.392°C, where eq. [16] is exact and the estimates of $Kp(h \rightarrow l_1g)$, $\Delta H^{oq}(h \rightarrow l_1g)$, $\Delta Cp^{oq}(h \rightarrow l_1g)$, and of $n = r$ are true and unbiased.

Bias 1 arises from assumption 1, because it is assumed in eq. [16] that $\Delta H^{ot}(h \rightarrow s_1g)$ is temperature-invariant with $\Delta Cp^{ot}(h \rightarrow s_1g) = 0$ over the extrapolated temperature range 2.798 to 30.666°C, where it is possible that the standard heat capacity change may have a small negative value. This bias is assessed using the datum $\Delta Cp^{ot}(h \rightarrow s_1g) = -8.0$ with SE 24 J mol^{-1}deg^{-1}, found but not significant for hydrogen sulfide hydrate with ice (9). Evaluation at 30.666°C, using eq. [16] with $\Delta H^{oq}(h \rightarrow s_1g) = 25\,732$ J/mol and a constant $\Delta Cp^{ot}(h \rightarrow s_1g) = -8.0$ J mol^{-1}deg^{-1}, gives $r = 5.863$ with SE 0.040: a result in good agreement with, and not significantly different from, the 5.840 with SE 0.019 listed in Table 2.

Bias 2 arises from assumption 2, because it is assumed in eq. [16] that $\Delta H^{ot}(s_1 \rightarrow l_1)$ is given by the Taylor's series eq. [17] over the extrapolated temperature range 2.798 – 30.666°C. Classical error theory (26) shows that the SE on

© 2000 NRC Canada

r at 30.666°C, due to errors on the Taylor's series parameters of eq. [17], is less than 0.0005 and is not significant.

The SE's on the standard enthalpy changes for *r* at 30.666°C are, 51 J/mol on $\Delta H^{ot}(h \rightarrow l_1 g)$, 108 J/mol on $\Delta H^{oq}(h \rightarrow s_1 g)$, and 15 J/mol on $\Delta H^{ot}(s_1 \rightarrow l_1)$, showing that the major contribution to the SE on *r* is always the SE on the estimate of $\Delta H^{oq}(h \rightarrow s_1 g)$.

In Table 2 it is shown that the value of *r* decreases monotonously with increasing temperature and asymptotically approaches its theoretical lower limit of 5.75, for a Structure I hydrate (11, 16), at a temperature above the quadruple point $Q(hl_1l_2g)$ at 30.770°C.

This means a continuous increase with temperature in the number of D_2S hydrate-former molecules per unit cell of $46D_2O$, from 7.510 with SE 0.022 at 2.798°C to about 7.875 with SE 0.025 at 30.666°C, asymptotically trending towards an upper limit of 8.0 (11, 16) above 30.770°C.

This proves that an increased fraction of cavities must be occupied by D_2S molecules in order to stabilize the solid D-hydrate lattice against collapse at higher temperatures. Although these numbers may be slightly biased, the overall effect of increasing temperature remains unchanged.

Dissociation of deuterium sulfide D-hydrate at 30.770°C, the quadruple point $Q(hl_1l_2g)$, occurs with 1.54% of empty and 98.46% of occupied cavities with SE 0.32% at the saturation activity of liquid D_2S (l_2). This fits in well with the work on hydrogen sulfide hydrate by Scheffer (8), who showed that hydrostatic pressure increased the temperature for hydrogen sulfide hydrate stability above $Q(hl_1l_2g)$ along the (hl_1l_2) three-phase line, where presumably empty cavities within the hydrate lattice were progressively being filled with additional H_2S at the higher pressures and temperatures.

We attempt to justify the use of the temperature invariant $\Delta H^{oq}(h \rightarrow s_1 g) = 25\,732$ J/mol for the hypothetical $\Delta H^{ot}(h \rightarrow s_1 g)$ above the quadruple point $Q(hs_1l_1g)$ at high temperatures where D-ice (s_1) is metastable with D-water (l_1). The major problem is resolved if it is justifiable to extrapolate the experimental heat capacities of D-ice between –74 and +3.82°C (24) using eq. [17] to provide valid heat capacities for metastable D-ice between 3.82 and 30.770°C. Applying classical error theory (26) to the D-ice measurements (24) shows that the SE on the standard enthalpy of D-ice at 30.666°C is 2.3 J/mol larger than the SE at 3.82°C. This error for extrapolation to 30.666°C is negligible compared with the SE of 0.2% or 13 J/mol, given by the authors (24), on the standard enthalpy for fusion of D-ice at 3.82°C. Thus, the use of eq. [17] is proven valid up to 30.666°C.

A minor problem is justification of extrapolation of $\Delta H^{oq}(h \rightarrow s_1 g)$, derived from measurements between –21 and 3.392°C (9, 14), to higher temperatures above the quadruple point $Q(hs_1l_1g)$. The low temperature measurements (9) show that $\Delta Cp^{ot}(h \rightarrow s_1 g)$ is zero within experimental error, with a non significant value of –8.0 with SE 24 J $mol^{-1}deg^{-1}$. It thus appears reasonable to assume that $\Delta Cp^{ot}(h \rightarrow s_1 g)$ is not significantly different from zero at higher temperatures, so that $\Delta H^{ot}(h \rightarrow s_1 g)$ is temperature invariant and is equal to $\Delta H^{oq}(h \rightarrow s_1 g)$. This means that up to 30.666°C the standard molar heat capacity of deuterium sulfide D-hydrate $D_2S \cdot rD_2O$ (h) is not significantly different from the standard molar heat capacity of deuterium sulfide gas plus the standard molar heat capacity of *r* moles of D-ice. This approximation seems reasonable in the absence of heat capacity data for deuterium sulfide D-hydrate.

Let us now assess internal evidence from the present measurements in an attempt to justify the use of a temperature invariant $\Delta H^{ot}(h \rightarrow s_1 g)$ between 2.798 and 30.666°C. Within the temperature range between 2.798 and 30.666°C, respectively, between 93.74% (7.510/8 = 1/1.0652) and 98.46% (7.877/8 = 1/1.0156), of the D-hydrate cavities are occupied by deuterium sulfide: over such a relatively small range of D-hydrate composition, $\Delta H^{ot}(h \rightarrow s_1 g)$, the standard enthalpy change for evaporation of one mole of D_2S hydrate-former from 1.0652 to 1.0156 mol of lattice cavities with the D-hydrate lattice forming D-ice may be expected to vary little. This is because the predominant enthalpy change arises from the evaporation of one mole of condensed deuterium sulfide from within the D-hydrate to form one mole of gaseous deuterium sulfide, and the associated minor enthalpy change arises from the assumed nearly athermal transformation of 6.125 to 5.840 mol of D_2O from solid D-hydrate into solid D-ice. At low temperatures below the quadruple point $Q(hs_1l_1g)$ down to –21°C (9), where the transformation of solid hydrate to solid ice probably involves more than 6.115 mol of H_2O, the derived value of $\Delta H^{ot}(h \rightarrow s_1 g)$ is invariant with temperature and $\Delta Cp^{ot}(h \rightarrow s_1 g)$ is zero within experimental error. Since the extrapolation of $\Delta H^{ot}(h \rightarrow s_1 g)$ above the quadruple point to higher temperatures involves transformation of fewer than 6.115 mol of D_2O solid D-hydrate to form solid D-ice, it appears that the value of $\Delta Cp^{ot}(h \rightarrow s_1 g)$ may be numerically even smaller and nearer to zero, and that $\Delta H^{ot}(h \rightarrow s_1 g)$ remains sensibly invariant with temperature.

The reason that the approximation of eq. [16] appears to work so well at higher temperatures probably depends on the real equality of the standard heat capacity of the D-hydrate $D_2S \cdot rD_2O$ to the sum of the standard heat capacities of one mole of D_2S gas and of *r* moles of D-ice, making $\Delta Cp^{ot}(h \rightarrow s_1 g)$ very near to zero at high temperatures, just as found experimentally (2, 9, 19, 20) at low temperatures. Apparently, large standard heat capacity changes and large biases of *r* away from the true *n* do not occur, even at our highest observed temperature 30.666°C.

In conclusion, the results for deuterium sulfide D-hydrate appear to provide a subsequent justification for the use of eqs. [16] and [17] with their assumptions at all temperatures along the (hl_1g) equilibrium line, to give estimates which are exact for $r = n$ at the lower quadruple point $Q(hs_1l_1g)$, and which are apparently a good approximation at higher temperatures up to the upper quadruple point $Q(hl_1l_2g)$.

References

1. D.N. Glew and E.A. Moelwyn-Hughes. Disc. Faraday Soc. **50**, 150 (1953).
2. D.N. Glew. Can. J. Chem. **38**, 208 (1960).
3. D.N. Glew. J. Phys. Chem. **66**, 605 (1962).
4. D.N. Glew, H.D. Mak, and N.S. Rath. *In* Hydrogen-bonded solvent systems. *Edited by* A.K. Covington and P. Jones. Taylor and Francis Ltd., London. 1968. p. 195.
5. R.H. Wright and O. Maass. Can. J. Res. **6B**, 94 (1932).
6. F.T. Selleck, L.T. Carmichael, and B.H. Sage. Ind. Eng. Chem. **44**, 2219 (1952).

© 2000 NRC Canada

7. R. de Forcrand and P. Villard. Compt. Rend. **106**, 849 (1888).
8. F.E.C. Scheffer. Proc. R. Acad. Sci. Amsterdam, **13**, 829 (1911).
9. F.E.C. Scheffer and G.Meyer. Proc. R. Acad. Sci. Amsterdam, **21**, 1204, (1919); **21**, 1338 (1919).
10. A.E. Korvezee and F.E.C. Scheffer. Rec. Trav. Chim. Pays-Bas, **50**, 256 (1931).
11. M.von Stackelberg and W. Jahns. Z. Elektrochem. **58**, 162 (1954).
12. E.C.W. Clarke and D.N. Glew. Can. J. Chem. **48**, 764 (1970).
13. E.C.W. Clarke and D.N. Glew. Can. J. Chem. **49**, 691 (1971).
14. C.W. Clarke and D.N. Glew. Can. J. Chem. **76**, 1119 (1998).
15. E.C.W. Clarke and D.N. Glew. Trans. Faraday Soc. **62**, 539 (1966).
16. D.W. Davidson. *In* Water: a comprehensive treatise. Vol. 2. *Edited by* F. Franks. Plenum Press, New York. 1973. p. 123.
17. D.N. Glew, H.D. Mak, and N.S. Rath. Can. J. Chem. **45**, 3059 (1967).
18. G.S. Kell. J. Phys. Chem. Ref. Data, **6**, 1109 (1977).
19. D.R. Hafemann and S.L. Miller. J. Phys. Chem. **73**, 1392 (1969).
20. D.R. Hafemann and S.L. Miller. J. Phys. Chem. **73**, 1398 (1969).
21. O. Redlich and J.N.S. Kwong. Chem. Rev. **44**, 233 (1949).
22. R.R. Spear, R.L. Robinson, Jr., and K.C. Chao. Ind. Eng. Chem. Fundam. **8**, 2 (1969).
23. N.E. Dorsey. Properties of ordinary water-substance. Reinhold Publishing Corp., New York. 1940. p. 462.
24. E.A. Long and J.D. Kemp. J. Am. Chem. Soc. **58**, 1829 (1936).
25. N.B. Vargaftik. Handbook of physical properties of liquids and gases. 2nd ed. Hemisphere Publishing Corp., New York. 1983. p. 84.
26. N.R. Draper and H. Smith. Applied regression analysis. 2nd ed. John Wiley & Sons, Inc., New York. 1981.

© 2000 NRC Canada

Synthesis and X-ray structures of amidinate, oxoamidate, and thioamidate complexes of boron

Pierre Blais, Tristram Chivers, Andrew Downard, and Masood Parvez

Abstract: The reactions of $PhBCl_2$ with Li[CE(N^{t}Bu)(^{n}Bu)] or Li[CS(N^{t}Bu)(NH^{t}Bu)] (1:1 molar ratio) in toluene at 23°C produced the heterocycles Ph(Cl)B(μ-N^{t}Bu)(μ-E)C(^{n}Bu) (**1a**, E = N^{t}Bu; **1b**, E = O; **1c**, E = S) or Ph(Cl)B(μ-N^{t}Bu)(μ-S)C(NH^{t}Bu) (**2**), which were characterized by ^{1}H, ^{11}B and ^{13}C NMR and by mass spectra. X-ray structural determinations revealed that **1a**, **1c** and **2** contain four-membered rings. In **2** the thioamidate ligand adopts an *N*,*S* bonding mode. Crystal data: **1a**, monoclinic, space group $P2_1$, a = 8.816(3), b = 11.311(2), c = 10.168(3) Å, β = 98.86(3)°, V = 1001.7(5) Å^3, Z = 2, R = 0.042, and R_w = 0.020; **1c**, monoclinic, space group $P2_1/n$, a = 7.617(2), b = 11.200(1), c = 19.568(2), β = 90.74(2)°, V = 1669.1(5) Å^3, Z = 4, R = 0.046, and R_w = 0.059; **2**, monoclinic, space group $P2_1/a$, a = 11.357(2), b = 12.289(2), c = 12.620(3) Å, β = 95.43(2)°, V = 1753.4(5) Å^3, Z = 4, R = 0.043, and R_w = 0.027.

Key words: boron, amidinate, oxoamidate, thioamidate, X-ray structures.

Résumé : Les réactions entre le $PhBCl_2$ et Li[(CE(N^{t}Bu)(^{n}Bu)] ou Li[CS(N^{t}Bu)(NH^{t}Bu)] (rapport molaire de 1:1), dans le toluène, à 23°C, conduisent à la formation d'hétérocycles Ph(Cl)B(μ-N^{t}Bu)(μ-E)C(^{n}Bu) (**1a**, E = N^{t}Bu; **1b**, E = O; **1c**, E = S) ou Ph(Cl)B(μ-N^{t}Bu)(μ-S)C(NH^{t}Bu) (**2**) que l'on a caractérisés par RMN du ^{1}H, ^{11}B et ^{13}C ainsi que par spectrométrie de masse. La diffraction des rayons appliquée aux produits **1a**, **1c** et **2** révèle qu'ils comportent des cycles à quatre chaînons. Dans le produit **2**, le ligand thioamidate adopte un mode de liaison *N*,*S*. Les données cristallographiques: **1a**, monoclinique, groupe d'espace $P2_1$, a = 8,816(3), b = 11,311(2) et c = 10,168(3)Å, β = 98,86(3)°, V = 1001,7(5)Å^3, Z = 2, R = 0,042 et R_w = 0,020; **1c**, monoclinique, groupe d'espace $P2_1/n$, a = 7,617(2), b = 11,200(1) et c = 19,568(2)Å, β = 90,74(2)°, V = 1669,1(5)Å^3, Z = 4, R = 0,046 et R_w = 0,059 et **2**, monoclinique, groupe d'espace $P2_1/a$, a = 11,357(2), b = 12,289(2) et c = 12,620(3) Å, β = 95,43(2)°, V = 1753,4(5) Å^3, Z = 4, R = 0,043 et R_w = 0,027.

Mots clés : bore, amidinate, oxoamidate, thiamidate, structures, diffraction des rayons X.

[Traduit par la Rédaction]

Introduction

There is an extensive literature of heterocyclic compounds involving boron–nitrogen (B-N) linkages (1). Four-membered rings are uncommon in comparison with larger ring sizes, but such systems are well established for three-coordinate boron when another heteroatom, e.g., Si(2), P(2–4), Te(5, 6), is incorporated into the ring.

Carbon-containing four-membered B-N heterocycles are relatively rare. Paetzold et al. (7) prepared the three-coordinate boron system $C_6F_5B(\mu\text{-}N^tBu)_2CPh_2$ by the [2+2] cycloaddition of $C_6F_5B \triangleq N^tBu$ and ^{t}BuN = CPh_2. A similar approach employing iso(thio)cyanates was used by Ansorge et al. (8) to create related four-coordinate boron systems. An interesting feature of the latter is the thermally induced isomerization of the *N*,*N*′-chelated complex to the unsymmetrical (*N*,*E*-chelation) isomer (Scheme 1). This process occurs more readily for E = S than for E = O and it is prevented by bulky *R* groups, e.g., ^{t}Bu (8).

An alternative route to $\overline{BNCN}$ heterocycles involves the reaction of BX_3 (X = Cl, Br) with Li[$CPh(NSiMe_3)_2$] which produces $X_2BCPh(NSiMe_3)_2$ (9). Although there have been extensive studies of amidinate complexes of the heavier Group 13 elements (Al, Ga, In, Tl) in recent years (10–18), investigations of boron derivatives are limited to this single report. The chloride was obtained as a yellow oil and the bromide gave yellow crystals, but no structural information was obtained (9).

Here we describe the synthesis and characterization of the series of $\overline{BNCE}$ (E = N, O, S) heterocycles **1a**–**c** by the route shown in eq. [1]. The preparation and X-ray structures of the hexameric reagents {Li[CE(N^{t}Bu)(^{n}Bu)]}$_6$ (E = O, S) were published very recently (19). Although a few transition-metal complexes of oxoamidate and thioamidate anions [RC(E)(NR′)]$^-$ have been reported (E = O (20), S (21)), none of them were generated from these anions by metathetical reactions. Furthermore, heterocycles **1b** and **1c** are, to our knowledge, the first examples of *p*-block element complexes

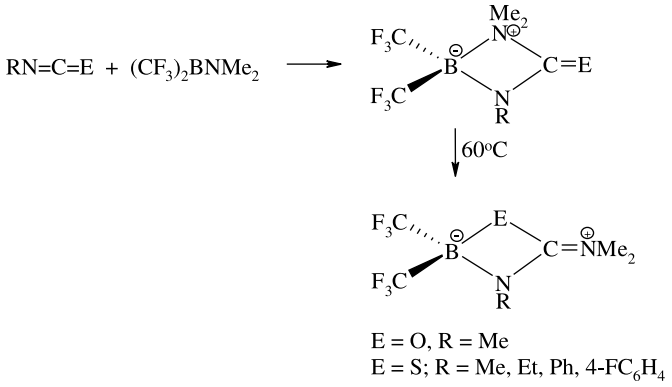
Accepted October 26, 1999.

P. Blais, T. Chivers,[1] A. Downard, and M. Parvez. Department of Chemistry, University of Calgary, Calgary, AB T2N 1N4, Canada.

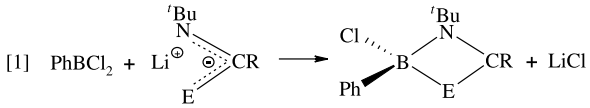
[1]Author to whom correspondence may be addressed. Telephone: (403) 220-5741. Fax: (403) 289-9488. e-mail: chivers@ucalgary.ca

 © 2000 NRC Canada

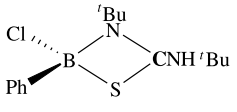
Scheme 1.



of these bidentate ligands. The structure of the related heterocycle **2** is included for comparison.



1a, E = N *t*Bu, R = *n*Bu
1b, E = O, R = *n*Bu
1c, E = S, R = *n*Bu



2

Experimental

The reagents *t*BuNCE (E = N*t*Bu, O, S), Li*n*Bu (2.5 M in hexane), *t*BuNH$_2$, and PhBCl$_2$ were all obtained from Aldrich and used as received. The reagents Li[CE(N*t*Bu)*n*Bu] were prepared by the addition of Li*n*Bu to an equimolar amount of *t*BuNCE (E = N*t*Bu, O, S) in toluene at 23°C (19, 22). LiNH*t*Bu was made by the reaction of dry *t*BuNH$_2$ with Li*n*Bu. All solvents were dried with appropriate drying agents and distilled. Deuterated solvents were degassed immediately before use. All reactions and manipulations of moisture and air-sensitive products were carried out using a glove box and Schlenk techniques under an atmosphere of high purity, dried argon.

^{1}H NMR spectra were recorded on a Bruker ACE200 spectrometer and the chemical shifts are reported relative to Me_4Si in C_6D_6. ^{11}B and ^{13}C NMR spectra were recorded on a Bruker AMX300 spectrometer and the chemical shifts are reported relative to $BF_3{\cdot}OEt_2$ in C_6D_6 and TMS in C_6D_6, respectively. Elemental analyses were provided by the Analytical Services Laboratory, Department of Chemistry, University of Calgary. IR spectra were obtained as Nujol mulls on a Mattson 4030 FTIR spectrophotometer. Mass spectra (EI, 70eV) were measured on a Kratos MS80RFA instrument.

Preparation of Ph(Cl)B(μ-N*t*Bu)$_2$C*n*Bu (1a)

A solution of PhBCl$_2$ (0.925 g, 5.82 mmol) in toluene (5 mL) was added dropwise via a stainless steel cannula to a solution of Li[C(N*t*Bu)$_2$*n*Bu] (1.267 g, 5.29 mmol) in toluene (10 mL) at 23°C. The mixture was stirred for 2 h to give a white precipitate and a pale yellow solution. Lithium chloride was removed by filtration and removal of solvent yielded a viscous yellow oil, which was washed with diethyl ether (2 × 5 mL) to give pale yellow crystals of **1a** (1.46 g, 4.36 mmol, 82%); mp 76–79°C. ^{1}H NMR (in C_6D_6, 25°C, δ): 8.1–7.2 (m, 5H, C_6H_5), 2.14 (m, 2H, CH_2), 1.60 (m, 2H, CH_2), 1.17 (s, 18H, $C(CH_3)_3$), 1.11 (m, 2H, CH_2), 0.73 (t, 3H, CH_3). ^{13}C NMR (in C_6D_6, 25°C, δ): 176.3 (s, $C(N^tBu)_2{}^nBu$), 134.0–128.2 (m, C_6H_5B-), 54.1 (s, -$C(CH_3)_3$), 31.6 (s, -$C(CH_3)_3$), 49.3 (s, $CH_2CH_2CH_2CH_3$), 30.4 (s, $CH_2CH_2CH_2CH_3$), 24.4 (s, $CH_2CH_2CH_2CH_3$), 6.4 (s, -$CH_2CH_2CH_2CH_3$). ^{11}B NMR (in C_6D_6, 25°C, δ): 6.8 (s). EIMS: *m/z* 334 (M^+, $C_{19}H_{32}N_2{}^{11}B^{35}Cl$; good agreement between calculated and observed isotopic distribution). Anal. calcd. for $C_{19}H_{32}N_2BCl$: C 68.16, H 9.65, N 8.37; found: C 67.76, H 9.97, N 8.45.

Preparation of Ph(Cl)B(μ-N*t*Bu)(μ-O)C*n*Bu (1b)

A solution of PhBCl$_2$ (0.889 g, 5.60 mmol) in toluene (5 mL) was added dropwise to a solution of Li[CO(N*t*Bu)*n*Bu] (0.885 g, 5.42 mmol) in toluene (10 mL) at 23°C. Observations and work-up procedure were similar to those described for **1a**. The crude product was washed with cold (–80°C) hexane (5 mL) (6 × 5 mL) to give **1b** as a yellow solid (1.03 g, 3.69 mmol, 68%); mp 111–112°C. ^{1}H NMR (in C_6D_6, 25°C, δ): 8.3–7.2 (m, 5H, C_6H_5), 1.93 (m, 2H, CH_2), 1.42 (m, 2H, CH_2), 1.14 (m, 2H, CH_2), 0.98 (s, 9H, $C(CH_3)_3$), 0.70 (t, 3H, CH_3). ^{13}C NMR (in C_6D_6, 25°C, δ): 184.2 (s, $CO(N^tBu)^nBu$), 136–127 (m, C_6H_5B-), 54.1 (s, -$C(CH_3)_3$), 29.9 (s, -$C(CH_3)_3$), 31.0 (s, -$CH_2CH_2CH_2CH_3$), 27.1 (s, -$CH_2CH_2CH_2CH_3$), 23.1 (s, -$CH_2CH_2CH_2CH_3$), and 14.5 (s, -$CH_2CH_2CH_2CH_3$). ^{11}B NMR (in C_6D_6, 25°C, δ): 11.6 (s). FAB–MS: *m/z* 280 [(M+H)$^+$]. Anal. calcd. for $C_{15}H_{23}NOBCl$: C 64.56, H 8.33, N 5.02; found: C 63.91, H 8.41, N 4.67.

Preparation of Ph(Cl)B(μ-N*t*Bu)(μ-S)C*n*Bu (1c)

A solution of PhBCl$_2$ (0.997 g, 6.28 mmol) in hexane (5 mL) was added dropwise to a solution of Li[CS(N*t*Bu)*n*Bu] (0.880 g, 4.91 mmol) in hexane (10 mL) at 23°C. Observations and work-up procedure were similar to those described for **1a**. The crude product was washed with diethyl ether (2 × 3 mL) to give **1c** as a yellow powder (0.455 g, 1.54 mmol, 31%); mp 67–69°C. ^{1}H NMR (in C_6D_6, 25°C, δ): 8.4–7.0 (m, 5H, C_6H_5), 2.23 (m, 2H, CH_2), 1.40 (m, 2H, CH_2), 1.11 (m, 2H, CH_2), 1.07 (s, 9H, $C(CH_3)_3$), 0.71 (t, 3H, CH_3). ^{13}C NMR (in C_6D_6, 25°C, δ): 203.7 (s, $CS(N^tBu)^nBu$), 136–128 (m, C_6H_5B-), 60.5 (s, -$C(CH_3)_3$), 29.5 (s, -$C(CH_3)_3$) and ($CH_2CH_2CH_2CH_3$), 37.0 (s, -$CH_2CH_2CH_2CH_3$), 22.8 (s, -$CH_2CH_2CH_2CH_3$), and 14.2 (s, -$CH_2CH_2CH_2CH_3$). ^{11}B NMR (in C_6D_6, 25°C, δ): 6.5 (s). EIMS: *m/z* 295 (M^+). Anal. calcd. for $C_{15}H_{23}NSBCl$: C 60.92, H 7.86, N 4.74; found: C 61.82, H 8.49, N 4.55.

Preparation of Ph(Cl)B(μ-N*t*Bu)(μ-S)CN(H)*t*Bu (2)

A solution of *tert*-butyl isothiocyanate (1.94 g, 16.8 mmol) in toluene (10 mL) was added dropwise to a slurry of LiNH*t*Bu (2.68 g, 33.9 mmol) in toluene (15 mL) at 20°C. The reaction mixture was stirred for 18 h. Solvent and

© 2000 NRC Canada

Table 1. Crystallographic data for **1a**, **1c,** and **2**.

	1a	**1c**	**2**
Formula	$C_{19}H_{32}N_2BCl$	$C_{15}H_{23}NBClS$	$C_{15}H_{24}N_2BClS$
*F*w	334.74	295.68	310.69
Space group	$P2_1$ (no. 4)	$P2_1/n$ (no. 14)	$P2_1/a$ (no. 14)
a, Å	8.816 (3)	7.617 (2)	11.357 (2)
b, Å	11.311 (2)	11.200 (1)	12.289 (2)
c, Å	10.168 (3)	19.568 (2)	12.620 (3)
β, deg	98.86 (3)	90.74 (2)	95.43 (2)
V, Å^3	1001.7 (5)	1669.1 (5)	1753.4 (5)
Z	2	4	4
T, °C	–103.0	–103.0	–103.0
λ, Å	0.71069	0.71069	0.71069
ρ_{calcd}, g cm^{-3}	1.110	1.177	1.177
μ, cm^{-1}	1.92	3.35	3.29
R^a	0.042	0.046	0.043
$R_w{}^b$	0.020	0.059	0.027

$^aR = \Sigma||F_o| - |F_c||/\Sigma|F_o|$.
$^bR_w = [\Sigma w\delta^2/\Sigma wF_o{}^2]^{1/2}$.

^{t}BuNH$_2$ were removed under vacuum and the product was washed with *n*-hexane (2 × 5 mL) to give $Li_2[CS(N^tBu)_2]$ as a very moisture-sensitive yellow powder (2.26 g, 67%). ^{1}H NMR (in C_6D_6, 25°C, δ) 1.18 [s, C(C*H*$_3$)$_3$].

A solution of $PhBCl_2$ (0.318 g, 2.00 mmol) in hexane (5 mL) was cooled to –35°C and added dropwise to a slurry of $Li_2[CS(N^tBu)_2]$ (0.400 g, 2.00 mmol) in hexane (10 mL) at –35°C. The reaction mixture was stirred for 5 h at –35°C. The mother liquor was decanted by cannula from the white precipitate and stored at –25°C for 3 days to give colourless crystals of **2** (0.055 g, 15%); mp 124–126°C. The precipitate was extracted with diethyl ether (2 × 20 mL) to give $(PhBS)_3$ (0.075 g, 31% based on boron); EIMS: *m*/*z* 360 (M^+). ^{1}H NMR (in C_6D_6, 25°C): δ 8.2–7.3 (m, 5H, C_6H_5), 5.2 (s, 1H, N*H*), 1.09 (s, 9H, C(C*H*$_3$)$_3$), 1.00 [s, 9H, C(C*H*$_3$)$_3$)]. ^{13}C NMR (in C_6D_6, 25 °C, δ): 172.3 [*C*S(N^{t}Bu)(NH^{t}Bu)], 136–128 (m, C_6H_5B), 56.3 [HN*C*(CH$_3$)$_3$], 54.6 [N*C*(CH$_3$)$_3$], 29.6 [HNC(*C*H$_3$)$_3$], 28.8 [NC(*C*H$_3$)$_3$]. ^{11}B NMR (in C_6D_6, 25°C, δ): 6.5 (s). EIMS: *m*/*z* 312 [(M+1)$^+$]. Anal. calcd. for $C_{15}H_{24}BClN_2S$: C 57.99, H 7.79, N 9.02; found: C 57.83, H 7.31, N 8.53.

X-ray analysis

Crystal data for **1a, 1c**, and **2** are summarized in Table 1.[2]

1a

A colourless, prismatic crystal (0.45 × 0.40 × 0.55 mm) was obtained from a mixture of pentane and diethyl ether (1:1) at 23°C. It was coated with epoxy and mounted on a glass fibre. Accurate cell dimensions and a crystal orientation matrix were obtained on a Rigaku AFC6S diffractometer by a least-squares fit of the setting angles of 25 reflections in the range 18.39° < 2θ < 23.96°. Intensity data were collected by the ω/2θ method using a scan speed of 4.0° min^{-1}, scan width (1.31 + 0.34 tan θ)°, and monochromatic MoK$_\alpha$ radiation in the range 4.0° < 2θ < 55.1°.

The intensities of 2443 unique reflections were measured of which 1346 had $I > 3\sigma(I)$. Data were corrected for Lorentz-polarization and absorption effects. The structure was solved by direct methods (23) and expanded using Fourier techniques (24). The non-hydrogen atoms were refined anisotropically. Hydrogen atoms were included but not refined. Scattering factors were those of Cromer and Waber (25) and allowance was made for anomalous dispersion (26). All calculations were performed using teXsan.[3]

1c

A colourless, prismatic crystal (0.50 × 0.48 × 0.45 mm) was obtained from pentane–Et_2O at –14°C. Data collection, structure solution and refinement procedures were similar to those described for **1a** except for the use of a different direct methods program (27). Range of data collected 4.0° < 2θ < 55.1°, scan speed 8.0° min^{-1}, scan width (1.57 + 0.34 tan θ)°, 4063 unique reflections of which 2431 had $I > 3\sigma(I)$.

2

A colourless, prismatic crystal (0.50 × 0.35 × 0.30 mm) was obtained from diethyl ether at –18°C. Data collection, structure solution and refinement procedures were similar to those described for **1c**. Range of data collected 4.0° < 2θ < 51.0°, scan speed 8.0° min^{-1}, scan width (1.63 + 0.34 tan θ)°, 4241 unique reflections of which 2330 had $I > 3\sigma(I)$.

Results and discussion

Compounds **1a–c** were obtained as moisture-sensitive pale yellow solids by the metathetical reaction illustrated in eq. [1]. They were characterized by elemental analyses and

[2] Copies of material on deposit may be purchased from: The Depository of Unpublished Data, Document Delivery, CISTI, National Research Council Canada, Ottawa, Canada K1A 0S2. Tables of hydrogen atom coordinates and bond lengths and angles involving hydrogen atoms have also been deposited with the Cambridge Crystallographic Data Centre and can be obtained on request from: The Director, Cambridge Crystallographic Data Centre, University Chemical Laboratory, 12 Union Road, Cambridge, CB2 1EZ, U.K.
[3] teXsan. Single crystal structure analysis software. Version 1.2. Molecular Structure Corp., The Woodlands, Tex. 1992.

© 2000 NRC Canada

Fig. 1. ORTEP drawing of PhB(Cl)(μ-N^{t}Bu)$_2$C^{n}Bu (**1a**).

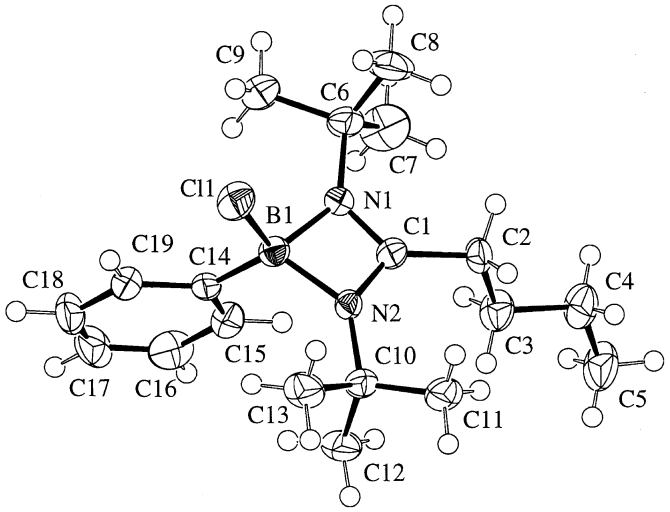
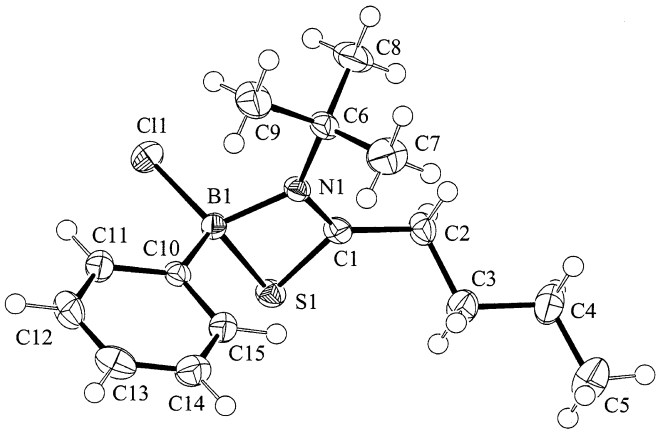


Fig. 2. ORTEP drawing of PhB(Cl)(μ-N^{t}Bu)(μ-S)C^{n}Bu (**1c**).



by ^{1}H, ^{13}C, and ^{11}B NMR spectra. The ^{11}B NMR chemical shifts are in the range δ 6–12 ppm consistent with tetracoordinate boron (28). The highest molecular ions observed in the EI and FAB mass spectra indicate monomeric structures in the solid state. We note, however, that four-coordinate boron compounds involving the [Me$_2$P(S)NR]$^-$ ligand, cf. [RC(S)N^{t}Bu]$^-$, exist in solution as an equilibrium mixture of monomers and dimers (29).

The related complex **2** was obtained unexpectedly, and in low yield, from the reaction of PhBCl$_2$ with Li$_2$[CS(N^{t}Bu)$_2$]. A major by-product of this reaction is (PhBS)$_3$ (30),[4] which accounts for the low yield of **2**.[5] Surprisingly, we were unable to obtain **2** from the reaction of PhBCl$_2$ with Li[CS(NH^{t}Bu)(N^{t}Bu)] (prepared from the reaction of ^{t}BuNCS with LiNH^{t}Bu in a 1:1 molar ratio). The ^{1}H and ^{13}C NMR spectra of **2** both show the presence of inequivalent N^{t}Bu environments and the ^{1}H NMR spectrum also exhibits a broad singlet at δ 5.2 attributable to the N*H* group. The ^{11}B NMR chemical shift for **2** is 6.5 ppm consistent with tetracoordinate boron.

Fig. 3. ORTEP drawing of PhB(Cl)(μ-N^{t}Bu)(μ-S)CN(H)^{t}Bu (**2**).

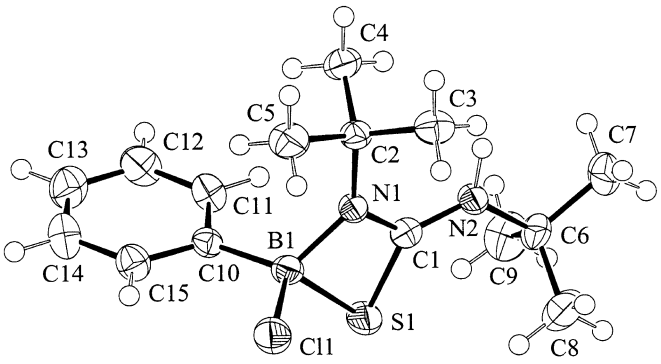


Table 2. Selected bond lengths (Å), bond angles (deg) for **1a**, **1c**, and **2**.

	1a	**1c**	**2**
B—C$_{ar}$[a]	1.589(6)	1.581(5)	1.581(4)
B—Cl	1.882(6)	1.847(4)	1.872(3)
B—N(1)	1.567(6)	1.571(5)	1.546(4)
B—E[b]	1.590(6)	2.032(4)	2.008(3)
C(1)—N(1)	1.321(6)	1.302(4)	1.323(3)
C(1)—E[b]	1.341(6)	1.740(4)	1.742(3)
C(1)—C(2)	1.522(7)	1.493(5)	—
N(1)—C(6)	1.491(5)	1.503(4)	1.495(3)
N(2)—C(10)	1.470(5)	—	—
C(1)—N$_{exo}$[c]	—	—	1.323(3)
C$_{Ar}$-B-Cl	113.8(4)	115.6(3)	113.2(2)
N(1)-B-E[b]	81.6(3)	83.7(2)	84.9(2)
B-N(1)-C(1)	89.2(4)	100.1(3)	99.9(2)
C(1)-N(1)-C(6)	132.5(4)	128.9(3)	127.8(2)
B-N(1)-C(6)	137.8(4)	131.3(3)	131.9(2)
B-E[b]-C(1)	87.6(4)	71.2(2)	71.4(1)
B-N(2)-C(10)	136.0(4)	—	—
C(1)-N(2)-C(10)	135.2(4)	—	—
N(1)-C(1)-E[b]	101.6(4)	105.0 (3)	103.7 (2)
N(1)-C(1)-C(2)	128.4(5)	131.3 (3)	—
E[b]-C(1)-C(2)	130.0(5)	123.7 (3)	—
N(1)-C(1)-N$_{exo}$	—	—	128.8 (3)
E[b]-C(1)-N$_{exo}$	—	—	127.4 (2)

[a] C$_{Ar}$ = *ipso* carbon of C$_6$H$_5$ group.
[b] **1a**, E = N(2); **1c**, E = S; **2**, E = S.
[c] N$_{exo}$ = exocyclic N atom.

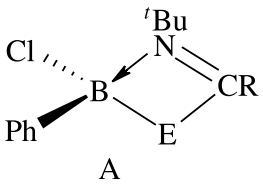
The monomeric, four-membered ring structures of **1a**, **1c**, and **2** were confirmed by X-ray crystallography (see Figs. 1–3). Numerous attempts to obtain crystals of **1b** suitable for X-ray crystallography were unsuccessful. Pertinent metrical parameters for these heterocyclic systems are compared in Table 2. All three ring systems are essentially planar with torsion angles (BNCE) of –1.9(4)°, 1.2(3)°, and –3.9(2)° for

[4] In one experiment a small amount of the five-membered ring (PhB)$_2$S$_3$ was isolated and identified by X-ray crystallography. This structure has been reported previously in a review (31).
[5] The metathetical reactions of Li$_2$[CSN^{t}Bu]$_2$ with other organometallic halides also produce the corresponding sulfides. For example, (Cp$_2$ZrS)$_2$ (32) and (Me$_2$SnS)$_3$ (33) were obtained from the reactions with Cp$_2$ZrCl$_2$ and Me$_2$SnCl$_2$, respectively, and identified by comparison of spectroscopic data with those reported in the literature (P. Blais and T. Chivers, unpublished results).

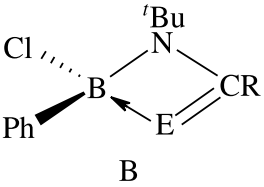
© 2000 NRC Canada

1a, **1c,** and **2**, respectively. The anionic ligand in **2** is chelated to boron in an *N*,*S* rather than *N*,*N*′ bonding mode consistent with the previous observations of Ansorge et al. (8) for related ligands in four-coordinate boron complexes.

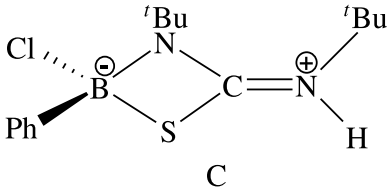
The C—N bond distances (1.321(6) and 1.341(6) Å) in the amidinate **1a** are almost equal, approximately intermediate between C—N double-bond and C—N(sp^2) single-bond values. The sums of the bond angles at the three-coordinate N and C centres are ca. 360° (as is the case for the other two heterocycles **1c** and **2**). These structural features indicate delocalized bonding in the NCN unit with approximately equal contributions from the two canonical forms **A** and **B** (E = N^{t}Bu). Consistently, the B—N bond lengths are also approximately equal (1.590(6) and 1.567(6) Å) and fall within the range of 1.55–1.61 Å found for B—N bonds involving four-coordinate boron linked to three-coordinate nitrogen (34). Interestingly, the endocyclic and exocyclic C—N bond lengths in **2** are identical at 1.323(3) Å. The shortness of the exocyclic bond suggests a significant contribution from the resonance form **C** to the overall structure (cf. Scheme 1 (8)).



A



B



C

The C—S bond lengths in **1c** and **2** are equal at 1.74 Å, which is close to the typical single-bond distance for sp^2-carbon atoms attached to two-coordinate sulfur (34). This observation and the relatively short (1.302(4) Å) C—N bond distance suggest that resonance form **A** (E = S) is a much more important contributor than **B** to the structure of **1c**. The B—S bond lengths in **1c** and **2** (2.032(4) and 2.008(3) Å, respectively) are somewhat longer than the mean single-bond value of 1.90 Å for four-coordinate boron attached to two-coordinate sulfur (34). This may reflect the relatively weak affinity of the hard Lewis acid boron for a soft Lewis base donor, sulfur, compared to nitrogen, a hard Lewis base centre.

The endocyclic bond angles at boron and carbon fall within the narrow ranges of 81.6(3)–84.9(2)° and 101.6(4)–105.0(3)°, respectively. However, there are substantial differences in the other two endocyclic bond angles for the S-containing rings **1c** and **2** compared to the corresponding values for **1a** as a result of the ability of two-coordinate sulfur to accommodate relatively small bond angles. Thus the endocyclic bond angles are ca. 71° at sulfur and ca. 100° at nitrogen in **1c** and **2**, cf. 88–89° at the N atoms in **1a**.

Conclusions

The first *p*-block element complexes of oxo- and thioamidate anions have been prepared by metathetical reactions using the novel reagents Li[CE(N^{t}Bu)(^{n}Bu)] (E = O, S). By analogy with the extensive chemistry of amidinates it is likely that this approach can be applied to the synthesis of a wide range of main group element and transition metal complexes of these hetero-bidentate ligands.

Acknowledgements

We thank the Natural Sciences and Engineering Research Council of Canada (NSERC) for financial support.

References

1. W. Maringgele. *In* The chemistry of inorganic homo- and heterocycles. Vol. 1. *Edited by* I. Haiduc and D.B. Sowerby. Academic Press, London, U.K. 1987. pp. 17.
2. W. Storch, W. Jackstiess, H. Nöth, and G. Winter. Angew. Chem. **89**, 494 (1977).
3. E. Niecke and W. Bitter. Angew. Chem. **87**, 34 (1975).
4. E. Niecke and W. Bitter. Chem. Ber. **109**, 415 (1976).
5. T. Chivers, X. Gao, and M. Parvez. Angew. Chem. Int. Ed. Engl..**34**, 2549 (1995).
6. H.-J. Koch, H.W. Roesky, S. Besser, and R. Herbst-Irmer. Chem. Ber. **126**, 571 (1993).
7. P. Paetzold, A. Richter, T. Thijssen, and S. Würtenburg. Chem. Ber. **112**, 3811 (1979).
8. A. Ansorge, D. Brauer, H. Bürger, F. Dörrenbach, T. Hagen, G. Pawelke, and W. Weuter. J. Organomet. Chem. **407**, 283 (1991).
9. C. Ergezinger, F. Weller, and K. Dehnicke. Z. Naturforsch. B: Chem. Sci. **43B**, 1621 (1988).
10. D. Kottmair-Maieron, R. Lechler, and J. Weidlein. Z. Anorg. Allg. Chem. **593**, 111 (1991).
11. R. Lechler, H.-D. Hausen, and J. Weidlein. J. Organomet. Chem. **359**, 1 (1989).
12. J. Barker, N.C. Blacker, P.R. Phillips, N.W. Alcock, W. Errington, and M.G.H. Wallbridge. J. Chem. Soc. Dalton Trans. 431 (1996).
13. R. Duchateau, A. Meetsma, and J.H. Teuben. J. Chem. Soc. Chem. Commun. 223 (1996).
14. (*a*) Y. Zhou and D.S. Richeson. Inorg. Chem. **35**, 2448 (1996); (*b*) Inorg. Chem. **35**, 1423 (1996).
15. Y. Zhou and D.S. Richeson. Inorg. Chem. **36**, 501 (1997).
16. M.P. Coles, D.C. Swenson, and R.F. Jordan. Organometallics, **16**, 5183 (1997).
17. M.P. Coles and R.F. Jordan. J. Am. Chem. Soc. **119**, 8125 (1997).
18. W.W. Schoeller, A. Sundermann, and M. Reiher. Inorg. Chem. **38**, 29 (1999).
19. T. Chivers, A. Downard, and G.P.A. Yap. Inorg. Chem. **37**, 5708 (1998).

© 2000 NRC Canada

20. F. Paul, J. Fischer, P. Oschenbein, and J.A. Osborn. Angew. Chem. Int. Ed. Engl. **32**, 1638 (1993).
21. (*a*) Th. Seitz, A. Muth, G. Huttner, Th. Klein, O. Walter, M. Fritz, and L. Zsolnai. J. Organomet. Chem. **469**, 155 (1994); (*b*) M. Vivanco, J. Ruiz, C. Floriani, A. Chiesi-Villa, and C. Rizzoli. Organometallics, **12**, 1802 (1993); (*c*) R.D. Adams, L. Chen, and W. Wu. Organometallics, **12**, 3812 (1993); (*d*) S. Gamborotta, M.L. Fiallio, C. Floriani, A. Chiesi-Villa, and C. Guastini. Inorg. Chem. **23**, 3532 (1984).
22. T. Chivers, A. Downard, and G.P.A. Yap. J. Chem. Soc. Dalton Trans. 2603 (1998).
23. H.-F. Fan. SAPI91: Structure analysis programs with intelligent control. Rigaku Corp. Tokyo.
24. P.T. Beurskens, G. Admiraal, G. Beurskens, W.P. Bosman, R. de Gelder, R. Israel, and J.M.M. Smits. DIRDIF94: The DIRDIF-94 program system. Technical report of the Crystallography Laboratory. University of Nijmegen, The Netherlands. 1994.
25. D.T. Cromer and J.T. Waber. International tables for X-ray crystallography. Vol. IV. The Kynoch Press, Birmingham. 1974. Table 2.2A. pp. 71–98.
26. J.A. Ibers and W.C. Hamilton. Acta Crystallogr. **17**, 781 (1964).
27. A. Altomare, M.C. Burla, M. Camalli, M. Cascarano, C. Giacovazzo, A. Guagliardi, and G. Polidori. SIR92. J. Appl. Crystallogr. **26**, 343 (1993).
28. H. Nöth and B. Wrackmeyer. *In* Nuclear magnetic resonance spectroscopy of boron compounds. Springer Verlag, Berlin. 1978. Chap. 7. pp. 74–101.
29. G. Muckle, H. Nöth, and W. Skorch. Chem. Ber. **109**, 2572 (1976).
30. W. Siebert. *In* The chemistry of inorganic homo- and heterocycles. Vol. 1. *Edited by* R. Steudel. Academic Press, New York. 1987. Chap. 5.
31. B. Krebs. Angew. Chem. Int. Ed. Engl. **22**, 113 (1983).
32. A. Shaver and J.M. McCall. Organometallics, **3**, 1823 (1984).
33. (*a*) B. Menzebach and P. Bleckmann. J. Organomet. Chem. **91**, 291 (1975); (*b*) H.J. Jacobsen and B. Krebs. J. Organomet. Chem. **136**, 333 (1977).
34. F.H. Allen, O. Kennard, D.G. Watson, L. Brammer, A.G. Orpen, and R. Taylor. J. Chem. Soc. Perkin Trans. (2), S1 (1987).

© 2000 NRC Canada

A kinetic modeling study of ethylene pyrolysis

John M. Roscoe, Alain R. Bossard, and Margaret H. Back

Abstract: A kinetic model is presented for the pyrolysis of ethylene at pressures ranging from 0.8 to 27 kPa and temperatures from 774 to 1023 K. The model is based on experimental measurements of C_2H_2, C_2H_6, C_3H_6, 1-C_4H_8, and 1,3-C_4H_6. In this temperature range the reaction is initiated by the disproportionation of C_2H_4 and the observed products result from reactions of the C_2H_3 and C_2H_5 radicals produced in this process. The C_2H_2 and 1,3-C_4H_6 result from reactions of C_2H_3 while C_2H_6, C_3H_6, and 1-C_4H_8 result from reactions of C_2H_5. C_2H_2 is produced exclusively by the decomposition of the C_2H_3 radical. This process is in its falloff region throughout the range of experimental conditions examined and the yield of C_2H_2 provides a measure of the degree of falloff. The production of 1,3-C_4H_6 is controlled by the reaction $C_4H_7 \rightarrow C_4H_6 + H$. The rate constants for this reaction were independent of pressure and are given as a function of temperature by $k = 2.2 \times 10^{13} \exp(-19.6 \times 10^3/T)$. Production of C_2H_6 is controlled by the reaction $C_2H_5 + C_2H_4 \rightarrow C_2H_6 + C_2H_3$. The rate constant for this reaction is given as a function of temperature by $k = 5.83 \times 10^{11} \exp(-14.6 \times 10^3/T)$. C_3H_6 is produced by decomposition of 2-C_4H_9 and is controlled kinetically by the isomerization reaction 1-$C_4H_9 \rightarrow$ 2-C_4H_9. The temperature dependence of the rate constants obtained for this reaction leads to a preexponential factor of approximately 3×10^{16} and an activation energy of approximately 200 kJ mol^{-1}. The yield of 1-C_4H_8 is controlled by 1-$C_4H_9 \rightarrow$ 1-C_4H_8 + H. The rate constants for this reaction were independent of pressure and are given as a function of temperature by $k = 2.97 \times 10^{12} \exp(-17.1 \times 10^3/T)$.

Key words: kinetic modeling, ethylene pyrolysis.

Résumé : On présente un modèle cinétique pour la pyrolyse de l'éthylène à des pressions allant de 0,8 à 27 kPa et à des températures allant de 774 à 1023 K. Le modèle est basé sur des mesures expérimentales de C_2H_2, C_2H_6, C_3H_6, but-1-ène et buta-1,3-diène. Dans cette plage de températures, la réaction est initiée par la dismutation du C_2H_4 et les produits observés résultent de réactions de radicaux C_2H_3 et C_2H_5 produit au cours de ce processus. La formation de C_2H_2 et le buta-1,3-diène résulte de réactions du C_2H_3 alors que la formation de C_2H_6, C_3H_6 et de but-1-ène résulte de réactions de C_2H_5. Le C_2H_2 ne se forme que par décomposition du radical C_2H_3; ce processus se retrouve dans la région de ralentissement dans toutes les conditions expérimentales étudiées et le rendement en C_2H_2 est une mesure du ralentissement. La production de buta-1,3-diène est contrôlée par la réaction $C_4H_7 \rightarrow C_4H_6 + H$. Les constantes de vitesse de cette réaction sont indépendantes de la pression et elle peuvent être exprimées comme une fonction de la température par l'équation $k = 2{,}2 \times 10^{13} \exp(-19{,}6 \times 10^3/T)$. La production de C_2H_6 est contrôlée par la réaction $C_2H_5 + C_2H_4 \rightarrow C_2H_6 + C_2H_3$. Les constantes de vitesse de cette réaction sont indépendantes de la pression et elle peuvent être exprimées comme une fonction de la température par l'équation $k = 5{,}83 \times 10^{11} \exp(-14{,}6 \times 10^3/T)$. La formation de C_3H_6 résulte de la décomposition du but-2-ène et, d'un point de vue cinétique, elle est contrôlée par la réaction d'isomérisation 1-$C_4H_9 \rightarrow$ 1-C_4H_8. La relation entre la température et les constantes de vitesse de cette réaction conduisent à un facteur préexponentiel d'environ 3 × 1016, une énergie d'activation d'environ 200 kJ mol^{-1}. Le rendement en but-1-ène est contrôlé par la réaction 1-$C_4H_9 \rightarrow$ 1-C_4H_8 + H. Les constantes de vitesse de cette réaction sont indépendantes de la pression et elles peuvent être exprimées en fonction de la température par l'équation $k = 2{,}97 \times 10^{12} \exp(-17{,}1 \times 10^3/T)$.

Mots clés : modélisation cinétique, pyrolyse de l'éthylène.

[Traduit par la Rédaction]

Introduction

The thermal reactions of hydrocarbons are important in combustion chemistry and petroleum processing. An understanding of the thermal decomposition of ethylene, the prototypical olefin, is essential for understanding the high temperature chemistry of other olefins. While the chemistry of saturated radicals such as C_2H_5 is reasonably well understood, a central issue in understanding the pyrolysis of olefins is elucidation of the chemistry of unsaturated radicals such as C_2H_3. These play a critical role at a much earlier stage in the thermal decomposition of olefins than in the corresponding reactions of saturated hydrocarbons. Indeed, it is the lack of well established kinetic parameters for the reactions of these unsaturated radicals that has prevented as comprehensive a description of olefin pyrolysis as has been developed for the thermal chemistry of saturated hydrocarbons.

The pyrolysis of olefins has been reviewed (1) and two limiting conditions are found for C_2H_4. At the high tempera-

Received October 14, 1999.

J.M. Roscoe.[1] Department of Chemistry, Acadia University, Wolfville, NS B0P 1X0, Canada.
A.R. Bossard and M.H. Back. Department of Chemistry, University of Ottawa, Ottawa, ON K1N 6N5, Canada.

[1]Author to whom correspondence may be addressed. Telephone: (902) 585-1353. Fax: (902) 585-1114. e-mail: jroscoe@acadiau.ca

© 2000 NRC Canada

tures characteristic of shock tube experiments, a comprehensive model has been developed (2) in which the reaction is initiated by decomposition of C_2H_4 via two channels: production of C_2H_2 + H_2 and production of C_2H_3 + H. Below about 1000 K, these reactions become very slow and the decomposition of C_2H_4 is initiated by its disproportionation to C_2H_5 and C_2H_3. This reaction has been extensively studied experimentally at temperatures between about 750 and 1000 K (3–13) and a kinetic model for the very early stages of the pyrolysis at about 900 K has been reported (14). The work which we present here extends that model to somewhat larger C_2H_4 conversions and to conditions which span a wide range of temperatures. This permits evaluation of the way in which the roles of key reactions in the process change with temperature and pressure over a significant range of these parameters and permits evaluation of Arrhenius parameters for those reactions that control the yields of the measured products.

Experimental

The kinetic modeling is based on the experiments of Bossard and Back (13) which provide an internally consistent data set for C_2H_2, C_2H_6, C_3H_6, C_4H_6, and 1-C_4H_8 at temperatures from 774 to 1023 K and pressures of 0.8 to 27 kPa. The experiments were performed in a static reaction vessel with chemical analysis by gas chromatography. The details of the methods used are given in the original publication (13). This provides experimental data obtained by methods which differ significantly from those upon which our earlier model was based (14) as well as giving data over a wide temperature range. It also includes results for the yield of C_2H_2 which was not measured in the experiments used for development of the earlier model. Knowledge of the C_2H_2 yield permits evaluation of the importance of decomposition of C_2H_3, information that is important in properly modeling other reactions of this radical which ultimately control the yields of 1,3-C_4H_6.

Kinetic modeling was done on a personal computer with a computer program which we have used in other work (14). It uses the DIFSUB integrator (15) to avoid stiffness instability and includes provision for first order sensitivity analysis. Rate constants were provided in the modified Arrhenius form

$$[1] \qquad k = AT^n \exp(-E_a/RT)$$

with the kinetic parameters A, n and E_a obtained from a variety of reviews and compilations (16–22). To the extent possible, data from reference (21) were used to improve internal consistency. When more recent direct experimental measurements of kinetic parameters were available and seemed to represent an improvement in accuracy, the more recent results were used. When the rate constant for a reaction was potentially subject to pressure falloff, this was evaluated using the Troe formalism (23) with the relations

$$[2] \qquad k = k_\infty \frac{P_r}{(1+P_r)} F, \qquad \text{where } P_r = \frac{k_0}{k_\infty}\frac{P}{RT}$$

Here, k_0 and k_∞ are the low pressure and high pressure limiting rate constants, respectively. The broadening factor F is given by

$$[3a] \qquad \log F = \frac{\log F_{cent}}{1+\left(\frac{\log P_r - 0.12}{0.85 - 0.67\log F_{cent}}\right)^2}, \qquad \text{when } P_r > 1$$

$$[3b] \qquad \log F = \frac{\log F_{cent}}{1+\left(\frac{\log P_r - 0.12}{0.65 - 1.87\log F_{cent}}\right)^2}, \qquad \text{when } P_r > 1$$

The value of the parameter F_{cent} varies with temperature and is specific to each reaction. The parameters needed in eqs. [2] and [3] were obtained from the same literature sources as the kinetic parameters where available.

Adjustment of the initial values of the rate constants for the reactions in the model was guided by sensitivity analysis and by the reported estimates of uncertainty of the kinetic parameters obtained from the literature. The number of reactions for which rate constants could be adjusted was limited by the number of reaction products for which measured yields were available. Rate constants were adjusted manually until the curves represented by the calculated composition appeared visually to represent the median trend of the experimental data points. The number of experimental measurements of composition as a function of time was generally insufficient to warrant the use of a statistical method such as least squares in assessing goodness of fit. In most cases, the sensitivity of the system to the rate constant being manually adjusted was sufficient to show a significant variation in the visual fit with a change of at most about 10% in the rate constant being fitted. The adjusted rate constants were finally constrained to fit eq. [1] except for those cases in which they had a clear dependence on pressure. The number of pressures for which data were available was too small to permit a quantitative analysis of the pressure falloff for those reactions having pressure sensitive rate constants.

Results and discussion

The full model consisted of 100 reactions, 96 of which corresponded to those evaluated in developing our earlier model (14). As in that work, many of these reactions had very small rates and negligibly small sensitivity coefficients for the reaction products for which experimental data were available. Such reactions were removed from the model if their removal did not appreciably alter the quality of the fit to the experimental data, provided they had not been shown to be important in our earlier model. This latter constraint is necessary because the earlier model was based on analytical data for H_2 and CH_4, two products for which information was not available in the experiments of Bossard and Back but which were used here.

The reduced model was larger than the reduced model presented in our earlier work and is given in Table 1. It consists of a total of 58 reactions, 27 of which are supplementary to those in the earlier model. Of these, 11 make an appreciable contribution to the measured products only at the higher temperatures examined. The quality of fit to the data provided by the model is indicated for three of the experimental data sets in Fig. 1. The kinetic parameters identi-

© 2000 NRC Canada

Table 1. Mechanism and rate constants.

Reaction	n	A (L mol^{-1} s^{-1})[a]	E_a (kJ mol^{-1})	Reference
Initiations:				
[4] 2 $C_2H_4 \rightarrow C_2H_3 + C_2H_5$	0	2.49×10^{12}	278	22, see text
[5] 1-$C_4H_8 \rightarrow CH_3 + C_3H_5$	0	1.00×10^{16}	305	24
[6] 1-$C_4H_8 \rightarrow C_2H_5 + C_2H_3$	0	1.30×10^{14}	290	14
[7][b] $C_5H_{10} \rightarrow C_2H_5 + C_3H_5$	0	1.00×10^{16}	296	25
H-transfer:				
[8] $CH_3 + C_2H_4 \rightarrow CH_4 + C_2H_3$	0	4.16×10^{9}	46.6	45
[9] $C_2H_5 + C_2H_4 \rightarrow C_2H_6 + C_2H_3$	0	5.83×10^{11}	121	This work
[10] $H + C_2H_4 \rightarrow H_2 + C_2H_3$	1.93	5.07×10^{4}	54.2	26
[11][c] $C_4H_7 + C_2H_4 \rightarrow$ 1-$C_4H_8 + C_2H_3$	0	1.00×10^{12}	125	Estimate
[12][b] $C_2H_3 + H_2 \rightarrow C_2H_4 + H$	0	2.06×10^{9}	34.7	26
[13][c] $C_2H_6 + H \rightarrow C_2H_5 + H_2$	1.50	1.44×10^{6}	31.0	45
Addition:				
[14] $CH_3 + C_2H_4 \rightarrow$ 1-C_3H_7	0	2.11×10^{8}	30.8	45
[15] $C_2H_5 + C_2H_4 \rightarrow$ 1-C_4H_9	2.44	3.97	22.4	27
[16] 1-$C_4H_9 + C_2H_4 \rightarrow$ 1-C_6H_{13}	0	2.34×10^{7}	28.0	16
[17] $C_2H_3 + C_2H_4 \rightarrow C_4H_7$	0	5.00×10^{8}	30.0	Estimate
[18] $H + C_2H_4 \rightarrow C_2H_5$	1.28	3.97×10^{6}	5.40	21[d]
[19] $C_3H_5 + C_2H_4 \rightarrow C_5H_9$	0	1.81×10^{8}	60.0	28
[20][b] $C_4H_7 + C_2H_4 \rightarrow$ 6-C_6H_{11}	0	5.00×10^{8}	30	Estimate
[21][c] $H + C_3H_6 \rightarrow$ 1-C_3H_7	0	1.30×10^{10}	13.6	29
[22][b] 1-$C_3H_7 + C_2H_4 \rightarrow$ 1-C_5H_{11}	0	6.31×10^{7}	31.0	17
[23][c] $C_4H_6 + H \rightarrow C_4H_7$	0	4.07×10^{10}	5.44	17
[24][c] $C_4H_6 + C_2H_3 \rightarrow C_6H_9$	–0.17	1.47×10^{9}	13.6	30
Radical decomposition:				
[–14] 1-$C_3H_7 \rightarrow CH_3 + C_2H_4$	–0.10	1.23×10^{13}	126	31
[–15] 1-$C_4H_9 \rightarrow C_2H_5 + C_2H_4$	0	1.06×10^{13}	116	27
[25] 2-$C_4H_9 \rightarrow C_3H_6 + CH_3$	1.06	2.67×10^{10}	129	32
[26] 2-$C_6H_{13} \rightarrow C_3H_6 +$ 1-C_3H_7	0	2.00×10^{13}	126	33
[–21] 1-$C_3H_7 \rightarrow C_3H_6 + H$	0	1.26×10^{13}	161	24
[–23] $C_4H_7 \rightarrow C_4H_6 + H$	0	2.16×10^{13}	163	This work
[27] $C_2H_3 \rightarrow C_2H_2 + H$	1.62	3.86×10^{8}	155	34[d]
[–18] $C_2H_5 \rightarrow C_2H_4 + H$	0	8.20×10^{13}	167	21[d]
[–17] $C_4H_7 \rightarrow C_2H_3 + C_2H_4$	0	2.00×10^{13}	171	14
[28] 1-$C_4H_9 \rightarrow$ 1-$C_4H_8 + H$	0	2.97×10^{12}	142	This work
[–16] 1-$C_6H_{13} \rightarrow C_2H_4 +$ 1-C_4H_9	0	2.51×10^{13}	120	14
[29][b] 3-$C_6H_{13} \rightarrow$ 1-$C_4H_8 + C_2H_5$	0	5.00×10^{12}	122	17
[30][b] 3-$C_6H_{13} \rightarrow C_5H_{10} + CH_3$	0	7.94×10^{13}	138	17
[31][b] *c*-$C_6H_{11} \rightarrow$ *c*-$C_6H_{10} + H$	0	2.00×10^{13}	160	Estimate
[–20][c] 6-$C_6H_{11} \rightarrow C_2H_4 + C_4H_7$	0	1.00×10^{13}	125	35
[32][c] 1-$C_5H_{11} \rightarrow C_2H_4 +$ 1-C_3H_7	0	2.51×10^{13}	120	17
[33][b] 3-$C_5H_{11} \rightarrow$ 1-$C_4H_8 + CH_3$	0	1.58×10^{14}	138	17
[34][b] *c*-$C_5H_9 \rightarrow$ *c*-$C_5H_8 + H$	0	2.00×10^{13}	160	Estimate
[35][c] 2-$C_3H_7 \rightarrow C_3H_6 + H$	1.83	6.50×10^{7}	148	36
[–24][c] $C_6H_9 \rightarrow C_4H_6 + C_2H_3$	0	1.00×10^{13}	120	Estimate
[36][c] *c*-$C_6H_9 \rightarrow$ *c*-$C_6H_8 + H$	0	2.00×10^{13}	160	Estimate
Isomerization:				
[37] 1-$C_4H_9 \rightarrow$ 2-C_4H_9	0	3.00×10^{16}	200	This work
[38] 1-$C_6H_{13} \rightarrow$ 2-C_6H_{13}	0	1.58×10^{9}	46	17
[39] $C_5H_9 \rightarrow$ *c*-C_5H_9	0	1.41×10^{11}	67.8	17
[40][b] 3-$C_6H_{13} \rightarrow$ 2-C_6H_{13}	0	1.00×10^{9}	46	Estimate
[41][b] 1-$C_5H_{11} \rightarrow$ 2-C_5H_{11}	0	1.20×10^{11}	84	37

© 2000 NRC Canada

Table 1 (*concluded*).

Reaction	n	A (L mol^{-1} s^{-1})[a]	E_a (kJ mol^{-1})	Reference
[42][b] 2-C_5H_{11} → 3-C_5H_{11}	0	1.00×10^{11}	84	Estimate
[43][b] 6-C_6H_{11} → c-C_6H_{11}	0	2.00×10^{11}	75	Estimate
[–43][b] c-C_6H_{11} → 6-C_6H_{11}	0	2.00×10^{13}	130	Estimate
[44][b] 2-C_6H_{13} → 3-C_6H_{13}	0	1.00×10^{9}	46	Estimate
[45][c] C_6H_9 → c-C_6H_9	0	2.00×10^{11}	75	Estimate
[–45][c] c-C_6H_9 → C_6H_9	0	2.00×10^{13}	130	Estimate
Termination:				
[46] 2 C_2H_5 → C_4H_{10}	0	1.15×10^{10}	0	45
[47] 2 C_2H_5 → C_2H_4 + C_2H_6	0	1.46×10^{9}	0	45
[48] 2 C_2H_3 → C_4H_6	0	7.23×10^{10}	0	38
[–6] C_2H_3 + C_2H_5 → 1-C_4H_8	0	1.60×10^{10}	0	18
[49] 2 CH_3 → C_2H_6	–1.10	3.26×10^{13}	1.33	39

[a]The values of the kinetic parameters given in the table are those used in the model calculations. They are not intended to imply a level of accuracy or precision in the numerical values.

[b]Reactions not included in the model of ref. 14.

[c]Reactions not included in the model of ref. 14 and only appreciable at high temperatures.

[d]The rate parameters are for the high pressure limit. The rate constants for these reactions were corrected for falloff.

fied in Table 1 as resulting from this work were obtained by fitting the rate constants for reactions having high, selective sensitivities to specific products so as to obtain optimal agreement with the experimental yields. The quality of fit obtained in such cases was well within the experimental uncertainty of the analytical data. However, the rate constants obtained in this way showed the normal experimental scatter about an Arrhenius plot. The kinetic parameters used in Table 1 result from these Arrhenius fits and the lack of exact agreement with the experimental data in Fig. 1 is a result of this scatter about the Arrhenius fits. While some of the Arrhenius plots appear curved, as will be seen later, the use of a nonlinear modified Arrhenius fit as defined in eq. [1] was not justified either by the number of experimental conditions or by the scatter of the kinetic data.

As in most attempts to infer detailed mechanisms for pyrolysis, some reactions must be evaluated for which experimental measurements of the relevant kinetic parameters are not available. We now outline how the parameters, which are indicated in Table 1 as estimates, were obtained.

The kinetic parameters for the reaction

[11] $C_4H_7 + C_2H_4 \rightarrow 1\text{-}C_4H_8 + C_2H_3$

were assumed to be similar to those for the corresponding reaction of C_2H_5.

[9] $C_2H_5 + C_2H_4 \rightarrow C_2H_6 + C_2H_3$

The measured product yields are not sensitive to variations of a factor of ±10 in the rate constant for reaction [11].

Weissman and Benson (40) estimate a preexponential factor of 2×10^8 L mol^{-1} s^{-1} and an activation energy lower limit of 8 kJ mol^{-1} for the reaction

[17] $C_2H_3 + C_2H_4 \rightarrow C_4H_7$

In our earlier model (14), we fixed the kinetic parameters for the subsequent reaction

[–23] $C_4H_7 \rightarrow C_4H_6 + H$

at the values given by Weissman and Benson (40) and adjusted the rate constant for reaction [17] to provide agreement with the measured yield of C_4H_6. We noted then that this decision was somewhat arbitrary since adjustment of the rate constant for either reaction [17] or [–23] would have served to fit the C_4H_6 yield. Reaction [17] was chosen as the one for which less was known about the kinetic parameters. Since our experiments were all made at temperatures within a few degrees of 900 K, we were unable to calculate an activation energy or preexponential factor. However, with an activation energy of 30 kJ mol^{-1}, typical of many radical additions to C_2H_4, our results suggested that the preexponential factor for reaction [17] would be 2.7×10^7 L mol^{-1} s^{-1}.

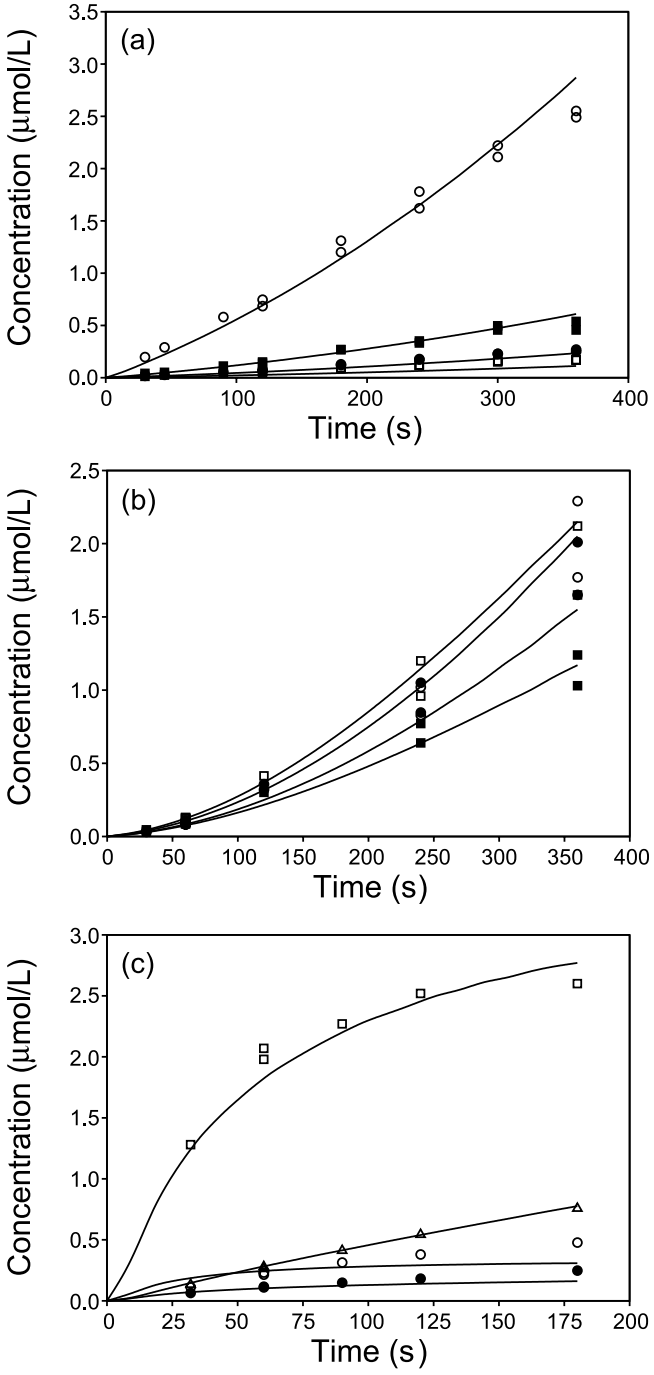
It was initially intended to fit the C_4H_6 yields in the current work by adjusting k_{17} at each temperature to determine whether the unexpectedly small rate constant for reaction [17] at 900 K was due to an unusually small preexponential factor or an unexpectedly large activation energy. It became clear that the overall magnitudes of the yields of most of the products could not be made large enough with reasonable values of the other rate constants unless the preexponential factor of reaction [17] was approximately 2×10^8 L mol^{-1} s^{-1} with our estimated activation energy of 30 kJ mol^{-1}. The yield of C_4H_6 could then be fitted satisfactorily at the lower temperatures by adjusting the value of k_{-23}. Above approximately 925 K, the general magnitudes of the predicted yields of the other products tended to be low unless the preexponential factor of reaction [17] was increased to approximately 5×10^8. This does not necessarily indicate that the preexponential factor suggested by Weissman and Benson is too small but may well indicate that our estimate of the activation energy is too large. However, the sensitivity of the system to the value of the rate constant for reaction [17] is not sufficient over the range of conditions for which data are available to permit unambiguous evaluation of the preexponential factor and activation energy of this reaction.

No information could be found in the literature for the reaction

[20] $C_4H_7 + C_2H_4 \rightarrow 6\text{-}C_6H_{11}$

© 2000 NRC Canada

Fig. 1. (*a*) Yields of reaction products in ethylene pyrolysis at 26.7 kPa and 774 K. The lines represent calculations using the model. The data points represent the experimental yields as follows: ○, C_3H_6; ■, 1-C_4H_8; ●, C_2H_6; □, C_4H_6. (*b*) Yields of reaction products in ethylene pyrolysis at 6.7 kPa and 853 K. The lines represent calculations using the model. The data points represent the experimental yields as follows: ○, C_3H_6; ■, 1-C_4H_8; ●, C_2H_6; □, C_4H_6. (*c*) Yields of reaction products in ethylene pyrolysis at 0.83 kPa and 974 K. The lines represent calculations using the model. The data points represent the experimental yields as follows: ○, C_3H_6; □, C_4H_6; ●, C_2H_6; △, C_2H_2.



We estimate its Arrhenius parameters to be similar to those for reaction [17]. This reaction only has a significant effect on the yield of C_4H_6 and its effect is significantly less sensitive than that of reaction [–23]. Its effect is more pronounced at low temperatures than at the higher ones.

The model contains three decomposition reactions of cyclic radicals.

[31] $c\text{-}C_6H_{11} \rightarrow c\text{-}C_6H_{10} + H$

[34] $c\text{-}C_5H_9 \rightarrow c\text{-}C_5H_8 + H$

[36] $c\text{-}C_6H_9 \rightarrow c\text{-}C_6H_8 + H$

Kinetic parameters for these reactions are scarce and varied. We used a preexponential factor of 2×10^{13} s^{-1} and an activation energy of 160 kJ mol^{-1} for all three reactions on the assumption that these would be similar to reactions [–21] or [28]. The calculations are not sensitive to the values of these rate constants.

Reaction [–24] has a modest effect on C_4H_6 and virtually no effect on any other

[–24] $C_6H_9 \rightarrow C_4H_6 + C_2H_3$

measured product. While there are no values available in the literature for its kinetic parameters, it is likely to be similar to reactions [–20] and [32]. On that basis, we estimate a preexponential factor of approximately 10^{13} s^{-1} with an activation energy of about 120 kJ mol^{-1}.

Reactions [40], [42], [43], [–43], [44], [45], and [–45] have very small effects on

[40] $3\text{-}C_6H_{13} \rightarrow 2\text{-}C_6H_{13}$

[42] $2\text{-}C_5H_{11} \rightarrow 3\text{-}C_5H_{11}$

[43] $6\text{-}C_6H_{11} \rightarrow c\text{-}C_6H_{11}$

[–43] $c\text{-}C_6H_{11} \rightarrow 6\text{-}C_6H_{11}$

[44] $2\text{-}C_6H_{13} \rightarrow 3\text{-}C_6H_{13}$

[45] $C_6H_9 \rightarrow c\text{-}C_6H_9$

[–45] $c\text{-}C_6H_9 \rightarrow C_6H_9$

the calculated yields of the measured products. The kinetic parameters for reactions [40], [42], and [44] were assumed to be the same as those for the other isomerization reactions of radicals with the same empirical formula. The kinetic parameters for reactions [43] and [45] were assumed to be the same as those for reaction [41], while those for reactions [–43] and [–45] were assumed to be similar to those for cleavage of an aliphatic C—C bond.

We now describe in some detail the selection of reactions whose rate constants were adjusted in fitting the model calculations to the experimental product yields. The yield of a product invariably showed a sensitive dependence on the rate constants of several reactions and this sensitivity frequently varied with temperature, pressure and reaction time. In the discussion which follows, the sensitivity of the model calculations to the rate constants of individual reactions is used to justify the selection of the reactions whose rate constants were adjusted. The results obtained by fitting these kinetic

© 2000 NRC Canada

Table 2. Rate constants for $C_2H_5 + C_2H_4 \rightarrow C_2H_6 + C_2H_3$.

Pressure (kPa)	Absolute temperature (K)	Rate constant (L mol^{-1} s^{-1})
26.7	774	5.0×10^{3}
13.3	774	7.0×10^{3}
6.7	774	6.0×10^{3}
6.7	824	1.2×10^{4}
3.33	824	1.1×10^{4}
1.63	824	8.0×10^{3}
6.7	853	2.0×10^{4}
3.33	853	2.0×10^{4}
1.63	853	2.0×10^{4}
3.33	925	5.0×10^{4}
1.63	925	5.0×10^{4}
1.63	974	2.0×10^{5}
0.83	974	2.5×10^{5}
1.63	1023	6.0×10^{5}
0.83	1023	6.0×10^{5}

parameters to obtain agreement with experiment are then presented.

The initiation step,

[4] $2C_2H_4 \rightarrow C_2H_3 + C_2H_5$

has received extensive study and the agreement among the experiments reported in the literature is good. These results are summarized in reference (22) and a linear Arrhenius fit to the collected data was used to obtain the kinetic parameters for this reaction quoted in Table 1. It seemed preferable to use this composite representation of the kinetic data in the literature rather than singling out a specific piece of work because of the good agreement among the experimental measurements made in several laboratories. While the selection of kinetic parameters for the initiation step is clearly a key decision in establishing the kinetic model, this reaction did not have a selective effect on any reaction product. Indeed, many other reactions in the model showed a much more sensitive and selective effect on the calculated yields of the measured products.

The reactions

[18] $H + C_2H_4 \rightarrow C_2H_5$

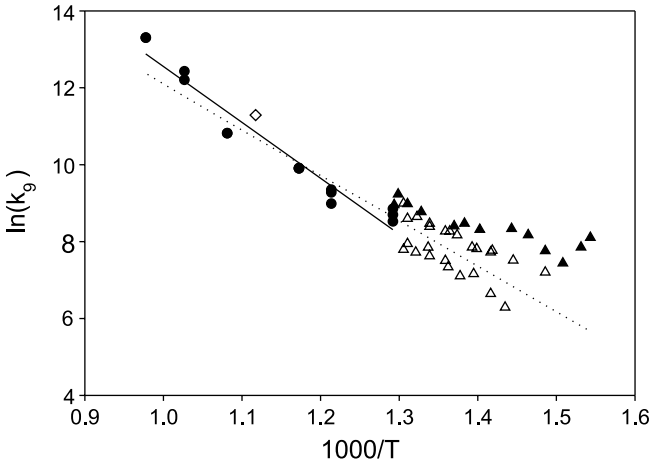
[–18] $C_2H_5 \rightarrow C_2H_4 + H$

[27] $C_2H_3 \rightarrow C_2H_2 + H$

were in their falloff region over the entire range of reaction conditions. Falloff corrections were calculated for reactions [18] and [–18] using the relation for F_{cent} given by Larson et al. (41) and microscopic reversibility. Examination of the calculated rates of reactions [18] and [–18] indicated that the reaction was virtually equilibrated. While the yields of many reaction products are sensitive to the choice of rate constant of either reaction [18] or [–18] individually, the calculated yields were not sensitive to the falloff calculation as long as the values of k_{18} and k_{-18} were consistent with the established thermochemistry of the C_2H_5 radical.

Initial estimates of the falloff corrections for the C_2H_3 radical were made using the relation for F_{cent} reported for reaction [27] by Knyazev and Slagle (34) with N_2 as the bath gas. The calculated yields were insensitive to the reverse of reaction [27] and it is therefore not included in the reduced model presented in Table 1. Below 925 K, none of the product yields were sensitive to the value of k_{27} while at this temperature and above, only the yield of C_2H_2 showed a consistently large and selective sensitivity to this rate constant. The yield of C_2H_2 could then be used to refine the estimate of the falloff correction for reaction [27] at the higher temperatures to give rate constants with a falloff correction appropriate to a bath gas of C_2H_4 rather than N_2. At the lower temperatures, where yields of C_2H_2 were not available, the falloff correction was calculated for N_2. This was felt to be sufficiently accurate since the calculated yields of the other products were very insensitive to the value of k_{27} at these temperatures. Unfortunately, the limited number of temperatures and pressures for which data were available prevents analysis of the falloff corrected values of k_{27} to obtain useful values of F_{cent} for C_2H_4 as a bath gas.

Fig. 2. Temperature dependence of k_9. ●, this work; ▲, ref. 43; ◇, ref. 9; △, ref. 42: Rate constants were measured by a relative method. The upper set of points use $C_2H_5 + C_3H_8 \rightarrow C_2H_6 + C_3H_7$ as the reference reaction. The rate constants are calculated using kinetic parameters for the reference reaction taken from reference 18. The total reference rate constant is taken as the sum of the rate constants for the two channels giving respectively 1-C_3H_7 and 2-C_3H_7. The lower set of points are based on C_2H_5 + iso-$C_4H_{10} \rightarrow C_2H_6 + C_4H_9$ as the reference reaction with kinetic parameters as in ref. 42. ·····, ref. 18.



The calculated yields of C_2H_6 showed consistently high sensitivity to the reaction

[9] $C_2H_5 + C_2H_4 \rightarrow C_2H_6 + C_2H_3$

None of the other product yields showed high sensitivity to this reaction. At the higher temperatures, reactions [18] and [–18] had an increasingly sensitive effect on the yield of C_2H_6 but the values of the rate constants for these reactions and their dependence on pressure were fixed as indicated earlier. Moreover, reactions [18] and [–18] have a sensitive effect on several products. This makes them unsuitable for use in fitting the yields of specific reaction products because the choice of product to use for fitting is ambiguous.

The yields of C_2H_6 could be exactly fitted over the entire range of reaction conditions by adjusting only the rate constant of reaction [9]. The values obtained are given in

© 2000 NRC Canada

Table 3. Rate constants for 1-$C_4H_9 \rightarrow$ 2-C_4H_9.

Pressure (kPa)	Absolute temperature (K)	Rate constant (s^{-1})
26.7	774	5.3×10^3
13.3	774	3.7×10^3
6.7	774	1.8×10^3
6.7	824	3.7×10^3
3.33	824	2.8×10^3
1.63	824	2.5×10^3
6.7	853	6.2×10^3
3.33	853	9.0×10^3
1.63	853	1.4×10^4
3.33	925	5.5×10^4
1.63	925	7.0×10^4
1.63	974	7.0×10^5
0.83	974	9.0×10^5
1.63	1023	3.5×10^6
0.83	1023	9.0×10^6

Table 2 and Fig. 2. Also shown in the figure are results taken from the literature. Our fitted values fall close to the recommendation of Tsang and Hampson (18) and, at the lower temperature, merge with the high temperature results of Ahonkhai et al. (42) and Zhang and Back (43). A single value at 900 K by MacKenzie et al. (9) falls within our combined uncertainties. A linear Arrhenius fit to our data leads to a preexponential factor of 5.83×10^{11} L mol^{-1} s^{-1} and an activation energy of 121 kJ mol^{-1} for this reaction.

The reaction product C_3H_6 arises from decomposition of the 2-C_4H_9 radical. However, its yield is kinetically limited by the isomerization of the 1-C_4H_9 radical. The reactions leading from the initiation reaction to C_3H_6 are therefore

[15] $C_2H_5 + C_2H_4 \rightarrow$ 1-C_4H_9

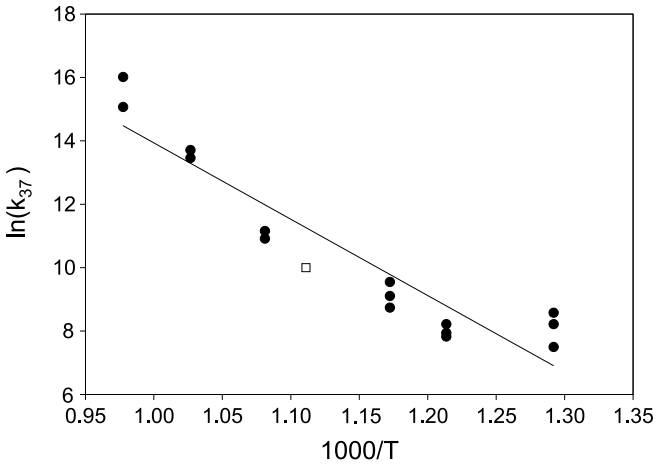
[37] 1-$C_4H_9 \rightarrow$ 2-C_4H_9

[25] 2-$C_4H_9 \rightarrow C_3H_6 + CH_3$

At all temperatures, the rate of reaction [25] is equal to that of reaction [37] and the sensitivity coefficient of reaction [25] is zero. The yield of C_3H_6 can be made to agree with the experimental value without appreciably altering the yields of the other measured products by adjusting the rate constant of reaction [37]. As the temperature increases, the number of reactions influencing the formation of C_3H_6 increases. However, the rate of reaction [25] is always equal to that of reaction [37] so adjustment of the rate constant for this reaction properly reflects the kinetic control of the C_3H_6 yield over the entire range of reaction conditions. The sensitivity coefficient for reaction [37] remains large throughout. Most of the additional reactions that increase in sensitivity consist of nearly equilibrated pairs of forward and reverse processes; therefore, their net sensitivity is determined by the difference between the forward and reverse sensitivity coefficients and is quite small. The effect of these reactions is therefore more a reflection of the relevant thermochemistry than of kinetic control.

The rate constants obtained as outlined above are listed in Table 3. While the rate constants obtained at temperatures below 853 K seem to show a systematic decrease with decreasing pressure, this may be an artefact resulting from the small number of pressures examined. The average deviation from the mean at the lowest two temperatures is of the same magnitude as that at the higher temperatures. The limited precision of these rate constants and the limited number of pressures used prevents any systematic examination of a pressure dependence for k_{37}. These rate constants are plotted in Arrhenius form in Fig. 3. Also shown in that plot is a single point obtained by MacKenzie et al. at 900 K (11) which fits very well into our results. The data lead to a preexponential factor of approximately 3×10^{16} and an activation energy of approximately 200 kJ mol^{-1}. However, within the scatter of the data, the activation energy could be uncertain by as much as ±30 kJ mol^{-1} with a consequent extrapolation uncertainty of as much as two orders of magnitude in the preexponential factor. The large activation energy is, however, consistent with the widely held view that isomerization of small free radicals is a slow process with a large activation energy.

Fig. 3. Temperature dependence of k_{37}. ●, this work; □, ref. 11.



The yield of 1-C_4H_8 is controlled by

[28] 1-$C_4H_9 \rightarrow$ 1-C_4H_8 + H

The only other reactions which have significant sensitivities for 1-C_4H_8 at the lower temperatures are

[15] $C_2H_5 + C_2H_4 \rightarrow$ 1-C_4H_9

[46] $2C_2H_5 \rightarrow C_4H_{10}$

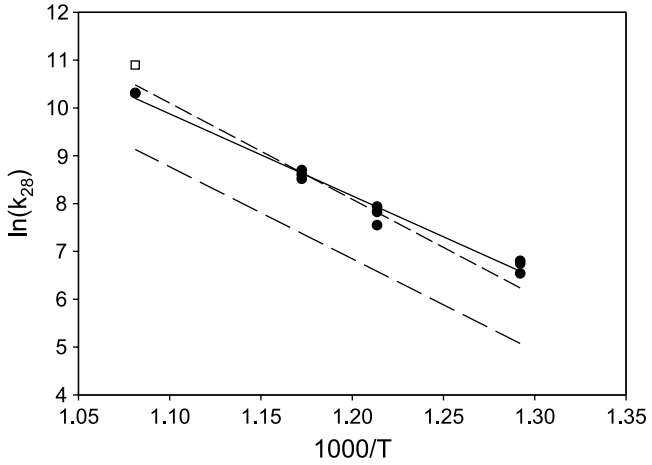
Reaction [15] is nearly equilibrated so its effect is governed by thermochemistry rather than kinetics and the rate constant for reaction [46] is sufficiently well established and insensitive to temperature that adjustment of its value would not be appropriate for fitting the experimental yields of 1-C_4H_8. The sensitivity coefficient for reaction [28] was consistently the largest of any reaction throughout the entire set of reaction conditions and the rate constant for that reaction was adjusted to bring the yields of 1-C_4H_8 calculated with the model into agreement with experiment. As the temperature increases, a substantial number of additional reactions begin to have a significant effect on the yield of 1-C_4H_8. The net effect is a decrease in the relative yield of 1-C_4H_8 and above 925 K the amounts formed were too small to measure

© 2000 NRC Canada

Table 4. Rate constants for 1-$C_4H_9 \rightarrow$ 1-C_4H_8 + H.

Pressure (kPa)	Absolute temperature (K)	Rate constant (s^{-1})
26.7	774	6.9×10^2
13.3	774	9.0×10^2
6.7	774	8.5×10^2
6.7	824	2.8×10^3
3.33	824	2.5×10^3
1.63	824	1.9×10^3
6.7	853	6.0×10^3
3.33	853	5.5×10^3
1.63	853	5.0×10^3
3.33	925	3.0×10^4
1.63	925	3.0×10^4

Fig. 4. Temperature dependence of k_{28}. ●, this work; □, ref. 11; — — —, ref. 44; – – –, ref. 24.



experimentally. The reaction that has the dominant effect on this reduction in C_4H_8 yield is

[5] 1-$C_4H_8 \rightarrow CH_3 + C_3H_5$

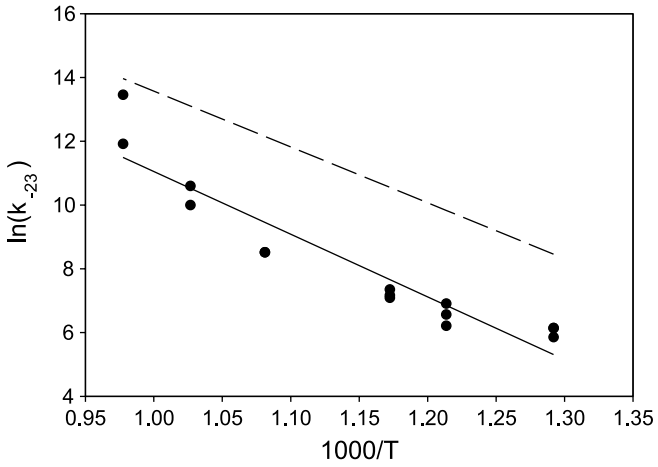
The sensitivity to this reaction is quite small at the lower temperatures. However, it has a sufficiently sensitive effect at the higher temperatures that inaccuracy in the value of k_5 could have an appreciable effect on the accuracy of the adjusted values of k_{28}. The other additional reactions which intervene at the higher temperatures are generally nearly equilibrated and their effect is largely due to thermochemical control rather than kinetic control.

The rate constants for reaction [28] obtained with the model are listed in Table 4 and plotted in Arrhenius form in Fig. 4. Also plotted in that figure are an Arrhenius fit to the experimental measurements by Lin and Back (44) and a single point measured at 900 K by MacKenzie et al. (11) as well as a line representing an estimate by Dean (24) of the Arrhenius parameters for this reaction. Our rate constants are in good agreement with the experimental results and roughly a factor of three above Dean's estimate. There is no apparent dependence of the rate constants on pressure within the precision of the data over the range of experimental conditions examined. An Arrhenius fit to our data leads to a

Table 5. Rate constants for $C_4H_7 \rightarrow C_4H_6$ + H.

Pressure (kPa)	Absolute temperature (K)	Rate constant (s^{-1})
26.7	774	4.6×10^2
13.3	774	4.6×10^2
6.7	774	3.5×10^2
6.7	824	1.0×10^3
3.33	824	7.1×10^2
1.63	824	5.0×10^2
6.7	853	1.6×10^3
3.33	853	1.3×10^3
1.63	853	1.2×10^3
3.33	925	5.0×10^3
1.63	925	5.0×10^3
1.63	974	2.2×10^4
0.83	974	4.0×10^4
1.63	1023	1.5×10^5
0.83	1023	7.0×10^5

Fig. 5. Temperature dependence of k_{-23}. ●, this work; — — —, ref. 40.



preexponential factor of 2.97×10^{12} s^{-1} and an activation energy of 142 kJ mol^{-1} for reaction [28]. This analysis is restricted to temperatures at and below 925 K because of the lack of measured yields of 1-C_4H_8 at the higher temperatures.

Butadiene is formed in the following sequence of reactions.

[17] $C_2H_3 + C_2H_4 \rightarrow C_4H_7$

[–23] $C_4H_7 \rightarrow C_4H_6 + H$

Neither reaction has well established kinetic parameters and the thermochemistry of the C_2H_3 radical is not as accurately known as that of C_2H_5 which played a significant role in determining the yields of C_2H_6, C_3H_6, and 1-C_4H_8. Reaction [17] plays a role in the production of several of the measured reaction products and this role varies with temperature. The rationale for estimating the rate constants for reactions [17] and [–17] was presented earlier. At the lower temperatures, the yield of C_4H_6 is not sensitive to the values of k_{17} and k_{-17} while at the higher temperatures the sensitiv-

© 2000 NRC Canada

ity to both reactions increases, with the positive sensitivity to k_{17} being significantly compensated by the negative sensitivity to k_{-17}. At the lower temperatures, the sensitivity to reaction [–23] dominates, therefore adjustment of k_{-23} provides a sensitive and selective means of fitting the calculated yield of C_4H_6 to the experimental yield. However, the sensitivity of this adjustment decreases with increasing temperature and is dependent to some degree on the estimates of kinetic parameters for reactions [17] and [–17]. For these reasons, the rate constants used for reaction [–23] in fitting the calculated yields of C_4H_6 to the experimental data are perhaps best regarded as estimates which may depend significantly on other parameters related to the reactions of C_2H_3 and C_4H_7.

The values of k_{-23} which provided agreement with the measured yields of C_4H_6 are presented in Table 5 and Fig. 5. Also shown in the figure is a line calculated from the Arrhenius parameters for reaction [–23] estimated by Weissman and Benson (40). Our results are approximately a factor of seven lower than their estimate with about the same activation energy. Our scatter is fairly large at the highest temperatures, possibly reflecting a problem resulting from the increased complexity of the dependence of the C_4H_6 yield on other reactions in the model. The uncertainty in the values of the kinetic parameters for some of the other reactions of C_2H_3 and C_4H_7 will almost certainly have a bearing on this behaviour. However, with these reservations in mind, our rate constants lead to an activation energy of 160 kJ mol^{-1} and a preexponential factor of 2.2×10^{13} s^{-1}, both of which are consistent with results for other hydrogen atom elimination reactions of hydrocarbon free radicals.

The model presented here provides a relatively concise description of the pyrolysis of ethylene at temperatures from about 750 to 1000 K. The rate constants obtained by fitting the yields calculated with the model to those measured experimentally give acceptable to good fits to Arrhenius plots. The parameters obtained from these plots are in excellent agreement with work in the literature where such comparisons are possible. The temperature dependence for the isomerization of the 1-C_4H_9 radical has been assessed for the first time. The results are in excellent agreement with a single published value of the rate constant at 900 K and lead to an expected large activation energy for the reaction. The isomerization appears to be in its falloff region at the lower temperatures at which it was examined. An estimate of the temperature dependence for the decomposition of the C_4H_7 radical to butadiene has been made which is in reasonable agreement with an estimate in the literature based on thermochemistry and group additivity. Work is needed to better define the thermochemistry of the C_2H_3 radical and the kinetics of its reactions in the presence of ethylene so that some of the uncertainties, particularly relative to the description of the yields of C_4H_6, can be resolved.

Acknowledgements

The experimental work upon which the model is based was supported by funding from the Department of Energy, Mines and Resources Canada. General support for the modelling was provided by an operating grant from the Natural Sciences and Engineering Research Council Canada.

References

1. T. Sakai. *In* Pyrolysis: theory and industrial practice. *Edited by* L.F. Albright, B.L. Crynes, and W.H. Corcoran. Academic Press, New York. 1983. pp. 89–116.
2. C.K. Westbrook, F.L. Dryer, and K.P. Schug. Symp. (Int.) Combust. Proc. **19**, 153 (1982).
3. M.L. Boyd, T.-M. Wu, and M.H. Back. Can. J. Chem. **46,** 2415 (1968).
4. M.P. Halstead and C.P. Quinn. Trans. Faraday Soc. **64**, 103 (1968).
5. M. Simon and M.H. Back. Can. J. Chem. **47**, 251 (1969).
6. M.H. Back and R. Martin. Int. J. Chem. Kinet. **11**, 757 (1979).
7. G. Ayranci and M.H. Back. Int. J. Chem. Kinet. **13**, 897 (1981).
8. G. Ayranci and M.H. Back. Int. J. Chem. Kinet. **15**, 83 (1983).
9. A.L. MacKenzie, P.D. Pacey, and J.H. Wimalasena. Can. J. Chem. **61**, 2033 (1983).
10. B.A. Collings, A.L. MacKenzie, and P.D. Pacey. React. Kinet. Catal. Lett. **26**, 31 (1984).
11. A.L. MacKenzie, P.D. Pacey, and J.H. Wimalasena. Can. J. Chem. **62**, 1325 (1984).
12. I.S. Jayaweera and P.D. Pacey. Int. J. Chem. Kinet. **20**, 719 (1988).
13. A.R. Bossard and M.H. Back. Can. J. Chem. **68**, 1401 (1990).
14. J.M. Roscoe, I.S. Jayaweera, A.L. MacKenzie, and P.D. Pacey. Int. J. Chem. Kinet. **28**, 181 (1996).
15. C.W. Gear. Numerical initial value problems in ordinary differential equations. Prentice–Hall, Englewood Cliffs, N.J. 1971.
16. J.A. Kerr and M.J. Parsonage. Evaluated kinetic data on gas phase addition reactions. Reactions of atoms and radicals with alkenes, alkynes and aromatic compounds. Butterworths, London. 1972.
17. D.L. Allara and R. Shaw. J. Phys. Chem. Ref. Data, **9**, 523 (1980).
18. W. Tsang and R.F. Hampson. J. Phys. Chem. Ref. Data, **15**, 1087 (1986).
19. W. Tsang. J. Phys. Chem. Ref. Data, **17**, 887 (1988).
20. W. Tsang. J. Phys. Chem. Ref. Data, **20**, 221 (1991).
21. D. L. Baulch, C.J. Cobos, R.A. Cox, P. Frank, G. Hayman, Th. Just, J.A. Kerr, T. Murrells, M.J. Pilling, J. Troe, R.W. Walker, and J. Warnatz. J. Phys. Chem. Ref. Data, **23**, 847 (1994).
22. F. Westley, J.T. Herron, D. Frizzell, R.F. Hampson, and W.J. Mallard. NIST Standard Reference Database 17-2Q98, 1998.
23. J. Troe. J. Phys. Chem. **83**, 114 (1979).
24. A.M. Dean. J. Phys. Chem. **89**, 4600 (1985).
25. T.C. Brown, K.D. King, and T.T. Nguyen. J. Phys. Chem. **90**, 419 (1986).
26. V.D. Knyazev, A. Bencsura, S.I. Stoliarov, and I.R. Slagle. J. Phys. Chem. **100**, 11346 (1996).
27. V.D. Knyazev and I.R. Slagle. J. Phys. Chem. **100**, 5318 (1996).
28. K.H. Ebert, H.J. Ederer, and G. Isbarn. Int. J. Chem. Kinet. **15**, 475 (1983).
29. W. Tsang. Ind. Eng. Chem. **31**, 3 (1992).
30. P.R. Westmoreland, A.M. Dean, J.B. Howard, and J.P. Longwell. J. Phys. Chem. **93**, 8171 (1989).
31. A. Bencsura, V.D. Knyazev, S.-B. Xing, I.R. Slagle, and D. Gutman. Symp. (Int.) Combust. Proc. **24**, 629 (1992).
32. J. Gang, M.J. Pilling, and S.H. Robertson. J. Chem. Soc. Faraday Trans. **93**, 1481 (1997).
33. F.E. Imbert and R.M. Marshall. Int. J. Chem. Kinet. **19**, 81 (1987).
34. V.D. Knyazev and I.R. Slagle. J. Phys. Chem. **100**, 16899 (1996).

© 2000 NRC Canada

35. S.M. Handford-Styring and R.W. Walker. J. Chem. Soc. Faraday Trans. **91**, 1431 (1995).
36. P.W. Seakins, S.H. Robertson, M.J. Pilling, I.R. Slagle, G.W. Gmurczyk, A. Bencsura, D. Gutman, and W. Tsang. J. Phys. Chem. **97**, 4450 (1993).
37. R.M. Marshall. Int. J. Chem. Kinet. **22**, 935 (1990).
38. A. Fahr, A. Laufer, R. Klein, and W. Braun. J. Phys. Chem. **95**, 3218 (1991).
39. S.H. Robertson, M.J. Pilling, D.L. Baulch, and N.J.B. Green. J. Phys. Chem. **99**, 13452 (1995).
40. M. Weissman and S.W. Benson. Int. J. Chem. Kinet. **16**, 307 (1984).
41. C.W. Larson, R. Patrick, and D.M. Golden. Combust. Flame, **58**, 229 (1984).
42. S.I. Ahonkhai, X.-H. Lin, and M.H. Back. Int. J. Chem. Kinet. **21**, 1 (1989).
43. H.-X. Zhang and M.H. Back. Int. J. Chem. Kinet. **22**, 21 (1990).
44. M.C. Lin and M.H. Back. Can. J. Chem. **44**, 2369 (l966).
45. D.L. Baulch, C.J. Cobos, R.A. Cox, C. Esser, P. Frank, Th. Just, J.A. Kerr, M.J. Pilling, J. Troe, R.W. Walker, and J. Warnatz. J. Phys. Chem. Ref. Data, **21**, 411 (1992).

© 2000 NRC Canada

Structure of 8-[4′-(3″-nitrobenzamido)benzamido]naphthalene-1,3,6-trisulfonate (NF-033), and molecular basis of its cellular toxicity

Arthur Camerman, Donald Mastropaolo, Peter Nickel, Andrew Hempel, and Norman Camerman

Abstract: The title compound is one of a large number of compounds related to the drug suramin which have been found to have anti-HIV properties. However, its toxicity to uninfected cells is high. We crystallized the compound, determined its structure, and investigated the molecular basis for its high toxicity. The crystals are monoclinic, *C*2/*c*, a = 28.614(1), b = 10.031(0), c = 24.051(1) Å, β = 98.36(2)°, Z = 8, convergence at R = 0.066 for 4264 reflections with $I > 2\sigma(I)$. The oxygen atoms of one of the sulfonate groups are disordered, as are several water molecules. Stereochemical comparisons with a segment of B-DNA have yielded a plausible explanation for the molecule's toxicity.

Key words: crystal structure, cellular toxicity, stereochemistry, NF-033.

Résumé : Le composé mentionné dans le titre est l'un de plusieurs composés apparentés à la suramine qui présente des propriétés anti-HIV. Toutefois, sa toxicité par rapport aux cellules qui ne sont pas infectées est élevée. On a cristallisé ce composé, on en a déterminé la structure et essayé de déterminer les bases moléculaires de sa toxicité élevée. Les cristaux sont monocliniques, groupe d'espace *C*2/*c*, avec a = 28,614(1), b = 10,031(0) et c = 24,051(1) Å, β = 98,36(2)°, Z = 8 et R = 0,066 pour 4264 réflexions avec $I > 2\sigma(I)$. Les atomes d'oxygène de l'un des groupes sulfonates sont désordonnés et c'est aussi le cas pour plusieurs molécules d'eau. Les comparaisons stéréochimiques avec un segment d'ADN-B ont permis de fournir une explication plausible pour la toxicité de la molécule.

Mots clés : structure cristalline, toxicité cellulaire, stéréochimie, NF-033.

Introduction

Suramin is a well-known antiprotozoal agent. Interest with respect to use in AIDS occurred because it had been reported (1) that suramin was a potent competitive inhibitor of the reverse transcriptase of a number of animal retroviruses. *In vitro* effectivity of suramin against HIV-1 virus in clinical doses was demonstrated (2) and short term clinical trials showed virustatic activity *in vivo* (3, 4). In the course of clinical trials for treatment of AIDS, suramin exhibited activity against both HIV-associated lymphoma and cutaneous Kaposi sarcoma (5), generating interest in the compound as a potential anticancer drug. Subsequently, clinical trials have shown suramin to have benefit in the treatment of a number of types of cancers, including some which are refractory to other treatments (6–11). A serious drawback to all suramin uses, however, is the drug's toxicity, which can be potentially life-threatening at the levels at which it is used for clinical chemotherapy. Suramin is thought to inhibit retroviruses by binding to the template/primer binding site of viral reverse transcriptase (RT) (1, 12); its toxicity results from similar binding to cellular DNA polymerases and other DNA-binding enzymes (12–14).

In an attempt to create more effective drugs, a large number of suramin derivatives have been synthesized and tested for their ability to inhibit HIV-1 RT, and for their toxicity to uninfected cells (15). The title compound, designated NF-033, had an anti-RT ID_{50} comparable to suramin, but was tenfold more toxic; indeed its toxicity in uninfected cells was the highest of all the analogues tested. We undertook crystallization and structure elucidation of NF-033 in order to investigate the stereochemical bases for its high toxicity.

Experimental

The structure was initially determined from room-temperature X-ray diffraction data. Because of some disorder, the data were recollected at low temperature, but the

Accepted October 28, 1999.

A. Camerman and D. Mastropaolo. Ardono Research, 8515-C 35 Ave. NE Seattle, WA 98115, U.S.A.
P. Nickel. Pharmazeutisches Institut, Universitat Bonn, Germany.
A. Hempel and N. Camerman.[1] Biochemistry Department, University of Toronto, Toronto, ON M5S 1A8, Canada.

[1]Author to whom correspondence may be addressed. Telephone: (416) 978-7027. Fax: (416) 978-8548.
e-mail: norman.camerman@utoronto.ca

© 2000 NRC Canada

Table 1. Crystal data and details of the structure determination.

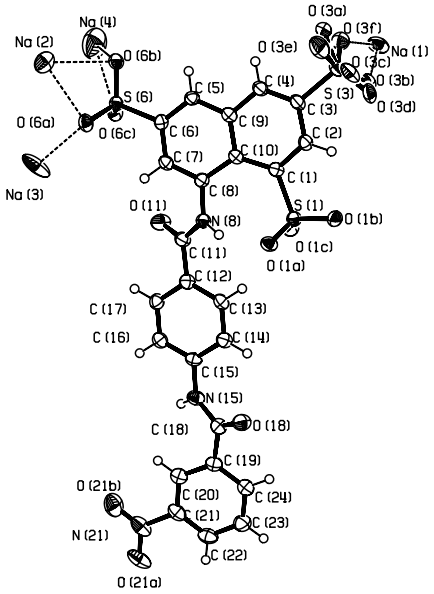
Crystal data	
Chemical formula	$C_{24}H_{15}N_3Na_3O_{13}S_3 \cdot 5H_2O$
Formula weight	718.54
Crystal system	Monoclinic
Space group	*C*2/*c* (No. 15)
a, *b*, *c* (Å)	28.614(1), 10.031(1), 24.051(1)
α, β, γ (°)	90, 98.36(2), 90
V (Å^3)	6829.9(5)
Z	8
D_{calc} (g/cm^3)	1.398
F(000)	2920
μ(MoK$_\alpha$) (1/cm)	3.18
Crystal size (mm)	0.15 × 0.25 × 0.61
Data collection	
Temperature (K)	96 ± 2
Radiation (Å)	MoK$_\alpha$ 0.71073
Theta min, max (°)	4.1, 26.4
Scan	ω
Dataset	*h* = 0:35; *k* = 0:12; *l* = –30:29
Uniq. data	6912
Observed data ($I > 2\sigma(I)$)	4464
Refinement	
N_{ref}, N_{par}	6912, 511
R, *S*	0.066, 1.06
wR (F_o^2)[a]	0.184
Max and av. shift/error	0.00, 0.00
Min and max resd. dens. (e/Å^3)	–1.20, 1.13

[a] $w=1/[\sigma^2(F_o^2) + (0.1148P)^2 + 6.7687P]$ where $P = (F_o^2 + 2F_c^2)/3$.

disorder remained. We report the results of the low temperature experiment.

Crystals were obtained by vapor diffusion of dioxane into an aqueous solution of NF-033. Data were collected at 96 K using a Nonius Kappa CCD diffractometer with rotating anode, MoK$_\alpha$ radiation and Nonius Kappa CCD software. The unit cell parameters were determined by a least-squares fit of the angular settings of all collected reflections. Processing was carried out using Denzo-SMN package (16). A total of 6912 unique reflections were measured and used in the structure analysis and refinement. The structure was solved and refined by SHELX97.[2] All non-hydrogen atoms, except for the water molecules and disordered oxygen atoms at S(3), were found from the best solution E-map. Refinement was by full-matrix least squares. Subsequently eight water molecules, six with partial occupancies, and six oxygen atoms of the disordered SO_3 group, also with partial occupancies, were found from a difference map. Hydrogen atoms positions were calculated geometrically and during the refinement were riding on parent atoms. No hydrogen atoms were fitted to water molecule oxygens. Crystal data and other pertinent information are presented in Table 1.[3]

Fig. 1. Labeled drawing of the molecular structure of the sodium salt of NF-033. Water molecules have been omitted for clarity.



Dispersion corrections and absorption coefficients were taken from International Tables for Crystallography (17), tables 6.1.1.4, 4.2.6.8, and 4.2.4.2 respectively. The final *R* factor converged at *R* = 0.066 for 4264 observed reflections with $I > 2\sigma(I)$, and *R* = 0.108 for all 6912 unique reflections. Atom coordinates and equivalent isotropic thermal parameters are shown in Table 2.

Results and discussion

Crystal and molecular structures

The asymmetric unit of the crystal consists of one molecule of NF-033, three sodium ions, and eight water molecules of which six have partial occupancies. The structure of NF-033 is shown in Fig. 1. The molecule consists of a naphthalene ring system and two phenyl rings, each linked by amide bonds, and overall the molecule is basically planar. The root mean square deviation of the atoms in the best plane passing through the three ring systems is 0.13 Å, and the maximum atomic deviation of the ring atoms from this plane is 0.28 Å (C(13)). The nitro group oxygen atoms are also coplanar with the phenyl ring; this is a consequence of the molecular packing, and to some degree π-electrons delocalization. The two amide groupings are also planar, and remarkably coplanar with each other. They are, however, not coplanar with the ring systems; calculation of all ring-amide torsion angles showed the terminal phenyl ring to be tilted about 33° to the amide, the middle phenyl ring to be tilted about 25.5° to each amide,

[2] G.M. Sheldrick. SHELX97. Program for the solution and refinement of crystal structures (1997). Univ. of Gottingen, Germany.

[3] Anisotropic temperature factors, hydrogen atom coordinates, and a stereoscopic diagram of the crystal packing have been deposited as supplementary material and may be purchased from: The Depository of Unpublished Data, Document Delivery, CISTI, National Research Council Canada, Ottawa, Ontario, Canada, K1A 0S2. With the exception of the anisotropic temperature factors, these have also been deposited with the Cambridge Crystallographic Data Centre and can be obtained on request from: The Director, Cambridge Crystallographic Data Centre, University Chemical Laboratory, 12 Union Road, Cambridge, CB2 1EZ, U.K.

© 2000 NRC Canada

Table 2. Atomic coordinates (× 10^4) and equivalent isotropic displacement parameters (Å^2 × 10^3).

Atom	*x*	*y*	*z*	U_{eq}[a]
C(1)	–844(1)	793(4)	–762(2)	24(1)
C(2)	–702(2)	1752(4)	–1112(2)	26(1)
C(3)	–364(2)	2701(4)	–916(2)	29(1)
C(4)	–166(2)	2725(4)	–366(2)	28(1)
C(5)	–95(2)	1897(4)	582(2)	25(1)
C(6)	–205(2)	997(4)	966(2)	24(1)
C(7)	–514(2)	–57(4)	796(2)	26(1)
C(8)	–746(1)	–168(4)	259(2)	24(1)
N(8)	–1087(1)	–1194(3)	157(1)	26(1)
C(9)	–299(1)	1769(4)	12(2)	24(1)
C(10)	–645(1)	752(4)	–172(2)	23(1)
C(11)	–1376(2)	–1573(4)	526(2)	30(1)
O(11)	–1371(1)	–1032(3)	992(1)	40(1)
C(12)	–1712(2)	–2685(4)	357(2)	27(1)
C(13)	–1907(2)	–2965(4)	–200(2)	28(1)
C(14)	–2239(2)	–3938(4)	–324(2)	30(1)
C(15)	–2390(1)	–4662(4)	114(2)	27(1)
N(15)	–2759(1)	–5618(3)	22(2)	32(1)
C(16)	–2194(2)	–4421(4)	666(2)	31(1)
C(17)	–1860(2)	–3427(4)	787(2)	30(1)
C(18)	–2898(2)	–6351(4)	–450(2)	31(1)
O(18)	–2706(1)	–6286(3)	–874(1)	38(1)
C(19)	–3294(2)	–7302(4)	–415(2)	30(1)
C(20)	–3349(2)	–7960(4)	82(2)	31(1)
N(21)	–3755(2)	–9665(4)	565(2)	44(1)
O(21A)	–4046(1)	–10578(3)	530(2)	53(1)
O(21B)	–3504(2)	–9366(4)	1012(2)	56(1)
C(21)	–3702(2)	–8916(4)	59(2)	34(1)
C(22)	–4005(2)	–9212(4)	–432(2)	36(1)
C(23)	–3950(2)	–8525(4)	–913(2)	41(1)
C(24)	–3596(2)	–7585(4)	–911(2)	36(1)
S(1)	–1287(1)	–297(1)	–1113(1)	26(1)
O(1A)	–1125(1)	–1661(3)	–977(1)	29(1)
O(1B)	–1319(1)	–23(3)	–1709(1)	31(1)
O(1C)	–1719(1)	29(3)	–896(1)	32(1)
S(3)	–193(1)	3891(1)	–1392(1)	47(1)
O(3A)	19(2)	5005(4)	–1052(2)	34(1)
O(3B)	–677(2)	4404(4)	–1704(2)	35(1)
O(3C)	61(2)	3294(4)	–1741(2)	40(1)
O(3D)	–313(4)	3273(8)	–1961(4)	37(2)
O(3E)	406(4)	3500(10)	–1314(5)	56(3)
O(3F)	–215(4)	5080(10)	–1254(4)	37(3)
S(6)	–14(1)	1191(1)	1693(1)	25(1)
O(6A)	180(1)	–83(3)	1897(1)	31(1)
O(6B)	339(1)	2243(3)	1765(1)	32(1)
O(6C)	–433(1)	1572(3)	1929(1)	30(1)
Na(1)	–942(1)	6502(2)	–1480(1)	47(1)
Na(2)	948(1)	748(2)	2464(1)	45(1)
Na(3)	0	–1716(2)	2500	68(1)
Na(4)	0	3543(5)	2500	101(1)
OW(1)	1298(2)	3062(5)	2453(2)	83(1)
OW(2)	886(2)	–1566(6)	2834(2)	110(2)
OW(3)	637(2)	4874(5)	2790(2)	56(2)
OW(4)	1699(4)	90(10)	3042(3)	152(6)
OW(5)	1550(4)	–3060(10)	2346(4)	127(6)
OW(6)	–2798(5)	–7610(20)	–1880(6)	110(9)
OW(7)	–2285(6)	1900(20)	–1644(7)	94(8)
OW(8)	–2079(7)	1270(20)	–2260(10)	85(6)

[a] U_{eq} = 1/3 (trace of the orthogonalized U_{ij} matrix).

and the naphthyl system to be tilted about 37.5° to the amide. These molecular features are shown in Fig. 2.

The 3-sulfonate group is disordered, with each oxygen atom occupying two positions at approximate ratios of 65:35. Bond lengths and angles in the rest of the molecule have normal values; the C—N distances of 1.354 and 1.362 Å reflect the delocalized character of the amide bonds. The negative charge at each SO_3 group is delocalized over the oxygen atoms. There is one intramolecular hydrogen bond in the structure, N(8)-H(8)···O(1A), with N···O distance of 2.75 Å and N-H···O angle of 152°. The other amide nitrogen is a donor in an intermolecular hydrogen bond, N(15)-H(15)···O(1C), with N···O distance of 2.81 Å and N-H···O angle of 150°.

Two sodium cations occupy general positions while the third occupies two special crystallographic positions with 0.5 occupancy in each. Each sodium ion is coordinated with six sulfonate, water and nitro group oxygen atoms, at distances ranging from 2.29–2.62 Å. Two water molecules (W1 and W2) are fully present in the crystal, while the other six have partial occupancies ranging from 0.25 to 0.76. Water oxygens O(W1)–O(W4) interact with sodium ions; the other water molecules do not appear to form intermolecular interactions.

Molecules of NF-033 are held together in dimers by two intermolecular hydrogen bonds and by extensive aromatic ring stacking involving nitrophenyl–naphthyl, phenyl–phenyl, and amide–amide π-electron interactions (Fig. 3). Parallel sets of dimers are stacked in infinite sheet structures, parallel to the (**a**, **b**) plane, held together within sheets by similar π-electron interactions. The sulfonic acid groups extend above and below the sheets; the spaces between sheets are occupied by the sodium ions and water molecules, which connect sheets through interactions with the sulfonates.

Molecular basis of toxicity

If the toxicity to uninfected cells of these types of compounds arises from binding to DNA-binding enzymes, it is likely the compounds bear stereochemical resemblance to DNA, although any such resemblance is not immediately obvious from the chemical structures. In order to reveal stereochemical similarities we have performed molecular superposition studies of NF-033 with segments of the sugar-phosphate backbone of a single strand of B-DNA.[4] The re-

[4] NF-033 was overlapped on a 3-nucleotide segment of a single strand of B-DNA by superposing the central C-C-N atoms of NF-033 with the B-DNA center O-P-O phosphate. In addition, to bring the ends of the molecules into the same plane, a naphthalene sulfonate S atom was superposed with a terminal DNA phosphorus atom. Two rotations were made to the NF-033 crystal structure conformation, both were 180° about C—C single bonds, thus leaving NF-033 planarity and conformational energy unchanged. These rotations brought an NF-033 carbonyl O and the terminal nitro group into approximation with a DNA phosphate oxygen and terminal phosphate group respectively.

© 2000 NRC Canada

Fig. 2. Edge-on view of NF-033, showing the relationship of the component planes.

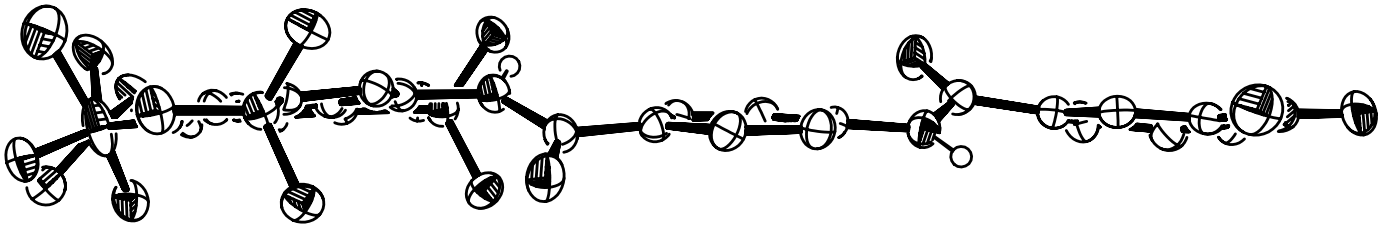


Fig. 3. Stereoscopic view of arrangement of NF-033 molecules as dimers.

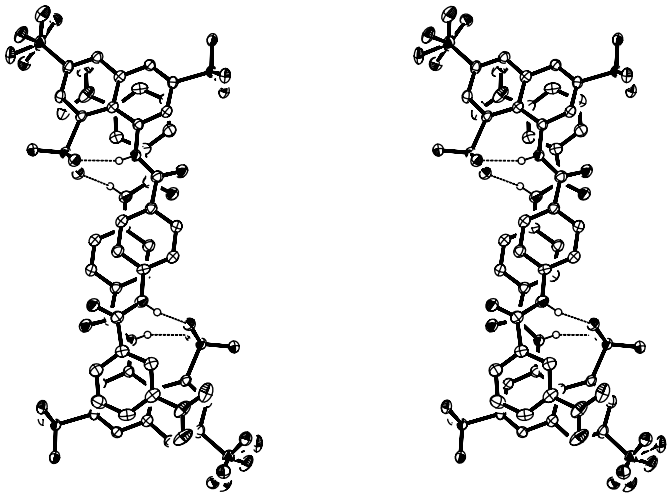
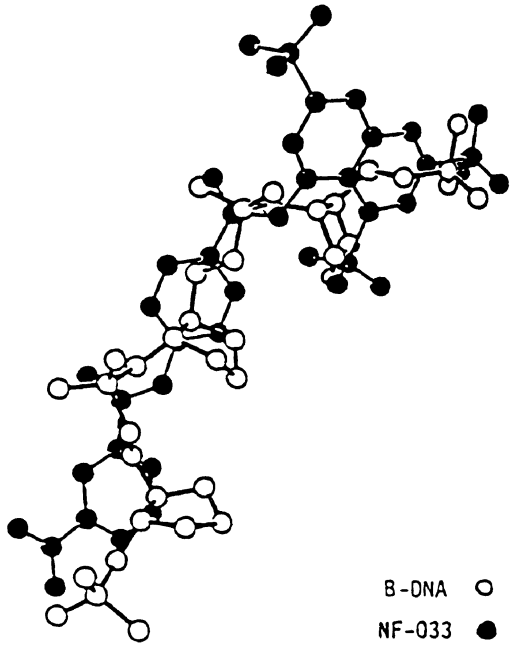


Fig. 4. Molecular superposition of NF-033 and a segment of the sugar-phosphate backbone of a single strand of B-DNA.



sults are shown in Fig. 4. Inspection of the figure reveals that NF-033's planar conformation fits the B-DNA helical conformation very well. Firstly, the molecular length of NF-033 is almost identical to the length of a three nucleotide segment of B-DNA. Secondly, there are close positionings of a number of chemically similar groups in the two molecules: the 3-sulfonate group with a DNA phosphate, a 1-sulfonate oxygen atom with a sugar hydroxyl oxygen, amide carbonyl oxygens with phosphate oxygens, and the NF-033 nitro group with a DNA phosphate. Additionally, the two phenyl groups in NF-033 are in the same neighborhoods as sugar rings in DNA. The molecular fits could possibly be additionally optimized by more extensive fitting procedures which allow for molecular flexibilities, but the fit is sufficient at this level to provide a plausible explanation of the molecular basis for NF-033 toxicity to uninfected cells, because the stereochemical similarities suggest how the molecule could interact with DNA polymerase and other DNA-binding enzymes. The results also indicate approaches to reducing toxicity in these molecules, by altering features which superpose with stereochemically similar groups in DNA.

Acknowledgements

This work was supported by grant AI40392 from the National Institutes of Health (AC) and by the National Cancer Institute of Canada with funds from Canadian Cancer Society (NC).

References

1. E. DeClercq. Cancer Lett. (Shannon, Irel.), **8**, 9 (1979).
2. H. Mitsuya, M. Popovic, R. Yarchoan, S. Matsushita, R. Gallo, and S. Broder. Science (Washington, D.C.), **226**, 172 (1984).
3. S. Broder, J. Collins, P. Markham, R. Redfield, D. Hoth, R. Gallo, R. Yarchoan, H. Lane, R. Klecker, H. Mitsuya, E. Gelmann, L. Resnick, and C. Myers. Lancet, ii, 627 (1985).
4. D. Rouvroy, J. Bodaerts, J.B. Habyarimana, D. Nzaramba, and P. Van De Perre. Lancet, i, 878 (1985).
5. A. Levine, P. Gill, J. Cohen, J. Hawkins, S. Formenti, S. Aquilar, P. Meyer, M. Krailo, J. Parker, and S. Rasheed. Ann. Intern. Med. **105**, 32 (1986).
6. C. Myers, M.R. Cooper, C.A. Stein, R.V. LaRocca, M. Walther, G. Weiss, P. Choyke, N. Dawson, S. Steinberg, M. Uhrich, J. Cassidy, D. Kohler, J. Trepel, and W. Linehan. J. Clin. Oncol. **10**, 881 (1992); M. Eisenberger, L. Reyno, D. Jodrell, V. Sinibaldi, K. Tkuczuk, R. Sridhara, E. Zuhowski, M. Lowitt, S. Jacobs, and M. Egorin. J. Nat. Cancer Inst. **85**, 611 (1993); K. Kobayashi, E. Vokes, L. Janish, N. Vogelzang, and M. Ratin. Proc. Am. Soc. Clin. Oncol. **13**, 140 (1994); M. Eisenberger, L. Reyno, V. Sinibaldi, R. Sridhara, M. Carducci, and M. Egorin. Cancer, **75**, 1927 (1995); E. Kehinde, T. Terry, N. Mistri, T. Horsburgh, D. Sandhu. and P. Bell. Cancer Surveys, **23**, 217 (1995).

© 2000 NRC Canada

7. R.V. LaRocca, C.A. Stein, R. Danesi, C. Jamis-Dow, G. Weiss, and C.E. Myers. J. Clin. Endocrinol. Metab. **71**, 497 (1990).
8. M. Pollack and M. Richard. J. Natl. Cancer Inst. **82**, 1349 (1990); M. Eisenberger and J. Fontana. J. Natl. Cancer Inst. **84**, 3 (1992); P. Andreotti, J.M. Lee, E. Greenspan, and H. Bruckner. Proc. Am. Soc. Clin. Oncol. **456**, 165 (1994).
9. R.V. LaRocca, M.R. Cooper, R. Danesi, C.A. Stein, and C.E. Myers. Eur. J. Cancer, **30A**, 718 (1994).
10. J. Fantini, J. Rognoni, M. Theveniau, G. Pommier, and J. Marvaldi. J. Cell Physiol. **143**, 468 (1990).
11. C. Taylor, R. Lui, R. Fanta, and S. Salmon. J. Natl. Cancer Inst. **84**, 489 (1992).
12. K. Ono, H. Nakane, and M. Fukushima. Eur. J. Biochem. **172**, 149 (1988).
13. Z. Spigelman, A. Dowers, S. Kennedy, D. DiSorbo, M. O'Brien, R. Barr, and R. McCaffery. Cancer Res. **47**, 4694 (1987).
14. A. Basu and M.J. Modak. Biochem. Biophys. Res. Commun. **128**, 1395 (1985).
15. K. Jentsch, G. Hunsmann, H. Hartmann, and P. Nickel. J. Gen. Virol. **68**, 2183 (1987).
16. Z. Otwinowski and W. Minor. Methods Enzymol. **276**, 307 (1997).
17. International Tables for Crystallography. Vol. C. Dordrecht: Kluwer Academic Publishers. 1992.

© 2000 NRC Canada

New abietane diterpenoids from the cones of *Larix kaempferi*

Hironori Ohtsu, Reiko Tanaka, Yasuko In, Shunyo Matsunaga, Harukuni Tokuda, and Hoyoku Nishino

Abstract: A new podocarpane diterpene, 7α,15-dihydroxypodocarp-8(14)-en-13-one (**1**) and eight new abietane diterpenes, abiet-8(14)-en-7α,13β,15,18-tetraol (**2**), 7α,13β,15-trihydroxyabiet-8(14)-en-18-oic acid (**3**), 13β,18-dihydroxyabiet-8(14)-en-7-one (**4**), 13β,15,18-trihydroxyabiet-8(14)-en-7-one (**5**), 7-oxo-13β-methoxyabiet-8(14)-en-18-oic acid (**7**), abiet-8(14)-en-7α,12α,13β,18-tetraol (**8**), 7α,12α,13β-trihydroxyabiet-8(14)-en-18-oic acid (**9**), and abiet-8(14)-en-7α,12α,13β,15,18-pentaol (**10**) were isolated from the $CHCl_3$ extract of the cones of *Larix kaempferi*. Their structures were determined on the basis of chemical and spectral evidence. The inhibitory effects of compounds **1–4** and **7–9** on Epstein–Barr virus early antigen (EBV–EA) activation induced by the tumor promoter, 12-*O*-tetradecanoylphorbol-13-acetate (TPA), were examined for a primary screening for anti-tumor promotors.

Key words: *Larix kaempferi*, Pinaceae, cones, abietane, EBV–EA.

Résumé : L'extraction au $CHCl_3$ de cônes de *Larix kaempferi* a permis d'isoler un nouveau diterpène de la série du podocarpane, le 7α,15-dihydroxypodocarp-8(14)-én-13-one (**1**) ainsi que huit nouveaux diterpènes de la série de l'abiétane, abiét-8(14)-ène-7α,13,β,15,18-tétraol (**2**), acide 7α,13β,15-trihydroxyabiét-8(14)-énoïque (**3**), 13β,18-dihydroxyabiét-8(14)-én-7-one (**4**), acide 13β,15,18-trihydroxyabiét-8(14)-én-7-one (**5**) 7-oxo-13β-méthoxyabiét08(14)-én-18-oïque (**7**), abiét-8(14)-ène-7α,12α,13β,18-tétraol (**8**), acide 7α,12α,13β-trihydroxyabiét-8(14)-én-18-oïque (**9**) et abiét-8(14)-ène-7α,12α,13β,15,18-pentaol (**10**). On a déterminé les structures en se basant sur des données chimiques et spectroscopiques. À titre d'évaluation primaire comme promoteurs d'effets antitumoraux, on a examiné les effets inhibiteurs des composés **1–4** et **7–9** sur l'activation de l'antigène primaire du virus d'Epstein–Barr (« EBV–EA ») induite par le promoteur tumoral, le 13-acétate de 12-*O*-tétradécanoylphorbol (« TPA »).

Mots clés : *Larix kaempferi*, Pinaceae, cônes, abiétane, « EBV–EA ».

[Traduit par la Rédaction]

Introduction

We have focused our attention on the biologically active constituents of the leaves, cones, and bark of coniferous trees which have been treated as wastes in the forestry industry. During the investigation of the chemical constituents of Pinaceae plants, we had reported that the leaves and bark of *Larix kaempferi* contained three new abietane-type diterpenes (1) and new cycloartane and lanostane-type triterpenes (2). Furthermore, we recently reported the isolation and structural elucidation of five new abietane-type diterpenes from the $CHCl_3$ extract of the cones of this tree (3, 4). Further fractionation of the extract led to the isolation of a new podocarpane diterpene (**1**) and eight new highly oxygenated abietane diterpenes (**2–5** and **7–10**), together with a known compound, 7-oxo-13β-hydroxyabiet-8(14)-en-18-oic acid (**6**).

Received October 26, 1999.

H. Ohtsu, R. Tanaka,[1] Y. In, and S. Matsunaga. Osaka University of Pharmaceutical Sciences, 4-20-1 Nasahara, Takatsuki, Osaka 569-1094, Japan.
H. Tokuda and H. Nishino. Kyoto Prefectural University of Medicine, Kamigyo-ku, Kyoto 602-0841, Japan.

[1]Author to whom correspondence may be addressed. Telephone: +81-726-90-1084. Fax: +81-726-90-1084. e-mail: tanakar@oysun01.oups.ac.jp

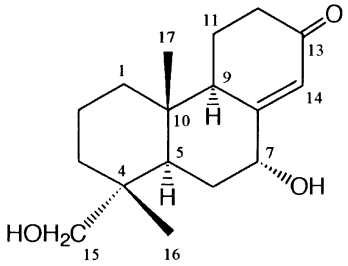
This paper deals with the structural elucidation of these new compounds. The inhibitory effects of compounds **1–4** and **7–9** on Epstein–Barr virus early antigen (EBV–EA) activation induced by the tumor promoter, 12-*O*-tetradecanoylphorbol-13-acetate (TPA), were examined for a primary screening for anti-tumor-promotors.

Results and discussion

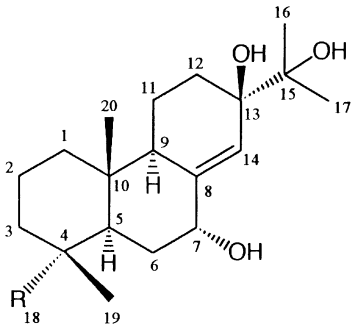
The preliminary silica gel column chromatography of the $CHCl_3$ extract of *L. kaempferi* had been reported previously (3). Rechromatography of EtOAc–MeOH (10:1) eluate (11.34 g) on silica gel, reversed-phase silica gel (ODS), and HPLC (ODS) furnished nine new diterpenes **1–5** and **7–10** as well as a known abietane (**6**). The known compound **6** was identified as 7-oxo-13β-hydroxyabiet-8(14)-en-18-oic acid by a comparison with literature data (5).

Compound **1** was assigned the molecular formula $C_{17}H_{26}O_3$ by HREIMS. The UV and IR spectra showed the presence of a hydroxyl group (ν_{max} 3375 cm^{-1}), an α,β-unsaturated ketone (λ_{max} 237 nm; ν_{max} 1684 cm^{-1}), and a trisubstituted double bond (ν_{max} 837 cm^{-1}). The ^1H and ^{13}C NMR spectra of **1** (Tables 1 and 2) revealed signals for two tertiary methyl groups, six methylene groups, two methine groups, two sp^3 quaternary carbons, an oxygenated methylene (δ_H 2.93 and 3.51 (each 1H, d, J = 11.0 Hz) ppm; δ_C

© 2000 NRC Canada

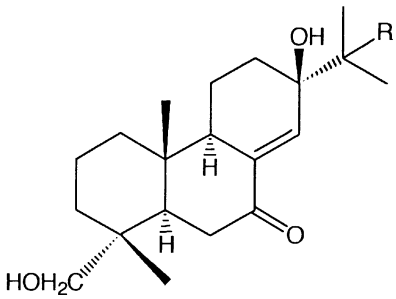


1



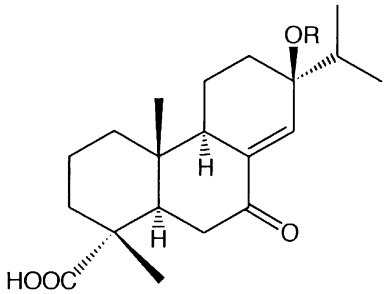
2 R = CH_2OH

3 R = COOH



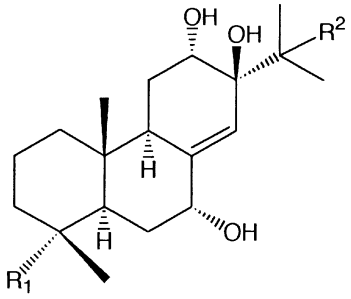
4 R = H

5 R = OH



6 R = H

7 R = Me



8 $R^1 = CH_2OH$, R^2 = H

9 R^1 = COOH, R^2 = H

10 $R^1 = CH_2OH$, R^2 = OH

70.2 (t) ppm), an oxygenated methine (δ_H 4.36 (1H, t, J = 3.0 Hz) ppm; δ_C 71.4 (d) ppm), and an α,β-unsaturated ketone (δ_H 5.94 (1H, d, J = 2.0 Hz) ppm; δ_C 127.5 (d), 164.1 (s), and 201.1 (s) ppm). Compound **1** was deduced to have one primary and one secondary hydroxyl group because treatment of **1** with Ac_2O-pyridine afforded a diacetate (**1a**). The planar structure of **1** was determined by a combination of ^1H–^1H COSY, HMQC and HMBC spectra (Fig. 1), which proved that **1** had a podocarpane skeleton bearing a primary hydroxyl group at C-4, a secondary hydroxyl group at C-7, and an α,β-unsaturated ketone at C-8(14)-13 positions. The relative stereochemistry of **1** was determined by NOESY experiment. In the NOESY spectrum, significant NOEs were observed for: (*i*) H-16 with H-17, (*ii*) H-7 with H-6α and H-6β, and (*iii*) a hydroxymethyl signal with H-3α and H-5α. Thus, the primary hydroxyl group was located at C-15, and the C-7 hydroxyl group had α-configuration. The absolute structure of **1** was determined by the CD exciton chirality method (6). As illustrated in Scheme 1, after protection of the primary hydroxyl group of **1** with a *t*-butyldimethylsilyl group, compound **1** was derived to *p*-chlorobenzoate (**1c**) (Scheme 1). The CD spectrum of **1c** (Fig. 2) showed a negative Cotton effect curve at 245 nm (Δε –20.4) and 223 nm (Δε +15.7). Therefore, the absolute configuration of C-7 of **1** was proved to be *R*, and the absolute stereostructure was as formulated in **1**.

HREIMS analysis of compound **2** revealed the molecular formula to be $C_{20}H_{34}O_4$. Its IR spectrum showed strong absorption for hydroxyl groups (ν_{max} 3340 cm^{-1}) and a trisubstituted double bond (ν_{max} 840 cm^{-1}). The ^1H and ^{13}C NMR spectra (Tables 1 and 2) suggested the presence of two tertiary methyl groups, a hydroxyisopropyl group (δ_H 1.18 and 1.23 (each 3H, s) ppm; δ_C 24.7 (q), 24.8 (q) and 76.0 (s) ppm), six methylene groups, two methine groups, two sp^3 quaternary carbons, a trisubstituted double bond, a primary hydroxyl group, a secondary hydroxyl group, and an oxygenated sp^3 quaternary carbon (δ_C 74.3 (s) ppm). Acetylation of **2** in usual manner gave a diacetate (**2a**). The molecular formula of compound **3** was assigned as $C_{20}H_{32}O_5$ by HREIMS and DEPT data. The IR spectrum suggested the presence of a carboxyl group (ν_{max} 3668–2869, 1697 cm^{-1}), and this was supported by esterification of **3** with diazomethane to afford a methyl ester (**3a**). The ^1H and ^{13}C NMR data of **3** closely resembled those of **2** except for the presence of a carboxyl group instead of a primary hydroxyl group in **2**. The relative structures of **2** and **3** were determined by analyzing their ^1H–^1H COSY, HMQC and HMBC spectra (Fig. 3), and the X-ray crystallographic analysis of **3** (Fig. 4). Then, the relative structures of **2** and **3** were proved to be abiet-8(14)-en-7α,13β,15,18-tetraol and 7α,13β,15-trihydroxyabiet-8(14)-en-18-oic acid, respectively. The absolute structures of **2** and **3** were determined by the following

© 2000 NRC Canada

Table 1. ^{1}H NMR (500 MHz) data for compounds **1**–**5** (TMS = 0).[a]

Position	1	2	3	4	5	HMBC data of **4** (H to C)
1α	1.16 m	1.08 ddd (12.5, 12.5, 3.5)	1.20 m	1.12 ddd (12.0, 12.0, 5.0)	1.12 ddd (12.0, 12.0, 5.0)	20
1β	1.73 m	1.72 ddd (12.5, 2.5, 2.5)	1.76 m	1.84 ddd (12.0, 3.0, 3.0)	1.82 ddd (12.0, 3.0, 3.0)	2
2	1.57 (2H) m	1.53 (2H) m	1.58 (2H) m	1.61 (2H) m	1.62 (2H) m	1, 4, 10
3α	1.68 m	1.53 m	1.88 m	1.51 m	1.50 m	2, 4
3β	1.21 ddd (11.5, 2.5, 2.5)	1.30 m	1.59 m	1.36 ddd (12.0, 4.0, 4.0)	1.36 ddd (12.0, 4.0, 4.0)	2, 4
5α	2.02 dd (13.0, 2.5)	1.81 dd (13.0, 3.0)	2.40 dd (13.0, 2.5)	1.90 dd (14.0, 5.0)	1.91 dd (14.0, 5.0)	4, 7, 9, 10, 18, 19, 20
6α	1.82 ddd (14.5, 2.5, 2.5)	1.64 m	1.45 dt (14.0, 2.5)	2.52 dd (18.8, 5.0)	2.53 dd (18.5, 5.0)	4, 5, 7, 10
6β	1.70 m	1.64 m	1.73 m	2.31 dd (18.8, 14.0)	2.32 dd (18.5, 14.0)	4, 5, 7, 8, 10
7β	4.36 t (3.0)	4.18 t (3.0)	4.14 t (3.0)	—	—	
9α	2.57 ddd (8.5, 5.8, 2.0)	2.12 ddd (8.3, 8.3, 2.5)	2.18 dd (8.3, 8.0)	2.03 m	2.04 m	5, 11
11α	2.04 m	1.64 m	1.64 m	1.75 m	1.77 m	9, 12
11β	1.75 m	1.64 m	1.64 m	1.46 m	1.50 m	9, 12
12α	2.26 ddd (16.0, 13.0, 5.5)	1.50 m	1.51 m	1.46 m	1.48 m	11, 13
12β	2.24 ddd (16.0, 4.5, 4.5)	1.65 m	1.66 m	1.73 m	1.85 m	11, 13
14	5.94 d (2.0)	5.90 br s	5.90 br s	6.73 dd (2.0, 2.8)	6.99 dd (1.5, 2.0)	7, 9, 12
15	2.93, 3.51 each d (11.0)	—	—	1.80 septet (7.0)	—	13, 16, 17
16	0.76 s	1.18 s	1.17 s	0.87 d (7.0)	1.15 s	13, 15
17	0.83 s	1.23 s	1.22 s	0.96 d (7.0)	1.24 s	13, 15
18	—	3.00, 3.36 each d (11.5)	—	3.11, 3.37 each d (11.0)	3.11, 3.37 each d (11.0)	3, 4, 5, 19
19	—	0.80 s	1.18 s	0.85 s	0.85 s	3, 4, 5, 18
20	—	0.85 s	0.83 s	0.87 s	0.88 s	1, 5, 9, 10

[a]Compounds **1**, **4**, and **5** were measured in $CDCl_3$, and **2** and **3** were measured in CD_3OD. δ in ppm; *J* (in parentheses) in Hz; assignments from ^{1}H–^{1}H COSY, HMQC, HMBC, and NOESY data.

chemical reactions: reduction of **3a** with $LiAlH_4$ gave compound **2**, followed by oxidation with $NaIO_4$ in CH_2Cl_2-H_2O to afford compound **1**. This chemical correlation indicated that the absolute structures of **2** and **3** were as formulated (Scheme 2).

Compound **4** was assigned the molecular formula $C_{20}H_{32}O_3$ by HREIMS. The UV and IR spectra showed the presence of hydroxyl groups (ν_{max} 3410 cm^{-1}), an α,β-unsaturated ketone (λ_{max} 245 nm; ν_{max} 1676 cm^{-1}), and a trisubstituted double bond (ν_{max} 1611 and 840 cm^{-1}). Signals were observed for two tertiary methyl groups, an isopropyl group, six methylenes, two methines, two quaternary carbons, a primary hydroxyl group (δ_H 3.11 and 3.37 (each 1H, d, *J* = 11.0 Hz) ppm; δ_C 70.8 (t) ppm), a tertiary hydroxyl group (δ_C 71.8 (s) ppm), and an α,β-unsaturated ketone (δ_C 200.4 (s) ppm) in the ^{1}H and ^{13}C NMR spectra (Tables 1 and 2). These spectral data were similar to those of a known compound, 7-oxo-13β-hydroxyabiet-8(14)-en-18-oic acid (**6**), except for the presence of a primary hydroxyl group instead of a carboxyl group of **6**. The HMBC data of **4** are listed in Table 1. From these spectral data, the structure of **4** was proved to be 13β,18-dihydroxyabiet-8(14)-en-7-one, the C-18 hydroxyl analog of **6**.

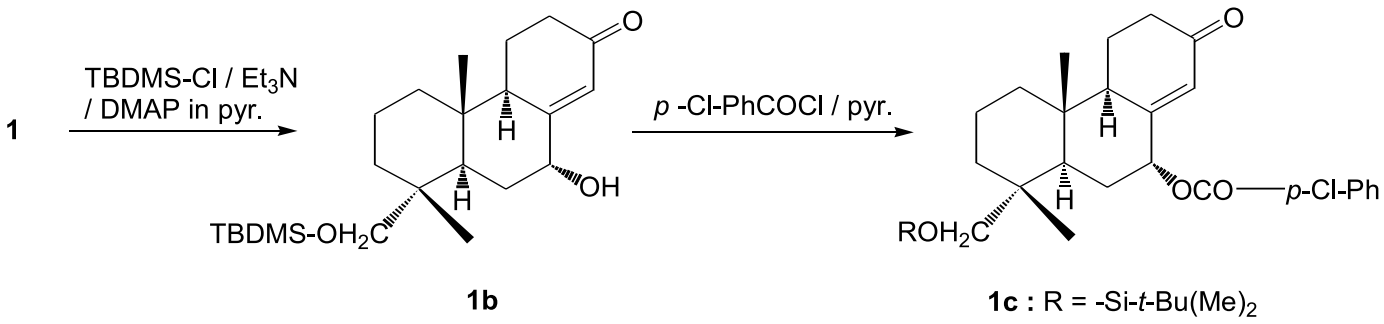
Compound **5** has the molecular formula $C_{20}H_{32}O_4$ by HREIMS and DEPT data. The ^{1}H and ^{13}C NMR data of **5** (Tables 1 and 2) closely resembled those of **4**, although two tertiary methyl signals of a hydroxyisopropyl group (δ_H 1.15 and 1.24 (each 3H, s) ppm; δ_C 23.9 and 24.7 (each q), 74.7 (s) ppm) were observed in **5** instead of an isopropyl group of **4**. These spectral data indicated that **5** should be a 15-hydroxyl derivative of **4**. This structure was supported by the HMBC spectrum of **5**. Therefore, the structure of **5** was proved to be 13β,15,18-trihydroxyabiet-8(14)-en-7-one.

Compound **7** was assigned the molecular formula $C_{21}H_{32}O_4$ by HREIMS. The IR, ^{1}H, and ^{13}C NMR spectra of **7** (Tables 2 and 3) were very similar to those of **6**, except that a tertiary methoxyl signal (δ_H 3.12 (3H, s) ppm; δ_C 75.5 (s) ppm) was observed in **7** instead of a tertiary hydroxyl group at C-13 in **6**. The EIMS spectrum of **7** showed a fragment ion peak at *m/z* 316.2009 corresponding to the loss of MeOH from the molecular ion. The linkage position for the methoxyl group was established as C-13 by HMBC correlation for the methoxyl proton to C-13, and the configuration of the methoxyl group was determined to be β because the methoxyl proton showed NOEs with H-11β and H-12β in the NOESY experiment. Therefore, the structure of **7** was proved to be 7-oxo-13β-methoxyabiet-8(14)-en-18-oic acid.

Compounds **8** and **9** have the molecular formula $C_{20}H_{34}O_4$ and $C_{20}H_{32}O_5$, respectively, based on the HREIMS and DEPT data. Acetylation of **8** with Ac_2O-pyridine gave a triacetate (**8a**), while **9** gave a methyl ester (**9a**) on treatment with diazomethane. The ^{1}H and ^{13}C NMR data (Tables 2 and 3) of **8** and **9** were similar, except for the presence of signals for a primary hydroxyl group (δ_H 2.99 and 3.37 (each d, *J* =

© 2000 NRC Canada

Scheme 1.



Scheme 2.

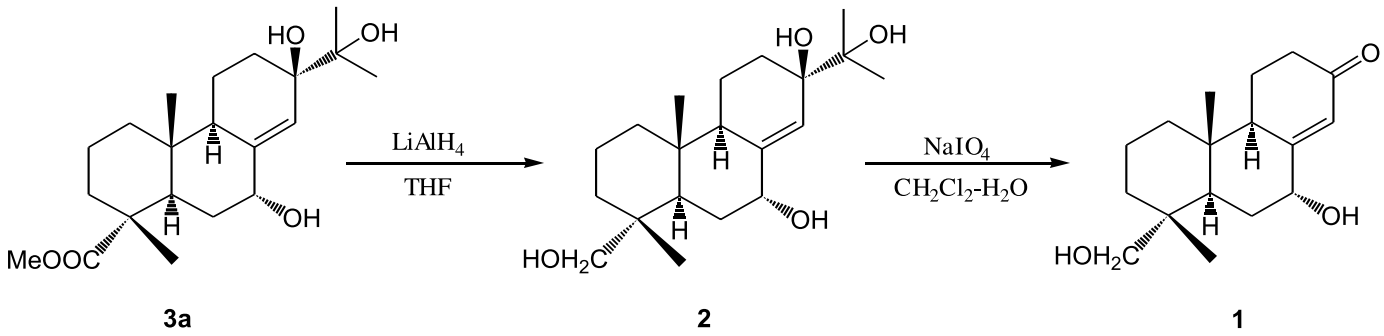


Fig. 1. HMBC correlations for **1**.

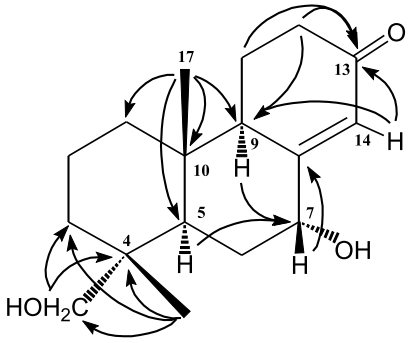
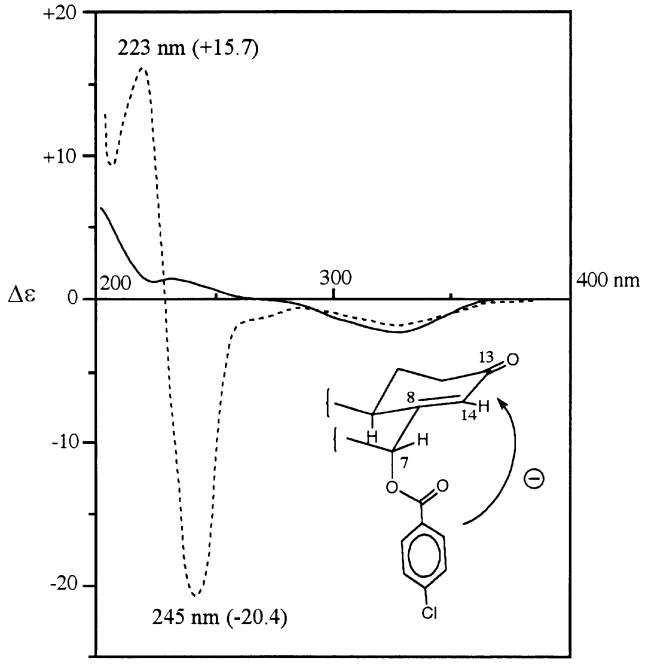


Fig. 2. CD spectra of **1** (——) and **1c** (– – –) in EtOH.



11.5 Hz) ppm; δ_C 71.9 (t) ppm) in **8**, and a carboxyl group (δ_C 184.5 (s) ppm) in **9**. The signals observed in common in their NMR spectra were as follows: two tertiary methyl groups, an isopropyl group, five methylene groups, two methine groups, two sp^3 quaternary carbons, two secondary hydroxyl group, a tertiary hydroxyl group, and a trisubstituted double bond. Comparison of these signal patterns with those of **2** and **3** showed that compounds **8** and **9** also contained 7α,13β-dihydroxyabiet-8(14)-en systems in their molecules. The secondary hydroxyl groups of **8** and **9** which appeared at δ_H 3.82 ppm were attributable to C-12 positions because these signals showed cross-correlations with C-9, C-11 and C-13 in the HMBC spectra. Configuration of the C-12 hydroxyl groups were determined to be α, based on the significant NOEs for H-12 with H-11α and H-11β in the NOESY experiments of **8** and **9** (Fig. 5). Therefore, the relative structures of **8** and **9** were elucidated as abiet-8(14)-en-7α,12α,13β,18-tetraol and 7α,12α,13β-trihydroxyabiet-8(14)-en-18-oic acid, respectively. The absolute structures of **8** and **9** were determined by CD spectra. Compounds **8** and **9a** were treated with benzoyl chloride in pyridine to give corresponding

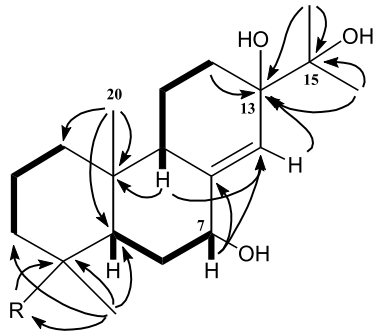
© 2000 NRC Canada

Table 2. ^{13}C NMR (125 MHz) data for compounds **1–5** and **7–10**.[a]

Position	1	2	3	4	5	7	8	9	10
1	38.6 t	40.0 t	39.6 t	38.4 t	38.5 t	37.8 t	39.7 t	39.3 t	39.7 t
2	18.0 t	19.3 t	19.2 t	17.9 t	17.9 t	17.8 t	19.3 t	19.3 t	19.2 t
3	34.7 t	36.5 t	38.0 t	35.1 t	35.1 t	36.8 t	36.5 t	38.7 t	36.5 t
4	37.7 s	38.6 s	47.9 s	37.8 s	37.7 s	46.0 s	38.7 s	47.9 s	38.7 s
5	38.8 d	41.5 d	43.2 d	42.5 d	42.5 d	44.3 d	41.8 d	43.6 d	41.8 d
6	28.7 t	30.3 t	32.9 t	37.0 t	37.0 t	38.7 t	30.4 t	33.0 t	30.2 t
7	71.4 d	73.9 d	73.6 d	200.4 s	200.3 s	199.4 s	74.1 d	74.0 d	73.9 d
8	164.1 s	145.7 s	145.5 s	138.6 s	139.3 s	140.4 s	144.4 s	144.4 s	146.5 s
9	47.0 d	48.3 d	48.4 d	51.6 d	51.4 d	51.5 d	43.7 d	43.9 d	43.5 d
10	39.4 s	39.1 s	38.8 s	35.6 s	35.6 s	35.6 s	39.3 s	39.0 s	39.0 s
11	20.3 t	18.7 t	18.5 t	18.4 t	18.9 t	18.3 t	26.3 t	26.2 t	26.7 t
12	36.7 t	30.3 t	30.2 t	29.5 t	30.0 t	26.9 t	70.9 d	70.9 d	72.3 d
13	201.1 s	74.3 s	74.3 s	71.8 s	73.7 s	75.5 s	72.3 s	72.4 s	72.0 s
14	127.5 d	129.2 d	129.4 d	139.8 d	136.9 d	139.6 d	127.9 d	128.1d	126.0 d
15	70.2 t	76.0 s	76.0 s	37.7 d	74.7 s	32.6 d	33.5 d	33.5 d	77.1 s
16	18.1 q	24.7 q	24.7 q	16.1 q	23.9 q	15.8 q	16.3 q	16.3 q	24.2 q
17	15.4 q	24.8 q	24.8 q	17.4 q	24.7 q	17.5 q	16.5 q	16.5 q	25.1 q
18	—	71.9 t	182.3 s	70.8 t	70.8 t	183.3 s	71.9 t	184.5 s	71.9 t
19	—	18.2 q	17.5 q	17.2 q	17.2 q	16.3 q	18.2 q	17.9 q	18.1 q
20	—	15.4 q	15.0 q	14.7 q	14.7 q	14.3 q	14.9 q	14.6 q	15.1 q
OMe	—	—	—	—	—	50.1 q	—	—	—

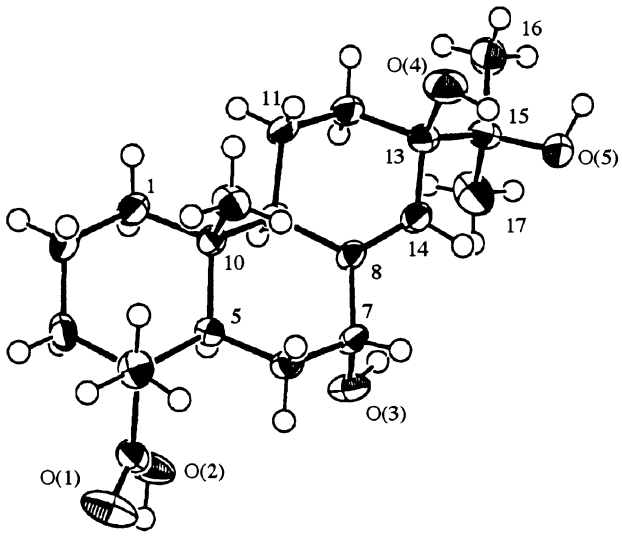
[a]Compounds **1**, **4**, **5**, and **7** were measured in $CDCl_3$, and **2**, **3**, and **8–10** were measured in CD_3OD. Assignments from DEPT, HMQC, and HMBC data.

Fig. 3. ^1H–^1H COSY (——) and HMBC (→) correlations for **2** and **3**.



2 : R = CH_2OH
3 : R = COOH

Fig. 4. ORTEP drawing of **3**.



tribenzoate (**8b**) and dibenzoate (**9b**), respectively (Scheme 3). The CD spectra of **8b** and **9b** (Fig. 6) showed the negative Cotton effects at 231 nm ($\Delta\varepsilon$ –22.7 and –15.7) which were in agreement with the wavelength of the allyl benzoate (7). Therefore, the absolute configurations of C-7 in **8b** and **9b** were proved to be *R*, and the absolute structures of **8** and **9** were established as depicted.

Compound **10**, the most polar substance in this series, was assigned the molecular formula $C_{20}H_{34}O_5$ by HREIMS and DEPT data. The ^1H and ^{13}C NMR spectra of **10** (Tables 2 and 3) were very similar to those of **2** and **8**. An oxygenated methylene signal at δ_H 3.00 and 3.38 ppm closely matched the H-18 signals of **2** and **8**, a signal at δ_H 4.23 ppm closely matched the H-7β signal of **2**, and a signal of δ_H 4.02 ppm matched the H-12β signal of **8**. Two tertiary methyl signals at 1.28 and 1.34 ppm were assigned to methyl signals of a hydroxyisopropyl group at C-13. Therefore **10** had hydroxyls at C-7α, C-12α, C-13β, C-15 and C-18, and the structure of **10** was proved to be abiet-8(14)-en-7α,12α,13β,15,18-pentaol.

Compounds **1–5** and **7–10** are new natural products and they all bear the abiet-8(14)-ene skeleton as a common structural unit. Among these compounds, the tetraols (**2** and **8**) and the pentaol (**10**), highly oxygenated abietanes having hydroxyls at C-7, C-12, C-13 C-15 and C-18 positions, are rare in nature.

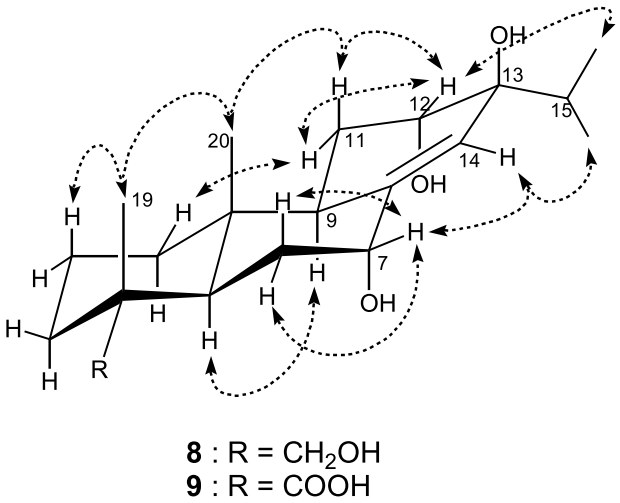
© 2000 NRC Canada

Table 3. [1]H NMR (500 MHz) data for compounds **7–10** (TMS = 0).[a]

Position	7	8	9	10
1α	1.21 ddd (13.0, 13.0, 5.0)	1.08 m (12.0, 12.0, 3.5)	1.20 m	1.09 ddd (13.0, 13.0, 2.5)
1β	1.84 ddd (13.0, 2.5, 2.5)	1.65 m (12.0, 3.5, 3.5)	1.68 m	1.66 m
2	1.64 (2H) m	1.58 (2H) m	1.58 (2H) m	1.55 (2H) m
3α	1.75 m	1.53 m	1.88 m	1.54 m
3β	1.75 m	1.30 m	1.58 m	1.30 m
5α	2.36 m	1.88 m	2.49 br s	1.87 m
6α	2.40 m	1.72 m	1.50 m	1.72 m
6β	2.40 m	1.60 m	1.70 m	1.64 m
7β	—	4.18 t (2.5)	4.15 br s	4.23 t (3.0)
9α	2.05 m	2.28 ddd (9.6, 7.6, 1.5)	2.28 dd (8.5, 8.5)	2.38 ddd (9.6, 8.0, 1.5)
11α	1.68 m	1.72 m	1.72 m	1.72 m
11β	1.54 m	1.89 m	1.92 m	1.87 m
12α	1.41 m	—	—	—
12β	1.70 m	3.82 dt (2.0, 3.5)	3.82 br s	4.02 dt (2.0, 3.5)
14	6.80 br s	5.78 t (1.5)	5.78 br s	5.89 t (1.5)
15	2.08 septet (7.0)	1.88 septet (6.5)	1.89 septet (6.5)	—
16	0.77 d (7.0)	0.97 d (6.5)	0.97 d (6.5)	1.28 s
17	0.89 d (7.0)	1.01 d (6.5)	1.00 d (6.5)	1.34 s
18	—	2.99, 3.37 each d (11.5)	—	3.00, 3.38 each d (11.5)
19	1.25 s	0.73 s	1.17 s	0.80 s
20	0.89 s	0.82 s	0.82 s	0.82 s
OMe	3.19 s	—	—	—

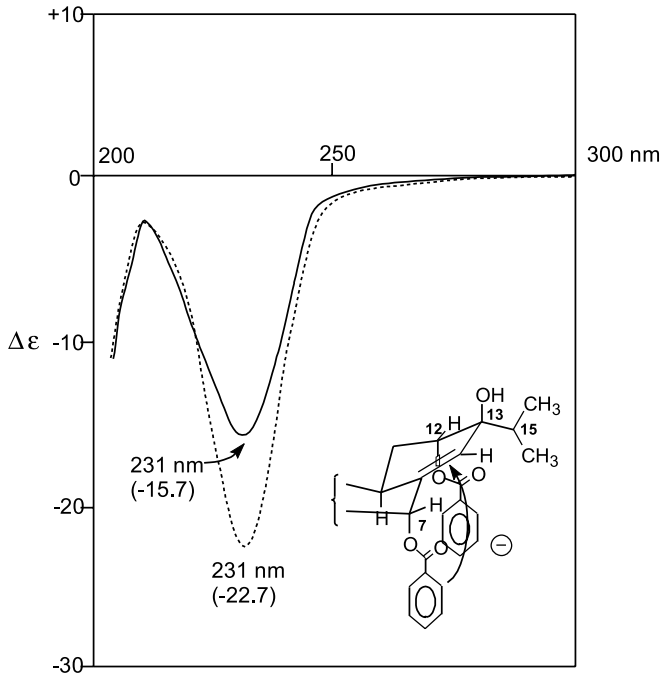
[a]Compound **7** was measured in $CDCl_3$, and **8–10** were measured in CD_3OD. δ in ppm, *J* (in parentheses) in Hz; assignments from [1]H–[1]H COSY, HMQC, HMBC, and NOESY data.

Fig. 5. NOESY correlations for **8** and **9**.



8 : R = CH_2OH
9 : R = COOH

Fig. 6. CD spectra of **8b** (– – –) and **9b** (——) in EtOH.



The inhibitory effects of **1–4** and **7–9** on EBV–EA activation induced by TPA were examined for a primary screening of anti-tumor-promoting activities and the results are shown in Table 4. All these compounds preserved the high viability of Raji cells, and showed moderate inhibitory effects on EBV–EA activation. Among them, compound **7** exhibited the most significant inhibitory effects on the activation (100% inhibition of activation at 1000 mol ratio/TPA, and more than 50% inhibition at 500 mol ratio/TPA), and was found to be more effective than that of β-carotene, a vitamin A precursor that has been intensively studied in cancer prevention using animal models (8).

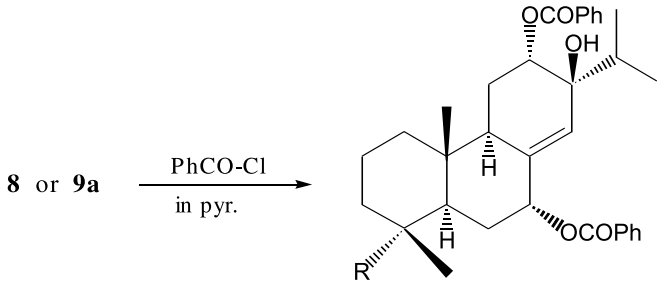
Experimental section

General experimental procedures

Melting points were determined on a Yanagimoto micro-melting-point apparatus and are uncorrected. Optical rota-

© 2000 NRC Canada

Scheme 3.



8b : R = CH_2OCOPh

9b : R = COOMe

tions were measured using a Jasco DIP-1000 digital polarimeter. UV spectra were recorded on a Hitachi 150-20 spectrophotometer and IR spectra were recorded using a Perkin-Elmer 1720X FT-IR spectrophotometer. CD spectra were recorded on a Jasco J-500A spectrometer. ^1H and ^{13}C NMR spectra were obtained on a Varian XL-300 and INOVA 500 spectrometer with standard pulse sequences operating at 300 and 500 MHz, and 74.5 and 125 MHz, respectively. EIMS and HREIMS were recorded on a Hitachi 4000H double focusing mass spectrometer (70 eV). Column chromatography was carried out over silica gel (70–230, and 230–400 mesh, Merck). Preparative HPLC was carried out using a TOSOH-system equipped with a CCPM-prep pump, a SC-8020 system controller, and a TSK-gel ODS-80Ts (21.5 × 300 mm). Fractions obtained from column chromatography were monitored by TLC (silica gel 60 F_{254}). Preparative TLC was carried out on Merck silica gel 60 F_{254} plates (20 × 20 cm, 0.5 mm in thickness).

Extraction and isolation

Fresh cones of *L. kaempferi* (1.45 kg), collected in July 1995, were cut off and treated with $CHCl_3$ (4 L × 5). The resulting $CHCl_3$ extract (123 g) was subjected to silica gel column chromatography (1). The EtOAc-MeOH (10:1) eluate (11.34 g), the most polar fraction in the preliminary silica gel column, was further subjected to silica gel column chromatography with EtOAc and EtOAc–MeOH (10:1 → 5:1) to yield EtOAc eluate (6.13 g) and EtOAc–MeOH (10:1) eluate (3.18 g). The EtOAc eluate was subjected to reversed-phase silica gel (ODS) column chromatography with MeOH–H_2O (75:25) and HPLC (ODS) with MeCN–H_2O (70:30) to give **1** (33 mg), **4** (25 mg), **5** (5 mg), **6** (106 mg), and **7** (18 mg). The EtOAc–MeOH (10:1) eluate was subjected to Sephadex LH-20 column chromatography with $CHCl_3$–MeOH (1:1) and ODS column chromatography with MeOH–H_2O (60:40) to yield **2** (25 mg), **3** (48 mg), **8** (6 mg), **9** (6 mg), and **10** (4 mg). Compound **6** was identified as 7-oxo-13β-hydroxyabiet-8(14)-en-18-oic acid by a comparison of its physical and spectral data with those reported in the literature (3).

*7α,15-Dihydroxypodocarp-8(14)-en-13-one (**1**):* Colorless needles, mp 153–154°C (*n*-hex-EtOAc); $[\alpha]_D^{23}$ –61.0°(*c* 0.44, EtOH); CD (*c* 7.81 × 10^{-5} M, EtOH) (Δε): 375 (0), 323 (–2.33), 260 (0) nm; UV (EtOH) λ_{max} (log ε): 237 (3.96) nm; IR (film) ν_{max}: 3375 (OH), 1684 (C=C-C=O), 1649, 1042, 837 (>C=CH-) cm^{-1}; ^1H and ^{13}C NMR: Tables 1 and 2; EIMS *m/z* (rel. int.): 278 $[M]^+$ (17), 260 (16), 151 (82), 123 (100), 81 (46), 67 (35); HREIMS *m/z*: 278.1882 $[M]^+$ (calcd. for $C_{17}H_{26}O_3$: 278.1880).

Table 4. Percentages of EBV–EA activation in the presence of compounds **1–4** and **7–9** with respect to positive control (100%).[a]

	Concentration (mol ratio/TPA)			
Compound	1000	500	100	10
1	11.7 (60)	55.5	81.0	100
2	9.8 (70)	52.3	83.4	100
3	5.6 (70)	49.7	80.1	96.7
4	11.7 (70)	54.9	88.0	100
7	0 (70)	46.2	82.1	100
8	7.4 (70)	50.5	82.9	100
9	6.6 (70)	50.1	81.4	100
β-Carotene	8.6 (70)	34.2	82.1	100

[a]Values represent relative percentages to the positive control value. TPA (32 pmol, 20 ng) = 100%. Values in parentheses are viability percentages of Raji cells.

*Acetylation of **1***

A mixture of compound **1** (5 mg) and Ac_2O (0.5 mL) in pyridine (0.5 mL) was kept at room temperature overnight. Evaporation of the solvent under reduced pressure gave a residue (6 mg), which was purified by preparative TLC (*n*-hex-EtOAc = 3:1) to furnish a diacetate (**1a**), 4.5 mg, as colorless oil, $C_{21}H_{30}O_5$; $[\alpha]_D^{23}$ –21.5°(*c* 0.28, EtOH); IR ν_{max} (film): 1735, 1732, 1237 (OAc), 1685 (>C=O), 835 cm^{-1}; ^1H NMR ($CDCl_3$) δ: 0.87 (3H, s, H-17), 0.89 (3H, s, H-16), 2.04 and 2.08 (each 3H, s, -OCOMe × 2), 3.61 and 3.92 (each 1H, d, *J* = 11.0 Hz, H-15), 5.49 (1H, t, *J* = 3.0 Hz, H-7 β), 6.08 (1H, d, *J* = 2.0 Hz, H-14) ppm; ^{13}C NMR ($CDCl_3$) δ: 15.9 (q, C-17), 17.7 (q, C-16), 17.9 (t, C-2), 20.4 (t, C-11), 20.9 and 21.4 (each q, -OCO*Me* × 2), 27.6 (t, C-6), 35.6 (t, C-3), 36.4 (s, C-4). 36.6 (t, C-12), 38.5 (t, C-1), 39.0 (s, C-10), 41.6 (d, C-5), 47.9 (d, C-9), 72.0 (t, C-15), 73.0 (d, C-7), 130.0 (d, C-14), 157.6 (s, C-8), 169.5 and 170.8 (each s, -O*C*OMe × 2), 199.9 (s, C-13) ppm; EIMS *m/z* (rel. int.): 362 $[M]^+$ (4), 320 (17), 302 (100), 260 (17), 242 (79), 229 (83), 121 (41), 43 (88).

Preparation of p-*chlorobenzoate (**1c**)*

A mixture of **1** (12 mg), Et_3N (10 μL), DMAP (3 mg), and TBDMS-Cl (10 mg) in dry CH_2Cl_2 (2 mL) was stirred for 48 h at room temperature. The reaction mixture was diluted with Et_2O and washed successively with aqueous $NaHCO_3$ and saturated brine solution, and dried with Na_2SO_4. The organic layer was concentrated under reduced pressure to give a residue (13 mg). Purification of the residue by preparative TLC (*n*-hex-EtOAc = 3:1) afforded a TBDMS ether of **1** (**1b**), 6 mg and **1**, 5 mg. **1b**: colorless oil, $C_{23}H_{40}O_3Si$; EIMS *m/z* (rel. int.): 392 $[M]^+$ (1), 376 (1), 349 (3), 335 (48), 305 (25), 243 (55), 148 (63), 105 (27), 75 (100). A solution of **1b** (4.8 mg) and *p*-chlorobenzoyl chloride (20 μL) in pyridine was stirred at room temperature for 24 h. After evaporation of the solvent under reduced pressure, the resulting product was purified by preparative TLC (*n*-hex-EtOAc = 3:1) to yield a *p*-chlorobenzoate (**1c**), 3.6 mg, as colorless oil, $C_{30}H_{43}O_4SiCl$; $[\alpha]_D^{23}$ –66.9°(*c* 0.28, $CHCl_3$); CD (*c* 8.40 × 10^{-5} M, EtOH) (Δε): 380 (0),

© 2000 NRC Canada

329 (–1.89), 287 (–0.6), 245 (–20.4), 234 (0), 223 (+15.7), 212 (+9.0) nm; UV (EtOH) λ_{max} (log ε): 240 (4.38) nm; ^{1}H NMR ($CDCl_3$) δ: –0.13 and –0.08 (each 3H, s, -Si-Me_2), 0.75 (9H, s, -Si-*t*-Bu), 0.80 (3H, s, H-16), 0.89 (3H, s, H-17), 2.99 and 3.32 (each 1H d, *J* = 11.0 Hz, H-15), 5.72 (1H, br s, H-7β), 6.14 (1H, d, *J* = 2.4 Hz, H-14), 7.40 and 7.93 (each 2H, d, *J* = 8.4 Hz, H-2′ and H-6′, H-3′ and H-5′) ppm; EIMS *m/z* (rel. int.): 531 $[M]^+$ (0.3), 530 $[M]^+$ (0.6), 473 (24), 373 (3), 317 (22), 243 (100), 213 (64), 173 (18), 139 (59), 73 (52).

*Abiet-8(14)-en-7α,13β,15,18-tetraol (**2**):* Colorless needles, mp 221–222°C (MeOH–H_2O); $[\alpha]_D^{23}$ –25.8°(*c* 0.57, EtOH); IR (film) ν_{max}: 3340 (OH), 2925, 1632, 840 (>C=CH-) cm^{-1}; ^{1}H and ^{13}C NMR: Tables 1 and 2; EIMS *m/z* (rel. int.): 338 $[M]^+$ (0.1), 320 (1), 302 (60), 279 (28), 262 (100), 149 (42), 123 (37), 109 (35), 59 (24); HREIMS *m/z*: 338.2449 $[M]^+$ (calcd. for $C_{20}H_{34}O_4$: 338.2455).

*Acetylation of **2***

A solution of **2** (6 mg) and Ac_2O (0.2 mL) in pyridine (0.2 mL) was kept at room temperature overnight. Work-up as usual afforded a residue (9 mg), which was purified by preparative TLC (*n*-hex-EtOAc = 1:2) to give a diacetate (**2a**), 5.2 mg, as colorless oil, $C_{24}H_{38}O_6$; $[\alpha]_D^{23}$ +26.5°(*c* 0.36, $CHCl_3$); IR (film) ν_{max}: 3473 (OH), 2929, 1738, 1733, 1245 (OAc), 839 (>C=CH-) cm^{-1}; ^{1}H NMR ($CDCl_3$) δ: 0.82 (3H, s, H-20), 0.88 (3H, s, H-19), 1.98 and 2.07 (each 3H, s, -OCOMe × 2), 3.60 and 3.90 (each 1H, d, *J* = 11.5 Hz, H-18), 5.36 (1H, t, *J* = 3.0 Hz, H-7β), 6.11 (1H, br s, H-14) ppm; ^{13}C NMR ($CDCl_3$) δ: 14.7 (q, C-20), 17.5 (t, C-11), 17.7 (q, C-19), 18.0 (t, C-2), 21.0 and 21.5 (each q, -OCO*Me* × 2), 24.2 and 24.3 (each q, C-16 and C-17), 27.5 (t, C-6), 29.3 (t, C-12), 35.8 (t, C-3), 36.3 (s, C-4), 37.6 (s, C-10), 38.5 (t, C-1), 41.8 (d, C-5), 47.7 (d, C-9), 72.3 (t, C-18), 73.6 (s, C-13), 74.6 (s, C-15), 74.7 (d, C-7), 131.2 (d, C-14), 140.3 (s, C-8), 169.9 and 170.9 (each q, -O*C*OMe × 2) ppm; EIMS *m/z* (rel. int.): 386 $[M - 2H_2O]^+$ (0.4), 363 (2), 344 (12), 326 (13), 304 (100), 244 (23), 229 (14).

*$NaIO_4$ oxidation of **2***

$NaIO_4$ (6 mg) was added to a solution of **2** (6 mg) in CH_2Cl_2–H_2O (3:1, 4 mL) and the mixture was stirred at room temperature for 24 h. After separation of the organic layer, the aqueous layer was extracted with CH_2Cl_2. The combined CH_2Cl_2 solution was dried with Na_2SO_4, and then concentrated. The resulting residue was purified by preparative TLC ($CHCl_3$–MeOH = 20:1) to afford a 13-keto derivative (4.2 mg), which was identical with compound **1**.

*7α,13β,15-Trihydroxyabiet-8(14)-en-18-oic acid (**3**)*: Colorless plates, $C_{20}H_{32}O_5$, mp 215–216°C (MeOH-H_2O); $[\alpha]_D^{23}$ –8.6° (*c* 0.64, EtOH); IR (film) ν_{max}: 3668–2869, 1697 (COOH), 3392 (OH), 841 (>C=CH-) cm^{-1}; ^{1}H and ^{13}C NMR: Tables 1 and 2; EIMS *m/z* (rel. int.): 316 $[M - 2H_2O]^+$ (100), 298 $[M - 3H_2O]^+$ (43), 276 (62), 270 (37), 237 (22), 183 (11), 150 (38), 110 (15); HREIMS *m/z*: 316.2027 $[M - 2H_2O]^+$ (calcd. for $C_{20}H_{28}O_3$: 316.2037).

*Methyl ester of compound **3** (**3a**)*

A solution of diazomethane in ether was added to a solution of **3** (15 mg) in ether (2 mL), and the mixture was allowed to stand over night. The removal of the solvent gave a residue (17 mg), which was purified by preparative TLC to give a methyl ester of **3** (**3a**), 14 mg, colorless oil, $C_{21}H_{34}O_5$; $[\alpha]_D^{23}$ –19.7° (*c* 0.27, $CHCl_3$); IR (film) ν_{max}: 3411 (OH), 1724, 1256 (COOMe), 1654, 831 cm^{-1}; ^{1}H NMR ($CDCl_3$) δ: 0.80 (3H, s, H-20), 1.17 (3H, s, H-19), 1.21 and 1.24 (each 3H, s, H-16 and H-17), 3.68 (3H, s, -COO*Me*), 4.21 (1H, t, *J* = 3.0 Hz, H-7β), 6.02 (1H, br s, H-14) ppm; ^{13}C NMR ($CDCl_3$) δ: 15.1 (q, C-20), 17.7 (q, C-19), 18.0 (t, C-11), 18.7 (t, C-2), 25.1 (q × 2, C-16 and C-17), 32.4 (t, C-6), 37.6 (t, C-3), 38.3 (s, C-10), 38.8 (t, C-1), 42.4 (d, C-5), 47.7 (d, C-9), 47.6 (s, C-4), 52.8 (q, -COO*Me*), 73.2 (d, C-7), 74.5 (s, C-13), 75.3 (s, C-15), 129.0 (d, C-14), 146.0 (s, C-8), 179.6 (s, C-18) ppm; EIMS *m/z* (rel. int.): 348 $[M - H_2O]^+$ (1), 330 (9), 290 (100), 247 (67), 230 (27), 181 (4), 123 (9), 110 (15).

*X-ray crystallographic analysis of **3***

Single crystals of **3** crystallized from MeOH–H_2O were $C_{20}H_{32}O_5$, Mr = 352.47, orthorhombic, space group $P2_12_12_1$, with unit cell dimensions *a* = 10.955(2), *b* = 24.122(3), *c* = 6.959(3) Å, *V* = 1839.1(9) $Å^3$, *Z* = 4, $D_{(calc)}$ = 1.273 g cm^{-1}. All unique reflections with 48.81° < 2θ < 49.93° were collected on a Rigaku AFC-5 diffractometer using graphite-monochromated Cu Kα radiation and employing ω–2θ scan mode. In 1831 collected reflections, 1681 reflections ($I > 2\sigma(I)$) were judged as observed and used for the structural determination and refinement. The structure was solved by direct methods and refined by full-matrix least-squares method with anisotropic thermal parameters using the SHELXL-97 programs.[2] The positions of H atoms were obtained from a difference Fourier map and were included in the final refinement. The residual factors were *R* = 0.040 and R_w = 0.135 for 1681 reflections. All calculation were performed using the teXsan.[3] List of atomic coordinates, thermal parameters, bond lengths and angles, the torsion angles, and the calculated and observed structure factors have been deposited.[4]

*$LiAlH_4$ reduction of **3***

A mixture of **3** (10 mg) and $LiAlH_4$ (17 mg) in dry THF (6 mL) was stirred at 40°C for 18 h. After deactivation of an excess of $LiAlH_4$ with H_2O, the reaction mixture was extracted with EtOAc. The EtOAc layer was washed successively with H_2O and saturated brine solution, and dried with Na_2SO_4. Evaporation of the solvent gave a residue (16 mg), which was purified by preparative TLC ($CHCl_3$–MeOH = 20:1) to afford the corresponding alcohol (5.5 mg) identical in all respects with compound **2**.

*13β,18-Dihydroxyabiet-8(14)-en-7-one (**4**)*: Colorless oil; $[\alpha]_D^{23}$ +8.9° (*c* 0.64, $CHCl_3$); UV(EtOH) λ_{max} (log ε): 245

[2] G.M. Sheldrick. Program for refinement of crystal structures. University of Gottingen, Germany (1997).
[3] Crystal Structure Analysis Package. Molecular Structure Corp. (1985 & 1992).
[4] Supplementary material has been deposited by the author with the Cambridge Crystallographic Data Centre and can be obtained on request from: The Director, Cambridge Crystallographic Data Centre, University Chemical Laboratory, 12 Union Road, Cambridge, CB2 1EZ, U.K.

© 2000 NRC Canada

(3.74) nm; IR (film) ν_{max}: 3410 (OH), 1676 (C=O), 1611, 840 (>C=CH-) cm^{-1}; ^1H and ^{13}C NMR: Tables 1 and 2; EIMS *m/z* (rel. int.): 320 $[M]^+$ (7), 277 $[M - C_3H_7]^+$ (100), 259 (7), 247 (15), 150 (6), 123 (35); HREIMS *m/z*: 320.2335 $[M]^+$ (calcd. for $C_{20}H_{32}O_3$: 320.2350).

*Acetylation of **4***

Using the same procedure as described for compound **1**, compound **4** (10 mg) was treated with Ac_2O (0.5 mL) in pyridine (0.5 mL) and purified by preparative TLC (*n*-hex-EtOAc = 1:2) to give a monoacetate (**4a**), 9 mg, colorless oil, $C_{22}H_{34}O_4$; $[\alpha]_D^{23}$ +6.2°(*c* 0.20, $CHCl_3$); IR (film) ν_{max}: 3460 (OH), 1740, 1236 (OAc), 1684 (C=O), 839 (>C=CH-) cm^{-1}; ^1H NMR ($CDCl_3$) δ: 0.88 (3H, s, H-20), 0.93 (3H, s, H-19), 0.87 and 0.97 (each 3H, d, *J* = 7.0 Hz, H-16 and H-17), 2.07 (3H, s, -OCOMe), 3.67 and 3.71 (each 1H, d, *J* = 11.0 Hz, H-18), 6.75 (1H, dd, *J* = 2.0, 2.8 Hz, H-14) ppm; ^{13}C NMR ($CDCl_3$) δ: 14.6 (q, C-20), 17.1 (q, C-19), 16.2 and 17.4 (each q, C-16 and C-17), 17.8 (t, C-2), 18.4 (t, C-11), 21.0 (q, -OCO*Me*), 29.5 (t, C-12), 35.6 (t, C-3), 36.5 (s, C-4), 37.2 (t, C-6), 37.8 (d, C-15), 38.3 (t, C-1), 38.5 (s, C-10), 44.0 (d, C-5), 51.5 (d, C-9), 71.8 (s, C-13), 72.0 (t, C-18), 138.5 (s, C-8), 139.8 (d, C-14), 171.0 (s, -O*C*OMe), 199.9 (s, C-7) ppm; EIMS *m/z* (rel. int.): 362 $[M]^+$ (4), 319 (61), 259 (23), 123 (94), 95 (26), 67 (28), 43 (100).

*13β,15,18-Trihydroxyabiet-8(14)-en-7-one (**5**)*: Colorless oil, $C_{20}H_{32}O_4$; $[\alpha]_D^{23}$ –8.3° (*c* 0.29, EtOH); CD (*c* 3.08 × 10^{-4} M, EtOH) (Δε): 400 (0), 341 (–0.42), 275 (0) nm; IR (film) ν_{max}: 3431 (OH), 1673 (C=O), 1611, 839 (>C=CH-) cm^{-1}; ^1H and ^{13}C NMR: Tables 2 and 3; EIMS *m/z* (rel. int.): 318 $[M - H_2O]^+$ (1), 303 (2), 278 (100), 250 (9), 138 (35), 123 (20), 109 (19), 95 (13), 59 (13); HREIMS *m/z*: 318.2180 $[M - H_2O]^+$ (calcd. for $C_{20}H_{30}O_3$: 318.2194).

*7-Oxo-13β-hydroxyabiet-8(14)-en-18-oic acid (**6**)*: Colorless oil; $C_{20}H_{30}O_4$; $[\alpha]_D^{23}$ –17.0° (*c* 0.29, $CHCl_3$); ^1H NMR ($CDCl_3$) δ: 0.85 and 0.96 (each 3H, d, *J* = 7.0 Hz, H-16 and H-17), 0.86 (3H, s, H-20), 1.23 (3H, s, H-19), 6.74 (1H, br s, H-14) ppm; ^{13}C NMR ($CDCl_3$) δ: 14.4 (q, C-20), 16.2 and 17.4 (each q, C-16 and C-17), 16.4 (q, C-19), 17.8 (t, C-2), 18.3 (t, C-11), 29.4 (t, C-12), 35.5 (s, C-10), 36.9 (t, C-3), 37.8 (d, C-15), 37.9 (t, C-1), 38.7 (t, C-6), 44.3 (d, C-5), 46.3 (s, C-4), 51.6 (d, C-9), 71.8 (s, C-13), 138.4 (s, C-8), 140.1 (d, C-8), 183.0 (s, C-18), 199.4 (s, C-7) ppm; EIMS *m/z* (rel. int.): 334 $[M]^+$ (19).

*13β-Methoxy-7-oxoabiet-8(14)-en-18-oic acid (**7**)*: Colorless oil, $[\alpha]_D^{23}$ +28.5° (*c* 0.38, $CHCl_3$); UV (EtOH) λ_{max} (log ε): 242 (3.81) nm; IR (film) ν_{max}: 3650 – 2640, 1695 (COOH), 1695 (>C=O), 1611, 856 (>C=CH-), 1466, 1389, 1236 cm^{-1}; ^1H and ^{13}C NMR: Tables 2 and 3; EIMS *m/z* (rel. int.): 348 $[M]^+$ (1), 316 $[M - MeOH]^+$ (1), 305 $[M - C_3H_7]^+$ (100), 259 (18), 137 (29), 109 (9), 79 (6), 43 (10); HREIMS *m/z*: 348.2285 $[M]^+$ (calcd. for $C_{21}H_{32}O_4$: 348.2299).

*Methyl ester of compound **7** (**7a**)*

Using the same procedure as described for compound **3**, a solution of compound **7** (5 mg) in ether (1 mL) was treated with diazomethane-ether and purified by preparative TLC (*n*-hex-EtOAc = 3:1) to give a methyl ester (**7a**), 3.8 mg, colorless oil, $C_{22}H_{34}O_4$; $[\alpha]_D^{23}$ +33.9° (*c* 0.64, $CHCl_3$); IR (film) ν_{max}: 2950, 2849, 1727 (COOMe), 1690 (>C=O), 1618, 832 (>C=CH-), 1462, 1251, 1233 cm^{-1}; ^1H NMR ($CDCl_3$) δ: 0.77 and 0.89 (each 3H, d, *J* = 7.0 Hz, H-16 and H-17), 0.88 (3H, s, H-20), 1.25 (3H, s, H-19), 3.18 (3H, s, C(13)-O*Me*), 3.66 (3H, s, -COO*Me*), 6.79 (1H, dd, *J* = 3.0, 2.0 Hz, H-14) ppm; EIMS *m/z* (rel. int.): 362 $[M]^+$ (9), 330 $[M - MeOH]^+$ (14), 319 (100), 259 (40), 235 (23), 181 (10), 137 (25), 83 (16).

*Abiet-8(14)-en-7α,12α,13β,18-tetraol (**8**)*: Colorless needles, mp 150–151°C (MeOH); $[\alpha]_D^{23}$ –17.7° (*c* 0.32, EtOH); IR (film) ν_{max}: 3375 (OH), 1634, 840 (>C=CH-) cm^{-1}; ^1H and ^{13}C NMR: Tables 2 and 3; EIMS *m/z* (rel. int.): 338 $[M]^+$ (1), 320 (27), 302 (19), 295 (100), 277 (69); HREIMS *m/z*: 338.2447 $[M]^+$ (calcd. for $C_{20}H_{34}O_4$: 338.2455).

*Acetylation of **8***

Using the same procedure as described for compound **1**, compound **8** (1.5 mg) was treated with Ac_2O (0.1 mL) in pyridine (0.1 mL) and purified by preparative TLC (*n*-hex-EtOAc = 2:1) to give a triacetate (**8a**), 1.2 mg, colorless oil, $C_{26}H_{40}O_7$; $[\alpha]_D^{23}$ +52.4°(*c* 0.16, EtOH); IR (film) ν_{max}: 3446 (OH), 1737, 1733, 1247 (OAc), 849 (>C=CH-) cm^{-1}; ^1H NMR ($CDCl_3$) δ: 0.81 (3H, s, H-19), 0.86 and 0.98 (each 3H, d, *J* = 7.0 Hz, H-16 and H-17), 0.88 (3H, s, H-20), 1.99, 2.00 and 2.08 (each 3H, s, -OCOMe), 3.61 and 3.88 (each 1H, d, *J* = 11.0 Hz, H-18), 5.00 (1H, dt, *J* = 2.0, 3.5 Hz, H-12β), 5.37 (1H, t, *J* = 3.0 Hz, H-7β), 5.94 (1H, t, *J* = 1.5 Hz, H-14) ppm; EIMS *m/z* (rel. int.): 421 $[M - C_3H_7]^+$ (1), 387 (1), 361 (34), 344 (22), 319 (24), 301 (35), 241 (100), 171 (45), 133 (21), 121 (21).

*Treatment of **8** with benzoyl chloride*

A mixture of compound **8** (0.6 mg) and benzoyl chloride (15 μL) in pyridine (0.2 mL) was stirred at room temperature overnight. After removal of the solvent under reduced pressure, the resulting residue was purified by preparative TLC (*n*-hex-EtOAc = 1:1) to give the corresponding tribenzoate (**8b**), 0.8 mg, colorless oil, $C_{41}H_{46}O_7$; CD (*c* 8.12 × 10^{-5} M, EtOH) (Δε): 270 (0), 231 (–22.67), 211 (–2.80) nm; ^1H NMR ($CDCl_3$) δ: 0.84 and 1.03 (each 3H, d, *J* = 7.0 Hz, H-16 and H-17), 0.94 (3H, s, H-19), 0.99 (3H, s, H-20), 3.79 and 4.18 (each 1H, d, *J* = 11.0 Hz, H-18), 5.31 (1H, br s, H-12β), 5.73 (1H, br s, H-7β), 6.21 (1H, br s, H-14), 6.85–7.90 (15H, -OCO-Ph × 3) ppm.

*7α,12α,13β-Trihydroxyabiet-8(14)-en-18-oic acid (**9**)*: Colorless powder, $C^{20}H^{32}O^5$; mp 220–222°C (MeOH–H_2O); $[\alpha]_D^{23}$ –10.1° (*c* 0.21, EtOH); IR (film) ν_{max}: 3450 (OH), 3200–2900, 1699 (COOH), 840 (>C=CH-) cm^{-1}; ^1H and ^{13}C NMR: Tables 2 and 3; EIMS *m/z* (rel. int.): 334 $[M-H_2O]^+$ (20), 316 $[M - 2H_2O]^+$ (64), 309 (31), 291 (22), 237 (43), 195 (28), 150 (44), 105 (28), 91 (42), 43 (100); HREIMS *m/z*: 334.2146 $[M - H_2O]^+$ (calcd. for $C_{20}H_{30}O_4$: 334.2140).

*Methyl ester of compound **9** (**9a**)*

Using the same procedure as described for compound **3**, a solution of compound **9** (3 mg) in ether (1 mL) was treated with diazomethane-ether and purified by preparative TLC (*n*-hex-EtOAc = 1:2) to give a methyl ester (**9a**), 2.3 mg,

© 2000 NRC Canada

colorless oil, $C_{21}H_{34}O_5$; IR (film) ν_{max}: 3450 (OH), 1733, 1237 (COOMe), 840 (>C=CH-) cm^{-1}; ^1H NMR ($CDCl_3$) δ: 0.78 (3H, s, H-20), 0.99 and 1.01 (each, 3H, d, J = 7.0 Hz, H-16 and H-17), 1.20 (3H, s, H-19), 3.69 (3H, s, -COOMe), 3.88 (1H, br s, H-12β), 4.20 (1H, br s, H-7β), 5.80 (1H, br s, H-14) ppm.

*Treatment of **9a** with benzoyl chloride*

Using the same procedure for compound **8**, a solution of compound **9a** (1.8 mg) in pyridine (0.5 mL) was treated with benzoyl chloride (20 μL) and purified by preparative TLC (*n*-hex-EtOAc = 1:1) to afford the corresponding dibenzoate (**9b**), 1.7 mg, colorless oil, $C_{35}H_{42}O_7$; CD (c 6.17 × 10^{-5} M, EtOH) (Δε): 285 (0), 231 (–15.72), 210 (–2.46) nm; ^1H NMR ($CDCl_3$) δ: 0.86 and 1.04 (each 3H, d, J = 7.0 Hz, H-16 and H-17), 0.90 (3H, s, H-20), 1.22 (3H, s, H-19), 5.31 (1H, br s, H-12β), 5.65 (1H, br s, H-7β), 6.21 (1H, br s, H-14), 6.99 – 8.08 (10H, -COO-Ph × 2) ppm.

Abiet-8(14)-en-7α,12α,13β,15,18-pentaol (**10**): Colorless powder, $C_{20}H_{34}O_5$; mp >300°C (MeOH–H_2O); $[\alpha]_D^{23}$ –23.0° (c 0.20, $CHCl_3$–MeOH = 1:1); IR (film) ν_{max}: 3340 (OH), 1632, 840 (>C=CH-) cm^{-1}; ^1H and ^{13}C NMR: Tables 2 and 3; EIMS *m/z* (rel. int.): 336 $[M - H_2O]^+$ (3), 318 (6), 300 (6), 278 (100), 260 (15), 229 (50), 123 (51), 109 (56), 81 (20), 59 (32); HREIMS *m/z*: 336.2304 $[M - H_2O]^+$ (calcd. for $C_{20}H_{32}O_4$: 336.2299).

Biological activities

The inhibition of EBV–EA activation was assayed using Raji cells (virus-nonproducer), the EBV genome-carrying human lymphoblastoid cells, that were cultivated in 10% FBS RPMI 1640 medium solution (Nacarai Tesque). The indicator cells (Raji) (1 × 10^6/mL) were incubated at 37°C for 48 h in 1 mL of the medium containing *n*-butyric acid (4 mM, inducer), 32 pmol of TPA (20 ng/mL; in DMSO), and a known amount of test compound in DMSO. Smears were made from the cell suspension. The activated cells were stained by high titer EBV–EA-positive sera from nasopharyngeal carcinoma (NPC) patients and were detected by a conventional indirect immunofluorescence technique. In each assay, at least 500 cells were counted and the experiments were repeated three times. The average EA induction was compared with that of positive control experiments with *n*-butyric acid plus TPA in which EA induction was ordinarily around 30%. The viability of cells was assayed by the Trypan Blue staining method reported previously (9).

Acknowledgments

The authors are grateful to Mr. Katsuhiko Minoura and Mrs. Mihoyo Fujitake of this University for NMR and MS measurements.

References

1. R. Tanaka, H. Ohtsu, and S. Matsunaga. Phytochemistry, **46**, 1051 (1997).
2. H. Ohtsu, R. Tanaka, T. Michida, T. Shingu, and S. Matsunaga. Phytochemistry, **49**, 1761 (1998).
3. H. Ohtsu, R. Tanaka, and S. Matsunaga. J. Nat. Prod. **61**, 406 (1998).
4. H. Ohtsu, R. Tanaka, and S. Matsunaga. J. Nat. Prod. **61**, 1307 (1998).
5. V.I. Bol'shakova, E.N. Shmidt, V.A. Pentegova, and V.I. Mamatyuk. Khim. Prir. Soedin. **5**, 571 (1986).
6. M. Koreeda, N. Harada, and K. Nakanishi. J. Am. Chem. Soc. **96**, 266 (1974).
7. N. Harada, J. Iwabuchi, Y. Yokota, H. Uda, and K. Nakanishi. J. Am. Chem. Soc. **103**, 5590 (1981).
8. A. Murakami, H. Ohigashi, and K. Koshumizu. Biosci. Biotech. Biochem. **60**, 1 (1996).
9. H. Tokuda, T. Konoshima, M. Kozuka, and T. Kimura. Cancer Lett. (Shannon, Irel.) **40**, 309 (1988).

© 2000 NRC Canada

On chirality measures and chirality properties

Noham Weinberg and Kurt Mislow

Abstract: It is shown that chiral zeroes are integral to all pseudoscalar functions, and that these functions, and thus the chirality properties that are described by them, are therefore normally unsuitable as chirality measures. The multidimensional nature of chirality properties is explored. Chirality measures for nonrigid objects and stochastic systems are discussed. It is shown that if the chirality of a nonrigid object is described as a time average of the chirality measures of its instant configurations, this time average is nonzero not only for chiral but also for achiral molecules. This paradox can be resolved if chirality measures are properly applied to nonrigid objects.

Key words: chirality, chiral zeroes, chirality measures, chirality properties.

Résumé : On démontre que les zéro chiraux font partie intégrale de toutes les fonctions pseudoscalaires et que ces fonctions, et en conséquence les propriétés de chiralité qu'elles décrivent, ne sont donc normalement pas des mesures adéquates de la chiralité. On a exploré la nature multidimensionnelle des propriétés de chiralité. On discute des mesures de chiralité pour les objets non rigides et les systèmes stochastiques. Si la chiralité d'un objet non rigide est décrite par une moyenne en fonction du temps de configurations instantanées, on démontre que cette moyenne en fonction du temps n'est pas égale à zéro non seulement pour les molécules chirales, mais aussi pour les molécules achirales. On peut résoudre ce paradoxe si les mesures de chiralité sont appliquées correctement aux objets non rigides.

Mots clés : chiralité, zéro chiraux, mesures de chiralité, propriétés de chiralité.

Introduction

More than a century ago, Guye (1) introduced a set of continuous functions designed to correlate a pseudoscalar property, i.e., optical rotation, with the structure of a chiral molecule. In effect, this was the first attempt to quantify chirality. Since then a number of other schemes have been suggested (see references in (2), as well as subsequent works (3)). Some of these approaches employ pseudoscalar functions that change sign under space inversion and thus would appear to lend themselves to the left–right classification of chiral objects. It has long been recognized, however, that left–right classifications are vitiated when such pseudoscalar functions as chirality polynomials assume a value of zero for chiral objects, the "chiral zero" (4). In the following two sections we show that chiral zeroes are integral to *all* pseudoscalar functions and that chirality properties therefore cannot normally be used as chirality measures. In the last section we analyze a paradoxical situation that arises when a chirality measure defined for a rigid object, such as a geometrical figure, is applied to a nonrigid one, such as a vibrating molecule, and define a chirality measure that is suitable for nonrigid objects and stochastic systems.

Accepted October 28, 1999.

N. Weinberg.[1] Department of Chemistry, University College of the Fraser Valley, Abbotsford, BC V2S 7M8, Canada.
K. Mislow.[1] Department of Chemistry, Princeton University, Princeton, NJ 08544, U.S.A.

[1]Authors to whom correspondence may be addressed. NW: Telephone: (604) 853-7441 x4493. Fax: (604) 855-7558. e-mail: weinbergn@ucfv.bc.ca. KM: Telephone: (609) 258-3941. Fax: (609) 258-6746. e-mail: kmislow@princeton.edu

Chirality measures

An object X (no matter whether physical or geometrical) is chiral if and only if it is not superposable on its mirror image $\overline{X}$ ($X \neq \overline{X}$) by a combination of rotations and translations. A chirality measure $\chi(X)$ is a real-valued function defined on a set Ω of objects X. It ranks the members of Ω in degrees of their chirality. The set Ω can be either discrete or continuous. We assume that Ω is a continuous set, any two elements of which can be connected by a continuous deformation.

The following would seem to be a set of natural requirements for a chirality measure $\chi(X)$:

1. Any two close objects, X_1 and X_2, are expected to have close degrees of chirality. Therefore,

[1] $\chi(X)$ is a continuous function on Ω

2. If X is superposable upon its mirror image $\overline{X}$ ($X \neq \overline{X}$), i.e. if it is achiral, then its degree of chirality is zero. That is,

[2] $X = \overline{X} \Rightarrow \chi(X) = 0$

3. Any two enantiomorphs, X and $\overline{X}$, are chiral to the same degree. That is,

[3*a*] $\chi(\overline{X}) = \chi(X)$ (scalar χ)

or

[3*b*] $\chi(\overline{X}) = -\chi(X)$ (pseudoscalar χ)

Of the two types of real-valued functions, scalar and pseudoscalar, that satisfy conditions [1]–[3], the latter might appear to have certain advantages as a chirality measure. First, condition [2] follows directly from [3*b*]. Second, the opposite signs assigned to the degrees of chiralities of

 © 2000 NRC Canada

enantiomorphs can be seen as a natural basis for a left–right classification of chiral objects. And, third, pseudoscalar functions [3*b*] are expected to have a direct connection to experimentally observed pseudoscalar properties, such as optical rotation.

There is, however, one more important constraint that has to be applied to $\chi(X)$: in order to properly measure chirality, this function is allowed to assume a value of zero only for achiral objects. That is,

[4] $\chi(X) = 0 \Rightarrow X = \overline{X}$

Combining [2] and [4], it follows that a proper chirality measure $\chi(X)$ equals zero *if and only if X* is achiral. That is,

[5] $\chi(X) = 0 \Leftrightarrow X = \overline{X}$

Accordingly, chiral zeroes, i.e., situations where $\chi(X) = 0$ for $X \neq \overline{X}$, are excluded.

Let us now return to the perceived advantages of pseudoscalar $\chi(X)$. It has been demonstrated (5) that, with rare exceptions of low-dimensional sets, a chiral object can be chirally connected to its enantiomorph, i.e., there always exists a path (a parametrized curve) $\Lambda \subset \Omega$ linking $X = X_0$ to $\overline{X} = X_1$ such that all $X_\lambda \in \Lambda$, $\lambda \in [0,1]$ are chiral. Along this path Λ, a pseudoscalar $\chi(X)$ can be considered as a real-valued continuous function defined on segment [0,1]. It changes its sign on this segment and therefore has to take a zero value somewhere within Λ, i.e., at some chiral X_λ. Thus $\chi(X)$ possesses chiral zeroes. It follows that, as a rule, *continuous pseudoscalar functions cannot be used as chirality measures in three and higher dimensions*. This conclusion renders questionable current and past attempts to formulate "chirality measures" on the basis of pseudoscalar functions.

An important exception obtains when a set of objects is split by its achiral subset into two disjoint subsets of chiral objects, such that any path connecting enantiomorphs must pass through the achiral boundary. Examples of such sets are the set of triangles of variable shape in two dimensions (6), the set of helices of variable pitch (7), and Ruch's models of class *a* (4). In such rare cases, a pseudoscalar $\chi(X)$ changes its sign only at the achiral boundary and is therefore suitable as a chirality measure.

Chirality properties

Optical rotation was the first recognized manifestation of chirality. Under identical conditions, enantiomers rotate the plane of polarization to the same degree but in opposite directions. The angle of rotation is therefore a pseudoscalar property. The situation is similar with respect to circular dichroism: ellipticity is a pseudoscalar property. Indeed, *all* manifestations of chirality are described by pseudoscalars. But, as stated in the previous section, pseudoscalar functions cannot normally be used as chirality measures. It follows that, as a rule, *chirality properties are unsuited as chirality measures*.

In this connection, we need to point out a key distinction between a chirality measure and a chirality property. The former is a mathematical construct that measures how far an object is from being achiral; even though this measure depends on a particular defining scheme, it is always associated with an isolated object and is independent of any external object or field. The latter, on the other hand, is an observable property that manifests itself through the difference in the interactions of a chiral object X and its enantiomorph $\overline{X}$ with a reference chiral object or field H, or, alternatively, through the difference in the interactions of X with enantiomorphs H and $\overline{H}$.

Let $P(X \circ H)$ represent a *scalar* property of a chiral complex $X \circ H$ or the result of the interaction of X with a chiral object or field H. Then an observed chirality property $\pi_H(X)$ can be expressed as a difference, either as

[6*a*] $\pi_H(X) = P(X \circ H) - P(\overline{X} \circ H)$

or as

[6*b*] $\pi_H(X) = P(X \circ H) - P(X \circ \overline{H})$

It follows from eq. [6*a*] that $\pi_H(X)$ is a pseudoscalar property. That is,

[7] $\pi_H(\overline{X}) = -\pi_H(X)$

Equations [6*a*] and [6*b*] are equivalent because $\overline{X} \circ H$ and $X \circ \overline{H}$ are enantiomorphous. Their different appearance only reflects the difference in the operations used to determine $\pi_H(X)$. For example, $\pi_H(X)$ in [6*a*] might represent the difference in retention times for enantiomers X and $\overline{X}$ on a chiral column H, while in [6*b*] it might represent the angle of rotation of plane-polarized light due to its interaction with X, found as a difference in phases of left and right circularly polarized waves, H and $\overline{H}$. The equivalence of definitions [6*a*] and [6*b*] implies that for each observable chiral property there should be two equivalent ways of experimental determination. For instance, the difference in retention times mentioned above can be equivalently found by chromatography of the same compound X through two enantiomeric columns, H and $\overline{H}$, and the angle of rotation can be found as a difference of phases of a left (or right) circularly polarized wave H as a result of its interaction with enantiomers X and $\overline{X}$.

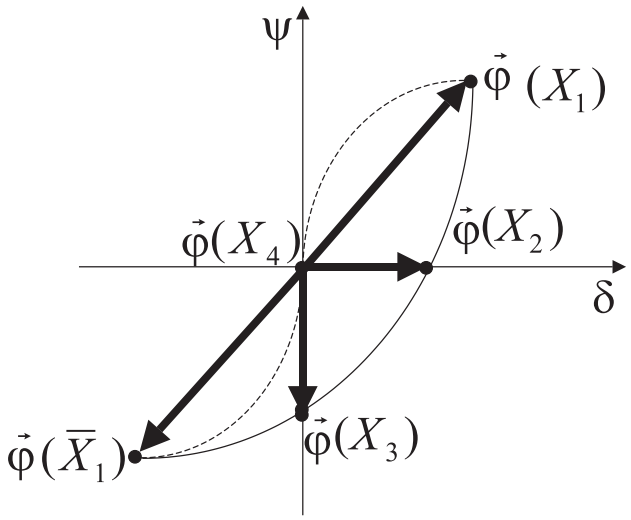
Depending on the conditions of measurement (temperature, wavelength, etc.) an object and its enantiomorph may have a scalar property of the same magnitude. That is, $P(X \circ H)$ and $P(\overline{X} \circ H)$ can be *accidentally* equal even for a chiral X. Thus, the fact that $\pi_H(X)$ equals zero does not necessarily mean that X is achiral. Chiral zeroes are therefore expected to occur for chirality properties.

This does not mean, however, that pseudoscalar properties fail to characterize a chiral object as chiral. The reason is that there are a virtually limitless number of such properties associated with a given object, and its observed chirality is therefore expressed as an infinite-dimensional pseudovector. This pseudovector remains nonzero if one, or even several, of its components vanish. Only for a truly achiral object is it the case that *all* of its individual pseudoscalar properties are zero, and hence that the whole chirality pseudovector is zero.

This statement may be illustrated by the example of optical rotation. Rotation angle δ and ellipticity ψ are known to be frequency-dependent, and at some frequencies become zero. They are related to the refractive index and absorption coefficient, the real and imaginary parts of the same complex quantity (8), and are therefore not independent. As a result, whenever δ takes on a value of zero in an isolated

© 2000 NRC Canada

Fig. 1. A chiral (solid line) and an achiral (dashed line) path connect enantiomorphs X_1 and $\overline{X}_1$. Pseudovector $\vec{\varphi}(X)$ (eq. [8*b*]) never turns zero on the chiral path even though one of its components turns zero for chiral objects: δ for X_3 and ψ for X_2. For an achiral object X_4, both δ and ψ are zero and $\vec{\varphi}(X) = 0$.



transition, the absolute value of ψ is near or at its maximum (the Cotton effect) (9). Thus, a complex pseudoscalar

[8*a*] $\varphi = \delta + i\psi$

or, equivalently, a two-dimensional pseudovector

[8*b*] $\vec{\varphi} = \begin{pmatrix} \delta \\ \psi \end{pmatrix}$

does not become zero for chiral molecules, but is identically zero for achiral molecules.

Similarly, if the entire function $\delta(\nu)$ that represents rotation angles for the whole range of frequencies ν is used, rather than a single value of δ taken at a particular frequency, the problem of chiral zeroes is also avoided since $\delta(\nu)$ is identically zero only for achiral molecules.

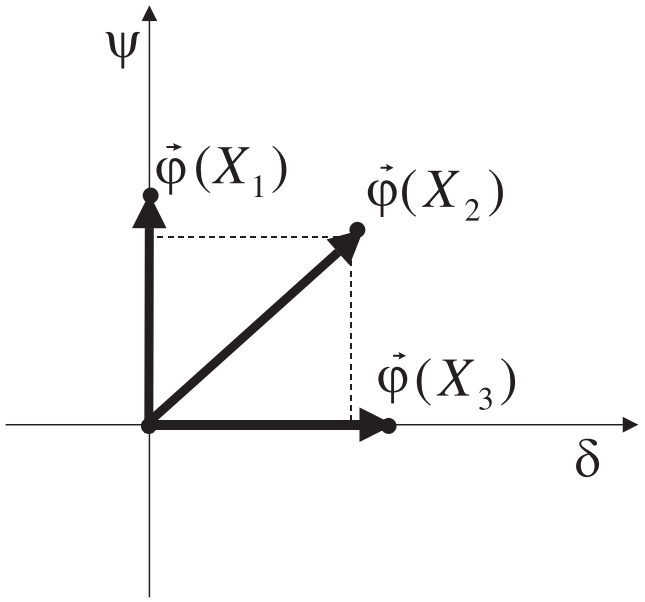
The above discussion suggests that a pseudovector $\vec{\chi}(X)$ can be continuously transformed into $\vec{\chi}(\overline{X}) = -\vec{\chi}(X)$ without passing through zero (Fig. 1), and that the problem of chiral zeroes can thus be avoided even though eq. [3*b*] is obeyed. It has to be added, however, that although a pseudovector $\vec{\chi}(X)$ can differentiate chiral objects from achiral ones, it cannot be directly used to compare their degrees of chirality because relations "greater than" or "less than" are not naturally defined for any two vectors (10). In other words, if chirality is described by $\vec{\chi}(X)$, it becomes impossible in many cases to say which of two objects is more chiral. To restore a linear ordering, one needs to use scalar quantities associated with pseudovectors, such as Euclidean norms

[9*a*] $\left\|\vec{\varphi}\right\| = \sqrt{\delta^2 + \psi^2}$

or

[9*b*] $\left\|\delta\right\| = \sqrt{\int_{\nu_{\min}}^{\nu_{\max}} [\delta(\nu)]^2 \, d\nu}$

Fig. 2. Chirality properties of three chiral objects, X_1, X_2, and X_3, are characterized by pseudovectors $\vec{\varphi}(X_1)$, $\vec{\varphi}(X_2)$, and $\vec{\varphi}(X_3)$, respectively. Optical rotation angle δ identifies X_3 as the most chiral object but fails to detect the chirality of X_1. Similarly, ellipticity ψ selects X_1 as the most chiral object but fails to detect the chirality of X_3. When δ and ψ are combined, however, and the norm $\left\|\vec{\varphi}\right\|$ (eq. [9*a*]) is used, all three objects are identified as chiral and X_2 is found to be the most chiral of the three.



Norms [9*a*] and [9*b*] are "well-behaved" scalar functions that obey conditions [1], [3*a*], and [5], and thus qualify as chirality measures.

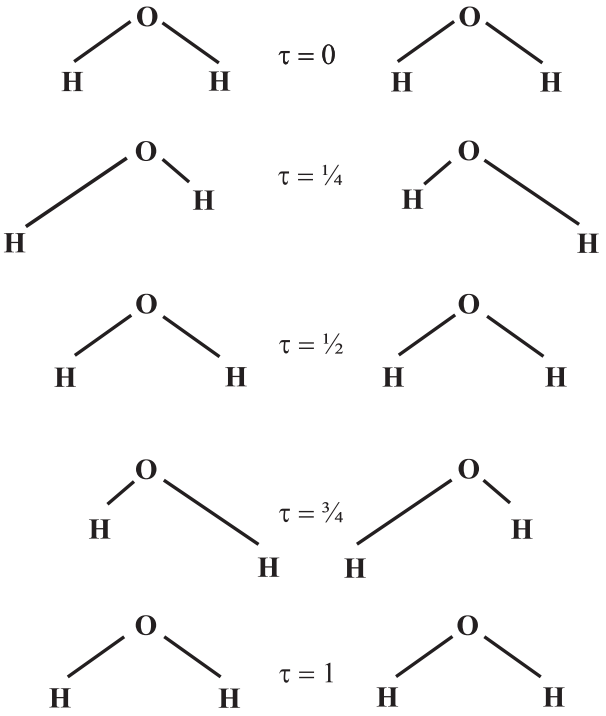
These considerations may be illustrated with the reference to Fig. 2. Three chiral objects, X_1, X_2, and X_3, are characterized by the pseudovector $\vec{\varphi}$ (eq. [8*b*]). If δ were to be chosen as the sole measure of chirality, the ranking would be $X_3 > X_2 > X_1$, with X_1 being "achiral" (zero optical rotation). Similarly, ψ as the sole measure of chirality would produce a different ranking, $X_1 > X_2 > X_3$, with X_3 now being "achiral" (zero ellipticity). Both rankings are clearly unacceptable, not only because they are mutually inconsistent but also because of the chiral zeroes. If, however, we use norm $\left\|\vec{\varphi}\right\|$ (eq. [9*a*]), for example, then this problem can be overcome because chiral zeroes no longer exist and the contributions of different chirality properties are integrated into a single chirality measure.

Chirality measures for nonrigid objects and stochastic systems

If a molecule such as methane is considered in a state of vibrational motion, most of its instantaneous configurations are chiral (7). Each such configuration is as probable as its enantiomorph, and the contributions from different configurations to the net observed chirality property will therefore cancel out on average. For this reason, no chirality properties are observed for such molecules. At the same time, however, in accordance with our earlier discussion, a chirality measure is a sign-preserving function on a set of instant configurations, and the contributions from different configurations therefore *cannot* cancel each other. Hence, if the

© 2000 NRC Canada

Fig. 3. An array of instant configurations **X** of a vibrating water molecule and its mirror-image array $\overline{\mathbf{X}}$.



chirality of a nonrigid object, such as a vibrating molecule, is described in terms of the time average of the chirality measures of its instant rigid configurations, *this time average is nonzero not only for a chiral but, paradoxically, even for any achiral molecule*.

This paradox can be avoided, however, if a chirality measure is defined for a nonrigid object as a whole rather than for its instant configurations.

We consider a nonrigid object **X** as a parametrized set of its instant rigid configurations X_τ:

$$\mathbf{X} = \{X_\tau;\ \tau \in T\}$$

Correspondingly, its enantiomorph $\overline{\mathbf{X}}$ can be represented as a set of the enantiomorphs $\overline{X}_\tau$of rigid configurations X_τ. That is,

$$\overline{\mathbf{X}} = \{\overline{X}_\tau; \tau \in T\}$$

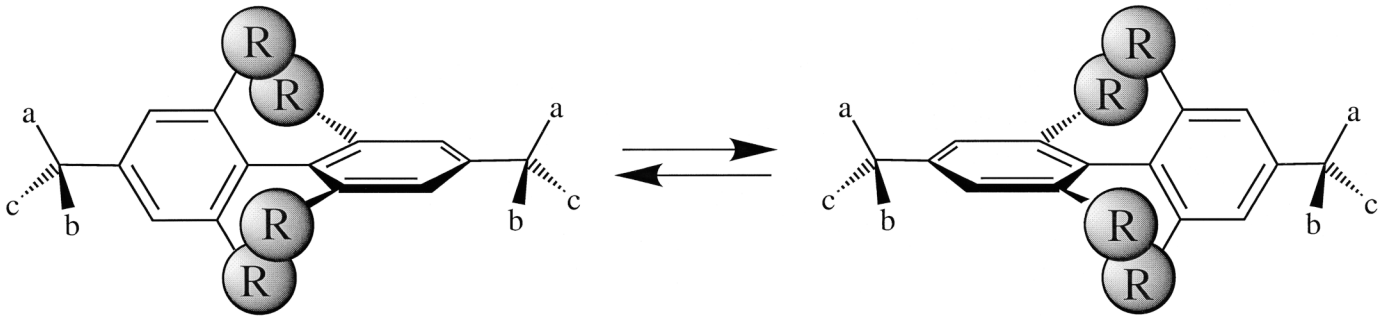
A congruency-based chirality measure χ (2b) is then defined for **X** as a minimum distance between **X** and $\overline{\mathbf{X}}$, for example as

$$[10] \qquad \chi(\mathbf{X}) = \frac{\int_{\tau\in T} \min_{\tau'\in T} \{dist(X_\tau, \overline{X}_{\tau'})\}\, d\tau}{\int_{\tau\in T} d\tau}$$

If **X** and $\overline{\mathbf{X}}$ differ only by a permutation of their elements, by virtue of [10] they are achiral. The following two examples serve as illustrations. Consider a vibrating water molecule in two-dimensional space (Fig. 3). Almost all instant configurations X_τ (except X_0, $X_{1/2}$, and X_1) are chiral in 2D. The entire array **X**, however, is achiral because $X_\tau = \overline{X}_{1-\tau}$ (e.g., $X_{1/4} = \overline{X}_{3/4}$, $X_{3/4} = \overline{X}_{1/4}$). Another example is a compound of the type 4-[(*R*)-*sec*-butyl]-4′-[(*S*)-*sec*-butyl]-2,2′,6,6′-tetramethylbiphenyl (Fig. 4) which consists entirely of chiral conformations (11). Instant configurations X_τ of this molecule are characterized by triples $\tau = (\tau_1, \tau_2, \tau_3)$, where τ_1 and τ_3 are torsion angles for phenyl-Cabc bonds and τ_2 is the torsion angle for the central phenyl-phenyl bond. Torsion angles τ_1, τ_2, and τ_3 can be changed to $-\tau_1$, $-\tau_2$, and $-\tau_3$ by internal rotations around the respective bonds. Although τ_2 cannot assume a value of zero (the two phenyl rings cannot become coplanar due to the presence of the bulky substituents R) it is nevertheless possible to transform τ_2 into $180^o - \tau_2$, which, by virtue of the symmetry of the rings and their R substituents, is equivalent to $-\tau_2$. As shown in Fig. 5, for any conformation X_τ of **X** with torsion parameter $\tau = (\alpha, \beta, \gamma)$ there exists another conformation of **X**, $X_{\tau'}$ with $\tau' = (-\gamma, -\beta, -\alpha)$, such that $X_\tau = \overline{X}_{\tau'}$. Therefore, in accordance with [10], $\chi(\mathbf{X}) = 0$, i.e. the discussed molecule is achiral even though it does not have a single achiral conformation.

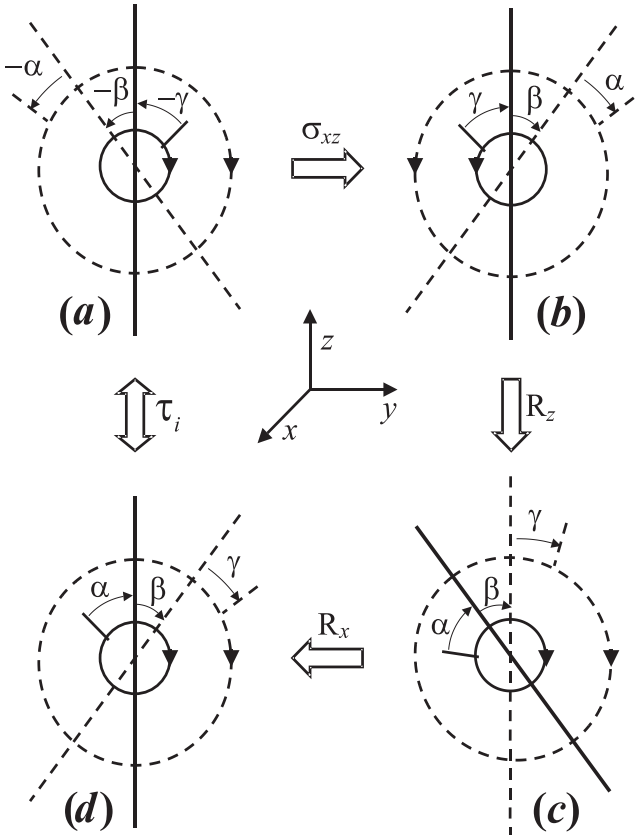
A similar approach applies to nonrigid stochastic systems, such as ensembles of molecules. The simplest example of this kind is a system that contains a statistically significant number *N* of monoatomic molecules (12), e.g., a mole of helium gas in a cubic box. Such a system can be described by its dynamic trajectory **X** in a 3*N*-dimensional configuration space. Practically every instant configuration, X_τ, acquired by the system at time τ, is bound to be chiral because random achiral arrangements of a large number of particles are highly improbable. The enantiomorphous configurations $\overline{X}_{\tau'}$ also belong to the configuration space but do not necessarily belong to the trajectory **X**. In accordance with the ergodic

Fig. 4. Schematic drawing of two enantiomorphous conformations of a biphenyl with bulky substituents (e.g., R = CH_3) in the 2,2′,6,6′ positions and enantiomorphous -Cabc groups (e.g., -$CH(CH_3)C_2H_5$) in the 4,4′ positions.



© 2000 NRC Canada

Fig. 5. Schematic side-view projection of conformations belonging to the molecular system of Fig. 4. Straight lines represent the edges of phenyl rings (substituents R are not shown); oriented circles represent -Cabc groups (the arrows point in the directions a → b → c). Solid lines represent parts of the molecule that are closer to the viewer; dashed lines represent the more distant ones. Conformations $X_{\tau'}$ (*a*) and X_{τ} (*d*) are interconverted by internal rotations τ_i. Conformation $X_{\tau'}$ (*a*) is converted to $\overline{X}_{\tau'}$ (*b*) by reflection σ_{xz} in the *xz* plane. A different view (*c*) of $\overline{X}_{\tau'}$ is obtained by a rigid 180° rotation R_z about the *z* axis. Conversion of $\overline{X}_{\tau'}$ (*c*) to X_{τ} (*d*) is achieved by rigid rotation R_x about the *x* axis by an angle β.



hypothesis (13), however, the trajectory **X** thoroughly covers the entire conformation space so that every point of the space that represents a structure with the same energy is infinitesimally closely approached by the trajectory. That is, for any configuration X_{τ} of **X** there always exists an infinitesimally close configuration $\overline{X}_{\tau'}$ of $\overline{\mathbf{X}}$. Thus, it follows from [10] that $\chi(\mathbf{X}) = 0$, i.e., that the system is achiral even though almost all of its instantaneous configurations are chiral.

Acknowledgments

We are indebted to a reviewer for drawing our attention to some relevant publications. We thank the National Science Foundation for the support of this work.

References

1. P.-A. Guye. C. R. Hebd. Seances Acad. Sci. (Paris) **110**, 714 (1890).
2. (*a*) A.B. Buda, T. Auf der Heyde, and K. Mislow. Angew. Chem. Int. Ed. Engl. **31**, 989 (1992); (*b*) N. Weinberg and K. Mislow. J. Math. Chem. **17**, 35 (1995).
3. For example, see: (*a*) M.A. Osipov, B.T. Pickup, and D.A. Dunmur. Mol. Phys. **84**, 1193 (1995); (*b*) H. Zabrodsky and D. Avnir. J. Am. Chem. Soc. **117**, 462 (1995); (*c*) M. Randic and M. Razinger. J. Chem. Inf. Comput. Sci. **36**, 429 (1996); (*d*) A. Cossé-Barbi and M. Raji. Struct. Chem. **8**, 409 (1997); (*e*) D.J. Klein and D. Babic. J. Chem. Inf. Comput. Sci. **37**, 656 (1997); (*f*) M. Petitjean. J. Math. Chem. **22**, 185 (1997); (*g*) B.B. Smirnov, A.V. Yevtushenko, and O.V. Lebedev. Zh. Org. Khim. **33**, 1129 (1997); (*h*) B.B. Smirnov, O.V. Lebedev, and A.V. Yevtushenko. Zh. Org. Khim. **33**, 1134, 1326, 1328, 1472 (1997); (*i*) P.G. Mezey. Int. J. Quantum Chem. **63**, 105 (1997); (*j*) P.G. Mezey. Comp. Math. Appl. **34**, 105 (1997); (*k*) P.G. Mezey. THEOCHEM. **455**, 183 (1998); (*l*) P.G.Mezey. Chirality, **10**, 173 (1998); (*m*) P.G. Mezey. J. Math. Chem. **23**, 65 (1998); (*n*) M.A. Osipov, B.T. Pickup, M. Fehervari, and D.A. Dunmur. Mol. Phys. **94**, 283 (1998); (*o*) A. Ferrarini and P.L. Nordio. J. Chem. Soc. Perkin Trans. 2, 455 (1998); (*p*) P. Le Guennec. J. Math. Chem. **23**, 429 (1998); (*q*) V.M. Markov, V.A. Potyomkin, and A.V. Belik. J. Struct. Chem. **39**, 407 (1998); (*r*) V.E. Kuzmin and A.G. Artemenko. J. Struct. Chem. **39**, 442 (1998); (*s*) S.É. Alikhanidi and V.E. Kuzmin, J. Struct. Chem. **39**, 447 (1998); (*t*) V.E. Kuzmin, V.A. Chelombitko, I.V. Yudanova, I.B. Stelmakh, and I.S. Rublev. J. Struct. Chem. **39**, 452 (1998); (*u*) L. Coffey, J.A. Drapala, and T. Erber. J. Phys. A: Math. Gen. **32**, 2263 (1999); (*v*) M. Petitjean. C. R. Acad. Sci. Paris, Serie IIc, **2**, 25 (1999); (*w*) M. Petitjean. J. Math. Phys. (N.Y.), **40**, 4587 (1999); (*x*) B.B. Smirnov, O.V. Lebedev, and A.V. Evtushenko. Acta Crystallogr. Sect. A: Fundam. Crystallogr. **A55**, 790 (1999).
4. E. Ruch. Angew. Chem. Int. Ed. Engl. **16**, 65 (1977).
5. (*a*) K. Mislow and P. Poggi-Corradini. J. Math. Chem. **13**, 209 (1993); (*b*) N. Weinberg and K. Mislow. Theor. Chim. Acta. **95**, 63 (1997).
6. K. Mislow. *In* Fuzzy logic in chemistry. *Edited by* D.H. Rouvray. Academic Press: San Diego. 1997. pp. 65–90.
7. K. Mislow. Top. Stereochem. **22**, 1 (1999).
8. D.J. Caldwell and H. Eyring. The theory of optical activity. Wiley-Interscience, NewYork. 1971. p. 21.
9. E. Charney. The molecular basis of optical activity. John Wiley and sons, New York. 1979.
10. H.G. Dales and W.H. Woodin. Super-real fields. Clarendon Press, Oxford. 1996. p. 2.
11. K. Mislow. Science (Washington, D.C.), **120**, 232 (1954). See also discussion in references (6, 7).
12. K. Mislow and P. Bickart. Isr. J. Chem. **15**, 1 (1976/77).
13. C. Truesdell. *In* Ergodic theories. *Edited by* P. Caldirola. Academic Press, New York. 1961. pp. 21–56.

© 2000 NRC Canada

A 2D deuterium NMR study of molecular reorientation in $(CH_3)_3E^+X^-$ onium salts

Andrew M. Wachner, Kenneth R. Jeffrey, and Glenn H. Penner

Abstract: Two dimensional deuterium NMR measurements are reported for three different onium salts $(CH_3)_3SeNO_3$-d_3, $(CH_3)_3TeI$-d_3, and $(CH_3)_3SI$-d_9. In these molecular solids with the general structure $(CH_3)_3E^+X^-$, three methyl groups are attached to the E atom. There is the possibility of reorientation of the methyls about their C_3 axes and reorientation of the whole tri-methyl group about the C_3' axis. From an analysis of the 2D NMR exchange spectra the angle between the E—C bonds and the rotation axis for trimethyl reorientation were determined. Exchange rates and spin lattice relaxation times are given for several temperatures, to show how the mixing times for the experiments were selected. The data presented for $(CH_3)_3TeI$-d_3, demonstrate that 2D techniques are sensitive to motions on a time scale an order of magnitude slower than that accessible using 1D line shape techniques.

Key words: deuterium NMR, molecular motion, onium salts, two dimensional spectra.

Résumé : On a effectué des mesures bidimensionnelles de RMN du deutérium pour trois sels onium différents, $(CH_3)_3SeNO_3$-d_3, $(CH_3)_3TeI$-d_3 et $(CH_3)_3SI$-d_9. Dans ces trois solides moléculaires comportant la structure générale $(CH_3)_3E^+X^-$, les trois groupes méthyles sont attachés à l'atome E. Il existe une possibilité de réorientation des groupes méthyles autour de leurs axes C_3 et de réorientation de l'ensemble du groupe triméthyle autour de l'axe C_3'. Sur la base d'une analyse du spectre d'échange RMN-2D, on a pu déterminer l'angle entre les liaisons E—C et l'axe de rotation pour la réorientation du triméthyle. On rapporte les vitesses d'échange et les temps de relaxation spin-réseau à plusieurs températures et ces données permettent de comprendre comment les temps de mélanges des expériences ont été choisis. Les données rapportées pour le $(CH_3)_3TeI$-d_3 démontrent que les techniques 2D sont sensibles aux mouvements sur une échelle de temps d'un ordre de grandeur inférieur à celle disponible à l'aide des techniques de formes de bandes en 1D.

Mots clés : RMN du deutérium, mouvement moléculaire, sels onium, spectres bidimensionnels.

[Traduit par la Rédaction]

Introduction

Two dimensional (2D) deuterium NMR has been used extensively to determine the nature of the molecular reorientation that is taking place in crystalline and amorphous solids (1–3). In the case of large finite angle jump reorientation, it has been shown that 2D deuterium NMR exchange spectra provide a model-independent method of measuring the angle of reorientation in many materials (4).

In previous work reported on the molecular dynamics of the onium salts (5) it was demonstrated, using one dimensional line shape analysis of spectra over a large temperature range and fitting to appropriate model simulations, that it was possible to determine certain bond angles and rates of reorientation. The present work is intended to confirm the results of the previous 1D study, using the model independent methods of Spiess (3), and to extend the results into the region of slower exchange rates not available to 1D line shape analysis techniques.

Deuterium is an ideal probe nucleus for the study of molecular dynamics because it can be treated as an isolated spin. The reason being that the strength of the quadrupolar interaction is 100–250 kHz while the strength of the dipolar interaction between spins is 1–2 kHz and as a result can be neglected. For the case of methyl groups, it is reasonable to assume that the electric field gradient at the deuterium site is axially symmetric along the C—D bond. The resonance frequency of the deuteron at the site of an axially symmetric electric field gradient is shifted as a result of the quadrupolar interaction by an amount

$$[1] \qquad \omega = \pm \frac{3}{8}\frac{e^2qQ}{\hbar}(3\cos^2\beta - 1)$$

where β is the angle between the carbon deuterium bond and the magnetic field axis and $e^2qQ/\hbar$ is the quadrupolar coupling. Because the angular dependence of the resonance frequency provides a direct measure of the orientation of a carbon deuterium bond, changes in the resonance frequency can be used to probe the reorientation that is taking place in a sample. Any change in the orientation of the bond vector will result in a change in the resonance frequency.

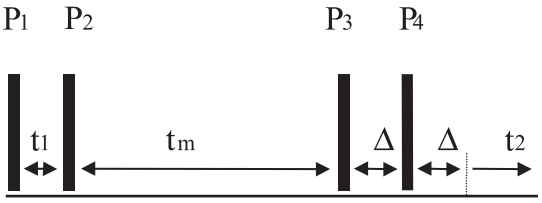
Accepted November 8, 1999.

A.M. Wachner and K.R. Jeffrey.[1] Guelph/Waterloo Program for Graduate Work in Physics, Department of Physics, University of Guelph, Guelph, ON N1G 2W1, Canada.
G.H. Penner. Guelph/Waterloo Centre for Graduate Work in Chemistry, Department of Chemistry, University of Guelph, Guelph ON N1G 2W1, Canada.

[1]Author to whom correspondence may be addressed. Telephone (519) 824-4120 ext 3909. Fax: (519) 836-9967. e-mail: KRJ@physics.uoguelph.ca

 © 2000 NRC Canada

Fig. 1. Stimulated Echo pulse sequence. To measure the sin–sin correlation select $P_1 = 90_y$, $P_2 = 45_{-x}$, $P_3 = 45_x$, $P_4 = 90_x$, and to measure the cos–cos correlation function select $P_1 = 90_y$, $P_2 = 90_{-y}$, $P_3 = 90_y$, $P_4 = 90_x$.



The 2D exchange experiment (2) provides a method of directly measuring the sin–sin and cos–cos two time single particle correlation functions given in eqs. [2] and [3].

$$[2] \qquad f_{cc}(t_1, t_m, t_2) \propto \langle \cos(\omega_1 t_1) \cos(\omega_2 t_2) \rangle$$

$$[3] \qquad f_{ss}(t_1, t_m, t_2) \propto \langle \sin(\omega_1 t_1) \sin(\omega_2 t_2) \rangle$$

where the angular brackets represent an ensemble average over the powder sample. Double Fourier transforming these functions leads to a 2D spectrum which can be analyzed to determine the nature of the reorientation that is taking place in the system. The appropriate 4 pulse sequence is shown in Fig. 1. The quadrupolar frequency ω_1 measured during the evolution time (t_1) is compared with the frequency ω_2 observed in the detection time (t_2) using the cos–cos and sin–sin correlation functions. Molecular reorientation during the mixing time (t_m) results in a loss of correlation and the creation of off-diagonal peaks in the 2D spectrum. To eliminate double quantum coherences and spectrometer imperfections the CYCLOPS (2) phase variations must be used with the above 2D exchange sequence. The pulse sequence shown in Fig. 1 is subject to a few constraints when used to measure 2D exchange spectra. The rate of exchange taking place in the system must be in the range (10^3–10^{-1} s^{-1}), to satisfy the requirements that no exchange takes place during the evolution time (t_1) and detection time (t_2) which is on the order of 1 ms. Sufficient exchange must take place during the mixing time (t_m) before the signal decays due to spin-lattice relaxation.

Using the method of Schmidt et al. (2) the above two correlation functions can be appropriately Fourier transformed and combined to produce a pure absorption mode spectrum. In the case of large finite angle jump reorientation, the spectra will contain two ellipses (3). By measuring the major and minor axis of these ellipses the jump angle can be determined from eq. [4],

$$[4] \qquad \alpha = \tan^{-1}\left(\frac{B}{A}\right)$$

where B is the minor axis, A is the major axis of the ellipse and α is the jump angle.

Experimental

All of the measurements were performed on a home built spectrometer using a Bruker (6.8 T) superconducting magnet with a deuterium resonance frequency of 44 MHz. Data accumulation was performed on a Nicolet Instruments 2090 III A digital oscilloscope that was interfaced with a 486 personal computer. Temperature control was maintained by regulating the flow of cold nitrogen gas over the sample and the current in a heater wrapped on a copper container surrounding the sample. The electronic feed back loop was able to maintain a stability of ±0.2°C over the duration of an experiment.

Samples of $(CH_3)_3SeI$-d_3, $(CH_3)_3TeI$-d_3, and $(CH_3)_3SI$-d_9 were prepared by reacting deuterated methyl iodide with $(CH_3)_2Se$, $(CH_3)_2Te$, and $(CH_3)_2S$ using the method outlined in the original paper (5). $(CH_3)_3SeNO_3$-d_3 was prepared by ion exchanging $(CH_3)_3SeI$-d_3.

Before a 2D spectra can be measured it is necessary to choose the appropriate temperature and the mixing time. One method to determine these quantities is to measure the sin–sin correlation function (f_{ss}) at several temperatures with several mixing times. These data can then be fit with eq. [5] to determine the exchange rate and the spin-lattice relaxation time (1).

$$[5] \qquad f_{ss}(t_1, t_2) = \frac{1}{n}\left\{tr\left[\sin(\omega_Q t_1)\right]\cdot tr\left[\sin(\omega_Q t_2)\right] - \left[1\cdot\sin(\omega_Q t_1)\cdot\left(\frac{\Pi}{\Omega}\cdot\sin(\omega_Q t_2)\right)\cdot 1\right] \exp(-n\Omega t_m)\right\}\exp\left(\frac{-t_m}{T_1}\right)$$

where ω_Q is a matrix with diagonal elements equal to the resonance frequency at the ith site. Π is an exchange matrix where each element Π_{ij} is the transition rate on going from site j to site i with the general condition that

$$\Pi_{ij} = \sum_j \Pi_{ij}, (i \neq j)$$

Equation [5] was also used to simulate the 2D spectra shown in the next section.

Results and discussion

The three salts that were analyzed in this study are $(CH_3)_3SeNO_3$-d_3, $(CH_3)_3TeI$-d_3, and $(CH_3)_3SI$-d_9. There is the possibility of both methyl group (CH_3) reorientation and rotation of the trimethyl $(CH_3)_3$ as previously discussed (5). The methyl group motion has a lower activation energy and occurs at lower temperatures. The 2D experiments reported in this paper explore the motion of the $E(CH_3)_3$ group in these compounds. The trimethyl group reorientation is shown in Fig. 2 and the relationship between the jump angle (α) and the angle (θ) between the E—CD_3 bond and the C_3' rotation axis, is given in eq. [5].

$$[5] \qquad \frac{\sqrt{3}}{2}\sin(\theta) = \sin\left(\frac{\alpha}{2}\right)$$

***Trimethylselenonium nitrate*-d_3:**

To determine the mixing time for the 2D spectra the sin–sin correlation function was measured as a function of the mixing time for 4 temperatures (0, –10, –20, and –30°C). A sample plot of this data at –30°C is shown in Fig. 3. The results of fitting with eq. [4] are summarized in Table 1. In

© 2000 NRC Canada

Fig. 2. Orientation of trimethyl group bonded to cation E^+ (S, Se, Te), the angle α is the jump angle measure in exchange experiments, θ is the angle between the methyl group and the C_3' rotation axis and β is the angle between the methyl group and the magnetic field orientation.

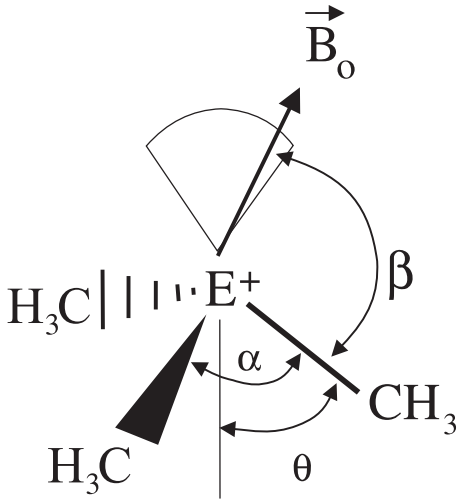


Fig. 3. Sin–sin correlation for $(CH_3)_3SeNO_3$ at –30°C.

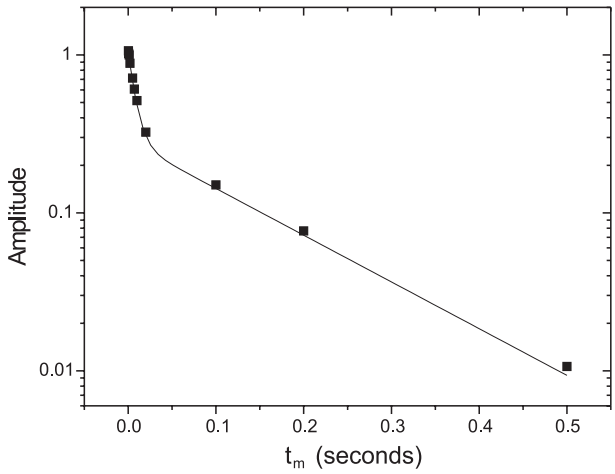


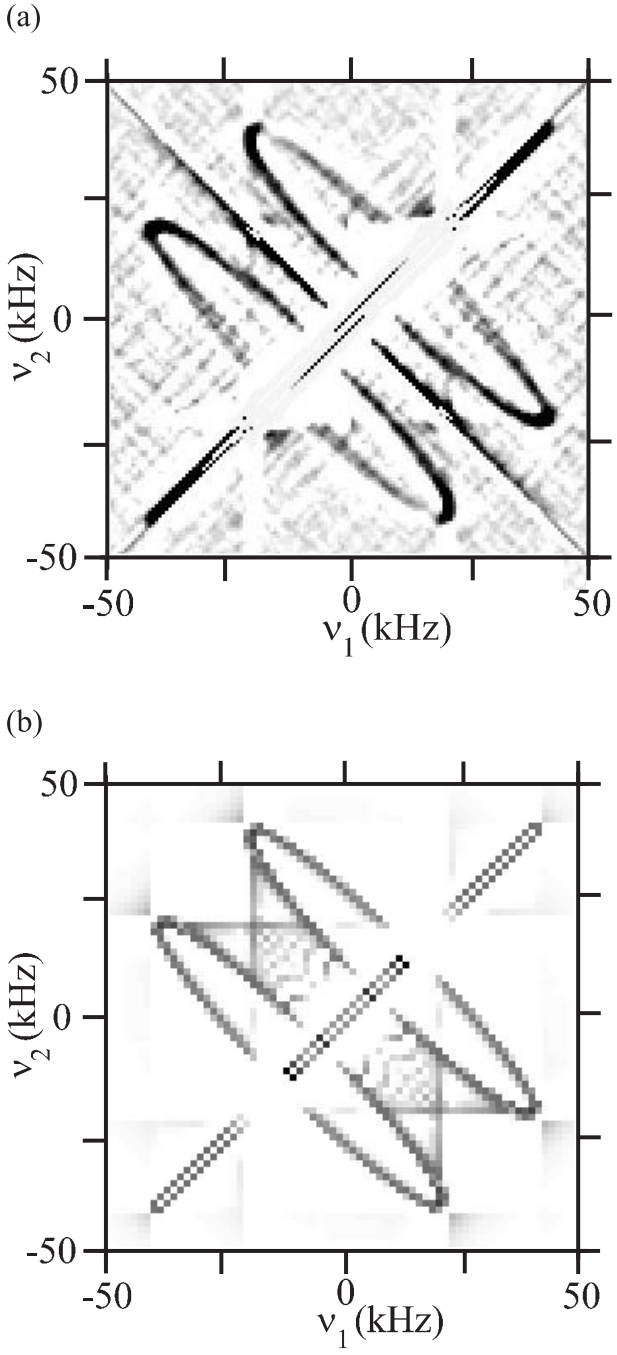
Fig. 3 the initial rapid decay is due to exchange while the longer decay is due to T_{1Q}.

To ensure that there is little exchange during the times t_1 and t_2 but appreciable reorientation during the mixing time (t_m) the 2D exchange experiment was performed at –30°C with a mixing time of 20 ms and 256 t_1 and t_2 values. A repetition rate of 0.5 s was used and 512 scans for each t_1 were collected to enhance the signal to noise ratio. The experimental and simulated spectra are shown in Figs. 4*a* and 4*b*. The spectra show that the elliptical ridge pattern has been well resolved, however the anti-diagonal has not been completely eliminated which indicates that there are some slight inconsistencies between the sin–sin spectrum and the cos–cos spectrum. These arise because of small differences in T_1 and T_{1Q} and a slight imbalance in the intensities of the two correlation functions. From the experimental 2D spectrum the reorientation angle (α) was determined to be 98.5 ± 0.5 degrees. This value is in good agreement with previous studies (5, 6) as shown in Table 2.

Table 1. Fitted parameters for $(CH_3)_3SeNO_3$.

Temperature (°C)	Exchange rate (s^{-1})	T_{1Q} (s)
0	5213	0.20
–10	2007	0.16
–20	361.3	0.17
–30	123.1	0.15

Fig. 4. $(CH_3)_3SeNO_3$ 2D exchange spectra at –30°C, (*a*) experimental, (*b*) simulation.



© 2000 NRC Canada

Table 2. Summary of bond (θ) and jump (α) angles for various $(CH_3)_3E^+X^-$ salts.

Sample	θ (2D NMR)	θ (1D NMR)	α (2D NMR)	α (1D NMR)	α (X-ray)
$(CH_3)_3SeNO_3$	60.6 ± 0.6	62.0 ± 0.5	98.0 ± 0.5	99.8 ± 0.5	98.5 ± 1
$(CH_3)_3TeI$	58.8 ± 0.7	—	95.6 ± 0.7	—	94.2 ± 0.1
$(CH_3)_3SI$	65.2 ± 0.5	65.0 ± 0.5	103.7 ± 0.5	103.4 ± 0.5	103 ± 1

Table 3. Fitted parameters for $(CH_3)_3SI$.

Temperature (°C)	Exchange rate (s^{-1})	T_{1Q} (ms)
–35	1900	5.2
–40	1500	4.8
–45	1100	4.0
–50	920	4.4

***Trimethylsulfonium iodide*-d_9:**

To determine the appropriate mixing time to use to obtain the 2D exchange spectrum for $(CH_3)_3SI$-d_9 the sin–sin correlation function was measured as a function of the mixing time for four temperatures. This data is given in Table 3. As the temperature decreases the exchange rate and the T_{1Q} value decrease as expected. At –50°C it is difficult to fit the two components of the decay since the two rates have similar values. However, the 2D exchange experiment was performed at –50°C so that the condition of no exchange during the detection and evolution times could be satisfied. Because T_{1Q} was so short a mixing time of 3 ms was selected, to permit exchange to occur during the mixing time and to limit the effects of T_{1Q} relaxation during the mixing time.

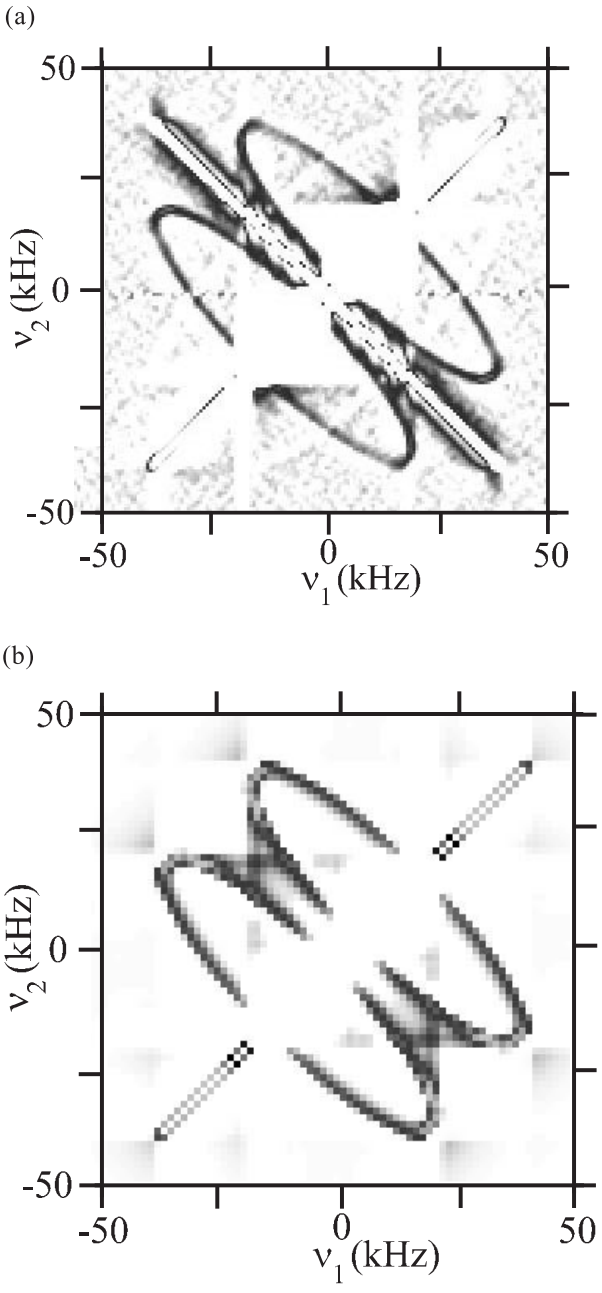
The 2D spectrum was obtained using 256 t_1 values and a repetition rate of 0.1 s. The final 2D spectrum is shown in Fig. 5*a* and the corresponding simulation is shown in Fig. 5*b*. From the experimental spectrum the jump angle (α) was determined to be 103.7 ± 0.5 degrees which is again in good agreement with earlier NMR (5) and X-ray work (7) as summarized in Table 2.

***Trimethyltelleronium iodide*-d_3:**

To determine the appropriate mixing time for $(CH_3)_3TeI$-d_3 the sin–sin correlation function was measured as a function of t_m at three temperatures. This data is summarized in Table 4. At the lower temperatures, 20°C and 50°C, only one component is present, this indicates that the exchange rate is very slow and cannot be distinguished from the spin alignment relaxation T_{1Q}. However at 75°C the two components in the decay are very distinct and the exchange rate is on the order of 100 s^{-1} which is ideal for the 2D exchange measurement. However the T_{1Q} value is quite long at 1.1s, which meant that the acquisition of the 2D data set was very time consuming.

The 2D spectrum was obtained using 128 t_1 values, a mixing time of 50 ms, a repetition rate of 5.3 s, and 256 scans were accumulated to improve the signal to noise ratio. The final spectrum is shown in Fig. 6*a*, along with a simulation in Fig. 6*b*. The spectrum shows that the ellipses have been resolved even though there is a significant amount of noise. This noise is largely thermal noise in the probe that is increased at high temperatures. From this spectrum the jump angle (α) was measured to be 95.6 ± 0.7 degree; this value is in good agreement with previous X-ray data (8) as shown in Table 2.

Fig. 5. $(CH_3)_3SI$ 2D exchange spectra at –50°C, (*a*) experimental, (*b*) simulation.



It should be noted that for each of the three onium salts studied the unit cell in the crystalline solid contains more that one formula unit (6–8). The crystal symmetry however demands that the molecular conformation is that same for

© 2000 NRC Canada

Fig. 6. $(CH_3)_3TeI$ 2D exchange spectra at 75°C, (*a*) experimental, (*b*) simulation.

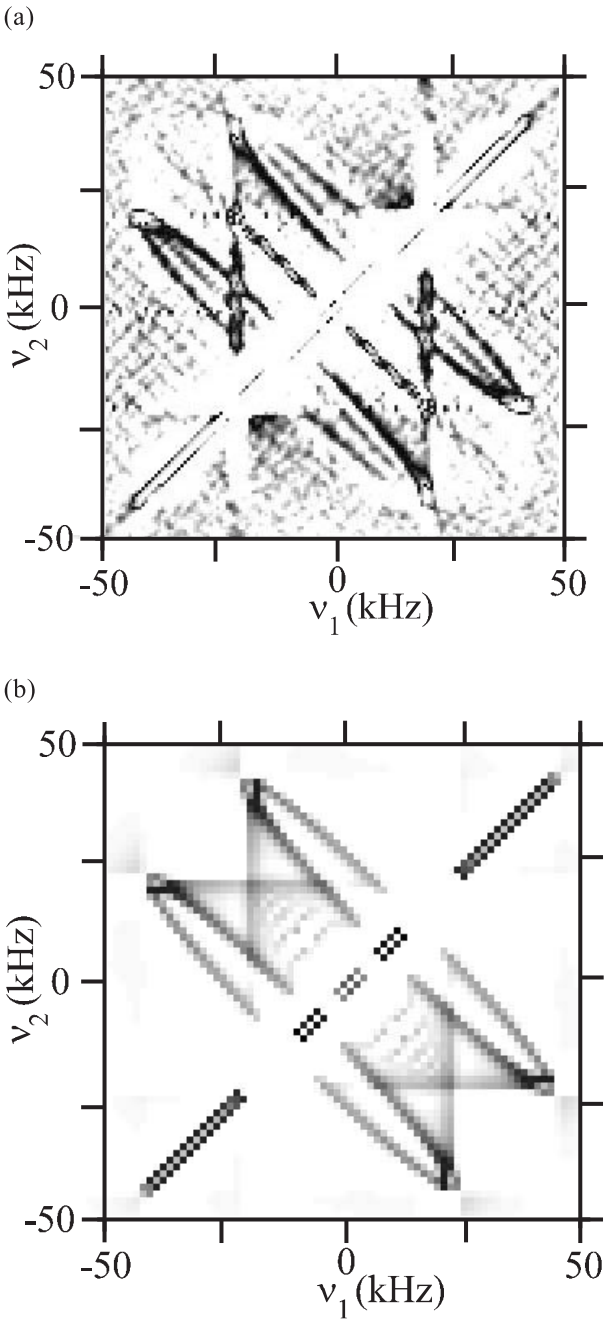


Table 4. Fitted parameters for $(CH_3)_3TeI$.

Temperature (°C)	Exchange rate (s^{-1})	T_{1Q} (s)
20	—	0.95
50	—	0.84
75	106	1.11

each formula unit. It is found that there are two crystallographically inequivalent carbon atoms in each $(CH_3)_3M^+$ ion but the bond lengths and C-M-C angles are nearly equally and the symmetry of the ion is nearly 3*m*. As a result the angles measured by NMR are averages over the two values obtained from X-ray diffraction.

Conclusions

It has been shown in this work that 2D exchange spectra provide a model independent method of determining the jump angle in several $(CH_3)_3E^+X^-$ odium salts. The jump angles obtained are in good agreement with previous studies. For the case of $(CH_3)_3TeI$-d_3 it was possible to determine the jump angle (α) using 2D exchange techniques where 1D line shape analysis methods failed because 2D spectral techniques are sensitive to motion on a slower time scale than 1D line shape techniques. Previously (5) it had not been possible to increase the temperature to the point where line shape changes in the 1D spectra could be observed and as a result model fitting was not possible.

Acknowledgments

The authors thank the Natural Sciences and Engineering Research Council of Canada for operating grant support (KRJ and GHP) and for graduate scholarship support (AMW).

References

1. H.W. Spiess. J. Chem. Phys. **72,** 12 (1980).
2. C. Schmidt, B.Blumich, and H.W. Spiess. J. Magn. Reson. **79**, 269 (1988).
3. K. Schmidt-Rohr and H.W. Spiess. Multidimensional solid state NMR and polymers. Academic Press Ltd., London. 1994.
4. S. Wefing and H.W. Spiess. J. Chem. Phys. **79**, 1219 (1988).
5. G.H. Penner, J.M. Polson, S.I. Daleman, and K. Reid. Can. J. Chem. **71**, 417 (1993).
6. H. Hope. Acta. Crystallogr. **20**, 610 (1966).
7. D.E. Zuccaro and J.D. McCullough. Z. Kristallogr. **112**, 401 (1959).
8. M.J. Collins, J.A. Ripmeester, and J.F. Sawyer. J. Am. Chem. Soc. **110**, 8583 (1988).

© 2000 NRC Canada

Pyrolysis gas chromatography – mass spectrometry of humic substances extracted from Canadian lake sediments

Helen A. Joly, Hongbo Li, and Nelson Belzile

Abstract: Humic substances (HS) were extracted with the aid of 0.1 M $Na_4P_2O_7$ and 0.5 M NaOH solutions from the sediments of four lakes located in the Sudbury area in Ontario, Canada, namely, Tilton, Clearwater, Silver and Ramsey Lake. The humic acid (HA) and fulvic acid (FA) extracts, purified and characterized using classical methods i.e., elemental analysis, FTIR spectroscopy, and CPMAS ^{13}C NMR (see N. Belzile, H.A. Joly, and H. Li. (1997)), were submitted to pyrolysis – gas chromatography – mass spectrometry (Py–GC–MS). The pyrolysates of the HA and FA extracts were found to be complex mixtures of at least 200 compounds. Results based on statistical analysis of the abundances of pyrolysis products (of known origin) revealed trends similar to those obtained from the classical bulk characterization techniques. The Py–GC–MS technique supported the observation, obtained from classical methods, that the chemical composition of HA extracts varied less significantly among the four lake sediments than for the FA extracts. The abundances of lignin and carbohydrate pyrolysates showed the highest variation among the FA extracts. Pyrolysis products originating from lignin, carbohydrates, proteins, and fatty acids were identified.

Key words: humic substances, humic acid, fulvic acid, pyrolysis, pyrolysis – gas chromatography – mass spectrometry, lake sediments.

Résumé : On a extrait des substances humiques (SH) à l'aide de solutions de $Na_4P_2O_7$ 0,1 M et de NaOH 0,5 M, à partir des sédiments de quatre lacs situés dans la région de Sudbury, en Ontario, Canada, à savoir, des lacs Tilton, Clearwater, Silver et Ramsey. Les acides humiques (AH) et fulviques (AF) isolés ont été purifiés et caractérisés à l'aide de méthodes classiques, comme l'analyse élémentaire, la spectroscopie IR à TF, et la RMN du ^{13}C à l'angle magique (« CPMAS ») (voir: N. Belzile, H.A. Joly et H. Li. (1997)) avant d'être soumis à une pyrolyse couplée à de la chromatographie gazeuse et à de la spectrométrie de masse (Py–CG–SM). On a trouvé que les pyrolysats des AH et AF extraits sont des mélanges complexes formés d'au moins 200 composés. Des résultats qui reposent sur une analyse statistique des abondances des produits de pyrolyse (d'origine connue) mettent en évidence des tendances semblables à celles obtenues à partir de techniques de caractérisation classique de la masse. Les résultats obtenus à l'aide de la technique de la Py–CG–SM sont en accord avec ceux obtenus à l'aide de méthodes classiques, selon lesquels la variation dans la composition chimique des AH extraits est moins importante que celle observée avec les AF. Les variations dans les abondances de la lignine et des hydrates de carbone dans les pyrolysats sont maximales avec les AF extraits. On a identifié les produits de pyrolyse qui tirent leur origine de la lignine, des hydrates de carbone, des protéines et des acides gras.

Mots clés : substances humiques, acide humique, acide fulvique, pyrolyse, pyrolyse – chromatographie gazeuse – spectrométrie de masse, sédiments de lacs.

[Traduit par la Rédaction]

1. Introduction

Organic matter (OM) in lake sediments is made up of a complex mixture of lipids, carbohydrates, proteins, and other biomaterials originating from the tissues of living benthic micro-organisms and the detritus of organisms formerly living in the lake and its watershed. In spite of the application of many analytical and spectroscopic methods, knowledge of their complex nature and composition is still limited. The methods most frequently used to characterize humic fractions, namely elemental analysis, visible, IR and NMR spectroscopy indicate the nature and origin of these compounds. More specifically, the atomic ratios H:C, O:C, and N:C, determined from elemental data, are indicators of the degree of aromaticity, carbohydrate content, and protein content, respectively. A comparison of these ratios to those reported for humic fractions from different origins is used to identify differences as well as to monitor the structural changes of humates in soils (1).

Characterization of humic substances (HS) by visible spectroscopy requires that the optical densities (E) of dilute aqueous solutions of HA and FA be recorded at 465 and

Received September 1, 1999.

H.A. Joly,[1] H. Li, and N. Belzile. Department of Chemistry and Biochemistry, Laurentian University, Ramsey Lake Road, Sudbury, ON P3E 2C6, Canada.

[1]Author to whom correspondence may be addressed. Telephone: (705) 675-1151 ext. 2333. Fax: (705) 675-4844. e-mail: hjoly@nickel.laurentian.ca

© 2000 NRC Canada

665 nm. The ratio of the optical density measured at two different wavelengths, E_4:E_6, has been shown to vary for humic materials of different soil types (2, 3). Furthermore, the E_4:E_6 ratio is thought to reflect (4): (*i*) the total carbon content of the HS, (*ii*) the number of aromatic residues versus the number of aliphatic residues, and (*iii*) the molecular weight of the HS, IR, and NMR spectroscopic studies of HS have also provided useful information concerning the types of functional groups present in the material. It has been shown that a comparison of the peak areas of the signals found in the aromatic and aliphatic regions of the ^{13}C NMR spectra of HS is indicative of the degree of aromaticity versus aliphaticity of the HS (5–8).

Another useful approach for obtaining information on the structure of HS involves degrading the macromolecular substance using an oxidative or reductive process (9–11) or a pyrolytic technique. The degradation products are recovered and identified with the aid of a suitable method, for example mass spectrometry. The degradation products give information concerning the residues originally present in the HS. In fact, the aromatic building blocks which make up the HS as well as some of the alkanes, fatty acids, and aliphatic chains have been identified by the degradation technique (12). Thermal degradation or pyrolysis has proven to be very useful in the identification of the substructures of macromolecules, especially HS (13–18). Of the various pyrolysis approaches known, pyrolysis – gas chromatography – mass spectrometry (Py–GC–MS) seems to be the most reliable as products can be separated by GC and identified by MS (15). It is also an advantageous technique with respect to the other degradation methods because: (*i*) the pyrolyser is a relatively inexpensive tool which can be easily coupled to a GC–MS, (*ii*) it can be applied to a large variety of samples, and (*iii*) little or no sample manipulation is required prior to analysis.

Pyrolysis is by no means an ideal technique for investigating the structural features of HS because the interpretation of the pyrograms can at times be difficult. Besides the fact that HS produce hundreds of degradation products, there is an added complication in that certain pyrolysis products undergo secondary reactions. Identification of the residues present in the original HS macromolecular structure requires an understanding of their behaviour under pyrolytic conditions. However time consuming the data analysis may be, it does provide a means of identifying the residues which make up the HS, information which the above mentioned conventional analytical techniques have not as of yet provided. Finally, the task of data analysis is facilitated as more pyrolysis studies of HS become available.

In an earlier study (12, 19), we used elemental analysis, visible spectroscopy (E_4:E_6 ratio), FTIR, and solid-state ^{13}C CPMAS NMR to study the composition and the chemical nature of HA and FA isolated from the sediment of four Sudbury Lakes. The results suggested that the HS extracted from the different lake sediments have similar chemical composition and structure suggesting that the factors influencing the formation and preservation of HS were similar in the lakes tested. The HS of lake sediments were found to contain a greater proportion of HA than FA. The higher H:C and O:C ratios found for FA extracts than for HA extracts suggested that the FA contained more carbohydrate and carboxylic functionalities. This was confirmed by the ^{13}C NMR spectra of the FA and HA extracts. Analysis of the NMR spectra also showed that the lake sediment FA and HA were highly aliphatic in nature. The FTIR spectra indicated, as did the NMR data, the presence of aromatic, aliphatic, O–alkyl, and carboxylic functionalities. However, no apparent structural differences were found between the FA and HA extracted from the lake sediments using the FTIR technique.

In the present study, the same HS extracted from the sediment of the four Sudbury lakes with the aid of 0.1 M $Na_4P_2O_7$ and 0.5 M NaOH were characterized using Py–GC–MS. A statistical analysis was applied to the abundances of the pyrolysis products to determine the significance of the pyrolytic trends observed for the different sediment samples. The pyrolytic results were compared to those obtained by the classical methods mentioned above.

Methodology

Sampling and extraction

A detailed description of the sampling sites, sample collection and the sequential extraction of organic matter is presented elsewhere (19). Sediment samples were collected from four different lakes located in the Sudbury Region (46° 25′ N, 81° 00′ W) namely, Tilton, Clearwater, Silver, and Ramsey. The four lakes chosen in this area differ in pH, levels of metal contamination, surrounding vegetation, and in the amount of dissolved organic matter in the water (19). Three sampling points were selected for each lake and surficial sediments were collected using a sediment grab. The sediments obtained from the three points were mixed to give one sample and air-dried at room temperature for seven days. The sediments were next ground and sieved through a 2 mm sieve. The dried sediment samples were treated with organic solvents to remove organic material trapped in the complicated macromolecular matrix. More specifically, 25.0 g of the sediment sample were placed in a Whatman extraction thimble, fitted into a Soxhlet extraction apparatus, and extracted with 300 mL of spectrograde solvent for 48 h. Two different solvents (*n*-hexane followed by chloroform) were used in the extraction process.

Although there are a number of classification schemes (20) for natural organic matter, the HS in this study have been defined with respect to their solubility in alkali and acid. More specifically, humic acid (HA) is defined as the fraction of the HS that is soluble in dilute alkali but is coagulated by acidification of the alkaline extract (below pH 2); fulvic acid (FA) is the fraction that remains in solution when the alkaline extract is acidified, that is, the fraction that is soluble in both dilute alkali and dilute acid. Humin is the fraction of the HS that cannot be extracted from the soil by dilute acid or base. The HA and FA were isolated from the residual sediment using the method introduced by Schnitzer and Schuppli (21, 22) for soil samples. The sediment was first shaken with a 0.1 M $Na_4P_2O_7$ solution, under a nitrogen atmosphere, for a period of 24 h. The solution was centrifuged (10 400 G) and filtered using a 0.45 μm Millipore membrane. The filtrate contained a mixture of FA and HA. Acidification of the filtrate with 6 N HCl resulted in the precipitation of the HA which was subsequently collected with

© 2000 NRC Canada

Table 1. Elemental ratios, E_4:E_6 ratios, and distribution of C determined by CPMAS ^{13}C NMR for the Sudbury area lake sediments.

	Elemental ratios				% Distribution of C determined by CPMAS ^{13}C NMR				
Sample	H:C	N:C	O:C	E_4:E_6 Ratio	Aliphatic 0–50[a]	O–alkyl 50–110	Aromatic 110–160	Carboxyl 160–190	Carbonyl 190–230
HA–$Na_4P_2O_7$									
T[b]	1.35	0.078	0.563	5.60	38.9	24	22.7	11.0	3.4
C	1.27	0.075	0.643	5.88	44	25.1	8.9	15.6	6.4
S	1.18	0.070	0.520	5.59	31.8	30.8	22.1	12.4	2.9
R	1.05	0.077	0.576	5.68	28.1	30.6	24.2	13.5	3.6
HA–NaOH									
T	1.43	0.085	0.509	4.23	43.7	30.5	11.1	14.7	6.6
C	1.36	0.080	0.516	4.47	45.4	31.4	9.2	10.8	3.2
S	1.36	0.076	0.470	4.66	44.0	27.8	9.2	12.8	6.2
R	1.30	0.083	0.486	4.54	44.4	24.4	11.2	12.9	7.2
FA-$Na_4P_2O_7$									
T	1.66	0.072	0.708	11.83	—	—	—	—	—
C	1.71	0.069	0.718	11.50	—	—	—	—	—
S	2.06	0.057	1.070	11.11	22.6	34.7	21.5	17.0	4.2
R	1.94	0.074	0.815	12.40	21.9	35.0	22.3	18.3	2.6
FA-NaOH									
T	1.84	0.098	0.710	9.85	—	—	—	—	—
C	1.73	0.091	0.671	8.81	—	—	—	—	—
S	1.66	0.089	0.630	10.21	23.5	37.1	19.1	17.9	2.4
R	1.67	0.105	0.642	11.03	34.1	31.0	8.6	21.2	5.1

[a]In ppm.

[b]T = Tilton Lake; C = Clearwater Lake; S = Silver Lake; R = Ramsey Lake.

the aid of vacuum filtration and further purified. The pH of the supernatant was adjusted to 8 with 5 N NaOH and the resulting solution dialyzed using dialysis tubing with a molecular weight cutoff of 3500 amu. The FA was recovered from the solution with the aid of a freeze dryer.

Next the residue resulting from $Na_4P_2O_7$ extraction was treated with a 0.5 M NaOH solution for a 24 h period. The FA and HA were recovered as described above for the $Na_4P_2O_7$ extract. The extraction process afforded two HA and two FA samples for each of the sediment samples studied, i.e., HA–$Na_4P_2O_7$, HA–NaOH, FA–$Na_4P_2O_7$, and FA–NaOH respectively.

Characterization

HA and FA extracts were characterized by classical techniques such as elemental analysis, visible (E_4:E_6) and infrared (FTIR) spectroscopy, and CPMAS ^{13}C-NMR (12, 19). The experimental details have been published elsewhere (19).

Pyrolysis – gas chromatography – mass spectrometry (Py–GC–MS)

The HA and FA fractions were also analyzed with the aid of a CDS Pyroprobe 1000 heated coil filament coupled to a Varian Saturn II gas chromatograph – ion trap mass spectrometer. Samples (450–900 µg) were pyrolyzed in quartz tubes (placed in the platinum coil of the pyroprobe) at 700°C for 10 s for FA and 20 s for HA. The pyrolysis unit – GC interface was maintained at 200°C. The pyrolyzed samples were swept into a gas chromatograph equipped with (*i*) a 1077 Split–Splitless capillary injector which was operated in split mode with a split ratio of ca. 75:1 and at a temperature of 250°C, and (*ii*) a Supelco SPB-5 bonded phase capillary column (30 m × 0.32 mm i.d., 0.25 µm film thickness). The column oven was programmed from an initial temperature of 50°C (isothermal, 2 min) to a final temperature of 250°C at a rate of 5°C per minute. The final hold period was 5 min. Ultrapure helium was used as the carrier gas with a column head pressure of 85 kPa. The GC–MS mass transfer line was set at 260°C. The mass spectrometer was operated at 70 eV in the electron impact mode with a manifold temperature of 220°C. Mass spectral scans ranging from *m/z* 450 to *m/z* 40 were recorded at a scan rate of 0.5 s/scan.

Identification was achieved by comparing the mass spectra of the pyrolysis products with standard mass spectra in the computer library (NIST), by comparing the GC–MS data with literature data (16), and (or) comparison with authentic standard compounds. The relative amount of the pyrolysis products ($\%P_i$) was calculated by dividing the areas counts obtained from electronic integration of individual peaks (AC_i) by the sum of the area counts of all the peaks in the chromatogram (ΣAC_i), eq. [1].

$$[1] \qquad \%P_i = (AC_i / \Sigma AC_i) \times 100$$

Results and discussion

The elemental ratios, H:C, N:C, and O:C, the E_4:E_6 ratios and CPMAS ^{13}C NMR spectroscopic data of the HA and FA extracts isolated from the sediment of four Sudbury area lakes, namely Tilton, Clearwater, Silver, and Ramsey Lake were the subject of an earlier report (19). The results are summarized in Table 1 for the purpose of comparison with the Py–GC–MS results presented below.

A Py–GC–MS analysis of the HA and FA samples isolated from the lake sediments was carried out according to

© 2000 NRC Canada

Fig. 1. The Total Ion Current (TIC) pyrogram (displayed in three windows, i.e., a, b, and c) of HA extracted from Ramsey Lake sediment with 0.1 M $Na_4P_4O_7$. Peak numbers correspond to those in Table 2.

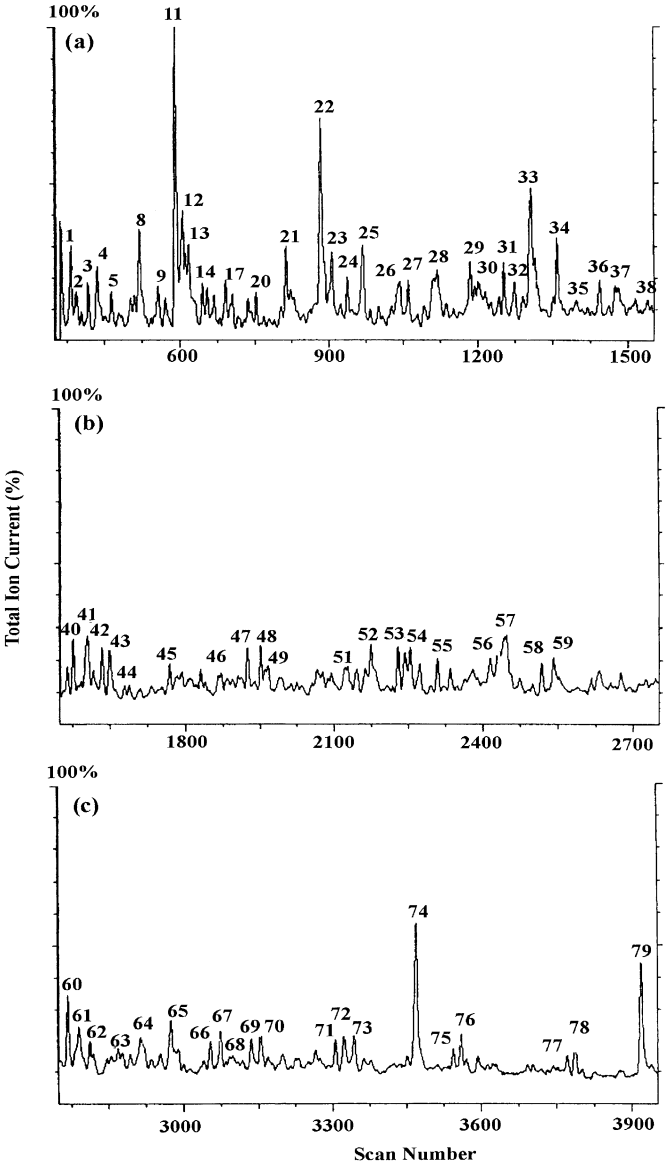
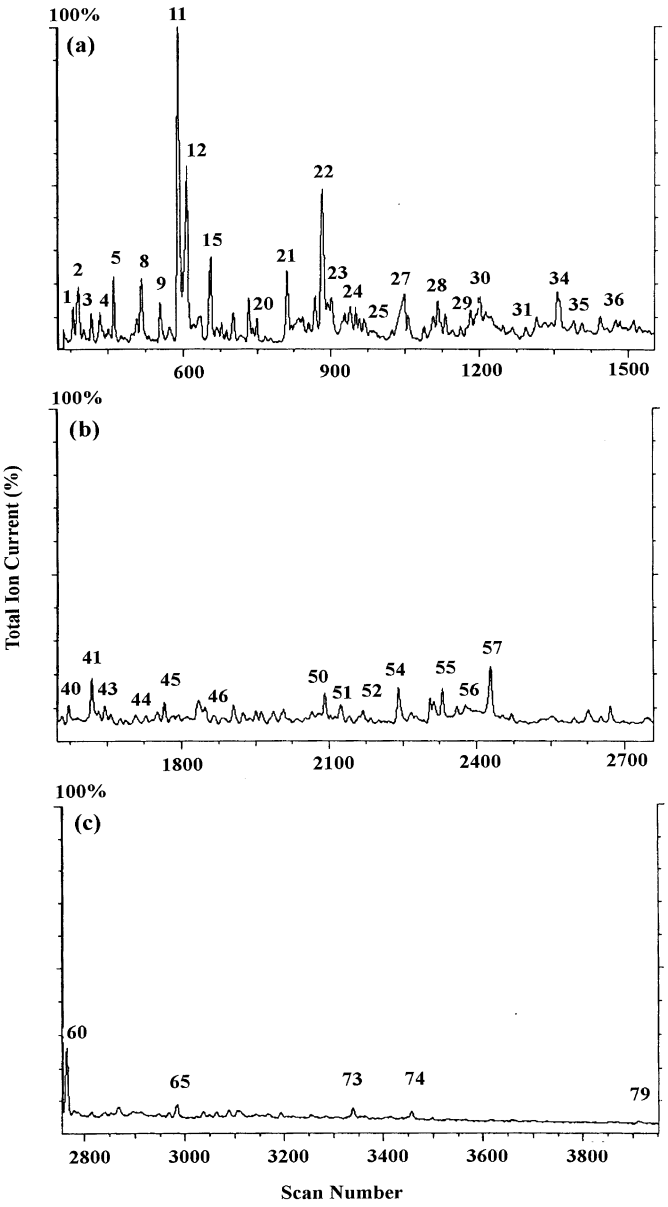


Fig. 2. The Total Ion Current (TIC) pyrogram (displayed in three windows, i.e., a, b, and c) of FA extracted from Ramsey Lake sediment with 0.1 M $Na_4P_4O_7$. Peak numbers correspond to those in Table 2.



the method provided by Chiavari et al. (16). The pyrolytic technique causes the thermal degradation of the FA and HA producing molecules of molecular mass range which are detectable by GC–MS. Representative total ion current (TIC) pyrograms of HA and FA extracted from the sediment of Ramsey Lake are given in Fig. 1 and 2. The same pyrolysis products were obtained whether the HS were extracted by NaOH or $Na_4P_2O_7$. However, the relative amounts of the products change and these changes will be discussed below.

Identification of the pyrolysis products

The pyrolysis products provide a fingerprint which aids in characterizing the original sample. An examination of the pyrograms (Fig. 1 and 2) indicates that there were more than 250 pyrolysis products in the pyrolysate of HA and approximately 200 products in the pyrolysate of FA. The complexity of the pyrograms is consistent with the fact that humic materials are complex heterogeneous macromolecular substances. The peaks corresponding to the main pyrolysis products were identified by comparing the GC and MS data to Py–GC–MS results published by Chiavari et al. (16). This could be done because the experimental set up was identical to that used by Chiavari and co-workers (16).

In order to facilitate identification of the products, authentic samples of phenol and indole were analyzed using the same GC–MS configuration as that used to study the pyroly-

© 2000 NRC Canada

sis products. The scan numbers (*SN*) obtained for the standards were compared to those reported for phenol and indole by Chiavari et al. (16). A correction was applied to the scan numbers in order to standardize the two studies, eq. [2]:

$$[2] \quad SN_{corr} = (SN_{phenol})_{exp} + (SN_r - SN_{phenol}) \times \frac{(SN_{indole})_{exp} - (SN_{phenol})_{exp}}{SN_{indole} - SN_{phenol}}$$

where $(SN_{indole})_{exp}$ and $(SN_{phenol})_{exp}$ are the scan numbers determined for indole and phenol in this study, SN_{indole} and SN_{phenol} are the scan number determined by Chiavari et al. (16) and SN_r is the scan number of a pyrolysis product in the pyrogram published by Chiavari et al. (16). Eq. [2] was used to predict the retention time of the reported pyrolysis products (16) under our experimental conditions (SN_{corr}). Twenty seven of the ninety-nine compounds were identified by comparing our data to the corrected scan numbers. For instance, 2-methylphenol, a pyrolysis product reported by Chiavari et al. (16) was found to have a scan number (SN_r) of 544. By using eq. [2] a SN_{corr} of 819 was calculated for 2-methylphenol. The product labelled **21** in Fig. 2 has a scan number of 811, very close to SN_{corr} for 2-methylphenol. The mass spectral data for the compound eluting at 811 is consistent with that of 2-methylphenol. The scan number, retention time, relative molecular weight, and the proposed origin of the products identified in the pyrolysates of the HA and FA samples have been listed in Table 2. Only peaks with an intensity ≥0.5% of the mixture were considered in the analysis. There are a number of products found in the pyrolysis of the sediment HS which were not observed in the soil humic acid pyrolysis. Their assignment was based on the comparison of the mass spectral data with spectra found in the NIST reference library and other published collections of Py–GC–MS data (23–25). The proposed identity of the pyrolysis products for the HA and or FA is found in column 6 of Table 2. In the cases where positive identification could not be made, the *m/z* of the main mass spectral fragments and their relative intensities to the base peak are presented.

Classification of the pyrolysis products according to their origin: Protein (P), Carbohydrate (C), Lignin (L), or Fatty acid (F)

In theory, the pyrolysis products can provide information on the structure of the HS. However, in practice this task is difficult because pyrolysis compounds can be products of secondary reactions. In addition, certain pyrolysis products are characteristic of many different types of biomaterials and of little use in identifying biological precursors. The interpretation of pyrolysis data is therefore complicated. Before the data can be used to elucidate the structure of HS, one must acquire a better understanding of the behaviour of the organic compounds likely to be present in HS under pyrolytic conditions.

Generally, the pyrolysis products obtained from HS can be classified according to their origin, i.e., protein (P), carbohydrate or structural polysaccharides (C), lignin (L), or fatty acids (F). Chiavari and Galletti (26) have identified the main pyrolysis products generated by 19 α-amino acids using Py–GC–MS. For instance, tryptophan produces indole, 3-methylindole, 3-ethylindole, and 2,3-dimethylindole on pyrolysis, while asparagine produces maleimide and succinimide. It follows that the alkylindoles and maleimide identified in the pyrolysis of the sediment HA and FA samples originate from proteinaceous material containing tryptophan and asparagine. The pyrolysis of proteins also yields N-containing heterocyclic compounds, alkylbenzonitriles, and some aromatic compounds such as benzene, toluene, styrene, phenol, etc. Polysaccharides are also incorporated into the macromolecular structure of HS. The pyrolysis of plant and soil polysaccharides produces a complex mixture of volatile, relatively low molecular weight compounds as well as anhydrosugars (27). Aldehydes and ketones of varying chain lengths, furans, and pyranones are also thought to originate from the pyrolysis of carbohydrate or structural polysaccharides. The pyrolysate of lignin contains primary pyrolysis products derived from the *p*-coumaryl, coniferyl, and (or) syringyl alcohol units depending on the type of lignin. These include phenol, 2-methoxyphenol, and 2,6-dimethoxyphenol. In addition, the thermal modification of functional groups of the basic phenolic units leads to a number of secondary products which can be attributed to lignin. Fatty acids (which are thought to be evaporation products) are known to produce alkylbenzenes and naphthalenes upon pyrolysis (27). The alkanes and alkenes may result from the decarboxylation of fatty acid moieties. Support for this interpretation comes from a study carried out by Saiz-Jimenez (28) where the protection of carboxylic groups by a methylation procedure greatly reduced the quantity of alkanes and alkenes observed in the pyrogram.

As many of the products observed in the pyrolysis of the HA and FA samples as possible were classified according to their origin (Table 2, column 9). This exercise again points to the complexity of characterizing the HS. There are many compounds which could originate from several sources. For instance, the alkanes can either come from the decarboxylation of fatty acids or are a product of evaporation. In other words, alkanes, synthesized by microorganisms can be trapped in the macromolecular matrix and released upon heating the HS. It should be noted that even though the FA and HA samples were previously treated with organic solvents to remove organic matter that was not covalently bound to the macromolecular structure small amounts could still have been trapped. Evidence for this comes from the detection of fatty acids in pyrolysates despite the fact that the HS were first treated with organic solvents (28).

In the pyrolysates of the HA and FA, 22 fragments were ascribed to lignin, 13 were labelled as protein markers, 8 originate from carbohydrate fragments and, finally, 4 peaks were identified as fatty acids. These results suggest that a variety of heterogeneous materials including lignins, proteins, polysaccharides, and fatty acids are components of the humic and fulvic acid molecules. In the case of the HA samples (Table 4, vide infra) approximately 12% of the pyrolysable organic matter is thought to originate from protein, 20% from lignin, 8% from carbohydrates, 6% from fatty acids. A similar analysis for the FA pyrolysate (Table 5, vide infra) shows that 19% of the matter originated from protein, 21% from lignin, 11% from carbohydrates and 0% from fatty acids. In a soil sample from an experimental

© 2000 NRC Canada

Table 2. Products identified in the pyrolysis of lake sediment HS.

Peak no.	SN_r [a]	SN_{corr} [b]	SN_{exp} [c]	M_r [d]	Proposed compound [e]	HA	FA	Proposed origin [f]
1			382	96	2-Furaldehyde	+	+	C
2			392	110	Acetylfuran	+	+	C
3	319	403	419	98	2,3-Dihydro-5-methylfuran-2-one – α-angelicalactone	+	+	C
4			438	95	C_2-alkylpyrrole	+	+	P
				107	C_2-alkylpyridine	+	+	P
5	359	473	463	95	Ethylpyrrole	+	+	P
6			502	106	C_2-alkylbenzene	+	—	U
7			509	—	110, 105, 92, 77, 67, 51, 43 (22, 100, 21, 63, 22, 49, 46)	+	—	U
8	381	517	520	110	Methyl-2-furaldehyde	+	+	C
9			552	110	110, 109, 93, 82, 66, 54, 53, 42 (22, 100, 40, 23, 20, 21, 21, 50)	+	+	U
10			572	—	119, 105, 91, 83, 79 (26, 100, 17, 18, 17)	+	—	U
			574	103	Benzonitrile	[g]	+	P
11	421	591	591	94	Phenol	+	+	L[h]
12	432	611	605	97	Maleimide	+	+	P
			614	120	C_3-alkylbenzene	+	—	U
13			618	140	Alkene (C_{10})	+	—	U
14			645	140	Alkene (C_{10})	+	—	U
15			652	112	2-Furancarboxylic acid[i]	+	+	C
16			668	—	120, 110, 109, 94, 82, 69, 52 (8, 14, 41, 13, 7, 33, 100)	+	+	U
17			689	120	C_3-alkylbenzene	+	+	U
18	490	719	705	118	Allylbenzene	+	[g]	L
19			737	—	110, 109, 97, 81, 67, 54, 53 (46, 66, 31, 12, 100, 60, 57)	+	[g]	U
			742	—	128, 127, 113, 98, 87, 69, 58, 43 (19, 47, 46, 34, 18, 89, 32, 100)	+	—	U
20			752	116	Indene	+	+	U
21	544	819	811	108	2-Methylphenol	+	+	L
22	582	889	880	108	4-Methylphenol	+	+	P
23	600	922	905	124	2-Methoxyphenol	+	+	L
24			935	154	Alkene (C_{11})	+	—	U
			939	131	α-Methylbenzyl cyanide	—	+	P
			949	140	140, 139, 112, 84, 67, 53 (15, 17, 39, 35, 100, 41)	—	+	U
			958	132	Methylbenzofuran	—	+	C
25			967	126	2-Methyl-3-hydroxypyran-4-one	[g]	+	C
			968	98	Furanmethanol	+	—	C
26			1043	100	100, 56, 55, 43, 42 (100, 95, 78, 37, 38)	+	+	U
27	678	1068	1059	117	Benzyl cyanide	+	+	P
28	709	1124	1117	122	Dimethylphenol	+	+	L
29	741	1184	1184	122	Ethylphenol	+	+	L
30			1194	122	C_2-phenol	+	+	U
			1201	128	Naphthalene	+	+	U
31	783	1261	1251	138	2-Methoxy-4-methylphenol	+	+	L
32			1272	168	Alkene (C_{12})	+	—	U
33			1304	110	Benzenediol	+	[g]	L
34	835	1358	1358	120	4-Vinylphenol	+	+	L
35	849	1383	1400	124	3-Methoxyphenol	+	+	L
36			1442	—	79, 78, 52, 51, 50 (100, 42, 46, 51, 31)	+	+	U
37			1473	140	Methoxybenzenediol	+	—	L
38			1539	152	4-Ethyl-2-methoxyphenol	+	—	L
39			1564	142	Methylnaphthalene	+	+	U
40	953	1576	1576	117	Indole	+	+	P
41			1604	182	Alkene (C_{13})	+	—	U
			1617	142	Methylnaphthalene	+	+	U
			1621	148	1,3-Benzofurandione	—	+	U
42			1634	184	Alkane (C_{13})	+	—	U
43	991	1649	1649	150	2-Methoxy-4-vinylphenol	+	+	L
44			1690	138	Dimethoxybenzene	+	+	L
45			1770	154	Dimethoxyphenol	+	+	L

© 2000 NRC Canada

Table 2 (*concluded*).

Peak no.	SN_r [a]	SN_{corr} [b]	SN_{exp} [c]	M_r [d]	Proposed compound [e]	HA	FA	Proposed origin [f]
46	1103	1853	1868	131	Methylindole	+	+	P
47			1924	196	Alkene (C_{14})	+	—	U
48			1951	—	148, 147, 71, 57, 43, 41 (14, 38, 62, 100, 84, 93)	+	—	U
49			1961	119	Hydroxybenzonitrile	+	—	P
			1965	154	Dimethylnaphthalene	+	+	U
50			2090	147	1*H*-Isoindol-1,3–2(*H*)-dione	—	+	U
51			2122	—	Alkene	+	—	U
	1241	2108	2127	133	2,3-Dihydro-3-methylindole	+	+	P
52			2162	133	Hydroxybenzeneacetonitrile	+	—	P
	1261	2145	2171	166	4′-Hydroxy-3′-methoxyacetophenone	+	+	L
53			2229	210	Alkene (C_{15})	+	—	U
54			2243	—	168, 167, 125, 69, 68, 43 (9, 12, 100, 34, 27, 71)	+	+	U
			2254	214	Alkane (C_{15})	+	—	U
			2273	—	173, 144, 115 (100, 33, 28)	+	—	U
55	1328	2269	2307	180	1-(4-Hydroxy-3-methoxyphenyl)-2-propanone – guaiacylacetone	+	+	L
56	1403	2409	2416	180	Propiovanillone	+	+	L
57			2432	—	161, 153, 118, 89, 77, 63, 51 (100, 41, 87, 82, 28, 64, 46)	+	+	U
			2445	168	4-Hydroxy-3-methoxybenzoic acid – vanillic acid[i]	+	+	L
			2448	170	C_3-naphthalene	+	—	U
58			2516	—	Alkene	+	—	U
59			2539	—	Alkane	+	—	U
60			2770	186	Biphenol	+	+	U
61	1614	2798	2791	196	3′,5′-dimethoxy-4′-hydroxyacetophenone – acetosyringone	+	—	L
			2791	224	Alkene (C_{16})	+	—	U
62			2813	226	Alkane (C_{16})	+	—	U
63			2895	—	Alkene	+	—	U
64			2914	—	Alkene	+	[g]	U
65	1665	2943	2972	210	1-(3,5-Dimethoxy-4-hydroxyphenyl)-2-propanone – syringylacetone	+	+	L
			2975	228	Tetradecanoic acid	+	—	F
66			3052	252	Alkene (C_{18})	+	—	U
67			3072	254	Alkane (C_{18})	+	—	U
68	1734	3020	3091	198	4-Hydroxy-3,5-dimethoxybenzoic acid – syringic acid[i]	+	—	L
69			3136	242	Pentadecanoic acid	+	—	F
70			3155	—	242, 241, 195, 177, 129, 97, 83, 69, 55, 41)(4, 5, 18, 31, 12, 17, 21, 27, 39, 55, 100)	+	—	U
71			3306	—	208, 138, 124, 110, 97, 83, 69, 55, 41 (5, 8, 16, 26, 53, 49, 44, 62, 100)	+	—	U
72			3328	—	Alkane	+	—	U
73			3343	195	195, 194, 193, 111, 110, 97, 96, 70 (14, 29, 23, 7, 16, 10, 18, 100)	+	+	U
74			3469	256	Hexadecanoic acid	+	+	F
75			3543	266	Alkene (C_{19})	+	—	U
76			3558	268	Alkane (C_{19})	+	—	U
77			3772	280	Alkene (C_{20})	+	—	U
78			3787	282	Alkane (C_{20})	+	—	U
79	2133	3758	3917	284	Octadecanoic acid	+	+	F

[a]The scan number of the products found in the pyrogram of Chiavari's study (1994).

[b]The corrected scan number of the product found in the pyrogram of Chiavari's study (1994), calculated using eq. [4].

[c]The scan number of the products found in the pyrogram of this study.

[d]Relative molecular weight.

[e]Mass spectral data is presented in the cases where identification of the compound was not possible. The values between parentheses represent the % abundance of the fragment with respect to the base peak.

[f]Proposed origin of the product: L = lignin, P = protein, F = fatty acid, C = carbohydrate, and U = unknown (many types of materials produce aromatic pyrolysis products therefore they are of little use in identifying biological precursors).

[g]Trace amounts were detected.

[h]Products also detected in the pyrolysis of amino acids.

[i]These are tentative assignments based on NIST standard spectra. Some concern exists because these aromatic carboxylic acids are very polar and may not freely elute from a GC column.

© 2000 NRC Canada

Table 3. Reproducibility of the relative amounts of the pyrolysis products.

Peak no.	Compounds	X^a (%)	SD^b (%)
1	2-Furaldehyde	2.4	0.1
3	2,3-Dihydro-5-methylfuran-2-one	0.7	0.1
4	Alkylpyridine–alkylpyrrole	0.8	0.1
5	Ethylpyrrole	0.3	0.1
8	Methyl-2-furaldehyde	3.7	0.2
11	Phenol	2.1	0.3
12	Maleimide	2.6	0.5
13	Alkene (C_{10})	2.1	0.4
14	Alkene (C_{10})	0.9	0.1
18	Allylbenzene	0.4	0.1
20	Indene	0.8	0.1
21	2-Methylphenol	1.0	0.3
22	4-Methylphenol	4.3	0.2
23	2-Methoxyphenol	0.2	0.2
24	Alkene (C_{11})	0.9	0.1
25	Furanmethanol	1.8	0.2
27	Benzyl cyanide	0.7	0.1
28	Dimethylphenol	0.6	0.1
29	Ethylphenol	0.7	0.1
31	2-Methoxy-4-methylphenol	0.1	0.1
32	Alkene (C_{12})	1.1	0.1
33	Benzenediol	1.5	0.3
34	4-Vinylphenol	0.6	0.1
35	3-Methoxyphenol	0.8	0.1
39	Methylnaphthalene	0.4	0.1
40	Indole	0.8	0.1
41	Alkene(C_{13})	1.6	0.2
42	Alkane(C_{13})	1.0	0.1
43	2-Methoxy-4-vinylphenol	0.7	0.2
46	Methylindole	0.5	0.1
47	Alkene (C_{14})	1.0	0.1
48	148, 147, 71, 57, 43, 41 (14, 38, 62, 100, 84, 93)	1.0	0.1
49	Dimethylnaphthalene	0.8	0.1
51	2,3-Dihydro-3-methylindole	0.7	0.1
52	4′-Hydroxy-3′-methoxyacetophenone	0.2	0.1
53	Alkene (C_{15})	1.0	0.1
55	1-(4-Hydroxy-3-methoxyphenyl)-2-propanone – guaiacylacetone	0.3	0.1
57	4-Hydroxy-3-methoxybenzoic acid – vanillic acid	1.7	0.3
58	Alkene	0.8	0.1
59	Alkane	0.7	0.1
61	3′,5′-Dimethoxy-4′-hydroxyacetophenone – acetosyringone	1.1	0.2
63	Alkene	1.0	0.1
64	Alkene	1.0	0.1
65	1-(3,5-Dimethoxy-4-hydroxyphenyl)-2-propanone – syringylacetone	0.4	0.1
66	Alkene (C_{18})	0.9	0.1
67	Alkane (C_{18})	1.2	0.1
68	4-Hydroxy-3,4-dimethoxybenzoic acid – syringic acid	0.8	0.1
72	Alkane	1.1	0.1
74	Hexadecanoic acid	2.8	0.2
76	Alkane (C_{19})	1.0	0.1
79	Octadecanoic acid	1.6	0.1
	Tetramethyloctadecanoic methyl ester[c]	0.7	0.1

[a]Average values of relative amounts of the pyrolysis resulting from three pyrolysis experiments. The HA extracted from the Tilton L. sediments with 0.5 M NaOH solution was used.

[b]Standard deviation.

[c]Only detected in the HA extracted from the sediment of Tilton Lake sediment with 0.5 M NaOH.

© 2000 NRC Canada

Table 4. Relative proportion of the pyrolysis products obtained from the NaOH and $Na_4P_2O_7$ extracted lake sediment humic acids.

Peak no.	Compound	Relative content (%GC peak area)[a]									
		NaOH extracts					$Na_4P_2O_7$ extracts				
		T	C	S	R	$X \pm SD^b$	T	C	S	R	$X \pm SD^b$
1	2-Furaldehyde	2.4	2.0	2.0	1.3	1.9 ± 0.5	1.8	1.5	2.8	2.1	2.1 ± 0.6
3	2,3-Dihydro-5-methylfuran-2-one	0.7	0.9	0.7	0.3	0.7 ± 0.3	1.9	0.6	0.9	0.9	1.1 ± 0.6
4	Alkylpyridine–alkylpyrrole	0.8	0.9	0.6	1.0	0.8 ± 0.2	0.8	1.2	1.5	1.3	1.2 ± 0.3
5	Ethylpyrrole	0.3	0.5	0.6	0.7	0.5 ± 0.2	0.4	0.5	0.5	0.6	0.5 ± 0.1
8	Methyl-2-furaldehyde	3.7	3.3	2.8	2.1	3.0 ± 0.7	3.1	3.2	3.2	2.1	2.9 ± 0.5
11	Phenol	2.1	2.6	4.2	4.5	3.4 ± 1.2	3.2	4.2	5.5	4.4	4.3 ± 0.9
12	Maleimide	2.6	3.7	3.1	2.6	3.0 ± 0.5	2.6	2.5	2.5	2.5	2.5 ± 0.1
13	Alkene (C_{10})	2.1	1.9	1.6	1.5	1.8 ± 0.3	2.3	1.7	2.1	1.7	2.0 ± 0.3
14	Alkene (C_{10})	0.9	0.8	0.9	0.9	0.9 ± 0.1	0.7	0.6	0.8	0.7	0.7 ± 0.1
18	Allylbenzene	0.4	0.6	0.6	0.5	0.5 ± 0.1	0.4	0.5	0.5	0.6	0.5 ± 0.1
20	Indene	0.8	0.7	0.7	0.9	0.8 ± 0.1	0.6	0.6	0.6	0.5	0.6 ± 0.1
21	2-Methylphenol	1.0	1.0	1.0	1.2	1.1 ± 0.1	1.4	0.9	1.9	1.7	1.5 ± 0.4
22	4-Methylphenol	4.3	4.4	6.1	7.0	5.5 ± 1.3	3.7	4.4	6.7	5.2	5.0 ± 1.2
23	2-Methoxyphenol	0.2	1.2	1.7	1.6	1.2 ± 0.7	0.4	1.3	1.7	1.1	1.1 ± 0.5
24	Alkene (C_{11})	0.9	0.9	1.0	1.0	1.0 ± 0.1	0.9	0.8	0.7	0.6	0.8 ± 0.1
25	Furanmethanol	1.8	1.7	1.6	1.3	1.6 ± 0.2	2.1	2.7	2.2	1.8	2.2 ± 0.4
27	Benzyl cyanide	0.7	0.6	0.5	0.7	0.7 ± 0.1	0.7	0.5	0.6	0.8	0.7 ± 0.1
28	Dimethylphenol	0.6	0.4	1.0	1.0	0.8 ± 0.3	0.6	1.0	1.6	1.0	1.1 ± 0.4
29	Ethylphenol	0.7	0.6	0.6	0.7	0.7 ± 0.1	0.4	0.6	1.0	0.8	0.7 ± 0.3
31	2-Methoxy-4-methyl phenol	0.1	1.1	1.4	1.7	1.1 ± 0.7	0.2	0.5	0.9	0.8	0.6 ± 0.3
32	Alkene (C_{12})	1.1	0.9	1.0	1.0	1.0 ± 0.1	1.1	0.9	0.7	0.9	0.9 ± 0.2
33	Benzenediol	1.5	1.1	1.4	0.4	1.1 ± 0.5	2.6	2.0	4.3	2.9	3.0 ± 1.0
34	4-Vinylphenol	0.6	1.3	1.2	2.1	1.3 ± 0.6	0.8	0.8	0.9	1.6	1.0 ± 0.4
35	Methoxyphenol	0.8	0.3	0.5	0	0.4 ± 0.3	0.5	0.3	0	0.4	0.3 ± 0.2
39	Methylnaphthalene	0.4	0.4	0.5	0.4	0.4 ± 0.1	0.3	0.3	0.6	0.4	0.4 ± 0.1
40	Indole	0.8	0.6	0.8	1.2	0.9 ± 0.3	0.7	0.5	0.7	0.9	0.7 ± 0.2
41	Alkene (C_{13})	1.6	1.3	1.3	1.1	1.3 ± 0.2	1.1	1.8	1.6	1.2	1.4 ± 0.3
42	Alkane (C_{13}	1.0	0.8	1.1	0.8	0.9 ± 0.2	0.8	0.8	1.1	0.8	0.9 ± 0.2
43	2-Methoxy-4-vinyl phenol	0.7	1.7	1.7	3.2	1.8 ± 1.0	0.8	1.3	1.1	1.4	1.2 ± 0.3
46	Methylindole	0.5	0	1.0	0.7	0.6 ± 0.4	0.4	0.3	0	0.3	0.3 ± 0.2
47	Alkene (C_{14})	1.0	0.9	0.9	0.8	0.9 ± 0.1	0.7	0.8	0.8	0.8	0.8 ± 0.1
48	?	1.0	0.8	0.9	0.8	0.9 ± 0.1	0.9	0.7	1.4	0.8	1.0 ± 0.3
49	Dimethylnaphthalene	0.8	0.6	0.5	0.3	0.6 ± 0.2	0.7	0.9	0.4	0.6	0.7 ± 0.2
51	2,3-Dihydro-3-methylindole	0.7	—	0.4	0.5	0.4 ± 0.3	0.8	0.7	0.7	—	0.6 ± 0.4
52	4′-Hydroxy-3′-methoxyacetophenone	0.2	1.2	1.0	1.2	0.9 ± 0.5	0.4	1.2	1.1	0.9	0.9 ± 0.4
53	Alkene (C15)	1.0	1.4	1.6	0.9	1.2 ± 0.3	1.1	1.3	0.9	0.8	1.0 ± 0.2
55	Guaiacylacetone	0.3	0.6	0.6	0.8	0.6 ± 0.2	0.3	0.5	0.5	0.6	0.5 ± 0.1
57	Vanillic acid	1.7	0.9	1.1	0.1	1.0 ± 0.7	2.1	0.7	0.8	0.3	1.1 ± 0.7
58	Alkene	0.8	0.8	0.9	0.8	0.9 ± 0.1	0.6	0.6	0.6	0.6	0.6 ± 0.0
59	Alkane	0.7	0.7	0.8	0.7	0.7 ± 0.1	0.7	0.7	0.6	0.6	0.7 ± 0.1
61	Acetosyringone	1.1	1.4	1.7	1.7	1.5 ± 0.3	1.0	1.0	1.1	1.2	1.1 ± 0.1
63	Alkene	1.0	1.0	1.0	1.5	1.1 ± 0.3	0.4	0.5	0.4	0.4	0.4 ± 0.1
64	Alkene	1.0	0.6	0.6	1.0	0.8 ± 0.2	0.6	0.7	0.2	0.5	0.5 ± 0.2
65	Syringylacetone	0.4	0.7	0.8	2.2	1.0 ± 0.8	1.8	1.2	1.1	1.0	1.3 ± 0.4
66	Alkene (C_{18})	0.9	0.8	0.9	0.7	0.8 ± 0.1	0.4	0.5	0.5	0.5	0.5 ± 0.1
67	Alkene (C_{18})	1.2	1.0	1.0	0.9	1.0 ± 0.1	1.0	1.2	0.7	0.9	1.0 ± 0.2
68	Syringic acid	0.8	0	0	0	0.2 ± 0.4	0.6	0.3	0	0	0.2 ± 0.3
72	Alkane	1.1	1.1	1.1	1.1	1.1 ± 0.0	0.9	0.9	0.9	0.7	0.9 ± 0.1
74	Hexadecanoic acid	2.8	3.7	3.1	6.4	4.0 ± 1.6	5.1	3.7	4.7	3.6	4.3 ± 0.7
76	Alkane (C_{19})	1.0	0.9	1.1	1.0	1.0 ± 0.1	0.8	0.7	0.6	0.6	0.7 ± 0.1
79	Octadecanoic acid	1.6	2.0	1.8	1.6	1.8 ± 0.2	2.8	1.7	1.4	2.5	2.1 ± 0.7

[a]The peak areas are related to the overall GC peak area which also includes unidentified substances T = Tilton Lake; C = Clearwater Lake; S = Silver Lake; R = Ramsey Lake.

[b]Average value ± standard deviation.

© 2000 NRC Canada

Table 5. Relative proportion of the pyrolysis products obtained from the NaOH and $Na_4P_2O_7$ extracted lake sediment fulvic acids.

		Relative content (%GC peak area)[a]									
		NaOH extracts					$Na_4P_2O_7$ extracts				
Peak no.	Compound	T	C	S	R	$X \pm SD$[b]	T	C	S	R	$X \pm SD$
1	2-Furaldehyde	1.7	2.4	1.4	1.5	1.8 ± 0.5	4.3	1.3	1.2	1.1	2.0 ± 1.6
3	2,3-Dihydro-methylfuran-2-one	5.4	1.7	1.1	1.1	2.3 ± 2.1	7.3	5.2	1.7	1.3	3.9 ± 2.9
4	Alkylpyridine–alkylpyrrole	2.8	1.9	1.8	2.2	2.2 ± 0.5	3.4	1.0	0.9	0.8	1.5 ± 1.3
5	Ethylpyrrole	1.2	0.5	1.4	1.3	1.1 ± 0.4	1.3	0.9	2.0	1.9	1.5 ± 0.5
8	Methyl-2-furaldehyde	3.8	5.7	3.9	3.1	4.1 ± 1.1	7.5	4.6	3.3	2.3	4.4 ± 2.3
11	Phenol	5.3	2.3	12	4.7	6.1 ± 4.2	10	5.7	15	14	11.2 ± 4.2
12	Maleimide	2.7	7.9	5.8	4.9	5.3 ± 2.2	2.6	2.1	9.0	9.6	5.8 ± 4.0
20	Indene	0.7	1.8	0.9	0.8	1.1 ± 0.5	0.9	1.2	0.8	0.9	1.0 ± 0.2
21	2-Methylphenol	1.5	2.0	4.2	1.5	2.3 ± 1.3	3.9	1.9	1.8	3.3	2.7 ± 1.0
22	4-Methylphenol	4.9	7.7	11	7.8	7.9 ± 2.9	6.7	3.8	9.5	9.2	7.3 ± 2.7
23	2-Methoxyphenol	1.7	2.2	2.5	2.1	2.1 ± 0.3	2.1	1.7	2.8	2.0	2.2 ± 0.5
25	2-Methyl-3-hydroxy-pyran-4-one	1.5	2.3	1.8	0.2	1.5 ± 0.9	0.6	2.4	0.7	0.7	1.1 ± 0.9
27	Benzyl cyanide	0	1.6	1.4	3.2	1.6 ± 1.3	0	2.3	0.7	1.2	1.1 ± 1.0
28	Dimethylphenol	0	1.9	1.7	0	0.9 ± 1.0	0.9	1.1	0	1.4	0.9 ± 0.6
29	Ethylphenol	0	0.5	1.4	1.0	0.7 ± 0.6	1.2	2.4	0.6	0.7	1.2 ± 0.8
31	2-Methoxy-4-methylphenol	0	0	0.8	0.9	0.4 ± 0.5	2.1	0	0	0	0.5 ± 1.1
32	Alkene (C_{12})	2.2	0.2	0.3	0	0.7 ± 1.0	2.1	2.2	0	0	1.1 ± 1.2
33	Benzenediol	0	0.7	0.4	0.6	0.4 ± 0.3	1.1	0	0	0	0.3 ± 0.6
34	4-Vinylphenol	0	0.3	3.0	1.7	1.3 ± 1.4	1.1	1.2	1.1	1.4	1.2 ± 0.1
35	3-Methoxyphenol	1.5	1.0	0.4	1.0	1.0 ± 0.5	0.5	2.0	0	0	0.6 ± 0.9
39	Methylnaphthalene	0.8	0.4	0.4	0.9	0.6 ± 0.3	0.3	0.3	0.6	0	0.3 ± 0.2
40	Indole	0.2	1.1	0.6	0.6	0.6 ± 0.4	2.7	0	0.4	0.7	1.0 ± 1.2
43	2-Methoxy-4-vinyl-phenol	1.2	0.6	0	0.6	0.6 ± 0.5	3.0	0.9	0.8	0.8	1.4 ± 1.1
46	Methylindole	0.4	0.9	0	0	0.3 ± 0.4	0	0.2	0	0	0.1 ± 0.1
51	2,3-Dihydro-3-methylindole	0.1	0	0.6	1.3	0.5 ± 0.6	1.0	0	0	0	0.3 ± 0.5
52	4′-Hydroxy-3′-methoxyacetophenone	0	1.0	1.4	1.1	0.9 ± 0.6	0.6	0	0.6	0	0.3 ± 0.4
55	Guaiacylacetone	0	0	1.5	1.3	0.7 ± 0.8	0.5	0	2.1	1.0	0.9 ± 0.9
57	Vanillic acid	0.2	0.4	1.7	0.5	0.7 ± 0.7	0.9	0	2.5	2.7	1.5 ± 1.3
64	Alkene	0	0	0	0.4	0.1 ± 0.2	0	0	0	0	0
65	Syringylacetone.	0.2	0	0	0.2	0.1 ± 0.1	0	0	0	0	0

[a]The peak areas are related to the overall GC peak area which also includes unidentified substances. T = Tilton Lake; C = Clearwater Lake; S = Silver Lake; R = Ramsey Lake.

[b]Average value ± standard deviation.

farm in Carpi (16), using the exact same experimental method, the relative amounts of protein, lignin, carbohydrate and fatty acid markers were 10%, 40%, 4.3%, and 0.5%, respectively.

Considering that only 50–70% of the pyrolysis products could be identified, any comparison and interpretation remain difficult. However, it is evident from this simple analysis that the carbohydrate content of the HA and FA extracted from lake sediment is considerably lower than that found for soils. The differences observed in the composition of lake sediment humics relative to those from soils might be partially due to the different circulation behaviour of aquagenic versus pedogenic organic matter in lakes. In addition, the FA appears to have a greater amount of products originating from proteinaceous material. This tendency was also observed in the N:C ratios for FA extracted by NaOH. Material which is high in nitrogen reflects a higher concentration of nonvascular aquatic plants (29). The presence of lignin derivatives can be related to terrestrial plants which are expected to contribute significantly to the pool of HS in small lakes surrounded by vegetation. A predominant proportion of phytoplanktonic material (30) would have been indicated by much higher percentages of protein (~50%) and carbohydrates (~30%).

Reproductibility of the Pyrolysis Data

Before making a quantitative comparison of the relative amounts of the pyrolysis products from the different lake sediments, the reproducibility of the relative amounts of the pyrolysis products was tested. This was done by pyrolyzing three samples of the same HA extracted with the aid of NaOH from Tilton Lake sediments. The relative amounts of 52 of the 94 compounds were determined for each of the 3 pyrolysis experiments by comparing the peak areas (eq. [1], vide infra). The average amount of each product generated in the pyrolysis and the standard deviation were calculated (Table 3). The average amounts of the pyrolysis products used to test the reproducibility range from 0.1 to 3.7%. As expected the largest errors occur for the compounds present in low concentration (≤0.5%). However, on average, standard deviations of about 13% were found for peaks larger than 0.5% of the total peak area. Therefore the reproducibility

© 2000 NRC Canada

was acceptable, considering the heterogeneity of the sample and the fact that often several compounds elute at virtually the same retention time.

FA and HA extracted from lake sediments

The FA and HA composition can first be compared in a qualitative fashion. Caution must always be exercised when comparing pyrograms because of their complexity. Often the peaks detected in the pyrograms represent a complex mixture of compounds with similar retention times. As a result, the mass spectrum is often a composite of two or three compounds making it difficult to interpret. We have been able to identify *94* major products in the pyrolysate of HA while *58* have been identified in the case of FA.

All of the products generated in the pyrolysis of the FA samples were detected in the TIC pyrograms of the HA samples, with the exception of the compounds eluting at a scan number of 939, 949, 958, 1621, and 2090. These products include α-methylbenzyl cyanide, an unknown compound, methylbenzofuran, 1,3-benzofurandione, and 1*H*-isoindol-1,3–2(*H*)-dione.

The pyrolysis of HA produced a number of products not detected in the pyrolysis of FA. Over half, i.e., 24 of the additional products generated in the pyrolysis of the HA samples were alkanes, alkenes, and alkylbenzenes. Hydroxybenzonitrile, hydroxybenzeneacetonitrile, methoxybenzenediol, furanmethanol, 4-ethyl-2-methoxyphenol, 3′,5′-dimethoxy-4′-hydroxyacetophenone, 4-hydroxy-3,5-dimethoxybenzoic acid, tetradecanoic acid, pentadecanoic acid, and eight unidentified compounds were also exclusively formed in the pyrolysis of the HA samples.

It should be noted that the major pyrolysis fragments of HA and FA were the same with the only difference being their relative proportion, Tables 4 and 5. Kuckuk et al. (18) observed a similar phenomenon in his study of HS extracted from peat and groundwater (Hannover, Germany).

The relative proportions of a number of products resulting from the pyrolysis of HA extracted from the four lake sediment samples by NaOH and $Na_4P_2O_7$ are given in Table 4. The average values of the pyrolysis products for the four lake sediments range from 0.2% for 4-hydroxy-3,5-dimethoxybenzoic acid to approximately 5% for 4-methylphenol in both the NaOH–extracted and $Na_4P_2O_7$–extracted HA. As was indicated above, the relative error associated with the reproducibility of the pyrolysis experiment is on average usually less than 13% for compounds which produce peaks larger than 0.5% of the total peak area. In comparing the relative amounts of each pyrolysis product for the respective lake sediments some small variations are apparent. For example, in the case of HA–NaOH, phenol, 2-methoxyphenol, 2-methoxy-4-methylphenol, 2-methoxy-4-vinylphenol, 4-hydroxy-3-methoxybenzoic acid, 1-(3,5-dimethoxy-4-hydroxyphenyl)-2-propanone, 4-hydroxy-3,5-dimethoxybenzoic acid, and hexadecanoic acid have relative deviations which are larger than 30%.

A chi-square goodness-of-fit test (31) was applied to the data to determine if there was a statistical difference in the composition of the pyrolysates of the different lake sediments. In the case of the HA–NaOH for the various lake sediments, the analysis showed that the pyrolysis products were formed in the same relative amounts at the 95% confidence level. The greatest variation in concentration was observed for phenol, 4-methylphenol, 2-methoxyphenol, 2-methoxy-4-methylphenol, 2-methoxy-4-vinylphenol, 4-hydroxy-3-methoxybenzoic acid, 1-(3,5-dimethoxy-4-hydroxyphenyl)-2-propanone, 4-hydroxy-3,5-dimethoxybenzoic acid, and hexadecanoic acid. Similarly, when the chi-square test was applied to the HA–$Na_4P_2O_7$ data, the concentration of only a few of the products formed during the pyrolysis varied significantly. These include 2,3-dihydromethylfuran-2-one, 4-methylphenol, benzenediol, 4-hydroxy-3-methoxybenzoic acid, and 4-hydroxy-3,5-dimethoxybenzoic acid. When the combined HA–NaOH and HA–$Na_4P_2O_7$ data were subjected to the chi-square goodness-of-fit test, the pyrolysis products were produced in the same relative amounts at the 95% confidence level. The statistical analysis confirmed that the variation in the composition of the HA collected from the different Sudbury area lakes (based on the pyrolysis data) is slight and that the material extracted using NaOH and $Na_4P_2O_7$ is virtually the same.

A similar conclusion can be reached when comparing the H:C, N:C, and O:C ratios determined for the HA extracted by $Na_4P_2O_7$ and NaOH (Table 1). The elemental ratios differ anywhere from 4–13%, with the largest deviations being observed for H:C and O:C ratios of HA extracted by $Na_4P_2O_7$. The changes detected in the H:C and O:C ratios suggest that there are small differences in the carbohydrate and aromatic composition of the HA. Finally, the major HA pyrolysis fragments in the lake sediments appear to be alkylbenzene (~2%), methyl-2-furaldehyde (~3%), phenol (~3.9%), maleimide (~2.8%), and 4-methylphenol (~5.2%).

The relative proportions of several of the pyrolysis products generated by the FA extracted from the four lake sediments using NaOH and $Na_4P_2O_7$ are presented in Table 5. The average values of the pyrolysis products ranged from 0.1% for 1-(3,5-dimethoxy-4-hydroxyphenyl)-2-propanone to 8% for 2-methylphenol in the FA-NaOH samples and from 0.1% for methylindole to 11% for phenol in the FA–$Na_4P_2O_7$ samples. The main FA pyrolysis products were 2,3-dihydro-methylfuran-2-one (~3.1%), methyl-2-furaldehyde (~4.2%), phenol(~8.6%), maleimide (5.5%), and 4-methylphenol (~7.6%).

The relative proportions of many of the pyrolysis products for the respective FA samples were clearly different which is supported by a chi-square goodness-of-fit test on the data. In fact, 2,3-dihydromethylfuran-2-one, phenol, maleimide, and allylbenzene could be rejected at a 90% confidence level. Large variations were observed for 2-methylphenol, 4-methylphenol, benzyl cyanide, dimethylphenol, 4-vinylphenol, and 1-(4-hydroxy-3-methoxyphenyl)-2-propanone in the case of the FA–NaOH and 2-furaldehyde, alkylpyridine, methyl-2-furaldehyde, 4-methylphenol, 2-methoxy-4-methylphenol, benzenediol, 3-methoxyphenol, 1*H*-indole, and 2,3-dihydro-3-methylindole in the case of FA–$Na_4P_2O_7$. Application of the chi-square test to the combined FA–NaOH and FA–$Na_4P_2O_7$ data suggests there is a difference in the material that was extracted using NaOH and $Na_4P_2O_7$. For example, the average percentage of phenol found in the NaOH extracts (6.1%) was lower than that of phenol found in the $Na_4P_2O_7$ extracts (11.2%). The probability that the relative amount of phenol formed is the same for the NaOH and

© 2000 NRC Canada

$Na_4P_2O_7$ extracts is 1%. In fact, the FA samples extracted with $Na_4P_2O_7$ produce more phenol upon pyrolysis in each case.

The FA samples differed from the HA samples in that their composition was variable. Moreover, the FA composition was dependent on the extractant used. The sediments were collected from lakes with different pH values, i.e., 4.0 (Silver Lake), 4.8 (Clearwater Lake), 5.6 (Tilton Lake), and 7.5 (Ramsey Lake). The carboxylic acid and phenolic hydroxyl groups of FA causes it to be relatively hydrophilic (24). Therefore, its solubility in water is expected to be higher than that of HA. The solubility of organic matter in the lake water was found to be dependent on pH. In fact, the dissolved organic matter increased as the pH of the lake increased (Table 1 in ref. 19). Presumably the soluble organic matter was primarily FA. This could explain why a significant variation in the relative amounts of the FA pyrolysis products was observed for samples taken from the different lakes.

A close examination of the data presented in Table 1 (vide supra) shows that the variation in N:C ratio determined for FA samples extracted from lake sediment was greater than that observed for the HA (cf. 9.3% vs. 5%). In other words, the protein content (which is related to the N:C ratio) was found to be more variable in the FA samples. Similar information can be obtained from the Py–GC–MS data in that the variation of the relative proportion of six of the eight pyrolysates generated by the proteinaceous material in FA found in the different lake sediments is greater than can be accounted for statistically. For the HA samples, the greatest variability in composition occurred for pyrolysis products originating from lignin.

The O:C ratio, as one might expect, is sensitive to carbohydrate content. The variation in the O:C ratio for FA extracted by $Na_4P_2O_7$ from the different lake sediments is four times greater than that observed for FA extracted with NaOH (0.36 vs. 0.08). Similarly, in regards to the Py–GC–MS data, large variations in the relative proportion of 3 of the 4 carbohydrate pyrolysates were detected for the FA–$Na_4P_2O_7$ material whereas only 1 carbohydrate pyrolysate deviated significantly from the norm in the FA–NaOH material indicating the greater variability of the carbohydrate content of the FA–$Na_4P_2O_7$ material. However, it must be taken into account that in the pyrolysis experiment, O-rich polysaccharides are converted to low molecular weight volatile products which elute before being analyzed which causes the carbohydrate content of the HS to be underestimated by pyrolysis.

The variation in the H:C ratios for FA extracted by $Na_4P_2O_7$ and NaOH, were found to be 10% and 5% respectively. The H:C ratios are thought to reflect the degree of aromaticity of the HS. Low H:C ratios are interpreted as meaning that the HS are highly aromatic in character. There are a few pyrolysis fragments originating from lignin, e.g., 2-methylphenol, 1-(4-hydroxy-3-methylphenyl)-2-propanone, 2-methoxy-4-methylphenol, and 3-methoxyphenol, which change significantly as a function of the FA sample. This change in composition of the lignin pyrolysis products could be related to the change in the H:C ratios observed for the FA samples. One again must exercise caution in using pyrolysis data to comment on aromatic:aliphatic ratios because of their sensitivity to pyrolysis temperatures (32).

Finally, from the cross polarization magic-angle spinning (CPMAS) ^{13}C NMR data we concluded that the most intense peak in the HA spectra was found at around 35 ppm, corresponding to the aliphatic C region. This is consistent with the pyrolysis data for the HA extracts in that the majority of the pyrolysates contain aliphatic carbons. In fact, approximately 20–22% of the pyrolysates were found to be long chain alkanes, alkenes, and fatty acids. For the FA extracts long chain hydrocarbons only represented 1% of the pyrolysates. This is in agreement with our finding that the most intense signal in the CPMAS ^{13}C NMR spectra occurs at 176 ppm (the carboxylic C region) rather than at 31 ppm as was observed in the HA spectra. An examination of the remaining pyrolysates (aromatic hydrocarbons, N-containing compounds, furans, phenols, guaiacols, syringols, etc.) is also consistent with finding peaks in the O–alkyl, aromatic, carboxyl, and carbonyl spectral regions.

Conclusions

In this study, organic matter was extracted from the sediment of four Sudbury area lakes, with 0.1 M $Na_4P_2O_7$, and 0.5 M NaOH solutions. The different fractions including FA and HA were characterized by Py–GC–MS. Several pyrolysis and evaporation products were identified in the pyrolysates of the HA (94) and FA (58) samples. The HS extracted from the different lake sediments gave similar pyrolysis products. One notable difference being the large number of alkanes, alkenes, and alkylbenzenes generated by the HA samples. The relative amounts of the pyrolysis products varied slightly between the HA samples whereas variation in the relative amounts of the FA pyrolysis products was significant according to a chi-square goodness-of-fit test. The pyrolysis products were related to the N:C ratios. Therefore it was interpolated that the protein content of the HA samples was similar in all four sediment samples while the FA protein composition differed for the lakes studied. The detection of pyrolysis products originating from lignin and carbohydrates indicates they are present in the humic macromolecular structure and reflects the contribution of terrestrial plants to the pool of natural HS.

Acknowledgements

The authors (N.B. and H.J.) would like to thank the Natural Sciences and Engineering Research Council (NSERC) of Canada for providing financial support. The technical support provided by Ms. Maria Kepes is also gratefully acknowledged.

References

1. C. Steelink. *In* Humic substances in soil, sediment and water. *Edited by* G.R. Aiken. Wiley, New York. 1985. pp. 457–476.
2. T. Koyama. Coal Sci. Adv. Chem. Ser. **55**, 43 (1966).
3. M. Schnitzer. *In* Soil biochemistry. Vol 2. *Edited by* D.W. Robertson and J.G.D. Lamb. Marcel Dekker, New York. 1971. pp. 60–95.
4. Y. Chen, N. Senesi, and M. Schnitzer. Soil Sci. Soc. Am. J. **42**, 352 (1977).
5. M.A. Wilson. Soil Sci. **32**, 167 (1981).

© 2000 NRC Canada

6. P.G. Hatcher, I.A. Breger, L.W. Dennis, and G.E. Maciel. *In* Aquatic and terrestrial humic materials. *Edited by* R.F. Christian and E.T. Gjessing. Ann Arbor Science, Ann Arbor. 1983. pp. 37–81.
7. R.L. Wershaw. *In* Humic substances in soil, sediment and water. *Edited by* G.R. Aiken. Wiley, New York. 1985. pp. 561–584.
8. R.L. Malcolm. *In* Humic substances II, in search of structure. *Edited by* M.H.B. Hayes, P. MacCarthy, R.L. Malcolm, and R.S. Swift. Wiley, New York. 1989. pp. 339–372.
9. J.P. Martin, K. Haider, and C. Saiz-Jimenez. Soil Sci. Soc. Am. Proc. **38**, 760 (1974).
10. S.M. Griffith and M. Schnitzer. *In* Humic substances II, in search of structure. *Edited by* M.H.B. Hayes, P. MacCarthy, R.L. Malcolm, and R.S. Swift. Wiley, New York. 1989. pp. 68–98.
11. M. Schnitzer. Soil Sci. **151**, 41 (1991).
12. H. Li. M.Sc. thesis. Laurentian University, Sudbury, Canada. 1995.
13. C. Saiz-Jimenez and J.W. De Leeuw. J. Anal. Appl. Pyrolysis, **9**, 99 (1986).
14. C. Saiz-Jimenez. Environ. Sci. Technol. **28**, 1773 (1994).
15. J.M. Alcaniz, A. Serés, and M. Gassiot-Matas. Agrochimica, **31**, 124 (1987).
16. G. Chiavari, G. Torsi, D. Fabbri, and G.C. Galletti. Analyst. **119**, 1141 (1994).
17. J.M. Bracewell, K. Haider, S.R. Larter, and H.-R. Schulten. *In* Humic substances II, in search of structure. *Edited by* M.H.B. Hayes, P. MacCarthy, R.L. Malcolm, and R.S. Swift. Wiley, New York. 1989. pp. 181–222.
18. R. Kuckuk, W. Hill, P. Burba, and A.N. Davies. Fresenius J. Anal. Chem. **350**, 528, (1994).
19. N. Belzile, H.A. Joly, and H. Li. Can. J. Chem. **75**, 14 (1997).
20. J. Buffle. *In* Complexation reactions in aquatic systems: An analytical approach. Ellis Horwood, Chichester. 1988. pp. 90–145.
21. M. Schnitzer and P. Schuppli. Soil Sci. Soc. Am. J. **53**, 1418 (1989).
22. M. Schnitzer and P. Schuppli. Can. J. Soil Sci. **69**, 253 (1989).
23. F. Martin, C. Saiz-Jimenez, and A. Cert. Soil Sci. Soc. Am. J. **43**, 309 (1979).
24. F. Martin, F.J. González-Vila, J.C. del Rio, and T. Verdejo. J. Anal. Appl. Pyrolysis, **28**, 71 (1994).
25. D. Fabbri, M. Mongardi, L. Montanari, G.C. Galletti, G. Chiavari, and R. Scotti. Fresenius J. Anal. Chem. **362**, 299 (1998).
26. G. Chiavari and G.C. Galletti. J. Anal. Appl. Pyrolysis, **24**, 123 (1992).
27. C. Saiz-Jimenez, J. Ortega-Calvo, and B. Hermosin. Naturwissenschaften, **81**, 28 (1994).
28. C. Saiz-Jimenez. Environ. Sci. Technol. **24**, 197 (1994).
29. P.A. Meyer and R. Ishiwatari. Org. Geochem. **20**, 867 (1993).
30. A.C. Sigleo, T.C. Hoering, and G.R. Helz. Geochim. Cosmochim. Acta, **46**, 1619 (1982).
31. R.L. Ott. *In* An introduction to statistical methods and data analysis. 4th ed. Wadsworth, Belmont. 1993.
32. F. Martin, J.C. del Rio, F.J. Gonzalez-Vila, and T. Verdejo. J. Anal. Appl. Pyrolysis, **31,** 75 (1995).

© 2000 NRC Canada

Infrared titration of aqueous NaOH by aqueous HCl

Jean-Joseph Max and Camille Chapados

Abstract: The titration of NaOH by HCl is achieved through infrared spectral measurement of the various mixtures. Factor Analysis (FA) is used to separate the spectra. Four principal spectra were necessary to perform the analysis: pure water, 2.09 M HCl, 2.23 M NaOH, and 2.60 M NaCl solvated water. Each of the 18 experimental spectra obtained was determined to be a linear combination of these principal spectra. The composition of the solutions retrieved from the IR analysis is identical to what was determined by the mass balance. The mean activity coefficient of HCl was calculated using the concentration of HCl obtained by IR and the activity obtained by pH measurements. It was found that the mean activity coefficient increased by a factor greater than 2 in the presence of 1 M NaCl. Because the water molecules associated to the ionic pair H^+/Cl^-, as observed by IR, are unmodified by the presence of the salt, such an increase cannot be attributed to a modification of the strong association of the water molecules to the pair of ions.

Key words: infrared spectroscopy; ATR; liquid; acidic solutions; alkaline solutions; aqueous solutions; factor analysis; principal spectra; HCl-, NaOH-, NaCl-solvated water; activity coefficient; IR titration.

Résumé : Le titrage d'une solution aqueuse de NaOH a été réalisé en mesurant le spectre infrarouge de différents mélanges et en utilisant l'analyse par facteurs. Quatre espèces principales ont été nécessaires pour réaliser cette analyse: l'eau pure, et des solutions de HCl (2.09 M), de NaOH (2.23 M) et de NaCl (2.60 M). Nous avons trouvé que chacun des 18 spectres expérimentaux obtenus est une combinaison linéaire des spectres de ces espèces principales. La composition de chacun des 18 mélanges obtenue par l'analyse par facteurs est la même que celle déterminée par la balance de masse. Le coefficient moyen d'activité du HCl a été calculé à partir des concentrations en HCl résultant des mesures infrarouge et des activités obtenues par mesure de pH. Les résultats ont montré que le coefficient moyen d'activité du HCl est multiplié par un facteur plus grand que 2 lorsque du NaCl (1 M) est ajouté à la solution. Puisque l'association de molécules d'eau avec la paire ionique H^+/Cl^-, telle qu'observée par infrarouge, n'est pas modifiée par la présence du sel, on en conclut que cet accroissement du coefficient d'activité de l'acide chlorhydrique ne peut être imputé à une modification de l'interaction forte des ions avec les molécules d'eau.

Mots clés : spectroscopie infrarouge; liquide; solutions acides; solutions alcalines; solutions aqueuses; analyse par facteurs; spectre principal; HCl-, NaOH- et NaCl-solvatés par de l'eau; coefficient d'activité; titrage IR.

Introduction

In previous papers (1, 2) (hereafter referred to as **I** and **II**) we studied aqueous solutions of NaCl and KCl using infrared (IR) spectroscopy and showed that in order to represent the species in 0 to 300 g/L solutions, only two principal spectra were necessary: that of pure water and that of a 300 g/L aqueous solution of salt. In **I,** we mentioned that liquid water and saline solutions are made of numerous species composed of clusters that may contain from 3 to 8, or even more, molecules of water. As the salt concentration of the solution is increased, the species are modified as two entities, forming what we call two types of species of water. This indicates that within the entire solubility range of the salts, saline solutions are composed of two types of species of water: pure water and NaCl- or KCl-solvated water. The two types of species of water are defined by the two eigenspectra, which indicates that the molecules within one type of species behave in the same manner. We use the term "eigenspectra" as an extension of the definition of Malinowski and Howery (3) to refer to principal spectra even when these spectra are not orthogonal.

Transmission spectra of aqueous solutions are difficult to obtain in the mid-IR region because in the 3–μm infrared region, the high absorptivity of water necessitates thin films. In contrast, ATR spectra of aqueous solutions do not require thin films and are easy to obtain. In **II** we compared the ATR spectra of KCl aqueous solutions to the real and imaginary refractive index spectra obtained by the Kramers–Krönig relation and reflection equations, and found that as long as the proper material is used for the ATR crystal and that the concentration of water is not drastically decreased compared to pure water, then the IR-ATR measurements as they appear directly reflect the chemistry of the sample.

Received July 13, 1999.

J.-J. Max[1] and C. Chapados.[2] Département de chimie-biologie, Université du Québec à Trois-Rivières, C.P. 500, Trois-Rivières, QC G9A 5H7, Canada.

[1]Current address: Scientech R&D, 2200 Sidbec-S, Trois-Rivières-O, QC G8Z 4H1, Canada.
[2]Author to whom correspondence may be addressed. Télephone: (819) 376-5052. Fax: (819) 376-5084. e-mail: Camille_Chapados@uqtr.uquebec.ca

© 2000 NRC Canada

In **I** it was established that it is possible to use only two eigenspectra to accurately subtract the water bands in the spectra of NaCl aqueous solution. Sodium monochloroacetate that was dissolved in the saline solution was used to test the procedure. After carefully subtracting the water spectra, a clean spectrum of the solute was retrieved, with no correction required to obtain a flat baseline. Spectral subtraction of water and baseline correction are difficulties encountered when working with IR spectra of aqueous solutions of biological (4) and other materials because the water spectrum does not remain constant but is influenced by the ions present, even though these ions do not absorb (5). Several complicated methods have been proposed to solve these problems (6–11). However, the method proposed in **I** is simple and requires no artifact to make the proper correction in order to obtain a flat baseline. This method has been tried successfully with several salts (1, 12), acids and bases (13–15).

A third paper (12) (**III**) confirmed the previous results by giving the equations that allow the interpolation and extrapolation of spectra of aqueous saline solutions. Given a spectrum of an aqueous solution obtained at one salt concentration, it is possible to calculate that spectrum at any other concentration. This development was necessary since binary salts dissolved in water are ionized and therefore do not absorb in the m-IR frequency range. The Beer-Lambert Law can therefore not be used directly. However, these samples were mixtures of two substances, one of which does not absorb but strongly influences the second. Applying factor analysis (FA) to aqueous salt solutions led to the following conclusions: (*i*) two types of species of water are present in the solutions; (*ii*) each spectrum is a linear combination of the spectra of the two types of species of water (pure water and salt solvated water); (*iii*) the intensity (in AU) of aqueous salt solutions is the sum of two intensities, each of which is proportional to the concentration of the respective type of species of water.

The development in **III** gave the relations as functions of the concentration of the non-absorbing species. By this scheme we calculated the virtual spectrum of "pure" KCl-solvated water. The latter is outside the solubility range of the salt but is present in the solution at concentrations lower than saturation. The "pure" KCl-solvated water contained no ordinary water, being composed of the two close-bound ions (cation and anion) and a mean of 5 molecules of water forming a cluster: $K^+(H_2O)_5Cl^-$. Using the data in **I** we also determined in **III** that NaCl in water behaves in the same manner, forming a cluster also containing a mean of 5 molecules of water: $Na^+(H_2O)_5Cl^-$. For other ions, the number of water molecules associated to them may be different than that obtained for KCl and NaCl (unpublished results).

The IR spectra of aqueous HCl and aqueous NaOH solutions at several concentrations were studied in **IV** (13). We found that each solution could be explained as a combination of two eigenspectra: pure water and HCl-solvated water, and pure water and NaOH-solvated water, respectively. Malic acid dissolved in acidic water and in basic water was used to illustrate the procedure. In both cases, two eigenspectra multiplied by the proper multiplying factors (MFs) (see Section 2.1) enabled the subtraction of the water spectra to produce the spectrum of malic acid in one case, and of sodium malate in the other. Both spectra were free of identifiable water bands. This result indicated that, for these solutions at least, it is possible to use the inter- and extrapolation procedure described in **III** to obtain the spectrum at a given concentration.

The object of the present study is to test the knowledge gained in **I**, **II**, **III**, and **IV** by performing a quantitative IR titration of NaOH by HCl, knowing that all the ions involved are either non-absorbing or very weakly-absorbing. Furthermore, these ions are in solution in a strong absorber: water. As the titration proceeds, the solvent that contains an increasing amount of NaCl, is successively basic, neutral, and acidic. The spectra obtained in the 14 to 0 pH range will be separated by FA to obtain the MFs in order to relate the concentration of the species to the values determined by the mass balance.

IR titration of aqueous glycine and of aqueous butyloxypropylaminodiacetic (BOPA) have previously been reported (14, 15). Good results have been obtained in both cases. In both cases, contrary to the one presented here, strong IR absorption bands of the solute varied with pH and served as good internal indicators of the ionic situation of the solution. The eigenspectra are constant throughout the pH range and indicates that the only types of species defined by these spectra are present in the solution. No intermediate species resulting from some interactions between the species are formed because the residues obtained are null for all the spectra. The situation is similar in the NaOH–HCl titration. For the latter, the situation is less evident because these species are not visible or only barely visible in IR but their interactions with water are observed.

For this base–acid titration where salt is formed one question comes to mind: what influence has salt on the measurements because it has been reported that the acidity and the ionic activity of aqueous solutions is greatly modified by the presence of salts (16, 17)? It has also been reported that the IR spectrum of aqueous HCl is greatly modified by the presence of binary salts (5). Electrolytes in an aqueous solution have been reported to influence the hydrolysis rate of esters (18). One of the aims of the present study is to examine the relationship between the IR spectroscopic characteristics of HCl-solvated water and the mean activity coefficient of HCl. The knowledge gained by the IR titration of NaOH by HCl may give some new insight into this age-old process and could determine the exact ionic composition of the solution as the titration proceeds.

2. Theoretical considerations

2.1. Factor analysis (FA)

The basic principles of FA applied to chemical analysis and the mathematical formulation of FA can be found in the book of Malinowski and Howery (3). The method of subtracting water bands from the spectrum of an aqueous solution is given in **I** for a binary salt and in **IV** for an acid and a base. It consisted of defining four eigenspectra: pure water and NaCl, HCl, and NaOH aqueous solutions. These four spectra are genuine but are not orthogonal spectra. The NaCl, HCl, and NaOH aqueous solutions contain an unknown amount of water organized as in pure water with the rest being organized as solvated water (**III**). S_e^p is the spec-

© 2000 NRC Canada

trum of pure water, $S_a^{M_a}$, $S_b^{M_b}$, and $S_c^{M_c}$ are the spectra of NaCl, HCl, and NaOH at the concentrations M_a, M_b, and M_c, respectively. With these four eigenspectra, FA was used on a series of 18 IR spectra (S_j) obtained in saline, acidic, and alkaline solutions. The MFs retrieved by FA are related to the concentration of the corresponding type of water in the sample. The MFs of each eigenspectrum in S_j are determined when the sum of the eigenspectra multiplied by their respective MF is compared to the experimental spectrum. The MFs are adjusted until a satisfactory fit is obtained. With the four eigenspectra $S_a^{M_a}$, $S_b^{M_b}$, $S_c^{M_c}$, S_e^P, the MFs obtained for the spectrum S_j are denoted $y_{aj}^{M_a}$, $y_{bj}^{M_b}$, $y_{cj}^{M_c}$, $y_{ej}^{M_aM_bM_c}$. The solutions used to obtain the three eigenspectra ($S_a^{M_a}$, $S_b^{M_b}$, $S_c^{M_c}$) contained some water organized as in "pure water." As a result, the MFs of pure water depend on the concentrations of the solutions used for the eigenspectra of the three other species and must be written: $y_{ej}^{M_aM_bM_c}$.

2.2. Calculation of Sample Composition from MFs

The composition of the sample is calculated from the MF values obtained by FA. The concentration of the three species **a**, **b** and **c** present in the solution are obtained by multiplying the MF value by the concentration of the solution used for the corresponding eigenspectrum. The solvent content of the samples is obtained by multiplying the amount of solvent in each of the four solutions used for the eigenspectra by its respective MF in the sample and calculating the sum of the four values obtained.

3. Experimental

3.1. Chemicals and Solutions

Deionized water was used to prepare the aqueous solutions. Sodium hydroxide (Fisher Scientific, purity 97%), and concentrated hydrochloric acid (Fisher Scientific, 38.0% w/w, density 1.19 g/mL, 12.40 M) were used to prepare the solutions of NaOH–, HCl–, and the NaOH–HCl mixtures. In order to produce the best spectra possible, high concentrations of titrant were used so as to avoid diluted solutions.

A stock solution of 1.12 M NaOH was prepared by weighing 11.2 ± 0.1 g of NaOH pellets in an empty 250 mL volumetric flask and completing the volume with water. The weight of the resulting solution was 260.1 ± 0.1g. The mixtures of NaOH and HCl were prepared by weighing an amount of aqueous 12.40 M HCl in empty 10 mL volumetric flasks. The volume of each sample was then completed to 10 mL with the stock solution of NaOH. The mass and pH of the samples were measured. The composition of each sample calculated from the mass balance is listed in Table 1.

The eigenspectra of NaOH, HCl, and NaCl used for FA were defined using the solutions obtained by weighing 0.8901, 2.0041, and 1.5189 g (± 0.0001 g), respectively in 10 mL volumetric flasks. Each sample was completed to 10 mL with water and the mass measured, giving: 10.8466, 10.2938, and 10.9484 g (± 0.0001 g), respectively. All samples produced homogeneous solutions.

For the pure solutions of NaOH and HCl in the 0 to 40 g/L range, we used the spectra reported in **IV**, whose pH had been measured using the method described below.

3.2. pH measurements

The pH was measured at room temperature (26.5 ± 0.3°C) with a pH meter (Omega model PHH-253) equipped with a combination electrode (Analytical Sensors, Inc., model PH10107B-03-B). Prior to any series of measurements a two-point calibration was carried out at pH = 2.00 and 7.00, or 7.00 and 10.00.

3.3. IR measurements

The IR measurements were obtained using a Model 510P Nicolet FT-IR spectrometer with a TGS detector. Two KBr windows isolate the measurement chamber from the outside. The samples were contained in a "Circle Cell" (SpectraTech, Inc.) equipped with a ZnSe crystal rod in an ATR configuration (making 11 internal reflections, the incident beam is at an angle of 45° with respect to the rod's axis). The spectral range of the ZnSe rod in the spectrophotometer is situated between 4800 and 650 cm^{-1}. The spectra were taken under a flow of nitrogen to ensure a low residue of CO_2 and water vapors in the spectrometer. For each spectrum, an accumulation of 100 scans with a resolution of 4 cm^{-1} was obtained. All measurements were taken at 26.5°C ± 0.3°C. The cell was carefully washed and dried before each measurement. Model 510P is a single-beam spectrometer and a background with the empty cell was taken before measuring each sample.

Due to the variation of the penetration depth with the wavelength, the use of an ATR configuration causes some modifications in the spectra compared to the transmission configuration. The depth of penetration is dependent on the wavelength, the angle of incidence, and the ratio of the refractive indices of the crystal to the sample (19). Nevertheless, for a sample with a constant refractive index (as a function of wavelength), the ratio of the depths of penetration for two given wavelengths is independent of both refractive indices and angle of incidence and depends only on the two wavelengths. From one spectrum to the other, the only possible variation may occur in the refractive index of the sample. The refractive index of aqueous KCl varies from 1.332 to 1.367 for concentrations 0 to 300 g/L (20). This minor variation will influence the IR ATR measurements but very little and has thus been disregarded in the present study. Since we deal only with ATR spectra, comparing them on a wavelength to wavelength basis, no major difficulty was encountered and no correction relative to this configuration was deemed necessary.

In **II** we demonstrated that the ATR spectrum of aqueous solutions and the spectrum recovered by the use of reflectance calculation and the Kramers-Krönig Relation ($k(\tilde{\nu})$ spectrum) are very similar. Their differences in shape are minor and only found at the top of the absorption band of the different components. The Anomalous Dispersion Effects neither mask nor create transformations in the ATR spectra of water when a binary salt is added. The Anomalous Dispersion Effects follow the pattern set by the transformation of the spectral characteristics of water when a salt is added. Since the modifications of the experimental ATR spectrum and the $k(\tilde{\nu})$ spectrum are proportional (**II**), it is not necessary to separate the optical effects of the ATR spectra beforehand to observe the sample's chemical modifications.

© 2000 NRC Canada

Table 1. Composition according to the balance of mass of the 10 mL aqueous solutions made with 1.12 M NaOH to which quantities of 12.40 M HCl were added (26.5 ± 0.3°C).

Mass of HCl 12.40 M (g)	Mass of the 10 mL sample (g)	pH	Concentrations (mol/L)		
			NaOH	NaCl	HCl
0.0000	10.3642	13.89	1.116	0.000	0.000
0.1089	10.3845	13.85	0.993	0.114	0.000
0.2374	10.3899	13.81	0.845	0.247	0.000
0.3037	10.3573	13.78	0.766	0.317	0.000
0.4225	10.3659	13.71	0.630	0.440	0.000
0.5164	10.3630	13.66	0.522	0.538	0.000
0.6208	10.3477	13.55	0.400	0.629	0.000
0.7325	10.3121	13.40	0.268	0.764	0.000
0.8623	10.3029	13.05	0.117	0.899	0.000
1.0027	10.3030	1.10	0.000	1.001	0.044
1.1290	10.3409	0.56	0.000	0.992	0.185
1.2323	10.3560	0.36	0.000	0.982	0.303
1.3640	10.3717	0.19	0.000	0.970	0.452
1.4628	10.3997	0.10	0.000	0.962	0.563
1.5891	10.4260	0.00	0.000	0.951	0.705
1.7110	10.4401	–0.10	0.000	0.940	0.844
1.9956	10.4874	–0.20	0.000	0.914	1.166
2.2283	10.5283	–0.25	0.000	0.894	1.430

The IR measurements consisted in obtaining the ATR background intensity: R_0, and the ATR sample intensity: R. The R/R_0 ratio produced intensity I for the spectral range being studied. Thereafter, data points (I ($\tilde{\nu}$) vs. $\tilde{\nu}$ (in cm^{-1})) were transferred to a Microsoft Excel spreadsheet program on a personal computer where the numerical treatments were performed. Intensities I were then transformed into log(1/I) that we designated as ATR Absorbance. No baseline correction was made.

3.4. Factor analysis

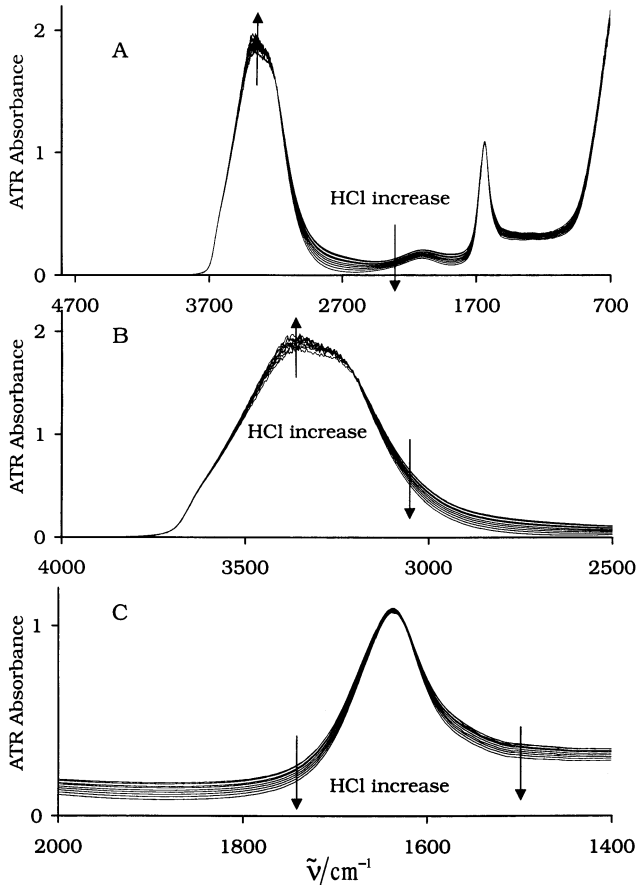
FA was applied to the series of spectra of aqueous NaOH and aqueous HCl. This was achieved using the eigenspectra and multiplying each by its MF. The MFs varied in order to obtain the fit that would best minimize the difference between the experimental and calculated spectra. The latter were obtained by adding the eigenspectra multiplied by their MFs. The minimization was monitored by using the least square fit procedure. The absorbance of water in the 3500–3100 cm^{-1} region and below 750 cm^{-1} was near saturation, resulting in a noisy signal in these frequency ranges. Consequently, these regions were eliminated in the least square fit procedure. Each mixture obtained by titration in the –0.3 to 14 pH range was composed of three components and as a result, three eigenspectra were sufficient to perform the analysis in each region.

4. Results and discussion

4.1. Spectra of 18 mixtures of NaOH and HCl

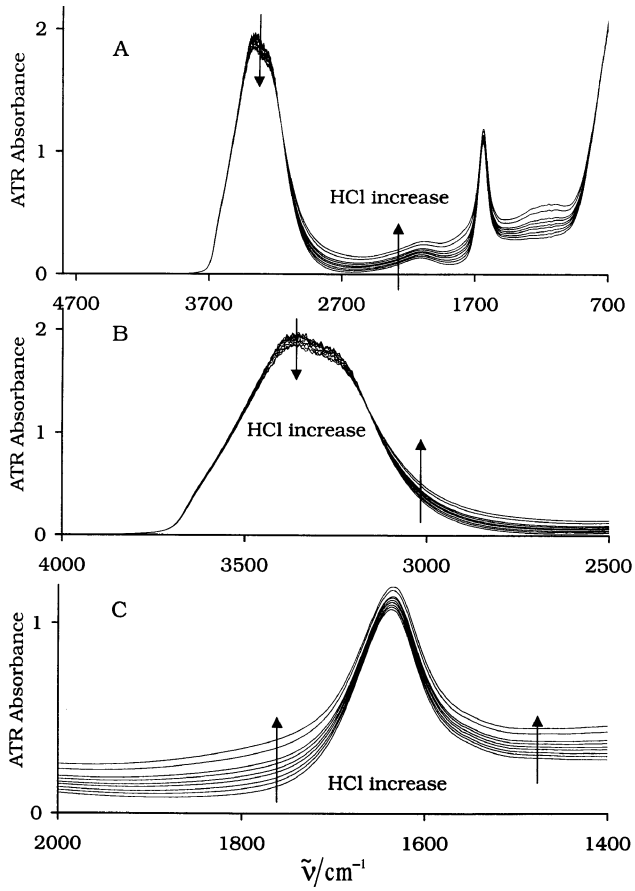
The spectra of the 18 samples reported in Table 1 are presented without modification in Figs. 1 and 2. To avoid confusion, the spectra of the alkaline solutions are given in Fig. 1 and the spectra of the acidic solutions are given in Fig. 2. Figures 1A and 2A show the spectra from 4800 to 700 cm^{-1}. Figures 1B and 2B show a blowup of the OH stretch region. In the latter, we observed that the central region of the band is not much displaced by the added HCl

Fig. 1. (A) IR-ATR spectra of the 9 mixtures of NaOH and HCl at pH higher than 7; (B) Expanded view of the OH stretching region; C) Expanded view of the OH deformation region.



© 2000 NRC Canada

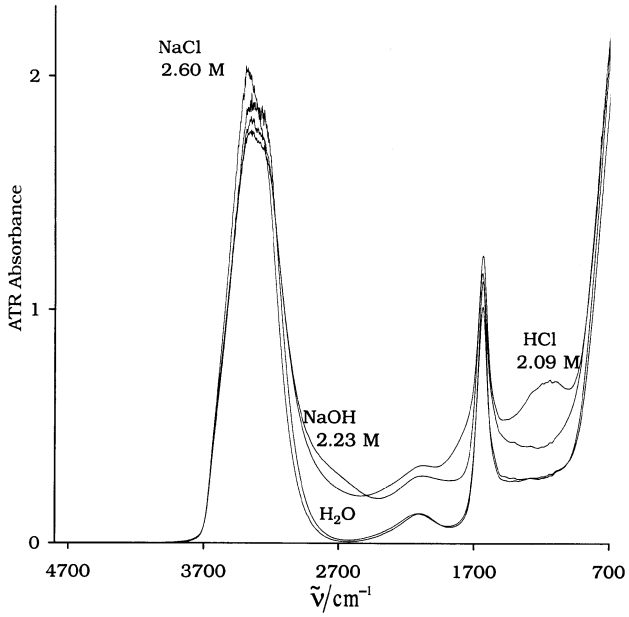
Fig. 2. (A) IR-ATR spectra of the 9 mixtures of NaOH and HCl at pH lower than 7; (B) Expanded view of the OH stretching region; C) Expanded view of the OH deformation region.



titrant, whereas the lower frequency far wing region is modified. Figures 1C and 2C display a blowup of the ν_2 water region. Within the resolution of 4 cm^{-1}, the ν_2 band center is not modified, although the far wing regions (high and low) are. As the pH decreases from 14 to 7, the intensity of the far wings decreases (Fig. 1C). Further decreasing the pH from 7 to –0.3, the intensity of the far wings increases (Fig. 2C). These modifications are in agreement with our previous studies. In **IV**, an increase in the HCl or NaOH content in pure water in turn increased the intensity of the far wings, as indicated by an apparent upward shift of the baseline. These modifications also confirm the results presented in **I,** where an increase in the NaCl content in pure water did not modify the apparent baseline. At the beginning of the titration of NaOH by HCl (pH = 13.89), an absorption is present in the far wings (the apparent baseline is high). Adding HCl neutralizes part of the samples' NaOH and therefore diminishes the NaOH content, which in turn lowers the far wings. When neutralization is reached, the sample is made of water and salt, both leading to low intensity far wings. Adding more HCl increases the sample's HCl content, therefore increasing the far wings.

The four eigenspectra used to deal with the base (NaOH) – acid (HCl) titration are provided in Fig. 3: pure water; 2.60 M NaCl; 2.09 M HCl; and 2.23 M NaOH. These spectra are uncorrected. All the spectra show large structureless

Fig. 3. The four eigenspectra: pure water; 2.60 M NaCl; 2.23 M NaOH; and 2.09 M HCl.



bands appearing in the same regions. Although the spectra are distinctly different, they display similar features in the strong absorption bands. This explains the difficulty of dealing with aqueous solutions.

4.2. MFs retrieved by FA for the IR titration of NaOH by HCl

Figure 4A illustrates the density of the samples as a function of the mass of the added 12.40 M HCl. The titration is divided into two regions. The first region is related to the mixtures of water, NaOH, and NaCl. The second region is related to the mixtures of water, NaCl, and HCl. In each region, within experimental error, the density is linear with the added titrant. It is easily demonstrated that this linearity stems from the linearity of the density of aqueous solutions in each of the three components, as a function of the respective concentration (in the 0–120 g/L range) (20). Consequently, as indicated in **III**, the equations of normalization, interpolation, and extrapolation can be used.

Figure 4B gives the MFs retrieved by factor analysis. The results were obtained by minimizing the intensity of the residues in the least square fit procedure. An example of the procedure can be found in Fig. 5A, where the situation at 0.7325 g of 12.40 M HCl was used for the exercise. The three species present are: pure, NaOH-, and NaCl-solvated water. The eigenspectra of these species (Fig. 3) are multiplied by the MFs given in Fig. 4B. The sum of the spectra is subtracted from the corresponding experimental spectrum given in Fig. 1. The residue observed at the bottom of Fig. 5A is a straight line at the 0.00 AU level. The residues, obtained for the 18 mixtures prepared for the titration, are illustrated in Fig. 5B. Except for the 3 μm region, the maximum and mean absolute absorbance of the residues were below 0.01 and 0.002, respectively. The minute residues obtained for all the samples indicate that FA procedure is adequate and that the results obtained are reliable.

© 2000 NRC Canada

Fig. 4. (A) Density (×) of the mixture of NaOH and HCl as a function of titrant; B) MFs retrieved for the solutions using the eigenspectra of Fig. 3: HCl (O) ; NaCl (Δ), NaOH (+), and pure water (◇).

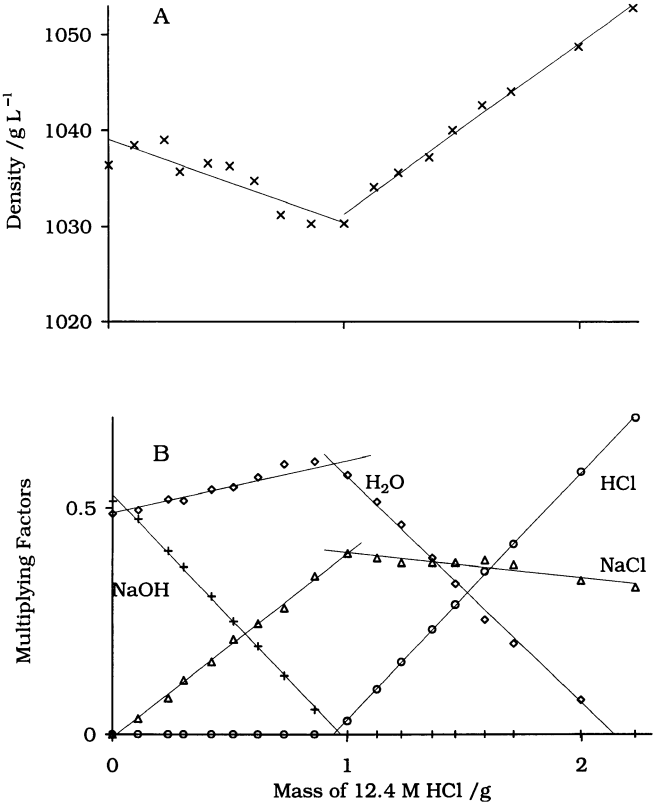
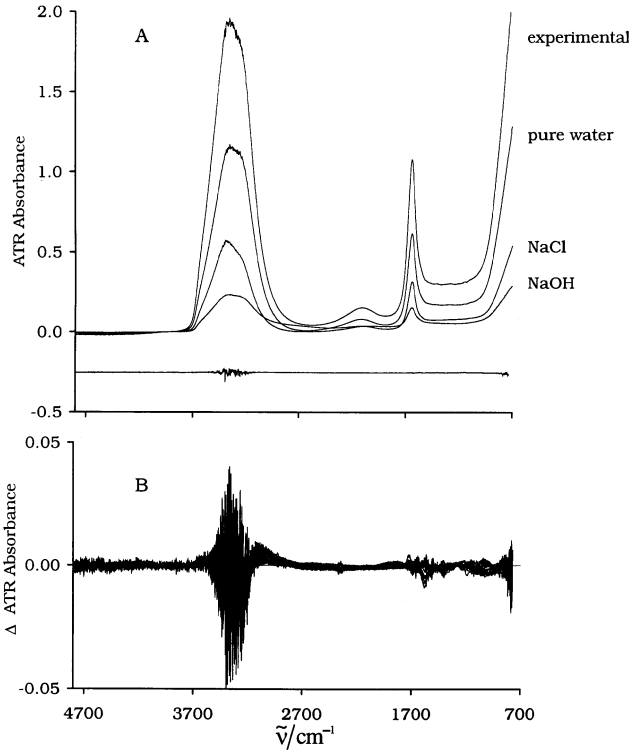


Figure 4B documents the results of the IR determination of the different species during the titration of NaOH by HCl. At the beginning of the titration, HCl reacted with NaOH to form H_2O and NaCl and therefore the MF of free NaOH decreased while the MF of NaCl increased. The two curves are linear functions of the amount of added titrant. No free HCl remained in the solution whose MF was zero. Once all NaOH was neutralized, the MF of free NaOH fell to zero while the MF of free HCl increased linearly when this substance was added to the solution. Since the samples were made with a constant volume, as the amount of titrant increased, the volume of the stock solution of NaOH in the sample decreased. Consequently, after neutralization of NaOH, the MF of NaCl slightly decreased (Fig. 4B).

4.3. Spectral differences between NaCl-, NaOH-, and HCl-solvated waters

The eigenspectra of pure water and solvated waters given in Fig. 3 are different. They were necessary and sufficient to perform FA on the series of samples throughout titration. This indicates that the four types of species of water defined by their respective eigenspectra are independent, that is: the interactions between the three types of species of water present at any time after the neutralization reaction are very weak. For example, after some titrant HCl has been added to the titrate NaOH, but before reaching the isoelectric point, aqueous NaOH, aqueous NaCl, and pure water are present in the solution at equilibrium. The NaCl-, NaOH-solvated waters, and pure water are the only water present in the solution. They are independent from each other (at the first order) because their eigenspectra, obtained with the pure solutions, are the only spectra used to recompose the spectra of the solution (Fig. 5A). If there were some interactions between the types of species of water, then the residue would not be at the zero level and this would indicate that one or more new species would be present in the solution. These new species would have genuine spectra different than the ones given in Fig. 3A. We have observed no such spectra. On other systems such intermediate spectra indicative of new species have been observed (unpublished results).

Fig. 5. (A) Example of FA decomposition of the sample at pH = 13.40. The top trace is the experimental spectrum. The three middle traces are the eigenspectra of water, 2.23 M NaOH, and 2.60 M NaCl multiplied by their respective MFs (Fig. 4B). The residue (shifted by –0.25 AU) is the difference between the top spectrum and the sum of the three others. (B) Residues of the 18 spectra of the NaOH–HCl mixtures. (Note the expanded intensity scale).



Schlöberg and Zundel reported that the spectra of 1M and 5 M HCl are modified by the presence of salts (5). They related the modifications of the water spectrum in the presence of ions to the action of a strong local electric field on the highly polarizable OH bonds. The results obtained by the present study of the IR titration of NaOH by HCl indicate that the spectral modifications observed are not caused by any modification in the spectrum of aqueous HCl, but represent the sum of the aqueous HCl and aqueous NaCl spectra in the low pH region and the sum of aqueous NaOH and of aqueous NaCl spectra in the high pH region.

The spectra given in Fig. 3 and the FA for the IR titration of NaOH by HCl (Fig. 4B) establish that the spectrum of aqueous NaCl cannot be represented by a combination of the

© 2000 NRC Canada

spectra of aqueous NaOH and aqueous HCl. Furthermore, the spectral characteristics of the NaCl-solvated water cannot be retrieved using the spectrum of NaOH-solvated water, nor with the spectrum of HCl-solvated water. This indicates that the solvation of NaCl by water does not produce isolated solvated ions, namely solvated Na^+ and solvated Cl^- in water. This confirms the results set forth in **III** where it was found that the pair Na^+/Cl^- formed a strong cluster with a mean of 5 molecules of water: Na^+-$(H_2O)_5$-Cl^-. We observed that the spectra for NaCl-, NaOH- and HCl-solvated waters are unchanged in the presence of the other types of species of water. This indicates that the organization Na^+-$(H_2O)_5$-Cl^- is not modified by the presence of HCl and that the structure of HCl–solvated water is unchanged when NaCl is present. Consequently, each pair of ions Na^+/Cl^-, Na^+/OH^-, and H_3O^+/Cl^- is associated to an amount of solvated water molecules and within each cluster the interactions of the ions with the water molecules are strong, while the interactions are weak between clusters. Strong interactions of the molecules imply modification of the intramolecular vibrations and result in significant spectral displacements.

4.4. Correlation between IR and mass balance results

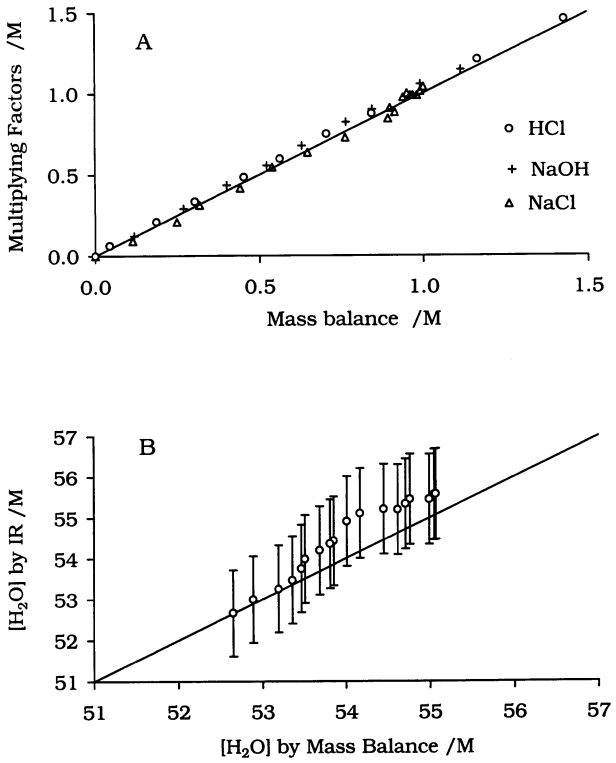
To make the correlation between the composition of NaCl, NaOH and HCl present in the sample calculated from the mass balance and that retrieved from the IR measurements, the MFs of Fig. 4B were taken and transformed into concentrations (Section 2.2). For instance, take the sample that originally contained 0.7325 g of 12.40 M HCl to which the NaOH solution was added. The MFs of this situation taken from Fig. 4B are: 0.280, 0.130, and 0.000 for NaCl, NaOH, and HCl, respectively. The concentrations of the original eigenspectra being 2.599, 2.225, and 2.086, then the concentrations of NaCl, NaOH, and HCl are 0.728, 0.289, and 0.000, respectively. The latter are the ordinates of the three points in Fig. 6A. From Table 1, the abscissas of these points are: 0.764, 0.268, and 0.000 (in mol/L), respectively. Similarly, the calculations are made for all the samples. The results given in Fig. 6A indicate that all the points are near the solid line, which is the theoretical slope for a perfect one to one correlation.

Figure 6B illustrates the correlation plot of the amount of water in the titration derived from the balance of mass and that retrieved from the IR analysis. Once again, all the points are in agreement with the theoretical slope. This indicates that FA is a reliable method of retrieving the right concentrations of NaOH, NaCl, HCl, and water in an aqueous solution from the IR spectra.

4.5. IR titration of NaOH by HCl

The concentration of the stock solution of NaOH can be obtained with the MFs provided in Fig. 4B. First, the complete neutralization of NaOH by HCl is obtained at the intercept of the two straight lines defined by the MFs of NaOH and HCl: 0.96 g of 12.4 M HCl. The amount of HCl added is determined by multiplying the mass by its concentration ([HCl] = 12.4 mol/L) and dividing the result by its density (d = 1.19 kg/L). The volume of the stock solution corresponding to this situation is then obtained by subtracting the volume of titrant (x/d) from the total volume (V). Finally, the concentration of the stock solution of NaOH is:

Fig. 6. Correlation plot between the concentrations obtained from the mass balance (Table 1) and that retrieved from the IR measurements. (A) for: HCl (O), NaOH (+), and NaCl (Δ); (B) H_2O with 2% error bars.



$$[1] \qquad [\mathrm{NaOH}] = \frac{\frac{x\,[\mathrm{HCl}]}{d}}{V - \frac{x}{d}} = \frac{[\mathrm{HCl}]}{\frac{Vd}{x} - 1}$$

Using the values [HCl] = (12.4 ± 0.1) M, d = (1190 ± 4) g/L, x = (0.96 ± 0.01) g, and V = (0.01000 ± 0.00005) L in eq. [1] we obtain a value of (1.09 ± 0.03) M for the concentration of NaOH. The concentration calculated directly from the mass of NaOH pellets is (1.086 ± 0.010) M. The result above indicates that IR titration produced the true concentration of NaOH with accuracy.

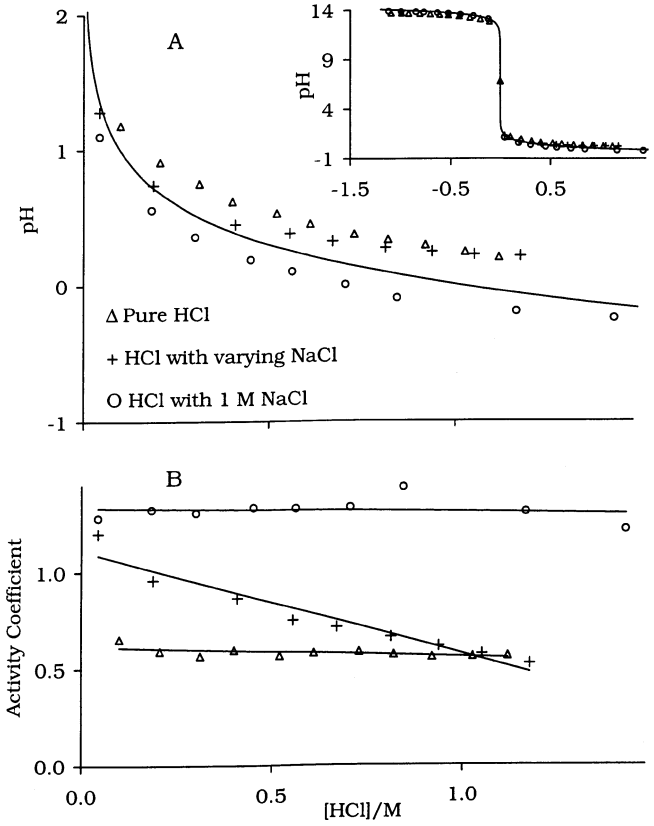
4.6. Rapid determination of NaOH, HCl, and NaCl concentrations in a solution by IR

The above titration was performed to establish that the three types of species of water simultaneously present in a solution are independent of each other. The present study shows that it is possible to obtain the accurate concentration of NaOH, NaCl, and HCl in water using a single IR spectrum. Therefore, a single spectrum of a given solution is sufficient to determine its ionic content.

The root mean square of the residue obtained in this series was 0.002 AU (Fig. 5B), to be compared to the absorbance level of HCl 2.09 M and NaOH 2.23 M near 2650 cm^{-1} (0.218 and 0.272, respectively, see Fig. 3). We can thus predict that for concentrations exceeding 10^{-2} M it is possible,

© 2000 NRC Canada

Fig. 7. (A) Plot of pH as a function of [HCl] in the samples in mol/L: pure (Δ), from titration of NaOH by HCl (O), and from titration of HCl by NaOH (+). The insert shows the full scale titration curve. The full lines are theoretical results for HCl with mean activity coefficient equal to unity. (B) Plot of the mean activity coefficient of HCl as a function of [HCl] calculated by eq. [2]. (Same symbols as in A). Full lines are linear fits in each case.



using IR, to obtain the titration of NaOH and HCl with an accuracy comparable to that of a volumetric titration. This method can be used to determine the concentration of NaOH and HCl in high-concentration solutions where it is often difficult to obtain these values rapidly. The lower limit of the determination depends on the IR apparatus used. This IR method can be automated to provide real time measurements. It would therefore be possible to monitor the variations of the concentrations of HCl, NaOH and NaCl in water in real time during a reaction involving either species, even in the presence of the other substances.

4.7. The activity coefficient and the IR spectrum of HCl

The activity and the specific conductivity of HCl have been reported to be greatly influenced by the presence of salt (5, 16, 17, 21, 22). The IR titration of NaOH by HCl presented here allows us to discuss the relation between the mean activity coefficient of aqueous HCl and its IR spectrum.

Estimating the activity of HCl or its acidity is no easy task (21, 22). Schwabe studied the relation between the acidity, activity, and pH according to conventional measurement techniques and the various sizes of different ionic species in water for several binary acids mixed with neutral salts (21). The purpose, in our study, is to determine whether or not there is a relation between the activity of HCl in water and the IR spectrum of aqueous HCl when a neutral salt is added (from 0 to 1 M NaCl). To this end, we used pH values obtained from a pH-meter.

Measurement by a pH-meter gives a representation of the activity of H^+ in the solution: pH ≈ paH = –log a_{H+} (21, 23). The mean activity coefficient of HCl (γ_{H^+/Cl^-}) is obtained through the usual relation:

$$[2] \qquad \gamma_{H^+/Cl^-} = \frac{a_{H^+}}{[H^+]} = \frac{10^{-pH}}{[H^+]}$$

The activity coefficients were retrieved from the pH measurements and the concentrations obtained from the IR measurements. In Fig. 7A, pH is a function of the concentrations of HCl retrieved by IR: neutralization of NaOH by HCl (O); neutralization of HCl by NaOH (+); and pure HCl (Δ). The values of the latter came from **IV**. The full line represents the theoretical curve for HCl where the mean activity coefficient is equal to unity. Figure 7A shows that the pH is lowered by adding a neutral salt (the salt comes from the neutralization of NaOH by HCl), passing from the values of pure HCl (Δ) to the values of HCl with NaCl (O). When HCl is neutralized by NaOH, the salt concentration varies and the mean activity coefficient varies with the concentration of the salt (Fig. 7A, +). The difference between the latter curve and that of pure HCl (Fig. 7A, Δ) is explained by the variation of the activity coefficient of HCl (21).

The results obtained by eq. [2] from the experimental values are illustrated in Fig. 7B in the 0.05 to 1.4 mol/L range where the mean activity coefficient of aqueous HCl is given as a function of HCl concentration. In the absence of NaCl (Δ data from **IV**), the mean activity coefficient of HCl is approximately constant at 0.6 from 0.1 M to 1.2 M HCl. In the presence of 1 M NaCl (○), the HCl mean activity coefficient is approximately 1.3. The mean activity coefficient of HCl is significantly increased when 1 M NaCl is present in the solution. Furthermore, when the concentration of salt increased in the HCl solution, the mean activity coefficient in the latter increased (+). This behavior and the range of value obtained are in agreement with that observed 30 years ago by Schwabe (21). The discussion about the exact value of the mean activity coefficient of HCl, its acidity (pwH, Hammet function, and other functions) (21, 22) is beyond the scope of this study.

The IR titration (Section 4.5) indicated that the spectra of NaCl-, NaOH-, and HCl-solvated waters were independent one from the other. Therefore the spectrum of HCl-solvated water is unchanged when NaCl-solvated water is present. From this we conclude that the structure of HCl-solvated water is stable and unchanged in the presence of NaCl-solvated water. Consequently, the variation of the mean activity coefficient of HCl is not related to a modification of the structure of the HCl-solvated water. This is true in the first order. Second order effects were not observed in the present study. Therefore, the activity of HCl in water is not related to its direct solvation by water. It could possibly de-

© 2000 NRC Canada

pend on the dynamics of the solvation. This effect is beyond the scope of the present study.

5. Conclusion

The species formed following the solvation of HCl, NaOH, and NaCl in water are stable in the concentration range 0 to 2 M for NaOH and HCl and 0 to 5.1 M for NaCl (higher concentrations have not been studied here). The spectra of water, NaOH-solvated water, NaCl-solvated water, and HCl-solvated water are all different and remain unchanged in the presence of the other species. The method of using four eigenspectra for the analysis of the IR spectra of mixtures of water, NaOH, HCl, and NaCl is accurate and gives the right composition of the samples. This is achieved even when the ionic species (H^+, Cl^-, Na^+, HO^-) dissolved in a strong absorber (H_2O) are either non-absorbing or very weakly-absorbing. Therefore, it is possible to titrate NaOH by HCl using their IR spectra even in the presence of NaCl. The four eigenspectra of water previously defined are necessary to this end. The result is a good first order approximation. IR spectra are well suited for measuring high concentrations of acids, bases, salts and their mixtures (14, 15, 24, 25). Furthermore, the IR spectrum, which is a non-destructive technique, can give precisely the ionization ratio which is difficult to obtain by means of usual techniques (22).

The addition of NaCl does not modify the structure of HCl-solvated water nor that of NaOH-solvated water. From the IR point of view, the ions of each of these three pairs are not solvated separately or independently of their respective counter ion. The mean activity coefficient of HCl is not related to its direct solvation by water. It possibly depends on the dynamics of the ionic solvation process which is a phenomenon that has not been studied here.

References

1. J.-J. Max, M. Trudel, and C. Chapados. Appl. Spectrosc. **52**, 234 (1998).
2. J.-J. Max and C. Chapados. Appl. Spectrosc. **53**, 1045 (1999).
3. E.R. Malinowski and D.G. Howery. Factor analysis in chemistry. Krieger R. E. Publishing Co., Malabar, Fla. 1989.
4. C. Chapados, S. Lemieux, and R. Carpentier. Biophys. Chem. **39**, 225 (1991).
5. D. Schlöberg and G. Zundel. Can. J. Chem. **54**, 2193 (1976).
6. F. Dousseau, M. Therrien, and M. Pezolet. Appl. Spectrosc. **43**, 538 (1989).
7. K. Rahmelow and W. Hübner. Appl. Spectrosc. **51**, 160 (1997).
8. W.B. Fischer, H.H. Eysel, O.F. Nielsen, and J.E. Bertie. Appl. Spectrosc. **48**, 107 (1994).
9. R.P. Paradkar and R.R. Williams. Appl. Spectrosc. **51**, 92 (1997).
10. A.H. Lipkus. App. Spectrosc. **42**, 395 (1988).
11. J.R. Powell, F.M. Wasacz, and R.J. Jakobsen. Appl. Spectrosc. **40**, 339 (1986).
12. J.-J. Max and C. Chapados. Appl. Spectrosc. **53**, 1601 (1999).
13. J.-J. Max and C. Chapados. Appl. Spectrosc. **52**, 963 (1998).
14. J.-J. Max, M. Trudel, and C. Chapados. Appl. Spectrosc. **52**, 226 (1998).
15. J.-J. Max, G. Bérubé, M. Trudel, S. Groleau, and C. Chapados. Langmuir, **14**, 5051 (1998).
16. B.F.Z. Reiff. Anorg. Allgem. Chem. **208**, 321 (1932).
17. S. Trautmann and L. Ambard. J. Chim. Phys. Phys.-Chim. Biol. **53**, 389 (1956).
18. P.T. McTigue and A.R. Watkins. Aust. J. Chem. **18**, 1943 (1965).
19. N.J. Harrick. Internal reflection spectroscopy. Interscience, New York. 1967. p. 43.
20. R.C. Weast. Handbook of chemistry and physics. 57th ed. CRC Press, Cleveland. 1977. pp. D252 and D218.
21. K. Schwabe. Electrochim. Acta. **12**, 67 (1967).
22. R.A. Cox and K. Yates. Can. J. Chem. **61**, 2225 (1983).
23. R.G. Bates. Determination of pH. Theory and practice. John Wiley and Sons, New York. 1973.
24. J. Baril, J.-J. Max, M. Trudel, and C. Chapados. 43rd International conference on analytical sciences and spectroscopy. Montréal, Que. 10 Aug. 1997.
25. C. Ménichelli, J.-J. Max, M. Trudel, and C. Chapados. 43rd International conference on analytical sciences and spectroscopy. Montréal, Que. 10 Aug. 1997.

© 2000 NRC Canada

Photoyellowing of peroxide-bleached lignin-rich pulps: a photochemical study on stilbene–hydroquinone chromophores issued from β-5 units of lignin during refining and (or) bleaching

Brigitte Ruffin and Alain Castellan

Abstract: The contribution of stilbene–parahydroquinone structures, formed from β-5 units during refining and bleaching, in photoreversion of peroxide-bleached high-yield pulps, was studied using 4′-benzyloxy-2,5-dihydroxy-3,3′-dimethoxystilbene (**I**), as a model compound. The various photoproducts formed during irradiation of **I** in solution or adsorbed on cellulose paper were identified. Isomerization of the stilbene double bond and oxidation of the hydroquinone into quinone were observed in solution, whereas in the solid state only the formation of the quinone was found to operate. Our attempts to detect and quantify stilbene–hydroquinones forming from β-5 units created on peroxide bleached mechanical pulp were not met with success.

Key words: lignin, stilbene, hydroquinone, lignin model compound, pulp, photoyellowing.

Résumé : La contribution des structures stilbène–parahydroquinone, formées à partir des unités β-5 durant le raffinage et le blanchiment de la pâte, au photojaunissement des pâtes mécaniques blanchies au peroxyde d'hydrogène a été étudiée à l'aide du 4′-benzyloxy-2,5-dihydroxy-3,3′-diméthoxystilbène (**I**). Les photoproduits formés sous irradiation de **I** en solution ou adsorbé sur papier de cellulose ont été identifiés. L'isomérisation de la double liaison stilbène ainsi que l'oxydation de l'hydroquinone en quinone ont été observées en solution, tandis qu'en phase solide, seule la formation de la quinone est notée. La détection et le dosage des unités stilbène-hydroquinone dans la pâte mécanique blanchie ne se sont pas révélés concluants.

Mots clés : lignine, stilbène, hydroquinone, composé modèle de la lignine, pâte, photojaunissement.

Introduction

High-yield pulps are obtained by mechanical refining of wood. This treatment causes some chemical modifications in the pulp and new chemical structures are formed. For example, phenylcoumaran (1, 2) and β-1 units (3) are turned into stilbenes by mechanochemistry, β-O-4 entities are converted into parahydroxybenzaldehyde (4), and coniferyl alcohols create α, β-unsaturated groups (5). Also acidic treatment generates stilbenes and phenylcoumarones (6) very sensitive to UV light (7, 8).

When lignin-rich pulps are bleached, new chromophores very sensitive to UV light are created. For example by the action of alkaline H_2O_2 bleaching solution, β-1 diol units are turned into stilbenes (9), α-carbonyl phenols were converted into hydroquinones (Dakin reaction) (10). In the same way, coniferaldehydes are transformed into methoxyhydroquinones (11). All these chromophores, hydroquinones in particular, were considered to have a key role in the photoyellowing of bleached mechanical pulps because hydroquinones, non-colored compounds, are easily oxidized into quinones (12), (very colored species). Lee and Sumimoto (13) suggested that parahydrobenzoquinone derivatives including a stilbene or biphenyl or diphenyl ether conjugated structures were the major chromophores responsible of the color reversion of pulps.

In a recent study (14), we performed a semi-quantitative evaluation, in peroxide-bleached high-yield pulps, of *p*-stilbene phenols formed from β-1 units and demonstrated that they are not the main contributors of the rapid photoyellowing of these pulps. The present article describes a similar approach on the photochemical behavior of chromophores including both parahydroquinone and stilbene entities. In that respect, the photochemical behavior of model **I** (Fig. 1) before and after catalytic hydrogenation and (or) acetylation was established and also a tentative evaluation of the content of this type of structure in peroxide-bleached softwood mechanical pulps was carried out.

Received August 6, 1999.

B. Ruffin and A. Castellan.[1] Laboratoire de Chimie des Substances Végétales, Institut du Pin, Université Bordeaux 1, 351, cours de la Libération, F-33405 TALENCE Cedex, France.

[1]Author to whom correspondence may be addressed. Telephone: (33) 5 56 84 62 80. Fax: (33) 5 56 84 64 22. e-mail: a.castellan@ipin.u-bordeaux.fr

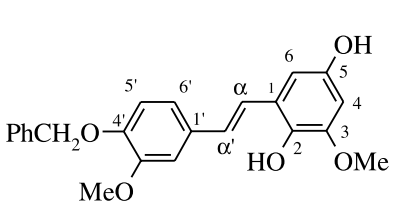
Experimental

1. General

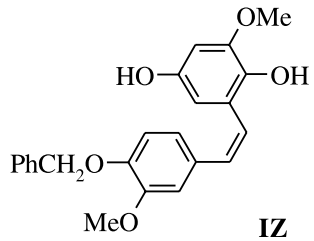
Melting points were measured with a Mettler FP62 heating block. NMR spectra were recorded on a Bruker DMP

© 2000 NRC Canada

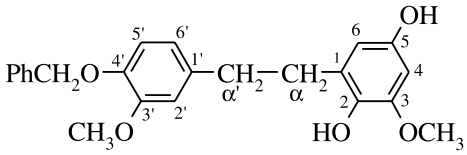
Fig. 1. Formulae of the studied compounds.



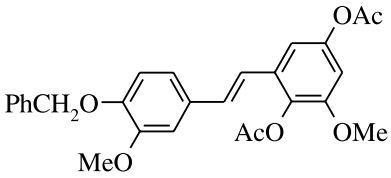
I



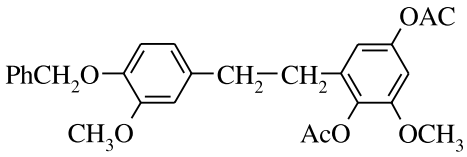
IZ



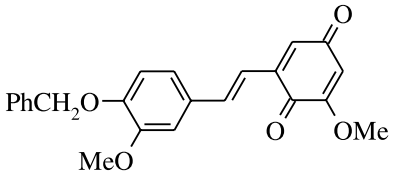
II



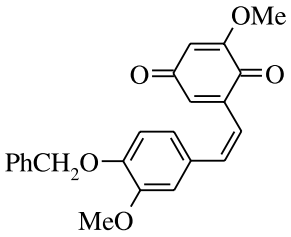
III



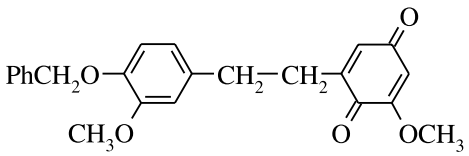
IV



IQ



IZQ



IIQ

200 (^{1}H, ^{13}C) spectrometer (reference Me_4Si, solvent $CDCl_3$). The IR and UV absorption spectra were respectively performed on a Perkin–Elmer Paragon 1000 PC and an Hitachi U-3300 spectrometers. Mass spectra were obtained using a VG Micromass Autospec Q instrument.

The chemicals were obtained from Aldrich and were used without further purification. The synthesized compounds were purified by column chromatography on silica gel 60 (70–200 mesh) using the appropriate eluents. The solid products were crystallized after chromatography.

2. Syntheses

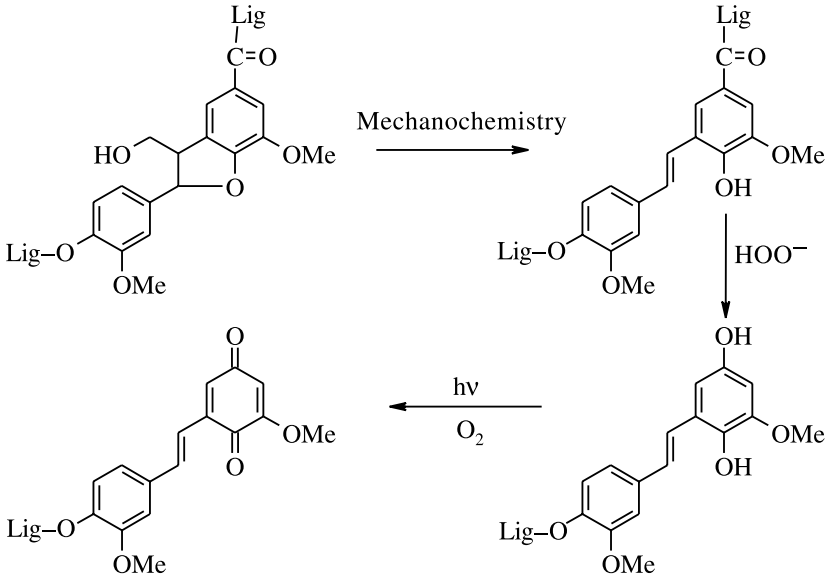
2.1 Stilbene derivatives

4′-benzyloxy-2,5-dihydroxy-3,3′-dimethoxystilbene (I)

*4′-benzyloxy-5-formyl-2-hydroxy-3,3′-dimethoxystilbene (**3**)*: Compounds **1** and **2** were prepared from vanillin by conventional methods respectively described in ref. 15 and 16. A *n*-butyl lithium solution in *n*-hexane (conc = 2.5 mol L^{-1}, 16 mmol) was added to a suspension of the phosphonium salt **2** (4.2 g, 8.0 mmol) in anhydrous THF (50 mL) under N_2 atmosphere and the mixture was stirred for 30 min at 0°C. The resulting red solution was treated with a solution of aldehyde **1** (1.6 g, 8.0 mmol) in anhydrous THF (40 mL). After being stirred for 3 h at room temperature, the THF was removed under vacuum, the residue was dissolved in CH_2Cl_2 and treated with hydrochloric acid (10%). The aqueous layer was extracted with CH_2Cl_2 (3 × 50 mL). The combined organic layers were washed with water, dried over $MgSO_4$, filtered, and concentrated. The residue was purified by chromatography on silica gel (eluent: CH_2Cl_2–EP) affording the expected *E* stilbene **3** as white crystals (1.15 g, yield 37%, mp 133°C). IR (KBr) ν : 950, 1010, 1080, 1140, 1260, 1520, 1600, 1690, 3400 cm^{-1}. ^{1}H NMR ($CDCl_3$) δ: 3.96 (s, 3H, OCH_3), 3.99 (s, 3H, OCH_3), 5.19 (s, 2H, OCH_2), 6.50 (s, 1H, OH), 6.88 (d, 1H, J = 8.24, $H_{5'}$), 7.04 (dd, 1H, J = 1.83 and 8.24, $H_{6'}$), 7.13 (d,1H, J = 1.83, $H_{2'}$), 7.2–7.5 (m, 8H, ArH), 7.71 (d, 1H, J = 1.52 H_4 or H_6), 9.88 (s, 1H, CHO) ppm. ^{13}C NMR ($CDCl_3$) δ: 56.1 (OCH_3), 56.4 (OCH_3), 71.0

© 2000 NRC Canada

Scheme 1. Formation of stilbenes via mechanochemistry and then quinones by photooxidation (**1**, **2**).



(OCH_2), 106.9 (CH ar.), 109,6 (CH ar.), 113.9 (CH ar.), 114.6 (CH ar.), 119.7 (CH ar.), 120.1 (=CH), 124.1 (C ar.), 127.3 (CH Bn), 127.9 (CH Bn), 128.6 (CH Bn), 129.2 (C ar.), 130.6 (=CH), 130.8 (C ar.), 134.2 (C Bn), 147.3 (C ar.), 148.3 (C ar.), 148.6 (C ar.), 149.8 (C ar.), 191.2 (CHO) ppm.

*4′-benzyloxy-2,5-dihydroxy-3,3′-dimethoxystilbene (**I**)*: A solution of compound **3** (600 mg, 1.4 mmol) in THF–water (30mL and 8 mL) under nitrogen atmosphere was treated with sodium carbonate (126 mg, 1.4 mmol) and oxygen peroxide (240 µL, 2.3 mmol). After being stirred at room temperature for 3 h, the reaction mixture was reacted with 1 mL of acetic acid. The aqueous layer was extracted with CH_2Cl_2 (3 × 30 mL). The combined organic layers were washed with water, dried over $MgSO_4$, filtered, and concentrated. The residue was purified by crystallization (CH_2Cl_2–EP) affording the expected *E* stilbene **I** as white crystals (360 mg, yield 62%, mp 150°C). UV λ_{max} (MeOH)/nm : 320 (ε/L mol^{-1} cm^{-1} 19 600). IR (KBr) ν : 960, 1000, 1080, 1130, 1260, 1510, 1600, 3400 cm^{-1}. ^1H NMR ($CDCl_3$) δ: 3.87 (s, 3H, OCH_3), 3.94 (s, 3H, OCH_3), 4.46 (s, 1H, OH), 5.14 (s, 2H, OCH_2), 5.55 (s, 1H, OH) 6.36 (d, 1H, H_4, *J* = 2.75 Hz), 6.60 (d, 1H, H_6, *J* = 2.75 Hz), 6.85 (d, 1H, $H_{5'}$, *J* = 8.22 Hz), 6.98 (dd, 1H, $H_{6'}$, *J* = 2.15 and 8.22 Hz), 7.00 (d, 1H, H_α or $H_{\alpha'}$, *J* = 16.45 Hz), 7.11 (d, 1H, $H_{2'}$, *J* = 2.15 Hz), 7.24 (d, 1H, H_α or $H_{\alpha'}$, *J* = 16.45 Hz), 7.25–7.6 (m, 5H, ArH) ppm. ^{13}C NMR ($CDCl_3$) δ: 56.1 (OCH_3), 56.2 (OCH_3), 71.0 (OCH_2), 98.7 (CH ar.), 103.4 (CH ar.), 109.5 (CH ar.), 114.0 (CH ar.), 120.0 (CH ar.), 120.8 (=CH), 123.8 (C ar.), 127.3 (CH Bn), 127.9 (CH Bn), 128.6 (CH Bn), 129.3 (=CH), 137.1 (C Bn), 137.6 (C ar.), 147.3 (C ar.), 148.0 (C ar.), 148.7 (C ar.), 149.8 (C ar.) ppm. MS (EI) *m/z* (%): 378 ($M^{+\cdot}$, 65), 287 (100), 255 (14), 227 (14), 91 (48). HPLC–MS (solvent acetonitrile, negative mode) *m/z*: 377 $(M - H)^-$.

*2,5-diacetoxy-4′-benzyloxy-3,3′-dimethoxystilbene (**III**)*: Compound **I** (200 mg, 0.43 mmol) in dichloromethane (40 mL) was refluxed under nitrogen in presence of acetic anhydride (1.2 mL, 1.2 mmol), triethylamine (0.17 mL, 1.2 mmol), and 4-dimethylaminopyridine (DMAP, 5 mg) for 4 h. The reacting mixture was treated with hydrochloric acid (10%) and extracted with dichloromethane. The organic layer was washed with water to neutrality, dried over magnesium sulfate and evaporated under reduced pressure. The reacting mixture, separated by chromatography (eluent: CH_2Cl_2–Et_2O, 95:5), followed by crystallization in ethanol afforded the expected *E* stilbene **III** as white crystals (204 mg, yield 93%, mp 158°C). IR (KBr) ν : 1030, 1080, 1140, 1180, 1210, 1270, 1510, 1590, 1760 cm^{-1}. UV λ_{max} (MeOH)/nm : 320 (ε/L mol^{-1} cm^{-1} 29 000). ^1H NMR ($CDCl_3$) δ: 2.31 (s, 3H, CH_3), 2.36 (s, 3H, CH_3), 3.81 (s, 3H, OCH_3), 3.93 (s, 3H, OCH_3), 5.18 (s, 2H, OCH_2), 6.66 (d, 1H, H_4, *J* = 2.75 Hz), 6.87 (d, 1H, $H_{2'}$, *J* = 8.24 Hz), 6.91 (d, H_α, *J* = 15.26 Hz), 6.96–7.05 (m, 3H, H_6, $H_{6'}$, and $H_{5'}$), 7.40 (d, $H_{\alpha'}$, *J* = 15.26 Hz), 7.3–7.5 (m, 5H, ArH) ppm. ^{13}C NMR ($CDCl_3$) δ: 20.5 (CH_3), 21.2 (CH_3), 56.1 (OCH_3), 56.2 (OCH_3), 71.0 (OCH_2), 104.9 (CH ar.), 110.1 (CH ar.), 110.2 (CH ar.), 113.9 (CH ar.), 119.4 (CH ar.), 119.9 (=CH), 127.2 (CH Bn), 127.9 (CH Bn), 128.6 (CH Bn), 130.5 (C ar.), 131.8 (=CH), 131.9 (C ar.), 135.1 (C ar.), 137.0 (C Bn), 148.5 (C ar.), 148.7 (C ar.), 149.7 (C ar.), 168.7 (C=O), 168.8 (C=O) ppm. MS (EI) *m/z* (%): 462 ($M^{+\cdot}$, 65), 432 (12), 371 (30), 329 (76), 299 (28), 287 (31), 255 (54), 227 (12), 91 (100), 43 (66).

*(Z)-4′-benzyloxy-2,5-dihydroxy-3,3′-dimethoxystilbene (**IZ**)*: By irradiation with UV light (λ ≈ 350 nm), compound **I** (50 mg, 0,13 mmol) in methanol (10 mL) solution degassed by bubbling nitrogen was converted to compound **IZ** ([**IZ**]:[**I**] = 90:10. The NMR data on **IZ** were obtained on the mixture after evaporation of the solvent and after subtracting the contribution of **I**. The electronic absorption spectrum of **IQ** was obtained with the diode array detector of the HPLC system (eluent: methanol). The mass spectrum of **IQ** was obtained using HPLC–MS technique with acetonitrile as eluent for the HPLC and electrospray for the ionization mode. UV λ_{max} (MeOH): 300 nm. ^1H NMR ($CDCl_3$) δ: 3.63 (s, 3H, OCH_3), 3.81 (s, 3H, OCH_3), 5.09 (s, 3H, OCH_2), 6.27 (d, 1H, H_4, *J* = 2.44 Hz), 6.35 (d, 1H,

© 2000 NRC Canada

H_6, J = 2.44 Hz), 6.55 (s, 2H, CH=CH), 6.76 (s, 1H), 6.77 (d, 1H, J = 1.83 Hz), 6.88 (d, 1H, J = 1.53 Hz), 7.25–7.45 (m, 5H, ArH) ppm. ^{13}C NMR ($CDCl_3$) δ: 55.7 (OCH_3), 56.1 (OCH_3), 70.9 (OCH_2), 98.8 (CH ar.), 106.9 (CH), 112.2 (CH), 113.4 (CH), 122.0 (CH), 122.9 (CH), 123.3 (CH), 127.3 (CH Bn), 127.4 (CH Bn), 127.9 (CH Bn), 128.6 (C ar.), 129.3 (C ar.), 130.2 (C ar.), 130.7 (C ar.), 137.1 (C ar.), 137.3 (C ar.), 147.4 (C ar.), 148.4 (C ar.) ppm. HPLC–MS (solvent acetonitrile, negative mode); *m/z*: 377 $(M - H)^-$.

2.2 Diphenyl ethane compounds

4′-benzyloxy-2,5-dihydroxy-3,3′-dimethoxydiphenylethane (II)

*4′-benzyloxy-5-formyl-2-hydroxy-3,3′-dimethoxydiphenylethane (**4**)*: Hydrogenation of compound **3** (500 mg, 1.28 mmol) in ethyl acetate (100 mL) containing 50 mg of $RhCl(PPh_3)_3$ was accomplished by treating the mixture under hydrogen pressure (180 bar, 1 bar = 10^5 Pa) for 5 h at 80°C. The mixture, after filtration on a silica gel to removed the catalyst, afforded a white solid (500 mg, yield 100%). ^{1}H NMR ($CDCl_3$) δ: 2.9 (s, 4H, CH_2-CH_2), 3.8 (s, 3H, OCH_3), 3.9 (s, 3H, OCH_3), 5.0 (s, 2H, OCH_2), 6.5 (s, 1H, OH), 6.6–7.4 (m, 10H, ArH), 9.8 (s, 1H, CHO) ppm.

*4′-benzyloxy-2,5-dihydroxy-3,3′-dimethoxydiphenylethane (**II**)*: A solution of compound **4** (300 mg, 0.8 mmol) in a mixture of THF (20 mL)–water (5 mL) was treated with potassium carbonate (72 mg, 0.8 mmol) and hydrogen peroxide (150 µL, 1.4 mmol). After being stirred at room temperature for 1 h, the reaction was stopped by addition of 1 mL of acetic acid. The residue was reacted with a solution of hydrochloric acid (10%). The aqueous layer was extracted with CH_2Cl_2. The combined organic layers were washed with water, dried over $MgSO_4$, filtered, and concentrated under vacuum. The residue was purified by crystallization in a mixture of CH_2Cl_2–petroleum ether (1v:1v) affording the expected stilbene **II** as a white solid (200 mg, yield 70%, mp 119°C). UV λ_{max} (MeOH)/nm : 270 (ε/L mol^{-1} cm^{-1} 6800). IR (KBr) ν : 730, 790, 1030, 1090, 1150, 1220, 1390, 1440, 1480, 1510, 2930, 3320 cm^{-1}. ^{1}H NMR ($CDCl_3$) δ: 2.86 (s, 4H, CH_2-CH_2), 3.85 (s, 3H, OCH_3), 3.88 (s, 3H, OCH_3), 4.80 (s, 1H, OH), 5.16 (s, 2H, OCH_2), 5.32 (s, 1H, OH), 6.17 (d, 1H, H_4, J = 2.64 Hz), 6.34 (d, 1H, H_6, J = 2.64 Hz), 6.72 (dd, 1H, $H_{6'}$, J = 1.95 and 8.10 Hz), 6.77 (d, 1H, $H_{2'}$, J = 1.95 Hz), 6.84 (d, 1H, $H_{5'}$, J = 8.10 Hz), 7.30–7.55 (m, 5H, ArH) ppm. ^{13}C NMR ($CDCl_3$) δ: 31.9 (CH_2), 35.4 (CH_2), 55.8 (OCH_3), 55.9 (OCH_3), 71.1 (OCH_2), 97.3 (CH ar.), 107.9 (CH ar.), 112.4 (CH ar.), 114.1 (CH ar.), 120.2 (CH ar.), 127.2 (CH Bn), 127.6 (CH Bn), 127.7 (C ar.), 128.4 (CH Bn), 135.4 (C ar.), 137.2 (C ar.), 137.3 (C ar.), 146.7 (C ar.), 148.3 (C ar.), 149.2 (C ar.) ppm. MS (EI) *m/z* (%): 380 ($M^{+\cdot}$, 30), 289 (35), 227 (40), 153 (33), 91 (100).

*2,5-diacetoxy-4′-benzyloxy-3,3′-dimethoxydiphenylethane (**IV**)*: Hydrogenation of **III** (300 mg, 0.72 mmol) in ethyl acetate (50 mL) containing 30 mg of $RhCl(PPh_3)_3$ was accomplished by treating the mixture under hydrogen pressure (180 bar, 1 bar = 10^5 Pa) for 5 h at 80°C. After filtration on silica gel, the solvent was removed under vacuum The compound **IV** was obtained as a white solid (300 mg, yield 100%, mp 130°C). UV λ_{max} (MeOH)/nm : 260 (ε/L mol^{-1} cm^{-1} 6900). IR (KBr) ν : 1030, 1090, 1140, 1180, 1220, 1510, 1760, 2930 cm^{-1}. ^{1}H NMR ($CDCl_3$) δ: 2.28 (s, 3H, CH_3), 2.33 (s, 3H, CH_3), 2.78 (s, 4H, CH_2-CH_2), 3.80 (s, 3H, OCH_3), 3.86 (s, 3H, OCH_3), 5.14 (s, 2H, OCH_2), 6.54 (d, 1H, H_4, J = 2.75 Hz), 6.61 (d, 1H, H_6, J = 2.75 Hz), 6.65 (dd, 1H, $H_{6'}$, J = 1.83 and 8.24 Hz), 6.69 (d, 1H, $H_{2'}$, J = 1.83 Hz), 6.82 (d, 1H, $H_{5'}$, J = 8.24 Hz), 7.25–7.50 (m, 5H, ArH) ppm. ^{13}C NMR ($CDCl_3$) δ: 20.6 (OAc), 21.2 (OAc), 32.4 (CH_2), 35.6 (CH_2), 55.9 (OCH_3), 56.1 (OCH_3), 71.2 (OCH_2), 104.3 (CH ar.), 112.0 (CH ar.), 112.3 (CH ar.), 114.2 (CH ar.), 120.2 (CH ar.), 127.3 (CH Bn), 127.8 (CH Bn), 128.6 (CH Bn), 134.6 (C ar.), 135.5 (C ar.), 135.7 (C ar.), 137.4 (C ar.), 146.5 (C ar.), 148.5 (C ar.), 149.5 (C ar.), 151.6 (C ar.), 168.9 (C=O), 169.4 (C=O) ppm. MS (EI): *m/z* (%): 464 ($M^{+\cdot}$, 51), 422 (12), 380 (27), 331 (30), 289 (27), 257 (11), 227 (34), 195 (37), 183 (27), 137 (77), 91 (100), 43 (48).

Compound **IV** was also prepared in quantitative yield by acetylation of compound **II** using the procedure described for the synthesis of compound **III**.

2,5,4′-trihydroxy-3,3′-dimethoxydiphenylethane (6)

*2,5-diacetoxy-4′-hydroxy-3,3′-dimethoxydiphenylethane (**5**)*: Hydrogenation of **III** (300 mg, 0.65 mmol) in anhydrous THF (50 mL) containing 30 mg of Pd–C was accomplished by treating the mixture under hydrogen pressure (80 bar, 1 bar = 10^5 Pa) for 24 h at 60°C. The mixture, after filtration on silica gel to removed the catalyst, afforded compound **5** (300 mg, yield 100%). ^{1}H NMR ($CDCl_3$) δ: 2.20 (s, 3H, OAc), 2.25 (s, 3H, OAc), 2.38 (s, 4H, CH_2-CH_2), 3.72 (s, 3H, OCH_3), 3.76 (s, 3H, OCH_3), 6.1–7.0 (m, 5H, ArH) ppm.

*2,5,4′-trihydroxy-3,3′-dimethoxydiphenylethane (**6**)*: A solution of **5** (300 mg, 0.8 mmol) in methanol (25 mL) was treated with K_2CO_3 (350 mg, 4 mmol). After being stirred at 90°C for 4h, the solution was reacted with a solution of hydrochloric acid (10%). The aqueous layer was extracted with CH_2Cl_2. The combined organic layers were washed with water, dried over $MgSO_4$, filtered, and concentrated. The reacting mixture was analyzed by ^{1}H NMR and by GC–MS after silylation. ^{1}H NMR ($CDCl_3$) δ: 2.20 (s, OAc), 2.41 (s, 4H, CH_2-CH_2), 3.75 (s, 3H, OCH_3), 3.78 (s, 3H, OCH_3), 6.0–7.0 (m, 5H, ArH) ppm. The observation of the peak at 2.20 ppm reveals the presence of compound **6Ac** (50%) in addition to compound **6** (50%). This proportion was also revealed by GC–MS when the mixture was silylated by treatment with pyridine (10 µL), BSTFA (100 µL) in dichloromethane. MS (EI) **6** silylated *m/z* (%): 433 ($(M - 1)^+$, 33), 223 (14), 209 (100), 193 (11), 75 (12), 73 (34). MS (EI) **6Ac** silylated *m/z* (%): 476 ($M^{+\cdot}$, 14), 434 (57), 209 (100), 179 (15), 75 (13), 73 (41). This spectra indicates the incorporation of two trimethylsilyl groups in the molecule, the OH in the 2 position being too hindered to be substituted by the bulky TMS group.

2.3 Formation of p*-quinonoid compounds*

Quinone diphenylethane (IIQ)

Oxidation with $NaIO_4$: A solution of compound **II** (100 mg, 0.26 mmol) in a mixture of acetic acid (12 mL) – water (8 mL) was treated with sodium periodate (85 mg, 0.40 mmol). After being stirred at room temperature for 4h,

© 2000 NRC Canada

the organic layer was extracted with dichloromethane, dried over $MgSO_4$, and reduced under vacuum. The expected compound **IIQ** was obtained as a pale yellow oil (100 mg, yield 100%). IR (NaCl film) ν : 2930, 1680, 1650, 1600, 1510, 1450, 1260, 1230, 1025, 790, 760 cm^{-1}. ^1H NMR ($CDCl_3$) δ: 2.75 (s, 4H, CH_2-CH_2), 3.82 (s, 3H, OCH_3), 3.88 (s, 3H, OCH_3), 5.13 (s, 3H, OCH_2), 5.88 (d, 1H, H_4, J = 2.44 Hz), 6.44 (d, 1H, H_6, J = 2.44 Hz), 6.65 (dd, 1H, $H_{6'}$, J = 2.14 and 8.24 Hz), 6.73 (d, 1H, $H_{2'}$, J = 2.14 Hz), 6.80 (d, 1H, $H_{5'}$, J = 8.24 Hz), 7.2–7.5 (m, 5H, ArH) ppm.

Oxidation with Fremy's salt: A solution of compound **II** (100 mg, 0.26 mmol) in methanol (20 mL) was treated with Fremy's salt $(KSO_3)_2NO$ (110 mg, 0.42 mmol) in water (5 mL) After being stirred at room temperature for 4h, the organic layer was extracted by dichloromethane, dried over $MgSO_4$, and reduced under vacuum. The expected compound **IIQ** was obtained as a pale yellow oil (100 mg, yield 100%).

Quinone stilbene (IQ): A solution of compound **I** (10 mg, 0.026 mmol) in acetonitrile was oxidized into quinone **IQ** by treatment under pressure of oxygen (20 bar, 1 bar = 10^5 Pa) at 60°C for 5 h. After evaporation of the solvent, the mixture was analyzed by HPLC and ^1H NMR. Products **I** and **IQ** were obtained in a 50:50 mixture. Various tentatives to isolate **IQ** as a pure compound by preparative chromatography were not successful due to the high reactivity of the quinone. So, the ^1H NMR spectrum of **IQ** was obtained from the reacting mixture spectrum by subtracting the contribution of compound **I**. The electronic absorption spectrum of **IQ** was obtained with the diode array detector on the HPLC system (eluent: methanol). The mass spectrum of **IQ** was obtained using HPLC–MS technique with acetonitrile as the eluent for the HPLC and electrospray for the ionization mode. This analysis did not allow the observation of the $(M - 1)^-$ peak as for **I**, but a peak was observed which corresponded to the addition of acetonitrile followed by the elimination of CO. UV λ_{max} (MeOH): 280 and 480 nm. ^1H NMR ($CDCl_3$) δ: 3.90 (s, 3H, OCH_3), 3.96 (s, 3H, OCH_3), 5.20 (s, 2H, OCH_2), 6.25 (d, 1H, H_4, J = 2.70 Hz), 6.55 (d, 1H, H_6, J = 2.70 Hz), 6.8–7.1 (4H, ArH and =CH), 7.25–7.6 (m, 6H, ArH and = CH) ppm. HPLC–MS (solvent acetonitrile, negative mode) *m/z*: 388 $(M + CH_3CN–CO–H)^-$.

Quinone stilbene (IZQ): The stilbene quinone **IZQ** formed by irradiation of **I** in non-degassed solutions was characterized by HPLC equipped with a diode array detector (eluent: methanol) and HPLC–MS technique with acetonitrile as eluent for the HPLC and electrospray for the ionization mode. As for **IQ**, this analysis did not allow the observation of the $(M - 1)^-$ peak, but a peak was observed which corresponds to the addition of acetonitrile followed by the elimination of CO. UV λ_{max} (MeOH): 270 and 470 nm. HPLC–MS (solvent acetonitrile, negative mode) *m/z* : 388 $(M + CH_3CN–CO–H)^-$.

3. UV–Irradiation of models I, II, III and IV adsorbed on cellulose matrix

Four paper sheets (3 cm × 3 cm) made from a kraft pulp (30 g/m^2) were separately impregnated with 2.0 mg of each compound in CH_2Cl_2 (1 mL) and dried with a nitrogen stream. The paper sheets were irradiated with three black light UV lamps (Mazdafluor TFWN 18) emitting mainly in the 350 nm wavelength range. The distance between the lamp and the sheets was 20 cm. The temperature of the irradiation was maintained at 25°C by a fan. The reflectance of the sheets backed with a black and white backgrounds were measured at appropriate irradiation time intervals. The absorption (K) given by the Kubelka–Munk theory (17) was calculated and plotted as the difference between non irradiated and irradiated samples versus irradiation time.

4. Attempt to detect stilbene–hydroquinone chromophore in bleached mechanical pulp

Peroxide bleaching of mechanical pulp (BMP) and acetylation

Unbleached softwood mechanical pulp (20 g), kindly provided by Dr. Petit-Conil (Centre Technique du Papier, Grenoble), was treated in a polyethylene bag with the bleaching liquor (200 mL) constituted by hydrogen peroxide (3% oven dry pulp, odp), NaOH (1.5% odp), $MgSO4{\cdot}7H_2O$ (0.5% odp), sodium silicate (3.5% odp), and DTPA (0.25% odp) at 60°C for 4 h. Then the pulp was filtered and bleached for a second time in the same conditions with fresh liquor (200 mL). At the end of the bleaching, the pulp was washed with distilled water and diluted hydrochloric acid to pH 4.5. Before acetylation, the pulp (1 g) was made alkaline by soaking it in a potassium carbonate solution (1 mol L^{-1}) for 15 min and filtrated under vacuum to remove the major part of the water. The pulp was then exposed to acetic anhydride vapor for 1 h and after was washed with water, ethanol and water to pH 4.5. At the end, the pulp was dried at 30°C for 24 h.

Hydrogenation of the acetylated BMP

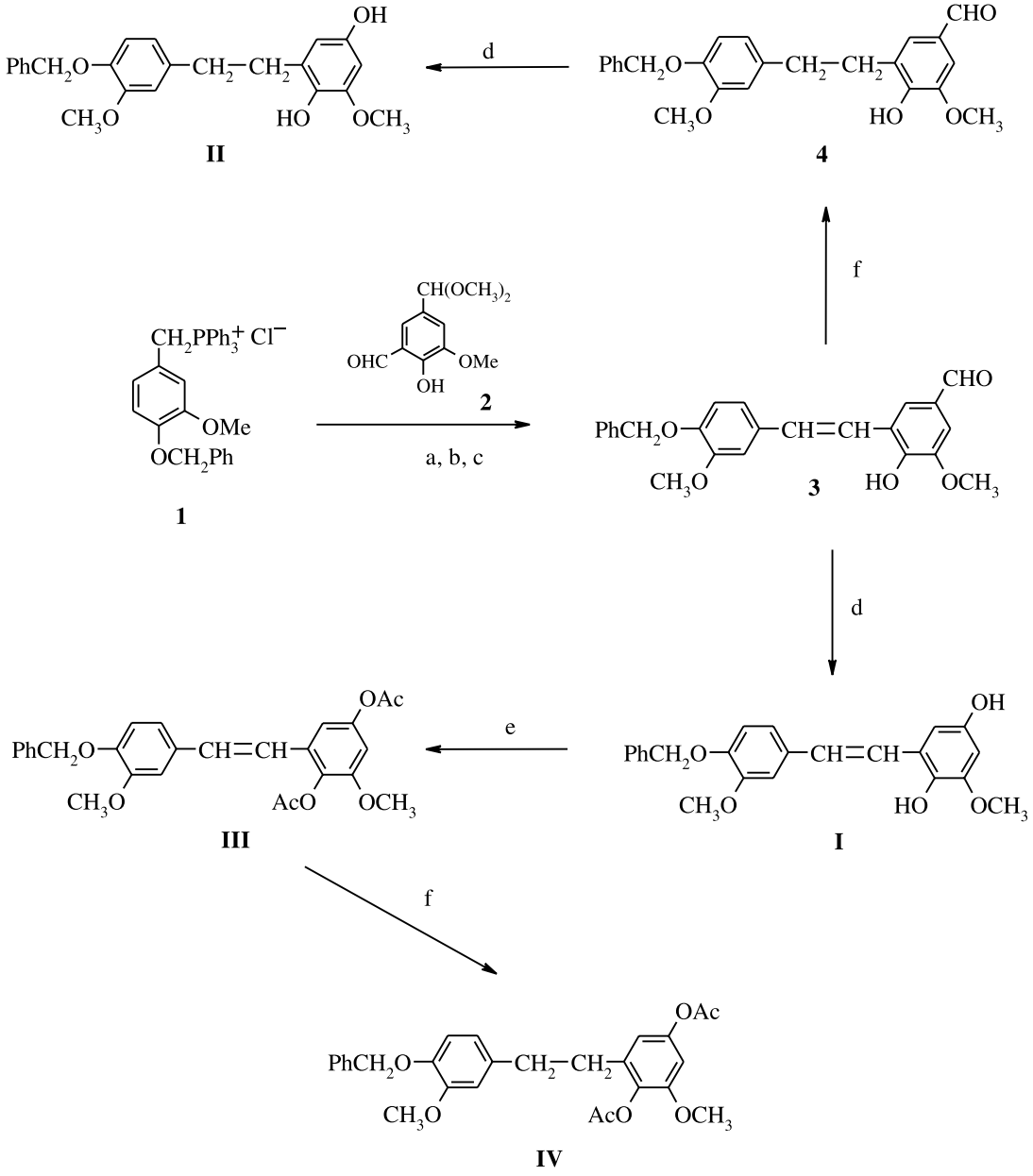
Hydrogenation of the pulp (300 mg) impregnated with a solution of $RhCl(PPh_3)_3$ (15 mg) in ethyl acetate (3 mL) was accomplished under 180 bar (1 bar = 10^5 Pa) of hydrogen pressure for 4 h at 60°C in presence of 3 mL of ethyl acetate in the bottom of the reactor as described previously (14). After cooling the reactor, the pulp was washed with ethyl acetate, methanol, and CH_2Cl_2 to remove the catalyst and then washed with water and dried at 40°C for 24 h.

Thioacidolysis and Acidolysis with $AlCl_3$

100 mg of pulp were treated with 20 mL of thioacidolysis solution (10 mL EtSH + 2.4 mL BF_3–Et_2O + 80 mL dioxan) at 100°C for 4 h under gentle magnetic stirring. After hydrolysis with diluted $NaHCO_3$ solution until pH 3–4, the reaction mixture was extracted with dichloromethane. The organic phase was washed with water, dried over magnesium sulfate, and evaporated under vacuum. The residue was dissolved in benzene (30 mL) and was treated with 10 mg of $AlCl_3$ at 90°C for 12 h, then the reacting mixture was hydrolyzed with water and extracted with CH_2Cl_2. The organic phase was dried over magnesium sulfate concentrated under vacuum and silylated with BTSFA (50 µL), pyridine (10 µL) in THF (50 µL) at room temperature. The silylated mixture was analyzed by GC–MS.

© 2000 NRC Canada

Fig. 2. Synthetic scheme of compounds **I**, **II**, **III**, and **IV**: (a) *n*-BuLi–DMF–THF; (b) **2**, THF; (c) HCl 10%; (d) H_2O_2–Na_2CO_3–THF–H_2O; (e) Ac_2O–NEt_3–DMAP–CH_2Cl_2; (f) H_2–$Rh(PPh_3)_3Cl$–ethyl acetate.



Results and discussion

1. Syntheses

The route chosen for the synthesis of compounds **I**, **II**, **III**, and **IV** is outlined in Fig. 2. The preparation of compound **I** which was similar to the Lee and Sumimoto (13) procedure, consists in the Wittig coupling between the ylide, generated by action of *n*-butyl lithium on the substituted benzyltriphenyl phosphonium chloride **1** (14), and the substituted salicylaldehyde **2** (16). The protection of the aldehyde group, needed for the coupling, was easily removed by treatment with hydrochloric acid at the end of the synthesis. Despite several attempts to improve the Wittig coupling e.g., by changing the reaction solvent, the yield was in our hands, lower (37%) than the one given by Lee (65%) (13) for the synthesis of a similar compound, but it was of the same order that we got for the syntheses of other lignin stilbene models (14). The hydroquinone **I** (*E* configuration) was obtained by Dakin reaction in mild conditions (room temperature and moderate pH given by the use of sodium carbonate). Compound **III** was synthesized in high yield (93%) by acetylation of compound **I**, using the catalytic action of 4-*N*,*N*-dimethylaminopyridine (DMAP) as for other lignin model compounds (18). Hydrogenation of compound **III**, was realized using experimental conditions set up previously for a study on the role of stilbenes issued from β-1 units on the photoyellowing of lignin rich pulps (14). Compound **II** which was prepared by catalytic hydrogenation of compound **3** followed by Dakin reaction at moderate pH, was quantitatively transformed into compound **IV** by acetylation.

Compound **IZ** was produced as a major product by irradiation of **I** in degassed methanol solution (Fig. 3). It was char-

© 2000 NRC Canada

Fig. 3. Synthetic scheme of compounds **IQ**, **IIQ**, and **IZ**: (a) $P(O_2)$ = 20 bar; (b) $NaIO_4$–acetic acid–water; (c) $(KSO_3)_2NO$–water.

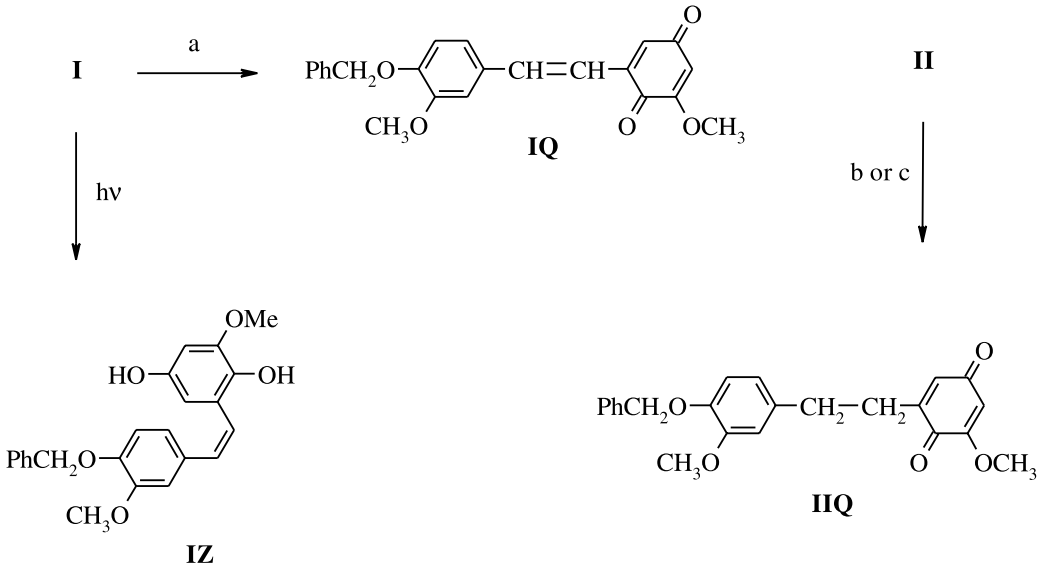
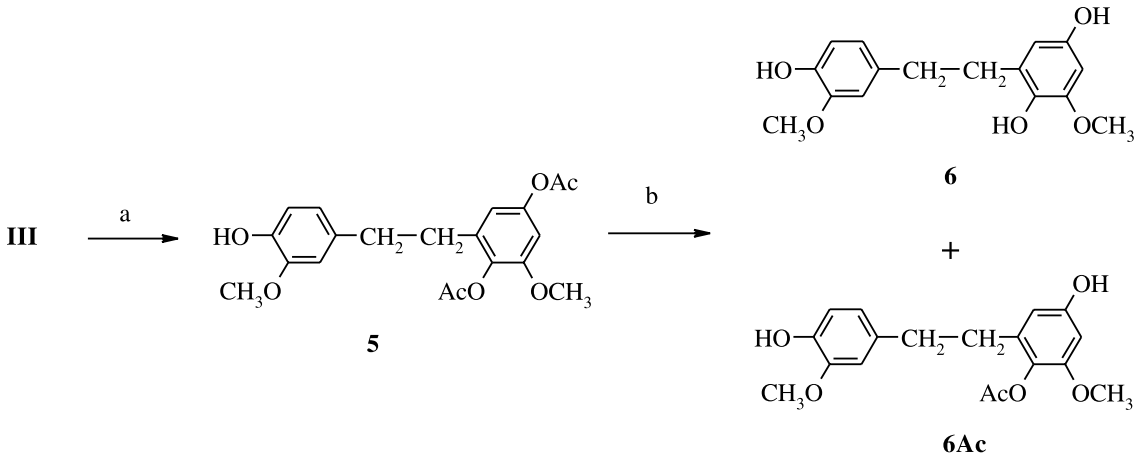


Fig. 4. Synthetic scheme of compound **6**: (a) H_2–Pd–C–THF; (b) K_2CO_3–methanol.



acterized by ^1H and ^{13}C NMR and HPLC–MS (electrospray in the negative mode) spectroscopies (see experimental part).

In contrast to compound **II**, which gave the *p*-quinone **IIQ** by oxidation by sodium periodate or Fremy's salt, compound **I** did not produce the quinone **IQ** using the same reagents. The latter compound, very reactive and sensitive to chromatographic phases and eluents was obtained by oxidation of **I** in acetonitrile by oxygen under pressure (20 bar, 1 bar = 10^5 Pa) at 60°C (Fig. 3). The structure of **IQ** was determined by ^1H NMR and HPLC–MS (electrospray in the negative mode) spectroscopies (see experimental part). The structure of **IZQ** was assigned by comparison of its HPLC–UV spectrum and its HPLC–MS peaks with those of the quinone isomer **IQ** (see experimental part).

In order to characterize the presence of stilbene–hydroquinone chromophores in bleached pulps, compounds **5** and **6** were synthesized. Following a procedure previously used (14), and due to the high reactivity of the stilbene and hydroquinone units, the pulp was acetylated and hydrogenated prior to thioacidolysis and acidolysis with aluminum trichloride. The diphenylethane incorporating hydroquinone entities obtained from the pulp after the degradative treatment were expected to be in the form of their acetates or trimethylsilyl derivatives. The mild deacetylation procedure, very efficient for lignin models (18), and applied to compound **5**, produced a mixture of compounds **6** and **6Ac** (50%–50%). This mixture was silylated and used for the GC–MS analysis of the pulps, because it is likely that these two structures will be detected if the stilbene hydroquinone entities would be present in the peroxide bleached pulp. It is noticeable that silylation of compound **6** was incomplete, the OH in the 2 position being too hindered to react with the bulky trimethylsilyl group.

2. Electronic absorption and emission spectroscopies

Absorption spectra

The electronic absorption spectra of the stilbenes **I**, **III** and of the diphenylethanes **II**, **IV** are reported on Fig. 5.

The two diphenylethanes present a significant absorption above 300 nm, so they can absorb the solar light and so they can give colored species and contribute to the yellowing of peroxide-bleached high-yield pulps as already shown (19). The presence of the stilbene double bond increases the ab-

© 2000 NRC Canada

Fig. 5. Electronic absorption spectra of compounds **I**, **II**, **III,** and **IV** in methanol solutions (left) and of compound **I** in acidic and alkaline methanol solutions (right).

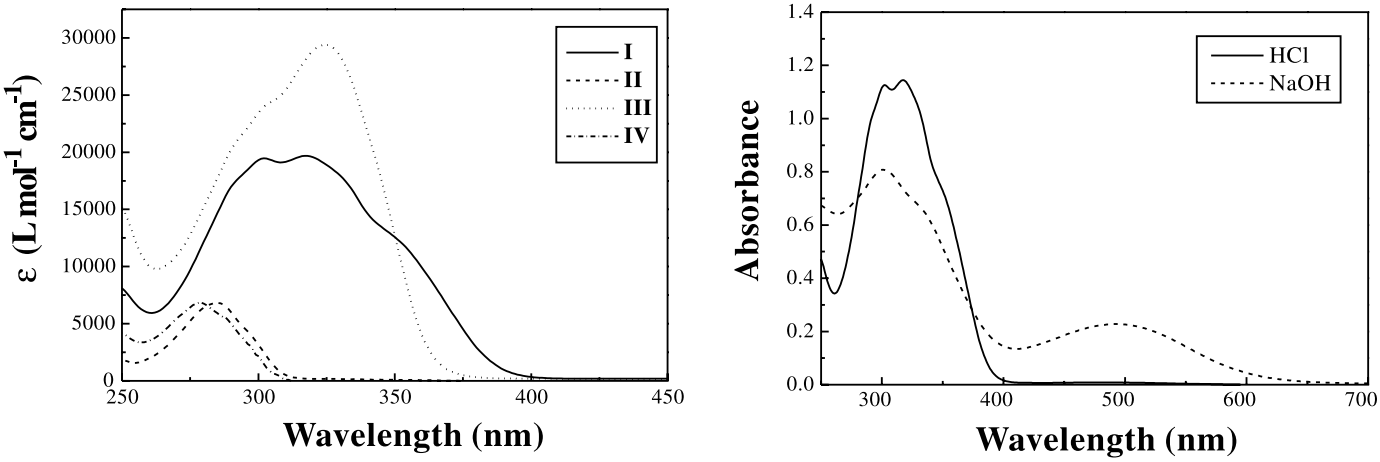
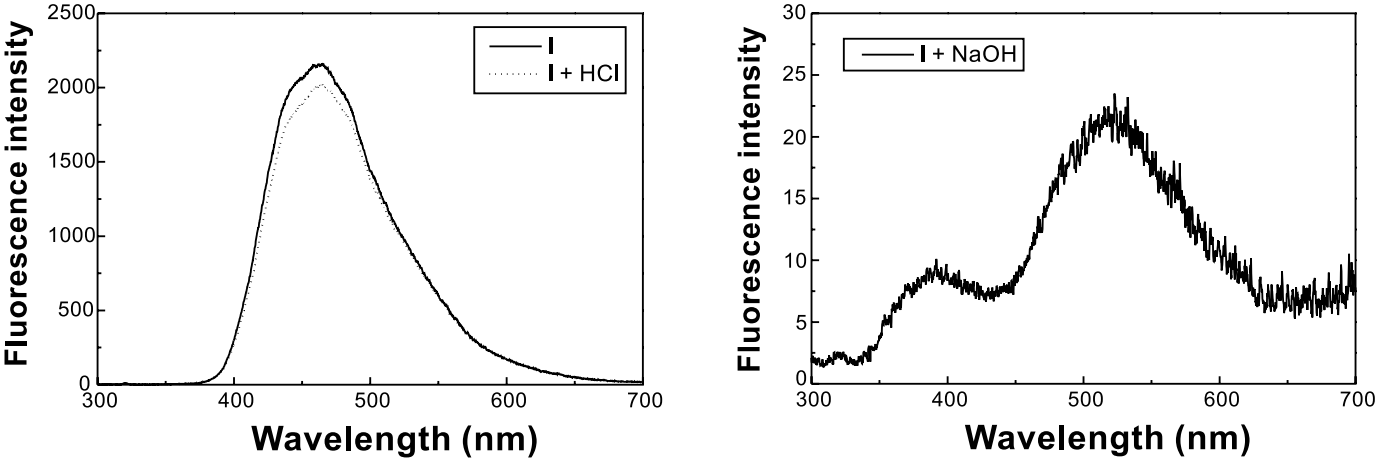


Fig. 6. Fluorescence emission spectra of compound **I** in ethanol solution. Left: neutral and acidic media; right: alkaline medium (λ_{exc} = 320 nm).



sorption above 300 nm compared to diphenylethanes, and so compound **I** which presents a very oxidizable phenol functional group, should be very sensitive to UV–irradiation. Moreover, phenols are in equilibrium with their phenolate anions and this equilibrium depends on the pH of the medium. In acidic or neutral media, the absorption of compound **I** is the same (Fig. 5). In contrast, in alkaline medium, compound **I** displays some absorption between 400 and 600 nm. The pulp industry usually produces papers with a basic reserve such as calcium carbonate for long term storage (20) but this alkaline treatment can induce a coloration of the materials if structures like compound **I**, which is ionized at pH 9, are present in lignin.

Fluorescence spectra

The interpretation of fluorescence spectra from wood, pulp, and paper samples is particularly cumbersome due to the physical heterogeneity and chemical complexity of the lignocellulosic matrix (21–23). Based on model studies (21, 22), it was shown that, in addition to cellulose emission, several chromophores of the lignin polymer are emitting in the region 330–430 nm. In contrast, the fluorophores at the origin of the emission of the pulp in the long wavelength range (430–530 nm) are still unknown. It is remarkable that the fluorescence emission, recorded for the stilbene **I** in neutral or acidic methanol solutions (Fig. 6), displays emission in this wavelength range (quantum yield ≈ 0.5 and lifetime ≈ 4 ns). This represents a bathochromic shift compared to other non-cyclic stilbene lignin models (22) and cyclic stilbene lignin model of the phenylcoumarone type (8*b*). In alkaline solution, the emission of compound **I** is shifted to longer wavelengths and its intensity is reduced, probably due to a highest reactive deactivation channel from the phenolate anion.

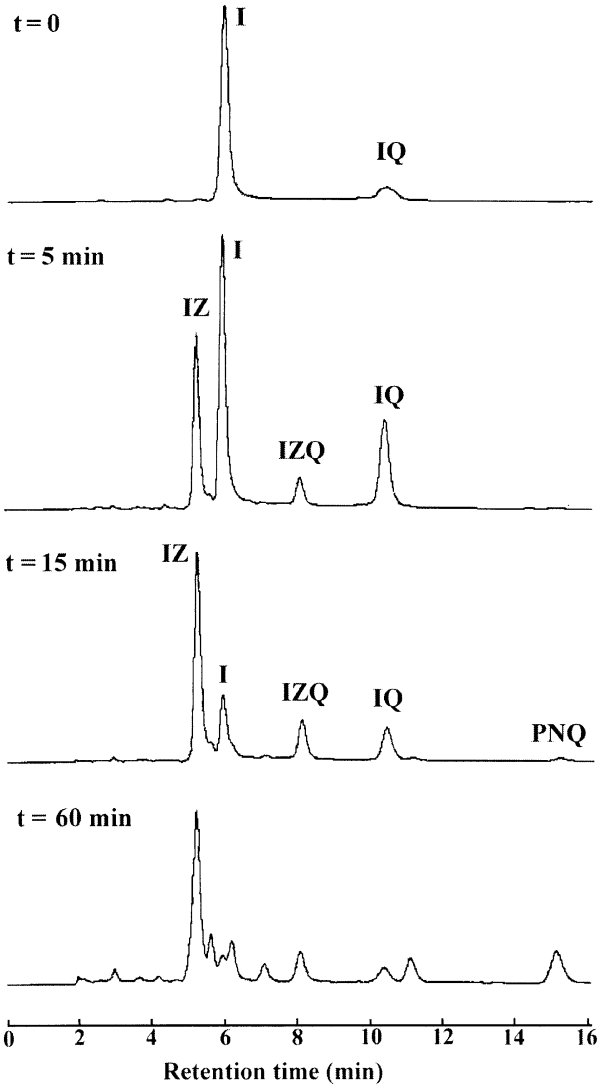
3. UV–irradiation of model I in solution

Compound **I** was irradiated in aerated methanol solutions (concentration ≈ 10^{-3} mol L^{-1}) with UV black lamps ($\lambda \approx 350$ nm). The irradiated solutions were analyzed by HPLC at different irradiaton times and some chromatogram traces are reported in Fig. 7.

The assignment of the HPLC peaks was carried out by comparison with samples analyzed by NMR and mass spectro-

© 2000 NRC Canada

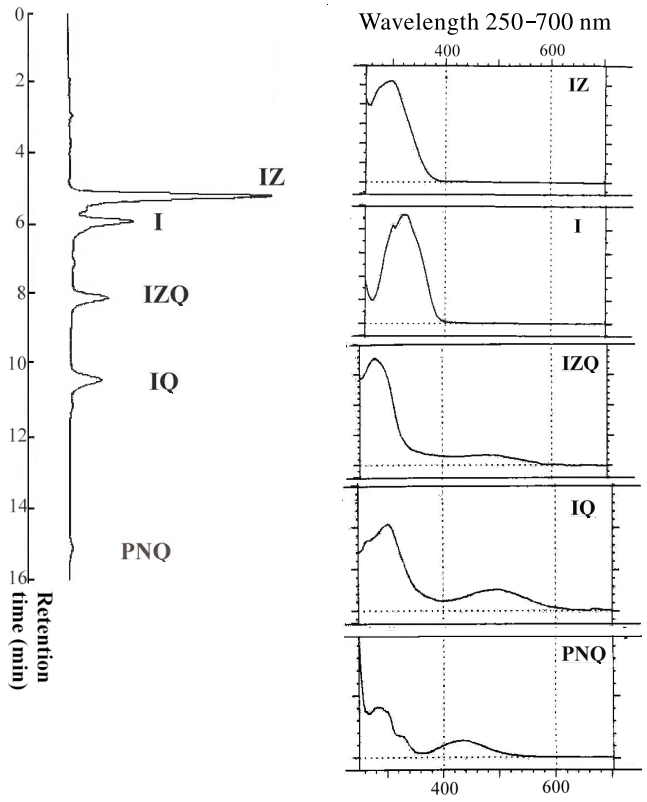
Fig. 7. HPLC analyses of photoproducts formed during irradiation of **I** in methanol.



scopies. The structure of the phenanthrene quinone derivative was assumed according to its UV absorption spectrum.

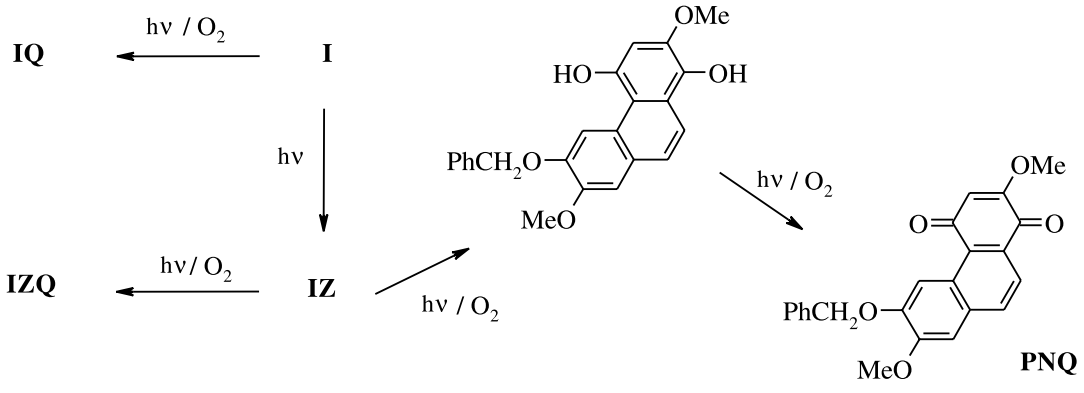
The UV absorption spectra of the photoproducts which were obtained with a diode array detector on the HPLC system are drawn in Fig. 8. One can observe a hypsochromic shift (20 nm) for the absorption of the **IZ** isomer compared to the *E* isomer (this shift was already found by Stomberg et al. (24) on other lignin stilbene-like structures). Also a shift to the short wavelength (10 nm) is observed for the quinone IZQ compared to the *E* quinone **IQ**, both for $n\pi^*$ visible and for $\pi\pi^*$ UV transitions.

Fig. 8. HPLC–UV analyses of photoproducts formed during irradiation of **I** in methanol.



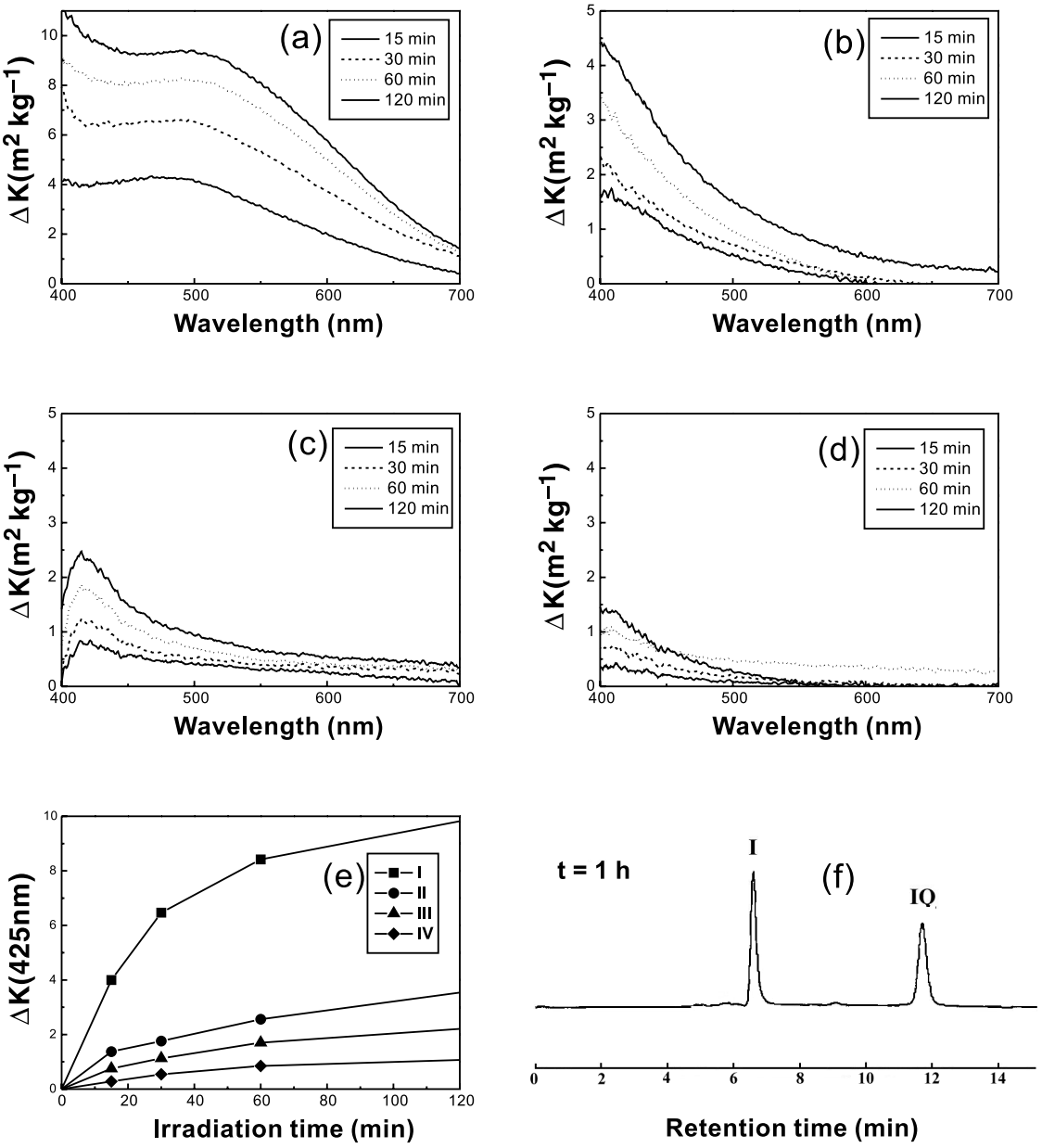
It is known that *Z* stilbenes are able to photocyclize to give phenanthrene derivatives (25). The dihydroxyphenanthrene formed by oxidative photocyclization of compound **IZ** might be transformed into p-phenanthrene quinone. The compound formed after 15 min of irradiation and having a retention time equal to 15 min might belong to this type of structure (Fig. 9). The photochemistry of compound **I** in methanol or acetonitrile solution is depicted in Fig. 9.

Fig. 9. Photoreactivity of compound **I** in solution.



© 2000 NRC Canada

Fig. 10. Irradiations of compounds adsorbed on cellulose paper. ΔK = absorption coefficient of irradiated paper – absorption coefficient of non irradiated paper. (*a*), (*b*), (*c*), (*d*): ΔK vs. λ for compounds **I**, **II**, **III**, and **IV** respectively.; (*e*) ΔK (425 nm) vs. irradiation time; (*f*) HPLC trace of extracted irradiated paper doped with compound **I**.



4. UV–irradiation of model I, II, III, and IV adsorbed on cellulose matrix.

The behavior of the lignin model compounds **I**, **II**, **III**, and **IV** adsorbed on cellulose paper were comparatively irradiated with UV light (see experimental part). The photocoloration was evaluated using the absorption coefficient given by the Kubelka–Munk theory (26). Fig. 10 (a–e) shows the difference of absorption coefficient (ΔK) of the lignin models adsorbed on cellulose paper before and after irradiation with UV light ($\lambda \approx 350$ nm) ranging from 5 min to 120 min. As observed for stilbenes formed from β-1 units (14), hydrogenated and acetylated chromophores display less variation of ΔK, which means less yellowing.

The kinetics confirm the great reactivity of compound **I**. Its coloration is reduced by acetylation. Hydrogenation of compound **I** followed by acetylation leads to a very stable compound **IV**. In contrast, hydrogenation of **I**, which gives hydroquinone structure **II**, is not sufficient enough to stop the yellowing completely. The variations of ΔK observed for compound **II** is reminiscent to what was observed for 2-methoxyhydroquinone in 2-hydropropylcellulose films (19).

After irradiation, the cellulose paper incorporating model **I** was extracted with solvent and analyzed by HPLC (Fig. 10*f*). Only the formation of quinone **IQ** is observed with no isomerization occurring. This is probably due the hydrogen bonding between the product and the cellulose

© 2000 NRC Canada

matrix which locks the configuration of the stilbene double bond. This confirms the key role of the environment in photochemical reactions.

5. Search for stilbene–hydroquinone chromophores in peroxide-bleached high-yield pulps

In order to assess and quantify the contribution of stilbene–hydroquinone chromophores in the photoreversion of high-yield pulps, we have attempted to find and quantify this structure in peroxide-bleached mechanical softwood pulp. For this purpose, we have used the same experimental procedure successfully set up for stilbenes emerging from β-1 lignin structures (14). In addition to the previous procedure, the pulp was first acetylated in the vapor phase in order to block the reactive hydroquinone groups. Even so, it was shown that catechol structures survive after the thioacidolysis (27). Therefore, after acetylation, hydrogenation, thioacidolysis with EtSH – BF_3–Et_2O in dioxane, and desulfurization with raney nickel, the organic residue was treated with $AlCl_3$ in benzene. The reacting mixture was analyzed by GC–MS. Careful inspection of the mass spectra of the chromatogram did not detect the silylated compounds **6** or **6Ac**. So, it seems that a mechanical treatment is not strong enough to produce structures resembling compound **I** by mechanochemistry in high-yield pulps. However, we can never neglect that the chemical treatment, used to liberate the stilbene chromophore before analyses, is not efficient enough if the chromophore is situated in the bulk of the lignin polymer.

Conclusions

We studied stilbene–paraquinone models formed by mechanochemistry from β-5 units during grinding and disk-refining of pulp. The contribution of these structures to the photoyellowing of bleached high-yield pulps was evaluated examining the photochemistry of model **I** which was hydrogenated and (or) acetylated. Photoproducts formed during irradiation of compound **I** were characterized. In particular, the isomerization of compound **I** into **IZ** was found to be the main process in solution. In aerated solution, the stilbenes **I** and **IZ** were oxidized in paraquinones **IQ** and **IZQ** respectively. The isomerization of **I** was not observed when adsorbed on cellulose paper, only the formation of quinone **IQ** was obtained. Comparative irradiation of different models, adsorbed on thin sheets of cellulose paper, showed the greatest reactivity of model **I**. Hydrogenation coupled with acetylation produced an efficient stabilization of this compound. The detection and quantification of stilbene–hydroquinone units, present in peroxide-bleached mechanical pulp, could not be determined. This might be due to inefficient mechanochemistry in pulp, as suggested by Zhu's studies (28), or it might be due to inappropriate experimental conditions necessary to liberate the acetylated hydroquinone diphenylethane entities, these structures being characteristic of the stilbene–hydroquinone units formed from β-5 elements in lignin.

References

1. D.Y. Lee, M. Matsuoka, and M. Sumimoto. Holzforschung, **44**, 415 (1990).
2. D.Y. Lee, M. Matsuoka, and M. Sumimoto. Fifth Intern. Symp. Wood Pulp. Chem. Raleigh, Proceedings, 21 (1989).
3. Z. Wu, M. Matsuoka, D.Y. Lee, and M. Sumimoto. Mokuzai Gakkaishi, **37**, 164 (1991).
4. D.Y. Lee and M. Sumimoto. Holzforschung, **44**, 347 (1990).
5. D.Y. Lee, S. Tachibana, and M. Sumimoto. Cellulose Chem. Technol. **22**, 201 (1988).
6. S. Li and K. Lundquist. Holzforschung, **53**, 39 (1999).
7. A. Castellan, N. Colombo, A. Nourmamode, J. Zhu, D. Lachenal, R.S. Davidson, and L. Dunn. J. Wood Chem. Technol. **10**, 461 (1990).
8. C. Noutary, P. Fornier de Violet, J. Vercauteren, and A. Castellan. Res. Chem. Intermed. (*a*) **21**, 223 (1995); (*b*) **21**, 247 (1995).
9. (*a*) A.J. Nonni and C.W. Dence. Holzforschung, **42**, 37 (1988); (*b*) W.J. Leigh, T.J. Lewis, V. Lin, and J.A. Postigo. Can. J. Chem. **74**, 263 (1996).
10. S. Omori and C.W. Dence. Wood Sci. Technol. **15**, 113 (1981).
11. G. Gellerstedt and R. Agnemo. Acta Chem. Scand. **B34**, 275 (1980).
12. I. Forsskåhl, J. Gustafsson, and A. Nybergh. Acta Chem. Scand. **B35**, 389 (1981).
13. D.Y. Lee and M. Sumimoto. Holzforschung, **45** (Supp.), 15 (1991).
14. B. Ruffin, A. Castellan, S. Grelier, A. Nourmamode, S. Riela, and V. Trichet. J. Appl. Polym. Sci. **69**, 2517 (1998).
15. J.G. Miller and C. Schuerch. Tappi J. **51**, 273 (1968).
16. F. Nakatsubo and T. Higuchi. Mokuzai Gakkaishi, **25**, 735 (1979).
17. J.A. Schmidt and C. Heitner. Tappi J. **76**, 117 (1993).
18. C. Jaeger, A. Nourmamode, and A. Castellan. Holzforschung, **47**, 375 (1993).
19. A. Castellan, A. Nourmamode, C. Jaeger, and I. Forsskåhl. Nordic Pulp Pap. Res. J. **8**, 239 (1993).
20. H.A. Carter. J. Chem. Educ. **73**, 1068 (1996).
21. A. Castellan, H. Choudhury, R.S. Davidson, and S. Grelier. J. Photochem. Photobiol. A: Chem. **81**, 117 (1994).
22. H. Tylli, I. Forsskåhl, and C. Olkkonen. J. Photochem. Photobiol. A: **87**, 181 (1995).
23. J.A. Olmstead and D.J. Gray. J. Pulp Pap. Sci. **23**, 571 (1997).
24. R. Stomberg, S. Li, K. Lundquist, and B. Albinsson. Acta Crystallogr. Sect.C: Cryst. Struct. Commun. **C54**, 1929 (1998).
25. N.J. Turro. *In* Modern molecular photochemistry. Benjamin Cumming Publ. Co., Menlo Park. (1978).
26. J.A. Schmidt and C. Heitner. Tappi J. **76**, 117 (1993).
27. X. Pan, D. Lachenal, C. Lapierre, and B. Monties. J. Wood Chem. Technol. **12**, 135 (1992).
28. J.H. Zhu, C. Archer, F. McNab, M.P. Andrews, G. Kubes, and D.G. Gray. J. Pulp Pap. Sci. **23**, J305 (1997).

© 2000 NRC Canada

Assisted hydrolysis of *cis*-2-(3-phenylthioureido)cyclopentane-carbonitrile in alkaline solution. Solvent dependent switch from hydrolysis to rearrangement of the iminothiooxopyrimidine intermediate

Ergun Atay, Iva B. Blagoeva, Francis L. Chubb, John T. Edward, Ivan G. Pojarlieff, and Maria M. Toteva

Abstract: The *cis* and *trans* isomers of 2-(3-phenylthioureido)cyclopentanecarbonitrile, **1**, and the respective carboxamides, **3**, and acids, **4**, have been prepared. Acid cyclization of both nitriles, faster with the *cis* isomer, gave the more stable *cis*-2-thiooxo-cyclopenta[*d*]pyrimidin-4-one, **7**. In base *cis*-**1** formed the *cis* 4-imino-2-thiooxopyrimidine **2** which in aqueous alkali broke down via **3** to the acid **4**; while in the presence of 66% acetonitrile **2** rearranged to the 4-phenyliminopyrimidine **5** to give as final product the thioureido acid **6** carrying no phenyl group. The ^{1}H NMR data for imino and phenylimino derivatives **2** and **5** showed strong bias for conformation **A** with 1-N pseudoaxial in the cyclopentane ring. Spectra of the *E* and *Z* isomers of the iminopyrimidine **2** under slow exchange could be recorded in DMSO-d_6. The phenylimino tautomer of **5** is observed in CD_3OD and in $CDCl_3$ with the *E* and *Z* isomers in a 1:1 ratio. In DMSO-d_6 the phenylamino tautomer **5a** is also detected. The first process in aqueous KOH, the conversion of nitrile *cis*-**1** into the imino intermediate **2**, reaches an equilibrium which shifts towards the nitrile at higher alkalinities because of ionization of the phenylthioureido group (K_e = [**2**]/[**1**] = 2.43 and pK_{AH} = 12.74). The cyclization of **1** to **2** is first order in [OH^-] while the slower breakdown of **2** is pH independent. The latter is 10^4 times faster than the hydrolysis of acetonitrile evidencing substantial anchimeric assistance. The change in the reaction route towards the rearranged phenyliminopyrimidine **5** upon addition of acetonitrile can be caused by the lower dielectric constant favouring the elimination step leading to the intermediate isothiocyanate, and by increased activity of OH^- accelerating the (presumably) second order elimination step as opposed to the pH-independent hydrolysis of the imino derivative **2**.

Key words: anchimeric assistance, phenylthioureido nitriles, iminothiooxopyrimidine tautomers, alkaline hydrolysis, solvent effects.

Résumé : On a préparé les isomères *cis* et *trans* du 2-(3-phénylthiouréido)cyclopentanecarbonitrile (**1**) et des carboxamides (**3**) et acides (**4**) correspondants. La cyclisation des deux nitriles, plus rapide pour l'isomère *cis*, conduit dans chaque cas à la *cis*-2-thiooxocyclopenta[*d*]pyrimidin-4-one (**7**), l'isomère le plus stable. En milieu basique, l'isomère **1**-*cis* conduit à la formation de la *cis*-4-imino-2-thiooxopyrimidine (**2**) qui, dans ces conditions, se décompose en acide **4** par le biais de **3**; toutefois, dans un milieu contenant 66% d'acétonitrile, le produit **2** se réarrange en 4-phényliminopyrimidine (**5**) qui se transforme pour fournir comme produit final l'acide thiouréido **6** où la groupe phenyle est absent. Les données de RMN du ^{1}H pour les dérivés imino et phénylimino **2** et **5** montrent que la conformation **A** est fortement favorisée, avec le 1-N en position axiale par rapport au cyclopentane. En opérant dans le DMSO-d_6, on a pu enregistrer les spectres des isomères *E* et *Z* de l'iminopyrimidine dans des conditions d'échange lent. Dans le CD_3OD et dans le $CDCl_3$, on peut observer le tautomère phénylamino de **5**; les isomères *E* et *Z* se trouvent dans un rapport de 1:1. On a aussi détecté le tautomère phénylamino **5a** dans le DMSO-d_6. Le premier processus réactionnel observé dans le KOH aqueux, la conversion du nitrile 1-*cis* en intermédiaire imino **2** atteint un équilibre qui, en raison de l'ionisation du groupe phénylthiouréido (K_e = [**2**]/[**1**] = 2,43 et pK_{AH} = 12,74), se déplace vers le nitrile à des niveaux d'alcalinité élevés. La cyclisation de **1** et **2** est du premier ordre en [OH^-] alors que la décomposition plus lente de **2** est indépendante du pH. Cette dernière réaction est 10^4 fois plus rapide que l'hydrolyse de l'acétonitrile; ceci confirme l'importance de l'assistance anchimérique. Le changement de la voie réactionnelle

Accepted October 25, 1999.

E. Atay, I.B. Blagoeva, I.G. Pojarlieff,[1] and M.M. Toteva. Institute of Organic Chemistry, Bulgarian Academy of Sciences, ul. Acad. G. Bonchev block 9, Sofia 1113, Bulgaria.
F.L. Chubb and J.T. Edward. Department of Chemistry, McGill University, 801 Sherbrooke St., Montreal, QC H3A 2K6, Canada.

[1]Author to whom correspondence may be addressed. Telephone: +359-2-7334-116. Fax: +359-2-700-225.
e-mail: ipojarli@orgchm.bas.bg

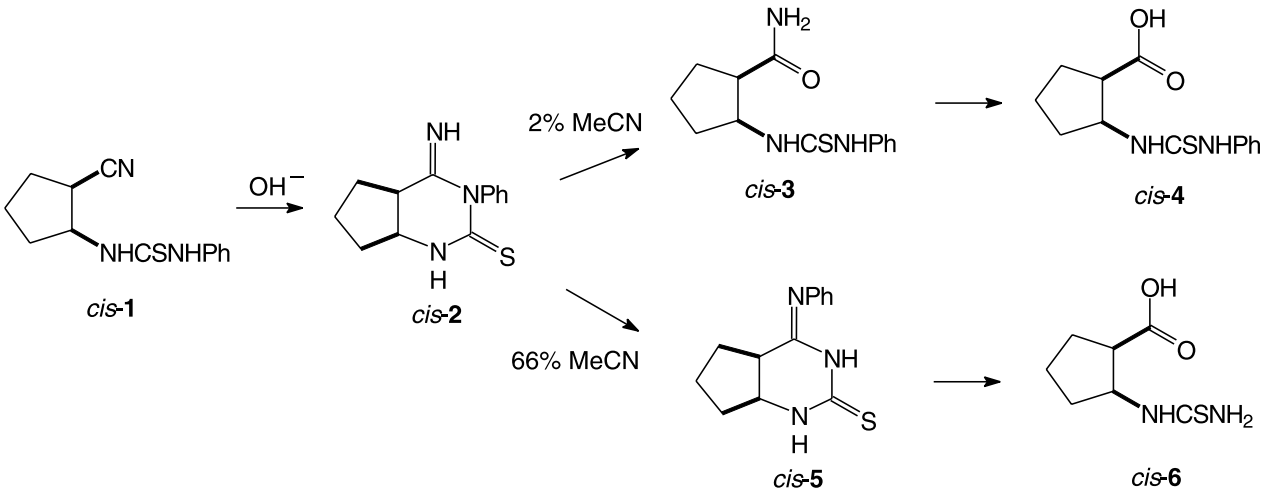
 © 2000 NRC Canada

conduisant à plus de phényliminopyrimidine réarrangée **5** par addition d'acétonitrile peut être provoqué par une baisse de constante diélectrique favorisant l'étape d'élimination qui conduit à l'intermédiaire isothiocyanate et par une activité accrue des ions OH^- qui augmente la vitesse de l'étape d'élimination que l'on croit être du deuxième ordre par opposition à l'hydrolyse du dérivé imino **2**, qui est indépendante du pH.

Mots clés : assistance anchimérique, nitriles phénylthiouréido, tautomères des iminothiooxopyrimides, hydrolyse alcaline, effets de solvant.

[Traduit par la Rédaction]

Scheme 1.



Introduction

Ureido or thioureido nitriles, readily available from amino nitriles, have been widely used (1) in the synthesis of aminopyrimidines, aminoimidazoles, or thiazoles. On a preparative level the ring-closure was found to be base catalyzed (2). The products of attack of the ω-nitrogen of the ureido group are formed from thioureido nitriles in neutral and basic media (3).

We now report that the hydrolysis of a nitrile group is anchimerically assisted by a suitably orientated β-phenylureido group as in *cis*-**1**. The latter compound, in 0.01 M aqueous alkali, converts into the amide **3** 10^4 times faster than acetonitrile (4). The hydrolysis is facilitated by the formation of the iminopyrimidine **2** as shown in Scheme 1.

However, hydrolysis of aminopyrimidine **2** to **3** and further to the phenylthiouredo acid **4** was observed in aqueous alkali with a low (1–2%) content of acetonitrile. When the concentration of MeCN was increased to 66% (v/v) the major products were the rearranged pyrimidine **5**, hydrolyzing ultimately to the thioureido acid **6** without the phenyl group.

Results and discussion

Preparation and configuration of 2-phenylthioureidocyclopentanecarboxylic acid and 4-oxo-2-thioxooctahydrocyclopenta[*d*]pyrimidine derivatives

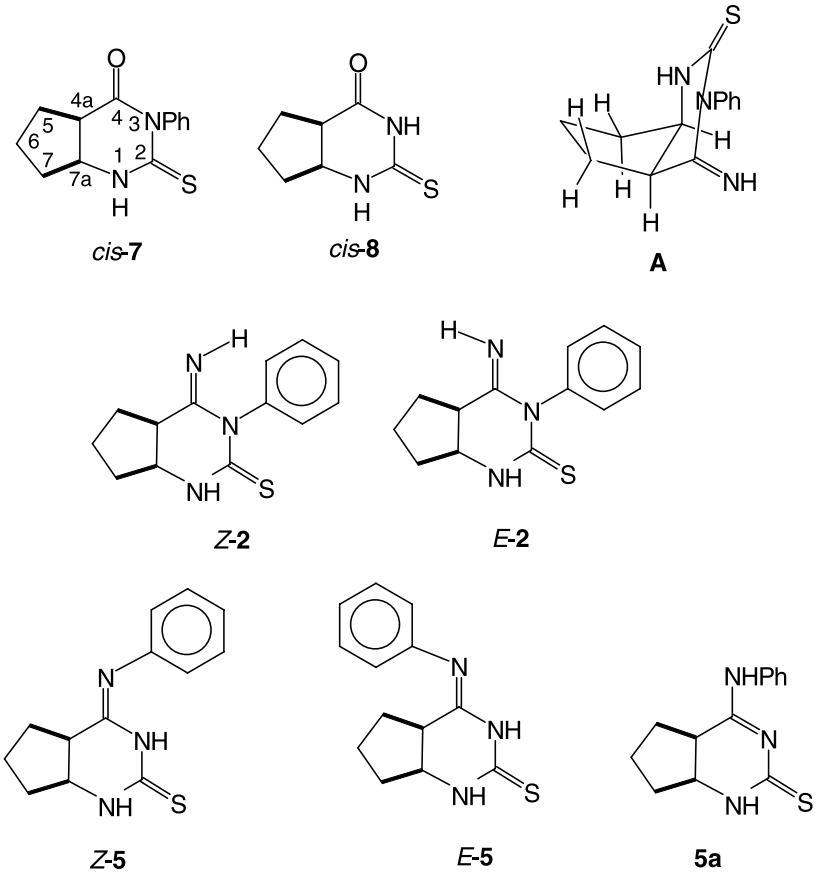
2-Aminocyclopentanecarbonitrile is obtained as a mixture of *cis* and *trans* isomers which have not yet been separated, but the phenylthioureido derivatives **1** are readily separated by column chromatography.

The configurations of the thioureido nitriles **1** were assigned from their behaviour in 1:2 HCl. Upon refluxing, the two isomers both cyclized in high yield to produce the single product *cis* 2-thiodihydrouracil **7** (Scheme 2). The latter has recently been obtained by cyclization of the respective *cis* thioureido ethyl ester in hydrochloric acid solution (5) and assigned as *cis* from bandwidths of the signals for 4a-H (ca. 25 Hz) and 7a-H (ca. 12 Hz) in the ^{1}H NMR (6). We proved this independently by double resonance experiments[2] which showed $J_{4a,7a}$ to be 6.5 Hz, which fell within the usual range for *cis* coupling in dihydrouracils (7). The 7a-H signal splittings due to the neighbouring methylene hydrogens were considerably smaller than those for 4a-H, indicating that the NH group is pseudoaxial in the presumably half-chair conformation of the cyclopentane ring. Cyclization of *cis* and *trans* **1** under milder conditions (2 h in 1 M HCl at 50°C) gave 86% and 15% *cis*-**7**, respectively. Whatever the reaction path from *cis*- or *trans*-**1** to *cis*-**7**, it can be safely assumed that the more readily cyclizing isomer has the same configuration as the ring product. Isomerization most likely occurs by acid catalyzed enolization which requires prior protonation of the carbonyl or imino function. It has been previously shown (8) that upon cyclization of ureido acids to dihydrouracils, isomerization occurs with the more basic ring compounds. Under the conditions used for obtaining the amides **3** on a

[2] Irradiation of H-6 of thiodihydrouracil decreased the 4a-H band by 6.5 Hz. Irradiation of 1-H sharpened the signal for 7a-H to a multiplet of 8 lines with couplings 6.6, 5.3, and 4.2 Hz. In the multiplet for 4a-H these couplings are 6.6, 7.8, and 9.0 Hz.

© 2000 NRC Canada

Scheme 2.



preparative scale (hydrolysis of the nitriles **1** in 60% sulfuric acid) the *cis* nitrile gave *cis* amide, shown by TLC to be free of the *trans* amide, while the *trans* nitrile hydrolyzed to a mixture of *cis* and *trans* isomers. Since the *trans* nitrile **1** and amide **3** are certainly more stable than *cis*-**1** and **3**, the isomerization must occur after the formation of a bicyclic derivative more stable in the *cis* configuration.

Greater stability of the *cis* isomer of dihydrouracil **7** can be understood by reference to the hydrindane system (bicyclo[4,3,0]nonane) (9). The *trans* hydrindane is more stable (ΔH) by 1.1 kcal mol^{-1} as the result of two conflicting forces: the unavoidable axial interactions in the *cis* isomer and the mismatch of torsion angles between the five and six membered rings. In a *trans* junction these can be accommodated by unfavourable greater puckering. Because dihydrouracils are considerably planar (10) with the torsion angles between the *trans* diequatorial bonds ca. 90°, *trans* fusion to a cyclopentane with an endocyclic torsion angle of ca. 45° would require considerable strain, which is apparently the main factor in determining the relative stability of the two isomers. Exclusive preference for *cis*-annelation has also been observed in the formation of 3-aryl-2,4-dioxo-octahydrocyclopenta[*d*]pyrimidines in a ring expansion reaction (6).

Acid *cis*-**4** was readily available by means of alkaline hydrolysis of *cis* dihydrouracil **7** while *trans* acid **4** was obtained under milder acid hydrolysis of *trans* nitrile **1** along with some *cis* dihydrouracil **7**. Acid *trans*-**4** has been isolated in high yield from the ethyl ester in an attempt to cyclize the latter under reflux in hydrochloric acid (5).

Preparation of 4-imino and 4-phenylimino-2-thiooxooctahydrocyclopenta[*d*]pyrimidine

When the hydrolysis of *cis* thioureido nitrile **1** was monitored by UV in aqueous alkaline media containing only 1–2% acetonitrile, a decrease of absorption at 245 nm due to NHCSNHPh and an accompanying increase in absorption at 267 nm were observed. The latter reached a maximum after which the absorption at 245 nm was restored in a slower process. Detailed product analysis (*vide infra*) showed that the intermediate formed broke down to amide *cis*-**3** and this in turn to *cis*-acid **4** with both compounds having the same UV absorption as the initial nitrile. The intermediate, expected to be the iminopyrimidine **2**, however, proved elusive. The usual work up gave the rearranged product, the phenyliminopyrimidine **5**. Its structure was deduced from the products of hydrolysis: in base the thioureido acid **6**, while in acid the known thiodihydrouracil **8** (11) without the phenyl group. Compounds **6** and **8** could be readily interconverted in acid or base as appropriate. Under the conditions described in the experimental section no isomerization was observed because ^{1}H NMR evidence demonstrated retention of *cis* configuration.

Under conditions where imines similar to **2** have been obtained from ureido nitriles our starting nitrile *cis*-**1** either remained unchanged (refluxing in benzene (3a,b)) or yielded the rearranged phenylimino product **5** directly (refluxing in methanol (3a) or in EtOH–EtONa (3c)). As the behaviour of *cis*-**1** in aqueous alkali could only be explained by the participation of imine **2** as depicted in Scheme 1, an attempt was

© 2000 NRC Canada

Table 1. ^{13}C NMR chemical shifts (in ppm) from TMS, in DMSO-d_6 solution

(a) Derivatives of cyclopentanecarboxylic acid											
Compound	COOH	CS	1-C	2-C	3-C	4-C	5-C	i-C	*o*-C	*m*-C	*p*-C
cis-**4**	175.1	179.9	45.8	56.6	31.0	21.4	27.4	139.2	124.0	128.5	122.7
cis-**6**	174.8	182.8	46.0	57.1	31.1	21.4	27.1	—	—	—	—
(b) Derivatives of 2-thio-1,2,3,4a,5,6,7,7a-octahydrocyclopenta[*d*]pyrimidines											
	4-C	2-C	4a-C	7a-C	5-C	6-C	7-C	i-C	*o*-C	*m*-C	*p*-C
cis-**7**	169.2	179.6	43.0	54.5	27.9	21.5	32.0	139.3	128.2	129.5	127.4
cis-**5**[a]	153.4	176.6	36.6	55.5	29.7	21.5	31.4	148.3	120.4	128.8	122.7
cis-**8**	169.3	177.2	41.6	55.4	27.7	21.6	32.2	—	—	—	—

[a]Resonances of the major isomer.

made to obtain it in this medium. To avoid the inconvenience of the limited solubility of *cis*-**1** in water, the experiment was carried out with 0.01 M KOH in a water–acetonitrile 1:2 mixture. Unexpectedly the reaction proceeded by the completely different course shown in Scheme 2. This meant that the rate of isomerization became faster than the rate of hydrolysis of the imine **2** to amide **3**. The procedure for obtaining the non-rearranged imine *cis*-**2** described in the experimental was based on the kinetic study of the hydrolysis of the nitrile **1**. Conditions were chosen where formation of *cis*-**2** was rapid and, at the moment of its maximum formation, the mixture was quenched in acid. The reaction is reversible and in acid unconverted nitrile was extracted from the aqueous solution. The water layer could be used as a stock solution of *cis*-**2**. The latter was isolated as a solid by rapid alkalization of the acid solution from which the nitrile has been removed, extraction with methylene chloride, and evaporation in vacuo. The ^1H NMR of the solid showed small admixtures of *cis*-**1** and the rearranged product *cis*-**5**, both most likely formed during the work up. In solution the imino compound converted into the phenylimino one with a rate dependant on the solvent. Rough estimates of the half lives (in min) were: 16 in DMSO, 130 in CD_3OD, and 400 in $CDCl_3$ (monitored by NMR at room temperature).

The structure of *cis*-**2** followed from the chemical transformations discussed above. The other possible structure, that of a iminothiazinone resulting from sulfur attack on the nitrile group can be refuted from the ^{13}C spectra of the final product of the transformations in Scheme 2. As shown in Table 1 the thioureido acid *cis*-**6** shows resonances for CS and COOH at 182.8 and 174.8 ppm respectively. It can be readily shown that the thiazine would ultimately afford an ureido thioacid for which resonances are expected at ca. 160 and 195 ppm for CO and CSOH (12). In DMSO the structurally similar R^*,R^*-2-methyl-3-ureidobutanoic acid showed resonances at 176.2 (COOH) and 158.5 ($NHCONH_2$).[3]

Tautomers and configurations of the imines.

The amidine moiety in iminopyrimidine *cis*-**2** is fixed and allows no tautomers. However, two geometrical isomers around the C=N bond are possible. According to Perrin (13) it is especially unusual to see separate forms such as *Z*-**2** and *E*-**2** (Scheme 2), since proton exchange interconverts them. Accordingly in CD_3OD and $CDCl_3$ the ^1H NMR spectrum showed only one, apparently time averaged, set of signals. In DMSO, however, spectra under fast and slow exchange were observed with various samples. Under fast exchange 1-H resonated at 9.26 ppm while =N*H* was hidden under the multiplet for the *m*-H and *p*-H at ca. 7.35 ppm, integrating for 4 protons. Under slow exchange 1-H gave rise to two signals: 9.38 (0.4H) and 9.15 (0.6H) ppm. The signals for =NH were at 8.59 (0.6H) and 6.58 (0.4H) ppm respectively. The 2 ppm upfield shift can be attributed to the ring current effect of the 3-phenyl group in the *Z*-isomer because the benzene ring is not in the plane of the heterocyclic ring in similar systems (14). Other samples showed intermediate exchange. On standing all of them converted cleanly into the phenyliminopyrimidine **5**, indicating that the initial spectra dealt with the same compound. In view of the rapid conversion in DMSO of **2** into **5** and the difficulty in controlling chemical exchange, further investigation was discontinued.

With compound **5** two tautomers are possible: the phenylimino and phenylamino isomers shown. Similar cyclic acylated phenylamidines such as 3-aryliminoisoindolinones have been found to be only in the phenylimino tautomeric form (15). This is also the predominant form with phenyliminopyrimidine **5**. An IR band at 1664 cm^{-1} is observed in $CHCl_3$ which is within the characteristic range for exocyclic C–N double bonds non-conjugated to an acyl group (16). Another feature is the upfield chemical shifts of the *o*- and *p*-protons and carbons of the phenyl ring which is due to better conjugation with the electron pair on nitrogen than is the case when interaction with an acyl group (C=S) is possible, as in **5a** (15) (see Tables 1 and 2). However, in DMSO a third set of signals could be detected which was assigned to the amino form **5a**. The assignment was supported by variable temperature measurements. Notably a doublet of the **5a** set at 7.89 ppm did not exchange with D_2O and coalesced with the *ortho* protons upon heating. That this belongs to the interchanging system is supported by the fact that at 383 K the *m*- and *p*-protons had already coalesced to sharp triplets while the signal for the *o*-protons at ca. 6.8 ppm was still broad due to the greater chemical shift difference (>1 ppm between the imino and amino forms). The greater significance of the amino form compared to the above mentioned isoindolinones can be attributed to the greater acidity of thioamides compared to ordinary amides. The isomer ratio is *E*-**5**:*Z*-**5**:**5a** = 7.5:1.5:1.

[3]Unpublished.

© 2000 NRC Canada

Table 2. ^{1}H NMR data for compounds in DMSO-d_6, chemical shifts from TMS (ppm), band widths, and couplings (Hz).[a]

(a) Derivatives of 2-phenylthioureidocyclopentanecarboxylic acid

Compound	1-H	2-H	*o*-H[c]	*m*-H[c]	*p*-H[d]	1′-NH	3′-NH
nitrile *cis*-**1**	3.53 quart bw 20.5	4.74 m[b]	7.50 d	7.32 t	7.11 t	8.06 d *J* ca. 7	9.60 s
in $CDCl_3$	3.62 bw 18.2	4.902 bw 33.1	[e]	7.47 t	[e]	6.19 d *J* 7.5	7.87 s
nitrile *trans*-**1**	3.060 quart bw 22.9	4.871 quin bw 29.7	7.397 d	7.303 t	7.117 t	7.99 d *J* 7.3	9.59 s
amide *cis*-**3**[f]	2.879 quart bw 22.2?	4.804 m[b]	7.432 d	7.303 t	7.087 t	7.64 d *J* 7.9	9.80 s
amide *trans*-**3**[g]	2.614 quart bw 22.8	4.66[b]	7.452 d	7.297 t	7.075 t	7.80[b]	9.41 s
acid *cis*-**4**[h]	2.993 quart bw 21.2	4.891[b] m	7.469 d	7.305 t	7.09 t	7.625 d *J* 8.3	9.696 s
acid trans-**4**[i]	2.709 quart bw 23	4.748[b]	7.423 d	7.297 t	7.076 t	7.93 d *J* ca. 6	9.44 s
cis-**6**[j]	2.924 quart bw 21.3	4.71[b]	—	—	—	7.47 d *J* 7	7.05 s 2H

(b) Derivatives of 2-thioxo-1,2,3,4a,5,6,7,7a-octahydrocyclopenta[*d*]pyrimidines

Compound	4a-H	7a-H	*o*-H[c]	*m*-H[c]	*p*-H[d]	1-NH	3-NH
4-oxo[k] *cis*-**7**	3.045 quart bw 23.3[l]	4.052 quart bw 15.9[m]	7.1 d	[n]	[n]	9.84	
4-oxo *cis*-**8**	2.770 quart bw 23.2	3.833 quart bw 19.0				9.49	10.93
4-imino[k] *cis*-**2**	3.039 sext bw 22.2	3.945[b] hw 11.5	7.088 d	7.37 t	7.317 t	9.26 s[o]	[p]
in CD_3OD	3.100 sext bw 24	4.042 hw 12.0	7.18 d	7.456 t	7.35 t		
in $CDCl_3$	3.118 sext bw 22.5	4.042 hw 12	7.295 d	[q]	[q]	7.21 s[r]	r
4-phenylimino *cis*-**5**-*E*[s]	2.584 bw 21	3.799[b] hw 10	6.752 d 7.7	7.299 t	7.029 t	8.87 s	10.51s
4-phenylimino cis-**5**-*Z*[s]	2.74	3.85	6.83 d	7.378	7.109	8.9 7s	9.99s
5a[s]	2.95	3.97	7.89 d	[t]	[t]	7.77 s	9.43 s
in CD_3OD **5a**-*E*[u]	2.760 sext bw 24	3.858 t bw 8	6.811 d	7.315 t	7.078 t		
5a-*Z*[u]		2.98[v]	4.02[v]	6.92[v]	7.404[v]	7.171[v]	
in $CDCl_3$ **5a**-*E*[u]	2.728 sext bw 22	3.912 bw 8.4	6.789 d	7.322 t	7.105 t	8.5 v.br.	7.239 7.1
5a-*Z*[u]		3.007 bw 22.3	4.052 bw 9.0	6.907 d	7.371 t	7.136 t	7.79 br

[a]The three methylene group gave complex peaks in the 1.4–2.2 ppm region.
[b]Unresolved.
[c]2H.
[d]1H.
[e]Part of multiplet 7.32–7.37 ppm.
[f]6.961 s, 7.448 s ppm $CONH_2$.
[g]6.87 s, 7.3 s ppm $CONH_2$.
[h]12.30 ppm COOH.
[i]12.22 ppm COOH.
[j]12.15 ppm COOH.
[k]3-phenyl, similar to data of ref. 9 except for $\delta_{1\text{-NH}}$ reported as 7.80 ppm.
[l]*J* = 6.6, 7.8 and 9.0 Hz.
[m]After removal of NH coupling by double resonance: *J* = 6.6, 5.3, and 4.2 Hz.
[n]Part of m 7.27–7.38 ppm.
[o]1H under fast exchange; under slow exchange 9.377 ppm 0.4H *Z*-isomer and 9.146 ppm 0.6H *E*-isomer.
[p]Imino group proton: under fast exchange 7.40 ppm; under slow exchange 8.59 ppm 0.6H *E*-isomer, 6.58 ppm 0.4H *Z*-isomer.
[q]Part of multiplet 7.39–7.55 ppm.
[r]2H, common signal for 1-H and the imino proton.
[s]*E*:*Z*:**5a** = 7.5:1.5:1.
[t]Could not be assigned.
[u]*E*:*Z* = 1:1.
[v]Broadened.

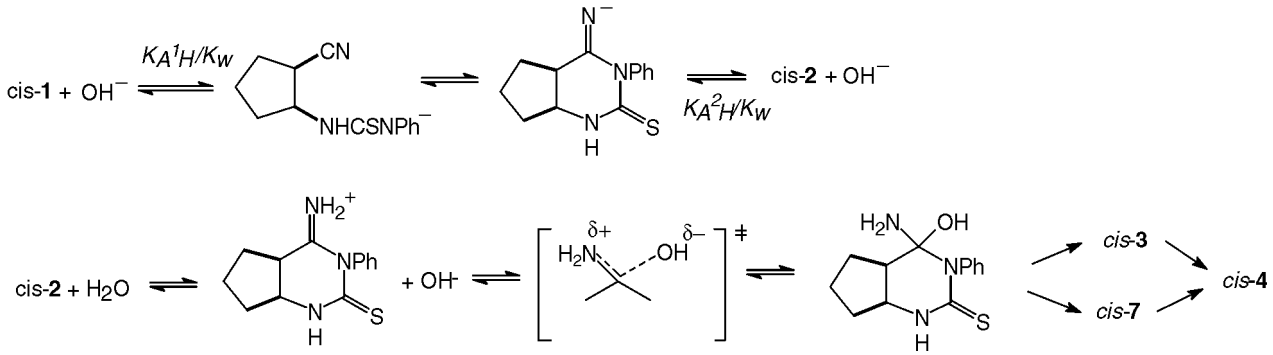
In CD_3OD only, a 1:1 ratio of the imino *Z* and *E* isomers was observed. The signals of one of the isomers were broadened, which is most likely due to exchange with the amino form. In $CDCl_3$ only two sets of signals, both sharp, in 1:1 ratio were observed. This could be due either to fast exchange with the amino isomer or to its absence in significant amounts.[4]

The assignment of *Z* or *E* configurations was based on the expected upfield shift of 4a-H and 7a-H caused by the ring current effect of the phenyl group, because in the *E*-isomer

[4]One of the referees has suggested that the doubling of the NMR resonances could be due to dimer-polymer equilibria. We believe that the amidines studied in ca. 0.04 M solutions are unlikely to give associates, particularly in DMSO and MeOH.

© 2000 NRC Canada

Scheme 3.



allylic strain will force it into a perpendicular position. Such an assignment readily explains the favouring of the *E*-isomer in DMSO: solvation at 3-NH will hinder the phenyl group in the *Z*-isomer. The conformation, *syn* or *anti,* of the **5a** isomer could not be assigned.

Noteworthy is the strong bias of *cis*-**2** for conformation **A** (Scheme 2) suggested by the bandwidths of the signals for protons 4a and 7a in DMSO: 22.2 and 11.5 Hz respectively. 7a-H is axial in the pyrimidine ring thus J_{HNH} will be 0–1 Hz (7) and pseudoequatorial in the cyclopentane ring so that the sum of 11.5 Hz has to be made up of three gauche couplings. The signals for the 4a- and 7a-protons in the imino tautomers of compound **5** were better resolved than those for the iminopyrimidine **2**. Again the bandwidths for the 7a-H signals are very small: 8.4–9.0 Hz in CD_3OD and $CDCl_3$. The signals are triplets which can be due to two couplings of ca. 4 Hz. This is the value of a *cis*-coupling in dihydrouracils in cases of a directed electronegativity effect (7), i.e., when an electronegative atom is *anti* to one of the coupled protons. In conformation **A,** shown on Scheme 2 for compound **2,** the ring nitrogen is *anti* to 4a-H and to the neighbouring *cis* cyclopentane ring proton which accounts for the low couplings. The coupling with the *trans* proton of the pentane ring with a torsion angle of ca. 90° can be close to zero and thus not seen. The sextets observed for 4a-H can be accommodated by two couplings of 9–10 Hz and one of ca. 4 Hz. The latter is of course $J_{4a,7a}$ while the large couplings are the expected ones with torsions of ca. 30 and 150° with the *cis* and *trans* cyclopentane ring protons, respectively.

Kinetics of alkaline hydrolysis of nitrile *cis*-1

The equilibrium nitrile cis-*1*-*imine* cis-*2*

As described above when the hydrolysis of *cis*-**1** in aqueous hydroxide is monitored by UV, the peak at 245 nm decreases while a new absorption at 267 nm appears due to *cis*-**2**. The latter then breaks down by a much slower process and the absorption at 245 nm is restored. Quantitative estimates showed that the conversion of *cis*-**1** into *cis*-**2** is incomplete and an equilibrium is established (Scheme 3). At an [OH^-] higher than 0.01 M the amount of *cis*-**2** at equilibrium decreased. This can be explained by considerable ionization of the phenylthioureido group.

Table 3. Absorbance ratios in 0.1 M HCl for determining K_e = [*cis*-**2**]/[*cis*-**1**] and pK_{AH} of the phenylthioureido group of nitrile *cis*-**2** (25.0°C and ionic strength of 1 M (KCl)).

[OH^-] (mol/dm^{-3})	$A_{295}{}^{a}/A_{265}{}^{b,c}$
0.00200	1.42
0.00400	1.43
0.00600	1.39
0.00800	1.38
0.0140	1.32
0.0160	1.29
0.0200	1.24
0.0400	1.05
0.100	0.785
0.160	0.68
0.200	0.634
0.320	0.538
0.400	0.511
0.520	0.502
1.00	0.474

[a] $A^\circ_{1,294}$ = 1 870, $A^\circ_{2,294}$ = 11 200.
[b] $A^\circ_{1,265}$ = 9810, $A^\circ_{2,265}$ = 4260.
[c] Ratios are averages from several experiments.

Defining K_e = [*cis*-**2**]/[*cis*-**1**] as the equilibrium constant between the neutral species, then upon considerable ionization of the thioureido group the apparent equilibrium between the stoichiometric concentrations is given by eq. [1]:

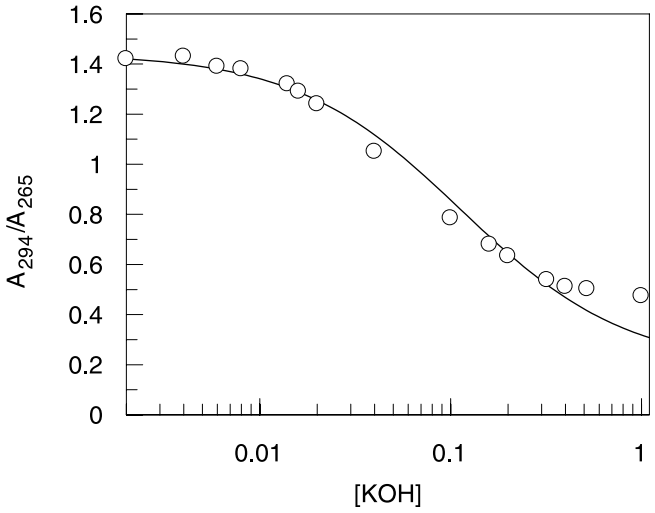
$$[1] \qquad K_{app} = \frac{[cis\text{-}\mathbf{2}]_{st}}{[cis\text{-}\mathbf{1}]_{st}} = \frac{K_e}{1 + [OH^-]K^N_{AH}/K_w}$$

The equilibrium mixture was analyzed by quenching the reaction mixture with hydrochloric acid at the moment of reaching the maximum of absorption at 267 nm, when the final products could still be neglected. HCl was added to a final concentration of ca. 0.1 M. Under these conditions the imine *cis*-**2** was fully protonated (pK_{BH^+} was determined spectrophotometrically to be 6.40 ± 0.11)[5] and hydrolysis is relatively slow. To avoid errors due to dilution, the equilibrium constant (K_e) and the dissociation constant for the CSNHPh group (K^N_{AH}) was determined from the ratio of the absorbances at two wave lengths:

[5] p*K* values for 4-imino-3-phenylhydantoins ranging from 6.1 to 6.5 have been reported in ref. 17.

© 2000 NRC Canada

Fig. 1. Semilogarithmic plot of A_{294}/A_{265} against [OH^-]. Curve is drawn by means of eq. [2] and parameters in text.

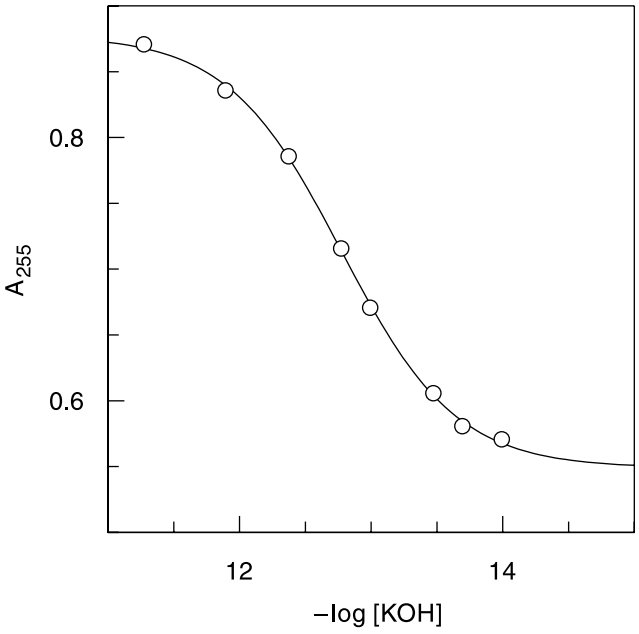


$$[2] \qquad \frac{A_{l1}}{A_{l2}} = \frac{A^{\circ}_{l1} + A^{\circ}_{21}K_e/(1 + K^N_{AH}[OH]/K_w)}{A^{\circ}_{l2} + A^{\circ}_{22}K_e/(1 + K^N_{AH}[OH]/K_w)}$$

where A^0_{ii} are the molar absorbances, the first subscript denoting the compound and the second one the wave length. A curve fit of the ratios A_{294}/A_{265} (Table 3) to eq. [2] in the interval 0.002 to 1 M KOH gave $K_e = 2.43 \pm 0.11$ and $K^N_{AH}/K_w = 18.0 \pm 2.1$ (I = 1 M (KCl)). Taking $K_w = 1 \times 10^{-14}$ and [OH^-] = a_{OH} gave a pK^N_{AH} of 12.74. These parameters resulted the fit shown in Fig. 1. The positive deviation of the points in 0.5 and 1 M KOH could be due to deprotonation of the amidine **2** (18) but attempts to include such an ionization in eq. [2] were unsuccessful.

Due to the rapid conversion of the nitrile *cis*-**1** in the region of ionization its p*K* could not be determined independently by spectroscopy. To check whether the value was reasonable, the p*K* for the ionization of the phenylthioureido group of the related amide *cis*-**3** was determined in KOH solutions (I = 1 M (KCl)). Again using –log [KOH] as the acidity function and $pK_w = 14$, a pK_{AH} of 12.78 ± 0.02 was obtained (Fig. 2).

Fig. 2. Determination of pK_{AH} for ionization of the phenylthioureido group in carboxamide *cis*-**3**.



$$[3] \qquad k_{obs} = k_f[OH^-]/(1 + K^N_{AH}[OH^-]/K_w) + k_f[OH^-]/K_e$$

The experimental data were fitted eq. [3] using the ionization and equilibrium constants found above as fixed parameters. This afforded $k_f = 4.24 \pm 0.08$ dm^3 mol^{-1} s^{-1} (Fig. 3). A $k_r$value of 1.74 dm^3 mol^{-1} s^{-1} was calculated from the equilibrium constant.

The kinetics observed indicate that the reactive form of *cis*-**2** is the ureide anion. According to the principle of microscopic reversibility the return path will involve the amidine anion.

The breakdown of the iminopyrimidine *cis*-**2** to products was found to be independent of the concentration of OH^- between 0.001 and 0.012 M KOH, where the observed first-order rates averaged to 2.21×10^{-4} s^{-1}. The somewhat higher rate observed in 0.1 M KOH indicates that a first order in [OH^-] process sets in. Actually, taking into account the lower fraction of *cis*-**2** at equilibrium in 0.1 M KOH, a lower pseudo-first-order constant should have been observed if only the pH-independent reaction took place. pH-independent rates are often encountered in the hydrolysis of amidines (18) in the alkaline region. The reaction can be formulated as attack of water on neutral iminopyrimidine, however, attack of OH^- on the protonated form as shown in Scheme 3 appears more appealing. The tetrahedral intermediate could either lose ammonia to give the pyrimidine **7** which would rapidly hydrolyze[6] to the acid **4**, or open the cycle to form the amide **3** which would then hydrolyze to the same acid **4**.[7] ^{1}H NMR of extracts of the acidified reaction mixture leaving *cis*-**2** as salt in the acid solution showed that the second route through the amide is preferred. After 110 min in 0.01 M KOH at room temperature (around two half-lives of *cis*-**2**) nitrile *cis*-**1** gave a mixture of *cis*-**3**:*cis*-

Rates of formation of imine *cis*-2 and its breakdown

The large difference in the rates of formation of *cis*-**2** from *cis*-**1** and the breakdown of the former allowed these to be measured as two separate first-order processes. The formation and breakdown were measured only up to 0.04 M KOH because of the considerable drop (due to the ionization of the ureido group at the higher alkalinities) in the amount of intermediate **2** formed at equilibrium. Furthermore, the rate of formation became too fast to measure by conventional means.

The cyclization of ureido nitrile **1** was found to be first order in [OH^-] at lower alkalinities. Taking into account the equilibria in Scheme 3, the following expression for the dependence of k_{obs} on [OH^-] can be derived:

[6] At pH 9.18 *cis*-**7** hydrolyzes with an observed rate of 0.0015 s^{-1}.
[7] Thin layer chromatography showed general retention of configuration. Only trace *trans* isomers of the products were found.

© 2000 NRC Canada

Scheme 4.

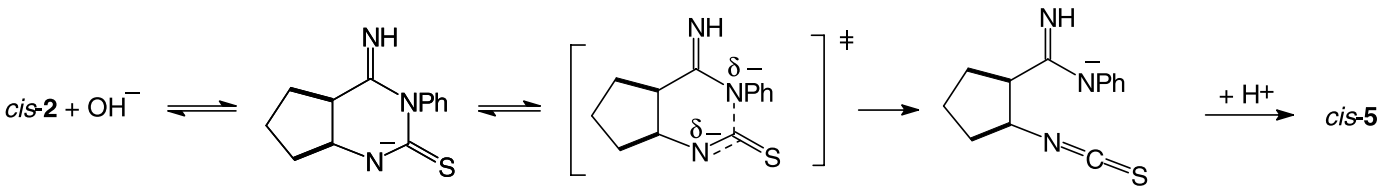
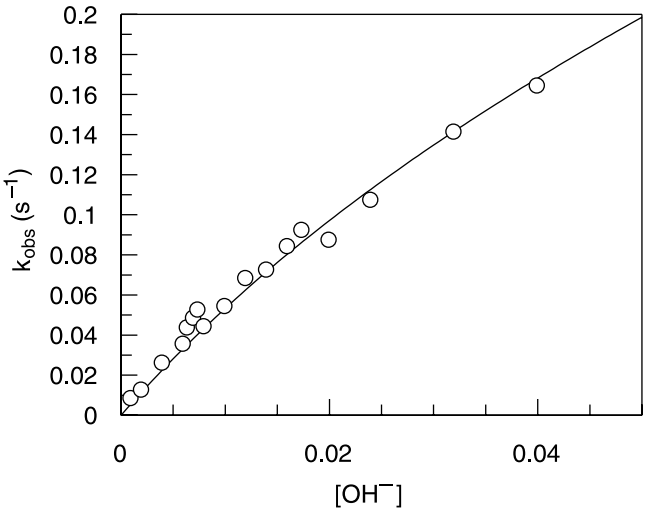


Fig. 3. Pseudo first order rate constants for the cyclization of nitrile **1**. Curve calculated by means of eq. [3] with parameters in text.



4:*cis*-**1** in a ratio of 57:30:13. After 7 h [*cis*-**3**]:[*cis*-**4**] = 19:81 and in 24 h the extract was pure acid *cis*-**4**.

In the introduction the magnitude of the anchimeric assistance to the alkaline hydrolysis of the nitrile group by the neighbouring phenylthioureido one is quoted as 1×10^4. This is estimated by comparing the rate of breakdown of *cis*-**2** with the second order rate constant of alkaline hydrolysis of acetonitrile. Another comparison could be provided by the hydrolysis of the nitrile group in *trans*-**1** which has a closer similarity with respect to steric and electronic influences. For 18 days at room temperature in aqueous 0.01 M KOH *trans*-**1** degraded only around 50%, the products were not, however, the amide *trans*-**3** or the acid *trans*-**4** (^{1}H NMR), and probably result from transformations of the thioureido group. If that time is compared with the half-life of *cis*-**2** of 50 min, the *trans* nitrile is at least 500 times more stable towards alkali.

Solvent effect on the breakdown of imine *cis*-2

The most likely transition states for the reaction of *cis*-**2** in water and in a mixture of water:acetonitrile (1:2 v/v) are shown on Schemes 3 and 4. The zero order in [OH^-] hydrolysis of **2** proceeds as suggested above as an attack by OH^- on the protonated form of the imine. On the other hand, the slow step in the isomerization is usually (19) a base catalyzed elimination giving the thioisocyanate shown on Scheme 4. The first reaction involves charge separation in the transition state while the second one dispersal of charge. Decreasing the dielectric constant by addition of acetonitrile will favour the second and disfavour the former reaction. Addition of a polar aprotic solvent will raise specifically the activity of the ground state of the elimination reaction (OH^-) and thus further accelerate elimination over hydrolysis.

Experimental

Unless otherwise stated IR-spectra are in nujol mulls on a Bruker IFS instrument, frequencies are in cm^{-1}, wavelengths are in nm. Instruments included a Bruker Spectrospin WM 250 NMR spectrometer (chemical shifts in ppm against TMS, couplings in Hz), a Jeol-D 300 mass spectrometer and a Unicam SP 800 UV spectrophotometer. Uncorrected melting points were determined in capillaries.

Inorganic reagents for kinetic measurements were of analytical grade and were used without further purification.

cis- *and* trans-*2-(-3-Phenylthioureido)cyclopentanecarbonitrile (**1**)*: The parent 2-aminocyclopentanecarbonitrile was prepared as a crude oil as follows. A solution of 2-amino-1-cyanocyclopentene (20) (7.3 g, 68 mmol) in methanol (100 mL) was made acid to bromocresol green with 1 N methanolic HCl. Sodium cyanoborohydride (4.9 g) was added by portions while the solution was kept acidic by the addition of more methanolic HCl. After stirring for 3 h the reaction mixture was concentrated. The residue was treated with 10% aqueous NaOH (68 mL) and NaCl (14 g), and taken up in dichloromethane (4 × 50 mL). It was removed from dichloromethane with 10% HCl (4 × 50 mL). The aqueous extract was made basic with 20% aqueous NaOH and extracted with dichloromethane (4 × 50 mL). The dichloromethane solution was dried (Na_2SO_4) and concentrated under reduced pressure to yield 2-aminocyclopentanecarbonitrile (6.53 g, 88%) as a colourless oil. IR (Nujol) ν_{max}: 3370, 3305 (NH), 2220 (CN) 1600 (NH_2).

A solution of phenylisothiocyanate (2.80 g, 21 mmol) in ether (5 mL) was slowly added to a solution of the above 2-aminocyclopentanecarbonitrile (2.2 g, 20 mmol) in ether (5 mL). A crystalline precipitate formed which was filtered and washed with petroleum ether to give the crude *cis* and *trans* isomers of **1** (4.4 g, 88%). The crude mixture (2 g) was chromatographed on 60 g "Florosil" with chloroform as the eluent. 50 mL fractions were taken and fractions 4 to 7 yielded the more mobile *cis* isomer while 9 to 25 yielded the

© 2000 NRC Canada

trans isomer. Crystallization from ethanol-water (2:1) yielded 0.67 g solid *cis*-**1** (mp 163–164°C). λ_{max} (H_2O): 245; IR (KBr disk) ν_{max}: 3230 (NH), 2232 (CN) 1546 (NHCSNHPh); MS *m/z*: 245. Anal. calcd. for $C_{13}H_{15}N_3S$: C 63.6, H 6.2; found: C 63.3, H 6.15. *trans*-**1** (1.07 g) had a mp 156–157°C. λ_{max} (H_2O): 244; IR (KBr disk) ν_{max}: 3295, 3181 (NH), 2240 (CN); MS *m/z*: 245. Anal. calcd. for $C_{13}H_{15}N_3S$: as above; found: C 63.25; H 6.5.

cis-*2-(3-Phenylthioureido)cyclopentanecarboxamide (*cis-***3***)*: The *cis* nitrile **1** (0.30 g, 1.2 mmol) was stirred in 60% sulfuric acid (5 mL). When solution was complete (1 h) it was diluted with water (15 mL) under cooling. The mixture was extracted with chloroform and the chloroform layer washed with 5% sodium carbonate and water, dried, and evaporated to dryness. TLC of the solid residue of *cis* amide **3** showed no appreciable admixture of the *trans* amide. Recrystallization from $CHCl_3$–petroleum ether yielded 0.15 g, 47% (mp 160–161°C after second crystallization). λ_{max} (H_2O): 245. IR (KBr disk) ν_{max}: 3388, 3356, 3277, 3165 (NH), 1662 ($CONH_2$), 1541 (NHCSNHPh). MS *m/z*: 263. Anal. calcd. for $C_{13}H_{17}N_3OS$: N 15.96; found N 15.54.

trans-*2-(3-Phenylthioureido)cyclopentanecarboxamide (*trans-***3***)*: The same procedure with *trans* nitrile **1** (0.30 g, 1.2 mmol) in which the dilution with water followed 5 min of stirring afforded, after two recrystallizations from chloroform-petroleum ether, 0.16 g (50%) of *trans*-**3** (mp 155–156°C, the crude product contained considerable amounts of the *cis* amide-**3** (determined by TLC)). λ_{max} (H_2O): 245. IR (KBr disk) ν_{max}: 3346, 3209 (NH), 1660, 1633 ($CONH_2$), 1541 (NHCSNHPh). Anal. calcd. for $C_{13}H_{17}N_3OS$: N 15.96; found N 15.95.

cis-*4-Oxo-1,2,3,4a,5,6,7,7a-octahydro-3-phenyl-2-thiooxocyclopenta[*d*]pyrimidine (*cis-***7***)*: (a) *cis* Nitrile **1** (0.305 g, 1.24 mmol) in 1:2 HCl (30 mL) was refluxed for 30 min. Cooling and filtering afforded 0.289 g (94%) of the crude thiouracil **7** (mp 267–269°C, ethanol, lit. mp 285–287°C (5)). λ_{max} (H_2O): 278; IR (Nujol) ν_{max}: 3171 (NH), 1711 (CO), 1564 (NHCSNPh); MS *m/z*: 246. Anal. calcd. for $C_{13}H_{14}N_2OS$: C 63.4; H 5.7; found: C 63.6; H 5.8. (b) Refluxing the *trans* nitrile **1** (60 mg, 0.24 mmol) in 1:2 HCl (30 mL) for 1 h, cooling, and standing overnight gave as precipitate 47 mg (78%) of pure (determined by ^{1}H NMR) *cis* pyrimidine **7**.

trans-*2-(3-Phenylthioureido)cyclopentanecarboxylic acid (*trans-***4***)*: Refluxing the nitrile *trans*-**1** (52 mg, 0.21 mmol) in 1:2 HCl for 30 min after cooling and standing overnight afforded 30 mg of a 4:1 mixture (^{1}H NMR) of the *cis* pyrimidine **7** and the *trans* acid **4**. Evaporating the mother liquor with a rotary evaporator yielded 19 mg, 34% of pure *trans* acid (mp 146–147°C, lit. mp 142–144°C(5)); λ_{max} (H_2O): 245; IR (KBr disk) ν_{max}: 3346, 3169 (NH), 1701, 1687 (CO), 1549 (NHCSNHPh). Anal. calcd. for $C_{13}H_{16}N_2O_2S$: C 59.1; H 6.1; N 10.6; found: C 59.0; H 6.32; N 10.8.

cis-*2-(3-Phenylthioureido)cyclopentanecarboxylic acid (*cis-***4***)*: The *cis* pyrimidine **7** (0.5 g, 2.03 mmol) dissolved easily in warm 0.5 M NaOH (20 mL). After acidifying the cooled solution with conc. HCl (2 mL) the *cis* acid **4** separated as a gum which crystallized rapidly to give 0.53 g. 99% of solid (mp 152–153°C, (chloroform-petroleum ether), resolidifies and melts again at 230°C). λ_{max} (H_2O): 245; IR (Nujol) ν_{max}: 3344, 3167 (NH), 1686 (CO), 1536 (NHCSNHPh). MS *m/z*: 264. Anal. calcd. for $C_{13}H_{16}N_2O_2S$: C 59.1; H 6.1; found: C 58.9; H 6.3.

cis-*4-Imino-1,2,3,4a,5,6,7,7a-octahydro-3-phenyl-2-thiooxocyclopenta[*d*]pyrimidine (*cis-***2***)*: The *cis* nitrile **1** (36 mg, 0.146 mmol) was dissolved by warming in acetonitrile (2 mL) and subsequently mixed with 0.01 M KOH (100 mL) at room temperature. After 3 min the mixture was transferred to a cooled separatory funnel containing ice and HCl, the amount of the latter dependant on the desired final acid concentration. The solution was extracted rapidly with dichloromethane (3 × 40 mL) in the course of five to eight min and passed through a fluted filter. The dry residues of the extracts amounted to 30–35% (by weight) of the starting material and consisted of (according to ^{1}H NMR) mixtures of the initial nitrile and the *cis* amide, the amount of the latter varying from trace to 30%). The aqueous layer was made alkaline (ca. 0.01 M in [OH^-]) and extracted twice rapidly with chloroform (ca. 12 min from the start of the experiment). The organic layer was filtered, dried with $MgSO_4$, and evaporated to give a solid, the iminopyrimidine *cis*-**2** (25 mg, containing up to ca. 15% the *cis* nitrile according to ^{1}H NMR). λ_{max} (H_2O): 267, (0.1 M HCl 295); IR ($CHCl_3$) ν_{max}: 3409, 3288, 3199b (NH), 1647 (C=N), 1528 (NCSNH).

cis-*4-Phenylimino-1,2,3,4a,5,6,7,7a-octahydro-3-phenyl-2-thiooxocyclopenta[*d*]pyrimidine (*cis-***5***)*: A solution of 0.5 g (2 mmol) of *cis*-2-(3-phenylthioureido)cyclopentyl cyanide in 80 mL of absolute methanol was refluxed for 3 h. The solvent was removed by a rotatory evaporator and the solid residue recrystallized from MeOH–MeCN to give 0.39 g (78%) of solid *cis*-**5** (mp 231–2°C). MS *m/e*: M^+ 245; λ_{max} (H_2O): 269, 242; IR (KBr disk) ν_{max}: 1670 (C=N), 1564 (δ NH), 1346 (NHCSNH), 3170, 3460 (NH); IR ($CHCl_3$) ν_{max}: 1664 (C=N) 1535 (δ NH), 1348 (NHCSNH), 3226, 3408 (NH). Anal. calcd. for $C_{13}H_{15}N_3S$: C 63.63, H 6.16, N 17.13, S 13.07; found: C 63.78, H 6.45, N 16.85, S 13.18.

cis-*1,2,3,4a,5,6,7,7a-Octahydro-4-oxo-2-thiooxocyclopenta[*d*]-pyrimidine (*cis-***8***)*: (a) From phenyliminopyrimidine *cis*-**5**. The phenyliminopyrimidine *cis*-**5** (0.37 g, 1.5 mmol) was dissolved with gentle heating in 30 mL of MeOH and 10 mL of MeCN. 40 mL of distilled water and 15 mL of 1M HCl were further added. The solution was left at ambient temperature for 75 min and then evaporated to dryness until HCl was completely removed in vacuo. Recrystallization from MeOH–petroleum ether afforded 0.180 g (80%) of solid (mp 198–9°C, lit. mp 206–208°C(11)); MS *m/e*: M^+ 170; IR (KBr disk) ν_{max}: 1693 (CO), 1362 (NHCSNH), 3182, 3460w (NH). Anal. calcd. for $C_7H_{10}N_2OS$: C 49.39; H 5.92; N 16.46; S 18.91; found C 49.50; H 6.03; N 16.77; S 18.91.

(b) From cyclization of *cis*-2-thioureidocyclopentanecarboxylic acid (*cis*-**6**). The acid *cis*-**6** (0.150 g) was dissolved in 8 mL of MeCN and 4 mL of MeOH. 12 mL of 1 M HCl were added and the mixture left at room temperature for 20 h. The solvent removed and the dry residue recrystallized from MeCN and petroleum ether to yield 0.085 g (63%) of

© 2000 NRC Canada

Table 4. Pseudo-first-order rate constants (s^{-1}) for the formation and breakdown of 4-imino-2-thiooxo-1,2,3,4a,5,6,7,7a-octahydrocyclopenta[*d*]pyrimidine *cis*-**2** in aqueous KOH and ionic strength 1.0 M (KCl) at 25°C.

$[OH^-]$ (mol/dm^{-3})	10^3 k_{obs} for formation	10^4 k_{obs} for breakdown
0.00031[a]	2.48	2.00
0.001	8.07	2.24
0.002	12.3	2.23
0.004	25.8	2.23
0.006	35.2	2.22
0.0064	43.4	2.21
0.007	48.2	2.11
0.0074	52.3	2.17
0.008	44.0	2.03
0.01	54.0	2.17
0.012	68.0	2.48
0.014	72.2	—
0.016	83.9	—
0.0174	92.0	—
0.02	87.1	—
0.024	107	—
0.032	141	—
0.04	164	—
0.1	—	3.90

[a]Experiment conducted at pH 10.49 in carbonate buffer 70% base.

solid *cis*-**8** (mp 197–199°C) identical with the above product according to spectral data and mixed mp.

cis-*2-Thioureidocyclopentanecarboxylic acid (*cis-***6***)*: (a) 0.31 g of phenyliminopyrimidine *cis*-**5** were dissolved by gentle heating in 20 mL of MeOH. 20 mL of aqueous 1 M KOH were added and the solution left at room temperature for 12 h. Most of the MeOH in the solution was removed on a rotary evaporator and the alkaline solution extracted twice with 20 mL portions of ether. The organic layers were dried and the solvent removed to yield an reddish-brown oil identified as aniline: M^+ 93; same IR and UV spectra as that of an authentic sample. The aqueous layer was neutralized with 2 equivalents of cationite Dowex 50x8 in H^+ form. The solution (pH two to three) was evaporated and the residue recrystallized twice from MeCN with addition of petroleum ether to yield 0.045 g (19%) of *cis*-**6** (mp 155–157°C). MS *m/e*: M^+ 188. λ_{max} (H_2O): 230 (log ϵ = 3.9), 280 (log ϵ = 3.1). IR (KBr disk) ν_{max}: 1635, 1560 (delta NH) 1703 (COOH), 3186, 3300, 3350 (NH,OH). Solution resulted a single spot on TLC and no admixtures were observable in the ^1H NMR spectrum. (b) 0.095 g of *cis*-**8** were dissolved in five mL of MeOH by gently heating and 10 mL of 1 M aqueous KOH added. Similar work up yielded 0.097 g of raw *cis*-**6** identical (according to ^1H NMR) to the product obtained in (a).

Kinetic measurements

The rates were measured under pseudo first order conditions in the thermostated cell compartment of a Unicam SP 800 spectrophotometer. The reactions were initiated by injecting 20 to 80 μL of a 10^{-2} to 10^{-3} M stock solution of the substrate in MeCN, to the preheated KOH solution of ionic strength 1 M (KCl). The conversion of *cis*-**1** into *cis*-**2** was monitored by the increase of absorption at 267 nm while the degradation of the latter was monitored by the decrease at the same wavelength. Pseudo-first-order rate constants (k_{obs}) were calculated by the least squares procedure from plots of either ln ($A_t - A_{inf}$) or ln ($A_{inf} - A_t$) (as appropriate) versus time, where A_{inf} was the absorbance after ten half-lives.

Equilibrium between the *cis* nitrile 1 and *cis* iminopyrimidine 2

Under the conditions of the rate experiments a solution of the *cis* nitrile **1** in MeCN was added to the preheated at 25.0°C KOH solution so that the final concentration of **2** was 7–8 × 10^{-5} M. When maximum absorption at 267 nm (λ_{max} (H_2O) of *cis*-**2**) was reached, the solution in the cell was acidified with a predetermined amount of HCl so that its final concentration was ca. 0.1 M and the spectrum of the solution taken immediately. The ratio [*cis*-**2**]:[*cis*-**1**] was determined from the ratio of the absorbances at the two wave lengths as well as the known extinction coefficients at these wavelengths of the two compounds in HCl solutions. Making the solution alkaline after the measurement restored the pre-acidification spectrum by better than 5%.

Product analysis

The course of the alkaline hydrolysis of *cis*-**1** was also followed by ^1H NMR in order to identify the products. For these large scale experiments the substrate was dissolved in an appropriate amount of MeCN so that when added to the KOH solution, the final concentration of MeCN equalled that in the kinetic experiment. After being kept at 25°C for the appropriate period of time, aliquots were acidified and extracted with dichloromethane, the solvent removed and the composition determined by ^1H NMR.

Determination of p*K*-values

(*a*) *cis*-Amide **3**. A solution (20 μL) of the amide (0.01 M) in MeCN was added to a 25.0°C (2.7 cm^{-1}) preheated solution of KOH (0.002 to 1 M, I = 1 M (KCl)) in a UV cell, and the absorbance measured at 255 nm. The pK was obtained by a nonlinear regression fit of the equation

$$K = (A_{AH} - A)[H^+]/(A - A_{A^-})$$

where A is the absorbance, A_{AH} and A_{A^-} the limiting absorbances at low and high basicity respectively. $[H^+]$ was assumed equal to antilog(14 – log $[OH^-]$).

(*b*) *cis*-Iminopyrimidine **2**. The compound was isolated as a solid as described above and as a solution prepared in MeOH which was kept cooled in ice/water. Aliquots (10 μL) were injected into UV cells containing 25.0°C preheated 0.1 M buffer solutions (formate, acetate, and phosphate) with I = 1 M (KCl). The absorbances were measured at 295 nm and the p*K* was calculated as above using the pH-values measured by means of a Radiometer pHM 84 Research pH-meter with a GK 2401 electrode.

© 2000 NRC Canada

Acknowledgements

We thank the National Foundation for Scientific Research of Bulgaria for funding this research and Dr. N. Vasilev for taking variable temperature NMR spectra.

References

1. (*a*) E.N. Zil'berman. *In* Reaktzii nitrilov, Khimiya, Moscow, 1972. Chap. 9; A.I. Mayers and J.C. Sircar. *In* The chemistry of the Cyano Group. *Edited by* S. Patai and Z. Rappoport. John Wiley, Chichester. 1970. pp. 341–421; (*b*) J.M. Balquist and F. I. Goetz. J. Heterocycl. Chem. **9,** 937 (1972).
2. K.W. Breukink and R.E. Verkade. Recl. Trav. Chim. Pays-Bas. **79**, 443 (1960).
3. (*a*) E.C. Taylor and R.V. Ravindranathan. J. Org. Chem. **27**, 2622 (1962); (*b*) T. Kinoshita, H. Wanatabe, S. Sato, and C. Tamura. Bull. Chem. Soc. Jpn. **53**, 442 (1980); (*c*) K. Takagi, H. Morita, and T. Aotsuka. Heterocycles, **26**, 175 (1987).
4. S. Wideqvist. Ark. Kemi. **10**, 265 (1956).
5. F. Fülöp, Z. Szakonyi, and G. Bernáth. J. Heterocycl. Chem. **34**, 1211 (1997).
6. G. Stájer, Z. Szöke-Molnár, G. Bernáth, and P. Sohár. Tetrahedron, **46**, 1943 (1990).
7. A.R. Katritzky, M.R. Nesbit, B.J. Kurtev, M. Lyapova, and I.G.Pojarlieff. Tetrahedron, **25**, 3807 (1969).
8. B. Kurtev, M. Lyapova, N. Berova, I. Pojarlieff, A. Orahovatz, P. Petrova, and N. Mollov. Comm. Dept. Chem. (Bulg. Acad. Sci.) **1** (1), 51 (1967).
9. E.L. Eliel, S.H. Wilen, and L.N. Mander. Stereochemistry of organic compounds. Wiley, New York. 1994. p. 773.
10. S. Furberg and L.H. Jensen. J. Am. Chem. Soc. **90**, 470 (1968); C.P. Rohrer and M. Sundaralingam. J. Chem. Soc. Chem. Commun. 746 (1968).
11. P. Sohár, Z. Szöke-Molnár, G. Stájer, and G. Bernáth. Magn. Reson. Chem. **27**, 959 (1989).
12. H.O. Kalinowski, S. Berger, and S. Braun. ^{13}C NMR Spektroskopie, G. Thieme Verlag, Stuttgart, 1984. Chap. 3.
13. C.L. Perrin. *In* The chemistry of amidines and imidates. Vol. 2. *Edited by* S. Patai and Z. Rappoport. Wiley, Chichester. 1991, p. 165.
14. L.D. Colebrook, H.G. Giles, and A. Rosowski. Tetrahedron Lett. 5239 (1972).
15. L.I. Spiessens and M.J.O. Anteneus. Bull. Soc. Chim. Belg. **91**, 763 (1982).
16. G. Barret and A. Foucaud. Bull. Soc. Chim. Fr. 4594 (1968).
17. V. Machacek, G. Svoboda, and V. Sterba. Coll. Czech. Chem. Commun. **52**, 140 (1987).
18. R.H. de Wolfe. *In* The chemistry of amidines and imidates. *Edited by* S. Patai. Wiley, Chichester. 1975, pp. 349–384.
19. A. Williams and K.T. Douglas. Chem. Rev. **75**, 627 (1975).
20. H.E. Schroeder and G.W. Rigby. J. Am. Chem. Soc. **71**, 2205 (1949).

© 2000 NRC Canada

Gas-phase luminescence of aromatic carbonyl compounds in excited nitrogen at atmospheric pressure[1]

Zhong-Ping Lin and Walter A. Aue

Abstract: Certain types of aroyl compounds such as benzaldehyde, acetophenone, benzophenone, and anthraquinone produce intense gas-phase luminescence in excited nitrogen at atmospheric pressure. This luminescence was measured in pressure ranges of 1.00–1.67 atm and temperature ranges of 343–473 K. A novel, radioactively (Ni-63) stimulated, high-voltage (≤1750 V/mm), low-current (≤35 nA) discharge in high-purity nitrogen was used for gas chromatographic detection and spectral excitation. The gas-phase luminescence spectra of about sixty aroyl compounds — introduced as gas chromatographic peaks — could thus be measured and compared with literature spectra obtained by conventional excitation in *condensed* phases. Only a few *gas*-phase spectra are available from the literature, and these did agree well with the spectra of this study. A speculative luminescence mechanism is proposed, in which ground-state N_2 becomes excited by collision with fast electrons. This is followed by efficient triplet–triplet energy transfer from $N_2(A\ ^3\Sigma_u^+)$ to the $n\rightarrow\pi^*$ excited aroyl compound.

Key words: aroyl phosphorescence, excited-nitrogen excitation, aroyl triplet–triplet excitation, aroyl luminescence detection, gas-phase phosphorescence spectra, gas-phase aroyl detection.

Résumé : En phase gazeuse, en présence d'azote excité, à pression atmosphérique, certains types de composés aroyles tels que le benzaldéhyde, l'acétophénone, la benzophénone et l'anthraquinone produisent une luminescence intense. On a mesuré cette luminescence à des pressions allant de 1,00 à 1,67 atm. et à des températures allant de 343 à 473 K. Pour la détection chromatographique et l'excitation spectrale, on a fait appel à une nouvelle décharge dans de l'azote purifié, stimulée d'une façon radioactive (Ni-63), à l'aide d'une tension élevée (≤1750 V/mm) et un faible courant (≤35 nA). On a ainsi pu mesurer les spectres de luminescence en phase gazeuse d'environ soixante composés aroyles — introduits sous la forme de pics chromatographiques — et on les a comparés avec des spectres rapportés dans la littérature et obtenus par une excitation conventionnelle dans des phases condensées. Dans la littérature, on ne retrouve que quelques spectres en phase gazeuse et ils sont en bon accord avec les spectres obtenus au cours de cette étude. On propose un mécanisme spéculatif pour la luminescence; il implique le passage de N_2 de l'état fondamental à l'état excité sous l'influence des collisions avec des électrons rapides. Cette excitation serait suivie d'un transfert d'énergie triplet-triplet efficace de $N_2(A\ ^3\Sigma_u^+)$ vers le composé aroyle excité $n\rightarrow\pi^*$.

Mots clés : phosphorescence d'aroyle, excitation par de l'azote excité, excitation triplet–triplet aroyle, détection de la luminescence aroyle, spectre de phosphorescence en phase gazeuse, détection aroyle en phase gazeuse.

[Traduit par la Rédaction]

Introduction

Photophysics and photochemistry of aromatic carbonyl molecules have been extensively studied, typically by optical excitation (1, 2) or electron impact (3, 4). Most investigations have been restricted to the condensed phases, in which these organic molecules often show photochemical or photophysical properties different from those observed in the gas phase. In this paper we report that a radioactively stimulated, high-voltage, low-current discharge in high-purity nitrogen was used to excite certain aromatic carbonyl compounds at *atmospheric* pressure and *high* temperature in the *gas* phase. The emission spectra of some sixty aroyl compounds were measured and compared with spectral data from other excitation systems (where available in the literature). Our objective was to develop an understanding of the general photophysical characteristics of these molecules under the specific gas-phase conditions of high temperature and atmospheric pressure, as well as to investigate their excitation, i.e., energy transfer mechanism.

Received October 8, 1998.

Z.-P. Lin[2] and W.A. Aue.[3] Department of Chemistry, Dalhousie University, Halifax, NS B3H 4J3, Canada.

[1]From the doctoral thesis of Z.-P. Lin (Dalhousie University, 1997).

[2]Present address: College of Pharmacy, Ohio State University, 500W 12th Ave., Columbus, OH 43210-1291

[3]Author to whom correspondence may be addressed. Telephone: (902) 494-7076(office); (902)494-3305(messages). Fax: (902) 494-1310. e-mail: auehot@hotmail.com

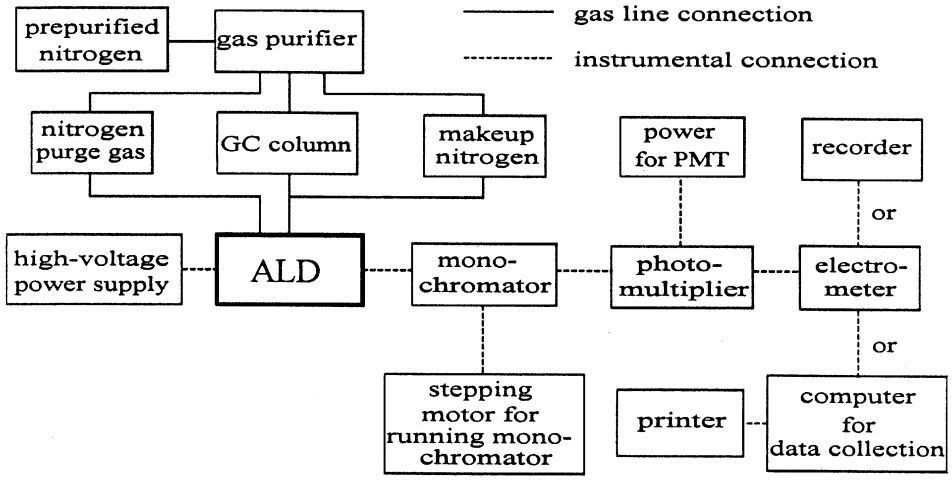
Experimental section

1. Experimental set-up

Figure 1 is a block diagram of the experimental set-up for obtaining gas-phase luminescence spectra. Nitrogen served

© 2000 NRC Canada

Fig. 1. Block diagram of the experimental set-up for obtaining gas-phase luminescence spectra of aroyl compounds. ALD = aroyl luminescence detector.



as GC carrier gas, purge gas and reagent gas for the "aroyl luminescence detector" (ALD). Prior to entering the injection port, nitrogen gas was purified by passage through molecular sieve 5A (Guild Corp., Bethel Park, Penn.) and heated zirconium sponge ("gas purifier"; Supelco, Bellefonte, Penn.). Carrier gas and make-up gas were mixed, if needed, with a doping gas at the entrance of the ALD. Purge gas was used to flush air or impurities out of the detector.

A 12 kV Spellman model HS5P30/CR/X769 (High Voltage Electronics Corp., Bronx, N.Y.), or a 5 kV Hipotronics model no. R10B (Brewster, N.Y.) DC high-voltage power supply was employed to polarize the ALD electrode. A current-limiting resistor of 5×10^6 ohm was installed between the DC power supply and the electrode for safety reasons.

The ALD signal (analyte luminescence) was measured with a Hamamatsu photomultiplier tube, typically an R-374 or R-268 PMT (Hamamatsu Corp., Middlesex, N.J.), and amplified with a Tracor electrometer (Tracor, Austin, Tex.). The signal was displayed on a Linear two-pen chart recorder, or stored in a computer for subsequent processing. Either Ditric (no longer in business) or Oriel (Stratford, Conn.) optical interference or colored-glass filters were used as needed.

2. Gases and chemicals

Nitrogen (prepurified, 99.998%), hydrogen (prepurified, 99.99%) and air (extra dry, maximum moisture 10 ppm) were the products of Linde Union Carbide Canada Ltd. (Toronto, Ont.). Argon of ultra-high-purity grade was obtained from Matheson Gas Products (Toronto, Ont.). All chemicals (95+% purity) were purchased from commercial sources, e.g., from Aldrich Chemical Company (Milwaukee, Wis.); Fluka Chemical Corp. (Ronkonkoma, N.Y.); or Sigma Chemical Company (St. Louis, Mo.). The chemicals were used without further purification.

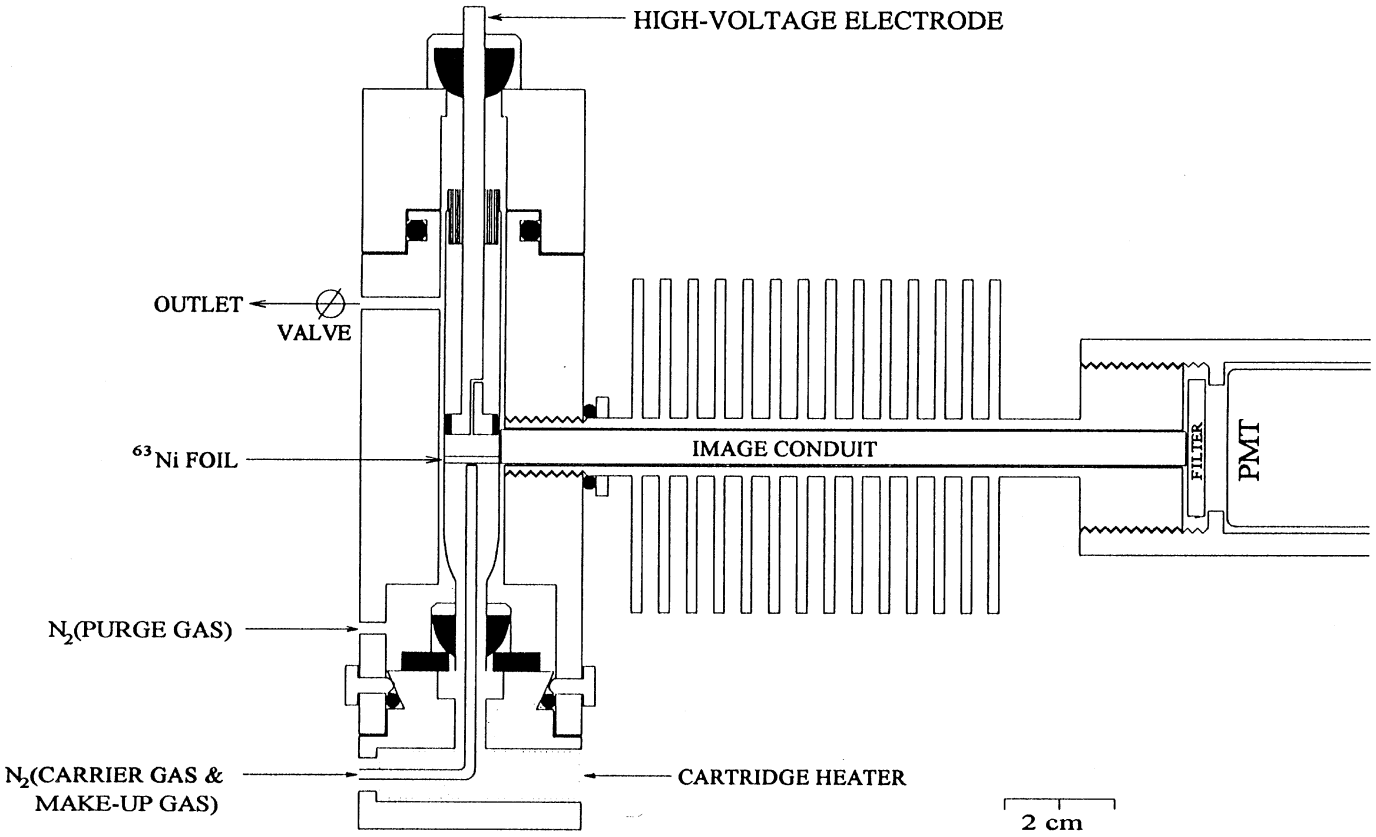
3. Aroyl Luminescence Detector

Both a single-channel and a triple-channel aroyl luminescence detector were used in this study. A detailed diagram of the single-channel ALD is shown in Fig. 2. The de novo design of this detector was based on the earlier described nitrogen-plasma photometric detector (NPPD) (5), which had been constructed by modifying a Shimadzu flame photometric detector (FPD). The two basic requirements in designing the new detector were (*i*) to ensure gas tightness, and (*ii*) to obtain maximal light output and throughput from the emission zone. Thus the detector cell was constructed with a 7.5 cm × 8 mm i.d. quartz tube of 1 mm thickness, which was fixed on the detector base with a Swagelock nut and a lab-made Teflon ferrule. A high-voltage electrode was inserted from the top of the detector into the quartz tube. The electrode was insulated from the detector body by a Teflon tube and a Swagelock fitting with Teflon ferrule. The distance between the polarized electrode and the nozzle (i.e., the detector jet, which also served as the grounded counter electrode) was adjustable, but was normally kept at 4 mm. A 1 mm high ^{63}Ni/Au cylindrical foil was held inside the quartz tube by friction fit, with the lower edge of the foil at the same level as the top of the nozzle. The detector volume was kept to 200 µL (and the luminescing zone much smaller than that), in order to maintain chromatographic peak resolution. A 6 in.(1in. = 25.4 mm) long, 6 mm o.d. high-quality glass image conduit (Edmund Scientific, Barrington, N.J.) was shielded from the room lights by an aluminum housing, inserted through the detector wall, and moved against the quartz tube to pick up as much light as possible. (The glass light guide was replaced by a quartz rod for any measurement — e.g., that of the nitrogen second-positive background system — for which UV transmission was important.) Enough space was left between the other end of the image conduit and the PMT to allow insertion of an optical filter (if needed). The detector was made light- and also gas-tight by silicone O-rings, Teflon ferrules, and Teflon stoppers. Even so, purge gas was required to flush traces of room air or other impurities out of the detector. The detector was exhausted through a long copper tube, which prevented the entry of light. A valve in the exhaust line kept the detector at a slight overpressure under normal operating conditions, in order to minimize back-diffusion of atmospheric oxygen. This valve was connected to a Matheson pressure gauge or to a MacLeod vacuum gauge for experiments run under other than the usual ambient pressure.

The triple-channel aroyl luminescence detector consisted of the detector cell, two photometric detection channels (together forming the "response-ratio channel"), and a "spectral

© 2000 NRC Canada

Fig. 2. Schematic of the single-channel aroyl luminescence detector.



channel." Figure 3 shows a diagram of the triple-channel ALD unit. The detector cell was constructed similar to that of the single-channel ALD. The two photometric channels consisted of a bifurcated optical glass fiber bundle (Item 77533; Oriel, Stratford, Conn.), with optical filters as needed, and two Hamamatsu R-268 PMTs installed in lab-made housings. An aluminum tube was used to hold the optical fiber bundle. It was positioned inside the light-guide housing, which ended in a lab-made spherical aluminum mirror of 31 mm diam. and 15 mm focal length. This aluminum mirror had a 6 mm diam. axial aperture (central hole) to accommodate the image conduit. The arrangement was inserted through the detector wall to a distance where the mirror would best focus the luminescence onto the slit of a monochromator in the spectral channel. This channel consisted of an aluminum tunnel connecting the detector body and the monochromator, of a quartz window installed at the end of the tunnel to make the detector gas-tight, and of a monochromator (vide infra for specs) with a Hamamatsu PMT to monitor the luminescence spectrum. The distances from the emission zone to the mirror on one side and the monochromator on the other could be adjusted. The purpose of adjustment was to focus the beam onto, and nigh fill the acceptance cone of, the monochromator aperture, so as to maintain optimal light throughput. To keep the photomultipliers and the monochromator cool, both the photometric detection channels and the spectral channel were equipped with water-flushed copper cooling coils. In addition, the spectral channel could be replaced by a PMT held in a water-cooled housing for more sensitive detection, as indicated at the lower right of Fig. 3. The whole detector was kept gas-tight by silicone O-rings and Teflon ferrules.

4. Spectral measurements

Repeated-injection mode

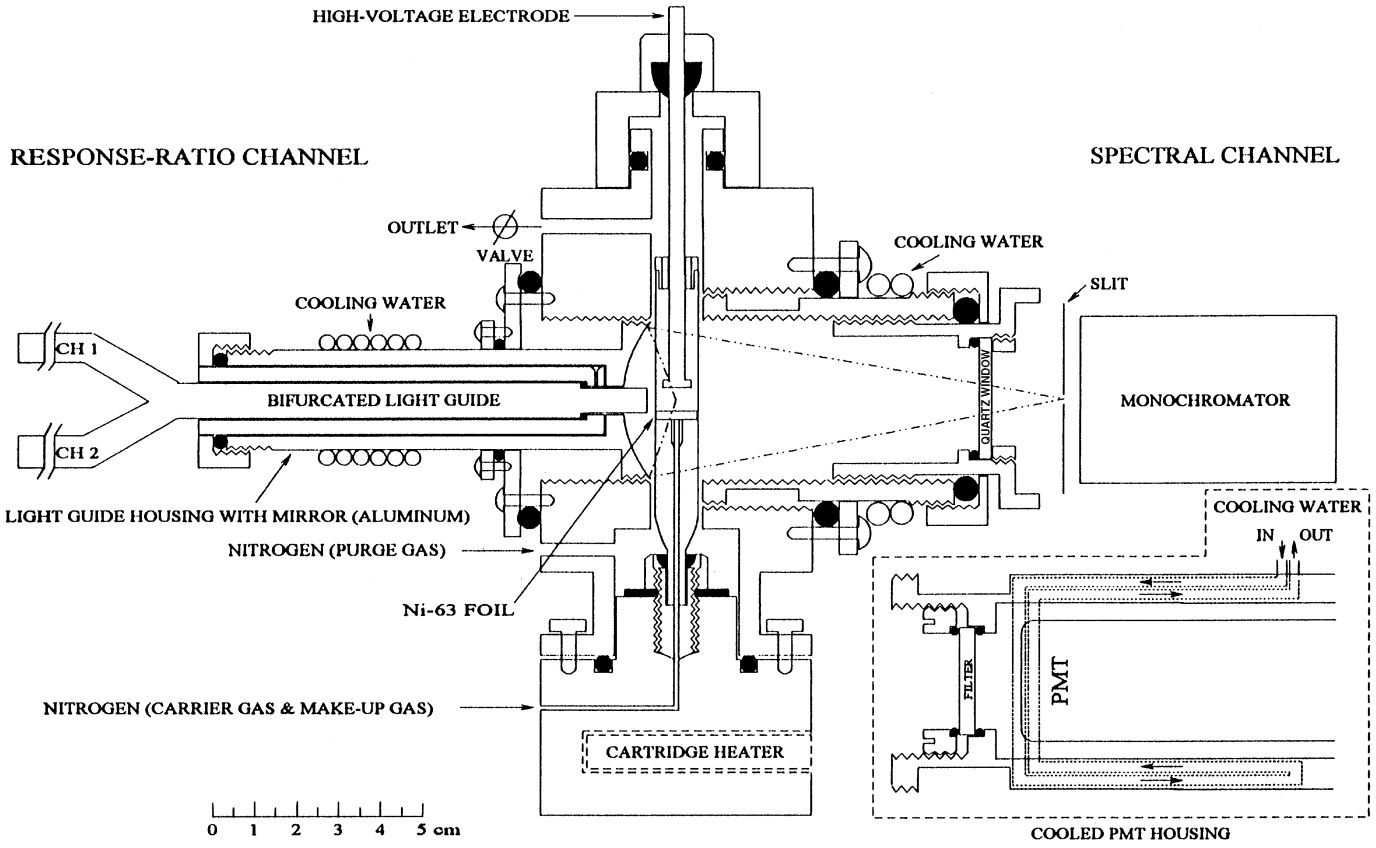
The image conduit of the single-channel ALD was replaced by a quartz rod of equal dimensions. Either a Jarrell–Ash model 82-415 quarter-meter monochromator of *f*/3.5 effective aperture ratio, with a 1180 grooves/mm grating blazed for 500 nm and fixed-width pairs of slits (0.5, 1, 2, or 4 mm; reciprocal dispersion 3.3 nm/mm); or an Oriel model 7155 filter monochromator (range 400–700 nm) for weakly emitting compounds, with slit options of 1, 2, 4, and 6 mm (corresponding to 11–40 nm bandpass at 550 nm), were employed to measure the spectra. In this mode, analytes were repeatedly injected while the wavelength drive was manually advanced.

Continuous-doping mode

In this mode, spectra were obtained from the quarter-meter monochromator described above. Liquid analytes were vaporized in a doping vessel to present a constant, nitrogen-diluted stream to the ALD. For solid compounds, the analytes were placed into a capillary tube, which was then inserted into the GC injection port and heated to produce a constant stream of analyte. The luminescence from the analyte was scanned with the help of an automatic wavelength drive.

© 2000 NRC Canada

Fig. 3. Schematic of the triple-channel aroyl luminescence detector.



Single-peak mode

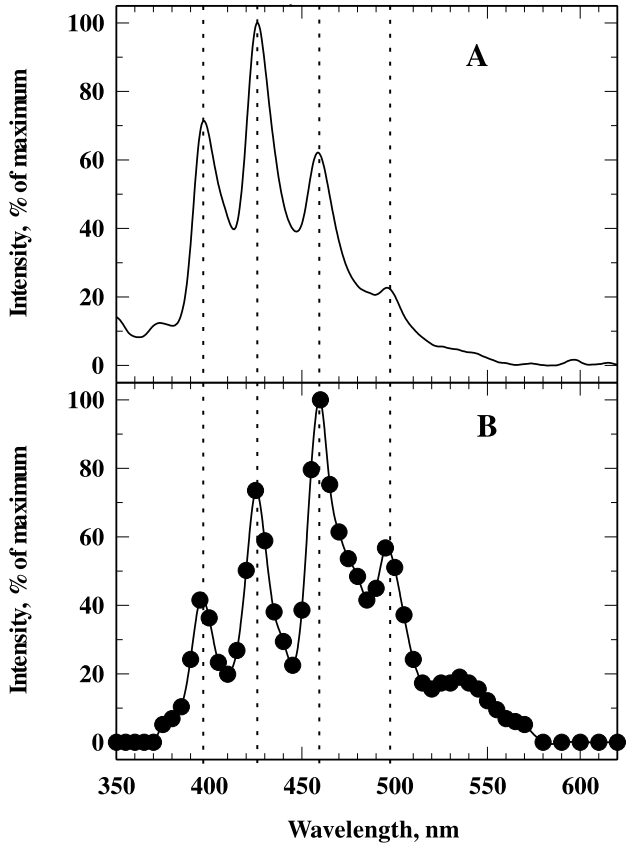
The triple-channel ALD and an Oriel model 77250 eighth-meter monochromator, *f*/3.7, with a no. 77298 grating (1200 lines/mm, 500 nm blaze) and 0.02–3.2 mm variable slits (reciprocal dispersion 6.4 nm/mm), were used in this mode. The single-peak scanning mode had been developed in our laboratory (6) for accurate spectral scans of GC peaks passing through a dual-channel FPD. An Oriel no. 77325 stepping motor, driven by a lab-built circuit with scan speeds from 0.25 to 315 nm/min, was used to record the spectra of luminescent GC peaks traversing the ALD. To correct for the analyte peak's first increasing and then decreasing concentration, the true intensity distribution of the spectrum was obtained by measuring the ratio of two channels. One was the dispersive spectral channel scanning through the desired wavelength region; the other a non-dispersive channel of constant wavelength (one of the response-ratio channels). The spectrum from the dispersive and the chromatogram from the non-dispersive channel were simultaneously recorded by a dual-channel program called CHROM 8 (7). The stored data were converted to an ASCII file and exported to a commercial program (SigmaPlot, Jandel Scientific, San Rafael, Calif.) for further manipulation.

The luminescence measurements were made by using one or more of three different recording modes. For strongly luminescing compounds such as benzaldehyde, the gas-phase spectrum was obtained with a Jarrell–Ash model 82-415 quarter-meter monochromator and (later) with an Oriel model 77250 eighth-meter monochromator (vide supra). The spectra from the two monochromators were equivalent, differing only in intensity distribution due to the distinctly different light transmission profiles of the two gratings (cf. Fig. 4). In most cases, the spectra reported are those obtained by the eighth-meter monochromator used in single-peak mode (i.e., by scanning a single chromatographic peak and employing dual-channel correction to account for the change in concentration profile during peak elution). For some weakly emitting compounds such as 1,4-naphthoquinone, a low-resolution device with a far higher light throughput, the Oriel "filter monochromator," was employed to map the spectra; and argon was added to the carrier gas to enhance aroyl luminescence.

For strongly luminescing compounds, a sample amount of 10 ng was typically required for injection into the triple-channel ALD system running in single-peak mode. However, spectra could still be measured from a peak of less than 10 ng, though with some loss in resolution (due to a wider slit and (or) a longer time constant). To secure as good a spectrum as possible from a single peak, samples corresponding in amount to the upper end of the linear calibration range were routinely introduced into the ALD. A background spectrum of pure nitrogen (the so-called second positive system) was always present at high amplification. To obtain spectra that accurately correlated spectral information with concentration, such a spectral background had to be subtracted from the raw spectrum as seen by the dispersive channel. While the "referenced" spectra of this study were corrected for the peak concentration profile and the nitrogen

© 2000 NRC Canada

Fig. 4. Gas-phase luminescence spectrum of benzaldehyde in excited nitrogen, as obtained from a 100 ng peak with the 1/8 meter grating monochromator (A); and by repeatedly injecting 100 ng benzaldehyde, with the 1/4 meter grating monochromator (B).



background, none were corrected for photomultiplier quantum yield, monochromator grating efficiency, or other instrumental parameters. Only the wavelength indicator on the monochromator was recalibrated from time to time with the help of a low-pressure mercury lamp. The slit width was usually set at 1 or 2 mm (about 6.6 and 13 nm bandpass, respectively), in accord with the innate spectral bandwidth.

Results and discussion

Selectivity

Very few types of organic compounds emitted light in the ALD. Only compounds containing an aroyl moiety in the form of an aromatic aldehyde, ketone, or quinone luminesced strongly. Most aromatic nitriles, esters, chlorides, alcohols, amines, and sulfides did not respond, even at the 1 µg level. Among aroyl-type compounds, particular ring substituents such as nitro-, amino-, and hydroxy- groups, as well as certain substituents in particular ring positions (mainly *ortho*), did severely depress or even eliminate luminescence. For these and other cases, a flame ionization detector (FID) was employed—in conjunction with temperature-programmed separation—to ensure that these organics did, in fact, properly elute from the GC column. Typical non-responding organic compounds are mentioned in Table 1, while Table 2 lists responding (and also some non-responding) aroyl compounds together with their relative luminescence intensities (vis-á-vis benzaldehyde), both according to structural similarity.

Table 1. Non-responding compounds in the ALD.

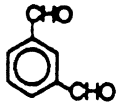
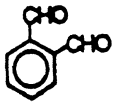
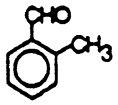
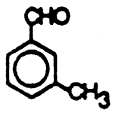
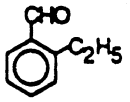
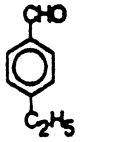
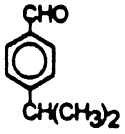
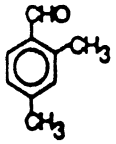
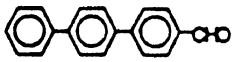
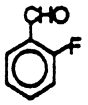
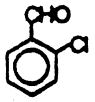
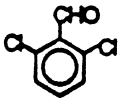
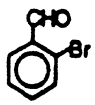
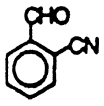
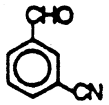
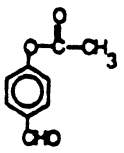
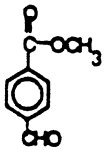
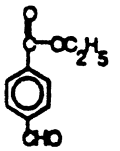
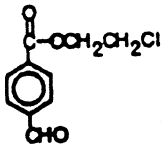
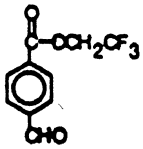
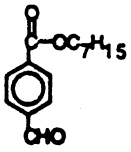
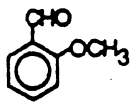
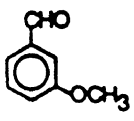
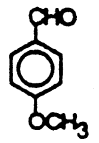
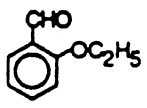
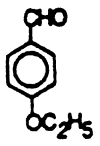
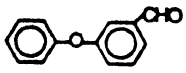
Aliphatic hydrocarbons	Fluoranthene
Aliphatic aldehydes	Pyrene
Aliphatic ketones	Benzo[*a*]pyrene
Aliphatic alcohols	2*H*-pyran-2-one
Aliphatic amines	Biacetyl
Aliphatic nitriles	Acetylacetone
Aliphatic sulfides	*p*-Benzoquinone
Aliphatic halides	Phenyl-1,4-benzoquinone
Aliphatic esters	Pyridazine
Aliphatic ethers	Pyrazine
Benzene	Pyrimidine
Nitrobenzene	Pyridine
1,3,5-Triethylbenzene	2,2′-Pyridil
Benzonitrile	Quinoxaline
Benzylether	Quinoline
Benzylchloride	Isoquinoline
Benzylalcohol	1-Benzosuberone
Benzylamine	Piperonal
Diphenylether	2-Phenyl-1,3-indandione
Diphenylsulfide	Benzalphthalide
Benzoylchloride	Furil
Phenylacetate	Benzil
Phenylacetaldehyde	Cumarin
Benzylacetate	Flavone
Phenylacetonitrile	3*H*-1,2-Benzodithiol-3-one
2-Phenylethylacetate	1,1′-Carbonyldiimidazole
Phenyl-2-propanone	3-Formylchromone
2-Phenylethylalcohol	3-Formyl-6-nitrochromone
3-Phenyl-1-propanol	2-Fluorene-carboxaldehyde
Naphthalene	Dibenzoylmethane
1-Methylnaphthalene	1-Benzoylacetone
Acenaphthene	*n*-Butyrophenone
Anthracene	Benzanthrone
Phenanthrene	Dibenzosuberenone

Spectra and interpretation

The photochemical behavior and photophysical properties of selected aromatic carbonyl compounds have been thoroughly studied both in condensed phases and in the gas phase. It is generally assumed that *unsubstituted* aromatic carbonyl compounds emit phosphorescence only, because the overall intersystem crossing $S_1 \rightarrow T_1$ is very efficient (8, 9). Some *substituted* aromatic carbonyl compounds also exhibit solely phosphorescence, while others display both phosphorescence and fluorescence (10). The triplet state gives rise to many photochemical reactions (11). The nature of the lowest excited state happens to be a subject of great interest. It is well established that T_1, the lowest excited triplet state of typical aromatic carbonyl compounds such as benzaldehyde or benzophenone, is $^3(n,\pi^*)$ both in non-polar solvents and in the gas phase. In contrast, T_1 of some substituted compounds that possess an electron-donating group at the para position is attributed to $^3(\pi,\pi^*)$ excitation (2, 12). The nature of the triplet state can be assigned to π,π^* or n,π^* based on several factors including (*i*) lifetime and polarization, (*ii*) electron

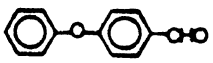
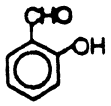
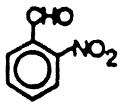
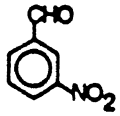
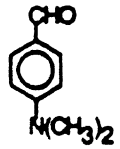
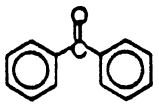
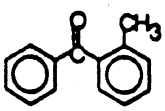
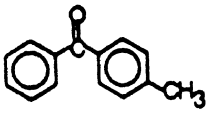
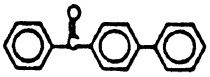
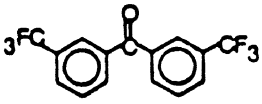
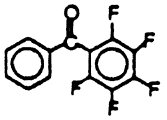
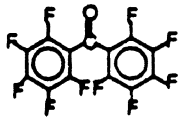
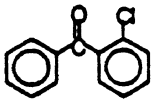
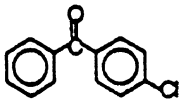
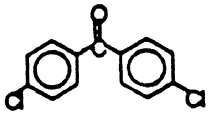
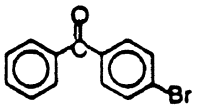
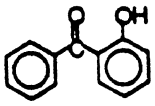
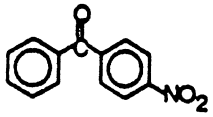
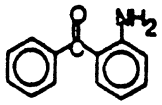
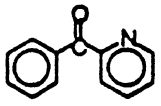
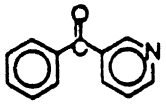
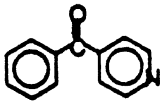
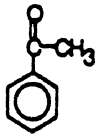
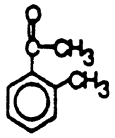
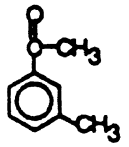
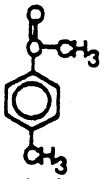
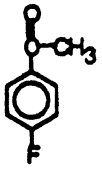
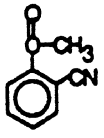
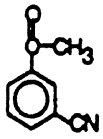
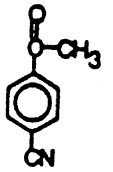
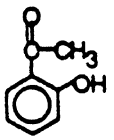
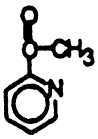
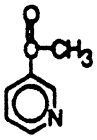
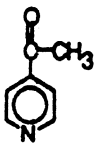
© 2000 NRC Canada

Table 2. Intensity of aroyl response in the ALD (as percent of benzaldehyde response).

 benzaldehyde (100)	 isophthalaldehyde (92)	 terephthal dicarbox-aldehyde (105)	 phthal dicarbox-aldehyde (0)	 2-methylbenz-aldehyde (0)
 3-methylbenz-aldehyde (125)	 4-methylbenz-aldehyde (120)	 2-ethylbenz-aldehyde (0)	 4-ethylbenz-aldehyde (138)	 4-isopropylbenz-aldehyde (165)
 2,4-dimethylbenz-aldehyde (0)	 biphenyl-4-carbox-aldehyde (0.2)	 2-fluorobenz-aldehyde (71)	 3-fluorobenz-aldehyde (75)	 4-fluorobenz-aldehyde (81)
 2-chlorobenz-aldehyde (10)	 4-chlorobenz-aldehyde (45)	 2,6-dichlorobenz-aldehyde (3)	 2-bromobenz-aldehyde (0)	 4-bromobenz-aldehyde (0)
 2-cyanobenz-aldehyde (0)	 3-cyanobenz-aldehyde (172)	 4-cyanobenz-aldehyde (100)	 4-acetoxybenz-aldehyde (45)	 methyl 4-formyl-benzoate (75)
 ethyl 4-formyl-benzoate (70)	 2-chloroethyl 4-formylbenzoate (61)	 2,2,2-trifluoro-ethyl 4-formyl-benzoate (73)	 n-heptyl 4-formyl-benzoate (60)	 2-methoxybenz-aldehyde (0)
 3-methoxybenz-benzoate (38)	 4-methoxybenz-aldehyde (7)	 2-ethoxybenz-aldehyde (0)	 4-ethoxybenz-aldehyde (2)	 3-phenoxybenz-aldehyde (0.5)

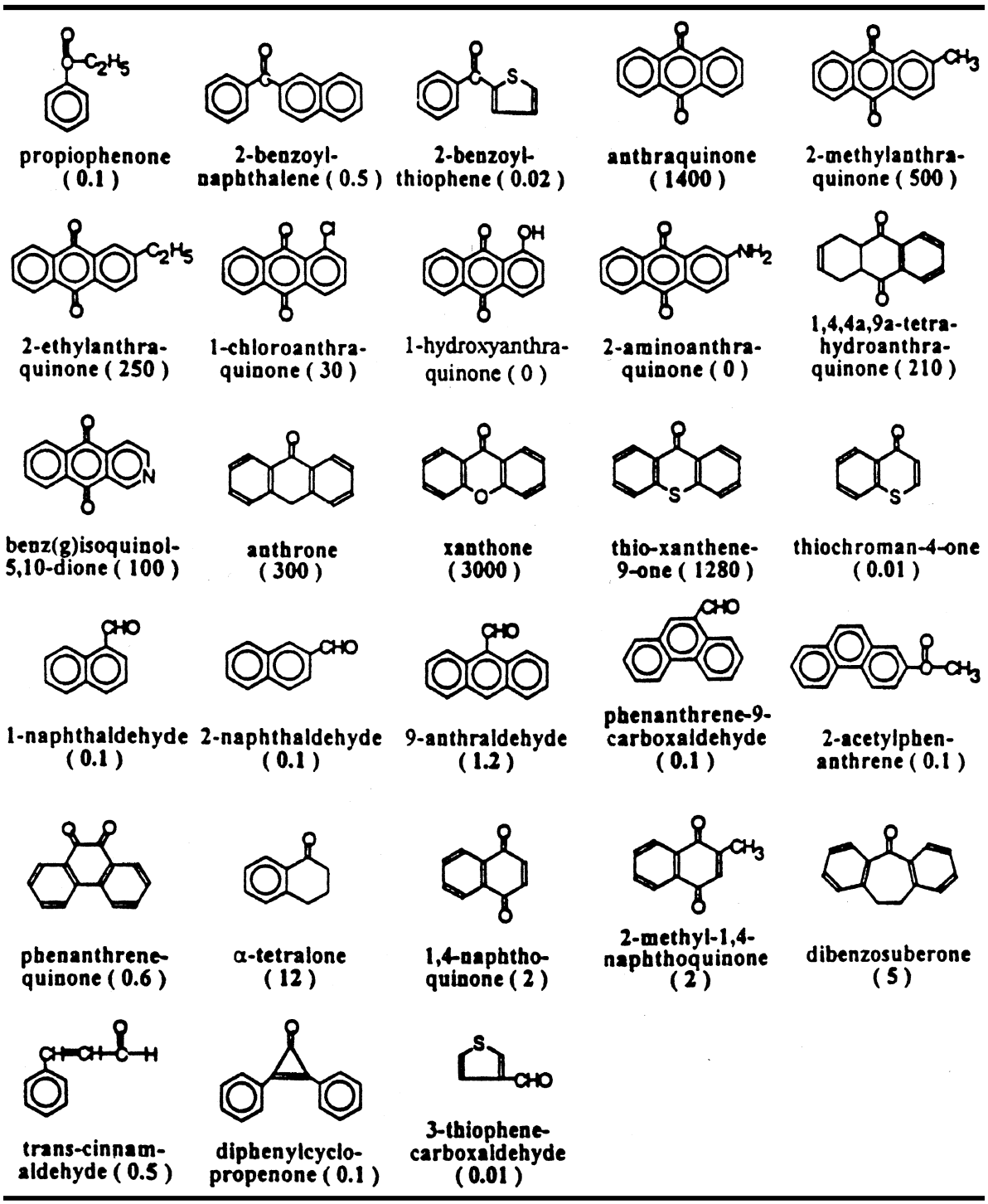
© 2000 NRC Canada

Table 2 (*continued*).

 4-phenoxybenz-aldehyde (0)	 2-hydroxybenz-aldehyde (0)	 2-nitrobenz-aldehyde (0)	 3-nitrobenz-aldehyde (0)	 4-nitrobenz-aldehyde (0)
 4-(dimethyl-amino)-benz-aldehyde (0)	 benzophenone (100)	 2-methylbenzo-phenone (0)	 4-methylbenzo-phenone (84)	 4-benzoyl-biphenyl (3.6)
 3,3'-bis(trifluoro-methyl)benzo-phenone (47)	 2,3,4,5,6-penta-fluorobenzo-phenone (0.02)	 decafluorobenzo-phenone (0)	 2-chlorobenzo-phenone (4)	 4-chlorobenzo-phenone (46)
 4,4'-dichloro-benzophenone (42)	 4-bromobenzo-phenone (0)	 2-hydroxybenzo-phenone (0)	 4-nitrobenzo-phenone (0)	 2-aminobenzo-phenone (0)
 2-benzoyl-pyridine (0.4)	 3-benzoyl-pyridine (1)	 4-benzoyl-pyridine (25)	 acetophenone (28)	 2-methylaceto-phenone (0)
 3-methylaceto-phenone (50)	 4-methylaceto-phenone (32)	 4-fluoroaceto-phenone (50)	 2-acetylbenzo-nitrile (0)	 3-acetylbenzo-nitrile (56)
 4-acetylbenzo-nitrile (134)	 2-hydroxyaceto-phenone (0)	 2-acetylpyridine (0.1)	 3-acetylpyridine (0.3)	 4-acetylpyridine (3)

© 2000 NRC Canada

Table 2 (*concluded*).



spin resonance, (*iii*) triplet-singlet splitting, (*iv*) vibrational structure, and (*v*) the heavy-atom solvent effect on the $n\rightarrow\pi^*$ absorption. It is very common that emission spectra from an n,π^* state of aromatic carbonyls will contain the C=O vibrational structure. All these findings are based on experiments carried out by using photon or electron impact for excitation. In this study, as well as in studies involving the ALD's predecessor (5, 13–15), it was found that only certain aromatic carbonyl compounds luminesce in this radioactively stimulated, high-voltage, low-current nitrogen discharge; others do not. It is therefore of substantial interest to investigate the photophysical properties of those aroyls that do luminescence in excited nitrogen, and to establish their excitation mechanism.

Benzaldehydes

Benzaldehyde, the simplest of the carbonyl-containing molecules, has been spectroscopically and photochemically

© 2000 NRC Canada

Table 3. Spectral characteristics of benzaldehyde and some substituted benzaldehydes.

Compound	Origin of $T_1(n,\pi^*) \rightarrow S_0$ transition, cm^{-1} (nm)	Substitutent shifts of $T_1(n,\pi^*) \rightarrow S_0$, cm^{-1} [a]
Benzaldehyde	25189 (397)	0
Isophthalaldehyde	24876 (402)	–313
Terephthaldicarboxaldehyde	23866 (419)	–1323
3-Methylbenzaldehyde	25126 (398)	–63
4-Methylbenzaldehyde	25316 (395)	+127
4-Ethylbenzaldehyde	25253 (396)	+64
4-Isopropylbenzaldehyde	25253 (396)	+64
2-Fluorobenzaldehyde	24510 (408)	–679
3-Fluorobenzaldehyde	24876 (402)	–313
4-Fluorobenzaldehyde	25381 (394)	+192
2-Chlorobenzaldehyde	24038 (416)	–1151
4-Chlorobenzaldehyde	25000 (400)	–189
2,6-Dichlorobenzaldehyde	24213 (413)	–976
3-Cyanobenzaldehyde	24631 (406)	–558
4-Cyanobenzaldehyde	24096 (415)	–1093
4-Acetoxybenzaldehyde	25253 (396)	+64
3-Methoxybenzaldehyde	25000 (400)	–189
4-Methoxybenzaldehyde	25381 (394)	+192
4-Ethoxybenzaldehyde	25445 (393)	+256
4-Methyl-formylbenzoate	24390 (410)	–799
4-Ethyl-formylbenzoate	24390 (410)	–799
4-(1-Chloroethyl)-formylbenzoate	24390 (410)	–799
4-(1,1,1-Trifluoroethyl)-formylbenzoate	24390 (410)	–799
4-Heptylformylbenzoate	24509 (408)	–680

[a]The + and – signs indicate blue and red shifts, respectively. The correct number of significant digits is indicated by the wavelength data (nm).

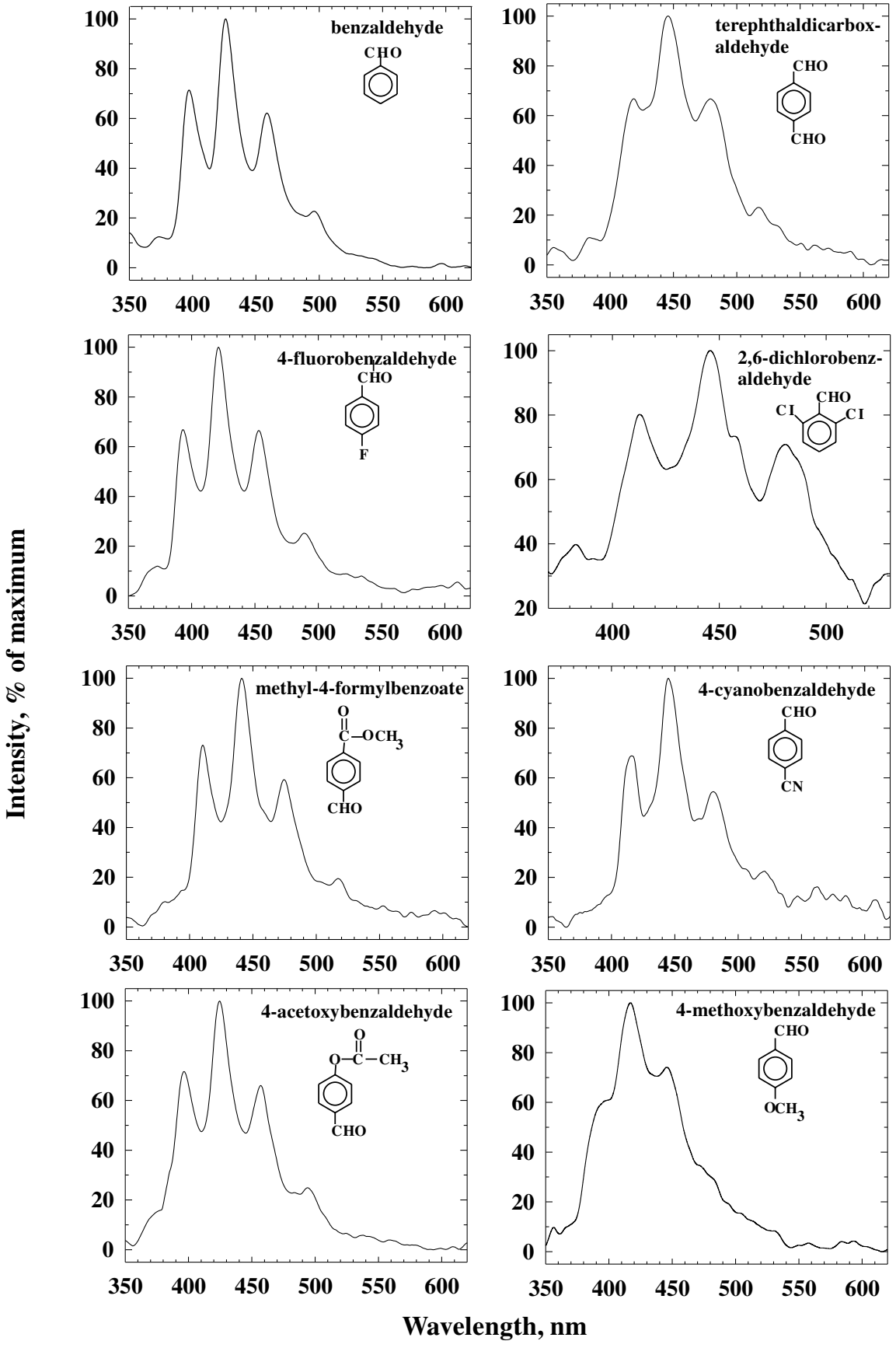
well investigated (1, 16–19), and these studies have served as the basis for understanding more complex aromatic carbonyl spectra. As mentioned before, the unsubstituted carbonyl-containing molecules usually emit phosphorescence only (10). The phosphorescence of benzaldehyde can be induced by optical excitation (2, 17–20), electron impact (3) or active nitrogen (21) in the condensed (2, 17, 18) or the gas phase (3, 21–24). The spectrum obtained in this investigation exhibits prominent peaks at 397, 427, 460, and 498 nm. This spectrum resembles the phosphorescence spectrum of benzaldehyde measured in a rigid medium (2) or in the gas phase (3, 21–24). The bands obtained in this study at high temperature and ambient pressure are, not surprisingly, somewhat broader than the ones measured at room temperature and reduced pressure in the gas phase. The C=O stretching progression with a spacing of about 1730 cm^{-1} appears prominent in the gas-phase luminescence spectrum. Based on the literature and these observations, then, the present spectrum is clearly that of benzaldehyde phosphorescence. Prominent peaks at 397, 427, 460 and 498 nm were assigned to the 0–0 band and progressions in the C=O stretching mode. The phosphorescence of benzaldehyde originates from the $T_1(n,\pi^*) \rightarrow S_0$ transition. $T_1(n,\pi^*)$ at 397 nm (25 189 cm^{-1} or 3.12 eV or 301 kJ/mol) is the lowest triplet state in benzaldehyde (2, 10). This assignment agrees with the previously reported assignment (2, 3), and is useful in locating $T(n,\pi^*)$ triplet states in substituted benzaldehydes.

The gas-phase luminescence spectra of benzaldehyde and of a selected few substituted benzaldehydes are shown in Fig. 5. The spectroscopic data for all investigated benzaldehydes of adequate luminescence are given in Table 3. For space reasons, however, Fig. 5 was only permitted to include those spectra that deviate most from that of benzaldehyde itself, or that are of particular interest for structural or spectroscopic reasons. Most spectra are quite similar to that of unsubstituted benzaldehyde, except for the spectral shift caused by the substituent(s). All of these spectra exhibit the same vibrational progression characteristic of the C=O stretching frequency (about 1700 cm^{-1}), and all can therefore be assigned to a $T_1(n,\pi^*) \rightarrow S_0$ transition. The spectroscopic data are in agreement with vapor phase data where such are available (23), or close to data obtained in nonpolar solvents (20). Electron-*donating* groups at the para-position cause a blue shift of the $T_1(n,\pi^*) \rightarrow S_0$ transition, whereas electron-*withdrawing* groups at the para-position cause a red shift (except for 4-fluorobenzaldehyde). On the other hand, the transitions are red-shifted in meta-substituted benzaldehydes relative to those of benzaldehyde. It is interesting to note that, while 4-fluorobenzaldehyde exhibits a large blue shift relative to benzaldehyde, the 2- and 3-fluorobenzaldehydes show a red shift. Fluorine thus behaves here like an alkyl or alkoxy group. This observation agrees with previous reports (20, 25).

Figure 6 shows the gas-phase phosphorescence spectrum of benzaldehyde at different temperatures. Within error limits, there is no change in wavelength and little if any change in relative band intensity. This means that the spectroscopic nature of benzaldehyde luminescence does not change with temperature (i.e., that there is no evidence of thermal activation). The emission intensity of phosphorescence increased

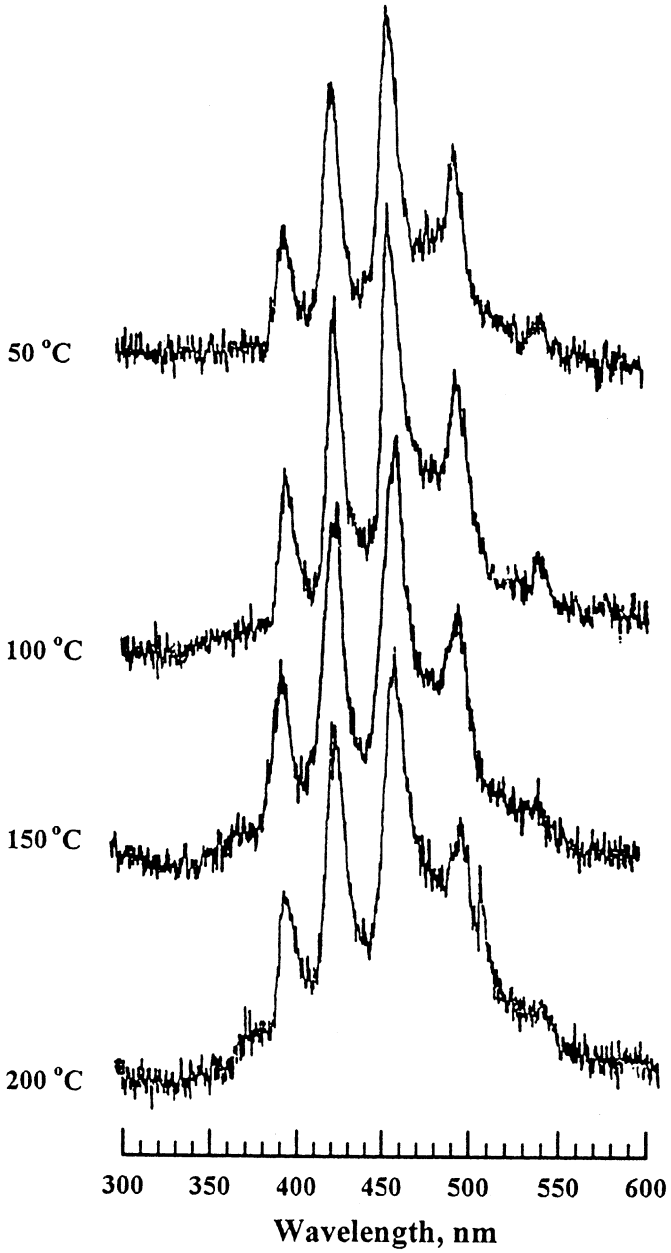
© 2000 NRC Canada

Fig. 5. Gas-phase luminescence spectra of selected benzaldehydes in excited nitrogen. Single-peak mode, 1/8 meter grating monochromator with R-374 PMT. Bandpass: 6.6 nm.



© 2000 NRC Canada

Fig. 6. Gas-phase luminescence spectra of benzaldehyde at different temperatures. Continuous-doping mode, 1/4 meter grating monochromator with R-374 PMT.

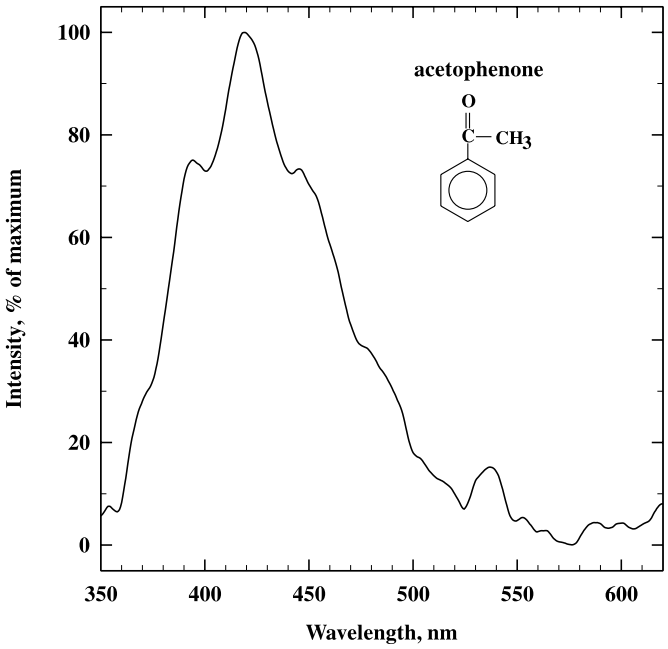


slightly as temperature increased (possibly because of the lower gas density), and the vibrational structure of the phosphorescence spectrum became slightly more diffuse (temperature broadening). The latter agrees with photophysical studies of other aroyl compounds in the gas phase (26, 27), but disagrees with studies in rigid media (28, 29).

Acetophenones

Acetophenone is the simplest aromatic ketone and has long been the subject of spectroscopic and photophysical studies (2, 23, 29–33). However, ambiguity remains concerning the assignment of the lowest triplet state of acetophenone (and of substituted acetophenones) in various environments (32, 34). The gas-phase luminescence spectrum of acetophenone is shown in Fig. 7; it is very similar to the spectra of several substituted acetophenones that could not be included here because of space limitations, but whose spectroscopic data are presented in Table 4. Figure 8 adds the spectra of two of the structurally related acetylpyridines (Note: 4-acetylpyridine looks much like 2-acetylpyridine). A severe loss of resolution is observed in these spectra compared to those of the benzaldehydes, because the slow torsional vibrations of the methyl group result in spectral congestion (33). The spectrum of acetophenone measured in this study exhibits peaks at ca. 394, 420, and 450 nm, and it shows a prominent C=O stretching vibrational progression with a spacing of about 1600 cm^{-1}. This spectrum is very similar in shape to that of acetophenone phosphorescence obtained in a rigid medium (2), the gas phase (23), or on Whatman no. 1 filter paper (29). Thus we conclude that the present gas-phase luminescence spectrum is mainly if not exclusively the phosphorescence spectrum of acetophenone. The lowest triplet state of acetophenone in the gas phase is of normal n,π^* character, because it is well known that n,π^*-type phosphorescence spectra exhibit a clear progression of the carbonyl vibration (10). The luminescence spectra of the substituted acetophenones are also considered to be phosphorescence spectra owing to their similarity to that of acetophenone.

Fig. 7. Gas-phase luminescence spectrum of acetophenone. Single-peak mode, 1/8 meter grating monochromator with R-374 PMT. Bandpass: 6.6 nm.



The 0–0 transitions of acetophenones are blue-shifted by electron-donating, red-shifted by electron-withdrawing groups at the para-position. The direction of shift parallels that of the substituted benzaldehydes. This similarity reflects the similar nature of the triplet state, which is T(n,π^*) for both benzaldehydes and acetophenones.

Benzophenones

Benzophenone has been investigated extensively as a triplet energy donor (1, 35), and its luminescence in various me-

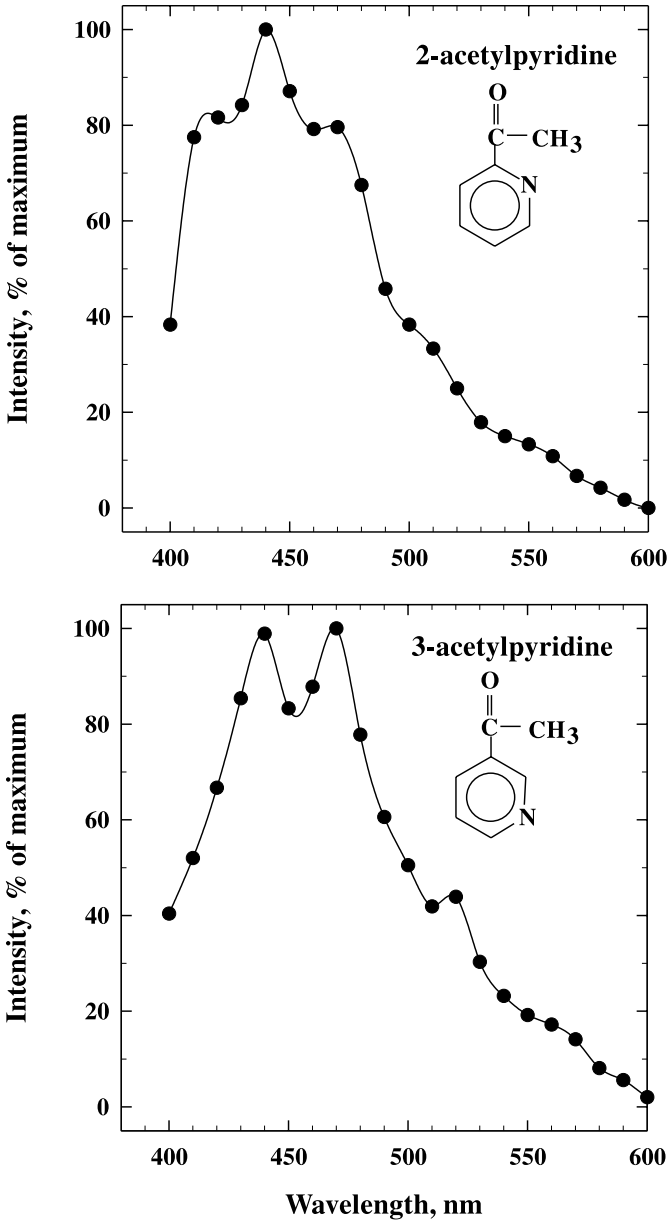
© 2000 NRC Canada

Table 4. Spectral characteristics of acetophenone and some substituted acetophenones.

Compound	Origin of phosphorescence, cm^{-1} (nm)	Substitutent shifts of 0–0 transitions, cm^{-1} [a]
Acetophenone	25381 (394)	0
3′-Methylacetophenone	25445 (393)	+64
4′-Methylacetophenone	25510 (392)	+129
4′-Fluoroacetophenone	25510 (392)	+129
3-Acetylbenzonitrile	24752 (404)	–629
4-Acetylbenzonitrile	24272 (412)	–1109
2-Acetylpyridine	24154 (414)	–1227
3-Acetylpyridine	22727 (440)	–2654
4-Acetylpyridine	24449 (409)	–932

[a]The + and – signs indicate blue and red shifts, respectively. Precision is indicated by wavelength (not wavenumber) digits.

Fig. 8. Gas-phase luminescence spectra of two acetylpyridine isomers. Repeated-injection mode, filter monochromator with R-268 PMT and 2 mm slit (bandpass ca. 13 nm).



dia was thoroughly studied (1, 2, 4, 8, 23, 29, 36, 37). In early papers it was reported that benzophenone shows solely phosphorescence from a $T_1(n,\pi^*)$ state in a rigid matrix at 77 K (1, 2, 36, 37). Sun et al. (26) demonstrated that the luminescence of benzophenone in CCl_4 solutions consists mainly of delayed fluorescence and phosphorescence originating from thermally equilibrated S_1 and T_1 states. The observation of delayed benzophenone fluorescence in solution (38, 39) and in rigid media (40) was confirmed by other researchers. Gated nanosecond time-resolved laser spectroscopy proved well suited to studying such luminescent processes of low quantum efficiency and (or) several competing modes of emission (39). The luminescence of benzophenone in the *gas* phase was first reported by Borisevich and Gruzinskii (41). Based on the appreciable overlap of the absorption and emission spectra, and on the long decay time of the emission, these authors concluded that the luminescence is thermally-activated delayed fluorescence (41). Dorokhin and Kotov (42) investigated the effect of temperature on the delayed luminescence of benzophenone, and showed that, as the temperature rises, the fraction of thermally activated delayed fluorescence in the total emission increases, similar to what had been reported for benzophenone in the condensed phase (26, 40). Itoh et al. (23) interpreted the gas-phase emission spectrum of benzophenone as being composed mainly of phosphorescence, accompanied by very weak E-type delayed fluorescence at shorter wavelengths. Inoue (4) measured the emission spectrum of benzophenone induced by electron impact, and assigned the spectrum to benzophenone phosphorescence with the origin at 390 nm (25 641 cm^{-1}).

Figure 9 shows the gas-phase luminescence spectrum of benzophenone in excited nitrogen. The spectra of various substituted benzophenones, including the benzoylpyridines, look very similar; they could not be reproduced here for space reasons. The ALD spectrum of benzophenone is very similar in shape to those spectra of benzophenone that had been assigned to mainly E-type fluorescence and phosphorescence (23, 26, 39, 40), but differs from the pure phosphorescence spectrum of benzophenone in rigid media (1, 2, 36, 37). It seems therefore reasonable to conclude that the gas-phase luminescence of benzophenone consists mainly of E-type fluorescence and phosphorescence with origins at about 380 nm (26 316 cm^{-1}) and 420 nm (23 809 cm^{-1}), respectively. Owing to the similarity of the substituted-

© 2000 NRC Canada

Fig. 9. Gas-phase luminescence spectrum of benzophenone. Single-peak mode, 1/8 meter grating monochromator with R-374 PMT. Bandpass: 12.6 nm.

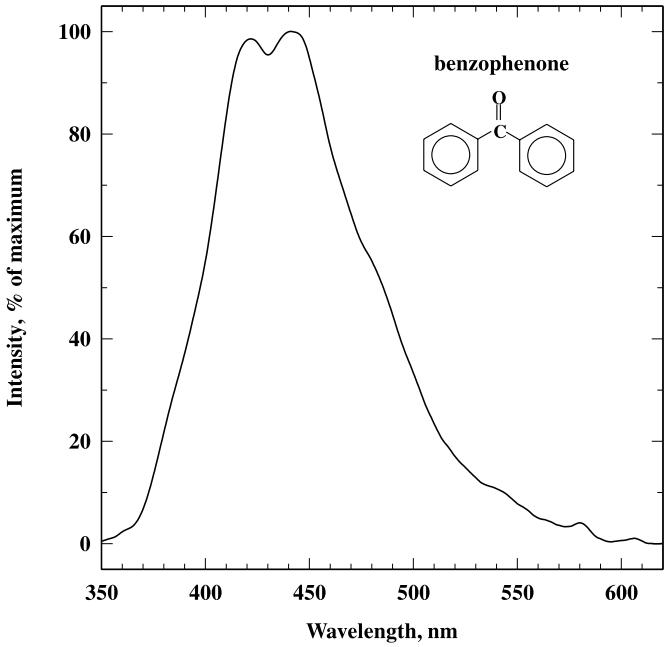
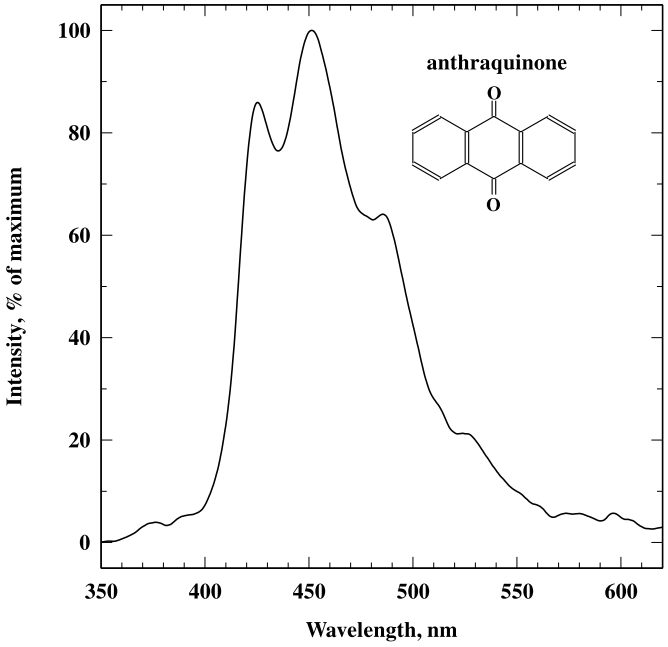


Fig. 10. Gas-phase luminescence spectrum of anthraquinone. Single-peak mode. 1/8 meter grating monochromator with R-374 PMT. Bandpass: 6.6 nm.



benzophenone spectra we tentatively assume that these, too, originated from a combination of E-type delayed fluorescence and phosphorescence. The substitutents shift only slightly the 0–0 transition of phosphorescence, but the direction of shift again parallels shifts observed in substituted benzaldehydes and acetophenones. Again, this similarity reflects the similar nature of the lowest triplet state for these three types of aromatic carbonyl compounds.

Anthraquinones

Anthraquinone is another aroyl compound whose photophysical and photochemical behavior was extensively investigated (43–56). The compound (9,10-anthraquinone by its complete name) shows comparatively strong emission in the visible region in various rigid media (16, 43, 45). This emission has been identified as phosphorescence from the lowest triplet state of the n,π^* type, originating at about 455 nm (22 000 cm^{-1}) (45–47, 50, 52). It is also known that anthraquinone exhibits weak emission in the gas phase. The gas-phase emission was obtained by Singh and Singh (53) and later by Longin (54) by discharge excitation. The former authors regarded the luminescence in the 420–540 nm region as fluorescence and that in the 590–690 nm region as phosphorescence, while Longin assigned the emission to dual fluorescence with origins at 421.4 and 422.7 nm. Later Rogozhin and co-workers (55) obtained highly resolved emission spectra of anthraquinone vapor at relatively high temperature. To clarify the nature of gaseous anthraquinone luminescence, emission and excitation spectra were measured and compared with those in the condensed phases by Itoh (56). Although the spectra obtained under different conditions differed with respect to band resolution and shape, the author's interpretation was that the emission of anthraquinone vapor consisted of $S_1(n,\pi^*) \rightarrow S_0$ fluorescence and $T_1(n,\pi^*) \rightarrow S_0$ phosphorescence, with origins at about 422 nm (23 700 cm^{-1}) and 455 nm (22 000 cm^{-1}), respectively.

In the present study, anthraquinone vapor exhibited very strong luminescence in excited nitrogen. Figure 10 shows the gas-phase luminescence spectrum of anthraquinone, to which the spectra of some substituted anthraquinones — which could not be printed here for editorial reasons — are very similar. Some of their spectroscopic data are found in Table 5. The main bands of the anthraquinone spectrum occur at around 425, 452, 487, and 530 nm. This spectrum is quite different from the phosphorescence spectra of anthraquinone obtained in rigid media and at low temperature (44, 46, 50), but very similar in respect to band position and shape to spectra obtained by Longin (54) and Itoh (56) in the gas phase. Hence, we presume that the anthraquinone spectrum in excited nitrogen consists of $S_1(n,\pi^*) \rightarrow S_0$ E-type fluorescence and T_1 $(n,\pi^*) \rightarrow S_0$ phosphorescence with origins at about 425 nm (23 529 cm^{-1}) and 452 nm (22 124 cm^{-1}), respectively. The prominent peaks at 452, 487, and 530 nm are assigned to the 0–0 band and progressions of the C=O stretching mode. From the 0–0 band position, the singlet–triplet energy gap, $\Delta E_{S-T,}$ is found to be 1405 cm^{-1}.

The gas-phase luminescence spectra of substituted anthraquinones are essentially identical to the spectrum of anthraquinone itself; they all exhibit the principal vibrational structure of the carbonyl stretching frequency (1590–1660 cm^{-1}) and can therefore be regarded as consisting of $S_1 \rightarrow S_0$ E-type fluorescence and $T_1 \rightarrow S_0$ phosphorescence from a T_1 state of n,π^* character. It is noteworthy that no significant wavelength shift has been observed among the anthraquinones tested (see Table 5).

© 2000 NRC Canada

Table 5. Spectral characteristics of anthraquinone and some substituted anthraquinones.

Compound	Origin of fluorescence, cm^{-1} (nm)	Origin of phosphorescence, cm^{-1} (nm)
Anthraquinone	23529 (425)	22124 (452)
2-Methylanthraquinone	23419 (427)	22124 (452)
2-Ethylanthraquinone	23419 (427)	22124 (452)
1-Chloroanthraquinone	23474 (426)	22124 (452)
1,4,4a,9a-Tetrahydroanthraquinone	23419 (427)	22124 (452)
Benz[*g*]isoquinolon-5,10-dione	23474 (426)	22124 (452)

1,4-Naphthoquinone and its 2-methyl derivative

1,4-Naphthoquinone is one of the prototype quinones and several studies were reported of its photophysical properties. Kuboyama and Yabe (45) recorded the strong visible emission of 1,4-naphthoquinone in a rigid glass solution at 77 K. This emission has been assigned to an n,π^*-type phosphorescence from the lowest triplet state. In the gas phase, 1,4-naphthoquinone shows weak emission. The first gas-phase emission spectra of 1,4-naphthoquinone were obtained in the presence of flowing benzene vapor by Singh and Singh (57), and later by Longin (54) by discharge excitation. Singh and Singh assigned the emission to fluorescence and phosphorescence with origins at 21 945 cm^{-1} (455 nm) and 18 782 cm^{-1} (532 nm), respectively, while Longin thought that the gas-phase emission consisted of two kinds of fluorescence with origins at 22 163 cm^{-1} (451.2 nm) and 21 974 cm^{-1} (455.1 nm). The carbonyl compounds, having a small singlet-triplet energy gap, often exhibit weak E-type delayed fluorescence (35). Itoh and Baba (58) took this into account in their assignment of the emitting states of 1,4-naphthoquinone. They investigated the temperature dependence of both the luminescence spectrum and the lifetime in the presence of foreign gases, and showed that the emission consists of phosphorescence and delayed fluorescence from the lowest triplet and singlet states at 20 460 cm^{-1} (488.8 nm) and 21 830 cm^{-1} (458.1 nm), respectively. In addition to the phosphorescence and E-type delayed fluorescence at low pressure (10^{-3}–10^{-1} Torr)(1 Torr = 133.3 Pa), these authors also reported a prompt fluorescence (59). It is known that the often non-fluorescent nature of aromatic carbonyl compounds is caused by a fast transition from S_1 to T_1; hence their speculation that the prompt fluorescence could be due to isoenergetic intersystem crossing from the lowest triplet to the lowest singlet state under collision-free conditions. More recently, Itoh (27) reported that the gas-phase emission spectrum of 1,4-naphthoquinone consists of dual phosphorescence from $T_1(n,\pi^*)$ and $T_2(n,\pi^*)$ with origins at 20 295 cm^{-1} (488.4 nm) and 20 475 cm^{-1} (492.0 nm), respectively (in addition to the weak E-type delayed fluorescence). This clarified the doublet structures in the main emission bands of 1,4-naphthoquinone vapor.

The emission spectrum of 2-methyl-1,4-naphthoquinone vapor was reported by Baruah et al. (60), and later by Itoh and Baba (58). The former authors interpreted the emission as consisting of fluorescence from an $S_1(n,\pi^*)$ state and phosphorescence from a $T_1(n,\pi^*)$ state, with origins at 22 075 cm^{-1} (453.0 nm) and 20 262 cm^{-1} (493.5 nm), respectively. The latter authors regarded the spectrum as consisting of $T_1(n,\pi^*) \rightarrow S_0$ phosphorescence and weak E-type delayed fluorescence from $S_1(n,\pi^*)$ with origins at 20 340 cm^{-1} (491.6 nm) and 21 950 cm^{-1} (455.6 nm), respectively.

Figure 11 shows the weak gas-phase luminescence spectra of 1,4-naphthoquinone and 2-methyl-1,4-naphthoquinone in excited nitrogen. The spectra lie entirely within the visible region (i.e., no emission below 400 nm). They consist of broad and diffuse bands located at about 450, 485, 525, and 575 nm for 1,4-naphthoquinone; and 455, 490, 530, and 580 nm for 2-methyl-1,4-naphthoquinone. These bands form a prominent C=O stretching progression. They resemble the corresponding gas-phase emission spectra obtained by Itoh (27) and Itoh and Baba (58, 59), and they also agree in band position with the spectra recorded in refs. 54, 57, and 60. We therefore consider the gas-phase luminescence spectra of 1,4-naphthoquinone and 2-methyl-1,4-naphthoquinone to consist of phosphorescence from $T_1(n,\pi^*)$ and E-type delayed fluorescence from $S_1(n,\pi^*)$, with origins at 22 222 cm^{-1} (450 nm) and 20 619 cm^{-1} (485 nm) for 1,4-naphthoquinone; and 21 978 cm^{-1} (455 nm) and 20 408 cm^{-1} (490 nm) for 2-methyl-1,4-naphthoquinone, respectively.

Xanthone and thioxanthone

Xanthone is one of a number of carbonyl compounds that exhibit anomalous emission behavior. Pownall and Huber (61) reported that the emission spectrum of xanthone in 3-methylpentane at 77 K is due to phosphorescence from a triplet n,π^* state with origin at 25 905 cm^{-1} (386 nm) and that it shows four fundamental vibrations with frequencies of 260, 530, 930 and 1665 cm^{-1}, while the polar-solvent phosphorescence originates from a triplet π,π^* state. Later, based on a study of xanthone emissions at about 2 and 77 K, Pownall et al. (62) concluded that xanthone exhibits "dual" phosphorescence at 77 K in a 3-methylpentane glass matrix, owing to emission from two triplet n,π^* states with origins at 25 905 cm^{-1} (386 nm) and 25 650 cm^{-1} (389 nm). They also reported the phosphorescence spectrum to be very sensitive to temperature. This phenomenon was confirmed by Terada and co-workers in a polyethylene matrix (63). However, the latter authors identified the lowest triplet state as π, π^*, which is in agreement with emissions from the crystal and from a diphenylmethane matrix at 1.5 K (64). Kanda and co-workers (65) reported that xanthone shows phosphorescence consisting of mainly three emission systems, whose origins are located at 25,751 cm^{-1} (389 nm), 25 766 cm^{-1} (388 nm) and 25 774 cm^{-1} (387 nm). They also gave a quantitative explanation for the origin of such multiple phosphorescence levels (66).

All these photophysical studies of xanthone were made in rigid media or crystals, with no reports available from the

© 2000 NRC Canada

Fig. 11. Gas-phase luminescence spectra of 1,4-naphthoquinone and 2-methyl-1,4-naphthoquinone. Repeated injection mode, filter monochromator with R-268 PMT and 2 mm slit (bandpass ca. 13 nm).

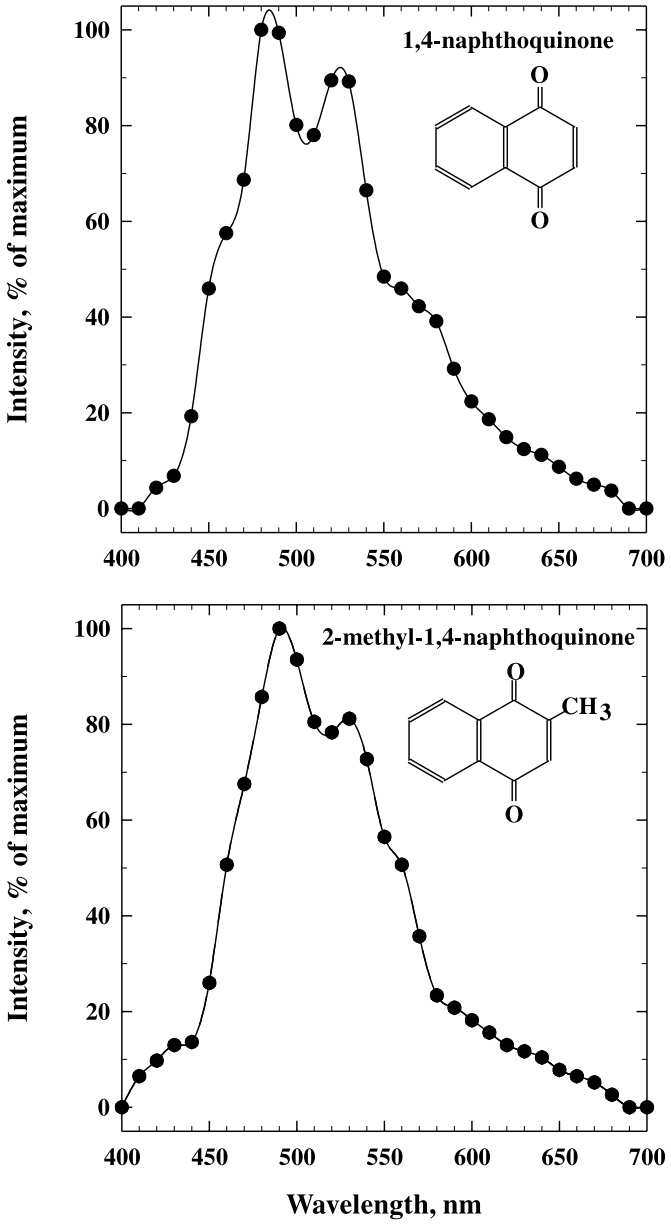
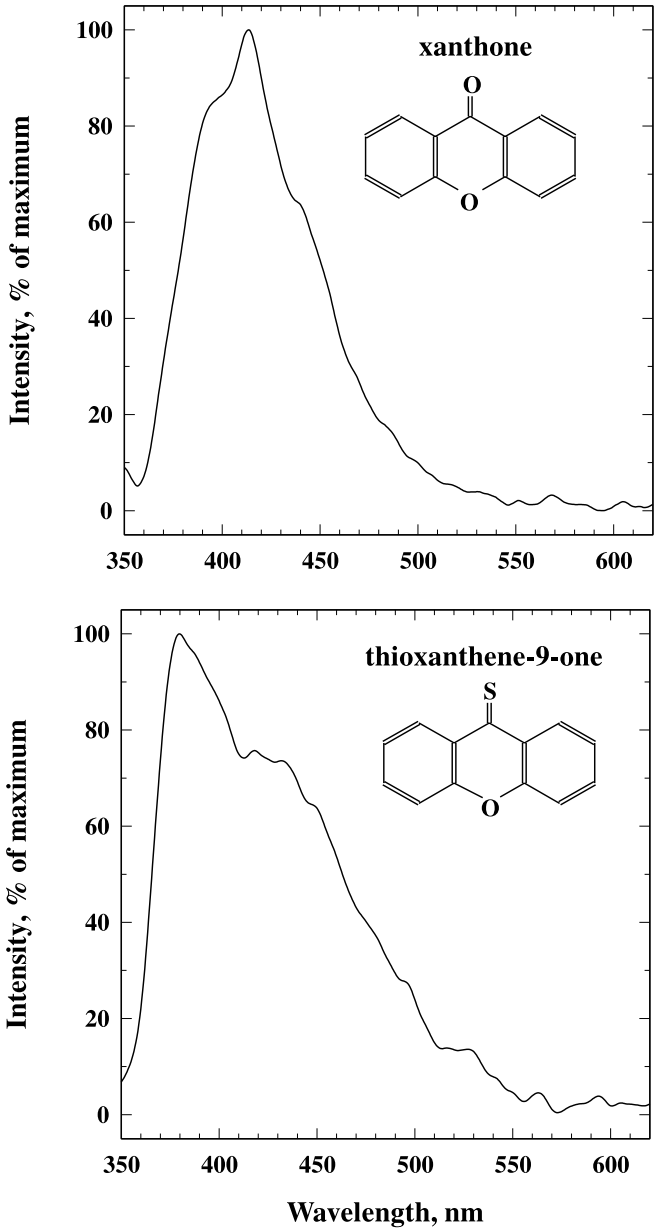


Fig. 12. Gas-phase luminescence spectra of xanthone and thioxanthene-9-one. Single-peak mode, 1/8 meter grating monochromator with R-374 PMT. Bandpass: 6.6 nm.

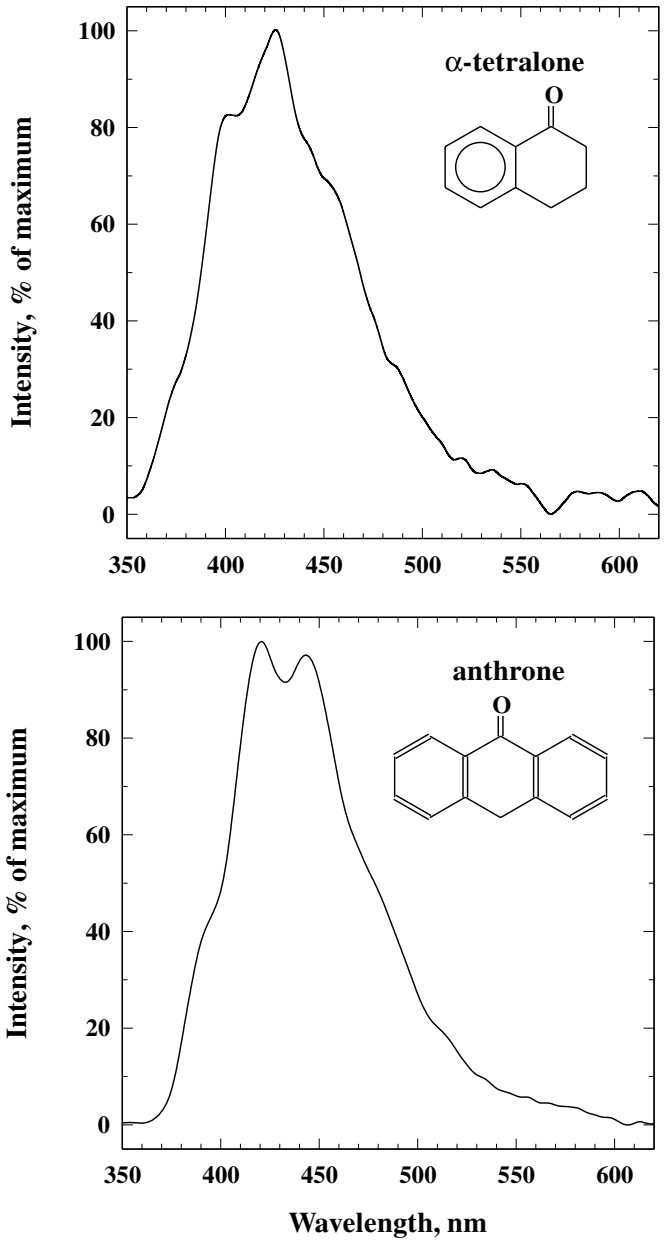


gas phase. In our study, xanthone luminesced strongly in excited nitrogen and turned out to be the strongest emitter among the sixty-odd compounds investigated. Figure 12 shows the gas-phase luminescence spectra of xanthone and thioxanthene-9-one in excited nitrogen. The emission of xanthone exhibits little structure and shows a maximum at about 24 154 cm^{-1} (414 nm) with two shoulders at about 25 773 cm^{-1} (388 nm) and 22 573 cm^{-1} (443 nm). These are also the main peaks in the phosphorescence spectrum of xanthone in 3-methylpentane at 77 K (61). It is therefore reasonable to conclude that the gas-phase luminescence of xanthone in excited nitrogen is due to phosphorescence from a $T_1(n,\pi^*)$ state, with the 0,0 band at about 25 773 cm^{-1} (388 nm). The bands at 24 154 cm^{-1} (414 nm) and 22 573 cm^{-1} (443 nm) are then the progressions of the C=O stretching mode. However, a more detailed analysis of vibrational structure cannot be made at this time due to spectrum congestion.

Thioxanthene-9-one also shows strong emission in excited nitrogen. Its gas-phase spectrum, but for the change in relative band intensity, resembles that of xanthone. (The agreement of wavelengths has been verified by making use of the "repeated-injection" mode — see Experimental — but the spectra are not shown here for space reasons.) Given this similarity, we suggest that the gas-phase emission spectrum of thioxanthene-9-one is caused by phosphorescence from a triplet n,π^* state with origin at about 26 316 cm^{-1} (380 nm). The 0–0 band is the strongest in the phosphorescence spec-

© 2000 NRC Canada

Fig. 13. Gas-phase luminescence spectra of α-tetralone and anthrone. Single-peak mode, 1/8 meter grating monochromator with R-374 PMT. Bandpass: 12.6 nm (tetralone) and 6.6 nm (anthrone).



trum of thioxanthene-9-one. This is in striking contrast to the case of xanthone, whose main radiative mechanism is possibly vibronic. This result differs substantially from the few condensed-phase emission data available on thioxanthene-9-one (67).

α-*Tetralone*

The phosphorescence behavior of this type of aromatic ketone is rather complex. Dual and even triple phosphorescence has been reported (65, 68–70). Several emission studies of α-tetralone have been done in rigid media (37, 69–71) or in a single durene crystal (72). It was reported that α-tetralone shows phosphorescence from a triplet n,π^* state with origin at about 25 450 cm^{-1} (393 nm) (37, 69–72). Kanda et al. (69) concluded that — unlike 1-indanone, which exhibits dual phosphorescence from a short-lived (1.5–2 ms) triplet n,π^* state and a long-lived (0.15–0.22 s) triplet state with mixed n,π^* and π,π^* character due to the reversible photochemical formation of the enolate anion — α-tetralone does not emit dual phosphorescence in accord with its lower acidity. This was, however, disputed by Chu and Kearns (70), who did manage to observe dual phosphorescence. They attributed the short-lived emission of α-tetralone to a $T_1(n,\pi^*)$ state, but considered the long-lived emission due to a mixture of photoreduction products. Their "authentic" phosphorescence spectrum of α-tetralone from the triplet n,π^* state contained three main peaks at about 25 253 cm^{-1} (396 nm) 23 641 cm^{-1} (423 nm) and 21 882 cm^{-1} (457 nm).

The emission spectrum of α-tetralone in the gas phase had not been reported before. Our spectrum (Fig. 13) was obtained in excited nitrogen to which argon had been added. (Note: the addition of argon was used in this study to boost the emission intensity of some rather weakly luminescing aroyl compounds such as α-tetralone, 9-anthraldehyde, and dibenzosuberone. Before using this technique for the acquisition of weak spectra, however, argon doping was thoroughly tested on such compounds as benzaldehyde and anthraquinone to ensure the absence of any change in wavelength and relative band intensity for both the aroyl analyte and the second-positive system of nitrogen. The *first*-positive system of nitrogen begins to show up under argon doping; however, this emission is extremely faint and does not compromise the spectral results.) The spectrum of α-tetralone shows little structure, with a maximum at 23 529 cm^{-1} (425 nm) and two shoulders at about 25 125 cm^{-1} (398 nm) and 21 925 cm^{-1} (456 nm). This spectrum is very similar in band position and relative intensity to the phosphorescence spectrum reported of α-tetralone in rigid media (37, 69, 70). We therefore tentatively assign the gas-phase luminescence spectrum of α-tetralone to phosphorescence from a $T_1(n,\pi^*)$ state with origin at about 25 125 cm^{-1} (398 nm). (Note that the undulations in Fig. 13 at $\lambda > 520$ nm are acquisition noise caused by the necessary high amplification.)

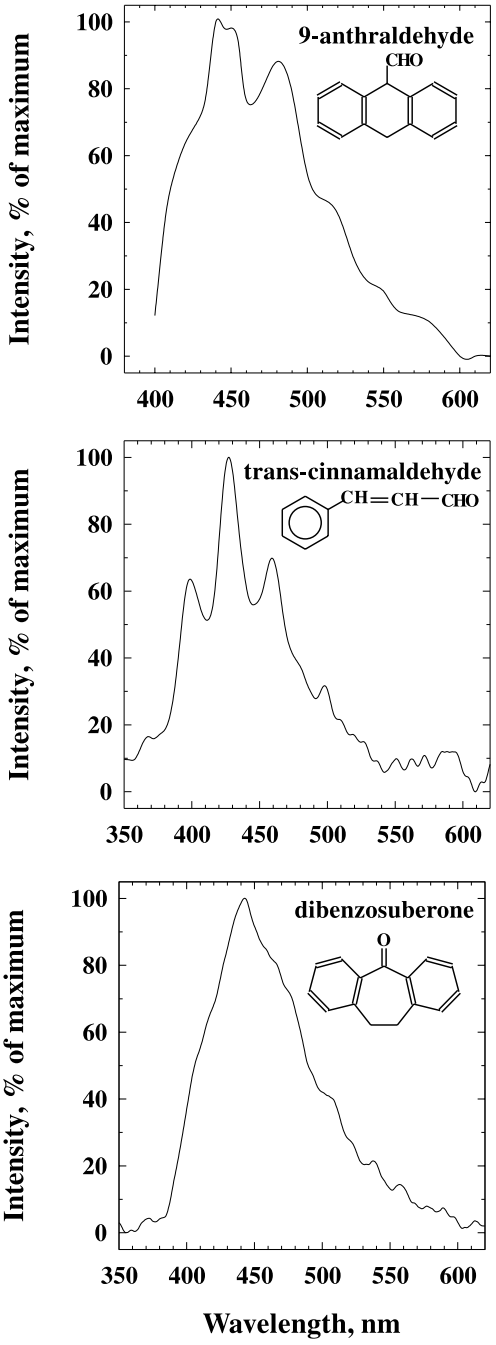
Anthrone

The photophysical and photochemical behavior of carbonyl compounds has been the subject of numerous studies, but among these anthrone received only very limited attention. It was reported that, in rigid media, anthrone exhibits phosphorescence from an n,π^* state with origin at 25 150 cm^{-1} (397.6 nm) (1, 37, 73). The other prominent peaks occur at about 23 331 cm^{-1} (430 nm), 21 739 cm^{-1} (460 nm), 20 202 cm^{-1} (495 nm), and 18 691 cm^{-1} (535 nm), and exhibit the pattern expected of aromatic C=O vibration (37).

Figure 13 shows the gas-phase luminescence spectrum of anthrone in excited nitrogen. It differs greatly from the pure phosphorescence spectrum of anthrone in rigid media (37), but is very similar in spectral shape and band position to the gas-phase luminescence spectrum of benzophenone in excited nitrogen, which was assigned to a mixture of E-type delayed fluorescence and phosphorescence. Given this similarity and the structural analogy between anthrone and benzophenone, the same assignment may be made for anthrone.

© 2000 NRC Canada

Fig. 14. Top: Gas-phase luminescence spectrum of 9-anthraldehyde. Repeated-injection mode, filter monochromator with R-268 PMT and 2 mm slit (bandpass ca. 13 nm), smoothed, and data points removed. Center: gas-phase luminescence spectrum of *trans*-cinnamaldehyde. Single-peak mode, 1/8 meter grating monochromator with R-374 PMT. Bandpass: 6.6 nm. Bottom: gas-phase luminescence spectrum of dibenzosuberone. Single-peak mode, 1/8 meter grating monochromator with R-374 PMT. Bandpass: 12.6 nm.



A similar comparison in regard to their photochemical behavior was made by Scaiano and Lee (74).

9-Anthraldehyde

Yang (75) reasoned, by analogy, that the triplet state of 9-anthraldehyde lies at the low value of 14 800 cm^{-1} (676 nm) and is π,π^* in nature. Warwick and Wells (76) confirmed the lowest π,π^* triplet state in 9-anthraldehyde by the oxygen perturbation technique. Hirayama (77) carried out kinetic studies relevant to the excited singlet and triplet states on eighteen anthracene-based carbonyl compounds in EPA at 77 K. He concluded that the 0–0 fluorescence band lies at 21 598 cm^{-1} (463 nm); and that the phosphorescence, which occurs from a triplet π,π^* state with origin at 13 790 cm^{-1} (725 nm), is very similar to that of anthracene in spectral shape and T_1 energy.

In excited nitrogen, 9-anthraldehyde shows relatively weak emission. The gas-phase luminescence spectrum of 9-anthraldehyde (Fig. 14) has two main peaks at 22 471 cm^{-1} (445 nm) and 20 833 cm^{-1} (480 nm), with two shoulders at about 24 096 cm^{-1} (415 nm) and 19 230 cm^{-1} (520 nm). This spectrum is very similar to the fluorescence spectrum in rigid media, both in spectral shape and band position. If the phosphorescence of 9-anthraldehyde occurred in the long-wavelength region (650–850 nm), we would not have observed it due to the limited wavelength range (400–700 nm) of the filter monochromator (which had to be used for this very weak emission).

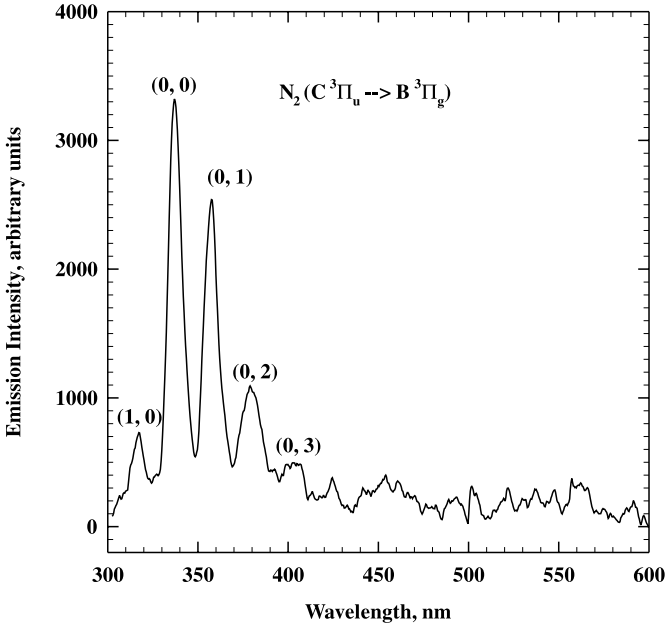
trans-*Cinnamaldehyde and dibenzosuberone*

To the best of our knowledge, the photophysical behaviors of *trans*-cinnamaldehyde and dibenzosuberone have not been investigated either in solution or in the gas phase. This is not surprising: dibenzosuberone is a rather obscure molecule, and the carbonyl group of the much more prominent *trans*-cinnamaldehyde does not adjoin the aromatic ring. (Thus considered, *trans*-cinnamaldehyde is an "aroyl" only by conjugation, not definition.) In this study, both compounds emitted weakly in excited nitrogen. The spectra of *trans*-cinnamaldehyde and dibenzosuberone are shown in Fig. 14. *trans*-Cinnamaldehyde emits a gas-phase spectrum similar to that of benzaldehyde, except for a slight red shift. The spectrum displays prominent peaks at about 25 063 cm^{-1} (399 nm), 23 366 cm^{-1} (428 nm), 21 739 cm^{-1} (460 nm), and 20 040 cm^{-1} (499 nm), and it shows a typical aromatic C=O vibrational spacing of 1674 cm^{-1}. We regard the present spectrum therefore to be that of *trans*-cinnamaldehyde phosphorescence from a $T_1(n,\pi^*)$ state. This means that the C=C group, which establishes conjugation between the carbonyl group and the benzene ring, does not appreciably alter the nature of the excited state as compared to that of benzaldehyde. However, it does lower the energy of the excited triplet state because of the conjugative effect (10). (Again, the spectral undulations above ca. 500 nm are random instrumental noise and should be disregarded.)

The gas-phase luminescence spectrum of dibenzosuberone exhibits a broad band with a maximum at about 22 573 cm^{-1} (443 nm); closest, perhaps, to that of anthrone. There is no literature available concerning the luminescence spectrum of dibenzosuberone. Since the luminescing compounds investigated in this study are all excited to the triplet state and emit mainly phosphorescence, we tentatively regard the gas-phase luminescence spectrum shown as that of dibenzosuberone phosphorescence. Also, since all compounds that gave note-

© 2000 NRC Canada

Fig. 15. Nitrogen background spectrum (second positive system) in the ALD.



worthy response in the ALD did so via n→π* (as opposed to π→π*) excitation, we presume dibenzosuberone to emit from a $T_1(n,\pi^*)$ state.

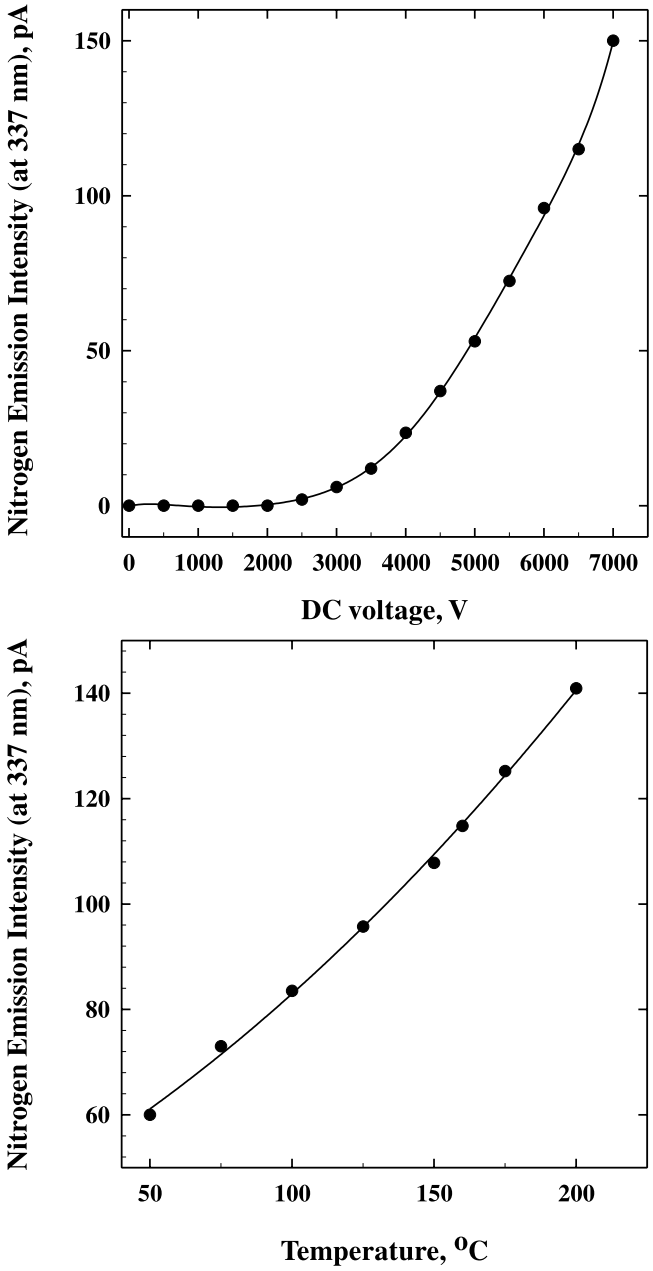
A speculative mechanism for luminescence of aroyl compounds in excited nitrogen

Background Luminescence in the ALD

Figure 15 shows the spectral background, i.e., the nitrogen luminescence of the ALD. The emission was scanned between 200 and 800 nm under various experimental conditions, and consisted solely of the well-known nitrogen "second positive" band system. This system results from the radiative decay of triplet-state nitrogen molecules, $N_2(C\ ^3\Pi_u) \rightarrow N_2(B\ ^3\Pi_g)$, and is seen in the 300–400 nm range, with the most intense band centered at 337.1 nm. It is very weak in the ALD**,** barely visible to the dark-adapted eye and instrumentally undetectable at the sensitivity setting used to record typically strong luminescence spectra. (However, when acquiring weaker spectra, the nitrogen background had to be subtracted, see Experimental.) The ALD differs markedly in this respect from the dielectric discharge system, in which a blue, flame-like nitrogen second-positive emission can be observed even under full room lights (78, 79). Figure 16 shows the intensity of the second-positive system's 0,0 band at 337.1 nm increasing with voltage and temperature. The nitrogen emission intensity was also measured as a function of pressure. As shown in Fig. 17, and as expected, the emission intensity of the nitrogen second-positive system increased as the pressure was lowered (even though the DC voltage had to be lowered simultaneously to avoid sparking).

The ALD is a radioactively stimulated, high-voltage, low-current (<35 nA) discharge. Thus, as expected, increasing its voltage did exponentially increase both its optical emission and its electrical current (5). (The current plots have been omitted to conserve space.) No other nitrogen emission could

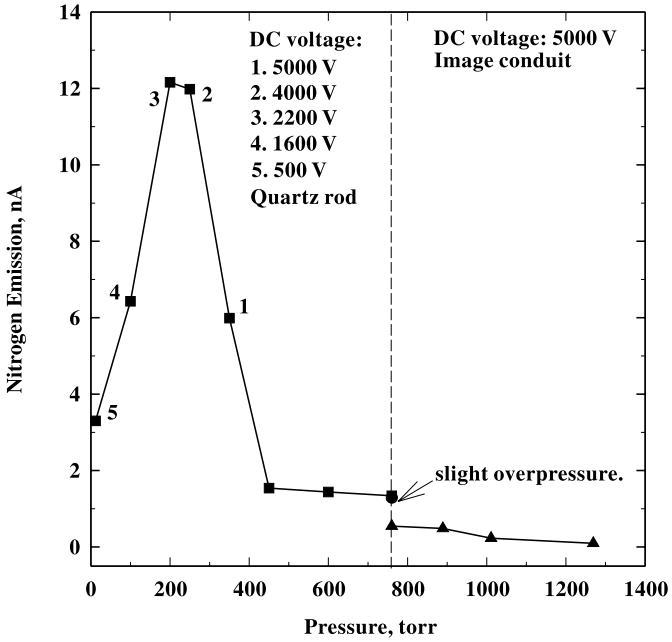
Fig. 16. Nitrogen second-positive emission at 337 nm as a function of applied DC voltage (top) and temperature (bottom).



be detected in the ALD system beside the nitrogen second-positive system, although a careful search for the possible nitrogen first-positive system, $N_2(B\ ^3\Pi_g) \rightarrow N_2(A\ ^3\Sigma_u^+)$, and the Vegard–Kaplan system, $N_2(A\ ^3\Sigma_u^+) \rightarrow N_2(X\ ^1\Sigma_g^+)$, was carried out. (Note: extremely faint traces of the nitrogen first-positive system do, however, show up when nitrogen is doped with argon.) Apparently, in pure nitrogen, the second-positive transition is able to generate only those low vibrational levels of the B state ($v < 6$) from which no visible emission is observed in the $N_2(B\ ^3\Pi_g) \rightarrow N_2(A\ ^3\Sigma_u^+)$ transition (80). The absence of the Vegard–Kaplan band system, $N_2(A\ ^3\Sigma_u^+) \rightarrow N_2(X\ ^1\Sigma_g^+)$, may be due to some rapid reactions of the $N_2(A\ ^3\Sigma_u^+)$ state, or to its meager overall yield in the ALD (cf. 78, 81).

© 2000 NRC Canada

Fig. 17. Nitrogen background emission in the ALD as a function of pressure. Note: Voltage settings at subambient pressure conditions are selected close to sparking. The quartz rod, used for the vacuum experiments, transmits more light at 337 nm than the image conduit.

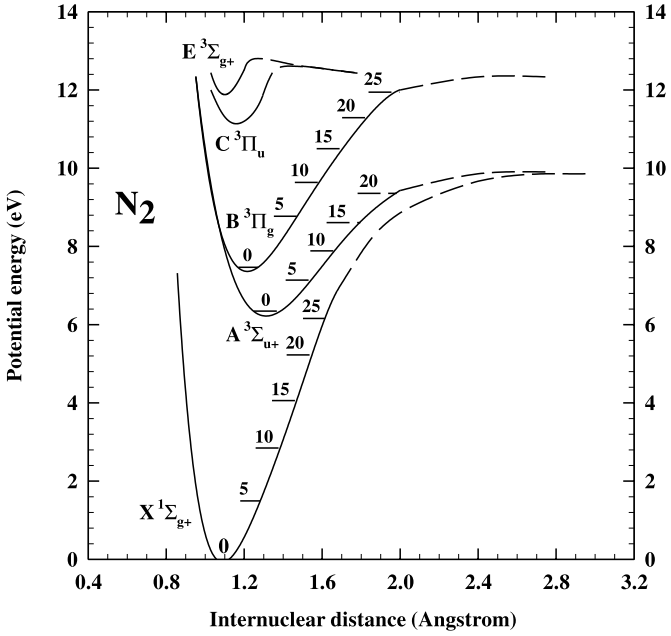


A partial energy-level diagram of dinitrogen and some of its excited states is shown in Fig. 18 for the reader's convenience. The first triplet state, metastable $N_2(A\ ^3\Sigma_u^+)$, with a long radiative lifetime ($\tau \leq 3.5$ s at low pressure) (82) and (at $v = 0$) 6.17 eV (594.9 kJ/mol) of energy above the $N_2(X\ ^1\Sigma_g^+)$ ground-state, can be obtained from electron exchange (83). The short-lived $N_2(B\ ^3\Pi_g)$ triplet state (τ ~10 ns) at 7.35 eV (708.7 kJ/mol) may also be excited from the singlet ground-state by electron exchange (83). The energetic $N_2(C\ ^3\Pi_u)$ state, with a radiative lifetime of 0.1 ms to 10 ns and 11.03 eV (1063.5 kJ/mol) of energy, may be populated by electron impact or triplet-triplet annihilation of $N_2(A\ ^3\Sigma_u^+)$ (84):

$$N_2(A\ ^3\Sigma_u^+) + N_2(A\ ^3\Sigma_u^+) \rightarrow N_2(X\ ^1\Sigma_g^+) + N_2(C\ ^3\Pi_u)$$

It has been observed under circumstances otherwise similar to those of the ALD, that (much weaker) luminescence of aroyl compounds can be observed even in the *absence* of an electric field (5), with the required energy being supplied by the beta rays emanating from the Ni-63 foil. Thus it is reasonable to assume that it is an excited state of nitrogen — as produced in the weak discharge of the ALD — that is causing aroyl excitation. This agrees with the fact that, on a relative basis, aroyl emission intensities are much stronger in the ALD than in the classical vacuum systems of the literature and that, furthermore, no other carrier (pure He, Ar, CO, and a host of other test gases) produced any aroyl emission in the ALD. Also, all excited aroyl states so far found to luminesce were of the $n \rightarrow \pi^*$ (as opposed to the $\pi \rightarrow \pi^*$) type. In the energy-transferring collision between triplet dinitrogen and singlet aroyl molecules, a preference for the larger and easier accessible *n* orbitals of carbonyl oxygen could be expected. While this "steric" explanation is clearly speculative,

Fig. 18. Partial energy-level diagram of N_2, showing species considered relevant to this study.



it would neatly serve to rationalize the conspicuous absence of $\pi \rightarrow \pi^*$ excitation in the ALD. That leaves the question which excited nitrogen species is(are) the source for aroyl emission, and what is the excitation process.

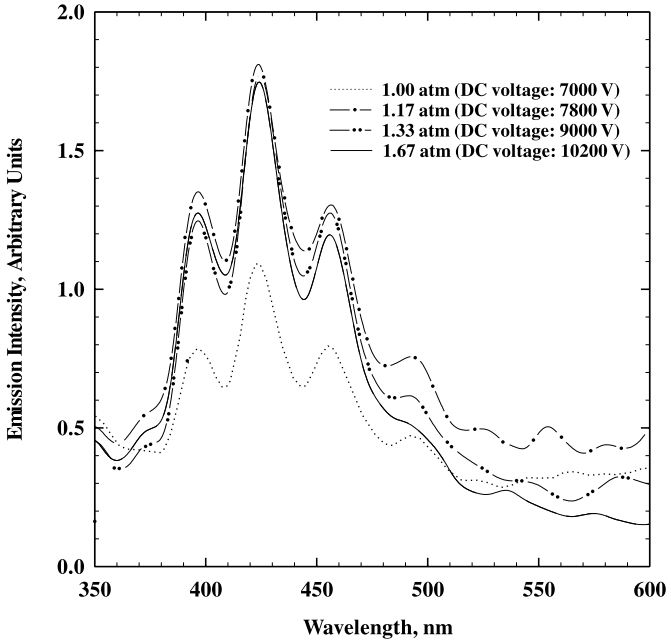
Energy transfer at atmospheric pressure

Generally, phosphorescence originates from excited molecules in their lowest triplet state and is distinguished by a long lifetime (10^{-4}–10 s). Therefore, collisional transfer of energy to molecules of the host gas, or to impurity molecules, is highly probable. At one atmosphere pressure, a molecule experiences close to 10^{10} collisions per second. As a consequence, metastable molecules typically lose their energy by collision before they have a chance to phosphoresce. In literature experiments, gas pressures much lower than ambient are therefore chosen to reduce the collision frequency and hence the collisional quenching of the desired phosphorescence.

In this study, aroyl compounds exhibit intense phosphorescence in the gas phase at atmospheric or even higher pressure. Figure 19 shows the effect of pressure on the relative intensity of gaseous benzaldehyde phosphorescence, as measured under conditions of *constant* nitrogen background emission. (Note: the nitrogen background emission is taken here as a comparative and convenient measure of the "strength" or optical emissivity of the excitation source under a particular set of conditions; it is therefore being held at the same value by correspondingly varying the DC voltage). Figure 19 clearly shows that, under thus "normalized" conditions, the emission intensity of benzaldehyde even increases slightly with increasing pressure. However, there is almost no effect of this pressure increase on spectral resolution. These observations can be rationalized in terms of the collisional excitation of benzaldehyde, with transfer of energy occurring from an excited state of nitrogen. High-purity nitrogen thus acts as both collision and excitation gas in the

© 2000 NRC Canada

Fig. 19. Pressure effect on the relative intensity of benzaldehyde gas-phase phosphorescence.



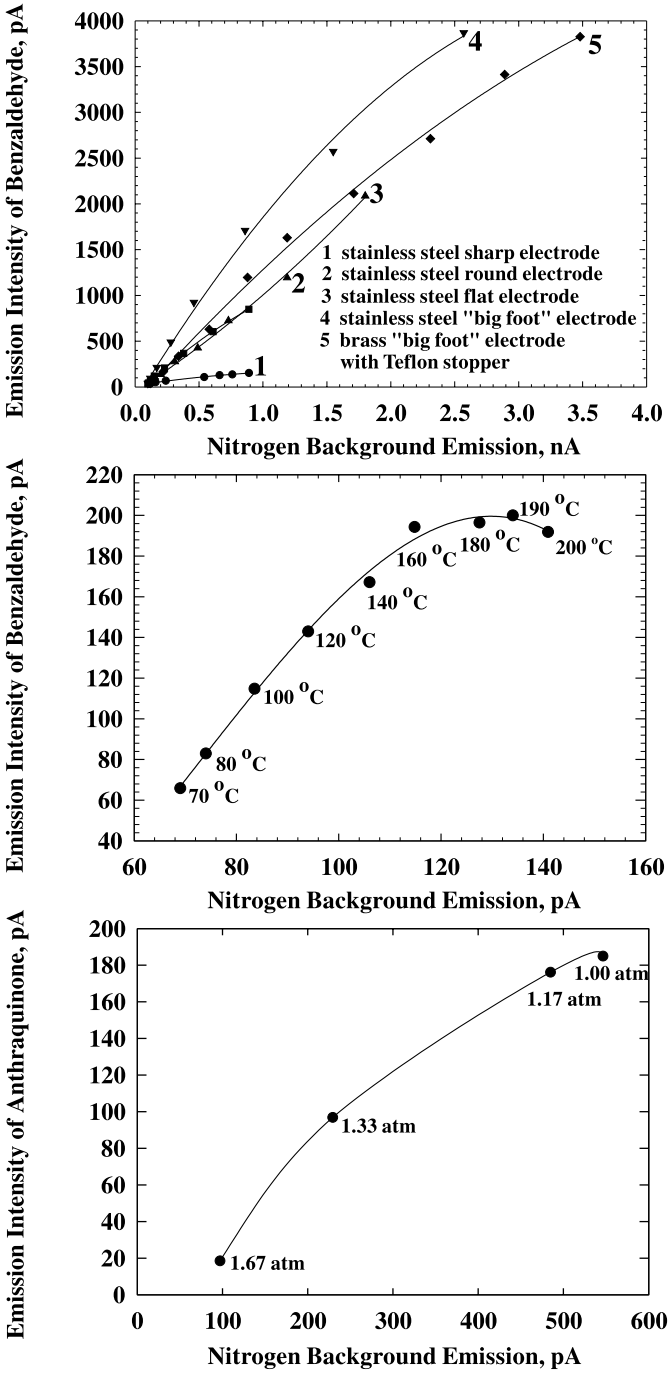
ALD (while the addition of any other molecular gas but induces quenching).

A speculative mechanism

The obvious question then becomes which nitrogen species is likely serving as the carrier of aroyl excitation energy. The weak background emission of the pure-nitrogen ALD originated solely from the so-called second positive system, $N_2(C\ ^3\Pi_u) \rightarrow N_2(B\ ^3\Pi_g)$. Therefore, the correlation between the nitrogen second-positive emission and the aroyl luminescence was checked by varying the applied DC voltage (from 0 to 7000 V), temperature (from 70 to 200 °C), and pressure (from 1.00 to 1.67 atm). The results are shown in Fig. 20 for either benzaldehyde or anthraquinone as test compound. By virtue of curvature, the data fail to implicate the C state, $N_2(C\ ^3\Pi_u)$, as being responsible for the collisional energy transfer to aroyl compounds (although they do not completely exclude it, either). In addition, the shorter (vacuum) lifetimes of $N_2(C)$ (0.1 ms–10 ns) and $N_2(B)$ (~10 ns) indicate that their concentrations may be small — a point reinforced by the (very weak) spectral background — and hence it is doubtful that $N_2(C)$ and (or) $N_2(B)$ would contribute significantly to aroyl excitation. The ALD, in contrast to other excitation sources, is a very "mild" discharge ($I \leq 35$ nA!). Furthermore, $N_2(A\ ^3\Sigma_u^+)$ has a much longer lifetime (≤3.5 s in high vacuum) and a greater stability toward deactivating collisions (83). Plus, its lower energy fits much better the excitation potential of typical aroyl compounds. $N_2(A)$ can therefore be speculatively considered to be the most likely carrier of excitation energy for aroyl luminescence in the ALD system.

In the literature, either metastable triplet state molecules, $N_2(A\ ^3\Sigma_u^+)$, or vibrationally excited ground-state molecules, $N_2(X\ ^1\Sigma_g^+)$, are believed to have served as principal energy carriers for *atomic* excitation in the nitrogen afterglow produced by electric discharges (78, 79). The technique of obtaining a relatively pure supply of $N_2(A\ ^3\Sigma_u^+)$ — with a minimum number of nitrogen atoms — by the reaction $Ar^*(^3P_{0,2}) + N_2 \rightarrow N_2(C)^* \rightarrow N_2(B)^* + h\nu \rightarrow N_2(A)^* + h\nu$ has been reported by Stedman, Setser and co-workers (82, 84, 85); and $N_2(A\ ^3\Sigma_u^+)$ generated by this source has been used as an efficient energy-transfer agent. Devolder et al.

Fig. 20. Emission intensity of aroyl compound versus nitrogen background for (top) DC voltage varied from 0 to 7000 V; (middle) temperature varied from 70 to 200°C; and (bottom) pressure varied from 1.00 to 1.67 atm. Note: different types of electrodes (91) are shown on top for general information; however, all other experiments of this study were carried out with electrode no. 5.



© 2000 NRC Canada

(21, 86, 87) observed phosphorescence of aromatic carbonyl compounds (but also of hydrocarbons!) in their reaction with active nitrogen, which was produced in a microwave discharge at low pressure. The excitation mechanism they proposed also involved the metastable $N_2(A\ ^3\Sigma_u^+)$ state.

Generally, high-energy discharges such as microwave sources produce large amounts of nitrogen atoms, which then rapidly recombine to form metastable $N_2(A\ ^3\Sigma_u^+)$. Electric discharges with a discharge current of about 11.2 mA produce very few nitrogen atoms (78). Instead, the $N_2(A\ ^3\Sigma_u^+)$ state is populated via initial excitation of nitrogen to the $N_2(C\ ^3\Pi_u)$ state. The formation of $N_2(A\ ^3\Sigma_u^+)$ is then believed to result from the following two steps, which are responsible for the appearance of the second positive and the first positive spectrum, respectively:

[1] $N_2(C\ ^3\Pi_u) \rightarrow N_2(B\ ^3\Pi_g)$ (second positive system)

[2] $N_2(B\ ^3\Pi_g) \rightarrow N_2(A\ ^3\Sigma_u^+)$ (first positive system)

In this study, a very mild, low-energy discharge with a discharge current of ≤35 nA — several orders of magnitude lower than the current mentioned in reference (78) — is used as the excitation source for nitrogen. We believe that ground-state N_2 is excited directly to the lowest triplet $N_2(A\ ^3\Sigma_u^+)$ state by collision with fast "secondary" electrons. These secondary electrons are produced by the β-induced ionization of N_2 (as well as by subsequent electron multiplication processes) and acquire their energy mainly from the electric field. (Note: electrons created directly by β-ray impact are, in fact, epithermal; however, they are slowed down quickly by collisions with nitrogen molecules.) Thus metastable $N_2(A\ ^3\Sigma_u^+)$ is assumed responsible for the excitation of aroyl molecules by an efficient triplet-triplet energy transfer process. $N_2(A\ ^3\Sigma_u^+)$ is also considered responsible for producing $N_2(C\ ^3\Pi_u)$ by an energy-pooling process (84), which is followed by the weak emission of the second positive system. In this manner, aroyl and background luminescence in excited nitrogen can be accounted for on the basis of the following mechanistic sequences:

1. Nitrogen is ionized (and occasionally excited) by β-particles from the ^{63}Ni source. Thus, $10^{\ 2}$–$10^{\ 3}$ secondary electrons are produced per β ray:

[3] $\beta + N_2(X\ ^1\Sigma_g^+) \rightarrow \beta' + N_2^+(X\ ^2\Sigma_g^+) + e^-$ (secondary electron)

[4] $\beta + N_2(X\ ^1\Sigma_g^+) \rightarrow \beta' + N_2(C\ ^3\Pi_u)$ (83) (minor process)

2. Singlet ground-state nitrogen is excited by secondary electrons (accelerated by ≤1750 V/mm) to produce $N_2(A\ ^3\Sigma_u^+)$:

[5] $N_2(X\ ^1\Sigma_g^+) + e^-$ (fast) $\rightarrow N_2(A\ ^3\Sigma_u^+) + e^-$ (slow)

3. This is followed by triplet–triplet energy transfer from $N_2(A\ ^3\Sigma_u^+)$ to an aroyl molecule (A):

[6] $N_2(A\ ^3\Sigma_u^+) + A(^1S_0) \rightarrow N_2(X\ ^1\Sigma_g^+) + A(^3T_1)$

and accompanied by some energy pooling of $N_2(A\ ^3\Sigma_u^+)$:

[7] $N_2(A\ ^3\Sigma_u^+) + N_2(A\ ^3\Sigma_u^+) \rightarrow N_2(X\ ^1\Sigma_g^+) + N_2(C\ ^3\Pi_u)$

4. Finally, the phosphorescence (or E-type delayed fluorescence) of aroyl compounds, and the emission of the second positive system of nitrogen take place:

[8] $A(^3T_1) \rightarrow A(^1S_0) + h\nu$ (phosphorescence, detector signal)

or

[9] $A(^3T_1) \rightarrow A(^1S_1)$ (intersystem crossing for close energy levels)

and

[10] $A(^1S_1) \rightarrow A(^1S_0) + h\nu$ (E-type fluorescence, detector signal)

plus

[11] $N_2(C\ ^3\Pi_u) \rightarrow N_2(B\ ^3\Pi_g)$ (second positive system, detector background)

It should again be noted that the metastable $N_2(A\ ^3\Sigma_u^+)$ state, which we propose to be the primary excitation source for the aroyl compounds of this ALD-based study, has long been used as a very efficient triplet-energy transfer agent, both in the gas phase (83, 81, 79, 82, 85–89) and in solid matrices at 4.2 K (90).

Conclusions

Phosphorescence in the gas phase is, as a rule, a very weak and very rare event. Almost all studies of the literature use reduced pressure in order to reduce quenching. In this study, however, very intense gas-phase $n\rightarrow\pi^*$ phosphorescence (or E-type delayed fluorescence) of certain types of aroyl compounds was observed in excited nitrogen at high temperature and atmospheric or higher pressure. A novel, radioactively stimulated, high-voltage, low-current (≤35 nA) discharge in high-purity nitrogen was used to excite the aroyl compounds. Our speculative luminescence mechanism for aroyl compounds suggests that ground-state N_2 is excited to the triplet metastable $N_2(A)$ state by collision with a fast electron, and that this is followed by efficient triplet-triplet energy transfer from $N_2(A\ ^3\Sigma_u^+)$ to the aroyl compound. Thus, for the experimentally ("sterically"?) favored $n\rightarrow\pi^*$ process, this novel excitation source can be used to produce large populations of aroyl triplet states in the gas phase. Such high concentrations of triplet states — which would otherwise be difficult to obtain at atmospheric pressure — can be put to good analytical (and perhaps other) use. The gas-phase luminescences of some sixty compounds were therefore recorded in an effort to assist such endeavors. As it turned out, most of the charted phosphorescences had never before been obtained in the gas phase. While only a few of these spectra could be reproduced in this manuscript because of space limitations, the fact that they can be obtained with ease from the ALD (91), and that some of the relevant spectral data can now be found in the Tables, should significantly

© 2000 NRC Canada

enlarge the analytical and physicochemical data base for their use.

Acknowledgements

This work was supported by the Natural Sciences and Engineering Research Council of Canada (NSERC) individual research grant A-9604. We thank C.G. Eisener for machining the ALD, Brian Millier for electronic help, and Jim Pincock for organic advice. Particular thanks are due to You-Zhi Tang, who obtained the first aroyl phosphorescence spectra from excited nitrogen (5), and who supplied this study with an initial list of relative aroyl responses.

References

1. V.L. Ermolaev. Sov. Phys. Uspekhi, **80**, 333 (1963).
2. D.R. Kearns and W.A. Case. J. Am. Chem. Soc. **88**, 5087 (1966).
3. A. Iuone and N. Ebara. Chem. Phys. Lett. **109**, 27 (1984).
4. A. Iuone. Chem. Lett. 2085 (1986).
5. Y.-Z. Tang. Doctoral thesis. Dalhousie University, Halifax. 1987.
6. H. Singh and W. A. Aue. J. Chromatogr. A, **746**, 43 (1996).
7. X.-Y. Sun. Doctoral thesis. Dalhousie University, Halifax. 1993.
8. N. Ohmori, T. Suzuki, and M. Ito. J. Phys. Chem. **92**, 1086 (1988).
9. T. Itoh. Chem. Phys. Lett. **151**, 166 (1988).
10. R.S. Becker. *In* Theory and interpretation of fluorescence and phosphorescence. Wiley–Interscience, New York. 1969.
11. J.A. Barltrop and J.D. Coyle. *In* Excited state in organic chemistry. John Wiley & Sons, New York. 1975.
12. T. Takemura and H. Baba. Bull. Chem. Soc. Jpn. **42**, 2756 (1969).
13. Y.-Z. Tang and W.A. Aue. J. Chromatogr. **409**, 243 (1987).
14. Y.-Z. Tang and W.A. Aue. Mikrochim. Acta, [Wien], **II**, 21 (1987).
15. Y.-Z. Tang and W.A. Aue. Mikrochim. Acta, [Wien], **II**, 29 (1987).
16. V.L. Ermolaev and A. Terenin. J. Chem. Phys. **55**, 698 (1958).
17. E.V. Donckt and C. Vogels. Spectrochim. Acta, **28A**, 1969 (1972).
18. L. Goodman, M. Lamotte, and M. Koyanagi, Chem. Phys. **47**, 329 (1980).
19. O. Sneh and O. Cheshnovsky. J. Phys. Chem. **95**, 7154 (1991).
20. E. Villa, A. Amirav, W. Chen, and E.C. Lim. Chem. Phys. Lett. **147**, 43 (1988).
21. P. Devolder. C.R. Acad. Sci., Ser. II: Mec., Phy., Chim., Sci., Terres Univers. **No. 4**, 133 (1985). Table 300.
22. M. Koyanagi and L. Goodman. Chem. Phys. **39**, 237 (1979).
23. T. Itoh, H. Baba, and T. Takemura. Bull. Chem. Soc. Jpn. **51**, 2841 (1978).
24. Y. Hirata and E.C. Lim. J. Chem. Phys. **72**, 5505 (1980).
25. S. Yamamoto, T. Ebata, and M. Ito. J. Phys. Chem. **94**, 5786 (1990).
26. Y.P. Sun, D.F. Sears, Jr., and J. Saltiel. J. Am. Chem. Soc. **111**, 706 (1989).
27. T. Itoh. J. Chem. Phys. **87**, 4361 (1987).
28. G. Yamaguchi, Y. Kakinoki, and H. Tsubomura. Bull. Chem. Soc. Jpn. **40**, 526 (1967).
29. G. Scharf and J.D. Winefordner. Talanta, **33**, 17 (1986).
30. R. Shimada and L. Goodman. J. Chem. Phys. **43**, 2027 (1965).
31. W.A. Case and D.R. Kearns. J. Chem. Phys. **52**, 2175 (1970).
32. S.K. Ghoshal, S.K. Sarkar, and G.S. Kastha. Bull. Chem. Soc. Jpn. **54**, 3556 (1981).
33. W. Siebrand, M.Z. Zgierski, A. Amirav, B. Fuchs, A. Penner, and E.C. Lim. J. Chem. Phys. **95**, 3074 (1991).
34. N.C. Yang, D.S. McClure, S.L. Murov, J.J. Houser, and R. Dusenbery. J. Am. Chem. Soc. **89**, 5466 (1967).
35. T. Nakayama, K. Sakural, and K. Hamanoue. J. Chem. Soc. Faraday Trans. **87**, 1509 (1991).
36. N.J. Turro. *In* Modern molecular photochemistry. Benjamin/Cummings, Menlo Park, Calif. 1978.
37. R. Shimada and L. Goodman. J. Chem. Phys. **43**, 2027 (1965).
38. R.E. Brown, L.A. Singer, and J.H. Parks. Chem. Phys. Lett. **14**, 193 (1972).
39. R.E. Brown, K.D. Legg, M.W. Wolf, and L.A. Singer. Anal. Chem. **46**, 1690 (1974).
40. P.F. Jones and A.R. Calloway. Chem. Phys. Lett. **10**, 438 (1971).
41. N.A. Borisevich and V.V. Gruzinskii. Dokl. Akad. Nauk SSSR, **175**, 852 (1967).
42. A.V. Dorokhin and A.A. Kotov. Opt. Spectrosc. **51**, 617 (1981).
43. G.N. Lewis and M. Kasha. J. Am. Chem. Soc. **66**, 2100 (1944).
44. C.A. Parker and C.G. Hatchard. Analyst, **87**, 664 (1962).
45. A. Kuboyama and S. Yabe. Bull. Chem. Soc. Jpn. **40**, 2475 (1967).
46. H.R. Drott and H.H. Dearman. J. Chem. Phys. **47**, 1869 (1967).
47. K.E. Drabe, H. Veenvliet, and D.A. Wiersma. Chem. Phys. Lett. **35**, 469 (1975).
48. O.S. Khall and L. Goodman. J. Phys. Chem. **80**, 2179 (1976).
49. T. Murao and T. Azumi. J. Chem. Phys. **70**, 4460 (1979).
50. K. Hamanoue, T. Nakayama, Y. Kajiwara, T. Yamaguchi, and H. Teranishi. J. Chem. Phys. **86**, 6654 (1987).
51. D.K. Palit, H. Pal, T. Mukherjee, and J.P. Mittal. J. Chem. Soc. Faraday Trans. **86**, 3861 (1990).
52. H.H. Dearman and A. Chan. J. Chem. Phys. **44**, 416 (1966).
53. S.N. Singh and R.S. Singh. Indian J. Pure Appl. Phys. **5**, 342 (1967).
54. P. Longin. C. R. Seances Acad. Sci. Ser. B: 271(4), 292 (1970); CA1970, 135644r.
55. K.L. Rogozhin, A.N. Rodionov, and D.N. Shigorin. Opt. Spektrosk. **52**, 952 (1982).
56. T. Itoh. Spectrochim. Acta, Part A, **42A**, 1083 (1986).
57. S.N. Singh and R.S. Singh. Indian J. Pure Appl. Phys. **5**, 394 (1967).
58. T. Itoh and H. Baba. Bull. Chem. Soc. Jpn. **52**, 3213 (1979).
59. T. Itoh and H. Baba. Chem. Phys. **51**, 179 (1980).
60. G.D. Baruah, S.N. Singh, and R.S. Singh. Bull. Chem. Soc. Jpn. **42**, 3572 (1969).
61. H.J. Pownall and J.R. Huber. J. Am. Chem. Soc. **93**, 6429 (1971).
62. H.J. Pownall, R.E. Connors, and J.R. Huber. Chem. Phys. Lett. **22**, 403 (1973).
63. T. Terada, M. Koyanagi, and Y. Kanda. Bull. Chem. Soc. Jpn. **53**, 352 (1980).
64. A. Chakrabarti and N. Hirota. J. Phys. Chem. **80**, 2966 (1976).
65. T. Terada, M. Koyanagi, and Y. Kanda. Chem. Phys. Lett. **72**, 408 (1980).
66. M. Koyanagi, T. Terada, and K. Nakashima. J. Chem. Phys. **89**, 7349 (1988).
67. K. Meier and H. Zweifel. J. Photochem. **35**, 353 (1986).
68. N.C. Yang and S. Murov. J. Chem. Phys. **45**, 4358 (1966).
69. Y. Kanda, J. Stanislaus, and E.C. Lim. J. Am. Chem. Soc. **91**, 5085 (1969).
70. N.Y.C. Chu and D.R. Kearns. J. Am. Chem. Soc. **94**, 2619 (1972).

© 2000 NRC Canada

71. G.W. Suter and U.P. Wild. Chem. Phys. **102**, 205 (1986).
72. A.M. Nishimura and J.S. Vincent. Chem. Phys. Lett. **13**, 89 (1972).
73. T.F. Hunter. Trans. Faraday Soc. **66**, 300 (1970).
74. J.C. Scaiano and C.W.B. Lee. J. Photochem. **20**, 327 (1982).
75. N.C. Yang. Pure Appl. Chem. **9**, 591 (1964).
76. D.A. Warwick and C.H.J. Wells. Spectrochim. Acta, Part A, **24A**, 589 (1968).
77. S. Hirayama. J. Chem. Soc. Faraday Trans. 1, **78**, 2411 (1982).
78. W.B. Dodge and R.O. Allen. Anal. Chem. **53**, 1279 (1981).
79. T. Yu, K. Tanabe, and J.D. Winefordner. Anal. Chem. Acta, **201**, 317 (1987).
80. O. Oldenberg. J. Opt. Soc. Am. **61**, 1092 (1971).
81. R. Brown and C.A. Winkler. Angew. Chem. **9** (3), 181 (1970).
82. J.A. Meyer, D.H. Klosterboer, and D.W. Setser. J. Chem. Phys. **55**, 2084 (1971).
83. A.N. Wright and C.A. Winkler. Active nitrogen. Academic Press, New York and London. 1968.
84. D.H. Stedman and D.W. Setser. J. Chem. Phys. **50**. 2256 (1969).
85. D.H. Stedman, J.A. Meyer, and D.W. Setser. J. Am. Chem. Soc. **90**, 6856 (1968).
86. P. Devolder. Spectrochim. Acta, **36A**, 783 (1980).
87. P. Devolder, O. Dessaux, and P. Goudmand. J. Photochem. **15**, 265 (1981).
88. J. Anketell and R.W. Nicholls. Rev. Prog. Phys. **33**, 269 (1970).
89. M.F. Golde and B.A. Thrush. Rev. Prog. Phys. **36**, 1285 (1973).
90. F. Valadier, E. Faure, R. Bergeron, and J. Janin. C. R. Acad. Sci. **265**, 1432 (1967).
91. Z.-P. Lin. Doctoral thesis. Dalhousie University, Halifax. 1997.

© 2000 NRC Canada

Characterization of phosphorus chemical shielding tensors in a phosphole tetramer: a combined experimental and theoretical study

Myrlene Gee, Roderick E. Wasylishen, Klaus Eichele, Gang Wu, T. Stanley Cameron, F. Mathey, and F. Laporte

Abstract: Phosphorus-31 1D NMR spectra of a stationary powder sample of a phosphole tetramer containing two phosphorus spin pairs have been obtained at 4.7 T and 9.4 T. In order to separate ^{31}P–^{31}P spin-spin coupling from anisotropic chemical shielding, 2D spin–echo NMR spectra have been acquired. Phosphorus-31 CPMAS NMR experiments indicate that the two spin pairs of the tetramer are equivalent and each may be treated as an isolated spin pair. Within a given spin pair, the difference between the isotropic chemical shifts of two directly bonded phosphorus nuclei is 1.7 ppm. As well, they are spin–spin coupled by both the indirect and direct interactions, $^1J(^{31}P, ^{31}P)$ = –362 Hz and R_{DD} = 1.80 kHz, respectively. The principal components and relative orientation of the two phosphorus chemical shielding tensors have been determined using the dipolar-chemical shift technique; however, since the dipolar tensor is axially symmetric, ambiguities in the chemical shielding tensor orientation relative to the molecular framework result. Using ab initio calculations and simulations of the 2D spin–echo spectra, many of these ambiguities have been resolved. The spans and skews of the phosphorus shielding tensors for all four three-coordinate phosphorus nuclei are the same within experimental error, 115 ppm and 0.70, respectively. Combined experimental and theoretical results indicate that the phosphorus shielding tensor orientations are dictated by the local environment. For both shielding tensors, the most shielded component, δ_{33}, is approximately 78° from the P—P bond and in the phosphole ring plane. The relative orientation of the δ_{33} components is described by a dihedral angle of 82°, similar to the dihedral angle of approximately 76° defining the twist of the phosphole rings about the bridging P—P bond.

Key words: solid-state ^{31}P NMR, phosphorus chemical shielding tensors, phosphole tetramer, ^{31}P–^{31}P spin pairs, ab initio calculations.

Résumé : On a enregistré à 4,7 T et à 9,4 T les spectres de RMN 1D du phosphore 31 à l'état solide à partir d'un échantillon d'un tétramère phosphole, sous forme de poudre, contenant deux paires de spin de phosphore. Dans le but de séparer les constantes de couplage spin-spin ^{31}P-^{31}P des blindages chimiques anisotropiques, on a enregistré également les spectres de RMN 2D spin écho. Les expériences de RMN CPMAS du phosphore-31 indiquent que les deux paires de spins du tétramère sont équivalentes et que chacune peut-être traitée comme une paire isolée. Pour une paire de spins donnée, la différence entre les déplacements chimiques isotropiques de deux noyaux phosphore directement liés est de 1,7 ppm. Les interactions directes et indirectes de ces noyaux donnent également un couplage spin–spin de $^1J(^{31}P, ^{31}P)$ = –362 Hz et R_{DD} = 1,80 kHz respectivement. Utilisant la technique de déplacement chimique-dipolaire, on a déterminé les composantes principales et l'orientation relative des deux tenseurs de blindage chimique; cependant, puisque le tenseur dipolaire est de symétrie axiale, il en résulte des ambiguïtés dans l'orientation du tenseur de blindage chimique par rapport au squelette moléculaire. Les calculs ab initio et les simulations de spectres 2D spin écho ont permis de résoudre plusieurs de ces ambiguïtés. L'envergure et l'obliquité des tenseurs de blindage chimique des quatre noyaux de phosphore tricoordonnés sont identiques, dans les limites des erreurs expérimentales, elles sont respectivement de 115 ppm et de 0,70. La combinaison des résultats expérimentaux et théoriques révèle que les orientations du tenseur de blindage du phosphore dépendent de l'environnement local. Pour les deux tenseurs de blindage, la composante la plus blindée, δ_{33}, est approximativement de 78° à partir de la liaison P—P et dans le plan du cycle du phosphole. L'orientation relative des composantes δ_{33} est décrite par un angle dièdre de 82°, semblable à l'angle dièdre de 76° approximativement définissant la torsion des cycles phosphole autour de la liaison P—P en pont.

Mots clés : RMN du ^{31}P à l'état solide, tenseurs de blindage chimique du phosphore, tétramère phosphole, paire de spins ^{31}P–^{31}P, calculs ab initio.

[Traduit par la Rédaction]

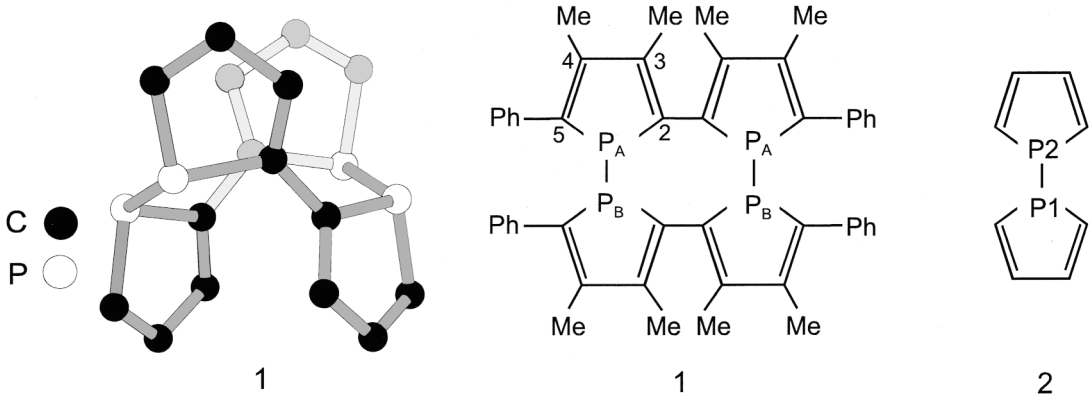
Received October 14, 1999.

M. Gee, R.E. Wasylishen,[1] K. Eichele, G. Wu, and T.S. Cameron. Department of Chemistry, Dalhousie University, Halifax, NS B3H 4J3, Canada.
F. Mathey and F. Laporte. Laboratoire Hétéroéléments et Coordination, CNRS URA 1499 DCPH Ecole Polytechnique, 91128 Palaiseau Cedex, France.

[1]Author to whom correspondence may be addressed. Telephone: (902) 494-2564. Fax: (902) 494-1310. e-mail: Roderick.Wasylishen@Dal.Ca

 © 2000 NRC Canada

Scheme 1. Molecular structure of the phosphole tetramer (**1**) and a three-dimensional representation of **1**. For clarity, the methyl and phenyl groups have been removed from the 3D representation. Molecule **2** has been used as a model system of **1** for the ab initio calculations.



Introduction

The phosphole tetramer, **1** (Scheme 1), was first synthesized in 1982 (1) and the X-ray crystal structure was reported subsequently (2). Solid-state NMR investigations of similar systems where two three-coordinate phosphorus nuclei are directly bonded are relatively rare (3). In the case of the phosphole tetramer, analysis of the ^{31}P NMR spectra acquired with cross polarization (CP) and magic angle spinning (MAS) revealed a difference in the isotropic phosphorus chemical shifts of 1.7 ppm with $^1J(^{31}P, ^{31}P)$ = –362 Hz (4, 5). Here, we use the presence of ^{31}P–^{31}P spin pairs to characterize the phosphorus chemical shift (CS) tensors via the dipolar-chemical shift NMR technique (6–8). In contrast to the earlier ^{31}P MAS NMR investigations (4, 5), we have fully analyzed NMR spectra of stationary samples obtained at different applied magnetic fields. We also demonstrate that analysis of the ^{31}P 2D spin–echo NMR spectrum of the phosphole tetramer is invaluable for refining the coupling parameters. In combination with ab initio calculations to verify the phosphorus shielding tensor orientations, this strategy of combining experimental and theoretical methods (7) is extremely powerful for accurately characterizing CS tensors in powdered samples. Inconsistencies between the NMR data (vide infra) and the original X-ray data (2) prompted a redetermination of the crystal structure.

Homonuclear Spin Pairs — Background Theory

The most reliable experimental method available for characterizing nuclear magnetic shielding tensors is single-crystal NMR (3*d*, 9). Unfortunately, single crystals of sufficient size and quality are frequently unavailable. However, the presence of isolated hetero- or homonuclear spin pairs in a molecule affords an opportunity to gain some information about the CS tensor orientation from NMR spectra of powdered samples by the application of dipolar-chemical shift NMR (6). As described below, the NMR spectra of a homonuclear spin pair will depend on the principal components of the chemical shielding tensor for each nucleus and the relative orientation of these tensors. In general, four transition frequencies with relative intensities P_i are observed for homonuclear spin-1/2 pairs (the two nuclei are labelled A and B respectively) (6, 10):

$$[1] \quad \nu_1 = \frac{1}{2}(\nu_A + \nu_B - A - D) \qquad P_1 = 1 - \frac{B}{D}$$

$$[2] \quad \nu_2 = \frac{1}{2}(\nu_A + \nu_B + A - D) \qquad P_2 = 1 + \frac{B}{D}$$

$$[3] \quad \nu_3 = \frac{1}{2}(\nu_A + \nu_B - A + D) \qquad P_3 = 1 + \frac{B}{D}$$

$$[4] \quad \nu_4 = \frac{1}{2}(\nu_A + \nu_B + A + D) \qquad P_4 = 1 - \frac{B}{D}$$

The frequencies ν_A and ν_B are given by

$$[5] \quad \nu_i(\theta, \phi) = \nu_0[1 - (\sigma^i_{11}\sin^2\theta\cos^2\phi + \sigma^i_{22}\sin^2\theta\sin^2\phi + \sigma^i_{33}\cos^2\theta)]$$

where ν_0 is the Larmor frequency, and σ_{11}, σ_{22}, and σ_{33} are the principal components of the chemical *shielding* tensor such that $\sigma_{11} \le \sigma_{22} \le \sigma_{33}$. In eq. [5], the polar angles θ and ϕ describe the orientation of the principal axis system (PAS) of the CS tensor with respect to the applied external magnetic field, $\mathbf{B}_0$ (Fig. 1). In practice, it is the chemical *shift* which is measured. It is related to the chemical shielding by $\delta = 10^6(\sigma_{ref} - \sigma)/(1 - \sigma_{ref})$, where σ_{ref} is the absolute nuclear magnetic shielding of the reference (328.35 ppm for the phosphorus atom of 85% H_3PO_4 (11) in the case of ^{31}P NMR studies). The principal components of the chemical shift tensor are defined such that $\delta_{11} \ge \delta_{22} \ge \delta_{33}$. The isotropic chemical shift, δ_{iso}, is $(\delta_{11} + \delta_{22} + \delta_{33})/3$ and the span and skew of the chemical shift tensor are defined as $\Omega = \delta_{11} - \delta_{33}$ and $\kappa = 3(\delta_{22} - \delta_{iso})/\Omega$, respectively (12). The terms *A*, *B*, and *D* in eqs. [1]–[4] are dependent on the isotropic indirect spin–spin coupling constant, J_{iso}, and the effective direct dipolar coupling constant, R_{eff}:

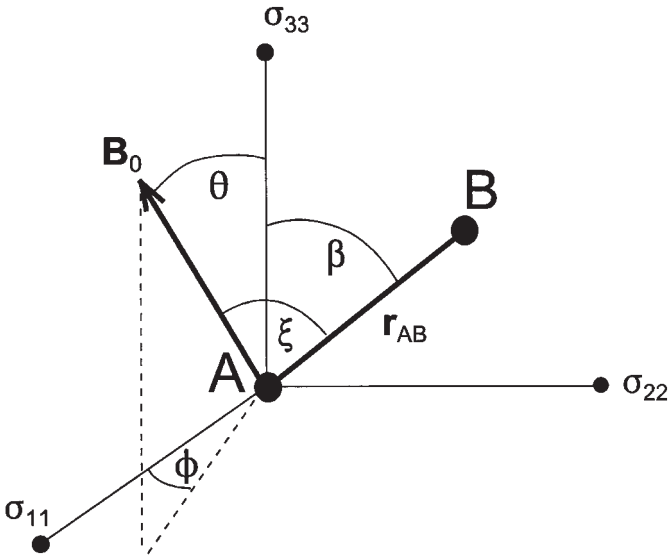
$$[6] \quad A = J_{iso} - R_{eff}(3\cos^2\xi - 1)$$

$$[7] \quad B = J_{iso} + \frac{1}{2}R_{eff}(3\cos^2\xi - 1)$$

$$[8] \quad D = [(\nu_A - \nu_B)^2 + B^2]^{\frac{1}{2}}$$

© 2000 NRC Canada

Fig. 1. An illustration of the angles which define the orientation of the applied magnetic field, $\mathbf{B}_0$, the internuclear vector, $\mathbf{r}_{AB}$, and the principal axis system of the chemical shielding tensor, indicated by σ_{11}, σ_{22}, and σ_{33}. The nuclei of the spin pair are labelled A and B.



where ξ is the angle between the internuclear vector, $\mathbf{r}_{AB}$, and $\mathbf{B}_0$ (Fig. 1), and R_{eff} is given by (10*e*):

$$[9] \qquad R_{eff} = R_{DD} - \frac{\Delta J}{3}$$

The dipolar coupling constant, R_{DD}, is dependent on the vibrationally averaged inverse cube of the internuclear distance, r_{AB}:

$$[10] \qquad R_{DD} = \frac{\mu_o}{4\pi} \frac{1}{\left\langle r_{AB}^3 \right\rangle} \gamma^2 \left(\frac{\hbar}{2\pi} \right)$$

In eq. [9], ΔJ is defined as the anisotropy in the indirect spin–spin coupling tensor, **J** (for an axially symmetric tensor).

The relative orientations of the CS tensors on each nucleus of the spin pair and $\mathbf{r}_{AB}$ are most conveniently described by the Euler angles, α, β, and γ, such that the rotation matrix to transform from the molecular frame of reference to the CS tensor PAS is (13):

$$[11] \qquad \mathbf{R}(\alpha, \beta, \gamma) = \mathbf{R}_{z'}(\gamma)\mathbf{R}_{y}(\beta)\mathbf{R}_{z}(\alpha)$$

where, for example, $\mathbf{R}_z(\alpha)$ is a rotation of α degrees about the z-axis. The axis z′ is the new z-axis generated by $\mathbf{R}_y(\beta)$.

In a microcrystalline powder sample, all possible orientations of the CS tensor PAS with respect to $\mathbf{B}_0$ are present; however, the NMR spectrum is still sensitive to the relative orientations of the CS and dipolar tensors (8). Unfortunately, difficulties can arise when one attempts to extract this orientational information from the NMR spectra of powder samples. In principle, the observed line shape will depend on two sets of CS tensor principal components, two sets of Euler angles, the **J** tensor, and R_{eff}. The analysis can be simplified by independent measurements of some parameters. For example, spectra obtained under conditions of rapid MAS provide the isotropic chemical shift and *J*-coupling constant. Bond lengths available from diffraction experiments provide a starting value for R_{eff} since $\Delta J/3$ is expected to be much smaller than R_{DD} (14). In some cases, trial and error analysis of NMR spectra obtained under conditions of slow MAS may provide a wealth of information (5, 15); however, we believe it is also prudent to analyze the NMR spectra of non–spinning samples. In the case of stationary samples, an independent measurement of the spin–spin coupling constants (R_{eff} and J_{iso}) can be obtained from the 2D spin–echo experiment, whereby the spin–spin coupling and the chemical shielding interactions can be separated for homonuclear spin pairs (3*a*). Nakai and McDowell (3*c*) have derived expressions for the free induction decays, $s(t_1)$ and $s(t_2)$, of the 2D spin–echo NMR experiment:

$$\begin{aligned} [12] \qquad s(t_1) = {} & \cos^2 2\xi \, [\exp(i\pi A t_1) + \exp(-i\pi A t_1)] \\ & + 1/2 \sin 2\xi \, (1 + \sin 2\xi) \, [\exp(i\pi\{D - A\}t_1) \\ & + \exp(-i\pi\{D - A\}t_1)] \\ & - 1/2 \sin 2\xi \, (1 - \sin 2\xi) \, [\exp(i\pi\{D + A\}t_1) \\ & + \exp(-i\pi\{D + A\}t_1)] \end{aligned}$$

$$\begin{aligned} [13] \qquad s(t_2) = {} & (1 - \sin 2\xi) \exp(i2\pi\nu_1 t_2) \\ & + (1 + \sin 2\xi) \exp(i2\pi\nu_2 t_2) \\ & + (1 + \sin 2\xi) \exp(i2\pi\nu_3 t_2) \\ & + (1 - \sin 2\xi) \exp(i2\pi\nu_4 t_2) \end{aligned}$$

where $\cos 2\xi = (\nu_A - \nu_B)/D$, $\sin 2\xi = B/D$ and the ν_is (i = 1 – 4) are given by eqs. [1]–[4]. Following Fourier transformation, the F1 projection of the 2D NMR spectrum is a Pake doublet with splittings dependent on the magnitudes and relative signs of R_{eff} and J_{iso}. The F2 projection is the normal 1D NMR spectrum of a stationary sample. Two dimensional spin–echo NMR spectroscopy has been used extensively to characterize homonuclear spin pairs in solids, especially ^{31}P–^{31}P systems such as Ph_2PPPh_2 (3*c*, 16), $Mes^*P = PMes^*$ (Mes^* = (2,4,6-tri-*tert*-butyl)phenyl) (3*a*), $[Mes^*NP\text{-}PPh_3][SO_3CF_3]$ (17), the pyrophosphate anion in $Na_4P_2O_7 \cdot 10H_2O$ (3*c*, 18), Lawesson's reagent, $(C_6H_4OCH_3PS_2)_2$ (19), and most recently in some molybdenum phosphine complexes (3*d*).

Despite the arsenal of experimental methods available for investigating spin pairs in powder samples, there is one fundamental property that prevents the unambiguous determination of the CS tensor orientation with respect to the molecular axis system, namely the axial symmetry of the dipolar tensor. Hence NMR spectra are invariant to simultaneous rotation of the two CS tensors about $\mathbf{r}_{AB}$. However, due to advances in computational chemistry, it is now possible to fix the orientations of chemical shielding tensors in the molecular framework with some confidence, provided one is dealing with first- and second-row elements. The present status of theoretical methods has been discussed in a number of recent reviews (20). It is well known that large basis sets are essential to obtain reliable results. Furthermore, methods capable of treating electron correlation are desirable for molecules containing multiple bonds or formal electron lone pairs. As well, relativistic effects may become important for heavier nuclei (21), but are unlikely to be sig-

© 2000 NRC Canada

nificant for phosphorus and influence CS tensor orientations. In an effort to deal with the electron correlation problem, researchers have used either Møller–Plesset (MP) perturbation theory (22) or density functional theory (DFT) (23). With advances in computation techniques and the advent of faster computers, the reliability of the calculations will continue to improve.

Experimental

The synthesis of the phosphole tetramer has been described previously (1).

Phosphorus-31 NMR spectra: All ^{31}P NMR spectra of stationary and MAS samples were acquired on Bruker MSL 200 (4.7 T), Chemagnetics CMX Infinity 200 (4.7 T), and Bruker AMX 400 (9.4 T) spectrometers operating at ^{31}P NMR frequencies of 81.03 MHz and 161.98 MHz, respectively. Cross polarization under the Hartmann–Hahn match condition and high power ^{1}H decoupling were used for all NMR experiments. At the lower field, double air bearing MAS probes were used with the sample packed in 7 mm o.d. (for the MSL) and 7.5 mm o.d. (for the CMX) zirconium dioxide rotors. For the stationary sample, 2180 transients were acquired with a ^{1}H $\pi/2$ pulse of 3.6 μs, contact time of 5 ms, and a recycle delay of 5 s, while 256 transients were acquired with the sample spinning at 1500 or 2000 Hz. A double air bearing MAS probe was used at the higher field as well, with the sample packed in a zirconium dioxide rotor (4 mm o.d.). A ^{1}H $\pi/2$ pulse of 3.6 μs with a contact time of 3 ms and a recycle delay of 10 s were used to acquire 458 transients. With MAS at 2000 or 4000 Hz, 512 transients were acquired. Gaussian line broadening of 20 to 100 Hz was applied before Fourier transformation. All ^{31}P NMR spectra are referenced to the primary standard, 85% H_3PO_4(aq) by setting the ^{31}P isotropic peak of solid $NH_4H_2PO_4$ to +0.8 ppm. Spectra of stationary samples at both fields were simulated using WSOLIDS, a program developed in this laboratory which incorporates the POWDER routine of Alderman et al. (24). Spectra of MAS samples were calculated using NMRLAB[2], which uses the Monte Carlo method to sample crystal orientations for powder averaging. In our calculations, 10 000 orientations were used. Gaussian line broadening of between 100 and 150 Hz was applied to the calculated spectra to approximate the experimental line broadening.

2D Spin–echo ^{31}P NMR spectrum: The 2D spin–echo NMR spectrum was acquired at 4.7 T (Bruker MSL 200) with a standard spin–echo pulse sequence using the phase cycling of Rance and Byrd (25) where the evolution time between the contact pulse and the π pulse (t_1) was incremented (3*c*). A ^{1}H $\pi/2$ pulse of 5.5 μs was used with a contact time of 5.5 ms and a recycle delay of 10 s. For each t_1 increment, 64 transients were acquired for a total of 64 increments. Gaussian line broadening of 200 Hz and 100 Hz were applied to the F1 and F2 projections respectively. The F1 projection was calculated using eq. [12] and eq. [13] with SpinEcho, a program developed in this laboratory. The experimental and calculated 2D NMR spectra were processed in magnitude mode.

X-ray data collection and processing: An orange crystal of approximate dimensions 0.10 × 0.10 × 0.10 mm, recrystallized from chlorobenzene, was mounted on a glass fibre. A Rigaku AFC5R diffractometer was used for all measurements. Calculations were performed using teXsan.[3] The orange crystals have cell dimensions a = 11.523 (4) Å, b = 23.083 (1) Å, c = 15.115 (1) Å, α = 89.99 (1)°, β = 92.71 (1)°, and γ = 89.99 (1)°. The merging R_{int} for the reflection data, merged on the assumption that the cell is monoclinic, is 3.04% for 244 equivalent reflections with $I > 5\sigma(I)$. The reflections for which $h = 2n + 1$ are weak in intensity and are generally diffuse. The strong reflections thus belong to a cell where a = 5.762 (1) Å. Both cells have systematic absences consistent with a space group $P2_1/c$. The molecule for the structure in the larger cell refines to R = 4.7%. The refinement used unit weights.

Computational details: Theoretical calculations were performed with the Gaussian 94 suite of programs[4] running on an IBM RISC/6000 computer. Using Restricted Hartree–Fock (RHF) theory and Gauge Independent Atomic Orbitals (GIAO) (26), the ^{31}P CS tensors were determined for the model geometry, **2** (Scheme 1), of the phosphole tetramer based on the X-ray crystallography results for half of the molecule where the methyl and phenyl groups are replaced by hydrogen atoms. A partial geometry optimization using RHF with the 6–311G basis set on all the atoms was carried out. The P—P bond length, the dihedral angle between the rings, and the C—H bond lengths were fixed at the X-ray structure values for the optimization. Shielding calculations were carried out using the 6–311++G(d,p) basis set on phosphorus and neighbouring nuclei, while the 6–311G basis set was used on the remaining atoms in order to keep computation time within reasonable limits (27). To compare with experimental results, the calculated phosphorus chemical shielding is converted to chemical shift by using the absolute shielding of 328.35 ppm for the phosphorus chemical shift reference, 85% H_3PO_4(aq) (11).

Results and discussion

Experimental determination of phosphorus CS tensors in the phosphole tetramer

The observed and calculated ^{31}P CP NMR spectra of stationary samples of the tetramer are shown in Fig. 2, while NMR spectra of MAS samples are shown in Figs. 3 and 4.

[2] B. Sun and R.G. Griffin. Unpublished results.
[3] teXsan for Windows version 1.05. Crystal structure analysis package. Molecular Structure Corp. (1997–8).
[4] M.J. Frisch, G.W. Trucks, H.B. Schlegel, P.M.W. Gill, B.G. Johnson, M.A. Robb, J.R. Cheeseman, T. Keith, G.A. Petersson, J.A. Montgomery, K. Raghavachari, M.A. Al-Laham, V.G. Zakrzewski, J.V. Ortiz, J.B. Foresman, J. Cioslowski, B.B. Stefanov, A. Nanayakkara, M. Challacombe, C.Y. Peng, P.Y Ayala, W. Chen, M.W. Wong, J.L. Andres, E.S. Replogle, R. Gomperts, R.L. Martin, D.J. Fox, J.S. Binkley, D.J. Defrees, J. Baker, J.P. Stewart, M. Head-Gordon, C. Gonzalez, and J.A. Pople. Gaussian 94, Revision B.2. Gaussian, Inc., Pittsburgh, Pa. 1995.

© 2000 NRC Canada

Table 1. Experimental and calculated CS principal components[a] for the phosphole tetramer.

	Site	δ_{iso}	δ_{11}[b]	δ_{22}[b]	δ_{33}[b]	Ω	κ
Experimental	P_A	–7.3	36	19	–77	113	0.7
	P_B	–9	35	18	–80	115	0.7
RHF[c]	P1	–49.7	29	–18	–160	189	0.5
	P2	–53.7	23	–21	–163	186	0.5

[a]All chemical shifts and Ωs are given in ppm.

[b]Estimated error on the principal components is ±5 ppm.

[c]GIAO were used with the 6–311++G(d, p) basis set on phosphorus and adjacent atoms. The 6–311G basis set was used on the remaining atoms. Calculated σ_{ii}s are converted to δ_{ii}s by using the absolute shielding of 328.35 ppm for the reference 85% H_3PO_4(aq) (11).

Fig. 2. Experimental and calculated ^{31}P NMR spectra of stationary samples of the phosphole tetramer acquired at (**a**) 4.7 T and (**b**) 9.4 T.

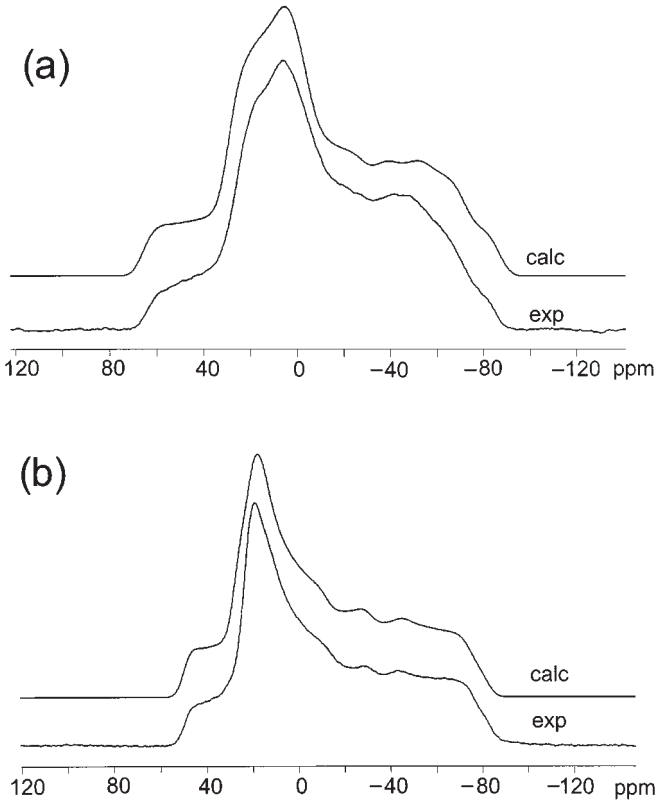
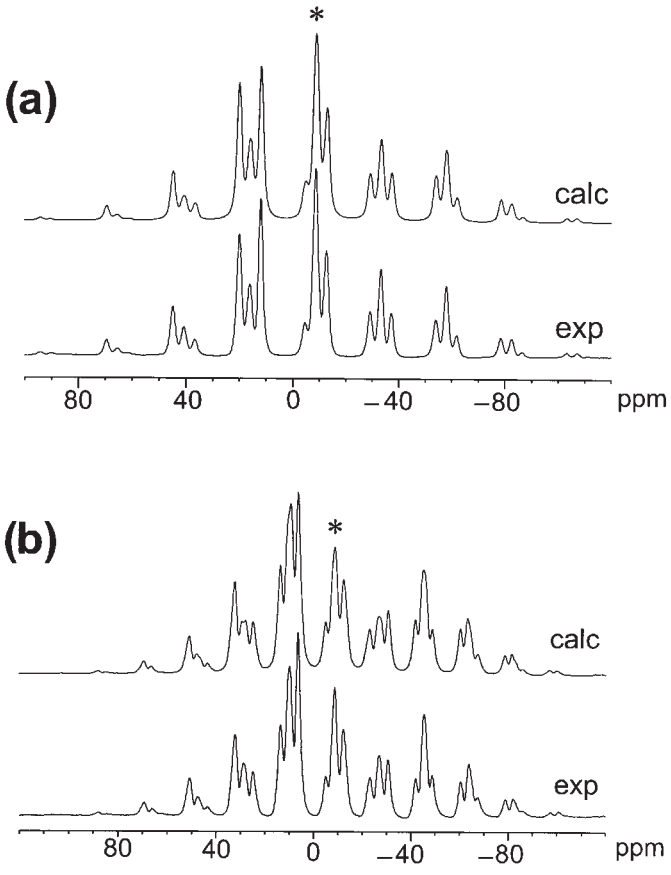


Fig. 3. Experimental and calculated ^{31}P NMR spectra of crystalline powder samples of the phosphole tetramer spinning at the magic angle, acquired at 4.7 T for sample spinning at (**a**) 2.0 kHz and (**b**) at 1.5 kHz. The asterisk indicates the average position of δ_{iso}.



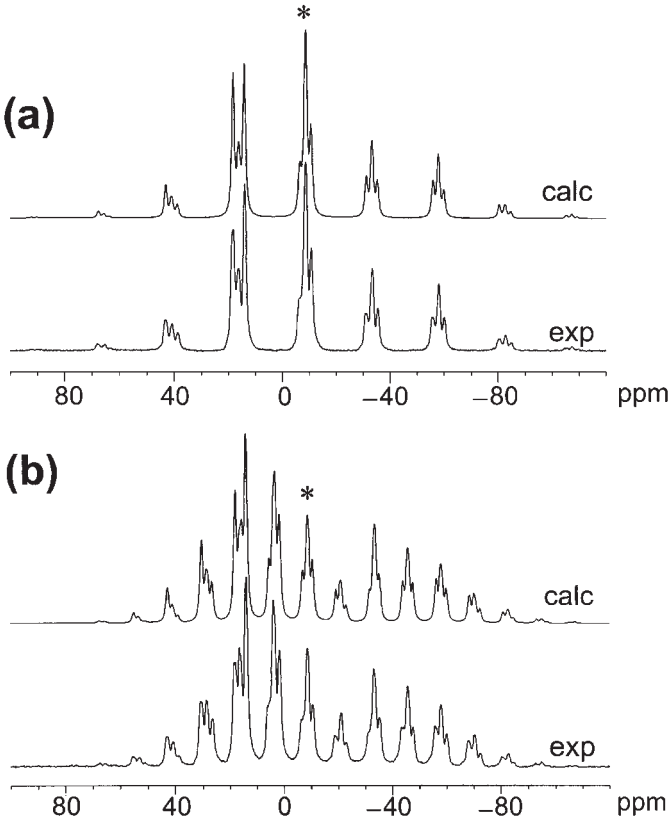
Best-fit parameters are given in Table 1. In the text to follow, a brief account of how these parameters were obtained is presented.

The ^{31}P CPMAS NMR spectra of the phosphole tetramer indicate the presence of a unique ^{31}P–^{31}P spin pair in the crystal (4, 5) and, as indicated in Table 1, the NMR spectra have been analyzed accordingly. However, in the previously reported crystal structure of the phosphole tetramer (2) there are two molecules in the asymmetric unit related by a pseudo mirror plane, hence four unique P—P bond lengths were reported; r = 2.198(6), 2.191(6), 2.201(6), and 2.175(6) Å (2). Given the reported X-ray structure, one would expect to see potentially eight different phosphorus sites in the ^{31}P MAS NMR spectrum; similarly up to 16 different methyl carbon sites could be anticipated in the ^{13}C MAS NMR spectrum. Experimentally, we observe only two unique ^{31}P sites at both 4.7 and 9.4 T. Carbon-13 CP MAS NMR spectra revealed two ^{13}C sites at both fields (δ_{iso} = 15.5 ± 0.1 ppm and 17.1 ± 0.1 ppm). This apparent disagreement between our NMR results and the reported X-ray data prompted a redetermination of the X-ray data. Repeated attempts were made to grow suitable single crystals; however, the best crystals obtained were less than ideal for X-ray diffraction. The R factor for our X-ray data is 0.047, compared to the R factor of 0.089 reported previously (2).

The space group obtained from the new X-ray data is $P2_1/c$ with the asymmetric unit consisting of one molecule, rather than a space group of $P\bar{1}$ with two molecules in the

© 2000 NRC Canada

Fig. 4. Experimental and calculated ^{31}P NMR spectra of crystalline powder samples of the phosphole tetramer spinning at the magic angle, acquired at 9.4 T for sample spinning at (**a**) 4 kHz and (**b**) 2 kHz. The asterisk indicates the average position of δ_{iso}.



asymmetric unit as had been previously reported (2), hence there are four crystallographically non-equivalent phosphorus sites and potentially eight non-equivalent methyl groups. In both cases, the unit cell contains four molecules. The molecular structure obtained from our X-ray data is essentially the same as the reported structure (2); however, our results indicate that the molecule contains a near perfect C_2 axis which relates the two pairs of phosphorus atoms (see Scheme 1). This reduces the number of different phosphorus sites from four to two and the number of different methyl carbons to four. Given that the isotropic ^{31}P chemical shifts of the two phosphorus sites only differ by 1.7 ppm (4, 5), it is not surprising that the four methyl carbons at the C_3 position (see Scheme 1) are isochronous; similarly for those at position 4.

Within the unit cell, pairs of phosphorus atoms related by the near perfect C_2 axis have very similar environments though the two atoms of each pair are in different environments. It would appear from the diffuse reflections for which $h = 2n + 1$ that there are stacking errors in the a direction. The molecules pack in layers approximately perpendicular to the a direction. Unfortunately there are too few reflections for which $h = 2n + 1$ (51 out of a total of 766) to test this suggestion. Using eq. [10], and an average P—P bond length of 2.192 Å from the new X-ray crystal structure, R_{DD} = 1.873 kHz with an estimated error of ±50 Hz, based on the error in the X-ray data. Also, with four phosphorus nuclei in each molecule, each ^{31}P–^{31}P spin pair is not truly isolated since there will be mutual dipolar coupling. From the internuclear distances between phosphorus nuclei that are not directly bonded to each other, the R_{DD}s are 233 Hz (r = 4.392 Å) and 169 Hz (r = 4.882 Å), hence the NMR spectral features are largely determined by the much larger dipolar coupling between directly bonded phosphorus nuclei rather than the phosphorus nuclei forming the other spin pairs in the molecule.

Before analyzing the 1D ^{31}P NMR spectra, R_{eff} is first independently measured by using the 2D spin–echo experiment. Fig. 5*a* shows the ^{31}P 2D spin–echo NMR spectrum of **1** with the experimental and calculated F1 projections shown in Figs. 5*b*–5*d* (the large central peak is an experimental artifact). Using J_{iso} = –362 Hz (4, 5), the best value of R_{eff} is 1.80 ± 0.05 kHz (Fig. 5*b*), which is in good agreement with the value calculated from the crystal structure. The difference, R_{eff} - R_{DD} = 73 ± 50 Hz, is very small and could arise from vibrational averaging and possibly anisotropy in the **J** tensor. The smaller dipolar couplings between the phosphorus nuclei that are not directly bonded to each other most likely contribute to line broadening; however, it is possible they could slightly modify the value of R_{eff}. The sensitivity of the F1 projection to R_{eff} can be seen in Fig. 5*c*, where the agreement between the calculated and experimental spectra is not as good using R_{eff} = R_{DD} = 1.873 kHz. As well, the poor fit in the simulation using $^1J(^{31}P, ^{31}P)$ = +362 Hz with R_{eff} = 1.80 kHz (Fig. 5*d*) indicates that R_{eff} and J_{iso} must have opposite signs. In fact, for $^1J(^{31}P, ^{31}P)$ to be positive, R_{eff} must be less than 1.20 kHz to obtain a satisfactory fit of the two most intense peaks, which seems unreasonable in light of previous investigations of ^{31}P–^{31}P spin-spin couplings (14). A negative J-coupling constant is consistent with INDO calculations of $^1J(^{31}P, ^{31}P)$ as a function of the dihedral angle, ϕ, between formal lone pairs (28). For example, the calculated $^1J(^{31}P, ^{31}P)$ in $(CH_3)_2P$-$P(CH_3)_2$, is –254 Hz for ϕ = 74°, which is similar to the dihedral angle for the phosphole tetramer (ϕ = 78°). Using these spin–spin coupling data (J_{iso} = –362 Hz and R_{eff} = 1.80 kHz), the experimental ^{31}P NMR spectra of a stationary sample shown in Fig. 2 were simulated to obtain the CS principal components given in Table 1 and tensor orientation information discussed below. The experimental error in the principal components of the two chemical shift tensors is estimated to be ±5 ppm. As a result, δ_{11}, δ_{22}, and δ_{33} are virtually identical for the two ^{31}P CS tensors; this is reasonable given that the isotropic shifts are different by only 1.7 ppm (4, 5). The NMR spectra of MAS samples, shown in Figs. 3 and 4, demonstrate that the quality of the simulations using these new parameters is comparable to previously published work (4, 5). Although the agreement between the calculated and experimental NMR spectra is good at both fields for stationary and MAS samples, there are some subtle differences between observed and calculated NMR spectra. These differences probably arise because neither of the two phosphorus spin pairs in the molecule are strictly isolated (i.e., these spin pairs interact with one another).

As detailed in the background section, it is possible to obtain some CS tensor orientation information from the NMR spectra of stationary samples. For the phosphole tetramer, the NMR lineshape is particularly sensitive to $\Delta\alpha$, which is

© 2000 NRC Canada

Fig. 5. (**a**) The 2D spin–echo ^{31}P NMR spectrum of the phosphole tetramer, acquired at 4.7 T. The calculated (dashed line) and experimental (solid line) F1 projections are shown for (**b**) R_{eff} = 1.80 kHz, J_{iso} = –362 Hz, which produce the best fit, (**c**) R_{eff} = R_{DD} = 1.873 kHz, J_{iso} = –362 Hz, and (**d**) R_{eff} = 1.80 kHz, J_{iso} = +362 Hz.

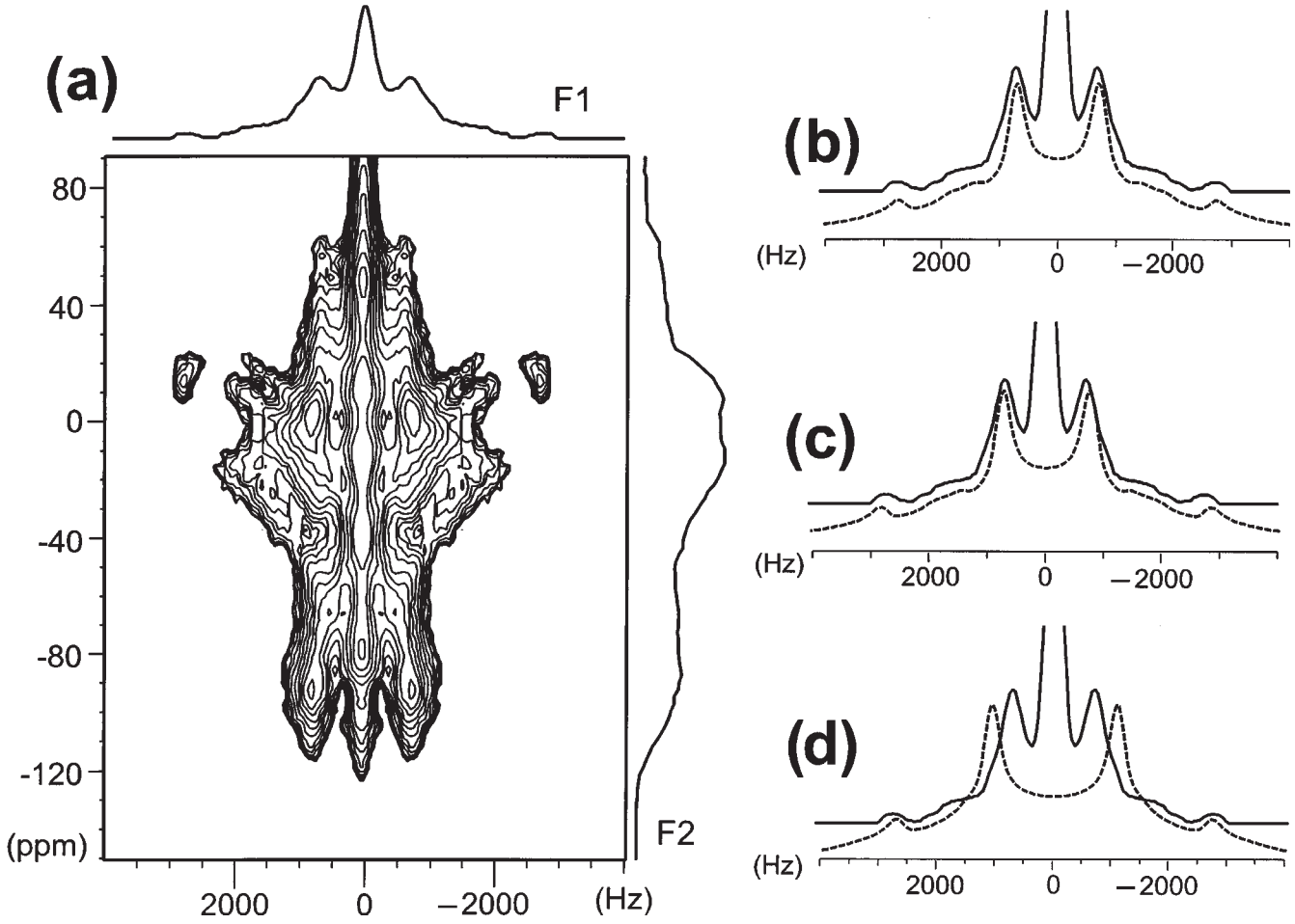
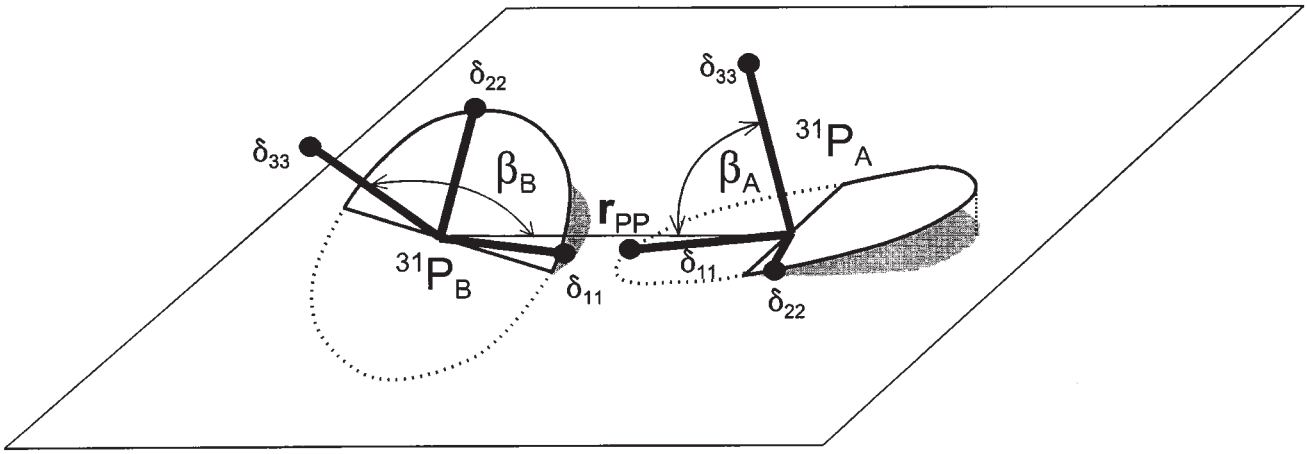


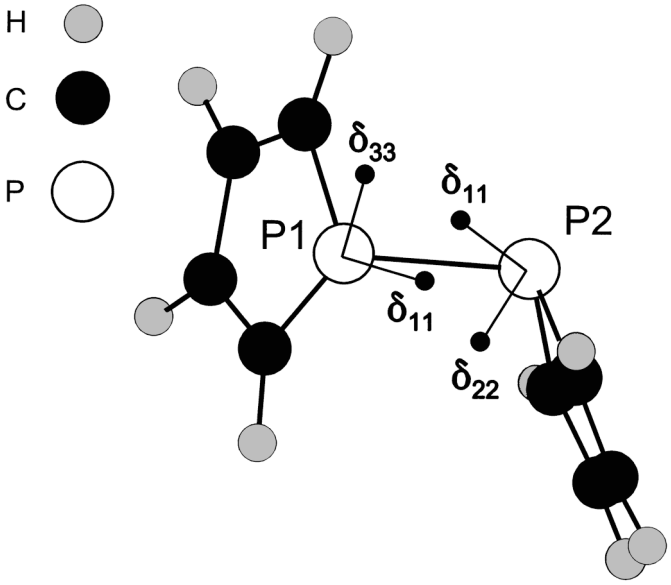
Fig. 6. The relative orientation of the two ^{31}P CS tensors in the phosphole tetramer, determined from simulation of the ^{31}P NMR spectra acquired at 4.7 T and 9.4 T for a stationary sample. For P_A, the Euler angles are α = 0°, β = 78°, and γ = 167°. For P_B, α = 82°, β = 78°, and γ = 167°.



the dihedral angle between the δ_{33} components of the two ^{31}P CS tensors. Best-fit calculated NMR spectra were obtained with $\Delta\alpha$ = 82 ± 3°. For both phosphorus CS tensors, the δ_{33} component is tipped away from the internuclear vector by β = 78 ± 5°. The relative orientation of the two ^{31}P CS tensors is illustrated in Fig. 6. In both cases, γ = 167 ± 5°

© 2000 NRC Canada

Fig. 7. The ^{31}P CS tensor orientations for **2** determined by ab initio calculations. For P1, δ_{22} is directed below the plane of the page, while for P2, δ_{33} is approximately out of the plane. In the case of P1, the δ_{11} and δ_{33} components are situated at angles of 19.3° and 79.1° respectively from the internuclear vector. For P2, δ_{11} is at an angle of 27.5° and δ_{33} at an angle of 79.0° from $\mathbf{r}_{PP}$.



places the least shielded component, δ_{11}, closest to $\mathbf{r}_{PP}$. Unfortunately, the ambiguities associated with the dipolar-chemical shift method prevent the determination of the absolute orientation of the CS tensor in the molecular frame of reference.

Ab Initio Calculations of Phosphorus Shielding Tensors.

As already mentioned, we use the ab initio calculations to fix the relative orientations (Fig. 6) in the molecular axis system (Fig. 7). Ab initio calculation results for the phosphorus chemical shielding tensors in the model system, **2**, for the phosphole tetramer are given in Table 1. The two phosphorus sites are labelled as P1 and P2 rather than P_A and P_B (Scheme 1) since it is not known how the two sites in the NMR spectra should be assigned to the molecule. In a partial optimization of the geometry, the P—C bond lengths and the ring bond angles were allowed to change, resulting in changes that were within the errors stated in the crystal structure (2). The calculated tensor orientations, depicted in Fig. 7, are similar for both P1 and P2 with respect to the local geometry about each phosphorus nucleus. The δ_{11} components are closest to the P—P bond at angles of 19.3° and 27.5° for P1 and P2, respectively while the δ_{33} component for P1 forms an angle of 79.1° with the internuclear vector, and the corresponding angle for P2 is 79.0°. The calculated orientations of δ_{11} and δ_{33} for both phosphorus nuclei are consistent with the experimental observations. In addition, the dihedral angle between the δ_{33} principal components is 87.8°, in good agreement with the value of 82° determined by analysis of ^{31}P NMR spectra. These ab initio calculations indicate that the δ_{33} components are not aligned in the general direction of the formal lone pairs, as had been previously suggested (4, 5). In fact, δ_{22} is closest to the direction of the formal lone pairs. For the phosphole tetramer, the δ_{33} components are in the plane of the respective phosphole rings and approximately perpendicular to the P—P bond. In the absence of single-crystal NMR data and (or) reliable first principles calculations, it is impossible to orient the CS tensors in the molecular frame.

With respect to the magnitudes of the principal components, the experimental and calculated results show similar trends (Table 1). The small calculated isotropic ^{31}P chemical shift difference (4 ppm) between the two sites is consistent with experiment. The calculations also predict that δ_{11} and δ_{22} are similar, while δ_{33} is quite distinct, as reflected in the skews of about 0.5, comparable to the skews of 0.7 observed experimentally. However, the calculated isotropic chemical shifts are too shielded by about 43 ppm and the spans are significantly larger than the experimental values. There are several possible reasons to account for these differences. First, a significant shift is anticipated due to the change in phase. For example, PH_3(g) is more shielded by 28 ppm compared to PH_3(l) (11) and P_4(g) is more shielded by 93.0 ppm compared to P_4(l) (29). In addition, the calculations are carried out on isolated gas phase molecules while the shielding will be affected by intermolecular interactions in the solid state. Another factor which may be responsible for part of the discrepancy between calculated and experimental results is the neglect of electron correlation in the RHF method. Inclusion of electron correlation has been shown to be important for obtaining good quantitative agreement between calculated and experimental shielding tensors in systems with formal lone pairs and multiple bonds (20). The importance of lone pairs in determining the chemical shielding in phospholes has been demonstrated recently in a series of ab initio calculations on phospholes and the phospholide ion (30). A recent investigation of some model phosphorus systems, for example PH_3, indicates that the inclusion of electron correlation in ab initio calculations yields improved results for isotropic chemical shielding (31). The use of a model geometry consisting of half of the phosphole tetramer may also contribute to this discrepancy. Given these factors, quantitative agreement between the experimental and ab initio values is not expected, and seemingly good calculated results may be due to the fortuitous cancellation of errors. Our primary goal with respect to ab initio calculations of chemical shielding tensors is to obtain the tensor orientation in the molecular frame of reference. Calculations on the model system H_2PPH_2 reveal that changes in the phosphorus tensor orientations are minor when various levels of theory (RHF or Møller–Plesset theory) are compared.[5]

The relative orientation of the δ_{33} components of the two phosphorus shielding tensors in the phosphole tetramer appears to be related to the relative orientation of the adjacent phosphole rings (see Fig. 7). In the crystal structure (2), the rings are arranged such that the ring planes are approximately parallel to each other and twisted about the bridging P—P bond. The dihedral angle between adjacent phosphole rings, ϕ_{ring}, ranges between 102°–105°, which can be equally well described by the supplement angle range of 75°–78°. This agrees well with the dihedral angle between the δ_{33}

[5] G.M. Bernard and R.E. Wasylishen. Unpublished results.

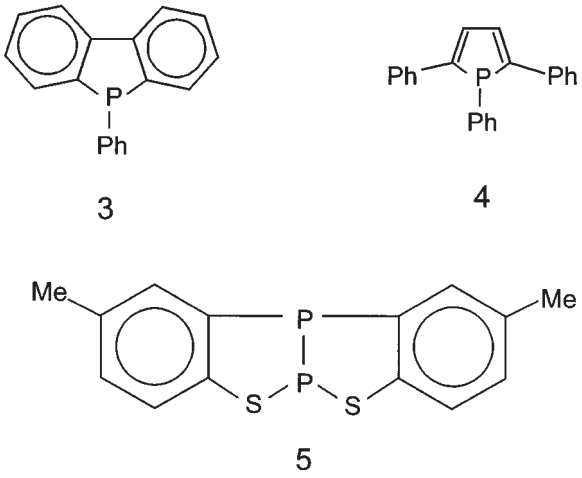
© 2000 NRC Canada

Table 2. Phosphorus CS tensor principal components[a] for some phospholes[b].

Compound	δ_{iso}	δ_{11}	δ_{22}	δ_{33}	Ω	κ	Ref.
5-phenyldibenzophosphole (two sites) (**3**)	–17.3	12	–19	–45	57	–0.1	34
	–19	9	–21	–45	54	–0.1	
1,2,5-triphenylphosphole (**4**)	0.7	30	–6	–22	52	–0.4	37
cis-2,10-dimethyl[1,2,3]benzothia-di-phospholo[2,3*b*][1,2,3] benzothiadiphosphole (**5**)	75.3 (PS_2)	129	122	–25	154	0.9	35
	53.7 (PC_2)	190	25	–54	244	–0.3	

[a]All chemical shifts and Ω are given in ppm.
[b]Structures are shown in Scheme 2.

Scheme 2. Molecular structures of compounds **3**, **4**, and **5** in Table 2.



components at each phosphorus nucleus, ϕ_{33}, which is 82° determined experimentally and 87.8° from ab initio calculations. This structure-tensor relationship can be further demonstrated by ab initio calculation of the phosphorus tensor orientations at various ϕ_{ring}. Further calculations on our model system using ϕ_{ring} = 0°, 70°, 110°, and 180° indicate that the δ_{33} components are oriented relative to the local geometry in a similar manner as shown in Fig. 7, with ϕ_{33} reflecting ϕ_{ring} (ϕ_{33} = 0°, 60.5°, 109.5°, and 180° for the corresponding ϕ_{ring} listed above).

There has been some discussion in the literature over the aromaticity of phospholes (32), recently revived by the synthesis of some planar phospholes (33). While ^{31}P solution NMR has been used routinely to characterize this important class of compounds, there are few comprehensive NMR investigations of the chemical shift (CS) tensors. The ^{31}P CS tensors of several phosphole derivatives have also been characterized recently by solid-state NMR (34). Comparison of the phosphorus CS tensors in phospholes (Table 2), reveals that δ_{33} in the phosphole tetramer is relatively shielded. For all phospholes investigated by ^{31}P solid-state NMR thus far, the spans of the phosphorus CS tensors are small compared with systems where the phosphorus nucleus is known to be participating in a delocalized electron framework. For example, the span of the ^{31}P CS tensors in Mes^*P = $PMes^*$ is 1239 ppm (3*a*) and in benzo-1,3,2-dithiaphospholium aluminum chloride, Ω = 779 ppm (36). In the latter two systems, the phosphorus environment is formally two-coordinate, hence the larger span may be attributed to efficient $n \rightarrow \pi^*$ mixing. This mixing is absent in systems where the phosphorus nucleus is formally three-coordinate.

Conclusions

The analysis of ^{31}P CP NMR spectra of a stationary sample of the phosphole tetramer as well as with MAS indicates that the principal components of the two ^{31}P CS tensors are virtually identical. Regarding the CS tensor orientation, the δ_{11} components of both CS tensors are approximately along the dipolar vector, while the δ_{33} components are tilted away at an angle of 78°, in addition to being twisted relative to each other by an angle of 82°. This latter angle is thought to reflect the relative orientation of the phosphole rings, which are related by a dihedral angle ranging from 75° to 78°. Ab initio results support the experimental conclusions and indicate that the δ_{33} components are not aligned with the formal lone pairs on the phosphorus nuclei. The characterization of the phosphorus CS tensors in the phosphole tetramer is greatly aided by the 2D spin–echo experiment as well as by employing ab initio calculations to suggest an orientation of the tensor in the molecular frame.

Acknowledgments

We are grateful to Guy M. Bernard, David L. Bryce, Scott Kroeker, Michael D. Lumsden, and Robert W. Schurko for many helpful comments and suggestions on this work. R. E. W. thanks the Natural Sciences and Engineering Research Council (NSERC) of Canada for operating and equipment grants and the Canada Council for a Killam Research Fellowship. M.G. acknowledges NSERC, the Izaak Walton Killam Trust, and the Walter C. Sumner Foundation for postgraduate scholarships. All NMR spectra were acquired at the Atlantic Region Magnetic Resonance Centre (ARMRC), which is also supported by NSERC.

References

1. F. Mathey, F. Mercier, F. Nief, J. Fischer, and A. Mitschler. J. Am. Chem. Soc. **104**, 2077 (1982).
2. J. Fischer, A. Mitschler, F. Mathey, and F. Mercier. J. Chem. Soc. Dalton Trans. 841 (1983).
3. (*a*) K.W. Zilm, G.G. Webb, A.H. Cowley, M. Pakulski, and A. Orendt. J. Am. Chem. Soc. **110**, 2032 (1988); (*b*) R. Challoner, C.A. McDowell, M. Yoshifuji, K. Toyota, and J.A. Tossell. J. Magn. Reson. Ser. A. **104**, 258 (1993); (*c*) T. Nakai and C.A. McDowell. J. Am. Chem. Soc. **116**, 6373 (1994); (*d*) K. Eichele, G.C. Ossenkamp, R.E. Wasylishen, and T.S. Cameron. Inorg. Chem. **38**, 639 (1999); (*e*) G.M. Bernard,

© 2000 NRC Canada

G. Wu, M.D. Lumsden, R.E. Wasylishen, N. Maigrot, C. Charrier, and F. Mathey. J. Phys. Chem. A. **103**, 1029 (1999).
4. G. Wu and R.E. Wasylishen. J. Chem. Phys. **99**, 6321 (1993).
5. G. Wu, B. Sun, R.E. Wasylishen, and R.G. Griffin. J. Magn. Reson. **124**, 366 (1997).
6. (*a*) D.L. VanderHart and H.S. Gutowsky. J. Chem. Phys. **49**, 261 (1968); (*b*) K.W. Zilm and D.M. Grant. J. Am. Chem. Soc. **103**, 2913 (1981); (*c*) R.E. Wasylishen, R.D. Curtis, K. Eichele, M.D. Lumsden, G.H. Penner, W.P. Power, and G. Wu. *In* Nuclear magnetic shieldings and molecular structure. *Edited by* J.A. Tossell. Kluwer Academic Publishers, Dordrecht. 1993, pp. 297–314.
7. G.M. Bernard, G. Wu, and R.E. Wasylishen. J. Phys. Chem. A. **102**, 3184 (1998).
8. K. Eichele and R.E. Wasylishen. J. Magn. Reson. Ser. A. **106**, 46 (1994).
9. (*a*) R.A. Santos, P. Tang, W.-J. Chien, S. Kwan, and G. Harbison. J. Phys. Chem. **94**, 2717 (1990); (*b*) R.A. Santos and G.S. Harbison. J. Am. Chem. Soc. **116**, 3075 (1994); (*c*) R.J. Iuliucci, C.G. Phung, J.C. Facelli, and D.M. Grant. J. Am. Chem. Soc. **118**, 4880 (1996); (*d*) K. Eichele, R.E. Wasylishen, K. Maitra, J.H. Nelson, and J.F. Britten. Inorg. Chem. **36**, 3539 (1997); (*e*) S. Kroeker, K. Eichele, R.E. Wasylishen, and J.F. Britten. J. Phys. Chem. B. **101**, 3727 (1997); (*f*) T. Vosegaard, E. Hald, V. Langer, H.J. Skov, P. Daugaard, H. Bildsøe, and H.J. Jakobsen. J. Magn. Reson. **135**, 126 (1998); (*g*) R. Iuliucci, C.P. Phung, J.C. Facelli, and D.M. Grant. J. Am. Chem. Soc. **120**, 9305 (1998).
10. (*a*) H. van Willigen, R.G. Griffin, and R.A. Haberkorn. J. Chem. Phys. **67**, 5855 (1977); (*b*) W.P. Power, and R.E. Wasylishen. Ann. Rep. NMR Spectrosc. **23**, 1 (1991); (*c*) R.D. Curtis, J.W. Hilborn, G. Wu, M.D. Lumsden, R.E. Wasylishen, and J.A. Pincock. J. Phys. Chem. **97**, 1856 (1993); (*d*) M.D. Lumsden, G. Wu, R.E. Wasylishen, and R.D. Curtis. J. Am. Chem. Soc. **115**, 2825 (1993); (*e*) R.E. Wasylishen. *In* Encyclopedia of nuclear magnetic resonance. *Edited by* D.M. Grant and R.K. Harris. John Wiley and Sons, Chichester. 1996, p. 1685.
11. C.J. Jameson, A.C. de Dios, and A.K. Jameson. Chem. Phys. Lett. **167**, 575 (1990).
12. J. Mason. Solid State Nucl. Magn. Reson. **2**, 285 (1993).
13. K. Schmidt-Rohr and H.W. Spiess. Multidimensional solid-state NMR and polymers. Academic Press, London. 1994. pp. 444–448.
14. K. Eichele, G. Wu, R.E. Wasylishen, and J.F. Britten. J. Phys. Chem. **99**, 1030 (1995).
15. (*a*) S. Dusold, E. Klaus, A. Sebald, M. Bak, and N.C. Nielsen. J. Am. Chem. Soc. **119**, 7121 (1997); (*b*) S. Dusold, W. Milius, and A. Sebald. J. Magn. Reson. **135**, 500 (1998); (*c*) S. Dusold and A. Sebald. Mol. Phys. **9**5 1237 (1998).
16. T. Nakai and C.A. McDowell. Chem. Phys. Lett. **217**, 234 (1994).
17. K. Eichele, R.E. Wasylishen, R.W. Schurko, N. Burford, and W.A. Whitla. Can. J. Chem. **74**, 2372 (1996).
18. S. Dusold, J. Kümmerlen, and A. Sebald. J. Phys. Chem. A. **101**, 5895 (1997).
19. T. Nakai and C.A. McDowell. Solid State Nucl. Magn. Reson. **4**, 163 (1995).
20. (*a*) D.B. Chesnut. Ann. Rep. NMR Spectrosc. **29**, 71 (1994); (*b*) A.C. de Dios. Prog. Nucl. Magn. Reson. Spectrosc. **29**, 229 (1996); (*c*) H. Fukui. Prog. Nucl. Magn. Reson. Spectrosc. **31**, 317 (1997); (*d*) G. Schreckenbach and T. Ziegler. Theor. Chem. **99**, 71 (1998); (*e*) C.J. Jameson. *In* Nuclear magnetic resonance — a specialist periodical report. *Edited by* G.A. Webb. Royal Soc. Chem., Cambridge, 1998. vol. 27, pp. 44–82; (*f*) T. Helgaker, M. Jaszuński, and K. Ruud. Chem. Rev. **99**, 293 (1999).
21. (*a*) P. Pyykkö. Chem. Rev. **88**, 563 (1988); (*b*) J. Li, G. Schreckenbach, and T. Ziegler. Inorg. Chem. **34**, 3245 (1995); (*c*) M. Kaupp, V.G. Malkin, O.L. Malkina, and D.R. Salahub. J. Am. Chem. Soc. **117**, 1851 (1995); (*d*) M. Kaupp, O.L. Malkina, and V.G. Malkin. J. Chem. Phys. **106**, 9201 (1997).
22. (*a*) J. Gauss. Chem. Phys. Lett. **191**, 614 (1992); (*b*) J. Gauss. Chem. Phys. Lett. **229**, 198 (1994).
23. M. Bühl, M. Kaupp, O.L. Malkina, and V.G. Malkin. J. Comput. Chem. **20**, 91 (1999).
24. D.W. Alderman, M.S. Solum, and D.M. Grant. J. Chem. Phys. **84**, 3717 (1986).
25 M. Rance and R.A. Byrd. J. Magn. Reson. **52**, 221 (1983).
26 (*a*) R. Ditchfield. Mol. Phys. **27**, 789 (1974); (*b*) K. Wolinski, J.F. Hinton, and P. Pulay. J. Am. Chem. Soc. **112**, 8251 (1990); (*c*) G. Rauhut, S. Puyear, K. Wolinski, and P. Pulay. J. Phys. Chem. **100**, 6310 (1996).
27. (*a*) D.B. Chesnut and K.D. Moore. J. Comput. Chem. **10**, 648 (1989); (*b*) D.B. Chesnut, B.E. Rusiloski, K.D. Moore, and D.A. Egolf. J. Comput. Chem. **14**, 1364 (1993).
28. S. Duangthai and G.A. Webb. Org. Magn. Reson. **21**, 199 (1983).
29. G. Heckmann and E. Fluck. Mol. Phys. **23**, 175 (1972).
30. D.B. Chesnut and L.D. Quin. J. Am. Chem. Soc. **116**, 9638 (1994).
31. D.B. Chesnut and E.F.C. Byrd. Heteroat. Chem. **7**, 307 (1996).
32. (*a*) F. Mathey. Chem. Rev. **88**, 429 (1988); (*b*) F. Mathey. Coord. Chem. Rev. **137**, 1 (1994).
33. (*a*) L. Nyulászi. J. Phys. Chem. **100**, 6194 (1996); (*b*) A. Dransfeld, L. Nyulászi, and P.v.R. Schleyer. Inorg. Chem. **37**, 4413 (1998); (*c*) F.G.N. Cloke, P.B. Hitchcock, P. Hunnable, J.F. Nixon, L. Nyulászi, E. Niecke, and V. Thelen. Angew. Chem. Int. Ed. **37**, 1083 (1998).
34. K. Eichele, R.E. Wasylishen, J.M. Kessler, L. Solujić, and J.H. Nelson. Inorg. Chem. **35**, 3904 (1996).
35. G. Wu, R.E. Wasylishen, W.P. Power, and G. Baccolini. Can. J. Chem. **70**, 1229 (1992).
36. R.D. Curtis, B.W. Royan, R.E. Wasylishen, M.D. Lumsden, and N. Burford. Inorg. Chem. **31**, 3386 (1992).
37. G.H. Penner and R.E. Wasylishen. Can. J. Chem. **67**, 1909 (1989).

© 2000 NRC Canada

$Mn(OAc)_3$-promoted hydroxylation of α-carbomethoxy-γ-lactones by molecular oxygen

Laurent Lamarque, Alain Méou, and Pierre Brun

Abstract: The $Mn(OAc)_3$-mediated hydroxylation of a series of α-carbomethoxy-γ-lactones by molecular oxygen is described. The reaction is regio- and stereoselective and gives α-carbomethoxy-α-hydroxy-γ-lactones.

Key words: manganese acetate, γ-lactones, hydroxylation, molecular oxygen.

Résumé : L'hydroxylation d'une série d'α-carbométhoxy-γ-lactones par l'oxygène moléculaire, en présence d'acétate de manganèse, est décrite. La réaction est régio- et stéréosélective et conduit à des α-carbométhoxy-α-hydroxy-γ-lactones.

Mots clés : acétate de manganèse, γ-lactones, hydroxylation, oxygène moléculaire.

Introduction

$Mn(OAc)_3$ promotes the oxidation of β-dicarbonyl compounds giving electrophilic radicals that have been extensively used for intra- and intermolecular annulation of unsatured compounds (1–5). It has also been reported that, in some cases, these radicals can react with molecular oxygen. For instance, Kurosawa (6, 7–10, 11, 12, 13, 14) has shown that when 1,1-diarylethene derivatives are reacted with β-keto esters, β-diketones, β-keto amides, β-keto sulfoxides, acetylacetonitrile, or pyrrolidine-2,3-dione and $Mn(OAc)_3$ in acetic acid, in the presence of molecular oxygen, depending on the temperature, either 1,2-dioxan-3-ols (room temperature) or 4,5-dihydrofurans (70°C) are formed. It has also been described by Shibasaki (15) that the electrophilic radical prepared by oxidation of a β-keto ester with $Mn(OAc)_3$ can be directly trapped by molecular oxygen and converted to a δ-hydroxy-β,γ-unsaturated-α-keto ester. Similar results were also observed in intramolecular reactions (16, 17). Recently, Nair (18) has shown that dialkyl malonates can be hydroxylated by cerium^{IV} ammonium nitrate (CAN) in methanol, under an air atmosphere.

Results and discussion

In a previous study, we described the formation of a mixture of the two lactones **1a** and **2a** when (+)-Δ^3-carene is reacted, under N_2, with monomethyl malonate in the presence of $Mn(OAc)_3$ (2.2 equiv.) (19). We later observed that, under an air atmosphere, the same reaction led to a third product identified as the α-carbomethoxy-α-hydroxy-γ-butyrolactone **3a** (Scheme 1, Table 1).

The formation of **3a** can be accounted for by the subsequent hydroxylation of the first formed lactone **1a** by atmospheric oxygen. Indeed, when pure lactone **1a** was reacted with $Mn(OAc)_3$ under an O_2 atmosphere, at 70°C in acetic acid, lactone **3a** and its epimer **4a** were obtained in higher yields (Table 2, entry 1).

As, to our knowledge, such $Mn(OAc)_3$-mediated hydroxylation of α-carbomethoxy-γ-lactones has not been described, we decided to study the behavior of a series of α-carbomethoxy-γ-lactones obtained previously (19) (Scheme 2). The reactions were realized in acetic acid until discoloration of the reaction medium (Mn^{III} reduced into Mn^{II}). In these conditions, although in most cases an excess of Mn^{III} was used, the reaction did not go to completion. Our results are summarized in Table 2.

The α-carbomethoxy-α-hydroxy-γ-lactones are formed as a mixture of the two epimers **3** and **4** which can be readily separated by flash chromatography.

Structural determinations

The structure and relative configuration of the major isomers **3a, 3c** were determined by X-ray crystallography. Upon catalytic hydrogenation, **3c** (known configuration) and **3d** gave the same hydroxylactone **3e** thus establishing unambiguously the structure of **3d** and **3e**. The configuration of **3b** is based upon the chemical shift of the carbon bearing the carbomethoxy and the hydroxyl group which happens, in each case, to be lower in **3** than in the respective isomer **4**. The structure of the minor isomers **4a–e** was ascertained by comparison of their ^1H and ^{13}C NMR spectra with those of the major isomers **3a–e**.

For each lactone tested, a high or very high selectivity in favor of the epimer in which the hydroxyl group is in a *cis* relationship with the vicinal hydrogen is obtained. This selectivity is similar to the one observed for the addition of

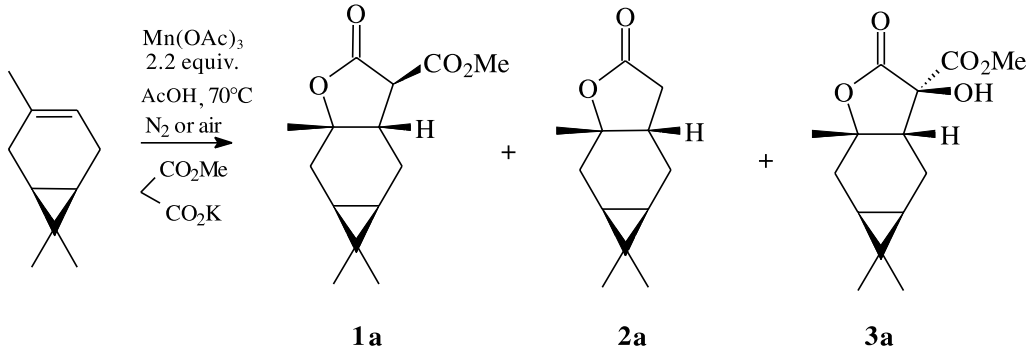
Accepted October 26, 1999.

L. Lamarque, A. Méou, and P. Brun.[1] Laboratoire de Synthèse Organique Sélective, associé au CNRS, GCOPL, ESA 6114, Université de la Méditerranée, 163 Avenue de Luminy, case 901, F-13288 Marseille Cedex 9, France.

[1]Author to whom correspondence may be addressed. Telephone: (33) 4 91 82 92 70. Fax: (33) 4 91 82 94 15. e-mail: brun@chimlum.univ-mrs.fr

 © 2000 NRC Canada

Scheme 1.



1a **2a** **3a**

Table 1. Mn^{III}-mediated addition of monomethyl malonate on (+)-Δ^3-carene. Relative ratio of lactones **1a**:**2a**:**3a**.

Atmosphere	**1a**:**2a**:**3a**	Yield (%)
N_2	35:65:0	57
Air	18:50:32[a]	56

[a]Accompanied by a trace of the epimeric α-carbomethoxy-α-hydroxy-γ-lactone **4a** (vide infra).

monomethyl malonate onto cycloalkenes and cycloalkadienes in the presence of $Mn(OAc)_3$ (19).

The influence of some experimental factors on the overall yield (**3**+**4**) has been investigated starting from lactone **1e** (entries 7–10): (*i*) in the absence of $Mn(OAc)_3$, no reaction is observed (entry 7); (*ii*) an enhanced yield is obtained when using less than 2.2 equiv. of $Mn(OAc)_3$ (compare entries 5 and 8); (*iii*) the reaction can be performed at room temperature by employing less than one equivalent of $Mn(OAc)_3$ (entry 9); (*iv*) the replacement of $Mn(OAc)_3$ by $Mn(OAc)_2$ (in situ generation of Mn^{III} salts) does not affect the course of the reaction (compare entries 5, 8, 9, 10).

The formation of these α-carbomethoxy-α-hydroxy-γ-butyrolactones can be explained by a mechanism similar to the one postulated by Nair (18): formation of a carbon-centered radical α- to the carbomethoxy group followed by reaction with molecular oxygen.

Such a radical could also explain the formation of 2-ethoxycarbonyl-4,4-diphenylbut-2-en-4-olide when monoethyl malonate is reacted with 1,1-diphenylethene in the presence of Mn^{III} (20). Although we do not have any evidence for the mechanism of the alcohol formation from a peroxyl radical, a mechanism similar to the one demonstrated for the formation of 2-hydroxymalonic acid when malonic acid is oxidized by Ce^{IV} in the presence of oxygen can be envisioned (21).

The decarbomethoxylation reaction of **3a** has been achieved using the Krapcho procedure (22) and gives the two epimeric α-hydroxy-γ-lactones **5a** + **5b** as a mixture (68:32) in good yield (84%). In the major epimer **5a**, the hydroxyl group is in a *cis* position with respect to the adjacent hydrogen (Scheme 3).

Conclusions

We have shown that α-carbomethoxy-α-hydroxy-γ-lactones can be prepared by Mn^{III}-mediated regioselective hydroxylation of α-carbomethoxy-γ-lactones using air or molecular oxygen as oxidant. Although some examples of such hydroxylations have been described using Ce^{IV}, it is the first case in which such a series of α-hydroxy-γ-lactones have been prepared using Mn^{III}. As exemplified by our results with Δ^3-carene, the overall transformation can be directly realized starting from the parent olefin by reaction with monomethyl malonate under an oxidative atmosphere in the presence of Mn^{III} (Table 1). Moreover, owing to the easy decarbomethoxylation of α-carbomethoxy-α-hydroxy-γ-lactones, this approach could be elaborated as a convenient two-step preparation of α-hydroxy-γ-lactones starting from olefins.

Table 2. Mn^{III}-mediated hydroxylation of α-carbomethoxy-γ-lactones **1a–f**. Relative ratio of lactones **3**:**4**.

Entry	**1**	Time (h)	$Mn(OAc)_3$ (equiv.)	T (°C)	**3**:**4**	Yield (%)[a]
1	**a**	24	2.2	70	66:34	36
2	**b**	3.5	2.2	70	87:13[b]	29
3	**c**	20	2.2	70	85:15	25
4	**d**	24	2.2	70	92:8	36
5	**e**	24	2.2	70	72:28	29
6	**f**	48	2.2	70	—	—[c]
7	**e**	20	0	70	—	—[d]
8	**e**	24	1.2	70	72:28	50
9	**e**	2.5	0.5	25	72:28	39
10	**e**	1.5	0.5[e]	70	72:28	37

[a]Chromatographic yield of pure isolated α-carbomethoxy-α-hydroxy-γ-lactones (**3** + **4**).

[b]**4b** was not isolated in a pure form but was identified by ^1H and ^{13}C NMR spectroscopy.

[c]Complex mixture of acetates and unidentified products.

[d]**1e** was recovered without significant loss.

[e]$Mn(OAc)_2$ was used instead of $Mn(OAc)_3$.

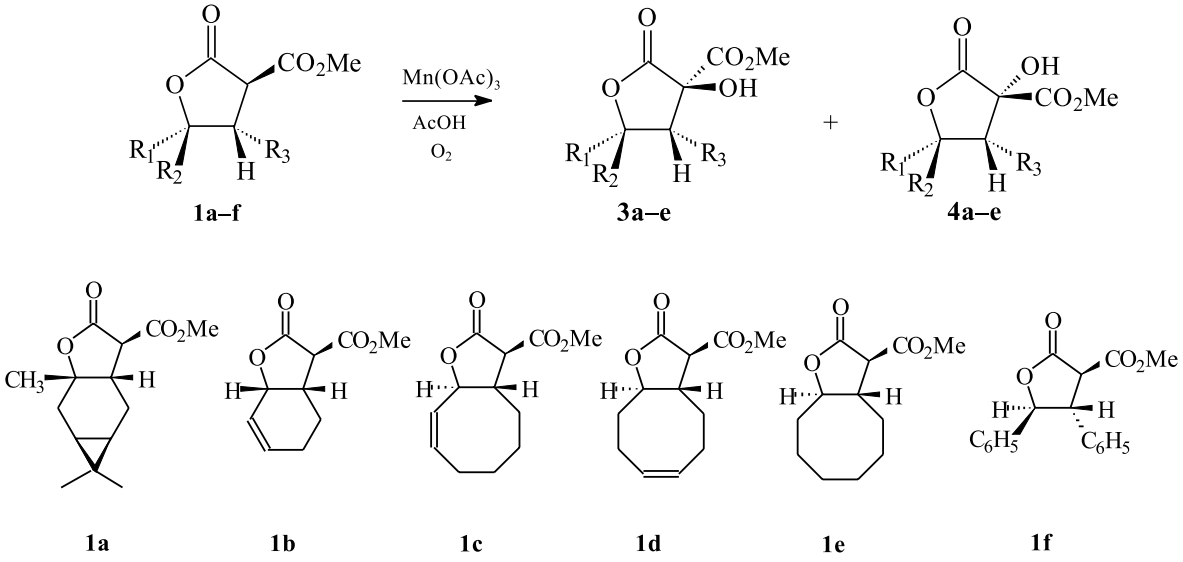
Experimental

General experimental procedures

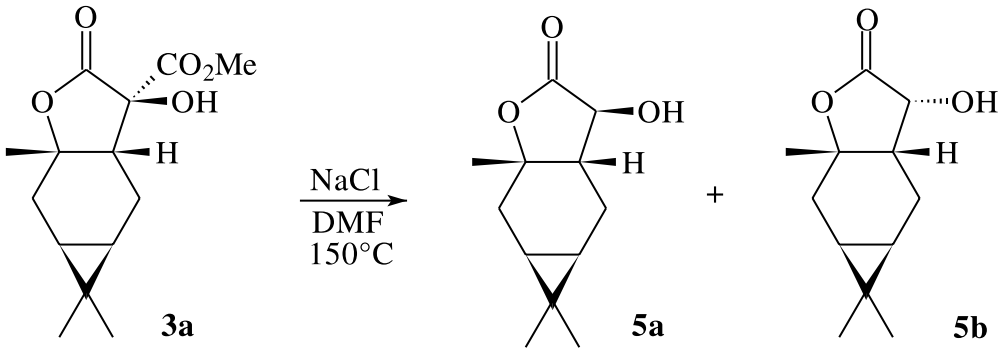
IR spectra were recorded on a Perkin–Elmer 297 apparatus, neat or in $CHCl_3$. ^1H NMR spectra were recorded in $CDCl_3$ on a Bruker AC 250 spectrometer operating at 250 MHz. Chemical shifts are reported in parts per million and are given in δ units; coupling constants are given in Hertz. We used the following symbols to report the multi-

© 2000 NRC Canada

Scheme 2.



Scheme 3.



plicity and shape of signals: s (singlet), d (doublet), t (triplet), m (multiplet). ^{13}C NMR spectra were recorded on the same spectrometer, operating at 62.5 MHz. Melting points were determined in capillary tubes using an Electrothermal IA 9100 apparatus. The progress of chromatographic separations was monitored by TLC on silica gel plates (Merck Kieselgel 60 F_{254}). Column flash chromatography was performed on silica gel (Merck Kieselgel 60H).

General procedure for hydroxylation

A two-necked 50 mL round-bottomed flask equipped with a reflux condenser was charged with α-carbomethoxy-γ-lactone **1** (1 mmol) and $Mn(OAc)_3{\cdot}2H_2O$ (see Table 2) in glacial acetic acid (10 mL). The solution was stirred for 10 min at room temperature under a stream of O_2 and the flask then placed in an oil bath at 70°C for the time indicated in Table 2. After cooling, the reaction mixture was poured into brine (40 mL) and extracted with Et_2O (4 × 10 mL). The organic layer was washed with a saturated $NaHCO_3$ solution to remove acetic acid and dried over $MgSO_4$. Removal of the solvent under reduced pressure at room temperature afforded an oily residue which was flash chromatographed (eluent: hexane–Et_2O gradient) to give the pure α-carbomethoxy-α-hydroxy-γ-lactones **3** and **4**.

*(1S,3S,5R,7R,8R)-1,4,4-Trimethyl-8-carbomethoxy-8-hydroxy-10-oxatricyclo[5.3.0.0^{3,5}]decan-9-one (**3a**)*: mp 221°C. IR ν_{max} cm^{-1} (KBr): 3480 (OH), 1760 (C=O, γ-lactone), 1740 (C=O, ester). ^{1}H NMR: δ ppm: 0.64–0.80 (m, 2H), 0.94 (dd, ^2J 15.3, ^3J 8.2 Hz, 1H), 0.97 (s, 3H), 1.03 (s, 3H), 1.07–1.17 (m, 1H), 1.56 (s, 3H), 1.66–1.77 (m, 1H), 2.26 (dd, ^2J 15.3, ^3J 7.0 Hz, 1H), 2.35 (d, ^3J 7.5 Hz, 1H), 3.93 (s, 3H), 4.10 (s, 1H). ^{13}C NMR: δ ppm: 14.69, 16.56, 17.89, 18.58, 20.45, 28.37, 28.73, 30.25, 50.89, 53.53, 83.02, 86.35, 170.68, 172.79.$[\alpha]^{20}_D$ = –38.4° (c 2.08, MeOH). Anal. calc. for $C_{14}H_{20}O_5$: C 62.66, H 7.52; found C 62.37, H 7.49.

*(1S,3S,5R,7R,8S)-1,4,4-Trimethyl-8-carbomethoxy-8-hydroxy-10-oxatricyclo[5.3.0.0^{3,5}]decan-9-one (**4a**)*: mp 132–134°C. IR, ν_{max} cm^{-1} (KBr): 3480 (OH), 1760 (C=O, γ-lactone), 1740 (C=O, ester). ^{1}H NMR: δ ppm: 0.49–0.59 (m, 1H), 0.67–0.90 (m, 3H), 0.91 (s, 3H), 0.94 (s, 3H), 1.46 (s, 3H), 2.05–2.20 (m, 2H), 2.48 (dd, ^3J 1.6, 5.6 Hz, 1H), 3.82 (s, 3H), 3.97 (s, 1H). ^{13}C NMR, δ ppm 14.43, 16.93, 17.67, 17.83, 18.27, 27.57, 27.98, 31.06, 45.82, 53.96, 79.03, 86.01,

© 2000 NRC Canada

171.73, 173.28. $[\alpha]^{20}_{578}$ = –18.1° (c 1.35, MeOH). Anal. calc. for $C_{14}H_{20}O_5$: C 62.66, H 7.52; found C 62.21, H 7.14.

(1S,6R*,7R*)-7-Carbomethoxy-7-hydroxy-9-oxabicyclo[4.3.0]-non-2-en-8-one (**3b**)*: mp 109°C. IR ν_{max} cm^{-1} (film): 3490 (OH), 1770 (C=O, γ-lactone), 1740 (C=O, ester). ^1H NMR: δ ppm: 1.44–1.53 (m, 2H), 1.87–2.01 (m, 1H), 2.04–2.20 (m, 1H), 2.46–2.55 (m, 1H), 3.81 (s, 3H), 4.49 (s, 1H), 5.01 (dd, ^3J 4.4, 5.3 Hz, 1H), 5.83–5.95 (m, 1H), 6.08–6.20 (m, 1H). ^{13}C NMR: δ ppm: 19.83, 23.59, 46.39, 53.48, 74.34, 81.11, 122.07, 135.35, 169.93, 172.20. Anal. calc. for $C_{10}H_{12}O_5$: C 56.60, H 5.70; found C 56.51, H 5.65.

(1R,8R*,9R*)-9-Carbomethoxy-9-hydroxy-11-oxabicyclo-[6.3.0] undec-2-en-10-one (**3c**)*: mp 158°C. IR ν_{max} cm^{-1} (film): 3500 (OH), 1780 (C=O, γ-lactone), 1745 (C=O, ester). ^1H NMR: δ ppm: 1.06–1.31 (m, 2H), 1.53–1.64 (m, 2H), 1.64–1.73 (m, 2H), 2.05–2.33 (m, 3H), 3.84 (s, 3H), 3.99 (s, 1H), 5.26 (ddd, ^3J 5.8, 7.0, ^4J 1.4 Hz, 1H), 5.55–5.67 (m, 1H), 5.76 (dd, ^3J 5.8, 10.7 Hz, 1H). ^{13}C NMR: δ ppm: 22.56, 23.78, 24.86, 27.90, 53.78, 56.03, 79.21, 80.19, 123.38, 129.88, 169.21, 172.80. Anal. calc. for $C_{12}H_{16}O_5$: C 59.99, H 6.71; found C 59.78, H 6.71.

(1R,8R*,9S*)-9-Carbomethoxy-9-hydroxy-11-oxabicyclo-[6.3.0]undec-2-en-10-one (**4c**)*: IR ν_{max} cm^{-1} (film): 3500 (OH), 1780 (C=O, γ-lactone), 1735 (C=O, ester). ^1H NMR: δ ppm: 1.25–1.90 (m, 6H), 2.12–2.35 (m, 2H), 2.35–2.45 (m, 1H), 3.80 (s, 1H), 3.90 (s, 3H), 5.32 (dd, ^3J 10.2, 5.8 Hz, 1H), 5.64–5.75 (m, 1H), 5.85 (dd, ^3J 5.8, 10.7 Hz, 1H). ^{13}C NMR: δ ppm: 21.26, 23.25, 24.84, 28.00, 53.28, 54.00, 79.41, 81.48, 128.88, 130.15, 170.47, 172.84. Anal. calc. for $C_{12}H_{16}O_5$: C 59.99, H 6.71; found C 59.81, H 6.69.

(1R,8R*,9R*)-9-Carbomethoxy-9-hydroxy-11-oxabicyclo-[6.3.0]undec-4-en-10-one (**3d**)*: mp 130°C. IR ν_{max} cm^{-1} (film): 3500 (OH), 1780 (C=O, γ-lactone), 1745 (C=O, ester). ^1H NMR: δ ppm: 1.13–1.28 (m, 2H), 1.47–1.59 (m, 1H), 1.75–1.88 (m, 1H), 2.08–2.36 (m, 4H), 2.48 (ddd, ^3J 3.8, 9.4, 12.9 Hz, 1H), 3.80 (s, 3H), 4.02 (s, 1H), 4.43 (ddd, ^3J 4.1, 10.6, 12.9 Hz, 1H), 5.54–5.72 (m, 2H). ^{13}C NMR: δ ppm: 20.87, 23.58, 26.31, 33.94, 50.60, 53.58, 81.45, 82.40, 129.51, 129.63, 169.78, 172.22. Anal. calc. for $C_{12}H_{16}O_5$: C 59.99, H 6.71; found C 59.79, H 6.64.

(1R,8R*,9S*)-9-Carbomethoxy-9-hydroxy-11-oxabicyclo-[6.3.0]undec-4-en-10-one (**4d**)*: IR ν_{max} cm^{-1} (film): 3500 (OH), 1780 (C=O, γ-lactone), 1745 (C=O, ester). ^1H NMR: δ ppm: 1.40–1.60 (m, 2H), 1.70–1.86 (m, 1H), 2.10–2.35 (m, 5H), 2.65 (ddd, ^3J 3.7, 7.9, 12.1 Hz, 1H), 3.73 (s, 1H), 3.82 (s, 3H), 4.46 (ddd, ^3J 3.7, 11.5, 12.1 Hz, 1H), 5.55–5.74 (m, 2H). ^{13}C NMR: δ ppm: 21.19, 23.73, 23.87, 33.78, 47.63, 54.13, 79.64, 84.83, 129.54, 130.06, 170.32, 171.26. Anal. calc. for $C_{12}H_{16}O_5$: C 59.99, H 6.71; found C 59.82, H 6.62.

(1R,8R*,9R*)-9-Carbomethoxy-9-hydroxy-11-oxabicyclo-[6.3.0]undecan-10-one (**3e**)*: mp 117°C. IR ν_{max} cm^{-1} (film): 3500 (OH), 1780 (C=O, γ-lactone), 1745 (C=O, ester). ^1H NMR: δ ppm: 1.10–1.90 (m, 10H), 2.10–2.30 (m, 2H), 2.41 (td, ^3J 3.6, 10.0, 10.0 Hz, 1H), 3.81 (s, 3H), 4.23 (s, 1H), 4.52 (td, ^3J 4.5, 10.0, 10.0 Hz, 1H). ^{13}C NMR: δ ppm: 23.06, 25.57, 27.13, 27.25, 27.85, 34.66, 52.16, 53.70, 81.93, 83.64, 169.67, 172.50. Anal. calc. for $C_{12}H_{18}O_5$: C 59.49, H 7.49; found C 59.22, H 7.33.

(1R,8R*,9S*)-9-Carbomethoxy-9-hydroxy-11-oxabicyclo-[6.3.0]undecan-10-one (**4e**)*: IR ν_{max} cm^{-1} (film): 3500 (OH), 1780 (C=O, γ-lactone), 1745 (C=O, ester). ^1H NMR: δ ppm: 1.10–2.05 (m, 10H), 2.10–2.30 (m, 2H), 2.60 (td, ^3J 3.5, 9.1, 9.1 Hz, 1H), 3.82 (s, 3H), 3.92 (s, 1H), 4.52 (td, ^3J 4.2, 9.1, 9.1 Hz, 1H). ^{13}C NMR: δ ppm: 22.58, 24.43, 24.47, 25.51, 27.14, 33.87, 49.09, 53.97, 79.99, 85.40, 170.80, 171.89. Anal. calc. for $C_{12}H_{18}O_5$: C 59.49, H 7.49; found C 59.19, H 7.23.

Procedure for the decarbomethoxylation of 3a

A 10 mL round-bottomed flask, equipped with a reflux condenser, was charged with **3a** (238 mg, 0.89 mmol), NaCl (79 mg, 1.35 mmol), and H_2O (30 μL, 1.66 mmol) in DMF (2 mL). The mixture was stirred for 3 h at 150°C. It was then cooled, poured into brine (10 mL), and extracted with Et_2O (4 × 5 mL). The organic layer was washed with brine and dried over $MgSO_4$. Removal of the solvent under reduced pressure at room temperature afforded an oily residue which was purified by flash chromatography (eluent: hexane–Et_2O gradient) to give α-hydroxy-γ-lactones **5a** and **5b** (84% yield).

*(1S,3S,5R,7R,8S)-1,4,4-Trimethyl-8-hydroxy-10-oxatricyclo-[5.3.0.0^{3,5}]decan-9-one (**5a**)*: IR ν_{max} cm^{-1} ($CHCl_3$): 3450 (OH), 1775 (C=O, γ-lactone). ^1H NMR: δ ppm: 0.42–0.94 (m, 3H), 0.91 (s, 3H), 0.94 (s, 3H), 1.36 (s, 3H), 2.00–2.23 (m, 3H), 2.37 (dd, ^3J 5.6, 9.8 Hz, 1H), 3.94 (m, 1H), 4.65 (d, ^3J 9.8 Hz, 1H). ^{13}C NMR: δ ppm: 14.56, 15.48, 16.64, 18.19, 18.45, 27.47, 28.00, 30.50, 41.60, 68.53, 85.28, 178.18.

*(1S,3S,5R,7R,8R)-1,4,4-Trimethyl-8-hydroxy-10-oxatricyclo-[5.3.0.0^{3,5}]decan-9-one (**5b**)*: IR ν_{max} cm^{-1} ($CHCl_3$): 3450 (OH), 1775 (C=O, γ-lactone). ^1H NMR: δ ppm: 0.42–0.94 (m, 3H), 0.91 (s, 3H), 0.98 (s, 3H), 1.35 (s, 3H), 2.00–2.23 (m, 3H), 2.25–2.35 (m, 1H), 4.15 (s, 1H), 4.47 (d, ^3J 7.0 Hz, 1H). ^{13}C NMR: δ ppm: 14.79, 17.55, 18.00, 18.48, 19.72, 28.34, 29.67, 30.08, 47.02, 73.25, 86.20, 177.79.

References

1. G.G. Melikyan. Synthesis, 833 (1993).
2. J. Iqbal, B. Bhatia, and N.K. Nayyar. Chem. Rev. **94**, 519 (1994).
3. P.I. Dalko. Tetrahedron, **51**, 7579 (1995).
4. B.B. Snider. Chem. Rev. **96**, 339 (1996).
5. W.J. de Klein. Organic synthesis by oxidation with metal compounds. *Edited by* W.J Mijs and C.R.H.I. de Jonge. Plenum Press, New York. 1986. pp. 261–314.
6. T. Yamada, Y. Iwahara, H. Nishino, and K. Kurosawa. J. Chem. Soc. Perkin Trans. 1, 609 (1993).
7. H. Nishino, S. Tategami, T. Yamada, J.D. Korp, and K. Kurosawa. Bull. Chem. Soc. Jpn. **64**, 1800 (1991).
8. C.-Y. Qian, T. Yamada, H. Nishino, and K. Kurosawa. Bull. Chem. Soc. Jpn. **65**, 1371 (1992).
9. C.-Y. Qian, H. Nishino, K. Kurosawa, and J.D. Korp. J. Org. Chem. **58**, 4448 (1993).
10. S. Tategami, T. Yamada, H. Nishino, J.D. Korp, and K. Kurosawa. Tetrahedron Lett. **31**, 6371 (1990).

© 2000 NRC Canada

11. C.-Y. Qian, H. Nishino, and K. Kurosawa. Bull. Chem. Soc. Jpn. **64**, 3557 (1991).
12. C.-Y. Qian, H. Nishino, and K. Kurosawa. J. Heterocycl. Chem. **30**, 209 (1993).
13. V.-H. Nguyen, H. Nishino, and K. Kurosawa. Tetrahedron Lett. **37**, 4949 (1996).
14. V.-H. Nguyen, H. Nishino, and K. Kurosawa. Tetrahedron Lett. **38**, 1773 (1997).
15. T. Ohshima, M. Sodeoka, and M. Shibasaki. Tetrahedron Lett. **34**, 8509 (1993).
16. P.A. Zoretic, M. Ramchandani, and M.L. Caspar. Synth. Commun. **21**, 915 (1991).
17. J.D. White and S.C. Jeffrey. Synlett, 831 (1995).
18. V. Nair, L.G. Nair, and J. Mathew. Tetrahedron Lett. **39**, 2801 (1998).
19. L. Lamarque, A. Méou, and P. Brun. Tetrahedron, **54**, 6497 (1998).
20. N. Fujimoto, H. Nishino, and K. Kurosawa. Bull. Chem. Soc. Jpn. **59**, 3161 (1986).
21. B. Neumann, S.C. Müller, M.J.B. Hauser, O. Steinbock, R.H. Simoyi, and N.S. Dalal. J. Am. Chem. Soc. **117**, 6372 (1995).
22. A.P. Krapcho. Synthesis, 805 (1982).

© 2000 NRC Canada

A short synthesis of both enantiomers of enterolactone

Mukund P. Sibi, Pingrong Liu, and Michael D. Johnson

Abstract: A short and efficient synthesis of both enantiomers of enterolactone, a mammalian lignan, is described. The overall yield for the natural enterolactone, over seven steps, was 19% and for its enantiomer 27%.

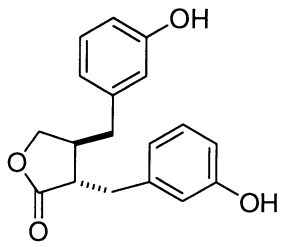
Key words: enterolactone, 4-diphenylmethyl-2-oxazolidinone, succinate, enantioselective synthesis.

Résumé : On décrit une synthèse courte et efficace des deux énantiomères de l'entérolactone, un lignane extrait de mammifères. Le rendement global en entérolactone naturelle après une synthèse en sept étapes est de 19% et il est de 27% pour son énantiomère.

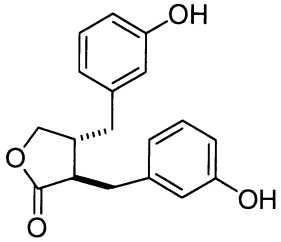
Mots clés : entérolactone, 4-diphénylméthyl-2-oxazolidone, succinate, synthèse énantiosélective.

[Traduit par la Rédaction]

Lignan natural products continue to receive attention due to their interesting biological profile (1). For example, enterolactone, a lignan present in human urine, has been shown to possess protective properties towards certain types of cancers (2). Neither enterolactone, nor its bioprecursor(s), secoisolariciresinol and matairesinol, are commercially available. Only a few routes to enantiomerically pure enterolactone have been reported (for racemic synthesis see ref. 3; for enantioselective synthesis see ref. 4). Availability of both enantiomers is important to establish biological efficacy. We have now developed a synthesis of enterolactone in both enantiomeric forms (**1**, **2**) in good overall yields. The novelty of the approach is that a single chiral auxiliary provides access to both targets and these details are presented in this article.



1 (+)-Enterolactone

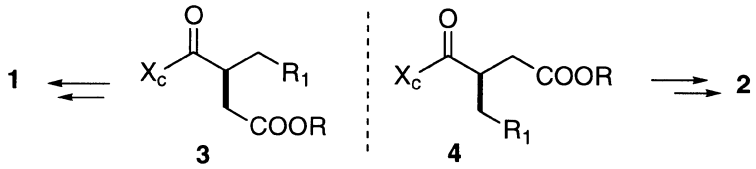


2 (–)-Enterolactone

We have been interested in developing a general methodology for the regio- and stereoselective functionalization of linear dicarboxylic acids and its application in natural product synthesis. The successful execution of this protocol in the synthesis of paraconic acid natural products (5) and seco lignans–peperomins (6), has been reported from our laboratory (for a similar strategy to butyrolactones involving the alkylation of acyloxazolidinones with halo acetates see ref. 7*a*; for another example of enolate alkylation leading to similar structures see ref. 7*b*). We were interested in extending the method to the synthesis of enterolactone enantiomers. The key step in the method was the preparation of the diastereomeric succinates **3** and **4** (R_1 = 3-methoxybenzyl) and chemoselective hydrolysis of the chiral auxiliary (X_c) followed by conversion to the target natural products (eq. [1]).

The synthesis of the unnatural (+)-enterolactone **1** is shown in Scheme 1. This involved the preparation of the monosubstituted succinate **3** in optically pure form by a stereoselective alkylation of a chiral imide. The sequence began by the acylation of the chiral oxazolidinone **5** (8)[2] with 3-methoxy dihydrocinnamoyl chloride under standard conditions to give **6** in excellent yield. Introduction of the acetate side chain was carried out using NaHMDS to provide the succinate **7** in good yield as a single diastereomer (for selected examples of alkylation using different bases leading

[1]



Accepted October 25, 1999.

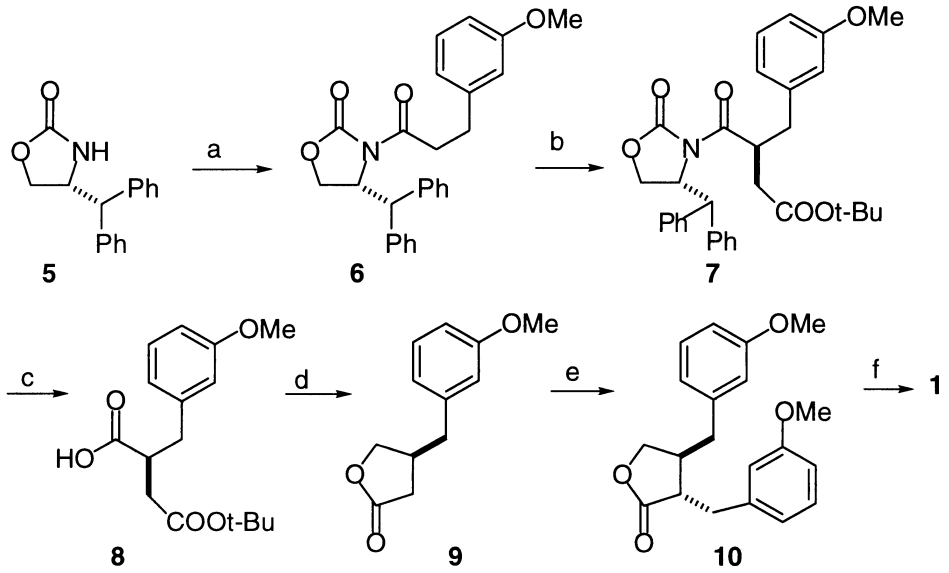
M.P. Sibi,[1] P. Liu, and M.D. Johnson. Department of Chemistry, North Dakota State University, Fargo, ND 58105-5516, U.S.A.

[1]Author to whom correspondence may be addressed. Fax: (701) 231-8831. e-mail: sibi@plains.nodak.edu

[2]For synthesis of the auxiliary see ref. 8*a*. This chiral auxiliary is available commercially from Aldrich Chemical Company. For applications of the auxiliary in synthesis see ref. 8*b*.

© 2000 NRC Canada

Scheme 1.



a, *n*-BuLi, THF, −78°C, $ClCO(CH_2)_2Ph$-3-OMe, 93%; b, 1.1 equiv. NaHMDS, −78 °C, ICH_2COOt-Bu, 85%; c, LiOH, H_2O_2, THF−H_2O, 0°C, 85%; d, (*i*) BH_3THF, THF, 0°C, 80%; (*ii*) PTSA, benzene, 92%; e, NaHMDS, THF, 3-OMe-$PhCH_2I$, −78°C to −54°C, 69%; f, BBr_3, CH_2Cl_2, 0°C to −18°C, 78%.

to succinates see ref. 9). Chemoselective removal of the chiral auxiliary was carried out using LiOH–H_2O_2 to furnish the succinate monoester **8** (85%) (10). The chiral auxiliary **5** could be recovered in >95% yield. Selective reduction of the carboxylic acid in the presence of the ester functionality using borane–THF followed by acid catalyzed cyclization gave the known lactone **9** in 74% overall yield over two steps (4b). The introduction of the second benzylic fragment onto **9** was carried out successfully by enolate generation with NaHMDS followed by treatment with 3-methoxy benzyl iodide to furnish **10**.[3] This procedure avoids the use of HMPA as reported by Doyle for the same alkylation using the corresponding benzyl bromide as the alkylating agent (4*b*). The lactone **10** was converted to the unnatural (+)-enterolactone **1** by demethylation using BBr_3. The spectral and analytical characteristics of **1** were identical to the data reported in the literature (4*a*, *b*). The overall yield for the unnatural isomer over seven synthetic steps was 27%.

The synthesis of the natural (–)-enterolactone **2** is shown in Scheme 2. The synthesis of this target involved the regio- and stereoselective alkylation of a succinate to provide **4** as the key step. To this end, acylation of **5** with the mono ethyl succinoyl chloride under standard conditions gave the succinate **11** in excellent yield. Treatment of **11** with 1.1 equiv. of NaHMDS in THF at –78°C for 75 min followed by quenching with 3-methoxybenzyl iodide furnished the mono alkylated succinate **12** in good chemical yield and high diastereoselectivity. Temperature and counterion play an important role in the generation of the enolate. When reactions were warmed to above –48°C after sodium enolate generation, cleavage of the chiral auxiliary was observed. Similarly, lithium enolates were found to be unstable at –78°C. The regioselectivity observed in enolate generation from **11** may be attributed to the increased acidity of these α-hydrogens adjacent to imide over the ester (for selective alkylation of a similar C-4 unit see ref. 11). The next step was the chemoselective hydrolysis of the imide. The rest of the synthesis followed the same sequence as described in Scheme 1. The overall yield for **2** was 19%.

In conclusion, we have developed an efficient strategy for the preparation of mammalian lignan enterolactone in either enantiomeric form using a single chiral auxiliary. The methodology is short and is amenable to scale up. The extension of the selective alkylation protocol to the synthesis of other lignans of biological interest is underway.

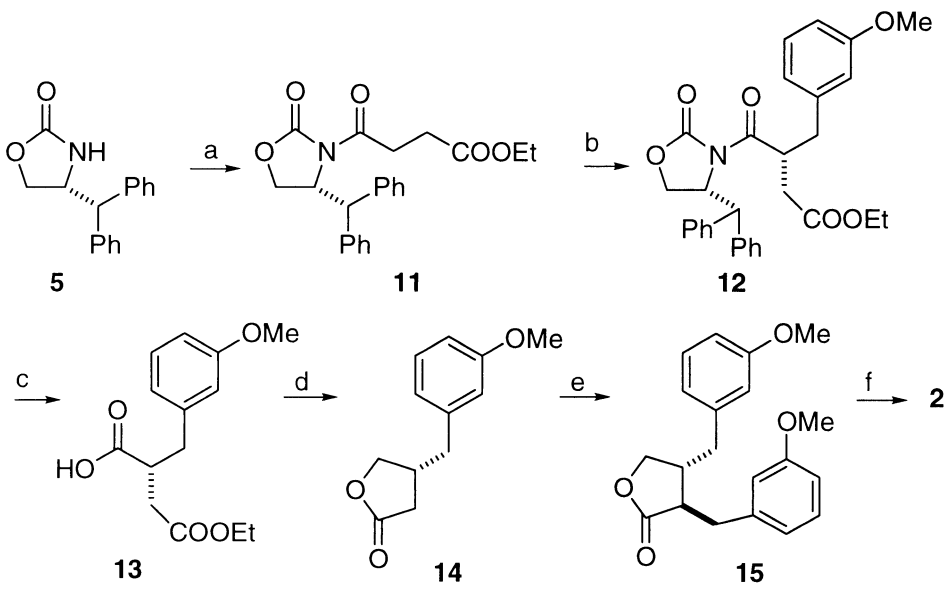
Experimental

Methylene chloride was distilled from calcium hydride. Tetrahydrofuran and benzene were distilled from benzophenone–ketyl prior to use. Thin layer chromatographic analyses were performed on silica gel Whatmann-60F glass plates and components were visualized by illumination with UV light or by staining with phosphomolybdic acid. Flash chromatography was performed using E. Merck silica gel 60 (230–400 mesh). All glassware was oven- and (or) flame-dried, assembled hot, and cooled under a stream of dry nitrogen or argon before use. Reactions with air sensitive materials were carried out by standard syringe techniques.

[3] On certain occasions less than 5% of the dialkylated product was also obtained.

© 2000 NRC Canada

Scheme 2.



a, *n*-BuLi, THF, −78°C, ethyl succinoyl chloride, 85%; b, 1.1 equiv. NaHMDS, -78°C to −54°C, 3-OMe-PhCH$_2$I, 60%; c, LiOH, H_2O_2, THF−H_2O, 0°C, 80%; d, (*i*) BH_3THF, THF, 0°C, 78%; (*ii*) PTSA, benzene, 97%; e, NaHMDS, THF, 3-OMe-PhCH$_2$I, −78°C to −54°C, 69%; f, BBr_3, CH_2Cl_2, 88%.

^{1}H NMR was recorded on a 400 or a 300 MHz spectrometer. ^{13}C NMR were recorded on a 400 (100) MHz and 300 (75) MHz spectrometers using broad band proton decoupling. Rotations were recorded on a JASCO-DIP-370 instrument. Elemental analyses were performed on a Perkin–Elmer Series II CHNS/O Analyzer 2400.

(4*R*)-4-(Diphenylmethyl)-3-[3-(3′-methoxyphenyl)propanoyl]-2-oxazolidinone (6)

4-Diphenylmethyl-2-oxazolidinone (**5**) (10.50 g, 41.52 mmol) in THF (160 mL) under N_2 was cooled to –78°C. *n*-BuLi (18.63 mL, 2.34 M in hexanes, 43.60 mmol) was then added dropwise over a period of 20 min. The reaction was stirred at that temperature for 30 min, then a solution of 3-methoxyhydrocinnamoyl chloride (9.07 g, 45.67 mmol) in THF (8 mL) was added dropwise over a period of 10 min. After stirring at –78°C for 2.5 h, the reaction mixture was quenched with saturated aqueous NH_4Cl (30 mL). The mixture was extracted with ethyl acetate. The organic layers were combined, washed with brine, dried over $MgSO_4$, and concentrated. The crude product was purified by flash column to afford the acylated product **6** (16.00 g, 93%). R_f 0.57 (50:50, EtOAc:hexanes). Colorless oil. $[\alpha]_D^{25}$ –95.98 (*c* 1.02, CH_2Cl_2). ^{1}H NMR (400 MHz, $CDCl_3$) δ: 2.89 (m, 2H), 3.18 (m, 2H), 3.82 (s, 3H), 4.38 (d, *J* = 5.36 Hz, 2H), 4.71 (d, *J* = 5.92 Hz, 1H), 5.33 (m, 1H), 6.79 (dd, *J* = 2.16, 8.32 Hz, 1H), 6.85 (m, 2H), 7.07–7.37 (m, 11H). ^{13}C NMR (100 MHz, $CDCl_3$) δ: 172.1, 159.8, 153.5, 142.3, 139.7, 138.1, 129.6, 129.4, 129.0, 128.8, 128.5, 128.0, 127.2, 121.1, 114.4, 111.8, 65.2, 56.4, 55.3, 51.0, 37.2, 30.4. Anal. calcd. for $C_{26}H_{25}NO_4$: C 75.16, H 6.06, N 3.37; found: C 75.35, H 5.72, N 3.29.

(4*R*)-4-(Diphenylmethyl)-3[(2*S*)-2-(*tert*-butyloxycarbonyl)methyl]3-(3′-methoxyphenyl)]-2-oxazolidinone (7)

Acyloxazolidinone **6** (13.50 g, 32.55 mmol) in THF (160 mL) under N_2 was cooled to –78°C. NaHMDS (35.81 mL, 1.0 M in THF, 35.81 mmol) was then added dropwise over a period of 40 min. The mixture was stirred at that temperature for 1 h. *tert*-Butyl iodoacetate (5.67 mL, 39.06 mmol) was added dropwise over a period of 8 min. After stirring at –78°C for 6 h, the reaction was quenched with saturated aqueous NH_4Cl (30 mL). The mixture was extracted with ethyl acetate. The organic layers were combined, washed with brine, dried over $MgSO_4$, and concentrated. The crude product was purified by flash column to afford the alkylated product **7** (14.66 g, 85%). R_f 0.63 (50:50, EtOAc:hexanes); mp 97–99°C. $[\alpha]_D^{25}$ –209.42 (*c* 1.21, CH_2Cl_2). ^{1}H NMR (400 MHz, $CDCl_3$) δ: 1.46 (s, 9H), 2.32, (dd, *J* = 4.56, 16.64 Hz, 1H), 2.58 (dd, *J* = 8.84, 12.88 Hz, 1H), 2.74 (dd, *J* = 9.96, 16.68 Hz, 1H), 2.96 (dd, *J* = 6.48, 12.92 Hz, 1H), 3.78 (s, 3H), 4.24 (t, *J* = 8.36 Hz, 1H), 4.37 (dd, *J* = 2.44, 9.16 Hz, 1H), 4.47 (m, 1H), 4.74 (d, *J* = 3.48 Hz, 1H), 5.14 (m, 1H), 6.76 (dd, *J* = 2.68, 8.32 Hz, 1H), 6.81 (m, 2H), 7.05 (d, *J* = 7.52 Hz, 2H), 7.18 (t, *J* = 7.80 Hz, 1H), 7.24–7.35 (m, 8H). ^{13}C NMR (100 MHz, $CDCl_3$) δ: 174.9, 171.4, 159.7, 152.9, 140.2, 139.8, 138.1, 129.8, 129.4, 128.8, 128.7, 128.3, 127.7, 127.0, 121.7, 114.5, 112.6, 80.8, 64.3, 56.7, 55.3, 50.0, 41.5, 38.2, 36.5, 28.2. Anal. calcd. for $C_{32}H_{35}NO_6$: C 72.57, H 6.66, N 2.64; found: C 72.64, H 6.82, N 2.62.

tert-Butyloxycarbonyl (2*S*)-(carboxymethyl)-3-(3′-methoxyphenyl)propionic acid (8)

Oxazolidinone **7** (2.00 g, 3.82 mmol) in THF (30 mL) and H_2O (10 mL) was cooled to 0°C. 30% H_2O_2 (1.56 mL,

© 2000 NRC Canada

15.28 mmol) was added dropwise over a period of 3 min. Then LiOH–H_2O (321 mg, 7.64 mmol) in H_2O (4 mL) was added dropwise over a period of 6 min. The mixture was stirred at 0°C for 1.5 h, then at room temperature for 3 h. The reaction mixture was cooled to 0°C before quenching with the solution of $NaHSO_3$ (2.00 g) in H_2O (5 mL). The mixture was acidified with HCl (1 M) and then made basic with NaOH (2 M) before being extracted with CH_2Cl_2. The organic layers were combined to recover the chiral auxiliary. The aqueous layer was acidified to pH = 2 with HCl (5 M) before extraction with ethyl ether. The organic layers were combined, washed with brine, dried over $MgSO_4$, and concentrated. The crude product was purified by flash column to afford the acid **8** (952 mg, 85%). R_f 0.33 (50:50-EtOAc:hexanes). Colorless liquid. $[\alpha]_D^{25}$ +150.0 (c 0.02, CH_2Cl_2). ^{1}H NMR (400 MHz, $CDCl_3$) δ: 1.41(s, 9H), 2.34 (dd, *J* = 4.39, 16.84 Hz, 1H), 2.55 (dd, *J* = 8.79, 16.84 Hz, 1H), 2.72 (dd, *J* = 10.62, 15.38 Hz, 1H), 3.09 (m, 2H), 3.78(s, 3H), 6.72–6.80 (m, 3H), 7.21 (t, *J* = 8.06 Hz, 1H), 11.45 (broad, 1H). ^{13}C NMR (100 MHz, $CDCl_3$) δ: 180.9, 171.1, 159.8, 139.7, 129.7, 121.5, 114.8, 112.2, 81.2, 55.2, 43.2, 37.4, 36.1, 28.1. Anal. calcd. for $C_{16}H_{22}O_5$: C 65.29, H 7.53; found: C 65.24, H 7.67.

(4*S*)-[(3-Methoxyphenyl)methyl]dihydro-2(3*H*)-furanone (9)

Reduction and lactonization

Acid **8** (1.00 g, 3.40 mmol) in dry THF (20 mL) under N_2 was cooled to 0°C. BH_3·THF (5.10 mL, 1 M in THF, 5.10 mmol) was then added dropwise over a period of 10 min. After stirring at that temperature for 1.5 h, the mixture was slowly warmed up to room temperature and stirred for another hour. The reaction mixture was cooled to 0°C before slow quench with methanol. The solvent was removed under reduced pressure, water was added, and CH_2Cl_2 was used to extract the organic compound. The organic layers were combined, washed with brine, dried over $MgSO_4$, and concentrated. The crude product was purified by flash column to afford alcohol (760 mg, 80%).

The alcohol (900 mg, 3.21 mmol) and PTSA (5 mg) in benzene (10 mL) under N_2 was heated to reflux for 2 h. The mixture was then cooled to room temperature. The mixture was washed with saturated aqueous $NaHCO_3$ and water before extracting with ethyl acetate and drying over $MgSO_4$. The extraction was concentrated and purified by flash column to afford the lactone **9** (608 mg, 92%). R_f 0.39 (50:50, EtOAc:hexanes). Pale yellow oil. $[\alpha]_D^{25}$ –6.76 (*c* 1.04, $CHCl_3$) (lit. (12) value: +6.40 (*c* 1.0, $CHCl_3$)) (also see ref. 4*a*). ^{1}H NMR (400 MHz, $CDCl_3$) δ: 2.29 (dd, *J* = 7.0, 17.44 Hz, 1H), 2.60 (dd, *J* = 8.08, 17.48 Hz, 1H), 2.74 (apt dd, *J* = 3.24, 7.0 Hz, 2H), 2.85 (m, 1H), 3.80 (s, 3H), 4.03 (dd, *J* = 6.2, 9.16 Hz, 1H), 4.33 (dd, *J* = 7.0, 9.16 Hz, 1H), 6.69 (d, *J* = 1.88 Hz, 1H), 6.73 (d, *J* = 7.52 Hz, 1H), 6.78 (dd, *J* = 1.88, 7.52 Hz, 1H), 7.23 (t, *J* = 7.76 Hz, 1H). ^{13}C NMR (100 MHz, $CDCl_3$) δ: 176.9, 160.0, 139.9, 129.9, 121.0, 114.7, 111.9, 72.7, 55.3, 39.1, 37.2, 34.3. Anal. calcd. for $C_{12}H_{14}O_3$: C 69.89, H 6.84; found: C 69.44, H 6.48.

(3*S*,4*S*)-3,4-Bis[(3-methoxyphenyl)methyl]dihydro-2(3*H*)-furanone (10)

To lactone **9** (0.45 g, 2.17 mmol) in THF (8 mL) under N_2 was cooled to –78°C. NaHMDS (3.25 mL, 1 M in THF, 3.25 mmol) was added dropwise over a period of 5 min. After stirring at that temperature for 1 h and 15 min, a solution of 3-methoxybenzyl iodide (1.16 g, 3.91 mmol) in THF (4 mL) was added dropwise over a period of 5 min. The reaction mixture was then warmed up to –54°C and stirred at this temperature for 22 h. The reaction mixture was quenched with saturated aqueous $NaHCO_3$ and extracted with diethyl ether. The organic layers were combined, washed with brine, dried over $MgSO_4$, and concentrated. The crude product was purified by column to afford the alkylated product **10** (490 mg, 69%). Pale yellow oil. $[\alpha]_D^{25}$ +42.0 (*c* 1.0, $CHCl_3$) (lit. (4*b*) value: $[\alpha]_D^{23}$ +40.9 (*c* 1.2, $CHCl_3$)). ^{1}H NMR (400 MHz, $CDCl_3$) δ: 2.43–2.62 (m, 4H), 2.90 (dd, *J* = 7.24, 13.96 Hz, 1H), 3.05 (dd, *J* = 5.08, 13.96 Hz, 1H), 3.76 (s, 3H), 3.77 (s, 3H), 3.83 (dd, *J* = 7.28, 16.40 Hz, 1H), 4.09 (dd, *J* = 7.52, 9.00 Hz, 1H), 6.53 (s, 1H), 6.59 (d, *J* = 7.60 Hz, 1H), 6.73–6.79 (m, 4H), 7.15–7.25 (m, 2H). ^{13}C NMR (100 MHz, $CDCl_3$) δ: 178.6, 159.9, 139.7, 139.4, 129.8, 129.7, 121.7, 121.0, 114.9, 114.5, 112.4, 111.9, 71.3, 55.3, 55.2, 46.4, 41.3, 38.6, 35.1.

(3*S*,4*S*)-3,4-Bis[(3-hydroxyphenyl)methyl]dihydro-2-(3*H*)-furanone 1: (+)-Enterolactone

Literature procedure as described in ref. 4*b* was used for the synthesis of **1**. Yield: 78%. Colorless solid. $[\alpha]_D^{25}$ +38.6 (*c* 0.24, $CHCl_3$) (lit. (4*b*) value: $[\alpha]_D^{23}$ +38.3 (*c* 0.24, $CHCl_3$)). ^{1}H NMR (300 MHz, acetone-d_6) δ: 2.46–3.00 (m, 6H), 3.06 (s, 1H), 3.85–4.06 (m, 2H), 6.59–6.78 (m, 6H), 7.06–7.16 (m, 2H), 8.29 (s, 1H). ^{13}C NMR (65 MHz, acetone-d_6) δ: 178.7, 158.4, 141.3, 140.8, 130.4, 130.3, 121.5, 120.6, 117.1, 116.4, 114.5, 114.2, 71.5, 46.8, 42.2, 38.7, 35.3.

(4*R*)-4-(Diphenylmethyl)-3-[3-(ethoxypropanoyl]-2-oxazolidinone (11)

A solution of **5** (10.00 g, 39.53 mmol) in THF (160 mL) under N_2 was cooled to –78°C. *n*-BuLi (17.38 mL, 2.5 M in hexane, 43.45 mmol) was added dropwise over a period of 20 min. The mixture was stirred at that temperature for 30 min. A solution of ethyl 4-chloro-4-oxobutyrate (6.75 mL, 47.40 mmol) in THF (8 mL) was added dropwise over a period of 10 min. After stirring at –78°C for 2.5 h, the reaction mixture was quenched with saturated aqueous NH_4Cl (30 mL). The mixture was extracted with ethyl acetate, washed with brine, dried over $MgSO_4$, and concentrated. The crude product was purified by column to afford the acylated product **11** (12.80 g, 85%). R_f 0.77 (50:50, EtOAC:hexanes). Colorless solid; mp 106°C. $[\alpha]_D^{25}$ –184.5 (*c* 0.12, CH_2Cl_2). ^{1}H NMR (400 MHz, $CDCl_3$) δ: 1.27 (t, *J* = 7.28, 3H), 2.58 (m, 2H), 3.04–3.25 (m, 2H), 4.15 (q, *J* = 7.28, 2H), 4.40–4.48 (m, 2H), 4.71 (d, *J* = 5.36, 1H), 5.30(m, 1H), 7.07–7.15 (m, 4H), 7.24–7.36 (m, 6H). ^{13}C NMR (100 MHz, $CDCl_3$) δ: 172.5, 171.7, 153.5, 139.6, 138.0, 129.4, 129.0, 128.8, 128.4, 128.0, 127.1, 65.2, 60.8, 56.3, 50.5, 30.9, 28.3, 14.3. Anal. calcd. for $C_{22}H_{23}NO_5$: C 69.28, H 6.08, N 3.67; found: C 69.14, H 6.07, N 3.72.

(4*R*)-4-(Diphenylmethyl)-3[(2*R*)-2-(ethoxycarbonyl)methyl]3-(3′-methoxyphenyl)]-2-oxazolidinone (12)

A solution of acyloxazolidinone **11** (5.80 g, 15.20 mmol) in THF (160 mL) under N_2 was cooled to –78°C. NaHMDS

© 2000 NRC Canada

(16.72 mL, 1 M in THF, 16.72 mmol) was added dropwise over a period of 25 min. After stirring at that temperature for 1 h and 15 min, a solution of 3-methoxybenzyl iodide (6.79 g, 22.80 mmol) in THF (20 mL) was added dropwise over a period of 30 min at –78°C. The mixture was allowed to warm up to –54°C slowly and stirred at this temperature for 22 h. The reaction mixture was quenched with saturated aqueous $NaHCO_3$ and extracted with diethyl ether. The organic layers were combined, washed with brine, dried over $MgSO_4$, and concentrated. The crude product was purified by column to afford alkylated product **12** (4.57 g, 60%). R_f 0.80 (50:50, EtOAc:hexanes). Colorless solid; mp 140°C. $[\alpha]_D^{25}$ –62.7 (*c* 0.11, CH_2Cl_2). ^{1}H NMR (400 MHz, $CDCl_3$) δ: 1.17 (t, *J* = 7.12 Hz, 3H), 2.11 (dd, *J* = 11.04, 13.16 Hz, 1H), 2.24 (dd, *J* = 3.48, 17.20 Hz, 1H), 2.72 (dd, *J* = 10.28, 17.20 Hz, 1H), 2.89 (dd, *J* = 4.04, 13.16 Hz, 1H), 3.79 (s, 3H), 4.01 (q, *J* = 7.12, 2H), 4.19–4.26 (m, 1H), 4.38–4.49 (m, 2H), 4.68 (d, *J* = 6.48 Hz, 1H), 5.37 (m, 1H), 6.76- 6.85 (m, 3H), 7.09–7.32 (m, 11H). ^{13}C NMR (100 MHz, $CDCl_3$) δ: 174.8, 172.4, 159.9, 153.4, 139.9, 139.7, 138.2, 129.6, 129.3, 129.0, 128.7, 128.6, 128.0, 127.2, 121.7, 114.6, 112.6, 65.5, 60.7, 56.7, 55.3, 51.6, 41.3, 37.6, 34.6, 14.2. Anal. calcd. for $C_{30}H_{31}NO_6$: C 71.84, H 6.23, N 2.79; found: C 71.41, H 6.33, N 2.78.

Ethoxycarbonyl-(2*R*)-(carboxymethyl)-3-(3′-methoxyphenyl)propionic acid (13)

Lithium hydroxide – H_2O_2 hydrolysis of the oxazolidinone **12** as described before gave the acid **13**. Yield: 80%. R_f 0.37 (50:50, EtOAc:hexanes). Colorless liquid. $[\alpha]_D^{25}$ +114.7 (*c* 0.034, CH_2Cl_2). ^{1}H NMR (400 MHz, $CDCl_3$) δ: 1.23 (t, *J* = 7.2 Hz, 3H), 2.39 (dd, *J* = 4.76, 16.84 Hz, 1H), 2.59–2.76 (m, 2H), 3.13 (m, 2H), 3.78 (s, 1H), 4.10 (q, *J* = 6.96 Hz, 2H), 6.75 (m, 3H), 7.20 (m, 1H). ^{13}C NMR (100 MHz, $CDCl_3$) δ: 180.5, 172.0, 159.9, 139.7, 129.8, 121.6, 114.9, 112.4, 61.1, 55.4, 43.1, 37.6, 34.9, 14.4. Anal. calcd. for $C_{14}H_{18}O_5$: C 63.15, H 6.81; found: C 62.92, H 7.18.

(4*R*)-[(3-Methoxyphenyl)methyl]dihydro-2(3*H*)-furanone (14)

A procedure as described for **9** was employed to obtain **14** from **13**. Reduction yield: 78%. Acid catalyzed cyclization yield: 97%. Colorless liquid. $[\alpha]_D^{25}$ +6.7 (*c* 1.66, $CHCl_3$).

(3*R*,4*R*)-3,4-Bis[(3-methoxyphenyl)methyl]dihydro-2(3*H*)-furanone (15)

A procedure as described for **10** was employed to obtain **15** from **14**. Yield: 69%. Colorless liquid. $[\alpha]_D^{25}$ –38.8 (*c* 1.06, $CHCl_3$) (lit. (4*b*) value $[\alpha]_D^{23}$ –39.2 (*c* 0.78, $CHCl_3$)).

(3*R*,4*R*)-3,4-Bis[(3-hydroxyphenyl)methyl]dihydro-2-(3*H*)-furanone 2: (–)-Enterolactone

A procedure as described for **1** was employed to obtain **2** from **15**. Yield: 88%. Colorless solid. $[\alpha]_D^{25}$ –38.3 (*c* 0.29, $CHCl_3$) (lit. (4*b*) value $[\alpha]_D^{23}$ –38.4 (*c* 0.25, $CHCl_3$)).

Acknowledgment

We thank North Dakota Oil Seed Council and North Dakota State University for providing financial support for this work. We thank Dr. Saumen Hajra for experimental assistance.

References

1. (*a*) J.L. Charlton. J. Nat. Prod. **61**, 1447 (1998); (*b*) M. Schottner, G. Spiteller, and D. Gansser. J. Nat. Prod. **61**, 119 (1998); (*c*) D.C. Ayres and J.D. Loike. *In* Lignans. Chemical, biological, and clinical properties.. Cambridge University, Cambridge. 1990. Chap. 3 & 4 and references cited therein; (*d*) R.S. Ward. Chem. Soc. Rev. **11**, 75 (1982); (*e*) R.S. Ward. Tetrahedron, **46**, 5029 (1990).
2. (*a*) S.R. Stitch, C.W. Funke, M.B. Groen, J. Leemhuis, J.K. Toumba, J. Vink, and G.F. Woods. Nature (London), **287**, 738 (1980); (*b*) A.P. Walters and J.T. Knowler. J. Reprod. Fertil. **66**, 379 (1982); (*c*) Y. Mousavi and H. Adlercreutz. J. Steroid Biochem. and Molec. Biol. **41**, 615 (1992); (*d*) A.M. Hutchins, J.W. Lampe, and J.L. Slavin. J. Am. Diet. Assoc. **95**, 769 (1995).
3. (*a*) A. Srikrishna, S. Venkateswarlu, and J.A. Sattigeri. Ind. J. Chem. Sect. B. **34**, 679 (1995); (*b*) M. Bambagiotti-Alberti, S.A. Coran, F.F. Vincieri, N. Mulinacci, and G.M.L. Pieraccini. Heterocycles, **27**, 2185 (1988); (*c*) M. Bambagiotti-Alberti, S.A. Coran, F.F. Vincieri, and P.L. Nostro. Heterocycles, **26**, 1735 (1998); (*d*) J.L Belletire and S.L. Fremont. Tetrahedron Lett. **27**, 127 (1986); (*e*) A. Pelter, R.S. Ward, P. Satyanarayana, and P. Collins. J. Chem. Soc. Perkin Trans. 1, 643 (1983); (*f*) K.K. Mahalanabis, M. Mumtaz, and V. Snieckus. Tetrahedron Lett. **23**, 3975 (1982). Synthesis of labelled materials. K. Waehaelae, T. Maekelae, R. Baeckstroem, G. Brunow, and T. Hase. J. Chem. Soc. Perkin Trans. 1, 95 (1986); N.D. Kirk, L.M. McLaughlin, A.M. Lawson, K.D.R. Setchell, and S.K. Patel. J. Chem. Soc. Perkin Trans. 1, 35 (1985).
4. (*a*) R. Chênevert, G. Mohammad-Ziarani, D. Caron, and M. Dasser. Can. J. Chem. **77**, 223 (1999); (*b*) J.W. Bode, M.P. Doyle, M.N. Protopopova, and Q.-L. Zhou. J. Org. Chem. **61**, 9146 (1996); (*c*) M.P. Doyle, M.N. Protopopova, Q.-L. Zhou, J.W. Bode, S.H. Simonsen, and V. Lynch. J. Org. Chem. **60**, 6654 (1995); (*d*) A. van Oeveren, J.F.G.A. Jansen, and B.L. Feringa. J. Org. Chem. **59**, 5999 (1994); (*e*) H. Yoda, H. Kitayama, T. Katagiri, and K. Takabe. Tetrahedron, **48**, 3313 (1992); (*f*) M. Asaoka, N. Fujii, K. Shima, and H. Takei. Chem. Lett. 805. (1988).
5. (*a*) M.P. Sibi, P.K. Deshpande, and A.J. La Loggia. Synlett, 343 (1996); (*b*) M.P. Sibi and J. Ji. Angew. Chem. Int. Ed. Engl. **36**, 274 (1997).
6. M.D. Johnson. M.S. thesis. North Dakota State University. 1999.
7. (*a*) J.L. Charlton and G. Chee. Can. J. Chem. **75**, 1076 (1997); (*b*) T. Nishi, M. Sakurai, S. Sato, M. Kataoka, and Y. Morisawa. Chem. Pharm. Bull. **37**, 2200 (1989).
8. (*a*) M.P Sibi, P.K. Deshpande, A.J. La Loggia, and J.W. Christensen. Tetrahedron Lett. **36**, 8961 (1995); (*b*) M.P. Sibi, C.P. Jasperse, and J. Ji. J. Am. Chem. Soc. **117**, 10779 (1995); (*c*) M.P. Sibi and J. Ji. J. Org. Chem. **61**, 6090 (1996); (*d*) M.P. Sibi, J. Lu, and J. Edwards. J. Org. Chem. **62**, 5864 (1997).
9. (*a*) H. Heitsch, H. Henning, H-W. Kleemann, W. Linz, W-U. Nickel, D. Ruppert, H. Urbach, and A. Wagner. J. Med. Chem. **36**, 2788 (1993); (*b*) D.E. Levy, F. Lapierre, W. Liang, W. Ye, C.W. Lange, X. Li, D. Grobelny, M. Casabonne, D. Tyrrell, K. Holme, A. Nadzan, and R.E. Galardy. J. Med. Chem. **41**, 199 (1998); (*c*) G.R. Gowravaram, B.E. Tomczuk, J.S. Johnson, D. Delecki, E.R. Cook, A.P. Ghose, A.M. Mathiowetz, J.C.

© 2000 NRC Canada

Spurlino, B. Rubin, D.L. Smith, T. Pulvino, and R.C. Wahl. J. Med. Chem. **38**, 2570 (1995).
10. (*a*) D.A. Evans, T.C. Britton, and J.A. Ellman. Tetrahedron Lett. **28**, 6141 (1987); (*b*) D.A. Evans; T.C. Britton, R.L. Dorow, and J.F. Dellaria Jr. Tetrahedron, **44**, 5525 (1988).
11. (*a*) D.A. Evans, J. Bartroli, and T.L. Shih. J. Am. Chem. Soc. **103**, 2127 (1981); (*b*) D.A. Evans, F. Urpi, T.C. Somers, J.S. Clark, and M.T. Bilodeau. J. Am. Chem. Soc. **112**, 8215 (1990); (*c*) D.A. Evans, M.T. Bilodeau, T.C. Somers, J. Clardy, D. Cherry, and Y. Kato. J. Org. Chem. **56**, 5750 (1991); (*d*) W. Oppolzer, P. Cintas-Moreno, O. Tamura, and F. Cardinaux. Helv. Chim. Acta, **76**, 187 (1993).
12. M.B. Groen and J. Leemhuis. Tetrahedron Lett. **21**, 5043 (1980).

© 2000 NRC Canada

Investigations on nonradiative transitions in different environments using excited (or ground state) 1,2,3,4-tetrahydroquinoline (THQ) as donor and ground state (or excited) 9-fluorenone (9FL) or 2-nitro-9-fluorenone (2N9FL) as acceptors

Avijit K. De and Tapan Ganguly

Abstract: By using steady state and time resolved spectroscopic techniques, investigations were made on the nature and mechanisms of different nonradiative processes involved within the excited donor (or acceptor) and ground state acceptor (or donor) in nonpolar *n*-heptane (NH), polar protic ethanol (EtOH), and polar aprotic acetonitrile (ACN) solvents at the ambient temperature as well as in EtOH rigid glassy matrix at 77 K. The bicyclic molecule 1,2,3,4-tetrahydroquinoline (THQ) was used as a donor (D) in the present investigation whereas 9-fluorenone (9FL) and 2-nitro-9-fluorenone (2N9FL) were chosen as electron acceptors (A). When the donor chromophore was excited in presence of an acceptor, highly exothermic electron transfer (ET) reactions seemed to occur from observed large negative driving energy (ΔG^0) values, measured by electrochemical techniques, Förster's type energy transfer, static quenching, etc. An attempt was made to estimate separately the contributions of static and dynamic quenching modes in the overall quenching mechanism of donor fluorescence by using a model of modified Stern–Volmer (SV) relation. From this relation it seemingly indicated that the major contribution in quenching originated from the static mode. When excited acceptors react with the ground state donor THQ it is primarily ET reactions that seem to occur. Observations of the transient absorption spectra, by laser flash photolysis techniques, of contact ion-pairs of the present D–A systems along with the triplet absorption spectra of the monomeric acceptor (9FL and 2N9Fl) corroborate our views regarding the occurrence of photoinduced ET reactions within the present reacting systems. At 77 K the combined effect of Förster type energy transfer and static quenching seems to be responsible for observed lowering of donor fluorescence emission intensity in presence of acceptors (9FL or 2N9FL). However, the phosphorescence lifetime measurements reveal that the triplet donor might be involved in photoinduced ET reaction with the unexcited acceptor in rigid glassy matrix at 77 K and this possibly causes the reduction in the phosphorescence band intensity of the donor THQ in presence of the latter one.

Key words: electron transfer, static quenching, fluorescence quenching, phosphorescence, energy transfer.

Résumé : Les méthodes de spectroscopie en régime stationnaire et résolue dans le temps ont été utilisées pour examiner la nature et le mécanisme de différents processus non-radiatifs qui existent dans les réactions entre un donneur (ou accepteur) éxcité et un accepteur (ou donneur) en état d'équilibre dans un solvant non-polaire *n*-heptane (NH), un solvant protique polaire éthanol (EtOH) et un solvant aprotique polaire acétonitrite (ACN) à la température ambiante et aussi dans une matrice vitreuse rigide (EtOH à 77 K). Une molécule à deux boucles, 1,2,3,4-tetracyanoquinoline (THQ) a été utilisée comme donneur dans cette étude, les molécules 9-fluorénone (9FL) et 2-nitro-9-fluorénone (2N9FL) ont été choisies comme accepteurs d'électrons. L'excitation d'un chromophore donneur en présence d'un accepteur semble entraîner des réactions éxothérmiques de transfert d'un électron (puisque la valeur de l'énergie de transfert, ΔG^0, mesurée par des méthodes électrochimimiques, est grande et négative); et aussi transfert d'énergie de type Förster, l'éxtinction statique, etc. On a aussi essayé d'évaluer séparément les contributions statiques et dynamiques de l'extinction de la fluorescence des donneurs, en utilisant un modéle de la relation Stern–Volmer (SV) modifié. Nous avons pu déduire à partir de cette relation, que la contribution majeure de l'extinction, a pour origine le mode statique. Les réactions entre les accepteurs excités avec le donneur THQ en état d'équilibre, semblent provoquer surtout des réactions de transfert d'un électron. Les observations des spectres d'absorption transitoires, par des techniques de photolyse par flash laser, des paires d'ion contact dans ces systémes D–A avec les spectres d'absorption des triplets de l'accepteur monomére (9FL et 2N9FL) confirment notre hypothése concernant l'existence de réactions ET photoinduites

Accepted October 26, 1999.

A.K. De. Department of Physics, Jadavpur University, Jadavpur, Calcutta-700 032, India.
T. Ganguly.[1] Department of Spectroscopy, Indian Association for the Cultivation of Science, Jadavpur, Calcutta-700 032, India.

[1]Author to whom correspondence may be addressed. Telephone: 91 033 473 4971/473 3073 X 266. Fax: 91 033 473 2805.
e-mail: sptg@mahendra.iacs.res.in

 © 2000 NRC Canada

à l'intérieur de ces systémes réactifs. À 77 K les effets de transfert de l'énergie de type Förster et l'extinction statique ensemble, semblent entraîner l'extinction de la fluorescence du donneur en présence des accepteurs (9FL ou 2N9FL). Mais les mesures de la durée de vie de la phophorescence montrent, que la réaction de transfért d'un électron, sous irradiation, entre le donneur triplet et les accepteurs en état d'équilibre, est possible dans une matrice vitreuse rigide à 77 K; ce qui vraisemblablement explique la diminution de l'intensité de la bande phosphorescence du donneur THQ en présence des accepteurs en état d'équilibre.

Mots clés : transfert d'électron, extinction statique, extinction de la fluorescence, phosphorescence, transfert d'énergie.

Introduction

In solutions the predominant mechanisms for the bimolecular fluorescence quenching of electronically excited molecules are generally through photoinduced ET (1–8), energy transfer (8–11) and static or transient (12, 13) effect. In nonpolar solvents there may be a charge transfer (CT) between the donor and acceptor molecules to produce a light emitting species such as exciplex. On the other hand in highly polar solvent like acetonitrile (ACN) it is a solvent separated radical ion pair (SSIP), a non-light emitting species, that is generally formed. Investigations were previously made on intermolecular/intramolecular ET reactions along with several other concurrent nonradiative processes (8, 9, 14–16). In these studies the emphasis was given mainly to the free energy (ΔG^0) dependence of the kinetic of charge separation (CS) and charge recombination (CR) processes in order to detect the Marcus inverted region (mir) in these systems. Testing of Marcus theory, especially in the cases of highly exothermic ET reactions, has become nowadays a useful practice. It is known (17–20) that ET rates and efficiencies are greatly influenced by several factors, of which solvent orientation dynamics is one. Most of the authors reported that in solution phase the intermolecular ET reactions, even in the highly exothermic cases, generally do not exhibit inverted behavior. From the experimental work Rehm and Weller (21) long ago established a correlation between the bimolecular dynamic fluorescence quenching rate constants, k_q and ΔG^0, for photoinduced ET reactions in cases of some typical electron donor-acceptor systems in ACN solvent. They showed that the correlation was in agreement with the prediction made by Marcus in his outstanding electron transfer theory but only in the normal region (endothermic or slightly exothermic region). They didn't observe inverted behavior, as proposed by Marcus, in the highly exothermic or exergonic region but instead observed a diffusion-limited rate (k_d) there. Mataga et al. (22) however, demonstrated the energy gap dependence in the inverted region but in the cases of the charge recombination only of the ion pair produced from intermolecular ET reactions. However, in cases of some intramolecular ET within some bichromophoric systems of organic donors and acceptors Marcus theory was found to be valid over the entire region (16, 23) of exothermicity. From the recent investigations made by our research group on some organic electron donor and acceptor systems it was observed (8) that the first order intermolecular ET (forward charge separation) rates within these systems seem to proceed through mir. In evaluating the first order rates within the D–A systems, the recently developed diffusion mediated theory (24) was considered. Lately studies, using steady state and time resolved spectroscopic techniques, on the effects of the protic and aprotic polar solvents on nonradiative transitions involving dimethyl substituted donors and well-known acceptor tetracyanoquinodimethane (TCNQ) (25) were made. From these investigations it was revealed that the ET reactions in both the polar solvents occur in mir. In nonpolar media (e.g., cyclohexane, *n*-heptane, etc.) generally low exothermicity (low negative ΔG^0 values) was reported (8). It is logical to presume that in this media ET reactions should proceed through downhill region. Thus studies on the nature of the photoinduced ET reactions within the different donor–acceptor systems in solvents of different polarities seem worthwhile because by changing the polarities of the surrounding media we could control the rates associated with electron transfer reactions.

Apart from searching the mir another interesting part of such type of investigation is that when the donor chromophore is excited in presence of a suitable acceptor, not only ET but several other nonradiative processes might also occur concurrently. The nature of these nonradiative processes originates due to interactions between the donor and acceptor molecules and may be different in different surrounding media having different polarities. Lack of systematic studies on such types of problems prompted us to undertake the present work. The present paper describes the studies made to reveal the nature of the mechanisms of the different nonradiative processes such as: ET, energy transfer, static quenching, etc., which might be involved with the 1,2,3,4-tetrahydroquinoline (THQ) and acceptors 9-fluorenone (9FL) and 2-nitro-9-fluorenone (2N9FL) in different solvents like *n*-heptane ($\varepsilon_s \sim 2.07$), EtOH ($\varepsilon_s \sim 24.55$), and ACN ($\varepsilon_s \sim 37.5$). The present donor THQ possesses a bicyclic structure where one ring is aromatic but the other has an alicyclic-like ring of flexible structure. Studies of photoinduced quenching reactions using this type of molecule as the donor species are not common. In the present work we examined the nature of photoinduced ET reactions and associated nonradiative processes in different polarity solvents. Studies were also made to detect Marcus inverted regions (which are not common phenomena in intermolecular cases) especially in highly polar environments (e.g., acetonitrile (ACN), ethanol (EtOH), etc). The fluorescence quenching studies by steady state/time resolved techniques, considering the various organic donor and acceptor systems, would seem to be very useful because these intermolecular studies would help to reveal the nature of the mechanism of intramolecular ET reactions when these donors and acceptors would be connected by various spacers. However, to build bichromophores only those donors and acceptors would be chosen which would be found to undergo, from intermolecular investigations, highly exothermic ET reactions in the Marcus inverted region (mir). It is well known that mir is a key to design molecular assem-

© 2000 NRC Canada

blies for artificial photosynthesis. Thus it is expected that these bichromophores might serve as efficient photoconducting materials or polymers (when bichromophoric units are connected through polymeric chains) which would be useful in photographic and xerographic industries, and also in developing molecular electronic devices.

An attempt was also made to correlate the rates associated with the several nonradiative processes, as discussed above, in the fluid solution at the ambient temperature and to examine the fate of these nonradiative processes in rigid glassy EtOH matrix at 77 K. The studies were made by using steady state and time resolved spectroscopic techniques. The low temperature investigations using the other two solvents NH and ACN as surrounding media were not possible as these media do not form glass at this low temperature.

Experimental

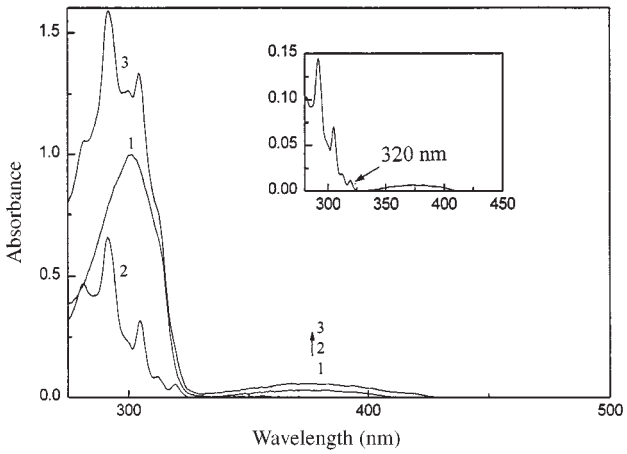
Materials and their purifications

The samples 1,2,3,4-tetrahydroquinoline (THQ), 9-fluorenone (9FL) and 2-nitro-9-Fluorenone (2N9FL), supplied by Aldrich were purified carefully by vacuum sublimation. The spectroscopic grade solvents acetonitrile (ACN), ethanol (EtOH), and *n*-heptane (NH) supplied by E. Marck were distilled under reduced pressure and tested for the absence of any emission in the wavelength region studied.

Experimental apparatus

The steady state electronic absorption and emission spectra of moderate to dilute (10^{-3}–10^{-6} M) solutions of the samples at ambient temperature were recorded by a Shimadzu UV-VIS spectrophotometer of model 2101PC and Hitachi F-4500 fluorescence spectrophotometer respectively. Fluorescence lifetimes of the samples were measured by using a time correlated single photon counting (TCSPC) fluorimeter, model 199 Edinburgh Instruments U.K., having conventional L format arrangement. The excitation source consists of an all metal coaxial N_2 flash lamp with an instrumental response function of about 1.2 ns FWHM at 30 kHz repitition rate. The fluorescence decays were analyzed by using deconvolution fit over the entire decay including the rising edge. The goodness of the fit was assessed with the help of some statistical parameters (e.g., χ^2) and Durbin–Watson (DW) values. Transient absorption spectra at the different delay times between the exciting and analyzing pulses were measured with the help of nanosecond flash photolysis setup (Applied Photophysics) comprised of Nd:YAG laser (DCR-11, Spectra Physics). The sample was excited by 355 nm laser light (third harmonic) (FWHM ~ 8ns). The pulsed Xe lamp of 250 W was used as probe. The photomultiplier (IP 28) output was fed into a storage oscilloscope (TDS-540 Tektronix, 500 MHz, 1 Giga sampling, GS, s^{-1}) and the storage data were transferred to a computer through a GPIB/IEEE interface. All the solutions used for the room temperature measurements were deoxygenated by a flushing argon gas stream for about 30 minutes. Electrochemical measurements were done by using PAR model 370-4 electrochemistry system incorporating a model 174A polarographic analyzer, model 175 universal programmer model RE0074X-Y recorder. Three electrode systems including SCE were used in the measurements. Tetraethylammonium perchlorate (TEAP) in ACN was used as supporting electrolyte. The fluorescence quantum yield (ϕ_f^0) of donor THQ in ACN fluid solution was determined at room temperature (296K) relative to that of 3-methylindole in CH solvent ($\phi_f^0 = 0.40 \pm 0.03$) (26). The necessary solvent corrections were made.

Fig. 1. Room temperature electronic absorption spectra in *n*-heptane (NH) of (1) THQ (2.5×10^{-5} mol dm^{-3}), (2) 9FL (2.77×10^{-4} mol dm^{-3}), and (3) mixture of THQ (2.5×10^{-5} mol dm^{-3}) and 9FL (2.77×10^{-4} mol dm^{-3}). Inset: 9FL (6.24×10^{-5} mol dm^{-3}) in *n*-heptane (NH) fluid solutions.



Results and discussion

1. Electronic absorption spectra at the ambient temperature

At the ambient temperature and in solvents of different polarities (e.g., NH, EtOH, and ACN) the electronic absorption spectra of THQ in presence of an acceptor (9FL or 2N9FL) show the superposition of the absorption bands of the individual donor and acceptor moieties (Fig. 1). This observation excludes the possibility of formation of ground state charge transfer (CT) complex within the reactants at the room temperature.

2. Fluorescence emission at the ambient temperature and quenching studies

(A) When the donor is excited to its S_1 level

The acceptor molecules (9FL or 2N9FL) used in the present investigation, cause drastic changes in the intensity of the donor (THQ) fluorescence emission spectra produced by singlet (S_1) excitation of the molecule. In nonpolar NH, polar protic EtOH, and polar aprotic ACN the fluorescence spectral intensity of THQ falls off remarkably without any noticeable spectral shift in the presence of both 9FL and 2N9FL molecules (Figs. 2*a*–2*c*). However, with the addition of the former quencher 9FL, a very weak but genuine long wavelength band is found to develop only in the highly polar ACN (ε_s ~37.5) environment, with concomitant reduction of the fluorescence emission band intensity of THQ (Fig. 2*a*). In the inset of Fig. 2*a*, the magnified version of this long wavelength band, whose envelope is around the 500–550 nm region, is shown. It is apparent from the figure that the long wavelength band, though very weak in nature, is forming at

© 2000 NRC Canada

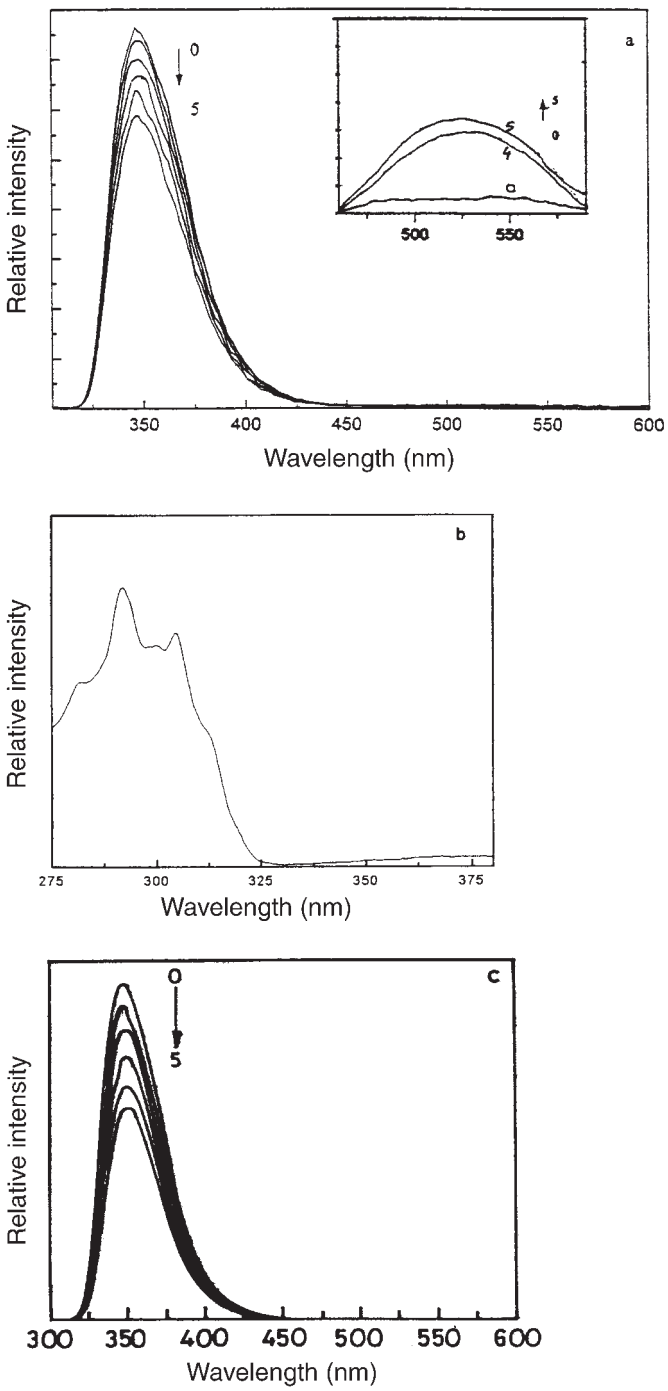


Fig. 2. (*a*) Fluorescence emission spectra of THQ donor (λ_{exc} = 320 nm) (to avoid inner filter effect) in ACN solvent of concentration (2.5×10^{-5} mol dm^{-3}) at 300 K in presence of acceptor 9FL whose concentrations (mol dm^{-3}) were: (0) 0, (1) 1.04×10^{-5}, (2) 2.08×10^{-5}, (3) 3.12×10^{-5} (4) 4.16×10^{-5}, (5) 6.24×10^{-5} (inset shows the magnified version of the longer wavelength band at 507 nm region); (*b*) Fluorescence excitation spectra of THQ donor (λ_{em} ~ 380 nm) in ACN solvent (~2.5×10^{-5} mol dm^{-3}) at 300 K in presence of acceptor 9FL (~6.24×10^{-5} mol dm^{-3}); (*c*) Fluorescence emission spectra of THQ donor (λ_{exc} = 320 nm) in ACN solvent of concentration (2.5×10^{-5} mol dm^{-3}) at 300 K in presence of acceptor 2N9FL whose concentrations (mol dm^{-3}) were: (0) 0, (1) 2.96×10^{-6}, (2) 5.92×10^{-6}, (3) 1.18×10^{-5}, (4) 1.78×10^{-5}, (5) 2.37×10^{-5}.

the expense of the fluorescence of the donor THQ molecules. As this band was not observed in nonpolar NH or in polar protic EtOH solvents, the band could not be assigned to the exciplex band which is generally formed in nonpolar environment. As it is known that 9FL fluoresces around the 510 nm region in ACN medium it is most likely that this long wavelength band (observed in only the ACN environment) might be due to the fluorescence of the acceptor 9FL and there is a high probability this might result from the $S_1^D \rightarrow S_1^A$ energy transfer process. The absence of this long wavelength band in the other two solvents (NH and EtOH), might be due to the non-fluorescent character of 9FL in these solvents. It seems the energy transfer might be of Förster type (dipole-dipole interaction) as this process generally sensitizes the acceptor fluorescence which was actually observed from the present steady state measurements. Fluorescence decay analysis of this band system was made by TCSPC technique monitoring at 508 nm wavelength. The value of fluorescence lifetime (τ) was found to be very similar to that of the acceptor 9FL (~14.6 ns). This observation corroborates our propositions, made from steady state measurements, that the long wavelength 500 nm band observed in the fluorescence emission spectra of THQ in presence of 9FL might be due to the fluorescence emission of 9FL resulting from the Förster type energy transfer process within the lowest excited singlet states (S_1) of the donor THQ and the lower lying corresponding level of the acceptor 9FL. Moreover the fluorescence excitation spectra of the mixture of THQ and 9FL in ACN corresponds to the absorption spectra of the same mixture (Fig. 2*b*). Thus from the comparison of the above two spectra the occurrence of Förster's energy transfer from the electronically excited THQ to 9FL is further confirmed. In the case of the other acceptor 2N9FL, such spectral argument in favor of occurrence of energy transfer is lacking possibly due to non-fluorescence behavior of this acceptor. However, it should be pointed out that in the present investigation the donor THQ chromophore was excited selectively at around 320 nm whereas the present acceptors, due to the low concentrations (~10^{-5} or 10^{-6} mol dm^{-3}) used in the present investigation, possess negligible absorbance (Fig. 1). In this way the competitive absorption by the acceptor 9FL (or 2N9FL) and its filtering effect on the donor emitted light were avoided. Furthermore as it has been discussed in Section 1, the ground state complex which might be responsible for the fluorescence quenching is also absent in the present case. Moreover an attempt was made to record fluorescence spectra of only 9FL in ACN solvent (choosing the same concentrations as were used in studying fluorescence quenching of the donor THQ

© 2000 NRC Canada

Table 1. Redox potential values, values of $E^{*}_{0,0}$,[a] Gibbs free energies (ΔG^0) for photoinduced electron transfer (ET) reactions within the present donor and acceptor molecules in highly polar solvents ACN at the ambient temperature.

Donors[a]	Acceptors[a]	$E^{OX}_{1/2}(D/D^+)$ (V)	$E^{RED}_{1/2}(A^-/A)$ (V)	$E^{*}_{0,0}$ (eV)	ΔG^0 (ACN) (eV)	ΔG^0 (EtOH) (eV)	ΔG^0 (*n*-heptane) (eV)
THQ	9FL	0.6	–1.28		1.88		
THQ*	9FL	0.6	–1.28	3.66	–1.78	–1.83	–0.24
THQ	2N9FL	0.6	–1.34		1.94		
THQ*	2N9FL	0.6	–1.34	3.66	–1.72	–1.77	–0.18
THQ	9FL*	0.6	–1.28	3.29	–1.41	–1.46	0.13
THQ	2N9FL*	0.6	–1.34	3.29	–1.35	–1.4	0.19
^{3}THQ*	9FL	0.6	–1.28	3.02		–1.14	
^{3}THQ*	2N9FL	0.6	–1.34	3.02		–1.08	

[a]The * denotes the excited singlet state S_1.

as shown above) by using 320 nm as an excitation wavelength. As expected, no 9FL fluorescence emission was observed. This indicates that the possibility of direct excitation of the acceptor 9FL when an excitation energy of 320 nm is used to excite the donor moiety is very slim.

Thus one of the processes responsible for nonradiative deactivation of the lowest excited singlet state S_1 of THQ in presence of the quenchers (electron acceptor) 9FL and 2N9FL in solvents of different polarities seems to be a Förster-type energy transfer process. However, THQ was found earlier (14, 27) to be a good electron donor and 9FL and 2N9FL are well known for their good electron accepting abilities (16, 28). Thus the possibility of the occurrence of photoinduced electron transfer (ET) reaction as a concurrent process with energy transfer within the present reacting systems could not be ruled out. Apart from these two basic quenching reactions several other nonradiative processes might also be responsible for the observed THQ fluorescence quenching, e.g., static or instantaneous (similar to static) quenching processes. Systematic studies were made on the present donor and acceptor molecules to reveal the mechanism of nonradiative processes involved within these reacting systems. The results obtained from the study have been described in details in the following sections.

(A1) Possibility of occurrence of photoinduced ET reactions within the present donor-acceptor systems

The half wave oxidation and reduction potentials of the donor THQ and the acceptor 9FL (or 2N9FL), denoted by $E^{OX}_{1/2}(D/D^+)$ and $E^{RED}_{1/2}$ (A^-/A) respectively, were measured in ACN environment by electrochemical techniques (see experimental section).

Using the Rehm–Weller relationship [1] the free energy change, ΔG^0, associated with radical ion pair formation could be computed from (21, 29)

$$[1] \qquad \Delta G^0 = E^{OX}_{1/2}(D/D^+) - E^{RED}_{1/2}(A^-/A) - E^{*}_{0,0} - C$$

Where $C = e^2/(4\pi\varepsilon_0\varepsilon_s R)$ is the Coulomb stabilization term which measures the gain in free energy due to stabilization of the ion pair compared to the free ions due to the proximity of the oppositely charged ions. $E^{*}_{0,0}$ is the (0,0) level of the lowest lying excited electronic singlet state (S_1) of the donor. ε_s is the static dielectric constant of the solvent. R is the distance of separation of the redox sites.

In highly polar ACN, ΔG^0 was estimated for the present donor-acceptor systems using the measured redox potential values. The Coulomb term was neglected in the calculations as its contribution in the highly polar ACN is very small (~ 0.06 eV) (16). The ΔG^0 values are listed in Table 1 where it can be seen that the ET reaction in ACN is highly exergonic ($\Delta G^0 < 0$) and hence energetically favorable when an excited donor reacts with ground state acceptors (9FL or 2N9FL). Positive values of ΔG^0, as found in the cases of the unexcited reactants (Table 1), clearly demonstrate the lack of occurrence of ET in the ground state. Moreover, when an excited acceptor chromophore undergoes an ET reaction with the ground state donor THQ, large negative ΔG^0 values (Table 1), though relatively smaller in magnitude than the corresponding values observed in the cases of D*–A pair, indicate the possibility of ET reactions even when the acceptor is excited.

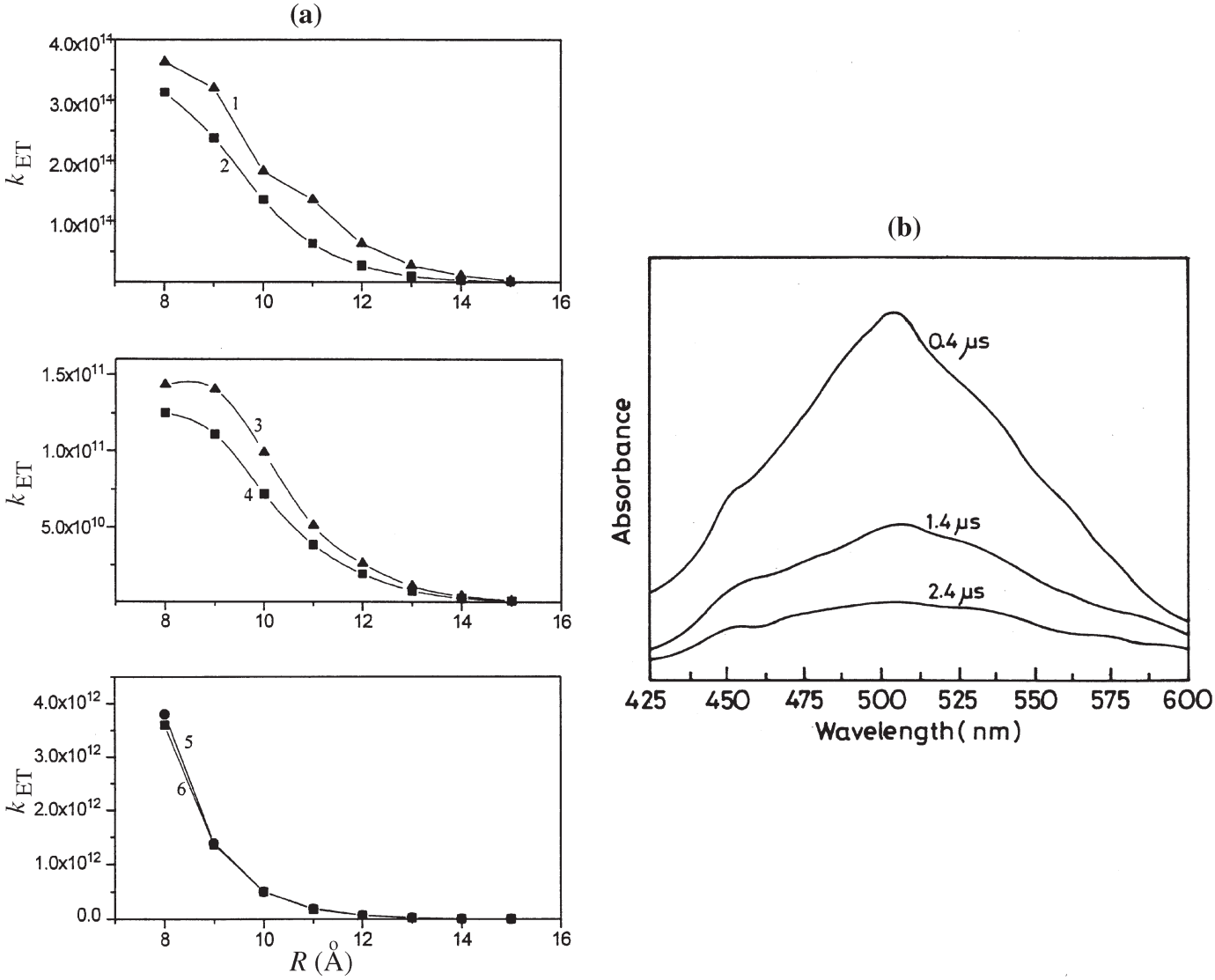
Because it is not possible to measure the redox potentials in the nonpolar NH and polar protic EtOH solvents, we estimated the ΔG^0 values in these solvents by considering the solvation energies in these media (30). However, in the two solvents the coulomb term is not negligible. In nonpolar NH solvent, the coulomb term we kept fixed at 0.2 eV as suggested by Weller (31) and in the case of EtOH we fixed it as 0.1 eV (32). The solvation energy ΔG^0_s was computed by using the relation [2] of Kavarnos and Turro (30)

$$[2] \qquad \Delta G^0_s = -\frac{e^2}{2}\left(\frac{1}{r_D} + \frac{1}{r_A}\right)\left(1 - \frac{1}{\varepsilon_s}\right)$$

From the values of ΔG^0 of the present D–A systems shown in Table 1, it is apparent that both in ACN and EtOH, the highly exothermic (large negative ΔG^0, $\Delta G^0 < 0$) ET reaction might occur within the present D*–A and D–A* systems (* denotes the first excited singlet state) whereas in nonpolar NH relatively much lower exothermicity ($\Delta G^0 \approx -0.24$ eV for THQ*–9FL and –0.18 eV for THQ*–2N9FL, (Table 1)) was observed. When the acceptors are excited, the possibility of occurrence of photoinduced ET reactions in this nonpolar environment appears to be slim from the thermodynamical point of view, as ΔG^0 acquires very low positive values, +0.13 and +0.19 eV in case of THQ–9FL* and THQ–2N9FL* systems respectively (Table 1). This region is known as endothermic region.

© 2000 NRC Canada

Fig. 3. (*a*) Variations of first order electron transfer rate constant (k_{ET}) with the distance of separation (R (Å)) between the present D and A molecules, where ΔG^0 in eV in (1) –1.72 in THQ* + 2N9FL + ACN, (2) –1.78 in THQ* + 9FL + ACN, (3) –1.77 in THQ* + 2N9FL + EtOH, (4) –1.83 in THQ* + 9FL + EtOH, (5) –0.18 in THQ*+ 2N9FL + NH, and (6) –0.24 in THQ* + 9FL + NH; (*b*) Transient absorption spectra of 9FL (excitation wavelength ~355 nm) (third harmonic of Nd:YAG laser system), obtained by laser flash photolysis techniques, in ACN at the ambient temperature in presence of the donor THQ at the different delay times. The delay times are shown on the graph.



We computed Marcus first order electron transfer rates k_{ET}, for the present D–A systems in different solvents by using the relation [3] as shown below.

$$[3] \qquad k_{ET} = \frac{2\pi}{\hbar} \frac{J^2}{\sqrt{4\pi k_B T \lambda}} \exp\left[-\frac{(\Delta G^0 + \lambda)^2}{4 k_B T \lambda}\right]$$

J is the transfer integral and λ is the reorganization energy parameter. J depends exponentially on the separation (between donor and acceptor) distance R through the expression

$$[3a] \qquad J^2 = J_0^2 \exp\left[-\beta\,(R - (r_D + r_A))\right]$$

J_0 denotes the transfer integral at $R = r_D + r_A$.

β is the attenuation coefficient with R.

The distance dependence of k_{ET} is computed from the relation [3] by assuming $J_0 = 100$ cm^{-1} and $\beta = 1$ Å^{-1} as proposed by Tachiya and Murata (24) and the variation is shown in Fig. 3*a*. It appears that in non-polar *n*-heptane (NH), k_{ET} is maximum at the encounter distance and decreases very fast with increase of separation distance between D and A. Thus it is logical to presume that at the

© 2000 NRC Canada

Table 2. Data on fluorescence lifetime of the fluorescer only (τ_0), Stern-Volmer constant (K_{SV}), dynamic fluorescence quenching rate constant (k_q), Förster's critical energy transfer distance (R_0), and Förster energy transfer rate constants (k_{FT}) for the present donor-acceptor pairs; the photoinduced ET rate constants (k_{ET}) for the present donor and acceptor systems; *R* is the reaction radius when the distance of separation between the donor and the acceptor molecules would be such that the probability of occurences of ET reactions will be maximum. (All the parameters mentioned above were measured at ambient temperature.)

System[a]	τ_0 (±0.04) (ns)	K_{SV}	l'	k_q (dm^3 mol^{-1} s^{-1})	R_0 (Å)	R (Å)	ΔG^0 (eV)	λ^b (eV)	k_{ET} (s^{-1})	k_{FT} × 10^{-10} (s^{-1})
THQ* + 2N9FL + ACN	2.3	15.6	1.0[c]	6.8×10^9	23	8	–1.72	1.32	3.63×10^{11}	2.45
THQ* + 9FL + ACN	2.3	535[d]	-	2.32×10^{11}[d]	16	8	–1.78	1.28	3.13×10^{11}	2.8
		773[e]		3.36×10^{11}[e]						
THQ* + 2N9FL + EtOH	2.33	21.4	0.99[c]	9.2×10^9	23	8	–1.77	1.26	1.43×10^{11}	2.45
THQ* + 9FL + EtOH	2.33	0.2	0.99[c]	8.6×10^8	16	8	–1.83	1.23	1.25×10^{11}	2.75
THQ* + 2N9FL + NH	1.023	7.69	0.99[c]	7.7×10^9	20	8	–0.18	0.3	3.7×10^{12}	2.44
THQ* + 9FL + NH	1.023	2.4	1.01[c]	8.7×10^9	13	8	–0.24	0.3	3.8×10^{12}	1.8
9FL* + THQ + ACN	14.6	800[d]		5.4×10^{10}[d]						
		720[e]		4.9×10^{10}[e]						

[a]The * denotes the first excited singlet state.

[b]$\lambda=\lambda_S+\lambda_I$ (see text), λ_S was computed by using dielectric continuum model. Quantum yield of donor THQ is 0.39 in ACN solvent.

[c]$l'=1+K[Q]$, *K* is the equilibrium constant for the ground state complex (see text).

[d]Computed from f_0/f versus [Q] plots.

[e]Computed from τ_0/τ versus [Q] plots.

contact distance ($r_D + r_A$) the probability of occurrence of ET reactions is maximum in non-polar NH.

In other two solvents ACN and EtOH, the rate was found to diminish slowly (Fig. 3) with increase of *R*, though the maximum value of k_{ET} was found at the encounter distance as it was observed in the case of non-polar environment.

Thus the value of reaction radius remains nearly the same (~8 Å) within the present reacting systems in solvents of different polarities used in the present investigation though the exothermicity of the ET reactions increases largely with the change of the environment from non-polar NH (~ –0.2 eV) to highly polar ACN (–1.78 eV) as it was shown above. As the magnitudes of the measured ΔG^0 values of all the present donor–acceptor systems in polar solvents (ACN and EtOH) are very close to each other (Table 2), the effect of ΔG^0 on the k_{ET} values, to show the energy gap dependence of Marcus inverted behavior, is not very clear. However inverted behavior was apparent from the observed values of λ, nuclear reorganization energy parameter, which was estimated from the relation [3*b*] shown below.

The total reorganization energy λ consists of two parts, λ_I and λ_S. The former is the contribution coming from intermolecular bond length changes and the latter one is the solvent reorganization energy (given by the expression [3*b*]) which was computed by using the dielectric continuum model as proposed by Marcus (8, 16),

$$[3b] \qquad \lambda_s = \frac{e^2}{4\pi\varepsilon_0}\left(\frac{1}{2r_D}+\frac{1}{2r_A}-\frac{1}{R}\right)\left(\frac{1}{\varepsilon_{op}}-\frac{1}{\varepsilon_S}\right)$$

where the meanings of the symbols are given elsewhere (16).

The radii of the oxidized donor (r_D) and the reduced acceptor (r_A) have been computed from the molecular volume of the neutral molecules (8).

We have chosen a fixed value of λ_I (= 0.3 eV) which is the characteristic value of organic donor and acceptor systems. The values of λ are shown in Table 2. In the present systems of donor and acceptor, λ values are found to be lower than $-\Delta G^0$ (Table 2) ($-\Delta G^0 > \lambda$) in polar environments (ACN and EtOH) which indicates the presence of Marcus inverted region. However, this phenomenon is very rare for intermolecular systems and so for conclusive evidence more investigations should be carried out with similar other donor–acceptor systems which possess different ΔG^0 values.

However, from the observed rate constant (k_{ET}) values (Table 2) it seemingly indicates that the electron accepting power of both the acceptors studied in the present investigation is nearly the same. Almost the same reduction potential values, obtained from the electrochemical measurements, of the two acceptors (Table 1) further corroborate our presumption.

For the direct evidence of the occurrences of photoinduced ET reactions the transient absorption spectra of the acceptor in presence of the donor THQ was measured by flash photolysis techniques. The results are described below.

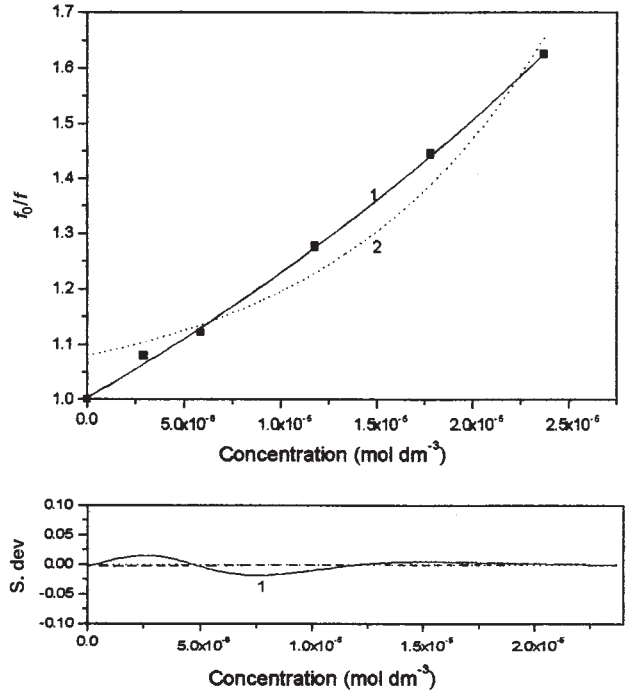
(A1.1) Transient absorption spectra

Pulsed laser excitation was performed at a wavelength of 355 nm with the help of a Nd:YAG laser system in order to excite only the acceptor moiety from the mixture of the donor THQ and the acceptor in ACN solvent. This excitation produced a transient species which absorbed at nearly 510 nm, along with a shoulder at around 450 nm region (Fig. 3*b*). Following the observations made earlier (16) the shoulder at 450 nm was assigned to the triplet-triplet absorption band of 9FL having lifetimes in the microsecond time scale. However we measured the transient absorption spectra of the fluorenone acceptors (9FL and 2N9FL) in ACN environment. The absorption band at about the same energy position (~450 nm) was found.

With an increase of the delay times between the exciting and analyzing pulses (Fig. 3*b*) the 510 nm band was observed to diminish very quickly relative to the 450 nm shoul-

© 2000 NRC Canada

Fig. 4. Plot of f_0/f versus [Q] for THQ donor and acceptor 9FL in EtOH solvent at the ambient temperature. The non-linear least square curve fitting procedure was used to treat the data according to the following models. (1) f_0/f = (exp (V[Q])) (1 + K_{SV}[Q])l' (both static and dynamic contributions are present, see text); the very nice fitting curve ($\chi^2 \approx 1.0$) is obtained (shown in the solid line); the standard deviation data was also shown. (2) f_0/f = exp (V[Q]) (only static part present) very poor fitting is obtained (shown by dotted line).



der. This shows the two different species should be responsible for these two bands. The band at 510 nm could be assigned to the band of contact ion-pair (CIP) of 9FL (or 2N9FL) radical anion according to what is known on the flash photolysis of fluorenone in ACN (33).

In comparing the magnitudes of the intensity ratio I_{450}/I_{510} at the different delay times, it can be seen that this ratio increases from 0.50 to 0.54 to 0.63 as the delay time increases from 0.4 to 1.4 to 2.4 μs (Fig.3*b*). It appears that the build up of monomeric triplet of 9FL (or 2N9FL) occurs in the same time interval during which the radical anionic species of it disappears. This might be due to the production of triplet of the fluorenone acceptor by the ion recombination mechanism.

The observations of transient absorption bands of ion-pair were in accord to our expectation as the large negative ΔG^0 values of the present D–A systems were found from the electrochemical measurements.

(A2) Possibility of occurrence of energy transfer

The existence of partial overlapping between the fluorescence emission spectra of the donor and the electronic absorption of the acceptors (9FL or 2N9FL) further confirms our proposition, as described in Section 2A, about the occurrence of nonradiative (Förster's type) energy transfer processes, along with photoinduced ET.

The rate constants, k_{FT}, associated with the nonradiative energy transfer process were computed by using the well known relation (8) and are listed in Table 2. For a particular donor–acceptor system k_{FT} values were found to remain nearly unchanged with the polarity of the environment (Table 2). These observations were in accord with our expectation for the Förster type energy transfer processes occurring within the present D*–A systems. It is relevant to point out that the contribution of the Dexter's exchange mechanism within the present reacting systems appears to be low in energy transfer process due to large Förster's critical transfer distance R_0 values (13–23 Å) though the values of $R$was chosen as 8 Å.

From a comparative study of the two rate constants k_{ET} and k_{FT} (Table 2) it could be seen that in the cases of all the donor-acceptor systems studied in the present investigation $k_{ET} > k_{FT}$. Thus in nonradiative transitions ET process plays a dominant role though as an associated process energy transfer is also present concurrently. This observation was made irrespective of the polarity of the environment.

(A3) Possibility of occurrence of static quenching process

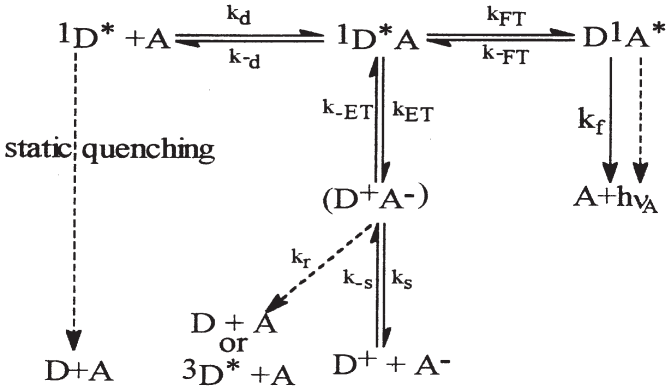
To examine the possibility of the presence of static quenching phenomena, apart from energy transfer and ET processes, Stern–Volmer (SV) plot of intensity variation as a function of quencher concentration was drawn for the D*–A pairs. By plotting f_0/f versus [Q], the upward curvature (Fig. 4) was found in each case except the system THQ*–9FL (* denotes the excited state S_1) in ACN where linear plot was observed. The positive deviations from the linearity indicate the possibility of the presence of static quenching. In case of THQ* + 9FL + ACN system the linear plot indicates that the dynamic quenching might be active in this system. To substantiate the fact another SV relation $\tau_0/\tau = 1 + K_{SV}[Q] = 1 + k_q\tau\,[Q]$ was plotted by using fluorescence lifetimes of the donor without and in presence of quencher (acceptor). As shown in the Table 2, no significant changes occur in the values of K_{SV} and k_q evaluating from intensity as well as lifetime plots, thus $f_0/f = \tau_0/\tau$. This observation shows that only dynamic quenching is operative within this D–A system. However, in the rest of the donor-acceptor systems, static quenching seems to play major role. In these systems the fluorescence lifetime of THQ remains more or less unaffected in presence of the acceptor, which suggests in favor of static quenching. However, electrochemical and transient absorption measurements indicate the possibility of the presence of dynamic quenching reactions also within the present reacting systems. Unaffected τ values of the donor THQ in presence of the acceptors might be due to the fact that large static effect may overwhelm the dynamic processes. Nevertheless, an attempt was made to dissect the static and dynamic quenching modes separately by using a model which is the modified form of SV relation. The modified relation is shown below:

$$[4] \qquad \frac{f_0}{f} = \exp(V[Q])(1 + K_{SV}[Q])l'$$

where V is the static parameter and $l' = 1 + K$[Q], where K is the equilibrium constant for the formation of ground state complex. V could provide us the information about the local distribution of the quencher around a fluorescer. Using non-

© 2000 NRC Canada

Scheme 1.



linear least square curve fitting procedure the data were treated according to eq. [4] and a nice fitted curve ($\chi 2$ = 1.01) (Fig. 4) was obtained. The values of V, K_{SV} and l' are obtained separately and presented in Table 2. As the values of K_{SV} were found to be small, it seems that the dynamic quenching though present has a minor role in quenching mechanism whereas large values (>500 dm^{-3} mol^{-1}) of V indicates the static component is so dominating over dynamic processes that the upward curvature of SV plot was obtained as a resulting effect. These observations are in accord to our speculations as discussed above. Thus, it could be presumed that within all the present systems of donor and acceptor studied (except THQ* + 9FL in ACN) at least three processes are involved in fluorescence quenching mechanism of THQ which are: static effect, energy transfer (Förster's type) and ET processes.

The values of K_{SV}, k_q and l' are listed in Table 2. As expected, l' values were found to be nearly one because this shows K = 0. As no ground state CT complex was visible in the electronic absorption spectra of the mixture of donor and acceptor in a solvent, it might be logical to presume that no such complex is formed. Scheme 1 depicts the photophysical processes within the present donor-acceptor systems when donor is excited at the ambient temperature.

Neglecting the dynamic part in the expression [4] we used another model f_0/f = exp (V[Q]) in which only static part is present. However this model exhibits very poor fitted curve (shown by dotted lines in Fig. 4). This indicates that to examine the fluorescence quenching data of the donor THQ in presence of the acceptor 9FL (or 2N9FL) the model expressed by the eq. [4], where both static and dynamic contributions are included, should be more appropriate.

(B) When the acceptor is excited to its S_1 *state*

The situation became simpler when the acceptor, instead of donor, was excited to its lowest excited singlet state in presence of the unexcited donor. As it could be seen from the Fig. 5, the excitation wavelength was chosen at 378 nm for exciting the fluorescence emission of 9FL. At this wavelength there is no absorption of the donor molecules, so the donor filtering effect on the acceptor emission will not be present. Moreover due to higher lying electronic excited singlet level S_1 of the donor THQ molecule, energy transfer from S_1 of the acceptor to this level is forbidden. With increase of donor concentration, the fluorescence emission of the acceptor 9FL was found to be reduced regularly without any noticeable spectral shift (Fig. 5). The reduction of 9FL fluorescence by the donor THQ obeys simple SV relation as evidenced from linear SV plot. Further the fluorescence lifetime (τ) of 9FL also decreases with increase of the concentration of THQ (Fig. 6).

Fig. 5. Fluorescence emission spectra of 9FL (λ_{exc} = 378 nm) in ACN solvent of concentration (1.66 × 10^{-4} mol dm^{-3}) at 300 K in presence of THQ whose concentrations (mol dm^{-3}) were: (0) 0, (1) 2.5 × 10^{-5}, (2) 1.25 × 10^{-4}, (3) 2.5 × 10^{-4}.

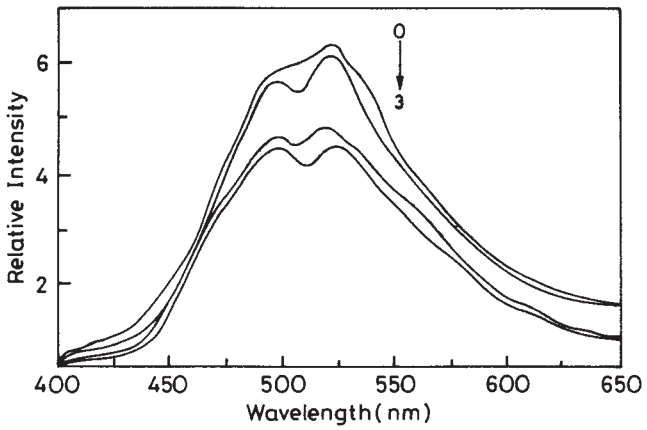
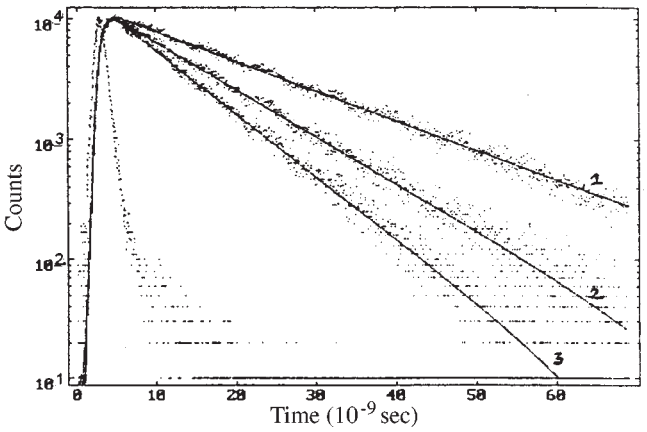


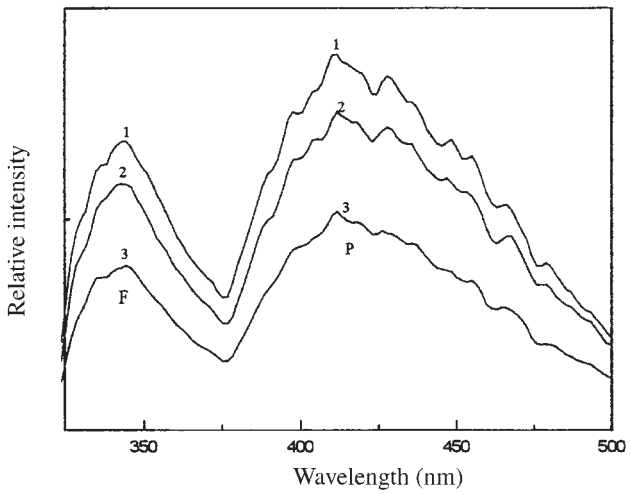
Fig. 6. Fluorescence decay curves (λ_{exc} = 378 nm, λ_{em} = 500 nm).associated with the lamp profile showing the single exponential decay of 9FL (3.61 × 10^{-4} mol dm^{-3}) in ACN in presence of THQ whose concentrations in mol dm^{-3} were: (1) 0, (2) 8.75 × 10^{-5}, and (3) 1.5 × 10^{-4} at room temperature. Their χ^2 values varied within 1.1 to 1.2 of each other.



Using two types of SV relations (from fluorescence intensity and fluorescence lifetime) K_{SV} and k_q were computed (Table 2). These quantities are found to be nearly the same (Table 2) and the relation $f_0/f \approx \tau_0/\tau$ holds. All these observations strongly suggest that when the acceptor moiety is excited, the quenching is of dynamic nature unlike the situation when the donor chromophore is excited where both static and dynamic type quenching might participate. Moreover, k_q for 9FL* + THQ system in ACN was found to be of the order of 10^{10} dm^3 mol^{-1} s^{-1} which is the upper limit (diffusion controlled limit) of the rate of photoinduced ET reaction. Thus it seems when excited acceptor reacts with

© 2000 NRC Canada

Fig. 7. Emission spectra of THQ donor (λ_{exc} = 320 nm) in EtOH rigid glassy matrix of concentration 2.5 × 10^{-5} mol dm^{-3} at 77 K in the presence of acceptor 9FL whose concentrations (mol dm^{-3}) were: (1) 0, (2) 2.25 × 10^{-5}, (3) 8.8 × 10^{-5}. F: fluorescence; P: phosphorescence.



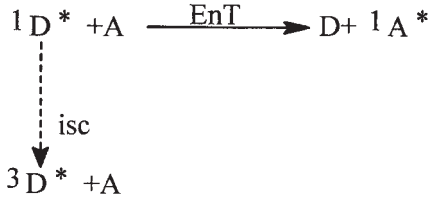
ground state donor, mainly ET process becomes operative. However, the similar experiment as above was not possible with the other acceptor 2N9FL due to lack of its fluorescence emission. The large negative ΔG^0 value (~ –1.41 eV) for 9FL* + THQ system, as shown in Table 1, substantiates the fact that the possibility of occurrence of ET within this system is high.

It is observed from the above findings that when the acceptor 9FL is excited in presence of the donor THQ molecule, the fluorescence quenching of the former species is observed to be of dynamic nature. 9FL quenching does not show any noticeable positive deviation in an SV plot. Following the observations made earlier by Eftink and Ghiron (12) it could be inferred that as 9FL is longer-lived species (longer fluorescence lifetime than THQ, Table 2) its fluorescence quenching by THQ may be ascribed due to the presence of dominating dynamic (collisional) processes. As it was observed in the case of acrylmide quenching of some longer-lived fluorescent molecules (12), in the quenching mechanism of 9FL fluorescence also it is possible that the dynamic component is so overwhelming (large K_{SV}) over the static one that the SV plots simply appears to be linear. However, the probable cause of the absence of static contribution in the quenching of fluorescence emission of THQ by 9FL is not comprehensible at the present stage of investigation. Further studies considering several other donor and acceptor systems might be helpful to understand this phenomena. Investigations in this direction are now underway.

3. Fate of the non-radiative processes due to lowering of temperature down to 77 K

At 77 K in EtOH rigid glassy matrix both the fluorescence and phosphorescence of THQ (λ_{exc} ~ 320 nm) gradually diminish with the increase of concentration of 9FL (or 2N9FL) (Fig. 7). ET, being a thermally activated process, seems to have less effect on fluorescence and phosphorescence emission quenching. However, it appears that another nonradiative channel energy transfer process of Förster's

Scheme 2.



type might be responsible for observed quenching at 77 K. Nearly same R_0 (≈26 Å) values, as observed at the ambient temperature, were obtained at this low temperature. Moreover, f_0/f versus [Q] plots clearly show positive deviation from linearity which seems to indicate that at 77 K, like the situation observed at the ambient temperature, static quenching is also present along with energy transfer and might be jointly responsible for nonradiative depletion of the donor's lowest excited singlet state. As ACN does not form glass, the above experiment was not possible with this solvent.

The quenching observed in the phosphorescence band intensity of a THQ donor in presence of acceptor 9FL (or 2N9FL) may not be due to triplet-triplet energy transfer process because of the large R_0 (~26 Å) value. This transfer requires the reactants to approach closer than 26 Å. One plausible explanation may be that with the increase of acceptor concentration, energy transfer (Förster) efficiency will be increased because more and more donor molecules will be involved in transferring their excitation energy to the singlet (S_1) of acceptors. Consequently the triplet of the donor, which is formed by isc process (another path for nonradiative depletion of donor lowest excited singlet), would be less populated resulting in the decreasing quantum yield of the phosphorescence of the donor. In Scheme 2, the possible non-radiative processes at 77 K within the present reacting systems are shown.

Another interesting finding is that the phosphorescence lifetime (τ_p) of the donor THQ (~3.4 s) was reduced considerably (~1.1 s) in presence of the acceptor 9FL (1.76 × 10^{-4} mol dm^{-3}). This indicates that the lifetime reduction was not only due to less population in the triplet level of the donor, as discussed above, but also because there is a possibility of the occurrence of ET reactions between the triplet state of the donor and ground state acceptor. This might cause noticeable reduction in the triplet lifetime of the former species. In favor of such a proposition the exothermicity of such reactions will be lowered by the difference between the first excited singlet and triplet states of the donor, but from the thermodynamic point of view there is a possibility of occurrence of ET reactions between the triplet donor THQ and the unexcited acceptor 9FL as the value of ΔG^0 is still negative, ~ –1.14 eV (Table 1) which is obtained from the relation (34–37)

$$\Delta G^0_{TET}(EtOH) = \Delta G^0_{SET}(EtOH) + \Delta E_{S_1-T_1}$$

$$\Delta G^0_{SET}(EtOH) = \Delta G^0_{SET}(ACN) + \Delta G^0_d$$

where,

$$\Delta G^0_d = \frac{e^2}{\varepsilon_S}\left(\frac{1}{2r_D} + \frac{1}{2r_A} - \frac{1}{R}\right) - \frac{e^2}{\varepsilon_{S'}}\left[\frac{1}{2r_D} + \frac{1}{2r_A}\right]$$

© 2000 NRC Canada

ΔG_d^0 is the ion pair destabilization energy due to the decrease in the polarity of the environment from ACN fluid solution at 296 K to EtOH glass at 77 K.

Similar quenching phenomena, both in phosphorescence intensity and the triplet lifetime of the donor THQ, were also observed in the presence of the other quencher 2N9FL. The ΔG^0 for this system was found to be around –1.08 eV. Thus at 77 K the triplet THQ seems to also be involved in ET reactions with this acceptor.

The above steady state and time resolved studies using TCSPC and flash photolysis methods at both the ambient temperature and at 77 K demonstrate the occurrences of photoinduced ET reactions along with several other nonradiative processes in the present reacting systems in solvents of different polarities, especially in those cases when one of the reactants is in the electronic excited state.

Concluding remarks

Steady state electronic absorption spectra observed at the ambient temperature do not exhibit any ground state CT complex between THQ and 9FL/2N9FL, irrespective of the polarity of the environment.

The large fluorescence quenching of the donor THQ molecule observed at the room temperature, in presence of the acceptors 9FL or 2N9FL, seemed to be due to the combined effect of static and dynamic processes involved in which the contribution of the former in the overall quenching mechanism appears to be significantly large. However, relatively weaker dynamic quenching processes, such as photoinduced ET and energy transfer (Förster mechanism) seemed to also be operative within the present reacting systems. Within these systems (D*–A) highly exothermic (large negative ΔG^0) ET reactions were observed both in the polar protic EtOH and aprotic ACN solvents. Conclusive evidence for the occurrence of inverted behavior in ET reactions was not observed due to the closer values of ΔG^0 in the present D–A systems. When the acceptor moiety was excited in presence of ground state THQ, the quenching was found to be primarily due to ET in ACN solvent. Observations of the transient absorption spectra of contact ion-pair of the acceptor radical anion provide us the direct evidence of occurrence of photoinduced ET reactions within the donor THQ and the acceptor 9FL or 2N9FL in ACN solvent. At 77 K, the combined effect of Förster type energy transfer and static quenching appears to be responsible for donor fluorescence quenching. The possibility of ET reactions between the triplet donor and ground state acceptor is hinted from the observed shortening of the donor phosphorescence lifetime (τ_p), and negative ΔG^0 values (<0).

Acknowledgements

We acknowledge for financial assistance by University Grants Commission to A.K.D. Special thanks are due to Dr. A. Samanta and S. Saha of Hyderabad Central University for fluorescence lifetime measurements. Thanks are also due to Prof. S. P. Ghosh of IACS for providing us with the facilities for electrochemical measurements; and thanks are also due to Dr Samita Basu of Saha Institute of Nuclear Physics, Calcutta for measurements of Transient absorption spectra by laser flash photolysis techniques. We like to express our heartiest thanks to the referees for their constructive criticisms and valuable suggestions. Special thanks are due to Professor Michel Boussuge of Ecole des Mines de Paris, Paris, France for helping us in preparing the french version of the abstract.

References

1. J. Chen, T. Ho, and C. Mou. J. Phys. Chem. **94**, 2889 (1990).
2. K.S. Peters and J. Lee. J. Phys. Chem. **96**, 8941 (1992).
3. R. Giasson, E.J. Lee, X. Zhao, and M.S. Wrighton. J. Phys. Chem. **97**, 2596 (1993).
4. S. Murata, M. Nishimura, S.Y. Matsuzaki, and M. Tachiya. Chem. Phys. Lett. **219**, 200 (1994).
5. S. Murata, S.Y. Matsuzaki, and M. Tachiya. J. Phys. Chem. **99**, 5354 (1995).
6. S.M. Hubig, T.M. Bockman, and J.K. Kochi. J. Am. Chem. Soc. **118**, 3842 (1996).
7. S. Murata and M. Tachiya. J. Chim. Phys. Phys-Chim. Biol. **93**,1577 (1996).
8. S. Sinha, R. De, and T. Ganguly. J. Phys. Chem. A. **101**, 2852 (1997).
9. B. Zelent, P. Messier, D. Gravel, S. Gauthier, and G. Durocher. J. Photochem. Photobiol. A. **40**, 145 (1987).
10. S. Sinha, R. De, T. Ganguly, A.K. De, and S.K. Nandy. J. Lumin. **75**, 99 (1997).
11. Z. Murtaza, D.K. Graff, A.P. Zipp, L.A. Worl, W.E. Johns, Jr., W.D. Bates, and T.J. Meyer. J. Phys. Chem. **98**, 10504 (1994).
12. M.R. Eftink and C.A. Ghiron. J. Phys. Chem. **80**, 186 (1976), and refs. therein.
13. S. Sinha, R. De, and T. Ganguly. Spectrochim. Acta Part A, **54A**, 145 (1998).
14. R. De, S. Bhattacharyya, and T. Ganguly. Spectrochim. Acta Part A, **50A**, 325 (1994).
15. S. Sinha, R. De, and T. Ganguly. J. Photochem. Photobiol. A: Chem. **112**, 13 (1998).
16. T. Ganguly, D.K. Sharma, S. Gauthier, D. Gravel, and G. Durocher. J. Phys. Chem. **96**, 3757 (1992).
17. J.J. Hopfield, J.N. Onuchic, and D.N. Beratan. J. Phys. Chem. **93**, 6350 (1989).
18. M.J. Weaver, G.E. McManis, W. Jarzeba, and P.F. Barbara. J. Phys. Chem. **94**, 1715 (1990).
19. B. Bagchi and G.R. Fleming. J. Phys. Chem. **94**, 9 (1990).
20. M. Maroncelli, J. Macinnis, and G.R. Fleming. Science (Washington, D.C.), **243**, 1674 (1989).
21. D. Rehm and A. Weller. Isr. J. Chem. **8**, 259 (1970).
22. N. Mataga, H. Shioyama, and Y. Kanda. J. Phys. Chem. **92**, 314 (1987).
23. J.R. Miller, L.T. Calcaterra, and G.L. Closs. J. Am. Chem. Soc. **106**, 3047 (1984).
24. M. Tachiya and S. Murata. J. Phys. Chem. **96**, 8441 (1992).
25. A.K. De, S. Sinha, S.K. Nandy, and T. Ganguly. J. Chem. Soc. Faraday Trans. **94**, 1695 (1998).
26. S.R. Meech and D. Phillips. Chem. Phys. **80**, 317 (1983).
27. P. Jana, G.K. Mallik, T. Ganguly, and S.B. Banerjee. Chem. Phys. Lett. **172**, 158 (1990).
28. K. Nokamura. J. Am. Chem. Soc. **102**, 7846 (1980).
29. D. Rehm and A. Weller. Ber Bunsen-Ges. Phys. Chem. **73**, 837 (1969).
30. G.J. Kavarnos and N.J. Turro. Chem. Rev. **86**, 401 (1986).
31. A. Weller. Z. Phys. Chem. **133**, 93 (1982).

© 2000 NRC Canada

32. H. Heitele, P. Finckh, S. Weeren, F. Pollinger, and M.E. Michel-Beyerle. J. Phys. Chem. **93**, 5173 (1989).
33. J. Gersdorf and J. Mattoy. J. Photochem. **28**, 405 (1985).
34. S. Sinha and T. Ganguly. J. Photochem. Photobiol. A, **117**, 83 (1998).
35. M.R. Wasielewski, D.G. Johnson, W.A. Svec, K.M. Kersey, and D.W. Minsek. J. Am. Chem. Soc. **110**, 7219 (1988).
36. G.L. Gains, M.P. O'Neil, W.A. Svec, M.P. Niemczyk, and M.R. Wasielewski. J. Am. Chem. Soc. **113**, 719 (1991).
37. Y. Sakata, H. Tsue, M.P. O'Neil, G.P. Wiederrecht, and M.R. Wasielewski. J. Am. Chem. Soc. **116**, 6904 (1994).

© 2000 NRC Canada

Thermodynamic properties of aqueous diethanolamine (DEA), *N*,*N*-dimethylethanolamine (DMEA), and their chloride salts: apparent molar heat capacities and volumes at temperatures from 283.15 to 328.15 K

Christopher Collins, Joelle Tobin, Dmitri Shvedov, Rom Palepu, and Peter R. Tremaine

Abstract: Apparent molar heat capacities $C_{p,\phi}$ and apparent molar volumes V_ϕ for aqueous diethanolamine $(HOC_2H_4)_2NH$, diethanolammonium chloride $(HOC_2H_4)_2NH_2Cl$, *N*,*N*′-dimethylethanolamine $(HOC_2H_4)(CH_3)_2N$, and *N*,*N*′-dimethylethanolammonium chloride $(HOC_2H_4)(CH_3)_2NHCl$ were determined from 283.15 to 328.15 K with a Picker flow microcalorimeter and vibrating tube densimeter. The experimental results have been analyzed in terms of Young's Rule with the Guggenheim form of the extended Debye–Hückel equation and appropriate corrections for chemical relaxation effects. These calculations lead to standard partial molar heat capacities and volumes for the neutral amines, $(HOC_2H_4)_2NH(aq)$ and $(HOC_2H_4)(CH_3)_2N(aq)$, and the ions $(HOC_2H_4)_2NH_2^+(aq)$ and $(HOC_2H_4)(CH_3)_2NH^+(aq)$ over the experimental temperature range.

Key words: standard partial molar volumes, standard partial molar heat capacities, diethanolamine, dimethyethanolamine, aqueous alkanolamine ionization.

Résumé : Faisant appel à un microcalorimètre à écoulement de Picker et à un densimètre à tube vibrant, on a déterminé les capacités calorifiques molaires apparentes, $C_{p,\phi}$, ainsi que les volumes molaires apparents, V_ϕ, de solutions aqueuses de diéthanolamine, $(HOC_2H_4)_2NH$, de chlorure de diéthanolammonium, $(HOC_2H_4)_2NH_2Cl$, de *N*,*N*′-diméthyléthanolamine, $(HOC_2H_4)(CH_3)_2NH$, et de chlorure de *N*,*N*′-diméthyléthanolammonium, $(HOC_2H_4)(CH_3)_2NH_2Cl$. Les résultats expérimentaux ont été analysés en fonction de la règle d'Young en utilisant la forme de Guggenheim de l'équation élargie de Debye–Hückel, en y apportant les corrections appropriées pour les effets de relaxation chimique. Ces calculs ont permis de déduire les capacités calorifiques et les volumes molaires partiels standards des amines neutres, $(HOC_2H_4)_2NH(aq)$ et $(HOC_2H_4)(CH_3)_2NH(aq)$ et de leurs ions $(HOC_2H_4)_2NH_2^+(aq)$, $(HOC_2H_4)(CH_3)_2NH_2^+(aq)$ sur toute la plage des températures expérimentales.

Mots clés : volumes molaires partiels standards, capacités calorifiques molaires partielles standards, diéthanolamine, diméthyléthanolamine, ionisation aqueuse d'alcanolamines.

Introduction

Aqueous alkanolamines are employed in industry for the removal of acidic components from natural and refinery gas streams, and as pH control agents in the steam generators of nuclear and thermal power stations. Thermodynamic properties of these species are needed to model speciation and vapour–liquid equilibria, and to develop predictive models for their behaviour at elevated temperatures and pressures. Diethanolamine (DEA) is important in the context of natural gas processing because it can be used when there is a significant quantity of carbonyl sulfide in the gas stream without forming irreversible reaction products. *N*,*N*′-Dimethylethanolamine (DMEA) is an example of a tertiary

Received June 16, 1999.

C. Collins, D. Shvedov,[1] and P.R.Tremaine.[2] Department of Chemistry, Memorial University of Newfoundland, St. John's, NF A1B 3X7, Canada.
J. Tobin and R. Palepu.[2] Department of Chemistry, St. Francis Xavier University, PO Box 5000, Antigonish, NS B2G 2W5, Canada.

[1]Present address: Alcan International Ltd., Kingston R&D Center, P.O. Box 8400, 945 Princess St., Kingston, ON K7L 5L9, Canada.
[2]Authors to whom correspondence may be addressed. PRT: Telephone: (709) 737-8744. Fax: (709) 737-3702. e-mail: tremaine@morgan.ucs.mun.ca; RP: Telephone: (902) 867-3886. Fax: (902) 867-2414. e-mail: rpalepu@stfx.ca

 © 2000 NRC Canada

alkanolamine used in gas processing applications to avoid the formation of aqueous carbamates. DMEA has also been considered as a candidate amine for use in the boilers of nuclear and thermal electric power stations as a pH additive.

Jones and Arnett (1) have reviewed the literature on DEA, DMEA, and other aqueous amines before 1974. More recent work in several laboratories has determined new values for the ionization constants (2, 3), enthalpies of ionization (2), viscosities (4), densities (4–6), and surface tension (4) of aqueous diethanolamine. Maham et al. (7) have measured the heat capacity of liquid DEA and DMEA over a range of temperatures.

Partial molar heat capacities and volumes of aqueous alkanolamines in their neutral and ionized forms are important parameters because they define the temperature and pressure dependance of the ionization constant, enthalpy of ionization and activity coefficients, respectively. Volumetric data leading to the standard partial molar volumes of DEA and DMEA have been reported by Maham et al. (5) and Zhang et al. (6) respectively. However, no measurements of the apparent molar heat capacities of aqueous DEA and its salts have been reported in the literature. Cobble and Turner (8) have determined apparent molar heat capacities for DMEA(aq) and its chloride salt at 298.15 K. No temperature-dependant studies have been reported.

Recently, our laboratories have undertaken a systematic program to determine pressure- and temperature-dependant thermodynamic properties of aqueous amines relevant to the natural gas and electric power industries (8–10). In this paper we report apparent molar heat capacities and volumes for diethanolamine, *N*,*N*′-dimethylethanolamine, and their chloride salts, leading to standard partial molar heat capacities and volumes for the neutral amines, DEA(aq) and DMEA(aq), and the ions, $(HOC_2H_4)_2NH_2^+$(aq) ($DEAH^+$(aq)) and $(CH_3)_2(HOC_2H_4)NH^+$(aq) ($DMEAH^+$(aq)), over the temperature range 283.15–328.15 K.

Experimental

Diethanolamine and *N*,*N*′-dimethylethanolamine (Aldrich, analytical reagent grade, 99+%) from freshly opened bottles were used without further purification. A stock solution of each amine was prepared by mass and then standardized by titration with HCl. The results agreed to within 0.1 mol percent. Stock solutions of diethanolammonium chloride and *N*,*N*′-dimethylethanolammonium chloride were prepared by adding a weighed excess of standard HCl solution to the standard amine solutions. More dilute solutions were prepared from the stock by mass, using boiled, deionized water. Nanopure water (resistivity >17 $M\Omega\cdot cm^3$) was used to prepare all solutions. NaCl solutions were prepared by mass after first drying the salt for 24 h at 120°C. HCl solutions were prepared from a 15 mol kg^{-1} stock solution (Fischer A.C.S. certified reagent grade) and standardized by titration against TRIS (tris(hydroxymethyl)aminoethane; Aldrich, 99.9+ %).

A Sodev CP-C flow microcalorimeter (11) and a Sodev 03D vibrating flow densitometer (12) equipped with platinum cells were employed in this work. The temperatures of the calorimeter and densitometer were independently controlled to ±0.01 K by two Sodev CT-L circulating baths. The thermistors (Omega, 44 107) used to measure the temperatures of calorimeter and densitometer were calibrated with a Hewlett–Packard 2804A quartz-crystal thermometer traceable to NBS standards. The densitometer was calibrated daily with pure water (13) and standard 1 mol kg^{-1} NaCl(aq) solution. The experimental values of $(1 - (c_p\rho / c_{p,1}^*\rho_1^*))$ for the standard NaCl(aq) were compared with literature values complied by Archer (14) to correct for a small heat-leak effect, according to method of Desnoyers et al. (15). Heat-leak correction factors (±0.005) were 1.025, 1.018, 1.007, and 1.001 at T = 283.15 K, 298.15 K, 313.15K, and 328.15 K. Here, $c_p\rho$ and $c_{p,1}^*\rho_1^*$ are the products of specific heat capacity and density of the solution and H_2O(l), respectively.

Results and discussion

Apparent Molar Properties

The experimental values for the heat capacity ratios $(1 - (c_p\cdot\rho/c_{p,1}^*\cdot\rho_1^*))$ and relative densities $(\rho - \rho_1^*)$ for diethanolamine and diethanolammonium chloride are listed in Tables 1–4, while those for *N*,*N*′-dimethylethanolamine and *N*,*N*′-dimethylethanolammonium chloride are listed in Tables 5–8. The tables also tabulate the experimental apparent molar volumes $V_{\phi,2}^{exptl}$ and heat capacities $C_{p,\phi,2}^{exptl}$, which were calculated from these results using densities and specific heat capacities of pure water taken from Hill (13). By definition,

$$[1] \qquad Y_\phi = (Y(sln) - 55.509\cdot Y_1^*) / (m_2 + m_3)$$

where Y_1^* is the molar heat capacity or volume of pure H_2O(l), m_2 is the molality of DEA(aq) or $DEAH^+Cl^-$(aq), and m_3 is the molality of excess hydrochloric acid, if present. The effect of the small amount of excess HCl was subtracted by applying Young's rule according to the procedure used by Hovey et al. (16, 17). Briefly, the contribution of each solute can be described by the expression (18, 19):

$$[2] \qquad Y_\phi = (m_2 / (m_2 + m_3))Y_{\phi,2} + (m_3 / (m_2 + m_3))Y_{\phi,3} + \delta$$

Here, $Y_{\phi,2}$ and $Y_{\phi,3}$ are the values for the hypothetical solution of the pure components with speciation and ionic strength identical to the mixture; and δ is an excess mixing term, which usually may be ignored in calculating the properties of the major components where there is a common cation or anion. Both $C_{p,\phi,3}$ and $V_{\phi,3}$ were calculated as functions of ionic strength and temperature from the equations for HCl reported by Hershey et al. (20) and Tremaine et al. (21), respectively. The resulting values of $C_{p,\phi,2}$ and $V_{\phi,2}$ for diethanolammonium chloride are tabulated in Tables 3 and 4 and for *N*,*N*′-dimethylethanolammonium chloride in Tables 7 and 8.

The ionization constants reported by Jones and Arnett (1) indicate the formation of diethanolamine is negligible in the diethanolammonium chloride solutions over the temperature range and molalities used in this investigation, in part because of the presence of excess HCl. No similar excess of NaOH was used to suppress the ionization of neutral species in the diethanolamine solutions. Therefore, the resulting $C_{p,\phi}$ and V_ϕ values for diethanolamine must be corrected for the reaction:

© 2000 NRC Canada

Table 1. Apparent molar heat capacities $C_{p,\phi,2}$ for aqueous diethanolamine where m_2 denotes molality; ρ_1^* and $c^*_{p,1}$ denote density and heat capacity of water; $C_{p,\phi}^{rel}$ is the relaxation contribution.

m_2 (mol kg^{-1})	α	$[1- c_p\rho/(c_{p,1}^*\rho_1^*)] \times 10^3$	$C_{p,\phi}^{exptl}$ (J K^{-1} mol^{-1})	$C_{p,\phi}^{rel}$ (J K^{-1} mol^{-1})	$C_{p,\phi,2}$ (J K^{-1} mol^{-1})
T = 283.15 K					
0.05324	0.0101	1.0244	307.43	2.33	308.3
0.11709	0.0068	2.2095	309.73	1.58	310.3
0.14647	0.0061	2.7490	309.60	1.41	310.1
0.21024	0.0051	3.9999	308.16	1.18	308.6
0.31166	0.0042	5.9900	306.97	0.97	307.3
0.40644	0.0036	7.9262	305.12	0.85	305.4
0.57840	0.0031	11.243	303.68	0.71	303.9
0.79515	0.0026	15.639	300.79	0.61	301.0
1.01020	0.0023	19.945	298.39	0.54	298.6
T = 298.15 K					
0.05324	0.0120	0.8516	323.87	1.56	325.3
0.11709	0.0081	1.8721	323.65	1.05	324.6
0.14647	0.0072	2.3304	323.84	0.94	324.7
0.21024	0.0060	3.3558	323.28	0.79	324.0
0.31166	0.0049	4.9464	323.06	0.65	323.6
0.40644	0.0043	6.4583	322.21	0.57	322.7
0.57840	0.0036	9.2334	320.62	0.47	321.0
0.79515	0.0031	12.677	319.13	0.40	319.5
1.01020	0.0027	16.130	317.52	0.36	317.8
T = 313.15 K					
0.05324	0.0134	0.7666	331.41	0.86	333.7
0.11709	0.0091	1.6229	333.24	0.58	334.8
0.14647	0.0081	1.9898	335.44	0.52	336.8
0.21024	0.0068	2.8690	333.96	0.43	335.1
0.31166	0.0056	4.0026	337.44	0.36	338.4
0.40644	0.0049	5.3825	335.06	0.31	335.9
0.57840	0.0041	7.4741	335.33	0.26	336.2
0.79515	0.0035	0.0106	332.57	0.22	333.4
1.01020	0.0031	0.0132	332.37	0.20	332.9
T = 328.15K					
0.05324	0.0146	0.6996	335.78	0.35	338.4
0.11709	0.0099	1.3440	343.71	0.24	345.5
0.14647	0.0088	1.6920	344.67	0.21	346.3
0.21024	0.0074	2.3453	346.25	0.18	347.6
0.31166	0.0060	3.7584	342.74	0.14	343.8
0.40644	0.0053	4.5556	345.34	0.13	346.3
0.57840	0.0044	6.6020	343.58	0.11	344.4
0.79515	0.0038	8.8875	343.34	0.09	344.0
1.01020	0.0034	11.260	342.58	0.08	343.2

Table 2. Apparent molar volumes of $V_{\phi,2}$ for aqueous diethanolamine, where m_2 denotes molality; $(\rho - \rho_1^*)$ denotes density relative to water.

m_2 (mol kg^{-1})	α	$(\rho - \rho_1^*) \times 10^3$ (g cm^{-3})	V_ϕ^{exptl} (cm^3 mol^{-1})	$V_{\phi,2}$ (cm^3 mol^{-1})
T = 283.15 K				
0.05324	0.0101	0.6621	92.67	92.71
0.11709	0.0068	1.4144	92.95	92.99
0.14647	0.0061	1.7765	92.87	92.90
0.21024	0.0051	2.5286	92.90	92.93
0.31166	0.0042	3.6856	93.00	93.02
0.40644	0.0036	4.7569	93.02	93.04

© 2000 NRC Canada

Table 2 (*concluded*).

m_2 (mol kg^{-1})	α	$(\rho - \rho_1^*) \times 10^3$ (g cm^{-3})	V_ϕ^{exptl} (cm^3 mol^{-1})	$V_{\phi,2}$ (cm^3 mol^{-1})
0.57840	0.0031	6.7218	92.92	92.93
0.79515	0.0026	9.1049	92.87	92.88
1.01020	0.0023	0.0115	92.77	92.78
T = 298.15 K				
0.05324	0.0120	0.6117	93.84	94.18
0.11709	0.0081	1.3336	93.87	94.10
0.14647	0.0072	1.6621	93.88	94.08
0.21024	0.0060	2.3693	93.89	94.06
0.31166	0.0049	3.4779	93.90	94.04
0.40644	0.0043	4.5132	93.86	93.98
0.57840	0.0036	6.3510	93.81	93.91
0.79515	0.0031	8.6087	93.75	93.84
1.01020	0.0027	0.0108	93.71	93.79
T = 313.15 K				
0.05324	0.0134	0.5956	94.54	94.92
0.11709	0.0091	1.3048	94.52	94.77
0.14647	0.0081	1.5864	94.81	95.04
0.21024	0.0068	2.3071	94.60	94.79
0.31166	0.0056	3.3475	94.74	94.89
0.40644	0.0049	4.3429	94.70	94.83
0.57840	0.0041	6.1191	94.64	94.75
0.79515	0.0035	8.2688	94.61	94.71
1.01020	0.0031	0.0104	94.56	94.65
T = 328.15 K				
0.05324	0.0146	0.6067	94.88	95.28
0.11709	0.0099	1.2930	95.18	95.45
0.14647	0.0088	1.5650	95.52	95.76
0.21024	0.0074	2.2243	95.56	95.77
0.31166	0.0060	3.2077	95.76	95.93
0.40644	0.0053	4.2071	95.60	95.75
0.57840	0.0044	5.9074	95.58	95.70
0.79515	0.0038	8.0256	95.50	95.60
1.0102	0.0034	9.9962	95.51	95.61

Table 3. Apparent molar heat capacities $C_{p,\phi}$ for aqueous diethanolammonium chloride + HCl. $F_3 = m(\text{HCl})/[m((HOC_2H_4)_2NH_2Cl) + m(\text{HCl})]$.

m_2 (mol kg^{-1})	m_3 (mol kg^{-1})	$[1 - c_p\rho/(c_{p,1}^*\rho_1^*)] \times 10^3$	$C_{p,\phi}^{exptl}$ (J K^{-1} mol^{-1})	$F_3 \times C_{p,\phi,3}$ (J K^{-1} mol^{-1})	$C_{p,\phi,2}$ (J K^{-1} mol^{-1})
T = 283.15 K					
0.05015	0.00750	3.9789	99.07	–18.54	135.2
0.10325	0.01417	8.0207	104.66	–16.90	138.2
0.16997	0.02026	12.836	112.51	–14.66	142.3
0.27893	0.03267	20.606	116.38	–14.09	145.8
0.35288	0.03439	25.408	122.65	–11.78	147.5
0.42410	0.03937	30.016	126.25	–11.13	150.1
0.47605	0.04911	33.633	125.37	–12.13	151.7
0.63189	0.05577	43.110	132.12	–10.27	155.0
0.77722	0.07307	52.087	133.33	–10.63	157.5
T = 298.15 K					
0.05015	0.00750	3.5220	138.38	–15.57	177.0
0.10325	0.01417	7.1603	141.52	–14.14	177.0
0.16997	0.02026	11.476	148.05	–12.24	179.4
0.27893	0.03267	18.370	152.66	–11.77	183.7

© 2000 NRC Canada

Table 3 (*concluded*).

m_2 (mol kg^{-1})	m_3 (mol kg^{-1})	$[1 - c_p\rho/(c_{p,1}^*\rho_1^*)] \times 10^3$	$C_{p,\phi}^{exptl}$ (J K^{-1} mol^{-1})	$F_3 \times C_{p,\phi,3}$ (J K^{-1} mol^{-1})	$C_{p,\phi,2}$ (J K^{-1} mol^{-1})
0.35288	0.03439	22.700	158.17	–9.85	184.4
0.42410	0.03937	26.861	160.95	–9.32	186.1
0.47605	0.04911	30.105	159.53	–10.18	187.2
0.63189	0.05577	38.658	165.57	–8.66	189.6
0.77722	0.07307	46.807	165.84	–9.02	191.3
T = 313.15 K					
0.05015	0.00750	3.334	153.45	–14.01	192.5
0.10325	0.01417	6.691	160.01	–12.66	196.4
0.16997	0.02026	10.836	164.81	–10.92	196.7
0.27893	0.03267	17.256	170.14	–10.46	201.8
0.35288	0.03439	21.113	178.67	–8.73	205.7
0.42410	0.03937	24.830	182.52	–8.25	208.5
0.47605	0.04911	27.961	179.81	–9.00	208.3
0.63189	0.05577	35.783	186.79	–7.64	211.6
0.77722	0.07307	43.448	186.26	–7.95	213.1
T = 328.15 K					
0.05015	0.00750	3.0235	175.00	–13.38	216.6
0.10325	0.01417	6.2718	175.20	–12.04	212.9
0.16997	0.02026	10.071	182.37	–10.34	215.7
0.27893	0.03267	16.208	185.33	–9.85	218.0
0.35288	0.03439	20.070	190.78	–8.20	218.4
0.42410	0.03937	23.775	193.24	–7.73	219.6
0.47605	0.04911	26.575	192.19	–8.42	221.3
0.63189	0.05577	34.378	196.80	–7.13	221.9
0.77722	0.07307	41.477	197.55	–7.39	224.2

Table 4. Apparent molar volumes V_ϕ for aqueous diethanolammonium chloride + HCl. $F_3 = m(\text{HCl})/[m((\text{HOC}_2\text{H}_4)_2\text{NH}_2\text{Cl}) + m(\text{HCl})]$.

m_2 (mol kg^{-1})	m_3 (mol kg^{-1})	$(\rho - \rho_1^*) \times 10^3$ (g cm^{-3})	V_ϕ^{exptl} (cm^3 mol^{-1})	$F_3 \times V_{\phi,3}$ (cm^3 mol^{-1})	$V_{\phi,2}$ (cm^3 mol^{-1})
T = 283.15 K					
0.05015	0.00750	2.0008	93.04	2.26	104.36
0.10325	0.01417	4.0514	94.04	2.11	104.55
0.16997	0.02026	6.5137	95.56	1.88	104.85
0.27893	0.03267	10.503	95.88	1.86	105.04
0.35288	0.03439	13.036	97.35	1.58	105.11
0.42410	0.03937	15.455	97.83	1.51	105.26
0.47605	0.04911	17.265	97.23	1.67	105.42
0.63189	0.05577	22.302	98.47	1.45	105.57
0.77722	0.07307	26.990	98.19	1.55	105.73
T = 298.15 K					
0.05015	0.00750	1.9085	94.82	2.37	106.27
0.10325	0.01417	3.8658	95.80	2.22	106.43
0.16997	0.02026	6.2473	97.15	1.97	106.52
0.27893	0.03267	10.046	97.55	1.95	106.80
0.35288	0.03439	12.484	98.99	1.66	106.82
0.42410	0.03937	14.821	99.42	1.59	106.91
0.47605	0.04911	16.585	98.75	1.75	107.00
0.63189	0.05577	21.427	99.98	1.53	107.14
0.77722	0.07307	25.945	99.67	1.63	107.26
T = 313.15 K					
0.05015	0.00750	1.8794	95.63	2.41	107.16
0.10325	0.01417	3.7992	96.69	2.25	107.40

© 2000 NRC Canada

Table 4. (*concluded*).

m_2 (mol kg^{-1})	m_3 (mol kg^{-1})	$(\rho - \rho_1^*) \times 10^3$ (g cm^{-3})	V_ϕ^{exptl} (cm^3 mol^{-1})	$F_3 \times V_{\phi,3}$ (cm^3 mol^{-1})	$V_{\phi,2}$ (cm^3 mol^{-1})
0.16997	0.02026	6.1028	98.24	2.00	107.70
0.27893	0.03267	9.8350	98.56	1.99	107.89
0.35288	0.03439	12.164	100.17	1.69	108.07
0.42410	0.03937	14.472	100.53	1.62	108.09
0.47605	0.04911	16.202	99.84	1.79	108.16
0.63189	0.05577	20.892	101.13	1.56	108.35
0.77722	0.07307	25.293	100.82	1.67	108.48
T = 328.15 K					
0.05015	0.00750	1.8834	95.97	2.34	107.62
0.10325	0.01417	3.7760	97.31	2.20	108.17
0.16997	0.02026	6.0492	98.96	1.96	108.56
0.27893	0.03267	9.7307	99.35	1.95	108.81
0.35288	0.03439	12.060	100.90	1.66	108.91
0.42410	0.03937	14.311	101.34	1.60	109.00
0.47605	0.04911	16.020	100.65	1.77	109.08
0.63189	0.05577	20.638	101.98	1.54	109.30
0.77722	0.07307	25.007	101.64	1.65	109.39

Table 5. Apparent molar heat capacities $C_{p,\phi,2}$ for aqueous *N,N′*-dimethylethanolamine where m_2 denotes molality; ρ_1^* and $c^*_{p,1}$ denote density and heat capacity of water; $C_{p,\phi}^{rel}$ is the relaxation contribution.

m_2 (mol kg^{-1})	α	$[1-c_p\rho/(c_{p,1}^*\rho_1^*)] \times 10^3$	$C_{p,\phi}^{exptl}$ (J K^{-1} mol^{-1})	$C_{p,\phi,2}^{relax}$ (J K^{-1} mol^{-1})	$C_{p,\phi,2}$ (J K^{-1} mol^{-1})
T = 283.15 K					
0.1011	0.0105	0.5420	367.30	4.45	366.7
0.1531	0.0086	0.8501	366.01	3.62	365.5
0.1965	0.0075	1.1034	365.57	3.20	365.1
0.2541	0.0067	1.4447	365.12	2.82	364.7
0.3002	0.0061	1.7381	364.23	2.59	363.8
0.4000	0.0053	2.4004	362.70	2.25	362.4
0.5031	0.0047	3.1640	360.73	2.01	360.4
0.5999	0.0043	3.8718	359.19	1.84	358.9
0.7958	0.0038	5.4679	355.95	1.60	355.7
1.0026	0.0034	7.2836	352.65	1.42	352.4
T = 298.15 K					
0.0499	0.0189	0.2547	368.74	4.69	369.8
0.1011	0.0133	0.5014	370.62	3.32	371.4
0.1531	0.0108	0.7598	370.27	2.70	370.9
0.1965	0.0096	0.9801	369.85	2.39	370.4
0.2541	0.0084	1.2585	369.75	2.10	370.2
0.3002	0.0077	1.5433	368.40	1.93	368.8
0.4000	0.0067	2.0311	368.33	1.68	368.7
0.5031	0.0060	2.6380	367.03	1.50	367.4
0.5999	0.0055	3.1928	366.21	1.37	366.5
0.7958	0.0048	4.3284	364.55	1.19	364.8
1.0026	0.0043	5.5782	362.89	1.06	363.1
T = 313.15 K					
0.1011	0.0157	0.4969	371.40	2.06	373.7
0.1531	0.0127	0.7522	370.43	1.68	372.3
0.1965	0.0113	0.9331	372.27	1.48	373.9
0.2541	0.0099	1.2426	370.51	1.31	372.0
0.3002	0.0091	1.4659	371.05	1.20	372.4
0.5031	0.0071	2.3411	372.21	0.93	373.2
0.5999	0.0065	2.7692	371.16	0.85	372.1

© 2000 NRC Canada

Table 5. (*concluded*).

m_2 (mol kg^{-1})	α	$[1-c_p\rho/(c_{p,1}^{*}\rho_1^{*})]$ × 10^3	$C_{p,\phi}^{exptl}$ (J K^{-1} mol^{-1})	$C_{p,\phi,2}^{relax}$ (J K^{-1} mol^{-1})	$C_{p,\phi,2}$ (J K^{-1} mol^{-1})
0.7958	0.0056	3.7383	370.10	0.74	370.9
1.0026	0.0050	4.7693	368.97	0.66	369.7
T = 328.15 K					
0.5999	0.0071	2.8001	373.96	0.41	375.3
0.7958	0.0062	3.5837	374.13	0.35	375.3
1.0026	0.0055	4.6570	373.28	0.32	374.3

Table 6. Apparent molar volumes $V_{\phi,2}$ for aqueous *N*,*N*′-dimethylethanolamine, where m_2 denotes molality; $(\rho - \rho_1^{*})$ denotes density relative to water.

m_2 (mol kg^{-1})	α	$(\rho - \rho_1^{*}) \times 10^3$ (g cm^{-3})	V_ϕ^{exptl} (cm^3 mol^{-1})	$V_{\phi,2}$ (cm^3 mol^{-1})
T = 283.15 K				
0.0499	0.0150	–0.1766	92.72	93.14
0.1011	0.0105	–0.3853	93.02	93.31
0.1531	0.0086	–0.5674	92.93	93.17
0.1965	0.0076	–0.7221	92.91	93.12
0.2541	0.0067	–0.9273	92.90	93.09
0.3002	0.0061	–1.0675	92.82	92.99
0.4000	0.0053	–1.3738	92.73	92.88
0.5031	0.0047	–1.6585	92.62	92.75
0.5999	0.0043	–1.8839	92.48	92.60
0.7958	0.0038	–2.3016	92.27	92.38
1.0026	0.0034	–2.6410	92.05	92.14
T = 298.15 K				
0.0499	0.0189	–0.2081	93.62	94.13
0.1011	0.0133	–0.4524	93.95	94.31
0.1531	0.0108	–0.6733	93.89	94.19
0.1965	0.0096	–0.8502	93.84	94.10
0.2541	0.0084	–1.0854	93.80	94.03
0.3002	0.0078	–1.2454	93.70	93.90
0.4000	0.0067	–1.6317	93.66	93.84
0.5031	0.0060	–1.9911	93.57	93.73
0.5999	0.0055	–2.3156	93.51	93.65
0.7958	0.0048	–2.8917	93.33	93.46
1.0026	0.0043	–3.4347	93.17	93.28
T = 313.15 K				
0.1011	0.0157	–0.4701	94.61	95.02
0.1531	0.0127	–0.6768	94.40	94.73
0.1965	0.0113	–0.9214	94.69	94.99
0.2541	0.0099	–1.1237	94.44	94.70
0.3002	0.0091	–1.3631	94.58	94.82
0.5031	0.0071	–2.3046	94.71	94.90
0.5999	0.0065	–2.5843	94.47	94.63
0.7958	0.0056	–3.3110	94.38	94.53
1.0026	0.0050	–3.9924	94.27	94.39
T = 328.15 K				
0.1531	0.0145	–0.7764	95.73	95.85
0.1965	0.0128	–0.9923	95.73	95.83
0.2541	0.0113	–1.3221	95.92	96.01
0.3002	0.0104	–1.5354	95.85	95.93
0.4000	0.0090	–2.0697	95.96	96.04
0.5031	0.0080	–2.4633	95.71	95.78

© 2000 NRC Canada

Table 6. (*concluded*).

m_2 (mol kg^{-1})	α	$(\rho - \rho_1^*) \times 10^3$ (g cm^{-3})	V_ϕ^{exptl} (cm^3 mol^{-1})	$V_{\phi,2}$ (cm^3 mol^{-1})
0.5999	0.0073	–2.8976	95.69	95.88
0.7958	0.0064	–3.9215	95.89	96.06
1.0026	0.0057	–4.6956	95.71	95.86

Table 7. Apparent molar heat capacities $C_{p,\phi}$ of aqueous *N*,*N*′-dimethylethanolammonium chloride + HCl. $F_3 = m(\text{HCl})/ [m(\text{DMEAH}^+\text{Cl}^-) + m(\text{HCl})]$.

m_2 (mol kg^{-1})	m_3 (mol kg^{-1})	$[1 - c_p\rho/(c_{p,1}^*\rho_1^*)] \times 10^3$	$C_{p,\phi}^{exptl}$ (J K^{-1} mol^{-1})	$F_3 \times C_{p,\phi,3}$ (J K^{-1} mol^{-1})	$C_{p,\phi,2}$ (J K^{-1} mol^{-1})
T = 283.15 K					
0.0510	0.00051	3.9165	119.18	–1.39	121.8
0.1024	0.00102	7.7861	122.45	–1.39	125.1
0.1500	0.00150	11.3150	124.09	–1.28	126.5
0.2015	0.00201	15.0335	125.25	–1.36	127.9
0.2493	0.00249	18.4292	127.58	–1.34	130.2
0.2981	0.00298	22.0066	126.06	–1.33	128.7
0.3999	0.00399	28.8997	130.06	–1.37	132.7
0.4996	0.00499	35.5634	132.16	–1.29	134.8
0.6635	0.00663	46.2088	134.07	–1.26	136.7
0.7949	0.00794	53.7590	140.34	–1.20	142.9
T = 298.15 K					
0.0510	0.00051	3.5287	156.12	–1.17	158.8
0.1024	0.00102	7.0056	159.45	–1.16	162.2
0.1500	0.00150	10.2517	158.54	–1.07	161.1
0.2015	0.00201	13.6541	159.28	–1.13	162.0
0.2493	0.00249	16.7467	160.27	–1.12	163.0
0.2981	0.00298	19.9610	159.79	–1.11	162.5
0.3999	0.00399	26.3082	162.47	–1.09	165.2
0.4996	0.00499	32.3887	163.99	–1.08	166.7
0.6635	0.00663	41.9185	166.81	–1.06	169.6
0.7949	0.00794	48.8392	172.02	–1.02	174.7
T = 313.15 K					
0.0510	0.00051	3.3414	175.62	–1.05	178.4
0.1024	0.00102	6.6278	178.22	–1.04	181.0
0.1500	0.00150	9.5661	179.08	–0.96	181.7
0.2015	0.00201	12.7983	179.14	–1.01	182.0
0.2493	0.00249	15.8242	178.65	–1.00	181.5
0.2981	0.00298	18.9280	177.70	–0.99	180.5
0.3999	0.00399	24.6084	182.52	–0.97	185.3
0.4996	0.00499	30.2285	184.61	–0.95	187.4
0.6635	0.00663	39.3270	185.70	–0.93	188.5
0.7949	0.00794	45.8720	190.32	–0.90	193.1
T = 328.15 K					
0.0510	0.00051	3.1829	186.34	–1.00	189.2
0.1024	0.00102	6.3348	188.35	–0.99	191.2
0.1500	0.00150	9.1709	191.30	–0.91	194.0
0.2015	0.00201	12.1465	193.54	–0.95	196.4
0.2493	0.00249	14.8714	194.16	–0.94	197.0
0.2981	0.00298	17.6409	195.15	–0.93	198.0
0.3999	0.00399	23.4949	195.02	–0.91	197.9
0.6635	0.00663	37.4651	199.09	–0.87	202.0
0.7949	0.00794	43.7047	203.42	–0.83	206.2

© 2000 NRC Canada

Table 8. Apparent molar volumes V_ϕ for aqueous *N*,*N*′-dimethylethanolammonium chloride + HCl. $F_3 = m(\mathrm{HCl})/[m(\mathrm{DMEAH^+Cl^-}) + m(\mathrm{HCl})]$.

m_2 (mol kg^{-1})	m_3 (mol kg^{-1})	$(\rho \times \rho_1^*) \times 10^3$ (g cm^{-3})	V_ϕ^{exptl} (cm^3 mol^{-1})	$F_3 \times V_{\phi,3}$ (cm^3 mol^{-1})	$V_{\phi,2}$ (cm^3 mol^{-1})
T = 283.15 K					
0.0510	0.00051	1.0170	104.91	0.17	105.76
0.1024	0.00102	1.9862	105.33	0.17	106.21
0.1500	0.00150	2.8693	105.55	0.16	106.37
0.2015	0.00201	3.8645	105.35	0.17	106.23
0.2493	0.00249	4.6989	105.59	0.17	106.47
0.2981	0.00298	5.6156	105.50	0.18	106.38
0.3999	0.00399	7.3979	105.65	0.18	106.53
0.4996	0.00499	9.0836	105.78	0.18	106.66
0.6635	0.00663	11.828	105.84	0.18	106.72
0.7949	0.00794	13.750	106.18	0.17	107.04
T = 298.15 K					
0.0510	0.00051	0.9444	106.56	0.18	107.42
0.1024	0.00102	1.8451	106.95	0.18	107.83
0.1500	0.00150	2.6803	107.05	0.17	107.88
0.2015	0.00201	3.5881	106.97	0.18	107.85
0.2493	0.00249	4.4203	106.96	0.18	107.84
0.2981	0.00298	5.2545	106.97	0.18	107.85
0.3999	0.00399	6.9122	107.13	0.18	108.02
0.4996	0.00499	8.5152	107.20	0.19	108.08
0.6635	0.00663	11.083	107.26	0.19	108.14
0.7949	0.00794	12.898	107.56	0.18	108.42
T = 313.15 K					
0.0510	0.00051	0.8870	108.13	0.18	109.00
0.1024	0.00102	1.7518	108.31	0.18	109.20
0.1500	0.00150	2.6161	107.92	0.17	108.75
0.2015	0.00201	3.4737	107.98	0.19	108.87
0.2493	0.00249	4.2345	108.16	0.19	109.05
0.2981	0.00298	5.0006	108.28	0.19	109.18
0.3999	0.00399	6.7063	108.10	0.19	108.99
0.4996	0.00499	8.2519	108.19	0.19	109.08
0.6635	0.00663	10.767	108.20	0.19	109.09
0.7949	0.00794	12.530	108.50	0.19	109.36
T = 328.15 K					
0.0510	0.00051	0.9099	108.26	0.17	109.15
0.1024	0.00102	1.7887	108.53	0.18	109.43
0.1500	0.00150	2.5647	108.87	0.17	109.72
0.2015	0.00201	3.4240	108.84	0.18	109.74
0.2493	0.00249	4.2593	108.65	0.18	109.55
0.2981	0.00298	5.0482	108.72	0.18	109.62
0.3999	0.00399	6.6329	108.90	0.19	109.80
0.6635	0.00663	10.575	109.12	0.19	110.02
0.7949	0.00794	12.323	109.39	0.18	110.26

[3] $(HOC_2H_4)_2NH(aq) + H_2O(l) \leftrightarrows (HOC_2H_4)_2NH_2^+(aq) + OH^-(aq)$

using Young's rule, (eq. [2]). The calculation for $C_{p,\phi,2}$ requires an additional term to account for the shift in the ionization constant caused by the temperature increment in the heat capacity measurement, $C_{p,\phi,2}^{rel}$, the "chemical relaxation" effect described by Mains et al. (22) and Woolly et al. (23), to yield the expression:

[4.1] $$C_{p,\phi}^{exptl} = (1 - \alpha)C_{p,\phi,2}[(HOC_2H_4)_2NH(aq)] + \alpha C_{p,\phi}((HOC_2H_4)_2NH_2Cl(aq)) + \alpha C_{p,\phi}(NaOH(aq)) - \alpha C_{p,\phi}(H_2O(l)) - \alpha C_{p,\phi}(NaCl(aq)) + C_{p,\phi,2}^{rel}$$

where

[4.2] $$C_{p,\phi,2}^{rel} = (\Delta_r \bar{H})^2\alpha(1 - \alpha) / (RT^2(2 - \alpha))$$

© 2000 NRC Canada

Fig. 1. The apparent molar heat capacities $C_{p,\phi,2}$ of diethanolamine from 283.15 to 328.15 K plotted as a function of molality. Symbols, experimental results; lines, global least-squares fit to eq. [7].

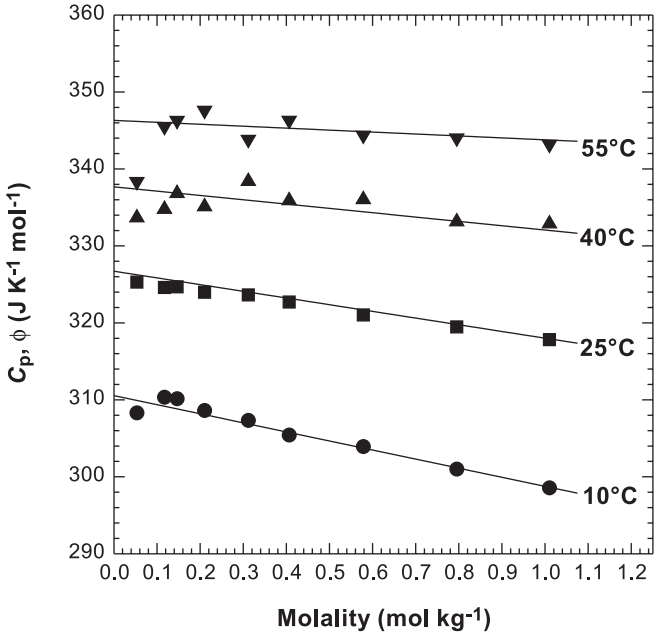
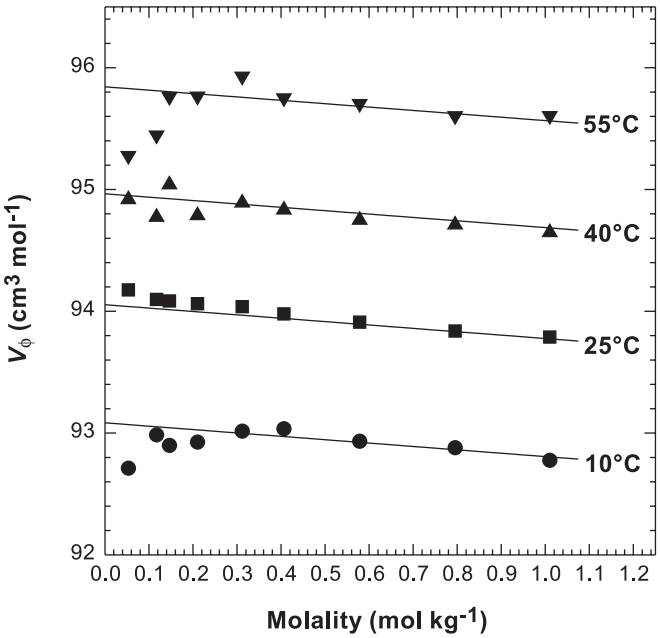
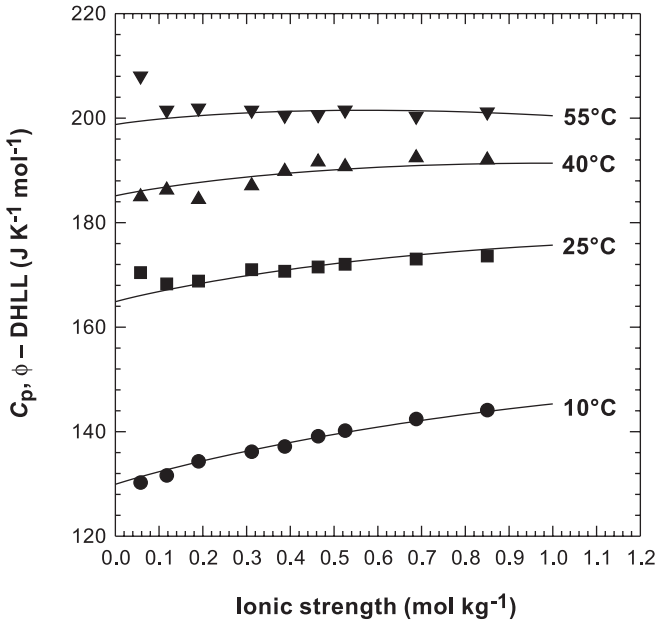


Fig. 2. The apparent molar volumes $V_{\phi,2}$ of diethanolamine from 283.15 to 328.15 K plotted as a function of molality. Symbols, experimental results; lines, global least-squares fit to eq. [8].



Here α is the fraction of stoichiometric $(HOC_2H_4)_2NH$ that is ionized and $\Delta_r\bar{H}$ represents the partial molar enthalpy of ionization of $(HOC_2H_4)_2NH$ at the molality and temperature of the $C_{p,\phi}^{exptl.}$ measurement. Eq. [4] is based on the generalized analysis by Mains et al. (22) for equilibria of the form AB ⇄ A + B. Because α is small under our experimental conditions, the partial molar properties of the minor species

Fig. 3. The apparent molar heat capacities $C_{p,\phi,2}$ of diethanolammonium chloride from 283.15 to 328.15 K plotted as a function of ionic strength I after subtracting the Debye–Hückel limiting law term. Symbols, experimental results; lines, least-squares global fit to eq. [11].



in eq. [4] were approximated by the values at infinite dilution, $Y_\phi \approx Y°$, $\Delta_r H \approx \Delta_r H°$. $\Delta_r H°$ at T = 298.15 K was taken from Jones and Arnett (1) and values for other temperatures were determined using $\Delta_r C_p^o$ at T = 298.15 K where:

$$[5]\quad \Delta_r C_p^o = C_p^o((HOC_2H_4)_2NH_2Cl(aq)) - C_p^o(Cl^-(aq)) + C_p^o(OH^-(aq)) - C_p^o((HOC_2H_4)_2NH(aq)) - C_p^o(H_2O(l))$$

$$[6]\quad \Delta_r H° = \Delta H°_{298.15} + \Delta_r C^o_{p,298.15}(T - 298.15)$$

For the purposes of this calculation $\Delta_r C_p^o$ was assumed constant over the temperature range. Values for $C_p^o((HOC_2H_4)_2NH(aq))$ and $C_p^o((HOC_2H_4)_2NH_2Cl(aq))$ were obtained from our own results. $C_p^o(H_2O(l))$ was taken from Jones and Arnett (1), and $C_p^o(Cl^-(aq))$ and $C_p^o(OH^-(aq))$ were obtained from values tabulated by Hovey et al. (17) The relaxation corrections $C_{p,\phi,2}^{rel}$ for the aqueous solutions of diethanolamine are listed in Table 1, along with the corrected values for $C_{p,\phi,2}$ (DEA (aq)). The results for $V_{\phi,2}$ and $C_{p,\phi,2}$ for DEA(aq) and $DEAH^+Cl^-(aq)$ are plotted in Figs. 1–4.

Identical procedures were used to analyse the data for *N*,*N*′-dimethylethanolamine and *N*,*N*′-dimethylethanolammonium chloride except that the excess of HCl(aq) in the solutions of the chloride was much lower. The results are found in Tables 5–8 and plotted in Figs. 5–8.

Data Treatment

The apparent molar properties of both amines could be closely described over the temperature range of 283.15 ≤ T ≤ 328.15 K using the following equations:

© 2000 NRC Canada

Fig. 4. The apparent molar volumes $V_{\phi,2}$ of diethanolammonium chloride from 283.15 to 328.15 K plotted as a function of ionic strength I after subtracting the Debye–Hückel limiting law term. Symbols, experimental results; lines, least-squares global fit to eq. [12].

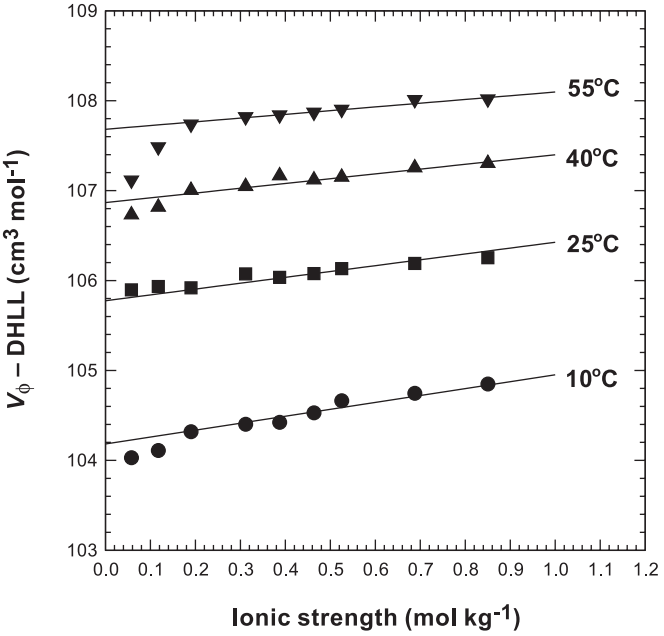


Fig. 5. The apparent molar heat capacities $C_{p,\phi,2}$ of *N*,*N*′-dimethylethanolamine from 283.15 to 328.15 K plotted as a function of molality. Solid symbols, experimental results; lines, global least-squares fit to eq. [8]; hollow symbols, Cobble and Turner (8).

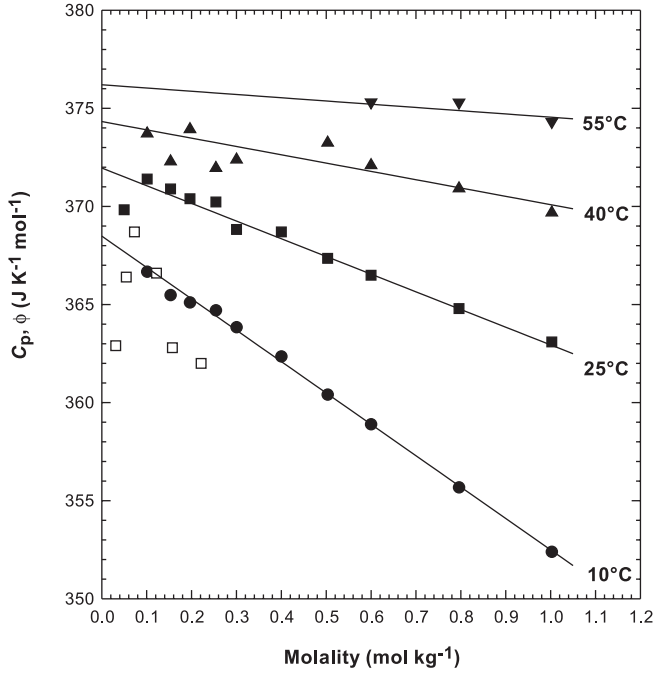


Fig. 6. The apparent molar volumes $V_{\phi,2}$ of *N*,*N*′-dimethylethanolamine from 283.15 to 328.15 K plotted as a function of molality. Solid symbols, experimental results; lines, global least-squares fit to eq. [9]; hollow symbols, from Zhang et al. (6) (corrected for the ionization of DMEA).

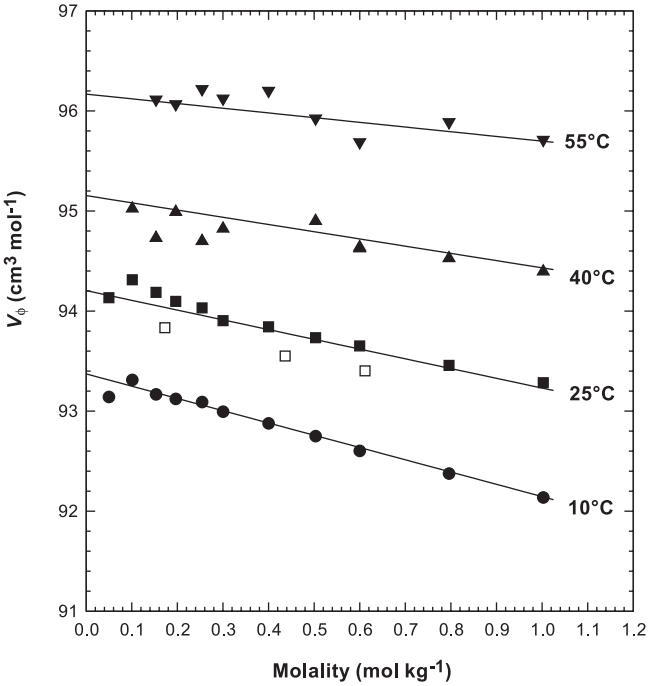
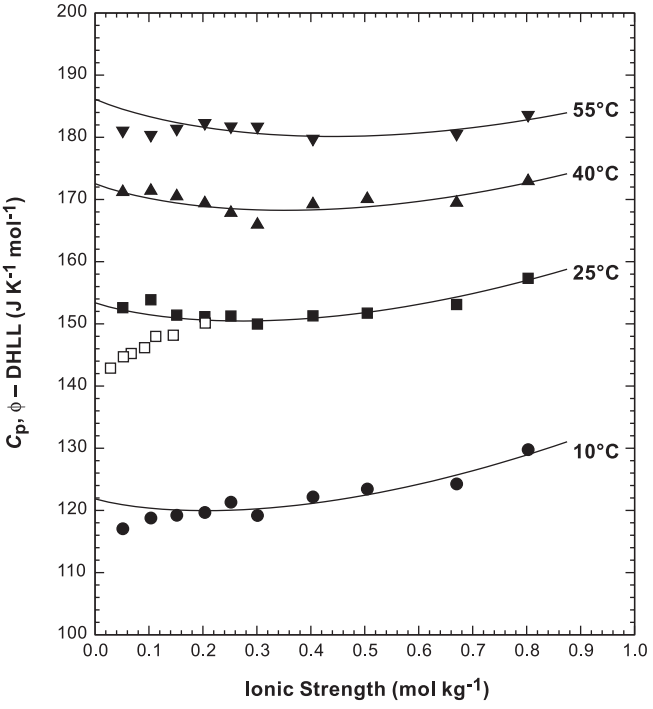
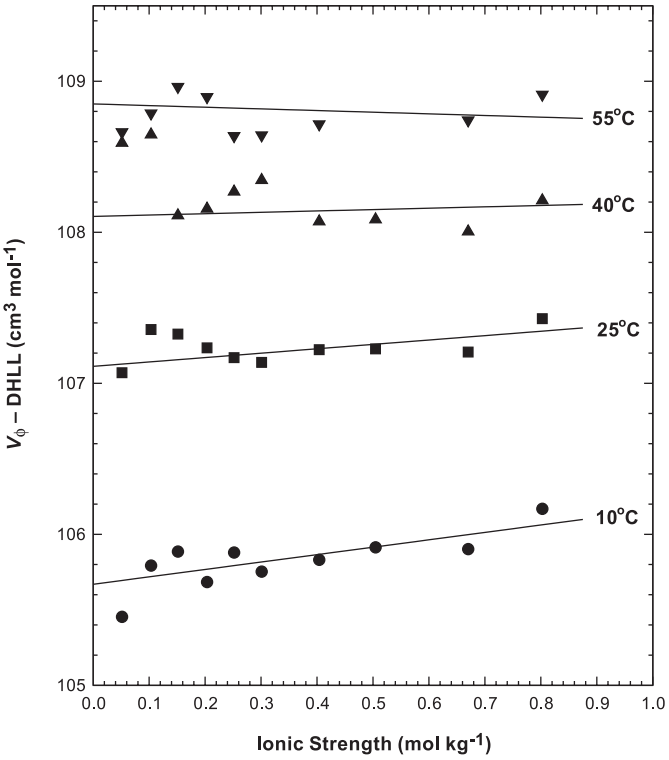


Fig. 7. The apparent molar heat capacities $C_{p,\phi,2}$ of *N*,*N*′-dimethylethanolammonium chloride from 283.15 to 328.15 K plotted as a function of ionic strength I after subtracting the Debye–Hückel limiting law term. Solid symbols, experimental results; lines, least-squares global fit to eq. [12]; hollow symbols, Cobble and Turner (8).



© 2000 NRC Canada

Fig. 8. The apparent molar volumes $V_{\phi,2}$ of *N*,*N*′-dimethylethanolammonium chloride from 283.15 to 328.15 K plotted as a function of ionic strength *I* after subtracting the Debye–Hückel limiting law term. Symbols, experimental results; lines, least-squares global fit to eq. [13].



$$[7] \quad C_{p,\phi,2} = C^{o}_{p,\phi,2} + (c_4 + c_5T)m + (c_6)m^2$$

$$[8] \quad V_{\phi,2} = V^{o}_{\phi,2} + (v_4 + v_5T)m$$

$$[9] \quad C^{o}_{p,\phi,2} = c_1 + c_2T + c_3 / (T - \Theta)^2$$

$$[10] \quad V^{o}_{\phi,2} = v_1 + v_2T + v_3 / (T - \Theta)$$

Here, the terms c_i and v_i are species-dependent fitting coefficients, and $\Theta = 228$ K is a solvent-dependent parameter associated with the anomalous behaviour of super-cooled water (24).

The functional dependence of the apparent molar heat capacities $C_{p,\phi,2}$ and volumes $V_{\phi,2}$ for the alkanolammonium salts were well represented by Debye–Hückel equations:

$$[11] \quad C_{p,\phi,2} = C^{o}_{p,2} + 1.5\omega A_c[I - 2I^{1/2} + 2 \ln (1 + I^{1/2})] / I + (c_4 + c_5T)I + (c_6)I^{3/2}$$

$$[12] \quad V_{\phi,2} = V^{o}_{2} + 1.5\omega A_v[I - 2I^{1/2} + 2 \ln (1 + I^{1/2})] / I + (v_4 + v_5T)I$$

where $I = \omega m = 1/2 \sum m_i z_i^2$, A_c in eq. [11], and A_v in eq. [12] are the Debye–Hückel limiting slopes for the heat capacity and for the volume, respectively, whose values were taken from the compilation by Archer and Wang (25).

The isothermal forms of eqs. [7–12] were fitted to the experimental results at each temperature by the Marquardt–Levenberg non-linear least-squares algorithm within the commercial software package SigmaPlot©, using weighting factors proportional to molality (9). The entire array of values at all temperatures and all molalities was then used to optimize the parameters in eqs. [7–12] in order to obtain a global fit to the data. The fitted parameters are listed in Tables 9–12, along with the overall standard deviations in $C_{p,\phi,2}$ and $V_{\phi,2}$, $\sigma_{C_p\phi}$, and $\sigma_{V\phi}$, respectively.

Table 9. Parameters for $C_{p,\phi}$ of diethanolamine and diethanolammonium chloride from global fits of eqs. [7–12].

	$C_{p,\phi}$ (J K^{-1} mol^{-1})	
Parameter	$(HOC_2H_4)_2NH$(aq)	$(HOC_2H_4)_2NH_2Cl$(aq)
c_1	238.2 ± 13.41	128.25 ± 16.07
c_2	0.3558 ± 0.0402	0.2890 ± 0.0485
c_3	–86 240 ± 6787	–243 800 ± 17 830
c_4	–70.03 ± 9.156	114.36 ± 15.44
c_5	0.2057 ± 0.0299	–0.3049 ± 0.0467
c_6	—	–12.6455 ± 6.1110
$\sigma_{Cp\phi}$	1.9	2.1

Table 10. Parameters for V_ϕ of diethanolamine and diethanolammonium chloride from global fits of eqs. [7–12].

	V_ϕ (cm^3 mol^{-1})	
Parameter	$(HOC_2H_4)_2NH$(aq)	$(HOC_2H_4)_2NH_2Cl$(aq)
v_1	78.709 ± 1.408	107.596 ± 1.254
v_2	0.0535 ± 0.003716	0.01140 ± 0.003412
v_3	–43.04 ± 20.36	–366.52 ± 17.03
v_4	–0.2775 ± 0.03587	3.0010 ± 0.7486
v_5	—	–7.88120 ± 0.002449
$\sigma_{V\phi}$	0.67	0.14

Table 11. Parameters for $C_{p,\phi,2}$ of *N*,*N*′-dimethylethanolamine and *N*,*N*′-dimethylethanolammonium chloride from global fits of eqs. [7–12].

	$C_{p,\phi,2}$ (J K^{-1} mol^{-1})	
Parameter	$(HOC_2H_4)(CH_3)_2N$(aq)	$(HOC_2H_4)(CH_3)_2NHCl$(aq)
c_1	392.76 ± 10.23	81.03 ± 16.47
c_2	–0.0346 ± 0.0303	0.3827 ± 0.0497
c_3	–47 068 ± 5365	–205 413 ± 7866
c_4	–91.350 ± 6.431	53.96 ± 15.87
c_5	0.2717 ± 0.0204	–0.2887 ± 0.0472
c_6	—	40.920 ± 6.847
$\sigma_{Cp\phi}$	0.9	1.5

Table 12. Parameters for $V_{\phi,2}$ of *N*,*N*′-dimethylethanolamine and *N*,*N*′- dimethylethanolammonium chloride from global fits of eqs. [7–12].

	$V_{\phi,2}$ (cm^3 mol^{-1})]	
Parameter	$(HOC_2H_4)(CH_3)_2N$(aq)	$(HOC_2H_4)(CH_3)_2NHCl$(aq)
v_1	69.83 ± 1.91	108.53 ± 2.461
v_2	0.07765 ± 0.00518	0.01101 ± 0.006738
v_3	85.68 ± 25.85	–329.54 ± 32.87
v_4	–5.9850 ± 0.9052	4.2656 ± 1.507
v_5	0.01681 ± 0.0030	–0.01333 ± 0.0050
$\sigma_{V\phi}$	0.11	0.17

© 2000 NRC Canada

Table 13. Standard state properties for diethanolamine and diethanolammonium chloride from 283.15 to 328.15 K from global fits of eqs. [7–12].

	$(HOC_2H_4)_2NH(aq)$		$(HOC_2H_4)_2NH_2Cl(aq)$	
T (K)	$C^o_{p,2}$ ($J\ K^{-1}\ mol^{-1}$)	V^o_2 ($cm^3\ mol^{-1}$)	$C^o_{p,2}$ ($J\ K^{-1}\ mol^{-1}$)	V^o_2 ($cm^3\ mol^{-1}$)
283.15	310.5 ± 2.0	93.08 ± 0.2	129.9 ± 2.0	104.18 ± 0.2
298.15	326.7 ± 1.2	94.06 ± 0.1	164.9 ± 2.0	105.77 ± 0.2
313.15	337.7 ± 3.0	94.96 ± 0.2	185.1 ± 4.0	106.87 ± 0.1
328.15	346.3 ± 2.0	95.84 ± 0.2	198.8 ± 4.0	107.68 ± 0.2

Table 14. Standard state properties of *N*,*N*′-dimethylethanolamine and *N*,*N*′-dimethylethanolammonium chloride from 283.15 to 328.15 K from global fits of eqs. [7–12].

	$(HOC_2H_4)(CH_3)_2N(aq)$		$(HOC_2H_4)(CH_3)_2NHCl(aq)$	
T (K)	$C^o_{p,2}$ ($J\ K^{-1}\ mol^{-1}$)	V^o_2 ($cm^3\ mol^{-1}$)	$C^o_{p,2}$ ($J\ K^{-1}\ mol^{-1}$)	V^o_2 ($cm^3\ mol^{-1}$)
283.15	367.5 ± 1.0	93.37 ± 0.2	121.9 ± 3.0	105.67 ± 0.2
298.15	372.9 ± 1.7	94.20 ± 0.2	153.4 ± 2.5	107.11 ± 0.2
313.15	375.4 ± 2.0	95.15 ± 0.3	172.5 ± 3.0	108.10 ± 0.3
328.15	376.7 ± 7.0	96.17 ± 0.3	186.1 ± 4.0	108.85 ± 0.3

Fig. 9. The standard partial molar heat capacities $C^o_{p,2}$ obtained from isothermal fitting at each temperature. ●, DMEA(aq); ■, DEA(aq); lines, global fits to eq. [9].

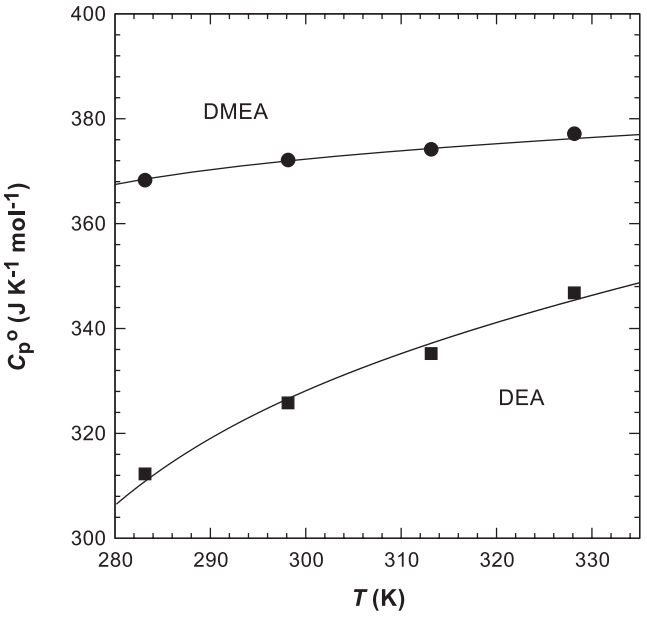
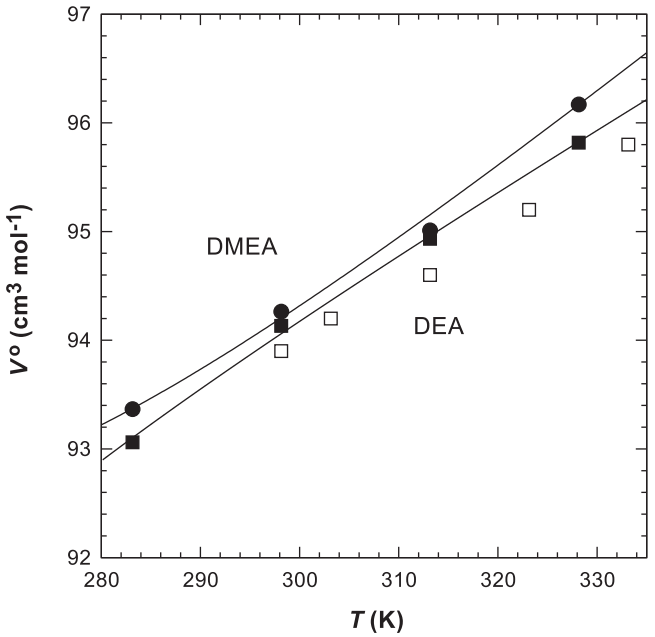


Fig. 10. The standard partial molar volumes V^o_2 obtained from isothermal fitting at each temperature. ●, DMEA(aq); ■, DEA(aq); □, DEA(aq) from Maham et al. (5); lines, global fits to eq. [10].



Discussion

The molality dependence of the apparent molar properties was found to be represented well by the treatment described above, as illustrated in Figs. 1–8. Values for the standard partial molar heat capacities and volumes from the global fit are tabulated in Tables 13 and 14 and plotted in Figs. 9–12. Data for the apparent molar volumes of diethanolamine at 298.15 K reported by Maham et al. (5), which are included in Fig. 10, agree with our results to within the combined experimental uncertainties. Values of the ionic properties of $C^o_p(DEAH^+(aq))$ and $V°(DEAH^+(aq))$, found in Table 15, were calculated on the conventional scale, $Y°(H^+(aq)) \equiv 0$, using expressions for $C^o_p(Cl^-(aq))$ and $V°(Cl^-(aq))$ taken from Hovey et al. (17). These are based on measurements on HCl(aq) by Tremaine et al. (21), Allred and Woolley (26), and Herrington et al. (27), and are consistent with recent measurements on $LaCl_3(aq)$ and $La(ClO_4(aq))$ by Tremaine and Xiao (28). The uncertainty limits in Tables 14 and 15 are estimates of *relative* accuracy, based on the 90% confidence lim-

© 2000 NRC Canada

Fig. 11. The standard partial molar heat capacities $C^{o}_{p,2}$ obtained from isothermal fitting at each temperature. ●, $DMEAH^{+}Cl^{-}$(aq); ■, $DEAH^{+}Cl^{-}$(aq); lines, global fits to eq. [9].

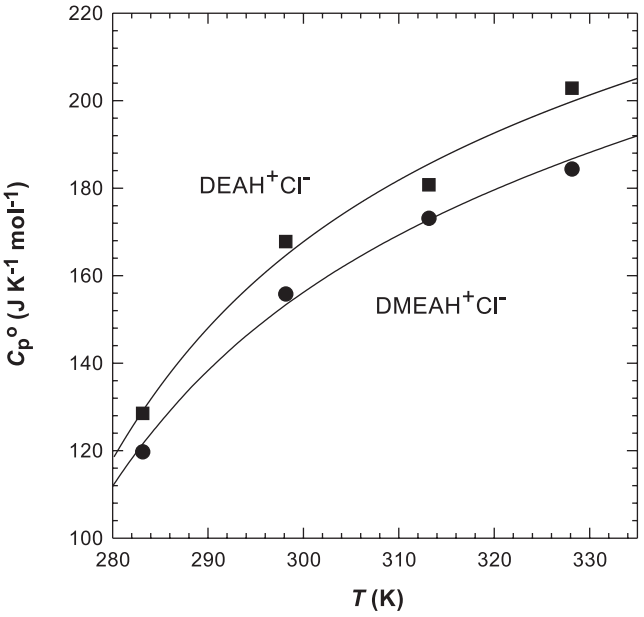


Fig. 12. The standard partial molar volumes V^{o}_{2} obtained from isothermal fitting at each temperature. ●, $DMEAH^{+}Cl^{-}$(aq); ■, $DEAH^{+}Cl^{-}$(aq); lines, global fits to eq. [10].

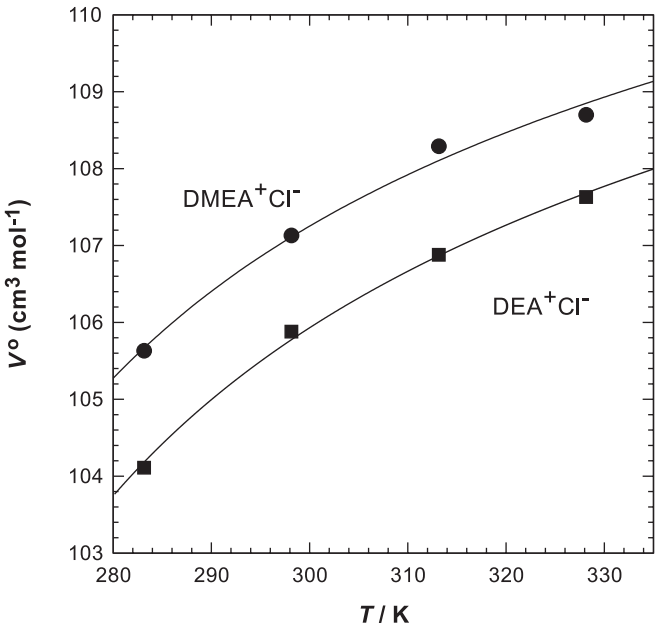


Table 15. Standard partial molar volumes and heat capacities of the diethanolammonium and *N,N′*-dimethylethanolammonium ions on the conventional scale, $Y°(H^{+}(aq)) = 0$.

	Cl^{-}(aq)		$(HOC_2H_4)_2NH_2^{+}$(aq)		$HOC_2H_4(CH_3)_2NH^{+}$(aq)	
	$C^{o}_{p,2}$	V^{o}_{2}	$C^{o}_{p,2}$	V^{o}_{2}	$C^{o}_{p,2}$	V^{o}_{2}
T (K)	(J K^{-1} mol^{-1})	(cm^3 mol^{-1})	(J K^{-1} mol^{-1})	(cm^3 mol^{-1})	(J K^{-1} mol^{-1})	(cm^3 mol^{-1})
283.15	–149.5	17.15	279 ± 2	87.0 ± 0.2	271 ± 3	88.5 ± 0.2
298.15	–126.2	17.80	291 ± 2	88.0 ± 0.2	280 ± 2	89.3 ± 0.2
313.15	–114.8	17.97	300 ± 4	88.9 ± 0.1	287 ± 2	90.1 ± 0.3
328.15	–110.2	17.74	310 ± 4	89.9 ± 0.2	296 ± 3	91.1 ± 0.3

its from the isothermal fits, the difference in standard state properties from the isothermal and global fits, and the performance of the equipment as the measurements were made. Further uncertainties in the *absolute* accuracy due to systematic errors in sample purity and calibration are estimated to be no more than ±1 J K^{-1} mol^{-1} and ±0.1 cm^3 mol^{-1}.

Aqueous diethanolamine is heavily hydrogen bonded and it is interesting to compare the experimental results at 298.15 K to those predicted by group additivity models, such as those developed by Guthrie (29), Perron and Desnoyers (30), and Cabani et al. (31). The predicted values for standard partial molar volumes from (29), $V°$(DEA(aq)) = 94.0 cm^3 mol^{-1}, and $V°(DEAH^{+}Cl^{-}(aq))$ = 107.5 cm^3 mol^{-1} are in excellent agreement with the experimental results in Table 13, 94 cm^3 mol^{-1} and 105.8 cm^3 mol^{-1} respectively. Ref. (30) does not have a value for the >NH or $>NH_2Cl$ groups, however Guthrie has reported values for C^{o}_{p}(>NH(aq)) that yield C^{o}_{p}(DEA(aq)) = 312 J K^{-1} mol^{-1}. This compares rather poorly to the experimental value C^{o}_{p}(DEA(aq)) = 327 J K^{-1} mol^{-1}. Applying the model to our earlier data on dimethylamine (DMA) (10), also yields a significant disagreement but of the opposite sign (292 J K^{-1} mol^{-1} vs. the experimental value of 260 J K^{-1} mol^{-1}). Similarly, it was not possible to chose a value for $>NH_2Cl$ group that gave agreement with the experimental results for the salts, $C^{o}_{p}(DEAH^{+}Cl^{-}(aq))$ = 165 J K^{-1} mol^{-1} and $C^{o}_{p}((CH_3)_2NH_2Cl(aq)$ = 104 J K^{-1} mol^{-1} to better than ±50 J K^{-1} mol^{-1}. The results from the group additivity model developed by Cabani et al. (31) are similar. The calculated values of C^{o}_{p} and $V°$ for DEA(aq), DMEA(aq), and dimethylamine are too positive by ~ 50 J K^{-1} mol^{-1}, and ~2 cm^3 mol^{-1} respectively. The sign of the deviation is consistent with the deviation reported by Cabani et al. (31) for bifunctional alkanolamines. Many authors have shown that C^{o}_{p} is sensitive to secondary solvation effects, while $V°$ primarily reflects the intrinsic volume of the solute molecule and effects in the primary solvation sphere. These results strongly suggest that the proximity to the hydrogen bonded amine or ammonium group acts by perturbing the secondary solvation sphere about the nearby alkyl or alkanol substituent.

© 2000 NRC Canada

Acknowledgements

This research was financially supported by the Natural Sciences and Engineering Research Council of Canada (NSERC). We are grateful to Mr. Rodney Clarke and Mr. Wei Xie for much assistance and helpful discussion while the measurements were in progress.

References

1. F.M. Jones and E.M. Arnett. Prog. Phys. Org. Chem. **11**, 263 (1974).
2. J.L. Oscarson, G. Wu, R.M. Faux, R.M. Izatt, and J.J. Christensen. Thermochim. Acta, **157**, 119 (1989).
3. J.M. Antelo, F. Arca, J. Casado, M. Sastre, and A. Varela. J. Chem. Eng. Data, **29**, 10 (1989).
4. E.B. Rinker, D.W. Oelschlager, A.T. Colussi, K.R. Henry, and O.C. Sandall. J. Chem. Eng. Data, **39**, 392 (1994).
5. Y. Maham, T.T. Teng, L.G. Hepler, and A.E. Mather. J. Solution Chem. **2**, 195 (1994).
6. F.Q. Zhang, H.P. Li, M. Dai, and J.P. Zhao. Thermochim. Acta, **254**, 347 (1995).
7. Y. Maham, L.G. Hepler, A.E. Mather, A.W. Hakin, and R.A. Marriott. J. Chem. Soc. Faraday Trans. **93**, 1747 (1997).
8. J.W. Cobble and P.J. Turner. Electric Power Research Institute Report NP-4209, 1985.
9. P.R. Tremaine, D. Shvedov, and C. Xiao. J. Phys. Chem. **101**, 409 (1997).
10. D. Shvedov and P.R. Tremaine. J. Solution Chem. **26**, 1113 (1997).
11. P. Picker, P.A. Leduc, R.R. Philip, and J.E. Desnoyers. J. Chem. Thermodyn. **3**, 631 (1971).
12. P. Picker, E. Tremblay, and C. Jolicoeur. J. Solution Chem. **3**, 377 (1974).
13. P.G. Hill.. J. Phys. Chem. Ref. Data, **19**, 1233 (1990).
14. D.G. Archer. J. Phys. Chem. Ref. Data, **21**, 793 (1992).
15. E. Desnoyers, C. de Visser, G. Perron, and P. Picker. J. Solution Chem. **5**, 605 (1976).
16. J.K. Hovey and P.R. Tremaine. Geochim. Cosmochim. Acta, **50**, 453 (1986).
17. J.K. Hovey, L.G. Hepler, and P.R. Tremaine. J. Phys. Chem. **92**, 1323 (1988).
18. P.J. Reilly and R.H. Wood. J. Phys. Chem. **73**, 4292 (1969).
19. T.F. Young and M.B. Smith. J. Phys. Chem. **58**, 716 (1954).
20. J.P. Hershey, R. Damesceno, and F.J. Millero. J. Solution Chem. **13**, 825 (1984).
21. P.R. Tremaine, K. Sway, and J.A. Barbero. J. Solution Chem. **15**, 1 (1986).
22. G.J. Mains, J.W. Larson, and L.G. Hepler. J. Phys. Chem. **88**, 1257 (1984).
23. E.M. Woolley and L.G. Hepler. Can. J. Chem. **55**, 158 (1977).
24. C.A. Angell. *In* Water: a comprehensive treatise. Vol. 7. *Edited by* F. Franks. Plenum Press, New York. 1982.
25. D.G. Archer and P. Wang. J. Phys. Chem. Ref. Data, **19**, 371 (1990).
26. G.C. Allred and E.M. Woolley. J. Chem. Thermodyn. **13**, 147 (1981).
27. T.M. Herrington, A.D. Pethybridge, and M.G. Roffey. J. Chem. Eng. Data, **30**, 264 (1985).
28. C. Xiao and P.R. Tremaine. J. Chem. Thermodyn. **28**, 43 (1996).
29. J.P. Guthrie. Can. J. Chem. **55**, 370 (1977).
30. G. Perron and J.E. Desnoyers. Fluid Phase Equilib. **2**, 239 (1979).
31. S. Cabani, P. Gianni, V. Mollica, and L. Lepori. J. Solution Chem. **10**, 563 (1981).

© 2000 NRC Canada

1999 Alfred Bader Award Lecture From early developments in multi-step organic synthesis on solid phases to multi-nuclear phthalocyanines[1]

Clifford C. Leznoff

Abstract: Early developments in solid phase organic synthesis are traced. Particular emphasis is placed on the use of cross-linked polystyrene in the first general method of monoblocking symmetrical difunctional compounds. The monoprotected polymer-bound symmetrical starting materials were then used in multi-step syntheses of a variety of compounds, particularly insect pheromones. Asymmetric synthesis on polymer supports was demonstrated. Diels–Alder and 1,3-dipolar additions on polymer supports proceeded readily as did macrocyclic formation of porphyrins and phthalocyanines. All of these reactions clearly showed that most organic chemical reactions could be performed on solid phases and laid the basis for the development of combinatorial chemistry. The first unsymmetrical phthalocyanine was prepared using the solid phase method and this led eventually to solution phase methods of preparing bi-, tri-, tetra-, and even a dendritic-like pentanuclear phthalocyanine.

Key Words: solid phase organic synthesis (SPOS), phthalocyanines.

Résumé : On retrace les développements de la synthèse organique en phase solide. On insiste sur l'utilisation du polystyrène réticulé dans la première méthode générale de bloquer une seule des deux fonctions de composés bifonctionnels symétriques. Les produits de départ symétriques reliés par une seule liaison à un polymère étaient ensuite utilisés dans des synthèses en plusieurs étapes d'une grande variété de composés, en particulier des phéromones d'insectes. La possibilité de réaliser des synthèses asymétriques sur des polymères solides a été démontrée. On a aussi montré que, sur des supports solides, on peut effectuer facilement des additions de Diels–Alder et des additions 1,3-dipolaires ainsi que la formation de macrocycles, comme les porphyrines et les phtalocyanines. Toutes ces réactions ont clairement démontré que la plupart des réactions organiques peuvent être réalisées en phases solides et ont servi de base au développement de la chimie combinatoire. La première phtalocyanine non symétrique a été préparée en faisant appel à la phase solide et ceci a conduit aux préparations, par des méthodes de phase en solution, de bi-, tri-, tétra- et même d'une phtalocyanine pentanucléaire de nature dendritique.

Mots clés : synthèse organique en phase solide (SOPS), phtalocyanines.

[Traduit par la Rédaction]

Introduction

Organic chemists have long been wedded to the practice of performing chemical reactions in homogeneous media. Hence, the idea that organic reactions could be performed on insoluble polymer supports was indeed revolutionary (1, 2). This concept was initially applied to solid phase synthesis of polypeptides (1, 3), polynucleotides (4–6), and later polysaccharides (7). These topics have been reviewed often (8–10). The general advantage of organic synthesis on insoluble polymer supports (usually cross-linked polystyrene) is particularly favourable for repetitive synthesis of like units such as the sequential addition of amino acids to a polymer support. Thus, polypeptides can be prepared on solid phases, whereby the only mechanical operations involved are stirring (or shaking), filtration, and washing. In some respects, these repetitive syntheses are easy in that only a very few different reactions at room temperature are required. It is so easy, in fact, that the process was automated even using pre-computer technology (11). Even so, difficulties abounded; however, multiple parallel synthesis of polypeptides using computer-controlled robotic systems is now routine (12, 13).

During this era, reagents attached to insoluble polymer supports, useful for organic synthesis, were developed. The work of Patchornik's group (14, 15) on the use of reagents for polypeptide synthesis was noteworthy. Polymer-bound reagents (15, 16) and catalysts (16, 17) in which the organic reagent or catalyst is bound to the polymer (with the organic substrate always remaining in solution) has found its place in many applications but is beyond the scope of this article.

Received December 18, 1999.

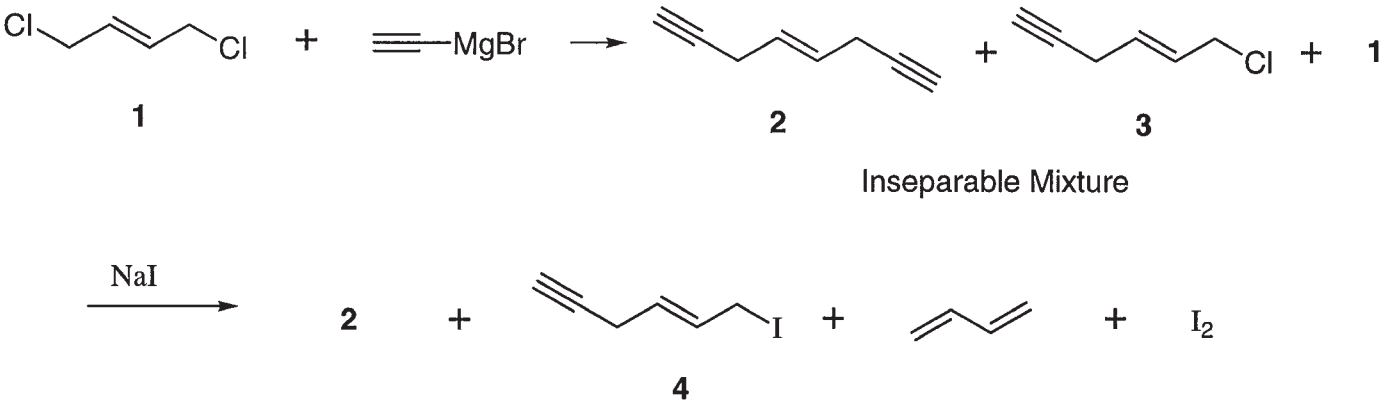
C.C. Leznoff.[2] Department of Chemistry, York University, Toronto, ON M3J 1P3, Canada.

[1]This paper is based on the Alfred Bader Award lecture presented May 30, 1999 by Professor Leznoff at the 82nd Annual Conference of the Canadian Society for Chemistry, Toronto, Ontario.

[2]Telephone: (416) 736-2100 ext. 33838. Fax: (416) 736-5936. e-mail: leznoff@yorku.ca

© 2000 NRC Canada

Scheme 1.



A post-doctoral fellowship in Letsinger's laboratory (2, 4) in 1964 piqued my curiosity to the possibility of using polymer supports in organic synthesis. Coincidentally, during our research project on the synthesis of annulenes in another post-doctoral sojourn in Sondheimer's group (18), we were faced with the problem of reacting *trans*-1,4-dichloro-2-butene (**1**) with ethynyl magnesium bromide. Invariably, an inseparable mixture of **1**, the bis reacted product *trans*-4-octen-1,7-diyne (**2**) and the desired *trans*-6-chloro-4-hexen-1-yne (**3**) was obtained. These compounds had very similar boiling points and they could not be separated by distillation. Ultimately, conversion of the mixture of **1–3** with NaI led to I_2, butadiene, **2**, and *trans*-6-iodo-4-hexen-1-yne (**4**) which was separable by distillation (Scheme 1). This problem led to the germination of an idea that insoluble polymer supports could be an advantage in addressing the whole concept of monoreactions of symmetrically difunctionalized organic compounds.

Insoluble polymers supports as blocking groups of symmetrically disubstituted compounds

Solid phase organic synthesis (SPOS) usually refers to general organic synthesis on polymer-supports, outside the repetitive syntheses of polypeptides, polynucleotides, and polysaccharides. The synthesis of a threaded rotaxane in 1967 (19) on a polymer support probably represents the first example of SPOS. Our own early efforts focussed on the use of polymer supports as monoblocking agents of completely symmetrical difunctional compounds. Monoreactions of reagents such as acetyl chloride with a compound such as 1,10-decanediol (**5**) in a 1:1 ratio would give 25% of the bis reacted product, 50% of the desired monoreacted product, and 25% of unreacted starting material. A large excess of (**5**), for example, would give mainly the desired monoreacted product and unreacted starting material but separating the minor product (the monoreacted product) from a sea of unreacted starting material could be difficult. This separation could be readily achieved, however, by simple filtration if the monoreacted product remained attached to an insoluble polymer and "fished out" of the excess starting material which could be recovered. The process would be particularly important for the longer chain symmetrical difunctional compounds such as **5**, as short chain monoreaction products of say ethylene glycol could be achieved by other methods such as ring opening reactions of ethylene oxide. Thus treatment of polymer-bound[3] phenylacetylchloride (**6**) (20) with a large excess of symmetrical diols (**5,** n = 2, 4, 6, 8, 10) gave the polymer-bound monoprotected diols (**7**). Subsequent reaction of **7** with chlorotriphenylmethane (TrCl) or dihydropyran (dhp) gave polymer-protected monoether **8**. Cleavage of **8** with NH_4OH gave polymer-bound phenylacetic acid (**9**) and the liberated monoprotected ethers of the symmetrical diols (**10**) (21, 22) (Scheme 2). Recovered **9** was converted back to **6** but the synthesis of **10** (n = 10) on once used **9** gave **10** in lower yield.

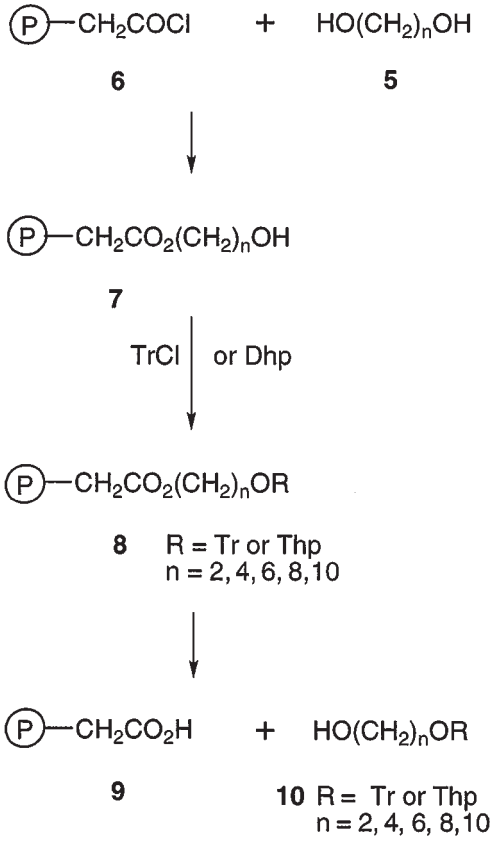
In order to obtain a more recyclable polymer, a polymer-bound trityl chloride[3] (**11**) was prepared by our direct lithiation method (23, 24). Treatment of **11** with symmetrical diols (**5**, n = 4, 7, 10) gave the polymer-bound monotrityl ether **12**. Acetylation gave the polymer-bound monotrityl monoacetates (**13**) which on acid cleavage gave polymer-bound trityl alcohol (**14**) and the desired symmetrical diol monoacetates (**15**) (23, 24) (Scheme 3). Polymer **14** was readily recyclable to give products in undiminished yield from used **14**.

The successful monoprotection of symmetrical diols encouraged us to explore the monoprotection of other symmetrical difunctional compounds, particularly symmetrical dialdehydes. For this purpose, a polymer-bound 1,2-diol (**16**) was developed (25). Treatment of **16** with terephthalaldehyde (**17**) gave the polymer-bound monoacetal (**18**). It should be noted that such a reaction in solution gives only bis acetal and unreacted **17** as the mono product is normally more reactive

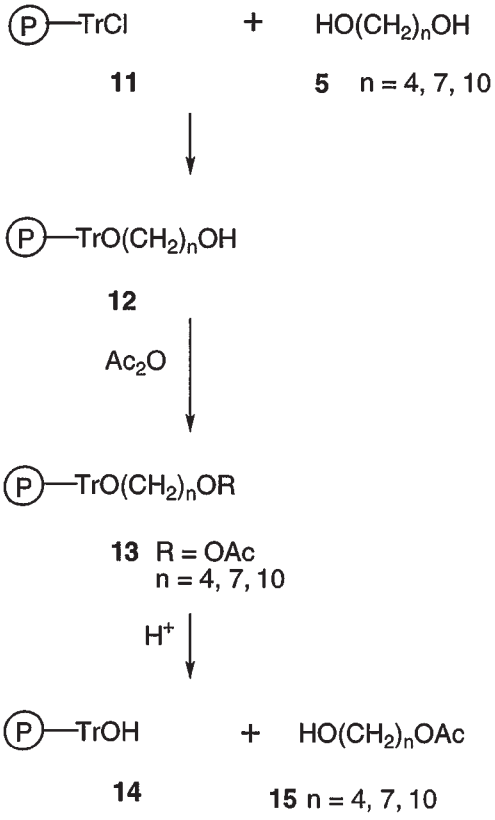
[3] The use of a ℗ used by Merrifield, Letsinger and others to represent the polymer has in recent times been replaced by a solid sphere. It is unlikely that the P could be confused for phosphate in the context used and the more currently used symbol, the solid grey or black sphere, could also be confused with current representations of solid metallic clusters, the latter use being more reasonable as the solid ball is solid like the cluster. In addition, the P can be replaced by Si for silica polymers and PEG for polyethylene glycol polymers, etc., and, hence, is more flexible. In this paper the polymer is, polystyrene, cross-linked with 1–3% divinylbenzene. In the trityl containing polymer (**11**), one phenyl group of the polymer is actually part of the trityl group.

© 2000 NRC Canada

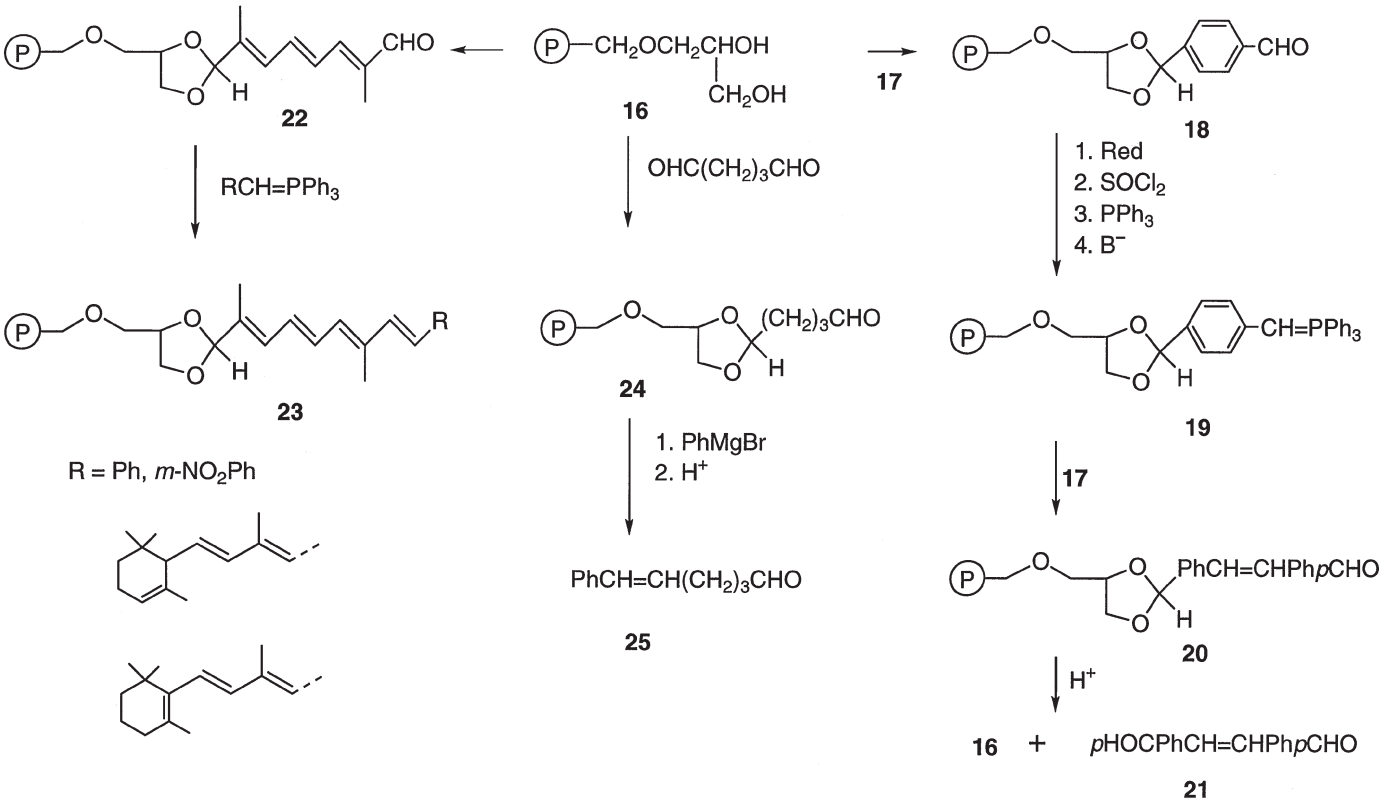
Scheme 2.



Scheme 3.

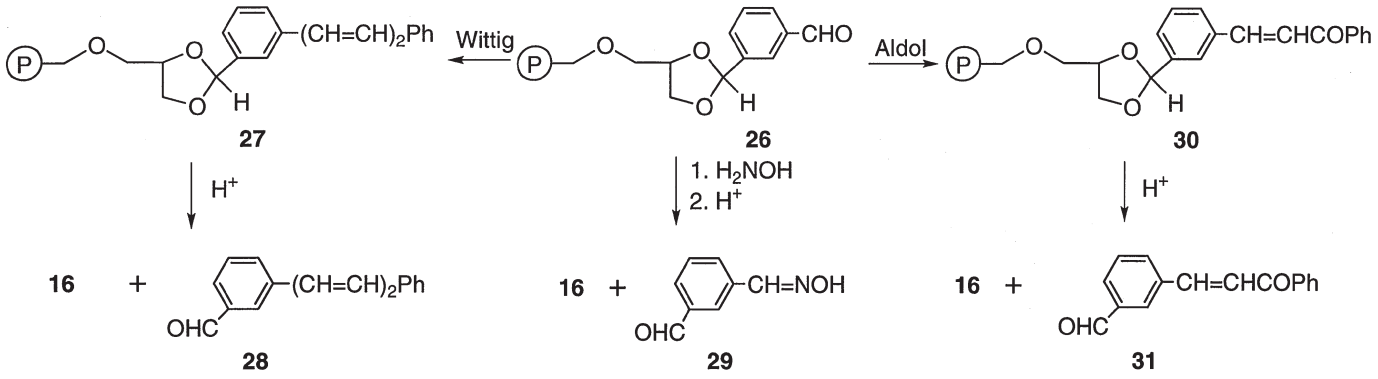


Scheme 4.

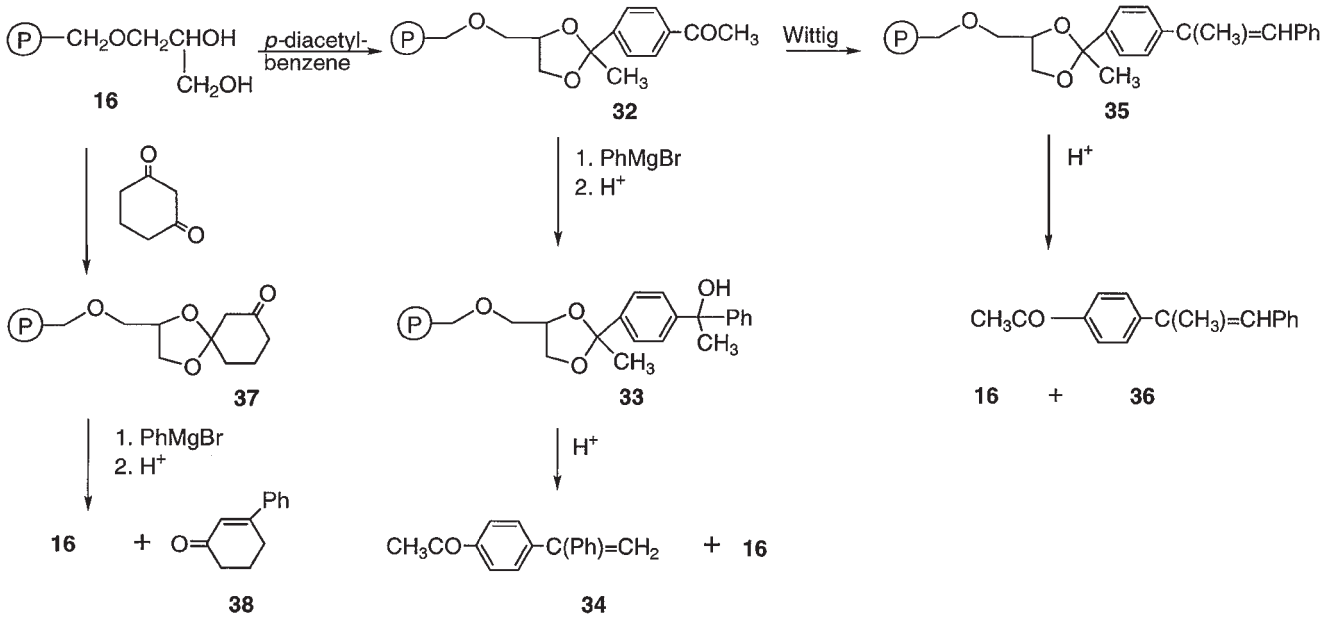


© 2000 NRC Canada

Scheme 5.



Scheme 6.



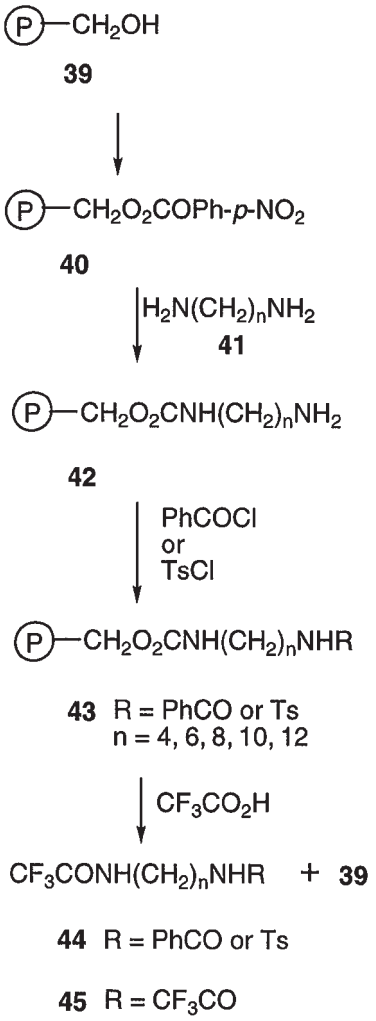
that the starting dial, containing two electron-withdrawing groups. Conversion of **18** to a polymer-bound Wittig reagent (**19**) in four steps and further reaction with symmetrical dial **17** led to polymer-bound **20**. Acid cleavage of **20** gave **16**, that could be recovered, and the symmetrical diformylstilbene (**21**) in the first multi-step (7 reactions) SPOS on polymer supports (26). Interestingly **18** was also converted to a helicene (27). A linear conjugated symmetrical dialdehyde, 2,7-dimethyl-2,4,6-octatrien-1,7-dial reacted with **16** to give the polymer-bound monoprotected **22**. The Wittig reaction of **22** gave the polymer-bound polyenes **23,** which on acid cleavage provided conjugated aldehydes, useful in carotenoid synthesis (28). Even symmetrical aliphatic dialdehydes may be monoprotected using **16** giving polymer-bound **24**, which with PhMgBr and acid cleavage, gives **25** (29) (Scheme 4). The symmetrical isophthalaldehyde can be monoprotected with **16** as well to give the polymer-bound monoblocked acetal **26**. Wittig reactions on **26** give the formyl diene **28** via polymer-bound butadiene **27**, oximation of **26** gives a polymer-bound acetal oxime which yields monooxime **29**, while an aldol condensation of **26** gives polymer-bound chalcone **30** and ultimately formyl chalcone **31** (25**)** (Scheme 5). In all cases recovered **16** is fully recyclable.

These formyl compounds **28**, **29**, and **31** and their *p*-analogs (25) are difficult to prepare in solution. Symmetrical diketones can be monoprotected with **16**. Thus, *p*-diacetylbenzene reacts with **16** to give the polymer-bound monoacetal (ketal) **32**, which with PhMgBr gives **33** and acid cleavage gives the *p*-acetylstyrene **34** (30). Alternatively, the Wittig reaction of **32** gives polymer **35** which liberates a *p*-acetylstilbene (**36**) (31). Symmetrical cyclic diketones such as 1,3-cyclohexanedione react with polymer **16** to give the monoprotected **37** which on Grignardization and acid cleavage liberates 3-phenyl-2-cylohexen-1-one (**38**) (Scheme 6). Again polymer **16** is recovered for reuse with undiminished capacity. Recently, polymer **16** has been used in palladium coupling reactions (32).

Other polymer-bound 1,2 and 1,3-diols were also used in similar reactions but the polymers were not always recyclable (33). Interestingly, the reverse of the procedures described

© 2000 NRC Canada

Scheme 7.



in Schemes 4–6 has been described recently in which a polymer-bound aldehyde has been used to monoblock symmetrical tetraols (34). Polymer-bound boronic acids have been used to selectively extract *cis*-diols from mixtures (35).

Polymer supports have been used to monoprotect symmetrical diamines. Thus, polymer-bound benzyl alcohol (**39**) on treatment with *p*-nitrophenyl chloroformate yielded the polymer-bound carbonate (**40**) which on reaction with the symmetrical diamines (**41**, n = 4, 6, 8, 10, 12) yielded the polymer-bound monoprotected carbamates (**43**). Subsequent treatment with benzoyl chloride or *p*-toluenesulfonyl chloride (TsCl) gave polymers **43**. Treatment of **43** with trifluoroacetic acid gave recyclable polymer **39**, the desired unsymmetrical amides (**44**, n = 4, 6, 8, 10, 12), and some bistrifluoroacetamide (**45**) of their respective diamines (36) (Scheme 7). The trifluoroacetamido groups of **44** are easily cleaved by mild base. Some recent examples using polymer-bound monoprotected symmetrical diamines in SPOS have been reported (37).

Symmetrical diesters, diacids, and diacid chlorides can be monoblocked most readily using diacid chlorides, which is general for both linear and aromatic diacid chlorides. Thus, polymer **39** readily reacts with a series of diacid chlorides ($ClOC(CH_2)_n$ $COCl$ (n = 2, 3, 4, 8)) to give the polymer-bound monoester mono-acid chlorides (**46**). These versatile monoblocked derivatives (**46**) may be treated with amines to give polymer-bound ester amides (**47**) which can be cleaved and esterified to the free methyl ester amides (**48**). Alternatively, **46** (n = 8) may be reduced selectively to methyl 10-hydroxydecanoic acid (**49**) (38, 39). Treatment of **46** with phenyl or butylmanganese iodide (40) gave polymers (**50**) resulting from selective addition to the acid chloride. Cleavage and methylation readily yielded **51** (41). In all cases, **39** was recovered and was recyclable. Similarly, aromatic diacid chlorides such as terephthaloyl and isophthaloyl chloride provided the ester alcohols **52** and aromatic ester amides **53** (Scheme 8). Polymer-bound monoester succinic acid was formed via succinic anlydride (42) and recently the malonic analog via Meldrum's acid (43) and other activated acids (44) were monoprotected using polymers. Only rigid diacids such as fumaric and 2-butyne-1,4-dioic acid can be reacted directly with a polymer support (45, 46) as intraresin reactions strongly interfere (47, 48).

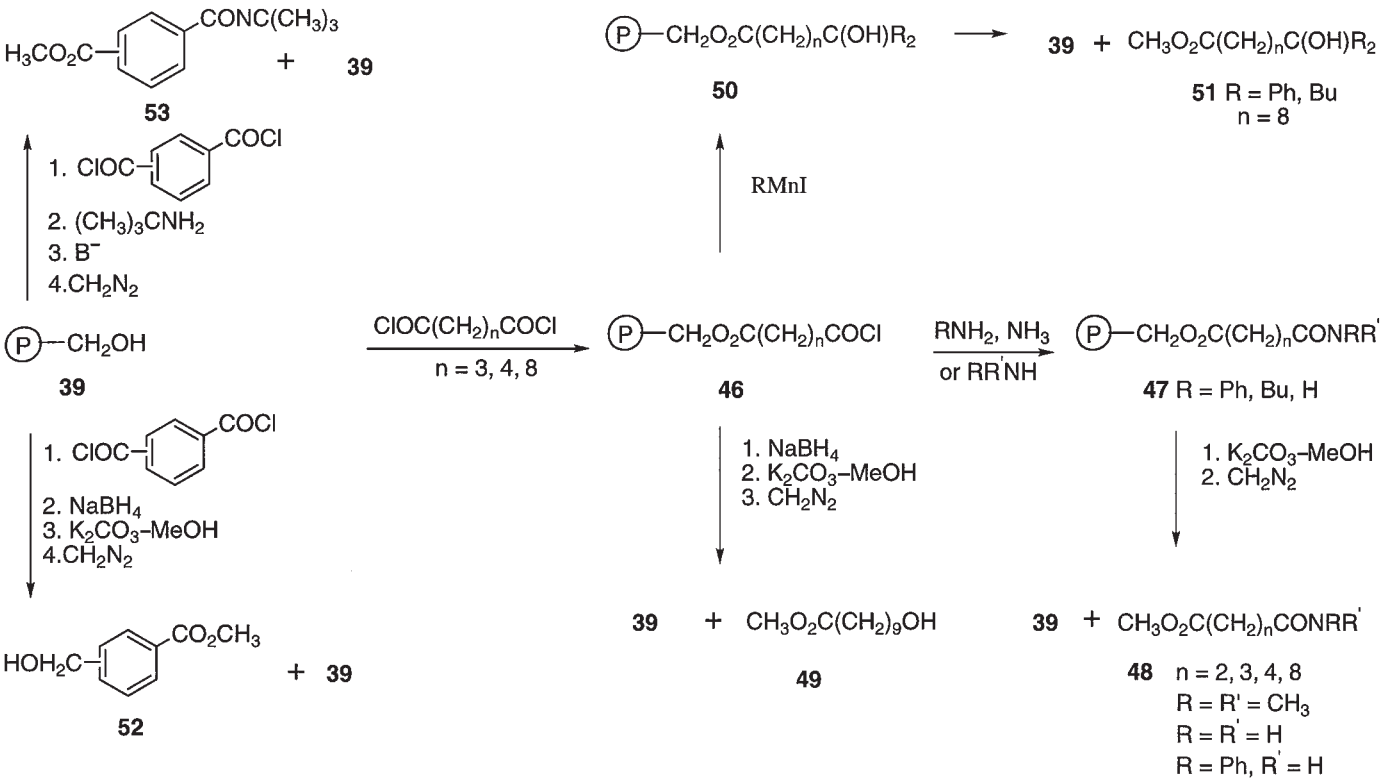
Dihydroxy aromatic compounds are also readily monoprotected using a polymer-bound benzoyl chloride (**54**). Thus, treatment of **54** with 2,7-dihydroxynaphthalene (**55**) gave the polymer-bound monoester mononaphthol (**56**), which on reaction with diazomethane and cleavage gave recovered polymer-bound benzoic acid (**57**) and 7-methoxy-2-naphthol (**58**). Simpler phenols such as resorcinol and hydroquinone also gave polymer-bound monoprotected phenols **59** which on alkylation gave **60** and cleavage yielded the *m*- or *p*-monoalkyl ethers of phenol (**61**) (50) (Scheme 9).

In all of the above examples, it is possible for the polymer support to react with both ends of the insoluble polymer support, the so called "double binding" problem. This problem has been discussed in some of the earliest reviews on SPOS (47–49) and in more recent reviews (49). Double binding can usually be diminished greatly by using a vast excess of starting symmetrical difunctional compound and indeed most of the examples listed show minimal double binding, but symmetrical diols can give up to 40% double binding and aliphatic diacids up to 100% double binding (47–50). Even when double binding occurs, it usually doesn't interfere in the reactions of SPOS but does reduce capacity. Although double binding can be eliminated by putting the polymer-bound functional group at a cross-linked position, capacity is reduced (23, 51).

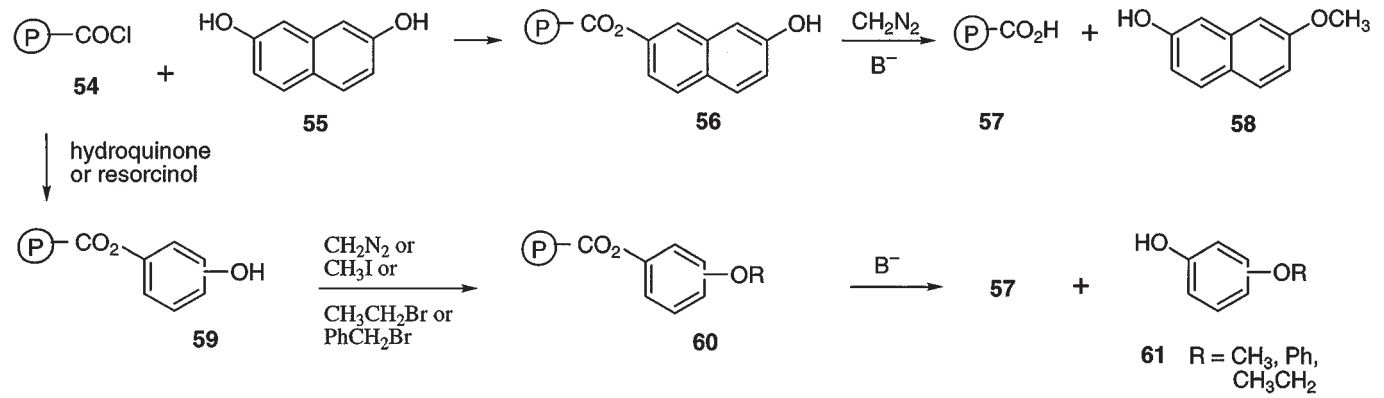
New methods of monoprotecting symmetrical difunctional compounds *in solution* have been developed, particularly with respect to diols (52–55), tetraols (56), dihydroxy-aromatic compounds (57, 58), dials (59, 60), diones (61), diamines (62–64), diesters (65, 66), diacids (67, 68), and dihalides (69, 70). Some of these methods still rely on statistical strategies using excess substrate (69, 70); others rely on specific properties of the monoprotected products such as precipitation (52*a*), solubility (54*b*), and enzymatic activity (55), while additional routes feature reactivity profiles (53), solid phase catalysis (54*c*, 65, 68), or alternative synthesis (69). All of these solution methods are, unfortunately, applicable not only to a specific symmetrical difunctional group, but to defined sub classes of that group and hence, are not general methods like the polymer support method. Despite this, specific methods are used more generally both

© 2000 NRC Canada

Scheme 8.



Scheme 9.



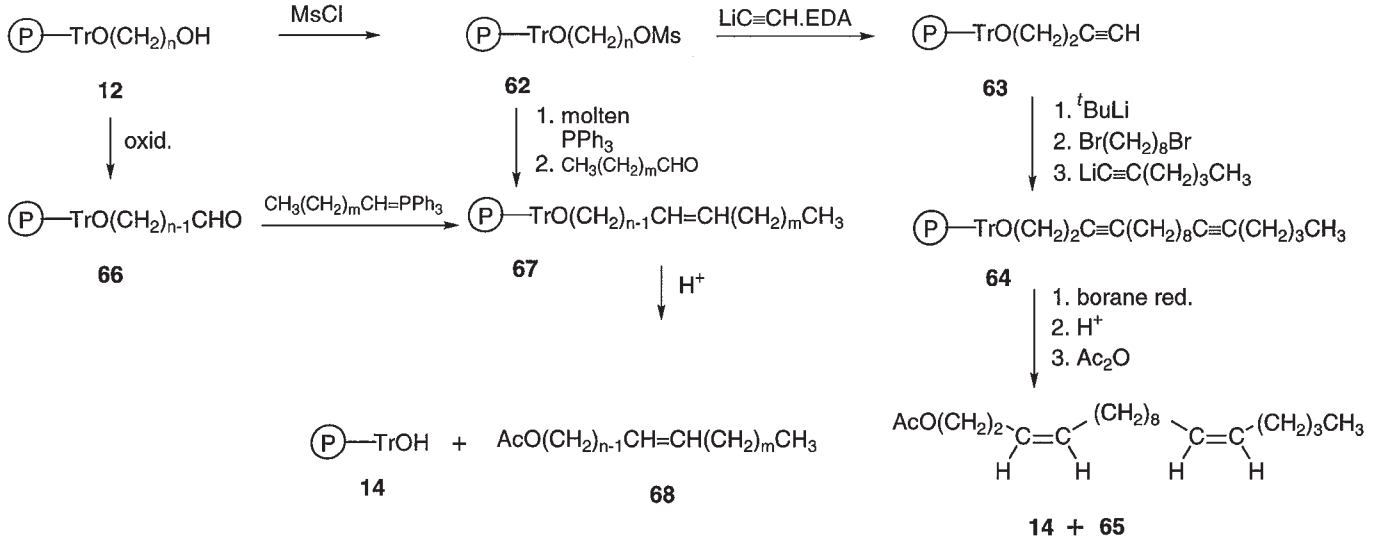
academically and industrially where a single particular difunctional compound can be monoblocked by methods peculiar to that compound. With the advent of combinatorial chemistry (71–73), it is important to have a general method of monoprotection of symmetrical substrates for elaboration into the preparation of chemistry libraries and this method is being used now in this context (37*b*, *c*).

Multi-step solid phase organic synthesis

The synthesis of polypeptides, polynucleotides, and polysaccharides all depend on the selective attachment to the polymer support of a difunctional compound containing two different functional goups. The monoblocking of symmetrical difunctional compounds, having two identical functional groups, on solid phases opened the way to using simple inexpensive materials in multi-step solid phase organic synthesis (SPOS). Although **21** (Scheme 4) was synthesized before in a multi-step synthesis, our major effort was devoted to SPOS of insect pheromones (74–80), which has been reviewed (77) previously. Three routes to insect pheromones on solid phases were paramount. Thus, polymer-bound trityl-blocked symmetrical diols (**12**) (23), were treated with mesyl chloride to yield to polymer-bound mesylate (**62**) which, in the alkyne route, reacted with lithioacetylide to

© 2000 NRC Canada

Scheme 10.



give the polymer-bound terminal alkyne (**63**, n = 2). Lithiation of **63**, followed by treatment with the symmetrical alkylating agent, 1,8-dibromooctane, gave the monoalkylated product, which was coupled with 1-lithio-1-hexyne to give the polymer-bound diyne (**64**). Although catalytic reduction of **64** with insoluble Pd or Pt catalysts was not possible, borane reduction proceeded even more easily than in solution as organoborane by-products were easily removed by simple filtration. Acid cleavage and acetylation readily gave **65**, an insect sex attractant of the lesser peach borer, *Synanthedon pictipes* (76, 77) (Scheme 10). Alternatively, polymer **12** can be oxidized with di-*tert*-butyl chromate to give the polymer protected ether aldehyde **66**. Reaction of **66** with Wittig reagents, the Wittig route, give a variety of polymer-bound insect pheromones **67**, containing up to 33% of the *E* isomer. On the other hand, in a "reverse" Wittig route, conversion of **62** with *molten* PPh_3 gave a polymer bound Wittig reagent, which on treatment with aliphatic aldehydes again gave **67** (n = 10, m = 2) with less than 9% of the *E* isomer. Acid treatment and acetylation of **67** gave recovered polymer **14** and insect attractants (**68**) (78) (Scheme 10). It is notable, in the alkyne route, that the polymer-bound synthesis uses two steps to monoreact symmetrical disubstituted substrates and a borane reduction step to such an advantage that this sequence cannot be readily performed in solution. Natural insect pheromones often contain mixtures of *E*, *Z* components so that the Wittig routes can be selected to give the desired mixture. The polymer support does affect the stereochemistry of the Wittig reactions (79). Large scale synthesis of pheromones using over 50 g of polymer supports and yielding up to 5 g of product have been reported (80). The synthesis of an insect pheromone using a polymer-bound silyl chloride and a more convenient Moffatt–Swern oxidation is interesting (81) as is the recent related polymer-supported Cadiot–Chodkiewicz coupling (82) giving conjugated unsymmetrical diynes, suitable for pheromones (82, 83).

One early example of a polymer-supported asymmetric synthesis (84) and high enantiomeric excesses (ee) achieved in solution (85) encouraged us to apply solid phases in asymmetric synthesis. Thus, Merrifield's polymer **69** reacted with the chiral blocked aminoalcohols **70** to give the polymer-bound chiral reagents **71**. Some unreacted chloro groups in **71** interfered with subsequent asymmetric synthesis, but these were converted to inactive methyl groups by treatment with NaI and reduction with tri-*n*-butyltin hydride. Deblocking with hydrazine gave the polymer-bound chiral reagents **72**. Treatment of **72** with cyclohexanone gave polymer-bound chiral imine **73** which on alkylation and cleavage gave the valuable recovered polymer-bound chiral reagent **72** and (*S*)-2-methylcylohexanone (**74**)(86). Alternatively, in the first example of an asymmetric protonation (87) on polymer supports (88), addition of racemic 2-methylcyclohexanone to **72** gave **73** which on deprotonation and asymmetric protonation gave **74** (Scheme 11). The ee of **74** was comparable to that obtained using solution methods (85). As in polypeptide syntheses, partially reacted substrates on the polymer may be carried forward and interfere in a polymer-supported multi-step synthesis and awareness of this problem (**71**→**72**) is a necessity.

Multi-step synthesis of cyclic compounds on solid phases became our next priority. Although a few Diels–Alder reactions had been performed on solid phases for mechanistic (89) or environmental purposes (89*d*), we wished to examine the effect of the polymer on regioselectivity in cycloaddition reactions (90). Thus, **69** reacted with acryloyl chloride to give polymer-bound acrylate (**75**), which on treatment with 1-phenyl-1,3-butadiene or methyl 2,4-pentadienoate gave the polymer-bound cyclohexenes **76** in good yield. Base cleavage and treatment with diazomethane gave a ratio of the *ortho* to *meta* Diels–Alders adducts **77,** similar to that achieved in solution, and hence the polymer support in this reaction did not affect the regiochemistry (Scheme 12). A polymer-bound chiral acrylate (**78**) was achieved by treatment of **69** with chiral 2-methyl-1,3-butanediol, esterification with acryloyl chloride, and blocking of unwanted primary alcohol groups with trityl chloride. Asymmetric Diels–Alder reactions of **78** using various titanium isopropoxy chlorides

© 2000 NRC Canada

gave the polymer-bound chiral cyclohexenes **79**. Reduction with $LiAlH_4$ liberated the free chiral 3-cyclohexenylmethanols **80** plus recovered polymer **39**.

In this example the polymer-bound asymmetric synthesis also yielded product having a similar ee to that achieved in solution and hence the bulk of the polymer did not aid in giving higher ee's (91). Again note that side reactions encountered in going from **69**→**78** caused difficulties in this synthesis, but it was possible to take countervailing measures (Scheme 12).

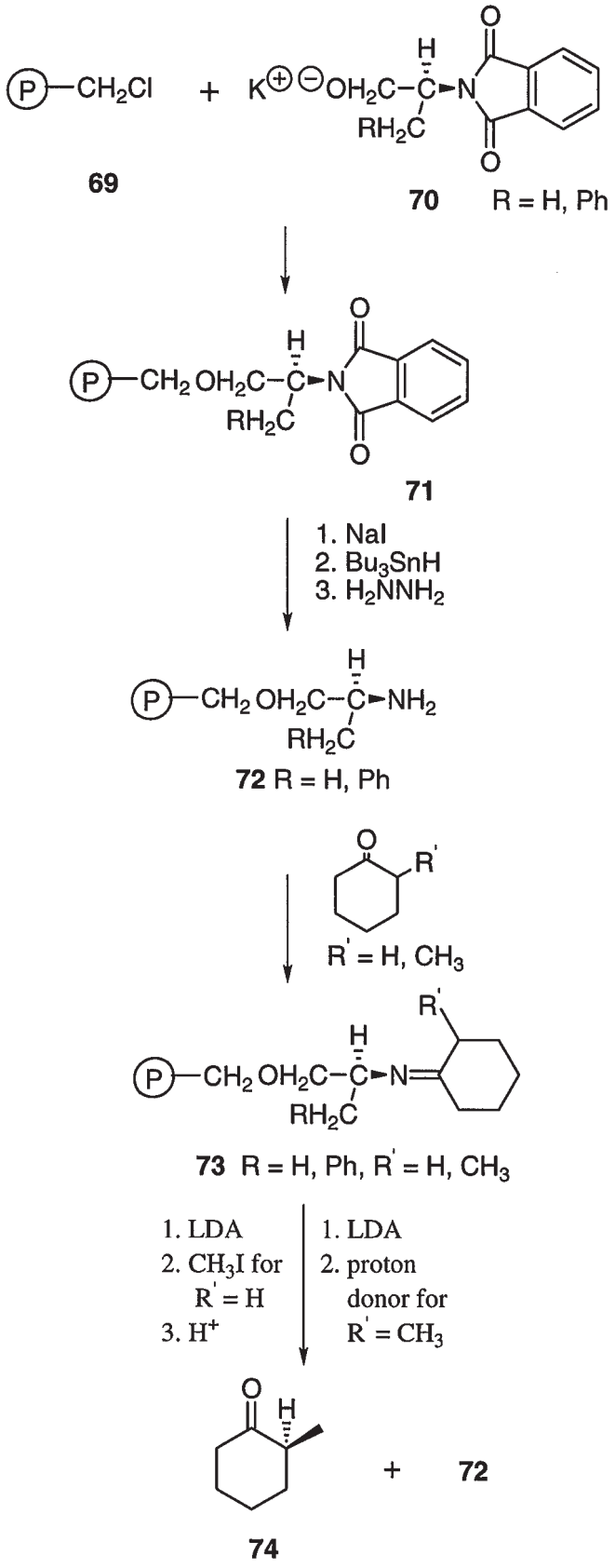
Cycloaddition of 1,3-dipolarophiles on polymer supported alkynes gave simple heterocyclic compounds. Thus, **39** was treated with propiolic acid (**81** R = H) or phenylpropiolic acid (**81** R = Ph) with an acid catalyst to give the polymer-bound alkynes **82**. The 1,3-dipolar addition (90) with benzonitrile *N*-oxide gave the polymer-bound isoxazoles **83** (from **82** R = H) and **84** (from **82** = Ph). Base cleavage of **83** and **84** and esterification with diazomethane gave the pure regioisomeric isoxazoles **85** and **86**. The regioselectivity of **86** via the solid phase method was opposite to that observed in solution and hence, polymer-supported reactions can be different than their solution analogs (92, 93) (Scheme 13).

A report on the synthesis in very low yield of an unsymmetrical tetraarylporphyrin in solution (94) led us to examine the syntheses of heterocyclic macrocyclic compounds on polymer supports. Thus, polymer-bound acid chloride **54** was treated with *m*- or *p*-hydroxybenzaldehyde (**87**) to give the polymer-bound aldehydes **88**. Treatment of **88** with pyrrole and excess tolualdehyde gave, after filtration from the excess symmetrical *meso*-tetratolylporphyrin produced, the unsymmetrical polymer-bound porphyrins **89**. Cleavage of **89** with base gave in higher yield the unsymmetrical *m*- and *p*-hydroxyphenyl tritolylporphyrins **90** (95) (Scheme 14). This synthesis represents another example of the "fishhook" principle (47), whereby the minor desired component **89** on the polymer is fished out from the major symmetrical product in solution.

Pure unsymmetrical phthalocyanines were virtually unknown prior to 1980 and hence the polymer supported synthesis of porphyrins, described above, is eminently suited to be applied to the more complex heterocyclic macrocycles, the phthalocyanines (Pcs). For example, polymer-supported monotrityl hexanediol (**12**) underwent an aromatic nucleophilic displacement reaction with 4-nitrophthalonitrile and a phase transfer reagent in nitrobenzene to give the polymer-bound phthalonitrile (**91**). Conversion of **91** with base and NH_3 gave the polymer-bound diiminoisoindoline (**92**). Treatment of **92** with a large excess of the isoindoline of 4-isopropoxyphthalonitrile gave the polymer-bound unsymmetrically substituted phthalocyanine **93** as the minor product and a large excess of the symmetrical phthalocyanine (Pc) (**94**). Again, simple filtration afforded pure **93** by the fishhook principle. Acid cleavage of **93** provided the first pure unsymmetrical Pc **95** (96) (Scheme 15). Other examples followed (97, 98).

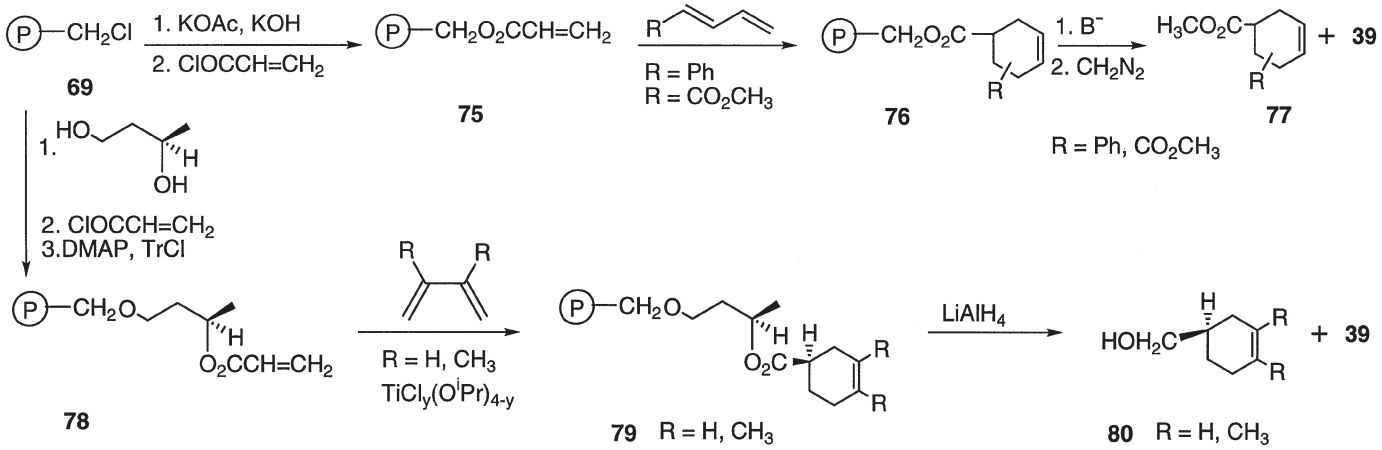
Our early forays into the use of polymer-supports as monoblocking agents of symmetrical difunctional compounds led us to develop multi-step synthesis of linear compounds, such as insect pheromones and carotenoids, cyclic and heterocyclic compounds, such as cyclohexanes and isoxazoles, chiral compounds, and finally macrocyclic

Scheme 11.

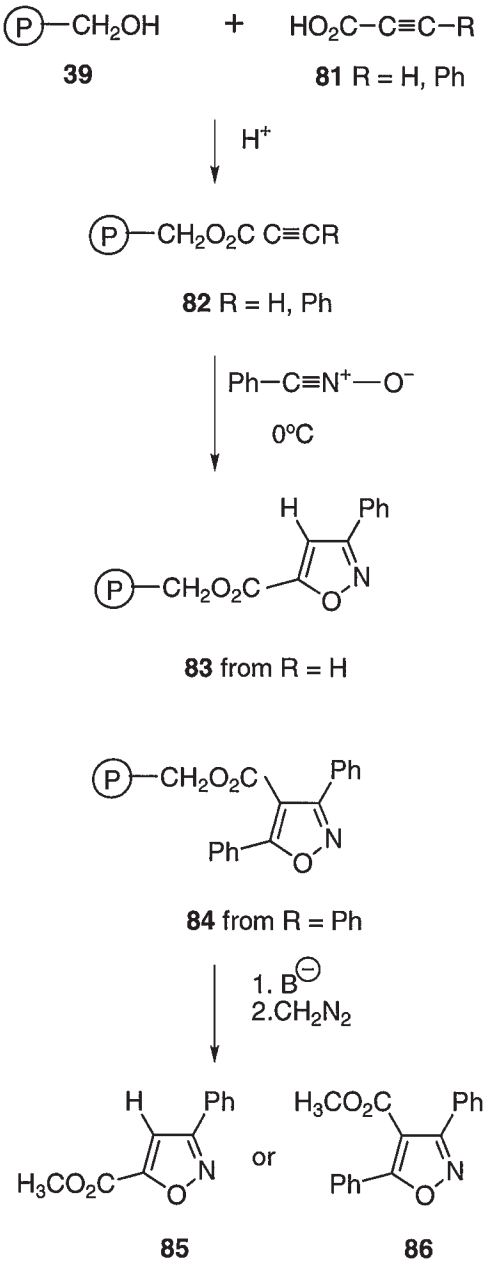


© 2000 NRC Canada

Scheme 12.

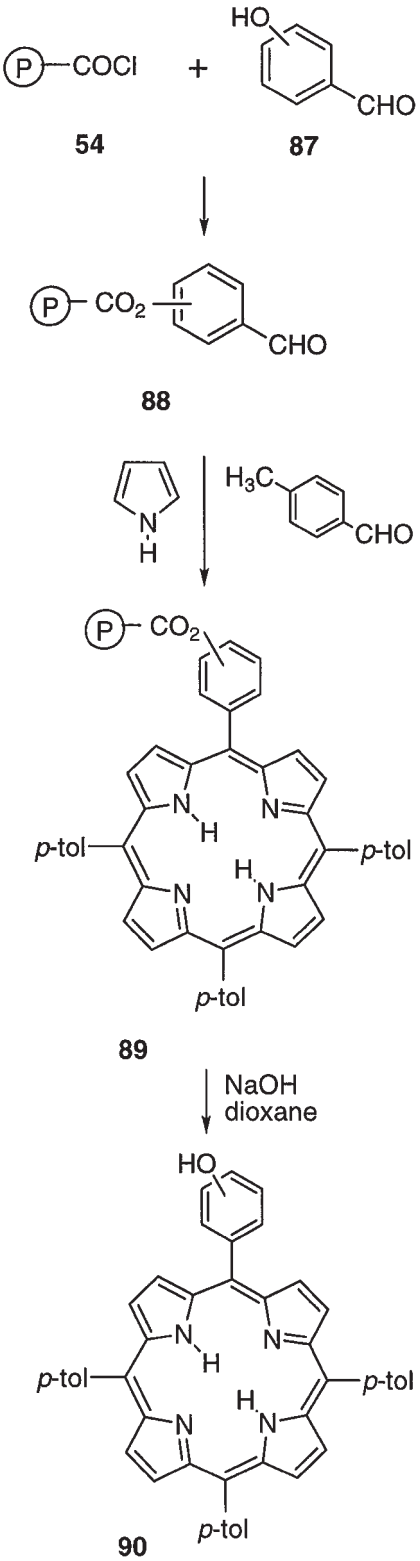


Scheme 13.

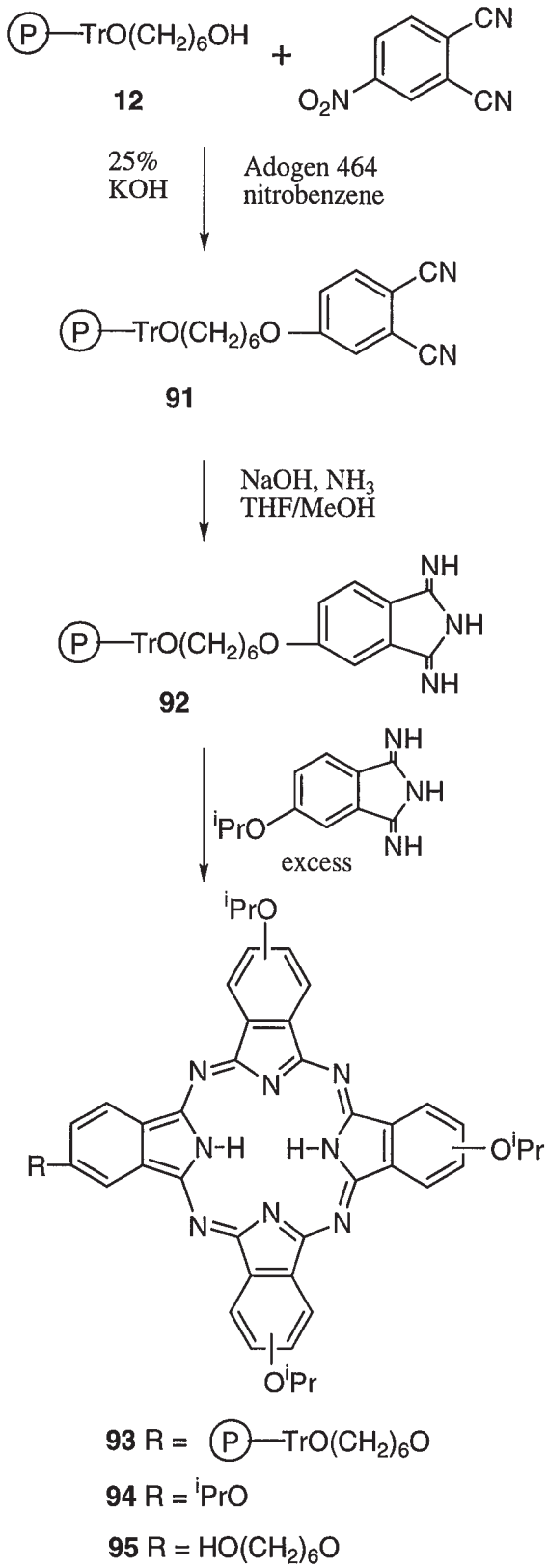


© 2000 NRC Canada

Scheme 14.

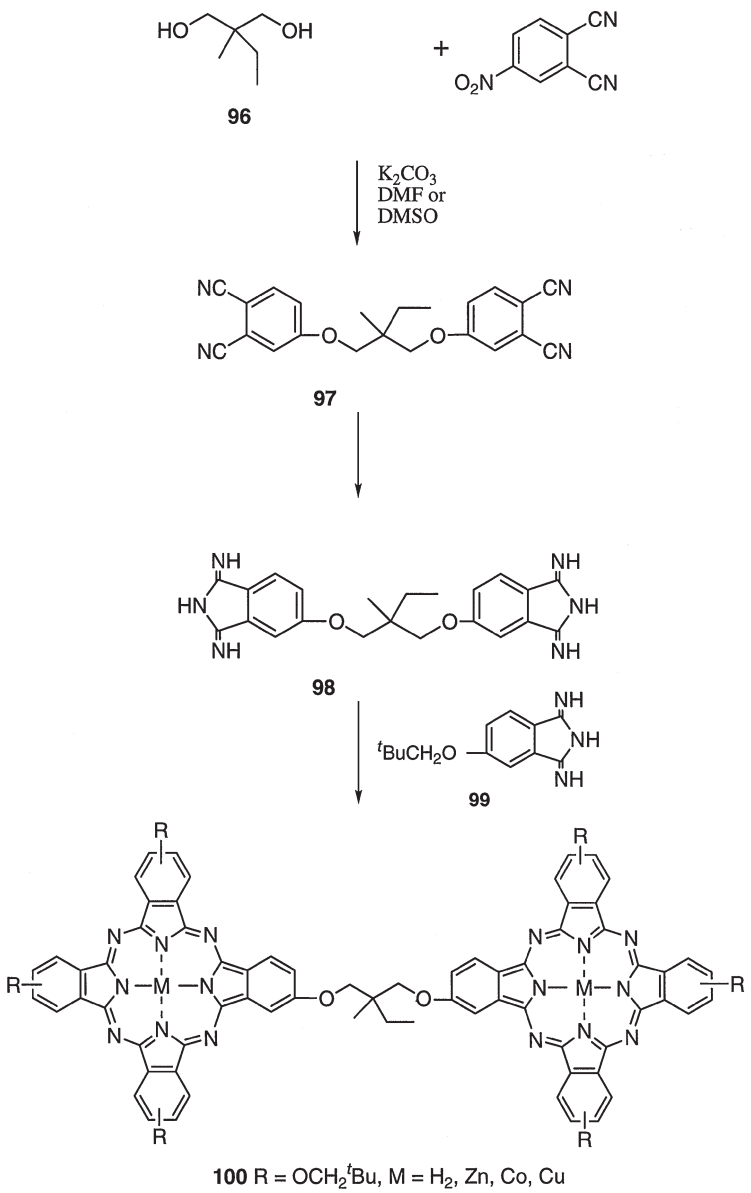


Scheme 15.



© 2000 NRC Canada

Scheme 16.



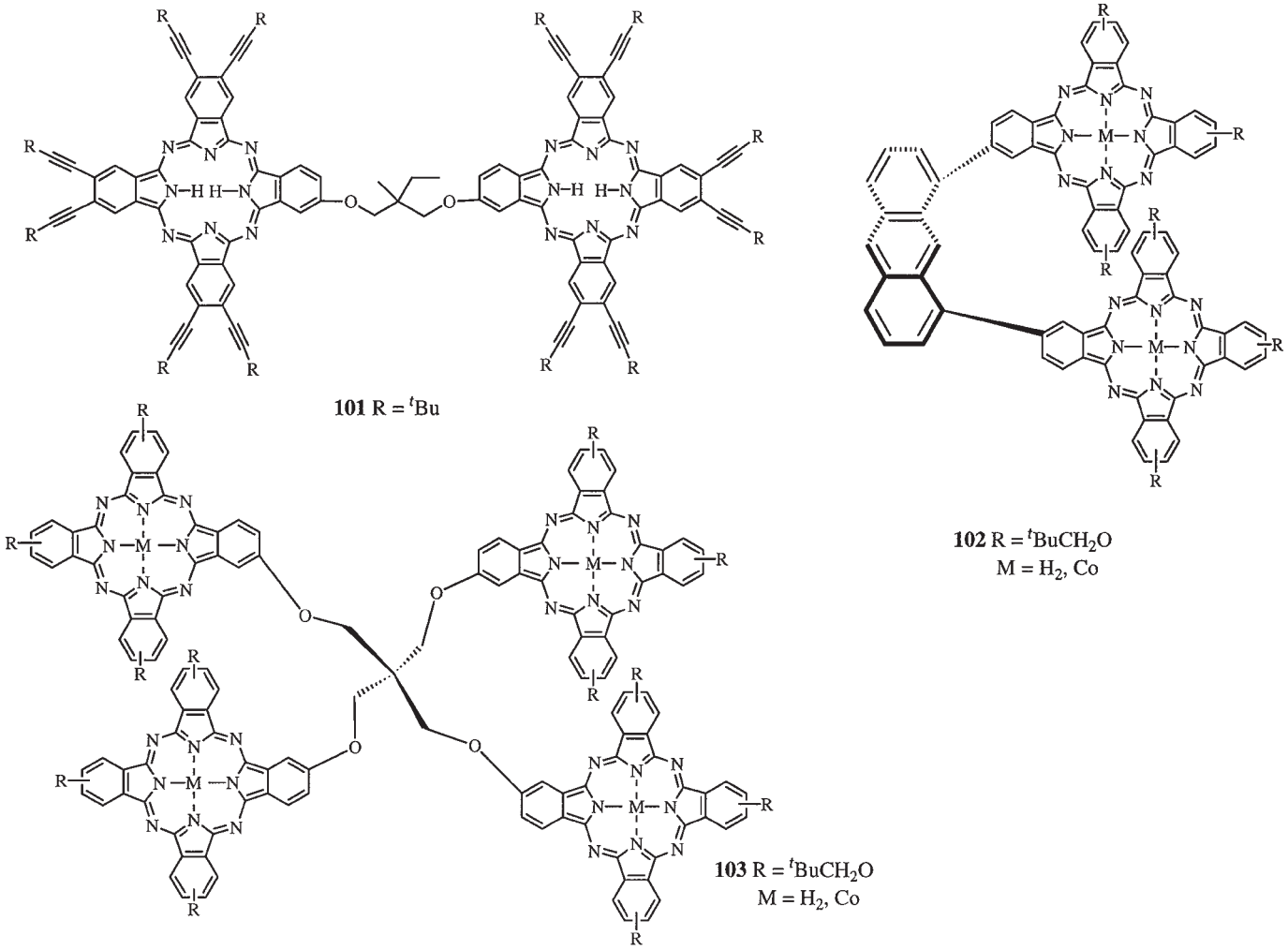
compounds such as porphyrins and phthalocyanines. Perhaps most importantly, it was demonstrated that a wide variety of common organic reactions could be performed readily on solid phases. These included ether and ester formation, Wittig and organometallic reactions, aldol condensations, oximation, amide formation, borane, borohydride and tin hydride reductions, non-chiral and chiral alkylations, mesylations, alkyne couplings, oxidations, Diels–Alder and 1,3-dipolar additions, and finally Rothemund type (99, 100) prophyrin and Linstead (101) phthalocyanine macrocyclic formations. Some more recent reactions that are noteworthy include the "traceless" attachment of substrates to polymer supports (102, 103), the four component Ugi reaction (104), the Pauson–Khand reaction (105), soluble palladium coupling reactions (106), and other protocols on solid phases (107). Other reactions are outlined in a number of early (47–49) and more recent reviews on SPOS (108, 109) and in reviews on the applications of polymer-supported synthesis in combinatorial chemistry (71–73, 109).

Phthalocyanines

Our synthesis of the first characterized unsymmetrically substituted Pc (96) whetted our appetite for further studies in phthalocyanine chemistry (110–113). During this time, it was shown that certain bridged binuclear porphyrins (114–116) were able to act as catalysts in the 4e-reduction of H_2O to hydrogen and oxygen, although the catalysts tended to decompose with time. Since it was known that Pcs are very much more robust than porphyrins and Pcs can even be used as paint coatings for automotibles, we embarked on a program to make hitherto unknown bridged binuclear phthalocyanines and study their electrocatalytic properties. To

© 2000 NRC Canada

Scheme 17.



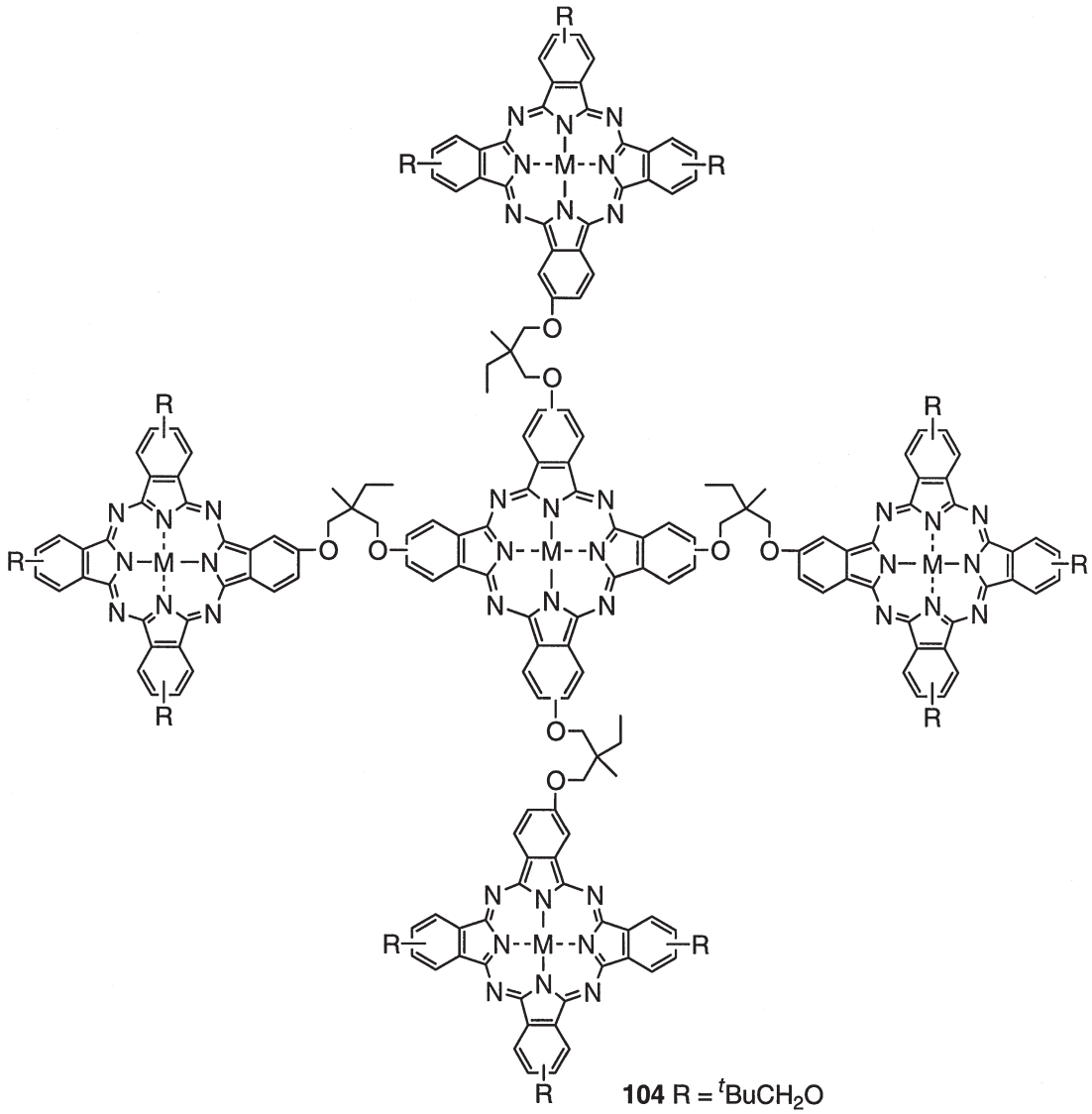
solubilize the rather insoluble pthhalocyanines, we used the bulky neopentoxy (2,2-dimethyl-1-propoxy) group as a solubilizing substituent. Since bridged binuclear Pcs are essentially unsymmetrical Pcs in which one substituent is simply another Pc group, our prior experience in synthesizing an unsymmetrical Pc on a polymer support served us well. Thus, treatment of 2-ethyl-2-methyl-1,3-propanediol (**96**) with base and 4-nitrophthalonitrile gave the bisphthalonitrile (**97**). Conversion of **97** to its bisdiiminoisoindoline (**98**) as before, followed by condensation with a large excess of the diiminoisoindoline (**99**) of 4-neopentoxyphthalonitrile, resulted in a mixture of a large amount of mononuclear 2,9,16,23-tetraneopentoxyphthalocyanine and some binuclear phthalocyanines (**100**) as a metal-free derivative into which various metals could be inserted (117, 118). Amusingly, gel permeation chromatography (94, 118), using the same 2% cross-linked polystyrene used in SPOS, was crucial in separating the mono- and binuclear Pcs in a final purification step (Scheme 16) in this and other polynuclear phthalocyanines (119–122). The method of synthesis of **100** gives the binuclear Pcs as a mixture of regioisomers which is actually beneficial as this mixture helps promote the solubility of **100**. More recently, we substituted the *tert*-butylalkynyl group for the neopentoxy group and we were able to make a binuclear Pc as the pure single isomer **101** (123) (Scheme 17).

Other rigid bridged binuclear Pcs based on attachment of Pcs to the 1,8-positions of anthracene (**102**) (124), naphthalene (125), and phenanthrene (126) were also synthesized (Scheme 17). Trinuclear (121), tetranuclear **103** (127) (Scheme 17), and even a dendriditic-like pentanuclear phthalocyanine (**104**) (128) succumbed to the synthetic anvil (Scheme 18). Cyclic voltammetry (128, 129) and Langmuir–Blodgett studies (130) of the polynuclear phthalocyanines yielded many insights on intraphthalocyanine interactions (128) including step by step oxidation–reductions of the Pcs rings. However, in all cases, the two electron reduction of O_2 to H_2O_2 was observed (most efficiently with tetranuclear Pc **104**).

Currently, we are interested in preparing polyalkynyl phthalocyanines (122*b*, 123, 131–33) for use in nonlinear optics (134) and in shifting the absorption maxima of Pcs towards longer wavelengths. To this end, the 2,3,9,10,16,

© 2000 NRC Canada

Scheme 18.



17,23,24-octaphenylethynylphthalocyanines **105** and **106** have been prepared. Phthalocyanine **105** is extremely insoluble, but again, the neopentoxy groups in **106** provide this very planar Pc with enough bulkiness to prevent aggregation and enhance solubility. The polyoctabutadiynyl Pc **107**, although soluble, is fairly unstable and decomposes slowly (135).

Conclusions

In the 1970's, SPOS was considered as unusual and impractical, but through the advent of combinatorial chemistry, has become an important endeavour in the 1990's. I have shown how our curiosity-driven research later came to have important practical considerations, and led us to develop a new interest in phthalocyanine chemistry, the applications of which are only now beginning to be realized.

Acknowledgement

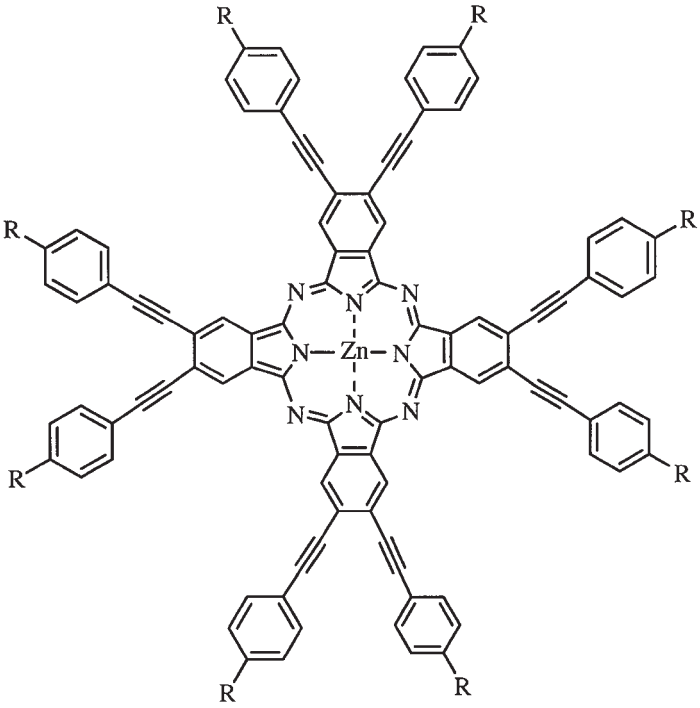
I would like to thank the many outstanding graduate students, postdoctoral fellows, research associates, and collaborators at York, as well as those at other institutions who have made this work possible and indeed enjoyable and whose names appear in the references quoted. We thank the Natural Sciences and Engineering Research Council of Canada for major support through operating, strategic, and collaborative grants. Other agencies supporting this research included the Petroleum Research Fund, the Ontario Ministry of the Environment, and the Office of Naval Research (U.S.A.).

References

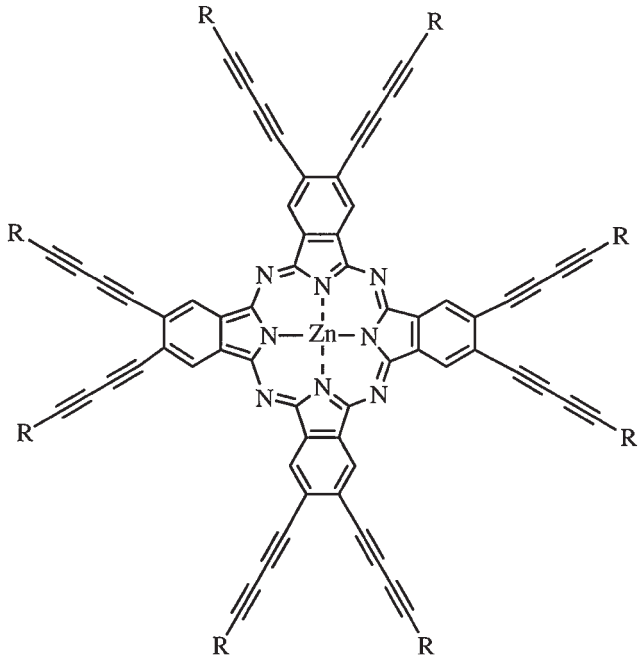
1. R.B. Merrifield. J. Am. Chem. Soc. **85**, 2149 (1963).
2. R.L. Letsinger and M.J. Kornet. J. Am. Chem. Soc. **85**, 3045 (1963).
3. R.B. Merrifield. Science (Washington, D.C.), **150**, 178 (1965).
4. (*a*). R.L. Letsinger and V. Mahadevan. J. Am. Chem. Soc. **87**, 3526 (1965); (*b*) R.L. Letsinger and V. Mahadevan. J. Am. Chem. Soc. **88**, 5319 (1966).
5. (*a*) F. Cramer and H. Koster. Angew. Chem. Int. Ed. Engl. **7**, 473 (1968); (*b*) H. Koster. Tetrahedron Lett. **13**, 1527 (1972).

© 2000 NRC Canada

Scheme 19.



105 R = H
106 R = ^{t}BuCH$_2$O



107 R = ^{t}BuCH$_2$O

6. (*a*) M.J. Gait and R.C. Sheppard. J. Am. Chem. Soc. **98**, 8514 (1976); (*b*) S.L. Beaucage and R.P. Iyer. Tetrahedron, **48**, 2223 (1992).
7. (*a*) J.M.J. Fréchet and C. Schuerch. J. Am. Chem. Soc. **93**, 492 (1971); (*b*) S.P. Douglas, D.M. Whitfield, and J.J. Krepinsky. J. Am. Chem. Soc. **113**, 5095 (1991); (*c*) S.J. Danishefsky, K.F. McClure, J.J. Randolph, and R.B. Ruggeri. Science (Washington, D.C.), **260**, 1307 (1993).
8. (*a*) G.B. Fields and R.L. Noble. Int. J. Pept. Protein Res. **35**, 161 (1990); (*b*) M.R. Pavia, T.K. Sawyer, and W.H. Moos. Bioorg. Med. Chem. Lett. **3**, 387 (1993).
9. (*a*) F.X. Montserra, A. Grandas, R. Eritja, and E. Pendroso. Tetrahedron, **50**, 2617 (1994).
10. (*a*). V. Amarnath and A.D. Broom. Chem. Rev. **77**, 183 (1977); (*b*) P.H. Seeberger and S.J. Danishefsky. Acc. Chem. Res. **31**, 685 (1998); (*c*) H.M.I. Osborn and T.H. Kwan. Tetrahedron, **55**, 1807 (1999).
11. (*a*) R.B. Merrifield, J.M. Stewart, and N. Jernberg. Anal. Chem. **38**, 1905 (1966); (*b*) B. Gutte and R.B. Merrifield. J. Am. Chem. Soc. **91**, 501 (1969); (*c*) J.M. Stewart and J.D. Young. Solid Phase Peptide Synthesis. W.H. Freeman, San Francisco. 1969; (*d*) E. Wunsch. Angew. Chem. Int. Ed. Engl. **10**, 786 (1971).
12. R.N. Zuckerman, J.M. Kerr, M.A. Siani, and S. Banville. Int. J. Pept. Protein Res. **40**, 497 (1992).
13. (*a*) G. Jung and A.G. Beck-Sickinger. Angew. Chem. Int. Ed. Engl. **31**, 367 (1992); (*b*) G.M. Gait. Solid phase oligonucleotide synthesis: a practical approach. IRL, Oxford. 1992.
14. M. Fridkin, A. Patchornik, and E. Katchalsky. J. Am. Chem. Soc. **88**, 3164 (1966).
15. A. Patchornik and M.A. Kraus. Pure Appl. Chem. **43**, 503 (1975).
16. (*a*) N.K. Mathur, C.K. Narang, and R.E. Williams. Polymer as aids in organic chemistry. Academic Press, New York. 1980; (*b*) P. Hodge. *In* Polymer supported reactions. *Edited by* P. Hodge and D.C. Sherrington. Wiley, New York. 1980. pp. 83–155. (*c*) J.M.J. Fréchet. Tetrahedron, **37**, 663 (1981); (*d*) W. Heitz. Adv. Polym. Sci. **23**, 2 (1977).
17. (*a*) D.C. Neckers, D.A. Kooistra, and G.W. Green. J. Am. Chem. Soc. **94**, 9284 (1972); (*b*) S.J. Shuttleworth, S.M. Allin, and P.K. Sharma. Synthesis, **1217**, (1997).
18. Y. Gaoni, C.C. Leznoff, and F. Sondheimer. J. Am. Chem. Soc. **90**, 4940 (1968).
19. I.T. Harrison and S. Harrison. J. Am. Chem. Soc. **89**, 5723 (1967).
20. T. Kusama and H. Hayatsu. Chem. Pharm. Bull. **18**, 319 (1970).
21. C. C. Leznoff and J.Y. Wong. Can. J. Chem. **50**, 2892 (1972).
22. J.Y. Wong and C.C. Leznoff. Can. J. Chem. **51**, 2452 (1972).
23. T.M. Fyles and C.C. Leznoff. Can. J. Chem. **54**, 935 (1976).
24. J.M.J. Fréchet and L.J. Nuyens. Can. J. Chem. **54**, 926 (1976).
25. C.C. Leznoff and J.Y. Wong. Can. J. Chem. **51**, 3756 (1973).
26. J.Y. Wong, C. Manning, and C.C. Leznoff. Angew. Chem. Int. Ed. Engl. **13**, 666 (1974).
27. J.M. Vanest, M. Gorsane, V. Libert, J. Pecher, and R.H. Martin. Chimia, **29**, 343 (1975).
28. C.C. Leznoff and W. Sywanyk. J. Org. Chem. **42**, 3203 (1977).
29. Z.-H. Xu and H. Cheng. Huaxue Tongbao, 14 (1985); Chem. Abstr. **103**, 105384b (1985).
30. Z.-H. Xu, C.R. McArthur, and C.C. Leznoff. Can. J. Chem. **61**, 1405 (1983).

© 2000 NRC Canada

31. C.C. Leznoff and Z.-H. Xu. Huaxue Tongbao, 16 (1983); Chem. Abstr. **99**, 194503d (1983).
32. S. Chamoin, S. Houldsworth, C.G. Kruse, W.I. Bakker, and V. Snieckus. Tetrahedron Lett. **39**, 4179 (1998).
33. (*a*) C.C. Leznoff and S. Greenberg. Can. J. Chem. **54**, 3824 (1976); (*b*) C. Bied-Charreton, J.P. Idoux, and A. Gaudemar. Nouv. J. Chim. **2**, 303 (1978); (*c*) P. Hodge and J. Waterhouse. J. Chem. Soc. Perkin Trans 1, 2319 (1983); (*d*) Q. Ren, W. Huang, and B. He. Huaxue Xuebao, **47**, 827 (1989); Chem. Abstr. **112**, 56903v (1990); (*e*) S. Chandrasekhan and M.B. Padmaja. Synth. Commun. **28**, 3715 (1998); (*f*) J. Chen and R. Xiao. Gaofenzi Tongxun, 467 (1986); Chem. Abstr. **106**, 214796v (1987).
34. S. Hanessian and H.K. Huynh. Synlett, 102, (1999).
35. (*a*) J.M.J. Fréchet and E. Seymour. Isr. J. Chem. **17**, 253 (1978); (*b*) J.M.J. Fréchet, L.J. Nuyens, and E. Seymour. J. Am. Chem. Soc. **101**, 433 (1979).
36. (*a*) D.M. Dixit and C.C. Leznoff. J. Chem. Soc. Chem. Commun. 798 (1977); (*b*) D.M. Dixit and C.C. Leznoff. Isr. J. Chem. **17**, 248 (1978).
37. (*a*) H. Boulen, B. Martens, and D. Wöhrle. Makromol. Chem. Rapid Comm. **1**, 753 (1980); (*b*) B.A. Dressman, L.A. Spangle, and S.W. Kaldor. Tetrahedron Lett. **37**, 937 (1996); (*c*) J.J. McNally, M.A. Youngman, and S. L. Dax. Tetrahedron Lett. **39**, 967 (1998).
38. C.C. Leznoff and J.M. Goldwasser. Tetrahedron Lett. **18**, 1875 (1977).
39. J.M. Goldwasser and C.C. Leznoff. Can. J. Chem. **19**, 1562 (1978).
40. G. Cahiez and J.F. Normant. Tetrahedron Lett. **18**, 3383 (1977).
41. C.C. Leznoff and V. Yedidia. Can. J. Chem. **58**, 287 (1980).
42. J.W. Apsimon and D.M. Dixit. Synth. Commun. **12**, 113 (1982).
43. B.C. Hamper, S.A. Kolodziej, and A.M. Scates. Tetrahedron Lett. **39**, 2047 (1998).
44. (*a*) G. Bhalay, P. Blaney, V.N. Palmer, and A.D. Baxter. Tetrahedron Lett. **38**, 8375 (1997); (*b*) A. Wahhab and J. Leban. Tetrahedron Lett. **40**, 235 (1979).
45. F. Gaviña, A.M. Costero, P. Gil, B. Palazon, and S.V. Luis. J. Am. Chem. Soc. **103**, 1797 (1981).
46. F. Gaviña, A.M. Costero, and S.V. Luis. J. Org. Chem. **49**, 4617 (1984).
47. (*a*) C.C. Leznoff. Chem. Soc. Rev. **3**, 65 (1974); (*b*) C.C. Leznoff. Acc. Chem. Res. **11**, 327 (1978).
48. (*a*) J.I. Crowley and H. Rapoport. Acc. Chem. Res. **9**, 135 (1976); (*b*) J. Rebek, Jr. Tetrahedron, **35**, 723 (1979); (*c*) A. Akelah and D.C. Sherrington. Chem. Rev. **81**, 557 (1981); (*d*) J.M.J. Fréchet. Tetrahedron, **37**, 663 (1981).
49. (*a*) J.S. Früchtel and G. Jung. Agnew. Chem. Int. Ed. Engl. **35**, 17 (1996); (*b*) I.W. James. Tetrahedron, **55**, 4855 (1999).
50. C.C. Leznoff and D.M. Dixit. Can. J. Chem. **55**, 3351 (1977).
51. T.M. Fyles, C.C. Leznoff, and J. Weatherston. Can. J. Chem. **56**, 1031 (1978).
52. (*a*) B. Castro, M. Ly, and C. Selve. Tetrahedron Lett. **14**, 4455 (1973); (*b*) J.H. Babler and M.J. Coghlan. Tetrahedron Lett. **20**, 1971 (1979); (*c*) S. David and A. Thieffry. J. Org. Chem. **48**, 441 (1983); (*d*) S.B. Fergusson and H. Alper. J. Chem. Soc. Chem. Commun. 1349 (1984); (*e*) P.G. McDougal, J.G. Rico, Y.-Im. On, and B.D. Condon. J. Org. Chem. **51**, 3389 (1986); (*f*) S.K. Kang, W.-S. Kim, and B.H. Moon. Synthesis, 1161 (1985); (*g*) F. Camps, J.M. Casamor, J. Coll, A. Guerrero, and M. Riba. Org. Prep. Proced. Int. **15**, 63 (1983).
53. (*a*) T. Nishiguchi and H. Taya. J. Am. Chem. Soc. **111**, 9102 (1989); (*b*) T. Nishiguchi. J. Org. Chem. **59**, 1191 (1994); (*c*) T. Nishiguchi, K. Kawamine, and T. Ohtsuka. J. Chem. Soc. Perkin Trans. 1, 153 (1992); (*d*) T. Nishiguchi, M. Kuroda, M. Saitoh, A. Nishida, and S. Fujisaki. J. Chem. Soc. Chem. Commun. 2491 (1995); (*e*). T. Nishiguchi, S. Fujisaki, M. Kuroda, K. Kajisaki, and M.Satoh. J. Org. Chem. **63**, 8183 (1998).
54. (*a*) V.E.M. Kaats-Richters, J.W. Zwikker, E.M.D. Keegstra, and L.W. Jenneskens. Synth. Commun. **24**, 2399 (1994); (*b*) D. Komiotis, B.L. Currie, G.C. LeBreton, and D.L. Venton. Synth. Commun. **23**, 531 (1993); (*c*) A. Ndibwami, S. Lamothe, D. Guay, R. Plante, P. Soucy, S. Goldstein, and P. Deslongchamps. Can. J. Chem. **71**, 695 (1993); (*d*) F. Freeman, D.S.H.L. Kim, and E. Rodriguez. J. Org. Chem. **57**, 1722 (1992); (*e*) J. Otera, N. Dan-Oh, and H. Nozaki. J. Chem. Soc. Chem. Commun. 1742, (1991); (*f*) U.P. Dhokte, V.V. Khau, D.R. Hutchison, and M.J. Martinelli. Tetrahedron Lett. **39**, 8771 (1998); (*g*) H. Ogawa, M. Amano, and T. Chihara. J. Chem. Soc. Chem. Commun. 495 (1998); (*h*) D. Wong and C.-J. Li. Synth. Commun. **28**, 507 (1998).
55. O. Hoville, T. Schmittberger, and D.D. Uguen. Tetrahedron Lett. **37**, 625 (1996).
56. (*a*) N.G. Lukyanenko and O.T. Melnik. Zh. Org. Khim. **24**, 2227 (1988); (*b*) G.D. Gamalevich, B.N. Morozov, A.L. Vlazyuk, and E.P. Serebryakov. Tetrahedron, **55**, 3665 (1999).
57. (*a*) K. Hollmann and M. Ecke. Z. Chem. **29**, 63 (1989); (*b*) M. Hayashi, K. Hiratani, S.-I. Kina, M. Ishii, and K. Saigo. Tetrahedron Lett. **39**, 6211 (1998); (*c*) J.R. Hwu, W.N. Tseng, J. Ghabre, P. Giza, and R.C.C. Huang. J. Med. Chem. **41**, 2994 (1998).
58. (*a*) R. Crux-Almanza, E.G. Pérez-Flores, and M. Avila. Synth. Commun. **20**, 1125 (1990); (*b*) D. Johnston. Chem. Ind. London, 1000 (1982); (*c*) J.E. Otis, Jr., T. Walle, H.B. Daniell, T.E. Gaffney, and D.R. Knapp. J. Med. Chem. **28**, 822 (1985).
59. (*a*) B.O. Brown and B.C.L. Weedon. Finn. Chem. Lett. 102 (1984); (*b*) C. Botteghi and F. Soccolini. Synthesis, 592 (1985).
60. (*a*) G.D. Hartman, B.T. Phillips, and W. Halczenko. J. Org. Chem. **50**, 2423 (1985); (*b*) G. Smith and G. Kruger. J. Org. Chem. **50**, 5759 (1985); (*c*) S. Michaud and J. Viala. Tetrahedron, **55**, 3019 (1999); (*d*) L.F. Tietze, H. Meier, and E. Voss. Synthesis, 274 (1988); (*e*) J. Hiratake, K. Shibata, N. Baba, and J. Oda. Synthesis, 278 (1988).
61. (*a*) T. Cuvigny, M. Larcheveque, and H. Normant. Synthesis, 857 (1978); (*b*) T. Volpe, G. Revial, M. Peau, and J. d'Angelo. Tetrahedron Lett. **27**, 2853 (1986); (*c*) M. C. Pirrung and D.S. Nunn. Tetrahedron Lett. **33**, 6591 (1992).
62. C.M. Hall and J.B. Wright. U.S. Patent 4, 128, 660 (1978); Chem. Abstr. **90**, 103668m (1979).
63. (*a*) G.L. Stahl, R. Walter, and C.W. Smith. J. Org. Chem. **43**, 2285 (1978); (*b*) M.M. Ponpipom. Carbohydr. Res. **113**, 45 (1983); (*c*) R. Houssin, J.-L. Bernier, and J.-P. Hénichart. Synthesis, 259 (1988); (*d*) K. Kaljuste and A. Unden. Tetrahedron Lett. **36**, 9211 (1995). (*e*) S.M. Hutchins and K.T. Chapman. Tetrahedron Lett. **36**, 2583 (1995). (*f*) G.J. Atwell and W.A. Denny. Synthesis, 1032 (1984).
64. W.C. Chou, M.-C. Chou, Y.-Y. Lu, and S.-F. Chen. Tetrahedron Lett. **40**, 3419 (1999).
65. J. Otera, N. Dan-Oh, and H. Nozaki. Tetrahedron, **49**, 3065 (1993).
66. (*a*) T.R. Hoye and N.E. Witowski. J. Am. Chem. Soc. **114**, 7291 (1992). (*b*) M. Lobell and M.P. Schneider. J. Chem. Soc. Perkin Trans. 1, 1713 (1993).
67. F.V. Brutcher, Jr. and H. Hinney. Tetrahedron Lett. **20,** 679 (1979).
68. H. Ogawa, T. Chihara, and K. Taya. J. Am. Chem. Soc. **107**, 1365 (1985).

© 2000 NRC Canada

69. C. Rogers and B.P. Keay. Can. J. Chem. **70**, 2929 (1992).
70. (*a*) R. Kikumoto, A. Tobe, H. Fukami, K. Ninomiya, and M. Egawa. J. Med. Chem. **27**, 645 (1984); (*b*) G.D. Diana, M.A. McKinlay, C.J. Brisson, F.S. Zalay, J.V. Miralles, and U.J. Salvador. J. Med. Chem. **28**, 748 (1985); (*c*) G.A. Kraus and K. Landgrebe. Synthesis, 885 (1984).
71. (*a*) H.M. Geysen, R.H. Melden, and S.J. Barteling. Proc. Nat. Acad. Sci. U.S.A. **81**, 3998 (1984); (*b*) R.A. Houghten. Proc. Nat. Acad. Sci. U.S.A. **82**, 5131 (1985); (*c*) A. Furka, F. Sebestyen, M. Asgedom, and G. Dibo. Int. J. Pept. Protein Res. **37**, 487 (1991); (*d*) K. Lam, S. Salmon, E. Hersh, V. Hruby, W. Kazmierski, and R. Knapp. Nature (London), **354**, 82 (1991); (*e*) S.H. DeWitt, J.S. Kiely, C.J. Stankovic, M.C. Schroeder, D.M.R. Cody, and M.R. Pavia. Proc. Nat. Acad. Sci. U.S.A. **90**, 6909 (1993).
72. (*a*) E.M. Gordon, R.W. Barrett, W.J. Dower, S.P.A. Fodor, and M.A. Gallop. J. Med. Chem. **37**, 1385 (1994); (*b*) F. Balkenhohl, C. von dem Bussche-Hünnefeld, A. Lansky, and C. Zechel. Angew. Chem. Int. Ed. Engl. **35**, 2288 (1996).
73. (*a*) A. Nefzi, J.R. Ostrech, and R.A. Houghton. Chem. Rev. **97**, 449 (1997); (*b*) J.A. Ellman. Acc. Chem. Res. **29**, 132 (1996); (*c*) S.H. DeWitt and A. Czarnik. Acc. Chem. Res. **29**, 114 (1996).
74. C.C. Leznoff and T.M. Fyles. J. Chem. Soc. Chem. Commun. 251 (1976).
75. C.C. Leznoff, T.M. Fyles, and J. Weatherston. Can. J. Chem. **55**, 1143 (1977).
76. P.I. Svirskaya and C.C. Leznoff. J. Chem. Ecol. **10**, 321 (1984).
77. C.C. Leznoff. *In* Biotechnology: applications and research. *Edited by* P.N. Cheremisinoff and R.P. Ouellette. Technomic Publ. Co., Lancaster, Penn. 1985. pp. 586–593.
78. T.M. Fyles, C.C. Leznoff, and J. Weatherston. Can. J. Chem. **56**, 1031 (1978).
79. (*a*). T.M. Fyles, C.C. Leznoff, and J. Weatherston. Can. J. Chem. **55**, 4135 (1977); (*b*) T.M. Fyles, C.C. Leznoff, and J. Weatherston. J. Chem. Ecol. **4**, 109 (1978).
80. P.I. Svirskaya, C.C. Leznoff, J. Weatherston, and J.E. Laing. J. Chem. Eng. Data, **24**, 152 (1979).
81. T.-H. Chan and W.-Q. Huang. J. Chem. Soc. Chem. Commun. 909 (1985).
82. J.M. Montierth, D.R. DeMario, M.J. Kurth, and N.E. Schore. Tetrahedron, **54**, 11741 (1998).
83. (*a*) P.I. Svirskaya, C.C. Leznoff, and W.L. Roelofs. Synth. Commun. **10**, 391 (1980); (*b*) P.I. Svirskaya, S.N. Maiti, A.J. Jones, B. Khouw, and C.C. Leznoff. J. Chem. Ecol. **10**, 795 (1984).
84. M. Kawana and S. Emoto. Tetrahedron Lett. 4855 (1972).
85. (*a*) D. Enders and H.E. Eichenauer. Angew. Chem. Int. Ed. Engl. **15**, 549 (1976); (*b*) A.I. Meyers, D.R. Williams, and M. Druelinger. J. Am. Chem. Soc. **98**, 3032 (1976); (*c*) J.K. Whitesell and M.A. Whitesell. J. Org. Chem. **42**, 377 (1977).
86. (*a*) P.M. Worster, C.R. McArthur, and C.C. Leznoff. Angew. Chem. Int. Ed. Engl. **18**, 221 (1979); (*b*) C.R. McArthur, P.M. Worster, J.-L. Jiang, and C.C. Leznoff. Can. J. Chem. **60**, 1836 (1982).
87. L. Duhamel and J.-C. Plaquevent. Bull. Soc. Chim. Fr. II-75 (1982).
88. C.R. McArthur, J.-L. Jiang, and C.C. Leznoff. Can. J. Chem. **60**, 2984 (1982).
89. (*a*) S.J. Blazka and H.J. Harwood. Polym. Prep. Am. Chem. Soc. Div. Polym. Chem. **16**, 633 (1975); (*b*) J. Rebek and F. Gaviña. J. Am. Chem. Soc. **96**, 7112 (1974); (*c*) F. Gaviña, P. Gil, and B. Palazón. Tetrahedron Lett. 1333 (1979); (*d*) T.J. Nieuwstad, A.P.G. Kieboom, A.J. Breijer, J. van der Linden, and H. van Bekkum. Recl. Trav. Chim. Pays-Bas **95**, 225 (1976).
90. V. Yedidia and C.C. Leznoff. Can. J. Chem. **58**, 1144 (1980).
91. M.D. Corbridge, C.R. McArthur, and C.C. Leznoff. React. Polym., **8**, 173 (1988).
92. K. Bust, M. Christl, R. Huisgen, W. Mack, and R. Sustmann. Chem. Ber. **106**, 3258 (1973).
93. M. Christl, R. Huisgen, and R. Sustmann. Chem. Ber. **106**, 3275 (1973).
94. R.G. Little, J. Anton, P. Loach, and J.A. Ibers. J. Heterocycl. Chem. **12**, 343 (1975).
95. C.C. Leznoff and P.I. Svirskaya. Angew. Chem. Int. Ed. Engl. **17**, 947 (1978).
96. (*a*) C.C. Leznoff and T.W. Hall. Tetrahedron Lett. **23**, 3023 (1982); (*b*) T.W. Hall, S. Greenberg, C.R. McArthur, B. Khouw, and C.C. Leznoff. Nouv. J. Chim. **6**, 653 (1982).
97. D. Wöhrle and G. Krawczyk. Polym. Bull. **15**, 193 (1986).
98. C.C. Leznoff, P.I. Svirskaya, B. Khouw, R.L. Cerny, P. Seymour, and A.B.P. Lever. J. Org. Chem. **56**, 82 (1991).
99. P. Rothemund. J. Am. Chem. Soc. **57**, 2010 (1935).
100. A.D. Adler, F.R. Longo, J.D. Finarelli, J. Goldmacher, J. Assour, and L. Korsakoff. J. Org. Chem. **32**, 476 (1967).
101. (*a*) R.P. Linstead and A.R. Rowe. J. Chem. Soc. 1022 (1934); (*b*) P.A. Barrett, D.A. Frye, and R.P. Linstead. J. Chem. Soc. 1157 (1938).
102. M.J. Plunkett and J.A. Ellman. J. Org. Chem. **60**, 6006 (1995).
103. (*a*) B.A. Lorsbach, R.B. Miller, and M.J. Kurth. J. Org. Chem. **61**, 8716 (1996); (*b*) M.J. Kurth, L.A.A. Randall, and K. Takenouchi. J. Org. Chem. **61**, 8755 (1996); (*c*) T. Ruhland, K. Anderson, and H. Pedersen. J. Org. Chem. **63**, 9204 (1998).
104. (*a*) I. Ugi, S. Lohberger, and R. Karl. *In* Comprehensive organic synthesis. *Edited by* B.M. Trost and I. Fleming. Pergamon, New York. 1991. Vol. 2. p. 1083; (*b*) B.P. Coppola, M.C. Noe, D.J. Schwartz, R.L. Il Abdon, and B.M. Trost. Tetrahedron, **50**, 93 (1994); (*c*) R.W. Armstrong, A.P. Combs, P.D. Tempest, S.D. Brown, and T.A. Keating. Acc. Chem. Res. **29**, 123 (1996).
105. (*a*) N.E. Schore and S.D. Najdi. J. Am. Chem. Soc. **112**, 441 (1990).
106. (*a*) M.S. Deshpande. Tetrahedron Lett. **35**, 5613 (1994); (*b*) B.J. Backes and J.A. Ellman. J. Am. Chem. Soc. **116**, 11171 (1994); (*c*) B.A. Lorsbach, J.T. Bagdanoff, R.B. Miller, and M.J. Kurth. J. Org. Chem. **63**, 2244 (1998).
107. (*a*) M.A. Blaskovich and M. Kahn. J. Org. Chem. **63**, 1119 (1998); (*b*) H.D. Piscopio, J.F. Miller, and K. Koch. Tetrahedron Lett. **39**, 2667 (1998); (*c*) C.W. Phoon and C. Abell. Tetrahedron Lett. **39**, 2655 (1998); (*d*) X. Du and R.W. Armstrong. J. Org. Chem. **62**, 5678 (1997).
108. (*a*) A.R. Brown, P.H.H. Hermkens, H.C.J. Ottenheijm, and D.C. Rees. Synlett, 817 (1998); (*b*) L.A. Thompson and J.A. Ellman. Chem. Rev. **96**, 555 (1996).
109. (*a*) Combinatorial peptide and nonpeptide libraries: a handbook. *Edited by* G. Jung. VCH, Weinheim. 1996; (*b*) Combinatorial chemistry. Synthesis and applications. *Edited by* S.R. Wilson and A.W. Czarnik. Wiley, New York. 1997.
110. C.C. Leznoff. *In* Phthalocyanines: properties and applications. *Edited by* C.C. Leznoff and A.B.P. Lever. VCH, New York. 1989. pp. 1–54.
111. C.C. Leznoff and A.B.P. Lever (*Editors*). Phthalocyanines: properties and applications. Vol. 1–4. VCH, New York. 1989, 1992, 1993, 1996.
112. F.H. Moser and A.L. Thomas (*Editors*). The Phthalocyanines. Vol. 1–2. CRC Press. Boca Raton, Fla. 1983.

© 2000 NRC Canada

113. N.B. McKeown. Phthalocyanine materials, synthesis, structure and function. Cambridge University Press, Cambridge. 1998.
114. (*a*) F.P. Schwartz, M. Gouterman, Z. Murjiana, and D.H. Dolphin. Bioinorg. Chem. **2**, 1 (1972); (*b*) J. Hiom, J.B. Paine, III, V. Zapf, and D. Dolphin. Can. J. Chem. **61**, 2220 (1983).
115. (*a*) J.P. Collman, F.C. Anson, S. Bencosme, A Chong, T. Collins, P. Denisevich, E. Evitt, T. Geiger, J.A. Ibers, G. Jameson, Y. Konai, C. Koval, K. Meier, P. Oakley, R.B. Pettman, E. Schmittov, and J. Sessler. *In* Organic synthesis today and tomorrow. *Edited by* B.M. Trost and C.R. Hutchinson. Pergamon, Oxford. 1981. pp. 29–45; (*b*) J.P. Collman, F.C. Anson, C.E. Barnes, C.S. Bencosme, T. Geiger, R.E. Evitt, R.P. Krch, K. Meier, and R.B. Pettman. J. Am. Chem. Soc. **105**, 2694 (1983).
116. (*a*) C.K. Chang. J. Am. Chem. Soc. **99**, 2819 (1977); (*b*) R. Karaman, S. Jeon, O. Almarsson, and T.C. Bruice. J. Am. Chem. Soc. **114**, 4899 (1992); (*c*) Z. Asfari, J. Vicens, and J. Weiss. Tetrahedron Lett. **34**, 627 (1992).
117. C.C. Leznoff, S. Greenberg, S.M. Marcuccio, P.C. Minor, P. Seymour, and A.B.P. Lever. Inorg. Chim. Acta. **89**, L35 (1984).
118. C.C. Leznoff, S.M. Marcuccio, S. Greenberg, A.B.P. Lever, and K.B. Tomer. Can. J. Chem. **63**, 623 (1985).
119. C.C. Leznoff, S. Greenberg, P.I. Svirskaya, K.B. Tomer, and A.B.P. Lever. Can. J. Chem. **63**, 3057 (1985).
120. E.S. Dodworth, A.B.P. Lever, P. Seymour, and C.C. Leznoff. J. Phys. Chem. **89**, 5698 (1985).
121. S. Greenberg, S.M. Marcuccio, C.C. Leznoff, and K.B. Tomer. Synthesis, 406 (1986).
122. (*a*) C.C. Leznoff, H. Lam, S.M. Marcuccio, W.A. Nevin, P. Janda, N. Kobayashi, and A.B.P. Lever. J. Chem. Soc. Chem. Commun. 699 (1987); (*b*) S. Vigh, H. Lam, P. Janda, A.B.P. Lever, C.C. Leznoff, and R.L. Cerny. Can. J. Chem. **69**, 1457 (1991).
123. H. Isago, D.S. Terekhov, and C.C. Leznoff. J. Porphyrins Phthalocyanines, **1**, 135 (1997).
124. H. Lam, S.M. Marcuccio, P.I. Svirskaya, S. Greenberg, A.B.P. Lever, C.C. Leznoff, and R.L. Cerny. Can. J. Chem. **67**, 1087 (1989).
125. C.C. Leznoff, H. Lam, W.A. Nevin, N. Kobayashi, P. Janda, and A.B.P. Lever. Angew. Chem. Int. Ed. Engl. **26**, 1021 (1987).
126. J. Li. Ph.D. Thesis, York University, Toronto, Canada. 1993.
127. W.A. Nevin, W. Liu, S. Greenberg, M.R. Hempstead, S.M. Marcuccio, M. Melnik, C.C. Leznoff, and A.B.P. Lever. Inorg. Chem. **26**, 891 (1987).
128. (*a*) W. Liu, M.R. Hempstead, W.A. Nevin, M. Melnik, A.B.P. Lever, and C.C. Leznoff. J. Chem. Soc. Dalton Trans. 2511 (1987); (*b*) W.A. Nevin, M.R. Hempstead, W. Liu, C.C. Leznoff, and A.B.P. Lever. Inorg. Chem. **26**, 570 (1987); (*c*) M.R. Hempstead, A.B.P. Lever, and C.C. Leznoff. Can. J. Chem. **65**, 2677 (1987).
129. (*a*) W.A. Nevin, M.R. Hempstead, W. Liu, C.C. Leznoff, and A.B.P. Lever. Inorg. Chem. **26**, 570 (1987); (*b*) W. Manivannan, W.A. Nevin, C.C. Leznoff, and A.B.P. Lever. J. Coord. Chem. **19**, 139 (1988); (*c*) P. Janda, N. Kobayashi, P.R. Auburn, H. Lam, C.C. Leznoff, and A.B.P. Lever. Can. J. Chem. **67**, 1109 (1989); (*d*) N. Kobayashi, H. Lam, W.A. Nevin, P. Janda, C.C. Leznoff, and A.B.P. Lever. Inorg. Chem. **29**, 3415 (1990); (*e*) N. Kobayashi, H. Lam, W.A. Nevin, P. Janda, C.C. Leznoff, T. Koyama, A. Monden, and H. Shirai. J. Am. Chem. Soc. **116**, 879 (1994).
130. J.H. Kim, T.M. Cotton, R.A. Uphaus, and C.C. Leznoff. Thin Solid Films, **159**, 141 (1988).
131. D.S. Terekhov, K.J.M. Nolan, C.R. McArthur, and C.C. Leznoff. J. Org. Chem. **61**, 3034 (1996).
132. (*a*) C.C. Leznoff, Z. Li, H. Isago, A.M. D'Ascanio, and D.S. Terekhov. J. Porphyrins Phthalocyanines, **3**, 406 (1999); (*b*) H. Isago, C.C. Leznoff, M.F. Ryan, R.A. Metcalfe, R. Davids, and A.B.P. Lever. Bull. Chem. Soc. Jpn. **71**, 1039 (1998); (*c*) K.J.M. Nolan and C.C. Leznoff. Synlett, 593 (1997).
133. (*a*) H. Naarmann and M. Hanack. Chem. Abstr. **115** P208923d (1991); (*b*) E.M. Maya, P. Haisch, P. Vazquez, and T. Torres. Tetrahedron, **54**, 4397 (1998).
134. H.S. Nalwa and J.S. Shirk. *In* Phthalocyanines: properties and applications, Vol 4. *Edited by* C.C. Leznoff and A.B.P. Lever, VCH, New York. 1996.
135. B. Suchozak. M.Sc. Thesis, York University, Toronto, Canada. 1999.

© 2000 NRC Canada

Solubility of the pesticide diuron in organic nonelectrolyte solvents. Comparison of observed vs. predicted values based upon Mobile Order theory

Karina M. De Fina, Tina L. Sharp, Michael A. Spurgin, Ivette Chuca, William E. Acree, Jr., Caroline E. Green, and Michael H. Abraham

Abstract: Experimental solubilities are reported at 25.0°C for diuron (also called 3-(3,4-dichlorophenyl)-1,1-dimethyl urea) dissolved in 49 different organic nonelectrolyte solvents containing ether-, chloro-, hydroxy-, ester-, methyl-, and *tert*-butyl-functional groups. Results of these measurements are used to test the applications and limitations of expressions derived from Mobile Order theory. For the 28 nonalcoholic solvents for which predictions could be made computations show that Mobile Order theory does provide fairly reasonable estimates of the saturation mole fraction solubilities. Average absolute deviation between predicted and observed values is 60.1%. Diuron solubilities in the alcohol solvents are used to calculate stability constants for presumed solute-solvent hydrogen bonds that are believed to occur in solution.

Key words: pesticide, diuron solubilities, organic nonelectrolyte solvents, solubility predictions.

Résumé: On a déterminé les solubilités expérimentales de la 1,1-diméthyl-3-(3,4-dichlorophényl)urée (nom générique, diuron), 25,0°C, dans divers solvants organiques non électrolytiques portant, comme substituants, des atomes de chlore, des groupes ester, éther, hydroxyle, méthyle et *tert*-butyle. On a utilisé les résultats de ces mesures pour évaluer les applications et les limitations d'expressions dérivées de la théorie de l'ordre mobile. Pour les 28 solvants non alcooliques pour lesquels il a été possible de faire des prédictions, les calculs montrent que la théorie de l'ordre mobile conduit à des évaluations assez raisonnables des solubilités exprimées en fractions molaires de saturation. La déviation absolue moyenne entre les valeurs prédite et observée est de 60,1%. Les solubilités du diuron dans les solvants alcooliques ont été utilisées pour calculer les constantes de stabilité des liaisons hydrogènes qui se produiraient en solution.

Mots clés: pesticide, solubilités du diuron, solvants organiques non électrolytiques, prédictions des solubilités.

[Traduit par la Rédaction]

Introduction

Solid-liquid equilibrium data of organic nonelectrolyte systems are becoming increasingly important in the petroleum industry, particularly in light of present trends towards heavier feedstocks and known carcinogenicity and mutagenicity of many of the larger polycyclic aromatic compounds. Solubility data for a number of polycyclic aromatic hydrocarbons (e.g., anthracene and pyrene) and heteroatom polynuclear aromatics (e.g., carbazole, dibenzothiophene, and xanthene) have been published in the recent chemical literature (for listing of references see Acree (1–3)). Despite efforts by experimentalists and scientific organizations, both in terms of new experimental measurements and critically-evaluated data compilations, there still exist numerous systems for which solubility data are not readily available.

To address this problem, researchers have turned to group contribution methods and semiempirical expressions to predict desired quantities. Group contribution methods have proved fairly successful in estimating solid solubility in pure and binary solvent mixtures from structural information (4–11). Practical application though, is limited to systems for which all group interaction parameters are known. Interaction parameters can be evaluated from liquid-vapor, liquid-liquid, and solid-liquid equilibria data. It is important that the data base contain as many different functional groups as possible, preferably with adequate representation from both mono- and multi-functional solute/solvent molecules to permit eval-

Received August 24, 1999.
K.M. De Fina, T.L. Sharp, M.A. Spurgin, I. Chuca, and W.E. Acree, Jr.[1] Department of Chemistry, University of North Texas, Denton, TX 76203-5070, U.S.A.
C.E. Green and M.H. Abraham. Department of Chemistry, University College London, 20 Gordon Street, London WC1H 0AJ, U.K.

[1]Author to whom correspondence may be addressed. (e-mail: Acree@unt.edu).

 © 2000 NRC Canada

uation of potential synergistic effects. The data base should contain sufficient experimental values near infinite dilution in the event that one wishes to determine separate interaction parameters for finite concentration and infinite dilution activity coefficient predictions.

Abraham and coworkers (12, 13) recently developed a general solvation equation that can be used in the correlation and understanding of physicochemical and biochemical phenomena. Physical properties that have been correlated include gas/solvent partition coefficients (as log L)

$$[1] \quad \log L = c + rR_2 + s\pi_2^H + a\sum\alpha_2^H + b\sum\beta_2^H + d \log L^{16}$$

and water/solvent partition coefficients (as log P)

$$[2] \quad \log P = c + rR_2 + s\pi_2^H + a\sum\alpha_2^H + b\sum\beta_2^H + vV_x$$

where R_2 and V_x refer to the excess molar refraction and McGowan volume of the solute, respectively, π_2^H is the solute dipolarity/polarizability descriptor, $\sum\alpha_2^H$ and $\sum\beta_2^H$ are measures of the solute's hydrogen bond acidity and hydrogen bond basicity, and L^{16} is the solute's gas-liquid partition coefficient on hexadecane at 298 K. For any given solvent, numerical values of the seven curve-fit coefficients (c, r, s, a, b, d, and v) are deduced by regressing experimental partition coefficient data in accordance with eqs. [1] and [2]. The input partition coefficients were sometimes calculated as the ratio of the solute molar solubilities in the organic solvent and water, $P = C_A^{org}/C_A^{aq}$, and as the ratio of the solute molar solubility in the organic solvent and vapor concentration, $L = C_A^{org}/C_A^{gas}$. Published papers have reported regressional coefficients for water (12, 13) and a few select organic solvents (13, 14)[2].

To increase the solubility database available for developing group contribution methods and general solvation correlations, we are in the process of measuring solubility data for several crystalline organic compounds. In the present communication, we report diuron (also called 3-(3,4-dichlorophenyl)-1,1-dimethyl urea) solubilities at 25°C in 49 different organic solvents of varying polarity and hydrogen bonding capability. Results of the measurements are used to further test the applications and limitations of predictive expressions derived from Mobile Order theory. A subsequent study[3] will use the experimental solubility data to determine the numerical values for diuron's solute descriptors based upon eqs. [1] and [2] and known solvent coefficients. At the present time, we have solvent coefficients for 27 of the organic solvents studied. Solute descriptors allow one to estimate biological properties involving blood-brain distribution (15), brain perfusion (16), water-skin permeation (17), tadpole narcosis (18), nasal pungency thresholds in man (19), upper respiratory tract irritation in mice (20), and eye irritation in mice (21) and man (22) from previously published correlation equations. Once the solute descriptors are calculated, we plan to use the remaining solubility data, together with other data, in the determination of c, r, s, a, b, d, and v values for additional organic solvents.

Materials and methods

Diuron (Sigma, 98%) was used as received. *n*-Hexane (Aldrich, 99%), *n*-heptane (Aldrich, HPLC), *n*-octane (Aldrich, 99+%, anhydrous), *n*-nonane (TCI, 99+%), *n*-decane (TCI, 99+%), *n*-hexadecane (Aldrich, 99%), cyclohexane (Aldrich, HPLC), methylcyclohexane (Aldrich, 99+%, anhydrous), cyclooctane (Aldrich, 99+%), 2,2,4-trimethylpentane (Aldrich, HPLC), *tert*-butylcyclohexane (Aldrich, 99+%), methanol (Aldrich, 99.9+%), ethanol (Aaper Alcohol and Chemical Comp., absolute), 1-propanol (Aldrich, 99+%, anhydrous), 2-propanol (Aldrich, 99+%, anhydrous), 1-butanol (Aldrich HPLC, 99.8+%), 2-butanol (Aldrich, 99+%, anhydrous), 1-pentanol (Aldrich, 99+%), 2-pentanol (Acros 99+%), 1-hexanol (Alfa Aesar, 99+%), 1-heptanol (Alfa Aesar, 99+%), 2-methyl-2-butanol (Acros, 99+%), 2-methyl-1-propanol (Aldrich, 99+%, anhydrous), 3-methyl-1-butanol (Aldrich, 99+%, anhydrous), 1-octanol (Aldrich, 99+%, anhydrous), 4-methyl-2-pentanol (Acros, 99+%), 2-ethyl-1-hexanol (Aldrich, 99+%), 2-methyl-1-pentanol (Aldrich, 99%), 2-methyl-2-propanol (Arco Chemical Comp., 99+%), 1-decanol (Alfa Aesar, 99+%), cyclopentanol (Aldrich, 99%), ethylene glycol (Aldrich, 99.8%, anhydrous), benzene (Aldrich, HPLC, 99.9+%), toluene (Aldrich, 99.8%, anhydrous), chlorobenzene (Aldrich, HPLC, 99.9+%), ethylbenzene (Aldrich, 99.8%, anhydrous), tetrahydrofuran (Aldrich, 99.9%, anhydrous), 1,4-dioxane (Aldrich, 99.8%, anhydrous), dibutyl ether (Aldrich, 99%), carbon tetrachloride (Aldrich, HPLC, 99.9+%), chloroform (HPLC, Aldrich, 99.9%), 1-chlorobutane (Sigma-Aldrich, HPLC, 99.5+%), 1-chlorooctane (Aldrich, 99%), chlorocyclohexane (Aldrich, 99%), dichloromethane (Aldrich, 99.8%, anhydrous), 1,2-dichloroethane (Aldrich, HPLC, 99.8%), ethyl acetate (Aldrich, HPLC, 99.9%), butyl acetate (Aldrich HPLC, 99.7%), and acetonitrile (Aldrich, 99.8%, anhydrous) were stored over molecular sieves and distilled shortly before use. Gas chromatographic analysis showed diuron to have a purity of 99.5 mole percent, and solvent purities to be 99.7 mole percent or better.

Excess solute and solvent were placed in amber glass bottles and allowed to equilibrate in a constant temperature water bath at 25.0 ± 0.1°C for at least three days (often longer). Attainment of equilibrium was verified both by repetitive measurements after several additional days and by approaching equilibrium from supersaturation by pre-equilibrating the solutions at a higher temperature. Aliquots of saturated diuron solutions were transferred through a coarse filter into a tared volumetric flask to determine the amount of sample and diluted quantitatively with 2-propanol for spectrophotometric analysis at either 254 nm (alkane solvents and dibutyl ether) or 286 nm (all other solvents) on a Bausch and Lomb Spectronic 2000. Concentrations of the dilute solutions were determined from a Beer–Lambert law absorbance vs. concentration working curve for nine standard solutions. The calculated molar absorptivity of

[2] M.H. Abraham, J. Le, and W.E. Acree, Jr. Manuscript in preparation.
[3] C.E. Green, M.H. Abraham, and W.E. Acree, Jr. Manuscript in preparation.

© 2000 NRC Canada

diuron at 254 nm varied slightly with concentration, ranging from a value of $\epsilon \approx 20\,950$ L mol^{-1} cm^{-1} (1.83×10^{-5} M) to $\epsilon \approx 19\,580$ L mol^{-1} cm^{-1} (9.16×10^{-5} M). At 286 nm the calculated molar absorptivity of $\epsilon \approx 1395$ L mol^{-1} cm^{-1} was constant over the concentration range of 1.97×10^{-4} M – 1.18×10^{-3} M. Molar solubilities in the six water-saturated solvents were determined in similar fashion, except that a known volume of sample was removed from the amber glass bottles for spectroscopic analysis.

Experimental molar concentrations were converted to (mass/mass) solubility fractions by multiplying by the molar mass of diuron, volume(s) of volumetric flask(s) used, and any dilutions required to place the measured absorbances on the Beer–Lambert law absorbance vs. concentration working curve, and then dividing by the mass of the saturated solution analyzed. Mole fraction solubilities were computed from (mass/mass) solubility fractions using the molar masses of the solute and solvent. Experimental mole fraction solubilities, X_A^{sat}, are listed in Tables 1 and 2 for diuron dissolved in 49 dry organic solvents and in six water-saturated organic solvents, respectively. Numerical values were obtained using diuron as received from the supplier, and they represent the average of between four and eight independent determinations. The measurements were reproducible to within ±2%. We did recrystallize several grams of the solid from methanol for solubility determinations in a few select solvents (benzene, methanol, heptane, tetrahydrofuran, chloroform, and butyl acetate). To within the stated experimental uncertainty of ±2%, there was no difference in the experimental solubilities using the recrystallized and unrecrystallized samples.

Results and discussion

Solvents listed in Table 1 include both noncomplexing alkanes and self-associating alcohols. Of the many solution models proposed in recent years, Mobile Order theory is perhaps the only one that is capable of describing solute behavior in such a wide range of solvent mixtures. The basic model (23–30) assumes that all molecular groups perpetually move, and that neighbors of a given kind of external atom in a molecule constantly change identity. All molecules of a given kind dispose of the same volume, equal to the total volume V of the liquid divided by the number N_A of molecules of the same kind, i.e., Dom A = V/N_A. The center of this domain perpetually moves. The highest mobile disorder is achieved whenever groups visit all parts of their domain without preference. Preferential contacts lead to deviations with respect to this "random" visiting. This is especially true in the case of hydrogen-bonding as specific interactions result in a specific orientation of the "donor" molecule with respect to an adjacent "acceptor" molecule.

In the case of an inert crystalline solute dissolved in a self-associating solvent, Mobile Order theory expresses the volume fraction saturation solubility, ϕ_A^{sat}, as

$$[3]\quad \ln \phi_A^{sat} = \ln a_A^{solid} - 0.5(1 - V_A/V_{solvent})\phi_{solvent} + 0.5 \ln [\phi_A^{sat} + \phi_{solvent}(V_A/V_{solvent})] - \phi_{solvent}^2 V_A(\delta'_A - \delta'_{solvent})^2(RT)^{-1} - r_{solvent}(V_A/V_{solvent})\phi_{solvent}$$

where the $r_{solvent}(V_A/V_{solvent})\phi_{solvent}$ term represents the contributions resulting from hydrogen-bond formation between the solvent molecules. For most of the published applications, $r_{solvent}$ was assumed to be unity for strongly associated solvents with single hydrogen-bonded chains such as monofunctional alcohols, to be two for water or diols, and to equal zero for non-associated solvents such as saturated hydrocarbons. A more exact value for alcoholic solvents can be calculated based upon

$$[4]\quad r_{solvent} = (K_{solvent}\ \phi_{solvent}/V_{solvent})/(1 + K_{solvent}\ \phi_{solvent}/V_{solvent})$$

with a numerical value of $K_{solvent} = 5000$ cm^3 mol^{-1} assumed for all mono-functional alcohols.

If complexation does occur between the crystalline solute and solvent

$$[5]\quad \ln \phi_A^{sat} = \ln a_A^{solid} - 0.5(1 - V_A/V_{solvent})\phi_{solvent} + 0.5 \ln [\phi_A^{sat} + \phi_{solvent}(V_A/V_{solvent})] - \phi_{solvent}^2 V_A(\delta'_A - \delta'_{solvent})^2(RT)^{-1} + \ln [1 + \phi_{solvent}(K_{ASolvent}/V_{solvent})]$$

then an additional term involving the solute–solvent equilibrium constant, $K_{ASolvent}$, must be introduced to describe the solubility enhancement that arises as a result of specific interactions. A slightly more complex expression applies in the case of solute complexation with a self-associating solvent. The expression's mathematical form depends to a large extent upon the number and type of hydrogen-bond acid and hydrogen-bond base functional groups in the solute molecule being studied. In the present case, diuron contains an -NC(O)NH- moiety which could conceivably act as both a hydrogen-bond base (through the lone electron pairs on the oxygen and nitrogen atoms) and hydrogen-bond acid.

Examination of the solubility data in Table 1 reveals that diuron is 10 times more soluble in dibutyl ether ($X_A^{sat} = 0.0005037$) than in the two saturated hydrocarbons, *n*-octane ($X_A^{sat} = 0.00002934$) and *n*-nonane ($X_A^{sat} = 0.00003615$) of comparable size. The large solubility enhancement observed by the introduction of the ether functional group into an alkane solvent suggests formation of a diuron – dibutyl ether association complex. If such complexation does occur then diuron's -NC(O)NH- functional group must act as a hydrogen-bond acid. The ether oxygen on dibutyl ether has no choice other than to act as a hydrogen-bond base. We do not believe, however, that the observed solubility enhancement results from complexation. As shown in the third and fourth columns of Table 1, eq. [3] of Mobile Order theory predicts the mole fraction solubility of diuron in dibutyl ether to within 9.1% without introducing any solute–solvent stability constants. Based upon these observations we feel that if diuron does interact specifically with alcohol solvent molecules in solution, the -NC(O)NH- functional group will act as a hydrogen-bond base, rather than as a hydrogen-bond acid.

An "O contribution" (see Ruelle et al. (29, 30))

$$[6]\quad O = \sum v_{Oi} \ln \{1 + K_{Oi} [(\phi_{solvent}/V_{solvent}) - v_{Oi} (\phi_A^{sat}/V_A)]\}$$

© 2000 NRC Canada

Table 1. Comparison between experimental diuron mole fraction solubilities and predicted values based upon mobile order theory.

Organic Solvent	$(X_A^{sat})^{exp,\ a}$	$(X_A^{sat})^{calc}$	% Dev[b]	$\Delta \ln X_A^{sat,\ c}$
n-Hexane	0.00001828	0.00002695	47.4	0.39
n-Heptane	0.00002703	0.00002428	–10.2	–0.11
n-Octane	0.00002934	0.00003100	5.7	0.06
n-Nonane	0.00003615	0.00004110	13.7	0.13
n-Decane	0.00004192	0.00004510	18.9	0.07
n-Hexadecane	0.00006794	0.00008515	25.3	0.23
Cyclohexane	0.00002676	0.00003135	17.2	0.16
Methylcyclohexane	0.00004661	0.00003820	–18.0	–0.20
Cyclooctane	0.00006082	0.00006239	2.6	0.03
2,2,4-Trimethylpentane	0.00002694	0.00001495	–44.5	–0.59
tert-Butylcyclohexane	0.00007557	0.00006969	–7.8	–0.08
Benzene	0.0008417	0.002276	170.4	0.99
Toluene	0.0008907	0.001076	20.8	0.19
Ethylbenzene	0.0007200	0.0009725	35.1	0.30
Chlorobenzene	0.001686	0.003156	87.2	0.63
Dichloromethane	0.002922	0.007678	162.8	0.97
1,2-Dichloroethane	0.004258	0.008415	97.6	0.68
Chloroform	0.005354	0.002087	–61.0	–0.94
Carbon tetrachloride	0.0002389	0.0004137	73.2	0.55
1-Chlorobutane	0.001086	0.0004240	–61.0	–0.94
1-Chlorooctane	0.001980	0.0009077	–54.2	–0.78
Chlorocyclohexane	0.001427	0.001369	–4.1	–0.04
Dibutyl ether	0.0005037	0.0005495	9.1	0.09
Tetrahydrofuran	0.03060	0.003008	–90.2	–2.32
1,4-Dioxane	0.007188	0.007564	5.2	0.05
Methanol	0.007681	0.007045[d]		
Ethanol	0.009406	0.009082[d]		
1-Propanol	0.01068	0.01024[d]		
2-Propanol	0.007700	0.01461[d]		
1-Butanol	0.01197	0.01186[d]		
2-Butanol	0.008521	0.008053[d]		
2-Methyl-1-propanol	0.008479	0.008273[d]		
2-Methyl-2-propanol	0.006467			
1-Pentanol	0.01402	0.01382[d]		
2-Pentanol	0.009004			
3-Methyl-1-butanol	0.01073			
2-Methyl-2-butanol	0.005469			
1-Hexanol	0.01442	0.01477[d]		
2-Methyl-1-pentanol	0.01122			
4-Methyl-2-pentanol	0.007564			
1-Heptanol	0.01506	0.01447[d]		
1-Octanol	0.01581	0.01520[d]		
2-Ethyl-1-hexanol	0.009674			
1-Decanol	0.01397	0.01418[d]		
Cyclopentanol	0.01437			
Ethylene glycol	0.00000009565			
Butyl acetate	0.009931	0.003288	–66.9	–1.11
Ethyl acetate	0.009135	0.006795	–25.6	–0.30
Acetonitrile	0.004296	0.02345	445.9	1.70
AVERAGE ABSOLUTE DEVIATIONS			60.1	0.52

[a]Numerical values represent the average of between four and eight independent determinations, with the measurements being reproducible to ±2%.

[b]Deviations (%) = $100[(X_A^{sat})^{calc} - (X_A^{sat})^{exp}]/(X_A^{sat})^{exp}$.

[c]$\Delta \ln X_A^{sat} = \ln (X_A^{sat})^{calc} - \ln (X_A^{sat})^{exp}$.

[d]Numerical values of K_{Oi} used were: K_{Oi} = 2500 cm^3 mol^{-1} for methanol; K_{Oi} = 6500 cm^3 mol^{-1} for ethanol; K_{Oi} = 10 000 cm^3 mol^{-1} for 1-propanol and 2-propanol; K_{Oi} = 12 000 cm^3 mol^{-1} for 1-butanol; K_{Oi} = 15 000 cm^3 mol^{-1} for 2-butanol; K_{Oi} = 18 000 cm^3 mol^{-1} for 1-pentanol; K_{Oi} = 25 000 cm^3 mol^{-1} for 2-methyl-1-propanol; K_{Oi} = 30 000 cm^3 mol^{-1} for 1-hexanol and 1-heptanol; and K_{Oi} = 32 000 cm^3 mol^{-1} for 1-octanol and 1-decanol.

© 2000 NRC Canada

Table 2. Comparison between experimental molar diuron solubilities, $(C_A^{sat})^{exp}$, measured in dry solvents and in water-saturated organic solvents.

Organic Solvent	$(C_A^{sat})^{exp}$ (Dry)[a]	$(C_A^{sat})^{exp}$ (Wet)
2-Methyl-1-propanol	0.09077	0.1329
1-Pentanol	0.1281	0.1533
1-Hexanol	0.1147	0.1340
1-Octanol	0.09980	0.1120
Ethyl acetate	0.09217	0.1577
Butyl acetate	0.07477	0.1032

[a]Molarities in the dry solvents were calculated from the experimentally measured mole fraction solubilities using the ideal molar volume approximation and V_{diuron} = 164.8 cm^3 mol^{-1}.

must be added to eq. [3] to describe the effect on the solubility of the H-bonds formed between the hydrogen-bond base sites on the solute and hydrogen-bond acid sites on the solvent. Each particular H-bond interaction like oxygen–alcohol (or nitrogen–alcohol) contributes to increase solubility, and is characterized by the group interaction stability constant K_{Oi}. For crystalline proton-acceptor solute molecules having limited solubility ($\phi_A^{sat} \approx 0$) the predictive expression becomes

$$[7] \quad \ln \phi_A^{sat} = \ln a_A^{solid} - 0.5(1 - V_A/V_{solvent})\phi_{solvent} + 0.5 \ln [\phi_A^{sat} + \phi_{solvent}(V_A/V_{solvent})] - \phi_{solvent}^2 V_A(\delta'_A - \delta'_{solvent})^2(RT)^{-1} - r_{solvent}(V_A/V_{solvent})\phi_{solvent} + \sum \nu_{Oi} \ln \{1 + K_{Oi}[(\phi_{solvent}/V_{solvent})\}$$

where ν_{Oi} is the number of active and independent type *i* proton-acceptor sites on the solute molecule. Equation [7] assumes specific interactions in solution, but not in the solid state. The crystalline phase in equilibrium with the saturated solution is taken to be pure diuron. The existence of molecular association complexes in solution does not necessarily require that the complex must also exist in the solid phase. Packing constraints in the crystalline phase may prevent the formation of solid molecular complexes.

The symbols δ'_A and $\delta'_{solvent}$ in eqs. [3], [5], and [7] denote the modified solubility parameters of the solute and solvent, respectively, V_i is the molar volume, and a_A^{solid} is the activity of the solid solute. This latter quantity is defined as the ratio of the fugacity of the solid to the fugacity of the pure hypothetical supercooled liquid. The numerical value of a_A^{solid} can be computed from

$$[8] \quad \ln a_A^{solid} = -\Delta H_A^{fus}(T_{mp} - T)/(RTT_{mp}) + (\Delta C_{p,A}/RT)(T_{mp} - T) - (\Delta C_{p,A}/T) \ln (T_{mp}/T)$$

the solute's molar enthalpy of fusion, ΔH_A^{fus}, and heat capacity difference, $\Delta C_{p,A}$, at the normal melting point temperature, T_{mp}. Contributions from nonspecific interaction are incorporated into Mobile Order theory through the $\phi_{solvent}^2 V_A(\delta'_A - \delta'_{solvent})^2(RT)^{-1}$ term. Ruelle and co-workers (26–30) have presented an impressive set of comparisons between experimental and predicted values for anthracene, naphthalene, pyrene, biphenyl, carbazole, benzil, *p*-benzoquinone, tricosane, octacosane, 10-nonadecanone, 11-heneicosanone, and 12-tricosanone solubilities in a wide range of both noncomplexing and complexing solvents to document the predictive ability of Mobile Order theory.

Predictive application of eqs. [3], [5], and [7] is relatively straightforward. First, an average numerical value of δ'_{diuron} = 24.57 MPa$^{1/2}$ is computed by requiring that each equation (with $r_{solvent}$ = 0 and (or) $K_{ASolvent}$ = 0) perfectly describes diuron mole fraction solubility data in *n*-hexane (δ'_{diuron} = 24.66 MPa$^{1/2}$), *n*-heptane (δ'_{diuron} = 24.46 MPa$^{1/2}$), and *n*-octane (δ'_{diuron} = 24.58 MPa$^{1/2}$). The numerical value of a_A^{solid} = 0.01590 is calculated using eq. [6] with ΔH_A^{fus} = 33 890 J mol^{-1} and T_{mp} = 429.7 K (31). The two heat capacity terms in eq. [8] were set equal to zero as we were unable to find heat capacity data for the subcooled liquid solute. A numerical value of V_{diuron} = 164.8 cm^3 mol^{-1} was used for the molar volume of the hypothetical subcooled liquid solute. The solute's molar volume was estimated using a group contribution method and molar volumes of dichlorobenzene and organic molecules having amide and methyl functional groups.

Table 1 summarizes the predictive ability of Mobile Order theory for the 28 different organic solvents for which both diuron solubility data and modified solubility parameters could be found. Solvent molar volumes and modified solubility parameters are listed in Table 3. We were unable to find modified solubility parameters for all of the secondary and branched alcohols. The modified solubility parameters account for only nonspecific interactions, and in the case of the alcoholic solvents the hydrogen-bonding contributions have been removed. Numerical values of $\delta'_{solvent}$ were obtained from published compilations (26, 27, 29, 30), and were either deduced by regressing actual solubility data of solid *n*-alkanes in organic solvents in accordance with the configurational entropic model of Huyskens and Haulait-Pirson (32) or estimated using known values for similar organic solvents. Examination of the entries in Table 1 reveals that Mobile Order theory does provide fairly reasonable (though by no means perfect) estimates of the solubility behavior of diuron in a wide range of nonalcoholic organic solvents. Average absolute deviation between predicted and observed values is 60.1%. Expressed on a natural logarithmic mole fraction scale, Mobile Order theory predicts the diuron solubilities to within an average absolute deviation of ±0.52 ln units. The arithmetic average of the ln X_A^{sat} difference is –0.06, which indicates a slight systematic error in the predicted values. Many solution models express the differences the between predicted and observed values in terms of the standard deviation. In the case of Mobile Order theory, the standard deviation for the diuron predictions is 0.75 ln units. We do note that Mobile order theory grossly overpredicts the solubility of diuron in acetonitrile. Similar failures were noted previously in the case of anthracene (33), fluoranthene (34), pyrene (34), and phenanthrene (35). We suspect that the overprediction results from either failure of the Scatchard–Hildebrand solubility parameter theory to describe the nonspecific interactions between acetonitrile and the various solutes, or perhaps from an incorrect value for this solvent's modified solubility parameter.

© 2000 NRC Canada

Table 3. Solvent and solute properties used in mobile order predictions.

Component (i)	V_i/(cm^3 mol^{-1})	δ'_i/(MPa$^{1/2}$)[a]
n-Hexane	131.51	14.56
n-Heptane	147.48	14.66
n-Octane	163.46	14.85
n-Nonane	179.87	15.07
n-Decane	195.88	15.14
n-Hexadecane	294.12	15.61
Cyclohexane	108.76	14.82
Methylcyclohexane	128.32	15.00
2,2,4-Trimethylpentane	166.09	14.30
Cyclooctane	134.9	15.40
tert-Butylcyclohexane	173.9	15.50
Benzene	89.4	18.95
Toluene	106.84	18.10
Ethylbenzene	123.1	18.02
Chlorobenzene	102.1	19.48
Dichloromethane	64.5	20.53
1,2-Dichloroethane	78.8	20.99
Chloroform	80.7	18.77
Carbon tetrachloride	97.08	17.04
1-Chlorobutane	105.0	17.12
1-Chlorooctane	171.1	18.00
Chlorocyclohexane	120.3	18.45
Dibutyl ether	170.3	17.45
Tetrahydrofuran	81.4	19.30
1,4-Dioxane	85.8	20.89
Methanol	40.7	19.25
Ethanol	58.7	17.81
1-Propanol	75.10	17.29
2-Propanol	76.90	17.60
1-Butanol	92.00	17.16
2-Butanol	92.4	16.60
2-Methyl-1-propanol	92.8	16.14
1-Pentanol	108.6	16.85
1-Hexanol	125.2	16.40
1-Heptanol	141.9	16.39
1-Octanol	158.3	16.38
1-Decanol	191.6	16.35
Butyl acetate	132.5	19.66
Ethyl acetate	98.5	20.79
Acetonitrile	52.9	23.62
Diuron[b]	164.8[c]	24.57[d]

[a]Tabulated values are taken from a compilation given in Ruelle et al. (26, 27, 29, 30).

[b]The numerical value of a_A^{solid} = 0.01590 was calculated from eq. [8] using ΔH_A^{fus} = 33 890 J mol^{-1} and T_{mp} = 429.7 K (31).

[c]Numerical value of V_{diuron} = 164.8 cm^3 mol^{-1} was estimated using a group contribution method and molar volumes of dichlorobenzene and molecules having amide and methyl functional groups.

[d]Numerical value was calculated using the measured diuron mole fraction solubilities in *n*-hexane, *n*-heptane, and *n*-octane, in accordance with Eqs. [3] and [5]; with $r_{solvent}$ = 0 and (or) $K_{ASolvent}$ = 0.

Alcoholic solvents were excluded from all statistical analyses because the observed mole fraction solubility was used to determine the K_{Oi} stability constant for each diuron–alcohol solvent pair in solution using eq. [7] with v_{oi} set equal to one. Hence, the numerical entries in the third column of Table 1 represent back-calculated mole fraction solubilities, rather than predicted values. The numerical value of K_{Oi} was found to increase with increasing alcohol size, ranging from a lower limit of about $K_{Oi} \approx 2500$ cm^3 mol^{-1} for methanol to an upper value of about $K_{Oi} \approx 32\,000$ cm^3 mol^{-1} for both 1-octanol and 1-decanol. This observation was not unexpected in that diuron is more soluble on a mole fraction basis in the larger alcohols than in the much smaller methanol and ethanol solvents. From a strictly mathematical point-of-view, this requires that the "O contribution" in eq. [7] must become larger with increasing alcohol. Moreover, the increased O contribution must offset the fact that the negative $-\phi^2_{solvent} V_A(\delta'_A - \delta'_{solvent})^2(RT)^{-1}$ term becomes more negative as $\delta'_{solvent}$ moves further away from δ'_{diuron}. This is what happens as one progresses in alcohol size from methanol to 1-decanol. The modified solubility parameter of methanol ($\delta'_{methanol}$ = 19.25 MPa$^{1/2}$) is much closer to the modified solubility parameter of diuron (δ'_{diuron} = 24.57 MPa$^{1/2}$) than is the modified solubility parameter of 1-decanol (δ'decanol = 16.35 MPa$^{1/2}$). Without the O contribution and without a larger K_{Oi} value, Mobile Order theory would have predicted that diuron would be significantly less soluble in 1-decanol than in methanol. Such predictions would be inconsistent with the observed mole fraction solubility data.

Readers are reminded that in evaluating the applicability of Mobile Order theory one must realize that many of these particular systems are highly nonideal, and that the experimental solubility data covers over a 1700-fold range in mole fraction. Had an ideal solution been assumed, then the predicted mole fraction solubility would be $X_A^{sat} = a_A^{solid} = 0.01590$ for each solvent. The ideal solution approximation corresponds to a considerably larger average absolute deviation of 17 590% between predicted and observed values for the nonalcoholic solvents studied.

Acknowledgements

Tina Sharp and Ivette Chuca thank the University of North Texas and the U. S. Department of Education for support provided under the Ronald E. McNair Postbaccalaureate Achievement Program. Michael Spurgin thanks the UNT Texas Academy of Math and Science (TAMS) for an undergraduate summer research fellowship. This work was funded in part by a travel award granted to C. E. Green by University College London, Graduate School Research Fund. We are also grateful to the European Commission for a studentship to C. E. Green, contract number SMT4-CT96-2114 (DG12-RSMT).

References

1. W.E. Acree, Jr. Polycyclic aromatic hydrocarbons in pure and binary solvents. IUPAC solubility data series, Vol. 54. Oxford University Press, Oxford, U.K. 1994.
2. W.E. Acree, Jr. Polycyclic aromatic hydrocarbons: binary nonaqueous systems: part 1 (solutes A–E). IUPAC solubility data series, Vol. 58. Oxford University Press, Oxford, U.K. 1995.
3. W.E. Acree, Jr. Polycyclic aromatic hydrocarbons: binary nonaqueous systems: part 2 (solutes F–Z). IUPAC solubility data series, Vol. 59. Oxford University Press, Oxford, U.K. 1995.

© 2000 NRC Canada

4. W.E. Acree, Jr. Int. J. Pharm. **18**, 47 (1984).
5. U. Domanska and T. Hofman. J. Solution Chem. **14**, 531 (1985).
6. U. Domanska. Fluid Phase Equilibr. **35**, 217 (1985).
7. R.S. Basu, H. Pham, and D.P. Wilson. Int. J. Pharm. **7**, 319 (1986).
8. A.B. Ochsner and T.D. Sokoloski. J. Pharm. Sci. **74**, 634 (1985).
9. R. Carta and S. Dernini. J. Chem. Eng. Data, **28**, 328 (1983).
10. W.E. Acree, Jr. and J.H. Rytting. Int. J. Pharm. **13**, 197 (1983).
11. A. Martin, P.L. Wu, A. Adjei, A. Beerbower, and J.M. Prausnitz. J. Pharm. Sci. **70**, 1260 (1981).
12. M.H. Abraham, H.S. Chadha, J.P. Dixon, and A.J. Leo. J. Phys. Org. Chem. **7**, 712 (1994).
13. M.H. Abraham, J. Andonian-Haftvan, J.P. Osei-Owasu, P. Sakellariou, J.S. Urieta, M.C. Lopez, and R. Fuchs. J. Chem. Soc., Perkin Trans. 2, 299 (1993).
14. M.H. Abraham, C.E. Green, W.E. Acree, Jr., C.E. Hernández, and L.E. Roy. J. Chem. Soc., Perkin Trans. 2, 2677 (1998).
15. M.H. Abraham, H.S. Chadha, and R.C. Mitchell. J. Pharm. Sci. **83**, 1257 (1994).
16. J.A. Gratton, M.H. Abraham, M.W. Bradbury, and H.S. Chadha. J. Pharm. Pharmacol. **49**, 1211 (1997).
17. M.H. Abraham, H.S. Chadha, and R.C. Mitchell. J. Pharm. Pharmacol. **47**, 8 (1995).
18. M.H. Abraham and C. Rafols. J. Chem. Soc., Perkin Trans. 2, 1843 (1995).
19. M.H. Abraham, R. Kumarsingh, J.E. Cometto-Muniz, and W.S. Cain. Arch. Toxicol. **72**, 227 (1998).
20. Y. Alarie, M. Schaper, G.D. Nielsen, and M.H. Abraham. Arch. Toxicol. **72**, 125 (1998).
21. M.H. Abraham, R. Kumarsingh, J.E. Cometto-Muniz, and W.S. Cain. Toxicol. in Vitro, **12**, 201 (1998).
22. M.H. Abraham, R. Kumarsingh, J.E. Cometto-Muniz, and W.S. Cain. Toxicol in Vitro, **12**, 403 (1998).
23. P.L. Huyskens and G.G. Siegel. Bull. Soc. Chim. Belg. **97**, 821 (1988).
24. G.G. Siegel, P.L. Huyskens, and G. Vanderheyden. Ber. Bunsen-Ges. Phys. Chem.**94**, 549 (1990).
25. P.L. Huyskens. J. Mol. Struct. **274**, 223 (1992).
26. P. Ruelle, C. Rey-Mermet, M. Buchmann, H. Nam-Tran, U.W. Kesselring, and P.L. Huyskens. Pharm. Res. **8**, 840 (1991).
27. P. Ruelle, M. Buchmann, H. Nam-Tran, and U.W. Kesselring. Int. J. Pharm. **87**, 47 (1992).
28. P. Ruelle, M. Buchmann, and U.W. Kesselring. J. Pharm. Sci. **83**, 396 (1994).
29. P. Ruelle, E. Sarraf, and U.W. Kesselring. Int. J. Pharm. **104**, 125 (1994).
30. P. Ruelle, E. Sarraf, L. Van den Berge, K. Seghers, M. Buchmann, and U.W. Kesselring. Pharm. Acta Helv. **68**, 49 (1993).
31. C. Plato and A.R. Glasgow, Jr. Anal. Chem. **41**, 330 (1969).
32. P.L. Huyskens and M.C. Haulait-Pirson. J. Mol. Liq. **31**, 135 (1985).
33. L.E. Roy, C.E. Hernández, and W.E. Acree, Jr. Polycyclic Aromat. Compd. **13**, 105 (1999).
34. L.E. Roy, C.E. Hernández, and W.E. Acree, Jr. Polycyclic Aromat. Compd. **13**, 205 (1999).
35. C.E. Hernández, K.M. De Fina, L.E. Roy, T.L. Sharp, and W.E. Acree, Jr. Can. J. Chem. **77**, 1465 (1999).

© 2000 NRC Canada

Excited state intramolecular proton transfer in 2-(2′-hydroxyphenyl)-1*H*-naphth-[2,3-*d*]-imidazole: effects of solvents and pH

Somes K. Das, G. Krishnamoorthy, and Sneh K. Dogra

Abstract: The solvent dependent study of absorption, fluorescence, and fluorescence excitation spectra of 2-(2′-hydroxyphenyl)-1*H*-naphth-[2,3-*d*]-imidazole (HPNI) have indicated the presence of different rotamers and tautomers in the S_0 and S_1 states. Similarity of the absorption and fluorescence spectra of HPNI in protic solvents with those of 2-(2′-methoxyphenyl)-1*H*-naphth-[2,3-*d*]-imidazole (MPNI) suggests that the normal emission is observed from the rotamers **2** and **4**, whereas the tautomer emission is observed from the tautomer **3**, formed by the excited state intramolecular proton transfer (ESIPT) in the rotamer **1** (Scheme 1). Ground state geometries of rotamers **1**, **2**, and the tautomer **3** were optimized using AM1 method. The results show that the rotamer **2** is the most stable and its stability further increases in polar and protic solvents due to the dipolar solvation interaction. The increase in the fluorescence quantum yield of the normal band when methanol or water is added to dioxane is due to: (*i*) the formation of rotamer **4**, where ESIPT is not possible and (*ii*) the decrease in the rate of non-radiative decay process. Very large red shifted fluorescence bands of the monocations of HPNI and MPNI in different solvents have been assigned to the charge transfer band.

Key words: 2-(2′-hydroxyphenyl)-1*H*-naphth-[2,3-*d*]-imidazole, ESIPT, prototropic reactions, fluorescence, 2-(2′-methoxyphenyl)-1*H*-naphth-[2,3-*d*]-imidazole.

Résumé : L'influence du solvant sur les spectres d'absorption, de fluorescence et d'excitation de fluorescence du 2-(2-hydroxyphényl)-1*H*-napht-[2,3-*d*]-imidazole (HPNI) suggère la présence de divers rotamères et tautomères dans les états S_0 et S_1. Les similarités entre les spectres d'absorption et de fluorescence du HPNI dans les solvants protiques et ceux du 2-(2-méthoxyphényl)-1*H*-naph-[2,3-*d*]-imidazole (MPNI) suggèrent que l'émission normale est observée à partir des rotamères **2** et alors que l'on observe l'émission tautomère à partir du tautomère **3** qui se forme par un transfert intramoléculaire de proton dans l'état excité (TIPEE) du rotamère **1** (Schéma **1**). Les géométries des rotamères **1** et **2** et du tautomère **3** dans leur état fondamental ont été optimisées à l'aide de la méthode AM1. Les résultats montrent que le rotamère **2** est le plus stable que sa stabilité est accrue par les solvants polaires et protiques en raison de l'interaction de solvatation dipolaire. L'augmentation du rendement quantique de fluorescence de la bande normale par addition de méthanol ou d'eau au dioxane résulte de: (*i*) la formation du rotamère **4** dans les cas où le TIPEE n'est pas possible; et (*ii*) de la diminution de la vitesse du processus de décroissance non radiative. Les importants déplacements vers le rouge des bandes de fluorescence des monocations du HPNI et du MPNI dans différents solvants ont été attribués à la bande de transfert de charge.

Mots clés : 2-(2-hydroxyphényl)-1*H*-napht-[2,3-*d*]-imidazole, TIPEE, réactions prototropiques, fluorescence, 2-(2-méthoxyphényl)-1*H*-naph-[2,3-*d*]-imidazole.

[Traduit par la Rédaction]

1. Introduction

The excited state intramolecular proton transfer (ESIPT) reactions have been an attractive topic of recent investigations as it is a possible mechanism for a number of photochemical (1–6) and photobiological processes (7). The main requirement of this process is that intramolecular hydrogen bonding should be present between the acidic and the basic moieties of the molecule in the ground state. Upon excitation to the first singlet state, the charge densities are changed on these basic centres, thereby drastically altering the acidic and the basic properties of these groups and thus leading to the intramolecular proton transfer. The acidic groups are in general -OH and -NH_2 and the basic groups are =N- and >C=O. Thus phototautomerism could be keto–enol or amine–imine tautomerization. It has been found that this process is extremely fast and requires nearly zero activation energy (7–10), and also occurs in frozen and solid states. Recently many molecules (1–12) showing ESIPT process have been investigated thoroughly and these molecules have been used in the action of many lasing dyes (13–18), polymer photostabilizers, (19) etc.

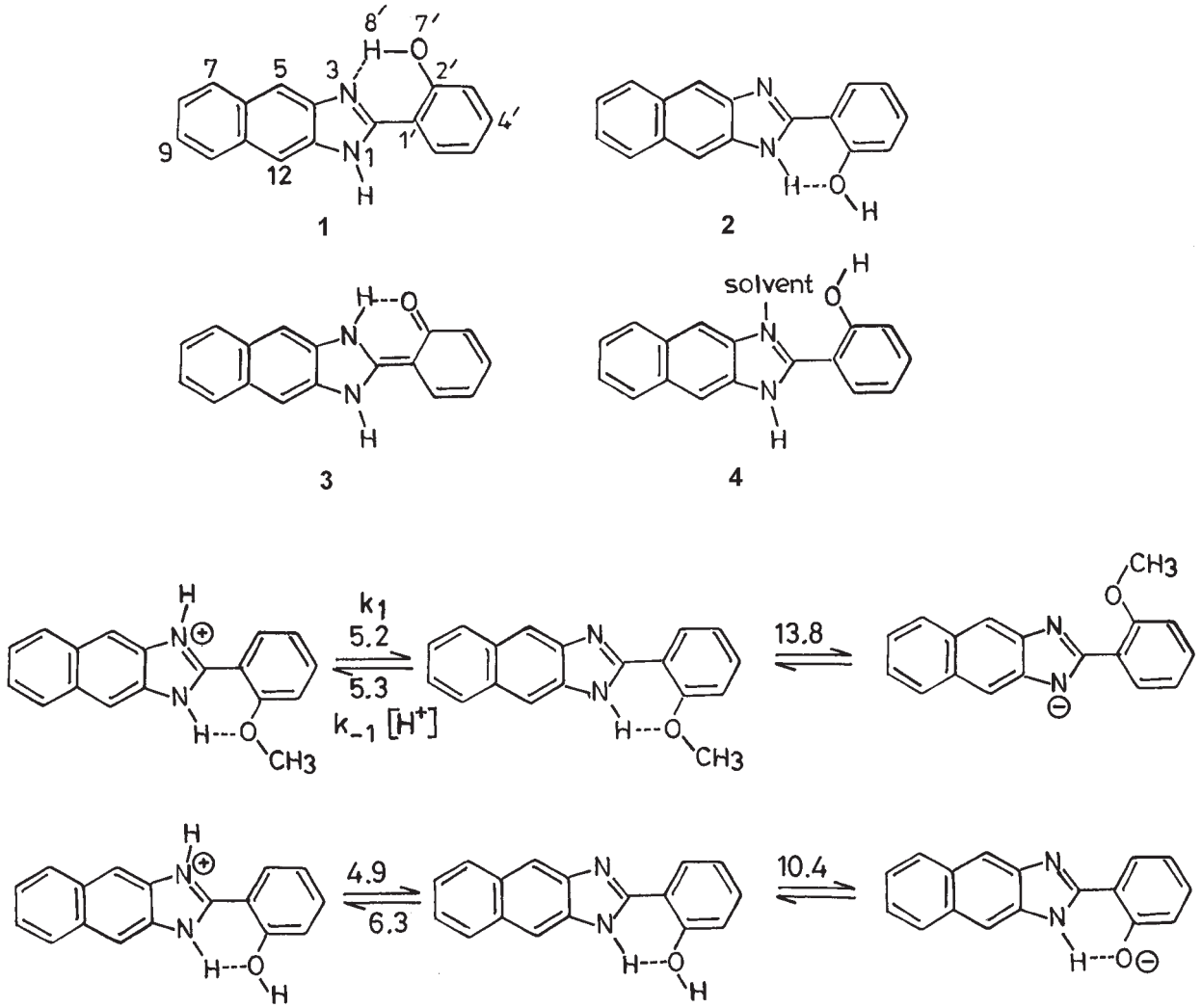
Received January 19, 1999.

S.K. Das, G. Krishnamoorthy, and S.K. Dogra.[1]
Department of Chemistry, Indian Institute of Technology Kanpur, Kanpur-208016, India.

[1]Author to whom correspondence may be addressed.
e-mail: skdogra@iitk.ernet.in

© 2000 NRC Canada

Scheme 1.



Recently we have studied ESIPT in a large number of molecules containing keto–enol (20–22) or amine–imine (23–25) phototautomerism and have started using these molecules as probes to study the characteristics of the organized assemblies (26–28). Some of these molecules exhibit dual fluorescence (20–23) and the others only one fluorescence band (24–25). Acuna et. al. (15) have shown that 2-(2′-hydroxyphenyl)benzimidazole (HPBI) molecule can be used as a tunable dye laser in the range of 440–470 nm. In continuation of our work in this area (ESIPT), we have synthesized HPNI and carried out this study from the following angles: (*i*) being a larger condensed ring (naphthalene), we are expecting that the low energy fluorescence band of HPBI will be further red shifted in HPNI and thus may provide a tunable dye laser range towards the red side of 470 nm; and (*ii*) HPNI will be more hydrophobic than HPBI. It will be present in the interior of the micelles, and thereby may provide the information about the core of the micelles and, (*iii*) effect of the increase in conjugation in the side of the imidazole moiety to the property of ESIPT. To supplement the above study, MPNI has also been synthesized and studied. Since MPNI will not show keto–enol tautomerization, the spectral characteristics of MPNI will help in assigning the spectra of HPNI to different species.

2. Materials and methods

HPNI and MPNI were synthesized by condensing 2,3-diaminonaphthalene and 2-hydroxy- and 2-methoxybenzoic acid (all from Aldrich) in polyphosphoric acid medium at 140°C as suggested in the literature (29). Both these compounds were purified by repeated crystallization from methanol. The purity of the compounds were checked by TLC, absorption spectra, NMR, and by getting similar fluorescence spectra in any one particular solvent when excited at different wavelengths. All the solvents were AnalR grades. Cyclohexane (S.D. Fine Chemicals), dioxane, ether, acetonitrile, methanol (all E. Merck), and ethanol were further purified according to the procedure suggested in the literature (30). Ethylacetate and *n*-butanol (E. Merck) were used as received. All these solvents were free from spurious emission when excited at the normal range. Triply distilled water was used for making aqueous solutions.

© 2000 NRC Canada

Table 1. Absorption band maxima (λ^{ab}_{max} (nm)) and logε_{max} (in parentheses) of MPNI in various solvents and at different hydrogen ion concentrations at 298 K. [MPNI] = 1×10^{-5} M.

Solvent (species)	λ^{ab}_{max} (nm) (logε_{max})						
Cyclohexane	382 (sh) (3.74)	363 (sh) (4.15)	342 (4.64)	330(sh) (4.49)	302 (sh) (3.91)	271 (4.86)	262 (sh) (4.76)
Ether	380 (sh) (3.70)	360 (sh) (4.20)	344 (4.65)	331 (sh) (4.50)	302 (sh) (3.99)	270 (4.98)	262 (sh) (4.80)
Dioxane	380 (sh) (3.70)	360 (sh) (4.22)	345 (4.63)	330 (sh) (4.47)	302 (sh) (3.98)	272 (4.86)	262 (sh) (4.75)
Ethylacetate	380 (sh) (3.69)	360 (sh) (4.19)	345 (4.64)	332 (sh) (4.50)	302 (sh) (4.00)	270 (4.80)	262 (sh) (4.80)
Acetonitrile	378 (sh) (3.70)	—	345 (4.63)	331 (sh) (4.50)	302 (sh) (3.99)	270 (4.89)	262 (sh) (4.75)
Methanol	376 (sh) (3.73)	—	341 (4.61)	330 (sh) (4.51)	302 (sh) (4.00)	270 (4.84)	260 (sh) (4.73)
Water (5% CH_3OH)	—	—	342 (4.50)	332 (sh) (4.41)	—	270 (4.81)	263 (sh) (4.51)
Monocation pH = 2.0	—	—	354 (4.64)	—	—	—	—
Monocation (CH_3OH) (1.0 M H_2SO_4)	352 (4.62)	340 (sh) (4.58)	—	—	—	—	—
Monocation (CH_3CN)(0.01–0.2M H_2SO_4)	352 (4.62)	338 (sh) (4.55)	—	—	—	—	—
Monocation (Dioxane)(0.74 M H_2SO_4)	352 (4.63)	340 (sh) (4.57)	—	—	—	—	—
Dication H_0 = –10.0	354 (4.61)	340 (sh) (4.52)	—				
Monoanion H_- = 15.7	—	—	346 (4.44)	—	—	—	—

Absorption spectra were recorded on a Shimadzu spectrophotometer model UV 190, equipped with a 135 U chart recorder. Fluorescence measurements were carried out on the scanning spectrofluorimeter, fabricated in our laboratory, and the details are available elsewhere (31). Fluorescence excitation spectra were recorded on Perkin–Elmer Luminescence Spectrophotometer Model LS 50B equipped with a Wipro Geneous PC 386X (both excitation and emission slit widths used were 2.5 nm). Fluorescence spectra were corrected according to the Parker's method (32). Fluorescence quantum yields were determined with solutions having absorbance less than 0.1 and using quinine sulphate in 0.1 N H_2SO_4 as a reference (33) (ϕ = 0.55). Excited state lifetimes were measured on a time correlated single photon counting nanosecond spectrofluorimeter, supplied by Applied Photophysics Limited (details are available in our recent paper (34)). Due to the poor solubility of HPNI in cyclohexane and water, saturated solutions were used. In other solvents, the concentrations of HPNI and MPNI were 1×10^{-5} M. In the study of prototropic reactions, the amount of methanol used did not exceed more than 5% (V/V) and the concentrations of the compounds were maintained at 1×10^{-5} M. pH in the range of 3–11 was maintained by adding appropriate amounts of NaOH and orthophosphoric acid. Modified Hammett's acidity functions (35) (H_o) for H_2SO4–H_2O solutions and Yagil's basicity scale (36) for NaOH–H_2O solutions were used for solutions with pH < 1 and pH > 13 respectively. pH of the solutions were measured on Toshniwal pH meter model CL 46A.

Results and discussion

3. MPNI

3.1 Effect of solvents on the spectral characteristics

Absorption band maxima (λ_{max}^{ab}), log ε_{max} (wherever MPNI is soluble), fluorescence band maxima (λ_{max}^{fl}), and fluorescence quantum yield (ϕ_{fl}) recorded in seven different solvents are compiled in Tables 1 and 2. Absorption spectrum (Fig. 1*a*) is not affected much with the change in the polarity of solvents, except that it is slightly blue shifted in water. The structured absorption spectrum of MPNI in nonpolar or weakly polar solvents is nicely described by a vibrational frequency of 1400 ± 50 cm^{-1}. The structure is lost as the polarity and hydrogen bonding capacity of the solvent increases.

The structured fluorescence spectrum (Fig. 2*a*) of MPNI in cyclohexane is also described by a vibrational frequency of 1450 ± 50 cm^{-1}. Similar to the absorption spectrum, structure is lost in highly polar and protic solvents. These results resemble the vibrational frequencies observed in the condensed aromatic hydrocarbons containing more than two rings and this vibrational frequency corresponds to the frequency of the dominant C-C vibrational modes (37). Further,

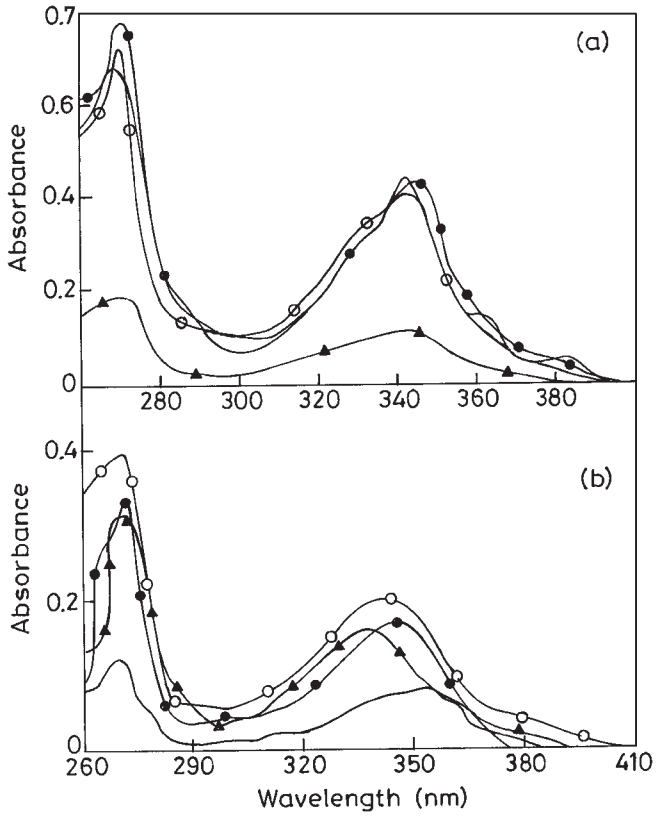
© 2000 NRC Canada

Table 2. Fluorescence band maxima (λ^{fl}_{max} (nm)) and lifetimes (τ, ns) and fluorescence quantum yields (ϕ_{fl}) in various solvents and at different hydrogen ion concentrations at 298 K. [MPNI] = 1×10^{-5} M. λ_{ex} = 350 nm.

Solvent (species)	λ^{fl}_{max}	(nm)				τ (ns)	ϕ_{fl}
Cyclohexane	383	405	432	458	492	—	0.37
Ether	388	407	432	461	497	—	0.30
Dioxane	392	413	437	463	498	4.4	0.30
Ethylacetate	395	412	434	464	—	3.6	0.24
Acetonitrile	394	417	438	—	—	4.1	0.22
Methanol	—	418	440	—	—	—	0.23
Water pH = 7.0	—	—	443	—	—	7.1	0.14
Monocation pH = 2.5	—	—	490	—	—	5.6[a]	0.02
Monocation (CH_3OH) (1.0 M H_2SO_4)	—	—	485	—	—	—	—
Monocation (CH_3CN) (0.2 M H_2SO_4)	—	—	480	—	—	—	—
Monocation (Dioxane) (0.74 M H_2SO_4)	—	—	485	—	—	—	—
Dication (H_o = –10.0)	—	—	435	—	—	—	—
Monoanion (H_- = 15.7)	—	—	443	—	—	—	0.11

[a] = λ_{em} = 480 nm

Fig. 1. Absorption spectra of (*a*) MPNI and (*b*) HPNI in different solvents at 298 K. [MPNI] or [HPNI] = 1×10^{-5} M. _____, cyclohexane (saturated solution); ·___·___·, acetonitrile; o___o___o, methanol; ▲___▲___▲, water (saturated solution).



the fluorescence band maxima and the fluorescence quantum yields observed in MPNI in all the solvents are independent of wavelength of excitation. This clearly indicates that the fluorescence is occurring from the most relaxed state in all the solvents and the solvent relaxation time is much smaller than the radiative lifetime as observed in other cases (38, 39). The fluorescence excitation spectra recorded at different emission wavelengths are similar to each other as well as to the absorption spectra. This suggests that not much change is observed in the geometry of MPNI, when excited to the S_1 state and similar vibrational frequencies observed in the absorption and the fluorescence spectra reflect the mirror image symmetry (37).

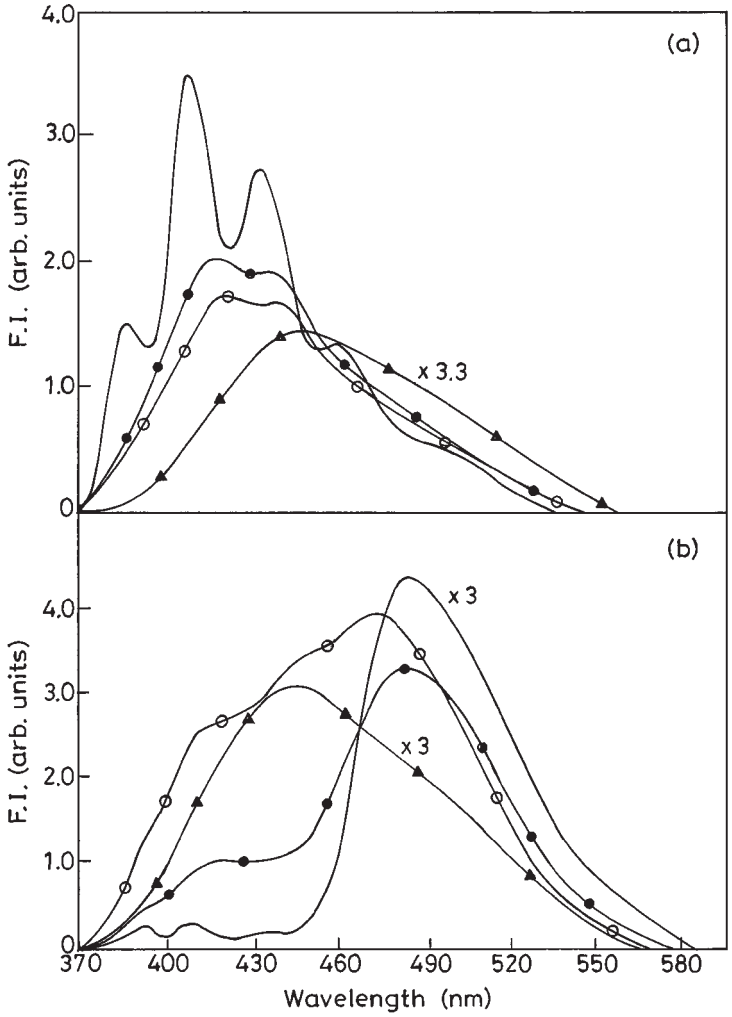
Excited state lifetimes of MPNI were measured at 440 nm by exciting at 337 nm in five different solvents. The fluorescence decay followed a single exponential in each case having χ^2 in the range of 1.0 ± 0.15 and nice autocorrelation function. Figure 3*a* depicts the fluorescence decay curve in water as a representative curve and the relevant data are compiled in Table 2. The results of lifetime data also substantiate the results of solvent study that similar to the ϕ_{fl}, the lifetimes are not much affected by the solvents except water.

3.2 Effect of pH on the spectral characteristics

The absorption and the fluorescence spectra of the various prototropic species of MPNI were recorded at different acid-base concentrations. The relevant data are mentioned in Table 1 and Table 2, whereas Scheme 1 depicts the various proton transfer reactions of MPNI in the ground and the first excited singlet states. Figures 4(*a*) and 4(*b*) depict the absorption and the fluorescence spectra of the different prototropic species of MPNI in aqueous medium. The data clearly show that MPNI is a neutral species in the pH range of 7–12; the monocation (MC) at pH < 2 and the monoanion (MA) above H_= 15. Red shifts observed in the absorption spectra of the MC and the MA in comparison to the neutral species are consistent with the protonation of the -N= atom and deprotonation of the >NH moiety, respectively (40). The fluorescence spectrum of MPNI remained unchanged in the basic range even up to H_= 16 (formation of the MA by deprotonating the >NH group), whereas the fluorescence spectrum of the MC is largely red shifted. Similar behaviour is also observed during the deprotonation and protonation reactions of 2-phenylbenzimidazole (41) (PBI) and thus supports the assignment of the respective spectrum to the formation of the MA and the MC. It has been established (42–44) that hardly any change is observed in the fluorescence spectra of the MCs of benzimidazoles if the transition involved is of π–π^* in nature and large red shifts are ob-

© 2000 NRC Canada

Fig. 2. Fluorescence spectra of (*a*) MPNI and (*b*) HPNI in different solvents at 298 K. [MPNI] or [HPNI] = 1×10^{-5} M. λ_{exc} = 350 nm. _____, cyclohexane; ·___·___·, acetonitrile; o___o___o, methanol; ▲___▲___▲, water (5% methanol).



served in the emission spectra of the MCs if the transition is of charge transfer in character. Fluorescence spectral data of the MC of MPNI, recorded in different solvents (Table 2), clearly established that the fluorescence spectrum of the MC of MPNI involves the charge transfer character, similar to some of the benzimidazoles (42, 43).

The pK_a values of the MC–N and the N–MA equilibria were calculated using absorption spectral data and the excited state pK_a (pK_a^*) value for the MC–N equilibrium has been determined using the fluorimetric titration method (Fig. 5). The pK_a^* for the N–MA equilibrium could not be determined because hardly any changes were observed either in the fluorescence band maxima or in the fluorescence intensities of MPNI. pK_a values are listed above the arrows and pK_a^* values below the arrows of the prototropic reactions given in Scheme 1. Similar to the spectral characteristics, pK_a values are also consistent with the prototropic reactions of PBI (41) and thus the addition of one benzo ring to BI does not affect the basicity of the =N- atom. Observation of similar pK_a and pK_a^* values for the MC–N equilibrium indicate that the equilibrium is not established in the S_1 state. Since the intersection point between the increase in the fluorescence intensity curve of $HMPNI^+$ and the decrease in the fluorescence intensity curve of neutral MPNI is at $I/I_o = 0.5$, it clearly suggests that no other reaction is taking place except protonation of MPNI and deprotonation of $HMPNI^+$ in the S_1 state. As pointed out by Schulman (45), the fluorimetric titration curves give the ground state pK_a values if the rate of the pseudo-first-order dissociation of an excited acid or protonation of an excited base is small (~10%) in comparison to the reciprocal of the lifetime of the excited acid or base and the rate of protonation of the excited conjugate base ($k_{-1}[H^+]$) or deprotonation of the excited conjugate acid is small (~10%) in comparison to the reciprocal of the lifetime of the excited base or acid. As mentioned above, since the prototropic equilibrium between $HMPNI^+$ and MPNI is not established during the lifetime of these conjugate acid-base pairs, it suggests that $k_1 < 1.8 \times 10^7$ s^{-1} and similarly $k_{-1}[H^+] < 1.4 \times 10^7$ s^{-1} at pH 2.

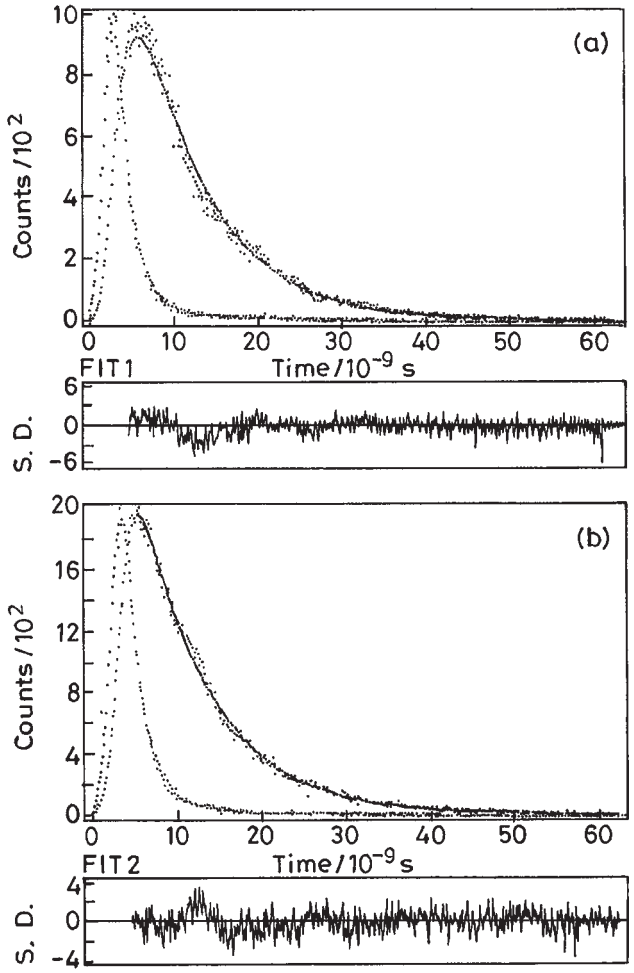
4. HPNI

4.1 Absorption Spectrum

The absorption characteristics of HPNI in different solvents are compiled in Table 3 and the spectra are shown in Fig. 1*b*. In the nonpolar and polar/aprotic solvents, the

© 2000 NRC Canada

Fig. 3. Fluorescence decay curve for (*a*) MPNI (*b*) HPNI in water. λ_{exc} = 337 nm. For MPNI, λ_{em} = 405 nm; for HPNI, λ_{em} = 490 nm.



absorption maxima are at ~342 and 350 nm, whereas in the polar/protic solvents, the band maximum is at ~343 nm with shoulders at ~360 and 380 nm. The tail part of the absorption spectrum is more stretched towards the red in the latter solvents and resembles the absorption spectrum of MPNI, where only one rotamer is expected.

The absorption spectrum of HPNI in pure water, methanol, and acetonitrile media under acidic and basic conditions have also been studied. Figure 6*a* only depicts the absorption spectra of these ionic species in methanol and the relevant data are compiled in Table 3. Under the mildly basic conditions (pH 13.5 in water and 0.6M NaOH in methanol), the red shifted absorption spectrum of HPNI in comparison to the neutral species can be assigned to the MA formed by deprotonating the -OH group. No further change was observed in the absorption spectrum of HPNI even up to H_= 16 in aqueous medium, indicating that the deprotonation of >NH does not occur in HPNI. The pK_a value for the N-MA equilibrium is found to be 10.4.

Under acidic conditions, the absorption spectrums of the neutral species in all the solvents are nearly similar to one another except water where there is only one absorption maximum (342 nm) and the structured band is replaced by a broad band with a maxima at ~340 nm and a shoulder at ~355 nm, as observed in the case of MPNI. The species so formed is the MC, obtained by the protonation of =N- atom. The pK_a value for the protonation reaction of HPNI is found to be 4.9. This is slightly lower than that of MPNI and could be due to the presence of intramolecular hydrogen bonding between = N- and hydroxyl proton. Small differences in the pK_a values for the hydroxy and methoxy derivatives have also been observed in HPBI(20) and 2-(2′-hydroxyphenyl)benzoxazole (HPBO) (46).

4.2 Fluorescence Spectrum

On excitation at 350 nm, dual fluorescence was observed in all the solvents. The relevant data are compiled in Table 4 and the fluorescence spectra in different solvents are shown in Fig. 2*b*. The fluorescence band maximum of the short wavelength (SW) band is red shifted and the long wavelength band (LW, tautomer, T-band) is blue shifted with increases in the polarity and hydrogen bonding capacity of the solvents. In water, the two bands are mixed to such an extent that it is very difficult to resolve them. The structure observed in the SW band of HPNI in nonpolar or weakly polar solvents is not as sharp as observed in MPNI. The fluorescence quantum yield of the SW band (ϕ_{fl}^{N}) increases under the above environments, whereas that of the tautomer band (ϕ_{fl}^{T}) remains nearly constant in polar/aprotic solvents but decreases with increases in the hydrogen bonding capacity of the solvents. The ϕ_{fl} of both the bands could not be measured in protic solvents because of their mixing. This is also evident from the fact that the band width at half the maximum height (BWHMH) is larger in protic solvents in comparison to that of aprotic solvents. No effect is observed on the fluorescence band maxima of both the bands (when excited with different wavelengths towards the red) but ϕ_{fl}^{T} decreases and ϕ_{fl}^{N} increases.

The fluorescence excitation spectra of HPNI have been recorded in all the solvents except *n*-butanol at seven different emission wavelengths in the range of 385–525 nm. Figure 7 depicts the above spectra in dioxane and methanol recorded only at two extreme wavelengths (i.e., 510 nm and 410 nm in dioxane and 490 nm and 390 nm in methanol are representative of the region 490–525 nm and 385–460 nm respecticely). It is clear from the results that the fluorescence excitation spectra recorded in the range of 490–525 nm are similar to the absorption spectrum of HPNI recorded in nonpolar and polar/aprotic solvents and those recorded in the range of 385–460 nm are similar to the absorption spectra of HPNI recorded in polar/aprotic solvents as well as to the absorption spectrum of MPNI. This difference clearly suggests that the normal and the tautomer emissions originate from two distinctly different species.

Excited state lifetimes of HPNI were measured at 405 nm (N-band) and 520 nm (T-band) in different solvents. The fluorescence decays observed in nonpolar and polar/aprotic solvents of the tautomer band follow a single exponential decay with χ^2 in the range of 1.0 ± 0.1, whereas double exponential decay is observed for the tautomer emission in dioxane containing even a slight amount (5%) of water. In case of the dioxane/water mixture, both the lifetimes (τ_{T1} and τ_{T2}) increase with an increase of water content. Amplitude of the short-lived component decreases and that of the long-lived component increases with an increase of water. The value of

© 2000 NRC Canada

Fig. 4. Absorption and fluorescence spectra of the different prototropic species of MPNI in water (5% methanol, V/V) at 298 K. [MPNI] = 1×10^{-5} M. _____, neutral; o___o___o, monoanion (H_- = 16.0) ; ·___·___·, monocation (pH = 3.0).

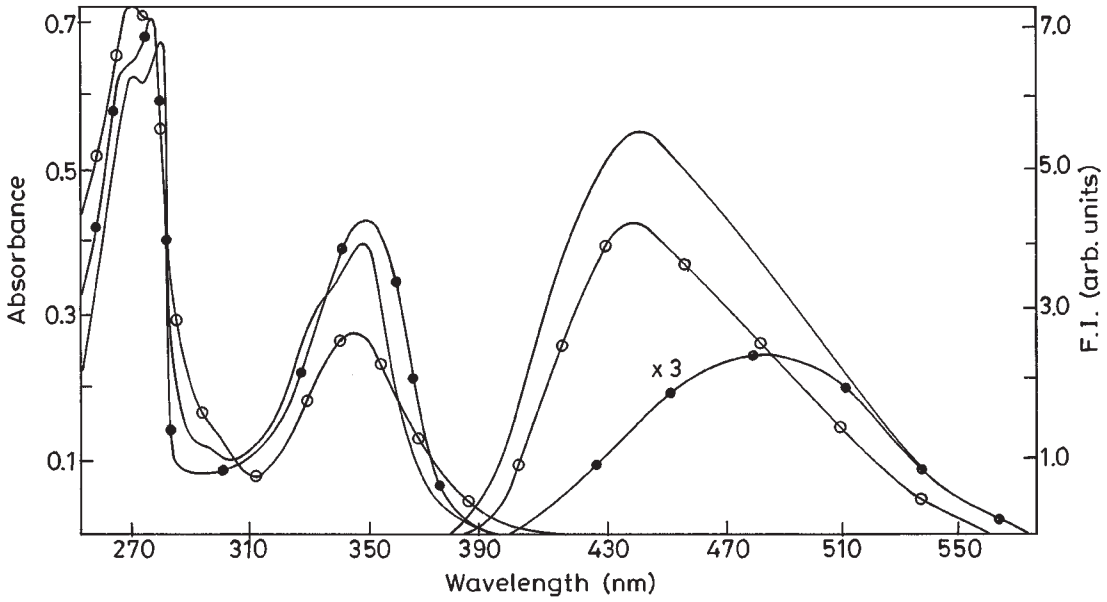
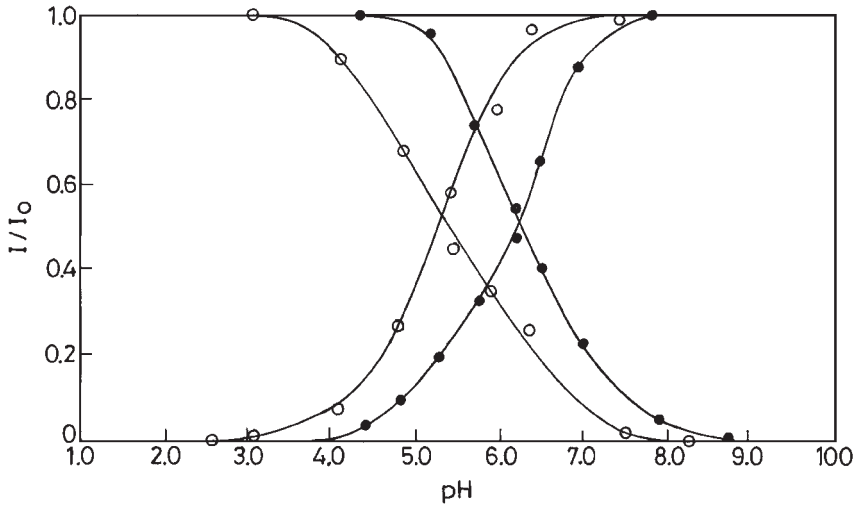


Fig. 5. Fluorimetric titration curves for the monocation – neutral equilibria of HPNI (·___·___·) and MPNI (o___o___o) in water (5% methanol V/V).



the longer component (τ_{T2}) in pure water nearly resembles that of MPNI in water. A single exponential is also observed for the fluorescence decay of the normal band in nonpolar and polar–aprotic solvents. In dioxane containing slight amount of water, the biexponential decay is observed in the normal emission. The lifetime of the fast-decaying component (τ_{f1}) remains nearly unchanged, whereas the value of the slow-decaying component (τ_{f2}) increases with increase of water content in dioxane. The amplitude of the fast-decaying component decreases whereas that of slow-decaying component increases under the above environment. Further, the values of τ_{T2} and τ_{f2} are nearly similar to each other but those of τ_{f1} are shorter than those of τ_{T1}. The relevant data are compiled in Table 5 and Fig. 3*b* represents the fluorescence decay of the tautomer emission in water as a representative plot.

The fluorescence spectra of HPNI in all the solvents under acidic conditions are largely red shifted and the red shift increases with the increase in polarity of the solvents. The fluorescence band maxima of all the ionic species of HPNI are independent of λ_{exc} (between 325 –370 nm in all these solvents). The fluorescence band maximum, as well as, BWHMH of HPNI do not change in the pH/H_o range of 2.5 to –7 in aqueous medium and up to 0.002–3.0 M acids in nonaqueous solvents. The fluorescence band maximum of the MC of HPNI and that of MPNI in the aqueous medium are nearly at the same wavelength. A large blue shift (447 nm) is observed at $H_o < -7$ in the fluorescence spectrum of the MC of HPNI, indicating the formation of the DC protonating the hydroxyl group (20). Under basic conditions, the fluorescence band maximum of HPNI observed in protic solvents are nearly at the same wavelength and are not dif-

© 2000 NRC Canada

Table 3. Absorption band maxima (λ^{ab}_{max} (nm)) and $\log\varepsilon_{max}$ (in parentheses) of HPNI in various solvents and at different hydrogen ion concentrations at 298 K. [HPNI] = 1×10^{-5} M.

Solvent	λ^{ab}_{max} (nm) ($\log\varepsilon_{max}$)							
Cyclohexane (saturated)	360	351	342	311	298	275	270	—
Ether	—	350 (4.16)	342 (4.10)	311 (3.64)	298 (3.53)	—	271 (4.39)	—
Dioxane	—	350 (4.34)	342 (4.31)	311 (3.90)	298 (3.84)	—	271 (4.61)	—
Ethylacetate	—	349 (4.24)	342 (4.22)	311 (3.77)	298 (3.68)	—	271 (4.53)	—
Acetonitrile	—	348 (4.23)	342 (4.21)	310 (3.75)	297 (3.64)	—	271 (4.53)	—
n-Butanol	380 (3.11)	—	342 (4.35)	310 (3.86)	297 (3.78)	—	272 (4.53)	—
Ethanol	380 (3.30)	—	342 (4.31)	310 (3.80)	297 (3.71)	—	272 (4.60)	—
Methanol	380 (3.60)	—	342 (4.31)	310 (3.85)	297 (3.77)	—	270 (4.60)	—
Water (pH = 7)	380 (3.60)	—	342 (4.31)	310 (3.85)	297 (3.77)	—	270 (4.60)	—
Monocation (pH = 0) (water)	—	—	342 (4.32)	—	—	274	—	—
Monocation (CH_3OH) (0.5 M H_2SO_4)	—	355 (4.27)	339 (4.33)	—	—	274	—	264
Monocation (C_2H_5OH) (0.002–1.0 M H_2SO_4)	—	360 (4.26)	340 (4.33)	—	—	274	—	264
Monocation (CH_3CN) (0.001–1.0 M H_2SO_4)	—	355 (4.27)	340 (4.33)	—	—	274	—	—
Dication (H_o = –10.3) (water)	—	—	342 (4.31)	—	—	273	—	—
Monoanion (water) pH = 13.5	380 (4.11)	365 (4.14)	345 (4.16)	—	—	—	—	—
Monoanion (CH_3OH) (NaOH = 0.6M)	382 (4.10)	367 (4.13)	345 (4.15)	—	—	—	—	—

ferent from that of neutral HPNI in water. The relevant data are compiled in Table 4 and the fluorescence spectra of the prototropic species are shown in Fig. 6*b*. The excited state pK_a value for the MC-N equilibrium has been determined with the help of fluorimetric titrations as shown in Fig. 5, whereas that of the N–MA equilibrium could not be determined as hardly any change in the band maximum or fluorescence intensity was observed with increase of pH. The pK^*_a values using the Forster cycle method could not be calculated because the absorption or the fluorescence spectra were representing two rotamers. The pK^*_a value from the fluorimetric titrations were given below the arrows of Scheme 1.

4.3 Spectral characteristics of HPNI in mixed solvents

Absorption spectrum of HPNI has been studied in dioxane–water and dioxane–methanol mixtures. The changes observed in the absorption spectra are only in the long wavelength band, whereas the other band systems at 310 nm and 297 nm are not affected. The 350 nm band maximum in pure dioxane is replaced by a 343 nm band with a shoulder at 380 nm when only 10% methanol or water is added to dioxane. Further addition of methanol or water does not lead to any change in the absorption spectrum. Figure 8*a* depicts the absorption spectra of HPNI in different proportion of dioxane–water (V/V) mixtures.

Dual fluorescence is observed in pure dioxane as said earlier. The ratio of ϕ^T_{fl}/ϕ^N_{fl} is 5 in pure dioxane. With the addition of only 10% methanol or water, the fluorescence intensity of the tautomer band measured at 520 nm decreases very sharply to 66% of that observed in pure dioxane, followed by slow decrease to 40% in pure water. On the other hand, the fluorescence intensity of the normal band increases very sharply by 6 times with the addition of only 20% water, remains nearly constant up to 70% of water, and then decreases to half of its maximum intensity. But it is still larger by a factor of three when compared to that in pure dioxane. This behaviour is different from that observed in HPBI (26), in the sense, that emission intensities of the tautomer and the normal bands of HPBI increased when water was added to dioxane. The fluorescence band maximum of the normal emission does not change much after a 20% addition of protic solvents to dioxane, but that of the tautomer band is blue shifted under similar environments. Similar to the results in the pure solvents, changing the excitation wavelength from 350 to 380 nm does not shift the band maxima of both the emissions, but fluorescence intensity of the normal band increases by a factor of 2, whereas not much

© 2000 NRC Canada

Fig. 6. (*a*) Absorption and (*b*) fluorescence spectra of the different prototropic species of HPNI in methanol at 298 K. [HPNI] = 1×10^{-5} M. _____, neutral; ·___·___·, monoanion ([NaOH] = 0.60 M); o___o___o, monocation ([H_2SO_4] = 1.0 M). λ_{ex} = 350 nm.

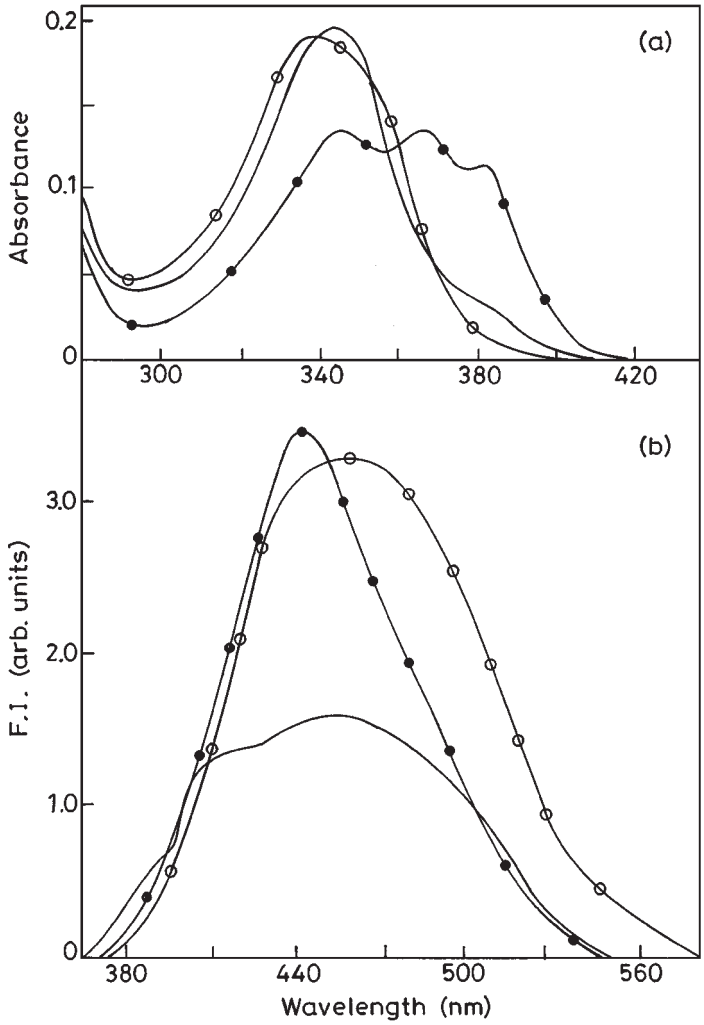


Table 4. Fluorescence band maxima (λ^{fl}_{max} (nm)) and fluorescence quantum yields (ϕ_{fl}) in various solvents and at different hydrogen ion concentrations at 298 K. [HPNI] = 1×10^{-5} M. λ_{exc} = 350 nm.

Solvent/species	Normal				Tautomer	
	λ^{fl}_{max}			ϕ^{N}_{fl}	λ^{fl}_{max}	ϕ^{T}_{fl}
Cyclohexane	388	415	437	—	488	—
Ether	389	413	—	—	488	0.156
Dioxane	388	416	—	0.027	488	0.135
Ethylacetate	388	412	437	0.081	486	0.174
Acetonitrile	389	412	437	0.119	486	0.141
n-Butanol	394	411	442	—	469	—
Ethanol	390	416	440	—	469	—
Methanol	—	416	442	—	466	—
Water pH = 8.0	—	—	447	—	—	—
Monocation pH = 2.5	—	—	492	—	—	—
Monocation (CH_3OH) 0.002–0.5 M H_2SO_4	—	—	462	—	—	—
Monocation (C_2H_5OH) 0.001–3.0 M H_2SO_4	—	—	464	—	—	—
Monocation (CH_3CN) 0.001–1.0 M H_2SO_4	—	—	480	—	—	—
Dication (H_o = –10.0)	—	—	447	—	—	—
Monoanion (water) (pH = 13.6)	—	—	445	—	—	—
Monoanion (CH_3OH) 0.6 M NaOH	—	—	444	—	—	—

© 2000 NRC Canada

Fig. 7. Fluorescence excitation spectra of 2-HPNI recorded at the emission wavelengths 410 nm and 510 nm in dioxane and 390 nm and 490 nm in methanol at 298 K. [HPNI] = 1×10^{-5} M. In methanol, _____, λ_{em} = 490 nm; ·___·___·, λ_{em} = 390 nm. In dioxane, Δ___Δ___Δ, λ_{em} = 510 nm; o___o___o, λ_{em} = 410 nm.

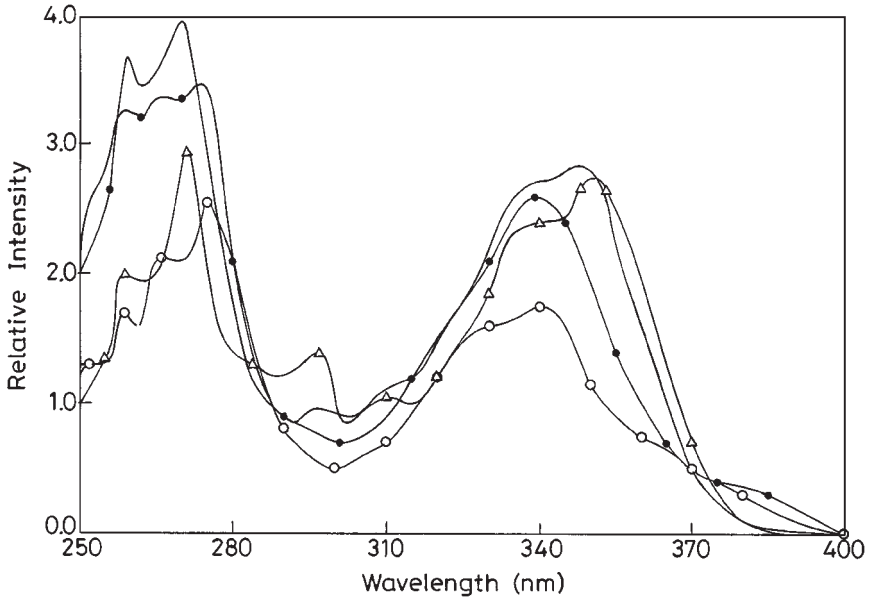


Table 5. Fluorescence lifetimes (ns) of the normal and tautomer fluorescence bands in different solvents at 298 K. λ_{exc} = 350 nm. Terms in the brackets represent amplitudes.

	λ_{em}	Single Exp		Double Exp		
Solvents	(nm)	χ^2	τ_f	χ^2	τ_{f1}	τ_{f2}
Normal band						
Dioxane	410	1.22	3.7	—	—	—
Ethylacetate	405	1.15	3.9	—	—	—
Acetonitrile	405	1.18	2.0	—	—	—
95% Dioxane	390	—	—	1.26	0.9(20)	4.8(80)
85% Dioxane	390	—	—	1.18	0.8(15)	5.9(85)
50% Dioxane	390	—	—	1.20	0.8(13)	6.7(87)
Water pH = 8	405	—	—	1.21	1.0(14)	7.1(86)
Monocation pH = 0.0	444	1.20	5.2	—	—	—
Monoanion pH = 13.0	445	1.20	4.3	—	—	—
Tautomer band						
Dioxane	525	1.2	1.04	—	—	—
Ethylacetate	525	1.15	1.36	—	—	—
Acetonitrile	505	1.29	1.24	—	—	—
95% Dioxane	510	—	—	1.15	1.49(89)	5.1(11)
85% Dioxane	530	—	—	1.19	1.3 (79)	5.9(21)
50% Dioxane	530	—	—	1.24	1.7(57)	6.8(49)
Water pH = 8.0	490	—	—	1.40	1.8(21)	7.54(79)
Monocation pH = 0.0	495	1.19	5.33	—	—	—

change is observed in the emission intensity of the tautomer band. Unlike that observed in pure solvents, the normal emission follows double exponential decay in mixed solvents (Table 5). Figure 8*b* depicts the fluorescence spectra of HPNI, whereas Fig. 9 shows the variation of the fluorescence intensities of both the bands when water is added to dioxane.

4.4 Quantum mechanical calculations

The PC MODEL 2 program (47) was used to find the starting geometries of the species **1**, **2**, and **3**. The ground state geometries of all the species were then fully optimized by the AM1 method (48) (QCMP 137, MOPAC 6/PC). It is evident from the data of Table 6 that the two rings (i.e., naphthimidazole and hydroxyphenyl), although connected by the intramolecular hydrogen bonding, are not completely coplanar in the rotamers **1** and **2**, whereas the tautomer **3** is planar. This is also reflected by the bond lengths between C_2 and C_1' in three different species. Energies of the rotamers **1** and **2** were also calculated by taking different dihedral angles (ϕ) and the energies so obtained are plotted as a function of angle ϕ in Fig. 10, which describes the potential energy

© 2000 NRC Canada

Fig. 8. (*a*) Absorption and (*b*) fluorescence spectra of HPNI in different proportions of dioxane–water mixtures at 298 K. [HPNI] = 1×10^{-5} M. _____, dioxane; ·___·___·, 98% dioxane; o___o___o, 94% dioxane; ▲___▲___▲, 80% dioxane; Δ___Δ___Δ, 50% dioxane; ×___×___×, 0% dioxane. λ_{exc} = 350 nm.

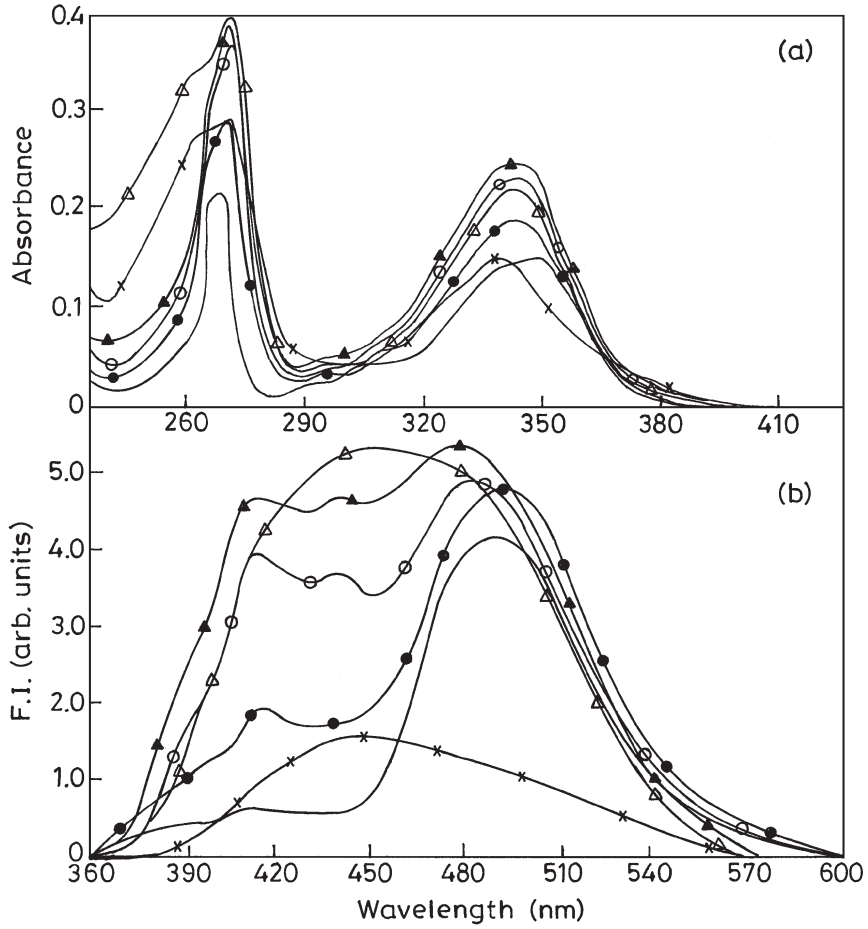


Table 6. Calculated properties of rotamers **1**, **2**, and tautomer **3** by the AM1 method in the ground state.

Properties	**1**	**2**	**3**
Energy (eV)	–3073.9996	–3074.02383	–3073.7032
Energy (eV) (solvated in MeOH)	–3074.01944	–3074.05625	–3073.75403
Dipole moment (μ) (Debye)	3.15	4.03	5.03
C_2—C_1' bond distance (A°)	1.465	1.465	1.401
Dihedral angle (ϕ) [C_3–C2–C_1'–C_2'] (deg)	42	145.2	1.7
Charge density	N_1 = 5.262	N_1 = 5.239	N_1 = 5.253
	N_3 = 5.169	N_3 = 5.150	N_3 = 5.244
	$O_{7'}$ = 6.249	$O_{7'}$ = 6.269	$O_{7'}$ = 6.411
	$H_{8'}$ = 0.750	$H_{8'}$ = 0.770	$H_{8'}$ = 0.687

curve for the interconversion of the rotamers **1** and **2** in the ground state. For the isolated molecule and in the ground state the barrier height for the interconversion of rotamer **2** to **1** is 7.43 kJ mol^{-1}. The dipolar solvation energy (49, 50) is calculated using the following relation:

$$E_{sol} = -[\mu_g^2/4\pi\varepsilon_o a^3] f(\varepsilon)$$

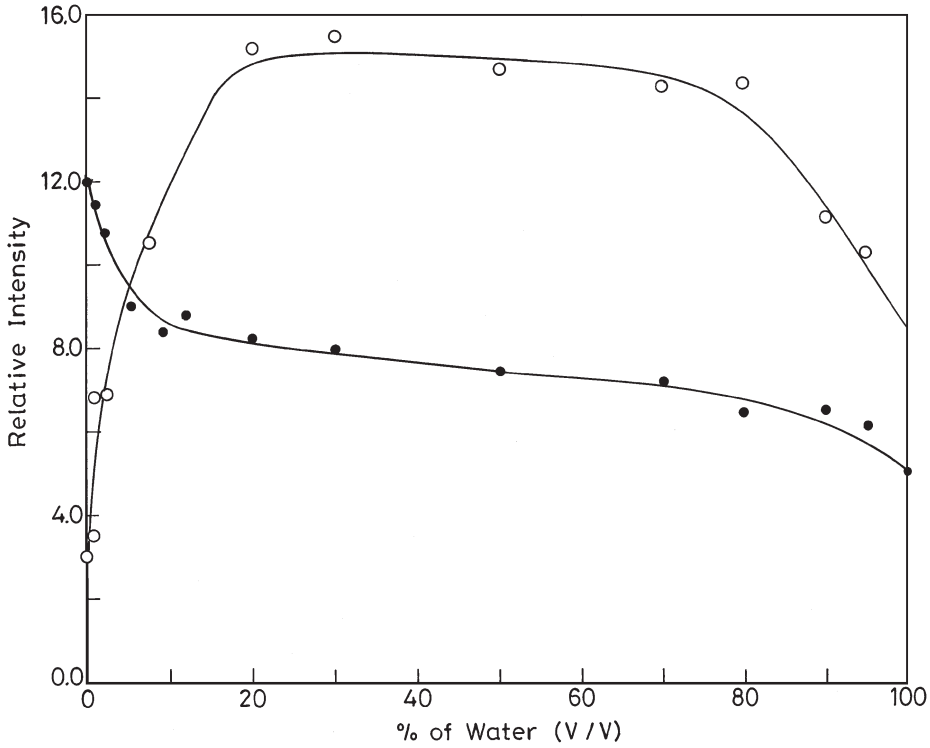
where $f(\varepsilon) = (\varepsilon - 1)/(2\varepsilon + 1)$, μ_g is the ground state dipole moment, a is the Onsager cavity radius, and ε is the dielectric constant of the solvent.

4.5 Discussion

The large red shifted absorption spectrum of HPNI in comparison to that of naphthalene (51) and similar to that of 2-(3′-hydroxy-2′-naphthyl)benzimidazole (4) (HNB), as well as, the vibrational frequencies in the absorption and fluorescence spectra of MPNI or in the normal emission of HPNI, are consistent with the spectral properties of the linearly condensed ring system (37, 51). The values of the molecular extinction coefficients of different bands and the fluorescence quantum yields are indicative of π–π^* transition in HPNI (37, 51). The resemblance of the absorption spectra of HPNI in protic solvents with that of MPNI clearly suggests

© 2000 NRC Canada

Fig. 9. Variation of fluorescence intensities of HPNI at 414 nm (o___o___o) and 520 nm (·___·___·) in different proportions of dioxane–water mixtures. λ_{exc} = 350 nm. [HPNI] = 1 × 10^{-5} M.



that the possibility of the formation of the MA of HPNI in polar/protic solvents (as suggested in the case of HPBI (52)) or of the tautomer as observed in case of 2-(3′-hydroxy-2′-pyridyl)benzimidazole (HPyBI (53)) in the ground state can be rejected. It may be proposed that 350 nm band belongs to the rotamer **1** and the 343 nm band with a shoulder at 380 nm can be assigned to the rotamer **2**.

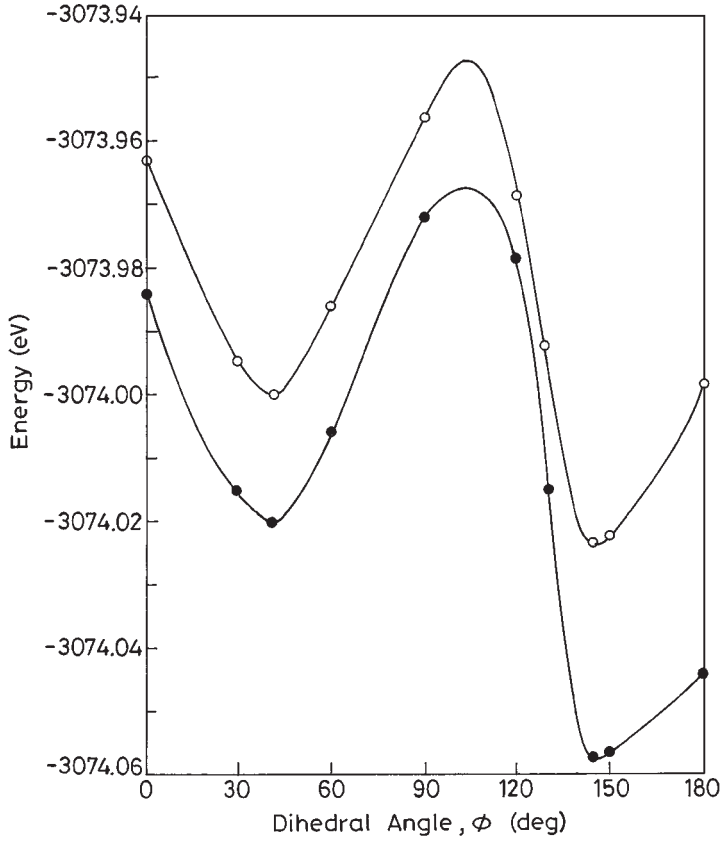
The absorption and the fluorescence spectra in different solvents, fluorescence excitation spectra recorded at different emission wavelengths, and two distinctly different lifetimes observed for the normal and the tautomer emissions clearly demonstrate the presence of at least two species in the ground state and excited state. Since the lifetimes observed for the two emission bands are different in all the solvents, it further suggests that the rotamers responsible for these emissions are not in equilibrium with each other in the S_1 state. Based on the earlier results in other molecules (12, 54), the tautomer emission in HPNI also results from the species **3**, formed from by the ESIPT in the rotamer **1**.

Based on the following results, the normal emission in nonpolar solvents is assigned only to the rotamer **2**: (*i*) the fluorescence excitation spectra recorded at normal band agree with the absorption spectra of MPNI where only one type of rotamer **2** is possible. AM1 calculations have further shown that the rotamer **1** is less stable by 13.0 kJ mol^{-1} compaired to the rotamer **2** for MPNI in the gaseous state. Similar behaviour has also been observed in HPyBI (3); (*ii*) the ϕ_{fl}^{N} increases with an increase in the excitation wavelength; (*iii*) in dry nonpolar solvents, the competition between the intra- and intermolecular hydrogen bonding is completely absent, and (*iv*) the rotamer **2** can not undergo ESIPT in any solvent.

The large increase in ϕ_{fl}^{N} in protic solvents can not be accounted for simply due to the increase in the population of the rotamer **2** over **1** by the polarity factor, as explained below. Semiempirical quantum mechanical calculations using the AM1 method (48) have shown (Table 6) that in isolated condition and in the ground state, the rotamer **2** is more stable than the rotamer **1** and the tautomer **3** by 2.33 and 30.79 kJ mol^{-1} respectively, whereas in methanol and water the rotamer **2** is more stable by 3.54 and 29.03; 3.57 and 28.98 kJ mol^{-1} respectively. Based on the Maxwell–Boltzmann's distribution, the additional stability of the rotamer **2** will increase its population over the rotamer **1**in the latter solvents by a factor of exp(–$\Delta E/RT$), i.e., approximately a 30% increase at 298 K in these solvents when compared to that in dioxane or cyclohexane. This will only increase ϕ_{fl}^{N} by 30% which is too small to account for a 4–5-fold increase observed in protic solvents. In other words, in strong hydrogen bonding solvents like alcohols and water, the population of the rotamer **4** will increase at the expense of the rotamer **1** (specially) and may be at the removal of the rotamer **2** also. In the presence of protic solvents, while the rotamer **2** continues to give normal fluorescence, an additional increase in the fluorescence intensity of the normal band arises from the rotamer **4**, formed from the rotamer **1** by disrupting the intramolecular hydrogen bond between =N- and the hydroxyl proton. Since the ESIPT process cannot take place in the rotamer **4**, the fluorescence occurring from it energetically will be similar to the normal fluorescence and thus will increase the fluorescence quantum yield. The results observed in dioxane–methanol and dioxane–water mixtures substantiate the above assignment. Similar enhancement of ϕ_{fl}^{N} has also been observed in other

© 2000 NRC Canada

Fig. 10. Potential energy curves for the interconversion of rotamer **1** and **2** of the HPNI molecule as isolated (o___o___o) and solvated (·___·___·) in the S_o state.



molecules (54, 55) and a similar mechanism has been proposed (9). The time dependence fluorescence decay of the normal emission in dioxane–water solution has also supported more than one species as being responsible for this emission. Unlike in pure solvents, the fluorescence decay of the tautomer emission in water or in dioxane containing water is always biexponential. The lifetime and the amplitude of the long-lived species increase with an increase in the amount of water. Since the lifetime of the long-lived species in the tautomer band is nearly equal to the lifetime of the long-lived species in the normal emission, as well as, it also resembles with that of MPNI in different solvents, it may be suggested that the biexponential decay observed in the tautomer band is due to the mixing of two emission bands as mentioned earlier i.e., tautomer emission and normal emission originating from the rotamer **2**. The smaller value of the amplitude of τ_{T2} in comparison to that of τ_{f2} could be due to the small proportion of the fluorescence intensity of the normal emission at ~500 nm. Lastly, the values of the lifetimes observed in the N-emission are different from each other and the lifetime of the fast-decaying component is smaller than that of the tautomer emission. This clearly suggests the fast-decaying lifetime is not from the tautomer emission and thus can be assigned to the species **4**.

Effect of pH: In each solvent, the fluorescence band of HPNI at an acid concentration of 0.001 M is very large red shifted in comparison to the normal emission of the neutral HPNI and emission follows a single exponential decay when monitored at either 445 nm or at 495 nm. This clearly establishes that there is only one kind of MC, formed by protonating the $=N_3$- atom. Although the fluorescence band maxima in different solvents at 0.001 M acid concentration are close to the tautomer emission band maxima in these nonaqueous solvents, the tautomer formation can be rejected on the following grounds: (*i*) it is well known that the aromatic alcohols become stronger acids on excitation and also the rate of deprotonation in aromatic alcohols is much greater in water than in alcoholic solvents such as methanol (40) or in polar–aprotic solvents. Had the deprotonation of hydroxyl group been occurred in the protic nonaqueous solvents, it should have also been observed in water. But the emission band observed from the species under acidic condition in aqueous medium is very large red shifted in comparison to the normal or the tautomer band in water under neutral condition. It also agrees with the emission band maximum noted in the MC of MPNI in water. Further the deprotonation of the hydroxyl group would have been the slowest in acetonitrile; (*ii*) no further change is observed in the fluorescence band maxima and BWHMH even up to 3 M H_2SO_4 in ethanol, 1M in acetonitrile, and H_o –6 in water, and (*iii*) the fluorescence excitation spectra resemble the absorption spectra of the MC of HPNI. Thus based on the above arguments and large red shifts observed in the fluorescence band maxima of the MC of MPNI with increase in the polarity of the solvents, the emission in the MC of HPNI

© 2000 NRC Canada

can also be assigned to the charge transfer band. A similar behavoiur has also been observed in the emission spectra of the MCs of benzimidazole and its alkyl derivatives (42, 44).

Under basic conditions and in all solvents, fluorescence excitation spectra overlap with the absorption spectra, fluorescence spectra exhibit normal Stokes shifted band, and emission in each solvent follows the single exponential decay. These observations suggest that emission at 445 nm is attributed to the MA, formed by the deprotonation of hydroxyl group. The pK_a and pK_a^* observed for the deprotonation of HPNI is lower than that of MPNI. This is because the former molecule involves the deprotonation of the -OH proton, whereas the latter one involves the deprotonation of the >NH proton. No further changes in the spectral characteristics of HPNI suggest that the bond between >NH and O^- is very strong and can not be broken even at $H_- = 16$. Similar behaviour is also observed in HPBI (20). This is further substantiated by the vibrational structure observed in the absorption spectrum of the MA of HPNI.

6. Conclusions

The following conclusions can be drawn from the above study: (*i*) in nonpolar solvents, the LW emission is observed from the tautomer **3**, formed by the ultrafast ESIPT processes from the rotamer **1**, whereas the normal emission is from the rotamer **2**. Rotamer **2** is predominant in nonpolar solvents, whereas in the protic solvents, species **4** may be more predominant; (*ii*) the fluorescence quantum yield of the normal emission increases in polar/protic solvents whereas that of the tautomer band nearly remains constant in polar/aprotic solvents, but decreases as the hydrogen bonding capacity of the solvent increases; (*iii*) the time-resolved studies have shown that rotamer **1** and **2** are distinctly different in the S_1 state and the equilibrium is not established between them in the excited state. Rotamers **2** and **4** on excitation give normal emission, where rotamer **1** on electronic excitation produces the tautomer **3** in the ultrafast time scale; (*iv*) the fluorescence spectrum of the MC involves the charge transfer band, whereas the fluorescence spectrum of the MA involves π–π^* transition.

Acknowledgement

The authors are grateful to the Department of Science and Technology, New Delhi for the financial support of Project no. SP/SI/H-39/96.

References

1. P.F. Barbara and H.F. Trommsdorff (*Editors*). Spectroscopy and dynamics of elementary proton transfer in polyatomic systems. Chem. Phys. (Special issue). **136** (1989); J. Phys. Chem. **95**, 10215 (1991).
2. K. Das, N Sarkar, A.K. Ghosh, D. Majumdar, D.N. Nath, and K. Bhattacharyya. J. Phys. Chem. **98**, 9126 (1994).
3. F.R. Prieto, M.C.R. Rodriguez, M.M. Gonzalez, and M.A.R. Fernandez. J. Phys. Chem. **98**, 8666 (1994).
4. A. Douhal, F. Amat-Guerri, A.U. Acuna, and K. Yoshihara. Chem. Phys. Lett. **217**, 619 (1994).
5. A. Douhal, F. Amat-Guerri, A.U. Acuna. J. Phys. Chem. **99**, 76 (1995), and refs. therein.
6. G.C. Lin, F.S. Awad, and M.A. El-Sayed. J. Phys. Chem. **95**, 10442 (1991).
7. B.J. Schwartz, I.A. Pateanu, and C.B. Harris. J. Phys. Chem. **96**, 359 (1993).
8. (*a*) N.P. Ernsting, Th. Arthem-England, M.A. Rodriguez, and W.J. Thiel. J. Chem. Phys. **97**, 3914 (1993); (*b*) Th. Arthem-England, T. Buttmann, N.P. Ernsting, M.A. Redriguez, and W.J. Thiel. Chem. Phys. **163**, 43 (1992).
9. F. Gai, R.L. Rich, and J.W. Petrich. J. Am. Chem. Soc. **116**, 735 (1994), and refs. therein.
10. M. Wiechmann, H. Port, W. Frey, F. Larmer, and J. Elsasser. Chem. Phys. Lett. **165**, 28 (1990).
11. A. Douhal, F. Amat-Guerri, M.P. Lillo, and A.U. Acuna. J. Photochem. Photobiol. A. Chem. **78**, 127 (1994).
12. A. Douhal, F. Lahmani, and A.H. Zewail. Chem. Phys. **207**, 477 (1996).
13. P.T. Chou, D. McMorrow, T.J. Aartsma, and M. Kasha. J. Phys. Chem. **88**, 5652 (1984).
14. A.U. Acuna, A. Costella, and J.M. Munoz. J. Phys. Chem. **90**, 2807 (1986).
15. A.U. Acuna, F. Amat, J. Catalan, A. Costella, J.M. Figuera, and J.M. Munoz. Chem. Phys. Lett. **132**, 567 (1986).
16. A. Costella, F. Amat, J. Catalan, A. Douhal, J.M. Figuera, J.M. Munoz, and A.U. Acuna. Opt. Commun. **64**, 457 (1987).
17. A.U. Acuna, F. Amat-Gueri, A. Costela, A. Douhal, J.M. Figuera, F. Florido, and R. Sastra. Chem. Phys. Lett. **187**, 98 (1991).
18. J. Sepiol, H. Bulaska, and A. Grabowski. Chem. Phys. Lett. **140**, 607 (1987).
19. W. Klopffer. Adv. Photochem. **10**, 311 (1977).
20. H.K. Sinha and S.K. Dogra. Chem. Phys. **102**, 337 (1986).
21. M. Krishnamoorthy and S.K. Dogra. J. Photochem. **32**, 235 (1986).
22. J.K. Dey and S.K. Dogra. J. Photochem. Photobiol. A. **66**, 15 (1992).
23. A.K. Mishra and S.K. Dogra. J. Photochem. **31**, 333 (1985).
24. J.K. Dey and S.K. Dogra. Chem. Phys. **149**, 97 (1990).
25. J.K. Dey and S.K. Dogra. Bull. Chem. Soc. Jpn. **64**, 3142 (1991).
26. S.K. Das, A. Bansal, and S.K. Dogra. Bull. Chem. Soc. Jpn. **70**, 307 (1997).
27. S.K. Das and S.K. Dogra. J. Chem. Soc. Faraday Trans. **94**, 139 (1998).
28. S. Santra and S.K. Dogra. J. Photochem. Photobiol. A: Chem. **101**, 221 (1997).
29. C.M. Orlando, J.G. Wirth, and D.R. Heath. J. Heterocycl. Chem. **7**, 1385 (1970).
30. J.A. Riddick and W.B. Bunger. *In* Techniques of chemistry. Vol. 8. Organic solvents. *Edited by* A. Wisseberger. Wiley–Interscience, New York. 1970. pp. 592, 644, 695.
31. M. Swaminathan and S.K. Dogra. Indian J. Chem. **22A**, 853 (1983).
32. C.A. Parker. *In* Photoluminesence of solutions with applications to photochemistry and analytical chemistry. Elsevier, Amsterdam. 1968.
33. G.G. Guilbault. *In* Practical fluorescence. Dekker, New York. 1971. p. 13.
34. G. Krishnamoorthy and S.K. Dogra. Chem. Phys. **243**, 45 (1999).
35. M.J. Jorgenson and D.R. Hartter. J. Am. Chem. Soc. **85**, 878 (1963).
36. G. Yagil. J. Phys. Chem. **71**, 1034 (1967).
37. J.B. Birks. *In* Photophysics of aromatic molecules. Wiley–Interscience, New York. Chap. 4. 1970.

© 2000 NRC Canada

38. N. Weichmann, H. Port, W. Frey, F. Larmer, and T. Elsasser. J. Phys. Chem. **95**, 1918 (1991).
39. E.W. Castrer, Jr., B. Bagchi, M. Maroncelli, S.P. Webb, A.J. Ruggiero, and G.R. Fleming..Ber. Bunsen-Ges Phys. Chem. **92**, 363 (1988).
40. J.F. Ireland and P.A.H. Wyatt. Adv. Phys. Org. Chem. **12**, 168 (1976).
41. A.K. Mishra and S.K. Dogra. Spectrochim. Acta Part A, **39A**, 609 (1983).
42. P.C. Tway and L.J.C. Love. J. Phys. Chem. **86**, 5223 and 5227 (1982).
43. M. Krishnamurthy, P. Phaniraj, and S.K. Dogra. J. Chem. Soc. Perkin Trans. II, 1917 (1986), and refs. therein.
44. H.K. Sinha and S.K. Dogra. J. Chem. Soc. Perkin Trans. II, 1465 (1987).
45. S.G. Schulman. *In* Fluorescence and phosphorescence spectroscopy. Pergamon Press, Oxford. 1977.
46. M. Krishnamurthy and S.K. Dogra. J. Photochem. **32**, 235 (1986).
47. J.C. Tai and N.L. Allinger. J. Am. Chem. Soc. **110**, 2050 (1988).
48. J. Delbene and H.H. Jaffe. J. Chem. Phys. **48**, 1801 (1968).
49. N. Mataga and T. Kubata. *In* Molecular interactions and electronic spectra. Marcel Dekker, New York. 1970.
50. J.F. Latard, R. Lapouynda, and W. Rettig. Chem. Phys. Lett. **222**, 2091 (1994).
51. H.H. Jaffe and M. Orchin. *In* Theory and applications of ultraviolet spectroscopy. John Wiley, New York. 1962. p. 301.
52. M. Mosquera, J.C. Pendo, M.C.R. Rodriguez, and F. Rodriguez-Proeto. J. Phys. Chem. **100**, 5398 (1996).
53. M. Mosquera, M.C.R. Rodriguez, and F. Rodriguez-Proeto. J. Phys. Chem. **101**, 2766 (1997).
54. P.T. Chou, M.L. Martinez, W.C. Cooper, D. McMorrow, S.T. Collino, and M. Khasa. J. Phys. Chem. **96**, 5203 (1992).
55. Y. Chen and P.L. Petrich. J. Phys. Chem. **97**, 1770 (1993).

© 2000 NRC Canada

A performance comparison between the CEP effective core potential/triple-split basis set approach and an all-electron computational method with emphasis on small Ti and V alkoxide complexes

Gustavo Larsen

Abstract: The structures of 30 neutral and positively charged small clusters were optimized and a number of hypothetical reaction pathways were investigated to compare the performance of the B3LYP/CEP-121G(d) Effective Core Potential/triple-split basis set method (ECP, method 1) and the B3LYP/6-311G(d) approach (method 2) for geometry optimizations. In addition, single point calculations at the B3LYP/CEP-121+G(d,p) (on geometries optimized by method 1) and at the B3LYP/6-311+G(d,p) (on optimized structures from methods 1 and 2) levels were also carried out. The augmented CEP-121G scheme is roughly 1.4 to 2.0 times computationally cheaper than full electron calculations, and is able to reproduce structures, infrared frequencies, thermochemical parameters and dipole moments predicted by the all-electron basis set employed in this study. From a practical viewpoint, the results confirm that ECPs can be used in combination with density functional methods, despite the fact that the former are typically generated via a Hartree–Fock approach.

Key words: CEP, Effective Core Potentials, alkoxides, DFT, Ti.

Résumé : On a optimisé les structures de 30 petits agrégats neutres ou chargés positivement et on a étudié un certain nombre de voies réactionnelles hypothétiques afin de pouvoir comparer la performance pour fins d'optimisation de la géométrie du potentiel effectif de coeur B3LYP/CEP-121-G(d) avec ensemble de base à triple dédoublement (« ECP », méthode 1) et l'approche B3LYP/6-311G(d) (méthode 2). De plus, on a effectué des calculs ponctuels aux niveaux B3LYP/CEP-121-G(d,p) (sur des géométries optimisées à l'aide de la méthode 1) et B3LYP/6-311+G(d,p) (sur des structures optimisées à l'aide des méthodes 1 ou 2). La méthode CEP-121-G améliorée est environ 1,4 à 2,0 fois moins coûteuse, d'un point de vue temps de calcul, que les calculs impliquant tous les électrons et elle permet de reproduire les structures, les fréquences infrarouges, les paramètres thermodynamiques et les moments dipolaires obtenus par l'ensemble de base comportant tous les électrons utilisé dans cette étude. D'un point de vue pratique, ces résultats confirment que l'on peut utiliser les ECP combinées aux méthodes de densité fonctionnelle même si celles-ci sont généralement générées par une approche de Hartree–Fock.

Mots clés : « CEP », potentiels effectifs de coeur, alcoolates, « DFT », Ti.

Introduction

A number of Effective Core Potential (ECP) methods for the treatment of inner shell electrons have been proposed in the past. In particular, the Hay and Wadt (1), the Cundari and Stevens (2), and the relativistic ECPs from Ross et al. (3) have gained popularity to evaluate both geometry and energetics of molecules containing post-second row elements. While all-electron Hamiltonians are generally preferred, an ECP approach is often a practical choice to study relatively large systems in which molecular structure and energetics of reactions involving similar species are sought.

Accepted September 15, 1999.

G. Larsen.[1] Department of Chemical Engineering, University of Nebraska, Lincoln NE 68588-0126, U.S.A.

[1]Telephone: (402) 472-9805. Fax: (402) 472-6989.
e-mail: glarsen@unlserve.unl.edu

Several authors have pointed to the fact that ECPs are generally adjusted to reproduce the properties of isolated atoms at the Hartree–Fock (HF) level, and that their use in density functional calculations (DFT) is not a priori justified (4, 5). This is chiefly due to the fact that exchange-correlation functionals are nonlinear with electron density, which results in core and valence contributions that are difficult to uncouple. However, Russo et al. (4) noted that all-electron basis sets such as 6-31G that implicitly contract the core often perform very well, and there is certainly no restriction as to their use in DFT studies. Indeed, these authors demonstrated that, for a small number of first-row transition metal complexes, the Hay and Wadt core potentials can be used in DFT studies to obtain accurate results. In any event, the combination of DFT methods with core potentials might constitute an important computational convenience if structures and energies are determined to be accurate, even if the theoretical justification for such approach is still a subject of debate. For example, Kovacs and Frenking (6) employed a

 © 2000 NRC Canada

Table 1. Recommended additional polarization and diffuse function types and their coefficients, according to standard nomenclature.[2]

	Element(s)										
	H			B, C, N, O, and F			P, S, Si, and Cl			Ti, V, and Br	
Polarization	P 1 1.00 1.1 1.0			D 1 1.00 0.8 1.0			D 1 1.00 0.5 1.0			F 1 1.00 0.5 1.0	
	Element(s)										
	H	B	C	N	O	F	Si	P	S	Cl	Ti,V,Br
Diffuse											
SP 1 1.00 y^a 1.0 1.0 (all)	—	3.15	4.38	6.39	8.45	10.76	3.31	3.48	4.05	4.83	5.00

[a]The *y* entries in each case are the tabulated values ($\times 10^2$) shown.

number of basis sets (primarily B3LYP and MP2) with relativistic and non-relativistic effective core potentials to study the structures of several Cu, Ti, Au, and Ag organometallic complexes. These authors found very good agreement among the geometries predicted by each method, even though they did not discuss the issue of the physical meaning of combining ECP and DFT methods. Similarly, Lee and Wright (7) studied the geometry and energetics of neutral and positively charged BBr_2 and BI_2 species using the Hay and Wadt (1) nonrelativistic ECPs in combination with hybrid density functionals. Again, these authors also did not discuss the physical appropriateness of a hybrid DFT/ECP approach. Another report on the practical aspects of adopting such hybrid methodology is that of Glukhovstev et al. (8). This group mentioned that the applicability of a combined DFT/ECP approach is beginning to be realized, and compared experimental data and relatively high-level calculations (QCISD(T), CCSD(T), etc.) with the DFT/ECP approach for a limited set of Fe complexes containing Fe—C bonds. Their findings on dissociation energies are encouraging, given that deviations from experimental values were well within experimental error. Another more recent report by Hay and Martin (9) deals with the structure and energetics of UF_6, NpF_6, and PuF_6 as evaluated by a hybrid DFT/ECP approach. Hay and Martin (9), who showed excellent awareness of the concern of transferring ECPs to DFT calculations, found that the local density (SVWN) and hybrid functional (B3LYP) presented the smallest deviations relative to experimentally determined structural parameters of these fluorides. In summary, while the combined use of high-quality ECPs and DFT methods is appealing from a computational efficiency viewpoint, studies leading to demonstrate the applicability of the technique are still in demand if the method is intended to enjoy some level of generality.

First-row transition elements represent an interesting case since the impact of neglecting relativistic terms when carrying out an all-electron calculation within the non-relativistic HF formalism on the accuracy of results may well be small, perhaps smaller than the errors associated with the introduction of an inert core. In the case of small Ti chloro-amine complexes, Baboul and Schlegel (10) chose to perform geometry optimizations at the B3LYP/6-311G(d) level, followed by high quality (modified G2 level) calculations to determine accurate atomization and dissociation energies. It has long been known that when energy differences between similar molecules are sought, and in which the splitting of species into atoms or elementary ions is not involved, triple-split basis sets augmented with diffuse and polarization functions are often able to describe the energetics of the system reasonably well.

Our interest stems from the need for a description of potential stable intermediates in the acid-catalyzed hydrolysis and condensation reactions of Ti and Si alkoxides to form mixed glasses via sol-gel chemistry (11). This issue clearly influenced the choice of certain complexes and molecules reported in this study. Titania-silica alcogels find use as high surface area amorphous solid catalysts and adsorbents.

Very recently, we used the sol-gel technique to prepare organic and inorganic TiO_2–SiO_2 materials, based on mixtures of tetraethylorthosilicate ($Si(OEt)_4$, TEOS) and permethylated oligosiloxane rings ($(Me_2SiO)_n$, n = 3–5) as the silicon source (11). To load such materials with Ti, $TiCl_2(i\text{-}OPr)_2$ was prepared in situ as previously reported (12). Such high-surface area materials display improved olefin epoxidation activities (13) relative to those found in alcogels where $Ti(i\text{-}OPr)_4$ is used as the Ti source instead (12).

There exist several difficulties associated with the tracking of Ti species formed early in the Ti alkoxides reactions with preformed silica alcogels, including the high reactivity of the former, and the low concentrations of Ti alkoxides in the sol to achieve high Ti dispersions. These two limitations render a number of spectroscopic techniques (e.g., EXAFS and EPR) ineffective to obtain reliable structural data on stable intermediates under realistic reaction conditions.

When studying Ti solution chemistry, the possibility of coordination expansion of the Ti center must be considered. Dimeric $TiCl_4$ and $TiCl_4$ complexes with chelating esters have been recognized for some time (14, 15). The formation

[2] M.J. Frisch, G.W. Trucks, H.B. Schlegel, G.E. Scuseria, M.A. Robb, J.R. Cheeseman, V.G. Zakrzewski, J.A. Montgomery, Jr., R.E. Stratmann, J.C. Burant, S. Dapprich, J.M. Millam, A.D. Daniels, K.N. Kudin, M.C. Strain, O. Farkas, J. Tomasi, V. Barone, M. Cossi, R. Cammi, B. Mennucci, C. Pomelli, C. Adamo, S. Clifford, J. Ochterski, G.A. Petersson, P.Y. Ayala, Q. Cui, K. Morokuma, D.K. Malick, A.D. Rabuck, K. Raghavachari, J.B. Foresman, J. Cioslowski, J.V. Ortiz, B.B. Stefanov, G. Liu, A. Liashenko, P. Piskorz, I. Komaromi, R. Gomperts, R.L. Martin, D.J. Fox, T. Keith, M.A. Al-Laham, C.Y. Peng, A. Nanayakkara, C. Gonzalez, M. Challacombe, P.M.W. Gill, B. Johnson, W. Chen, M.W. Wong, J.L. Andres, C. Gonzalez, M. Head-Gordon, E.S. Replogle, and J.A. Pople. Gaussian 98, Revision A.3. Gaussian, Inc., Pittsburgh, Pa. 1998.

© 2000 NRC Canada

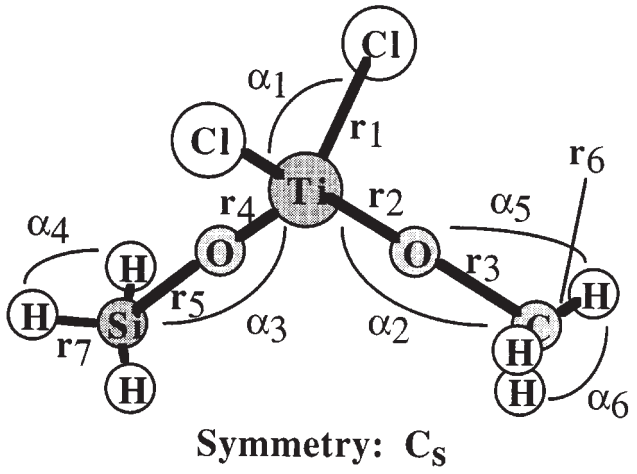
Table 2. List of fully optimized structures

Ti:	$TiCl(OCH_3)_3$, $TiCl_2(OCH_3)(OSiH_3)$, $TiCl_2(OCH_3)(HO^+SiH_3)$, $TiCl_2(OCH_3)(HO^+CH_3)$,
V:	$VO_2(OCH_3)$, $VO_2(OSiH_3)$, $VO_2(HO^+SiH_3)$, VO_2Cl
Non-transition element species:	B_2H_4, BF_3, S_2H_2, SH_2, SO_3, OCS, CH_3PH_2, CH_3OH, SiH_3OH, $CH_3OH_2^+$, CO, COF_2, $BrCH_3$, H_2O, H_3O^+, H_2O_2, NH_3, Cl_2, F_2, HF, HCl

Table 3. Selected geometrical parameters of the Ti chloroalkoxysiloxane structure shown in Fig. 1.

Method	r_1 (Å)	r_2 (Å)	r_3 (Å)	r_4 (Å)	r_5 (Å)	r_6 (Å)	r_7 (Å)	α_1 (°)	α_2 (°)	α_3 (°)	α_4 (°)	α_5 (°)	α_6 (°)
B3LYP/6-311G(d)	2.222	1.735	1.407	1.770	1.664	1.093	1.481	111.6	172.8	175.9	109.3	109.3	109.4
B3LYP/CEP-121G(d)	2.231	1.749	1.420	1.783	1.663	1.096	1.487	110.2	176.7	177.8	109.1	109.2	109.3

Fig. 1. Optimized structure of $TiCl_2(OCH_3)(OSiH_3)$. See Table 3.



of penta- and hexacoordinated $TiCl_4$-$(H_2CO)_n$ (n = 1 or 2) complexes is predicted by theory (16). Several hexacoordinated complexes of $TiCl_3$(i-OPr) with THF, diethylether, formaldehyde, and esters have been reported (17). Still, X-ray absorption studies of several Ti alkoxides in solution including Ti(i-OPr)$_4$, Ti(i-OAm)$_4$, and Ti(OEt)$_4$ reveal that their structures may or may not be tetrahedral (18). For example, Ti(i-OPr)$_4$ and Ti(i-OAm)$_4$ appear to adopt the conventional tetrahedral geometry, while Ti(OEt)$_4$ seems to be oligomeric (18). Based on an extensive literature search, we found no research describing the geometry of Ti chloroalkoxides in solution. Thus, this contribution is aimed at setting up the stage for studying the structure of Ti chloroalkoxides via theoretical methods. Emphasis is made on determining whether a hybrid (pseudopotentials and DFT), more computationally efficient method is appropriate to model the chemistry of such complexes. A more thorough study on the structure and energetics of tetra- and pentacoordinated Ti alkoxide species in acidic media will be presented in a separate paper. In addition, many other small molecules and hypothetical reactions involving Ti-free species were also studied, to confirm that the generalizations made in this contribution are unlikely to be case dependent. However, for some of the conclusions reached in this manuscript to be extended freely to other regions in the periodic table a more extensive study should be conducted. The ultimate goal of this paper is to determine what parameters are affected, relative to an all-electron method, when using an augmented ECP and triple-split basis set in combination with hybrid functionals on Ti and V complexes and on a number of simple molecules containing first- and second-row elements. Frequency and thermochemistry data, relative to the all-electron method adopted, are also reported. For "absolute" corrections to these parameters, the reader is referred to the comprehensive work of Scott and Radom (19).

Computational methods

The three-parameter Becke style hybrid functional (20), with the correlation functional of Lee et al. (21) was adopted. The ECPs from Cundari and Stevens (2), as built in the Gaussian 98 program[2] with a triple-split basis set (CEP-121G) were used. In order to compare the performance of this method with that of B3LYP/6-311G(d), one d-type polarization function was added to each first and second row element present in the molecule (or one f function for post second row atoms) for geometry optimizations. For single point energy calculations on optimized structures, this CEP-121G(d) basis set was further augmented by adding one p-type function to each hydrogen atom, and one suitable diffuse function to each heavy atom. The recommended auxiliary polarization and diffuse functions used in this study are presented in Table 1 in standard Gaussian® nomenclature.[2] In this study, the terminology adopted is B3LYP/CEP-121G(d) for geometry optimizations, and B3LYP/CEP-121+G(d,p) for single-point energy calculations. These are to be compared to the reference computational method adopted, namely B3LYP/6-311G(d), and B3LYP/6-311+G(d,p), respectively. In addition, single-point energy calculations at the B3LYP/6-311+G(d,p) level on CEP-121G(d) optimized structures were also carried out. Throughout this paper, each parameter (e.g., ΔE_{el}, μ, etc.) will generally carry a subscript such as "ref" (all-electron calculations), "CEP" (CEP-based computations), or "mix" (CEP-based optimized structures followed by a single-point all electron calculation). All calculations were carried out using Alpha-DEC Workstations with a single 667 MHz processor and 1 Gb SDRAM.

Results and discussion

Table 2 lists all molecules and ions evaluated in this study. Figure 1 shows the geometry of a representative Ti chloroalkoxysiloxane species, with a number of its structural parameters being presented in Table 3 for each geometry optimization method used. In all chemical species investigated in this work, key geometrical features (e.g., point group, similar dihedral angles, etc.) were always found to remain the same when going from the all-electron method to the ECP-based approach. The latter produced slightly larger

© 2000 NRC Canada

Table 4. Sample hypothetical reaction pathways: Energetics.

Reaction	ΔE_{el} (mHartrees)			$\Delta E_{ZPVE+therm.}$ (kcal/mol)		S_{tot}(cal k^{-1} mol^{-1})	
	Ref.	CEP	Mix	Ref.	CEP	Ref.	CEP
$TiCl(OMe)_3 + H_3SiOH + HCl >> TiCl_2(OMe)(OSiH_3) + 2H_3COH$	–15.6	–16.6	–14.4	2.65	2.59	0.24	0.10
$VO_2(OMe) + H_3SiOH >> VO_2(OSiH_3) + H_3COH$	–5.5	–5.1	–4.9	0.89	0.50	3.27	2.74
$VO_2(OSiH_3) + H_3O^+ >> VO_2(O^+HSiH_3) + H_2O$	–26.9	–21.6	–26.4	–0.74	–0.88	–5.87	–4.77
$VO_2Cl + H_3COH >> VO_2(OCH_3) + HCl$	7.7	8.5	6.8	–2.08	–2.00	–2.96	–2.51
$Cl_2 + 2H_2O >> H_2O_2 + HCl$	56.8	58.7	57.0	–2.87	–2.88	0.17	0.10
$14SH_2 + 2SO_3 >> 8S_2H_2 + 6H_2O$	–197.6	–221.6	–200.9	23.20	24.19	–60.64	–58.83
$S_2H_2 + 2H_2O >> 2SH_2 + H_2O_2$	104.2	102.4	104.3	–2.83	–2.88	2.29	2.19
$Cl_2 + 2HF >> F_2 + 2HCl$	134.9	132.2	135.0	–3.36	–2.74	1.17	1.22
$B_2H_4 + 5F_2 >> 4HF + 2BF_3$	–1339.8	–1294.4	–1339.6	7.60	7.40	–9.39	–8.96
$CO + F_2 >> COF_2$	–195.8	–184.7	–195.6	4.03	3.89	–33.67	–33.54

Fig. 2. Bond length relative deviations, R_{ref}/R_{CEP}, as a function of bond length for the reference method.

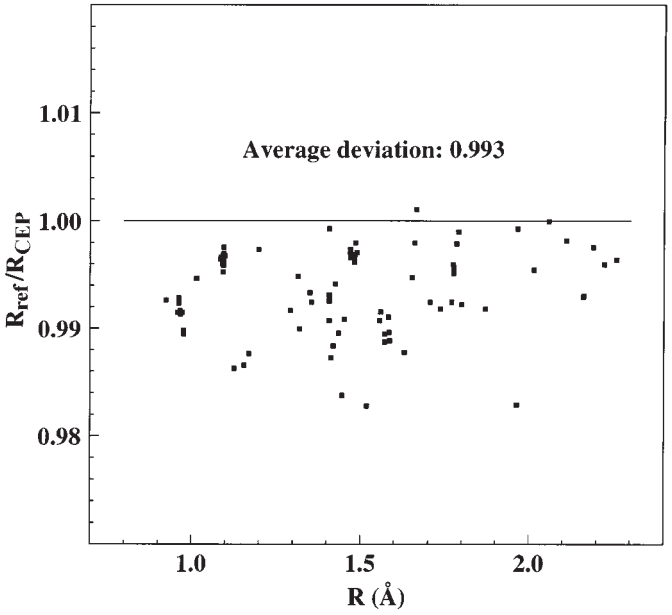
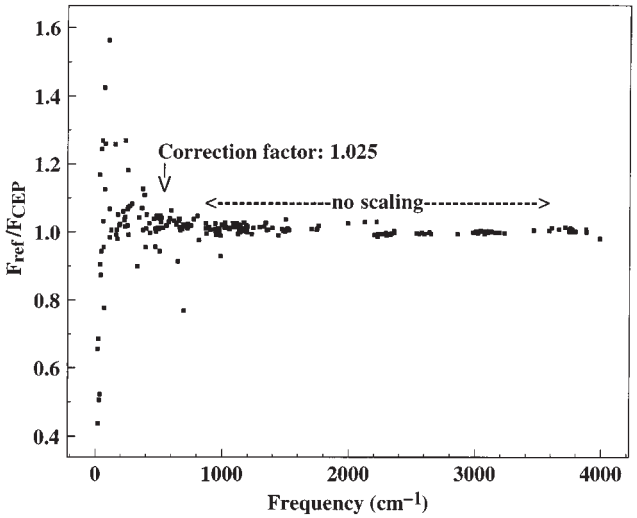


Fig. 3. Frequency relative deviations, F_{ref}/F_{CEP}, as a function of vibrational frequency for the reference method.



bond distances, and these deviations were always found to be consistent (Fig. 2 and Table 3).

Nearly 300 frequencies were animated and their values from the two methods were carefully compared (Fig. 3). Overall, the CEP method performs satisfactorily in this category as well, the only apparent drawback being the reproducibility of very low frequencies. This is known to be a problem that does not depend on the method of choice, because very low frequencies typically arise from the wagging or rocking of large groups, and small deviations in bond angles, distances, and bond orders necessarily translate into large frequency deviations. Though still very small, somewhat larger relative deviations were observed for the low-frequency vibrations involving heavier atoms (e.g., Cl, Si, Ti, V, and Br). Any partition of the range of frequencies produced by the calculations in this paper would be arbitrary. Nevertheless, it appears that the 400–900 cm^{-1} range (which is largely dominated by stretching frequencies involving post second row elements) should be scaled by a factor of 1.025 relative to B3LYP/6-311G(d), whereas differences between the two methods in the 1000–4000 cm^{-1} range are clearly small enough to recommend the use of B3LYP/CEP-121G(d) frequencies without scaling. As mentioned earlier, and since Scott and Radom (19) have reported on "absolute" scale factors (including values for the reference method selected here), adjustment of frequencies to results reported in ref. 5 becomes trivial. However, it must be mentioned that other authors have used calculated frequencies at the B3LYP/6-311G(d) level without scaling, since they appear to be in excellent agreement to experimental values for small Ti complexes (10). Again, in the absence of studies involving a number of other heavy atoms and the monitoring of thousands (instead of a few hundreds) of different vibrational modes, scale factors reported here should be taken with caution.

Table 4 shows thermodynamic data on a number of hypothetical reaction pathways. In general, all three methods yield comparable results. Relative deviations in the thermochemical parameters are shown in Figs. 4 and 5, with the lines S_{ref}/S_{CEP} and E_{ref}/E_{CEP} equal to one shown in the interest of clarity. These deviations were also small enough to recommend no scaling for ZPVE-corrected thermal energies

© 2000 NRC Canada

Fig. 4. $\Delta E_{ZPVE+therm}$ relative deviations (B3LYP/6-311G(d): B3LYP/CEP-121G(d)) as a function of $\Delta E_{ZPVE+therm}$ values from reference method.

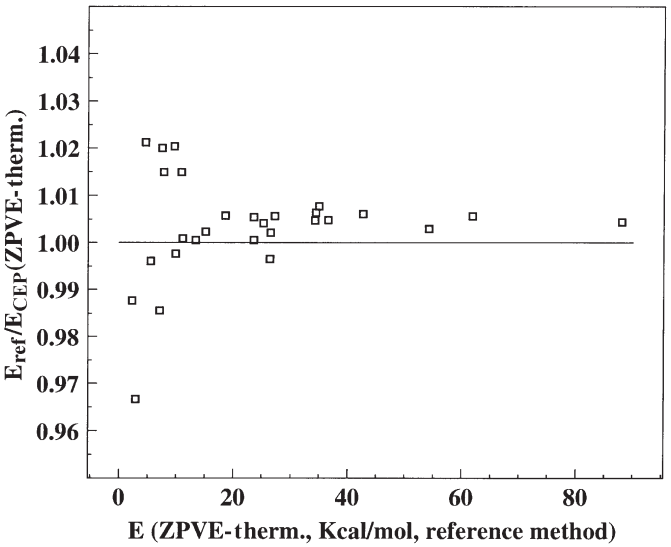


Table 5. Relative computational cost (B3LYP/6–311G(d) : B3LYP/CEP-121G(d)).

Molecule	Cost
$TiCl_2(OMe)(OSiH_3)$	1.16
VO_2Cl	2.03
$CBrH_3$	2.05
$VO_2(OMe)$	1.36

and entropies predicted by the augmented B3LYP/CEP method, relative to B3LYP/6-311G(d). The latter has been proposed to require scaling by a factor of 0.9806 for thermochemistry to yield accurate results (19), which indicates that a correction factor of 0.98 for values predicted at the B3LYP/CEP-121G(d) level should be adopted. In spite of the fact that the pool of species selected in this study is not very large, results from Table 4 appear to indicate that the B3LYP/6-311+G(d,p)//CEP-121G(d) single-point/geometry combined approach might be the most computationally efficient and reliable of all three.

Table 5 shows a few examples on the computational efficiency of the full-electron reference method and the augmented CEP approach. In practice, the situation is somewhat more favorable for the CEP method, since it was observed that a smaller number of cycles were normally required for tight convergence of the augmented CEP method.

Figure 6 shows the relative deviations in the dipole moments obtained from single-point calculations on optimized structures for both the "mix" and the "CEP" methods. In general, these can be considered small, and a "mix" approach does not improve the relative accuracy of the μ values to any significant extent. It should be mentioned however, that the predicted Mulliken populations derived from the CEP method differ considerably from those of the "mix" and the all-electron approach (see examples in Table 6). However, since atomic charge is not a quantum chemical observable, its evaluation via choosing a certain method is still somewhat arbitrary. For example, it has long been known that the Mulliken population analysis is essentially based on a balanced partition of the overlap region, but this does not necessarily translate into a very precise description of the electron density distribution. The differences between the two methods shown in Table 6 are thus expected, since the hybrid method obviously treats inner shells as a lump (core) contribution. Nevertheless, the "mix" approach (i.e., a hybrid optimization followed by an all-electron single point calculation) is clearly the method of choice if charge populations from all-electron methods are deemed more reliable. Note that in Table 6, Mulliken charges derived from the "mix" method do not differ significantly from those of the all-electron reference method.

Fig. 5. S_{ref}/S_{CEP} relative deviations as a function of S from reference thermochemistry calculations.

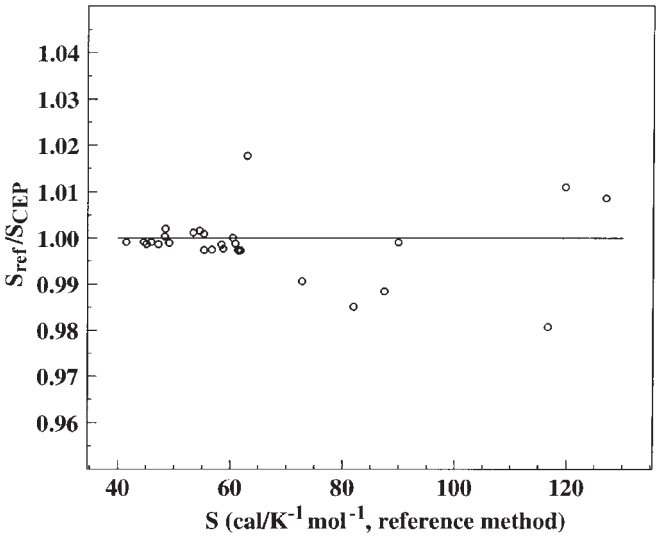
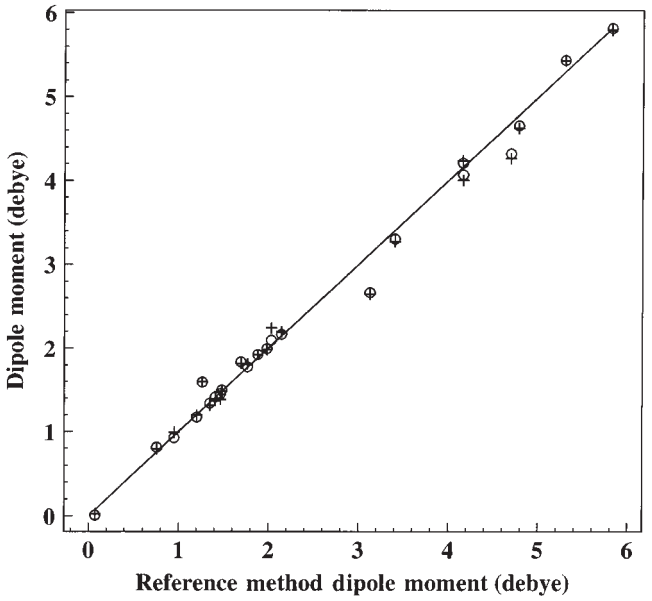


Fig. 6. Dipole moments from the CEP (○) and "mix" (+) methods as a function of dipole moments predicted by the B3LYP/6-311+G(d,p)//B3LYP/6-311G(d) reference method.



© 2000 NRC Canada

Table 6. Mulliken Population Analysis (heavy atoms[a]) for the clusters shown in Fig. 1.

	$TiCl(OCH_3)_3$			$VO_2(HO^+SiH_3)$			$TiCl_2(OCH_3)(OSiH_3)$		
Atom	Ref.	CEP	Mix	Ref.	CEP	Mix	Ref.	CEP	Mix
Ti	0.370	0.329	0.414	—	—	—	–0.330	0.495	–0.293
V	—	—	—	0.998	0.817	0.985	—	—	—
Si	—	—	—	0.745	0.686	0.748	0.790	0.477	0.785
Cl	–0.157	–0.400	–0.154	—	—	—	–0.040	–0.319	–0.030
O(=)	—	—	—	–0.194	–0.113	–0.190	—	—	—
O(=)	—	—	—	–0.190	–0.074	0.187	—	—	—
O(-C)	–0.337	–0.552	–0.369	—	—	—	–0.157	–0.431	–0.189
O(-Si)	—	—	—	–0.598	–0.644	–0.644	–0.230	–0.226	–0.252
C	–0.173	0.217	–0.154	—	—	—	–0.118	0.255	–0.117

[a]In some cases, there were be more than one non-equivalent O atom with double (=) or single (—) bond character in each molecule.

Finally, the issue of projected level of agreement between the proposed hybrid CEP/DFT approach and experiment, i.e. beyond a comparison between all-electron methods and CEP/DFT needs to be briefly discussed. At this point emphasis needs to be made on early transition and other heavy element work, because these represent an adequate reference to some of the species studied this work. The enthalpies of formation of several hydroxo-, and oxo- species of Fe, as well as FeS, $FeCH_2^+$, and $FeCH^+$ calculated (8) at the B3LYP level with the Stuttgart group (22) effective core potentials were found to be within experimentally determined values. As mentioned earlier, the combined ECP/B3LYP approach predicts vibrational frequencies and bond lengths that are in very good agreement with experiment for three uranide fluorides (9). In addition to these observations, one could stress the fact that since the all-electron method used in this study and the proposed hybrid CEP/B3LYP approach are in close internal agreement, comparisons between theoretical calculations at a good quality DFT/all-electron level with experiment should also provide a reliable model validation reference frame. For example, Ziegler (23) provided a comprehensive list of computations including a number of small first-row transition element molecules to show the accuracy of DFT methods for predicting bond energies and enthalpies of formation. It must be emphasized that thermochemistry data involving atomization and dissociation of molecules into elements or elementary ions constitute a particularly tough test that computations at a comparable level to the one used in the present work appear to pass (8, 22, 23). Thus, there is a priori no reason to believe that in reactions that do not involve atomization or fragmentation into elementary ions one should expect unusually large discrepancies between theory and experiment. Nevertheless, at least a limited set of very high level computations (e.g., G2) will be carried out in future studies dealing with Ti alkoxide condensations to further strengthen the validity of the proposed computational approach.

Conclusions

The use of DFT methods in combination with the ECPs from Cundari and Stevens (2) yield geometries and energetics that are in very good agreement with those derived from the classical B3LYP/6-311+G(d,p)//B3LYP/6-311G(d) approach. Calculated frequencies, thermochemistry, and geometrical parameters require essentially no scaling.

Acknowledgments

This work was supported by grants from the National Science Foundation (CTS-9733756), and the Nebraska Research Initiative.

References

1. P.J. Hay and W.R. Wadt. J. Chem. Phys. **82**, 299 (1985).
2. T.R. Cundari and W.J. Stevens. J. Chem. Phys. **98**, 5555 (1993).
3. R.B. Ross, J.M. Powers, T. Atashroo, W.C. Ermler, L.A. LaJohn, and P.A. Christiansen. J. Chem. Phys. **93**, 6654 (1990).
4. T.V. Russo, R.L. Martin, and P.J. Hay. J. Phys. Chem. **99**, 17085 (1995).
5. C. Van Wullen. Int. J. Quantum Chem. **58**, 147 (1996).
6. A. Kovacs and G. Frenking. Organometallics, **18**, 887 (1999).
7. E.P.F. Lee and T.G. Wright. J. Phys. Chem. A, **101**, 1374 (1997).
8. M.N. Glukhovstev, R.D. Bach, and C.J. Nagel. J. Phys. Chem. A, **101**, 316 (1997).
9. P.J. Hay and R.L. Martin. J. Chem. Phys. **109**, 3875 (1998).
10. A.G. Baboul and H.B. Schlegel. J. Phys. Chem. A, **102**, 5152 (1998).
11. E. Lotero, D. Vu, C. Nguyen, J. Wagner, and G. Larsen. Chem. Mater. **10**, 3756 (1998).
12. R. Neumann and M. Levin-Elad. J. Catal. **166**, 206 (1997).
13. D. Vu, C. Nguyen, M. Buechler-Skoda, R. Gill, and G. Larsen. Appl. Catal. A, **185**, 301 (1999).
14. I.W. Bassi, M. Calcaterra, and R. Intrito. J. Organomet. Chem. **127**, 305 (1977).
15. T. Poll, J.O. Mette, and G. Helmchen. Angew. Chem. Int. Ed. Engl. **24**, 112 (1985).
16. V. Branchadell and A. Oliva. J. Am. Chem. Soc. **114**, 4357 (1992).
17. H.-M. Gau, C.-S. Lee, C.C. Lin, M.-K. Jiang, Y.-C. Ho, and C.-N. Kuo. J. Am. Chem. Soc. **118**, 2936 (1996).
18. F. Babonneau, S. Doeuff, A. Leaustic, C. Sanchez, C. Cartier, and M. Verdaguer. Inorg. Chem. **27**, 3166 (1988).
19. A.P. Scott and L. Radom. J. Phys. Chem. **100**, 16504 (1996).
20. A.D. Becke. J. Chem. Phys. **98**, 5648 (1993).
21. C. Lee, W. Yang, and R.G. Parr. Phys. Rev. B: Condens. Matter, **37**, 785 (1988).
22. M. Dolg, U. Wedig, H. Stoll, and H. Preuss. J. Chem. Phys. **86**, 866 (1987).
23. T. Ziegler. ACS Symp. Ser. **677**, 369 (1998).

© 2000 NRC Canada

The solid-state structures of (–)-scopolamine free base, (–)-scopolamine methobromide, (–)-scopolamine hydrobromide trihydrate, and of the pseudopolymorphic forms of (–)-scopolamine hydrochloride anhydrate and 1.66hydrate[1]

Robert Glaser, Dror Shiftan, and Marc Drouin

Abstract: (–)-Scopolamine hydrochloride anhydrate gives crystals belonging to the orthorhombic space group $P2_12_12_1$ and at 293(2) K: a = 7.097(2), b = 10.686(2), c = 22.623(2) Å, V = 1715.7(6) Å^3, Z = 4, $R(F)$ = 0.039, and $R_w(F)$ = 0.053. (–)-Scopolamine hydrochloride 1.66hydrate yields crystals belonging to the tetragonal space group $P4_32_12$ and at 293(2) K: $a = b$ = 11.843(6), c = 26.211(4) Å, V = 3676(3) Å^3, Z = 8, $R(F)$ = 0.047, and $R_w(F^2)$ = 0.135. (–)-Scopolamine methobromide affords crystals belonging to the orthorhombic space group $P2_12_12_1$ and at 293(2) K: a = 7.0403(8), b = 10.926(2), c = 23.364(5) Å, V = 1797.2(6) Å^3, Z = 4, $R(F)$ = 0.039, and $R_w(F)$ = 0.052. The two hydrochloride pseudopolymorphs were isostructural to the corresponding two hydrobromide analogues. Both hydrohalide hydrated crystals have a water molecule occupying a general position of symmetry, and another water molecule occupying a special position of C_2-rotation symmetry. The hydrated hydrochloride salt also had an additional 0.322(17) partial occupancy water molecule (absent in the hydrobromide sesquihydrate) occupying another special position of C_2-rotation symmetry, i.e., the extra water molecule occupied the special position in statistically ca. one-third of the unit-cells to give a total hydrate stoichiometry of 1.66 molecules of water. While the two hydrohalide anhydrates exhibited extended tropate ester conformations (phenyl-ring antiperiplanar to oxirane moiety) vs. compact conformations (phenyl-ring near the scopine underside) for the two hydrated hydrohalides, all four displayed other common structural features: axial *N*-methyl stereochemistry, antiperiplanar methylol oxygen/aromatic C(*ipso*) relationships, and phenyl-ring eclipsing of the C(α)—H bond. The CPMAS ^{13}C NMR spectrum of (–)-scopolamine hydrobromide "trihydrate" shows it to be a conglomerate of (–)-scopolamine hydrobromide sesquihydrate plus two or more hydrated species (three ca. equal intensity carbonyl signals at 5.0 kHz spin-rate). High-speed rotor spinning (e.g., ca. 10 kHz and higher) causes a temperature-induced phase-transition to yield only the sesquihydrate form. The same transformation was noted with a 18 K rotor-temperature increase and an invariant 5.0 kHz spin-rate. The sesquihydrate spectrum remained after spin-rate decrease to 5.0 kHz, but the three component mixture 5.0 kHz spectrum was regenerated after three weeks sample storage within the capped rotor. The (–)-scopolamine free base crystalline melt CPMAS spectrum also shows a mixture of at least three hydrated species.

Key words: stereochemistry, X-ray crystallography, solid-state NMR, CPMAS, anticholinergic.

Résumé : Le chlorhydrate de la (–)-scopolamine anhydre forme des cristaux orthorhombiques du groupe d'espace $P2_12_12_1$ qui, à 293(2) K, présentent les caractéristiques suivantes: a = 7,097(2), b = 10,686(2) et c = 22,623(2) Å, V = 1715,7(6) A^3, Z = 4, $R(F)$ = 0,039 et $R_w(F)$ = 0,053. Le chlorhydrate de la (–)-scopolamine hydraté par 1,66 moles d'eau, existe sous la forme de cristaux tétragonaux du groupe d'espace $P4_32_12$ qui, à 293(2) K, présentent les caractéristiques suivantes: $a = b$ = 11,843(6) et c = 26,211(4) Å, V = 3676(3) A^3, Z = 8, $R(F)$ = 0,047 et $R_w(F^2)$ = 0,135. Le méthobromure de la (–)-scopolamine forme des cristaux orthorhombiques du groupe d'espace $P2_12_12_1$ qui, à 293(2) K, présentent les caractéristiques suivantes: a = 7,0403(8), b = 10,926(2) et c = 23,364(5) Å, V = 1797,2(6) A^3, Z = 4, $R(F)$ = 0,039 et $R_w(F)$ = 0,052. Les deux chlorhydrates pseudopolymorphes sont isostructuraux avec les deux bromhydrates correspondants analogues. Les cristaux des deux dérivés halogénés hydratés comportent une molécule d'eau qui occupe une position de symétrie générale et une autre qui occupe une position spéciale de symétrie de

Received August 23, 1999

R. Glaser[2] and D. Shiftan. Department of Chemistry, Ben-Gurion University of the Negev, Beer-Sheva 84105, Israel.
M. Drouin. Département de Chimie, Université de Sherbrooke, Québec, QC J1K 2R1, Canada.

[1]*This paper is dedicated to Professor Arthur S. Perlin on the occasion of his 77th birthday.*[3]

[2]Author to whom correspondence may be addressed. Telephone: +972 7 646 9812. Fax: +972 7 647 2943 (attn. Prof. Robert Glaser). e-mail: glaser@bgumail.bgu.ac.il

[3]"...הלומד על-מנת ללמד..." "*...he who learns in order to teach...*" Pirke Aboth, Chapter IV, verse 6.

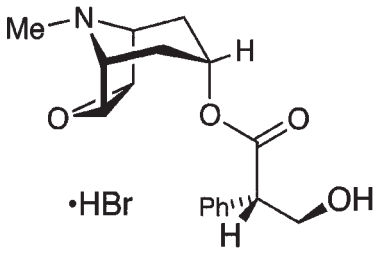
 © 2000 NRC Canada

rotation C_2. Le chlorhydrate hydraté comporte une fraction additionnelle de molécule d'eau (0,0322(17)) (absente dans le sesquihydrate du bromhydrate) qui, d'un point de vue statistique, occupe une autre position spéciale, soit le tiers des mailles élémentaires et il en résulte que la stoechiométrie totale de l'hydrate est égale à 1,66 molécules d'eau. Alors que la conformation de l'ester tropate des deux dérivés halogénés anhydres est de forme étendue (noyau phényle *antipériplanaire* par rapport à la portion oxirane), celle que l'on observe pour les deux dérivés halogénés hydratés se présente sous une forme compacte (avec un noyau phényle près de la partie inférieure de la scopine); les quatre présentent toutefois des caractéristiques structurales communes: stéréochimie *axiale* du *N*-méthyle, relation antipériplanaire entre l'oxygène du méthylol et le C(*ipso*) aromatique et le noyau phényle qui éclipse la liaison C(α)—H. Le spectre RMN du ^{13}C par la technique de la polarisation croisée avec rotation à l'angle magique (« CPMAS ») du bromhydrate de (–)-scopolamine « trihydraté » met en évidence qu'il s'agit d'un conglomérat de bromhydrate de (–)-scopolamine sesquihydraté en présence de d'au moins deux autres espèces hydratées (trois signaux d'intensités approximativement égales découlant de carbonyles, à une vitesse de spin de 5,0 kHz). Une vitesse de spin du rotor plus élevée (par exemple, environ 10 kHz ou plus) provoque une transition de phase induite par la température qui permet de n'observer que la forme sesquihydratée. On a observé la même transformation avec une augmentation de température de 18 K du rotor tout en maintenant la vitesse de spin à 5,0 kHz. Le spectre du sesquihydrate est conservé après une diminution de la vitesse de spin à 5,0 kHz; toutefois, après avoir conservé l'échantillon pendant trois semaines dans le rotor fermé, on régénère le spectre du mélange à trois composants à 5 kHz. Faisant appel à la technique de la polarisation croisée avec rotation à l'angle magique, on a déterminé le spectre RMN du ^{13}C de la base libre de la (–)-scopolamine fondue qui met aussi en évidence la présence d'un mélange d'au moins trois espèces hydratées.

Mots clés : stéréochimie, diffraction des rayons X, RMN à l'état solide par la technique de la polarisation croisée avec rotation à l'angle magique (« CPMAS »); anticholinergique.

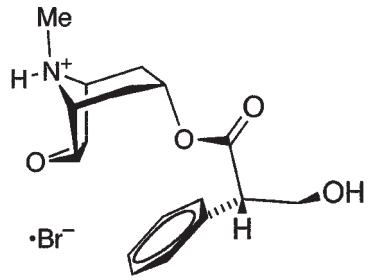
Introduction

(–)-Scopolamine hydrobromide [(–)-hyoscine hydrobromide, **1**] is a well known anticholinergic drug, and is also used in the treatment of motion sickness (1). (–)-Hyoscine is a tropane alkaloid natural product isolated from the belladonna plant *Hyoscyamus niger* (henbane) and consists of the (*S*)-(–)-tropic acid ester (2) of the 3-*endo*-substituted amino-alcohol scopine. Scopolamine has two stereogenic chirotopic (3) atoms: the relatively stereostable α-carbon and the stereolabile nitrogen.

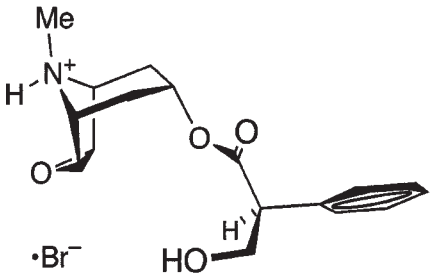


1

Pauling and Petcher (4) reported the first X-ray crystallographic single-crystal structure determination of (–)-hyoscine hydrobromide (**1**). It was described as a hemihydrate and the pictorial representation showed an *axial N*-methyl group, a "compact" conformation (phenyl-ring under the oxiranyl moiety, see iconic projection **2**), and an antiperiplanar (ca. 180°) phenyl – to – methylol-OH arrangement (4). Other stereochemical studies of this molecule, its derivatives, and analogues made use of this early X-ray determined structure (5–10), but no atomic coordinates were presented nor were any to be found in the *Cambridge Crystallographic Data Base*. In addition, it was reported that the structure converged only to an *R(F)* = 0.09 value upon refinement (4). A new single crystal X-ray diffraction analysis of **1** was undertaken by us to obtain the needed coordinates (11). However, this study produced a pseudopolymorph ((N*r*,Cα-*S*)-(–)-scopolamine hydrobromide anhydrate) with an "extended" solid-state conformation (see **3**, a 2D-iconic projection[4] of the X-ray determined 3D-structure) that was different from that depicted for the hemihydrate (11).



2



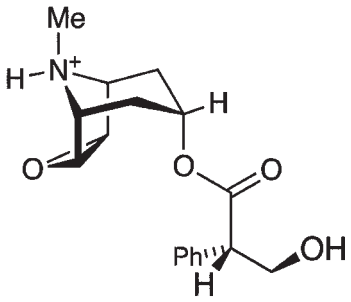
3

[4] CS-CHEMDRAW ULTRA 5.0 and CS-CHEM3D PRO 5.0. CambridgeSoft, Cambridge, Mass. 1999.

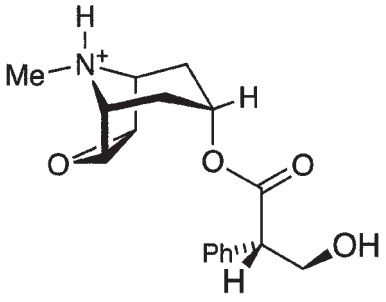
© 2000 NRC Canada

The trihydrate form of **1** is listed in the *United States Pharmacopeia 23 Official Monographs* (12). In a desire to obtain the structure of this hydrated crystal, **1** was recrystallized from water. The resulting crystal was a new pseudopolymorph in the form of a sesquihydrate (see iconic projection **2**), having a compact conformation (13). Both the crystal and molecular geometries of **2** were the same as that of the hemihydrate form reported earlier by Pauling and Petcher (4). Crystals of the hemihydrate were reported as belonging to the tetragonal $P4_12_12$ space group, and at presumed ambient temperature, a = 11.965(7), c = 26.52(2) Å, Z = 8, and $R(F)$ = 0.09. Those of the sesquihydrate differed in the left-handedness of the 4_3-screw in the tetragonal $P4_32_12$ space group, and at 293 K: a = 11.9667(8), c = 26.528(2) Å, Z = 8, and $R(F)$ = 0.051 (13). It is noted that all four of the reported pseudopolymorphs of **1** (the anhydrous form (11), hemihydrate (4), the sesquihydrate (13), and the trihydrate (12)) meet the USP requirements for water content, since only a maximum permissible weight loss of 13.0% after drying at 105°C for 3 h is stated, while no lower limits for weight loss are given (12).

NMR spectroscopy has been shown to be a useful tool to determine the stereochemistry of scopolamine and related compounds in solution. Under slow exchange limit (SEL) ^{1}H and ^{13}C NMR (acidic D_2O or CD_2Cl_2) conditions for the prototropic shift – nitrogen inversion epimerization mechanism, axial, and equatorial *N*-methyl diastereomers (**4a**, **4e**) can be observed for solutions of **1** (14). The major:minor, axial:equatorial *N*-methyl diastereomeric bias in D_2O became inverted in CD_2Cl_2 (14).



4a



4e

A recent solid-state CPMAS ^{13}C NMR study of crystalline scopolamine tertiary and quaternary ammonium salt analogues of known structures, clearly showed that the methylol (CH_2OH) chemical shift was diagnostic for the conformation about the C(carbonyl)—C(α) bond (15). In the synperiplanar (ca. 0°) O = C-C(α)-CH_2OH *compact* conformation, δ(CH_2OH) and δ(C = O) values were found to be closer to TMS than corresponding values in the *(+)*-synclinal (ca. +60°) O = C-C(α)-CH_2OH extended conformation (15). As a result of the solid-state CPMAS studies, the solution-state conformational preference about the C(carbonyl)—C(α) bond could then be ascertained from deconvolution of the weighted time-average values measured in various solvents (15). One axial *N*-methyl scopolammonium bromide phenyl-ring face is solvent exposed in the compact conformation predominating in D_2O medium, while both faces are solvent accessible in the *extended* major conformational contributor in CD_2Cl_2 solution (15). Similarly, the methylol OH group is more solvent exposed in the compact conformation predominating in D_2O medium, while it is near the scopine underside in the axial *N*-methyl scopolammonium bromide extended major conformational contributor in CD_2Cl_2 solution (15). The compact conformation has been described as the bioactive conformation based upon structural comparisons with other muscarinic receptor antagonists (16), and on modeling of ligand/muscarinic-m1 subtype receptor complexes (17).

The main impetus for this study was to obtain additional crystallographically determined scopolamine structures needed to define the linear correlationship between the O = C–C(α)–CH_2OH torsion angle and the δ(CH_2OH) and δ(C = O) solid-state CPMAS chemical shift values reported in our earlier study on the pseudopolymorphic forms of the hydrobromide drug (15). As a result, the structures of the analogous crystalline (–)-scopolamine hydrochloride anhydrate (**5**), (–)-scopolamine hydrochloride 1.66-hydrate (**6**), and (–)-scopolamine methobromide (**7**) were determined, and their details are reported herein. In addition, the solid-state CPMAS NMR characterization of (–)-scopolamine free base crystalline melt (**8**) and the hydrobromide trihydrate (**9**) are also described.

Experimental section

(–)-Scopolamine HBr, HCl, and methobromide were purchased from Sigma. (–)-Scopolamine HBr trihydrate and (–)-scopolamine free base crystalline melt were gifts of Phytex Australia Pty. Ltd., and another (–)-scopolamine HBr trihydrate sample was a gift of Boehringer Ingelheim KG.

Crystallography

(–)-Scopolamine hydrochloride anhydrate (**5**) and methobromide (**7**) were recrystallized by vapor diffusion of acetone into an abs ethanolic solution of the appropriate salt. (–)-Scopolamine HCl 1.66H_2O (**6**) was obtained by dissolving the hydrochloride anhydrate salt in water followed by slow evaporation to dryness. Intensity data from the clear colorless prism crystals were collected at 293(2) K on an Enraf–Nonius CAD-4 automatic diffractometer. Table 1 provides crystallographic and data collection details.

© 2000 NRC Canada

Table 1. Crystallographic details for (–)-scopolamine HCl anhydrate (**5**), (–)-scopolamine HCl 1.66H_2O (**6**), and (–)-scopolamine methobromide (**7**).

	5	**6**	**7**
Formula	$C_{17}H_{22}NO_4Cl$	$C_{17}H_{25.36}ClNO_{5.66}$	$C_{18}H_{24}NO_4Br$
FW (amu)	339.81	370.07	398.29
Space group	$P2_12_12_1$	$P4_32_12$	$P2_12_12_1$
a (Å)	7.097(2)	11.843(6)	7.0403(8)
b (Å)	10.686(2)	11.843(6)	10.926(2)
c (Å)	22.623(3)	26.211(4)	23.364(5)
V (Å^3)	1715.7(6)	3676(3)	1797.2(5)
Z	4	8	4
ρcalc (g cm^{-3})	1.316	1.337	1.472
Temperature (K)	293(2)	293(2)	293(2)
F(000)	723.66	1574	823.61
Linear abs coeff. (mm^{-1})	2.14	2.107	3.31
Min transmission factor	0.721	0.813	0.620
Max transmission factor	0.839	0.879	0.743
Crystal size (mm^3)	0.2 × 0.2 × 0.2	0.3 × 0.3 × 0.2	0.3 × 0.3 × 0.3
Radiation	Graphite-monochromated Cu Kα (λ = 1.54184 Å)	Graphite-monochromated Cu Kα (λ = 1.54184 Å)	Graphite-monochromated Cu Kα (λ = 1.54184 Å).
Collection range	$+h, +k, +l$ $0 \le h \le 7, 0 \le k \le 12,$ $0 \le l \le 25$	$+h, +k, +l$ $0 \le h \le 14, 0 \le k \le 10,$ $0 \le l \le 32$	$+h, +k, +l$ $0 \le h \le 8, 0 \le k \le 13,$ $0 \le l \le 28$
2θ max (°)	120	143.42	142.52
Scan type	θ/2θ	θ/2θ	θ/2θ
Scan speed (deg min^{-1})	2.7	2.7	2.7
Background time/scan time	0.25	0.25	0.25
Isotropic extinction coefficient (μm)	2.7(3)	0.0014(3)	1.4(7)
Unique data	1494	2154	2046
Unique data with $I_{net} \ge n\sigma(I_{net})$	1325 (n = 2.5)	1620 (n = 2.0)	1846 (n = 2.0)
No. of variables	209	239	218
No. of restraints	0	9	0
Max shift/σ	0.001	0.030	0.015
R indices (all data)[a]	$R(F) = 0.048$	$R(F) = 0.071$	$R(F) = 0.044$
$_wR$ indices (all data)[b]	$R_w(F) = 0.062$	$R_w(F^2) = 0.151$	$R_w(F) = 0.055$
Weighting factor, *w*	$(\sigma F_{obs}^2 + 0.0025F_{obs}^2)^{-1}$	$(\sigma^2F_{obs}^2+0.0833P^2+1.0651P)^{-1}$ where $P = (F_{obs}^2+2F_{calc}^2)/3$	$(\sigma F_{obs}^2 + 0.0050F_{obs}^2)^{-1}$
Final *R* indices[a] ($I_{net} \ge n\sigma(I_{net})$)	$R(F) = 0.041$ (n = 2.5)	$R(F) = 0.047$ (n = 2.0)	$R(F) = 0.039$ (n = 2.0)
Final $_wR$ indices[b] ($I_{net} \ge n\sigma(I_{net})$]	$R_w(F) = 0.059$ (n = 2.5)	$R_w(F^2) = 0.135$ (n = 2.0)	$R_w(F) = 0.052$ (n = 2.0)
Goodness of fit	1.04[c]	1.085[d]	1.06[c]
Largest diff. peak and hole (e.Å^{-3})	+0.27 and –0.18	+0.28 and –0.32	+0.58 and –0.39

[a]The final discrepancy index $R(F) = (\Sigma_i||F_{obs}|_i - |F_{calc}|_i|)/(\Sigma_i|F_{obs}|_i)$.

[b]The weighted value $R_w(F) = \mathrm{SQRT}[(\Sigma_i\{w_i(|F_{obs}|_i - |F_{calc}|_i)\}^2)/(\Sigma_i\{w_i(|F_{obs}|_i)\}^2)]$, and $R_w(F^2) = \mathrm{SQRT}[(\Sigma_i\{w_i(F_{obs}^2{}_i - F_{calc}^2{}_i)\}^2)/(\Sigma_i\{w_i(F_{obs}^2{}_i)\}^2)]$, where the particular weighting factor used is given in Table 1.

[c]Goodness of fit = SQRT[$(\Sigma_i\{w_i(|F_{obs}|_i - |F_{calc}|_i)\}^2)$/(no. of reflections – no. of parameters)].

[d]Goodness of fit = SQRT[$(\Sigma_i\{w_i(F_{obs}^2{}_i - F_{calc}^2{}_i)\}^2)$/(no. of reflections – no. of parameters)].

Cell constants and an orientation matrix for data collection, were obtained from a least-squares refinement using the setting angles of 24 carefully centered reflections in the range $40° \le 2\theta \le 50°$ for **5**, 26 reflections in the range $32° \le 2\theta \le 44°$ for **6**, and 24 reflections in the range $40° \le 2\theta \le 50°$ for **7**. Space group determination was based upon systematic absences, packing considerations, a statistical analysis of intensity distribution, and the successful solution and refinement of the structure. The NRCCAD program (18) was used for centering, indexing, and data collection. Two standard reflections were measured every 60 min.

The NRCVAX programs (19) were used for crystal structure solution (Cα-*S*-absolute configuration for the (–)-enantiomer (2, 11, 13)) by application of direct methods for **5**–**7**, and for refinement by full-matrix least squares on *F* (for **5** and **7**). Atomic scattering factors in the NRCVAX programs are from ref. 20. The *SHELX-97* program[5] was used for refinement by full-matrix least squares on F^2 (for **6**). The

[5] G.M. Sheldrick. SHELX-97. University of Göttingen, Göttingen, Germany. 1997.

© 2000 NRC Canada

absorption coefficients (μ) are listed in Table 1. Psi scans based empirical absorption corrections were made; the maximum and minimum transmission factors are given in Table 1. No significant decay was observed during data collection for **5**–**7**. Isotropic extinction coefficients were included in the refinement to account for secondary extinction effects (21); their values are given in Table 1.

Hydrogens for **5** and **7** were all geometrically placed and the respective final refinements included anisotropic thermal parameters for the non-hydrogen atoms, and isotropic thermal parameters for the hydrogen atoms. Structure determination of **6** afforded one water molecule at a fully occupied general position of symmetry, one water molecule at a fully occupied special position of C_2 symmetry, and one water molecule with 0.322(17) partial occupancy at a special position of C_2 symmetry (i.e., 13.288 total water molecules for the eight scopolamine HCl molecules in one complete unit cell, or $1.66H_2O$ for one scopolamine HCl molecule in the asymmetric unit). Hydrogens were all geometrically placed except for those on oxygen. Individual displacement parameters were fixed at $U(H) = 1.5 \times U_{eq}$ (C-methyl, OH) or $U(H) = 1.2 \times U_{eq}$ (C and N) and were treated as riding for refinement. The H_2O protons were calculated for the best hydrogen bond. Their positions were refined to fit the residual densities but restrained to have O—H set to 0.85 Å and H–O–H angle at 110.0° [$U(H) = 1.2 \times U_{eq}$]. The non-hydrogen atoms were refined anisotropically (with the exception of O(7) which was refined isotropically).

The $R(F)$ and $R_w(F)$ (or $R_w(F^2)$) final discrepancy indices at convergence for the $I_{net} \geq n\sigma(I_{net})$ (n = 2.5 for **5** and 2.0 for **6**, **7**) significant reflections, the number of restraints and variables, and the GoF are listed in Table 1 for **5**–**7**.

Molecular graphics

2D-iconic projections of the X-ray crystallographic (**2**, **3**, and Fig. 1) or molecular modeling (**11**–**17**) 3D-structures were generated using the combination of CS-Chem3D Pro 5.0 and CS-ChemDraw Ultra 5.0 programs.[4] Superimposition of molecular structures were performed with the MacMimic 3.0 program.[6]

NMR Spectroscopy

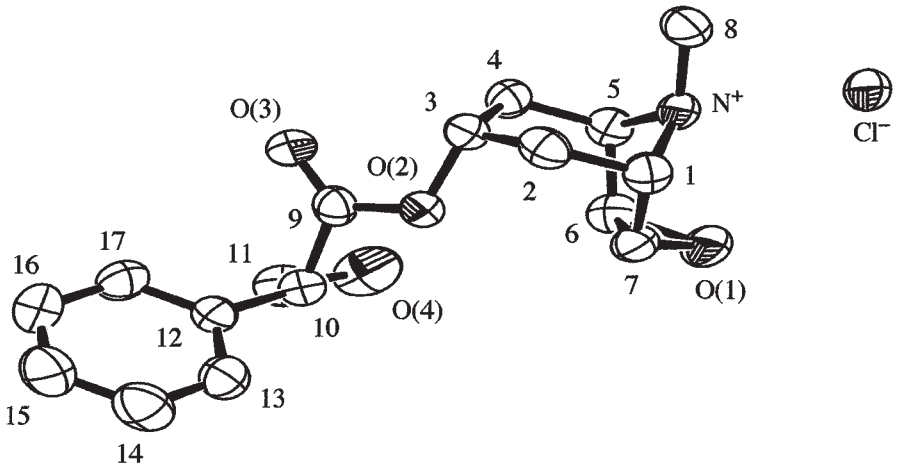
Solid-state CPMAS ^{13}C NMR spectra were recorded at 125.76 MHz at ambient temperature on a Bruker DMX-500 digital FT NMR spectrometer equipped with a BL-4 CPMAS probehead and a High Resolution/High Performance (HPHP) ^1H preamplifier for solids. Spectra were calibrated with an external spectral reference (glycine δ carbonyl = 176.03). A vacptppm (variable amplitude cross-polarization/two pulse phase modulation decoupling) pulse-program was used for CPMAS spectra. Vacptppmnqs (non-quaternary and non-methyl signal suppression) and cppi (22) pulse-programs were utilized to afford spectral-editing giving "quaternary-methyl-only" and "methylene-only" spectra, respectively. Nqs spectra used a 50 μs T_2 dipolar dephasing delay period. The fast inversion-recovery technique utilized a 20 s T_1 delay to afford spectra without methyl carbon signals. Samples were placed in 4 mm zirconia rotors, and spun at a rate of 11.0 kHz for all spectra (with the exception 5.0 kHz for cppi).

Results and discussion

Crystallographic details, non-hydrogen atom fractional coordinates for (–)-scopolamine hydrochloride anhydrate (**5**), (–)-scopolamine hydrochloride 1.66-hydrate (**6**), and (–)-scopolamine methobromide (**7**) are given in Tables 1–4, respectively.

(–)-Scopolamine hydrochloride anhydrate

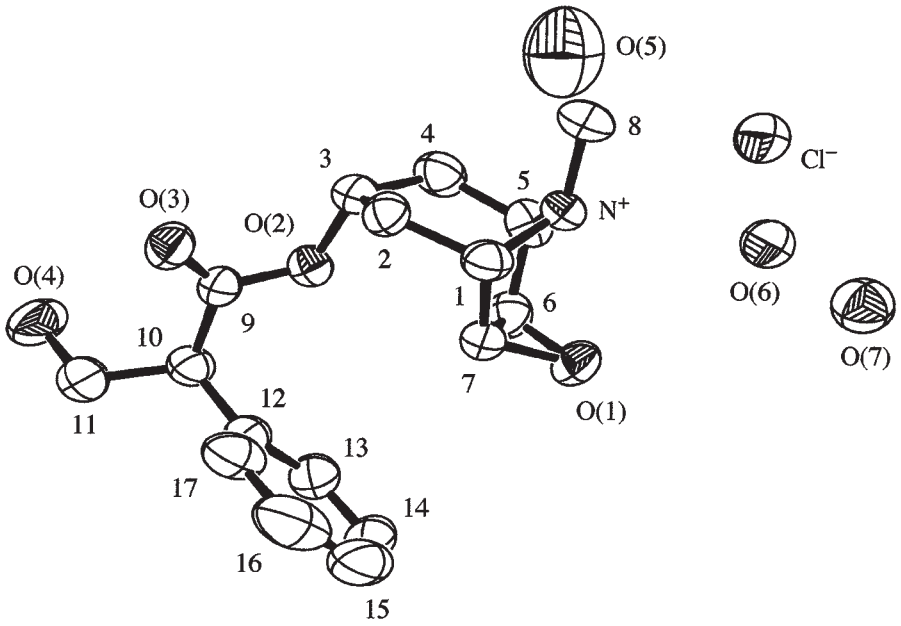
(–)-Scopolamine hydrochloride anhydrate (**5**) gave crystals belonging to the same space group and packed in the same motif as that previously reported (11) for the hydrobromide anhydrate analogue (**3**). The axial *N*-methyl scopolammonium cations in both HCl and HBr anhydrate salts were structurally the same as shown by superimposition[6] of non-hydrogen atoms in **5** (with the exception of the halide



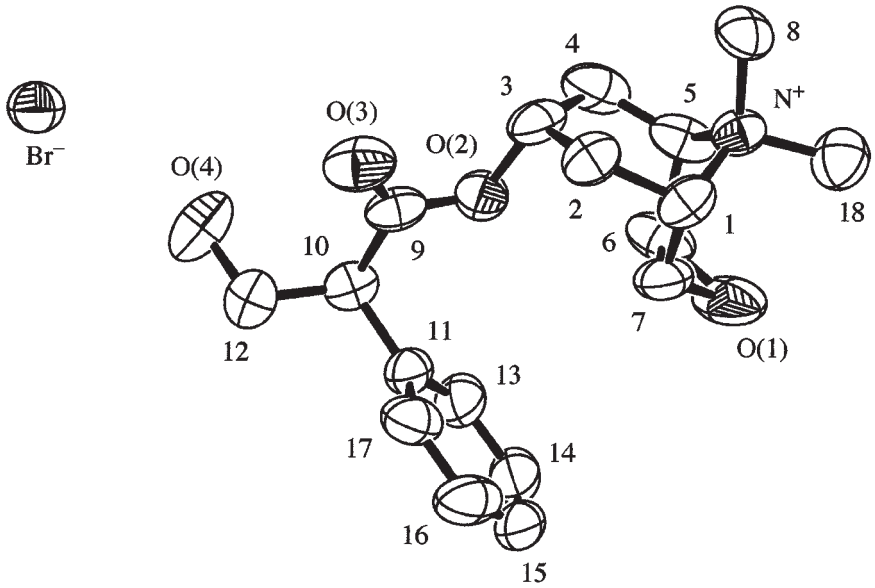
5

[6] A. Sundin. MACMIMIC 3.0. In-Star Software. Lund, Sweden. 1996.

© 2000 NRC Canada



6



7

anion) upon corresponding atoms in **3** to give a root mean square (RMS) difference of only 0.080 Å. Both **3** and **5** have extended conformations as shown by three characteristic torsion angles, e.g., 158.5(4)° antiperiplanar C(9)–O(2)–C(3)–C(2), –77.3(3)° *(–)*-synclinal C(9)–O(2)–C(3)–C(4), and 53.3(3)° *(+)*-synclinal O(3)–C(9)–C(10)–C(11) for **5**. In both **3** and **5**, the halide anion is hydrogen bonded to N(1). The Br···N(1),Cl···N(1) distances are 3.210, 3.070 Å, the Br···H(N1),Cl···H(N1) distances are 2.317, 2.175 Å, and the Br···H(N1)–N(1),Cl···H(N1)–N(1) angles are 133.0°, 146.1°.

In **3** and **5**, the perpendicular distance of nearest neighbors to the top and bottom faces of the phenyl ring best plane were ca. 3.0 Å or more away, thus enabling the phenyl ring to undergo a CPMAS ^{13}C NMR observed π-flip about the C(10)—C(12) bond axis (15). In the CPMAS ^{13}C NMR spectra of both **3** and **5**, the "off-axis" *ortho* and *meta* carbon atom signals appear as a broadened hump between relatively sharp signals arising from the "on-axis" *ipso* and *para* carbons (15). The phenyl-ring π-flip involves significant van der Waals contacts, and thus requires lattice deformations to permit ring dynamics (23). These occur in a different timeframe than that observed by X-ray crystallography, since the staccato rotation of the off-axis *ortho* and *meta* carbon atoms is not expressed in higher anisotropic thermal parameters for

© 2000 NRC Canada

Table 2. Fractional coordinates and anisotropic equivalent (B_{eq}) displacement parameters for (–)-scopolamine hydrochloride anhydrate (**5**); esd of last digit in parentheses.

Atom	*x*	*y*	*z*	B_{eq}[a]
Cl	0.6301(2)	0.5794(1)	–0.04089(4)	0.0449(5)
N(1)	0.2499(4)	0.5464(3)	0.0218(1)	0.032(1)
O(1)	0.4786(4)	0.4816(3)	0.1021(1)	0.048(2)
O(2)	–0.0669(4)	0.3696(2)	0.1322(1)	0.035(1)
O(3)	–0.2676(5)	0.2195(3)	0.1016(1)	0.046(1)
O(4)	0.1067(5)	0.0736(4)	0.1573(2)	0.068(2)
C(1)	0.1825(6)	0.5934(4)	0.0811(2)	0.035(2)
C(2)	–0.0278(6)	0.5680(4)	0.0856(2)	0.036(2)
C(3)	–0.0825(6)	0.4312(4)	0.0744(2)	0.036(2)
C(4)	0.0394(6)	0.3635(4)	0.0299(2)	0.037(2)
C(5)	0.2436(6)	0.4066(4)	0.0298(2)	0.033(2)
C(6)	0.3287(6)	0.3938(4)	0.0904(2)	0.038(2)
C(7)	0.2900(6)	0.5084(4)	0.1219(2)	0.037(2)
C(8)	0.1546(6)	0.5984(5)	–0.0308(2)	0.044(2)
C(9)	–0.1656(6)	0.2629(4)	0.1383(2)	0.035(2)
C(10)	–0.1269(6)	0.2063(4)	0.1986(2)	0.036(2)
C(11)	–0.0649(8)	0.0713(5)	0.1885(2)	0.048(2)
C(12)	–0.2974(6)	0.2198(4)	0.2387(2)	0.035(2)
C(13)	–0.2879(7)	0.2983(4)	0.2872(2)	0.042(2)
C(14)	–0.4360(8)	0.3143(5)	0.3243(2)	0.050(2)
C(15)	–0.6003(7)	0.2495(5)	0.3149(2)	0.053(2)
C(16)	–0.6143(8)	0.1693(6)	0.2677(2)	0.060(3)
C(17)	–0.4626(7)	0.1558(5)	0.2294(2)	0.048(2)

[a] B_{eq} is one-third of the trace of the orthogonalized *U*.

C(13, 14, 16, 17), as opposed to those for the on-axis *ipso* and *para* carbons C(12, 15). Crystalline Buscopan methanol solvate adduct (**10**) ((–)-hyoscine equatorial-*n*-butylbromide methanol solvate adduct (8)) also exhibits an extended conformation, and its phenyl ring also undergoes a π-flip as observed in the CPMAS ^{13}C NMR spectrum (15).

(–)-Scopolamine hydrochloride 1.66hydrate

(–)-Scopolamine hydrochloride 1.66hydrate (**6**) was crystallized from water giving 1.66hydrate crystals (**6**) belonging to the same tetragonal, $P4_32_12$ space group, and, with the exception of an additional O(7) labeled water, it packed in the same motif as that previously reported (13) for the hydrobromide sesquihydrate analogue (**2**). The axial *N*-methyl scopolammonium cations in both HCl and HBr hydrated salts were structurally identical, as shown by superimposition of non-hydrogen atoms in **6** (with the exception of halide anion and water oxygens) upon corresponding atoms in **2** to give an RMS difference of only 0.039 Å. Both **2** and **6** have compact conformations as shown by three characteristic torsion angles, e.g., 72.6(4)° *(+)*-synclinal C(9)–O(2)–C(3)–C(2), –164.7(3)° antiperiplanar C(9)–O(2)–C(3)–C(4), and 17.8(6)° synperiplanar O(3)–C(9)–C(10)–C(11) for **6**. Crystalline (–)-hyoscyamine hydrobromide (**11**) (6, 7), the optically active form of atropine hydrobromide (a deoxiranyl analogue), also exhibits a similar compact conformation.

Both hydrated crystals **2** and **6** have an O(5) labeled water molecule occupying a similar general position of symmetry, and an O(6) labeled water molecule occupying a special position of C_2-rotation symmetry. In addition, the hydrated hydrochloride (**6**) had a 0.322(17) partial occupancy O(7) labeled water molecule (absent in the hydrobromide sesquihydrate) occupying another special position of C_2-rotation symmetry, i.e., the extra water molecule occupied the special position in statistically ca. one-third of the unit-cells to give a total hydrate stoichiometry of 1.66 molecules of water. In **2** and **6**, the perpendicular distances of nearest neighbors to the top and bottom faces of the phenyl ring best plane were only ca. 2.5 Å (i.e., closer than those for the anhydrate), thus the phenyl ring is immobile (no π-flip, since six aromatic sharp ^{13}C NMR signals were clearly observed in the CPMAS spectrum) (15). Crystalline (–)-hyoscyamine hydrobromide (**11**) (6, 7) also does not show CPMAS evidence for a π-flip (15).

Table 3. Fractional coordinates and anisotropic equivalent (U_{eq}) displacement parameters for (–)-scopolamine hydrochloride 1.66hydrate (**6**); esd of last digit in parentheses.[a]

Atom	*x*	*y*	*z*	U_{eq}[b]
Cl	0.3811(1)	0.4284(1)	0.1681(1)	0.083(1)
N(1)	0.7343(3)	0.3883(3)	0.1706(1)	0.047(1)
O(1)	0.7722(3)	0.5834(2)	0.2026(1)	0.063(1)
O(2)	0.9097(2)	0.5228(2)	0.0632(1)	0.047(1)
O(3)	1.0714(3)	0.4436(3)	0.0368(1)	0.059(1)
O(4)	1.1417(4)	0.6348(3)	–0.0423(1)	0.089(1)
C(1)	0.8596(3)	0.4070(3)	0.1728(1)	0.046(1)
C(2)	0.9140(4)	0.3647(3)	0.1241(2)	0.048(1)
C(3)	0.8619(4)	0.4120(3)	0.0751(2)	0.051(1)
C(4)	0.7346(4)	0.4320(4)	0.0790(2)	0.059(1)
C(5)	0.6970(4)	0.4719(4)	0.1306(2)	0.053(1)
C(6)	0.7636(4)	0.5740(4)	0.1480(2)	0.054(1)
C(7)	0.8635(4)	0.5338(3)	0.1742(2)	0.048(1)
C(8)	0.6944(5)	0.2699(4)	0.1655(2)	0.069(1)
C(9)	1.0167(4)	0.5262(3)	0.0458(1)	0.045(1)
C(10)	1.0579(3)	0.6470(3)	0.0420(2)	0.047(1)
C(11)	1.1637(5)	0.6564(4)	0.0101(2)	0.068(1)
C(12)	1.0730(4)	0.6891(3)	0.0962(1)	0.048(1)
C(13)	1.0060(5)	0.7736(4)	0.1150(2)	0.067(1)
C(14)	1.0175(7)	0.8070(5)	0.1656(3)	0.106(3)
C(15)	1.0953(9)	0.7563(8)	0.1963(2)	0.114(3)
C(16)	1.1617(7)	0.6736(7)	0.1782(2)	0.101(3)
C(17)	1.1506(4)	0.6378(4)	0.1276(2)	0.066(1)
O(5)	0.4605(7)	0.3757(8)	0.0483(2)	0.176(3)
O(6)	0.5772(3)	0.4228(3)	0.2500	0.057(1)
O(7)	0.3740(10)	0.6260(10)	0.250	0.088(7)

[a] A 1.000 occupancy factor for all atoms with the exception of 0.322(17) for O(7).

[b] U_{eq} = (1/3)Σ(i) Σ (j) U(ij) a(i)* a(j)* a(i) a(j).

An extended hydrogen-bonding network perfuses the crystal lattice in both **2** and **6**. Comparisons of interatomic distances, angles, and torsion angles in the **2** and **6** hydrogen-bonding networks are presented in supplementary Table 7. A 2D-iconic representation of the 3D hydrogen-bonding scheme for **6** is depicted in Fig. 1. Atoms from within eight symmetry equivalent molecules are shown in this figure. The lower left-hand scopolammonium cation, left O(5), and left-middle chloride plus the O(6, 7) reside in the (*x*, *y*, *z*) symmetry equivalent molecule. The lower right-hand scopolammonium cation, right O(5), and right-middle chlo-

© 2000 NRC Canada

Table 4. Fractional coordinates and anisotropic equivalent (B_{eq}) displacement parameters for (–)-scopolamine methobromide (**7**); esd of last digit in parentheses.

Atom	*x*	*y*	*z*	B_{eq}[a]
Br	1.28918(7)	0.52528(5)	0.05567(2)	0.0501(2)
N(1)	0.2103(6)	–0.0689(3)	0.0691(1)	0.042(1)
O(1)	0.0836(6)	0.0198(7)	0.1702(2)	0.083(2)
O(2)	0.5088(6)	0.2201(3)	0.1046(1)	0.052(1)
O(3)	0.8214(6)	0.2403(5)	0.0904(2)	0.063(1)
O(4)	0.8796(7)	0.5167(4)	0.1219(2)	0.072(2)
C(1)	0.3628(8)	–0.0627(4)	0.1146(2)	0.046(1)
C(2)	0.5410(7)	–0.0008(5)	0.0898(2)	0.047(1)
C(3)	0.4969(9)	0.1233(4)	0.0619(2)	0.050(2)
C(4)	0.297(1)	0.1360(4)	0.0354(2)	0.063(2)
C(5)	0.1482(9)	0.0639(5)	0.0666(2)	0.053(2)
C(6)	0.1546(9)	0.1026(7)	0.1292(2)	0.063(2)
C(7)	0.2834(8)	0.0244(7)	0.1584(2)	0.056(2)
C(8)	0.2770(9)	–0.1164(4)	0.0118(2)	0.053(2)
C(9)	0.6790(8)	0.2700(4)	0.1147(2)	0.045(1)
C(10)	0.6639(7)	0.3693(4)	0.1601(2)	0.043(1)
C(11)	0.8496(8)	0.4355(5)	0.1690(2)	0.054(2)
C(12)	0.5865(8)	0.3095(4)	0.2143(2)	0.044(1)
C(13)	0.4037(9)	0.3319(6)	0.2319(2)	0.058(2)
C(14)	0.331(1)	0.2731(8)	0.2804(3)	0.078(3)
C(15)	0.439(2)	0.1947(6)	0.3108(3)	0.090(4)
C(16)	0.622(2)	0.1736(5)	0.2941(2)	0.074(3)
C(17)	0.696(1)	0.2287(4)	0.2453(2)	0.056(2)
C(18)	0.0470(9)	–0.1549(6)	0.0852(3)	0.064(2)

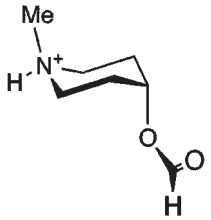
[a] B_{eq} is one-third of the trace of the orthogonalized *U*.

ride are in the (1 – *y*, 1 – *x*, 0.5 – *z*) symmetry equivalent molecule A. The upper right-hand scopolammonium cation (containing the O(4) label) is in the (–0.5 + *y*, 1.5 – *x*, 0.25 + *z*) symmetry equivalent molecule B. The upper left-hand scopolammonium cation (containing the O(4′) label) is in the (*x* – 1, *y*, *z*) symmetry equivalent molecule C. The far-left chloride and O(5′) is in the (*y*, *x*, –*z*) symmetry equivalent molecule D. The far-right chloride and O(5′) are in the (1 – *x*, 1 – *y*, 0.5 + *z*) symmetry equivalent molecule E. The upper right- and left-hand remote phenyl-R partial structures are in the respective (1 – *y*, 2 – *x*, 0.5 – *z*) and (*x* – 1, *y*, *z*) symmetry equivalent molecules F and G.

Inspection of the center of the figure shows a diamond-shaped cyclic network bisected by a C_2-axis. It involves chloride anions hydrogen-bonding to each of the O-H protons in the two specially positioned O(6), O(7) water molecules. The O(6)···O(7) and Cl···Cl(A) interatomic distances in the diamond arrangement are 3.40(2) and 5.348(3) Å, respectively (the perspective in Fig. 1 makes the Cl···Cl(A) distance appear smaller than that of O(6)···O(7)). The O(6)···Cl and O(7)···Cl hydrogen-bonding distances are quite similar (3.163(3) and 3.177(10) Å, respectively). The O(6) water molecule is very strongly anchored in the crystal since each of its two lone-pairs hydrogen-bond to scopolammonium $^{+}$N-H protons. Thermogravimetric analysis of the analogous HBr sesquihydrate (**2**) showed weight loss in two stages: ~4% at 90°C (1.0 H_2O), plus an additional ~2% at 102°C (0.5 H_2O) (13).

Chloride anions participate in four hydrogen-bonding interactions, e.g., Cl^- (the middle left-hand anion) is bound to protons on O(5), O(6), O(7) water molecules, and a methylol O(4B)-H proton. The general positioned O(5) water molecule has an O(5D) C_2-symmetry related neighbor (labeled O(5′) in the figure). These two oxygen atoms are 2.90(1) and 2.82(1) Å apart in hydrochloride **6** and hydrobromide **2**, respectively. In both **6** and **2**, they have the highest anisothermal thermal parameters of all the non-hydrogen atoms. Crystallographic C_2-symmetry considerations do not permit strong hydrogen-bonding between these stoichiometrically full water molecules (O(5), O(5D)). The O(5)–H(O51)···O(5D) angular arrangement cannot approach linearity, since H(O51D) in the C_2-symmetry related O(5D)–H(O51D)···O(5) counterpart would then lie almost on top of the H(O51) proton. The O(5)–H(O51)···O(5D)/O(5D)–H(O51D)···O(5) angles are thus rather shallow (only 117.9°).

The hydrogen-bonding network in the corresponding hydrobromide sesquihydrate **2** is identical to that found for **6** with the exception of the absence of specially-positioned O(7) and the obvious change of bromide anions for chlorides. The partial occupancy O(7) water molecule resides in a cavity surrounded by four scopolammonium cations. The cavity's boundaries are the two full cations in symmetry equivalent molecules B, C, and the phenyl rings (Ph-R) from the symmetry equivalent F, G cations depicted in Fig. 1. Nearest neighbors to O(7) are H(16F) (2.31 Å), H(10B) (2.70 Å), and H(13B) (2.75 Å). The O(7) position is unoccupied in the corresponding hydrobromide analogue **2**. A hydrogen-bonding network similar to that in **6** was modeled for **2** using data sets measured at 180 and 293 K temperature. The 5.428 Å Br···Br(A) interatomic distance and 3.260(3) Å O(6)···Br hydrogen-bonding distance in **2** using the 180 K data set (293 K data set: 5.401 and 3.259 Å, respectively) are indeed similar to values for corresponding parameters measured in **6** reported above (also at 293 K). A diamond-shaped network was then constructed placing a specially positioned O(7) oxygen "dummy atom" 3.260(3) Å away from each of the Br, Br(A) anions. Nearest neighbors in the hydrobromide calculated model were then measured and found to be H(16F) (2.17 Å), H(10B) (2.71 Å), and H(13B) (2.46 Å) from the 180 K data set, and H(16F) (2.15 Å), H(10B) (2.68 Å), and H(13B) (2.60 Å) from the 293 K data set.



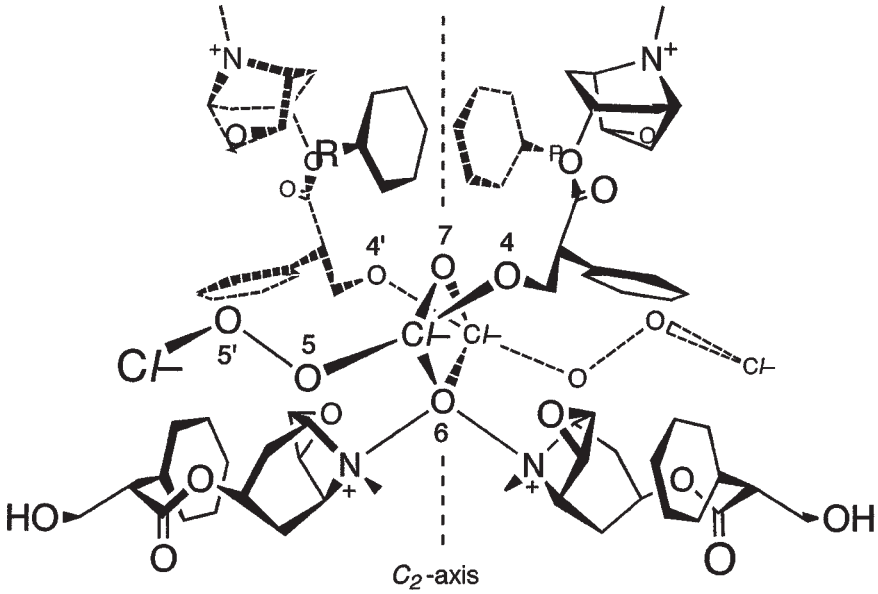
13

(–)-Scopolamine methobromide

(–)-Scopolamine methobromide (**7**) was crystallized by acetone vapor diffusion into abs. ethanol giving crystals belonging to a different space group (orthorhombic $P2_12_12_1$)

© 2000 NRC Canada

Fig. 1. Iconic projection of X-ray crystallographically determined structure of packing arrangement in the (–)-scopolamine HCl 1.66hydrate (**6**) crystal. The hydrogen-bonding network includes the O(5) labeled water molecule occupying a general position of symmetry (occupancy factor 1.000), and the O(6) and O(7) labeled water molecules both occupying special positions of C_2-symmetry (occupancy factors of 1.000 and 0.322(17), respectively) to afford a total stoichiometry of 1.66 water molecules. For clarity, two of the six scopolammonium cations are depicted only as partial structures (i.e., Ph-R).



than those obtained by crystallization of the corresponding methiodide (**12**) (monoclinic $P2_1$ (10)) from aqueous ethanol. However, the scopolammonium cations in both methohalide salts **7** and **12** are isostructural, as shown by superimposition of non-hydrogen atoms in **7** (with the exception of the halide anion) upon corresponding atoms in **12** to give an RMS difference of only 0.065 Å. Both **7** and **12** have compact conformations, similar to those of **2** and **6**, as shown by three characteristic torsion angles, e.g., 87.0(3)° (+)-synclinal-like C(9)–O(2)–C(3)–C(2), –148.4(4)° antiperiplanar-like C(9)–O(2)–C(3)–C(4), and 5.3(2)° synperiplanar O(3)–C(9)–C(10)–C(11) for **7**. The bromide anion is hydrogen-bonded to the methylol O(4)–H proton. In this arrangement, the Br···O(4) distance is 3.281 Å, the Br···H(O4) distance is 2.502 Å, and the Br···H(O4)–O(4) angle is 158.3°.

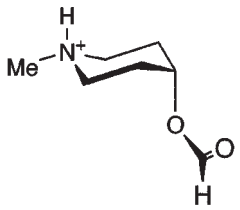
Placement of an equatorial *N*-methyl group [C(18)] in close juxtaposition to the transannular oxiranyl O(1) results in torque about the C(1)—N(1)/C(5)—N(1) bonds. As a result, C(8) is pushed away from O(1) and the axial *N*-methyl group [C(8)] is pushed inward towards C(2), C(4). This is clearly seen by an increase in the N(1)···O(1) interatomic distance: 2.693 and 2.728 Å in **7** and **12**, respectively, vs. 2.498 and 2.531 Å in **2** and **3**, respectively. It is also apparent in closing the C(2,4)···N(1)–C(8) angles: 88(1)° in **7** and 88.7(5)° in **12**, vs. 94.4(1)° in **2** and 96.5(6)° Å in **3**, respectively.

Stereochemistry of scopolamine-analogue models

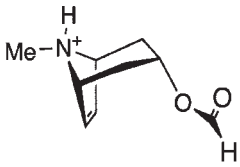
The tropate ester moiety in both scopine and tropine crystalline **2**, **3**, **5–7**, **10**, **11** all share common stereochemical features: a phenyl-ring *ortho* carbon eclipses the C(10)—H(10) bond, and there is an antiperiplanar C(12)–C(10)–C(10)–O(4) arrangement between the phenyl and the methylol oxygen. On the other hand, *N*-methyl groups on the scopine moiety are all axial in crystalline **2**, **3**, **5**, **6**, while they are equatorial in tropine-type alkaloids such as **11**. The effects of equatorial or axial *N*-methyl groups upon the molecular geometry of the scopine skeleton were recently investigated using RHF/6–31G* basis set ab initio[7] molecular modeling techniques (24). Due to *cis*-1,3-diaxial type interactions in the protonated axial *N*-methyl-3-*O*-formyl-piperidine model (see iconic projection **13** of the actual 3D-molecular model), the bulky axial *N*-methyl group is tilted outward away from each of the neighboring two axial C(2)—H/C(4)—H bonds (99.5(1)° C(2,4)···N(1)–C(8) angles), while the axial N—H bond is approximately parallel to these same axial *C*—H bonds in the equatorial *N*-methyl epimer (89.0(1)° C(2,4)···N(1)–H angles) (see projection **14**) (24). These calculations show that a consequence of both ethano- and etheno-bridge (see projection **15**) "pinching" of the piperidine moiety in N-protonated *O*-formyltropine is a tilt of the axial N-proton inward towards the neighboring two axial C—H bonds (81.9(1)° C(2,4)···N(1)–H angles) (24). Increased *cis*-1,3-diaxial interactions of the type noted above was assumed to be the cause of the lowered stability of the axial *N*-methyl N-protonated *O*-formyltropine model (96.4(1)°C(2,4)···N(1)–C(8) angles) relative to that of the equatorial epimer (24). On the other hand, a non-protonated (exomethylene) carbon or oxygen at the apex of a three-membered ring fused to the 6,7-positions of the *O*-formyltropine skeleton results in severe transannular interactions involving the neighboring equatorial *N*-methyl group. As a result, the axial N-H proton is pushed inward even closer towards its axial C-H neighbors (see projections **16** and **17**, C(2,4)···N(1)–H angles: 76.5(1)° in **16** and 78.1(1)° in **17**), whereas this close juxtaposition is reduced with the smaller

[7] MACSPARTAN PLUS 1.1.7. Wavefunction. Irvine, Calif. 1997.

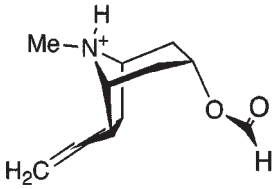
© 2000 NRC Canada



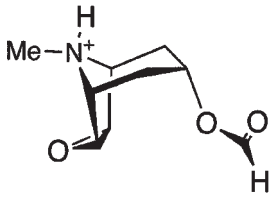
14



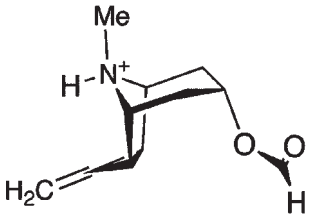
15



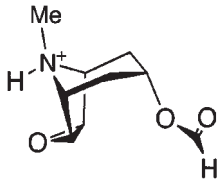
16



17



18



19

equatorial N-H proton. Transannular interactions result in the axial *N*-methyl diastereomeric models **18**, **19** (C(2,4)···N(1)–C(8) angles: 96.0(1)° in **18** and 97.6(1)° in **19**) being more stable than the epimeric equatorial cases (**16**, **17**) (24). Based upon these earlier theoretical studies, we suggest that the observation of *axial N*-methyl diastereomers for crystalline **2**, **3**, **5**, and **7** should be explained in terms of greater stability of the axial vs. the equatorial *N*-methyl epimer.

(–)-Scopolamine free base

Scopolamine free base (**8**) is utilized in transdermal patches to treat motion sickness (1, 25). CPMAS ^{13}C NMR spectroscopy provides insight into the solid-state stereochemistry of the crystalline melt, mp 58–61°C (monohydrate lit. (1) mp 59°). While only one carbonyl resonance (δ 170.6) was found for **8**, most other nuclei afforded multiple signals in the CPMAS spectrum. These multiple signals readily testify to a mixture of hydrated species in the crystallized melt. For example, four signals (δ 170.6 (high intensity) and three ca. 1:1:1 ratio lower intensity δ 46.8, 45.1, 43.6) were observed in the spectral-edited nqs (*n*on-*q*uaternary and non-methyl carbon *s*uppression) spectrum. The three almost-equal intensity resonances are all unequivocally assigned as more mobile *N*-methyl signals, since they diasppear in an inversion-recovery experiment (20 s T_1 delay). By analogy with the δ*C*H$_3$ 45.06 scopolamine hydrobromide equatorial *N*-methyl major diastereomer in CD_2Cl_2 solution (14), it is clear that all of the *N*-methyl groups are also equatorially disposed in the solid-state. Signals at δ 66.6, 65.9, and 64.6 were assigned to C(3) by analogy with the time-averaged δ 66.9 value reported (21) for C(3) in $CDCl_3$ solution. The δ 61.8 methylol C(11) signal found in the "methylene-only" spectral-edited cppi (cross polarization/polarization inversion) spectrum, is closer to TMS than those values noted above for alkoxy C(3). By analogy with our earlier CPMAS studies on scopolamine salts (15), $\Delta\delta > 0$ (where $\Delta\delta = \delta C(3) - \delta CH_2OH$) strongly suggests a compact conformation for the solid-state free base. In addition to tropate ester conformational interconversion, epimerization at the stereolabile nitrogen via nitrogen inversion can occur in solutions of the free base. The δ*C*H$_3$ 42.2 (15, 26) *N*-methyl, δC(3) 66.9 (26), and δC(11) 64.0 (24) values measured for the free base in $CDCl_3$ solution show that the dominant contributor to the weighted time-averaged free base **8** structure is very similar to the equatorial *N*-methyl compact conformation postulated for the crystalline solid. Similar to the case of the crystallographically determined structures **2**, **3**, **5**–**7**, **10**, **11** free base vicinal coupling constants ($^3J_{HH}$) show a bias for the antiperiplanar C(12)-C(10)-C(11)-O(4) conformation in solution (26).

(–)-Scopolamine hydrobromide trihydrate

The USP-grade, pharmacologically relevant trihydrate (12), like many other hydrate drugs, takes up or releases water upon exposure to air at various relative humidities (27). For example, at 25, 66, and 71 percent relative humidity

© 2000 NRC Canada

(18°C), the trihydrate (**9**) sample was reported to have 1.71, 2.31, and 2.55 moles of water, respectively (27). Solid-state CPMAS ^{13}C NMR spectroscopy was performed on two bona fide trihydrate samples. The 5.0 kHz spin-rate spectra (30 min acquisition) of each of these samples clearly showed signals from multiple species, i.e., the USP- EUP-grade trihydrate is not a single distinct entity. For example, three almost-equal intensity δ 173.5, 172.5, and 171.5 carbonyl signals were found for an 11.6% water content (Karl–Fischer) sample, while a ca. 1:1:2 ratio was measured for these same peaks for another supplier's sample. Increasing the spin-rate of the same 1:1:2 ratio sample to 11.5 kHz (50 min acquisition) afforded signal intensity reductions from two of the three species (e.g., carbonyl ratio now ca. 1:1:4, major species: sesquihydrate **2**). A further spin-rate increase to 13.5 kHz (10 min acquisition), afforded a spectrum identical in all respects to that of pure **2**. Single species **2** was still observed, rather than the original mixture of three components, upon reduction of the spin-rate to 5.0 kHz. After storing the capped rotor overnight, only the sesquihydrate species spectrum was measured at 5.0 kHz spin-rate. The original three component 5.0 kHz spin-rate spectrum was regenerated after ca. three weeks storage inside the capped rotor.

To ascertain if a centripetal pressure or rotor-friction temperature effect was at the root of this phase-transition phenomenon, the sample temperature within the rotor was determined at various rates of spin using the known lead nitrate (28) chemical shift temperature effect technique. The narrow line-widths observed in the ^{207}Pb NMR spectrum testified to a uniform temperature within the sample. The rotor-spinning air overcomes frictional heat felt by the spinning rotor at 5.0 kHz, since the internal temperature change was –0.8 K relative to the temperature of the non-spinning rotor. At 13.5 kHz spin-rate, the ^{207}Pb chemical shift increased by 15.8 ppm. The change in ^{207}Pb chemical shift as a function of spectrometer variable-temperature (VT) control panel setting was then measured. It was found that the VT setting had to be +18 K higher than the 295.3 K non-spinning rotor reference temperature to afford a +15.8 ppm δ^{207}Pb increase. The CPMAS spectrum of a fresh scopolamine hydrobromide trihydrate sample was measured at 5.0 kHz (three hydrated species seen), and the VT setting was then increased 18° to 313.3 K with invariant 5.0 kHz spin-rate. The same single sesquihydrate species **2** spectrum was observed under these conditions, showing a temperature effected phase-transition rather than one from increased centripetal force. Again, **2** remained as the sole observable species upon cooling the rotor back down to ambient temperature. It has been reported that the temperature effect of spinning in a 4 mm Bruker MAS probe with zirconia rotors could be fitted by a spin-rate to the second-power relationship (29).

Conclusions

The three new crystal structures reported above provided needed additional members in the series of scopine alkaloids investigated earlier by CPMAS ^{13}C NMR spectroscopy (15). In this series, the compact conformation (–)-scopolamine methobromide (**7**) played a very important role since it exhibited the smallest O(3)–C(9)–C(10)–C(11) torsion angle (5°). The γ-gauche effect was nicely seen by the δ 59.7 methylol C(11) and δ 61.4 alkoxy C(3) values measured for **7**, compared with the δ 65.5 methylol C(11) and δ 61.6 alkoxy C(3) values found for extended conformation Buscopan methanol solvate adduct (**10**) having the largest O(3)–C(9)–C(10)–C(11) torsion angle (61°) (15). While the reported dihydrate form (1) of scopolamine hydrochloride was not found, one can readily envision crystalline species containing up to a stoichiometric maximum of two water molecules per unit-cell. This dihydrate maximum hydration would arise from full occupancy of the special position of C_2 symmetry by the O(7) water molecule to afford a unit-cell consisting of two stoichiometrically half-molecules of water (O(6) and O(7)) plus one full O(5) water molecule.

Finally, the CPMAS NMR spectroscopic investigations of scopolamine free base monohydrate and hydrobromide trihydrate now show that these pharmacologically useful materials are really conglomerates of hydrated species. The diamond-shaped hydrogen-bonding network found for the hydrochloride 1.66hydrate (**6**) might be a very suitable model to explain the location of at least some of the water molecules in the trihydrate.

Supplemental information available

Hydrogen atom fractional coordinates for **5**–**7** (respective Tables 5–7), comparative non-hydrogen atom bond lengths, bond angles, and torsion angles in **5**–**7** (respective Tables 8–10); bonding parameters of hydrogen-bonding network in **2** and **6** (Table 11); and anisotropic thermal parameters for **5**–**7** (Tables 12–14).[8]

Acknowledgement

Thanks are extended to Dr. Lee T. Grady (Drug Standards Division, The United States Pharmacopeial Convention, Inc.), and Dr. Wilson H. De Camp (U. S. Food and Drug Administration) for encouragement to undertake this project. Gratitude is expressed to Dr. Reginald Smith (Phytex Australia Pty. Ltd.) for gifts of scopolamine HBr trihydrate and scopolamine free base, and to Dr. Manfred Psiorz (Boehringer Ingelheim KG) for the gift of scopolamine HBr trihydrate. Appreciation is extended to Dr. Stefan Steuernagel (Bruker Analytical Instruments, Rheinstetten, FRD) for assistance with the ^{207}Pb NMR spectroscopy. The Bruker DMX-500 spectrometer and related equipment at The University Laboratory for Magnetic Resonance (Ben-Gurion University of the Negev) were purchased with matching funds grants from the Israel Ministry of Science and Industry, while the solid-state CPMAS accessory, and HPHP solids ^{1}H preamplifier were purchased with matching funds grants from the Israel Academy of Sciences and Humanities Equipment Program and the Center for Natural Polysaccharides (BGU).

[8] Copies of material on deposit may be purchased from the Depository of Unpublished Data, Document Delivery, CISTI, National Research Council Canada, Ottawa, ON K1A 0S2, Canada.

© 2000 NRC Canada

References

1. Budavari, S. (*Editor*). The Merck Index. 12th ed. Merck & Co. Inc. Rahway, N.J. 1996. p. 1444, and refs. therein.
2. G. Fodor and G. Cserpreghy. J. Chem. Soc. 3222 (1961).
3. K. Mislow and J. Siegel. J. Am. Chem. Soc. **106**, 3319 (1984).
4. P.J. Pauling and T.J. Petcher. J. Chem. Soc. Chem. Commun. 1001 (1969).
5. J. Feeney, R. Foster, and E.A. Piper. J. Chem. Soc. Perkin Trans. 2, 2016 (1977).
6. P.J. Pauling and T.J. Petcher..Nature (London), **228**, 673 (1970).
7. von E. Kussäther and J. Hasse. Acta Crystallogr. Sect. B, **B28**, 2896 (1972).
8. M. Leger, M. Gadret, and A. Carpy. Acta Crystallogr. Sect. B, **B34**, 3705 (1978).
9. G. Guiseppetti, F. Massi, C. Tadini, A. Gallazzi, P.C. Vanoni, and M. Gaetani. Il Farmaco, Ed. Sc. **35**, 231 (1980).
10. R.B. Barlow, J.A.K. Howard, O. Johnson, and T.M. Sanders. Acta Crystallogr. Sect. C, **C43**, 671 (1987).
11. R. Glaser, J.-P. Charland, and A. Michel. J. Chem. Soc. Perkin Trans. 2, 1875 (1989).
12. The United States Pharmacopeia 23, The National Formulary 18, The United States Pharmacopeial Convention, Rockville, Md. 1994. pp. 1400–1402.
13. A. Michel, M. Drouin, and R. Glaser. J. Pharm. Sci. **83**, 508 (1994).
14. R. Glaser, Q.-J. Peng, and A.S. Perlin. J. Org. Chem. **52**, 2172 (1988).
15. R. Glaser, D. Shiftan, and M. Drouin. J. Org. Chem. **64**, 9217 (1999).
16. P. Pauling and N. Datta. Proc. Nat. Acad. Sci. U.S.A. **77**, 708 (1980).
17. F. Fanelli, M.C. Menziani, A. Carotti, and P.G. De Benedetti. Bioorg. Med. Chem. **2**, 195 (1994).
18. Y. Le Page, P.S. White, and E.J. Gabe. Proc. Am. Crystallogr. Hamilton Meet., 1986. Abs. PA23.
19. E.J. Gabe, Y. LePage, J.-P. Charland, F.L. Lee, and P.S. White. J. Appl. Cryst. **22**, 384 (1989).
20. Wilson, A.J.C. (*Editor*). International Tables for X-ray Crystallography. Vol C. Kluwer Academic Publishers. Dordrecht, The Netherlands. 1992. Tables 4.2.6.8 and 6.1.1.4.
21. A.C. Larson. Crystallographic computing. Munksgaard, Copenhagen. 1970. p. 291.
22. X. Wu and K.W. Zilm. J. Magn. Reson. **A102**, 205 (1993); J. Magn. Reson. **A104**, 119 (1993).
23. N.J. Clayden, D.W. Williams, and C.A. O'Mahoney. J. Chem. Soc. Perkin Trans. 2, 729 (1990).
24. R. Glaser, V. Khutorsky, and M. Shoken. Struc. Chem. **8**, 319 (1997).
25. Hebel, S.K. (*Editor*). *In* Drug facts and comparisons. Facts and comparisons. St. Louis. 1998. p. 1559.
26. C. Sarazin, G. Goethals, J.-P. Séguin, and J.-N. Barbotin. Magn. Reson. Chem. **29**, 291 (1991).
27. A. Lannung. Archiv. Pharmaci. Chem. **72**, 763 (1965).
28. A. Bielecki and D.P. Burum. J. Magn. Reson. **A116**, 215 (1995).
29. F.G. Riddell, R.A. Spark, and G.V. Günther. Magn. Reson. Chem. **34**, 824 (1996).

© 2000 NRC Canada

Theoretical studies of azulene and its derivatives

Bo-Cheng Wang, Yun-Shan Lin, Jian-Chuang Chang, and Pei-Yu Wang

Abstract: The results of ab initio calculations with the 6–31G basis sets on azulene and its derivatives (including azulenequinones and diazoazulenequinones) are presented in accordance with considerations of their structures and bonding. Azulene is a non-alternant compound with ten π electrons and has either a C_s or C_{2v} symmetry depending on the different carbon bonding. The semiempirical and HF ab initio calculations converge to a C_s symmetry and the DFT and MP2 calculations converge to a C_{2v} symmetry as a ground state structure of azulene. The CIS calculations describe the excited state of azulene and the first excitation energy ($S_0 - S_1$) is 533 nm (CIS/6–31+G*), which could illustrate the azure color of azulene. According to the geometry analysis, there are 16 geometrical isomers in azulenequinone conjugated diketones of azulene. Ab initio calculation with the 6–31G basis set generates 1,5- and 1,7-azulenequinone being the most stable isomers of azulenequinone. Theoretically, the relative stability of the bromination product of azulenequinones indicates that 7-bromo-1,5-azulenequinone and 3-bromo-1,7- azulenequinone (for monobromoazulenequinones) and 3,7-dibromo-1,5- azulenequinone and 3,5-dibromo-1,7-azulenequinone (for dibromoazulenequinones) are more stable isomers. The product of diazotization of amino- bromoazulenes is diazoazulenequinone in which a diazo group replaces a ketone group. Isomeric 1,8- and 1,2-diazoazulenequinones are the most stable isomers of diazoazulenequinone according to the theoretical consideration. Due to the resonance and relative stability, diazoazulenequinone may easily extrude nitrogen and form the corresponding triplet ketocarbene intermediate and electronic isomers that undergo photoreaction with THF leading to a polyether bridged azulene (crown type ether). The cyclic reactions in diazoazulenequinone are also studied.

Key words: azulene, azulenequinone, diazoazulenequinone, ab initio.

Résumé: Utilisant des ensembles de base 6–31G, on a effectué des calculs ab initio sur l'azulène et un certain nombre de ses dérivés, dont des azulènequinones et des diazoazulènequinones; les résultats sont présentés avec des considérations sur leurs structures et leurs modes de liaison. L'azulène est un composé non alternant comportant dix électrons π et de symétrie C_s ou C_{2v} selon les types de liaison des carbones. Les calculs semiempiriques et les calculs ab initio HF convergent vers une symétrie C_s alors que les calculs DFT et MP2 convergent vers une symétrie C_{2v} pour la structure de l'état fondamental de l'azulène. Les calculs CIS permettent de décrire l'état excité de l'azulène et la première énergie d'excitation ($S_0 - S_1$) est 533 nm (CIS/6–31+G*) qui pourrait expliquer la couler azur de l'azulène. Selon l'analyse géométrique, il existe seize isomères géométriques dans les dicétones conjuguées de l'azulènequinone. Les calculs ab initio avec l'ensemble de base 6–31G suggèrent que les 1,5- et 1,7-azulènequinones sont les isomères les plus stables. D'un point de vue théorique, les stabilités relatives des produits de bromation des azulènequinones indiquent que les bromo-1,5-azulènequinone et 3-bromo-1,7-azulènequinone (pour les monobromoazulènequinones) et les 3,7-dibromo-1,5-azulènequinone et 3,5-dibromo-1,7-azulènequinone (pour les dibromoazulènequinones) sont les isomères les plus stables. Le produit de diazotation des aminobromoazulènes est la diazoazulènequinone dans laquelle le groupe diazo remplace un groupe cétonique. Sur la base de considérations théoriques, les 1,8- et 1,2-diazoazulènequinones sont les isomères les plus stables des diazoazulènequinones. À cause de la résonance et de la stabilité relative, la diazoazulènequinone peut facilement éliminer de l'azote et conduire à la formation de l'intermédiaire triplet cétonecarbène correspondant et à ses isomères électroniques qui subissent des photoréactions avec le THF pour fournir un azulène à pont polyéther (éther de type couronne). On a aussi étudié les réactions cycliques des diazoazulènequinones.

Mots clés: azulène, azulènequinone, diazoazulènequinone, ab initio.

[Traduit par la Rédaction]

Introduction

In ancient Egypt, azulene derivatives were used for dying of cotton, since it has the natural blue color (called azure). Actually, azulene was generated from several kinds of plants through distillation, extraction, and other chemical treatment. In 1937, azulene, the parent compound, was synthesized by Plattner and Pfau (1) for the first time. About 30 years later, Nozoe (2) published a new method to synthesize azulene derivatives. In the meantime, the study of azulene

Received June 8, 1999.

B.-C. Wang,[1] Y.-S. Lin, J.-C. Chang, and P.-Y. Wang. Department of Chemistry, Tamkang University, Tamsui, Taiwan 251.
[1]Author to whom correspondence may be addressed. Telephone: +886-2-26215656 ext. 2813. Fax: +886-2-26209924.
e-mail: bcw@mail.tku.edu.tw

 © 2000 NRC Canada

has become one of the most popular topics in organic, inorganic, medicinal, and theoretical chemistry as well as in the dye industry.

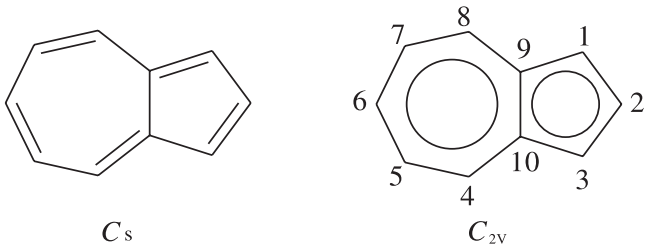
Azulene contains fused five-membered and seven-membered rings as a bicyclic structure and it is a nonalternant polycyclic aromatic compound with a 10 π electron system (3). Although azulene and naphthalene have the same 10 π electrons, they exhibit quite different properties in a number of respects.

For the last two decades, several theoretical studies of azulene have been published using semiempirical, ab initio, and DFT calculation methods (4–7). Recently, Kozlowski et al. (7) used both ab initio and DFT methods to determine the ground state structure and vibrational frequencies for azulene with C_s and C_{2v} symmetry. Experimentally, several attempts have been made to determine the molecular structure of azulene based on the X-ray analysis (8–10). Neither theoretical calculations nor experimental investigation have completely resolved the geometry of the ground state structure of azulene. Since azulene not only has a beautiful deep blue color, but also has a large dipole moment (μ = 0.8 – 1.08 D) and unusual photophysical properties, the excited states and electronic spectrum of azulene are of interest for theoretical and spectral studies (7). Natural compounds have a color due to the absorption of certain wavelengths of visible light. The particular structures necessary for this transition are unsaturated groups undergoing $\pi - \pi^*$ or $n - \pi^*$ transition. Azulene and its derivatives have a unique electronic structure for fluorescence properties. Michl and Thulstrup (11) described the color difference between anthracene and azulene by applying a simple MO picture to describe the electronic excitation energy.

Azulene with a diketone substituent is called azulenequinone. As early as 2700 B.C., quinone was used for Chinese medical, antifungal, antibiotic, or dyestuff purposes. The first unsubstituted azulenequinone was generated with an organic synthesis method by Morita (12) in 1980. Then Li and Scheuer (13) found the first natural occurrence of an azulenequinone, which was called guaiazulenequinone. Since azulenequinones contain a diketone substituent, they may have 16 structural isomers. Scott et al. (14) used theoretical calculations to predict the structures, spectral properties, relative stability, and reactivity for the selected isomers of azulenequinones. Various azulenequinones can be derived by nucleophilic reaction on bromoazulenequinones. Recently Nozoe et al. (15) discovered a standard procedure for the synthesis of 3-bromo-1,5- and -1,7-azulenequinones.

A replacement of a carbonyl C=O group by a diazo $C=N_2$ group gives diazoazulenequinone. As early as in the 1960s, diazoazulenequinone had been proposed by Hafner (16). Then, in 1974 Nozoe's group (17) obtained 2,6-azulenequinone-2-diazides by the diazotization of 2-amino-6-bromoazulene, which is one of the precursors of diazoazulenequinone. Recently, the new and efficient method to synthesize diazoazulenequinone was determined by Lin's group (18). They have also successfully isolated 2-diazo-2,6-azulenequinone and 2-diazo-2,4-azulenequinone (18). Particularly, these diazoazulenequinones could be used in the conjugated ketocarbene precursor of polyether bridged azulene reaction and as stabilizers for polymers as well as in the development of photo lithographic materials. Very recently, Lin's group (19) proposed a new method for the synthesis of polyether bridged azulene with three, four, and five THF (tetrahydrofuran) for 2-diazo-2,6-azulenequinone. This reaction is generated from azulenequinone diazides.

Fig. 1. Geometrical structure of azulene in C_s (bond alternate) and C_{2v} (bond equalized) symmetry.



The purpose of the present article is to study: the ground and the excited state of azulene, the relative stability of azulenequinone, bromoazulenequinone, diazoazulenequinone, and their isomers, and to predict the reactivity of diazoazulenequinone and the corresponding conjugated ketocarbene intermediates.

Computational methods

Ab initio calculations with the self-consistent field (SCF) theory using the standard Gaussian basis sets 6–31G, and second-order Møller–Plesset perturbation theory (MP2) as well as density function theory (DFT) using B3LYP/3–21G and B3LYP/6–31G were used to determine the optimized geometry of azulene. Ab initio calculations using the 6–31G basis sets were used to determine the electronic structure, the relative stability, and other physical properties for azulenequinones, bromoazulenequinones, and diazoazulenequinones. In order to study the electronic excited state and photochemistry properties, the configuration interaction with single excitations (CIS) with different basis sets (6–31+G and 6–31+G*) was used. The ab initio and DFT calculations were carried out on a version of the Gaussian 94 program[2], which was modified for an SGI workstation.

Results and discussion

Azulene

According to the bond analysis, azulene may have either the bond-equalized structure with C_{2v} symmetry or the bond-alternate structure with C_s symmetry (Fig. 1). Both semiempirical and ab initio calculations (HF with STO–3G and 3–21G) show the structure of azulene converged to a C_s structure (4, 14). Recently, Kozlowski et al. (7) performed

[2] M.J. Frisch, G.W. Trucks, H.B. Schlegel, P.M.W. Gill, B.G. Johnson, M.A. Robb, J.R. Cheeseman, T. Keith, G.A. Petersson, J.A. Montgomery, K. Raghavachari, M.A. Al-Laham, V.G. Zakrzewski, J.V. Ortiz, J.B. Foresman, J. Cioslowski, B.B. Stefanov, A. Nanayakkara, M. Challacombe, C.Y. Peng, P.Y. Ayala, W. Chen, M.W. Wong, J.L. Andres, E.S. Replogle, R. Gomperts, R.L. Martin, D.J. Fox, J.S. Binkley, D.J. Defrees, J. Baker, J.P. Stewart, M. Head-Gordon, C. Gonzalez, and J.A. Pople. Gaussian 94, Revision C.2, Gaussian, Inc., Pittsburgh, Pa. 1995.

© 2000 NRC Canada

Table 1. Calculated bond length (Å) of azulene for C_{2v} symmetry with different computational methods.

	HF/6–31G	MP2/6–31G	B3LYP/6–31G	B3LYP/6–31G*
C_2—C_3	1.396	1.422	1.409	1.404
C_3—C_{10}	1.400	1.422	1.411	1.405
C_4—C_{10}	1.386	1.404	1.394	1.393
C_4—C_5	1.388	1.414	1.400	1.398
C_5—C_6	1.389	1.414	1.401	1.399
C_9—C_{10}	1.488	1.527	1.507	1.500

calculations on azulene that are at higher level (B3LYP/3–21G, B3LYP/6–31G basis set) than any of the methods which have been used before. This calculation converges the structure of azulene to a C_{2v} symmetry and it provided the most accurate results. For the investigation of the optimized structure of azulene, Robertson (8) reported the X-ray data of azulene with the conclusion was that the symmetry of the molecule is C_{2v}. Table 1 shows the geometry optimization for C_{2v} symmetry of azulene with different computational methods. According to this result, the bond lengths in the five-membered ring and those in the seven-membered ring are approximately equal. Thus, we conclude that the electrons are delocalized in the five- and seven-membered rings respectively.

Since azulene has a beautiful azure color, it must have a $S_0 - S_1$ absorption in the visible region. In photochemical studies, azulene also has greatly interesting properties, e.g., the observed fluorescence corresponding to $S_2 - S_0$ transition. To investigate this special property of azulene, we performed the ab initio CIS calculation using the Gaussian 94 program with the 6–31+G and 6–31+G* basis sets. The first excitation energy ($S_0 - S_1$) is calculated to be at 518 nm (6–31+G) and 533 nm (6–31+G*) (Table 2). These values fall in the visible region and clearly illustrate the color of azulene. The experimental absorption peak is at 585 nm which is reasonably close to the theoretical value (20).

Table 2. Calculated transition frequency (nm) of azulene.

CIS/6–31+G	$S_0 - S_1$	518
	$S_{-1} - S_1$	307
	$S_0 - S_2$	236
CIS/6–31+G*	$S_0 - S_1$	533
	$S_{-1} - S_1$	316
	$S_0 - S_2$	238

Azulenequinones

The generic names of quinones are cyclohexadiendiones also commonly called *p*-benzoquinones. But they are named as some derivatives of aromatic systems: benzoquinones are derived from benzene, toluquinones from toluene, naphthoquinones from naphthalene. Azulenequinones are derived from azulene containing a diketone group spaced by one or more double bonds. The geometrical analysis shows that there are 16 possible geometrical isomers for azulenequinones, among them 11 azulenequinones which can be drawn by Kekule structures (also called classical azulenequinone) (Fig. 2) and five are nonclassical azulenequinones, which cannot be drawn in terms of simple Kekulé structures. However, Scott et al. (14) proposed their structures and relative stability with a semiempirical MINDO/3 calculation. The more quantitative results have not been reported. In the present work, we used the ab initio HF method with the 6–31G basis set to investigate the relative stability of these eleven classical azulenequinones only, since the nonclassical azulenequinones have smaller energy gap $\Delta\varepsilon$ (the energy gap between HOMO and LUMO) and higher heats of formation (ΔH_f) than the corresponding classical azulenequinones (14). Table 3 shows the energy, LUMO, HOMO, and $\Delta\varepsilon$ of azulenequinones which are generated by the ab initio calculations. The azulenequinones can be ranked from the lowest to the highest in order of their energy, computed at the Hartree–Fock level.

1,5 < 1,7 < 1,4 < 1,6 < 1,2 < 4,7 < 1,8 < 2,6 < 2,4 < 4,5 < 5,6

In conclusion, the relative stability of azulenequinone depends on the number of double bonds in the five-membered ring and the tropone ring. The structures of 1,5- and 1,7-azulenequinones contain one double bond in the five-membered ring and have a tropone unit in the seven-membered ring, which may stabilize the structure. The structure of 1,2-azulenequinone contains one double bond in the five-membered ring and the 1,2-diketone substitute that should increase the strain energy of the five-membered ring. Whereas 1,4-, 1,6-, and 1,8-azulenequinones have two double bonds in the five-membered ring (one double bond is located in the fusing junction), that decrease the stability of azulenequinone. Considering the structure, these azulenequinones have a tropone and a cyclopentadienone, which cannot be generated under normal laboratory conditions and is chemically unstable. 2,4- and 2,6-Azulenequinones contain a cyclopentadienone (which contains two double bonds in the five-membered ring) and do not have a typical tropone structure. Moreover, 4,5-, 4,7-, and 5,6-azulenequinones have a diketone substitute located in the seven-membered ring that should decrease the stability of azulenequinone. The calculation also indicated that 4,5-, 4,7-, and 5,6-azulenequinones are significantly non-planar, which should increase the strain energy and decrease the resonance energy. Concerning the aromaticity of plane, azulenequinones may obey the $4n + 2$ rule for free $p\pi$ electrons in five- and seven-membered rings. 1,5-, 1,7-, and 1,2-Azulenequinones have two and six $p\pi$ electrons in the five- and seven-membered rings respectively. Although 1,4-, 1,6-, and 1,8-azulenequinones have two (in the five-membered ring) and six (in the seven-membered ring) free $p\pi$ electrons, they include one double bond in the fused position of two rings. This should decrease the relative stability of azulenequinones.

According to the above calculations, 1,5- and 1,7-azulenequinones should be the most stable isomers in the azulenequinones. Morita et al. (21) synthesized 1,5- and

© 2000 NRC Canada

Fig. 2. Eleven Kekule structures of azulenequinone.

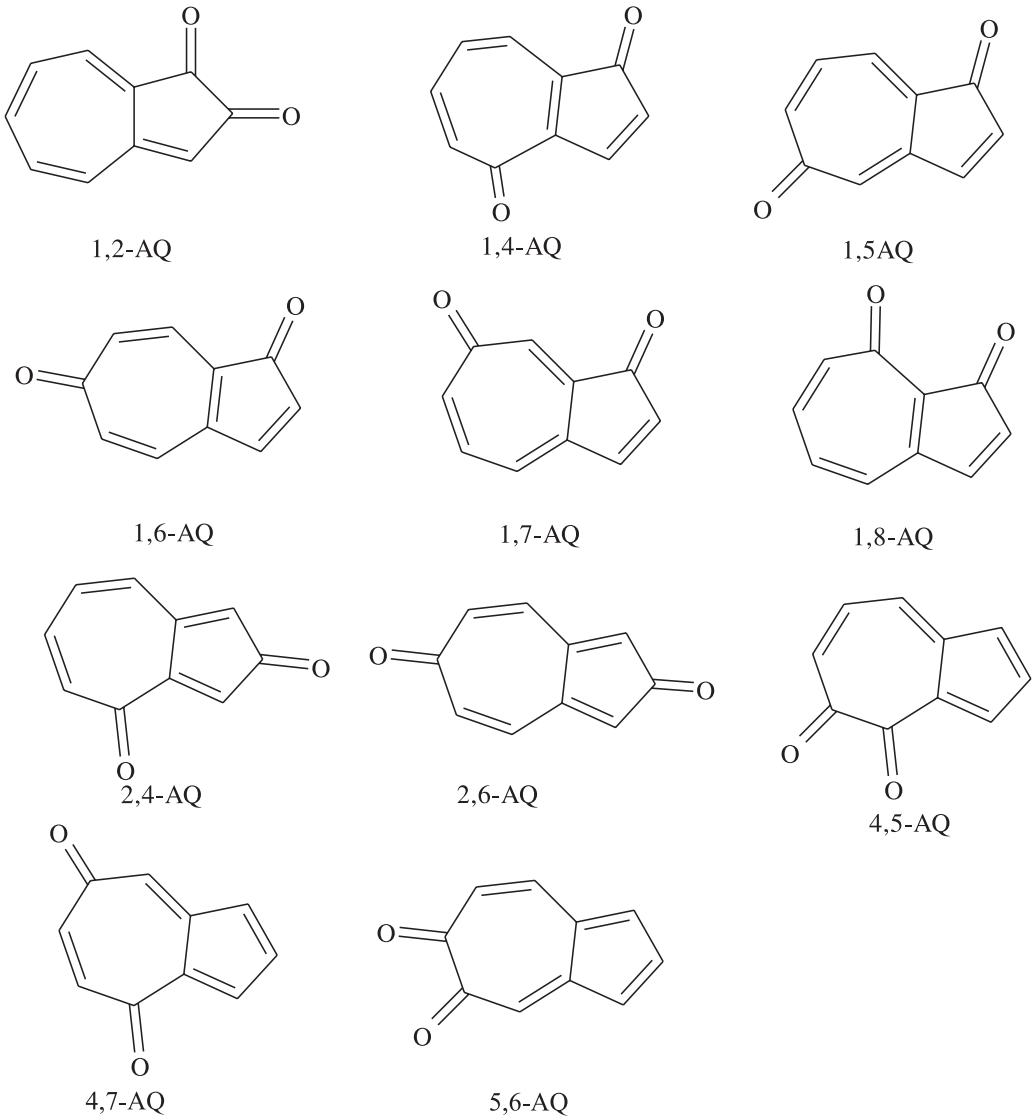


Table 3. Calculated energy, HOMO, LUMO (Hartree), and Δε (kcal/mol) for azulenequinones (AQ)[a].

Compd.	Energy	HOMO	LUMO	Δε
1,2-AQ	–531.62182	–0.2998	0.0087	194
1,4-AQ	–531.62731	–0.3185	0.0003	200
1,5-AQ	–531.63664	–0.3360	0.0179	222
1,6-AQ	–531.62354	–0.3168	–0.0060	195
1,7-AQ	–531.63427	–0.3244	0.0197	216
1,8-AQ	–531.61441	–0.3268	0.0023	206
2,4-AQ	–531.60805	–0.3243	–0.0138	195
2,6-AQ	–531.61212	–0.3341	–0.0125	202
4,5-AQ	–531.60376	–0.3366	–0.0092	205
4,7-AQ	–531.61728	–0.3445	–0.0092	210
5,6-AQ	–531.60283	–0.3195	–0.0055	197

[a]All calculations were performed using the ab initio HF method with the 6–31G basis set.

1,7- azulenequinones and Scott and Adams (22) isolated these azulenequinones as stable crystalline solids. On the other hand, 2,6- and 1,6-azulenequinones have been synthesized as the dimer and the naphtho fused form respectively, they could not be isolated as a stable compound. In conclusion, the 1,*n*-azulenequinones have the most favorable

© 2000 NRC Canada

Table 4. Calculated π-LUMO coefficients of 1,5- and 1,7-azulenequinones[a].

Compd	C-1	C-2	C-3	C-4	C-5	C-6	C–7	C-8	C-9	C–10
1,5-AQ	0.407	0.288	–0.472	0.015	0.321	0.437	–0.417	–0.372	0.463	–0.115
1,7-AQ	–0.379	–0.438	0.496	–0.270	–0.433	0.397	0.314	0.112	–0.290	0.410

[a]All calculations were performed using the ab initio HF method with the 6–31G basis set.

Table 5. Calculated energy (Hartree) and relative energy (kcal/mol) for dibromo-1,5- and -1,7-azulenequinone[a].

m,*n*-1,5-AQ	Energy	ΔE^b	*m*,*n*-1,7-AQ	Energy	ΔE^b
2,3	–5669.98535	0.85	2,3	–5669.98371	1.21
2,4	–5669.98240	2.70	2,4	–5669.98404	1.00
2,6	–5669.98157	3.23	2,5	–5669.98322	1.52
2,7	–5669.98483	1.18	2,6	–5669.97970	3.73
2,8	–5669.97694	6.13	2,8	–5669.96877	10.59
3,4	–5669.96665	12.59	3,4	–5669.97209	8.50
3,6	–5669.98339	2.08	3,5	–5669.98564	0.00
3,7	–5669.98671	0.00	3,6	–5669.98228	2.11
3,8	–5669.97858	5.10	3,8	–5669.97130	9.00
4,6	–5669.97760	5.72	4,5	–5669.97341	7.67
4,7	–5669.98239	2.71	4,6	–5669.98064	3.14
4,8	–5669.97348	8.30	4,8	–5669.96953	10.11
6,7	–5669.97351	8.28	5,6	–5669.97199	8.57
6,8	–5669.97338	8.36	5,8	–5669.96978	9.95
7,8	–5669.96371	14.43	6,8	–5669.96442	13.32

[a]All calculations were performed using the ab initio HF method with the 6–31G basis set.

[b]ΔE is the energy relative to 3,7–1,5-AQ and 3,5–1,7-AQ respectively.

Table 6. Calculated energy (Hartree)[a] and $S_0 - S_1$ transition frequency (nm) for *n*-bromo-1,5-AQ and *n*-bromo-1,7-AQ.

n-bromo-1,5-AQ	Energy	CIS ($S_0 - S_1$)	*n*-bromo-1,7-AQ	Energy	CIS ($S_0 - S_1$)
2	–3100.81097	311	2	–3100.80859	320
3	–3100.81272	315	3	–3100.81121	317
4	–3100.80864	315	4	–3100.81043	316
6	–3100.80772	318	5	–3100.80952	320
7	–3100.81111	317	6	–3100.80588	323
8	–3100.80319	337	8	–3100.79492	364

[a]All calculations were performed using the ab initio HF method with the 6–31G basis set.

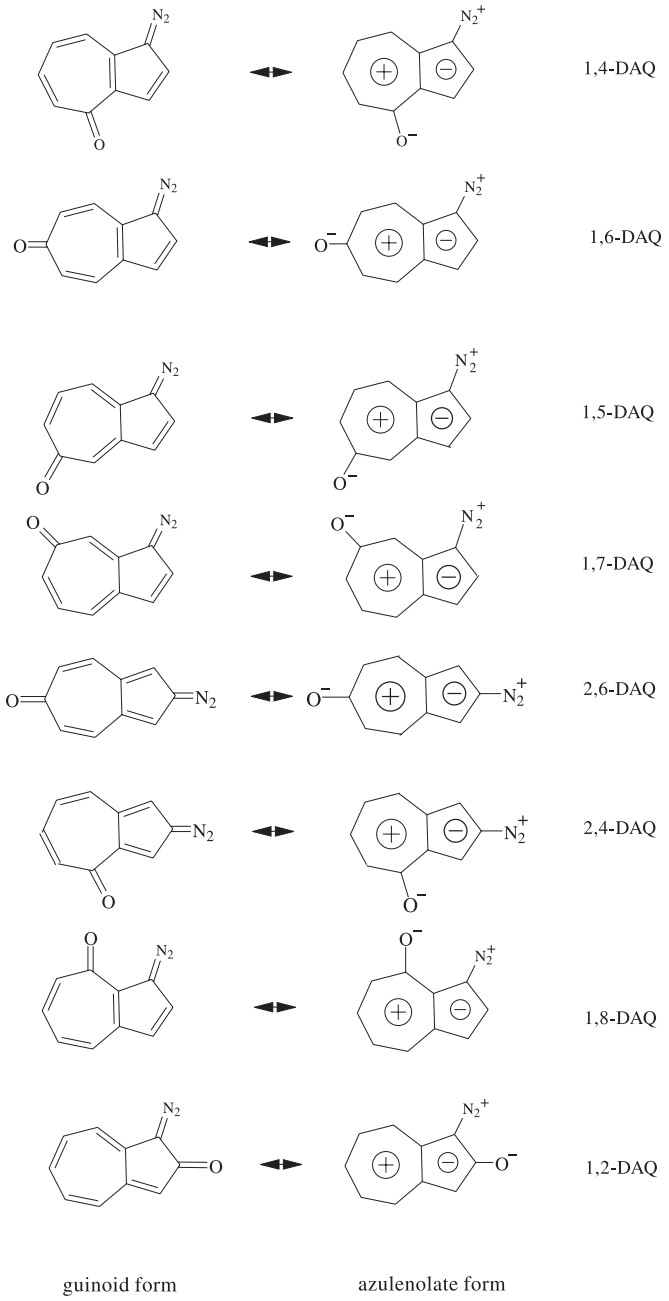
energy according to ab initio calculations and the experimental results confirmed the theoretical prediction in this azulenequinone study (21).

For the reactivity study of azulenequinone, the donor substitution (nucleophilic attack) should occur in the position with the largest π–LUMO coefficient. Table 4 shows the calculated π–LUMO coefficient of azulenequinone by the ab initio HF/6–31G calculation. 3, 7 and 3, 5 are the most possible positions for the nucleophilic attack in 1,5- and 1,7-azulenequinones, respectively. Experimentally, through repeated bromination in aqueous acetic acid, an azulenequinone affords a mixture of monobromoazulenequinone together with that of dibromoazulenequinones (24). These bromoazulenequinones could be the precursors for the formation reaction of polymers (23, 24). Actually, we select the most thermodynamically stable isomers 1,5- and 1,7-azulene- quinones as the precursors for the study of the bromoazulenequinone and dibromoazulenequinone isomers. The ab initio HF/6–31G calculated energy of six monobromoazulenequinones and 15 dibromoazulenequinones are given in Tables 5 and 6, respectively. The result shows that 3-bromo-1,5-azulenequinone and 3-bromo-1,7-azulenequinone are the major products for the bromination of 1,5- and 1,7-azulenequinones. Nozoe et al. (15) obtained 3-bromo-1,5-azulenequinone and 3-bromo-1,7-azulenequinone in agreement with the theoretical prediction. According to Table 5, 3,7-dibromo-1,5-azulenequinone and 3,5-dibromo-1,7-azulenequinone are the most stable isomers for dibromoazulenequinone in the ground state. 2,3-Dibromo-1,5-azulenequinone and 2,3-dibromo-1,7-azulenequinone are the next stable isomers of this compound. This theoretical prediction may provide the possible structures for organic chemists to design the new reaction path.

The electronic transition energy of $S_0 - S_1$ ($\pi - \pi^*$) is related to the color of the compound. Scott et al. (14) have obtained the π–HOMO/LUMO gap and colors of azulenequinones. Calculation results indicated that these compounds have intense-purple to blue-green colors. Table 6 shows the

© 2000 NRC Canada

Fig. 3. Kekule structures and resonance forms of diazoazulenequinones.



$S_0 - S_1$ electronic excitation energies of the monobromoazulenequinones, which are all in the UV region (between 311 nm and 364 nm).

Diazoazulenequinone

Anilines undergo diazotization under acidic condition to give diazonium ions as a reaction intermediate. Nozoe et al (17) and Lin and coworkers (18) have shown that the diazotization of 2-amino-6-bromo-1,3-dicyanoazulene to generate the diazoazulenequinone, which contained a conjugated ketone and diazo functional group, that endow a wide range of reactivity (18). While the symmetry consideration allow diazoazulenequinones to have 32 isomers, the Kekulé aromatic theory limits the possible structures of diazoazulenequinone to 22. Other isomers of diazoazulenequinone have nonclassical structure and are ignored in this study. The resonance structures of diazoazulenequinone may have a quinoid form or a diazonium azulenolate form. Due to the resonance, the structures of the aliphatic diazo compound are described as in Fig. 3. In quinoid form, none of the electron pairs can be delocalized into the functional group, which results in resonance structures containing a double bond between the azulene ring and the attached nitrogen. Azulenolate form presumes a positive charge on the diazo side and a negative charge on the carbonyl side. Since the five-membered ring of azulene contains a higher negative charge, the diazonium cation should be more stabilized on the five-membered ring. Therefore, in the calculations of relative stability of the diazoazulenequinone isomers, only those containing the diazo group located in the five-membered ring were considered. The ab initio HF calculation with the 6–31G basis set were used to generate the relative stability for these structures and the results are given as follows (Table 7):

Table 7. Calculated energy, HOMO, LUMO (Hartree) and Δε (kcal/mol) for diazoazulenequinones (DAQ)[a].

m,n-DAQ	Energy	HOMO	LUMO	Δε
1,2-DAQ	–565.58630	–0.2775	0.0412	200
1,4-DAQ	–565.58673	–0.2912	0.0326	203
1,5-DAQ	–565.57755	–0.2745	0.0456	201
1,6-DAQ	–565.58400	–0.2907	0.0284	200
1,7-DAQ	–565.57841	–0.2735	0.0434	199
1,8-DAQ	–565.59438	–0.2848	0.0433	206
2,4-DAQ	–565.58112	–0.2831	0.0265	194
2,6-DAQ	–565.57958	–0.2963	0.0261	202
4,5-DAQ	–565.56915	–0.2763	0.0165	184
4,7-DAQ	–565.56225	–0.2751	0.0187	184

[a]All calculations were performed using the ab initio HF method with the 6–31G basis set.

$$1,8 < 1,4 < 1,2 < 1,6 < 2,4 < 2,6 < 1,7 < 1,5 < 4,5 < 4,7$$

According to the above results, 1,8-, 1,4-, and 1,2-diazoazulenequinones have high chemical stability. But most of the diazoazulenequinones are derived from 2-amino-6-bromoazulenes and 2-amino-4-bromoazulenes, so that 2,6- and 2,4- should be the most probable diazoazulenequinone products (25). In a simple structural consideration, the relative stability of diazoazulenequinones depends on a tropone ring and a diazocyclopentadiene ring. Particularly, 1,8-, 1,4-, and 1,6-diazoazulenequinones contain a tropone unit and a diazocyclopentadiene ring. The azulenolate form should transfer the electron density to the ring and increase the aromatic character in the ring. Consequently, 2,4-, 2,6-, 1,7-, and 1,5-diazoazulenequinones contain a tropone unit and no cyclopentadiene, which may decrease the relative stability. As the result of the theoretical prediction, 4,5- and 4,7-diazoazulenequinones (diazo and carbonyl functions are located in the same ring) are nonplanar compounds and they may decrease the resonance energy and chemical stability.

For the geometrical structures of other possible isomers of diazoazulenequinone, like 1,2-quinondiazide, the diazo and the carbonyl group are brought closer sterically, which should

© 2000 NRC Canada

Fig. 4. Cyclic reaction of diazoazulenequinone.

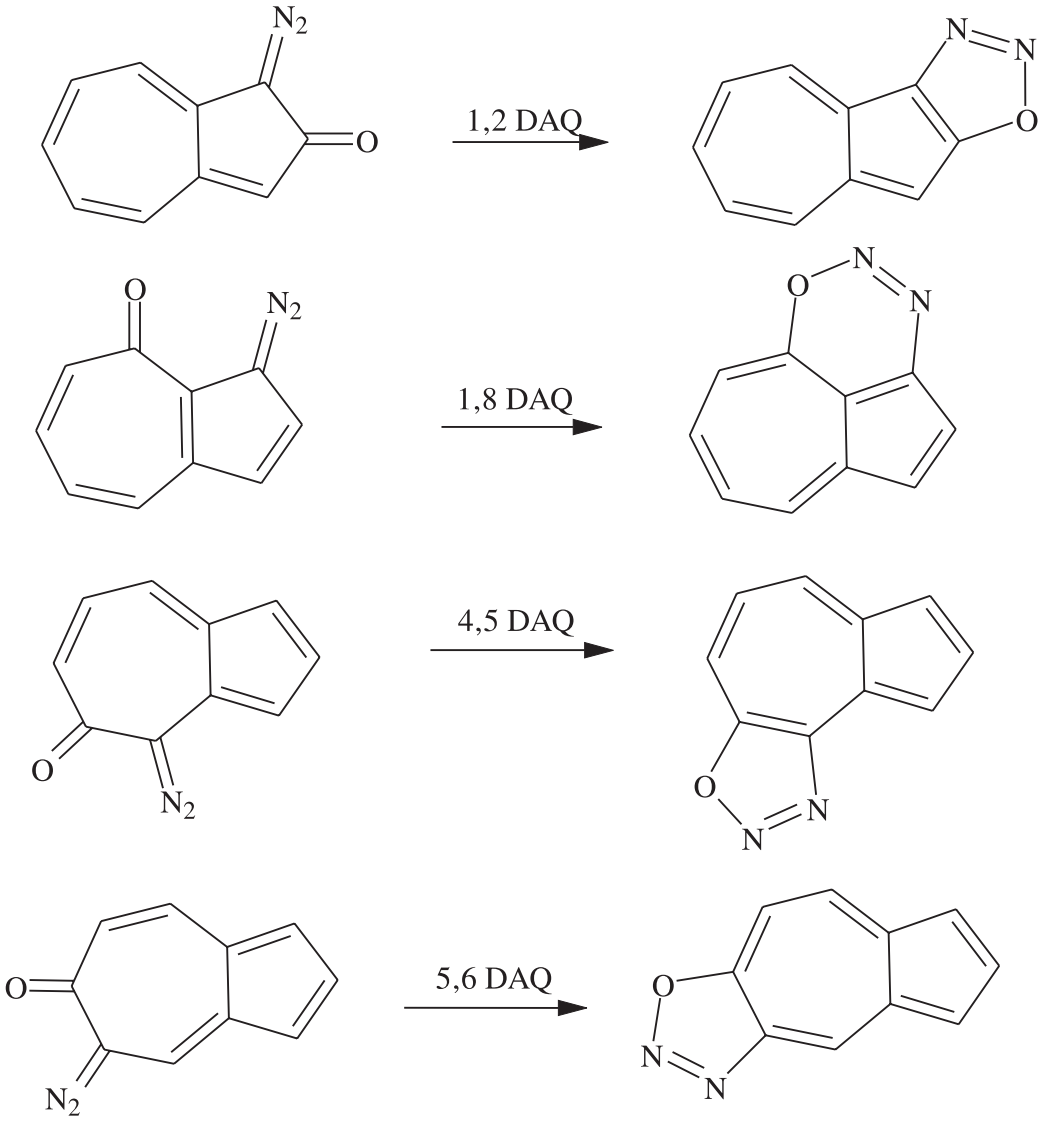


Table 8. Calculated energy (Hartree) and ΔE (kcal/mol) for m,*n*-DAQ cyclic reaction[a].

Compound	$E_{comp.}$	$E_{cyclic\ comp.}$	ΔE^b
1,2-DAQ	–565.58630	–565.53927	–30
1,8-DAQ	–565.59438	–565.59439	<0.01
4,5-DAQ	–565.56915	–565.55734	–7
5,6-DAQ	–565.58042	–565.56422	–10

[a]All calculations were performed using the.ab initio HF method with the 6–31G basis set.

[b]$\Delta E = E_{cyclic\ comp.} - E_{comp.}$.

be responsible for the partial interaction of the carbonyl oxygen with the nitrogen end atom of the diazo group to form a five-membered heterocycle. Blocher and Zeller (26) proposed that the *o*-quinone diazide (benzene) and *o*-quinone diazide (naphthalene) should favor the cyclic structure of the benzo-[1,2,3]-oxadiazole and naphtho-[2,3-*d*]-[1,2,3] oxadiazole, respectively. Accordingly, 1,2-, 1,8-, 4,5-, and 5,6-diazoazulenequinones have diazo and carbonyl groups in the neighboring positions which could result in cyclic reaction to provide the existence of a five- or a six- membered heterocycles, which are shown in Fig. 4. We study the relative preference for these cyclic reactions by theoretical calculations (Table 8). Since the energy difference is very small, only 1,8-diazoazulenequinone may favor the cyclic reaction to produce a six-membered ring heterocycle compound, which is an isomeric structure.

Diazotization of aniline gives a relatively stable arenediazonium salt. When arenediazonium ions are heated, the nitrogen extrusion is easy and the very reactive phenyl cation is produced. Similarly, diazotization of 2-amino-6-bromo-1,3-dicyanoazulene or 2-amino-4-bromo-1,3-dicyanoazulene produced a conjugated ketocarbene intermediate, which is a precursor for the reaction with THF. For the carbene studies, several results have been reported in the literature about the theoretical calculation to describe the energy difference between the singlet and triplet substituted carbenes (27–29). Carbenes contain two valence electrons. According to the electronic configuration analysis, the singlet ground state has

© 2000 NRC Canada

Fig. 5. Polyether bridged azulene.

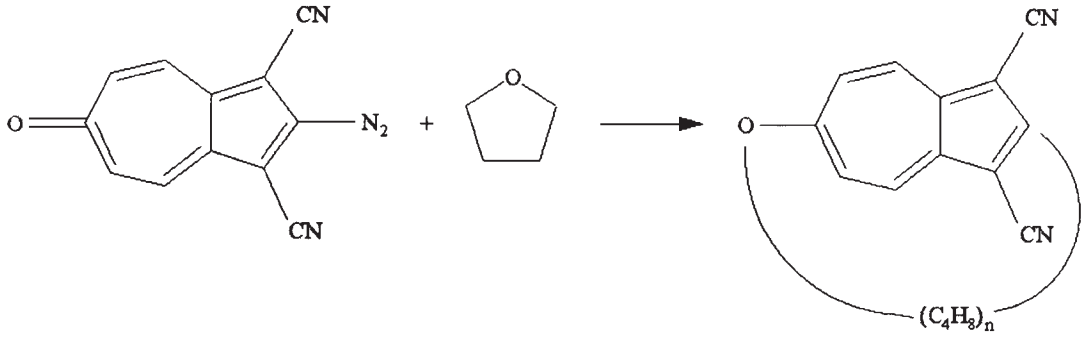
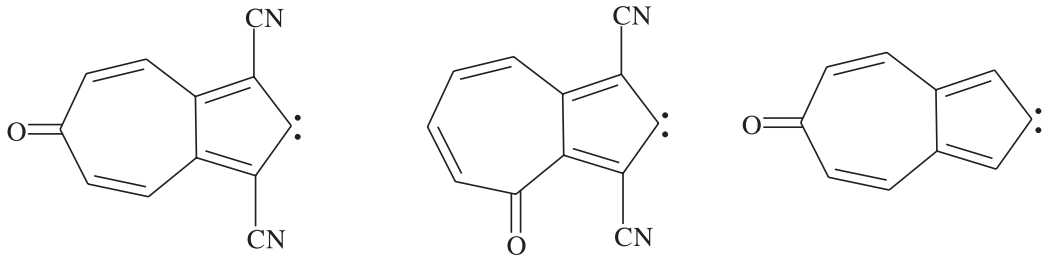


Table 9. Calculated energy for singlet and triplet ketocarbene intermediates.

Compd.	HF/6–31G(Hartree)	ΔE [a](kcal/mol)	Multiplicity
1	–640.03081	35	1
	–640.08613		3
2	–639.99841	96	1
	–640.15114		3
3	–456.63587	90	1
	–456.77866		3

[a] $\Delta E = E_{singlet} - E_{triplet}$.



1 2 3

a pair of spin coupled electrons localized on the sp^n orbital and the triplet ground state has one electron on the sp^n orbital and the other is on the $p\pi$ orbital. Thus, there is more $p\pi$ character in the triplet ground state, which should aid its electron delocalization. This conjugated ketocarbene intermediate has either singlet or triplet ground state. The results of the HF/6–31G calculations for this conjugated ketocarbene intermediate are shown in Table 9 in which triplet ketocarbene possesses a lower energy than that of singlet ketocarbene, by about 35 kcal/mol and 96 kcal/mol for conjugated 2,6- and 2,4-ketocarbenes with the 1,3-dicyano group, respectively. Furthermore, the conjugated ketocarbene should play an important role in the formation mechanism of polyether bridged azulene. Recently, diazoazulenequinone was found to undergo photoreactions with different numbers of THF substitutes leading to a polyether bridged azulene, such as diazoazulenequinone–3THF, diazoazulenequinone–4THF, and diazoazulenequinone–5THF (Fig. 5) (19). This polyether bridged azulene presents very special stereoselectivity in the reaction, and we are going to investigate this later.

Conclusions

The relative stability investigation shows that 1,5- and 1,7-azulenequinones are the most favorable (or stable) isomers, which depends on the number of double bonds in the five-membered ring and the tropone structure in the seven-membered ring. Bromination of 1,5- and 1,7-azulenequinones should produce 3-bromo-1,5-azulenequinine and 3-bromo-1,7-azulenequinone as monobromoazulenequinone, as well as 3,7-dibromo-1,5-azulenequinone and 3,5-dibromo-1, 7-azulenequinone as dibromoazulenequinone stable products, respectively.

The relative stability of diazoazulenequinones depends on a tropone unit and a diazocyclopentadiene ring. Thus, 1,8-, 1,4-, 1,2-, and 1,6-diazoazulenequinones are the favorable isomers. Due to the partial interaction of the carbonyl oxygen with the nitrogen end of the diazo group, it should form a heterocycle. 1,8-Diazoazulenequinone favors this cyclic reaction to give a six-membered ring heterocyclic compound.

Recently, the research on azulene and its derivatives has developed considerably and rapidly. Their chemical transformations along with the relative availability disclose a wide prospective for the production of various derivatives of heterocyclic compounds, polymers, and azulene. The results of the present calculation provide more accurate geometric structures, electronic structures, and spectroscopic data as well as other physical properties for azulene, azulenequinones, diazoazulenequinones, and bromoazulenequinones. They are

© 2000 NRC Canada

interesting precursors for the formation of azulene-based material and the starting material for the formation of polymers.

Acknowledgments

We thank Dr. Alexander Mebel and Prof. Yuan L. Chou for reading the manuscript and the National Science Council of ROC for support.

References

1. P.A. Plattner and A.S. Pfau. Helv. Chim. Acta, **20**, 224 (1937**)**.
2. T. Nozoe, K. Takase, and N. Shimazaki. Bull. Chem. Soc. Jpn. **37**, 1640 (1964).
3. A.G. Anderson and J.A. Nelson, Jr. J. Am. Chem. Soc., **72**, 3824 (1950).
4. R.C. Haddon and K. Raghavachari. J. Am. Chem. Soc. **104**, 351 (1982).
5. R.C. Haddon and K. Raghavachari. J. Chem. Phys. **79(2)**, 1093 (1983).
6. S. Grimme. Chem. Phys. Lett. **201**, 607 (1993).
7. P.M. Kozlowski, G. Rauhut, and P. Pulay. J. Chem. Phys. **103(13)**, 5650 (1995).
8. J.M. Robertson, H.M.M. Shearer, G.A. Sim, and D.G. Watson. Acta. Crystallogr. **15**, 1 (1962).
9. G.S. Pawley. Acta. Crystallogr. **18**, 560 (1965).
10. A.W. Hanson. Acta. Crystallogr. **19**, 19 (1965).
11. J. Michl and E.W. Thulstrup. Tetrahedron, **32**, 205 (1976).
12. T. Morita, M. Karasawa, and K. Takase. Chem. Lett. **2**, 197 (1980).
13. M.K.W. Li and P.J. Scheuer. Tetrahedron Lett. **25**, 587 (1984).
14. L.T. Scott, M.D. Rozeboom, K.N. Houk, Fukunaga, H.J. Lindner, and K. Hafner. J. Am. Chem. Soc. **102**, 5169 (1980).
15. T. Nozoe, H. Wakabayashi, K. Shindo, T. Kurihara, S. Ishikawa, and M. Kageyama. Chem. Lett. **1**, 25 (1995).
16. K. Hafner, K.H. Vöpel, G. Ploss, and C. König. Justus Liebigs Ann. Chem. **661**, 52 (1963).
17. T. Nozoe, T. Asao, H. Susumago, and M. Ando. Bull. Chem. Soc. Jpn. **47**, 1471 (1974).
18. W.C. Wun, T.C. Huang, S.J. Lin, B.B, Lin, T. Morita, and Y.S. Lin. J. Chin. Chem. Soc. **40**, 593 (1993).
19. Y.S. Lin, S.Y. Jiang, T.C. Huang, S.T. Lin, and Y.L. Chow. J. Org. Chem. **63**, 3364 (1998).
20. J.B. Birks. Chem. Phys. Lett. **17**, 370 (1972).
21. T. Morita, F. Ise, and K. Takase. Chem. Lett. **8**, 1303 (1982).
22. L.T. Scott and C.M. Adams. J. Am. Chem. Soc. **106**, 4857 (1984).
23. T. Nozoe and H. Takesita. Bull. Chem. Soc. Jpn. **69**, 1149 (1996).
24. T. Nozoe, H. Wakabayashi, K. Shindo, and S. Ishikawa. Chem. Lett. **1**, 27 (1995).
25. T. Nozoe, T. Asao, M. Yasunami, H. Wakui, T. Suzuki, and M. Ando. J. Org. Chem. **60**, 5919 (1995).
26. A. Blocher and K.P. Zeller. Angew. Chem. Int. Ed. Engl. **30**, 1476 (1991).
27. E.A. Carter and W.A. Goddard, III. J. Chem. Phys. **88(3)**, 1752 (1988).
28. N. Russo, E. Sicilia, and M. Toscano. J. Chem. Phys. **97**, 5031 (1992).
29. S.-J. Kim, T.P. Hamilton, and H.F. Schaefer, III. J. Chem. Phys. **94**, 2063 (1991).

© 2000 NRC Canada

Interaction of hydroxyphenyl alkyl ketones with β-cyclodextrin

Alicia Viviana Veglia and Rita Hoyos de Rossi

Abstract: Binding constants of β-cyclodextrin with six hydroxyphenyl alkyl ketones having a general structure Z-Ph-CO-$(CH_2)_n$CH$_3$ (Z = *o*-OH or *p*-OH and *n* = 0, 1, or 3) were measured at 25°C by UV–vis spectrophotometry. In all cases the formation of 1:1 host-guest complexes was established. NMR chemically induced shifts indicated mixed complexation modes. Equilibrium constants are around 200 M^{-1} for some of the compounds and for the others around 1000 M^{-1}. It is suggested that complexes with different geometries coexist in the solution with predominance of those with the aryl group ($K_{SCD} \approx 200$ M^{-1}) or alkyl group ($K_{SCD} \approx 1000$ M^{-1}) inside the cavity.

Key words: inclusion complex, β-cyclodextrin, hydroxyphenyl alkyl ketones, association constants, UV–vis spectrophotometry.

Résumé : Faisant appel à la spectrométrie UV–vis et opérant à 25°C, on a mesuré les constantes de fixation de la β-cyclodextrine avec six hydroxyphénylalkylcétones de structure générale Z-Ph-CO-$(CH_2)_n$CH$_3$ (Z = *o*-OH ou *p*-OH et *n* = 0, 1 ou 3). Dans chacun des cas, on a pu établir qu'il se forme des complexes hôte-invité 1:1. Les déplacements RMN induits chimiquement suggèrent l'existence de modes de complexation mixtes. Les constantes d'équilibre de certains de ces composés vont de 200 M^{-1} à 1000^{-1}. Ces données suggèrent que des complexes de géométries différentes coexistent en solution et qu'il y a prédominance de ceux dans lesquels les groupes aryle ($K_{SCD} \approx 200$ M^{-1}) ou alkyle ($K_{SCD} \approx 1000$ M^{-1}) se trouvent à l'intérieur de la cavité.

Mots clés : complexe d'inclusion; β-cyclodextrine; hydroxyphénylalkylcétone; constantes d'association; spectrophotométrie UV–vis.

Introduction

Cyclodextrins are doughnut-shaped molecules formed by six, seven, or eight glucose units (α, β, or γ) linked together covalently by glycosidic oxygen atoms. They have the secondary hydroxy groups on the wider rim of the cavity and the primary OH groups at the narrower one (1). They are able to form inclusion complexes with a great variety of compounds and this property is responsible for changes in reactivity and selectivity of organic reactions (2, 3). This property has been reported to have analytical implications ((4) and refs. therein).

Moreover, the interaction of cyclodextrins with organic compounds of different structures is a field of great interest because it may help in the understanding of the catalytic action of enzymes (5).

In previous work, we have studied the photochemical rearrangement of aryl esters of different alkyl chain lengths which lead to *ortho*- (**1**) and *para*- (**2**) hydroxyphenyl alkyl ketones (6, 7) in the presence of β-cyclodextrin (CD). We thought it would be of interest to determine the equilibrium constants for the association of **1** and **2** with CD in order to establish the effect of the position of the hydrophilic OH group and the length of the alkyl chain on the nature of the interaction.

Received October 1, 1999.

A.V. Veglia and R.H. de Rossi. Instituto de Investigaciones en Físico Química de Córdoba (INFIQC), Departamento de Química Orgánica, Facultad de Ciencias Químicas, Universidad Nacional de Córdoba, Ciudad Universitaria, 5000 Córdoba, Argentina. Telephone: 54-351-4334170/3. Fax: 54-351-4333030.
e-mail: aveglia@dqo.fcq.unc.edu.ar; ritah@dqo.fcq.unc.edu.ar

Results and discussion

Association constants determination. The addition of 10 mM of CD to aqueous solutions of substrates (S) **1** and **2** produces a bathochromic shift of about 3 nm in the UV–vis spectra. When the CD concentration is varied from 0–10 mM, there is not a well defined isosbestic point (Fig. 1 is representative). In all cases the corresponding blank of CD was subtracted. We did not find evidence for the formation of complexes with stoichiometry higher than 1:1, therefore we considered that the lack of an isosbestic point was probably due to some type of medium effect on the species (8). The addition of glucose in an equivalent weight of 10 mM CD did not produce any change on the absorbance of compounds **1** and **2,** which indicates that there are some specific interactions between the substrates and the CD.

The difference spectrum between a solution having the maximum of cyclodextrin concentration used (10 mM) and that without CD shows the wavelength (λ) of maximum absorbance differences (ΔA_{max}) in each case. These wavelengths which are collected in Table 1 were selected for the measurements.

The change in absorbance with the concentration of CD can be represented as in eq. 1

 © 2000 NRC Canada

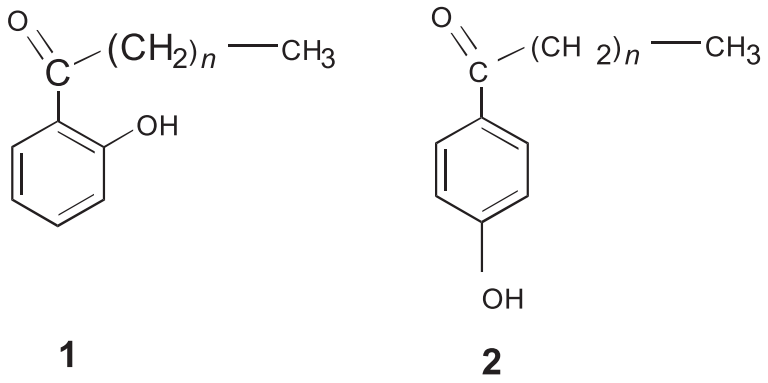
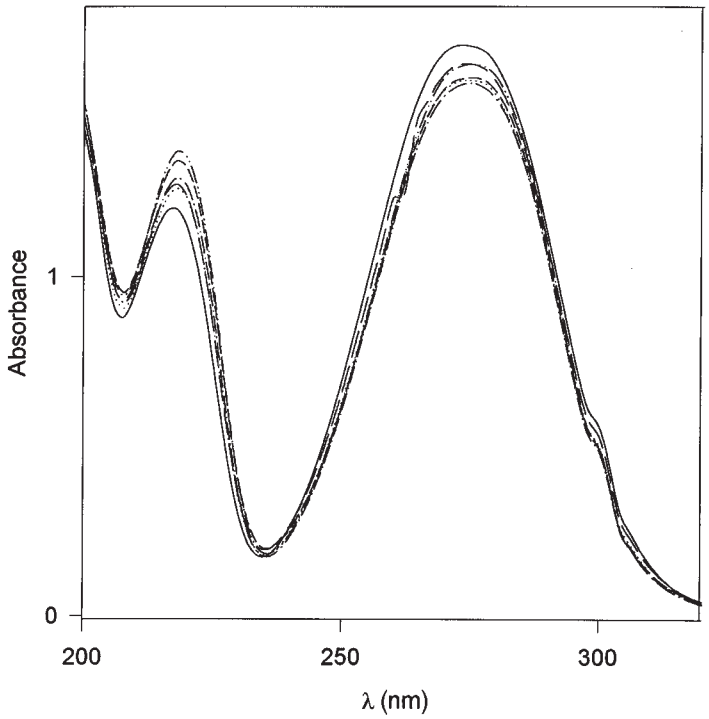


Fig. 1. UV–vis spectrum for *p*-hydroxyacetophenone (**2**, $n = 0$) 5×10^{-5} M with 0, 2, 4, 6, 8, and 10 mM of β-cyclodextrin, indicated in this order with lines —, — —,...., —. —, – – –, –.. –. At 224.6 nm the absorbance increases with the increase of β-cyclodextrin concentration.



$$[1] \qquad A = A_0 + \frac{\Delta A_{max} K_{SCD}[CD]}{(1 + K_{SCD}[CD])}$$

where A and A_0 are the absorbances at a given wavelength for the solutions with and without CD, ΔA_{max} represents the change in A between the complexed and free substrate, K_{SCD} is the association constant for the reaction described in eq. [2].

$$[2] \qquad S + CD \rightleftharpoons SCD$$

Alternatively, eq. [1] can be transformed into eq. [3] where Δε represents the difference in the extinction coefficients of the included and that of the free substrate.

$$[3] \qquad \frac{[S]_0[CD]}{\Delta A} = \frac{1}{K_{SCD}\Delta\varepsilon} + \frac{[CD]}{\Delta\varepsilon}$$

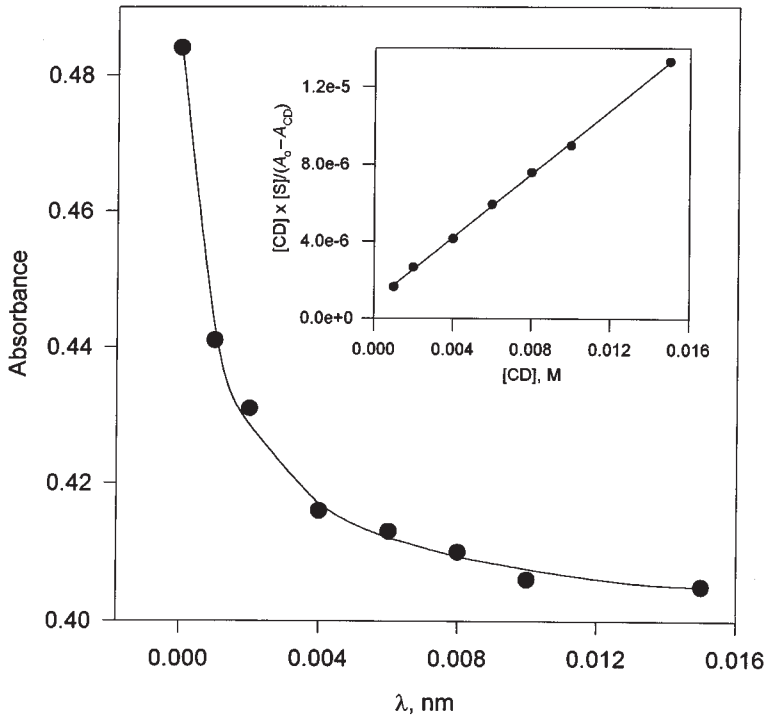
The measured values of absorbance were adjusted to eq. [1] (Fig. 2 is representative). The linear plot according to eq. [3] (Fig. 2 inset) confirms the 1:1 stoichiometric ratio (9). Both methods give the same value of K_{SCD} within experimental error.

© 2000 NRC Canada

Table 1. Equilibrium constants for the association of compounds **1** and **2** with β-cyclodextrin at 25°C in water.

Substrate	1 (n = 0)	2 (n = 0)	1 (n = 1)	2 (n = 1)	1(n = 3)	2 (n = 3)
λ(nm)	222.1	224.6	221.4	224.0	223.0 246.0	224.8 296.1
$K_{SCD}(M^{-1})$	239 ± 7	150 ± 20	150 ± 20	840 ± 200	890 ± 80	1300 ± 200
log K_{SCD}	2.38	2.18	2.18	2.92	2.95	3.11

Fig. 2. Absorbance of 7×10^{-5} M *o*-hydroxyvalerophenone (**1**, n = 3) as a function of β-cyclodextrin concentration at 246 nm. Inset: plot according to a linearized equation (see text eq. [3]).



For *o*-hydroxyvalerophenone (**1,** n = 3**)** and *p*-hydroxyvalerophenone (**2,** n = 3) the values of K_{SCD} reported in Table 1 are the average of the determination at two wavelengths, namely 223.0 nm and 246.0 nm for the former and 224.8 nm and 296.1 nm for the latter. For all the other substrates, there was only one wavelength where the ΔA_{max} is 0.1, so we used this value for equilibrium constant determination.

The K_{SCD} values determined in this study, for **1** and **2**, show better interaction with β-cyclodextrin relative to α-cyclodextrin, since the K_{SCD} values reported for substrates **2** with n = 0 and 3 and α-cyclodextrin were 14.9 and 41 M^{-1}, respectively (10). This behaviour ($K_{SCD}^{\beta} > K_{SCD}^{\alpha}$) was also observed for monosubstituted benzene derivatives (11).

The values of the K_{SCD} are in the range expected according to literature values (12). They can be grouped in two sets: one with K_{SCD} around 200 M^{-1} and one with K_{SCD} around 1000 M^{-1}.

The influence of the position of the hydroxyl group substituent of the aromatic rest can be observed from the dependence of the log K_{SCD} vs. the number of carbons (n) of the alkyl chain for the **1** and **2** series of compounds (Table 1). The polar group in the *para* position drives the change of the binding constant faster from ≈200 to ≈1000.

As in the literature (12), it is reasonable to infer, in the absence of 2:1 (S_2 : CD) complex, that the CD binding site is presumably the wider (secondary hydroxyl) end. In complexes between bencene derivatives and CD the orientation of the substrates in the cavity commonly observed (but not universally) is with the nonpolar group deeply inserted in the cavity of CD and the polar group located near the secondary hydroxyl's rim or it may even protude from the cavity (12).

The substrates studied here have a polar substituent (the OH group), a hydrophobic aromatic rest, and an acyl ($CO(CH_2)_nCH_3$) substituent with increasing hydrophobicity with n. Evidently the polar characteristics of these substituents are important in establishing the structure of the complexes with CD.

By the above general considerations, it is likely that in the case of the substrates studied here, the polar OH tend to be outside the cavity and the aryl part of the molecule or the acyl group is inside the cavity being the dispersive and hydrophobic interactions, the primarily driving force for the association in solution (13).

The fact that the OH group of S (S = **1** or **2**) probably is located near the wider rim forming hydrogen bonds with CD oxygen or interacting with the surrounding water shell, was

© 2000 NRC Canada

Table 2. Induced chemical shift values ($\Delta\delta$) in ^{1}H NMR spectra for proton signals of compounds **1** and **2** and phenylalkanoates complexed with β-cyclodextrin in relation to free substrates.[a]

Substrate	β-CD H_5	H_o[b]	H_p[c]	CH_3
1 (n = 0)	–0.028	–0.029	–0.002	–0.002
2 (n = 0)	0.07	–0.036	–0.022	–0.022
1 (n = 1)	0.01	–0.135	–0.038	0.033
2 (n = 1)	0.064	–0.023	–0.044	0.029
1 (n = 3)	0.002	–0.26	–0.053	–0.036
2 (n = 3)	–0.007	–0.065	–0.015	0.028
phenyl acetate	0.005	–0.018	0.02	0.011
phenylpropanoate	–0.010	–0.037	0.018	0.014
phenyl valerate	0.026	–0.163	0.062	0.078

[a]In D_2O at room temperature.

[b]H_o indicates the aromatic proton(s) in the *ortho* position of the -CO-$(CH_2)_n$$CH_3$ or -O-CO-$(CH_2)_n$$CH_3$ groups, being H_6 for **1** (2-hydroxyphenylketone), and H_2 and H_6 for **2** (4-hydroxyphenylketone) and for phenylalkanoates.

[c]H_p indicates the aromatic proton in the *para* position of the -O-CO-$(CH_2)_n$$CH_3$ or -CO-$(CH_2)_n$$CH_3$ group for phenylalkanoates and for **1** (2-hydroxyphenylketone), and H_3 and H_5 for **2** (4-hydroxyphenylketone).

also proposed for phenol and *p*-cresol from molecular mechanics, semiempirical methods, and circular dichroism (14).

The dependence of complex stability on the guest structure can provide information about the mode of inclusion. For instance, for a series of substrates containing the *trans*-cinnamoyl group (12), that have two potential binding sites, the phenyl and the side chain, binding constants around 1000 were interpreted as side chain inclusion.

The values for the binding constant determined in this work may indicate preferential aryl inclusion ($K_{ass} \approx 200$ M^{-1}) or alkyl inclusion ($K_{ass} \approx 1000$ M^{-1}). In the case of the complexes of other substituted phenols with β-CD (15), the relative hydrophobicity of the potential binding sites, determine which end of the guest molecules goes in. In the case of substrate **1** the fact that the OH is close to the hydrocarbon chain may be the reason why the predominance of complexes with the alkyl inside geometry takes place at a longer chain length than those for compounds **2**.

NMR determinations

The NMR (200 MHz) spectrum of compounds **1** and **2** were run in D_2O at the maximum possible concentration of the substrates which is 1.5 mM for **1** and **2** (n = 0) and 0.2 mM for all the other substrates. The CD concentration used was that required to have at least 70% of the substrate complexed, so the CD concentration was 2 mM for the substrates with K_{SCD} in the order of 1000, whereas for those with K_{SCD} in the order of 200, the CD concentration was 10 mM.

Table 2 shows some selected induced chemical shifts ($\Delta\delta$) which are those where the more significant changes were observed. Also included, for comparison, are the data for phenyl acetate, phenyl propionate, and phenyl valerate. The values obtained are in all cases small compared with data from the literature (16), so only limited information can be obtained from these data.

The reasons for the very small induced shifts observed in this study can be attributed to the low magnetic field of the available NMR instrument. An additional factor may be that the signals are the average of free and complexed substrates and the presence of mixed complexation modes (aryl and alkyl inclusion). Similar explanation was given to the small chemically induced shifts in the phenyl alkyl carboxylic acid series (n = 0 to 4) (11). For the later compounds it was demonstrated the formation of complexes with the phenyl group in and out the cavity.

The fact that for the compounds studied here the CIS are observed for the aryl as well as alkyl protons may indicate the presence in the solution of complexes with different geometries.

Experimental section

Reagents

The water was obtained from a Millipore apparatus. Compounds **1** and **2** were prepared or used as before (5,6). β-cyclodextrin (Roquete)was used as received.

Apparatus

The spectrophotometric determinations were carried out in a Shimadzu UV 260, controlling the temperature of the cell compartment at 25.0 ± 0.1°C with a Haake circulator. ^{1}H NMR spectra were recorded in a Bruker 200 FT instrument in D_2O solutions.

Acknowledgement

This research was supported in part by the Consejo Nacional de Investigaciones Cientificas y Técnicas (CONICET), Argentina, the Consejo Provincial de Investiagaciones Cientificas y Técnológicas (CONICOR), Córdoba, Argentina, the Secretaría de Ciencia y Tecnología de la Universidad Nacional de Córdoba (SECyT-UNC) and the Agencia Nacional de Promoción Científica y Tecnológica (FONCYT). We also wish to thank Ferromet for their donation of the β-cyclodextrin.

References

1. M.L. Bender and M. Komiyama. Cyclodextrin chemistry. Spinger–Verlag, Berlin. (1978); P. Bartolus, G. Kohler, and S. Monti. Coord. Chem. Rev. **125**, 261 (1993); D.F. Eaton. Tetrahedron, **43**, 1551 (1987).
2. R.H. de Rossi, M. Barra, and E.B. de Vargas. J. Org. Chem. **51**, 2157 (1986).

© 2000 NRC Canada

3. A.V. Veglia and R.H. de Rossi. J. Org. Chem. **53**, 5281 (1988); A.M. Sanchez, A.V. Veglia, and R.H. de Rossi. Can. J. Chem. **75**, 1151 (1997).
4. R.E. Galian, A.V. Veglia, and R.H. de Rossi. Analyst (Cambridge, UK), **123**, 1587 (1998).
5. R. Breslow and S.D. Dong. Chem. Rev. **98**, 1997 (1998).
6. A.V. Veglia, A.M. Sanchez, and R.H. de Rossi. J. Org. Chem. **55**, 4083 (1990).
7. A.V. Veglia and R.H. de Rossi. J. Org. Chem. **58**, 4941 (1991).
8. K.A. Connors. Binding constants. John Wiley & Sons, New York. 1987. p. 143.
9. A. Muñoz de la Peña, F. Salinas, I. Durán-Merás, and M.D. Moreno. Anal. Chem. **27**, 1893 (1994).
10. D.M. Davies, M.E. Deary, and D.I. Wealleans. J. Chem. Soc. Perkin Trans. 2, 193 (1998).
11. A. Grade, V. Rüdiger, H-J. Schneider, and K.A. Connors. J. Pharm. Sci. **86**, 236 (1997).
12. K.A. Connors. Chem. Rev. **97**, 1325 (1997).
13. J.L. Alderfer and A.V. Eliseev. J. Org. Chem. **62**, 8225 (1997).
14. G. Marconi, S. Monti, B. Mayer, and G. Köhler. J. Phys. Chem. **99**, 3943 (1995).
15. S. Divakar and M.M. Maheswaran. J. Incl. Phenom. Mol. Recognit. Chem. **27**, 113 (1997).
16. H-J. Schneider, F. Hacket, V. Rudiger, and H. Ikeda. Chem. Rev. **98**, 1755 (1998).

© 2000 NRC Canada

Medium-sized cyclophanes. part 51.[1] Acylation of [2.2]metaparacyclophanes: through-space electronic interactions between two benzene rings

Takehiko Yamato, Kiwamu Tokuhisa, and Hirohisa Tsuzuki

Abstract: The acylation of 8-methyl- (**1b**) and 8-methoxy[2.2]metaparacyclophane **1c** with 1.1 equiv. of acetyl chloride in CS_2 solution in the presence of aluminum chloride afforded 15-acetyl-8-methyl- (**2b**) and 12-acetyl-8-methoxy[2.2]metaparacyclophanes (**3c**) with 65 and 41% yields, respectively. The different orientations for the electrophilic substitution were observed to be dependant on the substituent at the 8 position. On the other hand, when the same reaction was carried out under the same reaction conditions with the corresponding 5-*tert*-butyl derivatives (**11**), *ipso*-acetylation at the *tert*-butyl group was observed along with acetylation on the *para*-benzene ring. The substituent effect on the 8-position was also observed in the present *ipso*-acetylation. The *ipso*-acylation at the *tert*-butyl group of 5-*tert*-butyl-8-methoxy[2.2]metaparacyclophane (**11c**) is attributed to the highly activated character of the aryl ring and the increased stabilization of a σ-complex intermediate arising from the dienone-type σ-complex intermediate possible in the case of a internal methoxy substituent. However, the present *ipso*-acetylation has not been observed in mild reaction conditions such as acetyl chloride in the presence of $TiCl_4$ catalyst due to deactivation of the second aromatic ring by the introduced acetyl group on the *para*-benzene ring. The mechanism of these novel reactions is also discussed.

Key words: cyclophanes, electrophilic aromatic substitution, regioselectivity, through-space electronic interaction, *ipso*-acylation.

Résumé : L'acylation des 8-méthyl- (**1b**) et 8-méthoxy[2.2]métaparacyclophanes (**1c**) avec 1,1 équivalents de chlorure d'acétyle, en solution dans le CS_2 et en présence de chlorure d'aluminium conduit aux 15-acétyl-8-méthyl- (**2b**) et 12-acétyl-8-méthoxy[2.2]métaparacyclophanes (**3c**) avec des rendements de 65 et 41% respectivement. La substitution électrophile se fait avec des orientations différentes suivant la nature du substituant en position 8. Par ailleurs, lorsqu'on a effectué la même réaction sur les dérivés 5-*tert*-butylés correspondants (**11**), on a observé une acétylation *ipso* au niveau du groupe *tert*-butyle en plus de l'acétylation sur le benzène en para. L'effet de substituant sur la position 8 a aussi été observée dans l'acétylation *ipso*. Cette acétylation *ipso* au niveau du groupe *tert*-butyle du 5-*tert*-butyl-8-méthoxy[2.2]métaparacyclophane (**11c**) est attribué au caractère fortement activé du noyau aromatique et à l'augmentation de la stabilisation d'un σ-complexe intermédiaire découlant d'un σ-complexe intermédiaire de type diénone qui peut se former dans le cas d'un substituant méthoxy en position interne. Toutefois, l'acétylation *ipso* n'a pas été observée dans les conditions douces, telles que celles impliquant le chlorure d'acétyle en présence d'un catalyseur comme le $TiCl_4$ en raison d'une désactivation du deuxième noyau aromatique par le groupe acétyle introduit sur le noyau benzénique para. On discute aussi du mécanisme de ces réactions nouvelles.

Mots clés : cyclophanes, substitution aromatique électrophile, régiosélectivité, interaction électronique à travers l'espace, acétylation *ipso*.

[Traduit par la Rédaction]

Received September 24, 1999.

T. Yamato[2] and K. Tokuhisa. Department of Applied Chemistry, Faculty of Science and Engineering, Saga University, Honjo-machi 1, Saga-shi, Saga 840–8502, Japan. **H. Tsuzuki.** Center of Environmental Analysis, Tohwa Institute for Science, Tohwa University, 1-1-1 Chikushigaoka, Minami-ku, Fukuoka-shi, Fukuoka 815–8510, Japan.

[1]Part 50. See Ref. 1.

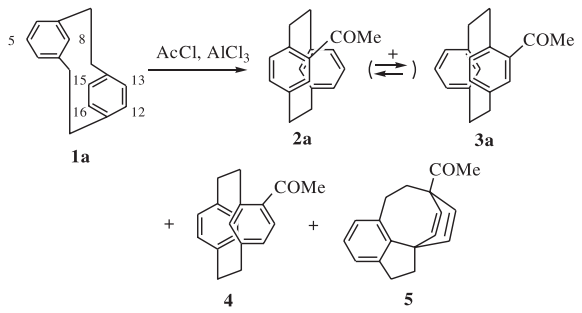
[2]Author to whom correspondence may be addressed. Telephone: (0952) 28-8679. Fax: (0952) 28-8591. e-mail: yamatot@cc.saga-u.ac.jp

Introduction

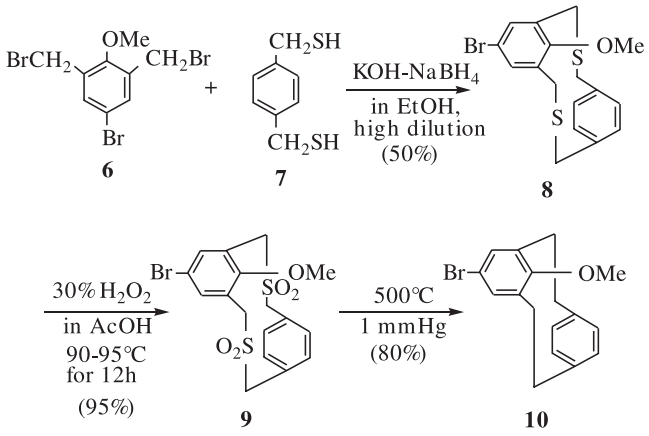
[2.2]MPCP (MPCP = metaparacyclophane) **1a** was first prepared by Cram et al. (2) via acid-catalyzed rearrangement of [2.2]paracyclophane. Later, **1a** became available owing to synthetic methods developed by other research groups (3). A versatile procedure, appropriate for the synthesis of substituted derivatives, makes use of 2,11-dithia[3.3]MPCP as a precursor (3*a*). The *meta*-bridged benzene ring of [2.2]MPCP **1a** has been shown to undergo conformational flipping (4) with a substantial energy barrier (ca. 20 kcal mol^{-1}). According to X-ray crystallographic studies of **1a** (5), the deformations of benzene rings are similar to those of the corresponding

© 2000 NRC Canada

Scheme 1.



Scheme 2.

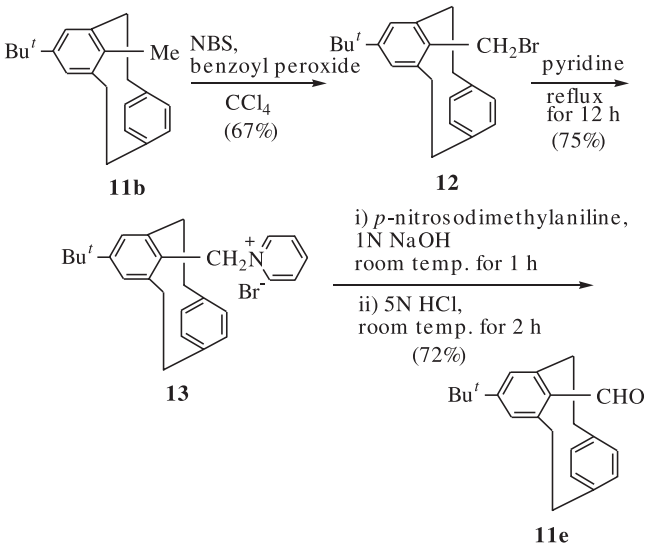


rings in *para*- and *meta*-[2.2]cyclophanes, with *para*- and *meta*-bridged rings bent in a boat- and a chair-like form, respectively. The angle between the two aromatic planes defined by the carbon atoms, 3, 4, 6, and 7, on one hand; and 12, 13, 15, and 16, on the other, is about 13°. It should be noted that the angle between the 11, 12, 16-plane and 10, 11-bond vector (or between 13, 14, 15-plane and 1, 14-bond vector) is even larger than the analogous angle in [2.2]paracyclophane. Introduction of substituents at the 8-position increases the strain in the molecule in comparison with unsubstituted [2.2]MPCP **1a**; the deformation of *para*-benzene ring of 8-methyl[2.2]MPCP was estimated to be 15° by our recent X-ray crystallography (6).

Cram and Hefelfinger reported (7) the acetylation of [2.2]MPCP **1a** with acetyl chloride in the presence of aluminum chloride to afford three kinds of monoacetylated derivatives **2a**, **3a**, and **4** along with the tetracyclic ketone **5**. However, since **2a** and **3a** equilibrate by ring rotation at room temperature, the orientation of acetylation to *para*-bridged benzene ring of **1a** has not yet been established.

Thus there is substantial interest in investigating the acetylation of 8-substituted [2.2]MPCPs, which might afford single mono-acetylated derivatives because the ring rotation of the meta-bridged benzene ring is impossible at room temperature. Also, in order to study the orientation of acetylation of *para*-bridged benzene ring in detail and the through-space electronic interactions between two benzene rings, we attempted to protect the 5-position of [2.2]-MPCPs by the bulky substituent, *tert*-butyl group. We report

Scheme 3.



here on the acylation of 5-*tert*-butyl 8-substituted [2.2]MPCPs.

Results and discussion

Synthesis of 8-substituted [2.2]MPCPs (1)

The preparation of 8-substituted [2.2]MPCPs (**1b** and **1c**) have already been described in an earlier paper (6) except 5-bromo-8-methoxy[2.2]MPCP (**10**). Preparation of **10** was carried out as shown in Scheme 2. The cyclization of 4-bromo-2,6-bis(bromomethyl)anisole (**6**) and 1,4-bis(mercaptomethyl)benzene (**7**) was carried out under highly diluted conditions in 10% ethanolic KOH in the presence of a small amount of $NaBH_4$, giving the desired 9-methoxy-2,11-dithia[3.3]MPCP (**8**) in 50% yield. Oxidation of **8** with 30% hydrogen peroxide in acetic acid, afforded the corresponding bissulfone **9** in 95% yield. Pyrolysis of **9** under reduced pressure (1 mm Hg (1 mm Hg = 133.322 Pa)) was carried out according to the reported method (8) to afford 8-methoxy[2.2]MPCP (**10**) in 80% yield.

Preparations of 5-*tert*-butyl-8-substituted [2.2]MPCPs (**11b**–**d**) were previously described (6). We have newly prepared 5-*tert*-butyl-8-substituted [2.2]MPCPs (**11e**–**g**) from 5-*tert*-butyl-8-methyl[2.2]MPCP (**11b**) as shown in Schemes 3 and 4.

Previously we reported (9) the conversion of 8-bromomethyl-16-methyl[2.2]metacyclophane to the corresponding 8-substituted 16-methyl derivatives in good yield. Thus, we have carried out the reaction of 5-*tert*-butyl-8-methyl[2.2]MPCP (**11b**) with *N*-bromosuccinimide in the presence of benzoyl peroxide in refluxing carbon tetrachloride; the desired 8-bromomethyl-5-*tert*-butyl[2.2]MPCP (**12**) was obtained in 67% yield. The reaction of 5-*tert*-butyl-8-(pyridiniomethyl)[2.2]MPCP bromide (**13**), which was easily prepared by the reaction of **12** with pyridine in 75% yield, with *p*-nitrosodimethylaniline was carried out at room temperature according to the Kröhnke's procedure (10) to give the corresponding nitrone in good yield. When the nitrone was treated with 5 N HCl solution at room temperature for

© 2000 NRC Canada

Table 1. Acetylation of 8-substituted [2.2]metaparacyclophanes **1** with acetyl chloride in the presence of aluminum chloride.[a]

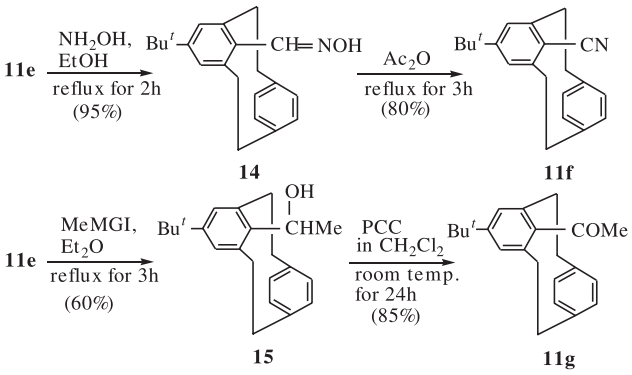
Run	Substrate	AcCl/**1** (mol/mol)	Recovery of **1**	Product (%)[b]
1	**1b**	1.1	30	**2b** (70) [65]
2	**1b**	3.1	0	**2b** (100) [87]
3	**1c**	1.1	5	**3c** (55) [41], **16c** (35) [23] **17c** (3) [+][c]
4	**1c**	3.1	0	**16c** (12) [5], **17c** (85) [65]

[a][$AlCl_3$]/[AcCl] = 1.5/1 (mol/mol).

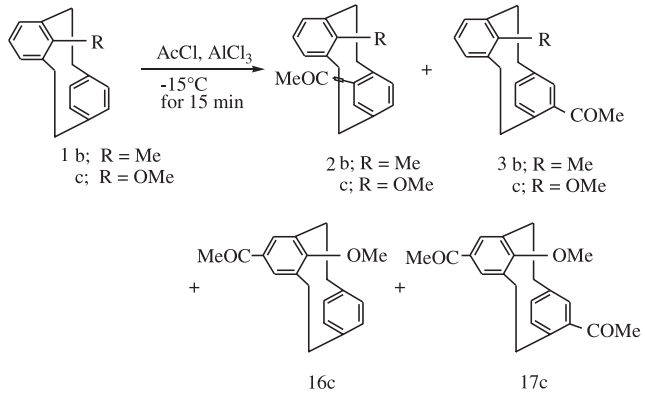
[b]Yields are determined by GLC. analysis. Isolated yields are shown in square bracket.

[c]Plus sign means that the yield of product was less than 1%.

Scheme 4.



Scheme 5.



2 h, the desired 5-*tert*-butyl-8-formyl[2.2]MPCP (**11e**) was obtained in 72% yield.

5-*tert*-Butyl-8-cyano[2.2]MPCP (**11f**) was obtained by the reaction of aldehyde **11e** with hydroxylamine followed by treatment of oxime **14** with boiling acetic anhydride in good yield. Reaction of aldehyde **11e** with methylmagnesium iodide afforded the corresponding alcohol **15** in 60% yield, which was converted to 8-acetyl-5-*tert*-butyl[2.2]MPCP **11g** in 85% yield by oxidation with PCC at room temperature for 24 h.

Acetylation of 8-substituted [2.2]MPCPs (1)

Acetylation of 8-methyl[2.2]MPCP (**1b**) with 1.1 equiv. of acetyl chloride in methylene dichloride solution in the presence of aluminum chloride afforded 15-acetyl substitution product **2b** in 65% yield along with starting compound. No acetyl substitution at the 12-position was observed. Same result was obtained in the case of 3 equiv. of acetyl chloride under the same reaction conditions to also afford 15-acetyl substitution product **2b** in 87% yield. In contrast, 8-methoxy derivative **1c** afforded a mixture of 12-acetyl substitution product **3c** and 5-acetyl derivative **16c** in 41 and 23% yield, respectively (Table 1). It was also found that the same tendency was observed in the diacetyl substitution in **1c** with 3 equiv. of acetyl chloride to give 5,12-diacetyl derivative **17c** in 65% yield.

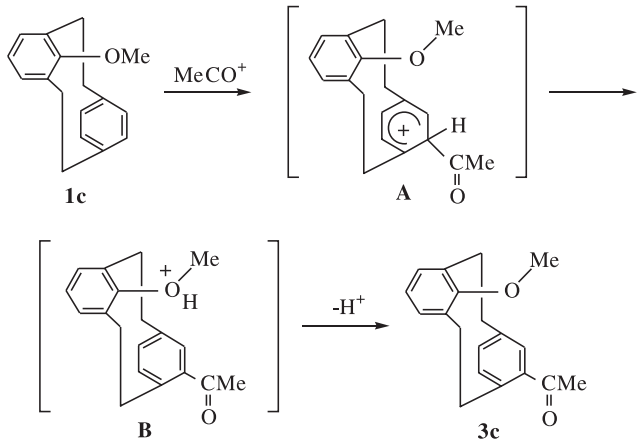
The structures of the products obtained in the present work were determined from their elemental analyses and spectral data. The ^1H NMR spectrum of **2b** in $CDCl_3$ shows a doublet (J = 2.0 Hz) at δ 6.44 for one aromatic C-16 proton, which is in a strongly shielding region of opposite meta-bridged benzene ring, and δ 7.11 and 7.16 for external aromatic C-13 and C-12 protons, respectively. On the other hand, the signals of two aromatic protons for C-15 and C-16 of **3c** were both observed at upper field of δ 5.96 and in turn the signals for external aromatic C-13 proton was deshielded at δ 7.62 by the neighbouring carbonyl group. These data strongly support the assignment of structure **2b** to 15-acetyl[2.2]MPCP and **3c** to 12-acetyl[2.2]MPCP.

Mechanism of acetylation

The different directive effects of 8-substituent to *para*-bridged benzene ring on the position of electrophilic substitution were first observed with these compounds. According to X-ray crystallographic studies of 8-methyl[2.2]MPCP (6), the 8-methyl group is located on the opposite *para*-bridged benzene ring which apparently sterically blocks electrophilic attack at 12,13-position. Therefore, internal attack of the electrophile on the *para*-bridged benzene ring of **1b** exclusively proceeds to give 15-acetyl derivative **2b**. On the other hand, with methoxy group at this position, acetylation occurs predominantly in the pseudo-geminal position in spite of the above steric hindrence. This pseudo-geminal directing effect of methoxy group might be attributed to the basicity and geometric availavility of the oxygen of the methoxy group. The oxygen is probably the strongest base in the medium. In the rate- and product-controlling step, the oxygen accepts a proton from the pseudo-geminal σ-complex (**A**) to form intermediate (**B**), and thus producing a pseudo-geminal substituted product **3c** as shown in Scheme 6. This result is consistent with Cram's reports (7, 11) that acetyl and nitro groups in the position of the [2.2]paracyclophane nucleous directed acetyl substitution to occur nearly exclusively in the 12-position to give the pseudo-geminal disubstituted hydrocarbon.

© 2000 NRC Canada

Scheme 6.



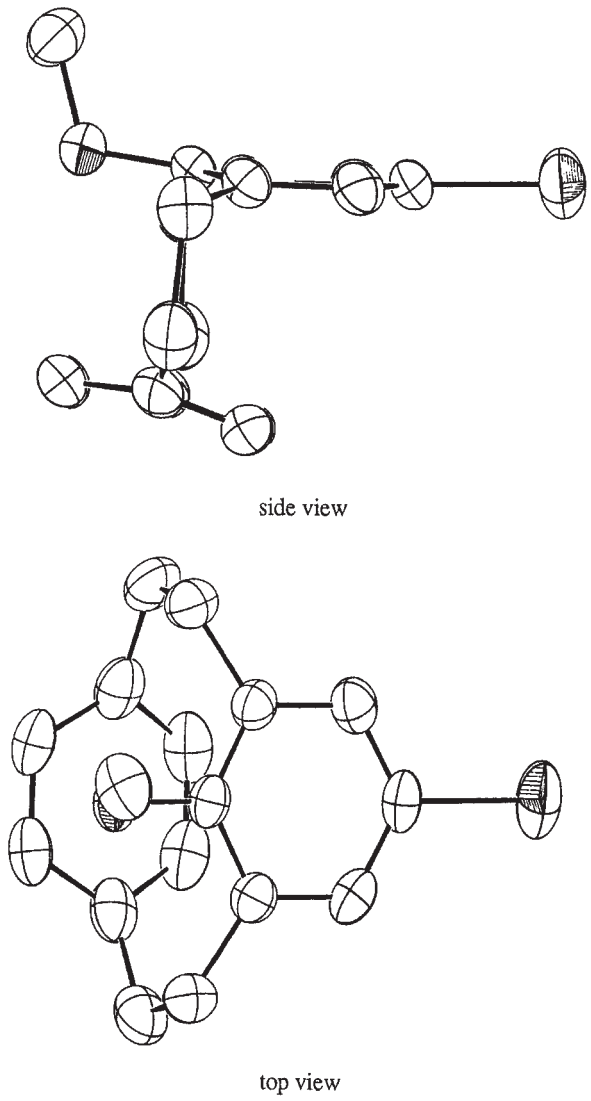
To confirm the present explanation of the regioselectivity on the acetylation of 8-substituted [2.2]MPCPs, we attempted to measure the X-ray analyses of [2.2]MPCPs. Fortunately, we have succeeded the single-crystal X-ray diffraction of 5-bromo-8-methoxy[2.2]MPCP (**10**).

Single colorless crystals of 5-bromo-8-methoxy[2.2]MPCP (**10**) suitable for X-ray crystallography were available by recrystallization from methanol. The perspective ORTEP drawing of **10** is illustrated in Fig. 1 with the atom numbering system. Compound **10** crystallized in the monoclinic space group $P2_1/a$. (No. 14). Two aromatic rings, which include the plane defined by the carbons, 3, 4, 6, and 7 and 11, 14, 15, and 16, tilt with a dihedral angle of about 12° and the strained form of the rings greatly differ with each other. The *meta*-benzene ring distorts like a boat shape and the carbons, 5 and 8, are out of the plane defined by the carbons, 3, 4, 6, and 7; the dihedral angle between the plane defined by the carbons, 3, 4, 6, and 7 and 3, 7, and 8 is about 11°. This value is much larger than the angle (about 5°) between the plane defined by the carbons, 3, 4, 6, and 7 and 4, 5, and 6. On the other hand, the *para*-benzene ring deforms like a roof shape and the dihedral angle between the plane defined by the carbons, 11, 12, 13, and 14, and 11, 14, 15, and 16, are about 16° which is closely similar to that in 8-methyl[2.2]MPCP (6). The oxygen, 1 is located just above the carbons, 12 and 13 and the intramolecular distance of the oxygen, 1 and the plane defined by the carbons, 11, 12, 13, and 14 is about 2.8 Å. Thus, according to X-ray crystallographic studies of **10**, the 8-methoxy group is located on the opposite *para*-bridged benzene ring which might assist in accepting a proton from the pseudo-geminal σ-complex (**A**) to form intermediate (**B**), thus electrophilic attack at the 12-position might preferentially occur.

Acylation of 5-*tert*-butyl-8-substituted [2.2]MPCPs (11)

In order to study this acetylation reaction more detail, we attempted to protect the 5-position of 8-substituted [2.2]MPCPs by the bulky substituent, *tert*-butyl group. The acetylation of 5-*tert*-butyl-8-methyl[2.2]MPCP (**11b**) with 1.2 equiv. of acetyl chloride in CS_2 solution in the presence of aluminum chloride afforded 15-acetyl-5-*tert*-butyl-8-methyl[2.2]MPCP (**18b**) in 86% yield along with trace amount of diacetylation product, 5,15-diacetyl-8-methyl[2.2]MPCP (**20**). Similarly,

Fig 1. Ortep drawing of 5-bromo-8-methoxy[2.2]meta-paracyclophane **10**. Thermal ellipsoids are drawn at the 50% probability level. All hydrogen atoms are omitted for clarify.



the reaction of 8-bromo derivative **11d** with acetyl chloride gave exclusively the corresponding 15-acetyl[2.2]MPCP (**18d**) in 61% yield. In contrast, when 5-*tert*-butyl-8-methoxy[2.2]MPCP (**11c**) was treated under the same reaction conditions, 12-acetyl-5-*tert*-butyl-8-methoxy[2.2]MPCP (**19c**) was obtained in 70% yield along with diacetylated prduct **17c** arising from the *ipso*-acetylation on the *tert*-butyl group at the 5-position (12,13).

The different orientation for the electrophilic substitution was observed depending on the substituent at 8 position. In contrast, the reaction of **11e**–**11g**, having electron-withdrawing groups such as formyl, cyano, and acetyl at the 8 position, did not afford any reaction product, and **11e**–**11g** were recovered in quantitative yield. It seems to assume that when R (in **11**) is electron donating, the σ-complex intermediate during the acetylation on the *para*-benzene ring could be stabilized by the through-space electronic interaction. In contrast, when R is electron-attracting groups such as CHO, CN, and Ac (e.g., in **11e**–**11g**), the σ-complex intermediate

© 2000 NRC Canada

Table 2. Acetylation of 5-*tert*-butyl[2.2]metaparacyclophanes **11** with acetyl chloride in the presence of aluminum chloride.[a]

Run	Substrate	R	Product (%)[b] **18**	**19**	Recovd.**11**
1	**11b**	Me	90 (86)[c,d]	0	6
2	**11c**	OMe	0	80 (70)[c,e]	5
3	**11d**	Br	80 (61)[c]	0	20
4	**11e**	CHO	0	0	100
5	**11f**	CN	0	0	100
6	**11g**	Ac	0	0	100

[a][AcCl]/**11** = 1.2/1 (mol/mol), [$AlCl_3$]/[AcCl] = 1.5/1 (mol/mol).

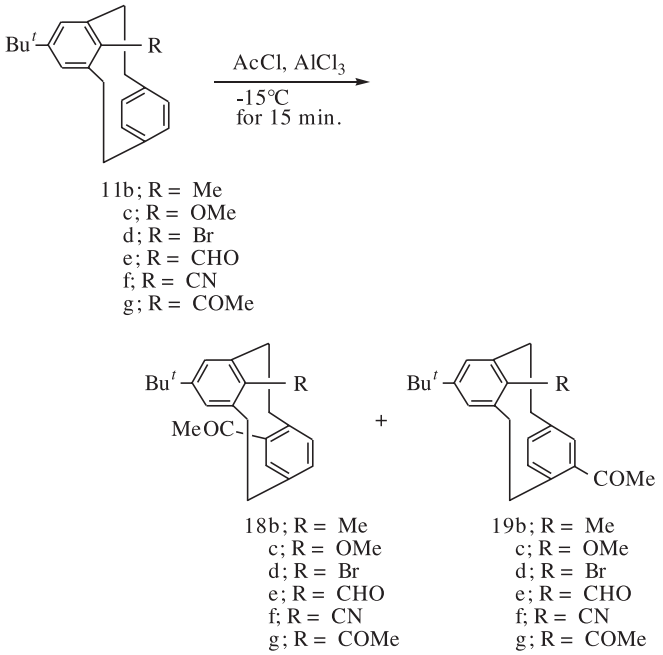
[b]Yields are determined by GLC analysis.

[c]Isolated yields are shown in parentheses.

[d]Trace amount of diacetylation product, 5,15-diacetyl-8-methyl[2.2]metaparacyclophane **20** was obtained.

[e]Diacetyl compound **17c** was obtained in 15% yield.

Scheme 7.

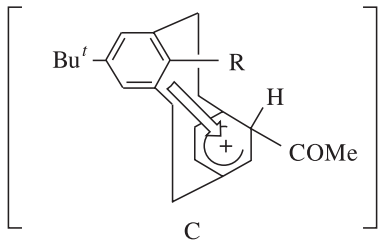


does not form because of deactivation of the *para*-benzene ring by these groups due to the through-space electronic interaction (13).

The acetylation of 5-*tert*-butyl-8-methoxy[2.2]MPCP (**11c**) with large excess (8.0 equiv.) of acetyl chloride in methylene dichloride solution in the presence of $AlCl_3$-$MeNO_2$ afforded diacetylated product **17c** in 85% yield arising from the *ipso*-acetylation on the *tert*-butyl group as well as the acetylation at 12-position of *para*-benzene ring. From the navigation of the reaction, it is clear that the the latter reaction was much faster than the former *ipso*-acetylation on the *tert*-butyl group since no formation of 5-acetyl-8-methoxy[2.2]MPCP (**16c**) has been observed under the reaction conditions used. It was also found that the *ipso*-acylation was completed within 30 minutes.

The *ipso*-acylation at the *tert*-butyl groups of 5-*tert*-butyl-8-methoxy[2.2]MPCP (**11c**) is attributed to the highly activated character of the aryl ring and the increased stabilization of a σ-complex intermediate arising from the dienone-type

Fig. 2. Through-space electronic interaction.



σ-complex intermediate possible in the case of an internally methoxy substituent (13). However, the present *ipso*-acetylation has not been observed in the mild reaction conditions such as acetyl chloride in the presence of $TiCl_4$ catalyst because of deactivation of the second aromatic ring by the introduced acetyl group on the *para*-benzene ring.

Similarly, acylation of **11c** with propionyl chloride and benzoyl chloride in the presence of $AlCl_3$-$MeNO_2$ led to the *ipso*-acylation at the *tert*-butyl group to give 5,12-diacyl-8-methoxy[2.2]MPCPs (**17h–i**) in quantitative yield, but longer reaction times (4 h) are required in the case of benzoylation. In contrast, in spite of prolonged reaction times and increased amounts of catalyst, the diacetylated compound **17j** was not obtained in the case of succinic anhydride, only the mono acylation product **19j** being obtained in quantitative yield.

In the MPCP system an initial σ-complex intermediate during the acetylation on the *para*-benzene ring would be stabilized by a through-space electronic interaction with the opposing *meta*-benzene ring, thus accelerating the reaction. However, in turn when *tert*-butyl group at 5-position is *ipso*-acylated, the deactivation of the second aromatic ring by the acyl group increased (13, 14).

Owing to electronic interaction between the two benzene rings and the considerable strain energy, [2.2]MPCP is prone to give isomerization and transannular cyclization reaction products under electrophilic reaction conditions (15). In fact, by treatment with $AlCl_3$-$MeNO_2$ in benzene 5-*tert*-butyl-8-methoxy[2.2]MPCP (**11c**) was isomerized to the strainless 5-*tert*-butyl-8-methoxy[2.2]metacyclophane (**21**) and then converted into the tetrahydropyrene **22**. This novel isomerization reaction might attributed to the methoxy group at the 8-position, which increase the strain in the molecule in

© 2000 NRC Canada

Table 3. Acylation of 5-*tert*-butyl-8-methoxy[2.2]metaparacyclophane **11c** with acylation reagents in the presence of Lewis acid.[a]

Run	Reagent	Reagent/**11c** (mol/mol)	Lewis acid[b]	Time (h)	Product (%)[c,d]
1	MeCOCl	8.0	A	0.5	**19c** (100) [85]
2	MeCOCl	8.0	B	0.5	**17c** (100) [90]
3	EtCOCl	8.0	B	0.5	**19h** (4), **17h** (96) [75]
4	PhCOCl	4.0	A	0.5	**19i** (100) [90]
5	PhCOCl	4.0	B	0.5	**19i** (60) **17i** (40)
6	PhCOCl	4.0	B	3.0	**19i** (15), **17i** (85) [70]
7	Succinic anhydride	1.2	B	2.0	**19j** (100) [90]
8	Succinic anhydride	4.0	B	2.0	**19j** (100) [87]

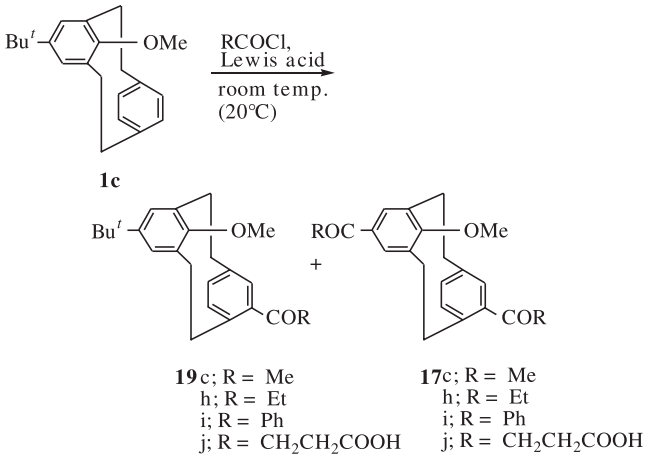
[a]The reaction temperature was 20°C.

[b]A = $TiCl_4$; B = $AlCl_3$-$MeNO_2$. [Lewis acid][Acylation reagent] = 1.5/1 (mol/mol).

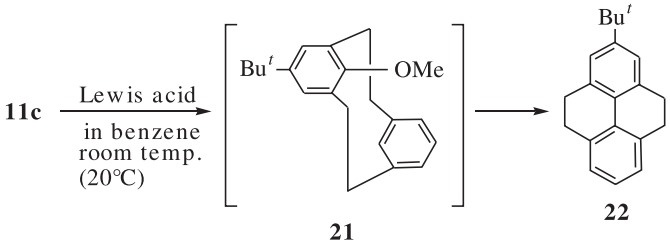
[c]Yields are determined by GLC analysis.

[d]Isolated yields are shown in square brackets.

Scheme 8.



Scheme 9.



comparison with the unsubstituted [2.2]MPCP **1a**. Therefore, the present acetylation in the system might compete with the transannular cyclization reaction to afford **22**.

However, under the present acylation conditions of 5-*tert*-butyl-8-methoxy[2.2]MPCP (**11c**), no formation of the isomerization and transannular cyclization reaction products has been observed. Only diacetylation product was obtained. This result strongly suggests that the acetylation at 12-position of *para*-benzene ring might occur much faster than the isomerization and transannular cyclization reaction to tetrahydropyrene. Thus acetylation product at *para*-benzene ring might deactivate the transannular cyclization reaction by the introduced acetyl group.

In conclusion, the different directive effects of 8-substituents on the *para*-bridged benzene ring on the position of electrophilic substitution were first observed with 8-substituted [2.2]MPCP derivatives. The presently developed procedure was further applied to the direct removal of a *tert*-butyl group by electrophilic substitution of 5-*tert*-butyl-8-methoxy[2.2]MPCP (**11c**) which are prone to give transannular reaction products under the electrophilic reaction conditions. The selective *ipso*-acylation of 5-*tert*-butyl-8-methoxy[2.2]MPCP (**11c**) can be attributed to the highly activated character of the aryl ring and the increased stabilization of the σ-complex intermediate arising from a dienone-type σ-complex intermediate possible in the case of a methoxy substituent. Further studies on the electrophilic substitution of 8-substituted [2.2]MPCPs **1** and **11** are now in progress.

Experimental

All melting points (Yanagimoto MP-S1) were uncorrected. Proton nuclear magnetic resonance (^{1}H NMR) spectra were recorded on a Nippon Denshi JEOL FT-270 spectrometer. Chemical shifts are reported as δ values (ppm) relative to internal Me_4Si. Mass spectra were obtained on a Nippon Denshi JMS-01SG-2 mass spectrometer at an ionization energy of 70 eV; *m*/*z* values reported include the parent ion peak. Infrared (IR) spectra were obtained on a Nippon Denshi JIR-AQ2OM spectrophotometer as KBr disks. Elemental analyses were performed by Yanaco MT-5. G.L.C. analyses were performed by Shimadzu gas chromatograph, GC-14A; Silicone OV-1, 2 m; programmed temperature rise, 12°C/min; carrier gas nitrogen, 25 mL/min.

Materials

2,6-Bis(bromomethyl)-4-bromoanisole (**6**) and 1,4-bis(mercaptomethyl)benzene (**7**) were prepared according the reported procedure (9). Preparations of 8-substituted [2.2]MPCPs (**1b**, **c**) and 5-*tert*-butyl-8-substituted [2.2]MPCPs (**11b**–**d**) were previously described (6).

© 2000 NRC Canada

*Preparation of 6-bromo-9-methoxydithia[3.3]metaparacyclophane (**8**)*: A solution of 2,6-bis(bromomethyl)-4-bromoanisole (**6**) (8.58 g, 23 mmol) and 1,4-bis(mercaptomethyl)benzene (**7**) (3.91 g, 23 mmol) in benzene (50 mL) and ethanol (50 mL) was added dropwise from a Hershberg funnel with stirring under nitrogen to a solution of potassium hydroxide (4.2 g, 28 mmol) and sodium borohydride (1.0 g, 26.4 mmol) in ethanol (4 L). When addition was complete (24 h), the reaction mixture was concentrated and the residue was extracted with CH_2Cl_2 (200 mL × 3). The combined extracts were washed with water, dried over Na_2SO_4 and concentrated. The residue was chromatographed over silica gel (Wako, C-300; 300 g) with benzene:hexane (1:1) as eluent to give a colorless solid. Recrystallization from hexane afforded 6-bromo-9-methoxy-2,11-dithia[3.3]metaparacyclophane (**8**) (4.4 g, 50%) as colorless prisms (hexane); mp 190–192°C; IR (KBr) ν_{max}: 2949, 2920, 1426, 1250, 1104, 1091 cm^{-1}; ^1H NMR ($CDCl_3$) δ: 3.30 (2H, d, *J* = 15.6), 3.32 (3H, s), 3.65 (2H, d, *J* = 15.6), 3.72 (2H, d, *J* = 13.2), 3.85 (2H, d, *J* = 13.2), 6.58 (2H, d, *J* = 1.0), 6.97 (2H, d, *J* = 1.0), 7.29 (2H, s); MS *m*/*z*: M^+ 380, 382. Anal. calcd. for $C_{17}H_{17}BrOS_2$: C 53.54, H 4.49; found: C 53.26, H 4.32.

*Preparation of 6-bromo-9-methoxy-2,11-dithia[3.3]metaparacyclophane-2,2,11,11-tetraoxide (**9**)*: A mixture of **8** (3.5 g, 9.19 mmol), 30% hydrogen peroxide (7.5 mL), and glacial acetic acid (54 mL) was heated at 85–90°C for 12 h. The reaction mixture was poured into a cold solution of sodium hydroxide (10 g) in water (140 mL) and the resulting paste was allowed to cool to room temperature. The prepicitate was filtered off and washed with water and a small amount of ethanol to afford 9-methoxy-2,11-dithia[3.3]metaparacyclophane-2,2,11,11-tetraoxide (**9**) (3.9 g, 95%) as colorless prisms; mp 135–137°C; ^1H NMR ($CDCl_3$-DMSO-d_6): 3.34 (3H, s), 3.80 (2H, d, *J* = 15.1), 4.34 (2H, d, *J* = 13.7), 4.43 (2H, d, *J* = 15.1), 4.50 (2H, d, *J* = 13.7), 6.83 (2H, d, *J* = 1.0), 7.23 (2H, d, *J* = 1.0) and 7.79 (2H, s); MS *m*/*z*: M^+ 444, 446. Anal. calcd. for $C_{17}H_{17}BrO_5S_2$: C 45.85, H 3.85; found: C 45.65, H 3.90.

*Pyrolysis of disulfone **9** to give 5-bromo-8-methoxy[2.2]metaparacyclophane (**10**)*: Pyrolysis of disulfone **9** was carried out in an apparatus consisting of a horizontal tube (15 mm in diameter) passing through two adjacent tube furnace, each of which 20 cm long. The first furnace provided a temperature that would induce sublimation of the sulfone; the second was used at a higher temperature (500°C) that would assure pyrolysis. A vacuum pump was connected at the exit from the second furnace. Disulfone **9** (1 g, 2.25 mmol) was pyrolyzed at 500°C under reduced pressure (1 mm Hg) in the above apparatus as follows. The sample of disulfone was placed in the first furnace and small glass beads were packed into the second furnace. The product which sublimed was collected and chromatographed on silica gel with hexane to yield the desired [2.2]metaparacyclophane. Recrystallization from methanol afforded 5-bromo-8-methoxy[2.2]metaparacyclophane (**10**) (571 mg, 80%) as colorless prisms; mp 144–146°C; ^1H NMR ($CDCl_3$) δ: 2.33–2.51 (4H, m), 2.66–2.76 (2H, m), 3.13 (3H, s), 3.13–3.19 (2H, m), 5.98 (2H, d, *J* = 2.0), 6.88 (2H, s) and 7.07 (2H, d, *J* = 2.0); MS *m*/*z*: M^+ 316, 318. Anal. calcd. for $C_{17}H_{17}BrO$: C 64.37, H 5.4; found: C 64.45, H 5.51.

*Preparation of 8-bromomethyl-5-*tert*-butyl[2.2]metaparacyclophane (**12**)*: After a mixture of **11b** (3.03 g, 9.55 mmol), *N*-bromosuccinimide (2.32 g, 13.06 mmol), and benzoyl peroxide (100 mg) in carbon tetrachloride (150 mL) was refluxed for 7 h, the formed precipitates were filtered off. The filtrate was washed with 10% sodium hydroxide and water. The organic layer was dried over sodium sulfate and evaporated in vacuo to leave the colorless solid which was recrystallized from hexane to give **12** (2.30 g, 67%) as colorless prisms; mp 163–164°C; IR (KBr) ν_{max}: 2970, 2920, 2850, 1580, 1550, 1500, 1470, 1455, 1440, 1355, 1320, 1220, 1190, 1180, 1105, 995, 935, 875, 815, 800 cm^{-1}; ^1H NMR ($CDCl_3$) δ: 1.32 (9H, s), 2.65–2.82 (6H, m), 3.16–3.20 (2H, m), 4.23 (2H, s), 5.77 (2H, d, *J* = 1.2), 6.81 (2H, s), 6.96 (2H, d, *J* = 1.2); MS *m*/*z*: M^+ 355, 357. Anal. calcd. for $C_{21}H_{25}Br$: C 70.59, H 7.05; found: C 70.69, H 7.11.

*Preparation of 5-*tert*-butyl-8-(pyridiniomethyl)[2.2]metaparacyclophane bromide (**13**)*: A mixture of 8-bromomethyl-5-*tert*-butyl[2.2]- metaparacyclophane (**12**) (250 mg, 0.70 mmol) and pyridine (10 mL) was boiled under reflux for 12 h. After the reaction mixture had cooled, hexane (10 mL) was added to give a solid which was washed with hexane to give the salt **13** (230 mg, 75%) as colorless prisms; mp 269–273°C; ^1H NMR ($CDCl_3$) δ: 1.33 (9H, s), 2.63–3.46 (8H, m), 5.80 (2H, s), 5.81 (2H, s), 6.95 (2H, s), 7.54 (2H, s), 7.85 (2H, dd, *J* = 6.0, 8.0), 8.24 (1H, dd, *J* = 8.0, 1.0), 8.94 (2H, dd, *J* = 6.0, 1.0); MS *m*/*z*: M^+ 435, 437. Anal. calcd. for $C_{26}H_{30}BrN$: C 71.55, H 6.93, N 3.21; found: C 71.30, H 6.88, N 3.22.

*Preparation of 5-*tert*-butyl-8-formyl[2.2]metaparacyclophane (**11e**)*: To a magnetically stirred solution of **13** (900 mg, 2.06 mmol) and *p*-nitrosodimethylaniline (342 mg, 2.28 mmol) in ethanol (25 mL) was added aqueous sodium hydroxide solution (900 mg in 2 mL water) at room temperature. After 5 min, the green solution turned to pale yellow solid precipitate. To the stirred reaction mixture was then added 10% aqueous HCl (20 mL) at room temperature. After a few min, the pale yellow suspension turned to reddish brown and a pale yellow solid precipitated. The reaction mixture was extracted with methylene dichloride; the extract was dried (Na_2SO_4) and evaporated under reduced pressure to leave a residue which was purified by column chromatography (silica gel) with hexane:benzene (1:1) as eluent to afford the colorless solid which was recrystallized from hexane to give aldehyde **11e** (430 mg, 72%) as colorless prisms; mp 102–104°C; IR (KBr) ν_{max}: 1650 (C = O) cm^{-1}; ^1H NMR ($CDCl_3$) δ: 1.32 (9H, s), 2.53–3.58 (8H, m), 5.80 (2H, d, *J* = 1.2), 6.80 (2H, s), 7.03 (2H, d, *J* = 1.2), 9.75 (1H, s); MS *m*/*z*: M^+ 292. Anal. calcd. for $C_{21}H_{24}O$: C 86.26, H 8.27; found: C 86.31, H 8.38.

*Reaction of **11e** with hydroxylamine — preparation of **14***: A mixture of **11e** (200 mg, 0.685 mmol), hydroxylamine (111.2 mg, 1.60 mmol), sodium hydroxide (64 mg, 1.60 mmol) and ethanol (20 mL) was refluxed for 2 h. After the reaction mixture was cooled, the solvent was removed in vacuo to leave the residue, which was washed with water and recrystallized from ethanol to give **14** (200 mg, 95%) as colorless prisms; mp 178–180°C; IR (KBr) ν_{max}: 3240, 2952, 1593, 1478, 1380, 1221, 956, 944, 888 cm^{-1}; ^1H NMR

© 2000 NRC Canada

($CDCl_3$) δ: 1.34 (9H, s), 2.57–2.70 (4H, m), 3.00–3.20 (4H, m), 5.80 (2H, d, *J* = 2.0), 6.83 (2H, s), 7.04 (2H, d, *J* = 2.0) and 8.03 (1H, s); MS *m/z*: M^+ 307. Anal. calcd. for $C_{21}H_{25}NO$: C 82.04, H 8.2, N 4.56; found: C 81.90, H 8.10, N 4.43.

*Preparation of 5-*tert*-butyl-8-cyano[2.2]metaparacyclophane (**11f**)*: A suspension of **14** (100 mg, 0.325 mmol) in acetic anhydride (10 mL) was refluxed for 3h. On cooling, the reaction mixture was poured into a large amount of water (100 mL), stirred for over night and extracted with methylene dichloride. The extract was washed with water (50 mL × 2), dried with Na_2SO_4, and evaporated in vacuo to leave a residue, which was recrystallized from hexane to give **11f** (75.1 mg, 80%) as colorless prisms; mp 119–121°C; IR (KBr) ν_{max}: 2208 (CN) cm^{-1}; ^1H NMR ($CDCl_3$) δ: 1.32 (9H, s), 2.55–2.65 (2H, m), 2.76–2.95 (4H, m), 3.26–3.35 (2H, m), 5.71 (2H, d, *J* = 2.0), 6.92 (2H, s), 7.33 (2H, d, *J* = 2.0); MS *m/z*: M^+ 289. Anal. calcd. for $C_{21}H_{23}N$: C 87.15, H 8.01, N 4.84; found: C 86.9, H 8.05, N 5.03.

*Reaction of **11e** with methylmagnesium iodide*: To a solution of MeMgI (prepared from methyl iodide (1.70 g, 12 mmol) and magnesium (243 mg, 10 mmol)) in ether (16 mL) was added a solution of **11e** (584 mg, 2 mmol) in ether (10 mL) dropwise under the conditions of gentle refluxing. After the reaction mixture was refluxed for an additional 3 h, it was quenched with 10% ammonium chloride and extracted with methylene dichloride (2 × 50 mL). The methylene dichloride extract was dried over Na_2SO_4 and evaporated in vacuo to leave the residue, which was which was chromatographed on silica gel with hexane:benzene (1:1) to afford a colourless solid. Recrystallization from hexane gave **15** (370 mg, 60%) as colorless prisms; mp 109°C; IR (KBr) ν_{max}: 3550, 2960, 2950, 2860, 1210, 1120, 1065, 790, 725 cm^{-1}; ^1H NMR ($CDCl_3$) δ: 0.93 (3H, d, *J* = 6.4), 1.31 (9H, s), 2.57–2.73 (5H, m), 3.10–3.18 (2H, m), 3.57–3.64 (1H, m), 4.69 (1H, d, *J* = 6.4), 5.80 (2H, s), 6.72 (2H, s), 7.05 (2H, s); MS *m/z*: M^+ 308. Anal. calcd. for $C_{22}H_{28}O$: C 85.66, H 9.15; found: C 85.46, H 9.35.

*Preparation of 8-acetyl-5-*tert*-butyl[2.2]metaparacyclophane (**11g**)*: To a suspension of $C_5H_5NH^+CrO_3Cl^-$ (2.30 g, 10.67 mmol) and CH_2Cl_2 (20 mL) was added a solution of **15** (1.0 g, 3.24 mmol) in CH_2Cl_2 (5 mL) at 0°C. The reaction mixture had been stirred at room temperature for 24 h. The reaction mixture was filtered and the filtrate was extracted with CH_2Cl_2 (30 mL × 3). The extract was dried over Na_2SO_4 and concentrated. The residue was subjected to silica-gel (Wako, C–300; 100 g) column chromatography using as eluent benzene to give the title compound **11g** (843 mg, 85%) as colorless prisms (hexane); mp 148–150°C; IR (KBr) ν_{max}: 1683 (C=O) cm^{-1}; ^1H NMR ($CDCl_3$) δ: 1.34 (9H, s), 1.97 (3H, s), 2.54–2.76 (6H, m), 3.20–3.29 (2H, m), 5.71 (2H, d, *J* = 1.2), 6.86 (2H, s) and 7.07 (2H, d, *J* = 1.2); MS *m/z*: M^+ 306. Anal. calcd. for $C_{22}H_{26}O$: C 86.23, H 8.55; found: C 86.36, H 8.45.

*Acetylation of **1** with acetyl chloride in the presence of aluminum chloride — typical procedure*: To a solution of **1c** (238 mg, 1 mmol) in CS_2 (12 mL) was added a solution of aluminum chloride (300 mg, 2.3 mmol) and acetyl chloride (94.2 mg, 1.2 mmol) in CS_2 (6 mL) at –15°C. After the reaction mixture was stirred at –15°C for 15 min, it was poured into a large amount of water. The organic layer was extracted with methylene dichloride. The extract was washed with 10% hydrochloric acid and water, dried with Na_2SO_4, and evaporated in vacuo to leave a residue, which was chromatographed on silica gel with benzene to give **3c** (114 mg, 41%) and **16c** (63 mg, 23%) as a colourless solid, respectively.

*12-Acetyl-8-methoxy[2.2]metaparacyclophane (**3c**)*: Colorless prisms (hexane); mp 162–163°C; IR (KBr) ν_{max}: 2965, 2932, 2820, 1671, 1461, 1436, 1428, 1352, 1286, 1255, 1235, 1206, 1171, 1018, 774 cm^{-1}; ^1H NMR ($CDCl_3$) δ: 2.66 (3H, s), 2.43–4.17 (8H, m), 3.13 (3H, s), 5.96 (2H, d, *J* = 2.4), 6.79 (3H, m), 7.62 (1H, s); MS *m/z*: M^+ 280. Anal. calcd. for $C_{19}H_{20}O_2$: C 81.40, H 7.19; found: C 81.73, H 7.17.

*5-Acetyl-8-methoxy[2.2]metaparacyclophane (**16c**)*: Colorless prisms (hexane); mp 140°C; IR (KBr) ν_{max}: 2923, 1666, 1588, 1412, 1358, 1286, 1200, 1184, 1155, 1013, 805, 727 cm^{-1}; ^1H NMR ($CDCl_3$) δ: 2.56 (3H, s), 2.49–3.19 (8H, m), 3.18 (3H, s), 5.81 (2H, d, *J* = 1.0), 7.09 (2H, d, *J* = 1.0), 7.39 (2H, s); MS *m/z*: M^+ 280. Anal. calcd. for $C_{19}H_{20}O_2$: C 81.40, H 7.19; found: C 81.57, H 7.16.

Reaction of **1b** with acetyl chloride in CS_2 was carried out using the same procedure as described above and details of the products and yields are compiled in Table 1.

*15-Acetyl-8-methyl[2.2]metaparacyclophane (**2b**)*: Colorless prisms (hexane); mp 133–135°C; IR (KBr) ν_{max}: 3045, 3000, 2970, 2922, 2853, 1669, 1555, 1478, 1456, 1444, 1436, 1350, 1257, 1197, 1170, 953, 776, 737, 722, 609 cm^{-1}; ^1H NMR ($CDCl_3$) δ: 1.76 (3H, s), 2.25 (3H, s), 2.64–4.00 (8H, m), 6.44 (1H, d, *J* = 2.0), 6.58 (1H, dd, *J* = 7.0, 2.0), 6.74 (1H, dd, *J* = 7.0, 2.0), 6.81 (1H, t, *J* = 7.0), 7.11 (1H, d, *J* = 7.3), 7.16 (1H, dd, *J* = 7.3, 2.0); MS *m/z*: M^+ 264. Anal. calcd. for $C_{19}H_{20}O$: C 86.32, H 7.63; found: C 85.90, H 7.61.

*5,12-Diacetyl-8-methoxy[2.2]metaparacyclophane (**17c**)*: Colorless prisms (ethanol); mp 142–143°C; IR (KBr) ν_{max}: 2926, 1669, 1355, 1289, 1257, 1197, 1160, 1015 cm^{-1}; ^1H NMR ($CDCl_3$) δ 2.57 (3H, s), 2.65 (3H, s), 2.37–3.28 (7H, m), 3.18 (3H, s), 4.16–4.27 (1H, m), 5.94 (2H, d, *J* = 2.0), 7.40 (1H, d, *J* = 2.4), 7.43 (1H, d, *J* = 2.4), 7.63 (1H, s); MS *m/z*: M^+ 322. Anal. calcd. for $C_{21}H_{22}O_3$: C 78.2, H 6.87; found: C 78.45, H 7.12.

*Acetylation of **11** with acetyl chloride in the presence of aluminum chloride — typical procedure*: To a solution of **11b** (278 mg, 1 mmol) in CS_2 (12 mL) was added a solution of aluminum chloride (300 mg, 2.3 mmol) and acetyl chloride (94.2 mg, 1.2 mmol) in CS_2 (6 mL) at –15°C. After the reaction mixture was stirred at –15°C for 15 min, the reaction mixture was treated as described above to give **18b** (275 mg, 86%) and trace amount of diacetylated product **20**.

*15-Acetyl-5-*tert*-butyl-8-methyl[2.2]metaparacyclophane (**18b**)*: Colorless prisms (hexane); mp 96–97°C; IR (KBr) ν_{max}: 2963, 2952, 2923, 1672, 1479, 1360, 1255, 1198, 880, 732, 620, 611 cm^{-1}; ^1H NMR ($CDCl_3$) δ: 1.17 (9H, s), 1.65

© 2000 NRC Canada

(3H, s), 2.11 (3H, s), 2.41–3.14 (7H, m), 3.97–4.09 (1H, m), 6.30 (1H, d, J = 1.6), 6.61 (1H, d, J = 2.4), 6.71 (1H, d, J = 2.4), 7.00 (1H, d, J = 7.7), 7.11 (1H, dd, J = 7.7, 1.6); MS m/z: M^+ 320. Anal. calcd. for $C_{23}H_{28}O$: C 86.20, H 8.81; found: C 86.22, H 9.10.

*5,15-Diacetyl-8-methyl[2.2]metaparacyclophane (**20**)*: Colorless prisms (hexane); mp 127–128°C; IR (KBr) ν_{max}: 1669 (C=O) cm^{-1}; ^1H NMR ($CDCl_3$) δ: 1.84 (3H, s), 2.10 (3H, s), 2.52 (3H, s), 2.60–2.90 (5H, m), 3.05–3.15 (1H, m), 3.20–3.30 (1H, m), 4.00–4.10 (1H, m), 6.42 (1H, d, J = 1.0), 7.12 (1H, d, J = 7.8), 7.16 (1H, d, J = 1.5), 7.18 (1H, dd, J = 7.8, 1.0), 7.40 (1H, d, J = 1.5); MS m/z: M^+ 306. Anal. calcd. for $C_{21}H_{22}O_2$: C 82.32, H 7.24; found: C 82.30, H 7.25.

Reaction of 8-substituted [2.2]metaparacyclophanes **11** with acetyl chloride in CS_2 or CH_2Cl_2 was carried out using the same procedure as described above and details of the products and yields are compiled in Table 2 and Table 3.

*12-Acetyl-5-*tert*-butyl-8-methoxy[2.2]metaparacyclophane (**19c**)*: Colorless prisms (hexane); mp 88–90°C; IR (KBr) ν_{max}: 2963, 2925, 1669, 1286, 1260, 1171, 1095, 1071, 1016, 802, 774 cm^{-1}; ^1H NMR ($CDCl_3$) δ: 1.31 (9H, s), 2.65 (3H, s), 3.13 (3H, s), 2.32–3.22 (7H, m), 4.15–4.22 (1H, m), 5.90 (2H, s), 6.74 (1H, d, J = 2.2), 6.79 (1H, d, J = 2.2), 7.60 (1H, s); MS m/z: M^+ 336. Anal. calcd. for $C_{23}H_{28}O_2$: C 82.10, H 8.39; found: C 82.30, H 8.35.

*15-Acetyl-5-*tert*-butyl-8-bromo[2.2]metaparacyclophane (**18d**)*: Colorless prisms (hexane); mp 115–120°C; IR (KBr) ν_{max}: 2963, 2932, 1668, 1428, 1352, 1199, 1008, 879, 734, 609 cm^{-1}; ^1H NMR ($CDCl_3$) δ: 1.24 (9H, s), 2.18 (3H, s), 2.40–3.27 (7H, m), 4.00–4.12 (1H, m), 6.35 (1H, d, J = 1.5), 6.71 (1H, d, J = 2.4), 6.76 (1H, d, J = 2.4), 7.27 (1H, d, J = 7.8), 7.38 (1H, dd, J = 7.8, 1.5); MS m/z: M^+ 384, 386. Anal. calcd. for $C_{22}H_{25}BrO_2$: C 68.57, H 6.54; found: C 68.22, H 6.50.

*5,12-Dipropionyl-8-methoxy[2.2]metaparacyclophane (**17h**)*: Colorless prisms (hexane); mp 92–93°C; IR (KBr) ν_{max}: 1680 (C=O) cm^{-1}; ^1H NMR ($CDCl_3$) δ: 1.24 (t, 3 H, J = 7.3), 1.26 (t, 3 H, J = 7.3), 2.35–2.60 (4H, m), 2.75–3.30 (7H, m), 3.15 (3H, s), 4.10–4.20 (1H, m), 5.93 (2H, s), 7.40 (1H, d, J = 2.4), 7.44 (1H, d, J = 2.4), 7.62 (1H, s); MS m/z: M^+ 306. Anal. calcd. for $C_{23}H_{26}O_3$: C 78.83, H 7.48; found: C 78.60, H 7.50.

*5-*tert*-Butyl-12-benzoyl-8-methoxy[2.2]metaparacyclophane (**19i**)*: Colorless oil; IR (NaCl) ν_{max}: 1660 (C=O) cm^{-1}; ^1H NMR ($CDCl_3$) δ: 1.34 (9H, s), 2.3–2.5 (4H, m), 2.63–2.75 (1H, m), 3.05–3.20 (2H, m), 3.13 (3H, s), 3.64–3.75 (1H, m), 5.95 (2H, s), 6.74 (1H, d, J = 2.4), 6.82 (1H, d, J = 2.4), 7.33–7.82 (6H, m); MS m/z: M^+ 398. Anal. calcd. for $C_{28}H_{30}O_2$: C 84.38, H 7.59; found: C 84.57, H 7.38.

*5,12-Dibenzoyl-8-methoxy[2.2]metaparacyclophane (**17i**)*: Colorless prisms (hexane:benzene (1:1)); mp 145–146°C; IR (KBr) ν_{max}: 1660, 1646 (C=O) cm^{-1}; ^1H NMR ($CDCl_3$) δ: 2.40–2.60 (4H, m), 2.73–2.83 (1H, m), 3.10–3.40 (2H, m), 3.25 (3H, s), 3.60–3.70 (1H, m), 6.10 (2H, s), 7.20–8.15 (13H, m); MS m/z: M^+ 446. Anal. calcd. for $C_{31}H_{26}O_3$: C 83.38, H 5.87; found: C 83.35, H 5.96.

*5-*tert*-Butyl-12-[(3-carboxyl)propionyl]-8-methoxy[2.2]metaparacyclophane (**19j**)*: Colorless prisms [hexane:benzene (3:1)]; mp 201–203°C; IR (KBr) ν_{max}: 3200–2500 (OH), 1711, 1677 (C=O) cm^{-1}; ^1H NMR ($CDCl_3$) δ: 1.31 (9H, s), 2.30–2.55 (4H, m), 2.70–2.90 (4H, m), 3.12 (3H, s), 3.10–3.32 (2H, m), 4.10–4.20 (2H, m), 5.90 (2H, s), 6.73 (1H, d, J = 2.0), 6.78 (1H, d, J = 2.0), 7.64 (1H, s); MS m/z: M^+ 494. Anal. calcd. for $C_{25}H_{30}O_4$: C 76.11, H 7.66; found: C 76.17, H 7.61.

*Crystallographic data for 5-bromo-8-methoxy[2.2]metaparacyclophane (**10**)*:

Crystal data

$C_{17}H_{17}BrO$, M = 317.23, Monoclinic, a = 13.883 (1), b = 12.7430 (11), c = 8.2263 (9) Å, β = 104.9466° (70), V = 1406.1 (2) $Å^3$ (by least-squares refinement on diffractometer angles for 25 automatically centered reflections), space group $P2_1/a$ (No. 14), Z = 4, D_x = 1.498 g/cm^3, colorless, prism, crystal size 0.40 × 0.30 × 0.25 mm, μ(Cu-K_α) = 39.0 cm^{-1}; total no. of unique reflections: 2204; R = 0.043, R_w = 0.070

Data correction and procedure

Enraf-Nonius CAD4 FR586 diffractometer, ω/2θ mode with ω scan width = 0.8 + 0.140 tan θ, scan speed 1.0 to 7.0 deg min^{-1}, graphite-monochromated Cu-K_α radiation; 2684 reflections were measured (4.8° = θ = 64.9°, $-h$, k, l). 2204 unique (merging R = 0.043 no absorption correction), Linear and approx. isotopic crystal decay, ca. –1.8% corrected during procedure.

Structure analysis and refinement

The structure was solved by direct method (MULTAN 11/80)[3]. Full-matrix least-squares refinement on F with all non-hydrogen atoms anisotropic and hydrogens isotropic fixed at Beq 4.0 $Å^2$. The weighting scheme is $\omega = 4F_0^2/[(\sigma I_0)^2 + 0.0016F_0^4]$. Final R and R_w values are 0.043, 0.070 (refined on F). All calculations were performed on a MicroVAX3100 using MolEN[4].

The refined non-hydrogen atomic coordinates are listed in Table 4 whilst the hydrogen coordinates, temperature factors (anisotropic for carbon atoms), scale factor, and secondary estimation coefficient are available, on request, from the Cambridge Crystallographic Data Centre.[5]

[3] P. Main, S.J. Fiske, S.E. Hull, L. Lessinger, G. Germain, J.P. DeClerq, and M.M. Woolfson. "MULTAN, a system of computer programs for the automatic solution of crystal structures for X-ray diffraction data." University of York, England. 1980.

[4] MolEN, an interactive structure solution procedure. Enraf-Nonius, Delft, The Netherlands. 1990.

[5] Hydrogen coordinates, temperature factors (anisotropic for carbon atons), scale factors, and secondary estimation coefficients have been deposited as supplementary material and may be purchased from: The Depository of Unpublished Data, Document Delivery, CISTI, National Research Council Canada, Ottawa, Ontario, Canada, K1A 0S2. These have also been deposited with the Cambridge Crystallographic Data Centre and can be obtained on request from: The Director, Cambridge Crystallographic Data Centre, University Chemical Laboratory, 12 Union Road, Cambridge, CB2 1EZ, U.K.

© 2000 NRC Canada

Table 4. Atomic coordinates with their estimated standard deviations in parentheses for 5-bromo-8-methoxy[2.2]metaparacyclophane **10** and the isotropic equivalent displacement parameters $B_{eq} = 4/3[a^2B_{11} + b^2B_{22} + c^2B_{33} + ac(\cos b)B_{13}]$.

atom	*x*	*y*	*z*	B_{eq}
BR1	0.97513(2)	0.05934(3)	0.76671(5)	5.553(9)
O1	0.5951(1)	–0.1878(1)	0.5635(2)	3.42(3)
C1	0.6501(2)	–0.1268(3)	1.0151(3)	4.75(6)
C2	0.6204(2)	–0.0559(2)	0.8538(3)	4.04(5)
C3	0.6967(2)	–0.0629(2)	0.7494(3)	3.16(5)
C4	0.7838(2)	–0.0047(2)	0.7931(3)	3.61(5)
C5	0.8590(2)	–0.0255(2)	0.7163(3)	3.53(5)
C6	0.8540(2)	–0.1096(2)	0.6078(3)	3.65(5)
C7	0.7675(2)	–0.1696(2)	0.5628(3)	3.21(4)
C8	0.6864(2)	–0.1380(2)	0.6225(3)	2.93(4)
C9	0.7686(2)	–0.2752(2)	0.4795(3)	4.02(5)
C10	0.8197(2)	–0.3594(2)	0.6089(4)	4.67(6)
C11	0.7887(2)	–0.3442(2)	0.7682(3)	4.01(5)
C12	0.6910(2)	–0.3620(2)	0.7734(3)	4.04(5)
C13	0.6473(2)	–0.3031(2)	0.8754(3)	4.02(5)
C14	0.7012(2)	–0.2238(2)	0.9777(3)	4.02(5)
C15	0.8046(2)	–0.2252(2)	0.9996(3)	4.35(5)
C16	0.8473(2)	–0.2832(2)	0.8985(3)	4.39(6)
C17	0.5396(2)	–0.1479(3)	0.4071(3)	4.62(6)

References

1. Part 50. T. Yamato, Y. Yamada, and M. Hirahara. J. Chem. Res. Synop. 724 (1999).
2. D.J. Cram. D.L. Helgeson, D. Lock, and L.A. Singer. J. Am. Chem. Soc. **88**, 1324 (1966).
3. (*a*) T. Hylton and V. Boekelheide. J. Am. Chem. Soc. **90**, 6887 (1968); (*b*) S.A. Sherrod and R.L. da Costa. Tetrahedron Lett. 2083 (1973); (*c*) V. Boekelheide, I.D. Reingold, and M. Tuttle. J. Chem. Soc. Chem. Commun. 406 (1973); (*d*) R.H. Mitchell and V. Boekelheide. J. Am. Chem. Soc. **96**, 1547 (1974); (*e*) S.A. Sherrod, R.L. da Costa, R.A. Barnes, and V. Boekelheide. J. Am. Chem. Soc. **96**, 1565 (1974); (*f*) R.H. Mitchell, T. Otsubo, and V. Boekelheide. Tetrahedron Lett. 219 (1975); (*g*) F. Vögtle. Chem. Ber. **102**, 3077 (1969); (*h*) P. Neumann and F. Vögtle. Synthesis, 85 (1973).
4. (*a*) D.T. Hefelfinger and D.J. Cram. J. Am. Chem. Soc. **92**, 1073 (1970); (*b*) D.T. Hefelfinger and D.J. Cram. J. Am. Chem. Soc. **93**, 4767 (1971); (*c*) S. Akabori, S. Hayashi, M. Mawa, and K. Shiomi. Tetrahedron Lett. 3727 (1969).
5. A. Renault, C. Cohen-Addad, J. Lajzerowicz-Bonneteau, J.P. Dutasta, and M.J. Cris. Acta Crystallogr. Sect. B: Struct. Sci. **43**, 480 (1987).
6. T. Yamato, J. Matsumoto, K. Tokuhisa, K. Tsuji, K. Suehiro, and M. Tashiro. J. Chem. Soc. Perkin Trans. 1, 2675 (1992).
7. D.T. Hefelfinger and D.J. Cram. J. Am. Chem. Soc. **93**, 4754 (1971).
8. (*a*) M. Tashiro and T. Yamato. J. Org. Chem. **46**, 1543 (1981); (*b*) M. Tashiro and T. Yamato. J. Org. Chem. **50**, 2939 (1985); (*c*) T. Yamato, J. Matsumoto, K. Tokuhisa, M. Kajihara, K. Suehiro, and M. Tashiro. Chem. Ber. **125**, 2443 (1992); (*d*) T. Yamato, A. Miyazawa, and M. Tashiro. Chem. Ber. **126**, 2505 (1993); (*e*) T. Yamato, A. Miyazawa, and M. Tashiro. J. Chem. Soc., Perkin Trans. 1, **126**, 3127 (1993); (*f*) T. Yamato, L.K. Doamekpor, K. Hasegawa, T. Furukawa, and M. Tashiro. J. Chem. Res. Synop. 168 (1995); J. Chem. Res. Miniprint, 1101 (1995).
9. (*a*) M. Tashiro and T. Yamato. J. Org. Chem. **46**, 4556 (1981); (*b*) M. Tashiro and T. Yamato. J. Org. Chem. **48**, 1461 (1983); (*c*) M. Tashiro and T. Yamato. J. Chem. Soc. Perkin Trans. 1, 2165 (1984).
10. F. Kröhnke. Angew. Chem. Int. Ed. Engl. **65**, 605 (1953).
11. D.J. Cram, R.B. Hornby, E.A. Truesdale, H.J. Reich, M.H. Delton, and J.M. Cram. Tetrahedron, **30**, 1757 (1974).
12. (*a*) R.B. Moodie and K. Schofield. Acc. Chem. Res. **9**, 287 (1976); (*b*) A. Fischer and R. Röderer. Can. J. Chem. **54**, 3978 (1976); (*c*) A. Fischer and K.C. Teo. Can. J. Chem. **56**, 258 (1978); (*d*) A. Fischer and K.C. Teo. Can. J. Chem. **56**, 1758 (1978); (*e*) H. Suzuki. Synthesis, 217 (1977); (*f*) P.C. Myhre and M. Beug. J. Am. Chem. Soc. **88**, 1568 (1966); (*g*) P.C. Myhre, M. Beug, and L.L. James. J. Am. Chem. Soc. **90**, 2105 (1968); (*h*) P.C. Myhre, M. Beug, K.S. Brown, and B. Östman. J. Am. Chem. Soc. **93**, 3452 (1971); (*i*) A. Fischer and R. Röderer. J. Chem. Soc. Chem. Commun. 798 (1975); (*j*) G.A. Olah and S.J. Kuhn. J. Am. Chem. Soc. **86**, 1067 (1964); (*k*) W. Verboom, A. Durie, R.J.M. Egberink, Z. Asfari, and D.N. Reinhoudt. J. Org. Chem. **57**, 1313 (1992); (*l*) E. Kelderman, L. Derhaeg, G.J.T. Heesink, W. Verboom, J.F.J. Engbersen, N.F. van Hulst, A. Persoons, and D.N. Reinhoudt. Angew. Chem. Int. Ed. Engl. **31**, 1075 (1992).
13. (*a*) M. Tashiro, S. Mataka, Y. Takezaki, M. Takeshita, T. Arimura, A. Tsuge, and T. Yamato. J. Org. Chem. **54**, 451 (1989); (*b*) T. Yamato, J. Matsumoto, M. Shigekuni, and M. Tashiro. J. Chem. Res. Synop. 198 (1993); (*c*) T. Yamato, J. Matsumoto, S. Kabu, Y. Takezaki, and M. Tashiro. J. Chem. Res. Synop. 44 (1993); (*d*) T. Yamato, H. Kamimura, K. Noda, and M. Tashiro. J. Chem. Res. Synop. 210 (1994); J. Chem. Res. Miniprint, 1152 (1994); (*e*) T. Yamato, K. Maeda, H. Kamimura, K. Noda, and M. Tashiro. J. Chem. Res. Synop. 310 (1995); J. Chem. Res. Miniprint, 1865 (1995); (*f*) T. Yamato, H.Kamimura, and T. Furukawa. J. Org. Chem. **62**, 7560 (1997); (*g*) T. Yamato, H. Kamimura, F. Zhang, and H. Tsuzuki. Can. J. Chem. **76**, 997 (1998).
14. (*a*) G.A. Olah. Acc. Chem. Res. **4**, 240 (1971); (*b*) F. Cacace, M.E. Crestoni, S. Fornarini, and D. Kuck. J. Am. Chem. Soc. **115**, 1024 (1993).
15. (*a*) N.L. Allinger, B.J. Gordon, H.-E. Hu, and R.A. Ford. J. Org. Chem. **32**, 2272 (1967); (*b*) T. Sato, E. Yamada, Y. Okamura, T. Amada, and K. Hata. Bull. Chem. Soc. Jpn. **38**, 1049 (1965); (*c*) M. Fujimoto, T. Sato, and K. Hata. Bull. Chem. Soc. Jpn. **40**, 600 (1967); (*d*) T. Sato, M. Wakabayashi, Y. Okamura, T. Amada, and K. Hata. Bull. Chem. Soc. Jpn. **40**, 2363 (1967); (*e*) T. Sato and K. Nishiyama. J. Chem. Soc. Chem. Commun. 220 (1973); (*f*) T. Sato, K. Nishiyama, S. Shimada, and K. Hata. Bull. Chem. Soc. Jpn. **44**, 2858 (1971); (*g*) S. Hayashi and T. Sato. Bull. Chem. Soc. Jpn. **45**, 2360 (1972).

© 2000 NRC Canada

Two novel Diels–Alder adducts from *Hippocratea celastroides* roots and their insecticidal activity

M. Jiménez-Estrada, R. Reyes-Chilpa, S. Hernández-Ortega, E. Cristobal-Telésforo, L. Torres-Colín, C.K. Jankowski, A. Aumelas, and M.R. Van Calsteren

Abstract: Two novel compounds, celastroidine A (**1**) and B (**2**), were isolated from the roots of *Hippocratea celastroides* K. Their structures were elucidated by spectroscopical and X-ray diffraction studies. Celastroidine A (**1**) ($C_{50}H_{74}O_5$) was identified as a Diels–Alder adduct of a triterpene plus a diterpene and celastroidine B (**2**) as a beyerane, a type of dimer of two diterpene ($C_{40}H_{60}O_4$). Both compounds could be formed in vivo by a Diels–Alder reaction. Celastroidine A showed some antifeeding activity against the stored grain insect *Sitophyllus zeamays*.

Key words: *Hippocratea celastroides*, Hippocrataceae, roots, Diels–Alder adducts, diterpenoids, triterpenoids, x-ray diffraction, insect antifeedants, stored grain insects, *Sitophyllus zeamays*, insecticidal plants, Diels–Alderase.

Résumé : Deux nouveaux terpènes, célastroïdines A (**1**) et B (**2**) ont été isolés à partir des racines d'*Hippocratea celastroides* K. Leurs structures ont été étudiées par des méthodes spectroscopiques (en particulier par RMN et rayons X). La célastroïdine A (**1**), un pentaterpène, a été identifié comme l'adduit du type de Diels–Alder entre des résidus di- et triterpéniques et la célastroïdine B (**2**) comme un dimère beyerane à C_{40} résultant de l'addition de deux unités diterpéniques réagissant en tant que diène et dièneophile. Les deux substances peuvent être formées in vivo suite à cette addition. La célastroïdine A (**1**) montre une activité bloquant le réflexe d'alimentation chez les insectes de stockage de grains *Sitophyllus zeamays*.

Mots clés : *Hippocratea celastroides*, hippocratacées, racines, adduits de Diels–Alder, diterpénoïdes, triterpénoïdes, diffraction des rayons X, antiappétants pour les insectes, insectes de stockage de grains, *Sitophyllus zeamays*, plantes insecticides, Diels–Aldérase.

Introduction

Hippocratea celastroides Kunth (also known as *H. acapulcensis*) is a shrubby vine which grows in the tropical deciduous forest in Mexico. The seeds and fruits are used in folk-medicine against head lice and skin mite parasites (1, 2). In a previous work, we reported that the organic extracts from the roots, especially acetone and methylene chloride extracts, have antifeeding activity against the stored grain insect *Sitophyllus zeamays*.[2] Chemical studies have shown that *H. celastroides* leaves contain the triterpenes: friedelin, friedelan-3β-ol (epifriedelinol), 3-oxo-lup-20-en-30-ol, and lup-20-en-3β,30-diol (3), meanwhile the roots contain the alditol galactitol.[2] Continuing our studies on *H. celastroides* roots, we wish now to report the isolation and structure elucidation of two novel compounds celastroidine A (**1**) and B (**2**) (Fig. 1), as well as the evaluation of their toxicity and antifeedant activity against *S. zeamays*.[3]

Toxicity and antifeeding properties of celastroidine A and B were examined against the stored grain pest *S. zeamays*. Celastroidine A (**1**) inhibited the feeding of the insect in 88.7%, but only increased mortality in 2%. On the other hand, celastroidine B (**2**) showed both low antifeeding activity (9.6%) and mortality (5.2%) rates. We have previously

Received September 8, 1999.

M. Jiménez-Estrada, R. Reyes-Chilpa, S. Hernández-Ortega, and E. Cristobal-Telésforo. Instituto de Química. Universidad Nacional Autónoma de México. Circuito Exterior, Ciudad Universitaria, Coyoacán, 04510, México D.F.
L. Torres-Colín. Instituto de Biología. Universidad Nacional Autónoma de México. Circuito Exterior, Ciudad Universitaria, Coyoacán, 04510, México D.F.
C.K. Jankowski,[1] A. Aumelas, and M.R. Van Calsteren. FESR Université de Moncton, Moncton, NB E1A 3E9, Canada.

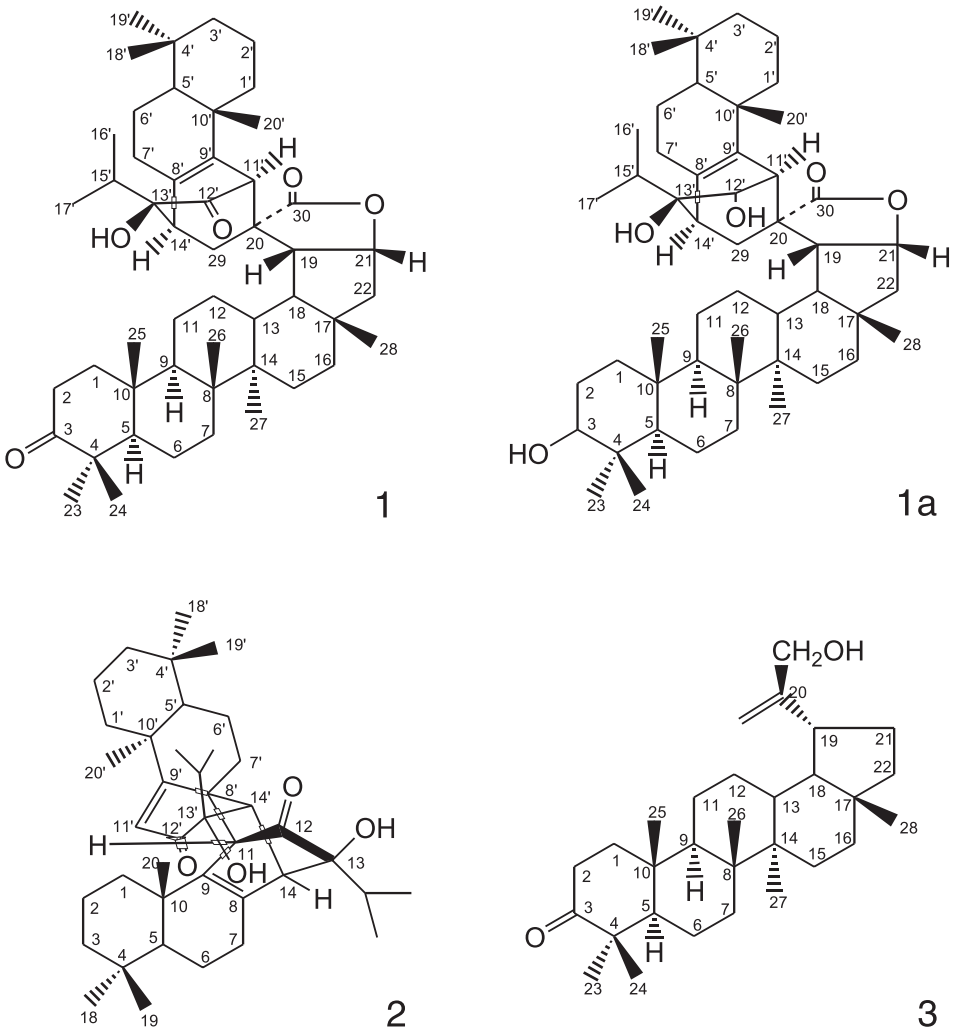
[1]Author to whom correspondence may be addressed. Département de chimie et biochimie, Université de Moncton, Moncton, NB E1A 3E9, Canada. Telephone (506) 858-4331. Fax:(506) 858-4541. e-mail: jankowc@umoncton.ca

[2]R. Reyes Chilpa, M. Jiménez-Estrada, E. Cristobal-Telésforo, L. Torres-Colín, M.A. Villavicencio, B.E. Pérez Escandón, and R. Mercado. Natural insecticides from *Hippocratea excelsa* and *Hippocratea celastroides*. Submitted to Economic Botany (1999).

[3]Tables of crystallographic details, atomic coordinates, anisotropic displacement coefficients, and bond distances and angles have been deposited and may be purchased from: The Depository of Unpublished Data, Document Delivery, CISTI, National Research Council Canada, Ottawa, Ontario, Canada, K1A 0S2. Tables of bond distances and angles and H coordinates have also been deposited with the Cambridge Crystallographic Data Centre and can be obtained on request from: The Director, Cambridge Crystallographic Data Centre, University Chemical Laboratory, 12 Union Road, Cambridge, CB2 1EZ, U.K.

 © 2000 NRC Canada

Fig. 1. Structure of celastroidine A (**1**) (and it's acetate (**1a**), celastroidine B (**2**), and 3-oxolup-20-en-30-ol (**3**).



reported that the total methylene chloride extract from *H. celastroides* roots has good antifeeding activity (70.3%) and low mortality (9.4%) when tested with *S. zeamays*.[2] The celastroidine A activity is quite similar and since is the most abundant component of this extract (~10.7%), and it seems to be its active principle.

Results and discussion

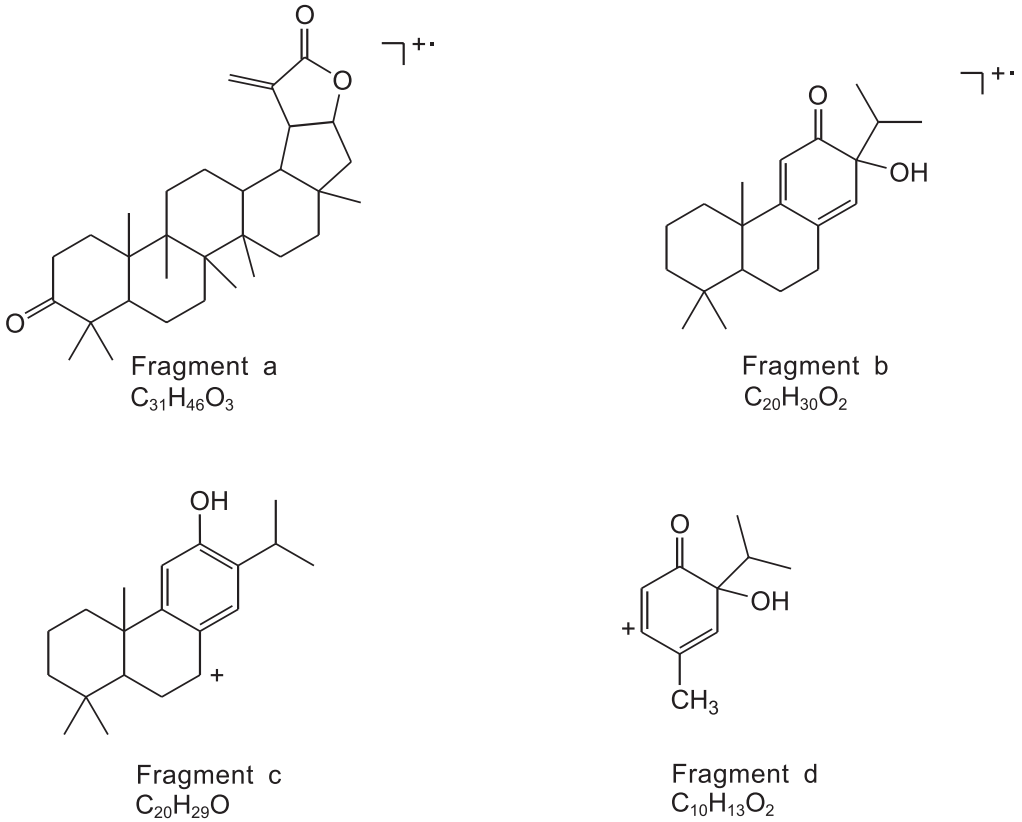
The methylene chloride root extract afforded celastroidine A (**1**) and B (**2**) in good yield. The petroleum ether extract produced celastroidine B and β-sitosterol. Celastroidine A was isolated as a white powder. According to spectral and X-ray diffraction evidence, the celastroidine A molecular structure corresponds to a Diels–Alder adduct of a triterpene on a diterpene (**1**). The IR spectrum showed absorption bands (cm^{-1}) for hydroxyl (3565) together with a lactone carbonyl (1759) and two ketones on the six member rings (1709 broad). The FAB mass spectrum confirmed the molecular mass at 754 corresponding to the formula $C_{50}H_{74}O_5$. Fragments of *m/z* 737 and 452 were attributed to the loss of water (MH^+–18), and to a lupen triterpene $C_{30}H_{42}O_3$ moiety (fragment **a**) as indicated in Fig. 2 from the protonated molecular ion. This last fragment also appeared in the EIMS and CIMS (as the quasimolecular ion). The difference among M^+ and fragment **a** accounts for *m/z* 302, equivalent to the molecular weight of a $C_{20}H_{32}O_2$ diterpene of the abietane type (fragment **b**). In addition, FABMS showed a peak at *m/z* 285 corresponding to fragment **c** originated from fragment **b** by loss of OH followed by ring aromatization. Fragment **d** (at *m/z* 165) could also be related to **b** (Fig. 2).

Structures **1** and **2** were supported by the ^{1}HNMR and ^{13}CNMR data. The assignment of their 1H and 13 C spectra was carried out from the analysis of a COSY, TOCSY, HSQC, and HMBC experiments (Table 1). The ^{13}C NMR (DEPT) spectrum of the compound **1** indicated 45 sp^3 carbon atoms, 11 methyls, 15 methylenes, 10 methines, nine quaternary C, and five sp^2 carbons (3 C=O, and 2 C=C).

Celastroidine A (**1**) has 11 methyl signals, five of them are part of the diterpene moeity, and six to the triterpene moiety. This part of the skeleton is related to lupene triterpenoids previously isolated from the same species (3). Further evidence came from comparison of ^{13}C NMR data of three compounds to those previously reported (3) (e.g., for 3-oxo-

© 2000 NRC Canada

Fig. 2. Fragmentation pattern of celastroidine A (FAB)



lup-20-en-30-ol (**3**) (Table 1, Fig. 1)). From this comparison, the signal at 217.9 ppm was readily assigned to the C-3 ketone. Therefore the signal at 213.4 ppm was assigned to the C-12′ ketone. This carbon showed couplings with H-11′ (2.92 ppm) and H-14′ (2.74 ppm).

Finally, the signal at 177.7 ppm was assigned to the C-30 carbonyl of a γ-lactone ring. This ring was indirectly confirmed by the presence of a tertiary carbon in position 21 whose ^{13}C (81.1 ppm) and ^{1}H (5.02 ppm) chemical shifts are typical of an ether or ester substitution. As expected, the COSY experiment showed interactions of H-21 proton with another tertiary proton (H-19 2.49 ppm) and with H-22 methylene protons (2.15 and 1.29 ppm). On the diterpene moiety the molecule bears one double bond and an isopropyl group. The C-8′—C-9′ double bond is unambiguously characterized by carbon signals at 136.1 and 134.9 ppm, respectively.

The isopropyl group was clearly identified with ^{1}H spectrum by the presence of two doublets for methyl groups at 0.84 (CH_3-16′) and 0.97 (CH_3-17′) ppm coupled to the H-15′ proton (1.78 ppm).

The bridge between diterpene and triterpene moieties was evidenced by HMBC and COSY experiments. For instance, H-14′ (2.74 ppm) on the diterpene side showed a long distance coupling with C-29 (23 ppm) on the triterpene side. The C-12′ signal showed couplings with H-11′ (2.92 ppm) and H-14′ (2.74 ppm).

Celastroidine A (**1**) did not hydrolyze under mild acidic conditions (HCl (aq)) and was recovered unaltered, excluding the possibility of an ether bridge presence. Acetylation under mild conditions with acetic anhydride in pyridine did not work, but the compound could be reduced with $NaBH_4$ in THF. The product **1a**, was a white solid. The IR spectrum did not show any carbonyl absorption, nevertheless hydroxyl bands were evident. The $^{1}HNMR$ spectrum showed a multiplet centered at 4.19 ppm which was assigned to the H-3 proton. This signal was duplicated and suggested a stereoisomer mixture. Two doublets, at 1.17 and 1.38 ppm, were assigned to C-16′ and C-17′. Other methyl signals appear among 1.2–1.4 ppm (7 singlets). The FAB mass spectrum showed the molecular ion at *m*/*z* 760 (3), and others similar to ***1*** fragments e.g., loss of water. Structure **1** was definitely confirmed by X-ray diffraction (Fig. 3).

Celastroidine B (**2**) was also isolated as a white powder. The IR spectrum showed two carbonyl absorptions at 1608 and 1712 cm^{-1} of a conjugated and deconjugated cyclohexenone respectively. Its molecular structure was deduced as **2** and corresponds to a $C_{40}H_{60}O_4$ diterpene dimer formed by a Diels–Alder reaction (Fig. 1). The PI mass spectrum obtained by FAB and EIMS showed the 100% ion at *m*/*z* 302 and the molecular mass at 604, therefore suggesting that compound ***2*** could be formed by attachment of two identical $C_{20}H_{30}O_2$ fragments. This retro-Diels–Alder fragment structure should be considered as a hypothetical diene (or dienophile) leading to formation of either **1** or **2**. This fragment is more intense (100%) for dimer **2** than for celestroidine A (**1**) (54%) for which it plays a role of diene only. A fragment of *m*/*z* 165 was also noticed and corresponds to structure **d** (Fig. 2).

$^{1}HNMR$ and $^{13}CNMR$ spectra (Table 2) suggested that the diterpene monomer has an abietane type skeleton, as already indicated for celastroidine A (**1**). All assignments were

© 2000 NRC Canada

Table 1. ^{13}C and ^{1}H NMR data of Celastroidine A (**1**) and 3-oxo-lup-20-en-30-ol (**3**). ($CDCl_3$, 27°C).

	1					**3**
C no.	δ_C (ppm)	δ_H (ppm)		*J* (Hz)		δ_C (ppm)
1	39.6	1.94 *eq*	13.2	7.3	4.7	39.9
		1.42 *ax*				
2	34.0	2.5 *ax*				34.1
		2.44 *eq*				
3	217.9	—				215.0
4	47.2	—				47.6
5	54.6	1.33				55.2
6	19.6	1.48				19.8
		1.48				
7	33.7	1.44				33.8
		1.44				
8	41.2	—				41.1
9	48.3	1.37				50.0
10	36.7	—				37.2
11	21.7	1.52 *eq*				21.7
		1.30 *ax*				
12	29.6	1.84 *ax*				29.8
		1.15 *eq*				
13	37.9	1.74				38.2
14	43.1					43.2
15	26.6	1.71				27.5
		1.10				
16	34.1	1.69				35.6
		1.40				
17	43.7	—				43.3
18	49.6	1.37				49.1
19	50.4	2.49	10.8	7.3		44.0
20	54.8	—				154.0
21	81.1	5.02	7.4	7.4	5.9	31.2
22	48.0	2.15 *eq*	13.0	7.6		39.4
		1.29 *ax*				
23	26.6	1.07				26.6
24	20.9	1.02				21.2
25	16.0	0.94				15.9
26	15.9	1.07				16.1
27	14.4	0.89				14.6
28	20.1	0.80				17.9
29	23.2	2.41				63.3
		1.76 *endo*	13.7	3.4		
30	177.7	—				107.1
1′	34.9	1.49 *eq*				
		1.40 *ax*				
2′	18.5	1.51				
		1.51				
3′	41.3	1.38				
		1.21				
4′	33.2	—				
5′	49.4	1.35				
6′	18.7	1.78				
		1.47				
7′	29.5	2.42 *ax*				
		2.16 *eq*				
8′	136.0	—				
9′	136.4	—				
10′	36.3	—				
11′	55.3	2.92				
12′	213.4	—				
13′	78.7	—				
14′	45.3	2.74	3.7	1.9		
15′	34.1	1.78				
16′	17.4	0.97	6.7			
17′	16.9	0.84	7.4			
18′	32.8	0.90				
19′	21.4	0.80				
20′	21.0	0.82				
OH13′	—	2.20				

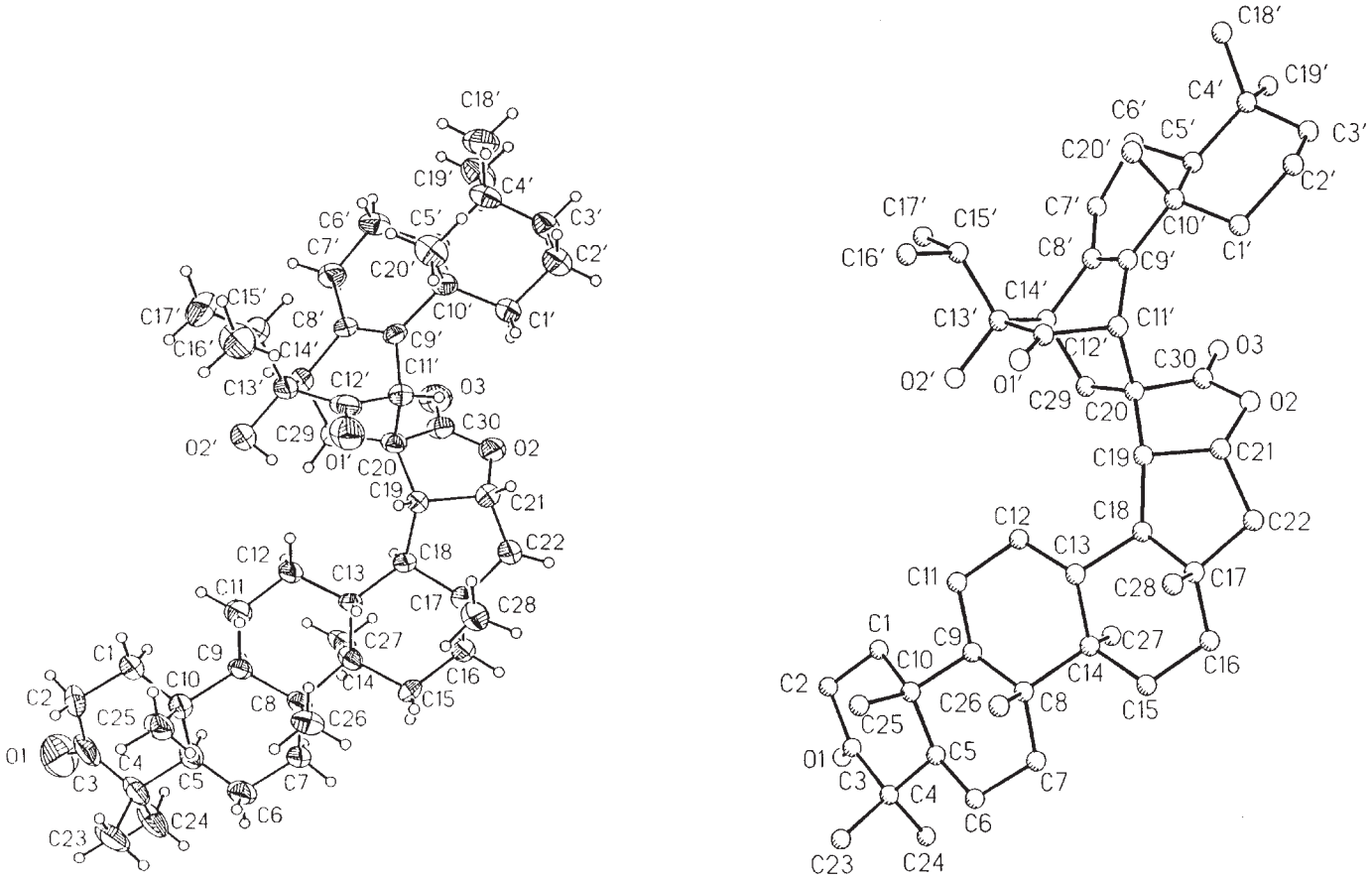
supported by homo- and heteronuclear NMR experiments. Two methine doublets at 3.11 ppm (*J* = 2.5 Hz) and 2.56 ppm (*J* = 2.5 Hz) integrating for one proton were assigned to H-14 and H-14′, respectively. Carbons C-14 and C-14′ bearing these protons, appeared at 45.4 and 43.3 ppm (Table 2). A singlet at 6.15 ppm was assigned to the vinylic proton H-11′ of the α,β-unsaturated ketone system. Carbons C-11′ and C-9′ supporting this double bond position were assigned at 120.0 (C-11′) and 172.6 ppm (C-9′). The second diterpene unit should bear a nonprotonated double bond as indicated by signals at 138.6 and 138.5, that corresponded to C-8 and C-9. A broad singlet at 3.46 ppm was assigned to H-11, while the carbon bearing this proton appeared at 57.8 ppm (CH). Two quaternary carbons appeared at 78.7 (C) and 76.1 (C) and correspond to C-13′ and C-13, respectively. Both carbons are substituted with a hydroxyl group. Ketone carbonyls on C-12′ and C-12 appeared at 200.6 and 213.4 ppm. A doublet at ~0.53 ppm was assigned to H-17′. Signals for nine additional methyls were also assigned as in the Table 1. The structure of *2* was confirmed by the X-ray diffraction studies (Fig. 4).

The preliminary molecular mechanics modeling of the stereochemistry of the central part of the celastroidine B (**2**) indicates a photochemical pathway for the retro Diels–Alder reaction leading to the monomeric dienone of fragment b-like structure. The mechanism of the formation and its stereoselectivity should be fully analyzed (endo/exo and specific diastereofacial stereochemistry of adducts).

Celastroidine A and B are Diels–Alder adducts. Several natural products, presumably arising from a Diels–Alder reaction, according to metabolic or enzymatic pathways, have previously been isolated from microorganisms, plants, and marine animals. These compounds included polyketides, terpenoids, and alkaloids (4). Involvement of the Diels–Alder reaction in biosynthesis has been suggested, but a definitive proof has been lacking due to unsuccessful attempts to obtain the corresponding enzymes or starting diene (5). Nevertheless, the isolation of a crude enzyme from the phytopathogenic fungus *Alternaria solanii* has recently been reported enable to catalyze the [4 + 2] cycloadditions (e.g., necessary to synthesize two solanopyrones phytotoxins) (4). Isolation of celastroidine A and B, therefore suggests that

© 2000 NRC Canada

Fig. 3. X-ray of celastroidine A (**1**).



H. celastroides roots could also bear enzymes able to catalyze Diels–Alder reactions.

Experimental

Hippocratea celastroides Kunth was collected near Tucumán (State of Morelos, Mexico). A voucher is deposited at MEXU Herbarium. The roots (1.610 kg) were ground and extracted at room temperature with petroleum ether, and CH_2Cl_2. The extracts were concentrated under reduced pressure. The CH_2Cl_2 extract (14.1 g) was dissolved with acetone obtaining a white precipitate (1.4 g). The precipitate was subjected to column chromatography on silica gel eluting with petroleum ether (pet et), CH_2Cl_2, and mixtures of these solvents. Two products were obtained. Fractions 24–72 eluted with a (7:3) mixture afforded a white powder (610 mg). This product was recrystallized from CH_2Cl_2–MeOH obtaining a crystalline solid (mp 198–9°C).. which was named as celastroidine A (**1**). The acetone soluble portion of the CH_2Cl_2 extract (12.7g) was subjected to CC (Silica Gel 60) eluting with pet et–CH_2Cl_2. Fractions 56–65 eluted with a mixture (8:2) yielded 224 mg of a white powder (mp 189–190°C) named as celastroidine B (**2**). Fractions 66–89 eluted with a mixture (8:2) afforded celastroidine A (902 mg) again. The pet et extract (6.18 g) under column chromatography (Silica Gel 60) and elution with mixtures of petroleum ether–ethyl acetate, also afforded celastroidine B, especially from fractions 30–42 eluted with a 9:1 mixture.

Insecticidal tests

Toxicity and antifeeding activity of isolated compounds against *Sitophyllus zeamays* was evaluated as described.[2]

Experimental NMR

Materials and methods

The samples were dissolved in $CDCl_3$ and all NMR experiments were recorded at 27° on Bruker spectrometers, operating at 300, 500, and 600 MHz for ^1H nucleus and up to 150 MHz for ^{13}C nucleus. Chemical shifts are quoted relative to the $CDCl_3$ resonance fixed at 7.24 ppm for the proton and 77.0 ppm for the carbon. The multiplicity of carbon signals was established by using the DEPT experiment.

DQF–COSY spectra (6) were collected into a 800 × 1024 data matrix with 32 scans per tl value and TOCSY (7) spectra were collected with a mixing time of 80 ms into a 512 × 1024 data matrix with 16 scans per tl value.

HSQC (8, 9) experiments were recorded with a delay of 3.5 ms ($^1J_{CH}$ = 143 Hz) and HSQC–TOCSY (10, 11) experiments with a mixing time for proton–proton transfer of 80 ms (400 × 1024) with 32 scans per tl value to identify the one-bond carbon–proton and the network of proton–proton conectivities, respectively. The HMBC experiment (400 × 10 240) was recorded with a delay of 50 ms with 64 scans per tl value to identify long range proton–carbon connectivities. All data were processed with the UXNMR software. For

© 2000 NRC Canada

Table 2. ^{13}C and ^{1}H NMR data of celastroidine B (**2**).

	2			
C no.	δC (ppm)	δH (ppm)	*J* (Hz)	
1	36.2	1.30 *eq*		
		1.08 *ax*		
2	18.4	1.53		
		1.46		
3	41.6	1.39		
		1.15		
4	33.1	—		
5	49.2	1.05	12.5	1.9
6	18.6	1.69 *eq*		
		1.34 *ax*		
7	29.4	2.09		
		2.00		
8	138.6	—		
9	138.5	—		
10	37.3	—		
11	57.8	3.46		
12	213.4	—		
13	76.1	—		
14	45.0	3.11	2.5	
15	34.6	1.60		
16	17.0	0.97	6.9	
17	17.6	0.96	7.4	
18	33.0	0.89		
19	21.3	0.76		
20	20.8	0.76		
1′	37.0	1.97 *eq*		
		1.40 *ax*		
2′	18.8	1.67		
		1.60		
3′	41.8	1.49		
		1.12		
4′	34.0	—		
5′	43.0	1.75	11.6	8.0
6′	16.4	2.08 *eq*		
		1.50 *ax*		
7′	30.9	1.98		
		1.91		
8′	48.4	—		
9′	172.6	—		
10′	42.0	—		
11′	120.0	6.15		
12′	200.6	—		
13′	78.7	—		
14′	43.3	2.56	2.4	
15′	37.0	1.50		
16′	15.4	0.94	6.3	
17′	16.2	0.53	6.7	
18′	32.9	0.95		
19′	21.1	0.95		
20′	26.5	1.0		
OH13	—	2.10		
OH13′		3.74		

DQF–COSY and TOCSY data, one zero filling and a π/4 phase-shifted sine bell window function were applied in both dimensions before Fourier transform. For HSQC, HSQC–TOCSY, and HMBC data, a zero filling and a π/2 phase-shifted sine bell window function were applied in F2 dimension and a linear prediction was applied to 1024 points in F1 dimension prior to processing. The assignment of ^{1}H and ^{13}C resonances of celastroidine A and B spectra was carried out from analysis of DQF–COSY, TOCSY, DEPT, HSQC, HSQC–TOCSY, and HMBC data. All 2D NMR data and additional spectral material are available on request from CKJ (Moncton, Canada).

Celastroidine A (1): $C_{50}H_{74}O_5$, white powder, mp 198–199°C, [α] = +7.5° ($CHCl_3$). IR (cm^{-1}), ν max, ($CHCl_3$): 3565, 2960, 2873, 1759, 1709, 1462, 1386, 1367, 1311, 1178, and 1145. MS (FAB^+) *m*/*z* (%): 755 $(M^+ + 1)_1$ (5) [$C_{50}H_{74}O_5$], 737 (20), 694 (10), 655 (4), 587 (2), 453 (7), 302 (45), 285 (63), 259 (30), 245 (17),165 (85), 91 (50), 81 (60), 69 (50), 43 (100).

Proton and carbon chemical shifts of **1** measured in $CDCl_3$ at 27°C are reported in Table 1.

X-Ray Structure Analysis Summary (Fig. 3)

Celastroidine A (1): Crystal data: $C_{50}H_{74}O_5$ from CH_2Cl_2, crystal dimensions 0.40 × 0.20 × 0.08 mm crystal system, monoclinic P2(1), cell parameters a = 6.940(1), b = 23.994(3), c = 14.009(5), β = 95.84(1) Å, Z = 2, V = 2320.6(9) $Å^3$, M_r = 840.0, D_{calc} = 1.202, μ = 1.606 mm^{-1}, F(000) = 912. Data collection: Siemens P4/PC, CuKα radiation (λ = 1.54178 Å), θ/2θ scan, scan range 3–110°, index range $0 \le h \le 7$, $0 \le k \le 25$, $-14 \le I \le 14.3238$ collected reflections and 2468 observed reflections [$F \ge 3\sigma(F)$]. Solution and refinement. The structure was solved by direct methods and refined by full-matrix least squares, function minimized $\Sigma[Fo - Fc]^2$, hydrogen atoms model $d_{C\text{-}H}$ = 0.96Å, common fixed isotropic U = 0.06 $Å^2$. Final values are R = 7.26, wR = 9.44, GOF = 1.47, weight $w^{-1} = \sigma^2 F + 0.0019 F^2$ secondary extinction correction χ = 0.0022(1), residual electron density: 0.27/ – 0.30 e/$Å^{-3}$.

Celastroidine B (2): white powder, mp 189–190°C. [α] = +55.5° ($CHCl_3$). IR (cm^{-1}) ν max, $CHCl_3$: 2937, 2875, 1712, 1608, 1602, 1462, 1373, 1155, 1022 MS(%) FAB^+ *m*/*z*: 605 (12) (M^++1), 586(4), 557(3), 487(2), 391(1), 303(43), 302(36), 286(27), 261(25), 245(10), 165(100), 123(32), 69(41), 55(29), 43(62), 41(40), 27(6). IE 70 eV *m*/*z*: 604(3), 543(2), 533(3), 344(3), 302(100), 285(15), 259(20), 260(15), 261(10), 245(10), 232(22), 217(6), 165(50), 123(11), 83(6), 69 (12), 71(12), 55(7), 57(7), 43(18).

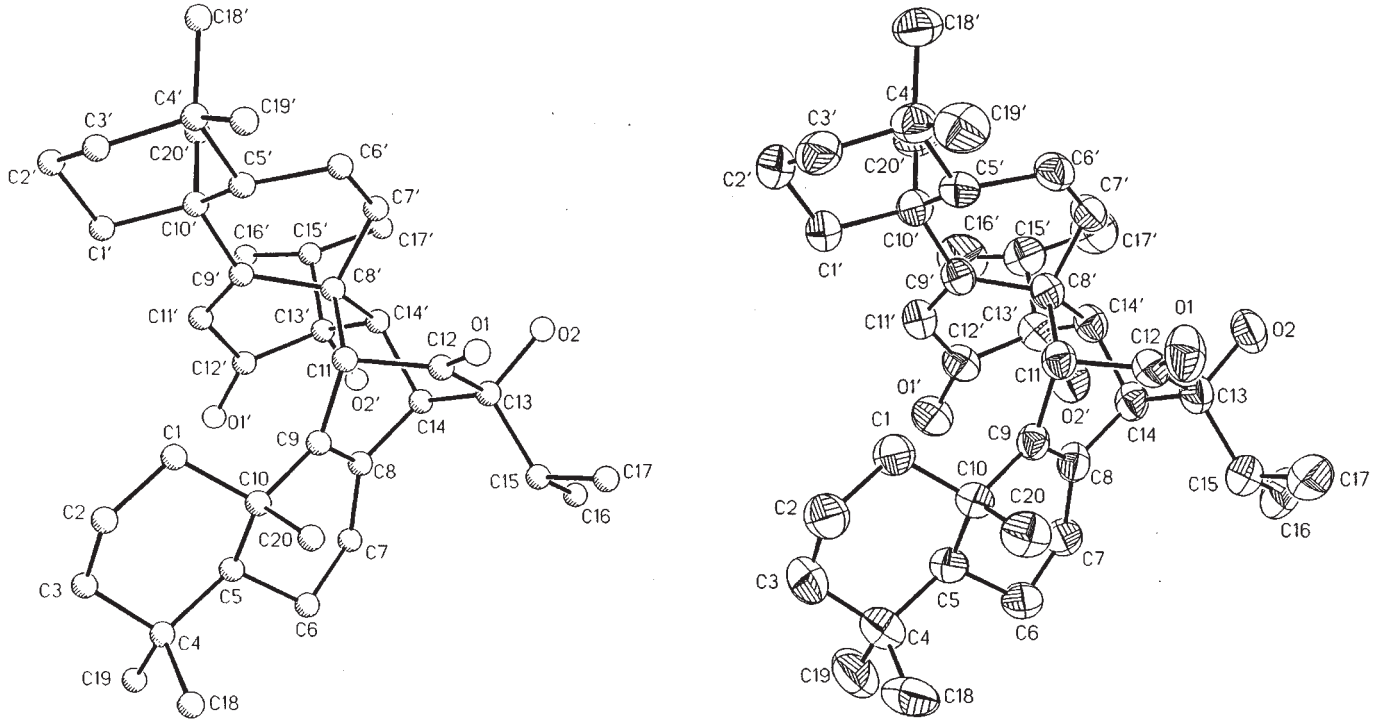
Proton and carbon chemical shifts of **2** measured in $CDCl_3$ at 27°C are reported in Table 2.

X-Ray Structure Analysis Summary (Fig. 3)

Celastroidine B (2): Crystal data: $C_{49}H_{60}O_4$, colorless and prism crystal of dimensions 0.40 × 0.24 × 0.16 mm, system orthorombic P2(1)2(1)2(1), cell parameters a = 10.589 (2), b = 15.607(3), c = 21.649(2) Å, Z = 4, V = 3577.7(9) $Å^3$, M_r = 604.9, D_{calc} = 1.123, μ = 0.542 mm^{-1}, F(000) = 1328. Data collection: Siemens P4/PC, CuKα radiation (λ = 1.54178 Å), θ/2θ scan, scan range 3–110°, index range $-11 \le h \le 0$, $-16 \le k \le 16$, $-22 \le I \le 0.4774$ reflections collected and 3659 ob-

© 2000 NRC Canada

Fig. 4. X-ray of celastroidine B (**2**).



served reflections [$F \geq 3\sigma(F)$]. Solution and refinement. The structure was solved by direct methods and refined by full-matrix least squares, function minimized $\Sigma[Fo - Fc]^2$, hydrogen atoms model $d_{C\text{-}H}$ = 0.96Å, common fixed isotropic U = 0.06Å^2. Final values are R = 5.88, wR = 8.58, GOF = 1.44, weight $w^{-1} = \sigma^2 F + 0.0018 F^2$ secondary extinction correction χ = 0.0021(5), residual electron density: 0.36/ – 0.29 e/Å^{-3}.

Acknowledgments

The authors are grateful to PREBELAC — The New York Botanical Garden and DGAPA-UNAM-(IN214996) for financing this project. We are grateful to I. Chavez, W. Matus, B. Quiroz, and L. Velasco for preliminary analysis. We thank M. A. Villavicencio and B.E. Pérez Escandón for performing the insecticidal assays.

References

1. P.C Standley and J.A. Steyermark. Hippocrateaceae in flora of Guatemala. Fieldiana Bot. **24**, 218 (1949).
2. J.C. Soto-Nuñez and M. Sousa. Plantas Medicinales de la Cuenca del Río Balsas. Serie Cuadernos del Instituto de Biología No. 25. Universidad Nacional Autónoma de México. México (1995).
3. A.G. González, I.L. Bazzochi, A.G. Ravelo, and J.G. Luis. Rev Latinoam. Quím. **20**, 17 (1989).
4. H. Oikawa, K. Katayama, Y. Suzuki, and A. Ichihara. J. Chem. Soc. Chem. Comm. 1321 (1995); D.H.R. Barton, K. Nakanishi, and D. Meth-Cohn. Comprehensive natural products chemistry. Vol. 1, 1999. pp. 367–408; K. Katayama, T. Kobayashi, H. Oikawa, M. Honma, and A. Ichitara. Biochim. Biophys. Acta, **1384**, 387 (1998); Y. Hano, T. Nomura, and S. Ueda. J. Chem. Soc. Chem. Commun. 610 (1990); D.E. Cane and L. Guanglin. J. Am. Chem. Soc. **117**, 6633 (1995); D.J. Witter and J.C. Vederas. J. Org. Chem. **61**, 2613 (1996); H. Oikawa, T. Kobayashi, K. Katayama, Y. Suzuki, and A. Ichihara. J. Org. Chem. **63**, 8748 (1998); H. Oikawa, T. Yokota, T. Abe, A. Ichihara, S. Sakamora, Y. Yoshizawa, and J.C. Vedeyas. J. Chem. Soc. Chem. Commun. 1282 (1989).
5. S. Laschat. Angew. Chem. Int. Ed. Engl. **35**(3), 289 (1996).
6. M. Rance, O.W. Sorensen, G. Bodenhausen, G. Wagner, R.R. Ernst, and M. Rance. J. Magn. Reson. **74**, 557 (1987).
7. G. Bodenhausen and D.J. Ruben. Chem. Phys. Lett. **69**, 185 (1980).
8. K. Wuthrich. Biochem. Biophys. Res. Commun. **117**, 479 (1983).
9. G. Wider and K. Wuthrich. J. Magn. Reson. **102**, 239 (1993).
10. L. Lerner and A. Bax. J. Magn. Reson. **69**, 375 (1986).
11. A. Bax and M. Summers. J. Am. Chem. Soc. **108**, 2093 (1986).

© 2000 NRC Canada

Synthesis and structural characterization of zirconium complexes containing aminodiolate ligands and their use as Lewis acid catalysts

Pengcheng Shao, Roland A.L. Gendron, and David J. Berg

Abstract: A series of aminodiols $RN(CH_2CH_2C(OH)R'_2)_2$ (R, R′ = Me, Me **4**; Me, Ph **5**; *tert*-butyl, Me **6**; *tert*-Bu, Ph **7**; (*S*)-PhCH(Me), Me **8**) were prepared by the Michael addition of a primary amine to methyl acrylate followed by reaction of the resulting aminodiester with excess methyl or phenyl lithium. Reaction of two equivalents of the aminodiols **4–8** with tetrabenzylzirconium afforded the zirconium bis(aminodiolates) **10–14** in excellent yield. Complex **11** (R, R′ = Me, Ph) adopts a *cis*, *fac*-octahedral geometry in solution and in the solid state. Complexes **10–14** are fluxional in solution by NMR spectroscopy: small substituents at nitrogen and large substituents at the alkoxide carbons slow the rate of exchange. The chiral complex **14** functions as a Lewis acid catalyst in the nitroaldol (Henry) reaction and the oxidation of geraniol by *tert*-butyl hydroperoxide with modest enantioselectivities (30 and 46% enantiomeric excess (ee), respectively).

Key words: diol, Michael addition, zirconium, synthesis, structure, fluxional, alkoxide, Lewis acid, catalysis.

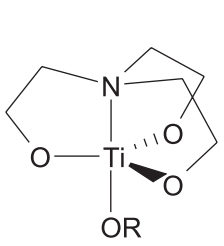
Résumé : On a préparé une série d'aminodiols, $RN(CH_2CH_2C(OH)R_2)_2$ (R, R′ = Me, Me **4**; Me, Ph **5**; *tert*-butyl, Me **6**; *tert*-butyl, Ph **7**; (*S*)-PhCH(Me), Me **8**), par le biais d'une addition de Michael d'une amine primaire sur l'acrylate de méthyle, suivie par une réaction de l'aminodiester qui en résulte avec un excès de méthyl ou de phényllithium. La réaction de deux équivalents des aminodiols **4–8** avec du tetrabenzylzirconium conduit aux bis(aminodiolates) de zirconium **10–14** avec d'excellents rendements. En solution ainsi qu'à l'état solide, le complexe **11** (R, R′ = Me, Ph) adopte une géométrie octaédrique *cis*, *fac*. En solution, la spectroscopie RMN indique que les complexes **10–14** sont en état de flux: des substituants de faibles tailles au niveau de l'azote et de taille importante au niveau des carbones des alcoolates ralentissent l'échange. Le complexe chiral **14** agit comme acide de Lewis pour catalyser la réaction de nitroaldol (Henry) et l'oxydation du géraniol par l'hydroperoxyde de *tert*-butyle avec des énantiosélectivités modestes (30 et 46% respectivement).

Mots clés : diol, addition de Michael, zirconium, synthèse, structure, fluxion, alcoolate, acide de Lewis, catalyse.

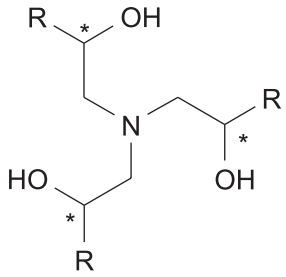
[Traduit par la Rédaction]

Introduction

Alkoxides (1), aryloxides (2), and siloxides (3) have been extensively used as ancillary ligands in group 4 organometallic chemistry. In addition, chelating biphenolates (4) and binaphtholates (5) have been employed, the latter being especially important in asymmetric catalysis due to its inherent C_2 symmetry. Chelating tripodal alkoxides based on triethanolamine have been extensively investigated by Verkade et al. (6) who demonstrated the hydrolytic stability of the chelate array in complexes such as **I**. Nugent has developed a C_3 chiral analog of **I**, using the homochiral triol **II**, which shows high catalytic enantioselectivity in the ring opening of meso epoxides by azidotrialkylsilanes (7).



I



II

Ligands such as those derived from triethanolamine or triol **II** are best suited to forming complexes with smaller metals such as titanium. In order to form monomeric zirconium complexes, additional steric bulk is required and this is most easily achieved by the introduction of two substituents at the alkoxide carbon. Replacement of one chelate arm by an alkyl group allows for further steric tuning by variation of the substituent at nitrogen and lowers the charge to two. This latter point is important because an aminodiolate ligand

Received October 26, 1999.

P. Shao, R.A.L. Gendron, and D.J. Berg.[1] Department of Chemistry, University of Victoria, P.O. Box 3065, Victoria, BC V8W 3V6, Canada.

[1]Author to whom correspondence should be addressed. Telephone: (250) 721-7161. Fax: (250) 721-7147. e-mail: DJBERG@UVIC.CA

© 2000 NRC Canada

Table 1. ^{1}H NMR spectra for aminodiesters **1–3** and aminodiols **4–8**.[a]

	*Me*N	*t-Bu*N	PhC*H*N	*Ph*CHN	*Me*CHN	NCH_2	CH_2CO	CO$_2$*Me*	CO*H*	C(O)*Me*$_2$	C(O)*Ph*$_2$
Aminodiester											
1	2.19			2.65 (t, 7.2)	2.41 (t, 7.2)	3.61					
2		1.01				2.78 (t, 7.6)	2.40 (t, 7.6)	3.62			
3			3.81 (q, 6.8)	7.27 (m)	1.33 (d, 6.8)	2.82 (dt)	2.40 (t, 7.0)	3.61			
				7.20 (m)		2.70 (dt)					
Aminodiol											
4	2.22					2.56 (t, 6.9)	1.61 (t, 6.9)		4.05 (br)	1.19	
5	2.22					2.36 (m)[b]	2.36 (m)[b]		5.22 (br)		7.38 (m)
											7.27 (m)
											7.18 (m)
6		0.95				2.58 (t, 6.9)	1.67 (t, 6.9)		4.54	1.22	
7		0.69				2.51 (m)[b]	2.47 (m)[b]		5.23		7.58 (*ortho*)
											7.13 (*meta*)
											7.00 (*para*)
8			3.93 (q)	7.3 (m)	1.36 (d)	2.68 (t)	1.60 (m)		4.19	1.10	
						2.57 (t)				1.00	

[a]Recorded at 360 MHz in $CDCl_3$; chemical shifts (δ) in ppm relative to TMS; multiplicity is not given for singlets.

[b]Overlapping resonances.

Table 2. ^{1}H NMR spectra for zirconium aminodiolates **10–14**.[a]

	*Me*N	*t-Bu*N	PhC*H*N	*Ph*CHN	*Me*CHN	NCH_2	CH_2CO	C(O)*Me*$_2$	C(O)*Ph*$_2$
10	2.14					3.46 (br t)	2.00 (br t)	1.52	
						3.40 (br t)	1.72[b]	1.48	
						1.20 (br)[b]	1.68[b]	1.28	
						1.3 (br)[b]	1.43[b]	1.22	
10[c]	2.20					2.50 (br)	1.60 (br)	1.33	
11[d]	1.56					3.14 (t, 12.4)	2.53 (dd, 15.3, 5.3)		8.25 (dd)
						2.94 (t, 12.3)	2.29 (dd, 15.2, 11.9)		8.19 (dd)
						1.38 (dd, 17.7, 5.5)	2.11 (dd, 14.0, 5.2)		6.7–7.7 (m)
						1.00 (dd, 12.7, 5.5)	1.93 (dd, 13.8, 5.1)		
12		1.11				2.90 (t, 6.7)	1.75 (t, 6.7)	1.25	
13	0.75					2.51 (br)	2.51 (br)		7.41 (d, 7.3)
									7.11 (t, 7.4)
									7.02 (d, 7.3)
14[e]			4.15 (q, 6.7)	7.0–7.3 (m)	1.54 (d, 6.7)	2.98 (m)	1.75 (m)	1.31	
						2.57 (m)	1.68 (m)	1.23	

[a]Recorded at 360 MHz in C_6D_6; chemical shifts (δ) in ppm relative to TMS; multiplicity and coupling constants (where measured) are given in brackets; singlets have not been denoted.

[b]Partially obscured.

[c]Recorded at 80°C.

[d]^{1}H–^{13}C COSY shows the following pairs of resonances are due to protons attached to the same carbon: 3.14, 1.00; 2.94, 1.38; 2.53, 2.29; 2.11, 1.93.

[e]Recorded at 70°C.

allows access to dialkyls, alkyl cations, imides, and many other important classes of compounds not possible for systems such as **I**. In this contribution, we describe the synthesis of several aminodiolate ligands and their zirconium coordination complexes. The nature of the alkoxide carbon and nitrogen substituents will be shown to control the fluxional behaviour of these complexes.

Experimental section

General procedures

All manipulations were carried out under an argon atmosphere, with the rigorous exclusion of oxygen and water, using standard glovebox (Braun MB150–GII) or Schlenk techniques. Tetrahydrofuran (THF), hexane, and toluene were dried by distillation from sodium benzophenone ketyl under argon immediately prior to use. Tetrabenzylzirconium was prepared according to the literature (8).

^{1}H, ^{13}C, and all variable temperature NMR spectra were recorded on a Bruker AC–300 or AMX–360 MHz spectrometer. Spectra were recorded in C_6D_6 or C_7D_8 solvent, previously distilled from sodium under argon, using 5 mm tubes fitted with a teflon valve (Brunfeldt). ^{1}H and ^{13}C NMR spectra were referenced to residual solvent resonances. ^{1}H NMR data for the ligands and their precursors are given in Table 1 while data for their zirconium complexes are listed in

© 2000 NRC Canada

Table 2; ^{13}C NMR data is given in the following section. Melting points were recorded using a Reichert hot stage and are not corrected. Elemental analyses were performed by Canadian Microanalytical, Delta, B.C. or Atlantic Microanalytical, Atlanta, Ga. Mass spectra were recorded on a Finnegan 3300 or a Kratos Concept H spectrometer using chemical ionization or electron impact (70 eV) sources, respectively.

Aminodiester preparation

The esters **1–3** were prepared by Michael addition of the appropriate amine to methyl acrylate. In a representative procedure, the amine (0.1 mol) was dissolved in 200 mL methanol in a 1 L round bottom flask fitted with a dropping funnel and reflux condenser. Dropwise addition of methyl acrylate (0.2 mol) over a period of 1 h followed by stirring at room temperature for 5 h was sufficient to complete the formation of ester **1**. In contrast, overnight reflux was necessary to complete the addition in the case of **3** and prolonged reflux (1 week) still resulted in a mixture of mono and diester for **2**. After cooling, methanol and any low boiling materials were removed by rotary evaporation using a water aspirator. The remaining liquids were then distilled under reduced pressure (0.1 Torr (1 Torr = 133.3 Pa)). In the case of **2**, the monoester was easily removed by fractional distillation leaving the pure diester as the higher boiling fraction.

*MeN($CH_2CH_2CO_2Me$)$_2$ (**1**)*: Yield: 95%; bp 120°C (0.1 Torr); $^{13}C(^1H)$ NMR ($CDCl_3$) δ: 172.8 (C=O), 52.4 (NCH_2), 51.5 (O*Me*), 41.7 (N*Me*), 32.3 (*CH_2*CO); MS(CI) *m*/*z*: 204 (M^+ +1, 100%), 130 (M^+ – (CH_2CO_2Me), 88%).

tert-*BuN($CH_2CH_2CO_2Me$)$_2$ (**2**)*: Yield: 52%; bp 110°C (0.1 Torr); $^{13}C(^1H)$ NMR ($CDCl_3$) δ: 173.1 (C=O), 55.1 (N*C*Me$_3$), 51.4 (O*Me*), 46.1 (NCH_2), 36.5 (*CH_2*CO), 27.1 (NC*Me*$_3$); MS(CI) *m*/*z*: 246 (M^+ +1, 92%), 230 (M^+ – Me, 15%), 188 (M^+ – *tert*-Bu, 80%), 172 (M^+ – (CH_2CO_2Me), 100%).

(S)-*PhMeC(H)N($CH_2CH_2CO_2Me$)$_2$ (**3**)*: Yield: 85%; bp 162–166°C (0.05 Torr); $^{13}C(^1H)$ NMR ($CDCl_3$) δ: 172.9 (C=O), 148.4 (*quat*-aryl*C*), 128.1 (aryl*C*), 127.6 (aryl*C*), 126.8 (aryl*C*), 58.9 (Ph*C*HN), 51.4 (O*Me*), 45.8 (NCH_2), 33.4 (*CH_2*CO), 16.2 (*Me*CHN).

Aminodiol preparation

Treatment of aminodiesters (**1–3**) with an excess of methyl or phenyllithium allowed isolation of a series of aminodiols (**4–8**). In a typical preparation, a 10-fold excess of methyl or phenyllithium was generated in situ from iodomethane and lithium or bromobenzene and *n*-butyllithium, respectively (diethyl ether solvent). The lithium reagent was then added by dropping funnel to a solution of the aminodiester in diethyl ether cooled to 0°C. The resulting turbid solution was stirred for 1 h at 0°C and allowed to warm to room temperature overnight. The reaction mixture was subsequently quenched with ice water, extracted with dichloromethane and the organic extract dried over anhydrous $MgSO_4$. Filtration and removal of the solvent under reduced pressure yielded the aminodiols as white crystals or colourless oils. The secondary amino alcohol **9** was obtained as a byproduct in the preparation of **8** and was separated by fractional distillation. Further drying over molecular sieves (4 Å) in toluene solution was carried out prior to reaction with tetrabenzylzirconium.

*MeN($CH_2CH_2C(OH)Me_2$)$_2$ (**4**)*: Colourless oil. Yield: 81%; $^{13}C(^1H)$ NMR ($CDCl_3$) δ: 70.6 (*C*OH), 53.9 (NCH_2), 41.9 (N*Me*), 38.8 (*CH_2*CO), 29.7 (C(OH)*Me*). MS(CI) *m*/*z*: 204 (M^+ +1, 100%), 186 (M^+ – OH, 11%), 130 (M^+ – ($CH_2C(OH)Me_2$), 71%). Anal. calcd. for $C_{11}H_{25}NO_2$: C, 64.98, H 12.39, N 6.89; found: C 65.31, H 11.90, N 7.14.

*MeN($CH_2CH_2C(OH)Ph_2$)$_2$ (**5**)*: White crystals. Yield: 48%; mp 170°C; $^{13}C(^1H)$ NMR ($CDCl_3$) δ: 147.2 (*quat*-aryl*C*), 128.1 (aryl*C*), 126.6 (aryl*C*), 125.8 (aryl*C*), 78.2 (*C*OH), 53.7 (NCH_2), 42.3 (N*Me*), 37.5 (*CH_2*CO); MS(CI) *m*/*z*: 480 (M^+ +29, 20%), 452 (M^+ +1, 100%), 374 (M^+ – Ph, 12%), 254 (M^+ – ($CH_2C(OH)Ph_2$), 5%). Anal. calcd. for $C_{31}H_{33}NO_2$: C 82.45, H 7.36, N 3.10; found: C 82.48, H 7.43, N 3.54.

tert-*BuN($CH_2CH_2C(OH)Me_2$)$_2$ (**6**)*: White crystals. Yield: 65%; mp 52°C; $^{13}C(^1H)$ NMR ($CDCl_3$) δ: 70.6 (*C*OH), 55.8 (N*C*Me$_3$), 46.5 (NCH_2), 42.4 (*CH_2*COH), 30.2 (C(OH)*Me*), 26.9 (NC*Me*$_3$); MS(CI) *m*/*z*: 274 (M^+ +29, 13%), 246 (M^+ +1, 100%), 230 (M^+ – Me, 21%), 172 (M^+ – ($CH_2C(OH)Me_2$), 78%). Anal. calcd. for $C_{14}H_{31}NO_2$: C 68.52, H 12.73, N 5.71; found: C 68.43, H 12.47, N 6.18.

tert-*BuN($CH_2CH_2C(OH)Ph_2$)$_2$ (**7**)*: White crystals. Yield: 75%; mp 120°C; $^{13}C(^1H)$ NMR ($CDCl_3$) δ: 147.5 (*quat*-aryl*C*), 128.1 (aryl*C*), 126.5 (aryl*C*), 125.9 (aryl*C*), 78.6 (*C*OH), 56.1 (N*C*Me$_3$), 47.2 (NCH_2), 40.0 (*CH_2*CO), 26.6 (NC*Me*$_3$); MS(CI) m/*z*: 512 (M^+ +29, 15%), 494 (M^+ +1, 100%), 296 (M^+ – ($CH_2C(OH)Ph_2$), 15%). A satisfactory elemental analysis was not obtained for this compound.

*(S)-PhMeC(H)N($CH_2CH_2C(OH)Me_2$)$_2$ (**8**)*: This compound was isolated as a sticky, colourless oil after column chromatography on silica gel (eluant: 95% ethyl acetate, 5% methanol). Yield: 62%; $^{13}C(^1H)$ NMR ($CDCl_3$) δ: 141.5 (*quat*-aryl*C*), 128.4 (aryl*C*), 128.1 (aryl*C*), 127.2 (aryl*C*), 70.5 (*C*OH), 58.2 (Ph*C*HN), 45.0 (NCH_2), 38.6 (*CH_2*CO), 29.6 (C(OH)*Me*), 29.3 (C(OH)*Me*), 14.7 (PhC*Me*N); MS(CI) *m*/*z*: 322 (M^+ +29, 12%), 294 (M^+ +1, 100%), 278 (M^+ – Me, 8%), 220 (M^+ – ($CH_2C(OH)Me_2$), 71%). Anal. calcd. for $C_{18}H_{31}NO_2$: C 73.68, H 10.65, N 4.77; found: C 72.58, H 10.40, N 5.22.

*(S)-PhMeC(H)NH($CH_2CH_2C(OH)Me_2$) (**9**)*: Colourless oil. ^1H NMR (C_6D_6) δ: 7.22–7.34 (5H, m, aryl*H*), 3.71 (1H, q, PhC(*H*)N), 3.6 (2H, br s, O*H* and N*H*), 2.73 (1H, dt, NCH_2), 2.69 (1H, dt, NCH_2), 1.62 (1H, dt, CH_2C(OH)), 1.48 (1H, dt, CH_2C(OH)), 1.39 (3H, d, PhC(*Me*)), 1.19 (3H, s, C(OH)*Me*), 1.07 (3H, s, C(OH)*Me*). The resonance at 3.6 ppm disappears after treatment with D_2O.

Zirconium complexes

Complexes **10–14** were prepared by adding a solution of two equivalents of aminodiol **4–8** in toluene to a stirred toluene solution of tetrabenzylzirconium. After stirring for 1 h, the volatiles were removed under reduced pressure and the crude solid product was recrystallized from a mixture of toluene and hexane.

© 2000 NRC Canada

*Zr{MeN(CH$_2$CH$_2$C(O)Me$_2$)$_2$}$_2$ (**10**)*: Yellow microcystalline powder. Yield: 96%; mp 206–212°C; ^{13}C(^{1}H) NMR (C_6D_6) **23°C** δ 73.7, 72.6 (*C*O); 58.0, 52.7 (N*C*H$_2$); 45.8 (N*Me*); 38.9, 38.8 (*C*H$_2$CO); 33.7, 33.1, 29.5 (br, two overlapping resonances), (C(O)*Me*); **80°C** δ 73.3 (*C*O), 56.0 (br, N*C*H$_2$), 46.1 (N*Me*), 39.3 (*C*H$_2$CO), 31.6 (C(O)*Me*); MS(EI) *m*/*z*: 493 (M^+, 31%), 407 (M^+ – CH$_2$CH$_2$C(O)Me$_2$, 81%), 114 (H$_2$CNCH$_2$CH$_2$C(O)Me$_2$, 100%). Anal. calcd. for $C_{22}H_{46}N_2O_4Zr$: C 53.51, H 9.39, N 5.67; found: C 53.71, H 9.28, N 5.94.

*Zr{MeN(CH$_2$CH$_2$C(O)Ph$_2$)$_2$}$_2$ (**11**)*: Colourless crystals. Yield: 90%; mp > 285°C; ^{13}C(^{1}H) NMR (C_6D_6) δ: 152.9, 151.2, 149.6, 149.4 (*quat*-aryl*C*); 126.3, 126.1, 126.0, 125.9 (*para*-aryl*C*); 129.3, 128.6, 128.5, 127.6, 127.3, 127.0, 126.7, 125.5 (*ortho*- and *meta*-aryl*C*); 83.7, 82.1 (*C*O); 58.3, 53.7 (N*C*H$_2$); 46.6 (N*Me*); 37.3, 36.5 (*C*H$_2$CO); MS(EI) *m*/*z*: 989 (M^+, 40%), 254 (H$_2$CNCH$_2$CH$_2$C(O)Ph$_2$, 100%). Anal. calcd. for $C_{62}H_{62}N_2O_4Zr$: C 75.19, H 6.31, N 2.83; found: C 75.51, H 6.37, N 2.78. Although X-ray analysis of this complex indicated (*vide infra*) that 1 equivalent of toluene was present in the crystals, grinding the product and exposure of the resulting powder to vacuum for 18 h was sufficient to remove this solvent.

*Zr{*tert-*BuN(CH$_2$CH$_2$C(O)Me$_2$)$_2$}$_2$ (**12**)*: Colourless crystals. Yield: 95%; ^{13}C(^{1}H) NMR (C_6D_6) δ: 76.7 (*C*O), 54.7 (N*C*Me$_3$), 43.6 (N*C*H$_2$), 42.6 (*C*H$_2$CO), 31.0 (NC*Me$_3$*), 28.8 (C(O)*Me$_2$*). Neither a satisfactory elemental analysis nor a mass spectrum could be obtained on this complex.

*Zr{*tert-*BuN(CH$_2$CH$_2$C(O)Ph$_2$)$_2$}$_2$ (**13**)*: Yellow crystals. Yield: 93%; mp 275–280°C; ^{13}C(^{1}H) NMR (C_6D_6) δ: 148.5 (*quat*-aryl*C*), 128.2 (aryl*C*), 126.9 (aryl*C*), 126.7 (aryl*C*), 85.9 (*C*O), 55.9 (N*C*Me$_3$), 45.4 (N*C*H$_2$), 42.0 (*C*H$_2$CO), 28.0 (NC*Me$_3$*); MS(EI) *m*/*z*: 1072 (M^+, 55%), 1057 (M^+ – Me, 100%), 1015 (M^+ – *tert*-Bu, 56%), 995 (M^+ – Ph, 12%), 877 (M^+ – CH$_2$CH$_2$CPh$_2$, 15%). A satisfactory elemental analysis was not obtained for this complex.

*Zr{(S)-PhMeC(H)N(CH$_2$CH$_2$C(O)Me$_2$)$_2$}$_2$ (**14**)*: Yellow microcrystalline powder. Yield: 92%; ^{13}C(^{1}H) NMR (C_6D_6) **70°**C δ: 144.1 (*quat*-aryl*C*), 128.7 (*ortho*-aryl*C*), 128.4 (*meta*-aryl*C*), 127.2 (*para*-aryl*C*), 75.4 (*C*O), 62.0 (Ph*C*HN), 46.5 (N*C*H$_2$), 40.5 (*C*H$_2$CO), 32.1 (C(O)*Me*), 30.6 (C(O)*Me*), 22.7 (PhC(*Me*)N); MS(EI) *m*/*z*: 673 (M^+, 100%), 658 (M^+ – Me, 82%). Anal. calcd. for $C_{36}H_{58}N_2O_4Zr$: C 64.15, H 8.67, N 4.15; found: C 64.28, H 8.31, N 4.13.

Lewis acid catalysis

Hetero Diels–Alder reaction

Ethyl vinyl ether was dried for several days over molecular sieves and then vacuum transferred (5 mL) to a Schlenk flask fitted with a Kontes valve. Under an argon atmosphere, 0.2 mL *trans*-crotonaldehyde was added to the ethyl vinyl ether solution followed by a solution of **14** (5 mol%) in 0.5 mL toluene. The flask was sealed and the reaction mixture was stirred at room temperature for 4 days. At the end of this period, the reaction vessel was opened to air and the solvent was removed by rotary evaporation (water aspirator, 35°C). Examination of the residue by ^{1}H NMR revealed the presence of trace *cis*-2-ethoxy-4-methyl-3,4-dihydro-2-pyran (9) δ: 6.20 (1H, dd, =C*H*CHMe, *J* = 6, 2 Hz), 4.87 (1H, dd, OC*H*(OEt), *J* = 9, 2 Hz), 4.53 (1H, m, =C*H*(O)). The remaining resonances of this product were obscured by unreacted starting material and free ligand signals.

Nitroaldol reaction

A solution of **14** (5 mol%) in 10 mL dry nitromethane was prepared under argon in a Kontes valve flask. Approximately 0.5 g of ArC(O)H (Ar = phenyl or β-naphthyl) was added, the flask sealed and the reaction mixture stirred at room temperature for up to 7 days. Samples were periodically removed and examined by ^{1}H NMR to monitor the progress of the reaction. At the end of each run, the solvent was removed under vacuum and the residue was chromatographed on silica gel using 75:25 CH_2Cl_2–hexane as eluant. The dinitro products eluted first along with any unreacted aldehyde followed by the β-nitroalcohol.

PhCH(OH)CH$_2$NO$_2$: ^{1}H NMR ($CDCl_3$) δ: 7.37 (5H, m, Ph*H*), 5.45 (1H, m, C*H*(OH)), 4.54 (2H, m, C*H*$_2$NO$_2$); ^{13}C(^{1}H) δ: 138.08 (*quat*-aryl*C*), 129.05, 129.00, 125.93 (aryl*C*), 81.21 (*C*H$_2$NO$_2$), 71.01 (*C*H(OH)). The ^{1}H and ^{13}C data agree with that reported in the literature (10, 11, 12).

PhCH(CH$_2$NO$_2$)$_2$: ^{1}H NMR ($CDCl_3$) δ: 8.09 (2H, d, Ph*H*), 7.63 (1H, m, Ph*H*), 7.35 (2H, m, Ph*H*), 4.76 (4H, dd, C*H*$_2$NO$_2$, *J* = 1.8, 7.0 Hz), 4.30 (1H, pentet, C*H*(CH$_2$NO$_2$)$_2$, *J* = 7.0 Hz); ^{13}C(^{1}H) δ: 133.88, 129.61, 128.49, 127.35 (aryl*C*), 76.73 (*C*H$_2$NO$_2$), 41.77 (*C*H(CH$_2$NO$_2$)$_2$). The ^{1}H and ^{13}C NMR data are very similar to those reported in the literature (13).

β-*NaphCH(OH)CH$_2$NO$_2$*: ^{1}H NMR ($CDCl_3$) δ: 7.85 (4H, m, β-naph*H*), 7.49 (2H, m, β-naph*H*), 7.42 (1H, d, β-naph*H*), 5.60 (1H, br d, C*H*(OH)), 4.61 (2H, m, C*H*$_2$NO$_2$); ^{13}C(^{1}H) δ: 135.40, 133.42, 133.19 (*quat*-β-naph*C*), 129.03, 128.07, 127.80, 126.74, 126.71, 125.35, 123.20 (β-naph*C*), 81.19 (*C*H$_2$NO$_2$), 71.16 (*C*H(OH)). Exact Mass MS, anal. calcd. for $C_{12}H_{11}NO_3$: 217.0739; found: 217.0743 amu.

β-*NaphCH(CH$_2$NO$_2$)$_2$*: ^{1}H NMR ($CDCl_3$) δ: 7.78–8.00 (4H, m, β-naph*H*), 7.49–7.68 (2H, m, β-naph*H*), 7.36 (1H, d, β-naph*H*), 4.85 (4H, d, C*H*$_2$NO$_2$, $^3J_{HH}$ = 7.2 Hz), 4.48 (1H, pentet, C*H*(CH$_2$NO$_2$)$_2$, $^3J_{HH}$ = 7.2 Hz); ^{13}C(^{1}H) δ: 133.31, 133.24, 131.37 (*quat*-β-naph*C*), 129.73, 127.92, 127.77, 127.04, 126.98, 124.22 (β-naph*C*), 76.73 (*C*H$_2$NO$_2$), 41.92 (*C*H(CH$_2$NO$_2$)$_2$). Exact Mass MS, anal. calcd. for $C_{13}H_{12}N_2O_4$: 260.0797; found: 260.0797 amu.

Geraniol oxidation

Geraniol (0.309 g, 2.0 mmol) was dissolved in 10 mL dry, distilled CH_2Cl_2 and a solution of **14** (0.050 g, 3.7 mol%) in 5 mL CH_2Cl_2 was added under argon in a Kontes flask. After stirring 10 min, 0.5 mL of a 5 M solution of *tert*-butyl hydroperoxide in decane was added via syringe (2.5 mmol). The flask was sealed and the reaction mixture stirred at room. Aliquots (1 mL) were withdrawn daily and examined by ^{1}H NMR to monitor the progress of the reaction. The reaction appeared to reach a plateau at 65% completion after 3 days so an additional 2.5 mL *tert*-butyl hydroperoxide was added. The reaction was stopped after 6 days at ca. 85% completion since no further conversion was evident. The reaction mixture was extracted with 10 mL water and the

© 2000 NRC Canada

CH_2Cl_2 phase was taken to dryness. Chromatography on silica gel using 50:50 Et_2O–hexane as eluant removed all traces of free ligand from the product but did not separate the geraniol from its epoxide. Geraniol epoxide was identified by NMR (14): ^1H ($CDCl_3$) δ: 5.00 (1H, m, =C*H*), 3.75–3.80 and 3.60–3.65 (2H, m, CH_2OH), 2.88 (1H, m, C*H*(O)), 1.98–2.08 (2H, m, =CHCH_2), 1.63 and 1.56 (3H, s and 3H, =C*Me*$_2$), 1.39–1.49 (2H, m, CH_2C(O)), 1.28 (3H, s, CH_2C*Me*(O)); $^{13}C(^1H)$ δ 132.10 (=*C*Me$_2$), 123.31 (=*C*HCH$_2$), 63.13 (*C*H(O)), 61.33 (*C*H_2OH), 59.27 (*C*H_2CMe(O)), 38.48 (=CH*C*H_2), 25.64 (CH_2C*Me*(O)), 23.64 (*C*H_2CH(O)), 17.61, and 16.71 (=C*Me*$_2$).

Epoxide cleavage with azidotrimethylsilane

Dry, distilled cyclohexene oxide (0.1 mL, 1 mmol) was added to a solution of **14** (0.037g, 5 mol%) dissolved in 5 mL toluene under argon in a Kontes flask. Neat azidotrimethylsilane (Aldrich, 0.13 mL, 1.0 mmol) was added to the stirred solution via syringe and the vessel was sealed. The reaction was allowed to continue until no cyclohexene oxide remained (^1H NMR, 4 days). Removal of the solvent under reduced pressure afforded a colourless, viscous oil which possessed an extremely complex NMR spectrum. This material was shown to contain cyclohexanol, cyclohexanone, and at least eight other compounds by GC analysis.

Determination of enantiomeric excess

Enantiomeric excesses were determined using Yb(hfc)$_3$ (hfc = 3-(heptafluoropropylhydroxymethylene)-(+)-camphorate), Aldrich). For the β-nitroalcohols, splitting of the resonances due to the α-hydrogens C*H*(OH)) was monitored as a function of lanthanide shift reagent (LSR) concentration. The ee's reported for these products are very crude estimates since the α-hydrogen resonances of the two enantiomers were only partially resolved. In the case of geraniol oxidation, the resonances due to the methyl groups of the two enantiomeric epoxides were fairly well resolved and better estimates of the ee was obtainable in this case (See Fig. S2 of the supporting information).

X-ray crystallographic studies

Crystallographic data for **11** is summarized in Table 3. Crystals of **11** (0.4 × 0.4 × 0.4 mm) were loaded into glass capillaries in the glove box and subsequently flame sealed. The crystals were transferred to a Nonius CAD4F diffractometer equipped with Mo Kα radiation. The unit cell of **11** was refined using 24 reflections in the 2θ range of 30–35°. An experimental density was not obtained because of the air sensitivity of the compound. Five standard reflections, measured periodically during data collection (4, 2, –12; 2, –6, 2; 3, 1, 11; 7, 0, 0; 0, 7, 0), showed less than a 3% decline in intensity during data collection. Intensity measurements were collected over one half of the sphere. After the usual data reduction procedures, including an absorption correction (max and min transmission: 0.9939, 0.8507) according to a measured PSI scan, the structure was solved by Patterson methods.[2] The refinements minimised $\Sigma w((|F_o| - |F_c|)^2)$ and proceeded normally using teXsan98.[3] Criteria for inclusion of reflections were $I > 3.0\sigma(I)$. The weighting scheme was determined by counting statistics using $w = 1/(\sigma^2(F) + 0.001F^2)$. Convergence was satisfactory: max shift/esd <0.01; the largest positive and negative peaks in the final difference map were 3.26 and –0.86 e/Å^3, respectively. A total of 630 parameters were refined; the toluene of solvation was refined as a rigid group. Hydrogen atoms were placed in calculated positions. No intermolecular contacts shorter than 3.5 Å were observed. The structural perspective plots were drawn using ZORTEP.[4] Complete tables of bond distances, angles, and anisotropic temperature parameters have been deposited as supplementary material.[5]

Table 3. Crystallographic data for **11**.

Formula	$C_{69}H_{70}N_2O_4Zr$
Fw	1082.54
Cryst syst	triclinic
Space group	$P\bar{1}$ (No. 2)
a (Å)	15.773(4)
b (Å)	10.889(2)
c (Å)	19.817(6)
α (°)	89.91(2)
β (°)	112.56(2)
γ (deg)	87.78(2)
V (Å^3)	3140.2(14)
Z	2
ρ (calcd.) (g cm^{-3})	1.145
μ (cm^{-1})	2.21
Radiation, λ (C)	Mo Kα, 0.7107
T	ambient
$2\theta_{max}$ (deg)	44.9
No. of observed reflections	8190
No. of unique reflections	6568
R^a, $R_w{}^b$	0.099, 0.169

$^aR = \Sigma(|F_o|-|F_c|)/\Sigma|F_o|$.
$^bR_w = [\Sigma w(|F_o|-|F_c|^2)/\Sigma w(|F_o|)^2]^{1/2}$.

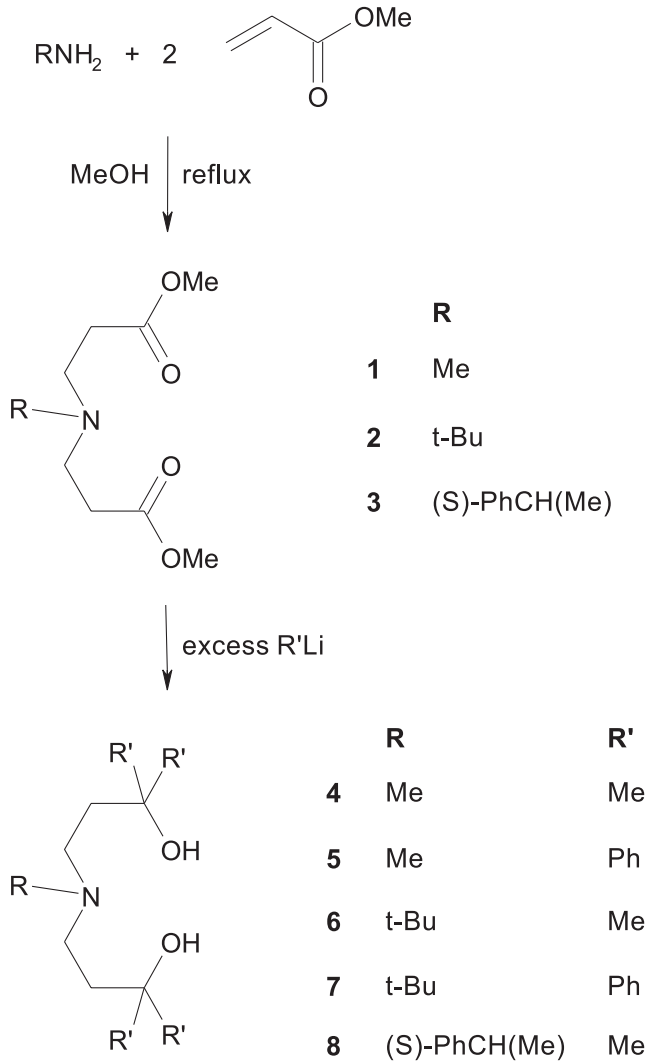
Results and discussion

The aminodiol ligands **4–8** were prepared in good yield by the two step procedure shown in Scheme 1. As might be expected, the rate of Michael addition to methyl acrylate is strongly dependent on the steric bulk of the amine. Thus, *tert*-butylamine fails to give complete conversion to the aminodiester even after 1 week at methanol reflux. Nevertheless, pure aminodiester **2** is easily obtained by fractional

[2] P.T. Beurskens, G. Admiraal, G. Beurskens, W.P. Bosman, R. De Gelder, R. Israel, and J.M.M. Smits. DIRDIF94: The DIRDIF94 Program System. Technical Report of the Crystallography Laboratory, University of Nijmegen, The Netherlands. 1994.
[3] Molecular Structure Corporation. teXsan for Windows Version 1.05. The Woodlands, Tex. 1998.
[4] L. Zsolnai. ZORTEP. University of Heidelberg, Germany. 1995.
[5] Complete atom labelling scheme, atomic positional parameters and B_{eq}, intramolecular distances and angles involving the nonhydrogen atoms, and anisotropic displacement parameters for **11**; as well as geraniol oxidation catalyzed by **14**: methyl region of the 1H NMR with added LSR (Yb(hfc)$_3$), have been deposited as supplementary material and may be purchased from: The Depository of Unpublished Data, Document Delivery, CISTI, National Research Council Canada, Ottawa, Ontario, Canada, K1A 0S2.

© 2000 NRC Canada

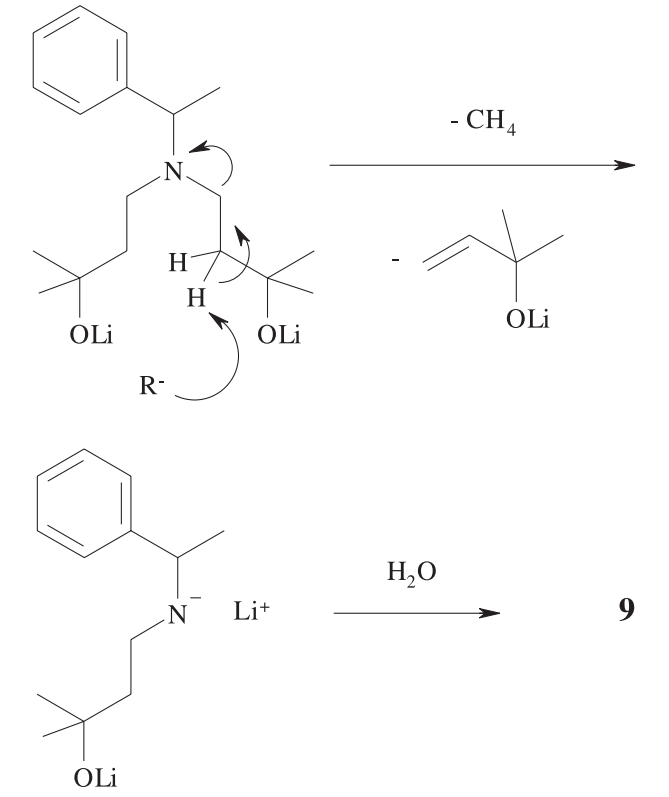
Scheme 1.



distillation of the reaction mixture. Treatment of aminodiesters **1**–**3** with a large excess of methyl or phenyl lithium afforded the aminodiols **4**–**8** after aqueous work up. In the case of **8**, a secondary amine byproduct (**9**) was also observed. Presumably, this product results from competing deprotonation of the protons α to the ester carbonyl by methyl lithium (Scheme 2). Attempts to prepare the R′ = Ph analog of **8** failed, possibly due to even more extensive α-deprotonation with phenyl lithium. The aminodiols bearing methyl alkoxide substituents were obtained as oils (**4**, **8**) or low melting solids (**6**) while those bearing phenyl substituents (**5**, **7**) were isolated as colourless crystals.

Addition of two equivalents of aminodiol **4**–**8** to tetrabenzylzirconium resulted in formation of the corresponding bis(ligand) complexes **10**–**14** (eq. 1). The complexes bearing methyl alkoxide substituents (**10**, **12**, and **14**) were extremely soluble in hexane and could not be purified by recrystallization. However, both **10** and **14** were isolated as analytically pure solids after removal of solvent. The phenyl substituted complexes, **11** and **13**, could be recrystallized from toluene–hexane mixtures.

Scheme 2.



[1] $2\ H_2L + Zr(CH_2Ph)_4 \rightarrow ZrL_2 + 4\ PhCH_3$

H_2L = **4–8** **10–14**

Molecular ions showing the expected isotopic distribution were observed for **10**, **11**, **13**, and **14**. Despite the observation of molecular ions by mass spectroscopy, dimeric and oligomeric solution structures are very common for zirconium alkoxides (15). However, cryoscopic molecular weight measurements on **10–14** indicated that these complexes are also monomeric in solution. Thus it appears that two aminodiolate ligands are sufficient to saturate the zirconium coordination sphere.

The monomeric solution structures of **10–14** greatly facilitate structural studies by NMR spectroscopy. Proton NMR evidence points to a *cis*, *fac*-octahedral (C_2) geometry (Fig. 1(*a*)) for both **10** and **11** since eight resonances are observed in the room temperature spectrum for the backbone CH_2 protons (Table 2). A *trans*, *fac* geometry (Fig. 1(*b*)) can be excluded since it would have C_{2h} symmetry and must therefore exhibit only four CH_2 resonances. Although a *trans*, *mer* ligand arrangement is also theoretically possible, the geometry of the aminodiolate ligand itself appears predisposed to form a *fac* donor arrangement. The *cis*, *fac* structure was confirmed in the solid state for **11** by an X-ray crystallographic study (*vide infra*).

The ^{1}H NMR resonances of **10** are not as sharp as those of **11** at room temperature suggesting that a dynamic process may be operative for the former. Indeed, when a NMR sample of **10** is heated, further broadening of the backbone

© 2000 NRC Canada

Fig. 1. Possible structures for zirconium bis(aminodiolate) complexes.

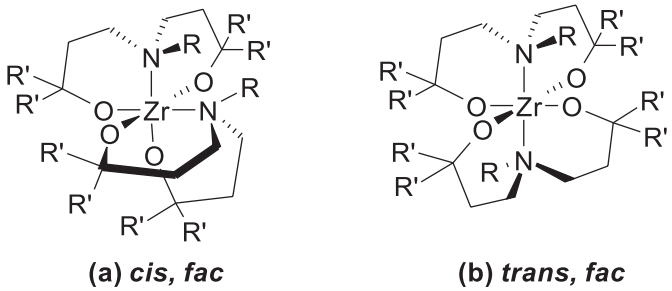
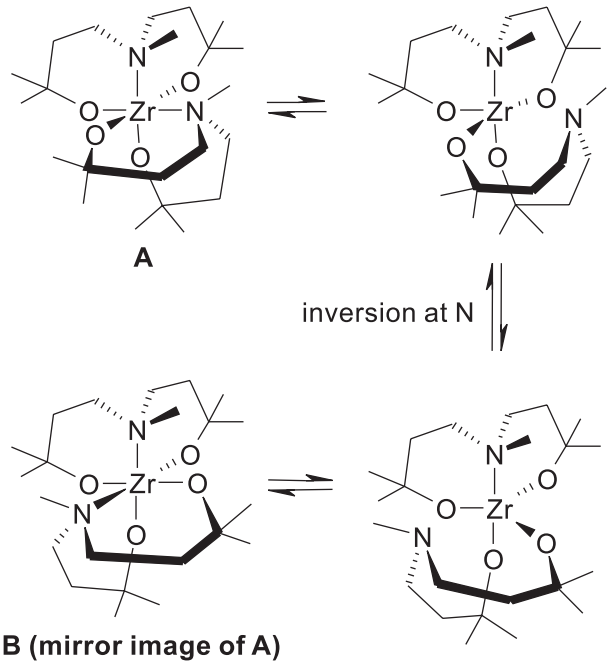
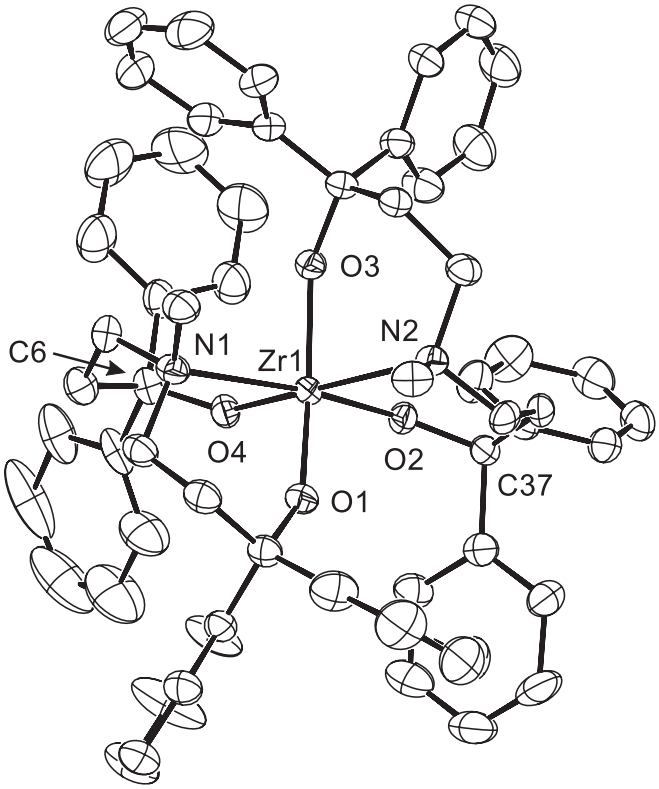


Fig. 2. A possible fluxional process for **10**.



resonances occurs leading to coalescence at 42°C. At 80°C, a simple spectrum is obtained which shows a single resonance integrating to eight protons for each chemically distinct CH_2 (Table 2). From the coalescence temperature, the free energy of activation for this process is calculated to be $\Delta G^{\ddagger} = 66.7 \pm 0.5$ kJ mol^{-1}.[6] A process that accounts for this behaviour is shown in Fig. 2. Amine dissociation to produce a five coordinate complex, followed by inversion at nitrogen and re-coordination exchanges all backbone CH_2 resonances of a given type. It should be noted that nitrogen inversion is required to exchange inequivalent protons on each backbone carbon; simple pseudorotation of the five coordinate intermediate can be ruled out since this will only exchange protons on different arms. Inversion at nitrogen is normally a low energy process (17) and dissociation of a single amine is also expected to require relatively little energy (18), so the low activation energy required to exchange the backbone protons is not surprising. A similar process has been proposed to account for the equivalence of the chelate arm resonances in the trigonal bipyramidal complex $Zr\{(Me_3Si)N(CH_2CH_2N(SiMe_3))_2\}\{CH_2Ph\}_2$ (19).

Fig. 3. ZORTEP plot (30% probability) of **11** (toluene of solvation omitted).



The ^{1}H NMR resonances of **11** also broaden on heating but in this case coalescence is not reached even at 110°C. The much higher barrier to exchange for **11** deserves some comment. Of the two processes involved, amine dissociation will be enhanced by steric congestion at the metal centre while nitrogen inversion may be hindered if it requires bulky substituents to pass by one another. Since the alkyl substituent at nitrogen is the same (methyl) in **10** and **11**, it seems reasonable to assume that amine dissociation will be favoured in **11** due to the phenyl substituents at the alkoxide carbon creating a more crowded coordination environment. Therefore the observation of a higher barrier to exchange can reasonably be ascribed to the second process, inversion at nitrogen. It is possible that the phenyl groups at the alkoxide carbon hinder the necessary rearrangement of the ligand required during inversion since they must pass by one another in order for the amine to recoordinate to the metal centre.

The simplicity of the NMR spectra for **12–14** (Table 2) indicates that these complexes are already undergoing a rapid fluxional process at room temperature. The presence of bulky groups at nitrogen (**12** and **13**, *tert*-butyl; **14**, α-methylbenzyl) likely leads to weaker amine binding which should enhance the rate of exchange. In fact, the observation

[6] The free energy of activation was calculated from the coalescence temperature (T_c) using the equal population, two site exchange equation: $\Delta G^{\ddagger} = (1.912 \times 10^{-2})(T_c)[9.972 + \log(T_c/\delta\nu)]$ in kJ mol^{-1} where $\delta\nu$ is the separation of the resonances in Hz at coalescence and T_c is in K (16). The error in $\Delta G^{\ddagger}$ was estimated to be ±0.5 kJ mol^{-1} assuming a liberal error of ±2°C in estimation of T_c.

© 2000 NRC Canada

Table 4. Selected bond distances and angles for **11**.[a]

Distances (Å)			
Zr(1)—O(1)	1.996(5)	Zr(1)—N(2)	2.562(5)
Zr(1)—O(2)	1.971(4)	O(1)—C(1)	1.399(9)
Zr(1)—O(3)	1.976(5)	O(2)—C(6)	1.412(8)
Zr(1)—O(4)	1.961(4)	O(3)—C(32)	1.415(8)
Zr(1)—N(1)	2.545(5)	O(4)—C(37)	1.406(7)
Angles (°)			
O(1)-Zr(1)-O(2)	101.9(2)	O(3)-Zr(1)-N(1)	82.8(2)
O(1)-Zr(1)-O(3)	147.0(2)	O(3)-Zr(1)-N(2)	77.9(2)
O(1)-Zr(1)-O(4)	100.0(2)	O(4)-Zr(1)-N(1)	171.5(2)
O(1)-Zr(1)-N(1)	78.2(2)	O(4)-Zr(1)-N(2)	79.5(2)
O(1)-Zr(1)-N(2)	82.8(2)	N(1)-Zr(1)-N(2)	108.4(2)
O(2)-Zr(1)-O(3)	100.9(2)	Z(1)-O(1)-C(1)	152.3(4)
O(2)-Zr(1)-O(4)	92.7(2)	Zr(1)-O(2)-C(6)	145.8(4)
O(2)-Zr(1)-N(1)	79.6(2)	Zr(1)-O(3)-C(32)	153.5(4)
O(2)-Zr(1)-N(2)	171.5(2)	Zr(1)-O(4)-C(37)	147.6(4)
O(3)-Zr(1)-O(4)	102.4(2)		

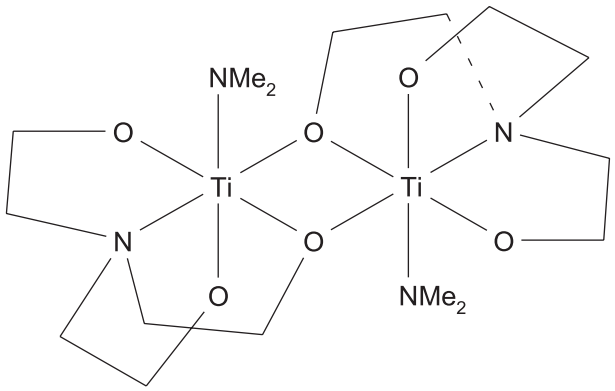
[a]Estimated standard deviations are given in parentheses.

that the ^{1}H NMR spectra for **12** and **14** remain sharp to –80°C may indicate that these complexes exist as ground state five coordinate structures similar to that shown in Fig. 2. At present, there is no evidence to distinguish this possibility from a fluxional six coordinate structure such as those shown in Fig. 1. The observation of fluxional behaviour for **13** even at room temperature appears to contradict the explanation given for the static behaviour of **11** at the same temperature. However, it is noteworthy that **13** is considerably more crowded than **11** and it is possible that exchange proceeds for **13** by dissociation of both amine nitrogens to give a four coordinate intermediate. In any case, further attempts to study the fluxional behaviour of this complex were hindered by its rather low solubility.

The solid state structure of **11** was investigated by X-ray crystallography. The structure is shown in Fig. 3 and significant bond lengths and angles are collected in Table 4. In agreement with the solution structure, the complex consists of a distorted *cis*, *fac*-octahedral coordination environment. The zirconium-amine nitrogen bond lengths in **11** (2.545(5), 2.562(5) Å) are shorter than might be predicted from the closely related five coordinate complexes $Zr\{(Me_3Si)N(CH_2CH_2N(SiMe_3))_2\}\{Cl\}\{CH(SiMe_3)_2\}$ and $Zr\{(Me_3Si)N(CH_2CH_2N(SiMe_3))_2\}\{BH_4\}_2$ (2.770(5) and 2.561(4), respectively) (20).[7] This is not surprising because the steric and electronic effects of the trimethylsilyl substituent at nitrogen combine to make this a much less basic amine than the methyl substituted amine in **11**. Obviously, the presence of a bulky alkyl group contributes to the very long Zr—N distances in $Zr\{(Me_3Si)N(CH_2CH_2N(SiMe_3))_2\}\{Cl\}\{CH(SiMe_3)_2\}$.

In comparison, the titanium-amine nitrogen bond in $\{Ti[NMe_2][N(CH_2CH_2O)_3]\}_2$ is only 2.270(2) Å, much shorter than that observed in **11**, even allowing for the difference in metal ionic radii (ca. 0.12 Å in six coordination) (6*a*, 21). However, the apical nitrogen of an atrane ligand is forced into close proximity with the metal in order to accommodate coordination of the three pendant alkoxide groups. Since the aminodiolate ligand in **11** possesses only two pendant alkoxide groups, the amine nitrogen is not constrained to a particular distance and can adopt a distance reflective of the strength of the amine binding.

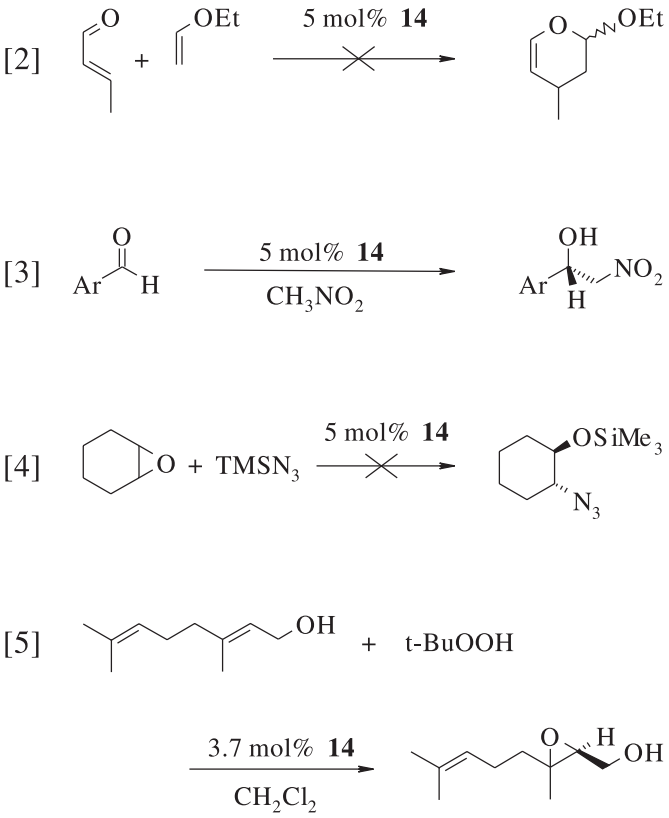
The zirconium-alkoxide oxygen distances in **11** (1.961(4)–1.996(5) Å) are very similar to those observed in the related six coordinate complexes, Zr[*O*-2,6-*tert*-$Bu_2C_6H_3]_2$[OCH(Me)NC_5H_3CH(Me)O][py] ($Zr\text{-}O_{aryloxide}$ = 2.006(5), 2.015(6); $Zr\text{-}O_{alkoxide}$ = 1.988(5), 2.034(5) Å) (22) and $Cp_2Zr(m\text{-}OCH_2(C_6H_4)CH_2O)ZrCp_2$ (1.946(6) Å) (1*b*). The Zr-O-C angles in **11** (145.8(4)°–153.5(4)°) are similar to those in the alkoxide-bridged zirconocene above (155.1(5)°). Interestingly, the Zr-O-C bond angles for the tridentate ligand in Zr[*O*-2,6-*tert*-$Bu_2C_6H_3]_2$[OCH(Me)NC_5H_3CH(Me)O][py] are only 126.7(6)° and 129.5(6)° while the $Zr\text{-}O\text{-}C_{aryl}$ angles in the same complex are nearly linear (172.8(5)°, 178.8(5)°). Presumably, the intermediate angles in **11** do not reflect any significant angular strain.



III

[7]Typically, five–coordinate zirconium complexes display bond lengths 0.06 C shorter than their six-coordinate analogues (24). The predicted Zr—N bond lengths for **11** based on these two complexes would therefore be 2.83 and 2.62 Å.

© 2000 NRC Canada



Verkade rationalized the *cis* arrangement of the amine and amide groups in **III** in terms of electronic properties of the ligands: strongly electron donating amide and amine groups preferring to occupy sites *trans* to the more electron withdrawing alkoxide ligands and *cis* with respect to one another (6). It is possible similar electronic factors are responsible for the *cis* disposition of the amine donors in **11** although steric effects cannot be ruled out.

Chiral complex **14** was also briefly screened for Lewis acid catalytic activity using four typical test reactions (eq. 2–5). The complex proved to be an effective catalyst for the nitroaldol (Henry) reaction (eq. 3)[8] and for the oxidation of geraniol with *tert*-butyl hydroperoxide (eq. 5). The nitroaldol reaction proceeded smoothly to give the β-nitroalcohols in good yield but low enantiomeric excess (Table 5). At longer reaction times (>48 h), in nitromethane as solvent, increasing amounts of the dinitro products $ArCH(CH_2NO_2)_2$ were obtained.

The oxidation of geraniol slowly proceeded over a period of 4 days and it was necessary to add excess *tert*-butyl hydroperoxide to achieve good yields. Nevertheless, the reaction does not proceed in the absence of **14** and the product is formed with very high selectivity (no other products derived from geraniol were detected at any stage of the reaction). That even moderate enantioselectivity is obtained (46% ee, Table 5) is somewhat surprising because ligand loss might be expected in the presence of a large excess of geraniol and *tert*-butyl hydroperoxide. Indeed, small amounts of free ligand were observed in the reaction mixture by ^1H NMR after one day.

Table 5. Lewis acid catalyst screen for **14**.

Reaction[a]	Yield (%)[b]	ee (%)[c]
Hetero-Diels Alder (eq. 2)	5[d]	—
Henry (eq. 3) Ar = Ph	70[e]	25
Ar = β-Naph	75[f]	30
Geraniol oxidation (eq. 4)	80[g]	46
Epoxide cleavage (eq. 5)	0	—

[a]25°C.
[b]Isolated yield.
[c]Determined using $Yb(hfc)_3$.
[d]96 h, ethyl viny ether.
[e]96 h, CH_2NO_2 solvent, 8% $PhCH(CH_2NO_2)_2$.
[f]70 h, CH_2NO_2 solvent, 15% β-$NaphCH(CH_2NO_2)_2$.
[g]7 days, CH_2Cl_2.

Attempts to carry out a hetero Diels–Alder reaction (eq. 2) or the addition of azidotrimethylsilane to cyclohexene oxide (7*a*) (eq. 4) using **14** as a catalyst failed. The hetero Diels–Alder reaction is particularly challenging because it requires a fine balance of Lewis acidity: catalysts that are too acidic (eq. $Yb(OTf)_3$) result in ethyl vinyl ether (dienophile) polymerization, while those that are too mild do not effect the reaction (23). Less than a 5% yield of the desired dihydropyran product was obtained after 4 days at room temperature using **14** as catalyst. No polymerization of ethyl vinyl ether was observed indicating that **14** is indeed a mild Lewis acid. This result is not surprising because the alkoxide groups are good donors and relatively low zirconium Lewis acidity is to be expected. In contrast, reaction of azidotrimethylsilane with cyclohexene oxide in the presence of **14** resulted in the slow consumption of the starting materials and formation of a complex mixture of products. GC analysis showed that at least 10 compounds were formed in significant amounts during this reaction. The reason for the lack of selectivity is not clear.

In summary, the aminodiolate ligands developed here form simple, monomeric zirconium complexes of good hydrocarbon solubility. The tendency towards amine dissociation and fluxional behaviour is dependent on the nature of the substituents at nitrogen and the alkoxide carbon. The most stable six coordinate geometry is obtained with small nitrogen substituents (e.g., methyl) and large alkoxide substituents (e.g., phenyl). The chiral complex **14** is a mild Lewis acid catalyst for the nitroaldol reaction and the oxidation of geraniol with low to moderate stereocontrol.

Acknowledgements

We thank Mrs. C. Greenwood for assistance in recording the NMR spectra and Dr. David McGillivray for obtaining the mass spectra. This research was supported by the NSERC (Canada) and a University of Victoria Internal Research Grant (to D.J.B.)

[8] Strictly speaking, the nitroaldol reaction is not an example of simple Lewis acid catalysis because the alkoxide groups must act as bases in the deprotonation of nitromethane. However, it is likely that coordination of the aldehyde also takes place and that this plays some role in rate acceleration.

© 2000 NRC Canada

References

1. See for example: (*a*) T.V. Lubben, P.T. Wolczanski, and G.D. Van Duyne. Organometallics, **3**, 977 (1984); (*b*) D.W. Stephan. Organometallics, **9**, 2718 (1990).
2. (*a*) S.L. Latesky, A.K. McMullen, G.P. Niccolai, and I.P. Rothwell. Organometallics, **4**, 902 (1985); (*b*) P.E. Fanwick, A.E. Ogilvy, and I.P. Rothwell. Organometallics, **6**, 73 (1987); (*c*) L.M. Kobriger, A.K. McMullen, P.E. Fanwick, and I.P. Rothwell. Polyhedron, **8**, 77 (1989).
3. (*a*) P.T. Wolczanski. Polyhedron, **14**, 3335 (1995); (*b*) R.E. LaPointe, P.T. Wolczanski, and J.F. Mitchell. J. Am. Chem. Soc. **108**, 6582 (1986).
4. A. van der Linden, C.J. Schaverien, N. Miejboom, C. Ganter, and A.G. Orpen. J. Am. Chem. Soc. **117**, 3008 (1995).
5. (*a*) M.T. Reetz, S.H. Kyung, C. Bolm, and T. Zierke. Chem. Ind. (London), 824 (1986); (*b*) D. Seebach, A.K. Beck, R. Imwinkelreid, S. Roggo, and A. Wonnacott. Helv. Chim. Acta, **70**, 954 (1987); (*c*) K. Mikami, Y. Motoyama, and M. Terada. J. Am. Chem. Soc. **116**, 2812 (1994).
6. (*a*) A.A. Naiini, W.M.P.B. Menge, and J.G. Verkade. Inorg. Chem. **30**, 5009 (1991); (*b*) A.A. Naiini, S.L. Ringrose, Y. Su, R.A. Jacobson, and J.G. Verkade. Inorg. Chem. **32**, 1290 (1993).
7. (*a*) W.A. Nugent. J. Am. Chem. Soc. **114**, 2768 (1992); (*b*) W.A. Nugent and R.L. Harlow. J. Am. Chem. Soc. **116**, 6142 (1994); (*c*) M. Bonchio, S. Calloni, F. Di Furia, G. Licini, G. Modena, S. Moro, and W.A. Nugent. J. Am. Chem. Soc. **119**, 6935 (1997).
8. U. Zucchini, E. Albizatti, and U. Giannini. J. Organomet. Chem. **26**, 357 (1971).
9. W.G. Dauben and H.O. Krabbenhoft. J. Org. Chem. **42**, 282 (1977).
10. P.B. Kisanga and J.G. Verkade. J. Org. Chem. **64**, 4298 (1999).
11. R. Ballini and G. Bosica. J. Org. Chem. **62**, 425 (1997).
12. S. Kiyooka, T. Tsutsui, H. Maeda, Y. Kaneko, and K. Isobe. Tetrahedron Lett. **36**, 6531 (1995).
13. M.D. Alcántara, F.C. Escribano, A. Gómez-Sánchez, M.J. Diánez, M.D. Estrada, A. López-Castro, and S. Pérez-Garrido. Synthesis, 64 (1996).
14. H. Lütjens, G. Wahl, F. Möller, P. Knochel, and J. Sundermeyer. Organometallics, **16**, 5869 (1997).
15. D.C. Bradley, R.C. Mehrotra, and D.P. Gaur. Metal alkoxides. Academic Press, London. 1978.
16. J. Sandstrom. Dynamic NMR spectroscopy. Pergamon, London. 1982.
17. J. March. Advanced organic chemistry. 3rd ed. Wiley and Sons, New York. 1985. p. 86.
18. (*a*) P. Shao, D.J. Berg, and G. Bushnell. Inorg. Chem. **33**, 3452 (1994); (*b*) L. DeCola, D.L. Smailes, and L.M. Vallarino. Inorg. Chem. **25**, 1729 (1986), and refs. therein.
19. (*a*) H.C.S. Clark, F.G.N. Cloke, P.B. Hitchcock, J.B. Love, and A.P. Wainwright. J. Organomet. Chem. **501**, 333 (1995); (*b*) A.D. Horton, J. de With, A.J. van der Linden, and H. van de Weg. Organometallics, **15**, 2672 (1996).
20. F.G.N. Cloke, P.B. Hitchcock, and J.B. Love. J. Chem. Soc. Dalton Trans. **1995**, 25.
21. R.D. Shannon. Acta Crystallogr. Sect. A: Cryst Phys. Diffr. Theor. Gen. Crystallogr. **A32**, 751 (1976).
22. C.H. Zambrano, A.K. McMullen, L.M. Kobriger, P.E. Fanwick, and I.P. Rothwell. J. Am. Chem. Soc. **112**, 6565 (1990).
23. C. Spino, L. Clouston, and D.J. Berg. Can. J. Chem. **75**, 1047 (1997).

© 2000 NRC Canada

Ethylene-polymerization by surface supported Cr(IV) species: possible reaction mechanisms revisited by theoretical calculations

Rochus Schmid and Tom Ziegler

Abstract: Possible reaction mechanisms of olefin polymerization catalyzed by surface supported Cr(IV) species have been investigated by first principles density functional theory (DFT). Pathways starting from neutral alkylidene or bisalkyl complexes were found to suffer from high ethylene insertion barriers, whereas a cationic system formed by protonation of the alkylidene show a low barrier for chain propagation.

Key words: density functional theory, alkylidene, olefin polymerization, Cr(IV) species.

Résumé : En faisant appel aux principes fondamentaux de la théorie de la densité fonctionnelle (TDF), on a évalué les divers mécanismes possibles pour la réaction de polymérisation des oléfines catalysées par des espèces Cr(IV) supportées par une surface. On a trouvé que les voies partant de complexes alkylidène ou bisalkyle neutres impliquent des barrières élevées pour l'insertion de l'éthylène alors qu'un système cationique formé par protonation de l'alkylidène ne présente qu'une faible barrière à la propagation de la chaîne.

Mots clés : théorie de la densité fonctionnelle, alkylidène, polymérisation d'oléfine, espèce Cr(IV).

[Traduit par la Rédaction]

Introduction

A number of industrially important ethylene polymerization processes depend on surface supported organometallic complexes, for example the Cr/SiO_2 catalysts developed by Phillips (1) and Union-Carbide (2). In contrast to the well defined, so-called "single site" homogeneous polymerization catalysts (3), neither the oxidation state nor the exact coordination environment of the active species are known with certainty (4). Therefore, the reaction mechanism for chain propagation and termination is often based on pure speculation. To solve this problem, homogeneous model systems of Cr(III) have been synthesized. Various N-donating bi- and tridentate ligands have been employed in order to model the hard coordination environment of a silica surface (5). Systems of Ti(III), V(III), and Cr(III) were found to be active in ethylene polymerization (6). Interestingly, these systems resemble the well known N-chelating ligands of early and late transition metal homogeneous polymerization catalysts (3). In addition to this strategy, well defined surface supported complexes can be studied. Recently, Amor Nait Ajjou and Scott (7) succeeded in the preparation of a silica-supported alkyl chromium(IV) system. After thermolysis of the bisalkyl complex, a new species is formed which polymerizes ethylene on the surface (8, 9). Our continuing interest in the mechanism of olefin polymerization (10) and our recent investigations of polymerization catalysts with occupied *d*-levels (footnote 3) (as it is the case for Cr(IV)) has prompted us to study the catalytic system discovered by Scott and coworkers (8, 9) by means of first principles calculations employing density functional theory (DFT) (11).

Computational details

All structures were fully optimized without symmetry constraints in a high-spin electronic state (spin unrestricted calculations) by standard optimization techniques with a gradient corrected functional (BP86 (12)) using the ADF 2.3 program package (13). Transition state searches were performed by linear transit calculations with a constrained reaction coordinate and subsequent use of a transition state search algorithm. First order scalar relativistic corrections were added to the total energy, since a perturbative approach is sufficient for first row transition metals (14). For Cr a triple-ζ Slater type basis set (3*s*, 3*p*, 3*d*, and 4*s* valence shells plus one 4*p* polarization function) was used and for Si a triple-ζ STO basis set (3*s* and 3*p* valence shell plus one 3*d* polarization function) was used. Non-metal atoms were described by a double-ζ STO basis with one 3*d* (C, N, and O) or one 2*p* (H) polarization function (15). The frozen core approximation was employed throughout. A set of auxiliary *s*, *p*, *d*, *f*, and *g* STO functions, centered on all nuclei, was used to fit the

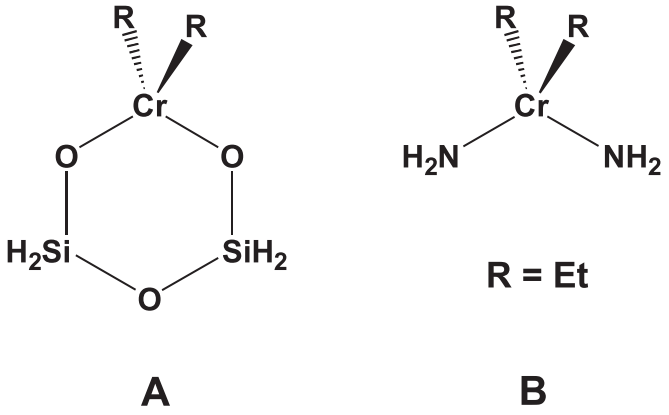
Received October 5, 1999.

R. Schmid[1] and T. Ziegler.[2] University of Calgary, Dept. of Chemistry, 2500 University Drive N.W., Calgary, AB T2N 1N4, Canada.

[1]Present address : Technische Universität München, Anorganisch-Chemisches Institut, D-85747, Garching, Germany.
[2]Author to whom correspondence may be addressed. Telephone: (403) 220-5368. Fax: (403) 289-9488.
[3]R. Schmid and T. Ziegler. Manuscript submitted for publication.

 © 2000 NRC Canada

Scheme 1. Model systems investigated.



molecular density and present Coulomb and exchange potentials accurately in each SCF cycle. This level of theory has been proven to be reliable for both structures and energetics of transition metal systems (16).

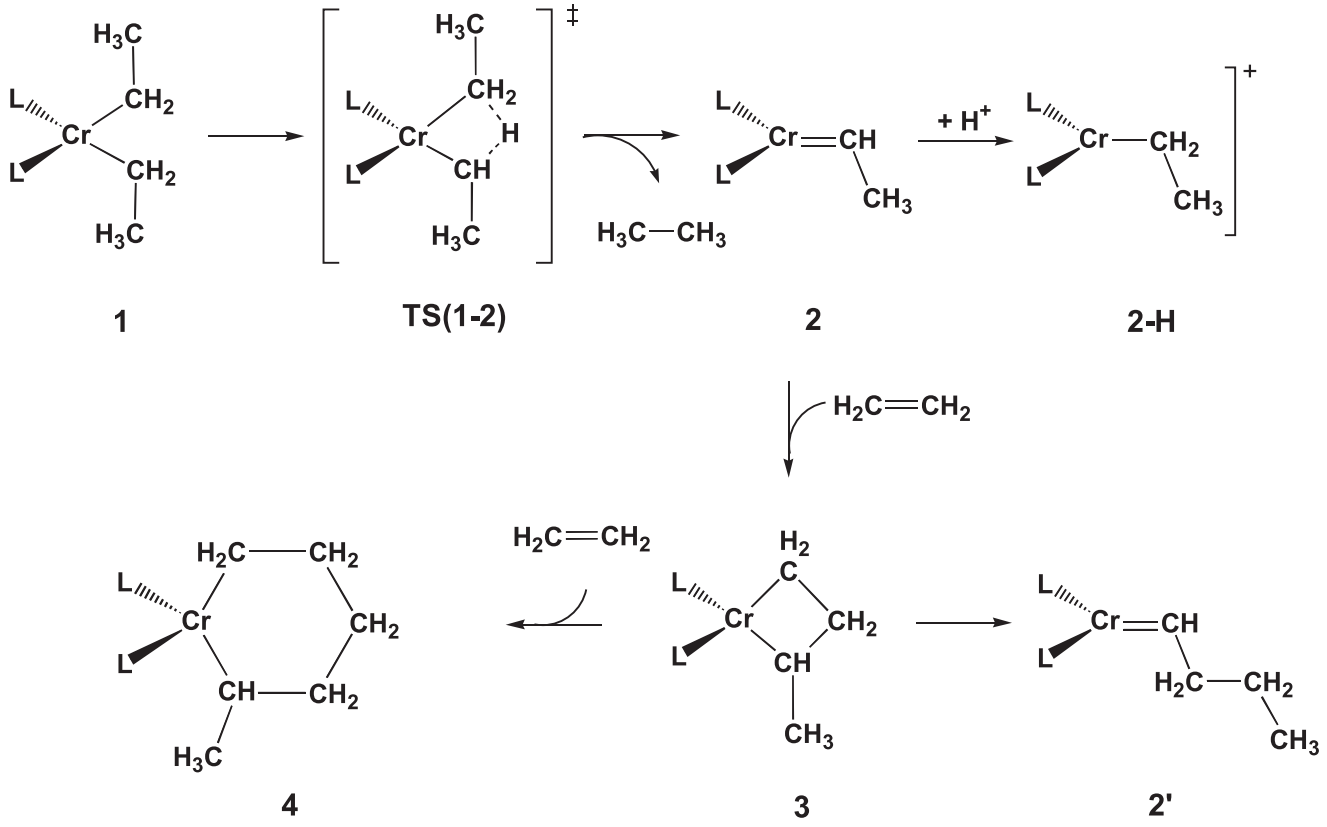
Results and discussion

Because of the large numeric effort with first principle methods in general, we limited ourselves to the model systems shown as **A** in Scheme 1. The neopentyl groups were reduced to an ethyl chain and the silica surface was simulated by two -O-SiH_2- units connected by an additional oxygen atom in order to include the "chelating" constraint present on the surface. Calculations with two amide ligands (**B**) were performed in order to compare with our results on systems of standard $[L_2MR]^+$ polymerization catalysts (footnote 3) and the findings of Theopold et al. (6).

Starting from homoleptic alkyls of Cr(IV) and dehydroxylated silica, Amor Nait Ajjou and Scott (7) could, depending on the conditions and the preconditioning of the silica, produce uniform surfaces with either one or two alkyl groups replaced by a Si-O unit. These bis or tris alkyl Cr(IV) complexes do not polymerize ethylene. However, by thermolysis of the $(\equiv SiO)_2CrR_2$ system with R = neopentyl (**1**) at only 60°C, one equivalent of neopentane is liberated and a new surface supported species is formed, which could either be a metallacycle or a rather unusual alkylidene-complex. Recent results on reactions with agents attacking specifically M=C bonds make it very plausible that the formed product is a surface stabilized alkylidenecomplex of Cr(IV) (**2**). In contrast to the bisalkyl complex (**1**), this new species polymerizes ethylene at room temperature (8). A mechanism of chain propagation has been proposed (Scheme 2), which is based on the assumption of an initial [2 + 2] addition of ethylene to the M=C bond under formation of a metalla-cyclobutane (**3**). A subsequent 1,3-hydrogen shift would reform the alkylidenecomplex (**2′**) with a chain length increased by one monomer.

Our calculations show that the initial step leading from the bis alkyl complex **1** to the alkylidenecomplex **2** is very endothermic (24.6 kcal/mol for **A**). Wu et al. (17) found a reaction energy for the equivalent methane elimination from $TiMe_4$ of 37.5 kcal/mol which is reduced for the sterically encumbered system $TiNp_4$ (Np = neopentyl) to 18.4 kcal/mol. For analogous reasons, a lower endothermicity of the

Scheme 2. Possible steps of ethylene polymerization starting from bisalkyl Cr(IV) complex **1**.



© 2000 NRC Canada

Table 1. Reaction energies for $L_2Cr(Et)_2 \rightarrow L_2Cr{=}CH\text{-}Me + Et$.

L_2		$E_{1\rightarrow 2}$ (kcal/mol)
$(NH_2)_2$	B	19.8
$(OH)_2$		21.3
$(OSiH_3)_2$		22
$O\text{-}SiH_2\text{-}O\text{-}SiH_2\text{-}O$	A	24.6

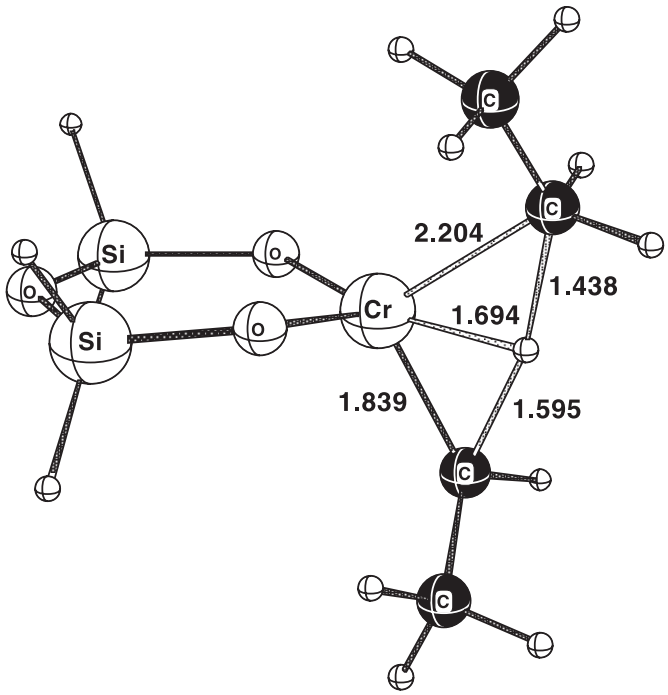
Table 2. Calculated total energies and relative reaction energies.

	A[a]		B[b]	
	E_{tot} (kcal/mol)	E_{rel} (kcal/mol)	E_{tot} (kcal/mol)	E_{rel} (kcal/mol)
1	0		0	
TS(1→2)	37.3	1: 37.3	37.1	1: 37.1
2	24.6	1: 24.6	19.8	1: 19.8
3	–14.1	2: –38.7	–19.2	2: –39.0
TS(3→2′)	42.2	3: 56.4	36.1	3: 55.3
2′	1.2	3: 15.3	–3.1	3: 16.1
TS(3→4)	7.7	3: 21.9	–1.2	3: 18.0
4	–46.6	3: –32.5	–51.0	3: –31.8
2-H	–198.2	2: –222.8	–219.9	2: –239.7
3-H	–221.4	2-H: –23.1	–238.1	2-H: –18.3
TS(3-H→2′-H)	–210.8	3-H: 10.5	–232.0	3-H: 6.2

[a] $O\text{-}SiH_2\text{-}O\text{-}SiH_2\text{-}O$ as co-ligand.

[b] Bis-amide systems.

Fig. 1. Transition state **TS(1→2)** for system **A** (important bond lengths are given in Å).



surface supported bis-neopentyl Cr-species can be expected. In addition, the entropic driving force from the formation of the volatile alkane can be estimated to contribute about –10 kcal/mol to the total free reaction energy. This makes the formation of alkylidene feasible (footnote 4, 18), especially because the alkane elimination on the support would be irreversible with complete alkane loss. In Table 1 the reaction energies for the alkylideneformation are given for **A**, **B**, and also intermediate model systems with OH and $OSiH_3$ as ligands. The thermodynamic energy difference for the step **1→2** is not significantly affected by the type of ligand, which justifies the use of **A** as a model for the surface supported system.

The calculated energies of all investigated stationary points for **A** and **B** are given in Table 2 with respect to the corresponding bisalkyl complex (**1**). The large kinetic isotope effect for **1→2** for α-deuterated alkyl complexes experimentally proves this to be a α-hydrogen transfer reaction (8). Kinetic measurements of this reaction suggest a two-step mechanism, which has been interpreted in terms of the formation of a stable Cr(VI) hydrido intermediate (9). Our calculations, however, show no preference for the latter and **TS(1→2)** is a direct hydrogen transfer with a barrier of 37.3 kcal/mol (**A**). No stationary point for a Cr(VI) hydrido species could be located. Similar barriers have been calculated by Wu et al. (17) for the alkane elimination from TiR_4 (R = Me: 41.2, R = Np: 32.8 kcal/mol) and also the geometry of the transition state closely resembles the one calculated for TiR_4 (Fig. 1). The Cr—C bond to the carbon atom in the forming ethylene molecule is elongated to 2.204 Å, whereas the generated alkylidene bond is shortened to 1.839 Å. The corresponding C—H bond length shows the opposite asymmetry. It is important to note that for the alkane elimination from TiR_4 the activation barrier was calculated to be less sensitive to the nature of the alkyl substituent than the reaction energy. Furthermore, our model (using ethyl) deviates from the real system for this initial activation process only, whereas in consecutive steps ethylene is a reasonable model for the growing polymer chain.

Ethylene can react with **2** in a [2 + 2] fashion to give a metallacycle **3** (8). This process occurs without any barrier and is about 40 kcal/mol exothermic by irrespective of the nature of the system (**A** or **B**). In the presence of ethylene, **3** must be seen as a strong thermodynamic sink and therefore represents the resting state of the system. A viable polymerization mechanism must allow for a repetitive olefin incorporation with reasonable barriers of activation. As shown in Scheme 2, a 1,3-hydrogen shift from **3** would lead to a alkylidene complex **2′** with a chain length increased by one monomer unit. It should be noted, however, that this hydrogen transfer is equivalent to the "activation" by thermolysis of **1**. Experimentally, it has been observed that for **1→2** elevated temperatures are necessary, but the polymerization occurs at room temperature. For both **A** and **B** our calculations show an activation barrier of about 55 kcal/mol for the hydrogen shift reaction, which is even larger than the barrier for **TS(1→2).** The ring strain in the four-membered metallacycle **3** does not lower the barrier. Figure 2 displays the transition state **TS(3→2′)** for **A**, which very much resembles the geometry in **TS(1→2)**. However, the structural deformations necessary for this 1,3-hydrogen transfer in the

[4] The estimation of the entropic contribution to ΔG is based on a reaction entropy (mostly rotational and translational contributions) of $\Delta S \sim 35$ cal mol^{-1} K^{-1} and a temperature of 300 K (see also Ref. 18).

© 2000 NRC Canada

Fig. 2. Transition state **TS(3→2′)** for system **A** (important bond lengths are given in Å).

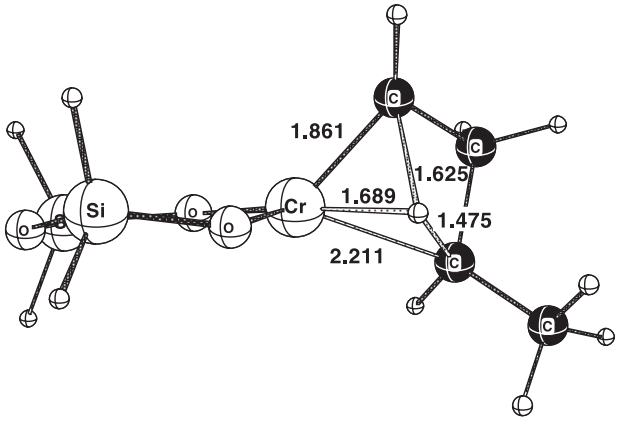
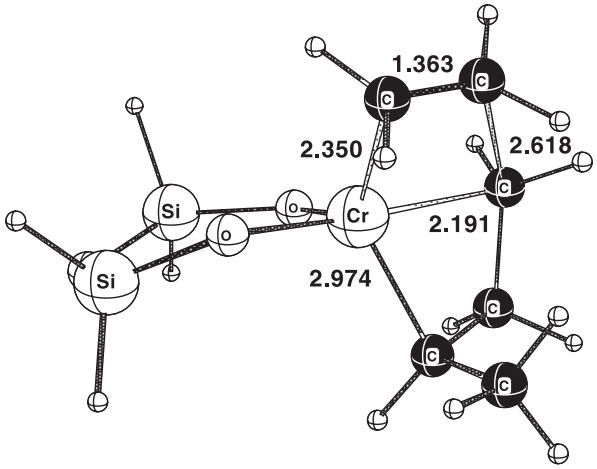


Fig. 3. Transition state **TS(3→4)** for system **A** (important bond lengths are given in Å).



metallacycle are much larger than for the corresponding **TS(1→2)** (Fig. 1), which explains the increase of 20 kcal/mol in the barrier. Our results do not support the sequence **2→3→2′** as a pathway for chain propagation in these systems.

Alternatively we considered direct ethylene insertion into one of the Cr—C bonds of **3**. We were not able to locate a stable olefin complex on the potential energy surface. However, with a barrier of 21.9 kcal/mol for **A** (18.0 kcal/mol for **B**) this is a more facile process than the 1,3-hydrogen shift reaction. The reaction leads directly to the metalla-cyclohexene **4**. Figure 3 shows the transition state **TS(3→4)** for system **A**. The thermodynamic exothermicity for the reaction step **3→4** is about 30 kcal/mol, again similar for systems **A** and **B**, and about 10 kcal/mol higher than the energy gain for the incorporation of ethylene into a linear alkyl chain. This is due to the release of ring strain when going from the four membered to the six membered ring.

Direct insertion mechanisms leading to larger and larger metallacycles have been discussed in the literature for the oligomerization of ethylene (18). It appears, however, to not be a viable pathway for chain propagation for the surface supported Cr(IV) systems considered here. A barrier of more than 20 kcal/mol for the insertion of ethylene into system **A** must be seen as prohibitive for polymerization. In addition, the consecutive insertion steps will suffer from lack of ring strain in the larger metallacycles, which will reduce the exothermicity while raising the insertion barrier. We did not investigate a 1,3-hydrogen shift reaction from **4**, which would reform an alkylidene complex similar to **2** with a chain length increased by two monomer units. Because of the similarity between the metalla-cyclohexane **4** and the bisethyl complex **1** this reaction can be expected to have an activation barrier of above 35 kcal/mol, which excludes this pathway as well.

Since all reaction steps including either a hydrogen transfer reaction or a direct insertion into a four coordinated Cr(IV) complex show very high activation barriers we suggest a possible alternative to explain the polymerization activity observed experimentally for the silica stabilized systems. Trace amounts of remaining acidic sites on the silica surface (Si-OH groups) are likely to protonize some of the alkylidene species, forming a cationic Cr(IV) alkyl complex **2-H**. Similar systems with two stabilizing auxilliary ligands are well known to effectively catalyze ethylene polymerization. In a recent theoretic investigation, Cr(IV) systems with a d^2-electron configuration have been found to be especially effective catalysts. For both systems **A** and **B** an olefin complex **3-H** is formed with respective ethylene binding energies of 23.1 (**A**) and 18.3 kcal/mol (**B**), respectively. The following step of the olefin insertion into the Cr—C bond proceeds with a very low activation barrier of only 10.5 kcal/mol for **A**. System **B** has, similar to the direct olefin insertion into the metalla-cyclopropane **3**, an even lower barrier of only 6.2 kcal/mol. For a detailed analysis of the electronic effects responsible for the low barrier in **B** we refer here to footnote 3.

Conclusions

We conclude from our calculations that any chain propagation pathways starting from the alkylidene complex **2**, involving either hydrogen transfer reactions or direct insertions into neutral bis-alkyl complexes, suffer from very high activation barriers. This might be altered by further surface-catalyst interactions, which are not accounted for in our calculations on model systems. However, by protonation of **2** a well known cationic alkylcomplexe **2-H** can be formed, which can act as an efficient ethylene polymerization catalyst with a very low activation barrier. This involves a standard reaction mechanism, which is known for a large number of known cationic homogeneous polymerization catalysts. Alternatively, the cationic alkyl could be formed by protonation of the metallacyclobutane species **3**.

Acknowledgements

We would like to thank Susannah L. Scott for discussions and suggestions helpful to this project. This investigation has been generously supported by Novacor Research and Technology Corporation (NRTC) of Calgary, and the Natural Sciences and Engineering Research Council (NSERC) of Canada.

© 2000 NRC Canada

References

1. J.P. Hogan. J. Polym. Sci. Part A1, **8**, 2637 (1970).
2. F.J. Karol, G.L. Karapinka, C. Wu, A.W. Dow, R.N. Johnson, and W.L. Carrick. J. Polym. Sci. Part A1, **10**, 2621 (1972).
3. (*a*) W. Spalek, M. Antberg, J. Rohrmann, A. Winter, B. Bachmann, P. Kiprof, J. Behm, and W.A. Herrmann. Angew. Chem. Int. Ed. Engl. **31**, 1347 (1992); (*b*) H.H. Brinzinger, D. Fischer, R. Mühlhaupt, B. Rieger, and R.M. Waymouth. Angew. Chem. Int. Ed. Engl. **34**, 1708 (1995); (*c*) M.J. Bochmann. J. Chem. Soc. Dalton Trans. 255 (1996).
4. A. Clark. Catal. Rev. Sci. Eng. **3**, 145 (1970).
5. (*a*) B.J. Thomas, S.K. Noh, G.K. Schulte, S.C. Sendlinger, and K.H. Theopold. J. Am. Chem. Soc. **113**, 893 (1991); (*b*) G. Bhandari, Y. Kim, J.M. McFarland, A.L. Rheingold, and K.H. Theopold. Organometallics, **14**, 738 (1995); (*c*) P.A. White, J. Calabrese, and K.H. Theopold. Organometallics, **15**, 5473 (1996).
6. (*a*) W.-K. Kim, M.J. Fevola, L.M. Liable-Sands, A.L. Rheingold, and K.H. Theopold. Organometallics, **17**, 4541 (1998); (*b*) P.H.M. Budzelaar, A.B. van Oort, and A.G. Orpen. Eur. J. Inorg. Chem. 1485 (1998).
7. J. Amor Nait Ajjou and S.L. Scott. Organometallics, **16**, 86 (1997).
8. J. Amor Nait Ajjou, S.L. Scott, and V. Paquet. J. Am. Chem. Soc. **120**, 415 (1998).
9. J. Amor Nait Ajjou, G.L. Rice, and S.L. Scott. J. Am. Chem. Soc. **120**, 13436 (1998).
10. (*a*) J.C.W. Lohrenz, T.K. Woo, and T. Ziegler. J. Am. Chem. Soc. **117**, 12793 (1995); (*b*) P.M. Margl, L. Deng, and T. Ziegler. Organometallics, **17**, 933 (1998); (*c*) P.M. Margl, L. Deng, and T. Ziegler. J. Am. Chem. Soc. **120**, 5517 (1998); (*d*) P.M. Margl, L. Deng, and T. Ziegler. J. Am. Chem. Soc. **121**, 154 (1999).
11. T. Ziegler. Chem. Rev. **91**, 651 (1991).
12. (*a*) A. Becke. Phys. Rev. A: At. Mol. Opt. Phys. **38**, 3098 (1988); (*b*) J.P. Perdew. Phys. Rev. B: Condens. Matter, **34**, 7406 (1986); (*c*) J.P. Perdew. Phys. Rev. B: Condens. Matter, **33**, 8822 (1986).
13. (*a*) E.J. Baerends, D.E. Ellis, and P. Ros. Chem. Phys. **2**, 41 (1973); (*b*) E.J. Baerends and P. Ros. Chem. Phys. **2**, 52 (1973).
14. (*a*) J.G. Snijders and E.J. Baerends. Mol. Phys. **36**, 1789 (1978); (*b*) J.G. Snijders, E.J. Baerends, and P. Ros. Mol. Phys. **38**, 1909 (1979).
15. J.G. Snijders, E.J. Baerends, and P. Vernoijs. At. Data Nucl. Data Tables, **26**, 483 (1982).
16. V. Jensen and K.J. Borve. Comput. Chem. **19**, 947 (1998).
17. Y.-D. Wu, Z.-H. Pend, and Z. Xue. J. Am. Chem. Soc. **11**8 9772 (1996).
18. R. Emrich, O. Heinemann, P.W. Jolly, C. Krüger, and G.P.J. Verhovnik. Organometallics, **16**, 1551 (1997).

© 2000 NRC Canada

A new short synthetic approach to chlorocyclopentenones related to cryptosporiopsin via a ring expansion strategy: first synthesis of a fungitoxic metabolite from *Sporormia affinis*[1]

Sidima Kabanyane, Andreas Decken, Chao-Mei Yu, and George M. Strunz

Abstract: A metabolite of the coprophilous fungus, *Sporormia affinis*, 2-*trans*-allyl-5-chloro-1-hydroxy-4-oxo-2-cyclopentene-1-carboxylic acid methyl ester, **2**, was synthesized in racemic form, by an eight-step sequence, in 11% overall yield. Departing from previous ring-contraction strategies for synthesis of chlorocyclopentenones in the cryptosporiopsin series, the key step in the new synthesis was ring expansion of a substituted cyclobutanone, the product of [2+2] cycloaddition of dichloroketene with methyl 2-trimethylsilyloxyhex-2-enoate.

Key words: *Sporormia affinis*, cryptosporiopsin, chlorocyclopentenone, dichloroketene, [2+2] cycloaddition, ring expansion, selenium dioxide.

Résumé : Nous avons synthétisé, sous forme racémique, en huit étapes et avec un rendement global de 11%, l'ester méthylique de l'acide 2-*trans*-allyl-5-chloro-1-hydroxy-4-oxocyclopent-2-ène-1-carboxylique, **2**, un métabolite du champignon coprophileux, *Sporormia affinis*. Les chlorocyclopentènones de la série de la cryptosporiopsine ont été synthétisées antérieurement par le biais d'une contraction de cycle. Par ailleurs, l'étape clé de la nouvelle synthèse consiste en une extension de cycle d'une cyclobutanone substituée, obtenue par une cycloaddition [2+2] du dichlorocétène sur l'ester méthylique de l'acide 2-trimethylsilyloxyhex-2-enoïque.

Mots clés : *Sporormia affinis*, cryptosporiopsine, chlorocyclopenténone, dichlorocétène, cycloaddition [2+2], extension de cycle, dioxyde de sélénium.

Isolation of the chlorine-containing fungitoxic cyclopentenone cryptosporiopsin (**1**) and several biogenetic congeners was reported by independent groups in 1969, from the coprophilous fungus *Sporormia affinis* (1*a*, cf. 1*b*), from a *Cryptosporiopsis* sp. (2), and from *Periconia macrospinosa* (3). In 1973, we published the first synthesis of cryptosporiopsin by a formally biomimetic route (4). The key step, based on the ring contraction of a phenolic precursor through the action of alkaline hypochlorite (5), was a capricious and low yield process. A subsequent synthesis, via a more readily controllable benzillic acid-type rearrangement of a suitably substituted quinone, produced the metabolite in better yield (6).

In this paper we describe a new concise synthetic approach (Scheme 1) to chlorine-containing cyclopentenones related to cryptosporiopsin, by way of ring expansion of a readily accessible cyclobutanone, a fundamental departure from the previously exploited ring contraction strategy. The methodology is employed towards the first reported synthesis of the *Sporormia affinis* metabolite, **2** (1*a*).

Cycloaddition of dichloroketene to the trimethylsilyl enol ether (**3**) of methyl 2-oxohexanoate appeared to offer a promising entry to a suitably substituted cyclobutane precursor. Dichloroketene is known to react with unsymmetrical olefins in a regiospecific manner, such that the most nucleophilic carbon of the olefin is always bonded to the *sp* hybridized carbon of the ketene (7). In the present instance, the reaction proceeded efficiently to give an 87% yield of a homogeneous product (**4**) hose regiochemistry was clearly evident from the mass spectral fragmentation pattern, and confirmed by NMR studies on a lower homologue (8). In the mass spectrum, ions corresponding to C_5H_8O and $C_7H_{12}O_3Cl_2Si$ were particularly diagnostic. The depicted relative stereochemistry follows from that established for a later intermediate (**7**) by nOe and X-ray diffraction studies.

The strategy for ring expansion of **4** as originally conceived, via fragmentation of an intermediate such as **6**, was thwarted by the failure of enol-ether **5** to react with dichlorocarbenoid species generated by several different methods (9) and under various conditions, including phase-transfer catalysis. Reaction of **4** with diazomethane, however, afforded a highly efficient alternative method of ring expansion. The regioselective reaction, conducted in ether containing a small amount of methanol, produced cyclopentanone (**7**), in almost

Received September 9, 1999.

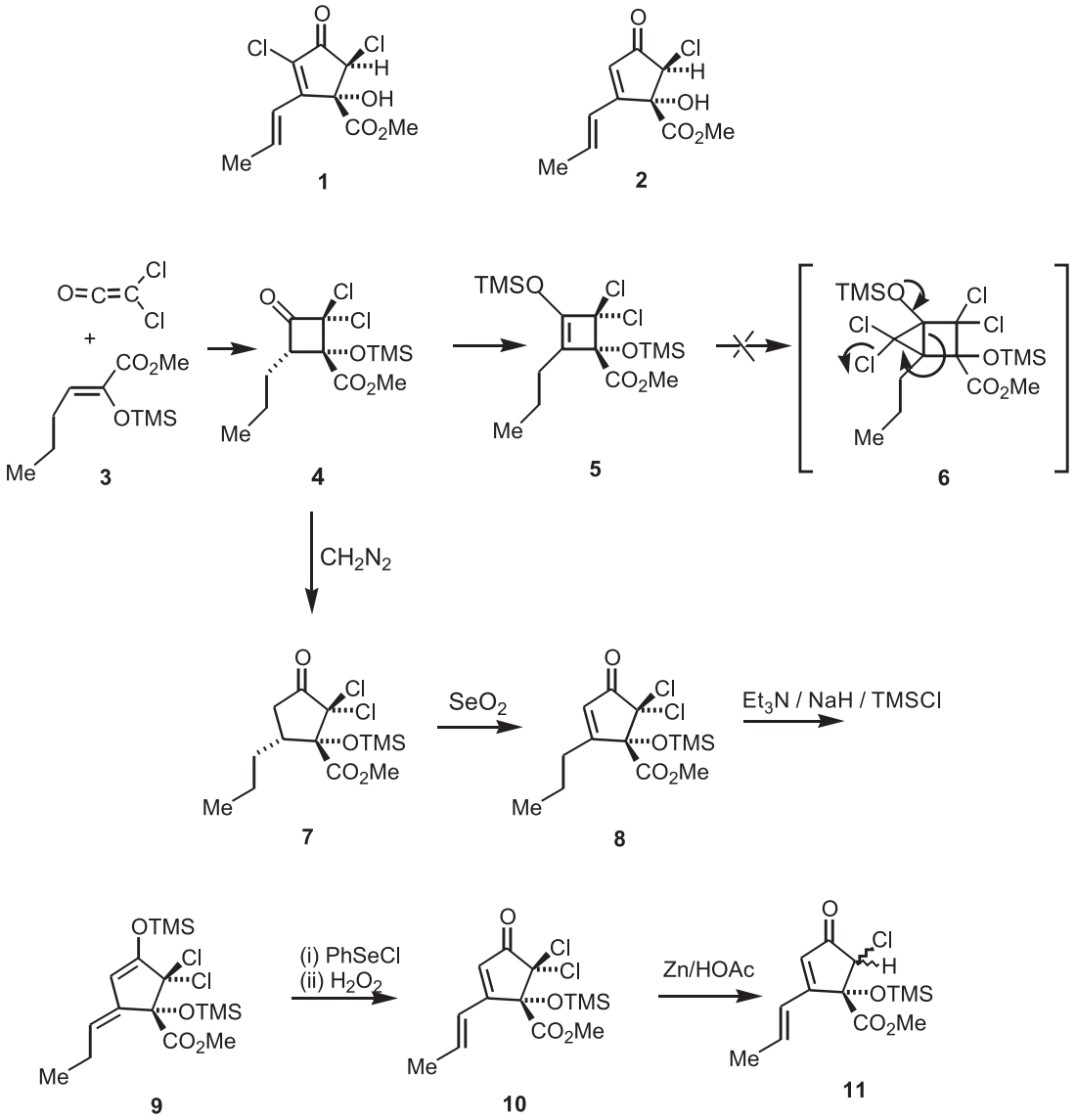
S. Kabanyane, A. Decken, C.-M. Yu, and G.M. Strunz.[2] Canadian Forest Service-Atlantic Forestry Centre, Natural Resources Canada, P.O. Box 4000, Fredericton, NB E3B 5P7, Canada and Chemistry Department, University of New Brunswick, Fredericton, NB E3B 6E2, Canada.

[1]*This paper is dedicated to the memory of Professor Larry Weiler (1942–1999), whose outstanding qualities as chemist, teacher, administrator and human being have contributed so much to chemistry and the Canadian chemical community.*

[2]Author to whom correspondence may be addressed. Telephone: (506) 452-3531. Fax: (506) 452-3525. e-mail: gstrunz@nrcan.gc.ca

© 2000 NRC Canada

Scheme 1.



quantitative yield (cf. 10). The relative stereochemistry of **7** (although not relevant to the outcome of the synthesis) was determined by ^{1}H NMR studies, in which significant nOe enhancement between the methyl ester protons and the C-5 methine hydrogen established their spatial proximity. An X-ray crystal structure analysis[3] confirmed this assignment, which also allowed the relative stereochemistry of precursor **4** and the *Z*-geometry of **3** to be inferred. Desaturation of cyclopentanone **7** could be accomplished by treatment of its trimethylsilyl enol ether with $Pd(OAc)_2$ (11), but the yield of the desired cyclopentenone product **8** was modest (~25%). A more direct and efficient procedure was developed with the observation that simply heating **7** with SeO_2 in toluene furnished **8** in 77% yield.

The additional (conjugated) side-chain unsaturation required for the synthesis was most effectively introduced via γ-phenylselenenylation (82%) of the trimethylsilyl enol ether, **9**, readily prepared (89%) from **8**. Oxidation to the selenoxide (12), followed by elimination then afforded the dienone **10** in 60% yield. Partial reduction of the *gem*-dichloride with zinc-acetic acid furnished **11**, and removal of the trimethylsilyl protecting group under mild conditions (13), produced the (racemic) *Sporormia affinis* product **2** in 38% yield (overall yield for the synthesis from methyl 2-oxohexanoate, ~11%). The identity of the product was verified by comparison of its spectra with data reported for the natural product (1*a*).

It is worth noting that although assignment of the relative configuration of **11** was not pursued, its conversion to the synthetic product **2** of known relative stereochemistry (also confirmed by nOe experiments with the dihydro derivative of **2**) was expected, being consistent with our previous observation (14) that treatment of cryptosporiopsin with methanol-d_1 in pyridine-d_5 effects exchange of the C-5 hydrogen

[3] A. Decken. Unpublished results.

© 2000 NRC Canada

without epimerization, i.e., the *anti* orientation of Cl and OH is the favored configuration for compounds in this series when formed under, or subjected to equilibrating conditions.

In summary, we have accomplished the first synthesis of the racemate of **2**, a fungitoxic metabolite of *Sporormia affinis*, using an efficient ring expansion strategy, that may also provide an entry to other chlorinated cyclopentenones in the cryptosporiopsin series. The methodology appears amenable to enantioselective modification, and this is currently under investigation in our laboratory.

Experimental

General

Melting points were determined on a hot-stage apparatus and are uncorrected. Infrared spectra were recorded in $CHCl_3$ on a Philips Pye Unicam PU9516 infrared spectrophotometer and as films on a Bruker IF-S25 FTIR spectrometer. The ultraviolet spectra were recorded on a Hewlett Packard Diode Array Spectrophotometer, Model 8452A. Mass spectra were recorded on a VG Autospec instrument. NMR spectra were recorded in $CDCl_3$ at ambient temperature on a Varian XL-200 spectrometer operating at a frequency of 200.068 MHz for ^1H, and at 25°C on a Varian Unity 400 operating at a frequency of 399.946 MHz for ^1H and 100.564 MHz for ^{13}C.

*Methyl 2-trimethylsilyloxyhex-2-enoate, **3***: The precursor for the title compound, methyl 2-oxohexanoate, was prepared as follows (cf. 15): The Grignard reagent, prepared in dry THF (30 mL) under nitrogen, from *n*-butyl bromide (1.5 mL, 1.91 g, 14 mmol) and magnesium turnings (400 mg, 16.5 mg-atom) was added dropwise at 0°C to a solution of dimethyl oxalate (2.0 g, 16.9 mmol) in dry THF (100 mL). The reaction mixture was set aside with stirring in a nitrogen atmosphere at 0°C for 2 h. It was then allowed to attain ambient temperature, before being diluted by addition of ether (100 mL). The mixture was washed with cold 5% HCl solution (3 × 50 mL) and brine and the organic phase was dried over $MgSO_4$ and evaporated to dryness *in vacuo*. The crude oily residue was purified by chromatography on a silica gel column (hexane:EtOAc, 10:1) to give methyl 2-oxohexanoate (1.88 g, 94% from bromide, 77% from oxalate) as a colorless oil. The keto ester was characterized spectroscopically; IR (film) ν_{max}: 2958, 1734, 1730, 900, and 650 cm^{-1}; ^1H NMR ($CDCl_3$, 200 MHz) δ 3.85 (3H, s), 2.85 (2H, t, J = 6.8 Hz), 1.75–1.60 (2H, m), 1.50–1.20 (2H, m), 0.90 (3H, t, J = 7.0 Hz).

A mixture of methyl 2-oxohexanoate (1.60 g, 11.1 mmol) and chlorotrimethylsilane (1.82 mL, 1.56 g, 14.4 mmol) in dry THF (10 mL) was added slowly to a solution of triethylamine (2.3 mL, 1.67 g, 16.5 mmol) in THF (20 mL). The mixture was heated under reflux in an atmosphere of dry nitrogen for 12 h, and after cooling to attain room temperature, it was diluted by addition of ether (50 mL). The resulting mixture was filtered through Celite and the filtrate was washed with with cold 5% HCl and brine. The organic layer was dried over $MgSO_4$ and concentrated under reduced pressure. Fractional distillation of the crude product afforded methyl 2-trimethylsilyloxyhex-2-enoate, **3**, (2.35 g, 98%) as a colorless oil: IR ($CHCl_3$) ν_{max}: 2985, 1720, 1650, 1230, 900, and 840 cm^{-1}; ^1H NMR (200 MHz, $CDCl_3$) δ: 6.07 (1H, t, J = 7.5 Hz), 3.75 (3H, s), 2.11 (2H, dd J = 7.5 and 14.8 Hz), 1.52–1.38 (2H, m), 0.95 (3H, t, J = 7.5 Hz) and 0.20 (9H, s); ^{13}C NMR δ: 165.3, 140.4, 123.7, 51.8, 27.8, 21.9, 13.9, 0.37; LREIMS *m/z* (relative intensity) (ion): 216 (6) $(M)^+$, 215 (8) $(M–H)^+$, 201 (100) $(M–CH_3)^+$, 187 (31) $(M–C_2H_5)^+$, 157 (14) $(M–CO_2CH_3)^+$, 89 (87) $(OSiMe_3)^+$, 73 (88) $(SiMe_3)^+$, 59 (15) $(CO_2CH_3)^+$.

*Methyl 2,2-dichloro-3-oxo-4-*n*-propyl-1-trimethylsilyloxycyclobutyl carboxylate, **4***: A solution of trichloroacetyl chloride (1.0 mL, 1.63 g, 8.96 mmol) in dry ether (20 mL) was added dropwise over a 4 h period under an argon atmosphere to a stirred suspension of activated zinc dust (16) (700 mg, 10.7 mg-atom) and methyl 2-trimethylsilyloxyhex-2-enoate (2.0 g, 9.24 mmol) in ether (50 mL) at ambient temperature. The reaction mixture was set aside with stirring for 12 h. It was then filtered, and the filtrate was evaporated *in vacuo* to about 10 mL. The residue was diluted by addition of pentane (50 mL) with vigorous stirring. The resulting suspension was set aside until the zinc salt separated, and the supernatent was decanted. The pentane solution was washed with cold 5% $NaHCO_3$ solution and brine, dried ($MgSO_4$) and distilled under reduced pressure.

The cyclobutane product, **4**, (2.64 g, 87%) was collected as a pale yellow oil, bp 89–92°C/1.4 Torr; IR (film) ν_{max}: 2960, 2878, 1818, 1755, 1460, 1292, and 846 cm^{-1}; ^1H NMR (400 MHz, $CDCl_3$) δ: 4.01 (1H, t, J = 7.6 Hz), 3.86 (3H, s), 1.80–1.71 (2H, m), 1.56–1.43 (2H, m), 0.93 (3H, t, J = 7.2 Hz), and 0.26 (9H, s); ^{13}C NMR δ: 194.7, 169.0, 128.3, 81.3, 62.9, 52.8, 27.7, 20.7, 13.8, and 1.3; LREIMS *m/z*: 311 $(M–CH_3)^+$.

*Methyl 4,4-dichloro-2-*n*-propyl-1,3-bistrimethylsilyloxycyclobut-2-ene carboxylate, **5***: To a stirred solution of cyclobutanone, **4**, (1.0 g, 3.06 mmol) in dry dimethoxyethane (20 mL) cooled to –70°C under argon was added 1,4 diazabicyclo[2.2.2]octane (140 mg, 1.25 mmol). Freshly distilled chlorotrimethylsilane (0.5 mL, 0.428 g, 3.94 mmol) was added by syringe via a septum, and the mixture was allowed to attain ambient temperature and stirred for 24 h. After dilution of the milky brown reaction mixture by addition of pentane (30 mL), it was filtered through Celite. The filtrate was washed successively with ice-cold 5% $NaHCO_3$ solution and brine and then dried over $MgSO_4$. The solvent was removed under reduced pressure and chromatography of the residue on silica gel (hexane:EtOAc, 5:1) afforded the trimethylsilyl enol ether, **5**, (1.03 g, 87%) as a colorless oil; IR (film) ν_{max}: 2950, 1743, 1642, and 851 cm^{-1}; ^1H NMR (200 MHz, $CDCl_3$) δ: 3.74 (3H, s), 2.20–2.00 (2H, m), 1.50–1.45 (2H, m), 0.82 (3H, t, J = 7.3 Hz), 0.33 (9H, s) and 0.26 (9H, s).

*Methyl 2,2-dichloro-3-oxo-5-*n*-propyl-1-trimethylsilyloxycyclopentane carboxylate, **7***: To a stirred solution of cyclobutanone, **4**, (1.0 g, 3.06 mmol) in dry ether (30 mL), cooled in an ice-bath, was added slowly a freshly prepared 0.22 M solution of diazomethane (29 mL, 6.38 mmol), followed by methanol (5 mL). The cooling bath was then removed and the mixture was set aside at ambient temperature for 30 min, when reaction was judged to be complete on the basis of TLC analysis. Addition of a few drops of acetic acid ensured

© 2000 NRC Canada

that no excess diazomethane remained, and the solution was then washed successively with saturated $NaHCO_3$ solution and brine. It was then dried over $MgSO_4$ and the amorphous material remaining after removal of solvent *in vacuo* was purified by flash chromatography on a column of silica gel (hexane:EtOAc, 5:1), affording the pure cyclopentanone, **7** (2.04 g, 98%) as fine crystals, mp 101–103°C; IR ($CHCl_3$) ν_{max}: 2989, 1780, 1750, 900, and 750 cm^{-1}; ^1H NMR (400 MHz, $CDCl_3$) δ: 3.84 (3H, s), 3.10–3.00 (1H, m), 2.75 (1H, dd, *J* = 18.9 and 8.9 Hz), 2.05 (1H, dd, *J* = 19.0 and 11.1 Hz), 1.60–1.20 (4H, m), 0.90 (3H, t, *J* = 7.4 Hz) and 0.25 (9H, s); ^{13}C NMR δ: 198.7, 167.9, 87.2, 87.0, 52.5, 38.9, 36.4, 32.5, 20.7, 14.1, and 1.6; HREIMS *m/z* (ion): 340.0665, M^+, (calcd. for $C_{13}H_{22}O_4Si^{35}Cl_2$: 340.0664).

*Methyl 5,5-dichloro-4-oxo-2-*n*-propyl-1-trimethylsilyloxy-cyclopent-2-ene carboxylate*, ***8***: A mixture of cyclopentanone (**7**) (1.0 g, 2.93 mmol) and selenium dioxide (467 mg, 4.21 mmol) in toluene was heated under reflux in an atmosphere of argon for 12 h. The reaction mixture was allowed to attain room temperature, and was then diluted by addition of hexane (50 mL) and filtered through Celite. The filtrate was evaporated to dryness *in vacuo*, and the residue was purified by chromatography on a column of silica gel (hexane:EtOAc, 10:1), affording cyclopentenone **8** (767 mg, 77%) as a pale yellow oil; IR (film) ν_{max}: 2960, 1755, 1743, and 851 cm^{-1}; UV λ_{max} (EtOH): 246 nm (ε = 10,900); ^1H NMR (400 MHz, $CDCl_3$) δ: 6.20 (1H, t, *J* = 1.5 Hz), 3.76 (3H, s), 2.25 (2H, ddd, *J* = 5.4, 7.3, and 16.5 Hz), 1.55 (2H, dt, *J* = 7.3 and 16.8 Hz), 0.98 (3H, t, *J* = 7.4 Hz) and 0.30 (9H, s); ^{13}C NMR δ: 189.9, 175.5, 168.8, 125.3, 124.9, 87.7, 53.4, 30.8, 19.8, 13.6, and 2.1; HREIMS *m/z* (ion): 323.0281, $(M–CH_3)^+$, (calcd for $C_{12}H_{17}O_4Si^{35}Cl_2$: 323.0273).

Preparation of silyl enol ether, ***9***: A solution of cyclopentenone, **8** (1.01 g, 2.98 mmol) and chlorotrimethylsilane (0.5 mL, 428 mg, 3.94 mmol) in dry tetrahydrofuran (10 mL) was added dropwise to a mixture of dry triethylamine (0.6 mL, 4.30 mmol) and sodium hydride (cf. 17) (7.2 mg, 0.30 mmol) in tetrahydrofuran (20 mL). The mixture was set aside with stirring at ambient temperature under an argon atmosphere for 30 min, and was then heated under reflux for 15 h. The reaction mixture was allowed to attain room temperature and was then diluted by addition of ether (100 mL) and filtered through Celite. The filtrate was washed successively with cold 5% HCl solution, saturated $NaHCO_3$ solution, and brine and then dried over $MgSO_4$. The solvent was removed under reduced pressure to yield the silyl enol ether, **9** (1.09 g, 89%) sufficiently pure to be used directly for the subsequent reaction; IR (film) ν_{max}: 2936, 1742, and 1225 cm^{-1}; ^1H NMR (400 MHz, $CDCl_3$) δ: 5.58 (1H, s), 5.20 (1H, t, *J* = 3.9Hz), 3.65 (3H, s), 2.10–2.00 (2H, m), 0.95 (3H, t, *J* = 7.0 Hz), 0.35 (9H, s), and 0.31 (9H, s); LREIMS *m/z* (relative intensity) (ion): 339 (6) $(M–^{35}Cl–H^{35}Cl)^+$, 321 (5) $(M–OSiMe_3)^+$, 295 (16), 279 (11), 205 (21), 89 (33) $(OSiMe_3)^+$, 73 (100) $(SiMe_3)^+$, 59 (21) $(CO_2CH_3)^+$.

Preparation of dienone, ***10***: To a solution of phenylselenenyl chloride (464 mg, 2.42 mmol) in dichloromethane (10 mL), cooled to –10°C, was added 1 M $TiCl_4$ (2.5 mL, 2.5 mmol). The mixture was cooled to to –78°C and a solution of silyl enol ether, **9**, (1.00 g, 2.43 mmol) in dichloromethane (20 mL) was gradually added from a dropping funnel over a 1 h period. The reaction mixture was stirred at –78°C for 4 h and was then allowed to warm up to ambient temperature. A cold saturated solution of NH_4Cl (30 mL) was added and the mixture was extracted with ether (3 × 50 mL). The extracts were washed with brine, dried ($MgSO_4$), and evaporated to dryness *in vacuo*. The residue was purified by flash chromatography on a column of silica gel (hexane:EtOAc, 10:1) furnishing the allylic phenyl selenide (980 mg, 82%) as a pale yellow oil; IR (film) ν_{max}: 2959, 1740, 1738, 1520, and 840 cm^{-1}; ^1H NMR (400 MHz, $CDCl_3$) δ: 7.4 (5H, m), 5.72 (1H, s), 3.66 (3H, s), 3.58 (1H, t, *J* = 6.7 Hz) 1.90–1.70 (2H, m), 0.90 (3H, t, *J* = 7.0 Hz), and 0.36 (9H, s); LREIMS *m/z* (relative intensity) (ion): 492 (8) (M^+), 477 (16) $(M–CH_3)^+$, 434 (3) $(MH–CO_2CH_3)^+$, 336 (23) $(M–PhSe)^+$, 322 (47), 294 (41) $(M–C_3H_6PhSe)^+$, 278 (100), 156 (37) $(PhSe)^+$, 93 (33), 89 (25), $(OSiMe_3)^+$,73 (82) $(SiMe_3)^+$.

The γ-phenyl selenide product (500 mg, 1.01 mmol) was dissolved in dry THF (10 mL). To the resulting solution, cooled to 0°C, was added 30% H_2O_2 solution (0.9 mL, ~7.9 mmol) and the mixture was set aside at 0°C with stirring for 2 h. The reaction mixture was then diluted by addition of ether (20 mL), and the solution was washed with saturated $NaHCO_3$ solution (2 × ~20 mL), dried ($MgSO_4$), and evaporated to dryness under reduced pressure. The residue was purified by chromatography on a column of silica gel (hexane:EtOAc, 10:1), furnishing the pure dienone, **10** (202 mg, 60%) as a pale yellow oil; IR (film) ν_{max}: 3440, 2954, 1740, 1738, 1600, 1200, and 956 cm^{-1}; UV λ_{max} (EtOH): 282 nm (ε = 16,800); ^1H NMR (400 MHz, $CDCl_3$) δ: 6.65 (1H, dt, *J* = 6.9 and 16.0 Hz), 6.30 (1H, s), 6.28 (1H, d, *J* = 15.8 Hz), 3.68 (3H, s), 1.90 (3H, d, *J* = 6.8 Hz), and 0.34 (9H, s); ^{13}C NMR δ: 189.8, 169.1, 165.9, 142.2, 123.2, 122.8, 89.6, 88.2, 53.5, 19.7, and 1.8; LREIMS *m/z* (relative intensity) (ion): 336 (8) (M^+), 320 (39) $(M–CH_3\text{-}H)^+$, 278 (75) $(MH\text{-}CO_2CH_3)^+$, 276 (79) $(M–CO_2CH_3\text{-}H)^+$, 242 (25) $(C_7H_{12}O_3Si^{35}Cl_2)$, 149 (100), 73 (82) $(SiMe_3)^+$.

Methyl 5-chloro-4-oxo-2-propenyl-1-trimethylsilyloxy-cyclopent-2-ene carboxylate, ***11***: The dienone **10** (300 mg, 0.99 mmol) was dissolved in 1:1 acetic acid-water (20 mL). Zinc powder (57 mg, 0.87 mg-atom) was added in one portion and the mixture was set aside with stirring at ambient temperature for 10 min. It was then diluted by addition of water (50 mL) and the mixture was extracted with ether (3 × 50 mL). The extracts were washed with saturated $NaHCO_3$ solution (3 × ~25 mL) and brine and then dried ($MgSO_4$) and evaporated to dryness under reduced pressure. The residue was purified by chromatography on a column of silica gel (hexane:EtOAc, 10:1), affording methyl 5-chloro-4-oxo-2-propenyl-1-trimethylsilyloxy-cyclopent-2-ene carboxylate, **11**, as a single epimer (183 mg, 68%); IR (film) ν_{max}: 2958, 2878, 1762, 1750, 1620, and 844 cm^{-1}; ^1H NMR (400 MHz, $CDCl_3$) δ: 6.80–6.60 (1H, m), 6.27 (1H, s), 6.20 (1H, d, *J* = 1.6 Hz), 4.45 (1H, s), 3.80 (3H, s), 1.95 (3H, dd, *J* = 1.6 and 5.9 Hz), and 0.24 (9H, s); ^{13}C NMR δ: 194.5, 169.5, 167.6, 141.5, 126.1, 123.4, 67.7, 67.5, 53.0, 19.6, and 1.0; LREIMS *m/z* (relative intensity) (ion): 303 (3) (MH^+), 287 (17) $(M–CH_3)^+$, 259 (6) $(M–C_3H_7)^+$, 243 (31) $(M–CO_2CH_3)^+$, 73 (100) $(SiMe_3)^+$.

© 2000 NRC Canada

Methyl 5-chloro-1-hydroxy-4-oxo-2-propenyl-cyclopent-2-ene carboxylate, Sporormia affinis *metabolite*, ***2***: To a cold stirred solution of methyl 5-chloro-4-oxo-2-propenyl-1-trimethylsilyloxy-cyclopent-2-ene carboxylate, **11** (180 mg, 0.59 mmol) in methanol (~25 mL) was added K_2CO_3 (98 mg, 0.71 mmol) in one portion. Stirring of the cooled reaction mixture was continued until no starting material remained (TLC analysis), and the mixture was then poured into cold water and extracted with ether (3 × 10 mL). The extracts were dried ($MgSO_4$) and evaporated to dryness *in vacuo*. The residue was purified by chromatography on a column of silica gel (hexane:EtOAc, 1:1), affording **2** (77 mg, 56%) as a colorless oil; IR (film) ν_{max}: 3470, 2908, 1742, 1710, 1663, and 838 cm^{-1}; UV λ_{max} (EtOH): 278 nm (ϵ = 23095); ^{1}H NMR (400 MHz, $CDCl_3$) δ: 6.70 (1H, dt, J = 6.8 and 16.0 Hz), 6.28 (1H, s), 6.24 (1H, d, J = 16 Hz), 4.60 (1H, s), 4.35 (1H, s, exchangeable with CD_3OD) 3.80 (3H, s) and 1.90 (3H, d, J = 6.7 Hz); ^{13}C NMR δ: 193.9, 171.2, 164.9, 141.4, 127.8, 123.2, 84.2, 67.1, 54.2, and 19.7; HREIMS *m*/*z* (ion): 230.0342 $(M)^+$, (calcd. for $C_{10}H_{11}O_4{}^{35}Cl$: 230.0346).

Acknowledgements

Financial support from Natural Resources Canada, Canadian Forest Service and from the Natural Sciences and Engineering Research Council of Canada is gratefully acknowledged. We thank Ms. Tammy Mallais for some technical support and Dr. Greg Lonergan, Research and Productivity Council, for providing the mass spectra.

References

1. (*a*) W.J. McGahren, J.H. van den Hende, and L.A. Mitscher. J. Am. Chem. Soc. **91**, 157 (1969); (*b*) W.J. McGahren and L.A. Mitscher. J. Org. Chem. **33**, 1577 (1968).
2. (*a*) G.M. Strunz, A.S. Court, J. Komlossy, and M.A. Stillwell. Can. J. Chem. **47**, 2087, 3700 (1969); (*b*) M.A. Stillwell, F.A. Wood, and G.M. Strunz. Can. J. Microbiol. **15**, 501 (1969).
3. D. Giles and W.B. Turner. J. Chem. Soc. C, 2187 (1969).
4. G.M. Strunz and A.S. Court. J. Am. Chem. Soc. **95**, 3000 (1973).
5. (*a*) A. Hantzsch. Chem. Ber. **20**, 2780 (1887); **22**, 1238 (1889); (*b*) C.J Moye and S. Sternhell. Tetrahedron Lett. 2411 (1964); Aust. J. Chem. **19**, 2107 (1966); (*c*) A.W. Burgstahler, T.B. Lewis, and M.O. Abdel-Rahmen. J. Org. Chem. **31**, 3516 (1966); (*d*) G.M. Strunz, A.S. Court, and J. Komlossy. Tetrahedron Lett. 3613 (1969).
6. G.B. Henderson and R.A. Hill. J. Chem. Soc. Perkin Trans. 1, 2595 (1983).
7. W.T. Brady. Tetrahedron, **37**, 2949 (1981).
8. C.M. Yu. Ph.D. thesis. University of New Brunswick, Fredericton. 1990.
9. E.V. Dehmlow. *In* Methoden der Organischen Chemie (Houben-Weyl), Band E19b. *Edited by* M. Regitz. Georg Thieme Verlag Stuttgart, 1989. pp. 1521–1537.
10. A.E. Greene and J.P. Deprés. J. Am. Chem. Soc. **101**, 4003 (1979).
11. Y. Ito, T. Hirao, and T. Saegusa. J. Org. Chem. **43**, 1011 (1978).
12. D.J. Clive. Tetrahedron, **34**, 1049 (1978).
13. D.T. Hurst and G. McInnis. Can. J. Chem. **43**, 2004 (1965).
14. G.M.Strunz, P.I. Kazinoti, and M.A. Stillwell. Can. J. Chem. **52**, 3623 (1974).
15. W.J. Middleton and E.M. Bingham. J. Org. Chem. **45**, 2883 (1980).
16. A.I. Vogel. Textbook of practical organic chemistry. 4th ed. Longman, New York. 1986. p. 318.
17. G. Stork and P.F. Hudrlik. J. Am. Chem. Soc. **90**, 4462 (1968).

© 2000 NRC Canada

Enantioselective synthesis of syringolide 2 from D-arabinose

Robert Chênevert and Mohammed Dasser

Abstract: Syringolide 2, a bacterial signal molecule which elicits active defence in resistant plants, has been synthesized in 9 steps from 2,3:4,5-di-*O*-isopropylidene-D-arabinose, a known derivative of D-arabinose.

Key words: syringolide, arabinose, synthesis.

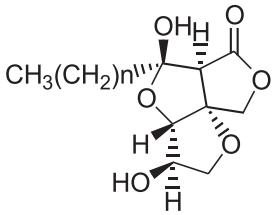
Résumé : Le syringolide 2, un signal moléculaire bactérien induisant une défense active chez les plantes résistantes, a été préparé en 9 étapes à partir du 2,3:4,5-di-*O*-isopropylidène-D-arabinose, un dérivé connu du D-arabinose.

Mots clés : syringolide, arabinose, synthèse.

Introduction

Syringolides 1 and 2, the first non-proteinaceous elicitors, were isolated from the plant pathogen bacterium *Pseudomonas syringea* pv. *tomato* by Sims and co-workers in 1993 (1). These elicitors trigger a hypersensitive defence response in soybean plants carrying a resistance gene (2). The hypersensitive defence phenomenon involves the localized cell death in the infected tissues and production of phytoalexins. Syringolides attract considerable interest since they have features in common with antigens recognized by the immune systems of vertebrates. Research on this defence mechanism could lead to cloning of disease-resistance genes and plant immunization through molecular genetic manipulation.

Four different strategies have been proposed for the synthesis of these C-glycosides possessing a new oxygen rich tricyclic structure. Syringolides have been synthesized from xylose (3–5), tartaric acid derivatives (6, 7), butenolides (8, 9), or via the Sharpless catalytic asymmetric dihydroxylation (10). In this paper, we report the enantioselective synthesis of syringolide 2 from D-arabinose.



Syringolide 1 (n=4)
Syringolide 2 (n=6)

Results and discussion

D-Arabinose (**1**) was transformed into di-*O*-isopropylidene-D-arabinose (**2**) in a three step sequence according to known procedures (11) (Scheme 1). Aldehyde **2** was reduced with $NaBH_4$ in ethanol to afford **3**. Alcohol **3** was protected by reaction with *p*-methoxybenzyl chloride (MPM-Cl) in the presence of NaH to give **4**. Regioselective deprotection of **4** was achieved by treatment with methanol under acidic catalysis (*p*-toluenesulfonic acid). The primary alcohol of **5** was selectively acylated with acetyl chloride in the presence of 2,4,6-collidine at –78°C. The Swern oxidation of **6** provided ketone **7**. The acetate group of **7** was selectively removed by transesterification with ethanol in diisopropyl ether in the presence of *Candida antarctica* lipase.

Acylation of **8** with the Meldrum's acid derivative **9** (12) in refluxing THF gave the unstable β-keto ester **10** (Scheme 2). Any attempt to purify **10** by chromatography on silica gel gave **11**, the product of the intramolecular Knoevenagel condensation; thus, **10** was stirred with silica gel in ethyl acetate – hexanes to give **11** in 71% yield for the two last steps. The *p*-methoxy-phenylmethyl (MPM) protecting group was removed by treatment with dichlorodicyanoquinone. All previous syntheses of syringolides invariably involved acid treatment of analogs of compound **12** to give syringolides in very low yields. Recently, Wong et al. (8) reported that the use of *p*-toluenesulfonic acid in large excess improved the yield of this rearrangement. Thus, treatment of **12** with a large excess of *p*-toluenesulfonic acid in acetone–water provided syringolide 2 (**13**) in 54% yield after recrystallization ($[\alpha]_D^{25}$ –75.1 ($CHCl_3$, *c* 0.06); litt. (1) $[\alpha]_D^{24}$ –75.91 ($CHCl_3$, *c* 0.22)). The spectroscopic data of the synthetic syringolide 2 (**13**) were identical to those reported in the literature.

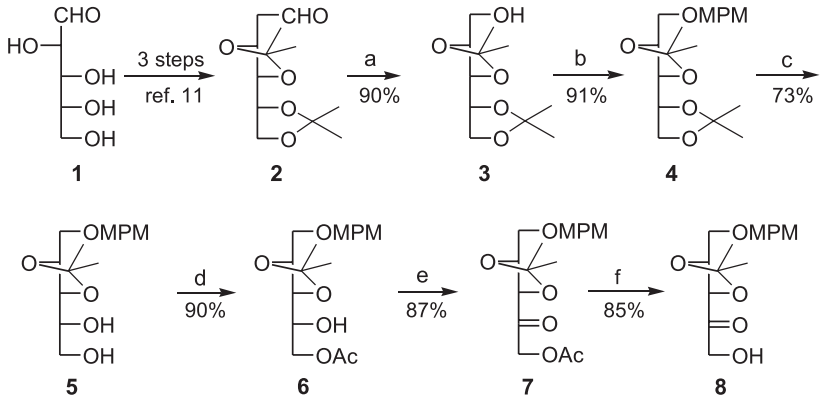
Received October 14, 1999.

R. Chênevert[1] and M. Dasser. Département de chimie, Faculté des sciences et de génie, Université Laval, Québec QC G1K 7P4, Canada.

[1]Author to whom correspondence may be addressed. Telephone: (418) 656-3283. Fax: (418) 656-7916.
e-mail: robert.chenevert@chm.ulaval.ca

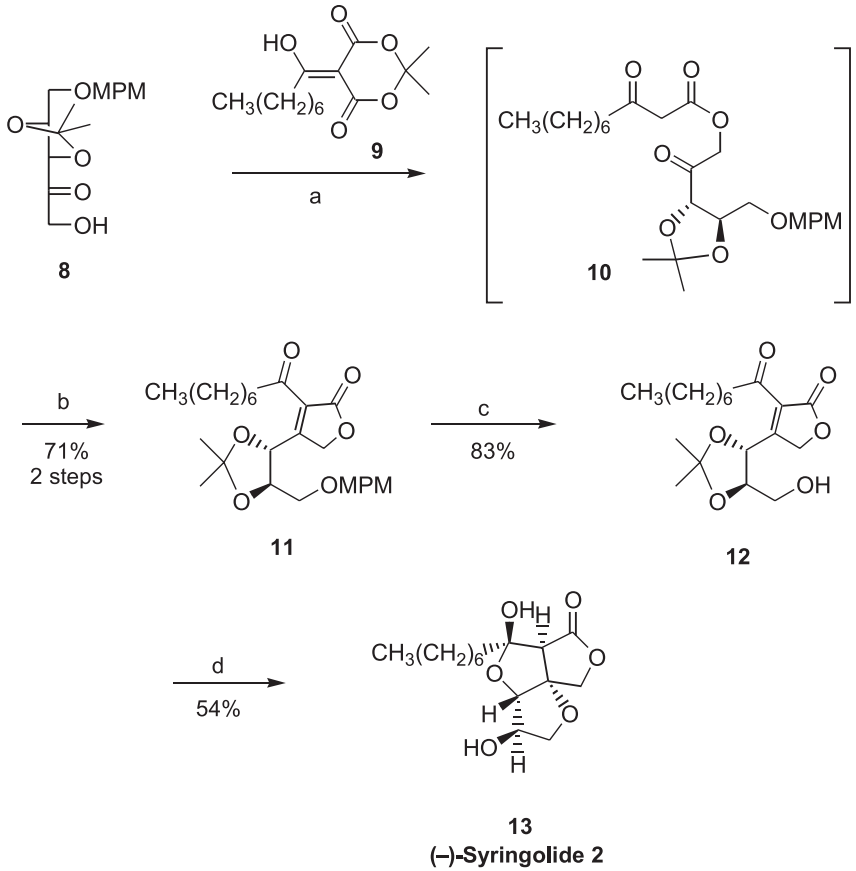
© 2000 NRC Canada

Scheme 1.



Scheme 1. Reagents: (a) $NaBH_4$, EtOH (b) NaH, p-methoxybenzyl chloride, DMF; (c) MeOH, TsOH; (d) AcCl, 2,4,6-collidine, -78°C; (e) $(COCl)_2$, DMSO; (f) *Candida antarctica* lipase, EtOH, diisopropyl ether.

Scheme 2.



Scheme 2. Reagents: (a) THF, reflux; (b) SiO_2, hexanes/EtOAc 9:1; (c) DDQ, CH_2Cl_2-H_2O; (d) TsOH, acetone-H_2O.

In conclusion, syringolide 2 has been synthesized in 9 steps and 15.3% overall yield from diisopropylidene-D-arabinose. Previous syntheses of syringolides from the sugar chiral pool involved the tedious and inefficient isomerization (~7% yield) of xylose to xylulose isolated as its acetonide. Both enantiomers of the starting material, arabinose, are readily

© 2000 NRC Canada

available at a reasonable cost. The use of *p*-toluenesulfonic acid in large excess greatly improved the yield of the last step (rearrangement of **12** to syringolide 2).

Experimental section

Candida antarctica lipase, fraction B (chirazyme L-2, carrier-fixed, lyo., 500 U/mg dry carrier) was purchased from Boehringer Mannheim. Melting points are uncorrected. NMR spectra were recorded at 300 MHz (^{1}H) and 75.44 MHz (^{13}C).

1,2:3,4-Di-*O*-isopropylidene-D-lyxitol (3)

Sodium borohydride (566 mg, 15.28 mmol) was added to a solution of aldehyde **2** (3.52 g, 15.29 mmol) in ethanol 95%. The mixture was stirred at room temperature for 6 h. The mixture was cooled to 0°C and acidified with 1 N HCl. The solvent was evaporated and the residue was dissolved in ether (200 mL), washed with 1 N HCl (30 mL), saturated aqueous $NaHCO_3$ (30 mL) and brine (2 × 20 mL). The organic layer was dried ($MgSO_4$) and evaporated. Flash chromatography on silica gel (EtOAc:hexane, 3:7) gave **3** (3.2 g, 90%) as a colorless oil. $[\alpha]_D^{25}$ –1.0 ($CHCl_3$, *c* 3.38); IR (neat) ν_{max}: 3700–3000, 3000–2800, 1380, 1370, 1300–1100 cm^{-1}; ^{1}H NMR ($CDCl_3$) δ: 4.05 (1H, dd, J_1 = 8.4 Hz, J_2 = 6.0 Hz), 3.92 (3H, m), 4.27 (1H, dd, J_1 = 11.7 Hz, J_2 = 4.3 Hz), 3.62 (2H, m), 2.75 (1H, s), 1.33 (3H, s), 1.31 (3H, s), 1.29 (3H, s), 1.25 (3H, s); ^{13}C NMR ($CDCl_3$) δ: 109.57, 109.20, 80.75, 78.65, 76.95, 67.62, 62.51, 26.77, 26.70, 26.42, 24.97; HRMS (CI, NH_3) *m/z*: calcd. for $C_{11}H_{21}O_5$: 233.1389 (MH^+), found 233.1393 ± 0.0007.

1,2:3,4-Di-*O*-isopropylidene-5-*O*-*p*-methoxybenzyl-D-lyxitol (4)

To a suspension of NaH (359.6 mg, 14.98 mmol) in dry DMF (10 mL) at 0°C and under dry nitrogen atmosphere was added dropwise a solution of **3** (2.23 g, 9.99 mmol) in DMF (50 mL). The mixture was stirred for 30 min at 0°C and the *p*-methoxybenzyl chloride (1.625 mL, 11.98 mmol) was added. The mixture was stirred for 1 h at 0°C and then overnight at room temperature. The mixture was then filtered through Celite and the filtrate was diluted with ether (300 mL), washed with water (3 × 60 mL). The organic phase was dried ($MgSO_4$) and evaporated. Flash chromatography on silica gel (ether:petroleum ether, 1:4) gave **4** (3.21 g, 91%) as a colorless oil. $[\alpha]_D^{25}$ +8.0 ($CHCl_3$, *c* 3.0); IR (neat) ν_{max}: 3090–3000, 2900–2800, 1380, 1370, 1300–1100 cm^{-1}; ^{1}H NMR ($CDCl_3$) δ: 7.24 (2H, d, *J* = 8.6 Hz), 6.84 (2H, d, *J* = 8.6 Hz), 4.50 (2H, s), 4.42–3.99 (3H, m), 3.86 (1H, m), 3.75 (3H, s), 3.70 (2H, m), 3.52 (1H, dd, J_1 = 10 Hz, J_2 = 6 Hz), 1.38 (3H, s), 1.36 (3H, s), 1.31 (3H, s), 1.29 (3H, s); ^{13}C NMR ($CDCl_3$) δ: 159.04, 130.95, 129.16, 113.55, 109.56, 109.39, 79.58, 77.57, 77.43, 72.93, 70.20, 67.39, 55.05, 26.92, 26.47, 25.10; HRMS (CI, NH_3) *m/z*: calcd. for $C_{19}H_{28}O_6$: 352.1886 (M^+), found 352.1893 ± 0.0010.

3,4-*O*-Isopropylidene-5-*O*-*p*-methoxybenzyl-D-lyxitol (5)

To a solution of diacetonide **4** (4.0 g, 11.34 mmol) in anhydrous methanol (40 mL) maintained at ~ 10°C was added *p*-toluenesulfonic acid (80 mg). The reaction was followed by thin layer chromatography (EtOAc; **4**, rf = 0.9; **5**, rf = 0.2, corresponding tetraol, rf = 0) and stopped after ~ 10 h. Triethylamine (1 mL) was added and the solvent was evaporated. Flash chromatography of the crude product (gradient from ether:hexane 1:1 to 4:1 and then pure MeOH) provided **5** (2.6 g, 73%) as a colorless oil along with starting material **4** (200 mg) and the corresponding tetraol (182 mg). $[\alpha]_D^{25}$ –15.52 ($CHCl_3$, *c* 1.15); IR (neat) ν_{max}: 3600–3100, 3000–2050, 2950–2850, 1380, 1370, 1300–1100 cm^{-1}; ^{1}H NMR ($CDCl_3$) δ: 7.17 (2H, d, *J* = 8.5 Hz), 6.80 (2H, d, *J* = 8.5 Hz), 4.45 (2H, s), 4.00 (1H, m), 3.72 (3H, s), 3.70–3.53 (5H, m), 3.46 (1H, dd, J_1 = 9.1 Hz, J_2 = 7.4 Hz), 1.30 (6H, s); ^{13}C NMR ($CDCl_3$) δ: 159.45, 129.56, 128.74, 113.85, 109.23, 80.51, 77.89, 73.48, 72.17, 70.20, 63.80, 55.13, 26.66; HRMS (CI, NH_3) *m/z*: calcd. for $C_{16}H_{24}O_6$ 312.1573 (M^+), found 312.1581 ± 0.0009.

1-*O*-Acetyl-3,4-*O*-isopropylidene-5-*O*-*p*-methoxybenzyl-D-lyxitol (6)

To a solution of **5** (1.83 g, 5.86 mmol) in dry CH_2Cl_2 (60 mL) cooled to –78°C was added freshly distilled 2,4,6-collidine (1.55 mL, 2 equiv.). After stirring for 5 min, acetyl chloride (0.55 mL, 1.2 equiv.) was added dropwise and the solution was stirred for 2 h at –78°C. Dichloromethane (200 mL) was added and the resulting organic phase was washed with 0.5 N HCl (1 × 50 mL), saturated aqueous $NaHCO_3$ (1 × 50 mL) and water (2 × 50 mL). The organic layer was dried ($MgSO_4$) and evaporated. Flash chromatography on silica gel (EtOAc:hexane, 3:7) gave **6** (1.87 g, 90%) as a colorless oil. $[\alpha]_D^{25}$ –1.0 ($CHCl_3$, *c* 2.45); IR (neat) ν_{max}: 3600–3150, 3010–2980, 2980–2800, 1740, 1380, 1370, 1300–1000 cm^{-1}; ^{1}H NMR ($CDCl_3$) δ: 7.24 (2H, d, *J* = 8.6 Hz), 6.87 (2H, d, *J* = 8.6 Hz), 4.52 (2H, s), 4.37 (1H, dd, *J* = 2.3 Hz), 4.06 (2H, m), 3.79 (4H, m), 3.70 (2H, m), 3.53 (1H, dd, J_1 = 9.3 Hz, J_2 = 6.7 Hz), 3.43 (1H, br s), 2.09 (3H, s), 1.36 (6H, s); ^{13}C NMR ($CDCl_3$) δ: 171.05, 159.31, 129.41, 129.11, 113.75, 109.37, 78.97, 78.51, 73.27, 70.98, 70.11, 66.08, 55.06, 26.67, 20.70; HRMS (CI, NH_3) *m/z*: calcd. for $C_{18}H_{26}O_7$: 354.1678 (M^+), found 354.1672 ± 0.0010.

(3*R*,4*R*)-1-Acetyl-3,4-isopropylidene-5-*p*-methoxybenzyl-1,3,4,5-tetrahydroxy-2-pentanone (7)

A solution of DMSO (872 µL, 11.33 mmol) in dichloromethane (6 mL) was added to a solution of oxalyl chloride (546 µL, 6.2 mmol) in dichloromethane (6 mL) at –78°C. The mixture was stirred for 20 min under dry nitrogen atmosphere. A solution of alcohol **6** (1.70 g, 4.783 mmol) in dichloromethane (50 mL) was added dropwise and the solution was stirred for 2 h at –78°C. Triethylamine (2.96 mL, 23.92 mmol) was added and the solution was allowed to reach room temperature. The reaction was diluted with dichloromethane (250 mL) and washed with water (40 mL), saturated aqueous $NaHCO_3$ (40 mL) and brine (3 × 40 mL). The organic phase was dried ($MgSO_4$) and evaporated. The crude product was purified by flash chromatography on silica gel (AcOEt:hexane, 3:7) to give ketone **7** (1.466 g, 87%) as a colorless oil. $[\alpha]_D^{25}$ –12.65 ($CHCl_3$, *c* 2.6); IR (film) ν_{max}: 3100–3000, 3000–2800, 1760, 1730, 1380, 1370, 1300–1100 cm^{-1}; ^{1}H NMR ($CDCl_3$) δ: 7.17 (2H, d, *J* = 8.6 Hz), 6.79 (2H, d, *J* = 8.6 Hz), 4.99 (1H, d, *J* = 17.8 Hz), 4.79 (1H, d, *J* = 17.8 Hz), 4.45 (2H, s), 4.26 (1H, d, *J* = 7.9 Hz), 4.20 (1H, m), 3.71 (3H, s), 3.64 (2H, dd, J_1 = 11.0 Hz, J_2 = 2.9 Hz), 3.51 (2H, dd, J_1 = 11.0 Hz,

© 2000 NRC Canada

J_2 = 5.1 Hz), 2.08 (3H, s), 1.39 (3H, s), 1.37 (3H, s); ^{13}C NMR ($CDCl_3$) δ: 202.46, 170.01, 159.13, 129.76, 129.18, 113.66, 111.34, 80.14, 77.38, 73.10, 69.18, 66.10, 55.08, 26.53, 25.97, 20.21. HRMS (CI, NH_3) *m*/*z*: calcd. for $C_{18}H_{24}O_7$: 352.1522 (M^+), found 352.1529 ± 0.0010.

(3*S*,4*R*)-3,4-Isopropylidene-5-*p*-methoxybenzyl-1,3,4,5-tetrahydroxy-2-pentanone (8)

Candida antarctica lipase (800 mg, total weigh enzyme on carrier, 500 U/mg dry carrier) and ethanol (1.0 mL, 17.0 mmol) were added to a solution of compound **7** (1.2 g, 3.4 mmol) in diisopropyl ether (30 mL) and the reaction mixture was stirred at room temperature. The reaction was followed by thin layer chromatography (ether:hexane, 1:1) and stopped when all the starting material was gone (~15 h). The reaction mixture was filtered and evaporated. Flash chromatography on silica gel (ether:hexane, 1:1) gave **8** (897 mg, 85%) as a colorless oil. $[\alpha]_D^{25}$ –7.7° ($CHCl_3$, *c* 1.45); IR (film) ν_{max}: 3600–3100, 3100–3000, 2990–2800, 1730, 1380, 1370, 1300–1100 cm^{-1}; ^{1}H NMR ($CDCl_3$) δ: 7.18 (2H, d, *J* = 8.6 Hz), 6.80 (2H, d, *J* = 8.6 Hz), 4.47 (2H, s), 4.44 (2H, m), 4.31 (1H, d, *J* = 8.0 Hz), 4.11 (1H, m), 3.72 (3H, s), 3.67 (1H, dd, J_1 = 3.1 Hz, J_2 = 10.7 Hz), 3.55 (1H, dd, J_1 = 5.2 Hz, J_2 = 10.7 Hz), 2.88 (1H, t, *J* = 5.0 Hz), 1.39 (3H, s), 1.34 (3H, s); ^{13}C NMR ($CDCl_3$) δ: 209.10, 159.21, 129.67, 129.22, 113.72, 111.36, 79.98, 76.90, 73.21, 69.23, 66.12, 55.13, 26.65, 26.01; HRMS (CI, NH_3) *m*/*z*: calcd. for $C_{16}H_{22}O_6$: 310.1416 (M^+), found 310.1421 ± 0.0009.

(1′*R*,2′*R*)-3-[1′,2′-(Isopropylidenedioxy)-3′-(*p*-methoxybenzyloxy)propyl]-2-octanoyl-2-buten-4-olide (11)

The octanoyl Meldrum's derivative **9** was prepared by stirring equimolar amounts of Meldrum's acid (2,2-dimethyl-1,3-dioxane-4,6-dione) and *n*-octanoyl chloride in dichloromethane at 0°C for 8 h.

A solution of alcohol **8** (380 mg, 1.224 mmol) and Meldrum's derivative **9** (397 mg, 1.469 mmol) in THF was brought to reflux during 3 h. The solvent was evaporated and the residue was dissolved in hexane:ethyl acetate 9:1 (15 mL) in the presence of silica gel (1 g). The mixture was stirred at room temperature for 18 h. Silica gel was filtered and the solvents were evaporated. Flash chromatography on silica gel (ethyl acetate:hexane, 3:7) gave **11** (402 mg, 71%) as a colorless oil. $[\alpha]_D^{25}$ –23.6 ($CHCl_3$, *c* 1.2); IR (film) ν_{max}: 3080–2990, 2990–2800, 1780, 1700, 1640, 1370, 1360, 1300–1100 cm^{-1}; ^{1}H NMR ($CDCl_3$) δ: 7.23 (2H, d, *J* = 8.6 Hz), 6.84 (2H, d, *J* = 8.6 Hz), 5.43 (1H, d, *J* = 8.2 Hz), 5.03 (1H, d, *J* = 19.8 Hz), 4.83 (1H, d, *J* = 19.8 Hz), 4.55 (1H, d, *J* = 11.6 Hz), 4.45 (1H, d, *J* = 11.6 Hz), 3.97 (1H, m), 3.78 (3H, s), 3.72 (2H, d, *J* = 4.8 Hz), 2.91 (2H, t, *J* = 7.0 Hz), 1.57 (2H, m), 1.43 (6H, s), 1.27 (8H, m), 0.86 (3H, t, *J* = 5.7 Hz); ^{13}C NMR ($CDCl_3$) δ: 196.56, 172.47, 170.08, 159.16, 129.69, 129.31, 126.71, 113.61, 110.96, 80.69, 73.76, 73.15, 69.78, 68.88, 55.10, 41.84, 31.53, 28.95, 28.87, 26.64, 23.03, 22.45, 13.92; HRMS (CI, isobutane) *m*/*z*: calcd. for $C_{26}H_{36}O_7$: 460.2461 (M^+), found 460.2464 ± 0.0014.

(1′*R*,2′*R*)-3-[3′-(Hydroxy)-1′,2′-(isopropylidenedioxy)propyl]-2-octanoyl-2-buten-4-olide (12)

Compound **11** (350 mg, 0.76 mmol) was dissolved in a mixture of CH_2Cl_2 (10 mL) and water (0.5 mL). DDQ (266 mg, 1.5 equiv.) was added and the mixture was stirred at room temperature. The reaction was followed by TLC and quenched after 4 h. The reaction mixture was diluted with CH_2Cl_2 (60 mL), filtered and washed with saturated aqueous $NaHCO_3$ (10 mL) and brine (3 × 10 mL). The organic layer was dried (Na_2SO_4) and evaporated. The crude product was purified by flash chromatography on silica gel (ethyl acetate:hexane, gradient 1:4 to 2:3) to give **12** (215 mg, 83%) as a colorless oil. $[\alpha]_D^{25}$ –60.0 ($CHCl_3$, *c* 1.6); IR (film) ν_{max}: 3600–3100, 2990–2800, 1790, 1710, 1620, 1370, 1360, 1300–1100 cm^{-1}; ^{1}H NMR ($CDCl_3$) δ: 5.39 (1H, d, *J* = 8.0 Hz), 5.10 (1H, d, *J* = 19.8 Hz), 4.85 (1H, d, *J* = 19.8 Hz), 3.96–3.80 (3H, m), 3.09 (1H, m), 2.92 (1H, m), 1.58 (2H, m), 1.45 (6H, s), 1.27 (8H, m) 0.97 (3H, t, *J* = 7.0 Hz); ^{13}C NMR ($CDCl_3$) δ: 198.75, 173.33, 169.74, 126.75, 110.54, 81.44, 73.82, 69.02, 61.42, 41.92, 31.49, 28.91, 28.84, 26.65, 23.04, 22.46, 13.93; HRMS (CI, NH_3) *m*/*z*: calcd. for $C_{18}H_{29}O_6$: 341.1964 (MH^+), found 341.1956 ± 0.0010.

Syringolide 2 (13)

A solution of **12** (140 mg, 0.411 mmol) and *p*-toluenesulfonic acid (782 mg, 10 equiv.) in acetone:water (1:1.2, 10 mL) was stirred for 56 h at room temperature. The solution was neutralized with saturated aqueous $NaHCO_3$ (2 mL) and extracted with ethyl acetate (3 × 20 mL). The organic layer was washed with brine (3 × 5 mL), dried over Na_2SO_4 and evaporated. The residue was redissolved in EtOAc (3 mL) and the solution was filtered through silica gel and evaporated. The product was washed with hexane to give syringolide 2 (95 mg, 77%) as a pale yellow solid. A fraction was recrystallized in pentane:ether 2:1 to give pure syringolide 2 (66.5 mg, 54%) as a colorless solid. Mp 122–123°C; $[\alpha]_D^{25}$ –75.1 ($CHCl_3$, c 0.06); lit. (1) mp 123–124°C $[\alpha]_D^{24}$ –75.91 ($CHCl_3$, *c* 0.22); IR (KBr) ν_{max}: 3600–3100, 2990–2800, 1770, 1300–1100 cm^{-1}; ^{1}H NMR (acetone-d_6) δ: 5.38 (1H, d, *J* = 1.9 Hz), 4.68 (1H, d, *J* = 10.2 Hz), 4.49 (1H, br s), 4.33 (1H, d, *J* = 10.2 Hz), 4.30 (1H, d, *J* = 4.2 Hz), 4.13 (1H, m), 3.94 (1H, dd, J_1 = 10.1 Hz, J_2 = 1.0 Hz), 3.83 (1H, dd, J_1 = 10.1 Hz, J_2 = 2.8 Hz), 3.10 (1H, s), 1.89 (2H, m), 1.70–1.40 (2H, m), 1.30 (8H, m), 0.87 (3H, t, *J* = 7.0 Hz); ^{13}C NMR (acetone-d_6) δ: 172.70, 108.72, 99.00, 92.16, 75.50, 75.32, 74.81, 59.63, 39.36, 32.40, 30.45, 29.40, 24.27, 23.15, 14.18. HRMS (CI, NH_3) *m*/*z*: calcd. for $C_{15}H_{25}O_6$: 301.1651 (MH^+), found 301.1657 ± 0.0009.

Acknowledgements

The authors would like to thank the Natural Sciences and Engineering Research Council of Canada (NSERC) for financial support.

References

1. S.L. Midland, N.T. Keen, J.J. Sims, M.M. Midland, M.M. Stayton, V. Burton, M.J. Smith, E.P. Mazzola, K.J. Graham, and J. Clardy. J. Org. Chem. **58**, 2940 (1993).
2. F. Schröder. Angew. Chem. Int. Ed. Engl. **37**, 1213 (1998).
3. C. Zeng, S.L. Midland, N.T. Keen, and J.J. Sims. J. Org. Chem. **62**, 4780 (1997).
4. H. Yoda, M. Kawauchi, K. Takabe, and K. Hosoya. Heterocycles, **45**, 1895 (1997).

© 2000 NRC Canada

5. J.P. Henschke and R.W. Rickards. Tetrahedron Lett. **37**, 3557 (1996).
6. J.L. Wood, S. Jeong, A. Salcedo, and J. Jenkins. J. Org. Chem. **60**, 286 (1995).
7. S. Kuwahara, M. Moriguchi, K. Miyagawa, M. Konno, and O. Kodama. Tetrahedron, **51**, 8809 (1995).
8. P. Yu, Q.G. Wang, T.C.W. Mak, and H.N.C. Wong. Tetrahedron, **54**, 1783 (1998).
9. J. Ishihara. T. Sugimoto, and A. Murai. Tetrahedron, **53**, 16029 (1997).
10. T. Honda, H. Mizutani, and K. Kanai. J. Org. Chem. **61**, 9374 (1996).
11. R. Ramage, A.M. MacLeod, and G.W. Rose. Tetrahedron, **47**, 5625 (1991).
12. Y. Oikawa, K. Sugano, and O. Yonemitsu. J. Org. Chem. **43**, 2087 (1978).

© 2000 NRC Canada

Pseudo-oxocarbons complexes — complexation of 2,4-bis(dicyanomethylene)-cyclobutane-1,3-dione dianion with copper. X-ray identification and electrochemical properties of the dianion and copper(I) and (II) complexes[1]

Paul-Louis Fabre, Christophe Pena, Anne Marie Galibert, Brigitte Soula, Gérald Bernardinelli, Bruno Donnadieu, and Paule Castan

Abstract: The compound $(Ph_4P)_2$(*trans*-cdcb)·$2H_2O$ (*trans*-$cdcb^{2-}$ = 2,4-bis(dicyanomethylene)-cyclobutane-1,3-dione dianion) has been synthesized and characterized by X-ray crystallography. Crystal data: triclinic, space group $P\bar{1}$, a = 10.829(2) Å, b = 11.297(2) Å, c = 11.515(2) Å, α = 79.61(1)°, β = 68.54(1)°, γ = 63.49(1)°, V = 1172.9(4) Å^3, Z = 1, R = 0.036, Rw = 0.047. With the dianion as a ligand, two complexes have been obtained and characterized by X-ray crystallography, UV–visible spectroscopy, and electrochemistry. The copper(II) complex [Cu(*trans*-cdcb)$(H_2O)_4$·$2H_2O]_n$ consists of polymeric chains with copper atoms bonded to two of the nitrile groups of the ligand. Crystal data: monoclinic, space group $P2_1/c$, a = 9.6366(6) Å, b = 7.1292(3) Å, c = 10.7018(6) Å, β = 99.603(4)°, V = 724.92(7) Å^3, Z = 2, R = 0.026, Rw = 0.041. The copper(I) complex[Cu_2(*trans*-cdcb)$(CH_3CN)_4$·$2CH_3CN]_n$ consists of polymeric chains with copper atoms bonded by all the four nitrile groups of the ligand. Crystal data: monoclinic, space group $P2_1/n$, a = 10.654(2) Å, b = 8.736(1) Å, c = 14.654(3) Å, β = 109.01(2)°, V = 1291.3(9) Å^3, Z = 2, R = 0.037, Rw = 0.041. In CH_3CN solution, the copper complexes are dissociated. Moreover, copper(II) is reduced into copper(I) by the dianion. Electrochemistry in the solid state (polymer coated electrode) showed the redox transitions of the different compounds.

Key words: pseudo-oxocarbons, X-ray diffraction, copper(II) complex, copper(I) complex, electrochemical behaviour.

Résumé : Le composé $(Ph_4P)_2$(*trans*-cdcb)·$2H_2O$ (*trans*-$cdcb^{2-}$ = dianion 2,4-bis(dicyanométhylène)-cyclobutane-1,3-dione) a été synthétisé et caractérisé par diffraction des rayons X. Données cristallographiques : triclinique, groupe d'espace $P\bar{1}$, a = 10.829(2) Å, b = 11.297(2) Å, c = 11.515(2) Å, α = 79.61(1)°, β = 68.54(1)°, γ = 63.49(1)°, V = 1172.9(4) Å^3, Z = 1, R = 0.036, Rw = 0.047. Avec le dianion comme ligand, deux complexes ont été obtenus et caractérisés par diffraction des rayons X, spectroscopie UV–visible et électrochimie. Le complexe du cuivre(II) [Cu(*trans*-cdcb)$(H_2O)_4$·$2H_2O]_n$ se présente comme une chaîne polymérique d'atomes de cuivre pontés par le ligand *trans*-cdcb et liés à deux des groupements nitrile du ligand. Données cristallographiques : monoclinique, groupe d'espace $P2_1/c$, a = 9.6366(6) Å, b = 7.1292(3) Å, c = 10.7018(6) Å, β = 99.603(4)°, V = 724.92(7) Å^3, Z = 2, R = 0.026, Rw = 0.041. Le complexe du cuivre(I) [Cu_2(*trans*-cdcb)$(CH_3CN)_4$·$2CH_3CN]_n$ se présente comme une chaîne polymérique d'atomes de cuivre liés aux quatre groupements nitrile du ligand. Données cristallographiques : monoclinique, groupe d'espace $P2_1/n$, a = 10.654(2) Å, b = 8.736(1) Å, c = 14.654(3) Å, β = 109.01(2)°, V = 1291.3(9) Å^3, Z = 2, R = 0.037, Rw = 0.041. En solution dans l'acétonitrile, les complexes du cuivre sont dissociés. De plus, le cuivre(II) est réduit en cuivre(I) par le dianion. Déposés sur une électrode recouverte d'un polymère, les composés sont électroactifs et présentent des processus redox.

Mots clés : pseudo-oxocarbones, diffraction des rayons X, complexe du cuivre(II), complexe du cuivre(I), électrochimie.

Received March 26, 1999.

P.L. Fabre,[2] C. Pena, A.M. Galibert, B. Soula, and P. Castan. Laboratoire de Chimie Inorganique, Université Paul Sabatier, 118 route de Narbonne, 31062 Toulouse Cedex 04, France.
G. Bernardinelli. Laboratoire de Cristallographie, Université de Genève, 24 Quai E. Ansermet, CH-1211 Geneva 4, Suisse.
B. Donnadieu. Laboratoire de Chimie de Coordination, UPR CNRS 8241, 205 route de Narbonne, 31077 Toulouse, France.

[1]This is Part 3 of the "Pseudo-oxocarbons complexes" series: see refs. 1 and 2 for the preceding parts of this series.
[2]Author to whom correspondence may be addressed. Telephone: 05-61-55-61-00. Fax: 05-61-55-61-18. e-mail: fabre@ramses.ups-tlse.fr

 © 2000 NRC Canada

Introduction

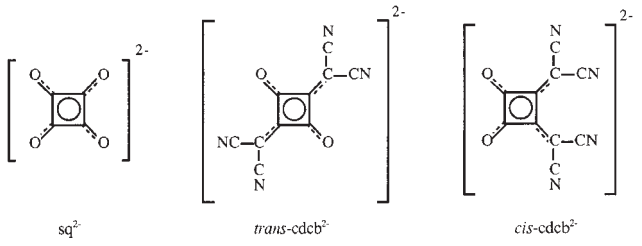
Magnetic interactions between paramagnetic centres can be propagated, not only through single atoms, but also through multi-atom bridges (3). Actually, metal dimers or chains with oxalate and dithiooxalate bridges have been known for some time, and relatively strong interactions have been observed. For example, the variable temperature magnetic susceptibility of $Cu(C_2O_4)\cdot 1/3H_2O$ was measured many years ago by a number of investigators (4), and more recently the symmetry factors governing the magnetic behavior of (μ-oxalato)copper(II) complexes were studied (5, 6).

Like oxalate, the squarate ion $C_4O_4^{2-}$ is an intriguing ligand because of its high symmetry and its electronic delocalization. Habenschuss and Gerstein's study (7) of the X-ray structure and magnetic properties of $Ni(C_4O_4)\cdot(H_2O)_2$ revealed an unexpected polymeric solid-state structure and a very low temperature ferromagnetic behaviour. In view of magnetic interactions between metal ions, a lot of copper(II) squarate complexes have been investigated (8–11).

Several species, derived from squarate entity, have been synthesized, in which one or more oxygen atoms have been substituted by other atoms or groups (sulfur, selenium, nitrogen or dicyanomethylene); they are called pseudo-oxocarbons. Among these pseudo-oxocarbons, our interest is focused on derivatives in which one or more oxygen atoms are replaced by dicyanomethylene, $C(CN)_2$, groups (12). They lead to brilliantly colored compounds which may be regarded as cyanine dyes. They are characterized by extensive π electron delocalization, interesting redox behaviour and, for some of them, intrinsic electrical conductivity.

These compounds can react with transition metals to lead to new complexes: molecular materials characterized by electron transport chains, compounds exhibiting magnetic exchange between metal ions, or electrochromic materials. We recently reported (1) on the first complex obtained with *cis*-cdcb^{2-} (3,4-bis(dicyanomethylene)-cyclobutane-1,2-dione dianion).[3] Regardless of the starting copper salt (Cu^I or Cu^{II}) used, only crystals of the copper(I) complex $[\{Cu_2(cdcb)(CH_3CN)_2\}_n]$ were obtained.

According to the synthetic pathway used with *trans*-cdcb^{2-} (2,4-bis(dicyanomethylene)-cyclobutane-1,3-dione dianion), the reduction of copper(II) may be prevented. Therefore copper(II), as well as copper(I), complexes of the dianion could be obtained. We report here on the syntheses and crystallographic investigations of the dianion *trans*-cdcb^{2-} itself and its Cu^I and Cu^{II} complexes. Electrochromic properties of *trans*-cdcb^{2-} and electrochemical behaviour of the two copper complexes are also presented.



Experimental

Reactants and methods

Squaric acid was purchased from Aldrich. CuI was prepared according to Inorganic Syntheses (13). All other chemicals and solvents were reagent grade. IR spectra were recorded in the solid state on nujol mulls or KBr pellets on a Perkin–Elmer 983 G spectrometer. UV–visible reflectance spectra were run in the solid state on a Perkin–Elmer Lambda 9 spectrophotometer. Magnetic susceptibility measurements in the 2–300 K temperature range were carried out with a Faraday-type magnetometer equipped with a continuous-flow Oxford Instruments cryostat. $HgCo(NCS)_4$ was used as a calibrant (susceptibility at 20°C, 16.44×10^{-6} cm^3 mol^{-1}). The molar susceptibilities were corrected for diamagnetism using Pascal's constants (14). The corrections were estimated at -1.5×10^{-5} cm^3 mol^{-1} for all the atoms of **3′**.

Powder conductivities were determined on compressed pellets with a Keithley 224 bridge.

Electrochemical measurements were carried out with a home-made potentiostat or an Autolab (EcoChemie) controlled by a PC computer at room temperature. The electrochemical cell (10 mL) was a conventional one with three electrodes: a working electrode, Pt (diameter 2 mm, EDI Tacussel) for rotating disk electrode experiments (LSV, linear sweep voltammetry) and Pt (disk diameter 0.5 mm) for cyclic voltammetry (CV) experiments; a counter electrode, Pt wire; and a reference electrode, double junction SCE. The experiments were carried out in CH_3CN–Bu_4NPF_6 (0.1 mol L^{-1}) under an argon atmosphere. CH_3CN and Bu_4NPF_6 (electrochemical grade) were used without further purification. A solution of Bu_4NPF_6 was scanned before use to check the purity of the solvent. The reported $E_{1/2}$ values were determined from stationary experiments at a rotating electrode (LSV).

Solid state electrochemistry was carried out according to the technique of polymer coated electrode (15, 16) which protects the electroactive substance from the solvent. The polymer coated electrode was prepared according to a reported procedure (16). A glassy carbon disk electrode (diameter 3mm, EDI Tacussel) was polished and sonicated in methanol and then one drop of a solution of the electroactive compound (50 mg in 5 mL of methanol) was applied to the electrode surface. After the electrode surface was air dried, one drop of the coating solution was added to overcoat the electrode surface. The coating solution was made of 1 g of polyacrylic acid (Aldrich, M_{ave} = 450 000) and 1 g of Bu_4NClO_4 in 15 mL of methanol. The electrode was again air dried. The electrochemical measurements were carried out in the same analytical cell using 0.1 mol L^{-1} CH_3CN–Bu_4NClO_4 as the solvent. The current interrupt method was used to measure the electrode potential in order to compensate for the ohmic drop (17).

[3] In precedent literature the name "carbodicyano" was given to the $C(CN)_2$ group and the acronym "cdcb" to the corresponding cyclobutanedione derivatives. According to the present use, we have adopted the name "dicyanomethylene" for the $C(CN)_2$ unit, but we have maintained the above acronym generally used by others.

© 2000 NRC Canada

Syntheses

*(i) Synthesis of 2,4-bis(dicyanomethylene)-cyclobutane-1,3-dione disodium salt [Na_2(trans-cdcb)·1/2H_2O] (**1**)*

This compound was obtained by reaction of malononitrile on 2,4-dianilinocyclobutene diylylium-1,3-diolate (18) by means of a method derived from that proposed by Seitz and co-workers (19).

To a solution of squaric acid (4.00 g, 0.035 mol) in 35 mL of DMF was added 6.52 g (0.070 mol) of aniline. The yellow solution was heated under reflux for 2 h and during this period a yellow precipitate appeared. Addition of 150 mL of water caused precipitation. The precipitate was separated by filtration and washed with water to remove the mono-adduct which is also obtained during the course of this synthesis. It was then washed several times with hot methanol to remove by-products. After exhaustive washing with warm DMF in order to remove the *cis*-isomer, the remaining yellow precipitate of 2,4-dianilinocyclobutenediylylium-1,3-diolate was dried and used without further purification (55%).

2,4-dianilinocyclobutenediylylium-1,3-diolate (5.30 g, 0.02 mol) was added by parts to a solution of sodium ethoxide (Na, 920 mg, 0.04 mol in dry ethanol 150 mL). After addition of malononitrile (2.64 g, 0.04 mol) the mixture was refluxed for 3 h. During this time the color changed from yellow to orange. After filtration, an orange precipitate was obtained. It was solubilized in 50 mL of hot water and the hot solution was filtered off. Orange needles of **1** were obtained by cooling the solution. Anal. calcd. for $C_{10}H_1N_4Na_2O_{2.5}$: C 45.65, H 0.38, N 21.29; found: C 45.20, H 0.31, N 21.00.

*(ii) [(Ph_4P)$_2$(trans-cdcb)]·2H_2O (**2**)*

This salt was prepared by mixing in 2:1 ratio Ph_4PBr and Na_2(*trans*-cdcb) in water. The orange solid which precipitated immediately was isolated and recrystallized from hot acetonitrile.

*(iii) [Cu(trans-cdcb)(H_2O)$_4$·2H_2O]$_n$ (**3**)*

This compound was obtained by reaction of **1** (0.131 g, 0.5 mmol) in water (25 mL) with $CuCl_2$·2H_2O (0.085 g, 0.5 mmol) in water (10 mL). From the first drops of **1** added to the copper salt, a violet precipitate appeared. This precipitate (**3a**) was filtered off. From the intensely violet filtrate solution, large bronze–violet crystals of **3** with a metallic lustre deposited. Out of the solution, these crystals became amorphous (**3′**) with loss of water. Recrystallization of **3a** or **3′** in water gave bronze–violet crystals of **3**. For **3′**: anal. calcd. for $C_{10}H_8CuN_4O_6$: C 34.94, H 2.35, N 16.30; found: C 33.72, H 2.45, N 16.10. This analysis agrees with the loss of two water molecules from **3**. Crystal structure of **3** is described.

*(iv) [Cu_2(trans-cdcb)(CH_3CN)$_4$·2CH_3CN]$_n$ (**4**)*

Method A: An aqueous solution of **1** (0.131 g, 0.5 mmol in 75 mL of water) was added dropwise to a solution of $CuCl_2$·2H_2O (0.085 g, 0.5 mmol) dissolved in a mixture of water–acetonitrile (5 and 150 mL). From the first drops of **1**, a red color appeared, then the solution became brown. After slow evaporation, orange crystals (**4**) were obtained.

Method B: An aqueous solution of **1** (0.131 g, 0.5 mmol in 50 mL of water) was added to a stoichiometric amount of CuI in acetonitrile (150 mL). The orange solution thus obtained deposited orange crystals (**4**) suitable for crystallographic analysis. **4** immediately became amorphous (**4′**) when the crystals were extracted from the solution. For **4′**: anal. calcd. for $C_{14}H_6Cu_2N_6O_2$: C 40.29, H 1.45, N 20.14; found: C 41.05, H 1.70, N 20.69. This analysis fits the loss of four acetonitrile molecules from **4**.

Crystallography

*X-ray structure determination of **2** and **3***

Selected crystal data, intensity measurements and structure refinement data for **2** and **3** are summarized in Table 1. Unit cell parameters and diffracted intensities were measured at 200 K on a Stoe–Stadi4 diffractometer with graphite monochromated CuKα radiation (λ = 1.5418 Å). For data collection of **3**, a crystal was immersed in RS 3000 oil (Riedel-de Haën) to prevent decomposition and mounted on a quartz fibre. The structure was solved by direct methods (MULTAN 87)[4] and refined by full-matrix least-squares with the XTAL 3.2 program (20). The data were corrected for Lorentz and polarization effects. Absorption corrections were applied with transmission factors ranging between 1.124–1.405 for **2** and 1.201–1.632 for **3**. Atomic scattering factors and anomalous dispersion terms are taken from reference 21. All coordinates of the H atom have been observed and refined using fixed U_{iso} at 0.04 Å^2 for **2** and **3**.

*X-ray structure determination of **4***

Selected crystal data, intensity measurements and structure refinement data for **4** are summarized in Table 1. To prevent decomposition during data collection, the crystal was immersed in RS 3000 oil (Riedel-de Haën) and mounted on a quartz fiber. Unit-cell parameters and diffracted intensities were measured at 160 K with the scan rotation phi mode on a Stoe-I.P.D.S. diffractometer equipped with an Oxford cryosystems cooler device. MoKα (λ = 0.71073 Å) was employed as X-ray source. The structure was solved by direct methods (SIR 92) (22) and refined by least-squares procedures on F_0. H atoms are calculated and not refined. Numerical absorption corrections applied are taken from footnote 5. Atomic scattering factors are taken from reference 21.

Results and discussion

A. Solution studies

As evidenced by conductivity measurements in water, in acetonitrile and DMF, the copper(I) and copper(II) complexes completely dissociate in solution at concentrations required for analytical studies. This is confirmed by electrochemical measurements in CH_3CN–Bu_4NPF_6 0.1 mol L^{-1} at concentration around 10^{-3} mol L^{-1}.

By linear sweep voltammetry at a rotating Pt electrode (Fig. 1), the voltammogram of the free *trans*-cdcb^{2-} ligand

[4] P. Main, S.J. Fiske, S.E. Hull, L. Lessinger, G. Germain, J.P. Declercq, and M.M. Woolfson. MULTAN 87, A system of Computer Programs for the Automatic Solution of Crystal Structures from X-ray Diffraction Data. Universities of York and Louvain-la-Neuve, 1987.
[5] X-Shape: a program for numerical absorption correction (version 2.01). STOE and Cie. GMBH Darmstadt. 1996.

© 2000 NRC Canada

Table 1. Summary of crystal data, intensity measurements, and structural refinement data for **2**, **3**, and **4**.

	2	3	4
Formula	$[P(C_6H_5)_4]_2[C_{10}N_4O_2]$ $2H_2O$ $C_{58}H_{44}N_4O_4P_2$	$[Cu(C_{10}N_4O_2)(H_2O)_4]$ $2H_2O$ $CuC_{10}H_{12}N_4O_8$	$[Cu_2(C_{10}N_4O_2)(C_2H_3N)_4]$ $2C_2H_3N$ $Cu_2C_{22}H_{18}N_{10}O_2$
Molecular weight	923.0	379.8	581.6
Crystal system	triclinic	monoclinic	monoclinic
Space group	$P\bar{1}$	$P21/c$	$P21/n$
a (Å)	10.829(2)	9.6366(6)	10.654(2)
b (Å)	11.297(2)	7.1292(3)	8.736(1)
c (Å)	11.515(2)	10.7018(6)	14.654(3)
α (°)	79.61(1)		
β (°)	68.54(1)	99.603(4)	109.01(2)
γ (°)	63.49(1)		
V (Å^3)	1172.9(4)	724.92(7)	1291.3(9)
Z	1	2	2
ρ_c (g cm^{-3})	1.31	1.74	1.50
F(000)	482	386	590
μ (mm^{-1})	1.271 (CuKα)	2.621 (CuKα)	1.691 (MoKα)
λ (Å)	1.5418	1.5418	0.71073
Temperature (K)	200	200	160
2Θ limits (°)	2–110	2–110	2.9–48.4
N° of measured reflections	3057	952	10028
N° of independant reflections	2878	891	1941
N° of observed reflections	2454	846	1698
Criterion for observed reflections	$\|F_o\| > 4\sigma(F_o)$	$\|F_o\| > 4\sigma(F_o)$	$\|F_o\| > 4\sigma(F_o)$
N° of parameters	374	125	200
Weighting scheme	$1/\sigma^2(F_o) + 0.0008(F_o^2)$	$1/[\sigma^2(F_o) + 0.0008(F_o^2)]$	Chebyshev[a]
Max. and min. ΔF (eÅ^{-3})	0.23, –0.23	0.24, –0.27	0.59, –0.75
"Goodness of fit" S	1.32(2)	1.30(3)	0.96
R, R_w	0.036, 0.047	0.026, 0.041	0.037, 0.041

[a]J.R. Carruthers and D.J. Watkin. Acta Crystallogr. Sect. A: Cryst. Phys. Diffr. Theor. Gen. Crystallogr. **A35**, 698 (1979).

shows two oxidation waves (full line) which appear monoelectronic and reversible as previously reported (23, 24):

$$\textit{trans}\text{-cdcb}^{2-} \rightleftharpoons \textit{trans}\text{-cdcb}^{\cdot -} + e^- \quad E^1_{1/2} = 0.255 \text{ V}$$

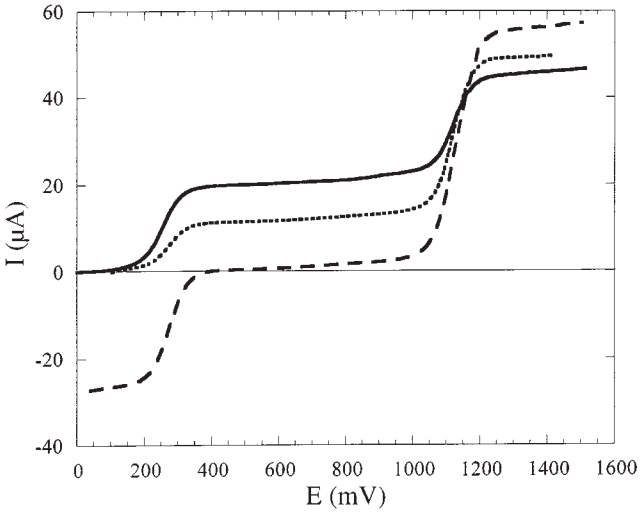
$$\textit{trans}\text{-cdcb}^{\cdot -} \rightleftharpoons \textit{trans}\text{-cdcb} + e^- \quad E^2_{1/2} = 1.129 \text{ V}$$

The *trans*-cdcb$^{\cdot -}$ radical anion is very stable. Its potential domain ($E^2_{1/2} - E^1_{1/2}$) depends on the solvent: 0.85 V in CH_3CN and 0.73 V in DMF. The *trans*-cdcb$^{\cdot -}$ radical anion is less stabilized in DMF than in CH_3CN. By exhaustive electrolysis of the dianion on the first plateau (0.6 V), the light orange solution turned deep red. Further electrolysis on the second plateau (1.4 V) yielded a transparent solution which is unstable. Only the first redox process is fully reversible and may be used for electrochromic applications.

The voltammogram (dotted line) of a saturated solution (6×10^{-4} mol L^{-1}) of the copper(I) complex (**4′**) presents the same pattern:

- a first oxidation wave ($E^1_{1/2}$ = 0.275 V) attributed to the first oxidation of the dissociated *trans*-cdcb^{2-} ligand, and
- a second oxidation wave ($E^2_{1/2}$ = 1.120 V) which is three times higher than the first one. The observed current ratio is in agreement with a process which involves the second oxidation ($E^2_{1/2}$ = 1.129 V) process of the dissociated *trans*-cdcb^{2-} ligand and the free copper(I) oxidation ($E_{1/2}$ = 1.04 V) into copper (II).

Fig. 1. Voltammograms at a rotating Pt disk electrode (diameter 2 mm, rotation speed 1000 rpm) in acetonitrile–Bu_4NPF_6 0.1 mol L^{-1}: $(Ph_4P)_2$(*trans*-cdcb) 1 mmol L^{-1} (——); copper(I) complex (**4′**) 0.6 mmol L^{-1} (⋯); copper(II) complex (**3′**) 1 mmol L^{-1} (– – –). Potentials are measured versus SCE.



© 2000 NRC Canada

As the dissociation of the complex gives two Cu^+ for one ligand, the ratio 1:3 was observed for the two oxidation waves:

$$Cu^+ \rightleftharpoons Cu^{2+} + e^- \qquad E_{1/2} = 1.04 \text{ V}$$

In this case, the invariance of the half-wave potentials is due to the dissociation of the copper(I) complex.

The voltammogram (dashed line) of a 10^{-3} mol L^{-1} solution of the copper(II) complex (**3′**) is slightly different but presents the same general pattern:

- a reduction wave ($E^1_{1/2}$ = 0.275 V) whose half-wave potential matches that of the first electron transfer of the free ligand and

- an oxidation wave ($E^2_{1/2}$ = 1.120 V) which is two times higher than the reduction wave. In the synthesis of **4**, method A, we might expect, through the dissociation of the complex, the oxidation of the *trans*-$cdcb^{2-}$ ligand by Cu^{2+} in CH_3CN solution. This oxidation reaction yields one *trans*-$cdcb^{\cdot -}$ radical anion and one Cu^+:

$$\textit{trans}\text{-}cdcb^{2-} + Cu^{2+} \longrightarrow \textit{trans}\text{-}cdcb^{\cdot -} + Cu^+$$

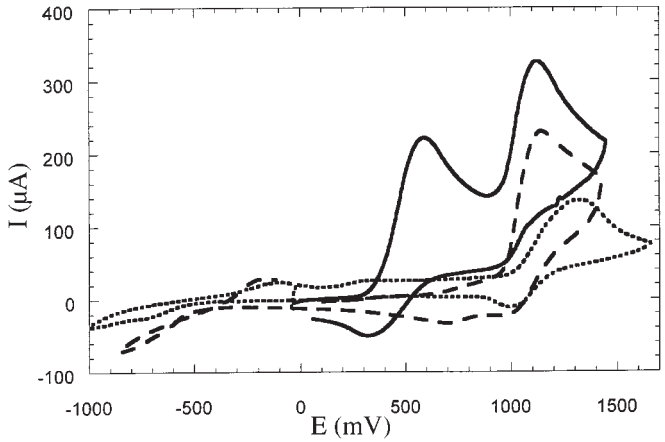
The recorded voltammogram agrees with this reaction: the reduction wave (one electron) is attributed to the reduction of the radical anion *trans*-$cdcb^{\cdot -}$ and the oxidation wave (one + one electron) is attributed to the oxidation of the radical anion *trans*-$cdcb^{\cdot -}$ and the oxidation of Cu^+ into Cu^{2+}.

From these studies, it appears that the copper complexes show low solubilities and that their dissolution implies dissociation and formation of $[Cu(CH_3CN)_4]^+$ in acetonitrile. The main question: is there a monomeric complex in solution?

The oxidation voltammograms of a Cu disk electrode were recorded as a function of *trans*-$cdcb^{2-}$ concentration. The displacement of the potential at a constant current was then related to the reactions occuring in solution (25). The variations of the potential versus the logarithm of the ligand concentration showed two linear domains: at a *trans*-$cdcb^{2-}$ concentration lower than 10^{-2} mol L^{-1}, a 1:1 complex may be expected, while at higher concentration the precipitate is formed. Unfortunately, the non-Nernstian behaviour of the electrode did not give reliable constant values: the complex formation constant of [Cu(*trans*-cdcb)]$^-$ is around 200. The solubility constant was determined from the voltammogram of a saturated solution (Fig. 1) by the measurement of the limiting current: K_s (Cu_2L) = 2×10^{-10}.

Polarographic measurements were carried out on the polymeric copper(II) complex which is synthesized in water in order to get information on its stability constants. In a typical experiment, a 10^{-4} mol L^{-1} solution of Cu^{2+} was analyzed by tast polarography as a function of *trans*-$cdcb^{2-}$ concentration. For a *trans*-$cdcb^{2-}$ concentration lower than 10^{-4} mol L^{-1}, only the Cu^{2+}–Cu(Hg) couple was observed. When the *trans*-$cdcb^{2-}$ concentration was increased, the polarographic wave turned into two waves, the first one related to the *trans*-$cdcb^{2-}$ concentration. With an increasing amount of *trans*-$cdcb^{2-}$, the copper(II) complex precipitated and the variations of the limiting current led to the determination of the solubility constant: K_s(CuL) = 3×10^{-7}. The splitting of the polarographic wave of the Cu^{2+}–Cu(Hg) couple showed the stabilization of a copper(I) complex as in the case of Cu^{2+}–Cu(Hg) reduction in presence of NH_3 (26). The variations of the half-wave potential versus the logarithm of the ligand concentration did not provide the evidence of the formation of a monomeric copper(II) complex.

Fig. 2. Cyclic voltammograms at a polymer coated glassy carbon disk electrode (diameter 3 mm) in CH_3CN–Bu_4NClO_4 0.1 mol L^{-1}: $(Ph_4P)_2$(*trans*-cdcb) (——); copper(I) complex (**4′**)(···); copper(II) complex (**3′**) (– – –); potential scan speed 0.05 V s^{-1}. Potentials are measured versus SCE.



B. Solid state studies

Bearing in mind the loss of solvent observed for the complexes **3** and **4**, only crystallographic measurements have been performed effectively on **3** and **4**. Spectroscopies, magnetic studies, as well as electrochemical measurements have been performed on **3′** and **4′**.

Least-squares fitting the μ_{eff} values of **3′** within the 2–300 K domain (1.929 at 300 K and 1.780 at 2 K) range to the Curie–Weiss law. This resulted C = 0.4607 cm^3 mol^{-1} K and Θ = –2.641 K. This magnetic behaviour can be easily understood when considering the very weak interaction between the copper(II) ions through the (μ-1,3) bismonodentate ligand (Cu···Cu = 13.1524(6) Å). However, we are not sure that the structure of **3** is retained in **3′**. Compound **4′** is diamagnetic as expected.

TCNQ[6] and its radical anion easily form metal salts (27) and Melby et al. (28) have reported the syntheses and conductivity properties of some TCNQ-transition metal complexes. The addition of dicyanomethylene groups $=C(CN)_2$ on the squarate ring leads to an extension of π delocalization and this ligand strongly looks like TCNQ. Moreover, charge-transfer salts, which are semiconductors, have been already obtained with cyanocroconates (C_5 pseudo-oxocarbon) (29). Considering the metallic lustre of **3′**, conductive properties may be expected. However, because its room temperature electrical conductivity on pressed pellets is 2×10^{-8} Ω^{-1} cm^{-1} it must be considered a poor conductor.

Solid state electrochemistry

Within the electroactive domain of the polymer coated electrode, the voltammograms were recorded by cyclic

[6] TCNQ = 7,7,8,8-tetracyano-*p*-quinodimethane.

© 2000 NRC Canada

voltammetry at a potential scan speed of 50 mV/s and starting towards anodic potential (Fig. 2). The voltammogram of the free *trans*-cdcb^{2-} ligand shows two oxidation processes (full line) which appear nearly reversible as in solution:

$$\textit{trans}\text{-cdcb}^{2-} \rightleftharpoons \textit{trans}\text{-cdcb}^{\cdot -} + e^- \quad E^1{}_p = 0.585 \text{ V}$$

$$\textit{trans}\text{-cdcb}^{\cdot -} \rightleftharpoons \textit{trans}\text{-cdcb} + e^- \quad E^2{}_p = 1.120 \text{ V}$$

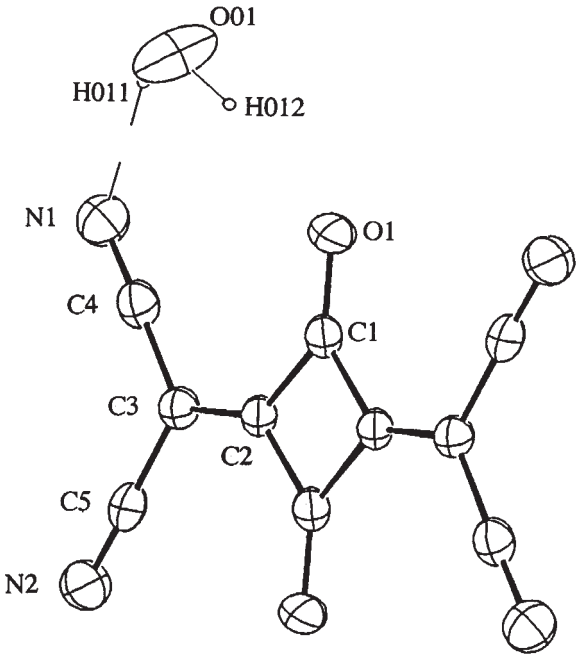
The oxidation process goes through the radical anion *trans*-cdcb$^{\cdot -}$, which must be stable. However, its potential domain ($E^2{}_p - E^1{}_p = 0.53$ V) is smaller than in solution (0.85 V in CH_3CN and 0.73 V in DMF). This is attributed to the *trans*-cdcb^{2-} ion-pairing in the solid phase, which is equivalent to a complexation and shifts the oxidation potential towards positive potentials. On the other hand, the second oxidation step is not displaced.

The voltammogram of the copper(II) complex (dashed line in Fig. 2) is different. The reduction of Cu^{2+} is observed around –0.5 V and on the anodic side only one oxidation process is observed. The potential of the oxidation peak is equivalent to that of the *trans*-cdcb$^{\cdot -}$/*trans*-cdcb oxidation peak. This indicates that the radical state of the ligand is unstable in the copper(II) complex. The voltammogram of the copper(I) complex (dotted line in Fig. 2) is similar to that of the copper(II) complex. On the cathodic side, the reduction of Cu^+ is observed around –0.5 V and on the anodic side only one oxidation process is also observed corresponding to the *trans*-cdcb$^{\cdot -}$/*trans*-cdcb oxidation potential. It can be pointed out that because the oxidation peak is large, it may involve the oxidation of the ligand and subsequent oxidation of Cu^+. The two complexes present the same electrochemical behaviour in the solid phase: the radical state of the ligand is unstable in both copper complexes and the oxidation of the ligand goes through a bielectronic transfer as in water.

Spectroscopies

The spectroscopic studies are related to **3′** and **4′**. The infrared study of several alkanes and cycloalkanecarbonitriles, and of their carbanions has been recently reported (30). Calculations confirm experimental data, with a marked decrease of nitrile band frequencies when going from the neutral molecule to the ionic form. We compare here the vibrational spectra of the free dianion of **1** with the spectra of the metal coordinated dianion. While the shift of the carbonyl or PO (in phosphine oxide) stretching frequencies is generally negative upon metal coordination, an increase in the frequency of the nitrile absorption appears to be quite a general phenomenon (31–34). This is expected due to the σ donation from the nitrogen lone pair of the nitrile which have antibonding character. Theoretical calculations involving the dianion (35) have shown that the negative charge is localized on the carbon atom bonded to the nitrile groups: the ligand may be considered as a nitrile rather than a cyanide ion. The vibrational spectrum of the dianion has already been reported (19). Two intense bands at 2223 and 2186 cm^{-1} are attributed to ν(CN) stretching frequencies. As expected for a nitrile group, the ν(CN) are shifted to higher frequencies in the copper(II) complex **3′**, i.e., at 2238 and 2206 cm^{-1}. Because the change from **3** to **3′** only consists of the loss of two crystallization water molecules, **3′** spectra are characteristic of complex **3**. In contrast, changing from **4** to **4′** results in a significant transformation of the copper atom environment. The metal, which is tetra-coordinated in **4**, is probably tri-coordinated in **4′**, surrounded by two nitrogen atoms from the ligands and one from an acetonitrile molecule. For **4′**, the ν(CN) are observed at 2197 and 2182 cm^{-1}, appreciably lower than those observed for the free dianion. We have already observed the same negative shift in the copper(I) complex obtained with the *cis*-ligand (1). This lowering of the CN stretching frequencies must not be related to the non-linearity of the Cu-N-C group, since this non-linearity is observed in both copper(I) and (II) complexes. Moreover, for the copper(I) complex **4′**, in the same region a band of weak intensity at 2296 cm^{-1} is attributed to the ν(CN) of acetonitrile, while the absorption band corresponding to free acetonitrile is observed at 2253 cm^{-1} (34, 36). It may be noticed that in **4′**, while the stretching frequencies of the nitrile group of *trans*-cdcb decrease upon complexation, the frequencies of the nitrile group of acetonitrile increase as expected. The vibrational assignments in the 1600–1400 cm^{-1} region are very difficult to make due to the strong coupling of the C=O and C=C oscillators. The band at 1604 cm^{-1} observed in the free ligand is shifted to 1568 cm^{-1} in **3′** but is unaffected in **4′**. In the same way, the two bands at 1462 and 1378 cm^{-1} in the free ligand are not affected upon complexation. In the far-infrared spectra of **3′** (450–200 cm^{-1}), the band observed at 436 cm^{-1} is assigned to the copper-oxygen stretching vibration. Nakagawa and Shimanouchi (32, 37) have carried out normal coordinate analyses of many $[M(H_2O)_4]^{n+}$ ions and indicate 440 and 442 cm^{-1} as the respective observed and calculated ν(Cu—O_{water}) values in $[Cu(H_2O)_4]^{2+}$. The 330 cm^{-1} band observed in the same spectrum is assigned to the metal-ligand stretching frequency (32–34, 37, 38).

Fig. 3. Structure of the dianion of $[(Ph_4P)_2(\textit{trans}\text{-cdcb})]\cdots 2H_2O$ (**2**).



© 2000 NRC Canada

Table 2. Selected interatomic distances (Å) and bond angles (°) with esd's in parentheses for **2**, **3** and **4.**

Crystal **2**					
O1—C1	1.238(4)	N1—C4	1.153(4)	N2—C5	1.149(5)
C1—C2	1.459(5)	C1—C2′	1.463(3)	C2—C3	1.393(4)
C3—C4	1.415(4)	C3—C5	1.421(5)		
O1-C1-C2	135.6(3)	O1-C1-C2′	134.1(3)	C2-C1-C2′	90.3(2)
C1-C2-C3	135.7(2)	C1-C2-C1′	89.7(2)	C1-C2′-C3′	134.5(3)
C2-C3-C4	122.3(3)	C2-C3-C5	120.8(2)	C4-C3-C5	116.7(3)
N1-C4-C3	178.5(3)	N2-C5-C3	178.5(3)		
Crystal **3**					
Cu—N1	2.357(2)	Cu—O01	2.015(2)	Cu—O02	1.937(2)
O1—C1	1.247(3)	C1—C2	1.458(4)	C1—C2′	1.454(4)
C2—C3	1.391(4)	C3—C4	1.422(4)	C3—C5	1.427(4)
N1—C4	1.146(3)	N2—C5	1.143(4)		
N1-Cu-O01	89.09(8)	N1-Cu-O02	92.61(8)	O01-Cu-O02	88.12(8)
Cu-N1-C4	156.2(2)	O1-C1-C2	134.0(2)	O1-C1-C2′	135.2(3)
C2-C1-C2′	90.8(2)	C1-C2-C3	133.8(2)	C1-C2-C1′	89.2(2)
C3-C2-C1′	137.0(3)	C2-C3-C4	120.3(3)	C2-C3-C5	121.8(2)
C4-C3-C5	118.0(2)	N1-C4-C3	178.4(3)	N2-C5-C3	178.3(3)
H011-O01-H012	117(4)	H021-O02-H022	108(4)		
H031-O03-H032	107(4)				
O1-C1-C2-C3	–3.2(5)	O1-C1-C2-C1′	178.5(3)		
C2-C1-C2′-C3′	178.3(3)	C2-C1-C2′-C1′	0.0(2)		
C1-C2-C3-C4	–11.7(4)	C1-C2-C3-C5	170.1(3)		
C1-C2′-C3′-C4′	165.8(3)	C1-C2′-C3′-C5′	–12.4(5)		
O01···O03 (1)	2.676(3)	O01-H011···O03 (1)	168(4)		
O02···N2 (2)	2.816(3)	O02-H021···N2 (2)	170(4)		
O02···O03 (3)	2.714(3)	O02-H022···O03 (3)	161(4)		
O03···O1 (4)	2.750(3)	O03-H032···O1 (4)	172(5)		
Crystal **4**					
Cu—N1	1.949(2)	Cu—N3	2.006(2)	Cu—N2	2.019(2)
Cu—N4	1.982(2)	N1—C11	1.130(4)	C11-C12	1.451(4)
N2—C21	1.141(3)	C21—C22	1.447(4)	N4—C2	1.149(3)
N3—C1	1.148(3)	C2—C3	1.417(3)	C1—C3′	1.407(3)
C4—C5	1.454(3)	C3—C4	1.393(3)	O1—C5	1.253(3)
N100—C100	1.136(4)	C100—C101	1.439(4)		
N1-Cu-N2	111.22(9)	N1-Cu-N3	115.74(9)	N2-Cu-N3	103.71(9)
N1-Cu-N4	119.59(8)	N2-Cu-N4	104.93(9)	N3-Cu-N4	99.81(8)
Cu-N1-C11	173.3(2)	Cu-N2-C21	171.6(2)	Cu-N3-C1	159.9(2)
Cu-N4-C2	162.5(2)	N3-C1-C3′	177.8(2)	N4-C2-C3	175.9(2)
C1′-C3-C2	116.1(2)	C1-C3-C4	122.3(2)	C2-C3-C4	121.5(2)
C3-C4-C5	134.6(2)	O1-C5-C4	135.3(2)	N1-C11-C12	179.0(3)
N2-C21-C22	179.2(3)	N100-C100-C101	178.5(3)		

The UV–visible region of the electronic spectrum of the ligand consists of a band at 430 nm. In the electronic spectra of **3′**, two bands are observed: the first at 487 nm is characteristic of the complexed ligand while the second broad band observed at 689 nm corresponds to *d–d* transitions. In the electronic spectra of **4′** only the band corresponding to an absorption within the ligand dianion is observed at 490 nm.

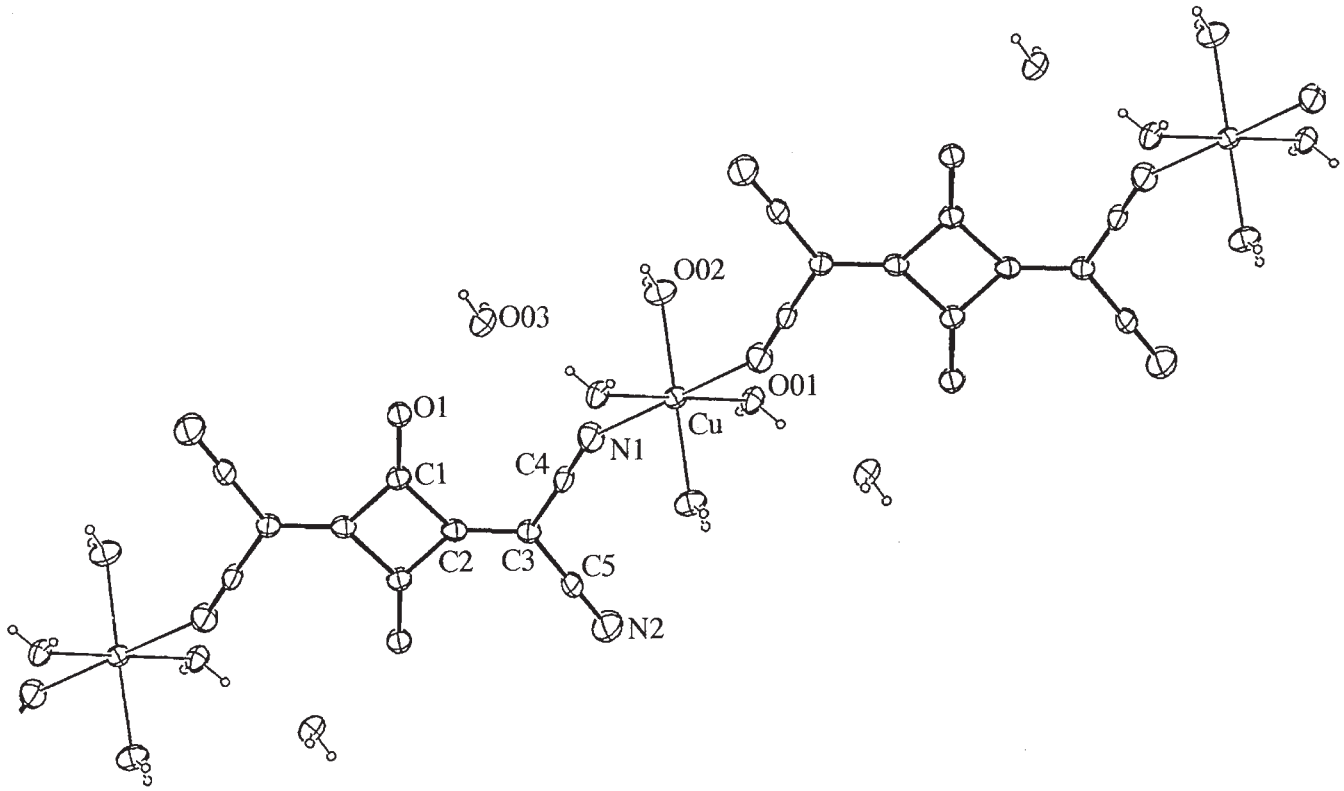
Structure of $[(Ph_4P)_2(trans\text{-}cdcb)]\cdot 2H_2O$ (2)

A view of the dianion, along with the numbering scheme, is shown in Fig. 3. Selected interatomic distances and bond angles are given in Table 2. The *trans*-$cdcb^{2-}$ ions are stacked along the b axis. The planar ring, which is nearly a square, is located around a crystallographic inversion center (0 0 1/2). This plane includes the atoms directly attached to it, O1 and C3. However, the dicyanomethylene group is slightly rotated about the C—C bonds. The mean plane through the five atoms of the dicyanomethylene group forms an angle of 2.71(3)° with the plane defined by the ring atoms. This deviation is in the order of those observed in the *cis*-$cdcb^{2-}$ salts (39, 40), and we can consider the occurrence of an intrinsically planar system.

The 1.459(5) Å distance C1—C2 is indicative of a perfectly π delocalized system. The 1.238(4) Å C1—O1 distance is normal for a carbonyl group. The 1.393(4) Å C(ring)—$C(CN)_2$ bond length is similar to the one observed in the isomeric *cis*-ligand regardless of whether it was

© 2000 NRC Canada

Fig. 4. Representation of the polymeric structure of $[Cu(trans\text{-}cdcb)(H_2O)_4 \cdot 2H_2O]_n$ (**3**).



coordinated or not. The structure of this planar ion indicates that all other bond distances observed are very similar to those observed for the *cis*-isomer, the only differing characteristic being a better π electron delocalization, as expected for symmetry. The distances and angles at the tetraphenylphosphonium ion are normal and are given as supplementary materials.[7]

Structure of $[Cu(trans\text{-}cdcb)(H_2O)_4 \cdot 2H_2O]_n$ (3)

A view of the molecule, along with the numbering scheme, is shown in Fig. 4. Selected bond lengths and angles are listed in Table 2. The structure of **3** is made of infinite chains located in the ac plane and parallel to the [101] direction (Fig. 4). These chains are built from $[Cu(trans\text{-}cdcb)(H_2O)_4]$ units and inside the chain the shortest Cu···Cu distance is 13.1524(6) Å (while the shortest interchain Cu···Cu is 7.1292(3) Å). A *trans*-cdcb unit bridges copper(II) ions acting in an *N*-bis(monodentate) mode. Each copper(II) ion situated on a crystallographic inversion center is octahedrally coordinated and the observed angles do not differ significantly from the ideal value (87.39(8)° to 92.61(8)°). However, the bond distances are notably different. The structure is better described as a (4 + 2) geometry and the important difference between equatorial and apical bond distances is indicative of an important Jahn–Teller effect associated with a semi-coordination of nitrogen of the cdcb ligand. The metal atom is linked to four water molecules in the equatorial plane and two nitrogen atoms from different cdcb are located at the apical sites. The copper—nitrogen distance of 2.357(2) Å is particularly longer than those already observed in copper(II)–nitrogen complexes (mean distance of ≅ 2 Å). Moreover, this distance is far from the Cu—N distances observed in the Cu(I) complex (crystal **4**) with the same ligand (2.019(2) and 1.982(2) Å) although the copper(I) ion is larger than the copper(II) ion. This structure may be related to that of the hexacoordinated copper(II) in $Cu(H_2O)_4(SO_4) \cdot H_2O$ (42) which involves a tetrahydrate copper(II) cation (Cu—O = 1.97 Å) and bridging semicoordinate SO_4^{2-} anion (Cu—O = 2.4 Å).

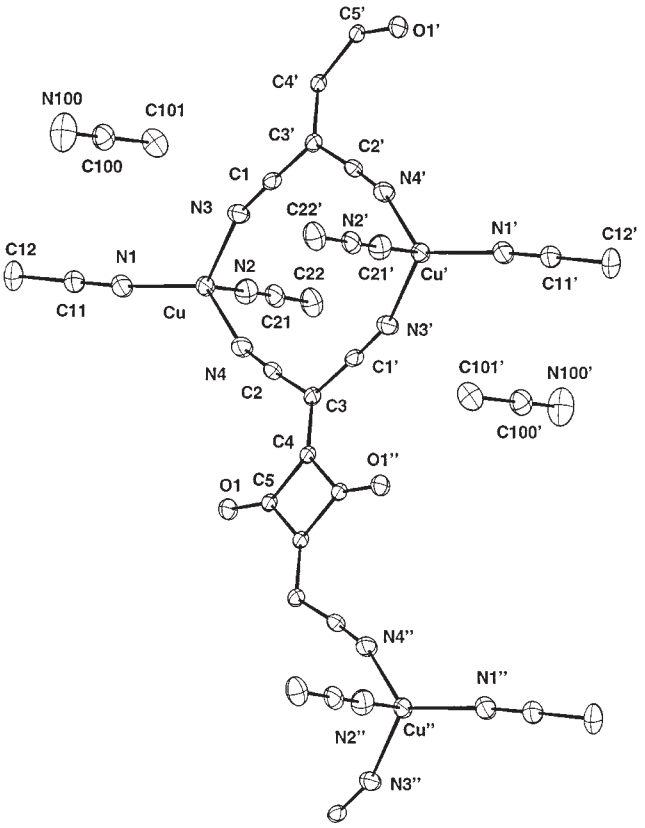
The *trans*-$cdcb^{2-}$ dianion is a potential multidentate ligand with coordination occurring by oxygen or nitrogen atoms, but more probably by nitrile groups. However, it may be underlined that contrary to the *cis* ligand, for which all the nitrile groups are involved in coordination, only two of the nitrogen atoms of the dicyanomethylene groups are coordinated in this complex. While the two nitrile groups are chemically distinct, they present similar C—N bond distances (1.146(3) and 1.143(4) Å for the bonded and nonbonded groups respectively) which are quite identical to those observed in compound **2**. The N1-C4-C3 and N2-C5-C3 angles at coordinated and non-coordinated cyanomethylene groups are 178.4(3)° and 178.3(3)° respectively. These values show that the cyanomethylene group is essentially linear as expected. However, the angle Cu-N1-C4 at 156.2(2)° deviates greatly from the expected value of 180°.

The square ring is planar with a crystallographic inversion center in the middle of the ring. However, while the deviation of the dicyanomethylene group from the ring is very

[7] The distances and angles at the tetraphenylphosphonium ion have been deposited as supplementary material and may be purchased from: The Depository of Unpublished Data, Document Delivery, CISTI, National Research Council Canada, Ottawa, Ontario, Canada, K1A 0S2.

© 2000 NRC Canada

Fig. 5. Structure of the unit of $[Cu_2(trans\text{-cdcb})(CH_3CN)_4\cdot 2CH_3CN]$ (**4**).



small in crystal **2**, the loss of planarity is important in crystal **3**. All the atoms of the dicyanomethylene group are coplanar and the dihedral angle between this plane and the square ring plane is 12.72(4)°. A similar deviation was observed in a copper(I) complex (1) obtained from the *cis*-ligand, but in the case of the *trans* ligand, it can't be explained by steric hindrance. Elsewhere, the bonds distances of the ligand are not affected by coordination.

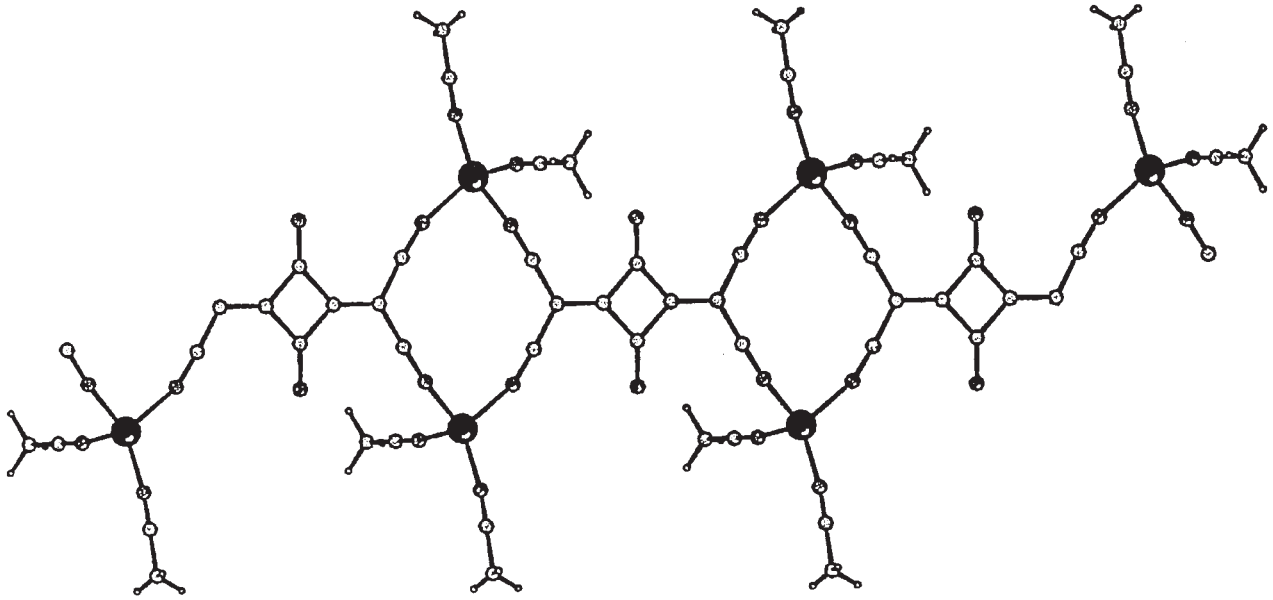
The hydrogen bond network involves the two water molecules located in the lattice, the bonded water molecules and the non-bonded nitrogen atoms of the cyano groups.

Structure of $[Cu_2(trans\text{-cdcb})(CH_3CN)_4\cdot 2CH_3CN]_n$ (4)

A view of the molecule, along with the numbering scheme, is shown in Fig. 5. Selected bond lengths and angles are listed in Table 2. The structure of **4** is made of infinite chains (Fig. 6). Within the chain, the geometry at copper(I) is nearly tetrahedral: the metal is linked to two acetonitrile ligands and two nitrogen atoms of two different dicyanomethylene groups belonging to two different *trans*-cdcb ligands. Moreover, two acetonitrile molecules are present in the lattice. The cation $[Cu(CH_3CN)_4]^+$ is easily obtained in acetonitrile. By substitution reaction on this cation, the tetrahedral geometry is most often retained. Actually, in the formation reaction of complex **4**, two acetonitrile molecules remain bonded to copper(I) and the two other molecules are present in the lattice.

It appears that there is little energetical difference between four-coordinated tetrahedral Cu(I) complexes and three-coordinated planar Cu(I) complexes. In the presence of soft donor atoms, the stereochemistry of copper(I) is very flexible: with the same metal and ligand stoichiometry, we may find complexes with different stereochemistries; otherwise, complexes with different stoichiometries may occur with the same ligand. Using *cis*-cdcb as the ligand, we obtained a planar tricoordinated copper(I) complex; with *trans*-cdcb as the ligand, we obtained a tetracoordinated complex. The Cu—N (*trans*-cdcb) distances (1.982(2) and 2.006(2) Å) are longer than those observed for Cu—N (*cis*-cdcb) (1.904(4) and 1.903(3) Å). Moreover, the Cu—N (acetonitrile) distances are also longer in the tetracoordinated complex. The study by Lippard et al. (42) of dichlorotris(triphenylphosphine)dicopper(I) complex, which contains both three- and four-coordinated copper(I), clearly reveals the shorter bond

Fig. 6. Representation of the polymeric structure of **4**.



© 2000 NRC Canada

lengths around the trigonal copper atom. A comparison of Cu—S distances in tetramethyl-thiourea copper(I) complexes (43, 44) produces similar results. These observations are in agreement with considerations based upon the steric repulsions around tetrahedrally or trigonally coordinated copper atoms. Out of the solvent, we observed the loss of four acetonitrile molecules during conversion from **4** to ***4′***. This implies the loss of the two non-coordinated solvent molecules and of two coordinated acetonitrile molecules (one on each copper atom) resulting in tricoordinated copper(I) atoms.

The *trans*-cdcb is potentially multidentate and acts as tetradentate in the present molecule. The four nitrogen atoms are linked to four different copper atoms, and, inside the chain, the shortest Cu···Cu distance is 6.796(1) Å.

While the Cu-N bonds are normal, bond distances of the ligand are not significantly affected by complexation as observed for complex **3**. The square ring is planar and an inversion center stands in the middle of the plane. The dihedral angle of the dicyanomethylene group from the mean plane is only 1.2° and lies in the order observed for the ligand. The angles Cu-N-C(acetonitrile) are normal (173.3(2)° and 171.6(2)°) and as expected; however, the values of Cu-N-C(cyanomethylene) (159.9(2)° and 162.5(2)°) are, as in the case of **3**, far from the expected 180° value.

The reaction of a Cu(II) salt with the *trans*-cdcb^{2-} ligand produces two different complexes, depending on the solvent used. In a water–CH_3CN mixture, the reduction of copper(II) occurs and leads to a copper(I) complex; in water alone, the copper(II) complex is obtained. While the redox potentials of the *trans*-cdcb^{2-} and *cis*-cdcb^{2-} dianions are of the same order of magnitude ($E^1_{1/2}$ = 0.255 V, $E^2_{1/2}$ = 1.129 V and $E^1_{1/2}$ = 0.243 V, $E^2_{1/2}$ = 1.068 V respectively) only a copper(I) complex has so far been obtained with the *cis*-dianion. This difference is attributed to kinetic effects.

Unfortunately, the copper complexes described in this paper dissociate in solution. In the solid state, electrochemical results showed that the complexes are electroactive and spectroelectrochemical experiments have yet to be carried out to determine the possible electrochromic properties of the complexes.

References

1. C. Pena, A.M. Galibert, B. Soula, P.L. Fabre, G. Bernardinelli, and P. Castan. J. Chem. Soc. Dalton Trans. 239 (1998).
2. F. Dumestre, B. Soula, A.M. Galibert, P.L. Fabre, G. Bernardinelli, B. Donnadieu, and P. Castan. J. Chem. Soc. Dalton Trans. 4131 (1998).
3. R.D. Willett, D. Gatteschi, and O. Kahn (*Editors*). Magneto-structural correlations in exchange coupled systems. Reidel, Dordrecht, Holland. 1985.
4. T.R. Felthouse, E. Laskowski, and D.N. Hendrickson. Inorg. Chem. **16**, 1077 (1979).
5. J.J. Girerd, M. Verdaguer, and O. Kahn. Inorg. Chem. **19**, 274 (1980).
6. M. Julve, M. Verdaguer, O. Kahn, A. Gleizes, and M. Piloche-Levisalles. Inorg. Chem. **22**, 368 (1983); **23**, 3808 (1984).
7. M. Habenschuss and B.C. Gerstein. J. Chem Phys. **61**, 852 (1974).
8. C. Robl and A. Weiss. Z. Naturforsch. B: Anorg. Chem. Org. Chem. **41b**, 1341 (1986).
9. X. Solans, M. Aguilo, A. Gleizes, J. Faus, M. Julve, and M. Verdaguer. Inorg. Chem. **29**, 775 (1990).
10. G. Bernardinelli, D. Deguenon, R. Soules, and P. Castan. Can. J. Chem. **67**, 1158 (1989).
11. I. Castro, J. Sletten, L.K. Glaerum, J. Cano, F. Lloret, J. Faus, and M. Julve. J. Chem. Soc. Dalton Trans. 3207 (1995).
12. A.J. Fatiadi. *In* Oxocarbons. *Edited by* R. West. Academic Press, New York. 1980. pp. 59–77.
13. G.B. Kauffman and R.P. Pinnell. Inorg. Synth. **VI**, 3 (1960).
14. P.W. Selwood. (*Editor*). Magnetochemistry. Interscience, New York. 1956.
15. E. Briot and F. Bedioui. Curr. Top. Electrochem. 87 (1997), and refs. therein.
16. C. Senaratne, J. Zhang, M.D. Baker, C.A. Bessel, and D.R. Rolison. J. Phys. Chem. **100**, 5849 (1996).
17. P. Cassoux, R. Dartiguepeyron, P.L. Fabre, and D. de Montauzon. Electrochim. Acta, **30**, 1485 (1985), and refs. therein.
18. E.W. Neuse and B.R. Green. J. Org. Chem. **39**, 3881 (1974).
19. B. Gerecht, T. Kämpchen, K. Köhler, W. Massa, G. Offermann, R.E. Schmidt, G. Seitz, and R. Sutrismo. Chem. Ber. **117**, 2714 (1984).
20. S.R. Hall and J.M. Steward (*Editors*). XTAL3.2 Users Manual. Universities of Western Australia and Maryland. 1992.
21. D.T. Cromer and J.T. Waber. International Tables for X-ray Crystallography. Vol. 4. Kynoch Press, Birmingham. 1974.
22. A. Altomare, G. Carascarano, G. Giacovazzo, A. Guargliardi, M.C. Burla, G. Polidori, and M. Camalli. J. Appl. Crystallogr. **27**, 435 (1994).
23. G. Farnia, B. Lunelli, F. Marcuzzi, and G. Sandonà. J. Electroanal. Chem. **404**, 261 (1996).
24. B. Lunelli, C. Corvaja, and G. Farnia. Trans. Faraday Soc. 67 (1971).
25. B. Trémillon. *In* Electrochimie analytique et réactions en solution. Masson, Paris. **2**, 248 (1993).
26. M. von Stackelberg and H. von Freyhold. Z. Elektrochem. Angew. Phys. Chem. **46**, 120 (1940).
27. A.R. Siedle. J. Am. Chem. Soc. **97**, 5931 (1975); P. Kathirgamanathan and D.R. Rosseinsky. J. Chem. Soc. Chem. Commun. 839 (1980).
28. L.R. Melby, R.J. Harder, W.R. Hertler, W. Mahler, R.E. Benson, and W.E. Moche. J. Am. Chem. Soc. **84**, 3374 (1962).
29. R.M. Doherty, J.M. Stewart, D. Mighell, C.R. Hubbard, and A.J. Fatiadi. Acta Crystallogr. Sect. B: Struct. Crystallogr. Cryst. Chem. **B38**, 589 (1982).
30. I.N. Juchnovski, J.A. Tsenov, and I.G. Binev. Spectrochim. Acta, **52**, 1145 (1996).
31. J. Reedijk, A.P. Zuur, and W.L. Groeneveld. Recl. Trav. Chim. Pays-Bas, **86**, 1127 (1967).
32. K. Nakamoto. *In* Infrared and raman spectra of inorganic and coordination compounds. J. Wiley & Sons, New York. **2**, 105 (1997).
33. W.E. Buschmann and J.S. Miller. Chem. Eur. J. **4**, 1731 (1998).
34. R. Bougon, P. Charpin, K.O. Christe, J. Isabey, M. Lance, M. Nierlich, J. Vigner, and W.W. Wilson. Inorg. Chem. **27**, 1389 (1988).
35. B. Lunelli and M.G. Giorgini. J. Mol. Struct. **218**, 303 (1990).
36. M. Kubota and D.L. Johnston. J. Inorg. Nucl. Chem. **29**, 769 (1967).
37. I. Nakagawa and T. Shimanouchi. Spectrochim. Acta, **20**, 429 (1964).
38. J. Reedijk and W.L. Groeneveld. Recl. Trav. Chim. Pays-Bas, **87**, 1079 (1968).
39. V. Busetti and B. Lunelli. J. Phys. Chem. **90**, 2052 (1986).

© 2000 NRC Canada

40. B. Lunelli and V. Busetti. J. Mol. Struct. **160**, 287 (1987).
41. J.N. Varghese and E.N. Maslen. Acta Crystallogr. Sect. B: Struct. Sci. **B41**, 184 (1985).
42. D.F. Lewis, S.J. Lippard, and P.S. Welcker. J. Am. Chem. Soc. **92**, 3805 (1970).
43. W.A. Spofford, E.A. Griffith, and E.L. Amma. J. Chem. Soc. Chem. Commun. 533 (1970).
44. M.S. Weininger, G.W. Hunt, and E.L. Amma. J. Chem. Soc. Chem. Commun. 140 (1972).

© 2000 NRC Canada

The effect of aspirin–HSA complexation on the protein secondary structure

J.F. Neault, A. Novetta-Delen, H. Arakawa, H. Malonga, and H.A. Tajmir-Riahi

Abstract: This study was designed to determine the secondary structure of human serum albumin (HSA) in the presence of aspirin in H_2O and D_2O solutions at physiological pH, using aspirin concentrations of 0.0001–5 mM with final protein concentration of 2% w/v. UV–vis spectra and Fourier transform infrared (FTIR) difference spectroscopy with its self-deconvolution, second derivative resolution enhancement, and curve-fitting procedures were applied to characterize the drug binding mode, the binding constant, and the protein secondary structure in the aspirin–HSA complexes. Spectroscopic evidence showed that no aspirin–protein interaction occurs at very low drug concentration (0.0001 mM), whereas at higher drug contents (0.001–0.1 mM) the aspirin anion binding (H-bonding) is mainly through the ε-amino NH_3^+ group with overall binding constant of $K = 1.4 \times 10^4$ M^{-1}. At high drug concentrations (1–5 mM), acetylation of Lys-199 was observed. Aspirin binding results in protein secondary structural changes from that of the α-helix 55% (free HSA) to 49%, β-sheet 22% (free HSA) to 31%, β-anti 12% (free HSA) to 4% and turn 11% (free HSA) to 16% in the aspirin–HSA complexes.

Key words: aspirin, protein, drug, binding mode, binding constant secondary structure, FTIR spectroscopy.

Résumé : Ce travail a comme objet de déterminer la structure secondaire de l'albumine de sérum humain (ASH) en présence d'aspirine, dans des solutions de H_2O ou de D_2O, au pH physiologique, à des concentrations d'aspirine allant de 0,0001 mM à 5 mM, avec une concentration finale de protéine de 2% p/v. On a utilisé la spectroscopie UV–vis et la spectroscopie infrarouge par transformée de Fourier (FTIR) différentielle en appliquant les méthodes d'autodéconvolution, d'augmentation de la résolution de la deuxième dérivée et d'ajustement des courbes pour caractériser le mode de fixation du médicament, la constante de fixation ainsi que la structure secondaire de la protéine dans les complexes aspirine-ASH. Les données expérimentales montrent qu'il ne se produit pas d'interaction aspirine-protéine à basses concentrations de médicament (0,0001 mM) alors que, à des concentrations plus élevées de médicament (de 0,001 à 0,1 mM), la fixation de l'anion de l'aspirine (fixation-H) se fait principalement par le biais du groupe ε-amino, NH_3^+, et que la constante globale de fixation, $K = 1{,}4 \times 10^4$ M^{-1}. À des concentrations élevées de médicament (1 à 5 mM), il se produit une acétylation de la Lys-199. La fixation de l'aspirine provoque des changements dans la structure secondaire de la protéine qui passe de 55% d'hélice-α (dans l'ASH libre) à 49%, de 22% de feuillet-β (dans l'ASH libre) à 31%, de 12% β-anti (dans l'ASH libre) à 4% et de 11% de décalement (dans l'ASH libre) à 16% dans les complexes aspirine-ASH.

Mots clés : aspirine, protéine, médicament, mode de fixation, constante de fixation, structure secondaire, spectroscopie IR à transformée de Fourier.

Introduction

Aspirin belongs to the nonsteroidal anti-inflammatory drugs and it is used extensively as a painkiller. It exerts an anti-inflammatory effect through selective acetylation of serine 530 on prostaglandin H_2 synthase (1). Aspirin has been shown previously to transfer its acetyl group to the ε-amino group of Lys-199 of human serum albumin under physiological conditions in vitro and in vivo and thus, this interaction increases the ability of HSA to bind the anionic drugs (2, 3). However, there has been no report on the effect of aspirin–HSA complexation on the protein secondary structure in aqueous solution.

Human serum albumin represents important and the most abundant protein constituent of blood plasma and serving as a protein storage component. Recently, the three-dimensional structure of human serum albumin was determined through X-ray crystallographic measurements (4). This globular protein consisting of a single polypeptide chain of 585 amino acids, which has many important physiological functions (5, 6). HSA considerably contributes to colloid osmotic blood pressure and realizes the transport and distribution of many molecules and metabolites such as fatty acids, amino acids, hormones, cations and anions, and many diverse drugs. It also makes possible to bind and carry through the bloodstream many drugs, which are poorly soluble in water (6). It has been shown that the distribution, free concentration, and the metabolism of various drugs can be significantly altered as a result of their bindings to HSA (7). Therefore, the inter-

Received October 12, 1999.

J.F. Neault, A. Novetta-Delen, H. Arakawa,[1] H. Malonga, and H.A. Tajmir-Riahi.[2] Department of Chemistry-Biology, University of Québec at Trois-Rivières, C.P. 500, Trois-Rivières, QC G9A 5H7, Canada.

[1]Dr. H. Arakawa was on sabbatical leave from Hokkaido Institute of Technology, Sapporo, Japan.

[2]Author to whom correspondence may be addressed. Telephone: (819) 376-5052. Fax: (819) 376-5084 (ext. 3321). e-mail: tajmirri@uqtr.uquebec.ca

© 2000 NRC Canada

action of aspirin with human serum albumin has major biochemical importance.

We now report the FTIR and UV–vis spectroscopic results on the interaction of aspirin with human serum albumin, in aqueous solution at physiological pH, using drug concentrations of 0.0001–5 mM with a final HSA (fatty acid free) concentration of 2% w/v. Spectroscopic evidence regarding the drug binding mode, drug binding constant, and the protein secondary structural changes are provided here. To our knowledge, our structural information provides the first spectroscopic evidence regarding aspirin–HSA interaction and should help to elucidate the nature of this biologically important complex formation in vitro and in vivo.

Materials and methods

Materials

Human serum albumin (fatty acid free) fraction V was purchased from Sigma Chemical Co., and used as supplied. Aspirin was from Sigma Chemical Co., and used without further purification. D_2O (99.98%) was from Aldrich Chemical Co. Other chemicals were of reagent grade.

Preparation of stock solution

Human serum albumin (fatty acid free) was dissolved in aqueous solution to 4% w/v (40 mg/mL) containing phosphate buffer and 0.05 M NaCl. The solutions of aspirin 0.2 μM to 10 mM were prepared by dissolving aspirin in double distilled water (pH 6–7). In the final step, the solution of drug was added dropwise to the protein solution with constant stirring to ensure the formation of homogeneous solution and to attain the desired drug concentrations of 0.0001–5 mM with a final protein concentration of 2% w/v. Equal volumes of aspirin and HSA solutions were incubated for 2 h at room temperature before spectral measurements. The deuterated samples were prepared in D_2O in the same way as described for H_2O solutions. The pH or pD of the solution was adjusted to 6.8–7.4 by the addition of NaOH or NaOD (0.1 M).

Absorption spectra

The absorption spectra were recorded on a Hewlett–Packard 8452A Diode Array Spectrophotometer.

FTIR spectroscopic measurements

Infrared spectra were recorded on a BOMEM DA3–0.02 Fourier transform infrared spectrometer equipped with a nitrogen cooled HgCdTe detector and a KBr beam splitter. Solution spectra were taken, using AgBr windows with resolution of 2 cm^{-1} and 100–500 scans. The subtraction of H_2O or D_2O from protein solution was carried out as reported in our previous reports (8). The difference spectra [(protein solution + aspirin anion solution) – (protein solution)] were generated using the polypeptide antisymmetric and symmetric C-H stretching bands (9), located at 2900–2800 cm^{-1} as internal standard. The protein C-H stretching vibrations exhibit no spectral changes upon drug interaction and they are cancelled on spectral subtraction. The accuracy of this method of subtraction was tested by using several control samples with the same protein or drug concentrations, that resulted in a similar flat baseline formation. However, a similar absorption scale was used, for the spectra of the free protein and its aspirin complexes as well as for the difference spectra produced here. This method allowed us to obtain meaningful spectral differences between the free protein and its drug complexes at different aspirin concentrations. Such spectral differences were used here, in order to characterize the nature of the drug–protein interaction.

Analysis of protein secondary structure

Determination of the secondary structure of HSA and its aspirin complexes was carried out on the basis of the procedure described by Byler and Susi (10). The protein secondary structure is determined from the shape of the amide I band, located at 1650–1660 cm^{-1}. Fourier self-deconvolution and second derivative resolution enhancement were applied to increase the spectral resolution in the region of 1700–1600 cm^{-1}. The second derivatives were produced using a point convolution of 11 or 13. The resolution enhancement resulting from self-deconvolution and the second derivative is such that the number and the position of the bands to be fitted are determined. In order to quantify the area of the different components of amide I contour, revealed by self-deconvolution and second derivative, a least-square iterative curve-fitting was used to fit the Lorentzian line shapes to the spectra between 1700–1600 cm^{-1}. Before curve-fitting was done, a straight baseline passing through the ordinates at 1700 and 1600 cm^{-1} was subtracted. The baseline is then modified again by the least-square curve-fitting, which allowed for a horizontal baseline to be adjusted as an additional parameter in order to obtain the best fit. It is known that no meaningful curve-fitting can be performed by simple examination of the original infrared spectra, that is why the self-deconvolution procedure has to be carried out first. The curve-fitting was done using a number of 25 simulations. The resulting curve fitted is analysed as follows: each Lorentzian band is assigned to a secondary structure according to the frequency of its maximum; α-helix (1656–1657 cm^{-1}), β-sheet (1616–1635 cm^{-1}), turn (1673–1678 cm^{-1}), random coil (1640–1645 cm^{-1}), and β-antiparallel (1684–1692 cm^{-1}). The area of all the component bands assigned to a given conformation are then summed and divided by the total area. The number obtained is taken as the proportion of the polypeptide chain in that conformation. These assignments are consistent with the previous values determined theoretically (9) and experimentally (10). The accuracy of this method was tested on several proteins of the known conformational contents (through X-ray diffraction analysis), such as cytochrome c (α-helix 49%) and RNase A (α-helix 27%) (11–13) that resulted in 2–3% differences. The data treatments of protein conformational analysis are also reported in our recent publication (8). The aspirin–protein binding constants were calculated based on the UV absorption method (14).

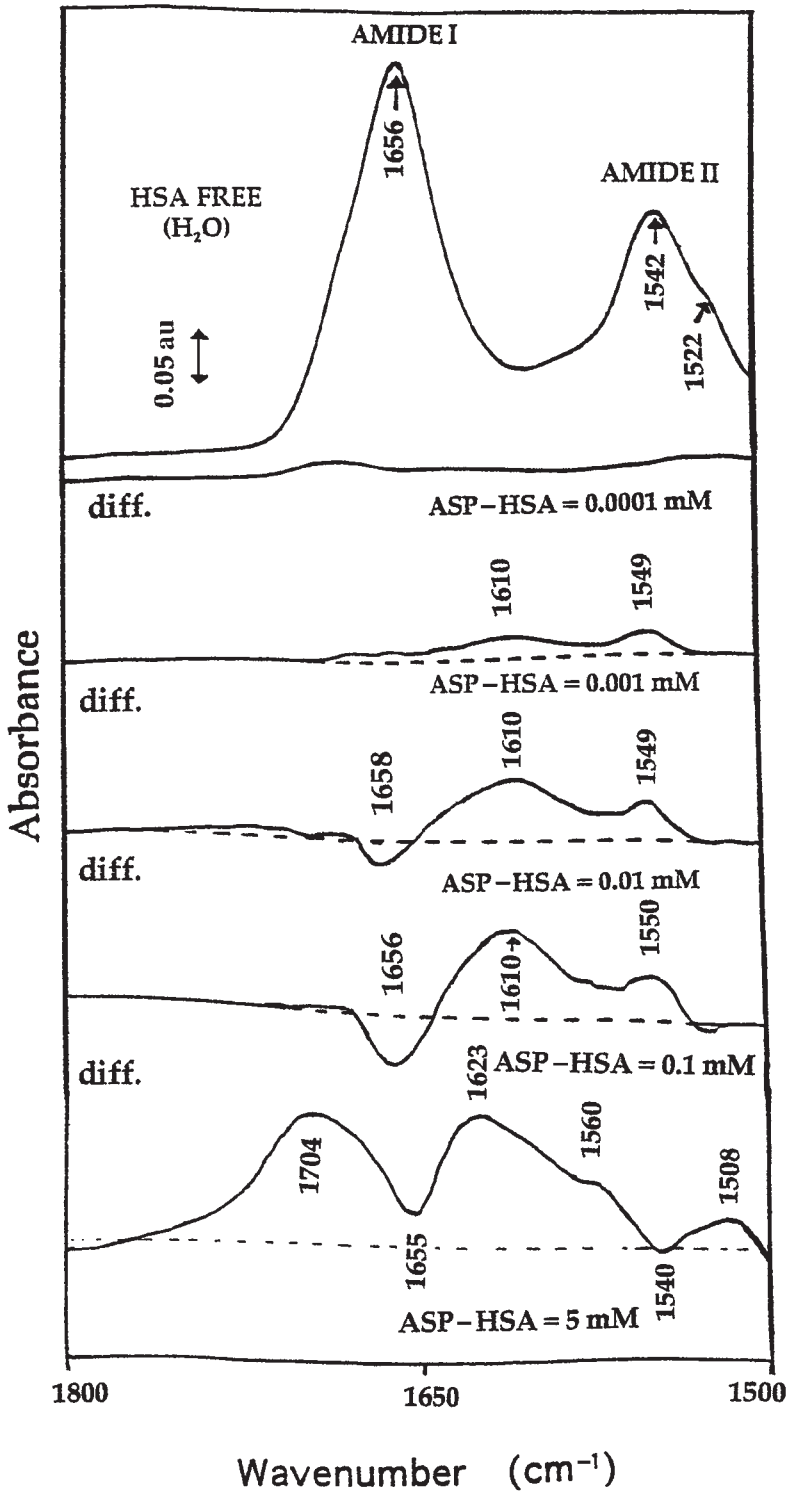
Results and discussion

Aspirin–HSA interaction

Since there was no major spectral shifting for the protein amide I band at 1656 cm^{-1} (mainly C=O stretch) and amide II band at 1542 cm^{-1} (C-N stretch coupled with N-H bending mode) (9, 10), the difference spectra [(protein solution +

© 2000 NRC Canada

Fig. 1. FTIR spectra (top first curve) and difference spectra [(protein solution + aspirin solution) – (protein solution)] (bottom four curves) of the free human serum albumin (HSA) and its aspirin anion complexes in aqueous solution at physiological pH with different drug concentrations in the region of 1800–1500 cm^{-1} (the baseline shown as broken lines).

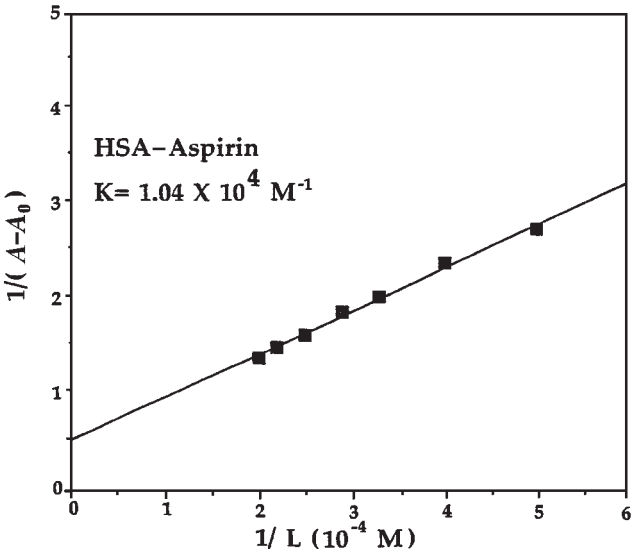


aspirin solution) – (protein solution)] were obtained in order to monitor the intensity variations of these vibrations and the results are shown in Fig. 1. The overall binding constants of the aspirin–HSA complexes were determined using UV absorption spectroscopy and the results are presented in Fig. 2. Similarly, the infrared self-deconvolution with second derivative resolution enhancement and curve-fitting procedures (10–13), were used to determine the protein secondary structure in the presence of aspirin anion and the results are given in Fig. 3 and Table 1.

At very low aspirin concentration (0.0001 mM), no spectral changes (intensity or shifting) occurred for the amide I

© 2000 NRC Canada

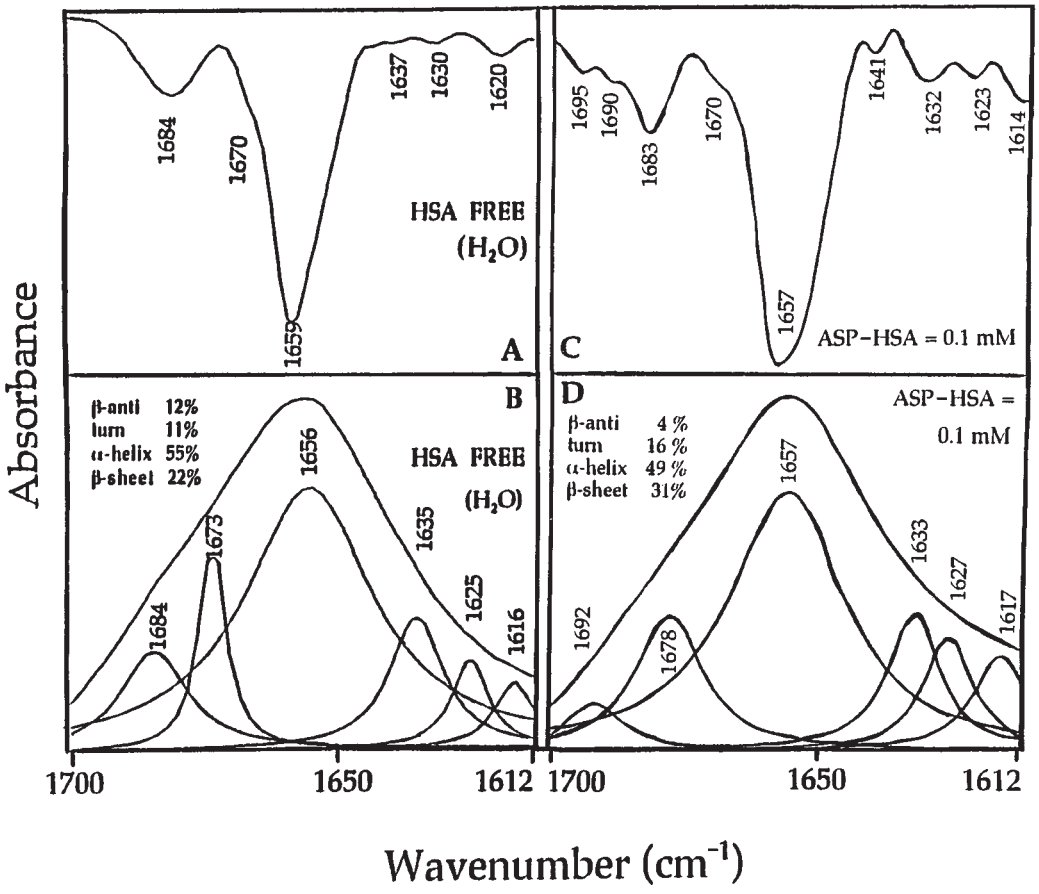
Fig. 2. The plot of $1/(A - A_0)$ vs. (1/L) for HSA and its aspirin complexes where A_0 is the initial absorption band of protein (275 nm) and A is the recorded absorption at different drug concentrations (L).



band at 1656 cm^{-1} and amide II band at 1542 cm^{-1}, as it is evident from the difference spectrum obtained at low drug concentration (Fig. 1, 0.0001 mM). This is indicative of no aspirin–HSA interaction at very low drug concentration. At higher drug content (0.001 mM), two weak positive features were observed at 1610 and 1549 cm^{-1}, due to an increase in the intensity of the amide II vibration and the alterations of the amide I vibration (Fig. 1, 0.001). The observd spectral changes are attributed to aspirin–HSA interaction through protein N-H group. Further evidence for aspirin interaction with the protein N-H group comes from the shift of the amide A (protein N-H stretching mode) (9, 10) at 3303 cm^{-1} towards a lower frequency at 3300 cm^{-1}, in the spectra of the drug–protein complexes. The band at 1522 cm^{-1}, in the spectrum of the free HSA, which is assigned to the tyrosine residue vibrational frequency (15–19), exhibited no spectral changes upon drug interaction (Fig. 1). This is indicative of no participation of the tyrosine moiety in the aspirin–protein complexation.

As drug concentration increased (0.01 and 0.1 mM), the two positive features at 1610 and 1540 cm^{-1} grew in intensities, while a negative feature was observed at 1658 and 1656 cm^{-1} (Fig. 1). The observed spectral changes (positive peaks) are due to continuation of drug binding to protein N-H group and the reduction of the protein α-helix structure (negative peak), upon aspirin–HSA complexation.

Fig. 3. Second derivative resolution enhancement and curve-fitted amide I region (1700–1612 cm^{-1}) and secondary structure determination of the free human serum albumin (curves A and B) and its aspirin complexes (curves C and D) in aqueous solution with 0.1 mM drug concentration.



© 2000 NRC Canada

Table 1. Secondary structure determination for the free HSA and its aspirin complexes in H_2O and D_2O at physiological pH with different drug concentrations (the values in the parentheses are from D_2O solution). The mean deviation was ±1.0–3.0% for the free protein and its aspirin complexes.

Amide I components (cm^{-1})	HSA Free H_2O (D_2O) (%)	HSA–aspirin 0.0001 mM (%)	HSA–aspirin 0.001 mM (%)	HSA–aspirin 0.01 mM (%)	HSA–aspirin 0.1 mM (%)
1684–1692	12 ± 1.0	10	4	4	4
β-Anti	(10 ± 1.0)				
1673–1678	11 ± 1.0	12	14	15	16
Turn	(13 ± 1.0)				
1656–1657	55 ± 3.0	54	53	50	49
α-Helix	(44 ± 3.0)				
1640–1645	(11 ± 1.0)	(12)	(12)	(13)	(14)
Random					
1635–1616	22 ± 2	24	29	31	31
β-Sheet	(22 ± 2)				

Additional evidence for the aspirin–HSA interaction also comes from the shift ($\Delta\nu$ = 10 cm^{-1}) of the aspirin anion C=O, C=C, and C-O stretching vibrations at 1770, 1746, 1609, 1598, and 1565 cm^{-1} towards lower frequencies, on aspirin complexation (spectrum is not shown).

The calculation of the overall binding constants were carried out using UV spectroscopy as reported (14). If the equilibrium for aspirin anion and HSA is established as

[1] HSA + aspirin $\Leftrightarrow$ HSA: aspirin K

The binding constant of aspirin anion complexes with HSA can be described as

$$[2] \qquad K = \frac{[\text{HSA:aspirin}]}{[\text{HSA}][\text{aspirin}]}$$

The double reciprocal plot of 1/[complexed aspirin] vs. 1/[aspirin] is linear (Fig. 2) and the binding constant (K) is calculated from the ratio of the intercept on the vertical coordinate axis to the slope (14). Concentrations of complexed aspirin were determined by subtracting absorbance of uncomplexed HSA at 275 nm from those of complexed HSA. Concentrations of free aspirin were determined by subtracting those of complexed drug from total drug used for the experiment. Our data of 1/[complexed aspirin] almost proportionally increased as a function of 1/[free aspirin], and the overall binding constant for the aspirin–HSA complexes was estimated to be K = 1.4 × 10^4 M^{-1} (Fig. 2).

The binding constant calculated for the aspirin–HSA complexes shows a weak aspirin–protein interaction with respect to the other strong drug–HSA complexes with binding constants ranging from 10^5 M^{-1} to 10^6 M^{-1} (7).

Recently, the interaction of inorganic anions such as F^-, Cl^-, Br^-, ClO_4^-, SO_4^{2-}, HPO_4^{2-} with human serum transferrin has been reported and a possible mode of action is suggested (20). Similarly, the binding constants of several inorganic and organic anions to cytochrome c were determined (21). A weak protein-anion interaction was found for these anions with overall binding constants of 10–100 M^{-1} (20, 21). A model for protein-anion binding was suggested in which the anion negative charged atom forms a stable hydrogen bonding with the protein NH groups (A^-...HN-protein), stabilizing the protein-anion complexes (21). On the other hand, oxyanions such as, VO_3^- (vanadate) showed marked affinity towards ε-amino NH_3^+ groups of human serum albumin with K ≃10^3 M^{-1} (22). On the basis of our infrared spectroscopic results that showed marked spectral similarities between the aspirin–HSA and VO_3–HSA complexes in the amide I and amide II regions, thus, one can assume a similar binding mode for both aspirin and vanadate anions in these anion-protein complexes at low anion concentrations (0.001–0.1 mM). The major spectral changes (shiftings and intensity variations) observed for the amide A band at 3300 cm^{-1} (protein N-H stretching) and the amide II band at 1545 cm^{-1} (C=N + N-H modes), are due to the formation of H-bonding between the positively charged protein N-H groups and the negatively charged aspirin anion oxygen atom (ε-amino NH_3^+..O^-), in these drug-HSA complexes.

However, at high aspirin concentrations (1–5 mM), acetylation of the Lys-199 occurs, which is accompanied by major spectral changes of the amide A at 3303, amide I at 1656, and amide II at 1542 cm^{-1}. The protein amide A band (N-H stretching) at 3303 cm^{-1} was shifted towards a lower frequency at 3295 cm^{-1}, the amide II band at 1542 cm^{-1} lost intensity and displaced toward lower frequency at 1540 cm^{-1} upon acetylation. The amide I band at 1656 cm^{-1} lost intensity and shifted towards a lower frequency at 1640 cm^{-1} (spectra not shown). The presence of a strong positive feature at 1704 cm^{-1} in the difference spectra of drug-HSA complexes is coming from the aspirin C=O stretching vibrations at 1770 and 1746 cm^{-1}, that were shifted towards lower frequencies upon acetyl group transfer (Fig. 1, 5 mM). These spectral changes are due to the acetylation of the lysine residue upon aspirin complexation. The acetylation of the Lys-199 of the HSA is well known (2, 3). Recent structural analysis of the HSA in the presence of aspirin anion shows that the aspirin binding is in sites I and II, where the Lys-199 is located (4, 23). Our spectroscopic results are in a good agreement with those of the literature reports that show acetylation of HSA occurs at high aspirin concentrations (2, 3). However, based on our infrared results alone, we can not locate the position of the lysine residue in order to establish the transfer of the acetyl group from aspirin to Lys-199.

A quantitative analysis of the HSA secondary structure in H_2O and D_2O is given in Table 1. The free protein contained major α-helix 55%, β-sheet 22%, turn structure 11%, and

© 2000 NRC Canada

β-antiparallel 12%. The β-sheet structure is composed of three components at 1616 cm^{-1} (inter β-strand), 1625 cm^{-1} (intra β-strand), and 1635 cm^{-1} (hydrated) (Fig. 3), that are consistent with the recent spectroscopic studies of the human serum albumin (24, 25). In D_2O solution, due to the isotopic substitution (D/H), the presence of a new component band at 1644 cm^{-1} in the spectrum of the free HSA was attributed to the contribution of the random structure 11% (Table 1). Upon aspirin complexation, the α-helix structure was reduced from 55% to 49%; the β-sheet increased from 22% to 31%; the β-anti changed from 12% to 4%, and the turn structure increased from 11% to 16% at high drug concentration in H_2O solution (Fig. 3 and Table 1, 0.1 mM). However, no major alterations were observed for the random structure on drug complexation (Table 1). The observed spectral changes are consistent with the major perturbations of the HSA secondary structure upon aspirin anion interaction. The secondary structural changes observed can be attributed to the interaction of the aspirin anion with the ε-amino NH_3^+ groups. The reduction of the α-helix in favor of the β-sheet structure is indicative of a partial unfolding of the protein structure, in the presence of aspirin anion at high drug concentration. Similar conformational transition from α-helix to β-sheet structure was observed for the protein unfolding, upon protonation and heat denaturation (26–28). At higher drug concentrations (1–5 mM), where acetylation of the lysine residue occurs, major loss of the intensity of the amide I band at 1656 cm^{-1} with an increase in the intensity of the band at 1637 cm^{-1} are observed (Fig. 1). These spectral changes are due to the reduction of the α-helix structure in favor of the β-sheet upon protein acetylation. Attempts to analyse the protein secondary structural changes upon acetylation (1 and 5 mM aspirin) were not successful, due to the overlapping of the protein amide I band at 1656 cm^{-1} with the aspirin C=O vibrational frequencies in the region 1700–1600 cm^{-1}.

In conclusion, the infrared spectroscopic results presented here for the first time, show that at low drug concentrations (0.001–0.1 mM), aspirin binds human serum albumin mainly through the polypeptide ε-amino NH_3^+ with overall binding constant $K = 1.4 \times 10^4$ M^{-1}. The low stabilities of the complexes formed are due mainly to the H-bonding interaction between protein polar groups and the anion donor atoms. At high drug contents (1–5 mM), acetylation of Lys-199 occurs. The aspirin–HSA complexation leads to the alterations of the protein secondary structure from that of the α-helix to β-sheet conformation. This study provides additional evidence regarding protein structural changes, induced by aspirin anion interaction.

Acknowledgements

This work is supported by grants from Natural Sciences and Engineering Research Council of Canada (NSERC) and Fonds pour la formation de chercheurs l'aide a la recherche (Québec) (FCAR).

References

1. P.J. Loll, D. Picotand, and M. Garavito. Nature (London), **2**, 637 (1995).
2. J.E. Walker. FEBS Lett. **66**, 173 (1976).
3. D. Hawkins, R.N. Pinckard, I.P. Crawford, and R.S. Farr. J. Clin. Invest. **48**, 536 (1969).
4. X.-M. He and D.C. Carter. Nature (London), **358**, 209 (1992).
5. A. Dugiaczyk, S.W. Law, and O.E. Dennison. Proc. Nat. Acad. Sci. U.S.A. **79**, 71 (1982).
6. T. Peters, Jr. Adv. Protein Chem. **37**, 161 (1985).
7. U. Kragh-Hansen. Pharmacol. Rev. **33**, 17 (1981).
8. J.F. Neault and H.A. Tajmir-Riahi. Biochim. Biophys. Acta, **1384**, 153 (1998).
9. S. Krimm and J. Bandekar. Adv. Protein Chem. **38**, 181 (1986).
10. M. Byler and H. Susi. Biopolymers, **25**, 469 (1986).
11. E. Goormaghtigh, V. Cabiaux, and J.M. Ruysschaert. Eur. J. Biochem. **193**, 409 (1990).
12. G. Vandenbussche, A. Clercx, T. Curstedt, J. Johansson, H. Jornvall, and J.M. Ruysschaert. Eur. J. Biochem. **203**, 201 (1992).
13. W.K. Surewicz, H.H. Mantsch, and D. Chapman. Biochemistry, **32**, 389 (1993).
14. I.M. Klotz and D.L. Hunston. Biochemistry, **16**, 3065 (1971).
15. Y.N. Chirgadze, O.V. Federov, and N.P. Trushina. Biopolymers, **14**, 679 (1975).
16. H. Matsuura, K. Hasegawa, and T. Miyazawa. Spectrochim. Acta Part A: **42A**, 1181(1986).
17. J.M. Olinger, D.M. Hill, R.J. Jakobsen, and R.S. Brody. Biochim. Biophys. Acta, **869**, 89 (1986).
18. H. Fabian, C. Schultz, J. Backmann, U. Hahn, W. Saenger, H.H. Mantsch, and D. Naumann. Biochemistry, **33**, 10725 (1994).
19. T. Yamamoto and M. Tasumi. J. Mol. Struct. **242**, 235 (1991).
20. W.R. Harris, A.M. Caffery, S. Abdollahi, and K. Trankler. Biochim. Biophys. Acta, **1383**, 197 (1998).
21. G. Battistuzzi, M. Borsari, and M. Sola. Arch. Biochem. Biophys. **339**, 283 (1997).
22. B.R. Nechay, L.B. Nanninga, and P.S.E. Nechay. Arch. Biochem. Biophys. **251**, 128(1986).
23. D.C. Carter and J.X. Ho. Adv. Protein Chem. **45**, 153 (1994).
24. L. Boulkanz, N. Balcar, and M.-H. Baron. Appl. Spectrosc. **49**, 1737 (1995).
25. E. Bramanti and E. Benedetti. Biopolymers, **38**, 639 (1996).
26. F.S. Parker. Applications of infrared, raman, and resonance spectroscopy in biochemistry. Plenum Press, New York. 1983.
27. W.K. Surewicz, M.A. Moscarello, and H.H. Mantsch. J. Biol. Chem. **262**, 8598 (1987).
28. I.E. Holzbaur, A.M. English, and A.A. Ismail. Biochemistry, **35**, 5488 (1996).

© 2000 NRC Canada

Benzooxirene, naphthooxirenes, and anthraceneoxirenes: the stabilization of the oxirene system by bond fixation in acenes. A comparison of ab initio and DFT in the investigation of annelated oxirenes

E. Lewars

Abstract: The effect on the stabilities of benzoannelated oxirenes (oxacyclopropenes) of variations in the C—C bond electron density (as measured by Löwdin bond order) was studied computationally. Benzo[*b*]oxirene (**4ox**), naphtho[2,3-*b*]oxirene (**5ox**), naphtho[1,2-*b*]oxirene (**6ox**), anthro[2,3-*b*]oxirene (**7ox**), and anthro[1,2-*b*]oxirene (**8ox**) were investigated using the DFT pBP/DN* method as implemented in the program Spartan. This method was chosen because with **4ox** it gave results similar to those from the much slower QCISD(T)/6–31G*//MP2(full)/6–31G* and MP4SDTQ/6–31G*//MP2(full)/6–31G* methods. The calculated barriers to oxirene ring opening for the "linear" **4ox**, **5ox**, and **7ox** (bond orders 1.35, 1.24, and 1.20, respectively) were 23.6, 39.9, and 46.6 kJ mol^{-1}, in contrast to the "angular" **6ox** and **8ox** (bond orders 1.50 and 1.59, respectively), with barriers of ca. 0 kJ mol^{-1}. The high-barrier vs. low-barrier series corresponds to the stabilities expected from the resonance structures of the oxirenes or their formal precursor acenes. Empirically, the ring-opening barriers were linearly related to the oxirene bond orders, and extrapolation to tetracene using this relationship gave a barrier of ca. 50 kJ mol^{-1}, which seems to be the limiting barrier in the linear series. In several cases the oxirene isomerized to a ketene without going through an oxo carbene (ketocarbene). Benzoannelation is only the second kind of substitution (after dimethyl substitution) that has been indicated, computationally, to be able to stabilize oxirenes.

Key words: oxirenes, ketocarbenes, benzooxirenes, AM1, ab initio, DFT.

Résumé : Faisant appel à des calculs théoriques on a déterminé l'effet (mesuré par l'ordre de liaison Löwdin) de variations de la densité électronique dans des liaisons C—C sur les stabilités d'oxirènes (oxacyclopropènes) portant un noyau benzénique. On a étudié les benzo[*b*]oxirène (**4ox**), naphto[2,3-*b*]oxirène (**5ox**), naphto[1,2-*b*]oxirène (**6ox**), anthro[2,3-*b*]oxirène (**7ox**) et anthro[1,2-*b*]oxirène (**8ox**) à l'aide de la méthode DFT pBP/DN* en relation avec le programme « Spartan ». On a choisi cette méthode parce que, avec le **4ox**, elle donne des résultats semblables à ceux obtenus avec les méthodes beaucoup plus lentes QCISD(T)/6–31G*//MP2(full)/6–31G* et MP4SDTQ/6–31G*//MP2(full)/6–31G*. Les barrières calculées pour l'ouverture de cycle des oxirènes « linéaires » **4ox**, **5ox** et **7ox** (ordres de liaison de 1,35, 1,24 et 1,20 respectivement) sont de 23,6, 39,9 et 46,6 kJ mol^{-1}; ces valeurs diffèrent grandement de celles calculées pour les produits « angulaires », **6ox** et **8ox**, (ordres de liaison de 1,50 et 1,59 respectivement) pour lesquels les barrières sont d'approximativement de 0 kJ mol^{-1}. Les séries à barrière élevée ou basse correspondent aux stabilités attendues sur la base des structures de résonance des oxirènes ou de leurs acènes précurseurs formels. D'un point de vue empirique, les barrières aux ouvertures de cycle sont reliées de façon linéaire aux ordres de liaison des oxirènes et une extrapolation au tétracène en faisant appel à cette relation conduit à une barrière d'environ 50 kJ mol^{-1} qui semble être la barrière limite dans la série linéaire. Dans plusieurs cas, l'oxirène s'isomérise en cétène sans passer par un oxocarbène (cétocarbène). La benzoannellation n'est que le deuxième type de substitution (après la substitution diméthyle) qui, sur la base de calculs, semble capable de stabiliser les oxirènes.

Mots clés : oxirènes, cétocarbènes, benzooxirènes, AM1, ab ititio, DFT.

Introduction

Oxirenes (oxacyclopropenes, **1**) are interesting for three reasons: there are very few reports of the preparation of any derivatives of this system (1), high-level computational investigations indicate that the very ability of the parent compound to exist is somewhat problematic (2, 3), with disubstitution by groups of widely different electronic proclivities stabilizing the ring only for the methyl case (4), and oxirenes appear to be involved in the important Wolff rear-

Received July 13, 1999.

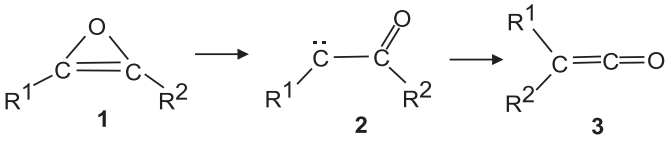
E. Lewars.[1] Department of Chemistry, Trent University, Peterborough, ON K9J 7B8, Canada. Adjunct Professor, Department of Chemistry, Queen's University, Kingston, ON K7L 3N6, Canada.

[1]Telephone: (705) 748-1404. Fax: (705) 748-1625. e-mail: elewars@trentu.ca

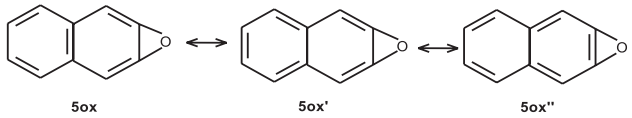
 © 2000 NRC Canada

rangement of diazoketones to oxo carbenes ("ketocarbenes") (5). Calculations indicate that benzo substitution stabilizes the oxirene system (6); on the other hand, push–pull substituents, which are effective in stabilizing another presumably antiaromatic (7) system, cyclobutadiene (8), apparently do not have such an effect on oxirene (9). The oxirene literature to 1983 has been reviewed (10).

Attempts to prepare oxirenes tend to be thwarted by the only known reaction of the system: rearrangement to oxo carbenes, **2**, which undergo facile rearrangement to ketenes, **3**, and in some cases may not even be discrete compounds (5, 10).



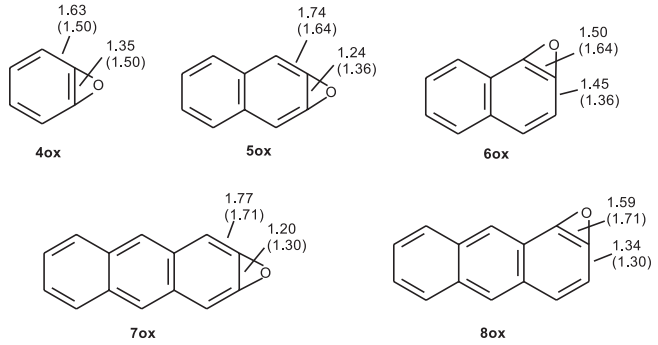
Since, besides dimethyl substitution (4), only fusion to a benzene ring has been shown (computationally) to inhibit this ring-opening, I addressed the question of the limits to stabilization of oxirenes by benzo-type annelation. The reasoning is based on the simple idea that to the extent that the electron density in the C—C double bond can be decreased, the electronic factor(s) (antiaromaticity?) that engenders instability will be ameliorated. Polycyclic acenes (naphthalene, anthracene, etc.) offer a choice of formal double bonds to which an oxirene ring may be attached. Figure 1 shows the oxirenes that are investigated here, **4ox**–**8ox**, and the relevant Löwdin bond orders (11) of the oxirenes and their formal precursor acenes. The bond orders clearly suggest that for **4ox**, **5ox**, and **7ox** the dimethyleneoxirane-type structure is a more accurate representation of the electron distribution than is the oxirene structure, e.g., **5ox** and **5ox′** rather than **5ox″**.



For the polybenzenoid acenes **5ox**–**8ox**, the main resonance form is expected to be that with the maximum number of benzenoid rings, as shown in Fig. 1.

In this paper I show that where "bond fixation" (12, 13) imposes a structure predominantly of the dimethyleneoxirane resonance form, the oxirene is strongly stabilized compared to molecules in which the main contribution is from the oxirene canonical form, and that the stabilization is correlated with the oxirene C—C bond order. I also show that density functional (DFT) calculations (14) on these molecules give results quite comparable to those from the much slower MP2 (15) method, the traditional workhorse for electron-correlated calculations on molecules of reasonable size.

Fig.1. Relevant Löwdin bond orders of oxirenes and (in parentheses) the corresponding acenes. In each case the resonance structure with the maximum number of formal benzene rings is shown. Bond orders are from HF/6–31G* single-point calculations on DFT pBP/DN* geometries.



Computational methods

Structures were constructed with the interactive model builder of the Spartan program[2] and subjected to a preliminary geometry optimization with molecular mechanics, which in relevant cases was also used to create the desired symmetry, then geometries and frequencies were calculated at the AM1 (16) level, giving reasonable geometries and Hessians for ab initio (17) and DFT (14) geometry optimizations. The ab initio calculations were at the HF/6–31G* level; the DFT calculations, designated pBP/DN*, employed the Becke–Perdew perturbational procedure (18) and the numerical DN* basis set (19). HF/6–31G* geometry optimizations were performed with Spartan version 3.1 on an SGI R4000 workstation, and the pBP/DN* calculations with Spartan version 5.0 on an SGI RS4000 workstation. The MP2 calculations were MP2 frozen core with the 6–31G* basis set, i.e., MP2(fc)/6–31G*, and were done by submitting AM1 geometries to the Gaussian 94W program[3] on a 200 MHz Pentium Pro computer with the Windows NT operating system.

Optimized HF and DFT geometries were subjected to frequency calculations (20) at the same level to verify that the structure was the desired relative minimum (no imaginary frequencies) or transition state (one imaginary frequency), and to obtain zero-point energies (ZPEs) to correct the frozen-nuclei energy. The frequency calculations for the HF/6–31G* geometries were done with Gaussian 92[4] on a Hewlett-Packard 9000/733 computer at the University of Toronto. For most of the MP2 structures frequency calculations

[2] Spartan, Version 3.1.3, Wavefunction Inc., 18401 Von Karman, Suite 370, Irvine, Calif. 1994.

[3] M.J. Frisch, G.W. Trucks, H.B. Schlegel, P.M.W. Gill, B.G. Johnson, M.A. Robb, J.R. Cheeseman, T. Keith, G.A. Petersson, J.A. Montgomery, K. Raghavachari, M.A. Al-Laham, V.G. Zakrzewski, J.V. Ortiz, J.B. Foresman, J. Cioslowski, B.B. Stefanov, A. Nanayakkara, M. Challacombe, C.Y. Peng, P.Y. Ayala, W. Chen, M.W. Wong, J.L. Andres, E.S. Replogle, R. Gomperts, R.L. Martin, D.J. Fox, J.S. Binkley, D.J. Defrees, J. Baker, J.P. Stewart, M. Head-Gordon, C. Gonzalez, and J.A. Pople. Gaussian 94 for Windows (G94W): Gaussian 94, Revision E.1. Gaussian, Inc., Pittsburgh, Pa. 1995.

[4] M.J. Frisch, G.W. Trucks, M. Head-Gordon, P.M.W Gill, M.W. Wong, J.B. Foresman, B.G. Johnson, H.B. Schlegel, M.A. Robb, E.S. Replogle, R. Gomperts, J.L. Andres, K. Raghavachari, J.S. Binkley, C. Gonzalez, R.L. Martin, D.J. Fox, D.J. Defrees, J. Baker, J.J.P. Stewart, and J.A. Pople. Gaussian 92, Revision C. Gaussian, Inc., Pittsburgh, Pa. 1992.

© 2000 NRC Canada

Table 1. Energies, zero-point energies (ZPEs), ZPE-corrected energies (hartrees), and relative energies (kJ mol^{-1}) of **4ox** and derived species (see Fig. 2). The basis is 6–31G* throughout. HF energies were corrected with HF/6–31G* ZPEs, and MP2, MP4, and QCI energies with MP2(fc)/6–31G* ZPEs; DFT ZPEs were calculated at the same DFT (pBP/DN*) level. The HF ZPEs have been multiplied by 0.9135 and the MP2(fc) ZPEs by 0.9670 (21); DFT ZPEs are uncorrected. NSP means the species was not a stationary point at that level; QCI calculations were impracticably long for **4k** and failed for **4tk**.

	HF	MP2(fc)	MP4SDTQ//MP2(full)	QCISD(T)//MP2(full)	DFT (pBP/DN*)
4ox	–304.21743	–305.16462	–305.24149	–305.23649	–306.21920
	0.07823	0.07823	0.07633	0.07633	0.07564
	–303.13920	–305.08639	–305.16516	–305.16016	–306.14356
	(0)	(0)	(0)	(0)	(0)
4c	–304.24169	–305.15887	–305.24384	–305.24386	NSP
	0.07722	0.07722	0.07573	0.07573	
	–304.16447	–305.08165	–305.16811	–305.16813	
	(–66.4)	(12.4)	(–7.7)	(–20.9)	
4k	–304.33871	–305.26820	–305.23184		–306.31940
	0.07853	0.07853	0.07694		0.07606
	–304.26018	–305.18967	–305.26890		–306.24334
	(–318)	(–271)	(–272)		(–272)
4tc	–304.19523	–305.14400	–305.23184	–305.22760	–306.20957
	0.07630	0.07630	0.07582	0.07582	0.07501
	–304.11893	–305.06770	–305.15602	–305.15178	–306.13456
	(53.2)	(49.1)	(24.0)	(22.0)	(23.6)
					(for **1ox** to **1k**)
4tk	–304.23542	–305.15851	–305.24326		**1c** was NSP
	0.07562	0.07562	0.07496		
	–304.15980	–305.08289	–305.16830		
	(–54.1)	(9.2)	(–8.2)		

were impractical, but the structures could be confidently assigned as minima or transition states from their relative energies and their resemblance to the corresponding HF and DFT species; the HF ZPE corrections were used for the MP2 structures. The MP2(full), MP4SDTQ, and QCISD(T) energies of **4ox** (Table 1) were corrected with ZPEs from MP2(fc)/6–31G* frequency calculations, which also verified the nature of the stationary points **4ox**, **4c**, **4k**, **4tc**, and **4tk** at the MP2(fc)/6–31G* level; the MP4 and QCI calculations were done on a 200 MHz Pentium Pro machine. For the anthracene derivatives the times for MP2 and even HF calculations were expected to be impracticably long, and only AM1 and DFT calculations were performed for these molecules. HF ZPEs were corrected by multiplying them by 0.9135 (21); the correction factor for the DFT pBP/DN* frequencies was expected (21) to be close to 1.0, and no correction was applied to these.

Gaussian geometries were visualized with Spartan and Gaussian frequencies were animated with Molwin[5] (Spartan has its own graphical interface). Löwdin bond orders were calculated with Spartan.

Results and discussion

Reliability of the computational methods: benzooxirene as a probe. Comparison of pBP/DN* and CCSD(T)/6–311G(df,p) for the parent oxirene

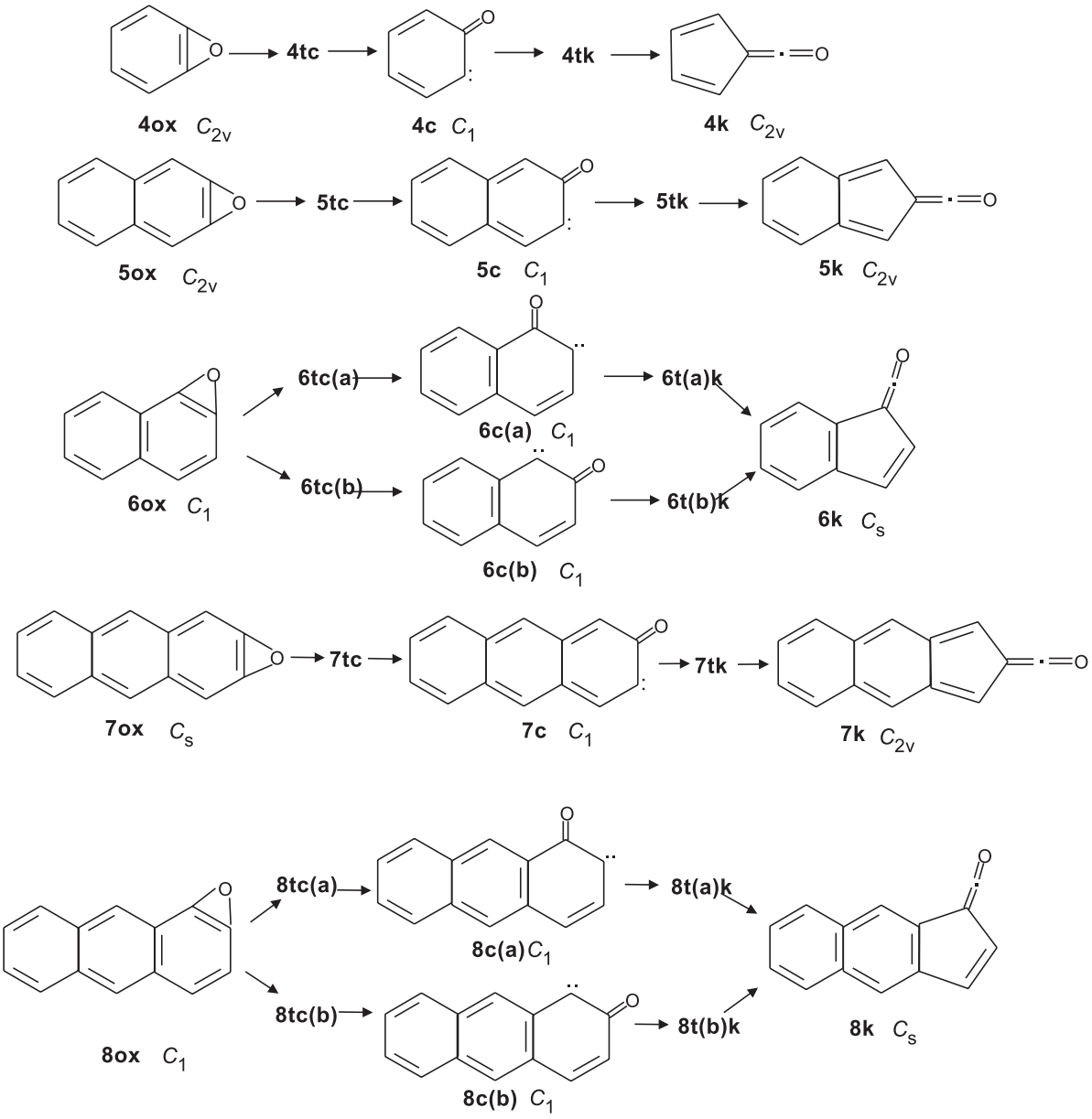
The isomerization reactions of interest for **4ox**–**8ox** are shown in Fig. 2. Table 1 shows the energy values for **4ox** and the species **4c**, **4k**, **4tc**, and **4tk** involved in its isomerization to the ketene. The energies of the carbene **4c** and the transition state **4tc** leading to it differ very slightly from those reported previously (6), because for the ZPEs MP2(full) (rather than MP2(fc)) frequencies and a slightly different correction factor were used in the earlier work. The results at the HF/6–31G*, MP2(fc)/6–31G*, MP4SDTQ/6–31G*//MP2(full)/6–31G*, QCISD(T)/6–31G*//MP2(full)/6–31G*, and DFT (pBP/DN*) levels appear (Table 1) to be converging toward a reaction profile in which **4ox** opens with a barrier of 22–24 kJ mol^{-1} to give **4k**, which lies 262–272 kJ mol^{-1} below the oxirene. The carbene **4c** is either not a stationary point (DFT; i.e., **4ox** rearranges directly to **4k**), or rearranges to **4k** with a very low barrier only. At the MP2 and MP4//MP2 levels **4c** and **4tk** have essentially the same energy without the ZPE; with the ZPE, **4tk** has 3 and 0.5 kJ mol^{-1} less energy than the carbene (for very low barriers a slightly negative barrier can result from applying a ZPE calculated at one level to a single-point energy from a higher-level calculation). The carbene, therefore, seems to be either nonexistent or a mere dimple on the potential energy surface, ca. 8–21 kJ mol^{-1} below the oxirene (the inversion seen at the MP2 level can be ascribed (6) to the known tendency of this method to overshoot in recovering correlation energy).

As a further test of the reliability of the pBP/DN* method for these species, for the parent oxirene (C_2H_2O) the reaction profile for this method was compared that reported (5) for the CCSD(T)/6–311G(df,p) profile. The main differences

[5] MolWin 2.3, P.V. Ganelin, Department of Chemistry, Catholic University of America, Washington, DC 20064. 1994.

© 2000 NRC Canada

Fig. 2. The species (oxirenes, carbenes, ketenes, transition states: **ox**, **c**, **k**, **t**) and reactions examined in this paper. All the transition states have C_1 symmetry; the symmetry of the other species is given.



between the curves (Fig. 3) were that for the CCSD(T) method the oxirene ring opens with a small (ca. 2 kJ mol^{-1}) barrier after which the energy falls to ca. –4 kJ mol^{-1} in the carbene region and then rises to ca. 21 kJ mol^{-1} for the hydrogen shift that leads to the ketene; for the pBP/DN* curve the oxirene opens without a barrier and the energy falls to ca. –25 kJ mol^{-1}, then rises to ca. 14 kJ mol^{-1}. If we accept the CCSD(T) results as definitive, then, at least for the parent system, the pBP/DN* level seems to somewhat overestimate the stability of the carbene and slightly underestimate the height of the critical barrier. Neither of these possible defects is relevant to the purpose for which the method was applied to the reaction profiles of **4ox**–**8ox**, namely, to observe the trends among these systems, and to obtain at least a semiquantitative estimate of the oxirene stabilities.

Comparison of the oxirenes 4ox–8ox using DFT (pBP/DN*)

DFT pBP/DN* calculations (Table 2 and Fig. 4) show that benxooxirene (**4ox**) and the "linear" species **5ox** and **7ox** have *relatively* high barriers to ring-opening (24, 40, and 46 kJ mol^{-1}) while the "angular" oxirenes **6ox** and **8ox** have very low barriers (ca. 1 kJ mol^{-1} or less; see below). This is as expected from the bond fixation view, where for **4ox**, **5ox**, and **7ox** the oxirene C—C bond has a relatively low bond order (ca. 1.2–1.4), while for **6ox** and **8ox** the oxirene C—C bond order is 1.6–1.7 (Fig. 1). Although it is a C—O bond rather than a C—C bond that is broken in oxirene ring opening, a high C—C bond order is expected to correlate with high electron density in the oxirene ring, i.e, with increased oxirene, rather than oxirane, character.

© 2000 NRC Canada

Table 2. Energies, zero point energies (ZPEs), and ZPE-corrected energies of the species discussed in this paper (see Fig. 2). AM1 energies were not ZPE-corrected; MP2 energies were corrected with HF/6–31G* ZPEs. The HF/6–31G* ZPEs shown are the calculated ones multiplied by a correction factor of 0.9135 (21); the DFT ZPEs shown are uncorrected. AM1 energies are heats of formation in kJ mol^{-1}; HF and DFT energies are in hartrees. Numbers in parentheses are relative energies in kJ mol^{-1} for a family of species (e.g., **4ox**, **4c**,..., **4tk**) at the same level (e.g., AM1). NSP means the molecule did not exist (was not a stationary point) at that level, and NF means the transition state was not found. Where the carbene is not a stationary point, the transition state for oxirene to carbene (e.g., **4tc** for DFT) really denotes the transition state for direct conversion of the oxirene to the ketene. The **7** and **8** species were not examined at the HF and MP2 levels.

	AM1	HF/6–31G*	MP2(fc)/6–31G*	DFT (pBP/DN*)
4ox	476	–304.21743	–305.16462	–306.21920
	(0)	0.07823	0.07823	0.07564
		–304.13920	–305.08639	–306.14356
		(0)	(0)	(0)
4c	382	–304.24169	–305.15887	NSP
	(–94)	0.07722	0.07722	
		–304.16447	–305.08165	
		(–66.4)	(12.4)	
4k	163	–304.33871	–305.26820	–306.31940
	(–313)	0.07853	0.07853	0.07606
		–304.26018	–305.18967	–306.24334
		(–318)	(–271)	(–262)
4tc	571	–304.19523	–305.14400	–306.20957
	(95)	0.07630	0.07630	0.07501
		–304.11893	–305.06770	–306.13456
		(53.2)	(49.1)	(23.6)
				(for **4ox** to **4k**)
4tk	398	–304.23542	–305.15851	**4c** was NSP
	(–78)	0.07562	0.07562	
		–304.15980	–305.08289	
		(–54.1)	(9.2)	
5ox	532	–456.88014	–458.32972	–459.91186
	(0)	0.12453	0.12453	0.12114
		–456.75561	–458.20519	–459.79072
		(0)	(0)	(0)
5c	478	–456.87571	–458.32916	NSP
	(–54)	0.12305	0.12305	
		–456.75266	–458.20611	
		(7.7)	(–2.4)	
5k	269	–456.97450	–458.41174	–459.99391
	(–263)	0.12450	0.12450	0.12130
		–456.85000	–458.28724	–459.87261
		(–248)	(–215)	(–215)
5tc	651	–456.83978	–458.29836	–459.89487
	(119)	0.12163	0.12163	0.11936
		–456.71815	–458.17673	–459.77551
		(98.4)	(74.7)	(39.9)
				(for **5ox** to **5k**)
5tk	NF	–456.87377	NF	**5c** was NSP
		0.12155		
		–456.75222		
		(8.9)		
6ox	574	–456.85981	–458.31809	–459.89800
	(0)	0.12369	0.12369	0.12104
		–456.73612	–458.19440	–459.77696
		(0)	(0)	(0)
6c(a)	428	–456.91491	–458.32946	NSP
	(–146)	0.12388	0.12388	
		–456.79103	–458.20558	
		(–144)	(–29.4)	

© 2000 NRC Canada

Table 2 (*continued*).

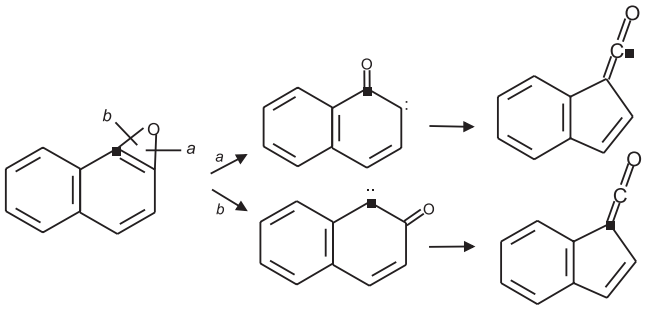
	AM1	HF/6–31G*	MP2(fc)/6–31G*	DFT (pBP/DN*)
6c(b)	434 (–140)	–456.91255 0.12376 –456.78879 (–138)	–458.31213 0.12376 –458.18837 (15.8)	NSP
6k	206 (–368)	–457.00512 0.12499 –456.88013 (–378)	–458.43816 0.12499 –458.31317 (–312)	–460.01679 0.12166 –459.89513 (–310)
6tc(a)	632 (58)	–456.85548 0.12320 –456.73228 (10.1)	–458.31020 0.12320 –458.18700 (19.4)	–459.89769 0.12010 –459.77759 (–1.65) (for **6ox** to **6k**)
6t(a)k	516 (–58)	–456.89857 0.12236 –456.77621 (–105)	–458.32575 0.12236 –458.20339 (–23.6)	**6c(a)** was NSP
6tc(b)	632 (58)	–456.85602 0.12314 –456.73288 (8.5)	–458.30693 0.12314 –458.18379 (27.9)	–459.89757 0.12050 –459.77707 (–0.3) (for **6ox** to **6k**)
6t(b)k	509 (–65)	–456.89992 0.12228 –456.77764 (–109)	–458.31823 0.12228 –458.19595 (–4.1)	**6c(b)** was NSP
7ox	615 (0)			–613.59400 0.16652 –613.42748 (0)
7c	576 (–39)			NSP
7k	377 (–238)			–613.66891 0.16581 –613.50310 (–199)
7tc	743 (128)			–613.57403 0.16428 –613.40975 (46.6)
7tk	NF			**7c** was NSP
8ox	676 (0)			–613.57591 0.16551 –613.41040 (0)
8c(a)	505 (–171)			–613.60715 0.16479 –613.44236 (–83.9)
8c(b)	511 (–165)			NSP
8k	281 (–395)			–613.70070 0.16619 –613.53451 (–326)

© 2000 NRC Canada

Table 2 (*concluded*).

	AM1	HF/6–31G*	MP2(fc)/6–31G*	DFT (pBP/DN*)
8tc(a)	716			–613.57644
	(40)			0.16501
				–613.41143
				(–2.7)
8t(a)k	599			–613.60468
	(–77)			0.16417
				–613.44051
				(–79.1)
8tc(b)	717			–613.57659
	(41)			0.16548
				–613.41111
				(–1.9)
				(for **8ox** to **8k**)
8t(b)k	593			**8c(b)** was NSP
	(–83)			

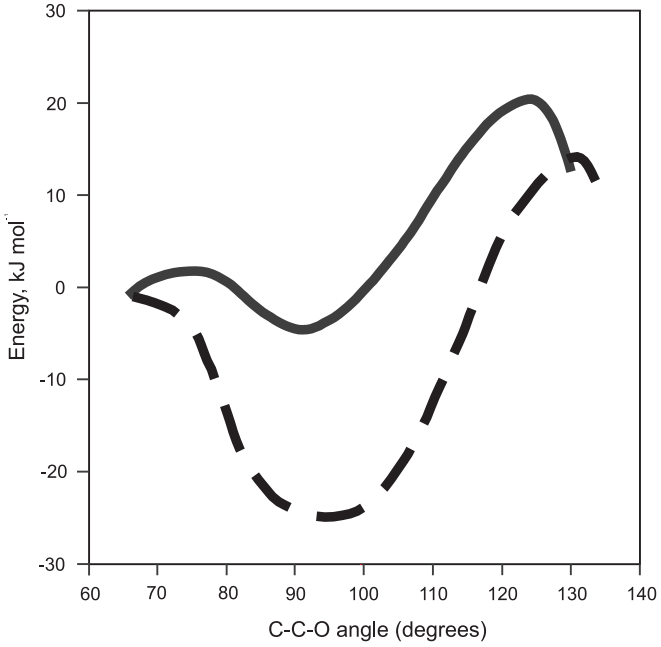
The nonlinear oxirenes **6ox** and **8ox** have two potential ring-opening modes, designated *a* and *b* in Fig. 4. These lead to different transition states and different putative carbenes (Fig. 2; the calculations indicate that the carbenes are either not stationary points, or have very low barriers for isomerization to the ketenes), but in the absence of isotopic labelling the ketenes are the same, e.g., for **6ox**.



The two modes have quite similar activation energies for **6ox** (–1.65 and –0.3 kJ mol^{-1} for modes *a* and *b*, respectively, with ZPE, and 0.81 and 1.1 without ZPE) and for **8ox** (–2.7 and –1.9 kJ mol^{-1} for modes *a* and *b*, respectively, with ZPE, and –1.4 and –1.8 kJ mol^{-1} without ZPE). The slightly negative barriers can be ascribed to errors in the DFT calculation caused by the grid or by the perturbational approximation in the pBP method. At the pBP/DN* level, only for mode *a* of **8ox** is a carbene (**8c(a)**, Fig. 2) an actual intermediate (a stationary point with all vibrational frequencies real); the barrier for conversion of the carbene to the ketene is 4.8 kJ mol^{-1}.

The correlation of the ring-opening barriers with the oxirene C—C Löwdin bond orders is shown in Fig. 5. The barriers for **6ox** and **8ox** have been simply set equal to zero. Although there is no clear theoretical basis for it, the empirical fact is that the linear relationship seen in Fig. 5 holds. An estimate of the ring-opening barrier of the linear tetracene oxirene was obtained from its calculated oxirene C—C Löwdin bond order and Fig. 5, bypassing a lengthy geometry optimization and frequency calculation on the transition state, which is not only big, but lacks symmetry

Fig. 3. Comparison of pBP/DN* (- - -) and CCSD(T)/6–311G(df,p) (5) (—) reaction profiles for the parent oxirene (C_2H_2O).

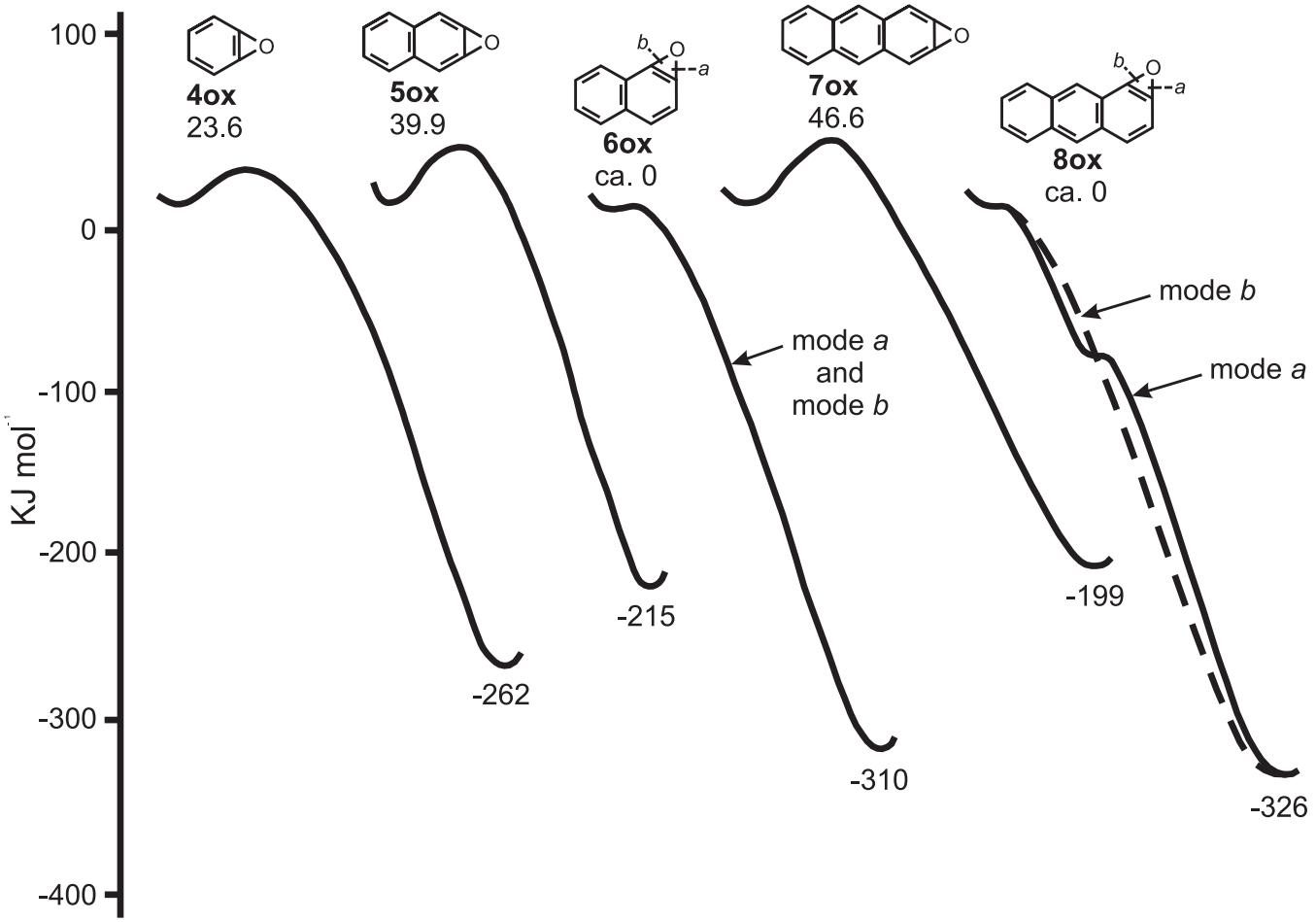


(the tetracene oxirene, slightly curved along the sequence of four benzene rings, has C_s symmetry). The barrier for the linear tetracene oxirene, with a bond order of 1.18, is estimated at 48 kJ mol^{-1}, only slightly higher than for the anthracene oxirene **7ox** (46.6 kJ mol^{-1}). Thus the ring-opening barrier for linear acene oxirenes appears to level off with four or five benzene rings, at about 50 kJ mol^{-1}. The borderline activation energy for observability at room temperature is about 100 kJ mol^{-1}, so it seems unlikely that any of these acene oxirenes will be isolable at room temperature. All of them, however, should be readily observable by matrix-isolation techniques.

These calculations indicate that not only can bond alternation in acenes be utilized to stabilize oxirenes, but that the

© 2000 NRC Canada

Fig. 4. Reaction profiles for the oxirenes **4ox**–**8ox** to give the corresponding ketenes, using the pBP/DN* method, with ZPE included. Only for ring-opening mode *a* of **8ox** was a carbene (**8c(a)**, Fig. 2) a stationary point. For **6ox** the activation energies denoted "ca. 0" are –1.65 and –0.3 kJ mol^{-1} for ring-opening modes *a* and *b*, respectively, with ZPE, and 0.81 and 1.1 without ZPE. For **8ox** the activation energies denoted "ca. 0" are –2.7 and –1.9 kJ mol^{-1} for ring-opening modes *a* and *b*, respectively, with ZPE, and –1.4 and –1.8 kJ mol^{-1} without ZPE. The barrier for conversion of **8c(a)** (the carbene formed by mode *a* ring opening) to the ketene was 4.8 kJ mol^{-1}.



oxirene system has the ability to impose on a benzene ring a large degree of bond alternation. This is seen for benzooxirene (6) and, more dramatically, for benzo*tris*oxirene **9** (Fig. 6). The *tris*oxirene is, judging by the bond orders, electronically essentially a cyclohexatriene. The bond orders (Löwdin bond orders calculated with the HF/6–31G* wavefunction using pBP/DN* geometries) are 1.84 and 1.05, and the bond lengths are not very different from those of a normal C—C double bond and a C—C single bond between sp^2 carbons: 1.316 Å and 1.401 Å (Fig. 6), cf. 1.32 Å and 1.48 Å, respectively (22). Molecule **9** appears not to have been previously studied, although related heterocyclopropene species, the silicon (23) and the nitrogen and boron (24) analogues, have been computationally investigated and show some bond fixation. In this work, **9** and **10** were found to be relative minima (no imaginary frequencies) of D_{3h} symmetry on the pBP/DN* hypersurface. That the bond fixation in **9** is largely due to the strong tendency of the oxirene system to exclude electrons from its C—C bond, rather than being mainly some kind of ring-strain effect, is shown by the fact that the corresponding benzo*tris*cyclopropene (**10**, Fig. 6) shows considerably less bond fixation: bond orders of 1.56 and 1.31, and bond lengths of 1.361 Å and 1.393 Å. The moderate degree of bond fixation in **10** found here is in accord with that reported in other computational studies of this molecule (23–25). The search for cyclohexatriene-like benzene rings is an active area of research (26), and **9**, with predicted bond lengths of 1.316 Å and 1.401 Å, evidently shows bond alternation comparable to that in the most cyclohexatriene-like "monobenzene" derivative whose geometry has been experimentally (X-ray analysis) confirmed: a *tris*-1,4-cyclobutadiyl-substituted benzene with bond lengths of 1.350 Å and 1.439 Å (27).

AM1, HF/6–31G* and MP2 calculations, compared to those at the DFT level

As shown above, a series of calculations (HF/6–31G*, MP2(full)/6–31G*, MP4SDTQ/6–31G*//MP2(full)/6–31G*, QCISD(T)/6–31G*//MP2(full)/6–31G* and pBP/DN* DFT; above) on **4ox** suggested that the reaction profile was converging at the last three levels, and that the DFT method was a practical way to obtain results similar to those at the much

© 2000 NRC Canada

Fig. 5. Correlation of DFT (pBP/DN*) ring-opening barriers with oxirene C—C Löwdin bond orders for **4ox**–**8ox**. Bond orders are from HF/6–31G* single-point calculations on DFT pBP/DN* geometries.

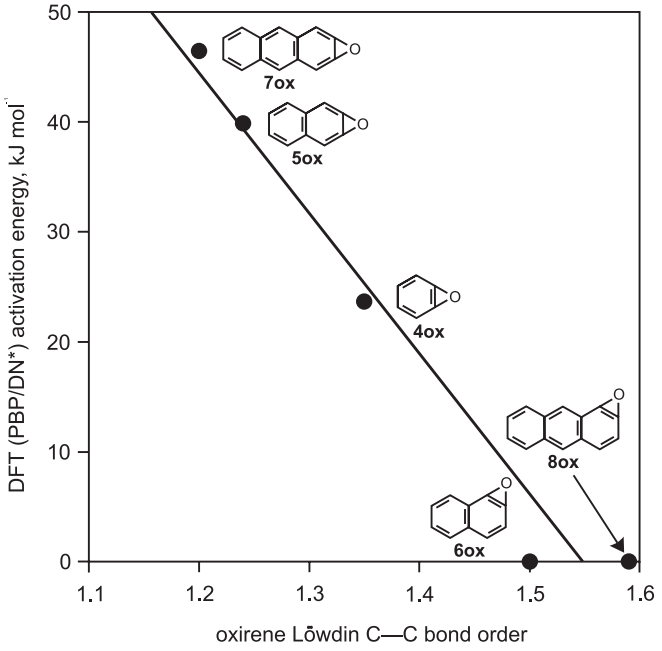
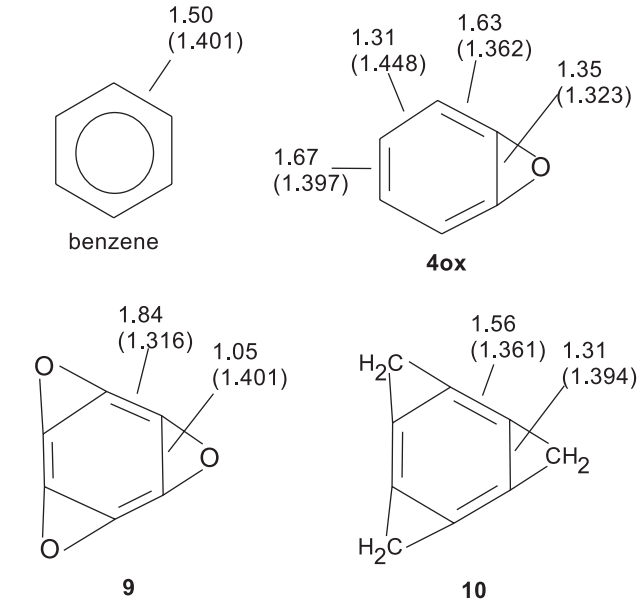


Fig. 6. Bond fixation in annelated benzenes. Löwdin bond orders and (in parentheses) bond lengths (Å) for benzene and oxirene-annelated and cyclopropane-annelated derivatives. Bond orders are from HF/6–31G* single-point calculations on DFT pBP/DN* geometries.



slower MP4SDTQ/6–31G*//MP2(full)/6–31G* and QCISD-(T)/6–31G*//MP2(full)/6–31G* levels. If we accept that the DFT calculations give realistic results for these systems, then we can judge the quality of the AM1, HF, and MP2 calculations by comparing them with the DFT ones. The main points of interest for **4ox**–**8ox** using these four methods (Table 2) are the height of the ring-opening barrier and the stability of the carbenes which might result from this opening (Fig. 2). The ring-opening barrier decreases almost monotonically from AM1 to DFT, and the changes are large: e.g., from 95 to 23.6 kJ mol^{-1} for **4ox**, and from 58 to essentially zero for **6ox**. Even the MP2 barrier is evidently unrealistically high: 49.1 cf. 23.6 for **4ox**, 74.7 cf. 39.9 kJ mol^{-1} for **5ox**, and 19.4 or 27.9 kJ mol^{-1} cf. essentially zero for and for **6ox**. The AM1 and (for **4ox**–**6ox**) the HF and MP2 calculations give the same ordering of barrier heights as do the DFT calculations, but the barriers are overestimated compared to the DFT results (greatly so for AM1).

The energies of the carbenes relative to the oxirenes, and the barrier to rearrangement of the carbenes to the ketenes, are also quite sensitive to the method. In all cases except **8c(a)** (Fig. 2) the DFT method predicts that the carbenes are not stationary points, but rather that the oxirene rearranges to the ketene without an intermediate (even for **8c(a)** the DFT barrier for rearrangement to the ketene is only 4.8 kJ mol^{-1}). AM1 and, to a lesser extent HF, overestimate (compared to DFT) the stability of the carbenes; for MP2 the barrier to carbene rearrangement to the ketene was low, in those cases where the transition state was found. All four methods agree that the ketenes lie ca. 200–400 kJ mol^{-1} below the oxirenes.

Conclusions

DFT calculations using the pBP/DN* method appear to be adequate to investigate the energetics of ring-opening of benzoannelated oxirenes; for benzooxirene the barrier is similar to that from QCISD(T)/6–31G* or MP4SDTQ/6–31G* calculations on MP2(full)/6–31G* geometries. The DFT calculations indicate that the stabilities of the oxirenes toward ring-opening increase with decreasing electron density in the C—C bond, as inferred from the calculated bond order, the barrier reaching about 50 kJ mol^{-1} for the linear anthracene oxirene or (estimated from bond order) tetracene oxirene. The tendency of the oxirene system to exclude electron density from the CC bond imposes strong bond alternation on annelated benzene rings: benzo*tris*oxirene is calculated to have distinct cyclohexatriene character. In most cases the carbene, the formal proximate product of ring-opening, is not a stationary point, but rather the oxirene is transformed in one step into the ketene. AM1, HF, and MP2 calculations overestimate the barrier to oxirene ring-opening.

Acknowledgements

Funds from Trent University's NSERC Committee on Research and Trent's Academic Innovation Fund, for the purchase of computers, are gratefully acknowledged. I thank the chemistry department of the University of Toronto for access to their HP computer.

References

1. M. Torres, J.L. Bourdelande, A. Clement, and O.P. Strausz. J. Am. Chem. Soc. **105**, 1698 (1983); C. Bachmann, T.Y. N'Guessan, F. Debû, M. Monnier, J. Pourcin, J.-P. Aycard, and H. Bodot. J. Am. Chem. Soc. **112**, 7488 (1990).

© 2000 NRC Canada

2. G. Vacek, B.T. Colegrove, and H.F. Schaefer. Chem. Phys. Lett. **177**, 468 (1991).
3. G. Vacek, J.M. Galbraith, Y. Yamaguchi, H.F. Schaefer, R.H. Nobes, A.P. Scott, and L. Radom. J. Phys. Chem. **98**, 8660 (1994).
4. J.E. Fowler, J.M. Galbraith, G. Vacek, and H.F. Schaefer. J. Am. Chem. Soc. **116**, 9311 (1994).
5. A.P. Scott, R.H. Nobes, H.F. Schaefer, and L. Radom. J. Am. Chem. Soc. **116**, 10159 (1994).
6. E. Lewars. J. Mol. Struct. (Theochem), **360**, 67 (1996).
7. N.L. Bauld, T.L. Welsher, J. Cessac, and R.L. Holloway. J. Am. Chem. Soc. **100**, 6920 (1978).
8. H.J. Lindner and B. von Gross. Chem. Ber. **107**, 598 (1974); R. Gompper, F. Hoisboer, W. Schmidt, and G. Seybold. J. Am. Chem. Soc. **95**, 8479 (1973).
9. E. Lewars. J. Mol. Struct. (Theochem), **391**, 39 (1997).
10. E. Lewars. Chem. Rev. **83**, 519 (1983).
11. M.A. Natiello and J.A. Medrano. Chem Phys. Lett. **105**, 180 (1984); **110**, 445 (1984).
12. M.J.S. Dewar and R.C. Dougherty. The PMO theory of organic chemistry. Plenum, New York. 1975. Chap. 3.
13. J. March. Advanced organic chemistry. Wiley-Interscience, New York. 1992. pp. 42–44.
14. F. Eckert and G. Rauhut. J. Am. Chem. Soc. **120**. 13478 (1998), refs. 25–43; E.R. Davidson. Int. J. Quantum Chem. **69**, 241 (1998); W. Kohn, A.D. Becke, and R.G. Parr. J. Phys. Chem. **100**, 12974 (1996); R.D. Parr and W. Yang. Ann. Rev. Phys. Chem. **46**, 701 (1995); C.W. Bauschlicher. Chem. Phys. Lett. **246**, 40 (1995).
15. W.J. Hehre, L. Radom, P.v.R. Schleyer, and J.A. Pople. Ab initio molecular orbital theory. Wiley-Interscience, New York. 1986. Chap. 2.
16. M.J.S. Dewar, E.G. Zoebisch, E.F. Healy, and J.J.P. Stewart. J. Am. Chem. Soc. **107**, 3902 (1985); W. Thiele. Tetrahedron, **44**, 7393 (1988).
17. W.J. Hehre, L. Radom, P.v.R. Schleyer, and J.A. Pople. Ab initio molecular orbital theory. Wiley-Interscience, New York. 1986; J.B. Foresman and A. Frisch. Exploring chemistry with electronic structure methods. 2nd ed. Gaussian Inc., Pittsburgh, Pa. 1996.
18. A.D. Becke. Phys. Rev. A. **38**, 3089 (1988); A.D. Becke. Phys. Rev. A: At. Mol. Opt. Phys. **33**, 2786 (1986); J.P. Perdew. Phys. Rev. B.: Condens. Matter, **33**, 8822 (1988).
19. B. Delley and D.E. Ellis. J. Chem. Phys. **76**, 1949 (1982).
20. W.J. Hehre, L. Radom, P.v.R. Schleyer, and J.A. Pople. Ab initio molecular orbital theory, Wiley-Interscience, New York. 1986. Section 6.3; J.B. Foresman and A. Frisch. Exploring chemistry with electronic structure methods. 2nd ed. Gaussian Inc., Pittsburgh, Pa. 1996. Chap. 4.
21. A.P. Scott and L. Radom. J. Phys. Chem. **100**, 16502 (1996).
22. Ref. 13, pp. 21, 31.
23. M. Eckert-Maksic, Z. Glasovac, and Z.B. Maksic. J. Organomet. Chem. **571**, 65 (1898).
24. A. Stanger. J. Am. Chem. Soc. **120**, 12034 (1998).
25. O. Mo, M. Yanez, M. Eckert-Maksic, and Z.B. Maksic. J. Org. Chem. **60**, 1638 (1995); L. Vujisic and D.L.J. Vuckovic. J. Serb. Chem. Soc. **58**, 641 (1993); W. Koch, M. Eckert-Maksic, and Z.B. Maksic. J. Chem. Soc., Perkin Trans. 2, 2195; K.K. Baldridge and J.S. Siegel. J. Am. Chem. Soc. **114**, 9583 (1992); Y. Apeloig, M. Karni, and D. Arad. NATO ASI Ser., Ser. C. 273 (Strain Its Implic. Org. Chem.), 457 (1989). CODEN: NSCSDW; ISSN: 0258–2023.
26. A.M. Rouhi. Chemical and engineering news. 1 April, 27 (1996); F. Cardullo, D. Guiffrida, F.H. Kohnke, F.M. Raymo, J.F. Stoddard, and D.J. Williams. Angew. Chem. Int. Ed. Engl. **35**, 339 (1996); E.D. Jemmis and B. Kiran. J. Org. Chem. **61**, 9006 (1996).
27. H-B. Bürgi, K.K. Baldridge, K. Hardcastle, N.L. Frank, P. Gantzel, J.S. Siegel, and J. Ziller. Angew. Chem. Int. Ed. Engl. **34**, 1454 (1995).

© 2000 NRC Canada

Electrocatalytic hydrogenation of lignin models at Raney nickel and palladium-based electrodes

André Cyr, Florence Chiltz, Paul Jeanson, Anna Martel, Louis Brossard, Jean Lessard, and Hugues Ménard

Abstract: The electrocatalytic hydrogenation (ECH) of β-O-4 lignin model compounds has been carried out at constant current at Raney nickel and palladium-based cathodes in aqueous sodium hydroxide solution at temperatures ranging from 25 to 75°C. It was found that the hydrogenolysis of phenolic β-arylethyl-aryl ethers with one β-O-4 linkage takes place at both types of electrodes to give a mixture of phenolic compounds. The ECH of 1-(4-hydroxy-3-methoxyphenyl)-2-(2-methoxyphenoxy)-1-ethanol (model **1**) at Raney nickel gives guaiacol (**9**), acetovanillone (**11b**), α-methylvanillyl alcohol (**12b**), and products derived from their further hydrogenation. The β-O-4 bond is more difficult to cleave upon replacing one hydrogen of the methylene group of **1** by a hydroxymethyl group (see **2**). However, model **4** with two β-O-4 linkages obtained by the introduction of an α-methylvanillyl group at the phenolic position of **1** is hydrogenolysed at the same rate as **1** at Raney nickel. Only the C—O aryl bond attached to the hydroxyethylphenol moiety is cleaved. At palladium, the hydrogenolysis of **1** requires only half of the theoretical amount of electricity due to the generation of chemisorbed hydrogen by dehydrogenation of **1** followed by hydrogenolysis of the resulting ketone. A general reaction scheme is proposed for the ECH of model **1**.

Key words: Lignins, lignin models, electrocatalytic hydrogenation, Raney nickel electrodes, palladium electrodes.

Résumé : L'hydrogénation électrocatalytique (HEC) de composés modèles contenant une(des) liaison(s) β-O-4 des lignines a été effectuée sur cathodes de nickel de Raney et de palladium dans des solutions aqueuses d'hydroxyde de sodium et à des températures variant de 25 à 75°C. L'hydrogénolyse, sur ces électrodes, d'éthers phénoliques β-aryléthyl-aryle ayant une liaison β-O-4 a donné un mélange de composés phénoliques. L'HEC du 1-(4-hydroxy-3-méthoxyphényl)-2-(2-méthoxyphénoxy)-1-éthanol (modèle **1**) sur nickel de Raney a donné le guaiacol (**9**), l'acétovanillone (**11b**), l'alcool α-méthylvanillique (**12b**) et des produits de leur hydrogénation subséquente. La liaison β-O-4 du modèle **2** dans lequel un des hydrogènes du groupe méthylène de **1** a été remplacé par un groupement hydroxyméthyle s'est avérée plus difficile à hydrogénolyser. Cependant, la vitesse d'hydrogénolyse, sur nickel de Raney, du modèle **4** ayant deux liaisons β-O-4 et obtenu par l'introduction d'un groupement α-méthylvanillyle sur la fonction phénol du composé **1** était la même que celle du modèle **1**. Seule la liaison C—O aryle fixée au reste hydroxyéthylphénol a été hydrogénolysée. Sur cathode de palladium, l'hydrogénolyse du modèle **1** n'a consommé que la moitié de la quantité théorique d'électricité dû à la formation d'hydrogène chimisorbé par déshydrogénation de **1** suivie de l'hydrogénolyse de la cétone ainsi formée. Un schéma général de réaction est proposé pour l'HEC du modèle **1**.

Mots clés : Lignines, modèles de lignines, hydrogénation électrocatalytique, électrodes de nickel de Raney, électrodes de palladium.

Introduction

Historically, chemical treatments of lignins, such as oxidation in alkaline nitrobenzene or permanganate solutions, hydrogenolysis, and ethanolysis (1) have given an insight into the lignin structure, but have also revealed the potential use of this biopolymer as a feedstock for the preparation of low molecular weight chemicals. Since most of the lignins generated by the pulp and paper industry are still exploited only as fuel, there is an economic interest to develop methods of cleaving lignins into valuable monomers (2). Generally, oxidative methods have the objective of producing vanillin and syringaldehyde. Typical oxidation treatments involve nitrobenzene (3), metal oxides (3), oxygen[2, 3], and

Received July 16, 1999.

A. Cyr, F. Chiltz, P. Jeanson, A. Martel, J. Lessard,[1] and H. Ménard.[1] Centre de recherche en électrochimie et électrocatalyse, Département de chimie, Université de Sherbrooke, Sherbrooke, QC J1K 2R1, Canada.
L. Brossard. Institut de recherche d'Hydro-Québec (IREQ), 1800 boul. Lionel-Boulet, Varennes, QC J3X 1S1, Canada.

[1]Authors to whom correspondence may be addressed. (JL) Telephone: (819) 821-7091. Fax: (819) 821-8017. e-mail: jlessard@courrier.usherb.ca. (HM) Telephone: (819) 821-7084. Fax: 819) 821-8017. e-mail: hmenard@courrier.usherb.ca

[2]H.B. Marshall and C.A. Sankey. U.S. Patent 2,516,827 (1945).
[3]J.R. Salvesen, D.L. Brink, D.G. Diddams, and P. Owzarski. U.S. Patent 2,434,626 (1948).

 © 2000 NRC Canada

electrolysis (4, 5).[4] Catalytic hydrogenation has also been studied as a method for production of phenolic monomers (6). A variety of catalysts have been used, including Raney nickel (7), copper chromite (8), supported rhodium (9, 10), ruthenium or palladium (11), and nickel boride[5]. Interesting compounds such as 4-*n*-propylguaiacol and dihydroconiferyl alcohol have been generated from aspen wood using Raney nickel (7) or supported rhodium (9, 10). With a palladium catalyst, a high selectivity has been reported for the formation of dihydroconiferyl alcohol (11). The use of nickel boride has led to the production of 4-ethylguaiacol and 4-ethylsyringol from wood.[5]

In a recent article (12), we prepared basic nonphenolic models of α-O-4 and β-O-4 bonds in lignins to demonstrate the potential of electrocatalytic hydrogenation (ECH) as an alternative method for lignin depolymerization. ECH is an advantageous combination of electrochemical and catalytic methods (for a review on ECH, see ref. 13). In ECH, chemisorbed hydrogen (H)M is generated in situ on the electrocatalyst surface by electroreduction of water at a low overpotential (rxn. [1]) and reacts with the adsorbed organic substrate (rxns. [2]–[4]). However, hydrogenation (rxns. [2]–[4]) competes with hydrogen desorption (rxns. [5] and (or) [6]) and this may decrease the current efficiency (13). This method of generating chemisorbed hydrogen allows one to carry out reactions similar to catalytic hydrogenation but at lower temperatures and pressures (13). Furthermore, the concentration of chemisorbed hydrogen can be controlled by adjustment of the current density.

[1] $2\ H_2O + 2\ e^- + M \rightarrow 2\ (H)M + 2\ OH^-$

[2] $R + M \rightleftharpoons (R)M$

[3] $(R)M + 2\ (H)M \rightleftharpoons (RH_2)M$

[4] $(RH_2)M \rightleftharpoons RH_2 + M$

[5] $(H)M + H_2O + e^- \rightarrow H_2 + M + OH^-$

[6] $(H)M + (H)\ M \rightleftharpoons H_2 + 2\ M$

ECH at electrodes made of Raney-type materials has been applied successfully to the selective hydrogenation of many types of molecules (13). In principle, all catalytic powders used in catalytic hydrogenation can also be used in ECH, provided that the catalyst can be immobilized on (or supported by) a conductive material or cast into a solid conductive piece. The simplest electrode set up is to spread the catalytic powder onto a conductive plate, but such a design is not fully satisfactory from a practical point of view. Several approaches have been developed to prepare electrodes from catalytic powders, including electromagnetic deposition (14), electrocodeposition (15), lanthanum phosphate polymerization,[6] and embodiment in a reticulated vitreous carbon support (16). The latter two methods have been used in this work.

As an extension of our previous work (12), we report in this paper the results of the ECH of phenolic lignin models (which are soluble in aqueous alkali) on Raney nickel and palladium-based electrodes. It has been recognized that the β-O-4 linkage (see **4** in Fig. 1) is the most important type of structural element in native lignins. We therefore studied the following models (see Fig. 1 for structures): (*i*) three compounds having one β-O-4 linkage and referred to as phenolic monoethers: 1-(4-hydroxy-3-methoxyphenyl)-2-(methoxyphenoxy)-1-ethanol (**1**), its hydroxymethyl derivative **2**, and its keto derivative **3**; (*ii*) phenolic diether **4** with two β-O-4 linkages; (*iii*) 1-(3,4-dimethoxyphenyl)-2-(methoxyphenoxy)-1-ethanol (**5**), a non-phenolic monoether (β-O-4 linkage); and (*iv*) 4-phenoxyphenol (**6**), a model of 4-O-5 linkages in which two aryl groups are directly bound to an oxygen atom. Raney nickel has proven to be a versatile hydrogenation electrocatalyst (13), and supported palladium was chosen in view of its well known activity in catalytic hydrogenolysis (17).

Experimental

Organic substrates and products

Phenolic monoethers **1** (18), **2** (19), **3** (18), and **5** (5) are known compounds and were synthesized according to published procedures. Phenolic diether **4** is also a known compound and was prepared from *O*-isopropyl-α-bromoacetovanillone (prepared according to ref. 20) by described procedures (18, 21). The following compounds (Fig. 2) were obtained from commercial sources: 4-phenoxyphenol (**6**), guaiacol (**9**), ethylphenol (**10a**), acetovanillone (**11b**), and 4′-hydroxypropiophenone (**11c**) from Aldrich; cyclohexanol (**7**) and phenol (**8**) from BDH; 4-ethylguaiacol (**10b**), 4-*n*-propylphenol (**10c**), and 4-*n*-propylguaiacol (**10d**) from Lancaster; 4′-hydroxyacetophenone (**11a**) from Eastman. The alcohols **12a, b** (Fig. 2) were prepared by catalytic hydrogenation of the corresponding ketone using nickel-aluminum alloy in 10% sodium hydroxide at 15°C (in situ generation of Raney nickel and chemisorbed hydrogen) (22). All compounds had ^{1}H NMR, ^{13}C NMR, IR, and mass spectral data in accordance with their structure.

Electrodes and electrolyses

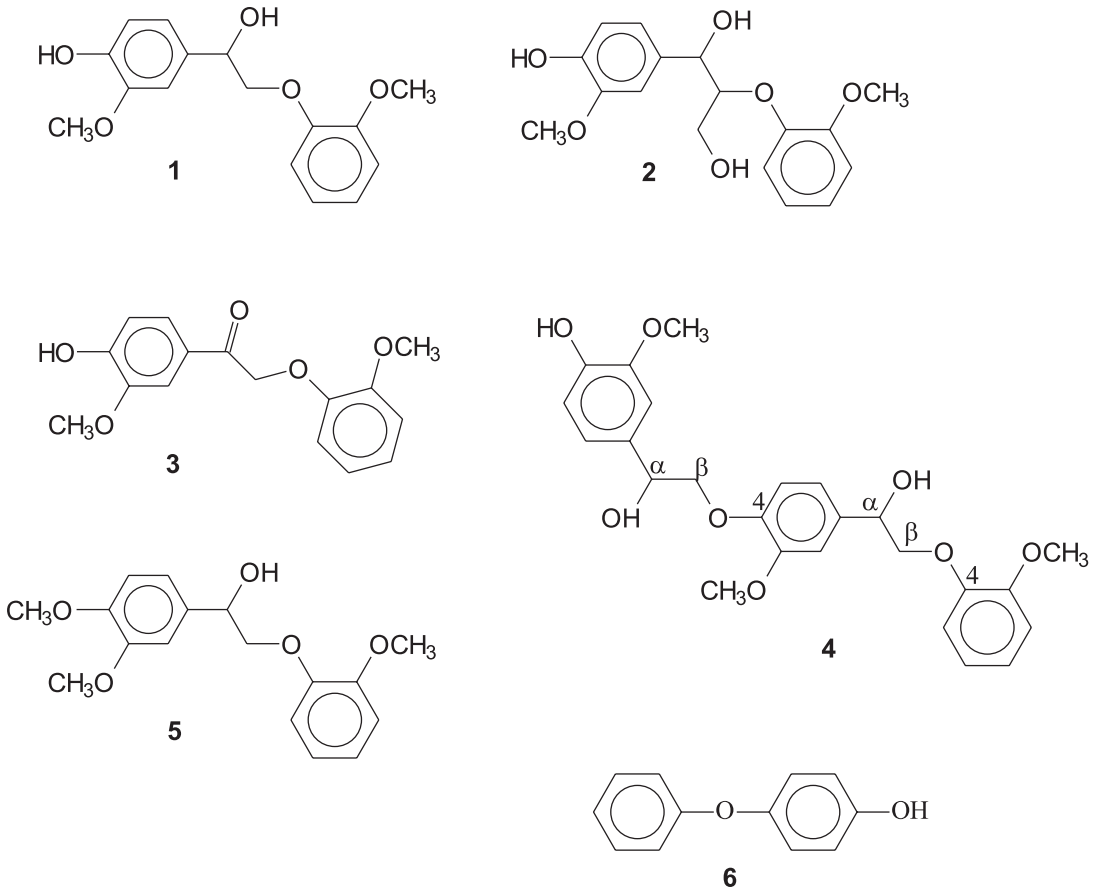
Raney nickel electrodes were made by mixing and grinding 45% of Raney alloy (Fluka), 45% of fractal nickel powder (Inco Type 250), and 10% of lanthanum phosphate[6]. About 40 g of this powder was pressed into a plate 3mm thick at about 1000 kg/cm^2 into a 5 × 71/2 cm^2 mould from which 2 × 21/2 cm^2 plates were cut. These plates were heated at 800°C for 4 h under an argon atmosphere. The electrical contact was made with a nickel stripe. The plates were leached in NaOH 30% at 75°C for 24 h to remove aluminum. In order to eliminate the chemisorbed hydrogen formed in the leaching process (reduction of water by aluminum), the Raney nickel plate was treated with a solution of *trans*-cinnamic acid (5 g in 200 mL of 1 M NaOH) at room temperature for at least 18 h (hydrogenation to phenylpropionic acid) prior to electrolysis.

The palladium-based electrode consisted of a 2 × 2.5 × 0.6 cm^3 piece of 100 ppi reticulated vitreous carbon (Electrosynthesis Co.) into which 0.20 g of catalyst

[4] J.H.P. Utley and C.Z. Smith. U.S. Patent 4,786,382 (1988).
[5] B. Loubinoux. French Patent 80 15272 (1980).
[6] J.-M. Lalancette, E. Potvin, and H. Ménard. U.S. Patent 4,886,591 (1989).

© 2000 NRC Canada

Fig. 1. Lignin models studies.



(palladium 5% on alumina from Aldrich) was embedded (16). This physical embodiment of the particles into the vitreous carbon reticulated structure occurred spontaneously when the powder was stirred in the catholyte solution for about one hour in the presence of the vitreous carbon matrix. The particles remained in contact with the carbon matrix despite vigorous stirring, provided that there was no sudden perturbation (16).

The electrolyses were carried out with a 410 Potentiostatic Controller coupled to a 640 digital coulometer (Electrosynthesis Co.). A two-compartment jacketed glass H-cell with a Nafion-324 membrane (E.I. duPont de Nemours & Co.) and condensers was connected to a temperature-regulated circulating bath. Both compartments were filled with 30 mL of 1 M NaOH (except for the electrolysis of **5**:1 M NaOH in 1:1 ethanol–water) and 0.75 mmol of organic substrate (0.38 mmol for compound **4** as it contains two β-O-4 links) was added to the catholyte stirred magnetically. A graphite rod was used as anode. A constant current was applied (5 or 20 mA) and samples of the catholyte were taken at regular intervals. The electrolysis of **1** at 75°C and 5 mA was conducted under a nitrogen atmosphere in order to avoid chemical degradation (23).

Work-up procedures and analyses

Part of the catholyte was neutralized with 10% acetic acid in water, then diluted to a fixed volume with 20% acetonitrile in water and analyzed by HPLC (C_{18} column packing, Beckman 100A pumps, Beckman 420 controller, Hitachi 100-40 spectrophotometer at λ = 272 nm, and HP3390A integrator) with the help of calibration curves for compounds **1**–**6**, **8**, **9**, **10a**–**c**, **11a**–**c** and **12a, b**. The best overall separation was achieved with the following eluent program at a flow rate of 1.0 mL/min: 90% of 4% acetic acid in water – 10% CH_3CN for 5 min, then adding 0.5% CH_3CN per min up to 45% CH_3CN.

Product identification was performed by GC–MS (Hewlett–Packard 5890, 30 m DB-5 column and HP5971 mass-selective detector) and complementary quantitative analyses were done by GC–FID (Perkin–Elmer 8500, 30m DB-1 capillary column and HP3390A integrator), when needed, using internal standards. Response factors were approximated for compounds for which authentic samples were not available (**10e**, **11d**, **12c**–**e**). The thermally unstable compounds **1, 2,** and **12a**–**e** were characterized as their acetate derivatives. Acetylation of the hydroxyl groups was accomplished overnight with a 1:1 pyridine – acetic anhydride mixture (24). For the GC analyses of the acetylated derivatives, part of the catholyte was neutralized with 1 M HCl then extracted with ethyl acetate, the organic layer was dried with magnesium sulfate and the solvent removed under vacuum.

Results and discussion

ECH at Raney nickel

The ECH of model **1** in alkaline solution was studied as a function of temperature and current density (Table 1). At

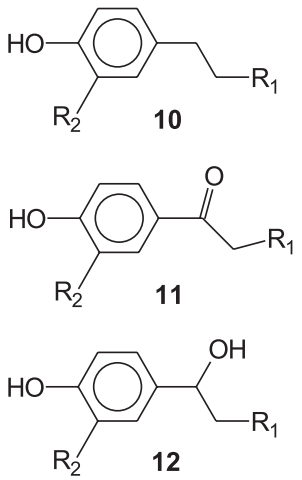
© 2000 NRC Canada

Table 1. Electrocatalytic hydrogenation (ECH) of model **1** at a Raney nickel electrode and in aqueous 1 M NaOH: yield (%) of products.

Products	T = 25°C Q^a = 18 F mol^{-1}		T = 50°C Q = 18 F mol^{-1}		T = 75°C Q = 18 F mol^{-1}	
	I =		I =		I =	
	5 mA	20 mA	5 mA	20 mA	5 mA	20 mA
Entry	1	2	3	4	5	6
Unreacted (**1**)	6.0	60	nd[b]	10	nd[b]	1.0
Cyclohexanol (**7**)	0.3	0	2.5	0.2	4.0	2.5
Phenol (**8**)	2.0	Traces	7.0	2.0	13	7.0
Guaiacol (**9**)	43	14	37	40	24	37
4-Ethylphenol (**10a**)	0.7	Traces	8.0	2.0	24	7.0
4-Ethylguaiacol (**10b**)	Traces	0	Traces	Traces	2.0	1.5
4′-Hydroxyacetophenone (**11a**)	Traces	Traces	1.2	0.6	3.0	2.0
Acetovanillone (**11b**)	1.3	1.6	7.0	7.0	5.0	12
4-(1-Hydroxyethyl)phenol (**12a**)	1.0	Traces	6.0	3.0	2.5	3.0
α-Methylvanillyl alcohol (**12b**)	41	21	21	31	4.0	18

[a]Q in F mol^{-1} is the charge corresponding to the number of moles of electrons per mole of substrate.
[b]Not detected.

Fig. 2. Compounds obtained from ECH of models **1** to **5**.



(a) $R_1 = H, R_2 = H$

(b) $R_1 = H, R_2 = OCH_3$

(c) $R_1 = CH_3, R_2 = H$

(d) $R_1 = CH_3, R_2 = OCH_3$

(e) $R_1 = CH_2OH, R_2 = OCH_3$

room temperature (entries 1 and 2), the hydrogenolysis of the β-O-4 bond occurs readily to give about equal amounts of guiacol (**9**) and α-methylvanillyl alcohol (**12b**) (see Figs. 1, 2, and 4 for structures) as expected and the electrohydrogenolysis is much less efficient at a current of 20 mA (entry 2: 40% conversion after a charge of 18 F mol^{-1}) than at a current of 5 mA (entry 1: 94% conversion). The effect of increasing the current becomes less and less important as the temperature is increased to 50°C (compare entries 3 and 4) then to 75°C (compare entries 5 and 6). At a given current, an increase of temperature leads to higher conversion rates and to further hydrogenation of guaiacol (**9**) to phenol (**8**) and cyclohexanol (**7**) and of α-methylvanillyl alcohol (**12b**) to 4-(1-hydroxyethyl)phenol (**12a**), 4-ethylguaiacol (**10b**) and 4-ethylphenol (**10a**) (compare entries 1 and 3, compare entries 2, 4, and 6). Thus, an increase of temperature and a lower current density favor the hydrogenation process (rxns. [2]–[4]) over hydrogen desorption (hydrogen evolution, rxns. [5] and (or) [6]) as observed with other substrates (13). As shown in Table 2, independent studies confirmed the hydrogenation, under the ECH conditions, of guaiacol (**9**) to phenol (**8**) and cyclohexanol (**7**) (entry 4), of phenol (**8**) to cyclohexanol (**7**) (entry 5), and of α-methylvanillyl alcohol (**12b**) to 4-(1-hydroxyethyl)phenol (**12a**), 4-ethylguaiacol (**10b**) and 4-ethylphenol (**10a**) (entry 1). Figure 3 (variation of the product distribution during the ECH of model **1** at 50°C and 5 mA) also shows that alcohol **12b** is hydrogenolysed further to 4-ethylphenol (**10a**).

It is noteworthy that, during the ECH of model **1**, acetovanillone (**11b**) was present along with methylvanillyl alcohol (**12b**) at the beginning of the electrolysis, whatever the temperature and the current. This is clearly seen in Fig. 3 which shows that an equimolar amount of ketone **11b** and alcohol **12b** was present after 2 F mol^{-1} in an electrolysis carried out at 50°C and 5 mA. Furthermore, the amount of ketone **11** formed is more important the higher the temperature (compare entries 2, 4, and 6 of Table 1). This demonstrates that a secondary benzyl alcohol can be dehydrogenated to the corresponding ketone on a polarized Raney nickel catalyst (reverse of rxns. [4], [3], and [2]) and that dehydrogenation

© 2000 NRC Canada

Table 2. Electrocatalytic hydrogenation, at a Raney nickel electrode and in aqueous 1 M NaOH, of compounds isolated from the ECH of model **1**: yield (%) of products.[a]

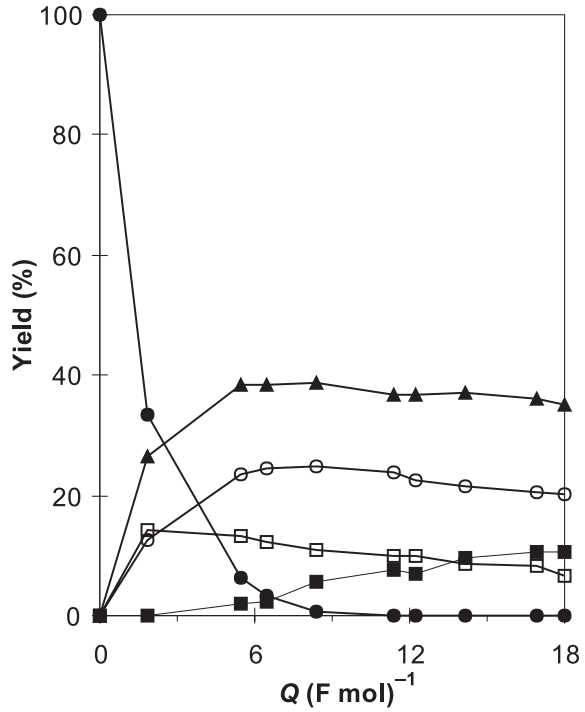
Products	Compound	**12b**	**11b**	**3**	**9**	**8**
	Q^b	18 F mol^{-1}	18 F mol^{-1}	8 F mol^{-1}	18 F mol^{-1}	18 F mol^{-1}
	Entry	1	2	3[c]	4	5
Cyclohexanol (**7**)		—	—	0	3.0	33
Phenol (**8**)		—	—	0	19	64
Guaiacol (**9**)		—	—	48	70	—
4-Ethylphenol (**10a**)		13	11	0	—	—
4-Ethylguaiacol (**10b**)		6.0	1.0	0	—	—
4′-Hydroxyacetophenone (**11a**)		3.5	2.0	1	—	—
Acetovanillone (**11b**)		21	1.8	27	—	—
4-(1-Hydroxyethyl)phenol (**12a**)		9.0	9.0	1.5	—	—
α-Methylvanillyl alcohol (**12b**)		38	53	15	—	—

[a]Experimental conditions: T = 50°C and I = 5.0 mA.

[b]Q in F mol^{-1} is the charge corresponding to the number of moles of electrons per mole of substrate.

[c]No unreacted **3** was detected.

Fig. 3. Evolution of the product distribution with the charge (F mol^{-1}) for the ECH of model **1** at a Raney nickel electrode at 50°C and 5mA: ● unreacted **1**, ▲ guaiacol (**9**), ○ α-methylvanillin (**12b**), ■ 4-ethylphenol (**10a**), □ acetovanillone (**11b**).

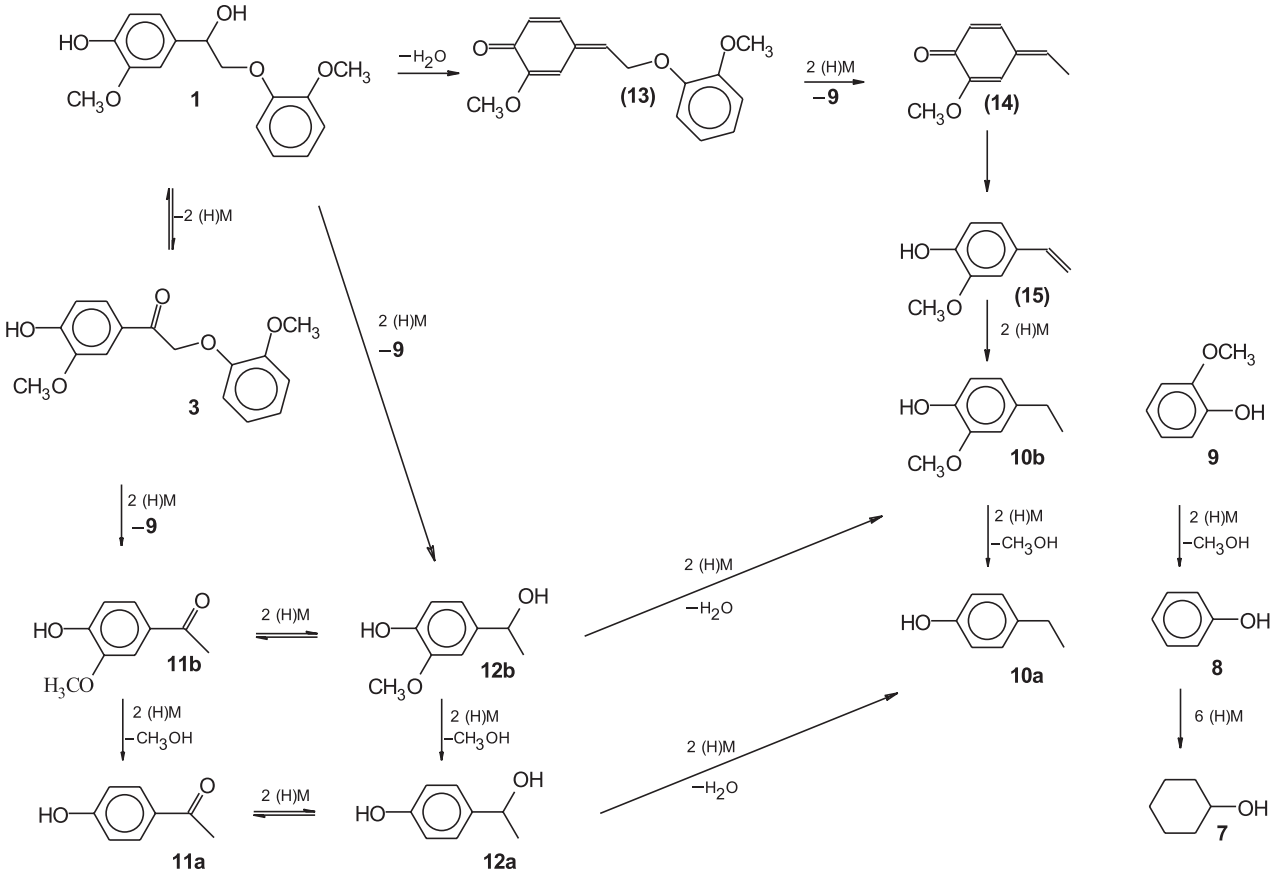


is faster at higher temperatures. The fact that dehydrogenation of a benzyl secondary alcohol could effectively take place under the electrolysis conditions was confirmed by carrying out the ECH of alcohol **12b** (Table 2, entry 1) under the same conditions (alcohol **12b** is stable under the electrolysis conditions in the absence of an electrode): acetovanillone (**11b**) is formed rapidly in the cell, then is slowly converted back to alcohol **12b** which, as already observed, is hydrogenolysed to 4-(1-hydroxyethyl)phenol (**12a**) (also dehydrogenated to 4′-hydroxyacetophenone (**11a**)), 4-ethylguaiacol (**10b**), and 4-ethylphenol (**10a**). After 18 F mol^{-1}, there was still 38% of alcohol **12b** and 21% of ketone **11b** present together with 9% of alcohol **12a**, 3.5% of ketone **11a**, 6% of 4-ethylguaiacol (**10b**), and 13% of 4-ethylphenol (**10a**). The ECH of ketone **11b** (entry 2) did give alcohol **12b** which is hydrogenolysed further to **12a** (also dehydrogenated to **11a**), **10b**, and **10a** as expected. Thus, there is a benzyl alcohol – ketone interconversion (dehydrogenation–hydrogenation) during the ECH of secondary alcohols at Raney nickel in aqueous alkali and this interconversion is faster the higher the temperature. Such dehydrogenation of alcohol **1** to ketone **3** during the ECH of **1** certainly occurs even if ketone **3** is not detected during the ECH of **1.** In fact, the electrohydrogenolysis of ketone **3** at 50°C and 5 mA occurs readily (Table 2, entry 3): after 8 F mol^{-1}, the conversion is complete and the products formed are: guaiacol (**9**) (48%); α-methylvanillyl alcohol (**12b**) (15%) together with acetovanillone (**11b**) (27%), its dehydrogenation product; 4-(1-hydroxyethyl)phenol (**12a**) (1.5%) and its dehydrogenation product, 4′-hydroxyacetophenone (**11a)** (1%). Ketone **3** also undergoes rapid degradation under the conditions used for ECH.

A scheme for the formation of most of the products isolated and detected in the ECH of **1** (Table 1) and in the ECH of some of the products isolated (Table 2), at a Raney nickel electrode, is shown in Fig. 4. Two possible pathways for the formation of α-methylvanillyl alcohol (**12b**) are illustrated: (1) direct hydrogenolysis of the β-O-4 bond of **1** (**1** → **12b** + guaiacol (**9**)), and (2) dehydrogenation of **1** to ketone **3** followed by its hydrogenolysis to acetovanillone (**11b**) and guaiacol (**9**), **11b** being hydrogenated to **12b** (**1** → **3** → **11b** → **12b**). The hydrogenolysis of ketone **3** should be faster than that of alcohol **1** because, in the former, the β-O-4 bond is conjugated to the carbonyl group of an acetophenone (to a π-electron system). So pathway (2) is probably the main route to alcohol **12b**. The two most probable routes to 4-ethylguaiacol (**10b**) are: (*i*) hydrogenolysis of α-methylvanillyl alcohol (**12b**) (**12b** → **10b**) and (or) (*ii*) dehydration of **1** to quinonemethide **13** followed by easy hydrogenolysis of the β-O-4 bond (**13** → **14** + **9**), then rapid tautomerization of **14** to the more stable styrene **15** which would be rapidly

© 2000 NRC Canada

Fig. 4. Reaction pathways for the formation of the various products in the ECH of model **1**.



hydrogenated to **10b**. The hydrogenolysis of the C—O aryl bond of quinonemethide **13** should be easy because the C—O bond is conjugated to the quinonemethide π-bond system. Quinonemethides **13** and **14** as well as styrene **15** were not detected during the ECH of model **1**, which means that, if pathway (*ii*) was occurring, their conversion is faster than their generation. Dehydrations similar to the dehydration of **1** to quinonemethide **13** were shown to occur under the drastic conditions of alkali pulping (25) but should be slower at temperatures of 75°C or lower (5). Finally, 4-ethylphenol (**10a**) might have been formed by demethoxylation of 4-ethylguaiacol (**10b**) and(or) by hydrogenolysis of 4-(1-hydroxyethyl)phenol (**12a**) and there are two possible routes to **12a**: **12b** → **12a** and(or) **11b** → **11a** → **12a**.

For the demethoxylation of 2-methoxyphenols (guaiacol (**9**) to phenol (**8**), 4-ethylguaiacol (**10b**) to 4-ethylphenol (**10a**), acetovanillone (**11b**) to 4′-hydroxyacetophenone (**11a**), α-methylvanillyl alcohol (**12b**) to 4-(1-hydroxyethyl)phenol (**12a**)), direct hydrogenolysis is not very probable due to the fact that the C—OCH_3 bond should be quite strong since the carbon is a sp^2 carbon and the C—O bond is not conjugated to a π-electron system. So demethoxylation most probably takes place on the less stable (nonaromatic) 6-methoxycyclohexa-1,4-dien-1-one tautomer (keto–enol tautomerism). Two routes are possible: (*i*) hydrogenolysis of the C—OCH_3 bond which should occur readily since the methoxy group is attached to a sp^3 carbon and the C—O bond is conjugated to a cyclohexadienone π-electron system; (*ii*) hydrogenation of the dienone to a 6-methoxycyclohexa-1,4-dien-1-ol followed by elimination of methanol. The fact that 2-methoxycyclohexanol was not detected during the ECH of guaiacol (**9**) to phenol (**8**) and cyclohexanol (**7**) (Table 2, entry 9) indicates that the hydrogenation of the aromatic ring takes place only after the methoxy group has been removed. As a matter of fact, cyclohexanol (**7**) was the only saturated compound detected in this study of ECH of model **1** and the other models.

The hydrogenolysis of the β-O-4 bond of model **2** with a hydroxymethyl group attached to the β carbon is more difficult than that of model **1** as shown by the lower conversion rates of entries 1 to 3 of Table 3. The mixture of compounds formed is more complex than that obtained from the ECH of **1** because compounds with a phenylpropane structure (**10c**, **10e**, **11c**, **11d**, **12c**, **12d**, **12e**) are formed in addition to those with a phenylethane structure (**10a**, **10b**, **11a**, **11b**, **12a**, **12b**) identified from the ECH of **1**. In the ECH of **2**, none of the compounds, besides guaiacol (**9**), is obtained with a high degree of selectivity. Compounds **12** (**12a**–**e**) were the most abundant with a total yield of 12% only (see Table 3, entry 2). Again, exhaustive electrolysis should favor compounds **10** (**10a**–**e**). Despite the relatively low yields, ECH appears more interesting than electrooxidation which causes much polymerization of **2** (and of **1** also) (5).

Expanding model **1** by adding a methylvanillyl alcohol unit to the phenolic end (see model **4** which has two β-O-4 bonds) appears to have little influence on the ease of hydrogenolysis. Indeed, (*i*) the extent of hydrogenolysis after a given charge (the current efficiency), for an ECH carried

© 2000 NRC Canada

Table 3. Electrocatalytic hydrogenation of model compounds **2**, **4**, and **6** at a Raney nickel electrode in aqueous 1 M NaOH: yield (%) of products.[a]

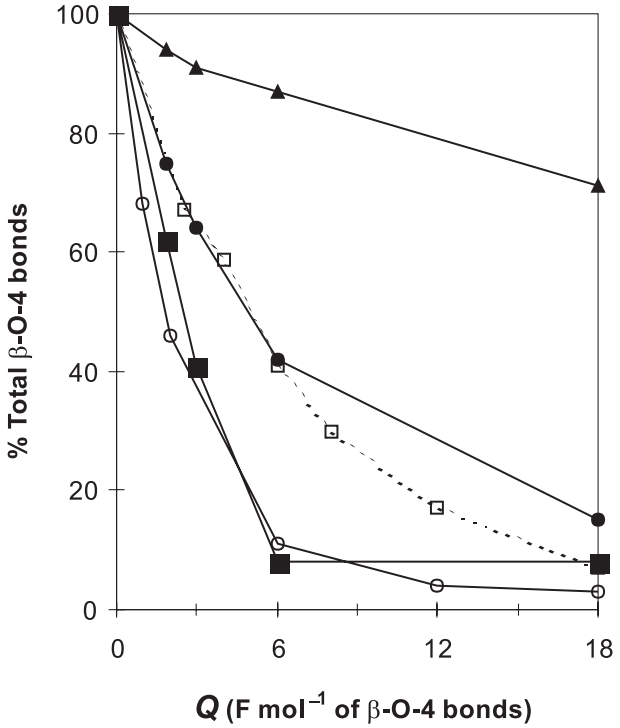
Products	Model	**2**			**4**	**6**
	T	25°C	50°C	75°C	75°C	50°C
	Q[b]		18 F mol^{-1}		18 F mol^{-1}	6 F mol^{-1}
	I	5 mA	5 mA	20 mA	20 mA	5 mA
	Entry	1	2	3	4[c]	5
Unreacted substrate		69	27	22	5.0	9.0
Cychohexanol (**7**)		0	0.5	1.0	0	0
Phenol (**8**)		0	3.5	5.0	9.0	84
Guaiacol (**9**)		11	26	29	15	—
4-Ethylphenol (**10a**)		0	0.8	2.5	9.0	—
4-Ethylguaiacol (**10b**)		0	0.5	1.0	0	—
4-n-Propylphenol (**10c**)		0	1.0	2.0	—	—
Dihydroconiferyl alcohol (**10e**)		0.1	0.6	1.0	—	—
4′-Hydroxyacetophenone (**11a**)		0	0	1.0	6.0	—
Acetovanillone (**11b**)		0.3	1.3	3.5	26	—
4-Hydroxypropiophenone (**11c**)		0	0.3	1.0	—	—
4′-Hydroxy-3′-methoxy-propiophenone (**11d**)		0.2	2.0	3.0	—	—
4-(1-Hydroxyethyl)phenol (**12a**)		0.2	0.8	1.5	13	—
α-Methylvannillyl alcohol (**12b**)		0.8	3.5	4.0	0.3	—
4-(1-Hydroxypropyl)phenol (**12c**)		0.7	2.5	2.0	—	—
1-(4-Hydroxy-3-methoxyphenyl)-1-propanol (**12d**)		1.3	3.0	2.5	—	—
1-(4-Hydroxy-3-methoxyphenyl)-1,3-propanediol (**12e**)		1.5	2.0	1.0	—	—

[a]Some compounds giving rise to GC–MS peaks could not be identified and they were not taken into account in the calculation of the yields.

[b]*Q* in F mol^{-1} is the charge corresponding to the number of moles of electrons per mole of β-O-4 bonds.

[c]Other products identified were ketone **4a** (2.0%), ketone **3** (2.0%), and model **1** (0.2%). There was as much as 7% of compound **1** accumulated after 3 F mol^{-1}.

Fig. 5. Influence of temperature and current on the rate of hydrogenolysis of model **4** : ▲ 25°C, 20 mA, ● 50°C, 20 mA, ■ 75°C, 20 mA, ○ 50°C, 5mA, □ model **1**: 50°C, 20 mA.



out at 50°C and at a current of 20 mA, is about the same for model **4** as for model **1** as shown in Fig. 5 and (*ii*) the product distribution after 18 F mol^{-1} for an ECH carried out at 75°C and a current of 20 mA is similar for model **4** (entry 4, Table 3) and model **1** (entry 6, Table 1). This is because the same type β-O-4 bond is hydrogenolysed in both model **4** and model **1**, the C—O aryl bond attached to a hydroxyethylphenol moiety. Figure 5 shows that the efficiency of hydrogenolysis increases with increasing temperature and decreases with increasing current as observed for the ECH of model **1**. Again dehydrogenation of secondary benzylic alcohols did occur as already noted since both the ketone resulting from dehydrogenation of model **4** and ketone **3** resulting from dehydrogenation of model **1** are formed in the ECH of **4**.

The fact that model **1** and its corresponding dehydrogenation product, ketone **3**, are formed in the ECH of **4** indicates that hydrogenolysis of one of the β-O-4 bonds, the C—O aryl bond attached to the hydroxyethylphenol moiety, is faster than the hydrogenolysis of the other β-O-4 bond, the C—O aryl bond attached to the *O*-alkylated hydroxyphenol moiety. In fact, model **5** in which the phenolic group had been methylated (structure akin to the *O*-alkylated hydroxyphenol moiety of model **4**) was recovered quantitatively after electrolysis under the same conditions as those used for the ECH of models **1**, **2**, and **4**. There are two possible explanations for the faster hydrogenolysis of the C—O aryl bond attached to the hydroxyethylphenolate moiety: (*i*) the hydrogenolysis takes place on the ketone resulting from

© 2000 NRC Canada

Table 4. Electrocatalytic hydrogenation of model **1** on palladium-based electrodes[a] in aqueous 1 M NaOH: yield (%) of products.[b]

Products	Electrode	Pd–C	Pd–C	Pd–Al_2O_3
	Q[c]	1 F mol^{-1}	18 F mol^{-1}	1 F mol^{-1}
	Entry	1	2	3
Unreacted substrate		nd[d]	nd[d]	nd[d]
Guaiacol (**9**)		33	41	51
Acetovanillone (**11b**)		42	24	51
4′-Hydroxyacetophenone		Traces	0.7	0
α-Methylvanillyl alcohol (**12b**)		Traces	14	0

[a]Pd 5% on charcoal or alumina in contact with a reticulated carbon matrix (see Experimental).

[b]Experimental conditions : 50°C and 5 mA. The lower mass balance for ECH on Pd–C compared to ECH on Pd–Al_2O_3 is due to the stronger adsorption of organics on charcoal than on alumina (16).

[c]Q in F mol^{-1} is the charge corresponding to the number of moles of electrons per mole of substrate.

[d]Not detected.

dehydrogenation of **4** and the dehydrogenation of the hydroxy group at the benzylic position of the electron-rich (negatively charged) phenolate ring is faster than that of the other benzylic alcohol; and (or) (*ii*) hydrogenolysis takes place from the quinonemethide resulting from elimination of the hydroxy group at the benzylic position of the phenolate ring which would indeed be faster than the elimination of the other benzylic alcohol because a negatively charged oxygen atom (phenolate anion) is a better electron donor than an alkoxy group.

The aryl-O-aryl bond of phenoxyphenol (**6**) is easily hydrogenolyzed to phenol at a Raney nickel cathode and at 50°C and 5 mA (Table 3, entry 5). This type of linkage is most frequent in the Kraft lignin (26). A study of the ECH of this compound as function of the electrode material has been reported elsewhere (16). It must be noted that phenol was the sole product formed. Neither benzene nor *p*-cresol were detected. Thus, only the C—Oaryl bond attached to the phenol ring was cleaved. This can be readily explained if the hydrogenolysis takes place via the cyclohexadienone tautomer in which the C—Oaryl bond is attached to a sp^3 carbon and conjugated to a cyclohexadienone π-electron system as suggested above for the demethoxylation of 2-methoxyphenols by ECH.

Finally, an electrolysis has been attempted on 2,2′-biphenyl which is representative of 5—5′ bonds in lignins. Such carbon–carbon bonds between two sp^2 carbons are particularly strong and, as expected, the unreacted substrate was quantitatively recovered.

ECH at palladium

The results are presented in Table 4. The ECH of model **1** at a cathode made of 5% Pd–C or 5% Pd–Al_2O_3 particles embedded in a matrix of reticulated vitreous carbon (16, see Experimental) gave an unexpected result (entries 1 and 3): the substrate was completely converted to guaiacol (**9**) and acetovanillone (**11b**) after only 1 F mol^{-1}, that is after consumption of only half of the theoretical amount of electricity required for complete hydrogenolysis. The reaction was quantitative with Pd–Al_2O_3 (entry 3) but the mass balance was 72% only with Pd–C due to the strong adsorption of organics on activated charcoal as reported previously (16). In a blank test performed under the same conditions as those of entry 3 (Pd–Al_2O_3) but with a nonpolarized electrode (open circuit), **1** was first dehydrogenated to ketone **3** (see Fig. 4). After a period of time corresponding to the duration of an electrolysis, some guaiacol (**9**) and acetovanillone (**11b**) were formed in small amounts thus showing that a small quantity of the hydrogen atoms generated at the surface of the palladium catalyst by dehydrogenation of **1** is used in the hydrogenolysis of ketone **3**. On the polarized catalyst, about 50% of the hydrogen atoms generated at the surface of the palladium electrode by dehydrogenation of **1** must have been used for the hydrogenolysis of ketone **3** in order to explain the low charge corresponding to 1 F mol^{-1} (50% of the theoretical charge) consumed for complete conversion of model **1**. Electrocatalytic hydrogenolysis of ketone **3** did indeed occur readily at these palladium cathodes to give guaiacol (**9**) and acetovanillone (**11b**) plus an unidentified compound resulting form the degradation of **3** in basic medium. Because of such degradation, the yield of **9** and **11b** was not determined. When an electrolysis at Pd–C was pursued up to 18 F mol^{-1} (entry 2), slow electrocatalytic hydrogenation of acetovanillone (**11b**) to alcohol **12b** did occur as shown by the decrease of the amount of **11b** and increase of the amount of **12b**.

Conclusions

Electrocatalytic hydrogenation has been applied successfully to the low-temperature hydrogenolysis of representative lignin phenolic models with β-O-4 bonds at Raney nickel and palladium electrodes in basic aqueous medium. The hydrogenolysis does not take place if the phenolic group is alkylated. This fact suggests that hydrogenolysis would occur on intermediates in which the C—O aryl bond is conjugated to a π-electron array such as in ketone **3** or quinonemethide **13**, and that the formation of those intermediates would be significantly faster with the electron-rich phenolate anion than with the *O*-alkylated derivative less rich in electrons. 4-Phenoxyphenol (**6**) is cleaved easily and exclusively to phenol at a Raney nickel electrode, showing that hydrogenolysis of a 4-O-5 linkage by ECH is also possible and most probably takes place on the cyclohexadienone tautomer of the phenol in which the C—O aryl bond is again conjugated to a π-electron array. The 4-O-5 type of linkage is abundant in Kraft lignins produced by the pulp and paper industry. The results of this paper infer that lignins could be

© 2000 NRC Canada

depolymerized and converted to useful basic organics by ECH.

Acknowledgments

Financial support from the Natural Sciences and Engineering Research Council of Canada and Hydro-Québec is gratefully acknowledged.

References

1. E. Adler. Wood Sci. Technol. **11**, 169 (1977).
2. A.F. Gogotov and V.A. Babkin. Chemistry Sustainable Development. **2**–**3**, 523 (1994).
3. C.-L. Chen. *In* Methods in lignin chemistry. *Edited by* S.Y. Lin and C.W. Dence. Springer–Verlag, Berlin. 1992. pp. 301–321.
4. O.J. Murphy, C.E Salinas, and G.D. Hitchens. Proc. Electrochem. Soc. **95**, 279 (1995).
5. L.V. Pardini, C.Z. Smith, J.H.P. Utley, R.R. Vargas, and H. Viertler. J. Org. Chem. **56**, 7305 (1991).
6. A. Sakakibara. *In* Methods in lignin chemistry. *Edited by* S.Y. Lin and C.W. Dence. Springer–Verlag, Berlin. 1992. pp. 350–368.
7. J.M. Pepper and W. Steck. Can. J. Chem. **41**, 2867 (1963).
8. E.E Harris, J. D'Ianni, and H. Adkins. J. Am. Chem. Soc. **60**, 1467 (1938).
9. J.M. Pepper and R.W. Fleming. Can. J. Chem. **56**, 896 (1978).
10. J.M. Pepper and P. Supathna. Can. J. Chem. **56**, 899 (1978).
11. J.M. Pepper and Y.W. Lee. Can. J. Chem. **47**, 723 (1969).
12. B. Mahdavi, A. Lafrance, A. Martel, J. Lessard, H. Ménard, and L. Brossard. J. Appl. Electrochem. **27**, 605 (1997).
13. J.M. Chapuzet, A. Lasia, and J. Lessard. *In* Electrocatalysis (frontiers of electrochemistry series). *Edited by* J. Lipkowski and P.N. Ross. VCH Publishers Inc., New York. 1998. pp. 155–196.
14. I.V. Kirilyus and M.A. Zhuk. Sov. Electrochem. **8**, 967 (1972).
15. G. Belot, S. Desjardins, and J. Lessard. Tetrahedron Lett. **25**, 5347 (1984).
16. P. Dabo, A. Cyr, J. Lessard, L. Brossard, and J. Lessard. Can. J. Chem. **77**, 1225 (1999).
17. R.L. Augustine. *In* Catalytic hydrogenation. Marcel Dekker, New York. 1965. p. 36.
18. R. Brezný and V. Mihálov. Cellulose Chem. Tech. **18**, 575 (1984).
19. F. Nakatsubo. *In* Methods in enzymology. Vol. 161. Biomass, part B. *Edited by* W.A. Wood and S.T. Kellogs. Academic Press, San Diego. 1988. pp. 57–65.
20. R.M. Romdhane, B. Carrier, M. Barelle, and C. Béguin. Holzforschung, **40**, 259 (1986).
21. J. Ralf, R.M. Ede, and A.L. Wilkins. Holzforschung, **40**, 23 (1986).
22. P.L. Cook. J. Org. Chem. **27**, 3873 (1962).
23. J. Gierer, F. Imsgard, and I. Norén. Acta Chem. Scand. **B 31**, 561 (1977).
24. K. Lunquist. *In* Methods in lignin chemistry. *Edited by* S.Y. Lin and C.W. Dence. Springer–Verlag, Berlin. 1992. p. 243.
25. J. Gierer. Wood Sci. Technol. **14**, 241 (1980).
26. W.G. Glasser, C.A. Barnett, P.C. Muller, and K.V. Sarkanen. J. Agric. Food Chem. **31**, 921 (1983).

© 2000 NRC Canada

Solid state stereochemistry of crown ethers: X-ray crystal structure and ^{13}C NMR studies of the LiNCS complex of 1,4,7,11-tetraoxacyclotetradecane

G.W. Buchanan, A.B. Driega, and G.P.A. Yap

Abstract: The title complex is asymmetric in the crystal due to the spatial orientation of the NCS function. The space group has been determined to be $P2_1$ with a = 9.496(3), b = 8.736(3), c = 9.676(3) Å, β = 117.859(5)°, and Z = 2. The solid state ^{13}C NMR spectrum is consistent with the lack of symmetry in the crystal and there is little evidence for large amplitude motion in the macrocycle as determined from the dipolar dephased spectrum.

Key words: macrocyclic crown ether, lithium complex.

Résumé : À l'état cristallin, le complexe mentionné dans le titre est asymétrique en raison de l'orientation spatiale de la fonction NCS. On a déterminé que le groupe d'espace est $P2_1$ avec a = 9,496(3), b = 8,736(3) et c = 9676(3) Å, β = 117,859(5)° et Z = 2. Le spectre RMN du ^{13}C à l'état solide est en accord avec un manque de symétrie dans le cristal et, sur la base du spectre déphasé dipolaire, il y a peu d'indications pouvant suggérer l'existence d'un mouvement de grande amplitude dans le macrocycle.

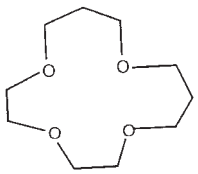
Mots clés : éther couronne macrocyclique, complexe de lithium.

[Traduit par la Rédaction]

Introduction

A number of publications from these laboratories (1–5) have dealt with large amplitude motion in crown ethers and their complexes in the solid state. To date, systems examined have been limited to 18-crown-6 complexes (1–3), a 12-crown-4 complex (4), as well as a benz-annelated 24-crown-8 molecule (5). In addition, the complementarity of X-ray crystallography and solid state NMR has been well demonstrated in the general area of solid state crown ether stereochemistry (6–8).

For complexation of the biologically important Li^+ ion, the 14-crown-4 ether system has the most nearly "ideal" cavity dimensions. Although the benz-annelated and cyclohexano-14-crown-4 systems have been studied in detail (7), no studies on any of the isomeric 14-crown-4 crown complexes themselves have appeared. In the present work, we report the synthesis and X-ray crystallographic study of the LiNCS complex of 1,4,7,11-tetraoxacyclotetradecane **1** (below), as well as a comparison of its solution phase and solid state ^{13}C NMR spectra.



1

Received August 23, 1999.

G.W. Buchanan[1] and A.B. Driega. Ottawa–Carleton Chemistry Institute, Department of Chemistry, Carleton University, 1125 Colonel By Drive, Ottawa, ON K1S 5B6, Canada.
G.P.A. Yap. Ottawa–Carleton Chemistry Institute, Department of Chemistry, University of Ottawa, 10 Marie Curie Avenue, Ottawa, ON K1N 6N5, Canada.

[1]Author to whom correspondence may be addressed. Telephone: (613) 520-3841. Fax: (613) 520-3749. e-mail: gwbuchan@ccs.carleton.ca

[2]Structure factor tables and anisotropic temperature factors have been deposited as supplementary material and may be purchased from: The Depository of Unpublished Data, Document Delivery, CISTI, National Research Council Canada, Ottawa, Ontario, Canada, K1A 0S2.

Results and discussion

The ORTEP plot of **1**.LiNCS. is presented in Fig. 1. In Fig. 2 are presented the normal (*a*) and dipolar dephased 50.3 MHz ^{13}C solid state Cross Polarized Magic Angle Spinning (CPMAS) spectra. Atomic bond lengths are collected in Table 1, with the bond angles and torsion angles appearing in Table 2. Crystallographic data are presented in Table 3 and the atomic coordinates in Table 4. Solution and solid state ^{13}C NMR chemical shifts are in Table 5. Structure factor tables and anisotropic temperature factors are available as supplementary data.[2]

(*i*) X-ray crystal structure

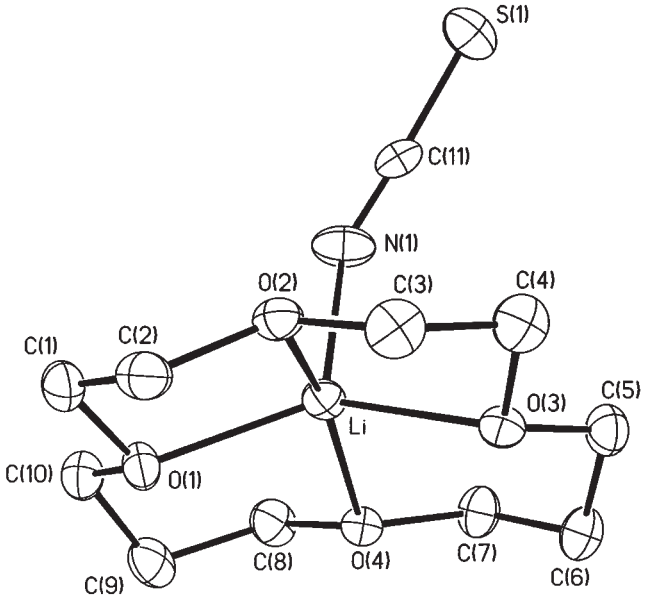
The ORTEP plot in Fig. 1 shows a structure which is symmetrical except for the spatial orientation of the thiocyanate function. Examination of the torsion angles in the Li.crown

 © 2000 NRC Canada

Table 1. Atomic bond lengths (Å) and angles (°).

(*a*) Bond lengths					
Li—O1	1.994(9)	Li—O4	2.012(9)	Li—N	2.031(9)
Li—O3	2.020(10)	Li—O2	2.068(9)		
N—C11	1.142(6)	O1—C10	1.420(7)	O1—C1	1.418(7)
O2—C2	1.414(6)	O2—C3	1.426(7)	O3—C5	1.414(6)
O3—C4	1.428(7)	O4—C7	1.434(6)	O4—C8	1.442(6)
S—C11	1.618(6)	C1—C2	1.499(9)	C3—C4	1.455(9)
C5—C6	1.497(8)	C6—C7	1.507(9)	C8—C9	1.534(8)
C9—C10	1.491(9)				
(*b*) Bond angles					
O1-Li-O4	92.1(3)	O1-Li-N	116.1(5)	O4-Li-N	99.8(4)
O1-Li-O3	138.1(4)	O4-Li-O3	92.8(4)	N-Li-O3	103.9(4)
O1-Li-O2	81.0(4)	O4-Li-O2	159.8(4)	N-Li-O2	100.3(4)
O3-Li-O2	80.2(3)	C11-N-Li	146.6(6)	C10-O1-C1	112.0(4)
C10-O1-Li	116.1(4)	C1-O1-Li	108.6(4)	C2-O2-C3	116.0(4)
C2-O2-Li	109.7(4)	C3-O2-Li	110.8(4)	C5-O3-C4	113.1(4)
C5-O3-Li	116.6(4)	C7-O4-C8	109.5(4)	C7-O4-Li	113.9(4)
C4-O3-Li	106.6(4)	C8-O4-Li	112.3(4)	O1-C1-C2	106.6(5)
O2-C2-C1	105.9(5)	O2-C3-C4	106.9(5)	O3-C4-C3	107.7(5)
O3-C5-C6	109.5(5)	C5-C6-C7	116.5(5)	O4-C7-C6	109.7(4)
O4-C8-C9	110.2(4)	C10-C9-C8	116.0(5)	O1-C10-C9	110.6(5)
N-C11-S	178.7(5)				

Fig. 1. ORTEP (50% thermal ellipsoids) plot for **1**.LiNCS.



ether unit only, shows that there is a plane of symmetry passing through O2-Li-O4, which effectively bisects the molecule. However, the overall structure lacks a symmetry element due to the fact that the O1-Li-N-C11 torsion angle is –143.4(9)°, while that for the O3-Li-N-C11 unit is 24.0(11)°. A significant difference from the expected opposite signs is also observed in the torsion angles for the N-Li-O2-C3 unit (105.6°) vs. the N-Li-O2-C2 (–125.1°) unit.

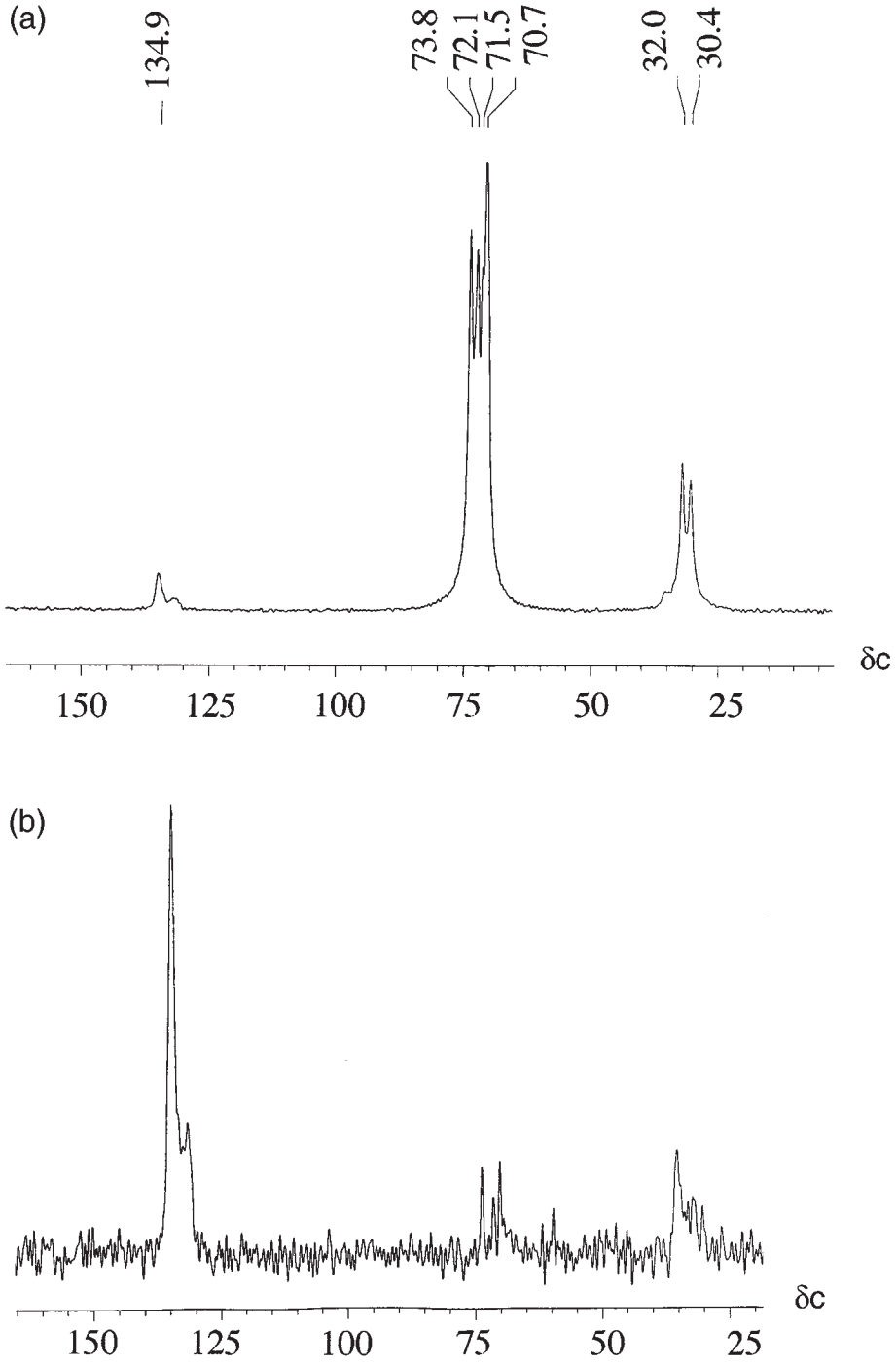
The lithium ion is coordinated by the four oxygens and the nitrogen in a distorted square-pyramidal geometry. The average Li—O bond distance of 2.023 Å is between the

Table 2. Torsion angles (°).

O1-Li-N-C11	–143.4(9)	O4-Li-N-C11	119.4(9)
O3-Li-N-C11	24.0(11)	O2-Li-N-C11	–58.4(11)
O4-Li-O1-C1	176.9(4)	O3-Li-O1-C1	–86.5(7)
N-Li-O1-C1	75.0(6)	O2-Li-O1-C1	–22.2(4)
O4-Li-O1-C10	49.7(5)	O3-Li-O1-C10	146.2(6)
N-Li-O1-C10	–52.3(6)	O2-Li-O1-C10	–149.4(4)
O1-Li-O2-C2	–10.0(4)	O4-Li-O2-C2	61.3(16)
O3-Li-O2-C2	132.4(4)	N-Li-O2-C2	–125.1(4)
O1-Li-O2-C3	–139.2(4)	O4-Li-O2-C3	–68.0(15)
O3-Li-O2-C3	3.1(4)	N-Li-O2-C3	105.6(5)
O1-Li-O3-C5	–141.3(7)	O4-Li-O3-C5	–45.1(5)
N-Li-O3-C5	55.8(5)	O2-Li-O3-C5	154.0(4)
O1-Li-O3-C4	91.3(7)	O4-Li-O3-C4	–172.4(4)
N-Li-O3-C4	–71.6(5)	O2-Li-O3-C4	26.7(4)
O1-Li-O4-C7	–175.8(4)	O3-Li-O4-C7	45.8(4)
N-Li-O4-C7	–58.8(5)	O2-Li-O4-C7	114.8(14)
O1-Li-O4-C8	–50.6(5)	O3-Li-O4-C8	171.0(3)
N-Li-O4-C8	66.4(5)	O2-Li-O4-C8	–120.0(15)
C10-O1-C1-C2	178.6(4)	Li-O1-C1-C2	49.1(6)
C3-O2-C2-C1	164.2(5)	Li-O2-C2-C1	37.9(6)
O1-C1-C2-O2	–57.6(6)	C2-O2-C3-C4	–157.6(5)
Li-O2-C3-C4	–31.8(5)	C5-O3-C4-C3	177.9(5)
Li-O3-C4-C3	–52.7(5)	O2-C3-C4-O3	56.0(6)
C4-O3-C5-C6	–177.7(5)	Li-O3-C5-C6	58.2(6)
O3-C5-C6-C7	–70.1(7)	C8-O4-C7-C6	171.8(5)
Li-O4-C7-C6	–61.5(6)	C5-C6-C7-O4	72.9(7)
C7-O4-C8-C9	–168.7(5)	Li-O4-C8-C9	63.7(6)
O4-C8-C9-C10	–69.8(7)	C1-O1-C10-C9	174.1(4)
Li-O1-C10-C9	–60.4(6)	C8-C9-C10-O1	66.4(7)
Li-N-C11-S	78.2(6)		

© 2000 NRC Canada

Fig. 2. 50.3 MHz ^{13}C CPMAS NMR spectra of **1**.LiNCS. (*a*) Normal. (*b*) Dipolar dephased.



mean value of 1.98 Å for tetrahedral complexes and 2.07 Å for pentacoordinated complexes with other macrocyclic ligands (9).

The O-C-C-O torsion angles in the complex are both within 4° of being perfectly gauche, in accordance with normal preferred complexation geometries for these units in related molecules (10–12). With respect to the overall conformation, it is of interest to compare the structure of the present complex with those found for other 14-crown-4 isomers. The crystal conformation of the uncomplexed isomeric 1,4,8,11-tetraoxacyclotetradecane has been determined at –150°C (12). A conformation having approximate twofold rotational symmetry was found. Stereochemistry in the CCCO and OCCO units was observed to be similar to that found herein, namely gauche type structures. For free 1,3,8,10-tetraoxacyclotetradecane, the crystal structure shows a rectangular centrosymmetric conformation (13).

(*ii*) ^{13}C NMR spectra

The general features of the solid state spectrum show the NCS peak at ca. 135 ppm, with the oxygenated aliphatic carbons in the 70–74 ppm range and the non-oxygenated

© 2000 NRC Canada

Table 3. Crystallographic data.

Formula	$C_{11}H_{20}LiNO_4S$
Formula weight	269.28
Temperature	213(2) K
Crystal system	monoclinic
Space group	*P*2(1)
a (Å)	9.496(3)
b (Å)	8.736(3)
c (Å)	9.676(3)
β	117.859(5)°
Volume (Å^3)	709.7(4)
Z (molecules/unit cell)	2
D_c (g/cm^3)	1.260
Crystal dimensions	0.2 × 0.2 × 0.2 mm
Radiation (λ, Å)	MoKα, 0.71073
Octants measured	*h* (–11 to 11), *k* (–11 to 10), *l* (0 to 12)
Theta range (°)	2.38 to 28.30
No. of unique reflections	2581
No. of reflections measured	3727
No. reflections with $I > 2\sigma(I)$	1441
R_1 ($I > 2\sigma(I)$)	0.0730
R_1 (all data)	0.0985
*WR*2 (all data)	0.1726
*WR*2 ($I > 2\sigma(I)$)	0.1658
Goodness of Fit	1.014
Maximum and minimum residual in final difference Fourier map (eÅ^{-3})	0.348 and –0.305

Table 4. Atomic coordinates (× 10^4) and equivalent isotropic displacement parameters (Å^2 × 10^3). *U*(eq) is defined as one third of the trace of the orthogonalized U_{ij} tensor.

	x	*y*	*z*	*U*(eq)
Li	1720(10)	8357(11)	7912(8)	32(2)
N	2265(6)	8947(6)	10136(6)	53(2)
O1	1133(4)	10073(4)	6382(4)	38(1)
O2	3905(4)	8690(4)	7973(4)	38(1)
O3	2455(4)	6162(4)	8097(4)	34(1)
O4	–573(4)	7746(4)	7110(4)	33(1)
S	4192(2)	8404(2)	13278(2)	57(1)
C1	2538(8)	10878(7)	6664(7)	48(2)
C2	3730(8)	9701(7)	6761(6)	49(2)
C3	4650(7)	7260(7)	8020(7)	44(2)
C4	4156(7)	6198(8)	8868(7)	46(2)
C5	1824(7)	5121(7)	8783(7)	46(2)
C6	45(7)	5110(7)	7867(7)	46(2)
C7	–805(7)	6526(7)	7974(7)	44(2)
C8	–1569(7)	9027(7)	7024(7)	48(2)
C9	–1594(7)	10209(7)	5841(7)	47(2)
C10	–84(8)	11070(7)	6301(7)	49(2)
C11	3049(6)	8713(6)	11437(6)	35(1)

carbons near 30 ppm. The multiplicity observed in the normal solid state spectrum is consistent with the lack of overall symmetry in **1**.LiNCS. Even though the C6 and C9 sites are relatively remote from the NCS group, there is a difference of 1.6 ppm in the chemical shift observed for these carbons (i.e., 30.4 vs. 32.0 ppm). With respect to the oxygenated carbons, one expects to see eight different resonances in the solid state spectrum. However only four of these resonances are resolved. The fact that these four lines are not of equal intensity also reflects the lack of overall symmetry in **1**.LiNCS.

The dipolar dephased spectrum shows little residual intensity for the protonated carbon resonances, which indicates that there is no substantial overall large amplitude motion in this complex. This is in contrast to some recent observations in these laboratories on the LiNCS complex of the isomeric 14-crown-4 system (1,4,8,11-tetraoxacyclotetradecane).[3]

In solution, the ^{13}C spectrum is consistent with the existence of rapid conformational averaging since only five resonances are observed (Table 5). Lowering the temperature to 200K produced no changes other than minor temperature dependent chemical shifts indicating that conformational interconversions remain fast on the NMR timescale.

With respect to assignments, one can employ the COSY, NOESY, and ^1J HETCOR experiments to obtain a partial assignment of connectivities. Specifically, one observes $^1H^1H$ COSY and NOESY connections between protons on C6 with those on C5 and C7 (and equivalently between protons on C9 with those on C8 and C10). A subsequent ^1H, ^{13}C, ^1J HETCOR experiment shows that ^{13}C resonances at 69.4 and 70.6 ppm connect to the protons on C5, C7, C8, and C10, thereby permitting distinction between these oxygenated carbons and the C1, C4 and C2, C3 sites.

Experimental

(*i*) Materials

The free crown ether **1** was synthesized via a reaction of 4-oxa-1,7-heptanediol (**A**) with diethylene glycol ditosylate. **A** was prepared by reduction of diethyl-4-oxa-heptanedioate (**B**) (15).

For the preparation of **B** the following procedure was employed. A round bottom flask was charged with 2-cyanoethyl ether (12.4 g, 0.1 mol) and 40 mL of 37% aqueous HCl. The flask was fitted with an efficient reflux condenser and the contents were heated to 80°C with stirring. The reaction quickly became exothermic, at which point heating was removed. After the boiling ceased (15 min) heating was resumed for 5 h. The solution was concentrated by rotary evaporation at 65°C and the residue was then titrated with hot acetone and filtered. After concentration by rotary evaporation at room temperature, an oil remained which fully crystallized after cooling overnight in a freezer. Recrystallization from a diethyletherpetroleum ether solvent pair yielded pure diacid in 93% yield, mp 59–60°C (reported (15) 60–61°C). ^{13}C NMR($CDCl_3$) δ_c: 175.1, 65.5, 34.2.

Esterification was accomplished by refluxing the diacid (16.5 g) for 2 h in absolute EtOH (175 mL) containing 1.6 g of concentrated H_2SO_4. The solution was then cooled and neutralized with 5% ethanolic KOH. Subsequently the mixture was poured into a separatory funnel with a suspension

[3] G.W. Buchanan, A.B. Driega, G.A. Facey, and C. Bensimon. In preparation.

© 2000 NRC Canada

Table 5. ^{13}C NMR chemical shifts (δ_c from TMS ± 0.1).

	1 ($CDCl_3$)	**1**.LiNCS ($CDCl_3$)	**1**.LiNCS(solid)
C1	(66.0)[a]	(68.2)[c]	70.7
C2	(66.5)[a]	(68.3)[c]	70.7
C3	(66.5)[a]	(68.3)[c]	70.7
C4	(66.0)[a]	(68.2)[c]	70.7
C5	(69.4)[b]	(70.9)[d]	(71.5)[e]
C6	30.0	29.2	(30.4)[f]
C7	(70.6)[b]	(72.3)[d]	(73.8)[e]
C8	(70.6)[b]	(72.3)[d]	(72.4)[e]
C9	30.0	29.2	(32.0)[f]
C10	(69.4)[b]	(70.9)[d]	(71.5)[e]
NCS		131.6	134.9

[a–f] Denotes possible assignment interchange.

containing $CHCl_3$ (125 mL) and H_2O (125 mL) and shaken. After allowing 20 min for separation, the organic layer was drawn off and the aqueous phase was extracted with $CHCl_3$ (2 × 100 mL). The combined organic extracts were concentated to a volume of ca. 100 mL by rotary evaporation, washed with saturated NaCl (100 mL), and dried over anhydrous Na_2SO_4. After filtration, solvent evaporation *in vacuo* gave the diester **B** as an oil (21.6 g). ^1H NMR (in $CDCl_3$ at 400 MHz): 1.24 ppm (6H, triplet), 2.55 ppm (4H, triplet), 3.71 ppm (4H, triplet), 4.13 ppm (4H, quartet); ^{13}C NMR ($CDCl_3$) δ_c: 171.2, 66.1, 60.2, 34.8, 13.9.

Reduction of **B** to **A** was accomplished in 90% yield in the following manner. To a cooled stirred solution of $LiAlH_4$ (4.9 g, 0.13 mol) in THF (175 mL) under an argon atmosphere, was added **B** (21.6 g, 0.1 mol) in 100 mL of THF over 90 min. The cooling was removed and the reaction mixture was stirred for an additional 45 min. Subsequently ca. 10 mL of 20% aqueous H_2SO_4 was added with stirring. Following filtration and drying over Na_2SO_4, the solvent was removed *in vacuo* at 50°C to yield 11.9 g of **A** as an oil, bp 110–115°C (0.3 Torr (1 Torr = 133.3 Pa)). Reported (16) bp 95–125°C (0.3 Torr). ^1H NMR: 1.84 ppm (4H, quintet), 3.57 ppm (4H, triplet),3.68 ppm (4H, triplet), 3.10 (2H, broad); ^{13}C NMR ($CDCl_3$) δ_c: 68.6, 60.2, 31.9.

Preparation of **1** was carried out as follows. A stirred solution of KOtBu (21.9 g, 0.02 mol) in a 3-neck flask equipped with a thermometer, condenser, and dropping funnel under nitrogen, was heated to 40°C while **A** (11.4 g, 0.085 mol) in THF (60mL) was added over 30 min. The mixture was brought to reflux and after 45 min, diethylene glycol ditosylate (17) (35.2 g., 0.085 mol) in THF (500mL) was added. A gummy precipitate was noticed which redissolved in a few hours. After a 6 day reflux, the mixture was cooled and filtered and the filtrate was concentrated *in vacuo*. The residue was titurated with hot pentane (5 × 15 mL) and from the pentane extracts was obtained 2.9 grams of an oil, judged to be ca. 75% pure by ^{13}C NMR. Purification was accomplished by vacuum distillation (0.1 mm Hg (1 mm Hg = 133.3 Pa)) in a Kugelrohr assembly with an oven temperature of 95 to 100°C. An overall yield of 12% (2.1 g of **1**) was obtained. ^1H NMR ($CDCl_3$) δ: 1.75 ppm (4H, quintet), 3.54 ppm (4H, triplet), 3.65 ppm (12H, multiplet); ^{13}C NMR ($CDCl_3$) δ_c: 70.6, 69.4, 66.5, 66.0, 30.1; MS (CI) *m/z*: 205 (M+1).

For the preparation of **1**.LiNCS, **1** (0.40g, 2.0 mmol) in 0.6 mL of ethyl acetate was added to LiNCS (0.17 g, 2.0 mmol) in hot ethyl acetate (7 mL). The solvent volume was then reduced by boiling to ca. 5 mL, with slow addition of acetone (1 mL) in order to maintain solution homogeneity. Heating was then removed and crystallization proceeded for a few hours at room temperature, followed by overnight in the freezer to give 0.26 g of colourless opaque crystals. These crystals were then redissolved in hot acetone and the solution was filtered. Slow recrystallization of the filtrate at 35 to 40°C in a loosely covered flask gave large hexagonal prisms of **1**.LiNCS, mp 235–237°C.

(*ii*) X-ray crystallographic studies and structure refinement

Suitable crystals were selected, mounted on thin glass fibres using viscous oil and cooled to the data collection temperature. Data were collected on a Bruker AX SMART 1k CCD diffractometer using 0.3° scans at 0, 90, and 180° in. Unit cell parameters were determined from 60 data frames collected at different sections of the Ewald sphere. Semi-empirical absorption corrections based on equivalent reflections were applied (18).

Unit cell parameters and systematic absences in the diffraction data are consistent with space groups $P2_1$ (No. 4) and $P2_1/m$ (No. 11). The occupancy of two and absence of inversion or a mirror plane in the molecule is consistent with the acentric option. Solution in $P2_1$ yielded chemically reasonable and computationally stable results of refinement. The structure was solved by direct methods, completed with difference Fourier syntheses and refined with full-matrix least -squares procedures based on F^2. All non-hydrogen atoms were refined with anisotropic displacement parameters and hydrogen atoms were treated as idealized contributions. All scattering factors and anomalous dispersion factors are contained in the SHEXTL 5.1 program library.

(*iii*) ^{13}C NMR spectra

Both solid and solution phase spectra were obtained using routine methods described previously (19). For the dipolar dephased ^{13}C CPMAS spectra, the ^1H decoupler was switched off for 40 μs before data acquisition. All solution NMR spectra were recorded using a Bruker AMX–400 spectrometer, while solid phase ^{13}C spectra were obtained with a Bruker ASX–200 system.

References

1. G.W. Buchanan, R.A. Kirby, J.A. Ripmeester, and C.I. Ratcliffe. Tetrahedron Lett. **28**, 4783 (1987).
2. G.W. Buchanan, C. Morat, C.I. Ratcliffe, and J.A. Ripmeester. J. Chem. Soc., Chem. Commun. 1306 (1989).
3. C.I. Ratcliffe, J.A. Ripmeester, G.W. Buchanan, and J.K. Denike. J. Am. Chem. Soc. **114**, 3294 (1992).
4. C.I. Ratcliffe, G.W. Buchanan, and J.K. Denike. J.Am. Chem. Soc. **117**, 2900 (1995).
5. G.W. Buchanan, A. Moghimi, and C.I. Ratcliffe. Can. J. Chem. **74**, 1437 (1996).
6. P.S. Belton, S.V. Tanner, K.M. Wright, M.P. Payne, M.R. Truter, and J.N. Wingfield. J. Chem. Soc. Perkin Trans. 2, 1307 (1985).

© 2000 NRC Canada

7. G.W. Buchanan, R.A. Kirby, and J.P. Charland. J. Am. Chem. Soc. **110**, 2477 (1988).
8. G.W. Buchanan. Progress in NMR spectroscopy, **34**, 327 (1999).
9. G. Shoham, W.N. Lipscomb, and U. Olsher. J. Am. Chem. Soc. **105**, 1247(1983).
10. M.J. Bovill, D.J. Chadwick, and I.O. Sutherland. J. Chem. Soc. Perkin Trans. 2, 1529 (1980).
11. A.B. Driega, G.W. Buchanan, and C. Bensimon. Can. J. Chem. **76**, 142 (1998).
12. P. Groth. Acta Chem. Scand. Ser. A, **A32**, 91 (1978).
13. W.I. Bassi, R. Scordamaglia, and L. Fiore. J. Chem. Soc. Perkin Trans. 2, 1726 (1972).
15. R.V. Christian Jr. and R.M. Hixon. J. Am. Chem. Soc. **70**, 1333 (1948).
16. Y. Liu, Y. Inoue, and T. Kahushi. Bull. Chem. Soc. Jpn. **63**, 3044 (1990).
17. M. Ouchi, Y. Inoue, Y. Liu, S. Nagamune, S. Nakamura, K. Wada, and T. Hakushi. Bull. Chem. Soc. Jpn. **63**, 1260 (1990).
18. R. Blessing. Acta Crystallogr. Sect. A: Fundam. Crystallogr. **A51**, 33 (1995).
19. G.W. Buchanan, M. Gerzain, G.A. Facey, and C. Bensimon. J. Mol. Struct. **471**, 95 (1998).

© 2000 NRC Canada

Crystal structure and ferromagnetic behavior of a *cis*-Co(II) complex with nitronyl nitroxide

Bai-Wang Sun, Qi-Hua Zhao, Dai-Zheng Liao, Zong-Hui Jiang, Shi-Ping Yan, Geng-Lin Wang, Xin-Kai Yao, and Hong-Gen Wang

Abstract: Bis(hexafluoroacetylacetonate)cobalt(II), $Co(hfac)_2$, reacted with the nitronyl nitroxide radical 2-(4-methylphenyl)-4,4,5,5-tetramethylimidazoline-1-oxyl-3-oxide, NITPhMe, to yield an octahedral adduct of formula $Co(hfac)_2(NITPhMe)_2$. The X-ray crystal structure shows that it crystallizes in the space group $P\bar{1}$, with a = 9.837(3), b = 11.618(3), c = 20.502(4) Å, α = 81.22(2), β = 87.93(2), γ = 72.24(3)°, V = 2205(1) Å^3, Z = 2. The mechanism of ferromagnetic exchange between cobalt(II) and the radical can be qualitatively understood in terms of a charge-transfer interaction (J being 25.7 cm^{-1}, the Hamiltonian is written in the form $\boldsymbol{H} = -2J(\boldsymbol{S}_{Rad1}\cdot\boldsymbol{S}_{Co} + \boldsymbol{S}_{Co}\cdot\boldsymbol{S}_{Rad2})$).

Key words: crystal structure, cobalt(II) complex, nitronyl nitroxide, magnetic property.

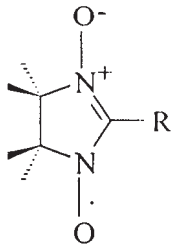
Résumé : Le bis(hexafluoroacétylacétonate) de cobalt(II), $Co(hfac)_2$, réagit avec le radical nitroxyde de nitronyle, 3-oxyde de 2-(4-méthylphényl)-4,4,5,5-tétraméthylimidazoline-1-oxyle, NITPhMe, et conduit à la formation d'un adduit octaédrique de formule $Co(hfac)_3$. La diffraction des rayons X permet de montrer que le produit cristallise dans le groupe d'espace $P\bar{1}$, avec a = 9,837(3), b = 11,618(3) et c = 20,502(4) Å, α = 81,22(2), β = 87,93(2) et γ = 72,24(3)°, V = 2205(1) Å^3 et Z = 2. D'un point de vue qualitatif, on peut comprendre le mécanisme d'échange ferromagnétique entre le cobalt(II) et le radical en fonction d'une interaction de transfert de charge pour laquelle J = 25,7 cm^{-1} et l'hamiltonien est de la forme $H = -2J(\boldsymbol{S}_{Rad1}\cdot\boldsymbol{S}_{Co} + \boldsymbol{S}_{Co}\cdot\boldsymbol{S}_{Rad2})$).

Mots clés : structure cristalline, complex du cobalt(II), nitroxyde de nitronyle, propriété magnétique.

[Traduit par la Rédaction]

Introduction

The nitronyl nitroxides, NITR = 2-*R*-4,4,5,5-tetramethylimidazoline-1-oxyl 3-oxide, with R = methyl, ethyl and phenyl, etc., have proven to be extremely versatile magnetic ligands toward metal ions (1–4). The general formula of NITR is



NITR

Received June 16, 1999.

B.-W. Sun, D.-Z. Liao, Z.-H. Jiang,[1] S.-P. Yan, and G.-L. Wang. Department of Chemistry, Nankai University, Tianjin, 300071, China.
Q.-H. Zhao. State Key Laboratory of Coordination Chemistry, Nanjing University, Nanjing Jiangsu, 210093 China.
X.-K. Yao and H.-G. Wang. Centre Laboratory of Nankai University, 300071, China.

[1]Author to whom correspondence may be addressed. Fax: +86-22-23502779. e-mail: coord@sun.nankai.edu.cn

Up to now, a number of nitronyl nitroxides compounds including copper(II) and manganese (II) have been synthesized, such as high-spin clusters (5), ferromagnetic chains (6), and compounds showing spontaneous magnetization (7). The mechanism of magnetic interaction in those compounds have been well discussed in recent years (1, 2, 8, 9). Very few cobalt – nitronyl nitroxides complexes have been reported, and relatively little work has been devoted to the study of the relationship between the structure and the magnetic properties in cobalt(II)–radical compounds(10–12).

In this contribution, we report a new adduct of formula $Co(hfac)_2(NITPhMe)_2$ (hfac = hexafluoroacetylacetonate, NITPhMe = 2-(4-methylphenyl)-4,4,5,5-tetramethylimidazoline-1-oxyl-3-oxide) which shows a moderate ferromagnetic coupling, J being 25.7 cm^{-1} (the Hamiltonian is written in the form $\boldsymbol{H} = -2J(\boldsymbol{S}_{Rad1}\cdot\boldsymbol{S}_{Co} + \boldsymbol{S}_{Co}\cdot\boldsymbol{S}_{Rad2})$). We wish to report here the crystal structure of this compound and the discussion of the subtle mechanism of exchange between cobalt(II) and nitroxide.

So far, there are three types of ferromagnetic interaction between metal and radical when oxygen of radical bound to metal have been reported. The first type is an axially coordinated nitroxide–copper compound (13): two magnetic orbitals, π^* of the radical and $dx^2 - y^2$ of copper(II), are orthogonal to each other, thus resulting in weak ferromagnetic interaction between copper and the radical. The second type is in a gadolinium(III)–radical compound (14): a fraction of π electron density in the radical transfers into the empty 6*s* orbital in the Gd(III) ion, thus leading to weak ferromagnetic coupling. The mechanism of ferromagnetic exchange reported

 © 2000 NRC Canada

in this paper belongs to a third type of ferromagnetic interaction pathway by MLCT charge transfer in metal–radical compounds (15).

Experimental

Synthesis

H_2hfac was purchased from Aldrich. Co(hfac)$_2$2H_2O (10) and NITPhMe radical (16) were prepared according to established procedure.

0.10 mmol (50.9 mg) of Co(hfac)$_2$2H_2O was dissolved in 20 mL of hot dry *n*-heptane, then 0.22 mmol (54.4 mg) of NITPhMe radical was added, and the solution was stirred for 10 min and filtered. After 6 h, dark green well-developed crystals were collected. The compound analyzed satisfactorily for Co(hfac)$_2$(NITPhMe)$_2$. Mp: 130–132 °C. Selected spectroscopic data: UV (nm): 375 ($\pi\rightarrow\pi^*$, ONCNO), 263 ($\pi\rightarrow\pi^*$, benzene), and 560 ($n\rightarrow\pi^*$, ONCNO). IR (KBr, cm^{-1}): 1650($\nu_{C\cdots O}$), 1466($\nu_{C\cdots O}$), and 1375($\nu_{N\text{-}O}$). Anal. calcd. for $C_{38}H_{40}N_4O_8F_{12}Co$: C 47.17, H 4.17, N 5.79, Co 6.09%; found: C 47.34, H 4.03, N 5.44, Co 6.32%.

Crystallographic data collection and structure determination

The structure was solved by direct methods using the program MULTAN. The Co-atom position was located in the initial *E*-maps. The other non-H-atoms were determined with successive difference-Fourier syntheses. The main feature of the present structure lay in the disorder and (or) thermal motion in the CF_3 groups. Nevertheless, it did not seriously affect the precision of the structural results, and the final refinement by full-matrix least-squares with anisotropic thermal parameters for non-H-atoms was converged with unweighted and weighted agreement factors of 0.070 and 0.071. The highest peak on the final difference-Fourier map was 0.45 e/Å^3. All data calculations were performed using the SDP-PLUS program system. Crystal data are reported in Table 1.

Table 1. Crystal data and parameters of data collection for Co(hfac)$_2$(NITPhMe)$_2$.

Formula	$C_{38}H_{42}N_4O_8F_{12}Co$
Formula weight	969.69
Crystal system	Triclinic
Space group	$P\bar{1}$
a (Å)	9.837(3)
b (Å)	11.618(3)
c (Å)	20.502(4)
α (°)	81.22(2)
β (°)	87.93(2)
γ (°)	72.24(3)
V (Å^3)	2205(1)
Z	2
D_c (Mg m^{-3})	1.46
Crystal dimensions (mm)	0.2 × 0.3 × 0.4
Temperature (K)	299 ± 1
Radiation (wavelength (Å))	Mo K_α (0.71073)
Monochromator	Graphite
Diffractometer	ENRAF–NONIUS CAD4
Scan method	$\omega - 2\theta$
Scan width (°)	$2 \le \theta \le 23$
Programs used	SDP-PLUS
F(000)	994
Measured reflection	6263
Independent reflections	5615
Observed reflections	2642 ($I \ge 3\sigma(I)$)
R^a	0.070
$R_w{}^b$	0.071
R^a (all data)	0.119
$R_w{}^b$ (all data)	0.118

$^aR = \Sigma||Fo| - |Fc|| / \Sigma |Fo|$.

$^bR_w = [\Sigma w(|Fo| - |Fc|)^2/\Sigma wFo^2]^{1/2}$, $w = 1$.

Physical measurements

Elemental analyses for C, H, and N were performed with a Perkin–Elmer Model 240 elemental analyzer. Metal content was determined by EDTA titration. IR spectra were recorded on a Shimadzu Model 408 IR spectrophotometer, using KBr pellets and the electronic spectra (in *n*-heptane) were measured on a Hitachi-240 spectrophotometer. Variable temperature magnetic susceptibilities were carried out at a field strength of 1.0 T with a vibrating sample magnetometer, Model CF-1 (sensitivity m = 10^{-4}emu). This equipment was built jointly by the Institute of Physics, Chinese Academy of Sciences, and the Laboratory of Louis-Neel CNRS, France. Diamagnetic corrections were made with Pascal's constants for all the constituent atoms. ESR spectra were measured with a JES-FEIXG ESR apparatus using the X-band.

Results and discussion

ESR spectra

The X-band powder ESR spectra at room temperature for the complex shows a broad band at the center of g = 2.1. It is clear that this feature reflects the exchange coupling between Co(II) and the radical. According to Kambe's approach (17), coupling the three spins S_{Rad1}–S_{Cot}–S_{Rad2}, $S_{Rad1} = S_{Rad2} = 1/2$ and $S_{Co} = 3/2$, yields one sextet, two quartets, and one doublet state. On the basis of Boltzmann's distribution, four states are all populated at room temperature. Thus, the broad ESR signal may be ascribed to the complex in these states.

Description of the structure

The cobalt atom is bound to two chelating hfac ligands and two nitroxides in a *cis*-octahedral configuration. A view of the molecular structure is given in Fig. 1. The final atomic positional parameters are listed in Table 2. Selected bond distances and angles are given in Table 3.

Three oxygen atoms of hfac (O_1, O_2, O_3) and one oxygen atom of the radical (O_6) form the equatorial plane, the M—O bond lengths being 2.071(6), 2.033(8), 2.046(7), and 2.058(6) Å, respectively. Another oxygen atom of hfac (O_4) and one oxygen atom from the second radical (O_5) occupy two axial positions, and the bond lengths are 2.073(7) and 2.107(8) Å, respectively. All these distances are typical for a cobalt(II) – nitroxide compound (10). The Co–O–N angles, which are relevant to the mechanism of exchange between metal and nitroxides, are 128.2(6) and 125.2(6)°. The

© 2000 NRC Canada

Fig. 1. ORTEP view of $Co(hfac)_2(NITPhMe)_2$ with the atom numbering scheme (ellipsoids at 30% probability level).

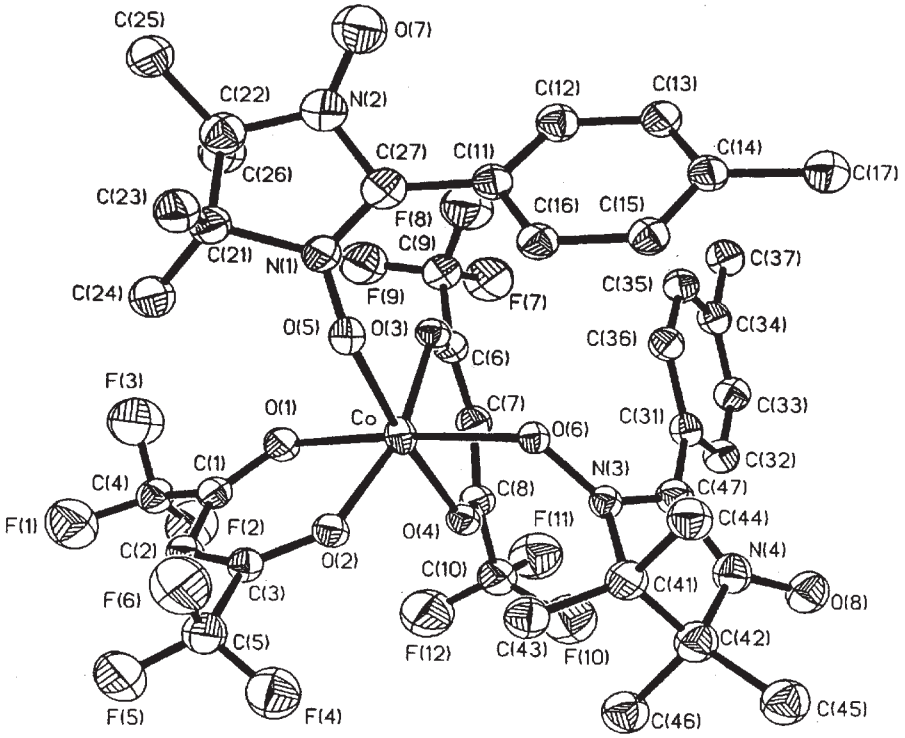
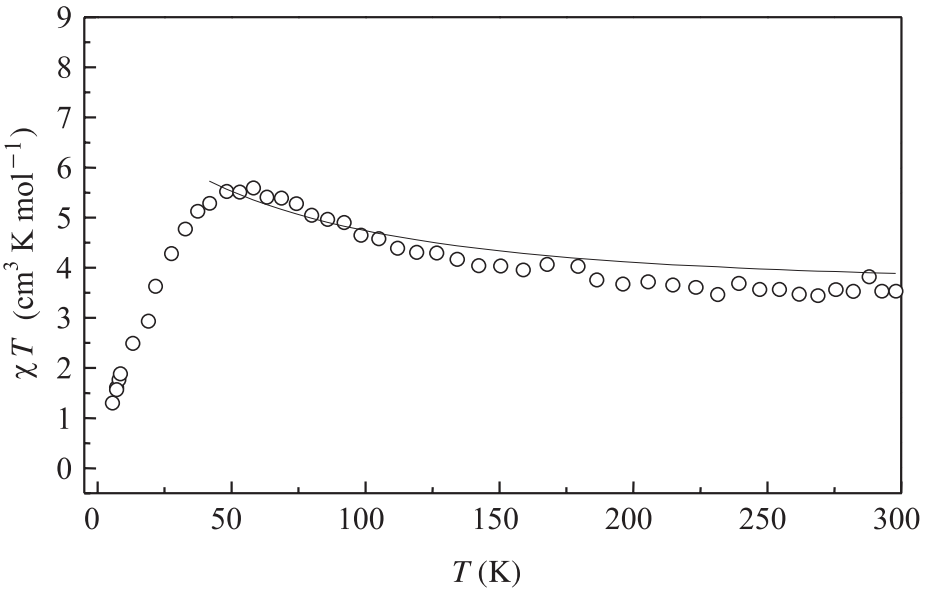


Fig. 2. Variable temperature magnetic susceptibility for $Co(hfac)_2(NITPhMe)_2$ in the form χT (cm^3 K mol^{-1}) vs. T (K). o: experimental data, _____: calculated curves.



ONCNO planes of two nitroxides make angles of 140.8(0.4) and 63.6(0.3)° with the equatorial plan, respectively. The phenyl rings of the two radicals make angles of 29.4(0.6) and 153.8(0.4)° with the planes of their radical five-member rings.

No significant intermolecular contacts are observed.

Magnetic Properties

In the case of the present complex, the cobalt(II) ion has a d^7 electron configuration with a distorted octahedral field and two unpaired electrons in d_{x2-y2} and d_{z2}, and one unpaired electron resides in the degenerate orbital (d_{xy}, d_{yz}, and d_{xz}). Therefore, at least one of them must have nonzero overlap with the radical π* orbital, and the coupling is expected to be an antiferromagnetic interaction according to the orthogonality of the magnetic orbital. But the experimental data of the title complex indicates a ferromagnetic interaction between cobalt(II) and the radical. Figure 2 shows the temperature dependence of the magnetic susceptibility of $Co(hfac)_2(NITPhMe)_2$ in the form χT vs. T. The room-temperature value of χT, 3.54 cm^3 K mol^{-1}, is very close to the value (3.45 cm^3 K mol^{-1} for g_{Co} = 2.4, g_{Rad} = 2.0) expected for the compound in the absence of exchange.

© 2000 NRC Canada

Table 2. Positional parameters and *B*(eq) for $Co(hfac)_2(NITPhMe)_2$[a].

Atom	*x*	*y*	*z*	*B*eq (Å^2)
Co	0.6125(2)	0.1803(1)	0.79175(8)	4.05(3)
F(1)	0.285(1)	0.6073(8)	0.8537(5)	12.4(3)
F(2)	0.1841(8)	0.4873(8)	0.8347(8)	17.5(5)
F(3)	0.278(1)	0.5773(9)	0.7655(6)	15.5(4)
F(4)	0.752(1)	0.2086(7)	1.0031(4)	12.3(3)
F(5)	0.667(1)	0.3968(7)	0.9963(4)	11.3(3)
F(6)	0.8441(9)	0.321(1)	0.9445(5)	14.2(3)
F(7)	0.2539(9)	0.1983(9)	0.6008(4)	12.6(3)
F(8)	0.4579(9)	0.212(1)	0.5761(4)	12.5(4)
F(9)	0.301(1)	0.3543(8)	0.6095(4)	11.4(3)
F(10)	0.276(2)	0.018(2)	0.9001(9)	13.3(6)
F(10′	0.289(2)	–0.027(1)	0.8792(9)	10.1(5)
F(11)	0.1438(8)	0.048(1)	0.8140(5)	17.8(3)
F(12)	0.159(1)	0.172(1)	0.8710(6)	16.8(4)
O(1)	0.4545(8)	0.3463(6)	0.7899(4)	5.5(2)
O(2)	0.6786(7)	0.2139(6)	0.8778(3)	4.5(2)
O(3)	0.5355(7)	0.1923(6)	0.6988(3)	4.7(2)
O(4)	0.4556(7)	0.1064(6)	0.8318(4)	4.7(2)
O(5)	0.7828(7)	0.2395(6)	0.7497(4)	5.0(2)
O(6)	0.7543(6)	0.0068(5)	0.8001(4)	4.3(2)
O(7)	0.861(1)	0.3164(9)	0.5272(5)	12.9(4)
O(8)	0.6281(9)	–0.3419(7)	0.8714(5)	8.3(3)
N(1)	0.7893(9)	0.2984(8)	0.6915(5)	5.4(3)
N(2)	0.820(1)	0.3346(9)	0.5857(6)	8.1(4)
N(3)	0.7374(8)	–0.0885(7)	0.8375(4)	4.0(2)
N(4)	0.6768(9)	–0.2544(8)	0.8721(5)	5.7(3)
C(1)	0.431(1)	0.4157(9)	0.8322(6)	4.8(3)
C(2)	0.508(1)	0.408(1)	0.8903(6)	5.2(3)
C(3)	0.632(1)	0.3082(9)	0.9031(6)	5.0(3)
C(4)	0.293(1)	0.515(1)	0.8226(8)	7.6(4)
C(5)	0.723(1)	0.309(1)	0.9625(7)	7.2(4)
C(6)	0.410(1)	0.187(1)	0.6878(6)	5.6(3)
C(7)	0.313(1)	0.151(1)	0.7340(6)	5.4(3)
C(8)	0.345(1)	0.114(1)	0.8007(6)	5.2(3)

Table 2 (*concluded*).

Atom	*x*	*y*	*z*	*B*eq (Å^2)
C(9)	0.356(1)	0.235(1)	0.6178(6)	6.8(4)
C(10)	0.233(1)	0.078(1)	0.8454(8)	8.0(4)
C(11)	0.884(1)	0.1111(9)	0.6340(6)	5.6(3)
C(12)	0.866(1)	0.064(1)	0.5765(7)	7.3(4)
C(13)	0.924(1)	–0.059(1)	0.5730(7)	6.5(4)
C(14)	1.000(1)	–0.139(1)	0.6275(6)	6.1(3)
C(15)	1.018(1)	–0.093(1)	0.6855(6)	5.8(3)
C(16)	0.960(1)	0.033(1)	0.6904(6)	5.4(3)
C(17)	1.065(1)	–0.275(1)	0.6254(7)	8.0(4)
C(21)	0.781(1)	0.431(1)	0.6795(7)	6.6(4)
C(22)	0.754(2)	0.460(1)	0.6026(7)	8.1(4)
C(23)	0.933(1)	0.430(1)	0.6994(8)	8.2(4)
C(24)	0.665(2)	0.504(1)	0.7214(8)	9.1(5)
C(25)	0.825(2)	0.549(1)	0.5655(9)	11.1(5)
C(26)	0.592(2)	0.497(2)	0.587(1)	12.4(6)
C(27)	0.830(1)	0.240(1)	0.6407(6)	8.3(4)
C(31)	0.5962(9)	–0.1477(9)	0.7526(5)	4.6(3)
C(32)	0.473(1)	–0.187(1)	0.7548(6)	5.5(3)
C(33)	0.405(1)	–0.178(1)	0.6950(6)	6.0(4)
C(34)	0.460(1)	–0.133(1)	0.6388(6)	5.8(3)
C(35)	0.579(1)	–0.095(1)	0.6367(6)	6.3(3)
C(36)	0.649(1)	–0.101(1)	0.6950(6)	6.1(3)
C(37)	0.383(1)	–0.119(1)	0.5707(7)	8.1(4)
C(41)	0.822(1)	–0.1427(9)	0.9011(6)	5.7(3)
C(42)	0.746(1)	–0.235(1)	0.9313(7)	7.1(4)
C(43)	0.846(1)	–0.051(1)	0.9376(7)	7.8(4)
C(44)	0.978(1)	–0.217(1)	0.8744(8)	8.7(5)
C(45)	0.824(2)	–0.352(1)	0.9721(8)	10.5(5)
C(46)	0.612(2)	–0.162(2)	0.9726(8)	11.3(6)
C(47)	0.665(1)	–0.1608(8)	0.8180(5)	6.6(3)

[a]Anisotropically refined atoms are given in the form of the isotropic equivalent displacement parameter defined as: *B*eq = (4/3) × [$a^2 \times \beta(1,1) + b^2 \times \beta(2,2) + c^2 \times \beta(3,3) + ab(\cos\gamma) \times \beta(1,2) + ac(\cos\beta) \times \beta(1,3) + bc(\cos\alpha) \times \beta(2,3)$]. Note: The multiplicities of atoms F(10) and F(10′ are 0.5, respectively. The multiplicities of the others are 1.

χT increases as temperature decreases, reaching a rounded maximum at about 60 K, corresponding to χT = 5.6 cm^3 K mol^{-1}. Below 60 K, χT decreases, reaching the value of 1.3 cm^3 K mol^{-1} at 4.2 K.

Since the magnetic behavior cannot be interpreted by the orthogonality of the magnetic orbital, it is necessary to consider that some other exchange interaction is operative in the title complex. Following Miller et al. (15, 18) and McConnell (19), we assumed a charge-transfer (CT) interaction from one of the 3*d* orbitals of the cobalt(II) ion to the SOMO (singly occupied molecular orbital) of the NITPhMe. Cobalt(II) ion with $t_{2g}^5 e_g^2$ has three single electrons in partially occupied molecular orbitals (POMO), while each radical has one electron in a nondegenerate π^* POMO. In the absence of spin interactions there are four possible ground states for this $s^1_{(Rad)}$–$d^7_{(Co(II))}$–$s^1_{(Rad)}$ spin system. The ferromagnetically coupled, GS_F, and antiferromagnetically coupled, GS_{AF}, states exist at equal energy (19). Spin interactions among the metal and radicals can stabilize either ferro- or antiferromagnetic coupling, i.e., lower either GS_F or GS_{AF}. The GS lowered has the greatest admixing with the lowest energy virtual charge transfer excited state. In the title complex, both ferromagnetic and antiferromagnetic CT excited states are possible (Fig. 3). However the splitting energy (Δ) maybe smaller than the electronic repulsion in the paired electrons (P), due to the strong negative contribution from π of hfac for the title complex (Δ < P) (20). From Hund's rule, the metal ion should prefer a high spin ground state. This means that a transfer will leave a higher spin multiplicity in cobalt(III), namely, the ferromagnetic CT excited state (S = 2) is energetically advantageous. The admixture of the ferromagnetic CT excited state results in a stabilization of the ferromagnetic interaction between Co(II) and radical.

To understand quantitatively the magnitudes of spin-exchange interaction between Co(II) and the radical, a magnetic analysis was performed with the susceptibility equation based on Heisenberg spin-exchange operator: $\boldsymbol{H} = -2J(\boldsymbol{S}_{Rad1}\boldsymbol{S}_{Co} + \boldsymbol{S}_{Rad2}\boldsymbol{S}_{Co}) - 2J'\boldsymbol{S}_{Rad1}\boldsymbol{S}_{Rad2}$ ($S_{Rad1} = S_{Rad2} = 1/2$ and $S_{Co} = 3/2$), where J is the interaction constant between Co(II) and the radical, and J' is the interaction constant between two radicals in the complex.

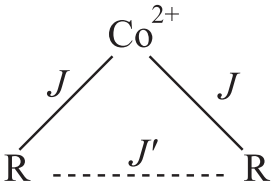
© 2000 NRC Canada

Table 3. Selected bond distances (Å) and angles (°) of $Co(hfac)_2(NITPhMe)_2$.

Atom 1	Atom 2	Distance	Atom 1	Atom 2	Distance
Co	O(1)	2.071(6)	O(1)	C(1)	1.24(1)
Co	O(2)	2.033(8)	O(2)	C(3)	1.24(1)
Co	O(3)	2.046(7)	O(3)	C(6)	1.29(1)
Co	O(4)	2.073(7)	O(7)	N(2)	1.28(2)
Co	O(5)	2.107(8)	O(8)	N(4)	1.25(1)
Co	O(6)	2.058(6)	O(4)	C(8)	1.25(1)
O(6)	N(3)	1.30(2)	O(5)	N(1)	1.30(1)

Atom 1	Atom 2	Atom 3	Angle	Atom 1	Atom 2	Atom 3	Angle
O(1)	Co	O(2)	86.1(3)	O(5)	Co	O(6)	85.9(3)
O(1)	Co	O(3)	82.5(3)	O(5)	N(1)	C(21)	123(1)
O(1)	Co	O(4)	84.5(3)	O(5)	N(1)	C(27)	121.0(9)
O(1)	Co	O(5)	100.5(3)	O(6)	N(3)	C(47)	123.5(8)
O(1)	Co	O(6)	173.5(3)	O(6)	N(3)	C(41)	121.5(9)
O(2)	Co	O(3)	165.8(3)	O(8)	N(4)	C(42)	123.6(9)
O(2)	Co	O(4)	96.9(3)	O(8)	N(4)	C(47)	123(2)
O(2)	Co	O(5)	84.7(4)	Co	O(1)	C(1)	127.5(6)
O(2)	Co	O(6)	93.4(3)	Co	O(2)	C(3)	127.1(6)
O(3)	Co	O(4)	90.5(3)	Co	O(3)	C(6)	122.7(7)
O(3)	Co	O(5)	89.0(4)	Co	O(4)	C(8)	123.1(7)
O(3)	Co	O(6)	98.9(3)	Co	O(5)	N(1)	128.2(6)
O(4)	Co	O(5)	174.8(3)	Co	O(6)	N(3)	125.2(6)
O(4)	Co	O(6)	89.2(3)	O(7)	N(2)	C(27)	125(2)

Scheme 1.

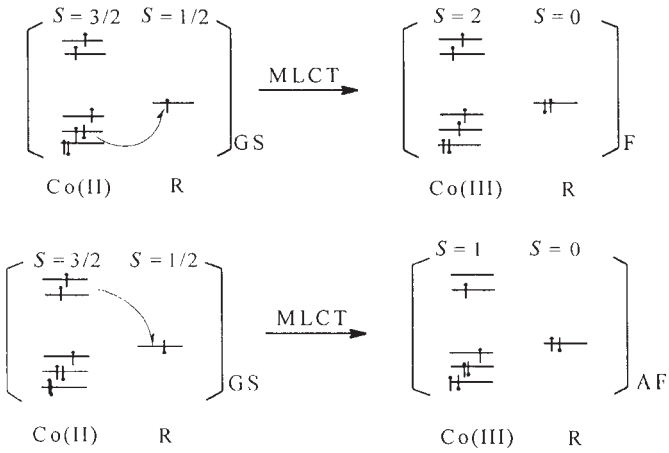


If the effect of J' is neglected and equal g values for Co(II) and the radical are used, the magnetic susceptibility data above 60 K are well simulated by eq. [2] based on the Heisenberg model (21)

$$[2] \qquad \chi M = \frac{Ng^2\beta^2}{4k(T-\theta)} \left\{ \left[\frac{10 + \exp(-5J/kT) + 10\exp(-2J/kT) + 35\exp(3J/kT)}{2 + \exp(-5J/kT) + 2\exp(-2J/kT) + 3\exp(3J/kT)} \right] (1-\rho) + 7\rho \right\} + N\alpha$$

where χ denotes the susceptibility per molar complex, θ is the intermolecular interaction, N is Avogadro's constant, β is the Bohr magneton, k is the Boltzmann constant, $N\alpha$ is the temperature-independent paramagnetism of the Co^{2+} ion. In addition, the data were corrected for the presence of a small proportion, ρ, of uncoupled spin center. We estimated the J value by taking data points above 60 K and fitted those values by using eq. [2] to obtain J = 25.7 cm^{-1} and g = 2.2, θ = –2 cm^{-1} and ρ = 0.002; F, defined here as $[(\chi T)_{obsd} - (\chi T)_{calcd}]^2/(\chi T)^2_{obsd}$, is then equal to 2×10^{-3}. The low-temperature magnetic behavior is difficult to analyze, because the Co(II) ion has unquenched orbital momentum. Since it ignores the effect of "spin-orbit" coupling within the $^4T_{1g}(F)$ ground term, the isotropic model is not strictly applicable for the estimation of exchange coupling, J, to the present complex. The $^4T_{1g}$ ground term for a Co(II) ion in an octahedral field yields $^4A_2$ + $^4B_1$ + $^4B_2$ terms in C_{2v} symmetry (idealized) each of them being split into two Kambe's doublets by spin-orbit coupling. Thus it is impossible to interpret the magnetic behavior of the

Fig. 3. Electronic structures of cobalt ion and radical.



© 2000 NRC Canada

complex below 60 K, where spin-orbit coupling plays a dominant role.

Acknowledgments

We wish to acknowledge grants from the National Natural Science Foundation of China (no. 29871019, no. 29631040) and the Research Fund for the Doctoral Program of Higher Education.

References

1. A. Caneschi, D. Gatteschi, R. Sessoli, and P. Rey. Acc. Chem. Res. **2**, 392 (1989).
2. A. Caneschi, D. Gatteschi, and P. Rey. Prog. Inorg. Chem. **39**, 331 (1991).
3. Z.H. Jiang, B.W. Sun, D.Z. Liao, G.L. Wang, F. Dahan, and J.P.Tuchagues. Inorg. Chim. Acta, **279**, 69 (1998).
4. Z.H. Jiang, B.W. Sun, D.Z. Liao, G.L. Wang, F. Dahan, and J.P. Tuchagues. Inorg. Chim. Acta, **279**, 76 (1998).
5. A. Caneschi, D. Gatteschi, J. Laugier, P. Rey, R. Sessoli, and C. Zanchini. J. Am. Chem. Soc. **110**, 2795 (1988).
6. C. Cabello, A. Caneschi, R.L. Carlin, D. Gatteschi, P. Rey, and R. Sessoli. Inorg. Chem. **29**, 2582 (1990).
7. A. Caneschi, D. Gatteschi, J.P. Renard, P. Rey, and R. Sessoli. Inorg. Chem. **28**, 2940 (1989).
8. F.L. Panthou, D. Luneau, R. Musin, L. Öhrström, A. Grand, P. Turek, and P. Rey. Inorg. Chem. **35**, 3484 (1996).
9. H. Oshio, T. Watanabe, A. Ohto, T. Ito, T. Ikoma, and S.T. Kubota. Inorg. Chem. **36,** 3014 (1997).
10. A. Caneschi, D. Gatteschi, J. Laugier, P. Rey, and R. Sessoli. Inorg. Chem. **27**, 1553 (1988).
11. A. Yamaguchi, T. Okuno, and K. Awaga. Bull. Chem. Soc. Jpn. **69**, 875 (1996).
12. C.F. Huang and H.H. Wei. J. Chin. Chem. Soc. (Taipei), **44**, 439 (1997).
13. A. Caneschi, D. Gatteschi, A. Grand, J. Laugier, L. Pardi, and P. Rey. Inorg. Chem. **27**, 1031 (1988).
14. A. Benelli, A. Caneschi, D. Gatteschi, L. Pardi, P. Rey, D.P. Shum, and R.L. Carlin. Inorg. Chem. **28**, 272 (1989).
15. J.S. Miller, A.J. Epstein, and W.M. Reiff. Acc. Chem. Res. **21**, 114 (1988).
16. E.F. Ullman, L. Call, and J.M. Osiecki. J. Org. Chem. **35**, 3623 (1970).
17. K. Kambe. J. Phys. Soc. Jpn. **5**, 48 (1950).
18. H.M. McConnell. Proc. Robert A. Welch Found. Conf. Chem. Res. **11**, 144 (1967).
19. J.S. Miller and A.J. Epstein. J. Am. Chem. Soc. **109**, 3850 (1987).
20. H.L. Schläfer and G. Gliemann. Basic principles of ligand field theory. Wiley–Interscience, London. 1969.
21. E. Sinn. Coord. Chem. Rev. **5**, 313 (1970).

© 2000 NRC Canada

Comparative electronic analysis between hydrogen transfers in the CH_4/CH_3^+, $CH_4/CH_3^\bullet$, and CH_4/CH_3^- systems: on the electronic nature of the hydrogen (H^-, $H^\bullet$, H^+) being transferred. II. Analysis of electron-pair interactions from intracule and extracule densities

Xavier Fradera, Miquel Duran, and Jordi Mestres

Abstract: The nature of the hydrogen transferred in the CH_3/CH_4^+, $CH_3/CH_4^\cdot$, and CH_3/CH_4^- systems is investigated by analyzing the topology of the contracted intracule and extracule electron-pair densities and their respective Laplacians. The CH_3/CH_4^+, $CH_3/CH_4^\cdot$, and CH_3/CH_4^- systems are taken as simple models for the study of hydride (H^-), hydrogen ($H^\cdot$), and proton (H^+) transfer reactions, respectively, under a constrained C—C distance. The study is focused on the comparison of the intracule and extracule densities at the intermediate structures for the three H-transfer reactions, complementing a previous investigation of the same model reactions based on the analysis of one-electron densities. The results obtained by analyzing the contracted electron-pair densities are consistent with those obtained from the analysis of one-electron densities. The electronic nature of the H atom being transferred in the three systems can be differentiated by the topologies of the corresponding intracule and extracule densities. However, the analysis underlies also the difficulties to interpretation of the topologies of contracted electron-pair densities, as different electron–electron interactions may contribute to the same point in the intracule or extracule spaces. In particular, for the systems studied, the contribution of the electron–electron interaction associated to the probability of having two electrons on the H being transferred is not reflected separately neither in the intracule nor in the extracule distributions. Nevertheless, the nature of the H being transferred can still be studied by comparing the importance of the electron–electron interactions associated to the probability of having one electron in C and one in the transferring H. The effects of inclusion of electron correlation are also discussed by means of (HF-CISD//HF) intracule and extracule density difference maps.

Key words: hydrogen transfer, electron-pair density, intracule density, extracule density, topological density analyisis.

Résumé : En se basant sur une analyse de la topologie des densités des paires d'électrons intracule et extracule contractées et de leurs laplaciens respectifs, on a étudié la nature de l'hydrogène qui est transféré dans les systèmes CH_3/CH_4^+, CH_3/CH_4^- et $CH_3/CH_4^\cdot$. On a considéré les systèmes CH_3/CH_4^+, CH_3/CH_4^- et $CH_3/CH_4^\cdot$ comme des modèles simples pour l'étude des réactions de transfert respectivement d'hydrure (H^-), d'hydrogène ($H^\cdot$) et de proton (H^+) dans des conditions où la distance C—C est restreinte. On a focalisé cette étude sur la comparaison des densités intracule et extracule au niveau des structures intermédiaires pour les trois réactions de transfert d'hydrogène; il s'agit donc d'un complément à l'étude antérieure des réactions du même modèle sur la base d'une analyse de densités à un électron. Les résultats obtenus sur la base d'une analyse des densités des paires d'électrons contractées sont en accord avec ceux obtenus sur la base d'une analyse de densités à un électron. Il est possible de distinguer la nature électronique de l'électron transféré dans les trois systèmes à partir des topologies des densités intracule et extracule correspondantes. Toutefois, l'analyse met aussi en relief les difficultés d'interpréter les topologies des densités de paires d'électrons contractées puisque différentes interactions électron–électron peuvent contribuer au même point des espèces intracule ou extracule. Dans les systèmes étudiés, on note en particulier que la contribution de l'interaction électron–électron associée à la probabilité de transfert de deux électrons d'un H n'est pas reflétée séparément ni dans les distributions ni intracule ni extracule. Toutefois, la nature du H qui est transféré peut quand même être étudiée en comparant l'importance des interactions électron–électron associées à la probabilité d'avoir un électron du C et de l'hydrogène qui est transféré. On discute aussi des effets d'inclusion de la corrélation d'électron à l'aide de cartes de

Received November 8, 1999.

X. Fradera and M. Duran.[1] Institute of Computational Chemistry, University of Girona, Girona, Catalonia, Spain.
J. Mestres.[1] Molecular Design & Informatics, N.V. Organon, 5340 BH Oss, The Netherlands.

[1]Author to whom correspondence may be addressed. (MD) Telephone: +34 972 418364. Fax: +34 972 418356. e-mail: quel@stark.udg.es. (JM) Telephone: +31 412 661456. Fax: +31 412 662539. e-mail: j.mestres@organon.oss.akzonobel.nl

 © 2000 NRC Canada

différences de densité intracule et extracule (HF-CISD//HF).

Mots clés : transfert d'hydrogène, densité de paires d'électrons, densité intracule, densité extracule, analyse topologique de la densité.

[Traduit par la Rédaction]

Introduction

Hydrogen transfers are one of the most usual reactions in biochemistry. From a formal point of view, these processes have been usually classified as proton, hydrogen, and hydride transfers. However, the particular electronic nature of the hydrogen being transferred has often been a matter of controversy. Some studies have analyzed the electronic characteristics associated to different types of hydrogen transfer. In a pioneering work, Swain et al. (1) established the basic differences between the transition states of hydride and proton transfer reactions in terms of bonding and electron charge density. Williams et al. (2), using qualitative molecular orbital theory, discussed the change in orbital energy when modifying the C—C distance and the C-H-C angle for hydride and proton transfers in model three-center C-H-C systems. Later, Pain and Williams (3) performed a theoretical comparison of primary deuterium kinetic isotope effects between hydride and proton transfers in the $HNCH_2/HCNH^+$ and $HNCH_2/HCNH^-$ systems.

The CH_4/CH_3^+, $CH_4/CH_3^{\cdot}$, and CH_4/CH_3^- systems can be taken as simple models for the formal transfer of a hydride (H^-), a hydrogen ($H^{\cdot}$), or a proton (H^+) between two carbon atoms:

[1] $$CH_4 + CH_3^+ \rightarrow [CH_3\text{-}H\text{-}CH_3]^+ \rightarrow CH_3^+ + CH_4$$

[2] $$CH_4 + CH_3^{\cdot} \rightarrow [CH_3\text{-}H\text{-}CH_3]^{\cdot} \rightarrow CH_3^{\cdot} + CH_4$$

[3] $$CH_4 + CH_3^- \rightarrow [CH_3\text{-}H\text{-}CH_3]^- \rightarrow CH_3^- + CH_4$$

Reaction [1] consists of the transfer of an H^- between two CH_3^+ fragments, through a $[CH_3\text{-}H\text{-}CH_3]^+$ intermediate structure. Accordingly, reaction [2] consists of the transfer of a $H^{\cdot}$ between two $CH_3^{\cdot}$ fragments through a $[CH_3\text{-}H\text{-}CH_3]^{\cdot}$ intermediate structure. Finally, reaction [3] illustrates the transfer of a H^+ between two CH_3^- fragments through a $[CH_3\text{-}H\text{-}CH_3]^-$ intermediate structure.

Several studies have considered the H^+ transfer between CH_4 and CH_3^- from a theoretical point of view (4–6). The transition state in this system is characterized by a symmetric linear structure, with a distance of ca. 2.9 Å between the two carbons involved in the proton transfer. The formal $H^{\cdot}$ transfer in the $CH_4/CH_3^{\cdot}$ system has also been studied both theoretically (7–12) and experimentally (13). The transition state in this system is also characterized by a symmetric linear structure, with a C—C distance of ca. 2.9 Å. However, for the hydride transfer between CH_4 and CH_3^+, the structure having the H^- midway between the two CH_3^+ fragments is not a transition state, but a minimum in the potential energy surface (14). The study of the hydride transfer in this system can be performed by constraining the potential energy surface to a C—C distance larger than ca. 2.4 Å (depending on the level of theory employed) found for the minimum energy structure (14).

Recently, we carried out a comparative study of the hydrogen transfers taking place in the CH_4/CH_3^+, $CH_4/CH_3^{\cdot}$, and CH_4/CH_3^- systems (15). For all cases, the C—C distance was frozen at 3.20 Å (6.05 au) in order to allow for straightforward comparison of the electronic characteristics of the hydrogen being transferred in the three systems. Despite the convenience for a proper comparative study, this constraint is not arbitrary but derived from the fact that hydrogen transfers in biological systems take normally place also under constrained C—C distances (16). Indeed, under this constraint, one cannot strictly speak of stationary points. Following the notation of our previous study (15), the point on the reaction coordinate where the hydrogen being transferred begins to notice the polarization effect of the acceptor CH_3 fragment will be formally referred to as *reactant complex* (RC), whereas the point where the hydrogen is midway between the two CH_3 fragments will be formally labelled as *transition state* (TS).

In the previous comparative analysis of one-electron densities between the CH_4/CH_3^+, $CH_4/CH_3^{\cdot}$, and CH_4/CH_3^- systems at the TS (15), contour maps of the electron density were used to compare the electronic characteristics of the three systems, at the HF, CISD, and MP2 levels of theory. It was found that the charge density at the H being transferred (H_t) decreases in the order $CH_4/CH_3^+ > CH_4/CH_3^{\cdot} > CH_4/CH_3^-$, in agreement with the formal hydride, hydrogen, and proton character of H_t in these systems. Moreover, the gradient vector field and Laplacian maps of the electron density for the three TS structures showed a progressive decrease of the size of the atomic basin of H_t and a stronger overlapping of the H_t *s* shell with the adjacent C shells, along the CH_4/CH_3^+, $CH_4/CH_3^{\cdot}$, and CH_4/CH_3^- series. Bader atomic charge populations were also reported for these systems. It was found that, at the HF level of theory, the atomic charges of H_t (–0.23, 0.05, and 0.35 for CH_4/CH_3^+, $CH_4/CH_3^{\cdot}$, and CH_4/CH_3^- respectively) deviate quite significantly from the formal assignment of –1, 0, and +1 to a hydride, hydrogen, and proton transfer, respectively. The effect of considering electron correlation effects was assessed by means of (MP2-HF) density difference maps. The difference maps, as well as the comparison of the H_t atomic charges obtained at the HF, CISD, and MP2 levels of theory, revealed that electron correlation reduces the electronic differences between the formal hydride, hydrogen, and proton transfer reactions. Finally, molecular quantum similarity measures (17) were used to measure the degree of electron redistribution suffered by the three systems when evolving from RC to TS, revealing that this redistribution is larger in hydride and hydrogen transfers than in proton transfers.

Even though the topological analysis of the one-electron density has been shown to be extremely useful in the elucidation of the electronic characteristics of atoms and molecules (18), some analysis based ultimately on the electron-pair density have appeared within the framework of the theory of Atoms in Molecules. In particular, some studies based

© 2000 NRC Canada

on the Fermi or exchange-correlation density have provided interesting insights on the electron-pair characteristics of molecules (19, 20). In contrast, the topological analysis of molecular intracule and extracule densities has received less attention (21, 22). However, the availability of new and efficient procedures to compute molecular intracule and extracule densities (23) allows nowadays to extend the usual analysis of one-electron densities to contracted electron-pair densities. Thus, while focusing on the TS's of the CH_3/CH_4^+, $CH_3/CH_4^{\cdot}$, and CH_3/CH_4^- model reactions at the Hartree-Fock (HF) and CISD levels of theory, this paper aims at investigating how the hydride, hydrogen and proton nature of the H being transferred in these systems is reflected in the corresponding electron-pair densities. The ultimate purpose of this work is to investigate whether intracule and extracule densities (24) can become useful in the electronic analysis of small and medium-sized molecules from an electron-pair perspective.

Methodological aspects

Ab initio molecular orbital HF wave functions for the TS's of CH_4/CH_3^+, $CH_4/CH_3^{\cdot}$, and CH_4/CH_3^- systems were taken from the results in Ref. 15. All calculations were performed with the 6–311++G** basis set (25) using the restricted HF method (RHF) for the closed-shell systems and the unrestricted HF method (UHF) for the open-shell system. For the closed-shell systems, single-point CISD/6–311++G** wave functions were generated, using both the molecular geometries optimized at the same level of theory in Ref. 15, and the molecular geometries optimized at the HF level. CISD wave functions calculated at the optimized CISD and HF geometries will be labelled as CISD and CISD//HF, respectively. These calculations were carried out by means of the Gamess program (26), in order to obtain the second-order density matrices required for the calculation of intracule and extracule densities at the CISD level of theory.

Intracule and extracule density maps were computed from the HF, CISD//HF and CISD wavefunctions, following the procedure described in Ref. 23. Integral neglect thresholds of 10^{-3} for the maps, and 10^{-5} for the exact location of the maxima, were used to discard integrals carrying little contribution to the total $I(\mathbf{r})$ and $E(\mathbf{R})$ densities.

The topological analysis of the one-electron density, $\rho(\mathbf{r})$, is a widely used tool for the interpretation of molecular electronic structure, and is the basis for a rigorous definition of an atom in a molecule (18). In practice, the electron-pair density, $\Gamma(\mathbf{r}_1,\mathbf{r}_2)$, should provide more direct information than its one-electron counterpart, including information about electron–electron interactions in molecules (27). However, due to its complexity, little is known about the topology of molecular electron-pair density functions. Alternatively, intracule, $I(\mathbf{r})$, and extracule densities, $E(\mathbf{R})$, can be used to reduce the dimensionality of the original electron-pair density while keeping an electron-pair character. The use of an interparticle separation or intracule coordinate, $\mathbf{r} = \mathbf{r}_1 - \mathbf{r}_2$, and a center of mass or extracule coordinate, $\mathbf{R} = (\mathbf{r}_1 + \mathbf{r}_2)/2$, allows to express the intracule and extracule densities as (24):

$$[4] \qquad I(\mathbf{r}) = \int \Gamma(\mathbf{r}_1, \mathbf{r}_2)\, \delta((\mathbf{r}_1 - \mathbf{r}_2) - \mathbf{r})\, d\mathbf{r}_1 d\mathbf{r}_2 \; ; \int I(\mathbf{r}) = \binom{N}{2}$$

and

$$[5] \qquad E(\mathbf{R}) = \int \Gamma(\mathbf{r}_1, \mathbf{r}_2)\, \delta\left(\frac{\mathbf{r}_1 + \mathbf{r}_2}{2} - \mathbf{R}\right) d\mathbf{r}_1\, d\mathbf{r}_2 \; ; \int E(\mathbf{R}) = \binom{N}{2}$$

respectively. On one hand, $I(\mathbf{r})$ distributions have the characteristic of always having a center of inversion at the origin, independent of the molecular symmetry, and being independent of any molecular translation. On the other hand, $E(\mathbf{R})$ distributions reflect the symmetry of the molecule. Both $I(\mathbf{r})$ and $E(\mathbf{R})$ integrate to the number of electron pairs in the molecule.

Although the topologies of atomic $I(\mathbf{r})$ and $E(\mathbf{R})$ distributions and the corresponding Laplacian functions have been studied in detail (28–33), calculations of anisotropic $I(\mathbf{r})$ and $E(\mathbf{R})$ densities for molecules have been few and focused mainly on diatomic molecules (34–40). However, HF $I(\mathbf{r})$ and $E(\mathbf{R})$ densities for some polyatomic molecules have been recently described in the literature (21, 22), and the corresponding Laplacian functions, $\nabla^2 I(\mathbf{r})$ and $\nabla^2 E(\mathbf{R})$, have also been investigated (22). It has been shown that the main topological features of molecular $I(\mathbf{r})$ and $E(\mathbf{R})$, and specially $\nabla^2 I(\mathbf{r})$ and $\nabla^2 E(\mathbf{R})$ distributions, can be understood in terms of electron–electron interactions, generated from the combination of electrons, each of them formally assigned to one of the atoms in the molecule (21, 22). Similarities between $I(\mathbf{r})$ and $E(\mathbf{R})$ densities for atoms and molecules have also been evaluated (41).

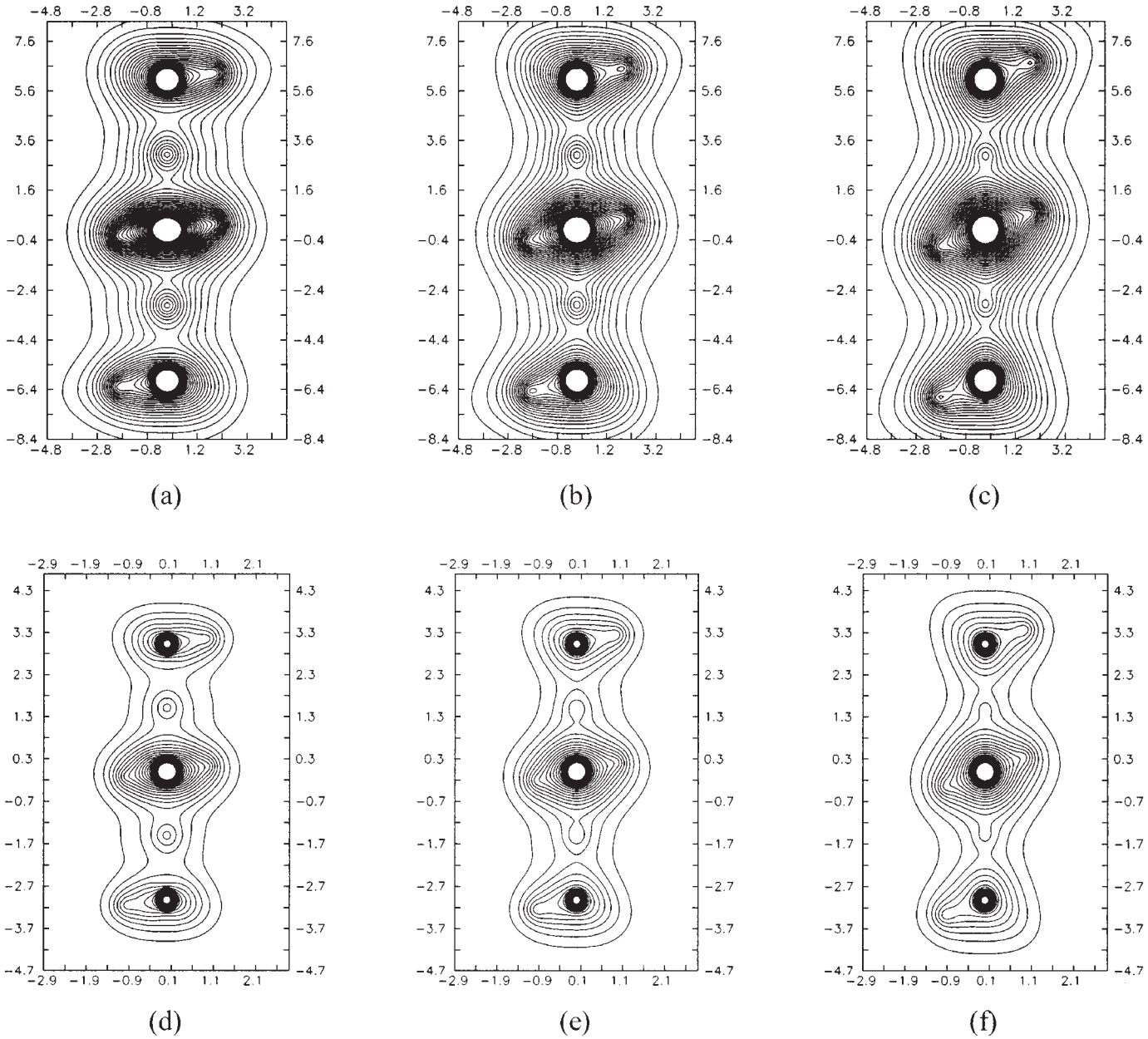
Results and discussion

Since the calculation of $I(\mathbf{r})$ and $E(\mathbf{R})$ density grids for small molecules at the HF and CISD levels of theory can now be routinely performed at a fairly low computational cost (21–23), it seems worthwhile to investigate the topologies of $I(\mathbf{r})$ and $E(\mathbf{R})$ densities for the CH_4/CH_3^+, $CH_4/CH_3^{\cdot}$, and CH_4/CH_3^- systems in order to study how they reflect the electronic differences between the three H-transfer processes. This analysis will be carried out at the TS's, because the molecular geometry at this point is the same for the three systems. Moreover, this point is illustrative enough of the electron rearrangements occurring along the reaction coordinate.

The discussion of the topological features of molecular $I(\mathbf{r})$ and $E(\mathbf{R})$ density distributions can be made by assigning a formal electron–electron interaction to each local maximum. Each electron–electron interaction will be labelled following a particular notation (22): $\{C_iC_j\}$ refers to electron–electron interactions between the two C atoms, $\{CH_t\}$ refers to electron–electron interactions between one of the C atoms and the H being transferred (H_t), and $\{C_{ii}\}$ and $\{H_{tt}\}$ refer to intraatomic interactions between electrons located on the same atom, C and H_t, respectively. Finally, the interaction labelled as $\{0\}$ refers to the maximum at the origin of each intracule and extracule density map. For the intracule densities, this interaction collects contributions from all the intraatomic pairs of electrons, which have a high probability of being close in space. For the extracule densities, the $\{0\}$ interaction is formed by the contributions of all the electron

© 2000 NRC Canada

Fig. 1. $I(\mathbf{r})$ and $E(\mathbf{R})$ topological maps for $[CH_3\text{-}H\text{-}CH_3]^+$, $[CH_3\text{-}H\text{-}CH_3]^{\cdot}$, and $[CH_3\text{-}H\text{-}CH_3]^-$ calculated at the HF level. (*a*) $I(\mathbf{r})$ for $[CH_3\text{-}H\text{-}CH_3]^+$, in contours of 0.05 au; (*b*) $I(\mathbf{r})$ for $[CH_3\text{-}H\text{-}CH_3]^{\cdot}$, in contours of 0.05 au; (*c*) $I(\mathbf{r})$ for $[CH_3\text{-}H\text{-}CH_3]^-$, in contours of 0.05 au; (*d*) $E(\mathbf{R})$ for $[CH_3\text{-}H\text{-}CH_3]^+$, in contours of 1 au; (*e*) $E(\mathbf{R})$ for $[CH_3\text{-}H\text{-}CH_3]^{\cdot}$, in contours of 1 au; (*f*) $E(\mathbf{R})$ for $[CH_3\text{-}H\text{-}CH_3]^-$, in contours of 1 au.



pairs being invariable upon a symmetry-inversion operation, provided that the molecular coordinates have been previously mass-centered. More electron–electron interactions arise by considering electrons formally assigned to terminal H atoms. However, these interactions are not considered relevant in order to investigate the electronic nature of H_t, and are not discussed. Furthermore, for the C atoms, the separate contributions of *core* and valence electrons are not resolved within this simple scheme, but they can be identified in the $\nabla^2 I(\mathbf{r})$ and $\nabla^2 E(\mathbf{R})$ distributions (*vide infra*).

Calculations at the HF level will be used for discussing the topologies of the $I(\mathbf{r})$ and $E(\mathbf{R})$ densities at the TS's for the three H-transfer model reactions. Since the electronic differences between hydride, hydrogen and proton transfers are overestimated at the HF level with respect to post-HF methodologies, the effect of adding Coulomb correlation energy at the CISD level will be discussed later by means of density difference maps.

Figure 1 shows the $I(\mathbf{r})$ and $E(\mathbf{R})$ density contour maps calculated at the HF level for the three TS's, labelled as $[CH_3\text{-}H\text{-}CH_3]^+$, $[CH_3\text{-}H\text{-}CH_3]^{\cdot}$, and $[CH_3\text{-}H\text{-}CH_3]^-$ for the CH_4/CH_3^+, $CH_4/CH_3^{\cdot}$, and CH_4/CH_3^- systems, respectively. First of all, the main topological features of the $I(\mathbf{r})$ maps will be assigned to the corresponding electron–electron

© 2000 NRC Canada

Table 1. Coordinates (z in au), intracule and extracule densities ($I(\mathbf{r})$ and $E(\mathbf{R})$, in au) for the $\{CH_t\}$ interaction localized in the $I(\mathbf{r})$ and $E(\mathbf{R})$ density maps of $[CH_3\text{-}H\text{-}CH_3]^+$, $[CH_3\text{-}H\text{-}CH_3]^{\cdot}$, and $[CH_3\text{-}H\text{-}CH_3]^-$. For the HF calculations, the contributions of the parallel ($\alpha\beta + \beta\alpha$) and antiparallel ($\alpha\alpha + \beta\beta$) spin components are also reported. For $[CH_3\text{-}H\text{-}CH_3]^+$ and $[CH_3\text{-}H\text{-}CH_3]^-$, CISD results are listed too. For all the systems, the distance between C and H_t is 3.024 au, and the center between the two atoms is located at 1.512 au in the molecular axis.

		Intracule		Extracule	
	Interaction	z	$I(\mathbf{r})$	z	$E(\mathbf{R})$
1a. $[CH_3\text{-}H\text{-}CH_3]^+$					
HF	$\{CH_t\}$	3.019	0.670	1.507	5.375
	$\{CH_t\}^{\alpha\beta+\beta\alpha}$	3.014	0.340	1.507	2.720
	$\{CH_t\}^{\alpha\alpha+\beta\beta}$	3.025	0.330	1.508	2.654
CISD	$\{CH_t\}$	3.019	0.658	1.485	5.241
1b. $[CH_3\text{-}H\text{-}CH_3]^{\cdot}$					
HF	$\{CH_t\}$	3.007	0.624	1.500	4.971
	$\{CH_t\}^{\alpha\beta+\beta\alpha}$	2.998	0.317	1.499	2.539
	$\{CH_t\}^{\alpha\alpha+\beta\beta}$	3.015	0.307	1.500	2.432
1c. $[CH_3\text{-}H\text{-}CH_3]^-$					
HF	$\{CH_t\}$	2.983	0.572	1.485	4.510
	$\{CH_t\}^{\alpha\beta+\beta\alpha}$	2.972	0.291	1.486	2.324
	$\{CH_t\}^{\alpha\alpha+\beta\beta}$	2.992	0.282	1.484	2.188
CISD	$\{CH_t\}$	2.976	0.595	1.490	4.660

interactions. Since the $I(\mathbf{r})$ maps for the three systems studied are equivalent from a topological point of view, this assignment is the same for $[CH_3\text{-}H\text{-}CH_3]^+$, $[CH_3\text{-}H\text{-}CH_3]^{\cdot}$, and $[CH_3\text{-}H\text{-}CH_3]^-$. Also, because of the symmetry inversion inherent to the intracule density distributions, only the upper half of each map needs to be discussed. For each map, the maximum located at 6.0 au on the vertical axis corresponds to the $\{C_iC_j\}$ interaction, while the maximum located at 3.0 au on the vertical axis can be assigned to the $\{CH_t\}$ interaction. Note that there are no maxima associated to the $\{H_{tt}\}$ and $\{C_{ii}\}$ interactions. Actually, these interactions, together with intraatomic contributions from the rest of H atoms, are responsible for the $\{0\}$ interaction at the origin. Other maxima which appear out of the vertical axis should be assigned to interactions between C and H atoms other than H_t.

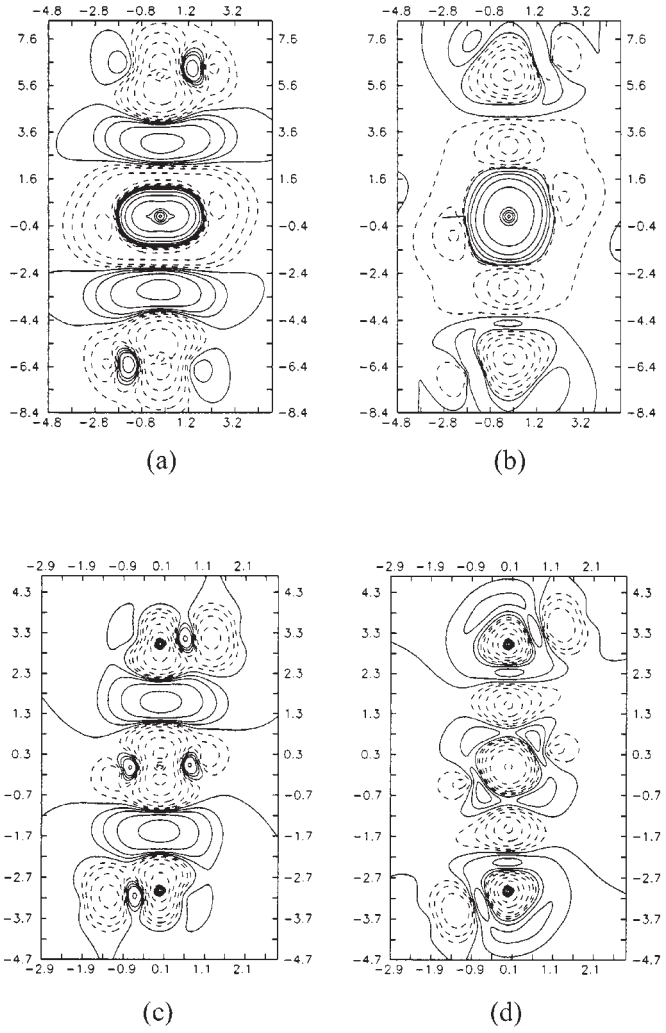
The $E(\mathbf{R})$ maps are also topologically equivalent for the three systems studied. Again, because of the symmetry of the molecule, only the upper half of the map will be discussed. For each map, the maximum at the origin, labelled as $\{0\}$, is assigned to the $\{C_iC_j\}$ and $\{H_{tt}\}$ interactions, together with other interactions between terminal H atoms related by a symmetry-inversion operation. The maximum located at 3.0 au on the vertical axis corresponds to a $\{C_{ii}\}$ interaction, whereas the maximum located at 1.5 au on the vertical axis of each map is assigned to a $\{CH_t\}$ interaction. Finally, there are also maxima out of the vertical axis, corresponding to interactions between C atoms and terminal H atoms.

The difficulty in analyzing the topology of the electron-pair $I(\mathbf{r})$ and $E(\mathbf{R})$ densities is reflected by the fact that, depending on the molecular geometry, several electron–electron interactions can contribute to the same point in the intracule or extracule space. For instance, for the analysis of the electronic differences between the formal hydride, hydrogen, and proton transfers, the $\{H_{tt}\}$ interaction would be the most important to analyze, since it can be directly related to the probability of having a pair of electrons on the H_t atom. However, it is not possible to isolate a maximum corresponding only to the $\{H_{tt}\}$ interaction in the $I(\mathbf{r})$ nor in the $E(\mathbf{R})$ density maps of the systems studied. In the $I(\mathbf{r})$ maps, all the intraatomic electron pairs always contribute to the $\{0\}$ interaction, making it impossible to assess the contribution of a single intraatomic electron–electron interaction. In the $E(\mathbf{R})$ maps, because of the molecular symmetry of the TS's, the $\{C_iC_j\}$ and $\{H_{tt}\}$ interactions also contribute exactly to the same point in space. However, the $\{CH_t\}$ interaction can be isolated both in the $I(\mathbf{r})$ and $E(\mathbf{R})$ maps for the three TS's. Thus, the electron-pair differences between the hydride, hydrogen, and proton transfers will be assessed by studying the maxima assigned to $\{CH_t\}$. In fact, a visual comparison of the topological maps in Fig. 1 reveals that the major differences among the $I(\mathbf{r})$ density maps, on one hand, and the $E(\mathbf{R})$ density maps, on the other hand, of the $[CH_3\text{-}H\text{-}CH_3]^+$, $[CH_3\text{-}H\text{-}CH_3]^{\cdot}$, and $[CH_3\text{-}H\text{-}CH_3]^-$ systems are found in the region where the topological maximum assigned to the maximum probability for the $\{CH_t\}$ interaction is located.

A more quantitative analysis can be made by comparing the heights of the maxima located in the $I(\mathbf{r})$ and $E(\mathbf{R})$ maps that are associated to the $\{CH_t\}$ electron–electron interaction. The values of those maxima for the three H-transfer model systems are reported in Table 1. The $I(\mathbf{r})$ values associated to this interaction are 0.67, 0.62, and 0.57, for $[CH_3\text{-}H\text{-}CH_3]^+$, $[CH_3\text{-}H\text{-}CH_3]^{\cdot}$, and $[CH_3\text{-}H\text{-}CH_3]^-$, respectively. The same trend is found for the $E(\mathbf{R})$ values, which are 5.37, 4.97, and 4.51, respectively. Thus, the $I(\mathbf{r})$ and $E(\mathbf{R})$ values associated to the $\{CH_t\}$ interaction at the TS decrease along the series of formal hydride, hydrogen, and proton transfer reactions. However, the fact that these values are similar for the three transfer reactions confirms that the electronic differences between the H_t atoms in the three transfer reactions are very subtle, in agreement with the results obtained from

© 2000 NRC Canada

Fig. 2. (HF-CISD//HF) $I(\mathbf{r})$ and $E(\mathbf{R})$ difference maps for $[CH_3\text{-}H\text{-}CH_3]^+$ and $[CH_3\text{-}H\text{-}CH_3]^-$. (*a*) $I(\mathbf{r})$ for $[CH_3\text{-}H\text{-}CH_3]^+$, in contours of 0.001×2^n, $n = 1,2,...$ au; (*b*) $I(\mathbf{r})$ for $[CH_3\text{-}H\text{-}CH_3]^-$, in contours of 0.001×2^n, $n = 1,2,...$ au; (*c*) $E(\mathbf{R})$ for $[CH_3\text{-}H\text{-}CH_3]^+$, in contours of 0.01×2^n, $n = 1,2,...$ au; (*d*) $E(\mathbf{R})$ for $[CH_3\text{-}H\text{-}CH_3]^-$, in contours of 0.01×2^n, $n = 1,2,...$ au.



the analysis of the one-electron densities (15). In fact, the importance of the $\{CH_t\}$ interaction is proportional to the probability of having simultaneously one electron at one of the C atoms and another electron at H_t. The analysis of the one-electron densities carried out in Ref. 15 showed that the Bader electron population decreases for H_t and increases for the C atoms, along the $[CH_3\text{-}H\text{-}CH_3]^+$, $[CH_3\text{-}H\text{-}CH_3]^{\cdot}$, and $[CH_3\text{-}H\text{-}CH_3]^-$ series. However, for the C atoms, the increase in one-electron density takes place mainly in the valence shell, rather than in the core region of the C atoms, and the value of $\rho(\mathbf{r})$ at the C nuclei decreases only slightly along the series of TS complexes. Thus, it can be assumed that the importance of the $\{CH_t\}$ interaction along this series depends mainly on the one-electron density at H_t, in agreement with the $I(\mathbf{r})$ and $E(\mathbf{R})$ values reported in Table 1. Finally, one has to take into account that the $\{CH_t\}$ interaction will also be affected by the Fermi correlation or exchange between electrons in the C and H_t atoms. However, Fermi correlation is expected to have only a minor effect on the height of the maxima associated to the $\{CH_t\}$ interaction.[2]

The values of the $I(\mathbf{r})$ and $E(\mathbf{R})$ maxima associated to the $\{CH_t\}$ interaction at the CISD level for $[CH_3\text{-}H\text{-}CH_3]^+$ and $[CH_3\text{-}H\text{-}CH_3]^-$ follow the same trends found at the HF level. However, the differences between the hydride and proton transfer are reduced, ranging from 0.098 at the HF level to 0.063 at the CISD level for the $I(\mathbf{r})$ values, and from 0.87 at the HF level to 0.58 at the CISD level for the $E(\mathbf{R})$ values. The effect of electron correlation is that it decreases the importance of the $\{CH_t\}$ interaction for $[CH_3\text{-}H\text{-}CH_3]^+$, and increases its importance for $[CH_3\text{-}H\text{-}CH_3]^-$, both with respect to the HF reference. This can be appreciated visually in the (HF-CISD//HF) density difference maps presented in Fig. 2, where the exaggeration of the ionic structures at the HF level is evident. As can be observed, the region corresponding to the $\{CH_t\}$ interaction in the $I(\mathbf{r})$ and $E(\mathbf{R})$ maps is positive for $[CH_3\text{-}H\text{-}CH_3]^+$, and negative for $[CH_3\text{-}H\text{-}CH_3]^-$, reflecting the HF exaggeration of the hydride and proton nature, respectively, of the H atom transferred in the two systems. Note that, for the rest of electron–electron interactions discussed previously (namely $\{0\}$, $\{C_{ii}\}$, and $\{C_iC_j\}$) the same trends are found in the $[CH_3\text{-}H\text{-}CH_3]^+$ and $[CH_3\text{-}H\text{-}CH_3]^-$ (HF-CISD//HF) density difference maps. For the $I(\mathbf{r})$ maps, it is also interesting to discuss the effect of including Coulomb correlation at the CISD level on the $\{0\}$ interaction. In fact, since this interaction collects contributions from all pairs of electrons close in space, Coulomb correlation always diminishes its importance, for any system. This is actually the case for $[CH_3\text{-}H\text{-}CH_3]^+$ and $[CH_3\text{-}H\text{-}CH_3]^-$. Interestingly, the shape of the positive region in the origin of the intracule density (HF-CISD//HF) difference maps suggests that, for $[CH_3\text{-}H\text{-}CH_3]^+$, CISD adds electron correlation mainly in a direction perpendicular to the molecular axis. On the other hand, for $[CH_3\text{-}H\text{-}CH_3]^-$, CISD adds electron correlation principally along the molecular axis. This is related to the larger accumulation of electron density on the valence shells of the carbon atoms for the latter system, as revealed by the analysis of the $\nabla^2 I(\mathbf{r})$ and $\nabla^2 E(\mathbf{R})$ functions (*vide infra*).

The exact locations of the $\{CH_t\}$ maxima in the $I(\mathbf{r})$ densities for the three TS's provide some additional information about the electronic characteristics of the H being transferred. The interelectron distance at which a given electron–electron interaction is found depends on the internuclear distance of the two atoms involved. In fact, for interactions between C atoms, the interelectron and internuclear distances are exactly coincident. However, for electron–electron interactions involving at least one H atom, the most probable interelectron distances are generally found to be slightly shorter than the corresponding internuclear distances, due to the high polarizability of the electron cloud in H atoms (22). Actually, this is the case for the $\{CH_t\}$ interaction, according to the HF results presented in Table 1. For the $\{CH_t\}$ interaction, the electron–electron distances associated to the maxima in the $I(\mathbf{r})$ maps are 0.005, 0.017, and 0.041 au shorter than the internuclear C–H_t distance, for $[CH_3\text{-}H\text{-}CH_3]^+$,

[2] X. Fradera, M. Duran, and J. Mestres. To be submitted.

© 2000 NRC Canada

$[CH_3\text{-}H\text{-}CH_3]^{\cdot}$, and $[CH_3\text{-}H\text{-}CH_3]^{-}$, respectively. The difference between the interelectron and internuclear distances for the formal hydride, hydrogen and proton transfers agree with the increasing polarizability of the hydrogen being transferred. For $[CH_3\text{-}H\text{-}CH_3]^{+}$ and $[CH_3\text{-}H\text{-}CH_3]^{-}$, the same trends are found at the CISD level, with differences between interelectron and internuclear distances of 0.005 and 0.048 au, respectively. In the $E(\mathbf{R})$ maps, the maxima associated to $\{CH_t\}$ interactions are located nearer to H_t than to the C atom, for the three systems. At the HF level, along the $[CH_3\text{-}H\text{-}CH_3]^{+}$, $[CH_3\text{-}H\text{-}CH_3]^{\cdot}$, and $[CH_3\text{-}H\text{-}CH_3]^{-}$ series, this maximum is found progressively closer to the H_t atom, in agreement with the progressive buildup of charge density in the valence shells of the C atoms. However, this trend is not followed at the CISD level of theory. Then, $[CH_3\text{-}H\text{-}CH_3]^{+}$ is the system with the $\{CH_t\}$ maximum located nearest to H_t.

Local maxima corresponding to the $\{CH_t\}$ interaction located in the parallel and antiparallel spin–spin components of the $I(\mathbf{r})$ and $E(\mathbf{R})$ densities calculated at the HF level are also reported in Table 1. The parallel components take into account $\alpha\alpha$ and $\beta\beta$ interactions, which are equivalent for the closed-shell systems, while the antiparallel component takes into account $\alpha\beta$ and $\beta\alpha$ interactions, which are always equivalent. For the three TS's, the $I(\mathbf{r})$ and $E(\mathbf{R})$ values associated to the points of maximum probability for an antiparallel $\{CH_t\}$ interaction are slightly larger than those associated to a parallel interaction. Furthermore, for the three TS's, the maximum probability for a parallel $\{CH_t\}$ interaction is found at a larger interelectron distance than the corresponding antiparallel interaction. The subtle differences between parallel and antiparallel $\{CH_t\}$ electron interactions are due to the Fermi correlation, which is present only for pairs of electrons of same spin. The differences between parallel and antiparallel interactions should be more important for intraatomic interactions, such as $\{C_{ii}\}$. On the other hand, for interatomic interactions at large distance, parallel and antiparallel interactions should be totally equivalent.

Recently, it has been found that a VB analysis is useful for the interpretation of intracule and extracule density difference maps between HF and CISD results.[3] Within this type of analysis, the points of maximum probability of finding a given electron–electron interaction can be assigned to formal valence bond structures, and the different weights of ionic and covalent VB structures at the HF and CISD levels of theory are reflected in the corresponding intracule and extracule density difference maps. Thus, for electron–electron interactions associated to ionic VB structures, positive values are found in the (HF-CISD//HF) difference maps, in agreement with the exaggeration of the ionic contributions to the molecular wavefunction at the HF level of theory. Inversely, negative values in the difference maps are found for electron–electron interactions associated to covalent VB structures.[4] Following the same interpretative scheme for the $[CH_3\text{-}H\text{-}CH_3]^{+}$ and $[CH_3\text{-}H\text{-}CH_3]^{-}$ systems, six VB structures (three covalent and three ionic) are needed for the description of a three-center bond with two or four electrons. At the TS, the six VB structures in the RC converge to three symmetric VB structures, namely, $C^{-}H^{+}C^{+}$ (= $C^{+}H^{+}C^{-}$), $C^{\cdot}H^{\cdot}C^{+}$ (= $C^{+}H^{\cdot}C^{\cdot}$), and $C^{+}H^{-}C^{+}$ for the $[CH_3\text{-}H\text{-}CH_3]^{+}$ system; and $C^{-}H^{+}C^{-}$, $C^{\cdot}H^{\cdot}C^{-}$ (= $C^{-}H^{\cdot}C^{\cdot}$), and $C^{-}H^{-}C^{+}$ (= $C^{+}H^{-}C^{-}$) for the $[CH_3\text{-}H\text{-}CH_3]^{-}$ system. Each of the VB structures of the two systems can be associated to an electron–electron interaction and, consequently, to a certain region in the intracule space. Thus, all the ionic structures, which can be associated to intraatomic interactions, contribute to furnish the maximum at the origin, labelled as $\{0\}$. The covalent structures can be associated to the $\{CH_t\}$ interaction, and contribute to the corresponding maximum in $I(\mathbf{r})$. Note that the $C^{\cdot}H^{\cdot}C^{-}$ structure (for the $[CH_3\text{-}H\text{-}CH_3]^{-}$ system) has an ionic and covalent character at the same time, and contributes to both the $\{0\}$ and $\{CH_t\}$ maxima. Finally, one must take into account that, although each ionic structure contributes to the maximum at the origin, the simultaneous presence of two or more ionic structures can make a contribution to other electron–electron interactions. Thus, the C^{-} and H^{-} structures together also contribute to the $\{CH_t\}$ maximum, while two symmetric C^{-} structures together contribute to the $\{C_iC_j\}$ maximum. A similar reasoning can be carried out for the $E(\mathbf{R})$ densities, with the difference that the contribution of the $\{C_{ii}\}$ interaction can be isolated into a pair of symmetric maxima in $E(\mathbf{R})$, while both $\{H_{ii}\}$ and $\{C_iC_j\}$ contribute to the origin of the extracule map and furnish the local maximum labeled as $\{0\}$.

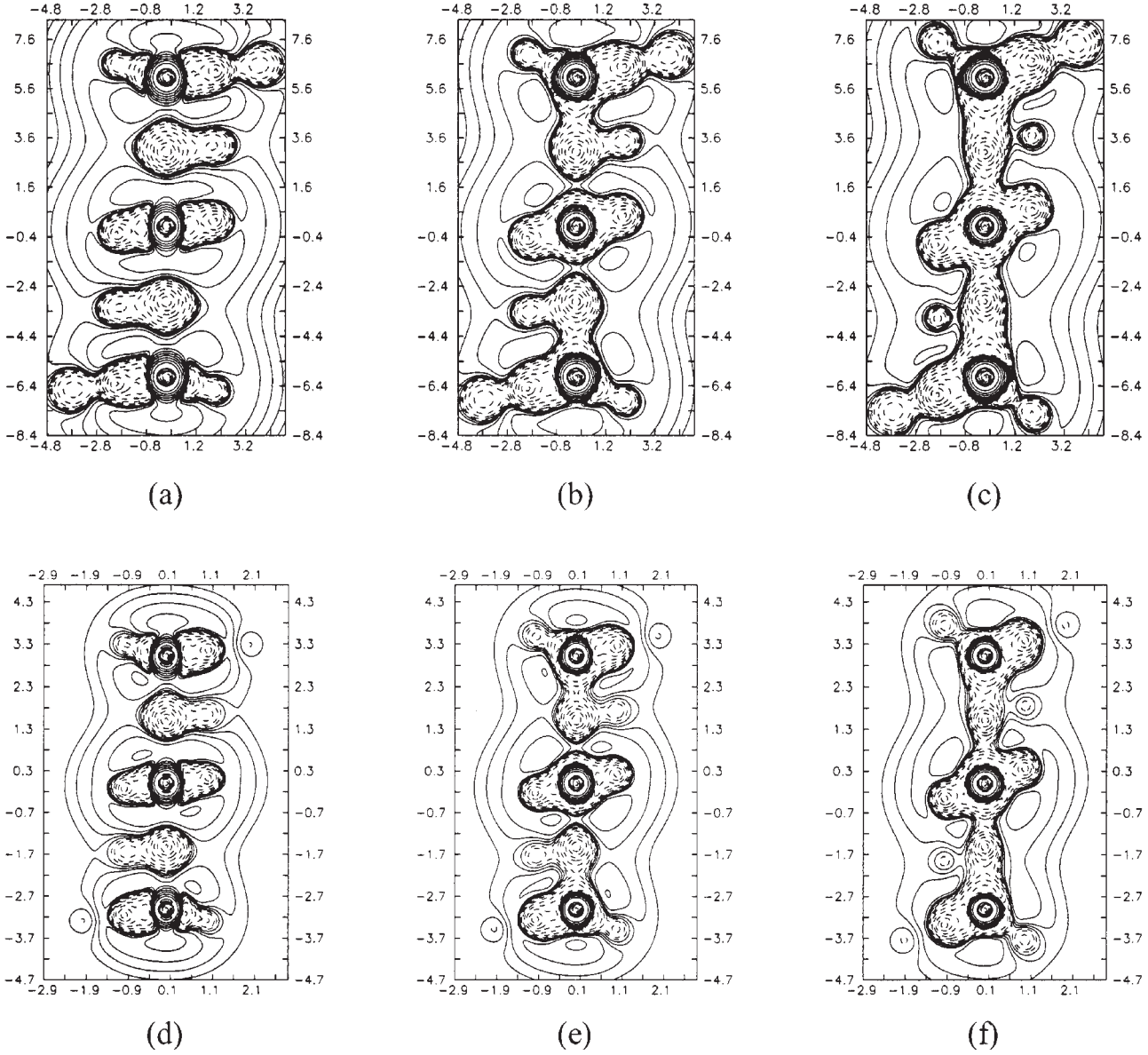
At the HF level of theory, the weights of ionic structures in the wave function are usually exaggerated. This overestimation is totally or partially corrected by post-HF methodologies, such as CISD. This trend can be reflected in the (HF-CISD//HF) difference maps of $I(\mathbf{r})$ and $E(\mathbf{R})$ densities for $[CH_3\text{-}H\text{-}CH_3]^{+}$ and $[CH_3\text{-}H\text{-}CH_3]^{-}$ (Fig. 2). The maxima at the origin of the intracule difference maps of the two systems (Figs. 2*a* and 2*b*) confirm that the contribution of the $\{0\}$ interaction, associated to the ionic VB structures, is greatly exaggerated at the HF level. Moreover, in the extracule (HF-CISD//HF) difference maps (Figs. 2*c* and 2*d*), local maxima appear in the positions assigned to $\{C_{ii}\}$ interactions, which can be associated to ionic C^{-} structures. Finally, for the $\{CH_t\}$ interaction, different trends are found for the two systems considered. In a valence bond language, the fact that electron correlation decreases the importance of this interaction for $[CH_3\text{-}H\text{-}CH_3]^{+}$ can be explained taking into account that, at the HF level, the contribution of the $C^{+}H^{-}C^{+}$ structure is exaggerated. On the other hand, for $[CH_3\text{-}H\text{-}CH_3]^{-}$, the increase of importance of the $\{CH_t\}$ interaction at the CISD level can be related to the overestimation of the contribution of the $C^{-}H^{+}C^{-}$ structure at the HF level. However, one must take into account that the importance

[3] X. Fradera, M. Duran, and J. Mestres. Submitted for publication.

[4] From a different point of view, it has been recently shown that considering electron correlation at the CISD level of theory increases the localization of electrons into each atom, while decreasing the electron delocalization between pairs of atoms, with respect to the HF approximation (20). For a pair of electrons shared between two atoms, A and B, electron localization is related to the probability of having each of the two electrons in a different atom, which corresponds to the covalent structure $A^{\cdot}\ B^{\cdot}$. In contrast, electron delocalization corresponds to the probability of the two electrons acting as a correlated pair, which can be at any of the atoms A or B, and corresponds to a pair of ionic structures, $A^{+}B^{-}$ and $A^{-}B^{+}$. Thus, the increasing electronic localization at the CISD level is related to the increasing contribution of the covalent VB structures to the molecular wave function.

© 2000 NRC Canada

Fig. 3. $\nabla^2 I(\mathbf{r})$ and $\nabla^2 E(\mathbf{R})$ topological maps for $[CH_3\text{-}H\text{-}CH_3]^+$, $[CH_3\text{-}H\text{-}CH_3]^{\cdot}$, and $[CH_3\text{-}H\text{-}CH_3]^-$ calculated at the HF level. (*a*) $\nabla^2 I(\mathbf{r})$ for $[CH_3\text{-}H\text{-}CH_3]^+$, in contours of 0.05×2^n, $n = 1,2,...$ au; (*b*) $\nabla^2 I(\mathbf{r})$ for $[CH_3\text{-}H\text{-}CH_3]^{\cdot}$, in contours of 0.05×2^n, $n = 1,2,...$ au; (*c*) $\nabla^2 I(\mathbf{r})$ for $[CH_3\text{-}H\text{-}CH_3]^-$, in contours of 0.05×2^n, $n = 1,2,...$ au; (*d*) $\nabla^2 E(\mathbf{R})$ for $[CH_3\text{-}H\text{-}CH_3]^+$, in contours of 1×2^n, $n = 1,2,...$ au; (e) $\nabla^2 E(\mathbf{R})$ for $[CH_3\text{-}H\text{-}CH_3]^{\cdot}$, in contours of 1×2^n, $n = 1,2,...$ au; (*f*) $\nabla^2 E(\mathbf{R})$ for $[CH_3\text{-}H\text{-}CH_3]^-$,.in contours of 1×2^n, $n = 1,2,...$ au.



of the $\{CH_t\}$ interaction depends also on the weight of the $C^-H^+C^+$ and $C^{\cdot}H^{\cdot}C^+$ structures for $[CH_3\text{-}H\text{-}CH_3]^+$, and the $C^-H^-C^+$ and $C^-H^{\cdot}C^{\cdot}$ structures for $[CH_3\text{-}H\text{-}CH_3]^-$. Unfortunately, the electron–electron interaction which reflects more directly the importance of the $C^+H^-C^+$ and $C^-H^+C^-$ structures is $\{H_{tt}\}$, which cannot be reflected separately in the intracule or extracule maps.

Finally, the Laplacians of the $I(\mathbf{r})$ and $E(\mathbf{R})$ densities for the systems studied are discussed. It is well known that the sign of the Laplacian of a function allows to detect where the function is locally concentrated (negative values) or locally depleted (positive values). For instance, zones of local charge concentration and depletion in atoms and molecules are revealed by means of the Laplacian of the one-electron density, $\nabla^2\rho(\mathbf{r})$ (18). This property gives $\nabla^2\rho(\mathbf{r})$ the ability of revealing the shell structure of atoms in molecules. Recently, it has been shown that the Laplacian functions of the intracule and extracule densities, $\nabla^2 I(\mathbf{r})$ and $\nabla^2 E(\mathbf{R})$, respectively, are also able to reveal the shell structure of atoms in molecules from an electron-pair perspective (22, 28, 41*a*). Moreover, many electron–electron interactions that are not reflected in the intracule or extracule density maps can be revealed in the maps of the corresponding Laplacian functions (22). $\nabla^2 I(\mathbf{r})$ and $\nabla^2 E(\mathbf{R})$ maps for $[CH_3\text{-}H\text{-}CH_3]^+$, $[CH_3\text{-}H\text{-}CH_3]^{\cdot}$, and $[CH_3\text{-}H\text{-}CH_3]^-$ calculated at the HF level are presented in Fig. 3.

Some electron–electron interactions between H atoms, not reflected in the $I(\mathbf{r})$ and $E(\mathbf{R})$ maps, are revealed in the Laplacian maps. However, the detection of these additional interactions is not relevant for the discussion of the electronic

© 2000 NRC Canada

nature of H_t. As in the $I(\mathbf{r})$ and $E(\mathbf{R})$ maps, the $\{H_{tt}\}$ interaction appears superimposed with other electron–electron interactions and cannot be isolated in the $\nabla^2 I(\mathbf{r})$ and $\nabla^2 E(\mathbf{R})$ maps. Nevertheless, Laplacian maps allow discussing in detail electron–electron interactions involving electrons of the carbon valence shell (22). When going from the hydride to the hydrogen and to the proton transfer, at the same time that the charge density at H_t decreases, there is an accumulation of charge density at the valence shell of the C atoms. This is reflected in the $\nabla^2 I(\mathbf{r})$ and $\nabla^2 E(\mathbf{R})$ maps of the three systems, for the electron–electron interactions involving pairs of electrons assigned to C atoms: $\{C_iC_j\}$ and $\{0\}$ in the intracule maps, and $\{C_{ii}\}$ and $\{0\}$ in the extracule maps. In the maps corresponding to $[CH_3\text{-}H\text{-}CH_3]^+$, these interactions reveal a negative shell, corresponding to the interaction between core electrons, surrounded by a positive shell. In contrast, for the same interactions, a second negative shell is found in the maps for the $[CH_3\text{-}H\text{-}CH_3]^{\cdot}$ and $[CH_3\text{-}H\text{-}CH_3]^+$ systems. For the interactions between C and H electrons, such as $\{CH_t\}$, no shell structure is found for any of the molecules studied. The progressive accumulation of charge density on the C-H_t-C region is also reflected in the $\nabla^2 I(\mathbf{r})$ and $\nabla^2 E(\mathbf{R})$ maps by the presence of negative Laplacian values connecting the different electron–electron interactions located on the vertical axis for $[CH_3\text{-}H\text{-}CH_3]^{\cdot}$, and specially for $[CH_3\text{-}H\text{-}CH_3]^+$.

Conclusions

The contracted electron-pair densities at the TS's corresponding to the formal hydrogen transfers in the CH_4/CH_3^+, $CH_4/CH_3^{\cdot}$, and CH_4/CH_3^- systems, constrained to a fixed C—C distance, have been investigated. The topological analysis of the corresponding intracule and extracule density and Laplacian functions complements, thus, a previous comparative electronic analysis of the same systems from the point of view of the one-electron density (15).

For the three systems considered, it has been shown that the topological characteristics of intracule and extracule densities can be readily interpreted in terms of formal electron–electron interactions. However, the $\{H_{tt}\}$ interaction, that could be directly related to the probability of having an electron pair in the H being transferred, cannot be isolated in the $I(\mathbf{r})$ or $E(\mathbf{R})$ distributions. Thus, the analysis of the electron-pair characteristics of the H being transferred has to be performed indirectly by analyzing the $\{CH_t\}$ interaction, whose contribution is more apparent in the $I(\mathbf{r})$ and $E(\mathbf{R})$ distributions. A comparative analysis of this interaction for the three systems shows that the nature of the hydrogen being transferred in each reaction is related to the heights of this maximum in each $I(\mathbf{r})$ or $E(\mathbf{R})$ map, although the differences between the formal hydride, hydrogen, and proton atoms transferred appear to be very subtle. The main shortcoming of this analysis is that the discussion of the electron-pair characteristics of H_t in terms of the $\{CH_t\}$ electron–electron interaction is not straightforward, because this interaction does not depend only on the nature of H_t, but depends also on the number of electrons present in C. The same difficulty arises when interpreting the differences between the HF and CISD $I(\mathbf{r})$ and $E(\mathbf{r})$ maps in terms of VB structures.

In summary, one can conclude that the topologies of intracule and extracule densities and their respective Laplacian functions are able to reflect the electron-pair characteristics of atoms and molecules. However, intracule and extracule densities present topologies considerably more complex than the one-electron densities, making the corresponding analysis more difficult. In addition, depending on the symmetry and size of the molecule studied, many different electron–electron interactions can contribute to the same regions of the intracule or extracule space. These drawbacks limit the current usefulness of topological analyses of intracule and extracule densities for molecules and complexes. More studies are required to find convenient tools for the analysis and interpretation of molecular contracted electron-pair densities that allow for unequivocally discriminating the contribution of the different electron–electron interactions.

Acknowledgements

This work has been supported by the Spanish DGICYT Project No. PB98-0457-C02-01. X. Fradera benefits from a doctoral fellowship from the University of Girona.

References

1. C.G. Swain, R.A. Wiles, and R.F.W. Bader. J. Am. Chem. Soc. **83**, 1945 (1961).
2. I.H. Williams, A.B. Miller, and G.M. Maggiora. J. Am. Chem. Soc. **112**, 530 (1990).
3. A.E. Pain and I.H. Williams. J. Chem. Soc. Chem. Commun. 1417 (1991).
4. (*a*) Z. Latajka and S. Scheiner. Int. J. Quantum Chem. **29**, 285 (1986); (*b*) S. Scheiner and Z. Latajka. J. Phys. Chem. **91**, 724 (1987); (*c*) A.D. Isaacson, L. Wang, and S. Scheiner. J. Phys. Chem. **97**, 1765 (1993).
5. R.V. Stanton and K.M. Merz Jr. J. Chem. Phys. **101**, 6658 (1994).
6. B. Kallies and R. Mitzner. J. Mol. Model. (Electronic Publication) **1**, 68 (1995).
7. M.J.S. Dewar and E. Haselbach. J. Am. Chem. Soc. **92**, 590 (1970).
8. M.T. Rayez-Meaume, J.J. Dannenberg, and J.L. Whitten. J. Am. Chem. Soc. **100**, 747 (1978).
9. M. Sana, G. Leroy, and J.L. Villaveces. Theor. Chim. Acta, **65**, 109 (1984).
10. E. Wünsch, J.M. Lluch, A. Oliva, and J. Bertrán. J. Chem. Soc., Perkin Trans. **2**, 211 (1987).
11. C. Musgrave, J.K. Perry, R.C. Merkle, and W.A. Goddard, III. Nanotechnology, **2**, 187 (1991).
12. (*a*) M.R. Pederson. Chem. Phys. Lett. **230**, 54 (1994); (*b*) D. Porezag and M.R. Pederson. J. Chem. Phys. **102**, 9345 (1995).
13. J.M. Tedder. Angew. Chim. Int. Ed. Engl. **21**, 401 (1982).
14. (*a*) J. Mestres, A. Lledós, M. Duran, and J. Bertrán. THEOCHEM, **260**, 259 (1992); (*b*) J. Mestres, M. Duran, and J. Bertrán. Theor. Chim. Acta, **88**, 325 (1994); (*c*) J. Mestres and P.C. Hiberty. New J. Chem. **20**, 1213 (1996).
15. J. Mestres, M. Duran, and J. Bertrán. Can. J. Chem. **74**, 1253 (1996).
16. R. Sustman, W. Sicking, and G.E. Schulz. Angew. Chem. Int. Ed. Engl. **28**, 1023 (1989).
17. E. Besalú, R. Carbó, J. Mestres, and M. Sola. Top. Curr. Chem. **173**, 31 (1995).

© 2000 NRC Canada

18. R.F.W. Bader. Atoms in molecules: a quantum theory. Oxford University Press, Oxford, U.K. 1990.
19. R.F.W. Bader and G.L. Heard. J. Chem. Phys. **111**, 8789 (1999); and refs. therein.
20. X. Fradera, M. Austen, and R.F.W. Bader. J. Chem. Phys. **103**, 304 (1999).
21. J. Cioslowski and G. Liu. J. Chem. Phys. **105**, 8187 (1996).
22. X. Fradera, M. Duran, and J. Mestres. J. Chem. Phys. **107**, 3576 (1997).
23. J. Cioslowski and G. Liu. J. Chem. Phys. **105**, 4151 (1996).
24. A.J. Coleman. Int. J. Quantum Chem. **S1**, 457 (1967).
25. (*a*) R. Krishan, J.S. Binkley, R. Seeger, and J.A. Pople. J. Chem. Phys. **72**, 650 (1980); (*b*) T. Clark, J. Chandreshakar, G.W. Spitznagel, and P. von Schleyer. J. Comput. Chem. **4**, 294 (1983); (*c*) M.J. Frisch, J.A. Pople, and J.S. Binkley. J. Chem. Phys. **80**, 3265 (1984).
26. M.W. Schmidt, K.K. Baldridge, J.A. Boate, S.T. Elbert, M.S. Gordon, J.H. Jensen, S. Koseki, N. Matsunaga, K.A. Nguyen, S.S. Su, T.L. Windus, M. Dupuis, and J.A. Montgomery. GAMESS, J. Comput. Chem. **14**, 1347 (1993).
27. E.R. Davidson. Reduced density matrices in quantum chemistry. Academic, New York, U.S.A. 1976.
28. C. Sarasola, L. Domínguez, M. Aguado, and J.M. Ugalde. J. Chem. Phys. **96**, 6778 (1992).
29. J. Wang and V.H. Smith Jr. Chem. Phys. Lett. **220**, 331 (1994).
30. H. Matsuyama, T. Koga, E. Romera, and J. Dehesa. Phys. Rev. A: At. Mol. Opt. Phys. **57**, 1759 (1998).
31. T. Koga, H. Matsuyama, E. Romera, and J. Dehesa. Phys. Rev. A: At. Mol. Opt. Phys. **57**, 4212 (1998).
32. A. Sarsa, F.J. Gálvez, and E. Buendía. J. Chem. Phys. **109**, 7075 (1998).
33. J. Cioslowski and G. Liu. J. Chem. Phys. **109**, 8225 (1998).
34. A.J. Thakkar, A.N. Tripathi, and V.H. Smith, Jr. Int. J. Quantum Chem. **26**, 157 (1984).
35. J. Wang, A.N. Tripathi, and V.H. Smith. J. Chem. Phys. **97**, 9188 (1992).
36. J. Wang, A.N. Tripathi, and V.H. Smith. J. Phys. B: At. Mol. Opt. Phys. **26**, 205 (1993).
37. J. Wang and V.H. Smith. Theor. Chim. Acta, **88**, 35 (1994).
38. J. Wang and V.H. Smith. Int. J. Quantum Chem. **49**, 147 (1994).
39. J. Cioslowski and G. Liu. J. Chem. Phys. **110**, 1882 (1999).
40. J. Cioslowski and G. Liu. J. Chem. Phys. **111**, 3401 (1999).
41. (*a*) X. Fradera, M. Duran, and J. Mestres. Theor. Chem. Acc. **99**, 44 (1998); (*b*) X. Fradera, M. Duran, and J. Mestres. Adv. Mol. Sim. **2**, 215 (1998).

© 2000 NRC Canada

Metabolism of analogs of the phytoalexin brassinin by plant pathogenic fungi

M. Soledade C. Pedras and Francis I. Okanga

Abstract: The metabolism of analogs of the cruciferous phytoalexin brassinin by the phytopathogenic fungi *Phoma lingam* (Tode ex Fr.) "virulent" and "avirulent" groups (sexual stage *Leptosphaeria maculans* (Desm.) Ces. et de Not.) and *Alternaria brassicae* (Berk.) Sacc. is reported. It was established that each pathogen detoxified methyl tryptamine dithiocarbamate, although yielding different metabolic products. While the biotransformation by virulent *P. lingam* proceeded to yield methyl 3a-hydroxy-3,3a,8,8a-tetrahydropyrrolo[2,3-*b*]indol-1(2H)-yl carbodithioate and indole-3-acetic acid as final products, avirulent *P. lingam* yielded indole-3-carboxylic acid via N_b-acetyltryptamine, and *A. brassicae* yielded N_b-acetyltryptamine, as final products. Furthermore, to establish the importance of the dithiocarbamate group in antifungal activity against *P. lingam* and *A. brassicae*, carbamates were compared with dithiocarbamates and it was established that carbamates were devoid of antifungal activity. These products, contrary to methyl tryptamine dithiocarbamate, showed no inhibitory activity against either pathogen.

Key words: *Alternaria brassicae*, brassinin, carbamates, detoxification, dithiocarbamates, *Leptosphaeria maculans*, *Phoma lingam*, phytoalexins.

Résumé : On a étudié le métabolisme d'analogues de la brassinine phytoalexine crucifère par *Alternaria brassicae* (Berk.) Sacc. et par les groupes « virulent » et « avirulent » des champignons phytopathogènes *Phoma lingam* (Tode ex Fr.) (stade sexuel *Leptosphaeria maculans* (Desm.) Ces. et de Not.). Il a été établi que chaque pathogène détoxifie le dithiocarbamate de la méthyltryptamine, même s'ils conduisent à ces produits de métabolisme différents. Alors que la biotransformation par le *P. lingam* virulent conduit au 3a-hydroxy-3,3a,8,8a-tétrahydropyrrolo[2,3-*b*]indol-1-(2*H*)-ylcarbodithionate de méthyle et à l'acide indole-3-acétique comme produits finaux, le *P. lingam* avirulent conduit à l'acide indole-3-carboxylique, via la N_b-acétyltryptamine, et *A. brassicae* conduit à la N_b-acétyltryptamine. De plus, afin d'évaluer l'importance du groupe dithiocarbamate dans l'activité antifongique contre *P. lingam* et *A. brassicae*, on a comparé les carbamates avec les dithiocarbamates et on a établi que les carbamates ne possèdent aucune activité antifongique. Contrairement à ce qui est observé avec le dithiocarbamate de la méthyltryptamine, ces produits ne présentent aucune activité inhibitrice contre l'un ou l'autre des pathogènes.

Mots clés : *Alternaria brassicae*, brassinine, carbamates, détoxification, dithiocarbamates, *Leptosphaeria maculans*, *Phoma lingam*, phytoalexines.

[Traduit par la Rédaction]

The role of phytoalexins in plant defense responses is becoming significantly better understood with the development of new transgenic and mutant organisms. For example, transformation of a fungus (*Cochliobolus heterostrophus*) nonpathogenic on pea (*Pisum sativum*) with a gene (cloned from the pea pathogen *Nectria haematococca*) responsible for detoxification of the pea phytoalexin pisatin, allowed the fungal transformant to become pathogenic on pea (1). These results indicated that the pisatin detoxifying gene was required for pathogenicity of *C. heterostrophus* on pea and that pisatin itself was a plant defense factor. On the other hand, a phytoalexin-deficient mutant of *Arabidopsis thaliana* showed significantly higher susceptibility to the fungus *Alternaria brassicicola* than wild-type parental plants; however, the reaction of the mutant to the pathogen *Botrytis cinerea* was similar to that of wild-type plants (2). Therefore, it is becoming indisputable that phytoalexins can be selectively inhibitory to plant pathogens and that plant pathogens can react differently to phytoalexins.

In instances where phytopathogens have been shown to react to plant defenses with metabolic detoxification, an environmentally attractive strategy to control such plant pathogens could involve application of selective inhibitors of those fungal enzymes utilized in detoxifying phytoalexins. Towards this end, we have been investigating the metabolism and detoxification (3) of cruciferous phytoalexins (4)[2] by

Received December 1, 1999.

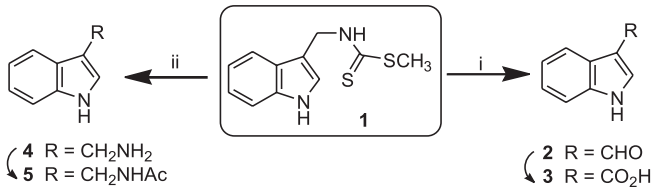
M.S.C. Pedras[1] and F.I. Okanga. Department of Chemistry, University of Saskatchewan, 110 Science Place, Saskatoon SK S7N 5C9, Canada.

[1]Author to whom correspondence may be addressed. Telephone: (306) 966-4772. Fax: (306) 966-4730.
e-mail: pedras@sask.usask.ca

[2]For a recent review see ref. 4.

© 2000 NRC Canada

Scheme 1.



(i) *Phoma lingam*,virulent; (ii) *P. lingam*, avirulent.

economically important phytopathogenic fungi, and have established that the phytoalexin brassinin (**1**) (5) was metabolized (6) and detoxified (7) by isolates of virulent and avirulent groups (8)[3] of the blackleg fungus (*Phoma lingam* (Tode ex Fr.) Desm., asexual stage of *Leptosphaeria maculans* (Desm.) Ces. et de Not. (Pleosporaceae)), one of the most important pathogens of the oilseeds rapeseed/canola (*Brassica napus*, *B. rapa*) (9).[4] These studies indicated that brassinin detoxification occurred via the so-called "virulent" route to yield **2** and **3** or "avirulent" route to yield **4** and **5**, depending on the isolate type, as depicted in Scheme 1 (7). In addition, due to studies with diverse dithiocarbamates (10), the dithiocarbamate group of brassinin (**1**) was thought to be essential for its antifungal activity.

Because methyl tryptaminedithiocarbamate (**6**) was significantly more inhibitory to *P. lingam* than brassinin, we examined its possible transformation by isolates of virulent and avirulent groups (8) of *P. lingam*. Furthermore, to establish the importance of the dithiocarbamate sulfur atoms, the corresponding carbamates of **1** and **6** were also examined and their antifungal activity established. A preliminary account of the metabolism of **6** by virulent type *P. lingam* was recently reported (11). Here we report for the first time the metabolism of **6** by avirulent type *P. lingam* and by *A. brassicae*, as well as the metabolism of methyl tryptamine carbamate (**16**) and N_b-carbomethoxyindole-3-methanamine (**17**) by both virulent and avirulent *P. lingam*. In addition, we propose a complete metabolic map of the metabolism of **6** by *P. lingam*, and compare the antifungal activities of brassinin (**1**), its homolog **6**, and corresponding carbamates **16** and **17**.

Results and discussion

The metabolism of methyl tryptamine dithiocarbamate (**6**) by virulent and avirulent isolates of *P. lingam* was investigated. Initially, experiments were carried out to compare the antifungal activity of dithiocarbamates **1** and **6**, as well as the time required for complete metabolism of **6**. Brassinin (**1**) was synthesized as previously described (7), and analog **6** was prepared as reported in the experimental. Fungal cultures and control medium were separately incubated with **1** (4×10^{-4} M) and **6** (2×10^{-4} M and 4×10^{-4} M) up to two weeks, and samples withdrawn at different times. Brassinin (**1**) was completely biotransformed within 2–4 days to yield the metabolites previously reported (6, 7). The HPLC chromatograms of extracts of cultures of either virulent or avirulent *P. lingam* incubated with methyl tryptamine dithiocarbamate (**6**) at the lower concentration (2×10^{-4} M) showed a decrease in the concentration of **6** as well as additional peaks not present in control cultures; however, at the higher concentration (4×10^{-4} M), no biotransformation occurred and the fungal mycelial growth was completely inhibited. These results established that methyl tryptamine dithiocarbamate (**6**) was biotransformed by either virulent (>14 days) or avirulent (ca. 4–6 days) types of *P. lingam* at a lower concentration (2×10^{-4} M), but at higher concentrations **6** inhibited primary metabolic steps, including mycelial growth (mycelial growth would resume upon dilution with culture medium). Therefore, biotransformation experiments to establish the structures of metabolites resulting from biotransformation of **6** were conducted at concentrations of 2×10^{-4} M.

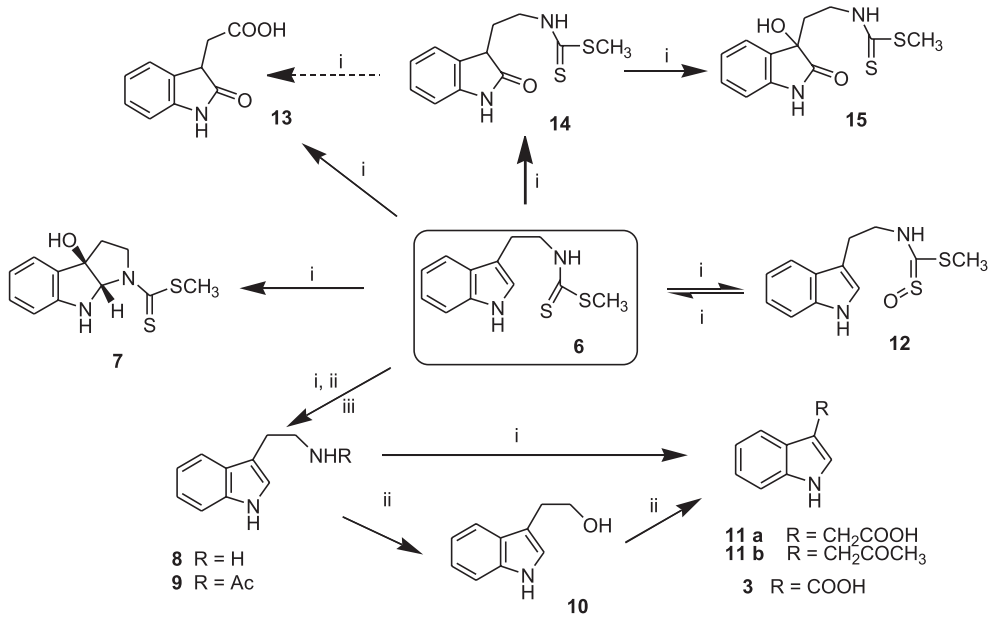
First, the biotransformation of methyl tryptamine dithiocarbamate (**6**) by virulent *P. lingam* was investigated. The metabolites were isolated by flash column chromatography and (or) preparative TLC as described in the experimental, and characterized by spectroscopic techniques (FTIR, ^{1}H NMR, ^{13}C NMR, MS). As a result of the biotransformation of **6**, eight metabolites were isolated and identified: methyl 3a-hydroxy-3,3a,8,8a-tetrahydropyrrolo[2,3-*b*]indol-1(2H)-yl carbodithioate (**7**), tryptamine (**8**), N_b-acetyltryptamine (**9**), indole-3-acetic acid (**11a**), methyl indole-3-acetate (**11b**), methyl tryptamine dithiocarbamate-*S*-oxide (**12**), 2-oxindole-3-acetic acid (**13**), and methyl 2-oxotryptamine dithiocarbamate (**14**). The isolated metabolites accounted for ca. 70% of the original amount of **6** after 14 days of incubation (Scheme 2); compounds **7** and **11a** were the major metabolites, representing ca. 65% of the total amount of isolated metabolites, followed by acetyltryptamine (**9**) (15%), and minor components **12**–**14** and methyl indole-3-acetate (less than 5%). The structure of each compound was deduced from analysis of spectroscopic data as previously described (11) and confirmed either by comparison of its spectroscopic data with those of authentic samples (**8** and **11a**), or corroborated by synthesis (**7**, **9**, **11b**, and **12–14**), as described in the experimental.

To further prove the sequence of the metabolic steps carried out by virulent *P. lingam*, compounds **7–9** and **11–14** were administered to fungal cultures and control medium and incubated for several days, the cultures were extracted and the resulting extracts analyzed by HPLC. Where the biotransformation led to detection of new compounds (**15**), i.e., not detected in the biotransformation of methyl tryptamine dithiocarbamate, scale up experiments were carried out to isolate and characterize them. Methyl 3a-hydroxy-3,3a,8,8a-tetrahydropyrrolo[2,3-*b*]indol-1(2H)-yl carbodithioate (**7**), indole-3-acetic acid (**11a**), and oxindole-3-acetic acid (**13**) underwent no further biotransformation on incubation with the fungus for up to 14 days. Tryptamine (**8**) was rapidly (within 24 h) biotransformed to give N_b-acetyltryptamine (**9**) and indole-3-acetic acid (**11a**). N_b-acetyltryptamine (**9**) was partially (ca. 50%) transformed to indole-3-acetic

[3] Although no formal reclassification has been carried out, virulent and avirulent isolates of *P. lingam* are now considered different species, see for example ref. 8.
[4] For a review on the blackleg fungus see for example, ref. 9.

© 2000 NRC Canada

Scheme 2.



(i) *Phoma lingam*,virulent; (ii) *P. lingam*, avirulent; (iii) *Alternaria brassicae*

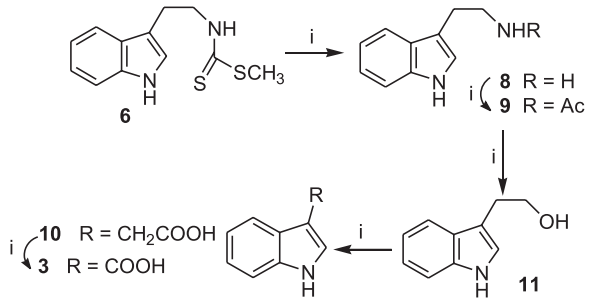
acid after 14 days of incubation. Methyl indole-3-acetate (**11b**) was biotransformed (within 48 h) into indole-3-acetic acid. Methyl tryptamine dithiocarbamate-*S*-oxide (**12**) was reduced (within 6 h) to methyl tryptamine dithiocarbamate (**6**). Methyl 2-oxotryptamine dithiocarbamate (**14**) yielded an apparently new metabolite which was isolated, characterized, and identified as methyl 3-hydroxy-2-oxotryptamine dithiocarbamate (**15**) based on a comparison of its spectroscopic data with those of its metabolic precursor **14**. In control experiments, each of the metabolites was stable in the cultures for up to 14 days of incubation.

The possible pathways for biotransformation of methyl tryptamine dithiocarbamate (**6**) and its metabolites by virulent *P. lingam* are shown in Scheme 2. There appear to be two major routes, one leading to acid **11** via tryptamine (**8**) and acetyltryptamine (**9**), and the other yielding dithiocarbamate **7**; neither **7** nor **11** appeared to be metabolized further. In addition, a minor pathway may lead to products **13** (≤1%) and **14** (≤1%). Although **14** appeared as a likely precursor of acid **13**, we did not detect **13** in cultures incubated with **14**. Surprisingly, although **6** is significantly more inhibitory to *P. lingam* than **12**, *S*-oxide **12** administered to fungal cultures was reduced to mostly **6**, in ca. 6 h. Control experiments indicated that **12** was stable under those incubation conditions for at least 48 h, suggesting that the transformation of **12** to **6** was an enzymatic process. Despite having investigated several biotransformations by fungi, this was the first time that we observed a reversible metabolic step in which one of the compounds (i.e., **6**) was clearly more inhibitory to the fungus. In this context, it is worthy to mention that structures such as **12**, i.e. containing a dithiocarbamate *S*-oxide, are rarely isolable and have been characterized mostly as mixtures (6, 12). Recently, however, the crystal structure of a stable dithiocarbamate *S*-oxide was determined by X-ray diffraction analysis (13). The *S*-oxide **12** is relatively more stable than the *S*-oxide of brassinin, perhaps due to the additional CH_2 group, which reduces the propensity for elimination of dithiocarbamic acid or equivalent. Although the decomposition of certain dithiocarbamate *S*-oxides was reported to lead mainly to the thiolocarbamates (sulfur extrusion), particularly in the presence of acid (12), we have not isolated such products from solutions containing **12**. Interestingly, the *S*-oxide **12** yielded oxindole **14** upon standing in acidic solvents such as $CDCl_3$; nonetheless, in fungal cultures **14** appeared to result from the enzymatic fungal transformation of **6**, since it was not detected in uninoculated control medium. Furthermore, similar to a previous observation with brassinin (**1**) (7), it was established during this process that, while **6** inhibited the synthesis of toxins produced by virulent *P. lingam*, neither dithiocarbamates **7** or **14** had noticeable effects.

Next, the biotransformation of methyl tryptamine dithiocarbamate (**6**) by avirulent *P. lingam* was examined; the biotransformation yielded indole-3-carboxylic acid (**3**), tryptamine (**8**), N_b-acetyltryptamine (**9**), tryptophol (**10**), and indole-3-acetic acid (**11a**). The total amount of isolated metabolites was ca. 70% of the initial amount of **6** after 4 days of incubation. Compounds **8**, **9**, and **11a** were also isolated from biotransformations with virulent isolates (Scheme 2). The structures of compounds **8**–**11a** were readily determined by comparison of their chromatographic and spectroscopic data (e.g., ^1H and ^{13}C NMR showed characteristic chemical shifts of indolyl moiety) with those of authentic samples. In order to establish the sequence of the biotransformation steps and hence the biotransformation pathway, each of the metabolites indole-3-carboxylic acid (**3**), tryptamine (**8**), N_b-acetyltryptamine (**9**), tryptophol (**10**), and indole-3-acetic acid (**11a**) were subjected to further incubation with

© 2000 NRC Canada

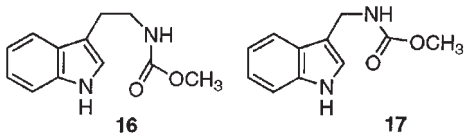
Scheme 3.



(i) *Phoma lingam* avirulent isolates.

avirulent *P lingam*. Indole-3-carboxylic acid (**3**) underwent no further transformation and was recovered unchanged from the cultures after 14 days. Tryptamine (**8**) was biotransformed via acetyltryptamine to tryptophol and indole-3-carboxylic acid. As expected, N_b-acetyltryptamine (**9**) yielded tryptophol and indole-3-carboxylic acid on further biotransformation by the fungus. Indole-3-acetic acid (**11a**) was completely transformed to indole-3-carboxylic acid (**3**), and tryptophol (**10**) was transformed (ca. 80%) to indole-3-carboxylic acid via indole-3-acetic acid, after 14 days incubation. In control experiments each of the compounds was stable in the cultures for at least 14 days. From these results, the pathway for biotransformation of methyl tryptamine dithiocarbamate (**6**) by avirulent *P. lingam* was inferred as shown in Scheme 3. Avirulent *P. lingam* biotransformed methyl tryptamine dithiocarbamate (**6**) through one major pathway to yield indole-3-carboxylic acid (**3**) via tryptamine (**8**), N_b-acetyltryptamine (**9**), tryptophol (**10**), and indole-3-acetic acid (**11a**).

Similarly, experiments carried out with *A. brassicae* incubated with tryptamine dithiocarbamate (**6**) at half of the concentration used in *P. lingam* cultures, showed that **6** was also completely metabolized by this pathogen in four days, to yield only two metabolites. These metabolites were identified as tryptamine (**8**) (less than 10%) and N_b-acetyltryptamine (**9**, ca. 70%). Importantly, it was established during these studies that dithiocarbamate **6** inhibited the production of the host-selective phytotoxin destruxin B by *A. brassicae.* In cultures incubated with tryptamine dithiocarbamate (**6**) the production of the toxin did not occur until complete metabolism of the compound by the fungus, while in control cultures the production of destruxin B occurred within 24 h.[5]



Methyl tryptamine carbamate (**16**) and N_b-carbomethoxyindole-3-methanamine (**17**) were chosen in order to probe the effect of substitution of oxygen for sulfur. Time-course experiments showed that methyl tryptamine carbamate (**16**) underwent little (<10%) transformation when incubated with virulent *P. lingam*. After 14 days incubation the major peak in the HPLC chromatogram of the neutral culture extract was that due to starting material (**16**) and phytotoxins produced by the fungus, while the acidic culture extract contained indole-3-acetic acid (**11a**). Further experiments showed that methyl tryptamine carbamate (**16**) was biotransformed by avirulent *P. lingam* (14 days) to yield two metabolites characterized by spectroscopic techniques and identified as tryptophol (**10**) and indole-3-carboxylic acid (**3**). Isolated metabolites accounted for ca. 40–50% of the initial amount of **16** after 14 days incubation.

Subsequent experiments with virulent *P. lingam* showed that N_b-carbomethoxyindole-3-methanamine (**17**) was biotransformed by the fungus, but compared to control cultures no additional metabolites (several known toxins (14) produced by the fungus were detected). Similar experiments with avirulent *P. lingam* indicated no biotransformation of N_b-carbomethoxyindole-3-methanamine by this fungal isolate. The compound was stable in the cultures with avirulent *P. lingam* for at least up to 14 days of incubation.

Bioassay results in liquid cultures inoculated with fungal spores and grown for 48 h before compound addition, indicated that methyl tryptamine dithiocarbamate (**6**) was more inhibitory to both virulent and avirulent *P. lingam* than brassinin (**1**); mycelial growth and metabolism of **6** were completely inhibited at 4×10^{-4} M, whereas brassinin caused a similar effect only at a concentration twice as high. However, the inhibitory effect of each compound decreased when fungal spores were incubated on solid medium containing either **1** or **6**. Nonetheless, as the results of Table 1 indicate, virulent *P. lingam* appeared more sensitive to **6** than to brassinin (**1**). It was observed that *P. lingam* spores germinated in 80–96 h on solid agar containing brassinin (at 5×10^{-4} M), but those spores germinated only after 100–120 h (results not shown) on solid agar containing **6** at similar concentration.

The results of bioassays of methyl tryptamine dithiocarbamate (**6**), methyl tryptamine carbamate (**16**), and N_b-carbomethoxyindole-3-methanamine (**17**) suggest that both the indole and the dithiocarbamate structural units are important for the antifungal activity of **6** against *P. lingam*. Compounds possessing the dithiocarbamate structural unit but lacking the indole unit such as methyl 2-oxotryptamine dithiocarbamate (**14**) and methyl 3a-hydroxy-3,3a,8,8a-tetrahydropyrrolo[2,3-*b*]indol-1(2*H*)-yl carbodithioate (**7**) were found to be much less active than methyl tryptamine dithiocarbamate (Table 1). Similarly, compounds possessing the indole unit but lacking the dithiocarbamate unit, such as methyl tryptamine dithiocarbamate-*S*-oxide (**12**) and indole-3-acetic acid (**11a**), were much less active. Furthermore, the growth and metabolism of *A. brassicae* was also strongly inhibited by **6**, as indicated by the results shown in Table 2; there was a significant inhibitory effect even at the lowest concentration. That is, **6** was more inhibitory to *A. brassicae* than to *P. lingam*. Finally, the bioassay results shown on Tables 1 and 2 indicate that none of the metabolic products of **6** displayed noticeable inhibitory activity against either *P. lingam* or *A. brassicae.*

[5] It was previously observed that brassinin caused a similar inhibitory effect on production of destruxins by *A. brassicae*, Pedras, M.S.C., unpublished results.

© 2000 NRC Canada

Table 1. Effect of brassinin (**1**), methyl tryptamine dithiocarbamate (**6**), and metabolites **3**, **7–14**, **16**, and **17** against virulent and avirulent *P. lingam* after 72 h incubation.

Compound	Concentration	% Inhibition[a]	
		Virulent	Avirulent
Brassinin (**1**)	5×10^{-4} M	34	100
	1×10^{-4} M	0	0
Indole-3-carboxylic acid (**3**)	5×10^{-4} M	NT	1
	1×10^{-4} M	NT	1
Methyl tryptamine dithiocarbamate (**6**)	5×10^{-4} M	100	100
	1×10^{-4} M	0	0
Methyl pyrrolo-indol-carbodithioate (**7**)	5×10^{-4} M	5	NT
	1×10^{-4} M	1	NT
Tryptamine (**8**)	5×10^{-4} M	1	1
	1×10^{-4} M	0	0
N_b-acetyltryptamine (**9**)	5×10^{-4} M	2	2
	1×10^{-4} M	0	0
Tryptophol (**10**)	5×10^{-4} M	NT	0
	1×10^{-4} M	NT	0
Indole-3-acetic acid (**11a**)	5×10^{-4} M	20	10
	1×10^{-4} M	5	0
Methyl indole-3-acetate (**11b**)	5×10^{-4} M	18	NT
	1×10^{-4} M	3	NT
Methyl tryptamine dithiocarbamate-*S*-oxide (**12**)	5×10^{-4} M	7	NT
	1×10^{-4} M	0	NT
Oxindole-3-acetic acid (**13**)	5×10^{-4} M	2	NT
	1×10^{-4} M	2	NT
Methyl 2-oxotryptamine dithiocarbamate (**14**)	5×10^{-4} M	3	NT
	1×10^{-4} M	3	NT
Methyl tryptamine carbamate (**16**)	5×10^{-4} M	6	1
	1×10^{-4} M	0	0
N_b-carbomethoxyindole-3-methanamine (**17**)	5×10^{-4} M	7	4
	1×10^{-4} M	0	0

[a] % inhibition = 100 – ((growth in treated / growth in control) × 100); results are means of at least three separate experiments conducted in triplicate; standard deviation ± 1.

Table 2. Bioassay of methyl tryptamine dithiocarbamate (**6**) and metabolites **8** and **9** against *A. brassicae* isolates after 72 h incubation.

Compound	Concentration	% Inhibition[a]
Methyl tryptamine dithiocarbamate (**6**)	5×10^{-4} M	100
	1×10^{-4} M	17
Tryptamine (**8**)	5×10^{-4} M	0
	1×10^{-4} M	0
N_b-acetyltryptamine (**9**)	5×10^{-4} M	0
	1×10^{-4} M	0

[a] % inhibition = 100 – ((growth in treated / growth in control) × 100); results are the mean of at least three separate experiments conducted in triplicate; standard deviation ± 1.

Virulent and avirulent *P. lingam* showed significant differences in their metabolism and detoxification of methyl tryptamine dithiocarbamate (**6**). The virulent isolates biotransformed methyl tryptamine dithiocarbamate (**6**) via two major and distinct pathways over a period of three weeks. The avirulent *P. lingam*, on the other hand, biotransformed methyl tryptamine dithiocarbamate (**6**) through one major pathway over a much shorter period (4–6 days). In both cases, however, the metabolism of dithiocarbamate **6** by virulent and avirulent *P. lingam* was a detoxification process. Importantly, the biotransformation pathways were somewhat different from those observed with brassinin; the transformation of **6** by virulent *P. lingam* occurred much slower (three weeks) than the transformation of brassinin (2–4 days). Furthermore, while brassinin (**1**) was detoxified by virulent *P. lingam* through one major pathway, to yield carboxylic acid **3** via aldehyde **2**, two major pathways occurred for detoxification of **6**, one which yielded **7** and the other one leading to indole-3-acetic acid (**11a**). On the other hand, both brassinin (**1**) and dithiocarbamate **6** were detoxified by avirulent *P. lingam* via acetylamines **5** and **9**, respectively, although acetylamine **5** was slowly oxidized to carboxylic

© 2000 NRC Canada

acid **3** via aldehyde **2**, whereas acetylamine **9** yielded carboxylic acid **3** via alcohol **10**.

Considering that brassinin (**1**) is produced by plants that virulent *P. lingam* attacks and colonizes, it is likely that virulent isolates have acquired very effective detoxification mechanisms to overcome this plant defense. The difference between the fungal metabolism of compounds **1** and **6** by virulent *P. lingam* may reflect the adaptation and specificity of the fungal enzymes involved in the detoxification of brassinin (**1**). Perhaps because those enzymes are not present in avirulent *P. lingam*, such differences are less obvious. These results, together with our previous studies (3), suggest that virulent *P. lingam* can detoxify dithiocarbamates effectively via pathways different from those followed by other species. Therefore, it should be possible to control virulent *P. lingam* with rationally designed inhibitors of dithiocarbamate detoxifying enzyme(s) without affecting other organisms.

Experimental

General

All chemicals were purchased from Sigma–Aldrich Canada Ltd., Oakville, ON. All solvents were HPLC grade and used as such, except for CH_2Cl_2 and $CHCl_3$ which were redistilled. TLC, and HPLC analyses were carried out as previously described (14).

NMR spectra were recorded on a Bruker AMX 300 or 500 spectrometer; for ^1H (300 or 500 MHz), δ values were referenced to CD_3OD (CD_2HOD at 3.31 ppm), CD_2Cl_2 ($CDHCl_2$ at 5.32 ppm), or $CDCl_3$ ($CHCl_3$ at 7.26 ppm), and for ^{13}C (75.5 or 125.8 MHz) referenced to CD_3OD (49.15 ppm), CD_2Cl_2 (54.00 ppm), or $CDCl_3$ (77.23 ppm). The multiplicities of ^{13}C NMR signals were determined based upon HMQC experiments.

Fungal cultures and bioassays

Phoma lingam virulent isolates BJ 125 and ENG 53, and avirulent isolate Unity, (virulent and avirulent isolates are considered a different species, although no formal reclassification has occurred) and *Alternaria brassica* isolates AB3 and IBJ were obtained from AAFC, G. Séguin-Swartz. Liquid cultures of *P. lingam* in 250 mL Erlenmeyer flasks containing 100 mL minimal medium inoculated with fungal spores at 2×10^9 per flask (15), and cultures of *A. brassicae* in 250 mL Erlenmeyer flasks containing 100 mL potato dextrose medium inoculated with fungal spores at 2.4×10^6 per flask (16), were used for the metabolism studies.

The antifungal activity of compounds **1** and **6**–**14** to *P. lingam* and *A. brassicae* was investigated using the mycelial radial growth bioassay previously reported (14). Each assay was conducted in triplicate and repeated at least three times.

Metabolism of methyl tryptamine dithiocarbamate (6)

Solutions of compounds under study (final concentration 2×10^{-4} M in cultures of *P. lingam*, and 1×10^{-4} M in cultures of *A. brassicae*) in DMSO (final concentration of DMSO in medium 0.5%, v/v) were administered separately to 48-hour-old liquid cultures and to uninoculated media. Cultures were incubated on a shaker at 150 rpm, at 24 ± 2°C. Samples (5–10 mL) were withdrawn immediately after addition of compound, and at different time intervals, and were either immediately frozen or filtered and extracted with Et_2O. The extracted broth was acidified to pH 2 with HCl and extracted with Et_2O, followed by neutralization with NaOH and extraction with $CHCl_3$ (containing 1% NH_4OH, (v/v)).

Isolation of metabolites of methyl tryptamine dithiocarbamate (6)

P. lingam *virulent isolate BJ 125*

From 10 flasks inoculated with fungal spores and incubated with methyl tryptamine dithiocarbamate (**6**) at 2×10^{-4} M for 14 days (final broth volume of 900 mL due to sampling over incubation period) neutral (60 mg) and acidic (75 mg) extracts were obtained. Preparative TLC (CH_2Cl_2:MeOH (97:3)) was carried out on the neutral extract to yield: methyl tryptamine dithiocarbamate (**6**, 10 mg), methyl 3a-hydroxy-3,3a,8,8a-tetrahydropyrrolo[2,3-*b*]indol-1(2*H*)-yl carbodithioate (**7**, 10 mg), N_b-acetyltryptamine (**9**, 5 mg), methyl tryptamine dithiocarbamate-*S*-oxide (**12**, 2 mg), 2-oxoindole-3-acetic acid (**13**, 1 mg), and methyl 2-oxotryptamine dithiocarbamate (**14**, 2 mg). Similarly, preparative TLC (CH_2Cl_2:MeOH (95:5)) carried out on the acidic extract afforded: indole-3-acetic acid (**11**, 5 mg) and methyl indole-3-acetate (**11b**, 1 mg). Similar results were obtained with isolate ENG 53.

Detection and isolation of tryptamine (**8**) in the biotransformation of methyl tryptamine dithiocarbamate (**6**): three flasks were inoculated with spores of *P. lingam* isolate BJ-125 and incubated with methyl tryptamine dithiocarbamate (**6**) as described above. Samples were taken immediately after adding the compound and subsequently every day over a period of 5 days. After 5 days the cultures were filtered, the combined broth (final broth volume of 280 mL due to sampling over incubation period) was extracted with diethyl ether to give a neutral extract. The broth was then basified to pH 10 with concentrated ammonia solution and extracted with $CHCl_3$:NH_4OH (98:2) to yield a basic extract (111 mg). The extracts were dried over Na_2SO_4, the solvent evaporated under reduced pressure and the basic residue analyzed by TLC ($CHCl_3$:MeOH:NH_4OH (80:20:1)). Preparative TLC ($CHCl_3$:MeOH:NH_4OH (80:20:1)) on the basic extract yielded 2 mg of tryptamine (**8**).

P. lingam *avirulent isolate Unity*

From five flasks inoculated with fungal spores and incubated with methyl tryptamine dithiocarbamate (**6**) at 2×10^{-4} M for five days (final broth volume of 350 mL due to sampling over incubation period) neutral (20 mg) and acidic extracts were obtained (16 mg). Preparative TLC (CH_2Cl_2:MeOH (96:4)) on the neutral extract led to the isolation of N_b-oxotryptamine (**9**, 2 mg), indole-3-acetic acid (**11a**, 2 mg), and tryptophol (**10**, 4 mg); prep. TLC on the acidic extract afforded indole-3-acetic acid (**11a**, 2 mg) and indole-3-carboxylic acid (**3**, 2 mg).

A. brassicae *IBJ and AB3*

From four flasks inoculated with fungal spores (two flasks per isolate) and incubated with methyl tryptamine dithiocarbamate (**6**) at 1×10^{-4} M for five days, from the

© 2000 NRC Canada

broth (final volume 120 mL per isolate) neutral (10 mg) and basic extracts (8 mg). Preparative TLC on the neutral extract led to the isolation of N_b-acetyltryptamine (**9**, 2 mg); prep. TLC on the basic extract afforded tryptamine (**8**, 1 mg). Similar experiments conducted in minimal medium yielded identical metabolites, but slower transformations were observed.

Biotransformation of metabolites of methyl tryptamine dithiocarbamate (6)

P. lingam *isolate BJ 125*

Methyl 3a-hydroxy-3,3a,8,8a-tetrahydropyrrolo[2,3-*b*]indol-1(2*H*)-yl carbodithioate (**7**), tryptamine (**8**), N_b-acetyltryptamine (**9**), indole-3-acetic acid (**11a**), methyl indole-3-acetate (**11b**), methyl tryptamine dithiocarbamate-*S*-oxide (**12**), oxindole-3-acetic acid (**13**), and methyl 2-oxotryptamine dithiocarbamate (**14**) were subjected to further biotransformation (final solution concentration of 2×10^{-4} M) by virulent *P. lingam*. If further biotransformation led to detection of new compounds, i.e., not detected in the biotransformation of methyl tryptamine dithiocarbamate, as in the case of **14**, scale up experiments were conducted to isolate and characterize them. All compounds were stable in uninoculated medium for at least 14 days, except for compound **12** which was kept in medium for no more than 48 h. The extracts were analyzed by HPLC and TLC.

Isolation of the metabolites of methyl 2-oxotryptamine dithiocarbamate (**14**): from eighteen flasks inoculated with fungal spores and incubated with methyl 2-oxotryptamine dithiocarbamate (**14**, final concentration 2×10^{-4} M) for 14 days, the broth (final volume 1700 mL) neutral extract (300 mg) was obtained; FCC (CH_2Cl_2:MeOH (95:5)) on the extract, followed by preparative TLC (ethyl acetate:hexane (80:20)) afforded methyl 3-hydroxy-2-oxotryptamine dithiocarbamate (**15**, 9 mg).

P. lingam *avirulent isolate Unity*

Indole-3-carboxylic acid (**3**), tryptamine (**8**), N_b-acetyltryptamine (**9**), tryptophol (**10**), and indole-3-acetic acid (**11a**) were subjected to further biotransformation (final concentration 2×10^{-4} M) by avirulent *P. lingam* as described above.

Biotransformation of methyl tryptamine carbamate (16)

P. lingam *virulent isolate BJ 125*

From eight flasks inoculated with fungal spores and incubated with methyl tryptamine carbamate (**16**, final concentration 2.0×10^{-4} M) in DMSO at 1×10^{-4} M for 14 days (broth final volume 750 mL) neutral (100 mg) and acidic extracts (110 mg). Preparative TLC (CH_2Cl_2:MeOH (95:5)) on the neutral extract led to isolation of recovered methyl tryptamine carbamate (**16**, 38 mg), phytotoxins, and lipid components. Preparative TLC on the broth acidic extract yielded indole-3-acetic acid (**11**, 2 mg), phytotoxins together with fatty acids.

P. lingam *avirulent isolate Unity*

From six flasks inoculated with fungal spores and incubated with methyl tryptamine carbamate (**16**, final concentration 2.0×10^{-4} M) in DMSO at 1×10^{-4} M for 14 days (broth final volume 550 mL) neutral (20 mg) and acidic extracts (110 mg) were obtained. Preparative TLC (CH_2Cl_2:MeOH (95:5)) on the neutral extract resulted in isolation of recovered methyl tryptamine carbamate (**16**, 2 mg), tryptophol (**10**, 2 mg), indole-3-carboxylic acid (**3**, 5 mg) together with unidentified UV-inactive components. The HPLC chromatograms of the acidic extract did not show UV active peaks of possible metabolites and was not fractionated further.

Syntheses and spectroscopic data of compounds

Methyl tryptamine dithiocarbamate (6)

Carbon disulfide (160 μL, 2.8 mmol) was added to a mixture of tryptamine (**8**, 320 mg, 2 mmol), triethylamine (360 μL), and pyridine (2 mL) at 0°C and the mixture stirred at 0°C for 1 hour. Methyl iodide (160 μL, 2.6 mmol) was added and the reaction mixture kept at 3°C for 15 h. The reaction mixture was then poured into 1.5 M H_2SO_4 (40 mL) and the crude product extracted with diethyl ether (3 × 50 mL). The combined extracts were successively washed with water (150 mL), saturated $NaHCO_3$ (150 mL), water (150 mL), and the ethereal solution dried over Na_2SO_4. Evaporation of the solvent under reduced pressure yielded 511 mg of crude product. Fractionation by flash column chromatography (CH_2Cl_2) yielded pure methyl tryptamine dithiocarbamate (**6**, 454 mg, 91%).

HPLC t_R = 20.4 min; ^{1}H NMR (500 MHz, $CDCl_3$) δ: 8.07 (1H, br s, D_2O exchangeable), 7.62 (1H, d, J = 8.0 Hz), 7.37 (1H, d, J = 8.0 Hz), 7.22 (1H, ddd, J = 8.0, 8.0, 1 Hz), 7.14 (1H, ddd, J = 8.0, 8.0, 1 Hz), 7.02 (1H, s), 7.00 (1H, br s, D_2O exchangeable), 4.04–4.07 (2H, m), 3.08–3.12 (2H, m), 2.56 (3H, s), and minor signals (ca. 1:4 intensity of the major ones) due to a rotamer at δ: 7.57 (d, J = 8.0 Hz), 3.74 (m), 2.68 (s); ^{13}C NMR (125.8 MHz, $CDCl_3$) δ 198.8 (s), 136.4 (s), 127.2 (s), 122.5 (d), 122.4 (d), 119.7 (d), 118.7 (d), 112.3 (s), 111.4 (d), 47.2 (t), 24.0 (t), 18.1 (q) and minor signals (ca. 1:4 intensity of the major ones) due to a rotamer at δ: 201.7 (s), 126.9 (s), 118.5 (d), 46.1 (t), 24.6 (t), 19.0 (q); FTIR (cm^{-1}): 3408, 3324, 2915, 1501, 1455, 1338, 1090, 934, 744; EIMS *m*/*z* (%): 250 (M^+, 6), 202 (68), 143 (63), 130 (100); FABMS *m*/*z* (%): 251 (M^+ + 1, 47), 144 (100); HREIMS *m*/*z*: calcd. for $C_{12}H_{14}N_2S_2$: 250.0598; found: 250.0600.

*Methyl 3a-hydroxy-3,3a,8,8a-tetrahydropyrrolo[2,3-*b*]indol-1(2*H*)-yl carbodithioate (7)*

Methyl tryptamine dithiocarbamate (**6**, 20 mg, 0.08 mmol) and Rose Bengal (8 mg, 0.008 mmol) were dissolved in 5% pyridine–methanol (5 mL) in a Pyrex test tube and irradiated with light (100 W halogen bulb) (17). Air was continuously bubbled through the solution while cooling in ice-water. After 2 h, the reaction mixture was transferred to a round bottom flask, dimethyl sulfide (200 μL) added and the solution stirred at room temperature; after two hours, the reaction mixture was diluted with toluene (5 mL) and the solvent evaporated under reduced pressure. Preparative TLC (CH_2Cl_2:MeOH (98:2)) on the crude reaction mixture yielded methyl 3a-hydroxy-3,3a,8,8a-tetrahydropyrrolo[2,3-*b*]indol-1(2*H*)-yl carbodithioate (**7**, 12.0 mg), 65% based on recovered starting material.

© 2000 NRC Canada

HPLC t_R = 14.5 min; $[\alpha]_D$ = +473 (CH_2Cl_2, *c* 0.14), obtained for the compound isolated from fungal metabolism of **6** (racemic synthetic material); ^{1}H NMR (300 MHz, CD_2Cl_2) δ: 7.33 (1H, d, *J* = 8.0 Hz), 7.18 (1H, ddd, *J* = 8.0, 8.0, and 1.0 Hz), 6.81 (1H, ddd, *J* = 8.0, 8.0, and 1.0 Hz), 6.64 (1H, d, *J* = 8.0 Hz), 5.71 (1H, s), 4.06–4.14 (1H, m), 3.28–3.37 (1H, m), 2.62 (3H, s), 2.52–2.59 (2H, m); ^{13}C NMR (75.5 MHz, $CDCl_3$) δ: 197.4 (s), 149.0 (s), 130.9 (d), 128.7 (s), 123.5 (d), 119.5 (d), 110.2 (d), 87.2 (d), 86.2 (s), 50.1 (t), 35.9 (t), 19.3 (q); FTIR (cm^{-1}): 3368, 3361, 2919, 2852, 1610, 1415, 1312, 1183, 1056, 949, 747; EIMS *m*/*z* (%): 266 (M^+, 100), 219 (21), 186 (45), 160 (41), 133 (61); HREIMS *m*/*z*: calcd. for $C_{12}H_{14}N_2OS_2$: 266.0548; found: 266.0547.

Methyl tryptamine dithiocarbamate-S-*oxide (**12**)*

Methyl tryptamine dithiocarbamate (**6**, 20 mg, 0.08 mmol) was dissolved in CH_2Cl_2 (2 mL) and the solution cooled to 0°C in ice-water. *m*-CPBA (18 mg, 0.08 mmol) was added to the solution and the reaction mixture stirred at 0°C for 30 min. After usual work up (addition of dimethyl sulfide, 500 μL, followed by successive washing with saturated $NaHCO_3$ and H_2O) the solvent was evaporated under reduced pressure, and the residue separated on TLC (CH_2Cl_2:MeOH (95:5)) to yield methyl tryptamine dithiocarbamate-*S*-oxide (**12**, 9 mg), 44% yield based on recovered starting material and methyl 2-oxotryptamine dithiocarbamate (**14**, 0.2 mg).

HPLC t_R = 11.6 min (broad); ^{1}H NMR (300 MHz, CD_2Cl_2) δ: 9.02 (br s, 1H, D_2O exchangeable), 7.57 (1H, d, *J* = 8.0 Hz), 7.36 (1H, d, *J* = 8.0 Hz), 7.16 (1H, ddd, *J* = 8.0, 8.0, 1.0 Hz), 7.09 (1H, ddd, *J* = 8.0, 8.0, 1.0 Hz), 7.02 (1H, s), 3.80 (1H, t, *J* = 7.0 Hz), 3.13 (1H, t, *J* = 7.0 Hz), 2.35 (3H, s); ^{13}C NMR (75.5 MHz, CD_2Cl_2) δ: 194.5 (s), 137.0 (s), 127.4 (s), 123.4 (d), 122.4 (d), 119.7 (d), 118.6 (d), 111.9 (d), 111.3 (s), 45.8 (t), 25.6 (t), 13.3 (q); FTIR (cm^{-1}): 3408, 3215, 2920, 2872, 1527, 1514, 1456, 1337, 905, 744; EIMS *m*/*z* (%): 266 (M^+, 2), 248 (7), 218 (5), 202 (8), 143 (59), 130 (100); HREIMS *m*/*z*: calcd. for $C_{12}H_{14}N_2OS_2$: 266.0548; found: 266.0447.

*Methyl 2-oxotryptamine dithiocarbamate (**14**)*

m-CPBA (52 mg, 0.24 mmol) was added to a solution of methyl tryptamine dithiocarbamate (**6**, 50 mg, 0.2 mmol) in CH_2Cl_2 (4 mL) cooled to 0°C, and the mixture stirred at 0°C. After 30 min a solution of *p*-toluene sulfonic acid (35 mg, 0.20 mmol) in methanol (0.5 mL) was added, the reaction mixture allowed to warm up to room temperature and kept stirring for 3 h. After usual work up, the solvent evaporated under reduced pressure, and the residue was subjected to preparative TLC (CH_2Cl_2:MeOH (97:3)) to yield methyl 2-oxotryptamine dithiocarbamate (**14**, 13 mg), 33% yield based on recovered starting material.

HPLC t_R = 12.5 min; $[\alpha]_D$ = –50 (CH_2Cl_2, *c* 0.08), for the compound isolated from fungal metabolism of **6** (racemic synthetic material); ^{1}H NMR (300 MHz, CD_2Cl_2) δ: 8.57 (1H, br s, D_2O exchangeable), 8.02 (1H, br s, D_2O exchangeable), 7.22–7.29 (2H, m), 7.07 (1H, dd, *J* = 8.0, 8.0 Hz), 6.92 (1H, d, *J* = 8.0 Hz), 4.04–4.10 (1H, m), 3.84–3.88 (1H, m), 3.55–3.59 (1H, m), 2.59 (3H, s), 2.38–2.45 (1H, m), 2.09–2.18 (1H, m); ^{13}C NMR (75.5 MHz, $CDCl_3$) δ: 199.0 (s), 180.7 (s), 140.9 (s), 128.9 (s), 128.4 (d), 124.1 (d), 123.0 (d), 110.1 (d), 45.4 (t), 45.0 (d), 28.7 (t), 18.0 (q); FTIR (cm^{-1}): 3234, 3204, 1700, 1619, 1519, 1470, 1335, 943, 751; EIMS *m*/*z* (%): 266 (M^+, 3), 218 (67), 159 (10), 146 (100), 133 (40); HREIMS *m*/*z*: calcd. for $C_{12}H_{14}N_2OS_2$: 266.0548; found: 266.0550.

*Methyl 3-hydroxy-2-oxotryptamine dithiocarbamate (**15**)*

HPLC t_R = 7.6 min; ^{1}H NMR (300 MHz, CD_3OD) δ 7.36 (1H, d, *J* = 8.0 Hz), 7.27 (1H, dd, *J* = 8.0, 8.0 Hz), 7.07 (1H, dd, *J* = 8.0, 8.0 Hz, 1H), 6.89 (1H, d, *J* = 8.0 Hz), 3.60–3.73 (2H, m), 2.50 (3H, s), 2.16–2.29 (2H, m); ^{13}C NMR (125.8 MHz, CD_3OD) δ: 199.8 (s), 181.6 (s), 142.5 (s), 132.5 (s), 130.7 (d), 125.2 (d), 123.8 (d), 111.4 (d), 76.5 (s), 43.0 (t), 36.6 (t), 17.8 (q); FTIR (cm^{-1}): 3305, 3271, 1715, 1622, 1471, 1188, 754; EIMS *m*/*z* (%): 282 (M^+, 5), 264 (7), 234 (15), 202 (8), 165 (15), 149 (100), 146 (25); FABMS *m*/*z* (%): 283 (M^+ + 1, 100), 269 (25), 217 (27), 158 (27); HREIMS *m*/*z*: calcd. for $C_{12}H_{14}N_2O_2S_2$: 282.0497; found: 282.0497.

*Methyl tryptamine carbamate (**16**)*

A solution of *N*,*O*-bis(trimethylsilyl)acetamide (1.5 mmol) in CH_2Cl_2 (1 mL) was added to a solution of tryptamine (**8**, 160 mg, 1.0 mmol) in CH_2Cl_2 (6 mL) under argon and the mixture stirred at 20°C for 1 hour (18). The reaction mixture was cooled to 0°C, and a solution of methyl chloroformate (1.5 mmol) in CH_2Cl_2 (1.5 mL) added. The reaction mixture was allowed to warm up to 20°C over 1 hour, stirred at 20°C for 1 h, cooled to 0°C, quenched with pH 7 buffer (10 mL), and extracted with diethyl ether (2 × 20 mL). The ether extract was washed with brine (40 mL), dried over Na_2SO_4, and evaporated under reduced pressure to afford methyl tryptamine carbamate (**16**, 187 mg), 86% yield.

HPLC t_R: 11.5 min; ^{1}H NMR (300 MHz, $CDCl_3$) δ: 8.13 (1H, br s, D_2O exchangeable), 7.61 (1H, d, *J* = 8.0 Hz), 7.38 (1H, d, *J* = 8.0 Hz), 7.23 (1H, dd, *J* = 8.0, 8.0 Hz), 7.14 (1H, dd, *J* = 8.0, 8.0 Hz), 7.03 (1H, s), 4.78 (1H, br s, D_2O exchangeable), 3.67 (3H, s), 3.53 (2H, m), 2.98 (2H, m); ^{13}C NMR (75.5 MHz, $CDCl_3$) δ: 157.1 (s), 136.5 (s), 127.3 (s), 122.2 (d), 122.1 (d), 119.5 (d), 118.7 (d), 112.9 (s), 111.2 (d), 52.0 (q), 41.4 (t), 25.8 (t); FTIR (cm^{-1}): 3409, 3322, 2945, 1700, 1524, 1457, 1261, 743; EIMS *m*/*z* (%): 218 (M^+, 29), 143 (38), 130 (100); HREIMS *m*/*z:* calcd. for 218.1055: $C_{12}H_{14}N_2O_2$; found: 218.1054.

N_b-*carbomethoxyindole-3-methanamine (**17**)*

Prepare as described for **16** with the following reagents: N,O-bis(trimethylsilyl)acetamide (3.5 mmol) in CH_2Cl_2 (3 mL), indole-3-methanamine (**4**, 415 mg, 2.8 mmol) in CH_2Cl_2 (10 mL); methyl chloroformate (3.5 mmol) in CH_2Cl_2 (3 mL); quenched with pH 7 buffer (20 mL), and extracted with diethyl ether (2 × 40 mL); N_b-carbomethoxyindole-3-methanamine (**17**, 430 mg), 74% yield.

HPLC t_R: 9.5 min; ^{1}H NMR (300 MHz, $CDCl_3$) δ: 8.13 (1H, br s, D_2O exchangeable), 7.66 (1H, dd, *J* = 8.0, 1.0 Hz), 7.39 (1H, dd, *J* = 8.0, 1.0 Hz), 7.23 (1H, ddd, *J* = 8.0, 8.0, 1.0 Hz), 7.13–7.18 (2H, m), 4.88 (1H, br s, D_2O exchangeable), 4.56 (2H, d, *J* = 5.0 Hz), 3.70 (3H, s); ^{13}C NMR (75.5 MHz, $CDCl_3$) δ: 157.1 (s), 136.5 (s), 126.5 (s), 123.0 (d), 122.4 (d), 119.8 (d), 118.8 (d), 113.1 (s), 111.4

© 2000 NRC Canada

(d), 52.2 (q), 36.8 (t); FTIR (cm^{-1}): 3407, 3322, 2950, 2870, 1699, 1521, 1457, 1258, 1236, 744; EIMS *m*/*z* (%): 204 (M^+, 100), 189 (36), 171 (10), 145 (18), 130 (83); HREIMS *m*/*z*: calcd. for $C_{11}H_{12}N_2O_2$: 204.0899; found: 204.0895.

Acknowledgements

Support for the authors' work was obtained from the Natural Sciences and Engineering Research Council of Canada and the University of Saskatchewan. We would like to thank Dr. G. Séguin-Swartz, Agriculture and Agri-Food Canada, Saskatoon Research Center, SK, for kindly providing isolates of *Phoma lingam* and *Alternaria brassicae.*

References

1. W. Schäfer, D. Straney, L. Ciuffetti, H.D. VanEtten, and O.C. Yoder. Science (Washington, D.C.), **246**, 247 (1989).
2. B.P.H.J. Thomma, I. Nelissen, K. Eggermont, and W.F. Broekaert. The Plant Journal, **19**, 163 (1999).
3. M.S.C. Pedras. Rec. Res. Dev. Phytochem. **2**, 259 (1998).
4. M.S.C. Pedras, F.I. Okanga, I.L. Zaharia, and A.Q. Khan. Phytochemistry, **53**, 161 (2000).
5. M. Takasugi, N. Katsui, and A. Shirata. J. Chem. Soc. Chem. Commun. 1077 (1986).
6. M.S.C. Pedras and J.L. Taylor. J. Org. Chem. **56**, 2619 (1991).
7. (*a*) M.S.C. Pedras, I. Borgmann, and J.L. Taylor. Phytochem. (Life Sci. Adv.) **11**, 1 (1992); (*b*) M.S.C. Pedras and J.L. Taylor. J. Nat. Prod. **56**, 731 (1993).
8. M.S.C. Pedras. Rec. Res. Dev. Agric. Food Chem. **2**, 513 (1998).
9. R.K Gugel and G.A. Petrie. Can. J. Plant Pathol. **14**, 36 (1992).
10. M.S.C. Pedras, A.K. Khan, K.C. Smith, and S.L. Stettner. Can. J. Chem. **75**, 825 (1997).
11. M.S.C. Pedras and F.I. Okanga. J. Org. Chem. **63**, 416 (1998).
12. Y. Segall and J.E. Casida. J. Agric. Food Chem. **31**, 242 (1983).
13. D. Chevrie and P. Metzner. Tetrahedron Lett. **39**, 8983 (1998).
14. M.S.C. Pedras and F.I. Okanga. J. Agric. Food Chem. **47**, 1196 (1999).
15. M.S.C. Pedras and A.Q. Khan. J. Agric. Food Chem. **44**, 3403 (1996).
16. M.S.C. Pedras and A.Q. Khan. Plant Science, **139**, 1 (1998).
17. M. Nakagawa, H. Okajima, and T. Hino. J. Am. Chem. Soc. **99**, 4424 (1977).
18. S. Raucher and D.S.A. Jones. Synth. Commun. **15**, 1025 (1985).

© 2000 NRC Canada

42-crown-14-based [2]catenane

Harry W. Gibson and Sang-Hun Lee

Abstract: A compound isolated from a synthesis directed toward 42-crown-14 (42C14) has been purified and characterized by means of IR, HPLC, NMR, MS, and DSC techniques. Its infrared spectrum contains no OH, tosylate, or unsaturated unit signals. The HPLC retention time of the compound differs from that of "42C14" and other crown ethers examined. The chemical shifts of the singlets in the ^{1}H and ^{13}C NMR spectra differ from those of poly(ethylene oxide)s (PEOs), and crown ethers. The FAB mass spectra contain signals attributable to a compound with twice the mass of 42C14 and the fragmentation pattern is consistent with [2]catenane **9** based on interlocked 42C14 units, because the next major signals generally correspond to 42C14 and its adducts. The DSC results showed that the compound, a colorless wax at room temperature, was amorphous with a glass transition temperature which was 80° higher than those of aliphatic crown ethers, which are crystalline compounds with melting points >40°C. Considering the high yield of the compound (8% in the reaction mixture as determined by NMR, 1.7% isolated), it is believed that sodium cation–crown ether–linear ether complexation was involved in templating its formation. Evidence for such complexation was also observed in the FAB MS.

Key words: catenanes, crown compounds, macrocycles, template synthesis, rotaxanes.

Résumé : Un composé a été isolé d'une synthèse effectuée dans le but d'obtenir l'éther 42-couronne-14 (42C14); on l'a purifié et caractérisé par des techniques de IR, CLHP, RMN, SM et d'analyse calorimétrique différentielle (ACD). Son spectre IR ne présente aucun signal correspondant à des groupes OH, tosylate ou insaturé. Le temps de rétention de ce composé en CLHP diffère de celui du « 42C14 » ou de tous les autres éthers couronnes étudiés. Les déplacements chimiques des singulets dans les spectres RMN du ^{1}H et du ^{13}C diffèrent de ceux des poly(oxydes d'éthylène) (POE) et des éthers couronnes. Les spectres de masse impliquant un bombardement avec des atomes rapides (BAR) comportent des signaux que l'on pourrait attribuer à un composé de masse double de celle du 42C14 et son patron de fragmentation est en accord avec le [2]caténane **9** dont la base serait des unités 42C14 reliées puisque les signaux majeurs suivants correspondent au 42C14 et à ses adduits. Les résultats d'ACD montrent que le composé, une cire incolore à la température ambiante, est amorphe avec une température de transition vitreuse qui est de 80°C plus élevée que celles des éthers couronnes aliphatiques qui sont des composés cristallins dont les points de fusion sont supérieurs à 40°C. Considérant le rendement élevé de ce composé (8% du mélange réactionnel sur la base de la RMN et 1,7% de produit isolé), on croit qu'une complexation du cation sodique avec l'éther couronne linéaire conduit à un gabarit impliqué dans sa formation. On a aussi observé des données pouvant supporter l'hypothèse d'une telle complexation dans le SM avec BAR.

Mots clés : caténanes, composés couronnes, macrocycles, synthèse sur gabarit, rotaxanes.

Introduction

Large crown ethers have been prepared in our laboratory using a "2+2" method (1). For example, the synthesis designed to produce 42-crown-14 (42C14) involves tri(ethylene glycol) ditosylate (**2**) addition to the sodium dianion (**1**) of tetra(ethylene glycol) in tetrahydrofuran (THF) (Scheme 1) to initially form α-oxy-ω-tosylate derivative **3**, which can either cyclize to form 21-crown-7 (21C7) (**4**) or react with more **1** to produce the undeca(ethylene glycol) dianion (**5**). **3** can also react with **2** to form deca(ethylene glycol) ditosylate (**6**). After chain extension from the reaction of **2** and **5** or **1** and **6**, the resultant oxytosylate **7** can afford 42C14 (**8**) through cyclization. **7** can react further with **1** and (or) **2** to form linear oligomers or polymers and crown ethers larger than 42C14. In fact, recent studies indicate that the product is a mixture of large crown ethers with 7n ethyleneoxy units, whose average size estimated by mass spectrometry corresponds to 84C28.[2] For this reason throughout the remainder of the discussion we will use quotation marks to denote the target of the synthesis, i.e., "42C14," so as not to misrepresent the material as a pure single compound.

The reaction mixture is typically purified by recrystallization before application of chromatography and other methods (1). In examining the mother liquors from such purifications, an NMR signal at 3.659 ppm caught our attention in repeated syntheses. This signal cannot be assigned to PEOs (see below) or crown ethers whose chemical shifts

Received September 27, 1999.

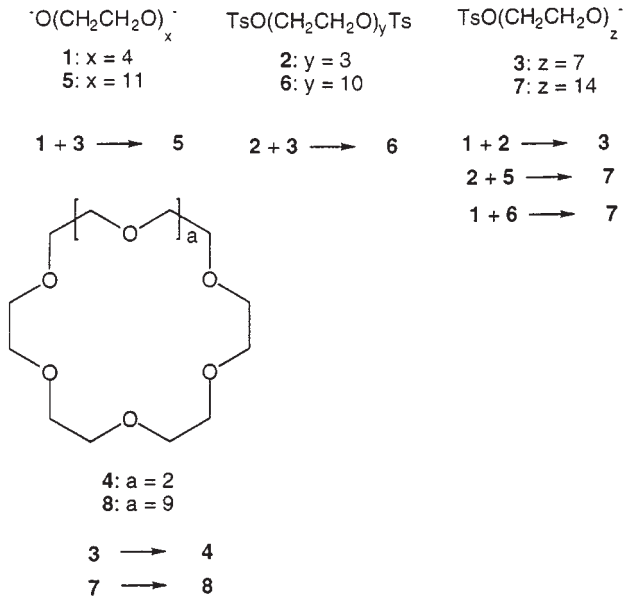
H.W. Gibson[1] and S.-H. Lee. Department of Chemistry, Virginia Polytechnic Institute and State University, Blacksburg, VA 24061–0212, U.S.A.

[1]Author to whom correspondence may be addressed. Telephone: (540) 231-5902. Fax: (540) 231-3255. e-mail: hwgibson@vt.edu.

[2]In collaboration with Prof. C. Booth et al. of the University of Manchester, U.K.

© 2000 NRC Canada

Scheme 1. Synthesis of 42C14 by "2+2" methodology.



under the same conditions range from 3.689 ppm for 18C6 up to 3.646 ppm for 60C20 (1, 2). We therefore set out to isolate and identify the source of this peak.

Results

A. Isolation

The isolation of the compound that gave rise to this signal was achieved by silica gel column chromatography of the mixture from the filtrate (after filtration of the "42C14") with acetone as eluent. In the ^{1}H NMR spectra in $CDCl_3$ the initial fractions gave several peaks, but consisted mainly of the 3.653 ppm signal, attributable to PEOs. The main peaks of the next fractions (nos. 16–55) appeared at 3.646 (PEOs) and 3.688 ppm (21C7). The peak at 3.659 ppm became a major peak of the later fractions (nos. 56–85). The spectra of last fractions (nos. 180–200) contained only a singlet at 3.659 ppm.

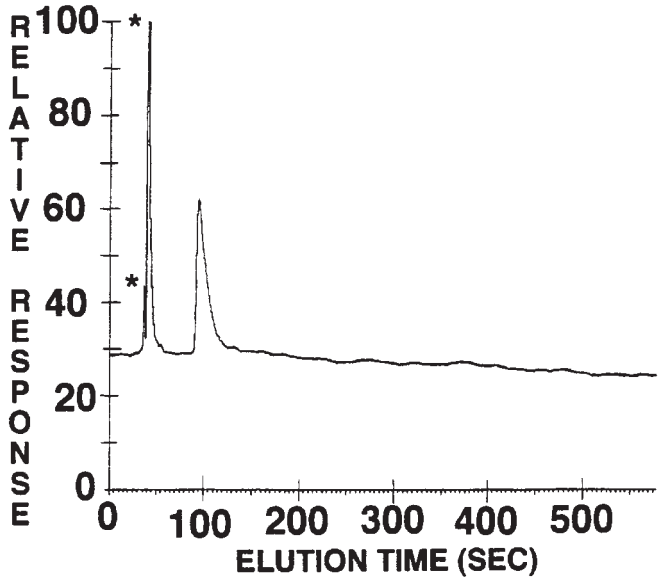
B. IR analysis

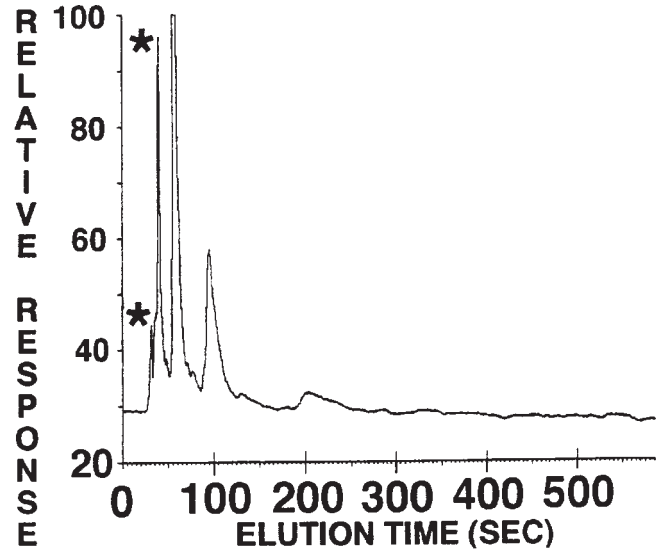
The infrared spectrum of the isolated compound did not contain OH or other extraneous signals; it was qualitatively the same as that of "42C14" or other aliphatic crown ethers.

C. HPLC analysis

The HPLC trace of the purified sample (Fig. 1*a*) does not contain the longer and shorter retention time impurities present in the starting mixture (Fig. 1*b*). It has a retention time of 93 s. As a reference point, 30C10 (3) has a retention time of 57 s under these conditions; 15C5 and 18C6 have shorter retention times. Furthermore, the major (~75%) peak in "42C14"[3] occurred at 105 s. Larger crown ethers have longer retention times.

Fig. 1. HPLC traces, H_2O:MeCN (70:30 v/v), 2 mL/min. Purified unknown, (*a*, top); crude starting mixture from filtrate, (*b*, bottom). Peaks that represent signals from the solvent are noted with an asterisk (*).





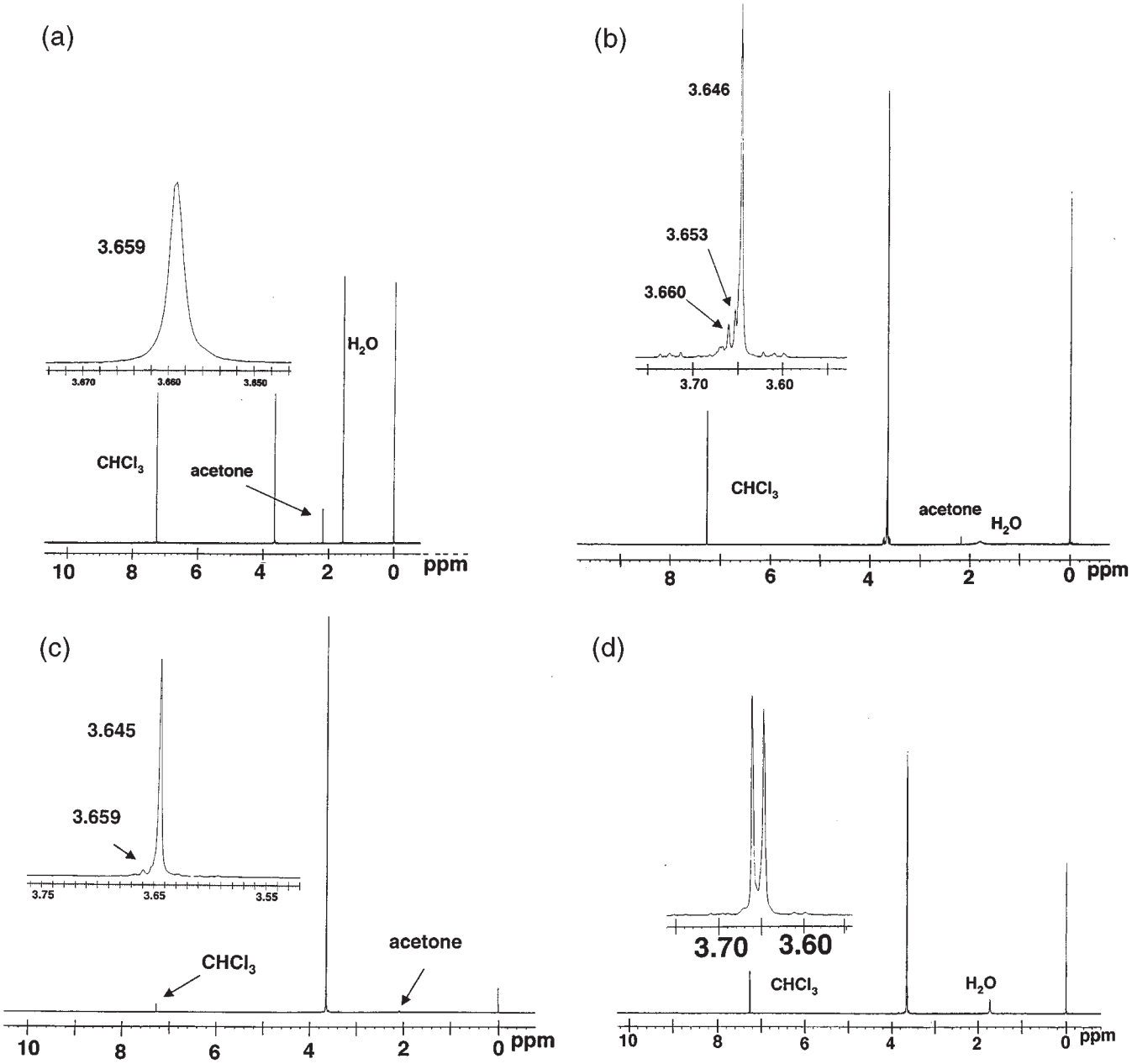
D. NMR analysis

The ^{1}H NMR spectrum of the purified sample is shown in Fig. 2*a*. It consists of a sharp singlet at 3.659 ppm without any side peaks or other signals as seen in PEOs (Fig. 2*b*). The spectrum of "42C14" (δ = 3.645 ppm) is shown in Fig. 2*c*. The spectrum of a mixture of the isolated material and "42C14" is shown in Fig. 2*d*; clearly the two can be readily distinguished. It is noteworthy that the signal for the new compound is downfield relative to "42C14."

[3] "42C14" in this case was synthesized following the "1+1" procedure of Chênevert and D'Astous (2) using hepta(ethylene glycol) and its ditosylate (4). The product was purified by column chromatography (ether, then ether:MeOH (1:1)) followed by recrystallization from toluene:hexane (1:8) twice. The HPLC trace contained peaks at shorter retention times as in Fig. 1*b*, corresponding to ca. 25% impurities. The identity of the major peak was verified by HPLC-mass spectrometry. Samples of "42C14" prepared by the method of ref. 1 also produced this same peak at 105 s along with longer retention time signals.

© 2000 NRC Canada

Fig. 2. 400 MHz ^{1}H NMR spectra in $CDCl_3$. (*a*) Purified unknown. (*b*) PEO (nominal molecular weight 1500). (*c*) "42C14"[3] (Note the small impurity signal at 3.659 ppm, corresponding to the present unknown). (*d*) Synthetic mixture of purified unknown + "42C14."[3]



The ^{13}C NMR spectrum of the new compound in $CDCl_3$ showed a single peak at 70.635 ppm (Fig. 3*a*) with no side peaks which appear in the case of linear PEOs (Fig. 3*b*). Compared to that of "42C14" (**8**) (δ = 70.555 ppm, corrected to $CDCl_3$, Fig. 3*c*) the ^{13}C NMR signal was shifted downfield by 0.080 ppm (reproducibility ±0.002 ppm). The spectrum of a mixture of the unknown and "42C14" (Fig. 3*d*) clearly shows the distinction between the two materials.

E. Mass spectrometric analysis

1. FAB in NBA/Cs$^+$ ion gun

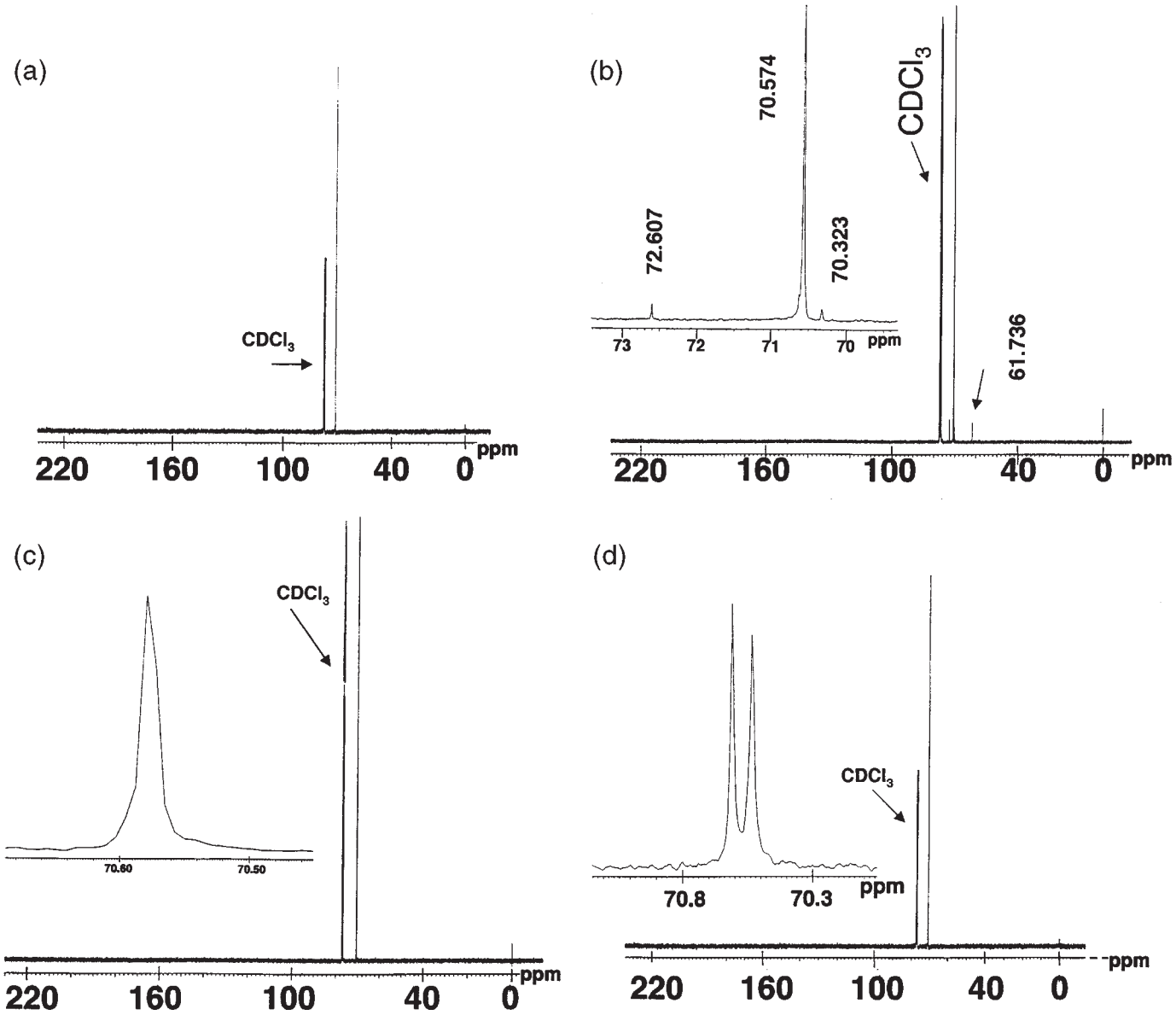
The FAB mass spectrum of the unknown from 3-nitrobenzyl alcohol (NBA) matrix using Cs^+ bombardment showed *m*/*z* = 617.4 and 639.3 ion peaks, i.e., most likely 42C14 (**8**) derived species, namely $[42C14 + H]^+$ and $[42C14 + Na]^+$, but no signals corresponding to other molecular ions were observed.

2. FAB in GLY/TFA

However, in the FAB mass spectrum from glycerol/1% trifluoroacetic acid (GLY/1% TFA) matrix using xenon bombardment (Fig. 4*a*), ions with *m*/*z* values of 1231.5, 1253.3 and 1269.2 were detected along with ions with *m*/*z* values of 617.4 ($[42C14 + H]^+$), 639.3 ($[42C14 + Na]^+$), and 655.3 ($[42C14 + K]^+$). In a matrix of GLY/NaI the sodium adduct peaks at *m*/*z* = 1253.2 and 639.5 were enhanced at the expense of the other signals (Fig. 4*b*). Similarly "42C14"[3] in GLY/1% TFA afforded the *m*/*z* = 617.4 (major), 639.3 (minor, 20% of 617.3), and 655.3 (minor, 20% of 617.3)

© 2000 NRC Canada

Fig. 3. 100 MHz ^{13}C NMR spectra in $CDCl_3$. (*a*) Purified unknown. (*b*) PEO (nominal molecular weight 1500). (*c*) "42C14."[3] (*d*) Synthetic mixture of purified unknown + "42C14."[3]



signals; with a GLY/NaI matrix the 617.4 and 655.3 peaks diminished into the noise. Notably in the spectra of the unknown (Fig. 4) the only other peak of significance is the *m*/*z* = 769.3 signal; there are no other fragments from the high mass signals, i.e., between *m*/*z* = 1231.5 and 769.3.

Upon increasing the amount of trifluoroacetic acid in the matrix (GLY/4% TFA) and changing over to Cs^+ ion bombardment, *m*/*z* = 1253.3 and 1269.2 ions were no longer detected (Fig. 5); only a strong *m*/*z* = 1231.7 ion was observed at high mass. Another new signal of lower intensity occurs at 1005.7, a strong signal was observed at *m*/*z* = 749.5 and there was also a new signal at *m*/*z* = 705.5. In the high resolution spectrum (Fig. 6) the *m*/*z* = 1231.7296 peak is consistent with $C_{56}H_{111}O_{28}$ = $(CH_2CH_2O)_{28}$ (calculated value = 1231.7262), with 2.7 ppm error; the isotopic peaks are present in approximately the abundances expected for this formula (M+1 and M+2 = 62 and 29%, respectively).

F. Thermal analysis

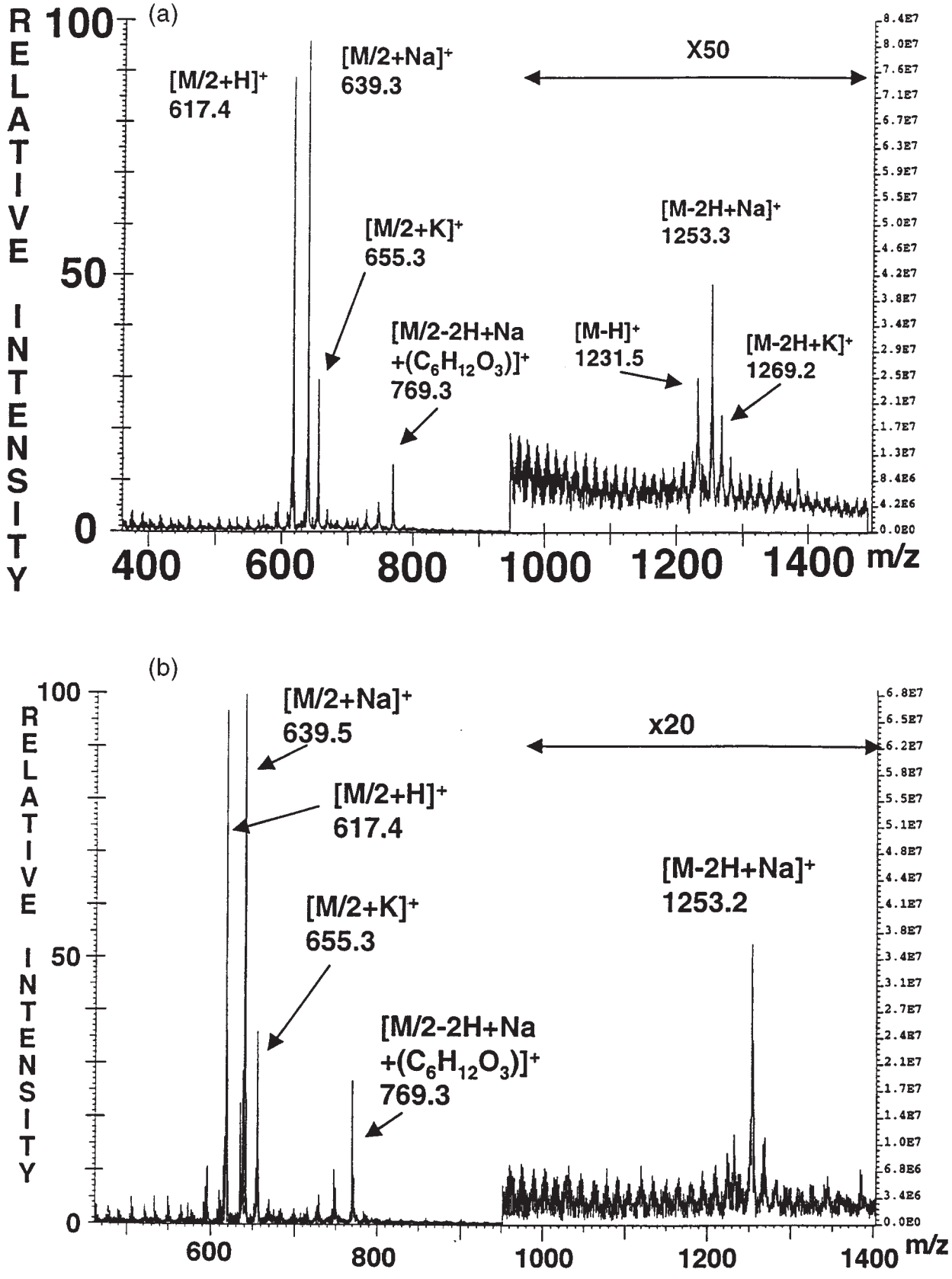
In the differential scanning calorimetric (DSC) traces (heating after slow cooling) the unknown compound displayed no melting endotherm or crystallization exotherm; the glass transition was observed at 13°C.

Discussion

Consideration of the results presented above has led us to conclude that the unknown compound is not a simple crown ether; the NMR chemical shifts conclusively argue against this; the mass spectral evidence to be discussed below supports this conclusion and the thermal properties also are inconsistent with the compound being a crown ether. The structure most consistent with these results is the [2]catenane (5) containing two 42C14 rings, i.e., **9**.

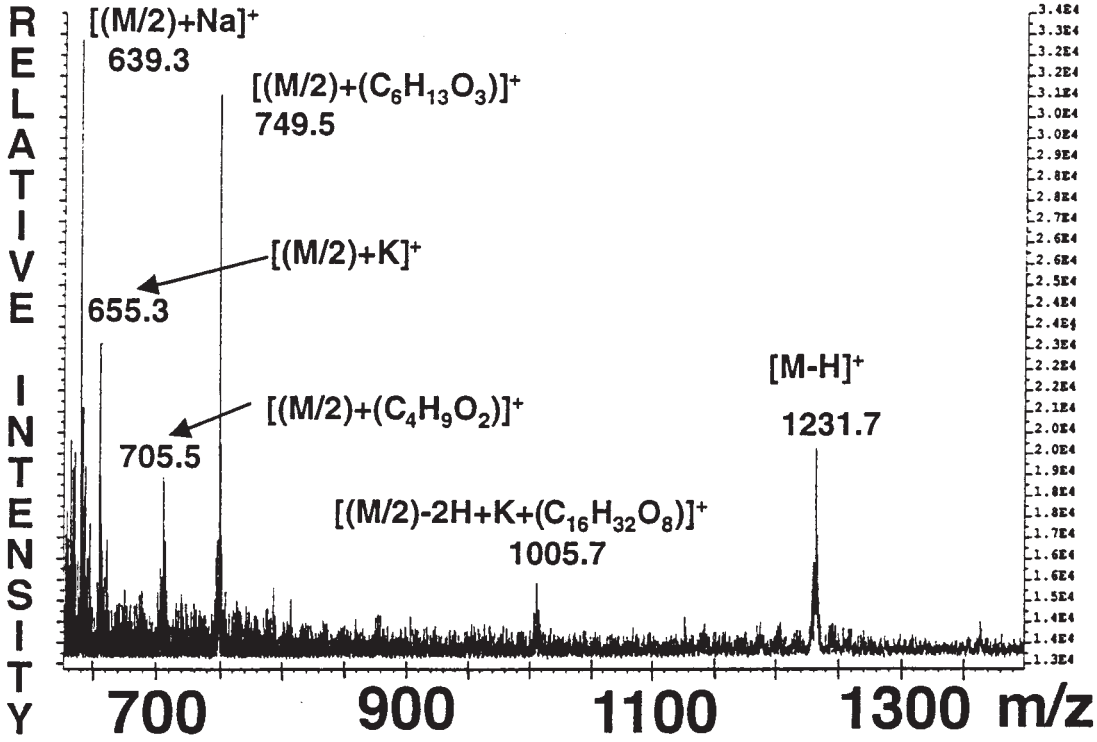
© 2000 NRC Canada

Fig. 4. FAB mass spectra of the purified unknown with xenon ionization from (*a*) GLY/1% TFA matrix. (*b*) GLY/NaI.

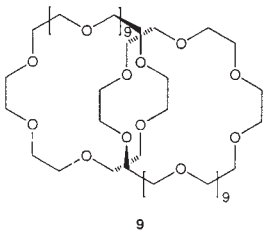


© 2000 NRC Canada

Fig. 5. FAB mass spectrum of purified unknown from GLY/4%TFA with Cs^+ ionization.



The results will now be discussed in detail in support of this assignment.



9

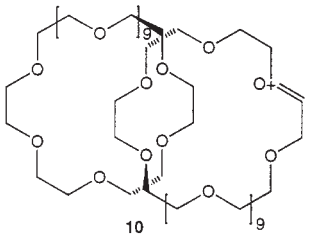
A. NMR results

In ^1H NMR downfield shifts relative to the individual components have been observed in hydrocarbon catenane systems (6). It was reasoned that because of the interlocked structure the intertwined segments of the macrocycles can not be solvated in the same manner as the unthreaded macrocycle and this lack of solvation results in the downfield shift of the ^1H NMR signal. In the present case the unknown exhibits a signal downfield from all the crown ethers larger than 30C10.

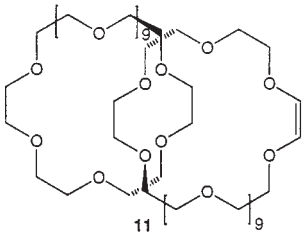
Similar shifts in ^{13}C NMR spectra have been observed in hydrocarbon catenanes relative to the individual macrocyclic components (6). These shifts to lower field were explained by interannular van der Waals interactions. In the present case again the signal of the unknown (70.635 ppm) appears well downfield from signals for crown ethers, both measured in our lab and those reported in the literature (70.53–70.44 ppm for crowns from 27C9 to 60C20 (2), and 70.30 for all large crowns (7) all in $CDCl_3$). Taken together, the NMR results conclusively argue against a crown ether structure for the unknown.

B. Mass spectral results

The lack of significant fragmentation signals between the high mass region and the low mass region corresponding to the component cyclic(s) constitutes classic mass spectral evidence for the catenane structure (8) that is now routinely sought (5). Thus, the m/z = 1231.5, 1253.3, and 1269.2 ions observed with the GLY/1% TFA matrix using xenon bombardment (Fig. 4*a*) are assigned to [**9**-H]$^+$ = **10**, [9–2H+Na]$^+$ = **11**·Na^+, and [9–2H+K]$^+$ = **11**·K^+. An alternative interpretation is that the high mass signals are due to formation of dimer structures from 42C14 in the gas phase; this possibility is inconsistent with the NMR results presented above and the thermal results presented below.



10

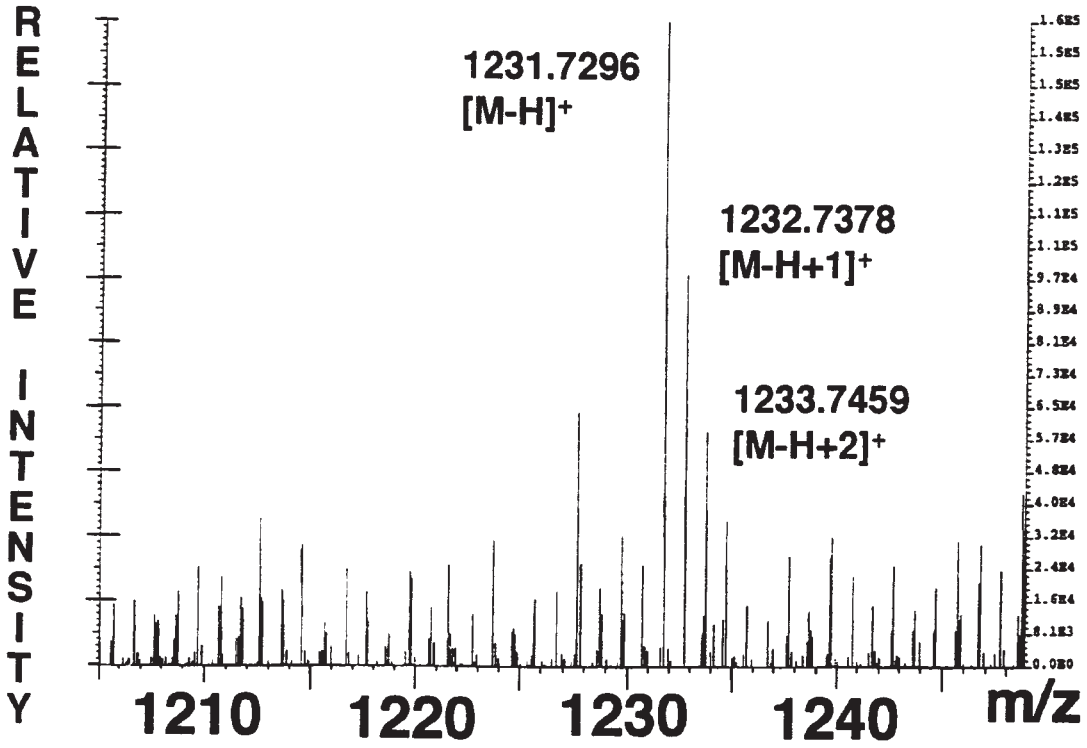


11

The observation of [M–H]$^+$ instead of M$^+$ in mass spectra of crown ethers is not unusual. In many cases of EI and FAB mass spectra of crown ethers [M+H]$^+$ and [M–H]$^+$ ions are detected instead of M$^+$ (9–12). In those cases, it is claimed that the [M+H]$^+$ ions are likely to exist in the form of open chains instead of closed rings (10). Therefore, there would be less chance to detect the [M+H]$^+$ ion peak of the 42C14-[2]catenane (**9**) because once a ring breaks down to the open chain, which is [(**9**/2)+H]$^+$ (assigned as [42C14 + H]$^+$ above), the charged linear species would dethread away from the

© 2000 NRC Canada

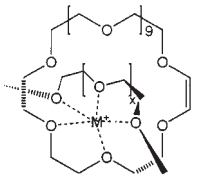
Fig. 6. High resolution FAB mass spectrum of purified unknown from GLY/4%TFA with Cs^+ ionization.



other 42C14 macrocycle. In contrast, $[M–H]^+$ ions of crowns are likely to retain the closed ring structure (9), so that the catenated $[M–H]^+$ ion **10** (*m*/*z* = 1231.5) could survive.

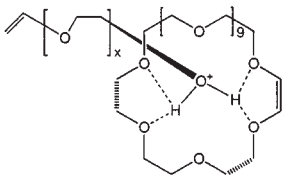
The observation of $[\mathbf{9}–2H+Na]^+$ and $[\mathbf{9}–2H+K]^+$ ions and the lack of $[\mathbf{9}+Na]^+$ and $[\mathbf{9}+K]^+$ peaks in Fig. 4 suggest that these latter metal ion complexes of the catenane are very readily converted to the former, i.e., $[\mathbf{11}+Na]^+$ and $[\mathbf{11}+K]^+$.

The modest peaks at *m*/*z* = 769.3 in Figs. 4*a* and 4*b* correspond to the $[(\mathbf{9}/2)–2H+Na+(C_6H_{12}O_3)]^+$ ion. This suggests that a neutral fragment derived from one 42C14 ring of the metal complexed catenane $[\mathbf{11}+Na]^+$ remains in the cavity of the other 42C14 because of template complexation by the metal ion, i.e., as pseudorotaxane **12** (13), until this species reaches the detector. A related phenomenon has been observed previously in the mass spectra of phenanthroline-Cu catenates, producing a Cu complex of two neutral acyclic species (14). And it appears to take place in catenanes based on cyclic amides (15). It is somewhat surprising that it has not been observed more frequently since the forces that lead to pseudorotaxane formation and thence catenation in solution should "live on" in the gas phase after one ring has been ruptured.



12: M = Na, x = 1
13: M = K, x = 6

In the mass spectra taken in GLY/4% TFA using Cs^+ ion bombardment (Figs. 5 and 6) only a strong $[\mathbf{9}–H]^+$ ion (**10**) was observed and no metal adducts. The high resolution results for this peak (*m*/*z* = 1231.7296, $C_{56}H_{111}O_{28}$ (calculated value = 1231.7262), 2.7 ppm error; isotopic peaks) support the molecular formula of the 42C14-[2]catenane (**9**). The peak at *m*/*z* = 1005.7 in Fig. 5 corresponds to $[(\mathbf{9}/2)–2H+K+(C_{16}H_{32}O_8)]^+$, presumably a complex of 42C14, K^+ and neutral linear $C_{16}H_{32}O_8$, i.e., pseudorotaxane **13**; indeed, the base peak in the spectrum corresponds to $[C_{16}H_{32}O_8+K]^+$, i.e., *m*/*z* = 391.3 (with intensity ca. 14 × *m*/*z* = 617.4). Again we speculate that **13** results from fragmentation of complex $[\mathbf{11}+K]^+$. Likewise the peaks at *m*/*z* = 705.5 and 749.5 may be due to pseudorotaxanes **14** and **15** derived from 42C14 and positively charged fragments $C_4H_9O_2^+$ and $C_6H_{13}O_3^+$, respectively, formed directly from catenane **9**.

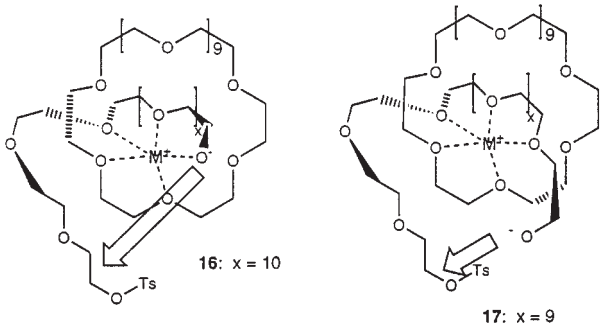


14: x = 1
15: x = 2

In fact the observation of species **12** and **13** in the gas phase suggests that the relatively high yield of the isolated compound (8% based on NMR analysis of the crude reaction mixture and 1.7% isolated) is a result of the same templating effect of the metal ions. It has been well known from the beginning (16), of course, that monocyclic crown syntheses are templated in this manner by bringing the ends of the linear precursors into proximity (17). The templating could occur between 42C14 and the paired sodium and alkoxide ions

© 2000 NRC Canada

(**16**) or alternatively by complexation of the metal ion and the crown ether at the center of the threaded (pseudorotaxane (13)) oxytosylate (**17**), allowing cyclization to give **9**; as the displacement reaction proceeds and alkoxides are consumed more free sodium ions will be available in solution to act as templating species. In this same way Sauvage and coworkers have utilized copper(I) ion as the templating agent in their elegant syntheses of phenanthroline/crown ether-based catenanes and knots (14, 17, 18), forming pseudorotaxane (13) intermediates in the process. Of course this latter templating situation is much more effective because of the rigidity of the components and the stronger complexation. Crown ether-based catenane templating with paraquat and derivatives as utilized by Stoddart et al. (19) and Becher et al. (20) in a variety of modes also relies on relatively high association constants to form the precursor pseudorotaxanes (13). Nonetheless the present results suggest that the proper choice of templating species (in excess) could lead to improved yields of aliphatic crown ether-based catenanes, especially if preformed crown ether were present initially in high concentration.



C. Thermal analysis

Aliphatic crown ethers are crystalline substances with melting points above room temperature that increase with ring size up to an asymptotic limit above 50°C (1, 2, 7). The glass transition temperatures of the crown ethers are quite low, around –67°C ~ –70°C (1), reflecting their flexible nature. The melting point of 81c27 (molecular weight 1188 Da) is reported to be 41°C (7*b*) and the melting point of 273c91 is 53°C (7*d*). If the present sample were 84c28 it would melt between these temperatures, probably ca. 45°C; thus, the catenane structural assignment is consistent with its amorphous character. It is known that large crown ethers crystallize in lamellar structures in which the macrocycles are once or twice folded (7). It is believed that due to the interlocked structure there would be little chance for such a crystalline arrangement in the solid state of the catenane, which consequently is completely amorphous. The interlocking is also expected to constrain the rings severely from a conformational point of view; thus, the fact that the glass transition temperature of the catenane is much (>80°C) higher than that for aliphatic crown ethers is not surprising.

Conclusions

The unknown compound isolated from the reaction aimed at 42C14 has been assigned the structure of a [2]catenane in which both rings are 42C14.

Experimental

Materials

Tri(ethylene glycol), tetra(ethylene glycol), NaH, *p*-toluenesulfonyl chloride (Aldrich) and THF (Mallinckrodt) were used as received. Tri(ethylene glycol) ditosylate (**2**) was synthesized (1) by the reaction of tri(ethylene glycol) with *p*-toluenesulfonyl chloride.

42C14-[2]catenane (9). NaH (7.6 g, 80% dispersed in oil, 0.25 mol) was washed with hexane and THF (80 mL) was added. To the suspension tetra(ethylene glycol) (12.14 g, 62.5 mmol) in THF (40 mL) was added slowly and tri(ethylene glycol) ditosylate (**2**, 14.34 g, 31.3 mmol) in THF (40 mL) was added to the mixture dropwise over 50 min while the mixture was stirred vigorously at reflux. The mixture was allowed to stir for 5 h and diluted to 850 mL with THF. Tri(ethylene glycol) ditosylate (14.45 g, 31.4 mmol) in THF (50 mL) was added to the refluxing mixture dropwise over 1 h. The mixture was refluxed for 28 h. The excess NaH was destroyed by addition of water and the salts were filtered off. After the evaporation of the solvent the crude product was recrystallized at –20°C. The crystals (crude crown ethers) were filtered and from the filtrate a light brown oil (9.0 g) was obtained. 2.3 g of the oil was separated into 200 fractions through a column (silica gel, 3 cm diameter, 30 cm length) using acetone as the eluent. Each fraction was checked by TLC and analyzed by NMR, if needed. 170 mg of colorless wax was obtained from the last 20 fractions; corrected to the total filtrate residue, this corresponds to a 1.7% yield.

Characterization techniques

NMR was done on a Varian Unity 400 spectrometer at ambient temperature with tetramethylsilane and $CDCl_3$ as the internal references for ^1H and ^{13}C NMR spectra, respectively. A Perkin–Elmer 283B IR spectrometer was used. For the HPLC analysis, an ISCO model 2350 HPLC instrument was used with a Novapak-C_{18} column eluted with a mixture of water and acetonitrile (75:25 by vol) with a flow rate of 2 mL/min; a refractive index detector (Waters, Differential Refractometer R401) was used. Thermal analysis was done on a Perkin–Elmer DSC-4 instrument at 5°C/min. The sample was heated to 150°C and cooled slowly to 0°C. The second heating was run at 5°C/min. The FAB mass spectra were obtained from the Midwest Center for Mass Spectrometry (MCMS) at the University of Nebraska-Lincoln and the Washington University Mass Spectrometry Resource (WUMSR), St. Louis, Missouri. The experimental conditions for the FAB mass spectrometry at the MCMS were as follows: Fisons VG ZAB mass spectrometer operating at 8 keV, ionization by a Cs^+ ion gun operating at 25 keV, matrix: 3-nitrobenzyl alcohol or glycerol/4% trifluoroacetic acid. The experimental conditions for the FAB mass spectrometry at WUMSR were as follows: Fisons VG ZAB SE double-focusing mass spectrometer operating at 8 keV, ionization by xenon gas at 1 mA, matrix: glycerol/1% trifluoroacetic acid. Samples were scanned over a mass range of 100 to 1500 at 10 s/decade; data collection and processing were done with the VG OPUS data system.

© 2000 NRC Canada

Acknowledgements

The authors acknowledge Donghang Xie and Nori Yamaguchi for their help with HPLC and DSC analyses and Caiguo Gong for data on "42C14."[3] Also we express our appreciation to the Midwest Center for Mass Spectrometry with partial support by the NSF, Biology Division (Grant No. DIR9017262) and the Washington University Mass Spectrometry Resource, an NIH Research Resource (grant no. P41RR0954). Finally, we gratefully acknowledge the NSF for financial support through grant CHE-95-21738.

References

1. H.W. Gibson, M.C. Bheda, P. Engen, Y.X. Shen, J. Sze, H. Zhang, M.D. Gibson, Y. Delaviz, S.-H. Lee, S. Liu, L. Wang, and D. Nagvekar. J. Org. Chem. **59**, 2186 (1994).
2. R. Chênevert and L. D'Astous. J. Heterocycl. Chem. **23**, 1785 (1986).
3. M. Bheda, J. Merola, W. Woodward, V. Vasudevan, and H.W. Gibson. J. Org. Chem. **59**, 1694 (1994).
4. E.M.D. Keegstra, J.W. Zwikker, M.R. Roest, and L.W. Jenneskens. J. Org. Chem. **57**, 6678 (1992).
5. For reviews of catenanes see the following: (*a*) G. Schill. Catenanes, rotaxanes and knots. Academic Press, New York. 1971; (*b*) H.W. Gibson, M.C. Bheda, and P.T. Engen. Prog. Polym. Sci. **19**, 843 (1994); (*c*) D.B. Amabilino and J.F. Stoddart. Chem. Rev. **95**, 2725 (1995); (*d*) J.-C. Chambron, C. Dietrich-Buchecker, and J.-P. Sauvage. *In* Large ring molecules. *Edited by* J.A. Semlyen. John Wiley and Sons, New York. 1996. pp. 155–190; (*e*) R. Jäger and F. Vögtle. Angew. Chem. Int. Ed. Engl. **36**, 931 (1997); (*f*) M. Beohradsky, F.M. Raymo, and J.F. Stoddart. Coll. Czech. Chem. Commun. **62**, 527 (1997); (*g*) S.A. Nepogodiev and J.F. Stoddart. Chem. Rev. **98**, 1959 (1998); (*h*) Molecular catenanes, rotaxanes and knots. *Edited by* J.-P. Sauvage and C.O. Dietrich-Buchecker. Wiley-VCH, Weinheim. 1999.
6. H. Fritz, E. Logemann, G. Schill, and T. Winkler. Chem. Ber. **109**, 1258 (1976); G. Schill, N. Schweickert, H. Fritz, and W. Vetter. Angew. Chem. Int. Ed. Engl. **22**, 889 (1983).
7. (*a*) K. Viras, Z.-G. Yan, C. Price, C. Booth, and A.J. Ryan. Macromolecules, **28**, 104 (1995); (*b*) Z. Yang, G.-E. Yu, J. Cooke, K. Viras, A. J. Ryan, and C. Booth. J. Chem. Soc. Faraday Trans. **92**, 3173 (1996); (*c*) Z. Yang, J. Cooke, K. Viras, P.A. Gorry, A.J. Ryan, and C. Booth. J. Chem. Soc. Faraday Trans. **93**, 4033 (1997); (*d*) J. Cooke, K. Viras, G.-E. Yu, T. Sun, T. Yonemitsu, A.J. Ryan, C. Price, and C. Booth. Macromolecules, **31**, 3030 (1998).
8. W. Vetter and G. Schill. Tetrahedron, **23**, 3079 (1967); W. Vetter, E. Logemann, and G. Schill. Org. Mass Spectrom. **12**, 351 (1977).
9. G. Podda, L. Corda, A.M. Maccioni, and P. Traldi. Org. Mass Spectrom. **21**, 395 (1986).
10. G. Podda, L. Corda, C. Anchisi, B. Pelli, and P. Traldi. Org. Mass Spectrom. **22**, 162 (1987).
11. M.A. Baldwin, K.J. Welham, I. Toth, and W.A. Gibbons. Org. Mass Spectrom. **23**, 697 (1988).
12. O. Curcuruto, P. Traldi, G. Moneti, L. Corda, and G. Podda. Org. Mass Spectrom. **26**, 713 (1991).
13. For reviews on pseudorotaxanes and rotaxanes see: refs. 5*a*–5*c*, 5*e*, 5*g* and 5*h*. D. Philp and J.F. Stoddart. Angew. Chem. Int. Ed. Engl. **35**, 1155 (1996); H.W. Gibson. *In* Large ring molecules. *Edited by* A.J. Semlyen. John Wiley and Sons, New York. 1996. pp. 191–262; A. Harada. Acta Polymer, **49**, 3 (1998); F.M. Raymo and J.F. Stoddart. Chem. Rev. **99**, 1643 (1999); E. Mahan and H.W. Gibson. *In* Cyclic polymers. 2nd ed. *Edited by* J.A. Semlyen. Thomson Science and Professional, London, U.K. in press.
14. F. Bitsch, G. Hegy, C. Dietrich-Buchecker, E. Leize, J.-P. Sauvage, and A. van Dorsselaer. New J. Chem. **18**, 801 (1994).
15. A.F. Johnston, D.A. Leigh, R.J. Pritchard, and M.D. Deegan. Angew. Chem. Int. Ed. Engl. **34**, 1209 (1995); in Fig. 3 a series of minor peaks from m/z = 535 to m/z = 765, all greater than the mass of the single macrocycle (535) and less than that of the [2]catenane ($[M+H]^+$ = 1069), may represent pseudorotaxane fragments.
16. C.J. Pedersen. J. Am. Chem. Soc. **89**, 7017 (1967).
17. For an exceptionally thorough review of the utilization of the concept of templating effects and a creative exposition of the possibilities that lie ahead see: T.J. Hubin, A.G. Kolchinski, A.L. Vance, and D.H. Busch. Adv. Supramol. Chem. **5**, 237 (1999).
18. C. Dietrich-Buchecker and J.-P. Sauvage. Chem. Commun. 615 (1999); D.J. Cárdenas, J.-P. Collin, P. Gaviña, J.-P. Sauvage, A. De Cian, J. Fischer, N. Armaroli, L. Flamigni, V. Vicinelli, and V. Balzani. J. Am. Chem. Soc. **121**, 5481 (1999); G. Rapenne, C. Dietrich-Buchecker, and J.-P. Sauvage. J. Am. Chem. Soc. **121**, 994 (1999), and refs. therein.
19. M. Asakawa, P.R. Ashton, V. Balzani, S.E. Boyd, A. Credi, G. Mattersteig, S. Menzer, M. Montalti, F.M. Raymo, C. Ruffilli, J.F. Stoddart, M. Venturi, and D.J. Williams. Eur. J. Org. Chem. 985 (1999); P.R. Ashton, A.M. Heiss, D. Pasini, F.M. Raymo, A.N. Shipway, J.F. Stoddart, and N. Spencer. Eur. J. Org. Chem. 995 (1999); D.B. Amabilino, P.R. Ashton, J.A. Bravo, F.M. Raymo, J.F. Stoddart, A.J.P. White, and D.J. Williams. Eur. J. Org. Chem. 1295 (1999), and refs. therein.
20. Z.-T. Li, P.C. Stein, J. Becher, D. Jensen, P. Mork, and N. Svenstrup. Chem. Eur. J. **2**, 624 (1996); Z.-T. Li and J. Becher. J. Chem. Soc. Chem. Commun. 639 (1996); Z.-Y. Li and J. Becher. SynLett. 557 (1997), and refs. therein.

© 2000 NRC Canada

Radicals from fragmentation of benzyloxymethoxycarbenes in solution

Nadine Merkley, Manal El-Saidi, and John Warkentin

Abstract: 2-Benzyloxy-2-methoxy-5,5-dimethyl-Δ^3-1,3,4-oxadiazolines, including the parent as well as *p*-substituted analogues, undergo thermolysis at 100°C in benzene to afford a mixture of products. Two primary fragmentations of the oxadiazolines were identified. The major pathway involves 1,3-dipolar cycloreversion to N_2 and the corresponding carbonyl ylides. The latter dissociate to acetone and the corresponding benzyloxy(methoxy)carbenes, which undergo fragmentation to $ArCH_2$ and MeOCO radical pairs that recombine to afford methyl arylacetates. Carbene dimers were not observed, showing that the fragmentation process is faster than carbene dimerization. A second fragmentation pathway observed for the oxadiazolines is an alternative cycloreversion to the corresponding benzyl methyl carbonate and 2-diazopropane. Products from diazopropane included acetone azine and, in some instances, traces of propene.

Key words: benzyloxy(methoxy)carbene, carbene, radical pair, rearrangement.

Résumé : Les 2-benzyloxy-2-méthoxy-5,5-diméthyl-Δ^3-1,3,4-oxadiazolines, y compris le produit fondamental ainsi que les analogues substitués en position *para*, donnent lieu à une thermolyse, à 100°C dans le benzène, qui conduit à un mélange de produits. On a identifié les deux fragmentations primaires des oxadiazolines. La voie principale implique une cycloréversion 1,3-dipolaire en N_2 et en ylures de carbonyles correspondants. Ces derniers se dissocient en acétone et en benzyloxy(méthoxy)carbènes correspondants qui se fragmentent en paires de radicaux $ArCH_2$ et MeOCO qui se recombinent pour donner des arylacétates de méthyle. On n'a pas observé la formation de dimères de carbènes ce qui démontre que le processus de fragmentation est plus rapide que la dimérisation des carbènes. Une deuxième voie de fragmentation observée pour les oxadiazolines est une cycloréversion alternative en 2-diazopropane et en carbonate de benzyle et de méthyle correspondant. Les produits résultant du diazopropane comprennent l'azine de l'acétone et, dans quelques cas, des traces de propène.

Mots clés : benzyloxy(méthoxy)carbène, carbène, paire de radicaux, réarrangement.

[Traduit par la Rédaction]

Introduction

There has been a resurgence of interest in the chemistry of dialkoxycarbenes (1) since the early work of Hoffmann (2), and Lemal et al. (3) with dialkoxycarbenes derived from norbornadien-7-one acetals. Much of the subsequent work was done by R.A. Moss and his group, who first generated dialkoxycarbenes from diazirines (4–10). Recently oxadiazolines (11) have also been used to generate dialkoxycarbenes, which were shown to react with a variety of unsaturated moieties including anhydrides (12), C60 (13–15), methylenecyclopropanes (16), alkynes (17, 18), fluorenone (19), α, β-unsaturated isocyanates (20, 21), a bisketene (22), and hexachlorocyclopentadiene (23), for example. They also attack aromatics substituted with electron-withdrawing groups to effect nucleophilic aromatic substitution (24).

Dialkoxycarbenes also undergo intramolecular rearrangements, at least in the gas phase in a mass spectrometer, to generate esters (25). Hoffmann et al. reported in 1972 that allyloxymethoxycarbene dissociates to allyl and methoxycarbonyl radicals in the gas phase (26). Intramolecular reactions of dialkoxycarbenes appeared to be slow in solution, the major products formed in the absence of a trap being the carbene dimers (4, 5, 27). However, a few cases of fragmentation of allyloxymethoxycarbenes to radical pairs, in solution at 110°C, were recently reported (28). In one of those cases, the carbene was intercepted with *tert*-butyl alcohol and the radicals were trapped with TEMPO. Thus the sequence oxadiazoline → carbene → radicals was established for the first time, ruling out a potential direct pathway from precursor to radicals.

We now report that the carbenes with a benzyloxy or *p*-substituted benzyloxy substituent ($ArCH_2O(MeO)C$:) also fragment to radicals in solution. Thermolysis of 2-benzyloxy-2-methoxy-5,5-dimethyl-Δ^3-1,3,4-oxadiazolines at 100°C in the presence of alcohols (ROH) affords orthoformates $(ArCH_2O)(MeO)(RO)CH$, formed by trapping $(ArCH_2O)(MeO)C$:. In the absence of a carbene trap however, the carbenes fragment to benzylic radicals and methoxycarbonyl radicals, both of which can be trapped with TEMPO. The radicals couple to afford methyl arylacetates, both in the presence or in the absence of TEMPO. Competing fragmentation of the oxadiazolines to the corresponding benzyl methyl carbonate and 2-diazopropane also occurs.

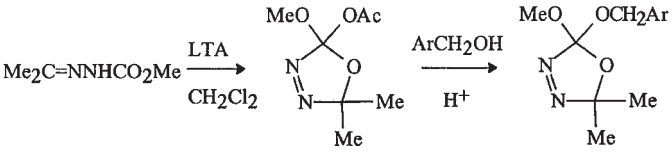
Received October 14, 1999.

N. Merkley, M. El-Saidi, and J. Warkentin.[1] Department of Chemistry, McMaster University, Hamilton, ON L8S 4L8, Canada.

[1]Author to whom correspondence may be addressed. Fax: (905) 525 2509. e-mail: warkent@mcmaster.ca

© 2000 NRC Canada

Scheme 1.



a: Ar= C_6H_5 ; **b**: Ar = 4-MeC_6H_4; **c**: Ar= 4-$MeOC_6H_4$; **d**: Ar= 4-ClC_6H_4; **e**: Ar= 4-$CF_3C_6H_4$; **f**: Ar= 4-$NO_2C_6H_4$

Methods, results, and discussion

Oxadiazolines **2** were prepared from the methoxycarbonyl hydrazone of acetone via 2-acetoxy-2-methoxy-5,5-dimethyl-Δ^3-1,3,4-oxadiazoline (**1**) by the exchange method (29), illustrated in Scheme 1. They were purified by chromatography on silica with a Chromatotron apparatus, and they were identified by means of ^{1}H and ^{13}C NMR spectroscopies at 200 and 50 MHz, respectively. Diastereotopicity of the CH_2 protons was evident. Moreover, the ^{13}C spectra are diagnostic for oxadiazolines of that type, with δ values near 137.5 for C-2 and 118.5 for C-5 (11). In the mass spectra, **2** afforded neither molecular ions nor M – N_2 ions.

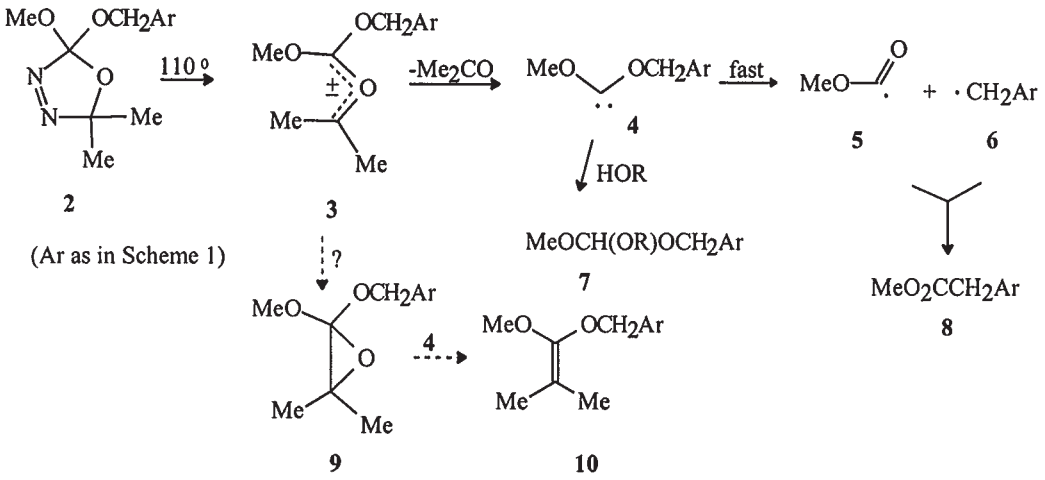
Thermolyses were carried out with degassed solutions in benzene-d_6 (initial oxadiazoline concentration 0.1 M) at 100 ± 0.1°C. Reaction products were examined by ^{1}H NMR spectroscopy before the tube was opened (in cases of small scale runs with NMR tubes) to facilitate recognition of initial products rather than those that might have arisen from rearrangements or hydrolyses during separation procedures. The reported yields (isol) are probably considerably lower than the chemical yields because reactions were run on a small scale (one mmol or less) and because of some difficulties with the separation of recognized products from one another and from minor co-products.

Scheme 2 outlines the overall thermolysis chemistry of the benzyloxymethoxy oxadiazolines, including some reactions that are included on the basis of analogy. The major first step is 1,3-dipolar cycloreversion to N_2 and carbonyl ylide **3**, supported by the finding that the rate constants for oxadiazoline thermolysis are relatively insensitive to the *para* substituent, and in the order *p*-NO_2 > *p*-CF_3 > *p*-Cl > *p*-H > *p*-Me > *p*-OMe (2.83, 2.62, 2.55, 2.35, 2.11, and 2.09, all × 10^{-5} s^{-1}). The reverse order would be expected if the thermolyses gave carbenes in one step, as proposed by Smith (30). The step forming **3** was assigned by analogy to instances in which a carbonyl ylide intermediate is mandatory, because a ketene acetal was among the products (27). Ylide **3** fragments to carbene **4**, possibly in competition with electrocyclic ring closure to oxirane (**9**) (19), from which a ketene acetal (**10**) might be generated by abstraction of the ring oxygen by the carbene (31). In the present cases, ketene acetals were not detectable in the crude reaction mixtures by ^{1}H NMR spectroscopy nor were any isolated. Thus, they were probably either formed in minor yields or they were absent altogether.

Intermediacy of carbenes **4** was conveniently demonstrated in a few cases by running thermolyses of oxadiazolines from which the alcohol ($ArCH_2OH$) used in the exchange reaction had not been removed. The excess alcohol trapped the carbene to afford the appropriate orthoformate (**7**, R = CH_2Ar). In other cases, *tert*-butyl alcohol (0.5 M) was used to intercept carbenes by converting them into analogous orthoformates **7** (R = *t*-Bu). Fragmentation of the carbenes to radicals **5** and **6** is apparently slower than trapping with *t*-BuOH at [*t*-BuOH] = 0.5 M. To estimate the rate constant for fragmentation of **4**, we modeled trapping of **4** with *t*-BuOH at 100°C with analogous trapping of (*p*-$MeOC_6H_4)_2C$: at ambient temperature (k = 0.4 × 10^9 M^{-1} s^{-1}) (32). Taking $k_{100°C}$ = 10^9 M^{-1} s^{-1} and the efficiency of trapping to be at least 98%, the estimated fragmentation rate constant for **4** is ≤10^7 s^{-1}. A fragmentation rate constant of 10^5 s^{-1} would be more than sufficient to prevent carbene dimerization in the absence of a carbene trap, because the carbene is generated very slowly from the oxadiazoline and its concentration must be extremely low. Dialkoxycarbenes that do not fragment to radicals generally do afford carbene dimers when generated in unreactive solvents (4, 5, 27).

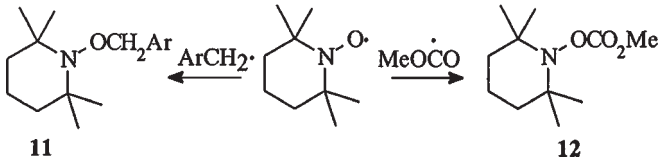
Radicals **5** and **6** must be born as a singlet pair (28), because the precursor carbene is a singlet lying below the triplet by more than 70 kcal mol^{-1} (4), and they couple to afford methyl arylacetates (**8**), Scheme 2. Only those radicals that have diffused out of the solvent cage in which they were born are trapped with TEMPO; in-cage coupling converts

Scheme 2.

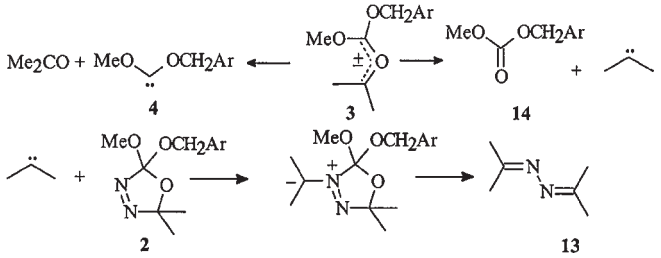


© 2000 NRC Canada

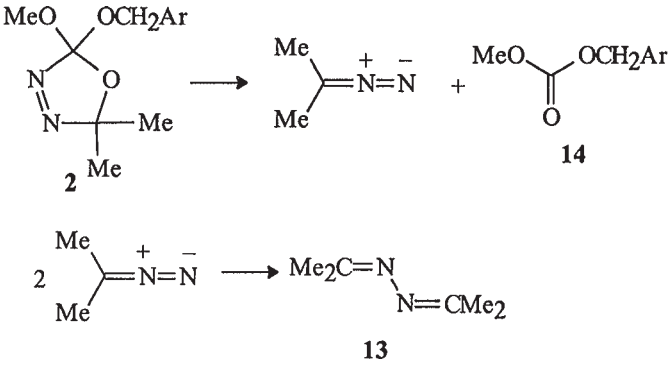
Scheme 3.



Scheme 4.



Scheme 5.



pairs to methyl arylacetate. In accord with that mechanism, small amounts (ca. 8% in the case of **1a**) of 1,2-diarylethanes, from coupling of benzylic radicals (**6**) in the absence of TEMPO, were indicated by GCMS although none could be isolated. Several other minor products, indicated in GC traces, were not identified.

Most of the methyl arylacetates (**8**) are well known although some had not been characterized by NMR spectroscopy. The NMR data are therefore included here. Esters **8b** and **8d** were also prepared independently by acid catalysed esterification of appropriate arylacetic acids. Their spectra agreed well with the spectra of corresponding **8** from oxadiazoline thermolysis.

Thermolysis of **2** in the presence of 2,2,6,6-tetramethyl-1-piperdinyloxy (TEMPO, 0.5 M)) afforded **11** and **12**. Those adducts, which arise from the coupling of methoxycarbonyl- and benzylic radicals with TEMPO, Scheme 3, constitute firm evidence for the intermediacy of radicals. The fact that ester **8a** and **11** were formed in approximately 1:1 ratio is not surprising, because 0.5 M TEMPO is not expected to compete with in-cage coupling. Formation of a fraction of the **8a** by a 1,2-rearrangement of carbene **4a** cannot be excluded from the experimental evidence. However, a computational study of allyloxyhydroxycarbene clearly indicated that homolysis of that carbene is strongly favoured over 1,2-rearrangement[2] and we assume that the same would be true for carbenes **4**.

A minor product obtained in some cases was acetone azine, **13**. It cannot be accommodated easily within the ylide mechanism of Scheme 1. Although fragmentation of the ylide intermediate to dimethylcarbene and carbonate, in competition with its fragmentation to dialkoxycarbene and acetone, could be proposed, the dimethylcarbene would then have to attack the oxadiazoline starting material to generate acetone azine, as in Scheme 4. An analogous process was proposed earlier for reactions with much higher initial oxadiazoline concentrations (33). It is now known that dimethylcarbene undergoes 1,2-H migration with $k = 1.4 \times 10^8\ s^{-1}$ at room temperature (34–36). That fast rearrangement, which is probably still faster at 100°C, makes it unlikely that acetone azine arises according to Scheme 4 and, for that reason, a second 1,3-dipolar cycloreversion (Scheme 5) of some oxadiazolines (37) is proposed. The mechanism is not firmly established, however. Although the appropriate carbonate **14** was obtained, its formation is not necessarily diagnostic for the alternate cycloreversion because reaction of **9** with **4** would afford the same carbonate, together with **10**. A comparison of the yields of azine and **10**, which might have helped, was not possible because the composite ^1H NMR spectra of the crude reaction mixture were too complicated to exclude low yields of the ketene acetals, which might not totally survive the reaction conditions in any case (27).

Authentic methyl benzyl carbonates **14b** and **14e**, prepared from the appropriate $ArCH_2OH$ and methyl chloroformate, gave NMR spectra in agreement with those of the corresponding **14** from oxadiazoline thermolysis.

The alternative cycloreversion reaction of the oxadiazolines to a carbonate ester and diazopropane is not well understood. It may be a general, although minor, competitor in other oxadiazoline thermolyses, which commonly produce traces of by-products that have not been identified.

Summary

2-Benzyloxy-2-methoxy-5,5-dimethyl-Δ^3-1,3,4-oxadiazolines undergo thermolysis at 100°C in benzene, by competing cycloreversions, affording either N_2 and a carbonyl ylide or 2-diazopropane and a carbonate ester. The carbonyl ylide fragments to acetone and a benzyloxy(methoxy)carbene, which fragments further to the methoxycarbonyl radical and a benzylic radical. Those radicals couple to afford methyl arylacetates. Formation of 2-diazopropane was inferred from the presence of acetone azine among the products.

Experimental

For product isolation, thermolyses were carried out with degassed solutions of substrate (1 mmol in 30 mL of dry benzene, 96 h) in a constant temperature oil bath at 100 ± 0.1°C. Products were isolated by means of centrifugal chromatography. For examination of a crude reaction mixture by NMR spectroscopy, thermolyses were run with degassed solutions in sealed NMR tubes (ca. 10 mg in 0.5 mL of C_6D_6). Unless otherwise indicated, the reported NMR data refer to

[2] D.L. Reid and J. Warkentin. Manuscript in preparation.

© 2000 NRC Canada

$CDCl_3$ solutions containing TMS. In the MS data, numbers in brackets are relative intensities.

Synthesis of oxadiazolines

Oxadiazolines **2** were prepared from a mixture of 2-acetoxy-2-methoxy-5,5-dimethyl-Δ^3-1,3,4-oxadiazoline (**1**, ca. 75%) and its acyclic isomer, methyl-2,3-diaza-4-methyl-4-acetoxypent-2-enoate (29) (ca. 25%) by treatment with the appropriate benzylic alcohol in dichloromethane containing acetic acid. For example, 3.6 mmol of **2** and 1.0 mmol of alcohol in CH_2Cl_2 (35 mL) containing acetic acid (1 mL) was refluxed for 48 h. Most of the solvent was removed with a rotary evaporator and the residue was stirred for one hour with 5% aqueous KOH. Extraction with CH_2Cl_2, drying over $MgSO_4$, and evaporation of the volatile components left the oxadiazolines in nearly pure form. Yields for the exchange step ranged from 60 to 90%, based on the alcohol. In some cases the analogous procedure, but with the alcohol in excess, gave an oxadiazoline containing about 20% of the alcohol. Thermolysis of those mixtures served as probes for the intermediacy of a carbene with the alcohol acting as a trap for it.

Oxadiazoline ***2a***: Oil, yield 89%. ^{1}H NMR δ: 1.48 (3H, s), 1.51 (3H, s), 3.43 (3H, s), 4.68 (1H, d, ^2J = –11.5 Hz), 4.78 (1H, d, ^2J = –11.5 Hz), 7.24–7.27 (5H, m). ^{13}C NMR δ: 23.9, 24.0, 51.9, 66.6, 119.3, 127.7, 127.8, 128.3, 136.6, 137.1. MS (CI, NH_3) *m*/*z*: 207 (40), 184 (29), 179 (12), 108 (100), 73 (12).

2b: Oil, 60% yield. ^{1}H NMR δ: 1.54 (3H, s), 1.57 (3H, s), 2.34 (3H, s), 3.48 (3H, s), 4.69 (1H, d, ^2J = –11 Hz), 4.79 (1H, d, ^2J = –11 Hz), 7.14 (2H, d, ^3J = 7 Hz), 7.24 (2H, d, ^3J = 7 Hz). ^{13}C NMR δ: 21.1, 24.0, 52.0, 66.6, 119.4, 127.9, 129.0, 133.6, 137.6, 142.6. MS (EI) *m*/*z*: 105 (100), 73 (59), 59 (10). MS (CI, NH_3) *m*/*z*: 198 (25), 147 (43), 122 (100), 73 (18), 58 (14).

2c: Oil, 77% yield. ^{1}H NMR δ: 1.55 (3H, s), 1.57 (3H, s), 3.48 (3H, s), 3.80 (3H, s), 4.66 (1H, d, ^2J = –13 Hz), 4.74 (1H, d, ^2J = –13 Hz), 6.87 (2H, d, ^3J = 9 Hz), 7.28 (2H, d, ^3J = 9 Hz). ^{13}C NMR δ: 23.9, 24.1, 51.9, 55.1, 66.4, 113.7, 119.2, 129.5, 130.2, 136.9, 159.3. MS (EI) *m*/*z*: 196 (10), 138 (32), 121 (100). MS (CI, NH_3) *m*/*z*: 267 ($(M + H)^+$, 4), 163 (100), 121 (78).

2d: Oil, 90% yield. ^{1}H NMR δ: 1.53 (3H, s), 1.58 (3H, s), 3.47 (3H, s), 4.72 (1H, d, ^2J = –11.8 Hz), 4.81 (1H, d, ^2J = –11.8 Hz), 7.30 (2H, d, ^3J = 5 Hz), 7.33 (2H, d, ^3J = 5 Hz). ^{13}C NMR δ: 24.0, 24.1, 51.9, 65.9, 119.4, 128.5, 129.0, 133.7, 135.3, 137.6. MS (EI) *m*/*z*: 127 (30), 125 (100), 89 (16), 73 (77), 59 (10). MS (CI, NH_3) *m*/*z*: 288 ($(M + NH_4)^+$, 8), 218 (11), 195 (8), 167 (5), 144 (33), 142 (100), 125 (25), 73 (26), 60 (26).

2e: Oil, 88% yield. ^{1}H NMR δ: 1.54 (3H, s), 1.59 (3H, s), 3.48 (3H, s), 4.83 (1H, d, ^2J = –8.2 Hz), 4.93 (1H, d, ^2J = –8.2 Hz), 7.46 (2H, d, ^3J = 8.1 Hz), 7.60 (2H, d, ^3J = 8.1 Hz). ^{19}F NMR ($CDCl_3$, $CFCl_3$) δ: –62.5 (s). ^{13}C NMR δ: 23.9, 24.2, 52.0, 65.9, 119.7, 125.3, 125.4, 127.6, 130.3, 136.9, 140.9. MS (EI) *m*/*z*: 159 (100), 140 (10), 127 (11), 109 (23), 84 (12), 73 (94), 59 (29). MS (CI, NH_3) *m*/*z*: 322 ($(M + NH_4)^+$, 6), 193 (10), 176 (100), 131 (15), 60 (52).

2f: Oil, 64% yield. ^{1}H NMR δ: 1.55 (3H, s), 1.58 (3H, s), 3.47 (3H, s), 4.94 (2H, m), 7.52 (2H, d, ^3J = 8.7 Hz), 8.21 (2H, d, ^3J = 8.7 Hz). ^{13}C NMR δ: 23.9, 24.3, 52.1, 65.5, 119.9, 123.6, 127.8, 136.9, 144.4, 147.6. MS (EI) *m*/*z*: 211 (8), 152 (17), 136 (40), 120 (16), 106 (10), 84 (31), 73 (100). MS (CI, NH_3) *m*/*z*: 299 ($(M + NH_4)^+$, 100), 282 ($(M + H)^+$, 8).

Orthoformate ***7a***: (R = *t*-Bu, Ar = benzyl). Yield 61%. ^{1}H NMR (C_6D_6) δ: 1.26 (9H, s), 3.21 (3H, s), 4.60 (2H, s), 5.36 (1H, s), 7.03–7.15 (5H, m). ^{13}C NMR (C_6D_6) δ: 28.8, 49.8, 65.1, 73.9, 109.5, 127.5, 128.4, 128.6, 139.6. MS (EI) *m*/*z*: 193 (17), 181 (61), 151 (36), 91 (100).

7c: (R = Ar = 4-methoxybenzyl) ^{1}H NMR δ: 3.36 (3H, s), 3.79 (6H, s), 4.56 (4H, s), 5.24 (1H, s), 6.86 (2H, d, ^3J = 8.7 Hz), 7.26 (2H, d, ^3J = 8.7 Hz). HRMS: calcd for $C_{18}H_{22}O_5$: 318.1467; found 318.1452.

7f: (R = Ar = 4-nitrobenzyl) ^{1}H NMR δ: 3.44 (3H, s), 4.78 (4H, s), 5.39 (1H, s), 7.52 (4H, d, ^3J = 8.7 Hz), 8.20 (4H, d, ^3J = 8.7 Hz).

Methyl phenylacetate ***8a***: (38) Oil, 20% yield. ^{1}H NMR δ: 3.60 (2H, s), 3.66 (3H, s), 7.25–7.35 (5H, m).

8b: (39) ^{1}H NMR δ: 2.30 (3H, s), 3.56 (2H, s), 3.64 (3H, s), 7.12 (5H, m). MS (EI) *m*/*z*: 164 (M^+, 27), 105 (95). MS (CI, NH_3) *m*/*z*: 182 $(M + NH_4)^+$.

8c: (40) Oil, 35% yield. ^{1}H NMR δ: 3.55 (2H, s), 3.67 (3H, s), 3.77 (3H, s), 6.84 (2H, d, ^3J = 8.5 Hz), 7.18 (2H, d, ^3J = 8.5 Hz). ^{13}C NMR δ: 40.1, 51.8, 55.1, 113.9, 125.9, 130.2, 158.6, 172.2.

8d: (39) Oil, 21% yield. ^{1}H NMR δ: 3.59 (2H, s), 3.69(3H, s), 7.20 (2H, d, ^3J = 8.5 Hz), 7.29 (2H, d, ^3J = 8.5 Hz). MS (EI) *m*/*z*: 186 ($(M + 2)^+$, 11), 184 (M^+, 22), 127 (40), 125 (80), 49 (100). MS (CI, NH_3) *m*/*z*: 204 (15), 202 ($(M + NH_4)^+$, 80), 125 (100).

8e: (footnote 3) Oil, 20% yield. ^{1}H NMR δ: 3.68 (2H, s), 3.70 (3H, s), 7.40 (2H, d, ^3J = 8.6 Hz), 7.58 (2H, d, ^3J = 8.6 Hz). ^{19}F NMR δ: ($CDCl_3$, $CFCl_3$): –62.5 (s). MS (EI) *m*/*z*: 159 (100). MS (CI, NH_3) *m*/*z*: 219 ($(M + H)^+$, 38), 176 (100).

8f: (41) Yield 19%. ^{1}H NMR δ: 3.72 (2H, s), 3.75 (3H, s), 7.46 (2H, d, ^3J = 8 Hz), 8.17 (2H, d, ^3J = 8 Hz). ^{13}C NMR δ: 40.7, 52.3, 123.5, 130.2, 145.2, 147.9. MS (EI) *m*/*z*: 195 (M^+, 12), 136 (79). MS (CI, NH_3) *m*/*z*: 196 ($(M + H)^+$, 40); HRMS: calcd for $C_9H_9NO_4$: 195.0532; found: 195.0531.

11: Thermolysis of **2a** (0.1 M) was carried out in the presence of excess TEMPO (0.5 M) in benzene at 110°C. After the solvent was evaporated some of the excess TEMPO was removed at ambient temperature with a vacuum pump. The TEMPO adducts of benzyl and of methoxycarbonyl were isolated by chromatography on silica, with a Chromatotron apparatus. It was difficult to separate **11** from excess

[3] P. Stahly. U.S. Patent 5,302,752 (1994).

© 2000 NRC Canada

TEMPO but rechromatography of an initial enriched fraction was successful. Yield 12%. ^{1}H NMR (C_6D_6) δ: 1.17 (6H, s), 1.28 (6H, s), 1.28–1.49 (6H, m), 4.89 (2H, s), 7.08–7.35 (5H, m). ^{13}C NMR (C_6D_6) δ: 17.4, 20.4, 33.3, 39.9, 79.3, 127.8, 128.5, 128.3, 138.7. GC/MS (EI) *m/z*: 247 (M^+, <1), 156 (100), 91 (45). Authentic **11** was prepared by heating a solution of di-*tert*-butylperoxide in toluene containing TEMPO. The NMR spectra in $CDCl_3$ matched those reported (42).

12: ^{1}H NMR (C_6D_6) δ: 1.15 (6H, s), 1.21 (6H, s), 1.24–1.77 (6H, m), 3.48 (3H, s). GC/MS (EI) *m/z*: 215 (M^+, 3), 200 (100), 83 (76), 55 (84).

14a: (43) 10% yield. ^{1}H NMR δ: 3.76 (3H, s), 5.14 (2H, s), 7.25–7.35 (5H, m). MS (EI) *m/z*: 155 (12), 107 (26), 91 (100). MS (CI, NH_3) *m/z*: 184 ($(M + NH_4)^+$, 100).

14b: 21% yield. ^{1}H NMR δ: 2.34 (3H, s), 3.76 (3H, s), 5.11 (2H, s), 7.15 (2H, d, ^3J = 8 Hz), 7.26 (2H, d, ^3J = 8 Hz). MS (EI) *m/z*: 180 (M^+, 95), 105 (100), 104 (97). MS (CI, NH_3) *m/z*: 198 ($(M + NH_4)^+$, 34), 122 (100).

14c: 25% yield. ^{1}H NMR δ: 3.76 (3H, s), 3.79 (3H, s), 5.08 (2H, s), 6.87 (2H, d, ^3J = 8.6 Hz), 7.31 (2H, d, ^3J = 8.6 Hz). MS (EI) *m/z*: 196 (M^+, 15), 180 (10), 122 (10), 121(100). HRMS: calcd for $C_{10}H_{12}O_4$: 196.0736; found 196.0744.

14e: 10% yield. ^{1}H NMR δ: 3.81 (3H, s), 5.21 (2H, s), 7.49 (2H, d, ^3J = 8 Hz), 7.63 (2H, d, ^3J = 8 Hz). ^{13}C NMR δ: 55.0, 68.5, 123.9 (q, $^1J_{C\text{-}F}$ = 271 Hz), 126.6, 128.1, 130.6 (q, $^2J_{C\text{-}F}$ = 32.4 Hz), 139.2, 155.6. ^{19}F NMR (CF_3Cl ref) δ: –62.7. MS (EI) *m/z*: 235 ($(M + 1)^+$, 21), 215 (18), 159 (100); MS (CI, NH_3) *m/z*: 252 $(M + NH_4)^+$.

14f: 12% yield. ^{1}H NMR δ: 3.83 (3H, s), 5.26 (2H, s), 7.55 (2H, d, ^3J = 8.7 Hz), 8.23 (2H, d, ^3J = 8.7 Hz). ^{13}C NMR δ: 55.1, 67.8, 123.7, 128.3, 142.4, 155.3 (one signal not seen, presumably superimposed). HRMS: calcd for $C_9H_9NO_5$ 211.0481; found 211.0482.

Acetone azine. ^{1}H NMR (C_6D_6) δ: 1.79 (3H, s), 1.81 (3H, s). The same spectrum was obtained with an authentic sample.

Rate constants for thermolysis of **2a–f** in C_6D_6 at 100°C were determined by means of ^{1}H NMR spectroscopy, with toluene as internal standard. Toluene did not react appreciably with radicals produced during the thermolyses. A sealed NMR tube containing the oxadiazoline (0.1 mmol) in C_6D_6 was withdrawn from the oil bath from time to time and cooled rapidly to room temperature before integration of the ^{1}H NMR spectrum. Typically, seven points were collected, covering the range from 0 to 87% of completion. The time scale was not corrected for the cooling and warm-up times. First order plots, which were linear, gave the rate constants reported in the text.

Acknowledgements

The authors gratefully acknowledge financial support in the form of a grant-in-aid from the Natural Sciences and Engineering Research Council of Canada. The assistance of Joseph P. Ross, who did some exploratory work on this project, is also greatly appreciated.

References

1. M. Regitz. Angew. Chem. Int. Ed. Engl. **35**, 725 (1996).
2. R.W. Hoffmann. Acc. Chem. Res. **18**, 248 (1985).
3. D.M. Lemal, E.P. Gosselink, and S.D. McGregor. J. Am. Chem. Soc. **88**, 582 (1966).
4. R.A. Moss, M. Wlostowski, S. Shen, K. Krogh-Jespersen, and A. Matro. J. Am. Chem. Soc. **110**, 4443 (1988).
5. C.-S. Ge, E.A. Jefferson, and R.A. Moss. Tetrahedron Lett. **34**, 7549 (1993).
6. R.A. Moss, M. Wlostowski, J. Terpinski, G. Kmiecik-Lawrynowicz, and K. Krogh-Jespersen. J. Am. Chem. Soc. **109**, 3811 (1987).
7. R.A. Moss and J.K. Huselton. J. Chem. Soc. Chem. Commun. 950 (1976).
8. R.A. Moss, C.M. Young, L.A. Perez, and K. Krogh-Jespersen. J. Am. Chem. Soc. **103**, 2413 (1981).
9. R.A. Moss, S. Shen, and M. Wlostowski. Tetrahedron Lett. **29**, 6417 (1988).
10. X.-M. Du, H. Fan, J.L. Goodman, M.A. Kesselmayer, K. Krogh-Jespersen, J.A. LaVilla, R.A. Moss, S. Shen, and R.S. Sheridan. J. Am. Chem. Soc. **112**, 1920 (1990).
11. M. El-Saidi, K. Kassam, D.L. Pole, T. Tadey, and J. Warkentin. J. Am. Chem. Soc. **114**, 8751 (1992).
12. B. Gregoire, M.-C. Carre, and P. Caubere. J. Org. Chem. **51**, 1419 (1986).
13. L. Isaacs and F. Diederich. Helv. Chim. Acta, **76**, 2454 (1993).
14. W.W. Win, M. Kao, M. Eiermann, J.J. McNamara, F. Wudl, D.L. Pole, K. Kassam, and J. Warkentin. J. Org. Chem. **59**, 5871 (1994).
15. R. González, F. Wudl, D.L. Pole, P.K. Sharma, and J. Warkentin. J. Org. Chem. **61**, 5837 (1996).
16. A. de Meijere, S.I. Kozhushkov, D.S. Yufit, R. Boese, T. Haumann, D.L. Pole, P.K. Sharma, and J. Warkentin. Liebigs Ann. 601 (1996).
17. K. Kassam, P. Venneri, and J. Warkentin. Can. J. Chem. **75**, 1256 (1997).
18. K. Kassam and J. Warkentin. Can. J. Chem. **75**, 120 (1997).
19. D.L. Pole and J. Warkentin. J. Org. Chem. **62**, 4065 (1997).
20. J.H. Rigby, A. Cavezza, and G. Ahmed. J. Am. Chem. Soc. **118**, 12848 (1997).
21. J.H. Rigby, A. Cavezza, and M.J. Heeg. J. Am. Chem. Soc. **120**, 3664 (1998).
22. J.D. Colomvakos, I. Egle, J. Ma, D.L. Pole, T.T. Tidwell, and J. Warkentin. J. Org. Chem. **61**, 9522 (1996).
23. J.A. Dunn, J. P. Pezacki, M. J. McGlinchey, and J. Warkentin. J. Org. Chem. **64**, 4344 (1999).
24. J.P. Ross, P. Couture, and J. Warkentin. Can. J. Chem. **75**, 1331 (1997).
25. D. Suh, D.L. Pole, J. Warkentin, and J.K. Terlouw. Can. J. Chem. **74**, 544 (1996).
26. R.W. Hoffmann, R. Hirsch, R. Fleming, and M.T. Reetz. Chem. Ber. **105**, 3532 (1972).
27. P. Couture, M. El-Saidi, and J. Warkentin. Can. J. Chem. **75**, 326 (1997).
28. P.C. Venneri and J. Warkentin. J. Am. Chem. Soc. **120**, 11182 (1998).
29. K. Kassam, D.L. Pole, M. El-Saidi, and J. Warkentin. J. Am. Chem. Soc. **116**, 1161 (1994).
30. W.B. Smith. J. Org. Chem. **60**, 7456 (1995).
31. J.P. Pezacki, P.D. Wood, T.A. Gadosy, J. Lusztyk, and J. Warkentin. J. Am. Chem. Soc. **120**, 8681 (1998).
32. E.J. Dix and J.L. Goodman. J. Phys. Chem. **98**, 12609 (1994).
33. D. Keus, M. Kaminski, and J. Warkentin. J. Org. Chem. **49**, 343 (1984).

© 2000 NRC Canada

34. D.A. Modarelli and M.S. Platz. J. Am. Chem. Soc. **113**, 8985 (1991).
35. S. Morgan, J.E. Jackson, and M.S. Platz. J. Am. Chem. Soc. **113**, 2782 (1991).
36. D.A. Modarelli, S. Morgan, and M.S. Platz. J. Am. Chem. Soc. **114**, 7034 (1992).
37. E.L. Tae, Z. Zhu, M.S. Platz, J.P. Pezacki, and J. Warkentin. J. Phys. Chem. A. **103**, 5336 (1999).
38. ^{1}H NMR ($CDCl_3$) Sadtler Standard NMR Spectra, Vol.1, No. 19 (1968). Sadtler Research Laboratories, Philadelphia, PA.
39. J.B. Lambert, H.W. Mark, and E.S. Magyar. J. Am. Chem. Soc. **99**, 3059 (1978).
40. R. Mohan and J.A. Katzenellenbogen. J. Org. Chem. **49**, 1238 (1984).
41. Beilstein's Handbuch der Organischen Chemie, **9**, 456.
42. T.J. Connolly, M.V. Baldoví, N. Motat, and J.C. Scaiano. Tetrahedron Lett. **37**, 4919 (1996).
43. D. Brillon and G.J. Sauve. J. Org. Chem. **55**, 2246 (1990).

© 2000 NRC Canada

Multidimensional conformational analysis of allyl methyl disulfide: a key component of garlic

Alvin C. Lin, Salvatore J. Salpietro, Eugen Deretey, and Imre G. Csizmadia

Abstract: Organosulfur compounds in garlic, like allyl methyl disulfide, have been found to be involved in antimutagenic, anticarcinogenic, antithrombotic, and lipid-lowering activities, and it has also been found to act as an antioxidant. Ab initio molecular computations were performed on dihydrogen disulfide (**1**) with respect to torsional angle $\tau_1 = \tau(H{\cdot}S{-}S{\cdot}H)$, hydrogen methyl disulfide (**2**) with respect to torsional angle $\tau_1 = \tau(H{\cdot}S{-}S{\cdot}CH_3)$, and allyl methyl disulfide (**3**) with respect to torsional angles $\tau_1 = \tau(H_3C_2{\cdot}CH_2{\cdot}S{-}S{\cdot}CH_3)$, $\tau_2 = \tau(H_3C_2{\cdot}CH_2{-}S{\cdot}S{\cdot}CH_3)$, and $\tau_3 = \tau(H_3C_2{-}CH_2{\cdot}S{\cdot}S{\cdot}CH_3)$. Potential energy curves (PEC) were obtained from **1** and **2**, i.e., $E = E(\tau_1)$, from which optimized structures were obtained at the HF/6–31G* level of theory. These optimized structures were used to investigate the potential energy hypersurface surface (PEHS) of **3**, i.e., $E = E(\tau_1,\tau_2,\tau_3)$. One-dimensional scans along τ_2 and τ_3 (where $\tau_1 = \pm 90°$; $\tau_1 = 180°$) were performed at the HF/3–21G* level of theory. From these scans, six lower energy pairs of enantiomeric minima (i.e., [$g^+g^+g^+$ | $g^-g^-g^-$], [g^+ag^- | g^-ag^+], [$g^+g^-g^+$ | $g^-g^+g^-$], [$g^+g^+g^-$ | $g^-g^-g^+$], [g^+ag^- | g^-ag^+], and [$g^+g^-g^-$ | $g^-g^+g^+$]) as well as 3 higher energy minima (i.e., [g^+g^+s | g^-g^-s], [g^+as | g^-as], and [$g{+}g^-s$ | g^-g^+s]) were optimized at $\tau_1 = \pm 90°$ at the HF/6–31G* and B3LYP/6–31G* levels of theory. The global minimum was determined to be the [$g^+g^-g^+$ | $g^-g^+g^-$] enantiomeric pair of conformers, and the fully symmetrical *anti-anti-anti* [*a a a*] structure was determined to be a second-order saddle point on the PEHS of **3**. Although there are no stereocentres in **3**, there is chirality in the conformational twist with respect to the [*a a a*] conformation through $\tau_1 = \tau_2 = \tau_3 = 180°$. Based on the energies and MO diagrams of the HUMO and LUMO +1 of **3**, the anticarcinogenic and cholesterol lowering activity mechanism of **3** is presented.

Key words: ab initio MO computations, allyl methyl disulfide, multidimensional conformational analysis (MDCA), anticarcinogenic, cholesterol lowering.

Résumé : Il a été observé que les composés organosulfurés de l'ail, comme le disulfure d'allyle et de méthyle, sont impliqués dans des activités antimutagènes, anticancérigènes, antithrombiques et d'abaissement du niveau des lipides; il a aussi été observé qu'ils peuvent agir comme antioxydant. On a effectué des calculs moléculaires ab initio sur le disulfure d'hydrogène (**1**) en fonction de l'angle de torsion $\tau_1 = \tau(H{\cdot}S{-}S{\cdot}H)$, sur le disulfure d'hydrogène et de méthyle (**2**) en fonction de l'angle de torsion $\tau_1 = \tau(H{\cdot}S{-}S{\cdot}CH_3)$ et sur le disulfure d'allyle et de méthyle (**3**) en fonction des angles de torsion $\tau_1 = \tau(CH_2 = CH{\cdot}CH_2{\cdot}S{-}S{\cdot}CH_3)$, $\tau_2 = \tau(CH_2 = CH{\cdot}CH_2{-}S{\cdot}S{\cdot}CH_3)$, et $\tau_3 = \tau(CH_2 = CH{-}CH_2{\cdot}S{\cdot}S{\cdot}CH_3)$. On a obtenu des courbes d'énergie potentielle (CEP) pour le passage de **1** à **2**, c'est-à-dire $E = E(\tau_1)$ à partir desquelles on a obtenu des structures optimisées au niveau HF/6–31G de la théorie. On a utilisé ces structures optimisées pour étudier la surface d'hypersurface d'énergie de potentiel (SHEP) de **3**, c'est-à-dire $E = E(\tau_1, \tau_2, \tau_3)$. Opérant au niveau HF/3–21G* de la théorie, on a effectué des balayages unidimensionnels le long de τ_2 et τ_3 (où $\tau_1 = \pm 90°$; τ_1 180°). À partir de ces balayages et opérant aux niveaux HF/6–31G* et B3LYP/6–31G* de la théorie, on a optimisé les six paires d'énergie les plus faibles des minima énantiomères (c'est-à-dire, [$g^+g^+g^+$ | $g^-g^-g^-$], [g^+ag^- | g^-ag^+], [$g^+g^-g^+$ | $g^-g^+g^-$], [$g^+g^+g^-$ | $g^-g^-g^+$], [g^+ag^- | g^-ag^+] et [$g^+g^-g^-$ | $g^-g^+g^+$]) ainsi que trois minima d'énergie plus élevée (soit, [g^+g^+s | g^-g^-s], [g^+as | g^-as], et [$g{+}g^-s$ | g^-g^+s]) à $\tau_1 = \pm 90°$. On a déterminé que le minimum global correspond à la paire énantiomère de conformères [$g^+g^-g^+$ | $g^-g^+g^-$] et que la structure complètement symétrique *anti-anti-anti* [*a a a*] est un point de selle du deuxième ordre sur la SHEP de **3**. Même s'il n'existe aucun stéréocentre dans **3**, il existe une chiralité dans la déformation conformationnelle par rapport à la conformation [*a a a*] lorsque $\tau_1 = \tau_2 = \tau_3 = 180°$. En se basant sur les énergies et les diagrammes d'OM des HO et BV +1 de **3**, on propose un mécanisme pour l'activité anticancérigène et d'abaissement du niveau de cholestérol résultant de **3**.

Mots clés: ab initio, calculs d'OM, disulfure d'allyle et de méthyle, analyse conformationnelle multidimensionnionnelle (ACMD), anticancérigène, abaissement du niveau de cholestérol.

[Traduit par la Rédaction]

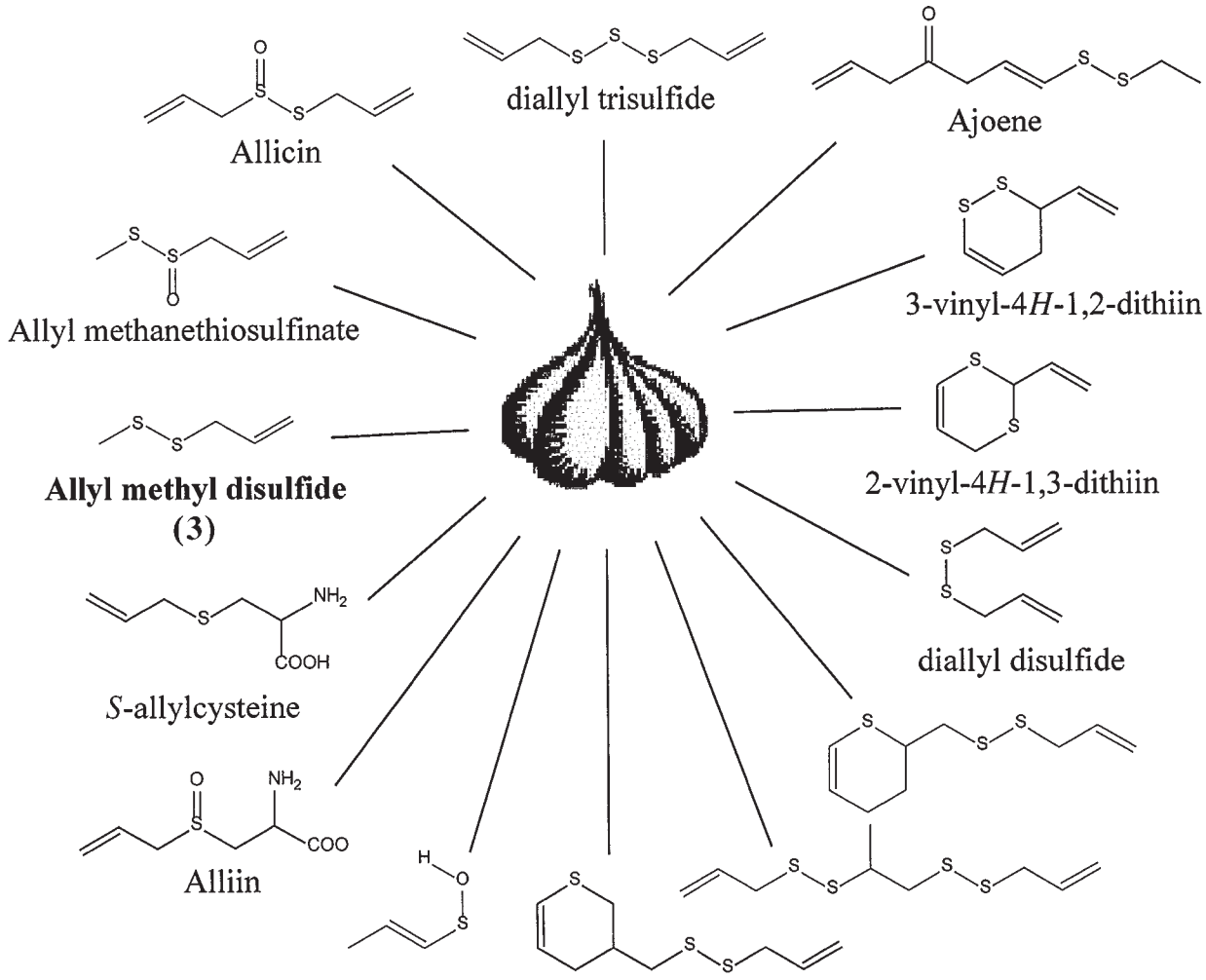
Received July 5, 1999.

A.C. Lin, S.J. Salpietro, E. Deretey, and I.G. Csizmadia.[1] Department of Chemistry, University of Toronto, Toronto, ON M5S 3H6, Canada.

[1]Author to whom correspondence may be addressed. Telephone/Fax: (416) 978-3598. e-mail: icsizmad@chem.utoronto.ca

 © 2000 NRC Canada

Fig. 1. Some organosulfur compounds found in garlic.



Introduction

Garlic has been one of the most popular medically researched plants, with over 1300 research articles in only the last 100 years (1). This growing interest is largely due to its therapeutic appeal, particularly in its anticarcinogenic, antimutagenic, antithrombotic, and lipid-lowering cardiovascular activities; and it has also been shown to act as an antioxidant. The following are a few examples. The title compound: allyl methyl disulfide and other allyl group-containing derivatives found in garlic were shown to inhibit benzo[*a*]pyrene-induced neoplasia of the forestomach and lungs of female mice (2). Other garlic constituents suggest effectiveness in binding to 7,12-dimethylbenz[*a*]anthracene, thereby preventing it from binding in vivo to DNA (3). Allicin (Fig. 1) and other organosulfur components in garlic extracts have been found to have significant radical scavenging capabilities (4–7), specifically a powerful scavenger of the OH radical (3). Garlic extracts have also been shown to have antimutagenic activity towards ionizing radiation, peroxides, adriamycin, and *N′*-methyl-*N′*-nitro-nitrosoguanidine (8). Allicin has also been found to inhibit platelet aggregation (9–13), along with ajoene, a colourless and odourless liquid isolated from methanolic extracts of fresh garlic (Fig. 1). In fact, ajoene actually inhibits aggregations even better than allicin in human whole blood (IC_{50} 60 μM vs. IC_{50} 90 μM) (14). In an other study, patients at risk of heart disease saw significant reductions in blood cholesterol and triglycerides levels after orally ingesting raw garlic daily (5g/day) for 2 to 3 months (15–19). A similar investigation also showed that a daily intake of garlic resulted in lower levels of cholesterol, triglycerides, low density lipoproteins, and very low density lipoproteins (commonly referred to as LDL, VLDL respectively) and an increase of high density lipoproteins (commonly referred to as HDL) (20). Garlic consumption has also significantly lowered the number of deaths due to gastric cancer in China (21), as well as in Italy (22), in comparison to regions with lower consumptions. Other anticancer effects have shown diallyl disulfide, the major constituent of garlic oil, to inhibit oxidative phosphorylation in hepatic mitochondria of mice (23).

It is interesting to note that although diallyl disulfide is the main constituent of garlic oil, it is diallyl trisulfide, a minor component, which is more reactive, and thus produces more of an inhibitory effect towards canine mammary tumor cells (24). Other trisulfides found in garlic include allyl methyl

© 2000 NRC Canada

Table 1. Optimized parameters for the conformational minima ($\lambda = 0$) of **1** (HSSH) computed at the HF/6–31G* level of theory.

Bond lengths		
H^1 — S^2	1.327	1.327
H^4 — S^3	1.327	1.327
S^2 — S^3	2.063	2.063
Bond angles		
H^1–S^2–S^3	99.12	99.12
S^2–S^3–H^4	99.12	99.12
Torsional angles		
$\tau_1 = H^1S^2–S^3H^4$	89.84	270.16 (–89.84)
Energies		
E (Hartree)	–796.174393	–796.174393

trisulfide, which has found to enhance glutathione *S*-transferase activity in mouse tissues (forestomach, small bowel mucosa, liver, and lung) (25).

Investigating the conformations of dihydrogen disulfide (**1**), hydrogen methyl disulfide (**2**), as well as the simplest allyl organosulfur component, allyl methyl disulfide (**3**), can hopefully provide a better understanding of its important role and the role of related compounds in biological processes. The structures of these three compounds are depicted below.

Stereochemical background

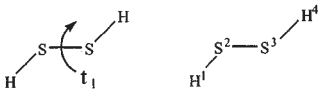
Disulfides (X·S–S·Y) have a torsional angle in the vicinity of 90°. This is manifested in previous computations reported on H·S–S·H and H·S–S·CH_3 (26–37). Geometrical parameters such as S—S, H—S, S—C bond lengths, HSS and SSC bond angles associated with the rotation about the S—S bond are summarized in Tables 1 and 2.

Table 2. Optimized parameters for the conformational minima ($\lambda = 0$) of **2** (HSS-CH_3) computed at the HF/6–31G* level of theory.

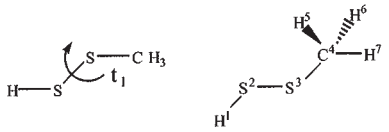
Bond lengths		
H^1 — S^2	1.328	1.328
S^2 — S^3	2.058	2.058
S^3 — C^4	1.814	1.814
C^4 — H^5	1.081	1.081
C^4 — H^6	1.081	1.081
C^4 — H^7	1.083	1.083
Bond angles		
H_1–S^2–S^3	99.54	99.54
S^2–S^3–C^4	102.72	102.72
S^3–C^4–H^5	110.80	111.16
S^3–C^4–H^6	111.16	110.80
S^3–C^4–H^7	106.24	106.24
Torsional angles		
$\tau_1 = \tau$ (H^1-S^2–S^3-C^4)	87.39	272.61 (–87.39)
S^2-S^3–C^4-H^5	57.37	65.32
S^2-S^3–C^4-H^6	294.68	302.63
S^2-S^3–C^4-H^7	176.02	183.98
Energies		
E (Hartree)	–835.2113839	–835.2113839

Computational methods

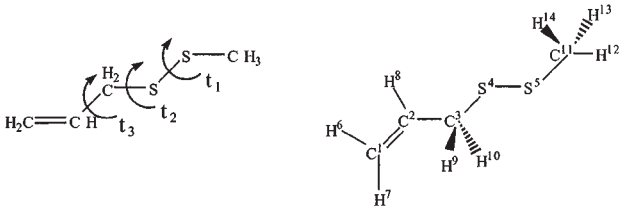
All potential energy curve (PEC) scans for **1** (dihydrogen disulfide), **2** (methyl hydrogen disulfide), and **3** (allyl methyl disulfide) were calculated using the GAUSSIAN 94 program[2] under tight optimization conditions using Berny Optimization algorithms (Opt = Z – Matrix, Tight). The PEC scans of **1** and **2** were calculated at the RHF/6–31G* level of



dihydrogen disulfide
1



hydrogen methyl disulfide
2



allyl methyl disulfide
3

[2] M.J. Frisch, G.W. Trucks, H.B. Schlegel, P.M.W. Gill, B.G. Johnson, M.A. Robb, J.R. Cheeseman, T. Keith, G.A. Petersson, J.A. Montgomery, K. Raghavachari, M.A. Al-Laham, V.G. Zakrzewski, J.V. Ortiz, J.B. Foresman, J. Cioslowski, B.B. Stefanov, A. Nanayakkara, M. Challacombe, C.Y. Peng, P.Y. Ayala, W. Chen, M.W. Wong, J.L. Andres, E.S. Replogle, R. Gomperts, R.L. Martin, D.J. Fox, J.S. Binkley, D.J. Defrees, J. Baker, J.P. Stewart, M. Head-Gordon, C. Gonzalez, and J.A. Pople. Gaussian 94, Revision E.1, E.2, C.3 and D.2., Gaussian, Inc., Pittsburgh, Pa. 1995.

© 2000 NRC Canada

Fig. 2. (A). PEC of **1** (dihydrogen disulfide) along $\tau_1 = \tau(H{\cdot}S\text{-}S{\cdot}H)$. (B). PEC of **II** (hydrogen methyl disulfide) along $\tau_1 = \tau(H{\cdot}S\text{-}S{\cdot}CH_3)$.

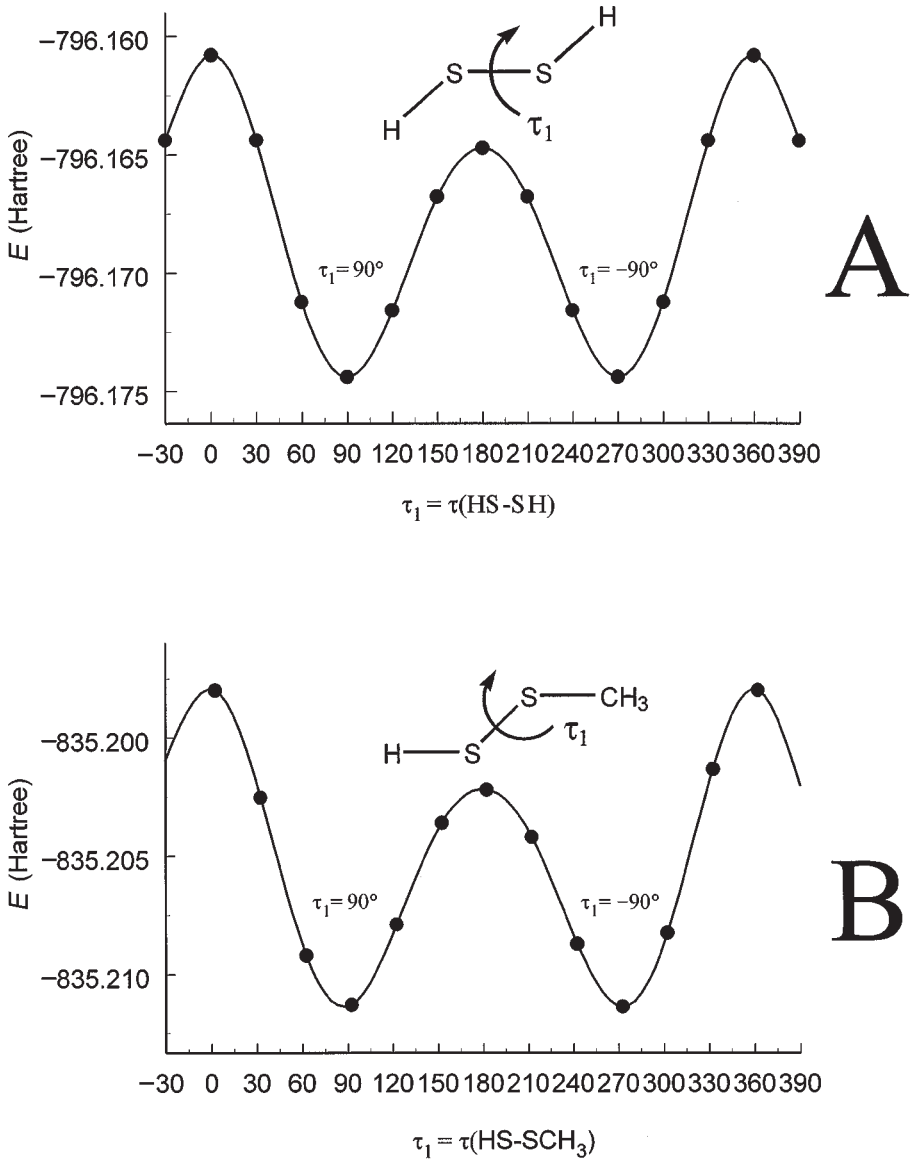
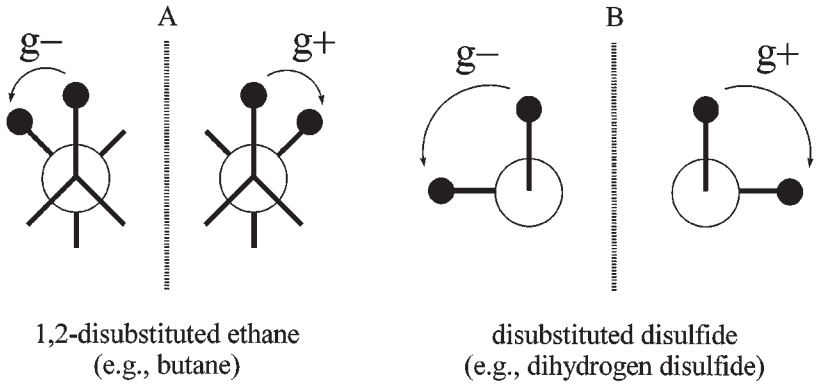
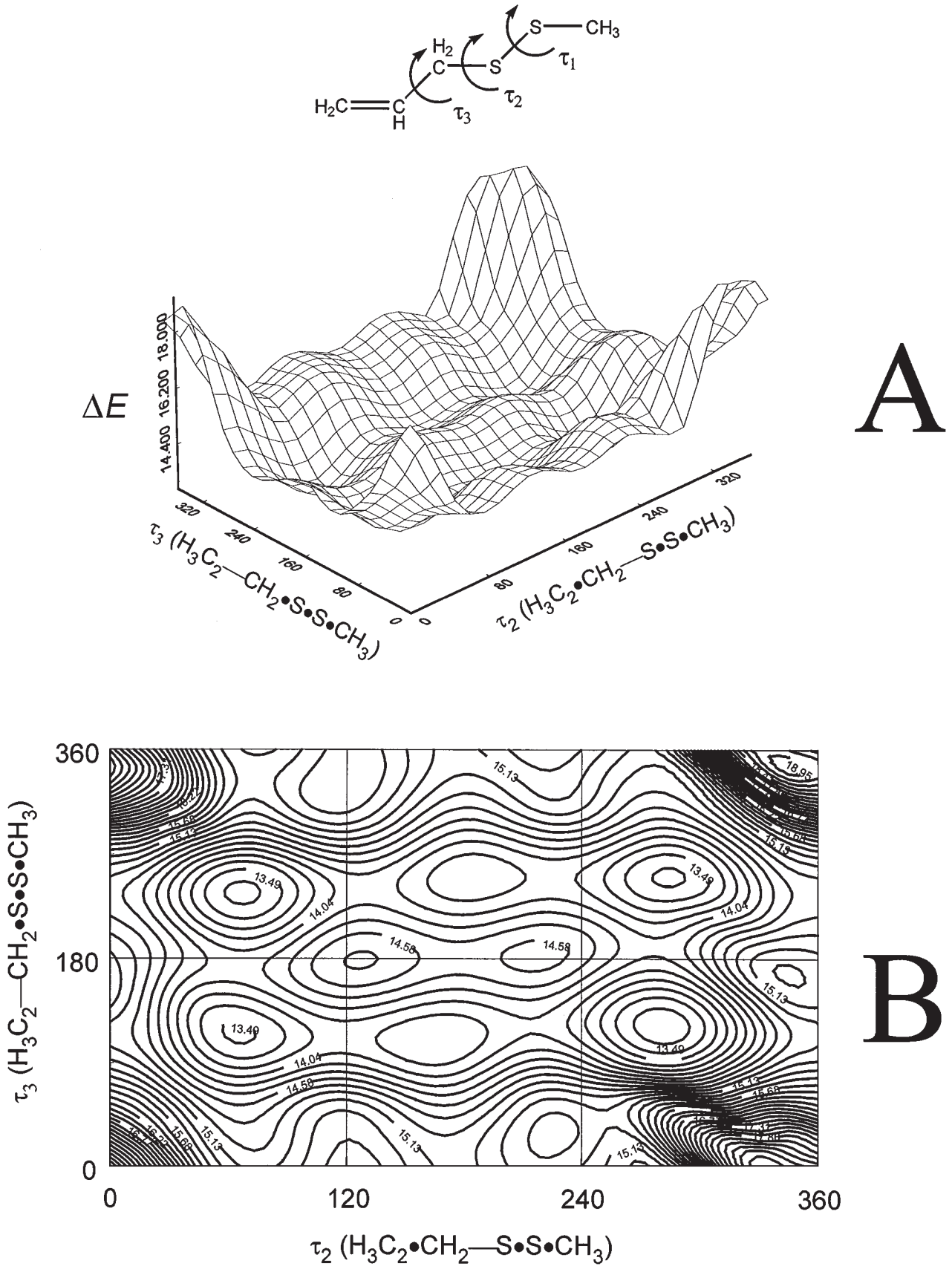


Fig. 3. (A). Enantiomeric relationship for the g^+ and g^- conformers of 1,2-disubstituted ethane (e.g., butane) and (B) of a disulfide (e.g., dihydrogen disulfide).



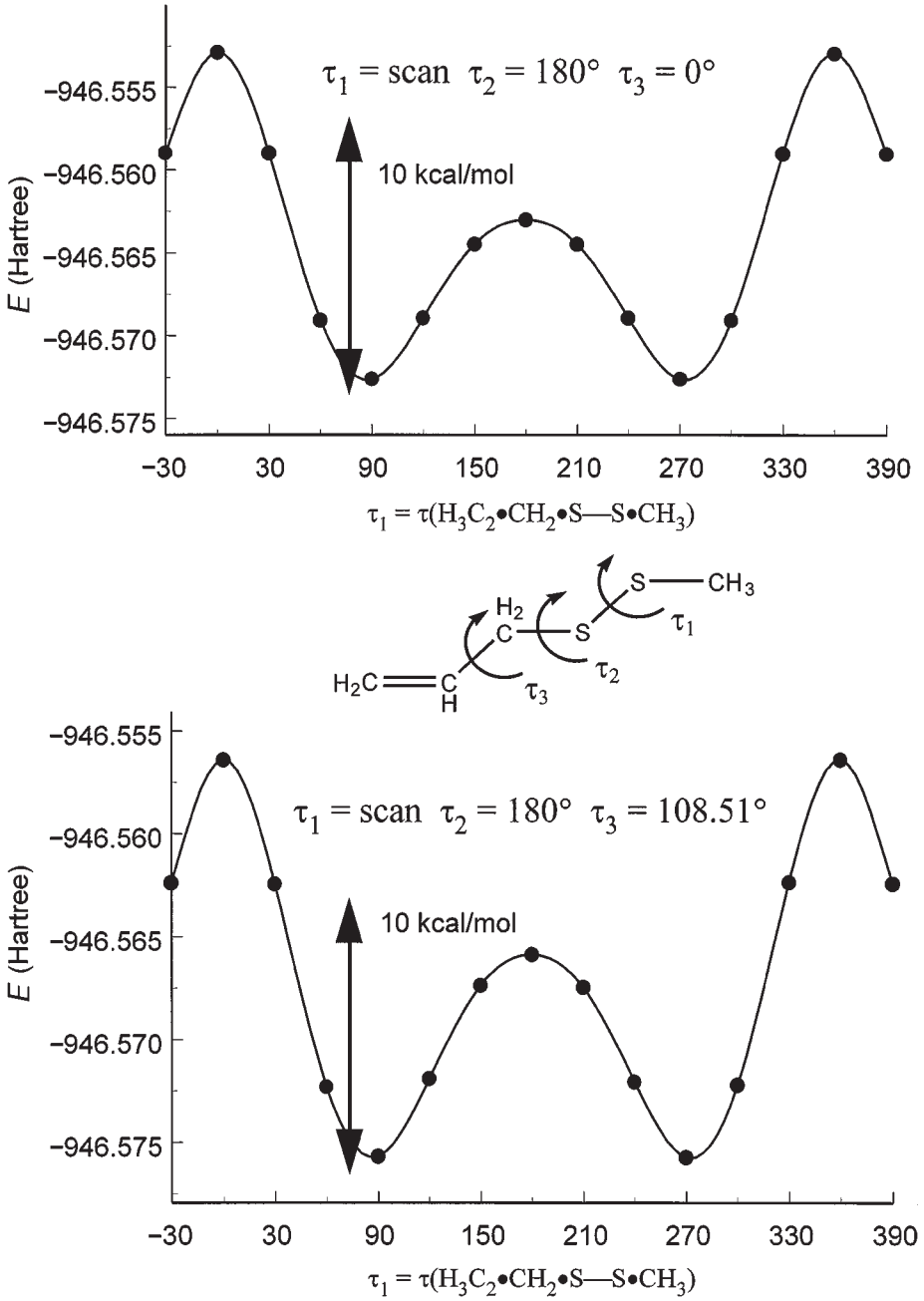
© 2000 NRC Canada

Fig. 4. Semiempirical PES of **3** (allyl methyl disulfide), where $E = E(\tau_2, \tau_3)$, at $\tau_1 = 90°$, showing both two-dimensional (A) and three-dimensional (B) representations.



© 2000 NRC Canada

Fig. 5. PEC's of **3** (allyl methyl disulfide) along $\tau_1 = \tau(H_3C_2{\cdot}CH_2{\cdot}S\text{-}S{\cdot}CH_3)$. Note that the minima are occurring at analogous torsional angles of $\tau_1 \approx +90°$ and $\tau_1 \approx -90°$.



theory, and the PEC scans of **3** were calculated at the RHF/3–21G* level of theory. All conformers of **1** and **2** were optimized at the RHF/6–31G* level of theory, whereas all structures of **3** were optimized at both the RHF/6–31G* and B3LYP/6–31G* levels of theory. At termination, all critical points had gradients $<1.5 \times 10^{-5}$ au. The semiempirical potential energy surface (PES) scan of **3** was calculated using MOPAC. All points generated from the PEC and PES scans were plotted using Axum 5.0A, and all molecular orbital diagrams were generated using Molden 3.6.

Results and discussion

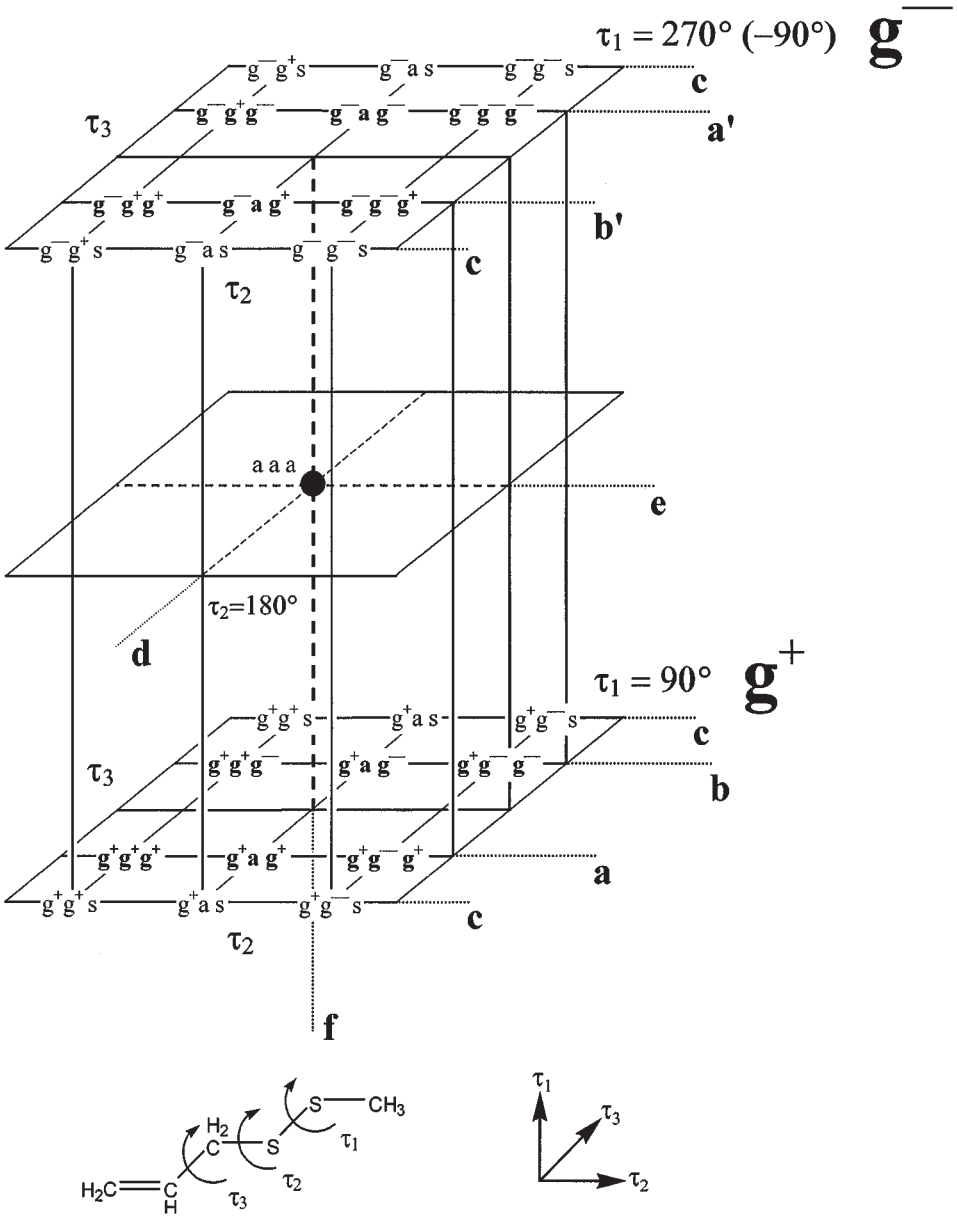
Multidimensional conformational analysis

Even after a first glance, it was apparently clear that allyl methyl disulfide (**3**) is more complex than its structure may suggest, largely because it contains three unique torsional angles $\tau_1 = \tau(H_3C_2{\cdot}CH_2{\cdot}S\text{–}S{\cdot}CH_3)$, $\tau_2 = \tau(H_3C_2{\cdot}CH_2\text{–}S{\cdot}S{\cdot}CH_3)$ and $\tau_3 = \tau(H_3C_2\text{–}CH_2{\cdot}S{\cdot}S{\cdot}CH_3)$. Based on these three torsional angles, the potential energy hypersurface (PEHS) of **3** needed to be explored, where

$$E = E(\tau_1, \tau_2, \tau_3)$$

© 2000 NRC Canada

Fig. 6. Topology of the PEHS of **3** (allyl methyl disulfide), where $E = E(\tau_1, \tau_2, \tau_3)$, indicating the notation of the 6 pairs of lower energy conformers in boldface, of the 3 pairs of higher energy conformers, and of the fully symmetrical *anti* structure. Note that the centre of symmetry (i.e., where $\tau_1 = \tau_2 = \tau_3 = 180°$) is denoted by a solid dot and corresponds to the [*a a a*] conformation shown in Fig. 8.



to determine its conformers. Thus, as a preliminary investigation, smaller disulfides, namely dihydrogen disulfide (**1**) and hydrogen methyl disulfide (**2**) were first examined. Specifically, ab initio PEC scan calculations on **1** and **2** and were performed with respect to their torsional angles: $\tau_1 = \tau(H{\cdot}S{-}S{\cdot}H)$ for **1,** and $\tau_1 = \tau(H{\cdot}S{-}S{\cdot}CH_3)$ for **2**. Not surprisingly, their PEC (Figs. 2A and 2B) showed that there are two minima at $\tau_1 \approx +90°$ (clockwise rotation) and $\tau_1 \approx -90°$ (counterclockwise rotation). These minima are enantiomeric in disulfides, analogous to the *gauche* conformers (i.e., g^+ and g^-) found in a 1,2-disubstituted ethane (e.g., butane), as illustrated in Fig. 3. (Note that although *gauche* (*g*) is a 60° torsional angle by convention, for the purposes of this investigation, an extension of the definition will include in the convention a 90° torsional rotation).

We then inferred that on the basis of the PEC of **1** and **2**, the value of τ_1 for **3** would be similar as well, namely $\tau_1 \approx \pm 90°$. The PEHS of **3**, i.e., $E = E(\tau_1,\tau_2,\tau_3)$, could now be investigated by first examining the PES of **3** when $\tau_1 = +90°$, i.e.,

$$E = E(\tau_2, \tau_3) \text{ for } \tau_1 = 90°$$

As a means of acquiring an idea of what this surface may look like, semiempirical PES scan calculations on **3** were performed using MOPAC at 30° rotational increments about torsional angles t_2 and τ_3, keeping τ_1 constant at +90°. From

© 2000 NRC Canada

Fig. 7. PEC's of **3** (allyl methyl disulfide) along $\tau_2 = \tau(H_3C_2{\cdot}CH_2\text{-}S{\cdot}S{\cdot}CH_3)$ illustrating that the chirality of **3** is due to the torsional twist along $\tau_1 = \tau(H_3C_2{\cdot}CH_2{\cdot}S\text{-}S{\cdot}CH_3)$.

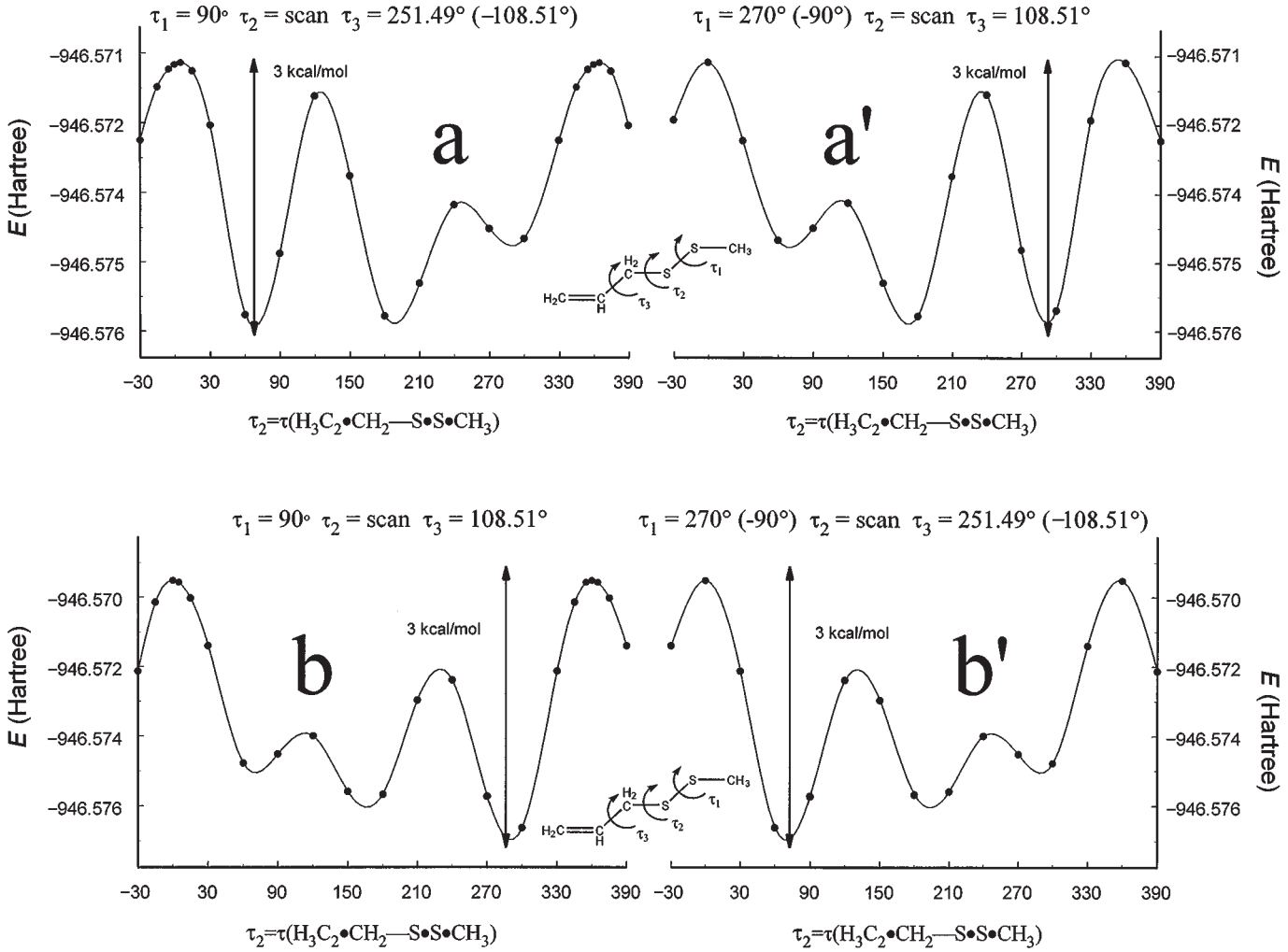
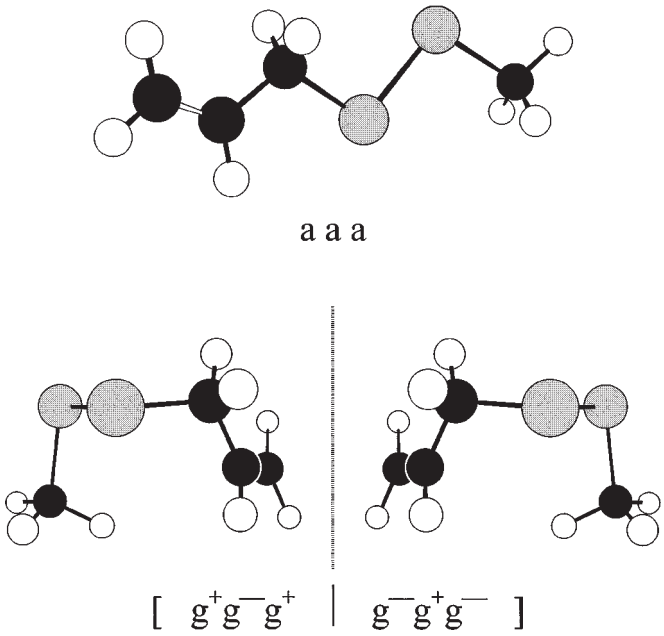
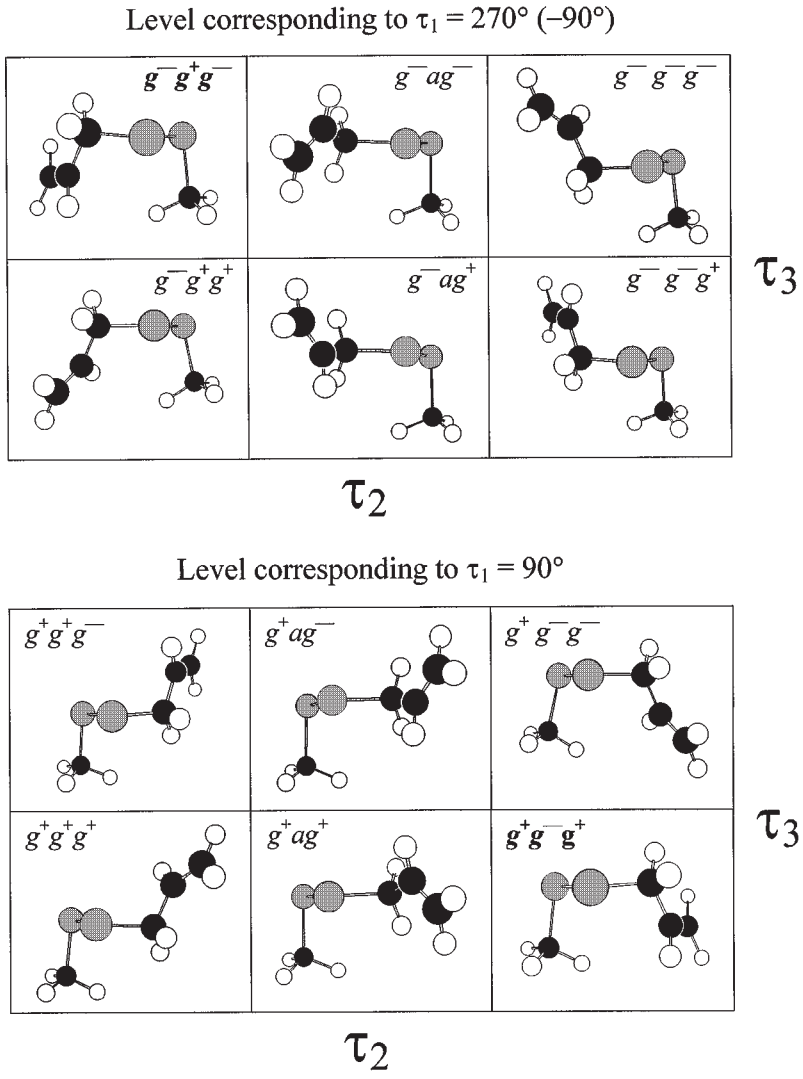


Fig. 8. Structures of the fully symmetrical *anti-anti-anti* [*a a a*] conformation ($\lambda = 2$) and the degenerate global minima [$g^+g^-g^+$] and [$g^-g^+g^-$] conformers ($\lambda = 0$). Note that the global minima conformers are enantiomeric and this relationship is denoted with the symbol " | ", indicating a mirror plane.



© 2000 NRC Canada

Fig. 9. Optimized structures of the six pairs of lower energy minima conformers ($\lambda = 0$) of **3** (allyl methyl disulfide) computed at the HF/6–31G* level of theory.



the pseudo three-dimensional landscape representation and the two-dimensional contour plot of the surface shown in Figs. 4A and 4B, there was a strong suggestion that there existed at least six energy minima for **3**. Therefore, to help verify these preliminary findings and to further investigate the PEHS of **3**, it was convenient to then carry out one-dimensional ab initio scans along the three torsional angles coordinates τ_1, τ_2, and τ_3.

As expected, scanning along τ_1 (Fig. 5) confirmed that the $\tau_1 = +90°$ and $\tau_1 = –90°$ platform levels on the PEHS of **3** can be regarded as equivalent if all other torsional angles (τ_2 and τ_3) are identical. These two levels are presented in Fig. 6. Scanning along τ_2 revealed that there are indeed six energy minima at $\tau_1 = 90°$ as well as at $\tau_1 = –90°$ as shown in Fig. 7. Furthermore, scanning along τ_2 also revealed that the PECs are chiral. From the four PEC cross-sectional scans along τ_2 (**a**, **b**, and **a′**, **b′**), presented in Figs. 6 and 7, one can clearly see that **a** (where $\tau_1 = 90°$ and $\tau_3 = –108.51°$ or 251.49°) is the nonsuperimposable image of **a′** (where $\tau_1 = –90°$ or 270°, and $\tau_3 = 108.51°$). Similarly, **b** (where $\tau_1 = 90°$ and $\tau_3 = 108.51°$) is the nonsuperimposable image of **b′** (where $\tau_1 = –90°$ or 270°, and $\tau_3 = –108.51°$ or 251.49°). Therefore, although **3** has no stereocentres, we can see that the chirality of **3** is due to the chirality of torsional twist. Each clockwise and counterclockwise twist about τ_1, τ_2, and τ_3 generates an enantiomeric pair (Fig. 8), and from Figs. 6 and 8, it is clear that there are six of these enantiomeric pairs of conformers on the PEHS of **3**. We were then able to obtain six enantiomeric pairs of conformers, illustrated in Fig. 9, and their optimized parameters are provided in Tables 3 and 4. These six structures are also represented on the PEHS of **3** in boldface symbols in Fig. 6. Because they are enantiomeric, each diagonally opposed pair is identical in energy, as illustrated in boldface numbers in Fig. 10. From Fig. 10, it also becomes apparently clear that the centre of symmetry of the PEHS of **3** is at $\tau_1 = \tau_2 = \tau_3 = 180°$, i.e., at the fully *anti-anti-anti* orientation (cf. [*a a a*] structure in Fig. 8). Therefore, if an imaginary line can be drawn through the fully *anti*-centre (i.e., [*a a a*] or $\tau_1 = \tau_2 = \tau_3 = 180°$) from one energy platform to the other on the PEHS of

© 2000 NRC Canada

Table 3. Optimized parameters and energy values for the six lower conformational minima[a] ($\lambda = 0$) of **3** (Allyl – SS – CH_3) computed at the HF/6–31G* level of theory.

$\tau_1 \approx 90°$	$g^+ g^+ g^+$	$g^+ a g^+$	$g^+ g^- g^+$	$g^+ g^+ g^-$	$g^+ a g^-$	$g^+ g^- g^-$
$\tau_1 \approx 270°$ (or –90°)	$g^- g^- g^-$	$g^- a g^-$	$g^- g^+ g^-$	$g^- g^- g^+$	$g^- a g^+$	$g^- g^+ g^+$
Bond lengths						
C^1 — C^2	1.318	1.319	1.319	1.318	1.319	1.318
C^2 — C^3	1.500	1.501	1.499	1.498	1.502	1.500
C^3 — S^4	1.832	1.834	1.830	1.832	1.834	1.832
S^5 — C^{11}	1.815	1.816	1.816	1.816	1.816	1.817
S^4 — S^5	2.054	2.052	2.052	2.052	2.053	2.054
C^1 — H^6	1.075	1.075	1.075	1.075	1.081	1.075
C^1 — H^7	1.077	1.077	1.076	1.076	1.081	1.077
C^2 — H^8	1.077	1.077	1.078	1.077	1.083	1.077
C^3 — H^9	1.083	1.082	1.086	1.082	1.081	1.082
C^3 — H^{10}	1.084	1.082	1.081	1.086	1.083	1.084
C^{11} — H^{12}	1.081	1.081	1.081	1.081	1.075	1.080
C^{11} — H^{13}	1.083	1.083	1.084	1.083	1.076	1.083
C^{11} — H^{14}	1.081	1.081	1.079	1.081	1.078	1.080
Bond angles						
C^1–C^2–C^3	124.17	124.24	124.18	124.24	124.16	123.45
C^2–C^3–S^4	114.14	108.85	114.62	113.96	108.93	115.45
C^3–S^4–S^5	103.62	103.23	104.07	104.18	103.01	104.12
S^4–S^5–C^{11}	102.94	103.21	103.69	102.72	103.10	103.40
C^2–C^1–H^6	121.41	121.46	121.47	121.46	121.45	121.49
C^2–C^1–H^7	122.09	121.96	121.90	121.97	121.93	122.01
C^1–C^2– H^8	119.89	119.86	119.91	119.97	119.80	119.62
C^3–C^2–H^8	115.93	115.90	115.91	115.79	116.03	115.92
C^2–C^3–H^9	111.15	110.94	110.50	111.41	111.30	110.75
C^2–C^3–H^{10}	110.81	110.91	111.36	110.68	110.62	110.91
S^4–C^3–H^9	108.13	107.71	103.18	109.50	108.90	103.72
S^4–C^3–H^{10}	104.53	109.56	108.74	103.09	108.38	107.64
S^5–C^{11}–H^{12}	110.68	110.68	110.60	110.83	110.70	110.57
S^5–C^{11}–H^{13}	106.42	106.41	106.15	106.37	106.43	106.20
S^5–C^{11}–H^{14}	111.40	111.40	111.13	111.38	111.40	111.62
H^6–C^1–H^7	116.50	116.59	116.63	116.57	116.62	116.50
H^9–C^3–H^{10}	107.70	108.80	107.96	107.74	108.65	107.92
H^{12}–C^{11}–H^{13}	109.35	109.31	109.18	109.31	109.33	109.21
H^{12}–C^{11}–H^{14}	109.92	109.96	110.27	109.90	109.91	109.81
H^{13}–C^{11}–H^{14}	108.99	108.99	109.40	108.95	108.97	109.34
Torsional angles						
$\tau_1 = \tau(C^3\text{-}S^4\text{–}S^5\text{-}C^{11})$	±87.67	±87.09	±93.14	±88.51	±88.32	±96.71
$\tau_2 = \tau(C^2\text{-}C^3\text{–}S^4\text{-}S^5)$	±73.43	±166.15	±287.93	±69.41	±189.08	±290.72
$\tau_3 = \tau(C^1\text{-}C^2\text{–}C^3\text{-}S^4)$	±118.70	±111.44	±119.78	±239.93	±249.42	±248.91
H^6- C^1–C^2- C^3	±179.53	±179.82	±179.17	±180.28	±180.11	±180.76
H^7-C^1–C^2- C^3	±0.54	±0.01	±0.62	±0.49	±0.02	±0.71
S^4-S^5–C^{11}-H^{12}	±58.58	±57.76	±57.21	±58.18	±58.68	±58.33
S^4-S^5–C^{11}-H^{13}	±177.29	±176.42	±175.52	±176.91	±177.39	±176.69
S^4-S^5–C^{11}-H^{14}	±295.97	±295.09	±294.39	±295.49	±296.05	±295.78
Energies						
E (Hartree)	–951.1242012	–951.1250546	–951.1261499	–951.1251593	–951.1248800	–951.1236829
ΔE (kcal/mol)	1.22	0.69	0.00	0.62	0.80	1.55

[a]The three symbols in $g^+g^+g^+$, $g^+a\ g^+$, … etc. are the conformational assignments for τ_1, τ_2, and τ_3, respectively.

© 2000 NRC Canada

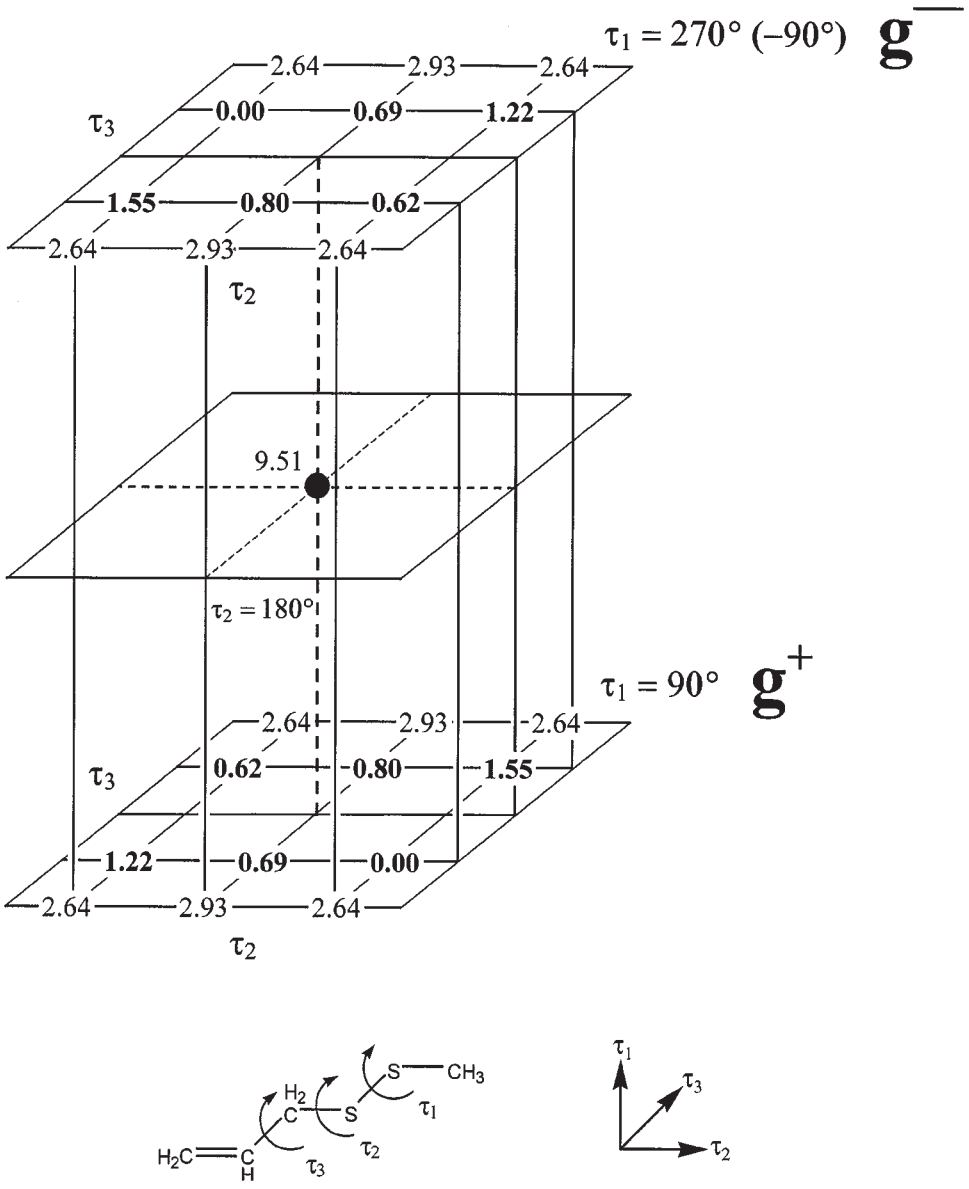
Table 4. Optimized parameters and energy values for the six lower conformational minima[a] ($\lambda = 0$) of **3** (Allyl – SS – CH_3) computed at the B3LYP/6–31G* level of theory.

$\tau_1 \approx 90°$	$g^+ g^+ g^+$	$g^+ a g^+$	$g^+ g^- g^+$	$g^+ g^+ g^-$	$g^+ a g^-$	$g^+ g^- g^-$
$\tau_1 \approx 270°$ (or –90°)	$g^- g^- g^-$	$g^- a g^-$	$g^- g^+ g^-$	$g^- g^- g^+$	$g^- a g^+$	$g^- g^+ g^+$
Bond lengths						
C^1 — C^2	1.334	1.335	1.335	1.334	1.335	1.334
C^2 — C^3	1.496	1.498	1.495	1.493	1.498	1.496
C^3 — S^4	1.864	1.867	1.862	1.866	1.837	1.864
S^5 — C^{11}	1.837	1.837	1.837	1.837	1.867	1.838
S^4 — S^5	2.082	2.081	2.080	2.079	2.082	2.082
C^1 — H^6	1.086	1.086	1.087	1.086	1.086	1.086
C^1 — H^7	1.088	1.088	1.088	1.088	1.088	1.088
C^2 — H^8	1.089	1.089	1.090	1.089	1.089	1.090
C^3 — H^9	1.095	1.094	1.098	1.094	1.093	1.096
C^3 — H^{10}	1.096	1.094	1.093	1.098	1.095	1.094
C^{11} — H^{12}	1.092	1.092	1.092	1.092	1.092	1.092
C^{11} — H^{13}	1.095	1.095	1.095	1.095	1.095	1.095
C^{11} — H^{14}	1.093	1.093	1.091	1.093	1.093	1.092
Bond angles						
C^1–C^2–C^3	124.30	124.24	124.06	124.11	124.03	124.54
C^2–C^3–S^4	113.85	108.85	114.29	113.61	108.27	114.94
C^3–S^4–S^5	103.82	103.23	104.20	104.43	103.55	104.19
S^4–S^5–C^{11}	103.21	103.21	103.71	103.01	103.41	103.73
C^2–C^1–H^6	121.62	121.46	121.68	121.68	121.65	121.70
C^2–C^1–H^7	121.86	121.96	121.65	121.72	121.69	121.78
C^1–C^2–H^8	119.99	119.86	119.94	119.98	119.82	119.70
C^3–C^2–H^8	115.71	115.90	115.99	116.13	116.13	115.75
C^2–C^3–H^9	111.99	110.94	111.36	111.88	111.70	111.27
C^2–C^3–H^{10}	111.36	110.91	111.74	111.63	111.47	111.75
S^4–C^3–H^9	107.37	107.71	102.27	108.67	108.67	103.30
S^4–C^3–H^{10}	103.85	109.56	108.41	107.59	107.59	106.86
S^5–C^{11}–H^{12}	110.69	110.68	110.64	110.86	110.73	110.60
S^5–C^{11}–H^{13}	106.03	106.41	106.87	105.98	106.05	105.83
S^5–C^{11}–H^{14}	111.47	111.40	110.81	111.40	111.41	111.56
H^6–C^1–H^7	116.52	116.59	116.67	116.61	116.65	116.52
H^9–C^3–H^{10}	107.93	108.80	108.22	108.02	109.03	108.18
H^{12}–C^{11}–H^{13}	109.39	109.31	109.30	109.35	109.39	109.28
H^{12}–C^{11}–H^{14}	110.13	109.96	110.55	110.13	110.13	110.03
H^{13}–C^{11}–H^{14}	108.03	108.99	109.55	109.01	109.02	109.44
Torsional angles						
$\tau_1 = \tau(C^3\text{-}S^4\text{–}S^5\text{-}C^{11})$	±87.88	±87.00	±91.61	±88.63	±88.45	±94.61
$\tau_2 = \tau(C^2\text{-}C^3\text{–}S^4\text{-}S^5)$	±72.37	±161.63	±290.28	±66.66	±192.22	±288.63
$\tau_3 = \tau(C^1\text{-}C^2\text{–}C^3\text{-}S^4)$	±115.01	±109.43	±117.29	±243.12	±251.86	±248.10
H^6-C^1–C^2-C^3	±180.15	±180.19	±179.72	±179.52	±179.73	±180.47
H^7-C^1–C^2-C^3	±0.24	±0.62	±0.14	±0.47	±0.65	±0.35
S^4-S^5–C^{11}-H^{12}	±58.12	±57.76	±57.76	±58.31	±58.39	±58.28
S^4-S^5–C^{11}-H^{13}	±176.66	±176.42	±176.07	±176.86	±176.96	±176.51
S^4-S^5–C^{11}-H^{14}	±295.18	±295.09	±294.77	±295.29	±295.45	±295.46
Energies						
E (Hartree)	–953.5985258	–953.5993372	–953.6005847	–953.5995770	–953.5991198	–953.5982672
ΔE (kcal/mol)	1.29	0.78	0.00	0.63	0.92	1.45

[a]The three symbols in $g^+g^+g^+$, $g^+a\ g^+$, … etc. are the conformational assignments for τ_1, τ_2, and τ_3, respectively.

© 2000 NRC Canada

Fig. 10. Topology of the conformational the PEHS of **3** (allyl methyl disulfide), where $E = E(\tau_1, \tau_2, \tau_3)$, indicating the relative energies in kcal/mol of the 6 pairs of lower energy conformers in boldface, of the 3 pairs of higher energy conformers, and of the fully symmetrical *anti* structure. Note that the centre of symmetry (i.e., where $\tau_1 = \tau_2 = \tau_3 = 180°$) is denoted by a solid dot, and corresponds to the [*a a a*] conformation shown in Fig. 8. The energy values were computed at the HF/6–31G* level of theory.



3, then the structures along such a line are enantiomers. Conversely, if an imaginary line joining two conformers cannot be drawn through the fully *anti*-centre, then the structures are diastereomers.

To denote the enantiomeric relationship of each pair of conformers, a convenient notation has been adopted, with the symbol " | " representing a mirror plane between two enantiomers. Therefore, as illustrated in Fig. 8, the $g^+g^-g^+$ conformer is enantiomeric to the $g^-g^+g^-$ conformer, i.e., $[g^+g^-g^+ \mid g^-g^+g^-]$.

From our previous study on the multidimensional conformational analysis of ethyl benzene (38), we remembered that when a planar moiety is rotated against a tetrahedral moiety, very often two minima result, one of them being higher (0° rotation) and the other being lower (90° rotation) in energy, as illustrated in Fig. 11. In the case of **3**, the planarity of the allyl group led us to believe that an analogous relationship was also present. For this reason, one-dimensional scans along τ_2 and τ_3 were performed, generating PEC's where,

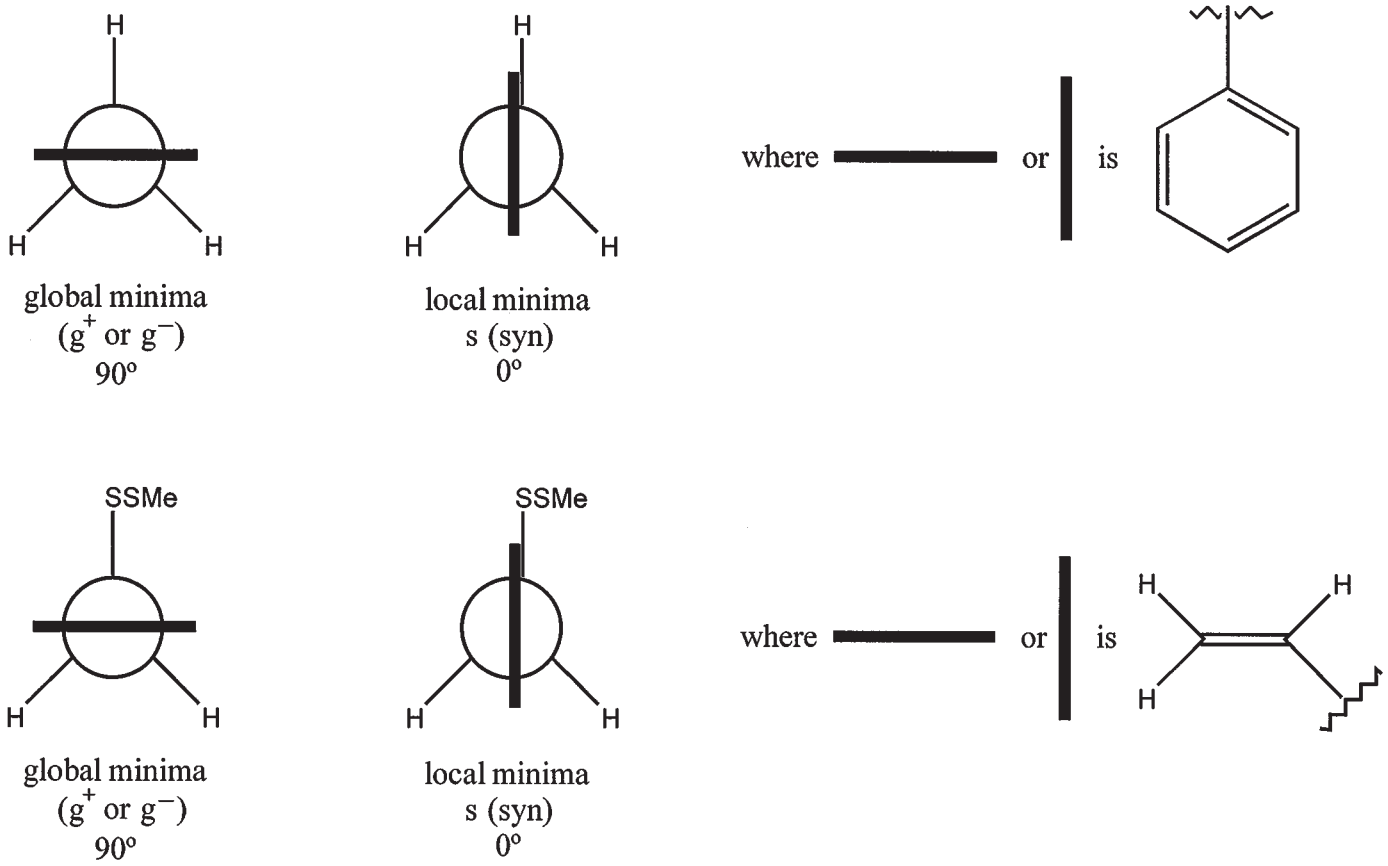
$$E = E(\tau_2)$$

and

$$E = E(\tau_3)$$

© 2000 NRC Canada

Fig. 11. Structural representation of ethyl benzene and **3** (allyl methyl disulfide) showing the two types of minima that result from rotating a planar moiety against a tetrahedral moiety.



respectively. Scanning along τ_2 (i.e., along **c** in Fig. 6) revealed that the possibility of three higher energy minima when the following constraint was applied: $\tau_1 = +90°$ and $\tau_3 = 0°$ (Fig. 12). On the same $\tau_1 = 90°$ platform of the PEHS of **3**, scanning along τ_3 confirmed that indeed there were three other higher energy minima. Therefore, just like in the case of ethyl benzene, the lower energy minima of **3** exist when the planar allyl moiety is perpendicular (90°) to the -H_2C—S- bond (*g*) and the higher minima exist when the same moiety is in alignment (*syn*) with that bond, as illustrated in Fig. 12. It is interesting to note that unlike the six pairs of lower minima, diastereomeric pairs were not found for these higher of conformers due to the internal symmetry at $\tau_3 = 0°$. The structures of these 3 higher minima are illustrated in Fig. 13, and their optimized parameters are provided in Tables 5 and 6. The relative energies for PEHS of **3** provided in Fig. 10 show, however, that the g^+ and g^- structures are enantiomers as manifested in the double degeneracy. Thus, on the basis of these one dimensional scans, six lower and three higher energy minima were optimized on both on the $\tau_1 = \pm 90°$ platforms. The global minimum conformer was found to be the enantiomeric [$g^+g^-g^+$ | $g^-g^+g^-$] pair of conformers, and their structures are shown in Fig. 8. As aforementioned, these diagonally opposed structures are enantiomeric in nature, and are therefore identical in energy.

Based on the enantiomeric relationship of the $\tau_1 = \pm 90°$ platforms, our ensuing investigation focused on the $\tau_1 = 180°$ platform of the PEHS of **3**, where the fully *anti* structure [*a a a*] of **3** can be found. As aforementioned, if an imaginary line joining two conformers of **3** can be drawn fully through *anti*-centre, then the structures are enantiomers. Thus, based on this relationship, enantiomeric pairs of **3** should exist, for example, between conformers along **d** on the $\tau_1 = 180°$ platform as shown in Fig. 6. Scanning along τ_3 (where $\tau_1 = 180°$ and $\tau_2 = 180°$) confirmed this enantiomeric relationship, as illustrated in the PEC shown in Fig. 14A. Furthermore, based on the relative energies provided in Fig. 10, the analogous rigid cross-sections along τ_3 at the $\tau_1 = \pm 90°$ platforms would not reveal this same element of symmetry due to the chirality created by the conformational twist about the -S—S- bond. It is interesting to note that the symmetrical cross-section shown in Fig. 14A is characteristic of rotating a bond connected to a prochiral centre. Allyl halides, which have been studied both experimentally (39–54) and computationally (55), are an example of compounds that contain such a bond.

The stereochemical significance of the fully symmetrical *anti* [*a a a*] structure of **3** (cf. the central achiral point or solid dot on the PEHS in Fig. 6) led us to its optimization, and the optimized parameters of this structure are summarized

© 2000 NRC Canada

Fig. 12. PEC of **3** (allyl methyl disulfide) along $\tau_2 = \tau(H_3C_2{\cdot}CH_2\text{-}S{\cdot}S{\cdot}CH_3)$ revealing the possiblity of three higher energy minima.

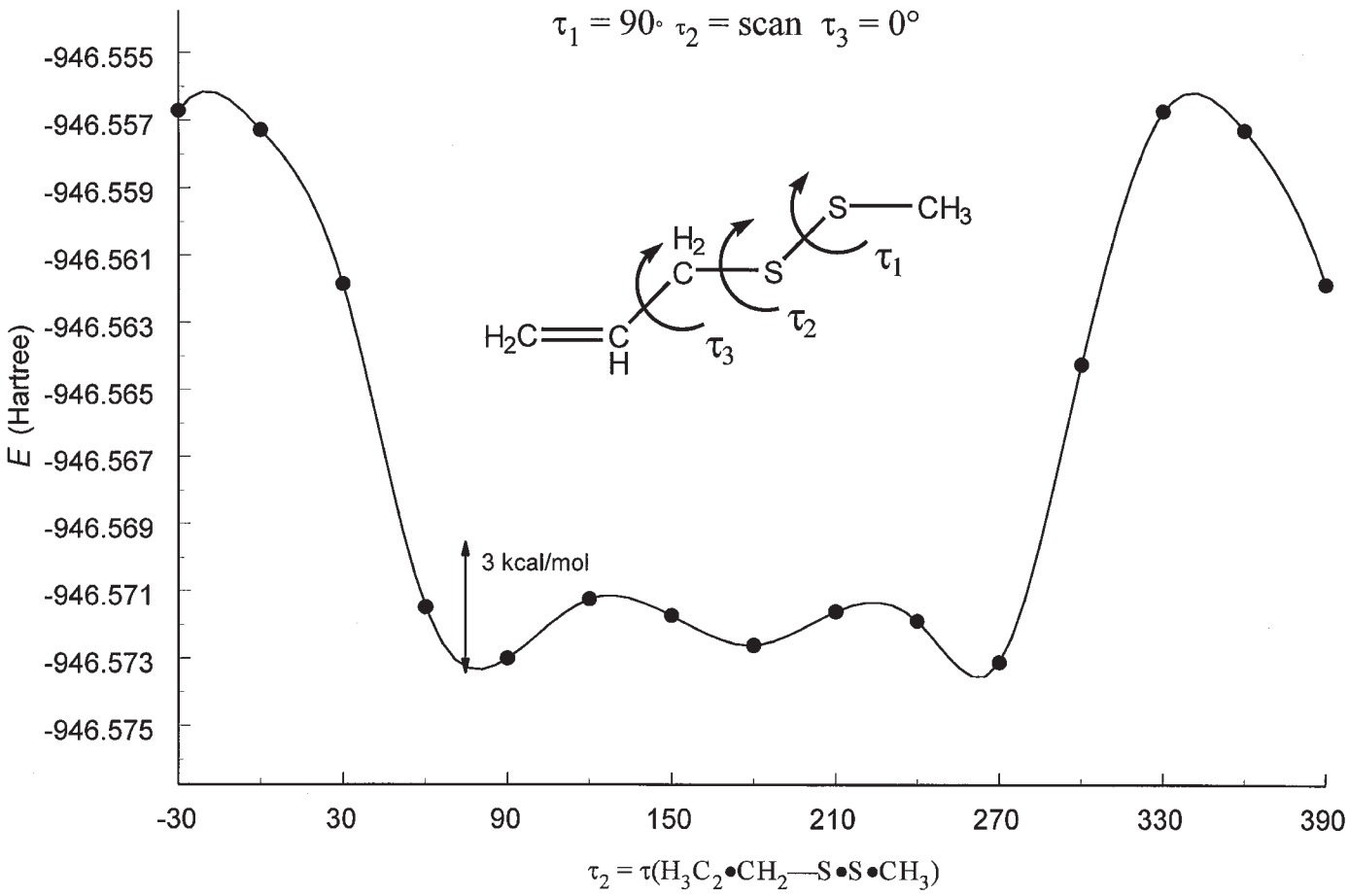
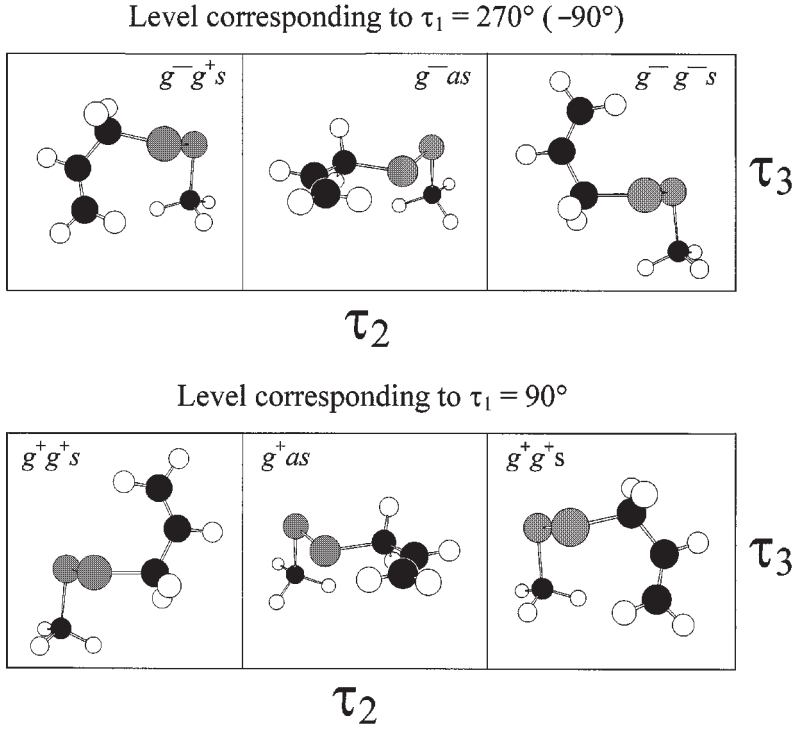


Fig. 13. Optimized structures of the three pairs of higher energy minima conformers ($\lambda = 0$) of **3** (allyl methyl disulfide) computed at the HF/6–31G* level of theory.



© 2000 NRC Canada

Table 5. Optimized parameters and energy values of the three pairs of higher conformational minima[a] ($\lambda = 0$) of **3** (Allyl – SS – CH_3) computed at the HF/6–31G* level of theory.

$\tau_1 \approx 90°$	$g^+ g^+ s$	$g^+ a s$	$g^+ g^- s$
$\tau_1 \approx 270°$ (or –90°)	$g^- g^- s$	$g^- a s$	$g^- g^+ s$
Bond lengths			
C^1 — C^2	1.317	1.318	1.318
C^2 — C^3	1.507	1.506	1.508
C^3 — S^4	1.821	1.826	1.823
S^5 — C^{11}	1.815	1.816	1.816
S^4 — S^5	2.055	2.052	2.054
C^1 — H^6	1.075	1.080	1.081
C^1 — H^7	1.074	1.083	1.084
C^2 — H^8	1.079	1.081	1.079
C^3 — H^9	1.084	1.075	1.075
C^3 — H^{10}	1.087	1.075	1.074
C^{11} — H^{12}	1.081	1.079	1.079
C^{11} — H^{13}	1.083	1.083	1.086
C^{11} — H^{14}	1.081	1.084	1.082
Bond angles			
C^1–C^2–C^3	128.01	128.17	128.02
C^2–C^3–S^4	117.59	113.62	117.89
C^3–S^4–S^5	103.86	101.84	104.06
S^4–S^5–C^{11}	102.67	103.10	104.48
C^2–C^1–H^6	120.60	120.57	120.70
C^2–C^1–H^7	122.57	123.14	122.40
C^1–C^2–H^8	118.91	118.82	118.78
C^3–C^2–H^8	113.07	113.02	113.17
C^2–C^3–H^9	109.87	109.63	109.09
C^2–C^3–H^{10}	109.44	109.20	110.20
S^4–C^3–H^9	108.72	108.13	104.73
S^4–C^3–H^{10}	104.20	108.78	107.75
S^5–C^{11}–H^{12}	110.82	110.69	110.71
S^5–C^{11}–H^{13}	106.35	106.37	105.98
S^5–C^{11}–H^{14}	111.35	111.43	111.33
H^6–C^1–H^7	116.83	116.29	116.90
H^9–C^3–H^{10}	106.35	107.28	106.52
H^{12}–C^{11}–H^{13}	109.32	109.33	109.11
H^{12}–C^{11}–H^{14}	109.92	109.94	110.23
H^{13}–C^{11}–H^{14}	108.98	108.99	109.37
Torsional angles			
$\tau_1 = \tau(C^3\text{-}S^4\text{–}S^5\text{-}C^{11})$	±89.48	±87.90	±90.57
$\tau_2 = \tau(C^2\text{-}C^3\text{–}S^4\text{-}S^5)$	±76.81	±178.16	±271.37
$\tau_3 = \tau(C^1\text{-}C^2\text{–}C^3\text{-}S^4)$	±5.87	±0.37	±12.08
H^6-C^1–C^2-C^3	±179.22	±180.12	±182.00
H^7-C^1–C^2-C^3	±0.83	±0.02	±1.65
S^4-S^5–C^{11}-H^{12}	±58.43	±58.37	±55.96
S^4-S^5–C^{11}-H^{13}	±177.14	±177.04	±174.15
S^4-S^5–C^{11}-H^{14}	±295.74	±295.71	±292.98
Energies			
E (Hartree)	–951.1219480	–951.1214844	–951.1219423
ΔE (kcal/mol)	2.64	2.93	2.64

[a]The three symbols in g^+g^+s, $g^+a\ s$, … etc. are the conformational assignments for τ_1, τ_2, and τ_3, respectively.

© 2000 NRC Canada

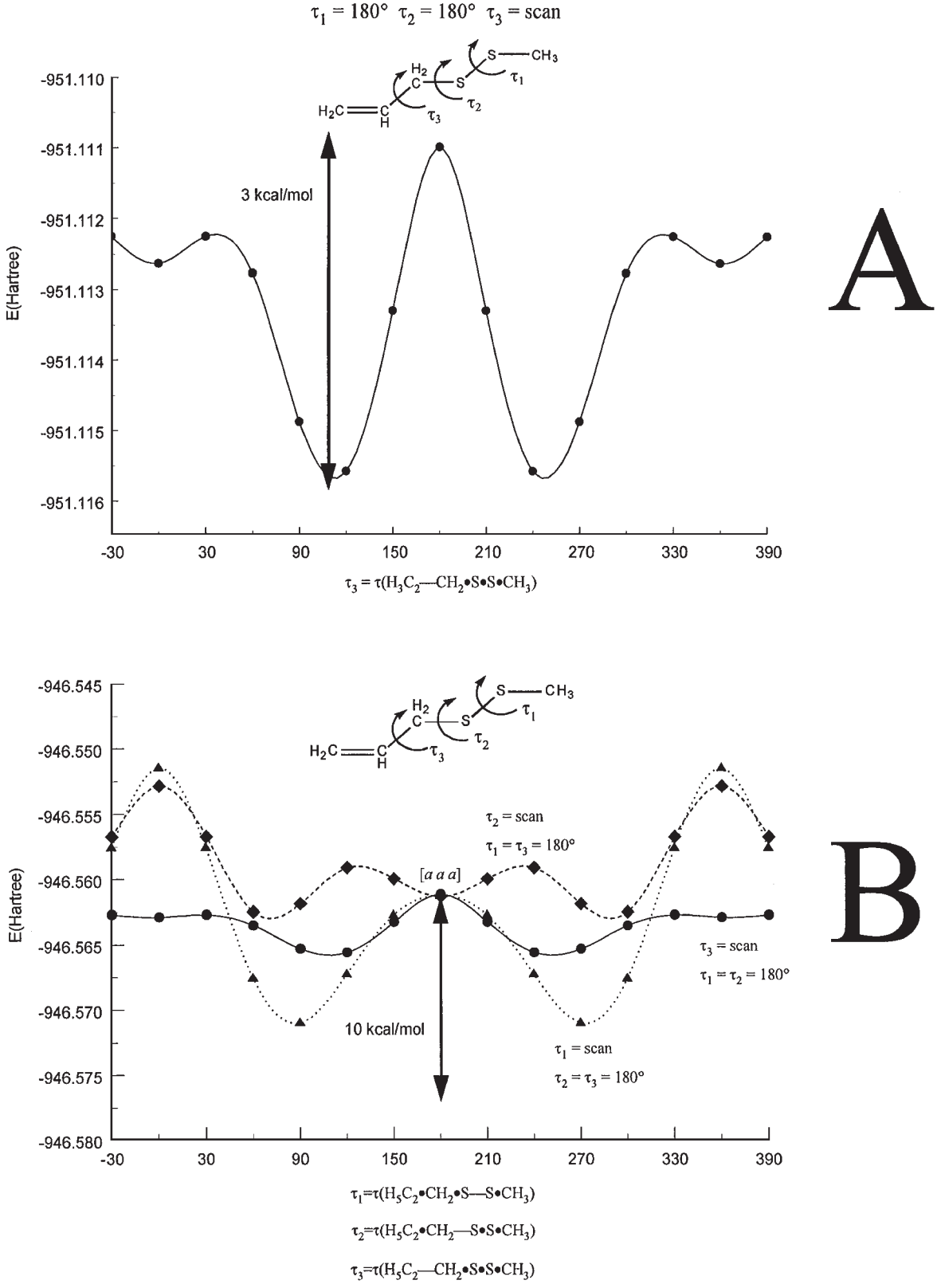
Table 6. Optimized parameters and energy values of the three higher conformational minima[a] ($\lambda = 0$) of **3** (Allyl – SS – CH_3) computed at the at the B3LYP/6–31G* level of theory.

$\tau_1 \approx 90°$	$g^+ g^+ s$	$g^+ a s$	$g^+ g^- s$
$\tau_1 \approx 270°$ (or –90°)	$g^- g^- s$	$g^- a s$	$g^- g^+ s$
Bond lengths			
C^1 — C^2	1.331	1.333	1.332
C^2 — C^3	1.507	1.504	1.508
C^3 — S^4	1.844	1.852	1.848
S^5 — C^{11}	1.836	1.837	1.837
S^4 — S^5	2.085	2.081	2.083
C^1 — H^6	1.086	1.086	1.086
C^1 — H^7	1.086	1.087	1.086
C^2 — H^8	1.092	1.091	1.092
C^3 — H^9	1.097	1.096	1.100
C^3 — H^{10}	1.100	1.097	1.095
C^{11} — H^{12}	1.092	1.092	1.092
C^{11} — H^{13}	1.095	1.095	1.095
C^{11} — H^{14}	1.093	1.093	1.091
Bond angles			
C^1–C^2–C^3	127.63	127.75	127.69
C^2–C^3–S^4	117.52	113.32	117.79
C^3–S^4–S^5	104.05	101.87	104.01
S^4–S^5–C^{11}	102.77	103.36	104.63
C^2–C^1–H^6	120.92	120.88	121.03
C^2–C^1–H^7	122.03	122.81	121.82
C^1–C^2–H^8	119.13	118.99	118.97
C^3–C^2–H^8	113.24	113.26	113.31
C^2–C^3–H^9	110.45	110.20	109.74
C^2–C^3–H^{10}	110.03	109.72	110.72
S^4–C^3–H^9	108.46	107.81	104.29
S^4–C^3–H^{10}	103.59	108.51	107.33
S^5–C^{11}–H^{12}	110.89	110.72	110.74
S^5–C^{11}–H^{13}	105.96	105.96	105.64
S^5–C^{11}–H^{14}	111.38	111.47	111.17
H^6–C^1–H^7	117.05	116.31	117.14
H^9–C^3–H^{10}	106.02	107.08	106.23
H^{12}–C^{11}–H^{13}	109.34	109.37	109.17
H^{12}–C^{11}–H^{14}	110.13	110.16	110.44
H^{13}–C^{11}–H^{14}	109.03	109.06	109.55
Torsional angles			
$\tau_1 = \tau(C^3\text{-}S^4\text{–}S^5\text{-}C^{11})$	±89.52	±87.94	±89.99
$\tau_2 = \tau(C^2\text{-}C^3\text{–}S^4\text{-}S^5)$	±77.18	±176.79	±271.77
$\tau_3 = \tau(C^1\text{-}C^2\text{–}C^3\text{-}S^4)$	±3.53	±1.16	±9.68
H^6-C^1–C^2-C^3	±179.58	±180.11	±181.69
H^7-C^1–C^2-C^3	±0.44	±0.06	±1.21
S^4-S^5–C^{11}-H^{12}	±58.48	±58.52	±57.80
S^4-S^5–C^{11}-H^{13}	±177.03	±177.01	±175.88
S^4-S^5–C^{11}-H^{14}	±295.48	±295.52	±294.63
Energies			
E (Hartree)	–9	–953.5954366	–953.5964362
ΔE (kcal/mol)	2.79	3.23	2.60

[a]The three symbols in g^+g^+s, $g^+a\ s$, … etc. are the conformational assignments for τ_1, τ_2, and τ_3, respectively.

© 2000 NRC Canada

Fig. 14. (A) PEC of **3** (allyl methyl disulfide) along $\tau_3 = \tau(H_3C_2\text{-}CH_2\cdot S\cdot S\cdot CH_3)$, computed at the HF/6–31G* level of theory. This symmetrical PEC is characteristic to the rotation about a bond connected to a prochiral centre. (B) Three PEC of **3** along $\tau_1 = \tau(H_3C_2\cdot CH_2\cdot S\text{-}S\cdot CH_3)$, $\tau_2 = \tau(H_3C_2\cdot CH_2\text{-}S\cdot S\cdot CH_3)$, and $\tau_3 = \tau(H_3C_2\text{-}CH_2\cdot S\cdot S\cdot CH_3)$, computed at the HF/3–21G* level of theory. Note that all three PEC cross through the fully symmetrical *anti-anti-anti* [*a a a*] structure (i.e., through $\tau_1 = \tau_2 = \tau_3 = 180°$) denoted by a solid dot, which is analogous to the one found on the PEHS in Figs. 6 and 10. The symmetrical [*a a a*] structure is above the global minimum by 9.51 kcal/mol computed at the HF/6–31G* level of theory.



© 2000 NRC Canada

Table 7. Optimized parameters and energy values of the fully symmetrical *anti-anti-anti* structure[a] ($\lambda = 2$) of **3** (Allyl – SS – CH_3) computed at the HF/6–31G* and B3LYP/6–31G* levels of theory.

a a a	HF/6–31G*	B3LYP/6–31G*
$\tau_1 = \tau_2 = \tau_3 = 180°$		
Bond lengths		
C^1 — C^2	1.332	1.332
C^2 — C^3	1.514	1.515
C^3 — S^4	1.821	1.840
S^5 — C^{11}	1.811	1.827
S^4 — S^5	2.088	2.133
C^1 — H^6	1.077	1.086
C^1 — H^7	1.077	1.088
C^2 — H^8	1.083	1.089
C^3 — H^9	1.083	1.096
C^3 — H^{10}	1.100	1.096
C^{11} — H^{12}	1.081	1.093
C^{11} — H^{13}	1.082	1.094
C^{11} — H^{14}	1.081	1.093
Bond angles		
C^1–C^2–C^3	123.44	123.60
C^2–C^3–S^4	109.69	109.28
C^3–S^4–S^5	98.036	97.32
S^4–S^5–C^{11}	98.14	97.65
C^2–C^1–H^6	121.27	121.32
C^2–C^1–H^7	122.17	122.14
C^1–C^2–H^8	119.30	119.20
C^3–C^2–H^8	117.26	117.19
C^2–C^3–H^9	110.66	111.01
C^2–C^3–H^{10}	110.66	111.01
S^4–C^3–H^9	108.70	108.70
S^4–C^3–H^{10}	108.70	108.70
S^5–C^{11}–H^{12}	110.94	111.14
S^5–C^{11}–H^{13}	106.30	105.84
S^5–C^{11}–H^{14}	110.94	111.14
H^6–C^1–H^7	116.56	116.54
H^9–C^3–H^{10}	108.37	108.10
H^{12}–C^{11}–H^{13}	109.20	109.16
H^{12}–C^{11}–H^{14}	110.16	110.28
H^{13}–C^{11}–H^{14}	109.20	109.16
Torsional angles		
$\tau_1 = \tau(C^3\text{-}S^4\text{–}S^5\text{-}C^{11})$	180.00	180.00
$\tau_2 = \tau(C^2\text{-}C^3\text{–}S^4\text{-}S^5)$	180.00	180.00
$\tau_3 = \tau(C^1\text{-}C^2\text{–}C^3\text{-}S^4)$	180.00	180.00
H^6 - C^1–C^2-C^3	180.00	180.00
H^7-C^1–C^2-C^3	0.00	0.00
S^4-S^5–C^{11}-H^{12}	61.39	61.62
S^4-S^5–C^{11}-H^{13}	180.00	180.01
S^4-S^5–C^{11}-H^{14}	298.60	298.40
Energies		
E (Hartree)	–951.1109930	–953.5839847
ΔE (kcal/mol)	9.51	10.42

[a]The three symbols in *a a a* is the conformational assignment for τ_1, τ_2, and τ_3, respectively.

Table 8. Frequencies, IR intensities, and Raman activities of the fully symmetrical *anti-anti-anti* structure[a] ($\lambda = 2$) of **3** (allyl methyl disufide) computed at the HF/6–31G* level of theory. Note that the negative frequencies (shown in bold) indicate a second-order saddle point.

Sequence no.	Frequency	IR intensity	Raman activity
1	**–135.137**	2.438	7.4531
2	**–53.6987**	5.085	0.4691
3	71.7456	0.2364	0.7763
4	109.1529	1.0256	0.6823
5	202.8809	0.158	0.0068
6	249.2133	0.8286	9.4262
7	290.9494	0.5426	4.0748
8	428.9482	0.6499	4.1958
9	583.5539	0.128	43.705
10	625.2566	14.3577	14.0827
11	778.5431	6.8805	20.5396
12	834.8552	11.0952	18.6932
13	1005.181	0.4693	4.4835
14	1014.844	1.1304	3.7825
15	1080.06	46.0608	4.2496
16	1086.157	3.8001	5.5871
17	1098.357	7.5271	4.8419
18	1122.276	11.3575	4.126
19	1229.46	7.7892	5.2152
20	1296.147	0.3256	5.188
21	1414.513	54.342	2.4157
22	1463.614	1.4544	32.0008
23	1517.589	13.1296	1.3622
24	1587.092	8.505	20.9257
25	1611.07	7.8827	22.6729
26	1628.881	13.1325	1.3858
27	1631.572	6.9816	18.2296
28	1872.835	3.4054	41.4831
29	3233.842	32.2431	131.318
30	3242.103	13.3708	72.0229
31	3290.226	8.5069	42.6385
32	3324.538	5.6295	112.7822
33	3326.529	9.9304	68.8955
34	3327.702	13.0164	71.9911
35	3350.012	2.4659	78.1458
36	3411.695	19.1185	98.9124

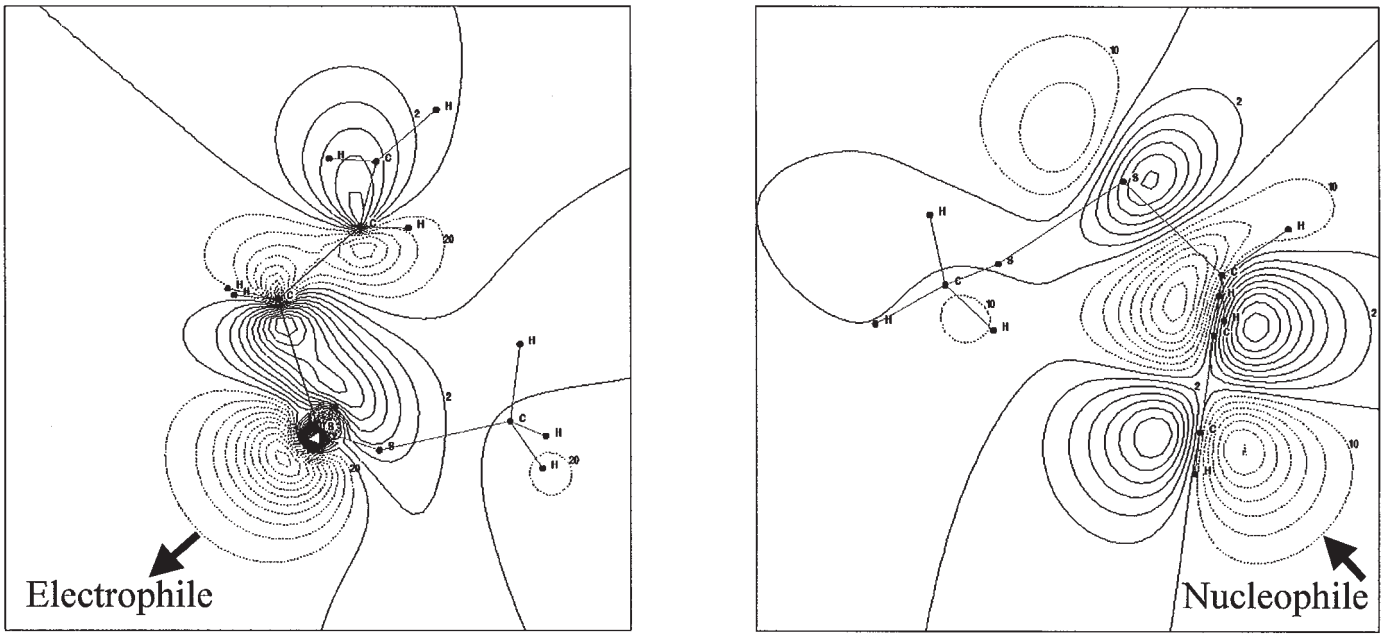
[a]The three symbols in *a a a* is the conformational assignment for τ_1, τ_2, and τ_3, respectively.

in Table 7. As illustrated in Fig. 14B, scanning along τ_3, τ_2, and τ_1 (i.e., shown in Fig. 6 as **d**, **e**, and **f** respectively) revealed that this [*a a a*] structure is a second-order saddle point ($\lambda = 2$), which was confirmed by a subsequent frequency calculation. We have provided the vibrational frequencies, IR intensities, and Raman activities of this fully *anti* structure of **3** in Table 8.

Finally, it is worthy to note that under the same basis set (i.e., 6–31G*), the level of theory (i.e., HF and B3LYP) had little influence on the relative optimized energies of both the higher and lower energy minima conformers of **3**, as Tables 3 to 6 illustrated. In fact, the energy difference between HF and B3LYP optimizations was within 0.3 kcal/mol for any given enantiomeric pair of conformers. For the global

© 2000 NRC Canada

Fig. 15. MO diagrams of the (A) HOMO and the (B) LUMO +1 orbitals of **3** (allyl methyl disulfide).



maximum conformation [*a a a*] of **3**, the level of theory had a slightly greater affect on the relative optimized energies, as the energy difference between the HF and B3LYP optimizations was 0.91 kcal/mol (Table 7).

Putative biomedical reaction mechanisms of allyl methyl disulfide

With a greater understanding of its structural behavior, the biological role of **3** was subsequently investigated. For the global minima conformers [$g^+g^-g^+$ | $g^-g^+g^-$], our examination of the HOMO (MO_{32}) and HOMO –1 (MO_{31}) orbitals revealed that they are almost energetically degenerate (MO_{32} = –0.23388 Hartree, and MO_{31} = –0.24048 Hartree); and likewise, the LUMO (MO_{33}) and LUMO +1 (MO_{34}) orbitals are similar in energy (MO_{33} = –0.02148 Hartree, and MO_{34} = –0.00129 Hartree). The relatively small negative energy values of the HOMO and HOMO –1 orbitals suggest that **3** can act as a nucleophile. Suprisingly, the energy values of the LUMO and LUMO +1 orbitals are negative, suggesting that **3** also has a strong tendency to accept electrons or act as an electrophile. Based on the similarities in energy values between the HOMO and HOMO –1 orbitals and between the LUMO and LUMO +1 orbitals, the shape of the MO will therefore largely determine which orbitals will be implicated in donating or accepting electrons in a reaction. By inspection, the HOMO and LUMO +1 orbitals would likely be involved as an electron donator and electron acceptor respectively, as shown in Fig. 15.

According to the HOMO and LUMO +1 diagrams of **3** shown in Fig. 15, one could envisage a mechanism of activity whereby allyl methyl disulfide (**3**) acts as both an electron donor and an electron acceptor, as illustrated in Fig. 16. According to Fig. 16A, disulfides like **3** lower cholesterol levels by reacting with squalene epoxide, a precursor in the biosynthesis of cholesterol. In a similar mechanism shown in Fig. 16B, the epoxy-based metabolite of the carcinogen dimethylbenz[*a*]anthracene could preferentially react with **3** instead of one of the DNA bases (e.g., guanine), thereby accounting for the anticarcinogenic activity of **3**.

Acknowledgements

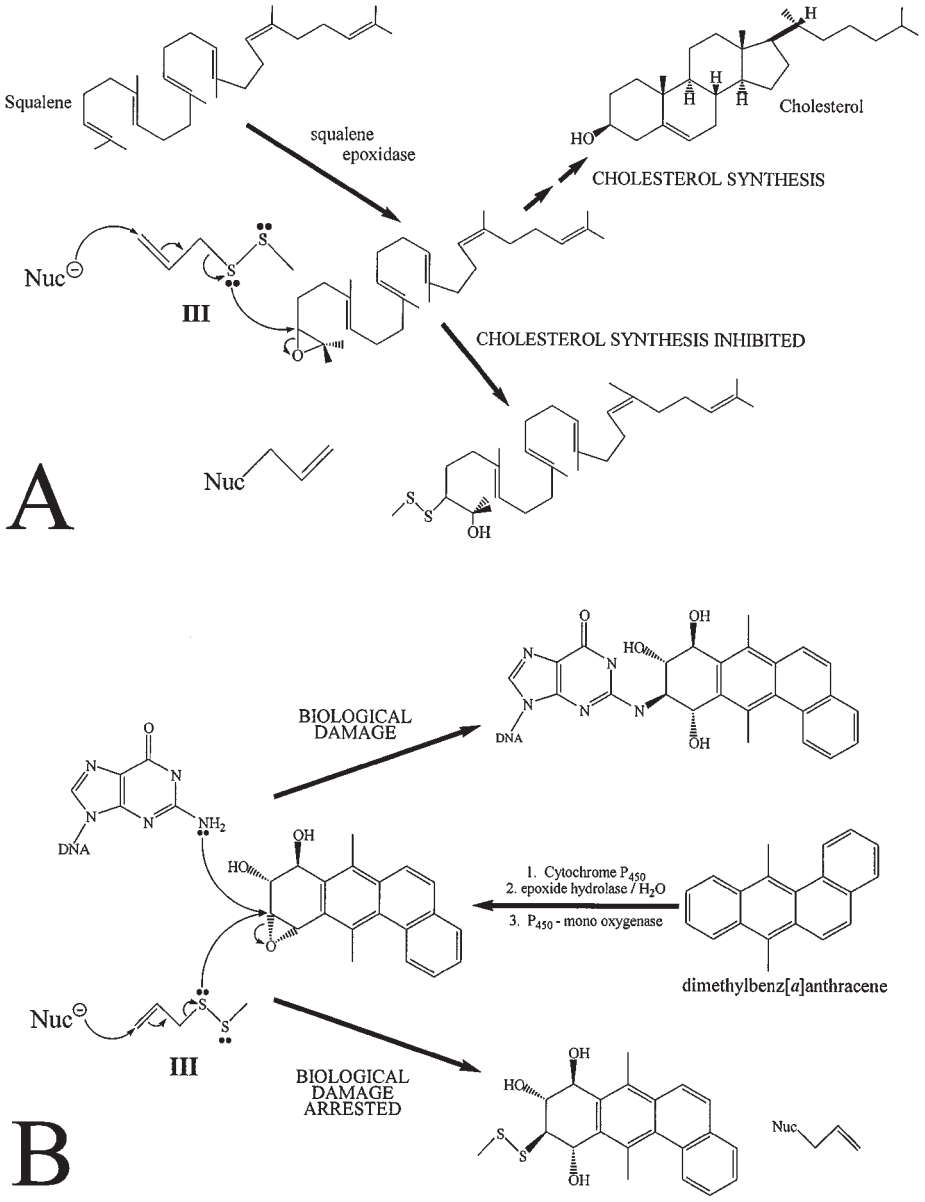
The authors wish to thank Dr. T.-H. Tang for his helpful discussions, as well as the National Cancer Institute (NCI) for the use of their services at the Frederick Biomedical Supercomputing Centre. The continuous financial support of the Natural Sciences and Engineering Research Council (NSERC) of Canada is gratefully acknowledged. Also, one of the authors (A.C. Lin) wishes to express his thanks to NSERC for the Undergraduate Student Research Award.

References

1. K.C. Agarwal. Med. Res. Rev. **16**, 111 (1996).
2. V.L. Sparnins, G. Barany, and L.W. Wattenberg. Carcinogenesis, **9**, 131, (1998).
3. H. Amagase and J.A. Milner. Carcinogenesis, **14**, 1627, (1993).
4. K. Prasad, V.A. Laxdal, M. Yu, and B.L Raney. Mol. Cell Biochem. **154**, 55 (1996).
5. B. Torok, J. Belagyi, B. Rietz, and R. Jacob. Arzneim. Forsch. **44**, 608 (1994).

© 2000 NRC Canada

Fig. 16. Putative biomedical mechanisms of the (A) cholesterol lowering and the (B) anticarcinogenic activity of **3** (allyl methyl disulfide).



6. J. Imai, N. Ide, S. Nagae, T. Moriguchi, H. Matsuura, and Y. Itakura. Planta Med. **60**, 417 (1994).
7. A. Rabinkov, T. Miron, L. Konstantinovski, M. Wilchek, D. Mirelman, and L. Weiner. Biochim. Biophys. Acta, **2**, 233 (1998).
8. S. Knasmuller, R. de Martin, G. Domjan, and A. Szakmary. Environ. Mol. Mutagen. **13**, 357 (1989).
9. A. Bordia. Atherosclerosis (Shannon, Irel.), **30**, 355 (1978).
10. J.Y. Vanderhoek, A.N. Makheja, and J.M. Bailey. Biochem. Pharmacol. **29**, 3169 (1980).
11. S.M. Mohammad and S.C. Woodward. Thromb. Res. **44**, 793 (1986).
12. R.R. Samson. Atherosclerosis (Shannon, Irel.), **44**, 199 (1982).
13. P.R. Mayeux, K.C. Agrawal, J.-S.H. Tou, B.T. King, H.L. Lippton, A.L. Hyman, P.J. Kadowitz, and D.B. McNamara. Agents Actions, **25,** 182 (1988).
14. L.D. Lawson, D.K. Ransom, and B.G. Hughes. Thromb. Res. **65,** 141 (1992).
15. G.S. Sainani, D.B. Desai, N.H. Gorhe, S.M. Nath, D.V. Pise, and P.G. Sainani. Ind. J. Med. Res. **69**, 776 (1979).
16. G.S. Sainani, D.B. Desai, and D.B. Moore. Lancett **ii**, 575 (1976); G.S. Sainani. Ind. J. Med. Res. **69**, 776 (1979).
17. S. Bhushan, S.P. Sharma, S.P. Singh, S. Agrawal, A. Indrayan, and P. Seth. Ind. J. Physiol. Pharmacol. **23**, 211 (1979).
18. R.C. Jain. Am. J. Clin. Nutr. **30**, 1380 (1977).
19. M.P. Ananad and A.S. Kochar. Int. Congr. Ser. Excerpta Med. 502 (1980).
20. B.H.S. Lau, F. Lam, and R. Wang-Cheng. Nutr. (N.Y.), Res. **7**, 139 (1987).
21. P. Xiyu. Chung hua Chung Liu Tsa Chih, **7**, 103 (1985).
22. E. Buiatti, D. Palli, A. Decarli, D. Amadori, C. Avellini, S. Bianchi, R. Biserni, F. Cipriani, P. Cocco, A. Giacosa, E.

© 2000 NRC Canada

Marubini, R. Putoni, C. Vindigni, J. Fraumeni, Jr., and W. Blot. Int. J. Cancer, **44**, 611 (1989).
23. E. George and J. Eapen. Biochem. Pharmacol. **23**, 931 (1974).
24. S.G. Sundaram and J.A. Milner. Cancer Lett. (Shannon, Irel.), **74**, 85 (1993).
25. V.L. Sparnins. A.W. Mott, G. Barany, and L.W. Wattenberg. Nutr. Cancer, **8**, 211 (1986).
26. A. Rauk. J. Am. Chem. Soc. **106**, 6517 (1984).
27. M. Aida and C. Nagata. Theor. Chim. Acta, **70**, 73 (1986).
28. R.S. Latinen, T.A. Pakkanen, and R. Steudel. J. Am. Chem. Soc. **109**, 710 (1987).
29. W. Zhao and S. Krimm. J. Mol. Struct. **224**, 7 (1990).
30. T.-K. Ha and W. Cencek. Chem. Phys. Lett. **182**, 519 (1991).
31. P. Császár, I.G. Csizmadia, W. Viviani, M. Loos, J.-L. Rivail, and A. Perczel. J. Mol. Struct. (Theochem), **455**, 107 (1998).
32. G. Winnewisser, M. Winnewisser, and W. Gordy. J. Chem. Phys. **49**, 3465 (1968).
33. (*a*) B. Beagley and K.T. McAloon. Trans. Faraday Soc. **67**, 3216 (1971); (*b*) A. Yokozeki and S.H. Bauer. J. Phys. Chem. **80**, 618 (1976); (*c*) D. Sutter, H. Dreizler, and H.D. Rudolph. Z. Naturforsch. **20a**, 1676 (1965).
34. R.L. Kuczkowski. J. Amer. Chem. Soc. **86**, 3617 (1964).
35. B. Beagely, G.H. Eckersley, D.P. Brown, and D. Tomlinson. Trans. Faraday Soc. **65**, 1 (1969).
36. E. Hirota. Bull. Chem. Soc. Jpn. **31**, 130 (1958).
37. R. Johansen, H.M. Seip, and W. Siebert. Acta Chem. Scand. Ser. A, **29**, 644 (1975).
38. Ö. Farkas, S.J. Salpietro, P. Császár, and I.G. Csizmadia. J. Mol. Struct. (Theochem), **367**, 25 (1996).
39. E. Hirota. J. Chem. Phys. **42**, 2071 (1965).
40. P. Meaken, D.D. Harris, and E. Hirota. J. Chem. Phys. **51**, 3775 (1965).
41. R.D. McLachlan and R.A. Nyquist. Spectrochim. Acta Part A, **24A**, 103 (1968).
42. J.R. Durig, M. Zhen, and T.S. Little. J. Chem. Phys. **81**, 4259 (1984).
43. J.R. Durig, M. Zhen, H.L. Heusel, P.J. Joseph, P. Groner, and T.S. Little. J. Chem. Phys. **81**, 4259 (1984).
44. J.R. Durig, T.J. Geyer, T.S. Little, and D.T. Durig. J. Mol. Struct. **172**, 165 (1988).
45. V. Santhanam, J. Sobhanadri, and S. Subramaiam. Pramana, **51**, 30 (1988).
46. J. Nieminen, J. Murto, and M. Rasanen. Spectrochim. Acta Part A, **47A**, 1495 (1991).
47. J.R. Durig, M.J. Lee, H.M. Badawi, J.F. Sullivan, and D.T. Durig. J. Mol. Struct. **266**, 59 (1992).
48. D.T. Durig, T.S. Little, T.G. Costner, and J.R. Durig. J. Mol. Struct. **266**, 277 (1992).
49. M.O. Bulanin. J. Mol. Struct. **347**, 73 (1995).
50. B.J. van der Vaken, W.A. Harrebout, D.T. Durig, W. Zhao, and J.R. Durig. J. Phys. Chem. A, **103**, 1976 (1999).
51. H.J. Bowen, A. Gilchrist, and L.E. Sutton. Trans. Faraday Soc. **34**, 1341 (1955).
52. A.A. Bothney-By and H. Gunther. Discuss. Faraday. Soc. **34**, 127 (1962).
53. E. Hirota. J. Mol. Spectrosc. **35**, 9 (1970).
54. Y. Niide, M. Takano, T. Satoh, and Y. Sasada. J. Mol. Spectrosc. **63**, 108 (1976).
55. J.R. Durig, H.Z. Qui, D.T. Durig, M. Zhen, and T.S. Little. J. Phys. Chem. **95**, 2745 (1991).

© 2000 NRC Canada

Organometallic oxides: preparation of the cluster $[(\eta\text{-}C_5Me_5)Mo]_4O_7$ by reduction of $[(\eta\text{-}C_5Me_5)MoCl(O)]_2(\mu\text{-}O)$ or $(\eta\text{-}C_5Me_5)MoCl_2(O)$

Frank Bottomley, Victor Sanchez, Robert C. Thompson, Olusola O. Womiloju, and Zhiqiang Xu

Abstract: Reduction of $[(\eta\text{-}C_5Me_5)MoCl(O)]_2(\mu\text{-}O)$ or $(\eta\text{-}C_5Me_5)MoCl_2(O)$ with sodium or magnesium amalgam, magnesium turnings, or tributyltin hydride produced $[(\eta\text{-}C_5Me_5)Mo]_4O_7$, with $[(\eta\text{-}C_5Me_5)Mo(O)(\mu\text{-}O)]_2$ as a co-product. $[(\eta\text{-}C_5Me_5)Mo]_4O_7$ was characterized by X-ray diffraction, mass spectrometry, ^{1}H NMR and IR spectroscopies, and magnetism. Crystals of $[(\eta\text{-}C_5Me_5)Mo]_4O_7$ contained a tetrahedral $[(\eta\text{-}C_5Me_5)Mo]_4$ unit (Mo—Mo = 2.909 (3) Å) with the Mo_4O_7 core having the structure $Mo_4(\mu_2\text{-}O(b))_3(\mu_2\text{-}O(c))_3(\mu_3\text{-}O(a))$ (**3**). Microcrystalline samples of $[(\eta\text{-}C_5Me_5)Mo]_4O_7$ were paramagnetic over the temperature range 2–300 K, with an effective moment of 1.26 μ_B at 300 K. $[(\eta\text{-}C_5Me_5)Mo]_4O_7$ was also paramagnetic in chloroform solution, over the temperature range 223–298 K, with an effective moment of 1.43 μ_B at 298 K. The ^{1}H NMR spectrum showed a broad resonance at 16.3 ppm ($\Delta\nu_{1/2}$ = 113 Hz) and two narrow resonances at 1.89 ppm and 1.69 ppm ($\Delta\nu_{1/2}$ = 5 Hz). The magnetism and NMR spectra showed that $[(\eta\text{-}C_5Me_5)Mo]_4O_7$ existed in two forms which were in equilibrium in solution. One form was paramagnetic (S = 1), with the Mo_4O_7 core having the geometry **3**, and the other was diamagnetic (S = 0), with the Mo_4O_7 core having the geometry **4**.

Key words: cluster, cyclopentadienyl, molybdenum, oxide, paramagnetism.

Résumé : La réduction du $[(\eta\text{-}C_5Me_5)MoCl(O)]_2(\mu\text{-}O)$ ou du $(\eta\text{-}C_5Me_5)MoCl_2(O)$ par de l'amalgame de sodium ou de magnésium, des tournures de magnésium ou de l'hydrure de tributylétain conduit à la formation de $[(\eta\text{-}C_5Me_5)Mo]_4O_7$ accompagné de $[(\eta\text{-}C_5Me_5)Mo(O)_2(\mu\text{-}O)]$ comme sous-produit. On a caractérisé le $[(\eta\text{-}C_5Me_5)Mo]_4O_7$ par diffraction des rayons X, de la spectrométrie de masse, des spectroscopies IR et RMN du ^{1}H ainsi que par magnétisme. Les cristaux de $[(\eta\text{-}C_5Me_5)Mo]_4O_7$ comprennent une unité tétraédrique de $[(\eta\text{-}C_5Me_5)Mo]_4$ (Mo—Mo = 2,909(3) Å dans laquelle le Mo_4O_7 fondamental possède la structure $Mo_4(\mu_2\text{-}O(b))_3(\mu_2\text{-}O(c))_3(\mu_3\text{-}O(a))$ (**3**). Les échantillons microcristallins de $[(\eta\text{-}C_5Me_5)Mo]_4O_7$ sont paramagnétiques sur la plage de température allant de 2 à 300 K. À des températures allant de 223 à 298 K, le $[(\eta\text{-}C_5Me_5)Mo]_4O_7$ est aussi paramagnétique en solution dans le chloroforme; à 298 K, le moment magnétique effectif est égal à 1,43 μ_B. Le spectre RMN du ^{1}H comporte une large bande de résonance à 16,3 ppm ($\Delta\nu_{1/2}$ = 113 Hz) et deux bandes de résonance étroites à 1,89 et 1,69 ppm ($\Delta\nu_{1/2}$ = 5 Hz). Le magnétisme et les spectres RMN démontrent que, en solution, le $[(\eta\text{-}C_5Me_5)Mo]_4O_7$ existe sous deux formes en équilibre. Une forme est paramagnétique (S = 1) dans laquelle le Mo_4O_7 fondamental possède la géométrie **3** et une autre forme, diamagnétique (S = 0), dans laquelle le Mo_4O_7 fondamental possède la géométrie **4**.

Mots clés : agrégat, cyclopentadiényle, molybdène, oxyde, paramagnétisme.

[Traduit par la Rédaction]

Introduction

We have been preparing organometallic clusters that exhibit exchange interactions between the metal atoms (1–3). Of particular interest were the oxide cubanes of general formula $[(\eta\text{-}C_5R_5)M(\mu_3\text{-}O)]_4$ (**1**) (3–6) and the adamantanes $[(\eta\text{-}C_5Me_5)M]_4(\mu_2\text{-}O)_6$ (**2**) (7, 8), which contain tetrahedra of *d*-block metal atoms. The cubanes $[(\eta\text{-}C_5R_5)Cr(\mu_3\text{-}O)]_4$ (R = H (4), Me (6), $R_5 = MeH_4$ (5)) were antiferromagnetic and $[(\eta\text{-}C_5Me_5)V(\mu_3\text{-}O)]_4$ was paramagnetic (3). The adamantanes $[(\eta\text{-}C_5Me_5)M]_4(\mu\text{-}O)_6$ (M = Ti, V) were diamagnetic (3, 7, 8). Because of the magnetic behaviour of $[(\eta\text{-}C_5R_5)M(\mu_3\text{-}O)]_4$ and $[(\eta\text{-}C_5Me_5)M]_4(\mu\text{-}O)_6$, we wished to prepare the molybdenum analogs $[(\eta\text{-}C_5Me_5)Mo(\mu_3\text{-}O)]_4$ and $[(\eta\text{-}C_5Me_5)Mo]_4(\mu\text{-}O)_6$.

The $[(\eta\text{-}C_5R_5)Cr(\mu_3\text{-}O)]_4$ clusters were prepared by mild oxidation of $(\eta\text{-}C_5R_5)_2Cr$ (4, 6, 9) and $[(\eta\text{-}C_5Me_5)V]_4(\mu\text{-}O)_6$ was first obtained by oxidation of $(\eta\text{-}C_5Me_5)_2V$ (7, 10, 11). However, oxidation of the only readily available low-valent $(\eta\text{-}C_5R_5)Mo$ derivatives, $[(\eta\text{-}C_5R_5)Mo(CO)_n]_2$ (n = 2, 3), gave either dimolybdenum oxo complexes (12–14), or the clusters

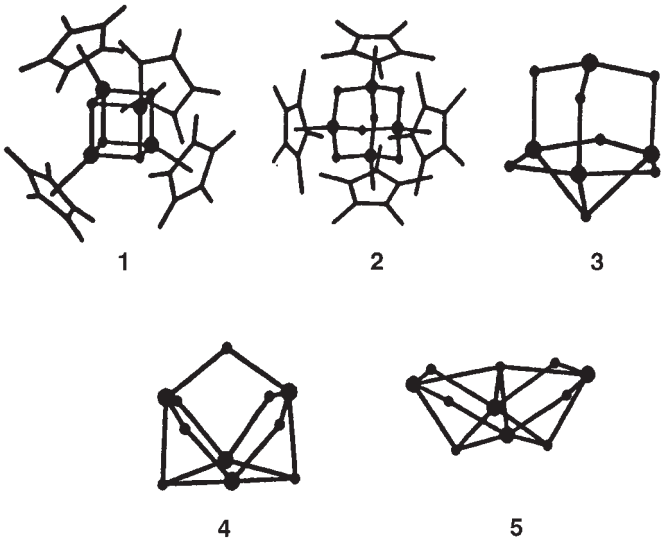
Received December 1, 1999

F. Bottomley[1] and O.O. Womiloju. Department of Chemistry, University of New Brunswick, Fredericton, NB E3B 6E2, Canada.
V. Sanchez, R.C. Thompson, and Z. Xu. Department of Chemistry, University of British Columbia, Vancouver, BC V6T 1Z1, Canada.

[1]Author to whom correspondence may be addressed. Telephone: (506) 458-7239. Fax: (506) 453-4981. e-mail: bottomly@unb.ca

© 2000 NRC Canada

$(\eta\text{-}C_5Me_5)_6Mo_8O_{16}$ (15) or $(\eta\text{-}C_5Me_5)_4Mo_5O_{11}$ (16). Recently we have been investigating the reductive aggregation of $(\eta\text{-}C_5Me_5)MCl_nA$ derivatives as a route to $[(\eta\text{-}C_5Me_5)M(\mu_3\text{-}A)]_4$ and $[(\eta\text{-}C_5Me_5)M]_4(\mu_2\text{-}A)_6$ clusters (A = N, O) (3, 17, 18). It was anticipated that reduction of $[(\eta\text{-}C_5Me_5)MoCl(O)]_2(\mu\text{-}O)$ (19, 20) would produce $[(\eta\text{-}C_5Me_5)Mo]_4(\mu\text{-}O)_6$ and reduction of $(\eta\text{-}C_5Me_5)MoCl_2(O)$ (19, 21) would produce $[(\eta\text{-}C_5Me_5)Mo(\mu_3\text{-}O)]_4$. However, we have found that reduction of $[(\eta\text{-}C_5Me_5)MoCl(O)]_2(\mu\text{-}O)$ or $(\eta\text{-}C_5Me_5)MoCl_2(O)$ gave the cluster $[(\eta\text{-}C_5Me_5)Mo]_4O_7$, which existed in paramagnetic and diamagnetic forms. The results are described in detail here.



Experimental

General information

All manipulations were performed using a standard double-manifold vacuum/argon line. Solvents were predried, stored on the vacuum line over a drying agent, and distilled directly onto reagents. The starting materials $(\eta\text{-}C_5Me_5)MoCl_2(O)$ and $[(\eta\text{-}C_5Me_5)MoCl(O)]_2(\mu\text{-}O)$ were prepared by the literature methods (19, 21–24). Sodium was freshly cut under argon and magnesium was flame dried under vacuum. Metal amalgams were prepared by using a syringe to add mercury to the predried metal under a counter flow of argon. Purification of the mercury was by washing with dilute nitric acid, then with distilled water until the washings were neutral, then with acetone. It was heated at 100°C under vacuum for 12 h before use.

Magnetic susceptibilities were measured on a Quantum Design (MPMS) SQUID magnetometer at the Advanced Materials and Process Engineering Laboratory (AMPEL) at the University of British Columbia. Measurements were made over the temperature range 2–300 K at an applied field of 10 000 G and susceptibilities were corrected for the background signal from the sample holder at all temperatures. Susceptibilities were corrected for the diamagnetism of all atoms using Pascal's constants (25) and are reported per mole of cluster. ^{1}H NMR spectra were measured on Varian XL200 or Unity 400 spectrometers. Mass spectra were measured by EI (70 eV) or by FAB methods, in the matrices specified, on a Kratos MS 50 instrument. IR spectra were measured as KBr pellets or Nujol mulls on a Perkin–Elmer 683 instrument. Extended Hückel molecular orbital calculations and molecular modeling were performed using the CAChe system.

Syntheses

Reaction of $[(\eta\text{-}C_5Me_5)MoCl(O)]_2(\mu\text{-}O)$ in toluene solution with sodium amalgam: formation of $[(\eta\text{-}C_5Me_5)Mo]_4O_7$

A solution of $[(\eta\text{-}C_5Me_5)MoCl(O)]_2(\mu\text{-}O)$ (1.34 g, 2.31 mmol) in toluene (100 cm^3) was added to sodium amalgam (0.61 g, 26.5 mmol sodium in 9 cm^3 mercury). The mixture was stirred vigorously for 14 h, during which time the solution changed color from wine-red to black-green and a grey precipitate (presumed to be sodium chloride) formed. The solution was decanted from the mercury and the residue washed twice with toluene (15 cm^3). The filtrate and washings were combined and set aside for 24 h to allow the suspended solids to settle. The mixture was then filtered three times, slowly, through acid-free Celite, giving a black residue and a black-green filtrate. The solution was reduced to a volume of 30 cm^3 under vacuum, frozen in liquid nitrogen and hexane (80 cm^3) was layered onto it. On setting aside at –25°C for two days, black $[(\eta\text{-}C_5Me_5)Mo]_4O_7$ precipitated. This was collected by filtration, washed with cold hexane (20 cm^3), and dried under vacuum. The product was recrystallized from toluene/hexane (20:80) at –25°C. Yield: 0.32 g, 26%, based on molybdenum.

Reaction of $(\eta\text{-}C_5Me_5)MoCl_2(O)$ in toluene solution with sodium amalgam: formation of $[(\eta\text{-}C_5Me_5)Mo]_4O_7$

A solution of $(\eta\text{-}C_5Me_5)MoCl_2(O)$ (2.16 g, 6.79 mmol) in toluene (100 cm^3) was added to sodium amalgam (1.61 g, 70.1 mmol sodium in 23.7 cm^3 mercury). The mixture was stirred vigorously for 14 h, during which time the solution changed color from brick-red to black-green and a grey precipitate (presumed to be sodium chloride) formed. Work-up of the reaction was the same as for the reduction of $[(\eta\text{-}C_5Me_5)MoCl(O)]_2(\mu\text{-}O)$ described above. Yield of $[(\eta\text{-}C_5Me_5)Mo]_4O_7$: 0.48 g, 27%, based on molybdenum.

Reaction of $[(\eta\text{-}C_5Me_5)MoCl(O)]_2(\mu\text{-}O)$ in tetrahydrofuran solution with tributyltin hydride: formation of $[(\eta\text{-}C_5Me_5)Mo]_4O_7$ and $[(\eta\text{-}C_5Me_5)Mo(O)(\mu\text{-}O)]_2$

To an ice-cold solution of $[(\eta\text{-}C_5Me_5)MoCl(O)]_2(\mu\text{-}O)$ (2.09 g, 3.6 mmol) in tetrahydrofuran (100 cm^3) was added $Bu^n{}_3SnH$ (2.2 cm^3, 2.4 g, 8.3 mmol) by syringe, against an argon purge. The mixture was stirred for 24 h at room temperature. The color of the solution changed from red to dark brown and $[(\eta\text{-}C_5Me_5)Mo]_4O_7$ precipitated. The mixture was filtered, giving a dark brown filtrate and a dark blue-green solid, which was washed with hexane and dried under vacuum. Yield: 0.42 g, 22%, based on molybdenum.

The dark-brown filtrate was reduced to a volume of 30 cm^3 under vacuum, then hexane (100 cm^3) was layered onto it, after which it was set aside for 24 h at –25°C. The orange crystals of $[(\eta\text{-}C_5Me_5)Mo(O)(\mu\text{-}O)]_2$ that precipitated were collected by filtration, washed with hexane (20 cm^3) and dried under vacuum. Yield: 0.29 g, 15%, based on molybdenum. IR: 913 cm^{-1} (vs, ν(Mo=O)), 713 cm^{-1}

© 2000 NRC Canada

Table 1. Crystal and refinement data for the four samples of $[(\eta\text{-}C_5Me_5)Mo]_4O_7$.

Crystal	A	B	C	D
Size (mm)	0.35 × 0.22 × 0.13	0.31 × 0.30 × 0.13	0.18 × 0.18 × 0.06	0.52 x 0.44 × 0.20
Source	$[(\eta\text{-}C_5Me_5)MoCl(O)]_2(\mu\text{-}O)$	$(\eta\text{-}C_5Me_5)MoCl_2(O)$	$(\eta\text{-}C_5Me_5)MoCl_2(O)$	$(\eta\text{-}C_5Me_5)MoCl_2(O)$
Diffractometer	Enraf–Nonius CAD4	Enraf–Nonius CAD4	Siemens P4/CCD	Rigaku AFC5R
a (Å)	11.056 (4)	11.042 (3)	11.1094 (3)	11.050 (9)
b (Å)	11.136 (4)	11.109 (4)	11.1807 (1)	11.092 (12)
c (Å)	18.489 (7)	18.425 (5)	18.4828 (4)	18.423 (14)
α (°)	83.61 (3)	83.59 (3)	83.331 (1)	83.55 (8)
β (°)	83.01 (3)	83.29 (2)	82.910 (1)	83.27 (7)
γ (°)	66.34 (3)	66.47 (2)	66.134 (1)	66.48 (7)
T (K)	295	293	300	253
$2\theta_{max}$ (°)	44.9	44.9	52.9	40.0
Scan	θ/2θ	θ/2θ	ω	θ/2θ
Reflexns. meas.	6158	6276	21239	4012
Uniq. reflexns.	5174	5289	7872	3844
Reflxns. with $I > n\sigma(I)$	3004	3411	4055	2126
n	1.0	1.0	2.0	1.0
Reflxns. used	2983	3393	4033	2072
Absorption correction	No	No	Multiple redundant data (T 0.80 – 0.94)	No
Params. ref.	269	443	467	265
R^a	0.107	0.087	0.080	0.072
$R_w{}^b$	0.125	0.112	0.083	0.085
GoF[c]	1.26	1.68	1.46	1.70
$(\Delta/\sigma)_{max}$ (parameter)	0.63 ($\eta\text{-}C_5Me_5$(3))	0.14 ($\eta\text{-}C_5Me_5$(3))	0.41 ($\eta\text{-}C_5Me_5$ (3))	0.49 ($\eta\text{-}C_5Me_5$ (3))
Δ_{max} (e Å^{-3}) (location)	1.95 ($\eta\text{-}C_5Me_5$(3))	1.26 (Mo(3))	1.03 ($\eta\text{-}C_5Me_5$ (3))	1.09 ($\eta\text{-}C_5Me_5$ (3))
Refinement	Mo aniso; C, O iso.	Mo, 3($\eta\text{-}C_5Me_5$) aniso; disordered $\eta\text{-}C_5Me_5$, O iso.	Mo, 3($\eta\text{-}C_5Me_5$) aniso; disordered $\eta\text{-}C_5Me_5$, O iso.	Mo aniso; C, O iso.

[a] $R = (\Sigma|\Delta F|/(\Sigma F_o)$.

[b] $R_w = [(\Sigma w(\Delta F)^2/(\Sigma w(F_o)^2]^{1/2}$.

[c] GoF = $\Sigma w(\Delta F)^2$/[(no. reflxns) – (no. params)].

(s, δ(O-Mo=O)) (lit. (19): 914, 713 cm^{-1}). ^{1}H NMR (200 MHz, C^2HCl_3 solution): singlet, 1.97 ppm (lit. for *cis*-$[(\eta\text{-}C_5Me_5)Mo(O)(\mu\text{-}O)]_2$: 1.93 ppm (14), 1.97 ppm (19)). MS (EI, 70 eV) (*m/e*, % abundance, assignment): 526, 74, $\{C_{20}H_{30}Mo_2O_4\}^+$ ($\{[(C_5Me_5)MoO_2]_2\}^+$), with the appropriate isotopic pattern and fragments.

Reaction of $(\eta\text{-}C_5Me_5)MoCl_2(O)$ in tetrahydrofuran solution with tributyltin hydride: formation of $[(\eta\text{-}C_5Me_5)Mo]_4O_7$

To an ice-cold solution of $(\eta\text{-}C_5Me_5)MoCl_2(O)$ (0.79 g, 2.5 mmol) in tetrahydrofuran (100 cm^3) was added $Bu^n{}_3SnH$ (4.2 cm^3, 4.51 g, 15.6 mmol) by syringe, against an argon purge. The mixture was stirred in an ice bath for 11 h, during which time the color of the solution changed from brick red to black-green. The solution was reduced to a volume of 30 cm^3 under vacuum, layered with hexane (60 cm^3) and set aside at –25°C for two days. The black precipitate of $[(\eta\text{-}C_5Me_5)Mo]_4O_7$ that formed was collected by filtration, washed twice with hexane (2 × 20 cm^3), and dried under vacuum. Yield: 0.22 g, 34%, based on molybdenum.

Reaction of $[(\eta\text{-}C_5Me_5)MoCl(O)]_2(\mu\text{-}O)$ in tetrahydrofuran solution with lithium nitride: formation of $[(\eta\text{-}C_5Me_5)Mo(O)(\mu\text{-}O)]_2$

A solution of $[(\eta\text{-}C_5Me_5)MoCl(O)]_2(\mu\text{-}O)$ (1.56 g, 2.68 mmol) in tetrahydrofuran (80 cm^3) was added to a suspension of lithium nitride (0.065 g, 1.87 mmol) in tetrahydrofuran (20 cm^3) and the mixture stirred for 14 h while warming to room temperature. The color of the solution changed from red to dark green. The mixture was then filtered through acid-free Celite and the volume of the filtrate reduced to 30 cm^3 under vacuum. The solution was then frozen in liquid nitrogen and hexane (60 cm^3) was layered onto it. On setting aside at –25°C for two days, a dark orange precipitate of $[(\eta\text{-}C_5Me_5)Mo(O)(\mu\text{-}O)]_2$ formed. This was collected by filtration, washed with cold hexane (20 cm^3), and dried under vacuum. It was recrystallized from toluene/hexane (20:80). Yield: 0.54 g, 38%, based on molybdenum. The product had identical spectroscopic properties to those given above for $[(\eta\text{-}C_5Me_5)Mo(O)(\mu\text{-}O)]_2$, obtained from $[(\eta\text{-}C_5Me_5)MoCl(O)]_2(\mu\text{-}O)$ and $Bu^n{}_3SnH$.

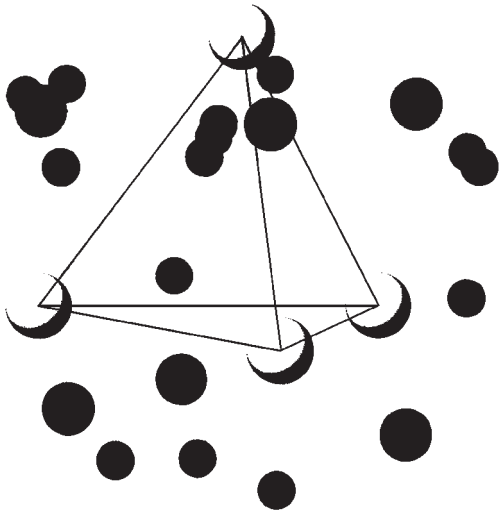
Characterization of $[(\eta\text{-}C_5Me_5)Mo]_4O_7$

X-ray diffraction

The crystals of $[(\eta\text{-}C_5Me_5)Mo]_4O_7$ used for X-ray diffraction experiment A (see Table 1) were obtained by setting aside saturated toluene solutions of the material produced by reduction of $[(\eta\text{-}C_5Me_5)MoCl(O)]_2(\mu\text{-}O)$ with sodium amalgam, at room temperature for 10 weeks. Crystals B, C, and D were obtained by setting aside saturated toluene solutions

© 2000 NRC Canada

Fig. 1. Sites of electron density greater than 1.0 e $Å^{-3}$ in a difference Fourier map of $[(\eta\text{-}C_5Me_5)Mo]_4O_7$ phased on the $[(\eta\text{-}C_5Me_5)Mo]_4$ unit, determined using data from crystal C.



of material produced by reduction of $(\eta\text{-}C_5Me_5)MoCl_2(O)$ with sodium amalgam, at room temperature for four days, 19 weeks and eight weeks, respectively. Data common to the four crystals: empirical formula = $C_{40}H_{60}Mo_4O_7$, M_r = 1036.67, class = triclinic, space group = $P\bar{1}$, D_c = 1.67 mg m^{-3}, Z = 2, MoKα radiation, λ = 0.71073 Å, μ(MoKα) = 12.0 cm^{-1}. Other details of the crystals, data collection, and refinements are given in Table 1.

Identification and refinement of the tetrahedral $[(\eta\text{-}C_5Me_5)Mo]_4$ unit of $[(\eta\text{-}C_5Me_5)Mo]_4O_7$ (Mo = 2.91 Å) was routine in all four of the determinations, but the oxygen atoms in the Mo_4O_7 core were severely disordered. This was unexpected, since the unit cell and distribution of intensities for $[(\eta\text{-}C_5Me_5)Mo]_4O_7$ were very similar to those of $[(\eta\text{-}C_5Me_5)M]_4(\mu\text{-}O)_6$ (M = Ti (8), V (7)) and $[(\eta\text{-}C_5Me_5)Cr(\mu_3\text{-}O)]_4$ (6), in which the M_4O_n cores were not disordered. Fig. 1 shows the 21 sites of electron density greater than 1.0 e $Å^{-3}$ in a difference Fourier synthesis phased on the $[(\eta\text{-}C_5Me_5)Mo]_4$ unit after isotropic refinement of the data from crystal C (Table 1). These sites were of three types. Four, designated O(a), with electron densities of 1.0 e $Å^{-3}$, bridged the three molybdenum atoms of each of the four Mo_3 faces of the tetrahedron. Eleven, designated O(b), with electron densities of 2.9–1.1 e $Å^{-3}$, bridged two molybdenum atoms and were located over the edges of each of the four Mo_3 faces of the tetrahedron. Six, designated O(c), with electron densities of 4.6–3.6 e $Å^{-3}$, bridged two molybdenum atoms and were located over the edges of the Mo_4 tetrahedron. It was found after many trials, which included structure **4**, that the correct geometry for the Mo_4O_7 core of $[(\eta\text{-}C_5Me_5)Mo]_4O_7$ was **3** (Fig. 2). The sites shown in Fig. 1 were observed because the μ_3-oxygen atom (O(a)) may bridge any of the four triangular faces of the tetrahedron, with the six μ_2-oxygen atoms (three O(b) and three O(c)) oriented accordingly. The short distance between oxygen atom sites of different orientations and further disorder in the $\eta\text{-}C_5Me_5$ ligand attached to Mo(3) prevented anisotropic refinement of these atoms. The refinements included the hydrogen atoms in fixed calculated positions, with C—H = 1.08 Å and $U_{eq}(H) = 0.01 + U_{eq}(C)$ (26). Tables of final parameters and derived distances and angles for all four crystals are available in the supplementary material.[2] The average metrical parameters are presented in Table 2 and a thermal ellipsoid plot of one orientation, using data from crystal C of Table 1, is shown in Fig. 3.

Fig. 2. Numbering scheme for the Mo_4O_7 core of $[(\eta\text{-}C_5Me_5)Mo]_4O_7$.

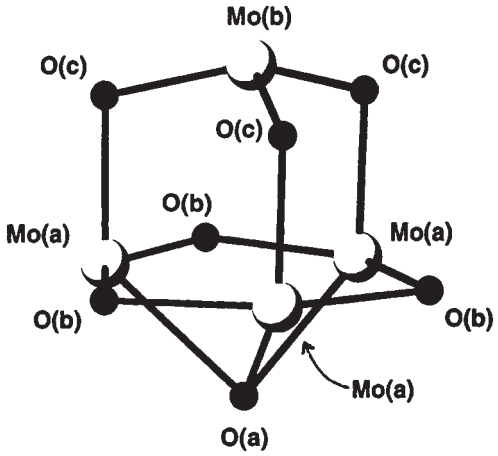
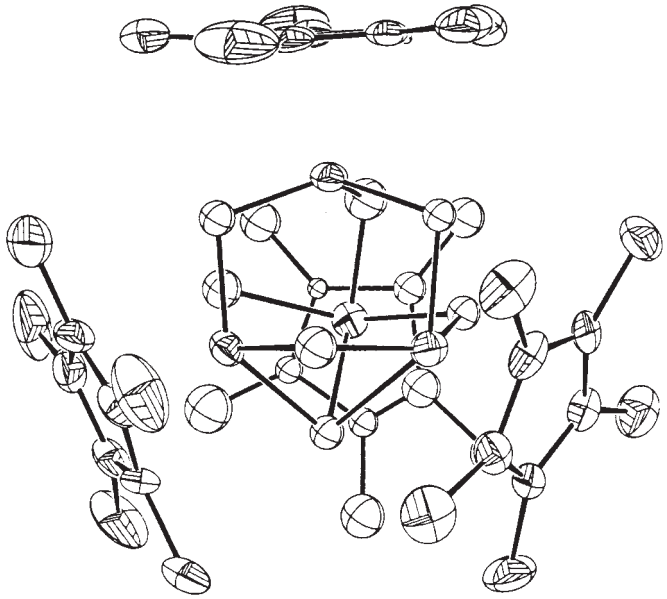


Fig. 3. Thermal ellipsoid plot of $[(\eta\text{-}C_5Me_5)Mo]_4O_7$. The data were taken from crystal C. Only one of the four orientations of the Mo_4O_7 core of the cluster is shown.



Mass spectra

The assignments of the ions observed in the FAB mass spectrum of $[(\eta\text{-}C_5Me_5)Mo]_4O_7$ are given in Table 3. Representative spectra in NOBA, thioglycerol, dithiothrei-

[2] The supplementary material has been deposited. Copies may be purchased from: The Depository of Unpublished Data, Document Delivery, CISTI, National Research Council of Canada, Ottawa K1A 0S2, Canada.

© 2000 NRC Canada

Table 2. Distances (Å) and angles (°) in $[(\eta\text{-}C_5Me_5)Mo]_4O_7$.

Crystal	A	B	C	D	Average
Number of oxygen sites	18	17	21	17	
Mo—Mo	2.914 (3)[a]	2.874 (3)	2.933 (2)	2.917 (5)	2.909 (3, 62, 24)[b]
Mo—Cp*[c]	2.07 (3)	2.06 (2)	2.07 (1)	2.06 (3)	2.07 (2, 3, 14)
Mo(a)—O(a)[d]	2.18 (6)	2.19 (3)	2.23 (5)	2.12 (6)	2.19 (5, 28, 42)
Mo(a)—O(b) (s)[e]	1.83 (7)	1.81 (5)	1.92 (4)	1.88 (5)	1.87 (5, 34, 35)
Mo(a)—O(b) (l)[e]	1.99 (7)	1.95 (5)	2.00 (4)	1.99 (5)	2.00 (5, 32, 35)
Mo—O(c)[f]	1.85 (4)	1.83 (5)	1.87 (3)	1.85 (5)	1.85 (4, 23, 39)
Mo(a)–O(a)–Mo(a)	84 (2)	82 (1)	82 (1)	87 (3)	83 (2, 9, 42)
Mo(a)–O(b)–Mo(a)	99 (3)	99 (3)	97 (2)	97 (3)	98 (3, 17, 35)
O(b)–Mo(a)–O(b)	136 (3)	137 (2)	138 (2)	136 (3)	137 (3, 16, 31)
Mo(a)–O(c)–Mo(b)	104 (2)	103 (2)	104 (1)	104 (3)	104 (2, 6, 39)
O(c)–Mo(b)–O(c)	112 (2)	111 (2)	112 (1)	111 (2)	111 (2, 22, 39)
Mo_3—O(a)[g]	1.38	1.43	1.45	1.28	1.39
Mo_3—O(b)[g]	–0.17	–0.21	–0.21	–0.02	–0.16
O(b)–Mo(a)–O(c)–Mo(b)[h]	67	70	70	67	68
O(c)—Mo_4(edge)[i]	0.02	0.07	0.09	–0.02	0.04

[a]Average distance or angle (average esd) for all orientations in the specified crystal.

[b]Average distance or angle (average esd maximum deviation from the average, number of distances averaged) for the four crystals.

[c]Cp* is the centroid of the C_5 ring of the η-C_5Me_5 ligand; the disordered η-C_5Me_5(3) in crystals B and C are excluded.

[d]See Fig. 2 for numbering scheme.

[e]Average of the alternating short (Mo(a)—O(b) (s)) and long (Mo(a)—O(b) (l)) distances of the $[Mo(a)(\mu\text{-}O(b))]_3$ ring, obtained by proceeding from the longest distance clockwise around the ring.

[f]Average of the Mo(a)—O(c) and Mo(b)—O(c) distances.

[g]Distance of O(a), or average distance of O(b), from the plane of the three Mo(a) atoms.

[h]O(b)–Mo(a)–O(c)–Mo(b) torsion angle.

[i]Distance of O(c) from the Mo(centroid)Mo(a)Mo(b) plane.

tol/dithioerythritol (magic bullet), and 2-nitrophenyl(octyl)ether as matrices are given in the supplementary material. There are seven naturally occurring isotopes of molybdenum: ^{92}Mo (natural abundance 14.8%), ^{94}Mo (9.3), ^{95}Mo (15.9), ^{96}Mo (16.7), ^{97}Mo (9.6), ^{98}Mo (24.1), ^{100}Mo (9.6). Thus, distinctive clusters of ions were observed. The isotopic distribution was calculated by simulation, using C, H, Mo, O, and Cl. The spectra were in excellent agreement with the structure of $[(\eta\text{-}C_5Me_5)Mo]_4O_7$ proposed below. Specifically, the parent ion $\{[(C_5Me_5)Mo]_4O_7\}^+$, was the most abundant of those ions with m/z > 400 and all $\{(C_5Me_5)_nMo_4O_7\}^+$ fragment ions for n = 3 – 0 were observed. Also observed were the fragment ions $\{(C_5Me_5)_nMo_3O_4\}^+$ (n = 3 – 0), derived from $[(C_5Me_5)Mo]_4O_7$ by loss of the $(C_5Me_5)Mo(b)(O(c))_3$ unit (see Fig. 2). A noticeable feature of all the mass spectra was the complete absence of the parent ions or fragments of $\{[(C_5Me_5)Mo]_4O_6\}^+$ or $\{[(C_5Me_5)MoO)]_4\}^+$.

^{1}H NMR spectra

The 200 MHz spectrum of $[(\eta\text{-}C_5Me_5)Mo]_4O_7$ ($C_6{}^2H_6$ solution, 298 K) is shown in Fig. 4. Three signals were observed: 16.3 ppm ($\Delta\nu_{1/2}$ = 113 Hz), 1.89 ppm ($\Delta\nu_{1/2}$ = 4 Hz), 1.69 ppm ($\Delta\nu_{1/2}$ = 5 Hz). The 400 MHz spectrum (C^2HCl_3 solution, 298 K) showed: 16.3 ppm ($\Delta\nu_{1/2}$ = 98 Hz), 1.99 ppm ($\Delta\nu_{1/2}$ = 3.5 Hz), 1.68 ppm ($\Delta\nu_{1/2}$ = 21 Hz). The assignments are discussed below.

Magnetism

The cluster $[(\eta\text{-}C_5Me_5)Mo]_4O_7$ was paramagnetic, with μ_{eff} = 1.26 μ_B at 300 K in the solid state and μ_{eff} = 1.43 μ_B at 298 K in C^2HCl_3 solution (Evans NMR method). The magnetic behavior is shown as a function of temperature in Figs. 5 and 6 and discussed below. Complete magnetic data are given in the supplementary material.[2]

Infrared spectra

In addition to absorption bands assigned to vibrations of the η-C_5Me_5 ligands, an intense band at 707 cm^{-1} (KBr pellet) was assigned to a vibration of the Mo_4O_7 core.

Analyses

Calculated for $C_{40}H_{60}Mo_4O_7$: C 46.3, H 5.8; found, C 40.1, H 5.8; C 40.5, H 5.3. The former microanalysis was by the University of British Columbia microanalytical facility. The latter was by Galbraith Laboratories, Knoxville, TN and was reproduced on a different sample. We have no explanation for the low carbon analyses. Fettinger et al. (27) attributed similar low carbon analyses for related molybdenum compounds to "incomplete combustion".

Results and discussion

Formation of $[(\eta\text{-}C_5Me_5)Mo]_4O_7$

The cluster $[(\eta\text{-}C_5Me_5)Mo]_4O_7$ was formed by reaction of a toluene solution of either $[(\eta\text{-}C_5Me_5)MoCl(O)]_2(\mu\text{-}O)$ or $(\eta\text{-}C_5Me_5)MoCl_2(O)$ with sodium amalgam, or by reaction of a tetrahydrofuran solution of the same complexes with tributyltin hydride. The coproduct $[(\eta\text{-}C_5Me_5)Mo(O)(\mu\text{-}O)]_2$ (14, 19, 26) was isolated from the reaction between $[(\eta\text{-}C_5Me_5)MoCl(O)]_2(\mu\text{-}O)$ and tributyltin hydride. The reaction between toluene solutions of $[(\eta\text{-}C_5Me_5)MoCl(O)]_2(\mu\text{-}O)$ or $(\eta\text{-}C_5Me_5)MoCl_2(O)$ and magnesium amalgam or between

© 2000 NRC Canada

Table 3. Mass spectrum of $[(\eta\text{-}C_5Me_5)Mo]_4O_7$.[a]

m/z (obs)[b]	Int (%)[c]	*m/z* (calc)[d]	Assignment
1057	0.8	1054	$\{(C_5Me_5)_3Mo_4O_7 + NOBA\}^+$
1036	16.6	1036	$\{(C_5Me_5)_4Mo_4O_7\}^+$
904	4.3	901	$\{(C_5Me_5)_3Mo_4O_7\}^+$
791	1.4	784	$\{(C_5Me_5)Mo_4O_7 + NOBA\}^+$
770	3.6	775	$\{(C_5Me_5)_2Mo_3O_4 + NOBA\}^+$
770	3.6	766	$\{(C_5Me_5)_2Mo_4O_7\}^+$
758	2.1	757	$\{(C_5Me_5)_3Mo_3O_4\}^+$
656	1.2	649	$\{Mo_4O_7 + NOBA\}^+$
634	2.2	640	$\{(C_5Me_5)Mo_3O_4 + NOBA\}^+$
634	2.2	631	$\{(C_5Me_5)Mo_4O_7\}^+$
618	4.9	622	$\{(C_5Me_5)_2Mo_3O_4\}^+$
599	2.4	602	$\{(C_5Me_5)_2Mo_2Cl_4\}^+$
585	1.4	580	$\{((C_5Me_5)MoClO)_2O\}^+$
564	0.8	567	$\{(C_5Me_5)_2Mo_2Cl_3\}^+$
545	1.2	545	$\{(C_5Me_5)_2Mo_2ClO_3\}^+$
545	1.2	544	$\{(C_5Me_5)Mo_2O_4 + NOBA\}^+$
527	9.8	526	$\{(C_5Me_5)_2Mo_2O_4\}^+$
511	2.0	510	$\{(C_5Me_5)_2Mo_2O_3\}^+$
511	2.0	505	$\{Mo_3O_4 + NOBA\}^+$
496	1.0	496	$\{Mo_4O_7\}^+$
496	1.0	497	$\{(C_5Me_5)_2Mo_2Cl\}^+$
485	2.5	487	$\{(C_5Me_5)Mo_3O_4\}^+$
466	1.3	467	$\{(C_5Me_5)Mo_2Cl_4\}^+$

[a]FAB, in a NOBA (3-$HOCH_2C_6H_4NO_2$, $C_7H_7NO_3$, M = 153) matrix.

[b]The most intense signal of the envelope of peaks in a single scan.

[c]$\{(NOBA)H\}^+ = 100$.

[d]Calculated using ^{96}Mo and ^{35}Cl.

tetrahydrofuran solutions of the same complexes and magnesium turnings also gave $[(\eta\text{-}C_5Me_5)Mo]_4O_7$, but the product was contaminated with insoluble impurities. Only $[(\eta\text{-}C_5Me_5)Mo(O)(\mu\text{-}O)]_2$ was isolated from the reaction between lithium nitride and $[(\eta\text{-}C_5Me_5)MoCl(O)]_2(\mu\text{-}O)$. The most convenient preparation of $[(\eta\text{-}C_5Me_5)Mo]_4O_7$ was the reduction of $[(\eta\text{-}C_5Me_5)MoCl(O)]_2(\mu\text{-}O)$ by sodium amalgam. The only difficulty was that repeated recrystallization was required to remove colloidal sodium chloride.

The reaction between $[(\eta\text{-}C_5Me_5)MoCl(O)]_2(\mu\text{-}O)$ and tributyltin hydride gave $[(\eta\text{-}C_5Me_5)Mo(O)(\mu\text{-}O)]_2$ (14, 19, 26) and the mass spectra of the crude products of all of the reactions which formed $[(\eta\text{-}C_5Me_5)Mo]_4O_7$ showed an ion envelope at *m/z* = 527, assigned to $\{(C_5Me_5)_2Mo_2O_4\}^+$ (see Table 3). The mass spectra also showed ion envelopes at *m/z* = 599 and 564. These were assigned to $\{(C_5Me_5)_2Mo_2Cl_4\}^+$ and $\{(C_5Me_5)_2Mo_2Cl_3\}^+$, respectively. The ^1H NMR spectra (benzene solution) of crude samples of $[(\eta\text{-}C_5Me_5)Mo]_4O_7$, prepared by any of the reactions, showed narrow resonances at 1.78 ppm and 1.83 ppm, assigned to $[(\eta\text{-}C_5Me_5)Mo(O)(\mu\text{-}O)]_2$ (14, 19) and $[(\eta\text{-}C_5Me_5)Mo(\mu\text{-}Cl)_2]_2$ (29, 30). Thus $[(\eta\text{-}C_5Me_5)Mo(O)(\mu\text{-}O)]_2$ was a coproduct of all the reactions. It is believed that $[(\eta\text{-}C_5Me_5)Mo(\mu\text{-}Cl)_2]_2$ was also a coproduct, but neither it, nor any other compound containing chlorine, was isolated in significant quantities. A probable reason for this is that monomeric $(\eta\text{-}C_5Me_5)MoCl_n$ (n = 2 (30), 3 (31), 4 (29, 32)) are insoluble in toluene or tetrahydrofuran and would therefore be removed in the first stage of work-up.

The formation of $[(\eta\text{-}C_5Me_5)Mo]_4O_7$ on reduction of either $[(\eta\text{-}C_5Me_5)MoCl(O)]_2(\mu\text{-}O)$ or $(\eta\text{-}C_5Me_5)MoCl_2(O)$ was very surprising. A cluster with an oxygen to molybdenum ratio of 1.75:1, containing no chloride and with a formal oxidation state of Mo_4^{18+}, was formed by treatment of $[(\eta\text{-}C_5Me_5)MoCl(O)]_2(\mu\text{-}O)$ (Mo^{5+}, O:Mo = 1.5:1, Cl:Mo = 1:1) or $(\eta\text{-}C_5Me_5)MoCl_2(O)$ (Mo^{5+}, O:Mo = 1:1, Cl:Mo = 2:1) with a powerful reducing agent. There were no extraneous sources of oxygen or chlorine. Thus a disproportionation involving both ligand exchange and electron exchange must have occurred. We observed a related disproportionation in the concurrent formation of $[(\eta\text{-}C_5Me_5)V]_4(\mu\text{-}O)_6$ and $[(\eta\text{-}C_5Me_5)V(\mu\text{-}Cl)_2]_3$ on reduction of $(\eta\text{-}C_5Me_5)VCl_2(O)$ (eq. [1]) (3).

$$[1]\quad 18(\eta\text{-}C_5Me_5)VCl_2(O) + 24/n[Red] \rightarrow 3[(\eta\text{-}C_5Me_5)V]_4(\mu\text{-}O)_6 + 2[(\eta\text{-}C_5Me_5)V(\mu\text{-}Cl)_2]_3 + 24/n[Red]Cl_n$$

In the present case, the products of the reactions between $[(\eta\text{-}C_5Me_5)MoCl(O)]_2(\mu\text{-}O)$ or $(\eta\text{-}C_5Me_5)MoCl_2(O)$ and sodium, magnesium or $Bu^n{}_3SnH$ were $[(\eta\text{-}C_5Me_5)Mo]_4O_7$, $[(\eta\text{-}C_5Me_5)Mo(\mu\text{-}Cl)_2]_2$ and $[(\eta\text{-}C_5Me_5)Mo(O)(\mu\text{-}O)]_2$. A reasonable scheme for the formation of these products is given by reactions [2]–[7].

$$[2]\quad (\eta\text{-}C_5Me_5)MoCl_2(O) + 1/n[Red] \rightarrow (\eta\text{-}C_5Me_5)MoCl(O) + 1/n[Red]Cl_n$$

© 2000 NRC Canada

Fig. 4. ^{1}H NMR spectrum (200 MHz, $C_6{}^2H_6$ solution, 298 K) of $[(\eta\text{-}C_5Me_5)Mo]_4O_7$.

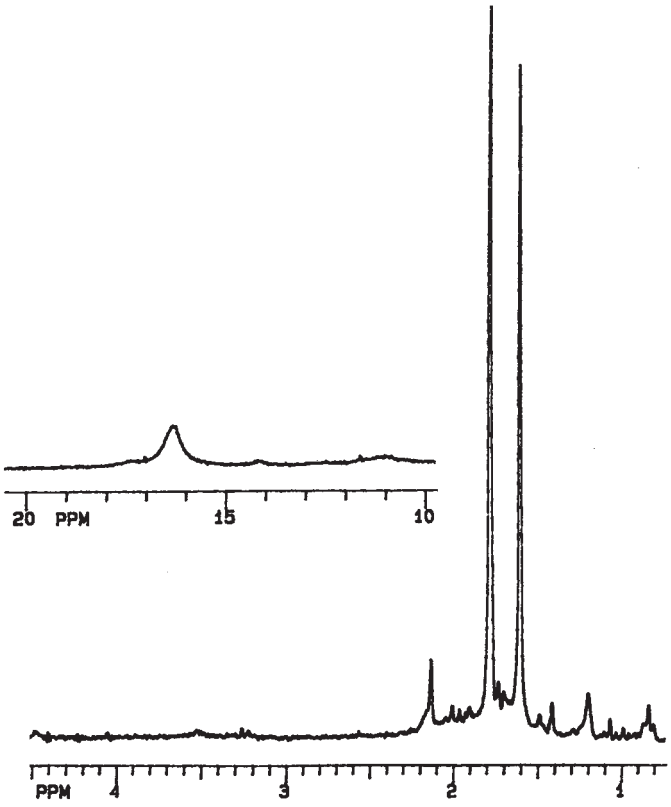
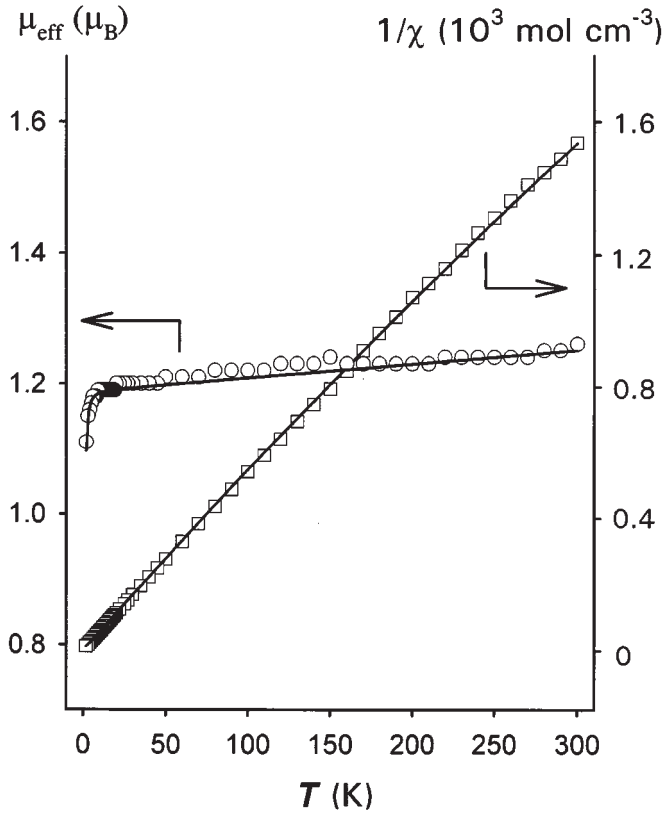


Fig. 5. Magnetic behaviour of $[(\eta\text{-}C_5Me_5)Mo]_4O_7$ in the solid state over the temperature range 2–300 K (lines calculated as described in the text).



[3] $2(\eta\text{-}C_5Me_5)MoCl(O) \rightarrow [(\eta\text{-}C_5Me_5)Mo(\mu\text{-}Cl)(\mu\text{-}O)]_2$

[4] $[(\eta\text{-}C_5Me_5)Mo(\mu\text{-}Cl)(\mu\text{-}O)]_2 \rightarrow (\eta\text{-}C_5Me_5)MoCl_2 + (\eta\text{-}C_5Me_5)MoO_2$

[5] $(\eta\text{-}C_5Me_5)MoCl_2(O) + (\eta\text{-}C_5Me_5)MoO_2 \rightleftharpoons [(\eta\text{-}C_5Me_5)MoCl(O)]_2(\mu\text{-}O)$

[6] $[(\eta\text{-}C_5Me_5)MoCl(O)]_2(\mu\text{-}O) + 2/n[Red] \rightarrow [(\eta\text{-}C_5Me_5)Mo(O)]_2(\mu\text{-}O) + 2/n[Red]Cl_n$

[7] $[(\eta\text{-}C_5Me_5)Mo(O)]_2(\mu\text{-}O) + (\eta\text{-}C_5Me_5)MoO_2 \rightarrow [(\eta\text{-}C_5Me_5)Mo]_4O_7$

The overall equation for the formation of $[(\eta\text{-}C_5Me_5)Mo]_4O_7$ from $[(\eta\text{-}C_5Me_5)MoCl(O)]_2(\mu\text{-}O)$ and sodium amalgam is [8] and based on this, the yield of $[(\eta\text{-}C_5Me_5)Mo]_4O_7$ was 40%. The overall equation for the formation of $[(\eta\text{-}C_5Me_5)Mo]_4O_7$ from $[(\eta\text{-}C_5Me_5)MoCl(O)]_2(\mu\text{-}O)$ and $Bu^n{}_3SnH$ is [9] and the yield of $[(\eta\text{-}C_5Me_5)Mo]_4O_7$ was 34% and of $[(\eta\text{-}C_5Me_5)Mo(O)(\mu\text{-}O)]_2$, 92%. The overall equation for the formation of $[(\eta\text{-}C_5Me_5)Mo]_4O_7$ from $(\eta\text{-}C_5Me_5)MoCl_2(O)$ and sodium amalgam is [10] and the yield was 61%.

[8] $6[(\eta\text{-}C_5Me_5)MoCl(O)]_2(\mu\text{-}O) + 8Na \rightarrow 2[(\eta\text{-}C_5Me_5)Mo]_4O_7 + [(\eta\text{-}C_5Me_5)Mo(O)(\mu\text{-}O)]_2 + [(\eta\text{-}C_5Me_5)Mo(\mu\text{-}Cl)_2]_2 + 8NaCl$

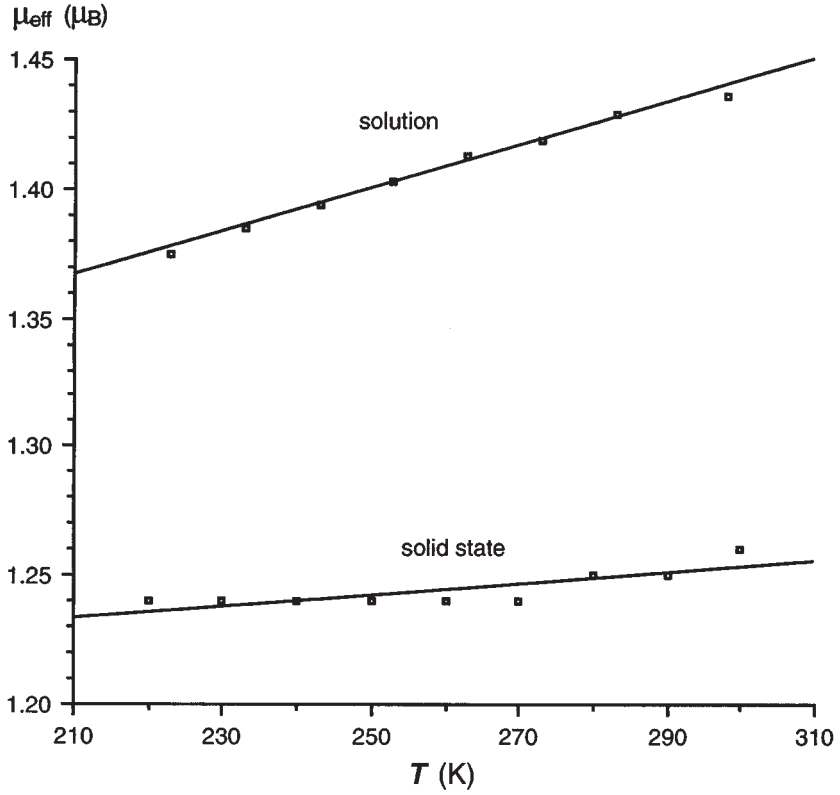
[9] $6[(\eta\text{-}C_5Me_5)MoCl(O)]_2(\mu\text{-}O) + 8Bu^n{}_3SnH \rightarrow 2[(\eta\text{-}C_5Me_5)Mo]_4O_7 + [(\eta\text{-}C_5Me_5)Mo(\mu\text{-}Cl)_2]_2 + [(\eta\text{-}C_5Me_5)Mo(O)(\mu\text{-}O)]_2 + 8Bu^n{}_3SnCl + 4H_2$

[10] $18(\eta\text{-}C_5Me_5)MoCl_2(O) + 20Na \rightarrow 2[(\eta\text{-}C_5Me_5)Mo]_4O_7 + [(\eta\text{-}C_5Me_5)Mo(O)(\mu\text{-}O)]_2 + 4[(\eta\text{-}C_5Me_5)Mo(\mu\text{-}Cl)_2]_2 + 20NaCl$

Reaction of $[(\eta\text{-}C_5Me_5)MoCl(O)]_2(\mu\text{-}O)$ with Li_3N gave $[(\eta\text{-}C_5Me_5)Mo(O)(\mu\text{-}O)]_2$, but no $[(\eta\text{-}C_5Me_5)Mo]_4O_7$, which indicated that Li_3N could not accomplish complete reduction of $[(\eta\text{-}C_5Me_5)MoCl(O)]_2(\mu\text{-}O)$ (reaction [6]). The cluster $[(\eta\text{-}C_5Me_5)Mo]_4(\mu\text{-}O)_6$ was not observed, presumably because the $[(\eta\text{-}C_5Me_5)Mo(O)]_2(\mu\text{-}O)$, produced by reaction [6], was captured by excess $(\eta\text{-}C_5Me_5)Mo(O)_2$ before dimerization occurred. The cubane cluster $[(\eta\text{-}C_5Me_5)Mo(\mu_3\text{-}O)]_4$ was not formed in any of the reactions, which indicated that none of the starting complexes or intermediates could be reduced to $(\eta\text{-}C_5Me_5)MoO$. Compounds of type $(\eta\text{-}C_5R_5)Mo^{III}O_mL_n$ have not been reported to our knowledge, presumably because it is not possible to reduce molybdenum to the oxidation state of III in compounds containing $\eta\text{-}C_5R_5$ and oxygen ligands. Therefore we are pessimistic that a $[(\eta\text{-}C_5P_5)Mo(\mu_3\text{-}O)]_4$ cubane can be synthesized.

© 2000 NRC Canada

Fig. 6. Comparison of the magnetic moment of $[(\eta\text{-}C_5Me_5)Mo]_4O_7$ in the solid state and in chloroform solution, over the temperature range 220–300 K.



Chemical properties of $[(\eta\text{-}C_5Me_5)Mo]_4O_7$

The cluster $[(\eta\text{-}C_5Me_5)Mo]_4O_7$ was a black, crystalline material which rapidly turned light brown on exposure to air. It was soluble in tetrahydrofuran and dichloromethane, moderately soluble in toluene and diethyl ether, but insoluble in hexane. These trends in solubility were similar to those of $[(\eta\text{-}C_5Me_5)M(\mu_3\text{-}O)]_4$ (M = V (3), Cr (6)), but in contrast to $[(\eta\text{-}C_5Me_5)V(\mu_3\text{-}N)]_4$ (18) and $[(\eta\text{-}C_5Me_5)M]_4(\mu\text{-}O)_6$ (M = Ti (8), V (7, 10)), which were very soluble in toluene and hexane. The reason for the differences in solubilities of these clusters is not clear, since they all have an essentially identical sheath of four $\eta\text{-}C_5Me_5$ ligands surrounding a tetrahedral Mo_4O_n core of similar size. The cluster reacted slowly with protonic reagents such as water or solvents such as chloroform to form a brown material that would not redissolve in any solvent. Evidence for the decomposition was the broadening of the signal at 16.3 ppm in the ^1H NMR spectrum, which was assigned to $[(\eta\text{-}C_5Me_5)Mo]_4O_7$, the appearance of a new signal at 11.5 ppm ($\Delta\nu_{1/2}$ = 440 Hz), and the formation of a precipitate. Decomposition also occurred in the solid state, unless the cluster was completely dry.

Structure of $[(\eta\text{-}C_5Me_5)Mo]_4O_7$ as determined by X-ray diffraction

The molecular structure of $[(\eta\text{-}C_5Me_5)Mo]_4O_7$ is shown in Fig. 3, the numbering scheme for the Mo_4O_7 core in Fig. 2 and the average distances and angles are given in Table 2. Because all of the crystals were small thin plates that did not diffract well and because of the severe disorder of the oxygen atoms, the accuracy of an individual determination was not high. However, this was compensated by the large number of independent measurements of a particular distance or angle.

It is seen from Table 2 and Fig. 3, that $[(\eta\text{-}C_5Me_5)Mo]_4O_7$ contained an essentially planar, six member $[Mo(a)(\mu\text{-}O(b))]_3$ ring, in which there was a long-short alternation of the Mo(a)—O(b) distances. The six-member ring was capped on one side by the μ_3-oxygen atom (O(a)) and on the other side by three μ_2-oxygen atoms (O(c)) which connected the Mo(a) atoms of the ring to the Mo(b) atom. The O(c) atoms were located over the edges of the tetrahedron of molybdenum atoms, with Mo(a), O(c), Mo(b), and the centroid of the molybdenum atoms, forming an essentially perfect plane. Because of the alternation in the Mo(a)—O(b) distances, the octahedral packing of the O(b) and O(c) atoms was distorted, the O(b)–Mo(a)–O(c)–Mo(b) torsion angle being 70° instead of 60°.

The Mo(a)—Mo(a) and Mo(a)—Mo(b) distances in $[(\eta\text{-}C_5Me_5)Mo]_4O_7$ should not be equal, because Mo(a) is seven-coordinate whereas Mo(b) is six (Figs. 2 and 3). Due to the disorder in the Mo_4O_7 core, only random variations in the Mo—Mo distances were observed; the average was 2.909 (3) Å. This distance is identical to that found in $(\eta\text{-}C_5R_5)_2(\eta\text{-}C_5R'_5)_2Mo_4(\mu_3\text{-}S)_4$ cubanes (2.902 (1) Å for R_5 = MeH_4, R′ = Me (33); 2.904 (1) Å for R = R′ = Pr^iH_4 (34, 35)). The determining factor in the Mo—Mo distance is the size and coordination number of oxygen or sulfur. Although sulfur is larger than oxygen, there are only four sulfur atoms in $(\eta\text{-}C_5R_5)_2(\eta\text{-}C_5R'_5)_2Mo_4(\mu_3\text{-}S)_4$ compared to seven oxygen atoms in $[(\eta\text{-}C_5Me_5)Mo]_4O_7$. The average Mo—Mo distance

© 2000 NRC Canada

for the three basal molybdenum atoms in $(\eta\text{-}C_5Me_5)_4Mo_5O_{11}$ was 2.731 (2) Å (16) and in $(\eta\text{-}C_5Me_5)_6Mo_8O_{16}$ it was 2.744 (1) Å (15). These distances are shorter than those in $[(\eta\text{-}C_5Me_5)Mo]_4O_7$ because the three basal molybdenum atoms were bridged by both three μ_2- and three μ_3-oxygen atoms. There are several triangular clusters of general formulae $[L_mMo(\mu_2\text{-}OR)]_3(\mu_3\text{-}OR)_n(\mu_3\text{-}O)$ (m = 2 for n = 1, m = 3 for n = 0, R = H, R′, or zero) with single Mo—Mo bonds, in which the range of Mo—Mo distances is 2.48–2.80 Å (36–39).

The average Mo—(μ_3-O(a)) distance in $[(\eta\text{-}C_5Me_5)Mo]_4O_7$ is 2.19 (5) Å, which is longer than the range of 1.95–2.05 Å observed in other molybdenum clusters containing the $[Mo(\mu_2\text{-}OR)]_3(\mu_3\text{-}O)$ unit (31, 37, 38, 40–45). The longer distance is ascribed to the planarity of the $[Mo(a)(\mu_2\text{-}O(b)]_3$ unit, which exerted steric pressure on the μ_3-oxygen.

An interesting feature of the $[(\eta\text{-}C_5Me_5)Mo(a)(\mu\text{-}O(b))]_3(\mu_3\text{-}O(a))$ unit of $[(\eta\text{-}C_5Me_5)Mo]_4O_7$ was the long-short alternation of the Mo(a)—O(b) distances on proceeding around the planar $[Mo(a)(\mu\text{-}O(b))]_3$ ring (Table 2). The overall average for the long Mo(a)—O(b) distances was 2.00 Å and for the short, 1.87 Å. A similar alternation appeared in the planar $[Mo(\mu\text{-}O)]_4$ rings of the polyoxometalates $[Mo_6O_{19}]^{2-}$ (46, 47), $[(\eta\text{-}C_5H_5)TiMo_5O_{18}]^{3-}$ (48), $[(\eta\text{-}C_5Me_5)Mo_6O_{18}]^-$ (49, 50), $[Mo_6O_{18}(N(\eta\text{-}C_5H_4))Fe(\eta\text{-}C_5H_5)]^{2-}$ (51) and $[W_6O_{18}(NAr)]^{2-}$ (52). Che et al. (48) ascribed this alternation to "off-center displacement of molybdenum atoms within a rigid, close-packed oxygen framework", a form of *trans* influence within the eight-membered $[Mo(\mu\text{-}O)]_4$ rings. This influence cannot be operative in the six-membered $[Mo(a)(\mu\text{-}O(b))]_3$ ring of $[(\eta\text{-}C_5Me_5)Mo]_4O_7$ and was not observed in any of the triangular $[L_mMo(\mu_2\text{-}OR)]_3(\mu_3\text{-}OR)(\mu_3\text{-}O)$ clusters, with the exception of $\{[(\eta\text{-}C_5H_5)Mo(CO)(\mu_2\text{-}CO)]_3(\mu_3\text{-}O)\}^+$, in which the Mo—($\mu_2$-CO) distances alternated, the shorter being 2.26 Å and the longer 2.49 Å (40). The alternation in the Mo—(μ_2-CO) distances was ascribed to an asymmetrical "freezing" of the fluxional migration of carbonyl ligands around the triangle of molybdenum atoms (40).

The cluster $[(\eta\text{-}C_5Me_5)Mo]_4O_7$ appears to be the first example of a molybdenum oxide with a tetrahedral $[(\eta\text{-}C_5Me_5)Mo]_4$ unit to be structurally characterized. The cubanes $\{(\eta\text{-}C_5R_5)_2(\eta\text{-}C_5R'_5)_2Mo4(\mu_3\text{-}A)_4\}^{n+}$ (**1**) have been structurally characterized for $R_5 = R'_5 = Pr^iH_4$, A = S or Se, n = 0 (53) and A = S, n = 1 or 2 (34, 35); $R_5 = MeH_4$, R′ = Me, A = S, n = 0 (34). The only oxides which have been structurally characterized are $(\eta\text{-}C_5Me_5)_4Mo_5O_{11}$ (16) and $(\eta\text{-}C_5Me_5)_6Mo_8O_{16}$ (15), which contain distorted tetrahedra, with only three of the molybdenum atoms carrying $\eta\text{-}C_5Me_5$ ligands.

Magnetic properties of $[(\eta\text{-}C_5Me_5)Mo]_4O_7$

The magnetism of $[(\eta\text{-}C_5Me_5)Mo]_4O_7$ in the solid state was determined using samples which were obtained by rapid precipitation from toluene solution on adding a large quantity of hexane. No macroscopic crystals were visible in these samples. The reciprocal susceptibility and magnetic moment are plotted as functions of temperature over the range 2–300 K in Fig. 5. The effective moment was 1.26 μ_B at 300 K and was virtually independent of temperature, except for a marked decrease at very low temperatures which indicated a weak zero field splitting. The cluster $[(\eta\text{-}C_5Me_5)Mo]_4O_7$ has an even number of electrons, and must therefore have zero or two unpaired electrons, corresponding to $S = 0$ or $S = 1$, respectively. In agreement with this, the cluster did not show any EPR signal at temperatures of 150 K and above. The observed moment was greater than zero, but it was very much less than the spin-only value for two unpaired electrons per cluster (2.83 μ_B). Therefore the data were treated as arising from a sample which was a mixture of two forms, one with $S = 0$ and one with $S = 1$.

The expression for the molar magnetic susceptibility, χ_m, of an $S = 1$ system with zero field splitting is given in eq. [11] (54), where $x = D(kT)^{-1}$ and $C = Ng^2\beta^2(kT)^{-1}$, D being the zero field splitting parameter. The data were modelled using eq. [12], with $g = 2.00$ and the temperature independent paramagnetism (*TIP*) for both forms, the fraction of the sample in the $S = 1$ form (P), and D as variables in a least-squares fitting procedure that minimized the function F, defined in eq. [13].

$$[11]\quad \chi_m = 3^{-1}C[(2e^{-x})(1 + 2e^{-x})^{-1} + 2(2x^{-1})(1 - e^{-x})(1 + 2e^{-x})^{-1}]$$

$$[12]\quad \chi^{calc} = P(\chi_m) + TIP$$

$$[13]\quad F = \left[1/n\sum_{i=1}^{n}((\chi_i^{obs} - \chi_i^{calc})^2(\chi_i^{obs})^{-2})\right]^{0.5}$$

The best fit was obtained with $D = 2.24$ (6) cm^{-1}, $TIP = 64\ (2) \times 10^{-6}$ and $P = 0.176$, for which parameters $F = 0.0085$. This analysis indicated that 17.6% of the sample had $S = 1$, the remainder $S = 0$. The good agreement between the calculated and observed data is shown by the low value of F, and is illustrated in Fig. 5. The magnetic behaviour of $[(\eta\text{-}C_5Me_5)Mo]_4O_7$ was also determined over the temperature range 223–298 K in chloroform solution, by the Evans NMR method (55, 56). The effective moment decreased linearly from 1.44 (±0.01) to 1.37 (±0.01) μ_B on cooling from 298 to 223 K. The decrease was completely reversed on warming from 223 K back to 298 K. Since $[(\eta\text{-}C_5Me_5)Mo]_4O_7$ must have either $S = 0$ or $S = 1$, the low magnetic moment in solution must be due to the sample being a mixture of two forms, one with $S = 0$ and one with $S = 1$, as discussed above for the solid state.

The magnetic behaviour in solution is compared to that in the solid state in Fig. 6. In the solid state, the form of $[(\eta\text{-}C_5Me_5)Mo]_4O_7$ having $S = 1$ was paramagnetic and the effective moment did not vary significantly with temperature over the range 220–300 K. The slope of the moment vs. temperature line for the solution sample is greater than the slope in the solid state, due to the change in the concentration of the paramagnetic form of $[(\eta\text{-}C_5Me_5)Mo]_4O_7$ with temperature. The reversibility of the change in moment with temperature showed that the two forms were in equilibrium with one another in solution. The system was treated as an equilibrium between a paramagnetic form of $[(\eta\text{-}C_5Me_5)Mo]_4O_7$ (which had $S = 1$ and a temperature independent spin-only moment of 2.83 μ_B) and a diamagnetic form. The standard eq. [14], relating magnetic susceptibility and moment, was used to calculate $\chi_{(S=1)}$ and the fraction of the sample which had $S = 1$ was then calculated using eq. [15]. It was determined

© 2000 NRC Canada

that 25.7% of the sample had $S = 1$ at 298 K and 23.4% at 223 K.

[14] $\mu_{B(S = 1)} = 2.828(\chi_{(S = 1)}T)^{0.5}$

[15] $P = \chi^{obs}(\chi_{(S = 1)})^{-1}$ ($\cong (\chi^{obs})T$)

^{1}H NMR spectra of $[(\eta\text{-}C_5Me_5)Mo]_4O_7$

The ^{1}H NMR spectrum (200 MHz) of a benzene solution of $[(\eta\text{-}C_5Me_5)Mo]_4O_7$ is shown in Fig. 4. The broad resonance at 16.3 ppm ($\Delta\nu_{1/2}$ = 113 Hz) was assigned to the protons of $\eta\text{-}C_5Me_5$ attached to an Mo_4O_7 core that had a magnetic moment. The narrow resonances at 1.89 ppm ($\Delta\nu_{1/2}$ = 4 Hz) and 1.69 ppm ($\Delta\nu_{1/2}$ = 5 Hz) were assigned to the protons of $\eta\text{-}C_5Me_5$ attached to a diamagnetic Mo_4O_7 core. The integrated intensity of the resonance at 1.89 ppm and the integrated intensity of the resonance at 1.69 ppm were in a 1:1 ratio. The integrated intensity of the resonance at 16.3 ppm and the sum of the integrated intensities of the resonances at 1.89 ppm and 1.69 ppm were in a ratio of approximately 1:1.4. At 400 MHz in C^2HCl_3 solution at 298 K, the resonances were at 16.3 ppm ($\Delta\nu_{1/2}$ = 98 Hz), 1.93 ppm ($\Delta\nu_{1/2}$ = 3.5 Hz), and 1.67 ppm ($\Delta\nu_{1/2}$ = 21 Hz). In this solvent, both the shift and the line-width of the resonance at 16.3 ppm decreased with increasing temperature. A plot of the reciprocal of the magnitude of the shift as a function of temperature was linear, as expected for a paramagnetic species (4, 57). The ^{1}H NMR spectrum therefore showed that there were two forms of $[(\eta\text{-}C_5Me_5)Mo]_4O_7$, one diamagnetic and one with a magnetic moment, which were in equilibrium in solution.

Structure of $[(\eta\text{-}C_5Me_5)Mo]_4O_7$ in the solid state and in solution

The geometry of the Mo_4O_7 core of $[(\eta\text{-}C_5Me_5)Mo]_4O_7$ can be described as $Mo_4(\mu_2\text{-}O(b))_3(\mu_2\text{-}O(c))_3(\mu_3\text{-}O(a))$ (**3**, C_3 symmetry, see Fig. 2). The only other M_4A_7 cores occur as $Mo_4(\mu_2\text{-}I(b))_4(\mu_2\text{-}I(c))(\mu_3\text{-}I(a))_2$ in $[Mo_4I_{11}]^{2-}$ (M = Mo (58–60), W (61)) (**4**, C_{2v} symmetry) and as $Ta_4(\mu_2\text{-}O(b))_4(\mu_3\text{-}O(a))_2(\mu_4\text{-}O)$ in $[(\eta\text{-}C_5Me_5)Ta]_2[(\eta\text{-}C_5Me_5)Ta(OH)]_2O_7$ (62) (**5**, C_{2v} symmetry). Conversion of **3** into **4** requires the formation of one Mo—O(a) bond, movement of two O(c) atoms into O(b) positions, and a relatively small distortion of the Mo_4 tetrahedron. Conversion of **3** into **5** requires the formation of one Mo—O(a) bond, two Mo—(μ_4-O) bonds, and a very large distortion of the Mo_4 tetrahedron.

In the ^{1}H NMR spectrum of $[(\eta\text{-}C_5Me_5)Mo]_4O_7$ (Fig. 4), the resonances at 1.89 ppm ($\Delta\nu_{1/2}$ = 4 Hz) and 1.69 ppm ($\Delta\nu_{1/2}$ = 5 Hz), which had a 1:1 intensity ratio, must be assigned to equal numbers of two types of $\eta\text{-}C_5Me_5$ attached to diamagnetic ($S = 0$) Mo_4O_7 and the resonance at 16.3 ppm ($\Delta\nu_{1/2}$ = 113 Hz) must be assigned to $\eta\text{-}C_5Me_5$ attached to paramagnetic ($S = 1$) Mo_4O_7. Therefore paramagnetic $[(\eta\text{-}C_5Me_5)Mo]_4O_7$ had an Mo_4O_7 core with the geometry **3** and diamagnetic $[(\eta\text{-}C_5Me_5)Mo]_4O_7$ had an Mo_4O_7 core with the geometry **4** or **5**. The magnetic results and the ^{1}H NMR spectra showed that the two forms of $[(\eta\text{-}C_5Me_5)Mo]_4O_7$ were in equilibrium with one another in solution, suggesting only a small change in the geometry of the Mo_4O_7 core. It is concluded that paramagnetic ($S = 1$) $[(\eta\text{-}C_5Me_5)Mo]_4O_7$, having an Mo_4O_7 core with the geometry **3**, was in equilibrium with diamagnetic ($S = 0$) $[(\eta\text{-}C_5Me_5)Mo]_4O_7$ having an Mo_4O_7 core with the geometry **4**. These two forms were also present in the solid state, although only **3** was obtained as macroscopic crystals. The cluster $[(\eta\text{-}C_5Me_4Et)Mo]_2[(SPh)Co]_2(\mu_3\text{-}S)_4$ had a mixture of $S = 1$, $S = 2$, and $S = 3$ forms in the solid state and also a contribution from $S = 0$ in solution (63). It is the only other cluster which behaved like $[(\eta\text{-}C_5Me_5)Mo]_4O_7$.

The energy levels for the cluster orbitals of $[(\eta\text{-}C_5H_5)Mo]_4O_7$ with the Mo_4O_7 core having the geometry **3** or **4** were calculated by the extended Hückel method. The calculation on $[(\eta\text{-}C_5H_5)Mo]_4O_7$ with the Mo_4O_7 geometry **3** (C_3 symmetry) used the distances: Mo—Mo = 2.909 Å, Mo(a)—O(a) = 2.175 Å, Mo(a)—O(bl) = 1.975 Å, Mo(a)—O(bs) = 1.920 Å, Mo(a)—O(c) = 1.90 Å, Mo(b)—O(c) = 1.78 Å. The energy level diagram for the cluster orbitals is shown in Fig. 7. This diagram predicts that $[(\eta\text{-}C_5H_5)Mo]_4O_7$, which has six cluster electrons, will have the ground state $1a^2\ 2a^2\ 1e^2\ 2e^0$ and $S = 1$. The results are in agreement with the observed paramagnetism ($S = 1$) of $[(\eta\text{-}C_5Me_5)Mo]_4O_7$ with the Mo_4O_7 geometry **3**.

The calculation on $[(\eta\text{-}C_5H_5)Mo]_4O_7$ with the Mo_4O_7 geometry **4** (C_{2v} symmetry) used the Mo—Mo distances found in $[Mo_4I_{11}]^{2-}$: Mo(a)—Mo(a) = 2.55 Å, Mo(b)—Mo(b) = 3.05 Å, Mo(a)—Mo(b) = 2.70 Å; and the Mo—O distances: Mo—O(a) = 2.10 Å, Mo—O(b) = Mo—O(c) = 1.90 Å (59). The ground state was predicted to be $1a_1^2\ 2a_1^2\ 1a_2^2\ 1b_1^0$ and $S = 0$, with a HOMO–LUMO gap of 0.183 eV (17.7 kJ mol^{-1}, 1478 cm^{-1}). This provides further evidence that the form of $[(\eta\text{-}C_5Me_5)Mo]_4O_7$ with the Mo_4O_7 geometry **4** was diamagnetic. The correlation between the orbital energy levels for the C_3 and C_{2v} geometry is shown in Fig. 7. This diagram was obtained by assuming that both **3** and **4** were derived from an Mo_4O_7 unit with T_d symmetry. The most striking feature of the diagram is the split in the 2e level on going from $[(\eta\text{-}C_5H_5)Mo]_4O_7$ with the C_3 geometry **3** to $[(\eta\text{-}C_5H_5)Mo]_4O_7$ with the C_{2v} geometry **4**. Two factors may be responsible for these changes in the energies of the orbitals: the formation of a new Mo—(μ_3-O) bond on going from **3** to **4** and changes in the extent of Mo—(μ_2-O) π-bonding.

Conclusions

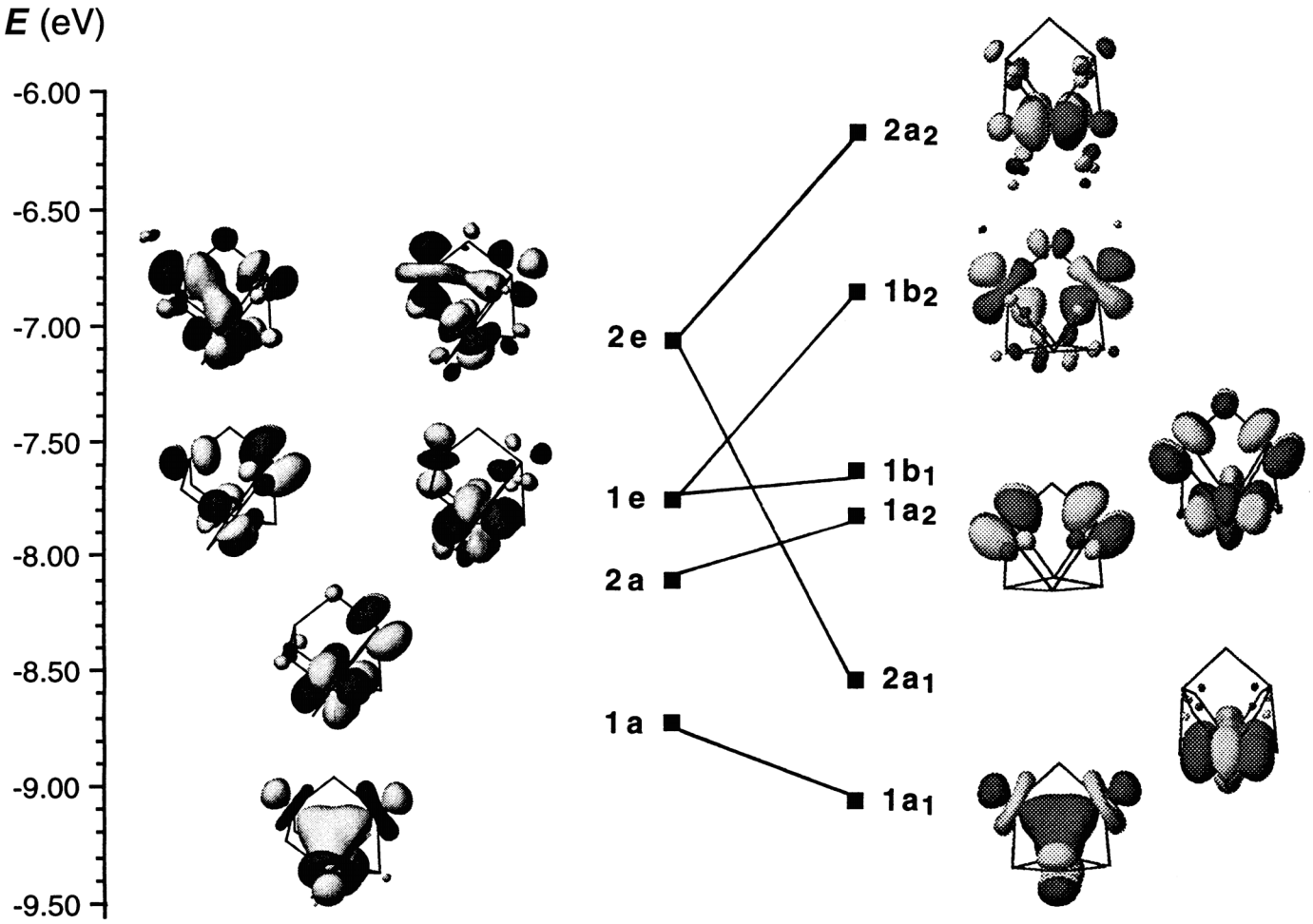
Disproportionation of $[(\eta\text{-}C_5Me_5)MoCl(O)]_2(\mu\text{-}O)$ or $(\eta\text{-}C_5Me_5)MoCl_2(O)$ on reduction by sodium or magnesium amalgam, magnesium turnings, or tributyltin hydride produced $[(\eta\text{-}C_5Me_5)Mo]_4O_7$. Crystals of $[(\eta\text{-}C_5Me_5)Mo]_4O_7$ contained a tetrahedral $[(\eta\text{-}C_5Me_5)Mo]_4$ unit with the Mo_4O_7 core having the geometry **3**. The magnetic moment and NMR spectra showed that $[(\eta\text{-}C_5Me_5)Mo]_4O_7$ existed in two forms, which were in equilibrium in solution. One form was paramagnetic ($S = 1$) $[(\eta\text{-}C_5Me_5)Mo]_4O_7$, with an Mo_4O_7 core which had the geometry **3** (C_3 symmetry). The other form was diamagnetic ($S = 0$) $[(\eta\text{-}C_5Me_5)Mo]_4O_7$ with an Mo_4O_7 core which had the geometry **4** (C_{2v} symmetry).

Acknowledgements

We thank Dr Andreas Decken (University of New Brunswick), Prof. T. Stanley Cameron (Dalhousie University), and Dr. James F. Britten (McMaster University) for collecting

© 2000 NRC Canada

Fig. 7. Correlation diagram for the energy levels of the cluster orbitals of $[(\eta\text{-}C_5H_5)Mo]_4O_7$ with Mo_4O_7 geometry **3** or **4**.



X-ray diffraction data, Daniel F. Drummond (University of New Brunswick) for assistance with the mass spectra, and Dr Larry A. Calhoun (University of New Brunswick) for helpful discussions on the NMR spectra. We are grateful to the Natural Sciences and Engineering Research Council of Canada (NSERC) for financial support to F. B. and R. C. T.

References

1. C.D. Abernethy, F. Bottomley, A. Decken, D.A. Summers, and R.C. Thompson. Organometallics, **17**, 1248 (1998).
2. C.D. Abernethy, F. Bottomley, A. Decken, and R.C. Thompson. Organometallics, **16**, 1865 (1997).
3. C.D. Abernethy, F. Bottomley, A. Decken, D.A. Summers, and R.C. Thompson. Organometallics, **18**, 870 (1999).
4. F. Bottomley, D.E. Paez, L. Sutin, P.S. White, F. Köhler, R.C. Thompson, and N.P.C. Westwood. Organometallics, **9**, 2443 (1990).
5. I.L. Eremenko, S.E. Nefedov, A.A. Pasynskii, B. Orazsakhatov, O.G. Ellert, Yu.T. Struchkov, A.I. Yanovsky, and D.V. Zagorevsky. J. Organomet. Chem. **368**, 185 (1989).
6. F. Bottomley, J. Chen, S.M. MacIntosh, and R.C. Thompson. Organometallics, **10**, 906 (1991).
7. F. Bottomley, C.P. Magill, and B. Zhao. Organometallics, **9**, 1700 (1990).
8. L.M. Babcock, V.W. Day, and W.G. Klemperer. J. Chem. Soc. Chem. Commun. 858 (1987).
9. F. Bottomley, D.E. Paez, and P.S. White. J. Am. Chem. Soc. **104**, 5651 (1982).
10. F. Bottomley, C.P. Magill, and B. Zhao. Organometallics, **10**, 1946 (1991).
11. M.R. Smith, P.T. Matsunaga, and R.A. Andersen. J. Am. Chem. Soc. **115**, 7049 (1993).
12. J.C. Stichbury, M.J. Mays, P.R. Raithby, M.-A. Rennie, and M.R. Fullalove. J. Chem. Soc. Chem. Commun. 1269 (1995).
13. K. Isobe, S. Kimura, and Y. Nakamura. J. Organomet. Chem. **331**, 221 (1987).
14. H. Arzoumanian, A. Baldy, M. Pierrot, and J.-F. Petrignani. J. Organomet. Chem. **294**, 327 (1985).
15. J.R. Harper and A.L. Rheingold. J. Am. Chem. Soc. **112**, 4037 (1990).
16. F. Bottomley, J. Chen, K.F. Preston, and R.C. Thompson. J. Am. Chem. Soc. **116**, 7989 (1994).
17. F. Bottomley and S. Karslioglu. Organometallics, **11**, 326 (1992).
18. C.D. Abernethy, F. Bottomley, A. Decken, and T.S. Cameron. Organometallics, **15**, 1758 (1996).
19. F. Bottomley, P.D. Boyle, and J. Chen. Organometallics, **13**, 370 (1994).
20. K. Umakoshi and K. Isobe. J. Organomet. Chem. **395**, 47 (1990).
21. J.M.B. Blanchard, Q. Chen, Y.-D. Chang, and M.B. Sponsler. Inorg. Chim. Acta, **221**, 147 (1994).

© 2000 NRC Canada

22. C.D. Abernethy, F. Bottomley, J. Chen, M.F. Kemp, T.C. Mallais, and O.O. Womiloju. Inorg. Synth. **32**, 207 (1998).
23. D. Chakraborty, M. Bhattacharjee, R. Krätzner, R. Siefken, H.W. Roesky, I. Usón, and H.-G. Schmidt. Organometallics, **18**, 106 (1999).
24. J.W. Faller and Y. Ma. J. Organomet. Chem. **368**, 45 (1989).
25. E. König. *In* Landolt-Börnstein, New Series, Vol. II/2. *Edited by* K.H. Hellwege and A.M. Hellwege. Springer–Verlag, Berlin. 1966.
26. E.J. Gabe, Y. LePage, J.P. Charland, F.L. Lee, and P.S. White. J. Appl. Crystallogr. **22**, 384 (1989).
27. J.C. Fettinger, D.W. Keogh, and R. Poli. J. Am. Chem. Soc. **118**, 3617 (1996).
28. E. de Jesús, A. Vázquez de Miguel, P. Royo, A.M.M. Lanfredi, and A. Tiripicchio. J. Chem. Soc. Dalton Trans. 2779 (1990).
29. F. Abugideiri, G.A. Brewer, J.U. Desai, J.C. Gordon, and R. Poli. Inorg. Chem. **33**, 3745 (1994).
30. R. Poli and A.L. Rheingold. J. Chem. Soc. Chem. Commun. 552 (1990).
31. A.A. Cole, J.C. Gordon, M.A. Kelland, R. Poli, and A.L. Rheingold. Organometallics, **11**, 1754 (1992).
32. M.L.H. Green, J.D. Hubert, and P. Mountford. J. Chem. Soc. Dalton Trans. 3793 (1990).
33. P.D. Williams and M.D. Curtis. Inorg. Chem. **25**, 4562 (1986).
34. J.A. Bandy, C.E. Davies, J.C. Green, M.L.H. Green, K. Prout, and D.P.S. Rodgers. J. Chem. Soc. Chem. Commun. 1395 (1983).
35. C.E. Davies, J.C. Green, N. Kaltsoyannis, M.A. MacDonald, J. Qin, T.B. Rauchfuss, C.M. Redfern, G.H. Stringer, and M.G. Woolhouse. J. Chem. Soc. Dalton Trans. 3779 (1992).
36. M.H. Chisholm, K. Folting, J.C. Huffman, and C.C. Kirkpatrick. Inorg. Chem. **23**, 1021 (1984).
37. K. Nakata, T. Yamaguchi, Y. Sasaki, and T. Ito. Chem. Lett. 983 (1992).
38. E. Benory, A. Bino, D. Gibson, F.A. Cotton, and Z. Dori. Inorg. Chim. Acta, **99**, 137 (1985).
39. M.H. Chisholm, F.A. Cotton, A. Fang, and E. Kober. Inorg. Chem. **23**, 749 (1984).
40. K. Schloter, U. Nagel, and W. Beck. Chem. Ber. **113**, 3775 (1980).
41. S.F. Gheller, T.W. Hambley, R.T.C. Brownlee, M.J. O'Connor, M.R. Snow, and A.G. Wedd. J. Am. Chem. Soc. **105**, 1527 (1983).
42. K.R. Rodgers, R.K. Murmann, E.O. Schlemper, and M.E. Shelton. Inorg. Chem. **24**, 1313 (1985).
43. D.T. Richens, L. Helm, P.-A. Pittet, A.E. Merbach, F. Nicolo, and G. Chapuis. Inorg. Chem. **28**, 1394 (1989).
44. A. Bino, F.A. Cotton, and Z. Dori. J. Am. Chem. Soc. **100**, 5252 (1978).
45. A. Bino, F.A. Cotton, and Z. Dori. J. Am. Chem. Soc. **101**, 3842 (1979).
46. H.R. Allcock, E.C. Bissell, and E.T. Shawl. Inorg. Chem. **12**, 2963 (1973).
47. P.L. Veya and J.K. Kochi. J. Organomet. Chem. **488**, C4 (1995).
48. T.M. Che, V.W. Day, L.C. Francesconi, M.F. Fredrich, W.G. Klemperer, and W. Shum. Inorg. Chem. **24**, 4055 (1985).
49. F. Bottomley and J. Chen. Organometallics, **11**, 3404 (1992).
50. A. Proust, R. Thouvenot, and P. Herson. J. Chem. Soc. Dalton Trans. 51 (1999).
51. J.L. Stark, V.G. Young, and E.A. Maatta. Angew. Chem. Int. Ed. Engl. **34**, 2547 (1995).
52. T.R. Mohs, G.P.A. Yap, A.L. Rheingold, and E.A. Maatta. Inorg. Chem. **34**, 9 (1995).
53. P. Baird, J.A. Bandy, M.L.H. Green, A. Hamnett, E. Marseglia, D.S. Obertelli, K. Prout, and J. Qin. J. Chem. Soc. Dalton Trans. 2377 (1991).
54. C.J. O'Connor. Prog. Inorg. Chem. **29**, 203 (1982).
55. D.F. Evans. J. Chem. Soc. 2003 (1959).
56. E.M. Schubert. J. Chem. Educ. **69**, 62 (1992).
57. G.N. La Mar, G.R. Eaton, R.H. Holm, and F.A. Walker. J. Am. Chem. Soc. **95**, 63 (1973).
58. J.C. Gordon and R. Poli. Acta Crystallogr. Sect. C: Cryst. Struct. Commun. **51**, 14 (1995).
59. F.A. Cotton and R. Poli. J. Am. Chem. Soc. **110**, 830 (1988).
60. S. Stensvad, B.J. Helland, M.W. Babich, R.A. Jacobson, and R.E. McCarley. J. Am. Chem. Soc. **100**, 6257 (1978).
61. J.D. Franolic, J.R. Long, and R.H. Holm. J. Am. Chem. Soc. **117**, 8139 (1995).
62. V.C. Gibson, T.P. Kee, and W. Clegg. J. Chem. Soc. Chem. Commun. 29 (1990).
63. M.A. Mansour, M.D. Curtis, and J.W. Kampf. Organometallics, **14**, 5460 (1995).

© 2000 NRC Canada

Peptide models XXVII. An exploratory ab initio study on the 21st amino acid side-chain conformations of *N*-formyl-L-selenocysteinamide (For-L-Sec-NH_2) and *N*-acetyl-L-selenocysteine-*N*-methylamide (Ac-L-Sec-NHMe) in their γ_L backbone conformation

Judith C. Vank, Carlos P. Sosa, Andras Perczel, and Imre G. Csizmadia

Abstract: Selenocysteine is expected to have 9 × 9 = 81 conformations [3 × 3 = 9 backbone: ψ (g^+,a,g^-) × ϕ (g^+,a,g^-) and 3 × 3 = 9 side-chain: χ_1 (g^+,a,g^-) × χ_2 (g^+,a,g^-)]. In the present study, all the torsional modes of the side-chain (χ_1: rotation about the C^α—C^β and χ_2: rotation about the C^β—Se bonds) were investigated in the relaxed γ_L backbone [(ϕ,ψ); (g^-,g^+)] conformation. Seven out of the nine expected minima were found at the RHF/3–21G level of theory for *N*-formyl-L-selenocysteinamide (For-L-Sec-NH_2) and *N*-acetyl-L-selenocysteine-*N*-methylamide (Ac-L-Sec-NHMe). The stabilization energy exerted by the -CH_2-SeH side-chain has been compared with that of -CH_2-SH and -CH_2-OH. Relative energies of the various conformers were also obtained via single point calculations at the B3LYP/6–31G(d,p) level of theory. Topological analysis of the electron density has been performed by Bader's Atoms in Molecule (AIM) approach using the results. The structures were also optimized at the B3LYP/6–31+G(d,p) level of theory.

Key words: selenocysteine side-chain conformations, ab initio MO study, Multidimensional Conformational Analysis (MDCA), Atoms in Molecules (AIM), Bader's electron density analysis.

Résumé : En théorie, la sélénocystéine peut avoir 9 × 9 = 81 conformations [3 × 3 = 9 squelettes: ψ(g^+,a,g^-) × ϕ(g^+,a,g^-) et 3 × 3 = 9 chaînes latérales: χ_1(g^+,a,g^-) × χ_2(g^+,a,g^-)]. Dans la présente étude, on a étudié tous les modes de torsion de la chaîne latérale (χ_1: rotation autour de C^α—C^β et χ_2: rotation autour des liaisons C^β—Se) dans la conformation détendue γ_L du squelette [(ϕ,ψ); (g^-,g^+)]. Opérant au niveau RHF/3–21G de la théorie, on a trouvé sept des neuf minima des *N*-formyl-L-sélénocystéinamide (For-L-Sec-NH_2) et *N*-acétyl-L-sélénocystéine-*N*-méthylamide (Ac-L-Sec-NHMe). On a comparé l'énergie de stabilisation exercée par la chaîne latérale -CH_2-SeH avec celles de -CH_2-SH et -CH_2-OH. On a obtenu les énergies relatives des divers conformères par le biais de calculs ponctuels au niveau B3LYP/6–31G(d,p) de la théorie. À l'aide de ces résultats, on a effectué une analyse topologique de la densité d'électrons à l'aide de l'approche de Bader des atomes dans la molécule. On a aussi optimisé les structures au niveau B3LYP/6–31+G(d,p) de la théorie.

Mots clés : sélénocystéine, conformations, chaîne latérale, étude d'OM ab initio, analyse conformationnelle multidimensionnelle, atomes dans la molécule, analyse, densité électronique, Bader.

[Traduit par la Rédaction]

1. Introduction

Selenocysteine is expected to exhibit a variety of side-chain/backbone interactions via hydrogen bonding and via intramolecular attractive non-covalent (i.e., charge transfer) interactions. This may occur between di- and tetracoordinated selenium from one side and oxygen or nitrogen atoms of neighbouring backbone amide groups from the other side. These interactions strongly affect the reactivity of selenocysteine and enhance the stability of a Se containing compound (1) analogously to sulfur–oxygen nonbonded interactions (2). They are also responsible for the high biological activity of the selenium, in particular selenoproteins and in nucleoside analogues. The conformation of the peptides

Received July 16, 1999.

J.C. Vank and I.G. Csizmadia.[1] Department of Chemistry, University of Toronto, Toronto, ON M5S 3H6, Canada.
C.P. Sosa. Silicon Graphics Computer System, 655 E Lone Oak Dr., Eagan, MN 55121, U.S.A.
A. Perczel. Institute of Organic Chemistry, Eotvos University, 112 Budapest, PO Box 32, H-1117, Hungary, and Department of Biochemistry, University of Oxford, South Parks Road, Oxford OX1 3QU, U.K.

[1]Author to whom correspondence may be addressed. Fax/Telephone: (416) 978-3598. e-mail: icsizmad@alchemy.chem.utoronto.ca

© 2000 NRC Canada

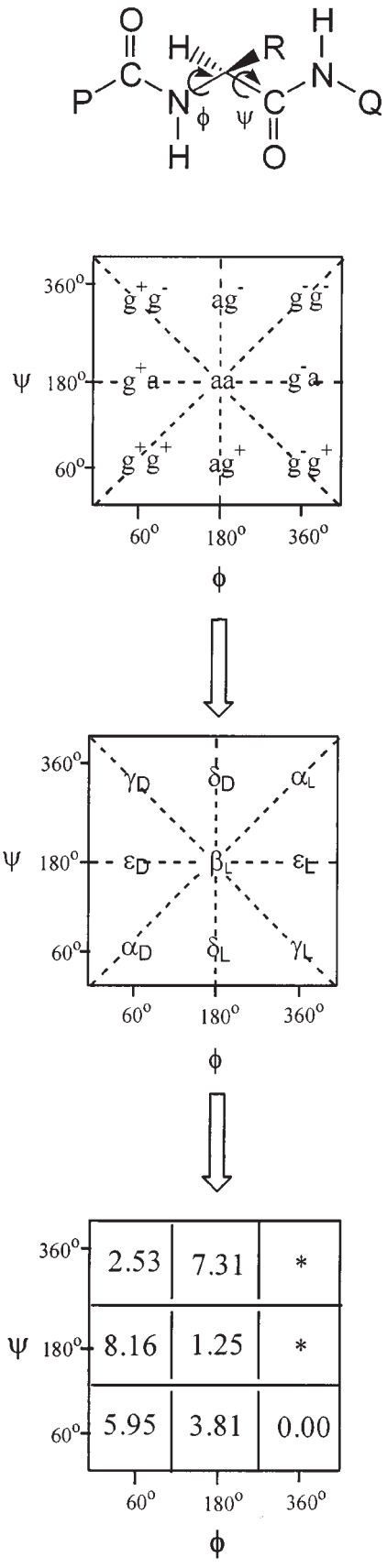


Fig. 1. Topological representation of the Ramachandran PES for an N- and C-protected amino acid (P and Q may be H or CH_3). The bottom matrix shows the relative energies for HCO-NH-CHMe-$CONH_2$ with *trans*-peptide bond computed at the RHF/3–21G level of theory.

Table 1. Total energy values of the component molecules for isodesmic reactions.

Molecular System		Energy (Hartree)
P-CONH-CH_2-CONH-Q	P = Q = H	–373.648790
	P = Q = Me	–451.2942433
CH_3-R where R = CH_2-SeH		–2467.271761
CH_3-H		–39.976877

as well as the conformation (i.e., folding) of proteins can be defined in terms of the conformations of the amino acid residues. In general, peptides with *trans*-peptide bonds are studied, therefore, ω is optimized in the vicinity of 180°. Each protein molecule is folded in a particular way to fulfill its biological function. It has been the working hypothesis for some time that the primary structure (i.e., the sequence of the amino acids) predetermines the secondary and tertiary structures (global fold) of proteins (3). The very fact that every protein has a different amino acid sequence and a different folding pattern strongly suggests that the influence of amino acid side-chains on protein folding must be great. The global minimum for all peptides containing a single amino acid residue that have been studied computationally so far is the γ_L conformation (4). This is illustrated for *N*-formyl-L-alaninamide in Fig. 1.

2. Computational method

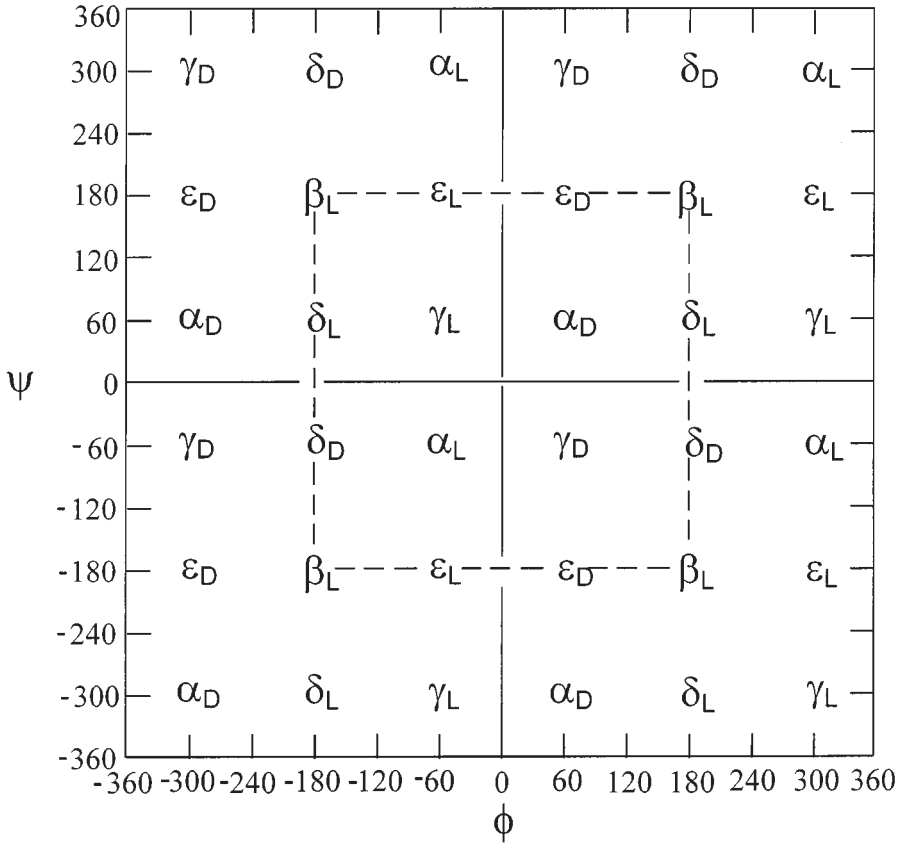
2.1 Conformational analysis

As a first approach, the nine side-chain conformations of the selenocysteine in its γ_L backbone conformation (cf. Ramachandran topology in Fig. 2) were determined, using the MDCA suggested input (5–7). The computation of the entire surface requires 12 × 12 = 144 SCF points if the grid search is executed by 30° increments. Although the resulting potential energy-surface is undoubtedly very visual, it also requires extensive CPU time. For this reason, in addition to geometry optimizations of the minima, only selected 1D cross-sections (i.e., potential energy curves: PEC) of the side-chain potential energy surface (PES) were generated. IUPAC–IUB recommended (8) the use of $-180° \le \chi_1 \le 180°$ and $-180° \le \chi_2 \le 180°$ torsional angles, where $0° \rightarrow +180°$ represents clockwise rotation and $0° \rightarrow -180°$ represents counterclockwise rotation.

However, occasionally for graphic presentation, we also use the traditional cut ($0° \le \chi_1 \le 360°$ and $0° \le \chi_2 \le 360°$) suggested previously by Ramachandran and Sasisekharan (9). The use of the latter is for sheer convenience since the nine minima are located within the traditional cut rather than on the edges and at its four corners (cf. Fig. 2).

© 2000 NRC Canada

Fig. 2. Topological representation of the Ramachandran map for an N- and C-protected amino acid PCO-NH-CHR-CO-NHQ (P and Q may be H or CH_3) showing two full cycles of rotation: $-360° \le \phi \le +360°$; $-360° \le \psi \le +360°$. The central box, denoted by broken line, represents the cut suggested by the IUPAC convention ($-180° \le \phi \le +180°$; $-180° \le \psi \le +180°$). The four quadrants denoted by solid lines are the conventional cuts (e.g., $0° \le \phi \le +360°$; $0° \le \psi \le +360°$). Most L-peptide residue exhibit nine unique conformations labeled as α_L, β_L, γ_L, δ_L, ε_L, α_D, γ_D, δ_D, and ε_D.



2.2 Molecular computations

To investigate the effects of side-chain/backbone conformational interactions, calculations were performed using GAUSSIAN 94[2] at RHF/3–21G (10) level of theory, which seemed suitable for the purpose of comparing similar results obtained for serine (11, 12) and even though the current trend is to rely on larger basis sets at a higher level of theory (13, 14). Single point calculations were carried out at B3LYP/6–31G(d,p) level of theory to compare to the relative energy values ($\Delta E_{rel.}$) computed at RHF/3–21G level of theory. The structures were also optimized at the B3LYP/6–31+G(d,p) level of theory.

2.3 Stabilization energies

The stabilization energies were calculated with respect to the γ_L backbone conformation of N- and C- protected glycine (15, 16) using the following isodesmic (same number of bonds) reaction, where P and Q may be H or CH_3 and R = CH_2-SeH.

$$\text{PCONH-CH}_2\text{-CONHQ} + \text{CH}_3\text{-R} \quad (\text{conformation } \gamma_L) \rightarrow \text{PCONH-CHR-CONHQ} + \text{CH}_3\text{-H} \quad (\text{conformation X})$$

The stabilization energy may be calculated as follows:

$$\Delta E_{\text{stabilization}} = \{E\,[\text{PCONH-CHR-CONHQ}]_X + E[\text{CH}_3\text{-H}]\} - \{E\,[\text{PCONH-CH}_2\text{-CONHQ}]_{\gamma L} + \text{CH}_3\text{-R}]\}$$

The components' energy values are summarized in Table 1.

The results of the structure optimizations, namely, geometrical parameters, total energies, relative energies, and stabilization energies as well as HOMO, LUMO energies obtained at the RHF/3–21G level of theory and B3LYP/6–31G(d,p)//RHF/3–21G are given in Table 2; similarly, the re-

[2] M.J. Frisch, G.W. Trucks, H.B. Schlegel, P.M.W. Gill, B.G. Johnson, M.A. Robb, J.R. Cheeseman, T. Keith, G.A. Petersson, J.A. Montgomery, K. Raghavachari, M.A. Al-Laham, V.G. Zakrzewski, J.V. Ortiz, J.B. Foresman, J. Cioslowski, B.B. Stefanov, A. Nanayakkara, M. Challacombe, C.Y. Peng, P.Y. Ayala, W. Chen, M.W. Wong, J.L. Andres, E.S. Replogle, R. Gomperts, R.L. Martin, D.J. Fox, J.S. Binkley, D.J. Defrees, J. Baker, J.P. Stewart, M. Head-Gordon, C. Gonzalez, and J.A. Pople. Gaussian 94, Revision E.1, E.2, C.3 and D.2. Gaussian, Inc., Pittsburgh, Pa. 1995.

© 2000 NRC Canada

Table 2. Ab initio RHF/3–21G and B3LYP/6–31G(d,p) results computed for various side-chain conformations of Ac-L-Sec-NHMe and For-L-Sec-NH_2 at the γ_L backbone conformation. Torsional angles (ϕ, ψ, χ_1, χ_2, ω_0, and ω_1) and bond angles ($\angle$) are given in degrees according to IUPAC–IUB convention. Distances are given in angstroms. INITIAL: initial side-chain conformation predicted by MDCA. CONVERGED: converged side-chain conformation calculated at RHF/3–21G level of theory.

INITIAL	$g^+ g^-$ $g^+ a$	$g^+ g^+$	$a g^-$	$a a$ $a g^+$	$g^- g^-$	$g^- a$	g^-g^+
CONVERGED	$g^+ a$	$g^+ g^+$	$a g^-$	$a g^+$	$g^- g^-$	$g^- a$	g^-g^+
Ac-L-Sec-NHMe							
ϕ	–85.93	–85.42	–86.52	–86.63	–86.91	–86.51	–87.34
ψ	65.81	62.74	71.20	72.29	70.22	69.37	68.48
χ_1	58.77	51.27	–168.55	–171.10	–54.80	–55.64	–67.42
χ_2	–124.04	68.35	–74.78	92.54	–58.18	–167.51	65.26
ω_0	–176.61	–174.97	–175.58	–176.46	–173.12	–174.62	–175.55
ω_1	–178.72	–179.64	–178.27	–178.35	–178.28	–178.58	–178.80
C13—Se16	1.9863	1.9802	1.9741	1.9765	1.9747	1.9822	1.9747
Se16—H17	1.4779	1.4654	1.4679	1.4759	1.4732	1.4722	1.4722
C11—O12	1.2237	1.2245	1.2241	1.2225	1.2217	1.2215	1.2215
O6···H19	2.0373	1.9981	2.0451	2.0706	2.0156	2.0277	2.0473
Se16···N7	3.2814	3.2487	4.2390	4.2353	3.2672	3.1472	3.3745
Se16···O12	3.0454	3.3315	3.4124	3.3381	4.6736	4.6834	4.6958
Se16···C11	3.3675	3.5341	3.4528	3.3861	4.3224	4.2815	4.3146
Se16···H8	2.7940	2.7211	4.5104	4.5159	3.0962	3.0753	3.4263
O12···H17	4.4363	2.4241	2.5683	4.5631	5.1213	5.1534	5.0978
$\angle$ Se16-H17···O12	16.23	115.64	112.57	28.32	64.25	63.41	66.01
$\angle$ Se16···H8-N7	110.61	113.32	68.01	67.48	90.87	84.88	78.63
ε_{HOMO} (Hartree)	–0.33644	–0.33739	–0.33035	–0.33231	–0.34166	–0.33796	–0.33850
ε_{LUMO} (Hartree)	0.16829	0.16380	0.16431	0.16441	0.15599	0.15820	0.15706
E^a (Hartree)	–2	–2878.6010140	–2878.5989039	–2878.5969858	–2878.5980902	–2878.5979009	–2878.5968000
$\Delta E^a_{rel.}$ (kcal mol^{-1})	1.50	0.00	1.32	2.52	1.83	1.95	2.64
$\Delta E^a_{stab.}$ (kcal mol^{-1})	–5.96	–7.46	–6.13	–4.93	–5.62	–5.51	–4.81
E^b (Hartree)	–2895.2532778	–2895.2533997	–2895.2475055	–2895.2467768	–2895.2474882	–2895.2461801	–2895.2451380
$\Delta E^b_{rel.}$ (kcal mol^{-1})	0.08	0.00	3.70	4.16	3.71	4.53	5.19
For-L-*sec*-NH2							
ϕ	–84.72	–83.97	–85.35	–85.51	–85.06	–84.97	–85.98
ψ	64.68	61.67	69.71	70.43	68.60	67.55	66.60
χ_1	58.69	51.25	–168.02	–171.04	–54.86	–56.42	–68.03
χ_2	–123.59	68.67	–75.12	94.21	–58.29	–168.21	66.05
ω_0	–171.37	–173.26	–175.06	–174.79	179.80	–175.33	–172.67
ω_1	–178.83	–179.84	–178.38	–178.57	–178.43	–178.80	–179.10
C9—Se12	1.9860	1.9798	1.9740	1.9766	1.9743	1.9819	1.9743
Se12—H13	1.4775	1.4656	1.4678	1.4758	1.4732	1.4720	1.4728
C7—O8	1.2200	1.2208	1.2204	1.2190	1.2182	1.2180	1.2180
O2···H15	2.0373	1.9998	2.0425	2.0634	2.0072	2.0214	2.0433

© 2000 NRC Canada

Table 2 (*concluded*).

INITIAL	$g^+ g^-$	$g^+ g^+$	$a\ g^-$	$a\ a$	$g^- g^-$	$g^-\ a$	$g^- g^+$
	$g^+\ a$			$a\ g^+$			
CONVERGED	$g^+\ a$	$g^+ g^+$	$a\ g^-$	$a\ g^+$	$g^- g^-$	$g^-\ a$	$g^- g^+$
Se12···N3	3.2809	3.2474	4.2399	4.2368	3.2697	3.1592	3.3828
Se12···O8	3.0614	3.3423	3.4100	3.3167	4.6738	4.6852	4.6939
Se12···C7	3.3692	3.5328	3.4590	3.3844	4.3234	4.2831	4.3142
Se12···H4	2.7978	2.7232	4.5129	4.5180	3.0810	3.0739	3.4244
O8···H13	4.4492	2.4416	2.5693	4.5549	5.1125	5.1461	5.1142
∠ Se12-H13 L O8	16.50	115.33	112.38	27.50	64.59	63.76	65.31
∠ Se12···H4-N3	110.28	113.04	67.92	67.45	91.89	85.65	79.21
ε_{HOMO} (Hartree)	–0.34074	–0.34174	–0.33433	–0.33609	–0.34548	–0.34185	–0.34237
ε_{LUMO} (Hartree)	0.16376	0.15952	0.15996	0.16074	0.15237	0.15497	0.15398
E^a (Hartree)	–2800.9530380	–2800.9555484	–2800.9532998	–2800.9513786	–2800.9524428	–2800.9521728	–2800.9512066
$\Delta E^a_{rel.}$ (kcal mol^{-1})	1.58	0.00	1.41	2.62	1.95	2.12	2.72
$\Delta E^a_{stab.}$ (kcal mol^{-1})	–5.88	–7.45	–6.04	–4.83	–5.50	–5.33	–4.73
E^b (Hartree)	–2816.6149892	–2816.6151803	–2816.6092504	–2816.6086200	–2816.6091907	–2816.6077504	–2816.6069365
$\Delta E^b_{rel.}$ (kcal mol^{-1})	0.12	0.00	3.72	4.13	3.76	4.66	5.17

[a]RHF/3–21G.
[b]B3LYP/6–31G(d,p)//RHF/3–21G.

sults of the full geometry optimization at B3LYP/6–31+G(d,p) level of theory are given in Table 3. The total, as well as the HOMO and LUMO energies are given in hartrees and the relative energies ($\Delta E_{rel.}$) and stabilization energies ($\Delta E_{stab.}$) are given in kcal mol^{-1} (using the conversion factor: 1 hartree = 627.5095 kcal mol^{-1}). The numbering system used for *N*-acetyl-L-selenocysteine-*N*-methylamide (P = Q = Me) and *N*-formyl-L-selenocysteinamide (P = Q = H) is shown in Fig. 3.

2.4 Topological analysis of electron densities

The topological analysis of electron density has been performed on the basis of Bader's theory of atoms in molecules (AIM) (17). In this theory, the topological properties of the electron density distribution were derived from the gradient vector field of the electron density $\nabla\rho(\mathbf{r})$ and on the Laplacian of the electron density $\nabla^2\rho(\mathbf{r})$. A critical point in the electron density, called the *bond critical point* (BCP), where $\nabla\rho = 0$, is formed for two interacting atoms in a molecule. A pair of gradient paths, which originate at a BCP and terminate at neighbouring nuclei define a *bond path*. The necessary condition for two atoms to be bonded to one another is therefore that their nuclei be linked by a bond path. The bond path is considered to be "a universal indicator of bonded interactions" (18). The method is widely used for the determination of hydrogen bonding (19).

3. Results and discussion

3.1. Structural characteristics

A relevant question is what atomic attributes does Se have that makes its presence necessary for enzyme activity and what accounts for the conformational differences of selenocysteine, if any, with respect to that of cysteine and serine? The similarities and differences of selenocysteine, cysteine, and serine hinge on the similarities and differences of the -CH_2SeH, -CH_2SH, and -CH_2OH groups. The Se atom is larger than that of S and O atoms and has a greater polarizability, hence it is a better nucleophile (20, 21). Since Se forms weaker σ-bonds than S, many reactions that involve the cleavage of C—Se, N—Se, or O—Se bonds are more rapid than cleavage of analogous bonds to sulfur (22, 23). The Se—C, Se—N, and Se—O bonds are shorter than the respective van der Waals contacts. Se is oxidized somewhat more easily to Se(IV) but with more difficulty to Se(VI) than the corresponding sulfur oxidations.

3.2 Conformational study

The nine side-chain conformations predicted by Multidimensional Conformational Analysis (MDCA) have been optimized at RHF/3–21G level of theory for N- and C-protected selenocysteine. For a non-ideal system, however, some of the expected conformers may disappear. This phenomenon is referred to as the annihilation of critical points (24, 25). The knowledge of all conformers with their relative energies ($\Delta E_{rel.}$) makes it possible to determine a conformational equilibrium distribution for the molecular system.

For φ and ψ input parameters, values characteristic for the γ_L conformation, –84.4° and +67.7° respectively (25), were used. However, they were allowed to relax during geometry optimization. The φ, ψ values thus are optimized, which

© 2000 NRC Canada

Table 3. Ab initio B3LYP/6–31+G(d,p) results computed for various side-chain conformations of Ac-L-Sec-NHMe and For-L-Sec-NH_2 at the γ_L backbone conformation. Torsional angles (ϕ, ψ, χ_1, χ_2, ω_0 and ω_1) and bond angles ($\angle$) are given in degrees according to IUPAC–IUB convention. Distances are given in angstroms. INITIAL: initial side-chain conformation predicted by MDCA. CONVERGED: converged side-chain conformation calculated at B3LYP/6–31+G(d,p) level of theory.

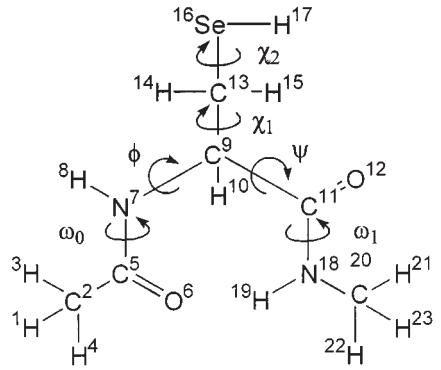
INITIAL	$g^+ g^-$ $g^+ a$	$g^+ g^+$	$a g^-$	$a a$ $a g^+$	$g^- g^-$	$g^- a$	$g^- g^+$
CONVERGED	$g^+ a$	$g^+ g^+$	$a g^-$	$a g^+$	$g^- g^-$	$g^- a$	$g^- g^+$
Ac-L-Sec-NHMe							
ϕ	–83.86	–84.62	–85.95	–86.90	–86.01	–85.29	–84.44
ψ	71.11	66.18	77.77	84.94	63.99	71.27	75.24
χ_1	54.85	47.87	–163.28	–161.60	–92.05	–58.73	–66.04
χ_2	–124.88	62.83	–72.84	72.55	–52.65	–174.27	55.29
ω_0	–177.15	–175.05	–178.63	178.57	–170.43	–174.87	–179.42
ω_1	–175.85	–178.42	–174.72	–174.51	–176.59	–175.97	–175.24
C13—Se16	1.9741	1.9652	1.9592	1.9621	1.9590	1.9710	1.9601
Se16—H17	1.4682	1.4633	1.4641	1.4668	1.4663	1.4641	1.4641
C11—O12	1.2322	1.2328	1.2319	1.2305	1.2311	1.2309	1.2308
O6···H19	2.0876	2.0419	2.1614	2.2911	2.0193	2.0744	2.1295
Se16···N7	3.2117	3.1899	4.2049	4.1985	3.2385	3.1701	3.3626
Se16···O12	3.1411	3.4301	3.5997	3.7355	4.6772	4.7192	4.7320
Se16···C11	3.4412	3.6042	3.4853	3.4961	4.3302	4.2850	4.3245
Se16···H8	2.6747	2.6224	4.5427	4.5759	2.8999	3.1093	3.4755
O12···H17	4.5206	2.4876	2.7787	4.7236	5.1200	5.1826	5.0751
$\angle$ Se16-H17···O12	16.54	118.16	112.34	40.67	64.40	63.66	68.24
$\angle$ Se16···H8-N7	113.10	115.20	64.34	62.07	100.37	84.16	75.21
E (Hartree)	–2	–2895.3008672	–2895.2982318	–2895.2965667	–2895.2982807	–2895.2976357	–2895.2969564
$\Delta E_{rel.}$ (kcal mol^{-1})	1.81	0.00	1.66	2.70	1.62	2.03	2.46
For-L-*sec*-NH2							
ϕ	–82.38	–83.36	–84.64	–86.28	–84.06	–84.07	–84.31
ψ	66.43	62.29	77.63	83.39	66.78	67.26	69.29
χ_1	54.96	48.51	–165.11	–162.61	–51.03	–59.26	–67.46
χ_2	–122.41	64.45	–73.40	74.35	–52.24	–176.94	56.36
ω_0	–171.44	–173.80	–172.21	–171.41	172.35	–179.26	–170.44
ω_1	–177.04	–179.45	–173.49	–171.96	–177.23	–177.06	–176.95
C9—Se12	1.9747	1.9649	1.9590	1.9615	1.9573	1.9700	1.9588
Se12—H13	1.4666	1.4632	1.4636	1.4669	1.4660	1.4636	1.4640
C7—O8	1.2277	1.2284	1.2277	1.2262	1.2267	1.2264	1.2265
O2···H15	2.1057	2.0870	2.2007	2.3080	2.0387	2.0784	2.1449
Se12···N3	3.2152	3.1950	4.2174	4.2094	3.2317	3.1787	3.3738
Se12···O8	3.1767	3.4435	3.5694	3.7080	4.6740	4.7101	4.7182
Se12···C7	3.4403	3.5914	3.4723	3.4983	4.3315	4.2872	4.3227
Se12···H4	2.6820	2.6341	4.5554	4.5746	2.8938	3.0875	3.4847

© 2000 NRC Canada

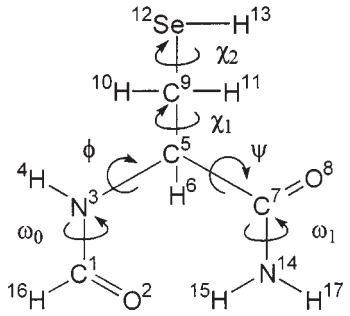
Table 3 (*concluded*).

INITIAL	$g^+ g^-$	$g^+ g^+$	$a g^-$	$a a$	$g^- g^-$	$g^- a$	$g^- g^+$
	$g^+ a$			$a g^+$			
CONVERGED	$g^+ a$	$g^+ g^+$	$a g^-$	$a g^+$	$g^- g^-$	$g^- a$	$g^- g^+$
O8···H13	4.5454	2.5147	2.7369	4.7182	5.1163	5.1637	5.1108
∠ Se12-H13···O8	17.44	117.46	112.83	39.61	64.41	64.02	66.35
∠ Se12···H4-N3	112.78	114.67	64.36	62.80	100.26	85.84	75.34
E (Hartree)	–2816.6583363	–2816.661098	–2816.6578393	–2816.6560339	–2816.6578482	–2816.6568683	–2816.6560593
$\Delta E_{rel.}$ (kcal mol^{-1})	1.73	0.00	2.05	3.18	2.04	2.66	3.16

Fig. 3. Ac-L-Sec-NHMe and For-L-Sec-NH_2 in their γ_L conformations. Torsional angles ω_0, ω_1, ϕ, ψ, χ_1, and χ_2 are shown.



N-Acetyl-L-Sec-*N*-methylamide



N-Formyl-L-Sec-amide

means that they change quantitatively but not qualitatively. The computations were carried out for both *N*-acetyl-L-selenocysteine-*N*-methylamide and *N*-formyl-L-selenocysteinamide.

From the nine legitimate side-chain conformations two legitimate conformations [($g^+ g^-$), ($a\ a$)] were annihilated and seven conformations have been located by geometry optimization [($a\ g^-$), ($g^- g^-$), ($g^+ a$), ($g^- a$), ($g^+ g^+$), ($a\ g^+$), ($g^- g^+$)] as illustrated in Fig. 4. The γ_L ($a\ a$) conformation has migrated to a different catchment region, to the γ_L ($a\ g^+$) minimum, and the γ_L ($g^+ g^-$) structure has migrated to the γ_L ($g^+ a$) minimum. This migration affected extensively the χ_1 and χ_2 values but only marginally the ϕ and ψ values, which were slightly shifted from the original input values. The relative energies ($\Delta E_{rel.}$) for *N*-acetyl-L-selenocysteine-*N*-methylamide and *N*-formyl-L-selenocysteinamide have been calculated at RHF/3–21G, B3LYP/6–31G(d,p)//RHF/3–21G and B3LYP/6–31+G(d,p) levels of theory and are also included in Table 2 and Table 3 respectively.

The obtained results agree with those obtained for *N*-acetyl-L-cysteine-*N*-methylamide[3] but differ from the corresponding serine (11) results as shown in Fig. 5.

The lower part of Fig. 5 also shows the calculated stabilization energies ($\Delta E_{stabil.}$). Side-chain R (CH_2-SeH) has a steric effect on the peptide backbone and it is important to determine whether the overall effect is stabilizing or

[3] M.A.. Zomora, H.A. Baldoni, A.M. Rodriguez, R.D. Enriz, C.P. Sosa, A. Perczel, A. Kucsman, O. Farkas, J.C. Vank, E. Deretey, and I.G. Csizmadia.. Submitted for publication.

© 2000 NRC Canada

Fig. 4. The annihilation of the two minima [(g^+ g^+), (a a)] on the side-chain PES of N- and C-protected selenocysteine. The two vertical arrows, pointing downward, indicate the shift in torsional angles during geometry optimization.

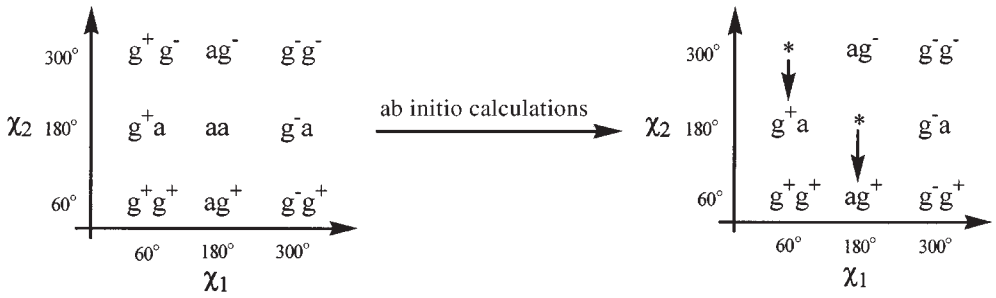


Fig. 5. Structures located on the side-chain PES of the γ_L backbone conformations of N- and C-protected serine, cysteine, and selenocysteine [HCO-NH-CH(CH_2-XH)-CO-NH_2]. The lower part of the figure collects the stabilization energies ($\Delta E_{stabil.}$), in kcal mol^{-1} units, exerted by the side-chain with respect to the glycine residue in its γ_L conformation.

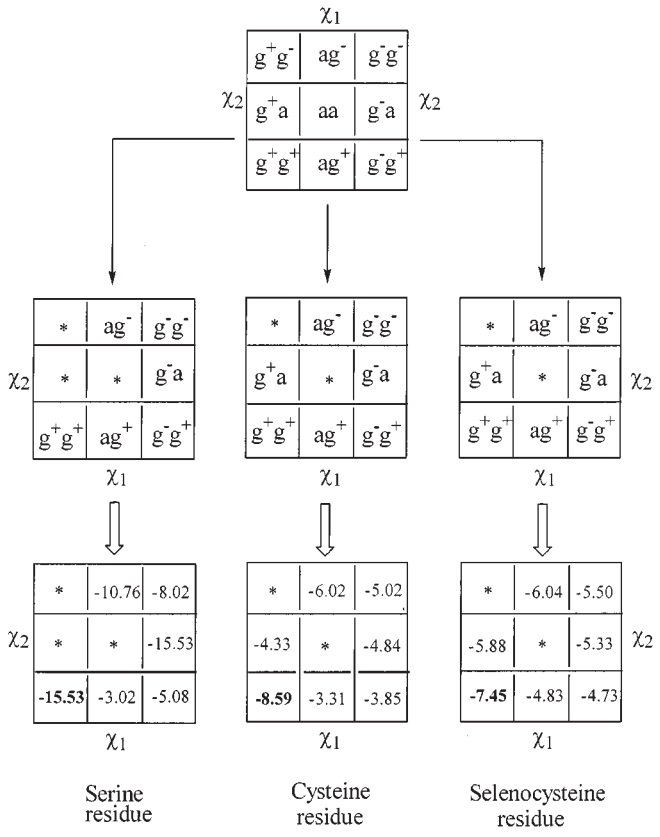
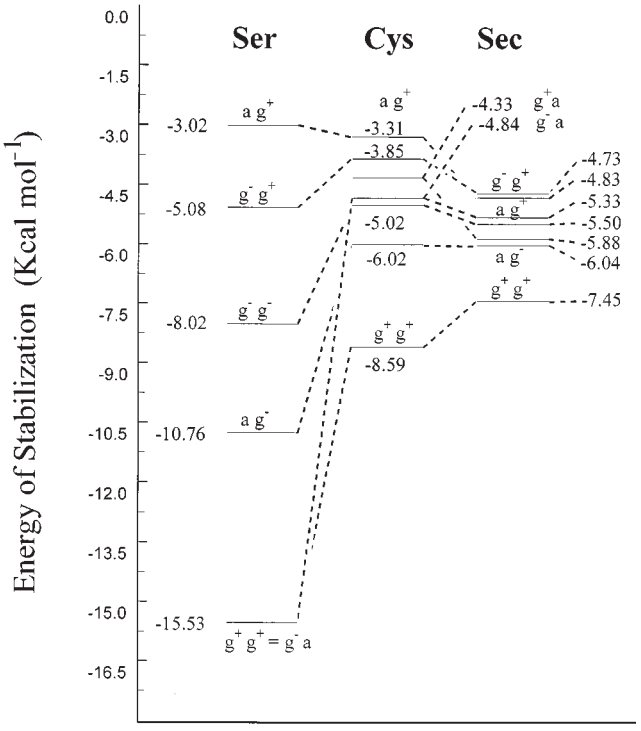


Fig. 6. Spectrum of conformational dependence of the side-chain stabilization energy on the γ_L backbone conformation of formyl ser-, cys-, and sec-amide.



destabilizing. If the side-chain R contains a polar group, such as -SeH (or -OH, -SH), then the special H-bonded interactions may have specific stabilizing effects. The isodesmic reactions were constructed with the aid of the total energies summarized in Table 2 and Table 3 and of the other component molecules involved (Table 1). The energies of the isodesmic reactions measure the relative stabilities of analogous compounds containing O, S, Se (Fig. 6), or relative stabilities of different amino acids [Gly (26), Ala (27), Val (14), Phe (28–30), Asp (31), Ser (11, 32, 33), Cys[3]] with respect to glycine (Fig. 7).

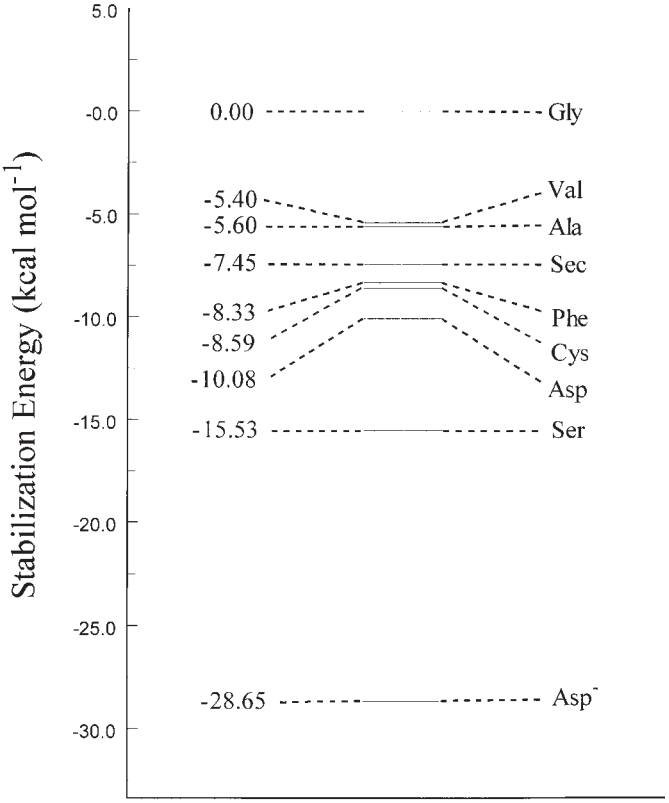
From Fig. 6 we can observe that the effect of the orientation of the side-chain with respect to the peptide backbone, going from serine to selenocysteine, is gradually decreasing. This is due to increase in the size of the atoms O → S → Se and the resulting gradual lengthening of C—O → C—S → C—Se bond lengths as well as the reduced hydrogen bonding ability in going from OH to SH all the way to SeH.

In general, *N*-acetyl-L-*sec*-*N*-methylamide shows a greater stabilizing effect than *N*-formyl-L-*sec*-amide, however, the difference between the (g^+ g^+) conformers is only 0.01 kcal mol^{-1} which seems insignificant. The difference between the (a g^+) conformers of *N*-acetyl-L-*sec*-*N*-methylamide and *N*-formyl-L-*sec*-amide is the largest (1.13 kcal mol^{-1}).

The (g^+ g^+) conformer was subjected to a torsional angle scan at RHF/3–21G, where χ_1 was fixed at 52° and χ_2 was rotated every 30° between $0° \le \chi_2 \le 360°$. The value of χ_1 = 52° was chosen arbitrarily, taking into consideration that χ_1 = 51.9° is the torsional angle value of the optimized (g^+ g^+)

© 2000 NRC Canada

Fig. 7. Relative side-chain stabilization energy values of various side-chains in the γ_L backbone conformation of HCO-NH-CHR-CO-NH_2. Most side-chains have several conformations but here only the one, which exerted the greatest stabilization, is shown.



side-chain conformation of serine and $\chi_1 = 52.657°$ is the torsional angle value of the optimized (g^+ g^+) side-chain conformation of cysteine. The variation of the total molecular energy with a single torsional angle (χ_2) leads to a Potential Energy Curve (PEC), $E = E(\chi_2)$. The scan (Fig. 8) shows the existence of two minima, which confirms the existence of (g^+ g^+) and (g^+ *a*) and the annihilation of (g^+ g^-) at least at the RHF/3–21G level of theory. A second and a third scan, namely in the vicinity of conformer (*a a)*, were carried out in which case first χ_2 was fixed at 180° and χ_1 was rotated every 10° between $165° \le \chi_1 \le 195°$.

Secondly χ_1 was fixed at 180° and χ_2 has been rotated every 10° between $155° \le \chi_2 \le 195°$ (Fig. 9*a, b*).

The two cross sections given in Fig. 9 clearly show that the (*a a*) conformation has indeed been anihilated. The (*a a*) conformer would exist if and only if both cross sections had a minimum energy point at or near 175°.

3.3 Intramolecular interactions

Intramolecular noncovalent attractive interactions exist between Se(II) or Se(IV) from one side and oxygen or nitrogen atoms from the other side. There is a strong dependence of the strength and length on the nature of the chalcogen atom, its valence state, and the electro-negativity of the attached substituents. These intra- and intermolecular contacts give rise to electrostatic effects, *d*-orbital participation and negative hyperconjugation (i.e., donation of an electron pair from the highest π or *n*-orbital of one center to the lowest lying σ^* orbital of the neighbouring center).

As presented in Fig. 10 the most important type of donor–acceptor interactions involve hydrogen bonding (i.e., O6···H19, O12···H17, Se16···H8 in *N*-acetyl-L-*sec*-*N*-methylamide as seen in **1b** and **1c** and O2···H15, O8···H13, Se12···H4 in *N*-formyl-L-*sec*-amide shown in **2b** and **2c** of Fig. 10). The hydrogen bonding between O6···H19 and O2···H15 is holding the backbone in the γ_L conformation and the last two structures of both molecules in Fig. 10 represent backbone/side-chain interactions.

Coordination or dative bonds (like those of Se16···O12 in *N*-acetyl-L-*sec*-*N*-methylamide, **1a** and Se12···O8 in *N*-formyl-L-*sec*-amide, **2a** of Fig. 10) may also form by the electron acceptor center (e.g., Se) with ligands donating electrons from lone-pairs or π orbitals (34, 35). In the case of the hydrogen bonding Brønsted complex (Fig. 10, **1c**, **2c**) the Se atom acquires a partial positive charge as it is accepting a proton. In contrast to the former, conformations **1a** and **2a** exhibit intramolecular Lewis complexes in which the Se acquires a partial negative charge, due to the transfer of electrons from the oxygen. In both *N*-acetyl-L-*sec*-*N*-methylamide and *N*-formyl-L-*sec*-amide, the interatomic distances between O6···H19, O12···H17 and O2···H15, O8···H13 are the shortest for the (g^+ g^+) conformations, which are the lowest in energy. Clearly, the geometrical proximity of the appropriate moieties in the (g^+ g^+) side-chain conformation is enhancing the intramolecular interaction, which in turn will lower the total molecular energy. In analyzing the (g^+ g^+) side-chain conformation, there seems to be no such correlation between the Se···N or Se···O interatomic distances and energy values.

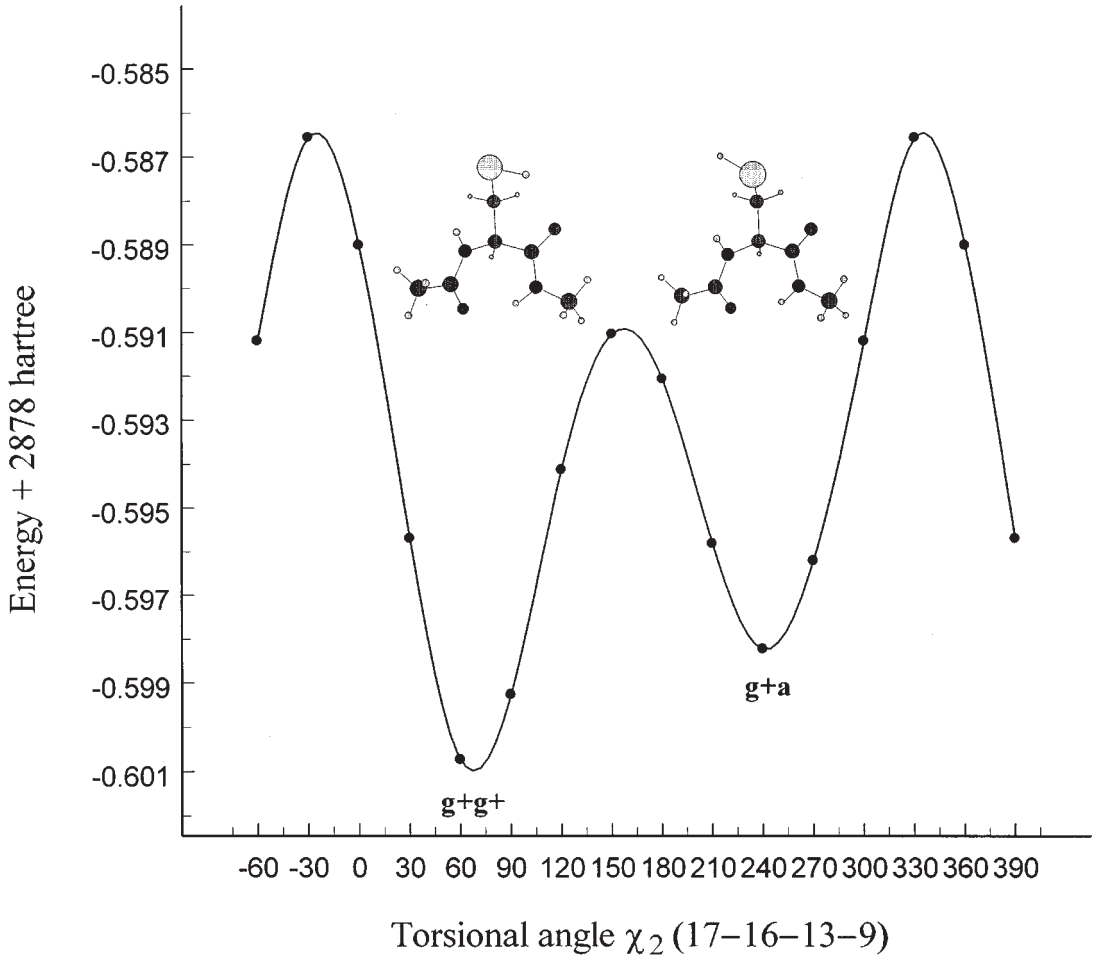
Comparing the data of Table 2 with known atomic radii, we can see that certain Se16···N7 [(g^+ *a*), (g^+ g^+), (g^- g^-), (g^- *a*), and (g^- g^+) conformations], Se16···O12 [(g^+ *a*), (g^+g^+), and (*a* g^+) conformations] distanes of *N*-acetyl-L-*sec*-*N*-methylamide and Se12···N3 [(g^+ *a*), (g^+ g^+), (g^- g^-), (g^- *a*), and (g^- g^+) conformations], Se12···O8 [(g^+ *a*), (g^+ g^+), and (*a* g^+) conformations] distances of *N*-formyl-L-*sec*-amide fall between the sums of the non-bonded radii and that of van der Waals radii. This may indicate noticeable interactions. Elongation of C9—Se12 and C7—O8 bond lengths may accompany the interactions between Se···O and elongation of C9—Se12 and N3—H4 suggests Se···N interaction.

In four of the seven structures [(g^- g^-), (*a* g^+), (g^- *a*), and (g^- g^+)] there seems to be no hydrogen bonding between the side-chain -SeH group and the peptide backbone. In both cases, the Se12···H4 and O8···H13 distances in *N*-formyl-L-*sec*-amide are quite large (between 3.4 and 5.1 Å). Unlike serine, where both (g^+ g^+) and (g^- *a*) conformers are the lowest in energy (having the same value, probably due to accidental degeneracy), the most stable conformer of *sec* is (g^+ g^+). The least favoured is (g^- g^+) closely followed by (*a* g^+), both of which show slight destabilizing effects due to the lack of H-bonding.

The hydrogen bonds were verified by the existence of bond critical points in the A-H···B region. This was carried out by Bader's Atoms in Molecules (AIM) topological analysis of the electron density computed at the B3LYP/6–31G(d,p)//RHF/3–21G level of theory. Three conformations:

© 2000 NRC Canada

Fig. 8. Energy as a function of torsional angle χ_2 in Ac-L-Sec-NHMe including the (g^+ g^+) and (g^+ a) conformations. The value of χ_2 was incremented in 30° steps while χ_1 was fixed at 52° and the remaining geometrical parameters of the molecule were subjected to full geometry optimization.



(g^+ g^+), (g^+ a), and (a g^-) exhibited such interactions as illustrated graphically in Figs. 11, 12, and 13, for For-Sec-NH_2. The computed values obtained for Ac-Sec-NHMe and For-Sec-NH_2 reveal that the density (ρ_b) at the bond critical points of the various bonds assume roughly the following values:

C = O ~ 0.40

N—H ~ 0.35

C—Se and Se—H ~ 0.15

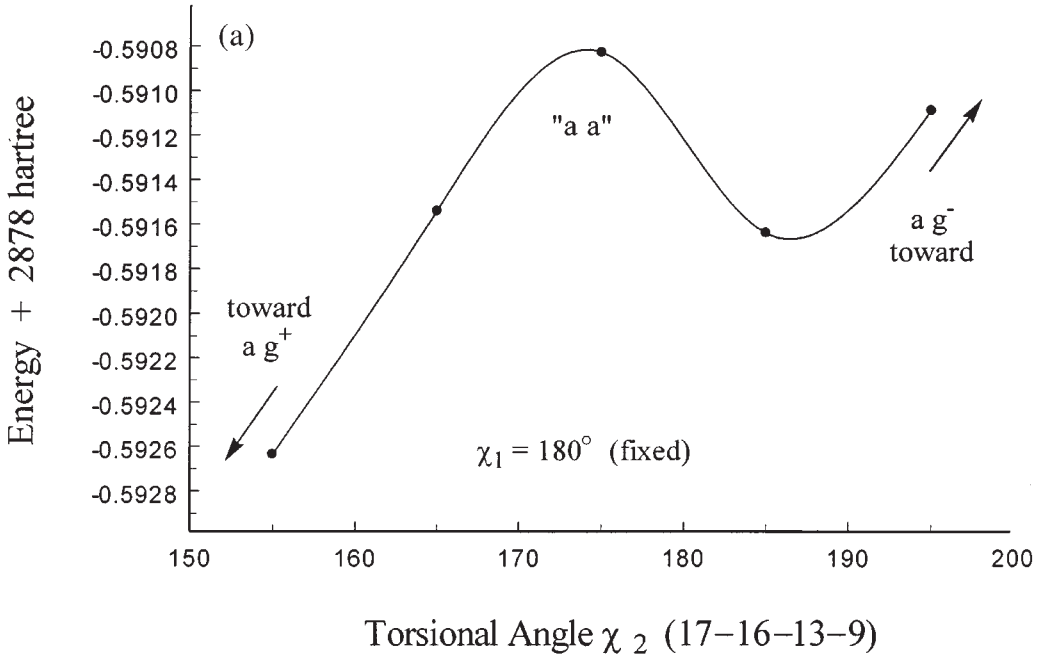
hydrogen bond ~ 0.01

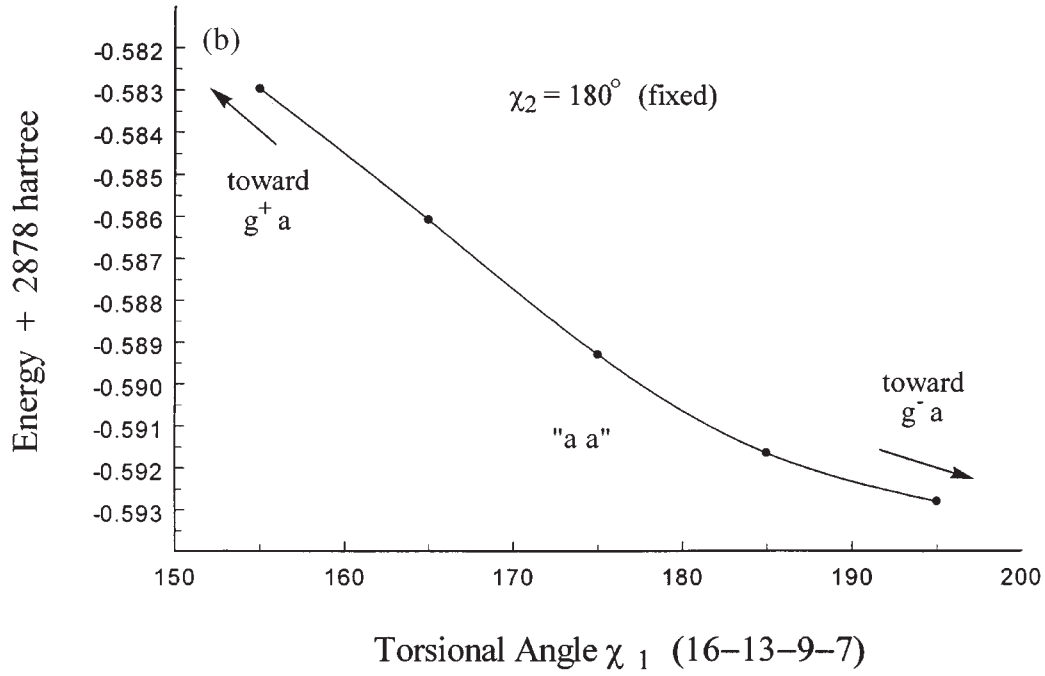
3.4 The effect of basis set and correlation energy on $\Delta E_{rel.}$

During the past decade it became clear by studying numerous N- and C-protected amino acids that the 3–21G basis set yielded fairly informative results at the HF level of theory (11, 12, 14–16, 25, 26–33) particularly when compared to large basis set MP2 calculations (14), while undoubtedly such qualitatively or sometime even semi-quantitatively acceptable results are fortuitous, nevertheless, they formed the basis of the advances in the 1990s. In all these compounds only C, H, N, and O atoms were present. It is of a fundamental question therefore whether such fortuitous results will persist when an O atom is replaced by a Se atom. Fig. 14 shows the relative energies of Ac-Sec-NHMe and For-Sec-NH_2 as computed at the RHF/3–21G and B3LYP/6–31G(d,p) levels of theory. The $\Delta E_{rel.}$ values of the two compounds are similar at the RHF/3–21G levels of theory. They are also comparable at the B3LYP/6–31G(d,p) levels. They all fall within a 3 Kcal/mol spread and the global minimum remains the same. However, when the DFT results are compared to those obtained at the RHF/3–21G level of theory, some differences may be noticed. Namely some of closely spaced levels are interchanged on the relative energy scale (Fig. 14) when one compares the RHF/3–21G and B3LYP/6–31+G(d,p) results. Nevertheless there seems to be no drastic change in stability. In conclusion, it is abundantly clear that for heavy elements, such as Se, one should aim to have better representation in terms of basis set and the inclusion of electron correlation than necessary for

© 2000 NRC Canada

Fig. 9. (*a*) Energy as a function of torsional angle χ_1 in Ac-L-Sec-NHMe in the vicinity of the annihilated (*a a*) conformation. The value of χ_1 was incremented in 10° steps from 165° → 195° while χ_2 was fixed at 180° and the remainder of the fragment subjected to full geometry optimization. (*b*) Energy as a function of torsional angle χ_2 in Ac-L-Sec-NHMe in the vicinity of the annihilated (*a a*) conformation. The value of χ_2 was incremented in 10° steps from 155° → 195° while χ_1 was fixed at 180° and the remainder of the fragment was subjected to full geometry optimization.





© 2000 NRC Canada

Fig. 10. Various types of intramolecular interactions in *N*-acetyl-L-selenocysteine-*N*-methylamide (above) and *N*-formyl-L-selenocysteinamide (below).

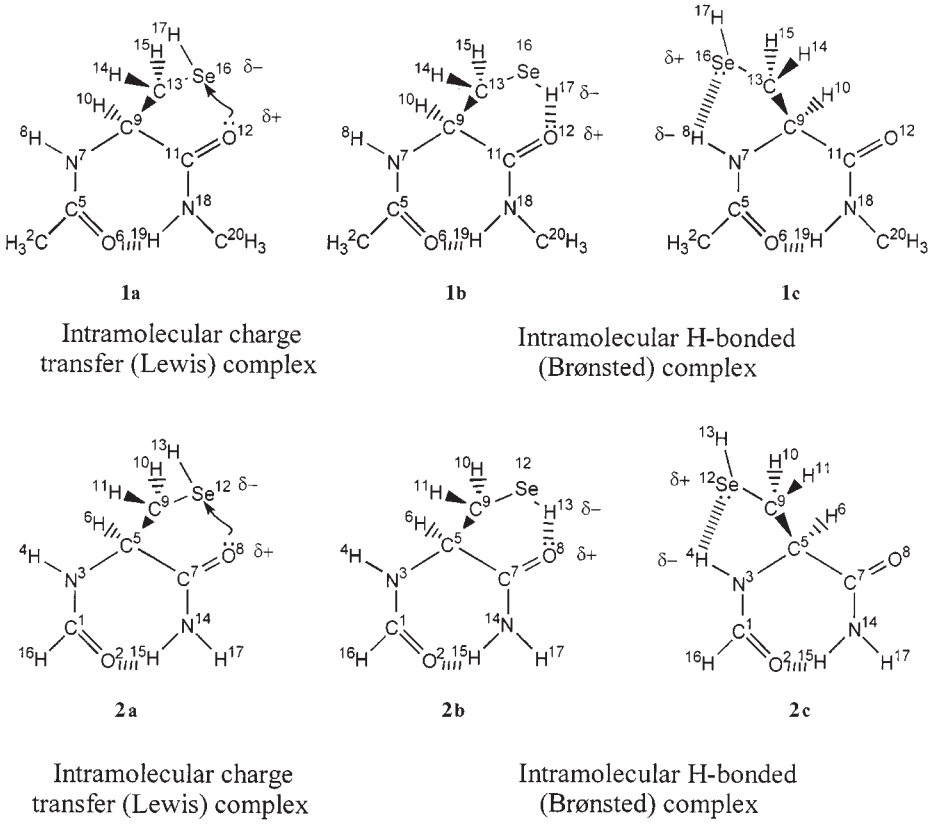


Fig. 11. The contour map of the Laplacian of the electron density for the (g^+ g^+) conformation of For-L-Sec-NH_2 calculated at the B3LYP/6–31+G(d,p)//RHF/3–21G level of theory. Bond paths are denoted by lines, bond critical points (BCPs) are denoted by black dots, ring critical points (RCPs) are denoted by open triangles, and the nuclei are denoted by crosses.

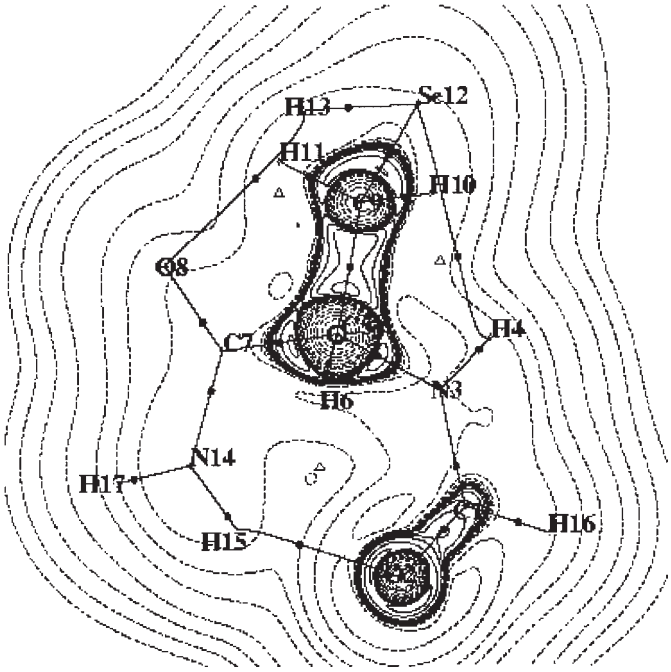
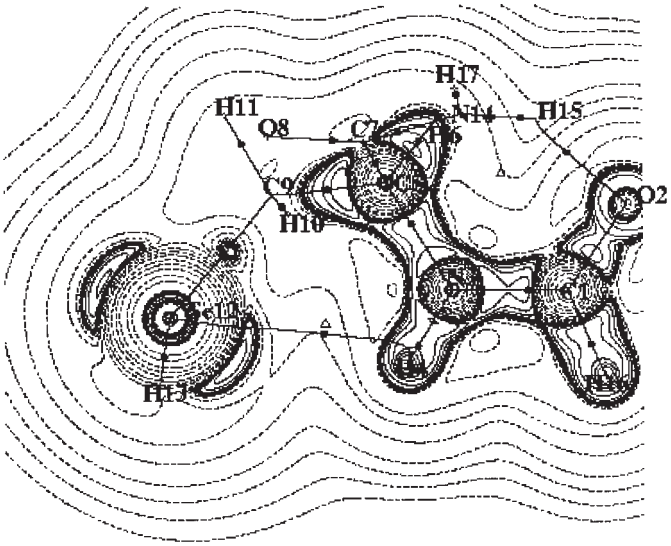


Fig. 12. The contour map of the Laplacian of the electron density for the (g^+ *a*) conformation of For-L-*sec*-NH_2 calculated at the B3LYP/6–31+G(d,p)//RHF/3–21G level of theory. Bond paths are denoted by lines, bond critical points (BCPs) are denoted by black dots, ring critical points (RCPs) are denoted by open triangles, and the nuclei are denoted by crosses.



© 2000 NRC Canada

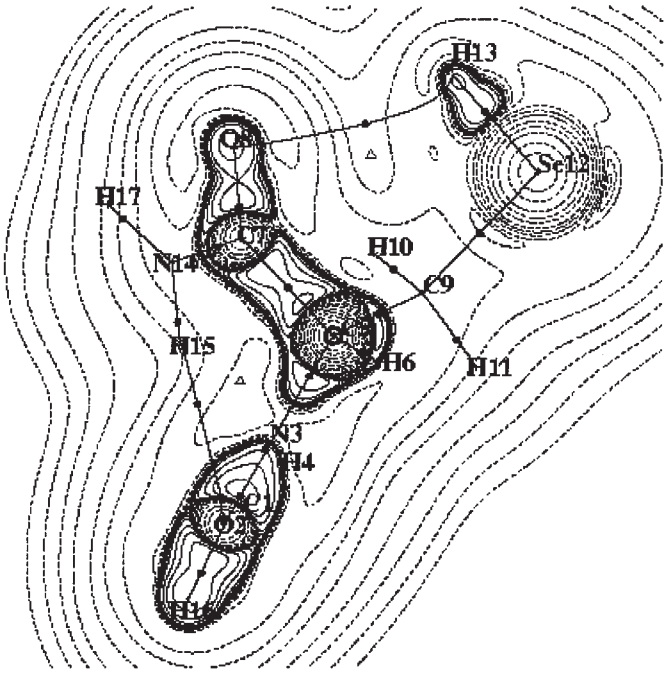


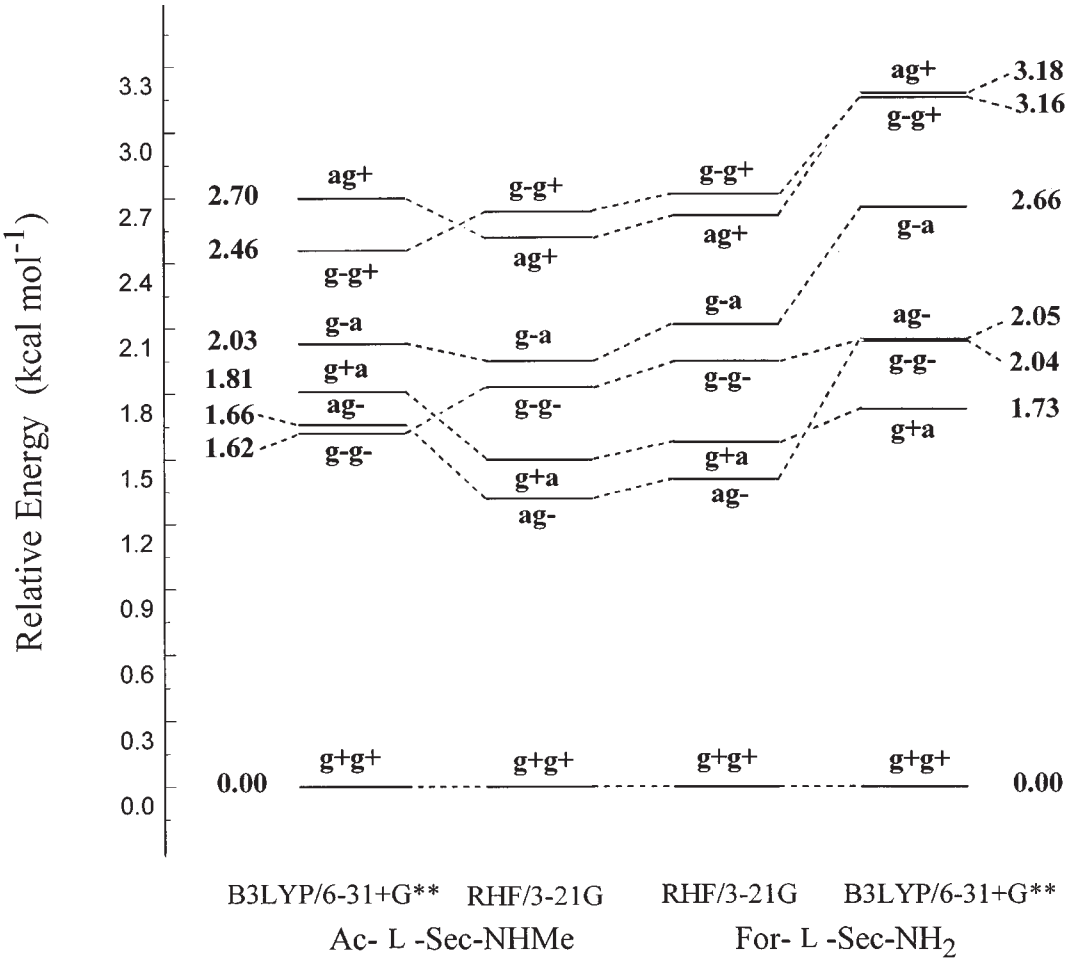
Fig. 13. The contour map of the Laplacian of the electron density for the ($a\ g^-$) conformation of For-L-Sec-NH_2 calculated at the B3LYP/6–31+G(d,p)//RHF/3–21G level of theory. Bond paths are denoted by lines, bond critical points (BCPs) are denoted by black dots, ring critical points (RCPs) are denoted by open triangles, and the nuclei are denoted by crosses.

simple amino acid residues, which only had C, H, N, and O. Such conclusions are in agreement with previous computations on other Se containing compounds (36).

Acknowledgements

The authors wish to thank Drs. T.-H. Tang and E. Deretey for helpful discussions. The continuous financial support of the Natural Sciences and Engineering Research Council of Canada (NSERC) is gratefully acknowledged. We would like to thank Silicon Graphics Inc. for providing computational resources at their facilities in Eagan, MN to carry out some of these calculations. We would also like to thank the NCI for the use of services at Frederick Biomedical Supercomputing Center.

Fig. 14. The role of basis set size and electron correlation in determining the relative energy ($\Delta E_{rel.}$) values of the various conformers for Ac-L-Sec-NHMe and For-L-Sec-NH_2.



© 2000 NRC Canada

References

1. R.M. Minyaev and V.I. Minkin. Can. J. Chem. **76**, 776 (1998).
2. A. Kucsman and I. Kapovits. *In* Organic sulfur chemistry. *Edited by* F. Bernardi, I.G. Csizmadia, and A. Mangini. Elsevier, Amsterdam. 1985. p. 191.
3. L. Stryer. Biochemistry. 3rd ed. W.H. Freeman and Co., New York. 1988.
4. A. Perczel and I.G. Csizmadia. Int. Rev. Phys. Chem. **14**, 127 (1995).
5. I.G. Csizmadia. General and theoretical aspects of the thiol group. *In* The chemistry of the thiol group. *Edited by* S.Patai. John Wiley and Sons, New York. 1974.
6. M.R. Peterson and I.G. Csizmadia. J. Am. Chem. Soc. **100**, 6911 (1978).
7. M.R. Peterson and I.G. Csizmadia. Progress of theoretical organic chemistry. Vol. 3. Elsevier, Amsterdam. 1982.
8. IUPAC–IUB Comission on Biochemical Nomenclature. Biochemistry, **9**, 3471 (1970).
9. I.G.N. Ramachandran and V. Sasisekharan. Adv. Protein Chem. **23**, 283 (1968).
10. J.S. Binkley, J.A. Pople, and W.J. Hehre. J. Am. Chem. Soc. **102**, 939 (1980).
11. O. Farkas, A. Perczel, J.F. Marcoccia, M. Hollosi, and I.G. Csizmadia. THEOCHEM. **331**, 27 (1995).
12. A. Perczel, O. Farkas, I. Jakli, and I.G. Csizmadia. THEOCHEM. **455**, 315 (1998).
13. R.F. Frey, J. Coffin, S.Q. Newton, M. Ramek, V.K.W. Cheng, F.A. Momany, and L. Schafer. J. Am. Chem. Soc. **114**, 5369 (1992).
14. G. Endredi, A. Perczel, O. Farkas, M.A. McAllister, G.I. Csonka, J. Ladik, and I.G. Csizmadia. THEOCHEM. **391**, 15 (1997).
15. W. Viviani, J.-L. Rivail, A. Perczel, and I.G. Csizmadia. J. Am. Chem. Soc. **115**, 8321 (1993).
16. M.A. McAllister, G. Endredi, W. Viviani, A. Perczel, P. Csaszar, J. Ladik, J.-L. Rivail, and I.G. Csizmadia. Can. J. Chem. **73**, 1563 (1995).
17. R.F.W. Bader. Atoms in molecules: a quantum theory. Clarendon Press, Oxford. 1990.
18. R.F.W. Bader. J. Phys. Chem. A, **102**, 7314 (1998).
19. (*a*) D.M. Whitefield and T.-H. Tang. J. Am. Chem. Soc. **115**, 9648 (1993)*;* (*b*) U. Koch and P.L.A. Popelier. J. Phys. Chem. **99**, 9747 (1995); (*c*) D.M. Whitefield, D. Lamba, T.-H. Tang, and I.G. Csizmadia. Carbohydr. Res. **286**, 17 (1996); (*d*) J.A. Platts, S.T. Howard, and B.R.F. Bracke. J. Am. Chem. Soc. **118**, 2726 (1996); (*e*) D.-C. Fang, P. Fabian, Z. Szekely, X.-Y. Fu,, T.-H. Tang, and I.G. Csizmadia. J. Mol. Struct. (Theochem*)*, **430** (1998); (*f*) P.L.A. Popelier. J. Phys. Chem. A, **102**, 1873 (1998).
20. H.J. Reich. Acc. Chem. Res. **12**, 23 (1979).
21. J.D. Odom. Struct. Bonding, **54,** 1 (1983).
22. H.J. Reich, S. Wollozitz, J.E. Trend, F. Chow, and D.F. Wendelboro. J. Org. Chem. **43**, 1697 (1978).
23. D.N. Jones, D. Mundy, and R.D. Whitehouse. Chem. Commun. 86 (1970).
24. J.G. Angyan, R. Daudel, A. Kucsman and I.G. Csizmadia. Chem. Phys. Lett. **136**, 1 (1987).
25. A. Perczel, O. Farkas, and I.G. Csizmadia. J. Comput. Chem. **17**, 821 (1996).
26. A. Perczel, J.G. Angyan, M. Kajtar, W. Viviani, J.-L. Rivail, J.F. Marcoccia, and I.G. Csizmadia. J. Am. Chem. Soc. **113**, 6256 (1991).
27. M.A. McAllister, A. Perczel, P. Csaszar, W. Viviani, J.-L. Rivail, and I.G. Csizmadia. THEOCHEM. **288**, 161 (1993).
28.. O. Farkas, M.A. McAllister, J.H. Ma, A. Perczel, M. Hollosi, and I.G. Csizmadia. THEOCHEM. **369**, 105 (1996).
29. A. Perczel, O. Farkas, and I.G. Csizmadia. Can. J. Chem. **75**, 1120 (1997).
30. I. Jakli, A. Perczel, O. Farkas, M. Hollosi, and I.G. Csizmadia. THEOCHEM. **455**, 303 (1998).
31. S.J. Salpietro, A. Perczel, O. Farkas, R.D. Enriz, and I.G. Csizmadia. THEOCHEM. **497**, 39 (2000).
32. A. Perczel, O. Farkas, and I.G. Csizmadia. THEOCHEM. **17**, 821 (1996).
33. A. Perczel, O. Farkas, I. Jakli, and I.G. Csizmadia. THEOCHEM. **455**, 315 (1998).
34. J.T.B.H. Jastrzebski and G. Van Vioten. Adv. Organomet. Chem. **35**, 241 (1993).
35. G.J. Gruter, G.P.M. van Kink, O.S. Akkerman, and F. Bickelhaupt. Chem. Rev. **95**, 2405 (1995).
36. (*a*) A. Nowek, R. Sims, P. Babinec, and J. Leszczynski. J. Phys. Chem. A, **102** (12), 2189, (1998); (*b*) J.S. Kwiatkowski, J. Leszczynski, and I. Teca. J. Mol. Struc. **436**–**437**, 451 (1997); (*c*) J.S. Kwiatkowski and J. Leszczynski. J. Phys. Chem. **100**, 941 (1996); (*d*) D. Venkateswarlu and J. Leszczynski. J. Phys. Chem. A, **102** (30), 6161 (1998).

© 2000 NRC Canada

Photoinduced birefringence in copolymers containing Disperse Red 1 and styrene

Gabriel Iftime, Lana Fisher, Almeria Natansohn, and Paul Rochon

Abstract: A series of copolymers of 4′-[[[2-(methacryloyloxy)ethyl]ethyl]amino]-4-nitroazobenzene (DR1M) and an optically "inert" styrene comonomer were tested for photoinduced birefringence. The level of saturated birefringence increased linearly with the content of DR1M in the copolymer. The birefringence per mole of azo chromophore was constant along the copolymer series.

Key words: azobenzene, photoinduced birefringence, copolymers, *trans-cis* isomerization.

Résumé : On a évalué le niveau de biréfringence photoinduite d'une série de copolymères du 4′-[[[2-(méthacryloyloxy)éthyl]éthyl]amino]-4-nitroazobenzène (DR1M) et d'un comonomère du styrène optiquement "inerte". Le niveau de biréfringence saturée augmente d'une façon linéaire avec la teneur en DR1M du copolymère. La biréfringence par mole de chromophore azo est constante pour toute la série de copolymères.

Mots clés : biréfringence photoinduite, copolymères, isomérisation *cis-trans*.

[Traduit par la Rédaction]

Introduction

Azo-based amorphous polymers are attracting much attention because they have proven to be good candidates for various optical applications. This research focuses on the utilization of amorphous (1) and liquid crystal polymers (2–3) as materials for photonic devices, mainly by photoinduced birefringence (4) and surface relief gratings (5–6) phenomena. The mechanism by which birefringence is obtained is based on photoinduced *trans-cis-trans* isomerization of the azobenzene groups, accompanied by their movement and re-arrangement perpendicular to the laser polarization direction. This "written" information can be "erased" locally by irradiation with circularly polarized light or globally by heating above the glass transition temperature (*Tg*) of the polymer film. Several structural factors were investigated and found to have an influence on the photo-driven orientation process. Among these factors are the polarity of the azobenzene groups (7), their bulkiness (8–9), the structure of the spacer between the azo group and the main chain (10), etc. One of the important factors is the concentration of the azo chromophore in the polymer film. To check this factor, several copolymer series containing azobenzene groups and optically "inert" groups were investigated. As expected, the photoinduced birefringence level increases with the increase of the concentration of the azo chromophore in the copolymer. However, some of the copolymers show a clear deviation from a postulated linear dependence, which has been assigned to a neighboring group effect. This phenomenon was first observed in poly{4′-[[[2-(methacryloyloxy) ethyl]ethyl]amino]-4-nitroazobenzene-*co*-methyl methacrylate} (poly(DR1M-*co*-MMA)) and poly{4′-[[[2-(acryloyloxy)ethyl]ethyl]amino]-4-nitroazobenzene-*co*-methyl methacrylate} (poly(DR1A-*co*-MMA)) (11). The structure of the monomers is given in Chart 1. Some form of dipolar interaction between the azo groups on the side chains that are next to each other appears to play a role in photo-orientation. The photoinduced birefringence calculated per azo unit in copolymers is higher at very low chromophore content than at high concentrations of DR1M (azo) groups. The effect is especially pronounced for a series of copolymers poly{4′-[[[2-(methacryloyloxy)ethyl]ethyl]amino]-4-nitroazobenzene-*co*-[[4-nitrophenyl-4′-[2-(methacryloyloxy)ethyl]benzoate]} (poly(DR1M-*co*-BEM)). The rigid ester group in BEM has a high dipole moment (about 7 D), comparable to the azo group in DR1M. The enhanced birefringence per azo unit was attributed to cooperative motion, i.e., the polar BEM group is being moved by the photoactivated DR1M motion. It was calculated that at low content of azo group in these polymers, up to 80% of the photoinduced birefringence may be due to the alignment of the optically inert polar comonomer groups (12). The explanation for this cooperative motion may be either a dipolar interaction or a steric factor or a combination of both. To understand which factor prevails (dipolar or steric interaction) one has to study each factor separately. Copolymers of DR1M with a less polar analogue of BEM, the NBEM with an ester group having a dipole moment of only 0.95 D but of comparable size to the BEM, were tested (13). In this case, there was much less cooperative motion, suggesting that polar interaction between the side group dipoles is more important, and that unlike in

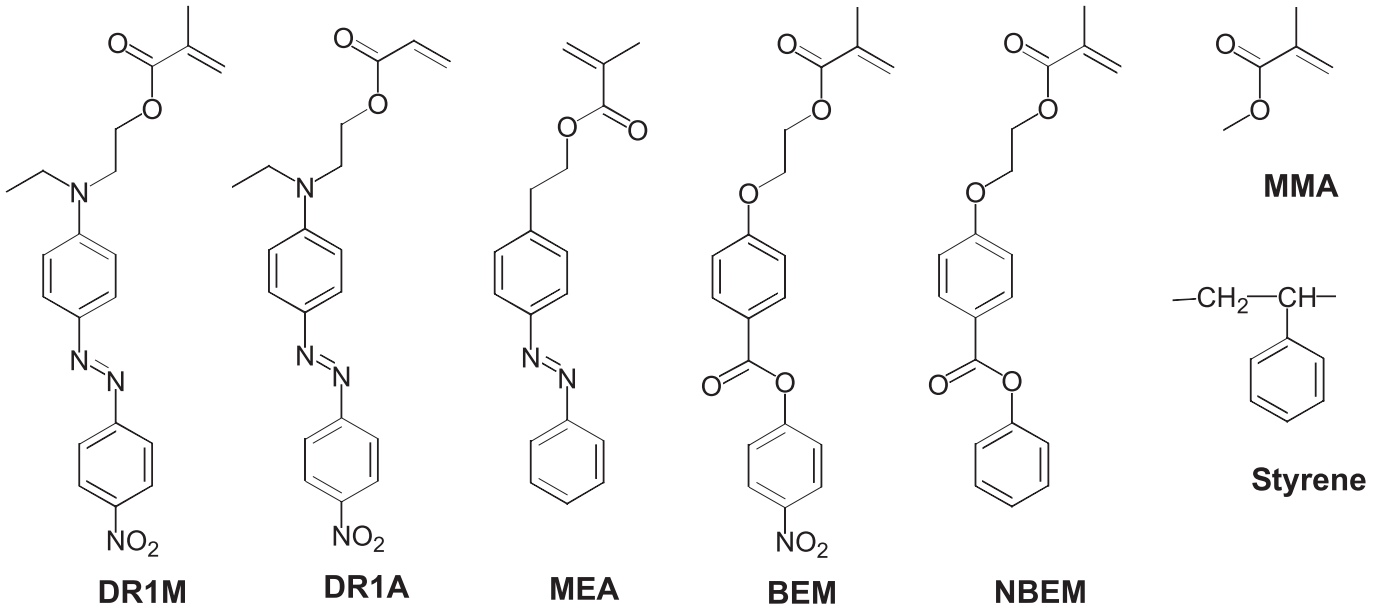
Received September 10, 1999. Published on the NRC Research Press website on March 27, 2000.

G. Iftime, L. Fisher, A. Natansohn.[1] Department of Chemistry, Queen's University, Kingston, ON K7L 3N6, Canada.
P. Rochon. Department of Physics, Royal Military College, Kingston, ON K7K 5LO, Canada.

[1]Author to whom correspondence may be addressed. Telephone: (613) 533-2008. Fax: (613) 533-6669. e-mail: natansoh@chem.queensu.ca.

© 2000 NRC Canada

Chart 1.



liquid crystals, the steric factor has probably a minor contribution in the cooperative motion of azobenzene and "inert" ester groups.

We report here the synthesis of a series of poly(DR1M-*co*-styrene) copolymers and their photoinduced birefringence. The nonpolar benzene group of the styrene comonomer is not expected to move in concert with the azobenzene and its steric effect is less important (its size being much smaller than that of the NBEM). Styrene can act as a diluent for the absorbing azobenzene group, allowing the use of thicker films in the photoinduced birefringence process.

Experimental

DR1M was prepared as previously reported, by reacting Disperse Red 1 (DR1) with methacryloyl chloride in the presence of triethylamine, in dry THF, under argon (14). The copolymers were obtained by free-radical polymerization in sealed ampoules, in dry toluene under argon atmosphere. Toluene and THF were dried over sodium with benzophenone indicator. Methacryloyl chloride was distilled under vacuum, triethyl amine and styrene were dried over calcium hydride. They were distilled prior to use and kept in sealed tubes under argon gas. The polymerization reactions were initiated with AIBN (5% of the total mass of the monomers), and were carried out at 60°C for four days. The copolymers were then isolated by precipitation in methanol. Purification was done by reprecipitation from THF/methanol, then by drying in a vacuum oven at 70°C overnight. ^{1}H-NMR spectra of the copolymers were measured on a Bruker AC-F 200 MHz spectrometer in deuterated dichloromethane solutions. Glass transition temperatures were measured on second heating scans on a Mettler TA-30 DSC instrument equipped with a TA-3000 processor at a scan rate of 10°C/min. UV–vis spectra of solutions and films of polymers were measured on a Shimadzu spectrophotometer. The average molecular weights and polydispersities of the polymers were estimated by gel permeation chromatography (polystyrene standard calibration), in THF, on a Waters liquid chromatograph equipped with a R410 differential refractometer. Films for birefringence measurements were prepared by spin coating solutions of polymers in THF onto clean glass microscope slides, and subsequently dried in an oven at 130°C for one hour to remove the THF. Films thickness ranging from 150 to 350 nm were determined with a Dektak profilometer. The densities of the films were measured as previously described (11). Optical anisotropy was induced using a linearly polarized 488 nm laser beam (100mW/cm^2) and measured using a diode laser beam at 670 nm.

Results and discussion

Synthesis and characterization of the polymers

For the purpose of this study, a series of nine copolymers with the DR1M molar fraction ranging from 0.10 to 1.00 were synthesized. They were obtained by free radical copolymerization of DR1M with styrene at various ratios in toluene at 60°C for four days. In all the reactions a 1g mixture of the two monomers (DR1M and styrene) at the indicated DR1M initial feed (molar fraction) were used. The yields for copolymers (g) are listed in Table 1. The copolymer compositions were determined by ^{1}H NMR. As an example the ^{1}H NMR spectrum of the copolymer **5** (46% mol DR1M) is shown in Fig. 1. The assignments were done by comparison with the spectra of the monomers. Glass transition temperatures (*Tg*) for all copolymers were between 97 and 113°C, as listed in Table 1.

In Fig. 2, the absorption maxima (λ_{max}) of the copolymers **1**–**9** in solution and in films are plotted as a function of copolymer composition. The electronic spectra for this copolymer series show a systematic shift of the λ_{max} to higher wavelength as the azo concentration decreases. The total shift in λ_{max} in films between polymer **1** containing 100% mol DR1M units and copolymer **9** containing only 10% mol DR1M units is about 17 nm. This shift is slightly less pronounced in solutions in chloroform (12 nm). This phenomenon

© 2000 NRC Canada

Table 1. Details of polymerization.

No.	Initial feed (mol fraction DR1M)	Yield (g)	Composition (mol fraction DR1M)	*Tg* (°C)	Mw	Mw/Mn
1	1.00	0.79	1.00	110	7800	1.57
2	0.90	0.73	0.93	108	14940	1.99
3	0.83	0.76	0.80	106	9960	1.71
4	0.75	0.65	0.65	102	8050	1.61
5	0.50	0.30	0.46	107	5820	1.37
6	0.40	0.21	0.38	113	6520	1.38
7	0.25	0.18	0.28	97	5610	1.30
8	0.17	0.12	0.16	100	6330	1.29
9	0.10	0.13	0.10	101	7300	1.34

Fig. 1. ^{1}H-NMR spectrum of poly(DR1M-*co*-styrene) copolymer **5** in CD_2Cl_2.

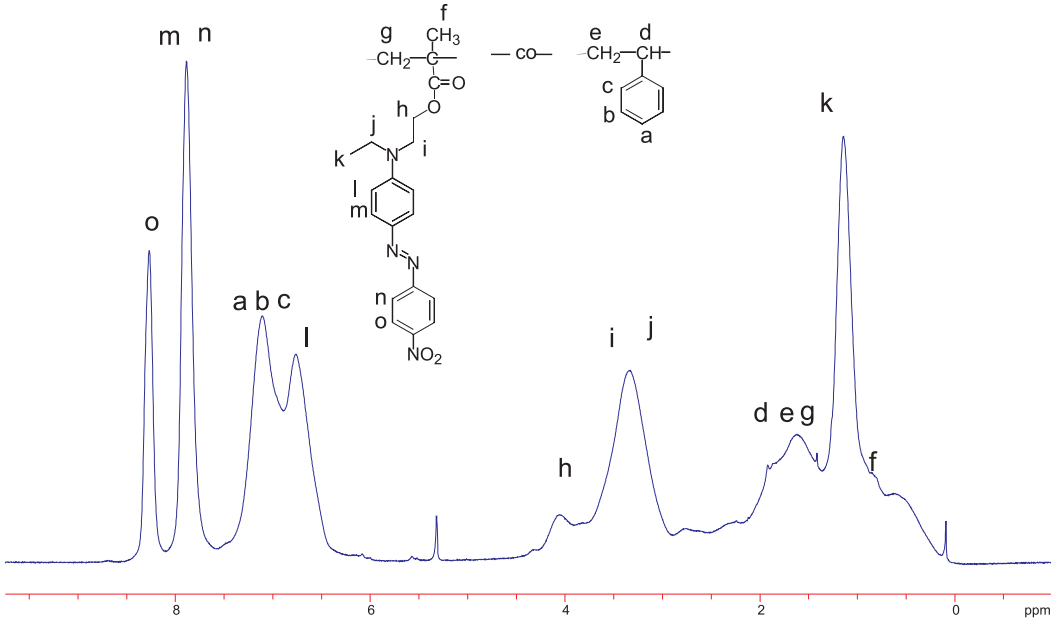
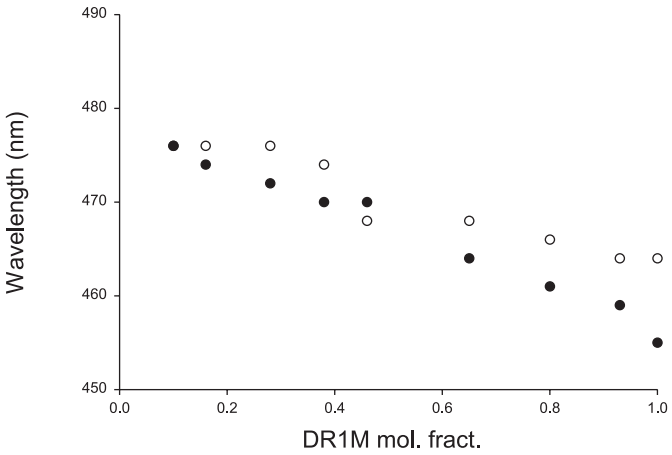


Fig. 2. Absorption maxima of poly(DR1M-*co*-styrene) copolymers in chloroform (○) and in film (●) as a function of composition.



was previously assigned to an antiparallel arrangement of the dipoles (DR1M units) (11). The higher the concentration of polar azo groups, the higher the probability of dipolar antiparallel interactions between neighboring azo groups. However, the effect observed in these copolymer films is slightly smaller than that reported for the poly(DR1M-*co*-MMA) series, where the shift was 22 nm. If this is the only effect responsible for the red shift in absorption maxima of the DR1M units when the azo concentration decreases, then one would expect the two polymer series to give similar results, this phenomenon being governed only by the concentration of DR1M groups in the copolymers.

A second effect that can be active here is the dipolar interaction of the DR1M groups with the comonomer structural units. If the comonomer structural unit is polar (as is the case for MMA) then it may behave as a polar solvent, causing a positive solvatochromic effect (red shift of the λ_{max}) as its concentration increases. The lower polarity of the styrene structural unit in the copolymers can be an explanation for the smaller shift of the λ_{max} observed in this series when compared with the poly(DR1M-*co*-MMA) series.

Photoinduced birefringence

Figure 3 shows a typical sequence of inducing and erasing birefringence for copolymer **5**. Birefringence is induced to a

© 2000 NRC Canada

Table 2. Parameters obtained by fitting the birefringence growth and decay curves to eqs. [1] and [2], respectively.

No.	A_n	B_n	k_a (s^{-1})	k_b (s^{-1})	C_n	D_n	E_n	k_c (s^{-1})	k_d (s^{-1})
1	0.94	0.06	0.44	0.016	0.11	0.10	0.79	0.41	0.011
2	0.92	0.08	0.61	0.018	0.12	0.09	0.79	0.46	0.009
3	0.75	0.25	0.39	0.029	0.11	0.10	0.79	0.35	0.010
4	0.95	0.05	0.49	0.016	0.15	0.12	0.73	0.42	0.011
5	0.96	0.04	0.98	0.013	0.17	0.16	0.67	0.30	0.010
6	0.96	0.04	0.76	0.010	0.20	0.15	0.65	0.45	0.013
7	0.96	0.04	0.65	0.007	0.19	0.17	0.64	0.42	0.011
8	0.97	0.03	0.98	0.008	0.21	0.18	0.61	0.45	0.011
9	0.93	0.07	1.07	0.021	0.26	0.21	0.53	0.50	0.012

Fig. 3. Write-erase profile for optically induced and erased birefringence of poly(DR1M-*co*-styrene) copolymer **5**.

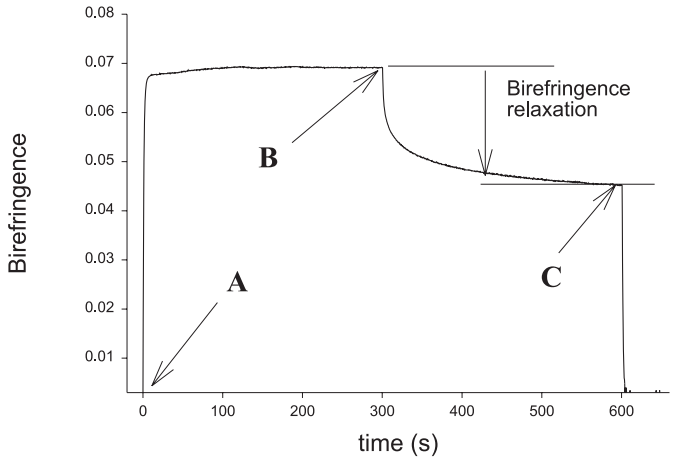
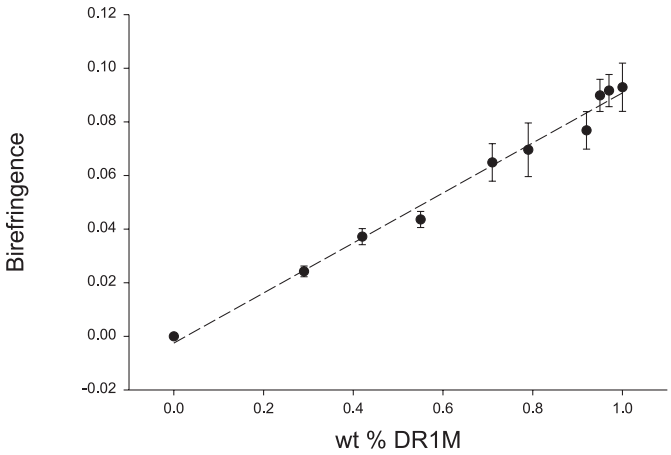


Fig. 4. Maximum induced birefringence (●) for the poly(DR1M-*co*-styrene) copolymer series as a function of DR1M weight fraction.



saturated level by a linearly polarized laser beam (488 nm, 100 mW/cm^2) at point A for 300 s. The relaxation starts at point B, when the laser beam is turned off for 300 s. At point C, the circularly polarized light is turned on and the birefringence is erased.

The maximum birefringence attained in the copolymer films after 300 s of writing is plotted as a function of DR1M content in Fig. 4. The photoinduced birefringence increases linearly with the DR1M content in the copolymer. This kind of graph has been previously observed for copolymers containing two different azo groups with one nonpolar azo unit, in poly{4′-[[[2-(methacryloyloxy)ethyl]ethyl]amino]-4-nitroazobenzene-*co*-4-[2-(methacryloyloxy)ethyl]azobenzene} (poly(DR1M-*co*-MEA)) (Chart 1) (15). In contrast, copolymers poly(DR1M-*co*-MMA), containing a more polar comonomer unit (MMA) showed a deviation from linearity at low content of DR1M. The results presented in Fig. 4 suggest that there is no cooperative effect in this copolymer series, and this can be explained by the low polarity of the styrene comonomer. No dipolar interactions between the two different structural units can occur.

The growth and the relaxation of the optically induced birefringence can be described by biexponential functions [1] and [2], respectively (8).

$$[1] \qquad \Delta n = A_n(1-\exp(-k_a t)) + B_n(1-\exp(-k_b t))$$

$$[2] \qquad \Delta n = C_n - \exp(-k_c t) + D_n - \exp(-k_d t) + E_n$$

Both growth and relaxation processes involve a "fast" process and a "slow" process. The parameter A_n in eq. [1] represents the contribution of the fast growth process with rate constant k_a. The parameter B_n, represents the slow growth with rate constant k_b. To compare the behavior of the different polymers, these parameters are normalized so that $A_n + B_n = 1$. Fitting results, presented in Table 2, show that the A_n and B_n parameters are relatively constant at levels of 0.95 and 0.05, respectively. The time constants k_a and k_b varied, but no particular trend could be found.

When the "writing" laser beam is turned off, the birefringence decays to a stable level. The relaxation process can be fit by a biexponential eq. [2]. C_n, D_n, and E_n are normalized constants. The parameter C_n represents the contribution of the fast relaxation process with rate constant k_c, and the parameter D_n, represents the slow relaxation with rate constant k_d. E_n represents the residual long-term birefringence, stable in time, if the birefringence is not erased optically or by heating. The relaxation time constants k_c and k_d extracted from the relaxation curve appear to be relatively constant, having values of approximately 0.40 and 0.010 s^{-1}, respectively.

The long term stability E_n, for the poly(DR1M-*co*-styrene) series decreases with the decrease of DR1M content in the copolymer, from 0.79 for polymer **1** (100% mol DR1M) to 0.53 for polymer **9** (0.10% mol DR1M). This means that the photoinduced birefringence in copolymers with lower content

© 2000 NRC Canada

Fig. 5. Long-term stable birefringence after relaxation (E_n) as a function of composition. (●) poly(DR1M-*co*-styrene), (○) poly(DR1M-*co*-MMA).

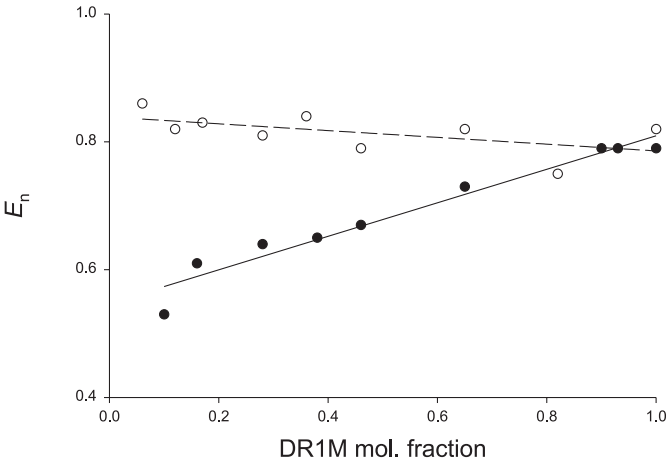
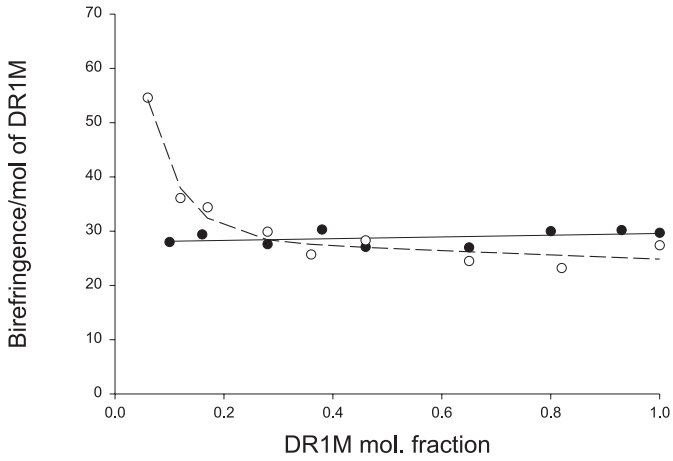


Fig. 6. Birefringence per mole of azo chromophore in copolymers as a function of composition. (●) poly(DR1M-*co*-styrene), (○) poly(DR1M-*co*-MMA).



of DR1M is less stable. The variation of the E_n parameter across the polymer series is shown in Fig. 5. There probably are at least two main separate processes that have an opposite influence to the long-term birefringence stability.

One relaxation process is due to the thermal *cis-trans* isomerization of the azobenzene groups that happen to be in the *cis* state when the writing laser beam is turned off. This phenomenon is specific to the azo groups, and has as an effect the randomization of the orientation of these groups.

A second factor is the dipolar interactions between the polar side groups. The local electric field existing in the film makes it difficult to move polar groups from their equilibrium position. This factor will enhance the stability of the photoinduced birefringence. For poly(DR1M-*co*-BEM) (12), where the polarity of the side group is similar, the sum of the two effects is relatively constant for the whole range of copolymer composition. In that case the stability is due to the fact that strong dipolar interactions exist at any content of azo chromophore in the copolymer. At high concentration, the interactions are mainly between DR1M neighboring groups, and at low concentrations, between DR1M and the polar BEM groups. In the poly(DR1M-*co*-styrene) series, the only polar group is the DR1M azo chromophore. In this case, the dipolar interactions between neighboring polar azo groups will be effective at high concentrations of the chromophore, giving a higher stability of the photoinduced birefringence (E_n parameter), as observed. At low concentrations of DR1M, the chromophores have mainly nonpolar styrene neighboring groups, and the chromophores will reorient independently since the nonpolar styrene group will not perturb the local electric field. The level of conserved birefringence is in this case lower at low DR1M concentrations in polymer.

A slight increase of the long-term stable birefringence with the content of azo chromophore was observed previously in the copolymer series containing as comonomer the NBEM group. NBEM has a low dipole moment but a similar size to the polar BEM groups. The increase of the long-term stable birefringence (E_n) as the concentration of DR1M increase is more pronounced in copolymers containing styrene. This suggests that the steric factor, i.e., the size of the comonomer groups, plays a role in the reorientation process. Indeed, the styrene group is much smaller than the NBEM group, which is similar in size to DR1M and BEM. This means that the azo groups have a higher degree of freedom, thus they are easier to randomize when a small side group is present.

The size of the MMA structural unit is similar to styrene. Relatively constant values were obtained for the E_n parameter for the poly(DR1M-*co*-MMA) series. For comparison, the E_n values obtained for poly(DR1M-*co*-MMA) are also plotted in Fig. 5 (11). For example, the ratio E_n (100% DR1M)/E_n(16% DR1M) is about 1.4 in poly(DR1M-*co*-styrene). The same ratio is 1 in poly(DR1M-*co*-MMA). This is probably due to the fact that the MMA group possesses a higher dipole moment than the styrene, so that at low content of DR1M, the dipolar interactions between DR1M and MMA can compensate the tendency of azo groups toward reorientation.

Another factor that may influence the relaxation process is the glass transition temperature (*Tg*) but the *Tg* for this series of copolymers is relatively constant at about 105°C, so no particular influence is expected.

The most useful comparison between this copolymer series and the copolymer series containing more polar comonomers, can be made by calculating the birefringence levels per azo unit. The molar density (MD) of the DR1M chromophore was calculated as follows

$$[3] \qquad MD = DF_w/M_{DR1M}$$

where D is the film density, F_w is the weight fraction of DR1M in the copolymer, and M_{DR1M} is the molecular weight of the azo chromophore. The film densities were measured as previously described (12). They show a linear increase from 1.05 g/cm^3 for the polystyrene (F_{DR1M} = 0) to 1.23 g/cm^3 for PDR1M (F_{DR1M} = 1, polymer **1**). The average contribution per mole of azo unit is obtained by dividing the maximum of photoinduced birefringence (at point B, in Fig. 3) by the calculated azo molar density (*MD*). Figure 6 shows the birefringence per azo chromophore in the poly(DR1M-*co*-styrene) copolymer series as a

© 2000 NRC Canada

function of copolymer composition. The birefringence per mole of dipole data is practically constant across the whole range of compositions. For comparison, the values obtained previously (11) for the poly(DR1M-*co*-MMA) series are also plotted in Fig. 6.

They show an increase up to two times at low content of DR1M. There is no explanation for this discrepancy at the present time. The poly(DR1M-*co*-styrene) data seem to suggest that there is little, if any, dipolar interaction between neighboring DR1M units, while the poly(DR1M-*co*-MMA) data indicated the presence of such interactions during photoisomerization. Verification of the measurement accuracy at very low DR1M composition in poly(DR1M-*co*-MMA) will be required.

Conclusions

A series of copolymers containing an azo chromophore DR1M, and an inert nonpolar and small group styrene, was synthesized and tested for the photoinduced birefringence. The levels of saturated birefringence and of conserved birefringence after relaxation increased linearly with the DR1M content in the copolymers. This is explained by the lack of dipolar interactions between the polar DR1M and the nonpolar styrene comonomer. The level of stable birefringence, conserved after relaxation, increased with the content of azo chromophore. This copolymer series shows a constant birefringence per DR1M unit. This result is in contrast with previously described copolymers containing polar optically inert groups (MMA). The level of stable birefringence is determined by the dipolar interactions between structural units. Steric factors have an influence as well, but to a lower extent than the dipolar interactions.

Acknowledgments

We thank the Natural Sciences and Engineering Research Council of Canada (NSERC) for partial funding of this research.

References

1. A. Natansohn and P. Rochon. Adv. Mater. (Weinheim Ger.). **11**, 1387 (1999).
2. C. Kulinna, S. Hvilsted, C. Hendann, H.W. Siesler, and P.S. Ramanujam. Macromolecules, **31**, 2141 (1998).
3. Y. Wu, Y. Demachi, O. Tsutsumi, A. Kanazawa, T. Shiono, and T. Ikeda. Macromolecules, **31**, 1104 (1998).
4. T. Todorov, L. Nikolova, and N. Tomova. Appl. Opt. **23**, 4309 (1984).
5. P. Rochon, E. Batalla, and A. Natansohn. Appl. Phys. Lett. **66**, 136 (1995).
6. D.Y. Kim, S.K. Tripathy, L. Li, and J. Kumar. Appl. Phys. Lett. **66**, 1166 (1995).
7. M.-S. Ho, A. Natansohn, C. Barrett, and P. Rochon. Can. J. Chem. **73**, 1773 (1995).
8. M.-S. Ho, A. Natansohn, and P. Rochon. Macromolecules, **28**, 6124 (1995).
9. A. Natansohn, P. Rochon, and S. Xie. Macromolecules, **25**, 5531 (1992).
10. X. Meng, A. Natansohn, and P. Rochon. J. Polym. Sci. Part B: Polym. Phys. **34**, 1461 (1996).
11. D. Brown, A. Natansohn, and P. Rochon. Macromolecules, **28**, 6116 (1995).
12. X. Meng, A. Natansohn, C. Barrett, and P. Rochon. Macromolecules, **29**, 946 (1996).
13. A. Natansohn, P. Rochon, X. Meng, C. Barrett, T. Buffeteau, S. Bonenfant, and M. Pezolet. Macromolecules, **31**, 1155 (1998).
14. P. Rochon, J. Gosselin, A. Natansohn, and S. Xie. Appl. Phys. Lett. **60**, 4 (1992).
15. M.-S. Ho, A. Natansohn, and P. Rochon. Macromolecules, **29**, 44 (1996).

© 2000 NRC Canada

Atomic properties of selected biomolecules. Part 1. The interpretation of atomic integration errors

Fiona M. Aicken and Paul L.A. Popelier

Abstract: Reliable atomic properties can be obtained via the theory of "Atoms in Molecules" (AIM) via integration over a finite volume. These integrations are challenging because of the variety and complexity of the shape of the AIM atoms. In practice the integration of a large number of atoms (100–1000, sampled from many molecules) yields integration errors $L(\Omega)$ of varying magnitude. We prove that it is impossible to predict the size of an angular Gauss–Legendre grid (outside the β sphere) that guarantees a pre-set error. Hence it is incorrect to assume that a large grid (~23 000 angular grid points) will automatically yield a low $L(\Omega)$ value. The erratic relationship between the integration error and the grid size prompts a statistical interpretation of atomic integration, at a purely practical level. More importantly we have investigated the relationship between $L(\Omega)$ and seven atomic properties which include volume, energy, and the magnitudes of five electrostatic multipole moments. The electronic population ($N(\Omega)$) and the volume ($v(\Omega)$) of carbon is linearly correlated with $L(\Omega)$, enabling the interpolation or extrapolation of $N(\Omega)$ and $v(\Omega)$. Other properties of carbon and other atoms (N, O, and S) yield low correlation coefficients but occasionally trends can be observed. For example, we find that some properties are systematically underestimated if $L(\Omega)$ is negative. This work has led to an estimate of safe error bars of atomic properties for atoms occurring in biological molecules with reasonably sized integration grids. The most stable properties were found to be the energy and the population. Finally, we have observed that the influence of the grid orientation is less if $L(\Omega)$ is small, and that population and energy are the least affected.

Key words: electron density, topology, atoms in molecules, atomic properties, amino acids.

Résumé : La théorie des « atomes dans les molécules » (ADM) couplée à une intégration sur un volume fini permet d'obtenir des propriétés atomiques fiables. Ces intégrations présentent un défi en raison de la variété et de la complexité de la forme des atomes dans les molécules. En pratique, l'intégration d'un grand nombre d'atomes (entre 100 et 1000 prélevés au hasard à partir de plusieurs molécules) conduisent à des erreurs d'intégration $L(\Omega)$ d'amplitudes diverses. On démontre qu'il est impossible de prédire la taille d'une grille angulaire de Gauss–Legendre (à l'extérieur de la sphère β) qui permettrait de garantir une erreur prédéterminée. Il est donc incorrect de faire l'hypothèse qu'une grande grille (grille angulaire à ≈ 23 000 points) conduira automatiquement à une faible valeur de $L(\Omega)$. La relation erratique entre l'erreur d'intégration et la taille de la grille conduit, à un niveau purement pratique, à une interprétation statistique de l'intégration atomique. D'un point de vue plus important, on a étudié la relation entre $L(\Omega)$ et sept propriétés atomiques qui comprennent le volume, l'énergie et les amplitudes de cinq moments multipolaires électrostatiques. On a établi une corrélation linéaire entre $L(\Omega)$ et la population et le volume électroniques du carbone, respectivement $N(\Omega)$ et $v(\Omega)$ ce qui permet de faire des interpolations ou extrapolations de $N(\Omega)$ et $v(\Omega)$. D'autres propriétés du carbone ainsi que d'autres atomes (N, O et S) donnent de faibles coefficients de corrélation, mais occasionnellement on peut observer des tendances. Par exemple, on a trouvé que quelques propriétés sont systématiquement sous-évaluées si la valeur de $L(\Omega)$ est négative. Ce travail a permis de faire une évaluation des limites d'erreur admissible des propriétés atomiques pour les atomes que l'on retrouve dans les molécules biologiques en utilisant des grilles d'intégration de taille raisonnable. On a trouvé que les propriétés les plus stables sont l'énergie et la population. Enfin, on a observé que l'influence de l'orientation de la grille est moins importante si $L(\Omega)$ est faible et que la population et l'énergie sont les moins affectées.

Mots clés : densité d'électrons; topologie; atomes dans les molécules; propriétés atomiques; acides aminés.

[Traduit par la Rédaction]

1. Introduction

Chemical insight is largely based on the ability to ascribe the characteristics of a molecule to its constituent atoms. Many schemes have been proposed to partition molecular properties into atomic contributions, but only one scheme originates from a comprehensive theory whose scope and depth is unique, called "Atoms in Molecules" (AIM) (1, 2). Using the topology of the electron density (ρ), this theory defines an atom as a bounded portion of real space, denoted

Received November 19, 1999. Published on the NRC Research Press website on March 27, 2000.

F.M. Aicken and P.L.A. Popelier.[1] Dept. of Chemistry, UMIST, P.O. Box 88, Sackville Street, Manchester M60 1QD, G.B.

[1]Author to whom correspondence may be addressed. Telephone: (+) 44 161 2004511. e-mail: pla@umist.ac.uk

© 2000 NRC Canada

by Ω. In contradistinction to partitioning methods defined in orbital space (3, 4) all information about a particular AIM atom is contained in its finite[2] volume. As a result the atom can be taken out of its chemical environment and compared with another atom originating from a different environment. In view of their finite shape (5), quantum mechanical roots (6), and basis set stability (7), AIM atoms are ideal for assessing the transferability of a molecular fragment (8). Moreover atomic properties, defined by AIM as integrations over the atomic volume, can be computed from experimental electron densities (9).

Integration of a property density over Ω yields atomic charges, dipole moments, quadrupole moments, volumes, energies, and other atomic properties. Atomic integration is a vital part of the practical application of AIM and since the development of the first integration algorithm (10) in the early eighties, several thousands of atoms have been integrated. When performed en masse atomic integration has led to remarkable results, such as the Transferable Atom Equivalent (TAE) method (11) and Quantitative Structure Property Relationships (QSPR) (12). Recently we have integrated a set of more than 700 atoms drawn from the 20 natural (free) amino acids and smaller derived molecules.[3] This data set comprises 57 molecules and is identical to the one studied before in connection with bond critical point properties (13).

Typically atomic integration is performed numerically. A typical integration algorithm either requires an a priori choice of a quadrature grid size, or a pre-set threshold for the integration error $L(\Omega)$. This quantity is defined below and must vanish for a perfect integration. It is important to point out that $L(\Omega)$ has no direct chemical meaning, i.e., it is not an atomic property of any relevance other than to measure the quality of the integration. In practice, when performing an integration one obtains a reasonable minimum $L(\Omega)$ value for a given CPU investment, without knowing how accurate the resulting atomic properties are. This paper attempts to answer the difficult question of what the error bars on atomic properties are. Some long overdue insight into this problem is warranted in view of the research activity of the AIM community. Indeed, according to a recent survey (14) more than 90 papers were published (by 60 different research groups), which contained substantial AIM contributions.

2. Atomic Integration

According to AIM a molecule is sub-divided into non-overlapping fragments, called atoms, which appear in the gradient vector field of the electron density. Each atom (Ω) is bounded by a surface (S) which satisfies a zero-flux boundary condition:

$$[1] \qquad \nabla\rho(\mathbf{r}) \cdot \boldsymbol{n}(\mathbf{r}) = 0 \qquad \forall\ \mathbf{r} \in S$$

An atomic property, $A(\Omega)$, is defined as a volume integral over the portion of real space the atom takes up, or

$$[2] \qquad A(\Omega) = \int_{\Omega} d\tau\ a(\mathbf{r})$$

where $a(\mathbf{r})$ is a property density. For example, $a(\mathbf{r})$ could be the charge density, $\rho(\mathbf{r})$, the dipole moment density, $\mathbf{r}_\Omega \rho(\mathbf{r})$, or the quadrupolar polarisation of an atomic density measured with respect to the z-axis, $(3z_\Omega^2 - \mathbf{r}_\Omega^2)\rho(\mathbf{r})$, where $\mathbf{r}_\Omega$ is a vector with origin at the nucleus inside the atom Ω.

In this work we monitor the following atomic properties: volume, energy, population, dipole, quadrupole, octopole, and hexadecupole moments. All atomic electrostatic moments are defined using the spherical tensor formalism (15), rather than the more common Cartesian multipole expansion (16). Although the spherical tensor formalism is mathematically more complex it has the advantage of generating $2\ell + 1$ non-redundant components for a moment of rank ℓ. A complete definition of the moments up to the hexadecupole moment has been given elsewhere (17). Here we list the definition of the moments Q_{lm} up to the quadrupole moment, $\ell = 2$, all in atomic units (au).

$$[3] \qquad Q_{00}(\Omega) = -\int_{\Omega} \rho(\mathbf{r})\, d\tau$$

$$[4] \qquad Q_{10}(\Omega) = -\int_{\Omega} z\rho(\mathbf{r})\, d\tau\ ;$$

$$Q_{11c}(\Omega) = -\int_{\Omega} x\rho(\mathbf{r})\, d\tau\ ;$$

$$Q_{11s}(\Omega) = -\int_{\Omega} y\rho(\mathbf{r})\, d\tau$$

$$[5] \qquad Q_{20}(\Omega) = -\int_{\Omega} \frac{1}{2}(3z^2 - r^2)\rho(\mathbf{r})\, d\tau\ ;$$

$$Q_{21c}(\Omega) = -\int_{\Omega} \sqrt{3}xz\,\rho(\mathbf{r})\, d\tau\ ;$$

$$Q_{21s}(\Omega) = -\int_{\Omega} \sqrt{3}yz\,\rho(\mathbf{r})\, d\tau\ ;$$

$$Q_{22c}(\Omega) = -\int_{\Omega} \frac{\sqrt{3}}{2}(x^2 - y^2)\rho(\mathbf{r})\, d\tau\ ;$$

$$Q_{22s}(\Omega) = -\int_{\Omega} \sqrt{3}xy\,\rho(\mathbf{r})\, d\tau$$

In this work we focus on the magnitude of the multipole moments, which is obtained by taking the square root of the sum of the squares of the components, or $Q_l = \sqrt{\sum_m Q_{lm}^2}$. This quantity does not depend on the orientation of the atom's axis system. The (electronic) population $N(\Omega)$ is trivially related to the monopole moment via $N(\Omega) = -Q_{00}(\Omega)$. The atomic volume is simply defined as $v(\Omega) = \int_{\Omega} d\tau$ and the atomic energy as $E(\Omega) = (1 + \gamma)\int_{\Omega} K(\mathbf{r})d\tau$ where $K(\mathbf{r})$ is a kinetic

[2] Strictly speaking the volume is not finite because atoms can extend to infinity at open sides. However, atoms are typically bounded by the $\rho = 0.001$ au contour envelope.
[3] F.M. Aicken and P.L.A. Popelier. In preparation.

© 2000 NRC Canada

Table 1. Atomic properties (in au) and integration error of C and S in methanethiol, N in ammonia, and O in water as a function of the number of quadrature points, $n_r(\beta)$.

Atom	$n_r(\beta)$	Error	Volume	Energy	Population	Dipole	Quadrupole	Octopole	Hexadecupole
C[a]	50	–0.00146	75.33	–37.9408	6.1134	0.0550	0.0945	3.3723	4.1366
C[a]	90	–0.00128	75.33	–37.9409	6.1134	0.0550	0.0945	3.3723	4.1366
N[a]	50	0.0011	140.30	–55.0728	7.9928	0.2151	1.5185	3.0025	6.3319
N[a]	90	0	140.30	–55.0718	7.9928	0.2151	1.5185	3.0025	6.3319
O[a]	50	–0.00428	149.46	–75.6585	9.1029	0.1620	0.8619	1.2036	3.7262
O[a]	90	0	149.46	–75.6628	9.1029	0.1620	0.8619	1.2036	3.7262
S[b]	90	–0.00776	212.12	–398.3435	15.9529	0.7926	3.3911	2.1017	5.3582
S[b]	150	0	212.12	–398.3513	15.9529	0.7926	3.3911	2.1017	5.3582

[a]Remaining quadrature values, ($n_\theta(\beta)$, $n_\phi(\beta)$, n_r, n_θ, n_ϕ) are set to (30, 40, 50, 130, 150).

[b]Remaining quadrature values, ($n_\theta(\beta)$, $n_\phi(\beta)$, n_r, n_θ, n_ϕ) are set to (30, 40, 70, 130, 150).

energy density (18) and γ is the virial ratio $< V > / < T >$ of the wave function. The integration error, $L(\Omega)$, is defined as $-\frac{1}{4}\int_\Omega \nabla^2 \rho(\mathbf{r}) d\tau$. Using Gauss' theorem it is straightforward to prove that the value of $L(\Omega)$ should be zero for a volume integral bounded by the zero-flux condition given in eq. [1]. The quantity $L(\Omega)$ measures the difference between the kinetic energy densities, $K(\mathbf{r})$ and $G(\mathbf{r})$(19) or $L(\Omega) = K(\Omega) - G(\Omega)$. To compute an atom's energy to within 1 kJ mol^{-1}, $L(\Omega)$ should be at most 4×10^{-4} au. An interesting question is whether this level of accuracy is necessary for the other atomic properties.

To address questions such as the one raised above we focus on three different carbon atoms, two nitrogen atoms, two oxygen atoms, and a sulfur, drawn from the data set described in the introduction. In particular we looked at the carbon in ethene, the carbon in methanethiol (CH_3SH) and the α carbon in alanine; the nitrogens in ammonia and alanine; the oxygens in the hydroxyl group of alanine and in water, and the sulfur in methanethiol. All the wave functions were generated using the GAUSSIAN94[4] program. The geometries were optimized at HF/6–31G(*d*) level with the single point calculation at B3LYP/6–311+G(2d,p) level. All integrations were carried out with the program MORPHY98,[5] which computes the atomic integral in spherical coordinates with a Gauss–Legendre quadrature in both the radial and angular integration variables. A separate grid is used for a sphere totally contained within the atom, traditionally called the β sphere (10).

There are six variables within the quadrature scheme, three variables within the β sphere and three outside this sphere. These six variables are denoted by ($n_r(\beta)$, $n_\theta(\beta)$, $n_\phi(\beta)$, n_r, n_θ, n_ϕ), where n_r is the number of quadrature points in the radial grid, and n_θ and n_ϕ the number of quadrature points in the angular grid, which consists of θ and ϕ. The atomic properties are influenced by both the size and the orientation of the integration grid atom relative to the atom's local axis system. We investigate both factors in turn.

3. Results and discussion

3.1 Grid size

A complete understanding of the dependence of the integration error $L(\Omega)$ on the quadrature grid would require a systematic scan through the six-dimensional space of integration variables ($n_r(\beta)$, $n_\theta(\beta)$, $n_\phi(\beta)$, n_r, n_θ, n_ϕ). To make this task more manageable we first focus on the β sphere. We have observed that $L(\Omega)$ is more dependent on the radial integration variable $n_r(\beta)$ than on the angular variables $n_\theta(\beta)$ and $n_\phi(\beta)$. In Table 1 we investigate the effect of an increase of the number of radial quadrature points, $n_r(\beta)$, for C, N, O, and S. Hydrogen atoms are omitted from this analysis because they do not have any core electrons and their $L(\Omega)$ values rarely exceed 10^{-4} au.

We see from Table 1 that only the atomic energy and $L(\Omega)$ are affected by the increase of $n_r(\beta)$. This effect can be explained by a well-known fact in the field of numerical analysis, namely that "high order is not the same as high accuracy" (20). In numerical integration high order translates only to high accuracy when the integrand is very smooth, in the sense of being well approximated by a polynomial. Both the Laplacian of the electron density, $\nabla^2\rho(\mathbf{r})$, which determines $L(\Omega)$, and the kinetic energy density $K(\mathbf{r})$ oscillate dramatically in the radial direction, near the nucleus. This explains why a large number of quadrature points are required to integrate the radial direction accurately. As the nuclear charge increases from C over N and O to S, more radial points are needed to obtain a good accuracy, i.e., a small $L(\Omega)$ value. Since $\nabla^2\rho(\mathbf{r})$ and $K(\mathbf{r})$ vary more smoothly along the angular integration variables values of $n_\theta(\beta) = 30$ and $n_\phi(\beta) = 40$ are sufficient. The fact that smoother functions are integrated better by modestly sized quadrature grids also explains why the electrostatic multipole moments do not change when $n_r(\beta)$ is increased. Indeed, the integrand for a multipole moment consists of ρ multiplied by a tensor (e.g., eq. [5]) and ρ decreases monotonically away from the nucleus, more smoothly than

[4] M.J. Frisch, G.W. Trucks, H.B. Schlegel, P.M.W. Gill, B.G. Johnson, M.A. Robb, J.R. Cheeseman, T. Keith, G.A. Petersson, J.A. Montgomery, K. Raghavachari, M.A. Al-Laham, V.G. Zakrzewski, J.V. Ortiz, J.B. Foresman, J. Cioslowski, B.B. Stefanov, A. Nanayakkara, M. Challacombe, C.Y. Peng, P.Y. Ayala, W. Chen, M.W. Wong, J.L. Andres, E.S. Replogle, R. Gomperts, R.L. Martin, D.J. Fox, J.S. Binkley, D.J. Defrees, J. Baker, J.P. Stewart, M. Head-Gordon, C. Gonzalez, and J.A. Pople. Gaussian 94, Gaussian Inc., Pittsburgh, Pa. 1995.

[5] Morphy98. A program written by P.L.A. Popelier with a contribution from R.G.A. Bone. UMIST, Manchester, England, EU. 1998.

© 2000 NRC Canada

Table 2. Atomic properties and integration error of the carbon in ethene as a function of the number of angular quadrature points, $n_\theta n_\phi$.[a]

$n_\theta n_\phi$ (n_θ, n_ϕ)	Error	Volume	Energy	Population	Dipole	Quadrupole	Octopole	Hexadecupole
900 (30,30)	0.00068	97.73	–38.0852	6.0638	0.0955	1.7270	2.6510	6.0203
1600 (40,40)	–0.00212	100.91	–38.0845	6.0664	0.0931	1.7191	2.7032	6.1190
2500 (50,50)	0.00096	98.82	–38.0853	6.0635	0.0958	1.7247	2.6475	5.9972
3600 (60,60)	0.00018	98.90	–38.0851	6.0642	0.0952	1.7224	2.6646	6.0154
4900 (70,70)	–0.00046	99.65	–38.0849	6.0649	0.0948	1.7243	2.6725	6.0762
6400 (80,80)	0.00034	99.03	–38.0852	6.0641	0.0953	1.7244	2.6588	6.0332
8100 (90,90)	–0.00004	99.26	–38.0851	6.0644	0.0950	1.7227	2.6668	6.0295
10000 (100,100)	–0.00001	99.29	–38.0851	6.0645	0.0951	1.7243	2.6645	6.0529
12100 (110,110)	0.00001	99.20	–38.0851	6.0644	0.0951	1.7239	2.6652	6.0399
14400 (120,120)	–0.00006	99.27	–38.0851	6.0645	0.0950	1.7233	2.6666	6.0365
16900 (130,130)	0.00011	99.20	–38.0851	6.0644	0.0952	1.7241	2.6628	6.0416
19600 (140,140)	–0.00011	99.29	–38.0851	6.0646	0.0950	1.7235	2.6676	6.0442
22500 (150,150)	0.00003	99.20	–38.0851	6.0644	0.0951	1.7238	2.6645	6.0397
Maximum difference		3.18	0.0008	0.0029	0.0027	0.0079	0.0557	0.1218
Mean		99.21	–38.0851	6.0645	0.0950	1.7237	2.6658	6.0420
Standard deviation		0.68	0.0002	0.0007	0.0006	0.0018	0.0131	0.0298

[a]Remaining quadrature values, ($n_r(\beta)$, $n_\theta(\beta)$, $n_\phi(\beta)$, n_r) are set to (50, 30, 40, 50).

Table 3. Atomic properties and integration error of the carbon in methanethiol (CH_3SH) as a function of the number of angular quadrature points, $n_\theta n_\phi$.[a]

$n_\theta n_\phi$ (n_θ, n_ϕ)	Error	Volume	Energy	Population	Dipole	Quadrupole	Octopole	Hexadecupole
900 (30,30)	–0.01102	78.50	–37.9381	6.1218	0.0634	0.1378	3.3733	4.4831
1600 (40,40)	0.00185	74.34	–37.9423	6.1116	0.0553	0.0981	3.3586	4.1320
2500 (50,50)	–0.00794	76.85	–37.9394	6.1199	0.0585	0.1059	3.3718	4.4421
3600 (60,60)	0.00119	74.47	–37.9410	6.1102	0.0535	0.0942	3.3872	4.0565
4900 (70,70)	–0.00413	75.91	–37.9399	6.1155	0.0560	0.0980	3.3824	4.2548
6400 (80,80)	–0.00041	75.07	–37.9408	6.1121	0.0547	0.0968	3.3825	4.0687
8100 (90,90)	–0.00222	75.70	–37.9403	6.1136	0.0545	0.0917	3.3786	4.1713
10000 (100,100)	–0.00142	75.22	–37.9410	6.1138	0.0559	0.0988	3.3706	4.1214
12100 (110,110)	–0.00348	75.67	–37.9406	6.1159	0.0565	0.0973	3.3684	4.2023
14400 (120,120)	–0.00151	75.29	–37.9408	6.1135	0.0555	0.0973	3.3755	4.1197
16900 (130,130)	–0.00251	75.52	–37.9404	6.1143	0.0553	0.0952	3.3781	4.1650
19600 (140,140)	–0.00058	75.27	–37.9407	6.1121	0.0539	0.0928	3.3823	4.0959
22500 (150,150)	–0.00211	75.47	–37.9405	6.1138	0.0550	0.0950	3.3797	4.1544
Maximum difference		4.16	0.0042	0.0116	0.0099	0.0461	0.0286	0.4266
Mean		75.64	–37.9405	6.1145	0.0560	0.0999	3.3761	4.1898
Standard deviation		1.06	0.0010	0.0032	0.0026	0.0119	0.0076	0.1324

[a]Remaining quadrature values, ($n_r(\beta)$, $n_\theta(\beta)$, $n_\phi(\beta)$, n_r) are set to (50, 30, 40, 50).

$\nabla^2\rho(\mathbf{r})$. Of course the smoothest integrand, the constant "1," occurs in the computation of the atomic volume. Consequently the atomic volume is invariant to an increasing value of $n_r(\beta)$.

Table 1 reveals that alteration of the β sphere radial grid has very little effect on the $L(\Omega)$ value of the carbon atom. For the other atoms, N, O, and S, there is a substantial improvement in the error of up two orders of magnitude. The energy suffers from an inaccurate grid within the β sphere, whereas all the other properties remain unchanged. Unsurprisingly sulfur, having the largest core, requires the largest value for $n_r(\beta)$. Apart from the fluctuations in both $\nabla^2\rho(\mathbf{r})$ and the energy the β sphere is very straightforward to integrate and $n_\theta(\beta)$, $n_\phi(\beta)$) = (30, 40) can be recommended for all atoms. We note that $n_r(\beta; C) = 50$, $n_r(\beta; N,O) = 90$ and $n_r(\beta; S) = 150$ yield satisfactory $L(\Omega)$ values and stable atomic properties. Therefore we conclude that the atomic core of most molecules of biological interest can be integrated with a number of points between 60 000 and 180 000, based on the product $n_r(\beta)\, n_\theta(\beta)\, n_\phi(\beta)$. Finally we have observed that the radial grid outside the β sphere has relatively little effect on the quality of the integration.[6]

Of the six parameters, ($n_r(\beta)$, $n_\theta(\beta)$, $n_\phi(\beta)$, n_r, n_θ, n_ϕ), that we are to investigate only the number of quadrature points in the angular grid outside the β sphere, denoted by n_θ and n_ϕ, remains. An angular grid is conveniently labelled as

[6]F.M. Aicken and P.L.A. Popelier. Unpublished results.

© 2000 NRC Canada

Table 4. Atomic properties and integration error of the α carbon in alanine as a function of the number of quadrature points, $n_\theta n_\phi$.[a]

$n_\theta n_\phi$ (n_θ, n_ϕ)	Error	Volume	Energy	Population	Dipole	Quadrupole	Octopole	Hexadecupole
900 (30,30)	–0.0101	46.35	–37.8638	5.6741	0.3497	0.4394	2.3001	2.6855
1600 (40,40)	–0.00933	46.61	–37.8638	5.6742	0.3481	0.4331	2.3468	2.4013
2500 (50,50)	–0.00525	46.53	–37.8635	5.6701	0.3688	0.3890	2.4026	2.7686
3600 (60,60)	–0.00378	46.16	–37.8647	5.6696	0.3702	0.4011	2.3498	2.5829
4900 (70,70)	–0.0019	45.83	–37.8652	5.6677	0.3594	0.4284	2.2776	2.3849
6400 (80,80)	–0.00281	46.13	–37.8646	5.6685	0.3629	0.4102	2.3655	2.3476
8100 (90,90)	–0.00382	46.20	–37.8645	5.6694	0.3629	0.4084	2.3488	2.4520
10000 (100,100)	–0.00195	45.92	–37.8649	5.6675	0.3597	0.4265	2.2918	2.4165
12100 (110,110)	–0.00314	46.13	–37.8647	5.6688	0.3623	0.4162	2.3211	2.4169
14400 (120,120)	–0.00397	46.16	–37.8648	5.6696	0.3636	0.4134	2.3201	2.4512
16900 (130,130)	–0.0018	45.96	–37.8648	5.6674	0.3608	0.4189	2.3024	2.4647
19600 (140,140)	–0.00315	46.10	–37.8647	5.6688	0.3610	0.4203	2.3194	2.3411
22500 (150,150)	–0.00282	46.06	–37.8648	5.6685	0.3611	0.4182	2.3153	2.4199
Maximum difference		0.78	0.0017	0.0065	0.0108	0.0504	0.1250	0.3837
Mean		46.16	–37.8645	5.6696	0.3608	0.4172	2.3278	2.4718
Standard deviation		0.22	0.0005	0.0022	0.0062	0.0134	0.0340	0.1293

[a]Remaining quadrature values, ($n_r(\beta)$, $n_\theta(\beta)$, $n_\phi(\beta)$, n_r) are set to (50, 30, 40, 50).

Table 5. Atomic properties and integration error of nitrogen in alanine as a function of the number of quadrature points, $n_\theta n_\phi$.[a]

$n_\theta n_\phi$ (n_θ, n_ϕ)	Error	Volume	Energy	Population	Dipole	Quadrupole	Octopole	Hexadecupole
900 (30,30)	–0.00075	111.86	–55.1060	7.9386	0.3536	1.2741	1.7005	4.7392
1500 (30,50)	–0.0012	112.50	–55.1049	7.9378	0.3533	1.2801	1.7131	4.7928
2100 (30,70)	–0.00107	112.42	–55.1056	7.9385	0.3537	1.2760	1.7013	4.7745
2700 (30,90)	–0.00146	112.35	–55.1055	7.9389	0.3529	1.2774	1.7017	4.7767
1500 (50,30)	–0.00242	111.99	–55.1047	7.9389	0.3511	1.2805	1.7135	4.7960
2500 (50,50)	–0.00219	112.49	–55.1054	7.9395	0.3517	1.2774	1.6972	4.8109
3500 (50,70)	–0.00219	112.49	–55.1054	7.9395	0.3517	1.2774	1.6972	4.8109
4500 (50,90)	–0.00143	112.31	–55.1054	7.9386	0.3530	1.2780	1.7040	4.7586
2100 (70,30)	–0.00170	111.89	–55.1050	7.9384	0.3525	1.2775	1.7106	4.7659
3500 (70,50)	–0.00214	112.53	–55.1054	7.9395	0.3522	1.2767	1.6987	4.8187
6300 (70,90)	–0.00198	112.46	–55.1056	7.9396	0.3520	1.2777	1.7018	4.7729
6300 (90,70)	–0.00168	112.45	–55.1051	7.9386	0.3528	1.2781	1.7119	4.7846
8100 (90,90)	–0.00177	112.34	–55.1055	7.9393	0.3525	1.2767	1.7020	4.7825
9900 (90,110)	–0.00141	112.32	–55.1053	7.9385	0.3532	1.2772	1.7078	4.7769
Maximum difference		0.67	0.0013	0.0018	0.0026	0.0064	0.0163	0.0795
Mean		112.31	–55.1053	7.9389	0.3526	1.2775	1.7044	4.7829
Standard deviation		0.23	0.0003	0.0005	0.0008	0.0016	0.0059	0.0218

[a]Remaining quadrature values, ($n_r(\beta)$, $n_\theta(\beta)$, $n_\phi(\beta)$, n_r) are set to (90, 30, 40, 90).

(n_θ, n_ϕ) and the number of points it contains is simply $n_\theta n_\phi$. Integration experience reveals that the angular grid outside β is the most important factor in the determination of the quality of the integration and the hardest to judge. The angular grid determines in which directions the integration rays are shot, away from the nucleus, hence this grid determines how the atomic boundaries are probed. The integration error $L(\Omega)$ is dependent on how well this probing is done.

The values of n_θ and n_ϕ were systematically varied to investigate what effect the grid has on the quality of the properties for each atom type. Tables 2, 3, and 4 show the values of the atomic properties and $L(\Omega)$ for a set of angular grids for the carbon in ethene, the carbon in methanethiol and the α carbon in alanine respectively. Table 5 shows the same information for the nitrogen in alanine, Table 6 for the hydroxyl oxygen in alanine, and Table 7 for the sulfur in methanethiol. The behavior of the integration error as a function of the number of angular grid points is given in Fig.1. This figure consists of six plots (*a* to *f*) with each corresponding to data in Tables 2 to 7 respectively.

Figure 1 clearly shows that the relationship between the integration error, $L(\Omega)$, and the number of angular grid points is not trivial. The naïve expectation that a larger grid leads to a $L(\Omega)$ value nearer to zero cannot be fulfilled. Rather we confirm that high order does not necessarily mean high accuracy. For example, a grid of 6400 points leads to $L(\Omega)$ = –0.00041 au (Table 3) while a grid of 22 500 points yields an integration error that is about five times higher. The carbons drawn from three very different chemical environments show a dampened oscillatory behaviour. These oscillations are also present in the integrations of the nitrogen

© 2000 NRC Canada

Fig. 1. Plots of the error, $L(\Omega)$, against the number of points in the angular grid, $n_\theta n_\phi$ for (*a*) the carbon in ethene, (*b*) the carbon in methanethiol, (*c*) the α carbon in alanine, (*d*) the nitrogen in alanine, (*e*) the hydroxyl oxygen in alanine, and (*f*) the sulfur in methanethiol. In Figs. 1*d* and 1*e* no curve could be drawn because the plots include degenerate points, i.e., two different grids leading to different $L(\Omega)$ values but with the same number of grid points.

Table 6. Atomic properties and integration error of the hydroxyl oxygen in alanine as a function of the number of angular quadrature points, $n_\theta n_\phi$.[a]

$n_\theta n_\phi$ (n_θ, n_ϕ)	Error	Volume	Energy	Population	Dipole	Quadrupole	Octopole	Hexadecupole
900 (30,30)	–0.00019	120.56	–75.9121	9.1227	0.1987	0.6580	0.5855	2.1733
1500 (30,50)	0.00013	120.20	–75.9122	9.1225	0.1976	0.6584	0.5871	2.1479
2100 (30,70)	0.00019	120.29	–75.9122	9.1224	0.1974	0.6586	0.5885	2.1448
2700 (30,90)	0.00017	120.31	–75.9122	9.1224	0.1974	0.6586	0.5896	2.1459
1500 (50,30)	–0.00014	120.39	–75.9120	9.1226	0.1985	0.6582	0.5867	2.1728
2500 (50,50)	0.00006	120.12	–75.9121	9.1225	0.1977	0.6586	0.5868	2.1510
3500 (50,70)	0.00012	120.15	–75.9121	9.1224	0.1975	0.6586	0.5880	2.1480
4500 (50,90)	0.0001	120.15	–75.9121	9.1224	0.1975	0.6586	0.5888	2.1478
2100 (70,30)	–0.0001	120.35	–75.9120	9.1226	0.1985	0.6581	0.5859	2.1704
3500 (70,50)	0.00008	120.06	–75.9121	9.1225	0.1977	0.6586	0.5873	2.1517
6300 (70,90)	0.00005	120.19	–75.9121	9.1224	0.1976	0.6586	0.5887	2.1509
6300 (90,70)	0.00013	120.16	–75.9121	9.1224	0.1974	0.6587	0.5884	2.1492
8100 (90,90)	0.00008	120.18	–75.9121	9.1224	0.1975	0.6586	0.5886	2.1502
9900 (90,110)	0	120.18	–75.9121	9.1225	0.1977	0.6585	0.5881	2.1527
Maximum difference		0.5000	0.0002	0.0003	0.0013	0.0007	0.0041	0.0285
Mean		120.24	–75.9121	9.1225	0.1978	0.6585	0.5877	2.1540
Standard deviation		0.13	0.0000	0.0001	0.0005	0.0002	0.0012	0.0101

[a]Remaining quadrature values, ($n_r(\beta)$, $n_\theta(\beta)$, $n_\phi(\beta)$, n_r) are set to (90, 30, 40, 90).

Table 7. Atomic properties and integration error of sulfur in methanethiol as a function of the number of angular quadrature points, $n_\theta n_\phi$.

$n_\theta n_\phi$ (n_θ, n_ϕ)	Error	Volume	Energy	Population	Dipole	Quadrupole	Octopole	Hexadecupole
2000 (40,50)	0.00119	211.64	–398.3515	15.9518	0.7959	3.3934	2.0803	5.2679
3250 (50,65)	0.00082	211.86	–398.3514	15.9522	0.7950	3.3924	2.0849	5.2995
4800 (60,80)	0.00054	212.12	–398.3514	15.9525	0.7939	3.3919	2.0923	5.3246
8000 (80,100)	0.00035	212.05	–398.3513	15.9527	0.7932	3.3917	2.0983	5.3500
12000 (100,120)	0.00026	212.10	–398.3513	15.9528	0.7929	3.3913	2.0996	5.3514
14300 (110,130)	0.00014	212.11	–398.3513	15.9529	0.7925	3.3917	2.1019	5.3671
19500 (130,150)	0.00015	212.12	–398.3513	15.9529	0.7926	3.3911	2.1017	5.3582
Maximum difference		0.48	0.0003	0.0011	0.0034	0.0023	0.0216	0.0992
Mean		212.01	–398.3513	15.9526	0.7936	3.3920	2.0947	5.3357
Standard deviation		0.17	0.0001	0.0004	0.0012	0.0008	0.0081	0.0357

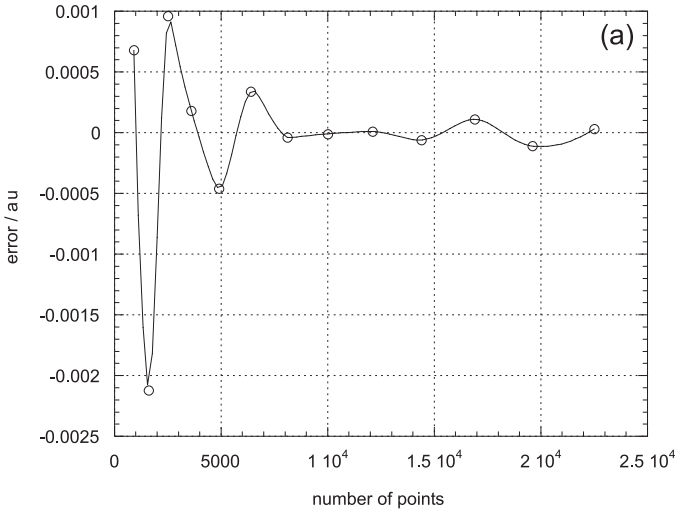
[a]Remaining quadrature values, ($n_r(\beta)$, $n_\theta(\beta)$, $n_\phi(\beta)$, n_r) are set to (150, 30, 40, 70).

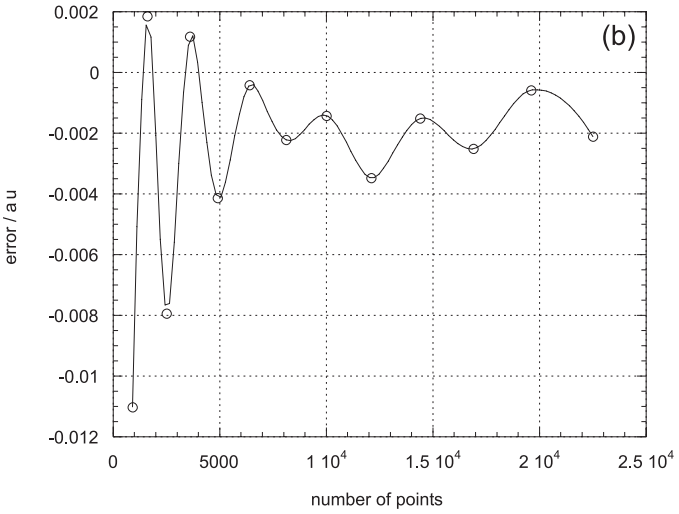
and the oxygen (Fig. 1*d*, *e*) but they are not shown by a curve. A curve could not be drawn because there are several instances where two different integration grids, with an equal number of points yield two different $L(\Omega)$ values. This phenomenon again proves the erratic relationship between $L(\Omega)$ and the number of grid points. For instance, the correlation coefficient for the data set of Fig. 1*d* (Table 5) is $R^2 = 0.01$.

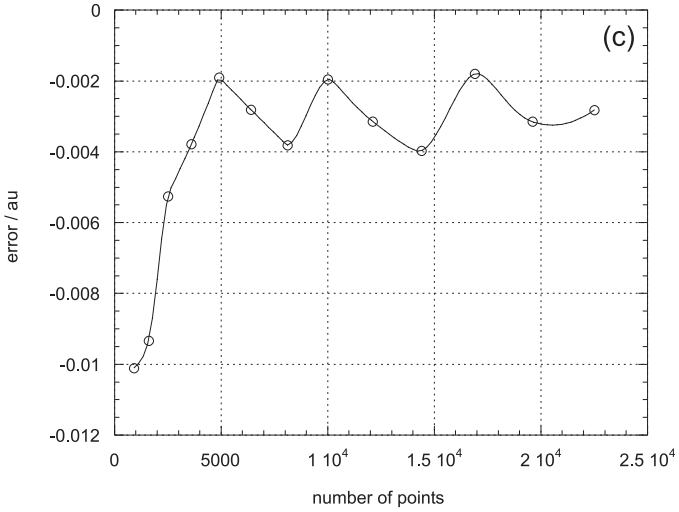
The behaviour of $L(\Omega)$ versus the size of the integration grid suggests a statistical interpretation of atomic integration. This approach is very practical and means that we regard an integration with any reasonable angular grid size as a "measurement" of the atomic properties of an atom. Grids with much fewer than a thousand points produce excessively high integration errors and should therefore be discarded. The statistical interpretation suggests the computation of the mean value ($\bar{x}$) of an atomic property and its standard deviation, σ. The latter quantity can serve as an error bar to the property. Both quantities, $\bar{x}$ and σ, together with range, defined as the difference between the minimum and maximum values of a property, are given in Tables 2–7.

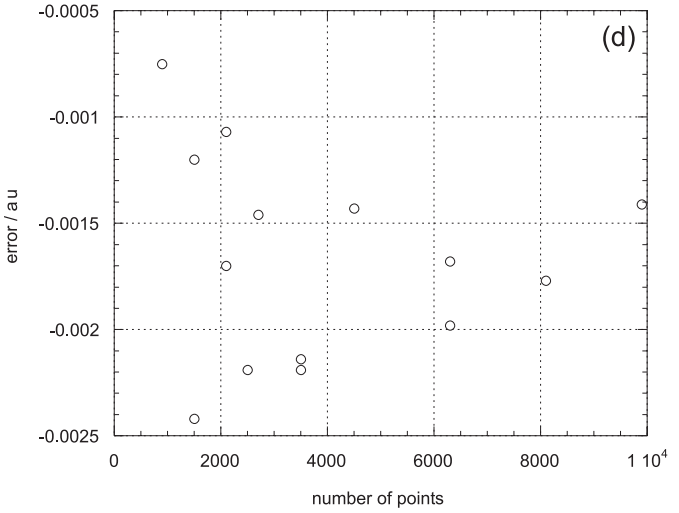
Although the statistical point of view may seem unorthodox for properties that are exactly obtainable in principle, it makes sense in practice, especially when a large set of atoms (order of hundreds) needs to be computed. There are three reasons why a statistical interpretation is appropriate at a practical level. The first reason is to enable the determination

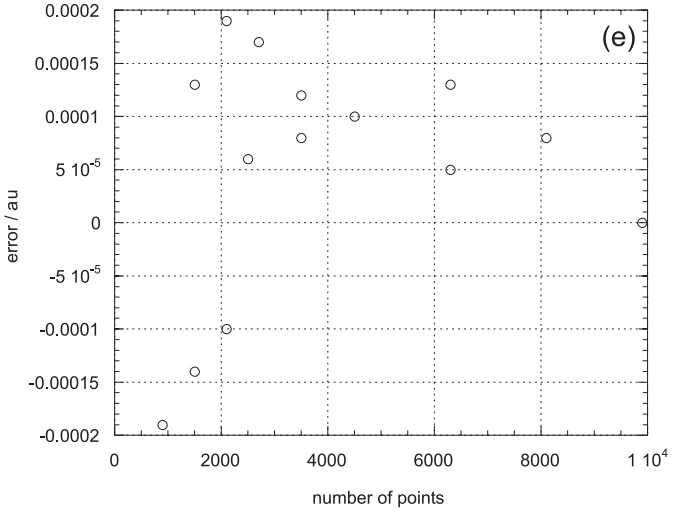
© 2000 NRC Canada

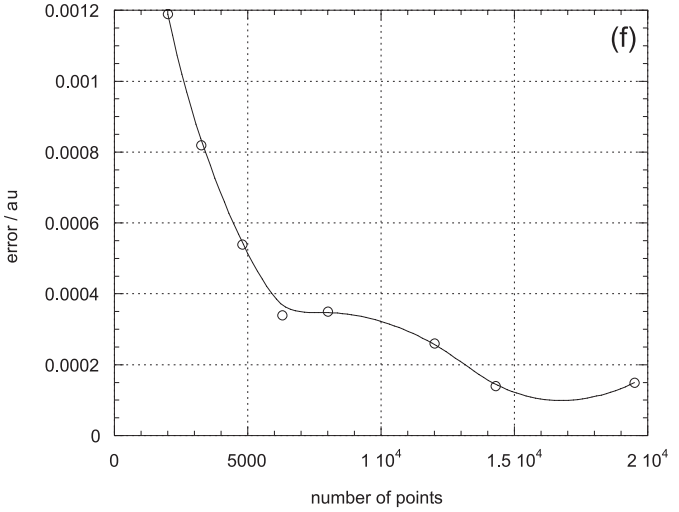






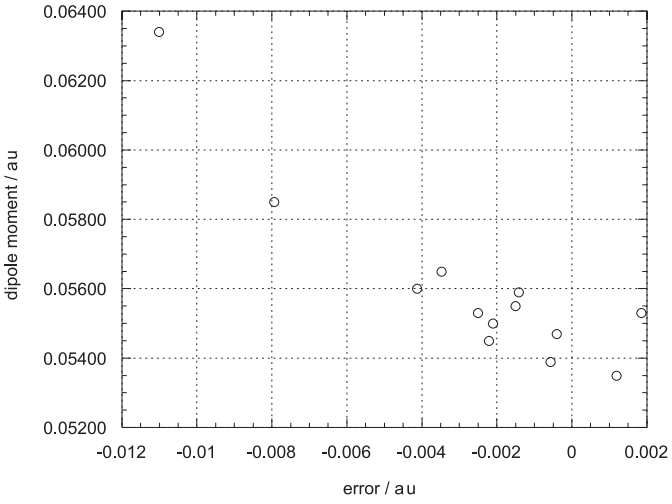






© 2000 NRC Canada

Fig. 2. Plot of the atomic dipole moment against $L(\Omega)$ for the carbon in methanethiol.



of a practical error bar of an atomic property in the classification of atoms via cluster analysis. Indeed, it makes no sense to subdivide a group of atoms if the resulting subgroups can actually not be distinguished because of their overlapping error intervals. The second reason is that the relation between the integration error $L(\Omega)$ and the grid size is erratic. The third reason is that, in general, the relation between $L(\Omega)$ and atomic properties is also erratic. We now discuss the second and the third reason in detail.

Given that $L(\Omega)$ is the ultimate judge of the integration quality, rather than the grid size, it is desirable to have an integration algorithm which reaches a pre-set $L(\Omega)$ value (21). To systematically attain a pre-set error one would like to improve a quadrature grid gradually, without discarding previously computed grid points. This systematic improvement is possible with Simpson's rule (or extended trapezoidal rules) but not with Gauss–Legendre quadrature. However the Gauss–Legendre quadrature is superior to a trapezoidal rule because it needs fewer grid points. Consequently one is faced with the dilemma that a more efficient integration technique uses a grid such that points evaluated in a lower order grid cannot be re-used in a higher order grid. Although some progress has been made in quadrature schemes that can be refined until a pre-set accuracy is reached, the question whether the maximum degree of exactness can actually be achieved in practice remains unsolved (20). Therefore one can only guess a grid size and hope that it will deliver the desired $L(\Omega)$ value. Often very large angular integration grids turn out be prohibitive. Moreover small grids can produce low integration errors. It is clear from Fig. 1 that a given $L(\Omega)$ value cannot be translated into a particular angular grid, so we prefer to view integration with typical quadrature grids as a "measurement" of an atomic property.

The third reason to adopt the statistical point of view is related to the following question: how low must $L(\Omega)$ be to obtain an atomic property with an acceptable error bar? A direct way to answer this question is to monitor the behaviour of atomic properties with the indicator of integration quality, $L(\Omega)$. A typical example is given in Fig. 2, which shows how the magnitude of the dipole moment, μ, varies with $L(\Omega)$ for the carbon in methanethiol. This example is representative for all properties except the electronic population of the carbon atoms. Naïvely one would expect that the property in question converges, possibly asymptotically, to an ideal value. Instead of this behaviour we recover in Fig. 2 a scatter plot with $R^2 = 0.821$. Systematic omission of data points can produce a correlation coefficient as low as 0.650. Accepting the quasi-random data pattern we conclude that the dipole moment's magnitude is bracketed, or $\mu = 0.0560 \pm 0.0099$ au. This error bar is rather large because two fairly large errors (two points on the left on Fig. 2, corresponding to 900 and 2500 grid points) have been included. When these results are excluded we find that $\mu = 0.0554 \pm 0.0014$ au. This recalculation shows that the original standard deviation, $\sigma = 0.0099$, which is listed in Table 3, is rather tolerant or safe. Indeed, as illustrated here, closer inspection of the integration data show that σ could easily be ten times smaller. However, we choose to err on the side of safety and quote the higher, more tolerant standard deviation. This level of safety is justified because of the difficulties in obtaining low $L(\Omega)$ values for carbons. Furthermore, in view of our cluster analysis of the atoms in amino acids (which will be published in Part 2) we want to incorporate a realistic cluster resolution.

Within the statistical framework we can prove in a different way that the number of grid points can be misleading in judging the quality of an atomic property. For example, in Table 2 we find that 900 points yield $L(\Omega) = 0.00068$ au, and 1600 points $L(\Omega) = -0.00212$ au However the discrepancy from the mean volume is 1.48 au for the former grid and 1.70 au for the latter. So properties deviate less from the mean value if $L(\Omega)$ is low rather than when the number of grid points is large.

It is clear from Tables 2–7 that, in general, the relative standard deviations of atomic properties can be ranked from the smallest to the largest as follows: energy < population < dipole < quadrupole < octupole < hexadecupole < volume. This means that energy and the population (and thus the monopole moment) are the most stable properties and that, on the other hand, volume is very dependent on the value of $L(\Omega)$. The maximum deviations from the mean generally follow this pattern.

It is also possible to propose error bars on atomic properties for C, N, O, and S from the standard deviations listed in Tables 2–7. Table 8 lists the most tolerant error bars σ (i.e., largest standard deviations found) for each atomic property of atoms C, N, O, and S. This means that two atoms that differ in one property by more than 3σ (as listed in Table 8) are definitely different, given that they were integrated with a feasible and typical quadrature grid with more than a thousand points. Hence this work provides useful results for clustering and transferability studies for a large set of atoms.

The slightly different values for an atomic property obtained by different angular grids however, are not completely without pattern. We observed the trend that, with few exceptions, a positive $L(\Omega)$ value tends to underestimate the volume, population, and octopole and hexadecupole moments,

© 2000 NRC Canada

Table 8. Estimated error bars (in au) on seven atomic properties for carbon, nitrogen, oxygen, and sulfur.

Atom	Volume	Energy	Population	Dipole	Quadrupole	Octopole	Hexadecupole
C	1.0	0.001	0.003	0.006	0.01	0.03	0.1
N	0.2	0.0003	0.0005	0.0008	0.002	0.006	0.02
O	0.1	$<10^{-4}$	0.0001	0.0005	0.0002	0.001	0.01
S	0.2	0.0001	0.0004	0.001	0.0008	0.008	0.04

Fig. 3. Plot of the electronic population $N(\Omega)$ against $L(\Omega)$ for the carbon in methanethiol.

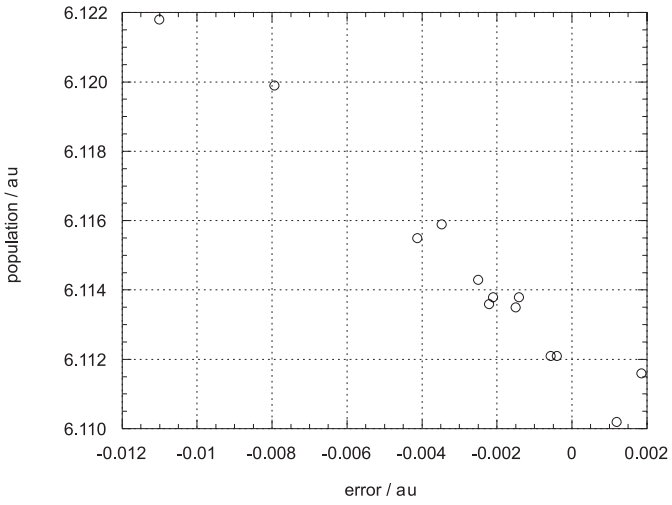
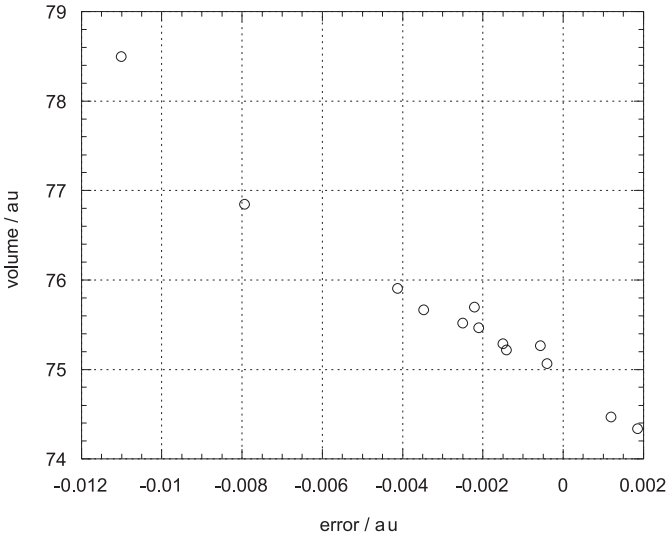


Fig. 4. Plot of the atomic volume $v(\Omega)$ against $L(\Omega)$ for the carbon in methanethiol.



while overestimating the magnitude of the energy, and the dipole and quadrupole moments. A negative error has the opposite effect. Regression analysis was carried out on the results to ascertain whether this trend was quantitative and therefore had predictive powers. Most properties were found to have no significant correlation with $L(\Omega)$ and could therefore not be used for interpolation or extrapolation.

The exceptions proved to be the population of the carbon atoms in the set and the volume of the carbon atom in methanethiol. Figure 3 shows the plot of the population, $N(\Omega)$, against $L(\Omega)$ for carbon in methanethiol. The corresponding R^2 value is 0.969. To check that the correlation observed was genuine, outlying points were removed, and R^2 was found to range from 0.945 to 0.987. The correlation coefficients are high enough to enable a meaningful interpolation to the desirable atomic property corresponding to $L(\Omega) = 0$. The regression equation is:

$$[6] \quad N(\Omega) = -0.90897\ L(\Omega)\ (\pm\ 0.049068) + 6.11207\ (\pm\ 0.00021)$$

It is clear that the ideal $N(\Omega)$ value is 6.11207 au, if $L(\Omega)$ is set to zero, which corresponds well with the result of the integration with the lowest error, which is 6.1121 au (see Table 3). A similar successful interpolation can be carried out with the volume of this carbon. Figure 4 shows the graph of the volume $v(\Omega)$ against $L(\Omega)$ where $R^2 = 0.966$ and the regression equation is:

$$[7] \quad v(\Omega) = -297.236\ L(\Omega)\ (\pm\ 16.812) + 74.853\ (\pm\ 0.072)$$

The ideal volume is thus predicted to be 74.853 au, which is 0.22 au lower (0.3%) than the best predicted value. A good estimate of the exact population of carbon in alanine (Fig. 5) can be made via extrapolation of the following regression equation:

$$[8] \quad N(\Omega) = -0.82405\ L(\Omega)\ (\pm\ 0.0491) + 5.66614\ (\pm\ 0.00013)$$

From this equation we predict that the population is 5.66614, which reduces the overall population, $\sum_{\Omega} N(\Omega)$, from 48.0087 to 48.0011. This means that the extrapolated population brings the overall population closer to the ideal value of 48.

We can also confirm the relationship reported before (22) between the overall sum of the integration errors of all atoms in a molecule $\sum_{\Omega} L(\Omega)$ and the deviation, $\Delta N(\Omega)$, of the sum of the populations, $\sum_{\Omega} N(\Omega)$, from the total population, N_{total}. The results from our data set of 57 molecules, including the twenty amino acids and smaller derived molecules[6] are plotted in Fig. 6.

© 2000 NRC Canada

Fig. 5. Plot of the electronic population $N(\Omega)$ against $L(\Omega)$ for the carbon in alanine.

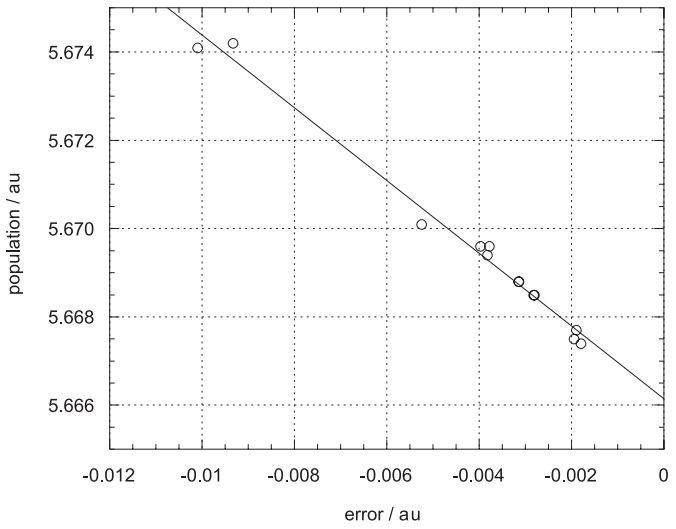
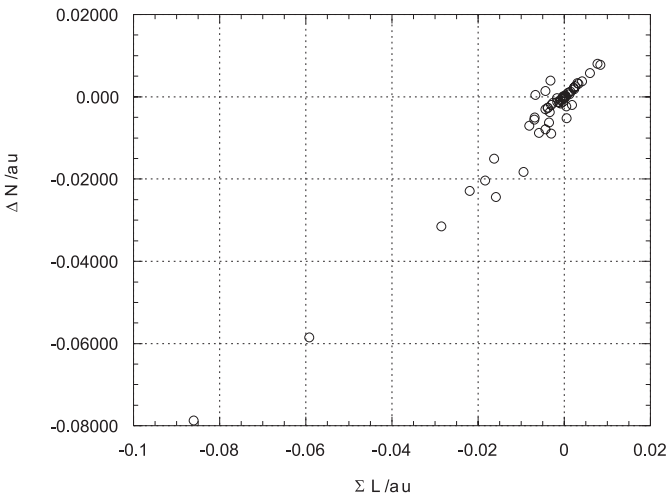


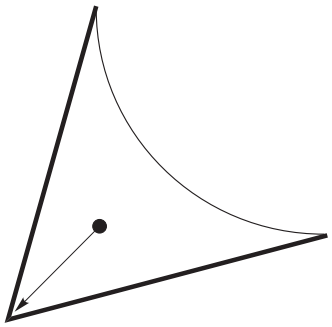
Fig. 6. Plot of the linear relationship between $\Delta N = N_{\text{total}} - \sum_{\Omega} N(\Omega)$ and $L(\Omega)$ for the 57 molecules of the data set, which includes the twenty amino acids and smaller derived molecules.



It should be pointed out that our current findings are not due to well-known inadequacies of atomic integration, such as the "leakage" phenomenon. This means that MORPHY has a special algorithm built in (23) that prevents an integration ray from penetrating into an adjacent basin due to incorrect truncation. Furthermore, MORPHY does not allow poor analytical representations of interatomic surfaces (23), for example when they contain ring critical points. These precautions make us believe that the effects we observe are genuine, although admittedly there are several integration parameters (23), other than the number of quadrature points, that we have not systematically varied. Rather, they were kept fixed in this work, at values that we associated with reliable and efficient integration practice in the course of the development of MORPHY.

A final comment is concerned with a speculative explanation for the oscillating behaviour of $L(\Omega)$ versus the number of grid points. It is well known that Gauss–Legendre quadrature requires an enormous amount of grid points to integrate reasonably a function that contains a cusp. A cusp is a continuous point where the left and right derivatives are not the same, hence the derivative is not defined at a cusp. In our case the cusp originates from the geometrical shape of the atom. A function that measures the distance from the nucleus to a point on the atomic boundary has no derivative with respect to the angular displacement at a cusp point. Figure 7 shows an example of a cusp in benzene. The so-called ring line, which is perpendicular to the molecular plane is a collection of cusp points. Indeed, an integration ray sweeping the atom (as marked by the arrow) would see its length increase when approaching the cusp line and then suddenly decrease having passed the cusp line. In other words, the geometry of the atom is not experienced as a smooth object by the integration ray. As a result the Gauss–Legendre quadrature needs to be very large. However, we suspect that a coarse grid will not detect the cusp as well as a fine grid and

Fig. 7. A schematic illustration of a (geometrical) cusp occurring in a typical ring atom such as carbon in benzene. The three interatomic surfaces bounding the carbon atom are outlined. The circle represents the nucleus and the arrow indicates an integration ray hitting the cusp.



hence accurate integrations can occur with small grids. Moderate grids may then detect the cusp better but they would not be large enough to handle it properly. However, very large grids should again be adequate, both in detecting the cusp and managing to integrate properties in its presence.

Although a cusp line appearing in ring system is a clear case, many atoms are bounded by interatomic surfaces that almost touch in long narrow tails. Such a geometrical feature may be viewed as a pseudo-cusp, i.e., a sudden change in the length of an integration ray upon angular displacement. Table 3 (or Fig. 1*b*) reveals the extent to which a cusp can affect the integration. There is a significant improvement in the quality of $L(\Omega)$ where the number of points is equal to 6 400 and again at 19 600.

© 2000 NRC Canada

Table 9. Atomic properties and integration error for oxygen in water as a function of grid size and orientation.[a]

Orientation	$n_\theta n_\phi$ (n_θ, n_ϕ)	Error	Volume	Energy	Population	Dipole	Quadrupole	Octopole	Hexadecupole
xy	2000 (40,50)	0.00023	148.92	–75.6627	9.1026	0.1607	0.8630	1.2005	3.7067
xy	4800 (60,80)	–0.00007	149.52	–75.6628	9.1030	0.1621	0.8621	1.2039	3.7228
xy	12000 (100,120)	0.00006	149.51	–75.6629	9.1029	0.1619	0.8619	1.2036	3.7240
xy	19500 (130,150)	0.00002	149.46	–75.6628	9.1029	0.1620	0.8619	1.2036	3.7262
xz	2000 (40,50)	0.00009	149.41	–75.6629	9.1029	0.1620	0.8619	1.2043	3.7409
xz	4800 (60,80)	0.00003	149.49	–75.6628	9.1029	0.1619	0.8620	1.2039	3.7224
xz	12000 (100,120)	0.00004	149.47	–75.6628	9.1029	0.1620	0.8620	1.2041	3.7251
xz	19500 (130,150)	0.00003	149.48	–75.6628	9.1029	0.1619	0.8619	1.2038	3.7258
yz	2000 (40,50)	0.00006	149.36	–75.6629	9.1029	0.1620	0.8621	1.2046	3.7241
yz	4800 (60,80)	0.00003	149.46	–75.6628	9.1029	0.1619	0.8619	1.2037	3.7224
yz	12000 (100,120)	0.00003	149.49	–75.6628	9.1029	0.1619	0.8620	1.2039	3.7232
yz	19500 (130,150)	0.00003	149.48	–75.6628	9.1029	0.1620	0.8620	1.2039	3.7260
	Maximum difference		0.60	0.0002	0.0004	0.0014	0.0011	0.0041	0.0342
	Mean		149.42	–75.6628	9.1029	0.1619	0.8621	1.2037	3.7241
	Standard deviation		0.16	0.0000	0.0001	0.0004	0.0003	0.0010	0.0074

[a]Remaining quadrature values, ($n_r(\beta)$, $n_\theta(\beta)$, $n_\phi(\beta)$, n_r) are set to (90, 30, 40, 50).

Table 10. Atomic properties and integration error for carbon in methanethiol (CH_3SH) as a function of grid size and orientation.[a]

Orientation	$n_\theta n_\phi$ (n_θ, n_ϕ)	L	Volume	Energy	Population	Dipole	Quadrupole	Octopole	Hexadecupole
xy	2000 (40,50)	–0.00592	76.70	–37.9394	6.1171	0.0565	0.0956	3.3753	4.4355
xy	4800 (60,80)	0.00055	74.87	–37.9409	6.1109	0.0530	0.0919	3.3878	4.0672
xy	12000 (100,120)	–0.0014	75.29	–37.9409	6.1136	0.0556	0.0975	3.3711	4.1162
xy	19500 (130,150)	–0.00246	75.50	–37.9405	6.1142	0.0555	0.0965	3.3792	4.1583
xz	2000 (40,50)	–0.00116	74.87	–37.9405	6.1124	0.0560	0.0930	3.3661	4.1881
xz	4800 (60,80)	0.00033	75.04	–37.9408	6.1110	0.0532	0.0903	3.3878	3.9992
xz	12000 (100,120)	–0.00082	75.35	–37.9406	6.1122	0.0541	0.0920	3.3793	4.1037
xz	19500 (130,150)	–0.00224	75.47	–37.9406	6.1142	0.0554	0.0969	3.3789	4.1235
yz	2000 (40,50)	0.00015	75.48	–37.9407	6.1112	0.0531	0.0912	3.3831	4.1209
yz	4800 (60,80)	–0.00344	75.56	–37.9408	6.1162	0.0584	0.1047	3.3758	4.2092
yz	12000 (100,120)	–0.00222	75.46	–37.9410	6.1148	0.0558	0.0959	3.3649	4.1688
yz	19500 (130,150)	–0.00146	75.33	–37.9408	6.1134	0.0550	0.0945	3.3723	4.1366
	Maximum difference		1.83	0.0016	0.0062	0.0054	0.0144	0.0229	0.4363
	Mean		75.41	–37.9406	6.1134	0.0551	0.0950	3.3768	4.1523
	Standard deviation		0.47	0.0004	0.0020	0.0016	0.0039	0.0074	0.1051

[a]Remaining quadrature values, ($n_r(\beta)$, $n_\theta(\beta)$, $n_\phi(\beta)$, n_r) are set to (50, 30, 40, 50).

3.2 Grid orientation

Finite grids produce properties that lack rotational invariance. This occurs because Gauss–Legendre quadrature samples the atom densely near the poles (θ near 0° or 180°) and the positive *x*-axis (φ near 0° or 360°). This effect can be illustrated by considering, for example, the four hydrogens in methane (24). By symmetry the hydrogens are expected to be identical but in practice they may not be, which can be explained as follows. The local axis system of a hydrogen atom is parallel to the molecular axis system, but the orientation of the hydrogen with respect to this axis system is of course different for each atom. The angular quadrature grids are constructed in the same way with respect to the local axis systems of the hydrogens, but each atom will have a different orientation with respect to this axis system. In other words, from the atom's point of view it is integrated via an angular grid with an orientation that is different for each hydrogen. Hence the molecular symmetry is not perfectly reflected in the atomic properties.

To assess the influence of grid orientation we have investigated carbon in methanethiol (Table 9) and oxygen in water (Table 10). In both cases we considered three different orientations, labeled *xy*, *xz*, and *yz*.[7] Carbon is generally harder to integrate than oxygen, presumably because it usually occurs tetra-coordinated, which leads to pseudo-cusps. Again the most stable properties are seen to be the energy and the population. It is clear that the same grid size leads to markedly different $L(\Omega)$ values dependent on the orientation, especially for carbon with its spike-like atomic tails. Such

[7]The Cartesian co-ordinates of the standard orientation were taken from the GAUSSIAN output file and the wave functions of the two new orientations were computed by interchanging the components of the axes alternately, i.e., the values of the *x*-axis and *y*-axis were exchanged as were those of the *x*-axis and *z*-axis. This resulted in one molecule lying in the *xy*-plane, one in the *xz*-plane and the third in the *yz*-plane.

© 2000 NRC Canada

Table 11. Comparison of the values of the atomic properties of the carbon in methanethiol (CH_3SH) for calculations with low $L(\Omega)$ with those computed at high values of $n_\theta n_\phi$.

Orientation	$n_\theta n_\phi$ (n_θ, n_ϕ)	L	Volume	Energy	Population	Dipole	Quadrupole	Octopole	Hexadecupole
yz	2000 (40,50)	0.00015	75.48	–37.940725	6.1112	0.0531	0.0912	3.3831	4.1209
xz	4800 (60,80)	0.00033	75.04	–37.940783	6.111	0.0532	0.0903	3.3878	3.9992
Difference		–0.00018	0.44	5.8×10^{-5}	0.0002	-1×10^{-4}	0.0009	–0.0047	0.1217
yz	19500 (130,150)	–0.00146	75.33	–37.940763	6.1134	0.055	0.0945	3.3723	4.1366
xz	19500 (130,150)	–0.00224	75.47	–37.940631	6.1142	0.0554	0.0969	3.3789	4.1235
Difference		0.00078	–0.14	–0.000132	–0.0008	–0.0004	–0.0024	–0.0066	0.0131

unpredictable variation reinforces our statistical point of view. A comparison of the standard deviations in Table 9 with those in Table 6, and of those in Table 10 with those in Table 3 reveals that the grid size and grid orientation have a similar effect on the variation of atomic properties. The effect on atomic properties of the variation of the integration grid with the same orientation can be larger than between identical grids with a different orientation.

Finally we prove that generally the difference between atomic properties is smaller for small values of $L(\Omega)$ rather than for a large number of points in the angular grid. To illustrate this phenomenon we list in Table 11 atomic properties for carbon in methanethiol. All the properties, with the exception of the volume and the hexadecupole, show a smaller deviation for low values of $L(\Omega)$ than for a high number of grid points. As such the orientation study also confirms that a larger grid does not necessarily lead to better results.

4. Conclusions

The practical integration of nearly a thousand atoms[6] in molecules of biological interest has prompted concern about the reliability or stability of the obtained atomic properties and about how many quadrature points are required to obtain sufficiently stable atomic properties. The only direct measure for the integration quality is $L(\Omega)$, a quantity without any chemical meaning. In other words, $L(\Omega)$ is not useful as an atomic property other than to assess the integration quality. It is straightforward to determine an integration grid that accurately integrates the β sphere inside C, N, O, and S. On the other hand predicting an angular grid outside the β sphere, with a number of points between approximately 1 000 and 25 000, and that guarantees a low $L(\Omega)$ value, is virtually impossible. The naïve view that a feasibly large grid leads to low $L(\Omega)$ values proves to be wrong. Instead we find that $L(\Omega)$ depends on the number of grid points according to nontrivial patterns, which may exhibit oscillatory behaviour. Consequently, from a practical point of view, we regard an atomic integration as a "measurement" of an atomic property, which has an error bar associated with it. Based on systematic calculations we are able to present safe error bars for seven atomic properties for the most common atoms occurring in biological molecules, i.e., C, N, O, and S. The integrations of hydrogen usually yield $L(\Omega)$ values well below 10^{-4} au and can hence be considered as perfect.

We also investigated the dependence of seven atomic properties on $L(\Omega)$, i.e., volume, energy, and the magnitudes of five electrostatic moments. Whereas atomic properties and $L(\Omega)$ are typically poorly correlated, the electronic populations of carbon tends to correlate linearly with $L(\Omega)$. This fact can be used to interpolate and extrapolate the population corresponding to $L(\Omega) = 0$, resulting in the ideal value. In spite of the lack of correlation some properties are systematically overestimated by a negative $L(\Omega)$ value, and others underestimated. Finally we have observed that the influence of the grid orientation is reduced if $L(\Omega)$ is small.

References

1. R.F.W. Bader. Atoms in molecules: a quantum theory. Clarendon Press, Oxford. 1990.
2. P.L.A. Popelier. Atoms in molecules. An introduction. Pearson Education, Harlow. 1999.
3. E. Kapuy, C. Kozmutza, and R. Daudel. Theor. Chim. Acta, **56**, 259 (1980).
4. R.E. Christoffersen. Adv. Quant. Chem. **6**, 333 (1972).
5. R.F.W. Bader, P.L.A. Popelier, and T.A. Keith. Angew. Chem. Int. Ed. Engl. **33**, 620 (1994).
6. R.F.W. Bader, S. Srebrenik, and T.T. Nguyen-Dang. J. Chem. Phys. **68**, 3680 (1978).
7. K.B. Wiberg and P.R. Rablen. J. Comput. Chem. **14**, 1504 (1993).
8. P.L.A. Popelier and R.F.W. Bader. J. Phys. Chem. **98**, 4473 (1994).
9. T. Koritsanszky, R. Flaig, D. Zobel, H.G. Krane, W. Morgenroth, and P. Luger. Science (Washington, D.C.), **279**, 356 (1998).
10. F.W. Biegler-König, T.T. Nguyen-Dang, Y. Tal, R.F.W. Bader, and A.J. Duke. J. Phys. B: At. Mol. Opt. Phys. **14**, 2739 (1981).
11. C.M. Breneman, T.R. Thompson, M. Rhem, and M. Dung. Comput. Chem. **19**, 161 (1995).
12. C.M. Breneman and M. Rhem. J. Comput. Chem. **18**, 182 (1997).
13. S.E. O'Brien and P.L.A. Popelier. Can. J. Chem. **77**, 28 (1999).
14. P.L.A. Popelier, F.M. Aicken, and S.E. O'Brien. Specialist periodical report, R. Soc. Chem. 2000, to appear in June.
15. A.J. Stone and R.J.A. Tough. Chem. Phys. Lett. **110**, 123 (1984).
16. K.E. Laidig. J. Phys. Chem. **97**, 12760 (1993).
17. S.L. Price, A.J. Stone, and M. Alderton. Mol. Phys. **52**, 987 (1984).
18. R.F.W. Bader and H.J.T. Preston. Int. J. Quantum Chem. **3**, 327 (1969).
19. R.F.W. Bader. Atoms in molecules: a quantum theory. Clarendon Press, Oxford. 1990. p. 147.
20. W.H. Press, B.P. Flannery, S.A. Teucholsky, and W.T. Vetterling. Numerical Recipes. 2nd ed. Cambridge University Press, Cambridge. 1992.
21. J.M. Perez-Jorda, A.D. Becke, and E. San-Fabian. J. Chem. Phys. **100**, 6520 (1994).
22. A.M. Grana and R.A. Mosquera. J. Chem. Phys. 1999, 6606 (1999).
23. P.L.A. Popelier. Comput. Phys. Commun. **108**, 180 (1998).
24. P.L.A. Popelier. Mol. Phys. **87**, 1169 (1996).

© 2000 NRC Canada

Excess molar volumes and viscosities of binary mixtures of some *n*-alkoxyethanols with propylamine at 298.15 K

Amalendu Pal, Sanjay Sharma, and Harsh Kumar

Abstract: Excess molar volumes (V^E_m) and dynamic viscosities (η) for five (alkoxyethanol + propylamine) mixtures have been measured as a function of composition at 298.15 K and atmospheric pressure. The alkoxyethanols were 2-methoxyethanol, 2-(2-methoxyethoxy)ethanol, 2-(2-ethoxyethoxy)ethanol, 2-(2-butoxyethoxy)ethanol, and 2-{2-(2-methoxyethoxy)ethoxy}ethanol. The excess molar volumes V^E_m are all negative over the whole composition range. The viscosity data have been correlated by the methods of Kendall and Monroe, Grunberg and Nissan, Tamura and Kurata, Hind, Katti and Chaudry, and with McAllister correlations. From the experimental data, deviations in the viscosity ($\Delta\eta$) have been calculated. The results are discussed in terms of the interaction between components.

Key words: excess volume, viscosity, binary mixtures.

Résumé : Opérant à 298,15 K et à la pression atmosphérique, on a mesuré les volumes molaires en excès (V^E_m) et les viscosités dynamiques (η) de cinq mélanges (alkoxyéthanol + propylamine) en fonction de la composition. Les alkoxyéthanols utilisés sont: 2-méthoxyéthanol; 2-(2-méthoxyéthoxy)éthanol; 2-(2-éthoxyéthoxy)éthanol; 2-(2-butoxyéthoxy)éthanol et 2-{2-(2-méthoxyéthoxy)éthoxy}éthanol. Les volumes molaires en excès (V^E_m) sont négatifs à toutes les compositions. On a pu établir une corrélation entre les données de viscosité en faisant appel aux méthodes de corrélation de Kendall et Monroe, Grunberg et Nissan, Tamura et Kurata, Hind, Katti et Chaudry et de McAllister. À partir des données expérimentales, on a calculé les déviations dans la viscosité ($\Delta\eta$). On discute des résultats en fonction de l'interaction entre les composants.

Mots clés : volume en excès, viscosité, mélanges binaires.

Introduction

In continuation of our program of research on thermodynamic, acoustic, and transport properties of binary mixtures containing oxygen (-O-) and hydroxyl (-OH) functional groups (1–4), we report here new experimental data of the excess molar volumes (V^E_m) and viscosities (η) of binary solvent mixtures containing 2-methoxyethanol, 2-(2-methoxyethoxy)ethanol, 2-(2-ethoxyethoxy)ethanol, 2-(2-butoxyethoxy)ethanol, and 2-{2-(2-methoxyethoxy)ethoxy}ethanol with propylamine over the whole composition range at 298.15 K and atmospheric pressure. Investigations into the literature have shown that excess properties of binary mixtures of butylamine, dibutylamine, or tributylamine with a straight-chain, branched-chain, or cyclic ether have previously been studied by several authors (5–9). They have analyzed the results in terms of different correlating equations or Flory's theory that gave a better understanding about the association behaviour of the amine and the ether. Recently, few studies involving binary mixtures of propylamine with 1-alkanol have been carried out by some other authors (10–12). The present study was therefore undertaken to assess the effects of increasing the alkyl group size with a common polar head group, and of inserting oxyethylene groups with a common alkyl group in alkoxyethanol. An attempt is also made to interpret the results in terms of intermolecular interactions between amine and alkoxyethanol.

Received September 3, 1999. Published on the NRC Research Press website on March 27, 2000.

A. Pal,[1] S. Sharma,[2] and H. Kumar. Department of chemistry, Kurukshetra University, Kurukshetra 136 119, India.

[1]Author to whom correspondence may be addressed. Fax: +(91)-01744-21639. e-mail: kuru@doe.ernet.in

[2]Present address: Department of Chemistry, Regional Engineering College, Kurukshetra 136 119, India.

Experimental

Material

The propylamine and ethylene glycol monomethyl ether samples were obtained from Merck–Schuchardt with stated purities of >99% and 99.5% and were dried and fractionally distilled (13, 14). The origin and purities of other liquids used have been described (15, 16). All liquids were stored in dark bottles over 4 Å molecular sieves (Fluka, AG) to reduce water content. Prior to measurements, all liquids were partially degassed under vacuum. The densities, and viscosities of these liquids are measured and compared at (298.15 ± 0.01) K and atmospheric pressure with their corresponding literature values (14, 17–23) as shown in Table 1. The densities of pure liquids were measured with a bicapillary pycnometer that gave an accuracy of 5 parts in 10^5.

© 2000 NRC Canada

Table 1. Densities and viscosities of the pure components at 298.15 K.

	$\rho \times 10^{-3}$ (kg m^{-3})		η (mPa s)	
Component	Expt.	Lit.	Expt.	Lit.
Propylamine	0.7122	0.7121 (14)	0.356	0.353 (14)
2-Methoxyethanol	0.9602	0.96024 (14)	1.532	1.60 (14)
		0.96020 (17)		1.5414 (22)
		0.96016 (23)		
2-(2-Methoxyethoxy)ethanol	1.0164	1.0167 (14)	3.448	3.480 (14)
		1.01445 (18)		
2-(2-Ethoxyeyhoxy)ethanol	0.9839	0.9841 (14)	3.828	3.85 (14)
		0.983589 (20)		
		0.98387 (21)		
2-(2-Butoxyethoxy)ethanol	0.9479	0.948016 (20)	5.052	
		0.94916 (21)		
2-{2-(2-Methoxyethoxy)ethoxy} ethanol	1.0430	1.04310 (18)	6.252	6.253 (19)
		1.04524 (19)		

Apparatus and procedure

Excess molar volumes, which are reproducible to ±0.003 $\times 10^6$ m^3 mol^{-1}, were measured by means of a continuous dilution dilatometer in fashion similar to that described by Dickinson et al. (24). Details of its calibration and operational procedures have been described previously (25). Each run covered just over half of the mole fraction range, giving an overlap between two runs.

The kinematic viscosities of both the pure liquids and liquid mixtures were measured with a calibrated Ubbelohde suspended-level viscometer. Experimental details have been given previously (26, 27). Care was taken to prevent evaporation during the measurements. Four or five sets of readings for the flow times were taken for each liquid and the arithmetic mean was taken for the calculation of viscosity. The measured values of kinematic viscosities (ν) were converted to dynamic viscosities (η) after multiplication by the density. The values of η obtained are reproducible to 3×10^{-3} mPas. The flow time was measured with an accurate stop watch with a resolution of 0.01 s. The mole fraction of each mixture was obtained with an accuracy of 1×10^{-4} from the measured apparent masses of the components. All apparent masses were corrected for buoyancy. All the molar quantities were based upon the relative atomic mass table of 1986 issued by IUPAC (28). All the measurements were carried out in a thermostat-controlled well-stirred water bath, whose temperature was controlled to ±0.01 K.

Results

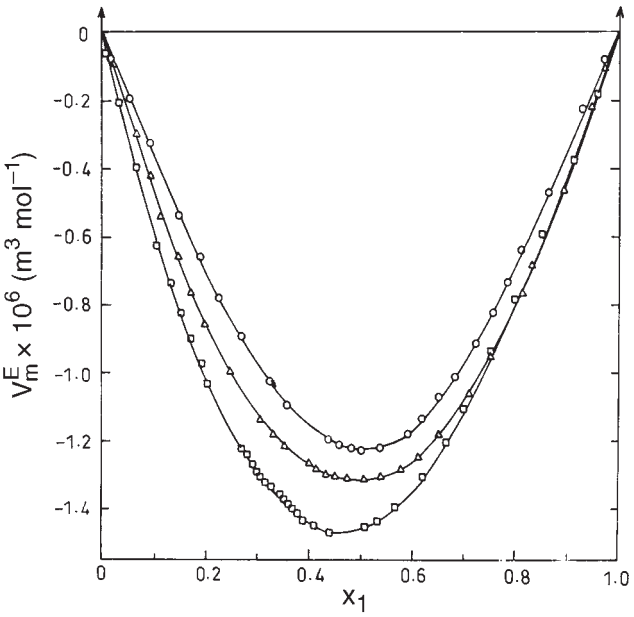
Results of measurements of excess molar volumes for all the binary mixtures at number of mole fractions at 298.15 K are given in Table 2 and are graphically represented in Figs. 1 and 2.

The viscosities were fitted to a polynomial of type:

$$[1] \qquad \eta = \sum_{i=1}^{n} A_i x_1^{\,i}$$

by the method of least squares with equal weights assigned to each point. The values of coefficients A_i and standard deviations σ are listed in Table 3(a).

Fig. 1. Experimental excess molar volumes for propylamine (2) + 2-methoxyethanol (1), ○; 2-(2-methoxyethoxy)ethanol (1), △; 2-{2-(2-methoxyethoxy)ethoxy}ethanol (1), □. Continuous curves were calculated from eq. [5].



The densities of the mixtures were obtained from the densities of the pure components and measurements on V_m^E for their binary mixtures according to the equation:

$$[2] \qquad \rho = (x_1M_1 + x_2M_2)/(V_m^E + x_1V_1 + x_2V_2)$$

where M_1 and M_2 represent molar masses.

The deviation in viscosity $\Delta\eta$ from a linear dependence on mole fraction average has been calculated from the following relation:

$$[3] \qquad \Delta\eta = \eta - x_1\eta_1 - x_2\eta_2$$

where x_1 and x_2 are the mole fractions, η is the dynamic viscosity of the mixtures and η_1 and η_2 are the viscosities of components 1 and 2, respectively. The estimated accuracy of ρ is about 1×10^{-1} kg m^{-3}.

© 2000 NRC Canada

Table 2. Excess molar volumes for (*n*-alkoxyethanol + propylamine) systems at 298.15 K.

x_1	$V_m^E \times 10^6$ (m^3 mol^{-1})	x_1	$V_m^E \times 10^6$ (m^3 mol^{-1})	x_1	$V_m^E \times 10^6$ (m^3 mol^{-1})
2-Methoxyethanol (1) + propylamine (2)					
0.0232	–0.079	0.4408	–1.197	0.7257	–0.912
0.0554	–0.194	0.4615	–1.205	0.7601	–0.818
0.0934	–0.325	0.4868	–1.222	0.7879	–0.731
0.1531	–0.528	0.4996	–1.225	0.8156	–0.634
0.1913	–0.654	0.5394	–1.215	0.8649	–0.469
0.2275	–0.769	0.5904	–1.176	0.9325	–0.223
0.2729	–0.891	0.6232	–1.128	0.9742	–0.078
0.3288	–1.023	0.6543	–1.074		
0.3603	–1.086	0.6888	–1.009		
2-(2-Methoxyethoxy)ethanol (1) + propylamine (2)					
0.0179	–0.087	0.3561	–1.216	0.6149	–1.238
0.0643	–0.303	0.4025	–1.273	0.6538	–1.184
0.0906	–0.423	0.4225	–1.285	0.7142	–1.059
0.1163	–0.540	0.4358	–1.298	0.7538	–0.949
0.1462	–0.661	0.4486	–1.304	0.8119	–0.763
0.1746	–0.762	0.4718	–1.306	0.8353	–0.684
0.2024	–0.864	0.4733	–1.312	0.8908	–0.457
0.2495	–1.001	0.5090	–1.313	0.9471	–0.223
0.3050	–1.135	0.5380	–1.300	0.9756	–0.101
0.3312	–1.180	0.5779	–1.282		
2-(2-Ethoxyethoxy)ethanol (1) + propylamine (2)					
0.0220	–0.161	0.3457	–1.521	0.5627	–1.530
0.0695	–0.478	0.3666	–1.551	0.5889	–1.490
0.1240	–0.779	0.3727	–1.556	0.6107	–1.450
0.1645	–0.971	0.3855	–1.577	0.6356	–1.379
0.1922	–1.092	0.4247	–1.606	0.7285	–1.115
0.2446	–1.275	0.4450	–1.607	0.7712	–0.955
0.2759	–1.363	0.4736	–1.606	0.8481	–0.644
0.3022	–1.430	0.4937	–1.601	0.8848	–0.486
0.3268	–1.486	0.5154	–1.588	0.9396	–0.252
0.3288	–1.488	0.5374	–1.566	0.9718	–0.118
2-(2-Butoxyethoxy)ethanol (1) + propylamine (2)					
0.0063	–0.038	0.2798	–1.201	0.4995	–1.416
0.0197	–0.115	0.2929	–1.237	0.5294	–1.404
0.0682	–0.382	0.2957	–1.244	0.5500	–1.375
0.0873	–0.485	0.3153	–1.279	0.5818	–1.340
0.1043	–0.570	0.3432	–1.328	0.6470	–1.234
0.1282	–0.683	0.3666	–1.365	0.6834	–1.148
0.1485	–0.765	0.3694	–1.368	0.7277	–1.028
0.1941	–0.943	0.3876	–1.385	0.7672	–0.909
0.2076	–0.997	0.3943	–1.393	0.8003	–0.798
0.2239	–1.048	0.4118	–1.406	0.8531	–0.606
0.2583	–1.153	0.4256	–1.418	0.9119	–0.369
0.2727	–1.184	0.4708	–1.427		
2-{2-(2-Methoxyethoxy)ethoxy}ethanol (1) + propylamine (2)					
0.0075	–0.054	0.3022	–1.289	0.5108	–1.451
0.0305	–0.200	0.3061	–1.298	0.5332	–1.430
0.0643	–0.394	0.3207	–1.325	0.5648	–1.392
0.1075	–0.620	0.3252	–1.332	0.6195	–1.302
0.1335	–0.733	0.3442	–1.364	0.6638	–1.203
0.1537	–0.821	0.3511	–1.384	0.7017	–1.097
0.1747	–0.902	0.3586	–1.385	0.7511	–0.943
0.1910	–0.966	0.3671	–1.402	0.8000	–0.782

© 2000 NRC Canada

Table 2 (*concluded*).

x_1	$V^E_m \times 10^6$ (m^3 mol^{-1})	x_1	$V^E_m \times 10^6$ (m^3 mol^{-1})	x_1	$V^E_m \times 10^6$ (m^3 mol^{-1})
0.2086	–1.028	0.3776	–1.414	0.8550	–0.590
0.2734	–1.220	0.3894	–1.427	0.9107	–0.370
0.2790	–1.234	0.4148	–1.449	0.9576	–0.185
0.2937	–1.271	0.4410	–1.165		

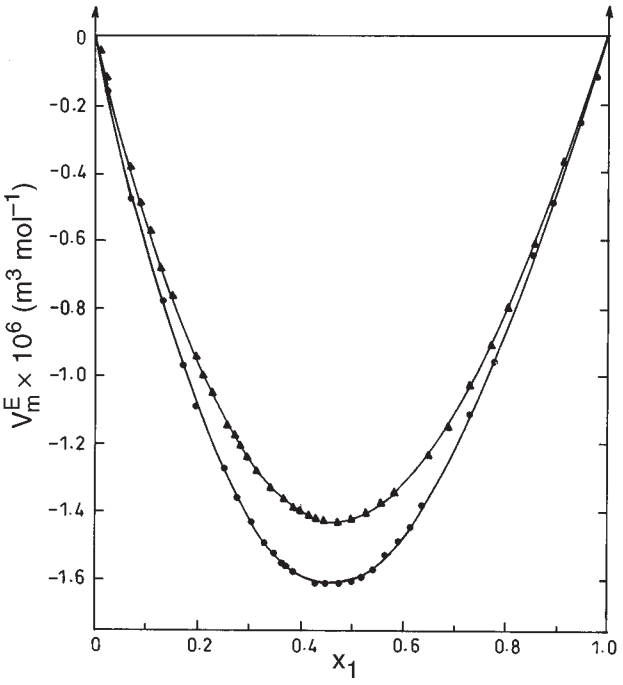


Fig. 2. Experimental excess molar volumes for propylamine (2) + 2-(2-ethoxyethoxy)ethanol (1), ●; 2-(2-butoxyethoxy)ethanol (1), ▲. Continuous curves were calculated from eq. [5].

On the basis of the theory of absolute reaction rate (29), the excess energies of activation ΔG^{*E} for viscous flow were obtained with the expression:

$$[4] \qquad \Delta G^{*E} = RT\{\ln (\eta V/\eta_2 V_2) - x_1 \ln (\eta_1 V_1/\eta_2 V_2)\}$$

where V is the molar volume of mixture and V_1 and V_2 represent molar volumes of the components 1 and 2. R and T have their usual meaning. Data on derived densities, viscosities and energies of activation for viscous flow for the different binary mixtures at 298.15 K are given in Table 4. The values of V^E_m, $\Delta\eta$, and ΔG^{*E} for each mixture have been fitted to the Redlich–Kister (30) polynomial equation:

$$[5] \qquad F(x) = x_1 x_2 \sum_{i=1}^{n} A_i (x_1 - x_2)^i$$

Values of the coefficients A_i and standard deviations are summarized in Table 3(b).

Correlating equations

Several relations have been proposed to evaluate the dynamic viscosity η of liquid mixtures by using classic laws of mixing representative of the viscosity of binary mixtures with an empirical adjustable parameter. In the literature, there are several laws of mixing, which can be classified according to the numbers of adjustable parameters used to account for the deviation from an ideal mixture. We will consider here some of the more commonly used semi-empirical models for analyzing viscosity of liquid mixtures based on zero, one and two parameters. An attempt has been made to check the suitability of the equation for experimental data fits by taking into account the number of empirical adjustment-coefficients.

One of the earliest and more effective equation to describe the dynamic viscosity of binary liquid mixtures as a function of those of the pure components is due to Kendall and Monroe (31) which has no parameter is expressed as

$$[6] \qquad \eta = (x_1 \eta_1^{1/3} + x_2 \eta_2^{1/3})^3$$

The equations of Grunberg–Nissan, Tamura and Kurata, Hind, and Katti and Chaudry have one adjustable parameter. Grunberg and Nissan provided the following empirical equation containing one adjustable parameter (32). The expression is

$$[7] \qquad \ln \eta = x_1 \ln \eta_1 + x_2 \ln \eta_2 + x_1 x_2 G_{12}$$

where G_{12} is a parameter proportional to the interchange energy. Tamura and Kurata developed the following expression for viscosity of binary mixtures (33):

$$[8] \qquad \eta = x_1 \phi_1 \eta_1 + x_2 \phi_2 \eta_2 + 2(x_1 x_2 \phi_1 \phi_2)^{1/2} T_{12}$$

where T_{12} is the interaction parameter and ϕ_1 and ϕ_2 are the volume fractions. Hind et al. (34) suggested the following equation:

$$[9] \qquad \eta = x_1^2 \eta_1 + x_2^2 \eta_2 + 2x_1 x_2 H_{12}$$

where H_{12} is attributed to unlike pair interactions.

Katti and Chaudry (35) derived the following equation:

$$[10] \qquad \ln \eta V = x_1 \ln V_1 \eta_1 + x_2 \ln V_2 \eta_2 + x_1 x_2 W_{vis}/RT$$

where V_i is molar volume of pure component i and W is an adjustable parameter.

McAllister's two-parameter equation (36), based on Eyring's theory of absolute reaction rates (37), takes into account interactions both of like and unlike molecules by a two-dimensional three-body model. The equation is:

$$[11] \qquad \begin{aligned} \ln \nu = {} & x_1^3 \ln \nu_1 + 3x_1^2 x_2 \ln Z_{12} + 3x_1 x_2^2 \ln Z_{21} \\ & + x_2^3 \ln \nu_2 - \ln (x_1 + x_2 M_2/M_1) \\ & + 3x_1^2 x_2 \ln (2/3 + M_2/3M_1) \\ & + 3x_1^2 x_2 \ln (1/3 + 2M_2/3M_1) + x_2^3 \ln (M_2/M_1) \end{aligned}$$

where Z_{12} and Z_{21} are interaction parameters and M_i and ν_i are the molecular mass and kinematic viscosity of pure component i.

© 2000 NRC Canada

Table 3.

(a) Coefficients A_i of eq. [1] for viscosity η (mPa s) and standard deviations σ

Propylamine (2) +	A_1	A_2	A_3	A_4	A_5	σ
2-Methoxyethanol (1)	0.3793	0.3835	2.4888	–1.2618	–0.4751	0.004
2-(2-Methoxyethoxy)ethanol (1)	0.4016	0.4100	6.2914	–1.8841	–1.8377	0.013
2-(2-Ethoxyethoxy)ethanol (1)	0.3925	0.5700	7.2996	–2.9893	–1.5112	0.016
2-(2-Butoxyethoxy)ethanol (1)	0.3896	0.7060	9.8825	–3.7780	–2.2486	0.022
2-{2-(2-Methoxyethoxy)ethoxy} ethanol (1)	0.3812	1.1292	9.2101	0.2549	–4.8997	0.015

(b) Coefficients A_i of eq. [5] and standard deviations σ

Propylamine (2) +		A_1	A_2	A_3	A_4	A_5	σ
2-Methoxyethanol (1)	$V^E_m \times 10^6$ (m^3 mol^{-1})	–4.8858	–0.1691	1.6673	0.3565		.003
	Δη (mPa s)	0.2409	1.1308	0.2338	–0.5098	–0.1395	.002
	ΔG^{*E} (J mol^{-1})	2912.736	1433.845	–828.1564	–921.997	794.4005	11
2-(2-Methoxyethoxy)ethanol (1)	$V^E_m \times 10^6$ (m^3 mol^{-1})	–5.2523	0.1379	–0.2635	0.2811	–1.1918	.003
	Δη (mPa s)	–0.2876	2.8238	0.3575	–1.3088	2055.317	.003
	ΔG^{*E} (J mol^{-1})	5019.816	1212.029	–2160.085	–1057.528		10
2-(2-Ethoxyethoxy)ethanol (1)	$V^E_m \times 10^6$ (m^3 mol^{-1})	–6.3932	1.2276	0.8239	0.5854	–0.2646	.003
	Δη (mPa s)	–0.2278	3.1358	0.2202	–1.4656	1561.787	.003
	ΔG^{*E} (J mol^{-1})	5675.186	704.991	–1861.172	–867.502		14
2-(2-Butoxyethoxy)ethanol (1)	$V^E_m \times 10^6$ (m^3 mol^{-1})	–5.6675	0.8530	0.3184	0.0616	0.2451	.003
	Δη (mPa s)	4.3859	0.5078	–2.1212	–0.3755	1484.480	.002
	ΔG^{*E} (J mol^{-1})	7140.844	4.7606	–1577.714	–896.961		10
2-{2-(2Methoxyethoxy)ethoxy}	$V^E_m \times 10^6$ (m^3 mol^{-1})	–5.8237	1.0453	1.0594	0.1748	–0.9399	.003
ethanol (1)	Δη (mPa s)	–1.2746	4.6546	0.2945	–1.6723	0.3635	.003
	ΔG^{*E} (J mol^{-1})	7286.882		–1927.764	–42.953	1792.323	12

To perform a numerical comparison of the correlating capability of eqs. [6–11] we calculated the standard percentage deviation (σ%) using the relation

$$[12] \quad \sigma(\%) = [1/(n - k) \times \Sigma(100(\eta_{exp} - \eta_{cal})/\eta_{exp})^2]^{1/2}$$

where n represents the number of experimental data and k the number of numerical coefficients in the respective equations.

Discussion

Figures 1 and 2 show that V^E_m values for all mixtures are negative over the whole mole fraction range. The value of V^E_m decreases with the addition of an OC_2H_4 group at the middle of the ether molecules, whereas V^E_m increases in the sequence 2-(2-methoxyethoxy)ethanol > 2-(2-butoxyethoxy)ethanol > 2-(2-ethoxyethoxy)ethanol. This behaviour may be compared with the V^E_m results for mixtures *n*-alkoxyethanols with alcohols (38–43); V^E_m decreases as the alkyl chain length as well as the polar head group of the alkoxyethanol increases. The large negative values of V^E_m is the result of contributions from several factors such as (*i*) the breakdown of self associated structure of alkoxyethanol and amine, (*ii*) the intermolecular hydrogen bond formation in the alkoxyethanol and the amine molecules, and (*iii*) specific interaction between alkoxyethanol and amine. With increasing the polar head group of the alkoxyethanol, interactions between unlike molecules become more important: V^E_m decreases and becomes more negative for the larger *n*-alkoxyethanols. In the same homologous series the algebraic values of V^E_m at $0.1 < x_1 < 0.8$ for the three binary systems with propylamine are in the order 2-(2-ethoxyethoxy)ethanol > 2-(2-butoxyethoxy)ethanol > 2-(2-methoxyethoxy)ethanol. The negative contribution to the V^E_m with 2-(2-ethoxyethoxy)ethanol caused due to strong association by hydrogen bonding and complex forming interaction giving higher negative values compared with those of the other two mixtures

Figure 3 shows that η increases with increase in the mole fraction x_1 of alkoxyethanol for all mixtures. Viscosities of all alkoxyethanol–propylamine binary mixtures increase with an increase in the alkyl group size as well as the polar head group in alkoxyethanol. The deviations in viscosity (Δη) and excess energies of activation for viscous flow (ΔG^{*E}) are represented in Figs. 4 and 5. All the mixtures show negative deviations from mole fraction linearity except small positive deviations in high mole fraction region of alkoxyethanol in alkoxyethanol + propylamine systems. The magnitude of negative deviations increases with increasing polar head group as well as the alkyl chain length of alkoxyethanol. This sequence, highly related to the strengthening of the heteroassociation of molecule with the increase of a $-OC_2H_4$ group in 2-methoxyethanol, is also observed for the excess molar volumes V^E_m of these mixtures. The values of ΔG^{*E} are positive for all the mixtures and increase with increasing the alkyl chain end length as well as the polar head group of alkoxyethanol. The positive values of ΔG^{*E} are attributed to the large size and cohesive energy difference between the two unlike components.

The positive η, Δη, and ΔG^{*E} are an indication of specific interactions (44, 45). In fact, the strong positive deviations in the viscosity for 2-{2-(2-methoxyethoxy)ethoxy}ethanol + propylamine, and 2-(2-butoxyethoxy)ethanol + propylamine

© 2000 NRC Canada

Table 4. Densities, viscosities, and excess energies of activation for viscous flow of (*n*-alkoxyethanols + propylamine) systems at 298.15 K.

x_1	$\rho \times 10^{-3}$ (kg m^3)	η (mPa s)	ΔG^{*E} (J mol^{-1})	x_1	$\rho \times 10^{-3}$ (kg m^3)	η (mPa s)	ΔG^{*E} (J mol^{-1})
2-Methoxyethanol (1) + propylamine (2)							
0.0294	0.7199	0.387	98	0.5165	0.8502	1.031	731
0.0662	0.7298	0.415	134	0.5599	0.8609	1.106	748
0.0845	0.7348	0.431	160	0.5942	0.8692	1.166	756
0.1053	0.7404	0.448	178	0.6575	0.8842	1.265	732
0.1391	0.7497	0.482	233	0.6877	0.8912	1.309	710
0.1936	0.7646	0.540	313	0.7452	0.9043	1.384	644
0.2423	0.7780	0.600	393	0.8042	0.9174	1.442	538
0.2765	0.7873	0.644	442	0.8424	0.9258	1.470	451
0.3210	0.7993	0.708	512	0.8852	0.9352	1.495	343
0.3635	0.8107	0.775	580	0.9064	0.9398	1.505	285
0.3989	0.8200	0.835	635	0.9584	0.9523	1.522	127
0.4418	0.8312	0.909	689	0.9794	0.9556	1.527	65
0.4845	0.8421	0.974	705				
2-(2-Methoxyethoxy)ethanol (1) + propylamine (2)							
0.0255	0.7240	0.399	140	0.5252	0.9100	1.953	1269
0.0563	0.7380	0.444	233	0.5736	0.9236	2.163	1250
0.0879	0.7521	0.493	315	0.6235	0.9369	2.386	1212
0.1249	0.7681	0.562	432	0.6581	0.9457	2.523	1156
0.1605	0.7831	0.634	531	0.7072	0.9576	2.718	1064
0.2036	0.8006	0.735	655	0.7563	0.9689	2.892	940
0.2453	0.8169	0.842	758	0.7974	0.9779	3.020	816
0.2996	0.8371	1.010	904	0.8476	0.9882	3.165	649
0.3405	0.8515	1.159	998	0.8779	0.9942	3.225	525
0.3854	0.8668	1.334	1111	0.9088	1.0000	3.297	405
0.4144	0.8763	1.455	1163	0.9387	1.0055	3.351	276
0.4488	0.8871	1.601	1207	0.9526	1.0080	3.375	215
0.4769	0.8957	1.726	1235				
2-(2-Ethoxyethoxy)ethanol (1) + propylamine (2)							
0.0118	0.7178	0.374	56	0.5112	0.8969	2.092	1414
0.0312	0.7269	0.412	186	0.5558	0.9079	2.317	1409
0.0523	0.7366	0.448	273	0.5903	0.9159	2.488	1381
0.0786	0.7484	0.495	371	0.6330	0.9253	2.695	1325
0.0990	0.7573	0.533	437	0.6711	0.9331	2.869	1254
0.1259	0.7687	0.590	534	0.7054	0.9398	3.013	1171
0.1728	0.7878	0.701	691	0.7412	0.9464	3.154	1071
0.2037	0.7999	0.789	805	0.7802	0.9532	3.297	948
0.2298	0.8097	0.868	890	0.8328	0.9617	3.464	756
0.2646	0.8223	0.986	1003	0.8664	0.9667	3.549	615
0.3048	0.8362	1.133	1113	0.8935	0.9706	3.616	498
0.3392	0.8475	1.272	1180	0.9187	0.9740	3.674	387
0.4055	0.8680	1.566	1325	0.9388	0.9768	3.712	291
0.4419	0.8784	1.745	1379	0.9709	0.9805	3.779	143
0.4758	0.8877	1.917	1412				
2-(2-Butoxyethoxy)ethanol (1) + propylamine (2)							
0.0104	0.7175	0.381	107	0.4782	0.8761	2.460	1780
0.0212	0.7230	0.404	189	0.5424	0.8891	2.900	1761
0.0381	0.7313	0.440	300	0.5729	0.8947	3.115	1734
0.0898	0.7551	0.562	596	0.6163	0.9023	3.404	1662
0.1063	0.7622	0.602	666	0.6419	0.9064	3.571	1608
0.1290	0.7717	0.668	785	0.6779	0.9120	3.790	1511
0.1640	0.7854	0.780	953	0.7205	0.9181	4.031	1374
0.1944	0.7967	0.884	1074	0.7508	0.9221	4.193	1265

© 2000 NRC Canada

Table 4 (*concluded*).

x_1	$\rho \times 10^{-3}$ (kg m^3)	η (mPa s)	ΔG^{*E} (J mol^{-1})	x_1	$\rho \times 10^{-3}$ (kg m^3)	η (mPa s)	ΔG^{*E} (J mol^{-1})
0.2231	0.8067	1.003	1206	0.7957	0.9277	4.402	1077
0.2623	0.8196	1.178	1357	0.8278	0.9314	4.535	930
0.3079	0.8334	1.400	1493	0.8577	0.9347	4.647	784
0.3270	0.8389	1.505	1550	0.8744	0.9364	4.703	698
0.3856	0.8545	1.851	1683	0.9181	0.9407	4.837	464
0.4114	0.8609	2.011	1720	0.9513	0.9437	4.925	278
0.4443	0.8686	2.230	1760	0.9752	0.9458	4.986	141
2-{2-(2-Methoxyethoxy)ethoxy}ethanol (1) + propylamine (2)							
0.0053	0.7157	0.369	54	0.3651	0.8950	1.935	1697
0.0087	0.7179	0.378	91	0.4217	0.9151	2.362	1791
0.0251	0.7285	0.415	214	0.4710	0.9312	2.749	1817
0.0368	0.7359	0.440	281	0.5445	0.9530	3.350	1781
0.0680	0.7548	0.514	458	0.5740	0.9610	3.599	1747
0.0810	0.7624	0.549	534	0.6281	0.9748	4.032	1638
0.1050	0.7761	0.617	661	0.6683	0.9843	4.359	1540
0.1254	0.7872	0.682	772	0.7088	0.9932	4.660	1412
0.1752	0.8130	0.861	1011	0.7716	1.0061	5.104	1180
0.2146	0.8321	1.034	1194	0.8120	1.0137	5.359	1005
0.2627	0.8538	1.279	1388	0.8595	1.0220	5.626	776
0.2934	0.8669	1.456	1495	0.8867	1.0265	5.774	640
0.3347	0.8835	1.724	1625	0.9185	1.0315	5.920	468

Fig. 3. Experimental viscosities for propylamine (2) + 2-methoxyethanol (1), ○; 2-(2-methoxyethoxy)ethanol (1), △; 2-(2-ethoxyethoxy)ethanol (1), ●; 2-(2-butoxyethoxy)ethanol (1), ■; 2-{2-(2-methoxyethoxy)ethoxy}ethanol (1), □. Continuous curves were calculated from eq. [1].

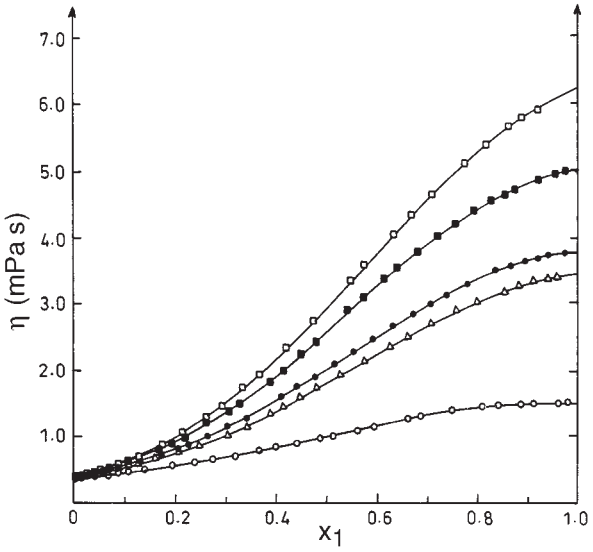
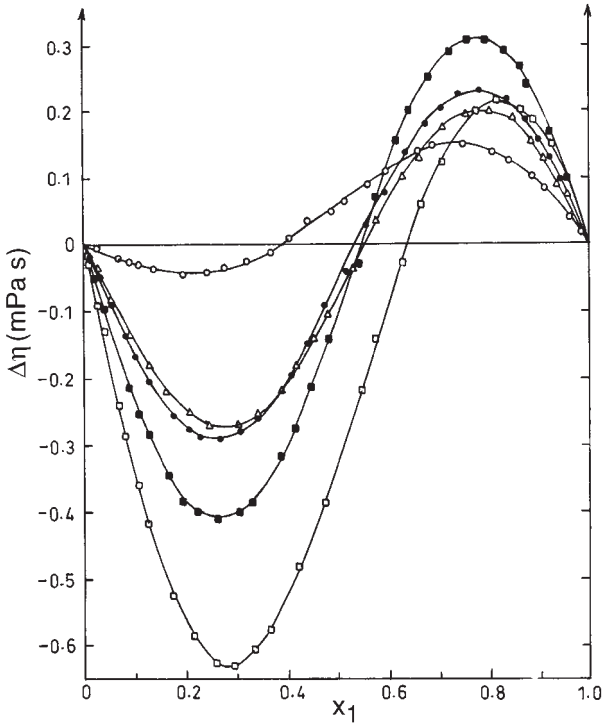


Fig. 4. Experimental viscosity deviations for propylamine (2) + 2-methoxyethanol (1), ○; 2-(2-methoxyethoxy)ethanol (1), △; 2-(2-ethoxyethoxy)ethanol (1), ●; 2-(2-butoxyethoxy)ethanol (1), ■; 2-{2-(2-methoxyethoxy)ethoxy}ethanol (1), □. Continuous curves were calculated from eq. [5].



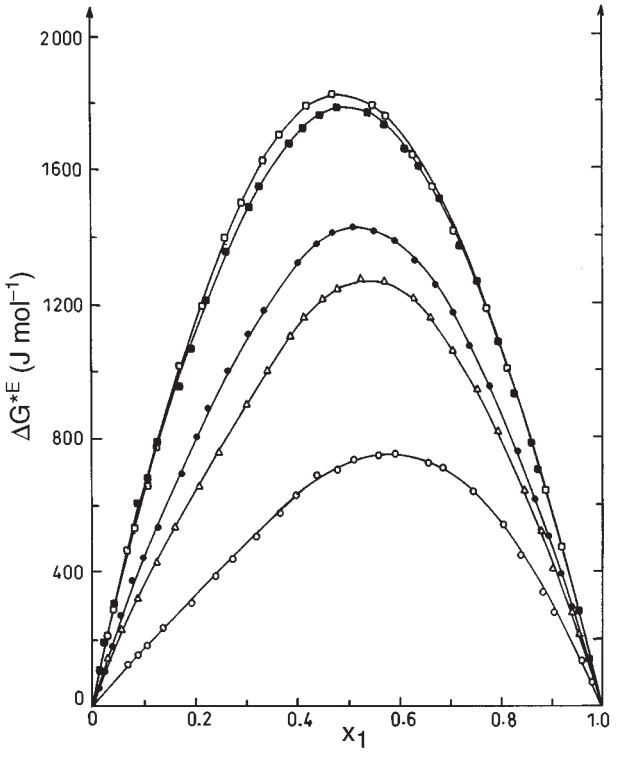
when mixture is rich in alkoxyethanol are observed. But negative deviations in viscosity are observed which regularly increase as the polar head group size or viscosity of the alkoxyethanol is increased. This suggests that the strength of intermolecular hydrogen bonding is not the factor influencing the viscosity deviation of liquid mixtures. The molecular size and shapes of the components also play an equally important role. Their behaviour also finds support from the

© 2000 NRC Canada

Table 5. Values of the parameters and standard percentage deviations for (*n*-alkoxyethanol + propylamine) systems represented by eqs. [7–11] and [6–11].

	eq. 6	eq. 7		eq. 8		eq. 9		eq. 10		eq. 11		
Propylamine (2) +	σ%	G_{12}	σ%	C	σ%	H_{12}	σ%	W_{vis}/RT	σ%	Z_{12}	Z_{21}	σ%
2-Methoxyethanol (1)	13.88	1.18	3.21	0.97	6.95	0.92	7.09	1.12	3.19	1.82	0.92	0.88
2-(2-Methoxyethoxy)ethanol(1)	17.50	1.92	2.78	1.12	9.09	1.32	10.00	1.93	2.80	3.62	1.53	1.58
2-(2-Ethoxyethoxy)ethanol (1)	19.82	2.70	1.62	1.16	7.98	1.78	10.99	2.85	1.76	5.78	2.78	1.30
2-(2-Butoxyethoxy)ethanol (1)	18.60	2.13	1.97	1.14	9.05	1.48	10.43	2.21	1.87	4.04	1.81	1.46
2-{2-(2Methoxyethoxy)ethoxy}ethanol (1)	21.67	2.59	1.33	1.19	9.19	1.76	11.48	2.81	1.49	5.37	2.59	1.22

Fig. 5. Experimental excess energies of activation for viscous flow for propylamine (2) + 2-methoxyethanol (1), ○; 2-(2-methoxyethoxy)ethanol (1), △; 2-(2-ethoxyethoxy)ethanol (1), ●; 2-(2-butoxyethxy)ethanol (1), ■; 2-{2-(2-methoxyethoxy)ethoxy}ethanol (1), □. Continuous curves were calculated from eq. [5].



negative values of excess molar volumes. The large negative values of V_m^E and Δη were also observed for propylamine + 1-alkanol mixture (10) which were interpreted as strong H-bonding between unlike component molecules.

Table 5 gives the results of the correlating eqs. [6–11]. The values of the different adjustable parameters induced in eqs. [6–11] were determined for the systems using a least squares method, with equal weights assigned to each point. These values are reported in Table 5 together with the percentage standard deviations (σ%) between the calculated and experimental values. The values of σ are in the range from 13.9 to 21.7% for eq. [6] without any adjustable parameter; from 1.3 to 12.0% for single parameter eqs. [7–10]; from 0.9 to 1.6% for two parameters eq. [11]. As can be clearly seen by the results of eqs. [7–10] in Table 5, the two eqs. [7] and [10] of Grunberg–Nissan and Katti, and Chaudry give nearly identical results. They both represent the behaviour of the binary mixture satisfactorily as compared to Tamura and Kurata (33), and Hind et al. (34) (eqs. [8] and [9]). The equation of Kendall and Monroe (31) (eq. [6]) without any adjustable parameter is less suitable as the values of σ% are higher than that of the one parameter eqs. [7–10]. Use of the two parameters (eq. [11]) reduces the σ% values significantly below that of single-parameter equations. From this study, it can be concluded that the correlating ability significantly improves for these non-ideal systems as the number of adjustable parameters is increased.

Acknowledgement

The authors acknowledge financial support from the Council of Scientific and Industrial Research (Grant No. 01(1428)/96/EMR-II) for this work.

References

1. A. Pal and A. Kumar. J. Solution Chem. **28**, 153 (1999).
2. A. Pal and S. Sharma. J. Chem. Eng. Data, **44**, 212 (1999).
3. A. Pal and G. Dass. J. Pure Appl. Ultrasonics, **21**, 9 (1999).
4. A. Pal and G. Dass. J. Solution Chem. **28**, 237 (1999).
5. T.M. Letcher and A. Goldon. J. Chem. Eng. Data, **41**, 629 (1996).
6. I.L. Acevedo, M.A. Postigo, and M. Katz. J. Solution Chem. **27**, 977 (1988).
7. T.M. Letcher, U. Domanska, and P. Govender. J. Chem. Thermodyn. **26**, 681 (1994); **26**, 1019 (1994).
8. T.M. Letcher and U. Domanska. J. Chem. Thermodyn. **26**, 553 (1994); **26**, 1241 (1994).
9. S.G. Patel and S.L. Oswal. J. Chem. Soc. Faraday Trans. **88**, 2497 (1992).
10. S.L. Oswal and H.S. Desai. Fluid Phase Equilib. **149**, 359 (1998).
11. I. Farnandez, M.I. Paz-Andrade, M. Pintos, F. Sarmiento, and R. Bravo. J. Chem. Thermodyn. **15**, 581 (1983).
12. D. Papaioannou and C. Panayiotou. J. Chem. Eng. Data, **40**, 202 (1995).
13. T.M. Letcher. J. Chem. Thermodyn. **4**, 159 (1972).
14. J.A. Riddick, W.B. Bunger, and T.K. Sakano. Organic solvents: physial properties and method of purifications. 4th ed. Wiley Interscience, New York. 1986.
15. A. Pal and Y.P. Singh. J. Chem. Thermodyn. **28**, 1197 (1996).
16. A. Pal, H. Kumar, A. Kumar, and G. Dass. Fluid Phase Equilib. **166**, 245 (1999).
17. D. Venkatesulu, P. Venkatesu, and M.V. Prabhakara Rao. J. Chem. Eng. Data, **42**, 365 (1997).
18. G. Douhéret, P. Lajoie, M.I. Davis, J.L. Ratliff, J. Ulloa, H. Høiland, and I.J. Fjellanger. J. Chem. Soc. Faraday Trans. **91**, 2291 (1995).

© 2000 NRC Canada

19. A. Henni, P. Tontiwachwuthikul, and A. Chakma. J. Chem. Eng. Data, **44**, 101 (1999).
20. G. Douhéret, C. Salgado, M.I. Davis, and J. Loya. Thermochim. Acta, **207**, 313 (1992).
21. J.C. Cobos. Ph.D. thesis. Universidad de Valladolid, Spain. 1987.
22. P.K. Muhuri and D.K. Hazra. J. Chem. Eng. Data, **40**, 582 (1995).
23. G. Roux, G. Perron, and J.E. Desnoyers. J. Solution Chem. **7**, 639 (1978).
24. E. Dickinson, D.C. Hunt, and I.A. McLure. J. Chem. Thermodyn. **7**, 731 (1975).
25. A. Pal and Y.P. Singh. J. Chem. Thermodyn. **26**, 1063 (1994).
26. A. Pal and W. Singh. J. Chem. Eng. Data, **42**, 234 (1997).
27. A. Pal and A. Kumar. J. Chem. Eng. Data, **43**, 143 (1998).
28. IUPAC, IUPAC Commission on Atomic weights and Isotopic Abundances 1985. Pure Appl. Chem. **58**, 1677 (1986).
29. R.I. Bearman and P.F. Jones. J. Chem. Phys. **12**, 1432 (1960).
30. O. Redlich and A.T. Kister. Ind. Eng. Chem. **40**, 345 (1948).
31. J. Kendall and K.P. Monroe. J. Am. Chem. Soc. **39**, 1787 (1917).
32. L. Grunberg and A.H. Nissan. Nature (London), **164**, 799 (1949).
33. M. Tamura and M. Kurata. Bull. Chem. Soc. Jpn. **25**, 32 (1952).
34. R.K. Hind, E. McLaughin, and U.R. Ubbelohde. Trans Faraday Soc. **56**, 328 (1960).
35. P.K. Katti and M.M. Chaudry. J. Chem. Eng. Data, **9**, 442 (1964).
36. R.A. McAllister. AIChE J. **6**, 427 (1960).
37. S. Glasstone, K.J. Laidler, and H. Eyring. The theory of rate process. McGraw–Hill, New York. (1941).
38. A. Pal and G. Dass. Indian J. Chem. **38A**, 237 (1999).
39. J.C. Cobos, I.A. Garcia, C. Casanova, G. Roux-Desgranges, and J.-P.E. Grolier. Thermochim. Acta, **131**, 73 (1988).
40. A. Pal and A. Kumar. Acoust. Lett. **20**, 203 (1997).
41. K.Y. Ramana Reddy, K. Rambabu, T. Devarajulu, and A. Krishnaiah. Phys. Chem. Liq. **31**, 9 (1996).
42. A. Pal and W. Singh. J. Chem. Thermodyn. **28**, 1369 (1996).
43. J.C. Cobos, C. Casanova, G. Roux-Desgranges, and J.-P.E. Grolier. J. Chem. Thermodyn. **19**, 791 (1987).
44. R. Palepu, J. Oliver, and B. Mackinnon. Can. J. Chem. **63**, 1024 (1985).
45. R.J. Fort and W.R. Moore. Trans. Faraday Soc. **62**, 1112 (1966).

© 2000 NRC Canada

Kinetics of acetal and orthobenzoate hydrolysis as probes of cyclodextrin–guest binding

Oswald S. Tee, Samer M. I. Hussein, Isabelle E. Turner, and Ogaritte J. Yazbeck

Abstract: Acid-catalyzed hydrolysis of acetophenone dimethyl acetal (ADMA) and trimethyl orthobenzoate (TMOB) is retarded by cyclodextrins (CDs): α-CD, β-CD, hp-β-CD = "hydroxypropyl-β-cyclodextrin", and γ-CD. The observed first order rate constants (k_{obs}) vary with [CD] in the manner expected for 1:1 binding between the substrates and the CDs. Similar behaviour was found recently for the hydrolysis of benzaldehyde dimethyl acetal (BDMA). With β-CD and hp-β-CD, the binding of all three substrates (BDMA, ADMA, TMOB) is strong and the CD-bound forms have very little reactivity. By contrast, substrate binding by α-CD is much weaker, and the CD-bound forms have appreciable, though reduced, reactivity. Substrate binding by γ-CD is also relatively weak, but the bound substrates have very low reactivities. The hydrolysis reactions of ADMA, TMOB, and BDMA have been evaluated as kinetic probes of the binding of guests to CD hosts. For α-CD, β-CD, and hp-β-CD, the addition of guests reduces the amount of free CD and thereby alleviates retardation of the hydrolysis by the CD. The resultant increases in hydrolysis rates can be analyzed to provide estimates of CD–guest dissociation constants, K_G. For aliphatic alcohols and ketones binding to β-CD and hp-β-CD, all three probe reactions provide values of K_G that agree well with each other and with literature values determined by other methods. The approach does not work well with α-CD because of its much weaker binding of the kinetic probes and their less pronounced dependence of k_{obs} on [α-CD]. In the case of γ-CD, the approach cannot be used because added guests cause a further lowering in the rate of hydrolysis, suggesting the formation of an unreactive ternary (substrate·CD·guest) complex.

Key words: acetal, hydrolysis, cyclodextrin, host–guest, binding.

Résumé : L'hydrolyse acidocatalysée du diméthylacétal de l'acétophénone (« ADMA ») et de l'orthobenzoate de triméthyle (« TMBO ») est ralentie par les cyclodextrines (CD), α-CD, β-CD, hp-β-CD (= hydroxypropyl-β-cyclodextrine) et γ-CD. L'influence de la [CD] sur les constantes de vitesse du premier ordre observées (k_{obs}) correspond à celle que l'on peut attendre en faisant l'hypothèse qu'il y a formation d'un complexe 1:1 entre les substrats et les CD. On a observé un comportement semblable récemment pour l'hydrolyse de l'acétal diméthylique du benzaldéhyde (« BDMA »). Avec la β-CD et la hp-β-CD, la fixation des trois substrats (BDMA, ADMA et TMOB) est forte et les formes liées aux CD n'ont qu'une faible réactivité. Par opposition, la fixation des substrats par l'α-CD est beaucoup plus faible et les formes liées aux CD sont assez réactives, même si celles-ci sont réduites. La fixation des substrats par la γ-CD est aussi relativement faible; toutefois, les substrats ainsi liés ont de très faibles réactivités. Les réactions d'hydrolyse des ADMA, TMOB et BDMA ont été évaluées comme sondes cinétiques de la fixation des invités aux CD hôtes. Pour les α-CD, β-CD et hp-β-CD, l'addition de molécules invitées réduit la quantité de CD libre et il en résulte que la CD atténue la diminution de la vitesse d'hydrolyse. L'analyse de l'augmentation qui en résulte dans les constantes de vitesse permet d'obtenir des évaluations des constantes de dissociation CD–hôte, K_G. Pour la fixation d'alcools et de cétones sur les β-CD et hp-β-CD, les trois réactions sondes conduisent à des valeurs de K_G qui sont en accord les unes avec les autres ainsi qu'avec les valeurs déterminées par d'autres méthodes rapportées dans la littérature. Cette approche ne donne pas de bons résultats avec l'α-CD en raison du fait que les sondes cinétiques se fixent beaucoup plus faiblement et que l'influence de la [α-CD] sur k_{obs} est beaucoup plus faible. Dans le cas de la γ-CD, il est impossible d'utiliser cette approche parce que les hôtes supplémentaires provoquent une diminution supplémentaire dans la vitesse d'hydrolyse; ceci suggère qu'il y a formation d'un complexe ternaire (substrat-CD-invité) qui n'est pas réactif.

Mots clés : acétal, hydrolyse, cyclodextrine, hôte–invité, fixation.

[Traduit par la Rédaction]

Received November 23, 1999. Published on the NRC Research Press website on March 27, 2000.

O.S. Tee,[1] S.M.I. Hussein, I.E. Turner, and O.J. Yazbeck. Department of Chemistry and Biochemistry, Concordia University, Montréal, QC H3G 1M8, Canada.

[1]Author to whom correspondence may be addressed. Telephone: (514) 848-3348. Fax: (514) 848-2868. e-mail: ostee@vax2.concordia.ca.

Introduction

Competitive inhibition kinetics (1) are widely used in enzymology to quantify the binding of substrate analogues and transition state analogues to enzymes (2). To a limited extent, similar methodology has been employed for assessing the binding of guests to cyclodextrin (CD) hosts (3). For example, VanEtten et al. (4) studied the inhibition of CD-induced ester cleavage and obtained estimates of dissociation

 © 2000 NRC Canada

Fig. 1. Effects of cyclodextrins on rates of hydrolysis: ADMA and β-CD ■, TMOB and β-CD □, ADMA and hp-β-CD ●. The data for TMOB and hp-β-CD are not shown in the interests of clarity. The curves are calculated from eq. [4], with constants from Table 1.

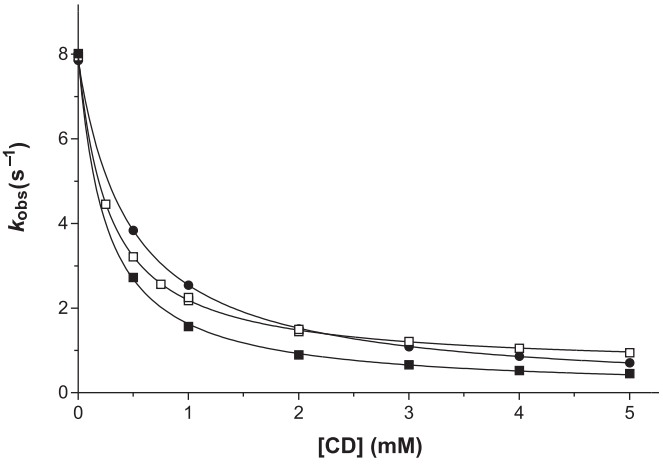
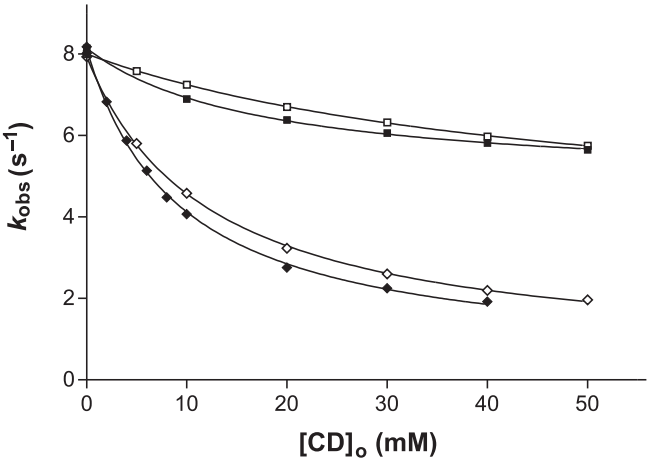


Fig. 2. Effects of cyclodextrins on rates of hydrolysis: ADMA and α-CD □, TMOB and α-CD ■, ADMA and γ-CD ◇, TMOB and γ-CD ◆. The curves are calculated from eq. [4], with constants from Table 1.



constants of CD–guest complexes (K_G, eq. [1]). We have used a similar approach on many occasions (5), although with a different form of data analysis from VanEtten's.

$$[1] \qquad CD + G \underset{K_G}{\overset{K_f}{\rightleftharpoons}} CD{\cdot}G;\ K_G = [CD][G]/[CD{\cdot}G] = 1/K_f$$

The basis of normal "inhibition" methods is that addition of an inhibitor (= guest, G), which binds to the catalyst (enzyme or CD host), reduces the concentration of the free catalyst, and so reduces the rate of the catalyzed reaction. Appropriate analysis of the rate reductions in terms of the amount of added guest then affords an estimate of the catalyst–guest dissociation constant (K_G)[2], or its inverse, the formation constant (K_f) (6).

Recently, we showed that the same approach can be used for a probe reaction that is retarded, rather than catalyzed, by cyclodextrins (CDs) (7). The acid-catalyzed hydrolysis of benzaldehyde dimethyl acetal (BDMA) is strongly retarded by binding to β-CD, hp-β-CD, and γ-CD, but less so by α-CD.[3] In simple cases, the addition of guests lowers the concentration of free CD, reduces the amount of CD-bound substrate, and so *increases* the rate of acetal hydrolysis. Analysis of the rate increases as a function of [guest] can be used to estimate K_G for the CD–guest complexation (7).

In the present paper we report studies of the effects of the same four CDs on the hydrolysis of two more substrates, acetophenone dimethyl acetal (ADMA) and trimethyl orthobenzoate (TMOB), as well as extensive studies of the use of the hydrolysis of BDMA, ADMA, and TMOB as kinetic probes of the binding of alcohols and ketones to CDs, using the methodology of "inhibition kinetics." We have also tried another way of analyzing the rate data to find K_G values. This work is part of our ongoing search for fast[4] and reliable methods of estimating the dissociation constants of host–guest complexes formed by CDs (5, 7).

Results

As found previously for BDMA (7), the acid-catalyzed hydrolysis of acetophenone dimethyl acetal (ADMA) and of trimethyl orthobenzoate (TMOB) are both sharply retarded by β-CD and hp-β-CD (Fig. 1), but much less so by α-CD and γ-CD (Fig. 2). The fitted curves in Figs. 1 and 2 are derived from the normal model for saturation kinetics (5, 7) which allows for 1:1 binding between the substrate (S) and the CD, reaction of the free substrate, eq. [2], and reaction of a substrate–CD complex (S·CD), eq. [3]. For this model the predicted variation of k_{obs} with [CD] is given by eq. [4], assuming that [CD] >> [S·CD] < $[S]_o$, which was valid for all experiments.

$$[2] \qquad S \xrightarrow{k_u} \text{products}$$

$$[3] \qquad S + CD \underset{K_S}{\rightleftharpoons} S{\cdot}CD \xrightarrow{k_c} \text{products}$$

$$[4] \qquad k_{obs} = \frac{(k_u K_S + K_c[CD])}{(K_S + [CD]}$$

Table 1 contains the parameters obtained from fitting eq. [4] to the data for ADMA and TMOB, and used to calculate the curves in Figs. 1 and 2. As seen by the standard errors and correlation coefficients, the fits to the data are good to excellent. Table 1 also contains parameters for BDMA, deter-

[2] In enzymology, K_G is usually referred to as an inhibition constant, K_I (1, 2).

[3] The three parent cyclodextrins are α-cyclodextrin (α-CD), β-cyclodextrin (β-CD), and γ-cyclodextrin (γ-CD), composed of six, seven, and eight glucose units, respectively (3). We also use hydroxypropyl-β-cyclodextrin (hp-β-CD), which is β-CD that has been reacted with propylene oxide so that most of its primary hydroxyl groups are alkylated (3*e*).

[4] Acetal hydrolysis was chosen as a kinetic probe because it is a fast reaction that came be monitored easily in dilute aqueous acid. The broad features of the reaction are well-known and will not be discussed here. Background references can be found in ref. (7).

© 2000 NRC Canada

Table 1. Constants for the effects of cyclodextrins on the acid-catalyzed hydrolysis of ADMA, TMOB, and BDMA.[a]

Cyclodextrin	k_u (s^{-1})	K_S (mM)	k_c (s^{-1})	r	N
(*a*) Acetophenone dimethyl acetal (ADMA)[b]					
α-CD	8.00	49.3 ± 1.6	3.52 ± 0.08	0.9999	7
β-CD	8.02 ± 0.04	0.247 ± 0.006	0.0507 ± 0.0296	0.9999	7
hp-β-CD	7.86 ± 0.01	0.473 ± 0.002	0.0284 ± 0.0082	1.0000	7
γ-CD	7.93	12.3 ± 0.3	0.444 ± 0.063	0.9999	7
(*b*) Trimethyl orthobenzoate (TMOB)[c]					
α-CD	8.14	17.3 ± 0.9	4.81 ± 0.06	0.9997	6
β-CD	7.94	0.281 ± 0.004	0.573 ± 0.018	0.9999	11
hp-β-CD	8.39	0.459 ± 0.004	0.216 ± 0.013	1.0000	5
γ-CD	8.12 ± 0.06	9.30 ± 0.47	0.394 ± 0.128	0.9994	10
(*c*) Benzaldehyde dimethyl acetal (BDMA)[c, d]					
α-CD	3.70 ± 0.01	46.5 ± 3.1	0.588 ± 0.118	0.9990	21
β-CD	3.62 ± 0.02	2.26 ± 0.05	0[e]	0.9992	12
hp-β-CD	3.60 ± 0.01	3.64 ± 0.03	0[e]	0.9999	12
γ-CD	3.66 ± 0.01	51.3 ± 0.4	0[e]	0.9997	19

[a]At 25°C. Values of K_S and k_c were obtained by nonlinear fitting of eq. [4], usually with k_u fixed at the observed value. Where k_u is presented with errors, it was fitted. The errors cited are standard errors, r is the correlation coefficient, and N is the number of data points. Several examples of the data and fitted curves are shown in Figs. 1 and 2.

[b]In 0.010 M aqueous HCl.

[c]In 0.100 M aqueous HCl.

[d]Taken from ref. (7).

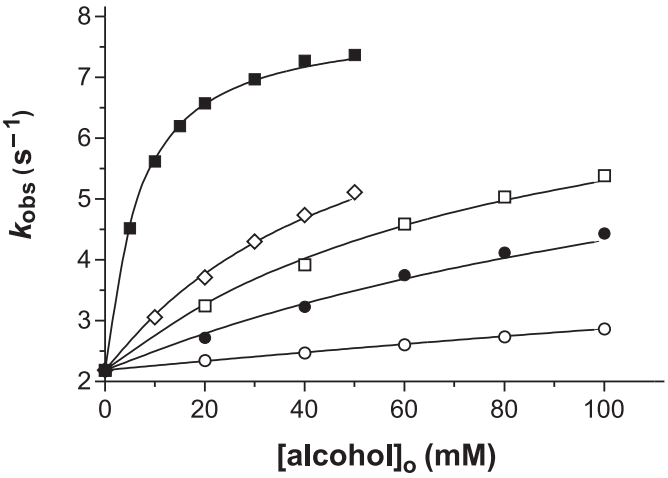
[e]Value fixed at zero. With k_c as a parameter, nonlinear fitting gave values indistinguishable from zero, and closely similar values of K_S. For details, see ref. (7).

mined earlier (7), which are included for comparative purposes, and which were necessary for binding studies discussed later. Note that in the case of the hydrolysis of BDMA, three of the CDs give values of k_c that are indistinguishable from zero, and such is almost the case for ADMA reacting in the presence of β-CD or hp-β-CD (Table 1).

We have carried out a large number of kinetic studies of the effects of guests on the CD-retarded hydrolysis of BDMA, ADMA, and TMOB, to ascertain the feasibility of using the rates of these reactions for estimating dissociation constants of CD–guest complexes. As remarked in the introduction, the addition of a guest, which binds to the CD in competition with the reacting substrate, should lead to an *increase* in k_{obs}, because $k_c < k_u$. Such behaviour has been observed for the hydrolysis of all three substrates in the presence of α-CD, hp-β-CD, and β-CD, with aliphatic alcohols and ketones as guests. Some examples involving the hydrolysis of TMOB, showing the effects of added alcohols and ketones, are presented in Figs. 3 and 4. Comparable behaviour has been found for the hydrolysis of ADMA and BDMA (some examples for BDMA were presented earlier (7)).

Substantial rate increases, such as those displayed in Figs. 3 and 4, can be analyzed to estimate the dissociation constants (K_G) of cyclodextrin–guest (CD·G) complexes using an approach developed some years ago (5*a*). The basis of the approach is utilization of eq. [5], derived from a rearrangement of eq. [4], to find [CD] from k_{obs} measured in the presence of an added guest, G. Using established parameters k_u, k_c, and K_S (Table 1), values of [CD] are calculated for

Fig. 3. Effects of alcohols on the rate of hydrolysis of TMOB in the presence of 1.00 mM β-CD: cyclohexanol ■, 1-pentanol ◇, *tert*-butanol □, 1-butanol ●, 2-propanol ○. The curves are calculated with K_G values from Table 2.



several $[G]_o$, and then estimates of K_G are evaluated, through the use of eq. [6],[5] and averaged. Calculations are carried out in a spreadsheet, as described earlier (5*a*, *c*).

$$[5] \qquad [CD] = \frac{(k_{obs} - k_u)K_S}{(k_c - k_{obs})}$$

$$[6] \qquad K_G = \frac{[CD]([G]_o - [CD]_o + [CD])}{([CD]_o - [CD])}$$

[5]Equation [6] is derived from the definition of K_G in eq. [1], along with the substitution of $[CD] = [CD]_o - [CD\cdot G]$ and $[G] = [G]_o - [CD\cdot G] = [G]_o - ([CD]_o - [CD])$.

© 2000 NRC Canada

Table 2. Dissociation constants (K_G, in mM) of CD–guest complexes determined using inhibition kinetics and the kinetics of hydrolysis of the probes ADMA, TMOB, and BDMA.[a]

Guest	ADMA	TMOB	BDMA[b]	literature
(*a*) β-CD and alcohols[c]				
1-Propanol	184 ± 7	171 ± 7	216 ± 7	200 – 270
2-Propanol	189 ± 2	163 ± 6	218 ± 8	127 – 263
1-Butanol	41.4 ± 4.7	45.1 ± 2.7	54.7 ± 4.2	36.2 – 60.2
	42.4 ± 4.7	36.9 ± 3.3	48.7 ± 1.1	
1-Pentanol	12.8 ± 0.3	11.2 ± 0.6	15.3 ± 0.1	13.2 – 15.8
1-Hexanol	4.07 ± 0.18	3.76 ± 0.12	4.00 ± 0.05	3.57 – 4.84
1-Heptanol	1.27 ± 0.01	1.25 ± 0.06	1.38 ± 0.24	1.41 – 1.52
3-Hexanol	16.2 ± 0.6	14.6 ± 0.2	17.2 ± 0.6	17.7
tert-Butanol	20.3 ± 1.0	18.4 ± 1.4	21.5 ± 0.4	17.9 – 24.0
Cyclohexanol	1.51 ± 0.09	1.44 ± 0.06	1.44 ± 0.14	1.39 – 2.17
		1.32 ± 0.03	1.47 ± 0.23	
(*b*) Hp-β-CD and alcohols[d]				
1-Propanol		310 ± 22	334 ± 10	173, 319
1-Butanol		75.1 ± 1.4	77.5 ± 2.0	64.0
1-Pentanol		22.4 ± 1.4	23.5 ± 0.6	16.6
1-Hexanol		7.33 ± 0.33	6.22 ± 0.27	5.41, 4.37
1-Heptanol		2.29 ± 0.19	1.44 ± 0.14	1.51
3-Hexanol		29.3 ± 1.0	23.9 ± 0.7	20.8
Cyclohexanol		4.07 ± 0.12	3.97 ± 0.09	2.19, 3.66
(*c*) β-CD and ketones[e]				
Acetone		224 ± 29	142 ± 38	367
2-Butanone		91.7 ± 9.1	61.4 ± 19.6	107
			48.9 ± 21.1	
			56.0 ± 12.9	
2-Pentanone		32.2 ± 0.9	34.4 ± 3.3	39.0
			27.6 ± 3.4	
2-Hexanone		11.2 ± 1.8	10.3 ± 1.8	16.4
2-Heptanone		5.07 ± 0.32	4.76 ± 0.21	
2-Octanone		1.87 ± 0.13	1.73 ± 0.03	
3-Pentanone[f]		51.1 ± 2.27		56.9
3-Hexanone[f]	19.8 ± 0.3	21.8 ± 1.0	19.7 ± 0.2	21.2
		18.4 ± 1.4		
3-Heptanone		7.88 ± 0.52		9.62
3-Octanone		3.37 ± 0.27		3.76
4-Heptanone		8.84 ± 0.23		8.79
Cyclopentanone	20.0 ± 0.4	16.2 ± 0.6	18.4 ± 1.5	19.6
Cyclohexanone	2.30 ± 0.24	2.50 ± 0.06	2.88 ± 0.14	2.51
	2.56 ± 0.05	2.63 ± 0.17	2.82 ± 0.05	
Cycloheptanone		0.801 ± 0.040		0.635
Cyclooctanone		0.530 ± 0.040		0.484

[a]At 25°C. The CD-retarded hydrolysis of ADMA was in 0.010 M aqueous HCl; that of TMOB and of BDMA were in 0.100 M aqueous HCl. Multiple entries for a particular guest reflect separate results from different experiments or different researchers.

[b]Values for BDMA and ketones were obtained in this work; those for BDMA and alcohols are taken from ref. (7).

[c]Literature values for β-CD and alcohols are given as the range of the most reasonable values to be found in Matsui and coworkers (8), two recent reviews (9), and other sources cited in ref. (7).

[d]Literature values for hp-β-CD and alcohols are from a method based on the inhibition of basic ester cleavage by the CD or a fluorescent probe displacement method (5*c*).

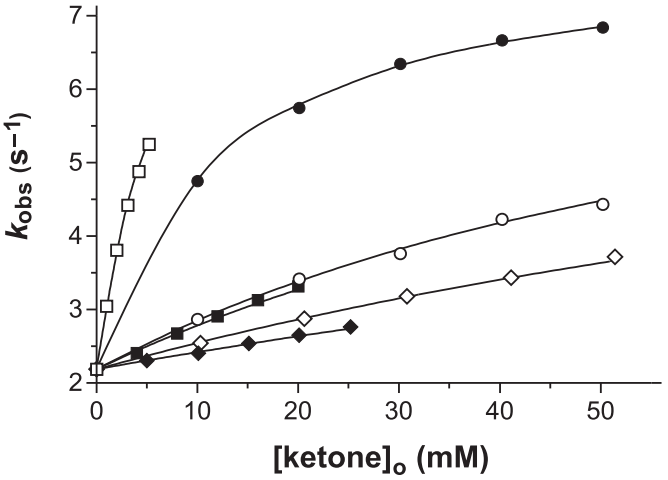
[e]Literature values for β-CD and ketones were obtained from the inhibition of CD-induced ester cleavage or from a fluorescent probe displacement method (5*d*). There are fewer entries for ketones and ADMA because of spectral interference by the ketone guest at the wavelength used to monitor the hydrolysis reaction (see text).

[f]The entry for this 3-isomer in Table 1 of ref. (7) is mislabelled as the 2-isomer.

Table 2 presents a large number of K_G values for the binding of aliphatic alcohols and ketones to β-CD and hp-β-CD, obtained through the use of eqs. [5] and [6], and the hydrolysis of ADMA, TMOB and BDMA as probes. Table 2 also contains literature values for comparison: those for alcohols binding to β-CD are taken primarily from Matsui and co-

© 2000 NRC Canada

Fig. 4. Effects of ketones on the rate of hydrolysis of TMOB in the presence of 1.00 mM β-CD: cycloheptanone □, cyclohexanone ●, cyclopentanone ○, 3-hexanone ■, 2-pentanone ◇, 3-pentanone ◆. The curves are calculated with K_G values from Table 2.



workers (8) and two recent compilations (9)[6] (most of the other values were determined in this laboratory by one or more different methods (5, 7)).

Attempts to use ADMA and TMOB hydrolysis to probe guest binding to α-CD gave results that were variable and hence unreliable, as found previously for BDMA (7). Equally disappointing, experiments on guest binding to γ-CD were unsuccessful since small *decreases* in the rates of hydrolysis of the kinetic probes were observed, instead of the increases that are required for simple 1:1 CD–guest binding.

In addition to the "spreadsheet" analysis, which was used to obtain the K_G values in Table 2, we have examined use of an expression which relates [CD] to the initial concentration of the guest. Expansion of eq. [6] leads to a quadratic in [CD] whose solution is given by eq. [7]. For several different $[G]_o$, non-linear fitting of eq. [7] to the values of [CD], calculated from eq. [5], was used to get an estimate of K_G. Table 3 presents several values obtained in this way, and Fig. 5 shows examples of the variation of [CD] with $[G]_o$, along with the fitted curves described by eq. [7]. It will be noted that the K_G values resulting from fitting to the quadratic solution are essentially identical to those obtained from the spreadsheet treatment, though with smaller standard errors (Table 3).

$$[7] \qquad [CD] = \{-B + (B^2 + 4K_G.[CD]_o)^{1/2}\}/2,$$

$$\text{where } B = ([G]_o - [CD]_o + K_G).$$

Discussion

The present work expands greatly on our initial study of the effects of CDs on the hydrolysis of BDMA (7). Similar behaviour has now been found for ADMA and TMOB (Table 1), and all three hydrolysis reactions can be used as kinetic probes of CD–guest binding, at least for β-CD and hp-β-CD (Table 2). Before discussing some aspects of this usage, we make a few remarks about the substrate binding and how it relates to the rate reductions.

Table 3. Dissociation constants (K_G, in mM) of β-CD–uest complexes, as calculated by the spreadsheet method and quadratic method.[a]

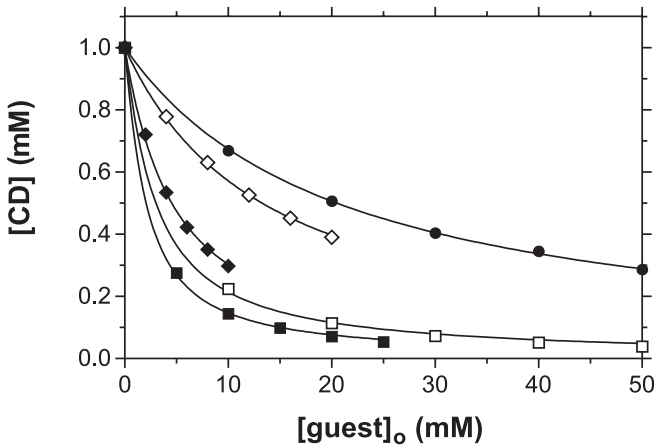
Guest	Spreadsheet method[b]	Quadratic method[c]
1-Propanol	184 ± 7	182 ± 3
2-Propanol	189 ± 2	190 ± 1
1-Butanol	42.6 ± 4.6	43.7 ± 1.7
	42.4 ± 4.7	43.5 ± 1.8
1-Pentanol	12.8 ± 0.3	12.8 ± 0.1
1-Hexanol	4.07 ± 0.18	4.05 ± 0.07
1-Heptanol	1.27 ± 0.01	1.27 ± 0.01
3-Hexanol	16.2 ± 0.6	16.0 ± 0.2
tert-Butanol	20.3 ± 1.0	20.6 ± 0.4
Cyclohexanol	1.51 ± 0.09	1.57 ± 0.03
3-Hexanone	19.8 ± 0.3	19.7 ± 0.2
Cyclopentanone	20.0 ± 0.4	20.0 ± 0.2
Cyclohexanone	2.30 ± 0.24	2.51 ± 0.09
	2.56 ± 0.05	2.54 ± 0.01

[a]At 25°C, in aqueous solution. From the effect of added guests on the kinetics of hydrolysis of ADMA in the presence of 1.00 mM β-CD, in 0.010 M aqueous HCl.

[b]The spreadsheet method refers to application of eq. [5] to the kinetic data and estimation of K_G values with eq. [6] in a spreadsheet, as described elsewhere (5, 7).

[c]The quadratic method entails fitting K_G in eq. [7] to [CD] values calculated using eq. [5].

Fig. 5. Variation of [CD] with $[guest]_o$, calculated from the variation of the rates of hydrolysis of ADMA in the presence of total $[\beta\text{-CD}]_o$ = 1.00 mM. The symbols are: cyclopentanone ●, 1-pentanol ◇, 1-hexanol ◆, cyclohexanone □, cyclohexanol ■. The curves are drawn with the quadratic equation in eq. [7] and fitted K_G values (See Table 3).



Substrate binding

Table 4 contains constants for the binding of BDMA, ADMA, and TMOB, expressed as $pK_S = -\log K_S = -\Delta G°/RT$ to reflect binding energies. Also in the Table, for comparative purposes, are other values from the literature (9). As

[6]The extensive supplementary material for ref. (9*a*) is currently available on the world-wide web at: http://www.pharmacy.wisc.edu/facstaff/sciences/CONNORS_supp.pdf.

© 2000 NRC Canada

Table 4. Constants for the binding of simple phenyl-substituted guests to cyclodextrins.[a]

Ph-X	α-CD	β-CD	hp-β-CD	γ-CD
Ph-$CH(OMe)_2$	1.33	2.65	2.44	1.29
Ph-$CMe(OMe)_2$	1.31	3.61	3.33	1.91
Ph-$C(OMe)_3$	1.76	3.55	3.34	2.03
Ph-H	1.38	2.17		0.96, 1.02
Ph-OH	1.29	1.96, 2.11		
Ph-$OCOCH_3$	1.66	1.94, 2.14[b]		
Ph-CH_2OH	1.33[b]	1.70[b]		
Ph-CH_2NH_2	1.24	1.84[c]		
Ph-COCH3	1.10[d]	2.09[d]	2.15[d]	
Ph-$CH_2CH_2NH_2$	1.41			
Ph-CH_2CH_2OH		2.15		
Ph-$CH(CH_3)NH_2$		1.91		
Ph-$CH(CH_3)OH$	1.12[d]	2.02[d], 2.15	2.19[d]	
Ph-Ph	1.40[e]			
Ph-X (mean)[f]	1.40 ± 0.25	1.98 ± 0.67		1.34 ± 0.35

[a]At 25°C. The constants are values of $pK_d = -\log K_d = \log K_f$, where K_d has units of molarity. The first three rows, for BDMA, ADMA, and TMOB, are from the K_S values in Table 1. For the next 11 derivatives, the values are taken from literature compilations (9), or as noted.

[b]From ref. (8*a*) or (8*b*).

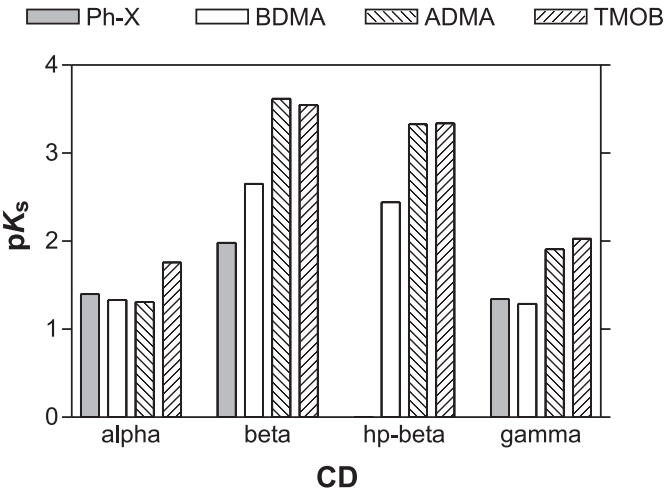
[c]Unpublished work from this laboratory.

[d]Determined in this laboratory (5*d*, 7).

[e]Value for biphenyl minus 0.30, for the statistical correction (10).

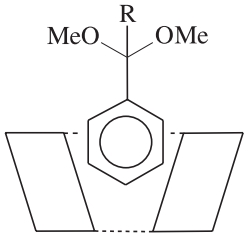
[f]The mean values for Ph-X, calculated by Gadre et al. (10), are based on the following number of derivatives: α-CD 15, β-CD 14, γ-CD 5.

Fig. 6. The relative strengths of binding of Ph-$CH(OMe)_2$, Ph-$CMe(OMe)_2$, and Ph-$C(OMe)_3$ to CDs, compared to the mean values for other phenyl-substituted derivatives.

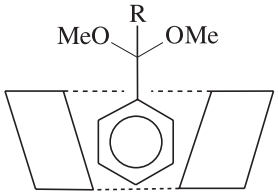


seen there, for all three substrates the strength of binding follows the order: α-CD < β-CD ~ hp-β-CD > γ-CD. This order is typical for benzenoid compounds derivatives (7, 9), and to emphasize the point, Table 4 has the mean values of pK_S determined by Gadre et al. (10) for phenyl-substituted derivatives binding through their phenyl groups.[7] Compared to the mean values for Ph-X derivatives, the pK_S values for Ph-$CH(OMe)_2$, Ph-$CMe(OMe)_2$, and Ph-$C(OMe)_3$ are very similar in some cases, but appreciably higher in others. These trends are most clearly seen from the bar graphs in Fig. 6.

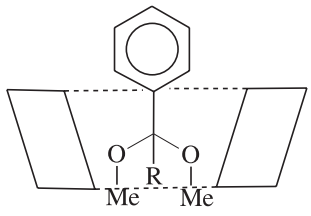
For binding to α-CD, the pK_S values of all three substrates are close to the mean value, consistent with the idea that they bind by their phenyl groups and sit more or less "perched" in the mouth of the CD cavity, as structure **1**. By contrast, substrate binding to β-CD is stronger than that of the mean of other phenyl derivatives, especially for $PhCMe(OMe)_2$ and $PhC(OMe)_3$, suggesting the involvement of some additional interactions. Conceivably, the substrates sit more deeply and snugly in the β-CD cavity, with some attractive interactions between the rim and the substituents (structure **2**). Alternatively, the stronger binding, particularly of ADMA and TMOB, may arise from binding of the substrates to β-CD with their substituents deep inside the CD cavity (structure **3**).



1



2



3

[7]The derivatives considered did not include carboxylic acids because they bind most strongly through their carboxyl groups (9, 10).

© 2000 NRC Canada

Because of its wider cavity (3), one expects γ-CD to show weaker binding than β-CD or hp-β-CD, and such is the case for all three substrates (Table 4). However, in the case of $PhCMe(OMe)_2$ and $PhC(OMe)_3$, their binding to γ-CD is stronger than expected from the mean value for other derivatives, which also may indicate additional interactions with the cavity rim (**2**) or that the substituents are buried inside the CD cavity (**3**).

Reactivity of CD-bound forms

The complexation of BDMA, ADMA, and TMOB by CDs reduces their reactivities in acid-catalyzed hydrolysis significantly (Figs. 1 and 2; Table 1). In the case of α-CD, the reactivities are attenuated by factors of k_u/k_c = 6.3, 2.3, and 1.7, respectively whereas with β-CD and hp-β-CD, both of which bind the substrates much more strongly, the rate reductions are by factors 14 to much more than 270. In the case of BDMA and the two β-CDs, the bound forms are essentially unreactive (Table 1). Even though γ-CD does not bind as strongly as β-CD, it also leads to large rate decreases by a factors of 18, 21, and much more.

In terms of our usual model of transition state stabilization (11), the low reactivities of the CD-substrate complexes mean that the hydrolysis transition states are bound less strongly than the substrates to the CDs ($k_u/k_c = K_{TS}/K_S > 1$). Previously, in our paper on BDMA hydrolysis (7), we argued that this weak transition state binding may be a consequence of the transition state being cationic, and CDs do not bind simple cations as well as neutrals. The same factor was later adopted by Iglesias and coworkers (12) to explain the rate-retarding effects of β-CD on the acid-catalyzed hydrolysis of phenylpropyl nitrites (12*a*) and on the nitrosation of the enol of benzoylacetone (12*b*). In the case of α-CD, where the substrates are most likely bound with their reactive groups exposed to the aqueous medium (**1**), this factor alone may be responsible for the relatively modest rate reductions. However, in the case of the two β-CDs, the much larger reductions in reactivity may result because the substrates are bound deeper within the CD cavity (**2**), and possibly with their substituents buried (**3**). In the latter case, the reactive groups would be more or less completely screened from the aqueous acidic medium and thus quite unreactive. Similar considerations apply to γ-CD, which also causes large rate reductions, even though its binding of the substrates is not as strong (Table 1).

Cyclodextrin–guest binding

In Table 2 are K_G values for various alcohols and ketones binding to β-CD and hp-β-CD, determined using the hydrolysis reactions of ADMA, TMOB, and BDMA as kinetic probes, and data analysis based on eqs. [5] and [6]. For these two CDs, the method works well in most cases, as can be appreciated from the calculated curves in Figs. 3 and 4, the standard errors, and comparisons with the literature values. The only sizeable deviations from the literature values are for quite small guests where the K_G values are large and less easily determined (5*c*, 5*d*, 6), and where there is a greater possibility of the guest not completely impeding the binding of the substrate. In the case of small ketones, like acetone and 2-butanone, there can be an additional problem of spectral interference, as outlined below.

In Table 2, under the column marked ADMA there are several blank entries for ketone guests. In these cases, kinetic experiments were unsatisfactory due to spectral interference by the ketones at the wavelength of 244 nm, used to monitor the appearance of the hydrolysis product, acetophenone. A similar problem was noted for the hydrolysis of BDMA to benzaldehyde, monitored at 252 nm, and it is the probable cause of the fairly large errors for acetone and 2-butanone, which must be added in high concentrations because they bind weakly. Generally speaking, however, the problem was less severe with BDMA than it is with ADMA and so there are more results for ketones under the column labelled BDMA in Table 2. There is no comparable problem of spectral interference when using the hydrolysis of TMOB as the probe because this reaction was monitored at 228 nm.

Previously, we found that the use of BDMA hydrolysis to probe guest binding to α-CD gave results that were not particularly reproducible and therefore unreliable (7). We have found the same to be true for the use of the hydrolysis of ADMA and TMOB. In all three cases, the difficulty is due to the low sensitivity of k_{obs} to [α-CD] (eg., Fig. 2) which arises because the values of k_c and k_u are not greatly different from one another, unlike the situation with β-CD or hp-β-CD (Table 1). As a consequence, relatively small errors in k_{obs} translate to larger errors in [α-CD] and even larger errors in estimates of K_G (7).

Our hopes of finding a new and fast method for assessing guest binding to γ-CD were not realized. None of several binding studies with γ-CD were successful since we observed decreases in the rates of hydrolysis of the probes, instead of the increases that are required for simple 1:1 CD–guest binding. As remarked previously (7), these decreases could arise from the formation of unreactive ternary complexes, composed of substrate, CD, and guest.

Conclusions

Cyclodextrins cause appreciable retardation of the acid-catalyzed hydrolysis of benzaldehyde dimethyl acetal, acetophenone dimethyl acetal, and trimethyl orthobenzoate. Using these three hydrolysis reactions as quantitative probes of CD–guest binding works very well for β-CD and hp-β-CD because these two CDs bind the substrates tightly and cause drastic reductions in their rates of hydrolysis. By contrast, the approach works poorly for α-CD because it does not bind the substrates strongly or reduce the substrate reactivities greatly. With γ-CD the approach is not applicable because added guests cause further reductions in the rates of hydrolysis, not increases, possibly due to formation of ternary (substrate·CD·guest) complexes. The findings also serve to emphasize that to be successful, competition methods for estimating host–guest binding must involve a host and probe that bind together tightly, so that little host or probe need be used, and that the host–probe binding should evoke a large response in some easily measurable property (5*c*, 6).

Experimental

The cyclodextrins were purchased from the Aldrich Chemical Co. or Wacker–Chemie (Munich), and used as supplied.

© 2000 NRC Canada

As previously (5, 7), the hydroxypropyl-β-cyclodextrin used was the Wacker product Beta W 7 HP 0.9, with an average molecular weight of 1500, corresponding to alkylation of six of the seven primary hydroxyl groups of β-CD by 2-hydroxypropyl groups. The substrates (BDMA, TMOB, and ADMA = (1,1-dimethoxy-ethyl)-benzene), alcohols, and ketones were all of the best grades available from Aldrich. Hydrochloric acid solutions were made by dilution of standard 1.00 M solutions obtained from American Chemicals Ltd (Montreal).

Hydrolysis reactions were initiated by 1:1 mixing in a stopped-flow spectrophotometer. Since the orthoester TMOB and the acetal ADMA both hydrolyze slowly but appreciably in water, the substrate solutions were made fresh for each set of kinetic runs, and made slightly basic with a drop of aqueous NaOH solution. These substrate (S) solutions (100 μM) were made up by dilution of a 0.10 M stock solutions in spectral grade acetonitrile, so as to give $[S]_o$ = 50 μM, after 1:1 mixing in the stopped-flow apparatus. For the experiments with varying $[CD]_o$ (eg., Fig. 1), one syringe of the stopped-flow apparatus contained 2 × 0.100 (or 0.010 M) aqueous HCl, and the other syringe held the substrate (100 μM) and the CD at twice the concentration desired in the final, reacting solution.

For the "inhibition" experiments, with fixed $[CD]_o$ and varying $[guest]_o$, one syringe contained 2 × $[CD]_o$ and 0.20 M aqueous HCl, and the other had the acetal (100 μM) and 2 × $[guest]_o$. The values of $[CD]_o$ were usually as follows: α-CD, 20.0 or 30.0 mM; β-CD, 1.00, 2.00, or 5.00 mM; hp-β-CD, 5.00 mM; γ-CD, 20.0 mM. The different values were chosen with regard to the K_S values of the CDs. The ranges of varying $[guest]_o$ used can be judged using the examples shown in Figs. 3, 4, and 5, and from those employed in previous studies involving the same guests (5, 7).

The hydrolysis of BDMA, ADMA, and TMOB was followed by monitoring the appearance of their products in the UV region: benzaldehyde at 252 nm, acetophenone at 244 nm, methyl benzoate at 228 nm. Pseudo-first-order rate constants were calculated from absorbance increases, measured using an Applied Photophysics SX17MV stopped-flow apparatus in the usual way (7). As explained in our initial study of BDMA (7), the first 5% of the absorbance trace was ignored to allow for the induction period that is a feature of acetal hydrolysis. The observation cell of the apparatus was kept at 25.0 ± 0.1°C.

Non-linear fitting of eqs. [4] and [7] was carried out with commercial software: GraphPad Prism, version 2.01. The estimation of dissociation constants of CD–guest complexes using the spreadsheet method and inhibition kinetics has been described in detail in previous publications (5, 7). The use of eq. [7] is described in the main text.

Acknowledgements

This work was made possible by an operating grant and an equipment grant from the Natural Sciences and Engineering Research Council of Canada. We thank Mr. Alexei Fedortchenko for some preliminary experiments and for frequent technical advice. OST is grateful to Dr. Chris Easton and his colleagues at the Research School of Chemistry of the Australian National University for their hospitality and for the award of a Visiting Fellowship during a leave of absence spent in Canberra.

References

1. (*a*) A. Fersht. Enzyme structure and mechanism. 2nd ed. W.H. Freeman, New York. 1985. p. 107; (*b*) I.H. Segel. Enzyme kinetics: behavior and analysis of rapid equilibrium and steady state enzyme systems. Wiley–Interscience, New York. 1975. Chap. 3; (*c*) K.F. Tipton. *In* Enzymology: LABFAX. *Edited by* P.C. Engel. Academic Press, San Diego. 1996. Chap. 4.
2. (*a*) R. Wolfenden. Acc. Chem. Res. **5**, 10 (1972); (*b*) R. Wolfenden and W.M. Kati. Acc. Chem. Res. **24**, 209 (1991).
3. (*a*) M.L. Bender and M. Komiyama. Cyclodextrin chemistry. Springer–Verlag, New York. 1978; (*b*) W. Saenger. Angew. Chem. Int. Ed. Engl. **19**, 344 (1980); (*c*) J. Szejtli. Cyclodextrins and their inclusion complexes. Akademiai Kiado, Budapest, 1982; (*d*) R.J. Clarke, J.H. Coates, and S.F. Lincoln. Adv. Carbohydr. Chem. Biochem. **46**, 205 (1988); (*e*) J. Szejtli. Cyclodextrin technology. Kluwer, Dordrecht. 1988; (*f*) S. Li and W.C. Purdy. Chem. Rev. **92**, 1457 (1992); (*g*) J. Szejtli. Chem. Rev. **98**, 1743 (1998).
4. R.L. VanEtten, J.F. Sebastian, G.A. Clowes, and M.L. Bender. J. Am. Chem. Soc. **89**, 3242 (1967).
5. (*a*) O.S.Tee, M. Bozzi, J.J. Hoeven, and T.A. Gadosy. J. Am. Chem. Soc. **115**, 8990 (1993); (*b*) O.S. Tee, T.A. Gadosy, and J.B. Giorgi. J. Chem. Soc. Perkin Trans. 2, 1705 (1993); (*c*) O.S. Tee, T.A. Gadosy, and J.B. Giorgi. Can. J. Chem. **74**, 736 (1996); (*d*) O.S. Tee, A.A. Fedortchenko, P.G. Loncke, and T.A. Gadosy. J. Chem. Soc. Perkin Trans. 2, 1243 (1996); (*e*) O.S. Tee and J.B. Giorgi. J. Chem. Soc. Perkin Trans. 2, 1013 (1997).
6. K.A. Connors. Binding constants: the measurement of molecular complex stability. John Wiley & Sons, New York. 1987.
7. O.S. Tee, A.A. Fedortchenko, and P. Lim Soo. J. Chem. Soc. Perkin Trans. 2, 123 (1998).
8. (*a*) Y. Matsui and K. Mochida. Bull. Chem. Soc. Jpn. **52**, 2808 (1979); (*b*) Y. Matsui, T. Nishioka, and T. Fujita. Top. Curr. Chem. **128**, 61 (1985).
9. (*a*) K.A. Connors. J. Pharm. Sci. **84**, 843 (1995); (*b*) M.V. Rekharsky and Y. Inoue. Chem. Rev. **98**, 1875 (1998).
10. A. Gadre, V. Rüdiger, H-J. Schneider, and K.A. Connors. J. Pharm. Sci. **86**, 236 (1997).
11. (*a*) O.S. Tee. Adv. Phys. Org. Chem. **29**, 1 (1994); (*b*) A.J. Kirby. Angew. Chem. Int. Ed. Engl. **35**, 707 (1996).
12. (*a*) E. Iglesias. J. Am. Chem. Soc. **120**, 13057 (1998); (*b*) E. Iglesias, V. Ojea-Cao, L Garcia-Rio, and J.R. Leis. J. Org. Chem. **64**, 3954 (1999).

© 2000 NRC Canada

Excess molar volumes and viscosities of binary mixtures of triethylene glycol dimethyl ether (triglyme) with chloroalkanes at 298.15 K

Amalendu Pal and Gurcharan Dass

Abstract: Excess molar volumes (V^E_m) and viscosities (η) for mixtures of triethylene glycol dimethyl ether + dichloromethane, + trichloromethane, and + tetrachloromethane have been determined at 298.15 K and atmospheric pressure over the whole concentration range. From the experimental results, deviations in viscosities ($\Delta \ln \eta$) have been calculated. These properties were fitted to the polynomial relations to obtain the coefficients and the standard deviations. The results have been analysed in terms of molecular interactions between components.

Key words: experiments, data, excess volume, viscosity deviation, binary mixtures.

Résumé : Opérant à 298,15 K, à pression atmosphérique et sur l'ensemble de la plage de concentration, on a mesuré les volumes molaires en excès (V^E_m) et les viscosités (η) de mélanges de l'éther diméthylique du triéthylèneglycol additionné de dichlorométhane, de trichlorométhane ou de tétrachlorométhane. Sur la base des résultats expérimentaux, on a calculé les déviations dans les viscosités ($\Delta \ln \eta$). On a ajusté ces propriétés aux relations polynomiales pour obtenir les coefficients et les déviations standards. On a analysé les résultats en fonction d'interactions moléculaires entre les composants.

Mots clés : expériences, données, volume en excès, déviation de la viscosité, mélanges binaires.

[Traduit par la Rédaction]

Introduction

This is a part of an ongoing program of research in which we study thermodynamic, acoustic, and transport properties of binary mixtures containing alkoxyethanols as one of the components (1–4). The results on excess properties of volume, and viscosity for binary mixtures of *n*-butoxyethanols with chloroalkanes (2–4) were explained by considering the specific interactions between the components. In continuation of these investigations we report here the excess molar volume (V^E_m) and viscosity deviations ($\Delta \ln \eta$), at 298.15 K and atmospheric pressure, of binary mixtures of triethylene glycol dimethyl ether (triglyme) + dichloromethane (DCM), + trichloromethane (TCM), and + tetrachloromethane (TC). Investigations into the literature have shown that excess properties of binary mixtures containing chloroalkanes have previously been studied by several authors (5–7). The present study was therefore undertaken in order to compare the excess molar volumes and deviations in viscosity of triethylene glycol dimethyl ether + chloroalkanes with those of the results for diethylene glycol dimethyl ether + chloroalkanes (8) by the addition of an OC_2H_4 unit, for species with a common alkyl chain.

Received February 26, 1999. Published on the NRC Research Press website on March 27, 2000.

A. Pal[1] and G. Dass. Department of Chemistry, Kurukshetra University, Kurukshetra 136119, India.

[1]Author to whom correspondence to be addressed. Fax: +(91)-01744-21639. e-mail: kuru@doe.ernet.in

Experimental

Materials

Materials were the same origin and purity as used in earlier studies (2). Triethylene glycol dimethyl ether (Acros, U.S.A., 99+%) was fractionally distilled with sodium under reduced nitrogen gas pressure, and only the middle fraction was collected. Karl–Fischer titration gave water contents of 0.01 mass%. The densities and viscosities of these liquids are compared with their corresponding literature values (8–11) in Table 1. All liquids were stored in dark bottles over molecular sieves (Fluka, AG) to reduce water content. Before the measurements, all liquids were partially degassed under vacuum.

Apparatus and Procedure

The excess molar volumes were measured by means of a continuous-dilution dilatometer in fashion similar to that described by Dickinson et al. (12). Details of its calibration, experimental setup, and operational procedure have been described previously (13). The measured excess molar volumes were reproducible to $\pm 0.003 \times 10^6$ m^3 mol^{-1}. Each run covered just over half of the mole fraction range, giving an overlap between two runs. The mole fraction of each mixture was obtained with a precision of 1×10^{-4} from the measured apparent masses of the components. All apparent masses were corrected for buoyancy. All molar quantities are based on the relative atomic mass table of 1986 issued by IUPAC (14).

The kinematic viscosities in both the pure liquids and their mixtures were measured at 298.15 K and atmospheric

 © 2000 NRC Canada

Table 1. Densities and viscosities of the pure components at 298.15 K

Component	$\rho \times 10^{-3}$ (kg m^{-3})		η (mPa s)	
	Expt.	Lit.	Expt.	Lit.
Triethylene glycol dimethyl ether	0.9807	0.98067 (9)	1.950	1.96 (10)
Dichloromethane	1.3165	1.3162 (8)	0.406	0.410 (8)
		1.31678 (11)		0.4043 (11)
Trichloromethane	1.4794	1.4791 (8)	0.532	0.537 (8)
		1.47970 (11)		0.5357 (11)
Tetrachloromethane	1.5843	1.5843 (8)	0.905	0.900 (8)
		1.58436 (11)		0.9004 (11)

Table 2. Excess molar volumes for (triethylene glycol dimethyl ether + chloroalkane) systems at 298.15 K

x_1	$V_m^E \times 10^6$ (m^3 mol^{-1})	x_1	$V_m^E \times 10^6$ (m^3 mol^{-1})	x_1	$V_m^E \times 10^6$ (m^3 mol^{-1})
Triethylene glycol dimethyl ether (1) + dichloromethane (2)					
0.0215	–0.054	0.2160	–0.386	0.5836	–0.331
0.0467	–0.117	0.2467	–0.405	0.6788	–0.249
0.0759	–0.177	0.2690	–0.418	0.7597	–0.182
0.1164	–0.250	0.2777	–0.422	0.8262	–0.123
0.1309	–0.275	0.3149	–0.435	0.8811	–0.077
0.1479	–0.301	0.3541	–0.440	0.9318	–0.041
0.1685	–0.341	0.3809	–0.432		
0.1808	–0.349	0.4319	–0.420		
0.2142	–0.386	0.4851	–0.395		
Triethylene glycol dimethyl ether (1) + trichloromethane (2)					
0.0034	–0.020	0.2997	–0.897	0.5823	–0.611
0.0404	–0.247	0.3220	–0.890	0.6647	–0.487
0.0734	–0.422	0.3450	–0.879	0.7479	–0.366
0.1242	–0.622	0.3920	–0.853	0.7511	–0.362
0.1611	–0.733	0.4322	–0.817	0.8492	–0.223
0.2049	–0.825	0.4480	–0.798	0.9158	–0.121
0.2472	–0.874	0.5016	–0.727	0.9614	–0.060
Triethylene glycol dimethyl ether (1) + tetrachloromethane (2)					
0.0128	–0.013	0.2382	–0.196	0.4935	–0.260
0.0323	–0.033	0.2515	–0.207	0.5625	–0.245
0.0574	–0.057	0.2813	–0.220	0.6065	–0.231
0.0789	–0.077	0.3000	–0.229	0.6869	–0.196
0.0934	–0.089	0.3250	–0.239	0.7856	–0.133
0.1262	–0.118	0.3479	–0.250	0.8857	–0.069
0.1624	–0.149	0.3933	–0.255	0.9356	–0.033
0.2128	–0.186	0.4553	–0.260		

pressure, by using an Ubbelohde suspended-level viscometer (15), which was calibrated with doubly distilled water and benzene. The detailed procedure was described previously (16). Care was taken to prevent evaporation during the measurements. An average of four or five sets of readings for the flow times for each fluid were taken for the purpose of the calculation of viscosity. The measured values of kinematic viscosites (ν) were convereted to dynamic viscosites (η) after multiplication by the density. The values of η obtained were reproducible to 3×10^{-3} mPa s. The flow-time measurements were made with an accurate stopwatch with a precision of 0.01 s. The densities of pure liquids were measured with a bicapillary pycnometer, which gave an accuracy of 5 parts in 10^{-5}. The pycnometer was calibrated at 298.15 K and atmospheric pressure with twice-distilled water. All the measurements were carried out in a thermostatically controlled, well-stirred water bath, whose temperature was controlled to ±0.01 K.

Results

The experimental data of the excess molar volumes for triethylene glycol dimethyl ether + dichloromethane, trichloromethane, and tetrachloromethane for a number of mole fractions at atmospheric pressure and 298.15 K are reported in Table 2. The plots of excess molar volume together with the smoothing curves are given in Fig. 1.

From the measured values of excess molar volumes, densities of liquid mixtures were calculated using the following equation:

© 2000 NRC Canada

Table 3. Densities and viscosities for the (triethylene glycol dimethyl ether + chloroalkane) systems at 298.15 K

x_1	$\rho \times 10^{-3}$ (kg m^{-3})	η (mPa s)	x_1	$\rho \times 10^{-3}$ (kg m^{-3})	η (mPa s)
Triethylene glycol dimethyl ether (1) + dichloromethane (2)					
0.0122	1.3058	0.436	0.4705	1.0805	1.371
0.0214	1.2983	0.451	0.5389	1.0623	1.476
0.0430	1.2808	0.496	0.5879	1.0505	1.549
0.0736	1.2582	0.575	0.6389	1.0393	1.645
0.1008	1.2397	0.621	0.6782	1.0313	1.669
0.1590	1.2046	0.752	0.7651	1.0152	1.787
0.2062	1.1798	0.868	0.8030	1.0089	1.823
0.2482	1.1600	0.960	0.8785	0.9972	1.897
0.3121	1.1332	1.078	0.9474	0.9877	1.920
0.3987	1.1024	1.247			
Triethylene glycol dimethyl ether (1) + trichloromethane (2)					
0.0083	1.4712	0.569	0.4686	1.1550	1.717
0.0278	1.4523	0.622	0.5236	1.1304	1.766
0.0552	1.4269	0.702	0.5853	1.1052	1.809
0.0851	1.4005	0.795	0.6310	1.0879	1.836
0.1347	1.3596	0.962	0.7080	1.0612	1.868
0.1950	1.3141	1.160	0.7445	1.0495	1.893
0.2410	1.2823	1.295	0.8071	1.0307	1.901
0.2903	1.2507	1.425	0.8627	1.0152	1.918
0.3545	1.2131	1.559	0.9174	1.0010	1.934
0.4174	1.1798	1.678	0.9853	0.9845	1.949
Triethylene glycol dimethyl ether (1) + tetrachloromethane (2)					
0.0041	1.5798	0.912	0.4494	1.2222	1.590
0.0202	1.5622	0.952	0.5000	1.1934	1.646
0.0485	1.5325	1.000	0.5522	1.1655	1.696
0.0921	1.4893	1.080	0.6149	1.1341	1.750
0.1704	1.4188	1.198	0.6542	1.1155	1.790
0.2242	1.3749	1.288	0.7187	1.0867	1.826
0.2579	1.3490	1.333	0.7623	1.0683	1.846
0.2736	1.3374	1.364	0.8533	1.0324	1.891
0.3237	1.3018	1.437	0.8992	1.0155	1.913
0.3887	1.2590	1.520	0.9312	1.0040	1.929

[1] $$\rho = (x_1M_1 + x_2M_2)/(V_m^E + x_1V_1 + x_2V_2)$$

where M_1 and M_2 represent molar masses.

The deviations of the viscosities from the ideal mixture values can be calculated from the following relationship (17–19):

[2] $$\Delta \ln \eta = \ln \eta - [\, x_1 \ln \eta_1 + x_2 \ln \eta_2]$$

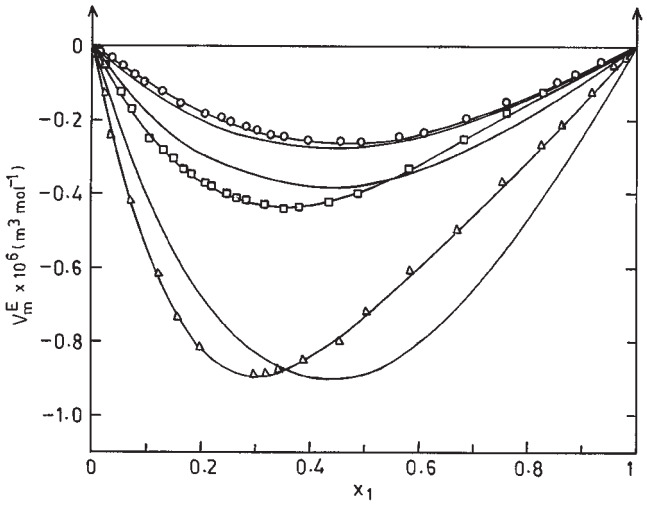
where x_1 and x_2 are the mole fractions, η is the dynamic viscosity of the mixtures, and η_1 and η_2 are the viscosities of components 1 and 2. The derived densities, and viscosities for the three systems at 298.15 K are shown in Table 3. The estimated accuracy of ρ is about 1×10^{-1} kg m^{-3}.

The values of V_m^E and $\Delta \ln \eta$ for each mixture have been fitted to the Redlich–Kister (20) polynomial equation:

[3] $$F = x_1x_2 \sum_{i=1}^{m} A_i(x_1 - x_2)^{i-1}$$

where A_i is the polynomial coefficient and m is the polynomial degree. The values of the coefficients (A_i) obtained by the least-squares method with each points weighted equally are given in Table 4 along with standard deviations (σ).

Fig. 1. Experimental excess molar volumes for triethylene glycol dimethyl ether (1) + dichloromethane (2), □; + trichloromethane (2), △; and + tetrachloromethane (2), ○. Continuous curves were calculated from eq. [3] for experimental data and from PFP theory.



© 2000 NRC Canada

Table 4. Coefficients A_i and standard deviations σ for least-squares representations by eq. [3]

Triethylene glycol dimethyl ether (1) +		A_1	A_2	A_3	A_4	A_5	σ
Dichloromethane (2)	$V^E_m \times 10^6$ (m^3 mol^{-1})	–1.543	1.203	–0.304	–0.122	0.338	0.003
	Δ ln η (mPa s)	1.865	–0.854	0.636	–0.218		0.008
Trichloromethane (2)	$V^E_m \times 10^6$ (m^3 mol^{-1})	–2.915	2.742	–1.660	–0.073	0.452	0.003
	Δ ln η (mPa s)	2.177	–1.599	0.596	0.134		0.008
Tetrachloromethane (2)	$V^E_m \times 10^6$ (m^3 mol^{-1})	–1.034	0.260	0.275			0.002
	Δ ln η (mPa s)	0.864	–0.251	–0.083	–0.178	0.314	0.004

Table 5. Parameters of pure components and Prigogine–Flory–Patterson theory (χ_{12}) at 298.15 K

	$\alpha \times 10^{-4}$ (K^{-1})	$\kappa_T \times 10^7$ (kPa^{-1})	$V^* \times 10^6$ (m^3 mol^{-1})	$P^* \times 10^6$ (J m^{-3})	T^*	$\tilde{V}$	$\tilde{T}$	$\chi_{12} \times 10^6$ (J m^{-3})
Triethylene glycol dimethyl ether	9.72 (9)	7.05[a]	146.28	634	5315	1.2419	0.0561	
Dichloromethane	13.91 (11)	10.26 (11)	48.77	707	4430	1.3227	0.0673	–24.6
Trichloromethane	12.6 (11)	9.98 (11)	62.13	635	4644	1.2987	0.0642	–47.6
Tetrachloromethane	12.29 (11)	10.80 (11)	75.10	567	4695	1.2928	0.0635	–1.3

[a]Calculated from eq. $\kappa_T = \kappa_S + TV\alpha^2/C_{P,m}$; values $C_{P,m}$ calculated from group additivity and κ_S from footnote 2.[2]

In each case, the optimum number of coefficients was ascertained through an examination of the variation of the standard deviation with *m*:

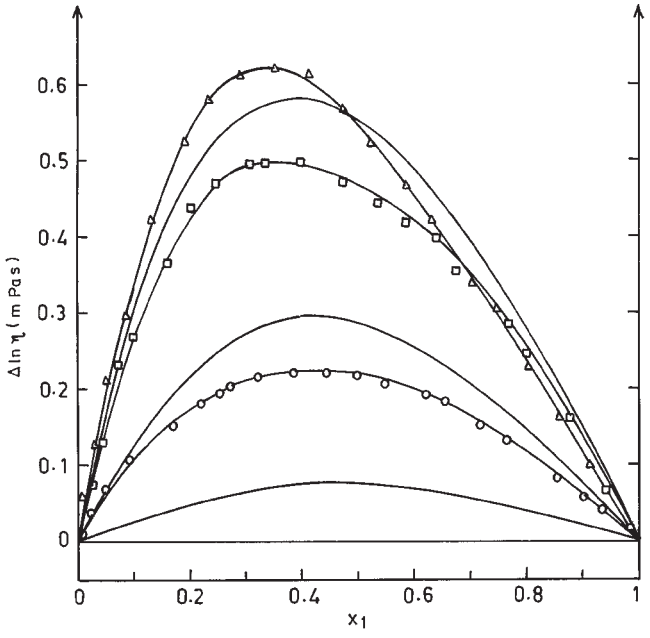
$$[4] \qquad \sigma = [\sum (F_{cal} - F_{obs})^2/(n_{obs} - m)]^{1/2}$$

where n_{obs} is the number of measurements. *F* denotes either V^E_m or Δ ln η. For the mixtures, $\sigma(V^E_m) < 0.003$, in accord with the precision attainable with the dilatometer used.

Figure 1 shows that V^E_m values for these three mixtures are negative over the whole mole fraction range. The behaviour is similar for a diethylene glycol dimethyl ether (8) but with a marked decrease in V^E_m here. The value of V^E_m decreases as the chain length of the hydrophilic moiety $-OC_2H_4-$ increases. The magnitude of V^E_m is the result of contributions from different effects: (*i*) specific interactions due to possible association between the glyme and the chloroalkane molecules, (*ii*) contraction due to molar volume and free volume difference of unlike molecules, and (*iii*) possible association and (or) by hydrogen bonding and other complex forming interactions. It is important to note that a considerable amount of volume contraction is observed for the triglyme (1) + TCM (2) system. This reflects the possible chemical interactions between the oxygen and hydrogen atom of TCM.

The Prigogine–Flory–Patterson (PFP) (21–26) theory was used to correlate the V^E_m results for the present mixtures. The values of the parameters for the pure liquid components required in the PFP theory obtained from Flory's formalism are listed in Table 5. In the prediction of V^E_m values by PFP theory the interaction parameter χ_{12} is needed, this is usualy determined using H^E values. Since values of H^E are not available for these mixtures, the χ_{12} parameter was adjusted by fitting the experimental V^E_m results over the whole mole fraction range. Values of χ_{12} obtained from the PFP theory are listed in the last column of Table 5 and Fig. 1 gives the results estimated from the theory together with the experimental values. The much larger negative values of χ_{12} parameter for the triethylene glycol dimethyl ether (tri-EGDME) + trichloromethane (TCM) systems indicate the possible chemical interaction as suggested from the V^E_m results.

Fig.2. Experimental viscosity deviations for triethylene glycol dimethyl ether (1) + dichloromethane (2), □; + trichloromethane (2), △; and + tetrachloromethane (2), ○. Continuous curves were calculated from eq. [3] for experimental data and from Bloomfield and Dewan data (Bloomfield and Dewan, 1971).



We have determined the η and calculated Δ ln η at 298.15 K as shown in the Fig. 2. The positive values of Δ ln η would imply that the mixture is more viscous than (*i*) the corresponding ideal mixtures and (*ii*) the specific interactions

[2] A. Pal and A. Kumar. Indian J. Pure Appl. Phys. **37**, 810 (1999).

© 2000 NRC Canada

(27), as corroborated by the negative V^{E}_{m} values. There are different expressions available in the literature to calculate η. Here we have applied the method of Bloomfield and Dewan (28).

Bloomfield and Dewan developed an expression from the combination of the theories of free volume and absolute reaction rate. This expression is written

$$[5] \qquad \Delta \ln \eta = f(\tilde{v}) - \Delta G^{R}/RT$$

Where $f(\tilde{v})$ is the characteristic function of the free volumes defined by

$$[6] \qquad f(\tilde{v}) = 1/(\tilde{v} - 1) - x_1/(\tilde{v}_1 - 1) - x_2/(\tilde{v}_2 - 1)$$

and ΔG^{R} is the residual energy of mixing, calculated with the following expression (29):

$$[7] \qquad \Delta G^{R} = \Delta G^{E} + RT(x_1 \ln x_1/\phi_1 + x_2 \ln x_2/\phi_2)$$

The excess free energy can be obtained from the statistical theory of liquid mixtures proposed by Flory and co-workers (23) and is given by the following expression:

$$[8] \qquad \begin{aligned} \Delta G^{E} = {} & x_1 P_1^{*} V_1^{*}[1/\tilde{v}_1 \\ & - 1/\tilde{v} + 3\tilde{T}_1 \ln \{(\tilde{v}_1^{1/3} - 1)/(\tilde{v}^{1/3} - 1)\}] \\ & + x_2 P_2^{*} V_2^{*}[1/\tilde{v} - 1/\tilde{v} \\ & + 3\tilde{T}_2 \ln \{(\tilde{v}_2^{1/3} - 1)/(\tilde{v}^{1/3} - 1)\}] \\ & + (x_1 \theta_2 V_1^{*} \chi_{12})/\tilde{v} \end{aligned}$$

where the various symbols used have their usual meanings.

Using the χ_{12} values from fitting values of V^{E}_{m} and Table 5, ΔG^{R} and $f(\tilde{v})$ were estimated, and finally $\Delta \ln \eta$, according to the Bloomfield and Dewan relationship, which was compared with the experimental data as shown in Fig.2.

Acknowledgement

Financial support (grant no. SP/SI/H-16/94) of this work by the Department of Science and Technology (DST), New Delhi is gratefully acknowledged.

References

1. A. Pal and W. Singh. J. Chem. Eng. Data, **41**, 888 (1996); **40**, 1130 (1995); **41**, 181 (1996).
2. A. Pal and W. Singh. Fluid Phase Equilib. **129**, 211 (1997).
3. A. Pal and A. Kumar. Fluid Phase Equilib. **143**, 241(1998).
4. A. Pal and A. Kumar. Indian J. Chem. Sec. A: Inorg. Bio-inorg. Phys. Theor. Anal. **38A**, 275 (1999).
5. S.C. Sharma, J. M. Joshi, and Y. Singh. J. Chem. Thermodyn. **21**, 331 (1989).
6. A. Spanedda, L. Lepori, and E. Matteoli. Fluid Phase Equilib. **69**, 209 (1991).
7. A. Inglese. Thermochim. Acta, **199**, 173 (1992).
8. M.E. de Ruiz Holgado, C.R. de Schaefer, E.L. Arancibia, and M. Katz. Fluid Phase Equilib. **95**, 299 (1994).
9. C.A. Tovar, E. Carballo, A. Claudio, Cerdeiriña, and L. Romani. J. Chem. Eng. Data, **42**, 1085 (1997).
10. W.J. Wallace, C.S. Shephard, and C. Underwood. J. Chem. Eng. Data, **13**, 11 (1968).
11. J.A. Riddick, W.B. Bunger, and T.K. Sakano. Techniques of chemistry, Vol. 2, 4th ed. Wiley–Interscience. 1986.
12. E. Dickinson, D.C. Hunt, and I.A. McLure. J. Chem. Thermodyn. **7**, 731 (1975).
13. A. Pal and Y.P. Singh. J. Chem. Thermodyn. **26**, 1063 (1994).
14. IUPAC, Commission on Atomic Weights and Isotopic Abundances. Pure Appl. Chem. **58**, 1677 (1986).
15. F.A. Conclaves, J. Kestin, and J.V. Sengers. Int. J. Thermophys. **12,** 1013 (1991).
16. A. Pal and W. Singh. J. Chem. Eng. Data, **42**, 234 (1997).
17. S. Arrhenius. Z. Phys. Chem. Stoechiom. Verwandtschaftsl. **1**, 285 (1887).
18. A. Aucejo, M. Cruz Burguet, R. Munoz, and M. Sanchotello. J. Chem. Eng. Data, **41**, 508 (1996)
19. R.S. Ramadevi, P. Venkatesu, and M.V.P. Rao. J. Chem. Eng. Data. **41**, 479 (1996).
20. O. Redlich and A.T. Kister. Ind. Eng. Chem. **40**, 345 (1948).
21. D. Patterson and G. Delmas. Discuss. Faraday Soc. **49**, 98 (1970).
22. I. Prigogine. The molecular theory of solution. North Holland, Amsterdam. 1957.
23. P.J. Flory. J. Am. Chem. Soc. **87**, 1833 (1965).
24. A. Abe and P.J. Flory. J. Am. Chem. Soc. **87**, 1838 (1965).
25. M. Costas and M.J. Patterson. J. Solution Chem. **11**, 807 (1982).
26. B. Riedl and G. Delmas. Can. J. Chem. **61**, 1876 (1983).
27. R.J. Fort and W.R. Moore. Trans. Faraday Soc. **62**, 1112 (1966).
28. V.A. Bloomfield and R.K. Dewan. J. Phys. Chem. **75** (20), 3113 (1971).
29. B. Celda, R. Gavara, and J.E. Figueruelo. J. Chem. Eng. Data, **32**, 31 (1987).

© 2000 NRC Canada

Solubility of diphenyl sulfone in organic nonelectrolyte solvents. Comparison of observed vs. predicted values based upon Mobile Order theory

Karina M. De Fina, Tiffany T. Van, Kristin A. Fletcher, and William E. Acree, Jr.

Abstract: Experimental solubilities are reported at 25.0°C for diphenyl sulfone dissolved in 25 different organic nonelectrolyte solvents containing ether-, chloro-, hydroxy-, ester, methyl-, and *tert*-butyl-functional groups. Results of these measurements, combined with previously reported diphenyl sulfone solubilities taken from the chemical literature, are used to test the applications and limitations of expressions derived from Mobile Order theory. For the 34 solvents for which predictions could be made, computations show that mobile order theory does provide fairly reasonable estimates of the saturation mole fraction solubilities. Average absolute deviation between predicted and observed values is 49.3%. In comparison, the average absolute deviation is 5 500% when ideal solution behavior is assumed.

Key words: diphenyl sulfone solubilities, organic nonelectrolyte solvents, solubility predictions.

Résumé : Opérant à 25,0°C, on a mesuré les solubilités expérimentales de la diphénylsulfone en solution dans vingt-cinq solvants organiques non électrolytiques qui comprennent des groupes substituants éther, chloro, hydroxyle, ester, méthyle et *tert*-butyle. On a utilisé les résultats de ces mesures, combinés aux valeurs retrouvées dans la littérature pour la solubilité de la diphénylsulfone, pour vérifier les applications et les limitations d'expressions dérivées du modèle de l'ordre mobile. Les trente-quatre solvants pour lesquels il a été possible de faire des calculs montrent que le modèle de l'ordre mobile conduit à des évaluations assez raisonnables des solubilités en fraction molaire de la saturation. La déviation absolue moyenne entre les valeurs prévues et observées est de 49,3%. Pour fins de comparaison, la déviation absolue moyenne est de 5 500% lorsqu'on fait l'hypothèse que le comportement de la solution est idéal.

Mots clés : solubilités de la diphénylsulfone, solvants organiques non électrolytiques, prévisions des solubilités.

Introduction

Solvation energies for solutes dissolved in organic nonelectrolyte solvents are important in thermodynamic modeling in that they provide valuable information in regards to the interaction of the solute with surrounding solvent molecules. Solvation energies can also be used to predict partition coefficients of solutes between water and an immiscible organic solvent and to estimate organic solvent – air partition coefficients, both of which are important properties in understanding the fate and transport of organic chemicals in the environment. There exists in the published chemical literature a fairly large body of experimental solubility and partition coefficient data for organic solvents such as 1-octanol and *n*-hexadecane. Sizeable solubility and partition coefficient databases are also available for several of the saturated alkane solvents, and for benzene, toluene, chloroform, and carbon tetrachloride. Very little experimental data has been published for solutes dissolved in many of the other organic solvents commonly encountered in chemical and engineering applications. Sparcity of experimental data seriously hinders development and testing of predictive linear free energy relationships (LFERs) for most of the individual solvents.

Proposed LFERs have taken several different mathematical forms, depending upon whether one wishes to predict gas/organic solvent partition coefficients (as log L) (1)

$$[1] \qquad \log L = c + r\cdot R_2 + s\cdot\pi_2^H + a\cdot\sum\alpha_2^H + b\cdot\sum\beta_2^H + l\cdot\mathrm{Log}\ L^{16}$$

$$[2] \qquad \log L = c + d\cdot\delta_2 + s\cdot\pi_2^H + a\cdot\sum\alpha_2^H + b\cdot\sum\beta_2^H + l\cdot\mathrm{Log}\ L^{16}$$

$$[3] \qquad \log L = c + r\cdot R_2 + q\mu_2^2 + a\cdot\sum\alpha_2^H + b\cdot\sum\beta_2^H + l\cdot\mathrm{Log}\ L^{16}$$

and water/organic solvent partition coefficients (as log P) (1–3)

Received November 10, 1999. Published on the NRC Research Press website on March 27, 2000.

K.M. De Fina, T.T. Van, K.A. Fletcher, and W.E. Acree, Jr.[1] Department of Chemistry, University of North Texas, Denton, TX 76203-5070, U.S.A.

[1]Author to whom correspondence may be addressed. e-mail: acree@unt.edu

© 2000 NRC Canada

Table 1. Comparison between experimental diphenyl sulfone mole fraction solubilities and predicted values based upon Mobile Order theory.

Organic solvent	$(X_A^{sat})^{exp,a}$	Data ref.	$(X_A^{sat})^{calc}$	% Dev[b]
n-Hexane	0.000524	12	0.000515	–1.7
n-Heptane	0.000593	12	0.000574	–3.2
n-Octane	0.000672	12	0.000714	6.3
n-Nonane	0.000745	12	0.000920	23.5
n-Decane	0.000819	12	0.001000	22.1
n-Hexadecane	0.001411	12	0.001773	25.7
Cyclohexane	0.000872	12	0.000724	–17.0
Methylcyclohexane	0.000882	This work	0.000862	–2.3
Cyclooctane	0.00126	This work	0.00133	5.6
2,2,4-Trimethylpentane	0.000497	12	0.000372	–25.2
tert-Butylcyclohexane	0.00114	This work	0.00147	28.9
Squalane	0.00194	This work	0.00400	106.2
Dibutyl ether	0.00414	This work	0.00941	127.3
Methyl *tert*-butyl ether	0.00932	This work		
Tetrahydrofuran	0.1051	This work	0.0446	–57.6
1,4-Dioxane	0.0902	This work	0.0844	–6.5
Methanol	0.00491	12	0.00134	–72.7
Ethanol	0.00535	12	0.00113	–78.9
1-Propanol	0.00527	12	0.00113	–78.6
2-Propanol	0.00349	12	0.00152	–56.4
1-Butanol	0.00527	12	0.00137	–74.0
2-Butanol	0.00436	12	0.000837	–80.8
2-Methyl-1-propanol	0.00397	This work	0.000542	–86.3
2-Methyl-2-propanol	0.00423	This work	0.000386	–90.9
1-Pentanol	0.00532	12	0.00130	–75.6
2-Pentanol	0.00453	This work		
3-Methyl-1-butanol	0.00453	This work		
2-Methyl-2-butanol	0.00550	This work		
1-Hexanol	0.00528	12	0.00102	–80.7
2-Methyl-1-pentanol	0.00449	This work		
4-Methyl-2-pentanol	0.00450	This work		
1-Heptanol	0.00498	12	0.00115	–76.9
1-Octanol	0.00484	12	0.00128	–73.6
2-Ethyl-1-hexanol	0.005304	This work		
1-Decanol	0.00466	This work	0.00150	–67.8
Cyclopentanol	0.00943	This work		
Butyl acetate	0.03410	This work	0.04382	28.5
Ethyl acetate	0.04458	This work	0.07724	73.3
Methyl acetate	0.04978	This work		
1,2-Dichloroethane	0.1093	This work	0.09048	–17.2
1-Chlorobutane	0.02253	This work	0.00770	–65.8
1-Chlorooctane	0.01183	This work	0.01457	23.2
Chlorocyclohexane	0.02541	This work	0.02135	–16.0

[a]Numerical values represent the average of between four and eight independent determinations, with the measurements being reproducible to ±1.5%.

[b]Deviations (%) = $100[(X_A^{sat})^{calc} - (X_A^{sat})^{exp}]/(X_A^{sat})^{exp}$.

$$[4] \quad \log P = c + r\cdot R_2 + s\cdot\pi_2^H + a\cdot\sum\alpha_2^H + b\cdot\sum\beta_2^H + v\cdot V_x$$

$$[5] \quad \log P = c + d\cdot\delta_2 + s\cdot\pi_2 + a\cdot\alpha_2 + b\cdot\beta_2 + v\cdot V_x$$

where R_2 and V_x refer to the excess molar refraction and McGowan volume of the solute, respectively, π_2^H (and π_2) is the solute dipolarity/polarizability descriptor, and $\sum\alpha_2^H$ (and α_2) and $\sum\beta_2^H$ (and β_2) are measures of the solute's hydrogen-bond acidity and hydrogen-bond basicity, respectively. δ_2 is a polarizability parameter which was preset by Kamlet et al. (4) to 0.0 in the case of nonpolychlorinated aliphatic solutes, to 0.5 for polychlorinated aliphatic solutes, and to 1.0 for aromatic solutes. Numerical values of the solute descriptors are available in several published tabulations for 500+ common organic molecules and inorganic gas solutes (3–6). For any given solvent, numerical values of the various curve-fit coefficients (*c*, *r*, *s*, *a*, *b*, *d*, *l*, *q*, and *v*) are

© 2000 NRC Canada

Table 2. Solvent and solute properties used in Mobile Order predictions.

Component (i)	V_i (cm^3 mol^{-1})	δ_i' (MPa$^{1/2}$)[a]
n-Hexane	131.51	14.56
n-Heptane	147.48	14.66
n-Octane	163.46	14.85
n-Nonane	179.87	15.07
n-Decane	195.88	15.14
n-Hexadecane	294.12	15.61
Cyclohexane	108.76	14.82
Methylcyclohexane	128.32	15.00
Cyclooctane	134.9	15.40
2,2,4-Trimethylpentane	166.09	14.30
tert-Butylcyclohexane	173.9	15.50
Squalane	525.0	16.25
Dibutyl ether	170.3	17.45
Tetrahydrofuran	81.4	19.30
1,4-Dioxane	85.8	20.89
Methanol	40.7	19.25
Ethanol	58.7	17.81
1-Propanol	75.10	17.29
2-Propanol	76.90	17.60
1-Butanol	92.00	17.16
2-Butanol	92.4	16.60
2-Methyl-1-propanol	92.8	16.14
2-Methyl-2-propanol	94.3	15.78
1-Pentanol	108.6	16.85
1-Hexanol	125.2	16.40
1-Heptanol	141.9	16.39
1-Octanol	158.3	16.38
1-Decanol	191.6	16.35
Butyl acetate	132.5	19.66
Ethyl acetate	98.5	20.79
1,2-Dichloroethane	78.8	20.99
1-Chlorobutane	105.0	17.12
1-Chlorooctane	171.1	18.00
Chlorocyclohexane	120.3	18.45
Diphenyl sulfone[b]	161.5[c]	23.65[d]

[a]Tabulated values are taken from a compilation given in Ruelle and coworkers (16, 17, 19, 20).

[b]The numerical value of a_A^{solid} = 0.1100 was calculated from eq. [9] using ΔH_A^{fus} = 21 780 J mol^{-1} and T_{mp} = 398.2 K.[2]

[c]Numerical value of $V_{dpsulfone}$ = 161.5 cm^3 mol^{-1} was estimated using the known molar volumes of dimethyl sulfoxide, diphenyl sulfide, and dimethyl sulfide.

[d]Numerical value was calculated using the measured diphenyl sulfone mole fraction solubilities in *n*-hexane, *n*-heptane, and *n*-octane, in accordance with eqs. [6] and [8] (with $r_{solvent}$ = 0 and (or) $K_{ASolvent}$ = 0).

deduced by regressing experimental partition coefficient data in accordance with eqs. [1]–[5]. At the present time coefficients are available for only 50 or so different water/organic solvent and gas/solvent systems (2, 3, 7–11). Equations [1]–[5] allow one to estimate water/organic solvent and gas/solvent partition coefficients for systems for which the solute descriptors and curve-fit coefficients are known.

If correlation equations are to be developed for still more organic solvents, then additional experimental data must be measured. Activity coefficients, partition coefficients, and saturation solubilities for a mininum of 40 or so different solutes are required to derive meaningful correlation equations. Moreover, the solutes used should span as wide of a range of solute descriptor values as possible. To increase the solubility database available for developing LFERs, we are in the process of measuring solubility data for polycyclic aromatic hydrocarbons (PAHs), polycyclic aromatic nitrogen hetero-atoms (PANHs), and other crystalline sulfur-containing nonelectrolyte solutes. In the present communication, we report diphenyl sulfone solubilities at 25°C in 25 different organic solvents containing ether-, chloro-, hydroxy-, ester, methyl-, and *tert*-butyl-functional groups. This brings the number of organic solvents for which we have reported diphenyl sulfone solubility data up to 43. Previously we had reported diphenyl sulfone solubilities in water and in eight alkane and ten alcohol solvents (12). Results of the measurements are used to further test the applications and limitations of predictive expressions derived from Mobile Order theory. Lack of enthalpy of fusion data for diphenyl sulfone prevented us from using Mobile Order theory at the time our first set of diphenyl sulfone solubility data was published.

Materials and methods

Diphenyl sulfone (Aldrich, 97%) was recrystallized several times from methanol. Methylcyclohexane (Aldrich, 99+%, anhydrous), *tert*-butylcyclohexane (Aldrich, 99+%), cyclooctane (Aldrich, 99+%), squalane (Aldrich, 99%), dibutyl ether (Aldrich, 99%), 2-pentanol (Acros Organics, distributed by Fisher Scientific, 99+%), 2-methyl-2-butanol (Acros, 99+%), 2-methyl-1-propanol (Aldrich, 99+%, anhydrous), 3-methyl-1-butanol (Aldrich, 99+%, anhydrous), 4-methyl-2-pentanol (Acros Organics, 99+%), 2-ethyl-1-hexanol (Aldrich, 99+%), 2-methyl-1-pentanol (Aldrich, 99%), 1-decanol (Alfa Aesar, 99+%), cyclopentanol (Aldrich, 99%), 1,4-dioxane (Aldrich, 99.8%, anhydrous), tetrahydrofuran (Aldrich, 99.9%, anhydrous), methyl *tert*-butyl ether (Arco, 99.9+%), ethyl acetate (Aldrich, HPLC, 99.9%), 2-methyl-2-propanol (Arco Chemical Co. 99+%), 1,2-dichloroethane (Aldrich, HPLC, 99.8%), 1-chlorobutane (Sigma–Aldrich, HPLC, 99.5+%), 1-chlorooctane (Aldrich, 99%), chlorocyclohexane (Aldrich, 99%), methyl acetate (Aldrich, 99.5%, anhydrous) and butyl acetate (Aldrich HPLC, 99.7%) were stored over molecular sieves before use. Gas chromatographic analysis showed solvent purities to be 99.7 mole % or better.

Excess solute and solvent were placed in amber glass bottles and allowed to equilibrate in a constant temperature water bath at 25.0 ± 0.1°C for at least three days (often longer). Attainment of equilibrium was verified both by repetitive measurements after several additional days and by approaching equilibrium from supersaturation by pre-equilibrating the solutions at a higher temperature. Aliquots of saturated diphenyl sulfone solutions were transferred through a coarse filter into a tared volumetric flask to determine the amount of sample and diluted quantitatively with methanol (or 2-propanol in the case of the larger alkane solvents) for spectrophotometric analysis at 267 nm on a Bausch and Lomb Spectronic 2000. Concentrations of the dilute solutions were determined from a Beer–Lambert law

© 2000 NRC Canada

absorbance vs. concentration working curve for nine standard solutions. The concentration of diphenyl sulfone in the standard solutions varied from 2.08×10^{-4} M to 9.35×10^{-4} M. The calculated molar absorptivity of the standard solutions varied slightly over the concentration range, from $\epsilon \approx 1850$ L mol^{-1} cm^{-1} (2.08×10^{-4} M) to $\epsilon \approx 1750$ L mol^{-1} cm^{-1} (9.35×10^{-4} M).

Experimental molar concentrations were converted to (mass/mass) solubility fractions by multiplying by the molar mass of diphenyl sulfone, volume(s) of volumetric flask(s) used, and any dilutions required to place the measured absorbances on the Beer–Lambert law absorbance vs. concentration working curve, and then dividing by the mass of the saturated solution analyzed. Mole fraction solubilities were computed from (mass/mass) solubility fractions using the molar masses of the solute and solvent. Experimental diphenyl sulfone solubilities, X_A^{sat}, in 25 organic solvents studied are listed in Table 1. Numerical values represent the average of between four and eight independent determinations, with the measurements being reproducible to ±1.5%. For each solvent studied, all experimental measurements fell within ±1.5% of the average value listed in Table 1.

Results and discussion

Solvents listed in Table 1 include both noncomplexing alkanes and self-associating alcohols. Of the many solution models proposed in recent years, mobile order theory is perhaps the only one that is capable of describing solute behavior in such a wide range of solvent mixtures. The basic model (13–20) assumes that all molecular groups perpetually move, and that neighbors of a given kind of external atom in a molecule constantly change identity. All molecules of a given kind dispose of the same volume, equal to the total volume V of the liquid divided by the number N_A of molecules of the same kind, i.e., Dom A = V/N_A. The center of this domain perpetually moves. The highest mobile disorder is achieved whenever groups visit all parts of their domain without preference. Preferential contacts lead to deviations with respect to this "random" visiting. This is especially true in the case of hydrogen-bonding as specific interactions result in a specific orientation of the "donor" molecule with respect to an adjacent "acceptor" molecule.

In the case of an inert crystalline solute dissolved in a self-associating solvent, Mobile Order theory expresses the volume fraction saturation solubility, ϕ_A^{sat}, as

$$[6]\quad \ln \phi_A^{sat} = \ln a_A^{solid} - 0.5(1 - V_A/V_{solvent})\phi_{solvent} + 0.5 \ln [\phi_A^{sat} + \phi_{solvent}(V_A/V_{solvent})] - \phi_{solvent}^2 V_A(\delta'_A - \delta'_{solvent})^2(RT)^{-1} - r_{solvent}(V_A/V_{solvent})\phi_{solvent}$$

where the $r_{solvent}(V_A/V_{solvent})\phi_{solvent}$ term represents the contributions resulting from hydrogen-bond formation between the solvent molecules. For most of the published applications, $r_{solvent}$ was assumed to be unity for strongly associated solvents with single hydrogen-bonded chains such as monofunctional alcohols, to be two for water or diols, and to equal zero for nonassociated solvents such as saturated hydrocarbons. A more exact value for alcoholic solvents can be calculated based upon

$$[7]\quad r_{solvent} = (K_{solvent}\phi_{solvent}/V_{solvent})/(1 + K_{solvent}\phi_{solvent}/V_{solvent})$$

with a numerical value of $K_{solvent} = 5\,000$ cm^3 mol^{-1} assumed for all monofunctional alcohols.

If complexation does occur between the crystalline solute and solvent

$$[8]\quad \ln \phi_A^{sat} = \ln a_A^{solid} - 0.5(1 - V_A/V_{solvent})\phi_{solvent} + 0.5 \ln [\phi_A^{sat} + \phi_{solvent}(V_A/V_{solvent})] - \phi_{solvent}^2 V_A(\delta'_A - \delta'_{solvent})^2(RT)^{-1} + \ln [1 + \phi_{solvent}(K_{ASolvent}/V_{solvent})]$$

then an additional term involving the solute–solvent equilibrium constant, $K_{ASolvent}$, must be introduced to describe the solubility enhancement that arises as a result of specific interactions. A slightly more complex expression applies in the case of solute complexation with a self-associating solvent. The symbols δ'_A and $\delta'_{solvent}$ denote the modified solubility parameters of the solute and solvent, respectively, V_i is the molar volume, and a_A^{solid} is the activity of the solid solute. This latter quantity is defined as the ratio of the fugacity of the solid to the fugacity of the pure hypothetical supercooled liquid. The numerical value of a_A^{solid} can be computed from

$$[9]\quad \ln a_A^{solid} = -\Delta H_A^{fus}(T_{mp} - T)/(RTT_{mp}) + (\Delta C_{p,A}/RT)(T_{mp} - T) - (\Delta C_{p,A}/T) \ln (T_{mp}/T)$$

the solute's molar enthalpy of fusion, ΔH_A^{fus}, and heat capacity difference, $\Delta C_{p,A}$, at the normal melting point temperature, T_{mp}. Contributions from nonspecific interaction are incorporated into mobile order theory through the $\phi_{solvent}^2 V_A(\delta'_A - \delta'_{solvent})^2(RT)^{-1}$ term. Ruelle and coworkers (16–20) have presented an impressive set of comparisons between experimental and predicted values for anthracene, naphthalene, pyrene, biphenyl, carbazole, benzil, *p*-benzoquinone, tricosane, octacosane, 10-nonadecanone, 11-heneicosanone, and 12-tricosanone solubilities in a wide range of both noncomplexing and complexing solvents to document the predictive ability of Mobile Order theory.

Predictive application of eqs. [6] and [8] is relatively straightforward. First, an average numerical value of $\delta'_{dpsulfone} = 23.65$ MPa$^{1/2}$ is computed by requiring that each equation (with $r_{solvent} = 0$ and (or) $K_{ASolvent} = 0$) perfectly describes diphenyl sulfone mole fraction solubility data in *n*-hexane ($\delta'_{dpsulfone} = 23.63$ MPa$^{1/2}$), *n*-heptane ($\delta'_{dpsulfone} = 23.63$ MPa$^{1/2}$), and *n*-octane ($\delta'_{dpsulfone} = 23.70$ MPa$^{1/2}$). The numerical value of $a_A^{solid} = 0.1100$ is calculated using eq. [9] with $\Delta H_A^{fus} = 21780$ J mol^{-1} and $T_{mp} = 398.2$ K.[2] The two heat capacity terms in eq. [9] were set equal to zero as we were unable to find heat capacity data for the subcooled liquid solute. A numerical value of $V_{dpsulfone} = 161.5$ cm^3 mol^{-1} was used for the molar volume of the hypothetical subcooled liquid solute. The solute's molar volume was estimated as the twice the molar volume of dimethyl sulfoxide ($V_{dmso} = 70.96$ cm^3 mol^{-1})

[2] J.W. McCargar. Unpublished data.

© 2000 NRC Canada

plus the molar volume of diphenyl sulfide ($V_{dpsulfide}$ = 166.62 cm^3 mol^{-1}) minus twice the molar volume of dimethyl sulfide ($V_{dmsulfide}$ = 73.52 cm^3 mol^{-1}). The calculation assumes that there is no change in volume for transferring the two oxygen atoms from dimethyl sulfoxide to diphenyl sulfide.

Table 1 summarizes the predictive ability of Mobile Order theory for the 34 different organic solvents for which both diphenylsulfone solubility data and modified solubility parameters could be found. Solubility data for diphenyl sulfone dissolved in several of the alkane and alcohol solvents were taken from an earlier study (12). Solvent molar volumes and modified solubility parameters are listed in Table 2. The modified solubility parameters account for only nonspecific interactions, and in the case of the alcoholic solvents the hydrogen-bonding contributions have been removed. Numerical values of $\delta'_{solvent}$ were obtained from published compilations (16, 17, 19, 20), and were either deduced by regressing actual solubility data of solid *n*-alkanes in organic solvents in accordance with the configurational entropic model of Huyskens and Haulait-Pirson (21) or estimated using known values for similar organic solvents. Examination of the entries in Table 1 reveals that Mobile Order theory does provide fairly reasonable (though by no means perfect) estimates of the solubility behavior of diphenyl sulfone in a wide range of organic solvents. Average absolute deviation between predicted and observed values is 49.3%. Expressed on a natural logarithmic mole fraction scale, Mobile Order theory predicts the diphenyl sulfone solubilities to within ±0.77 ln units. The arithmetic average of the ln X_A^{sat} difference is –0.56, which indicates a systematic underprediction in the predicted value. Many solution models express the difference between the predicted and observed in terms of the standard deviation. In the case of Mobile Order theory, the standard deviation for the diphenyl sulfone predictions is 1.03 ln units.

It is noted that eq. [6] did underpredict the solubility of diphenyl sulfone in all of the alcohol solvents, thus suggesting the possibility that the solute does interact specific with alcohol molecules. Based upon the molecular structure of diphenyl sulfone, it is very likely that the alcohol's acidic OH hydrogen atom can be involved in H-bond formation with one of the lone electron pairs on either of the two oxygen atoms of the sulfone functional group. If this does happen, then one would need to know the stability constant for the diphenyl sulfone – alcohol complex to estimate the enhanced solubility that would result from the molecular complexation. Readers are reminded that in evaluating the applicability of Mobile Order theory one must realize that many of these particular systems are highly nonideal, and that the experimental solubility data covers over a 200-fold range in mole fraction. Had an ideal solution been assumed, then the predicted mole fraction solubility would be X_A^{sat} = a_A^{solid} = 0.1100 for each solvent. The ideal solution approximation corresponds to a considerably larger average absolute deviation of 5 500% between predicted and observed values.

Acknowledgement

Research supported in part by the University of North Texas Research Council. The authors thank Jim W. McCargar of Baldwin-Wallace College for measuring the enthalpy of fusion of diphenyl sulfone.

References

1. M.H. Abraham, G.S. Whiting, R.M. Doherty, and W.J. Shuely. J. Chromatogr. **518**, 329 (1990).
2. P. Meyer and G. Maurer. Ind. Eng. Chem. Res. **32**, 2105 (1993).
3. P. Meyer and G. Maurer. Ind. Eng. Chem. Res. **34**, 373 (1995).
4. M.J. Kamlet, R.M. Doherty, M.H. Abraham, Y. Marcus, and R.W. Taft. J. Phys. Chem. **92**, 5244 (1988).
5. M.H. Abraham. Chem. Soc. Rev. **22**, 73 (1993).
6. M.H. Abraham. J. Phys. Org. Chem. **6**, 660 (1993).
7. M.H. Abraham, C.E. Green, W.E. Acree, Jr., C.E. Hernández, and L.E. Roy. J. Chem. Soc. Perkin Trans. 2, 2677 (1998).
8. M.H. Abraham, J. Le, W.E. Acree, Jr., and P.W. Carr. J. Phys. Org. Chem. **12**, 675 (1999).
9. M.H. Abraham, J. Le, and W.E. Acree, Jr. Collect. Czech. Chem. Commun. **64**, 1748 (1999).
10. M.H. Abraham, H.S. Chadha, J.P. Dixon, and A.J. Leo. J. Phys. Org. Chem. **7**, 712 (1994).
11. M.H. Abraham, J. Andonian-Haftvan, J.P. Osei-Owasu, P. Sakellariou, J.S. Urieta, M.C. Lopez, and R. Fuchs. J. Chem. Soc. Perkin Trans. 2, 299 (1993).
12. K.A. Fletcher, C.E. Hernández, L.E. Roy, K.S. Coym, and W.E. Acree, Jr. Can. J. Chem. **77**, 1214 (1999).
13. P.L. Huyskens and G.G. Siegel. Bull. Soc. Chim. Belg. **97**, 821 (1988).
14. G.G. Siegel, P.L. Huyskens, and G. Vanderheyden. Ber. Bunsen–Ges. Phys. Chem. **94**, 549 (1990).
15. P.L. Huyskens. J. Mol. Struct. **274**, 223 (1992).
16. P. Ruelle, C. Rey-Mermet, M. Buchmann, H. Nam-Tran, U.W. Kesselring, and P.L. Huyskens. Pharm. Res. **8**, 840 (1991).
17. P. Ruelle, M. Buchmann, H. Nam-Tran, and U.W. Kesselring. Int. J. Pharm. **87**, 47 (1992).
18. P. Ruelle, M. Buchmann, and U.W. Kesselring. J. Pharm. Sci. **83**, 396 (1994).
19. P. Ruelle, E. Sarraf, and U.W. Kesselring. Int. J. Pharm. **104**, 125 (1994).
20. P. Ruelle, E. Sarraf, L. Van den Berge, K. Seghers, M. Buchmann, and U.W. Kesselring. Pharm. Acta Helv. **68**, 49 (1993).
21. P.L. Huyskens and M.C. Haulait-Pirson. J. Mol. Liq. **31**, 135 (1985).

© 2000 NRC Canada

Synthesis, solid state structure, and solution behaviour of the lighter lanthanide bis(trimethylsilyl)amido chlorides, $[Ln\{N(SiMe_3)_2\}_2(THF)(\mu\text{-}Cl)]_2$ (Ln = Ce, Nd)

David J. Berg and Roland A.L. Gendron

Abstract: The synthesis of $[Ln\{N(SiMe_3)_2\}_2(THF)(\mu\text{-}Cl)]_2$ (Ln = Ce, **1**; Nd, **2**) by reaction of sodium bis(trimethylsilyl)amide (2 equiv.) with $LnCl_3$ is reported. The same complexes were also isolated from the ligand redistribution reactions of $Ln[N(SiMe_3)_2]_3$ and $LnCl_3$ (2:1 ratio) in THF at 80°C. The crystal structure of **2**, determined by X-ray diffraction, revealed a centrosymmetric dimer with bridging chlorides and pentacoordinate metal centres. ^{1}H NMR studies show that the solid state structure is not maintained in solution. NMR evidence for the presence of $Ln[N(SiMe_3)_2]_3$ and two other bis(trimethylsilyl)amide containing species, presumably $Ln[N(SiMe_3)_2]Cl_2(THF)_x$ and $Ln[N(SiMe_3)_2]_2Cl(THF)_y$, is presented.

Key words: lanthanide, amide, neodymium, cerium, crystal structure, X-ray, nuclear magnetic resonance, redistribution.

Résumé : On a effectué la synthèse du $[Ln\{N(SiMe_3)_2\}_2(THF)(\mu\text{-}Cl)]_2$ (Ln = Ce, **1**; Nd, **2**) par réaction du bis(triméthylsilyl)amide (2 équiv.alents) avec du $LnCl_3$. On a aussi isolé les mêmes complexes à partir de réactions de ligands de $Ln[N(SiMe_3)_2]_3$ et $LiCl_3$ (rapport 2:1) dans le THF à 80°C. La structure cristalline du produit **2**, déterminée par diffraction des rayons X, met en évidence la présence d'un dimère centrosymétrique comportant des atomes de chlore agissant comme pont et des centres métalliques pentacoordinés. Les études de RMN du ^{1}H montrent que la structure solide n'est pas maintenue en solution. On rapporte des données de RMN qui mettent en évidence la présence de $Ln(N(SiMe_3)_3]_3$ et de deux autres espèces contenant du bis(triméthylsilyl)amide, probablement du $Ln[N(SiMe_3)_2]Cl_2(THF)_x$ et $Ln[N(SiMe_3)_2]Cl(THF)_y$.

Mots clés : lanthanide, amide, néodyme, cérium, structure cristalline, rayons X, résonance magnétique nucléaire, redistribution.

[Traduit par la Rédaction]

Introduction

The incorporation of anionic ligands into lanthanide complexes is usually achieved by metathetical reactions between a lanthanide halide or alkoxide and a salt of the ligand (eqs. [1], [2]). While often useful, there are many instances when pure products can not be obtained by this method due to incomplete substitution of the leaving group or formation of an anionic "ate" complexes (an addition reaction, eq. [3]) (for some representative examples see ref. (1)). A protonolysis reaction between an acidic, protonated form of the incoming ligand and strongly basic anionic leaving groups is an attractive alternative in many cases, particularly when the leaving group has little propensity to coordinate to the product complex (eq. [4]). Bis(trimethylsilyl)amido complexes are attractive alternative precursors because the amido group is quite basic and the bis(trimethylsilyl)amine that is formed is noncoordinating and volatile, making its removal straightforward.

[1] $3\ M^+L^- + LnCl_3 \rightarrow LnL_3 + 3\ M^+Cl^- \downarrow$ (M = Li, Na, K)

[2] $3\ M^+L^- + Ln(OAr)_3 \rightarrow LnL_3 + 3\ MOAr \downarrow$ (Ar = 2,6-*t*-$Bu_2C_6H_3$)

[3] $3\ M^+L^- + LnCl_3 \rightarrow [LnL_3Cl]^-\ M^+ + 2\ M^+Cl^- \downarrow$ (M = Li, Na, K)

[4] $3\ HL' + LnL_3 \rightarrow LnL'_3 + 3\ HL$ (L = $N(SiMe_3)_2$)

The synthesis of mixed ligand complexes of the lanthanides by methathetical reactions is even more challenging because controlled substitution of the leaving groups is difficult and ligand redistribution often occurs under these conditions. (2) The successful isolation of mixed bis(trimethlsilyl)amido chloride complexes $[Ln\{N(SiMe_3)_2\}_2(THF)(\mu\text{-}Cl)]_2$ (Ln = Eu, Gd, Yb) by Aspinall et al. (3) using metathesis is noteworthy

Received December 8, 1999. Published on the NRC Research Press website on March 31, 2000.

D.J. Berg[1] and R.A.L. Gendron. Department of Chemistry, University of Victoria, P.O. Box 3065, Victoria, BC V8W 3V6, Canada.

[1]Author to whom correspondence may be addressed. Telephone: (250) 721-7161. Fax: (250) 721-7147. e-mail: DJBERG@UVIC.CA

 © 2000 NRC Canada

Table 1. Crystallographic data for **2**.

Formula	$C_{16}H_{44}N_2OSi_4ClNd$
Fw (dimer)	1145.14
Cryst syst	monoclinic
Space group	$P\ 2_1/n$ (no. 14)
a (Å)	15.210(2)
b (Å)	12.074(1)
c (Å)	16.621(3)
β (deg)	112.62(1)
V (Å^3)	2817.6(4)
Z	2 (dimers)
ρ (calcd) (g cm^{-3})	1.35
μ (cm^{-1})	21.1
Radiation, λ (Å)	Mo Kα, 0.7107
T	ambient
$2\theta_{max}$ (deg)	45.0
No. obsd reflcns	3667
No. of unique reflcns	2880
R [a], R_w [b]	0.047, 0.049

[a] $R = \Sigma(|F_o| - |F_c|)/\Sigma|F_o|$.
[b] $R_w = [\Sigma w(|F_o| - |F_c|^2)/\Sigma w(|F_o|)^2]^{1/2}$.

because the products are suitable precursors to other mixed ligand complexes by protonolysis of the two silylamido groups. However, these authors did not attempt to isolate the analogous complexes for the lighter lanthanides because they assumed that these complexes would be too coordinatively unsaturated to exist as simple dimers. In this contribution we demonstrate that bis(amido) complexes of these metals are accessible both by metathesis or redistribution reactions.

Results and discussion

Synthesis

The bis(trimethylsilyl)amido chloride complexes $[Ln\{N(SiMe_3)_2\}_2(THF)(\mu\text{-}Cl)]_2$ (Ln = Ce, **1**; Ln = Nd, **2**) were initially prepared by stirring two equiv. of sodium bis(trimethylsilyl)amide with the appropriate trichloride in THF for 48 h, followed by filtration to remove NaCl, removal of the solvent and recrystallization of the residue from hexane at –30°C (eq. [5]). In agreement with earlier observations (2, 3), complexes **1** and **2** were more intensely coloured (**1**, canary yellow; **2**, lilac) and more soluble than their tris(amido) analogues, $Ln[N(SiMe_3)_2]_3$. The crystals are also easily distinguishable from the tris(amido) complexes by their form: both **1** and **2** are isolated as well-formed prisms, while the tris(amido) complexes of all the lanthanides form feathery needles.

$$[5]\quad 2\ Na^+[N(SiMe_3)_2]^- + LnCl_3 \xrightarrow{THF} [Ln\{N(SiMe_3)_2\}_2(THF)(\mu\text{-}Cl)]_2 + 2\ Na^+Cl^-$$

Ln = Ce (**1**), Nd (**2**)

Small amounts of the tris(amido) complexes were always isolated along with **1** and **2** during recrystallization but these products were very easy to separate. It is noteworthy that pure crystalline **1** and **2** inevitably produced some of the tris(amido) product during recrystallization supporting facile redistribution in solution. This fact was confirmed by ^{1}H NMR (vide infra) and by the successful synthesis of **1** and **2** from $LnCl_3$ and $Ln[N(SiMe_3)_2]_3$ by redistribution (eq. [6]). The yields obtained by redistribution were comparable to those obtained by metathesis.

$$[6]\quad 2\ Ln[N(SiMe_3)_2]_3 + LnCl_3 \xrightarrow[80°C]{THF} 3/2\ [Ln\{N(SiMe_3)_2\}_2(THF)(\mu\text{-}Cl)]_2$$

Ln = Ce (**1**), Nd (**2**)

Table 2. Selected bond distances and angles for **2**[a].

Distances (Å)	
Nd(1)—Cl(1)	2.791(3)
Nd(1)—Cl(1)′	2.854(3)
Nd(1)—O(1)	2.496(7)
Nd(1)—N(1)	2.300(8)
Nd(1)—N(2)	2.335(8)
N(1)—Si(1)	1.702(9)
N(1)—Si(2)	1.732(9)
N(2)—Si(3)	1.705(9)
N(2)—Si(4)	1.707(9)
Angles (deg)	
Cl(1)–Nd(1)–Cl(1)′	73.66(10)
Cl(1)–Nd(1)–O(1)	144.1(2)
Cl(1)–Nd(1)–N(1)	99.0(2)
Cl(1)–Nd(1)–N(2)	108.2(2)
Cl(1)′–Nd(1)–O(1)	76.2(2)
Cl(1)′–Nd(1)–N(1)	107.0(2)
Cl(1)′–Nd(1)–N(2)	136.7(2)
O(1)–Nd(1)–N(1)	108.2(3)
O(1)–Nd(1)–N(2)	81.3(3)
N(1)–Nd(1)–N(2)	115.1(3)
Nd(1)–Cl(1)–Nd(1)′	106.3(1)
Nd(1)–N(1)–Si(1)	122.4(5)
Nd(1)–N(1)–Si(2)	115.9(4)
Nd(1)–N(2)–Si(3)	129.2(5)
Nd(1)–N(2)–Si(4)	110.2(4)
Si(1)–N(1)–Si(2)	121.5(5)
Si(3)–N(2)–Si(4)	120.6(5)

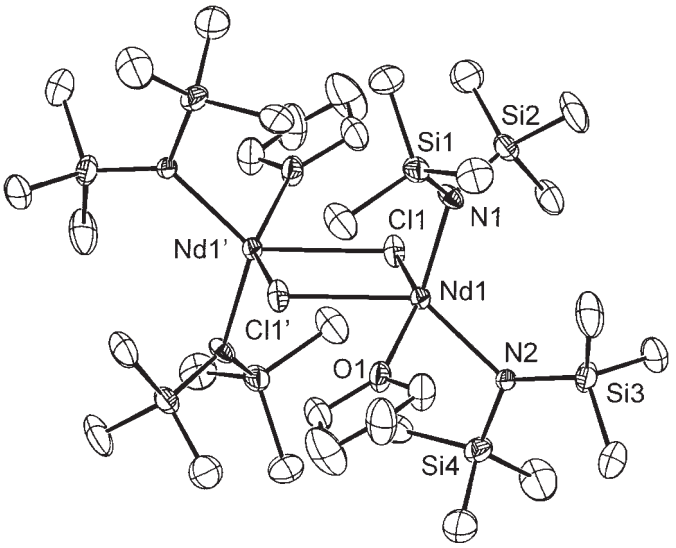
[a]Estimated standard deviations are given in parentheses.

Solid-state structure of $[Nd\{N(SiMe_3)_2\}_2(THF)(\mu\text{-}Cl)]_2$ (2)

The solid state structure of the neodymium complex **2** was determined by X-ray crystallography. Crystallographic data for **2** is summarized in Table 1, selected bond distances and angles are given in Table 2, and the structure is shown in Fig. 1. The complex is dimeric in the solid state and consists of two five-coordinate metal centres bridged by chloride ions. The geometry at the metal is approximately trigonal bipyramidal with one chloride and two amido ligands defining the equatorial plane. The observed structure is isostructural with those previously reported for the Gd and Yb analogues (3). The metal–ligand bond distances in **2** are,

© 2000 NRC Canada

Fig. 1. ZORTEP plot (30% probability) of **2**.



on average, 0.06 and 0.14 Å larger than those found in the Gd and Yb complexes, respectively in keeping with the difference in ionic radii for these metals (0.04 and 0.11 Å, respectively) (4). The only significant differences between this structure and those for Gd and Yb is that the Ln–N–Si angles span a much wider range (110.2(4)–129.2(5)° vs. 117.4(3)–123.5(3)°) and the bridging chlorides display greater asymmetry (Δ = r(Ln-Cl) – r(Ln-Cl′) = 0.063(4) (Nd), 0.025(6) (Gd), 0.023(6) (Yb) Å) in complex **2**. The greater asymmetry in the chloride bridges is surprising because **2** is clearly the least sterically crowded of the three structures. A comparison of the Ln—Cl distances reveals that the shorter Nd—Cl distance in **2** is consistent with that predicted from the earlier Gd and Yb structures (predicted: 2.78(1) Å from both the Yb and Gd structures; observed: 2.791(3) Å). (4) In contrast, the longer Nd—Cl distance in **2** is significantly greater than expected based on the Gd and Yb structures (predicted: 2.80(1) Å; observed: 2.854(3) Å).

Solution behaviour

The solution behaviour of **1** and **2**, monitored in d_5-bromobenzene by variable temperature ^{1}H NMR spectroscopy (Figs. 2 and 3), clearly indicates that the solid state structure is not maintained in solution. For both complexes, five resonances were observed throughout the temperature range studied (20–125°C). The two smaller resonances (**D** and **E**) were established as THF signals by exchange with d_8-THF. One of the larger resonances (**B**) was established as due to $Ln[N(SiMe_3)_2]_3$ by addition of a large excess of the authentic tris(amido) complex. The remaining two resonances are tentatively assigned as the mono (**A**) and bis(amido) (**C**) complexes, $Ln[N(SiMe_3)_2]Cl_2(THF)_x$ and $Ln[N(SiMe_3)_2]_2Cl(THF)_y$, respectively on the basis of integration. It is not possible to know the state of aggregation of these two complexes in solution or the extent to which they are solvated by THF, although it is extremely unlikely that either exists as a base-free monomer. If it is assumed that these are the only species present then a plausible solution equilibrium is given in eq. [7].[2]

Fig. 2. Plot of chemical shift (ppm) vs. $1/T$ (× 1000 K^{-1}) for **1**. Assignments: $Ce[N(SiMe_3)_2]Cl_2(THF)_x$ (**A**), $Ce[N(SiMe_3)_2]_3$ (**B**), $Ce[N(SiMe_3)_2]_2Cl(THF)_y$ (**C**), α-CH_2THF (**D**), and β-CH_2THF (**E**).

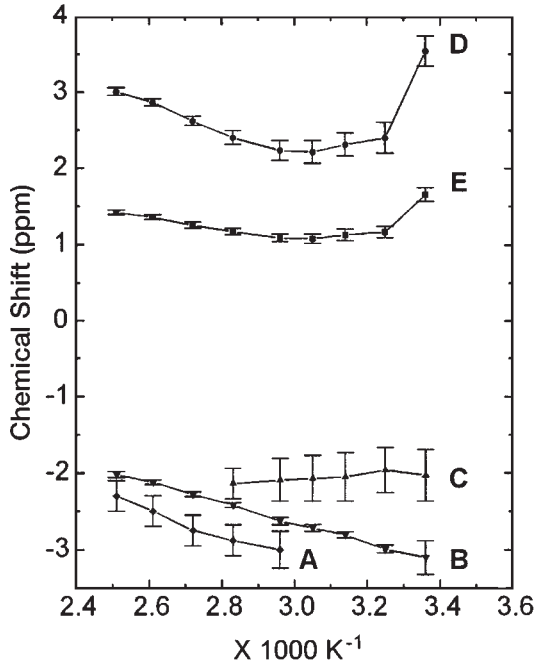
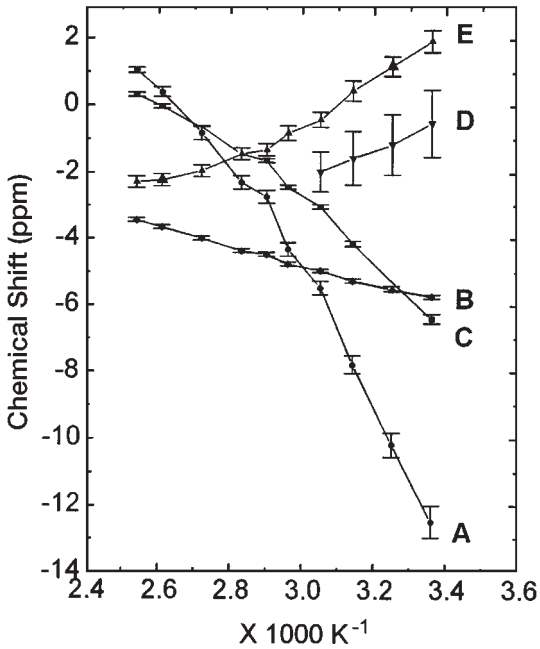


Fig. 3. Plot of chemical shift (ppm) vs. $1/T$ (× 1000 K^{-1}) for **2**. Assignments: $Nd[N(SiMe_3)_2]Cl_2(THF)_x$ (**A**), $Nd[N(SiMe_3)_2]_3$ (**B**), $Nd[N(SiMe_3)_2]_2Cl(THF)_y$ (**C**), α-CH_2THF (**D**) and β-CH_2THF (**E**).

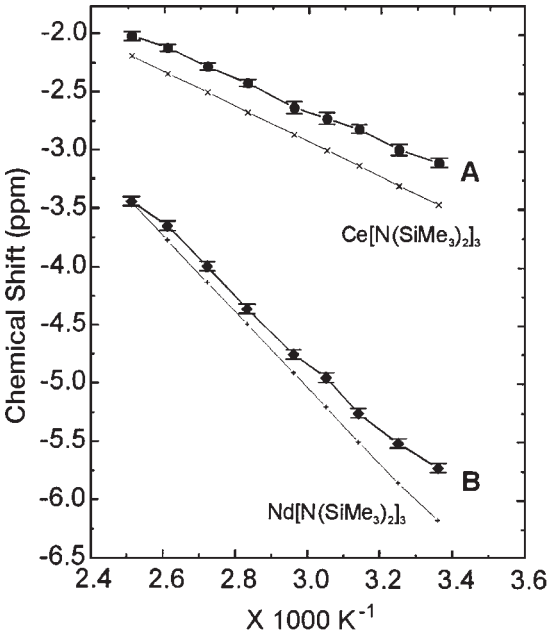


The silylamide integration ratio of $Ln[N(SiMe_3)_2]_3$ (**B**) relative to $Ln[N(SiMe_3)_2]Cl_2(THF)_x$ (**A**) remains approximately

[2] $LnCl_3$ may also form but this product cannot be observed by NMR and there was no visual evidence for its formation.

© 2000 NRC Canada

Fig. 4. Plot of chemical shift (ppm) vs. $1/T$ (× 1000 K^{-1}) for the $Ln[N(SiMe_3)_2]_3$ resonances of **1**(**A**) and **2** (**B**) and pure $Ln[N(SiMe_3)_2]_3$ (Ln = Ce (×), Nd (+)).



3:1 at all temperatures which is what would be expected based on eq. [7].

$$[7] \quad 2\ Ln[N(SiMe_3)_2]_2Cl(THF)_y \rightleftharpoons Ln[N(SiMe_3)_2]_3 + Ln[N(SiMe_3)_2]Cl_2(THF)_x$$

Resonances **A**–**C** for **1** follow nearly linear behaviour throughout the temperature range sampled. This is consistent with each resonance being due to a single well-defined species. The resonances due to the THF (**D**–**E**) do show curvature over this temperature range. The temperature dependence of the amido resonances for **2** show greater curvature although the resonance due to $Nd[N(SiMe_3)_2]_3$ (Fig. 3, **B**) is close to linear. The temperature dependence of the $Ln[N(SiMe_3)_2]_3$ resonances for **1** and **2** are compared with those for separate samples of pure $Ln[N(SiMe_3)_2]_3$ in Fig. 4. The close similarity between these plots confirms the assignments made in Fig. 2 and 3.[3] In addition, since the resonances in Fig. 4 are essentially unperturbed from those of pure $Ln[N(SiMe_3)_2]_3$, the forward and reverse reaction rates in eq. [7] must be slow on the NMR timescale over the entire temperature range studied.

The results presented here indicate that it is possible to isolate pure solid bis(amido) chloride complexes such as **1** and **2** for the lighter lanthanides. However, in solution ligand redistribution occurs readily so that mono and tris(amido) species are also present. This does not necessarily preclude the use of these complexes as precursors to other mixed ligand systems by protonolysis reactions. However, in cases where the reaction proceeds rapidly and irreversibly (for example, giving an insoluble product), it is useful to remember that this kinetic product may be derived from any of the three amido species present in solution.

Experimental

General procedures

All manipulations were carried out under an argon atmosphere, with the rigorous exclusion of oxygen and water, using standard glovebox (Braun MB150-GII) or Schlenk techniques. Tetrahydrofuran (THF) and hexane were dried by distillation from sodium benzophenone ketyl under argon immediately prior to use. $Ln[N(SiMe_3)_2]_3$ (Ln = Ce, Nd) were prepared according to the literature (5).

Variable temperature ^1H NMR spectra were recorded on a Bruker WM-250 MHz spectrometer. Spectra were recorded in C_6D_5Br dried over 4 Å molecular sieves for one week, using 5 mm tubes fitted with a teflon valve (Brunfeldt). The sample was allowed to equilibrate for 15 min at each temperature prior to recording the spectrum. Melting points were recorded using a Reichert hot stage and are not corrected. Elemental analyses were performed by Canadian Microanalytical, Delta, B.C. Mass spectra were recorded on a Kratos Concept H spectrometer using an electron impact (70 eV) source.

Preparation of $[Ln\{N(SiMe_3)_2\}_2(THF)(\mu\text{-}Cl)]_2$

In a typical preparation, a solution of sodium bis(trimethylsilyl)amide (2 equiv.) was added to a stirred suspension of $LnCl_3$ under argon at room temperature. The solution was stirred for 48 h and the solvent was removed under reduced pressure. The solid residue was extracted into hexane, filtered through a Celite pad to remove NaCl, and crystallized in the glovebox at –30°C. Generally this resulted in a large mass of block-like crystals of the bis(amide) surrounded by fine needles of $Ln[N(SiMe_3)_2]_3$. The smaller tris(amide) crystals can usually be removed with the mother liquor by a Pasteur pipette. Although the larger bis(amide) crystals are more soluble, they are slow to redissolve so washing with cold hexane is an ideal way to wash off the smaller tris(amide) needles.

Alternatively, the complexes were prepared in comparable yield by heating a THF solution of two equiv. $Ln[N(SiMe_3)_2]_3$ with one equiv. of $LnCl_3$ in a sealed Kontes flask at 80°C overnight. All solids dissolved on heating and remained in solution after the reaction mixture was cooled back to room temperature. The THF solvent was removed under reduced pressure and the residue was recrystallized from hexane in the glove box as described above. Complexes **1** and **2** are readily accessible on a 10 g scale by either preparative route.

*$[Ce\{N(SiMe_3)_2\}_2(THF)(\mu\text{-}Cl)]_2$ (**1**)*

Canary yellow prisms. Yield: 65%, mp. 151–153°C. Anal. calcd. for $C_{32}H_{88}N_4O_2Si_8Cl_2Ce_2$: C 33.81, H 7.80, N 4.93%; found: C 33.39, H 7.94, N 4.78%.

[3] The small difference in chemical shift between pure $Ln[N(SiMe_3)_2]_3$ and that formed in the equilibrium of eq. [7] is likely a result of differences in the concentrations of the paramagnetic ions, which will exhibit differences in bulk susceptibility.

© 2000 NRC Canada

*[Nd{N(SiMe$_3$)$_2$}$_2$(THF)(μ-Cl)]$_2$ (**2**)*

Deep lilac prisms. Yield: 81%, mp. 147–149°C. MS(EI): m/z 499 (10%, Nd{N(SiMe$_3$)$_2$}$_2$Cl$^+$), 464 (100%, Nd{N(SiMe$_3$)$_2$}$_2^+$), 449 (10%, [Nd{N(SiMe$_3$)$_2$}$_2$ – CH$_3$]$^+$), 434 (10%, [Nd{N(SiMe$_3$)$_2$}$_2$ – 2 CH$_3$]$^+$), 419 (10%, [Nd{N(SiMe$_3$)$_2$}$_2$ – 3 CH$_3$]$^+$), 302 (10%, Nd{N(SiMe$_3$)$_2$}$^+$) amu. Anal. calcd. for $C_{32}H_{88}N_4O_2Si_8Cl_2Nd_2$: C 33.56, H 7.75, N 4.89%; found: C 33.21, H 7.59, N 4.71%.

X-ray crystallographic studies

Crystallographic data for **2** is summarized in Table 1. Crystals of **2** (0.5 × 0.5 × 0.5 mm) were loaded into glass capillaries in the glove box and subsequently flame sealed. The crystals were transferred to a Nonius CAD4F diffractometer equipped with MoKα radiation. The unit cell of **2** was refined using 24 reflections in the 2θ range of 38–42. An experimental density was not obtained because of the air sensitivity of the compound. Six standard reflections, measured periodically during data collection (9, 0, 7; 7, 0, 1; 8, 9, 0; 0, 7, 1; 0, 0, 8; 3, 5, 7) showed a 10% decline in intensity during data collection. Intensity measurements were collected over one quarter of the sphere. After the usual data reduction procedures, including an absorption correction (max/min transmission: 0.9939, 0.8507) according to a measured PSI scan, the structure was solved by Patterson methods.[4] The refinements minimized $w((F_o - F_c)^2)$ and proceeded normally using teXsan98.[5] Criteria for inclusion of reflections were $I > 3.5\sigma(I)$. The weighting scheme was determined by counting statistics using $w = 1/(\sigma^2(F) + 0.001F^2)$.

Convergence was satisfactory: max shift/esd < 0.01; the largest positive and negative peaks in the final difference map were 1.64 and –0.97 e/Å^3, respectively. A total of 227 parameters were refined. Hydrogen atoms were placed in calculated positions. No non-hydrogen intermolecular contacts shorter than 3.5 Å were observed. The structural perspective plots were drawn using ZORTEP.[6] Complete tables of bond distances, angles, and anisotropic temperature parameters have been deposited as supplementary material.[7]

Acknowledgements

We thank Mrs. C. Greenwood for assistance in recording the NMR spectra and Dr. David McGillivray for obtaining the mass spectra. This research was supported by the Natural Sciences and Engineering Research Council of Canada (NSERC) and a University of Victoria Internal Research Grant (to D.J.B.).

References

1. (*a*) S.A. Cotton, F.A. Hart, M.B. Hursthouse, and A.J. Welch. J. Chem. Soc. Chem. Commun. 1225 (1979); (*b*) H. Schumann and J. Müller. Angew. Chem. Int. Ed. Engl. **17**, 276 (1978); (*c*) A.L. Wayda and W.J. Evans. J. Am. Chem. Soc. **100**, 7119 (1978); (*d*) H. Schumann. Angew. Chem. Int. Ed. Engl. **23**, 474 (1984); (*e*) P.N. Hazin, J.W. Bruno, and G.K. Schulte. Organometallics. **9**, 416 (1990); (*f*) H. Schumann, P.R. Lee, and J. Loebel. Chem. Ber. **122**, 1897 (1989); (*g*) J. Holton, M.F. Lappert, D.G. Ballard, R. Pearse, J.L. Atwood, and W.E. Hunter. J. Chem. Soc. Dalton Trans. 4554 (1979).
2. T.D. Tilley, A. Zalkin, R.A. Andersen, and D.H. Templeton. Inorg. Chem. **20**, 551 (1981).
3. H.C. Aspinall, D.C. Bradley, M.B. Hursthouse, K.D. Sales, N.P.C. Walker, and B. Hussain. J. Chem. Soc. Dalton Trans. 623 (1989).
4. R.D. Shannon. Acta Crystallogr. Sect. A: Cryst. Phys. Diffr. Theor. Gen. Crystallogr. **A32**, 751 (1976).
5. D.C. Bradley, J.S. Ghotra, and F.A. Hart. J. Chem. Soc. Dalton Trans. 1021 (1973).

[4] P.T. Beurskens, G. Admiraal, G. Beurskens, W.P. Bosman, R. De Gelder, R. Israel, and J.M.M. Smits. DIRDIF94: The DIRDIF94 Program System. Technical Report of the Crystallography Laboratory, University of Nijmegen, The Netherlands. 1994.
[5] Molecular Structure Corporation. teXsan for Windows Version 1.05. The Woodlands, Texas. 1998.
[6] L. Zsolnai. ZORTEP. University of Heidelberg, Germany. 1995.
[7] Copies of material on deposit may be purchased from the Depository of Unpublished Data, Document Delivery, CISTI, National Research Council of Canada, Ottawa, ON K1A 0S2, Canada.

© 2000 NRC Canada

Solubility of hexachlorobenzene in organic nonelectrolyte solvents. Comparison of observed vs. predicted values based upon Mobile Order model

Karina M. De Fina, Tiffany T. Van, and William E. Acree, Jr.

Abstract: Experimental solubilities are reported at 25.0°C for hexachlorobenzene dissolved in 42 different organic nonelectrolyte solvents containing ether-, chloro-, hydroxy-, ester, methyl-, and *tert*-butyl-functional groups. Results of these measurements are used to test the applications and limitations of expressions derived from Mobile Order model. For the 33 solvents for which predictions could be made computations show that Mobile Order model does provide fairly reasonable estimates of the saturation mole fraction solubilities. Average absolute deviation between predicted and observed values is 210%. In comparison, the average absolute deviation is 2 060% when ideal solution behavior is assumed.

Key words: hexachlorobenzene solubilities, organic nonelectrolyte solvents, solubility predictions.

Résumé : Opérant à 25,0°C, on a mesuré les solubilités expérimentales de l'hexachlorobenzène en solution dans quarante-deux solvants organiques non électrolytiques qui comprennent des groupes substituants éther, chloro, hydroxyle, ester, méthyle et *tert*-butyle. On a utilisé les résultats de ces mesures pour vérifier les applications et les limitations d'expressions dérivées du modèle de l'ordre mobile. Les trente-trois solvants pour lesquels il a été possible de faire des calculs montrent que le modèle de l'ordre mobile conduit à des évaluations assez raisonnables des solubilités en fraction molaire de la saturation. La déviation absolue moyenne entre les valeurs prévues et observées est de 210%. Pour fins de comparaison, la déviation absolue moyenne est de 2 060% lorsqu'on fait l'hypothèse que le comportement de la solution est idéal.

Mots clés : solubilités de l'hexachlorobenzène, solvants organiques non électrolytiques, prévisions des solubilités.

Introduction

Solid–liquid equilibrium data of organic nonelectrolyte systems are becoming increasingly important in the petroleum industry, particularly in light of present trends towards heavier feedstocks and known carcinogenicity and (or) mutagenicity of many of the larger polycyclic aromatic compounds. Solubility data for a number of polycyclic aromatic hydrocarbons (e.g., anthracene and pyrene) and heteroatom polynuclear aromatics (e.g., carbazole, dibenzothiophene, and xanthene) have been published in the recent chemical literature (for listing of references see Acree (1–3)). Despite efforts by experimentalists and scientific organizations, both in terms of new experimental measurements and critically evaluated data compilations, there still exist numerous systems for which solubility data are not readily available.

To address this problem, researchers have turned to group contribution methods and semiempirical expressions to predict desired quantities. Group contribution methods have proved fairly successful in estimating solid solubility in pure and binary solvent mixtures from structural information (4–11). Practical application though, is limited to systems for which all group interaction parameters are known. Interaction parameters can be evaluated from liquid–vapor, liquid–liquid, and solid–liquid equilibria data. It is important that the data base contain as many different functional groups as possible, preferably with adequate representation from both mono- and multifunctional solute/solvent molecules to permit evaluation of potential synergistic effects. The data base should contain sufficient experimental values near infinite dilution in the event that one wishes to determine separate interaction parameters for finite concentration and infinite dilution activity coefficient predictions.

Abraham and coworkers (12, 13) recently developed a general solvation equation that can be used in the correlation and understanding of physicochemical and biochemical phenomena. Physical properties that have been correlated include gas/solvent partition coefficients (as log L)

$$[1] \qquad \log L = c + r\cdot R_2 + s\cdot\pi_2^H + a\cdot\sum\alpha_2^H + b\cdot\sum\beta_2^H + d\cdot\log L^{16}$$

and water/solvent partition coefficients (as log P)

Received October 27, 1999. Published on the NRC Research Press website on April 4, 2000.

K.M. De Fina, T.T. Van, and W.E. Acree, Jr.[1] Department of Chemistry, University of North Texas, Denton, TX 76203-5070, U.S.A.

[1]Author to whom correspondence may be addressed. e-mail: acree@unt.edu

© 2000 NRC Canada

[2] $$\log P = c + r\cdot R_2 + s\cdot\pi_2^H + a\cdot\sum\alpha_2^H + b\cdot\sum\beta_2^H + v\cdot V_x$$

where R_2 and V_x refer to the excess molar refraction and McGowan volume of the solute, respectively, π_2^H is the solute dipolarity–polarizability descriptor, and $\sum\alpha_2^H$ and $\sum\beta_2^H$ are measures of the solute's hydrogen-bond acidity and hydrogen-bond basicity. For any given solvent, numerical values of the seven curve-fit coefficients (*c*, *r*, *s*, *a*, *b*, *d*, and *v*) are deduced by regressing experimental partition coefficient data in accordance with eqs. [1] and [2]. The input partition coefficients were sometimes calculated as the ratio of the solute molar solubilities in the organic solvent and water, $P = C_A^{org}/C_A^{aq}$, and as the ratio of the solute molar solubility in the organic solvent and vapor concentration, $L = C_A^{org}/C_A^{gas}$. Published papers have reported curve-fit coefficients for water (12, 13) and a few select organic solvents (13).

To increase the solubility database available for developing group contribution methods and general solvation correlations, we are in the process of measuring solubility data for polycyclic aromatic hydrocarbons (PAHs), polycyclic aromatic nitrogen heteroatoms (PANHs), and other crystalline nonelectrolyte solutes. In the present communication, we report hexachlorobenzene solubilities in 42 different organic solvents at 25°C. Results of the measurements are used to further test the applications and limitations of predictive expressions derived from Mobile Order model. Subsequent studies will use the experimental hexachlorobenzene solubilities, along with other published activity coefficient and solubility data, in developing gas/liquid partition and water/organic solvent partition correlations based upon eqs. [1] and [2].

Materials and methods

Hexachlorobenzene (Aldrich, 99%) was recrystallized several times from methanol. *n*-Hexane (Aldrich, 99%), *n*-heptane (Aldrich, HPLC), *n*-octane (Aldrich, 99+%, anhydrous), *n*-nonane (TCI, 99+%), *n*-decane (TCI, 99+%), *n*-hexadecane (Aldrich, 99%), cyclohexane (Aldrich, HPLC), methylcyclohexane (Aldrich, 99+%, anhydrous), 2,2,4-trimethylpentane (Aldrich, HPLC), *tert*-butylcyclohexane (Aldrich, 99+%), dibutyl ether (Aldrich, 99%), methanol (Aldrich, 99.9+%), ethanol (Aaper Alcohol and Chemical Comp., absolute), 1-propanol (Aldrich, 99+%, anhydrous), 2-propanol (Aldrich, 99+%, anhydrous), 1-butanol (Aldrich HPLC, 99.8+%), 2-butanol (Aldrich, 99+%, anhydrous), 1-pentanol (Aldrich, 99+%), 2-pentanol (Acros 99+%), 1-hexanol (Alfa Aesar, 99+%), 1-heptanol (Alfa Aesar, 99+%), 2-methyl-2-butanol (Acros, 99+%), 2-methyl-1-propanol (Aldrich, 99+%, anhydrous), 3-methyl-1-butanol (Aldrich, 99+%, anhydrous), 1-octanol (Aldrich, 99+%, anhydrous), 4-methyl-2-pentanol (Acros, 99+%), 2-ethyl-1-hexanol (Aldrich, 99+%), 2-methyl-1-pentanol (Aldrich, 99%), 1-decanol (Alfa Aesar, 99+%), cyclopentanol (Aldrich, 99%), 1,4-dioxane (Aldrich, 99.8%, anhydrous), tetrahydrofuran (Aldrich, 99.9%, anhydrous), methyl *tert*-butyl ether (Arco, 99.9+%), ethyl acetate (Aldrich, HPLC, 99.9%), 2-methyl-2-propanol (Arco Chemical Co. 99+%), 1,2-dichloroethane (Aldrich, HPLC, 99.8%), 1-chlorobutane (Sigma–Aldrich, HPLC, 99.5+%), 1-chlorohexane (Aldrich, 99%), 1-chlorooctane (Aldrich, 99%), chlorocyclohexane (Aldrich, 99%), methyl acetate (Aldrich, 99.5%, anhydrous), and butyl acetate (Aldrich HPLC, 99.7%) were stored over molecular sieves before use. Gas chromatographic analysis showed solvent purities to be 99.7 mole % or better.

Excess solute and solvent were placed in amber glass bottles and allowed to equilibrate in a constant temperature water bath at 25.0 ± 0.1°C for at least three days (often longer). Attainment of equilibrium was verified both by repetitive measurements after several additional days and by approaching equilibrium from supersaturation by preequilibrating the solutions at a higher temperature. Aliquots of saturated hexachlorobenzene solutions were transferred through a coarse filter into a tared volumetric flask to determine the amount of sample and diluted quantitatively with 2-propanol for spectrophotometric analysis at 291 nm on a Bausch and Lomb Spectronic 2000. Concentrations of the dilute solutions were determined from a Beer–Lambert law absorbance vs. concentration working curve for nine standard solutions. The concentration of hexachlorobenzene in the standard solutions varied from 1.41×10^{-3} M to 3.54×10^{-3} M. The calculated molar absorptivity of the standard solutions varied slightly over the concentration range, from $\epsilon \approx 230$ L mol^{-1} cm^{-1} (1.41×10^{-3} M) to $\epsilon \approx 222$ L mol^{-1} cm^{-1} (3.54×10^{-3} M). Experimental hexachlorobenzene solubilities, X_A^{sat}, in 42 organic solvents studied are listed in Table 1. Numerical values represent the average of between four and eight independent determinations, with the measurements being reproducible to ±1.5%. For each solvent studied, all experimental measurements fell within ±1.5% of the average value listed in Table 1.

Results and discussion

Solvents listed in Table 1 include both noncomplexing alkanes and self-associating alcohols. Of the many solution models proposed in recent years, Mobile Order model is perhaps the only one that is capable of describing solute behavior in such a wide range of solvent mixtures. The basic model (14–21) assumes that all molecular groups perpetually move, and that neighbors of a given kind of external atom in a molecule constantly change identity. All molecules of a given kind dispose of the same volume, equal to the total volume *V* of the liquid divided by the number N_A of molecules of the same kind, i.e., Dom $A = V/N_A$. The center of this domain perpetually moves. The highest mobile disorder is achieved whenever groups visit all parts of their domain without preference. Preferential contacts lead to deviations with respect to this "random" visiting. This is especially true in the case of hydrogen-bonding as specific interactions result in a specific orientation of the "donor" molecule with respect to an adjacent "acceptor" molecule.

In the case of an inert crystalline solute dissolved in a self-associating solvent, Mobile Order model expresses the volume fraction saturation solubility, ϕ_A^{sat}, as

[3] $$\ln \phi_A^{sat} = \ln a_A^{solid} - 0.5(1 - V_A/V_{solvent})\phi_{solvent} + 0.5 \ln [\phi_A^{sat} + \phi_{solvent}(V_A/V_{solvent})] - \phi_{solvent}^2 V_A(\delta'_A - \delta'_{solvent})^2(RT)^{-1} - r_{solvent}(V_A/V_{solvent})\phi_{solvent}$$

© 2000 NRC Canada

Table 1. Comparison between experimental hexachlorobenzene mole fraction solubilities and predicted values based upon Mobile Order model.

Organic solvent	$(X_A^{sat})^{exp,a}$	$(X_A^{sat})^{calc}$	%Dev[b]
n-Hexane	0.00262	0.00289	10.3
n-Heptane	0.00314	0.00307	–2.2
n-Octane	0.00371	0.00349	–5.9
n-Nonane	0.00410	0.00404	–1.5
n-Decane	0.00460	0.00425	–7.6
n-Hexadecane	0.00681	0.00601	–11.7
Cyclohexane	0.00295	0.00357	21.0
Methylcyclohexane	0.00387	0.00390	0.8
2,2,4-Trimethylpentane	0.00252	0.00238	–5.6
tert-Butylcyclohexane	0.00471	0.00523	11.0
Dibutyl ether	0.00440	0.0127	188.6
Methyl *tert*-butyl ether	0.00320		
Tetrahydrofuran	0.00592	0.0220	271.6
1,4-Dioxane	0.00397	0.0208	423.9
Methanol	0.0000902	0.000861	854.5
Ethanol	0.000236	0.00140	493.2
1-Propanol	0.000398	0.00179	349.7
2-Propanol	0.000298	0.00206	591.3
1-Butanol	0.000667	0.00229	243.3
2-Butanol	0.000521	0.00183	251.2
2-Methyl-1-propanol	0.000533	0.00149	179.5
2-Methyl-2-propanol	0.000517	0.00126	143.7
1-Pentanol	0.00103	0.00251	143.7
2-Pentanol	0.000860		
3-Methyl-1-butanol	0.000770		
2-Methyl-2-butanol	0.00120		
1-Hexanol	0.00144	0.00243	68.8
2-Methyl-1-pentanol	0.00140		
4-Methyl-2-pentanol	0.00143		
1-Heptanol	0.00190	0.00277	45.8
1-Octanol	0.00238	0.00308	29.4
2-Ethyl-1-hexanol	0.00174		
1-Decanol	0.00380	0.00364	–4.2
Cyclopentanol	0.000920		
Butyl acetate	0.00365	0.0193	428.8
Ethyl acetate	0.00211	0.0200	847.9
Methyl acetate	0.00148		
1,2-Dichloroethane	0.00286	0.0213	644.8
1-Chlorobutane	0.00383	0.0119	210.7
1-Chlorohexane	0.00508	0.0149	193.3
1-Chlorooctane	0.00606	0.0149	145.9
Chlorocyclohexane	0.00610	0.0168	175.4

[a]Numerical values represent the average of between four and eight independent determinations, with the measurements being reproducible to ±1.5%.

[b]Deviations (%) = $100[(X_A^{sat})^{calc} - (X_A^{sat})^{exp}]/(X_A^{sat})^{exp}$.

where the $r_{solvent}(V_A/V_{solvent})\phi_{solvent}$ term represents the contributions resulting from hydrogen-bond formation between the solvent molecules. For most of the published applications, $r_{solvent}$ was assumed to be unity for strongly associated solvents with single hydrogen-bonded chains such as monofunctional alcohols, to be two for water or diols, and to equal zero for nonassociated solvents such as saturated hydrocarbons. A more exact value for alcoholic solvents can be calculated based upon

$$[4]\quad r_{solvent} = (K_{solvent}\phi_{solvent}/V_{solvent})/(1 + K_{solvent}\phi_{solvent}/V_{solvent})$$

with a numerical value of $K_{solvent}$ = 5 000 cm^3 mol^{-1} assumed for all monofunctional alcohols.

If complexation does occur between the crystalline solute and solvent

$$[5]\quad \ln \phi_A^{sat} = ln\ a_A^{solid} - 0.5(1 - V_A/V_{solvent})\phi_{solvent} + 0.5 \ln [\phi_A^{sat} + \phi_{solvent}(V_A/V_{solvent})] - \phi_{solvent}^2 V_A(\delta'_A - \delta'_{solvent})^2(RT)^{-1} + \ln [1 + \phi_{solvent}(K_{ASolvent}/V_{solvent})]$$

then an additional term involving the solute–solvent equilibrium constant, $K_{ASolvent}$, must be introduced to describe the solubility enhancement that arises as a result of specific interactions. A slightly more complex expression applies in the case of solute complexation with a self-associating solvent. The symbols δ'_A and $\delta'_{solvent}$ denote the modified solubility parameters of the solute and solvent, respectively V_i is the molar volume, and a_A^{solid} is the activity of the solid solute. This latter quantity is defined as the ratio of the fugacity of the solid to the fugacity of the pure hypothetical supercooled liquid. The numerical value of a_A^{solid} can be computed from

$$[6]\quad \ln a_A^{solid} = -\Delta H_A^{fus}(T_{mp} - T)/(RTT_{mp}) + (\Delta C_{p,A}/RT)(T_{mp} - T) - (\Delta C_{p,A}/T) \ln (T_{mp}/T)$$

the solute's molar enthalpy of fusion, ΔH_A^{fus}, and heat capacity difference, $\Delta C_{p,A}$, at the normal melting point temperature, T_{mp}. Contributions from nonspecific interaction are incorporated into Mobile Order model through the $\phi_{solvent}^2 V_A(\delta'_A - \delta'_{solvent})^2(RT)^{-1}$ term. Ruelle and coworkers (17–21) have presented an impressive set of comparisons between experimental and predicted values for anthracene, naphthalene, pyrene, biphenyl, carbazole, benzil, *p*-benzoquinone, tricosane, octacosane, 10-nonadecanone, 11-heneicosanone, and 12-tricosanone solubilities in a wide range of both noncomplexing and complexing solvents to document the predictive ability of Mobile Order model.

Predictive application of eqs. [3] and [5] is relatively straightforward. First, an average numerical value of $\delta'_{hexclbz}$ = 20.10 MPa$^{1/2}$ is computed by requiring that each equation (with $r_{solvent}$ = 0 and (or) $K_{ASolvent}$ = 0) perfectly describes hexachlorobenzene mole fraction solubility data in *n*-hexane ($\delta'_{hexclbz}$ = 20.24 MPa$^{1/2}$), *n*-heptane ($\delta'_{hexclbz}$ = 20.07 MPa$^{1/2}$), and *n*-octane ($\delta'_{hexclbz}$ = 20.00 MPa$^{1/2}$). The numerical value of a_A^{solid} = 0.01943 is calculated using eq. [6] with ΔH_A^{fus} = 23 850 J mol^{-1} and T_{mp} = 505.0 K (22). The two heat capacity terms in eq. [6] were set equal to zero as we were unable to find heat capacity data for the subcooled liquid solute. A numerical value of $V_{hexclbz}$ = 155.6 cm^3 mol^{-1} was used for the molar volume of the hypothetical subcooled liquid solute. The solute's molar volume was estimated as the molar volume of liquid 1,2-dichlorobenzene (V_{diclbz} = 112.8 cm^3 mol^{-1}) plus four times the difference between the molar

© 2000 NRC Canada

Table 2. Solvent and solute properties used in Mobile Order predictions.

Component (i)	V_i (cm^3 mol^{-1})	δ_i' (MPa$^{1/2}$)[a]
n-Hexane	131.51	14.56
n-Heptane	147.48	14.66
n-Octane	163.46	14.85
n-Nonane	179.87	15.07
n-Decane	195.88	15.14
n-Hexadecane	294.12	15.61
Cyclohexane	108.76	14.82
Methylcyclohexane	128.32	15.00
2,2,4-Trimethylpentane	166.09	14.30
tert-Butylcyclohexane	173.9	15.50
Dibutyl ether	170.3	17.45
Tetrahydrofuran	81.4	19.30
1,4-Dioxane	85.8	20.89
Methanol	40.7	19.25
Ethanol	58.7	17.81
1-Propanol	75.10	17.29
2-Propanol	76.90	17.60
1-Butanol	92.00	17.16
2-Butanol	92.4	16.60
2-Methyl-1-propanol	92.8	16.14
2-Methyl-2-propanol	94.3	15.78
1-Pentanol	108.6	16.85
1-Hexanol	125.2	16.40
1-Heptanol	141.9	16.39
1-Octanol	158.3	16.38
1-Decanol	191.6	16.35
Butyl acetate	132.5	19.66
Ethyl acetate	98.5	20.79
1,2-Dichloroethane	78.8	20.99
1-Chlorobutane	105.0	17.12
1-Chlorohexane	138.1	18.00
1-Chlorooctane	171.1	18.00
Chlorocyclohexane	120.3	18.45
Hexachlorobenzene[b]	155.6[c]	20.10[d]

[a]Tabulated values are taken from a compilation given in Ruelle and coworkers. (17, 18, 20, 21).

[b]The numerical value of a_A^{solid} = 0.01943 was calculated from eq. [6] using ΔH_A^{fus} = 23 850 J mol^{-1} and T_{mp} = 505.0 K (22).

[c]Numerical value of $V_{hexclbz}$ = 155.6 cm^3 mol^{-1} was estimated using the known molar volumes of 1,2-dichlorobenzene and chlorobenzene.

[d]Numerical value was calculated using the measured hexachlorobenzene mole fraction solubilities in *n*-hexane, *n*-heptane, and *n*-octane, in accordance with eqs. [3] and [5] (with $r_{solvent}$ = 0 and (or) $K_{ASolvent}$ = 0).

volumes of 1,2-dichlorobenzene and chlorobenzene (V_{clbz} = 102.1 cm^3 mol^{-1}). The difference represents the calculated incremental group value for replacing one of the hydrogen atoms on chlorobenzene with a chlorine atom.

Table 1 summarizes the predictive ability of Mobile Order model for the 33 different organic solvents for which both hexachlorobenzene solubility data and modified solubility parameters could be found. Solvent molar volumes and modified solubility parameters are listed in Table 2. The modified solubility parameters account for only nonspecific interactions, and in the case of the alcoholic solvents, the hydrogen-bonding contributions have been removed. Numerical values of $\delta'_{solvent}$ were obtained from published compilations (17, 18, 20, 21), and were either deduced by regressing actual solubility data of solid *n*-alkanes in organic solvents in accordance with the configurational entropic model of Huyskens and Haulait-Pirson (23) or estimated using known values for similar organic solvents. The predicted values do depend upon the numerical values assumed for the various input parameters. Computations using slightly different numerical values for a_A^{solid} and the molar volume of hexachlorobenzene (± 5 cm^3 mol^{-1}) indicate that the predicted value can vary by 10–15% as a result of small changes in these two input parameters. This would be true of any predictive thermodynamic model that uses solubility parameters and bases activity coefficients upon the thermodynamic properties of the hypothetical subcooled liquid solute.

Examination of the entries in Table 1 reveals that Mobile Order model does provide fairly reasonable estimates of the solubility behavior of hexachlorobenzene in a wide range of organic solvents. Average absolute deviation between predicted and observed values is 210%. Expressed on a natural logarithmic mole fraction scale, Mobile Order model predicts the hexachlorobenzene solubilities to within ±0.87 ln units. Readers are reminded that in evaluating the applicability of Mobile Order model one must realize that many of these particular systems are highly nonideal, and that the experimental solubility data covers over a 75-fold range in mole fraction. Had an ideal solution been assumed, then the predicted mole fraction solubility would be $X_A^{sat} = a_A^{solid}$ = 0.01943 for each solvent. The ideal solution approximation corresponds to a considerably larger average absolute deviation of 2 060% between predicted and observed values.

Acknowledgement

Research supported in part by the University of North Texas Research Council.

References

1. W.E. Acree, Jr. Polycyclic aromatic hydrocarbons in pure and binary solvents. IUPAC solubility data series, Vol. 54. Oxford University Press, Oxford, U.K. 1994.
2. W.E. Acree, Jr. Polycyclic aromatic hydrocarbons: binary nonaqueous systems: part 1 (solutes A–E). IUPAC solubility data series, Vol. 58. Oxford University Press, Oxford, U.K. 1995.
3. W.E. Acree, Jr. Polycyclic aromatic hydrocarbons: binary nonaqueous systems: part 2 (solutes F–Z). IUPAC solubility data series, Vol. 59. Oxford University Press, Oxford, U.K. 1995.
4. W.E. Acree, Jr. Int. J. Pharm. **18**, 47 (1984).
5. U. Domanska and T. Hofman. J. Sol. Chem. **14**, 531 (1985).
6. U. Domanska. Fluid Phase Equilibr. **35**, 217 (1985).
7. R.S. Basu, H. Pham, and D.P. Wilson. Int. J. Pharm. **7**, 319 (1986).
8. A.B. Ochsner and T.D. Sokoloski. J. Pharm. Sci. **74**, 634 (1985).
9. R. Carta and S. Dernini. J. Chem. Eng. Data, **28**, 328 (1983).
10. W.E. Acree, Jr. and J.H. Rytting. Int. J. Pharm. **13**, 197 (1983).
11. A. Martin, P.L. Wu, A. Adjei, A. Beerbower, and J.M. Prausnitz. J. Pharm. Sci. **70**, 1260 (1981).
12. M.H. Abraham, H.S. Chadha, J.P. Dixon, and A.J. Leo. J. Phys. Org. Chem. **7**, 712 (1994).

© 2000 NRC Canada

13. M.H. Abraham, J. Andonian-Haftvan, J.P. Osei-Owasu, P. Sakellariou, J.S. Urieta, M.C. Lopez, and R. Fuchs. J. Chem. Soc. Perkin Trans. 2, 299 (1993).
14. P.L. Huyskens and G.G. Siegel. Bull. Soc. Chim. Belg. **97**, 821 (1988).
15. G.G. Siegel, P.L. Huyskens, and G. Vanderheyden. Ber. Bunsen–Ges. Phys. Chem. **94**, 549 (1990).
16. P.L. Huyskens. J. Mol. Struct. **274**, 223 (1992).
17. P. Ruelle, C. Rey-Mermet, M. Buchmann, H. Nam-Tran, U.W. Kesselring, and P.L. Huyskens. Pharm. Res. **8**, 840 (1991).
18. P. Ruelle, M. Buchmann, H. Nam-Tran, and U.W. Kesselring. Int. J. Pharm. **87**, 47 (1992).
19. P. Ruelle, M. Buchmann, and U.W. Kesselring. J. Pharm. Sci. **83**, 396 (1994).
20. P. Ruelle, E. Sarraf, and U.W. Kesselring. Int. J. Pharm. **104**, 125 (1994).
21. P. Ruelle, E. Sarraf, L. Van den Berge, K. Seghers, M. Buchmann, and U.W. Kesselring. Pharm. Acta Helv. **68**, 49 (1993).
22. S.C. Mraw and D.F. O'Rourke. J. Chem. Thermodyn. **13**, 199 (1981).
23. P.L. Huyskens and M.C. Haulait-Pirson. J. Mol. Liq. **31**, 135 (1985).

© 2000 NRC Canada

Dissolution of organic solvents from painted surfaces into water

J.C. Wren, D.J. Jobe, G.G. Sanipelli, and J.M. Ball

Abstract: The presence of volatile iodine in containment buildings is one of the major safety concerns in the potential event of nuclear reactor accidents. Organic impurities in containment water, originating from various painted structural surfaces and organic materials, could have a significant impact on iodine volatility following an accident. To determine the source and magnitude of organic impurities and their effects on time-dependent iodine volatility, the dissolution for organic constituents from paints used in reactor buildings has been studied under postulated accident conditions. The studies of the organic dissolution from carbon steel coupons coated with zinc-primed vinyl, epoxy-primed polyurethane or epoxy paints over the temperature range 25–90°C are reported. Relatively large activation energies were measured for the release of the principal organic compounds from painted surfaces, suggesting it is the release of the solvents from the paint matrix rather than their diffusion through the solution that is the rate determining step for the dissolution mechanism. The similarities in the values of activation energies for the dissolution of different organic compounds from the paints suggest the release rate is independent of the nature of the painted surface or the type of organic being released from the surface. These two observations indicate that it may be possible to write a generalized rate expression for the release of organic compounds from painted surfaces in containment following an accident. The possible implications of these results for predicting iodine volatility in containment are also discussed.

Key words: dissolution kinetics, organic solvents, painted surfaces, reactor accidents.

Résumé : La présence d'iode volatil dans les enceintes de confinement est une des préoccupations majeures en matière de sécurité dans les cas d'accidents de réacteurs nucléaires. Les impuretés organiques présentes dans l'eau de confinement, qui pourraient provenir de divers matériaux organiques et de surfaces structurales peintes, pourraient avoir des répercussions significatives sur la volatilité de l'iode après un accident. Dans le but de déterminer la source et l'amplitude des impuretés organiques ainsi que leurs effets sur la volatilité de l'iode en fonction du temps, on a étudié la dissolution des constituants organiques des peintures utilisées dans les édifices des réacteurs dans les conditions prévues en cas d'accident. On rapporte les résultats d'études, effectuées à des températures allant de 25 à 90°C, sur la dissolution des produits organiques provenant d'échantillons d'acier au carbone recouverts peintures époxy, au vinyle avec couche d'apprêt au zinc ou au polyuréthane avec couche d'apprêt époxy. On a déterminé que les énergies d'activation sont relativement élevées pour la libération des principaux produits organiques des surfaces peintes; cette observation suggère que l'étape déterminante du mécanisme de dissolution est probablement la libération des solvants à partir de la matrice de peinture plutôt que leur diffusion à travers la solution. Les similarités dans les valeurs des énergies d'activation pour la dissolution de différents composés organiques à partir des peintures suggèrent que la vitesse de libération est indépendante de la nature de la surface peinte ou du type de composé organique libéré de la surface. Ces deux observations indiquent qu'il serait vraisemblablement possible de définir une expression de vitesse généralisée permettant de décrire la libération des composés organiques, à partir de surfaces peintes sur les enceintes de confinement, à la suite d'un accident. On discute aussi des implications possibles de ces résultats pour prédire la volatilité de l'iode dans les enceintes de confinement.

Mots clés : cinétique de dissolution, solvants organiques, surfaces peintes, accidents dans des réacteurs.

[Traduit par la Rédaction]

I. Introduction

The time-dependent airborne concentration of iodine in the reactor containment building is one of the most important parameters used to evaluate the potential radiological consequences of a nuclear reactor accident. The parameter is important because of the large inventory of iodine in irradiated nuclear fuel, and the radiological impact to public dose from an airborne emission of volatile ^{131}I species which could be released to the outside atmosphere through contain-

Received January 25, 1999. Published on the NRC Research Press website on April 06, 2000.

J.C. Wren,[1] D.J. Jobe,[2] G.G. Sanipelli, and J.M. Ball. AECL, Chalk River Laboratories, Fuel Chemistry Branch, Chalk River, ON K0J 1J0, Canada.

[1]Author to whom correspondence may be addressed. Telephone: (613) 584-3311. Fax: (613) 584-1220. e-mail: wrenc@aecl.ca
[2]Present address: College of Pharmacy and Nutrition, University of Saskatchewan, Saskatoon, Sask.

 © 2000 NRC Canada

ment leakage or controlled venting. The behaviour of iodine under containment accident conditions has thus been a subject of extensive studies for the nuclear industry world-wide including Atomic Energy of Canada Limited (AECL) for many years. Recent critical reviews on iodine behaviour (1–3) and references therein provide a comprehensive technical background on this subject.

The results of these studies have established that iodine behaviour in containment would depend strongly on the pH and the steady-state concentration of water radiolysis products such as ·OH, O_2^-:, and H_2O_2 in the containment sump water, both of which influence the rate of conversion of non-volatile I^- to volatile I_2 (1, 2, 4–7). Under accident conditions, organic impurities in containment water (or the sump), could significantly affect the pH and the concentrations of the water radiolysis products via the following reactions (1, 2, 4–7):

[1] $R + \cdot OH \rightarrow R\cdot + H_2O$

[2] $R\cdot + O_2 \rightarrow RO_2\cdot \rightarrow \rightarrow R'\cdot$, alcohols, aldehydes, acids and CO_2

where R and R· represent an organic compound and corresponding organic radical dissolved in water. Organic iodides would also be formed thermally and radiolytically through aqueous phase reactions of I_2 with the organic impurities:

[3] $R\cdot + I_2/HOI \rightarrow RI + I\cdot$

The formation and decomposition of organic iodides will influence iodine volatility by changing the steady-state concentration of volatile I_2. Some organic iodides are also volatile, and would contribute directly to the volatile iodine component in containment.

Although there are many different organic surfaces and impurities in containment, those that are dissolved in aqueous solutions and undergoing reactions [1] to [3] would have the largest effect on iodine volatility (1, 2). Consequently, the relative rates for the release of organic impurities from painted surfaces to the aqueous phase, and their subsequent degradation to organic acids and organic iodides, are important parameters required to describe iodine behaviour following an accident. The objective of the current study is to establish one of these parameters; the release rate of organic impurities into the sump water. The dissolution kinetics of organic solvents from paints have been studied using carbon steel coupons coated with zinc-primed vinyl, epoxy-primed polyurethane, or epoxy paint in a temperature range of 25–90°C. The studied temperature range is that expected in containment following an accident, and the vinyl, polyurethane, and epoxy paints have been used to coat the containment surfaces of CANDU®[3] nuclear generating stations. The results of the dissolution study are presented in this paper.

II. Experimental

The studies were performed under controlled temperature conditions in glass cells containing water at 25, 40, 60, 70, and 90°C. The temperature of the cell was controlled by either a circulating-water bath or heating tape. The solution pH was held constant at either pH = 5 or pH = 10 using a 0.1 mol dm^{-3} H_3BO_3–NaOH buffer. All solutions were made using filtered water from a Millipore Filtration System.

II.A Coatings and coupons

Release of organic compounds into both the aqueous and gas phases from painted surfaces immersed in water was studied using cylindrical carbon steel coupons coated with zinc-primed vinyl, epoxy-primed polyurethane, or epoxy coatings. The constituents of these paints as supplied by the manufacturer are listed in Table 1.

The coupons (geometric surface area = 5.7 cm^2) were sandblasted and within two hours spray-coated with the appropriate coating(s). For the zinc primer, a layer of approximately 0.015 cm was applied while for the other coatings, a thickness of approximately 0.025 cm was used. The epoxy-coated coupons and epoxy-primed-polyurethane-coated coupons were stored for 9 and 60 months, respectively, while the zinc-primed-vinyl-coated coupons were stored for various periods (15 days to 36 months). The coupons were stored in a ventilated area at room temperature (i.e., under conditions that did not inhibit solvent release by evaporation). The thinners used in applying the paints contained toluene, xylenes, methyl isobutyl ketone (MIBK), or 1,1,1-trichloroethane.

At the end of many of the dissolution experiments performed at 90°C there was evidence for blistering of the paint. The vinyl paint was particularly susceptible, with immersion resulting in the whole coupon surface being covered with blisters, 1 to 2 mm in diameter, and in some cases, exposure of the carbon steel on the edges of the coupon. A layer of the vinyl polymer was peeled, revealing yellow discoloration underneath, and ethanol and 2-propanol, the major solvent constituents of the zinc primer base undercoating, were observed in solution. Blistering was not observed at lower temperatures.

II.B Reaction vessel apparatus

Glass vessels were prepared from 500 cm^3 beakers, with final total volumes of 375 cm^3. These beakers were modified to accommodate a thermowell in the liquid phase for thermocouple readings, and a screw-on Teflon Mininert septum valve for sampling. The Mininert valve consisted of a push-type Teflon valve and a replaceable septum. The Teflon valve provided a seal when not sampling whereas the septum provided the only other seal when taking samples and allowed multiple punctures during the study. For studies at 60, 70, and 90°C the glass vessels were inserted into insulated machined-out aluminum cylinders, wrapped with heating tape. The temperature difference between the aluminum wall and the liquid phase was approximately 1 to 2°C. At 25 and 40°C, the glass vessels were kept in a circulating water bath.

The glass vessels, containing 60-cm^3 of air-sparged and buffered solutions, were heated to temperature at which point a single painted coupon was added to each vessel. Blank runs, for which no coupon was added to a vessel, were also conducted. There was no intentional mixing of the gas or liquid phase during the runs except when l.0-cm^3 gas and aqueous samples were removed using a Hamilton gas-tight syringe.

[3] CANDU is a registered trademark of Atomic Energy of Canada Limited.

© 2000 NRC Canada

Table 1. Constituents of the zinc primer, vinyl, epoxy, and polyurethane paints.[a]

Paint	Ingredients[b]	wt %
INTERVINUX VM HB (Vinyl paint)		
	Methyl ethyl ketone	15–40
	Ethyl 3-ethoxy propionate	10–30
	Tricresyl phosphate	3–7
	Xylene	1–5
	Methyl isobutyl ketone	1–5
	Silica amorphous	1–5
	Ferric/ferrous oxide	1–5
Thinner		
	Methyl isobutyl ketone	30–60
	Toluene	30–60
CARBOLINE CARBOZINC 11 (Zinc primer)		
Part A (base)[c]		
	Ethanol	30
	2-Propanol	20
	Silica	15
	2-Butoxy ethanol	10
	Aluminum silicate	10
	Ethyl silicate	10
	Methanol	10
	Pigment	5
	Methyl silicate	5
	Mica	5
	Water	4.4
Part B (zinc filler)[c]		
	Zinc dust	97
	Zinc oxide dust	3
Thinner #21		
	2-Propanol	100
Thinner #26		
	1-Methoxy-2-propanol	>1
	2-Ethoxy butanol	>1
AMERCOAT 66 (Epoxy paint)		
Part A (cure)[d]		
	Polyamide resin	<75
	Xylene	<30
	Triethylene tetramine	<5
Part B (resin)[d]		
	Epoxy resin	<25
	Methyl isobutyl ketone	<10
	Xylene	<10
	Methyl *n*-amyl ketone	<10
	2-Butoxyethanol	<5
	Talc	<40
	Titanium dioxide	<10
	Iron oxide	<10
	Amercoat 7 (thinner)	No Data provided
NORMAC NR-5S (Polyurethane paint)		
Part A[e]		
	Polyether polyol	42–60
	Methylene bis-(4-cyclohexylisocyanate)	2.1–3.6
	1,1,1-Trichloroethane	35–55
Part B[e]		
	Dihydro-2(3H)-furanone	35–60
	4-4′-Methylene dianiline	42–50

© 2000 NRC Canada

Table 1 (*concluded*).

Paint	Ingredients[b]	wt %
Thinner		
	1,1,1-Trichloroethane	96.5
	Diethylene ether	2.5
	1,2-Butylene oxide	0.5
	Nitromethane	0.3

[a]Paint compositions provided by manufacturers.

[b]Only hazardous materials are listed. Paint is up to 30% solids (vinyl-chloride, vinyl-acetate co-polymer) by volume.

[c]One gallon part A (base) mixed with 8 kg (zinc filler). Thinner added as required.

[d]One part A (hardener) mixed with 4 parts B (resin). Thinner added as required.

[e]One part A mixed with 0.15 parts B. Thinner added as required.

II.C Analyses

The gas-phase concentrations of the organic compounds were determined using a Model 3700 Varian Gas Chromatograph (GC) equipped with a HNU Model PI-52 photoionization detector. The GC was routinely calibrated using gas mixtures of known composition. Gas-phase constituents were identified using a Hewlett Packard (HP) Model 5890 GC fitted with a HP Series 5972 mass selective detector. The detection limit of the GC for the organic molecules was 0.05 $\times 10^{-6}$ mol dm^{-3}.

The concentrations of the aqueous-phase carbonyl species were determined using a Waters' HPLC (High Performance Liquid Chromatography) system, following derivatization by 2,4-dinitrophenylhydrazine (DNPH) (8). The aqueous organic species detected by this method were formaldehyde, acetaldehyde, acetone, methyl ethyl ketone, *n*-heptan-2-one, and MIBK. The detection limits of the HPLC/derivatization method ranged from 0.5×10^{-6} to 1×10^{-6} mol dm^{-3} for aldehydes and ketones and from 4×10^{-6} to 10×10^{-6} mol dm^{-3} for organic acids. The concentrations of aromatic compounds were too low to be detected by direct injections. At the end of each test, the pH was measured and the liquid sent for chloride analyses by ion chromatography. The statistical measurement uncertainties ($\pm 1\ \sigma$ with 95% confidence limits) of the gas and aqueous phase analysis were 12 and 5%, respectively, except for low concentrations near the detection limits.

During a typical experiment, one of the coupons was placed in the reaction flask containing the solution and the flask was sealed with a screwed septum cap. This arrangement provided a surface area to volume ratio in the aqueous phase (A_{surf}/V_{aq}) of ~0.095 cm^{-1} and a gas to aqueous volume ratio (V_g/V_{aq}) of approximately 5.25.

Both gas and aqueous samples were taken periodically using micro-syringes and analyzed for organic content; from every half an hour to an hour at 90°C to every 24 h at 25°C. Because of the small sampling volumes, the total reduction in the aqueous volumes due to sampling was no more than 8% by the end of the test. A test lasted until a steady-state was reached or up to 20 days.

III. Results

III.A Dissolution and partitioning of organic compounds between gas and aqueous phases

A number of organic compounds were found in the gas and aqueous phases in the presence of the three coatings. MIBK is common to all coatings as it was present in either the paint, the undercoating (e.g., it is not present in the polyurethane paint, but was present in the epoxy undercoating), or the thinner. One organic compound that appears in the epoxy and vinyl tests but is absent from the list of the manufacturer's ingredients is acetone. This component must have been present as either an impurity (present in the MIBK) or as a product of hydrolysis or oxidation of one of the other components. A number of other lower-weight aliphatic aldehydes and ketones which may be by-products of reactions or impurities were also identified. Components of the thinners, such as aromatic (toluene and *m*-xylene) and chlorinated (1,1,1-trichloroethane) hydrocarbons were also observed. For the organic compounds detected in the aqueous phase, the following sequence was observed for their concentrations in the presence of the three surfaces:

Epoxy: acetone > MIBK > *n*-heptan-2-one > *m*-xylene

Vinyl: acetone ≅ MIBK ≅ MEK ≅ acetaldehyde > formaldehyde

Polyurethane: MIBK > formaldehyde

while in the gas phase:

Epoxy: *m*-xylene > MIBK ≅ *n*-heptan-2-one > acetone

Vinyl: MIBK > *m*-xylene > toluene

Polyurethane: MIBK > *m*-xylene >> 1,1,1-trichloroethane

The different order of abundance in the gas and aqueous phases is due to different partition coefficients of these compounds, where the partition coefficient (H) is defined as the ratio of the *aqueous* to the *gas*-phase concentration at equilibrium, and is related to the equilibrium constant K (Henry's law constant) obtained from the free energy, by the relationship $H = K(RT)$.

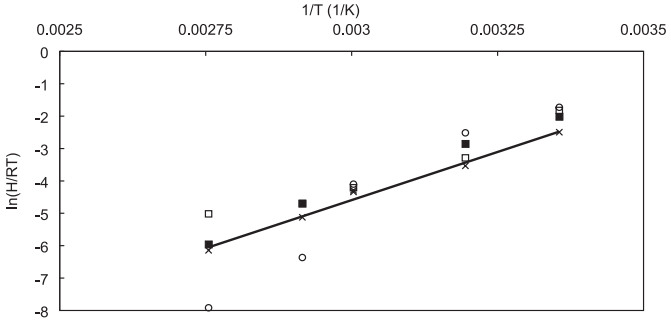
The equilibration of these organic compounds between the gas and aqueous phases in a shallow pool should be quite rapid and thus the concentrations of organic compounds in the gas phase should reflect those in the aqueous phase. This was confirmed experimentally by injecting MIBK at the bottom of an aqueous solution and then analyzing the gas phase for MIBK as a function of time. Equilibrium was obtained within 10 min, much faster than the time scale of these

© 2000 NRC Canada

Table 2. Values for the partition coefficient (H) for MIBK at 25, 40, 60, 70, and 90°C.

	H			
Temperature (°C)	Vinyl	Epoxy	Polyurethane	Water
25	330	204	440	400
40	150	76	210	97
50	—	—	—	83
60	38	36	46	41
70	26	17	4.9	26
90	7.8	6.5	1.1	20

Fig. 1. Plot of ln (H) versus 1/T(K) for the distribution of MIBK between the gas and aqueous phases in the absence of any surface (□) and in the presence of the epoxy (×), vinyl (■), and polyurethane (○) surfaces.



thermal dissolution studies. The fast equilibrium between the gas and aqueous phases enabled us to use both the aqueous- and gas-phase data to determine the dissolution rates.

The partition coefficient of MIBK as a function of temperature, measured in water in the absence of a painted surface, is listed in Table 2. Similar values, generally within a factor of two (which is within experimental uncertainties) were obtained using painted coupons as the source of MIBK. These values are also listed in Table 2. Note that the uncertainties are greater for lower partition coefficients (i.e., at higher temperatures).

A least-squares fit of ln (H/RT) versus 1/T(K) (Fig. 1) using all of the data in Table 2 yields a $\Delta H° = -(59 \pm 6)$ kJ mol^{-1} and $\Delta S° = -(214 \pm 16)$ J mol^{-1} K^{-1} for the transfer of MIBK from the gas phase to the aqueous phase using the slope and intercept, respectively (MIBK(g) = MIBK(aq)).

$$[4] \qquad \Delta G° = -RT \ln (H/RT) = \Delta H° - T\Delta S°$$

$$[5] \qquad \ln (H) - \ln (RT) = -(\Delta H°/R)\ (1/T) + \Delta S°/R$$

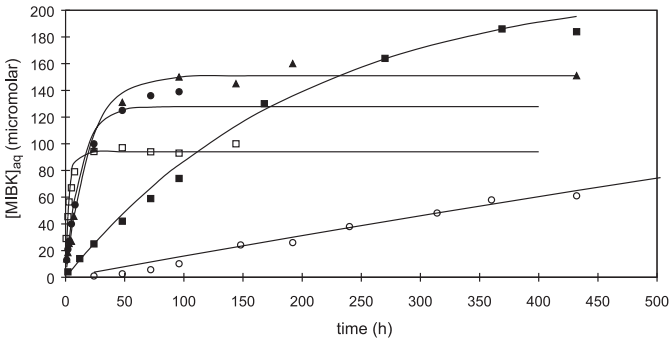
A similar analysis of the data obtained for *n*-heptan-2-one and acetone during the epoxy test gives the results in Table 3. The values for $\Delta H°$ are compared to literature values for the same compounds obtained from Ref. 9. $\Delta S°$ values for the ketones were not readily available from the literature, therefore $\Delta S°$ values for organic compounds having similar heats of vapourization e.g., ethanol and methanol are provided for comparison in Table 3 (10).

Table 3. Values of $\Delta H°$ and $\Delta S°$ for the gas–liquid phase partitioning of various organics in water.

Organic	$\Delta H°$ (kJ mol^{-1})	$\Delta S°$ (J K^{-1} mol^{-1})	Reference
MIBK	–(59 ± 6)	–(214 ± 16)	This study
	–1.4[a]		(9)
acetone	–(69 ± 13)	–(245 ± 13)	This study
	–46		(9)
n-heptan-2-one	–(57 ± 18)	–(210 ± 5)	This study
	–37		(9)
methanol	–46	–107	(10)
ethanol	–54	–134	(10)

[a]Both the reported partition coefficient and the reported activation energy are very low in comparison to those for similar compounds.

Fig. 2. Aqueous-phase concentrations of MIBK in the presence of the epoxy surface (pH = 10) at 25 (○), 40 (■), 60 (▲), 70 (●), and 90°C (□). The lines drawn through the data are those calculated using eq. [14].



III.B Dissolution of MIBK from coatings

To assess the release of organic compounds from the coatings under containment conditions, it is best to study the release of one representative compound common to all coatings. Since MIBK is present in varying degrees in all of the coatings (it is not present in the polyurethane coating per se., but is present in the epoxy undercoating), the MIBK data have been used to obtain the dissolution kinetics. The dissolution kinetics of MIBK from vinyl, epoxy, and polyurethane surfaces were studied at 25, 40, 60, 70, and 90°C. Some of the results are shown in Figs. 2 to 6. For each coating, additional analysis included several other organic compounds, ranging from other ketones (acetone, *n*-heptan-2-one), to aromatic compounds (*m*-xylene, toluene) and halogenated hydrocarbons (trichloroethylene, chloroform). All of these species showed dissolution kinetics very similar to MIBK.

Comparing the time dependent concentration profiles for the various surfaces, it appears that the final steady-state MIBK concentrations, which were far below the solubility limit of MIBK in water, depend on both coating type and paint aging. MIBK dissolution also follows the rate laws derived from the simple mechanism:

$$[6] \qquad \text{MIBK(ab)} \rightarrow \text{MIBK(aq)}$$

© 2000 NRC Canada

Fig. 3. Gas-phase concentrations of MIBK in the presence of the epoxy surface (pH = 10) at 25 (○), 40 (■), 60 (▲), 70 (●), and 90°C (□). The lines drawn through the data are those calculated using eq. [14].

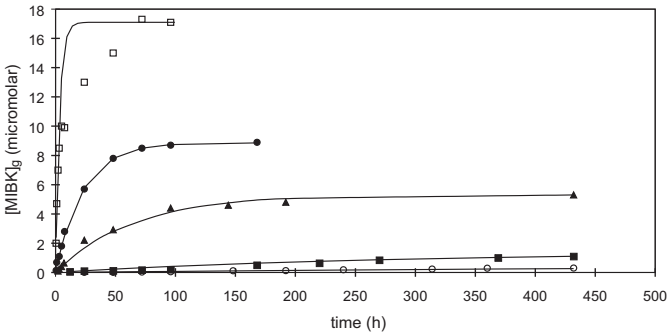


Fig. 4. Normalized concentrations of MIBK in the presence of the epoxy surface (pH = 10) at 25 (○), 40 (■), 60 (▲), 70 (●), and 90°C (□). The lines drawn through the data are those calculated using eq. [14] normalized to the steady-state concentration.

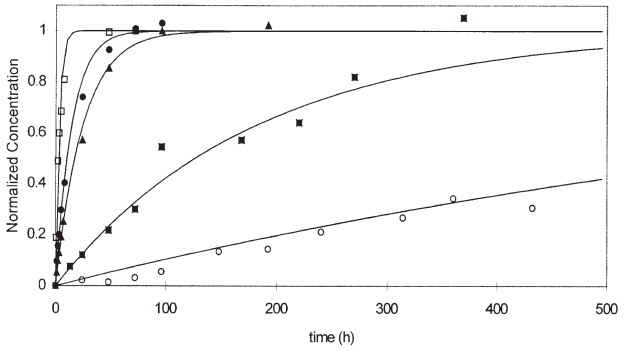


Fig. 5. Normalized concentrations of MIBK in the presence of the polyurethane surface (pH = 5) at 25 (○), 40 (■), 60 (▲), 70 (●), and 90°C (□). The lines drawn through the data are those calculated using eq. [14] normalized to the steady-state concentration.

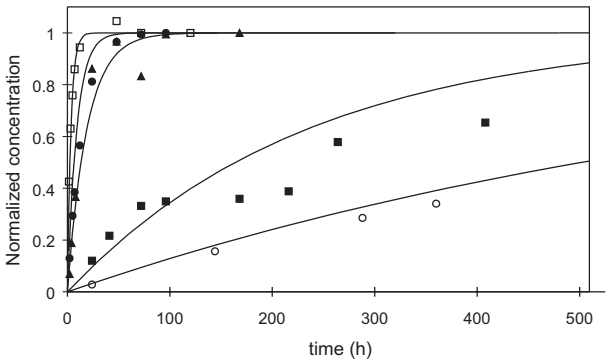
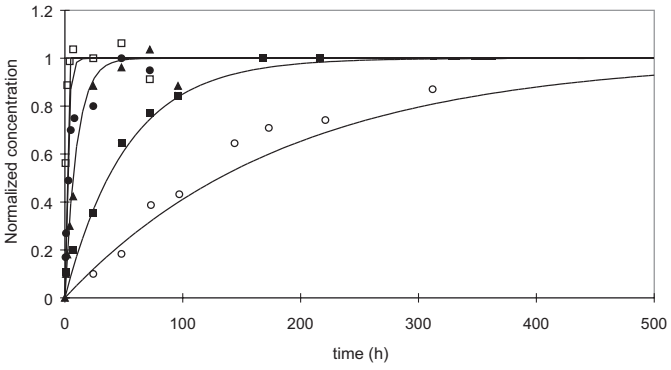


Fig. 6. Normalized concentrations of MIBK in the presence of the vinyl surface (pH = 10) at 25 (○), 40 (■), 60 (▲), 70 (●), and 90°C (□). The lines drawn through the data are those calculated using eq. [14] normalized to the steady-state concentration.



[7] MIBK(aq) ↔ MIBK(g)

where aq, ab, and g in the brackets represent aqueous, absorbed, and gas phase, respectively. Assuming a fast equilibrium for eq. [7] leads to the following equation for the concentration of MIBK in solution, $[MIBK(aq)]_t$ (μmol dm^{-3}):

$$[8] \quad [MIBK(aq)]_t = [MIBK(aq)]_\infty \cdot (1 - \exp(-kt))$$

$$[9] \quad = \alpha(1 - \exp(kt))$$

and for the gas-phase concentration of MIBK, $[MIBK(g)]_t$ (μmol dm^{-3}):

$$[10] \quad [MIBK(g)]_t = \frac{1}{H}[MIBK(aq)]_\infty (1 - \exp(-kt))$$

$$[11] \quad = \beta(1 - \exp(kt))$$

where k is the dissolution rate constant (s^{-1}), α and β are proportional constants, H is the partition coefficient, and $[MIBK(aq)]_\infty$ (μmol dm^{-3}) is the final MIBK concentration present in the water at the end of dissolution, and is related to the amount of MIBK present in the paint polymer initially, $[MIBK(ab)]_0$.

Table 4 shows the values of k and $[MIBK(aq)]_\infty$ that result from fitting eq. [8] to the observed time-dependent aqueous-phase concentrations for the epoxy, vinyl, and polyurethane surfaces. The amount of MIBK originally on the surface $[MIBK(ab)]_0$ is also shown in the table. $[MIBK(ab)]_0$ was calculated using the measured partition coefficient of MIBK in water at the appropriate temperature, (see Table 2), the surface area of the coupon, and the appropriate liquid and gas volumes. The aqueous-phase data for the test in the presence of the epoxy surface at pH = 10 is shown graphically in Fig. 2 while the gas-phase data for the same test is shown in Fig. 3. The lines drawn through the data are those predicted by eqs. [9] and [11] using the k and $[MIBK(aq)]_\infty$ values given in Table 4. In general, the calculated lines reproduce the data extremely well, indicating the simple mechanism represented by reactions [6] and [7] adequately describes the dissolution process.

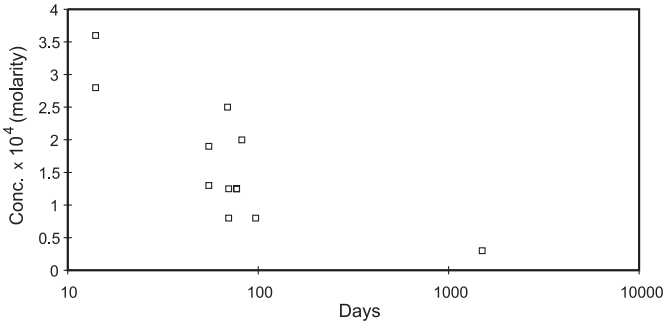
From Table 4 (Fig. 2), it can be seen that the final steady-state concentration for MIBK, $[MIBK(aq)]_\infty$, in the presence of a painted surface varies from one test to another. The range of the final concentration is more than expected from the variations in paint thickness which were kept small. This variance is considered to be mainly due to the difference in

© 2000 NRC Canada

Table 4. Values for the parameters resulting from the fit of eq. [14] to the time-dependent aqueous-phase MIBK concentration data.

Surface	pH	T (°C)	k (h^{-1})	$[MIBK(ab)]_o$ (nmol cm^{-2})	$[MIBK(aq)]_\infty$ (μmol dm^{-3})
Epoxy	5	25	0	1770	160
		40	0	3100	270
		60	0.051	1850	150
		70	0.074	1710	130
		90	0.3	1300	94
	10	25	0	1440	130
		40	0.01	3450	300
		60	0.041	1600	130
		70	0.074	1710	130
		90	0.33	830	60
Polyurethane	5	25	0	460	42
		40	0.01	760	66
		60	0.052	1230	100
		70	0.11	1580	120
		90	0.28	1530	110
	10	25	0	660	60
		40	0	1500	130
		60	0.028	1720	140
		70	0.069	1840	140
		90	0.33	1800	130
Vinyl	5	25	0	3650	330
		40	0.01	1500	130
		60	0.084	2300	200
		70	0.14	1640	130
		90	0.77	1480	80
	10	25	0.01	3650	330
		40	0.019	1380	120
		60	0.1	3080	250
		70	0.41	2100	160
		90	1.7	1080	78

Fig. 7. The final steady-state concentration of MIBK released from vinyl-painted coupons as a function of the aging of paint.



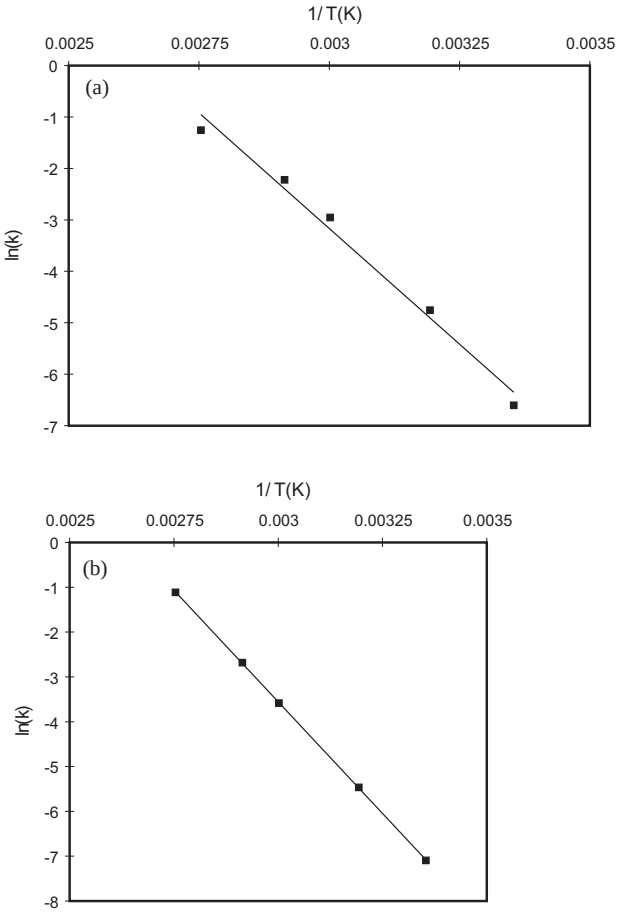
the amount of solvent initially in the paint polymer, and related to the degree of aging of the paint. The maximum concentration of MIBK released into the aqueous phase from the vinyl painted coupons is shown as a function of paint aging in Fig. 7. Data obtained at different pH values and temperatures are all included in the figure. (We do not have enough data to establish the effect of aging for the other paints.) Although the data show large scatter, the effect of aging on the final concentration can be seen clearly. Therefore, it is assumed that the initial MIBK concentration within the coating surface controls the maximum MIBK concentration in solution and that the MIBK content in the coating decreases with aging due to evaporative losses.

To compensate for this aging effect in the graphical presentation, the concentrations of MIBK were normalized by dividing by final steady-state concentration. A plot of the normalized data for the epoxy, polyurethane, and vinyl surfaces can be found in Figs. 4–6, respectively. Only the initial data are shown for low temperature tests due to the variable time frame over which the tests were conducted, i.e., tests at 25°C take much longer to reach steady-state than tests performed at 90°C. The lines drawn through the data are those calculated using eq. [9] normalized to the final steady-state concentration.

The solution pH appears to have only a minor effect on the dissolution of MIBK. For most of the data, the dissolution behaviour of MIBK at pH 5 is not that much different than that at pH 10. For the most part, the time-dependent dissolution curves at the two pHs parallel each other for the three surfaces at the various temperatures; although generally, the dissolution curves at pH = 10 yield slightly higher final concentrations. This is unlikely to be a consequence of small variations in the painted samples, because the higher of the two final concentrations would be expected to be dis-

© 2000 NRC Canada

Fig. 8. Arrhenius plot of the dissolution rate constants observed for MIBK from polyurethane painted coupons, using (*a*) gas-phase data and (*b*) aqueous-phase data.



tributed randomly between the two pH values, which is not the case. It may be possible that the results obtained from the DNPH derivatization are pH dependent.

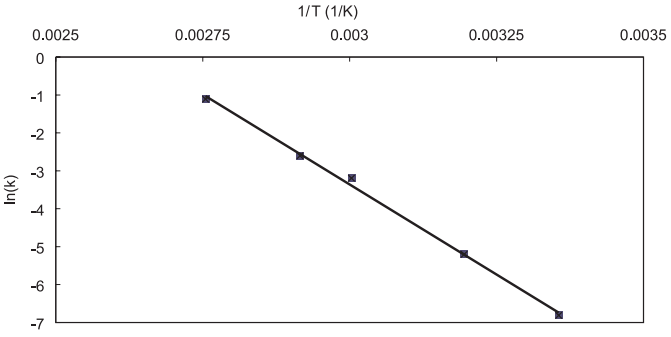
As can be seen in Figs. 4–6, the effect of temperature on dissolution is as expected, increasing the dissolution rate for MIBK sharply as the temperature increases. The dissolution rate constant for MIBK from polyurethane measured as a function of temperature is shown in an Arrhenius plot, i.e., ln k versus (1/T), in Fig. 8, where the slope of the plot provides the activation energy (E_a) of the dissolution process:

$$[12] \quad k = A \exp(-E_a/RT)$$

The rate constants obtained using the gas-phase data are nearly identical with those obtained from the aqueous-phase data for all paints studied. Arrhenius plots of the dissolution constants from epoxy and vinyl paints are shown in Figs. 9 and 10, respectively.

The activation energies determined from Arrhenius plots for the dissolution of MIBK are listed in Table 5. Table 5 includes data from all three surfaces at pH = 5 and 10 using both the aqueous and gas-phase measurements. The errors on E_a listed in Table 5 are those associated with the slopes based on a least-squares (Arrhenius) fit of the ln (k) and 1/T(K) values listed in Table 4. Except for some of the results obtained in the presence of the polyurethane surface,

Fig. 9. Arrhenius plot of the dissolution rate constants observed for MIBK from epoxy-painted coupons, using aqueous-phase data.



the E_a values are within experimental error of each other, yielding an average of E_a = 82 ± 11 kJ mol^{-1}.

We have also analyzed the data for acetone and *m*-xylene and obtained the activation energies for the dissolution of these compounds; E_a = 83 ± 3 and 65 ± 4 kJ mol^{-1} respectively, similar to those observed for MIBK.

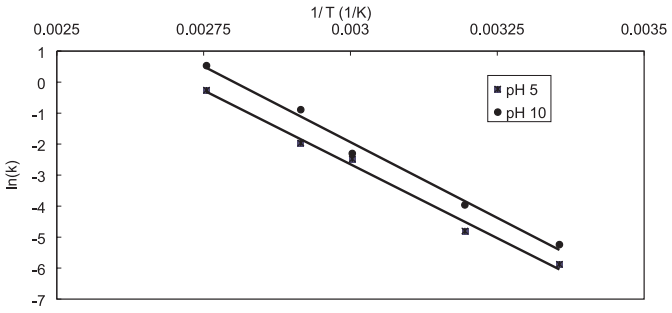
IV. Discussion

Unlike the dissolution of a pure solid, the release of MIBK from the painted surface does not involve the rupture or hydrolysis of chemical bonds within the structure of the solid, but rather occurs through the diffusion of the organic compound out of the paint matrix. A typical final concentration for MIBK in the experiments is ~100 μmol dm^{-3}. For the 60 cm^3 of water, this indicates an overall release of ~6 μmoles or 4 × 10^{18} molecules of MIBK per coupon (surface area = 5.7 cm^2). Typical BET (Brunauer, Emmett and Teller) surface area measurements have shown that small organic molecules like pyridine usually occupy an adsorbed surface area of 26 × 10^{-16} cm^2 (11); therefore, it would have required a surface with an area of ~1 × 10^4 cm^2 to have released this amount of MIBK as an adsorbed monolayer. This is ~2000 times more than the surface area of the coupon; therefore, MIBK must be diffusing out of the paint matrix.

Except for one of the results obtained in the presence of the polyurethane surface, the E_a values are within experimental error of each other yielding an average of 82 ± 11 kJ mol^{-1}. The similar values of E_a obtained for the three surfaces imply that the diffusion of the organic solvents through the matrix is relatively independent of the chemical composition of the matrix of the paint. Furthermore, the absolute dissolution rate constants are very similar for the three surfaces, indicating that, for a given substrate (in this case sandblasted carbon steel), the painted surface area does not vary significantly with the type of paint. This is important, for if this assumption is valid, it is possible that a general expression can be used to predict the release rate and time dependent concentrations for MIBK from a painted surface, provided the surface concentration and temperature are known. This assumption can be extended one step further. Fits of the Arrhenius equation to the data obtained for acetone and *m*-xylene yield E_a = 83 ± 3 and 65 ± 4 kJ mol^{-1}, respectively. These values are similar to that obtained for

© 2000 NRC Canada

Fig. 10. Arrhenius plot of the dissolution rate constants observed for MIBK from vinyl-painted coupons, using aqueous-phase data.



MIBK, which suggests that the dissolution rate is also independent of the type of organic compound.

The mechanism for the release of organic compounds from paint surfaces exposed to water is believed to be assisted by, and dependent upon, the rate of diffusion of water through the paint matrix.[4] This is supported by the fact that coupons aged several years (cf. the polyurethane coupons used in this study) retain significant quantities of solvents, but readily lose these solvents upon exposure to water. It is also supported by the observation that the dissolution rate appears to be independent of chemical nature of the organic compound. Finally, the water assisted dissolution is suggested by the measured activation energies. Diffusion of water through a layer of paint should have a large activation energy (E_a), typically between 50 and 100 kJ mol^{-1} (12), whereas the diffusion of a molecule away from the surface should be smaller, typically 10–20 kJ mol^{-1} (13, 14). The relationship between the adsorption of water by a polymer coating, and the release of solvents is discussed in detail elsewhere (See footnote 4). Briefly however, the apparent first order kinetic behaviour observed for the release of solvents from painted surfaces exposed to water is analogous to that observed for surface evaporation of a solvent from a solid to a final equilibrium concentration in the gas phase. The initial boundary conditions and physical processes assumed in deriving the solvent evaporation model in Ref. 15 (i.e., concentration of the diffusing species constantly decreasing in the solid and increasing outside of the solid) were consistent with our experimental conditions, and result in the first-order kinetics behaviour observed in our experiments.

The effect of radiation on the rate of dissolution of the organic compounds was negligible, although radiation rapidly decomposed the organic compounds once they had been released into the aqueous phase. This is consistent with studies described in Refs. 1 and 2. Release of MIBK from coupons in which dissolution followed a period of irradiation appeared to have the same rate constant, although the final concentrations of MIBK in solution were smaller. Solutions in contact with painted coupons that were irradiated subsequent to a dissolution period were found to yield increased gas-phase concentrations of acetaldehyde, acetone, and MEK; and reduced concentrations of MIBK. The former three compounds were found to arise as a result of decomposition of dissolved MIBK. Toluene and xylene were not observed, because the small amounts present decomposed to phenol derivatives (and to some extent to organic acids), which are non-volatile and difficult to detect in the gas phase by conventional GC techniques.

Table 5. Activation energies for the dissolution of MIBK from different painted surfaces.

Surface	Phase	pH	E_a (kJ mol^{-1})
Epoxy[a]	Aqueous	5	79 ± 5
	Aqueous	10	78 ± 3
	Gas	10	75 ± 7
	Aqueous	5	75 ± 5
Polyurethane	Aqueous	10	83 ± 0.3
	Gas	5	85 ± 5
	Gas	10	108 ± 10 (91 ± 3)[b]
	Aqueous	5	82 ± 5
Vinyl	Aqueous	10	73 ± 6
	Gas	5	72 ± 4
	Gas	10	72 ± 8

[a]Gas phase data was not obtained for pH 5.

[b]This number was obtained from 40, 60, 70, and 90°C data only.

From these observations, we concluded that irradiation at the total absorbed doses and dose rates (0.13 Gy s^{-1}) used here does *not* have a significant impact on the chemistry of the paint coating per se, although it decomposes the organic solvents that have been released to solution, affecting their concentrations observed in the aqueous and gas phases. A factor not considered in this study but which should be investigated further, is the impact of the thickness of the coating on the release rate. Presumably, as with aging time, there should be some dependence of the release rate on thickness, because it should affect the amount of MIBK originally in the coating for the surface. Also, a thicker coating may increase the length of the pathway that the organic solvent takes through the paint matrix before reaching the surface. Therefore, a study of the activation energy as function of paint thickness for one of the coatings is required to determine the effect of coating thickness on the E_a for the dissolution process (See footnote 4).

The studies on the radiolysis of organic compounds presented in Refs. 4–6 have shown that, compared to the dissolution rate, the rate of the radiolytic decomposition of organic solvents in the aqueous phase would be very fast under postulated accident containment conditions in which the radiation dose rate is expected to be in the range of 1–10 kGy h^{-1} immediately following an accident but fall off exponentially with time. These relative rates of organic dissolution and organic radiolysis have been observed in integral tests performed in the intermediate-scale Radioiodine Test Facility[5] (1, 2, 7, 16). These studies show that, (*i*) the

[4] J.M Ball, J.C. Wren, and J.R. Mitchell. Manuscript in preparation.

[5] The Radioiodine Test Facility is an intermediate scale (350 dm^{-3}) facility which provides a combination of potential reaction media (gas phase, aqueous phase and variety of surfaces) and conditions (pH, temperature, radiation, initial concentrations and speciation of iodine), simulating a reactor containment building following an accident. The RTF is equipped with various on-line sensors to follow various chemical and physical properties as a function of time. A description of the RTF and test procedures can be found in refs. (1), (2), (7), and (16).

© 2000 NRC Canada

radiolysis of organic compounds from paint coatings will occur primarily in the aqueous phase and not on the surface, and (*ii*) under reactor accident containment conditions, the rates of radiolytic decomposition of organic compounds and formation of organic iodides are much faster than the rate of organic dissolution. The slower rate for organic dissolution is the principal parameter determining the pH reduction rate. Differences in the composition of the surfaces result in small variations in the rate of pH change because of the differences in the overall radiolysis production rate of organic acids and CO_2 from the different paint constituents.

The implication of these studies on modelling the effects of organic impurities on the time dependent iodine volatility in containment following an accident is that the dissolution process appears to be the rate-determining step for the changes in pH, dissolved oxygen concentration and organic iodide concentration observed when aqueous solutions containing CsI are irradiated in the presence of painted surfaces. Consequently, detailed kinetic mechanisms for the radiolytic decomposition of organic compounds and organic iodide formation may not be necessary.

V. Conclusions

The release of organic solvents from a variety of painted coupons exhibits pseudo-first order behaviour. Values of *k*, the pseudo-first order rate constant for solvent release, are relatively insensitive to solvent type, the effect of radiation, and water pH, and are similar in magnitude for various surfaces at a given temperature. Relatively large activation energies were measured for the release of organic compounds from painted surfaces. This suggests that it is the release from the paint-matrix rather than diffusion through the solution that is the rate determining step for the dissolution mechanism. The similarities in the values of activation energies for the dissolution of different organic compounds from the paint further suggests the release rate is relatively independent of the nature of the painted surface or the type of organic compound being released from the surface. Based on these two observations, it may be possible to write a generalized rate expression for the release of organic compounds from painted surfaces in containment during an accident.

Thermodynamic values have been obtained for the partitioning of the major constituents found in paints used to coat the containment surfaces of several CANDU® nuclear generating stations. Under the conditions of these experiments, the distribution of organic compounds between the gas and aqueous phases is rapid relative to the dissolution of these organic compounds from the paint matrix. All of these constituents have large negative ΔS values (Table 3) for the distribution equilibrium, suggesting the reverse process (i.e., partitioning of the organic compound from the aqueous to the gas phase) is entropy driven.

This work, in combination with the study on the radiolysis of organic compounds (4–6) and various integral effects test results from the intermediate scale Radioiodine Test Facility (1, 2, 7, 16), has established that dissolution of organic compounds from a painted surface into water is a key rate controlling step for any changes in the iodine volatility due to organic reactions, i.e., pH change and organic iodide formation. Since the release rate appears to be largely independent of the nature of the paint for a given surface substrate, it may be possible that a generalized expression for the dissolution rate for compounds will be sufficient to describe the kinetics of pH change and organic iodide information in containment.

Acknowledgements

The authors would like to acknowledge K. Weaver at Ontario Power Generation and G. Glowa, A. Tarr, and J. Halliday at AECL for reviewing this document and for their helpful discussions. This work was funded by the COG (CANDU Owners Group) R&D Program, Working Party 06, Containment Behaviour under the joint participation of Ontario Power Generation, Hydro Quebec, New Brunswick Power and AECL.

References

1. J.C. Wren, J.M. Ball, and G.A. Glowa. Nucl. Technol. **129**, 297 (2000).
2. J.C. Wren, J.M. Ball, and G.A. Glowa. Nucl. Technol. **125**, 337 (1999).
3. R.M. Sellers. *In* Proceedings of the specialists' workshop on iodine chemistry in reactor safety. Harwell, U.K., September 1985. *Edited by* A.M. Deane and P.E. Potter. Atomic Energy Research Establishment, AERE- R1197491. 1986. p. 91.
4. P.A. Driver, G.A. Glowa, and J.C. Wren. Rad. Phys. Chem. **57**, 37 (2000).
5. G.A. Glowa, P.A. Driver, and J.C. Wren. Rad. Phys. Chem. **58**, 49 (2000).
6. J.C. Wren and G.A. Glowa. Accepted in Rad. Phys. Chem. (2000).
7. J.M. Ball, W.C.H. Kupferschmidt, and J.C. Wren. *In* Proceedings of the fourth CSNI/OECD workshop on the chemistry of iodine in reactor safety. Wurenlingen, Switzerland, June 1996. *Edited by* S Guntay. Paul Sherrer Institute. 1997. p. 63.
8. R.J. Kieber and K. Mopper. Environ. Sci. Technol. **24**, 1477 (1990).
9. J. Staudinger and P.V. Roberts. Crit. Rev. Environ. Sci. Technol. **26**, 205 (1996).
10. D.D. Wagman, W.H. Evans, V.B. Parker, R.H. Schumm, I. Halow, S.M. Bailey, K.L. Churney, and R.L. Nuttall. J. Phys. Chem. Ref. Data, **11**, Supplement 2 (1982).
11. M.A. Rahman and A.K. Ghosh. J. Colloid Interface Sci. **77**, 50 (1980).
12 T. Skouulikidis and A Ragoussis. Corrosion (Houston), **88**, 666 (1992).
13. L. Bonoli and P.A. Witherspoon. J. Phys. Chem. **72**, 2532 (1968).
14. E. Oelkers. Geochim. Cosmochim. Acta, **55**, 3515 (1991).
15. J. Crank. *In* The mathematics of diffusion. 2nd ed. Clarendon Press, Oxford. 1975. p. 60.
16. W.C.H. Kupferschmidt, J.B. Buttazoni, G.J. Evans, B.L. Ford, A.S. Palson, R. Portman, and G.G. Sanipelli. *In* Proceedings of the Third CSNI Workshop on Iodine Chemistry in Reactor Safety, Tokai-mura, Japan, September 1991. Japan Atomic Energy Research Institute Report, JAERI - M 92-012. 1992. p. 212.

© 2000 NRC Canada

Metal ion–biomolecule interactions. Part 22.[1] Cr(III)-catalyzed isotopic hydrogen exchange in methylimidazoles[2]

Omoshile Clement, Ikenna Onyido, and Erwin Buncel

Abstract: The detritiation kinetics of the Cr(III) complexes **1** and **3**–**6** have been studied in aqueous buffers at 35°C, using the liquid scintillation counting technique. Results for **5** and **6** provide benchmark kinetic data for N-T/N-H exchange under the experimental conditions of the study and have aided in the delineation of N-T/N-H from C-T/C-H exchange in the parallel reactions observed experimentally. Curved first-order plots obtained for **1**, **3**, and **4** were treated to yield rate constants for two parallel exchange reactions k^{A}_{obs} and k^{B}_{obs} for the "fast" and "slow" processes, respectively. The "fast" process has been assigned to C(2)-H exchange in **1**, competing N-H and C(2)–H exchange in **3**, and N-H exchange in **4**. In all cases, the "slow" process is associated with C(4,5)-H exchange. Identification of exchange sites in **1**, **3**, and **4** was made possible by the consideration of the results of an IR spectroscopic study of hydrogen-deuterium exchange, comparison of the extent of ^{3}H incorporatation in different complexes in the tritiation experiments, and a careful analysis of the exchange kinetic data. Analysis of the rate data indicates that Cr(III) significantly enhances C(2)-H exchange in **1** and **3**, while C(4,5)-H exchange, hitherto reported in the literature only under drastic reaction conditions, was observed for **1**, **3**, and **4** under the mild conditions of the present study. Quantitation of the effect of Cr(III) coordination on ^{3}H exchange in imidazole-type nuclei was achieved fully in **1**; giving k^{M^+} values of 6×10^3 and 7×10^2 $M^{-1}s^{-1}$ for C(2)-H and C(4,5)-H exchange, respectively. Using the literature value for k^{H^+}, the second-order rate constant for C(2)-H exchange under H^+ catalysis, 2.9×10^2 $M^{-1}s^{-1}$, it follows that Cr(III) is ca. 20 times better as a catalyst for C(2)-H exchange in 1-methylimidazole than H^+, providing the first example of a metal ion being more effective than a proton in these processes. Comparison of the results obtained with **1** with literature results for **2** shows a very large (ca. 3×10^5-fold) difference in the catalytic activities of Cr(III) and Co(III), favouring the former. The dichotomy in the effectiveness of the two metal ions in catalyzing ^{3}H exchange in the imidazole nucleus has been ascribed to differences in (*i*) extent of M^{n+}—N bond polarization (and the consequent effect on ligand C-H acidity); (*ii*) electronic configuration; (*iii*) crystal field stabilization and activation energies; and (*iv*) importance of metal–ligand π back-bonding. The study highlights the diversity of factors and complexity of interactions involved in determining the role of metal ions in biological systems, especially where such processes involve complex formation between metal ions and heterocyclic fragments of biomolecules.

Key words: metal ion–biomolecule interactions, methylimidazole, isotopic hydrogen exchange, catalysis by chromium.

Résumé : Opérant à 35EC, dans des tampons aqueux et faisant appel à la technique de comptage de scintillation liquide, on a étudié la cinétique de détritiation des complexes de Cr(III) 1 et 3-6. Les résultats pour 5 et 6 sont des données cinétiques de référence pour l'échange N-T/N-H dans les conditions expérimentales de l'étude et ils ont permis de délimiter les échanges N-T/N-H et C-T/C-H dans les réactions parallèles observées expérimentalement. Les courbes du premier ordre obtenues pour les composés 1, 3 et 4 ont permis de tirer les constantes de vitesse pour les deux réactions d'échange parallèles k^{A}_{obs} et k^{B}_{obs} qui correspondent respectivement aux réactions "rapide" et "lente". On a attribué la réaction rapide à l'échange C(2)-H du composé 1 qui est en compétition avec celle du N-H, à l'échange C(2)-H du composé 3 et à l'échange N-H du composé 4. Dans chacun des cas, la réaction lente est associée à l'échange C(4,5)-H. L'identification des sites d'échange des produits 1, 3 et 4 a été rendue possible en prenant en considération les résultats d'une étude de l'échange hydrogène-deutériun par spectroscopie IR, en faisant une comparaison du taux d'incorporation du 3H dans divers complexes au cours d'expériences de tritiation et une analyse soignée des données cinétiques. L'analyse des données relatives aux vitesses indique que le Cr(III) augmente de façon significative l'échange C(2)-H des composés 1 et 3. Par ailleurs, dans les conditions douces utilisées dans cette étude, on a pu observer l'échange C(4,5)-H avec les produits 1, 3 et 4; jusqu'à maintenant, cet échange n'avait été rapporté

Received January 10, 2000. Published on the NRC Research Press website on April 6, 2000.

O. Clement[3] and E. Buncel.[4] Department of Chemistry, Queen's University, Kingston, ON K7L 3N6, Canada.
I. Onyido. Center for Agrochemical Technology, University of Agriculture, Makurdi, Nigeria.

[1]for Part 21 see ref. 53.
[2]This paper is dedicated to the memory of Professor Jack Hirst.
[3]Present address: Molecular Simulations Inc., 9685 Scranton Road, San Diego, CA 92121, U.S.A.
[4]Author to whom correspondence may be addressed. Fax: (613) 533–6669.

 © 2000 NRC Canada

dans la littérature que pour des réactions impliquant des conditions drastiques. Dans le cas du composé 1, il a été possible de quantifier l'effet de la coordination du Cr(III) sur l'échange du 3H dans un noyau imidazole type; pour les échanges respectivement du C(2)-H et C(4,5)-H, les valeurs de k^{M^+} sont égales à 6 x 103 et 7 x 102 M^{-1} s^{-1}. Utilisant une valeur de k^{H^+} tirée de la littérature, la constante de deuxième ordre pour l'échange C(2)-H dans des conditions de catalyse par H^+ est de 2,9 x 102 M^{-1} s^{-1} et il en découle que le Cr(III) est un catalyseur approximativement 20 fois plus efficace que le H+ pour l'échange C(2)-H dans le 1-méthylimidazole; cette observation correspond au premier cas dans lequel un ion métallique est plus efficace qu'un proton dans ce type de procédé. Une comparaison entre les résultats obtenus avec le composé 1 et ceux rapportés dans la littérature pour le composé 2 met en évidence qu'il existe une très grande différence (rapport de 1 à 3 x 105 en faveur du Cr) entre les activités catalytiques de Cr(III) et Co(III). La dichotomie entre les efficacités des deux ions métalliques dans la catalyse de l'échange du 3H dans le noyau imidazole a été attribuée à des différences dans (i) le degré de polarisation de la liaison M^{n+}—N (et l'effet qui en découle sur l'acidité du C-H du ligand); (*ii*) la configuration électronique; (*iii*) la stabilisation du champ cristallin et les énergies d'activation et (*iv*) l'importance de la liaison B en retour métal-ligand. L'étude met en évidence la diversité des facteurs et la complexité des interactions impliquées dans la détermination du rôle des ions métalliques dans les systèmes biologiques, particulièrement dans les processus qui impliquent la formation d'un complexe entre des ions métalliques et des portions hétérocycliques de biomolécules.

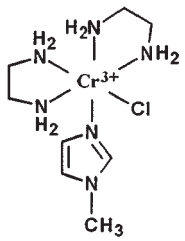
Mots clés : interactions ions métalliques/biomolécules; méthylimidazole; échange d'hydrogène isotopique; catalyse par le chrome.

[Traduit par la Rédaction]

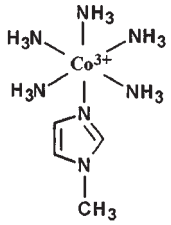
Introduction

The imidazole nucleus and similar heterocyclic residues occur in nature as key structural components of many biologically important molecules such as proteins, enzymes, nucleic acids, some vitamins, and high-energy molecules (e.g., ATP). These biomolecules are fundamental to a variety of life processes (1, 2); their key function in biological reactions is thought to involve binding through their donor (N, O, S) heteroatoms to mediating or interacting metal ions (3).

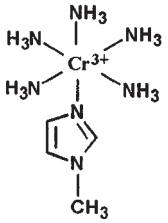
Studies in our laboratories have focussed in part on two important aspects of metal ion-biomolecule interactions, which bear direct relevance to, and would facilitate the understanding of, the physiological roles of metal ions in living systems. Firstly, we have been involved in the study of the interactions of biomolecules with heavy metal ions like mercury and cadmium, utilizing the heterocyclic residues of the DNA framework as model systems, to elucidate the molecular basis for the toxic effects of heavy metal ions (4, 5). Secondly, we have devoted considerable effort to the investigation of isotopic hydrogen exchange reactions of some five-membered heterocyclic biomolecules like imidazole, histidine, and thiazole. The C(2)-H in these heterocycles of interest is relatively acidic; their exchange in different environments has been utilized as probes of biological function (6). Our studies in this area have revealed interesting structure-reactivity relationships (7, 8) and have also firmly established that in the presence of the proton and metal ions, the prevailing order of reactivity in isotopic hydrogen exchange is protonated >> metal ion-coordinated >> neutral forms of the substrates (7*b*, 9–11). In quantitative terms, metal ions are generally ca. 10^3–10^5 times less effective than H^+ as catalysts, but they enhance reactivity by a factor of 10^4–10^6 relative to the neutral (uncomplexed) substrates. We



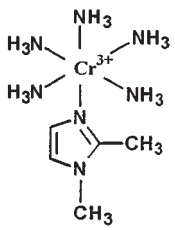
1



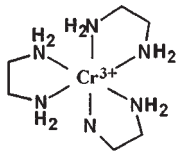
2



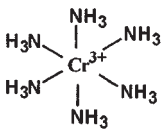
3



4



5



6

© 2000 NRC Canada

Table 1. Comparison of the amounts of tritium incorporation in Cr(III) and Co(III) complexes **1**–**6** at 35°C on treatment with HTO.[a]

Complex	Wt. of complex used (mg)	Vol. of HTO used (μL)	Specific Activity (Theoretical)[b]	Specific Activity (Experimental)
$[Cr(en)_2(MeIm)Cl]Cl_2 \cdot 2H_2O$ (**1**)	24.1	80	0.51	2.60
$[Co(NH_3)_5MeIm](ClO_4)_3$ (**2**)[c]	15.0	20	0.21	0.04
$[Cr(NH_3)_5MeIm](ClO_4)_3 \cdot H_2O$ (**3**)	8.1	20	0.12	0.26
$[Cr(NH_3)_5DMeIm]ClO_4$ (**4**)	10.4	20	0.16	0.06
$[Cr(en)_3]Cl_3 \cdot 3H_2O$ (**5**)	10.7	20	0.20	0.02
$[Cr(NH_3)_6](NO_3)_3$ (**6**)	10.3	10	0.18	0.002

[a]Results represent measured tritium content in complexes **1**–**6** following treatment with HTO and washing with 4 × 1 mL aliquots of distilled, deoinized water.

[b]Calculation is based on exchange of *en*/NH_3 and aquo hydrogens as well as C(2)-H of imidazole moiety, where applicable.

[c]Tritiation was done for 30 h at 60°C (see ref. 10*b*).

Table 2. First-order rate constants (k_{obs}) for the detritiation of **5** and **6** in aqueous buffers at 35°C following treatment with HTO under standard conditions.

		10^{-4} k_{obs} (s^{-1})	
pH	$10^9[OH^-]/M$[a]	**5**	**6**
3.19	0.03	—	1.16
3.45	0.06	—	1.76
3.76	0.12	2.95	—
4.55	0.70	9.30	—
4.76	1.00	—	9.20
4.84	1.43	—	13.20
5.00	2.00	13.00	—

[a]Obtained using pK_w (35.0°C) = 13.684 (see ref. 17).

also note that similar trends have been reported in the literature (12).

Recently, we reported in a preliminary communication (13) the first observation of a metal ion-coordinated imidazole complex, *cis*-$[Cr(en)_2(MeIm)Cl]Cl_2$ (en = ethylenediamine, MeIm = 1-methylimidazole), **1**, in which catalysis by Cr(III) was found to be more effective than by H^+, the ratio k^{M^+}/k^{H^+} being 20. In a related study (10*b*) with $[Co(NH_3)_5(MeIm)](ClO_4)_3$, **2**, we obtained $k^{M^+}/k^{H^+} \leq 10^{-4}$. Together, the studies showed clearly that (*i*) Co(III) is a much poorer catalyst than H^+, and (*ii*) the net effect of Cr(III) in promoting hydrogen exchange in 1-methylimidazole is substantially different in magnitude and direction when compared to Co(III). The present work elaborates on the preliminary study reported in our earlier communication (13). An understanding of the various factors that could influence the catalytic effectiveness of metal ions is sought; a causal relationship has been established between the effective charge at N(3) and the C(2)-H acidity of the imidazole nucleus (vide infra).

Kinetic data for the detritiation of the *substitution-inert* (14) complex cations *cis*-$[Cr(en)_2(MeIm)Cl]^{2+}$ (**1**), $[Cr(NH_3)_5MeIm]^{3+}$ (**3**), and $[Cr(NH_3)_5DMeIm]^{3+}$, and {DMeIm = 1,2-dimethylimidazole} (**4**), under experimental conditions similar to our earlier studies (7, 9, 10) are presented, thus enabling direct comparison with results obtained in previous work. The exchange kinetics of tritiated $[Cr(en)_3]^{3+}$ (**5**) and $[Cr(NH_3)_6]^{3+}$ (**6**) were also undertaken in order to obtain reliable data on the direct effect of Cr(III) on N-T/N-H exchange, thus establishing a basis for comparison with the results obtained for the same process in **1**, **3**, and **4**. There has been continuing interest in the biochemistry of the complexes of Cr(III) with nucleic and amino acids because of the importance of this metal in carbohydrate metabolism (15, 16).

The results show clearly that the ring hydrogens of 1-methylimidazole are significantly activated towards isotopic exchange through Cr(III) coordination, to the extent that the otherwise relatively inert C(4,5)-H is observed to undergo exchange under the relatively mild conditions of the study. The relationship between M^{n+}—N σ bond polarization and the electronic structure of the catalytic entity as well as the relative importance of crystal field effects and metal–ligand π back-bonding, highlight the complex nature of the physiological chemistry of (especially) transition metal ions in living systems and the diverse and complex interactions which determine reactivities and selectivities in these systems.

Results

Tritiation experiments

Details of the labelling of the complexes with ^3H, prior to detritiation experiments, are described in the Experimental Section. The tritiation data presented for **1**–**6** in Table 1 clearly demonstrate a hierachy of activities. In all cases, the experimental activities of the ^3H-labelled Cr(III) complexes containing the imidazole moiety, i.e., **1**, **3**, and **4**, are significantly higher than those without imidazole (**5** and **6**). This observation suggests that isotopic exchange in **1**, **3**, and **4** involves the ring hydrogens in addition to the ammine (*en* or NH_3), which is clearly corroborated by the curved first-order plots exhibited by these substrates in the detritiation kinetics presented below. Comparing the experimental activity of 3 to that of its Co(III) analogue, **2**, investigated earlier (10*b*), it is observed that ^3H incorporation in **3** effected for 10 h at 35°C is appreciably greater than in **2** achieved after 30h at the higher temperature of 60°C.

The C(4,5)-H in **2** were shown (10*b*) in H/D exchange experiments to be non-exchanging under the more demanding experimental conditions (p*D* 7.77–10.46, 60°C) of the study (p*D* = (measured pH) + 0.4 at room temperature). The higher tritium incorporation of **3** relative to **2** is therefore suggestive of the involvement of C(4,5)-H exchange in **3**. The results of these tritiation experiments, especially comparing the amounts of tritium incorporation in **2** and **3**, point to a difference in the action of Cr(III) relative to Co(III) in these processes.

© 2000 NRC Canada

Table 3. First-order rate constants (s^{-1}) for parallel exchange processes (k^A_{obs} and k^B_{obs}) for **1**, **3**, and **4** in aqueous buffers at 35°C following treatment with HTO under standard conditions.

		1		**3**		4	
pH	$10^9[OH^-]/M^a$	$10^{-4}\ k^A_{obs}$	$10^{-4}\ k^B_{obs}$	$10^{-4}\ k^A_{obs}$	$10^{-4}\ k^B_{obs}$	$10^{-4}\ k^A_{obs}$	$10^{-4}\ k^B_{obs}$
3.76	0.12	—	—	2.04	0.27	2.82	0.49
4.14	0.30	0.19	—	—	—	—	—
4.42	0.54	—	—	4.90	0.25	—	—
4.56	0.75	0.21	—	—	—	6.37	0.54
4.84	1.43	—	—	8.70	0.24	—	—
5.01	2.00	—	—	11.2	0.23	13.5	0.40
5.46	6.0	0.45	0.17	—	—	—	—
6.08	25.0	1.47	0.27	—	—	—	—
6.52	69.0	4.30	0.57	—	—	—	—

[a]Obtained using pK_w (35.0°C) = 13.684 (see ref. 18).

Fig. 1. Plot of k_{obs} *vs.* $[OH^-]$ for the detritiation of **6** at 35°C. A similar plot was obtained for **5**.

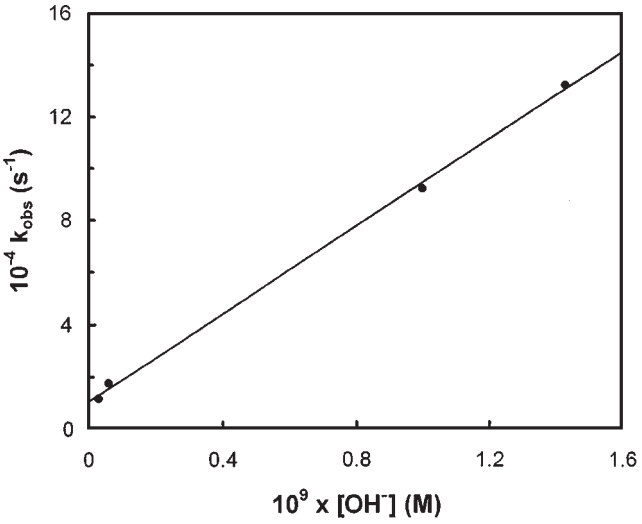
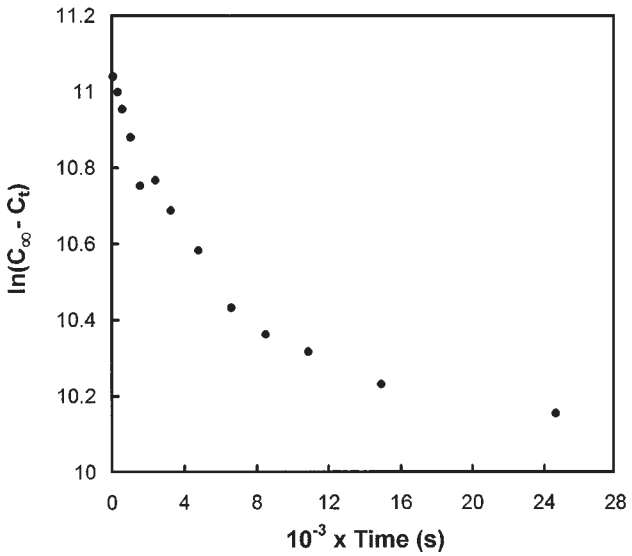


Fig. 2. Plot of ln $(C_\infty - C_t)$ vs. t for the detritiation of **1** at 35°C. Similar plots were obtained for **3** and **4**.



Kinetic Studies

Detritiation of **1** and **3**–**6** following treatment with HTO under standard conditions was performed in aqueous buffers at 35°C under first-order conditions with the substrate in significant deficit with respect to the buffer components, using the liquid scintillation counting technique (7*b*). In all cases, the reactions were monitored for at least 3 half-lives.

For exchange reactions of **1**, **3**, and **4**, the plots of ln $(C_\infty - C_t)$ vs. time were curved (where C_∞ and C_t are the counts in dpm at infinity and time t, respectively). However, for the simple N-T/N-H exchange reactions of the Cr(III)-ammine complexes complexes **5** and **6**, linear first order plots of ln $(C_\infty - C_t)$ vs. time were obtained, allowing a direct determination of the relevant k_{obs} values (Table 2). The second order rate constants (k^{M^+}) for the N-T/N-H exchange reactions in **5** and **6**, were obtained from slopes of the plots of k_{obs} vs. $[OH^-]$, see e.g., Fig.1.

Two peculiar kinetic features which facilitate the identification of exchange sites (vide infra) were noted in experiments involving **1**, **3**, and **4**. Specifically for **1**, the initial counts (dpm) in the kinetic experiments were unusually high. More generally, first-order plots for **1**, **3**, and **4** were curved (see Fig. 2 for a typical plot), indicating the occurrence of two parallel first-order processes (19). Treatment of the curved plots according to the method of Frost and Pearson (20) separated the two parallel rate processes to afford the observed first-order rate constants for the fast (k^A_{obs}) and slow (k^B_{obs}) exchange reactions. These are assembled in Table 3.

The kinetic expression for the exchange process in these substrates is given by eq. [1] (12, 15, 18) from which eq. [2] follows, k^{M^+} being the second-order rate constant for the exchange reaction of the complex.

$$[1] \qquad \text{Rate} = k^{M^+}[\text{Substrate}][OH^-]$$

$$[2] \qquad k_{obs} = k^{M^+}[OH^-]$$

The corresponding second-order rate constants k^{M^+} are gathered in Table 4 together with those for **5** and **6**. Figure 3 shows a plot of k_{obs} vs. $[OH^-]$ for the fast and slow processes in **1**. Values of k^B_{obs} for **3** and **4** are insensitive to $[OH^-]$ in the range of pH investigated; the pH range in each case was determined in separate experiments as the optimum range in

© 2000 NRC Canada

Table 4. Second-order rate constants ($M^{-1}s^{-1}$) for the detritiation of **1**–**6** at 35°C (following treatment under standard conditions) from the relevant plots of k_{obs} *vs.* [OH^-].

	1	**2**[a]	**3**	**4**	**5**	**6**
k^{M^+}	—	—	—	—	5.0×10^5	8.2×10^5
$k_A^{M^+}$ [b]	6.0×10^3	1.8×10^{-2}	4.7×10^5 [c]	5.7×10^5	—	—
$k_B^{M^+}$ [d]	7.1×10^2	—	[e]	[e]	—	—

[a]This value at 35°C was estimated from data originally obtained at 60°C in a previous study (see ref. 10*b*).

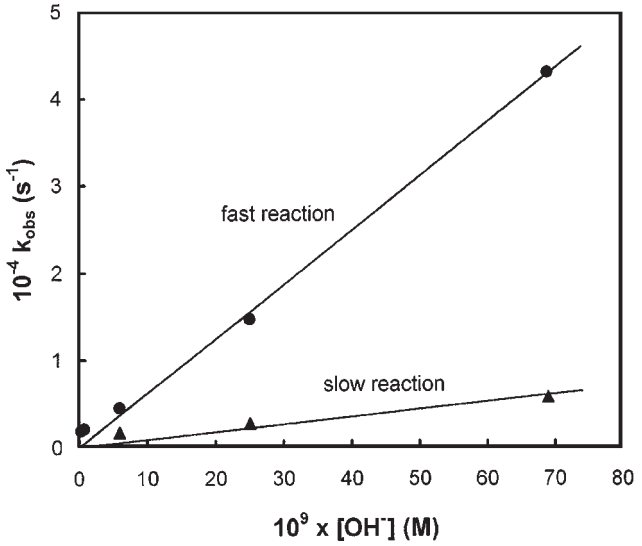
[b]Second-order rate constant for the fast exchange process.

[c]This value represents a composite rate constant for N–T/N–H and C(2)-T/C(2)-H exchange processes; it is inferred that the rate constant for C(2)-T/C(2)-H exchange is > 6×10^3 $M^{-1}s^{-1}$ (see text).

[d]Second-order rate constant for the slow exchange process.

[e]First-order rate constant values for these complexes are independent of [OH^-] (see text).

Fig. 3. Plots of k_{obs} *vs.* [OH^-] for the fast (k_{obs}^A) and slow (k_{obs}^B) processes in **1**; these enable evaluation of $k_A^{M^+}$ and $k_B^{M^+}$ values given in Table 4 (see text).



which the complex of interest remained stable throughout the duration of the kinetic investigation.

The kinetic peculiarities highlighted above not only aid the identification of exchange sites in the complexes of interest but also enable the assignment of the "fast" and "slow" processes to definitive kinetic events within the context of several possibilities.

Infra-red (IR) spectroscopic studies

Hydrogen-deuterium exchange in **1** and **3**, as well as in the model substrates **5**, **6**, imidazole (Im), and MeIm was examined by IR spectroscopy. The model substrates **5** and **6** provide internal standards for N-D and C-D IR frequencies in the complexes of interest. IR spectroscopy performed on the attached ligands in **1** and **3**, following H/D exchange, provide evidence for ring C-H/C-D exchange and enable identification of N-H/N-D (*en* or NH_3) and C-H/C-D (ring) frequencies in the exchanged complexes. The results are given in Table 5. Moreover, IR spectra from a kinetic experiment with **3** reveal that while all amine N-H had exchanged at infinite reaction time, residual aromatic C-H bands remain due to incomplete deuteration of the imidazole moiety. It was ensured that the experimental conditions for H/D exchange were similar to those for detritiation kinetic studies to enable comparison. The C=C (1620 cm^{-1}) and C=N (1530 cm^{-1}) stretching bands of the imidazole ring, not shown in Table 5, persisted throughout the reaction time for **1** and **3**. Similarly, stretching frequencies for N-CH_3 of **1** and **3** (2800–2950 cm^{-1}) and for *en* of **1** (3000 cm^{-1}) were unchanged at infinite reaction time, thus providing clear evidence that the aliphatic protons, whether CH_2- in **1** or N-CH_3 in **1** and **3**, did not exchange under the conditions of the study. Diagnostic deuterium bands for N-D at 2470, 2438, and 2295 cm^{-1}, and C-D at 2360 and 2340 cm^{-1}, were observed for **3** in Table 5; these shift to 2380 and 2304 cm^{-1} for N-D and C-D, respectively, in **1**.

For IR experiments involving the free ligand 1-methylimidazole, parallel ^1H and ^2H NMR experiments were undertaken under the conditions specified in the Experimental Section to confirm exchange at C(2), C(4), and C(5) positions of the ligand. This information has enabled the confident assignment of N-H/N-D and C-H/C-D bands in the IR spectra of the complexes as accomplished in Table 5.

Discussion

Rate data and identification of C–H(T) vs. N–H(T) exchange sites

While identification of exchange sites by ^3H NMR spectroscopy has proven an invaluable tool, especially in substrates that are potentially capable of exchanging at multiple sites (11, 21) this useful technique with its unique advantage of providing explicit structural information could not be utilized in the present study because of the paramagnetic nature of Cr(III) which renders its complexes unamenable to NMR investigations.

The IR studies presented above clearly show that N-T/N-H (*en* or NH_3) and C-T/C-H (ring) exchange occurs in **1**, **3**, and **4**. For the ring protons, there is evidence in the literature, from deuteration (12*d*, 17*a*), and detritiation (12*b*, 12*e*) studies, that C(2)-H in imidazoles is much more acidic than other ring hydrogens. A practical challenge offered by the present study is the identification of exchange site(s) in **1**, **3**, and **4** in the absence of the diagnostic advantage offered by ^3H NMR spectroscopy.

As pointed out earlier, detritiation kinetics provide evidence for two parallel first-order processes in **1**, **3**, and **4**, for which subsequent dissection and analysis afforded second-order rate constants ($M^{-1}s^{-1}$) for the fast reactions ($k_A^{M^+}$) as follows: 6.0×10^3 (**1**), 4.7×10^5 (**3**), and 5.7×10^5 (**4**). For the slow reaction of **1**, a value of $k_B^{M^+} = 7.1 \times 10^2$ $M^{-1}s^{-1}$

© 2000 NRC Canada

Table 5. IR frequencies for free imidazoles and Cr(III) complexes before and after deuteration.[a]

Frequencies	ImH[b]	MeIm[c]	**1**	**3**	**5**	**6**
Aliphatic ν_{CH}	—	2950m	3000vs	2960w	3000m	—
	—	2920m	2976vs	2923w	2952m	—
	—	—	2907vs	2854w	2892m	—
	—	—	2802s	—	—	—
Aromatic ν_{CH}	3124	3142sh	3117vs	3156sh	—	—
	3105	3107m	—	3134sh	—	—
Aromatic ν_{CD}	2372sh	2366m	2304m	2366m	—	—
	2347sh	2320w–m	—	2338w–m	—	—
Aromatic ν_{CH}/ν_{CD} [d]	1.33	1.33	1.35	1.33	—	—
	1.34	1.34	—	1.34	—	—
ν_{NH}	3021	—	3204vs	3320vs	3207vs	3317vs
	—	—	—	3263vs	3156vs	3250vs
	—	—	—	3189s	3083s	3186vs
ν_{ND}	2325	—	2380m	2470s	2401s	2435s
	—	—	2205s	2428sh	2344m	2352s
	—	—	—	2290m	2288m	2295sh
ν_{NH}/ν_{ND} [e]	1.30	—	1.35	1.34	1.34	1.36
	—	—	—	1.35	1.35	1.38
	—	—	—	1.39	1.35	1.39

[a]Units in cm^{-1}; sh = shoulder, w = weak, w–m = weak to medium, s = strong, vs = very strong; data obtained using BOMEM MB-200 FTIR.

[b]ImH = imidazole; data taken from M. Cordes and J.L. Walter, Spectrochim. Acta, **24A**, 231 (1968).

[c]MeIm = 1-methylimidazole.

[d]Ratio of ring CH and CD stretching frequencies.

[e]Ratio of NH and ND stretching frequencies.

was obtained. Corresponding $k_B^{M^+}$ values for **3** and **4** could not be obtained from the observed k_{obs}^B values which remained insensitive to [OH^-] in the pH range investigated. The second-order rate constant for the single N-T/N-H exchange process (k^{M^+}, $M^{-1}s^{-1}$) was calculated as 5.0×10^5 and 8.2×10^5 for **5** and **6**, respectively. It would be expected, to a first approximation, that the rates of en N-T/N-H exchange in **1** and **5** would be similar, since substitution of 1-methylimidazole and chlorine in **5** to yield **1** would presumably have moderate but compensating effects on N-T/N-H exchange (13, 22). In the same vein, rates of amine N-T/N-H exchange in **3**, **4**, and **6** are expected to be closely similar. While these expectations were realized in the latter group (see Table 4), there is a ca. 10^2-fold difference in the k^{M^+} values of **1** and **5**, favouring **5**. This difference in rates is good evidence that the fast process in **1** cannot be due to N-T/N-H exchange. The unusually high counts (dpm) obtained in the initial assay of **1** (vide supra) show that N-T/N-H exchange had occurred by the time that first experimental point was acquired and accords with the ca. 10^2-fold difference in $k_A^{M^+}$ between **1** and **5** noted above.

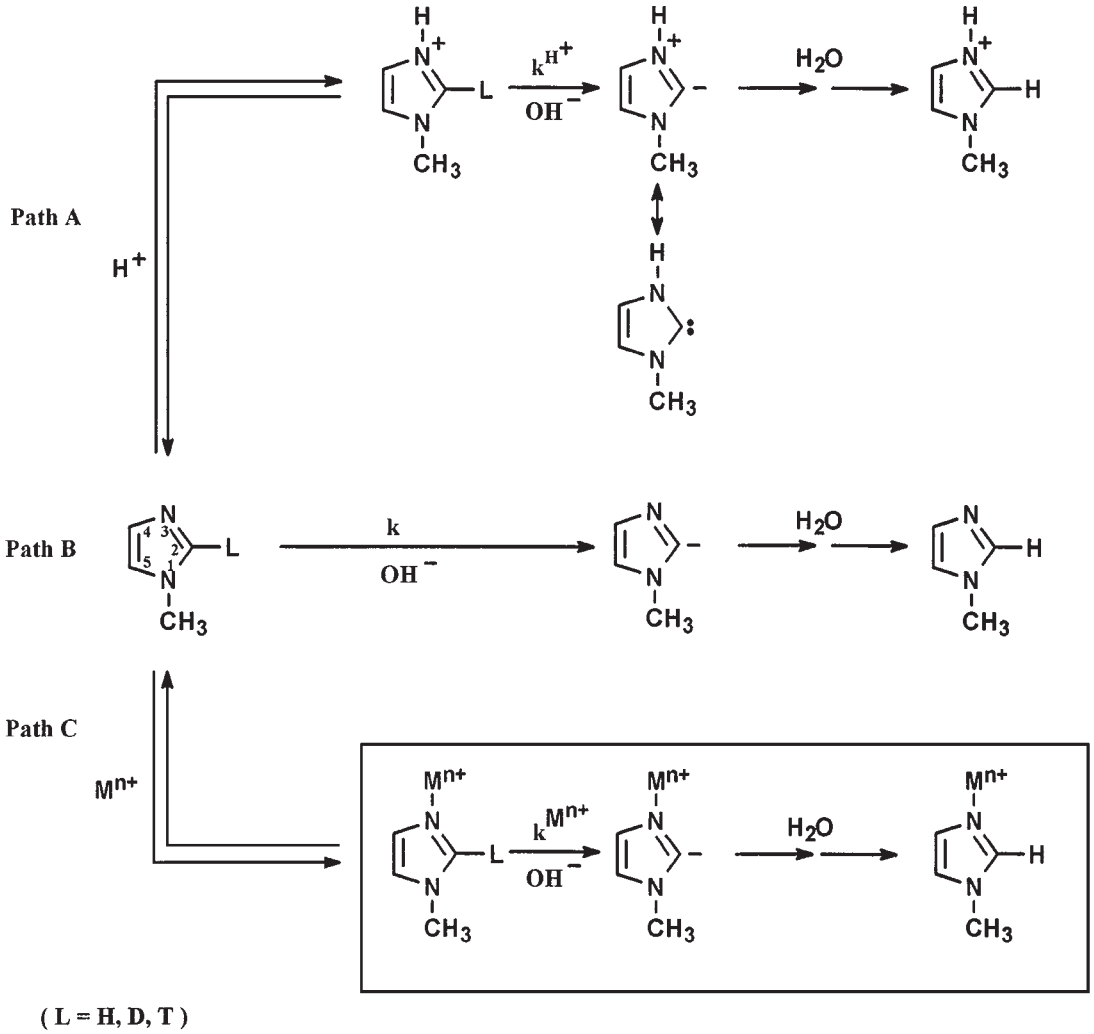
The fast and slow processes in **1** are thus assigned to C(2)-T and C(4,5)-T exchange, respectively, based on the substantial difference between the acidities of C(2)-H and C(4,5)-H already documented in the literature (12, 17*c*). We are unable to specify with certainty which position is favoured, C(4) or C(5), in the slow exchange, although inductive and field effects would reasonably argue for preference for C(4) over C(5). It is important however to note that in cases where additional structural factors operate, as reported recently in the case of $[Pt(en)(Th)_2]Cl_2.2H_2O$ (Th = thiazole) (10*a*) in which the α-carbanionic intermediate formed on deprotonation at C(5) is stabilized by the adjacent sulfur atom, inductive/field effects could become less significant in determining exchange site preferences (23).

We focus next on consideration of rate data for **4**. Methyl substitution at C(2) in this substrate, absent in **1** and **3**, precludes exchange at C(2). It is therefore reasonable to assign the two first-order rate processes observed for **4** to N-T/N-H (fast) and C(4,5)-T/C(4,5)-H (slow) exchange. The value of $k_A^{M^+} = 5.7 \times 10^5\ M^{-1}s^{-1}$ obtained for N-T/N-H exchange in **4** compares reasonably well with the value of $8.2 \times 10^5\ M^{-1}s^{-1}$ measured for **6**. The slight (1.4-fold) difference in rates, favouring **6**, may be ascribed to the reduced acidity of NH_3 protons in **4** due to the replacement of one NH_3 with the more basic 1-methylimidazole. The first-order rate constant for the slow process, attributed to C(4,5)-H exchange, is independent of [OH^-] and hence the corresponding second-order rate constant ($k_B^{M^+}$) could not be obtained, contrasting with the situation in **1**. From the data in Table 2, it is noted that data acquisition was restricted to the pH range 3.8–5.0 due to concern for stability of **3** and **4**, as opposed to experiments with **1** whose stability permitted investigations in the pH range of 4.1–6.5. In particular, it is also noted that for **1**, $k_B^{M^+}$ was evaluated from first-order rate data acquired in the moderate pH region of 5.5–6.5, well beyond the pH region in which data for **3** and **4** were acquired.

It is possible that at the low pH in which data for **3** and **4** were acquired and in which [OH^-] is very low, C(4,5)-H exchange prefers an alternative pathway, not shown in Scheme 1 (vide infra), in which the abstracting base is H_2O. This appears reasonable, considering the preponderance of

© 2000 NRC Canada

Scheme 1.



H_2O molecules in the reaction system, and would explain the constant values of k_{obs}^{B} obtained for C(4,5)-H exchange in **3** and **4**. If this explanation is correct, then second order rate constants for water-catalyzed exchange of C(4,5)-H, $k_{H_2O}^{M^+}$, can be obtained as 4.5×10^{-7} M^{-1} s^{-1} and 4.8×10^{-7} $M^{-1}s^{-1}$ for **3** and **4**, respectively, noting that the concentration of water in H_2O is 55.5 M. The very large difference between $k_B^{M^+}$ for **1** (7.1×10^2 $M^{-1}s^{-1}$) and $k_{H_2O}^{M^+}$ for **3** and **4** (ca. 4.7×10^{-7} $M^{-1}s^{-1}$), the rate constants for detritiation of C(4,5)-T in these complexes, reflects the very large differences in the kinetic basicities of the two species, OH^- and H_2O. A similar observation of pH-independent first-order rate constants at low pH (pH 3–6) at 163°C has been reported by Wong and Keck (17*a*) for H/D exchange in 1-methylimidazole in D_2O; hence a precedent exists for this phenomenon in isotopic exchange studies. Although these authors made no attempt to rationalize this observation, the fact that it is reproduced in this study with **3** and **4** at the much lower temperature of 35°C consistently assigns a catalytic role to Cr(III).

The value of $k_A^{M^+} = 4.7 \times 10^5$ $M^{-1}s^{-1}$ obtained for **3** lies in the same domain as that observed for the same process in **4**; it is therefore reasonable to assign this fast process in **3** to N-T/N-H exchange. However, the possibility that this value of $k_A^{M^+}$ is a composite one for both C(2)-T/C(2)-H and N-T/N-H exchange can also not be discounted easily, given the conclusive demonstration (24) that the graphical procedure utilized in separating the two parallel rate processes is insensitive to, and therefore unsuited for use in, rate processes that differ from each other by less than a factor of 4. It is noted that the slow exchange in this substrate has been ascribed to C(4,5)-H abstraction. We point to the fact that C(2)-H abstraction should be favoured in **3**, relative to **1** for which $k_A^{M^+} = 6.0 \times 10^3$ M^{-1} s^{-1}, since the presence of the more basic *en* groups in **1** would modulate the acidifying effect of Cr(III) on the imidazole ring protons, compared to the effect of the less basic NH_3 in **3**. Thus we can justifiably estimate $k_A^{M^+} > 6 \times 10^3$ M^{-1} s^{-1} for **3**.

In summary, the foregoing analysis of the kinetic results provides quantitative data for C(2)-H and C(4,5)-H exchange in **1** as well as qualitative evidence for C(2)-H exchange in **3** and C(4,5)-H exchange in **3** and **4**. A catalytic role by Cr(III) in isotopic exchange of the ring hydrogens of **1**, **3**, and **4** is thus established. The importance and magnitude of the relevant rate constants are considered further below, to

© 2000 NRC Canada

Table 6. Comparison of kinetic effects of protonation versus metal ion-coordination in detritiation of several imidazole-type heterocycles.

Heterocycle	Metal ion	k^{H^+}/k^{M^+} [a]	k^{M^+}/k [b]	Ref.
Imidazole	Co(III)	$\geq 8 \times 10^2$	$\sim 1 \times 10^3$	10*b*
1-Methylimidazole	Co(III)	$\geq 1 \times 10^4$	$\sim 1 \times 10^3$	10*b*
	Cr(III)	0.05	$\sim 2 \times 10^7$	This work
1-Methyhistidine	Pd(II)	2.5×10^5	—	12*d*
	$CH_3Hg(II)$	$\geq 1 \times 10^3$	—	12*d*
1-Methylinosine	Cu(II)	8.2×10^2	1.1×10^6	26*c*
	Ag(I)	4.5×10^4	2.1×10^6	26*c*
1-Methylguanosine	Cu(II)	3.8×10^2	5.6×10^6	26*c*
5′-Adenosine monophosphate	Cu(II)	1.1×10^3	—	28
3′-Adenosine monophosphate	Ag(I)	1.3×10^2	—	28
Thiazole	Pt(II)	$\geq 10^3$	ca. 10^6	10*a*

[a]The k^{H^+}/k^{M^+} ratio is known as the proton activating factor (see ref. 12*b*).

[b]The k^{M^+}/k ratio is known as the metal activating factor (see ref. 12*b*).

include a discussion of the superior catalytic activity of H^+ relative to the general effects expressed by metal ions in these processes.

Exchange mechanism, reaction pathways, and the catalytic effects of M^{n+} and H^+

The mechanism for isotopic exchange of C(2)-H in imidazoles and related heterocycles is generalized in Scheme 1. A similar mechanism can be written for C(4)-H and C(5)-H exchange, although a significant difference that exists for exchange at these latter sites is the absence of the ylide intermediate-carbene resonance shown in path A of Scheme 1; the intermediate for proton abstraction at C(4) and C(5) would bear a localized negative charge at these positions. Paths A and B represent the reaction pathways in buffer solutions, with the protonated (path A) and neutral (path B) forms of the substrate being the reactive species. Addition of soluble salts of metal ions to buffered solutions of the ligand introduces an additional pathway (path C) in which the reactive species is the metal-complexed ligand. This pathway is often complicated because kinetically labile (11, 14, 25, 26) metal ion-ligand complexes which are derived in situ set up multiple dissociation equilibria with uncertain stoichiometries (9–11). When the ligand has a free N(3)-H, additional exchange pathways, not shown in Scheme 1, are also possible involving mainly anionic species obtained at high pH through deprotonation of the pyrrole-like N-H; such derived species, whether bound to metal ions or not, can in principle undergo isotopic exchange (10*b*, 12, 27). In all cases, the rate-determining step involves proton abstraction from the reactive species. Rate-pH profiles of various types have been reported (12, 26) and these can, in principle, provide useful information regarding the identity of the reactive species lying along the reaction coordinate. Rate-pH profiles can, in some cases, reveal the presence of unreactive species (12*b*).

The Cr(III)-imidazole complexes presented in this paper, in addition to those involving Co(III) and Pt(II) reported earlier (9*b*, 10*a*), are substitution-inert complexes (11, 27) which were synthesized, isolated and fully characterized prior to kinetic measurements. Direct rate measurements were performed on the isolated complexes under optimized experimental conditions, hence the ensuing discussion simplifies to a consideration of the boxed-in portion of Scheme 1. As required by that mechanism, the kinetic expression for the process is given by eq. [1] and [2] (12, 15, 17). The linear plots of k_{obs} vs. $[OH^-]$ obtained according to eq. [2] (Fig. 3) provide second-order rate constants for C(2)-H ($k_A^{M^+}$) and C(4,5)-H ($k_B^{M^+}$) exchange. The effect of Cr(III)-coordination on C(2)-T abstraction by OH^- in **1**, as compared to the effect of protonation of 1-methylimidazole for the same process, can now be discussed.

The value of $k^{H^+} = 1.0 \times 10^4\ M^{-1}s^{-1}$ at 85°C from our previous study (7*a*) of C(2)-T exchange in protonated 1-methylimidazole ($MeImH^+$) is reasonably close to $k_A^{M^+} = 6.0 \times 10^3\ M^{-1}s^{-1}$ measured at 35°C for the same process in **1** in our present study. This comparison of rates of C(2)-T exchange in $MeImH^+$ and **1** already shows qualitatively that Cr(III) is more effective than H^+ in activating C(2)-H exchange. Using the E_a value of 16.5 kcal mol^{-1} measured (12*e*) for the closely analogous process of detritiation of [8-^{3}H]-adenine, one obtains $k^{H^+} = 2.9 \times 10^2\ M^{-1}\ s^{-1}$ for the $MeImH^+$ system at 35°C. A comparison of the effects of H^+ and Cr(III) on C(2)-H exchange shows that Cr(III) is ca. 20 times more effective than H^+ as a catalyst for C(2)-H exchange. Furthermore, the C(4,5)-H exchange observed in this study under the mild experimental conditions employed (pH 4.1–6.5, 35°C) occurs only under very drastic conditions (pH ~ 12, 100–160°C) when catalysed by H^+ (17). These facts clearly show that Cr(III) is a superior catalyst to H^+ for isotopic exchange of the ring protons of the imidazole nucleus, thus providing the first demonstration of the order of catalytic activity $M^{n+} > H^+$ ($\equiv k^{H^+}/k^{M^+} < 1$) in this class of reaction. Previous studies involving metal ions such as Co(III), Pd(II), $CH_3Hg(II)$, Cu(II) and Ag(I) have consistently yielded the kinetic condition $k^{H^+}/k^{M^+} >> 1$ (10, 12, 26*c*, 28).

Data from this and earlier studies which compare the kinetic effect of protonation versus metal ion coordination in detritiation of several imidazole-type heterocycles are presented in Table 6. The ratios k^{H^+}/k^{M^+} and k^{M^+}/k are the so-called proton activating factor and metal activating factor, respectively (12*b*). What is quite clear from Table 6 (see also refs. 7, 9–11, 13) is that metal ions promote isotopic hydrogen exchange in these heterocycles by factors of 10^3–10^6 relative to the reaction of the neutral substrates, while they

© 2000 NRC Canada

are 10^2–10^5 times inferior to H^+ as catalyst. That is to say, the condition $k^{H^+} >> k^{M^+}$ generally holds. The only apparent exception to this trend is the behaviour of Cr(III) reported in this paper; this observation therefore critically points to the necessity for expanding the scope of transition metal ions investigated so that a wide range of metal ion characteristics (e.g., charge, size, electronic configuration, redox potential, etc.) can be factored into a discussion of metal ion effects in these systems.

The kinetic and thermodynamic rationale for the superiority of H^+ over M^{n+} as catalysts for isotopic exchange has been discussed in detail elsewhere (7, 10*b*) and need not be repeated here. However, additional evidence on the different modes of stabilization of the carbanionic intermediates which lie along the reaction coordinate is provided in the present work. The rate ratio for C(2)-H over C(4,5)-H exchange under H^+ catalysis is ~ 10^4 and this can be understood on the basis of the fact that the ylide intermediate formed on C(2)-H abstraction is resonance-stabilized (path A, Scheme 1), while the corresponding carbanions obtained through C(4,5)-H abstraction are stabilized principally through an inductive/field effect. Under Cr(III) catalysis, the rate ratio for C(2)-H over C(4,5)-H exchange diminishes to ca. 10. This levelling effect by Cr(III) accords with the metal ion exerting largely an inductive effect on the exchange process (10*a*), in which case C(2)-H abstraction is still favoured over C(4,5)-H, but not overwhelmingly so. The higher value of ~ 2×10^2 obtained for this ratio with thiazole exchanging under Pt(II) catalysis reflects, in part, the extra stabilization of the carbenoid intermediate by the sulfur atom; additionally clear differences exist between Cr(III) and Pt(II) in terms of electronic charge, electronic configuration and the magnitude of electrostatic effects which combine to make the former more effective in inducing and transmitting inductive and field effects.

Cr(III) versus Co(III) Activation

The results of Brodsky et al. (29) show that Co(III)-bound 1-methylimidazole in the complex ion $[Co(en)_2(MeIm)OH]^{2+}$ undergoes sluggish deuteration at C(2)-H (pH 12, room temperature) with $t_{1/2}$ = 16 h. These results extrapolate to reactivity ratios of ca. 2×10^{-5}:1:20 for catalysis of C(2)-H exchange by Co(III), H^+, and Cr(III) respectively. The above comparison involves ^3H out of the ligand in H_2O for $[Cr(en)_2(MeIm)Cl]^{2+}$ (**1**), and similarly for $MeImH^+$, but ^2H into the ligand for $[Co(en)_2(MeIm)OH]^{2+}$ in D_2O. If assumptions of approximate values for the solvent isotope effect and the substrate isotope effect are made, then the rate effect disfavouring Co(III) becomes even larger by a factor of ca. 10. Our recent study (10*b*) of the detritiation of $[Co(NH_3)_5MeIm]^{3+}$ (**2**), gives k^{M^+} = 0.15 $M^{-1}s^{-1}$ (pH 7.8–10.5, 60°C) which again extrapolates to reactivity ratios of ca. 6×10^{-5}:1:20 for Co(III), H^+, and Cr(III) respectively. Hence it is clear that compared to H^+, Cr(III) catalyzes C(2)-H exchange in imidazoles while Co(III) exerts an inhibitory role. Comparing the effects of the two metal ions, it is seen that Cr(III) is a ca. 3×10^5-fold better catalyst than Co(III), thus mimicking enzyme activation and inactivation consequent upon changes in the metal ion identity at the enzyme active site, at constant ionic radius and electrical charge.

A close examination of the data in Table 6 reveals a diversity of kinetic effects of different metal ions which are not readily correlated with properties of the ions, i.e., charge-type, redox potential, ionic size, etc. It becomes apparent therefore that the net effect of metal ions on reactivity in these systems is the resultant of a complex interplay of a number of factors which presumably operate on a delicate balance. A qualitative consideration of these factors is considered a profitable exercise to aid an understanding of metal ion effects in these reactions and provide a rational framework for the discussion of the intervention roles played by metal ions in biological systems.

Factors governing the catalytic effects of electrophiles ($E^+ = H^+, R^+, M^{n+}$) in C/H exchange

Magnitude of positive charge developed at N(3) by protonation and coordination

Norris et al. (30) have shown that when the imidazole nucleus is treated in simple electrostatic terms, the fractional positive charge (Z_i) on the imidazole N(3) is related to ΔpK_a as given in eq. [3], in which the standard is 1-methylimidazolium ion with unit positive charge.

$$[3] \qquad Z_i = \Delta pK_a/7.1$$

These authors demonstrated also that a plot of C(2) chemical shift as a function of Z_i for the series in which E^+ (electrophile) = (*i*) CH_3^+, (*ii*) CH_3Hg^+, (*iii*) $Co(NH_3)_5^{3+}$, and (*iv*) zero substituent shows a positive linear correlation which indicates enhanced lability of C(2)-H with increasing positive charge at N(3). It is significant that the order that emerges from this treatment is CH_3^+ (a good model for H^+) > CH_3Hg^+ ~ $Co(NH_3)_5^{3+}$. Thus the fractional positive charge at N(3) in metal complexes is lower than when the coordinating species to the ligand is CH_3^+ (and by extension H^+); evidently, almost the same amount of fractional charge is placed on N(3) by CH_3Hg^+ as by $Co(NH_3)_5^{3+}$, even though the latter species carries with it an associated (nominal) 3+ charge.

There is strong evidence in the literature which supports the hypothesis of Norris et al. (30), showing that the acidifying effect of M^{n+} is far less than that of H^+, partly because of the non-polarisable nature of H^+ and also because the positively charged centre is effectively removed from N(3) and is located on M^{n+} itself. The pK_a values of C(2)-H which measure the intrinsic acidity of different heterocycles collected from a number of sources in our previous paper (10*b*) are consistent with this idea. Rowan et al. (31) reported ^1H NMR chemical shift differences ($\Delta\delta$) of 1 and 0.5 ppm for C(2)-H of imidazole upon coordination to H^+ and Co(III) respectively while the observed (32) decrease in electron density follows the order: H^+ > Co(III) > Rh(III). Furthermore, the pK_a values of –1.7, 7.3, and 1.7 measured (11*d*, 33) for the acid–base equilibrium of eq. [4] for M = H^+, Cu(II) and Co(III) respectively clearly show that the metal ions are poorer Lewis acids than the proton.

$$[4] \qquad M(H_2O)_z^{n+} \rightleftarrows M(H_2O)_{z-1}(OH^-)^{(n-1)+} + H^+$$

From pK_a values of related protolytic equilibria involving Cr(III) and Co(III) complexes (34–36), it is apparent that,

© 2000 NRC Canada

generally, Cr(III) has a greater acidifying effect than Co(IIII) in situations where no structural features are called into play.

An explanation based solely on the simple model of E^+—N σ bond polarization cannot adequately account for the order of electrophile-induced reactivities given in Table 6 and additional factors and effects have to be considered in rationalizing the observed differences. In the following we focus on the very large difference in the effects of Cr(III) and Co(III) (Table 6) when there is a marginal difference in their acidifying effects on heterocycles, favouring Cr(III).

Electronic structure of M^{n+} and differences in crystal field stabilization energy (CFSE)

The data in Table 6, although limited in scope, already demonstrate a wide variety of electronic structures of metal ions encountered in our studies. To evaluate the contribution of electronic structure to reactivity, we focus on the Cr(III)/Co(III) pair which presents a relatively constant set of properties such as electrical charge on ion, ionic radius, and ionization energies but which differ in their electronic configuration within the first row of transition metals, i.e., d^3 for Cr(III) and d^6 for Co(III).

The differing reactivities of Cr(III) and Co(III) complexes in substitution and isotopic exchange reactions have been discussed in some detail (37–39). The general framework resulting from the application of the crystal field theory (CFT) to reactivity (38, 39) can be summarized as follows: (*i*) Cations with large crystal field stabilization energies (CFSE) are likely to have large crystal field activation energies (CFAE) with respect to substitution (39) or dissociative (38*a*) processes, with CFAE defined as in eq. [5]. (*ii*) For a dissociative process, e.g., one in which part of the ligand is

[5] CFAE = CFSE (transition state) – CFSE (initial state)

removed in the transition state as is the case with isotopic hydrogen (H/D) or water exchange, the cation with the largest CFSE has the most to lose in the transition state (39).

A formally analogous process to that described in the present study is ammine isotopic exchange in Cr(III) and Co(III) complexes shown in eq. [6]. The observed rate ratio

[6] $(NH_3)_5M^{n+}NH_3 + OD^- \rightarrow [(NH_3)_5M^{n+}NH_2^{\delta-} \cdots\cdots H \cdots\cdots OD]^{\#} \rightarrow (NH_3)_5M^{n+}NH^-_2 + H\text{-}OD$

favours Cr(III) over Co(III) by a factor of 1.5 which is qualitatively in accord with expectations on the basis of CFT and CFSE though smaller than predicted (38*a*); i.e., for d^3 Cr(III), CFSE = 1.2Δ while for d^6 (low spin) Co(III), CFSE = 2.4Δ. It is noteworthy that for the second row transition metals a rate difference of 3×10^3 was measured for $Ru(NH_3)_6^{3+}$ and $Rh(NH_3)_6^{3+}$, favouring Ru(III) (38*a*), consistent with larger crystal field strengths for second row transition metals than their first row counterparts.

The rate-determining step for isotopic exchange in the present system can be described as in eq. [7], where L represents the imidazole ligand from which tritium is

[7] $M^{n+}L\text{-}T + OH^- \rightarrow [M^{n+}L^{\delta-} \cdots\cdots T \cdots\cdots OH]^{\#} \rightarrow M^nL^- + T\text{-}OH$

removed at C-2 (or at any carbon for that matter). The analogy with ammine isotopic exchange (eq. [6]) is obvious though any electronic effect resulting from interaction of the unshared electron pair on the ligand and the *d* orbital system of the metal would be modulated in eq. [7] relative to eq. [6]. However, this would be counteracted by the fact that proton transfers from carbon centers are much more demanding energetically than transfers from electronegative atoms such as nitrogen (23*c*, 40, 41). In conclusion, C(2)-H isotopic exchange in Cr(III) complexes such as **1** (eq. [7]) is predicted to be more favorable than for Co(III) complexes (e.g., **2**) on the basis of a greater loss in crystal field stabilization energy in the rate determining transition state of the Co(III) system.

The importance of metal to ligand π back-bonding

The electronic structures of Cr(III) and Co(III) reveal differences in their capacity for π-bonding. With a d^3 configuration, Cr(III) is mainly σ-withdrawing, engaging mainly in electrostatic interactions while the d^6 structure of Co(III) predisposes the metal ion to act via a combination of σ + π (covalent) interactions (14, 27, 37*a*). As a consequence, Cr(III) complexes show very little tendency to π-back bonding (42). On the other hand, the low spin d^6 complexes of Co(III) participate in π-bonding with electron acceptor ligands (42*b*, 43). Since imidazole-type ligands are fairly good π-acceptors (44), they can accept d electrons from Co(III). Two consequences of π-back bonding can be considered. (*i*) The Co(III)-N (M^{n+}—N) bond (vide supra) is weakened resulting in poorer M^{n+}—N bond polarization with the consequent attenuation of the ring H acidities of the coordinated ligand. This ground state effect predicts lower intrinsic acidity of the ring hydrogens of Co(III)-bound imidazoles relative to their Cr(III) counterparts. (*ii*) A kinetic effect can be envisaged. Metal-to-ligand π-back donation would accentuate the electron density of the imidazole nucleus; in turn, the effect would disfavour attack by the approaching base thus raising the energy of the transition state for the reaction of the Co(III) complex. These two effects, acting individually or in concert, will favour isotopic hydrogen exchange in Cr(III) imidazole complexes relative to their Co(III) counterparts.

Concluding remarks

The present results involving Cr(III) as catalyst for isotopic hydrogen exchange in imidazoles enlarge the scope of reactivities of metal ions encountered in these systems and provide the first example of a metal ion being more effective as a catalyst than H^+. Comparison of Cr(III) and Co(III) as catalysts shows that the former is ca. 10^5 times more effective than the latter. It has been shown that at constant electronic charge and ionic size, factors such as: M^{n+}—N σ bond polarisation, electronic structure of M^{n+}, crystal field stabilization energy of M^{n+}, as well as crystal field activation energy of the reaction, and the ability of M^{n+} to participate in π back donation, all acting in the right direction can qualitatively account for the observed rate difference in the exchange reactions of Cr(III) and Co(III) imidazole complexes. The underlying significance of the present work is that it highlights the diversity of factors at play in determining

© 2000 NRC Canada

metal ion effects in the exchange reactions of heterocycles of biological importance, and emphasizes a holistic approach in the consideration of the biochemistry of metal ions.

Experimental

Materials

Anhydrous chromium trichloride (99%), 1-methylimidazole (MeIm,99%), 1,2-dimethylmidazole (DMeIm, 98%), 1,2-diaminoethane (99%), tetramethylsulfone (99%), D_2O (99.9% atom D), and trifluoromethanesulfonic acid (anhydrous, 98%) were purchased from Aldrich. DMSO-d_6 (99.9%) and CDCℓl_3 (99.8%) were Cambridge Isotopes products while HTO (1 Ci/mL) and HP-Ready Solvent liquid scintillant were obtained from NEN Du Pont and Beckman Instruments, respectively. Potassium hydrogen phthalate was oven-dried at 110°C for 48h before use. Solutions of NaOH and HCl were freshly prepared and were standardized before use. The starting complexes $[Cr(NH_3)_6](NO_3)_3$ (45), $[Cr(NH_3)_5Cl]Cl_2$ (45), $[Cr(en)_3]Cl_3{\cdot}3H_2O$ (46), *cis*-$[Cr(en)_2Cl_2]Cl{\cdot}H_2O$ (47), and $[Cr(NH_3)_5OSO_2CF_3](CF_3SO_3)_2$ (48) were synthesized and purified according to literature procedures.

Physical measurements

IR spectra for samples in KBr disks were obtained on a Bruker IFS 85 or Bomen-MB 120 FTIR spectrophotometer. UV-visible spectra were run on Cary 3 and Beckman Lamba-5 spectrophotometers, while ^1H and ^2H NMR spectra, where applicable, were recorded on Bruker AC-200 and AM-400 spectrometers. ^3H assays were performed on a Beckman LS5801 liquid scintillation counter. Melting points were determined on a Hoover Mel-Temp II apparatus and are uncorrected; elemental analyses were performed by the Canadian Microanalytical Services, Delta, B.C. All pH values are room temperature measurements obtained on a Beckman ΦpH meter calibrated with standard aqueous buffers of pH 4 and 7 (BDH). Buffer solutions in the pH range of study were prepared at room temperature according to the procedure of Perrin (49). Values of pH at 35°C were obtained by applying the temperature correction factor as described in the literature (50).

Hydrogen–deuterium exchange measurements

H/D exchange in Cr(III) ammine and methylimidazole complexes

A known quantity of the relevant complex (**1**, **3**, **5**, or **6**) was dissolved in D_2O (99.9%) in a glass-stoppered 25 mL test tube. The resulting solution, whose pH was adjusted to the desired value with either 1 M NaOD or 1 M D_2SO_4, was shaken vigourously before immersing in an oil-bath equilibrated at 35°C. 200 μL aliquots of the reaction mixture were withdrawn at known intervals, placed in a 50 mL round bottomed flask and lyophilized to remove excess D_2O. The resulting solid was ground with ca. 200 mg of IR-grade KBr; the IR spectrum of the sample was taken in KBr disks and compared with that of the undeuterated complex.

H/D Exchange in MeIm

A sample of 2.5 M solution of MeIm in D_2O (p*D* 11.77) was placed in an oil-bath operating at 35°C. Aliquots (1 mL) were withdrawn at known intervals into 10 mm diameter long-neck test tubes and extracted with 3 × 1 mL portions of $CHCl_3$. The extract was dried with anhydrous Na_2SO_4 and solvent removed under vacuum. IR (neat) and ^1H NMR (DMSO-d_6) spectra were then taken. To provide definitive information concerning exchange sites in the substrate, the ^2H NMR spectrum of a sample of MeIm in D_2O (pD 11.77) kept at 85°C was taken in $CHCl_3$ with a drop of DMSO-d_6 as internal reference. Exchange at C(2), C(4), and C(5) was observed under these conditions. The IR spectrum of the exchanged ligand provided a standard that aided assignment of bands in the complexes given in Table 5.

Tritiation of complexes

The procedure for tritiating the complexes has been published previously (7*a*, 51). Typically, 10–20 mg of the complex to be tritiated was dissolved in ca. 100 μL of freshly distilled DMSO in a heavy-walled glass ampoule stoppered with a rubber septum. HTO (10–80 μL, 1 Ci/mL) was added with a gas-tight syringe. The contents of the glass ampoule were frozen in liquid N_2 and evacuated, sealed and suspended in an oil-bath maintained at 35°C for 10–12 h. The ampoule was then removed, opened into a 25 mL pear-shaped flask and washed with 1 mL of distilled H_2O to remove labile ^3H. The solvent was removed by lyophilization. Further aliquots, usually three, of 1 mL H_2O were added and lyophilized until the activity of the lyophilized H_2O became negligible. A stock solution of the tritiated complex was then prepared by dissolving a known amount in <1 mL of freshly distilled DMSO in a test tube which was firmly stoppered and carefully stored in a refrigerator.

Kinetic measurements

Rates of detritiation of **1** and **3**–**6** were studied in aqueous buffer solutions (pH 3–6.6) following a procedure published previously (7, 10*b*). In general, the kinetics were performed under first-order conditions and reactions were monitored for at least 3 half-lives. Pseudo first-order and second-order rate constants were obtained as described in the Results section.

Synthesis of complexes

*cis-$[Cr(en)_2(MeIm)Cl]Cl_2{\cdot}2H_2O$ (**1**).* A mixture of MeIm (0.4 mL, 5.06 mmol) and *cis*-$[Cr(en)_2Cl_2]Cl{\cdot}H_2O$ (1.5 g, 5.06 mmol) in H_2O (5 mL) was stirred for 5 h at room temperature. Absolute EtOH (150 mL) was then added and the resulting solution was evaporated to dryness to yield a violet coloured solid, which was recrystallized from EtOH:H_2O (2:1 v/v). The violet hygroscopic needles obtained were washed successively with absolute EtOH and Et_2O, and dried in vacuo, yield 0.91 g (45%), mp 175–177°C (dec.); $\lambda_{max}(\varepsilon)$ in H_2O: 380, 520 nm (49, 57 M^{-1} cm^{-1}). Anal calc. for $C_8H_{27}N_6O_2Cl_3Cr$: C 24.21, H 6.56, N 21.18; found: C 23.07, H 6.66, N 21.00.

*$[Cr(NH_3)_5MeIm](ClO_4)_3{\cdot}H_2O$ (**3**).* This was prepared by a modification of the method of Curtis and Lawrence (52).

© 2000 NRC Canada

Reaction of $[Cr(NH_3)_5OSO_2CF_3](CF_3SO_3)_2$ (48) (0.5 g, 1.02 mmol) with neat MeIm (15 mL, 0.19 mol) under stirring at 40°C for 4 h produced a yellowish solution, which was decanted into a 400 mL beaker and treated with a mixture of absolute EtOH (10 mL) and Et_2O (200 mL). Upon leaving overnight, a thin film of yellow oil was formed which was recovered and treated with EtOH (5 mL) to give a yellow crystalline solid. The solid product was filtered, washed successively with EtOH (3 × 10 mL) and Et_2O (10 mL), and dried in air to yield 0.23g (46%) of the triflate complex $[Cr(NH_3)_5MeIm](CF_3SO_3)_3$. Further treatment of the triflate complex (0.163 g, 0.29 mmol) in H_2O (1 mL) with conc. $HClO_4$ (1 mL) with cooling in ice resulted in a crystalline yellow product which was filtered and washed successively with EtOH and Et_2O. The crude product was recrystallized from conc. $HClO_4$ to give the yellow light-sensitive crystals of the perchlorate complex in almost quantitative yield 0.16 g (95%), which darkens and decomposes > 200°C; λ_{max} (ε) in H_2O: 356, 469 nm (31, 35 $M^{-1}cm^{-1}$) Anal calcd. for $C_4H_{23}N_7O_{13}Cl_3Cr$: C 8.92, H 4.29, N 18.30; found: C 8.39, H 3.97, N 18.68.

*$[Cr(NH_3)_5DMeIm](ClO_4)_3$ (**4**).* This complex was obtained by a procedure (48) similar as for **3**. Reaction of $[Cr(NH_3)_5OSO_2CF_3](CF_3SO_3)_2$ (0.86 g, 1.75 mmol) and DMeIm (15 mL, 0.17 mol) gave small golden yellow crystalline plates, yield 0.20 g (26%), which darken and decompose > 200°C; λ_{max} (ε) in H_2O: 355, 471 nm (34, 42 $M^{-1}cm^{-1}$). Anal. calcd. for $C_5H_{23}N_7O_{12}Cl_3Cr$: C 11.29, H 4.33, N 18.44; found: C 11.32, H 4.20, N 18.21.

Stability of the complexes

It was essential to establish that complexes **1**, **3**, and **4** remained stable under the experimental conditions of the kinetic study. Two sets of experiments were undertaken to ascertain this fact. (*i*) Solutions of the complexes were repetitively scanned by UV–visible spectrophotometry in the pH range 5–6 at 35°C for 24 h, representing the most extreme conditions under which detritiation conditions were undertaken. Resulting spectra confirmed the stability of the complexes under the specified conditions. (*ii*) Colour changes in complexes of the type *cis*-$[Cr(III)(en)_2XY]$ are diagnostic of competitive and/or preferential side reactions. In the isotopic exchange reactions of *cis*$[Cr(en)_2(MeIm)Cl]^{2+}$, the violet colour of the complex remained unchanged throughout the duration of the experiments (pH 4–6.5, 35°C) both in the tritiation experiments (≤10 h) and in H/D exchange monitored by IR (≤12 h).

Acknowledgements

We thank the Natural Sciences and Engineering Research Council of Canada (E.B.) and the Canadian International Development Agency (I.O. and O.C.) for supporting this work. Discussions with Prof. Donal Macartney are also acknowledged.

References

1. A. Fersht. Enzyme structure and mechanisms. W.H. Freeman and Co., New York. 1985.
2. (*a*) M.N. Hughes. The inorganic chemistry of biological processes. Wiley, London. 1982. pp. 15, 139; (*b*) C.A. Matuszak and A.J. Matuszak. J. Chem. Ed. **53**, 281 (1976); (*c*) R.J. Sundberg and R.B. Martin. Chem. Rev. **74**, 471 (1974).
3. (*a*) E. Buncel, E.J. Dunn, and R.Nagelkerke. *In* Metal ions in biology and medicine. Vol. 4. *Edited by* J. Anastasspoulou, P. Collery, J.C. Etienne, and T. Theophanides. John Libbey, London. 1992; (*b*) A.S. Brill. Transition metals in biochemistry, in Molecular biology, biochemistry and biophysics. Vol. 26. *Edited by* A. Kleinzeller, G.F. Springer, and H.E. Wittman. Springer–Verlag, Berlin. 1977; (*c*) H. Sigel. Metal ions in biological systems. Vol. 6. Marcel Dekker, New York. 1976; (*d*) A.E. Martell and R.M. Smith (*Editors*). Critical stability constants. Plenum, New York. 1982.
4. (*a*) A.R. Norris, E. Buncel, and S.E. Taylor. J. Inorg. Biochem. **16**, 279 (1982); (*b*) E. Buncel, C. Boone, and H.A. Joly. Inorg. Chim. Acta, **125**, 167 (1986); (*c*) L.J.S. Vandewater, W.J. Racz, A.R. Norris, and E. Buncel. Can. J. Physiol. Pharmacol. **61**, 1487 (1983).
5. (*a*) E. Buncel, A.R. Norris, W.J. Racz, and S.E.Taylor. Inorg. Chem. **20**, 98 (1981); (*b*) E. Buncel, A.R. Norris, S.E. Taylor, and W.J. Racz. Can. J. Chem. **60**, 3033 (1982); (*c*) E. Buncel, C. Boone, H. Joly, R. Kumar, and A.R. Norris. J. Inorg. Biochem. **25**, 61 (1985); (*d*) E. Buncel, R. Kumar, and A.R. Norris. Can. J. Chem. **64**, 442 (1986).
6. (*a*) G.S. Baldwin, S.G. Waley, and E.P. Abraham. Biochem. J. **179**, 459 (1979); (*b*) A.E.G. Cass, H.A.O. Hill, J.V. Bannister, and W.H. Bannister. Biochem. J. **183**, 127 (1979); (*c*) D.H. Meadows. Methods Enzymol. **26**, 638 (1972); (*d*) H.H. Rütterjans and O. Pongs. Eur. J. Biochem. **18**, 313 (1971); (*e*) M. Washabaugh and W.P. Jencks. J. Am. Chem. Soc. **111**, 683 (1989).
7. (*a*) E. Buncel, H.A. Joly, and J.R. Jones. Can. J. Chem. **64**, 1240 (1986); (*b*) E. Buncel, H.A. Joly, and D.C. Yee. Can. J. Chem. **67**, 1426 (1989).
8. (*a*) F. Terrier, A.-P. Chatrousse, J.R. Jones, S.W. Hunt, and E. Buncel. J. Phys. Org. Chem. **3**, 684 (1990); (*b*) J.R. Jones, S. Hunt, F. Terrier, and E. Buncel. J. Chem. Soc. Perkin Trans. 2, 295 (1992).
9. (*a*) E. Buncel, J.R. Jones, H.A. Joly, and I. Onyido. *In* Synthesis and applications of isotopically labelled compounds 1988. *Edited by* T.A. Baillie and J.R. Jones. Elsevier, Amsterdam. 1989. pp. 219–224; (*b*) E. Buncel, O. Clement, F. Yang, H.A. Joly, J.R. Jones, and I. Onyido. *In* Synthesis and applications of isotopically labelled compounds 1991. *Edited by* E. Buncel and G.W. Kabalka. Elsevier, Amsterdam. 1992. pp. 309–316.
10. (*a*) E. Buncel and O. Clement. J. Chem. Soc. Perkin Trans. 2, 1333 (1995); (*b*) E. Buncel, F. Yang, R.Y. Moir, and I. Onyido. Can. J. Chem. **73**, 772 (1995).
11. H.A. Joly. Ph.D. thesis. Queens University, Kingston, Canada. 1987.
12. (*a*) J.A. Elvidge, J.R. Jones, C. OBrien, E.A. Evans, and H.C. Sheppard. Adv. Heterocycl. Chem. **16**, (1974); (*b*) J.R. Jones and S.E. Taylor. Chem. Soc. Rev. **10**, 329 (1981); (*c*) R.B. Martin and Y. Miriam. Metal Ions Biol. Syst. **8**, 57 (1979); (*d*) B. Noszal, V. Scheller-Krattiger, and R.B. Martin. J. Am. Chem. Soc. **104**, 1078 (1982); (*e*) J.R. Jones and S.E. Taylor. J. Chem. Soc. Perkin Trans. 2, 1587 (1979); (*f*) J.R. Jones and S.E. Taylor. J. Chem. Soc. Perkin Trans. 2, 1253 (1979); (*g*) J.R. Jones and S.E. Taylor. J. Chem. Soc. Perkin Trans. 2, 441 (1980).
13. E. Buncel, O. Clement, and I. Onyido. J. Am. Chem. Soc. **116**, 2679 (1994).
14. F.A. Cotton and G. Wilkinson. Advanced inorganic chemistry. 5th ed. Wiley Interscience, New York. 1988. pp. 1283–1334.

© 2000 NRC Canada

15. (*a*) S. Ojada, M. Taniyana, and H. Ohha. J. Inorg. Biochem. **17**, 41 (1982); (*b*) J.A. Cooper, L.F. Blackwell, and P.D. Buckley. Inorg. Chim. Acta, **92**, 23 (1984); (*c*) C.E. Green, R.J. Bianchine, and I. Legg. Inorg. Chem. ***23***, 2713 (1984); (*d*) H. Oki and K. Otsuka. Bull. Chem. Soc. Jpn. **49**, 1841 (1976); (*e*) H. Oki. Bull. Chem. Soc. Jpn. **50**, 680 (1977).
16. (*a*) W. Mertz. Science (Washington, D.C.), **213**, 1332 (1981); (*b*) J.A. Cooper, B.F. Anderson, P.D. Buckley, and L.F. Blackwell. Inorg. Chim. Acta, **91**, 1, (1984); (*c*) W. Mertz. Nutr. Rev. **33**, 129 (1975).
17. H.L. Clever. J. Chem. Ed. **25**, 231 (1968).
18. (*a*) J.L. Wong and J.H. Keck, Jr. J. Org. Chem. **39**, 2398 (1974); (*b*) Y. Takeuchi, H.J.C. Yeh, K.L. Kirk, and L.A. Cohen. J. Org. Chem. **43**, 3565 (1978).
19. J.R. Jones and S.E. Taylor. Int. J. Chem. Kinet. **12**, 131 (1980).
20. A.A. Frost and R.G. Pearson. Kinetics and mechanism, 2nd ed. Wiley, New York. 1997. pp. 162–164.
21. (*a*) J.A. Elvidge, J.R. Jones, V.M.A. Chambers, and E.A. Evans. *In* Isotopes in organic chemistry. *Edited by* E. Buncel and C.C. Lee. Elsevier, Amsterdam. 1978. Vol. 4, 1; (*b*) V.M.A. Chambers, E.A. Evans, J.A. Elvidge, and J.R. Jones. Tritium nuclear magnetic resonance spectroscopy. Review 19. The Radiochemical Centre, Amersham. 1978.
22. J.W. Palmer and F. Basolo. J. Phys. Chem. **64**, 778 (1960).
23. (*a*) R.A. Olofson, D.S. Kemp, J.M. Landesberg, and R.A. Coburn. Tetrahedron, **26**, 685 (1970), and refs. therein; (*b*) A. Streitweiser, Jr., E. Juaristi, and L.L. Nebanzahl. *In* Comprehensive carbanion chemistry. *Edited by* E. Buncel and T. Durst. Elsevier, Amsterdam. 1980. p. 323; (*c*) E. Buncel. Carbanions: mechanistic and isotopic aspects. Elsevier, Amsterdam. 1975. ch. 2; (*d*) O. Attanasi. J. Heterocycl. Chem. **14**, 95 (1977).
24. E. Buncel, J.P. Davey, G.J. Buist, J.R. Jones, and K.D. Perring. J. Chem. Soc. Perkin Trans. 2, 169 (1990).
25. F. Basolo and J. Johnson. Coordination chemistry. 1st ed. Wiley, New York. 1964.
26. K.F. Purcell and J.C. Kotz. Inorganic chemistry. Sanders, London. 1977.
27. (*a*) J.R. Jones and S.E.Taylor. J. Chem. Soc. Perkin Trans. 2, 1773 (1979); (*b*) D.H. Buisson, J.R. Jones, and S.E. Taylor. J. Chem. Soc. Chem. Commun. 856 (1975); (*c*) R. Stewart and R. Srinivasan. Acc. Chem. Res. **11**, 271 (1978); (*d*) J.A. Elvidge, J.R. Jones, C. OBrien, E.A. Evans, and J.C. Turner. J. Chem. Soc. Perkin Trans. 2, 432 (1973).
28. J.A. Elvidge, J.R. Jones, R. Salih, M. Shandala, and S.E. Taylor. J. Chem. Res. (M), 2375 (1980).
29. N.R. Brodsky, N.M. Nguyen, N.S. Rowan, C.B. Storm, R.J. Butcher, and E. Sin. Inorg. Chem. **23**, 891 (1984).
30. A.R. Norris, E. Buncel, and S.E. Taylor. J. Inorg. Biochem. **16**, 279 (1982).
31. N.S. Rowan, C.B. Storm, and R. Rowan, III. J. Inorg. Biochem. **14**, 59 (1981).
32. (*a*) D.K. Lavallee, M.D. Baughman, and M.N. Phillips. J. Am. Chem. Soc. **99**, 718 (1977); (*b*) D.K. Lavallee and E.B. Fleisher. J. Am. Chem. Soc. **94**, 2583 (1972).
33. R.B. Martin. J. Am. Chem. Soc. **89**, 2502 (1967).
34. (*a*) F. Woldbye. Acta Chem. Scand. **12**, 1079 (1958); (*b*) J. Bjerrum and S.E. Rasmussen. Acta. Chem. Scand. **6**, 1265 (1952).
35. (*a*) A.J. Cunningham, D.A. House, and H.K.J. Powell. Aust. J. Chem. **21**, 3061 (1970); (*b*) S.C. Chan and K.Y. Hui. Aust. J. Chem. **21**, 3061 (1968); (*c*) J.E. Earley and W. Alexander. J. Am. Chem. Soc. **92**, 2294 (1970).
36. J.A. Winter, D. Caruso, and R.E. Shepherd. Inorg. Chem. **27**, 1086 (1988).
37. (*a*) F. Basolo and R.G. Pearson. Mechanisms of inorganic reactions. Wiley, New York. 1968; (*b*) I.B. Bersuker. Electronic structure and properties of transition metal compounds. Wiley, New York. 1996.
38. (*a*) J.W. Palmer and F. Basolo. J. Inorg. Nucl. Chem. **16**, 279 (1960); (*b*) F. Basolo, J.W. Palmer, and R.G. Pearson. J. Am. Chem. Soc. 82, 1073 (1960); (*c*) R.G. Pearson, N.C. Stellwagen, and F. Basolo. J. Am. Chem. Soc. 82, 1077 (1960).
39. J. Burgess. Metal ions in solution. Ellis Horwood, Chichester. 1978. 326ff.
40. A.J. Kresge. Pure Appl. Chem. **53**, 189 (1981), and refs. therein.
41. H.F. Koch. Acc. Chem. Res. **17**, 137 (1984), and refs. therein.
42. (*a*) H. Van Dam, G. Boxhoorn, D.J. Stufkens, and A. Oskam. Inorg. Chim. Acta, **53**, 1235 (1981); (*b*) R.G. Pearson and F. Basolo. J. Am. Chem. Soc. **78**, 4878 (1956).
43. R. Benedix, J. Reinhold, and H. Henning. Inorg. Chim. Acta, **40**, 47 (1980).
44. A.R. Katritzky. (*Editor*). Handbook of heterocyclic chemistry. Pergamon. 1986.
45. W.C. Fernelius. (*Editor*). Inorg. Synth. **2**, 138 (1946).
46. (*a*) G.G. Schlessinger. Inorganic laboratory preparations. Chemical Publishing Co. Inc., **1**, 172 (1962); (*b*) C.L. Rollinson and J.C. Bailar, Jr. J. Am. Chem. Soc. **65**, 250 (1943).
47. W.C. Fernelius. (*Editor*). Inorg. Synth. **2**, 200 (1946).
48. N.E. Dixon, G.A. Lawrence, P.A. Lay, and A.M. Sargeson. Inorg. Chem. **23**, 2940 (1984).
49. D.D. Perrin. Aust. J. Chem. **16**, 572 (1963).
50. D.D. Perrin. Aust. J. Chem. **17**, 484 (1964).
51. J.B. Davey. Ph.D. thesis. University of Surrey, Guildford. 1984.
52. N.J. Curtis and G.A. Lawrence. Inorg. Chim. Acta, **100**, 275 (1985).
53. O. Clement, D.H. Macartney, and E. Buncel. Inorg. Chim. Acta, **264**, 117 (1997).

© 2000 NRC Canada

Calodendroside A: a taxifolin diglucoside from the stem bark of *Ochna calodendron*

Bernard Blaise Messanga, Beibam Luc Sondengam, and Bernard Bodo

Abstract: A new flavanone diglucoside, calodendroside A (**1**), was isolated from the methanolic extract of the stem bark of *Ochna calodendron* (Ochnaceae) and its structure elucidated as (2*R*,3*R*) taxifolin-3-*O*-glucosyl-(1→2)-glucoside by means of chemical and spectroscopic evidence including ^{1}H-^{1}H and ^{1}H-^{13}C COSY NMR. The connection of the two sugar moities was determined by the use of the heteronuclear multiple bond connectivities experiment (HMBC). To our knowledge, the present report is the first describing the isolation of a flavonoid diglucoside from a member of the Ochnaceae family.

Key words: *Ochna calodendron*, Ochnaceae, stem bark, flavanone diglucoside, calodendroside A.

Résumé : L'étude chimique de l'extrait au méthanol des écorces du tronc de *Ochna calodendron* (Ochnacées) a conduit à l'obtention d'une nouvelle flavanone diglucosée de nom systématique: (2*R*,3*R*) taxifolin-3-*O*-glucosyl-(1→2)-glucoside (**1**). La structure de ce nouveau dérivé naturel a pu être élucidée grâce à l'analyse des spectres de COSY ^{1}H-^{1}H et ^{1}H-^{13}C. L'enchaînement des deux sucres a particulièrement été défini grâce à l'analyse du spectre de corrélation à longue distance ^{1}H-^{13}C, en mode inverse (HMBC). A notre connaissance, ce rapport représente la première communication décrivant la présence d'un diglucoside de flavonoide dans la famille des Ochnacées.

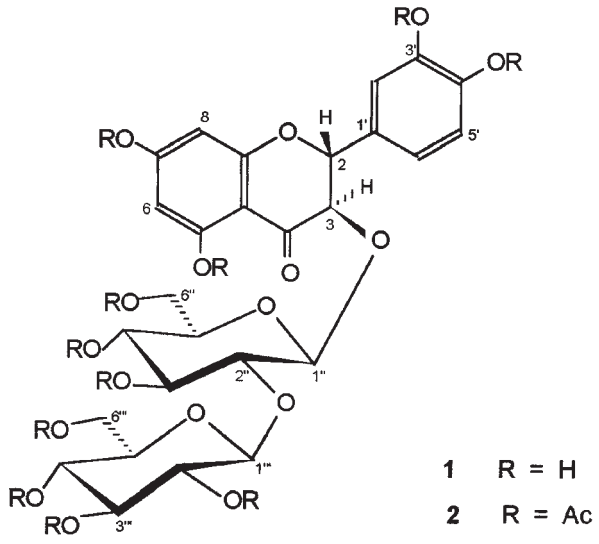
Mots clés : *Ochna calodendron*, ochnacées, écorces du tronc, flavanone diglucosée, calodendroside A.

Introduction

Ochna calodendron (Gilg. and Mildbr. (Ochnaceae)) is one of the ten species of the genus *Ochna* reported in Cameroon. Major constituents previously isolated from this genus were isoflavonoids (1), flavone monoglycosides (2) and biflavonoids (3–6). We recently described the isolation from the stem bark of *O. calodendron* of three chalcone dimers, namely, calodenone, calodenin A, and lophirone K (7, 8). In continuation of our phytochemical investigation on this plant, we have isolated a new flavonoid diglucoside, calodendroside A (**1**), the structure of which is described herein.

Results and discussion

The MeOH extract of the stem bark of *O. calodendron* was chromatographed on a reverse-phase gel column (RP-2) with H_2O–MeOH gradient as eluent, yielding fourteen fractions (E_1–E_{14}). Further purification of fractions E_4–E_7 by a combination of reverse-phase Si gel (RP-8) and Sephadex LH20 column, afforded calodendroside A (**1**).



1 R = H

2 R = Ac

Compound (**1**) was isolated as an amorphous yellow powder and exhibited a green color with Fe^{+3} and a positive Molisch test. The molecular formula $C_{27}H_{32}O_{17}$ was deduced from the pseudomolecular ion at 629.1347 observed in the HRFAB mass spectrum. On acetylation (Ac_2O–pyridine) calodendroside A gave an undecaacetate (**2**) the IR spectrum of which showed no OH absorption. Acidic (2 N methanolic HCl, 1 h) and almond emulsion hydrolysis of **1** yielded D-glucose and an aglycone which was identified as the known dihydroflavonol (+)-taxifolin (2*R*,3*R*) by comparison of the

Received November 18, 1999. Published on the NRC Research Press website on April 12, 2000.

B.B. Messanga[1] and B.L. Sondengam. Department of Organic Chemistry, Faculty of Science, University of Yaoundé I, P.O. Box 812 Yaoundé, Cameroun.
B. Bodo. Laboratoire de Chimie des Substances Naturelles, Muséum National d'Histoire Naturelle — CNRS — ESA 8041, 63 Rue Buffon. 75005 Paris, France.

[1]Author to whom correspondence may be addressed. Telephone: (237) 23 53 87. Fax: (237) 23 53 86. e-mail: bmessanga@hotmail.com

© 2000 NRC Canada

Table 1. ^{1}H- and ^{13}C-NMR data for calodendroside A (**1**) (DMSO-d_6, 300 Mz, TMS).

	1				
Position	δ_C	m	δ_H	m	*J* (Hz)
Taxifolin					
2	81.0	d	5.35	d	11.1
3	74.0	d	4.66	d	11.1
4	193.1	s	—	—	—
4a	100.4	s	—	—	—
5	163.6	s	—	—	—
6	96.3	d	5.86	brs	—
7	168.5	s	—	—	—
8	95.4	d	5.90	brs	—
8a	162.0	s	—	—	—
1′	126.9	s	—	—	—
2′	115.5	d	6.68	brs	—
3′	145.7	s	—	—	—
4′	145.2	s	—	—	—
5′	114.6	d	6.69	brs	—
6′	118.7	d	6.85	m	—
3-*O*-Glucosyl					
1″	100.3	d	4.62	d	7.0
2″	81.2	d	3.48	m	—
3″	65.1	d	3.40	m	—
4″	71.7	d	3.62	m	—
5″	69.8	d	3.74	m	—
6″	62.2	t	3.40	m	—
			2.98	m	—
2″-*O*-Glucosyl					
1‴	102.5	d	4.60	d	7.6
2‴	75.3	d	2.98	m	—
3‴	65.9	d	3.62	m	—
4‴	71.8	d	3.62	m	—
5‴	70.1	d	3.40	m	—
6‴	63.0	t	3.40	m	—
			3.24	m	—

optical rotation ($[\alpha]_D^{18}$ +21.1° (*c* = 0.56, EtOH), +24.6° (*c* = 0.57, acetone)) and the ^{1}H- and ^{13}C- NMR spectra with those of an authentic sample.

The ^{1}H-NMR spectrum of calodendroside A (**1**) confirmed the presence of a taxifolin aglycone characterized by two doublet signals at δ 5.35 (*J* = 11.1 Hz) and 4.66 (*J* = 11.1 Hz) assigned to H-2 and H-3 respectively, two doublet signals at δ 5.86 (brd) and δ 5.90 (brd) assigned to H-6 and H-8 respectively and signals for three aromatic protons on the B-ring showing the ABX-type coupling [δ 6.68 (brd, H-2′), δ 6.69 (m, H-5′), δ 6.85 (m, H-6′)] (Table 1). The presence of two glycosyl units was suggested by two characteristic doublet signals correspondig to two anomeric protons at δ 4.62 (d, *J* = 7.0 Hz, H-1²) and δ 4.60 (d, *J* = 7.2 Hz, H-1‴). Each carbohydrate spin system was assigned by ^{1}H-^{1}H and ^{1}H-^{13}C COSY NMR experiments (Table 1). ^{1}H-^{13}C long-range correlations were observed in the heteronuclear long-range COSY spectra (HMBC) between H-1″ (δ 4.62) and C-3 (δ 74.0) and between H-1‴ (δ 4.60) and C-2″ (δ 81.2). This indicated a glucopyranosyl unit, linked glycosidically with the C-3 oxygen of the aglycone and linked further through its C-2 oxygen to the anomeric centre of a second glucopyranosyl unit. This sustitution pattern agreed with the deshielding effet, +8 ppm, observed for C-2″ carbon signal (Table 1) as compared to the signal of an unsubstituted 3-*O*-glucosyl. The large coupling constants (7.0 and 7.6 Hz) observed for the anomeric H-1″ and H-1‴ respectively indicated a β-configuration for both of them (Table 1). Based on these data, calodendroside A has been characterized as (2*R*,3*R*) taxifolin-3-*O*-β-D-glucopyranosyl-(1→2)-*O*-β-D-glucopyranoside (**1**). To our knowledge, this is the first paper describing the characterization of a flavanone diglycoside from a member of the Ochnaceae family.

Experimental section

General experimental procedures

IR spectra were registered on a Nicolet Impact 400D spectrometer. NMR spectra were recorded on a Bruker AC 300 spectrometer (^{1}H-, 300 MHz; ^{13}C-, 75 MHz; DMSO-d_6). Long-range ^{1}H-^{13}C COSY NMR spectra were obtained with *J* = 7 Hz. Positive FAB mass spectra were obtained on a ZAB-HF mass spectrometer. Column chromatography was carried out on silanized silica 60 gel RP-2 (70–230 mesh) Merk, on Lichroprep RP-8 (40–63) Merk, and on Sephadex LH20 (Pharmacia) using a H_2O–MeOH gradient. Elutions were checked by TLC (silica 60 F_{254}, Merk) using H_2CCl_2:MeOH (3:1) as solvent system. TLC was visualized under UV (254 nm) and spraying an ethanolic vanillin – sulfuric acid solution followed by heating.

Plant material

Stem bark of *O. calodendron* (8 kg) was extracted with MeOH exhaustively. The extract was concentrated to dryness under reduced pressure to afford a brownish material (45 g) which was re-extracted with a EtOAc. The soluble portion was concentrated to dryness and chromatographed on a RP-2 column. Elution with H_2O–MeOH gradient, starting with pure water, gave fourteen fractions (E_1–E_{14}). Purification of fractions E_4–E_7 on RP-8 column eluted with a mixture of H_2O:MeOH (4:6) yielded three fractions (E_{47}a, E_{47}b, and E_{47}c). Fraction E_{47}b (0.72g) was further purified on a Sephadex LH20 column eluted with MeOH to yield calodendroside A which was re-chromatographed on a RP-8 using H_2O:MeOH (1:1) as eluent, to give pure **1** (45 mg).

calodendroside A [taxifolin-3-O-β-*D-glucopyranosyl-(1→2)*-O-β-*D-glucopyranoside]* (**1**): $[\alpha]_D^{28}$ –92° (MeOH, *c* = 1.0) ; IR (KBr) ν: 3420, 2625, 1705, 1640, 1598, 1450, 1370, 1201, 1198, 950, 840 cm^{-1}; HR-FABMS $[M + H]^+$ 629.1347 (calcd. for $C_{27}H_{32}O_{17}$, 629.1355); ^{1}H- and ^{13}C-NMR data see Table 1.

calodendroside A undecaacetate (**2**): Acetylation of calodendroside A by Ac_2O:pyridine and usual treatment yielded **2**: ^{1}H-NMR (DMSO-d_6, 300 MHz) δ 1.90–2.35 (33H, m, OAc), 4.00–4.85 (14H, m, sugar protons), 4.90 (1H, d, *J* = 12.1 Hz, H-3), 5.72 (1H, d, *J* = 12.0 Hz, H-2), 6.22 (1H, d, *J* = 1.8 Hz, H-8), 6.13 (1H, d, *J* = 2.0 Hz, H-6), 6.98–7.05 (3H, m, B-ring protons) ppm; HR-FABMS $[M + H]^+$ 1091.2017 (calcd for $C_{49}H_{54}O_{28}$, 1091.2023); EIMS m/*z*: $M^{+\cdot}$ absent, 1048 [19, M – Ac]$^+$, 760 [36, M – Ac_4]$^+$, 636 [2,

© 2000 NRC Canada

$GlucAc_3$ – $GlucAc_4]^+$, 349 [26, $GlucAc_4]^+$, RDA fragments 236 [100, A and B-ring].

*Acid hydrolysis of **1***. Acid hydrolysis of **1** with 2 N methanolic HCl gave (+)-taxifolin (UV, TLC and $[\alpha]_D$ comparison with an authentic marker) and a sugar which was identified as glucose by PC in BAW (*n*-butanol:HOAc H_2O; 4:1:5) compared with an authentic marker (R_f: glucose 0.18, $[\alpha]_D^{20}$ = +52.4°). The sugar was detected by spraying with anisidine phtalate and *p*. anisidine phosphate. The identity of the sugar was confirmed by comparative GLC of the trimethyl ether compared with an authentic marker (R_t: glucose1.0).

Acknowledgements

We gratefully acknowledge the constructive cooperation of Professor Raphaël Ghogomu (Laboratoire de Chimie Organique, Cameroon) and Alain Blond (Laboratoire de Chimie du Muséum, France) during the course of this study. We also wish to thank Mr. Nole of the "Institut Médical des Plantes Médicinales du Cameroun" for identification and collection of the plant material. The authors are indebted to the "Centre d'Analyse du CNRS de Lyon" for the FAB measurements.

References

1. C. Rao Venkata and D. Gunnasekar. Indian J. Chem. Sect. B: Org. Chem. Incl. Med. Chem. **28 B (9)**, 780 (1989).
2. F. Mohammad, H.M. Taufeed, M. Ilyas, W. Rahman, and J. Chopin. Indian J. Chem. Sect. B: Org. Chem. Incl. Med. Chem. **21 B (9)**, 167 (1982).
3. K. Mohd, K.N. Ahmad, M. Ilyas, and R. Wasiur. Indian J. Chem. Sect. B: Org. Chem. Incl. Med. Chem. **22 B (6)**, 608 (1983).
4. K. Mohammad, N.A. Khan, A.M. Sarwar, and M. Ilyas. Phytochemistry, **26**, 1171 (1987).
5. M. Okigawa, N. Kawano, M. Aqil, and W. Rahman. Tetrahedron Lett. **22**, 2003 (1973).
6. M. Okigawa, N. Kawano, M. Aqil, and W. Rahman. J. Chem. Soc. Perkin Trans. 1, 580 (1976).
7. B.B. Messanga, T.R. Ghogomu, B.L. Sondengam, M.T. Martin, and B. Bodo. J. Nat. Prod. **55**, 243 (1992).
8. B.B. Messanga, T.R. Ghogomu, B.L. Sondengam, M.T. Martin, and B. Bodo. Phytochemistry, **35**, 791 (1994).

© 2000 NRC Canada

Titrage infrarouge de l'acide phosphorique

Jocelyn Baril, Jean-Joseph Max et Camille Chapados

Résumé : Le titrage par spectroscopie infrarouge (IR) de l'acide phosphorique par l'hydroxyde de sodium a été fait à des pH variant entre 0,18 et 13,4 dans le but d'obtenir les spectres des espèces ioniques pures et d'en déterminer la distribution en fonction du pH. Après la soustraction des spectres d'eau neutre, d'eau acide et d'eau basique, l'analyse par facteurs (AF) appliquée sur la série de spectres a été utilisée pour atteindre le but fixé. Les espèces ioniques les plus abondantes sont : H_3PO_4 (pH 0 à 4), $H_2PO_4^-$ (pH 0 à 9), HPO_4^{-2} (pH 4 à 14) et PO_4^{-3} (pH 9 à 14). Trois complexes, présents en faible quantité, ont pu être observés : H_3PO_4–$H_2PO_4^-$ (pH 0 à 4), $H_2PO_4^-$–HPO_4^{-2} (pH 4 à 9) et HPO_4^{-2}–PO_4^{-3} (pH 9 à 14). Les constantes d'équilibre de ces espèces avec les molécules parentes sont respectivement 0,65, 0,63 et 0,4 L/mol. Nous avons également trouvé de l'eau résiduelle qui forme, avec les espèces ioniques, des hydrates. Les pK_a obtenus à partir du titrage IR ont été utilisés pour calculer, en fonction du pH, la concentration théorique des quatre espèces ioniques principales. La courbe de distribution résultante est semblable à celle qui fut obtenue par IR.

Mots clés : spectroscopie infrarouge, FT-IR, solutions aqueuses, analyse par facteurs, titrage, acide phosphorique, pH.

Abstract: The titration of phosphoric acid by sodium hydroxide was performed by infrared (IR) spectroscopy with the objective of obtaining the infrared spectra of the pure ionic species and determining their abundance as a function of pH. In the series of spectra, taken in the pH range of 0.18–13.4, the subtraction of neutral water, acidic water, and basic water was made. Factor analysis (FA) was then applied to the series of spectra to obtain the objective. First, we found the four most abundant species : H_3PO_4 (pH 0–4), $H_2PO_4^-$ (pH 0–9), HPO_4^{-2} (pH 4–14), and PO_4^{-3} (pH 9–14). Secondly, we found three complexes in small quantities : H_3PO_4–$H_2PO_4^-$ (pH 0–4), $H_2PO_4^-$–HPO_4^{-2} (pH 4–9), and HPO_4^{-2}–PO_4^{-3} (pH 9–14). The equilibrium constants of these species with the parent molecules are 0.65, 0.63, and 0.4 L/mol, respectively. Thirdly, we found residual water that was closely bound to the ionic species which formed hydrates. The pK_a values obtained from the IR titration were used to obtain the theoretical concentration of the four principal species as a function of pH. The resulting distribution curve was found to be coincident with the distribution curve obtained by IR.

Key words : infrared spectroscopy, FT-IR, aqueous solutions, factor analysis, titration, phosphoric acid, pH.

1 Introduction

Nous avons entrepris depuis quelques temps le titrage acide–base en utilisant la spectroscopie infrarouge (titrage IR) de façon à évaluer cette technique dans de telles situations. Nous voulions voir, entre autres, comment cette technique se compare aux techniques classiques de titrage acide–base et aux autres techniques comme la spectroscopie Raman. Nous avons déjà fait le titrage de la glycine qui est un acide aminé (1) et de l'acide butoxy-propyl-amine-diacétique (BOPA) qui est un surfactant de la famille des glycinates (2). Pour ce faire, nous avons utilisé une cellule ATR avec un cristal de ZnSe en nous assurant que les phénomènes optiques ne modifiaient pas l'analyse du signal IR (3).

Reçu le 22 novembre 1999. Publié sur le site Web des Presses scientifiques du CNRC le April 14, 2000.

J. Baril, J.-J. Max[1] et C. Chapados.[2] Département de chimie-biologie, Université du Québec à Trois-Rivières, Trois-Rivières, QC G9A 5H7, Canada.

[1]Adresse actuelle : Scientech R&D, 2200, Sidbec–S, Trois-Rivières–Ouest, Qc G8Z 4H1, Canada.
[2]Auteur auquel la correspondance doit être adressée. Tél. : (819) 376-5052. Téléc. : (819) 376-5084. Mél. : Camille_Chapados@uqtr.uquebec.ca

La difficulté d'un titrage IR réside dans la forte absorptivité de l'eau qui est le solvant utilisé pour ces titrages. Lors de ces titrages nous avons de l'eau acide, de l'eau basique, de l'eau saline et de l'eau neutre. Nous avons montré que ces différents types d'eau ont une signature spectrale IR unique (4–6) qui peut être utilisée pour faire la soustraction quantitative des bandes d'absorption de l'eau afin d'obtenir le spectre du chromophore en fonction du pH.

Lors du titrage, plusieurs espèces ioniques sont présentes simultanément et leurs spectres respectifs se superposent. Pour les séparer, nous avons utilisé la méthode d'analyse par facteurs (AF). Cette méthode, qui est décrite par Malinowski et Howery (7), conduit à des facteurs abstraits dont l'interprétation est souvent difficile. Nous avons surmonté cette difficulté en imposant des contraintes qui rendent les spectres réels (8). Pour la glycine et le BOPA, nous avons montré que cette méthode fonctionne bien (1, 2). Lors des titrages, les espèces se succèdent tout en se chevauchant, mais comme nous partons d'une solution connue, il est possible de faire la séparation des espèces en séparant directement les spectres. Un chiffrier électronique comme Excel de Microsoft permet de faire cette opération sans difficulté (2, 6).

La glycine et le BOPA sont des acides organiques faibles qui ont des bandes carbonyles caractéristiques qui évoluent en fonction du pH. Bien que nous utilisions l'ensemble du

© 2000 CNRC Canada

spectre (de 4800 à 700 cm^{-1}) pour les besoins du titrage, la variation des bandes carbonyles permet de bien faire la séparation des spectres des espèces ioniques.

Les acides inorganiques ont moins de bandes dans la région de l'IR moyen, et le titrage IR de ces acides est plus difficile. Malgré ces difficultés, nous avons montré qu'il était possible de faire le titrage de l'acide chlorhydrique par le NaOH et les résultats que nous avons obtenus sont excellents, malgré le fait que les constituants n'absorbent pas ou très peu dans l'IR. Ce sont les variations dans le spectre de l'eau qui servent de témoin lors d'un tel titrage IR.

Afin de vérifier que le titrage d'un acide inorganique complexe qui possède plusieurs constantes d'équilibre peut se faire en IR, nous avons choisi l'acide phosphorique qui a trois pK_a. Cet acide est important dans l'industrie et le groupe phosphate se trouve dans plusieurs molécules biologiques. Dans la nature, certaines eaux contiennent de l'acide phosphorique (H_3PO_4) qui est un acide faible. En fonction du pH, le H_3PO_4 s'ionise pour former successivement du $H_2PO_4^-$, du HPO_4^{-2} et du PO_4^{-3}. Une solution aqueuse d'acide phosphorique constitue un mélange complexe contenant plusieurs espèces ioniques en équilibre dans l'eau. La mesure des constantes d'équilibre de l'acide phosphorique en solution aqueuse a fait l'objet de plusieurs travaux (9–18). Dans ces travaux, les auteurs ont fait varier le degré de dissociation de l'acide phosphorique en solution aqueuse, en ajoutant une base forte ou un acide fort. L'activité des espèces dans la solution, qui est fonction de la concentration de ces espèces et de leur coefficient d'activité, a été déterminée par des mesures électrochimiques. Dans ces mesures, il faut tenir compte de la force ionique de la solution. Les mesures électrochimiques ne permettent pas une mesure directe de la concentration des espèces en solution qui doit être obtenue de façon indirecte.

Les spectres IR des quatre espèces ioniques du H_3PO_4 aqueux ont déjà été obtenus par transmission (19, 20). Les quatre espèces ioniques ont un nombre de bandes différent et des fréquences d'absorption caractéristiques. Malgré ces travaux, le titrage par IR n'a pas été effectué et c'est l'objet du présent travail.

Dans un titrage acide–base comme celui qui est l'objet de ce travail, la solution passe d'un milieu acide à un milieu basique. L'eau est influencée par la présence de ces ions et va donner de l'eau acide, de l'eau neutre et de l'eau basique (4, 5). L'eau acide est de l'eau qui contient des protons (H^+) sous la forme d'ions H_3O^+ (ou $H_5O_2^+$) auxquels sont associés un certain nombre de molécules d'eau. De la même façon, l'eau basique et l'eau salée contiennent respectivement des ions OH^- et Na^+ et Cl^- pour donner de l'eau avec des caractéristiques propres qui se manifestent par des spectres différents dans la région du continuum d'absorption entre 2900 et 2000 cm^{-1} (voir section 4.3 et la figure 3A). Même dans des mélanges, ces espèces donnent des spectres constants qui peuvent être soustraits. Dans les solutions acides qui contiendraient du sel, les spectres de l'eau acide, de l'eau neutre et de l'eau salée sont soustraits successivement par la méthode de l'AF afin d'obtenir des spectres sans ces types d'eau. Nous procédons de la même façon pour l'eau basique.

Par la suite, l'AF sera utilisée pour obtenir les spectres IR des espèces ioniques de l'acide phosphorique et leur distribution en fonction du pH. Les courbes de distribution des espèces ainsi obtenues seront comparées à celles calculées à l'aide des équations d'équilibre.

2 Considérations théoriques

2.1 Courbes de titrage volumétrique

2.1.1 Définition du problème

L'acide phosphorique est un triacide qui possède trois pK_a. dont les équilibres sont :

$$[1] \qquad H_3PO_4 \overset{K_1}{\underset{H^+}{\rightleftharpoons}} H_2PO_4^- \overset{K_2}{\underset{H^+}{\rightleftharpoons}} HPO_4^{-2} \overset{K_3}{\underset{H^+}{\rightleftharpoons}} PO_4^{-3}$$

Les équations nécessaires pour obtenir les courbes de titrage volumétrique ont été développées pour le titrage IR de la glycine en solution aqueuse qui est un acide avec deux pK_a (1) et le BOPA qui est un glycinate avec trois pK_a et qui peut exister sous forme cationique (2). Tout comme ce dernier, l'acide phosphorique possède trois pK_a mais ne possède pas de forme cationique. Comme l'acide phosphorique est une situation différente des deux cas précédents, nous ne pouvons utiliser les équations qui ont été développées pour eux. Il nous faut par conséquent développer un jeu d'équations adéquat pour cet acide.

Deux situations doivent être considérées pour le titrage en solution aqueuse : l'ajout d'une base forte et l'ajout d'un acide fort. Pour simplifier le développement mathématique, l'addition de la base forte et de l'acide fort seront considérées comme étant simultanées, même si expérimentalement ce n'est pas le cas. Après le développement, les espèces seront séparées. Nous avons :

$$[2] \qquad \begin{array}{cccccc} H_3PO_4 & + H_2O & + NaOH & + HCL & & \\ A & D & C_1 & C_{-1} & & \end{array}$$

$$\rightarrow \begin{array}{cccccc} H_3PO_4 & + H_2PO_4^- & + HPO_4^{-2} & + PO_4^{-3} & & \\ y_1 & y_2 & y_3 & y_4 & & \end{array}$$

$$+ \begin{array}{ccccc} H^+ & + OH^- & + Cl^- & + Na^+ & + H_2O \\ x & x' & c' & c & d \end{array}$$

Le membre de gauche de l'équation 2 contient les différentes espèces dans la solution avant mélange : le produit à titrer (H_3PO_4), la solution aqueuse titrante d'acide fort (HCl) et la solution aqueuse titrante de base forte (NaOH). La base forte et l'acide fort sont complètement dissociés dans l'eau et seul le produit à titrer pourra se trouver sous ses différentes formes ioniques à l'équilibre. Le membre de droite de l'équation 2 représente la situation à l'équilibre.

La deuxième ligne de l'équation 2 indique les quantités molaires des espèces impliquées dans le titrage. Les quantités à gauche (A, C_1, C_{-1} et D) sont celles des ingrédients originaux du mélange et sont donc connues. Les quantités à droite (y_1 à d) sont les valeurs que nous allons déterminer.

© 2000 CNRC Canada

2.1.2 Les équations

(a) Les relations d'équilibre : Les constantes de dissociation s'écrivent en fonction des équations d'équilibre entre les formes ioniques du H_3PO_4 et celles de l'eau. En première approximation, le coefficient d'activité de chaque espèce est considéré comme étant égal à 1.

$$[3] \quad K_1 = \frac{[H_2PO_4^-][H^+]}{H_3PO_4}$$

$$[4] \quad K_2 = \frac{[HPO_4^{2-}][H^+]}{H_2PO_4^-}$$

$$[5] \quad K_3 = \frac{[PO_4^{-3}][H^+]}{HPO_4^{-2}}$$

$$[6] \quad K_w\,[H_2O] = K_0 = [H^+][OH^-]$$

où K_1, K_2 et K_3 sont les trois constantes d'équilibre de l'acide phosphorique et K_w est la constante d'ionisation de l'eau dont la valeur est 1.00×10^{-14} à 25°C (21). Pour simplifier les équations, $[H^+]$ est utilisé à la place de $[H_3O^+]$.

Soit *V*, le volume total de la solution. La quantité molaire de chacune des espèces en solution est obtenue des équations 3 à 6 :

$$[7] \quad y_2 = [H_2PO_4^-]\,V = y_1K_1\frac{V}{x}$$

$$[8] \quad y_3 = [HPO_4^{-2}]\,V = y_1K_1K_2\left(\frac{V}{x}\right)^2$$

$$[9] \quad y_4 = [PO_4^{-3}]\,V = y_1K_1K_2K_3\left(\frac{V}{x}\right)^3$$

$$[10] \quad x' = [OH^-]\,V = K_0\frac{V^2}{x}$$

(b) La conservation des espèces : Les relations pour la conservation des espèces s'écrivent :

$$[11] \quad A = y_1 + y_2 + y_3 + y_4$$

$$[12] \quad C_{-1} = c'$$

$$[13] \quad C_1 = c$$

La quantité d'eau, *d*, ne varie pas beaucoup d'un échantillon à l'autre, et en première approximation, elle sera considérée comme constante.

(c) La relation d'électroneutralité : La solution est électriquement neutre en tout temps, c'est-à-dire :

$$[14] \quad y_2 + 2y_3 + 3y_4 + x' + c' = x + c$$

2.1.3 Résolution du problème

(a) Répartition des espèces en fonction du pH : En utilisant les équations 7 à 9 et 11, et en remplaçant x/V par $[H^+]$, on obtient :

$$[15] \quad y_1 = \frac{A}{1 + \frac{K_1}{[H^+]} + \frac{K_1K_2}{[H^+]^2} + \frac{K_1K_2K_3}{[H^+]^3}}$$

$$[16] \quad y_2 = \frac{A}{\frac{[H^+]}{K_1} + 1 + \frac{K_2}{[H^+]} + \frac{K_2K_3}{[H^+]^2}}$$

$$[17] \quad y_3 = \frac{A}{\frac{[H^+]^2}{K_1K_{2\,1}} + \frac{[H^+]}{K_2} + \frac{K_3}{[H^+]}}$$

$$[18] \quad y_4 = \frac{A}{\frac{[H^+]^3}{K_1K_2K_{3\,1}} + \frac{[H^+]^2}{K_2K_3} + \frac{[H^+]}{K_3} + 1}$$

Les concentrations relatives des quatre espèces ioniques de l'acide phosphorique en fonction du pH sont obtenues en divisant les équations 15 à 18 par *A* et en remplaçant $[H^+]$ par 10^{-pH}.

(b) Évaluation de la quantité de titrant à partir de la concentration en $[H^+]$: L'acide fort et la base forte réagissant pour former de l'eau et un sel neutre, seule la différence entre la quantité d'acide fort et de base forte influence la valeur du pH et la répartition des espèces ioniques (en négligeant la variation éventuelle des coefficients d'activité en présence d'un sel neutre). Cette différence est donnée par $C_1 - C_{-1}$. En utilisant les équations 12 et 13, nous obtenons :

$$[19] \quad C_1 - C_{-1} = c - c'$$

Et en utilisant les équations 7 à 10 et 14 et 15, nous obtenons :

$$[20] \quad C_1 - C_{-1} = A\,\frac{\frac{K_1}{[H^+]} + \frac{2K_1K_2}{[H^+]^2} + \frac{3K_1K_2K_3}{[H^+]^3}}{1 + \frac{K_1}{[H^+]} + \frac{2K_1K_2}{[H^+]^2} + \frac{3K_1K_2K_3}{[H^+]^3}} + V\,\frac{K_0}{[H^+]} - x$$

(c) Évaluation de la quantité de matière à partir de la masse de solution utilisée : Soient M_1 et M_{-1}, les masses molaires de la base BOH et de l'acide HC. Soient ε_1 et ε_{-1}, leur masse relative dans les solutions de titrant utilisées, et m_1 et m_{-1}, la masse de solution titrante introduite dans l'échantillon. Les quantités molaires de base (C_1) et d'acide (C_{-1}) s'écrivent :

$$[21] \quad C_1 = m_1\frac{\varepsilon_1}{M_1} \qquad \text{et} \qquad C_{-1} = m_{-1}\frac{\varepsilon_{-1}}{M_{-1}}$$

De même, soient M_2, ε_2 et m_2, respectivement la masse molaire de l'acide phosphorique (*A*), sa masse relative dans la solution mère et la masse de solution mère dans l'échantillon. Par définition, nous avons :

$$[22] \quad A = m_2\frac{\varepsilon_2}{M_2}$$

© 2000 CNRC Canada

En combinant les équations 20 à 22, nous obtenons :

$$[23]\quad m_1\frac{\varepsilon_1}{M_1}-m_{-1}\frac{\varepsilon_{-1}}{M_{-1}}=m_2\frac{\varepsilon_2}{M_2}\frac{\dfrac{K_1}{[H^+]}+\dfrac{2K_1K_2}{[H^+]^2}+\dfrac{3K_1K_2K_3}{[H^+]^3}}{1+\dfrac{K_1}{[H^+]}+\dfrac{2K_1K_2}{[H^+]^2}+\dfrac{3K_1K_2K_3}{[H^+]^3}}+V\frac{K_0}{[H^+]}-x$$

2.1.4 Paramètres expérimentaux

Pour simplifier l'écriture des équations, nous introduisons l'indice δ pour remplacer l'indice de ε, *m* et *M* du titrant utilisé : δ = 1 correspond à la solution alcaline et δ = –1, à la solution acide. La solution au problème est facile lorsque le titrage est effectué en conservant constant le volume (*V*) de l'échantillon. Par conséquent, la masse m_2 est fonction des masses m_δ et *m*, la masse totale de l'échantillon.

(a) La masse du titrant en fonction du pH : Le volume total (*V*) reste toujours constant. On mesure la masse de la solution titrante m_δ et la masse totale *m* résultant du mélange lorsque le volume est complété. La masse m_2 correspond donc à $m_2 = m - m_\delta$. Expérimentalement, la masse totale *m* n'est pas constante. En effet, la densité du mélange dépend de la quantité de titrant. La variation de la densité de l'échantillon est approximativement linéaire avec la quantité de titrant ajouté :

$$[24]\quad m=\rho V=\rho_0 V+\Delta\rho V=\rho_0 V+\rho_\delta m_\delta$$

Dans l'équation 24, le terme ρ_δ est un paramètre sans dimension ($\rho_\delta = \Delta\rho\ V/m_\delta$), choisi pour simplifier les expressions mathématiques. En l'utilisant et puisque $m_2 = m - m_\delta$, on a :

$$[25]\quad m_2=\rho_0 V-(1-\rho_\delta)m_\delta$$

Nous introduisons maintenant la restriction qu'un seul titrant est utilisé à la fois. À partir des équations 23 et 25, nous obtenons :

$$[26]\quad \delta m_\delta\frac{\varepsilon_\delta}{M_\delta}=[\rho_0 V-(1-\rho_\delta)m_\delta]\frac{\varepsilon_2}{M_2}\frac{\dfrac{K_1}{[H^+]}+\dfrac{2K_1K_2}{[H^+]^2}+\dfrac{3K_1K_2K_3}{[H^+]^3}}{1+\dfrac{K_1}{[H^+]}+\dfrac{2K_1K_2}{[H^+]^2}+\dfrac{3K_1K_2K_3}{[H^+]^3}}+V\frac{K_0}{[H^+]}-x$$

En isolant m_δ de l'équation 26, nous obtenons :

$$[27]\quad m_\delta=V\frac{\rho_0\dfrac{\varepsilon_2}{M_2}\left[\dfrac{K_1 10^{pH}+2K_1K_2 10^{2pH}+3K_1K_2K_3 10^{3pH}}{1+K_1 10^{pH}+2K_1K_2 10^{2pH}+3K_1K_2K_3 10^{3pH}}\right]+K_0 10^{pH}-10^{-pH}}{\delta\dfrac{\varepsilon_\delta}{M_\delta}+(1-\rho_\delta)\dfrac{\varepsilon_2}{M_2}\left[\dfrac{K_1 10^{pH}+2K_1K_2 10^{2pH}+3K_1K_2K_3 10^{3pH}}{1+K_1 10^{pH}+2K_1K_2 10^{2pH}+3K_1K_2K_3 10^{3pH}}\right]}$$

Cette équation donne la valeur de la masse de titrant en fonction du pH. Le résultat est alors la courbe de titrage volumétrique.

La valeur de la constante de dissociation de l'eau K_0 dépend de la concentration de l'eau (équation 6) et peut différer de la valeur usuelle de $1.00 \times 10^{-14}/55.5$. L'équation 27 indique que cette correction n'affectera la valeur de m_δ qu'aux valeurs élevées du pH.

2.1.5 La concentration de l'eau

En appliquant la relation de conservation des espèces OH^- à l'équation 2, nous obtenons l'expression $x' + d = C_1 + D$. La quantité d'eau, *d*, à l'équilibre est calculée à partir de :

$$[28]\quad [H_2O]=\frac{d}{V}=\frac{m_1\varepsilon_1}{V M_1}+\frac{(1-\varepsilon_2)}{M_{H_2O}}\frac{m_\delta}{V}\frac{(1-\varepsilon_2)(1-\rho_\delta)+(1-\varepsilon_\delta)}{M_{H_2O}}-\frac{K_0}{[H^+]}$$

L'équation 28 permet de vérifier que la concentration de l'eau reste approximativement constante pour la série d'échantillons.

2.2 Analyse par facteur (AF)

L'AF est effectuée en deux étapes : premièrement, en faisant la soustraction des bandes dues à l'eau, et deuxièmement, en faisant la séparation des espèces ioniques de l'acide phosphorique.

2.2.1 Soustraction des bandes d'eau

La soustraction des bandes d'absorption dues à l'eau est effectuée en utilisant un spectre propre à chacun des trois types d'eau observés : eau acide, eau neutre et eau basique (2, 4, 6). La soustraction est faite en donnant la valeur maximale des facteurs multiplicatifs (FM) affectés au spectre propre de chacun des types d'eau avec la seule contrainte de ne pas avoir d'absorption négative.

© 2000 CNRC Canada

2.2.2 Détermination du nombre d'espèces et de leur spectre propre respectif

Une fois la soustraction des bandes d'eau effectuée, l'évolution du spectre de l'échantillon en fonction du pH permet de déterminer le nombre d'espèces principales retrouvées dans l'ensemble des échantillons. L'apparition, la disparition et les changements d'intensité des bandes d'absorption peuvent être directement reliés à une espèce. Le choix des spectres propres S_i, correspondant à chacune des espèces ioniques pures, est effectué, dans un premier temps, en recherchant le spectre dont les bandes caractéristiques de l'espèce sont d'intensité maximale dans la série d'échantillons (2, 4–6). Il se peut que l'une ou l'autre des espèces ne se trouve à l'état pur dans aucun des échantillons. Dans ce cas, le spectre propre sera obtenu en retranchant une fraction du spectre propre d'une espèce voisine (2).

2.2.3 La décomposition en facteurs

Une fois la séparation des espèces effectuée, pour chaque spectre S_j de la série d'échantillons, nous retranchons une certaine proportion FM_i^j de chacun des spectres propres S_i. Le résidu est obtenu par :

$$[29] \quad R_j = S_j - \sum_i FM_i^j \; S_i$$

où j correspond à l'échantillon et i à l'espèce ionique. La somme des carrés de R_j doit être la plus faible possible. Nous obtenons ainsi des FM bruts.

2.2.4 Vérification

Les résidus indiquent s'il n'y pas d'autre espèce présente dans la série. Lorsque d'autres espèces sont détectées, le spectre propre de celles-ci est introduit dans l'AF et les FM de toutes les espèces sont réajustés.

2.2.5 Normalisation

La décomposition en facteurs, par minimisation du résidu R_j conduit, pour tout j, à :

$$[30] \quad S_j = \sum_i FM_i^j \times S_i$$

La masse m_2 de solution mère, contenue dans chacun des échantillons, varie d'un échantillon à l'autre. La masse de titrant m_δ et la masse totale de la solution m ont été mesurées. La différence entre ces deux quantités correspond à la masse m_2 de la solution mère d'acide phosphorique dans l'échantillon. Le FM correspond à la fraction du spectre propre retranché du spectre de l'échantillon. Le spectre propre S_i contient une masse m_2^i de la solution mère et le spectre de l'échantillon S_j, une masse m_2^j. Il faut donc normaliser les FM pour une même quantité d'acide phosphorique. Les spectres propres sont normalisés (S_i^0), par rapport à la masse M_2^0 qui correspond à la masse m_2 de l'échantillon qui ne contient pas de titrant :

$$[31] \quad S_i^0 = S_i \times \frac{m_2^0}{m_2^i}$$

Les FM correspondants à la série de spectres propres normalisés sont obtenus par la relation :

$$[32] \quad FM_i^{j0} = FM_i^j \times \frac{m_2^i}{m_2^0}$$

avec cette relation, pour chacun des spectres expérimentaux S_j, nous obtenons :

$$[33] \quad S_j = \sum_i FM_i^{j0} \times S_i^0$$

La normalisation des spectres S_j par rapport à m_2^0 est effectuée par la relation :

$$[34] \quad S_j^0 = S_j \times \frac{m_2^0}{m_2^j}$$

En utilisant les équations 32 à 34, nous obtenons :

$$[35] \quad S_j^0 = \sum_i FM_i^j \times \frac{m_2^i}{m_2^j} \times S_i^0$$

À partir de l'équation 35, nous déduisons que les FM normalisés sont obtenus par la relation :

$$[36] \quad FM_i^{jN} = FM_i^j \times \frac{m_2^i}{m_2^j}$$

Ainsi, les facteurs obtenus avec l'équation 36 correspondent aux concentrations normalisées des différentes espèces présentes en solution relativement à la masse de la solution mère d'acide phosphorique m_2^j contenue dans l'échantillon.

3 Partie expérimentale

3.1 Substances utilisées et solutions

Une solution aqueuse à 85% p/p d'acide phosphorique (P.M. 98,00) 99,999%, densité 1685 g/L provenant de chez Aldrich Chemical Co. (n° de catalogue 34,524–5) ainsi que de l'eau déminéralisée (pH 6,8), ont été utilisées pour la préparation d'une solution mère à 0,715 M en H_3PO_4. La solution mère a été préparée en pesant 20,6165 g de H_3PO_4 dans un ballon jaugé de 250 mL complété au trait de jauge avec de l'eau déminéralisée pour un poids total de solution de 257,9 g. Le pH de cette solution était de 1,12. Une solution à 50% p/p de NaOH ainsi qu'une solution de HCl concentrée 37% p/p (densité 1,19 g/mL, Fisher Scientific) ont été utilisées comme titrants.

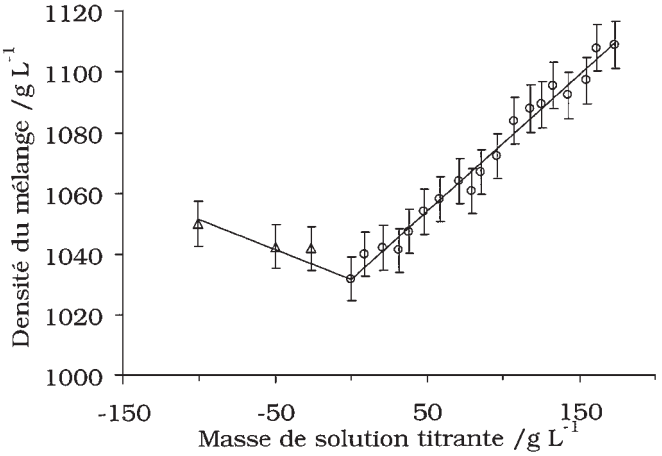
Vingt-deux échantillons, couvrant la gamme de pH entre 0,18 et 13,35, ont été préparés en pesant premièrement l'acide fort ou la base forte dans un ballon jaugé de 10,00 ± 0,04 mL, puis en complétant le volume avec la solution mère d'H_3PO_4. La masse totale de chaque échantillon a été mesurée. Les solutions étaient homogènes. Chaque échantillon était divisé en deux parties : une pour la mesure en IR et l'autre pour la mesure du pH.

3.2 Mesures de pH

Le pH a été mesuré à la température ambiante (26,5 ± 0,3°C) avec un pH mètre Omega, modèle PHH-253, équipé d'une électrode combinée (Analytical Sensors, Inc., modèle PH10107B-03-B). L'appareil a été calibré avec trois solutions tampons de pH 2.00, 7.00 et 10.00. La mesure du pH a été prise après un temps de stabilisation de 20 min.

© 2000 CNRC Canada

Fig. 1. Densité de H_3PO_4 en solution en fonction de la masse du titrant : HCl (37% p/p (Δ)) et NaOH (50,8%) p/p (○).



3.3 Mesures IR

Les mesures IR ont été effectuées avec un spectromètre FT-IR Nicolet, modèle 510P. Deux fenêtres de KBr isolaient la chambre de mesure qui était purgée avec un courant d'azote en continu pour réduire le CO_2 et la vapeur d'eau atmosphérique. Les mesures ont été prises à 26,5 ± 0,3°C dans une cellule cylindrique ATR munie d'un cristal de ZnSe (11 réflexions, SpectraTech). Chaque mesure correspond à la moyenne de 20 balayages avec une résolution de 4 cm^{-1}. La cellule était lavée et séchée pour obtenir un spectre de fond avant chaque mesure des solutions. Les spectres ont été obtenus des différents types d'eau : déminéralisée, basique et acide. Pour les deux derniers, des solutions aqueuses de NaOH 2,23 M et de HCl 1,54 M ont été utilisées.

3.4 Traitement des données

Les données obtenues du FT-IR ont été transférées sur micro-ordinateur où elles ont été traitées avec le chiffrier Microsoft Excel 97. Après la soustraction des différents types d'eau, les lignes de base n'ont pas été corrigées. Les spectres propres des espèces ioniques ont ensuite été déterminés avec la méthode mentionnée dans la section 2.2. L'AF, qui a été réalisée avec le même chiffrier, utilisait comme critère d'optimisation la minimisation de la différence quadratique, avec la contrainte de ne pas avoir de valeur d'intensité négative (hors des zones de bruit).

4 Résultats et discussion

4.1 La densité du mélange en fonction de la masse de titrant

La figure 1 montre la relation entre la densité ρ des échantillons et la masse de titrant m_δ. Les masses avec les signes négatifs représentent les échantillons avec HCl (Δ, $-m_{-1}$) et celles avec les signes positifs, ceux avec NaOH (O, $+m_1$). Cette relation est représentée par deux droites de pentes différentes : l'une, pour les échantillons avec HCl, ρ_{-1} = 0,20; l'autre, pour ceux avec NaOH, ρ_1 = 0,44. Ces valeurs seront utilisées dans le calcul des courbes théoriques de titrage volumétrique et de distribution des espèces ioniques. Les barres d'erreur proviennent des incertitudes sur le volume et la masse de l'échantillon et sur la concentration des solutions titrantes.

4.2 Les spectres bruts

La figure 2A présente 13 des 22 spectres de solutions aqueuses d'acide phosphorique obtenus entre les pH 0,18 et 13,35. Les bandes situées entre 1350 et 700 cm^{-1} varient en fonction de la composition ionique de la solution. Les variations spectrales dans la région entre 3700 et 3000 cm^{-1} sont dues à l'eau qui passe d'un milieu acide à un milieu alcalin.

4.3 Analyse par facteurs des différents types d'eau

La figure 3A présente les spectres des trois types d'eau utilisés pour la soustraction de l'absorption de l'eau. Les caractéristiques spectrales de l'eau changent en fonction du pH. Les trois bandes principales de l'eau changent peu de position, mais l'absorptivité change beaucoup dans les solutions de NaOH et de HCl entre 2900 et 1700 cm^{-1} et entre 1500 et 950 cm^{-1} (4, 22). La bande du groupement phosphate est affectée par l'absorptivité de l'eau qui doit donc être soustraite afin d'obtenir l'absorptivité réelle de ce groupement (2, 4–6).

La figure 2B présente les spectres obtenus après la soustraction des différents types d'eau. La ligne de base de chacun des 22 spectres se situe au niveau du zéro d'absorbance, ce qui indique que la soustraction de l'absorption de l'eau est adéquate. Les bandes résiduelles situées vers 2920 et 1590 cm^{-1} (fig. 2B) sont des bande d'eau d'un autre type que celles qui furent soustraites et sont attribuées à de l'eau complexée aux ions phosphates. Cet aspect sera discuté plus loin.

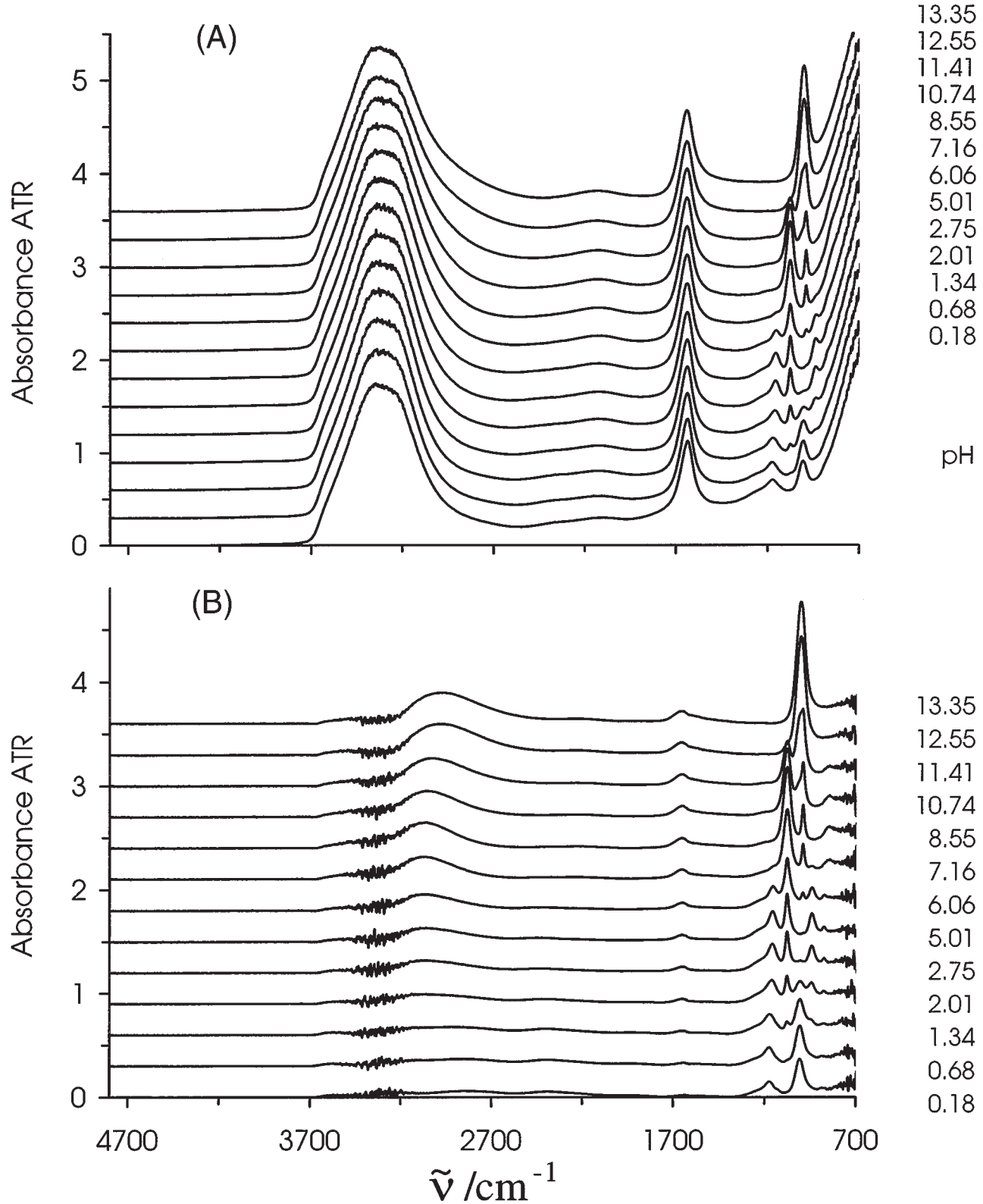
Les FM obtenus lors de la soustraction des bandes d'eau sont donnés sur la figure 3B. L'évolution de ces facteurs est approximativement linéaire par parties, dans trois régions distinctes délimitées par les masses de 55,5 et 157 g/L de NaOH à 50%.

Dans la région I, de –100 à 55,5 g/L (100 g/L de HCl à 55,5 g/L de NaOH), il y a une certaine quantité d'eau acide dans la solution. Lorsque l'acide chlorhydrique est ajouté, on s'attend effectivement à ce que de l'eau acide soit présente. Il est intéressant de noter que la quantité d'eau acide est non nulle dans la solution mère d'acide phosphorique. Cela signifie qu'une certaine portion de l'acide est dissociée en H_3O^+ et $H_2PO_4^-$. À 55,5 g/L de NaOH ajouté (fig. 3B), il n'y a plus d'eau acide, ce qui indique que la concentration d'ion hydronium est très faible ($[H^+] < 0,01$) (23). La masse de 55,5 ± 0,5 g/L de solution de soude caustique à 50% de concentration en poids correspond à 1,00 ± 0,01 équivalent molaire d'acide phosphorique en solution. On en conclut que l'acide phosphorique se dissocie dans l'eau et est en équilibre avec les ions H_3O^+ et $H_2PO_4^-$ et que l'ion $H_2PO_4^-$ ne se dissocie que très peu en H_3O^+ et HPO_4^{-2}. Une fois la première neutralisation de l'acide phosphorique atteinte, la concentration en ions hydroniums reste très faible et n'est pas observée par IR. Ce résultat est en accord avec les petites valeurs des constantes de deuxième et de troisième dissociations de l'acide phosphorique.

Dans la région II, de 55,5 à 157 g/L de NaOH à 50%, il y a une certaine quantité d'eau basique dans la solution, et cette quantité croît au fur et à mesure de l'addition du NaOH. Cette eau ne peut provenir des ions HO^- qui proviendraient de la dissociation du NaOH dans l'eau, car le pH est inférieur à 12,5. Nous attribuons cette situation aux groupements

© 2000 CNRC Canada

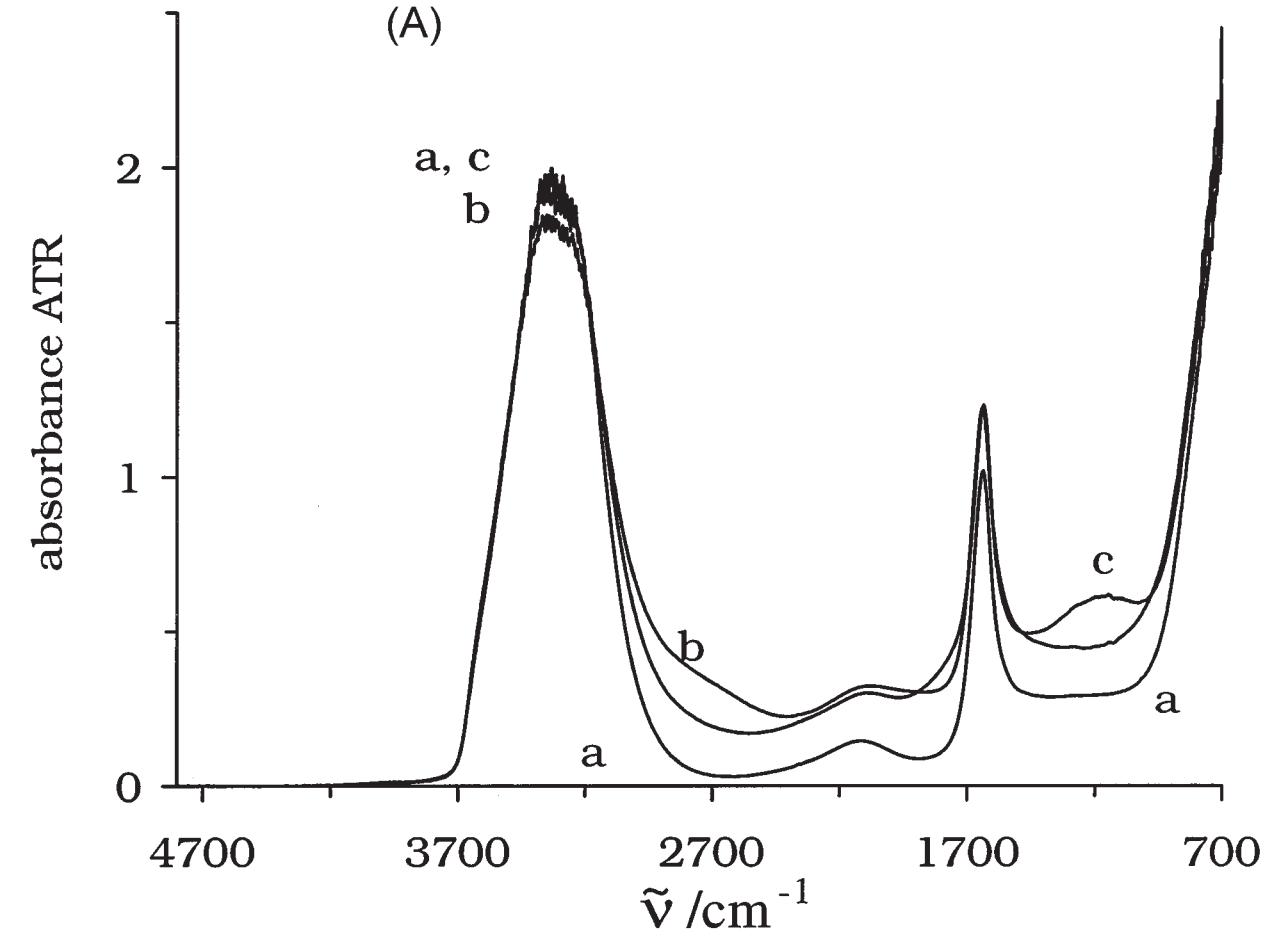
Fig. 2. (A) Spectres IR de 13 des 22 solutions aqueuses d'H_3PO_4 à différents pH. (B) Spectres IR après la soustraction des bandes d'eau. Chaque spectre est décalé de 0.3 UA par rapport au précédent, excepté celui à pH 0.18.

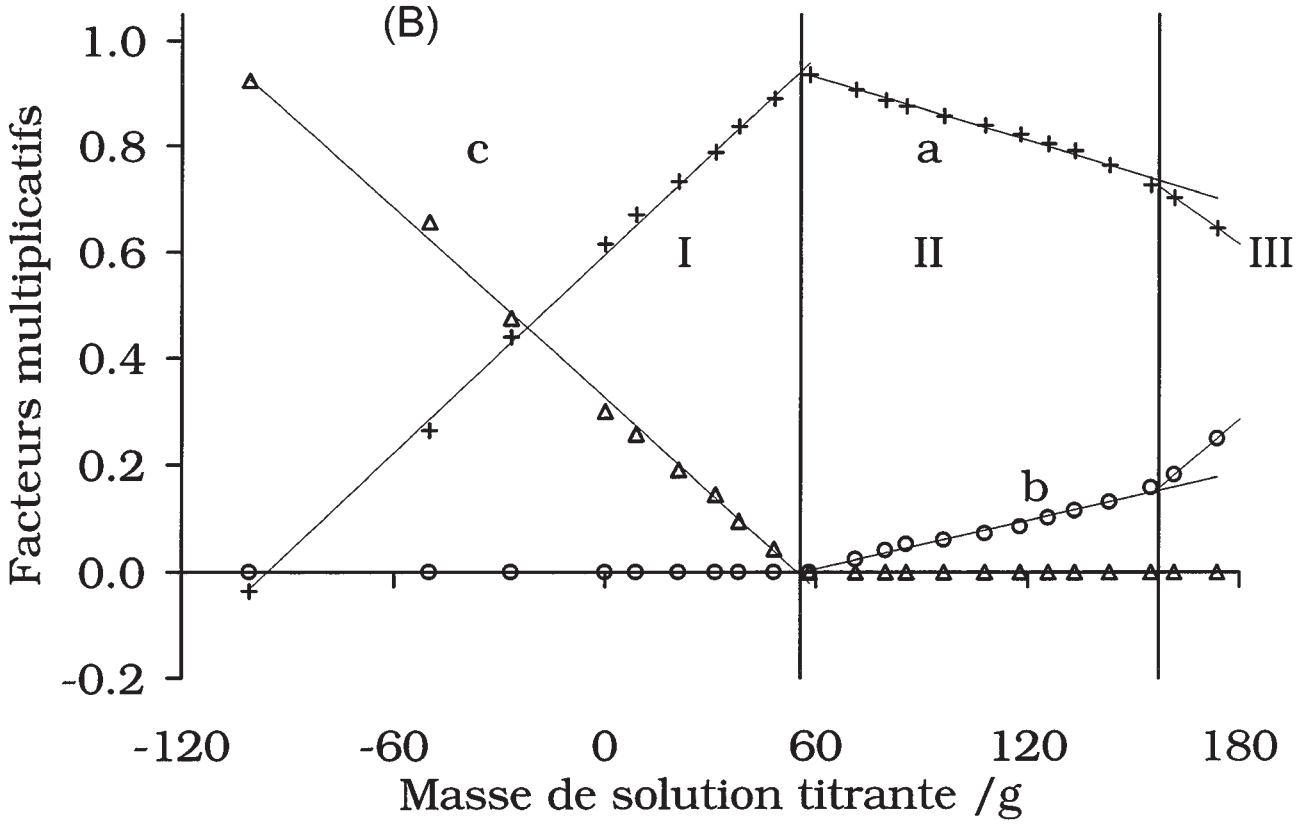


chargés négativement -PO^- (il y a trois PO^- dans O-P-$(O^-)_3$) qui agiraient sur l'eau comme le ferait l'ion HO^-.

Dans la région III, à partir de 157 ± 1 g/L de NaOH ajouté, le changement de pente dans la variation du FM de

© 2000 CNRC Canada





© 2000 CNRC Canada

Fig. 3. (A) Spectres des types d'eau utilisés pour la soustraction des bandes d'eau : *a*, eau neutre (pH 6.8); *b*, NaOH 2.23 M (pH > 14); *c*, HCl 1.54 M (pH –0.17). (B) Facteurs multiplicatifs (FM) utilisés pour cette soustraction : eau neutre (+), eau acide (Δ) et eau basique (○).

l'eau basique est nettement visible sur la figure 3B (bien que seulement deux points expérimentaux soient disponibles). La masse de 157 ± 1 g/L de solution aqueuse de NaOH à 50% correspond à 3,00 ± 0,02 équivalents molaires d'acide phosphorique. Le changement de pente observé dans la quantité d'eau basique est donc en relation avec la présence d'ions HO^- libres, une fois la troisième neutralisation de l'acide phosphorique atteinte.

Les concentrations des solutions titrantes acide et alcaline utilisées sont différentes, de même que les solutions utilisées pour les spectres propres de l'eau acide et de l'eau basique. Lorsque la normalisation en regard de ces concentrations est effectuée, la variation du FM de l'eau acide en solution présente une cassure au point correspondant à la solution mère. L'absence de cassure observée sur la figure 3B au point d'abscisse 0 est fortuit.

4.4 Analyse par facteurs des ions phosphates

4.4.1 Détermination des spectres propres des espèces ioniques les plus abondantes

L'analyse des spectres en fonction du pH (fig. 2B) permet de distinguer la présence de quatre espèces phosphates principales. Les spectres des échantillons à pH 0,44, 8,55 et 13,35 sont choisis comme spectres propres des espèces ioniques H_3PO_4, HPO_4^{-2} et PO_4^{-3}. Comme aucun spectre ne représente l'espèce $H_2PO_4^-$ pure, nous avons utilisé le spectre de l'échantillon à pH 5.01 sur lequel une fraction (0,045) du spectre propre de l'espèce HPO_4^{-2} a été retranchée.

4.4.2 Résultats de l'analyse par facteurs avec quatre espèces

Les FM obtenus avec les quatre spectres propres sont présentés sur la figure 4A. La figure 5A montre les 22 résidus représentant la différence entre les spectres expérimentaux (fig. 2B) et les spectres calculés. Le niveau de bruit est élevé entre 3500 et 3100 cm^{-1} à cause de la forte absorption de l'eau dans les spectres originaux (fig. 2A). Pour cette raison, seule la différence quadratique des régions entre 4800 et 3600 cm^{-1} et 2950 et 900 cm^{-1} a été utilisée pour la détermination des FM. Sur la figure 4A, la diminution de H_3PO_4 avec l'augmentation de la quantité de HCl est due à la diminution de la quantité d'acide phosphorique, puisque le même volume est conservé pour les échantillons. Cette diminution (fig. 4A) disparaît lorsque les FM sont normalisés à une même quantité d'acide phosphorique (fig. 4B).

La figure 5A montre des résidus non négligeables dans la région de 1100 cm^{-1}. Ces bandes de faible intensité n'ont pu être soustraites avec les quatre spectres propres utilisés. Ces bandes montrent une régularité en fonction du pH et sont attribuées à la formation de complexes.

La figure 6A montre les spectres propres normalisés à 1 M des quatre espèces ioniques les plus abondantes de l'acide phosphorique. Ces spectres, qui furent utilisés pour l'AF, ne peuvent être obtenus par combinaison des autres spectres propres et sont, par conséquent, orthogonaux.

4.4.3 Spectres propres des trois complexes

Sur l'ensemble des résidus de la figure 5A, on distingue trois séries de spectres qui sont attribués à autant de complexes. La figure 6B montre les spectres propres des trois complexes normalisés à 1 M en équivalent phosphate et qui ont été tirés des spectres obtenus à pH 2,01; 6,64 et 11,41. Comme les spectres des espèces principales ont été pris en dehors de la zone d'influence des complexes, tous les spectres présentés sur la figure 6 sont normalisés et orthogonaux.

4.4.4 Résultats de l'analyse par facteurs avec sept espèces

La figure 5B montre les résidus lorsque les sept spectres ont été utilisés dans l'AF. Les quatre premiers viennent de la figure 6A et les trois autres, de la figure 6B. Les FM obtenus avec ces spectres sont présentés sur la figure 4B (équation 36, section 2.2.5). Suite à l'AF, les résidus de la figure 5B, qui sont nuls pour l'ensemble des spectres, indiquent que sept spectres principaux sont donc nécessaires et suffisants pour décrire la totalité de la série de 22 solutions.

4.4.5 Distribution normalisée des espèces ioniques

Les FM bruts, FM_i^j, ont été normalisés avec l'équation 36 pour exprimer une même quantité d'acide phosphorique. La quantité de titrant a été transformée en équivalent titrant *P* par :

$$[37] \quad P = \delta \frac{\dfrac{m_\delta \varepsilon_\delta}{M_\delta}}{\dfrac{(m - m_\delta)\,\varepsilon_2}{M_2}}$$

Le résultat de ces opérations est donné sur la figure 4B où les droites correspondent aux régressions linéaires des concentrations relatives des quatre espèces principales de l'acide phosphorique en fonction de la quantité de titrant. La pente et l'ordonnée à l'origine de ces droites sont données dans le tableau 1. Les pentes unitaires indiquent que la transformation d'une espèce principale en une autre s'effectue dans le rapport 1:1. Ceci est en accord avec le processus classique de neutralisation d'un acide faible par une basse forte. L'acide phosphorique (H_3PO_4, △), d'abord partiellement dissocié, se transforme en anion ($H_2PO_4^-$, ○) pour ensuite se transformer en (HPO_4^{-2}, +) et finalement en (PO_4^{-3}, ×). Ces transformations sont à peu près proportionnelles à la quantité de titrant (pentes unitaires), car l'abondance des complexes indiqués par des symboles pleins reste très faible.

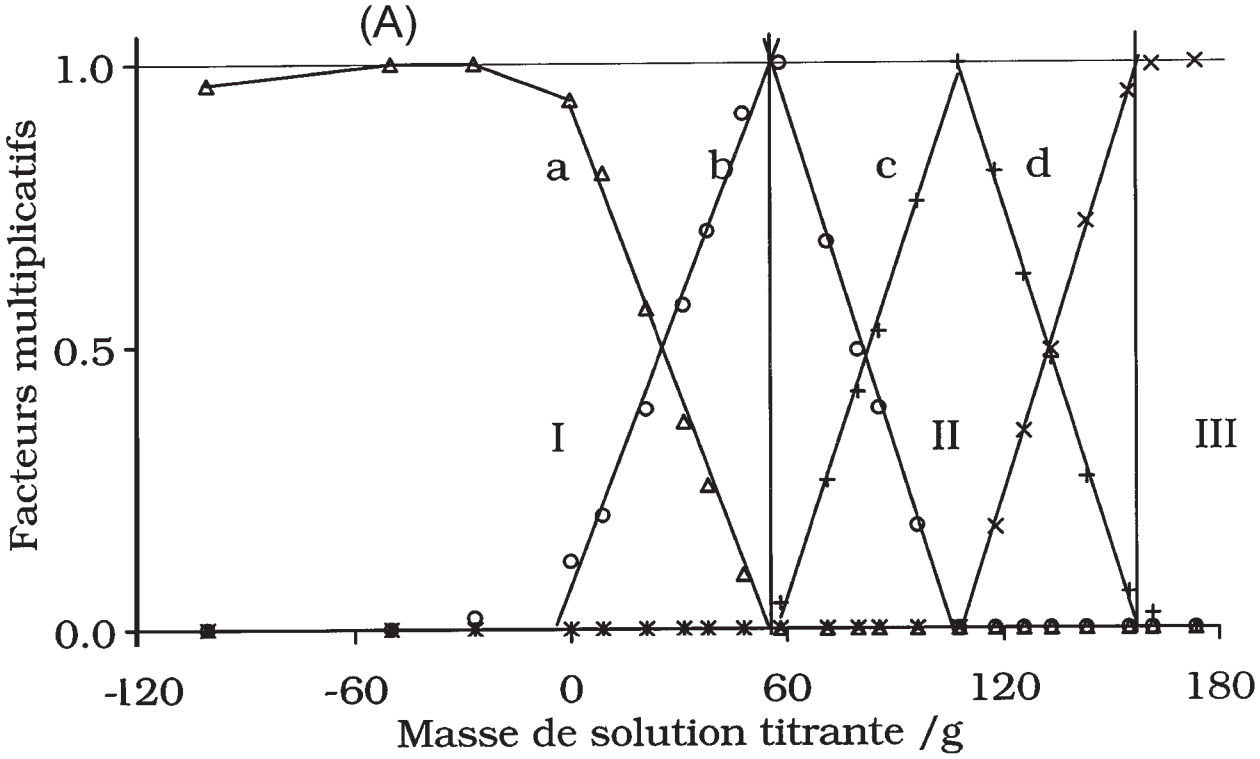
Les trois complexes sont représentés par les symboles pleins sur la figure 4B : H_3PO_4 –$H_2PO_4^-$ (▲), $H_2PO_4^-$ –HPO_4^{-2} (●) et HPO_4^{-2} –PO_4^{-3} (■). La transformation des complexes n'est pas proportionnelle à la quantité de titrant, mais obéit aux équilibres suivants :

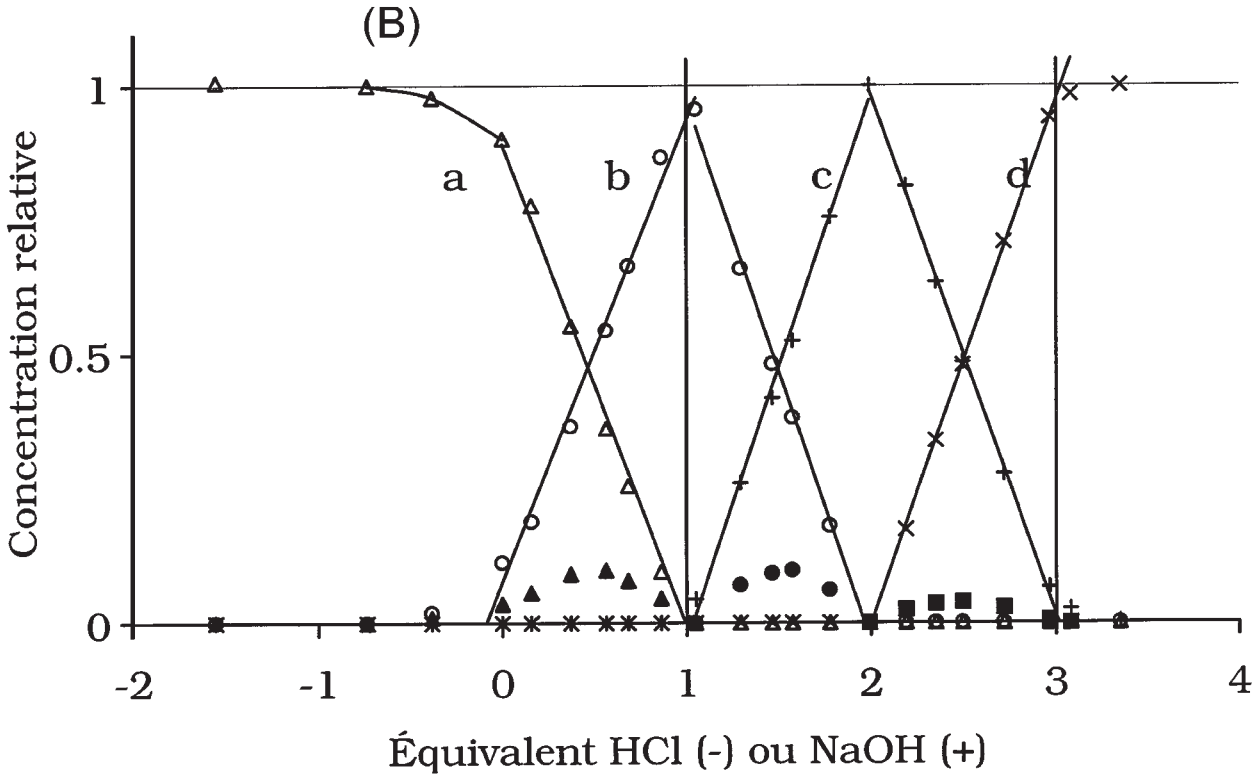
$$[38] \quad H_3PO_4 + H_2PO_4^- \rightleftharpoons H_5(PO_4)_2^-$$

$$K_{12} = 0{,}65 \pm 0{,}14 \text{ L/mol}$$

© 2000 CNRC Canada

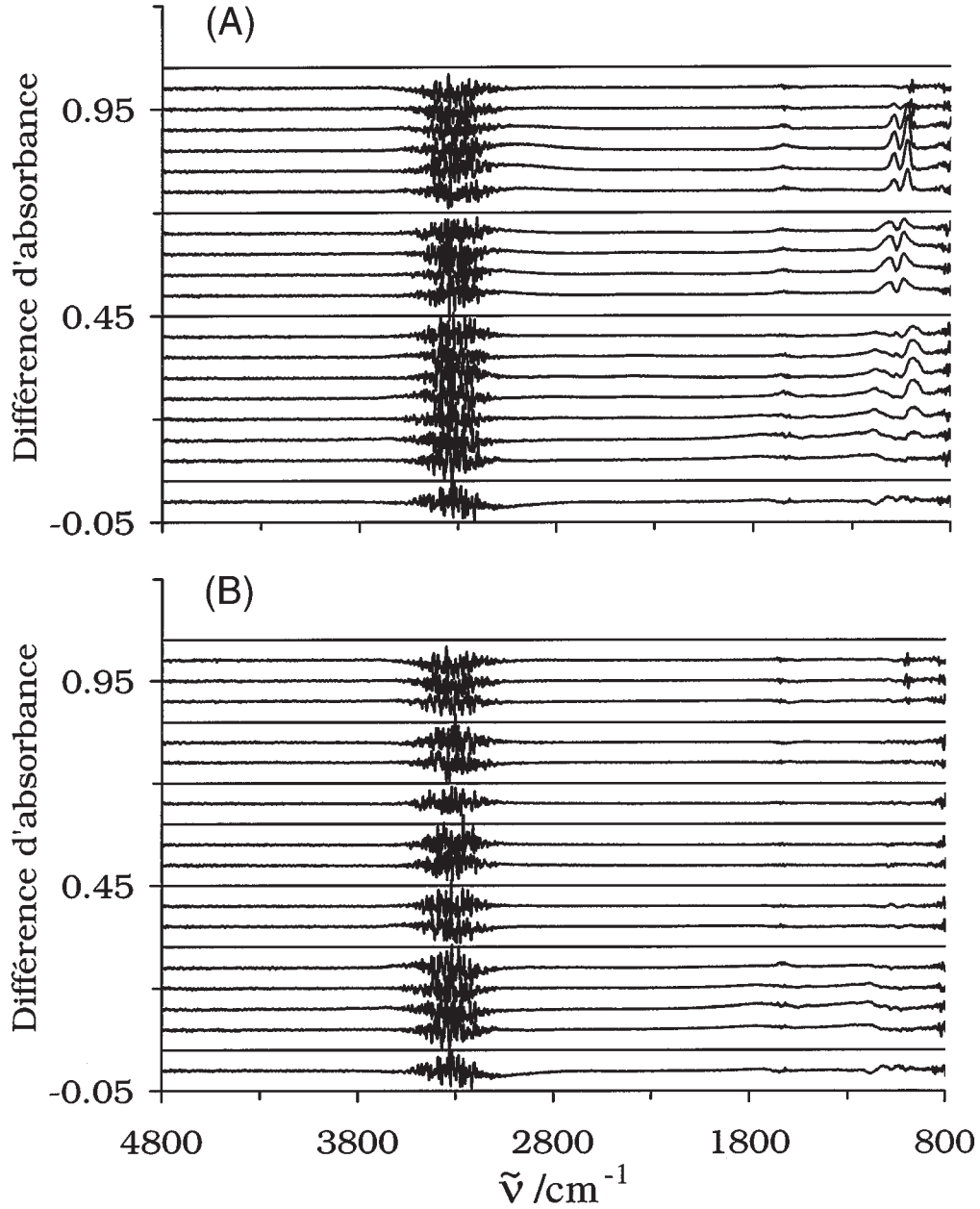
Fig. 4. Facteurs : Δ, H_3PO_4; ○, $H_2PO_4^-$; +, HPO_4^{-2} et ×, PO_4^{-3}. Concentration relative des sept espèces ioniques de H_3PO_4 en fonction de la quantité de titrant (équivalent HCl (–) ou NaOH (+)) : quatre espèces principales (même que A) et trois complexes : ▲, H_3PO_4–$H_2PO_4^-$; ●, $H_2PO_4^-$–HPO_4^{-2} et ■, HPO_4^{-2}–PO_4^{-3}. Les symboles représentent les valeurs expérimentales et les lignes, la régression linéaire.





© 2000 CNRC Canada

Fig. 5. Spectres des résidus : (A), avec les quatre espèces ioniques principales; (B), avec les sept espèces.



[39] $H_2PO_4^- + HPO_4^{-2} \rightleftharpoons H_3(PO_4)_2^{-3}$

$K_{23} = 0{,}63 \pm 0{,}04$ L/mol

[40] $HPO_4^{-2} + PO_4^{-3} \rightleftharpoons H(PO_4)_2^{-5}$

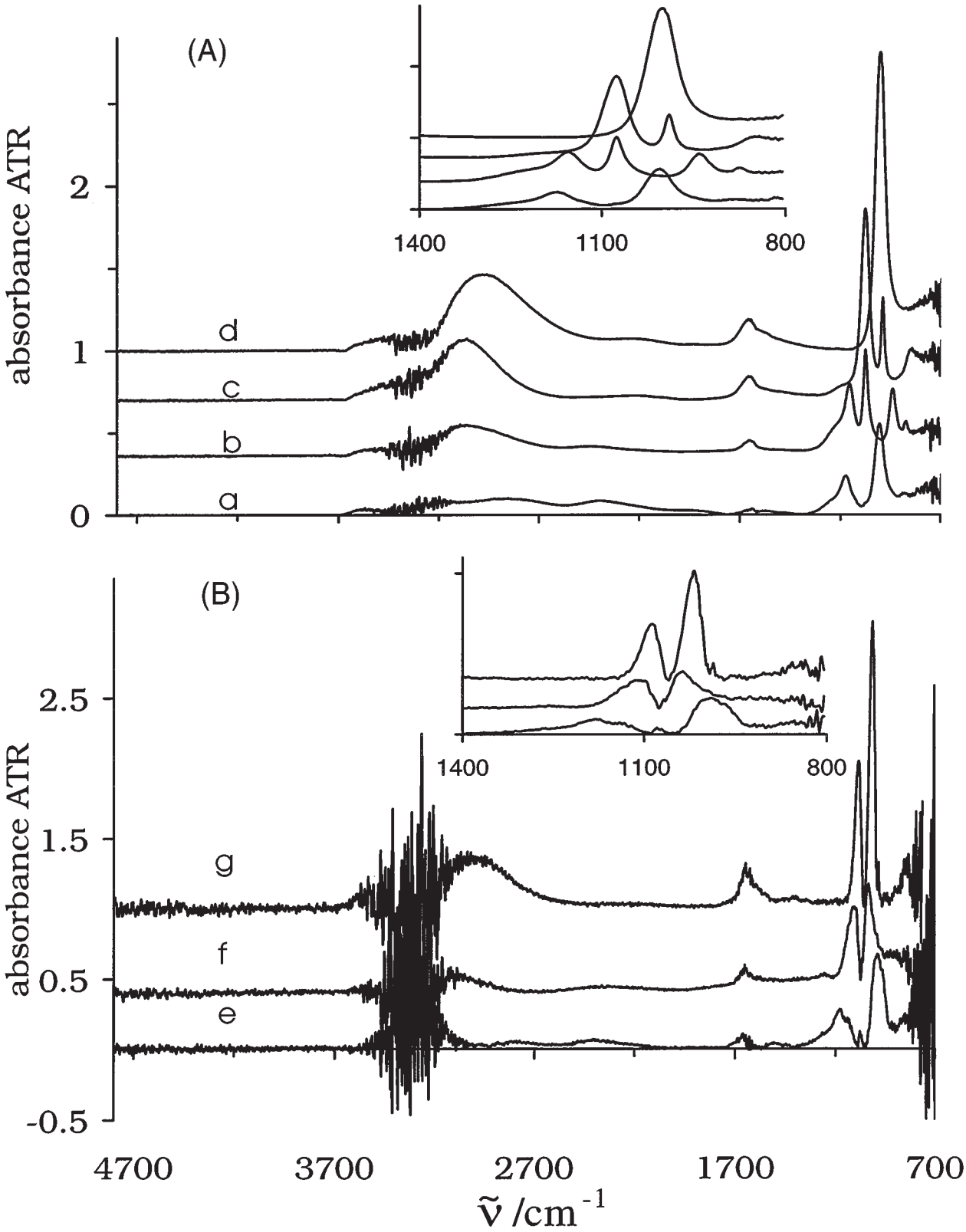
$K_{34} = 0{,}4 \pm 0{,}2$ L/mol

À droite des équations, se trouvent les constantes d'équilibre obtenues. L'étude de ces complexes a fait l'objet de travaux antérieurs en électrochimie et en pression de vapeurs (10, 24, 25). Le présent travail est le premier qui fournit des mesures spectroscopiques montrant l'existence de ces complexes en solution aqueuse.

Pour la constante d'équilibre [38], Childs a obtenu une valeur qui varie selon le coefficient d'activité entre 0 et 100 L/mol (10), Selvaratnam et Spiro ont obtenu une valeur de 3 L/mol (24) et Elmore et al. (25) ont obtenu une valeur de 1,263 L/mol. La valeur de 0,65 L/mol que nous avons obtenue par la présente analyse faite en IR est donc raisonnable. Pour la constante d'équilibre [39], Childs a obtenu 2,7 ± 2,5 L/mol (10). La valeur obtenue par IR se situe à l'intérieur de la marge d'erreur de Childs. Comme ce dernier et les autres auteurs ne parlent pas de la constante d'équilibre [40], nous serions les premiers à en faire état. Bien que la valeur que nous avons obtenue pour cette dernière soit légèrement inférieure aux deux précédentes, elle est du même ordre de grandeur. Comme les valeurs des constantes d'équilibre que nous avons déterminées le furent par des mesures spectroscopiques directes de quantité, ces valeurs sont entichées de moins d'erreurs que celles obtenues par les mesures électrochimiques et de tension de vapeurs et sont, par conséquent, plus précises et plus fiables que ces dernières.

© 2000 CNRC Canada

Fig. 6. (A) Spectres molaires des quatre espèces ioniques de l'acide phosphorique les plus abondantes : *a*, H_3PO_4; *b*, $H_2PO_4^-$; *c*, HPO_4^{-2}; *d*, PO_4^{-3}. (B) Spectres molaires des trois complexes : *e*, H_3PO_4–$H_2PO_4^-$; *f*, $H_2PO_4^-$–HPO_4^{-2}; *g*, HPO_4^{-2}–PO_4^{-3}.



© 2000 CNRC Canada

Tableau 1. Résultats de la régression linéaire de la distribution normalisée de l'acide phosphorique en fonction de l'équivalent titrant.[a]

Titrant	Espèce ionique	Symboles	Pente	Ordonnée à l'origine	Coefficient de corrélation
NaOH	H_3PO_4	Δ	–0,8820	0,8904	0,9923
NaOH	$H_2PO_4^-$	○	0,9854	0,0217	0,9958
NaOH	$H_2PO_4^-$	○	–1,0388	2,0733	0,9950
NaOH	HPO_4^{-2}	+	0,9999	–1,0513	0,9953
NaOH	HPO_4^{-2}	+	–0,9540	2,9230	0,9980
NaOH	PO_4^{-3}	×	0,9604	–1,9552	0,9994

[a]Les droites sont présentées à la figure 5B.

Tableau 2. Valeurs des pK_a de l'acide phosphorique en solution aqueuse.

Travaux antérieurs		Ce travail		
À dilution infinie	À force ionique semblable à ce travail	Volumétrique[a]	IR[b]	Force ionique
2,146[c]	1,87±0,04[f]	1,95±0,05	1,86±0,05	0,45
2,12[d]	—	—	—	—
7,198[e]	6,25±0,02[f]	6,46±0,05	6,50±0,05	1,5
7,21[d]	—	—	—	—
12,35	10,84±0,03[f]	11,34±0,05	11,42±0,05	2,95
12,67[d]	—	—	—	—

[a]Valeurs déterminées à partir de la figure 7B.

[b]Valeurs obtenues à partir de la courbe distribution IR des concentrations relatives en fonction du pH, figure 7A.

[c]Référence 12.

[d]Référence 21.

[e]Référence 9.

[f]Référence 14.

Tableau 3. Paramètres pour le calcul de la courbe de titrage volumétrique théorique.[a]

M_1 (g/mol)	M_{-1} (g/mol)	M_2 (g/mol)	ε_1 (g/g ± 0,003)	ε_{-1} (g/g ± 0,005)	ε_2 (g/g ± 0,0003)	ρ_0 (g/L ± 2)	ρ_1 (g/L ± 0,01)	ρ_{-1} (g/L ± 0,04)	V (L)	K_0
40	36,5	98	0,50	0,37	0,068	1032	0,44	0,2	0	$9{,}72 \times 10^{-15}$

[a]M_1, M_{-1} et M_2 sont les masses molaires de la basse, de l'acide et d'H_3PO_4 respectivement. ε_1, ε_{-1} et ε_2 sont les concentrations (p/p) de la base, de l'acide et d'H_3PO_4 (solution stock) respectivement. ρ_0 est la densité de la solution stock d'H_3PO_4. ρ_1 et ρ_{-1} sont des paramètres sans dimension en relation avec la variation de densité (voir section 2.1.4 et figure 7). V est le volume de chaque échantillon et K_0 correspond à la constante de dissociation de l'eau calculée en prenant la concentration moyenne de l'eau: 54,04 *M*.

4.5 Courbe de distribution en fonction du pH : titrage IR et les pK_a

La figure 7A présente la distribution normalisée des concentrations des espèces en fonction du pH : H_3PO_4 (△); $H_5(PO_4)_2^-$ (▲); $H_2PO_4^-$ (○); $H_3(PO_4)_2^{-3}$ (●); HPO_4^{-2} (+); $H(PO_4)_2^{-5}$ (■); et PO_4^{-3} (×). Puisque l'abondance des trois espèces secondaires est faible, on peut en première approximation conserver les équations d'équilibre 3 à 5. De ces équations, on montre que le pH à l'équipartition de deux espèces principales en équilibre est égal au pK_a de cet équilibre. Le tableau 2 présente les valeurs des pK_a de l'acide phosphorique, obtenues à partir de l'AF des spectres et celles obtenues par titrage volumétrique. À partir des valeurs obtenues pour les pK_a et des équations 15 à 18, 22, 25 et 27, on calcule les courbes de distribution théoriques correspondant aux équilibres 3 à 5 (seules les espèces principales sont ainsi calculées). La figure 7A montre que les résultats obtenus par ces calculs (traits pleins) et les résultats expérimentaux (indiqués par des symboles) se superposent. La présence des trois sous-espèces dont la concentration relative est inférieure à 10%, influence peu l'allure des courbes. Ceci indique que l'AF est une méthode qui permet d'obtenir les constantes de dissociation d'un composé en utilisant les bandes IR caractéristiques des différentes espèces ioniques.

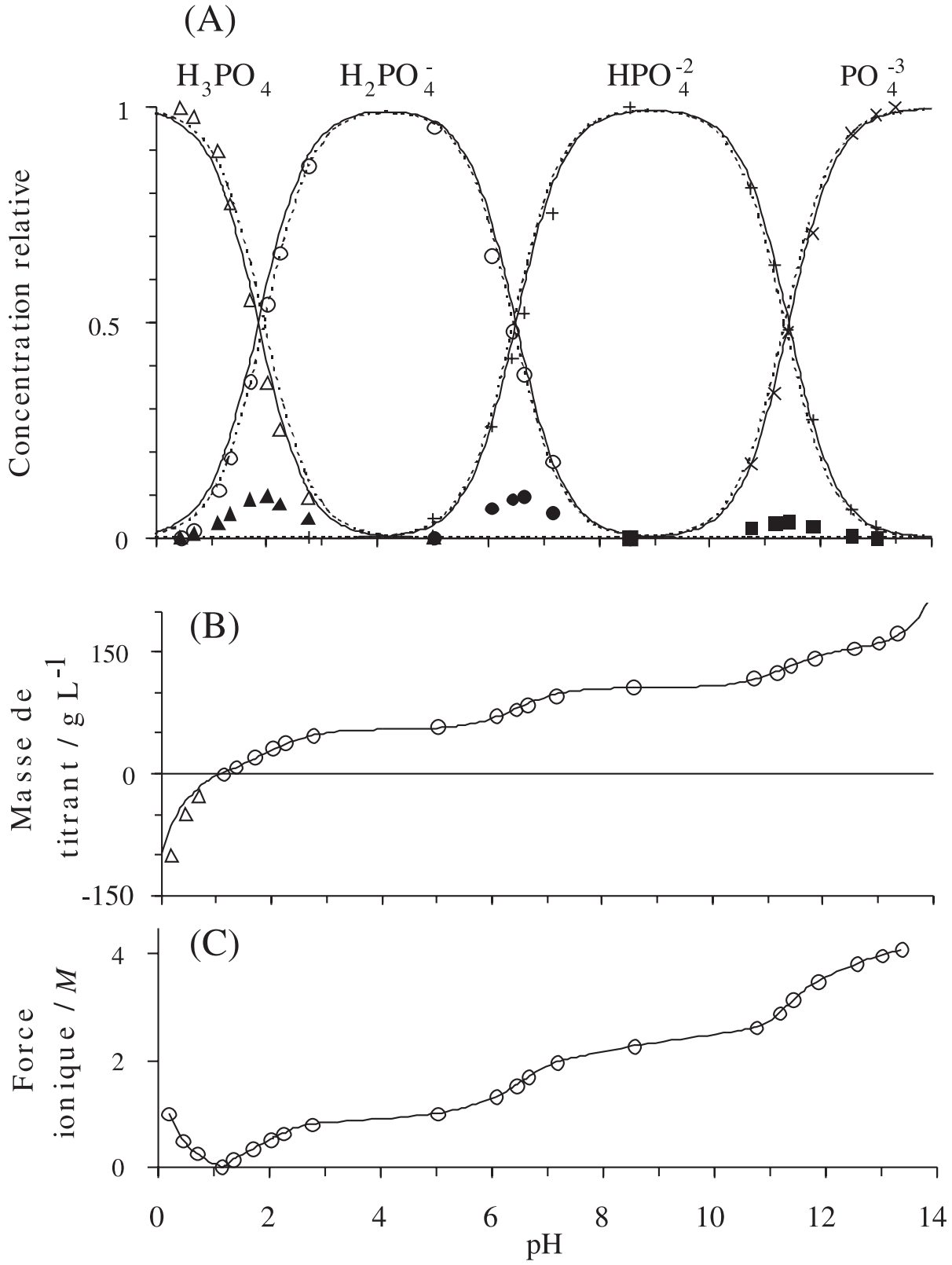
Nos résultats pour les pK_a sont comparés à ceux de la littérature à dilution infinie dans le tableau 2. Les faibles différences entre les deux séries de valeurs s'expliquent par l'influence de la force ionique sur les coefficients d'activité des espèces en solution. Ces différences s'estompent lorsque nous comparons nos résultats aux valeurs de pK_a obtenues à force ionique égale (tableau 2). La force ionique de la solution aqueuse d'acide phosphorique 7% p/v a varié lors du titrage de 0 à 4,0 M entre les pH 0,18 et 13,35 (fig. 7C). Lorsque les forces ioniques sont aussi élevées, les coefficients d'activité peuvent varier de façon importante.

4.6 Le titrage volumétrique

La quantité d'eau dans les échantillons était de 54,0 ± 0,5 M comparativement à 55,5 M pour l'eau pure dans les conditions normales. Cette concentration moyenne conduit à une valeur de $9{,}72 \times 10^{-15}$ pour K_0. Le tableau 3 donne l'ensemble des paramètres permettant de calculer la courbe de titrage volumétrique théorique avec l'équation 27. Ce calcul est effectué de manière itérative afin d'ajuster les valeurs des

© 2000 CNRC Canada

Fig. 7. Relations de H_3PO_4 en fonction du pH. (A) Distribution relative des espèces ioniques. Les symboles indiquent les valeurs obtenues par IR. La ligne continue (—) est obtenue à partir des équations d'équilibre et des pK_a déterminés par IR; la ligne hachurée (—) est obtenue à partir des pK_a déterminés par titrage volumétrique. (B) Courbe de titrage volumétrique : calculée (—) et observée (HCl, Δ; NaOH, ○). (C) Force ionique en fonction du pH.



© 2000 CNRC Canada

Tableau 4. Position (cm^{-1}) des bandes vibrationnelles des espèces ioniques de l'acide phosphorique.[a]

$OP(OH)_3 \equiv H_3PO_4$			$O_2P(OH)_2^- \equiv H_2PO_4^- - Na^+$			$O_3P(OH)^{-2} \equiv HPO_4^{-2} - 2Na^+$			$PO_4^{-3} - 3Na^+$			H_2O (liq.)[f]	
Raman	Infrarouge		Raman	Infrarouge		Raman	Infrarouge		Raman	Infrarouge		IR	Attribution
[c]	[c]	Ce travail Fig. 4A, spectre *a*	[c]	[c]	Ce travail Fig. 4A, spectre *b*	[c]	[c]	Ce travail Fig. 4A, spectre c	[c]	[c]	Ce travail Fig. 4A, spectre *d*		
	3000–2700 I	3535 tf, tl		3000–2800 I, l	3500 tf, tl		3000–2900 I, l	3415 tf, tl		3000–2900 I, l	3460 tf, tl	ν_3 : 3405 ν_1 : 3210	ν OH : H_2O
		3230 tf, tl			3060 tf, tl			3066 f, tl			2969 f, tl		ν OH : H_2O
		2847 tf, tl			2860 tf, l			2800 tf, tl			2666 tf, tl		ν OH : H_2O, POH
	2370 m	2393 tf, tl		2380 m, l	2440 tf, tl		2380 f	2340 tf,tl					ν OH : POH
								2166 tf, tl		2280 tf	2234 tf, tl	$\nu_2+\nu_{lib}$: 2130	Comb. Eau + ν OH : H_2O, POH
		1922 tf, tl			1900 tf, tl						~1900 tf, tl		Comb. Eau + ν OH : H_2O, POH ?
	1780 f			1810 f			1830 tf						?
		1638 tf			1650 tf			1652 f			1654 f	ν_2 : 1637	Défo. HOH
		1574 tf, ép									1500 tf, ép		Comb.
		1471 ttf, ép			1500 tf, tl			1500 tf, ép					Comb.
	1250 f	1251 tf, ép		1230 I	1233 tf, ép		1230 f	1197 tf, l					δ POH
1190 f,p	1165 tI ; 1178[e]	1173 f											ν P–O
1079–1052 f,p	1074–1066 tf	1133 tf, ép											Comb
			1150[d]	1150 tI 1159[e]	1156 f	1081 dp 1080[d]	1076 f 1080[e]	1077 I	1026–1014 dp	1082[b] ; 1004 tI ; 1009[e]	1001 tI		ν P-O anti
			1069 I, p 1074[c]	1072 tI 1078[e]	1076 m								ν P-O sym
		1070 tf, ép											δ POH
1008 f, dp	1007 tI l010[e]	1005 m	947 f, dp 940[d]	947 tI 941[e]	940 f								ν P-(OH) anti
						976 p 987[d]	988 m, ét 991[e]	990 m	980[b] ; 936 p				ν P-O sym
890 I, p	885 I	881 tf	880 I, p 874[d]	878 I	874 tf	865 p 805[d]	862 f	846 f					ν P-(OH) sym
		817 tf											Comb.
500 dp				514		537 dp				515[b] ; 573			δ OPO
390			380			394 dp							δ OPO
345									363[b] ; 420				δ OPO

[a]Abréviations : I, intense; m, moyenne; f, faible; t, très; l, large; ét, étroite; ép, épaulement; p, polarisée; dp, dépolarisée; sym, symétrique; anti, antisymétrique.
[b]28.
[c]19.
[d]26.
[e]27.
[f]29.

© 2000 CNRC Canada

Tableau 5. Comparaison des positions (cm^{-1}) des bandes infrarouges des complexes de l'acide phosphorique avec celles des espèces ioniques pures.[a]

C_{3v}		C_{2v}		C_{3v}		T_d	
H_3PO_4	$H_5(PO_4)_2^- - Na^+$	$H_2PO_4^- - Na^+$	$H_3(PO_4)_2^{-3} - 3Na^+$	$HPO_4^{-2} - 2Na^+$	$H(PO4)_2^{-5} - 5Na^+$	$PO_4^{-3} - 3Na^+$	Attribution
Fig. 4A, spectre *a*	Fig. 4B, spectre *e*	Fig. 4A, spectre *b*	Fig. 4B, spectre *f*	Fig. 4A, spectre *c*	Fig. 4B, spectre *g*	Fig. 4A, spectre *d*	
3535 tf, tl		3500 tf, tl		3415 tf, tl	3500 tf, tl	3460 tf, tl	ν OH : H_2O
3230 tf, tl	3290 tf, tl	3060 tf, tl	3100 tf, tl	3066 tf, tl	3000 tf, tl	2969 f, tl	ν OH : H_2O
2847 tf, tl	2790 tf, tl	2860 tf, tl		2800 tf, tl	~ 2700 tf, ép	2666 f, tl	ν OH : H_2O, POH
2393 tf, tl	2400 tf, tl	2440 tf, tl	2349 tf, tl	2340 tf, tl			ν OH : POH
				2166 tf, tl	2225 tf, tl	2234 tf, tl	Comb. Eau + ν OH : H_2O, POH
1922 tf, tl		1900 tf, tl				~1900 tf, tl	Comb. Eau + ν OH : H_2O, POH ?
			1775 tf, tl				Comb.
1638 tf	1661 tf	1650 tf	1649 tf	1652 tf	1640 tf	1654 f	δ HOH
1574 tf, ép						1500 tf, ép	Comb.
1471 tf, ép	1500 tf	1500 tf, tl	1500 tf, tl	1500 tf, ép	~ 1400 tf, tl		Comb.
1251 tf, ép	1250 tf, ép	1233 tf, ép	1257 tf, l	1197 tf, l			δ POH
1173 f	1180 f						ν P = O
1133 tf, ép	1147 tf, ép						Comb.
			1136 tf, ép				
		1156 f	1108 f	1077 I	1087 f	1001 tI	ν P–O anti
		1076 m	1036 f		1017 m		ν P–O sym
1070 tf, ép	1075 tf						δ POH
1005 m	991 f	940 f					ν P–(OH) anti
			~990 tf, ép	990 m	986 tf, ét	936 ia	ν P–O sym
	967 tf, ép						
881 tf	855 tf	874 tf		846 f	850 tf		ν P–(OH) sym
817 tf							Comb.

[a]La symétrie indiquée est celle des espèces ioniques pures et ne tient pas compte de la position des hydrogènes. Abréviations : I, intense; m, moyenne; f, faible; t, très; l, large; ét, étroite; ép, épaulement; p, polarisée; dp, dépolarisée; dég, dégénérée; sym, symétrique; anti, antisymétrique; ia, inactive.

pK_a de façon que l'erreur quadratique entre les valeurs théoriques et expérimentales soit minimale. Les valeurs ainsi obtenues sont présentées dans le tableau 2. Les différences entre ces résultats et ceux obtenus par IR sont minimes et se trouvent à l'intérieur de la marge d'erreur. La figure 7B montre que la courbe théorique du titrage volumétrique calculée à partir de l'équation 2 (trait plein) et les points expérimentaux (Δ pour le HCl et ○ pour le NaOH) se superposent.

4.7 Les spectre IR des espèces ioniques de l'acide phosphorique

4.7.1 Attribution des bandes IR des quatre espèces principales

La figure 6 montre les spectres IR normalisés des espèces ioniques de l'acide phosphorique dans la région de pH entre 0 et 14. Le tableau 4 donne la position et l'attribution des bandes des quatre espèces ioniques principales (fig. 6A) en les comparant avec les valeurs de la littérature (19, 26–29). La position des bandes les plus intenses correspond assez bien avec les valeurs de la littérature. Cependant, comme nous avons soustrait trois types d'eau, les spectres des espèces principales se trouvent débarrassés des bandes intenses d'eau, ce qui permet d'avoir une meilleure définition des bandes pour lesquelles nous obtenons avec plus de précision la valeur des positions et des maxima. Nous observons également une certain nombre de bandes de combinaison qui n'ont pas encore été rapportées.

Sur chaque spectre des espèces principales nous avons identifié un certain nombre de bandes d'eau. Cette eau est différente de l'eau neutre, acide et basique qui ont été soustraites. Cette eau résiduelle se trouve complexée aux espèces ioniques. En comparant la surface de la bande OH d'élongation (~2900 cm^{-1}) avec celle de l'eau (fig. 3A, spectre *a*) nous arrivons aux résultats suivants : pour un ion PO_4^{-3}, nous obtenons 14 molécules d'eau; pour un ion HPO_4^{-2}, nous obtenons 9 molécules d'eau; pour un ion $H_2PO_4^-$, nous obtenons 5 molécules d'eau et pour la molécule H_3PO_4, nous obtenons 4 molécules d'eau. Pour les hydrates solides de ces ions, le nombre de molécules d'eau par ion est le suivant et est donné dans le même ordre : 12, 12, 2 et 0,5 (21). Il est intéressant de constater que les valeurs obtenues en milieu aqueux se comparent aux valeurs des hydrates solides et indiquent que nos résultats sont valables. Nous sommes les premiers à obtenir des valeurs d'hydrates en milieux aqueux pour l'acide phosphorique et ses sels. Cette méthode peut s'appliquer à d'autres substances mais dépend grandement de la précision de la soustraction des spectres d'eau. À

© 2000 CNRC Canada

mesure que la précision de cette opération cruciale va augmenter, la qualité des résultats va s'améliorer.

4.7.2 Attribution des bandes IR des trois complexes

Le spectre molaire des trois complexes situés aux pK_a des espèces principales est présenté sur la figure 6B. La position des bandes et leur attribution sont données sur le tableau 5. Cette attribution est basée sur celle des espèces principales, puisque les bandes des complexes se trouvent dans la fourchette des bandes des espèces principales. Comme il n'y a pas de bandes qui apparaissent dans des régions autres que celles où apparaissent les bandes des espèces principales, les complexes seraient formés des deux molécules parentes attachées bout à bout. Bien que nous ne puissions déterminer avec certitude la symétrie des complexes, elle serait inférieure ou égale à la symétrie de l'espèce principale qui a la plus basse symétrie. Sur le spectre des complexes nous observons des bandes d'eau dont l'intensité est voisine de celle des espèces principales (fig. 6A). Cette eau serait intimement liée aux complexes pour former un super complexe.

5 Conclusion

Nous avons présenté le titrage par spectroscopie IR de l'acide phosphorique par l'hydroxyde de sodium. Après avoir débarrassé les spectres originaux des spectres de l'eau neutre, de l'eau acide et de l'eau basique, l'AF a permis d'obtenir les spectres des espèces ioniques et de déterminer leur abondance en fonction du pH. Les spectres des quatre espèces ioniques principales qui ont été obtenus sont plus nets et plus précis que ceux qui ont été publiés jusqu'à présent. Trois complexes phosphates peu abondants ont été observés pour la première fois en IR, bien que la présence de deux d'entre eux ait été déduite de mesures potentiométriques et conductométriques. Ces complexes, dont l'abondance maximale se trouve aux pK_a de deux espèces ioniques principales, sont composés de ces espèces.

Les spectres ont été normalisés à 1 M afin de bien comparer les intensités des bandes des différentes espèces ioniques. Plusieurs bandes de faible intensité ainsi que des bandes d'eau ont été observées pour la première fois. Ces dernières ont été attribuées à de l'eau complexée aux espèces ioniques tandis que les premières sont attribuées à des bandes de combinaison. Le nombre de molécules d'eau par ion phosphate qui fut trouvé est comparable à celui des hydrates solides. C'est la première fois qu'on rapporte la présence d'hydrates observés par IR en milieux aqueux.

Nous rapportons également la distribution des espèces ioniques, en fonction du pH, de l'acide phosphorique que nous avons obtenue par IR. Cette distribution est en parfait accord avec celle qui résulte du calcul basé sur les équilibres thermodynamiques. Les pK_a de l'acide phosphorique ont été obtenus de deux façons : par mesure directe en IR des concentrations des espèces ioniques et par ajustement des courbes de titrage volumétrique expérimental et théorique. Les valeurs obtenues par les deux méthodes concordent et sont en accord avec la littérature.

On a déterminé les constantes d'équilibre de trois complexes formés par deux espèces ioniques de l'acide phosphorique dont deux avaient été déduites de mesures électrochimiques. Les valeurs obtenues pour les constantes sont en accord avec les valeurs déjà publiées. De plus les valeurs que nous rapportons ont été obtenues de mesures directes de quantités molaires et sont, par conséquent, fiables et précises.

6 Bibliographie

1. J.-J. Max, M. Trudel et C. Chapados. Appl. Spectrosc. **52**, 226 (1998).
2. J.-J. Max, G. Bérubé, M. Trudel, S. Groleau et C. Chapados. Langmuir, **14**, 5051 (1998).
3. J.-J. Max et C. Chapados. Appl. Spectrosc. **53**, 1045 (1999).
4. J.-J. Max et C. Chapados. Appl. Spectrosc. **52**, 963 (1998).
5. J.-J. Max, M. Trudel et C. Chapados, Appl. Spectrosc. **52**, 234 (1998).
6. J.-J. Max, C. Ménichelli et C. Chapados. J. Phys. Chem. A 104, 2845 (2000).
7. E.R. Malinowski et D.G. Howery. Factor analysis in chemistry. R.E. Krieger, Malabar, Fla. 1989.
8. C. Chapados et M. Trudel. Biophys. Chem. **47**, 267 (1993).
9. R.G. Bates et S.F. Acree. J. Res. Natl. Bur. Stand. **30**, 129 (1943).
10. C.W. Childs. J. Phys. Chem. **73**, 2956 (1969).
11. R.E. Mesmer et C.F. Base, Jr. J. Solution Chem. **3**, 307 (1974).
12. K.S. Pitzer et L.F. Silvester. J. Solution Chem. **5**, 269 (1976).
13. D.R. Migneault et R.K. Forcé. J. Solution Chem. **17**, 987 (1988).
14. J.P. Hershey, M. Fernandez et F.J. Millero. J. Solution Chem. **18**, 9, 875 (1989).
15. C.A. Vega et M. Romero. J. Chem. Eng. Data. **39**, 294 (1994).
16. J.I. Partanen et P.O. Minkkinen. Acta Chem. Scand. **50**, 1081 (1996).
17. V.P. Vasil'ev, L.A. Kochergina et S.V. Dushina. Russ. J. Inorg. Chem. **40**, 58 (1995).
18. C. Jiang. Chem. Eng. Sci. **51**, 5, 689 (1996).
19. A.C. Chapman et L.E. Thirlwell. Spectrochim. Acta, **20**, 937 (1964); A.C. Chapman, D.A. Long et D.T.L. Jones. Spectrochim. Acta, **21**, 633 (1965).
20. Von E. Steger et K. Herzog. Z. Anorg. Allg. Chem. **331**, 169 (1964).
21. R.C. Weast (*Éditeur*). Handbook of chemistry and physics. 57^{ième} éd. CRC Press, Cleveland, Ohio, 1977.
22. D. Schlöberg et G. Zundel. Can. J. Chem. **54**, 2193 (1976).
23. J.-J. Max et C. Chapados. Can. J. Chem. **78**, 64 (2000).
24. M. Selvaratnam et M. Spiro. Trans. Faraday Soc. **61**, 360 (1965).
25. K.L. Elmore, J.D. Hatfield, R.L. Dunn et A.D. Jones. J. Phys. Chem. **69**, 3520 (1965).
26. P. Haufe. J. Solution Chem. **14**, 73 (1985).
27. R. Vonash, B. Lendl et R. Kellner. Analyst, **122**, 525 (1997).
28. G. Herzberg. Molecular spectra and molecular structure. II. Infrared and Raman spectra of polyatomic molecules. Van Nostrand Company, Princeton, N.J. 1945.
29. J.-J. Max et C. Chapados. Appl. Spectrosc. **53**, 1601(1999).

Liste des symboles utilisés

Symbole	Signification
A	Quantité totale (en mol) d'acide phosphorique dans l'échantillon
c	Quantité (en mol) de Na^+ dans l'échantillon
c'	Quantité (en mol) de Cl^- dans l'échantillon
C	Quantité de NaOH (en mol) ajouté à l'échantillon

© 2000 CNRC Canada

C Quantité de HCl (en mol) ajouté à l'échantillon
d Quantité (en mol) d'eau à l'équilibre dans l'échantillon
D Quantité totale d'eau (en mol) initialement dans l'échantillon
FM_i^j Facteur multiplicatif brut de l'espèce i dans le spectre S_j
$FM_i^{j\,0}$ Facteur multiplicatif associé au spectre propre normalisé S_i^0 dans le spectre S_j de l'échantillon j
$FM_i^{j\,N}$ Facteur multiplicatif normalisé de l'espèce principale i dans l'échantillon j
K_1 Constante de première dissociation de l'acide phosphorique
K_2 Constante de seconde dissociation de l'acide phosphorique
K_3 Constante de troisième dissociation de l'acide phosphorique
K_{12} Constante de complexion $H_3PO_4 + H_2PO_4^- \rightleftharpoons H_5(PO_4)_2^-$
K_{23} Constante de complexion $H_2PO_4^- + HPO_4^{-2} \cdot H_3(PO_4)_2^{-3}$
K_{34} Constante de complexion $HPO_4^{-2} + PO_4^{-3} \rightleftharpoons H(PO_4)_2^{-5}$
K_0 Constante de dissociation de l'eau : $1{,}805 \times 10^{-16}$ à 25,0°C
m Masse totale de l'échantillon (en g)
m_2 Masse de solution mère d'acide phosphorique mise dans l'échantillon (en g)
m_δ Masse de solution titrante ajoutée à l'échantillon (en g)
m_2^0 Masse de l'échantillon sans titrant
m_2^i Masse de solution mère dans l'échantillon i
M_1 Masse molaire de la base forte (NaOH) : 40,00 g/mol
M_{-1} Masse molaire de l'acide fort (HCl) : 36,46 g/mol
M_2 Masse molaire de l'acide phosphorique : 97,99 g/mol
M_{H_2O} Masse molaire de l'eau : $18{,}015_2$ g/mol
P Équivalent titrant
R_j Spectre résiduel : différence entre les spectres expérimental et calculé pour l'échantillon j
S_i Spectre de l'espèce principale i pour l'analyse par facteur
S_j Spectre de l'échantillon j
S_i^0 Spectre de l'espèce i normalisé par rapport à la masse de l'échantillon sans titrant m_2^0
V Volume total de chaque échantillon (en L)
x Quantité (en mol) de H^+ à l'équilibre dans l'échantillon
x' Quantité (en mol) de OH^- à l'équilibre dans l'échantillon
y_1 Quantité (en mol) de H_3PO_4 à l'équilibre dans l'échantillon
y_2 Quantité (en mol) de $H_2PO_4^-$ à l'équilibre dans l'échantillon
y_3 Quantité (en mol) de HPO_4^{-2} à l'équilibre dans l'échantillon
y_4 Quantité (en mol) de PO_4^{-3} à l'équilibre dans l'échantillon
δ sélectionne le titrant utilisé : base, $\delta = +1$; acide, $\delta = -1$
ε_2 concentration relative d'acide phosphorique dans la solution mère (p/p)
ε_δ concentration relative de la solution de titrant (p/p)
ρ_0 Densité de la solution mère d'acide phosphorique (en g/L)
ρ Densité de l'échantillon (en g/L)
ρ_δ Coefficient sans dimension de la variation de la densité de l'échantillon avec la quantité de titrant : $\rho_\delta = (\rho - \rho_0)\, V/m_\delta$

© 2000 CNRC Canada

Correlation of rates of uncatalyzed and hydroxide-ion catalyzed ketene hydration. A mechanistic application and solvent isotope effects on the uncatalyzed reaction

John Andraos and A. Jerry Kresge

Abstract: Rates of hydration of a number of ketenes were measured in neutral and basic solution using flash photolytic techniques, and rate constants for their uncatalyzed, k_{uc}, and hydroxide-ion catalyzed, k_{HO}, reactions were determined. These results, plus additional data from the literature, were found to provide the remarkably good correlation log k_{uc} = –3.21 + 1.14 log k_{HO}, which spans 10 orders of magnitude in reactivity and includes 31 ketenes. This good correlation implies that uncatalyzed and hydroxide-ion catalyzed ketene hydraton occur by similar reaction mechanisms, which for the hydroxide-ion catalyzed process is known to involve nucleophilic attack on the carbonyl carbon atom of the ketene. Rate constants for phenylhydroxyketene, on the other hand, do not fit this correlation, which suggests that the mechanistic assignment upon which these rate constants are based may not be correct. Solvent isotope effects on these uncatalyzed ketene hydrations are weak; most are less than k_H/k_D = 2. It is argued that these isotope effects are largely, if not entirely, secondary in nature and that they are consistent with both a reaction mechanism in which nucleophlic attack of a single water molecule on the ketene carbonyl carbon atom produces a zwitterionic intermediate and also a mechanism that avoids this intermediate by passing through a cyclic transition state involving several water molecules.

Key words: ketene hydration, rate correlation, nucleophilic attack, solvent isotope effects, phenylhydroxyketene.

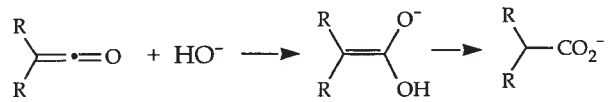
Résumé : Faisant appel à des techniques de photolyse éclair et opérant en solutions neutre et basiques, on a mesuré les vitesses d'hydratation d'un certain nombre de cétènes; on a aussi déterminé les constantes de vitesse de leurs réactions non catalysées, k_{uc}, et catalysées par l'ion hydroxyde, k_{OH}. On a trouvé que ces résultats, en combinaison avec des données additionnelles tirées de la littérature, permettent d'obtenir une corrélation relativement bonne, log k_{uc} = –3,21 + 1,14 log k_{OH}, qui couvre dix ordres de grandeur de réactivité et qui inclut trente et un cétènes. Cette bonne corrélation implique que les hydratations du cétène non catalysée ainsi que catalysée par l'ion hydroxyde se produisent par des mécanismes réactionnels similaires; dans le cas du processus catalysé par l'ion hydroxyde, il est admis que la réaction implique une attaque nucléophile sur l'atome de carbone du carbonyle du cétène. Par ailleurs, les constantes de vitesse du phénylhydroxycétène ne suivent pas la corrélation; ceci suggère que l'attribution mécanistique sur laquelle ces constantes de vitesse sont basées n'est peut-être pas correcte. Les effets isotopiques de solvant sur ces hydratations non catalysées du cétène sont faibles; dans la plupart des cas, $k_H/k_D \leq 2$. On croit que ces effets isotopiques sont en grande partie, si ce n'est pas totalement, de nature secondaire et qu'ils sont en accord à la fois avec un mécanisme réactionnel dans lequel l'attaque nucléophile d'une seule molécule d'eau sur l'atome de carbone du carbonyle du cétène produit un intermédiaire zwitterionique ainsi qu'avec un mécanisme qui évite cet intermédiaire en passant par un état de transition cyclique impliquant plusieurs molécules d'eau.

Mots clés : hydratation du cétène, corrélation de vitesse, attaque nucléophile, effets isotopiques du solvant, phénylhydroxylcétène.

[Traduit par la Rédaction]

Introduction

The generally accepted reaction mechanism for the hydroxide-ion catalyzed hydration of ketenes to carboxylate ions consists of nucleophilic addition of hydroxide to the carbonyl carbon atom of the ketene, followed by ketonization of the carboxylic acid enolate ion thus formed, eq. [1] (1).

[1] 

Received November 8, 1999. Published on the NRC Research Press website on April 14, 2000.

J. Andraos and A.J. Kresge.[1] Department of Chemistry, University of Toronto, Toronto, ON M5S 3H6, Canada.

[1]Author to whom correspondence may be addressed. Telephone: (416) 978–7259. Fax: (416) 978–7259. e-mail: akresge@chem.utoronto.ca

© 2000 NRC Canada

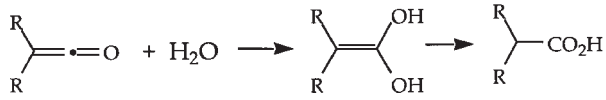
Nucleophilic attack is directed at the lowest unoccupied molecular orbital of the ketene, **1**, which lies in the ketene



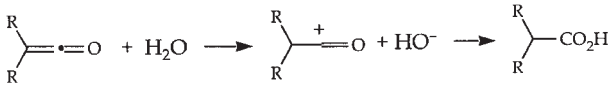
1 *2*

molecular plane, and large groups attached to the ketene β-carbon atom interfere substantially with approach of the nucleophile. The large steric rate retardations introduced in this way are in fact a hallmark of this reaction, and they provide some of the principal evidence upon which this reaction path is based.

A similar mechanism is believed to operate in uncatalyzed ketene hydration, with a water molecule acting as the nucleophile and enol and carboxylic acid replacing enolate and carboxylate ions, as shown in eq. [2]. Water, however, is

[2] 

an acid as well as a nucleophile, and another mechanism is in principle possible, in which proton transfer from a water molecule to the ketene β-carbon atom is followed by conversion of the ensuing acylium ion to a carboxylic acid, eq. [3].

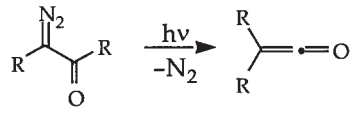
[3] 

The mode of initial attack in this case is electrophilic addition to the highest occupied molecular orbital of the ketene, **2**, and, because this orbital is perpendicular to the ketene molecular plane, steric effects can be expected to be quite different from, and much less severe than, those on the nucleophilic reaction of eq. [2].

It was observed (1, 2) that substituent effects on the rate constant for uncatalyzed ketene hydration, k_{uc}, are remarkably similar to those for the hydroxide-ion catalyzed reaction, k_{HO}, and this similarity was used to support a common nucleophilic mechanism for both processes. We have now expanded the somewhat limited data upon which this earlier observation was based by determining k_{uc} and k_{HO} for a number of additional ketenes, and we have found that these values, plus data already in the literature, provide a remarkably good correlation between these two rate constants spanning ten orders of magnitude in reactivity.

We have also found a striking exception to this correlation, which suggests that the mechanistic assignment upon which this exception is based may not be correct.

The ketenes whose rate constants were measured in the present study were generated by photo-Wolff reactions of the corresponding α-diazocarbonyl compounds, eq. [4]. Because the hydration reactions were rapid, flash photolytic methods were used.

[4] 

Experimental Section

Materials

The α-diazocarbonyl compounds used as photo-Wolff reaction substrates were prepared by standard methods. Their spectra conformed to their structures and agreed with literature values. Details are available in the theses of references 3 and 4.

All other materials were best-available commercial grades.

Kinetics

Flash photolytic rate measurements were made using conventional (microsecond) (5) and laser (nanosecond, λ = 248 nm) (6) systems that have already been described. The ketene hydration reactions were followed by monitoring the decrease in ketene absorbance at λ = 215 nm for the aliphatic ketenes and at λ = 260–300 nm for the aromatic ketenes. The temperature of all solutions upon which rate measurements were made was controlled at 25.0 ± 0.05°C. The rate data so obtained conformed to the first-order rate law well, and observed first-order rate constants were obtained by non-linear least squares fitting of an exponential function.

Results

All rate measurements were made in wholly aqueous solution at an ionic strength of 0.10 M, maintained by adding $NaClO_4$ as required.

Rate profiles for ketene hydration reactions in aqueous solution typically show extensive uncatalyzed plateaus, with no base catalysis up to pH = 10–11, and correspondingly weak, or often absent, acid catalysis. Uncatalyzed hydration rate measurements were consequently made in neutral unbuffered solutions containing no added acid or base. For each substrate, 10–25 replicate determinations were made. The results are summarized in the theses of references 3 and 4, and average values are listed in Table 1.

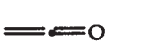
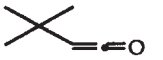
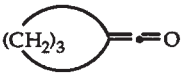
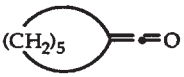
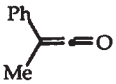
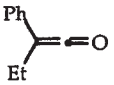
Some rate measurements of the uncatalyzed reaction were also made in D_2O solution. These values are also summarized in the theses of references 3 and 4, and the solvent isotope effects that they produce when combined with their H_2O counterparts, $(k_{uc})_{H_2O}/(k_{uc})_{D_2O}$, are listed in Table 1.

Rate measurements of the hydroxide-ion catalyzed ketene hydration reaction were made in dilute sodium hydroxide solutions. For each substrate, 5 to 6 different sodium hydroxide concentrations were used, spanning a 5– to 25–fold variation in [NaOH], and replicate measurements were made at each concentration. The results are summarized in the theses of references 3 and 4.

In all cases, observed first-order rate constants increased linearly with hydroxide ion concentration, and the data were

© 2000 NRC Canada

Table 1. Rate constants for uncatalyzed, k_{UC}, hydroxide-ion catalyzed, k_{HO}, and hydronium-ion catalyzed, k_H, hydration of ketenes in aqueous solution at 25°C.[a]

Ketene	k_{uc}/s^{-1}	$(k_{uc})_{H_2O}/(k_{uc})_{D_2O}$	$k_{HO}/M^{-1}s^{-1}$	$k_H/M^{-1}s^{-1}$	Ref
	3.65×10^1	1.59	5.26×10^4	1.01×10^4	7,8
	9.66×10^1	1.88	3.29×10^4	3.98×10^3	3,9,20
	1.46×10^1	2.01	1.68×10^4	4.77×10^3	4,7
	4.09×10^2	-	-	3.13×10^5	3
	1.11×10^2	3.39	3.89×10^4	2.14×10^4	3
	2.30×10^1	2.04	6.24×10^3	2.78×10^3	3
	2.35×10^1	1.91	6.08×10^3	-	3
	4.77×10^3	1.44	1.22×10^6	-	9
	5.57×10^1	1.55	2.03×10^4	-	4
	1.03×10^1	1.48	6.05×10^3	-	10

therefore analyzed by least-squares fitting of eq [5]. The resulting hydroxide-ion catalytic coefficients are listed in Table 1.

$$[5] \qquad k_{obs} = k_{uc} + k_{HO}[HO^-]$$

This analysis also produced uncatalyzed reaction rate constants, k_{uc}, and these were nicely consistent with the more precise values of this rate constant determined directly in neutral solution.

Some rate measurements were also made in dilute perchloric acid solution, using several different acid concentrations of each substrate and making replicate measurements at each acid concentration. These results are summarized in reference 3. Observed first-order rate constants increased linearly with acid concentration, and the data were analyzed by least squares fitting of the H^+ analog of eq [5]. The hydronium-ion catalytic coefficients so obtained, k_H, are also listed in Table 1. The uncatalyzed reaction rate constants produced by this analysis were once again nicely consistent with results determined in neutral solution.

Discussion

Correlation

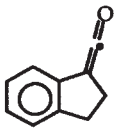
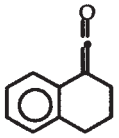
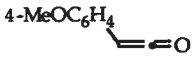
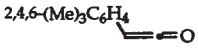
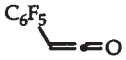
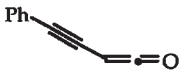
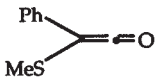
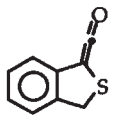
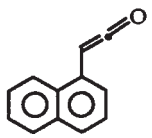
The ketenes examined here, plus others for which aqueous solution hydration rate constants are available from the literature, are assembled in Table 1. These ketenes possess a wide variety of substituents, which produces a wide range of hydration reactivity: the range covered is 2×10^{10} in k_{HO} and 5×10^{10} in k_{uc}. And yet these widely different rate constants generate the remarkably good correlation shown in Fig. 1. Linear least squares analysis[2] of the data gives $\log k_{uc} = -(3.21 \pm 0.22) + (1.14 \pm 0.04)\log k_{HO}$, with a root-mean-square deviation in $\log k_{uc}$ of 0.271, which corresponds to 0.37 kcal mol^{-1} in free energy of activation.

This good correlation implies that the various substituents present in these ketenes are affecting the uncatalyzed and

[2] The analysis was performed using simple weighting with both $\log k_{uc}$ and $\log k_{HO}$ subject to (the same) uncertainty (22).

© 2000 NRC Canada

Table 1 (*continued*).

	1.96×10^3	1.18	8.42×10^5	-	11
	1.03×10^2	1.60	6.30×10^4	-	4
	2.90×10^3	-	1.13×10^6	-	12
	1.10×10^2	1.51	6.78×10^4	4.67	4,12,21
	8.28×10^0	-	4.34×10^3	-	12
	2.76×10^3	1.42	1.13×10^6	-	10
	5.76×10^3	2.09	2.31×10^6	2.09×10^4	4, 20
	7.15×10^4	2.84	1.98×10^7	1.61×10^5	4, 20
	1.02×10^2	1.59	1.89×10^4	-	10, 11
	2.21×10^5	1.17	1.66×10^7	-	13
	2.95×10^3	-	1.25×10^6	-	12

hydroxide-ion catalyzed reactions in the same way. As pointed out in the Introduction above, this could hardly be possible if one reaction involved nucleophilic attack and the other involved electrophilic attack. Since there is good evidence that the hydroxide-ion catalyzed reaction is a nucleophilic process (1) — it is, in fact, difficult to conceive of a different role for the hydroxide ion — it follows that the uncatalyzed reaction is a nucleophilic process as well.

This conclusion is supported by the much poorer correlation of k_{UC} with rate constants for hydronium-ion catalyzed ketene hydration, k_H, shown in Fig. 2. Linear least squares analysis[3] of these data gives log k_{UC} = –(3.69 ± 1.97) + (1.54 ± 0.52) log k_H, with a root-mean-square deviation in log k_{UC} of 1.08, which corresponds to 1.47 kcal mol^{-1} in free energy of activation and is 4.0 times the deviation given by the k_{UC}–k_{HO} correlation. The hydronium-ion catalyzed reaction, of course, involves electrophilic attack on the ketene β-carbon atom and has very different steric requirements than nucleophilic attack of water or hydroxide ion on the ketene carbonyl carbon atom (1).

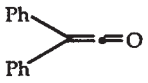
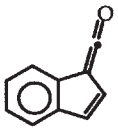
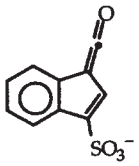
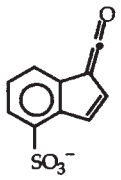
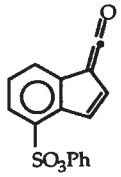
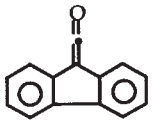
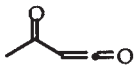
An Exception

Figure 1 shows that the point for phenylhydroxyketene provides an apparent exception to the good k_{UC}–k_{HO} correlation. This point lies 1.77 below the correlation line, which is equivalent to 2.41 kcal mol^{-1} in free energy of activation and

[3] This analysis was also performed using simple weighting with both log k_{UC} and log k_H subject to (the same) uncertainty (22).

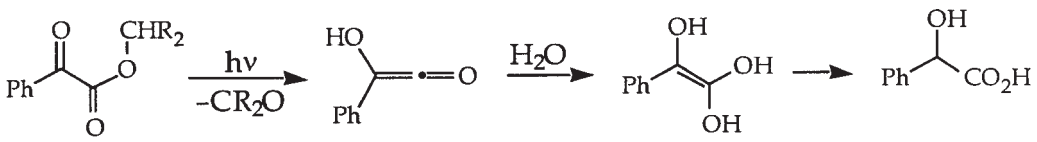
© 2000 NRC Canada

Table 1 (*continued*).

	2.75×10^2	1.27	6.11×10^4	-	9
	9.0×10^5	-	4.8×10^7	-	14
	1.2×10^6	-	3.8×10^7	-	15
	1.57×10^7	1.39	2.25×10^9	-	6
	2.82×10^6	1.22	8.77×10^7	-	6
	9.89×10^6	1.17	2.00×10^8	-	6
	1.07×10^5	1.35	3.47×10^6	-	16
	1.54×10^6	1.10	1.86×10^8	-	17

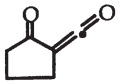
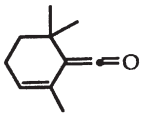
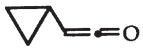
is more than six times the root-mean-square deviation of the 31 points upon which this correlation is based. The probability that such a deviant point would occur by chance is ca. 10^{-9}.

The ketene providing this errant point was generated by Norrish type II photoelimination of benzoylformic acid esters, and hydration of this ketene provided the enol of mandelic acid, as shown in eq. [6] (23). In acidic and neutral solutions, ketonization of this enol is considerably slower than hydration of the ketene, and both transient species could be easily observed and a rate constant for uncatalyzed hydration of the ketene could be quite firmly established. In basic solution, however, the rates of ketene hydration and enol ketonization became comparable. In such a situation, assignment of rate constants to molecular processes becomes notoriously difficult (24), and it now seems likely that the hydroxide-ion catalyzed process then believed to be ketene hydration was actually enol ketonization, with ketene hydration occurring only in the more basic region not investigated. The true value of k_{HO} for this ketene would consequently be less than the number assigned, and that would move the errant point closer to the correlation line.

[6] 

© 2000 NRC Canada

Table 1 (*concluded*).

	1.40×10^{6}	-	7.53×10^{7}	-	**18**
	2.97×10^{-4}	2.32	1.04×10^{-1}	7.03	**19**
	3.04×10^{2}	2.58	2.48×10^{5}	-	**20**

[a] Ionic strength = 0.10 M

Fig. 1. Relationship between rate constants for the uncatalyzed, k_{uc}, and hydroxide-ion catalyzed, k_{HO}, hydration of ketenes in aqueous solution at 25°C. The triangle, representing phenylhydroxyketene, is not included in the correlation that produces the line drawn through the data.

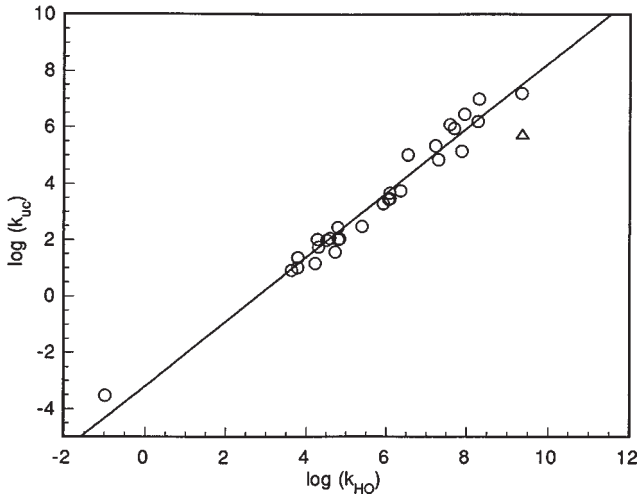
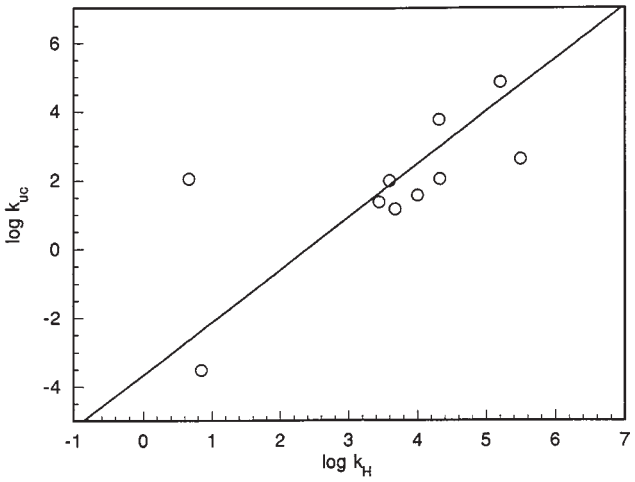


Fig. 2. Relationship between rate constants for the uncatalyzed, k_{UC}, and hydronium-ion catalyzed, k_H, hydration of ketenes in aqueous solution at 25°C.

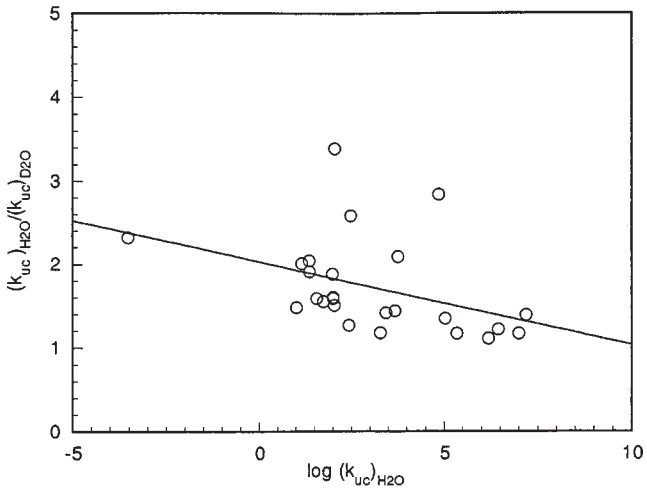


Isotope effects

The solvent isotope effects on uncatalyzed ketene hydration generated by the measurements made here in H_2O and D_2O solution, plus other values of this isotope effect determined in wholly aqueous solution available from the literature, are assembled in Table 1 and are displayed in Fig. 3. Although there is a fair amount of scatter, these isotope effects do appear to increase in strength with decreasing ketene reactivity as measured by $\log(k_{uc})_{H_2O}$; linear least squares analysis gives $(k_{uc})_{H_2O}/(k_{uc})_{D_2O} = (2.03 \pm 0.18) - (9.92 \pm 4.60) \times 10^{-2} \log(k_{uc})_{H_2O}$.[4]

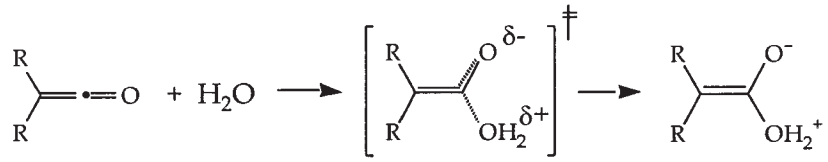
It may be seen that these isotope effects are all rather weak: the strongest is only $k_H/k_D = 3.4$ and most are less than $k_H/k_D = 2.0$. Much stronger isotope effects would be expected for the electrophilic reaction mechanism of eq. [3] in which water is acting as an acid delivering a proton to the β-carbon atom of the ketene. In addition to the sizeable primary isotope effect component expected for proton transfer to carbon, this mechanism would produce a secondary effect

Fig. 3. Solvent isotope effects on uncatalyzed ketene hydration in wholly aqueous solution at 25°C.



[4] This analysis was performed using simple weighting with uncertainty in $(k_{uc})_{H_2O}/(k_{uc})_{D_2O}$ only.

© 2000 NRC Canada

[7] 

in the normal direction ($k_H/k_D > 1$) generated by solvation of the hydroxide ion being formed in this reaction (25). Strong isotope effects consistent with this expectation have in fact been observed for such reactions in other systems, e.g., $k_H/k_D = 7.5$ for hydron transfer from water to the β-carbon atom of isobutyrophenone enolate ion (26), $k_H/k_D = 6.5$ to 9.1 for the corresponding reactions of a series of ynolate ions (12), and $k_H/k_D = 7.1$ for that of the enolate dianion of fluorene-9-carboxylic acid (16). The present isotope effects therefore argue against an electrophilic mechanism for uncatalyzed ketene hydration.

These isotope effects, on the other hand, are consistent with a nucleophilic mechanism. The simplest variant of such a mechanism would involve a single water molecule and give a zwitterionic product, as shown in eq. [7]. Since no bonds to isotopically substituted hydrogen are broken or made in this process, there would be no primary component in the isotope effect on such a process. There would, however, be two secondary components: one produced by solvation of the negative charge being generated on the ketene oxygen atom and another produced by the change from neutral to positively-charged oxygen-hydrogen bonds in the attacking water molecule. The maximum value of the latter secondary component can be estimated as $1/\ell^2$, where $\ell(= 0.69)$ is the fractionation factor for a fully positively charged oxgyen-hydrogen bond (25*b*). This gives $(k_H/k_D)_{max} = 2.1$. It is more difficult to estimate the other one of these secondary isotope effect components because, although it is known that a fully negatively charged oxygen atom, such as that in the hydroxide ion, is solvated by three water molecules whose solvating oxygen-hydrogen bonds have fractionation factors $\phi \cong 0.7$ (25), the negative charge in this case is partly delocalized into the ketene double bond and the rest of the molecule. It is likely, however, that this secondary component can contribute as much as another factor of two, raising the overall maximum value to $k_H/k_D = 4$ and easily accommodating the range of isotope effects listed in Table 1.

In addition to the reaction mechanism of [eq.] 7 giving a zwitterionic product, other nucleophilic mechanisms may be written in which the zwitterion is avoided by proton transfer from the attacking water to the ketene oxygen atom through a cyclic array of several intervening water molecules. Such mechanisms are favored by *ab initio* calculations (27) and there is evidence that the hydration of ketenes in organic solvents involves more than one water molecule (28), although, of course, in purely aqueous solution the reaction order in water cannot be determined. At any rate, protons are transferred in such mechanisms, but it is unlikely that this will add much of a primary component to the overall isotope effect. In a proton transfer such as this, where the transfer is between electronegative atoms and is accompanied by heavy-atom reorganization, protonic and heavy-atom motion appear to be uncoupled, with proton transfer taking place in a rapid step either before or after the heavy-atom reorganization; protonic motion consequently does not contribute to the rate-determining reaction coordinate, and there is, therefore, no primary isotope effect (29). Even in situations where proton transfer is isolated and the only heavy-atom motion is diffusional encounter of proton donor and acceptor or separation of proton transfer products, proton transfer is not fully rate-determining and solvent isotope effects are small (30). Cyclic ketene hydration mechanisms avoiding zwitterionic products are therefore likely to show small, if any, primary isotope effects. Neutralization of the zwitterionic charge, moreover, will diminish the secondary effects produced by charge generation as described above, and the overall solvent isotope effects will be small, just like those for the zwitterionic mechanism. Small isotope effects should therefore be characteristic of uncatalyzed ketene hydration proceeding by nucleophilic attack of water on the ketene carbonyl carbon atom, no matter what the detailed reaction mechanism is.

Acknowledgements

We wish to thank Professor S. D. Christian for his generosity in providing us with a computer program that performs linear least squares analysis on data with both dependent and independent variables subject to error. We are also grateful to the Natural Sciences and Engineering Research Council of Canada for financial support of this work.

References

1. T.T. Tidwell. Ketenes. Wiley–Interscience, New York, 1995. pp. 571–587.
2. T.T. Tidwell. Acc. Chem. Res. **23**, 273 (1990).
3. J. Andraos. M.Sc. Thesis, University of Toronto, Toronto. 1989.
4. J. Andraos, Ph.D. thesis, University of Toronto, Toronto. 1992.
5. Y. Chiang, M. Hojatti, J.R. Keeffe, A.J. Kresge, N.P. Schepp, and J. Wirz. J. Am. Chem. Soc. **109**, 4000 (1987).
6. J. Andraos, Y. Chiang, C.-G. Huang, A.J. Kresge, and J.C. Scaiano. J. Am. Chem. Soc. **115**, 10605 (1993).
7. J. Andraos and A.J. Kresge. J. Photochem. Photobiol. A: Chem. **57**, 165 (1991).
8. Y. Chiang, A.J. Kresge, and V.V. Popik. J. Chem. Soc., Perkin 2, 1107 (1999).
9. A.D. Allen, A.J. Kresge, N.P. Schepp, and T.T. Tidwell. Can. J. Chem. **65**, 1719 (1987).
10. J. Andraos, Y. Chiang, S.J. Eustace, A.J. Kresge, S.W. Paine, V.V. Popik, and K. Sung. Can. J. Chem. **77**, 459 (1999).
11. J. Andraos and Y. Chiang. Unpublished work.
12. Y. Chiang, A.J. Kresge, and V.V. Popik. J. Am. Chem. Soc. **117**, 9165 (1995).
13. Y. Chiang, E.A. Jefferson, A.J. Kresge, and V.V. Popik. J. Am. Chem. Soc. **121**, 11330 (1999).
14. B. Urwyler and J. Wirz. Angew. Chem. Int. Ed. Engl. **29**, 790 (1990).
15. J.-I. Kim, B. Urwyler, and J. Wirz. J. Am. Chem. Soc. **116**, 954 (1994).

© 2000 NRC Canada

16. J. Andraos, Y. Chiang, A.J. Kresge, and V.V. Popik. J. Am. Chem. Soc. **119**, 8417 (1997).
17. Y. Chiang, H.-X. Guo, A.J. Kresge, and O.S. Tee. J. Am. Chem. Soc. **118**, 3386 (1996).
18. Y. Chiang, A.J. Kresge, V.A. Nikolaev, and V.V. Popik. J. Am. Chem. Soc. **119**, 11183 (1997).
19. A.D. Allen, A. Stevenson, and T.T. Tidwell. J. Org. Chem. **54**, 2843 (1989).
20. A.D. Allen, J. Andraos, A.J. Kresge, M.A. McAllister, and T.T. Tidwell. J. Am. Chem. Soc. **114**, 1878 (1992).
21. J. Andraos, A.J. Kresge, and N.P. Schepp. Can. J. Chem. **73**, 539 (1995).
22. D. York. Can. J. Phys. **44**, 1079 (1966); S.D. Christian and E.E. Tucker. J. Chem. Ed. **61**, 788 (1984); S.D. Christian, E.E. Tucker, and E. Enwall. Am. Lab. (Fairfield, Conn.) **18**, (16) 41 (1986).
23. Y. Chiang, A.J. Kresge, V.V. Popik, and N.P. Schepp. J. Am. Chem. Soc. **119**, 10203 (1997).
24. R. Bonneau, J. Wirz, and A.D. Zuberbühler. Pure Appl. Chem. **69**, 979 (1997); J. Andraos. Can. J. Chem. **77**, 565 (1999).
25. (*a*) V. Gold and S. Grist. J. Chem. Soc. Perkin 2, 89 (1972); (*b*) W.J. Albery. *In* Proton transfer reactions. *Edited by* E.F. Caldin and V. Gold. Chapman and Hall, London. 1975, Chap. 9; A.J. Kresge, R.A. More O'Ferrall, and M.F. Powell. *In* Isotopes in organic chemistry. Vol. 7. *Edited by* E. Buncel and C.C. Lee. Elsevier, Amsterdam. 1987, Chap. 4.
26. Y. Chiang, A.J. Kresge, and P.A. Walsh. Z. Naturforsch. **44a**, 406 (1989).
27. M.T. Nguyen and A.F. Hegarty. J. Am. Chem. Soc. **106**, 1552 (1984); J. Andraos, A.J. Kresge, M.R. Peterson, and I.G. Csizmadia. J. Mol. Struct. (Theochem), **232**, 155 (1991); J. Andraos and A.J. Kresge. J. Mol. Struct. (Theochem), **233**, 165 (1991); M.A. McAllister, A.J. Kresge, and I.G. Csizmadia. J. Mol. Struct. (Theochem), **258**, 399 (1992); P.N. Skancke. J. Phys. Chem. **96**, 8065 (1992); M.T. Nguyen and G. Raspoet. Can. J. Chem. **77**, 817 (1999).
28. P.J. Lillford and D.P.N. Satchell. J. Chem. Soc. B, 889 (1968); D.P.N. Satchell and R.S. Satchell. Chem. Soc. Rev. **4**, 231 (1975); N.L. Poon and D.P.N. Satchell. J. Chem. Soc. Perkin Trans. 2, 1381 (1983); N.L. Poon and D.P.N. Satchell. J. Chem. Soc. Perkin Trans. 2, 1485 (1986).
29. C.G. Swain, D.A. Kuhn, and R.L. Schowen. J. Am. Chem. Soc. **87**, 1553 (1965); R.L. Schowen. Prog. Phys. Org. Chem. **9**, 275 (1972); R. Eliason and M.M. Kreevoy. J. Am. Chem. Soc. **100**, 7037 (1978).
30. N.Å. Bergman, Y. Chiang, and A.J. Kresge. J. Am. Chem. Soc. **100**, 5954 (1978); M.M. Cox and W.P. Jencks. J. Am. Chem. Soc. **100**, 5956 (1978); H. Fischer, F.X. DeCandis, S.D. Ogden, and W.P. Jencks. J. Am. Chem. Soc. **102**, 1340 (1980); M.M. Cox and W.P. Jencks. J. Am. Chem. Soc. **103**, 572 (1981).

© 2000 NRC Canada

COMMUNICATIONS

Reductive deposition of Au^{3+}(aq) on oxidized silicon surfaces

Şefik Süzer and Ömer Dag

Abstract: X-ray photoelectron spectroscopy (XPS) is used to determine the oxidation state of gold deposited from an aqueous solution of $AuCl_4^-$ on to various oxidized surfaces of silicon. Although the observed Au4f signal decreased with the thickness of the oxide layer, the oxidation state of Au was determined as 0 for all the samples analyzed. From the angular dependence of the Si2p and Au4f signals it was determined that Au is deposited on top of the oxidized surfaces of metallic silicon. It is postulated that from an aqueous solution of $AuCl_4^-$, gold would deposit in its zerovalent form on to any surface due to its large and positive electrochemical reduction potential ($\varepsilon^\circ_{red}(Au^{3+}/Au)$ = +1.50 V) and the substrate plays a role only in providing active deposition sites. To further support the proposal, it is shown that the same process takes place even in inert and hydrophobic polypropylene substrates. Similarly, it is also shown that more gold deposits if the surface of the polypropylene is made less hydrophobic (but probably more active) via the industrially used corona discharge treatment.

Key words: XPS, gold, electroless deposition, oxidized silicon surface.

Résumé : On a utilisé la spectroscopie photoélectronique aux rayons X pour déterminer l'état d'oxydation de l'or déposé à partir d'une solution aqueuse de $AuCl_4^-$ sur diverses surfaces oxydées de silicium. Même si le signal observé pour Au4f diminue avec l'épaisseur de la couche d'oxyde, on a déterminé que l'état d'oxydation de l'or est égal à zéro pour tous les échantillons analysés. En se basant sur la dépendance angulaire des signaux Si2p et Au4f, on a déterminé que l'or se déposé au sommet des surfaces oxydées du silicium métallisé. On a fait l'hypothèse que, à partir d'une solution aqueuse de $AuCl_4^-$, l'or se déposerait dans sa forme zérovalente sur toutes les surfaces en raison de son potentiel de réduction électrochimique élevé et positif [$\varepsilon^\circ_{red}(Au^{3+}/Au)$ = +1,50 V]. Pour appuyer cette hypothèse, on montre que le même processus se produit même dans des substrats inertes et polypropyléniques hydrophobes. De la même manière, on a démontré qu'il y a plus d'or qui se dépose si la surface de polypropylène est rendue moins hydrophobe (mais probablement plus réactive) par le biais d'un traitement industriel par effluve.

Mots clés: spectroscopie photoélectronique à rayons X, dépôt sans électrode, surface de silicium oxydée.

Introduction

Interest in the chemistry of gold has renewed due especially to the ability of molecular self-assembly of aliphatic thiols on gold colloids (1) and also to form clusters in nm scales with potentially useful optical, optoelectronic, and material properties (2–4). Successful methods of preparation usually involve vapour-deposition or deposition from solution via chemical and (or) electrochemical routes. An electroless deposition of zerovalent gold nano-clusters was reported using electroactive poly(3-alkylthiophenes) from a solution of the polymer and $AuCl_4^-$ in nitromethane (5). Similar studies were reported using other electroactive polymers, such as, polyaniline and polypyrrole (6). The same group later reported on the uptake of gold and palladium from acidic solution of $AuCl_3$ and $PdCl_2$ using electroactive polymer-SiO_2 nano-composites (7). In a recent study it was claimed that porous silicon could be utilized for reductive deposition of gold nano-clusters again from an aqueous solution $AuCl_4^-$ (8). In our XPS investigation of metal ions deposited on the surface of silica tubes for atom-trapping atomic absorption spectrometric determinations, we had also reported that Au was deposited in its zerovalent state both from the vapour phase of the flame and also from the aqueous solution of $AuCl_4^-$ (9). In a later study in which we had also examined Mn and Bi, we claimed that reductive deposi-

Received November 16, 1999. Published on the NRC Research Press web site on March 27, 2000

Ş. Süzer[1] and Ö. Dag. Bilkent University, Chemistry Department, 06533 Ankara, Turkey.

[1]Author to whom correspondence may be addressed. Telephone: 90-312-266-4946. Fax: 90-312-266-4579. e-mail: suzer@fen.bilkent.edu.tr

© 2000 NRC Canada

Table 1. XPS data of the $AuCl_4^-$ deposited from a 10^{-5} M aqueous solution on to silicon with different oxide thickness and polypropylene substrates.

Sample	Binding energy (eV) and atomic abundances (in parenthesis)				
		Si2p			
	$Au4f_{7/2}$	Si°	Si^{4+}	C1s	O1s
Si/SiO_x (reference)	—	99.7	102.4[a]		
		(0.78)	(0.22)		
Si/SiO_2 (~3 nm)	84.0	99.7	103.3[a]		
	(0.03)	(0.57)	(0.43)		
Si/SiO_2 (~5 nm)	84.0	99.7	103.7[a]		
	(0.02)	(0.25)	(0.75)		
Si/SiO_2 (~10 nm)	84.0	99.7	104.3[a]		
	(0.01)	(0.12)	(0.88)		
PP (as is)	84.0	—	—	285.0	532.0
	(0.001)			(1.00)	(0.06)
PP (corona treated)	84.0	—	—	285.0	532.0
	(0.0005)			(1.00)	(0.15)

[a]The energy difference between the Si^0 and Si^{4+} levels (the chemical shift) increases as the oxide layer becomes thicker due to the differential charging of the layers (12).

tion of gold was mainly dictated by its electrochemical reduction potential rather than the properties of the substrate (10). In this contribution we demonstrate this property of gold by depositing zerovalent gold from aqueous $AuCl_4^-$ solution on to different substrates.

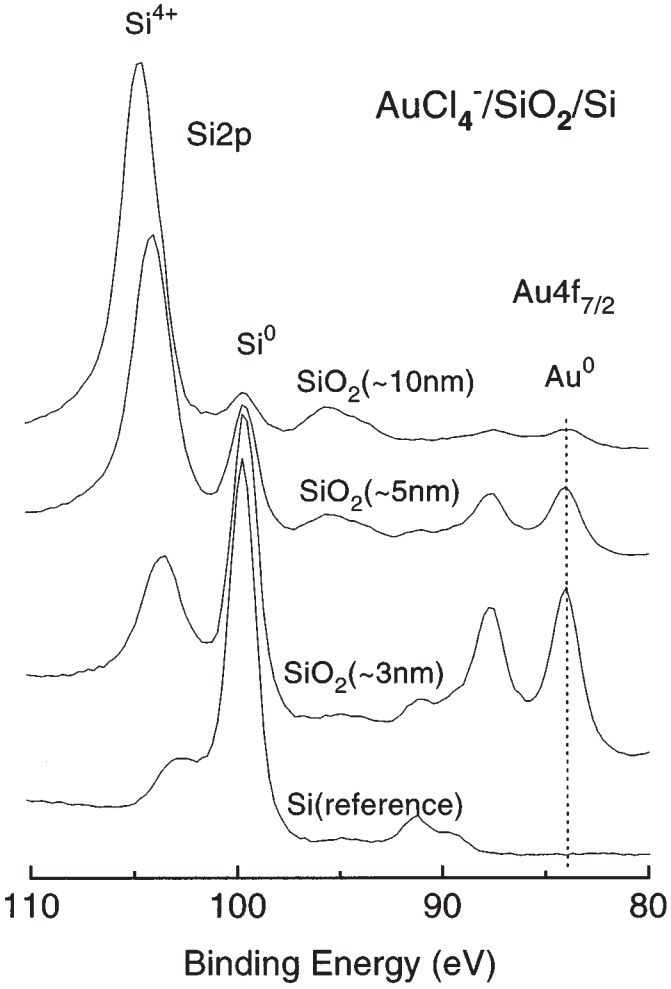
Experimental

Si wafers with their polished surfaces are used to deposit gold from a dilute ca. 10^{-5} M aqueous solution of $AuCl_4^-$. Si samples were cut into 5 × 15 mm slices and cleaned by 10% HF before thermal treatment and analysis. Different oxide thicknesses were obtained by heating the substrate in air at different temperatures or for different periods. The substrates were then immersed into the solution for 10 h without stirring after which they were washed with acetone, dried in air, and inserted into the spectrometer. A Kratos ES300 spectrometer with MgK X-rays was used for XPS analysis. The X-ray anode power is kept below 40 W to reduce the possibility of reduction under severe X-ray bombardment (11). SEM images were obtained using a Jeol 6400 electron microscope.

Results and discussion

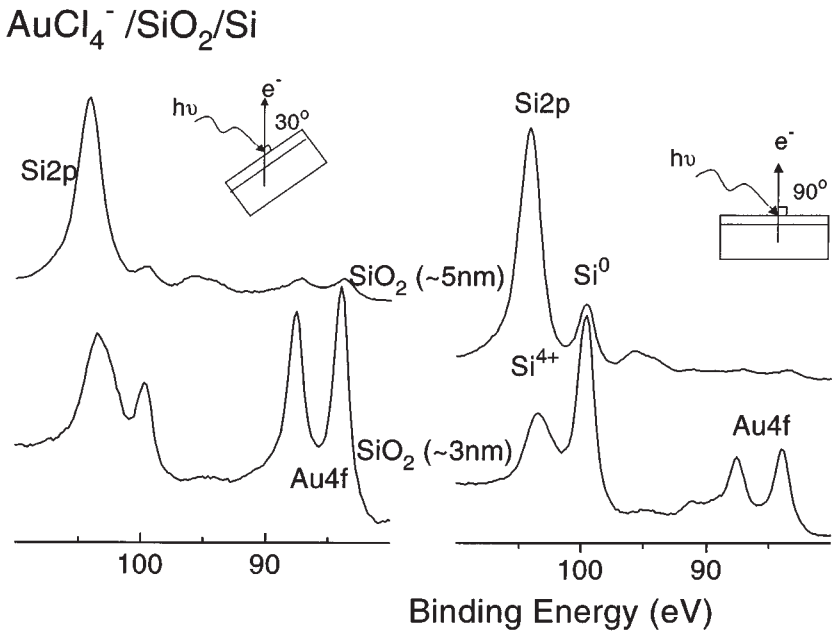
Figure 1 displays the Si2p and Au4f region of the XPS spectra of gold deposited on to silicon wafers containing approximately 3, 5, and 10 nm oxide layers and the relevant data are given in Table 1. One of the relevant observations in this investigation is that the oxidation state of gold is zero in all samples. Secondly, it is observed that the Au4f signal decreases as thickness of the oxide layer is increased. At normal electron take-off angle, the sampling depth of XPS using the MgKα X-rays is around 10 nm which can be further reduced by decreasing this electron take-off angle (11, 12). Figure 2 displays Si2p and Au4f signals recorded at normal (90°) and 30° electron take-off angles from two gold deposited samples containing ca. 3 and 5 nm oxide layers,

Fig. 1. Si2p–Au4f region of the XPS spectra of oxidized silicon surfaces containing gold deposited from a 10^{-5} M aqueous solution of $HAuCl_4$. A spectrum of a reference Si is also given for comparison.



© 2000 NRC Canada

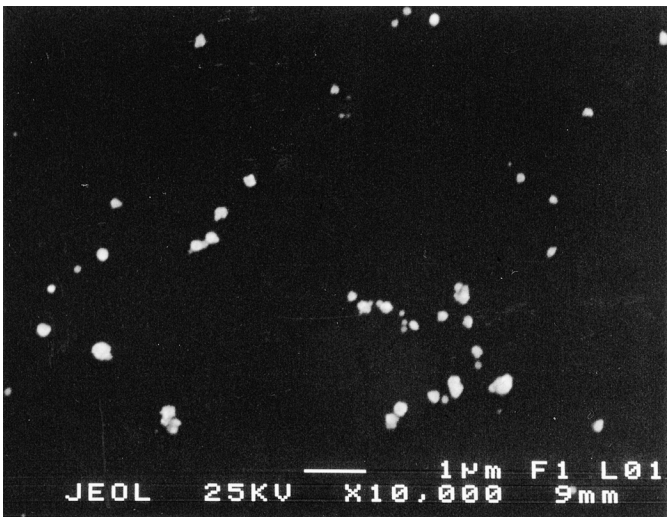
Fig. 2. Si2p–Au4f region of XPS spectra of two samples recorded at two different take-off angles.



respectively. As can be seen from the figure the intensity of the $Si^0$2p signal goes down and the intensity of the Si^{4+}2p and the $Au^0$4f signals go up indicating that Au is on top of the Si^{4+} layer and is not in direct contact with the underlying Si^0 substrate. The SEM image of the samples indicate that gold is deposited on the surface of the substrate as colloidal particles of varying sizes of less than 100 nm as shown in Fig. 3.

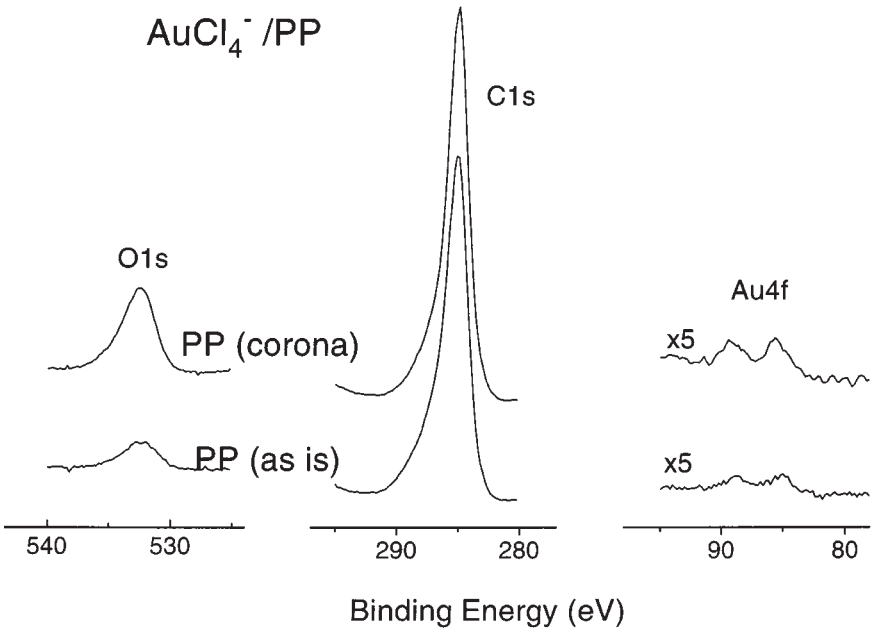
Two important questions arise: (*i*) why does gold deposit in its zerovalent state as opposed to deposition in ionic form, and (*ii*) why do we get seemingly more deposition when we have a thinner oxide layer? The first can be related to the large and positive reduction potential of Au^{3+}, $\varepsilon^{\circ}_{red}(Au^{3+}/Au)$ = +1.50 V in aqueous solutions which is inherent to gold. The second, however, must be related to the activity of the substrate surfaces (voids, defects, pores, reduction centres, or domains etc.). Since the thicker oxide layers are obtained by the corresponding longer heating/annealing times the number of active sites must also be diminished during this process. Hence we propose that gold would deposit as zerovalent form its aqueous solution on to any substrate as long as there are active reducing sites. This of course brings the more difficult question related to the nature of the surface reducing agents at this point which we can only speculate about. The role of the substrate surface is only important, if active sites are present or created which may facilitate this deposition. As a result the claim of Coulthard et.al. (8) that porous silicon is utilized as a reducing agent for reductive deposition of gold must be interpreted as the porous silicon providing ample active sites. This point is further supported by our observation that this deposition even takes place on relatively inert and hydrophobic substrates like polyethylene and (or) polypropylene as shown in Fig. 4. It is also interesting that relatively more gold is deposited if the surface of the polypropylene is made less hydrophobic

Fig. 3. SEM image of gold deposited on silicon containing an approximately 5 nm oxide layer.



© 2000 NRC Canada

Fig. 4. O1s, C1s, and Au4f regions of XPS spectra of gold deposited from a 10^{-5} M aqueous solution of $HAuCl_4$ on polypropylene and corona-treated polypropylene.



via the corona treatment which increases the number of -COH (hydroxyl groups) as well as other active sites like defects on the surface (13) as also shown in Fig. 4. Further investigations are definitely needed to identify/clarify the mechanism of the process.

References

1. C.S. Weisbecker, M.V. Merritt, and G.M. Whitesides. Langmuir, **12**, 3763 (1996).
2. G. Schmid. Clusters and Colloids, VCH, Weinheim, 1994.
3. U. Kreibig and M. Vollmer. Optical properties of metal clusters. Springer, Berlin, 1995.
4. R.L. Whetten, M.N. Shafigullin, J.T. Khoury, T.G. Schaaff, I. Vezmar, M.M. Alvarez, and A. Wilkonson. Acc. Chem. Res. **32**, 397 (1999).
5. M.S.A. Abdou and S. Holdrich. Chem. Mater. **8**, 26 (1996).
6. K.G. Noeh, T.T. Young, N.T. Looi, E.T. Kang, and K.L. Tan. Chem. Mater. **9**, 2906 (1997).
7. K.G. Noeh, K.K. Tan, P.L. Goh, S.W. Huang, E.T. Kang, and K.L. Tan. Polymer, **40**, 887 (1999).
8. I. Coulthard, S. Degen, Y.-J. Zhu, and T.K. Sham. Can. J. Chem. **76**, 1707 (1998).
9. Ş. Süzer, N. Ertas, S. Kumser, and O.Y. Ataman. Appl. Spectrosc. **51**, 1537 (1997).
10. Ş. Süzer, N. Ertas, and O.Y. Ataman. Appl. Spectrosc. **53**, 479 (1999).
11. D. Briggs and M.P. Seah. Practical surface analysis. Vol. 1. *In* Auger and X-ray photoelectron spectroscopy. 2nd ed. Wiley, Chichester. 1996.
12. S. Iwata and A. Ishizaka. J. Appl. Phys. **79**, 6653 (1996).
13. Ş. Süzer, A. Argun, O. Vatansever, and O. Aral. J. Appl. Polym. Sci. **74**, 1846 (1999).

© 2000 NRC Canada

ERRATUM

Erratum: Assisted hydrolysis of *cis*-2-(3-phenylthioureido)cyclopentane-carbonitrile in alkaline solution. Solvent dependent switch from hydrolysis to rearrangement of the iminothiooxopyrimidine intermediate

Ergun Atay, Iva B. Blagoeva, Francis L. Chubb, John T. Edward, Ivan G. Pojarlieff, and Maria M. Toteva

Ref.: Canadian Journal of Chemistry, 78: 84–94.

The interested reader should take note of the following addition

Acknowledgements

We also thank Dr. Diana Gash for preparing 2-aminocyclopentanecarbonitrile.

The authors apologize for the omission in the published paper.

Received March 20, 2000. Published on the NRC Research Press website on March 29, 2000.

E. Atay, I.B. Blagoeva, I.G. Pojarlieff, and M.M. Toteva. Institute of Organic Chemistry, Bulgarian Academy of Sciences, ul. Acad. G. Bonchev block 9, Sofia 1113, Bulgaria.
F.L. Chubb and J.T. Edward. Department of Chemistry, McGill University, 801 Sherbrooke St., Montreal, QC H3A 2K6, Canada.

© 2000 NRC Canada

Analysis of the electrode kinetics of Ni(II) reduction at the DME in the presence of nicotine

M.S. Crespo-Pinilla, A.B. Infante, and F. Mata-Pérez

Abstract: A study of the prewave of the Ni^{2+} – nicotine system was carried out under the experimental conditions when the influence of electroreduction of nicotine is negligible. The kinetics of Ni(II) reduction in nicotine media on the dropping mercury electrode were studied by direct current Tast polarography (DC_TP) via the determination of the Koutecky's parameter, χ and the influence of different variables was analyzed. An electrochemical study of the prewave was also made by using various polarographic techniques. Values of χ depend on the nicotine concentration, pH, ionic strength (ψ-effect), and on the nature of the supporting electrolyte. The αn product (α = transfer coefficient, n = number of electrons) and the stoichometric number,ν, were determined. The prewave is interpreted as a surface reaction, the main features of the mechanism being its catalytic nature. The discharge is a two electron step and reaction between species of opposite charge is rate-determining.

Key words: catalytic, prewave, polarography, nickel(II), nicotine.

Résumé : Opérant dans des conditions expérimentales dans lesquelles l'influence de l'électroréduction de la nicotine est négligeable, on a réalisé une étude du système Ni^{2+} – nicotine dans la prévague. Faisant appel à la polarographie en système Tast à courant direct (« DC_TP »), on a étudié la cinétique de la réduction du Ni(II) dans un milieu de nicotine sur une électrode de mercure tombante par le biais de la détermination des paramètres χ de Koutecky et on a analysé l'influence des diverses variables. On a aussi effectué une étude électrochimique dans la prévague en faisant appel à diverses techniques polarographiques. Les valeurs de χ dépendent de la concentration de nicotine, du pH, de la force ionique (effet ψ) et de la nature de l'électrolyte de support. On a déterminé le produit αn (α = coefficient de transfert; n = nombre d'électrons) et le nombre de stoechiométrie,ν. On interprète la prévague en termes d'une réaction de surface dont le mécanisme est caractérisé principalement par une nature catalytique, une décharge qui se fait en une étape de deux électrons et pour lequel l'étape qui détermine la vitesse est la réaction entre des espèces de charges opposées.

Mots clés : catalyse, prévague, polarographie, nickel(II), nicotine.

Introduction

Electrocatalysis of metal ion reduction on mercury by adsorbed ligands has been the subject of a recent review (1) from which a number of important features can be noted. First, the method of direct current polarography has been the most popular as well as being the most informative method (especially from the theoretical aspect). Usually the limiting catalytic current is analyzed, since it is not complicated by the kinetics of electron transfer. Moreover, using the DME, it is possible to exclude the stage of metal crystallization, so that attention can be focused on the catalytic reaction. Besides, in polarography, the catalytic process is frequently separated, in its potential, from the noncatalytic process, resulting in the formation of so-called prewaves. In this way, Ni^{2+}–pyridine is one of the model systems. That system has been studied by us (2) and our experience with it and other systems (3, 4) supports the use of the Kouctecky's parameter, χ, as an experimental rate constant. The study of the dependence of χ on the different experimental variables is a good method for understanding the mechanism of this type of reaction.

There is a previous work of Moskatov et al. (5) about the ultrasensitive detection of nicotine, Nc, via the electroreduction of nickel(II) in its presence. A later study (6) deals with the determination of the stability constant of the nickel(II) – nicotine complex, and involves a study of the influence of both the Nc and Ni^{2+} concentration and also of the pH on the catalytic current. A qualitative scheme for the reaction has also been proposed.

However, the kinetics and mechanism of the formation of the electrochemically active complex which is responsible for the appearance of the prewave have not been explained satisfactorily. Hence, the behaviour of Ni^{2+} species at the dropping mercury electrode (DME) in media containing nicotine species is even now an open question. This work was undertaken to clarify the question by studying the kinetics of the Ni^{2+} – Nc system.

Received June 17, 1999. Published on the NRC Research Press website on April 19, 2000.

M.S. Crespo-Pinilla, A.B. Infante, and F. Mata-Pérez.[1]
Departamento de Química Física, Facultad de Ciencias, Universidad de Valladolid, E - 47005 - Valladolid, Spain.

[1]Author to whom correspondence should be addressed. Fax: 34-983-423013.

Experimental

The experimental conditions were optimized to resolve both the prewave and prepeak of Ni^{2+} induced by Nc. Chemicals used were Merck ($Ni(NO_3)_2$) and Panreac ($LiNO_3$, $NaNO_3$, KNO_3, $CsNO_3$, KOH, and HNO_3) of analytical grade. Nicotine (Merck for synthesis) was purified by vacuum distillation

© 2000 NRC Canada

(about 10 mmHg) at 150ºC. Solutions were prepared from water purified by passage through a Milli-Q system from Millipore. Experiments were performed in the presence of excess Ni^{2+} species ($5.0 \times 10^{-3} - 2.5 \times 10^{-2}$ mol dm^{-3}), with the concentration of Nc ranging from 1.0×10^{-5} to 1.0×10^{-4} mol dm^{-3}. An excess of electrolyte in the solutions was achieved by using KNO_3 (alternatively $LiNO_3$, $NaNO_3$, or $CsNO_3$), providing a constant ionic strength condition, I (0.06–0.2 mol dm^{-3}). To avoid hydrolysis of Ni^{2+}, the pH of the solutions was kept between 3.0 and 8.0. The acidity was adjusted to the desired values by using very dilute solutions of HNO_3 and KOH. Oxygen was removed from the probe solutions with a stream of purified nitrogen for 15 min (and for a further 1 min before each new experiment). The polarographic cell was thermostated from 20 to 35 (±0.1)ºC.

The electrode process was studied by using DC tast (DC_TP), normal pulse (NDP), and differential pulse polarography (DPP). All techniques were implemented with a Tacussel microprocessor unit connected to an automatic polarographic stand equipped with a DME, a Pt wire auxiliary electrode, and a SCE as the reference electrode. The drop time was maintained mechanically at 3.5 s except when studying its effect in DC_TP, when it was changed from 0.5–3.5 s. The potential scan rate was 5 mV/s and the voltage range was between –0.1 and –1.6 V. The DPP pulse amplitude was 50 mV. pH measurements were made with a Radiometer 51 instrument (pH meter, accuracy: ±0.01 pH units).

Because of the sensitivity of catalytic prewaves to the experimental conditions, the heights of both the prewave and prepeak was recorded several times under a set of given conditions. The agreement between the experimental values was, in general, satisfactory and their average was taken.

Results

Nc proved to be polarographically inactive in the supporting electrolyte, viz. KNO_3 up to 0.5 mol dm^{-3} at pH in the range 3.0–8.0. Addition of Ni^{2+} to the electrolyte caused Nc to induce one Ni^{2+} prewave in DC_TP, however. The half-wave potential ($E_{1/2}$) for the prewave was –0.70 ± 0.02 V, compared to –1.13 ± 0.02 V for the reduction wave of Ni^{2+} in the absence of nicotine.

The temperature coefficients obtained for the prewave (9–15% deg^{-1}) point to the catalytic character of the prewave. Moreover, no dependence of i_k (limiting current for the prewave) on $h^{1/2}$ (h = corrected height of the mercury column) was found, which confirms that the prewave has an unambiguous catalytic character. The main Ni^{2+} wave is diffusion-controlled under the experimental conditions of this study. This was shown by the linear dependence of i_d (limiting current for the main wave) with $h^{1/2}$.

For these experiments, the height of the prewave was less than 20% of the height of the main Ni^{2+} wave. Under these circumstances, the kinetic or catalytic limiting currents are proportional to the concentration of the Ni^{2+} species which are responsible for the appearance of the main wave. Consequently, it was verified that i_k values vary linearly with the concentration of Ni^{2+}. The dependence of i_k on the drop life time, t, is also relevant. The values of log i vs. log t are straight lines for both the prewave and the main Ni^{2+} wave. From the slopes, the direct proportionality between i_d and $t^{1/6}$ (Ilkovic's equation) was verified, while it was found that the i_k values are proportional to $t^{2/3}$.

All our results support the catalytic character of the prewave. Also, the location of its $E_{1/2}$ value as compared with the main wave indicates that the prewave is due to Ni^{2+} complexes with Nc species, where Ni^{2+} is reduced at a potential lower than that required to reduce it in the Ni^{2+} complex present in the supporting electrolyte.

Increasing the stoichiometric concentration of Nc species in the solution raised the limiting current for the prewave to about 30% of the limiting current for the reduction wave of Ni^{2+} in the absence of Nc. This could be due to the limiting adsorption of Nc on the DME or, alternatively, to an autoinhibition effect (Nc absorbs strongly on the DME surface and therefore inhibits the electrode reaction). This behavior is contradictory with that of most reported prewaves for metal ions, where the maximum limiting current (at a high ligand catalyst concentration) virtually coincides with the limiting diffusion current for the metal ion concerned. A similar behavior has been observed for prewaves and prepeaks of Ni^{2+} in the presence of Nc by using NPP and DPP, respectively.

It seems reasonable to consider the appearance of a prewave as a special case of irreversibility of the overall wave. So, from our prior investigations (2, 3), the ratio i_k/i_d was taken as a function $F(\chi)$ of the Koutecky's parameter, χ (7, 8). In practice, the values of $F(\chi)$ were determined experimentally and the χ values were obtained by simulation using the following equation

$$[1] \qquad F(\chi) = \left(\frac{7\pi}{12}\right)^{\frac{1}{2}} \chi \exp\left(\frac{7}{12}\chi^2\right) erfc\left[\left(\frac{7}{12}\right)^{\frac{1}{2}} \chi\right]$$

The meaning of the parameter χ depends on the rate-determining step of the mechanism, explaining the appearance of the prewave. In all cases, χ actually has all the characteristics of an experimental rate constant; implying that we are employing a relaxation method. On the other hand, it is well known that the analysis of the influence of different variables (e.g., concentrations, pH, ionic strength, temperature, etc.) on the experimental rate constant is a usual method to elucidate the reaction mechanism.

Here, the Koutecky theory of polarographic kinetic currents can be applied with the assumption that the condition $[Nc]/K_2 << 1$ is realized, K_2 being the stability constant of the polarographically active compound (PAC), so that the following equation can be derived (9)

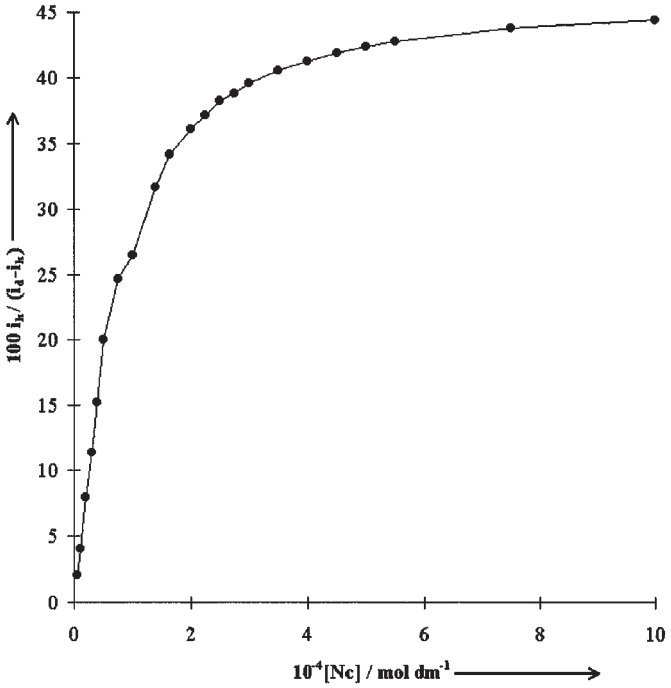
$$[2] \qquad \chi = \frac{i_k}{i_d - i_k} = \sqrt{\frac{12}{7}\frac{k_r t}{K_2}} \frac{[Nc]}{K_1 + [Nc]}$$

where K_1 and K_2 are the stability constants of the $[NiNc]^{2+}$ and $[NiNcNO_3]^{1+}$ complexes, respectively, and k_r is the rate constant of the rate-determining step (eq. [6]). The χ values are satisfactorily fitted by eq. [2], as Fig.1(*b*) shows, this being an additonal support of the mechanism that is proposed.

From the DC_TP records, the dependence of $i_k/(i_d - i_k)$ on the Nc concentration (in the range $0–10^{-3}$ mol dm^{-3}) was obtained (Fig. 1(*a*)). By using DPP, the peak currents increase with the Nc concentration (in the same range) with a curve

© 2000 NRC Canada

Fig. 1(*a*). Effect of the Nc concentration ($1.0 \times 10^{-5} - 1.5 \times 10^{-4}$ mol dm^{-3}) on the limiting current of the Ni^{2+} prewave, i_k, recorded by DC_TP. [Ni^{2+}] = 1.0×10^{-2} mol dm^{-3}. pH = 5.0. I = 0.1 mol dm^{-3} KNO_3. Temp = 25°C.



similar to Fig. 1(*a*). Accurate values of χ were obtained for the different concentrations of Nc. Analysis of these results (Fig. 1(*b*)) leads to the following equation

$$[3] \qquad \chi = \frac{a\,[\mathrm{Nc}]}{1 + b\,[\mathrm{Nc}]}$$

a = 4893.62

b = 15832.6

r_{xy} = 0.9966

For a PAC formed between the adsorbate $[Ni(H_2O)_x^{2+}]_{ES}$ and the depolarizer (Nc in this case), Čaja et al. (10) gave the following equation for Koutecky's parameter

$$[4] \qquad \chi = k\theta_{Nc}$$

where θ_{Nc} is the surface concentration on the DME of the depolarizer and k includes a number of parameters, e.g., the rate constant for the PAC formation and the ψ potential of the double layer. Equation [3] has the formal structure of the Langmuir isotherm and the χ values can be used for fitting the adsorption isotherm of Nc on the DME. Moreover, these results confirm our previous findings (vide supra) concerning the nature of the mechanism causing the prewave, explained via a surface process.

The sensitivity of the isotherm to experimental conditions, especially to the drop formation time, should be noted. This allows us to conclude that, under our experimental conditions, the Langmuir adsorption model is valid. In Fig. 1(*a*), the results actually fit to a linear function for [Nc] $\leq 1.0 \times 10^{-4}$ mol dm^{-3} (Henry's isotherm), which is consistent with a linear dependence of χ on the Nc concentration. For these circumstances, the reaction takes place partially or completely in the adsorption layer under the conditions of Henry's isotherm. On the other hand, the linear dependence of χ on $t^{1/2}$ (Fig. 2) strongly suggests that adsorption on the DME surface very quickly attains equilibrium (11). This fact supports the surface nature assumed for the PAC forming the prewave. A linear dependence of the limiting current, i_k, on the Ni^{2+} concentration was found (Fig. 3). This explains

Fig. 1(*b*). Dependence of Kouctecky's parameter χ on the Nc concentration at the same conditions.

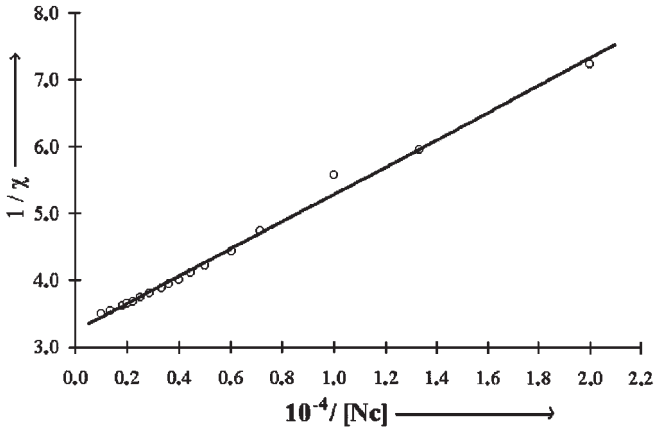
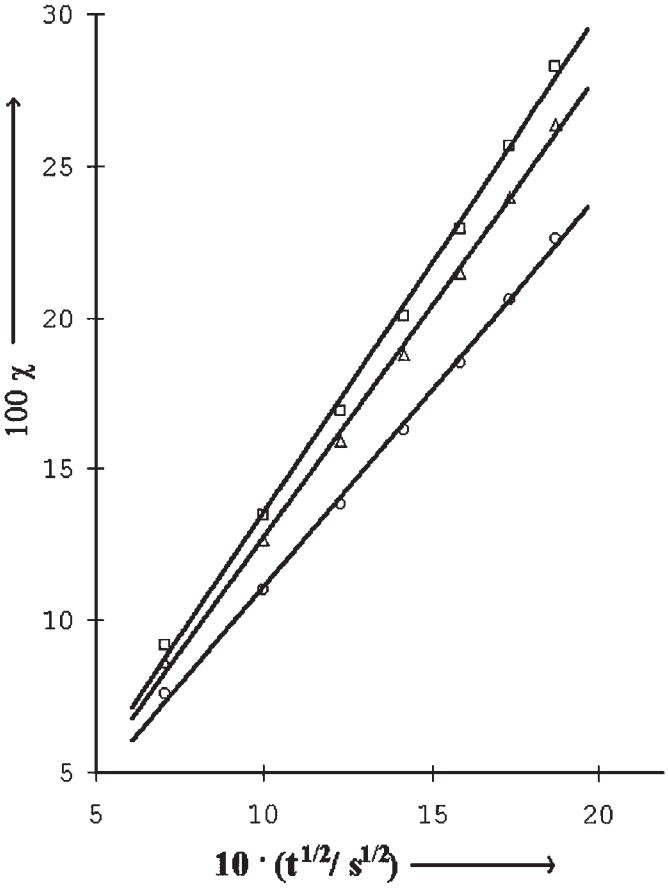
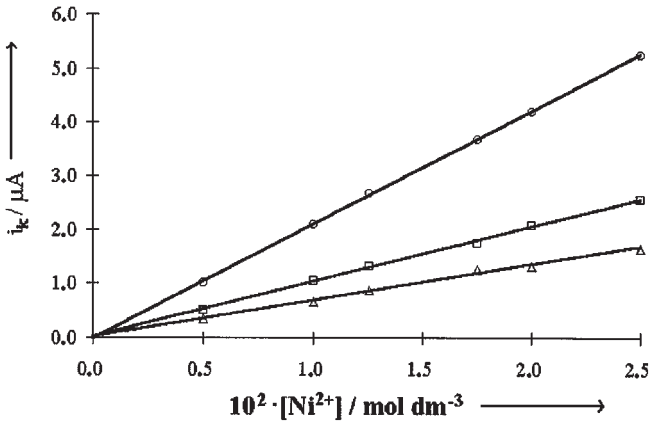


Fig. 2. Dependence of χ on the drop life time. [Ni^{2+}] = 1.0×10^{-2} mol dm^{-3}. pH = 5.0. Temp = 25°C. I = 0.1 mol dm^{-3} KNO_3. [Nc]: (○) 1.65×10^{-4}; (△) 3.5×10^{-4}; and (□) 7.5×10^{-4} mol dm^{-3}.



© 2000 NRC Canada

Fig. 3. Dependence of the prewave limiting current, i_k, on the Ni^{2+} concentration. pH = 5.0. I = 0.1 mol dm^{-3} KNO_3. Temp = 25°C. [Nc]: (△) 1.0 × 10^{-5}; (□) 2.0 × 10^{-5}; and (○) 5.0 × 10^{-5} mol dm^{-3}.



the fact that no changes were observed for the χ values (DC_TP) when the Ni^{2+} concentration was changed from 5.0 × 10^{-3} to 2.5 × 10^{-2} mol dm^{-3}.

In this work, the pH is affected by both the protonation of Nc and the hydrolysis of the Ni^{2+} species, the latter being important for pH > 8.0. All experiments were conducted in the range 5.0 < pH < 8.0. If one takes into account the pK_a values for Nc (12), under these conditions, both the alkaline form and the monoprotonated form of Nc are present in solution, with the latter increasing when the pH decreases. From the dependence of Koutecky's parameter, χ, on the activity, a_{H+} (Fig. 4), one can conclude that in the PAC the alkaline form of Nc is involved. On the other hand, given the distribution of the electronic charge density on the pyridine and pyrrolidine rings, the PAC could be adsorbed on the DME via the pyridinic N-atom. This is consistent with the existence of bridge compounds, Py-Ni^{2+} (13, 14), on the DME surface.

The dependence of χ on the ionic strength (I) was also studied in the range 0.06–0.2 mol dm^{-3}, KNO_3 being the supporting electrolyte. A tentative fit of ln χ vs. $\sqrt{I}/(1+\sqrt{I})$ was made by using Guggenheim's correction (15) of the Debye–Hückel theory. In Fig. 5(*a*), the fit function is given. These results strongly suggest the existence of a kinetic salt effect for the reaction. A value of about –11.5 was found for the $z_+ \times z_-$ product. The anomalously high value of this product could be the result of the limited validity of the Debye–Hückel–Guggenheim formula for interpreting the activity coefficients of reacting molecules and of the transition state. The unambiguous negative value of this product shows that the process responsible for the prewave is controlled by a reaction between two species of opposite charge.

A decrease in the kinetic limiting current (i_k) with an increase in the ionic strength reflects the ψ-effect on the rate of chemical reactions taking place in the immediate vicinity of the electrode. Figure 5(*b*) shows the plot of ln χ vs. ψ. The ψ values were taken from Russell's table (16) for the potential value (vs. SCE) of –0.90 ± 0.02 V. This potential corresponds to the limiting current for the prewave when serious interferences are not predicted (17). A charge of +1.04 was found for the PAC. Russell's table has been used by a

Fig. 4. Dependence of χ on proton activity. [Ni^{2+}] = 1.0 × 10^{-2} mol dm^{-3} KNO_3. Temp = 25°C. [Nc] = 1.0 × 10^{-3} mol dm^{-3}.

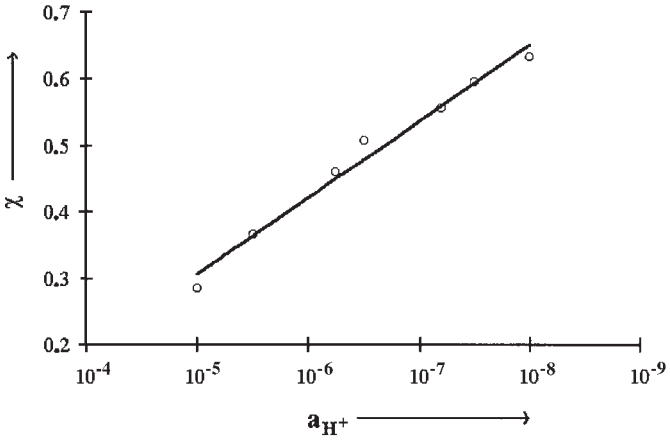
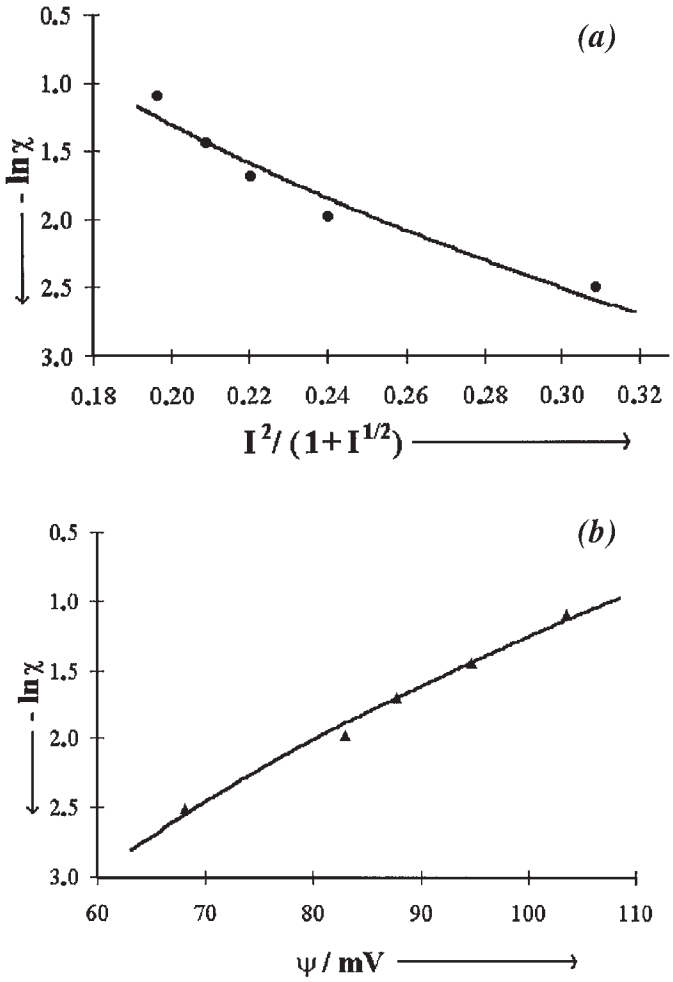


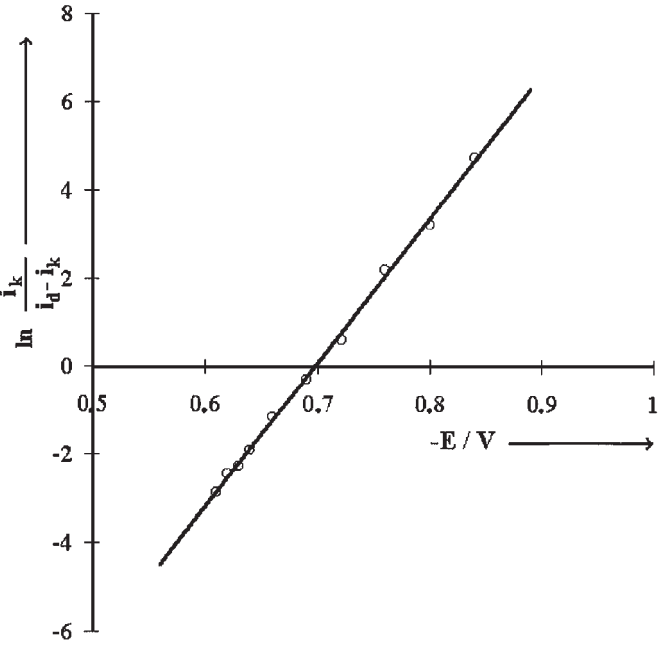
Fig. 5. Dependence of ln χ on: (*a*) the ionic strength (•), and (*b*) the potential of the Helmholtz plane (▲). [Nc] = 5.0 × 10^{-5} mol dm^{-3}. [Ni^{2+}] = 1.0 × 10^{-2} mol dm^{-3}. pH = 5.0. Temp = 25°C.



number of researchers. However, the ψ values of Russell's table were obtained for the mercury – aqueous NaF interface according to the Gouy–Champman theory, with the assumption

© 2000 NRC Canada

Fig. 6. Analysis of the irreversibility of the polarographic curve (DC_TP) for the prewave. [Ni $^{2+}$] = 1.0×10^{-2} mol dm^{-3}. pH = 5.0. I = 0.1 mol dm^{-3} KNO_3. Temp = 25°C. [Nc] = 4.5×10^{-3} mol dm^{-3}.



of no specific adsorption of sodium or fluoride ions. The adsorption of nicotine might drastically change the properties of the double layer. For all these reasons, the ψ values are only an approximation to the actual potential on the outer Helmholtz plane for a given electrolyte (KNO_3) under our experimental conditions. Hence, the preceding conclusions about the ψ-effect have to be taken with caution.

It is well known (18) that an increase in the concentration of anions of the supporting electrolyte, which are surface-active, gives rise to an increase in the limiting currents of the prewaves. Wroblowa et al. (19) have shown that the adsorption of NO_3^- is not important for $[NO_3^-] \leq 0.5$ mol dm^{-3}. Hence, at the experimental conditions of this work, the adsorption of NO_3^- on the DME will have little effect on the magnitude of Koutecky's parameter. The only relevant role of the anionic species of the supporting electrolyte appears to be the charge of the PAC. This may be due to the association of Ni^{2+} species with anions in the surface layer (8). The effect of the cation of the supporting electrolyte on the χ values is noticeable. The χ values increase when the concentration of MNO_3 (M = Cs^+, K^+, Na^+, and Li^+) is decreased. The magnitude of this effect is proportional to the inverse of the cation size, which is consistent with specific cation adsorption.

For comparative purposes, the effect of temperature on χ was studied. Both the activation enthalpy, $\Delta H^{\neq}$ (27.8 kJ mol^{-1}), and the activation entropy, $\Delta S^{\neq}$ (–166.5 J K^{-1} mol^{-1}), were determined for [Nc] = 1.0×10^{-3} mol dm^{-3}, the rest of the experimental conditions being the same as in Fig. 1. The magnitude of $\Delta H^{\neq}$ for gravity dropping conditions is smaller by using DC_TP, while the absolute values of $\Delta S^{\neq}$ undergoes an important increase. This fact means that adsorption also plays an important role in affecting the activation parameters.

Changes of the $E_{1/2}$ values with the drop time, t, were observed, which is a sign of the irreversibility of the electrode process responsible for the appearance of the prewave.

Consequently, the irreversibility of the polarographic curve was analyzed (20) by plotting $i_k/i_d - i_k$ vs. $-E$ (i_k = the prewave current for a given potential; i_d = the prewave limiting current). A linear profile was found in all cases (Fig. 6), this being characteristic of a fully irreversible process. From the slope of those plots, the product αn can be obtained, n being the number of electrons participating in the charge transfer process and α the transfer coefficient. If it is assumed that α = 0.5, from our findings, the n values range from 1.5 to 1.8. This means that an average value of b = 0.03 can be predicted for the slope of the Tafel equation, which is consistent with a catalytic mechanism in the prewave.

The overpotential, η, at a given potential, E, is defined as the difference between this potential and the reversible potential. η is taken as the potential at the point where the base line intersects the bottom part of the extrapolated slope of the prewave. The method described by Bard and Faulkner (21) was used to calculate the exchange current, i_o. It was verified that $i_d - i_k/i_k$ vs. η is a linear function in the Tafel region under our experimental conditions (the correlation coefficients being, in all cases, $r_{xy} > 0.99$). From the respective intercepts, the i_o values were obtained. Plots of ln i_o vs. ln $[Ni^{2+}]$ are linear. The slopes are 1.0, an additional positive feature of the analysis.

When $\eta \rightarrow 0$, the kinetic order of the rate-determining step, p, and the stoichometric number, ν, were determined (22). These findings mean that the step which controls the reaction is a bimolecular process and that it does not repeat itself in the mechanism.

Formal mechanism

The dependence of the χ values on the Nc concentration shows that charge transfer is not (23) the rate-determining step for the mechanism responsible for the appearance of the prewave. On the contrary, the form of eq. [3] is consistent with a surface origin of the prewave. Moreover, the dependence of χ on the nature of the cation species of the supporting electrolytes is an additional proof of this.

Figure 4 confirms that the alkaline form of Nc is the adsorbed species on the DME. From FTIR studies (11), it has been shown that the sulfur atom is attracted to the electrode surface by strong chemical interaction forces and not through electrostatic interactions, as proposed by Parsons and Symons (24). So, the Nc species is actually adsorbed on the electrode surface, ES (denoted by $[Nc]_{ES}$).

In a former paper (3), the mechanism explaining the main wave was discussed. It consists of diffusion and dehydration (acid catalyzed) by partial loss of water molecules of the $Ni(H_2O)_6^{2+}$ species, and the discharge of the $Ni(H_2O)_x^{2+}$ ($2 < x < 4$) species on the DME. For all systems previously studied, in the mechanisms explaining the origin of the prewaves, the $Ni(H_2O)_x^{2+}$ species is involved. The mechanism for the appearance of the prewave is stated as follows

© 2000 NRC Canada

[5] $[Ni(H_2O)_x^{2+}]_H + [Nc]_{ES} \rightleftarrows [Ni(H_2O)_{x-1}Nc^{2+}]_{ES} + H_2O$

[6] $[Ni(H_2O)_{x-1}Nc^{2+}]_{ES} + [NO_3^-]_H \xrightarrow{\text{slow}} [Ni(H_2O)_{x-2}NcNO_3^+]_{ES} + H_2O$

PAC

[7] $[Ni(H_2O)_{x-2}NcNO_3^+]_{ES} \xrightarrow{2e^-} Ni(Hg) + Nc + NO_3^- + (x-2)H_2O$

H = Helmholtz plane (reaction plane)
ES = Electrode surface

It consists of a reaction between $Ni(H_2O)_x^{2+}$ species and adsorbed Nc to give a compound (eq. [5]). Reactions of this type are well known (25) and they are very fast in the bulk solution. Hence, it is reasonable to expect that the step of eq. [5] almost instantaneously reaches equilibrium conditions. The assumption of the formation of this compound is supported by the existence of bridge Ni^{2+}-Py compounds on the DME surface (13, 14).

Čaja et al. (10) assume, for similar systems, that the rate-determining step is the reaction between hexaaquonickel ion in the bulk solution and the adsorbed amine on the DME surface. We think, however, that the surface nature of the prewave is not a conclusive proof of that formulation. In fact, when the alkaline form of the amine is the kinetically active species (e.g., pyridine and pyridine derivatives), the amine concentration at the Helmholtz plane equals the value of this magnitude at the surface electrode because the alkaline form of the amine has no ionic charge. So, the dependence of Koutecky's parameter, χ, on the surface concentration of amine may arise from this. On the other hand, Čaja et al. (10) have not taken into account the adsorption of Ni^{2+} species on the DME surface.

We have assumed that the rate-determining step is the reaction between $[Ni(H_2O)_x^{2+}]_{ES}$ species and nitrate ions at the Helmholtz plane (reaction plane) to give the PAC. This assumption is consistent with both the association of Ni^{2+}-NO_3^- on the (surface) layer (8) and that the adsorption of nitrate ions is not important under the experimental conditions of this work (19).

This formulation is also supported by the small magnitude of the reaction rates of the exchange reactions (10, 26). The latter is probably not enough to consider eq. [6] to be the rate-determining step. But there are some other reasons which argue for this, such as $p = 2$ for the molecularity of the rate-determining step. Also, activation entropy values which were constantly found to be negative support the assumption that eq. [6] is the rate-determinining step. Hence, eq. [6] is formulated involving two ionic species of opposite sign, consistent with the observed salt kinetic effect and also with the ψ-effect.

The experimental value of +1.04 for the electric charge of the PAC could be a consequence of the NO_3^- effect. On the other hand, the existence of Ni^{2+} coordination complexes, in which NO_3^- participates, has been confirmed (27).

The analysis of the irreversibility of the prewave provides certain values for the αn product, which points to a two-electron transfer reaction at the DME. This fact is consistent with a value of +1 for the ionic charge of the PAC in the formulation of eq. [7]. It should also be noted that the catalytic character of the prewave is implied in the formulation of this mechanism, because the discharge of the PAC regenerates the Nc and nitrate ions.

References

1. Ya.I. Tur'yan. J. Electroanal. Chem. **338**, 31 (1992).
2. F. Mata and M.S. Crespo. Z. Phys. Chem. (Leipzig). **260**, 1033 (1979).
3. F. Mata and M.S. Crespo. Z. Phys. Chem. (Leipzig). **260**, 1042 (1979).
4. R.M. Villamañan and F. Mata-Pérez. Can. J. Chem. **69,** 599 (1991).
5. I.I. Moskatov, Ya.I. Tur'yan, and V.N. Sirko. Izv. Vyssh. Uchebn. Zaved. Pishch. Tekhnol. **5**, 137 (1980).
6. Ya.I. Tur'yan and I.I. Moskatov. Zh. Obshch. Khim. **51**, 1412 (1981).
7. J. Weber and J. Koutecky. Collect. Czech. Chem. Commun. **20**, 980 (1955).
8. J. Koutecky and J. Cizet. Collect. Czech. Chem. Commun. **21**, 836 (1956); **50**, 196 (1956).
9. Ya.I. Tur'yan. Elektrokhimiya, **19**, 1615 (1983).
10. J. Čaja, H.C. McDonald, Jr., E. Kirowa-Einsner, L.R. McCoy, and H.B. Mark, Jr. J. Phys. Chem. **76**, 1170 (1972).
11. R.L. McCoy and H.B. Mark. J. Phys. Chem. **73**, 953 (1969).
12. Handbook of Chemistry and Physics. 76th Edition. *Edited by* D.R. Lide. CRC Press. 1981. p. D-162.
13. Ya.I. Tur'yan and O.N. Malyavinskaya. J. Electroanal. Chem. **23**, 69 (1969).
14. Ya.I. Tur'yan and O.N. Malyavinskaya. Elektrokhimiya, **8**, 64 (1972); **8**, 836 (1972).
15. E.A. Guggenheim and J.C. Turgeon. Trans. Faraday Soc. **51,** 747 (1955).
16. C.R. Russell. J. Electroanal. Chem. **6**, 486 (1963).
17. L.R. McCoy, H.B. Marck, and L. Gierst. J. Phys. Chem. **72**, 4637 (1968).
18. L. Gierst, L. Vanderbergen, E. Nicolas, and A. Traboni. J. Electrochem. Soc. **113**, 1025 (1966).
19. H. Wroblowa, Z. Kovac, and J. O'M Bockris. Trans. Faraday Soc. **51,** 747 (1955); **61**, 1523 (1965).
20. J. Heyrovsky and J. Kůta. Principles of polarography. Academic Press, New York. 1966. p. 214.
21. A.J. Bard and L.E. Faulker. Electrochemical Methods. John Wiley and Sons, New York. 1980. p. 110.
22. P. Delahay. Double layer and electrode kinetics. Interscience, New York. 1965. pp. 165–185.
23. J. Dandoy and L. Gierst. J. Electroanal. Chem. **2**, 836 (1961).
24. R. Parsons and P.C. Symons. Trans. Faraday Soc. **64**, 1077 (1968).
25. R.H. Holyer, C.D. Hubbard, S.F.A. Kettle, and R.G. Wilkins. Inorg. Chem. **4**, 929 (1965).
26. S. Funahashi and M. Tanaka. Inorg. Chem. **8**, 2159 (1969).
27. A.M. Bond. J. Phys. Chem. **75**, 2640 (1971).

© 2000 NRC Canada

Synthesis of 2,3-disubstituted norbornadienes

Geoffrey K. Tranmer, Carol Yip, Sean Handerson, Robert W. Jordan, and William Tam

Abstract: Various 2,3-disubstituted norbornadienes that can hardly be made by the traditional Diels–Alder method were synthesized by double lithium halide exchange of 2,3-dibromonorbornadiene in moderate to good yields.

Key words: 2,3-disubstituted norbornadienes, Diels–Alder reaction, lithium halide exchange.

Résumé: Faisant appel à un double échange de lithium/halogénure sur le 2,3-dibromonorbornadiène, on a réalisé la synthèse, avec des rendements allant de modérés à bons, de divers norbornadiènes 2,3-disubstitués qui peuvent à peine être fabriqués par la méthode traditionnelle de Diels–Alder.

Mots clés: norbornadiènes 2,3-disubstitués, réaction de Diels–Alder, échange lithium halogénure.

Introduction

During our study of the effect of a C-3 substituent on regio- and stereoselectivity in the intramolecular 1,3-dipolar cycloaddition of norbornadiene-tethered nitrile oxides (Scheme 1) (1), we came across a problem for the synthesis of the 2,3-disubstituted norbornadienes (**1**). Most of the literature syntheses of 2,3-disubstituted norbornadienes rely on Diels–Alder reactions between cyclopentadiene and highly activated acetylenes (2–6). Less activated or unactivated acetylenes are poor dienophiles in Diels–Alder reactions, thus limiting the substituents on the norbornadiene ring system to electron-withdrawing groups. In this paper, we report a more general and simple procedure for the synthesis of 2,3-disubstituted norbornadienes **8** and **9** with a variety of substituents (E_1 and E_2) (Scheme 2).

2,3-Disubstituted norbornadienes are important compounds, which have found a place as key intermediates in the synthesis of many natural products, such as prostaglandin endoperoxides PGH_2 and PGG_2 (7), *cis*-trikentrin B (8), and β-santalol (9, 10). 2,3-Disubstituted norbornadienes also serve in the reversible photoinduced isomerization of norbornadiene derivatives into the corresponding quadricyclanes (11–14). Extensive investigation of 2,3-disubstituted norbornadienes–quadricyclanes interconversion for solar energy storage has demonstrated the efficiency and switching potential of these reversible systems (15–17).

Received December 8, 1999. Published on the NRC Research Press website on April 19, 2000.

G.K. Tranmer, C. Yip, S. Handerson, R.W. Jordan, and W. Tam.[1] Guelph-Waterloo Centre for Graduate Work in Chemistry and Biochemistry, Department of Chemistry and Biochemistry, University of Guelph, Guelph, ON N1G 2W1, Canada.

[1]Author to whom correspondence may be addressed. Telephone: (519) 824-4120, ext. 2268. Fax: (519) 766-1499. e-mail: tam@chembio.uoguelph.ca

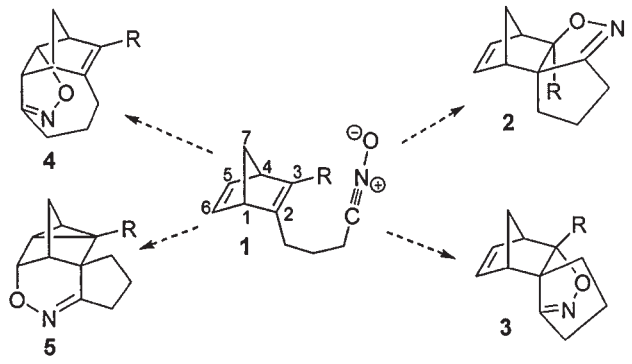
Results and discussion

Schlosser and co-workers (18) and Brandsma and co-worker (19) have shown independently that deprotonation of a vinyl hydrogen of norbornadiene **6** can be achieved by the use of Schlosser's base, a mixture of *n*-butyllithium (^{n}BuLi) and potassium or sodium *tert*-butoxide (^{t}BuOK or ^{t}BuONa). Trapping of the metalated norbornadiene **10** with electrophiles leads to the formation of 2-substituted norbornadienes (**11**) (Scheme 3). This method has been used in the synthesis of 2,3-dibromonorbornadiene (**7**) (20). We have modified the procedure to achieve a more reliable large-scale (10–20g scale) synthesis of 2,3-dibromonorbornadiene (**7**) (Scheme 4). After deprotonation of norbornadiene with Schlosser's base, 1,2-dibromoethane (0.5 equiv) was added to the norbornadienyl potassium (**10**) at –78°C, and the reaction mixture was stirred at –40°C for 1.5 h. At this point, 0.5 equiv. of 2-bromonorbornadiene (**12**) would have been formed together with the remaining 0.5 equiv. of norbornadienyl potassium (**10**). We found that the temperature control is very important at this stage. If the temperature was too low or too high, the yield of the reaction was very poor. The Br in **12** enhances the acidity of its adjacent vinyl hydrogen, and the leftover norbornadienyl potassium (**10**) is basic enough to remove that proton to generate **13**. Trapping of **13** with excess 1,2-dibromoethane leads to the formation of 2,3-dibromonorbornadiene (**7**).

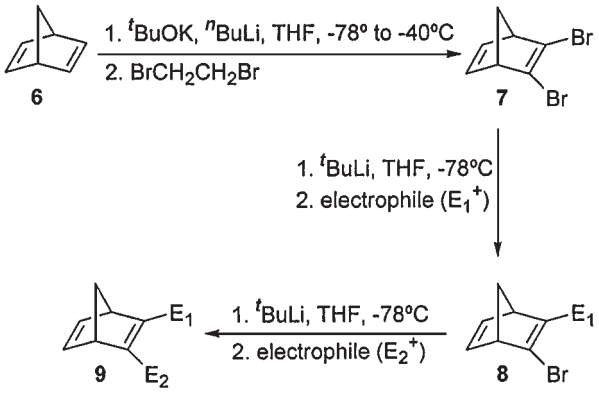
Monolithium-halide exchange of the 2,3-dibromonorbornadiene (**7**) with ^{t}BuLi (2 equiv) produces 2-bromo-3-lithionorbornadiene (**14**). Trapping of this organolithium with water (Table 1, entry 1) gave **8a**, and trapping with alkyl halides (entries 2–5) and benzyl bromide (entry 6) afforded the corresponding 2,3-disubstituted norbornadienes (**8b**–**8f**) in moderate to good yields. The disubstituted analogs **8d** and **8e** have been used in the synthesis of C-2, C-3-disubstituted norbornadiene-tethered nitrile oxides **1** (Scheme 1) in our studies of intramolecular 1,3-dipolar cycloadditions (1). We prepared 2,3-disubstituted norbornadienes with heteroatoms (Si, Cl, I, and Sn) by trapping the 2-bromo-3-lithionorbornadiene (**14**) with silyl chlorides (entries 7 and 8), tosyl chloride (entry 9), iodine (entry 10), and tributyltin chloride

© 2000 NRC Canada

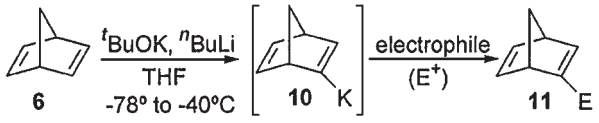
Scheme 1.



Scheme 2.



Scheme 3.



(entry 11). In reacting with the intermediate 2-bromo-3-lithionorbornadiene (**14**), ethyl chloroformate (entry 12) provided the corresponding ester **8l**, aldehydes (entries 13 and 14) afforded secondary alcohols **8m** and **8n**, and ketones (entries 15 and 16) gave tertiary alcohols **8o** and **8p**. In all these cases, we saw no evidence for the intermediacy of norbornenyne (**15**) (21) (Scheme 5).

A second lithium halide exchange of bromide **8b** followed by trapping with 1-bromohexane (Table 2, entry 1), 1,4-dibromobutane (entry 2), trimethylsilyl chloride (entry 3), tosyl chloride (entry 4), iodine (entry 5), ethyl chloroformate (entry 6), and acetone (entry 7) provided in moderate to good yields a broad range of 2,3-disubstituted norbornadienes (**9a**–**9g**) with various functional groups. Trapping of bromides **8c** and **8d** with 1,4-dibromobutane (entry 8) and methyl chloroformate (entry 9), respectively, led to the formation of 2,3-disubstituted norbornadienes **9h** and **9i**, which are precursors of the norbornadiene-tethered nitrile oxides in our studies of 1,3-dipolar cycloadditions (1).

In conclusion, we have developed a simple and convenient access to a variety of 2,3-disubstituted norbornadienes that can hardly be prepared by traditional Diels–Alder methodology. Analogs **8a**–**8p** are very useful precursors for the synthesis of many other 2,3-disubstituted norbornadienes. Obviously, instead of the second lithium halide exchange as discussed above to provide 2,3-disubstituted norbornadienes such as **9a**–**9i**, one could presumably couple the bromides **8** with organotin compounds (for the Stille coupling see refs. (22) and (23)), with organoboron compounds (for the Suzuki coupling see ref. (24)), with alkenes (for the Heck reaction see ref. (25)), and with 1-alkynes (for the Castro–Stephens–Sonogashira coupling see ref. (26)) to generate broad classes of vinyl, aryl, and alkynyl norbornadienes. We are currently investigating these coupling reactions in the synthesis of novel conjugated norbornadiene-based polymers. Studies on asymmetric lithium halide exchange of 2,3-dibromonornadiene (**7**) by precomplexation of ^{t}BuLi with a chiral base are also underway in our laboratory and will be reported in due course.

Experimental

General Information

All reactions were carried out in an atmosphere of dry nitrogen at ambient temperature unless otherwise stated. Standard column chromatography was performed on 230–400 mesh silica gel (obtained from Silicycle) by use of flash column chromatography techniques (27). Analytical thin-layer chromatography (TLC) was conducted on Merck precoated silica gel 60 F_{254} plates. All glassware was flame dried under an inert atmosphere of dry nitrogen. Infrared spectra were taken on a Bomem MB-100 FTIR spectrophotometer. ^{1}H and ^{13}C NMR spectra were recorded on a Varian Gemini-200 or a Bruker-400 spectrometer. Chemical shifts for ^{1}H NMR spectra are reported in parts per million (ppm) from tetramethylsilane with the solvent resonance as the internal standard (deuterochloroform: δ 7.26). Chemical shifts for ^{13}C NMR spectra are reported in parts per million (ppm) from tetramethylsilane with the solvent as the internal standard (deuterochloroform: δ 77.0). High resolution mass spectra were done by Mass Spectrometry Laboratory Services Division at the University of Guelph. Elemental analyses were performed by Canadian Microanalytical Service Ltd., British Columbia or by Quantitative Technologies Inc., New Jersey.

Reagents

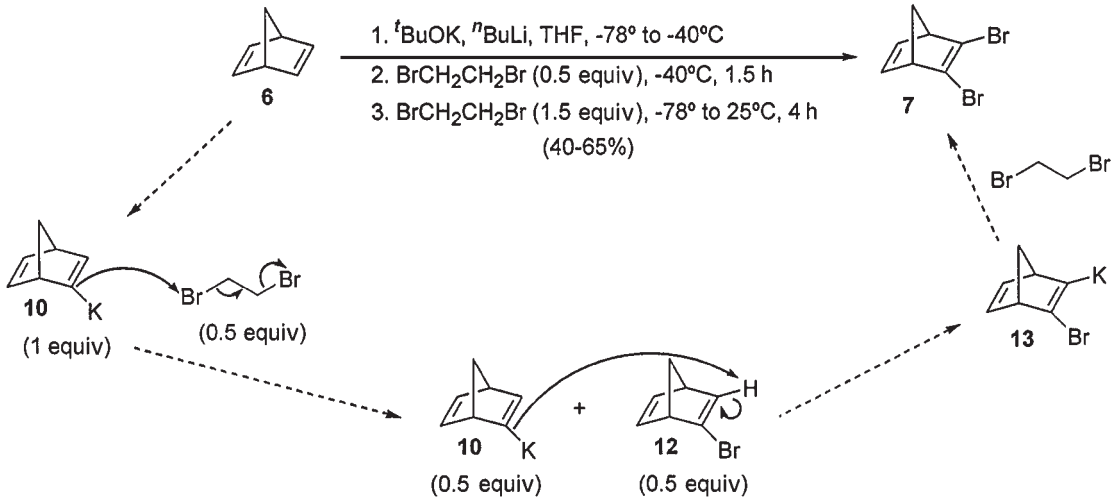
Unless stated otherwise, commercial reagents were used without purification. THF was purified by distillation from potassium/benzophenone under dry nitrogen. 1,2-Dibromoethane, 1-iodohexane, 1,4-dibromobutane, chlorotrimethylsilane, acetone, acetaldehyde, and methyl chloroformate were purified by distillation from 4 Å molecular sieves under dry nitrogen.

2,3-Dibromonorbornadiene (7)

Norbornadiene **6** (35.0 mL, 324 mmol) was added to a flame-dried 3-neck flask containing potassium *tert*-butoxide (18.7 g, 167 mmol) and THF (240 mL), which was cooled at –78°C (cryobath). *n*-Butyllithium (66.0 mL, 2.5M, 165 mmol) was added dropwise through a dropping funnel over 2 h, which the temperature was maintained below –70°C. The mixture was stirred at –65°C for 30 min. then at –40°C for 30 min. After the mixture was cooled to –78°C, 1,2-dibromoethane (7.20 mL, 83.5 mmol) was added, and

© 2000 NRC Canada

Scheme 4.

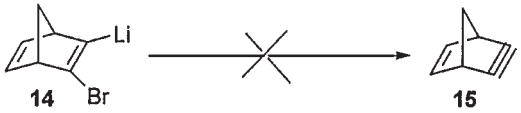


the mixture was stirred at –40°C for 1.5 h. Excess 1,2-dibromoethane (21.6 mL, 250 mmol) was then added at –70°C. The brown mixture was stirred at –40°C for 2 h then at room temperature for 4 h. After quenching the mixture with saturated ammonium chloride (150 mL) and water (300 mL), the aqueous layer was extracted with diethyl ether (4 × 300 mL), and the combined organic layers were washed sequentially with water (500 mL) and brine (500 mL) and dried over magnesium sulfate. The solvent was removed by rotary evaporation, and the crude product was purified by vacuum distillation to give three fractions. The first fraction (20–30 torr (1 torr = 133.322 Pa) at 40–60°C) contained mainly the excess 1,2-dibromoethane and norbornadiene. The second fraction (10–15 torr (1 torr = 133.322 Pa) at 50–60°C) contained 2-bromonorbornadiene and 2,3-dibromonorbornadiene in a ratio of 2:1 as determined by ^{1}H NMR. The third fraction (6–9 torr (1 torr = 133.322 Pa) at 80–100°C) contained pure 2,3-dibromonorbornadiene **7** (13.6 g, 54.4 mmol, 65%) as colorless oil. R_f: 0.67 (hexanes). ^{1}H NMR ($CDCl_3$, 400 MHz) δ: 6.88 (s, 2H), 3.61 (m, 2H), 2.45 (dd, 1H, J = 6.3, 1.1 Hz), 2.18 (dt, 1H, J = 6.3, 1.4 Hz). ^{13}C NMR ($CDCl_3$, 100 MHz) δ: 141.2, 133.0, 72.0, 58.6. Spectral data were identical to those reported in the literature (20).

*2-Bromonorbornadiene (**8a**)*

tert-Butyllithium (1.04 mL, 1.7M, 1.77 mmol) was added to a flame-dried flask containing dibromide **7** (222 mg, 0.887 mmol) in THF (4 mL) at –78°C. After the yellow mixture was stirred for 15 min, distilled water (0.50 mL, 28.0 mmol) was added at –78°C. The mixture was stirred at –78°C for 30 min. then at room temperature for 1 h. After quenching the mixture with water (5 mL), the aqueous layer was extracted with diethyl ether (3 × 10 mL), and the combined organic layers were washed sequentially with water (10 mL) and brine (10 mL) and dried over magnesium sulfate. The solvent was removed by rotary evaporation and the crude product was purified by column chromatography (hexanes) to give **8a** (93.2 mg, 0.545 mmol, 61%) as colorless oil. Note: **8a** is not very stable and it turned to blackened oil upon standing at room temperature for a few days.

Scheme 5.



R_f: 0.69 (hexanes). ^{1}H NMR ($CDCl_3$, 400 MHz) δ: 6.89 (dd, 1H, J = 5.2, 3.2 Hz), 6.78 (dd, 1H, J = 5.2, 3.2 Hz), 6.65 (d, 1H, J = 3.2 Hz), 3.61 (br. s, 1H), 3.48 (br. s, 1H), 2.67 (dt, 1H, J = 6.0, 1.6 Hz), 2.07 (dt, 1H, J = 6.0, 1.6 Hz). ^{13}C NMR ($CDCl_3$, 100 MHz) δ: 142.9, 141.8, 139.6, 136.6, 73.9, 58.2, 51.6. Spectral data were identical to those reported in the literature (20).

*2-Bromo-3-methylnorbornadiene (**8b**)*

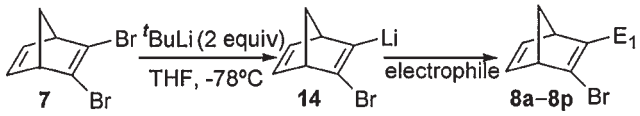
tert-Butyllithium (17.3 mL, 1.7M, 29.4 mmol) was added to a flame-dried flask containing dibromide **7** (3.67 g, 14.7 mmol) in THF (40 mL) at –78°C. After the yellow mixture was stirred for 1 h, methyl iodide (2.30 mL, 36.8 mmol) was added at –78°C. The mixture was stirred at –78 °C for 30 min then at room temperature for 2 h. After quenching the mixture with water (40 mL), the aqueous layer was extracted with diethyl ether (3 × 50 mL), and the combined organic layers were washed sequentially with water (100 mL) and brine (100 mL) and dried over magnesium sulfate. The solvent was removed by rotary evaporation and the crude product was purified by bulb-to-bulb distillation (15–20 torr (1 torr = 133.322 Pa) at 70–80°C) to give **8b** (2.39 g, 12.9 mmol, 88%) as colorless oil. R_f: 0.74 (hexanes). IR (neat, NaCl) cm^{-1}: 2973 (s), 2939 (s), 2905 (w), 2869 (w), 1639 (w), 1557 (w), 1439 (m), 1376 (w), 1262 (w). ^{1}H NMR ($CDCl_3$, 400 MHz) δ: 6.87 (dd, 1H, J = 5.0, 2.9 Hz), 6.78 (m, 1H), 3.47 (m, 1H), 3.36 (br. s, 1H), 2.21 (dt, 1H, J = 6.0, 1.5 Hz), 2.02 (dt, 1H, J = 6.0, 1.7 Hz), 1.76 (s, 3H). ^{13}C NMR ($CDCl_3$, 100 MHz) δ: 147.6, 142.1, 141.5, 128.7, 71.4, 57.9, 55.2, 15.4. Anal. calcd. for C_8H_9Br: C 51.92, H 4.90; found C 51.90, H 4.84.

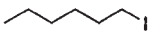
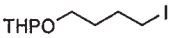
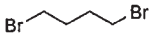
*2-Bromo-3-hexylnorbornadiene (**8c**)*

tert-Butyllithium (9.70 mL, 1.7M, 16.5 mmol) was added to a flame-dried flask containing dibromide **7** (1.87 g, 7.48 mmol) in THF (25 mL) at –78°C. After the yellow mixture was

© 2000 NRC Canada

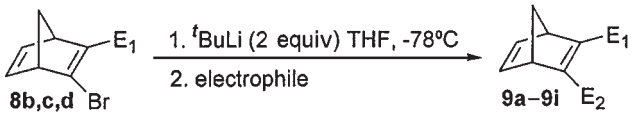
Table 1.

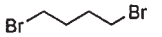
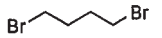


Entry	Electrophile	Norbornadiene	E_1	Yield (%)
1	H_2O	**8a**	H	61
2	MeI	**8b**	Me	88
3		**8c**	^{n}Hexyl	87
4		**8d**	$(CH_2)_4OTHP$	90
5		**8e**	$(CH_2)_4Br$	53
6	BnBr	**8f**	CH_2Ph	63
7	Me_3SiCl	**8g**	$SiMe_3$	88
8	$^t BuMe_2SiCl$	**8h**	$SiMe_2{}^t Bu$	77
9	TsCl	**8i**	Cl	75
10	I_2	**8j**	I	82
11	Bu_3SnCl	**8k**	$SnBu_3$	73
12	EtOC(O)Cl	**8l**	COOEt	61
13	CH_3CHO	**8m**	$CH(OH)CH_3$	83
14	PhCHO	**8n**	CH(OH)Ph	70
15	CH_3COCH_3	**8o**	$C(OH)(CH_3)_2$	73
16	PhCOPh	**8p**	$C(OH)Ph_2$	66

stirred for 1 h, 1-iodohexane (2.00 mL, 13.6 mmol) was added at –78°C. The mixture was stirred at –78 °C for 90 min then at room temperature for 2 h. After quenching the mixture with water (50 mL), the aqueous layer was extracted with diethyl ether (4 × 50 mL), and the combined organic layers were washed sequentially with water (100 mL) and brine (100 mL) and dried over magnesium sulfate. The solvent was removed by rotary evaporation and the crude product was purified by bulb-to-bulb distillation (1–2 torr (1 torr = 133.322 Pa) at 60°C for 1 h) to remove excess 1-iodohexane, then 0.3 torr (1 torr = 133.322 Pa) at 100°C) to give **8c** (1.66 g, 6.50 mmol, 87%) as colorless oil. R_f: 0.85 (hexanes). IR (neat, NaCl) cm^{-1}: 3068 (w), 2958 (s), 2929 (s), 2857 (s), 1633 (w), 1557 (w), 1466 (m), 1378 (w), 1297 (m), 1263 (w), 1224 (w); ^{1}H NMR ($CDCl_3$, 400 MHz) δ: 6.86 (m, 1H), 6.75 (m, 1H), 3.47 (m, 1H), 3.43 (m, 1H), 2.24–2.08 (m, 3H), 2.03 (dt, 1H, J = 5.9, 1.7 Hz), 1.44–1.24 (m, 8H), 0.89 (t, 3H, J = 6.8 Hz). ^{13}C NMR ($CDCl_3$, 100 MHz) δ: 151.3, 141.90, 141.87, 129.0, 71.5, 57.9, 53.5, 31.6, 29.2, 28.8, 26.4, 22.6, 14.1. HRMS *m/z* for $C_{13}H_{19}Br$: calcd. 254.0671; found 254.0677.

Table 2.



Entry	E_1	Electrophile	Norbornadiene	E_2	Yield (%)
1	Me		**9a**	^{n}Hexyl	80
2	Me		**9b**	$(CH_2)_4Br$	41
3	Me	Me_3SiCl	**9c**	$SiMe_3$	71
4	Me	TsCl	**9d**	Cl	73
5	Me	I_2	**9e**	I	60
6	Me	EtOC(O)Cl	**9f**	COOEt	77
7	Me	MeCOMe	**9g**	$C(OH)Me_2$	80
8	^{n}Hexyl		**9h**	$(CH_2)_4Br$	54
9	$(CH_2)_4OTHP$	MeOC(O)Cl	**9i**	COOMe	74

*2-Bromo-3-(4-tetrahydropyranyloxybutyl)norbornadiene (**8d**)*

tert-Butyllithium (24.0 mL, 1.7M, 40.8 mmol) was added to a flame-dried flask containing dibromide **7** (5.10 g, 20.4 mmol) in THF (41 mL) at –78°C. After the yellow mixture was stirred for 30 min, 1-iodo-4-tetrahydropyranyloxybutane (4.43 g, 15.6 mmol) was added at –78°C. The mixture was stirred at –78°C for 1 h then at room temperature for 20 h. After quenching the mixture with water (80 mL), the aqueous layer was extracted with diethyl ether (3 × 80 mL), and the combined organic layers were washed sequentially with water (100 mL) and brine (100 mL) and dried over magnesium sulfate. The solvent was removed by rotary evaporation and the crude product was purified by column chromatography (EtOAc:hexanes = 1:19) to give **8d** (6.01 g, 18.4 mmol, 90%) as colorless oil. R_f: 0.35 (EtOAc:hexanes = 1:19). IR (neat, NaCl) cm^{-1}: 3067 (w), 2939 (s), 2867 (s), 1633 (w), 1558 (m), 1440 (m), 1352 (m), 1323 (w), 1297 (m), 1260 (m), 1224 (w), 1201 (m), 1137 (m), 1120 (m), 1077 (m), 1033 (m). H NMR ($CDCl_3$, 400 MHz) δ: 6.84 (dd, 1H, J = 4.9, 2.9 Hz), 6.73 (dd, 1H, J = 4.9, 2.9 Hz), 4.55 (m, 1H), 3.85 (m, 1H), 3.71 (m, 1H), 3.51–3.42 (m, 3H), 3.37 (m, 1H), 2.27–2.10 (m, 3H), 2.01 (dm, 1H, J = 5.9 Hz), 1.80 (m, 1H), 1.70 (m, 1H), 1.59–1.42 (m, 8H). ^{13}C NMR ($CDCl_3$, 100 MHz) δ: 150.9, 141.8 (2), 129.3, 98.8, 98.7, 71.5, 67.2, 62.24, 62.22, 57.9, 53.3, 30.7, 29.1, 28.9, 25.4, 23.13, 23.11, 19.61, 19.59. HRMS *m/z* for $C_{16}H_{23}BrO_2$: calcd. 326.0882; found 326.0886.

© 2000 NRC Canada

*2-Bromo-3-(4-bromobutyl)norbornadiene (**8e**)*

tert-Butyllithium (8.20 mL, 1.7M, 13.9 mmol) was added to a flame-dried flask containing dibromide **7** (1.60 g, 6.40 mmol) in THF (30 mL) at –78°C. After stirring the reaction mixture for 1 h, the resulting yellow reaction mixture was added to a flame-dried flask containing 1,4-dibromobutane (5.50 mL, 46.1 mmol) in THF (30 mL) at –78°C. The mixture was stirred at –78°C for 1 h then at room temperature for 12 h. After quenching the mixture with water (100 mL), the aqueous layer was extracted with diethyl ether (4 × 50 mL), and the combined organic layers were washed sequentially with water (100 mL) and brine (100 mL) and dried over magnesium sulfate. The solvent was removed by rotary evaporation and the excess 1,4-dibromobutane was removed by bulb-to-bulb distillation (4 torr (1 torr = 133.322 Pa) at 70°C for 4 h) and the crude product was purified by column chromatography (hexanes) to give **8e** (1.04 g, 3.40 mmol, 53%) as colorless oil. R_f: 0.50 (EtOAc:hexanes = 1:9). IR (neat, NaCl) cm^{-1}: 3066 (w), 2973 (m), 2937 (s), 2866 (w), 1632 (w), 1557 (w), 1451 (w), 1296 (s), 1249 (w). ^1H NMR ($CDCl_3$, 400 MHz) δ: 6.85 (dd, 1H, *J* = 5.1, 2.9 Hz), 6.76 (dd, 1H, *J* = 4.6, 3.0 Hz), 3.47 (m, 1H), 3.44 (m, 1H), 3.40 (t, 2H, *J* = 6.6 Hz), 2.28–2.12 (m, 3H), 2.04 (dt, 1H, *J* = 6.0, 1.7 Hz), 1.78 (m, 2H), 1.57 (m, 2H). ^{13}C NMR ($CDCl_3$, 100 MHz) δ: 150.3, 141.9, 141.8, 129.9, 71.6, 57.9, 53.3, 33.7, 31.8, 28.1, 24.8. HRMS *m*/*z* for $C_{11}H_{14}Br_2$: calcd. 303.9463; found 303.9460.

*2-Benzyl-3-bromonorbornadiene (**8f**)*

tert-Butyllithium (19.0 mL, 1.7M, 32.3 mmol) was added to a flame-dried flask containing dibromide **7** (4.0 g, 16 mmol) in THF (48 mL) at –78°C. After the yellow mixture was stirred for 1.2 h, benzyl bromide (2.85 mL, 24.0 mmol) was added at –78°C. The mixture was stirred at –78 °C for 2 h then at room temperature for 22 h. After quenching the mixture with water (25 mL), the aqueous layer was extracted with diethyl ether (4 × 25 mL), and the combined organic layers were washed sequentially with water (25 mL) and brine (25 mL) and dried over magnesium sulfate. The solvent was removed by rotary evaporation and the excess benzyl bromide was by vacuum bulb-to-bulb distillation (5 torr (1 torr = 133.322 Pa) at 120°C for 3 h). The crude product was purified by column chromatography (hexanes) to give **8f** (2.62 g, 10.0 mmol, 63%) as yellow oil. R_f: 0.85 (EtOAc:hexanes = 1:9). IR (neat, NaCl) cm^{-1}: 3064 (m), 3027 (s), 2976 (s), 2938 (s), 2867 (s), 1630 (m), 1601 (m), 1557 (m), 1494 (s), 1453 (s), 1428 (w), 1297 (s), 1264 (m), 1224 (m), 1168 (w), 1087 (w), 1074 (m), 1029 (s), 1010 (m). ^1H NMR ($CDCl_3$, 400 MHz) δ: 7.31–7.20 (m, 3H), 7.12 (dm, 2H, *J* = 7.2 Hz), 6.81 (dd, 1H, *J* = 4.9, 3.0 Hz), 6.55 (dd, 1H, *J* = 4.9, 2.9 Hz), 3.57 (d_{AB}, 1H, *J* = 14.9 Hz), 3.55 (br. s, 1H), 3.48 (d_{AB}, 1H, *J* = 14.9 Hz), 3.30 (m, 1H), 2.21 (dt, 1H, *J* = 6.0, 1.5 Hz), 2.00 (dt, 1H, *J* = 6.0, 1.6 Hz). ^{13}C NMR ($CDCl_3$, 100 MHz) δ: 149.7, 142.0, 140.9, 137.5, 129.9, 128.8, 128.3, 126.2, 71.4, 57.9, 53.4, 35.7. HRMS *m*/*z* for $C_{14}H_{13}Br$: calcd. 260.0201; found 260.0189.

*2-Bromo-3-trimethylsilylnorbornadiene (**8g**)*

tert-Butyllithium (1.01 mL, 1.7M, 1.72 mmol) was added to a flame-dried flask containing dibromide **7** (215 mg, 0.862 mmol) in THF (4 mL) at –78°C. After the yellow mixture was stirred for 30 min, chlorotrimethylsilane (0.27 mL, 2.10 mmol) was added at –78°C. The mixture was stirred at –78°C for 1 h then at room temperature for 1 h. After quenching the mixture with water (5 mL), the aqueous layer was extracted with diethyl ether (3 × 10 mL), and the combined organic layers were washed sequentially with water (10 mL) and brine (10 mL) and dried over magnesium sulfate. The solvent was removed by rotary evaporation and the crude product was purified by column chromatography (hexanes) to give **8g** (185 mg, 0.762 mmol, 88%) as colorless oil. R_f: 0.88 (EtOAc:hexanes = 1:19). IR (neat, NaCl) cm^{-1}: 2957 (s), 2938 (s), 1571 (s), 1549 (s), 1296 (s), 1248 (s), 1022 (m), 836 (s). ^1H NMR ($CDCl_3$, 400 MHz) δ: 6.83 (dd, 1H, *J* = 5.0, 3.2 Hz), 6.70 (dd, 1H, *J* = 5.0, 3.2 Hz), 3.73 (br. s, 1H), 3.54 (br. s, 1H), 2.14 (dt, 1H, *J* = 6.1, 1.5 Hz), 1.94 (dt, 1H, *J* = 6.1, 1.5 Hz), 0.15 (s, 9H). ^{13}C NMR ($CDCl_3$, 100 MHz) δ: 147.6, 147.2, 142.7, 141.0, 72.3, 61.4, 55.7, –1.7. HRMS *m*/*z* for $C_{10}H_{15}SiBr$: calcd. 242.0127; found 242.0124.

*2-Bromo-3-tert-Butyldimethylsilylnorbornadiene (**8h**)*

tert-Butyllithium (1.00 mL, 1.7M, 1.70 mmol) was added to a flame-dried flask containing dibromide **7** (212 mg, 0.847 mmol) in THF (4 mL) at –78°C. After the yellow mixture was stirred for 30 min, *tert*-butyldimethylsilyl chloride (338 mg, 2.24 mmol) was added at –78°C. The mixture was stirred at –78°C for 1 h then at room temperature for 1 h. After quenching the mixture with water (5 mL), the aqueous layer was extracted with diethyl ether (3 × 10 mL), and the combined organic layers were washed sequentially with water (10 mL) and brine (10 mL) and dried over magnesium sulfate. The solvent was removed by rotary evaporation and the crude product was purified by column chromatography (hexanes) to give **8h** (187 mg, 0.655 mmol, 77%) as colorless oil. R_f: 0.88 (EtOAc:hexanes = 1:19). IR (neat, NaCl) cm^{-1}: 2953 (s), 2928 (s), 2855 (s), 1570 (s), 1548 (s), 1470 (m), 1296 (s), 1249 (s), 1019 (s), 835 (s). ^1H NMR ($CDCl_3$, 400 MHz) δ: 6.85 (dd, 1H, *J* = 4.9, 3.1 Hz), 6.72 (dd, 1H, *J* = 4.9, 2.9 Hz), 3.77 (br. s, 1H), 3.55 (br. s, 1H), 2.18 (d, 1H, *J* = 6.1 Hz), 1.94 (dm, 1H, *J* = 6.1 Hz), 0.88 (s, 9H), 0.18 (s, 3H), 0.15 (s, 3H). ^{13}C NMR ($CDCl_3$, 100 MHz) δ: 148.8, 146.1, 142.9, 140.9, 72.4, 61.7, 56.7, 26.7, 18.4, –5.4, –5.8. HRMS *m*/*z* for $C_{13}H_{21}SiBr$: calcd. 284.0596; found 284.0597.

*2-Bromo-3-chloronorbornadiene (**8i**)*

tert-Butyllithium (1.00 mL, 1.7M, 1.70 mmol) was added to a flame-dried flask containing dibromide **7** (213 mg, 0.852 mmol) in THF (4 mL) at –78°C. After the yellow mixture was stirred for 30 min, *p*-toluenesulfonyl chloride (345 mg, 1.81 mmol) was added at –78°C. The mixture was stirred at –78°C for 45 min then at room temperature for 1 h. After quenching the mixture with water (5 mL), the aqueous layer was extracted with diethyl ether (3 × 10 mL), and the combined organic layers were washed sequentially with water (10 mL) and brine (10 mL) and dried over magnesium sulfate. The solvent was removed by rotary evaporation and the crude product was purified by column chromatography (hexanes) to give **8i** (130 mg, 0.635 mmol, 75%) as colorless oil. R_f: 0.76 (hexanes). ^1H NMR ($CDCl_3$, 400 MHz) δ: 6.89 (m, 2H), 3.60 (m, 1H), 3.52 (m, 1H), 2.43 (dtd, 1H, *J* = 6.3,

© 2000 NRC Canada

1.6, 0.3 Hz), 2.19 (dt, 1H, J = 6.3, 1.9 Hz). ^{13}C NMR ($CDCl_3$, 100 MHz) δ: 144.0, 141.6, 141.1, 128.3, 71.5, 57.8, 56.8. Spectral data were identical to those reported in the literature (20).

*2-Bromo-3-iodonorbornadiene (**8j**)*

tert-Butyllithium (1.00 mL, 1.7M, 1.70 mmol) was added to a flame-dried flask containing dibromide **7** (213 mg, 0.854 mmol) in THF (3 mL) at –78°C. After the yellow mixture was stirred for 30 min, iodine (456 mg, 1.80 mmol), in a separate flame-dried flask containing 4Å molecular sieves (550 mg) and THF (1 mL), was added via a cannula at –78°C. The mixture was stirred at –78°C for 45 min then at room temperature for 1 h. After quenching the mixture with saturated sodium thiosulfate (5 mL), the aqueous layer was extracted with diethyl ether (3 × 10 mL), and the combined organic layers were washed sequentially with water (10 mL) and brine (10 mL) and dried over magnesium sulfate. The solvent was removed by rotary evaporation and the crude product was purified by column chromatography (hexanes) to give **8j** (207 mg, 0.699 mmol, 82%) as pale-yellow oil. R_f: 0.77 (hexanes). IR (neat, NaCl) cm^{-1}: 2993 (s), 2940 (s), 2867 (w), 1573 (s), 1551 (w), 1291 (s), 1220 (w), 711 (s). ^{1}H NMR ($CDCl_3$, 400 MHz) δ: 6.87 (m, 2H), 3.71 (m, 1H), 3.62 (m, 1H), 2.44 (dm, 1H, J = 6.4 Hz), 2.14 (dm, 1H, J = 6.4 Hz). ^{13}C NMR ($CDCl_3$, 100 MHz) δ: 141.9, 141.4, 140.8, 105.0, 72.5, 61.9, 59.0. HRMS m/z for C_7H_6BrI: calcd. 295.8700; found 295.8697.

*2-Bromo-3-tributylstannylnorbornadiene (**8k**)*

tert-Butyllithium (1.05 mL, 1.7M, 1.79 mmol) was added to a flame-dried flask containing dibromide **7** (233 mg, 0.894 mmol) in THF (4 mL) at –78°C. After the yellow mixture was stirred for 30 min, tributyltin chloride (0.61 mL, 2.25 mmol) was added at –78°C. The mixture was stirred at –78°C for 45 min then at room temperature for 1 h. After quenching the mixture with water (5 mL), the aqueous layer was extracted with diethyl ether (3 × 10 mL), and the combined organic layers were washed sequentially with water (10 mL) and brine (10 mL) and dried over magnesium sulfate. The solvent was removed by rotary evaporation and the crude product was purified by column chromatography (hexanes) to give **8k** (299 mg, 0.649 mmol, 73%) a$s colorless oil. R_f: 0.89 (hexanes). IR (neat, NaCl) cm^{-1}: 2956 (s), 2930 (s), 2870 (m), 2853 (m), 1566 (m), 1541 (s), 1463 (m), 1294 (s), 1009 (s), 874 (w). ^{1}H NMR ($CDCl_3$, 400 MHz) δ: 6.85 (dd, 1H, J = 5.1, 3.0 Hz), 6.65 (dd, 1H, J = 5.1, 2.9 Hz), 3.74 (br. s, 1H), 3.51 (br. s, 1H), 2.19 (dm, 1H, J = 6.0 Hz), 1.98 (dm, 1H J = 6.0 Hz), 1.49 (m, 6H), 1.29 (m, 6H), 1.00 (t, 6H, J = 8.0 Hz), 0.88 (t, 9H, J = 7.2 Hz). ^{13}C NMR ($CDCl_3$, 100 MHz) δ: 151.2, 148.9, 142.6, 141.3, 73.1, 60.3, 57.5, 29.1, 27.2, 13.7, 9.7. HRMS m/z for $C_{19}H_{33}SnBr$: calcd. 460.0788; found 460.0792.

*2-Bromo-3-ethoxycarbonylnorbornadiene (**8l**)*

tert-Butyllithium (1.20 mL, 1.7M, 2.04 mmol) was added to a flame-dried flask containing dibromide **7** (219 mg, 0.876 mmol) in THF (2.4 mL) at –78°C. After stirring the mixture for 1 h, the resulting yellow mixture was added to a flame-dried flask containing ethyl chloroformate (0.40 mL, 4.18 mmol) in THF (2 mL) at –78°C. The mixture was stirred at –78°C for 3 h. After quenching the mixture with water (15 mL), the aqueous layer was extracted with diethyl ether (4 × 15 mL), and the combined organic layers were washed sequentially with water (20 mL) and brine (20 mL) and dried over magnesium sulfate. The solvent was removed by rotary evaporation and the crude product was purified by column chromatography (EtOAc:hexanes = 1:19) to give **8l** (130 mg, 0.535 mmol, 61%) as colorless oil. R_f: 0.70 (EtOAc:hexanes = 1:4). IR (neat, NaCl) cm^{-1}: 2980 (m), 2943 (m), 2872 (w), 1718 (s), 1717 (s), 1704 (s), 1699 (s), 1695 (s), 1559 (m), 1368 (m), 1310 (s), 1290 (s), 1277 (s), 1249 (s), 1235 (s), 1203 (w), 1150 (m), 1101 (s), 1086 (s), 1024 (w). ^{1}H NMR ($CDCl_3$, 400 MHz) δ: 6.90 (dd, 1H, J = 4.9, 3.0 Hz), 6.84 (m, 1H), 4.21 (m, 2H), 3.99 (m, 1H), 3.67 (m, 1H), 2.30 (dt, 1H, J = 6.6, 1.5 Hz), 2.11 (dt, 1H, J = 6.7, 1.6 Hz), 1.30 (t, 3H, J = 7.1 Hz). ^{13}C NMR ($CDCl_3$, 100 MHz) δ: 163.7, 148.4, 143.0, 142.0, 140.4, 71.7, 61.6, 60.4, 52.0, 14.2. Anal. calcd. for $C_{10}H_{11}BrO_2$: C 49.41, H 4.56; found C 49.23, H 4.58.

*2-Bromo-3-(1-hydroxyethyl)norbornadiene (**8m**)*

tert-Butyllithium (0.50 mL, 1.7M, 0.850 mmol) was added to a flame-dried flask containing dibromide **7** (106 mg, 0.424 mmol) in THF (2 mL) at –78°C. After the yellow mixture was stirred for 45 min, acetaldehyde (0.10 mL, 2.88 mmol) was added at –78°C. The mixture was stirred at –78°C for 1 h. After quenching the mixture with water (5 mL), the aqueous layer was extracted with diethyl ether (3 × 10 mL), and the combined organic layers were washed sequentially with water (10 mL) and brine (10 mL) and dried over magnesium sulfate. The solvent was removed by rotary evaporation and the crude product was purified by column chromatography (EtOAc:hexanes = 1:4) to give **8m** (75.9 mg, 0.353 mmol, 83%, 1:1 inseparable mixture of diastereomers) as colorless oil. R_f: 0.33 (EtOAc:hexanes = 1:4); IR (neat, NaCl) cm^{-1}: 3354 (br. s), 3069 (w), 2973 (s), 2939 (s), 2869 (s), 1628 (m), 1558 (m), 1449 (m), 1368 (m), 1327 (m), 1296 (s), 1268 (m), 1224 (m), 1209 (m), 1091 (s), 1062 (s), 1030 (m), 1009 (m). ^{1}H NMR ($CDCl_3$, 400 MHz) δ: 6.86–6.76 (m, 2H), 4.70 (q, 0.5H, J = 6.2 Hz), 4.69 (q, 0.5H, J = 6.2 Hz), 3.72 (br. s, 0.5H), 3.68 (br. s, 0.5H), 3.50 (br. s, 1H), 2.16 (m, 1H), 2.04 (m, 1H), 1.87 (br. s, 1H), 1.62 (br. s, 1H), 1.33 (d, 1.5H, J = 6.4 Hz), 1.11 (d, 1.5H, J = 6.5 Hz). ^{13}C NMR ($CDCl_3$, 100 MHz) δ: 152.6, 152.4, 142.9, 142.5, 141.4, 141.2, 130.4, 130.2, 71.8, 71.3, 64.6, 64.5, 58.2, 58.1, 50.0, 49.5, 20.8, 18.9. Anal. calcd. for $C_9H_{11}BrO$: C 50.26, H 5.15; found C 50.09, H 5.16.

*2-Bromo-3-(1-hydroxybenzyl)norbornadiene (**8n**)*

tert-Butyllithium (1.10 mL, 1.7M, 1.87 mmol) was added to a flame-dried flask containing dibromide **7** (212 mg, 0.849 mmol) in THF (4.2 mL) at –78°C. After the yellow mixture was stirred for 1 h, benzaldehyde (0.10 mL, 0.98 mmol) was added at –78°C. The mixture was stirred at –78°C for 2 h. After quenching the mixture with water (15 mL), the aqueous layer was extracted with diethyl ether (4 × 15 mL), and the combined organic layers were washed sequentially with water (15 mL) and brine (15 mL) and dried over magnesium sulfate. The solvent was removed by rotary evaporation and the crude product was purified by column chromatography (EtOAc:hexanes = 1:9) to give **8n**

© 2000 NRC Canada

(164 mg, 0.592 mmol, 70%, 1:1 inseparable mixture of diastereomers) as colorless oil. R_f: 0.55 (EtOAc:hexanes = 1:4). IR (neat, NaCl) cm^{-1}: 3395 (s), 3064 (m), 3028 (m), 2992 (s), 2939 (s), 2869 (m), 1626 (m), 1602 (w), 1557 (w), 1494 (m), 1449 (s), 1299 (s), 1266 (m), 1224 (m), 1127 (w), 1037 (s), 1021 (s), 1002 (s). ^{1}H NMR ($CDCl_3$, 400 MHz) δ: 7.42–7.22 (m, 5H), 6.88 (dd, 0.5H, *J* = 5.0, 3.0 Hz), 6.82 (dd, 0.5H, *J* = 5.0, 3.0 Hz), 6.58 (dd, 0.5H, *J* = 4.9, 3.0 Hz), 6.22 (dd, 0.5H, *J* = 4.9, 2.9 Hz), 5.70 (br. s, 0.5H), 5.68 (d, 0.5H, *J* = 2.7 Hz), 3.58 (br. s, 0.5H), 3.55 (br. s, 1H), 3.47 (br. s, 0.5H), 2.26 (dm, 0.5H, *J* = 2.0 Hz), 2.19 (dm, 0.5H, *J* = 6.2 Hz), 2.09 (dm, 0.5H, *J* = 6.2 Hz), 2.03 (d, 0.5H, *J* = 3.4 Hz), 1.98 (dd, 1H, *J* = 6.2, 1.3 Hz). ^{13}C NMR ($CDCl_3$, 100 MHz) δ: 151.3, 151.1, 142.7, 142.5, 141.5, 141.1, 139.2, 139.0, 132.0, 130.9, 128.4, 128.2, 127.4, 127.3, 125.6, 125.5, 72.1, 70.4, 70.3, 70.0, 58.2, 58.1, 50.8, 49.6. Anal. calcd. for $C_{14}H_{13}BrO$: C 60.67, H 4.73; found C 60.83, H 4.71.

*2-Bromo-3-(2-hydroxypropyl)norbornadiene (**8o**)*

tert-Butyllithium (1.05 mL, 1.7M, 1.79 mmol) was added to a flame-dried flask containing dibromide **7** (199 mg, 0.797 mmol) in THF (4.0 mL) at –78°C. After the yellow mixture was stirred for 1 h, acetone (0.40 mL, 5.4 mmol) was added at –78°C. The mixture was stirred at –78 °C for 2 h. After quenching the mixture with water (15 mL), the aqueous layer was extracted with diethyl ether (4 × 15 mL), and the combined organic layers were washed sequentially with water (15 mL) and brine (15 mL) and dried over magnesium sulfate. The solvent was removed by rotary evaporation and the crude product was purified by column chromatography (EtOAc:hexanes = 1:9) to give **8o** (0.133 mg, 0.580 mmol, 73%) as colorless oil. R_f: 0.45 (EtOAc:hexanes = 1:4). IR (neat, NaCl) cm^{-1}: 3400 (s), 3122 (w), 3069 (w), 2975 (s), 2937 (s), 2869 (m), 1614 (m), 1557 (m), 1463 (m), 1363 (s), 1296 (s), 1269 (m), 1249 (m), 1232 (m), 1170 (s), 1141 (s), 1058 (m). ^{1}H NMR ($CDCl_3$, 400 MHz) δ: 6.87(dd, 1H, *J* = 5,0, 3.3 Hz), 6.80 (dd, 1H, *J* = 5.0, 2.9 Hz), 3.67 (m, 1H), 3.47 (m, 1H), 2.17 (dt, 1H, *J* = 6.1, 1.5 Hz), 2.13 (br. s, 1H), 1.94 (dt, 1H, *J* = 6.1, 1.7 Hz), 1.38 (s, 3H), 1.37 (s, 3H). ^{13}C NMR ($CDCl_3$, 100 MHz) δ: 154.1, 142.2, 141.6, 126.0, 71.9, 70.7, 60.2, 53.0, 28.1, 28.0. Anal. calcd. for $C_{10}H_{13}BrO$: C 52.42, H 5.72; found C 52.61, H 5.70.

*2-Bromo-3-(1,1-diphenyl-1-hydroxymethyl)norbornadiene (**8p**)*

tert-Butyllithium (1.20 mL, 1.7M, 2.04 mmol) was added to a flame-dried flask containing dibromide **7** (225 mg, 0.902 mmol) in THF (4.5 mL) at –78°C. After the yellow mixture was stirred for 1 h, benzophenone (204 mg, 1.12 mmol) was added at –78°C. The mixture was stirred at –78°C for 3 h. After quenching the mixture with water (15 mL), the aqueous layer was extracted with diethyl ether (4 × 15 mL), and the combined organic layers were washed sequentially with water (20 mL) and brine (20 mL) and dried over magnesium sulfate. The solvent was removed by rotary evaporation and the crude product was purified by column chromatography (EtOAc:hexanes = 1:19) to give **8p** (210 mg, 0.594 mmol, 66%) as colorless oil. R_f: 0.40 (EtOAc:hexanes = 1:9). IR (neat, NaCl) cm^{-1}: 3560 (m), 3061 (m), 2938 (m), 2868 (m), 1557 (w), 1492 (s), 1448 (s), 1329 (m), 1295 (s), 1259 (w), 1210 (w), 1163 (m), 1032 (s), 1017 (s). ^{1}H NMR ($CDCl_3$, 400 MHz) δ: 7.34–7.25 (m, 10H), 6.79 (dd, 1H, *J* = 4.7, 3.0 Hz), 6.48 (dd, 1H, *J* = 4.8, 2.9 Hz), 3.58 (m, 1H), 3.41 (m, 1H), 2.98 (s, 1H), 2.36 (dt, 1H, *J* = 6.2, 1.5 Hz), 1.95 (dt, 1H, *J* = 6.3, 1.7 Hz). ^{13}C NMR ($CDCl_3$, 100 MHz) δ: 153.0, 143.81, 143.77, 142.5, 140.2, 129.7, 128.1, 128.0, 127.6, 127.5, 80.7, 70.3, 60.7, 54.5. HRMS *m/z* for $C_{20}H_{17}BrO$: calcd. 352.0463; found 352.0461.

*2-Hexyl-3-methylnorbornadiene (**9a**)*

tert-Butyllithium (0.96 mL, 1.7M, 1.63 mmol) was added to a flame-dried flask containing bromide **8b** (151 mg, 0.817 mmol) in THF (4 mL) at –78°C. After the yellow mixture was stirred for 20 min, 1-bromohexane (0.25 mL, 1.78 mmol) was added at –78°C. The mixture was stirred at –78°C for 45 min then at room temperature for 1 h. After quenching the mixture with water (5 mL), the aqueous layer was extracted with diethyl ether (3 × 10 mL), and the combined organic layers were washed sequentially with water (10 mL) and brine (10 mL) and dried over magnesium sulfate. The solvent was removed by rotary evaporation and the crude product was purified by column chromatography (hexanes) to give **9a** (124 mg, 0.652 mmol, 80%) as colorless oil. R_f: 0.83 (hexanes). IR (neat, NaCl) cm^{-1}: 2970 (s), 2938 (s), 2870 (s), 1558 (w), 1440 (m), 1378 (w), 1295 (m), 715 (s). ^{1}H NMR ($CDCl_3$, 400 MHz) δ: 6.74 (m, 2H), 3.29 (br. s, 1H), 3.20 (br. s, 1H), 2.13 (m, 1H), 2.02 (m, 1H), 1.88 (dt, 1H, *J* = 5.6, 1.5 Hz), 1.82 (dm, 1H, *J* = 5.6 Hz), 1.69 (s, 3H), 1.40–1.17 (m, 8H), 0.87 (t, 3H, *J* = 6.8 Hz). ^{13}C NMR ($CDCl_3$, 100 MHz) δ: 146.3, 142.8, 142.6, 142.1, 70.9, 55.2, 53.2, 31.8, 28.9, 28.0, 27.4, 22.6, 14.2, 14.1. Anal. calcd. for $C_{14}H_{22}$: C 88.35, H 11.65; found C 88.04, H 11.69.

*1-Bromo-4-(3-methyl-2-norbornadienyl)butane (**9b**)*

tert-Butyllithium (30.0 mL, 1.7M, 51.0 mmol) was added to a flame-dried flask containing bromide **8b** (4.40 g, 23.8 mmol) in THF (120 mL) at –78°C. After stirring the mixture for 1 h, the resulting yellow mixture was added to a flame-dried flask containing 1,4-dibromobutane (18.0 mL, 151 mmol) in THF (120 mL) at –78°C. The mixture was stirred at –78°C for 30 min then at room temperature for 12 h. After quenching the mixture with water (300 mL), the aqueous layer was extracted with diethyl ether (4 × 150 mL), and the combined organic layers were washed sequentially with water (150 mL) and brine (150 mL) and dried over magnesium sulfate. The solvent was removed by rotary evaporation and the crude product was purified by vacuum distillation to give two fractions. The first fraction (4–6 torr (1 torr = 133.322 Pa) at 70–80°C) contained mainly the excess 1,4-dibromobutane. The second fraction (0.4–1 torr (1 torr = 133.322 Pa) at 60–80°C) contained **9b** (2.35 g, 9.74 mmol, 41%) as colorless oil. R_f: 0.54 (hexanes). IR (neat, NaCl) cm^{-1}: 3066 (w), 2963 (s), 2932 (s), 2862 (m), 1557 (w), 1438 (m), 1376 (w), 1301 (m), 1249 (w), 1230 (w), 1202 (w). ^{1}H NMR ($CDCl_3$, 400 MHz) δ: 6.74 (m, 2H), 3.38 (t, 2H, *J* = 7.0 Hz), 3.29 (br. s, 1H), 3.22 (m, 1H), 2.17 (m, 1H), 2.06 (m, 1H), 1.89 (dt, 1H, *J* = 5.7, 1.5 Hz), 1.84 (m, 1H), 1.74 (m, 2H), 1.69 (br. s, 3H), 1.52 (m, 2H). ^{13}C NMR ($CDCl_3$, 100 MHz) δ: 145.3, 143.5, 142.7, 142.1,

© 2000 NRC Canada

70.9, 55.3, 53.1, 33.9, 32.1, 27.0, 25.9, 14.2. HRMS *m/z* for $C_{12}H_{17}Br$: calcd. 240.0514; found 240.0516.

*2-Methyl-3-trimethylsilylnorbornadiene (**9c**)*

tert-Butyllithium (0.99 mL, 1.7M, 1.68 mmol) was added to a flame-dried flask containing bromide **8b** (156 mg, 0.845 mmol) in THF (4 mL) at –78°C. After the yellow mixture was stirred for 20 min, chlorotrimethylsilane (0.27 mL, 2.13 mmol) was added at –78°C. The mixture was stirred at –78°C for 45 min then at room temperature for 1 h. After quenching the mixture with water (5 mL), the aqueous layer was extracted with diethyl ether (3 × 10 mL), and the combined organic layers were washed sequentially with water (10 mL) and brine (10 mL) and dried over magnesium sulfate. The solvent was removed by rotary evaporation and the crude product was purified by column chromatography (hexanes) to give **9c** (106 mg, 596 mmol, 71%) as colorless oil. R_f: 0.79 (hexanes). IR (neat, NaCl) cm^{-1}: 2965 (s), 2933 (s), 2864 (s), 1608 (m), 1556 (m), 1439 (w), 1299 (s), 1247 (s), 835 (s), 709 (s). ^1H NMR ($CDCl_3$, 400 MHz) δ: 6.72 (dd, 1H, *J* = 5.2, 3.1 Hz), 6.67 (dd, 1H, *J* = 5.2, 2.9 Hz), 3.63 (br. s, 1H), 3.27 (br. s, 1H), 1.93 (s, 3H), 1.83 (dm, 1H, *J* = 6.0 Hz), 1.77 (dm, 1H, *J* = 6.0 Hz), 0.08 (m, 9H). ^{13}C NMR ($CDCl_3$, 100 MHz) δ: 164.4, 143.6, 141.5, 140.9, 71.6, 57.9, 54.5, 18.1, –0.9. Anal. calcd. for $C_{11}H_{18}Si$: C 74.08, H 10.17; found C 74.38, H 10.13.

*2-Chloro-3-methylnorbornadiene (**9d**)*

tert-Butyllithium (1.00 mL, 1.7M, 1.70 mmol) was added to a flame-dried flask containing bromide **8b** (159 mg, 0.860 mmol) in THF (4 mL) at –78°C. After the yellow mixture was stirred for 20 min, *p*-toluenesulfonyl chloride (259 mg, 1.36 mmol) was added at –78°C. The mixture was stirred at –78°C for 45 min then at room temperature for 1 h. After quenching the mixture with water (5 mL), the aqueous layer was extracted with diethyl ether (3 × 10 mL), and the combined organic layers were washed sequentially with water (10 mL) and brine (10 mL) and dried over magnesium sulfate. The solvent was removed by rotary evaporation and the crude product was purified by column chromatography (hexanes) to give **9d** (88.3 mg, 0.628 mmol, 73%) as colorless oil. R_f: 0.78 (hexanes). IR (neat, NaCl) cm^{-1}: 2970 (s), 2938 (s), 2870 (m), 1670 (w), 1646 (m), 1440 (m), 1295 (s), 1015 (s). ^1H NMR ($CDCl_3$, 400 MHz) δ: 6.87 (dd, 1H, *J* = 4.9, 2.9 Hz), 6.79 (dd, 1H, *J* = 4.9, 2.9 Hz), 3.37 (br. s, 1H), 3.35 (br. s, 1H), 2.19 (dt, 1H, *J* = 6.0, 1.6 Hz), 2.01 (dt, 1H, *J* = 5.6, 2.0 Hz), 1.75 (s, 3H). ^{13}C NMR ($CDCl_3$, 100 MHz) δ: 143.6, 142.0(2), 139.6, 71.0, 56.3, 54.8, 13.7.

*2-Iodo-3-methylnorbornadiene (**9e**)*

tert-Butyllithium (0.97 mL, 1.7M, 1.65 mmol) was added to a flame-dried flask containing bromide **8b** (152 mg, 0.822 mmol) in THF (4 mL) at –78°C. After the yellow mixture was stirred for 20 min, iodine (437 mg, 1.72 mmol) was added at –78°C. The mixture was stirred at –78°C for 30 min then at room temperature for 1 h. After quenching the mixture with saturated sodium thiosulfate (5 mL), the aqueous layer was extracted with diethyl ether (3 × 10 mL), and the combined organic layers were washed sequentially with water (10 mL) and brine (10 mL) and dried over magnesium sulfate. The solvent was removed by rotary evaporation and the crude product was purified by column chromatography (hexanes) to give **9e** (115 mg, 0.496 mmol, 60%) as colorless oil. R_f: 0.79 (hexanes). IR (neat, NaCl) cm^{-1}: 2970 (s), 2938 (s), 2870 (m), 1646 (w), 1558 (w), 1440 (m), 1295 (s), 1163 (m), 715 (s). ^1H NMR ($CDCl_3$, 400 MHz) δ: 6.86 (dd, 1H, *J* = 4.9, 2.9 Hz), 6.75 (dd, 1H, *J* = 4.9, 3.0 Hz), 3.58 (br. s, 1H), 3.37 (br. s, 1H), 2.19 (dt, 1H, *J* = 6.0, 1.6 Hz), 1.99 (dt, 1H, *J* = 6.0, 1.6 Hz), 1.80 (s, 3H). ^{13}C NMR ($CDCl_3$, 100 MHz) δ: 155.4, 142.3, 141.1, 100.2, 72.0, 61.0, 55.2, 18.5. HRMS *m/z* for C_8H_9I: calcd. 231.9751; found 231.9760.

*2-ethoxycarbonyl-3-methylnorbornadiene (**9f**)*

tert-Butyllithium (1.10 mL, 1.7M, 1.87 mmol) was added to a flame-dried flask containing bromide **8b** (158 mg, 0.852 mmol) in THF (2.0 mL) at –78°C. After stirring the mixture for 1 h, the resulting yellow mixture was added to a flame-dried flask containing ethyl chloroformate (0.38 mL, 4.0 mmol) in THF (2.5 mL) at –78°C. The mixture was stirred at –78°C for 3 h. After quenching the mixture with water (15 mL), the aqueous layer was extracted with diethyl ether (4 × 15 mL), and the combined organic layers were washed sequentially with water (20 mL) and brine (20 mL) and dried over magnesium sulfate. The solvent was removed by rotary evaporation and the crude product was purified by column chromatography (EtOAc:hexanes = 1:9) to give **9f** (109 mg, 0.655 mmol, 77%) as colorless oil. R_f: 0.50 (EtOAc:hexanes = 1:4). IR (neat, NaCl) cm^{-1}: 2978 (m), 2939 (m), 2870 (w), 1702 (s), 1632 (m), 1558 (w), 1370 (m), 1331 (m), 1314 (m), 1295 (s), 1249 (m), 1237 (s), 1189 (m), 1146 (m), 1101 (m), 1066 (m), 1047 (m), 1019 (w). ^1H NMR ($CDCl_3$, 400 MHz) δ: 6.86 (dd, 1H, *J* = 5.0, 3.0 Hz), 6.70 (dd, 1H, *J* = 4.9, 3.2 Hz), 4.14 (m, 2H), 3.86 (br. s, 1H), 3.37 (br. s, 1H), 2.19 (s, 3H), 2.02 (dm, 1H, *J* = 6.4 Hz), 1.92 (dm, 1H, *J* = 6.4 Hz), 1.26 (t, 3H, *J* = 7.1 Hz). ^{13}C NMR ($CDCl_3$, 100 MHz) δ: 169.4, 165.9, 144.0, 140.3, 138.3, 70.8, 59.6, 58.0, 50.9, 17.1, 14.3. Anal. calcd. for $C_{11}H_{14}O_2$: C 74.13, H 7.92; found C 73.99, H 7.95.

*2-(2-Methyl-3-norbornadienyl)-2-propanol (**9g**)*

tert-Butyllithium (0.80 mL, 1.7M, 1.4 mmol) was added to a flame-dried flask containing bromide **8b** (116 mg, 0.627 mmol) in THF (3.0 mL) at –78°C. After the yellow mixture was stirred for 1 h, acetone (0.35 mL, 4.8 mmol) was added at –78°C. The mixture was stirred at –78 °C for 3 h. After quenching the mixture with water (15 mL), the aqueous layer was extracted with diethyl ether (4 × 15 mL), and the combined organic layers were washed sequentially with water (20 mL) and brine (20 mL) and dried over magnesium sulfate. The solvent was removed by rotary evaporation and the crude product was purified by column chromatography (EtOAc:hexanes = 1:4) to give **9g** (82 mg, 0.50 mmol, 80%) as colorless oil. R_f: 0.45 (EtOAc:hexanes = 1:4). IR (neat, NaCl) cm^{-1}: 3384 (s), 3063 (m), 2971 (s), 2932 (s), 2864 (s), 1557 (w), 1448 (m), 1372 (m), 1299 (s), 1250 (m), 1236 (m), 1174 (m), 1132 (m), 1112 (m), 1023 (w). ^1H NMR ($CDCl_3$, 400 MHz) δ: 6.76 (m, 2H), 3.48 (m, 1H), 3.16 (m, 1H), 1.92 (s, 3H), 1.89 (dm, 1H, *J* = 5.7 Hz), 1.75 (dm, 1H, *J* = 5.7 Hz), 1.53 (br. s, 1H), 1.34 (s, 3H), 1.32 (s, 3H). ^{13}C NMR ($CDCl_3$, 100 MHz) δ: 150.3, 143.0, 142.9,

© 2000 NRC Canada

141.9, 72.4, 70.0, 57.6, 52.5, 29.2, 28.8, 15.9. HRMS *m/z* for $C_{11}H_{16}O$: calcd. 164.1201; found 164.1206.

*2-(4-bromobutyl)-3-hexylnorbornadiene (**9h**)*

tert-Butyllithium (7.50 mL, 1.7M, 12.8 mmol) was added to a flame-dried flask containing bromide **8c** (1.48 g, 5.80 mmol) in THF (30 mL) at –78°C. After stirring the mixture for 1 h, the resulting yellow mixture was added to a flame-dried flask containing 1,4-dibromobutane (4.50 mL, 37.7 mmol) in THF (30 mL) at –78°C. The mixture was stirred at –78°C for 1 h then at room temperature for 12 h. After quenching the mixture with water (100 mL), the aqueous layer was extracted with diethyl ether (4 × 50 mL), and the combined organic layers were washed sequentially with water (100 mL) and brine (100 mL) and dried over magnesium sulfate. The solvent was removed by rotary evaporation and the excess 1,4-dibromobutane was removed by bulb-to-bulb distillation (2.5 torr (1 torr = 133.322 Pa) at 65°C for 2 h) and the crude product was purified by column chromatography (hexanes) to give **9h** (980 mg, 3.15 mmol, 54%) as colorless oil. R_f: 0.50 (EtOAc:hexanes = 1:9). IR (neat, NaCl) cm^{-1}: 3063 (w), 2960 (s), 2928 (s), 2857 (s), 1557 (w), 1456 (m), 1378 (w), 1303 (m), 1249 (w). ^{1}H NMR ($CDCl_3$, 400 MHz) δ: 7.26 (m, 2H), 3.39 (t, 2H, *J* = 6.9 Hz), 3.29 (m, 2H), 2.21–1.95 (m, 4H), 1.87 (dt, 1H, *J* = 5.6, 1.6 Hz), 1.84 (dm, 1H, *J* = 5.6 Hz), 1.76 (m, 2H), 1.56–1.22 (m, 10H), 0.88 (t, 3H, *J* = 6.8 Hz). ^{13}C NMR ($CDCl_3$, 100 MHz) δ: 147.6, 145.6, 142.5, 142.3, 71.0, 53.3, 53.0, 33.9, 32.3, 31.7, 29.0, 28.1, 27.5, 27.1, 26.1, 22.6, 14.1. HRMS *m/z* for $C_{17}H_{27}Br$: calcd. 310.1297; found 310.1303.

*2-methoxycarbonyl-3-(4-tetrahydropyranyloxybutyl)norbornadiene (**9i**)*

tert-Butyllithium (14.0 mL, 1.7M, 23.8 mmol) was added to a flame-dried flask containing bromide **8d** (3.00 g, 9.17 mmol) in THF (17.0 mL) at –78°C. After stirring the mixture for 1 h, the resulting yellow mixture was added to a flame-dried flask containing methyl chloroformate (3.0 mL, 39 mmol) in THF (7.0 mL) at –78°C. The mixture was stirred at –78°C for 3 h. After quenching the mixture with water (20 mL), the aqueous layer was extracted with diethyl ether (4 × 20 mL), and the combined organic layers were washed sequentially with water (25 mL) and brine (25 mL) and dried over magnesium sulfate. The solvent was removed by rotary evaporation and the crude product was purified by column chromatography (EtOAc:hexanes = 1:9) to give **9i** (2.07 g, 6.76 mmol, 74%) as colorless oil. R_f: 0.55 (EtOAc:hexanes = 1:4). IR (neat, NaCl) cm^{-1}: 2941 (s), 2868 (m), 1700 (s), 1695 (s), 1558 (w), 1435 (m), 1342 (m), 1295 (s), 1238 (s), 1200 (m), 1163 (m), 1138 (m), 1119 (m), 1103 (m), 1074 (s), 1034 (s), 1022 (m). ^{1}H NMR ($CDCl_3$, 400 MHz) δ: 6.85 (dd, 1H, *J* = 5.0, 3.0 Hz), 6.67 (dd, 1H, *J* = 4.7, 3.3 Hz), 4.55 (m, 1H), 3.86–3.84 (m, 2H), 3.72 (m, 1H), 3.69 (s, 3H), 3.50–3.48 (m, 2H), 3.37 (m, 1H), 2.76–2.64 (m, 2H), 2.01 (dm, 1H, *J* = 6.4 Hz), 1.94 (dm, 1H, *J* = 6.4 Hz), 1.80 (m, 1H), 1.69 (m, 1H), 1.61–1.44 (m, 8H). ^{13}C NMR ($CDCl_3$, 100 MHz) δ: 173.3, 166.2, 143.8, 140.7, 138.5, 98.81, 98.78, 71.0, 67.2, 62.30, 62.27, 55.9, 51.0, 50.9, 30.7, 29.9, 29.3, 25.4, 23.5, 19.64, 19.62. Anal. calcd. for $C_{18}H_{26}O_4$: C 70.56, H 8.55; found C 70.67, H 8.52.

Acknowledgements

We thank the Natural Sciences and Engineering Research Council of Canada (NSERC) and the University of Guelph for generous financial support of our program. GKT thanks the Ontario government for a graduate scholarship.

References

1. C. Yip, S. Handerson, R. Jordan, and W. Tam. Org. Lett. **1**, 791 (1999).
2. H.L. Holmes. Org. React. **4**, 60 (1948).
3. B.M. Trost, I. Fleming, and L.A. Paquette. Comprehensive organic synthesis. Vol. 5. Pergamon, Oxford. 1991. Chap. 4.1.
4. K. Ishihara, S. Kondo, H. Kurihara, and H. Yamamoto. J. Org. Chem. **62**, 3026 (1997), and refs. therein.
5. E.J. Corey and T.W. Lee. Tetrahedron Lett. **38**, 5755 (1997), and refs. therein.
6. T. Nishikubo, A. Kameyama, K. Kishi, and Y. Mochizuki. J. Polym. Sci. Part A: Polym. Chem. **32**, 2765 (1994), and refs. therein.
7. E.J. Corey, M. Shibasaki, K.C. Nicolaou, C.L. Malmsten, and B. Samuelesson. Tetrahedron Lett. 737 (1976).
8. M. Lee, I. Ikeda, T. Kawabe, S. Mori, and K. Kanematsu. J. Org. Chem. **61**, 3406 (1996).
9. K. Sato, O. Miyamoto, S. Inoue, and K. Honda. Chem. Lett. 1183 (1981).
10. H. Monti, C. Corriol, and M. Bertrand. Tetrahedron Lett. **23**, 5539 (1982).
11. W.G. Dauben and R.L. Cargill. Tetrahedron, **15**, 197 (1961).
12. G.S. Hammond, N.J. Turro, and A. Fisher. J. Am. Chem. Soc. **83**, 4674 (1961).
13. N.J. Turro, W.R. Cherry, M.F. Manfred, and M.J. Mairbach. J. Am. Chem. Soc. **99**, 7390 (1977).
14. H. Tomioka, Y. Hamano, and Y. Izawa. Bull. Chem. Soc. Jpn. **60**, 821 (1987).
15. E.E. Bonfantini and D.L. Officer. J. Chem. Soc. Chem. Commun. 1445 (1994).
16. M. Maafi, C. Lion, and J.J. Aaron. New J. Chem. **20**, 559 (1996).
17. V.A. Chernoivanov, A.D. Dubonosov, V.A. Bren, V.I. Minkin, A.N. Suslov, and G.S. Borodkin. Mol. Cryst. Liq. Cryst. **297**, 239 (1997).
18. M. Stäble, R. Lehmann, J. Kramaø, and M. Schlosser. Chimia, **39**, 229 (1985).
19. H.D. Verkruijsse and L. Brandsma. Recl. Trav. Chim. Pays-Bas, **105**, 66 (1986).
20. J. Kenndoff, K. Polborn, and G. Szeimies. J. Am. Chem. Soc. **112**, 6117 (1990).
21. P.G. Gassman and I. Gennick. J. Am. Chem. Soc. **102**, 6864 (1980).
22. W.J. Scott and J.K. Stille. J. Am. Chem. Soc. **108**, 3033 (1986).
23. V. Farina, V. Krishnamurthy, and W.J. Scott. Org. React. **50**, 1 (1997).
24. N. Miyaura and A. Suzuki. Chem. Rev. **95**, 2457 (1995).
25. R.F. Heck. *In* Comprehensive organic synthesis. Vol. 4. *Edited by* B.M. Trost and I. Fleming. Pergamon Press, New York. 1991. pp. 883–863.
26. K. Sonogashira. *In* Comprehensive organic synthesis. Vol. 3. *Edited by* B.M. Trost and I. Fleming. Pergamon Press, New York. 1991. pp. 521–549.
27. W.C. Still, M. Kahn, and A. Mitra. J. Org. Chem. **43**, 2923 (1978).

© 2000 NRC Canada

Crystallographic and spectroscopic studies of adducts of indium (III) iodide with two cyclic ketones

M.A. Brown and D.G. Tuck

Abstract: Indium(III) iodide forms a 1:1 adduct with 9-xanthenone, of quasi-tetrahedral structure; triclinic, a = 10.805(4), b = 11.494(4), c = 7.493 (2) Å, α = 104.12(3), β = 106.35(3), γ = 91.165(3)°, V = 860.8(5) Å^3, Z = 2, space group $P\bar{1}$. With 9-fluorenone, the adduct has 1:2 stoichiometry, and approximately D_{3h} symmetry in the InI_3O_2 kernel; the structure is triclinic, a =11.212(2), b = 16.504(3), c = 7.537(2) Å, α = 94.57(2), β = 109.05(1), γ = 91.165(15)°, V = 1312.6(4) Å^3, Z = 2, space group $P\bar{1}$. The solid structures, and the solution chemistry, are compared with those of related neutral derivatives of indium(III) halides.

Key words: Indium(III) iodide, solution chemistry, crystal structures, adducts.

Résumé : L'iodure d'indium(III) forme un adduit 1:1 avec la 9-xanthénone de structure pratiquement tétraédrique; triclinique, groupe d'espace $P\bar{1}$, avec a = 10,805(4), b = 11,494(4) et c = 7,493(2) Å, α = 104,12(3), β = 106,35(3) et γ = 91,165(3)°, V = 860,8(5) Å^3, Z = 2. Avec la 9-fluorénone, l'adduit est de stoechiométrie 1:2 et de symétrie approximativement D_{3h} dans le noyau InI_3O_2; la structure est triclinique, groupe d'espace $P\bar{1}$, avec a = 11,212(2), b = 16,504(3) et c = 7,537(2) Å, α = 94,57(2), β = 109,05(1) et γ = 91,165(3)°, V = 1312,6(4) Å^3, Z = 2. On compare les structures solides et la chimie en solution avec celles de dérivés neutres apparentés d'halogénures d'indium(III).

Mots clés : iodure d'indium(III), chimie en solution, structures cristallines, adduits.

[Traduit par la Rédaction]

Introduction

Structural and spectroscopic studies of the neutral and anionic derivatives of the indium(III) halides have done much to help in elucidating the possible modes of coordination for such molecules in both solution and crystalline phases (1). A recent paper from this laboratory re-examined earlier work on triphenylphosphine and bis(diphenylphosphino)ethane (dppe) adducts of indium(III) iodide, and showed that the species in solution are related to, but not necessarily identical with, those in the solid phase (2). Similar conclusions were reached in analogous studies of gallium(III) iodide derivatives (3).

In addition to the intrinsic interest of such work, the solution behaviour of the neutral adducts of indium(III) halides is fundamental to an understanding of electron transfer reactions involving these compounds and substituted ortho- and paraquinones (4). It proved impossible to obtain crystals of the quinone adducts, and we have therefore studied the structure and spectroscopy of analogous compounds with the cyclic ketones xanthone (9-xanthenone) and 9-fluorenone, which form 1:1 and 1:2 adducts respectively in the solid state.

Received September 21, 1999. Published on the NRC Research Press website on May 3, 2000.

M.A. Brown and D.G. Tuck.[1] Department of Chemistry and Biochemistry, University of Windsor, Windsor, ON N9B 3P4, Canada.

[1]Author to whom correspondence may be addressed. Telephone (519) 253-4232 ext. #3541. Fax: (519) 973-7098. e-mail: dgtuck@uwindsor.ca

Experimental section

General techniques

Indium(III) iodide was prepared by reacting gram quantities of the elements in refluxing xylene (5). Xanthone and fluorenone were used as supplied (Aldrich, 98% pure). Solvents were distilled from suitable drying agents, and stored over molecular sieves.

Microanalysis was by Canadian Microanalytical Services Ltd. Carbon-13 and proton NMR spectra were recorded on a Bruker AC300L instrument ($\delta(Me_4Si)$ = 0), and infrared spectra on a Nicolet 3DX spectrometer.

Preparative

(i) Xanthone

Xanthone (0.20 g, 1.02 mmol) and InI_3 (0.50 g, 1.01 mmol) were dissolved in tetrahydrofuran (50 mL) and the solution was stirred under nitrogen for 12 h at room temperature. The volume of the solution was reduced by 50%; addition of *n*-hexane (10 mL) led to opalescence and on subsequent cooling a pale yellow solid precipitated. This was recrystallized from $CHCl_3$ to give pale yellow crystals of the 1:1 adduct, $InI_3(C_{13}H_8O_2)$. Anal. calcd. for $C_{13}H_8InI_3$: C 22.6, H 1.17; found: C 23.6, H 1.25. Yield 0.42 g, 61%. This compound is highly sensitive to moisture.

© 2000 NRC Canada

Table 1. Summary of crystal intensity data, collection, and structural refinement for $InI_3(C_{13}H_8O_2)$ **(1)** and $InI_3(C_{13}H_8O)_2$ **(2)**.

	1	**2**
Chemical formula	$C_{13}H_8O_2InI_3$	$C_{26}H_{16}O_2InI_3$
M	691.74	855.92
Crystal system	triclinic	triclinic
Space group	$P\bar{1}$	$P\bar{1}$
a (Å)	10.805(4)	11.212(2)
b (Å)	11.494(4)	16.504(3)
c (Å)	7.493(2)	7.537(2)
α (°)	104.12(3)	94.57(2)
β (°)	106.35(3)	109.05(1)
γ (°)	91.165(15)	91.165(15)
V (Å^3)	860.8(5)	1312.6(4)
Z	2	2
F(000)	620	792
D_c (g cm^{-3})	2.66	2.17
Crystal dimensions (mm)	0.1 × 0.1 × 0.1	0.1 × 0.1 × 0.1
μ (cm^{-1})	6.73	4.45
2θ max (°)	50.0	50.0
Total reflections measured	3223	4896
Unique data used ($I \geq 3\sigma(I)$)	3044	4896
T (°C)	23	23
No. of parameters	191	160
Ratio observations/parameters	7.2	12.4
R	0.058	0.048
R_w	0.067	0.039
Maximum shift/error in final cycle	0.68	2.09
Maximum, minimum peaks in final difference map (eÅ^{-3})	0.99, –1.20	0.78, –0.99

(ii) Fluorenone

In a similar reaction involving InI_3 (0.50 g, 1.01 mmol) and fluorenone (0.20 g, 1.1 mmol), the solution became red after about 30 min. Evaporation of the solvent after 12 h stirring gave orange-red crystals suitable for X-ray crystallography. This product is the 1:2 adduct, $InI_3(C_{13}H_8O)_2$. Anal. calcd. for $C_{26}H_{16}O_2InI_3$: C 36.5, H 1.88; found: C 36.5, H 1.87. Yield 0.38 g, 81% based on fluorenone.

Crystallographic analysis

The procedures for both $InI_3(C_{13}H_8O_2)$ **(1)** and $InI_3(C_{13}H_8O)_2$ **(2)** were essentially identical. A suitable crystal on a glass fibre was mounted in a Rigaku AFC6S diffractometer, equipped with graphite monochromated Mo-Kα radiation (λ = 0.71069 Å) and a rotating anode generator. Cell constants, and orientation matrices for data collection, were obtained from least-squares refinements, using 20 carefully centred reflections in the range $12.61 < 2\theta < 19.62°$. In each case, the space group was uniquely identified as $P\bar{1}$ (No. 2) by the lack of systematic absences, and this was confirmed by subsequent solution and refinement of the structures. Details of the intensity collection are given in Table 1. The intensities of three representative reflections were measured after every 150 reflections, and a linear correction factor was applied to correct for decay. Absorption corrections were made using PSI scan, and the values were also corrected for Lorentz and polarization effects. The structure was solved by direct methods, and expanded using Fourier techniques. In refining **1**, all non-hydrogen atoms were refined anisotropically, but for **2**, only In, I, and O were so treated due to the restricted data available. In both cases, hydrogen atoms on carbon were included in ideal positions (r = 0.95 Å), but were not refined. The final Fourier difference map calculations showed no peaks of chemical significance.

Neutral-atom scattering factors were taken from Cromer and Waber (6). Anomalous dispersion effects were included in the calculations (7); the values for $-f'$ and $-\Delta f''$ were those published by Cromer (8). All calculations were performed using the TEXSAN[2] crystallographic software package. The structures of the molecules are shown in Figs. 1 and 2, positional parameters are in Tables 2 and 4, and important bond distances and angles in Tables 3 and 5.

Tables of hydrogen-atom coordinates and thermal parameters and anisotropic thermal parameters for other atoms, other other bond distances and angles, and least-squares planes are available as supplementary data.[3]

[2] TEXSAN–TEXRAY structure and analysis package. Molecular Structure Corporation, The Woodlands, Tex. 1985.

[3] This supplementary data can be purchased from: The Depository of Unpublished Data, Document Delivery, CISTI, National Research Council Canada, Ottawa, Ontario, Canada, K1A 0S2. Tables of hydrogen atom coordinates and structural data have also been deposited with the Cambridge Crystallographic Data Centre and can be obtained on request from: The Director, Cambridge Crystallographic Data Centre, University Chemical Laboratory, 12 Union Road, Cambridge, CB2 1EZ, U.K.

© 2000 NRC Canada

Fig. 1. The molecular structure of $InI_3(C_{13}H_8O_2)$, showing the numbering system; ORTEP diagram, with 30% probability ellipsoids.

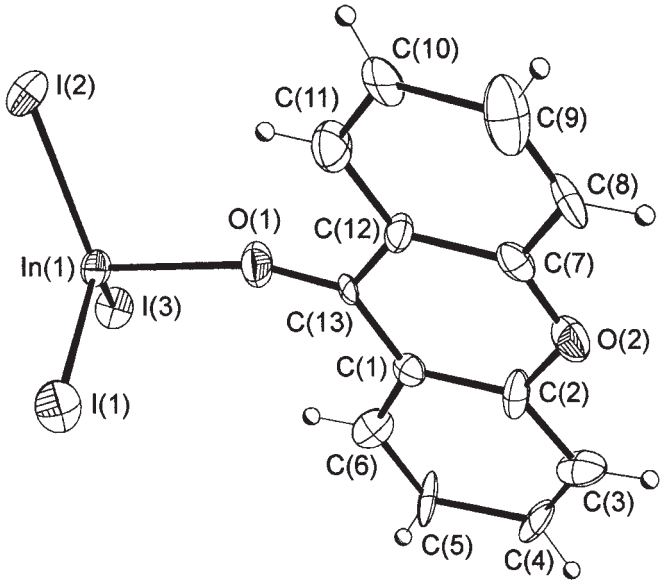


Table 2. Positional parameters and isotropic thermal parameters for the non-hydrogen atoms of $InI_3(C_{13}H_8O_2)$ **(1)**.

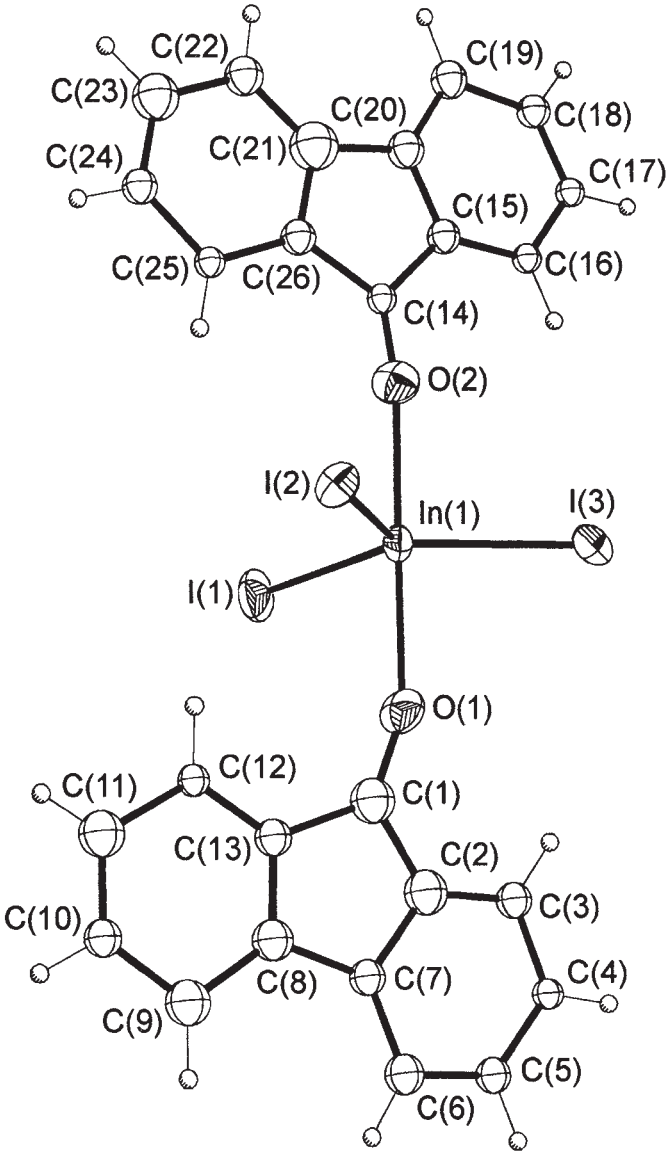
Atom	*x*	*y*	*z*	*B*(eq)
I(1)	0.1983(3)	0.8962(2)	0.0827(3)	5.9(1)
I(2)	–0.0019(2)	0.8171(2)	0.5035(2)	5.6(1)
I(3)	0.3926(2)	0.9732(2)	0.7101(2)	5.00(9)
In(1)	0.2107(2)	0.8626(2)	0.4256(2)	3.35(7)
O(1)	0.2925(2)	0.6754(2)	0.3837(2)	5(1)
O(2)	0.473(3)	0.360(3)	0.1751(2)	5(1)
C(1)	0.476(2)	0.575(3)	0.301(2)	3(1)
C(2)	0.534(5)	0.465(2)	0.229(3)	4(1)
C(3)	0.661(3)	0.448(6)	0.220(3)	6(2)
C(4)	0.734(3)	0.549(5)	0.278(8)	5(1)
C(5)	0.673(4)	0.668(3)	0.344(4)	5(1)
C(6)	0.552(3)	0.673(5)	0.353(3)	5(1)
C(7)	0.350(3)	0.362(3)	0.172(4)	4(1)
C(8)	0.2816(3)	0.259(3)	0.102(2)	5(1)
C(9)	0.1527(3)	0.2634(4)	0.093(3)	8(2)
C(10)	0.0776(3)	0.3683(3)	0.1622(3)	7(2)
C(11)	0.145(5)	0.4758(4)	0.2361(3)	6(2)
C(12)	0.277(6)	0.469(5)	0.2325(4)	3(1)
C(13)	0.346(3)	0.580(5)	0.310(4)	3(1)

Results and discussion

Crystallographic studies

The structure of the xanthone adduct of InI_3 (Fig. 1) demonstrates quasi-tetrahedral symmetry, which is rare for neutral adducts of indium(III) halides, and especially unusual when the ligand is an oxygen-donor, since such ligands typically form 1:2 or 1:3 complexes (1). The In—I bond distances are in the normal range for analogous four-coordinate adducts (r = 2.68 ± 0.04 Å (9)), but slightly lower by approx. 0.02 Å than those in substituted phosphino com-

Fig. 2. The molecular structure of $InI_3(C_{13}H_8O)_2$, showing the numbering system; ORTEP diagram, with 30% probability ellipsoids.



plexes (2). Other noteworthy features are the range of values, 2.654(2)–2.672(1) Å, and the fact that the sum of the angles at the indium atom is 648.8° which is significantly different from that calculated for tetrahedral coordination (657°).

The In—O bond distance, 2.1872(6) Å, is close to that in compounds with strongly polar In—O bonds; for example, r(In—O)(av) = 2.22(1) Å in In(TBSQ)Br_2pic$_2$(10) TBSQ (= 3,5-di-*tert*-butyl-1,2-semiquinonate; pic = 4-methylpyridine), 2.128(7) Å in In($O_2C_6Cl_4$)Clpic$_3$ (11), and 2.124(3) and 2.164(3) in $InCl_2$(acac)py$_2$ (12) (acac = 2,4-pentanedionate). These last three molecules are six-coordinate, and lower values of r(In—O) are to be expected in four-coordinate species in the light of related studies (cf. ref. 10). The C=O bond distance in the xanthone moiety is 1.25(5) Å, which is the same within experimental uncertainty as the value reported for 1,3,4,6,7,9-hexachloroxanthenone, 1.211(13) Å (13);

© 2000 NRC Canada

Table 3. Important bond distances (Å) and angles (°) in $InI_3(C_{13}H_8O_2)$ **(1)**.

Atom	Atom	Distance (Å)		Atom	Atom	Distance (Å)
I(1)	In(1)	2.654(2)		O(2)	C(2)	1.38(5)
I(2)	In(1)	2.672(1)		O(2)	C(7)	1.32(5)
I(3)	In(1)	2.6572(8)		C(1)	C(2)	1.38(4)
In(1)	O(1)	2.1872(6)		C(7)	C(12)	1.41(6)
O(1)	C(13)	1.25(5)				
Atom	**Atom**	**Atom**	**Angle (°)**	**Atom**	**Atom**	**Atom**	**Angle (°)**
I(1)	In(1)	I(2)	119.87(3)	I(2)	In(1)	O(1)	95.13(7)
I(1)	In(1)	I(3)	115.78(4)	I(3)	In(1)	O(1)	102.49(4)
I(1)	In(1)	O(1)	97.33(5)	In(1)	O(1)	C(13)	159(2)
I(2)	In(1)	I(3)	118.23(4)	C(2)	O(2)	C(7)	120(3)

Table 4. Positional parameters and isotropic thermal parameters for the non-hydrogen atoms of $InI_3(C_{13}H_8O)_2$ **(2)**.

Atom	*x*	*y*	*z*	*B*(eq)
I(1)	0.3281(1)	0.24365(9)	0.4339(2)	5.85(7)
I(2)	0.2927(1)	0.36989(8)	–0.0956(2)	5.44(6)
I(3)	0.3358(1)	0.09308(8)	–0.1210(2)	5.69(7)
In(1)	0.3173(1)	0.23139(8)	0.0744(2)	3.73(6)
O(1)	0.537(1)	0.2479(8)	0.183(2)	6.2(6)
O(2)	0.096(1)	0.2029(8)	–0.015(2)	6.2(6)
C(1)	0.646(2)	0.274(1)	0.280(2)	4.0(4)
C(2)	0.760(1)	0.227(1)	0.326(2)	3.5(3)
C(3)	0.774(2)	0.147(1)	0.279(2)	4.6(4)
C(4)	0.893(2)	0.117(1)	0.343(2)	5.2(4)
C(5)	0.989(2)	0.166(1)	0.446(3)	6.2(5)
C(6)	0.981(2)	0.250(1)	0.489(2)	4.9(4)
C(7)	0.861(2)	0.280(1)	0.432(2)	3.6(4)
C(8)	0.810(2)	0.360(1)	0.453(2)	4.4(4)
C(9)	0.880(2)	0.431(1)	0.547(2)	5.8(5)
C(10)	0.799(2)	0.497(1)	0.544(3)	7.0(6)
C(11)	0.677(2)	0.497(1)	0.462(3)	6.1(5)
C(12)	0.616(2)	0.423(1)	0.369(2)	5.5(5)
C(13)	0.687(2)	0.358(1)	0.370(2)	3.9(4)
C(14)	–0.018(2)	0.206(1)	–0.065(2)	3.5(3)
C(15)	–0.110(1)	0.138(1)	–0.153(2)	3.6(4)
C(16)	–0.088(2)	0.057(1)	–0.192(2)	5.4(5)
C(17)	–0.187(2)	0.006(1)	–0.274(3)	7.7(6)
C(18)	–0.302(2)	0.031(1)	–0.311(3)	7.3(6)
C(19)	–0.334(2)	0.115(1)	–0.280(2)	5.5(5)
C(20)	–0.228(2)	0.167(1)	–0.196(2)	4.2(4)
C(21)	–0.221(2)	0.255(1)	–0.137(2)	3.6(4)
C(22)	–0.311(2)	0.311(1)	–0.143(2)	5.5(4)
C(23)	–0.271(2)	0.392(1)	–0.070(3)	5.9(5)
C(24)	–0.149(2)	0.412(1)	0.007(3)	6.5(5)
C(25)	–0.053(2)	0.358(1)	0.018(2)	4.7(4)
C(26)	–0.094(1)	0.278(1)	–0.058(2)	3.9(4)

there does not appear to have been a structural determination of unsubstituted xanthone. There are no other significant differences between the coordinated xanthone and hexachloroxanthenone.

The reaction between indium(III) iodide and 9-fluorenone yields the 1:2 adduct, whose molecular structure in the solid state is based on an InI_3O_2 kernel of approximate D_{3h} symmetry (O1-In-O2 = 173.8(4°); sum of I-In-I angles = 360°). The In—I bond distances in this case are longer on average than in **1**, but significantly smaller than in the analogous phosphino derivatives $(InI_3(PPh_3)_2$, *r*(In—I) = 2.707(1) Å (2); $InI_3(PMePh_2)_2$, *r*(In—I) = 2.736(4), 2.762(2), and 2.776(2) Å (14); $[InI_3(dppe)]_3$, *r*(In—I) = 2.729(2), 2.730(2), and 2.766(3) Å (2); $(InI_3)_3(dppe)_2$ *r*(In—I) = 2.731(15) Å (15)), all of which have the same trigonal bipyramidal stereochemistry at the indium centre. The increased In—I bond distance between four and five-coordinate species is in keeping with earlier observations (9), but the significant reduction on replacing a phosphorus ligand with an oxygen donor is surprising. It seems unlikely that this is due solely to the effect of inter-ligand repulsion, since all the neutral ligands in question are quite bulky.

The In—O bonds in this molecule (*r* = 2.33(1), 2.37(1) Å) are substantially longer than in the xanthone adduct (see above), in keeping with the increased coordination number, while the C=O bonds in the coordinated ketone are identical within experimental error with that in free 9-fluorenone (1.21(2) and 1.25(2), compared with 1.220(4) Å (16)). These interdependent results indicate a relatively weak ketone → metal donation, in which case the tightening of the In—I bonds relative to those in the substituted phosphino derivatives can be ascribed to a higher positive charge at the metal in the former case.

A comparison with recent results on the 1:1 adducts of these ligands with $AlCl_3$(17) supports the argument that coordination is weak in the bis-fluorenone derivative of InI_3. The C=O bond in $AlCl_3$(fluorenone) is shorter than in the free ligand by ca 0.07 Å, and a similar result is found for the xanthenone analogue (ca. 0.05 Å). With adducts of InI_3, as noted above, there is no significant change in *r*(C=O), implying that coordination to $AlCl_3$ is stronger, in keeping with the higher charge density on the smaller metal atom. Similarly, the changes in ν(C=O) on coordination to InI_3 are ca. 5 cm^{-1} for both ligands, and these are also lower than the comparable values in the 1:1 adducts with $AlCl_3$.

We note finally an important common feature in the adducts of these cyclic ketones with both $AlCl_3$ and InI_3, namely the non-linear In—O=C bonding. The bond angles at oxygen are 159(2) and 164(2)° (av) for InI_3 and xanthone and 9-fluorenone respectively, while the values in the corresponding $AlCl_3$·L compounds are 160.0(7) and 150.2(3)° (17). This has important effects in the spectroscopic properties of

© 2000 NRC Canada

Table 5. Bond distances (Å) and angles (°) in $InI_3(C_{13}H_8O)_2$ (2).

Atom	Atom	Distance (Å)		Atom	Atom	Distance (Å)
I(1)	In(1)	2.644(2)		O(2)	C(14)	1.21(2)
I(2)	In(1)	2.684(2)		C(1)	C(2)	1.46(2)
I(3)	In(1)	2.666(2)		C(1)	C(13)	1.49(2)
In(1)	O(1)	2.33(1)		C(14)	C(15)	1.46(2)
In(1)	O(2)	2.37(1)		C(14)	C(26)	1.50(2)
O(1)	C(1)	1.25(2)				

Atom	Atom	Atom	Angle (°)	Atom	Atom	Atom	Angle (°)
I(1)	In(1)	I(2)	116.82(6)	I(3)	In(1)	O(2)	88.9(3)
I(1)	In(1)	I(3)	124.60(6)	O(1)	In(1)	O(2)	173.8(4)
I(1)	In(1)	O(1)	87.4(3)	In(1)	O(1)	C(1)	161(1)
I(1)	In(1)	O(2)	88.9(3)	In(1)	O(2)	C(14)	166(1)
I(2)	In(1)	I(3)	118.56(6)	O(1)	C(1)	C(2)	127(2)
I(2)	In(1)	O(1)	92.2(3)	O(1)	C(1)	C(13)	127(2)
I(2)	In(1)	O(2)	93.9(3)	O(2)	C(14)	C(15)	127(2)
I(3)	In(1)	O(1)	89.1(3)	O(2)	C(14)	C(26)	128(2)
C(2)	C(1)	C(13)	106(2)	C(15)	C(14)	C(26)	105(1)

these adducts, and of the related substituted paraquinonate derivatives (4, 17).

Solution chemistry

The formation of InI_3L and InI_3L_2 with xanthone and 9-fluorenone respectively under essentially identical preparative conditions parallels a number of earlier reports in which slight changes in ligand, or solvent, were shown to affect the stoichiometry of the adduct (1, 2, 3, 18, 19). The underlying phenomenon is the existence of the solution equilibria.

$$[1] \qquad InX_3 \rightleftarrows InX_3L \rightleftarrows InX_3L_2 \rightleftarrows InX_3L_3$$

whose overall balance depends on the factors noted. In studies of the substituted phosphino derivatives of GaI_3, ^{31}P NMR spectroscopy proved to be useful in investigating the solution chemistry, and in particular processes such as eq.[1]. The ^{13}C spectra of xanthone and InI_3 (xanthone) are identical except for a small shift in *C*=O, from 177.06 to 178.95 ppm (Me_4Si = 0), and the analogous values for fluorenone and InI_3(fluorenone)$_2$ are 195.66 and 196.93 ppm. These changes are too small to allow any meaningful study of solution processes by ^{13}C NMR spectroscopy.

At first sight, it is surprising that two such apparently similar ligands as xanthone and 9-fluorenone should give adducts of different stoichiometry, and in the absence of quantitative studies (see above) it is tempting to seek an explanation based on steric or electronic effects. Before embarking on any discussion of such concepts, it should be recalled that the reaction of InI_3 and triphenylphosphine in ethyl acetate gave $InI_3(PPh_3)_2$ as the only product, but that attempts to recrystallise this compound from the same solvent gave a crystalline equimolar mixture of $InI_3(PPh_3)$ and $InI_3(PPh_3)_2$, while recrystallisation from cyclohexane yielded only $InI_3(PPh_3)$ (2,19). These results emphasize how finely balanced are the energetics of eq. [1]. In the present case, the slight structural and spectroscopic changes in xanthone and 9-fluorenone on complexation indicate the formation of weak complexes, so that the dissociation of InI_3L_2 to InI_3L and L, and the consequent formation of adducts of differing stoichiometry, is not surprising. Extended studies of solvent effects, and of the stoichiometry of adducts of InI_3 and different cyclic ketones, might well produce results similar to those with substituted phosphines (2, and refs. therein): it is not our intention to pursue such investigations.

Acknowledgements

This work was supported in part by Research Grants (to D.G.T.) from the Natural Sciences and Engineering Research Council of Canada. We thank Prof. S.J. Loeb for help with the X-ray crystallography.

References

1. D.G. Tuck. The chemistry of aluminium, gallium, indium and thallium. *Edited by* A.J. Downs. Blackie, London. 1993. Chap. 8, p. 430.
2. M.A. Brown, D.G. Tuck, and E.J. Wells. Can. J. Chem. **74**, 1535 (1997).
3. M.A. Brown, J.A. Castro, and D.G. Tuck. Can. J. Chem. **75**, 333 (1997).
4. M.A. Brown, B.R. McGarvey, and D.G. Tuck. J. Chem. Soc. Dalton Trans. 354 (1998).
5. B.H. Freeland and D.G. Tuck. Inorg. Chem. **15**, 476 (1976).
6. D.T. Cromer and J.T. Waber. International tables for X-ray crystallography. Vol. 4. Kynoch Press, Birmingham. 1974. Table 2.2A.
7. J.H. Ibers and W.C. Hamilton. Acta Crystallogr. **17**, 781 (1964).
8. D.T. Cromer. International tables for X-ray crystallography. Vol. 4. Kynoch Press, Birmingham.
9. M.A. Brown and D.G. Tuck. Inorg. Chim. Acta, **247**, 135 (1996).
10. T.A. Annan, R.K. Chadha, P. Doan, D.H. McConville, B.R. McGarvey, A. Ozarowski, and D.G. Tuck. Inorg. Chem. **29**, 3936 (1990).
11. T.A. Annan and D.G. Tuck. Can. J. Chem. **67**, 1807 (1989).
12. J.G. Contreras, F.W.B. Einstein, and D.G. Tuck. Can. J. Chem. **52**, 1793 (1974).

© 2000 NRC Canada

13. M. Soderholm, V. Sonnerstam, R. Sonnerstam, and T.-B. Palm. Acta Crystallogr. Sect. B: Struct. Crystallogr. Cryst. Chem. **32**, 3013 (1976).
14. W. Clegg, N.C. Norman, and N.L. Pickett. Acta Crystallogr. Sect. C: Cryst. Struct. Commun. **C50**, 36 (1994).
15. I.A. Degnan, N.W. Alcock, S.M. Roe, and M.G.H. Wallbridge. Acta Crystallogr. Sect. C: Cryst. Struct. Commun. **C48**, 995 (1992).
16. H.R. Luss and D.L. Smith. Acta. Crystallogr. Sect. B: Struct. Crystallogr. Cryst. Chem. **B28**, 884 (1972).
17. D.L. Boucher, M.A. Brown, B.R. McGarvey, and D.G. Tuck. J. Chem. Soc. Dalton Trans. 3445 (1999).
18. A.J. Carty and D.G. Tuck. J. Chem. Soc. A, 1188 (1996).
19. A.J. Carty and D.G. Tuck. Prog. Inorg. Chem. **19**, 245 (1975).

© 2000 NRC Canada

The synthesis of hydroxysmirnovine

Veejendra K. Yadav, Philip Williams, and Michael Benn

Abstract: The synthesis of *N*-(4-acetamidobutyl)-*N*-((*Z*)-4-hydroxy-3-methyl-2-butenyl) guanidine confirmed this as the structure of the natural product hydroxysmirnovine.

Key words: hydroxysmirnovine, synthesis, naturally occurring guanidines.

Résumé : Comme suite à la synthèse de la *N*-(4-acétamidobutyl)-*N*-[(*Z*)-4-hydroxy-3-méthylbutén-2-yl]guanidine, cette structure est attribuée à l'hydroxysmirnovine, un produit naturel.

Mots clés : hydroxysmirnovine, synthèse, guanidines naturelles.

[Traduit par la Rédaction]

Introduction

In the course of an investigation of the constituents of *Galega orientalis* Lam. cv. Gale, "Fodder Galega", a plant being considered as a cold-hardy crop for Northern Canada, we isolated two compounds which we identified as hemiterpenoidal guanidines: the known smirnovine, and its previously unknown (*Z*)-4-hydroxy derivative (**1**), which we named hydroxysmirnovine (1).

We confirmed the identity of the former by synthesis, while that of the latter rested upon its spectrometric characterization. The biological role of these guanidines is unknown and, as their isolation was tedious, we decided to develop a synthesis of hydroxysmirnovine with the intention of obtaining material for biological testing as well as checking the proposed structure.

Results and discussion

As for the synthesis of smirnovine, our general strategy was to assemble the appropriate secondary amine and then elaborate it into the guanidine (see Scheme). Guided by the Leonard and Playtis synthesis of hydroxygalegine (2), we utilized the [4 + 2] cycloaddition reaction of 1-chloro-1-nitrosocyclohexane with isoprene to make the dihydro-1,2-oxazine (**2**), the ring system of which might be cleaved to generate the (*Z*)-4-amino-2-methyl-2-buten-1-ol fragment of **1**.

Alkylation of **2** with *N*-(4-bromobutyl)phthalimide provided **3,** after which the phthalimido group was replaced by hydrazinolysis, and subsequent acetylation to afford **4**. The reductive ring scission of **4** proved more troublesome than we had expected for the dihydrooxazine was recovered unchanged from a variety of treatments with zinc dust in acetic acid, with or without heating, and including the addition of hydrochloric acid (3, 4). However, treatment with aqueous sulfuric acid and zinc dust, at room temperature, smoothly converted **4** into the desired secondary amine **5**.

The guanidination procedure which we had developed for the synthesis of smirnovine, involving sequential treatment of the secondary amine with phenyl cyanate and ammonia-ammonium nitrate (1), gave a very low yield of material with the spectroscopic properties expected for **1**. Apparently 1,2-elimination from the intermediate phenyl imidate to form a cyanamide predominated over the desired nucleophilic ammonolysis. We therefore resorted to the method recently described by Lipton (5) and treated **5** with *N*,*N*′-bis(*tert*-butoxycarbonyl)-thiourea (**6**) in the presence of a stoichiometric amount of Mukaiyama's reagent (**7**). This gave the desired bis(*tert*-butoxycarbonyl)guanidine (**8**), albeit in low yield (25%, ca. 40% based on recovered **5**). Probably, as a referee has suggested, this step could be further improved by using Goodman's new procedure for the guanidinylation of amines (9). However, we completed our synthesis at this point by treating **8** with trifluoroacetic acid in dichloromethane. Passage of the reaction product through an anion exchange column (OH form) then afforded the desired compound (**1**), which had identical spectrometric (^{1}H-, and ^{13}C NMR) properties with those of the hydroxysmirnovine which we had isolated from *G. orientalis*.

Received December 1, 1999. Published on the NRC Research Press website on May 5, 2000.

V.K. Yadav. Chemistry Department, Indian Institute of Technology, Kanpur, 208016, India.
P. Williams and M. Benn.[1] Chemistry Department, The University of Calgary, Calgary, AB T2N 1N4, Canada.

[1]Author to whom correspondence may be addressed. Telephone: (403) 220-5352. Fax: (403) 289-9488. e-mail: benn@ucalgary.ca

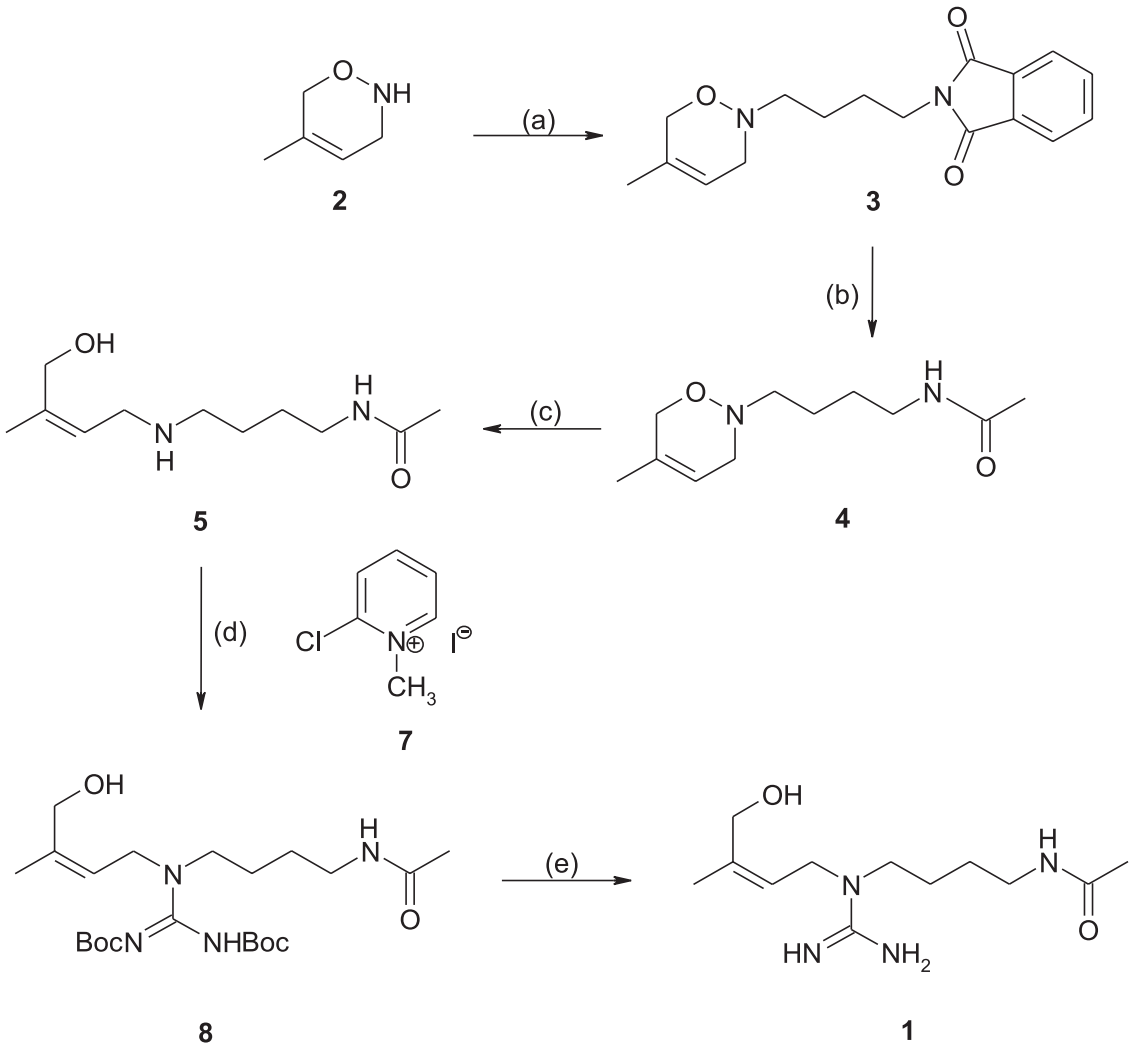
Experimental

Instrumentation

NMR spectra reported here were recorded, using a Bruker DRX-400 spectrometer. For samples dissolved in $CDCl_3$, the spectra were referenced to residual $CHCl_3$ at 7.27 ppm, or the centre line of the $CDCl_3$ resonance at 77 ppm; for solutions in D_2O the signals were referenced to the methyl resonances (δ_H and δ_C = 0) of sodium trimethylsilylpropionate-[2,3-$^2H_4$]. TLC was performed using Merck silica gel 60 F-254, 0.2 mm on aluminum sheeting (Cat. 5562).

© 2000 NRC Canada

Scheme 1.



3,6-Dihydro-5-methyl-N-*(4-phthalimidobutyl)-2*H-*1,2-oxazine (3)*: To a solution of *N*-(4-bromobutyl)phthalimide (1.40 g, 4.96 mmol) (6) and 5-methyl-3,6-dihydro-1,2-oxazine hydrochloride (**2**, 2.01 g, 14.8 mmol) (7) in acetonitrile (100 mL) was added anhydrous sodium carbonate (2.5 g, 24 mmol), and the mixture was boiled under reflux for 16 h. The reaction mixture was then cooled and poured into ice-water (ca. 300 mL). After extraction with chloroform (4 × 50 mL) and removal of solvent from the combined, dried (Na_2SO_4) organic extracts, the reaction product (**3**) was purified by flash chromatography on a column of silica gel 60. The pure product (**3**) eluted with hexane – ethyl acetate (3:1 v/v) and was obtained as a white crystalline solid (1.33 g, 4.63 mmol 89%), mp 82–84°C. MS 300.1472, calcd. for $C_{17}H_{20}N_2O_3$: 300.147. NMR δ_H: 7.84 (2H, m), 7.71 (2H, m), 5.49 (1H, m), 4.15 (2H, v br s), 3.71 (2H, t, J = 7.1 Hz); 3.18 (2H, br m), 2.73 (2H, t, J = 7.1 Hz), 1.77 (2H, pt, J = 7.1 Hz), 1.66 (2H, pt, J = 7.1 Hz); δ_c 168.8 (2C, s), 134.2 (2C, d), 133.7 (2C, s), 132.6 (s), 123.6 (2C, d), 118.0 (d), 72.1 (t), 58.3 (t), 55.3 (t), 38.2 (t), 26.7 (t), 24.7 (t), and 18.4 (q).

N-*(4-acetamidobutyl)-2,3-dihydro-5-methyl-2*H-*1,2-oxazine (4)*: Hydrazine hydrate (345 mg, 6.9 mmol) was added to a solution of **3** (1.03 g, 3.4 mmol) in ethanol (30 mL) and the mixture was boiled under reflux for 3 h, at the end of which time analytical TLC (hexane – ethyl acetate 3:2 v/v) revealed no residual starting material. The mixture was filtered

© 2000 NRC Canada

and the filter cake washed with cold ethanol. The filtrate and washings were then evaporated to dryness and the solid residue was dissolved in pyridine (3 mL). Acetic anhydride (3.5 mL) was added, and the mixture left at room temperature overnight. The reddish reaction mixture was evaporated under vacuum, a process which was repeated twice more after adding water (ca. 1 mL), and the residue was then stirred with saturated aqueous sodium carbonate solution (4 mL), and extracted with chloroform (3 × 5 mL). The combined chloroform extracts were dried (Na_2SO_4) and evaporated to leave an oily residue (760 mg) which crystallized when stored overnight in a refrigerator. Recrystallization of this material from acetone-hexane afforded **4** as fine colourless needles, mp 120°C (512 mg, 2.41 mmol, 71%). NMR δ_H 5.99 (1H, br s, exchanged with D_2O), 5.50 (1H, br s), 4.16 (2H, v br s), 3.24 (q, becoming t with D_2O, J = 6.8 Hz), 3.18 (4H, br m), 2.70 (2H, t, J = 6.8 Hz), 1.94 (3H, s), 1.64 (3H, s, on 2H, m), and 1.58 (2H, pt, J = 6.8 Hz); δ_c 169.9 (s), 133.3 (s), 117.5 (d), 71.7 (t) 58.1 (t), 54.8 (t), 39.5 (t), 27.4 (t), 24.5 (t), 23.3 (q), and 18.0 (q).

N,N-*(4-acetamidobutyl)((Z)-4-hydroxyl-3-methyl-2-butenyl)amine (**5**)*: Zinc dust (700 mg, 11 mmol) was added over 1 h to a stirred solution of **4** (100 mg, 4.7 mmol) in 1 M aqueous sulfuric acid (13 mL). More zinc dust (400 mg, 6 mmol) was added over the next 30 min, and, finally, another portion (200 mg, 3 mmol) over the next 15 min. The reaction mixture was stirred for a further 1 h, then filtered and the residual zinc was washed with water (2 × 2 mL). The combined filtrate and washings were chilled in an ice-water bath and made alkaline (to pH ca. 10, indicator paper) with aqueous ammonia (d = 0.88). The solution was then diluted with ethanol (ca. 5 mL) and evaporated to dryness under reduced pressure (bath < 35°C). More ethanol (5 mL) and chloroform (5 mL) were added to the residue and the mixture taken to dryness as before. The residual solid was then extracted with chloroform (4 × 7 mL), the combined extracts were dried (Na_2SO_4) and evaporated under reduced pressure to yield **5** as a colourless oil, homogeneous by TLC and NMR analyses, (95 mg, 4.4 mmol, 94%). NMR δ_H 6.20 (1H, br s), 5.48 (1H, t, J = 6.7 Hz), 4.05 (2H, s), 3.20 (4H, m), 2.61 (2H, t, J = 6.7 Hz), 1.94 (3H, s) 1.76 3H, (s), and 1.52 (4H, br m); δ_c 170.2 (s), 142.0 (s), 123.2 (d), 62.8 (t), 48.5 (t), 46.2 (t), 39.2 (t), 27.1 (t), 26.9 (t), 23.2 (q), and 22.5 (q).

N-*(4-acetamidobutyl)* N-*((Z)-4-hydroxyl-3-methyl-2-butenyl) N′N″-bis-(*tert-*butoxycarbonyl) guanidine (**8**)*: Mukaiyama's reagent (*N*-methyl-2-chloropyridinium iodide (Aldrich Chem. Co.) **7**, 104 mg, 0.41 mmol) was added to a solution of the amine **5** (72.4 mg, 0.34 mmol) and *N*,*N*′-bis-(*tert*-butoxycarbonyl)thiourea (**6**) (112 mg, 0.41 mmol) in dichloromethane (3.5 mL), and the mixture was stirred at room temperature for 42 h. Initially a sticky solid was present but this was replaced by a free-floating crystalline solid. The suspension was filtered, and the yellow solid was washed with dichloromethane. The combined filtrate and washings were evaporated to a solid residue which was taken up in a little methanol and this solution was then passed through a column of Dowex-1 ion exchange resin (OH form, 20–50 mesh, 1.0 × 10 cm). The column was washed with methanol and the combined eluates and washings were evaporated under reduced pressure to yield a solid residue (85 mg). Flash column chromatography of this material with chloroform containing increasing amounts of methanol (0–20% v/v) eluted a substance which was homogeneous by TLC R_F 0.12 (silica gel, chloroform – methanol 95:5 v/v) and NMR analyses, (24 mg, 0.053 mmol, 15%) with more of this product (20 mg) in a fraction which contained small amounts of impurities). NMR δ_H 5.24 (1H, t, J = 7.1 Hz), 4.10 (2H, s), 4.05 (2H, d, J = 7.1 Hz), 3.35 (2H, t, J = 7.2 Hz), 3.25 (2H, q, becoming t with D_2O, J = 6.8 Hz), 1.96 (3H, s), 1.82 (3H, br s), 1.66 (2H, pt, J = 7.2 Hz), and 1.46 (18 H, s on 2 H, m); δ_c 170.4 (s), 154.9 (s), 140.0 (s) 120.7 (t), 80.9 (s), 61.2 (t), 45.9 (t), 38.7 (t), 37.6 (t), 28.1 (q, 6C), 26.4 (t), 24.7 (t), 23.1 (q), and 21.6 (q).

The dichloromethane-insoluble yellow solid was also dissolved in methanol and passed through a column of Dowex-1 resin (OH form). Evaporation of the eluates and washings gave a residue (58 mg) whose H-1 NMR spectrum revealed it to be a mixture of **5** and 2-chloropyridine.

N-*(4-acetamidobutyl)* N-*((Z)-4-hydroxy-3-methyl-2-butenyl) guanidine, Hydroxysmirnovine (**1**)*: The bis-BOC guanidine (**8**) (24 mg, 0.053 mmol) was dissolved in dichloromethane (4 mL) to which trifluoroacetic acid (6 drops) was added and the mixture was boiled under reflux for 5 h, after which TLC revealed the reaction to be complete. The solvent and excess trifluoroacetic acid were stripped off under reduced pressure, and the residue was dissolved in methanol and passed through a column of Dowex-1 resin (OH form) and the column washed with methanol. Evaporation of the eluates yielded **1** as a colourless oil (13 mg, 0.051 mmol, 95%), whose spectrometric properties (H-1 and C-13 NMR, and MS) were the same as those of the natural hydroxysmirnovine (1) δ:$_H$ (D_2O) 5.38 (1H, t, J = 6.7 Hz), 4.16 (2H,s) 4.05 (2H, d, J = 6.7 Hz), 3.35 (2H, t, J = 6.8 Hz), 3.20 (2H, t, J = 6.8Hz), 1.99 (3H,s), 1.82 (3H, br s), 1.66 (2H, pt, J = ~7 Hz), and 1.55 (2H, pt J = ~7 Hz); δ_C (D_2O) 176.9 (s), 159.3 (s), 142.2 (s), 124.0 (d), 62.8 (t), 50.9 (t), 48.9 (t), 41.7 (t), 28.4 (t), 26.8 (t), 24.7 (q), and 23.5 (q).

Acknowledgements

Financial support for this work was provided by the Natural Sciences and Engineering Research Council of Canada, through a grant in aid of research to M. Benn. We also wish to thank Mr. Jack Ho for the preparation of some *N*-(4-bromobutyl)-phthalimide.

References

1. M.H. Benn, G. Shustov, L. Shustova, W. Majak, Y. Bai, and N. Fairey. J. Agric. Food Chem. **44**, 2779 (1996).
2. N.J. Leonard and A.J. Playtis. J. Chem. Soc. Chem. Commun. 133 (1972).
3. O. Wichterle and J. Novak. Coll. Czech. Chem. Commun. **15**, 309 (1950).
4. G. Kresze, M.M. Weiss, and W. Dittel. Justus Liebigs Ann. Chem. 203 (1984).
5. Y.F. Yong, J.A. Kowalski, and M.A. Lipton. J. Org. Chem. **62**, 1540 (1997).
6. T.A. Crabb, A. Patel, F.R. Newton, and T.J. Cholerton. J. Chem. Soc. Perkin Trans 1, 191 (1985). (This compound is

© 2000 NRC Canada

commercially available, e.g., Aldrich Chem. Co; Fluka Chemie A.G.; and Lancaster Synthesis.)
7. F.G. Ridell. Tetrahedron, **31**, 523 (1975).
8. E.J. Iwanowicz, M.A. Pass, and J. Lin. Synth. Commun. **23**, 1443 (1993).
9. (*a*) K. Feichtinger, C. Zapf, H.L. Sings, and M. Goodman. J. Org. Chem. **63**, 3804 (1998); (*b*) K. Feichtinger, H.L. Sings, T.J. Baker, K. Matthews, and M. Goodman. J. Org. Chem. **63**, 8432 (1998).

© 2000 NRC Canada

Diphenylboron complexes of the enol tautomers of arylpyruvic acids. Crystal and molecular structure of triethylammonium (2-nitrophenyl)pyruvato-diphenylboron(1-)[1]

Wolfgang Kliegel, Jens O. Pokriefke, Steven J. Rettig, and James Trotter

Abstract: Synthesis has been carried out of 15 examples of anionic diphenylboron complexes of arylpyruvic acids, and the structures of the compounds have been determined from spectroscopic data and from X-ray analysis of one of the compounds. Crystals of **5j** are monoclinic, $P2_1/n$, a = 9.5566(10), b = 15.961(3), c = 16.6382(6) Å, β = 99.3239(10)°, and Z = 4, at 180 K. The structure was solved by direct methods and refined by full-matrix least-squares procedures to $R(F^2)$ = 0.056 for 6662 CCD data. **5j** contains a triethylammonium cation and an anion containing a planar five-membered OBOCC ring, with cation and anion linked by an N-H···O hydrogen bond. Spectroscopic data and bond distances establish that the pyruvate ligand is the enol-tautomeric state.

Key words: arylpyruvic acids, enol tautomers, boron complexes, diphenylboron chelates, organoborate salts, crystal structure.

Résumé : On a réalisé la synthèse de quinze complexes diphénylbore anioniques d'acides arylpyruviques et on en a déterminé les structures à partir de données spectroscopiques et de diffraction des rayons X. Les cristaux du composé **5j** sont monocliniques, groupe d'espace $P2_1/n$, avec a = 9,5566(10), b = 15,961(3) et c = 16,6382(6) Å, β = 99,3239(10)° et Z = 4, à 180 K. On a résolu la structure par des méthodes directes et on l'a affinée par la méthode des moindres carrés (matrice entière) jusqu'à des valeurs de $R(F^2)$ = 0,056 pour 6662 données CCD. Le composé **5j** contient un cation triéthylammonium et un anion qui comporte un cycle planaire OBOCC à cinq chaînons; le cation et l'anion sont liés par une liaison hydrogène N-H···O. Les données spectroscopiques et les longueurs des liaisons permettent d'établir que le ligand pyruvate est dans l'état tautomère énolique.

Mots clés : acides acylpyruviques, tautomères énoliques, complexes du bore, chélates diphénylbore, sels organoborates, structure cristalline.

[Traduit par la Rédaction]

Introduction

Arylpyruvic (2-oxo-3-arylpropanoic) acids, **1**, which are significant products and intermediates in the metabolism of amino acids like phenylalanine, tyrosine, or tryptophane (1) exhibit keto-enol tautomerism (2–6). Both tautomers have been identified in spectroscopic and chemical experiments, as for example about 90% of the keto form **1** in aqueous solution, or almost exclusive presence of the enol form **2** in DMSO solution (3–5). For the solid state, the enol form **2** has been found recently by an X-ray crystallographic analysis of the structure of phenylpyruvic acid (7).

Boric acid reacts with the enol tautomer of arylpyruvic acids trapping the enol form in solution (2). This reaction is used in the spectrophotometric analysis of arylpyruvates in biological and clinical chemistry, and was introduced as the "enol-borate-method" in the determination of enzymatic activities or of the concentration of substrates or products in many biochemical reactions that involve an arylpyruvic acid as an educt, intermediate, or product (8). The enol-borate 2:1-complex, **3**, first suggested by Knox and Pitt (2), had been defined on the grounds of spectrophotometric studies. From the preceding and fundamental work of Böeseken and coworkers (9) it is generally known that the conductivity of boric acid solutions can be enhanced also by 2-oxocarbonic acids, presumably mainly by virtue of the hydrated carbonyl group, enabling the borate complex formation, although the possibility of enolization was considered, too.

To corroborate the assumption of an enol-borate complex structure we report here the synthesis of the anionic diphenylboron chelate complexes of several arylpyruvic acids, carried out in the course of our investigations on organoboron

Received January 5, 2000. Published on the NRC Research Press website on May 8, 2000.

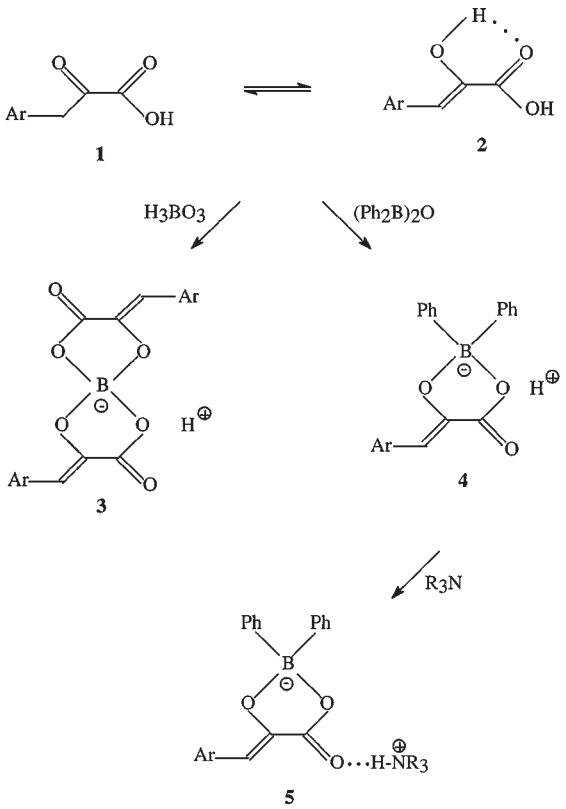
W. Kliegel and J.O. Pokriefke. Institut für Pharmazeutische Chemie der Technischen Universität Braunschweig, Beethovenstrasse 55, 38106 Braunschweig, Germany.
S.J. Rettig and J. Trotter.[2] Department of Chemistry, University of British Columbia, 2036 Main Mall, Vancouver, BC V6T 1Z1, Canada.

[1]Structural studies of organoboron compounds. Part LXXI. Previous paper in this series: ref. 10.

[2]Author to whom correspondence may be addressed. Telephone: (604) 822-4865. Fax: (604) 822-2847. e-mail: jtrt@xray4.chem.ubc.ca

© 2000 NRC Canada

Scheme 1.



5	Ar	R_3N
a	C_6H_5	Et_3N
b	C_6H_5	$MeN(CH_2)_4$
c	C_6H_5	$MeN(CH_2)_5$
d	C_6H_5	$N(C_2H_4)_3N$
e	C_6H_5	4-Me_2N-C_5H_4N
f	4-OH-C_6H_4	$MeN(CH_2)_4$
g	4-OH-C_6H_4	$MeN(CH_2)_5$
h	4-OH-C_6H_4	$N(C_2H_4)_3N$
i	4-OH-C_6H_4	4-Me_2N-C_5H_4N
j	2-O_2N-C_6H_4	Et_3N
k	2-O_2N-C_6H_4	$MeN(CH_2)_4$
l	2-O_2N-C_6H_4	$MeN(CH_2)_5$
m	2-O_2N-C_6H_4	$N(C_2H_4)_3N$
n	2-O_2N-C_6H_4	4-Me_2N-C_5H_4N
o	C_6H_5	$(C_6H_{11})_2NH$

chelate complexes (10), and the unambiguous structural proof by X-ray crystallographic analysis of the trialkylammonium salt of such a borate complex.

Experimental

General procedures

Arylpyruvic acids were commercial products. Oxybis(diphenylborane) was prepared according to literature methods (11). All reactions were carried out under normal conditions, without protective gas atmosphere. Melting points (uncorrected): Büchi SMP 20 apparatus. IR: Philips PU 9800 FT-IR-Spectrometer, V 3.00 and ATI Mattson Genesis Series FT-IR™ Rev. I, ATI Unicam. ^{1}H NMR: Varian EM 390. ^{11}B NMR: Bruker AC 200. Elemental analyses: Carlo Erba CHNO elemental analyzer 1106; boron titrimetrically after Schöniger-oxidation with Metrohm-Potentiograph E 536/Dosimat 655.

4-Arylmethylene-2,2-diphenyl-1,3-dioxa-2-boratacyclopentan-5-one, tertiary ammonium salts (5)

General procedure: The arylpyruvic acid **1/2** (5 mmol) and oxybis(diphenylborane) (0.87 g, 2.5 mmol) are dissolved in 5 mL of ethanol under slight heating. After cooling to room temperature the amine (5 mmol) is added. Crystallization starts spontaneously or upon cooling. The product is analytically pure in most of the cases, or is recrystallized from absolute ethanol.

The compounds **5** give a blue colored solution upon the addition of diphenylcarbazone in ethanol, indicating the presence of the chelated diphenylborenium (Ph_2B^+) ion (12).

2,2-Diphenyl-4-phenylmethylene-1,3-dioxa-2-boratacyclopentan-5-one, triethylammonium salt (5a)

From phenylpyruvic acid (0.82 g, 5 mmol) and triethylamine (0.51 g, 5 mmol). Yield: 1.83 g (85%) of colorless crystals; mp 154°C. IR (KBr, cm^{-1}): 1667 (C=O), 1654 (C=C); ^{1}H NMR (90 MHz, $CDCl_3$–TMS) δ (ppm): 0.93 (t, J = 7 Hz, 3 CH_3), 2.37–2.93 (m, 3 NCH_2), 6.00 (s, C=CH), 6.87–7.77 (m, 13 aromatic H), 7.87 (d, J = 7 Hz, 2 aromatic H), 9.67 (s, broad, exchangeable, NH); ^{11}B NMR (64 MHz, $CDCl_3$–Et_2OBF_3) δ (ppm): 8.7 ($w_{1/2}$ = 385 Hz). Anal. calcd. for $C_{27}H_{32}BNO_3$: C 75.53, H 7.51, B 2.52, N 3.26; found: C 75.56, H 7.55, B 2.53, N 3.18.

2,2-Diphenyl-4-phenylmethylene-1,3-dioxa-2-boratacyclopentan-5-one, 1-methylpyrrolidinium salt (5b)

From phenylpyruvic acid (0.82 g, 5 mmol) and 1-methylpyrrolidine (0.43 g, 5 mmol). Yield: 1.72 g (83%) of colorless crystals; mp 155°C. IR (KBr, cm^{-1}): 1672 (C=O), 1645 (C=C); ^{1}H NMR (90 MHz, $CDCl_3$–TMS) δ: (ppm): 1.73 (m, $(CH_2)_2$), 2.37 (s, CH_3), 2.77 (m, CH_2NCH_2), 6.13 (s, C=CH), 7.00–7.80 (m, 13 aromatic H), 7.97 (d, J = 7 Hz, 2 aromatic H), 9.27 (s, broad, exchangeable, NH); ^{11}B NMR (64 MHz, $CDCl_3$–Et_2OBF_3), δ (ppm): 11.1 ($w_{1/2}$ = 470 Hz). Anal. calcd. for $C_{26}H_{28}BNO_3$: C 75.56, H 6.83, B 2.62, N 3.39; found: C 75.63, H 6.86, B 2.66, N 3.24.

2,2-Diphenyl-4-phenylmethylene-1,3-dioxa-2-boratacyclopentan-5-one, 1-methylpiperidinium salt (5c)

From phenylpyruvic acid (0.82 g, 5 mmol) and 1-methylpiperidine (0.50 g, 5 mmol). Yield: 1.67 g (78%) of

© 2000 NRC Canada

colorless crystals; mp 130°C. IR (KBr, cm^{-1}): 1666 (C=O), 1596 (C=C); ^1H NMR (90 MHz, $CDCl_3$–TMS), δ (ppm): 0.93–1.80 (m, $(CH_2)_3$), 1.90–3.33 (m, CH_2NCH_2), 2.30 (s, CH_3), 6.10 (s, C=CH), 6.83–7.83 (m, 13 aromatic H), 7.93 (d, J = 7 Hz, 2 aromatic H), 9.4 (s, very broad, exchangeable, NH); ^{11}B NMR (64 MHz, $CDCl_3$–Et_2OBF_3), δ (ppm): 10.1 ($w_{1/2}$ = 385 Hz). Anal. calcd. for $C_{27}H_{30}BNO_3$: C 75.89, H 7.08, B 2.53, N 3.28; found: C 75.77, H 7.12, B 2.54, N 3.21.

2,2-Diphenyl-4-phenylmethylene-1,3-dioxa-2-boratacyclopentan-5-one, 1-aza-4-azoniabicyclo[2.2.2]octane salt (5d)

From phenylpyruvic acid (0.82 g, 5 mmol) and 1,4-diazabicyclo[2.2.2]octane (0.56 g, 5 mmol). Yield: 2.04 g (93%) of colorless crystals; mp 182°C. IR (KBr, cm^{-1}): 1668 (C=O), 1645 (C=C); ^1H NMR (90 MHz, DMSO-d_6–TMS), δ (ppm): 3.00 (s, $N(CH_2CH_2)_3N$), 4.67 (s, broad, exchangeable, NH), 5.87 (s, C=CH), 6.90–7.57 (m, 13 aromatic H), 7.87 (d, J = 7 Hz, 2 aromatic H); ^{11}B NMR (64 MHz, DMSO-d_6–Et_2OBF_3), δ (ppm): 10.7 ($w_{1/2}$ = 428 Hz). Anal. calcd. for $C_{27}H_{29}BN_2O_3$: C 73.65, H 6.64, B 2.46, N 6.36; found: C 73.69, H 6.66, B 2.48, N 6.15.

2,2-Diphenyl-4-phenylmethylene-1,3-dioxa-2-boratacyclopentan-5-one, 4-dimethylaminopyridinium salt (5e)

From phenylpyruvic acid (0.82 g, 5 mmol) and 4-dimethylaminopyridine (0.61 g, 5 mmol). Yield: 1.98 g (88%) of colorless crystals; mp 199°C. IR (KBr, cm^{-1}): 1684 (C=O), 1647 (C=C); ^1H NMR (90 MHz, DMSO-d_6–TMS), δ (ppm): 3.13 (s, 2 CH_3), 5.87 (s, C=CH), 6.70–7.63 (m, 13 aromatic H), 6.90 and 8.17 (d and d, AA′BB′, J = 7 Hz, 4 pyridine-H), 7.87 (d, J = 7 Hz, 2 aromatic H), 13.20 (s, broad, exchangeable, NH); ^{11}B NMR (64 MHz, DMSO-d_6–Et_2OBF_3), δ (ppm) 10.6 ($w_{1/2}$ = 342 Hz). Anal. calcd. for $C_{28}H_{27}BN_2O_3$: C 74.68, H 6.04, B 2.40, N 6.22; found: C 74.76, H 6.05, B 2.39, N 6.13.

4-(4′-Hydroxyphenyl)methylene-2,2-diphenyl-1,3-dioxa-2-boratacyclopentan-5-one, 1-methylpyrrolidinium salt (5f)

From (4-hydroxyphenyl)pyruvic acid (0.90 g, 5 mmol) and 1-methylpyrrolidine (0.43 g, 5 mmol). Yield: 1.93 g (90%) of colorless crystals; mp 207°C. IR (KBr, cm^{-1}): 1670 (C=O), 1653 (C=C); ^1H NMR (90 MHz, DMSO-d_6–TMS), δ (ppm): 2.00 (m, $(CH_2)_2$), 3.00 (s, CH_3), 3.27 (m, CH_2NCH_2), 3.67 (s, broad, exchangeable, NH), 5.93 (s, C=CH), 6.90 and 7.83 (d and d, AA′BB′, J = 7 Hz, 4 H of hydroxyphenyl), 7.07–7.70 (m, 10 aromatic H), 9.40 (s, broad, exchangeable, OH); ^{11}B NMR (64 MHz, DMSO-d_6–Et_2OBF_3), δ (ppm): 8.6 ($w_{1/2}$ = 428 Hz). Anal. calcd. for $C_{26}H_{28}BNO_4$: C 72.74, H 6.57, B 2.52, N 3.26; found: C 72.56, H 6.72, B 2.57, N 3.11.

4-(4′-Hydroxyphenyl)methylene-2,2-diphenyl-1,3-dioxa-2-boratacyclopentan-5-one, 1-methylpiperidinium salt (5g)

From (4-hydroxyphenyl)pyruvic acid (0.90 g, 5 mmol) and 1-methylpiperidine (0.50 g, 5 mmol). Yield: 1.46 g (66%) of colorless crystals; mp 170°C. IR (KBr, cm^{-1}): 1665 (C=O), 1655 (C=C); ^1H NMR (90 MHz, DMSO-d_6–TMS), δ (ppm): 1.77–2.00 (m, $(CH_2)_3$), 2.70 (s, CH_3), 2.80 - 4.37 (m, CH_2NCH_2, NH, exchangeable), 5.77 (s, C=CH), 6.74 and 7.67 (d and d, AA′BB′, J = 9 Hz, 4 H of hydroxyphenyl), 6.90–7.57 (m, 10 aromatic H), 9.17 (s, exchangeable, OH); ^{11}B NMR (64 MHz, DMSO-d_6–Et_2OBF_3), δ (ppm): 11.2 ($w_{1/2}$ = 470 Hz). Anal. calcd. for $C_{27}H_{30}BNO_4$: C 73.15, H 6.82, B 2.44, N 3.16; found: C 73.14, H 6.86, B 2.50, N 3.16.

4-(4′-Hydroxyphenyl)methylene-2,2-diphenyl-1,3-dioxa-2-boratacyclopentan-5-one, 1-aza-4-azoniabicyclo[2.2.2]octane salt (5h) (• EtOH)

From (4-hydroxyphenyl)pyruvic acid (0.90 g, 5 mmol) and 1,4-diazabicyclo[2.2.2]octane (0.56 g, 5 mmol). Yield: 2.24 g (89%) of colorless crystals; mp 190°C. IR (KBr, cm^{-1}): 1672 (C=O), 1654 (C=C); ^1H NMR (90 MHz, DMSO-d_6–TMS), δ (ppm): 1.02 (t, J = 6 Hz), 3.00 (s, $N(CH_2CH_2)_3N$), 3.43 (q, J = 6 Hz), 4.20 (s, broad, exchangeable, NH, OH), 5.73 (s, C=CH), 6.73 and 7.67 (d and d, AA′BB′, J = 12 Hz, 4 H of hydroxyphenyl), 6.97–7.53 (m, 10 aromatic H), 9.17 (s, broad, exchangeable, OH); ^{11}B NMR (64 MHz, DMSO-d_6–Et_2OBF_3), δ (ppm): 10.8 ($w_{1/2}$ = 470 Hz). Anal. calcd. for $C_{27}H_{29}BN_2O_4 + C_2H_5OH$: C 69.47, H 6.83, B 2.16, N 5.59; found: C 69.87, H 7.16, B 2.17, N 5.58.

4-(4′-Hydroxyphenyl)methylene-2,2-diphenyl-1,3-dioxa-2-boratacyclopentan-5-one, 4-dimethylaminopyridinium salt (5i)

From (4-hydroxyphenyl)pyruvic acid (0.90 g, 5 mmol) and 1,4-dimethylaminopyridine (0.61 g, 5 mmol). Yield: 2.10 g (90%) of colorless crystals; mp 207°C. IR (KBr, cm^{-1}): 1692 (C=O), 1648 (C=C); ^1H NMR (90 MHz, DMSO-d_6–TMS), δ (ppm): 3.13 (s, 2 CH_3), 5.80 (s, C=CH), 6.77 and 7.70 (d and d, AA′BB′, J = 7 Hz, 4 H of hydroxyphenyl), 6.90 and 8.13 (d and d, AA′BB′, J = 7 Hz, 4 H of pyridine), 7.00–7.57 (m, 10 aromatic H), NH and OH detected only by exchange; ^{11}B NMR (64 MHz, DMSO-d_6–Et_2OBF_3), δ (ppm): 9.4 ($w_{1/2}$ = 428 Hz). Anal. calcd. for $C_{28}H_{27}BN_2O_4$: C 72.12, H 5.84, B 2.32, N 6.00; found: C 71.90, H 5.96, B 2.30, N 5.87.

4-(2′-Nitrophenyl)methylene-2,2-diphenyl-1,3-dioxa-2-boratacyclopentan-5-one, triethylammonium salt (5j)

From (2-nitrophenyl)pyruvic acid (1.05 g, 5 mmol) and triethylamine (0.51 g, 5 mmol). Yield: 1.68 g (78%) of yellow crystals; mp 160°C. IR (KBr, cm^{-1}): 1678 (C=O), 1634 (C=C), 1518 and 1321 (N=O); ^1H NMR (90 MHz, $CDCl_3$-d_6–TMS), δ (ppm): 1.23 (t, J = 7 Hz, 3 CH_3), 3.00 (q, J = 7 Hz, 3 NCH_2), 6.63 (s, C=CH), 7.00–7.90 (m, 13 aromatic H), 9.00 (d, J = 7 Hz, 1 H of nitrophenyl), 9.75 (s, broad, exchangeable); ^{11}B NMR (64 MHz, $CDCl_3$–Et_2OBF_3), δ (ppm): 12.6 ($w_{1/2}$ = 335 Hz). Anal. calcd. for $C_{27}H_{31}BN_2O_5$: C 68.37, H 6.59, B 2.29, N 5.91; found: C 68.38, H 6.73, B 2.34, N 5.87. Crystals suitable for X-ray analysis were obtained by slow crystallization from chloroform – petroleum ether.

4-(2′-Nitrophenyl)methylene-2,2-diphenyl-1,3-dioxa-2-boratacyclopentan-5-one, methylpyrrolidinium salt (5k)

From (2-nitrophenyl)pyruvic acid (1.05 g, 5 mmol) and 1-methylpyrrolidine (0.43 g, 5 mmol). Yield: 1.72 g (75%) of yellow crystals; mp 136°C. IR (KBr, cm^{-1}): 1678 (C=O), 1638 (C=C), 1516 and 1336 (N=O); ^1H NMR (90 MHz,

© 2000 NRC Canada

Table 1. Crystallographic data.[a]

Compound	**5j**
Formula	$(C_6H_{16}N^+)(C_{21}H_{15}BNO_5^-)$
fw	474.36
Crystal system	Monoclinic
Space group	$P2_1/n$
a (Å)	9.5566(10)
b (Å)	15.961(3)
c (Å)	16.6382(6)
β (°)	99.3239(10)
V (Å^3)	2504.4(4)
Z	4
ρ_{calc} (g/cm^3)	1.258
F(000)	1008
Radiation	Mo
μ (cm^{-1})	0.86
Crystal size (mm)	0.20 × 0.30 × 0.35
Correction factors[b]	0.71–1.00
φ sweep range (deg) (χ = –90°)	0 –190
ω sweep range (deg) (χ = –90°)	–22 to 18
Oscillation width (deg)	0.5
Data images, exposure time	462, 50 s
$2\theta_{max}$ (deg)	60.0
Total reflections	23428
Unique reflections	6662
R_{merge}	0.037
No. with $I \geq 3\sigma(I)$	3260
No. of variables	440
R (F) ($I \geq 3\sigma(I)$)	0.036
R_w (F^2) (all data)	0.056
gof	1.37
Max Δ/σ (final cycle)	0.0003
Residual density (e/Å^3)	–0.39 to 0.46

[a]Temperature 180 K, Rigaku/ADSC CCD diffractometer, Mo K_α (λ = 0.71069 Å), graphite monochromator, takeoff angle 6.0°, aperture 94.0 × 94.0 mm at a distance of 39.2 mm from the crystal, $\sigma^2(F^2) = (C + B)/Lp^2$ (C = scan count, B = background count), function minimized $\Sigma w(|F_o^2| - |F_c^2|)^2$ where $w = 1/\sigma^2(F_o^2)$, $R(F) = \Sigma||F_o| - |F_c||/\Sigma|F_o|$, $R_w(F^2) = (\Sigma w(|F_o^2| - |F_c^2|)^2/\Sigma w|F_o^2|^2)^{1/2}$, and gof = $[\Sigma w(|F_o^2| - |F_c^2|)^2/(m - n)]^{1/2}$.

[b]Includes crystal decay (if any), absorption, and scaling corrections performed in a single step.

$CDCl_3$–TMS), δ (ppm): 1.90 (m, $(CH_2)_2$), 2.67 (s, CH_3), 3.07 (m, CH_2NCH_2), 6.63 (s, C=CH), 7.00–8.00 (m, 13 aromatic H), 9.97 (d, J = 7 Hz, 1 H of nitrophenyl), 9.80 (s, broad, exchangeable, NH); ^{11}B NMR (64 MHz, $CDCl_3$–Et_2OBF_3), δ (ppm): 12.0 ($w_{1/2}$ = 428 Hz). Anal. calcd. for $C_{26}H_{27}BN_2O_5$: C 68.14, H 5.94, B 2.36, N 6.11; found: C 68.20, H 6.03, B 2.38, N 5.98.

4-(2′-Nitrophenyl)methylene-2,2-diphenyl-1,3-dioxa-2-boratacyclopentan-5-one, methylpiperidinium salt (5l)

From (2-nitrophenyl)pyruvic acid (1.05 g, 5 mmol) and 1-methylpiperidine (0.50 g, 5 mmol). Yield: 1.93 g (82%) of orange-yellow crystals; mp 141°C. IR (KBr, cm^{-1}): 1688 (C=O), 1633 (C=C), 1525 and 1323 (N=O); ^{1}H NMR (90 MHz, $CDCl_3$–TMS), δ (ppm): 1.00–2.00 (m, $(CH_2)_3$), 2.50 (s, CH_3), 2.80–4.00 (m, CH_2NCH_2), 6.60 (s, C=CH), 6.90–8.20 (m, 13 aromatic H), 8.93 (d, J = 7 Hz, 1 H of nitrophenyl), NH detected only by exchange; ^{11}B NMR (64 MHz, $CDCl_3$–Et_2OBF_3), δ (ppm): 10.5 ($w_{1/2}$ = 342 Hz). Anal. calcd. for $C_{27}H_{29}BN_2O_5$: C 68.65, H 6.20, B 2.29, N 5.93; found: C 68.77, H 6.23, B 2.29, N 6.11.

4-(2′-Nitrophenyl)methylene-2,2-diphenyl-1,3-dioxa-2-boratacyclopentan-5-one, 1-aza-4-azoniabicyclo[2.2.2]octane salt (5m)

From (2-nitrophenyl)pyruvic acid (1.05 g, 5 mmol) and 1,4-diazabicyclo[2.2.2]octane (0.56 g, 5 mmol). Yield: 2.13 g (88%) of yellow crystals; mp 184°C. IR (KBr, cm^{-1}): 1675 (C=O), 1631 (C=C), 1517 and 1332 (N=O); ^{1}H NMR (90 MHz, DMSO-d_6–TMS), δ (ppm): 3.10 (m, $N(CH_2CH_2)_3$), 3.53 (s, C=CH), 7.00–8.00 (m, 13 aromatic H), 8.80 (d, J = 7 Hz, 1 H of nitrophenyl); ^{11}B NMR (64 MHz, DMSO-d_6–Et_2OBF_3), δ (ppm): 8.6 ($w_{1/2}$ = 470 Hz). Anal. calcd. for $C_{27}H_{28}BN_3O_5$: C 66.82, H 5.81, B 2.23, N 8.66; found: C 67.11, H 5.95, B 2.24, N 8.61.

4-(2′-Nitrophenyl)methylene-2,2-diphenyl-1,3-dioxa-2-boratacyclopentan-5-one, 4-dimethylaminopyridinium salt (5n)

From (2-nitrophenyl)pyruvic acid (1.05 g, 5 mmol) and 4-dimethylaminopyridine (0.61 g, 5 mmol). Yield: 2.26 g (91%) of a yellow powder; mp 214°C. IR (KBr, cm^{-1}): 1686 (C=O), 1646 (C=C), 1515 and 1320 (N=O); ^{1}H NMR (90 MHz, DMSO-d_6–TMS), δ (ppm): 3.20 (s, 2 CH_3), 6.20 (s, C=CH), 6.97 and 8.20 (d and d, AA′BB′, J = 7 Hz, 4 H of pyridine), 7.03–8.00 (m, 13 aromatic H), 8.80 (d, J = 7 Hz, 1 H of nitrophenyl), NH detectable only by exchange; ^{11}B NMR (64 MHz, DMSO-d_6–Et_2OBF_3), δ (ppm): 11.2 ($w_{1/2}$ = 428 Hz). Anal. calcd. for $C_{28}H_{26}BN_3O_5$: C 67.89, H 5.29, B 2.18, N 8.84; found: C 67.88, H 5.41, B 2.19, N 8.29.

2,2-Diphenyl-4-phenylmethylene-1,3-dioxa-2-boratacyclopentan-5-one, dicyclohexylammonium salt (5o)

From phenylpyruvic acid (0.87 g, 5 mmol) and dicyclohexylamine (0.91 g, 5 mmol). Yield: 0.37 g (15%) of colorless crystals; mp 173°C. IR (KBr, cm^{-1}): 1677 (C=O), 1645 (C=C); ^{1}H NMR (90 MHz, $CDCl_3$–TMS), δ (ppm): 0.67–2.20 (m, 2 $(CH_2)_5$), 2.97 (m, CH-N-CH), 5.97 (s, C=CH), 6.87–7.80 (m, 13 aromatic H), 7.90 (d, J = 7 Hz, 2 H of aromatic H), NH_2 detected only by exchange; ^{11}B NMR (64 MHz, $CDCl_3$–Et_2OBF_3), δ (ppm): 10.6 ($w_{1/2}$ = 385 Hz). Anal. calcd. for $C_{33}H_{40}BNO_3$: C 77.80, H 7.91, B 2.12, N 2.75; found: C 77.87, H 7.99, B 2.18, N 2.64.

X-ray crystallographic analysis of 5j

Crystallographic data appear in Table 1. The final unit-cell parameters were obtained by least-squares based on 13215 reflections with 2θ = 4.0–60.1°. The data were processed,[3] corrected for Lorentz and polarization effects, and absorption (based on analysis of symmetry-equivalent data).

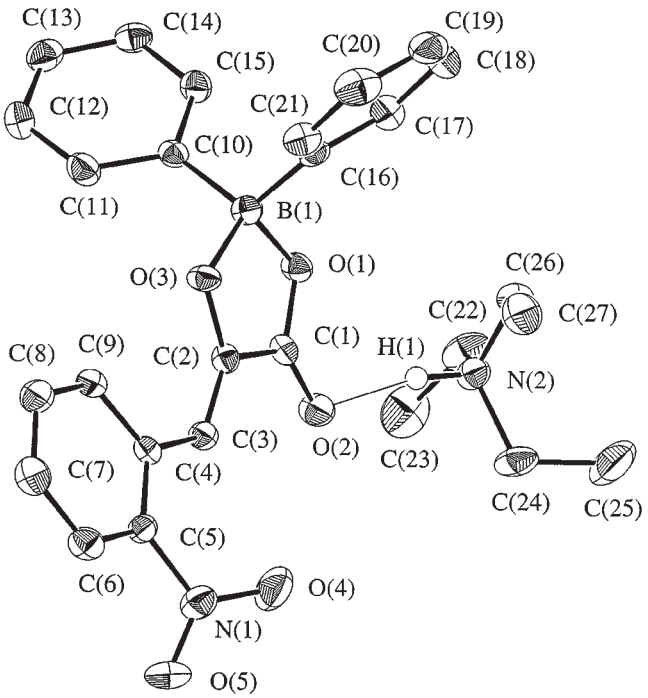
[3] teXsan: Crystal structure analysis package. Unix version 1.7. Molecular Structure Corporation, The Woodlands, TX, U.S.A. 1995; and d*TREK: Area Detector Software. Molecular Structure Corporation, The Woodlands, TX, U.S.A. 1997.

© 2000 NRC Canada

Table 2. Selected bond lengths (Å) and angles (°), with estimated standard deviations in parentheses.

Bond Lengths (Å)		Bond Angles (°)	
		Anion	
B(1)—O(1)	1.553(2)	O(1)-B(1)-O(3)	101.2(1)
B(1)—O(3)	1.513(2)	C(10)-B(1)-C(16)	114.2(1)
O(1)—C(1)	1.309(2)	O(1)-C(1)-C(2)	109.5(1)
O(3)—C(2)	1.341(2)	O-B-C	109.5–111.4(1)
C(2)—C(3)	1.339(2)	B-O-C	110.1–110.3(1)
B(1)—C(10)	1.622(2)	O(3)-C(2)-C(1)	108.8(1)
B(1)—C(16)	1.601(2)		
C(1)—C(2)	1.498(2)		
C(1)—O(2)	1.224(1)		
		Cation	
N(2)—C	1.502–1.516(2)	C-N-C	109.7–114.2(1)
C—C	1.505–1.510(2)		

Fig. 1. View of the structure of **5j**; 50% probability thermal ellipsoids are shown for the non-hydrogen atoms.



The structures were solved by direct methods, the coordinates of the non-hydrogen atoms being determined from *E*-maps or from subsequent difference Fourier syntheses. The non-hydrogen atoms were refined with anisotropic thermal parameters, and the hydrogen atoms were refined with isotropic thermal parameters. No corrections for secondary extinction were necessary. Neutral atom scattering factors for all atoms and anomalous dispersion corrections for the non-hydrogen atoms were taken from the *International Tables for X-Ray Crystallography* (13). Selected bond lengths and angles are listed in Table 2. Complete tables of atomic coordinates and equivalent isotropic thermal parameters, anisotropic thermal parameters, bond lengths and angles, torsion angles, intermolecular contacts, and least squares planes are included as supplementary material.[4]

Results and discussion

From the reaction of various arylpyruvic acids **1/2** (Ar = phenyl, 4-hydroxyphenyl, 2-nitrophenyl) with diphenylborinic acid anhydride (oxybis(diphenylborane)) in ethanol, the corresponding diphenylboron chelate complexes **4** could not be isolated. After addition of a tertiary amine, however, the respective salts **5** crystallized from the solution. A selection of different sufficiently basic amines was used with the intention of finding a compound with good crystallizing qualities, making possible an X-ray analysis of an example of **5**. The tertiary amines gave the salts **5a–n** in near-quantitative amounts, whereas dialkylamines did not give satisfactory yields of crystalline compounds (one example (**5o**) is included here, 15% yield). Use of primary amines was omitted because of possible azomethine formation; arylpyruvic acids and other α-ketocarbonic acids react with primary amines and diphenylborinic acid to give five-membered boron chelates with an N→B coordination.[5]

The compounds **5** have elemental analyses and ^{1}H NMR spectroscopic data consistent with the postulated diphenylborinate complex salt. The intact diphenylboron moiety is indicated by rechelatization of the Ph_2B^+ ion with diphenylcarbazone, resulting in a blue color reaction (12). A boron chelate system as in **5** is also confirmed by the ^{11}B NMR spectra, which all display typical signals for a tetracoordinated boron nucleus around $\delta(Et_2OBF_3) \sim 10$ ppm (14). In the infrared spectra of **5**, strong absorption bands between 1653 and 1688 cm^{-1} and less-intense bands between 1631 and 1654 cm^{-1} indicate the carboxyl-C=O and the enol-C=C stretching vibrations, respectively. The enol character of the arylpyruvate ligands is demonstrated by one-proton signals of the corresponding O-C=CH moiety in the ^{1}H NMR spectra of **5** between δ(TMS) 5.73 and 6.63 ppm. Crystallization tests with the different substituted arylpyruvato boron com-

[4] Copies of material on deposit may be purchased from the Depository of Unpublished Data, Document Delivery, CISTI, National Research Council Canada, Ottawa, Canada K1A 0S2.
[5] W. Kliegel and J. Graumann. Unpublished results.

© 2000 NRC Canada

pounds revealed that the triethylammonium salt of the 2-nitrophenylpyruvate complex, **5j**, gave the best crystals suitable for an X-ray analysis.

The structure of **5j** contains cation-anion pairs (triethylammonium cations and boron-containing anions), linked by an N(2)-H···O(2) hydrogen bond between the amine nitrogen atom and the carboxyl C=O of the arylpyruvato ligand (Fig. 1): N···O = 2.793(2), N-H = 0.97(1), H···O = 1.84(1) Å, N-H···O = 167(1)°; the somewhat bent N-H···O arrangement may be the result of steric interaction with neighboring groups such as the C(16)-C(21) phenyl ring, and of the orientation of the triethylammonium ion within the crystal lattice and the resulting packing forces.

The anion contains a five-membered boron chelate ring, OBOCC, which is almost exactly planar, and is similar to the boron chelate ring system in compounds of type **6** (10). Maximum atomic displacement from the mean ring plane is only 0.004(2) Å for the B atom, and the maximum torsion angle in the ring is only 0.4(1)°; the ring conformation is a very slight B-envelope. The exocyclic methylene system is also almost planar, although with slightly larger displacements from exact planarity; maximum atomic displacements are 0.015(1) Å for C(2) and 0.04 Å for the less-precisely determined H atom bonded to C(3). The torsion angle about the C=C double bond is 1.8(2)° (for O(3)-C(2)-C(3)-C(4)), so that the configuration around the C=C double bond of the enol function is (*Z*), as in the (free ligand) phenylpyruvic acid. The phenyl groups are all approximately planar, that containing the nitro group showing the largest deviations from exact planarity (maximum atomic displacement 0.014(1) Å); this ring makes an angle of 17° with the methylene plane, and the nitro group is rotated 37.3° out of the phenyl plane, presumably as a result of steric interaction with the methylene H atom.

The C(2)—O(3) and C(2)—C(3) bond distances of 1.341(1) and 1.339(2) Å, respectively, point out clearly the enol-tautomeric state of the ligand, with considerable loss of the double bond character of the carbonyl-C=O and the appearance of the neighboring enol-C=C double bond. The estimated C—O π-bond order is 0.35 from plots of bond length vs. π-bond order (15), or 0.32 from calculation (16). The C=C bond length is normal for Ar-C=C bonds (17), with a calculated π-bond order of 0.998 (16). These C—O and C=C bond lengths in **5j** are similar to those in the enol system in crystalline pyruvic acid, **2** (Ar = phenyl), where the C—O and C=C bond distances are 1.355 and 1.339 Å, respectively, (7).

A considerable difference between the enolate and carboxylate C—O bond lengths in the five-membered chelate ring (C(2)—O(3) = 1.341(4), C(1)—O(1) = 1.309(2) Å) demonstrates the more-pronounced π-bond participation in the latter, and corresponds to the weaker coordinative O—B bond from the carboxylate oxygen atom to boron (O(1)—B = 1.553(2) Å), compared to that from the enolate oxygen to boron (O(3)—B = 1.513(2) Å). Two diphenylboron complexes of type **6** (10) show similar bond length variations, B—O = 1.554(2), 1.551(3) Å for the weaker bonds, and 1.532(2), 1.518(3) Å for the stronger; the C—O distances have corresponding (although not statistically significant) differences, C—O = 1.312(2), 1.304(3) vs. 1.309(2), 1.296(3) Å. A tetrahedral arrangement about the boron atom includes a slightly compressed O-B-O angle of 101.2(1)°, a consequence of the relatively narrow bite of the bidentate ligand, and similar to the corresponding angles in the complexes of type **6** (O-B-O from 99.4 to 100.4°) (10). The C(1)—C(2) bond, 1.498(2) Å, is slightly long for a C(sp^2)—C(sp^2) bond (17), but this is not unexpected as a result of intra-ring angles of 108.8 and 109.5(1)°, and exocyclic angles of 123.1 and 126.5(1)°.

The ion pairs are linked by van der Waals interactions. These include two possibly significant intermolecular C-H···O interactions: C···O = 3.493(2) and 3.399(2) Å, H···O = 2.50 and 2.52(2) Å, C–H···O = 164 and 160(1)°. There are also five intra-anion C-H···O contacts involving methylene and phenyl hydrogen atoms and the nitro and ring oxygen atoms: C···O = 2.721(2)–2.950(2) Å, H···O = 2.23–2.52(2) Å, C–H···O = 96–123(1)°.

The X-ray analysis of **5j** thus proves the expected five-membered chelate anion, and supports the suggestions made for the chelate ring type in arylpyruvatoborate complexes like **3**, with an exocyclic positioning of the enolic C=C moiety, different from the many known borate complexes of 1,3-dicarbonyl compounds which incorporate an endocyclic enolic C=C group (19). To the best of our knowledge **5j** is the first structurally characterized example of an arylpyruvatoborate complex.

Acknowledgements

We thank the Natural Sciences and Engineering Research Council of Canada and the Fonds der Chemischen Industrie, Frankfurt am Main, for financial support. We are grateful to the Chemische Institute der Technischen Universität Braunschweig for ^{11}B NMR spectra, and Peter G. Jones for a reference to the literature.

References

1. (*a*) H. Bickel, F.P. Hudson, and L.I. Woolf (*Editors*). Phenylketonuria and some other inborn errors of amino acid metabolism. Georg Thieme, Stuttgart. 1971; (*b*) P. Felig. Amino acid metabolism in man. Annu. Rev. Biochem. **44**, 933 (1975); (*c*) A. Meister. Biochemistry of the amino acids. Vol. I and II. Academic Press, New York. 1964; (*d*) W.L. Nyhan (*Editor*). Heritable Disorders of amino acid metabolism. John Wiley, New York. 1974.
2. W.E. Knox and B.M. Pitt. J. Biol. Chem. **225**, 675 (1957).
3. P.O. Larsen and E. Wieczorkowska. Acta Chem. Scand. Ser. B, **B28**, 92 (1974).
4. O. Sciacovelli, A. Dell'Atti, A. De Giglio, and L. Cassidei. Z. Naturforsch. C: J. Biosci. **31 C**, 5 (1976).
5. L. Cassidei, A. Dell'Atti, and O. Sciacovelli. Z. Naturforsch. C: J. Biosci. **31 C**, 641 (1976).
6. L. Cassidei, A. Dell'Atti, and O. Sciacovelli. Z. Naturforsch. C: J. Biosci. **31 C**, 1 (1980).
7. N. Okabe and C. Inubushi. Acta Crystallogr. Sect. C: Cryst. Struct. Commun. **C53**, 1449 (1997).
8. W. Kliegel. Bor in biologie, medizin und pharmazie. Springer, Berlin. 1980. pp. 92–94.
9. J. Böeseken and A. Niks. Recl. Trav. Chim. Pays-Bas, **59**, 1062 (1940); and lit. cited therein.
10. J. Grünefeld, W. Kliegel, S.J. Rettig, and J. Trotter. Can. J. Chem. **77**, 439 (1999).

© 2000 NRC Canada

11. (*a*) R. Neu. Chem. Ber. **87**, 802 (1954); (*b*) G.N. Chremos, H. Weidmann, and H.K. Zimmermann. J. Org. Chem. **26**, 1683 (1961).
12. (*a*) R. Neu. Z. Anal. Chem. **176**, 334 (1960); (*b*) B. Friese and F. Umland. Anal. Chim. Acta, **96,** 303 (1978).
13. (*a*) International tables for X-ray crystallography. Kynoch Press. Birmingham, U.K. (present distributor Kluwer Academic Publishers: Boston, Mass. U.S.A.). 1974. Vol. IV. pp. 99–102; (*b*) International tables for crystallography. Kluwer Academic Publishers. Boston, Mass. U.S.A. 1992. Vol. C. pp. 200–206.
14. (*a*) H. Nöth and B. Wrackmeyer. Nuclear magnetic resonance spectroscopy of boron compounds. Springer, Berlin. 1978; (*b*) R. Köster. Organoborverbindungen III. Vol. XIII/3c, *Edited by* Houben-Weyl. Thieme, Stuttgart. 1984.
15. G. Häfelinger. Chem. Ber. **103**, 2922 (1970).
16. J.P. Paolini. J. Comput. Chem. **11**, 1160 (1990).
17. F.H. Allen, O. Kennard, D.G. Watson, L. Brammer, A.G. Orpen, and R. Taylor. J. Chem. Soc. Perkin 2, **S1** (1987).
18. (*a*) H. Steinberg. Organoboron chemistry. Vol. I. Boron-oxygen and boron-sulfur compounds. John Wiley, New York. 1964; (*b*) I. Bally and A.T. Balaban. Stud. Cercet. Chim. **17**, 431 (1969); (*c*) K. Niedenzu and K.C. Buschbeck (*Editors*). Borverbindungen. Teil 16. Gmelin Handbuch der Anorganischen Chemie. Vol. 48. Springer, Berlin. 1977.

© 2000 NRC Canada

Antiviral activity of arylnaphthalene and aryldihydronaphthalene lignans

Christopher Cow, Carmen Leung, and James L. Charlton

Abstract: A practical method for large scale synthesis of 1-arylnaphthalene and 1-aryl-1,2-dihydronaphthalene lignans is described. The method makes use of the classic Stobbe condensation followed by regioselective reactions that provide access to both the common and retrolactone lignans, e.g., **2** and **3**. A total of 25 compounds, many of which are known natural products, were prepared and their antiviral activity against human cytomegalovirus measured.

Key words: lignan, Stobbe, arylnaphthalene, antiviral.

Résumé : On décrit une méthode pratique de réaliser des synthèses à grande échelle de 1-arylnaphtalène et de 1-aryl-1,2-dihydronaphtalène lignanes. La méthode fait appel à la condensation classique de Stobbe suivie de réactions régiosélectives qui conduisent aussi bien aux lignanes normales que rétrolactoniques, par exemple **2** et **3**. On a ainsi préparé vingt-cinq composés, dont plusieurs sont des produits naturels connus, et on a mesuré leur activité antivirale vis-à-vis le cytomégalovirus humain.

Mots clés : lignane, Stobbe, arylnaphtalène, antiviral.

[Traduit par la Rédaction]

Introduction

Lignans are natural products that are well known for their broad spectrum of medicinal properties (1–4). They are found in many plant species and are believed to be derived from the dimerization of two phenyl propanoid units at the central carbons of their side chains (see Scheme 1) (4).

Further cyclization of lignans can lead to cyclolignans, such as 1-arylnaphthalenes, **1**, (as well as reduced 1-arylnaphthalenes and dibenzocyclooctadienes). Natural 1-arylnaphthalene lignans often feature a γ-lactone ring at the 2,3-position most commonly oriented as in structure **2**, but also found as in **3** (retrolactone) (see Scheme 1) (4).

A recent review of the antiviral activity of lignans (5) prompted us to carry out a more extensive study of the antiviral activity of several 1-arylnapthalene and 1-aryl-1,2-dihydronaphthalene lignans, and their analogs. Although several excellent methods for the synthesis of arylnaphthalene lignans have been published (1–4, 6, 7), we sought a simple method that would yield both 1-arylnaphthalene and 1-aryl-1,2-dihydronaphthalene compounds. The general method that we have used is shown in Scheme 2.

The method is short, convergent, and the purification of intermediates is relatively straightforward. Although the classic Stobbe condensation (first step) is well known (8), it appears that the route from the Stobbe diester **5** to the 1-aryl-1,2-dihydroanthracenes **7** has not previously been investigated. DDQ oxidation of **7** led to the arylnaphthalene diesters **8** that could be regioselectively hydrolysed and reduced to form the lactones **2** or **3**. The dihydrodiesters **7** and **8,** and the lactones **2** and **3**, were tested for antiviral activity against human cytomegalovirus using a standard plaque reduction assay.

Received October 20, 1999. Published on the NRC Research Press website on May 8, 2000.

C. Cow, C. Leung, and J.L. Charlton.[1] Department of Chemistry, University of Manitoba, Winnipeg, MB R3T 2N2, Canada.

[1]Author to whom correspondence may be addressed. Telephone: (204) 474-9267. Fax: (204) 474-7608. e-mail: charltn@cc.umanitoba.ca

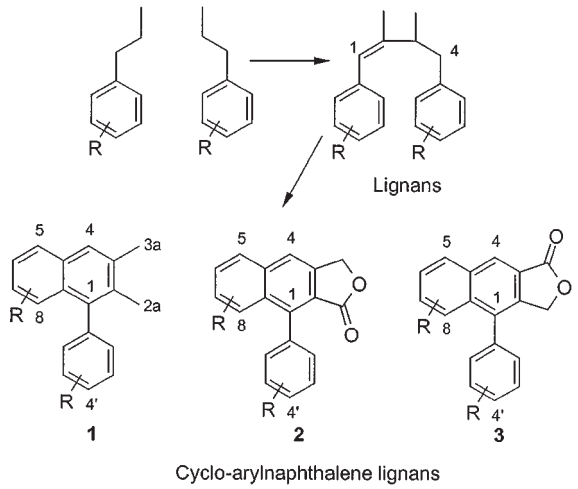
Results and discussion

The classic Stobbe condensation of diethyl succinate with piperonal (3,4-methylenedioxybenzaldehyde) (**a**), veratraldehyde (3,4-dimethoxybenzaldehyde) (**b**) and 3,4,5-trimethoxybenzaldehyde (**c**) was used to prepare the corresponding mono-acids **4a**–**c** (8, 9) The crude mono-acids were esterified to the diethyl esters **5a**–**c** (9) followed by short path distillation under vacuum. Each of the diesters was treated with strong base (LDA) and condensed with each of the three aromatic aldehydes (except for the reaction of **5c** with veratraldehyde) to provide a library of eight alcohols, **6aa**–**6ca**, and **6cc**. It was necessary to quench the condensations with acetic acid at low temperature to prevent lactonization and elimination reactions from occurring. The alcohols were not purified or characterized but were immediately dissolved in trifluoroacetic acid and stirred at room temperature for one hour to form the eight 1-aryl-1,2-dihydronaphthalenes **7aa**–**7ca** and **7cc**. Although there are many methods for the preparation of 1-aryltetralin and 1-aryldihydronaphthalene lignans in the literature, we could find no precedent for this direct and relatively straightforward preparation of 1-aryl-1,2-dihydronaphthalenes from the Stobbe diesters **5**.

Aromatization of the dihydronaphthalenes **7** was accomplished using dicyanodichloro-*p*-benzoquinone (DDQ) in refluxing toluene. This worked well for compounds **7aa**–**7bc** but did not work for the more hindered derivatives **7ca** and

 © 2000 NRC Canada

Scheme 1.



7cc, presumably due to steric crowding. The naphthalenes **8aa**–**8bc** could all be recrystallized from the crude reaction mixtures using $CHCl_3$–hexanes as solvent.

The selective hydrolysis of 1-arylnaphthalene diesters similar to **8** has been described in the literature (6). We found that hydrolysis using KOH in methanol–water gave the six mono-acids **9aa**–**9bc** in good yield. Formation of the lactones **2** was accomplished by reducing **9** using borane–dimethylsulfide in THF followed by lactonization in acid. In this way, lactones **2aa** (Taiwanin C), **2ab** (Chinensin), **2ac** (dehydroanhydropodophyllotoxin), **2ba** (Justicidin B), **2bb,** and **2bc** (7-deoxydiphyllin) were prepared. Formation of the retrolactones **3** was accomplished by reducing the ester group using sodium borohydride – lithium chloride in diglyme at 120°C followed by lactonization in acid. The lactones **3aa** (Justicidin E), **3ab** (Retrochinensin), **3ac** (5′-methoxyretrocinensin), **3ba** (Retrojusticidin B), **3bb,** and **3bc** were prepared.

Most of the compounds represented by structures **2**, **3**, **7**, and **8** were tested for their ability to inhibit human cytomegalovirus virus using a standard plaque reduction assay. The cytotoxicities of the compounds were also measured using a tetrazolium salt MTT (10). Seven compounds had EC_{50}s in the low micromolar range (EC_{50}/TC_{50}: **7aa** 25/ >37 μM; **7ac** 1.4/ >25 μM; **7bc** 22/ >33 μM; **2aa** 1.2/ >19 μM; **2ac** 1.4/ >2.0 μM; **3ab** 63/50 μM; **3ba** 7.2/ >65 μM). Most of the remaining compounds did not show substantial antiviral activity at their solubility limit (ca. 50 μM).

Conclusions

A simple, convergent procedure has been developed for the synthesis of 1-arylnaphthalene and 1-aryl-1,2-dihydronaphthalene lignans and lignan analogs. The compounds prepared were screened for activity against human cytomegalovirus using a standard plaque reduction assay. While antiviral activity was found, the activity did not extend into the nanomolar range and was often paired with high cytotoxicity. Only **2aa** (Taiwanin C) and **3ba** (Retrojusticidin B) had a clear antiviral window.

Experimental

General methods

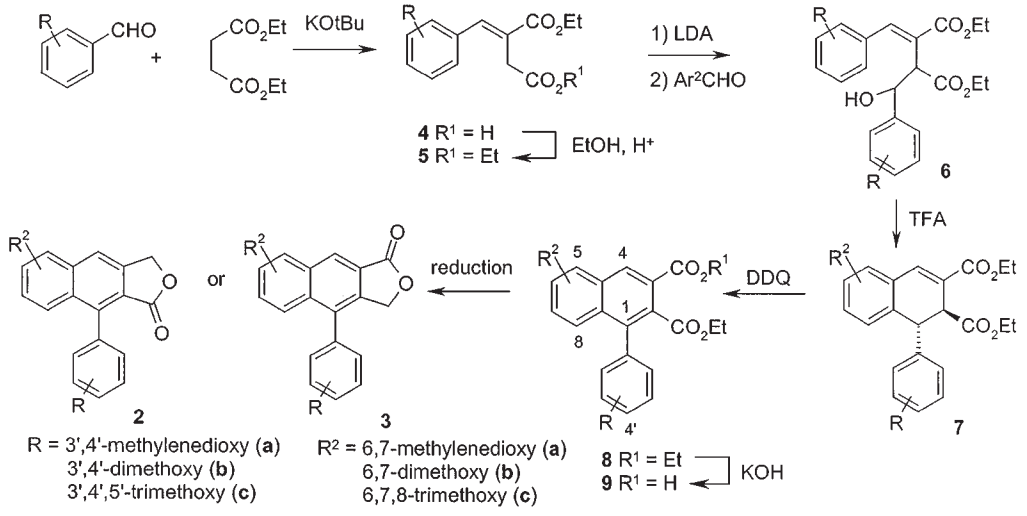
The general experimental procedures and instrumentation have been described in a previous publication (12).

Stobbe condensation – general procedure

tert-Butyl alcohol was charged to a 500 mL flask, and then potassium metal (1.2 equiv., ca. 0.5 M) was cut into pieces and added to the flask. The mixture was heated at reflux until the potassium metal had disappeared (ca. 1 h), and then was cooled to room temperature. Diethyl succinate (2.0 equiv.) and the substituted benzaldehyde (1.0 equiv.) were dissolved in *tert*-butyl alcohol (30 mL), and this mixture added, with stirring, via a dropping funnel over 20 min. The dropping funnel was rinsed with *tert*-butyl alcohol, and the reaction mixture stirred at room temperature for 3 h, during which time a yellow precipitate formed.

The mixture was poured into 10% HCl (100 mL) in a separatory funnel and extracted with EtOAc (3 × 100 mL). The organic layers were combined and washed with satu-

Scheme 2.



© 2000 NRC Canada

rated aqueous $NaHCO_3$ (3 × 100 mL). The basic extracts were combined, acidified with concentrated HCl, and extracted into fresh EtOAc (3 × 50 mL). This second organic extract was washed with water (10 mL), dried over anhydrous magnesium sulfate, filtered, and evaporated to give crude product, which was reacted in the next step without further purification.

*Stobbe acid – **4a***

Piperonal (3,4-methylenedioxybenzaldehyde, 15 g, 100 mmol), potassium metal (4.7 g, 120 mmol), *tert*-butyl alcohol (250 mL), and diethyl succinate (33 mL, 200 mmol), following the general procedure gave a crude product as a light yellow oil (14.0 g, 50% yield).

*Stobbe acid – **4b***

Veratraldehyde (3,4-dimethoxybenzaldehyde, 20 g, 120 mmol), potassium metal (5.6 g, 144 mmol), *tert*-butyl alcohol (250 mL), and diethyl succinate (42 mL, 240 mmol), following the general procedure gave a crude product as a light yellow oil (29.7 g, 77% yield).

*Stobbe acid – **4c***

3,4,5-Trimethoxybenzaldehyde (20 g, 102 mmol), potassium metal (4.8 g, 123 mmol), *tert*-butyl alcohol (250 mL), and diethyl succinate (34 mL, 204 mmol), following the general procedure gave crude product as a yellow oil (27.2 g, 82% yield).

Esterification reaction – general procedure

The crude acid-ester **4** was dissolved in anhydrous EtOH (100 mL, ca. 0.4 M), concentrated H_2SO_4 was added (catalytic amount) and the mixture was heated at reflux for 16 h. The majority of the ethanol was removed on a rotary evaporator, the mixture poured into saturated aqueous NaCl (150 mL) and extracted with EtOAc (3 × 50 mL). The organic extracts were combined and washed with saturated aqueous $NaHCO_3$ (3 × 50 mL) and water (50 mL). The mixture was dried over anhydrous magnesium sulfate, filtered, and evaporated to give a yellow oil. This crude oil was purified by short path, high vacuum (0.01 mm Hg) distillation to give the product.

*Stobbe diester – **5a***

Crude acid **4a** (14.0 g, 50.3 mmol), concentrated H_2SO_4 (2.5 mL), and ethanol (100 mL) gave **5a** as a clear pale yellow distillate (10.7 g, 70% yield). ^{1}H NMR (300 MHz, $CDCl_3$) δ 7.78 (s, 1H, Ar-C*H*=C), 6.8–6.9 (m, 3H, Ar-*H*), 5.99 (s, 2H, O-CH_2-O), 4.26 (q, 2H, *J* = 7.1 Hz, CH=C-CO_2-C$H_2$$CH_3$), 4.19 (q, 2H, *J* = 7.1 Hz, CO_2-C$H_2$$CH_3$), 3.53 (s, 2H, C$H_2$-$CO_2$Et), 1.32 (t, 3H, *J* = 7.1 Hz, $CO_2CH_2CH_3$), 1.26 (t, 3H, *J* = 7.1 Hz, $CO_2CH_2CH_3$); ^{13}C NMR ($CDCl_3$, 75 MHz) δ 171.1 (*C*=O), 167.4 (*C*=O), 148.2, 147.9, 141.4, 128.9, 124.9, 123.9, 109.1, 108.5, 101.4, 61.0, 60.9, 33.8, 14.3, 14.2; EIMS *m*/*z* = 306 [M^+] (base), 261, 232, 203, 175, 159; HRMS calcd. for $C_{16}H_{18}O_6$: 306.1103, found: 306.1084.

*Stobbe diester – **5b***

Crude acid **4b** (19.0 g, 64.5 mmol), concentrated H_2SO_4 (2.5 mL), and ethanol (100 mL) gave **5b** as a clear yellow distillate (16.0 g, 77% yield). ^{1}H NMR (300 MHz, $CDCl_3$) δ 7.78 (s, 1H, Ar-C*H*=C), 6.7–7.0 (m, 3H, Ar-*H*), 4.22 (q, 2H, *J* = 7.1 Hz, CH=C-CO_2-C$H_2$$CH_3$), 4.14 (q, 2H, *J* = 7.2 Hz, CO_2-C$H_2$$CH_3$), 3.85 (s, 3H, OC$H_3$), 3.83 (s, 3H, OC$H_3$), 3.53 (s, 2H, C$H_2$), 1.29 (t, 3H, *J* = 7.1 Hz, $CO_2CH_2CH_3$), 1.22 (t, 3H, *J* = 7.2 Hz, $CO_2CH_2CH_3$); ^{13}C NMR ($CDCl_3$, 75 MHz) δ 171.1 (*C*=O), 167.3 (*C*=O), 149.5, 148.6, 141.4, 127.5, 124.2, 122.4, 112.0, 110.9, 60.8, 60.7, 55.7, 55.6, 33.7, 14.1, 14.0; EIMS *m*/*z* = 322 [M^+] (base), 276, 249, 175; HRMS calcd. for $C_{17}H_{22}O_6$: 322.1416, found: 322.1436. The preparation of this compound has been previously reported (8).

*Stobbe diester – **5c***

Crude acid **4c** (27.2 g, 83.8 mmol), concentrated H_2SO_4 (4.0 mL), and ethanol (100 mL) gave **5c** as a clear pale yellow distillate (15.7 g, 53% yield). ^{1}H NMR (300 MHz, $CDCl_3$) δ 7.78 (s,1H, Ar-C*H*=C), 6.59 (s, 2H, Ar-*H*), 4.24 (q, 2H, *J* = 7.13 Hz, CO_2-CH_2-CH_3), 4.14 (q, 2H, *J* = 7.13 Hz, CO_2-CH_2-CH_3), 3.83 (s, 3H, *p*-O-CH_3), 3.81 (s, 6H, *m*-O-CH_3), 3.52 (s, 2H, CH_2-CO_2), 1.30 (t, 3H, *J* = 7.12 Hz, O-CH_2CH_3), 1.22 (t, 3H, *J* = 7.13 Hz, O-CH_2CH_3); ^{13}C NMR ($CDCl_3$, 75 MHz) δ171.0 (*C*=O), 167.1 (*C*=O), 153.0, 141.6, 138.5, 130.3, 125.5, 106.2, 60.9, 60.8, 60.6, 55.9, 33.8, 14.0_3, 14.0_1; EIMS *m*/*z* = 352 [M^+] (base), 278, 263, 205; HRMS calcd. for $C_{18}H_{24}O_7$: 352.1522, found: 352.1509. The preparation of this compound has been previously reported (8).

Dihydronaphthalene diesters – general method

Lithium diisopropylamide (1.2 equiv.) was prepared by addition of *n*-BuLi (1.2 equiv., 2.5 M in hexanes) to diisopropylamine (1.3 equiv.) in freshly distilled THF at –70°C. The solution was warmed briefly to 0°C, then recooled to –70°C. A solution of the diester **5** (1 equiv.) in THF was added dropwise through a plug (ca. 1 g) of activated alumina, which was then rinsed with THF. On addition of the diester, the solution turns orange to deep red; this colour persists until the reaction is quenched. The mixture was stirred for 10 min, then a solution of the aldehyde (**a**, **b**, or **c**) in THF was added, and stirring was continued for 1 h. The reaction was quenched with glacial acetic acid at –70°C, then warmed to room temperature.

The mixture was extracted with EtOAc (3 × 20 mL), washed with water (20 mL), dried over anhydrous magnesium sulfate, filtered, and evaporated on the rotary evaporator at 30–40°C. The residue was subjected to high vacuum for 1/2 h to remove solvent, then excess trifluoroacetic acid (TFA) (3–4 mL) was added and the solution stirred at room temperature for 1 h. The reaction was poured into saturated aqueous $NaHCO_3$ and extracted into EtOAc (3 × 20 mL). The organic extracts were washed with saturated aqueous $NaHCO_3$ (3 × 10 mL) and water (10 mL), dried over anhydrous magnesium sulfate, filtered and evaporated. The products were isolated by flash column chromatography on silica gel using 20–30% (depending on the polarity of the final product) EtOAc–hexane as the eluant. The product appears as a fluorescent spot on thin layer chromatography (silica) under UV light.

*Dihydronaphthalene diester – **7aa***

Diester **5a** (1.00 g, 3.28 mmol), diisopropylamine (597 μL, 4.26 mmol), *n*-BuLi (1.79 mL of 2.2 M, 3.94 mmol), piperonal (516 mg, 3.44 mmol), and TFA

© 2000 NRC Canada

(3 mL) were used in the general method above. Flash column chromatography on silica gel using 20% EtOAc–hexanes gave diester **7aa** (684 mg, 48% yield) as a yellow oil, which foamed under vacuum. ^{1}H NMR (300 MHz, $CDCl_3$) δ 7.58 (s, 1H, Ar-C*H*=C), 6.81 (s, 2H, Ar-*H*), 6.67 (d, 1H, *J* = 7.5 Hz, Ar-*H*), 6.60 (s, 1H, Ar-*H*), 6.53 (dd, 1H, *J* = 1.9, 7.5 Hz, Ar-*H*), 6.52 (s, 1H, Ar-*H*), 5.95 (s, 2H, O-CH_2-O), 5.88 (m (AB), 2H, O-CH_2-O), 4.56 (d, 1H, *J* = 3.0 Hz, C*H*-CO_2Et), 4.21 (m (2 overlapping doublets of quartets), 2H, *J* = 7.1 Hz, CH=C-CO_2C$H_2$$CH_3$), 4.08 (m (2 overlapping doublets of quartets), 2H, *J* = 7.2 Hz, CH-CO_2C$H_2$$CH_3$), 3.93 (d, 2H, *J* = 3.1 Hz, C*H*-Ar), 1.29 (t, 3H, *J* = 7.1 Hz, CH_2CH_3), 1.16 (t, 3H, *J* = 7.1 Hz, CH_2CH_3); ^{13}C NMR (75 MHz, $CDCl_3$) δ 172.2 (*C*=O), 166.6 (*C*=O), 149.4, 147.7, 147.1, 146.4, 137.1, 136.3, 132.0, 125.5, 123.2, 120.8, 109.7, 108.9, 108.2, 108.1, 101.5, 101.0, 61.2, 60.8, 47.4, 46.2, 14.3, 14.1; EIMS *m*/*z* = 438 [M^+], 410, 364 (base), 319, 292; HRMS calcd. for $C_{24}H_{22}O_8$: 438.1315, found: 438.1311.

*Dihydronaphthalene diester – **7ab***

Diester **5a** (1.26 g, 4.1 mmol), diisopropylamine (692 μL, 4.9 mmol), *n*-BuLi (1.8 mL of 2.5 M, 4.5 mmol), 3,4-dimethoxybenzaldehyde (814 mg, 4.9 mmol), and TFA (4 mL) were used in the general method above. Flash column chromatography on silica gel using 30% EtOAc–hexanes gave diester **7ab** (1.01 g, 54% yield) as a yellow oil, which foamed under vacuum. ^{1}H NMR (300 MHz, $CDCl_3$) δ 7.58 (s, 1H, Ar-C*H*=C), 6.82 (s, 2H, Ar-*H*), 6.70 (d, 1H, *J* = 8.4 Hz, Ar-*H*), 6.66 (d, 1H, *J* = 2.0 Hz, Ar-*H*), 6.61 (s, 1H, Ar-*H*), 6.50 (dd, 1H, *J* = 2.0, 8.1 Hz, Ar-*H*), 5.96 (s, 2H, O-CH_2-O), 4.58 (d, 1H, *J* = 3.4 Hz, C*H*-CO_2Et), 4.21 (m (2 overlapping doublets of quartets), 2H, *J* = 7.0 Hz, CH=C-CO_2C$H_2$$CH_3$), 4.08 (m (2 overlapping doublets of quartets), 2H, *J* = 7.7 Hz, CH-CO_2C$H_2$$CH_3$), 3.98 (d, 1H, *J* = 3.4 Hz, C*H*-Ar), 3.82 (s, 3H, O-CH_3), 3.80 (s, 3H, O-CH_3), 1.29 (s, 3H, *J* = 7.0 Hz, CH_2CH_3), 1.15 (s, 3H, *J* = 7.0 Hz, CH_2CH_3); ^{13}C NMR (75 MHz, $CDCl_3$) δ 172.3 (*C*=O), 166.5 (*C*=O), 149.3, 148.9, 147.9, 146.9, 136.9, 134.7, 132.2, 125.5, 123.5, 119.8, 111.1, 110.9, 109.7, 108.7, 101.4, 61.1, 60.7, 55.9, 55.8, 47.3, 46.1, 14.3, 14.1; EIMS *m*/*z* = 454 [M^+], 380 (base), 335, 308; HRMS calcd. for $C_{25}H_{26}O_8$: 454.1628, found: 454.1647.

*Dihydronaphthalene diester – **7ac***

Diester **5a** (751 mg, 2.4 mmol), diisopropylamine (446 μL, 3.2 mmol), *n*-BuLi (1.3 mL of 2.5 M, 2.9 mmol), 3,4,5-trimethoxybenzaldehyde (483 mg, 2.5 mmol), and TFA (4 mL) were used in the general method above. Flash column chromatography on silica gel using 30% EtOAc–hexanes gave diester **7ac** (495 mg, 42% yield) as a yellow oil, which foamed under vacuum. ^{1}H NMR (300 MHz, $CDCl_3$) δ 7.57 (s, 1H, Ar-C*H*-C), 6.81 (s, 1H, Ar-*H*), 6.61 (s, 1H, Ar-*H*), 6.26 (s, 2H, Ar-*H*), 5.96 (m (AB), 2H, O-CH_2-O), 4.55 (d, 1H, *J* = 4.0 Hz, C*H*-CO_2Et), 4.21 (m (2 overlapping doublets of quartets), 2H, *J* = 7.0 Hz, CH=C-CO_2C$H_2$$CH_3$), 4.08 (m (2 overlapping doublets of quartets), 2H, *J* = 7.4 Hz, CH-CO_2C$H_2$$CH_3$), 3.98 (d, 2H, *J* = 3.7 Hz, C*H*-Ar), 3.78 (s, 3H, *p*-OCH_3), 3.75 (s, 6H, 2 × *m*-OCH_3) 1.29 (t, 3H, *J* = 7.1 Hz, CH_2CH_3), 1.14 (t, 3H, *J* = 7.1 Hz, CH_2CH_3); ^{13}C NMR (75 MHz, $CDCl_3$) δ 172.3 (*C*=O), 166.5 (*C*=O), 153.1, 149.3, 146.8, 137.8, 136.9, 136.8, 131.9, 125.4, 123.6, 109.7, 108.7, 104.9, 101.5, 61.1, 60.7 (both ethyl CH_2 carbons), 56.1, 47.2, 46.5, 14.3, 14.0; EIMS *m*/*z* = 484 [M^+], 410 (base), 365, 338; HRMS calcd. for $C_{26}H_{28}O_9$: 484.1733, found: 484.1718.

*Dihydronaphthalene diester – **7ba***

Diester **5b** (1.70 g, 5.31 mmol), diisopropylamine (1.04 mL, 7.4 mmol), *n*-BuLi (2.98 mL of 2.5 M, 6.86 mmol), piperonal (911 mg, 6.07 mmol), and TFA (4 mL) were used in the general method above. Flash column chromatography on silica gel using 20% EtOAc–hexanes gave diester **7ba** (1.08 g, 42% yield) as a yellow oil, which foamed under vacuum. ^{1}H NMR (300 MHz, $CDCl_3$) δ 7.65 (s, 1H, Ar-C*H*=C), 6.86 (s, 1H, Ar-*H*), 6.66 (d, 1H, *J* = 8.0 Hz, Ar-*H*), 6.62 (s, 1H, Ar-*H*), 6.50 (dd, 1H, *J* = 1.7, 8.0 Hz, Ar-*H*), 6.48 (d, 1H, *J* = 1.7 Hz, Ar-*H*), 5.88 (m (AB), 2H, O-CH_2-O), 4.60 (d, 1H, *J* = 2.7 Hz, C*H*-CO_2Et), 4.21 (q, 2H, *J* = 7.0 Hz, CH=C-CO_2C$H_2$$CH_3$), 4.10 (m (2 overlapping doublets of quartets), 2H, *J* = 7.0 Hz, CH-CO_2C$H_2$$CH_3$), 3.94 (d, 2H, *J* = 2.7 Hz, C*H*-Ar), 3.90 (s, 3H, OCH_3), 3.82 (s, 3H, OCH_3) 1.30 (t, 3H, *J* = 7.0 Hz, CH_2CH_3), 1.16 (t, 3H, *J* = 7.0 Hz, CH_2CH_3); ^{13}C NMR (75 MHz, $CDCl_3$) δ 172.3 (*C*=O), 166.6 (*C*=O), 150.8, 148.2, 147.7, 146.4, 137.1, 136.7, 130.1, 124.3, 122.9, 120.8, 112.0, 111.8, 108.2, 108.1$_6$ 101.0, 61.2, 60.7, 56.1, 56.0, 47.6, 45.8, 14.3, 14.1; EIMS *m*/*z* = 454 [M^+], 380 (base), 335, 308); HRMS calcd. for $C_{25}H_{28}O_8$: 454.1627, found: 454.1624

*Dihydronaphthalene diester – **7bb***

Diester **5b** (1.00 g, 3.11 mmol), diisopropylamine (611 μL, 4.36 mmol), *n*-BuLi (1.8 mL of 2.5 M, 4.03 mmol), 3,4-dimethoxybenzaldehyde (574 mg, 3.45 mmol), and TFA (4 mL) were used in the general method above. Flash column chromatography on silica gel using 30% EtOAc–hexanes gave diester **7bb** (694 mg, 46% yield) as a yellow oil, which foamed under vacuum. ^{1}H NMR (300 MHz, $CDCl_3$) δ 7.64 (s, 1H, Ar-C*H*=C), 6.87 (s, 1H, Ar-*H*), 6.69 (d, 1H, *J* = 8.4 Hz, Ar-*H*), 6.64 (s, 2H, Ar-*H*), 6.47 (dd, 1H, *J* = 2.0, 8.1 Hz, Ar-*H*), 4.62 (d, 1H, *J* = 3.0 Hz, C*H*-CO_2Et), 4.18 (m (2 overlapping doublets of quartets), 2H, *J* = 7.0 Hz, CH=C-CO_2C$H_2$$CH_3$), 4.06 (m (2 overlapping doublets of quartets), 2H, *J* = 7.0 Hz, CH-CO_2C$H_2$$CH_3$), 3.96 (d, 2H, *J* = 3.0 Hz, C*H*-Ar), 3.90 (s, 3H, OCH_3), 3.81 (s, 3H, OCH_3), 3.80 (s, 3H, OCH_3), 3.78 (s, 3H, OCH_3), 1.29 (t, 3H, *J* = 7.1 Hz, CH_2CH_3), 1.15 (t, 3H, *J* = 7.2 Hz, CH_2CH_3); ^{13}C NMR ($CDCl_3$, 75 MHz) δ 172.5 (*C*=O), 166.6 (*C*=O), 150.7, 148.9, 148.1, 147.9, 137.0, 135.1, 130.4, 124.4, 123.2, 119.8, 111.7, 111.3, 110.6, 110.3, 61.2, 60.8, 56.1, 56.0, 55.9, 55.8$_8$, 47.5, 45.8, 14.3, 14.1; EIMS *m*/*z* = 470 [M^+], 396 (base), 351, 324; HRMS calcd. for $C_{26}H_{30}O_8$: 470.1941, found: 470.1965.

*Dihydronaphthalene diester – **7bc***

Diester **5b** (1.10 g, 3.11 mmol), diisopropylamine (672 μL, 4.79 mmol), *n*-BuLi (2.0 mL of 2.2 M, 4.43 mmol), 3,4,5-trimethoxybenzaldehyde (724 mg, 3.69 mmol), and TFA (5 mL) were used in the general method above. Flash column chromatography on silica gel using 30% EtOAc–hexanes gave diester **7bc** (804 mg, 44% yield) as a yellow

© 2000 NRC Canada

oil, which foamed under vacuum. ^{1}H NMR (300 MHz, $CDCl_3$) δ 7.64 (s, 1H, Ar-C*H*=C), 6.88 (s, 1H, Ar-*H*), 6.66 (s, 1H, Ar-*H*), 6.24 (s, 2H, Ar-*H*), 4.62 (d, 1H, *J* = 3.4 Hz, C*H*-CO_2Et), 4.23 (m (2 overlapping doublets of quartets), 2H, *J* = 6.8 Hz, CH=C-$CO_2CH_2CH_3$), 4.09 (m (2 overlapping doublets of quartets), 2H, *J* = 7.4 Hz, CH-$CO_2CH_2CH_3$), 4.00 (d, 2H, *J* = 3.0 Hz, C*H*-Ar), 3.92 (s, 3H, OCH_3), 3.84 (s, 3H, OCH_3), 3.79 (s, 3H, OCH_3), 3.73 (s, 6H, 2 × *m*-OCH_3), 1.30 (t, 3H, *J* = 7.1 Hz, CH_2CH_3), 1.16 (t, 3H, *J* = 7.2 Hz, CH_2CH_3); ^{13}C NMR (75 MHz, $CDCl_3$) δ 172.4 (*C*=O), 166.6 (*C*=O), 153.1, 150.7, 148.3, 138.2, 136.9, 130.0, 124.4, 123.4, 112.1, 111.6, 104.9, 61.2, 60.8, 60.7, 56.1, 56.0_6 (2 × OCH_3), 47.5, 46.3, 14.3, 14.1 (one quaternary carbon not observed, may be obscured by peak at 136.9); EIMS *m*/*z* = 500 [M^+], 426 (base), 381, 354; HRMS calcd. for $C_{27}H_{32}O_9$: 500.2046, found: 500.2049.

*Dihydronaphthalene diester – **7ca***

Diester **5c** (1.01 g, 2.87 mmol), diisopropylamine (523 μL, 3.73 mmol), *n*-BuLi (1.9 mL of 1.76 M, 3.44 mmol), piperonal (443 mg, 2.95 mmol), and TFA (4 mL) were used in the general method above. Flash column chromatography on silica gel using 30% EtOAc–hexanes gave diester **7ca** (498 mg, 36% yield) as a yellow oil, which foamed under vacuum. ^{1}H NMR (300 MHz, $CDCl_3$) δ 7.62 (s, 1H, Ar-C*H*=C), 6.70 (s, 1H, Ar-*H*), 6.49–6.62 (m, 3H), 5.85 (m (AB), 2H, O-CH_2-O), 4.93 (bs, 1H, C*H*-CO_2Et), 4.19 (q, 2H, *J* = 7.0 Hz, CH=C-$CO_2CH_2CH_3$), 4.09 (m (2 overlapping doublets of quartets), 2H, *J* = 7.1 Hz, CH-$CO_2CH_2CH_3$), 3.94 (d, 2H, *J* = 1.0 Hz, C*H*-Ar), 3.90 (s, 3H, OCH_3), 3.85 (s, 3H, OCH_3), 3.61 (s, 3H, OCH_3), 1.28 (t, 3H, *J* = 7.0 Hz, CH_2CH_3), 1.18 (t, 3H, *J* = 7.0 Hz, CH_2CH_3); ^{13}C NMR (75 MHz, $CDCl_3$) δ 171.8 (*C*=O), 166.5 (*C*=O), 152.7, 151.3, 147.5, 146.2, 144.3, 137.0, 136.9, 127.1, 124.5, 123.3, 120.5, 108.4, 108.1, 108.0, 100.9, 61.2, 60.9, 60.8, 56.1, 56.0, 46.9, 39.3, 14.3, 14.1; EIMS *m*/*z* = 484 [M^+], 410, 352 (base), 278, 263, 205; HRMS calcd. for $C_{26}H_{28}O_9$: 484.1733, found: 484.1753.

*Dihydronaphthalene diester – **7cc***

Diester **5c** (3.01 g, 8.50 mmol), diisopropylamine (1.55 mL, 11.05 mmol), *n*-BuLi (6.0 mL of 1.76 M, 10.2 mmol), 3,4,5-trimethoxybenzaldehyde (1.68 g, 8.56 mmol), and TFA (5 mL) were subjected to the general method above. Flash column chromatography on silica gel using 30% EtOAc–hexanes gave diester **7cc** (704 mg, 16% yield) as a yellow oil, which foamed under vacuum. ^{1}H NMR (300 MHz, $CDCl_3$) δ 7.62 (s, 1H, C*H*=C-CO_2Et), 6.71 (s, 1H, Ar-*H*), 6.28 (s, 2H, 2 × Ar-*H*), 5.00 (d, 1H, *J* = 1.2 Hz, C*H*-CO_2Et), 4.23 (2 overlapping quartets, 2H, *J* = 7.1 Hz, CO_2-CH_2CH_3), 4.12 (2 overlapping quartets, 2H, *J* = 7.2 Hz, CO_2-CH_2CH_3), 4.06 (d, 1H, *J* = 1.2 Hz, C*H*-Ar), 3.89 (s, 3H, OCH_3), 3.88 (s, 3H, OCH_3), 3.77 (s, 3H, OCH_3), 3.72 (s, 6H, 2 × *m*-OCH_3), 3.67 (s, 3H, OCH_3), 1.31 (t, 3H, *J* = 7.1 Hz, CH_2CH_3), 1.19 (t, 3H, *J* = 7.2 Hz, CH_2CH_3); ^{13}C NMR ($CDCl_3$, 75 MHz) δ 171.7 (*C*=O), 166.5 (*C*=O), 152.9, 152.7, 151.4, 144.2, 138.4, 136.7, 127.1, 124.9, 123.2, 108.2, 104.6, 61.2, 60.8_4, 60.7_7, 60.7_1, 56.0 (4 × OCH_3), 46.2, 39.4, 14.3, 14.1 (one quaternary carbon not observed); EIMS *m*/*z* = 530 [M^+], 456 (base), 411, 384, 196; HRMS calcd. for $C_{28}H_{34}O_{10}$: 530.2152, found: 530.2129.

Aromatization – formation of arylnapthalene diesters – general procedure

The dihydronaphthalene diesters **7** were dissolved in toluene (ca. 0.015 M), then dicyanodichloroquinone (DDQ, 1.2 equiv.) was added, and the mixture was heated at reflux for 2–5 h. The reaction mixture was cooled to room temperature, and quenched by addition of 100 mL 0.1 M KOH. The product was extracted into 60 mL EtOAc (60 mL) and washed with aqueous KOH (0.1 M, 2 × 50 mL). The aqueous layer was extracted with additional EtOAc (2 × 50 mL), the organic layers combined and washed with water (20 mL) and saturated aqueous NaCl (20 mL). The solution was dried over anhydrous magnesium sulfate, filtered, and evaporated. The resulting red-brown residue was dissolved in the minimum amount of dichloromethane, then passed through a filter column of silica gel using 30% EtOAc–hexanes as the eluant and evaporated. Further purification, to get better than 95% purity by HPLC, required recrystallization from $CHCl_3$–hexanes.

*Arylnaphthalene diester – **8aa***

Diester **7aa** (656 mg, 1.5 mmol), DDQ (409 mg, 1.8 mmol) was heated at reflux in toluene (20 mL) for 5 h, and worked up as in the general method above to give **8aa** (571 mg, 87% yield) as off-white crystals; mp = 171–172°C; ^{1}H NMR (300 MHz, $CDCl_3$) δ 8.38 (s, 1H, C*H*=C-CO_2Et), 7.23 (s, 1H, Ar-*H*), 6.8–6.9 (m, 4H, Ar-*H*), 6.06 (s, 2H, O-CH_2-O), 6.03 (m (AB), 2H, O-CH_2-O), 4.39 (q, 2H, *J* = 7.1 Hz, CO_2-CH_2CH_3), 4.12 (q, 2H, *J* = 7.1 Hz, CO_2-CH_2CH_3), 1.40 (t, 3H, *J* = 7.1 Hz, CO_2-CH_2CH_3), 1.11 (t, 3H, *J* = 7.1 Hz, CO_2-CH_2CH_3); ^{13}C NMR (75 MHz, $CDCl_3$) δ 168.9 (*C*=O), 166.0 (*C*=O), 150.3, 148.7, 147.3, 136.9, 132.3, 130.6_4, 130.5_9, 129.9, 129.8_6, 123.9, 123.4, 111.0, 108.1, 104.9, 103.3, 101.7, 101.2, 61.5, 61.1, 14.3, 13.9 (one quaternary carbon not detected; perhaps under 147.3); EIMS *m*/*z* = 436 [M^+] (base), 391, 363; HRMS calcd. for $C_{24}H_{20}O_8$: 436.1158, found: 436.1140.

*Arylnaphthalene diester – **8ab***

Diester **7ab** (838 mg, 1.85 mmol), DDQ (503 mg, 2.21 mmol) was heated at reflux in toluene (10 mL) for 3 h, and worked up as in the general method above to give **8ab** (826 mg, 99% yield) as off-white crystals. ^{1}H NMR (300 MHz, $CDCl_3$) δ 8.37 (s, 1H, C*H*=C-CO_2Et), 7.21 (s, 1H, Ar-*H*), 6.94 (d, 1H, *J* = 8.0 Hz, Ar-*H*), 6.87 (dd, 1H, *J* = 2.0, 8.0 Hz, Ar-*H*), 6.86 (s, 1H, Ar-*H*), 6.85 (s, 1H, Ar-*H*), 6.04 (s, 2H, O-CH_2-O), 4.38 (q, 2H, *J* = 7.0 Hz, CO_2-CH_2CH_3), 4.07 (2s, 2H, *J* = 7.0 Hz, CO_2-CH_2CH_3), 3.94 (s, 3H, OCH_3), 3.84 (s, 3H, O-CH_3), 1.39 (t, 3H, *J* = 7.1 Hz, CO_2-CH_2CH_3), 1.03 (t, 3H, *J* = 7.1 Hz, CO_2-CH_2CH_3); ^{13}C NMR (75 MHz, $CDCl_3$) δ 169.0 (*C*=O), 165.9 (*C*=O), 150.1, 148.6, 148.5_9, 148.4, 137.1, 132.3, 130.5, 129.8, 129.4, 123.3, 122.7, 113.6, 110.7, 104.8, 103.3, 101.6, 61.4, 61.0, 55.9 (2 × OCH_3), 14.2, 13.8 (one quaternary carbon not detected); EIMS *m*/*z* = 452 [M^+] (base), 407, 379, 363, 335; HRMS calcd. for $C_{25}H_{24}O_8$: 452.1471, found: 452.1470.

*Arylnaphthalene diester – **8ac***

Diester **7ac** (464 mg, 0.96 mmol), DDQ (260 mg, 1.15 mmol) was heated at reflux in toluene (10 mL) for 3 h,

© 2000 NRC Canada

and worked up as in the general method above to give **8ac** (414 mg, 90% yield) as off-white crystals; mp = 178–182°C; ^{1}H (300 MHz, $CDCl_3$) δ 8.39 (s, 1H, C*H*=C-CO_2Et), 7.24 (s, 1H, Ar-*H*), 6.91 (s, 1H, Ar-*H*), 6.55 (s, 2H, Ar-*H*), 6.07 (s, 2H, O-CH_2-O), 4.39 (q, 2H, *J* = 7.1 Hz, CO_2-CH_2CH$_3$), 4.10 (q, 2H, *J* = 7.2 Hz, CO_2-CH_2CH$_3$), 3.92 (s, 3H, *p*-OCH_3), 3.83 (s, 6H, 2 × *m*-OCH_3), 1.40 (t, 3H, *J* = 7.2 Hz, CO_2-CH$_2$CH_3), 1.03 (t, 3H, *J* = 7.1 Hz, CO_2-CH$_2$CH_3); ^{13}C NMR (75 MHz, $CDCl_3$) δ 169.0 (*C*=O), 165.9 (*C*=O), 152.9, 150.2, 148.8, 137.6, 137.3, 132.5, 132.0, 130.3, 130.0, 129.9, 123.4, 107.7, 104.9, 103.3, 101.8, 61.5, 61.1, 61.0, 56.2, 14.3, 13.9; EIMS *m*/*z* = 482 [M^+] (base), 410, 393, 365; HRMS calcd. for $C_{26}H_{26}O_9$: 482.1576, found: 482.1566.

*Arylnaphthalene diester – **8ba***

Diester **7ba** (914 mg, 2.01 mmol), DDQ (548 mg, 2.4 mmol) was heated at reflux in toluene (10 mL) for 5 h, and worked up as in the general method above to give **20** (878 mg, 97% yield) as off-white crystals; mp = 195–197°C; ^{1}H NMR (300 MHz, $CDCl_3$) δ 8.43 (s, 1H, C*H*=C-CO_2Et), 7.24 (s, 1H, Ar-*H*), 6.79–6.92 (m, 4H, Ar-*H*), 6.02, 6.07 (2s, 2H, O-CH_2-O, hindered rotation), 4.39 (q, 2H, *J* = 7.1 Hz, CO_2-CH_2CH$_3$), 4.13 (q, 2H, *J* = 7.1 Hz, CO_2-CH_2CH$_3$), 4.03 (s, 3H, OCH_3), 3.79 (s, 3H, O-CH_3), 1.40 (t, 3H, *J* = 7.1 Hz, CO_2-CH$_2$CH_3), 1.10 (t, 3H, *J* = 7.1 Hz, CO_2-CH$_2$CH_3); ^{13}C NMR (75 MHz, $CDCl_3$) δ 169.1 (*C*=O), 166.1 (*C*=O), 151.7, 150.5, 147.4, 147.3, 136.4, 130.7, 130.6, 130.4, 129.5, 128.5, 123.9, 123.2, 110.9, 108.1, 107.3, 105.3, 101.2, 61.4, 61.1, 56.1, 55.9, 14.3, 13.9; EIMS *m*/*z* = 452 [M^+] (base), 407, 379; HRMS calcd. for $C_{25}H_{24}O_8$: 452.1471, found: 452.1525.

*Arylnaphthalene diester – **8bb***

Diester **7bb** (594 mg, 1.33 mmol), DDQ (363 mg, 1.59 mmol) was heated at reflux in toluene (10 mL) for 3 h, and worked up as in the general method above to give **8bb** (586 mg, 99% yield) as off-white crystals; mp = 127–128°C; ^{1}H NMR (300 MHz, $CDCl_3$) δ 8.43 (s, 1H, C*H*=C-CO_2Et), 7.24 (s, 1H, Ar-*H*), 6.85–7.00 (m, 4H, Ar-*H*), 4.39 (q, 2H, *J* = 7.1 Hz, CO_2-CH_2CH$_3$), 4.09 (dq, 2H, *J* = 2.4, 7.1 Hz, CO_2-CH_2CH$_3$), 4.03 (s, 3H, OCH_3), 3.95 (s, 3H, OCH_3), 3.85 (s, 3H, OCH_3), 3.76 (s, 3H, O-CH_3), 1.40 (t, 3H, *J* = 7.1 Hz, CO_2-CH$_2$CH_3), 1.05 (t, 3H, *J* = 7.1 Hz, CO_2-CH$_2$CH_3); ^{13}C NMR (75 MHz, $CDCl_3$) δ 169.3 (*C*=O), 166.1 (*C*=O), 151.7, 150.5, 148.6, 148.5, 136.6, 130.6, 129.6, 129.4, 128.5, 123.2, 122.7, 113.6, 110.8, 107.3, 105.4, 61.4, 61.1, 56.1, 56.0, 55.9$_4$, 55.8$_7$, 14.3, 13.9 (one quaternary carbon not observed; perhaps under 129.4); EIMS *m*/*z* = 468 [M^+] (base), 423, 395; HRMS calcd. for $C_{26}H_{28}O_8$: 468.1784, found: 468.1794.

*Arylnaphthalene diester – **8bc***

Diester **7bc** (538 mg, 1.08 mmol), DDQ (293 mg, 1.29 mmol) was heated at reflux in toluene (20 mL) for 2 h, and worked up as in the general method above to give **8bc** (535 mg, 100% yield) as off-white crystals; mp = 148–149°C; ^{1}H NMR (300 MHz, $CDCl_3$) δ 8.44 (s, 1H, C*H*=C-CO_2Et), 7.24 (s, 1H, Ar-*H*), 6.93 (s, 1H, Ar-*H*), 6.61 (s, 2H, Ar-*H*), 4.39 (q, 2H, *J* = 7.1 Hz, CO_2-CH_2CH$_3$), 4.12 (q, 2H, *J* = 7.1 Hz, CO_2-CH_2CH$_3$), 4.03 (s, 3H, OCH_3), 3.92 (s, 3H, OCH_3), 3.84 (s, 6H, 2 × *m*-OCH_3), 3.79 (s, 3H, O-CH_3), 1.40 (t, 3H, *J* = 7.1 Hz, CO_2-CH$_2$CH_3), 1.04 (t, 3H, *J* = 7.1 Hz, CO_2-CH$_2$CH_3); ^{13}C NMR (75 MHz, $CDCl_3$) δ 169.2 (*C*=O), 166.0 (*C*=O), 152.9, 151.8, 150.6, 137.6, 136.7, 132.6, 130.2, 130.0, 129.5, 128.5, 123.2, 107.6, 107.3, 105.4, 61.4, 61.1, 61.0, 56.2, 56.1, 56.0, 14.3, 13.9; EIMS *m*/*z* = 498 [M^+], 425, 409, 322, 196 (base); HRMS calcd. for $C_{27}H_{30}O_9$: 498.1890, found: 498.1899.

Formation of arylnapthalene mono-acids – general procedure

The arylnaphthalene diesters **8** were dissolved in MeOH (20 mL, ca. 0.05 M), aqueous KOH (0.4 M, 1.2 equiv.) was added, and the mixture was heated at reflux for 3 h. The mixture was cooled, quenched by addition of 10% HCl until precipitation occurred (pH of <2), then the mixture extracted into EtOAc (3 × 20 mL). The organic layers were combined and extracted with 3 × 20 mL (sat.) $NaHCO_3$. This basic extract was washed with EtOAc (20 mL), then acidified and extracted with ethyl acetate (3 × 10 mL), backwashing with 10 mL of water. The mixture was dried over anhydrous magnesium sulfate, filtered, and evaporated to give a powdery white solid.

*Acid – **9aa***

Arylnaphthalene diester **8aa** (356 mg, 0.82 mmol) and KOH (6 mL, 0.4 M, 2.4 mmol) were subjected to the general procedure described above, producing **9aa** (291 mg, 87% yield) as a fine white powder. ^{1}H NMR (300 MHz, acetone-d_6) δ 11.40 (br. s, 1H, CO_2*H*), 8.49 (s, 1H, C*H*=C-CO_2H), 8.00 (s, 1H, Ar-*H*), 7.48 (s, 1H, Ar-*H*), 6.97 (d, 1H, *J* = 7.7 Hz, Ar-*H*), 6.83 (s, 1H, Ar-*H*), 6.80 (d, 1H, *J* = 1.3 Hz, Ar-*H*), 6.76 (dd, 1H, *J* = 1.7, 7.7 Hz, Ar-*H*), 6.18 (2s, 2H, O-CH_2-O, hindered rotation), 6.09 (m (AB), 2H, O-CH_2-O), 4.02 (q, 2H, *J* = 7.1 Hz, CO_2-CH_2CH$_3$), 1.05 (t, 3H, *J* = 7.1 Hz, CO_2-CH$_2$CH_3); ^{13}C NMR (75 MHz, acetone-d_6) δ 168.5 (*C*=O), 166.9 (*C*=O), 151.2, 149.6, 148.2, 137.4, 132.7, 131.9, 131.4, 130.6$_2$, 130.5$_5$, 124.5, 124.3, 111.5, 108.5, 105.4, 103.1, 102.9, 102.1, 60.9, 14.0 (one quaternary carbon not observed); EIMS *m*/*z* = 408 [M^+], 362 (base), 290, 260, 232, 174; HRMS calcd. for $C_{22}H_{16}O_8$: 408.0845, found: 408.0823.

*Acid – **9ab***

Arylnaphthalene diester **8ab** (602 mg, 1.33 mmol) and KOH (4 mL, 0.4 M, 1.6 mmol) were subjected to the general procedure described above, producing **9ab** (491 mg, 87% yield) as a fine white powder. ^{1}H NMR (300 MHz, $CDCl_3$) 8.49 (s, 1H, C*H*=C-CO_2H), 7.25 (d, 1H, *J* = 2.8, Ar-*H*), 6.8–7.0 (m, 5H, Ar-*H*), 6.07 (s, 2H, O-CH_2-O), 4.09 (2 overlapping quartets, 2H, *J* = 7.1 Hz, CO_2-CH_2CH$_3$), 3.95 (s, 3H, OCH_3), 3.86 (s, 3H, OCH_3), 1.09 (t, 3H, *J* = 7.1 Hz, CO_2-CH$_2$CH_3); ^{13}C NMR (75 MHz, $CDCl_3$) δ 170.7 (*C*=O), 169.1 (*C*=O), 150.9, 149.1$_0$ 149.0$_9$, 148.8, 137.7, 131.3, 131.2, 130.1, 129.6, 123.1, 122.1, 113.9, 111.1, 105.4, 103.8, 101.8, 61.6, 56.3 (2 × OCH_3), 14.2 (one quaternary carbon not observed); EIMS *m*/*z* = 424 [M^+], 378 (base), 335, 291, 248; HRMS calcd. for $C_{23}H_{20}O_8$: 424.1158, found: 424.1152.

© 2000 NRC Canada

*Acid – **9ac***

Arylnaphthalene diester **8ac** (840 mg, 1.74 mmol) and KOH (6 mL, 0.4 M, 2.4 mmol) were subjected to the general procedure described above, producing **9ac** (644 mg, 82% yield) as a fine white powder. ^{1}H NMR (300 MHz, $CDCl_3$) δ 8.48 (s, 1H, C*H*=C-CO_2H), 6.92 (s, 1H, Ar-*H*), 6.56 (s, 2H, Ar-*H*), 6.08 (s, 2H, O-CH_2-O), 4.10 (2 overlapping quartets, 2H, *J* = 7.1 Hz, CO_2-CH_2CH$_3$), 3.93 (s, 3H, *p*-OCH_3), 3.83 (s, 6H, 2 × *m*-OCH_3), 1.07 (t, 3H, *J* = 7.1 Hz, CO_2-CH$_2$CH_3); ^{13}C NMR (75 MHz, $CDCl_3$) δ 169.9 (*C*=O), 168.7 (*C*=O), 150.6, 152.9, 148.8, 137.7, 137.5, 132.6, 132.2, 131.0, 130.5, 129.7, 107.7, 105.0, 103.4, 101.8, 61.3, 61.0, 56.2, 13.8 (one quaternary carbon not detected); EIMS *m*/*z* = 454 [M$^+$], 408 (base), 393, 380, 365; HRMS calcd. for $C_{24}H_{22}O_9$: 454.1264, found: 454.1285.

*Acid – **9ba***

Arylnaphthalene diester **8ba** (877 mg, 1.94 mmol) and KOH (6 mL, 0.4 M, 2.4 mmol) were subjected to the general procedure described above, producing **9ba** (613 mg, 74% yield) as a fine white powder. ^{1}H NMR (300 MHz, $CDCl_3$) δ 8.52 (s, 1H, C*H*=C-CO_2H), 6.92 (d, 1H, *J* = 8.0 Hz, Ar-*H*), 6.88 (s, 1H, Ar-*H*), 6.86 (d, 1H, *J* = 1.0 Hz, Ar-*H*), 6.83 (dd, 1H, *J* = 1.3, 8.0 Hz, Ar-*H*), 6.04 (m (AB), 2H, O-CH_2-O, hindered rotation), 4.14 (q, 2H, *J* = 7.1 Hz, CO_2-CH_2CH$_3$), 4.03 (s, 3H, O-CH_3), 3.80 (s, 3H, O-CH_3), 1.15 (t, 3H, *J* = 7.1 Hz, CO_2-CH$_2$CH_3); ^{13}C NMR (75 MHz, $CDCl_3$) δ 170.9 (*C*=O), 168.8 (*C*=O), 152.1, 150.5, 147.4, 147.3, 136.5, 131.2, 130.6, 130.5, 130.4, 128.4, 123.8, 121.6, 110.9, 108.1, 107.5, 105.4, 101.2, 61.2, 56.1, 55.9, 13.9; EIMS *m*/*z* = 424 [M$^+$], 378 (base), 306, 291, 276; HRMS calcd. for $C_{23}H_{20}O_8$: 424.1158, found: 424.1159.

*Acid – **9bb***

Arylnaphthalene diester **8bb** (906 mg, 1.94 mmol) and KOH (6 mL, 0.4 M, 2.4 mmol) were subjected to the general procedure described above, producing **9bb** (763 mg, 90% yield) as a fine white powder. ^{1}H NMR (300 MHz, acetone-d_6) δ 11.32 (br. s, 1H, CO_2*H*), 8.51 (s, 1H, C*H*=C-CO_2H), 7.55 (s, 1H, Ar-*H*), 7.06 (d, 1H, *J* = 8.0 Hz, Ar-*H*), 6.96 (s, 1H, Ar-*H*), 6.93 (d, 1H, *J* = 2.0 Hz, Ar-*H*), 6.88 (dd, 1H, *J* = 2.0, 8.0 Hz, Ar-*H*), 4.01 (q, 2H, *J* = 7.1 Hz, CO_2-CH_2CH$_3$), 4.00 (s, 3H, OCH_3), 3.87 (s, 3H, OCH_3), 3.82 (s, 3H, OCH_3), 3.72 (s, 3H, OCH_3), 1.02 (t, 3H, *J* = 7.2 Hz, CO_2-CH$_2$CH_3); ^{13}C NMR (75 MHz, $CDCl_3$) δ 171.3 (*C*=O), 169.0 (*C*=O), 152.0, 150.5, 148.6, 148.4, 136.7, 131.2, 130.5, 130.4, 129.3, 128.3, 122.7, 121.6, 113.5, 110.7, 107.4, 105.4, 61.2, 56.0, 55.9, 55.7 (2 × OCH$_3$), 13.8; EIMS *m*/*z* = 440 [M$^+$], 394 (base), 307; HRMS calcd. for $C_{24}H_{24}O_8$: 440.1471, found: 440.1469.

*Acid – **9bc***

Arylnaphthalene diester **8bc** (621 mg, 1.25 mmol) and KOH (6 mL, 0.4 M, 2.4 mmol) were subjected to the general procedure described above, producing **9bc** (516 mg, 88% yield) as a fine white powder. ^{1}H NMR (300 MHz, acetone-d_6) δ 11.25 (br. s, 1H, CO_2*H*), 8.54 (s, 1H, C*H*=C-CO_2H), 7.56 (s, 1H, Ar-*H*), 7.03 (s, 1H, Ar-*H*), 6.64 (s, 2H, Ar-*H*), 4.03 (q, 2H, *J* = 7.0 Hz, CO_2-CH_2CH$_3$), 4.01 (s, 3H, OCH_3), 3.84 (s, 6H, 2 × *m*-OCH_3), 3.81 (s, 3H, OCH_3), 3.75 (s, 3H, OCH_3), 1.03 (t, 3H, *J* = 7.0 Hz, CO_2-CH$_2$CH_3); ^{13}C NMR (75 MHz, acetone-d_6) δ 168.9, 167.1, 153.9, 152.9, 151.8, 138.7, 137.3, 133.3, 130.6, 130.0, 129.3, 124.1, 108.7, 108.3, 106.0, 61.0, 60.6, 56.4, 56.0, 55.7, 14.0 (one quaternary carbon not observed); EIMS *m*/*z* = 470 [M$^+$], 424 (base), 409, 381, 363; HRMS calcd. for $C_{25}H_{26}O_9$: 470.1577, found: 470.1568.

Formation of arylnaphthalene lactones – general procedure

The arylnaphthalene mono-acids **9** were dissolved in dry THF (ca. 0.05 M) under nitrogen, a borane-dimethylsulfide solution (2.0 M in ether, 10 equiv.) added, and the mixture stirred at room temperature for 2 h. The reaction was quenched with 3% HCl–EtOH (prepared by addition of 0.5 mL acetyl chloride to 9.5 mL of anhydrous ethanol), then the solvent removed on a rotary evaporator. Anhydrous ethanol (20 mL) was added and evaporated, the solid residue dissolved in chloroform and washed with saturated aqueous $NaHCO_3$ (3 × 10 mL) to remove any remaining acid. The organic extract was washed with water (10 mL), dried over anhydrous magnesium sulfate, filtered, and evaporated to give a white powder. Further purification, to get better than 95% purity by HPLC, involved recrystallization from $CHCl_3$–hexanes.

*Taiwanin C – **2aa***

Arylnaphthalene acid **9aa** (99 mg, 0.24 mmol) and BH_3–DMS (1.2 mL, 2.4 mmol) were subjected to the above conditions to give taiwanin C (**2aa**) (70 mg, 82% yield) as a white powder. ^{1}H NMR (300 MHz, $CDCl_3$) δ 7.68 (s, 1H, C*H*=C-CH_2O), 7.19 (s, 1H, Ar-*H*), 7.11 (s, 1H, Ar-*H*), 6.95 (d, 1H, *J* = 7.7 Hz, Ar-*H*), 6.80 (s, 1H, Ar-*H*), 6.77 (d, 1H, *J* = 1.3, 7.7 Hz, Ar-*H*), 6.08 (s, 2H, O-CH_2-O), 6.06 (2 s, 2H, O-CH_2-O, hindered rotation), 5.37 (s, 2H, CH_2-O-C=O); ^{13}C NMR (75 MHz, $CDCl_3$) δ 169.7 (*C*=O), 149.9, 148.6, 147.6, 147.5, 140.1, 139.8, 134.6, 130.5, 123.5, 128.3, 119.0, 118.9, 110.5, 108.2, 103.7 (broad, 2 carbons), 101.8, 101.2, 68.0; EIMS *m*/*z* = 348 [M$^+$] (base), 319, 289, 261; HRMS calcd. for $C_{20}H_{12}O_6$: 348.0634, found: 348.0629. ^{1}H NMR data identical to that published previously (12, 13).

*Chinensin – **2ab***

Arylnaphthalene acid **9ab** (198 mg, 0.47 mmol) and BH_3–DMS (2.3 mL, 4.7 mmol) were subjected to the above conditions to give Chinensin (**2ab**) (166 mg, 97% yield) as a white powder. ^{1}H NMR (300 MHz, $CDCl_3$) δ 7.69 (s, 1H, C*H*=C-CH_2O), 7.20 (s, 1H, Ar-*H*), 7.12 (s, 1H, Ar-*H*), 7.02 (d, 1H, *J* = 8.0 Hz, Ar-*H*), 6.88 (dd, 1H, *J* = 1.7, 8.4 Hz, Ar-*H*), 6.86 (d, 1H, *J* = 1.7 Hz, Ar-*H*), 6.07 (s, 2H, O-CH_2-O), 5.37 (2s, 2H, CH_2-O-C=O), 3.97 (s, 3H, O-CH_3), 3.87 (s, 3H, O-CH_3); ^{13}C NMR (75 MHz, $CDCl_3$) δ 169.7 (*C*=O), 149.9, 148.9, 148.6, 148.5, 140.5, 139.8, 134.6, 130.5, 127.2, 122.5, 118.9, 118.8, 113.4, 110.8, 103.7, 103.6, 101.8, 67.9, 55.9, 55.8; EIMS *m*/*z* = 364 [M$^+$] (base); HRMS calcd. for $C_{21}H_{16}O_6$: 364.0947, found: 364.0958. ^{1}H NMR data identical to that published previously (12).

*Dehydroanhydropodophyllotoxin – **2ac***

Arylnaphthalene acid **9ac** (201 mg, 0.44 mmol) and BH_3–DMS (2.2 mL, 4.4 mmol) were subjected to the above conditions to give dehydroanhydropodophyllotoxin (**2ac**)

© 2000 NRC Canada

(122 mg, 70% yield) as a white powder. ^{1}H NMR (300 MHz, $CDCl_3$) δ 7.70 (s, 1H, C*H*=C-CH_2O), 7.20 (s, 1H, Ar-*H*), 7.12 (s, 1H, Ar-*H*), 6.55 (s, 2H, Ar-*H*), 6.09 (s, 2H, O-CH_2-O), 5.38 (2s, 2H, CH_2-O-C=O), 3.97 (s, 3H, *p*-OCH_3), 3.84 (s, 6H, 2 × *m*-OCH_3); ^{13}C NMR (75 MHz, $CDCl_3$) δ 169.6 (*C*=O), 152.9, 150.0, 148.6, 140.4, 139.8, 137.8, 134.6, 130.3 (broad, 2 carbons), 119.1, 118.7, 107.3, 103.7, 103.6, 101.8, 68.0, 60.9, 56.1; EIMS *m*/*z* = 394 [M^+] (base), 379; HRMS calcd. for $C_{22}H_{18}O_7$: 394.1052, found: 394.1041. ^{1}H NMR data identical to that published previously (14).

Justicidin B – ***2ba***

Arylnaphthalene acid **9ba** (273 mg, 0.65 mmol) and BH_3–DMS (3.2 mL, 6.5 mmol) were subjected to the above conditions to give justicidin B (**2ba**) (223 mg, 95% yield) as a white powder. ^{1}H NMR (300 MHz, $CDCl_3$) δ 7.69 (s, 1H, C*H*=C-CH_2O), 7.18 (s, 1H, Ar-*H*), 7.10 (s, 1H, Ar-*H*), 6.96 (d, 1H, *J* = 7.7 Hz, Ar-*H*), 6.84 (d, 1H, *J* = 2.0 Hz, Ar-*H*), 6.83 (dd, 1H, *J* = 2.0, 7.7 Hz, Ar-*H*), 6.08, 6.03 (2s, 2H, O-CH_2-O, hindered rotation), 5.37 (2s, 2H, CH_2-O-C=O), 4.04 (s, 3H, OCH_3), 3.80 (s, 3H, OCH_3); ^{13}C NMR (75 MHz, $CDCl_3$) δ 169.9 (*C*=O), 151.7, 150.0, 147.4$_9$, 147.4$_6$, 139.5$_5$, 139.4$_6$, 133.1, 128.8, 128.3, 123.4, 118.4, 118.2, 110.5, 108.1, 106.0, 105.8, 101.2, 68.0, 56.0, 55.8; EIMS *m*/*z* = 364 [M^+] (base); HRMS calcd. for $C_{21}H_{16}O_6$: 364.0947, found: 364.0958. ^{1}H NMR data identical to that published previously (15).

Lactone – ***2bb***

Arylnaphthalene acid **9bb** (304 mg, 0.69 mmol) and BH_3–DMS (3.4 mL, 6.9 mmol) were subjected to the above conditions to give lactone **2bb** (250 mg, 95% yield) as a white powder. ^{1}H NMR (300 MHz, $CDCl_3$) δ 7.71 (s, 1H, C*H*=C-CH_2O), 7.19 (s, 1H, Ar-*H*), 7.15 (s, 1H, Ar-*H*), 7.04 (d, 1H, *J* = 8.4 Hz, Ar-*H*), 6.96 (dd, 1H, *J* = 2.0, 8.2 Hz, Ar-*H*), 6.93 (dd, 1H, *J* = 2.0 Hz, Ar-*H*), 5.38 (2s, 2H, CH_2-O-C=O), 4.05 (s, 3H, OCH_3), 3.98 (s, 3H, OCH_3), 3.88 (s, 3H, OCH_3), 3.79 (s, 3H, OCH_3); ^{13}C NMR (75 MHz, $CDCl_3$) δ 169.9 (*C*=O), 151.8, 150.0, 148.9, 148.5, 139.9, 139.6, 133.1, 128.8, 127.1, 122.6, 118.3, 118.1, 113.4, 110.8, 106.0 (broad, 2 carbons), 68.0, 56.0$_5$, 55.9$_6$, 55.8$_0$, 55.7$_7$; EIMS *m*/*z* = 380 [M^+] (base), 365; HRMS calcd. for $C_{22}H_{20}O_6$: 380.1260, found: 380.1256. ^{1}H NMR data identical to that published previously (13).

7-Deoxydiphyllin – ***2bc***

Arylnaphthalene acid **9bc** (191 mg, 0.41 mmol) and BH_3–DMS (2.0 mL, 4.1 mmol) were subjected to the above conditions to give lactone **2bc** (233 mg, 80% yield) as a white powder. ^{1}H NMR (300 MHz, $CDCl_3$) δ 7.72 (s, 1H, C*H*=C-CH_2O), 7.20 (s, 1H, Ar-*H*), 7.15 (s, 1H, Ar-*H*), 6.62 (s, 2H, 2 × Ar-*H*), 5.40 (2s, 2H, CH_2-O-C=O), 4.06 (s, 3H, OCH_3), 3.98 (s, 3H, OCH_3), 3.85 (s, 6H, 2 × *m*-OCH_3), 3.80 (s, 3H, OCH_3); ^{13}C NMR (75 MHz, $CDCl_3$) δ 169.7 (*C*=O), 152.9, 151.9, 150.1, 139.9, 139.5, 137.8, 133.2, 130.2, 128.6, 118.3, 118.2, 107.4 (broad, 2 carbons), 106.0, 68.0, 61.0, 56.2, 56.1, 55.9; EIMS *m*/*z* = 410 [M^+] (base), 395; HRMS calcd. for $C_{23}H_{22}O_7$: 410.1365, found: 410.1376. ^{1}H NMR data identical to that published previously (16).

Formation of arylnaphthalene retrolactones – general procedure

The arylnaphthalene mono-acids, **9**, sodium borohydride (10–15 equiv.), and lithium chloride (10–15 equiv.) were charged to a 25 mL flask as powders, then diglyme (10 mL) was added and the resulting mixture was heated at ~120°C for 3–16 h. The mixture was cooled and quenched with 10% HCl (10 mL), which was stirred for 1.5 h. The product was extracted into EtOAc (3 × 20 mL) and washed with saturated aqueous $NaHCO_3$ (3 × 10 mL) to remove any remaining acid. The organic extract was washed with water (10 mL), dried over anhydrous magnesium sulfate, filtered, and evaporated to give a white powder. Recrystallization from $CHCl_3$–hexanes provided a white powder, which was a mixture of the desired lactone and the corresponding diol as a side product from over-reduction. The lactone was purified by recrystallization from hot EtOH (95%), providing crystals that were >90% pure by HPLC.

Justicidin E – ***3aa***

Arylnaphthalene acid **9aa** (125 mg, 0.31 mmol), $NaBH_4$ (174 mg, 4.6 mmol), LiCl (194 mg, 4.6 mmol) were used in the general procedure above (16 h reflux time) to give justicidin E (**3aa**) (20.5 mg, 19.2% yield) as colourless crystals. ^{1}H NMR (300 MHz, $CDCl_3$) δ 8.26 (s, 1H, C*H*=C-CO_2), 7.30 (s, 1H, Ar-*H*), 7.09 (s, 1H, Ar-*H*), 6.97 (d, 1H, *J* = 8.4 Hz, Ar-*H*), 6.80 (s, 1H, Ar-*H*), 6.79 (dd, 1H, *J* = 1.6, 8.4 Hz, Ar-*H*), 6.09 (s, 2H, O-CH_2-O), 6.08 (2s, 2H, O-CH_2-O, hindered rotation), 5.20 (AB doublet, 2H, Δδ = 17.6 Hz, *J* = 15.0 Hz, C-CH_2-O); ^{13}C NMR (75 MHz, $CDCl_3$) δ 171.4 (*C*=O), 150.5, 148.4, 148.2, 147.7, 138.4, 133.4, 132.7, 131.3, 129.6, 124.7, 122.7, 121.6, 109.6, 109.0, 105.2, 102.0, 101.8, 101.4, 69.4; EIMS *m*/*z* = 348 [M^+] (base), 319, 233; HRMS calcd. for $C_{20}H_{12}O_6$: 348.0634, found: 348.0604. ^{1}H NMR spectral properties identical with those previously reported (6,12).

Retrochinensin – ***3ab***

Arylnaphthalene acid **9ab** (311 mg, 0.73 mmol), $NaBH_4$ (277 mg, 7.3 mmol), LiCl (309 mg, 7.3 mmol) were used in the general procedure above (5 h reflux time) to give retrochinensin (**3ab**) (165.7 mg, 62.3%; 86.2 mg, 32.4% yield after recrystallization from 95% EtOH) as colourless crystals. ^{1}H NMR (300 MHz, $CDCl_3$) δ 8.23 (s, 1H, C*H*=C-CO_2), 7.28 (s, 1H, Ar-*H*), 7.09 (s, 1H, Ar-*H*), 7.03 (d, 1H, *J* = 8.2 Hz, Ar-*H*), 6.89 (dd, 1H, *J* = 1.9, 8.1 Hz, Ar-*H*), 6.84 (d, 1H, *J* = 1.9 Hz, Ar-*H*), 6.08 (s, 2H, O-CH_2-O), 5.19 (AB doublet, 2H, Δδ = 17.8 Hz, *J* = 14.8 Hz, C-CH_2-O), 3.97 (s, 3H, O-CH_3), 3.88 (s, 3H, O-CH_3); ^{13}C NMR (75 MHz, $CDCl_3$) δ 171.4 (*C*=O), 150.4, 149.3, 148.9, 148.3, 138.3, 133.4, 132.9, 131.2, 128.5, 124.5, 121.6, 112.2, 111.7, 105.2, 102.0, 101.8, 69.5, 56.0$_4$, 55.9$_9$ (one quaternary carbon not observed); EIMS *m*/*z* = 364 [M^+] (base), 350, 335, 319; HRMS calcd. for $C_{21}H_{16}O_6$: 364.0947, found: 364.0927. ^{1}H NMR spectral properties identical with those previously reported (17).

5′-Methoxyretrochinensin – ***3ac***

Arylnaphthalene acid **9ab** (407 mg, 0.89 mmol), $NaBH_4$ (334 mg, 8.9 mmol), LiCl (378 mg, 8.9 mmol) were used in the general procedure above (5 h reflux time) to give 5′-

© 2000 NRC Canada

methoxyretrochinensin (**3ac**) (250.7 mg, 71.5%; 163 mg, 46.5% yield after recrystallization from 95% EtOH) as colourless crystals. ^{1}H NMR (300 MHz, $CDCl_3$) δ 8.26 (s, 1H, C*H*=C-CO_2), 7.30 (s, 1H, Ar-*H*), 7.10 (s, 1H, Ar-*H*), 6.54 (s, 2H, Ar-*H*), 6.10 (s, 2H, O-CH_2-O), 5.22 (s, 2H, CH_2-O-C=O), 3.96 (s, 3H, *p*-OCH_3), 3.86 (s, 6H, 2 × *m*-OCH_3); ^{13}C NMR (75 MHz, $CDCl_3$) δ 171.3 (*C*=O), 153.7, 150.5, 148.4, 138.1, 137.9, 133.2, 133.0, 131.6, 131.2, 124.7, 121.6, 106.2, 105.2, 102.0, 101.9, 69.4, 61.0, 56.3; EIMS *m*/*z* = 394 [M^+] (base), 379, 363; HRMS calcd. for $C_{22}H_{18}O_7$: 394.1052, found: 394.1060. ^{1}H NMR spectral properties identical with those previously reported (18).

*Retrojusticidin B – **3ba***

Arylnaphthalene acid **9ba** (152 mg, 0.36 mmol), $NaBH_4$ (203 mg, 5.4 mmol), LiCl (226 mg, 5.4 mmol) were used in the general procedure above (16 h reflux time) to give retrojusticidin B (**3ba**) (139.9 mg, 83%; 52.8 mg, 40.3% yield after recrystallization from 95% EtOH) as colourless crystals. ^{1}H NMR (300 MHz, $CDCl_3$) δ 8.28 (s, 1H, C*H*=C-CO_2), 7.28 (s, 1H, Ar-*H*), 7.09 (s, 1H, Ar-*H*), 6.98 (d, 1H, *J* = 8.2 Hz, Ar-*H*), 6.84 (s, 1H, Ar-*H*), 6.83 (d, 1H, *J* = 8.2 Hz, Ar-*H*), 6.10, 6.07 (2s, 2H, O-CH_2-O, hindered rotation), 5.22 (s, 2H, CH_2O-C=O), 4.04 (s, 3H, O-CH_3), 3.86 (s, 3H, O-CH_3); ^{13}C NMR (75 MHz, $CDCl_3$) δ 171.5 (*C*=O), 151.9, 150.0, 148.2, 147.6, 137.9, 131.8, 131.5, 129.8, 129.7, 124.1, 122.7, 121.3, 109.4, 109.0, 107.6, 104.0, 101.4, 69.4, 56.0, 55.9; EIMS *m*/*z* = 364 [M^+] (base), 335; HRMS calcd. for $C_{21}H_{16}O_6$: 364.0947, found: 364.0943. ^{1}H NMR spectral properties identical with those previously reported (19).

*Retrolactone – **3bb***

Arylnaphthalene acid **9bb** (187 mg, 0.54 mmol), $NaBH_4$ (203 mg, 5.4 mmol), LiCl (227 mg, 5.4 mmol) were used in the general procedure above (16 h reflux time) to give retrolactone **3bb** (105.2 mg, 51%; 60.1 mg, 29.3% yield after recrystallization from 95% EtOH) as colourless crystals. ^{1}H NMR (300 MHz, $CDCl_3$) δ 8.29 (s, 1H, C*H*=C-CO_2), 7.29 (s, 1H, Ar-*H*), 7.12 (s, 1H, Ar-*H*), 7.06 (d, 1H, *J* = 8.1 Hz, Ar-*H*), 6.95 (d, 1H, *J* = 8.2 Hz, Ar-*H*), 6.91 (s, 1H, Ar-*H*), 5.22 (d, 2H, *J* = 6.2 Hz, CH_2O-C=O), 4.05 (s, 3H, O-CH_3), 4.00 (s, 3H, O-CH_3), 3.89 (s, 3H, O-CH_3), 3.83 (s, 3H, O-CH_3); ^{13}C NMR (75 MHz, $CDCl_3$) δ 171.5 (*C*=O), 151.9, 150.0, 149.3, 148.9, 137.8, 132.1, 131.6, 129.8, 128.6, 124.0, 121.5, 121.3, 112.2, 111.6, 107.6, 104.1, 69.5, 56.0 (2 carbons, OCH_3), 55.9, 55.8; EIMS *m*/*z* = 380 [M^+] (base), 351; HRMS calcd. for $C_{22}H_{20}O_6$: 380.1260, found: 380.1267. ^{1}H NMR spectral properties identical with those previously reported (13).

*Retrolactone – **3bc***

Arylnaphthalene acid **9bc** (310 mg, 0.66 mmol), $NaBH_4$ (250 mg, 6.6 mmol), and LiCl (280 mg, 6.6 mmol) were used in the general procedure above (3 h reflux time) to give retrolactone **3bc** (230.5 mg, 85.1%; 143.6 mg, 53.0% yield after recrystallization from 95% EtOH) as colourless crystals. ^{1}H NMR (300 MHz, $CDCl_3$) δ 8.26 (s, 1H, C*H*=C-CO_2), 7.27 (s, 1H, Ar-*H*), 7.13 (s, 1H, Ar-*H*), 6.60 (s, 2H, Ar-*H*), 5.24 (s, 1H, CH_2O-C=O), 4.04 (s, 3H, O-CH_3), 3.96 (s, 3H, O-CH_3), 3.86 (s, 6H, 2 × O-CH_3), 3.84 (s, 3H, O-CH_3); ^{13}C NMR (75 MHz, $CDCl_3$) δ 171.4, 153.7, 152.0, 150.1, 137.8, 137.6, 132.2, 131.6, 131.3, 129.8, 124.1, 121.3, 107.6, 106.2, 104.1, 69.5, 60.9, 56.3, 56.0, 55.9; EIMS *m*/*z* = 410 [M^+] (base), 395, 379; HRMS calcd. for $C_{23}H_{22}O_7$: 410.1365, found: 410.1382. ^{1}H NMR spectral properties identical with those previously reported (13).

Acknowledgements

We are grateful to the Natural Sciences and Engineering Research Council of Canada, Boehringer Ingelheim (Canada) Ltd., Bio-Méga Research Division, and the University of Manitoba for financial support of this project. We also thank Nathalie Dansereau for assaying the compounds in cell culture.

References

1. R.S. Ward. Nat. Prod. Rep. **14**, 43 (1997).
2. R.S. Ward. Nat. Prod. Rep. **12**, 183 (1995).
3. R.S. Ward. Nat. Prod. Rep. **10**, 1 (1993).
4. D.C. Ayres and J.D. Loike. *In* Lignans: chemical, biological and clinical properties. Cambridge University Press, Cambridge. 1990.
5. J.L. Charlton. J. Nat. Prod. **61**, 1447 (1998).
6. A. Padwa, J.E. Cochran, and C.O. Kappe. J. Org. Chem. **61**, 3706 (1996), (also see references 49–51 of this article).
7. T. Ogiku, S. Yoshida, H. Ohmizu, and T. Iwasaki. J. Org. Chem. **60**, 4585 (1995), (also see references 2–7 of this article).
8. W.S. Johnson and G.H. Daub. *In* Organic reactions. Vol VI, John Wiley and Sons, Inc., New York. pp. 1–73.
9. D.C. Ayres, B.G. Carpenter, and R.C. Denney. J. Chem. Soc. 3578 (1965).
10. C. Lawetz and M. Liuzzi. Antiviral Res. **39**, 35 (1998).
11. J.L. Charlton, G.L. Plourde, K. Koh, and A.S. Secco. Can. J. Chem. **68**, 2022 (1990).
12. T. Hattori, H. Tanaka, Y. Okaishi, and S. Miyano. J. Chem. Soc. Perkin Trans. 1, 235 (1995).
13. R. Stevenson and J.V. Weber. J. Nat. Prod. **52**, 367 (1989).
14. A. San Feliciano, M. Medarde, R.P. Lamamie de Clairac, J.L. López, P. Puebla, D. García Gravalos, P. Ruiz Lázaro, and T. García de Quesada. Arch. Pharm. (Weinheim, Ger.), **326**, 421 (1993).
15. M. Okigawa, T. Maeda, and N. Kawano. Tetrahedron, 4301 (1970).
16. T. Ukita, Y. Nakamura, A. Kubo, Y. Yamamoto, M. Takahashi, J. Kotera, and T. Ikeo. J. Med. Chem. **42**, 1293 (1999). The ^{1}H NMR of **2bc** given in two other references is incorrect.
17. T. Ogiku, S. Yoshida, H. Ohmizu, and T. Iwasaki. J. Org. Chem. **60**, 4585 (1995) and T. Iwasaki, K. Kondo, T. Kuroda, Y. Moritani, S. Yamagata, M. Sugiura, H. Kikkawa, O. Kaminuma, and K. Ikezawa. J. Med. Chem. **39**, 2696 (1996).
18. S. Ghosal and S. Banerjee. J. Chem. Soc. Chem. Commun. 165 (1979).
19. S. Takano, S. Otaki, and K. Ogasawara. Tetrahedron Lett. **26**, 1659 (1985).
20. A. Pelter, R.S. Ward, P. Satyanarayana, and P. Collins. Tetrahedron Lett. **23**, 571 (1982).

© 2000 NRC Canada

Substituent effects on stability of oxiranes, oxirenes, and dioxiranes

Kuangsen Sung

Abstract: Homodesmotic reactions were designed to study substituent effects on stability of oxiranes, oxirenes, and dioxiranes. Good or fair correlation between their homodesmotic stabilization energies and Taft's dual-substituent-parameters has been found. Oxiranes are stabilized by σ-donating and π-donating substituents but destabilized by σ-accepting and π-accepting substituents. The π-effects on oxiranes are comparable to σ-effects for π-acceptor substituents and are much stronger than σ-effects for π-donor substituents. Oxirenes are stabilized by σ-donating, π-donating, and π-accepting substituents but destabilized by σ-accepting substituents. The π-effects on oxirenes are stronger than σ-effects. Oxirenes with strong π-donor substituents such as F, OH, and NH_2, or strong σ-donor substituents such as Li and Na are neither real molecules nor transition states. Dioxiranes are stabilized by σ-donating and π-donating substituents but destabilized by σ-accepting and π-accepting substituents. The π-effects on dioxiranes are stronger than σ-effects for π-donor substituents, but weaker than σ-effects for π-acceptor substituents

Key words: oxirane, oxirene, dioxirane, homodesmotic reaction, substituent effect.

Résumé : On a mis au point des réactions homodesmotiques orientées vers l'étude des effets de substituant sur la stabilité des oxiranes, oxirènes et dioxiranes. On a observé des corrélations allant de bonnes à correctes entre les énergies de stabilisation homodesmotiques et les paramètres à doubles substituants de Taft. Les oxiranes sont stabilisés par les substituants σ-donneurs et π-donneurs, mais ils sont déstabilisés par les substituants σ- ou π-accepteurs. Les effets π sur les oxiranes sont comparables aux effets σ pour les substituants π-accepteurs et ils sont beaucoup plus forts que les effets σ pour les substituants π-donneurs. Les oxirènes sont stabilisés par les substituants σ-donneurs, π-donneurs et π-accepteurs, mais ils sont déstabilisés par les substituants σ-accepteurs. Pour les oxirènes, les effets π sont plus forts que les effets σ. Les oxirènes portant des substituants fortement π-donneurs, tel que F, OH et NH_2, ou des substituants fortement σ-donneurs, tel que Li et Na, ne sont ni des molécules ni des états de transition. Les dioxiranes sont stabilisés par des substituants σ-donneurs et π-donneurs, mais ils sont déstabilisés par des substituants σ-accepteurs et π-accepteurs. Dans le cas des dioxiranes, les effets π sont plus forts que les effets σ pour les substituants π-donneurs, mais ils sont plus faibles que les effets σ pour les substituants π-accepteurs.

Mots clés : oxirane, oxirène, dioxirane, réaction homodesmotique, effet de substituant.

[Traduit par la Rédaction]

Introduction

The substituent effects on structures and stability of a variety of organic compounds such as ketenes (1*a*–*c*), isocyanates (1*d*), imines (1*d*), allenes (1*c*, 2), cyclopropanes (3), diazirines (1*c*, 4*a*–*b*), diazomethanes (1*c*, 4*c*–*e*), alkanes (3*c*), alkenes (3*a*, 3*c*, 5), alkynes (3*a*, 5*b*), 1,3-dienes (6*a*), cyclopropenes (1*c*), carbonyl compounds (5*a*, 6*b*), and carbocations (7) have been extensively studied by ab initio calculations in recent years. Recently we have studied substituent effects on stablity of ketenimines, nitriles, and isocyanides by ab initio calculations (8). In the article, the same method is applied to study substituent effects on stability of oxiranes, oxirenes, and dioxiranes.

Received December 3, 1999. Published on the NRC Research Press website on May 8, 2000.

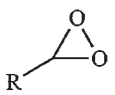
K. Sung.[1] Department of Chemistry, National Cheng Kung University, Tainan, Taiwan, ROC.

[1]Telephone: 886-6-2757575 ext. 65338. Fax: 886-6-2740552. e-mail: kssung@mail.ncku.edu.tw

Oxiranes **1** are well-known intermediates and most of attention has been focused on their preparation, reaction, and stereochemistry (9). Since most of them can be isolated and stay stable at room temperature, their stability is not chemists' major concern and their substituent-stability relationship still remain intact.



1

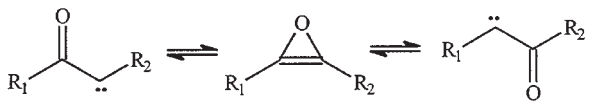


5

Oxirenes **2** are a class of highly strained heterocycles whose instability and high reactivity have made isolation or direct detection difficult (10). From thermal and photochemical experiments with unsymmetrically substituted diazo ketones and from label scrambling in isotopically labeled diazo ketones, ketocarbene **3** – ketocarbene **4** interconversion has been found and explained by existence of the oxirene (11). Later, the oxirenes were observed by means of matrix-isolation techniques and laser flash photolysis experiments

© 2000 NRC Canada

(10*a*, *b*). Will substituents destabilize oxirenes and make them become unreal? Will substituents stabilize oxirenes and allow them to be isolated and to stay isolated at higher temperature for longer time?



3 **2** **4**

Dioxiranes **5** with a smallest cyclic peroxide system were first isolated at low temperature in 1972 (12*a*). Since then, they have proven to be powerful oxygen transfer reagents of unusual synthetic utility (12). Most of them are generated in situ since they were reported to be explosive and unstable. In 1985, Murray and Jeyaraman were able to prepare a solution of ca. 0.1 M dimethyl dioxirane in acetone (12*b*). Methyl(trifluoromethyl)dioxirane was prepared in this way as a 0.8 M solution in $CF_3C(O)CH_3$ (12*c*). Recently difluorodioxirane was isolated and stable even at 22°C for more than 12 h (12*d*). Clearly, stability is one of major concerns for chemists to do the dioxirane chemistry.

Hammett equation and its extensions [1] described substituent effects on reaction rates (*k*) or equilibrium constants (*K*), and there exits a linear free energy relationship between the two sets of effects (13). The phenomena and concept have been applied to substituent effects on isodesmic and homodesmotic stabilization energies of cyclopropanes, ethylenes, acetylenes, benzenes, allenes, ketenimines, nitriles and isocyanides (2*a*, 3*a*, 8). Since entropy changes of isodesmic and homodesmotic reactions are so small as to be negligible, it is reasonable that isodesmic and homodesmotic stabilization energies are directly correlated with substituent constants (σ). [2] Both sign and magnitude of σ for a substituent are a measure of its capacity to perturb its environment electronically. Substituent constants σ_p and σ_m may involve both inductive and resonance contributions of substituents, but Taft's dual-substituent-parameters (DSP) provide a good way to divide the substituent constant (σ) into σ_I for inductive contribution only and σ_R for resonance contribution only (14). Therefore, in this article we study substituent effects on stability of oxiranes, oxirenes, and dioxiranes by ab initio calculations and by correlating the stabilization energies with Taft's DSP.

[1] $$m \log (K/K_0) = m\,\Delta\Delta G = \log (k/k_0) = \Delta\Delta G^{\ddagger} = \rho\sigma = \rho_I\sigma_I + \rho_R\sigma_R$$

[2] $$\Delta E \text{ (for isodesmic and homodesmotic reactions)} = \rho\sigma = \rho_I\sigma_I + \rho_R\sigma_R$$

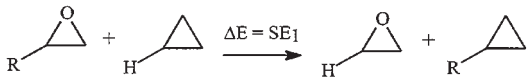
The isodesmic reaction is one in which the total number of each type of bond is identical in the reactants and products, but there may be changes in the relationship of one bond to another (15*a*). The homodesmotic reaction is defined as a reaction in which not only is the number of bonds of each type conserved, but the number of carbon atoms with zero, one, two, or three hydrogen atoms is also conserved (15*b*). The isodesmic and homodesmotic reactions are widely used in theoretical studies because errors in the energies of reactants and products are more likely to cancel, thereby allowing simple computational approaches to give accurate estimates of heats of reactions (15*c*). Generally speaking, a substituted reactant of one type is more stable than a substituted product of the other type if the isodesmic or homodesmotic reaction is endothermic; a substituted product of one type is more stable than a substituted reactant of the other type if the reaction is exothermic.

Computation

All the calculations reported here were performed with Gaussian94 program (16). Geometry optimizations were carried out at level of HF/6–31+G* without any symmetry restriction. After geometry optimizations were performed, analytic vibration frequencies were calculated at the same level to determine the nature of the located stationary points. Thus all the stationary points found were properly characterized by evaluation of the harmonic frequencies. Single point energies of the optimized structures were carried out by density functional theory (DFT) at level of B3LYP/6–311+G(2d,p)//HF/6–31+G*, and energies of all the stationary points were calculated at the same level with scaling zero-point vibration energies included. A scaling factor of 0.8929 for zero-point vibration energies is used according to the literature (1*b*, 1*c*, 15*a*).

Results

Substituent effects on stability of oxiranes were studied with a homodesmotic reaction [3], which measures stabilizing effect of a substituent, R, on oxirane relative to the effect of the substituent on cyclopropane. The stabilization energies (SE_1) were correlated with Taft's DSP to study how

[3] 

substituents influence the stability of oxiranes via inductive and resonance routes (Table 1). Two independent parameters (σ_I and σ_R) of Taft's DSP were taken from Charton's compendium (17). Since both π-donors and π-acceptors can cause stabilization, one must treat them separately. Therefore, substituents were divided into two categories, π-donating and π-accepting substituents. In each category, values of σ_I and σ_R of the substituents were correlated with substituent stabilization energies by eq. [4]. In a category of π-donating substituents, eight substituents were chosen and their Taft's dual-substituent-parameters have a fair correlation with the stabilization energies (SE_1) of oxiranes with $r^2 = 0.85$ and sey = 1.45. [5] The sey means standard deviation of estimated stabilization energies. Coefficients of σ_I and σ_R are –0.20 and –10.14, respectively. In a category of π-accepting substituents, six substituents were chosen and a correlation between the oxirane stabilization energies (SE_1) and their Taft's dual-substituent-parameters is fair with $r^2 = 0.72$ and sey = 0.94. [5] Coefficients of σ_I and σ_R are –4.63 and –3.07, respectively.

[4] $$SE = \rho_I\sigma_I + \rho_R\sigma_R + \text{constant}$$

© 2000 NRC Canada

Table 1. Calculated energies (B3LYP/6–311+G(2d,p)//HF/6–31+G*) (hartrees) of oxiranes and cyclopropanes and SE_1 (kcal/mol) of the homodesmotic reaction [3].

R	σ_I	σ_R	*E* (oxiranes)	*E* (cyclopropanes)	SE_1
H	0	0	–153.78303	–117.85536	0
CH_3	–0.01	–0.16	–193.08941	–157.15630	3.41
C(O)H	0.25	0.20	–267.12972	–231.20505	–1.88
$CH=CH_2$	0.11	–0.15	–231.17437	–195.24354	1.98
ethynyl	0.29	–0.04	–229.93662	–194.01099	–1.28
CO_2H	0.30	0.11	–342.40329	–306.48007	–2.79
CF_3	0.40	0.11	–490.93411	–455.01073	–2.69
CN	0.57	0.08	–246.04488	–210.12391	–4.20
C1	0.47	–0.25	–613.41866	–577.48701	2.50
NH_2	0.17	–0.80	–209.14650	–173.20806	6.76
NO_2	0.67	0.10	–358.34413	–322.42083	–2.74
OH	0.24	–0.62	–229.03093	–193.09178	7.20
F	0.54	–0.48	–253.06656	–217.12886	6.29

Table 2. Calculated energies (B3LYP/6–311+G(2d,p)//HF/6–31+G*) (hartrees) of oxirenes and cyclopropenes and SE_2 (kcal/mol) of the homodesmotic reaction [7].

R	σ_I	σ_R	*E* (oxirenes)	*E* (cyclopropenes)	SE_2
H	0	0	–116.60235	–116.60235	0
CH_3	–0.01	–0.16	–191.80859	–155.91122	4.31
C(O)H	0.25	0.20	–265.84727	–229.95112	3.55
$CH=CH_2$	0.11	–0.15	–229.89930	–194.00118	–4.78
ethynyl	0.29	–0.04	–228.65785	–192.76510	1.41
CO_2H	0.30	0.11	–341.11735	–305.22460	1.41
CF_3	0.40	0.11	–489.63563	–453.75205	–4.34
CN	0.57	0.08	–244.75864	–208.87169	–2.23
Phenyl	0.12	–0.11	–383.54940	–347.65233	4.12
NO_2	0.67	0.10	–357.03779	–321.15453	–4.54

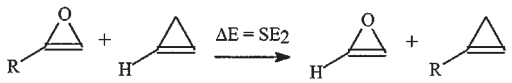
π donors (F, Cl, OH, NH_2, vinyl, ethynyl, CH_3, H) :

$$SE_1 = (-0.20)\,\sigma_I + (-10.14)\,\sigma_R + 0.23 \quad [5]$$
$$r^2 = 0.95, \quad \text{sey} = 1.45$$

π acceptors (CO_2H, CN, C(O)H, NO_2, CF_3, H) :

$$SE_1 = (-4.63)\,\sigma_I + (-3.07)\,\sigma_R - 0.38 \quad [6]$$
$$r^2 = 0.72, \quad \text{sey} = 0.94$$

Substituent effects on stability of oxirenes were studied with a homodesmotic reaction [7], which measures stabilizing effect of a substituent, R, on oxirene relative to the effect of the substituent on cyclopropene. To study how inductive and resonance effects of the substituents influence the stability of oxirenes, Taft's DSP was applied and correlated with the stabilization energies (SE_2) by eq. [4] (Table 2).

[7] 

In the category of π-donating substituents, five substituents were chosen and their Taft's dual-substituent-parameters have a good correlation with oxirene stabilization energies (SE_2) with $r^2 = 0.96$ and sey = 0.58. [8] Coefficients of σ_I and σ_R are 1.90 and –30.02, respectively. In the category of π-accepting substituents, six substituents were chosen and a correlation between the oxirene stabilization energies (SE_2) and Taft's dual-substituent-parameters is fair with $r^2 = 0.71$ and sey = 2.25. [9] Coefficients of σ_I and σ_R are –10.75 and +28.73, respectively. Oxirenes with substituents like F, OH, NH_2, Li, and Na are no longer stationary points in their potential energy surfaces at level of HF/6–31+G*. In other words, they are neither local minima nor transition states.

π donors (ethynyl, vinyl, methyl, phenyl, H) :

$$SE_2 = (1.90)\,\sigma_I + (-30.02)\,\sigma_R - 0.03 \quad [8]$$
$$r^2 = 0.96, \quad \text{sey} = 0.58$$

π acceptors (CO_2H, CN, C(O)H, NO_2, CF_3, H) :

$$SE_2 = (-10.75)\,\sigma_I + (28.73)\,\sigma_R + 0.03 \quad [9]$$
$$r^2 = 0.71, \quad \text{sey} = 2.25$$

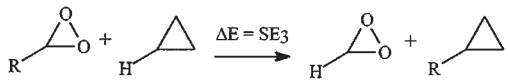
Substituent effects on stability of dioxiranes were studied with a homodesmotic reaction [10], which measures stabilizing effect of a substituent, R, on dioxirane relative to the effect of the substituent on cyclopropane. To study how inductive and resonance effects of the substituents influence the stability of dioxiranes, Taft's DSP was applied and correlated with the stabilization energies (SE_3) by eq. [4] (Table 3). In the category of π-donating substituents, eight substituents were

© 2000 NRC Canada

Table 3. Calculated energies (B3LYP/6–311+G(2d,p)//HF/6–31+G*) (hartrees) of dioxiranes and cyclopropanes and SE_3 (kcal/mol) of the homodesmotic reaction [10].

R	σ_I	σ_R	*E* (dioxiranes)	*E* (cyclopropanes)	SE_3
H	0	0	–189.64739	–117.85536	0
CH_3	–0.01	–0.16	–228.96000	–157.15630	7.32
C(O)H	0.25	0.20	–302.99137	–231.20505	–3.58
$CH=CH_2$	0.11	–0.15	–267.04356	–195.24354	5.01
ethynyl	0.29	–0.04	–265.79960	–194.01099	–2.15
CO_2H	0.30	0.11	–378.26272	–306.48007	–5.89
CF_3	0.40	0.11	–526.79359	–455.01073	–5.75
CN	0.57	0.08	–281.90202	–210.12391	–8.73
C1	0.47	–0.25	–649.28481	–577.48701	3.62
NH_2	0.17	–0.80	–245.02266	–173.20806	14.16
NO_2	0.67	0.10	–394.20114	–322.42083	–7.35
OH	0.24	–0.62	–264.91017	–193.09178	16.54
F	0.54	–0.48	–288.93821	–217.12886	10.87

chosen and their Taft's dual-substituent-parameters have a fair correlation with dioxirane stabilization energies (SE_3) with r^2 = 0.86 and sey = 2.94. [11] Coefficients of σ_I and σ_R are –4.93 and –21.92, respectively. In the category of π-accepting substituents, six substituents were chosen and a fair correlation between the dioxirane stabilization energies (SE_3) and Taft's dual-substituent-parameters is found with r^2 = 0.87 and sey = 1.43. [12] Coefficients of σ_I and σ_R are –11.78 and –2.77, respectively.

[10] 

π donors (F, Cl, OH, NH_2, vinyl, ethynyl, CH_3, H) :

$$SE_3 = (-4.93)\,\sigma_I + (-21.92)\,\sigma_R + 1.18 \quad [11]$$
$$r^2 = 0.86, \quad \text{sey} = 2.94$$

π acceptors (CO_2H, CN, C(O)H, NO_2, CF_3, H) :

$$SE_3 = (-11.78)\,\sigma_I + (-2.77)\,\sigma_R - 0.64 \quad [12]$$
$$r^2 = 0.87, \quad \text{sey} = 1.43$$

Discussion

The Hammett equation and its extensions and modifications consider an induced perturbation in a reaction center A by a substituent B through a hydrocarbon framework H, that is, A-H-B (13). The present study examines an induced perturbation in a reaction center A directly by a substituent B, that is, A-B. In this article, the stabilization energies of homodesmotic reactions were correlated with Taft's DSP. Any deviation from the correlation analysis could result from through-space intramolecular interaction between reaction center A and substituent B. However, errors in the energies of reactants and products are more likely to cancel in well-designed homodesmotic reactions.

There is a fair correlation (r^2 = 0.85) between SE_1 and Taft's DSP for oxiranes with π-donating substituents. [5] The σ_I coefficient (–0.20) is too small and within standard deviation. The σ_R coefficient (–10.14) implies that π-donating substituents stabilize oxiranes. The π-donating effects outweigh σ-effects on stability of oxiranes with π-donating substituents.

There is also a fair correlation (r^2 = 0.72) between SE_1 and Taft's DSP for oxiranes with π-accepting substituents. [6] The σ_I coefficient is –4.63, indicating that σ-donating substituents stabilize oxiranes while σ-accepting substituents destabilize them. The σ_R coefficient is –3.07, indicating that π-donating substituents stabilize oxiranes while π-accepting substituents destabilize them. The π-effects on oxirane stability are comparable to σ-effects for π-acceptor substituents

Oxiranes have a strong electronegative oxygen atom on a 3-membered ring and that makes two other carbon atoms on the ring electron-deficient. Therefore, both σ-donating and π-donating substituents would enrich electron density of the ring carbons and cause stabilization. Conversely, both σ-accepting and π-accepting substituents would deplete electron density of the ring carbons and cause destabilization.

As to oxirenes with π-donating substituents, a good correlation (r^2 = 0.96) between SE_2 and Taft's DSP was obtained. [8] The σ_I coefficient (1.90) is so small and within standard deviation. The σ_R coefficient (–30.02) implies that π-donating substituents stabilize oxirenes. The π-donating effects outweigh σ-effects on stability of oxirenes with π-donating substituents. Regarding oxirenes with π-accepting substituents, there is a fair correlation (r^2 = 0.71) between SE_2 and Taft's DSP. [9] The σ_I coefficient is –10.75, indicating that σ-donating substituents stabilize oxirenes while σ-accepting substituents destabilize them. The σ_R coefficient is 28.73, indicating that π-accepting substituents stabilize oxirenes. The π-accepting effects outweigh σ-effects on stability of oxirenes with π-accepting substituents.

It was reported that parent oxirene is 11.3 kJ mol^{-1} more stable than its formylcarbene isomer at level of MP3/6–31G** (18). However, at level of HF/6–31+G*, strong π-donor substituents such as F, OH, and NH_2 make oxirenes become unreal. The same thing happens to oxirenes with strong σ-donating substituents such as Li and Na.

Correlation between dioxirane stabilization energies (SE_3) and Taft's dual-substituent-parameters is fair (r^2 = 0.86 and sey = 2.94) for dioxiranes with π-donating substituents. [11] The σ_I coefficient of –4.93 indicates that σ-donating substituents stabilize dioxiranes while σ-accepting substituents

© 2000 NRC Canada

destabilize them. The σ_R coefficient of –21.92 implies that π-donating substituents stabilize dioxiranes. The π-donating effects outweigh σ-effects on stability of dioxiranes with π-donating substituents.

There is also a fair correlation (r^2 = 0.87) between SE_3 and Taft's DSP for dioxiranes with π-accepting substituents. [12] The σ_I coefficient is –11.78, indicating that σ-donating substituents stabilize dioxiranes while σ-accepting substituents destabilize them. The σ_R coefficient is –2.77, indicating that π-donating substituents stabilize dioxiranes while π-accepting substituents destabilize them. The σ-effects outweigh π-effects on stability of dioxirane with π-accepting substituents.

Dioxiranes have two strong electronegative oxygen atoms on a 3-member ring and that causes the other carbon atom on the ring to be electron-deficient. It turns out that any effort to compensate electron density of the electron-deficient carbon on the ring would stabilize the dioxiranes. Therefore, both σ-donors and π-donors stabilize dioxiranes while both σ-acceptors and π-acceptors destabilize them.

The methyl group is a weak σ-donor (σ_I = –0.01) and a medium π-donor (σ_R = –0.16), so the methyl group has a stabilization effect (SE_3 = +7.32 kcal/mol) on dioxiranes. This is consistent with an experiment result that dimethyldioxirane was isolated and prepared as a solution storable at –20°C for several days (12*b*). The trifluoromethyl group is a medium σ-acceptor (σ_I = 0.40) and a medium π-acceptor (σ_R = 0.11), so the trifluoromethyl group has a destabilization effect (SE_3 = –5.75 kcal/mol) on dioxiranes. This is also consistent with an experiment result that methyl(trifluoromethyl)dioxirane was found to be markedly more reactive and unstable than dimethyldioxirane (12*c*). The fluorine substituent is a strong σ-acceptor (σ_I = 0.54) but it is a strong π-donor (σ_R = –0.48). The fluorine substituent should have a higher stabilization effect (SE_3 = +10.87 kcal/mol) on dioxiranes since π-donating effects outweigh σ-effects on stability of dioxiranes with π-donating substituents. Actually, difluorodioxirane has been isolated at 22°C recently and it is stable at 22°C for more than 12 h (12*d*).

Conclusions

Substituent effects on the stability of oxiranes, oxirenes, and dioxiranes can be found by correlation between their stabilization energies (SE_1, SE_2, and SE_3) and Taft's dual-substituent-parameters. As to substituent effects on the stability of oxiranes, σ-donating substituents stabilize them while σ-accepting substituents destabilize them; π-donating substituents stabilize them while π-accepting substituents destabilize them. The π-effects on oxiranes are comparable to σ-effects for π-acceptor substituents and are much stronger than σ-effects for π-donor substituents.

Regarding substituent effects on the stability of oxirenes, σ-donating substituents stabilize them while σ-accepting substituents destabilize them. Both π-donating and π-accepting substituents stabilize them. The π-effects on oxirenes are stronger than σ-effects. Oxirenes with strong π-donor substituents such as F, OH, and NH_2 and strong σ-donor substituents such as Li and Na are neither real molecules nor transition states at level of HF/6–31+G*.

As far as substituent effects on the stability of dioxiranes are concerned, σ-donating substituents stabilize them while σ-accepting substituents destabilize them; π-donating substituents stabilize them while π-accepting substituents destabilize them. The π-effects on dioxiranes are stronger than σ-effects for π-donor substituents, but π-effects on dioxiranes are weaker than σ-effects for π-acceptor substituents

Acknowledgements

Financial support by National Science Council of Taiwan, Republic of China (NSC 89-2113-M-006-005) are gratefully acknowledged. We thank the National Center For High-performance Computing of Taiwan for computer time.

References

1. (*a*) T.T. Tidwell. Ketenes. John Wiley & Sons, New York. 1996; (*b*) L. Gong, M.A. McAllister, and T.T. Tidwell. J. Am. Chem. Soc. **113**, 6021 (1991); (*c*) M.A. McAllister and T.T. Tidwell. J. Org. Chem. **59**, 4506 (1994); (*d*) M.A. McAllister and T.T. Tidwell. J. Chem. Soc. Perkin Trans. 2, 2239 (1994).
2. (*a*) P. Furet, R.L. Matcha, and R. Fuchs. J. Phys. Chem. **90**, 5571 (1986); (*b*) C. Lambert, P.v.R. Schleyer, and E.-U. Wurthwein. J. Org. Chem. **58**, 6377 (1993).
3. (*a*) A. Greenberg and T.A. Stevenson. J. Am. Chem. Soc. **107**, 3488 (1985); (*b*) T. Clark, G.W. Spitznagel, R. Klose, and P.v.R. Schleyer. J. Am. Chem. Soc. **106**, 4412 (1984); (*c*) K.B. Wiberg, and K.E. Laidig. J. Org. Chem. **57**, 5092 (1992); (*d*) D. Cremer and E. Kraka. J. Am. Chem. Soc. **107**, 3811 (1985).
4. (*a*) C. Liang and L.C. Allen. J. Am. Chem. Soc. **113**, 1878 (1991); (*b*) P.L. Muller-Remmers and K. Jug. J. Am. Chem. Soc. **107**, 7275 (1985); (*c*) J.M. Goodman, J.J. James, and A. Whiting. J. Chem. Soc. Perkin Trans. 2, 109 (1994); (*d*) F. Wang, M.A. Winnik, M.P. Peterson, and I.G. Csizmadia. THEOCHEM., **232**, 203 (1991); (*e*) S.D. Kahn, W.J. Hehre, and J.A. Pople. J. Am. Chem. Soc. **109**, 1871 (1987).
5. (*a*) N. Heinrich, W. Koch, G. Frenking, and H. Schwarz. J. Am. Chem. Soc. **108**, 593 (1986); (*b*) J.D. Dill, A. Greenberg, and J.F. Liebman. J. Am. Chem. Soc. **101**, 6814 (1979).
6. (*a*) K.B. Wiberg and R.E. Rosenberg. J. Am. Chem. Soc. **112**, 1509 (1990); (*b*) K.B. Wiberg, C.M. Hadad, P.R. Rablen, and J. Cioslowski. J. Am. Chem. Soc. **114**, 8644 (1992).
7. J.C. White, R.J. Cave, and E.R. Davidson. J. Am. Chem. Soc. **110**, 6308 (1988).
8. (*a*) K. Sung. J. Chem. Soc. Perkin Trans. 2, 1169 (1999); (*b*) K. Sung. J. Org. Chem. **64**, 8984 (1999).
9. (*a*) T. Katsuki and V.S. Martin. Org. React. (N.Y.) **48**, 1 (1996); (*b*) J.K. Crandall and M. Apparu. Org. React. (N.Y.) **29**, 345 (1983); (*c*) D. Swern. Org. React. (N.Y.) **7**, 378 (1953).
10. (*a*) C. Bachmann, T.Y. N'Guessan, F. Debu, M. Monnier, J. Pourcin, J.-P. Aycard, and H. Bodot. J. Am. Chem. Soc. **112**, 7488 (1990); (*b*) K. Tanigaki and T.W. Ebbesen. J. Phys. Chem. **93**, 4531 (1989); (*c*) F. Turecek, D.E. Drinkwater, and F.W. Mclafferty. J. Am. Chem. Soc. **113**, 5958 (1991); (*d*) E.G. Lewars. Chem. Rev. **83**, 519 (1983).
11. (*a*) R.A. Cormier. Tetrahedron Lett. **21**, 2021 (1980); (*b*) S.A. Matlin and P.G. Sammer. J. Chem. Soc. Perkin Trans. 1, 2623 (1972); (*c*) M.A. Blaustein and J.A. Berson. Tetrahedron Lett. **22**, 1081 (1981); (*d*) K.P. Zeller. J. Chem. Soc. Chem.

© 2000 NRC Canada

Commun. 317 (1975); (*e*) K.-P. Zeller. Angew. Chem. Int. Ed. Engl. **16**, 781 (1970); (*f*) U. Timm, K.-P. Zeller, and H. Meier. Tetrahedron, **33**, 463 (1977).
12. (*a*) R.I. Talbott and P.G. Thompson. U.S. Patent 3 632 606 (1972); (*b*) R.W. Murray and R. Jeyaraman. J. Org. Chem. **50**, 2847 (1985); (*c*) R. Mello, M. Fiorentino, O. Sciacovelli, and R. Curci. J. Org. Chem. **53**, 3890 (1988); (*d*) A. Russo and D.D. DesMarteau. Angew. Chem. Int. Ed. Engl. **32**, 905 (1993).
13. N. Isaacs. Physical organic chemistry. 2nd ed. Longman Scientific & Technical, England. 1995.
14. S. Ehrenson, R.J.C. Brownlee, and R.W. Taft. Prog. Phys. Org. Chem. **10**, 1 (1973); (*b*) R.D. Topsom. Prog. Phys. Org. Chem. **12**, 1 (1976).
15. (*a*) J.B. Foresman and A. Frisch. Exploring chemistry with electronic structure methods. 2nd ed. Gaussian Inc., Penn. 1996; (*b*) P. George, M. Trachtman, C.W. Bock, and A.M. Brett. Tetrahedron, **32**, 317 (1976); (*c*) W.J. Hehre, L. Radom, P.v.R. Schleyer, and J.A. Pople. Ab initio molecular orbital theory. John Wiley & Sons, New York. 1986.
16. M.J. Frisch, G.W. Trucks, H.B. Schlegel, P.M.W. Gill, B.G. Johnson, M.A. Robb, J.R. Cheeseman, T.A. Keith, G.A. Pertersson, J.A. Montgomery, K. Raghavachari, M.A. AlLaham, V.G. Zakrzewski, J.V. Ortiz, J.B. Foresman, J. Cioslowski, B.B. Stefanov, A. Nanayakkara, M. Challacombe, C.Y. Peng, P.Y. Ayala, W. Chen, M.W. Wong, J.L. Andres, E.S. Replogle, R. Gomperts, R.L. Martin, D.J. Fox, J.S. Binkley, D.J. Defrees, J. Baker, J.P. Stewart, M. Head-Gordon, C. Gonzales, and J.A. Pople. Gaussian 94, Revision D2. Gaussian, Inc., Pittsburgh, Pa. 1995.
17. M. Charton. Prog. Phys. Org. Chem. **13**, 119 (1981).
18. W.J. Bouma, R.H. Nobes, L. Radom, C.E. Woodward. J. Org. Chem. **47**, 1869 (1982).

© 2000 NRC Canada

Trans alkenylpyridine and alkenylamine complexes of platinum

Michael P. Shaver, Christopher M. Vogels, Andrew I. Wallbank, Tracy L. Hennigar, Kumar Biradha, Michael J. Zaworotko, and Stephen A. Westcott

Abstract: Addition of *cis*-cyclooctene (coe) to K_2PtCl_4 gives *trans*-$[PtCl_2(coe)]_2$ (**1**), which reacts with excess coe to give *trans*-$PtCl_2(coe)_2$ (**2**). Compound **2** was characterized by an X-ray diffraction study and crystals were found to be triclinic, a = 5.7838(5), b = 7.4347(6), c = 9.9972(9) Å, α = 83.924(1), β = 87.844(2), γ = 73.546(1)°, Z = 1, with space group $P\bar{1}$. Addition of 4-vinylpyridine (4vp) to **1** gave *trans*-$PtCl_2(4vp)_2$ (**5**) which was also characterized by an X-ray diffraction study. Crystals of **5** were monoclinic, a = 8.2255(6), b = 12.8254(10), c = 6.9624(5) Å, β = 98.8230(10)°, Z = 2, with space group $P2_1/c$. Although alkenylamines react with **1** to give a mixture of products, addition of one equivalent of apve ($H_2NCH_2CH_2CH_2OCH{=}CH_2$) to **1** cleanly afforded the organometallic product *trans*-$PtCl_2(coe)(thmo)$ (thmo = tetrahydro-2-methyl-1,3-oxazine) arising from a metal-catalyzed intramolecular hydroamination of the starting alkenylamine. Initial investigations into the functionalization of metal complexes containing pendant alkene groups have shown that catecholborane can be added in some cases, using a rhodium catalyst, to give the corresponding organoboronate ester platinum compounds.

Key words: alkenylamines, alkenylpyridines, hydroamination, hydroboration, platinum.

Résumé : L'addition du *cis*-cyclooctène (coe) au K_2PtCl_4 conduit à la formation de *trans*-$[PtCl_2(coe)]_2$ (**1**) qui réagit avec un excès de coe pour fournir le *trans*-$PtCl_2(coe)_2$ (**2**) que l'on a caractérisé par une étude de diffraction des rayons X. On a trouvé que les cristaux sont tricliniques, groupes d'espace $P\bar{1}$, *avec* a = 5,7838(5), b = 7,4347(6) et c = 9,9972(9) Å, α = 83,924(1), β = 87,844(2) et γ = 73,545(1)° et Z = 1. L'addition de 4-vinylpyridine (4vp) au composé **1** fournit le *trans*-$PtCl_2(4vp)_2$ (**5**) que l'on a aussi caractérisé par diffraction des rayons X. Les cristaux de **5** sont monocliniques, groupe d'espace $P2_1/c$, avec a = 8,2255(6), b = 12,8254(10) et c = 6,9624(5) Å, β = 98,8230(10)° et Z = 2. Même si les alcénylamines (L) réagissent avec **1** pour fournir un mélange de produits, l'addition d'un équivalent d'apve ($H_2NCH_2CH_2CH_2OCH{=}CH_2$) à **1** fournit proprement le produit organométallique *trans*-$PtCl_2(coe)(thmo)$ (thmo = tétrahydro-2-méthyl-1,3-oxazine) qui provient d'une hydroamination intramoléculaire catalysée par un métal de l'alcénylamine de départ. Des études initiales sur la fonctionnalisation de complexes métalliques contenant des groupes alcènes ont montré que sous l'influence d'un catalyseur de rhodium, on peut, dans certains cas, additionner du catécholborane pour obtenir les esters organoboronates du platine correspondants.

Mots clés : alcénylamines, alcénylpyridines, hydroamination, hydroboration, platine.

[Traduit par la Rédaction]

Introduction

Cisplatin, *cis*-$PtCl_2(NH_3)_2$, is an anti-cancer agent used extensively for the treatment of testicular and ovarian tumours, and has moderate use in the treatment of neck, bladder and lung tumours (1–6). Unfortunately, widespread application of this compound has been limited by numerous drawbacks including nausea, myelosuppression of bone marrow, renal tubular necrosis leading to kidney failure, loss of high frequency hearing, and neuropathy. These side effects, coupled with the low solubility of cisplatin in water, have resulted in a large influx of research into derivatives of cisplatin in an attempt to overcome some of these limitations. With this in mind, we have prepared a number of *trans* platinum complexes containing alkenylamine and alkenylpyridine ligands and hypothesize that further hydroboration of the pendant C=C moieties in these complexes may prove to be a facile route to making novel platinum compounds containing biologically-active boronic acid groups. Platinum complexes containing alkenylamines and

Received December 22, 1999. Published on the NRC Research Press website on May 8, 2000.

M.P. Shaver, C.M. Vogels, A.I. Wallbank, and S.A. Westcott.[1] Department of Chemistry, Mount Allison University, Sackville, NB E4L 1G8, Canada.
T.L. Hennigar, K. Biradha, and M.J. Zaworotko.[2, 3] Department of Chemistry, St. Mary's University, Halifax, NS B3H 3C3, Canada.

[1]Author to whom correspondence may be addressed. Telephone: (506) 364-2351. Fax: (506) 364-2313. e-mail: swestcott@mta.ca
[2]Current address: Department of Chemistry, University of South Florida, Tampa, FL 33620–5250, U.S.A.
[3]Author to whom correspondence about crystallography may be addressed.

 © 2000 NRC Canada

alkenylpyridines are also of interest as these ligands can coordinate to the metal centre via either the nitrogen lone pair or the alkene moiety.

Experimental

Reagents and solvents used were obtained from Aldrich Chemicals. THF, hexane, and diethyl ether were distilled from sodium benzophenone ketyl. Methylene chloride and chloroform were distilled from CaH_2. Potassium tetrachloroplatinate was obtained from Johnson Matthey Ltd. $RhCl(PPh_3)_3$ was prepared as described elsewhere (7). NMR spectra were recorded on a JEOL JNM-GSX270 FT NMR spectrometer. ^1H NMR chemical shifts are reported in ppm and referenced to residual protons in deuterated solvent at 270 MHz. $^{11}B\{^1H\}$ NMR chemical shifts are referenced to external $F_3B{\cdot}OEt_2$ at 87 MHz. $^{13}C\{^1H\}$ NMR chemical shifts are referenced to solvent carbon resonances as internal standards at 68 MHz. Multiplicities are reported as (s) singlet, (d) doublet, (t) triplet, (q) quartet, (quint) quintet, (m) multiplet, (br) broad, and (ov) overlapping. Infrared spectra were obtained using a Mattson Polaris FT-IR spectrometer and reported in cm^{-1}. Melting points were measured uncorrected with a Mel-Temp apparatus. Microanalyses for C, H, and N were carried out at Desert Analytics (Tucson, AZ).

Preparation of $[PtCl_2(coe)]_2$ (1)

$[PtCl_2(coe)]_2$ (**1**) was prepared by modification of a known procedure (8). Potassium tetrachloroplatinate (300 mg, 0.70 mmol) was dissolved in a water isopropanol mixture (10 :7 mL). A catalytic amount of tin chloride (3.8 mg, 0.02 mmol) was added to the red solution along with an excess of *cis*-cyclooctene (3.0 mL, 23.0 mmol). After 5 days, the yellow solution was decanted from a small amount of black precipitate. Compound **1** was extracted from the aqueous phase with 15 mL of methylene chloride and filtered to afford a clear yellow solution. The solvent was removed in vacuo to give a yellow solid and a small amount of yellow liquid. The liquid was dissolved in hexane (10 mL) and decanted to afford a bright yellow powder. Yield: 158 mg (58%). A yellow–orange precipitate appeared in the hexane phase after 3 days. The hexane was decanted and the solid dried. Yield: 53 mg (79% total); mp 190°C (decomposition). Spectroscopic NMR data (in $CDCl_3$): ^1H δ:1.35 (br s, 8H), 1.52 (br s, 8H), 2.18 (br d, $J_{H\text{-}H}$ = 5 Hz, 8H), 5.78 (br, 4H); $^{13}C\{^1H\}$ δ: 26.1, 27.4, 28.9, 109.2 (br). IR (nujol): 762, 817, 868, 955, 1031, 1125, 1170, 1230, 1378, 1464, 2859, 2915.

Yellow crystals of **2** could be isolated from solutions of **1** in the presence of excess coe. The mp was found to be 178°C (decomposition). Spectroscopic NMR data (in $CDCl_3$): ^1H δ: 1.45 (br s, 8H), 1.62 (br s, 8H), 2.29 (br d, $J_{H\text{-}H}$ = 5 Hz, 8H), 5.94 (br, 4H); $^{13}C\{^1H\}$ δ: 26.3, 27.6, 29.2, 113.3 (br). IR (nujol): 762, 818, 953, 1125, 1170, 1233, 1317, 1354, 1380, 1427, 1467, 1529, 2845, 2884, 2972. The formation of this monomer has been reported previously (8). Interestingly, C and H elemental analyses from this previous study varied over time, suggesting loss of the second coe ligand to give **1** is facile even in the solid state.

Preparation of *trans*-$PtCl_2$(coe)(2vp) (3)

2-Vinylpyridine (14 mg, 0.13 mmol) in 3 mL of CH_2Cl_2 was added dropwise at 0°C to a solution of *trans*-$[PtCl_2(coe)]_2$ (50 mg, 0.07 mmol) in 15 mL of CH_2Cl_2. The reaction was stirred for 4 h at which point solvent was removed under vacuum to afford a yellow solid which was washed with ether (2 × 2 mL) and hexane (3 × 5 mL). Yield: 26 mg (40%); mp 187°C (decomposition). Spectroscopic NMR data (in $CDCl_3$): ^1H δ: 1.43 (s, 4H), 1.80 (br s, 4H), 2.22–2.49 (ov m, 4H), 5.53 (m, $J_{H\text{-}Pt}$ = 70 Hz, 2H), 5.83 (d, $J_{H\text{-}H}$ = 8 Hz, 1H), 6.06 (d, $J_{H\text{-}H}$ = 15 Hz, 1H), 7.31 (t, $J_{H\text{-}H}$ = 5 Hz, 1H), 7.72 (m, 2H), 8.12 (d of d, $J_{H\text{-}H}$ = 15, 5 Hz, 1H), 8.68 (d, $J_{H\text{-}H}$ = 5 Hz, $J_{H\text{-}Pt}$ = 35 Hz, 1H); $^{13}C\{^1H\}$ δ: 26.1, 27.9, 29.0, 94.5 ($J_{C\text{-}Pt}$ = 153 Hz), 121.7, 123.2, 124.0, 135.2, 138.7, 150.3, 156.7. IR (nujol): 761, 793, 939, 957, 1108, 1127, 1163, 1229, 1377, 1465, 1562, 1602, 2857, 2897, 2941, 2966. Elemental analysis calcd. for $PtCl_2C_{15}H_{21}N$: C 37.42, H 4.41, N 2.91; found: C 37.68, H 4.50, N 3.01.

Preparation of *trans*-$PtCl_2$(coe)(4vp) (4)

4-Vinylpyridine (60 mg, 0.56 mmol) in 5 mL of CH_2Cl_2 was added dropwise to a stirred solution of **1** (200 mg, 0.27 mmol) in 15 mL of CH_2Cl_2 at 0°C. The solvent was removed under vacuum after 4 h to afford a yellow solid which was washed with hexane (3 × 5 mL). Spectroscopic NMR data (in $CDCl_3$): ^1H δ: 1.47 (s, 6H), 1.83 (br s, 2H), 2.36 (br s, 2H), 2.54 (br s, 2H), 5.55 (br d, $J_{H\text{-}H}$ = 11 Hz, $J_{H\text{-}Pt}$ = 64 Hz, 2H), 5.61 (d, $J_{H\text{-}H}$ = 11 Hz, 1H), 6.06 (d, $J_{H\text{-}H}$ = 19 Hz, 1H), 6.68 (d of d, $J_{H\text{-}H}$ = 11, 5 Hz, 1H), 7.40 (d, $J_{H\text{-}H}$ = 5 Hz, 2H), 8.78 (d, $J_{H\text{-}H}$ = 5 Hz, $J_{H\text{-}Pt}$ = 27 Hz, 2H); $^{13}C\{^1H\}$ δ: 26.4, 28.3, 29.4, 94.4 ($J_{C\text{-}Pt}$ = 158 Hz), 122.3, 122.9, 133.3, 148.3, 151.7. Attempts to isolate **4** for elemental analysis were complicated by disproportionation in solution to give **1** and **5**.

Preparation of *trans*-$PtCl_2(4vp)_2$ (5)

4-Vinylpyridine (25 mg, 0.24 mmol) in 1 mL of CH_2Cl_2 was added dropwise to a stirred solution of **1** (45 mg, 0.06 mmol) in 7 mL of CH_2Cl_2. The mixture was cooled to 0°C for 2 days and the resultant off-white precipitate was filtered and dried under vacuum. Yield: 43 mg (75%); mp 264°C (decomposition). Spectroscopic NMR data (in $CDCl_3$): ^1H δ: 5.60 (d, $J_{H\text{-}H}$ = 11 Hz, 2H), 6.02 (d, $J_{H\text{-}H}$ = 19 Hz, 2H), 6.58 (d of d, $J_{H\text{-}H}$ = 19, 11 Hz, 2H), 7.18 (d, $J_{H\text{-}H}$ = 8 Hz, 4H), 8.84 (br d, $J_{H\text{-}H}$ = 6 Hz, $J_{H\text{-}Pt}$ = 30 Hz, 4H); $^{13}C\{^1H\}$ δ: 121, 122, 133, 147, 155. IR (nujol): 666, 846, 991, 1206, 1417, 1435, 1499, 1546, 1616, 2943. Elemental analysis calcd. for $PtCl_2C_{14}H_{14}N_2$: C 35.29, H 2.97, N 5.88; found: C 34.72, H 2.99, N 5.69.

Preparation of *trans*-$PtCl_2$(coe)(4chp) (6)

4-(3-Cyclohexen-1-yl)pyridine (89 mg, 0.56 mmol) in 5 mL of CH_2Cl_2 was added dropwise to a stirred solution of **1** (200 mg, 0.27 mmol) in 15 mL of CH_2Cl_2 at 0°C. The reaction was allowed to proceed for 4 h at which point the solvent was removed under vacuum. The resultant orange oil was dissolved in 1 mL of CH_2Cl_2 after which 5 mL of hexane was added and the reaction mixture stored at 0°C for 18 h. The precipitate was collected and determined to be **7** by NMR spectroscopic data. The solvent was removed from the filtrate to afford a bright yellow solid. Spectroscopic

© 2000 NRC Canada

NMR data (in $CDCl_3$) for **6**: ^{1}H δ: 1.46 (m, 6H), 1.76 (ov m, 4H), 2.15 (s, 2H), 2.32 (m, 4H), 2.53 (m, 2H), 2.89 (s, 1H), 5.66 (d, $J_{H\text{-}H}$ = 8 Hz, $J_{H\text{-}Pt}$ = 72 Hz, 2H), 5.72 (s, 2H), 7.29 (d, $J_{H\text{-}H}$ = 5 Hz, 2H), 8.73 (br d, $J_{H\text{-}H}$ = 5 Hz, $J_{H\text{-}Pt}$ = 32 Hz, 2H); ^{13}C{^{1}H}δ: 25.0, 26.3, 28.1, 28.5, 29.3, 31.8, 39.5, 94.1 ($J_{C\text{-}Pt}$ = 156 Hz), 124.0, 125.4, 127.3, 151.2, 153.2. Attempts to isolate **6** were complicated by disproportionation in solution to give **1** and **7**.

Preparation of *trans*-$PtCl_2(4chp)_2$ (7)

4-(3-Cyclohexen-1-yl)pyridine (45 mg, 0.29 mmol) in 1 mL of CH_2Cl_2 was added dropwise to a stirred solution of **1** (50 mg, 0.07 mmol) in 15 mL of CH_2Cl_2. The solvent was removed under vacuum after the reaction was allowed to proceed for 5 h. The resultant yellow oil was dissolved in 1 mL of CH_2Cl_2 after which addition of hexane (3 mL) to the solution produced an off-white precipitate. Yield: 53 mg (68%); mp 272°C (decomposition). Spectroscopic NMR data (in $CDCl_3$): ^{1}H δ 1.60 (m, 4H), 1.93 (m, 4H), 2.25 (m, 4H), 2.87 (br s, 2H), 5.77 (s, 4H), 7.16 (d, $J_{H\text{-}H}$ = 5 Hz, 4H), 8.75 (d, $J_{H\text{-}H}$ = 5 Hz, $J_{H\text{-}Pt}$ = 32 Hz, 4H); ^{13}C{^{1}H} δ 25.1, 28.6, 32.0, 39.5, 123.9, 125.6, 127.4, 153.1, 159.2. IR (nujol): 719, 829, 1069, 1212, 1244, 1422, 1616, 2936. Elemental analysis calcd. for $PtCl_2C_{22}H_{26}N_2$: C 45.21, H 4.49, N 4.79; found: C 44.83, H 4.26, N 4.62.

Preparation of *trans*-$PtCl_2(aa)_2$ (8)

Allylamine (18 mg, 0.32 mmol) in 3 mL of CH_2Cl_2 was added to a stirred solution of **1** (50 mg, 0.07 mmol) in 10 mL of CH_2Cl_2 at 0°C. Within 30 min a yellow precipitate had formed and was collected by suction filtration. Yield: 37 mg (72%); mp 214°C (decomposition). Spectroscopic NMR data (in $CDCl_3$): ^{1}H δ: 3.49 (d, $J_{H\text{-}H}$ = 5 Hz, 4H), 5.37 (d of d, $J_{H\text{-}H}$ = 11, 5 Hz, 2H), 5.97 (m, 4H), 8.18 (br s, 4H); ^{13}C{^{1}H} δ: 44.2, 123.7, 131.9. IR (nujol): 722, 1018, 1108, 1566, 1603, 2928. Elemental analysis calcd. for $PtCl_2C_6H_{14}N_2$: C 18.95, H 3.72, N 7.37; found: C 18.95, H 3.97, N 7.23. Complex **8** eventually decomposes in solution to give a number of unidentified products.

Preparation of *trans*-$PtCl_2$(coe)(chea) (9)

2-(1-Cyclohexenyl)ethylamine (35 mg, 0.28 mmol) in 15 mL of CH_2Cl_2 was added to a solution of **1** (100 mg, 0.13 mmol) in 10 mL of CH_2Cl_2 at 0°C. The reaction was allowed to proceed for 3 h at which point solvent was removed under vacuum to afford an orange oil. The oil was dissolved in 1 mL of CH_2Cl_2 after which hexane (10 mL) was added and the reaction mixture cooled to 0°C. After 18 h, a pale yellow precipitate was collected by suction filtration and found to be a mixture of products by NMR spectroscopy. The solvent was allowed to evaporate from the filtrate over 48 h to afford bright yellow needles which were collected and dried under vacuum. Yield: 70 mg (52%); mp 122°C. Spectroscopic NMR data (in $CDCl_3$): ^{1}H δ: 1.43 (m, 6H), 1.59 (ov m, 4H), 1.78 (br s, 2H), 1.92 (br s, 2H), 2.01 (br s, 2H), 2.24 (br m, 4H), 2.39 (ov m, 2H), 3.09 (m, $J_{H\text{-}H}$ = 8 Hz, 2H), 3.72 (br s, $J_{H\text{-}Pt}$ = 59 Hz, 2H), 5.30 (d, $J_{H\text{-}H}$ = 11 Hz, $J_{H\text{-}Pt}$ = 81 Hz, 2H), 5.55 (s, 1H); ^{13}C{^{1}H} δ: 22.4, 22.8, 25.5, 26.4, 27.9, 28.1, 29.5 ($J_{C\text{-}Pt}$ = 41 Hz), 39.7, 42.7, 93.6 ($J_{C\text{-}Pt}$ = 158 Hz), 126.5, 132.8. IR (nujol): 722, 1001, 1231, 1377, 1461, 1579, 2841, 2968. Elemental analysis calcd. for $PtCl_2C_{16}H_{29}N$: C 38.31, H 5.84, N 2.79; found: C 38.72, H 5.92, N 2.86.

Preparation of *trans*-$PtCl_2$(coe)(thmo) (10)

Tetrahydro-2-methyl-1,3-oxazine (14 mg, 0.14 mmol) in 3 mL of CH_2Cl_2 was added dropwise to a solution of **1** (50 mg, 0.07 mmol) in 10 mL of CH_2Cl_2 at 0°C. Solvent was removed after 4 h to afford a yellow oil which was triturated with hexane (3 × 5 mL) and dried under vacuum to afford a yellow solid. Yield: 25 mg (40%); mp 98°C. Spectroscopic NMR data (in $CDCl_3$): ^{1}H δ: 1.37 (br s, 6H), 1.70 (ov m, 6H), 2.13 (br s, 2H), 2.29 (br s, 2H), 3.39 (m, 2H), 3.70 (t, $J_{H\text{-}H}$ = 16 Hz, 1H), 3.92 (m, 1H), 4.45 (br s, 1H), 4.60 (m, 2H), 5.27 (m, 2H); ^{13}C{^{1}H} δ: 22.3, 25.6, 25.9, 27.4, 27.6, 28.9, 48.4, 86.5, 92.9 ($J_{C\text{-}Pt}$ = 140 Hz). IR (nujol): 815, 846, 963, 1017, 1059, 1099, 1139, 1230, 1378, 1461, 2889, 3216, 3433. Elemental analysis calcd. for $PtCl_2C_{13}H_{25}NO$: C 32.71, H 5.28, N 2.93; found: C 33.10, H 5.23, N 2.90.

Catalyzed hydroboration of *trans*-$PtCl_2(4vp)_2$ (5) with catecholborane

Under an atmosphere of dinitrogen, *trans*-$PtCl_2(4vp)_2$ (25 mg, 0.05 mmol) was suspended in 1 mL of $CDCl_3$ with 7 mol% of Wilkinson's catalyst, $RhCl(PPh_3)_3$. Catecholborane (14 mg, 0.12 mmol) in 0.5 mL of $CDCl_3$ was added dropwise to the stirred suspension and the reaction mixture was allowed to stand for 48 h and then analyzed by NMR spectroscopy. Spectroscopic NMR data (in $CDCl_3$): ^{1}H δ: 1.22 (t, $J_{H\text{-}H}$ = 8 Hz), 1.50 (d, $J_{H\text{-}H}$ = 8 Hz), 1.64 (t, $J_{H\text{-}H}$ = 8 Hz), 2.12 (s), 2.69 (q, $J_{H\text{-}H}$ = 8 Hz), 3.03 (ov), 5.29 (s), 5.38 (s), 5.63 (m), 7.0 (m), 8.74 (d, $J_{H\text{-}H}$ = 5 Hz); ^{11}B{^{1}H} δ: 7.0 (s), 7.8 (s), 12.3 (s), 29.0 (s), 23.2 (br), 35.0 (br).

Catalyzed hydroboration of *trans*-$PtCl_2(4chp)_2$ (7) with catecholborane

Under an atmosphere of dinitrogen, *trans*-$PtCl_2(4chp)_2$ (52 mg, 0.09 mmol) was dissolved in 1 mL of $CDCl_3$ with 7 mol% catalyst. Catecholborane (24 mg, 0.20 mmol) in 0.5 mL of $CDCl_3$ was added dropwise to the stirred solution and the reaction was allowed to proceed for 48 h and then analyzed by NMR spectroscopy. Spectroscopic NMR data (in $CDCl_3$): ^{1}H δ: 1.45–1.59 (ov m), 2.00–2.18 (ov m), 2.66 (m), 6.92–7.39 (ov m), 8.75 (d, $J_{H\text{-}H}$ = 5 Hz), 8.88 (d, $J_{H\text{-}H}$ = 5 Hz); ^{11}B{^{1}H} δ: 12.3 (s), 23.0 (s), 36.3 (br); ^{13}C{^{1}H} δ 21.2 (br, C-B), 21.8 (br, C-B), 27.1, 27.2, 27.7, 33.3, 33.7, 34.1, 43.6, 44.4, 112.6, 112.8, 121.6, 122.9, 124.0, 148.2, 148.3, 153.5, 159.4.

The platinum aminoboronate ester was formed in situ as described in the previous procedure and removed from the dinitrogen atmosphere. Addition of 0.5 mL of D_2O to this product resulted in a convincing change in the solution's appearance from brown to orange in colour. Spectroscopic NMR data (in $CDCl_3$): ^{1}H δ: 1.48–1.58 (ov m), 1.99 (m), 2.18 (m), 2.65 (m), 6.70 (d, $J_{H\text{-}H}$ = 5 Hz), 6.88 (d, $J_{H\text{-}H}$ = 5 Hz), 7.09–7.21 (ov m), 7.39 (m), 8.73 (d, $J_{H\text{-}H}$ = 5 Hz); ^{11}B{^{1}H} δ: 19.6 (s, $B(OH)_3$), 36.9 (br); ^{13}C{^{1}H} δ 21.2 (br, C-B), 22 (br, C-B), 27.1, 27.2, 27.6, 33.0, 33.6, 33.7, 43.6, 44.3, 115.6, 120.9, 124.0, 148.2, 153.2, 159.5.

© 2000 NRC Canada

Table 1. Crystallographic data collection parameters for *trans*-$PtCl_2(coe)_2$ (**2**) and *trans*-$PtCl_2(4vp)_2$ (**5**).

Complex	**2**	**5**
Formula	$C_{16}H_{28}Cl_2Pt$	$C_{14}H_{14}Cl_2N_2Pt$
fw	486.37	476.26
Crystal system	triclinic	monoclinic
Space group	$P\bar{1}$	$P2_1/c$
a (Å)	5.7838 (5)	8.2255 (6)
b (Å)	7.4347 (6)	12.8254 (10)
c (Å)	9.9972 (9)	6.9624 (5)
α (°)	83.924 (1)	—
β (°)	87.844 (2)	98.8230 (10)
γ (°)	73.546 (1)	—
V (Å^3)	409.95 (6)	725.81 (9)
Z	1	2
ρ_{calcd} (g cm^{-3})	1.970	2.179
Crystal size (mm)	0.15 × 0.20 × 0.20	0.15 × 0.20 × 0.20
Temperature (K)	183 (2)	193 (2)
Radiation	MoKα (λ = 0.71073)	MoKα (λ = 0.71073)
μ, (mm^{-1})	8.869	10.021
Total reflections[a]	2602	4464
Total unique relections	1807	1689
No. of variables	88	88
Largest difference peak/hole (e Å^{-3})	1.061/–1.889	0.624/–1.177
R^b	0.0232	0.0188
R_w	0.0606	0.0480
GoF[c]	0.575	1.093

[a] $I_o > 3\sigma(I_o)$.
[b] $R = \Sigma||F_o| - |F_c||/\Sigma|F_o|$; $R_w = [\Sigma(w(|F_o| - |F_c|)^2/\Sigma(w|F_o|)^2]^{1/2}$.
[c] $[\Sigma(w(|F_o| - |F_c|)^2/(NO - NV)]^{1/2}$.

X-ray crystallographic data for 2 and 5

Crystals of **2** and **5** suitable for X-ray diffraction studies were obtained by crystallization from solutions of methylene chloride at 5°C. A summary of the crystal data and parameters for data collection is given in Table 1. Data were collected at 183 K (for **2**) and 193 K (for **5**) on a Siemens SMART/CCD diffractometer equipped with an LT-II low temperature device. Diffracted data were corrected for absorption using the SADABS[4] program. SHELXTL was used for structure solution and refinement was based on F^2.[5] All non-hydrogen atoms were refined anisotropically. Hydrogen atoms were fixed at calculated positions and refined isotropically on the basis of the corresponding carbon atoms [*U*(H) = 1.2*U*eq(C)]. Selected bond distances and angles are given in Tables 2 and 4 and final atomic coordinates in Tables 3 and 5. Complete tables of bond distances and angles, final atomic coordinates, and anisotropic displacement parameters have been deposited as supporting material.[6]

Results and discussion

As part of our ongoing research into making novel aminoboron platinum complexes, we decided to initially prepare a number of unsaturated *trans* amine and pyridine complexes from the monoalkene dimer *trans*-$[PtCl_2(coe)]_2$ (**1**) (coe = η^2 – C_8H_{14}) (8). The starting organometallic dimer, which is soluble in common organic solvents, was readily prepared by the addition of *cis*-cyclooctene to aqueous solutions of K_2PtCl_4, and appears to be indefinitely stable in the solid state. A recent paper examining reaction mechanisms for alkene exchange with *trans*-$[PtCl_2(C_2H_4)]_2$ suggests that a two-step process incorporating *trans*-$PtCl_2(C_2H_4)_2$ might be occurring in the steady state (9). Indeed, the analogous disubstituted alkene complex *trans*-$PtCl_2(coe)_2$ (**2**) could be crystallized in minor amounts (<10%) by addition of excess coe to **1** (10).

We have carried out an X-ray diffraction study on **2** which shows the platinum metal centre in a square plane with the cyclooctene ligands lying *trans* to one another. The structure of **2** is shown in Fig. 1, summary of the crystallographic data presented in Table 1, pertinent bond distances and angles given in Table 2, and atomic coordinates provided in Table 3. Platinum–carbon bond distances of 2.258(4) and 2.278(4) Å are somewhat longer than analogous Pt(II) complexes where a chloride ligand lies *trans* to the alkene group. For instance, average bond lengths of 2.128(19), 2.13(2),

[4] G.M. Sheldrick. SADABS Univ. Gottingen (1996).
[5] G.M. Sheldrick. SHELXTL Release 5.03; Siemens Analytical X-ray Instruments Inc., Madison, Wis. (1994).
[6] A complete set of data may be purchased from: The Depository of Unpublished Data, Document Delivery, CISTI, National Research Council Canada, Ottawa, Ontario, Canada, K1A 0S2. Tables of coordinates, bond distances and angles, and alternative views of **2** and **5** have also been deposited with the Cambridge Crystallographic Data Centre, University Chemical Laboratory, 12 Union Road, Cambridge, CB2 1EZ, U.K.

© 2000 NRC Canada

Table 2. Selected bond distances (Å) and angles (°) for *trans*-$PtCl_2(coe)_2$ (**2**).[a]

Bond distances	
Pt(1)—C(2)#1	2.258(4)
Pt(1)—C(2)	2.258(4)
Pt(1)—C(1)#1	2.278(4)
Pt(1)—C(1)	2.278(4)
Pt(1)—Cl(1)	2.3107(10)
Pt(1)—Cl(1)#1	2.3107(10)
C(1)—C(2)	1.389(5)
C(1)—C(8)	1.499(6)
C(2)—C(3)	1.492(6)
C(3)—C(4)	1.543(6)
C(4)—C(5)	1.532(6)
C(5)—C(6)	1.550(6)
C(6)—C(7)	1.536(6)
C(7)—C(8)	1.547(6)
Bond angles	
C(2)-C(1)-C(8)	125.2(4)
C(1)-C(2)-C(3)	123.8(4)
C(2)-C(3)-C(4)	109.5(3)
C(5)-C(4)-C(3)	114.6(3)
C(4)-C(5)-C(6)	116.4(4)
C(7)-C(6)-C(5)	115.2(4)
C(6)-C(7)-C(8)	115.4(4)
C(1)-C(8)-C(7)	112.2(4)
Cm-Pt1-Cl(1)[b]	85.7

[a]Symmetry transformations used to generate equivalent atoms: #1 –x, –y, –z.

[b]Cm is in the middle of the C(1)—C(2) bond.

and 2.12(2) Å have been reported for $K[PtCl_3(C_2H_4)]$ (11), $PtCl(C_6H_2Me_3)(\eta^4\text{-}C_8H_{12})$ (12), and $[PtCl_2(C_7H_{12})]_2$ (13), respectively. However, the Pt—C bond distance in **2** is similar to that reported for the double bond *trans* to the mesityl group ($C_6H_2Me_3$) in the previous example (cf. 2.30(2) Å). The carbon–carbon bond distance of 1.389(5) Å shows the expected weakening of the double bond due to π-backbonding from the metal to the empty π^* orbital of the alkene (14).

Addition of neutral ligands (L) to either **1** or **2** will give complexes of the type *trans*-$PtCl_2(coe)L$ and, upon addition of a second equivalent of ligand, the disubstituted species *trans*-$PtCl_2L_2$ (15). Reactions with alkenylpyridine and alkenylamine ligands are of special interest because coordination of these ligands to a transition metal can occur via either the alkene moiety and (or) the nitrogen lone pair.

Alkenylpyridines

A number of transition metal complexes (16–23) containing alkenylpyridine ligands have been reported. For example, addition of 2-vinylpyridine (2vp = 2-$NC_5H_4CH{=}CH_2$) to $[Cu(NCCH_3)_4][ClO_4]$ gave the binuclear complex $[Cu_2(\mu\text{-}2vp)_2(2vp)_2][ClO_4]_2$ where two of the alkenylpyridine ligands use the nitrogen and the alkene to bond to two respective metal centres (16). For this study we decided to prepare *trans* complexes from three commercially available alkenylpyridines (Fig. 2).

Table 3. Atomic coordinates ($\times 10^4$) and equivalent isotropic displacement coefficients for *trans*-$PtCl_2(coe)_2$ (**2**). *U*(eq) is defined as one third of the trace of the orthogonalized U_{ij} tensor.

	x	*y*	*z*	*U*(eq)
Pt(1)	0	0	0	16(1)
Cl(1)	3265(2)	–1340(1)	1394(1)	24(1)
C(1)	2409(7)	–1393(6)	–1674(4)	19(1)
C(2)	1241(7)	–2656(5)	–1051(4)	18(1)
C(3)	–681(8)	–3230(6)	–1703(4)	22(1)
C(4)	464(9)	–5041(6)	–2393(5)	26(1)
C(5)	2532(9)	–4921(6)	–3369(5)	26(1)
C(6)	2023(9)	–3197(7)	–4444(4)	27(1)
C(7)	3150(9)	–1635(6)	–4166(4)	26(1)
C(8)	1883(8)	–391(6)	–3057(4)	23(1)

Table 4. Selected bond distances (Å) and angles (°) for *trans*-$PtCl_2(4vp)_2$ (**5**).[a]

Bond distances	
Pt(1)—N(1)	2.020(3)
Pt(1)—N(1)#1	2.020(3)
Pt(1)—Cl(1)	2.2996(8)
Pt(1)—Cl(1)#1	2.2996(8)
N(1)—C(5)	1.350(4)
N(1)—C(1)	1.352(4)
C(1)—C(2)	1.373(5)
C(2)—C(3)	1.398(5)
C(3)—C(4)	1.403(5)
C(3)—C(6)	1.473(5)
C(4)—C(5)	1.368(5)
C(6)—C(7)	1.330(6)
Bond Angles	
N(1)-Pt(1)-N(1)#1	180.0
N(1)-Pt(1)-Cl(1)	89.92(8)
N(1)#1-Pt(1)-Cl(1)	90.08(8)
N(1)-Pt(1)-Cl(1)#1	90.08(8)
N(1)#1-Pt(1)-Cl(1)#1	89.92(8)
Cl(1)-Pt(1)-Cl(1)#1	180.0
C(5)-N(1)-C(1)	117.9(3)
C(5)-N(1)-Pt(1)	120.0(2)
C(1)-N(1)-Pt(1)	122.1(2)
N(1)-C(1)-C(2)	122.2(3)
C(1)-C(2)-C(3)	120.3(3)
C(2)-C(3)-C(4)	116.8(3)
C(2)-C(3)-C(6)	120.4(3)
C(4)-C(3)-C(6)	122.8(3)
C(5)-C(4)-C(3)	119.9(3)
N(1)-C(5)-C(4)	122.8(3)
C(7)-C(6)-C(3)	125.0(4)

[a]Symmetry transformations used to generate equivalent atoms: #1 (–x + 1), (–y + 1), –z.

Previous work has shown that attempts to prepare *cis*-$PtCl_2(2vp)_2$ (20) from K_2PtCl_4 resulted in the formation of several products where both the alkene and nitrogen groups are involved in bonding to platinum. Likewise, efforts to generate the *trans* derivative from *trans*-$PtCl_2(NCCH_3)_2$ have also proven unsuccessful (23). Although we were also unable to generate *trans*-$PtCl_2(2vp)_2$ from addition of 2vp to

© 2000 NRC Canada

Table 5. Atomic coordinates (× 10^4) and equivalent isotropic displacement coefficients for *trans*-$PtCl_2(4vp)_2$ (**5**). *U*(eq) is defined as one third of the trace of the orthogonalized U_{ij} tensor.

	x	*y*	*z*	*U*(eq)
Pt(1)	5000	5000	0	20(1)
Cl(1)	3695(1)	5692(1)	2403(1)	31(1)
N(1)	6632(3)	6188(2)	343(4)	21(1)
C(1)	6151(4)	7197(3)	253(5)	24(1)
C(2)	7255(4)	8005(3)	531(5)	25(1)
C(3)	8945(4)	7804(3)	909(5)	25(1)
C(4)	9427(4)	6754(3)	1009(5)	25(1)
C(5)	8261(4)	5985(3)	711(5)	24(1)
C(6)	10133(5)	8671(3)	1204(6)	33(1)
C(7)	11757(5)	8568(4)	1365(6)	44(1)

trans-$[PtCl_2(coe)]_2$ (**1**), the novel organometallic complex *trans*-$PtCl_2(coe)(2vp)$ (**3**), which is soluble in common organic solvents such as methylene chloride, could be isolated in moderate yield (40%). Steric congestion around the nitrogen atom in 2-vinylpyridine presumably inhibits addition of a second equivalent of this ligand to the metal centre. The ^{1}H NMR spectrum for **3** shows a shift for the pyridine ring's α-carbon proton from 8.54 ppm for free 2vp to 8.68 ppm in the complex. Coupling ($J_{H\text{-}Pt}$ = 35 Hz) to the ^{195}Pt nucleus (14) is also observed for this resonance. Shifts for the alkenyl peaks are also observed by ^{1}H NMR spectroscopy for this complex, suggesting that the alkenyl group may lie directly above the plane of the platinum atom (15).

The corresponding 4-vinylpyridine (4vp = 4-$NC_5H_4CH{=}CH_2$) complex, *trans*-$PtCl_2(coe)(4vp)$ (**4**), was prepared by addition of 2 equivalents of 4vp to **1**, along with minor amounts of the disubstituted product *trans*-$PtCl_2(4vp)_2$ (**5**) and unreacted **1**. For complex **4**, the diagnostic shift from 8.56 ppm for free 4vp to 8.78 ppm is observed in the ^{1}H NMR spectrum, along with coupling to platinum ($J_{H\text{-}Pt}$ = 27 Hz), for the pyridine ring's α-carbon protons. Complex **5** could be readily prepared by the addition of excess 4vp to **1**. Although NMR spectroscopic data show similar trends upon complexation to platinum, unambiguous assignment of **5** is based upon an X-ray diffraction study. The molecular structure of **5** is shown in Fig. 3, relevant bond angles and distances in Table 4, and atomic coordinates in Table 5. The platinum atom lies in a distorted square plane with two Cl atoms and two 4vp N atoms coordinated to the metal centre in a *trans* geometry. The Pt—Cl and Pt—N bond distances of 2.2996(8) and 2.020(3) Å, respectively, are similar to those reported for *cis*-$PtCl_2(4vp)_2$ (21). Bond lengths of 1.330(6) Å are typical for uncomplexed C—C double bonds. The alkenylpyridines are planar with bond distances and angles similar to those observed in other transition metal pyridine derivatives (21).

The organometallic complex *trans*-$PtCl_2(coe)(4chp)$ (**6**) (4chp = 4-(3-cyclohexen-1-yl)pyridine) and the disubstituted compound *trans*-$PtCl_2(4chp)_2$ (**7**) were readily prepared from reaction of the cyclooctene dimer **1** with 2 and 4 equivalents of 4chp, respectively, (24). Complex **6** has the diagnostic shift for the α-hydrogens of the pyridine group in the ^{1}H NMR spectrum (8.49 ppm for free 4chp to 8.73 ppm for **6**) along with coupling to the ^{195}Pt nucleus ($J_{H\text{-}Pt}$ = 72 Hz). The cyclohexenyl groups in **7** resulted in this complex having increased solubility in common organic solvents as compared to **5**.

Fig. 1. Molecular structure of *trans*-$PtCl_2(coe)_2$ (**2**).

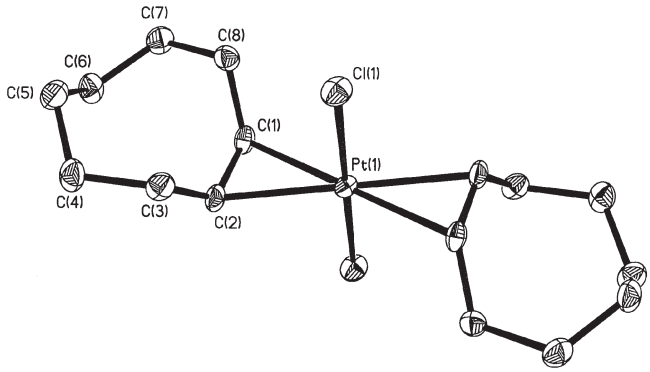
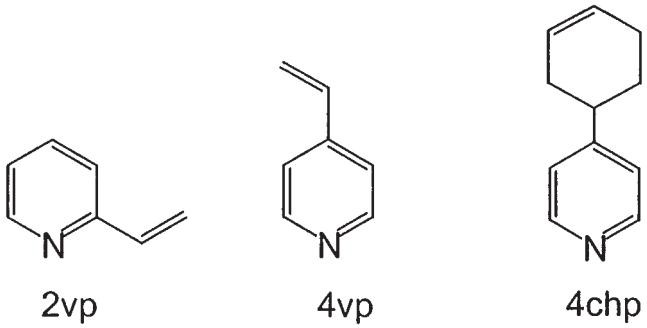


Fig. 2. Alkenylpyridines.



Alkenylamines

The synthesis of platinum complexes containing neutral and protonated alkenylamines has been reported previously (25–28). For example, addition of allylamine (aa = $NH_2CH_2CH{=}CH_2$) to acidic solutions of $[PtCl_4]^{2-}$ are known to give zwitterionic $PtCl_3(CH_2{=}CHCH_2NH_3)$ where only the C=C group of the alkenylamine is coordinated to the platinum centre (14, 25). In the absence of protonation, or by treatment with NaOH, the above complex can be transformed into a neutral alkenylamine species where the ligand is capable of coordinating in a chelating bidentate manner through both the alkene moiety and the nitrogen lone pair (26). Another allylamine complex has been reported in which the ligand bridges two metal centres by binding to one metal via the nitrogen atom and to the other platinum using the alkene group (29). We have found that addition of aa to *trans*-$[PtCl_2(coe)]_2$ (**1**) afforded the novel diamine complex *trans*-$PtCl_2(aa)_2$ (**8**) in high yield (72%). Complex **8** is only sparingly soluble in common organic solvents such as methylene chloride. The amine hydrogens appear as a broad peak in the ^{1}H NMR spectrum and shift from 1.23 for free allylamine to 8.18 ppm in **8**. Likewise, the broad methylene peak shifts from 3.36 to 3.49 ppm upon complexation. The vinyl peaks, however, remain relatively unchanged suggesting that coordination of the allylamine ligand occurs through the nitrogen atom only. IR data supports this hypothesis as the C=C π stretch found in free allylamine at 1637 cm^{-1} only shifts to 1603 cm^{-1} when the ligand coordinates to Pt(II). For metal complexes containing the

© 2000 NRC Canada

Fig. 3. Molecular structure of *trans*-$PtCl_2(4vp)_2$ (**5**).

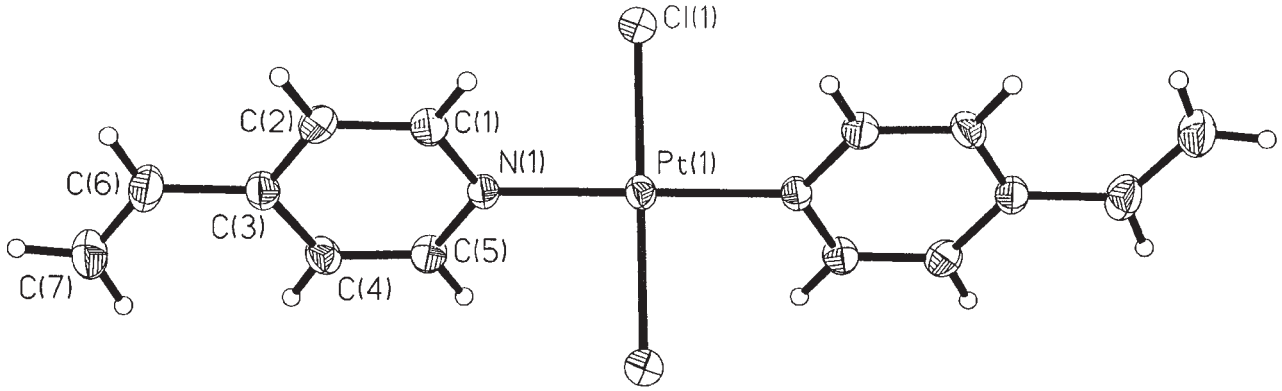
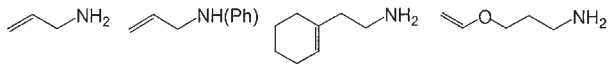


Fig. 4. Alkenylamines.



protonated alkenylamine ligands, where the alkene is directly bound to the metal centre, this band appears near 1500 cm^{-1} (26). Efforts to prepare the monoamine complex *trans*-$PtCl_2$(coe)(aa) have proven unsuccessful.

We have attempted to prepare platinum complexes with other alkenylamines (Fig. 4) in an effort to confirm the bonding modes in these unique ligands. Unfortunately, no reaction was observed between dimer **1** and secondary amine *N*-allylaniline (aA = $NH(Ph)CH_2CH{=}CH_2$). The increased steric bulk of this amine, as compared with allylamine, presumably precludes coordination to the metal centre. Conversely, *trans*-$PtCl_2$(coe)(chea) (**9**) was prepared by addition of 2-(1-cyclohexenyl)ethylamine (chea) to dimer **1**. As with the other monoamine complexes, the $^{13}C\{^1H\}$ NMR spectrum for **9** exhibits a singlet for the sp^2 carbons of the coe ligand at 93.6 ppm with diagnostic ^{195}Pt satellites ($J_{C\text{-}Pt}$ = 158 Hz). Unfortunately, treatment of **1** with four equivalents of chea led to a complex mixture of products, even at low temperatures.

Addition of aminopropylvinylether (apve = $H_2NCH_2CH_2CH_2OCH{=}CH_2$) to *trans*-$[PtCl_2(coe)]_2$ (**1**) gave the unexpected product *trans*-$PtCl_2$(coe)(thmo) (**10**) (thmo = tetrahydro-2-methyl-1,3-oxazine) in moderate yields (40%). The formation of thmo presumably arises from a platinum mediated intramolecular hydroamination of the starting apve group (30). A proposed mechanism for this reaction is shown in Fig. 5 (31). Coordination of the alkene group to the metal centre activates it towards nucleophilic attack by the amine group. Selective attack at the carbon α to the ether oxygen affords an alkylplatinum intermediate. Subsequent hydrogen abstraction from the ammonium group yields an alkylmetal hydride intermediate which undergoes reductive elimination to produce free thmo and the coordinatively unsaturated metal species '$PtCl_2$(coe)'. This complex, or unreacted **1**, rapidly traps free thmo to give *trans*-$PtCl_2$(coe)(thmo). This reaction is specific for the hydroamination product as no other apve derivatives were observed. Further work in this area will concentrate on examining the hydroamination of *N*-substituted apve derivatives, the results of which will be reported in due course.

Hydroboration of Metal Complexes

We hypothesize that hydroboration of pendant alkenyl groups in the above mentioned alkenylamine and alkenylpyridine compounds, followed by aqueous workup, should give novel platinum complexes containing boronic acids, $-B(OH)_2$ (32). Compounds containing boronic acids have extensive biological activity (33) as well as facilitate the transport of molecules across lipid bilayers (34, 35). As hydroborations of the starting alkenylamines and alkenylpyridines are known to give a number of unwanted products (36, footnote 7), this present methodology is advantageous in that coordination of the ligand to the metal centre deactivates the lone pair of nitrogen.

Initial work was conducted on the monoalkene complexes **3**, **4**, **6**, and **9**. Not surprisingly, however, hydroborations of these complexes always gave complex product distributions arising from attack of the borane at the metal centre following initial loss of the labile cyclooctene ligand. We therefore decided to concentrate our efforts on functionalizing the disubstituted analogues and proceeded by using the fully characterized pyridine complex *trans*-$PtCl_2(4vp)_2$ (**5**). Reactions of **5** with catecholborane (HBcat, cat = $O_2C_6H_4$), using 7 mol% of $RhCl(PPh_3)_3$ (37), gave mixtures of *anti*-Markovnikov (45% by ^1H NMR spectroscopy) and Markovnikov (45%) hydroboration products, products derived from a dehydrogenative borylation/hydrogenation (5% each) pathway, as well as some decomposition to platinum metal. Dehydrogenative borylation is basically a mechanism that replaces one of the alkene hydrogens with a Bcat group while generating H_2; this latter species accounts for the observation of products containing hydrogenated 4-ethylpyridine. The complex product distributions observed in these reactions is somewhat surprising in light of the fact that hydroborations of styrene derivatives ($ArCH{=}CH_2$) using HBcat can give exclusive formation of either the Markovnikov ($ArCH(Bcat)CH_3$) or *anti*-Markovnikov ($ArCH_2CH_2Bcat$) products depending upon the choice of catalyst (37, 38).

It is plausible that the numerous products observed in hydroborations of **5** may be arising from the low solubility

[7] C.M. Vogels, P.E. O'Connor, M.P. Shaver, T.E. Phillips, K.J. Watson, and S.A. Westcott. unpublished results.

© 2000 NRC Canada

Fig. 5. Intramolecular hydroamination of aminopropylvinylether.

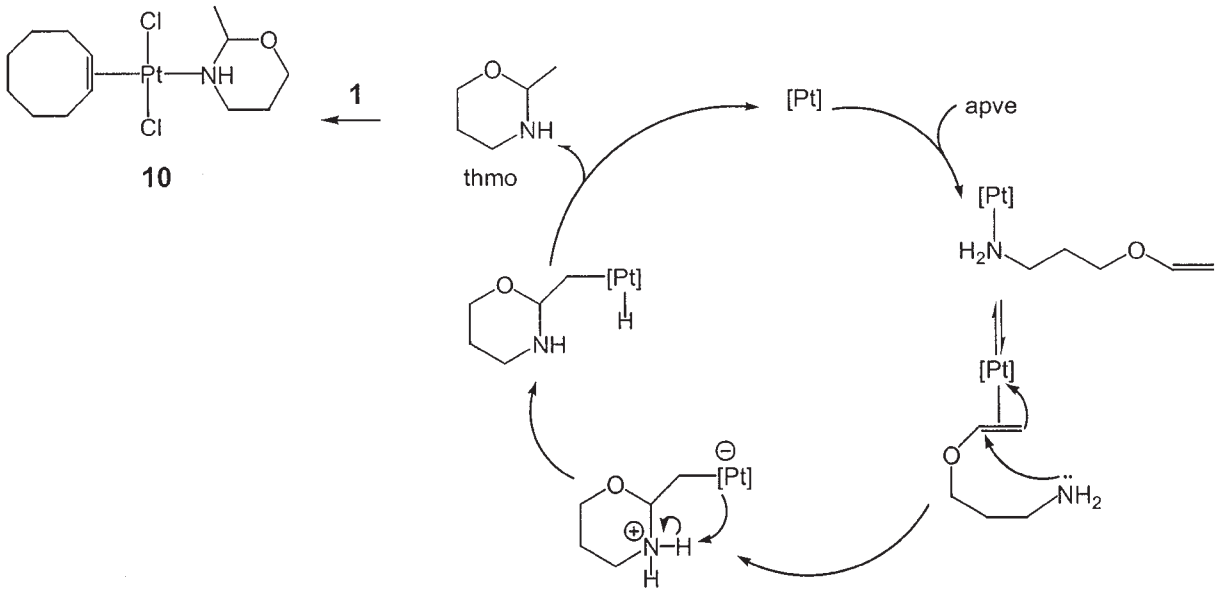
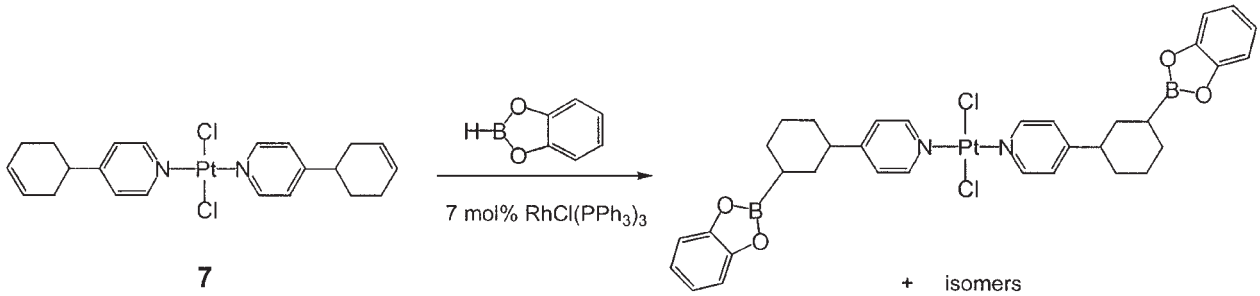


Fig. 6. Hydroboration of *trans*-$PtCl_2(4chp)_2$ (**7**) with catecholborane.



of the starting platinum material in organic solvents. We therefore decided to investigate the catalyzed hydroboration of organic soluble *trans*-$PtCl_2(4chp)_2$ (**7**). Addition of HBcat to **7** employing 7 mol% $RhCl(PPh_3)_3$ as a catalyst gave the desired hydroborated product (Fig. 6) as ascertained by multinuclear NMR spectroscopy. The diagnostic peak at 36 ppm in the $^{11}B\{^1H\}$ NMR spectrum suggests the formation of an organoboronate ester (38). Further evidence that the 1,2-disubstituted alkene is being reduced is indicated by the disappearance of the vinylic peak in the ^1H NMR spectrum. Preliminary results attempting to convert the hydroborated product to the corresponding boronic acid compound have also proven successful. However, because of the disubstituted nature of the alkene, it appears that this reaction is not selective as regioisomers are present as observed by ^1H and $^{13}C\{^1H\}$ NMR spectroscopy. We are currently examining the full scope of this reaction in an effort to improve selectivities and will report our results in due course.

Conclusions

We have prepared a number of *trans* platinum alkenylpyridine and alkenylamine complexes from the organometallic dimer *trans*-$[PtCl_2(coe)]_2$ (coe = *cis*-cyclooctene). Coordination in all cases appears to proceed through the nitrogen lone pair and not the alkene moiety. Several novel organometallic complexes of the type *trans*-[PtCl(coe)L] (L = alkenylpyridine or alkenylamine) have also been prepared and characterized. Initial investigations into the functionalization of the pendant alkene groups have shown that catecholborane can be added to these complexes, using a rhodium catalyst, to give the corresponding organoboronate ester platinum compounds.

Acknowledgements

Thanks are gratefully extended to the Natural Sciences and Engineering Research Council of Canada, St. Mary's University, and Mount Allison University for financial support and Johnson Matthey Ltd. for the generous supplies of platinum salts. We also wish to thank Dan Durant, Roger and Marilyn Smith, and John E. Marcone (DuPont Co.) for their expert technical assistance, Dr. Hilary Jenkins (SMU) for help with the X-ray crystallography, and Drs. Terri Bright, Sabine Weiguny and Giuliano Muccin (BASF) for the generous gift of aminopropylvinylether. Anonymous reviewers are thanked for helpful suggestions.

© 2000 NRC Canada

References

1. R. Young, B. Chabner, S. Hubbard, R. Fischer, R. Bender, T. Anderson, and V. de Vita. Proc. Am. Soc. Clin. Oncol. **19**, 378 (1978).
2. E. Wong and C.M. Giandomenico. Chem. Rev. **99**, 2451 (1999).
3. E.R. Jamieson and S.J. Lippard. Chem. Rev. **99**, 2467 (1999).
4. J. Reedijk. Chem. Rev. **99**, 2499 (1999).
5. H. Kawai, Y. Kitano, M. Mutoh, and G. Hata. Chem. Pharm. Bull. **41**, 357 (1993).
6. U. Bierbach and N. Farrell. J. Biol. Inorg. Chem. **3**, 570 (1998), and refs. therein.
7. J.A. Osborn and G. Wilkinson. Inorg. Synth. **28**, 77 (1990).
8. E. Kuljian and H. Frye. Z. Naturforsch. B: Anorg. Chem. Org. Chem. Biochem. Biophys. Biol. **20b**, 204 (1965).
9. M.R. Plutino, S. Otto, A. Roodt, and L.I. Elding. Inorg. Chem. **38**, 1233 (1999).
10. J.F. Harrod. Inorg. Chem. **4**, 428 (1965).
11. J.A.J. Jarvis, B.T. Kilbourn, and P.G. Owston. Acta. Crystallogr. Sect. B: Struct. Crystallogr. Cryst. Chem. **B27**, 366 (1971).
12. K.A. Fallis, G.K. Anderson, and N.P. Rath. Organometallics, **12**, 2435 (1993).
13. J. Bordner and D.W. Wertz. Inorg. Chem. **13**, 1639 (1974).
14. F.R. Hartley. The chemistry of platinum and palladium. John Wiley & Sons, New York. 1973.
15. C.M. Vogels, H.L. Wellwood, K. Biradha, M.J. Zaworotko, S.A. Westcott. Can. J. Chem. **77**, 1196 (1999).
16. M. Munakata, S. Kitagawa, H. Simono, T. Emori, and H. Masuda. J. Chem. Soc. Chem. Commun. 1798 (1987).
17. L.M. Engelhardt, P.C. Healy, J.D. Kildea, and A.H. White. Aust. J. Chem. **42**, 185 (1989).
18. R. Settambolo, S. Scamuzzi, A. Caiazzo, and R. Lazzaroni. Organometallics, **17**, 2127 (1998).
19. D. Thomas, W. Baumann, A. Spannenberg, R. Kempe, and U. Rosenthal. Organometallics, **17**, 2096 (1998).
20. A. Kasahara, K. Tanaka, and T. Izumi. Bull. Chem. Soc. Jpn. **42**, 1702 (1969).
21. M. Kubiak and J. Kuduk-Jaworska. Acta. Crystallogr. Sect. C: Cryst. Struct. Commun. **C42**, 1703 (1986).
22. J. Kuduk-Jaworska. Pol. J. Chem. **59**, 705 (1985).
23. A.G.M.M. Hossain and K. Ogura. Indian. J. Chem. **35A**, 373 (1996).
24. M.J. Bloemink, R.J. Heetebrij, J. Ireland, G.B. Deacon, and J. Reedijk. JBIC J. Biol. Inorg. Chem. **1**, 278 (1996).
25. R.G. Denning, F.R. Hartley, and L.M. Venanzi. J. Chem. Soc. A 324 (1967), and refs. therein.
26. D.B. Brown, A.R. Khokhar, M.P. Hacker, J.J. McCormack, and W.M. Stalick. Inorg. Chim. Acta. **67**, 45 (1982).
27. J. Viljanen, K.D. Klika, R. Sillanpää, and J. Arpalahti. Inorg. Chem. **38**, 4924 (1999).
28. E.I. Montero, S. Díaz, A.M. González-Vadillo, J.M. Pérez, C. Alonso, and C. Navarro-Ranninger. J. Med. Chem. **42**, 4264 (1999).
29. A.V. Kotov and L.N. Essen. Zh. Neorg. Khim. **15**, 2188 (1970).
30. C.M. Vogels, P.G. Hayes, M.P. Shaver, S.A. Westcott. Chem. Commun. (Cambridge), 51 (2000).
31. T.E. Muller and M. Beller. Chem. Rev. **98**, 675 (1998).
32. H.C. Brown. Hydroboration. Wiley–Interscience, New York. 1962.
33. C. Morin. Tetrahedron, **50**, 12521 (1994).
34. P.R. Westmark, S.J. Gardiner, and B.D. Smith. J. Am. Chem. Soc. **118**, 11093 (1996).
35. M. Takeuchi, T. Imada, S. Shinkai. J. Am. Chem. Soc. **118**, 10658 (1996).
36. A. Dicko, M. Montury, and M. Baboulene. Tetrahedron Lett. **28**, 6041 (1987).
37. I. Beletskaya and A. Pelter. Tetrahedron, **53**, 4957 (1997).
38. S.A. Westcott, H.P. Blom, T.B. Marder, and R.T. Baker. J. Am. Chem. Soc. **114**, 8863 (1992).

© 2000 NRC Canada

Glycosidase-catalyzed hydrolysis of 2-deoxyglucopyranosyl pyridinium salts: effect of the 2-OH group on binding and catalysis

Kelly S. E. Tanaka, Jiang Zhu, Xicai Huang, Francesco Lipari, and Andrew J. Bennet

Abstract: Three 2-deoxy-α-D-glucopyranosyl pyridinium tetrafluoroborates were tested for their binding affinity to a range of α-glucosidases and α-mannosidases. The α-isoquinolinium salt (**11**) binds approximately 275–fold more tightly to yeast α-glucosidase than does the isomeric quinolinium salt (**12**). In addition, compound **11** binds to the yeast enzyme approximately two-fold tighter than the corresponding glucopyranosyl isoquinolinium salt (**9**). The (k_{cat}/k_{hyd}) values for the yeast α-glucosidase-catalyzed reactions of **11** and **9** are 1.6×10^5 and 2.0×10^9, respectively, when compared to the spontaneous uncatalyzed reactions. Thus, the interaction of the 2-OH group in compound **9** with the yeast enzyme's active site generates a relative transition state stabilization of about 23.5 kJ mol^{-1}. For both compounds **11** and **12**, the observed rate accelerations for the yeast α-glucosidase-catalyzed hydrolysis, relative to the spontaneous reaction in solution, (k_{cat}/k_{hyd}) are identical within experimental error.

Key words: glycosidase, inhibitor, 2-deoxyglucose, pyridinium, catalysis.

Résumé : On a évalué les affinités de liaison de trois fluoroborates de 2-désoxy-α-D-glucopyranosyl pyridinium avec un ensemble d'α-glucosidases et d'α-mannosidases. Le sel d'α-isoquinoléinium (**11**) se lie approximativement 275 fois fortement à l'α-glucosidase de la levure que le sel quinoléinium isomère (**12**). De plus, le composé **11** se lie à l'enzyme de la levure approximativement deux fois mieux que le sel du glucopyranosyl isoquinoléinium correspondant (**9**). Les valeurs de (k_{cat}/k_{hyd}) pour les réactions des composés **11** et **9** catalysées par l'α-glucosidase de la levure sont égales respectivement à $1{,}6 \times 10^5$ et $2{,}0 \times 10^9$ lorsqu'on les compare aux réactions spontanées non catalysées. On en déduit que l'interaction du groupe 2-OH du composé **9** avec le site de l'enzyme de la levure génère une stabilisation relative de l'état de transition d'environ 23,5 kJ mol^{-1}. Pour chacun des composés **11** et **12**, les accélérations de vitesse observées pour les hydrolyses catalysées par l'α-glucosidase de la levure, comparées à la réaction spontanée en solution (k_{cat}/k_{hyd}) sont identiques aux erreurs expérimentales près.

Mots clés : glucosidase, inhibiteur, 2-désoxyglucose, pyridinium, catalyse.

Introduction

Recent advances in the rapidly growing field of glycobiology have provided insights into the fundamental importance of glycoproteins, glycolipids, and oligosaccharides in a myriad of biological events (1). Clearly, glycoconjugate-processing enzymes play a crucial role in the scheme of these various biological events (2). As a key subclass of glycoconjugate-processing enzymes, glycosidases are the focus of ongoing research aimed at the discovery of new glycosidase inhibitors (3). One class of naturally occurring glycosidase inhibitors are carbohydrate mimics that contain an endocyclic amino group, the so-called "imino-sugars" (4), a notable example of which is 1-deoxynojirimycin (DNJ, **1**) a compound that has the same hydroxyl configuration as 1-deoxyglucose (5). In general, imino-sugars are good inhibitors of glycosidase enzymes, probably due to protonation at physiological pH of the secondary amine of the imino-sugar, thus generating a cation mimic of the glucosyl oxacarbenium ion (**2**) which emulates the glycosylation transition state structure (3, 6).

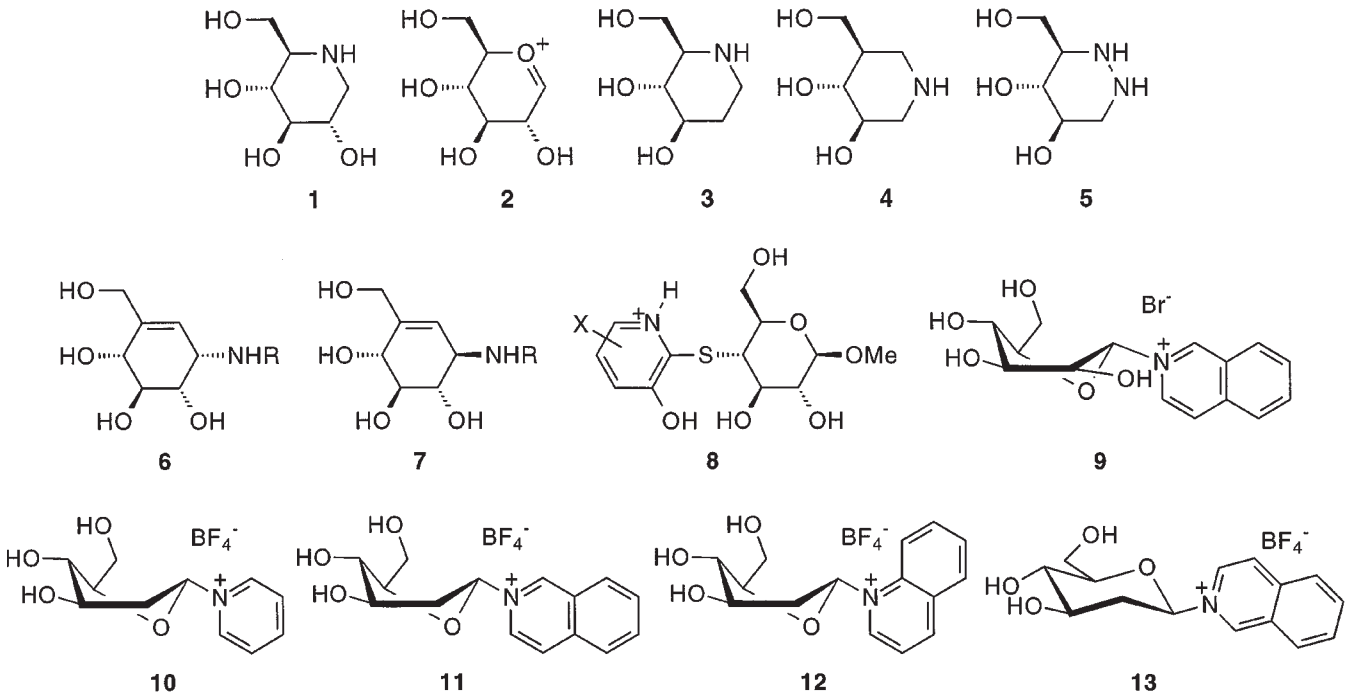
New glycosidase inhibitors isolated from natural sources are often prototypes for the design and synthesis of analogues as potential therapeutic agents. For example,

Received October 15, 1999. Published on the NRC Research Press website on May 8, 2000.

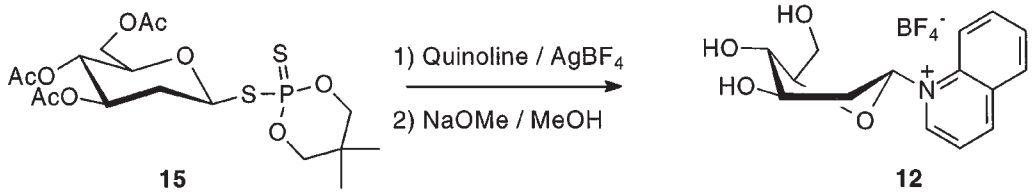
K.S.E. Tanaka,[1] J. Zhu, X. Huang,[2] and A.J. Bennet.[3] Department of Chemistry, Simon Fraser University, Burnaby, British Columbia, V5A 1S6, Canada.
F. Lipari.[4] McGill Cancer Centre, McGill University, 3655 Drummond Street, Montréal, QC H3G 1Y6, Canada.

[1]Current address: Department of Biochemistry, Albert Einstein College of Medicine, 1300 Morris Park Avenue, Bronx, NY 10461, U.S.A.
[2]Current address: Conjuchem, 225 President-Kennedy Avenue, Montréal, QC H2X 3Y8, Canada.
[3]Author to whom correspondence may be addressed. Telephone: (604) 291-3532. Fax: (604) 291-3765. e–mail: bennet@sfu.ca
[4]Current address: Boehringer Ingelheim (Canada) Ltd. BioMéga Research Division, 2100 Cunard Street, Laval, QC H7S 2G5, Canada.

© 2000 NRC Canada



Scheme 1.



isofagomine (**4**) an analogue of the natural product fagomine (**3**) isolated from buckwheat seeds (7) has recently been synthesized and shown to be a potent inhibitor (K_i = 0.11 μM) of the almond-emulsion β-glucosidase (8). Yet another related compound, 1-azafagomine (**5**) is a good inhibitor of both yeast α-glucosidase (K_i = 3.9 μM) and almond-emulsion β-glucosidase (K_i = 0.65 μM) (9).

A separate class of nitrogen-containing natural products is the "amino-sugars" which possess an exocyclic rather than endocyclic amino group (4). One such family of amino-sugar glycosidase inhibitors is the validamycins. which contain the critical valienamine structural motif (**6**). An example of this type of glycosidase inhibitor is the tight binding natural product acarbose (10, 11). Various epimeric analogues of valienamine, i.e., epi-valienamine (**7**) have also been synthesized and tested as potential β-glycosidase inhibitors (12).

Using an alternative strategy, Knapp et al. (13) explored the effectiveness of substituted 3-hydroxypyridines (**8**) rather than the more customary carbohydrate-based compounds as glycosylation TS mimics. The tightest binding of these aromatic compounds (**8**, X = H) was shown to be a weak competitive inhibitor (K_i = 0.8 mM) of *Agrobacterium* β-glucosidase (13).

Natural substrates generally are bound much more weakly to enzymes than the corresponding natural inhibitors (14), and as a result of this, the design of potential reversible glycosidase inhibitors rarely, if ever, exploit the modification of a natural substrate structure. Most glycosidase-catalyzed reactions are, however, monitored using nonnatural substrates that contain an aromatic aglycon leaving group. In 1985, Hosie and Sinnott (15) reported that yeast α-glucosidase efficiently catalyzes the hydrolysis of α-D-glucopyranosyl pyridinium bromides with an apparent binding constant (K_m) for the isoquinolinium substrate (**9**) of 6.6 μM. Thus, this man-made substrate binds to yeast α-glucosidase more tightly than the naturally occurring inhibitor DNJ (**1**) (K_i = 13 μM) (16).

Given that the C-2 hydroxyl-group of glycosides is critical for efficient glycosidase-catalyzed hydrolysis of carbohydrate substrates (17), we decided to test whether 2-deoxyglucopyranosyl pyridinium salts would retain the tight binding interactions exhibited by their 2-hydroxy counterparts, while simultaneously becoming more resistant to enzyme-catalyzed hydrolysis. Accordingly, the 2-deoxy-α- and β-glucopyranosyl pyridinium salts **10**, **11**, **12**, and **13** were synthesized, and their binding affinities and hydrolytic stabilities were evaluated for various glucosidase and mannosidase enzymes.

Results and discussion

The route used for the synthesis of **12** is shown in Scheme 1. This synthetic scheme involves a silver-promoted S_N2 reaction and is similar to the synthetic route employed for the production of both **10** and **11** (18).

Presented in Table 1 are the inhibition constants (K_i) measured for the interaction of **10**, **11**, **12**, and **13** with several

© 2000 NRC Canada

Table 1. Dissociation constants (μM) measured for the binding of 2-deoxyglucopyranosyl pyridinium salts to various glycosidases.[a]

Enzyme and Source	**10**	11	12	13
α-Glucosidase — yeast[b]	107 (8)	2.9 (0.5)	800[c]	—
α-Glucosidase — rice[d,e]	141 (52)	44 (7)	NI[f]	—
β-Glucosidase — almonds[b]	—	—	—	7400 (800)
α-Mannosidase — almonds[b]	31000[g]	8000[h]	—	–
α-Mannosidase — yeast[d]	NI[i]	NI[j]	—	—

[a]Data were analyzed using nonlinear least-squares regression; estimate of standard error in brackets.
[b]Temperature = 25°C.
[c]Determined as a K_m value that was estimated using five concentrations of **12** between 0.112 mM and 2.52 mM, estimated error 25%.
[d]Temperature = 37°C.
[e]Slow onset to maximal binding.
[f]No inhibition detected at 1.1 mM.
[g]Value estimated using two concentrations of **10** (3.5 and 8.4 mM); estimated error 15%.
[h]Value estimated using two concentrations of **11** (1.3 and 2.5 mM); estimated error 40%.
[i]No inhibition detected at 5.0 mM.
[j]No inhibition detected at 1.0 mM.

Table 2. Rate constants (k_{cat} and k_{hyd}) for the glycosidase-catalyzed and the spontaneous hydrolyses of 2-deoxyglucopyranosyl pyridinium salts at 25°C.

	9	11	12
Yeast α-glucosidase (k_{cat}) s^{-1}	0.52[a]	7.1×10^{-3}[b]	5.5[c]
Spontaneous hydrolysis (k_{hyd}) s^{-1}	2.6×10^{-10} [d]	4.58×10^{-8} [e]	3.14×10^{-5} [f]
Rate acceleration (k_{cat}/k_{hyd})	2.0×10^{9}	1.6×10^{5}	1.8×10^{5}

[a]Value taken from ref. 15.
[b]Calculated from relative k_{cat} values measured in comparison to compound **9** (15), estimated error 5%.
[c]Calculated from relative k_{cat} values measured in comparison to compound **9** (15), estimated error 25%.
[d]Extrapolated from a $pK_a(B–H^+)$ value of 5.38 and eq. [3] taken from ref. 22*a*.
[e]Value extrapolated from kinetic data measured between 55–95°C.[5]
[f]Value measured directly at 25°C.[5]

glycosidases. A Lineweaver–Burk plot of the kinetic data for yeast α-glucosidase-catalyzed hydrolysis of 4-nitrophenyl α-D-glucopyranoside in the presence of various concentrations of **11** is illustrated in Fig. 1. When detailed kinetic measurements were possible (K_i < 200 μM), only competitive inhibition of the glycosidases by the test compounds was observed. Consequently, these compounds are binding in a reversible manner to the enzyme active site. Table 2 presents the measured k_{cat} values for yeast α-glucosidase-catalyzed hydrolysis of **9**, **11**, and **12**. Also given in Table 2 are the corresponding spontaneous first-order reaction rates (k_{hyd}).

Hosie and Sinnott (15) proposed that yeast α-glucosidase-catalyzed hydrolysis of glucopyranosyl pyridinium salts occurs via the mechanism depicted in Scheme 2, a process in which glucosylation (k_{gluc}) is rate-limiting for k_{cat}, and a kinetically significant nonchemical step (k_2) is rate-limiting for k_{cat}/K_m.

The same scheme must hold for the reactions of the 2-deoxy salts, since: (*i*) k_{cat} for **12** is about 800–fold greater than k_{cat} for **11** (Table 2), thus k_{degluc} cannot be rate limiting (i.e., $k_{degluc} > k_{gluc}$); and (*ii*) k_{cat}/K_m for **11** and **12** are within a factor of three of each other and consequently, $_{kgluc}$ is not the major rate limiting step for k_{cat}/K_m. The apparent K_m for an enzyme-catalyzed reaction is given by eq. [1], where Σ[ES] is the sum of all enzyme bound species (14). Thus, the only two enzyme-bound species which contribute to the apparent K_m or K_i values are ES and ES′ (Scheme 2).

$$[1] \qquad K_m = \frac{[E][S]}{\sum[ES]}$$

Notably, the apparent dissociation constants measured for binding of **11** (K_i = 2.9 μM) and its 2-OH analogue [K_m = 6.6 μM (15); K_m = 7.7 μM (19)] to yeast α-glucosidase indicate that removal of the 2-hydroxyl moderately enhances the free energy for association by about 2 kJ mol^{-1} at 25°C.

The orientation of the aromatic ring is a critical variable for binding affinity of these compounds to the yeast enzyme. Specifically, fusion of a second aromatic ring onto the pyridinium compound (**10**) gives **11** and **12**, and this change causes either an increase of 8.9 kJ mol^{-1} (**11**) or a decrease of 5.0 kJ mol^{-1} (**12**) in the free energy of binding to the enzyme. An identical trend in K_i values (**11** < **10** < **12**) is also apparent for inhibition of the rice α-glucosidase, despite the attenuated potency of these compounds with this enzyme (Table 1).

It is presumed that the origin of the tight binding between the yeast enzyme and **11** results from strong hydrophobic interactions between the active-site and the isoquinoline ring. Lemieux (20) has stressed the important contribution to binding free energy that occurs as ordered water molecules

[5]J. Zhu and A.J. Bennet. Unpublished data.

© 2000 NRC Canada

Scheme 2.

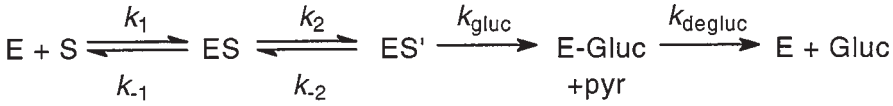
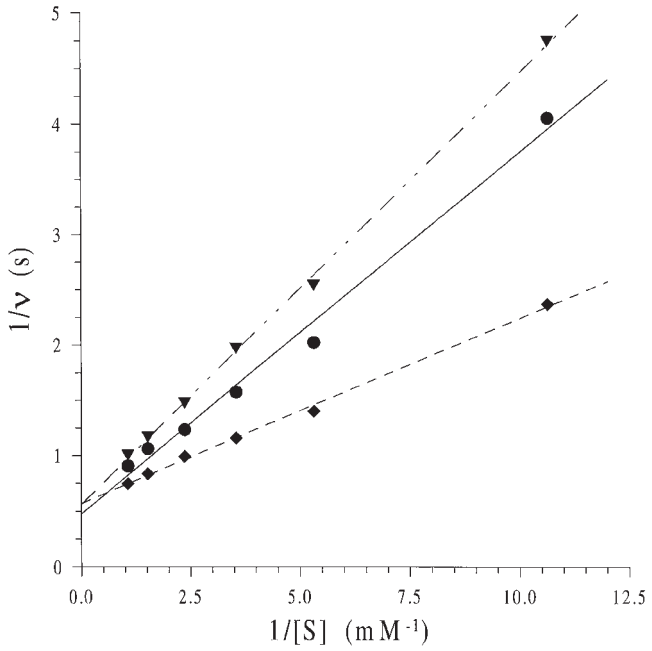


Fig. 1. Lineweaver–Burk plot for the inhibition of yeast α-glucosidase-catalyzed hydrolysis of 4-nitrophenyl α-D-glucopyranoside (**S**) by 2-deoxy-α-D-glucopyranosyl isoquinolinium tetrafluoroborate; symbols represent different concentrations of **11**: ◆ 1.57 μM, ● 3.77 μM, and ▼ 6.91 μM. Kinetic data measured at concentrations of **11** of 0.00 and 0.63 μM have been omitted for clarity.



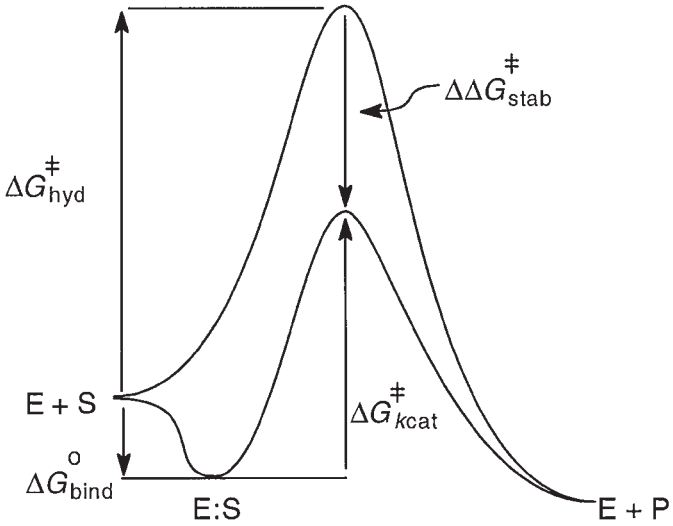
surrounding nonpolar surfaces in solution are liberated into bulk solution when a hydrophobic moiety binds to a biological receptor. Carbohydrate–protein interactions of this nature have been discussed by Wong (21) in terms of providing a favourable entropic contribution towards the free energy for binding of hydrophobic groups.

Another potential source of the tight binding of these compounds may be that their ground state conformations are $^1S_3$ skew-boats rather than the usual $^4C_1$ chair (18, 22), and thus, if these α-glucosidase enzymes bind substrates in non-chair conformations, it is to be expected that conformationally biased compounds such as **9**, **10**, and **11** will display lower binding constants (K_ms) than the natural substrates.

The β-epimer of **11**, 2-deoxy-β-D-glucopyranosyl isoquinolinium bromide (**13**), is a mediocre inhibitor of almond-emulsion β-glucosidase (K_i = 7.4 mM). Therefore, it is clear that the attachment of an extended aromatic ring onto the anomeric carbon of a carbohydrate analogue will not guarantee an increase in binding affinity of glucosidase inhibitors.

Both mannosidases investigated, namely the retaining enzyme from almond and the inverting enzyme from yeast, showed either weak or no affinity for the 2-deoxyglucopyranosyl pyridinium salts, suggesting that the 2-OH group is important for binding to α-mannosidases. However, since kinetic studies using the parent α-mannopyranosyl pyridinium

Scheme 3.



salts have not been reported, no definite conclusions concerning the mannosidase enzymes can be made at this time.

The yeast α-glucosidase hydrolysis of compound **11** is roughly 73 times less than for the glucosyl salt **9** (Table 2), a rate difference that corresponds to a $\Delta\Delta G^{\ddagger}_{kcat}$ (Scheme 3) of around 10.6 kJ mol^{-1}. A similar $\Delta\Delta G^{\ddagger}_{kcat}$ of 9.7 kJ mol^{-1} is observed for barley α-glucosidase-catalyzed hydrolysis of maltose (23). This similarity is not too surprising given that both enzymes are members of glycosidase family 31 (24). For members of other glycosidase families, the removal of a 2-OH group from the substrate can lead to larger differences in $\Delta\Delta G^{\ddagger}_{kcat}$. For example, the β-glucosidase from *Agrobacterium* gives a value for $\Delta\Delta G^{\ddagger}_{kcat}$ of 22 kJ mol^{-1} for the hydrolysis of 4-nitrophenyl β-D-glucopyranoside when compared to its 2-deoxy derivative (25).

At the present time, a more detailed analysis of the magnitude of $\Delta\Delta G^{\ddagger}_{kcat}$ is unwarranted since X-ray crystallographic 3-D structure analysis has not been reported for any member of the α-glucosidase family 31.

The spontaneous hydrolysis of **11** occurs approximately 176-fold more rapidly than that of the corresponding glucoside (Table 2) (18, 22*a*). From this, it can be concluded that removal of the 2-OH group reduces $\Delta\Delta G^{\ddagger}_{stab}$ by approximately 23.5 kJ mol^{-1} (i.e., 176 × 79–fold) for the yeast enzyme-catalyzed process. Furthermore, yeast α-glucosidase accelerates the hydrolysis of both **11** and **12** (the best and worst inhibitors, respectively) by similar amounts (Table 2). Therefore, the differential hydrophobic interactions that occur in the enzyme-substrate complexes for **11** and **12** are maintained at their respective α-glucosidase-catalyzed hydrolysis TSs, and the free energy differences associated with the measured k_{cat}/k_{hyd} rate accelerations ($\Delta G^{\ddagger}_{kcat} - \Delta G^{\ddagger}_{hyd}$, Scheme 3) are indistinguishable. In other words, the nonspe-

© 2000 NRC Canada

cific, hydrophobic interactions of the quinoline (and isoquinoline) moiety with the yeast enzyme's active site are of a similar magnitude in both the enzyme–substrate complex and the rate limiting glucosidation transition state, and as a consequence, the observed rate acceleration must be caused by an increase in binding of the 2-deoxyglucose unit to the glucosidase-catalyzed transition state relative to the E–S complex.

Materials and methods

All reagents and procedures used for the measurement of enzymatic binding constants with compounds **10**, **11**, and **13** were identical to those described previously (26, 27). Quinoline was purchased from Aldrich and purified by recrystallization of its hydrogen sulfate salt from HOAc–Et_2O, followed by neutralization and fractional distillation at atmospheric pressure.

All new compounds were fully characterized using NMR spectroscopy. All observed resonances in the NMR spectra were fully assigned using ^{1}H–homonuclear (28) and ^{1}H–^{13}C-heteronuclear (29) chemical shift correlated NMR spectroscopy techniques. All coupling constants (J) are listed in hertz (Hz). Synthesis of the substrate α-D-glucopyranosyl 4′-bromoisoquinolinium bromide (19) and the 2-deoxy compounds **10** (18), **11** (18), and **13** (30) were accomplished according to published procedures.

3,4,6-Tri-*O*-acetyl-2-deoxy-α-D-*arabino*-hexopyranosyl quinolinium tetrafluoroborate (14)

Silver tetrafluoroborate (0.63 g, 3.1 mmol) was added to a solution of the 2-thiono-1,3-dioxa-2-phosphorinane **15** (18) (1.50 g, 3.1 mmol) in quinoline (2 mL) and dichloromethane (1.5 mL). After the solution had stirred at rt for 2 h, the silver salts were precipitated by the addition of methanol (250 mL). Following filtration, the solvent was removed under reduced pressure. The resulting residue was dissolved in a minimum volume of methanol and subsequent addition of diethyl ether (500 mL) resulted in precipitation of the product. This procedure was repeated and the final colourless powder was crystallized from methanol–ether to give **14** (0.83 g, 53%), mp 111–113°C. ^{1}H NMR (400 MHz, D_2O) δ: 2.00, 2.17, 2.26 (s, 9 H, 3 × CH_3), 2.86 (ddd, 1 H, $J_{2a,1}$ = 4.2, $J_{2a,2e}$ = 15.4, $J_{2a,3}$ = 7.3, H-2a), 3.02 (ddd, 1 H, $J_{2e,1}$ = 6.2, $J_{2e,3}$ = 4.2, H-2e), 4.23 (dd, 1 H, $J_{6a,5}$ = 3.0, $J_{6a,6b}$ = 12.6, H-6a), 4.29 (ddd, 1 H, $J_{5,4}$ = 6.5, $J_{5,6b}$ = 6.7, H-5), 4.66 (dd, 1 H, H-6b), 5.21 (t, 1 H, $J_{4,3}$ + $J_{4,5}$ = 12.4, H-4), 5.53 (ddd, 1 H, $J_{3,4}$ = 5.6, H-3). 7.28 (dd, 1 H, H-1), 8.07 (ddd, 1 H, $J_{5',6'}$ = 7.9, $J_{6',7'}$ = 7.0, $J_{6',8'}$ = 0.7, ArH-6′), 8.19 (dd, 1 H, $J_{3',2'}$ = 6.2, $J_{3',4'}$ = 8.2, ArH-3′), 8.30 (ddd, 1 H, $J_{5',7'}$ = 1.4, $J_{7',8'}$ = 8.7, ArH-7′), 8.43 (dd, 1 H, $J_{2',4'}$ = 1.4, ArH-4′), 8.50 (brd, 1 H, ArH-5′), 9.26 (brd, 1 H, ArH-8′), 9.52 (dd, 1 H, ArH-2′). Anal. calcd. for $C_{21}H_{24}BF_4NO_7$: C 51.52, H 4.94, N 2.86; found: C 51.50, H 4.87, N 2.72.

2-Deoxy-α-D-*arabino*-hexopyranosyl quinolinium tetrafluoroborate (12)

A solution of sodium methoxide (4 equiv) in methanol (10 mL) was added in one portion, with stirring, to an ice-cold solution of **14** (0.12 g, 2.5 mmol) in methanol (15 mL) that was maintained under an inert atmosphere. After stirring for 15 min, the resulting solution was neutralized by the addition of I-120 Amberlite resin (H^+-form) (2.5 g). After an additional 3 min, a solution of HBF_4 in ether (35% w/v, 1 mL) was added and the resultant acidic solution was filtered directly into cold anhydrous ether (–78°C, 250 mL). The ensuing cloudy solution was kept in a freezer (–16°C) for 24 h. After decanting the solvent, addition of acetonitrile (5 mL) to the solid residue gave a clear solution. Subsequent addition of anhydrous ether (250 mL) gave a cloudy solution and this suspension was placed into a freezer (–16°C). After 48 h, the resultant colourless, hygroscopic solid was filtered and dried to give an analytically pure sample of **12** (0.65 g, 71%). ^{1}H NMR (400 MHz, D_2O) δ 2.63 (ddd, 1 H, $J_{2a,1}$ = 5.3, $J_{2a,2e}$ = 15.4, $J_{2a,3}$ = 9.9, H-2a), 2.92 (dt, 1 H, $J_{2e,1}$ + $J_{2e,3}$ = 8.3, H-2e), 3.41 (ddd, 1 H, $J_{5,6a}$ = 2.3, $J_{5,6b}$ = 5.7, $J_{5,4}$ = 8.6, H-5), 3.67 (dd, 1 H, $J_{6a,6b}$ = 12.5, H-6a), 3.71 (t, 1 H, $J_{4,3}$ + $J_{4,5}$ = 16.0, H-4), 3.82 (dd, 1 H, H-6b), 4.25 (ddd, 1 H, $J_{3,2e}$ = 4.3, $J_{3,4}$ = 7.6, H-3). 7.16 (brt, 1 H, $J_{2e,1}$ = 4.0, H-1), 7.99 (brt, 1 H, $J_{5',6'}$ + $J_{6',7'}$ = 15.4, ArH-6′), 8.07 (dd, 1 H, $J_{2',3'}$ = 6.2, $J_{3',4'}$ = 8.1, ArH-3′), 8.22 (brt, 1 H, $J_{6',7'}$ + $J_{7',8'}$ = 16.2, ArH-7′), 8.35 (brd, 1 H, $J_{5',6'}$ = 8.2, ArH-5′), 8.55 (brd, $J_{7',8'}$ = 9.2, ArH-8′), 9.16 (brd, 1 H, ArH-4′), 9.43 (brd, 1 H, ArH-2′). Anal. calcd. for $C_{15}H_{18}BF_4NO_4$: C 49.62, H 5.00, N 3.86; found: C 49.46, H 5.19, N 4.09.

Measurement of k_{cat} values

The k_{cat} value for yeast α-glucosidase-catalyzed hydrolysis of **11**, relative to that for **9**, was measured under saturation conditions ([**11**] = 303 μM and [**9**] = 110 μM) in 50 mM phosphate buffer (pH 6.8, 0.1% w/v BSA) at 25°C. The relative rate of formation of isoquinoline from the two substrates was monitored at 337 nm. Yeast α-glucosidase-catalyzed hydrolysis of **12** was monitored (using an identical enzyme concentration to that from the experiments with both **9** and **11**) at 320 nm in 50 mM phosphate buffer (pH 6.8, 0.1% w/v BSA) at 25°C. The kinetic parameters V_{max} and K_m were calculated using a nonlinear least-squares fit of the initial rate vs. concentration data. The relative k_{cat} value for α-glucosidase-catalyzed hydrolysis of **12** was calculated from the observed V_{max} values and the measured Δ(ε) values for **11** and **12** at the respective wavelengths used to monitor their hydrolysis reactions (**11**, Δ(ε) = 2010 at 337 nm; **12**, Δ(ε) = 2770 at 320 nm).

Acknowledgments

The authors are grateful to the Natural Sciences and Engineering Research Council of Canada (NSERC) and the British Columbia Health Research Foundation for financial support. In addition, the authors would like to thank NIH for a grant (GM 31265, to Dr. A. Herscovics) that supports research on the yeast α-mannosidase enzyme. Finally, we would like to thank Dr. T. E. Kitos for editorial assistance with this manuscript.

References

1. R.A. Dwek. Chem. Rev. **96**, 683 (1996).
2. P. Sears and C.-H. Wong. Angew. Chem. Int. Ed. Eng. **38**, 2300 (1999).

© 2000 NRC Canada

3. (*a*) G. Legler. Adv. Carbohydr. Chem. Biochem. **48**, 319 (1990); (*b*) M.L. Sinnott. Chem. Rev. **90**, 1171 (1990); (*c*) J.D. McCarter and S.G. Withers. Curr. Opin. Struct. Biol. **4**, 885 (1994).
4. A.D. McNaught. Adv. Carbohydr. Chem. Biochem. **52**, 43 (1997).
5. (*a*) S. Inouye, T. Tsuruoka, and T. Niida. J. Antibiot. **19**, 288 (1966); (*b*) A.B. Hughes and A.J. Rudge. Nat. Prod. Rep. 135 (1994).
6. D.E. Koshland. Biol. Rev. Cambridge Philos. Soc. **28**, 416 (1953).
7. M. Koyama and S. Sakamura. Agric. Biol. Chem. **38**, 1111 (1974).
8. T.M. Jespersen, W. Dong, M.R. Sierks, T. Skrydstrup, I. Lundt, and M. Bols. Angew. Chem. Int. Ed. Eng. **33**, 1778 (1994).
9. M. Bols, R.G. Hazell, and I.B. Thomsen. Chem. Eur. J. **3**, 940 (1997).
10. (*a*) Y. Kameda and S. Horii. J. Chem. Soc. Chem. Commun. 746 (1972); (*b*) Y. Kameda and S. Horii. J. Chem. Soc. Chem. Commun. 747 (1972).
11. B. Svensson and M.R. Sierks. Carbohydr. Res. **227**, 29 (1992).
12. (*a*) J.C. McAuliffe, R.V. Stick, D.M.G. Tilbrook, and A.G. Watts. Aust. J. Chem. **51**, 91 (1998); (*b*) J.C. McAuliffe and R.V. Stick. Aust. J. Chem. **50**, 193 (1997); (*c*) S. Ogawa, C. Uchida, and Y. Shibata. Carbohydr. Res. **223**, 279 (1992).
13. S. Knapp, Y. Dong, K. Ruptiz, and S.G. Withers. Bioorg. Med. Chem. Lett. **5**, 763 (1995).
14. A. Fersht. Enzyme structure and mechanism. 2nd. ed. W.H. Freeman and Co., New York. 1985.
15. L. Hosie and M.L. Sinnott. Biochem. J. **226**, 437 (1985).
16. G. Hanozet, H.-P. Pircher, P. Vanni, B. Oesch, and G. Semenza. J. Biol. Chem. **256**, 3703 (1981).
17. *(a)* B.W. Sigurskjold, B. Duus, and K. Bock. Acta. Chem. Scand. **45**, 1032 (1991); (*b*) J.D. McCarter, M.J. Adam, and S.G. Withers. Biochem. J. **286**, 721 (1992).
18. J. Zhu and A.J. Bennet. J. Am. Chem. Soc. **120**, 3887 (1998).
19. X. Huang, K.S.E. Tanaka, and A.J. Bennet. J. Am. Chem. Soc. **119**, 11147 (1997).
20. R.U. Lemieux. Acc. Chem. Res. **29**, 373 (1996).
21. C.-H. Wong. Acc. Chem. Res. **32**, 376 (1999).
22. (*a*) L. Hosie, P.J. Marshall, and M.L. Sinnott. J. Chem. Soc. Perkin Trans. 2, 1121 (1984); (*b*) R.U. Lemieux and A.R. Morgan. Can. J. Chem. **43**, 2205 (1965).
23. T.P. Frandsen and B. Svensson. Plant Mol. Biol. **37**, 1 (1998).
24. (*a*) B. Henrissat. Biochem. J. **280**, 309 (1991); (*b*) B. Henrissat. Biochem. J. **293**, 781 (1993); (*c*) B. Henrissat and A. Bairoch. Biochem. J. **316**, 695 (1996).
25. M.N. Namchuk and S.G. Withers. Biochemistry, **34**, 16194 (1995).
26. K.S.E. Tanaka and A.J. Bennet. Can. J. Chem. **76**, 431 (1998).
27. F. Lipari and A. Herscovics. Biochemistry, **38**, 1111 (1999).
28. A.E. Derome and M.P. Williamson. J. Magn. Reson. **88, 177 (1990).**
29. A. Bax and S. Subramanian. J. Magn. Reson. **67**, 565 (1986).
30. X. Huang, C. Surry, T. Hiebert, and A.J. Bennet. J. Am. Chem. Soc. **117**, 10614 (1995).

© 2000 NRC Canada

Superamidines 2. Synthesis of the bulky ligand *N,N′*-bis-(2,6-diisopropylphenyl)-trifluoroacetamidine and its molybdenum carbonyl complex[1]

René T. Boeré, Vicki Klassen, and Gotthelf Wolmershäuser

Abstract: *N,N′*-bis-(2,6-diisopropylphenyl)trifluoroacetamidine has been prepared for the first time from 2,6-diisopropylaniline and the trifluoroacylation reagent TFAP via the imidoylchloride. The crystal structure of the amidine was determined, indicating that it crystallizes in the *Z-anti* tautomer, in contrast to the nonfluorinated analogue, which is *E-anti* in the solid state. In solution, as indicated by NMR spectroscopy, it exists in two isomeric forms. The amidine reacts with $Mo(CO)_6$ to produce a coordination complex with $Mo(CO)_3$ in which the ligand is also in the *Z-anti* geometry, the metal is η^6-coordinated to the imino-2,6-diisopropylphenyl ring, and the amino N-H unit is directed towards the metal, as determined by a single-crystal X-ray structure. Unlike the analogous nonfluorinated acetamidine, there is no indication of an intermediate in which the neutral amidine is coordinated in a monodentate fashion to an $Mo(CO)_5$ unit, which we now attribute to the predominant geometry of the ligand, both in the solid state and in solution, being *Z-anti*. The high steric bulk of this superamidine ligand apparently prevents the formation of a metal–metal bonded $Mo_2(amidinate)_4$ as observed previously in a redox reaction between *N,N′*-diphenylbenzamidine and $Mo(CO)_6$ under similar thermal reaction conditions.

Key words: trifluoromethyl, superamidine, amidine, molybdenum, carbonyl, coordination.

Résumé : On a réalisé la première synthèse de la *N,N′*-bis-(2,6-diisopropylphényl)-trifluoroacétamidine à partir de la 2,6-diisopropylaniline et du réactif de trifluoroacétylation, TFAP, par le biais du chlorure d'imidoyle. On a déterminé la structure cristalline de l'amidine qui indique qu'elle cristallise sous la forme du tautomère *Z-anti*, qui diffère de la situation avec l'analogue non fluoré qui, à l'état solide, existe sous la forme *E-anti*. Sur la base des données de R.M.N., en solution, il existe dans les deux formes isomères. L'amidine réagit avec le $Mo(CO)_6$ pour donner un complexe de coordination avec le $Mo(CO)_3$ dans lequel, selon la structure déterminée par diffraction des rayons X sur un cristal unique, le ligand est aussi dans une géométrie *Z-anti*, le métal forme une η^6-coordination avec le noyau imino-2,6-diisopropylphényle et l'unité N-H de l'amino est orientée vers le métal. Contrairement à ce qui a été observé avec l'acétamidine analogue non fluorée, il ne semble pas exister d'intermédiaire dans lequel l'amidine neutre serait coordinée de façon monodentate avec une unité de $Mo(CO)_5$; on attribue maintenant cette situation à la géométrie prédominante du ligand qui est *Z-anti* tant à l'état solide qu'en solution. Le grand encombrement stérique qui l'on retrouve dans ce ligand superamidine empêche la formation d'un $Mo_2(amidinate)_4$ avec liaison métal-métal comme on l'a observé antérieurement dans une réaction redox entre la *N,N′*-diphénylbenzamidine et le $MO(CO)_6$ dans des conditions de réactions semblables.

Mots clés : trifluorométhyle, superamidine, amidine, molybdène, carbonyle, coordination.

Introduction

Amidines and amidinate anions are useful ligands in the general development of coordination chemistry (1, 2), and their complexes with the Group 13 elements catalyze the polymerization of ethylene (3–5). We have recently reported the preparation of the first *N,N′*-disubstituted amidines containing the 2,6-diisopropylphenyl (Dip) substituent on nitrogen (6). Such "super-bulky" substituents were originally developed to stabilize low-coordinate main-group elements of the third and subsequent periods. It is our contention that the use of super-bulky substituents with conventional nitrogen-based ligands will lead to unique patterns of reactivity. So far, we have demonstrated that it is possible to synthesize

Received June 24, 1999. Published on the NRC Research Press website on May 10, 2000.

This paper is dedicated to Professor Christopher J. Willis on the occasion of his 65th birthday.

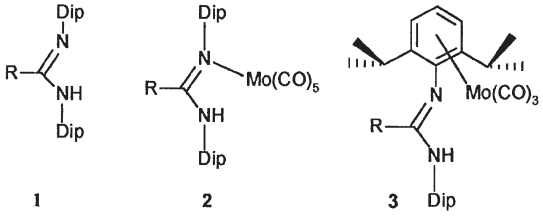
R.T. Boeré[2] and V. Klassen. Department of Chemistry, University of Lethbridge, Lethbridge, AB T1K 3M4, Canada.
G. Wolmershäuser. Fachbereich Chemie der Universität Kaiserslautern, Erwin-Schrödinger-Straße, D-67663 Kaiserslautern, Germany.

[1]Part of this work was presented at the 15th International Symposium on Fluorine Chemistry, UBC, Vancouver, B.C., August 2–7, 1997.

[2]Author to whom correspondence may be addressed. Telephone: (403) 329-2045. Fax: (403) 329-2057. e-mail: boere@uleth.ca

 © 2000 NRC Canada

amidines **1a-c** with Dip groups on nitrogen. The ligands dissolve in typical NMR solvents ($CDCl_3$) as at least two isomeric forms, and so far, three different isomers have been detected in the solid state by X-ray crystallography (6). However, whereas analogous nonbulky amidines such as *N*,*N*′-diphenylbenzamidine produce quadruply bonded dimolybdenum(II) compounds (7) in thermal reactions with $Mo(CO)_6$ in hydrocarbon solvents, under these conditions the superamidines have only provided two different kinds of neutral coordination compounds. Thus superamidine **1a** reacts with molybdenum carbonyl in hot *n*-heptane to produce an N-coordinated $LMo(CO)_5$ complex **2a**, but on further reaction this complex loses two further CO molecules to form the half-sandwich $LMo(CO)_3$ complex **3a**. By contrast, amidines **1b**, **c** form $LMo(CO)_3$ complexes **3b**, **c** with no detectable intermediates in thermal reactions with $Mo(CO)_6$ (6).



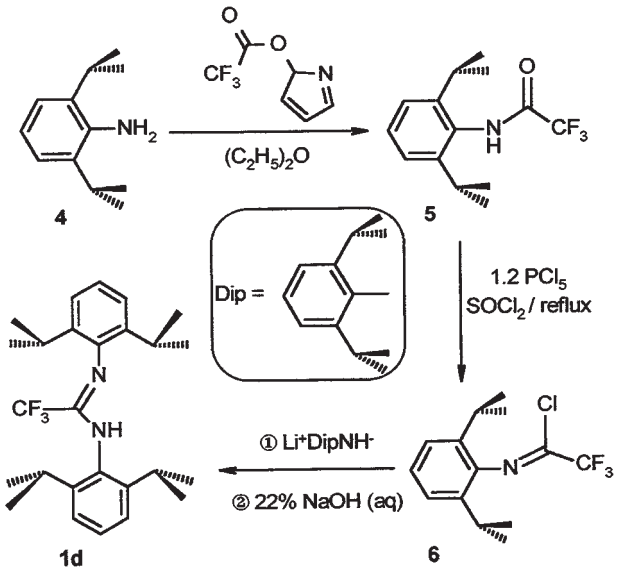
In this work we report results on a further superamidine with Dip groups on N and a trifluoromethyl substituent on the central carbon atom, **1d**. The structure and reactivity of this compound is distinct from that of its unfluorinated analogue **1a**, and more closely resembles that of the aryl derivatives **1b**, **c**, apparently for structural rather than electronic reasons. In thermal reactions of **1d** with $Mo(CO)_6$ the only observed product is the $LMo(CO)_3$ complex **3d**.

Results and discussion

Ligand synthesis

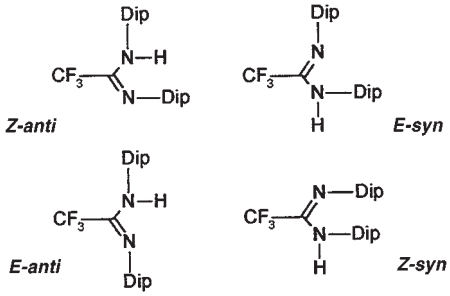
Our synthesis follows the basic methodology outlined by Maringgele and Meller (8) for the synthesis of several *N*,*N*′-diaryl-*N*′-trimethylsilyltrifluoroacetamidines (i.e., with the remaining hydrogen on N being replaced with an $Si(CH_3)_3$ group). Each step of the procedure required extensive optimization, and in particular, differed significantly from that of the nonfluorinated analogues **1a-c**. The synthetic route is outlined in Scheme 1, and the particulars of each step are detailed in the Experimental section. Commercially available 2,6-diisopropylaniline, **4**, was converted to the corresponding amide of trifluoroacetic acid, **5**, using the trifluoroacylation reagent 2-(trifluoroacetoxy)pyridine (TFAP) (9). Dehydration and chlorination using 1.2 equiv of PCl_5 in refluxing $SOCl_2$ produced the imidoylchloride, **6**, which was isolated and purified by vacuum distillation in 63% yield. Maringgele and Meller (10) obtained a variety of *N*-aryltrifluoromethylimidoyl chlorides as byproducts in only 10–20% yield from reactions of amides with BCl_3. The ^{19}F NMR chemical shifts of these imidoyl chlorides are found at $\delta = -71.0$ to -72.0 ppm, in excellent agreement with the –71.48 ppm we find in the NMR spectrum of **6**.

Scheme 1.



The imidoylchloride does not react directly with a second equiv of **4** as the nonfluorinated analogues do (6). Instead, the lithium anilide was produced, and this reacted with the imidoyl chloride to produce the desired amidine directly. However we have found that to purify this raw product conversion first to the hydrochloride, followed by reforming the free amidine, **1d**, using 23% sodium hydroxide solution was required. All of these compounds are new, and have been fully characterized by elemental analysis, mass spectroscopy as well as ^1H and ^{13}C NMR spectroscopy. The details are given in the Experimental section.

Scheme 2.



Isomers and tautomers

In $CDCl_3$ solution, **1d** exists in two isomeric forms as shown by ^1H, ^{13}C, and ^{19}F NMR spectroscopy. Previously reported trifluoroacetamidines with a variety of nonbulky aryl groups also show isomerism in solution (8). For example, an amidine with a 2,6-dimethylphenyl group on one nitrogen and a phenyl group on the other displays two singlets at $\delta = -61.9$ and -60.4 ppm in the ^{19}F NMR spectrum (8). Similarly in **1d** there are two closely spaced singlets at $\delta = -67.24$ and -66.84 ppm. The difference in absolute shift is attributable to protonation vs. silylation at the amino nitrogen.

We have previously shown that superamidines can exist in a variety of isomeric and tautomeric forms (6). The four possible isomers of the trifluoromethyl derivative are shown in Scheme 2, using the nomenclature devised by Perrin (11)

© 2000 NRC Canada

Fig. 1. PLUTO diagram of **1d**, showing the atom numbering scheme. The ligand is in the *Z-anti* conformation. The rotationally disordered CF_3 group has been modeled by two trigonal F_3 units with occupancy of 0.85, F(1)-F(3), and 0.15, F(4)-F(6).

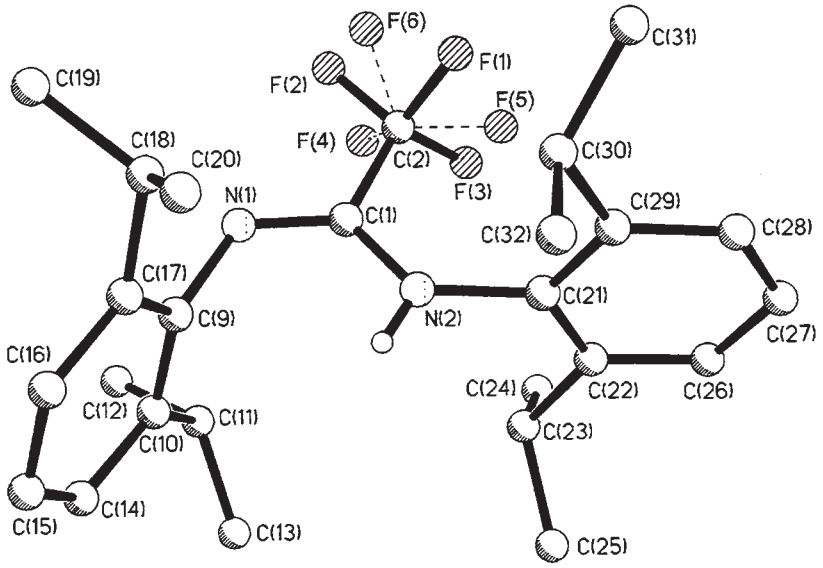


Table 1. Crystal data and structure refinement.[a]

Compound	**1d**	**3d**
Formula	$C_{26}H_{35}F_3N_2$	$C_{29}H_{35}F_3MoN_2O_3$
FW	432.56	612.53
T (K)	293(2)	293(2)
Crystal system	Monoclinic	Monoclinic
Space group	C2/*c*	$P2_1/n$
a (Å)	17.4663(17)	12.0559(11)
b (Å)	14.6527(12)	16.5327(10)
c (Å)	20.7594(15)	15.3228(14)
β (°)	106.654(10)	95.270(11)
V (Å^3)	5090.1(7)	3041.2(4)
Z	8	4
D_c (mg/m^3)	1.129	1.338
Crystal	colourless block	yellow plate
Size (mm)	0.40 × 0.34 × 0.30	0.60 × 0.26 × 0.08
Rfl. Collected (R_{int})	21505 (0.0403)	26067 (0.0338)
Data / restraints / parameters	3871 / 30 / 301	4787 / 0 / 364
Final *R* [$I > 2\sigma(I)$]	*R*1 = 0.0421, *wR*2 = 0.0943	*R*1 = 0.0287, *wR*2 = 0.0653
Gof (all data)	0.992	0.946

[a]Weighting schemes used: **1d**, $w = 1/[\sigma^2(Fo^2) + (0.0500P)^2]$; **3d**, $w = 1/[\sigma^2(Fo^2) + (0.0420P)^2]$ where $P = (Fo^2 + 2Fc^2)/3$.

based on the Cahn–Ingold–Prelog sequence rules. The lowest-energy isomer of **1d**, as minimized in an AM1 calculation, is the *Z-anti* form. Relative to this, the tautomeric *E-syn* isomer lies only 1.2 kJ mol^{-1} higher in energy, while the *Z-syn* isomer lies 11.0, and the *E-anti* 26.7 kJ mol^{-1} higher in energy. Calculations on **1a**, however, indicate that the *E-anti* isomer for the methyl ligand **1a** lies only 15.5 kJ mol^{-1} higher than *Z-anti*. These calculations do not factor in the energy of hydrogen bonding, which apparently can stabilize the *E-anti* form as seen in the solid state for the methyl analogue **1a**. The typical energy of a single H-bond is ~20 kJ mol^{-1} (12). We have determined the single-crystal X-ray structure of **1d** (see Fig. 1), which indicates that it crystallizes preferentially as the *Z-anti* isomer. There are no short intermolecular contacts in the crystal. Apparently the steric bulk of a trifluoromethyl group is sufficiently large to cancel out the energetic advantage for the formation of an H-bonded dimer, which is possible only in the *E-anti* conformation. Important bond distances and angles are listed in Table 1.

Häfelinger and Kuske (13) have defined the parameter $\Delta_{CN} = d(C—N) - d(C=N)$ for the central N—C—N linkage found in all amidines, using crystallographic structural data. This parameter ranges from 0 in the structure of **1a**, to 0.178 Å in 2,6-*cis*-dimethylpiperidyl-*N*-phenyl-2,2-dimethylpropionamidine, an amidine where conjugation is minimized due to bulky substituents on nitrogen and carbon (d(C—N) = 1.441(5); d(C=N) = 1.263(5) Å), and which crystallizes in

© 2000 NRC Canada

Table 2. Selected interatomic distances and angles.

Distances (Å)		Angles (°)	
1d			
N(1)—C(1)	1.270(2)	C(1)-N(1)-C(9)	119.49(15)
N(2)—C(1)	1.364(2)	C(1)-N(2)-C(21)	128.55(15)
Δ_{CN}[a]	0.094	N(1)-C(1)-N(2)	126.85(16)
N(1)—C(9)	1.426(2)	N(1)-C(1)-C(2)	115.45(17)
N(2)—C(21)	1.444(2)	N(2)-C(1)-C(2)	117.68(18)
C(1)—C(2)	1.509(3)		
N(2)—H(2)	0.92(2)		
3d			
N(1)—C(1)	1.270(3)	N(1)-C(1)-N(2)	128.1(2)
N(2)—C(1)	1.343(3)	N(1)-C(1)-C(2)	113.5(2)
Δ_{CN}[a]	0.073	N(2)-C(1)-C(2)	118.4(2)
C(1)—C(2)	1.527(3)	C(1)-N(1)-C(9)	126.6(2)
N(1)—C(9)	1.402(3)	C(1)-N(2)-C(21)	128.3(2)
N(2)—C(21)	1.454(3)	C(33)-Mo(1)-C(34)	83.63(13)
N(2)—H(2)	0.88(3)	C(33)-Mo(1)-C(35)	82.96(14)
Mo(1)—C(33)	1.940(3)	C(34)-Mo(1)-C(35)	85.77(16)
Mo(1)—C(34)	1.912(4)	Mo(1)-H(1)-N(1)	
Mo(1)—C(35)	1.947(4)		
Mo(1)—H(2)	3.14(3)		

[a] $\Delta_{CN} = d(\text{C-N}) - d(\text{C=N})$.

the rarely observed *Z-syn* form (14). In the crystal structure of **1d**, $\Delta_{CN} = 0.094$, the largest we have yet observed for a superamidine structure. The metric parameters of **1d** otherwise closely parallel those of **1c**, the only other superamidine so far which crystallizes exclusively in the *Z-anti* form, for which $\Delta_{CN} = 0.057$ (6). The C—N single bonds in **1c** and **1d** are identical within experimental error at 1.364 Å. Thus the origin of the larger Δ_{CN} value in **1d** is the *shorter* C=N double bond, which at 1.270(2) is almost 0.04 Å shorter in the fluorinated amidine. However, these values are not unprecedented. In the structure of *N′-p*-bromophenyl-*N*-(*p*-tolyl)acetamidine, which crystallizes in the *E-anti* isomer, *d*(C–N) = 1.366(8) and *d*(C=N) = 1.273(8) Å, leading to a $\Delta_{CN} = 0.093$ (15).

Reaction with $Mo(CO)_6$

Amidine **1d** was heated with $Mo(CO)_6$ in refluxing *n*-heptane under an atmosphere of N_2. The course of the reaction was easily monitored by solution infrared spectroscopy and we observed that **1d** reacted slowly, with no observable evidence by solution IR spectroscopy of any intermediate, to the final product, a bright yellow crystalline solid, which was produced in 25% yield. The structure of the compound was indicated by ^{1}H NMR and IR spectroscopy to be a half-sandwich "piano-stool" complex of $Mo(CO)_3$, in which the metal is coordinated to one of the electron-rich aromatic rings of the ligand rather than through nitrogen. In the ^{1}H NMR spectrum, the signals due to the aromatic hydrogen atoms of one of the diisopropylphenyl groups are shifted 1.45–1.49 ppm upfield, while the other signals remain at the same chemical shift. In the free ligand, the *meta* and *para* hydrogen resonances are not distinguishable, but in the complex, the upfield-shifted signals show a resolved pseudo-triplet for the *para* and a resolved pseudo-doublet for the *meta* hydrogen atoms, in the expected 1:2 intensity ratio. The magnitude of these shifts are typical of those observed for η^6-arenes coordinated to an $Mo(CO)_3$ unit. The solution IR spectrum (Table 3) showed three bands in the carbonyl-stretching region, a very strong singlet at about 1966 cm^{-1}, and a slightly less intense doublet centred at about 1885 cm^{-1}. This is the pattern expected for a *fac*-octahedral tricarbonyl metal complex with highly asymmetric coligands (16).

Table 3. Solution IR data.[a]

Compound	ν(N-H) (cm^{-1})	ν(N-C-N) (cm^{-1})	ν(C≡O) (cm^{-1})
1d	3453, 3356	1657	—
3d		1665	1971, 1906, 1883

[a] *n*-Heptane solution in 0.2 mm NaCl solution cell.

The single-crystal X-ray structure of **3d** is presented in Fig. 2. The same "baseball catcher's mitt," structure is observed as previously obtained for the methyl **3a** and tolyl **3b** structures, in which the amidine ligand, itself in the *Z-anti* tautomer, has "caught" the $Mo(CO)_3$ fragment with the inside face of the imino-bearing ring. With respect to the C(1)=N(1) double bond, the metal complex also has *Z* symmetry. The N-H of the amino group corresponds to the "catcher's thumb," and there is a close contact of 3.14(3) Å between H(1) and Mo, less than a reasonable guess at the sum of their van der Waals' radii (the van der Waals radius for molybdenum is not contained in standard compilations; we have used values of neighbouring elements to provide this estimate). The similarity in structures of **3d**, **3a**, and **3b** is striking. The amidine unit in **3d** is bent further away from the molybdenum atom than in **3a**. This is evidenced by a 5° larger N(1)-C(1)-N(2) angle, and a 3° smaller N(1)-C(1)-C(2) angle. Other metric parameters between the two structures are extremely similar.

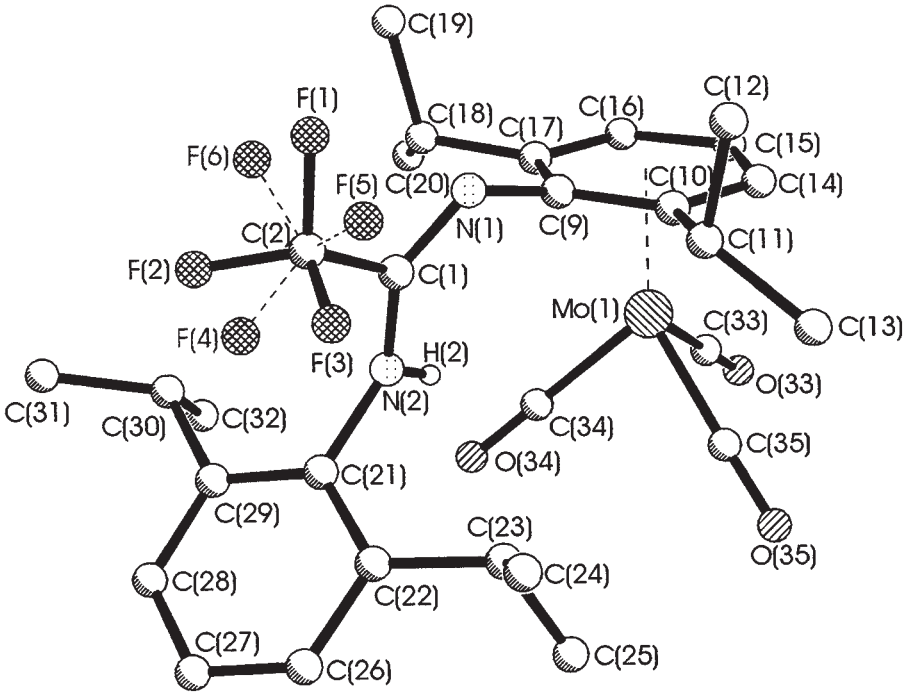
Progress of reaction with $Mo(CO)_6$

The thermal reactions with $Mo(CO)_6$ of all the superamidines that we have studied do not go on to the formation of bridged multiply bonded dimolybdenum species (6, 7). This is undoubtedly due to the high steric bulk of the Dip groups. The question that remains, however, is why **1d** reacts more like the aryl amidines **1b** and **1c**, in going directly to an η^3-$Mo(CO)_3$ complex, than the methyl amidine **1a**, which first forms an N-bonded $Mo(CO)_5$ complex, and only on further heating produces the η^3-$Mo(CO)_3$ complex?

We believe that this difference in reactivity can be traced to the structural forms of the free ligand in the solid state and in solution. Only **1a** crystallizes in the *E-anti* form as an H-bonded dimer, unlike **1b**, **1c**, and **1d**. Furthermore, **1a** is much less soluble in *n*-heptane than the others, undoubtedly due to the dimer structure. Thus visual inspection of the thermal reaction of **1a** with $Mo(CO)_6$ clearly shows that undissolved ligand is present during much of the course of the reaction. This is different from what is observed for the other three superamidines, which dissolve readily as the temperature of the solvent is increased. We hypothesize that if the three more soluble amidines dissolve in the *Z-anti* geometry they have in the solid, reaction of ligand in this configuration promotes conversion to the η^6-$Mo(CO)_3$ complex. On the other hand, if the hexacarbonyl reacts with a

© 2000 NRC Canada

Fig. 2. PLUTO diagram of **3d**, showing the atom numbering schemes. The ligand is also in the *Z-anti* conformation, with the Mo atom coordinated to the inside of the aryl ring attached to the imino nitrogen atom. The rotationally disordered CF_3 group has been modeled by two trigonal F_3 units with occupancy of 0.87, F(1)-F(3), and 0.13, F(4)-F(6).



hydrogen-bonded dimer in the *E-anti* geometry before this can isomerize to the *Z-anti* form, it forms a metal complex in which this geometry is preserved. We have previously shown that conversion of the η^1-$Mo(CO)_5$ complex to the η^6-$Mo(CO)_3$ complex is accompanied by *E* to *Z* ligand isomerism (6).

Is there any evidence that the amidines exist in solution in the *Z-anti* form? Consider the combined NMR spectroscopic parameters presented in Table 4 for all the species we have so far prepared. The proton (and ^{19}F, where applicable) NMR parameters of the *dominant* species in $CDCl_3$ solution for the free amidines in each case are strikingly similar to those of the metal tricarbonyl derivatives. If, as seems likely, the latter dissolve in the *Z-anti* geometry found in the solid state, the correspondence of the NMR spectoscopic parameters supports this isomer as the predominant form of the free ligand in $CDCl_3$ as well. Furthermore, this is also the lowest energy form in the gas phase as indicated by MO calculations.

The differences that do exist between the NMR spectroscopic parameters of free ligand and complex are readily attributed to variations in ring shielding effects. Thus the ^1H signal of the amino NH atom is further upfield in the ligand, where in the *Z-anti* form it experiences ring current shielding from the Dip group on the imino nitrogen. Similarly, one CH_3 group is significantly further upfield than the rest. Assuming that the Dip group on the amino nitrogen rocks back and forth on the C—N bond, one set of methyl groups would also experience ring current shielding from the ring attached to the imino nitrogen. In the $Mo(CO)_3$ complexes, both types of anomalously shielded protons revert to more normal chemical shifts. This is consistent with the metal carbonyl unit blocking the aromatic ring that is responsible for the shielding effect.

Experimental section

General

2,6-diisopropylaniline, 2-hydroxypyridine, trifluoroacetic anhydride, thionyl chloride, phosphorus pentachloride, *n*-butyl lithium (Aldrich), and molybdenum carbonyl (Strem) were commercial products, and used as received, except that the aniline was vacuum distilled and stored under nitrogen before use. Solvents were reagent grade, and distilled from sodium wire (toluene, THF), P_2O_5 (CH_2Cl_2), or $LiAlH_4$ (*n*-heptane). 2-(Trifluoroacetoxy)pyridine (TFAP) was prepared from 2-hydroxypyridine and trifluoroacetic anhydride by the literature method (9). Reactions involving metal carbonyl and organolithium reagents were performed under an atmosphere of purified N_2 using a dry-box, Schlenk ware, and vacuum-line techniques; all other procedures were performed in vessels open to the atmosphere but protected by $CaCl_2$ drying tubes. Infrared spectra were recorded on a BOMEM MB102 Fourier transform spectrometer, and are KBr pellets unless otherwise specified. NMR spectra were acquired at 250.13 (^1H) and 62.90 (^{13}C) MHz on a Bruker AC250-F spectrometer referenced to TMS, and on a Bruker AMX300 at 282.41 (^{19}F) MHz referenced to external C_6F_6 in C_6D_6 at –163.00 ppm on the $CFCl_3$ scale, and are in $CDCl_3$ unless otherwise specified. Mass spectra were recorded by the Mass Spectrometry Center, University of Alberta, Canada and in the Fachbereich Chemie, Universität Kaiserslautern. Elemental analyses were performed by MHW

© 2000 NRC Canada

Table 4. ^{1}H and ^{19}F NMR chemical shifts.

Compound	NH	Aromatic	X	^{i}Pr CH[a]	^{i}PrCH[a]	^{i}Pr CH_3[b]	^{i}Pr CH_3[b]	^{i}Pr CH_3[b]	^{i}Pr CH_3[b]
1a major[c,d]	5.40	7.29–7.04m	1.88[f]	3.23	3.21	1.32	1.26	1.19	1.04
1a minor[c,d]	5.51	buried	1.84[f]	3.31 br	2.95 br	buried between 1.35 and 1.15			
1b major[c]	5.67	7.29–6.97 m	2.27[g]	3.24	3.16	1.34	1.23	0.98	0.88
1b minor[c]	6.88	buried	buried	3.45 br	3.00 br	buried 1.4–1.2		buried 1.0–0.8[j]	
1c major[c]	5.66	7.35–6.70 m	3.74[h]	3.23	3.16	1.34	1.23	0.99	0.90
1c minor[c]	6.89	buried	buried	3.37 br	2.93 br	buried 1.1–1.3		buried	0.8
1d major[e]	5.50	7.34–7.06 m	–67.24[i]	3.18	3.03	1.34	1.27	1.20	1.00
1d minor[e]	6.05	buried	–66.84[i]	3.25 br	2.82 br	buried between 1.4–1.2			
2a[c]	7.37	7.4–7.16 m	1.42[f]	3.16	3.15	1.42	1.30	1.27	1.11
3a[c]	7.98	7.35–7.17 m, 5.82 tr, 5.60 d	1.79[f]	3.19	2.81	1.29	1.25	1.24	1.22
3b[c]	8.20	7.29–6.96 m, 5.79–5.66 m	2.27[g]	3.17	2.85	1.28	1.27	1.20	0.86
3c[c]	8.18	7.29–7.06 m, 6.69 d, 5.79–5.66 m	3.74[h]	3.17	2.84	1.28	1.27	1.20	0.88
3d[e]	8.07	7.37–7.17 m, 5.89 t, 5.57 d	–67.54[i]	3.14	2.72	1.28	1.27	1.26	1.22

[a]Heptet with J ≅ 7 Hz.
[b]Doublet with J ≅ 7 Hz.
[c]Ref. (6).
[d]There is evidence for a third species as well, with a single sharp ^{i}Pr CH signal, which could be the H-bonded dimer in solution.
[e]This work.
[f]δCH_3 group on amidine backbone.
[g]δCH_3 group on 4-position of phenyl ring.
[h]δCH_3O group on 4-position of phenyl ring.
[i]δCF_3 group, ^{19}F NMR.
[j]Upfield doublet is evident centred on 0.80 ppm.

Laboratories, Phoenix, AZ, U.S.A. and by the analytical services of the Fachbereich Chemie, Universität Kaiserslautern.

Preparation of $CF_3C\{O\}NH(2,6\text{-}^iPrC_6H_3)$, 5

2,6-Diisopropylaniline (90.9 g, 513 mmol) in 250 mL of dry diethyl ether was added drop wise to TFAP (98.0 g, 513 mmol) in 300 mL of the same solvent, with cooling to maintain 23°C. After stirring 20 h, the solvent was removed, and the residues extracted with 1.6 L of dH_2O by vigorous stirring for 2 h, filtering and drying to give 128.6 g of pure **5** (471 mmol, 92% yield), mp 158–159°C. An analytical sample was obtained by recrystallizing from ethanol. IR: ν(N-H) 3254, ν(C=O) 1709 cm^{-1}. ^{1}H NMR: 7.54 (s, 1 H, conc. depend.), 7.40–7.20 (m, 3 H), 2.95 (hept, 6.9 Hz, 2 H), 1.19 (d, 6.9 Hz, 12 H. ^{13}C NMR: 157.11 (quart, 37 Hz), 146.17, 129.63, 128.10, 123.98, 116.34 (quart, 289 Hz), 28.83, 23.58. ^{19}F NMR: –75.47 (s, CF_3). Mass spec: 272.8 (M^+, 34%), 258 (M–CH_3^+, 12%), 204 (M–CF_3^+, 100%). Anal. calcd. for $C_{14}H_{18}F_3NO$: C 61.5, H 6.6, N 5.1%; found: C 61.5, H 6.7, N 5.2%.

Preparation of $4\text{-}CF_3C\{Cl\}N(2,6\text{-}^iPr_2C_6H_3)$, 6

5 (20.0 g, 73.2 mmol) was refluxed in 15 mL of $SOCl_2$ (excess) for 0.5 h (oil bath at 80–90°C), after which one equiv of PCl_5 (15.2 g, 73.2 mmol) was added in small increments. After a further 1.5 h reflux and NMR monitoring of the reaction, a further 2.5 g (12 mmol) PCl_5 was added, which after 3 h led to complete consumption of **5**. The bath temperature was raised to 140°C and the remaining $SOCl_2$ was distilled off. The residues were fractionally distilled under vacuum, producing **6** as a colourless liquid, bp 48°C / 4 × 10^{-2} mbar (13.5 g, 46.3 mmol, 63% yield). IR (neat): ν(X=N) 1703, ν(X–Φ) 1287, 1217, 1165. ^{1}H NMR: 7.20–7.18 (m, 3 H), 2.62 (hept, 6.9 Hz, 2 H), 1.18 (d, 6.9 Hz, 12 H). ^{13}C NMR: 140.47, 135.93, 133.94 (quart, 49 Hz), 126.35, 123.47, 116.65 (quart, 277 Hz), 28.64, 22.97. ^{19}F NMR: –71.48 (s, CF_3). Mass spec: 290.7 (M^+ on ^{35}Cl, 29%), 256 (M–Cl^+, 75%), 240 (M–CH_4Cl), 177 ($C_6H_3{}^iPr_2NH_2^+$, 48%), 162 ($C_6H_3{}^iPr_2^+$, 100%). Anal. calcd. for $C_{14}H_{17}ClF_3N$: C 57.64, H 5.87, N 4.80%; found: C 57.57, H 5.85, N 5.00%.

Preparation of $CF_3C\{N\text{-}2,6\text{-}^iPr_2C_2H_3\}NH(2,6\text{-}^iPr_2C_6H_3)$, 1d

210 mL of 1.5 M *n*BuLi (hexane solution) was added via cannula to 44 mL (233 mmol) of 2,6-diisopropylaniline in 500 mL of THF in a 1 L flask equipped with a reflux condenser. After stirring a further 30 min, 68 g (233 mmol) of **6** in 200 mL THF was added dropwise with cooling. After stirring 30 min, the mixture was heated to reflux for 10 h, filtered, and the filtrate evaporated. The resulting oil was treated with 1 L of 95% ethanol followed by 600 mL *c*HCl. After evaporation to dryness, the residues were divided into five parts, each dissolved in 200 mL ethanol, reacted with 200 mL of 23% NaOH, and extracted three times with 100 mL of toluene. The toluene phase was washed with NH_4Cl and then water, and evaporated to an oil. Extended pumping on this oil produced crystals, which could be recrystallized from *n*-heptane, to give 16 g of colourless crystals of **1d** (38 mmol, 16% yield). An analytical sample was produced by recrystallizing a second time from *n*-heptane, mp 94–98°C. IR: ν(N-H) 3451, 3358, ν(N-C-N) 1655 cm^{-1}. ^{1}H NMR: 7.37–7.06 (m, 6H), 5.50 (s, 1 H), 3.18 (hept, 6.9 Hz, 2H), 3.03 (hept, 6.7 Hz, 2 H), 1.34 (d, 6.8 Hz, 6 H), 1.27 (d, 6.8 Hz, 6 H), 1.20 (d, 6.7, 6 H), 1.00 (d, 6.7 Hz, 6 H). ^{13}C NMR: 147.51, 143.28 (quart, 33 Hz),

© 2000 NRC Canada

140.62, 138.17, 131.18, 129.03, 123.46, 118.10 (quart, 279 Hz), 28.48, 25.32, 24.16, 22.41, 22.10. ^{19}F NMR: –67.24 (s, CF_3, major species), –66.84 (s, CF_3, minor species). Mass spec: 432.27486 (M^+, 57%), 389 (M–^{i}Pr$^+$, 79%), 256 (M-$C_6H_3{}^i Pr_2NH^+$, 100%), 214 ($CF_3NC_6H_3{}^i Pr^+$, 13%), 177 ($C_6H_3{}^i Pr_2NH_2^+$, 73%). Anal. calcd. for $C_{26}H_{35}F_3N_2$: C 72.19, H 8.16, N 6.48%; found: C 71.95, H 7.99, N 6.59%.

Preparation of η^6-[CF_3C{N-2,6-$^i Pr_2C_6H_3$}NH(2,6-$^i Pr_2C_6H_3$)]Mo(CO)$_3$, 3d

Three grams (6.9 mmol) of **7** and 1.83 g (6.9 mmol) of $Mo(CO)_6$ were loaded under N_2 into a side-arm flask under N_2. One hundred fifty millilitres of dry *n*-heptane was then added, and the mixture heated to reflux. Progress of the reaction was monitored by solution IR, and heating discontinued after 42 h. Removal of the solvent followed by recrystallization from *n*-heptane provided 1.02 g (1.7 mmol, 25% yield) of **3d** as bright yellow crystals, which were analytically pure, mp 145°C dec. IR: ν(N-H) 3462, 3208, ν(C=O) 1969, 1865, ν(N-C-N) 1665 cm^{-1}. ^{1}H NMR: 8.07 (s, 1 H), 7.37–7.17 (m, 3 H), 5.89 (t, 6.5 Hz, 1 H), 5.57 (d, 6.5 Hz, 2 H), 3.14 (hept, 6.8 Hz, 2 H), 2.72 (hept, 6.9 Hz, 2 H), 1.28 (d, 6.9 Hz, 6 H), 1.27 (d, 6.8 Hz, 6 H), 1.26 (d, 6.9, 6 H), 1.22 (d, 6.8 Hz, 6 H). ^{13}C NMR spectrum not obtained due to sample instability. ^{19}F NMR: –67.54 (s, CF_3). Mass spec: 614.16607 (M^+ based on ^{98}Mo, 31%), 558 (M–2CO$^+$, 4%), 530 (MoL$^+$, 100%), 486 (MoL–^{i}Pr$^+$, 2%), 432 (L$^+$, 36%), 389 (L–^{i}Pr$^+$, 62%), 256 (M-$C_6H_3{}^i Pr_2NH^+$, 72%), 177 ($C_6H_3{}^i Pr_2NH_2^+$, 56%). Anal. calcd. for $C_{26}H_{35}F_3MoN_2O_3$: C 56.86, H 5.76, N 4.57%; found: C 57.00, H 5.60, N 4.65%.

Crystallography

Data collected on a Stoe IPDS diffractometer using monochromated Mo K_α radiation (0.71073 Å) by the ϕ-oscillation method. An analytical absorption correction was carried for **3d**, but no correction was necessary for **1d**. Both structures were solved by direct methods using SHELXS-97 (17) and refined by full-matrix least-squares on F^2 using SHELXL-97 (18) using all reflections. For **1d** all the hydrogen atoms except the one attached to N were localized geometrically and a riding model was used for refinement. The CF_3 group is rotationally disordered and was modeled by two trigonal F_3 units with occupancies of 0.85 and 0.15. For **3d**, all the hydrogen atoms were localized, and a similar disorder model was applied to the F_3 unit, with refined occupancies of 0.87 and 0.13.[3]

Electronic structure calculations

All calculations were performed using the AM1 method as implemented in HyperChem 5.1 running on a Pentium II computer under Windows 95 (19).

Acknowledgments

The Natural Sciences and Engineering Research Council of Canada, the University of Lethbridge research fund, and the Alexander von Humboldt-Foundation supported this work. R.T.B wishes to thank Prof. Dr. O.J. Scherer and Dr. G. Wolmershäuser for their hospitality during a sabbatical leave at Kaiserslautern and acknowledges the access given to the facilities of the Fachbereich Chemie of the University. We thank staff at the Chemistry Department of the University of Calgary for acquiring the ^{19}F NMR spectra, and one of the referees for many helpful suggestions.

References

1. G.A. Dushenko, I.E. Mikhailov, A. Zschunke, G. Reck, B. Schulz, C. Mugge, and V.I. Minkin. Mendeleev Comm. 67 (1999).
2. A. Kasani, R.P.K. Babu, K. Feghali, S. Gambarotta, G.P.A. Yap, L.K. Thompson, and R. Herbst-Irmer. Chem. Eur. J. **5**, 577 (1999).
3. A. Littke, N. Sleiman, C. Bensimon, D.S. Richeson, G.P.A. Yap, and S.J. Brown. Organometallics, **17**, 446 (1998).
4. M.P. Coles and R.F. Jordan. J. Am. Chem. Soc. **119**, 8125 (1997).
5. S. Dagorne, L.A. Guzei, M.P. Coles, and R.F. Jordan. J. Am. Chem Soc. **122**, 274 (2000).
6. R.T. Boeré, V. Klassen, and G. Wolmershäuser. J. Chem. Soc. Dalton Trans. 4147 (1998).
7. F.A. Cotton, T. Inglis, M. Kilner, and T.R. Webb. Inorg. Chem. **14**, 2023 (1975).
8. W. Maringgele and A. Meller. Z. Anorg. Allg. Chem. **445**, 107 (1978).
9. T. Keumi, M. Shimada, T. Morita, and H. Kitajima. Bull. Chem. Soc. Jpn. **63**, 2252 (1990).
10. W. Maringgele and A. Meller. Monatsh. Chem. **110**, 63 (1979).
11. C.L. Perrin. *In* The chemistry of the amidines and imidates. Vol. 2. *Edited by* S. Patai and Z. Rappoport. Wiley, Chichester. 1991. Ch. 3, p. 152.
12. P. Atkins. Physical chemistry, 6th ed. Freeman, N.Y. 1998. p. 666.
13. G. Häfelinger and K.H. Kuske. *In* The chemistry of the amidines and imidates. Vol. 2. *Edited by* S. Patai and Z. Rappoport. Wiley, Chichester. 1991. Ch. 1, pp. 1–100.
14. G. Gilli and V. Bertolasi. J. Am. Chem. Soc. **101**, 7704 (1979).
15. E. Cisazk, M. Gdaniec, and Z. Kosturkiewicz. Acta Crystallogr. **B43**, 1362 (1978).
16. C.M. Lukehart. *In* Fundamental transition metal organometallic chemistry. Brooks/Cole, Monterey, CA. 1985. p. 81.
17. G. Sheldrick. SHELXS-97, University of Göttingen. 1997.
18. G. Sheldrick. SHELXL-97, University of Göttingen. 1997.
19. HyperChem Pro Release 5.1. HyperCube, Waterloo, Ontario.

[3] Detailed structure reports including the H-atom positions and the anisotropic temperature factors have been deposited. Copies of materials on deposit may be purchased from the Depository of Unpublished Data, Document Delivery, CISTI, National Research Council Canada, Ottawa, Canada K1A 0S2.

© 2000 NRC Canada

Solution multinuclear (^{31}P,^{111}Cd,^{77}Se) magnetic resonance studies of cadmium complexes of heterocyclic aromatic thiones and the structure of [tetrakis(2(1*H*)-pyridinethione)cadmium] nitrate, $[Cd(C_5H_5NS)_4](NO_3)_2$

Umarani Rajalingam, Philip A.W. Dean, and Hilary A. Jenkins

Abstract: The complex salts $CdL_4(O_3SCF_3)_2$ (L = 2(1*H*)-pyridinethione (Py2SH), 4(1*H*)-pyridinethione (Py4SH), or 2(1*H*)-quinolinethione (Q2SH)) have been synthesized by the stoichiometric reaction of $Cd(O_3SCF_3)_2$ and the appropriate thione. Both ambient-temperature ^{13}C and reduced-temperature ^{111}Cd NMR of $CdL_4(O_3SCF_3)_2$ in solution are consistent with L being bound through sulfur. Reduced-temperature NMR (^{31}P, ^{77}Se, ^{111}Cd, as appropriate) of mixtures of $CdL_4(O_3SCF_3)_2$ and $Cd(EPCy_3)_4(O_3SCF_3)_2$ (E = Se, Cy = *c*-C_6H_{11}) and of $Cd(EPCy_3)_4(O_3SCF_3)_2$ (E = S, Se) and L in solution provides evidence for various $[CdL_n(EPCy_3)_{4-n}]^{2+}$. Similarly, reduced-temperature metal NMR of $[CdL_4]^{2+}$ and $[CdL'_4]^{2+}$ (L, L′ = Py2SH, Py4SH, Q2SH; L ≠ L′) in solution shows the formation of $[CdL_nL'_{4-n}]^{2+}$. Thus it has been demonstrated that at reduced temperature $[CdL_4]^{2+}$ is intact in solution and exchange of L is slow on the timescale of the metal chemical shift differences. From the NMR studies of $Cd(EPCy_3)_4(O_3SCF_3)_2$ (E = S, Se):L mixtures, the binding preferences are found to be L > $EPCy_3$ in solution. Similarly, from the reduced temperature metal NMR spectra of mixtures where L and L′ compete for Cd(II) in solution, the binding preferences are Py4SH > Py2SH > Q2SH. The structure of $Cd(Py2SH)_4(NO_3)_2$ (**4**) has been determined by single crystal X-ray analysis. Colorless crystals of **4** are tetragonal, I4(1)/*acd* with 8 molecules per unit cell of dimensions *a* = 18.660(3), *c* = 15.215(3) Å. The structure is comprised of recognizable NO_3^- anions and $[Cd(Py2SH)_4]^{2+}$ cations. In the cations, which have S_4 symmetry, the ligands are *S*-bound. A network of NH···O hydrogen bonds links the cations and anions.

Key words: aromatic heterocyclic thiones, cadmium complexes, phosphine chalcogenides, ^{111}Cd, ^{31}P, ^{77}Se NMR, X-ray crystallography.

Résumé : On a réalisé la synthèse des sels complexes $CdL_4(O_3SCF_3)_2$ (L = 1*H*-pyridine-2-thione (Py2HS), 1*H*-pyridine-4-thione (Py4SH) ou 1*H*-quinoléine-2-thione (Q2SH) en procédant à une réaction stoechiométrique du $Cd(O_3SCF_3)_2$ avec la thione appropriée. Les spectres RMN du ^{13}C à la température ambiante et du ^{111}Cd à température réduite des $CdL_4(O_3SCF_3)_2$ en solution sont en accord avec liaison du L par le biais de l'atome de soufre. Les spectres RMN (^{31}P, ^{77}Se ou ^{111}Cd suivant le cas) de mélanges de $CdL_4(O_3SCF_3)_2$ et de $Cd(EPCy_3)_4(O_3SCF_3)_2$ (E = Se, Cy = cyclo-C_6H_{11}) à température réduite ainsi que ceux de $Cd(EPCy_3)_4(O_3SCF_3)_2$ (E = S, Se) en présence de L en solution mettent en évidence la présence de divers ions $[CdL_n(EPCy_3)_{4-n}]^{2+}$. De la même manière, la RMN des métaux de $[CdL_4]^{2+}$ et de $[CdL'_4]^{2+}$ (L, L′ = Py2SH, Py4SH ou Q2SH; L ≠ L′), en solution et à température réduite, montre qu'il y a formation de $[CdL_nL'_{4-n}]^{2+}$. On a donc ainsi démontré que, à température réduite, le $[CdL_4]^{2+}$ est intact en solution et que l'échange de L est lent à l'échelle de temps des différences de déplacement chimique des métaux. À partir des études RMN sur des mélanges de $Cd(EPCy_3)_4(O_3SCF_3)_2$ (E = S, Se):L, on a trouvé que, en solution, les préférences de fixation sont L > $EPCy_3$. De la même manière, sur la base de spectres RMN des métaux à température réduite, de mélanges en solution dans lesquels L et L' sont en compétition pour le Cd(II), on a pu établir que les préférences de fixation sont Py4SH > Py2SH > Q2SH. On a déterminé la structure du $Cd(Py2SH)_4(NO_3)_2$ (**4**) par diffraction des rayons X par un cristal unique. Les cristaux incolores du produit **4** sont tétragonaux, groupe d'espace I4(1)/*acd*, avec huit molécules par maille élémentaire dont les dimensions sont *a* = 18,660(3) et *c* = 15,215(3) Å. Dans la structure on peut reconnaître des anions NO_3^- et des cations $[Cd(Py2SH)_4]^{2+}$. Dans les cations, de symétrie S_4, les ligands sont liés au soufre. Un réseau de liaisons hydrogènes NH···O relie les cations et les anions.

Received January 10, 2000. Published on the NRC Research Press website on May 11, 2000.

U. Rajalingam,[1] P.A.W. Dean,[2] and H.A. Jenkins.[3] Department of Chemistry, University of Western Ontario, London, ON N6A 5B7, Canada.

[1]Present address: Vice-President, Urecoats Technologies Inc., 4100, North Powerline Business Park, Pompano Beach, FL 33073, U.S.A.

[2]Author to whom correspondence may be addressed. Telephone: (519) 679-2111 ext. 86331. Fax: (519) 661-3022. e-mail: pawdean@julian.uwo.ca

[3]Current address: Department of Chemistry, Saint Mary's University, Halifax, NS B3H 3C3, Canada.

 © 2000 NRC Canada

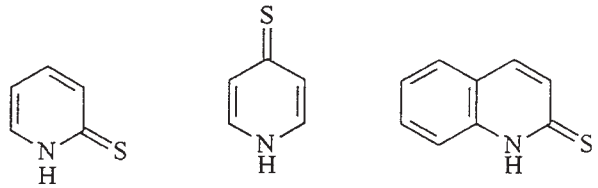
Mots clés : thiones d'hétérocycles aromatiques, complexes du cadmium, chalcogénures de phosphine, RMN du ^{111}Cd, du ^{31}P et du ^{77}Se, cristallographie.

[Traduit par la Rédaction]

Introduction

The cysteine-rich protein metallothionein has a role in the detoxification of cadmium, a wide-spread environmental pollutant (1). In metallothionein, the cadmium ions are bound by cysteinyl sulfur atoms to give thiolate clusters (2). Although no antidote is yet available for cadmium poisoning, it seems likely that any antidote will have one or more sulfur atoms to compete with the donor atoms of the metallothionein. Thus a detailed understanding of the cadmium–sulfur bond is desirable. Previous contributions to this area from these laboratories have included synthetic, structural, and solution NMR spectroscopic studies of cadmium–thiolate (and –selenolate) complexes (3), as well as of thiobenzoato-complexes (4), and solution NMR studies of complexes of phosphine sulfides (and selenides) (5).

In the present paper we turn our attention to homoleptic complexes of cadmium with the heterocyclic thiones[4] 2(1*H*)-pyridinethione (Py2SH), 4(1*H*)-pyridinethione (Py4SH), and 2(1*H*)-quinolinethione (Q2SH).[5] Hitherto, these complexes have received little attention. To our knowledge, no information is available on the behaviour of such complexes in solution, and no structural analyses are available.[6] However, the synthesis of $Cd(Py2SH)_4(NO_3)_2$ has been reported (9). This compound is isomorphous with the Co(II) analogue, which, from its *d-d* spectrum, contains a cation with a tetrahedral CoS_4 kernel. Also, solution ^{1}H and ^{13}C NMR data have been presented for the mixed-ligand complexes $Cd(Py2SH)_2X_2$ (X = Cl, Br) and $Cd(Py4SH)_2Cl_2$ (as well as $Cd(Py2S)_2$) in DMSO-d_6 at ambient probe temperature (10).



Py2SH Py4SH Q2SH

Experimental

Methods and materials

All manipulations were carried out under an atmosphere of dry N_2(g) in a glove box or with a vacuum:N_2(g) manifold, or under an atmosphere of Ar(g) in a glove bag. Analar grade solvents (MeCN, $CHCl_3$, CH_2Cl_2, Me_2CO, Et_2O) were dried over 3 A molecular sieves and deoxygenated using Ar prior to use.

Pyridine-2-thione (Acros or Aldrich) and quinoline-2-thione (Aldrich) showed no significant impurities by ^{1}H and (or)^{13}C NMR and were used as received. Pyridine-4-thione (Acros or Aldrich) was used after repeated recrystallization from toluene–methanol. Literature methods were used to convert $Cy_3P{\cdot}CS_2$ (Strem) into Cy_3PS (5*b*) and Cy_3PSe (11),[7] and for synthesis of anhydrous $Cd(O_3SCF_3)_2$ ($Cd(trif)_2$) by dehydration of the hydrate produced from the metal oxide and aqueous CF_3SO_3H (12). The metal triflate was weighed out in the glove box.

$Cd(Py2SH)_4(O_3SCF_3)_2$ (1)

To a solution of pyridine-2-thione (0.074 g, 0.67 mmoL) in $CHCl_3$ (3.0 mL) was added a solution of $Cd(trif)_2$ (0.066 g, 0.16 mmoL) in MeCN (1 mL). Diethyl ether was layered onto the clear reaction mixture until slight turbidity was seen. The reaction vial was tightly sealed and kept in a freezer at –15°C. After a week, the first crop of white block shaped crystals was separated by filtration, washed with cold Et_2O, and vacuum dried. Yield: 0.070 g (64%), mp: 144–146°C. Further crops, up to a quantitative yield, can be obtained by further addition of Et_2O to the initial filtrate. ^{13}C NMR spectrum (CH_2Cl_2 or Me_2CO): 167.4 (C-2), 133.7 (C-3), 140.5 (C-4), 119.6 (C-5), and 142.4 (C-6). Anal. calcd for $C_{22}H_{20}Cd\ F_6N_4O_6S_6$: C 30.90, H 2.36, N 6.55; found: C 31.20, H 2.20, N 6.48.

*Synthesis of $Cd(Py4SH)_4(O_3SCF_3)_2$ (**2**)*

Pyridine-4-thione (0.074 g, 0.67 mmoL) was dissolved in $CHCl_3$ (8.0 mL). To the clear yellow solution $Cd(trif)_2$ (0.066 g, 0.16 mmoL) in acetonitrile (1 mL) was added. The bright yellow colour faded. Diethyl ether was layered onto the clear solution until slight turbidity was seen. The reaction mixture was sealed tightly and kept in a freezer at –15°C. After two weeks, a first crop of pale yellow flaky crystals was separated by filtration, washed with cold Et_2O, and vacuum dried. Yield: 0.097 g (89%); mp 178–180°C. Anal. calcd. for $C_{22}H_{20}Cd\ F_6N_4O_6S_6$: C 30.90, H 2.36, N 6.55; found: C 31.26, 31.28, H 2.21, 2.27, N 6.41, 6.63. ^{13}C NMR (Me_2CO): 180.1(C-4), 137.0 (C-2), and 131.0 (C-3). (^{13}C NMR of free Py4SH (Me_2CO): 188.5(C-4), 133.0 (C-2), 130.0(C-3)).

*Synthesis of $Cd(Q2SH)_4(O_3SCF_3)_2$ (**3**)*

Cadmium triflate (0.066 g, 0.16 mmol) in acetonitrile (1 mL) was added to the intense yellow solution of quinoline-2-thione (0.105 g, 0.65 mmol) in $CHCl_3$ (3 mL). The reaction mixture quickly turned light yellow. Diethylether (3 mL) was added and the clear solution was kept at room temperature for slow crystallization. After three days, the product, as yellow needles, was collected by filtration, washed with Et_2O, and dried under vacuum. Yield: 0.140 g (82.8%); mp 192–194°C. ^{13}C NMR (CH_2Cl_2): 139.08, 133.39, 129.89,

[4] Complexes of thiones in general have been little studied compared with thion*ates* (6).
[5] Free Py2SH and Py4SH are involved in tautomeric equilibria, e.g., ref. 7.
[6] Structural data are available for several heterocyclic aromatic thion*ates* of cadmium (8).
[7] Cy = *c*-C_6H_{11}

© 2000 NRC Canada

Table 1. Crystal data and structure refinement for $[Cd(Py2SH)_4](NO_3)_2$, **IV**.

Formula	$C_{20}H_{20}CdN_6O_6S_4$
fw	681.06
Crystal system	Tetragonal
Space group	*I*4(1)/*acd*
a (Å)	18.660(3)
c (Å)	15.215(3)
V (Å^3)	5298(2)
Z	8
ρ_{calcd} (g cm^{-3})	1.708
Crystal size (mm)	0.25 × 0.23 × 0.18
Temperature (K)	294(2)
Radiation	MoKα (λ = 0.71073 Å)
μ (cm^{-1})	11.87
Data collection method	hemisphere
θ range (deg)	2.18 to 24.99
Total unique reflections measured	1167
Total observed reflections[a]	914
Data/restraints/parameters	1162/0/86
Final max Δ/σ	0.000
Max res. density/hole (e Å^{-3})	0.870, –0.375
R^b	0.0274
$R_w{}^b$	0.0771
GoF	1.021

[a] $I > 2\sigma I$.

[b] $R = \Sigma(||F_o| - |F_c||)/\Sigma|F_o|$; and $R_w = [\Sigma w(F_o^2 - F_c^2)^2/\Sigma wF_o^4]^{1/2}$, with $w = 1/[\sigma^2(F_o^2) + (0.0580p)^2 + 0.0000p]$, where $p = (F_o^2 + 2F_c^2)/3$.

[c] GoF = $[\Sigma w(F_o^2 - F_c^2)^2/(n - p)]^{1/2}$, where n is the number of reflections and p is the number of parameters refined.

128.56, 127.26, 118.46, and 174.4 (C-2). (^{13}C NMR of free Q2SH: 138.8, 135.4, 131.2, 127.7, 124.6, 122.8, 115.7, and 180.9 (C-2)). Anal. calcd. for $C_{38}H_{28}CdF_6N_4O_6S_6$: C 43.2, H 2.65, N 5.3; found: C 43.60, H 2.51, N 5.24.

*$Cd(Py2SH)_4(NO_3)_2$ (**4**)*

Pyridine-2-thione (0.72 g, 6.47 mmol) was dissolved in methanol(10 mL) under an atmosphere of Ar(g). To the clear solution was added at room temperature a solution of $Cd(NO_3)_2 \cdot 4H_2O$ (0.52 g, 1.69 mmol) in MeOH (1 mL). Light yellow needle-shaped crystals formed in ca. 10 min. The crystals(1.08 g, 88.8%) were collected by filtration, washed with ice-cold MeOH (2 mL), and vacuum dried. The crystals appear to decompose above 158°C but become a yellowish liquid in the range 170–172°C. Anal. calcd. for $C_{20}H_{20}N_6O_6S_4Cd$: C 35.27, H 2.95, N 12.33; found: C 35.39, H 2.78, N 12.28. The data crystal for X-ray analysis was obtained during the synthesis.

A similar synthetic route has been given in ref. 9.

*$[Cd(SePCy_3)_4](O_3SCF_3)_2$ (**5**)*

To a solution of Cy_3PSe (0.252 g, 0.700 mmol) in 3 mL of 50% v/v Me_2CO:CH_2Cl_2 was added, with stirring, solid $Cd(trif)_2$ (0.066 g (0.161 mmol)). When the cadmium salt had dissolved, Et_2O (ca. 4 mL) was layered onto the mixture, which was then refrigerated (–15°C) overnight. The white crystals of $[Cd(SePCy_3)_4](O_3SCF_3)_2$ were separated by filtration, washed with ice-cold Et_2O, and vacuum dried. Yield: 0.262 g (88%). The product was pure by ^{31}P, ^{77}Se, and ^{111}Cd NMR. The NMR data are included in Table 2.

Compounds **1**–**5** were air-stable when dry.

Table 2. Atomic coordinates (× 10^4) and equivalent isotropic displacement parameters (Å^2 × 10^3) for $[Cd(Py2SH)_4](NO_3)_2$ (**4**).

Atom	*x*	*y*	*z*	*U*(eq)
Cd(1)	–5000	7500	3750	45(1)
S(1)	–4058(1)	6822(1)	4592(1)	59(1)
N(1)	–4076(1)	5637(1)	5521(1)	51(1)
C(1)	–4479(1)	6196(1)	5238(1)	43(1)
C(2)	–5190(2)	6202(1)	5511(2)	55(1)
C(3)	–5454(2)	5666(2)	6034(2)	61(1)
C(4)	–5015(2)	5114(2)	6311(1)	57(1)
C(5)	–4325(2)	5115(2)	6053(2)	59(1)
N(2)	–2500	4744(2)	5000	69(1)
O(1)	–3055(1)	4406(2)	5102(2)	115(1)
O(2)	–2500	5402(2)	5000	96(1)

Note: *U*(eq) is defined as one third of the trace of the orthogonalized *Uij* tensor.

NMR Spectra: ^{13}C NMR spectra were obtained at ambient probe temperature using a Varian Gemini-200 spectrometer system equipped with a 5 mm probe. The field was preshimmed, and then spectra of samples in protiated solvents were measured without a ^{2}D field/frequency lock. Field drift was negligible. 63.59-MHz ^{111}Cd{^{1}H} NMR spectra were obtained using a Varian XL-300 spectrometer system and inverse-gated decoupling to avoid the negative Overhauser effect. (In the more usual ^{113}Cd region, artifacts were present in the frequency range of interest; no primary isotope effect is expected between ^{111}Cd and ^{113}Cd NMR spectra.). The metal NMR spectra were measured with samples in protiated solvents in 10 mm o.d. NMR tubes and a preshimmed field. Again, no ^{2}*D* field/frequency lock was used, field drift being negligible. The samples were referenced to external 0.1 M $Cd(ClO_4)_2$(aq) at ambient probe temperature (294 ± 2 K). The same spectrometer system, with continuous decoupling, was used to obtain ^{31}P{^{1}H} and ^{77}Se{^{1}H} NMR spectra at 121.42 and 57.20 MHz, respectively, in an analogous manner. The external references were 85% H_3PO_4 and pure Me_2Se, respectively, at 296 ± 2 K. Concentrations of samples in 10 mm o.d. NMR tubes were prepared on the basis of mass of sample/volume of solvent, normally 1.6 × 10^{-4} mol/3 mL of solvent (= 0.053 mol/L of solvent) for starting cadmium complexes. In mixing experiments, additional cadmium complexes were added as solids to the existing volume of solution, leading to an increase in the total cadmium concentration. For reduced temperature NMR spectra, 30 min was allowed for thermal equilibration at each temperature.

X-ray structure determination

A crystal of **4** from the synthesis was cut to appropriate size, 0.25 × 0.23 × 0.18 mm, and mounted on a glass fibre. Crystal data and refinement parameters for **4** are listed in Table 1, the final positional parameters and equivalent isotropic thermal parameters are given in Table 2 and selected interatomic distances and angles are listed in Table 5. One full hemisphere of data were collected on a Nonius Kappa-CCD

© 2000 NRC Canada

system. Unit cell parameters were calculated from reflections obtained from 15 consecutive data images collected at phi intervals of one degree using DENZO v.1.9 (13) Systematic absences indicated the tetragonal space group $I4_1acd$, and this was borne out by successful refinement of the structure. Data were scaled using Scalepack (13) and no other absorption coefficient were applied. Full-matrix least-squares refinement on F^2 was performed after solving using Patterson methods and the solution package SHELXTL 5.03 (14). Anisotropic thermal parameters were applied to all non-hydrogen atoms and hydrogen atoms themselves were generated in ideal positions, although all five could be found in a difference Fourier. The Cd atoms sit on a four-fold inversion centre, while N(2) (nitrate) is on a two-fold axis. The largest residual peak was associated with the nitrate anion (0.870 eÅ^{-3}). In the final stages of refinement, $R1$ = 2.74% and $wR2$ = 7.71%.

Substitution reactions of $[M(EPCy_3)_4]^{2+}$ (M = Zn or Cd, E = S or Se) with thiones

In an Ar-filled glove bag, each equivalent of the thione was added at room temperature to a solution of the cadmium complex (0.053 mol of complex/L of 50% v/v Me_2CO–CH_2Cl_2) in a 10 mm o.d. NMR tube. The NMR tube was the transferred to the precooled NMR probe.

Elemental microanalyses:

Carbon, hydrogen, and nitrogen microanalyses were performed by Guelph Chemical Laboratories Ltd.

Results and discussion

Syntheses

Reactions of $Cd(O_3SCF_3)_2$ with a slight excess of the ligands Py2SH, Py4SH, and Q2SH in acetonitrile-chloroform under Ar(g) produced crystalline $CdL_4(O_3SCF_3)_2$ (L = Py2SH, Py4SH, and Q2SH in compounds **1**, **2**, and **3**, respectively) when the reaction mixture was layered with Et_2O and kept at –15°C. Crystallization occurred within 0.5 h for **3**, within one week for **1**, and within two weeks for **2**. The reaction of Py2SH with a slight excess of $Cd(NO_3)_2{\cdot}4H_2O$ in MeOH under Ar(g) at room temperature yielded the known compound (9) $Cd(Py2SH)_4(NO_3)_2$ (**4**) in crystalline form.

NMR Spectra

*(a) Studies of **1**, **2**, and **3***

The compounds **1**–**3** had sufficient solubility in many organic solvents (Me_2CO, MeCN, MeOH, CH_2Cl_2, DMF) to allow at least solution ^{13}C NMR studies at ambient temperature. In addition, they have in common the weakly coordinating triflate anion, which simplifies comparison of their metal NMR spectra in particular. Compound **4** has poor solubility in many solvents, e.g., CH_2Cl_2, MeOH, Me_2CO, although it is quite soluble in DMF.

In the ^{13}C NMR spectrum of **1**–**3**, the thione carbon is shielded relative to the free ligand (Experimental section) due to the aromatization of the pyridyl ring. At ambient probe temperature, the shielding is 12.8 ppm for **1**,[8] 8.4 ppm for **2**, and 6.5 ppm for **3**. The shielding is consistent with coordination of cadmium at sulfur, which should decrease the double-bond character of the thione. and increase the double-bond character of the N to (thione) C linkage, thus aromatizing the heterocyclic rings.

The ^{111}Cd NMR spectra of **1** and **2** in 50% v/v Me_2CO:CH_2Cl_2 at 189 K consist of single resonances with δ_{Cd} (approximate $\Delta\nu_{1/2}$) of 603 (45 Hz) and 622 (25 Hz). The solubility of **3** under these conditions is poor, but its resonance is probably a weak signal observed at $\delta_{Cd} \approx 566$. At ambient probe temperature, signals that are shielded and broader are observed for all three complexes, suggesting partial dissociation. The assignments of resonances that are single lines call for confirmation. Ligand mixing experiments (see below) show that the signals observed in the low temperature spectra are due to CdL_4^{2+} for **1** and **2** and strongly support a similar assignment for **3**.

The ^{111}Cd chemical shifts of **1**–**3** fall in, or close to, the range that has been established for the CdS_4 kernel (16). Thus the thiones act as S-donors in **1**–**3**, as is commonly the case (6, 8*a*, *b*), and as has been suggested for the cation in **4** on the basis of its isomorphism with the Co(II) analogue for which a CoS_4 kernel has been established from *d-d* spectroscopy (9). We note that a rough inverse correlation exists between the ^{111}Cd chemical shifts of **1**–**3** and the values of pK_a for LH^+ (pK_a = –1.07, 1.50, –1.53 for LH^+, L = Py2S, Py4S, and Q2S, respectively, (17)).

(b) Studies of cadmium complexes with mixed ligands

(i) The systems $[Cd(SePCy_3)_4]^{2+}$–$[CdL_4]^{2+}$ and $[Cd(SePCy_3)_4]^{2+}$–L (L = Py2SH, Py4SH, Q2SH): At 189 K,[9] the ^{31}P and metal NMR spectra of $[Cd(SePCy_3)_4]^{2+}$ in 50% v/v Me_2CO:CH_2Cl_2 (Table 3) are a singlet with ^{77}Se and $^{111/113}Cd$ (av) satellites, and a quintet (from ^{111}Cd–^{31}P coupling), respectively. These are consistent with earlier data (5*a*, *b*). The ^{77}Se NMR spectrum, which has not been reported previously, consists of a doublet (from $^1J(^{77}Se\text{-}^{31}P)$) with $^{111/113}Cd$ satellites (from $^1J(^{111/113}Cd\text{-}^{77}Se)$) : δ_{Se} = –403.6, $^1J(^{77}Se\text{-}^{31}P)$ = 549 Hz, $^1J(^{111/113}Cd\text{-}^{77}Se)$ = 248 Hz (Table 3). As **1** is added to the solution of **5**, a total of three new $SePCy_3$-containing species is observed by a combination of ^{31}P, ^{77}Se, and ^{111}Cd NMR. Their NMR spectra (Table 3) characterize them as $[Cd(Py2SH)_{4-n}(SePCy_3)_n]^{2+}$ (n = 1–3), with n increasing as $SePCy_3$:Py2SH increases in the mixtures. Thus the whole series $[Cd(Py2SH)_{4-n}(SePCy_3)_n]^{2+}$ (n = 0–4) has been characterized, proving that, like $[Cd(SePCy_3)_4]^{2+}$, the homoleptic complex formed between Cd(II) and Py2SH in solution is four-coordinate, $[Cd(Py2SH)_4]^{2+}$.

When Py2SH is added incrementally to **5** in 50% v/v Me_2CO:CH_2Cl_2, the ^{31}P NMR spectrum at –189°C shows first the formation of $[Cd(Py2SH)(SePCy_3)_3]^{2+}$, as confirmed by the observation of the appropriate quartet (from $^1J(^{111}Cd\text{-}^{31}P)$) in the corresponding ^{111}Cd NMR spectrum. However, with increased addition of Py2SH, separate ^{31}P NMR signals are not observed for $[Cd(Py2SH)_2(SePCy_3)_2]^{2+}$ and $[Cd(Py2SH)_3(SePCy_3)]^{2+}$, although the ^{111}Cd NMR spectrum shows the separate signals from these two species. Evidently

[8] $\delta_{C\text{-}2}$ (free Py2SH) = 180.2 (15).

© 2000 NRC Canada

Table 3. NMR spectral parameters for $[CdL_n(SePCy_3)_{4-n}]^{2+}$ (L = Py2SH, Py4SH, or Q2SH[a]) in 50% Me_2CO:CH_2Cl_2 v/v at 189 K.

L[a]	*n*	δ_P[b]	δ_{Cd}[c]	δ_{Se}[d]	$^1J(^{77}Se\text{-}^{31}P)$[e] (Hz)	$J(^{111/113}Cd\text{-}^{31}P)_{Ave}$[f] (Hz)	$J(^{111}Cd\text{-}^{77}Se)$[g] (Hz)
Cy_3PSe	4	66.4	519[h]	–403.6	549	57	248
	–[i]	61.4		–466.4	671		
Py2SH	0		603				
	1	?	595	–443.6	543[j]		
	2	64.8	574[k]	–430.1	546	44	165
	3	65.6	550[l]	–416.0	548	50	205
Py4SH		0	621				
	1	64.2	604	[m]	[n]	[n]	[n]
	2	64.3	582[k]	–463.3	557	42	177
	3	65.3	552[l]	–416.4	553	49	211
Q2SH	2	65.3	540[k]	–435.1	540	44	[n]
	3	65.9	544[l]	–423.7	544	51	172

[a]Py2SH = 2(1*H*)-pyridinethione; Py4SH = 4(1*H*)-pyridinethione; Q2SH = 2(1*H*)-quinolinethione.
[b]Estimated error ±0.1 ppm.
[c]Estimated error ±0.3 ppm; reproducibility ~ ±1 ppm
[d]Estimated error ±0.3 ppm or better.
[e]From the ^{31}P NMR spectrum, except as noted; estimated error ±3 Hz.
[f]From the ^{31}P NMR spectrum; estimated error ±1 Hz.
[g]From the ^{77}Se NMR spectrum; estimated error ±1 Hz.
[h]Quintet, from $^1J(^{111}Cd\text{-}^{31}P)$.
[i]Free ligand.
[j]From the ^{77}Se NMR spectrum; estimated error ±5.
[k]Triplet, from $^1J(^{111}Cd\text{-}^{31}P)$.
[l]Quartet, from $^1J(^{111}Cd\text{-}^{31}P)$.
[m]Not measured.
[n]Not observed.

the two ^{31}P NMR spectra are coincident. In increasingly Py2SH-rich mixtures, a broad ^{31}P NMR signal from $SePCy_3$ appears. This part of spectrum becomes increasingly sharper as it comprises increasingly more of the total intensity. At Py2SH:**5** = 4.1:1, the ^{31}P NMR spectrum (now sharp) provides evidence for free $SePCy_3$ only (δ_P = 61.4, $^1J(^{77}Se\text{-}^{31}P)$ = 671 Hz). At this point, no ^{111}Cd NMR signal from $[Cd(Py2SH)_4]^{2+}$ is observed; **1** seems to have crystallized out completely over the time taken for the experiment. However, it is evident that Py2SH is a stronger ligand to Cd(II) than $SePCy_3$.

Essentially identical results to those obtained for **1**:**5** and Py2SH:**5** mixtures are observed for **2** or **3**:**5** and Py4SH or Q2SH:**5** mixtures, except that no evidence could be obtained for $[Cd(Q2SH)_3(SePCy_3)]^{2+}$. (Q2SH-rich complexes are poorly soluble at –189°C.) NMR spectral parameters for the new complexes observed are given in Table 3. Both Py4SH and Q2SH are better ligands towards Cd(II) than $SePCy_3$.

(ii) The systems $[Cd(SPCy_3)_4]^{2+}$:L (L = Py2SH, Py4SH, Q2SH):
Mixed-ligand complexes containing Cy_3PS were detected by NMR in experiments where the free thiones were added to $[Cd(SPCy_3)_4]^{2+}$ (preformed in situ in Me_2CO:CH_2Cl_2 (1:1 v/v) from Cy_3PS and $Cd(trif)_2$). At 189 K,[9] the ^{31}P NMR spectrum of $[Cd(SPCy_3)_4]^{2+}$ consists of a singlet with $^{111/113}Cd$ satellites, while the ^{111}Cd NMR spectrum consists of a quintet (from $^2J(^{111}Cd\text{-}^{31}P)$). These are in concert with data for the same complex in SO_2(l) at 203–209 K (5*a*, *b*).

When one equiv. of Py2SH is added to $[Cd(SPCy_3)_4]^{2+}$ at 189 K, the ^{31}P NMR and ^{111}Cd NMR spectra provide evidence for $[Cd(Py2SH)_1(SPCy_3)_3]^{2+}$ and $[Cd(Py2SH)_2(SPCy_3)_2]^{2+}$. Details of the NMR spectra of these two new species are given in Table 4. With the addition of second equiv. of Py2SH, the relative intensities of the spectra of the individual species that are observed shift in favour of those that are more Py2SH-rich. A new broad signal appears in the ^{31}P NMR spectrum at ~68 ppm, and the signal observed for Cy_3PS at 64 ppm is broad. Under the same conditions the ^{111}Cd NMR spectrum provides evidence for $[Cd(Py2SH)_2(SPCy_3)_2]^{2+}$. When a third equiv. of Py2SH is added, the ^{31}P NMR signal from $[Cd(SPCy_3)_4]^{2+}$ finally disappears, and the relative intensities of the broad signals at ~ 68 ppm and from free Cy_3PS increase. A signal attributable to $[Cd(Py2SH)_3(SPCy_3)_1]^{2+}$ is observed in the ^{111}Cd NMR spectrum. Evidently ligand exchange between free Cy_3PS and Cy_3PS coordinated in $[Cd(Py2SH)_2(SPCy_3)_2]^{2+}$ and $[Cd(Py2SH)_3(SPCy_3)_1]^{2+}$ occurs at a rate sufficient to broaden (or possibly collapse) the ^{31}P NMR spectra of the species involved, but not sufficient to collapse their ^{111}Cd NMR spectra. With the addition of a fourth equiv. of Py2SH, insoluble crystals, presumably $[Cd(Py2SH)_4](trif)_2$, separated and the now sharp singlet of Cy_3PS alone appears. This experiment confirms that Cd–Py2SH complex is four-coordinate in solution and also shows that Py2SH can completely displace Cy_3PS from Cd(II).

Results for addition of Py4SH and Q2SH to $[Cd(SPCy_3)_4]^{2+}$ at 189 K, were very similar to those observed for the corresponding addition of Py2SH, except that of the complexes containing Q2SH, only that with *n* = 3 gave a sharp ^{31}P NMR spectrum. Details of the NMR

© 2000 NRC Canada

Table 4. NMR spectral parameters for $[CdL_n(SPCy_3)_{4-n}]^{2+}$ (L = Py2SH, Py4SH, or Q2SH[a]) in 50% Me_2CO:CH_2Cl_2 v/v at 189 K.

L[a]	*n*	δ_P[b]	δ_{Cd}[c]	$^2J(^{111/113}Cd\text{-}^{31}P)_{Ave}$[d] (Hz)
Cy_3PS	4	69.9	588[e]	48
	–[f]	64.4		
Py2SH	0		603[g]	
	1	?	605[h]	
	2	68.2	600[h]	[i]
	3	69.1	597[j]	42
Py4SH		0	622	
	1	[k]	612	[k]
	2	67.8[h]	602	[i]
	3	69.0	597[j]	39
Q2SH	1	[k]	590[h]	[k]
	2	[k]	594[h]	[k]
	3	69.3	588[j]	41

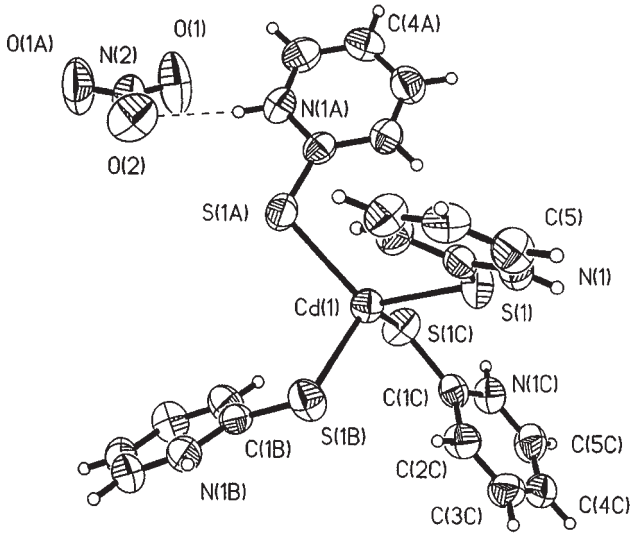
[a]Py2SH = 2(1*H*)-pyridinethione; Py4SH = 4(1*H*)-pyridinethione; Q2SH = 2(1*H*)-quinolinethione.
[b]Estimated error ±0.1 ppm.
[c]Estimated error ±0.3 ppm; reproducibility ~ ±1 ppm.
[d]From the ^{31}P NMR spectrum; estimated error ±1 Hz.
[e]Quintet, from $^1J(^{111}Cd\text{-}^{31}P)$.
[f]Free ligand.
[g]At 185 K.
[h]Broad resonance; no fine structure observed.
[i]Could not be measured with certainty.
[j]Quartet, from $^1J(^{111}Cd\text{-}^{31}P)$.
[k]Not observed.

spectra are included in Table 4. Again it is evident that the thiones can displace Cy_3PS from Cd(II).

(iii) The complexes $[Cd(Py2SH)_{4-n}L_n]^{2+}$ (L = Py4SH or Q2SH): The observation of slow exchange NMR spectra for many complexes $[CdL_{4-n}(EPCy_3)_n]^{2+}$ (E = S or Se) (see above) proves that in these complexes intermolecular exchange of the phosphine chalcogenide is slow, but does not provide evidence about the lability of the thione ligands. To obtain information pertinent to the latter point, and also to further confirm four-coordination of $[CdL_4]^{2+}$, reduced-temperature[9] ^{111}Cd NMR spectra of complexes with mixed thione ligands have been studied, again using a 1:1 (v/v) Me_2CO:CH_2Cl_2 as solvent.

Mixtures of **1** and **2** were prepared by adding **2** incrementally to a solution of **1** in 1:1 (v/v) Me_2CO:CH_2Cl_2. By varying the **1**:**2** ratio, a total of five singlets was observed by ^{111}Cd NMR for the mixtures at 189 K. The extreme chemical shifts are those of the parent complexes $[Cd(Py2SH)_4]^{2+}$ (603.4 ppm) and $[Cd(Py4SH)_4]^{2+}$ (624.0 ppm). The intervening resonances at δ_{Cd} = 609.6, 614.5, and 618.4 are readily assigned to $[Cd(Py2SH)_{4-n}(Py4SH)_n]^{2+}$, with *n* = 1, 2, and 3, respectively. These assignments can be confirmed by expressing the chemical shifts in terms of pairwise interactions (18).

Fig. 1. A view of the cation in $[Cd(Py2SH)_4](NO_3)_2$ (**4**), showing one of the cation···nitrate hydrogen bonds. Non-hydrogen atoms are shown as 50% probability thermal ellipsoids.



A similar experiment with mixtures of **1** and **3** also yields a total of five singlet resonances, δ_{Cd} = 603.4, 596.2, 586.9, 576.1, and 566.0. These can be assigned to $[Cd(Py2SH)_{4-n}(Q2SH)_n]^{2+}$, with *n* = 0, 1, 2, 3, and 4, respectively.

The observation of separate ^{111}Cd NMR signals for the complexes with mixed thiones shows that intermolecular exchange of the thiones is slow on the timescale of $\Delta\delta_{Cd}$ at 189 K.[10] Further the total of five signals observed when two thiones are mixed confirms that the thione complexes are of general formula $[CdL_4]^{2+}$ in solution, consistent with the results obtained using mixtures of thiones and Cy_3PE (see above).

(iv) Competition between thiones for complexation to Cd(II): At 189 K, the ^{111}Cd NMR spectrum of a mixture with Cd(trif)$_2$:Py2SH:y4SH = 1:4:1 in Me_2CO:CH_2Cl_2 (1:1, v/v) shows broad signals corresponding to $[Cd(Py2SH)_{4-n}(Py4SH)_n]^{2+}$ with *n* = 1 and *n* = 2. On the other hand, the analogous spectrum of a mixture in which Cd(trif)$_2$:Py2SH:Py4SH = 1:1:4 shows only the sharp signal of $[Cd(Py4SH)_4]^{2+}$ at 623 ppm. This experiment shows that towards Cd(II) the ligating ability is Py4SH > Py2SH.

After addition of free Q2SH to a 1:1 mixture of $[Cd(Py2SH)_4]^{2+}$:$[Cd(Q2SH)_4]^{2+}$ in Me_2CO:CH_2Cl_2 (1:1, v/v) until (total L)/M > 6, broad signals corresponding to the mixed thione species are seen in ^{111}Cd NMR at 189 K. Clearly Py2SH can compete with Q2SH for coordination to Cd(II) even when Q2SH/Cd > 4. Conversely, when free Py2SH was added to a 1:1 mixture of $[Cd(Py2SH)_4]^{2+}$ and $[Cd(Q2SH)_4]^{2+}$ until (total L)/M > 6, the metal NMR spectrum at 189 K shows only the resonance of $[Cd(Py2SH)_4]^{2+}$ at 603 ppm. Thus Q2SH cannot compete with Py2SH for coordination to Cd(II) when Py2SH/Cd > 4. Therefore for the three different thione ligands donor ability towards Cd(II) is

[9]Rapid exchange occurs at ambient probe temperature, and fine structure is lost.
[10]An alternative explanation that only exchange of Py2SH is slow, or that only exchanges of Py4SH and Q2SH are slow, seems highly improbable.

© 2000 NRC Canada

Table 5. Bond distances (Å) and bond angles (deg) for $[Cd(Py2SH)_4](NO_3)_2$ (**4**).

Bond distances	(Å)
Cd(1)—S(1)	2.5163(7)
S(1)—C(1)	1.716(2)
N(1)—C(5)	1.349(3)
N(1)—C(1)	1.356(3)
C(1)—C(2)	1.390(3)
C(2)—C(3)	1.368(4)
C(3)—C(4)	1.383(4)
C(4)—C(5)	1.345(4)
N(2)—O(1)	1.222(3)
N(2)—O(2)	1.229(6)
Bond angles	**(deg)**
S(1)-Cd(1)-S(1A)[a]	118.81(3)
S(1)-Cd(1)-S(1B)[b]	105.01(2)
S(1)-Cd(1)-S(1C)[c]	105.01(2)
S(1A)-Cd(1)-S(1B)	105.01(2)
S(1A)-Cd(1)-S(1C)	105.01(2)
S(1B)-Cd(1)-S(1C)	118.81(3)
C(1)-S(1)-Cd(1)	108.30(8)
C(5)-N(1)-C(1)	123.7(2)
N(1)-C(1)-C(2)	116.0(2)
N(1)-C(1)-S(1)	116.9(2)
C(2)-C(1)-S(1)	127.1(2)
C(3)-C(2)-C(1)	120.8(2)
C(2)-C(3)-C(4)	120.5(3)
C(5)-C(4)-C(3)	118.5(3)
C(4)-C(5)-N(1)	120.4(3)
O(1)-N(2)-O(1A)[d]	117.9(4)
O(1)-N(2)-O(2)	121.1(2)
O(1A)-N(2)-O(2)	121.1(2)

[a]Symmetry operators: –x + 1 – 2, –y + 3/2, z + 1 – 1.
[b]Symmetry operators: –y + 1/4, x + 5/4, –z + 3/4.
[c]Symmetry operators: y – 5/4, –x + 1/4, –z + 3/4.
[d]Symmetry operators: –x – ½, y, –z + 1.

Py4SH > Py2SH > Q2SH, the order of the basicities of the ligands (see above).

Crystal structure of $[Cd(Py2SH)_4](NO_3)_2$ (4)

The crystal structure of **4** consists of recognizable $[Cd(Py2SH)_4]^{2+}$ cations and NO_3^- anions. Figure 1 shows the structure of the cation. Selected bond angles and bond distances are listed in Table 5.

In the cations the ligands behave as S-donors, as is usual for this ligand (6, 8*a*). The point group symmetry of $[Cd(Py2SH)]_4^{2+}$ is S_4, the point group symmetry of the CdS_4 core being D_{2d}. The Cd—S bond distance is 2.5163(7) Å and S-Cd-S bond angles are 105.01(2) and 118.81(3)°, there being a tetragonal compression of the core. The Cd—S distance may be compared with, for example, 2.496(6)–2.56(1) Å reported (19) for $[Cd(Me_2tu)_4](NO_3)_2$, and 2.516(2)–2.556(3) found (20) for various salts of homoleptic thiolate anions, $[Cd(SR)_4]^{2-}$.[11]

In the ligand, the C(1)-N(1)-C(5) bond angle is 123.7(2)°, implying that the proton is bonded to nitrogen and not to sulfur (22). The bond distance C(1)—S(1) is 1.716(2) Å, slightly longer than the value of 1.692(2) Å found (23) by X-ray diffraction[12] for free *2*(1*H*)-pyridinethione. Accompanying this increase are slight reductions of the C(1)—C(2) and C(3)—C(4) bond distances (1.390(3) and 1.383(4) Å compared with 1.417(4) and 1.399(4) Å in the free ligand) consistent with increasing aromatization of the pyridyl ring as the thione character of the C—S linkage is reduced. Also observed on complexation are changes in the angles subtended at C(1): the C(2)-C(1)-S(1) angle increases to 127.1(2)°, from 124.3(2)° in the free ligand, the N(1)-C(1)-S(1) angle decreases to 116.9(2)°, from 120.6(2)° in the free ligand, and there is a slight increase in the N(1)-C(1)-C(2) angle compared with the free ligand (to 116.0(2)° from 115.0°). The skeleton of the thione is planar (mean deviation 0.007 Å), and the dihedral angle between the C_5NS and C(1)-S(1)-Cd(1) planes is 20.2°.

It is interesting to note that the point group symmetry of the cations (S_4) is one of the two ideal possibilities that have been recognized (23) for $[M(SPh)_4]^{n-}$ (the other possibility is D_{2d}).[13] The anion with M = Cd and n = 2 is isoelectronic with the cation in **4**. For the anions of S_4 symmetry, a tetragonal compression is uniformly observed (23*b*), and such a compression is found here for $[Cd(Py2SH)]_4^{2+}$ also. A similar compression is evident in data for $[M(Py2SH)_4](BF_4)$ (M = Cu or Ag), although it has not been remarked upon (25). The Cu(I) and Ag(I) complexes have less regular symmetry than is observed here for $[Cd(Py2SH)]_4^{2+}$, however.

The $[Cd(Py2SH)]_4^{2+}$ cations stack in columns in the *c* direction, with a Cd···Cd distance of 7.607(1) Å. The anions, which have C_{2v} symmetry, occupy channels between the columns of cations. Extending the parallel between $[Cd(Py2SH)_4]^{2+}$, and $[M(SPh)_4]^{n-}$, a two-fold disorder of the heterocyclic rings about their C(1)-C(4) axes might be anticipated in the former. However, the NO_3^- anions are "docked" between two adjacent cations in such a way that O(2) is positioned to take part in two symmetry-related weak hydrogen bonds, to one N-*H* on each of the two cations (H(1A)···O(2) = 2.223 Å, N(1)-H(1A)-O(2) = 172(1)°, H(1A)-O(2)-H(1D) = 159(1)°). (One such hydrogen bond is shown in Fig. 1.) This hydrogen bonding network presumably prevents disorder of the pyridyl groups.[14]

Acknowledgments

We thank Dr. M. Jennings, Manager of the X-Ray Crystallographic Service at UWO, for considerable assistance with

[11]A 1995 review of all structurally characterized coordination compounds of cadmium (21) found average values of the Cd—S distance to be 2.546 and 2.527 Å for complexes of mono- and bi-dentate sulfur donors, respectively.
[12]Values obtained by neutron diffraction are given in ref. 22 also.
[13]A recent discussion of this topic is provided in ref. 24.
[14]Supplementary material may be purchased from: The Depository of Unpublished Data, Document Delivery, CISTI, National Research Council of Canada, Ottawa ON, Canada, K1A 0S2. These have also been deposited with the Cambridge Crystallographic Data Center, and can be obtained on request from: The Director, Cambridge Crystallographic Data Center, University Chemical Laboratory, 12 Union Road, Cambridge, CB2 1EZ, U.K.

© 2000 NRC Canada

presentation of crystallographic material. This work was funded in part by a Research Grant from the Natural Sciences and Engineering Research Council of Canada to PAWD.

References

1. (*a*) J.H.R. Kägi and A. Schaffer. Biochemistry, **27**, 8509 (1988); (*b*) I. Bremner. Experientia Suppl. **52**, 81 (1987).
2. A.H. Robbins and C.D. Stout. *In* Metallothioneins. *Edited by.* M.J. Stillman, C.F. Shaw, III, and K.T. Suzuki. VCH, New York. 1992. Ch. 3, and refs. therein.
3. (*a*) P.A.W. Dean, N.C. Payne, J.J. Vittal, and Y. Wu. Inorg. Chem. **32**, 4632 (1993); (*b*) P.A.W. Dean and J.J. Vittal. *In* Metallothioneins. *Edited by* M. J. Stillman, C.F. Shaw, III, and K.T. Suzuki. VCH, New York. 1992. Ch. 14 and refs. therein; (*c*) G.K. Carson and P.A.W. Dean. Inorg. Chim. Acta, **66**, 37 (l982); (*d*) G.K. Carson, P.A.W. Dean, and M.J. Stillman. Inorg. Chim. Acta, **56**, 59 (l98l); **108**, 71 (1985).
4. (*a*) P.A.W. Dean, J.J. Vittal, D.C. Craig, and M.L. Scudder. Inorg. Chem. **37**, 1661 (1998); (*b*) J.J. Vittal and P.A.W. Dean. Acta Crystallogr. Sect. C: Cryst. Struct. Commun. **54**, 319 (1998); (*c*) J.J. Vittal and P.A.W. Dean. Inorg. Chem. **35**, 3089 (1996); (*d*) J.J. Vittal and P.A.W. Dean. Inorg. Chem. **31**, 791 (1993).
5. (*a*) P.A.W. Dean. Can. J. Chem. **59**, 322l (l98l); *(b)* P.A.W. Dean and L. Polensek. Can. J. Chem. **58**, l627 (l980); (*c*) P.A.W. Dean and M.K. Hughes. Can. J. Chem. **58**, l80 (l980).
6. E.S. Raper. Coord. Chem. Rev. **153**, 199 (1996); **165**, 475 (1997).
7. M. Witanowski and L. Stefaniak. Bull. Polish Acad. Sci. Chem. **35**, 305 (1987).
8. *(a)* E.S. Raper. Coord. Chem. Rev. **129**, 91(1994); **61**, 115 (1985); (*b*) E. Block, E,M. Gernon, H. Kang, G. Ofori-Okai, and J. Zubieta. Inorg. Chem. **28**, 1263 (1989); *(c)* M.B. Hursthouse, O.F.Z. Khan, M. Mazid, M. Motevalli, and P. O'Brien. Polyhedron, **9**, 541 (1990); *(d)* R. Castro, J.A. Garcia-Vasquez, J. Romero, A. Sousa, R. Pritchard, and C.A. McAuliffe. J. Chem. Soc. Dalton Trans. 1115 (1994).
9. B.P. Kennedy and A.B.P. Lever. Can. J. Chem. **50**, 3488 (1972).
10. R. Shunmugam and D.N. Sathyanarayana. J. Coord. Chem. **14**, 27 (1985).
11. P.A.W. Dean. Can. J. Chem. **57**, 754 (1979).
12. G.R. Hedwig and A.J. Parker. J. Am. Chem. Soc. **96**, 6589 (1974).
13. Z. Otwinowski and W. Minor. Methods Enzymol. **27**, Part A, 307 (1997).
14. SHELXTL Reference Manual, Version 5.03, Siemens Energy and Automation, Inc., Analytical Instrumentation, Wisconsin, U.S.A. 1996.
15. L. Stefaniak. Org. Magn. Reson. **12**, 379 (1979).
16. M.F. Summers. Coord. Chem. Rev. **86**, 43 (1988).
17. S. Stoyanov, T. Stoyanova, L. Antonov, P. Karagiannidis, and P. Akrivos. Monatshefte fur Chemie, **127**, 495 (1996), and refs. therein.
18. T. Vladimiroff and E.R. Malinowski. J. Chem. Phys. **46**, 1830 (1967).
19. P.F. Rodesiler, N.G. Charles, E.A.H. Griffith, and E.L. Amma. Acta Crystallogr. Sect. C: Cryst. Struct. Commun. **39**, 1350 (1983).
20. (*a*) D. Swenson, N.C. Baenziger, and D. Coucouvanis. J. Am. Chem. Soc. **100**, 1932 (1978); (*b*) N. Ueyama, T. Sugawara, K. Sasaki, A. Nakamura, S. Yamashita, Y. Wakatsuki, H. Yamazaki, and N. Yasuoka. Inorg. Chem. **27**, 741 (1988); (*c*) E. Block, M. Gernon, H. Kang, G. Ofori-Okai, and J. Zubieta. Inorg. Chem, **28**, 1263 (1989); (*d*) A. Silver, S.A. Koch, and M. Miller. Inorg. Chem. Acta, **205**, 9 (1993).
21. C.E. Holloway and M. Melnik. Main Group Chemistry, **18**, 451 (1995).
22. U. Ohms, H. Guth, A. Kutoglu, and C. Scheringer. Acta Crystallogr. Sect. B: Struct. Crystallogr. Cryst. Chem. **38**, 831 (1982).
23. (*a*) S.A. Koch and L.E. Maelia. J. Am. Chem. Soc. **105**, 5944 (1983); (*b*) L.E. Maelia, M. Millar, and S.A. Koch. Inorg. Chem. **31**, 4594 (1992).
24. B.F. Ali. Ph.D. thesis. School of Chemistry, University of New South Wales, 1998. Ch. 5.
25. G. Giusti, G. Geier, A. Currao, and R. Nesper. Acta Crystallogr. Sect. C: Cryst. Struct. Commun. **52**, 1914 (1996).

© 2000 NRC Canada

Redox chemistry of the selenium coronand, 1,5,9,13-tetraselenacyclohexadecane, and a mechanistic study of the electron transfer reaction of its Cu(II) complex

Raymond J. Batchelor, Frederick W.B. Einstein, Ian D. Gay, Jian-Hua Gu, B. Mario Pinto, and Xue-Min Zhou

Abstract: The crystal structure of Cu(16Se4)$(SO_3CF_3)_2$ (**1**) shows a centrosymmetric complex having tetragonally distorted octahedral coordination about Cu with *trans*-axial triflate ligands; Cu—O 2.464(5) Å. The stereochemistry of the coronand is *c*,*t*,*c*; Cu—Se 2.4592(9), 2.4553(9) Å. **1**: T = 190 K; fw = 845.83; space group $P2_1/n$; Z = 2; a = 8.220(2), b = 10.965(4), c = 14.657(5) Å; V = 1273.4 Å^3; R_f = 0.037 for 1708 data ($I_o \geq 2.5\sigma(I_o)$) and 152 variables. When recrystallized from $MeNO_2$–Et_2O **1** undergoes an electron-transfer reaction to give Cu(I) as well as the intermediate radical cation $[16Se4]^{\cdot+}$ and the stable dication $[16Se4]^{2+}$. The crystal structure of a mixed MeCN–CH_2Cl_2 solvate of $[(16Se4)][SO_3CF_3]_2$ (**2**) revealed the $[16Se4]^{2+}$ cation which displays two transannular Se—Se bonds of 2.5916(15) and 2.6689(15) Å, linking three of the Se atoms in an approximately linear relationship. The central Se atom of this grouping also has a close contact to the fourth Se atom of the molecule of 3.3941(20) Å. **2**·solv: T = 195 K; fw = 828; space group $P\bar{1}$; Z = 2; a = 9.015(2), b = 12.850(3), c = 13.835(3) Å; α = 63.98(2), β = 74.71(2), γ = 73.59(2)°; V = 1363.3 Å^3; R_f = 0.042 for 2098 data ($I_0 \geq 2.5\sigma(I_0)$) and 254 variables. A solid-state ^{77}Se NMR spectrum of **2** shows 4 lines, with isotropic shifts ranging from 173 to 737 ppm. The line widths are all different, and we obtain a tentative assignment by attributing this to differences in dipolar coupling to ^{19}F. Significant differences in chemical shift anisotropy are observed for the various selenium atoms. UV–visible absorption spectroscopy has been used to characterize **1** and its reduction products. **1** absorbs at 560, 464, and 310 nm. Reaction of **1** with the free ligand 16Se4 leads to the disappearance of these peaks, and the growth of a new peak at 320 nm. Oxidation of 16Se4 by $NOBF_4$ produced a transient peak at 320 nm, and subsequently a peak at 256 nm. From the dependence of intensity on 16Se4 concentration, we infer that the former arises from a dimeric species; we assign the lines to the radical cations $(16Se4)_2^{+\cdot}$ and $16Se4^{+\cdot}$, respectively. Electrochemical studies have been carried out on **1** and on 16Se4. Cyclic voltammetry of **1** shows a two-step reduction to Cu(II)$L^{+\cdot}$ (L = 16Se4) and subsequently to Cu(I)L^+. Electrochemical oxidation of 16Se4 leads to $16Se4^{+\cdot}$ and $16Se4^{2+}$. Spectroelectrochemical studies showed that oxidation to $16Se4^{+\cdot}$ gives rise to a band at 256 nm, as seen in chemical oxidation, and at high concentrations a band at 322 nm is also seen, supporting the assignment of this species to the dimeric radical cation. The EPR spectrum of **1** in CH_3NO_2 solution gave an isotropic g value of 2.053 with hyperfine constants A_{iso}^{Cu} = 75 G and A_{iso}^{Se} = 65 G. The low temperature EPR spectrum of **1**, measured at –148°C in CH_3NO_2:toluene (1:1 v/v), gave values of $g_{//}$ = 2.085, $A_{//}^{Cu}$ = 160 G; $g_{\perp}$ = 2.049, $A_{\perp}^{Cu}$ = 46 G. An EPR spectrum of **1** in CH_3NO_2 in the presence of added 16Se4 showed a decrease in intensity of the signals attributable to **1** and the emergence of new signals that are presumed to arise from a species with radical cation character. We have carried out kinetic studies on the reaction between **1** and 16Se4. It is found that the reaction is first order in each of these species, second order overall. The reaction stoichiometry is 2 Cu(16Se4)$^{2+}$ + 16Se4 → 2 Cu(16Se4)$^+$ + $16Se4^{2+}$. These results can be explained by the simple mechanism Cu(II)L^{2+} + L ⇌ $L^{+\cdot}$ + Cu(I)L^+, followed by Cu(II)L^{2+} + $L^{+\cdot}$ → L^{2+} + Cu(I)L^+. The activation energy is found to be 35 kJ mol^{-1}.

Key words: selenium coronands, Cu(II) complex, redox chemistry, mechanism, electron transfer.

Résumé : La structure cristalline du Cu(16Se4)$(SO_3CF_3)_2$ (**I**) indique qu'il s'agit d'un complexe centrosymétrique comportant une coordination octaédrique déformée de façon tétragonale autour du Cu avec des ligands triflates dans la position *trans*-axiale; Cu—O = 0,2464(5)Å. La stéréochimie du coronand est *c*,*t*,*c*; Cu—Se = 2,4592(9) et 2,4553Å. Pour le composé **1**, à T = 190 K, fw = 845,83; groupe d'espace $P2_1/n$; Z = 2; a = 8,220(2), b = 10,965(4) et c = 14,657(5) Å, V = 1273,4Å^3; R_f = 0,037 pour 1708 données ($I_0 \geq 2,5\sigma(I_0)$) et 152 variables. Par recristallisation d'un mélange $MeNO_2$–Et_2O, le composé **1** subit une réaction de transfert d'électron qui fournit du Cu(I) ainsi que le cation

Received December 8, 1999. Published on the NRC Research Press website on May 12, 2000.

R.J. Batchelor, F.W.B. Einstein, I.D. Gay, J.-H. Gu, B.M. Pinto,[1] and X.-M. Zhou. Department of Chemistry, Simon Fraser University, Burnaby, BC V5A 1S6, Canada.

[1]Author to whom correspondence may be addressed. Telephone: (604) 291-4327. Fax: (604) 291-3765. e-mail: bpinto@sfu.ca

 © 2000 NRC Canada

radical intermédiaire $[16Se4]^{+\cdot}$ et le dication stable $[16Se4]^{2+}$. La structure cristalline d'un produit de solvatation mixte $MeCN–CH_2Cl_2$ et $[(16Se4)][SO_3CF_3]_2$ (**2**) révèle que le cation comporte deux liaisons Se—Se transannulaires de 2,5916(15) et 2,6689(15) Å qui relient trois des atomes de Se dans une relation approximativement linéaire. L'atome de Se central de ce groupe est aussi en contact assez intime [distance de 3,394(20) Å] avec le quatrième atome de Se de la molécule. Le produit de solvatation mixte, à T = 195K, f_w = 828; groupe d'espace $P\bar{1}$, Z = 2; a = 9,015(2), b = 12,850(3) et c = 13,835(3) Å, α = 63,98(2), β = 74,71(2) et γ = 73,59(2)°; V = 1363,3 Å^3; R_f = 0,042 pour 2098 données ($I_0 \geq 2{,}5\sigma(I_0)$) et 254 variables. Le spectre RMN du ^{77}Se du produit **2** à l'état solide présente quatre raies avec des déplacements isotropes allant de 173 à 737 ppm. Les largeurs de raies sont toutes différentes et il est possible de faire des attributions préliminaires en faisant l'hypothèse que ces résultats sont dus à des différences de couplage dipolaire avec le ^{19}F. On a observé des différences marquées dans l'anisotropie du déplacement chimique pour les divers atomes de sélénium. On a utilisé la spectroscopie d'absorption UV–visible ainsi que les produits de réduction pour caractériser le produit **1**. Le produit **1** absorbe à 560, 464 et 310 nm. La réaction de **1** avec un ligand libre 16Se4 conduit à la disparition de ces bandes et au développement d'une nouvelle bande à 320 nm. L'oxydation du 16Se4 par du $NOBF_4$ provoque l'apparition d'une bande transitoire à 320 nm qui est suivie d'une bande à 256 nm. Sur la base de la dépendance de l'intensité sur la concentration de 16Se4, on en déduit que la première bande découle d'une espèce dimère et on attribue les bandes respectivement au cation radical [16Se4] et au dication stable $[16Se4]^{2+}$. On a effectué des études électrochimiques sur le composé **1** et sur le 16Se4. La voltammétrie cyclique de **1** démontre qu'il s'agit d'une réduction en deux étapes conduisant au $Cu(II)L^{+\cdot}$ (L = 16Se4) et subséquemment au $Cu(I)L^+$. Les études spectroélectrochimiques montrent que l'oxydation en 16Se4 donne lieu l'apparition d'une bande à 256 nm, comme on l'a observé au cours de l'oxydation chimique, et que, à concentrations élevées, on observe aussi l'apparition d'une bande à 322 nm qui favorise l'attribution de cette espèce au cation radical dimère. Le spectre RPE du composé **1** en solution dans le CH_3NO_2 donne une valeur isotrope de g de 2,053 avec des constantes hyperfines A_{iso}^{Cu} = 75G et A_{iso}^{Se} = 65G. Le spectre RPE du composé **1** à basse température, mesuré à –148°C dans un mélange 1:1 v/v de CH_3NO_2:toluène permet de tirer des valeurs de $g_{//}$ = 2,085, $A_{//}^{Cu}$ = 160 G; $g_{\perp}$ = 2,049, $A_{\perp}^{Cu}$ = 46 G. Un spectre RPE du composé **1**, dans du CH_3NO_2, en présence de 16Se4 ajouté, montre qu'il y a diminution de l'intensité des signaux attribuables à **1** et l'émergence de nouveaux signaux que l'on attribue à une espèce ayant un caractère cation radical. On a aussi effectué des études cinétiques sur la réaction du composé **1** avec le 16Se4. On a trouvé que la réaction est du premier ordre pour chacune des espèces et que la réaction globale est du deuxième ordre. La stoechiométrie de la réaction est: $2Cu(16Se4)^{2+} + 16Se4 \rightarrow 2\ Cu(16Se4)^{+} + 16Se4^{2+}$. Ces résultats peuvent être expliqués par le mécanisme simple $Cu(II)L^{2+} + L \rightleftharpoons L^{+\cdot} + Cu(I)L^{+}$ suivi par $Cu(II)L^{2+} + L^{+\cdot} \rightarrow L^{2+}\ Cu(I)L^{+}$. L'énergie d'activation est de 35 kJ mol^{-1}.

Mots clés : coronands au sélénium, complexe Cu(II), chimie redox, mécanisme, transfert d'électron.

Introduction

We have been active in the study of the synthesis and conformational analysis of selenium coronands (1, 2). We have also described the synthesis and properties of polymer-bound selenium coronands (3), and the metal-ion complexation of selenium coronands (4, 6). To date, we have reported the structure of the Cu(II) complex of 1,5,9,13-tetraselenacyclohexadecane (16Se4) (4), and the stereochemical analysis of Pd(II) complexes of 16Se4 and 24Se6 (5). We have also reported the study of the adducts of 16Se4 with Cu(I) triflate and Hg(II) cyanide (6), and communicated our results on Cu(I), Cu(II), and Pd(II) complexes of 16Se4 and other selenium coronands (7). Several other reports of complexes of 16Se4, with Rh(III), Co(III) and Ir(III) (8); Pd(II) and Pt(II) (9); Ni (II), Ag (I), Cr (III), Ru (II), and Ru (III) (10) have appeared. Metal-ion complexation by mono- and di-selena (11), and tetraselena (12) macrocyclic ligands containing additional heteroatoms has also been reported.

The rich redox chemistry exhibited by metal complexes of sulfur coronands (13) promised an exciting period of discovery with complexes of the heavier congeners. In the first report of a selenium coronand complex (4), we described a Cu(II) complex of 16Se4, $[Cu(16Se4)][SO_3CF_3]_2$ (**1**), which underwent an unprecedented electron-transfer reaction in coordinating organic solvents to give Cu(I) as well as the intermediate radical cation $[16Se4]^{+\cdot}$ and the stable dication $[16Se4]^{2+}$. The salts $[16Se4]^{2+}([SO_3CF_3]^-)_2$ (**2**) and $[Cu(16Se4)][SO_3CF_3]$ (a polymeric Cu(I) adduct) (6) were isolated from these solutions by selective crystallization. We now report the detailed mechanistic investigation of this electron-transfer reaction, using electrochemistry, spectroelectrochemistry and kinetic analysis. We also include the full structural details for **1** and **2** as well as the ^{77}Se solid state NMR spectrum of **2**.

Experimental

General information

Melting points were determined on a Fisher–Johns melting-point apparatus and are uncorrected. Solvents were distilled before use and were dried, as necessary, by literature procedures. Microanalyses were performed by M. K. Yang of the Simon Fraser University Microanalytical Laboratory.

Spectroscopy

^{1}H NMR spectra were recorded on a Bruker AMX-400 NMR spectrometer operating at 400.13 MHz. Chemical shifts are given with respect to $SiMe_4$. Saturation transfer experiments were performed on **2** in $(CD_3)_2CO$ at 180 K, in the difference mode with a saturating power of 50 dB and saturating times of 0.1 to 0.5 s. The solid state ^{77}Se NMR spectrum was recorded on an instrument (built in-house)

© 2000 NRC Canada

operating at a field of 1.4 T. This produces a resonance frequency of 11.4 MHz. Spectra were excited by using single-contact Hartmann–Hahn cross polarization. The matched radio frequency field strength was 40 kHz. The same field strength was used for proton decoupling during data acquisition. The sample was spun at the magic angle at frequencies of 2–3 kHz. The magic angle was correctly set within ±0.1° by optimizing the line width on a well-crystallized sample of $(t\text{-}Bu_2Sn)_2Se_2$. Chemical shifts were measured relative to long cylindrical samples of aqueous H_2SeO_3. These were converted to shifts based on the standard Me_2Se by use of literature data.

EPR spectra were recorded on a Varian E-4 spectrometer equipped with a temperature controller. The magnetic field was calibrated with DPPH (g = 2.0036) (14). For experiments at ambient temperature, nitromethane was used as the solvent; for experiments at low temperature, nitromethane:toluene (1:1 v/v) was used. The concentration of the Cu(II) complex was 1×10^{-3} M. Measurements were obtained on samples sealed in melting point capillaries that were in turn placed in EPR tubes. In a separate experiment, a mixture of **1** (1×10^{-2} M) in CH_3NO_2 was treated with 16Se4 (1×10^{-2} M) at room temperature and the changes were monitored. Spectra were simulated with Simfonia (WINEPR, Bruker). The spectrum at ambient temperature was simulated using Lorentzian lineshapes with line width/G = 11 + m + m^2, where m is the nuclear spin z-component (–3/2, –1/2, 1/2, 3/2). The spectrum at low temperature was simulated using Gaussian lineshapes with a line width of 32 G.

IR spectra were recorded on a Bomem FT-IR spectrometer. All UV-visible spectra were measured on a Hewlett–Packard HP 89500 UV/VIS Chem Station or a Hewlett-Packard HP 8452 Diode Array Spectrophotometer. The temperature was controlled at 25°C with a thermostat, unless otherwise stated.

Electrochemistry

Cyclic voltammograms of N_2-purged solutions, under an atmosphere of N_2, were recorded on a PAR™ Model 170 or a PAR™ Model 173/175 Electrochemistry System. The reference electrode was an aqueous saturated calomel electrode (SCE) with a Luggin capillary. The working electrode was a platinum plate and the counter electrode was a platinum wire. For the kinetic analysis, cyclic voltammograms were obtained from a single scan for each concentration and each scan rate, and the surface of the electrode was cleaned with a tissue after every scan.

Controlled potential electrolysis, in continuously N_2-purged, stirred solutions, was carried out in a two-compartment electrochemical cell with a sintered-glass partition. The working and counter electrodes were Pt gauze and the reference electrode was aqueous saturated calomel with a Luggin capillary. Tetraethylammonium perchlorate (TEAP, 0.1 M) was used as the electrolyte. The species in solution were characterized by UV–visible spectroscopy; aliquots were withdrawn with a syringe and transferred into a UV cuvette. The coulometer was calibrated with MeCN solutions of ferrocene.

Cyclic voltammetry (CV) during electrolysis was carried out in a two compartment cell with two potentiostats. A PAR™ Model 170 Electrochemistry System was used for electrolysis and a PAR™ Model 173/175 Electrochemistry System was used for cyclic voltammetry. The working and counter electrodes for electrolysis were both Pt gauze. The compartment for electrolysis contained the working electrode, another Pt electrode for CV, and the SCE. 16Se4 (3.3 mM in MeCN) was electrolyzed at 1.2 V and 1.8 V. The species in solution were monitored by UV–visible spectroscopy; aliquots were withdrawn with a syringe and transferred into a UV cuvette. When the absorbance maximum of interest became the predominant peak, the CV scan was started.

Convolution analysis of cyclic voltammograms (15) was carried out after digitization of the data.

Spectroelectrochemistry

The working electrode was an optically transparent Pt-film electrode, fabricated by evaporating Pt powder (using a tungsten filament) onto quartz plates, which were then annealed in a muffle furnace at 550°C for 2 h (16–18). The UV–visible spectrum of the electrode had a broad window for UV–visible light (λ = 200–800 nm; absorbance = 0.5 – 0.6). A AgI/Ag reference electrode was prepared by dipping a thin silver plate into melted AgI in a crucible until a thin film of AgI was obtained. The counter electrode was a Pt wire kept in a glass tube with a sintered end to prevent the species generated on the counter electrode from interfering with the observation of species at the working electrode.

The electrolyses of N_2-purged solutions were carried out, under an atmosphere of N_2, in a UV cuvette. Repeated UV–visible scans were started as soon as the desired potentials (determined by CV) were applied to the electrodes.

Chemical generation of radical cations

Stock solutions of 16Se4 and $NOBF_4$, in freshly distilled MeCN, were prepared, the latter in a glove bag under N_2. The 16Se4 solution was transferred by pipette into a quartz UV cuvette which was then sealed with a septum. N_2 was bubbled through the stirred 16Se4 solution for 15 min, after which the $NOBF_4$ solution was added with a 25 μL syringe. When half of the solution had been added, the repeated scanning of the spectrum was begun.

Kinetic analysis

Flasks were flushed with N_2 before use and CH_2Cl_2 was freshly distilled from P_2O_5 under N_2. A UV cuvette containing an N_2-purged solution of the Cu(II) complex (**1**) was sealed with a septum, under N_2. An N_2-purged solution of 16Se4 was stored under N_2 in a vial, sealed with a septum. The reaction was initiated by injecting the 16Se4 solution with a 25 μL syringe into a stirred solution of **1** in the cuvette. When half of the solution had been added, the repeated scanning of the spectrum was begun, and this point was taken as t = 0 in the data treatment. The variations in intensities of the absorbance bands of the complex and intermediate with time were monitored. Three separate runs were performed for a given substrate concentration.

Synthesis

*$[Cu(16Se4)][SO_3CF_3]_2$ (**1**)*

Under N_2, 16Se4 (1) (45 mg, 0.093 mmol) in dry acetone (2 mL) was added to $Cu(SO_3CF_3)_2$ (18) (34 mg, 0.093 mmol)

© 2000 NRC Canada

in dry acetone (1 mL). The mixture was stirred for 10 min at ambient temperature. Reddish-black crystals were precipitated from the solution by the addition of dry diethyl ether (2 mL) and cooling to 0°C. The crystals were collected by filtration (34 mg, 45%). Recrystallization by diethyl ether vapor diffusion into a CH_2Cl_2 solution afforded 17 mg of reddish-black needles. UV ($MeNO_2$), λ (ϵ): 466 (2193), 556(shoulder) nm; IR (cm^{-1}, KBr) 2940, 1450, 1270, 1235, 1160–1170, 1040, 650, 550. Anal. calcd. for $C_{14}H_{24}CuF_6O_6S_2Se_4$: C 19.88, H 2.83; found: C 19.87, H 2.74.

*[16Se4][SO_3CF_3]$_2$ (**2**)*

Under N_2, 16Se4 (1) (28.7 mg, 0.059 mmol) in MeCN:CH_2Cl_2 (1 mL; 1:1 v/v) was added to $Cu(SO_3CF_3)_2$ (19) (21.4 mg, 0.059 mmol) in MeCN:CH_2Cl_2 (1 mL; 1:1 v/v). The mixture was stirred for 5 min at ambient temperature. CH_2Cl_2 (0.5 mL) was added followed by cooling to 0°C (1 h), and then to –20°C in a refrigerator (overnight). Pale yellow crystals were collected by filtration and washed with CH_2Cl_2 to give **2** (23 mg; 50%). Mp 192–3°C dec. UV (MeCN), λ_{max} (ϵ): 223 (9315) nm; IR (cm^{-1}, KBr) 2940, 1450, 1270, 1235, 1165, 1035, 645, 545. ^{1}H NMR ($(CD_3)_2CO$; RT) δ(ppm): 1.97–2.05, 2.06–2.12, 2.30–2.45, 2.62–2.73, 2.73–2.88, 3.1–3.5 (br), 3.57–3.77 (complex multiplets). ^{1}H NMR ($(CD_3)_2CO$; 180 K) δ(ppm): 1.80–1.98, 2.15–2.32, 2.32–2.48 (complex br. multiplets, β-CH_2s); 2.52–2.72 (complex br. multiplet, α- + β-CH_2s), 2.72–2.88, 2.88–3.02, 3.50–3.68, 3.78–3.95 (complex br. multiplets, α-CH_2s). CP-MAS δ^{77}Se (±1 ppm; ref Me_2Se): 173 ($W_{1/2}$ = 85 Hz), 419 ($W_{1/2}$ = 120 Hz), 502 ($W_{1/2}$ = 140 Hz), 737 ($W_{1/2}$ = 110 Hz). Anal. calcd. for $C_{14}H_{24}F_6O_6S_2Se_4$: C 21.5, H 3.09. Anal. calcd. for $C_{15.67}H_{25.67}Cl_{0.67}F_6N_{0.67}O_6S_2Se_4$ (**2** + 0.67MeCN + 0.33CH_2Cl_2): C 22.45, H 3.10, N 1.11; found: C 22.69, H 3.05, N 1.08.

X-ray crystallography

A reddish-black colored, plate-shaped crystal of **1** was mounted on a pyrex fiber with 5-minute epoxy. A yellow plate-shaped crystal grown from a MeCN:CH_2Cl_2 solution of **2** was sealed in a capillary tube. Intensity data (Mo K_α/graphite monochromator) were collected at 190 K for **1** and at 195 K for **2** using an Enraf Nonius CAD-4F diffractometer equipped with an in-house modified low temperature attachment. The data were corrected for absorption by the Gaussian integration method. Data reduction also included Lorentz and polarization corrections.

For **1**, appropriate coordinates and anisotropic displacement parameters were refined for the non-hydrogen atoms. Hydrogen atoms were placed in calculated positions (C—H, 0.95 Å) with assigned isotropic displacement parameters proportionate to the equivalent isotropic values for their respective carbon atoms — on which they were made to ride during refinement. A single parameter was refined for the hydrogen atom isotropic displacement and its shift applied to the individual values. The final full matrix least-squares refinement included 152 parameters for 1708 reflections ($I \geq 2.5\sigma(I)$). The maximum |shift/error| in the final cycle of refinement was 0.01. The largest peak in the final difference map was 1.0(2) eÅ^{-3} occurring 0.9 Å from Se(1).

In the case of **2** the crystal contained solvent of crystallization. The solvent region exhibited disorder which was modelled with partial occupancy by a molecule of MeCN (0.885(6)) or a molecule of CH_2Cl_2 (0.115). The H-atoms of the CH_2Cl_2 were omitted. A correlated orientational disorder of one of the $SO_3CF_3^-$ anions was observed and was modelled by two independent orientations. Ultimately, a single parameter was refined which accounted for the relative occupancy (constrained to total **1**) of both MeCN:CH_2Cl_2 and the two orientations of the disordered anion. Appropriate component SO_3 or CF_3 fragments were refined as rigid groups. The S—C bond lengths, C-S-O bond angles, and S-C-F bond angles were restrained by their respective mean values. The bond distances within the solvent molecules and the N-C-C bond angle were also restrained by representative values. Within the anions, anisotropic displacements for pairs of bonded atoms were restrained to have the same along-bond components. Anisotropic displacement parameters were refined for all the non-hydrogen atoms except for those of the solvent molecules and those of the minor orientation of the disordered $SO_3CF_3^-$. The latter were assigned isotropic displacement parameters derived from the equivalent isotropic displacement parameters for the major orientation. Subsequently a single parameter was refined for the isotropic displacement for this $SO_3CF_3^-$ component and its shifts were applied to the individual values. Three isotropic displacement parameters for the non-hydrogen atoms of the solvent molecules were refined — one for each pair of nearest complementarily disordered neighbours. The hydrogen atoms were treated as in **1**, above, except that two parameters were refined for their isotropic displacements — one for the H-atoms of the cation and another for those of the MeCN molecule. The latter were initially placed in calculated positions using peak positions from an electron density difference map to specify their orientation. Final full matrix least-squares refinement included 254 parameters for 2098 reflections ($I_o \geq 2.5\sigma(I_o)$) and 41 restraints. The maximum |shift/error| in the last cycle of refinement (0.1) occurred among the parameters for the disordered solvent. The maximum |shift/error| among the parameters of the cation was 0.01. The maximum peak in the final difference map was 0.7(2) eÅ^{-3} and was 1.1 Å from Se(1).

For both structures weighting schemes (20) were applied such that $< w(|F_o| - |F_c|)^2 >$ was near constant as a function of both $|F_o|$ and $(\sin\theta/\lambda)^2$. Complex scattering factors for neutral atoms (21) were used in the calculation of structure factors. The programs used for data reduction, structure solution and graphical output were from the NRCVAX Crystal Structure System (22). The program suite CRYSTALS (23) was employed in the refinement. Computations were carried out on MicroVAX-II, 80486, and Pentium computers. Crystal and refinement data for the structures are shown in Table 1. Fractional coordinates are given in Tables 2 (**1**) and 3 (**2**).

Results and discussion

Synthesis

The complex (1,5,9,13-tetraselenacyclohexadecane)copper(II) trifluoromethanesulfonate, [Cu(16Se4)][SO_3CF_3]$_2$ (**1**), was synthesized by the addition of 16Se4 to an acetone solution of $Cu(SO_3CF_3)_2$. Reddish-black needles of **1** were precipitated

© 2000 NRC Canada

Table 1. Crystallographic data for the structure determinations of $[Cu(16Se4)][SO_3CF_3]_2$ (**1**) at 190 K, and $[16Se4][SO_3CF_3]_2 \cdot 0.89MeCN \cdot 0.11CH_2Cl_2$ (**2**·solv), at 195 K.

	1	**2**·solv
Formula	$CuSe_4S_2F_6O_6C_{14}H_{24}$	$Se_4Cl_{0.23}S_2F_6O_6N_{0.89}C_{15.89}H_{26.66}$
Crystal system	monoclinic	triclinic
fw	845.83	828
Space group	$P2_1/n$	$P\bar{1}$
a (Å)[a]	8.220(2)	9.015(2)
b (Å)	10.965(4)	12.850(3)
c (Å)	14.657(5)	13.835(3)
α (°)		63.98(2)
β (°)	105.44(2)	74.71(2)
γ (°)		73.59(2)
T (K)	190	195
V (Å^3)	1273.4	1363.3
Z	2	2
ρ_c (g cm^{-3})	2.206	2.017
λ(Mo Kα$_1$) (Å)	0.70930	0.70930
μ(Mo Kα) (cm^{-1})	67.5	55.5
Crystal dimension (mm)	0.15 × 0.31 × 0.43	0.08 × 0.22 × 0.23
transmssn[b]	0.139–0.476	0.352–0.659
2θ range (°)	4–50	4–42
R_F[c]	0.037	0.042
R_{wF}[d]	0.046	0.043

[a]The unit cells were determined from 25 well-centered reflections (**1**, 32° ≤ 2θ ≤ 40°; **2**·solv, 30° ≤ 2θ ≤ 40°).

[b]The data were corrected for absorption by the Gaussian integration method.

[c]$R_F = \Sigma(|F_o| - |F_c|)/\Sigma|F_o|$, for: 1708 (**1**), 2098 (**2**·solv) data ($I_o \geq 2.5\sigma(I_o)$).

[d]$R_{wF} = [\Sigma(w(|F_o| - |F_c|)^2)/\Sigma(wF_o^2)]^{1/2}$. $w = [a_0t_0(x) + a_1t_1(x) + a_2t_2(x)]^{-1}$; **1**: a_0 = 19.2921, a_1 = 24.3042, a_2 = 7.6223; **2**: a_0 = 3.6177, a_1 = 4.6072, a_2 = 2.3161; $x = |F_o|/F_{max}$; t_n are the polynomial functions of the Chebyshev series, ref. J.R. Carruthers and D.J. Watkin. Acta Crystallogr. Sect. A: Cryst. Phys. Diffr. Theor. Gen. Crystallogr. **A35**, 698 (1979).

Table 2. Fractional atomic coordinates and equivalent isotropic temperature factors (Å^2) for the non-hydrogen atoms of $[Cu(16Se4)][SO_3CF_3]_2$ (**1**) at 190 K.

Atom	x	y	z	U_{eq}[a]
Se(1)	0.53800(9)	0.60813(6)	0.65123(4)	0.0280
Se(5)	0.20388(8)	0.56471(6)	0.44608(4)	0.0255
Cu	0.50000	0.50000	0.50000	0.0216
S	0.67024(19)	0.76039(14)	0.38712(11)	0.0251
F(1)	0.8532(6)	0.8700(5)	0.5381(3)	0.061
F(2)	0.8375(8)	0.9651(5)	0.4091(4)	0.077
F(3)	0.6285(7)	0.9651(5)	0.4702(5)	0.078
O(1)	0.5551(6)	0.8051(5)	0.3025(3)	0.041
O(2)	0.8181(6)	0.7045(5)	0.3736(4)	0.049
O(3)	0.5904(7)	0.6970(5)	0.4492(4)	0.049
C(1)	0.7501(9)	0.8976(7)	0.4541(5)	0.038
C(2)	0.3094(9)	0.6036(7)	0.6681(5)	0.037
C(3)	0.1987(10)	0.7051(7)	0.6128(5)	0.041
C(4)	0.2129(9)	0.7228(6)	0.5117(5)	0.033
C(6)	0.1833(8)	0.6407(6)	0.3232(4)	0.030
C(7)	0.1912(9)	0.5524(7)	0.2446(4)	0.038
C(8)	0.3675(10)	0.5090(6)	0.2473(4)	0.036

[a]U_{eq} is the cube root of the product of the principal axes of the thermal ellipsoid.

from solution by the addition of Et_2O. Compound **1** is unstable in coordinating organic solvents such as MeCN, $MeNO_2$, Me_2CO, or THF. Indeed, prolonged reaction of 16Se4 and $Cu(SO_3CF_3)_2$ followed by precipitation with Et_2O yielded colorless crystals of $[Cu(16Se4)][SO_3CF_3]$ (a polymeric Cu(I) adduct) (6). Dissolution of **1** in CH_2Cl_2:MeCN (1:1) for 5 min at room temperature, followed by cooling, gave yellow crystals that were identified crystallographically as the salt $[16Se4]^{2+}([SO_3CF_3]^-)_2$. We note that the autoreduction of Cu(II) complexes of macrocyclic tetrathiaethers has been observed (24), although earlier reports (25) of such complexes did not note this phenomenon.

Crystal structures

[Cu(16Se4)][SO$_3$CF$_3$]$_2$ (1)

The molecular structure of **1**, shown in Fig. 1, displays tetragonally distorted octahedral coordination typical of Cu(II) species. Oxygen atoms of the $SO_3CF_3^-$ anions occupy the more weakly bound axial positions. The Cu atom is situated on a crystallographic center of inversion. Selected bond distances and angles are given in Table 4. Additional data are presented as supplementary material (Tables S1–S5). The configuration and conformation of the complex are analogous to those of the thia ether complex $[Cu(16S4)][ClO_4]_2$ (26). The configuration of the complex (**1**) can be described as *ctc*, denoting the relative orientations as *cis*, *trans*, *cis*, with respect to the coordination plane of the coronand, of successive pyramidal donor atom environments. The same stereochemistry of ligation has also been observed in the crystal structures of *trans*-$[RhCl_2(16Se4)][BF_4]$ (27), and $[M(16Se4)][PF_6]_2 \cdot 2MeCN$ (M = Pd, Pt) (28). In marked contrast to the latter, the crystal structures of $[Pd(16Se4)][BF_4]_2$ and

© 2000 NRC Canada

Table 3. Fractional atomic coordinates and equivalent isotropic temperature factors (Å^2) and site occupancies for the non-hydrogen atoms of [16Se4][SO_3CF_3]$_2$·0.89MeCN·0.11CH_2Cl_2 (**2**·solv), at 195 K.

Atom	*x*	*y*	*z*	U_{eq}[a]	Occ.[b]
Se(1)	0.34830(12)	0.84619(9)	0.35418(9)	0.0254	—
Se(2)	0.40635(12)	0.64494(8)	0.51509(9)	0.0316	—
Se(3)	0.01258(13)	0.82722(9)	0.30077(9)	0.0341	—
Se(4)	0.26665(12)	1.05658(8)	0.19757(8)	0.0299	—
S(1)	0.2565(3)	0.23245(21)	0.39975(20)	0.0309	—
F(1)	0.1587(11)	0.4478(5)	0.2689(6)	0.089	—
F(2)	0.1828(11)	0.3196(6)	0.2056(6)	0.082	—
F(3)	0.3866(11)	0.3667(7)	0.2103(6)	0.092	—
O(1)	0.3713(8)	0.1372(5)	0.3790(6)	0.039	—
O(2)	0.3053(9)	0.2866(6)	0.4537(6)	0.045	—
O(3)	0.1023(9)	0.2103(7)	0.4388(7)	0.062	—
C(13)	0.2451(13)	0.3462(7)	0.2655(6)	0.045	—
S(2)	0.6105(3)	0.64518(22)	0.18005(22)	0.0362	0.885(6)
F(4)	0.8797(10)	0.7097(8)	0.1083(8)	0.108	0.885(6)
F(5)	0.8922(10)	0.5248(7)	0.1738(7)	0.140	0.885(6)
F(6)	0.8288(9)	0.6311(8)	0.0199(5)	0.090	0.885(6)
O(4)	0.5588(10)	0.5476(5)	0.1866(7)	0.086	0.885(6)
O(5)	0.5436(9)	0.7571(4)	0.1042(5)	0.070	0.885(6)
O(6)	0.6139(10)	0.6456(7)	0.2821(4)	0.083	0.885(6)
C14	0.8101(5)	0.6274(5)	0.1184(5)	0.051	0.885(6)
S(20)	0.691(3)	0.6767(21)	0.1869(20)	0.044(7)	0.115(6)
F(104)	0.751(10)	0.658(6)	–0.001(3)	0.115(7)	0.115(6)
F(105)	0.877(7)	0.516(6)	0.123(6)	0.115(7)	0.115(6)
F(106)	0.631(8)	0.527(6)	0.130(6)	0.115(7)	0.115(6)
O(104)	0.672(8)	0.590(3)	0.2968(22)	0.083(7)	0.115(6)
O(105)	0.824(6)	0.732(5)	0.156(5)	0.083(7)	0.115(6)
C(114)	0.740(5)	0.591(3)	0.106(3)	0.058(7)	0.115(6)
C(1)	0.2175(11)	0.9041(8)	0.4666(7)	0.0266(24)	—
C(2)	0.2907(12)	0.8482(8)	0.5687(8)	0.0293(25)	—
C(3)	0.3103(13)	0.7150(9)	0.6237(9)	0.040(3)	—
C(4)	0.2152(13)	0.6081(10)	0.5070(9)	0.044(3)	—
C(5)	0.2108(12)	0.5966(9)	0.4038(9)	0.038(3)	—
C(6)	0.0518(12)	0.6550(9)	0.3656(9)	0.036(3)	—
C(7)	0.1252(14)	0.8394(10)	0.1566(9)	0.048(3)	—
C(8)	0.1481(12)	0.9642(9)	0.0773(9)	0.036(3)	—
C(9)	0.2910(12)	0.9988(9)	0.0823(9)	0.037(3)	—
C(10)	0.4848(12)	1.0793(9)	0.1645(9)	0.036(3)	—
C(11)	0.5931(12)	0.9661(8)	0.2107(8)	0.032(3)	—
C(12)	0.5476(12)	0.8944(9)	0.3320(8)	0.032(3)	—
N	0.1757(16)	0.8240(9)	–0.1437(10)	0.068(4)	0.885(6)
C(15)	0.2311(15)	0.7318(9)	–0.0857(10)	0.049(4)	0.885(6)
C(16)	0.2937(19)	0.6157(10)	–0.0115(12)	0.069(4)	0.885(6)
Cl(1)	0.162(4)	0.783(3)	–0.151(3)	0.068(4)	0.115(6)
Cl(2)	0.357(4)	0.639(3)	0.0161(25)	0.069(4)	0.115(6)
C(17)	0.238(10)	0.637(3)	–0.066(6)	0.049(4)	0.115(6)

[a] U_{eq} is the cube root of the product of the principal axes of the thermal ellipsoid.
[b] Occupancies not listed are 1.0.

[Pd(16Se4)][BF_4]Cl (5), display *ccc* stereochemistry of the complex cations. NMR results indicated that, in aqueous solution, the [Pd(16Se4)]$^{2+}$ ion exists as an equilibrium mixture of *ctc* and *ccc* forms. The other possible configurations for coron and complexes of 16Se4, *ttt* and *cct*, have not been definitively observed (5).

*[16Se4][SO_3CF_3]$_2$·0.88MeCN·0.12CH_2Cl_2 (**2**·solv)*

The salt **2** co-crystallizes with a non-stoichiometric ratio of the solvent molecules from MeCN:CH_2Cl_2 (1:1 v/v). [16Se4]$^{2+}$ exists in the crystal as a discrete molecular dication, shown in Fig. 2. Selected bond distances and angles for **2** are given in Table 5. Additional data are presented as supplementary material (Tables S6-S9). The two transannular Se—Se bonds are nearly colinear. This configuration, in which the positive

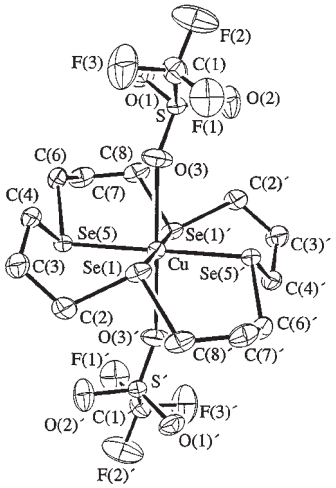
© 2000 NRC Canada

Table 4. Selected intramolecular distances (Å) and angles (°) for $[Cu(16Se4)][SO_3CF_3]_2$ (**1**) at 190 K.

Bond distances (Å)			
Se(1)—Cu	2.4592(9)	Se(1)—C(2)	1.961(8)
Se(1)—C(8)′[a]	1.962(6)	Se(5)—Cu	2.4553(9)
Se(5)—C(4)	1.974(7)	Se(5)—C(6)	1.951(6)
Cu—O(3)	2.464(5)		
Bond angles (°)			
Cu-Se(1)-C(2)	101.86(20)	Cu-Se(1)-C(8)′	107.29(21)
C(2)-Se(1)-C(8)′	95.0(3)	Cu-Se(5)-C(4)	101.05(19)
Cu-Se(5)-C(6)	104.80(21)	C(4)-Se(5)-C(6)	93.3(3)
Se(1)-Cu-Se(5)	91.60(3)	Se(1)-Cu-O(3)	82.73(13)
Se(5)-Cu-O(3)	90.12(12)	Cu-O(3)-S	147.3(4)

[a]′ indicates the symmetry related position $1 - x$, $1 - y$, $1 - z$.

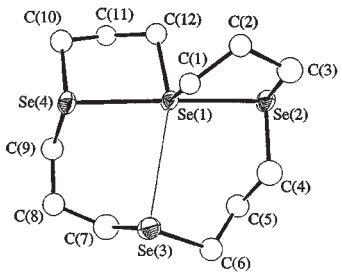
Fig. 1. Molecular structure of $[Cu(16Se4)][SO_3CF_3]_2$ (**1**) (Reproduced with permission from J. Am. Chem. Soc. **112**, 3706–3707 (1990).)



charges are delocalized over three selenium centers, is preferred over a two center transannular bond, as observed in the dication of 1,5-diselenacyclooctane (29), or the S—S transannular bond in the analogous dithiacyclooctane dication (30). The bonds to the central Se atom (Se(1)) are arranged in a pseudo-trigonal-bipyramidal geometry typical of tetracoordinate Se(IV), having the more electron withdrawing substituents ($Se^{\delta+}$) in the axial positions and the non-bonding electron pair in the equatorial plane. Similar nearly linear Se-Se-Se arrangements, displaying comparable Se—Se bond lengths, have been observed previously in the tris (selenourea) dication (31) (Se—Se 2.664(2) Å) and 6a-selenaselenophthene and its derivatives (2.548(3)–2.583(3) Å) (32).

The Se(1)—Se(3) contact distance (3.3941(20) Å), which is significantly less than twice the accepted Van der Waals radius of Se (3.8 Å), suggests a weak secondary interaction between these atoms. Although this contact could merely represent a constraint of the ring's size and its preferred conformation, the associated angles at both Se(1) and Se(3) are consistent with an attractive interaction. Se(3) is roughly trans to the Se(1)—C(12) bond (Se(3)-Se(1)-C(12) 160.2(3)°) and approximately orthogonal to the other bonds to Se(1)

Fig. 2. Molecular structure of $[16Se4][SO_3CF_3]_2 \cdot 0.89 MeCN \cdot 0.11CH_2Cl_2$ (**2**·solv) (Reproduced with permission from J. Am. Chem. Soc. **112**, 3706–3707 (1990).)



(Se(3)-Se(1)-C(1) 87.8(3)°; Se(3)-Se(1)-Se(2) 101.16(5)°; Se(3)-Se(1)-Se(4) 76.36(5)°). Thus, the environment of Se(1) might be better described as tending towards Ψ-octahedral with the lone pair trans to the Se(1)-C(1) bond. Furthermore, the Se(3)—-Se(1) vector makes angles with the bonds to Se(3) which describe a reasonable pyramidal environment for this selenium center (C(6)-Se(3)-Se(1) 94.4(3)°; C(7)-Se(3)-Se(1) 87.5(4)°). This secondary interaction may be a significant contributing factor to the overall asymmetry of the molecule, and thus indirectly to the inequality of the Se(1)—Se(2) (2.5916(15) Å) and Se(1)—Se(4) (2.6689(15) Å) bond lengths.

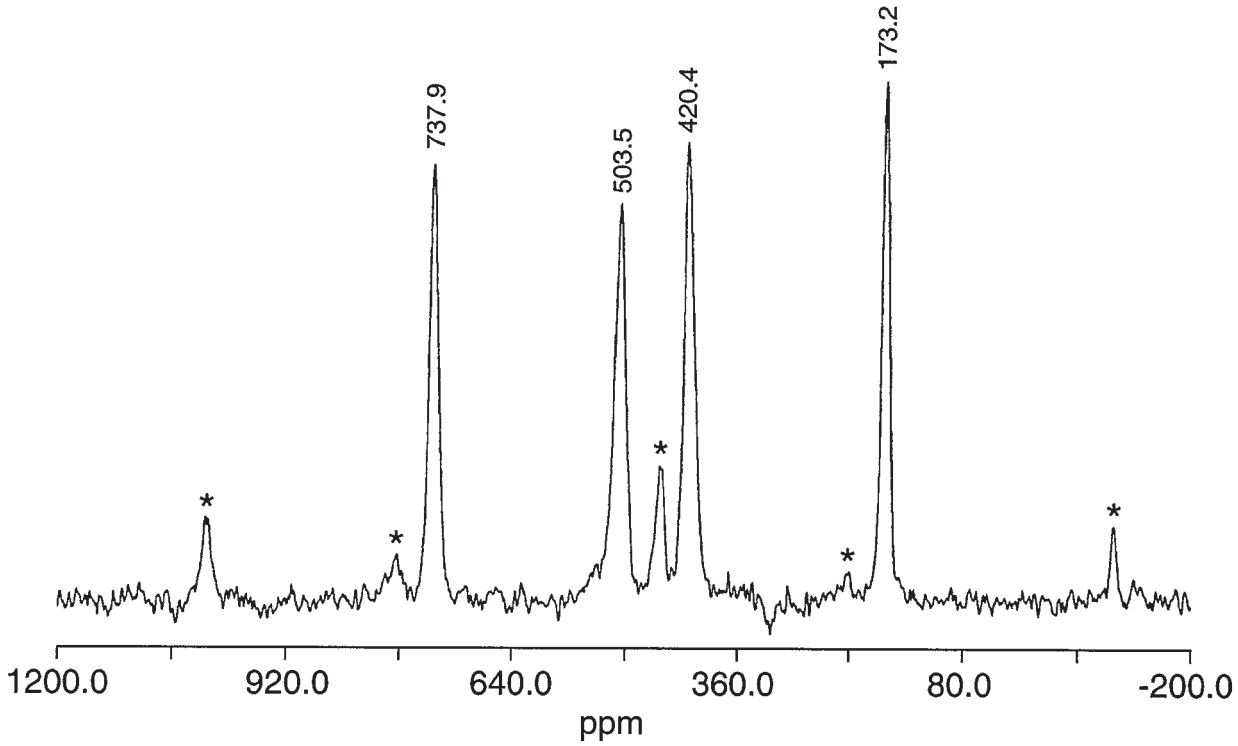
A few Se—O distances (3.152(7) Å Se(2)—O(2)′, where ′ = $1 - x$, $1 - y$, $1 - z$; 3.271(6) Å Se(2)—O(6); 3.299(8) Å Se(1)—O(6); 3.328(9) Å Se(3)—O(3)″, where ″ = $-x$, $1 - y$, $1 - z$) and one Se—F distance (3.294(7) Å Se(4)—F(2)‴, where ‴ = x, $1 + y$, z) are slightly shorter than the respective sums of the Van der Waals radii (3.42 Å and 3.37 Å). These are consistent with reasonable dipolar electrostatic attraction between cation and anion. The fact that Se(2) has two such Se-O interactions, whereas Se(4) has only one weaker Se-F interaction, would also appear to correlate with the asymmetry in the Se—Se bond lengths, in that the shorter of these bonds, Se(1)—Se(2), should be associated with slightly greater positive charge on Se(2) than on Se(4). The interionic interactions are clearly weaker than the S-O interactions in the triflate salt of the 1,5-dithiacyclooctane dication (30) (S—O 2.682(6) Å, cf. sum of Van der Waals radii 3.32 Å) in which the positive charge is more localized. Similarly, in the crystal structure of the tetrafluoroborate salt (acetonitrile solvate)

© 2000 NRC Canada

Table 5. Selected intramolecular distances (Å) and angles (°) for $[16Se4]^{2+}$ in $[16Se4][SO_3CF_3]_2 \cdot 0.89MeCN \cdot 0.11CH_2Cl_2$ (**2**·solv), at 195 K.

Bond distances (Å)			
Se(1)—Se(2)	2.5916(15)	Se(1)—Se(4)	2.6689(15)
Se(1)—C(1)	1.978(11)	Se(1)—C(12)	1.969(12)
Se(2)—C(3)	1.969(13)	Se(2)—C(4)	1.954(14)
Se(3)—C(6)	1.952(10)	Se(3)—C(7)	1.945(12)
Se(4)—C(9)	1.976(14)	Se(4)—C(10)	1.974(11)
Se(1)—Se(3)	3.3941(20)		
Bond angles (°)			
Se(2)-Se(1)-Se(4)	175.54(5)	Se(2)-Se(1)-C(1)	85.79(24)
Se(2)-Se(1)-C(12)	96.8(3)	Se(4)-Se(1)-C(1)	90.39(24)
Se(4)-Se(1)-C(12)	86.3(3)	C(1)-Se(1)-C(12)	102.0(5)
Se(1)-Se(2)-C(3)	92.3(3)	Se(1)-Se(2)-C(4)	88.9(3)
C(3)-Se(2)-C(4)	96.6(5)	C(6)-Se(3)-C(7)	95.2(5)
Se(1)-Se(4)-C(9)	96.6(3)	Se(1)-Se(4)-C(10)	89.1(3)
C(9)-Se(4)-C(10)	95.3(5)		

Fig. 3. Solid-state ^{77}Se CP-MAS NMR spectrum of $[16Se4][SO_3CF_3]_2 \cdot 0.89$ MeCN·$0.11CH_2Cl_2$ (**2**·solv). The peaks marked with asterisks are spinning side bands.



of the dication of 1,5-diselenacyclooctane (29), relatively strong Se-F interactions (2.81(1) and 2.89(2) Å) are observed.

While the formation of radical monocations and dications of polythiaethers is documented (33), and Musker et al. (34) have reported the oxidation of dithiacyclooctane derivatives by Cu (II) complexes, the present study reports the first selenium coronand dication resulting from an electron-transfer reaction of a metal-selenium coronand complex. The structures of other cyclic selena cations have also been reported, e.g. the radical monocation and dication of 1,2,4-triselena–3,5-diazacyclopentane (35), Se_8^{2+} and Se_{10}^{2+} (36, 37).

NMR Studies of 2

The ^1H NMR spectrum of the dication, $16Se4^{2+}$, in Me_2CO at ambient temperature consisted of several sharp, complex multiplets. Upon cooling these broadened and, at 180 K, the spectrum showed broad multiplets (reported in the Experimental section) as well as other unresolved broad peaks, suggesting a slow exchange process that had not reached the slow exchange limit. Saturation-transfer experiments at 180 K only permitted a partial assignment of the signals to α- and β-CH_2s.

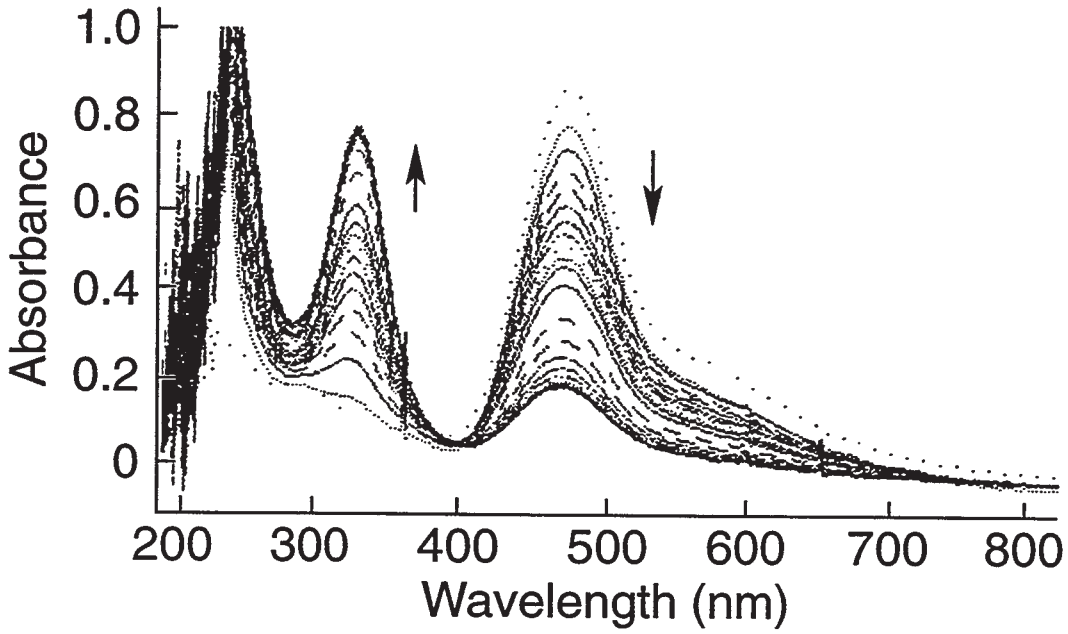
The solid-state CP-MAS ^{77}Se NMR spectrum of **2**·solv is shown in Fig. 3. Unfortunately, this is a difficult sample for

© 2000 NRC Canada

Table 6. Solid-state ^{77}Se CP-MAS NMR data of $[16Se4][SO_3CF_3]_2 \cdot 0.89MeCN \cdot 0.11CH_2Cl_2$ (**2**·solv).

Isotropic shift (ppm)	Width (Hz)	$\Sigma(r_{Se—F})^{-3}$ (Å^{-3})	Assignment	$\Delta\sigma$ (ppm)
173	73	0.0013	Se(1)	766 ± 25
420	152	0.0055	Se(2)	≤ 370
505	168	0.0086	Se(4)	509 ± 80
737	103	0.0035	Se(3)	771 ± 15

Fig. 4. UV–visible spectra of $[Cu(16Se4)][SO_3CF_3]_2$ (7.8×10^{-5} M) in CH_2Cl_2 in the presence of 16Se4 (1.78×10^{-5} M). The dotted line is the original spectrum of $[Cu(16Se4)][SO_3CF_3]_2$. The spectra were taken at intervals of 60 s.



solid-state NMR analysis, in that the proton T_1 times are long and a relaxation delay of 60 s was required. Figure 3 shows four lines, corresponding to the four unique selenium atoms in the asymmetric unit. These cover a surprisingly wide range of isotropic shift, given the chemical similarity of Se(2) and Se(4). The lines are of different widths, and have differing chemical shift anisotropies, as evidenced by spinning sidebands of varying intensities.

A tentative assignment can be made based on the varying linewidths, and on the fact that ^{19}F is not decoupled. Strong F-F dipolar coupling will render the Se-F dipolar coupling homogeneous (38) and thus a contributor to the ^{77}Se linewidth. Table 6 shows the average linewidths for each line, obtained from the spectrum shown in Fig. 3, and a second spectrum obtained at a lower spinning speed (3.0 kHz). Table 6 also shows the summation of $(r_{Se—F})^{-3}$ which should be a measure of the dipolar coupling. This sum was evaluated from the crystallographic data, including distances out to 6 Å. There is a reasonable correlation between width and the dipolar sum, leading us to make the tentative assignments shown. These assignments have the merit of giving Se(2) and Se(4) the closest pair of isotropic shifts, as would be expected on chemical grounds.

It is possible to estimate the chemical shift anisotropy from the intensities of the spinning sidebands (39). In Table 6, we give this as $\Delta\sigma = \sigma_{11} - \sigma_{33}$ for the various selenium atoms. For the line at 420 ppm no sidebands are observed, and the value given is an upper limit, based on the noise level of the spectrum. The uncertainties in the anisotropies are considerable because of the low intensities of the sidebands. The poor relaxation characteristics of this sample made measurements at lower spinning speeds, required for the determination of accurate anisotropies, impractical.

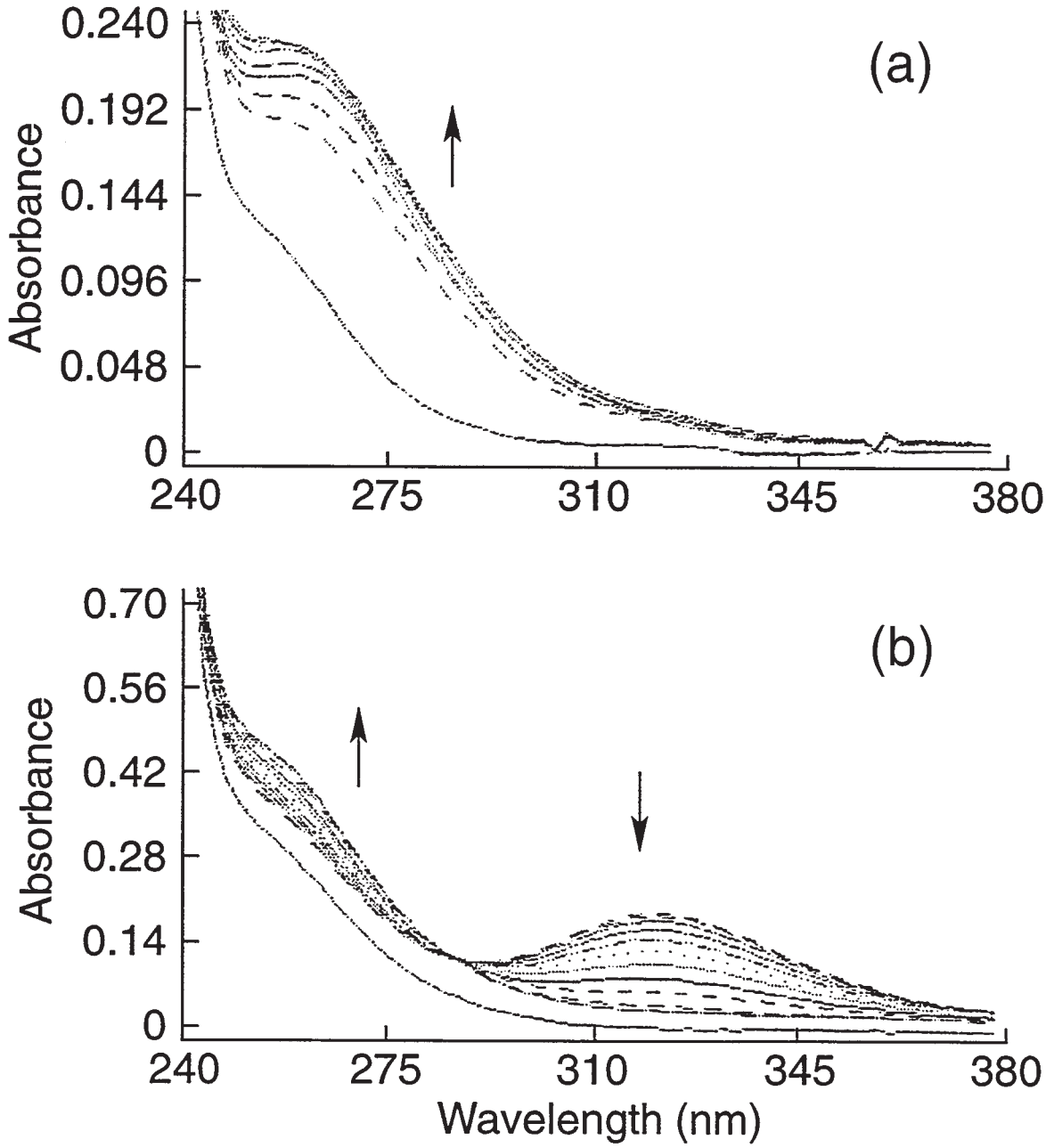
UV–visible spectroscopic studies of 1 and the radical cations of 16Se4

The UV–visible absorption spectrum of **1** in CH_2Cl_2 solution showed three absorption bands; λ_{max}(nm (ϵ)): 560 (2957), 464 (11920), 310 (1267). Addition of the ligand 16Se4 into a CH_2Cl_2 solution of **1** initiated a time dependent process, in which the intensities of the above absorption peaks decreased, together with a concomitant increase in the intensity of a new peak at 320 nm (Fig. 4). Similar behavior was also observed in a mixture of EtOH and THF.

To characterize the species that absorbs at 320 nm, 16Se4 was oxidized by $NOBF_4$ in CH_3CN solution in a UV-cell, and the mixture was monitored by UV–visible spectroscopy as soon as the $NOBF_4$ solution was added to the solution containing 16Se4. Continuous scanning was carried out at intervals of 300 s. In a typical experiment in which the concentrations of 16Se4 and $NOBF_4$ were both 5.3×10^{-4} M, a new absorption peak appeared at 320 nm whose intensity grew to a maximum value, following which it decreased, and a new peak appeared at 256 nm. There was an isosbestic

© 2000 NRC Canada

Fig. 5. UV–visible spectra of the 16Se4 radical cation recorded as a function of time. The radical cation was prepared by mixing 16Se4 with $NOBF_4$ in CH_3CN: (*a*) [$NOBF_4$] = 2.05 × 10^{-5} M; [16Se4] = 1.87 × 10^{-4} M. (*b*) [$NOBF_4$] = 2.05 × 10^{-5} M; [16Se4] = 5.62 × 10^{-4} M. The spectra were taken at intervals of 300 s. The bottom trace is the original spectrum of 16Se4.



point at about 290 nm, indicating the presence of at least two interconverting species.

Further experiments revealed that the above peak variation was dependent on the initial concentration of 16Se4. Thus, $NOBF_4$ in CH_3CN was added separately to solutions of 16Se4 of different concentrations, and UV–visible spectra were recorded as a function of time for each concentration (Table S10). At the lowest concentration of 16Se4 (1.87 × 10^{-4} M, entry 1), a peak at 256 nm was observed but the peak at 320 nm was almost absent. However, the absorption peak at 320 nm became more and more significant as the 16Se4 concentration increased (Fig. 5). At the highest concentration (entry 5), the peak at 320 nm first rose to a maximum and then fell, with a concomitant increase in intensity of the peak at 256 nm.

Oxidation of 16Se4 by $NOBF_4$ is a one-electron transfer reaction that yields the radical cation, $16Se4^{+\cdot}$. The spectroscopic results show that this radical cation is relatively stable and can be observed by UV–visible spectroscopy at room temperature. This is the first time that a selenium coronand radical cation has been detected in static conditions, to the best of our knowledge. The stability of $16Se4^{+\cdot}$ may be attributed to two-center three-electron (2c/3e) interactions (40, 41), which are well documented for the radical cations of thioethers (33*a*, 42–51) but not for the case of selenoethers (52). According to frontier molecular orbital theory (53), the

© 2000 NRC Canada

doubly and singly occupied non-bonding orbital would interact with one another to give bonding (σ) and *anti*-bonding (σ*) molecular orbitals which are occupied by three electrons. Such interactions between Se atoms, as shown in eq. [1], could be intramolecular and (or) intermolecular in nature.

[1] 

The absorption band at 320 nm is assigned to a σ–σ* transition of a dimeric radical cation, in which the 2c/3e bond is formed through interactions of an oxidized selenium in 16Se4 with a neutral selenium from another 16Se4, because the dimer is observed only at high concentrations. The absorption band at 256 nm is attributed to a σ–σ* transition of 2c/3e bonds formed through intramolecular (transannular) interactions, because it is observed at low concentrations of 16Se4.

The UV–visible absorption bands are correlated with the strength of the 2c/3e bonds and the position of the absorbance maximum of a σ–σ* transition is expected to depend on the extent of *p* orbital overlap and, therefore, the distance between the two interacting atoms (54, 55). The X-ray crystal structure of the dication $16Se4^{2+}$ shows bond distances between Se atoms that are within the sum of the covalent radii of Se, as was the case with other dications containing nearly linear Se-Se-Se arrangements (31, 32), and this species absorbs at 256 nm. This supports our assignment of the peak at 256 nm to a σ–σ* transition of a 2c/3e bond from a radical cation with transannular Se-Se interactions, and that at 320 nm to a σ–σ* transition from an intermolecular Se—Se bond formed in a dimeric radical cation.

EPR spectroscopy of 1

Analysis and simulation of the room temperature EPR spectrum of **1** in CH_3NO_2 solution gave an isotropic *g* value of 2.053 with hyperfine constants A^{Cu}_{iso} = 75G and A^{Se}_{iso} = 65 G. The low temperature EPR spectrum of **1**, measured at –148°C in CH_3NO_2:toluene (1:1 v/v), gave values of $g_{//}$ = 2.085, $A^{Cu}_{//}$ = 160 G; $g_{\perp}$ = 2.049, $A^{Cu}_{\perp}$ = 46 G. An EPR spectrum of **1** in CH_3NO_2 in the presence of added 16Se4 showed a decrease in intensity of the signals attributable to **1** and the emergence of new signals that overlapped with those of **1**, making analysis difficult. The new signals are presumably due to a species with radical cation character.

Electrochemistry of 1 and 16Se4

*Cyclic voltammetry of **1***

A cyclic voltammogram of **1** in CH_2Cl_2 on a Pt electrode was recorded. Over the scanning potential range from 1.6 to 0.3 V then back to 1.6 V, two redox waves were observed. The first redox wave with $E_{1/2}$ = 0.67 V vs. SCE at a scan rate of 20 mV/s showed an increase in the cathodic-anodic peak separation, ΔE_p, and a decrease in the ratio of anodic to cathodic current when the scan rate was increased. A plot of cathodic peak current i_c versus $\nu^{1/2}$ was linear, suggesting that the electrode reactions were diffusion controlled. The second redox wave appeared at $E_{1/2}$ = 1.06 V (ν = 20 mV/s). We tentatively assign the former to the redox pair $Cu(II)L^{+\cdot}/Cu(I)L^{+}$ (L = 16Se4) and the latter to the redox pair $Cu(II)L^{2+}/ Cu(II)L^{+\cdot}$. As the potential was swept in the cathodic direction up to –1.0 V, two more irreversible reduction peaks were seen at 0.087 V and –0.65 V. These peaks were attributed to the Cu(I)L/Cu redox couple, possibly due to the reduction of monomeric and polymeric Cu(I) complexes (6).

It is well known that Cu(I) undergoes a quick disproportionation reaction (56); for example, in aqueous solution the cyclic voltammogram of Cu(II) is irreversible. However, the cyclic voltammogram of **1** suggests that the redox reaction is partially chemically reversible over the timescale of the potential sweep, although the ΔE_p is large. The chemical reversibility may arise from the ability of chalcogen atoms to stabilize Cu(I) ions (57).

The large ΔE_p observed in the cyclic voltammogram of **1** suggests a kinetically quasi-reversible electrode process, which may result from the fact that electron transfer is slow. It may also suggest that electron transfer is not the sole process that takes place (58). Since changing the oxidation state from Cu(II) to Cu(I) would be accompanied by a significant configurational change (59, 60), it is possible that the spatial reorganization or conformational changes of 16Se4 may also contribute (61, 62).

Cyclic voltammetry of 16Se4

A typical cyclic voltammogram of 16Se4, measured on a platinum working electrode in CH_3CN solution, is shown in Fig. 6*a*. The potential scanning range was from 0 to 1.6 V vs. SCE. Two waves were observed with $E_{1/2}$ = 0.508 V, ΔE_p = 175 mV, and 1.41 V, ΔE_p = 150 mV at a scan rate of 50 mV/s. A plot of anodic peak current i_{a1} or i_{a2} versus $\nu^{1/2}$ was linear, suggesting that the electrode reactions were diffusion controlled. These two waves correspond to the following two redox reactions:

[2] $16Se4 - e \rightarrow 16Se4^{+\cdot}$

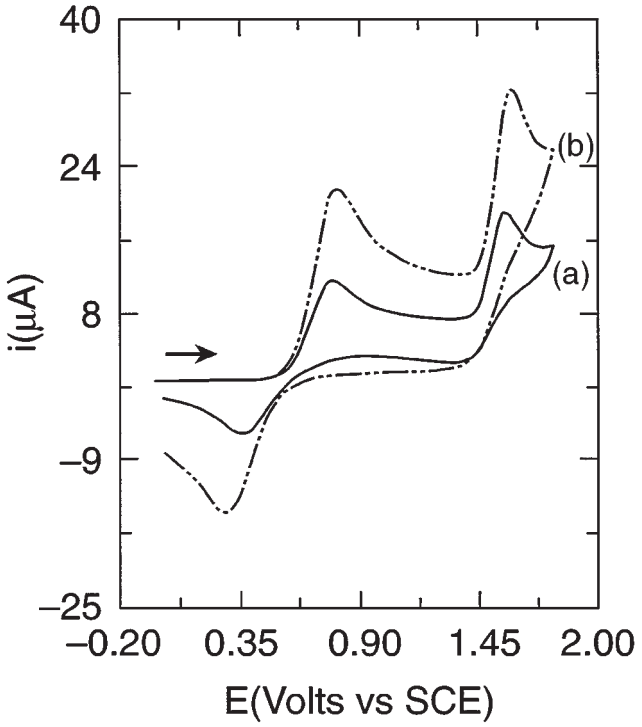
[3] $16Se4^{+\cdot} - e \rightarrow 16Se4^{2+}$

The separations between anodic and cathodic peak potentials were scan rate dependent, the peak separations increasing as the scan rate increased (compare Fig. 6*b* vs. 6*a*). This indicates that the electrode process is a quasi-reversible process. As the scan rates exceeded 200 mV/s (not shown), the redox reaction (3) became kinetically irreversible, as manifested by the disappearance of the second cathodic peak on the return scan. On the other hand, slow scan rates also altered the appearance of the cyclic voltammogram. At a scan rate of 5 mV/s (not shown), the second oxidation peak as well as the cathodic peak disappeared; the current plateaued after the first oxidation peak, but the first cathodic peak was still observed on the return scan. This behavior suggested complications arising from chemical reactions in solution.

To gain a better insight of the solution chemical reactions, we performed the cyclic voltammetry of 16Se4 at several initial concentrations with a scanning potential range of 0–1.2 V vs. SCE, in which only the first redox pair $16Se4/16Se4^{+\cdot}$ was of concern (data not shown). The results showed that for a given scan rate, as the initial concentrations were increased, the anodic current peak shifted to a

© 2000 NRC Canada

Fig. 6. Cyclic voltammograms of 16Se4 (1mM) in CH_3CN recorded at scan rates: (*a*) 50 mV/s; (*b*) 200 mV/s. Working electrode: Pt. Reference electrode: SCE. Electrolyte: 0.1 M tetraethylammonium perchlorate.



more positive potential while the cathodic current peak shifted to a more negative potential. In addition, the ratio of cathodic to anodic current became less than 1. Apparently, the solution chemical reactions become more significant at higher concentrations of 16Se4, affecting the concentration of the radical cation $16Se4^{+\cdot}$ and, in turn, the recovery of 16Se4 on the reverse scan. This behavior is consistent with the depletion of 16Se4 at the electrode surface by reaction with $16Se4^{+\cdot}$. The cyclic voltammetry data for the redox pair $16Se4/16Se4^{+\cdot}$ were further analyzed by convolution transformation by a numerical integration technique (15), using eq. 4.

$$[4] \qquad I(k\Delta t) = \frac{1}{\pi} \sum_{j=1}^{j=k} \frac{\Gamma(k-j+1/2}{(k-j)!} \Delta t^{1/2} i(j\Delta t)$$

where $I(k\Delta t)$ is the convolution transformation ($I(t)$) of the experimental $i(t)$; $\Gamma(x)$ is the Gamma function of x. The results are shown in Figs. 7 and S1. These plots show that the redox system is not reversible in general because none of the forward and backward curves is superimposable. Furthermore, the maximum of the $I(t)$ function is scan rate dependent; at the lowest scan rate, the $I(t)$ function attained its largest value. Figures 7 and S1 show that the reduction of the oxidized product is a time dependent phenomenon: faster scans resulted in more recovery, as shown by the overlapped curves ($I(t)$) of forward and backward scans at the starting point of convolution voltammetry; slower scans gave rise to less recovery, as shown by separated curves for the forward and backward scans at the starting point of convolution voltammetry. Concentration effects were also shown by the convolution transformation: more recovery of 16Se4 was achieved on the reverse scan for low initial 16Se4 concentrations, consistent with the observation of the i_c/i_a ratio from cyclic voltammetry (compare Fig. 7 vs. Fig. S1).

Comparison of the X-ray structures of 16Se4 and the 16Se4 dication shows that there are significant structural differences in these two molecules. 16Se4 has most of the C—Se bonds in *gauche* conformations (1). However, in the 16Se4 dication three selenium atoms are co-linear (4). In such an arrangement, the positive charges are on the two outside selenium atoms to achieve the best separation. The fourth selenium atom interacts with the central selenium atom with van der Waals forces so that the positive charges are dispersed among the four selenium atoms. This is probably also the case in solution, so that positive charges are delocalized among the selenium atoms, as suggested by Asmus et al. (40) for the case of lower sulfur analogues. Since the oxidation of $16Se4^{+\cdot}$ to $16Se4^{2+}$ occurs at higher potential, the formation of the dication of 16Se4 through disproportionation is unlikely.

Spectroelectrochemistry.

Electrolysis of a CH_3CN solution of 16Se4 indicated a concentration-dependent phenomenon (Fig. 8). When the concentration of 16Se4 was about 10^{-4} M, only the peak at 256 nm was observed. However, at a concentration of 16Se4 of about 10^{-3} M, peaks at both 322 nm and 256 nm were observed. This indicates that the species absorbing at 322 nm is only formed when the concentration of 16Se4 is high. A plot of the logarithm of the absorbance at 256 nm versus that at 322 nm gave a straight line with a slope of about 1 (ca. 0.88, $R = 0.99$). Once again, we suggest that the species absorbing at 322 nm is a dimeric radical cation $(16Se4)_2^{+\cdot}$, because it is formed only at high concentrations of 16Se4.

Coulometric studies of 16Se4 and cyclic voltammetry of 16Se4 under electrolysis.

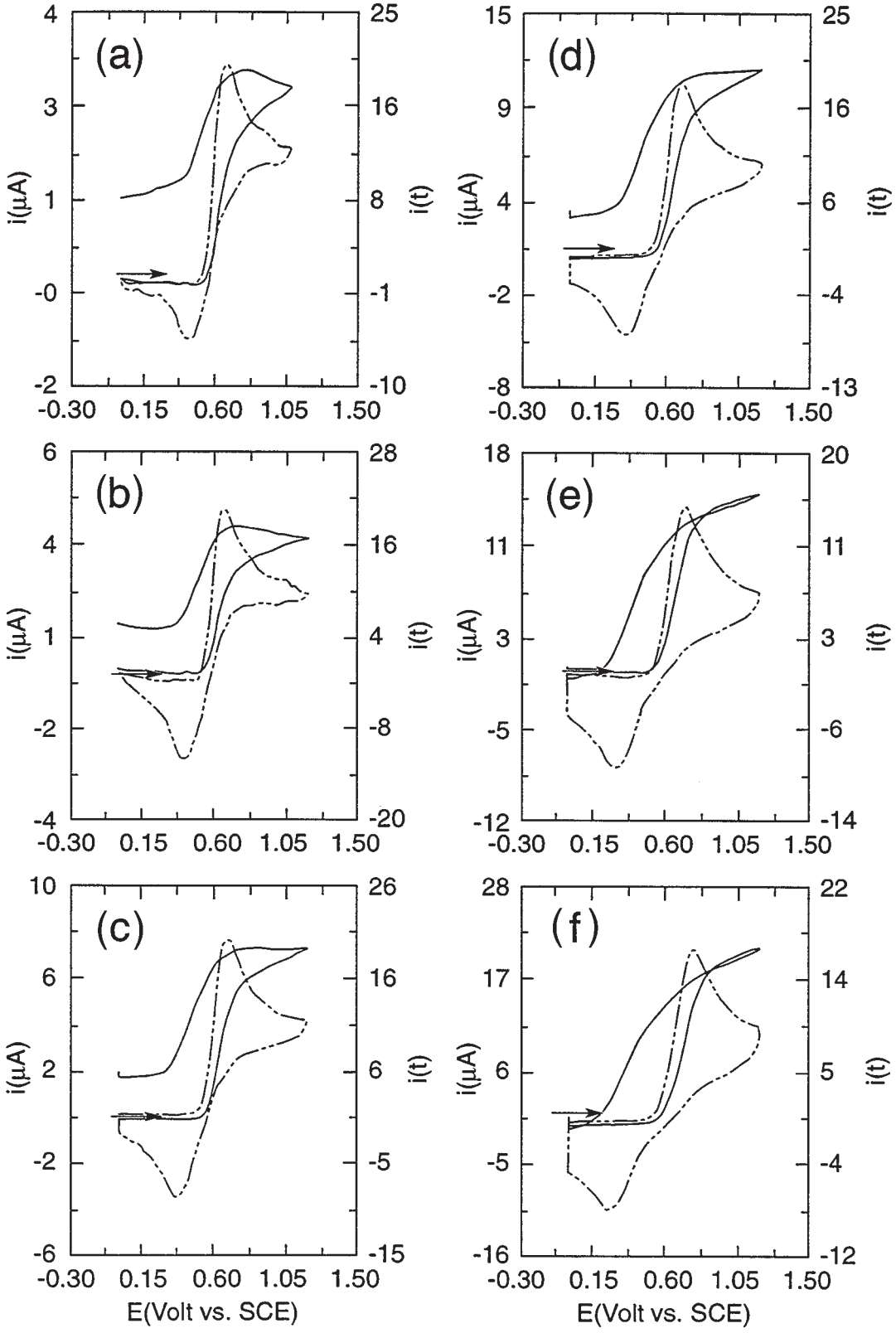
Electrolysis of 16Se4 at a pair of Pt gauze electrodes was undertaken. Two applied potentials (0.8 and 1.8 V vs. SCE) were chosen to effect oxidation of 16Se4 to the radical cation (one electron-transfer) and to the dication (two-electron transfer), as determined by cyclic voltammetry. These studies were performed while monitoring the electrolyte by UV–visible spectroscopy. The results of the experiments are given in the supplementary material.

Cyclic voltammetry experiments were performed on solutions of 16Se4 in CH_3CN that were being simultaneously electrolyzed with an applied potential of 1.2 V. Two sets of working electrodes were used. One set was a pair of Pt gauze electrodes for electrolysis; the other was a Pt microelectrode for cyclic voltammetry. The results of the experiments are described in the supplementary material.

The results of coulometry on 16Se4 support the contention that the dication, $16Se4^{2+}$ is formed by consecutive oxidation of $16Se4^{+\cdot}$; i. e., 16Se4 is first oxidized to $16Se4^{+\cdot}$, then to $16Se4^{2+}$. At the applied potential of 0.8 V, which is higher than the first anodic peak potential (E^1_{ap}) but lower than the second anodic peak potential (E^2_{ap}) on the cyclic voltammogram, no $16Se4^{2+}$ should be produced electrochemically because the potential is not anodic enough to oxidize $16Se4^{+\cdot}$. Therefore, at that potential the total number of

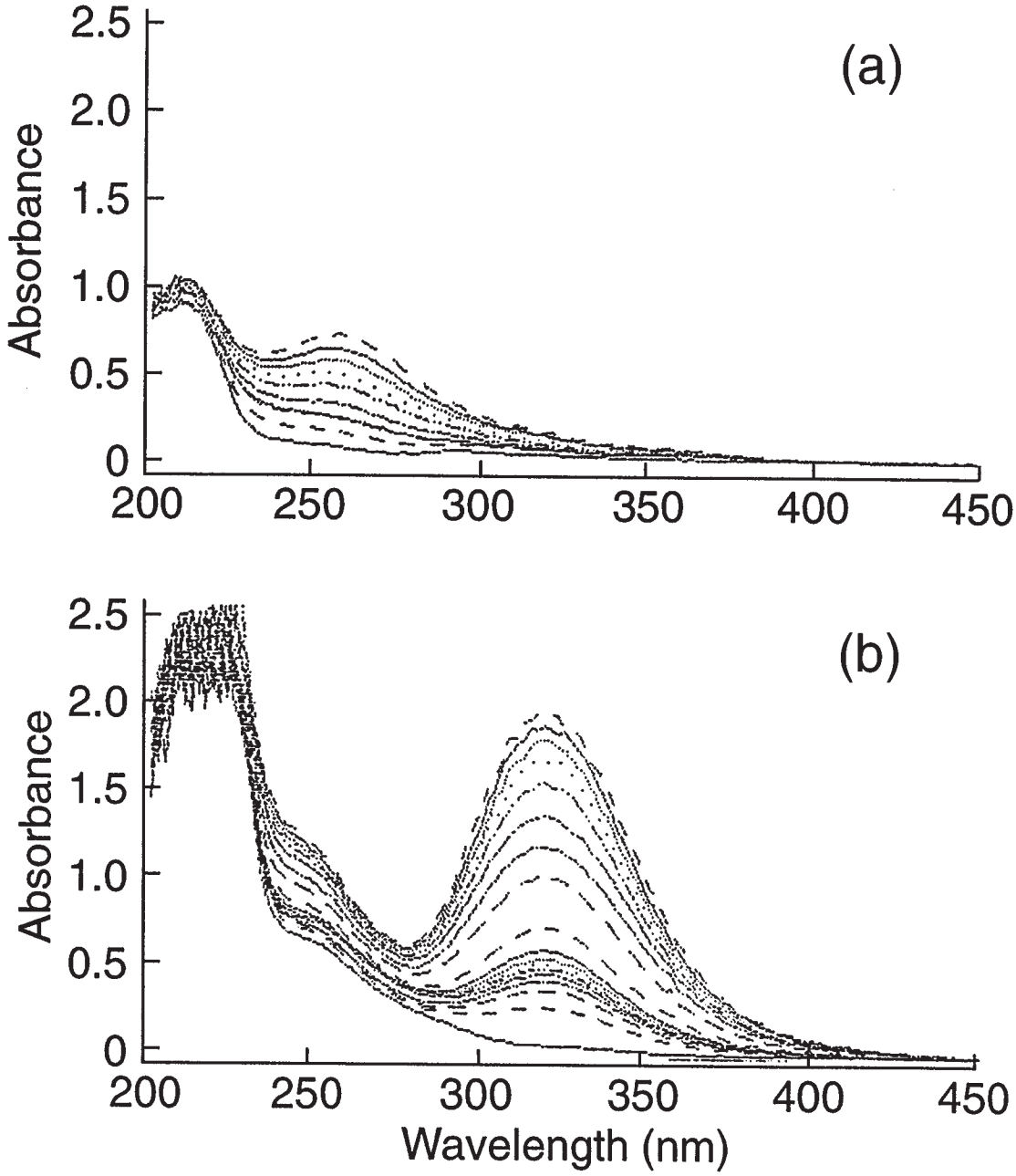
© 2000 NRC Canada

Fig. 7. Convolution transformation of voltammograms of 16Se4 for the first redox pair. Concentration of 16Se4 1.2 mM. (*a*) 0.01 V/s; (*b*) 0.02 V/s; (*c*) 0.05 V/s; (*d*) 0.1 V/s; (*e*) 0.2 V/s; (*f*) 0.5 V/s. The solid lines indicate the cyclic voltammograms and the dashed lines indicate the corresponding convolution transformation voltammograms.



© 2000 NRC Canada

Fig. 8. UV–visible spectra of 16Se4 on a Pt transparent electrode. The applied potential was 1.2 V vs. AgI/Ag. (*a*) [16Se4] = 1.02 × 10^{-4} M; (*b*) [16Se4] = 1.02 × 10^{-3} M. Electrolyte: 0.1 M tetraethylammonium perchlorate in CH_3CN. In each case, the lowermost curve is the initial curve.



electrons involved in the reaction should be one. However, if there were a disproportionation reaction, the total number of electrons involved in the reaction would be two even if the applied potential for electrolysis was not anodic enough to oxidize $16Se4^{+\cdot}$ to $16Se4^{2+}$, because 16Se4 could be regenerated through reaction (5).

[5] $$16Se4^{+\cdot} + 16Se4^{+\cdot} \rightleftharpoons 16Se4^{2+} + 16Se4$$

The results show that only one electron is involved in the electrolysis at a potential of 0.8 V vs. SCE, and two electrons are involved at a potential of 1.8 V, which unequivocally shows that the whole process of oxidizing 16Se4 to $16Se4^{2+}$ is a two-step oxidation, and that each step is a single electron transfer process. Combining all the information from UV–visible spectroscopy, cyclic voltammetry, spectroelectrochemistry, and coulometry, the fate of the radical cation, $16Se4^{+\cdot}$, may be summarized as in Scheme 1.

Kinetic analysis

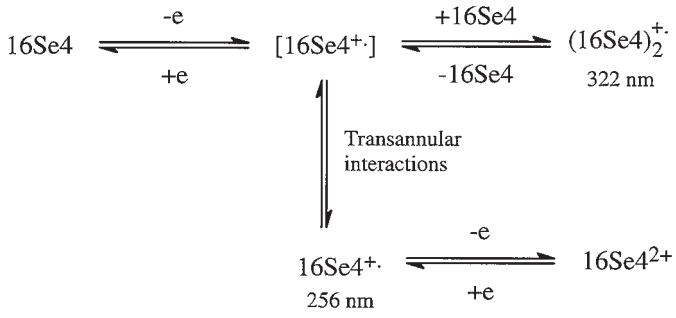
Rate law.

We have established that **1** undergoes a redox reaction with free ligand:

[6] $$2\ Cu(16Se4)^{2+} + 16Se4 \rightarrow 2\ Cu(16Se4)^{+} + 16Se4^{2+}$$

© 2000 NRC Canada

Scheme 1.



For simplicity the anion is not shown. The reaction was shown to be first order with respect to each of the reagents and to conform to the rate law as shown in eq. [7] (see supplementary material).

[7] $\text{Rate} = k_1\,[\text{Cu(II)}L^{2+}][L]$

The rate constant at 298 K is $(1.31 \pm 0.03) \times 10^3\ \text{M}^{-1}\text{s}^{-1}$ and the activation parameters are $\Delta H^{\#} = 32 \pm 2\ \text{kJmol}^{-1}$ and $\Delta S^{\#} = -103 \pm 10\ \text{Jmol}^{-1}\text{K}^{-1}$.

Reaction mechanism.

On the basis of the collective information described in the foregoing sections, we propose the following mechanism:

[8] $$\text{Cu(II)L}^{2+} + \text{L} \underset{k_{-1}}{\overset{k_1}{\rightleftharpoons}} \text{L}^{+\cdot} + \text{Cu(I)L}^{+}$$

[9] $$\text{Cu(II)L}^{2+} + \text{L}^{+\cdot} \overset{k_2}{\rightarrow} \text{L}^{2+} + \text{Cu(I)L}^{+}$$

The driving force for the reaction is presumably the formation of the thermodynamically more stable Cu(I) complex (6).

Conclusions

We have discovered a redox reaction between the Cu (II) complex of 16Se4 (**1**) and the free ligand 16Se4, which gives rise to a Cu(I) complex and the dication of 16Se4. The reaction products have been isolated and characterized by X-ray crystallography. Further investigation of the redox reaction by UV–visible spectroscopy, cyclic voltammetry, coulometry, and spectroelectrochemistry shows that, in the initial stages, the redox reaction is first order with respect to the concentrations of **1** and 16Se4, and the stoichiometry of the reaction is 2:1. The intermediates in the reaction have been characterized by UV–visible spectroscopy and electrochemical studies, and have been shown to be monomeric and dimeric radical cations of 16Se4 that absorb at 320 nm and 256 nm, respectively. Electrochemical studies have ruled out the disproportionation reaction of $16\text{Se4}^{+\cdot}$ as a possible pathway to give the dication, 16Se4^{2+}. The dication is formed instead through two consecutive one electron transfer steps, as depicted in Scheme 1.

Acknowledgements

We are grateful to S. Holdcroft and P.W. Percival for helpful discussions and to the Natural Sciences and Engineering Research Council of Canada for financial support.

Supplementary material available

Additional details of the structure determination of **1** and **2**·solv, and tables of additional bond lengths, angles, torsion angles, coordinates, isotropic temperature factors for the hydrogen atoms, anisotropic thermal parameters (11 pages); tables of calculated and observed structure factors for **1** and **2**·solv (36 pages); the concentration dependence of absorbance bands for $NOBF_4$ oxidation of 16Se4 (Table S10); details of the coulometric and electrolysis studies; details of the kinetic analysis; the convolution transformations at a higher concentration of 16Se4 (Fig. S1), and the cyclic voltammograms under electrolysis (Fig. S2) may be purchased from: The Depository of Unpublished Data, Document Delivery, CISTI, National Research Council Canada, Ottawa, Ontario, Canada, K1A 0S2.

References

1. R.J. Batchelor, F.W.B. Einstein, I.D. Gay, J.-H. Gu, B.D. Johnston, and B.M. Pinto. J. Am Chem. Soc. **111**, 6582 (1989).
2. I. Cordova-Reyes, E. VandenHoven, A. Mohammed, and B.M. Pinto. Can. J. Chem. **73**, 113 (1995).
3. I. Cordova-Reyes, H. Hu, J.-H. Gu, E. VandenHoven, A. Mohammed, S. Holdcroft, and B.M. Pinto. Can. J. Chem. **74**, 533 (1996).
4. R.J. Batchelor, F.W.B. Einstein, I.D. Gay, J.-H. Gu, B.M. Pinto, and X.-M. Zhou. J. Am. Chem. Soc. **112**, 3706 (1990).
5. R.J. Batchelor, F.W.B. Einstein, I.D. Gay, J.-H. Gu, B.M. Pinto, and X.-M. Zhou. Inorg. Chem. **35**, 3667 (1996).
6. R.J. Batchelor, F.W.B. Einstein, I.D. Gay, J.-H. Gu, and B.M. Pinto. J. Organomet. Chem. **411**, 147 (1991).
7. B.M. Pinto, R.J. Batchelor, F.W.B. Einstein, I.D. Gay, J.-H. Gu, and X.-M. Zhou. 76th Canadian Society for Chemistry Conference, Sherbrooke, Quebec. June, Abstr. 683 (1993).
8. (*a*) P.F. Kelly, W. Levason, G. Reid, and D.J.Williams. J. Chem. Soc. Chem. Commun. 1716 (1993); (*b*) W. Levason, J.J. Quirk, and G. Reid, J. Chem. Soc. Dalton Trans. 3713 (1996).
9. N.R. Champness, P.F. Kelly, W. Levason, G. Reid, A.M.Z. Slawin, and D.J. Williams. Inorg. Chem. **34**, 651 (1995).
10. (*a*) D.G. Booth, W. Levason, J.J. Quirk, G. Reid, and S.M. Smith. J. Chem. Soc. Dalton Trans. 3493 (1997); (*b*) M.K. Davies, W. Levason, and G. Reid, J. Chem. Soc. Dalton Trans. 2185 (1998); (*c*) W.G. Levason, G. Reid, and S.M. Smith. Polyhedron, **16**, 4253 (1997); (*d*) W. Levason, J.J. Quirkk, G. Reid, and S.M. Smith. J. Chem. Soc. Dalton Trans. 3719 (1997).
11. (*a*) H. Xu, W. Li, and X. Liu. Youji Huaxue, **13**, 52 (1993); (*b*) T. Kumagai and S. Akabori. Chem. Lett. 1667 (1989); (*c*) C. Bornet, R. Amardeil, P. Meunier, and J.C. Daran. J. Chem. Soc. Dalton Trans. 1039 (1999).
12. For example: (*a*) W.-P. Li, J. Wu, J.-G. Zhang, X.-F. Liu, and H.-S. Xu. Youji Huaxue, **16**, 436 (1996); (*b*) W.-P. Li, X.-F. Liu, and H.-S. Xu. Huaxue Xuebao, **52**, 1082 (1994); (*c*) W.-P. Li, X.-F. Liu, X.-R. Lu, and H.-S. Xu. Gaodeng Xuexiao Huaxue Xuebao, **52**, 1082 (1994); (*d*) W.-P. Li, J. Wu, X.-F. Liu, and H.-S. Xu. Gaodeng Xuexiao Huaxue Xuebao, **16**,

© 2000 NRC Canada

1558 (1995); (*e*) Y.-Q. Huang, S.-Z. Hu, W.-P. Li, X.-F. Liu, and H.-S. Xu. Jiegou Huaxue, **14**, 267 (1995); (*f*) W.-P. Li, X.-F. Liu, H.-S. Xu, Y.-Q. Huang, and S.-Z. Hu. Chin. J. Chem. **13**, 47 (1995); (*g*) Y. Liu, S.-P. Dong, Y. Inoue, and T. Wada. J. Chem. Res. Synop. 284 (1999); (*h*) A. Mazouz, P. Meunier, M.M. Kubicki, B. Hanquet, C.B. Amardeil, and A. Zahidi. J. Chem. Soc. Dalton Trans. 1043 (1997).

13. For example: (*a*) D.B. Rorabacher, M.M. Bernado, A.M.Q. Vande Linde, G.H. Leggett, B.C. Westerby, M.J. Martin, and L.A. Ochrymowycz. Pure Appl. Chem. **60**, 501 (1988); (*b*) M. Schröder. Pure Appl. Chem. **60,** 517 (1988); (*c*) S.R. Cooper. Acc. Chem. Res. **21**, 141 (1988); (*d*) M.J. Martin, J.F. Endicott, L.A. Ochrymowycz, and D.B. Rorabacher. Inorg. Chem. **26**, 3012 (1987); (*e*) A.J. Blake, R.O. Gould, A.J. Holder, T.I. Hyde, and M. Schröder. Polyhedron, **8**, 513 (1989); (*f*) A.J. Blake, R.O. Gould, J.A. Greig, A.J. Holder, T.I. Hyde, and M. Schröder. J. Chem. Soc. Chem. Commun. 876 (1989); (*g*) D.B. Rorabacher, M.M. Bernardo, M.J. Heeg, R.R. Schroeder, and L.A. Ochrymowycz. Inorg. Chem. **31**, 191 (1992).
14. T. Denguchi. J. Chem. Phys. **32**, 1584 (1960).
15. A.J. Bard and L.R. Faulkner. Electrochemical methods: Fundamentals and applications. John Wiley & Sons, New York. 1980.
16. N. Winograd. *In* Laboratory techniques in electroanalytical chemistry. *Edited by* P.T. Kissinger. Marcel Dekker, New York. 1984. pp. 321–335.
17. T. Kuwana, R.K. Darlington, and D.W. Leedy. Anal. Chem. **36**, 2023 (1964).
18. W. vonBenken and T. Kuwana. Anal. Chem. **42**, 1114 (1970).
19. P.G. Moniotte, A.J. Hubert, and P. Teyssie. J. Organomet. Chem. **88**, 115 (1975).
20. J.R. Carruthers and D.J. Watkin. Acta Crystallogr. Sect. A: Cryst. Phys. Diffr. Theor. Gen. Crystallogr. **A35**, 698 (1979).
21. International tables for X-ray crystallography. Kynoch, Birmingham, England. 1975. Vol. IV, p. 99.
22. E.J. Gabe, Y. LePage, J-P. Charland, F.L. Lee, and P.S. White. NRCVAX — An interactive program system for structure analysis. J. Appl. Crystallogr. **22**, 384 (1989**)**.
23. D.J. Watkin, J.R. Carruthers, and P.W. Betteridge. CRYSTALS, Chemical cystallography laboratory, Univ. of Oxford, Oxford, England. 1984.
24. V.V. Pavlishchuk, K.B. Yatsimirskii, P.E. Strizhak, and J. Labuda. Inorg. Chim. Acta. **164**, 65 (1989).
25. For example: B.V. Gorewit and W.K. Musker. J. Coord. Chem. **5**, 67 (1976).
26. V.B. Pett, L.L. Diaddario, Jr., E.R. Dockal, P.W. Corfield, C. Ceccarelli, M.D. Glick, L.A. Ochrymowycz, and D.B. Rorabacher. Inorg. Chem. **22**, 3661 (1983).
27. P.F. Kelly, W. Levason, G. Reid, and D.J. Williams. J. Chem. Soc. Chem. Commun. 1716 (1993).
28. N.R. Champness, P.F. Kelly, W. Levason, G. Reid, A.M.Z. Slawin, and D.J. Williams. Inorg. Chem. **34**, 651 (1995).
29. H. Fujihara, R. Akaishi, T. Erata, and N. Furukawa. J. Chem. Soc. Chem. Commun. 1789 (1989).
30. F. Iwasaki, N, Toyoda, R. Akaishi, H. Fujihara, and N. Furukawa. Bull. Chem. Soc. Jpn. **61**, 2563 (1988).
31. S. Hauge. Acta Chem. Scand. A. **33**, 317 (1979).
32. A. Hordvik and J.A. Porten. Acta Chem. Scand. A, **27**, 485 (1973), and refs. therein.
33. For example: (*a*) K.D.Asmus. Acc. Chem. Res. **12**, 436 (1979). W.K. Musker. Acc. Chem. Res. **13**, 200 (1980); (*b*) M. Tamaoki, M. Serita, Y. Shiratori, and K. Itoh. J. Phys. Chem. **93**, 6052 (1989); (*c*) T. Drewello, C.B. Lebrilla, K.-D. Asmus, and H. Schwarz. Angew. Chem. Int. Ed. Engl. **28**, 1275 (1989).
34. (*a*) W.K. Musker and T.L. Wolford. J. Am. Chem. Soc. **98**, 3055 (1976); (*b*) W.K. Musker, M.M. Olmstead, and R.M. Kessler. Inorg. Chem. **23**, 1764 (1984).
35. E.G. Awere, J. Passmore, P.S. White, and T. Klapotke. J. Chem. Soc. Chem. Commun. 1415 (1989).
36. R.K. McMullan, D.J. Prince, and J.D. Corbett. Inorg. Chem. **10**, 1749 (1971).
37. R.C. Burns, W.-L. Chan, R.L. Gillespie, W.-C. Luk, J.F. Sawyer, and D.R. Slim. Inorg. Chem. **19**, 1432 (1980).
38. M.M. Maricq and J.S.Waugh. J. Chem. Phys. **70**, 3300 (1979).
39. J. Herzfeld and A. Berger. J. Chem. Phys. **73**, 6021 (1980).
40. K.-D. Asmus, D. Bahnemann, C.-H. Fischer, and D. Veltwisch. J. Am. Chem. Soc. **101**, 5322 (1979).
41. T. Bally. *In* Radical ionic systems-properties in condensed phases. *Edited by* A. Lund and M. Shiotani. Kluwer Academic, Dodrecht. 1991.
42. R.O.C. Norman, B.C. Gilbert, and D.K.C Hodgeman. J. Chem. Soc. Perkin Trans. 2, 1748 (1973).
43. K.-D. Asmus, M. Bonifacic, and H. Mockel. J. Chem. Soc. Perkin Trans. 2, 675 (1975).
44. K.-D. Asmus, H.A. Gills, and G.G. Teather. J. Phys. Chem. **82**, 2677 (1978).
45. K.-D. Asmus, M. Göbl, and M. Bonifacic. J. Am. Chem. Soc. **106,** 5984 (1984).
46. K.-D. Asmus and M. Bonifacic. J. Org. Chem. **51**, 1216 (1986).
47. K.-D. Asmus, T. Drewello, C.B. Lebrilla, and H. Schwarz. Angew. Chem. Int. Ed. Engl. **28**, 1275 (1989).
48. S.F. Nelsen, R.W. Alder, R.B. Sessions, K.-D. Asmus, K.-O. Hiller, and M. Göbl. J. Am. Chem. Soc. **102**, 1429 (1980).
49. K.-O. Hiller, B. Masloch, M. Göbl, and K.-D. Asmus. J. Am. Chem. Soc. 2734 (1981).
50. W.K. Musker and P.B. Roush. J. Am. Chem. Soc. **98**, 6745 (1976).
51. W.K. Musker, T.L. Wolford, and P.B. Roush. J. Am. Chem. Soc. **100**, 6416 (1978).
52. F. Williams and K. Nishikida. Chem. Phys. Lett. **34**, 302 (1975).
53. T.A. Albright, J.K. Burdett, and M.-H. Whangbo. Orbital interactions in chemistry. John Wiley & Sons, New York. 1985.
54. M.H. Cohen. Phys. Rev. **101**, 1432 (1956).
55. M.C.R. Symons. Faraday Discuss. Chem. Soc. **63**, 280 (1978).
56. A. McAuley. Coord. Chem. Rev. **5**, 245 (1970).
57. S.G. Murray and F.R. Harthley. Chem. Rev. **81**, 365 (1981).
58. W.K. Musker, M.M. Olmstead, and R.M. Kessler. Inorg. Chem. **23**, 3266 (1984).
59. D.B. Rorabacher, E.R. Dockal, T.E. Jones, W.F. Sokol, R.J. Engerer, and L.A. Ochrymowycz. J. Am. Chem. Soc. **98**, 4322 (1976).
60. D.B. Rorabacher, N.E. Meagher, K.L. Juntunene, P.V. Robandt, G.H. Leggett, C.A. Salhi, B.C. Dunn, R.R. Schroeder, and L.A. Ochrymowycz. Pure Appl. Chem. **65**, 573 (1993).
61. C.A. Salhi, Q.Yu, M.J. Heeg, N.M. Villeneuve, K.L. Juntunen, R.R. Schroeder, L.A. Ochrymowycz, and D.B. Rorabacher. Inorg. Chem. **34**, 6053 (1995).
62. N.M. Villeneuve, R.R. Schroeder, L.A. Ochrymowycz, and D.B. Rorabacher. Inorg. Chem. **36**, 4475 (1997).

© 2000 NRC Canada

Nuclear magnetic shielding tensors for the carbon, nitrogen, and selenium nuclei of selenocyanates — a combined experimental and theoretical approach

Guy M. Bernard, Klaus Eichele, Gang Wu, Christopher W. Kirby, and Roderick E. Wasylishen

Abstract: The principal components of the carbon, nitrogen, and selenium chemical shift (CS) tensors for several solid selenocyanate salts have been determined by NMR measurements on stationary or slow magic-angle-spinning powder samples. Within experimental error, all three CS tensors are axially symmetric, consistent with the expected linear geometry of these anions. The spans (Ω) of the carbon and selenium CS tensors for the selenocyanate anion ($SeCN^-$) are approximately 300 and 800 ppm, respectively, much less than the corresponding values for carbon diselenide (CSe_2). This difference is a consequence of the difference in the CS tensor components perpendicular to the C_∞ symmetry axes in these systems. Ab initio calculations show that the orbital symmetries of these compounds are a significant factor in the shielding. For CSe_2, efficient mixing of the σ and π orbitals results in a large paramagnetic contribution to the total shielding of the chemical shielding tensor components perpendicular to the molecular axis. Such mixing is less efficient for the $SeCN^-$, resulting in a smaller paramagnetic contribution and hence in greater shielding in directions perpendicular to the molecular axis.

Key words: selenocyanates, solid-state NMR, carbon shielding tensors, nitrogen shielding tensors, selenium shielding tensors, ab initio calculations.

Résumé : À partir de mesures RMN sur des échantillons de poudre stationnaires ou à rotation lente à l'angle magique de plusieurs sélénocyanates solides, on en a déterminé les principaux composant des tenseurs des déplacements chimiques (DC) du carbone, de l'azote et du sélénium. Dans les limites des erreurs expérimentales, les trois tenseurs des DC sont axialement symétriques, ce qui est en accord avec la géométrie linéaire attendue pour ces anions. Les plages, Ω, des tenseurs du carbone et du sélénium pour l'anion sélénocyanate ($SeCN^-$), sont approximativement de 300 et de 800 ppm respectivement, des valeurs beaucoup plus faible que les valeurs correspondantes observées dans le disélénure de carbone (CSe_2). Cette différence est une conséquence de la différence dans les composants du tenseur DC qui sont perpendiculaire aux axes de symétrie C_2 dans ces systèmes. Des calculs ab initio montrent que les symétries des orbitales de ces composés sont un facteur important dans le blindage. Pour le CSe_2, une combinaison efficace des orbitales σ et π conduit à une contribution paramagnétique importante au blindage total des composantes du tenseur de blindage chimique perpendiculaires à l'axe moléculaire. Une telle combinaison est moins efficace pour le $SeCN^-$; il en résulte que la contribution paramagnétique est plus faible et, en conséquence, que le blindage est plus grand dans les directions perpendiculaires à l'axe moléculaire.

Mots clés : sélénocyanates, RMN à l'état solide, tenseurs de blindage du carbone, tenseurs de blindage de l'azote, tenseurs de blindage du sélénium, calculs ab initio.

Introduction

The selenocyanate ligand ($SeCN^-$) has been of considerable interest because of its ambidentate nature (1). That is, it may coordinate to a metal through the nitrogen, the selenium, or by various bridging modes. In the absence of diffraction data, NMR spectroscopy may provide the most reliable information concerning the coordination and structure of these ligands. A review by Duddeck provides an overview of the ^{77}Se NMR literature including the results of several solution NMR studies of organic selenocyanate compounds (2). Carbon-13 and nitrogen-14 or -15 NMR results for selenocyanates have been discussed in several reviews (3, 4). The coordination of metal atoms with several selenocyanate anions has been investigated by solution NMR (5, 6). An analogous study of the thiocyanate anion in copper(I) complexes was conducted using solid-state ^{13}C

Received January 27, 2000. Published on the NRC Research Press website on May 12, 2000.

G.M. Bernard, K. Eichele, G. Wu, C.W. Kirby, and R.E. Wasylishen.[1] Department of Chemistry, Dalhousie University, Halifax, NS B3H 4J3, Canada.

[1]Author to whom correspondence may be addressed. Telephone: (902) 494-2564. Fax: (902) 494-1310. e-mail: Roderick.Wasylishen@Dal.Ca

© 2000 NRC Canada

NMR (7). In addition to providing insight into the coordination mode of the cation in these complexes, this study showed that conclusions about coordination to the metal drawn from solution NMR studies cannot always be extended to solids.

With four NMR-active nuclei, ^{13}C, ^{14}N, ^{15}N, and ^{77}Se, much information may be gained from solid-state NMR studies of $SeCN^-$. For example, internuclear distances may be determined from dipolar interactions, and information about the bonding modes of $SeCN^-$ is available from isotropic chemical shifts and spin–spin coupling constants. Also, examination of stationary powder samples provides the principal components of the chemical shift (CS) tensors, which potentially contain a wealth of structural information. Before embarking on a solid-state NMR study of selenocyanate–metal complexes, it is important to understand the shielding tensors for the uncoordinated ligand. Towards this end, we present the results of solid-state NMR studies of the carbon, nitrogen, and selenium CS tensors for selenocyanate salts $M^+[SeCN]^-$, M = K, NH_4, or NMe_4. Also presented are the preliminary results of a solid-state ^{13}C NMR study of a related compound, potassium cyanate. The interpretation of the observed magnetic shielding tensors is aided by high-level ab initio calculations.

Selenocyanate anions are thought to be linear; the selenocyanate ion of a copper complex which had been reported as bent (8) has recently been shown to be linear (9). Linear systems are ideal for a study of nuclear magnetic shielding since, in the absence of intermolecular effects, the orientation of the axially symmetric CS tensor is known exactly and the unique component of the CS tensor, along the C_∞ symmetry axis, is dependent only on the diamagnetic term of the shielding (*vide infra*). The relative simplicity of these systems allows one to identify the specific molecular orbitals (MOs) responsible for the paramagnetic shielding.

Although carbon and nitrogen shielding tensors are available for most functional groups, corresponding data for selenium are not as widespread (10). The first comprehensive experimental study of selenium CS tensors was that of Collins et al. (11). A surprising feature of the selenocyanate ligands is that the spans of the carbon and selenium CS tensors are much smaller than those of CSe_2 (12). With high-level ab initio calculations on $SeCN^-$ and CSe_2, the MOs responsible for the different magnetic shielding in these closely related compounds were identified.

Background theory

It is convenient to discuss the nuclear magnetic shielding (σ) of nuclei in linear molecules or ions using Ramsey's theory (13). In this model, the magnetic shielding is expressed as the sum of diamagnetic (σ^d) and paramagnetic (σ^p) components (14):

$$[1] \qquad \sigma_{ii} = \sigma_{ii}^{d} + \sigma_{ii}^{p}$$

where

$$[2] \qquad \sigma_{ii}^{d} = \frac{\mu_0}{4\pi}\frac{e^2}{2m}\left\langle 0\right| \sum_k \frac{r_k^2 - r_{ki}^2}{r_k^3} \left|0\right\rangle$$

and

$$[3] \qquad \sigma_{ii}^{p} = \frac{-\mu_0}{4\pi}\frac{e^2}{2m^2}\sum_{n>0}\frac{1}{E_n - E_0}[\left\langle 0\right| \sum_k \frac{\boldsymbol{l}_{ki}}{r_k^3}\left|n\right\rangle\left\langle n\right| \boldsymbol{l}_{ki} \left|0\right\rangle + \left\langle 0\right| \sum_k \boldsymbol{l}_{ki}\left|n\right\rangle\left\langle n\right| \sum_r \frac{\boldsymbol{l}_{ki}}{r_k^3} \left|0\right\rangle]$$

In the above equations, μ_0 is the permeability of free space, e and m are the electron charge and rest mass, respectively, while $\langle 0|$ and $\langle n|$ represent ground and excited electronic states of the molecule with electronic energy E_0 and E_n, respectively. The position vector for electron k is defined by $\boldsymbol{r}_k$ and $\boldsymbol{l}_{ki}$ is the angular momentum operator. Equations 2 and 3 describe the shielding in the directions of the principal components of the chemical shielding tensor and are valid only if the nucleus of interest is chosen as the gauge origin. Expressions for the off-diagonal elements of the chemical shielding tensor and for different gauge origins have been derived (14, 15).

The contribution to shielding from σ^d (eq. [2]) is always positive, leading to increased shielding relative to the bare nucleus. Because σ^d depends only on the ground electronic state of the molecule, it can be calculated accurately at relatively low levels of theory and hence is expected to be essentially invariant to basis set size or to the effects of electron correlation. Gierke and Flygare (16) have shown that σ^d may be approximated if the molecular structure is known. For example, the shielding for nucleus A in the x-direction may be approximated by:

$$[4] \qquad \sigma_{xx}^{d} \approx \sigma_{av}^{d}(\text{free atom}) + \frac{\mu_0}{4\pi}\frac{e^2}{2m}\sum_{B\neq A}\frac{Z_B}{r_{AB}^3}(y_B^2 + z_B^2)$$

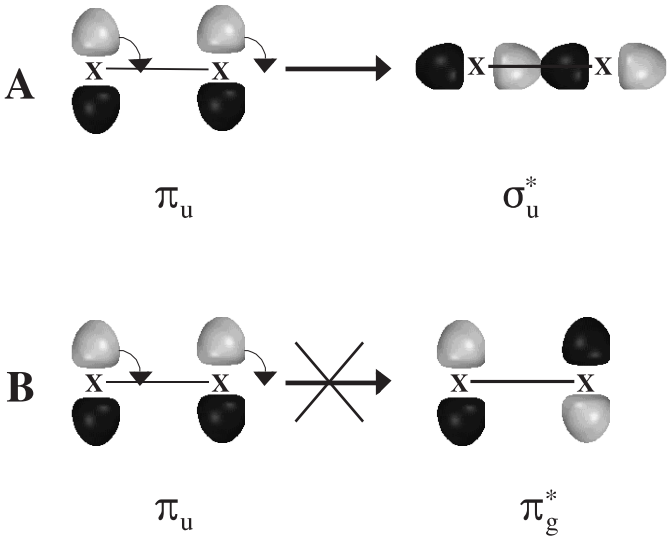
where σ_{av}^{d}(free atom) is the shielding for the "free" atom. The summation is carried out over all other atoms in the molecule, Z_B is the atomic number of the atom being summed, y_B and z_B are the Cartesian coordinates of the atoms which are a distance r_{AB} from the origin (the site of the observed nucleus). The remaining tensor components may be approximated by cyclic permutations of eq. [4]. In linear molecules, the component of the chemical shielding tensor along the C_∞ axis is labelled $\sigma_\parallel$ while the two components perpendicular to this axis are labelled $\sigma_\perp$. Since $\sigma_\parallel^p = 0$ for the nuclei of linear molecules, it follows from eq. [4] that:

$$[5] \qquad \sigma_\parallel = \sigma_\parallel^d \approx \sigma_{av}^d \quad (\text{free atom})$$

The paramagnetic term (eq. [3]) is a second-order electronic property which depends on the mixing of ground and excited electronic states of the molecule. These states correspond approximately to the occupied and unoccupied MOs (17). The paramagnetic term is usually negative and is inversely proportional to the difference in the electronic energy of the orbitals undergoing mixing. Contributions to σ^p arise from induced electron motion in the plane perpendicular to the direction of the applied magnetic field such that charge appears to rotate (17). This can be understood by considering the action of the angular momentum operator in eq. [3]. For example, consider $\boldsymbol{l}_z|p_x\rangle$; the operator $\boldsymbol{l}_z$ rotates p_x by 90° about the z-axis. Thus, there is an effective mixing between p_x and p_y. Mixing of MOs can only occur between occupied and unoccupied MOs with magnetic-dipole allowed symmetry. This is shown graphically in Fig. 1.

© 2000 NRC Canada

Fig. 1. Examples of magnetic-dipole allowed (A) and forbidden (B) mixing of orbitals for a hypothetical diatomic molecule with an applied magnetic field perpendicular to the page.



Mixing of π_u and σ_u^* MOs (Fig. 1A) is magnetic-dipole allowed, but mixing of π_u and π_g^* MOs (Fig. 1B) is forbidden by symmetry. Hence, significant deshielding is expected in directions perpendicular to the symmetry planes of occupied and virtual MOs that have the proper symmetry for mixing, and that are separated by a small energy difference. It is of interest to point out that a related discussion of nuclear shielding in terms of electronic current density conveniently leads to equivalent partitioning of the diamagnetic and paramagnetic terms (eqs. [1]–[3]) (18).

In eqs. [1]–[5], σ denotes the magnetic *shielding* relative to the bare nucleus such that $\sigma_{33} \geq \sigma_{22} \geq \sigma_{11}$. While ab initio methods calculate shielding, experimentally one measures a chemical *shift* (δ_{ii}) relative to a given reference with the convention $\delta_{11} \geq \delta_{22} \geq \delta_{33}$. The two are related by:

$$[6] \qquad \delta_{ii} = \frac{\nu_{ii} - \nu_{ref}}{\nu_{ref}}(10^6) = \frac{\sigma_{ref} - \sigma_{ii}}{1 - \sigma_{ref}}$$

where ν_{ii} and ν_{ref} are the resonance frequencies of the principal tensor components for the nucleus of interest and for the reference sample, respectively. Since $1 - \sigma_{ref} \approx 1$, $\delta_{ii} \approx \sigma_{ref} - \sigma_{ii}$. In the ensuing sections the experimental results will be discussed in terms of chemical shifts and the theoretical results will be discussed in terms of chemical shielding. The experimental data are related to those calculated by ab initio methods by using an absolute shielding scale for the nucleus of interest (19). Absolute shielding scales for carbon (20), nitrogen (21), and selenium (22) have been established by Jameson and coworkers.

It is convenient to discuss the NMR line shape of static powder samples in terms of the span, $\Omega = \sigma_{33} - \sigma_{11} \approx \delta_{11} - \delta_{33}$, and the skew, $\kappa = 3(\sigma_{iso} - \sigma_{22})/\Omega = 3(\delta_{22} - \delta_{iso})/\Omega$(23). With a few exceptions (24), $\sigma_\parallel > \sigma_\perp$ and $\kappa = +1.0$ for linear molecules with perfect axial symmetry.

Experimental

Ammonium selenocyanate (25) and tetramethylammonium selenocyanate (26) were prepared according to literature methods. Potassium cyanate and potassium selenocyanate were purchased from Aldrich and used without further purification.

Natural abundance ^{13}C, ^{15}N, and ^{77}Se NMR spectra were obtained on Bruker MSL-200 and AMX-400 NMR spectrometers (B_0 = 4.7 and 9.4 T, respectively). Samples were packed into 7 and 4 mm o.d. zirconium oxide rotors. Cross polarization (CP) and high-power proton decoupling were employed in acquiring all NMR spectra, except for KSeCN, where spectra were acquired after a single pulse. Unless otherwise noted, recycle delays were 5 s. Carbon chemical shifts were referenced to tetramethylsilane by setting the high-frequency isotropic peak of solid adamantane to 38.56 ppm (27). Nitrogen chemical shifts were referenced to $NH_3(\ell$, 293 K) by setting the NMR peak of the ammonium ion in solid $^{15}NH_4NO_3$ to +23.8 ppm. The chemical shift for $CH_3NO_2(\ell)$, another common nitrogen chemical shift reference, is 380.20 ppm with respect to $NH_3(\ell$, 293 K) (28). Selenium chemical shifts were referenced to $Se(CH_3)_2(\ell)$ by setting the ^{77}Se NMR peak of solid $(NH_4)_2SeO_4$ to +1040.2 ppm (11).

NMR spectra of MAS samples were analyzed by the method of Herzfeld and Berger (29) using the program HBA. Spectra of stationary samples were analyzed with the program WSOLIDS, which incorporates the POWDER algorithm of Alderman et al. (30). Both programs were developed in this laboratory and run on IBM compatible microprocessors.

Ab initio calculations of the carbon, nitrogen, and selenium chemical shielding tensors were performed with the Gaussian 98 suite of programs[2] mounted on an IBM RS/6000 computer. The chemical shielding tensors for all compounds were calculated at the Hartree–Fock (HF) level of theory using the gauge-independent atomic orbitals (GIAO) method (31) with the 6–311+G* basis set. The basis-set dependence of these results was determined by calculating the chemical shielding tensors for CSe_2 and $SeCN^-$ with basis sets[3] ranging from 3–21G to cc-pVQZ (32). The effects of electron correlation

[2] M.J. Frisch, G.W. Trucks, H.B. Schlegel, G.E. Scuseria, M.A. Robb, J.R. Cheeseman, V.G. Zakrzewski, J.A. Montgomery, Jr., R.E. Stratmann, J.C. Burant, S. Dapprich, J.M. Millam, A.D. Daniels, K.N. Kudin, M.C. Strain, O. Farkas, J. Tomasi, V. Barone, M. Cossi, R. Cammi, B. Mennucci, C. Pomelli, C. Adamo, S. Clifford, J. Ochterski, G.A. Petersson, P.Y. Ayala, Q. Cui, K. Morokuma, D.K. Malick, A.D. Rabuck, K. Raghavachari, J.B. Foresman, J. Ciolowski, J.V. Ortiz, B.B. Stefanov, G. Liu, A. Liashenko, P. Piskorz, I. Komaromi, R. Gomperts, R.L. Martin, D.J. Fox, T. Keith, M.A. Al-Laham, C.Y. Peng, A. Nanayakkara, C. Gonzalez, M. Challacombe, P.M.W. Gill, B. Johnson, W. Chen, M.W. Wong, J.L. Andres, C. Gonzalez, M. Head-Gordon, E.S. Replogle, and J.A. Pople. Gaussian 98, Revision A.4. Gaussian, Inc. Pittsburgh, Pa. 1998.

[3] Basis sets were obtained from the Extensible Computational Chemistry Environment Basis Set Database, Version 1.0, as developed and distributed by Molecular Science Computing Facility, Environmental and Molecular Sciences Laboratory which is part of the Pacific Northwest Laboratory, P.O. Box 999, Richland, Washington 99352, USA, and funded by the U.S. Department of Energy. The Pacific Northwest Laboratory is a multi-program laboratory operated by the Batelle Memorial Institute for the U.S. Department of Energy under contract DE-AC06–76RLO 1830. Contact David Feller or Karen Schuchardt for further information.

© 2000 NRC Canada

Table 1. Experimental carbon, nitrogen, and selenium chemical shift tensors for some solid cyanate salts.[a]

Compound	Nucleus	δ_{iso}[b]	δ_{11}	δ_{22}	δ_{33}	Ω[c]	κ[d]
KOCN	^{13}C	130.2	—	—	—	—	—
NH_4SCN[e]	^{13}C	133.1	240	240	–81	321	1.00
NH_4SeCN	^{13}C	125.7[f]	228	226	–77	305	0.99
NMe_4SeCN	^{13}C	119.1[g]	215	212	–70	285	0.98
NH_4SCN[e]	^{15}N	211.0	349	349	–66	415	1.00
NMe_4SeCN	^{15}N	255[h]	401	401	–38	439	1.00
KSeCN	^{77}Se	–282.6[i]	25	–23	–849	874	0.89
NH_4SeCN	^{77}Se	–255.9	26	–15	–778	804	0.9
NMe_4SeCN	^{77}Se	–299.4	–40	–40	–814	854	1.00

[a]All chemical shift values are in ppm. Uncertainties are estimated to be less than 0.5 ppm for δ_{iso}; those of the individual components are estimated to be on the order of 2–3% of the total span of the tensor.

[b]δ_{iso} may not be exactly equal to the average of the individual tensor components since the values of the former were obtained from the isotropic peak of an MAS sample.

[c]Span $\Omega = \delta_{11} - \delta_{33}$.

[d]Skew $\kappa = 3(\delta_{22} - \delta_{iso})/\Omega$.

[e]Ref. 39.

[f]From MAS spectra: $\chi(^{14}N) = -2.6 \pm 0.3$ MHz; $^1J(^{14}N, ^{13}C) = 15 \pm 3$ Hz.

[g]From MAS spectra: $\chi(^{14}N) = -2.6 \pm 0.3$ MHz; $^1J(^{77}Se, ^{13}C) = 260 \pm 30$ Hz; methyl groups: $\delta_{iso} = 56.1$ ppm.

[h]Tetramethylammonium: $\delta_{iso} = 47.3$ ppm.

[i]Surface solvated: –297.5 ppm.

on these two compounds were investigated by calculating the chemical shielding tensors at the second-order Møller–Plesset (MP2) level of theory (33). The geometries used in these calculations are from a high-level ab initio geometry optimization of $SeCN^-$ (34), a neutron diffraction study of NH_4SCN (35), a microwave study of SeCO (36), and an IR study of CSe_2 (37). To facilitate comparison, experimental chemical shifts (δ) were converted to chemical shielding (σ) according to $\sigma(exp) = \sigma(ref) - \delta(exp)$. The carbon shielding in TMS(ℓ, 300 K) was taken to be 188.1 ppm (20), that for nitrogen in NH_3(ℓ, 293 K) was taken to be 264.5 ppm (21) and that for the selenium in $Se(CH_3)_2$(ℓ) was taken to be 1769 ppm (22). The latter value is an approximate non-relativistic value. That is, in deriving the absolute shielding scale for selenium, it was assumed that σ(free ^{77}Se atom) = 2998 ppm (38).

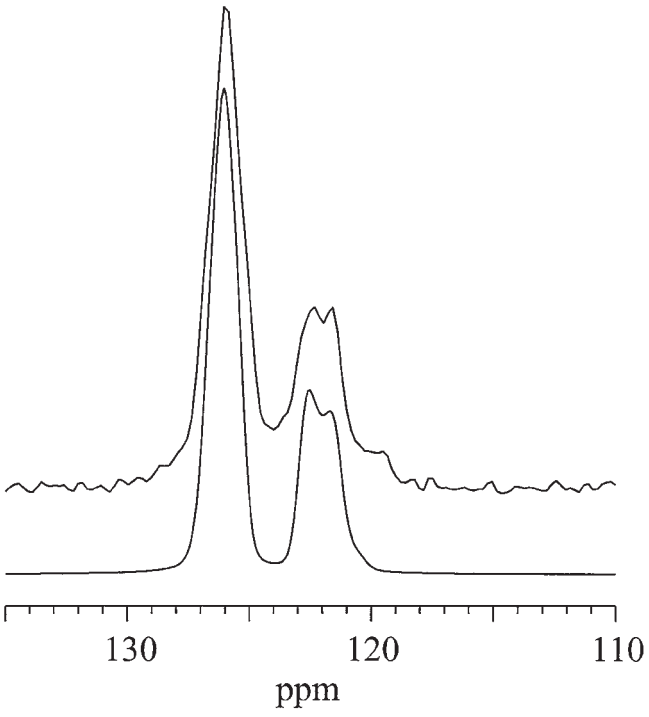
Results and discussion

Observed chemical shift and spin–spin coupling data determined from stationary and MAS powder samples of solid selenocyanate salts investigated in this study are collected in Table 1. Included for comparison are data obtained from a previous ^{13}C and ^{15}N NMR study of ammonium thiocyanate (39).

Carbon-13 NMR spectra

The ^{13}C NMR spectrum of an MAS sample of solid ammonium selenocyanate is shown in Fig. 2. The spinning sidebands of the experimental spectrum have been added to the isotropic peak to produce the spectrum expected at the high-spinning limit. The asymmetric doublets arise because the carbon is directly bonded to the quadrupolar ^{14}N nucleus ($I = 1$, natural abundance = 99.64%). Although the isotropic ^{13}C chemical shift can be accurately determined from the spectrum of an MAS sample, it is more difficult to extract the principal components of the carbon chemical shift tensors from spinning sidebands because the presence of the dipolar interaction with ^{14}N nuclei must be considered (40).

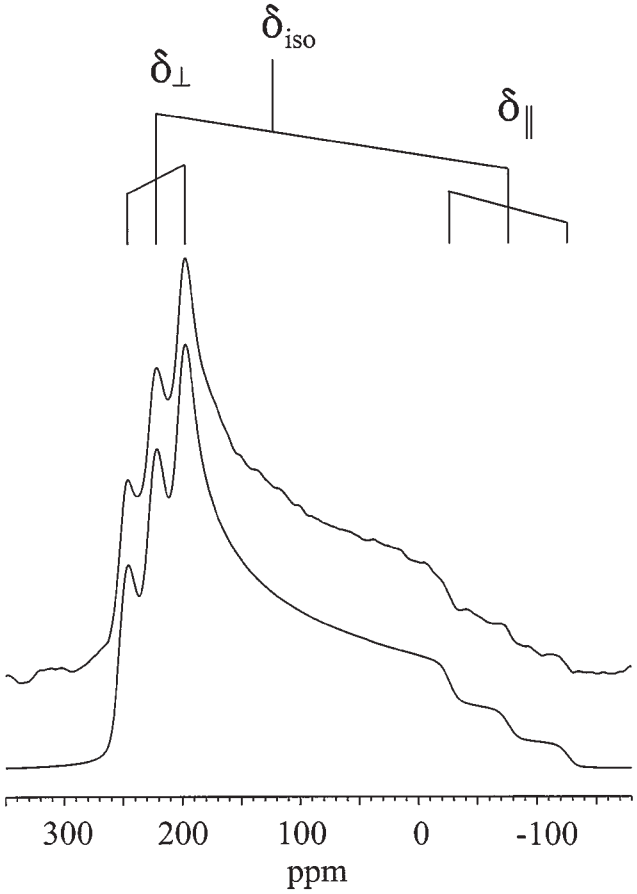
Fig. 2. Isotropic region of the experimental (top) and calculated (bottom) ^{13}C NMR spectra of NH_4SeCN acquired at 4.7 T with a spinning frequency of 3320 Hz; 7455 transients were acquired.



The ^{13}C NMR spectrum of a stationary powder sample of NH_4SeCN is shown in Fig. 3. As well as being perturbed by anisotropic shielding, the ^{13}C NMR line shape is modified by the ^{14}N, ^{13}C dipolar interaction. The splittings at $\delta_\perp$ and $\delta_\parallel$ are R_{DD} and $2R_{DD}$, respectively (41). The ^{14}N, ^{13}C direct dipolar coupling constant (R_{DD}) is defined as

© 2000 NRC Canada

Fig. 3. Experimental (top) and calculated (bottom) ^{13}C NMR spectra of a stationary powder sample of NH_4SeCN at 4.7 T; 20549 transients were acquired. The splitting of the parallel and perpendicular components arise from the dipolar interaction with ^{14}N.



$$[7] \qquad R_{DD} = \frac{\mu_0}{4\pi}\frac{\hbar}{2\pi}\gamma(^{13}C)\,\gamma(^{14}N)\left\langle r_{CN}^{-3}\right\rangle$$

where $\langle r_{CN}\rangle$ is the motionally averaged C—N bond length. The splittings due to R_{DD} for crystallites oriented such that $\delta_\perp$ is parallel to $\mathbf{B}_0$ are clearly seen at high frequency in Fig. 3; although it is not as well resolved, the effect of R_{DD} on the spectra of crystallites oriented such that $\delta_\parallel$ is parallel to $\mathbf{B}_0$ are also observed at low frequency. From the fit of the NMR spectrum of a stationary powder sample, R_{DD} = 1250 ± 20 Hz, corresponding to r_{CN} = 1.205 ± 0.007 Å. This is significantly longer than the value of r_{CN} determined from an early X-ray diffraction study of KSeCN (42), 1.117 Å, but is in agreement with the results of an ab initio study (34). In principle, the quadrupolar interaction with ^{14}N should also be considered in the fit, but it has been shown (39–41) that this interaction has only minor effects on the positions of the critical frequencies in spectra of stationary samples acquired at the external magnetic fields used in this study. From the dipolar coupling, and assuming that the largest component of the ^{14}N EFG tensor is along the C,N bond with an asymmetry of zero, analysis of the spectrum of an MAS sample (Fig. 2) yields $C_Q(^{14}N)$ = –2.6 ± 0.3 MHz. This value is in excellent agreement with the value reported for the NCS^- anion, $|C_Q(^{14}N)|$ = 2.3 MHz (43).

The ^{13}C NMR spectrum of an MAS sample of NMe_4SeCN (not shown) contains some smaller peaks, attributed to ^{13}C nuclei bonded to the ^{77}Se nucleus (natural abundance = 7.58%, I = 1/2). The value of $^1J_{iso}(^{77}Se, ^{13}C)$ is estimated to be 260 ± 30 Hz. These satellite peaks are not resolved in the spectrum of NH_4SeCN (Fig. 2), a consequence of the broader lines. The line shape of the asymmetric doublet in the ^{13}C NMR spectrum of an MAS sample of NMe_4SeCN cannot be simulated as well as that of NH_4SeCN (Fig. 2); this may be caused by the onset of self-decoupling of the ^{14}N (44). The ^{13}C NMR spectrum of a stationary sample of NMe_4SeCN is dominated by the contribution from the four methyl groups, but the splittings due to $R_{DD}(^{14}N, ^{13}C)$ in the high-frequency region of the spectrum are well resolved. With these features and with the isotropic chemical shift obtained from the spectra of MAS samples, analysis of the spectrum is possible, yielding the principal components of the carbon CS tensors summarized in Table 1. From the ^{14}N, ^{13}C dipolar splittings observed in the high-frequency region, R_{DD} = 1180 ± 30 Hz, corresponding to r_{CN} = 1.23 ± 0.01 Å. This value is slightly longer than the value of 1.205 Å obtained for NH_4SeCN. While the difference is only slightly greater than the experimental error, the longer value obtained for NMe_4SeCN is probably a consequence of greater librational motion of the selenocyanate anion of the latter salt. Note that motion of the N—C bond will result in partial averaging of $R_{DD}(^{14}N, ^{13}C)$ and an apparent lengthening of r_{CN}.

For the ^{13}C MAS NMR spectrum of KOCN, recycle delays in excess of one hour were used, but the signal-to-noise ratio was still very low, precluding any analysis for the compound at natural abundance. Hence only the isotropic chemical shift was determined. The value of δ_{iso}, 130.2 ppm, is within experimental error of the value determined for KOCN dissolved in D_2O, 129.7 ppm (45).

Nitrogen-15 NMR spectra

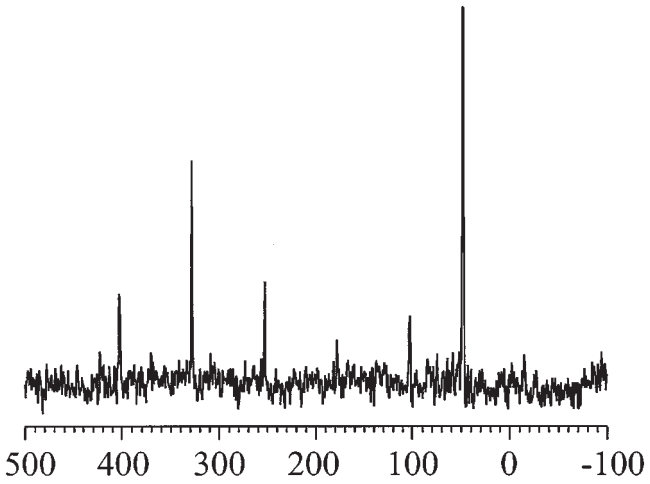
The ^{15}N MAS NMR spectrum of NMe_4SeCN (Fig. 4) consists of an intense peak at 47.3 ppm, due to NMe_4^+, and a weaker, spinning rate invariant peak at 255.0 ppm due to $SeCN^-$. The spinning sidebands of the latter peak were analyzed by the Herzfeld–Berger method to obtain the span of the nitrogen CS tensor, Ω = 439 ± 10 ppm. This value is within experimental error of the value obtained for NH_4SCN, 415 ± 15 ppm (39). The average nitrogen shielding for $SeCN^-$ in solid NMe_4SeCN is 44 ppm less than the value for SCN^- of solid NH_4SCN. In aqueous solutions, the shielding of the nitrogen nuclei of $SeCN^-$ dissolved in D_2O (46) decreases by 30 ppm compared to that of the nitrogen nuclei of SCN^- dissolved in H_2O (47).

Selenium-77 NMR spectra

Selenium-77 NMR spectra of MAS samples of NMe_4SeCN are shown in Fig. 5. The isotropic ^{77}Se chemical shift is comparable to that of KSeCN measured in solution (6). The experimental spectra of the selenocyanates were simulated via a non-linear least-square implementation of the method of Herzfeld and Berger (29); the resulting data are summarized in Table 1. These simulations indicate large

© 2000 NRC Canada

Fig. 4. Experimental ^{15}N NMR spectrum of solid NMe_4SeCN acquired at 9.4 T with a spinning frequency of 3040 Hz. 10 000 transients were acquired, with a recycle time of 30 s.



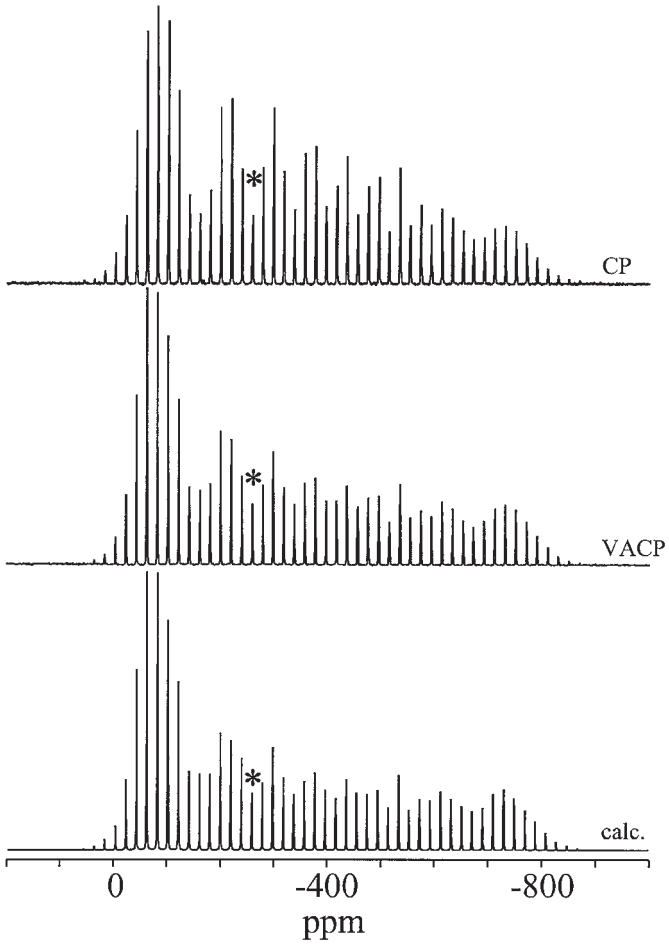
anisotropies in the ^{77}Se CS tensors, making the observation of spectra of stationary powder samples difficult. Non-axially symmetric CS tensors are not precluded by the linear $SeCN^-$ anion, since the positions of the cations in the crystal lattice may affect the shielding. For example, the crystal structure of KSeCN shows that the potassium atoms are not arranged symmetrically about the selenium (42). Chemical shift tensors determined from the analysis of spinning sideband intensities in spectra of slow-spinning MAS samples are subject to significant errors if the tensor is approximately axially symmetric (48). In light of the above and considering the errors associated with the experimental data, the values quoted in Table 1 do not conclusively determine the symmetry of the selenium CS tensor. In cases where cross-polarization was used to obtain the spectra, further artifacts could be introduced in the spinning sideband intensities from anisotropy in the cross-relaxation stage of the experiment (49). For example, clear differences were observed for NMe_4SeCN in regular CP experiments (Fig. 5, top) and experiments employing variable-amplitude cross-polarization (50) (see Fig. 5, middle). In the spectrum obtained with regular CP, the intensities of the spinning sidebands in the neighbourhood of the isotropic peak (indicated with an asterisk) are much stronger relative to the higher-order spinning sidebands about the position of $\delta_\perp$ and $\delta_\parallel$ than are those obtained with VACP. The latter spectrum agrees much better with the calculated spectrum. This effect is probably due to the offset dependence of the Hartmann–Hahn matching condition (50). In spite of the possible errors and artifacts, it is clear that the selenium CS tensors do not deviate significantly from axial symmetry (the maximum deviation in κ is estimated to be 10%). In the ensuing discussion, we will assume that the carbon, nitrogen, and selenium tensors are axially symmetric, consistent with our experimental data.

Ab initio calculations

Carbon and nitrogen shielding tensors for $SeCN^-$ and related molecules

The calculated carbon and nitrogen chemical shielding tensor components are listed in Tables 2 and 3, respectively.

Fig. 5. Experimental and calculated ^{77}Se MAS NMR spectra of solid NMe_4SeCN at 9.4 T and a spinning frequency of 1500 Hz. Top: regular cross-polarization experiment with 3000 scans and 10 ms contact time. Middle: variable-amplitude cross-polarization experiment with 2532 scans and 15 ms contact time. Bottom: calculated spectrum with $\delta_{11} = \delta_{22} = -40$ ppm, $\delta_{33} = -814$ ppm. The isotropic peaks are indicated with an asterisk.



For comparison, the chemical shift values of the experimental data have been converted to chemical shielding (see experimental section). While the observed spans for the carbon CS tensors of SCN^- and $SeCN^-$ are similar (321 to 285 ppm), the span is significantly greater for SeCO (399 ppm) and CSe_2 (506 ppm). These experimental trends are reproduced by the highest level ab initio computations that we can presently apply to all three molecules, HF/6–311+G*. Likewise, ab initio calculations correctly predict a larger span for the nitrogen nucleus of the $SeCN^-$ anion than for that of the SCN^- anion.

The calculated isotropic carbon chemical shielding for $SeCN^-$ plotted against basis set size is shown in Fig. 6 (top). This figure indicates that the calculated isotropic shielding is converging to a value which is approximately 15 ppm less than the experimental value. Similar results were obtained for the calculated shielding of the nitrogen of $SeCN^-$ (Table 3) and the carbon of CSe_2 (Table 2).

The calculated carbon chemical shielding tensor components parallel to the bond are invariant to basis set size or to

© 2000 NRC Canada

Table 2. Carbon chemical shielding tensors for CSe_2, SeCO, and for some cyanate salts.[a]

Compound	Method	σ_{iso}	$\sigma_\perp$	$\sigma_\parallel$	Ω
KOCN	Exp	57.9	—	—	—
OCN^-	HF/6–311+G*	58.7	–57	290	347
NH_4SCN[b]	Exp	55.0	–52	269	321
SCN^-	HF/6–311+G*	42.7	–81	290	371
NH_4SeCN	Exp	62.4	–40	265	305
NMe_4SeCN	Exp	69.0	–27	258	285
$SeCN^-$	HF/6–311+G*	26.7	–106	292	398
	MP2/6–311+G*	65	–49	293	342
SeCO	Exp[c]	34	–99	300	399
	HF/6–311+G*	–4	–151	289	440
CSe_2	Exp[d]	–21.8	–190	316	506
	HF/6–311+G*	–121	–329	295	624
	MP2/6–311+G*	8	–137	298	435

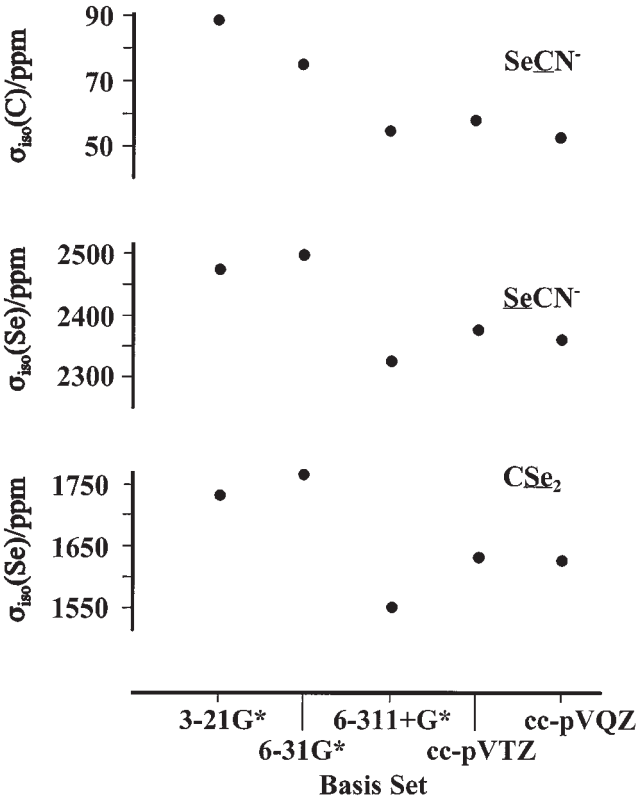
[a]See the footnotes to Table 1 for details on experimental data.

[b]From reference 39. Values reported in Table 1 of this reference are slightly different from those shown here, since the values were based on an earlier absolute shielding scale for carbon.

[c]From reference 56(*a*), Vol. 25, p.48. A comparable value of σ_{iso}, 31.5 ppm, has also been reported from a solution-state study (reference 57).

[d]The individual tensor components were calculated from the experimental values of σ_{iso} (reference 57) and Ω (reference 12) according to $\sigma_\perp = \sigma_{iso} - (1/3)\Omega$ and $\sigma_\parallel = \sigma_{iso} + (2/3)\Omega$.

Fig. 6. Isotropic carbon and selenium chemical shielding, calculated at the HF level, plotted against the basis set used for the calculation. The scale for the abscissa is qualitative.



the effects of electron correlation, reflecting the fact that there is no paramagnetic contribution to this component of the chemical shielding tensor. However, the experimental values of $\sigma_\parallel$ are approximately 30 ppm less than the calculated values, perhaps a consequence of intermolecular effects. Calculations on a larger portion of the crystal lattice would be instructive but are not practical at this time given the computational requirements. In addition to intermolecular effects, vibrational effects are a factor, although these are expected to be fairly small for carbon and nitrogen (51). For example, Lounila et al. (52) calculated a vibrational correction of $\sigma_{iso} = -2.4$ ppm for the carbon of CSe_2. For molecules containing large atoms, relativistic effects (53) may become significant (*vide infra*), even for the calculated shielding of neighbouring nuclei (54).

Table 3. Nitrogen chemical shielding tensors for some cyanate salts.[a]

Compound	Method	σ_{iso}	$\sigma_\perp$	$\sigma_\parallel$	Ω
OCN^-	HF/6–311+G*	223.4	162	347	185
NH_4SCN[b]	Exp	53.5	–85	331	416
SCN^-	HF/6–311+G*	19.3	–144	346	490
NMe_4SeCN	Exp	9.5	–137	303	440
$SeCN^-$	HF/6–311+G*	–32.3	–221	345	566
	MP2/6–311+G*	32.0	–125	346	471

[a]See the footnotes to Table 1 for details on experimental data.

[b]From reference 39.

The chemical shielding tensors for the carbon and nitrogen nuclei of $SeCN^-$ as well as that for the carbon of CSe_2 were calculated at the MP2 level (Tables 2 and 3). In all cases, the isotropic shielding values calculated at the MP2 level are significantly greater than the corresponding HF values, and are generally greater than the experimental values, reflecting the fact that the effects of electron correlation are not considered in HF calculations but are often overestimated by MP2 (55). A particularly large electron correlation effect is expected for the carbon of CSe_2 because of its multiple bonding (56). The large deshielding (57) and span (12) reported for the carbon of CSe_2 are in agreement with our calculations, as well as with those of an earlier computational study (52).

© 2000 NRC Canada

Table 4. Selenium chemical shielding tensors for CSe_2, SeCO, and for some selenocyanate salts.[a]

Compound	Method	σ_{iso}	$\sigma_{\perp}$	$\sigma_{\parallel}$	Ω
NH_4SeCN	Exp	2025	1764	2547	783
NMe_4SeCN	Exp	2067	1809	2583	774
$SeCN^-$	HF/6–311+G*	2343	2009	3011	1002
	MP2/6–311+G*	2443	2160	3010	850
SeCO	Exp[b]	2347	2018	3006	988
	Exp[c]	2216	1887	2875	988
	HF/6–311+G*	2327	1986	3008	1022
CSe_2	Exp[d]	1438	701[e]	2911	2210
	HF/6–311+G*	1547	816	3009	2193
	MP2/6–311+G*	1816	1220	3007	1787

[a]See the footnotes to Table 1 for details on the experimental data.

[b]From reference 56(*a*), Vol. 25, p. 48.

[c]The isotropic value is from a solution-state study (reference 57). The chemical shielding tensor components were calculated from this value and the experimental value of Ω (reference 56(*a*), Vol. 25, p. 48) according to $\sigma_{\perp} = \sigma_{iso} - (1/3)\Omega$ and $\sigma_{\parallel} = \sigma_{iso} + (2/3)\Omega$.

[d]Components of the chemical shielding tensor are calculated from the experimental values of σ_{iso} (reference 57) and Ω (reference 12); see footnote *c* above.

[e]A value of $\sigma_{\perp} = 1068$ ppm, determined from a solid state NMR study at –90°C, has also been reported (reference 63).

Selenium chemical shielding tensors for $SeCN^-$ and related molecules

The existence of an absolute shielding scale for selenium (22) combined with experimental data on simple molecules has prompted several theoretical groups to investigate selenium chemical shielding tensors. For example, the selenium shielding for CSe_2 has been calculated at the CHF (12), HF/IGLO (55), MP2/GIAO (55, 58), CCD (58), and DFT (59) levels of theory. Recently Lounila et al. reported the results of a detailed computational study of this molecule, which included DFT and CAS calculations (52). Such calculations are challenging, a consequence of the large chemical shielding range of selenium (60) and of the fact that selenium shielding is subject to relativistic effects (53). The progress of selenium shielding calculations has been reviewed recently (56).

The calculated selenium chemical shielding tensors are listed in Table 4. The calculated results are more dependent on basis set size than are those of carbon and nitrogen (Fig. 6), reflecting the greater chemical shift range of selenium compared to those of carbon (3) or nitrogen (61). Figure 6 shows that the calculated isotropic selenium chemical shielding for both $SeCN^-$ and CSe_2 are converging to values which are significantly shielded compared to experimental values. Ab initio calculations are performed on isolated molecules, which may result in significant discrepancies between calculated and experimental results, since selenium is known to be susceptible to medium effects. For example, the isotropic shielding for gaseous H_2Se is 126.6 ppm greater than that for this compound in the liquid state, which in turn is shielded by 11.4 ppm compared to its value in the solid (62). For CSe_2, the gas-phase shielding is 74.7 ppm greater than that for the same molecule in its liquid phase (63).

An electron correlation effect of 100 ppm is predicted for $SeCN^-$, based on the results of calculations at the MP2 level. The effect is more significant for CSe_2; σ_{iso} calculated at the MP2 level is 269 ppm greater than the value calculated at the HF level (Table 4). Chesnut has noted that isotropic chemical shielding constants calculated at various orders of Møller–Plesset theory converge such that the infinite-order Møller–Plesset calculated shielding may be approximated by (64):

$$[8] \qquad \sigma_{iso} = \frac{1}{3}\sigma_{HF} + \frac{2}{3}\sigma_{MP2}$$

Substituting our calculated values for CSe_2 (Table 4), we obtain a value of $\sigma_{iso} = 1726$ ppm, close to the value calculated with the CAS method, 1755.2 ppm (52).

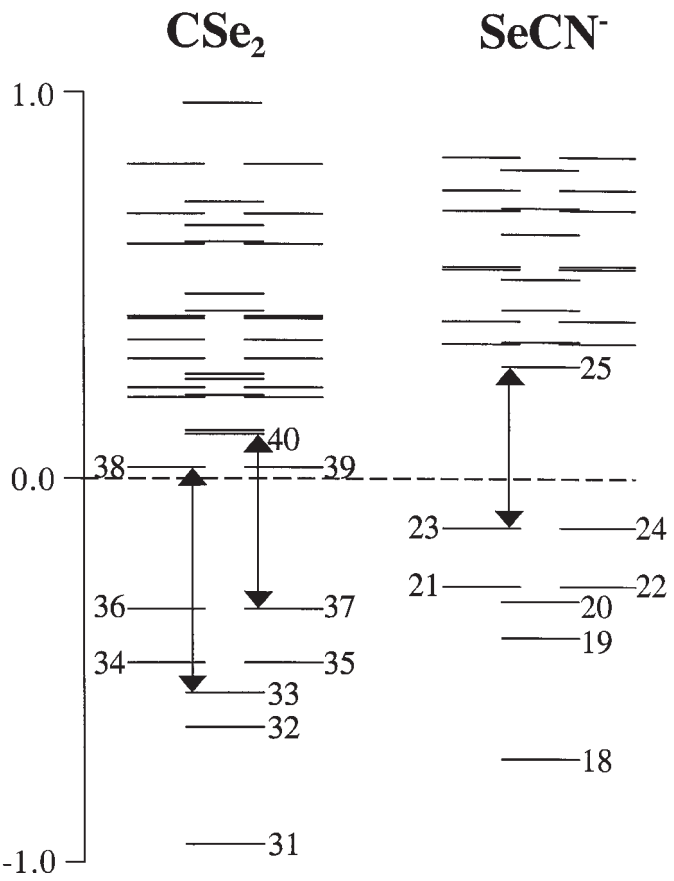
In the absence of intermolecular effects $\sigma_{\parallel} \approx \sigma^d_{av}$ (free atom) (eq. [5]). Our calculated values of $\sigma_{\parallel}$ (Table 4) are comparable to the non-relativistic value of σ^d_{av} (free Se), 2998 ppm (38), reflecting the fact that first-order molecular properties can usually be calculated accurately. Experimental values of $\sigma_{\parallel}$ for the selenocyanate salts are significantly smaller than the calculated values. This difference is attributed to intermolecular effects. A paramagnetic contribution to $\sigma_{\parallel}$ in the selenocyanate salts arises from the fact that, with the neighbouring nuclei such as potassium in KSeCN, the selenium atoms are not in a perfectly linear environment and hence the assumption that $\sigma^p_{\parallel} = 0$ is no longer strictly valid.

A comparison of the selenium chemical shielding tensors for $SeCN^-$ and CSe_2.

One might expect the selenium chemical shielding tensors for Se=C=N$^-$ and Se=C=Se to be similar, but this is not the case (Table 4). Particularly surprising is the large difference in the spans — that of CSe_2 is almost three times greater than the spans of the selenocyanates. This is remarkable given that selenium is directly bonded to carbon in both cases. The difference cannot be attributed to the charge on $SeCN^-$, since the span of SeCO (65) is comparable to those of the selenocyanate salts. These large differences are reproduced qualitatively by the calculations. In particular, we note that agreement between the experimental and calculated spans of SeCO is very good. Since the experimental span of SeCO was determined from spin-rotation data (65), it is that of an isolated molecule and is thus ideal for comparison with calculated values. To a first approximation, the span of the chemical shielding tensor is invariant to the effects of

© 2000 NRC Canada

Fig. 7. Molecular orbital energy levels (in hartrees) for CSe_2 and $SeCN^-$, calculated at the HF/cc-pVQZ level. Molecular orbitals below the dashed line are occupied. Some of the MOs have been labelled for reference.



relativity (52), and thus may be the best gauge of the accuracy of non-relativistic calculations.

The large difference in the spans of the selenium chemical shielding tensors for CSe_2 and $SeCN^-$ is a consequence of a large difference in their respective $\sigma_\perp$ values because $\sigma_\parallel$ does not vary greatly amongst linear molecules. The contribution to the span from σ^d can be estimated from eq. [4]. For $SeCN^-$, $\sigma^d_\parallel$ = 2998 ppm and $\sigma^d_\perp$ = 3078 ppm, giving a span in σ^d of 80 ppm. Similarly, a span of 151 ppm is predicted for σ^d of CSe_2. These numbers are much smaller and opposite in sign to those observed for σ^p. Thus, to understand the large difference between the spans of CSe_2 and $SeCN^-$, one must consider $\sigma^p_\perp$.

One of the factors contributing to $\sigma^p_\perp$ is the number of MOs undergoing mixing, since eq. [3] is a summation. Figure 7 shows the energies for the highest occupied and lowest unoccupied MOs of $SeCN^-$ and CSe_2, calculated at the HF level using the cc-pVQZ basis set. Although the energy difference between the highest occupied and lowest unoccupied MOs are comparable for the two compounds, there are more low-lying unoccupied MOs for CSe_2 than for $SeCN^-$. However, we must also consider the symmetry of these MOs, since mixing will only occur between MOs with magnetic-dipole allowed symmetry. These are indicated with arrows in Fig. 7.

Fig. 8. MOs 33 and 38 (or 39) for CSe_2, illustrating the magnetic-dipole allowed $\sigma_u \rightarrow \pi^*_u$ mixing for an applied magnetic field perpendicular to the page.

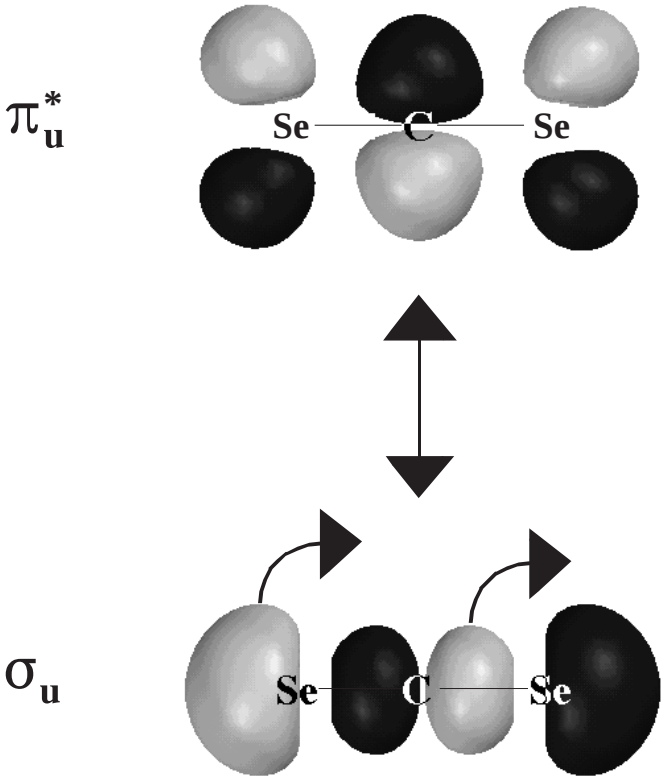


Figure 8 illustrates that MO 33 with σ_u symmetry can mix with degenerate MOs 38 or 39, with π^*_u symmetry. Because of the favourable symmetry, these MOs are expected to be a major factor in the deshielding observed in the direction perpendicular to the C_∞ axis of CSe_2. In Fig. 9, MO 36 (or degenerate MO 37) of CSe_2, with π_g symmetry, is shown along with MO 40, which has σ^*_g symmetry. Figures 8 and 9 illustrate the importance of symmetry in considering contributions to σ^p. Although MOs 36 and 37 are only separated by 0.46 hartrees from MO 40, compared to 0.57 hartrees separating MO 33 from MOs 38 and 39, the shape of the latter is much more favourable for mixing.

Figure 10 demonstrates why the selenium chemical shielding tensor for $SeCN^-$ has a large span which nevertheless is much smaller than that for CSe_2. The illustrated MOs, occupied π MO 23 (or degenerate MO 24) and unoccupied σ^* MO 25, have a relatively small difference in energy, 0.42 hartrees, but the symmetry of the MOs clearly is not as favourable for mixing here. Hence, these MOs are expected to be a significant factor in the deshielding perpendicular to the C_∞ axis of the anion, but the lower symmetry makes mixing much less favourable than in the case of CSe_2.

In summary, the smaller span of the chemical shielding tensor of $SeCN^-$ compared to that of CSe_2 may be attributed to two factors. The selenocyanate anion has fewer low-lying unoccupied MOs which can mix with occupied MOs and contribute to $\sigma^p_\perp$, and the mixing of most of those MOs separated by a small energy difference are not magnetic-dipole allowed. The latter may be attributed to the lower symmetry

© 2000 NRC Canada

Fig. 9. MOs 36 (or 37) and 40 of CSe_2, illustrating the magnetic-dipole allowed $\pi_g \rightarrow \sigma_g^*$ mixing for an applied magnetic field perpendicular to the page.

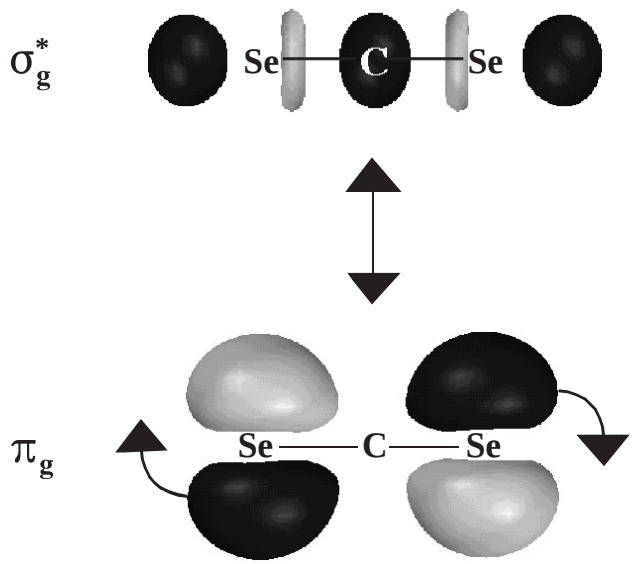
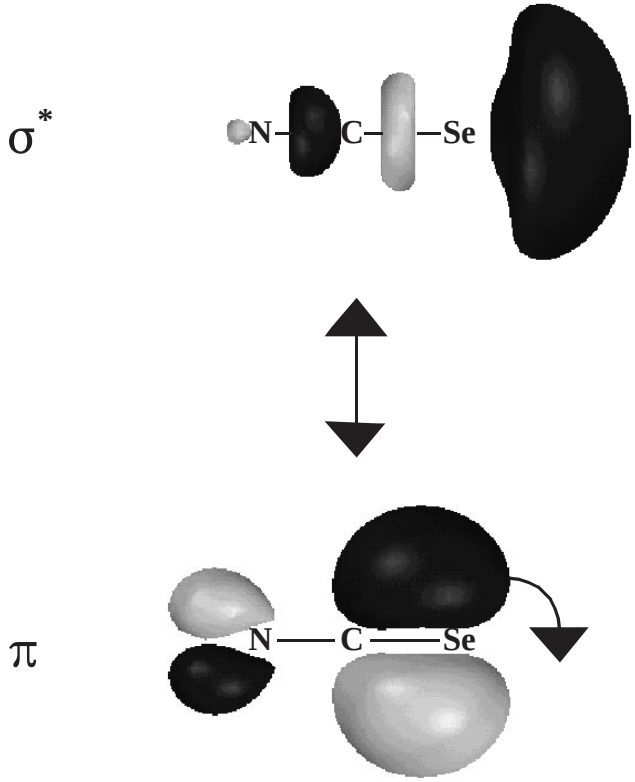


Fig. 10. MOs 23 (or 24) and 25 of CSe_2, illustrating the magnetic-dipole allowed $\pi \rightarrow \sigma^*$ mixing for an applied magnetic field perpendicular to the page.



of $SeCN^-$ ($C_{\infty v}$), compared to that of CSe_2 ($D_{\infty h}$). This conclusion is supported by the observation that the chemical shielding tensor for SeCO, which also has $C_{\infty v}$ symmetry, is comparable to that of $SeCN^-$. Finally we note that, although we have not explicitly discussed the spans of the carbon shielding tensors for $SeCN^-$ and CSe_2 (Table 2), the different spans of these shielding tensors may also be explained as above. For example, the mixing of MOs 33 with MOs 38 and 39 of CSe_2, which contributes to σ^p of the selenium chemical shielding tensor, will also be an important factor in the paramagnetic component of the carbon shielding perpendicular to the C_∞ symmetry axis.

Conclusions

The carbon, nitrogen, and selenium chemical shift tensors for several solid selenocyanate salts have been characterized by NMR. Within experimental error, the chemical shift tensors are axially symmetric. A notable result of this study is the observation that the spans of the carbon and selenium CS tensors for $SeCN^-$ are much smaller than those for CSe_2, a consequence of the smaller paramagnetic term in the shielding perpendicular to the C_∞ axis of $SeCN^-$ compared to that of CSe_2. High-level ab initio calculations show that the smaller paramagnetic term results from the lower symmetry of the MOs of $SeCN^-$ and from the fact that there are fewer low-lying unoccupied MOs for $SeCN^-$ compared to CSe_2. The shielding parallel to the C_∞ axis of $SeCN^-$ is less than expected for linear molecules, suggesting that this component is sensitive to intermolecular effects. This work has shown that multinuclear magnetic resonance studies of solids can offer much information about solid selenocyanate salts; it is hoped that this study will encourage further studies of these and related ligands.

Acknowledgments

We are grateful to Tenkir Asfaw for help in the preparation of a sample of ammonium selenocyanate. We thank Martine Ziliox for her help in initially setting up the VACP experiments on our Bruker AMX-400. We are grateful to members of the solid-state NMR group at Dalhousie University for many helpful suggestions and to Andrew D. Phillips for his help with the preparation of the molecular orbital diagrams. The financial assistance of the Natural Sciences and Engineering Research Council (NSERC) of Canada is gratefully acknowledged. GMB acknowledges NSERC, the Izaak Walton Killam Trust, and the Walter C. Sumner Foundation for postgraduate scholarships. Spectra were acquired at the Atlantic Region Magnetic Resonance Centre, which is also supported by NSERC.

References

1. (*a*) J.L. Burmeister. Coord. Chem. Rev. **1**, 205 (1966); (*b*) J.L. Burmeister. Coord. Chem. Rev. **3**, 225 (1968); (*c*) J.L. Burmeister. Coord. Chem. Rev. **105**, 77 (1990).
2. H. Duddeck. Prog. Nucl. Magn. Reson. Spectrosc. **27**, 1 (1995).
3. H.-O. Kalinowski, S. Berger, and S. Braun. Carbon-13 NMR spectroscopy. John Wiley and Sons, Chichester. 1988.
4. (*a*) N. Logan. *In* Applications of ^{14}N NMR data in the study of inorganic molecules. *Edited by* M. Witanowski and G.A. Webb. Plenum Press, N.Y. 1973. Ch. 6; (*b*) M. Witanowski, L. Stefaniak, and G.A. Webb. Annu. Rep. NMR Spectrosc. **11b**, 1

© 2000 NRC Canada

(1981); (*c*) M. Witanowski, L. Stefaniak, and G.A. Webb. Annu. Rep. NMR Spectrosc. **18**, 1 (1986); (*d*) M. Witanowski, L. Stefaniak, and G.A. Webb. Annu. Rep. NMR Spectrosc. **25**, 1 (1993).

5. J.A. Kargol, R.W. Crecely, and J.L. Burmeister. Inorg. Chem. **18**, 2532 (1979).
6. W.-H. Pan, J.P. Fackler, Jr., J.A. Kargol, and J.L. Burmeister. Inorg. Chim. Acta, **44**, L95 (1980).
7. N. Zumbulyadis and H.J. Gysling. J. Am. Chem. Soc. **104**, 3246 (1982).
8. M. Dunaj-Jurčo, M. Kabešová, V. Kettmann, I. Císařová, and D. Mikloš. Acta Crystallogr. Sect. C: Cryst. Struct. Commun. **C49**, 1476 (1993).
9. R.E. Marsh. Acta Crystallogr. Sect. B: Struct. Sci. **B54**, 503 (1998).
10. T.M. Duncan. A compilation of chemical shift anisotropies. Farragut Press, Chicago. 1990. p. M-5.
11. M.J. Collins, C.I. Ratcliffe, and J.A. Ripmeester. J. Magn. Reson. **68**, 172 (1986).
12. J. Jokisaari, P. Lazzeretti, and P. Pyykkö. Chem. Phys. **123**, 339 (1988).
13. (*a*) N.F. Ramsey. Phys. Rev. **77**, 567 (1950); (*b*) N.F. Ramsey. Phys. Rev. **78**, 699 (1950).
14. G.A. Webb. *In* Encyclopedia of nuclear magnetic resonance. *Edited by* D.M. Grant and R.K. Harris. John Wiley and Sons, Chichester. 1996. p. 4307.
15. (*a*) W.H. Flygare. Molecular structure and dynamics. Prentice-Hall, Englewood Cliffs, N.J. Ch. 6; (*b*) C.J. Jameson and J. Mason. *In* Multinuclear NMR. *Edited by* J. Mason. Plenum Press, N.Y. 1987. Ch. 3; (*c*) G.A. Webb. *In* Nuclear magnetic shieldings and molecular structure. NATO ASI Series. Vol. 386. *Edited by* J.A. Tossell. Kluwer Academic Publishers, Dordrecht. 1993. p. 1; (*d*) K. Eichele, R.E. Wasylishen, J.F. Corrigan, N.J. Taylor, and A.J. Carty. J. Am. Chem. Soc. **117**, 6961 (1995).
16. T.D. Gierke and W.H. Flygare. J. Am. Chem. Soc. **94**, 7277 (1972).
17. (*a*) C.J. Jameson and H.S. Gutowsky. J. Chem. Phys. **40**, 1714 (1964); (*b*) J.B. Grutzner. *In* Recent advances in organic NMR spectroscopy. *Edited by* J.B. Lambert and R. Rittner. Norell Press, Landisville, N.J. 1987, Ch. 2.
18. K.B. Wiberg, J.D. Hammer, K.W. Zilm, J.R. Cheeseman, and T.A. Keith. J. Phys. Chem. A, **102**, 8766 (1998).
19. C.J. Jameson. *In* Encyclopedia of nuclear magnetic resonance. *Edited by* D.M. Grant and R.K. Harris. John Wiley and Sons, Chichester. 1996. p. 1273.
20. A.K. Jameson and C.J. Jameson. Chem. Phys. Lett. **134**, 461 (1987).
21. C.J. Jameson, A.K. Jameson, D. Oppusunggu, S. Wille, P.M. Burrell, and J. Mason. J. Chem. Phys. **74**, 81 (1981).
22. C.J. Jameson and A.K. Jameson. Chem. Phys. Lett. **135**, 254 (1987).
23. J. Mason. Solid State Nucl. Magn. Reson. **2**, 285 (1993).
24. H.S.P. Müller and M.C.L. Gerry. J. Chem. Phys. **103**, 577 (1995).
25. K. Geisler, E. Nobst, C. Müller, and E. Bulka. Z. Chem. **22**, 113 (1982).
26. J. Songstad and L.J. Stangeland. Acta Chem. Scand. **24**, 804 (1970).
27. W.L. Earl and D.L. VanderHart. J. Magn. Reson. **48**, 35 (1982).
28. P.R. Srinivasan and R.L. Lichter. J. Magn. Reson. **28**, 227 (1977).
29. J. Herzfeld and A.E. Berger. J. Chem. Phys. **73**, 6021 (1980).
30. D.W. Alderman, M.S. Solum, and D.M. Grant. J. Chem. Phys. **84**, 3717 (1986).
31. (*a*) R. Ditchfield. Mol. Phys. **27**, 789 (1974); (*b*) K. Wolinski, J.F. Hinton, and P. Pulay. J. Am. Chem. Soc. **112**, 8251 (1990); (*c*) G. Rauhut, S. Puyear, K. Wolinski, and P. Pulay. J. Phys. Chem. **100**, 6310 (1996).
32. For carbon and nitrogen, see T.H. Dunning, Jr. J. Chem. Phys. **90**, 1007 (1989); for selenium, see A.K. Wilson, D.E. Woon, K.A. Peterson, and T.H. Dunning, Jr. J. Chem. Phys. **110**, 7667 (1999).
33. M.J. Frisch, M. Head-Gordon, and J.A. Pople. Chem. Phys. Lett. **166**, 281 (1990).
34. P.W. Schultz, G.E. Leroi, and J.F. Harrison. Mol. Phys. **88**, 217 (1996).
35. J.W. Bats and P. Coppens. Acta Crystallogr. Sect. B: Struct. Crystallogr. Cryst. Chem. **B33**, 1542 (1977).
36. M. LeGuennec, G. Wlodarczak, J. Demaison, H. Bürger, M. Litz, and H. Willner. J. Mol. Spectrosc. **157**, 419 (1993).
37. H. Bürger and H. Willner. J. Mol. Spectrosc. **128**, 221 (1988).
38. G. Malli and C. Froese. Int. J. Quantum Chem. Symp. I, 95 (1967).
39. R.M. Dickson, M.S. McKinnon, J.F. Britten, and R.E. Wasylishen. Can. J. Chem. **65**, 941 (1987).
40. (*a*) B.H. Suits, J. Šepa, and D. White. J. Magn. Reson. Ser. A, **120**, 88 (1996); (*b*) J. Šepa, R.J. Gorte, B.H. Suits, and D. White. Chem. Phys. Lett. **252**, 281 (1996); (*c*) G. Wu and R.E. Wasylishen. J. Phys. Chem. **97**, 7863 (1993).
41. (*a*) K. Eichele, M.D. Lumsden, and R.E. Wasylishen. J. Phys. Chem. **97**, 8909 (1993); (*b*) M.D. Lumsden, R.E. Wasylishen, K. Eichele, M. Schindler, G.H. Penner, W.P. Power, and R.D. Curtis. J. Am. Chem. Soc. **116**, 1403 (1994).
42. D.D. Swank and R.D. Willett. Inorg. Chem. **4**, 499 (1965).
43. T. Asaji, R. Ikeda, and D. Nakamura. J. Magn. Reson. **31**, 437 (1978).
44. (*a*) R.W. Schurko, R.E. Wasylishen, and J.H. Nelson. J. Phys. Chem. **100**, 8057 (1996); (*b*) C.-G. Hoelger, E. Rössler, B. Wehrle, F. Aguilar-Parrilla, and H.-H. Limbach. J. Phys. Chem. **99**, 14271 (1995); (*c*) A.C. Olivieri. J. Magn. Reson. **82**, 342 (1989).
45. G.E. Maciel and D.A. Beatty. J. Phys. Chem. **69**, 3920 (1965).
46. M.N. Akhtar, A.A. Isab, and A.R. Al-Arfaj. J. Inorg. Biochem. **66**, 197 (1997).
47. M. Witanowski, L. Stefaniak, S. Szymański, and H. Januszewski. J. Magn. Reson. **28**, 217 (1977).
48. N.J. Clayden, C.M. Dobson, L.-Y. Lian, and D.J. Smith. J. Magn. Reson. **69**, 476 (1986).
49. G. Jeschke and G. Grossmann. J. Magn. Reson. Ser. A, **103**, 323 (1993).
50. (*a*) O.B. Peersen, X. Wu, I. Kustanovich, and S.O. Smith. J. Magn. Reson. Ser. A, **104**, 334 (1993); (*b*) G. Metz, M. Ziliox, and S.O. Smith. Solid State Nucl. Magn. Reson. **7**, 155 (1996).
51. Y. Ishii, T. Terao, and S. Hayashi. J. Chem. Phys. **107**, 2760 (1997).
52. J. Lounila, J. Vaara, Y. Hiltunen, A. Pulkkinen, J. Jokisaari, M. Ala-Korpela, and K. Ruud. J. Chem. Phys. **107**, 1350 (1997).
53. (*a*) P. Pyykkö and J.-P. Desclaux. Acc. Chem. Res. **12**, 276 (1979); (*b*) P. Pyykkö. Chem. Rev. **88**, 563 (1988).
54. (*a*) W. Kutzelnigg, Ch. van Wüllen, U. Fleischer, R. Franke, and T.V. Mourik. *In* Nuclear magnetic shieldings and molecular structure. NATO ASI Series, Vol. 386. *Edited by* J.A. Tossell. Kluwer Academic Publishers, Dordrecht. 1993. p. 141; (*b*) M. Kaupp, V.G. Malkin, O.L. Malkina, and D.R. Salahub. J. Am. Chem. Soc. **117**, 1851 (1995); (*c*) M. Kaupp, O.L. Malkina, and V.G. Malkin. J. Chem. Phys. **106**, 9201

© 2000 NRC Canada

(1997); (*d*) T. Baba and H. Fukui. J. Chem. Phys. **110**, 131 (1999).
55. M. Bühl, W. Thiel, U. Fleischer, and W. Kutzelnigg. J. Phys. Chem. **99**, 4000 (1995).
56. (*a*) C.J. Jameson and A.C. de Dios. *In* Nuclear magnetic resonance — a specialist periodical report. *Edited by* G.A. Webb. Royal Society of Chemistry, Cambridge, UK. 1999. Vol. 28. Ch. 2, and previous volumes in this annual series; (*b*) C.J. Jameson. *In* Modeling NMR chemical shifts. *Edited by* J.C. Facelli and A.C. de Dios. American Chemical Society, Washington. 1999. Ch. 1.
57. W. Gombler. Z. Naturforsch. B: Anorg. Chem. Org. Chem. **36b**, 1561 (1981).
58. M. Bühl, J. Gauss, and J.F. Stanton. Chem. Phys. Lett. **241**, 248 (1995).
59. G. Schreckenbach, Y. Ruiz-Morales, and T. Ziegler. J. Chem. Phys. **104**, 8605 (1996).
60. H.C.E. McFarlane and W. McFarlane. *In* Multinuclear NMR. *Edited by* J. Mason. Plenum Press, N.Y. 1987. Ch. 15.
61. J. Mason. *In* Multinuclear NMR. *Edited by* J. Mason. Plenum Press, N.Y. 1987. Ch. 12.
62. G. Facey, R.E. Wasylishen, M.J. Collins, C.I. Ratcliffe, and J.A. Ripmeester. J. Phys. Chem. **90**, 2047 (1986).
63. Q. Chen, D.L. Freeman, J.D. Odom, and P.D. Ellis. Poster abstracts. 36th Experimental NMR Conference. Boston. 1995. p. 333.
64. D.B. Chesnut. Chem. Phys. Lett. **246**, 235 (1995).
65. C.J. Jameson. *In* Nuclear magnetic resonance — a specialist periodical report. *Edited by* G.A. Webb. Royal Society of Chemistry, Cambridge, UK. 1995. Vol. 25, p. 48.

© 2000 NRC Canada

An exploratory ab initio study on the conformations of ethylguanidine in its neutral [CH_3-CH_2-NH-C(=NH)NH_2] and protonated [CH_3-CH_2-NH-C(NH_2)$_2$] forms

Melody L. Mak, Salvatore J. Salpietro, R. Daniel Enriz, and Imre G. Csizmadia

Abstract: To explore the conformation intricacies of the guanidine group in the arginine side chain, ab initio computations have been carried out with ethylguanidine and the ethyl guanidinium ion. HF computations have been performed using 3–21G and 6–31G basis sets and DFT calculations were carried out at the B3LYP/6–31G(*d*) level of theory. The ethyl guanidinium ion has a single isomer due to its internal symmetry, although this structure has at least three conformations. However, several structures were found and optimized for ethylguanidine, involving the *endo*- and *exo*- orientation of the lone NH and torsional angle χ_6, as well as the torsional modes associated with χ_4 and χ_5. Torsional angle χ_5 gives rise to *s-cis* and *s-trans* structures.

Key words: ethylguanidine, ethylguanidinium ion, ab initio MO, arginine side-chain, conformational analysis.

Résumé : Dans le but d'étudier les problèmes reliés à la conformation du groupe guanidine dans la chaîne latérale de l'arginine, on a effectué des calculs ab initio sur l'éthylguanidine et l'ion éthylguanidinium. Les calculs HF ont été effectués à l'aide d'ensembles 3–21G et 6–31G alors que les calculs DFT ont été effectués au niveau B3LYP/6–31G(*d*) de la théorie. L'ion éthylguanidinium ne comporte qu'un seul isomère en raison de la symétrie interne de l'ion guanidinium même si cette structure comporte au moins trois conformations. Toutefois, on a trouvé et optimisé plusieurs structures pour l'éthylguanidine qui impliquent une orientation *endo*- et *exo*- du NH seul avec des angles de torsion χ_6 ainsi que des modes de torsion associés à χ_4 et χ_5. L'angle de torsion χ_5 conduit aux structures *s-cis* et *s-trans*.

Mots clés : éthylguanidine, ion éthylguanidinium, OM ab initio, chaîne latérale de l'arginine, analyse conformationnelle.

[Traduit par la Rédaction]

1. Introduction

Arginine is an amino acid with a positive charge at neutral pH due to its polar guanidinium group side-chain. The typical pK_a value of arginine is 12.0, the highest pK_a of all amino acids. Arginine is, therefore, important in salt bridge coupling, which is part of certain docking processes.

Arginine plays significant roles in a number of biological processes. For example, it is part of the tripeptide arginyl – glycyl – aspartic acid (RGD) which is found in adhesive proteins of extracellular matrices (1). This tripeptide serves as a cell recognition site in fibronectin. Although the cell attachment sequence is similar in different adhesive proteins, cells have the ability to distinguish them individually due to the specificity of receptors called integrins (2). Each integrin is able to recognize one RGD-containing ligand. Consequently, RGD-containing protein is extremely useful in the identification of these receptors.

Arginine is the source of nitric oxide (NO) in biological systems. NO is a free radical which serves as an intracellular second messenger and an intercellular messenger that regulates neighbouring, and possibly distant cells (3). NO takes part in many biological processes such as vasodilation, platelet aggregation, and adhesion (4–6). NO is also involved in various aspects of the central nervous system (CNS) such as the modification of pain perception, mediation of long-term potentiation and memory, controlling the cerebral blood flow, and in neurodegeneration following cerebral ischaemia (7–10). One of the two equivalent nitrogens of the terminal guanidine in L-arginine undergoes five-electron oxidation in the presence of the enzyme NO synthase (NOS), yielding NO and L-citrulline (4–6).

Current studies agree with the hypothesis that L-arginine is converted to NO by NOS in consecutive phases resulting in a multi-step mechanism (11–16). Studies by Marletta et al. (17) suggested that *N*-hydroxylation of L-arginine initiates the synthesis of NO. The discovery that the initial monooxygentation product N^G-hydroxy-L-arginine (L-NHA)

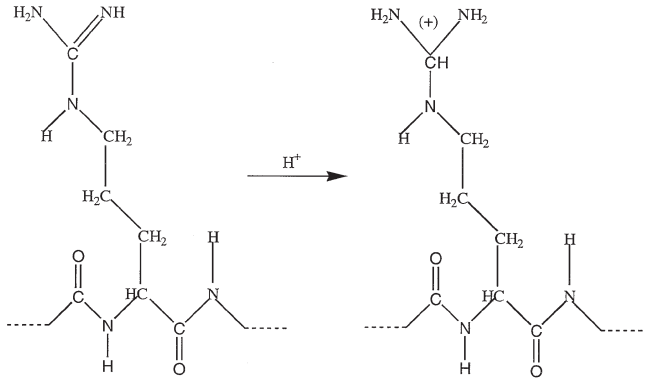
Received November 10, 1999. Published on the NRC Research Press website on May 12, 2000.

M.L. Mak, S.J. Salpietro, and I.G. Csizmadia.[1] Department of Chemistry, University of Toronto, Toronto, ON M5S 3H6, Canada.
R.D. Enriz. Departamento de Quimica, Universidad Nacional de San Luis, 5700 San Luis, Argentina.

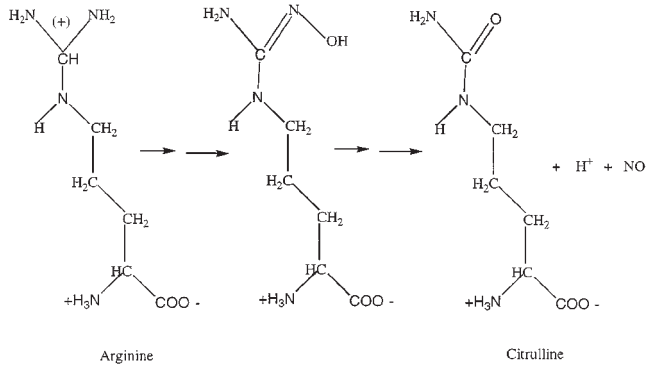
[1]Author to whom correspondence may be addressed.
e-mail: icsizmad@chem.utoronto.ca

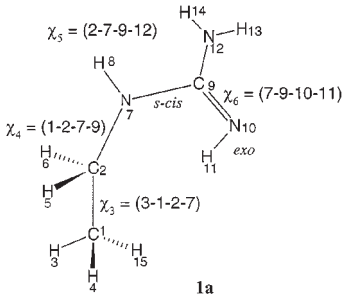
© 2000 NRC Canada

Scheme 1.



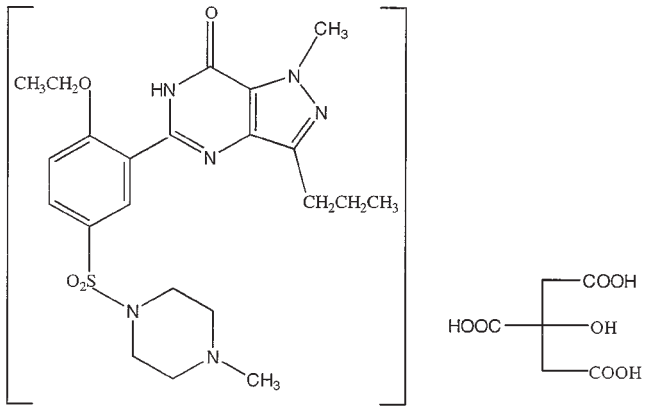
Scheme 2.

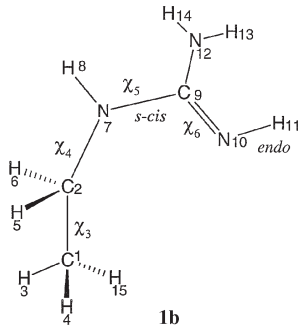




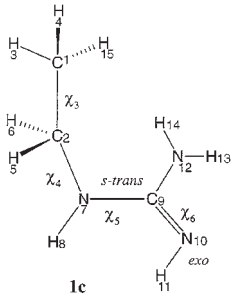
1a

Scheme 3.





1b



1c

is oxidized only at the guanidine nitrogen that has the hydroxyl group (16) agrees with the mechanism proposed by Marletta et al. (17). The oxidation of *N*-hydroxyguanidine, as an L-NHA model, was first studied by Fukuto et al. (13). Recently, the nitric oxide – cyclic guanosine monophosphate (cGMP) signal transduction system is regarded as an ubiquitous pathway for intra- and intercellular communication (18, 4). It was also discovered that endogeneous vasodilators, such as acetylcholine, have no direct action on the vascular smooth muscle, but act on endothelial cells. Upon the action of vasodilators, the cells release NO, which is a "labile factor" that diffuses into the overlying smooth muscles. The smooth muscles underlying the blood vessel walls are relaxed by NO which spreads by diffusion (18, 3–6, 19*a*). For example, the release of NO by the cavernous nerves, which induces the relaxation of smooth muscles in the corpus cavernosum during sexual stimulation, has prompted the recent development of sildenafil citrate, or VIAGRA®, in treatment of erectile dysfunction.

N-methyl guanidine has been used as a model compound for arginine to study the mechanism of NO release using ab initio molecular computations (19*b*).

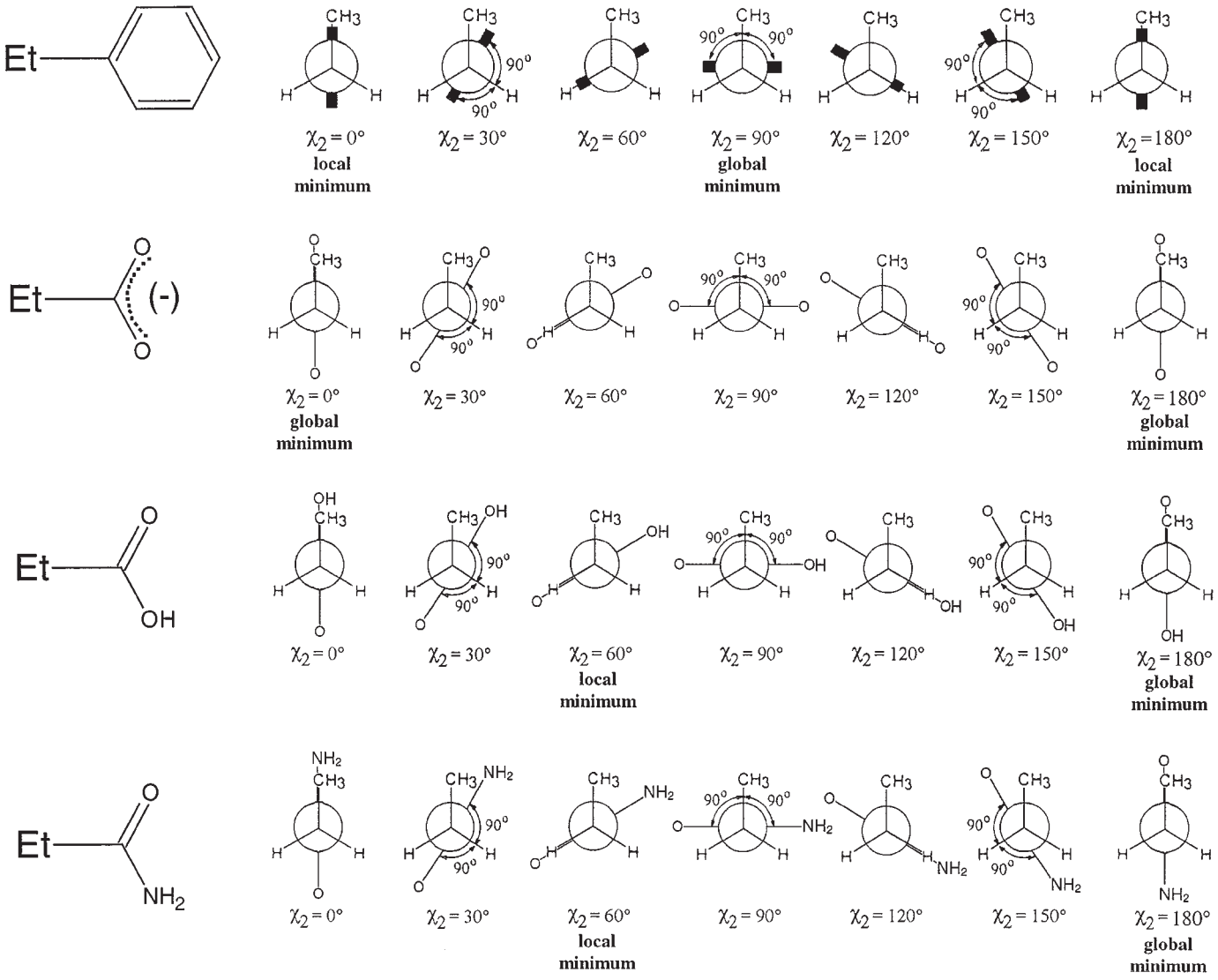
Previous work has already been done regarding the conformations of simple amino acids such as glycine and alanine (20). Other amino acids with more complicated side chains, such as phenylalanine (Phe) (21), serine (Ser) (22–24), cysteine (Cys) (footnote 2), selenocysteine (Sec) (25), aspartic acid (Asp) (26), and asparagine (Asn) (27) have also been studied. With the exception of proline (Pro) (28), all 19 chiral amino acids are expected to have nine different backbone conformations.

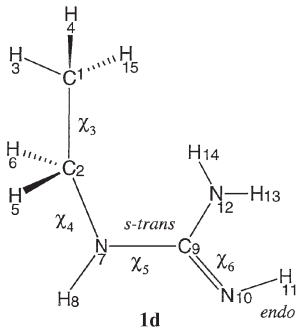
Ethylguanidine (**1**) and ethylguanidinium ion (**2**) are the terminal portions of the side chain (R-group) of the arginine

[2] M.A. Zamora, H.A. Baldoni, A.M. Rodriguez, R.D. Enriz, C.P. Sosa, A. Perczel, A. Kucsman, Ö. Farkas, E. Deretey, J.C. Vank, and I.G. Csizmadia. J. Am. Chem. Soc. (in preparation).

© 2000 NRC Canada

Scheme 4.





1d

residue in *N*-formyl-argininamide (**3**) and its side chain terminal *N*-protonated form (**4**), respectively. Arginine can be divided into two portions: the backbone, which is analogous to glycine (or alanine), and the side chain, which is an alkyl guanidine.

Due to the large number of conformations of the amino acid side chain, even if it is of a modest size, it is simply not practical to optimize the entire structure before we have a preliminary knowledge about the intricacy of its conformations. As an appropriate model one may study **1** instead of **3** or, in a similar fashion, **2** in order to better understand the behavior of **4**.

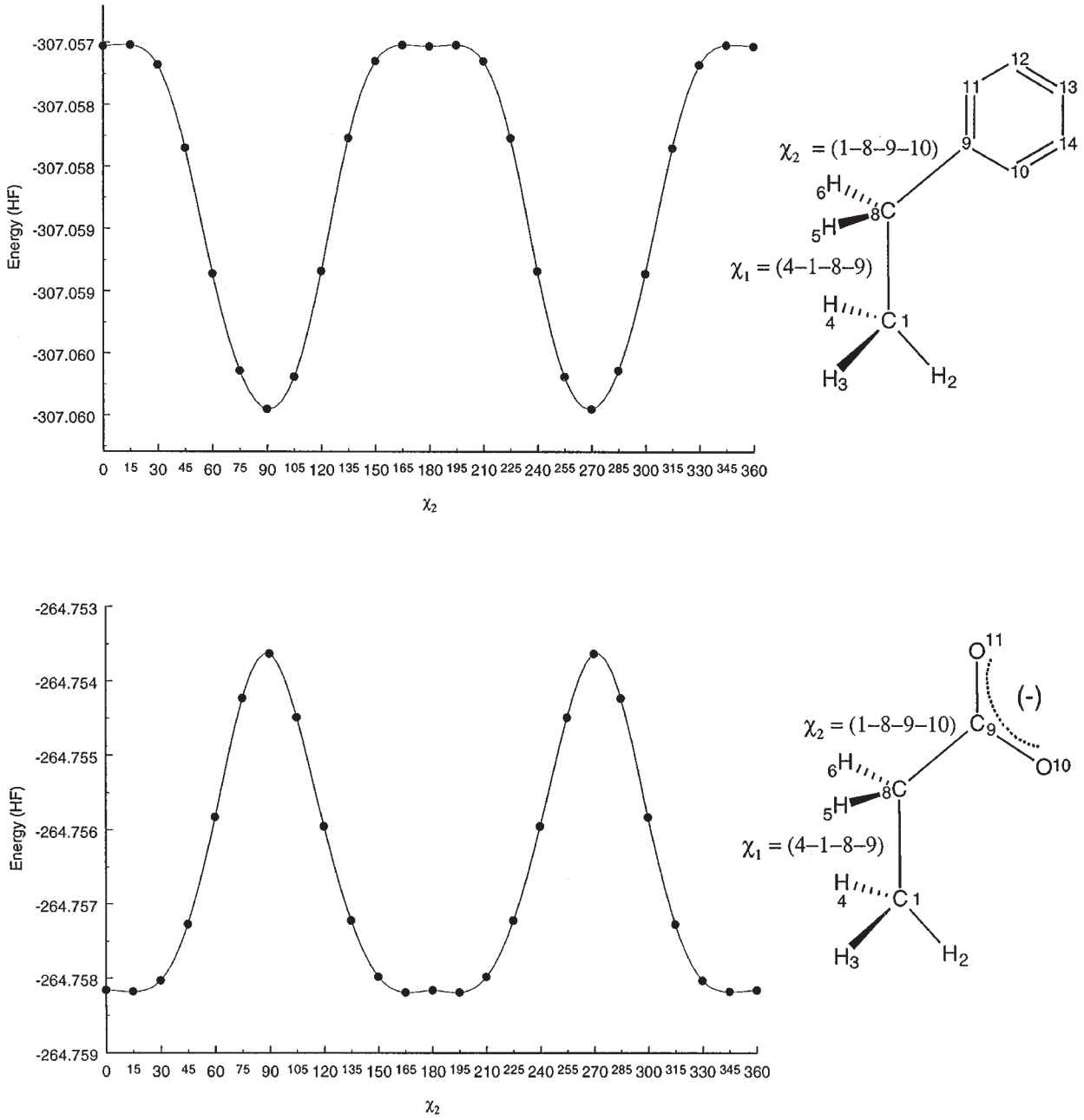
The two torsional modes of motion (rotation about the C—C and C—N bonds) are labeled as χ_3 and χ_4 respectively in all four structures (**1**–**4**) even though structures **1** and **2** have no χ_1 and χ_2 torsional modes.

2. Computational methods

Quantum chemical calculations involving geometry optimizations were carried out using the Gaussian 94 program at the Hartree Fock (HF) and DFT levels of theory using various basis sets. The following two basis sets have been employed for HF calculations: 3–21G and 6–31G. Geometries optimized at the HF level were subjected to further geometry optimization using DFT calculation at the B3LYP/6–31G(*d*) level of theory. Points calculated by the 1D-scan for the $E = E(\chi_4)$ potential energy curve (PEC) of

© 2000 NRC Canada

Fig. 1. Potential energy curve $E = E(\chi_2)$ of ethylbenzene (top) and that of propionate ion (bottom) both calculated at HF/3-21G.



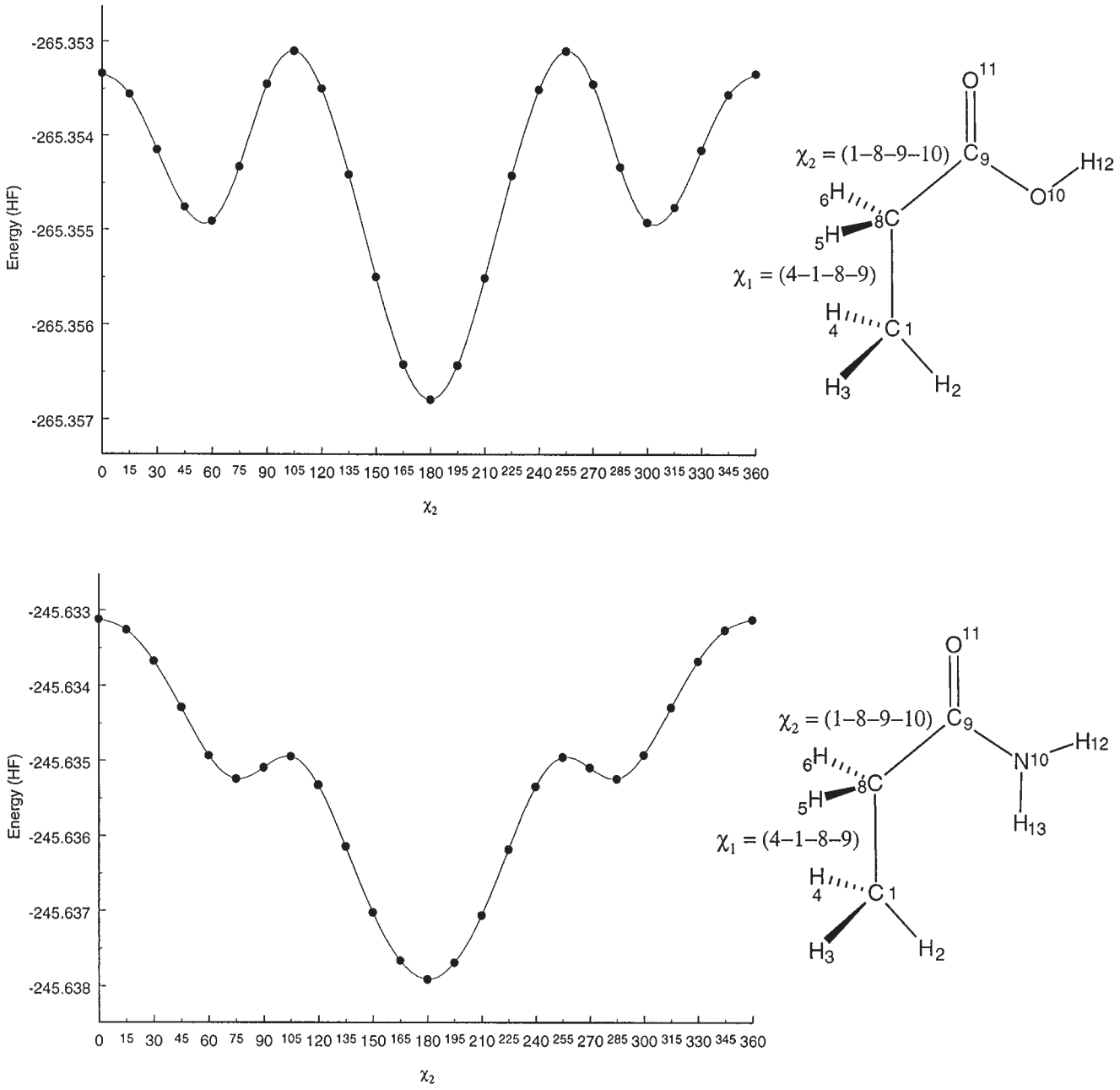
1a was obtained at the HF/6–31G level of theory and the $E = E(\chi_5)$ PEC of **2** was obtained at the HF/3–21G level of theory. Surface points generated by 2D–PES scans were calculated at HF/3–21G level of theory. All curves and surface points obtained were plotted using the Axum 5.0c program.

3. Results and discussion

When a planar moiety is twisted about a single bond with respect to a tetrahedral moiety, in principle six minima may appear. Some of these conformations are shown schematically in Scheme 4. In all cases shown, the methyl group was staggered (i.e., $\chi_1 = 60°$). For the case of ethyl benzene (29) only two unique minima were shown to exist; one at $\chi_2 = 0°$ (the plane of the phenyl ring eclipsed with the C—C bond) and the other one at $\chi_2 = 90°$ (the plane of the phenyl ring being perpendicular to the C—C bond). The global minimum was found to be the one in which the planar moiety was perpendicular to the C—C bond ($\chi_2 = 90°$). Of course, both of these minima occurred twice in full 360° rotation due to the fact that the two sides of the benzene ring were identical. The potential energy curve of the other symmetrical compound, namely the propionate ion, is the exact mirror image of that associated with ethyl benzene, where the minimum of one is the maximum of the other (Fig. 1). The two asymmetrical compounds, propionic acid and

© 2000 NRC Canada

Fig. 2. Potential energy curve $E = E(\chi_2)$ of propionic acid (top) and that of propionamide ion (bottom) both calculated at HF/3-21G.



propionamide, give rise to a global minimum when they are in the *anti* conformation and local minima in the *gauche* conformations. (Fig. 2)

In the case of ethylguanidine (**1**) and the ethylguanidinium ion (**2**), there are two torsional angles χ_3 and χ_4. The dihedral numbering is in accord with the amino acid convention (corresponding to χ_1 and χ_2 in ethylbenzene). These are two kinds of bonds, C—C and C—N, with respect to which the guanidine group could be either eclipsed or perpendicular.

3.1 Energetic considerations

3.1.1 Ethylguanidine

Figure 3 shows the torsional potential, with varying χ_4, for ethylguanidine in its *s-cis*/*exo* **1a** structure calculated using the HF/6–31G level of theory. The global minimum occurs at 180° (the *anti* form). For all four structures (**1a**, **1b**, **1c**, and **1d**) g^+, a, and g^- were shown to have energy minima. We optimized these minima using three levels of theory (Hartree Fock 3–21G, 6–31 G, and DFT/B3LYP). The results are summarized in Table 1.

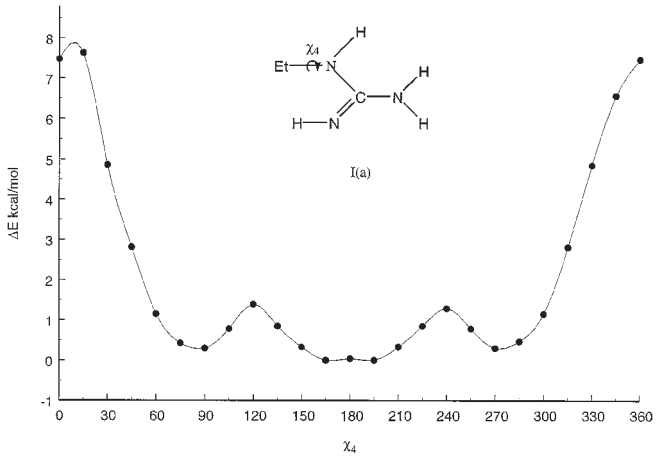
The ethyl rotation as characterized by the PES of the type $E = E(\chi_3, \chi_4)$ for the structures **1a**, **1b**, **1c**, and **1d** are presented in Figs. 4, 5, 6, and 7 respectively. Although the four surfaces are noticeably different, the three-fold periodicity of the CH_3 rotation (along χ_3) is fully apparent. The relative stabilities of these $4 \times 3 = 12$ structures are illustrated in Fig. 8. One can observe that the *gauche* conformation of **1b** is the global minimum, and that its *anti* conformation is of a relatively low energy comparing to the other three *anti*

© 2000 NRC Canada

Table 1. Optimized torsional angle (χ_4) and energy values of the conformational minima ($\lambda = 0$) of structures **1a**, **1b**, **1c**, and **1d** using various basis sets at the HF and DFT level of theory.

Structure	Basis set	Optimized Parameters			
		(χ_4)	E_{min} (hartree)	ΔE (kcal/mol)	$\Delta\Delta E$ (kcal/mol)
1a	HF/3–21G	82.27	–280.6102467	1.35	0.09
		168.67	–280.6101103	1.44	0.00
		–74.59	–280.6098721	1.59	0.15
	HF/6–31G	78.29	–282.0620464	0.92	0.44
		171.21	–282.0627458	0.49	0.00
		–78.22	–282.0620465	0.92	0.44
	B3LYP/6–31G(d)	75.48	–283.9874326	0.10	0.30
		177.36	–283.9879119	0.40	0.00
		–81.42	–283.9865861	0.43	0.83
1b	HF/3–21G	79.38	–280.6124011	0.00	0.97
		162.46	–280.6108520	0.97	0.00
		–79.41	–280.6124010	0.00	0.97
	HF/6–31G	84.26	–282.0635187	0.00	3.98
		168.25	–282.0630562	0.29	0.00
		–84.12	–282.0635189	0.00	0.29
	B3LYP/6–31G(d)	76.14	–283.9877135	0.27	0.27
		173.42	–283.987277	0.00	0.00
		–76.27	–283.9877134	0.27	0.27
1c	HF/3–21G	100.76	–280.6079228	2.81	0.06
		157.14	–280.607826	2.87	0.00
		–64.80	–280.6085254	2.43	0.44
	HF/6–31G	75.57	–282.0599067	2.27	0.39
		–179.98	–282.060534	1.87	0.00
		–85.42	–282.0598876	2.28	0.41
	B3LYP/6–31G(d)	67.85	–283.9857075	0.98	0.43
		179.73	–283.9850151	1.42	0.00
		–67.97	–283.9857073	0.99	0.43
1d	HF/3–21G	63.05	–280.6087256	2.31	0.44
		189.70	–280.6080244	2.75	0.00
		–62.95	–280.6087256	2.31	0.44
	HF/6–31G	77.53	–282.0603108	2.01	0.41
		–179.94	–282.0609655	1.60	0.00
		–77.30	–282.0603107	2.01	0.41
	B3LYP/6–31G(d)	65.46	–283.9856017	1.05	3.17
		179.94	–283.9805551	4.22	0.00
		–65.66	–283.9856012	1.05	3.17

Fig. 3. Potential energy curve $E = E(\chi_4)$ of structure **1a** calculated at HF/6-31G.

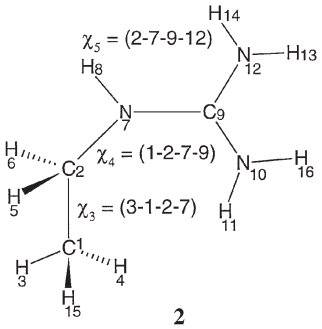


forms. The *anti* conformation of **1d** is highest in energy. It is also interesting to note that the energy difference between the *anti* and *gauche* forms of **1d** is the greatest, whereas this energetic difference is the smallest in **1b**.

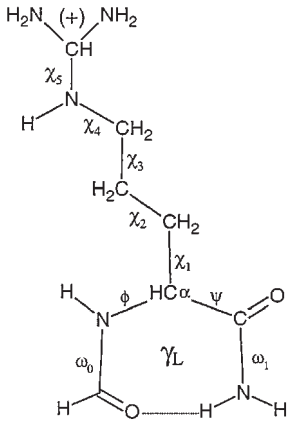
3.1.2 Ethylguanidinium ion

The protonated form of the ethylguanidine (**1**) is the ethyl guanidinium ion (**2**). Due to the internal symmetry of the N-$C(NH_2)_2^+$ moiety, this species has only one arrangement, unlike **1** which has four: **1a**, **1b**, **1c**, and **1d**. Consequently, only the ethyl rotation $E = E(\chi_3, \chi_4)$ is important, of which the 1D cross-section $E = E(\chi_4)$ predominates. The energy values for the 1D-scan are computed at the HF/3–21G level of theory. This PEC is depicted in Fig. 9. The $E = E(\chi_3, \chi_4)$ PES is depicted in Fig. 10. The PEC has a pattern similar to those seen in Fig. 2. Another PEC cross-section of the PEHS $E = E(\chi_5)$ is of particular interest since it interconnects the *s-cis* and *s-trans* conformers. However, in the case of the

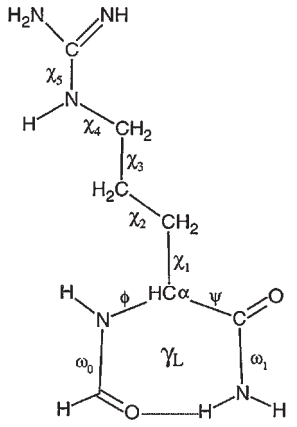
© 2000 NRC Canada



2



3



4

protonated form they become degenerate as shown in Fig. 11. It is interesting to note that the curve (Fig. 11) is analogous to that of Et-COO(-) of Fig. 1. The principal results of the geometry optimizations achieved at these levels of theory are summarized in Table 2.

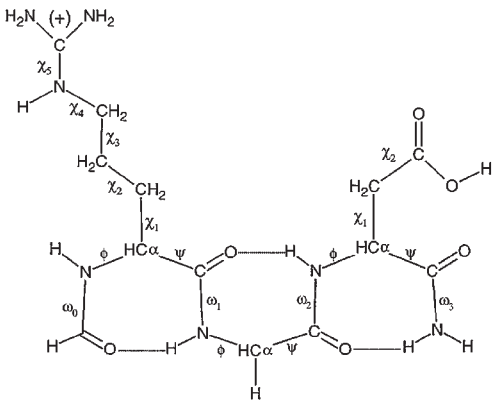
For the proton affinity (PA) we may recognize that a number of values may be calculated. There is only one PEC for the protonated form (**2**) but there are four PECs for (**1**). Two vertical proton affinity values may be identified using these PECs. The two vertical ones involve g→g and a→a. These values are summarized in Table 3.

Table 2. Optimized torsional angles (χ_4) and energy values of the conformational minima ($\lambda = 0$) of structure **2** CH_3-CH_2-NH-$C(NH_2)_2$ using various basis sets at the HF and DFT level of theory.

Basis set	Optimized Parameters		
	(χ_4)	E_{min} (hartree)	ΔE (kcal/mol)
3–21G	81.79	–281.0413070	0.61
	179.52	–281.0422726	0
	–82.59	–281.0413097	0.60
6–31G	85.00	–282.4864891	0.91
	179.98	–282.4879377	0
	–85.06	–282.4864888	0.91
B3LYP/6–31G(d)	90.52	–284.3914612	0.37
	179.94	–284.3920511	0
	–90.54	–284.3914611	0.37

Table 3. Proton affinities (in kcal/mol) for the 3 conformational minima of structures **1a**, **1b**, **1c,** and **1d** at HF/6–31G and B3LYP/6–31G(*d*) levels of theory.

Conformation	Base	HF/6–31G	B3LYP/6–31G(d)
g^+	**1a**	266.34	253.53
	1b	265.42	253.36
	1c	267.70	254.61
	1d	267.43	254.68
a	**1a**	266.81	253.60
	1b	266.62	254.00
	1c	268.20	255.42
	1d	267.93	258.22
g^-	**1a**	266.34	254.43
	1b	265.42	253.36
	1c	267.69	254.61
	1d	267.43	254.68

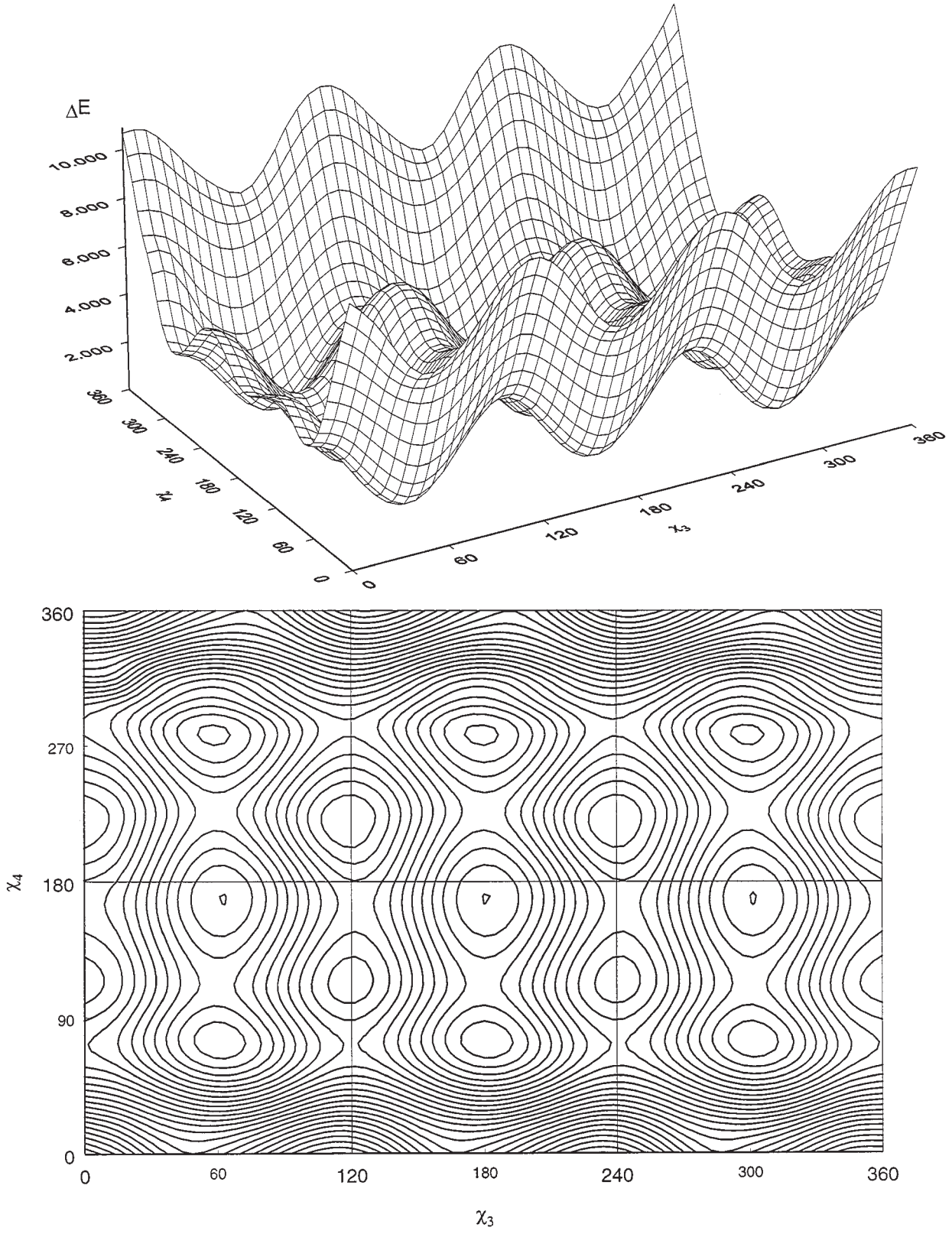


5

The first ab initio proton affinities were computed in Toronto (30) in 1968. A collection of relative proton affinities was compiled by Lias et al. (31) in 1984. In 1993, Radom (32) provided state-of-the-art calculation of various proton affinities, some of which involved saturated nitrogen compounds. Note that the present proton affinities are generated for illustrative purposes only and not for state of the art

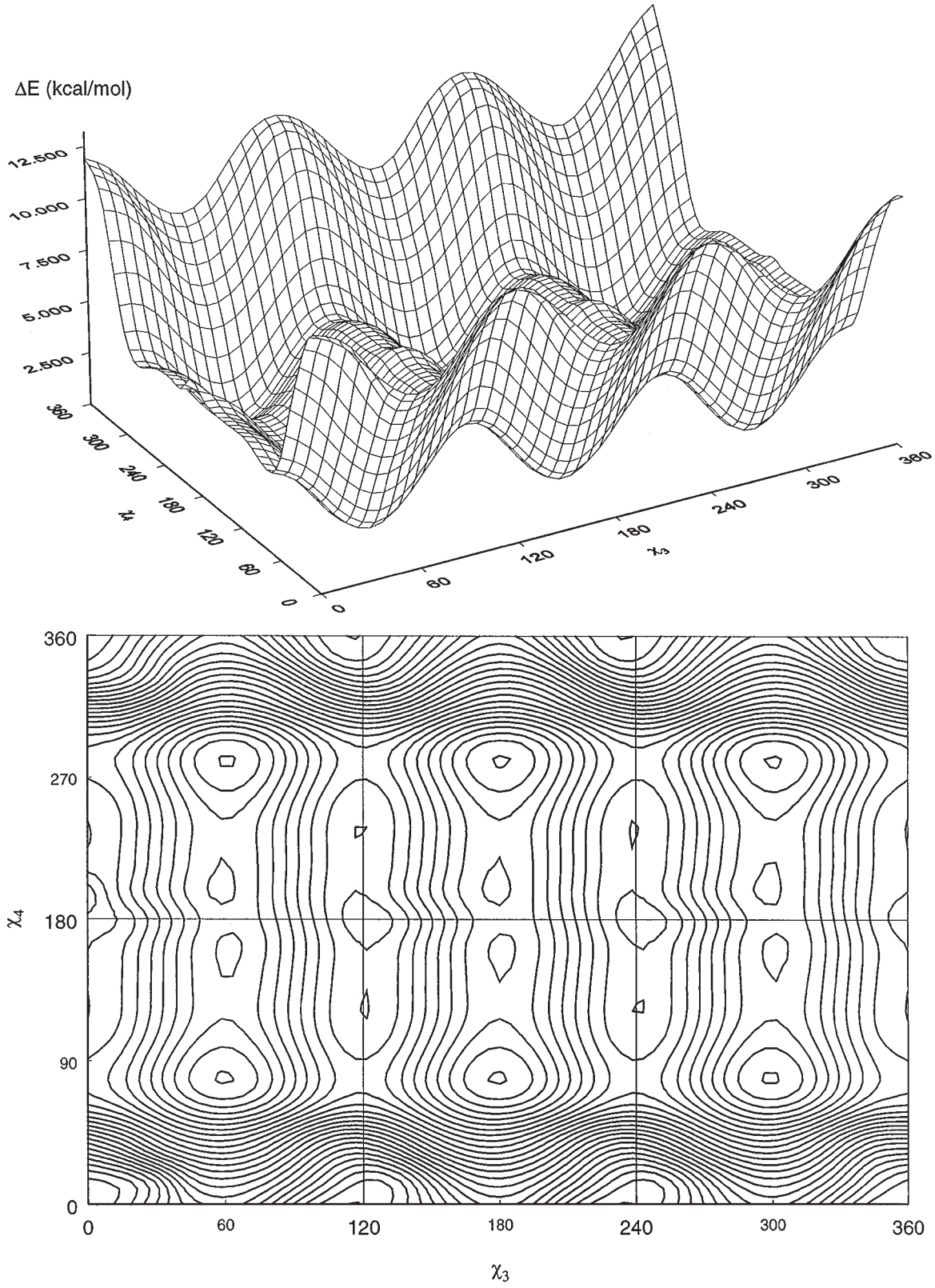
© 2000 NRC Canada

Fig. 4. Conformational potential energy surface $E = E(\chi_3, \chi_4)$ of structure **1a** as landscape (top) and projected contour plot (bottom) calculated at HF/3-21G.



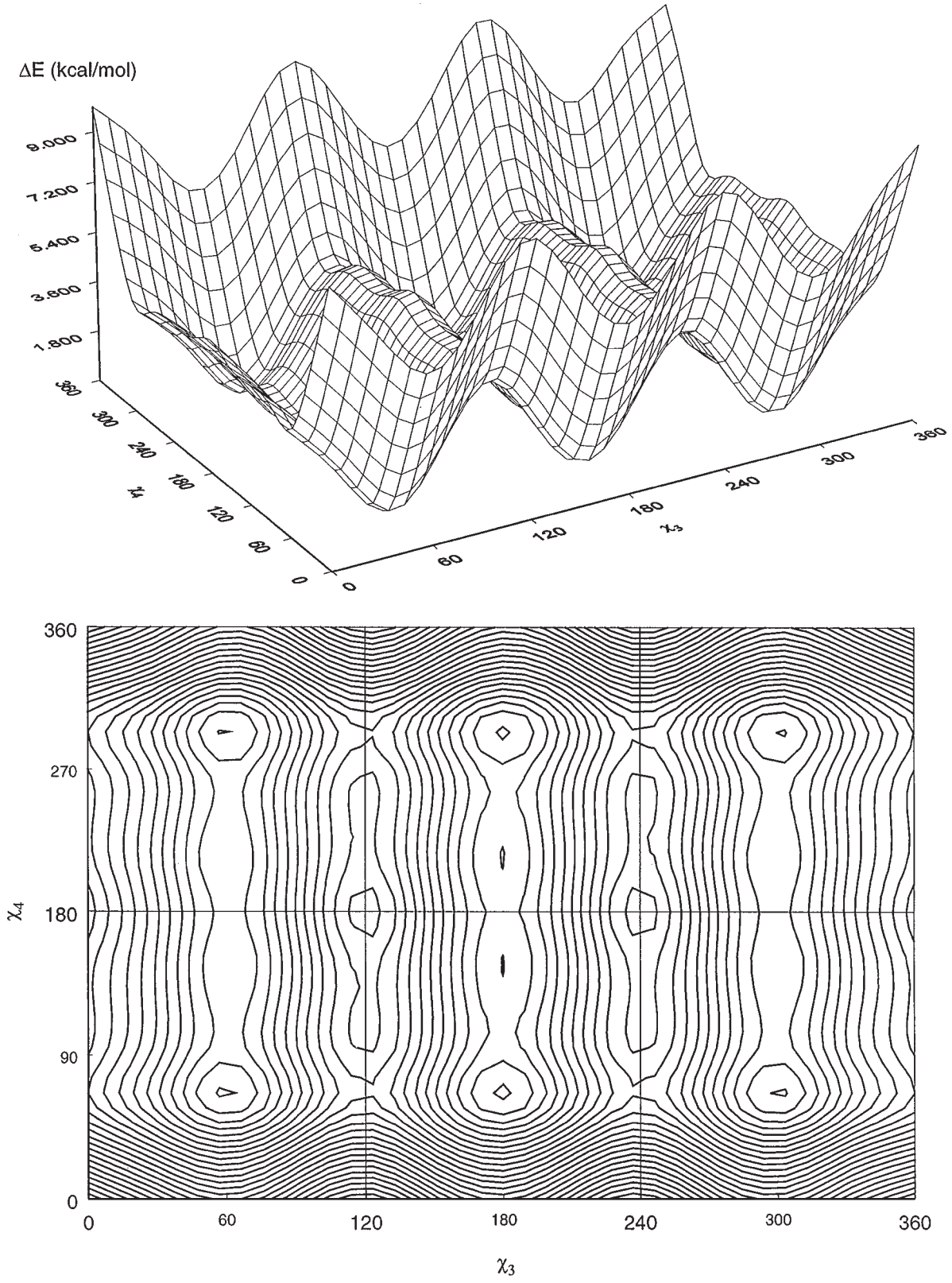
© 2000 NRC Canada

Fig. 5. Conformational potential energy surface landscape (top) $E = E\chi_3, \chi_4)$ of structure **1b** and projected contour plot (bottom) calculated at HF/3-21G.



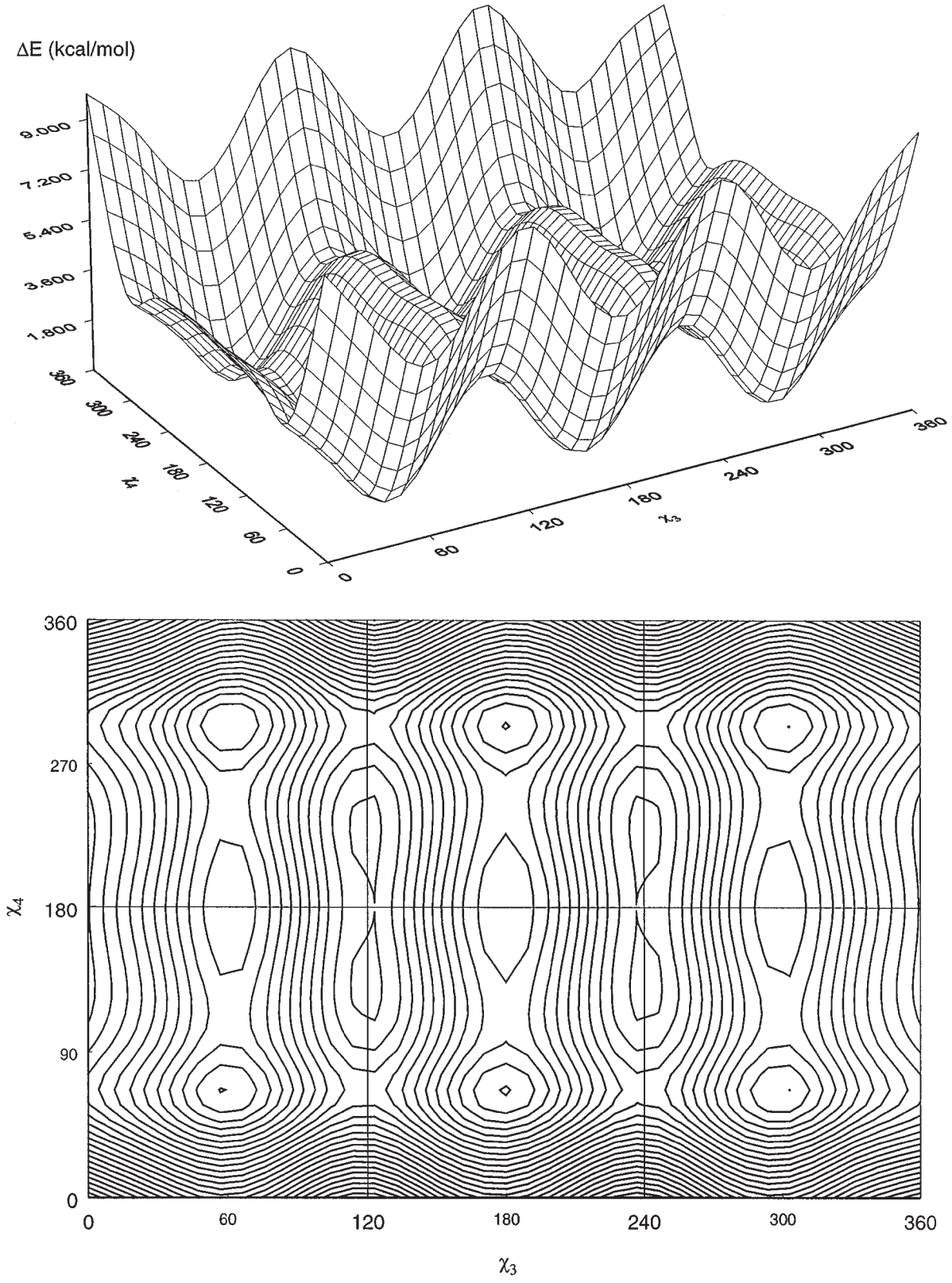
© 2000 NRC Canada

Fig. 6. Conformational potential energy surface landscape (top) $E = E(\chi_3, \chi_4)$ of structure **1c** and projected contour plot (bottom) calculated at HF/3-21G.



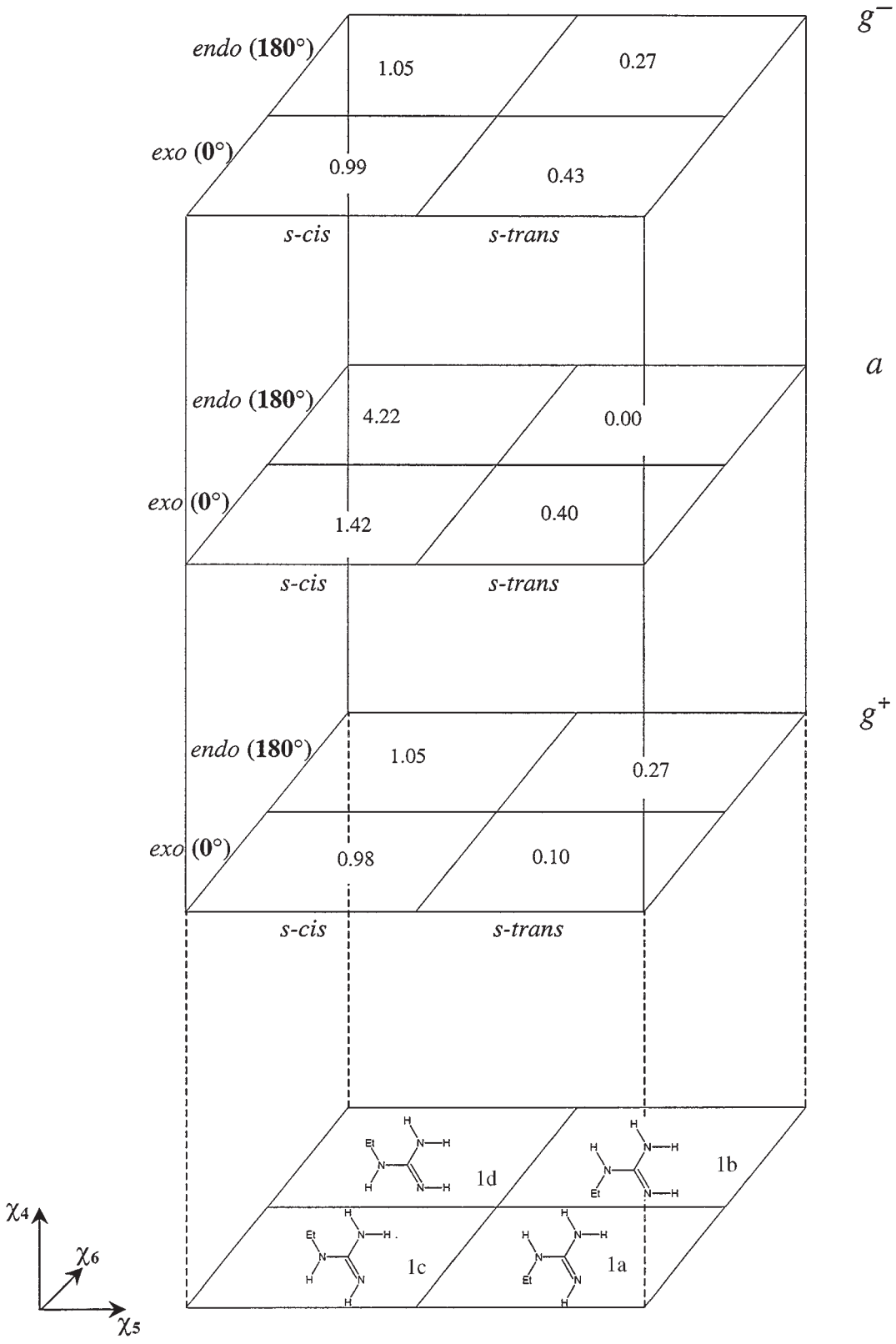
© 2000 NRC Canada

Fig. 7. Conformational potential energy surface landscape (top) $E = E(\chi_3, \chi_4)$ of structure **1d** and projected contour plot (bottom) calculated at HF/3-21G.



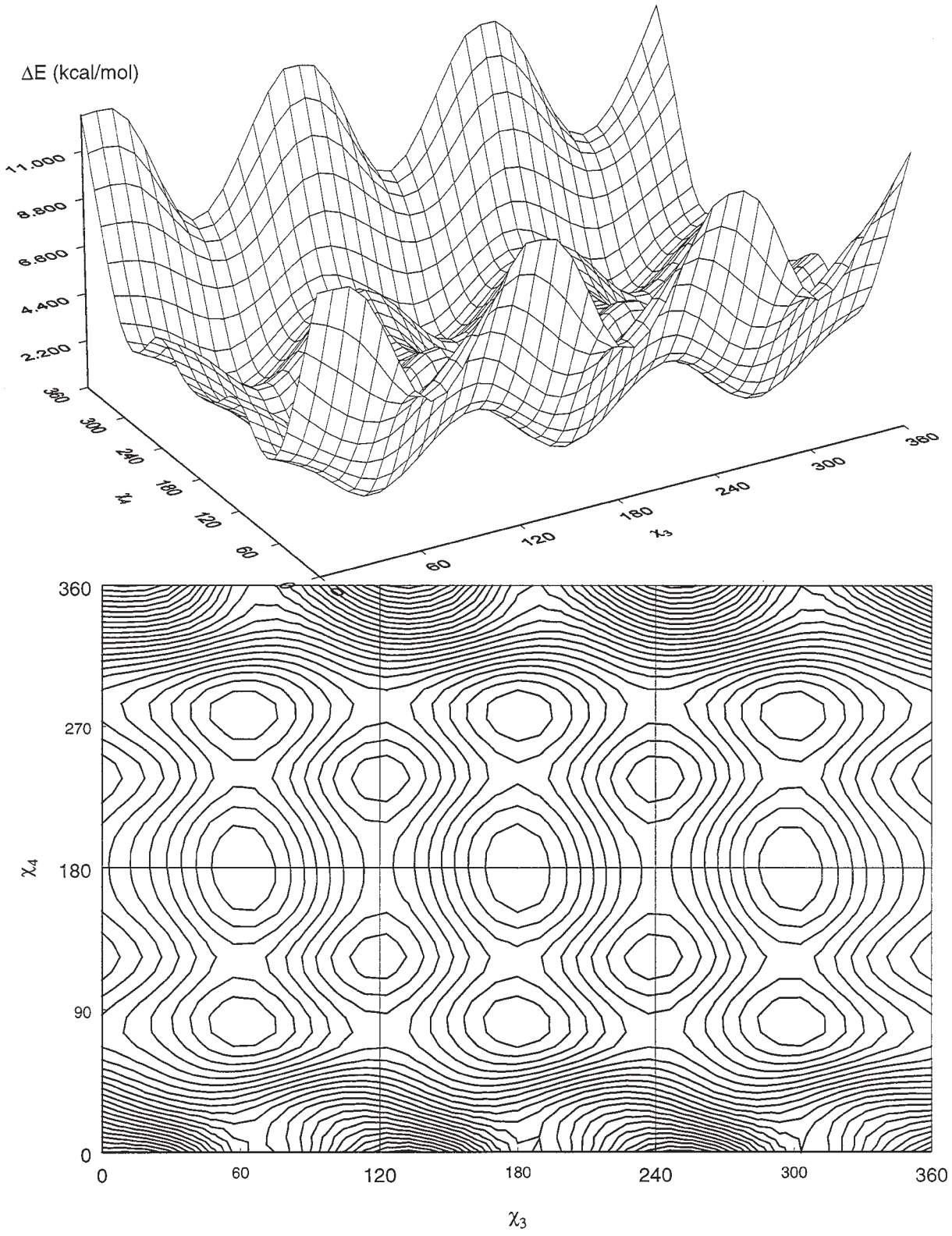
© 2000 NRC Canada

Fig. 8. Topological representation of the $E = E(\chi_4, \chi_5, \chi_6)$ Potential energy hypersurface for compound **1**. Energy differences were computed at the B3LYP/6-31G(*d*) level of theory.



© 2000 NRC Canada

Fig. 10. Conformational potential energy surface landscape (top) $E = E(\chi_3, \chi_4)$ of structure **2** and projected contour plot (bottom) calculated at HF/3-21G.



© 2000 NRC Canada

Fig. 9. Potential energy curve $E = E(\chi_4)$ of structure **2** calculated at HF/3-21G.

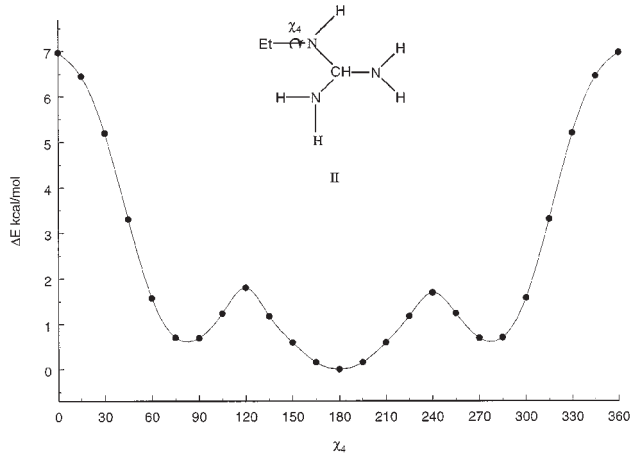
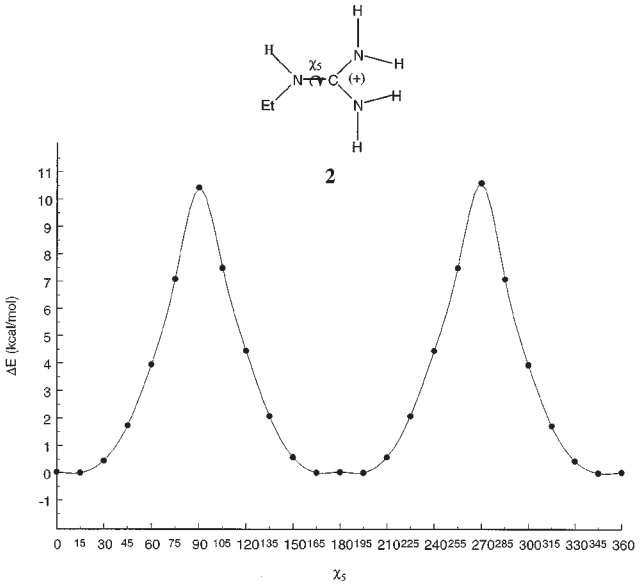


Fig. 11. Potential energy curve $E = E(\chi_5)$ of structure **2** calculated at HF/3-21G.



accuracy. It is worthy to mention, however, that at least the trend in proton affinities is apparent when one compares the values at the HF level with those of the DFT level of theory. These values are to show that different conformations give different proton affinities. Proton affinity is defined with a positive sign and is actually the deprotonation energy of the conjugated acid. The a→a and the g→g vertical deprotonation energies are shown in Fig. 12 and Fig. 13 respectively. In this way, one can determine the order of relative acidities of the four protons in the guanidinium ion (Fig. 14).

Proton affinities of amino acids are studied in detail (33) and the deprotonation of side chain protonated arginine (34) has also been investigated. It has also been pointed out that the proton at the first N—H bond of side chain-protonated

Fig. 12. Vertical proton affinity values for the transition a→a calculated at HF/6-31G.

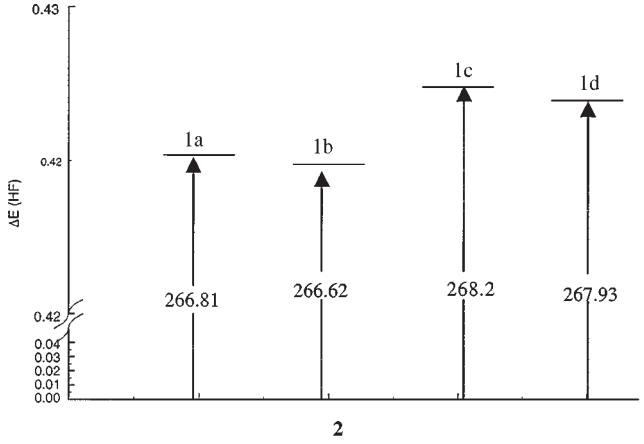
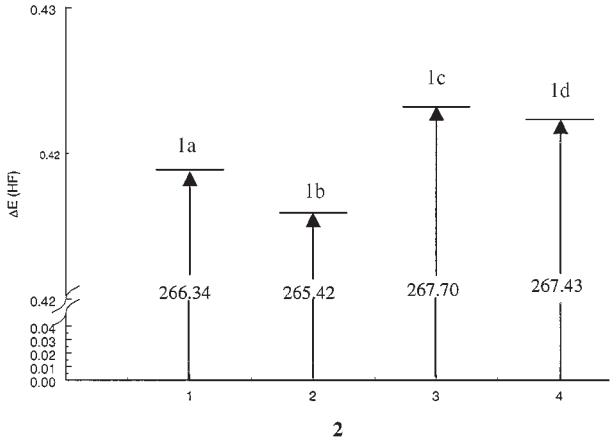


Fig. 13. Vertical proton affinity values for the transition g→g calculated at HF/6-31G.



arginine (N^7—H^8 in **2**) can also deprotonate if the lone pair formed in the deprotonation is stabilized by backbone→side chain hydrogen bonding. Other reactions of the arginine side chain have also been investigated (19*b*, 35) recently.

3.2 Geometrical considerations

For the ease of identification of the various geometrical parameters, the symbolic *z*-matrix is given in Table 4. Tables 5, 6, 7, and 8 (Supplementary material)[3] summarize optimized geometrical parameters for **1a**, **1b**, **1c**, and **1d**. It may be interesting to compare how some parameters remain virtually unchanged with conformational variation while others vary noticeably.

Table 9 (Supplementary material)[3] gives the geometrical parameters for **2**. It is noteworthy to compare what happens to the C=N double bond of **1**, upon protonation, leading to ethylguanidinium ion (**2**).

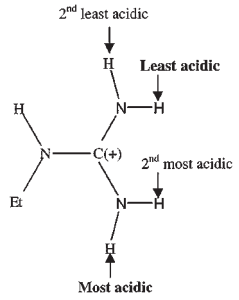
3.2.1 Ethylguanidine

Ethylguanidine has four stereoisomeric forms, as shown in Fig. 8; they are *s-cis*/*endo*, *s-cis*/*exo*, *s-tran*/*endo*, and

[3] Supplementary material may be purchased from: The Depository of Unpublished Data, Document Delivery, CISTI, National Research Council Canada, Ottawa, Ontario, Canada, K1A 0S2.

© 2000 NRC Canada

Fig. 14. Hierarchy of acidity of the four protons of ethylguanidium ion.



s-trans/*exo*. The *cis–trans* relationship is assigned with respect to the orientation of the ethyl moiety around the torsional angle χ_5, and the *exo–endo* relationship is assigned according to the orientation of the hydrogen double bonded to the nitrogen (N^{10}=H^{11}). If the hydrogen is pointing out of plane, the isomer is assigned *exo*, with χ_6 = 180°; similarly, if the hydrogen is pointing towards the plane, the isomer is assigned *endo*, χ_6 = 0°. One can compare C^9=N^{10} (B9) and C^9—N^{12} (B11) bond lengths of **1** with the C—N bond lengths of **2**, and deduce the extent of the double bond nature. The C^9—N^{12} and C^9—N^{10} bond lengths (1.340) of **2** are between the lengths of the C^9=N^{10} bond and the C^9—N^{12} bond of **1**. The difference between these two bond lengths is the greatest in all three conformations of **1c**. So, the single bonds C^9—N^{10} and C^9—N^{12} of **2** have more "double bond" character than the single bond C^9—N^{12} of **1**.

3.2.2 Ethylguanidinium ion

While the guanidinium ion is symmetrical, ethylguanidinium is not. Presence of the ethyl moiety makes all five hydrogens of guanidinium ion inequivalent. The four hydrogens for deprotonation can lead to four isomers of the neutral ethylguanidine.

The lengths of N—H bonds of the guanidino end are identical, indicating that the positive charge is delocalized. It is also worth noting that N_{10}—H_{11} (B10) of **2** is the shortest of the four NH_2 hydrogens although H_{11} is the most acidic of the four (Fig. 14). Therefore, the N—H bond length is not governed by acidity (i.e., electronic effects), but rather by the orientation of the ethyl moiety (i.e., steric effects). N^{10}—H^{11} is *syn* with respect to the ethyl group and is therefore sterically the closest to the aliphatic group.

4. Acknowledgements

The continuous financial support of the Natural Sciences and Engineering Research Council (NSERC) of Canada is gratefully acknowledged. We would also like to thank the NCI for the use of services at Frederick Biomedical Supercomputing Center.

References

1. E. Ruoslahti and M.D. Pierschbacher. Science (Washington, D.C.), **238**, 491 (1987).
2. R.O. Hynes. Cell (Cambridge, Mass.), **48**, 549 (1987).
3. P.K. Moore and R.L.C. Handy. Trends Pharmacol. Sci. **18**, 204 (1997).
4. F. Murad, B.A. Weissman, A. Allon, and S. Shapira (*Editors*). Biochemical, pharmacological and clinical aspects of nitric oxide. Plenum Press, New York. 1995. pp. 1–11.
5. M.A. Marletta. J. Biol. Chem. **268** (17), 12231 (1993).
6. A.R. Butler, F.W. Flitney, and D.L.H. Williams. Trends Pharmacol. Sci. **16**, 18 (1995).
7. M.D. Black, E.K. Matthews, and P.P.A. Humphrey. Neuropharmacology, **33** (11), 1357 (1997).
8. Chol Lipton, Lei Pan, Sucher Chen, Singel Loscalzo, Stamler. Nature (London), **364**, 626 (1993).
9. V.L. Dawson, T.M. Dawson, E.D. London, D.S. Bredt, and S.H. Snyder. Proc. Natl. Acad. Sci. U.S.A. **88**, 6368 (1991).
10. W. Wutian and L. Linxi. Neurosc. Lett. **153**, 121 (1993).
11. J.F. Kerwin and M. Heller. Med. Res. Rev. **14**, 23 (1994).
12. N.M. Olken and M.A. Marletta. Biochemistry, **32**, 9677 (1993).
13. J.M. Fukuta, D.J. Stuehr, and P.L. Feldman. J. Med. Chem. **36**, 2666 (1993).
14. J.S. Valentine, J.N. Burstyn, and L.D. Margernum. *In* Oxygen complexes and oxygen activation by transition metals. *Edited by* A.E. Martell, D.T. Martella, and D.T. Sawyer. Plenum Press, New York. 1988. pp. 175–187.
15. D.J. Stuehr, N.S. Kwon, C.F. Nathan, O.W. Griffith, P.L. Feldman, and J. Wiseman. J. Biol. Chem. **266**, 6259 (1991).
16. D.J. Stuehr and O.W. Griffith. Adv. Enzymol. Relat. Areas Mol. Biol. 297 (1992).
17. M.A. Marletta, P.S. Yoon, R. Ivengar, C.D. Leaf, and J.S. Wishnok. Biochemistry, **27**, 8706 (1988).
18. T. Dalkara and M.A. Moskowitz. *In* Biochemical, pharmacological and clinical aspects of nitric oxide. *Edited by* B.A. Weissma, A. Allon, and S. Shapira. Plenum Press, New York. 1995. pp. 189–194.
19. (*a*) S. Moncada, R.M.J. Palmer, and E.A. Higgs. Pharmacol. Rev. **43**, 109 (1991); (*b*) M.B. Santillan, G.M. Ciuffo, E.A. Jauregui, and I.G. Csizmadia. THEOCHEM, **468**, 223 (1999).
20. (*a*) A. Perczel, J.G. Angyan, M. Kajtar, W. Viviani, J.L. Rivail, J.F. Marcoccia, and I.G. Csizmadia. J. Am. Chem. Soc. **113**, 6256 (1991); (*b*) M.A. McAllister, A. Perczel, P. Császár, W. Viviani, J.L. Rivail, and I.G. Csizmadia. THEOCHEM, **288**, 161 (1993).
21. (*a*) Ö. Farkas, M.A. McAllister, J.H. Ma, M. Hollósi, and I.G. Csizmadia. THEOCHEM, **369**, 105 (1996); (*b*) A. Perczel, Ö. Farkas, and I.G. Csizmadia. Can. J. Chem. **75,** 1120 (1997); (*c*) I. Jakli, A. Perczel, Ö. Farkas, M. Hollosi, and I.G. Csizmadia. THEOCHEM, **455**, 303 (1998).
22. (*a*) Ö. Farkas, J.F. Marcoccia, M. Hollósi, and I.G. Csizmadia. THEOCHEM, **331**, 27 (1995); (*b*) A. Perczel, Ö. Farkas, and I.G. Csizmadia. J. Comput. Chem. **17**, 821 (1996).
23. A. Perczel, Ö. Farkas, and I.G. Csizmadia. J. Am. Chem. Soc. **118**, 7809 (1996).
24. A. Perczel, Ö. Farkas, and I.G. Csizmadia. THEOCHEM, **455**, 303 (1998).
25. J.C. Vank, C.P. Sosa, A. Perczel, and I.G. Csizmadia. Can. J. Chem. **78**, 395 (2000).
26. S.J. Salpietro, A. Perczel, Ö. Farkas, R.D. Enriz, and I.G. Csizmadia. THEOCHEM, **497**, 37 (2000).
27. M. Berg, S.J. Salpietro, and I.G. Csizmadia. THEOCHEM, (in press).
28. H.A. Baldoni, A.M. Rodriguez, M.A. Zamora, G.N. Zamarbide, R.D. Enriz, Ö. Farkas, P. Csaszar, L.L. Torday, C.P. Sosa, I. Jakli, A. Perczel, J.G. Papp, M. Hollosi, and I.G. Csizmadia. THEOCHEM, **465**, 79 (1999).
29. Ö. Farkas, S.J. Salpietro, P. Csaszar, and I.G. Csizmadia. THEOCHEM, **367**, 25 (1996).

© 2000 NRC Canada

30. A.C. Hopkinson, N.K. Holbrook, K. Yates, and I.G. Csizmadia. J. Chem. Phys. **49**, 3596 (1968).
31. S.G. Lias, J.F. Liebman, and R.D. Levin. J. Phys. Chem. Ref. Data, **13**, 695 (1984).
32. B.J. Smith and L. Radom. J. Am. Chem. Soc. **115**, 4885 (1993).
33. Z.B. Maksic and B. Kovacevic. Chem. Phys. Lett. **307**, 497 (1999).
34. Z.B. Maksic and B. Kovacevic. J. Chem. Soc. Perkin Trans. 2, 2926 (1999).
35. C. Kozmutza, E.M. Evleth, L. Udvardi, and J. Pipek. Acta Biol. Hung. **49**, 219 (1998).

© 2000 NRC Canada

Cyclic five-membered phosphinate esters as transition state analogues for obtaining phosphohydrolase antibodies

Gabriel Hum, Krista Wooler, Jeremy Lee, and Scott D. Taylor

Abstract: Two novel cyclic five-membered phosphinate esters (**6** and **7**) were synthesized and used as transition state analogues (TSAs) for raising phosphohydrolase antibodies. The key step in the syntheses was a McCormack reaction between (2-chloroethyl)dichlorophosphite and 1,4-diphenyl-1,3-butadiene to form isomeric cyclic phosphinyl chlorides which upon further elaboration yielded the TSAs. X-ray crystal structures of two cyclic phosphinate TSA precursors (**14a** and **14b**) show highly compressed CPC bond angles of 94°–97° indicating that the CPC bond angles in **6** and **7** are significantly distorted towards the ideal trigonal bipyramidal equatorial–apical transition state angle of 90° formed during phosphate ester hydrolysis. Antibodies were raised to **6** and **7** using standard hybridoma technology. One antibody, Jel 541, an IgM class antibody, was obtained that was capable of catalyzing the hydrolysis of phosphonate substrate **9** and, to a much lesser extent, phosphate substrate **8**. This antibody bound TSA **6** approximately 100 times more tightly than TSA **7** as determined by solid phase radio immune assays. The activity of the antibody-catalyzed reaction was completely inhibited by the presence of TSA **6**. Although the relative instability and poor solubility of Jel 541 made it impossible to perform a detailed kinetic analysis of the antibody-catalyzed reactions, these results demonstrate that phosphohydrolase antibodies can indeed be obtained using cyclic five membered phosphinates as haptens.

Key words: transition state analogues, phosphate ester hydrolysis, catalytic antibodies.

Résumé : On a réalisé la synthèse de deux nouveaux esters phosphinates formant un cycle à cinq chaînons (**6** et **7**) et on les a utilisés comme analogues de l'état de transition (AET) pour la production d'anticorps de la phosphohydrolase. L'étape clé de la synthèse est une réaction de McCormack entre le dichlorophosphite de 2-chloroéthyle et le 1,4-diphénylbuta-1,3-diène pour former les chlorures de phosphinyle cycliques isomères qui, par réaction ultérieure, conduisent aux AET. Les structures cristallines des deux phosphinates cycliques précurseurs dAET (**14a** et **14b**), telles que déterminées par diffraction des rayons X, montrent que les angles de liaison CPC sont fortement comprimés (94–97°) et ceci indique que les angles de liaison dans les composés **6** et **7** sont fortement déformés vers l'angle idéal de 90° de l'état de transition trigonal bipyramidal équatorial-axial qui caractérise l'hydrolyse des esters phosphates. Des anticorps ont été produits à l'aide des produits **6** et **7** en faisant appel à la technologie hybridome standard. On a obtenu un anticorps, Jel 541, un anticorps de la classe IgM, capable de catalyser l'hydrolyse d'un substrat phosphonate **9** et, à un degré moindre, celle du substrat phosphonate **8**. Sur la base d'essais radioimmunologiques en phase solide, cet anticorps se lie à l'AET **6** environ 100 fois plus fortement que l'AET **7**. L'activité de la réaction catalysée par l'anticorps est complètement inhibée par la présence de l'AET **6**. Même si l'instabilité relative et la mauvaise solubilité du Jel 541 empêchent toute analyse cinétique détaillée des réactions catalysées par l'anticorps, ces résultats démontrent qu'il est possible d'obtenir des anticorps de la phosphohydrolase en utilisant des phosphinates cycliques à cinq chaînons comme haptènes.

Mots clés : analogues d'états de transition, hydrolyse d'esters phosphates, anticorps catalytiques.

Introduction

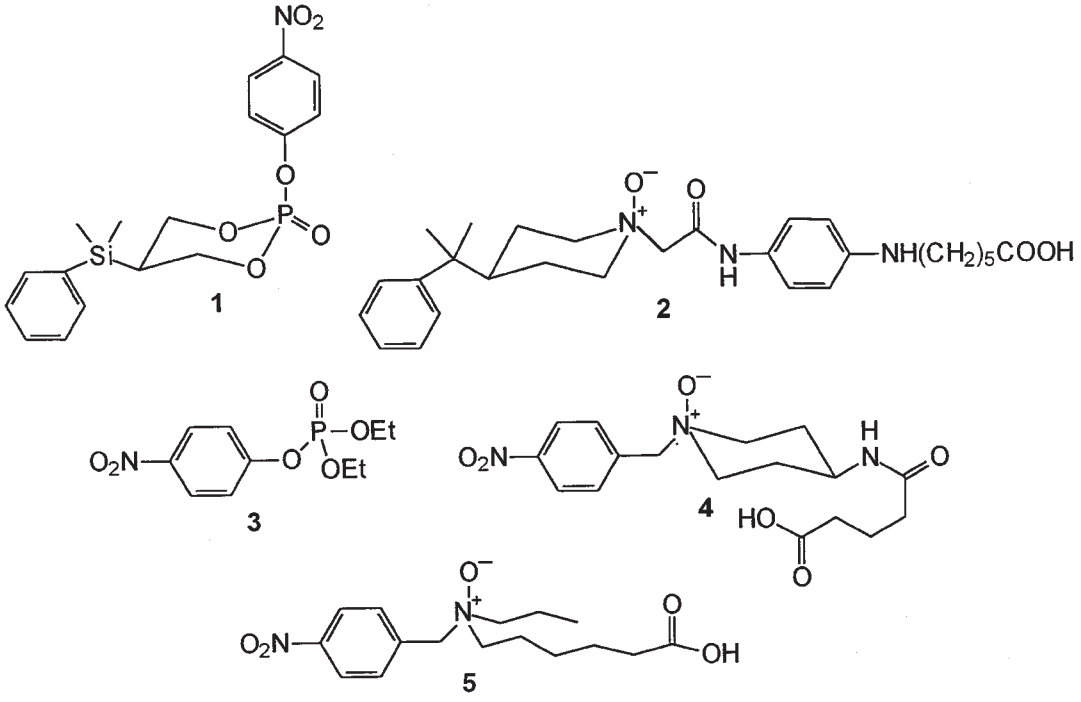
Recently, several reports have appeared describing antibodies capable of hydrolyzing phosphate triesters (1–4). Interest in generating these antibodies, as well as phosphonate-hydrolyzing abzymes, is mainly due to their potential as therapeutic agents in the treatment or prevention of organophosphorus poisoning such as paraoxon, tabun, sarin etc. The most common means of obtaining catalytic antibodies is to raise antibodies to compounds that mimic the transition state of the reaction of interest. In general, phosphate triesters and phosphonate diesters hydrolyze via pentavalent,

Received December 15, 1999. Published on the NRC Research Press website on May 12, 2000.

G. Hum and S.D. Taylor.[1,2] Department of Chemistry, University of Toronto, Mississauga Campus, 3359 Mississauga Rd. N, Mississauga, ON L5L 1C6, Canada.
K. Wooler and J. Lee. Dept. of Biochemistry, University of Saskatchewan, 107 Wiggins Rd., Saskatoon, SK S7N 5E5, Canada.

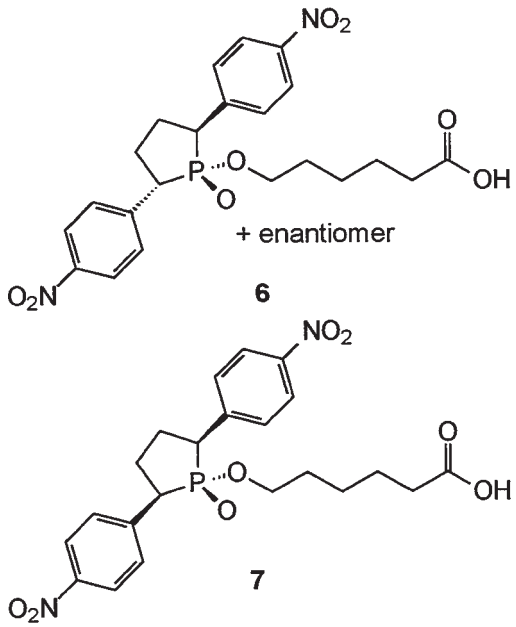
[1]Current address: Department of Chemistry, University of Waterloo, 200 University Avenue West, Waterloo, ON N2L 3G1, Canada.
[2]Author to whom correspondence may be addressed. Telephone: (519) 888-4567 ext. 3325. Fax: (519) 746-0435.
e-mail: s5taylor@sciborg.uwaterloo.ca

© 2000 NRC Canada



trigonal bipyramidal (TBP) transition states or intermediates (5). However, most TBP species are either too toxic or too unstable in aqueous solution to be used as haptens for immunization. Consequently, recent reports on phosphotriesterase antibodies have utilized a bait and switch approach (1–4) using tetrahedral N-oxides as transition state analogues (TSAs). For example, Rosenblum et al. (1) have reported antibodies capable of catalyzing the hydrolysis of the phosphotriester **1** with a rate enhancement of ~360-fold by raising antibodies to the N-oxide **2**. Janda and coworkers (2–4) have reported the generation of antibodies capable of catalyzing the hydrolysis of the insecticide paraoxon, **3**, utilizing employing N-oxides **4** and **5** as haptens. With the cyclic hapten **4**, the largest rate enhancement obtained was ~500-fold (2, 3). The rate enhancement was only 56-fold using the less constrained hapten **5** (4). On the basis of these results, Janda and coworkers (4) concluded that constrained haptens elicit superior catalysts for paraoxon hydrolysis.

As part of our research program on antibody-catalyzed reactions, we became interested in examining new haptens for obtaining phosphohydrolase antibodies. It has been known for many years that phosphate or phosphonate esters contained in a five-membered ring can be as much as 10^8-times more reactive than their acyclic analogues (5–8). This phenomenon has been studied in detail and has been attributed mainly to these species having strained bond angles at phosphorus approaching that of the ideal TBP equatorial–apical transition state configuration (5–9). Applying this knowledge to TSA design, we propose that cyclic five-membered phosphinic acids could be used as TSAs for raising phosphohydrolase abzymes. To test this strategy we have designed two isomeric cyclic 5-membered phosphinate esters, **6** and **7**, as TSAs for the hydrolysis of model phosphonate and phosphate esters **8** and **9** (Scheme 1). Several features of these TSAs warrant mention. First, compounds **6** and **7** should have highly compressed endocyclic C—P—C bond angles of



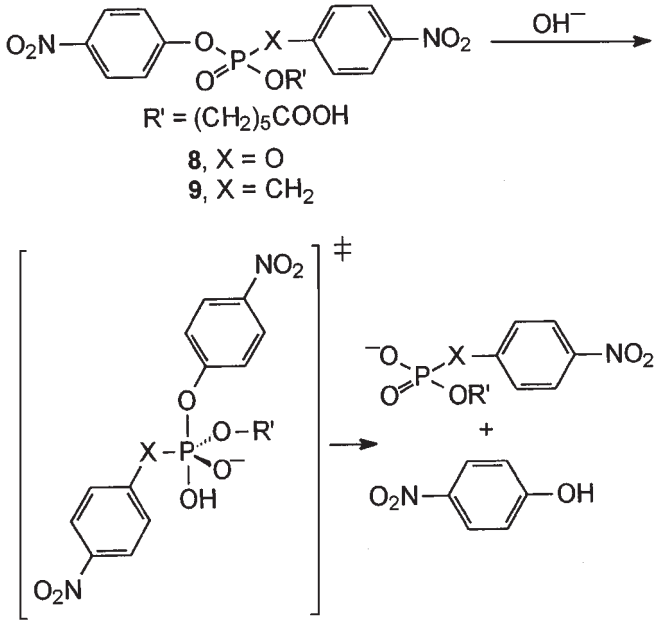
about 95°–98° (9, 10). Thus, when antibodies raised to **6** or **7** bind acyclic substrates **8** or **9**, the ArX—P—OAr bond in **8** or **9** will be compressed from the unstrained tetrahedral angle (109°) to a strained angle of 95°–98° (towards the optimal unstrained TBP transition state angle of 90°) analogous to that found in the highly reactive cyclic, five-membered phosphate and phosphonate esters. This will result in the induction of strain or stress upon the bound substrate thus preventing the substrate from falling into a thermodynamic "pit" upon binding to the abzyme. Attack of hydroxide or water at phosphorus will result in the formation of the unstrained TBP transition state. Second, although **8** and **9** are neutral, the highly polar nature of the phosphoryl bond (11) should result in the generation of complementary residues in

© 2000 NRC Canada

the antibody binding site which will aid in the stabilization of the negatively charged TBP transition state. Third, by utilizing both the *trans* (**6**, phenyl groups *trans* to one another) and *cis* (**7**, phenyl groups *cis* to one another) isomers of the TSA, crucial antigenic determinants can be ascertained. For example, if an antibody raised to the *cis* hapten binds equally well to the *trans* hapten (or vice versa) then this would imply that the antibody does not bind strongly to both phenyl rings and would probably not catalyze the reaction. Finally, both TSAs have a hexanoic acid linker arm for attaching the TSAs to carrier proteins which is necessary for immunization. The linker arm is attached to the phosphorus atom and not the aryl rings to minimize any interference by the linker arm with antibody recognition of the aryl rings.

In this report we present the synthesis of *trans* and *cis* 2,5-diarylphospholanate TSAs (**6** and **7**) and our attempts to obtain phosphohydrolase antibodies using these compounds as haptens.

Scheme 1.



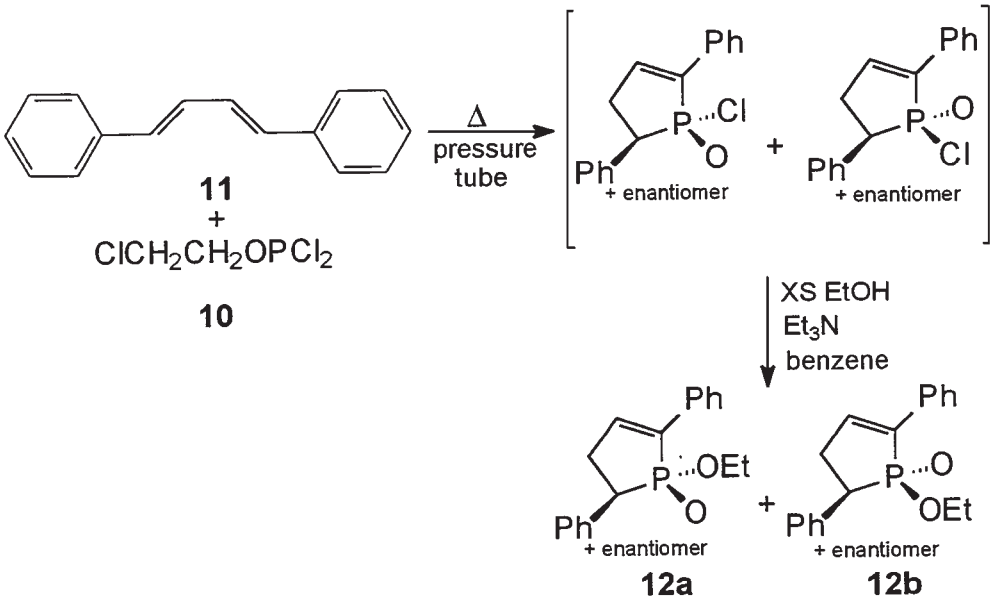
Results and discussion

Synthesis of transition state analogues 6 and 7

Although there are a variety of methods for synthesizing cyclic five-membered phosphinates (12, 13), we chose to employ a McCormack reaction since this is the most common and versatile means of constructing this class of compounds (13, 14). The McCormack reaction involves a cycloaddition reaction between a P(III) halide or in situ-generated phosphenium ion (15) and a 1,3-diene. Although this reaction usually proceeds more readily with phosphenium ions, we chose instead to employ Moedritzer's modification (16) of the McCormack reaction, which employs 2-chloroethyldichlorophosphite as the P(III) halide and directly produces cyclic phosphinyl chlorides which can be reacted in situ with alcohols to form the esters. For our purposes, 1,4-diphenyl-1,3-butadiene would be employed as the diene. However, there are very few examples in the literature of McCormack reactions between 1,4-diaryl-1,3-butadienes and P(III) halides and, in all cases reported to date, only alkylphosphonic dichlorides have been used yielding phospholes (17–19) or phospholenium salts (20). McCormack reactions between diaryl-1,3-butadienes and chlorophosphites have never been reported.

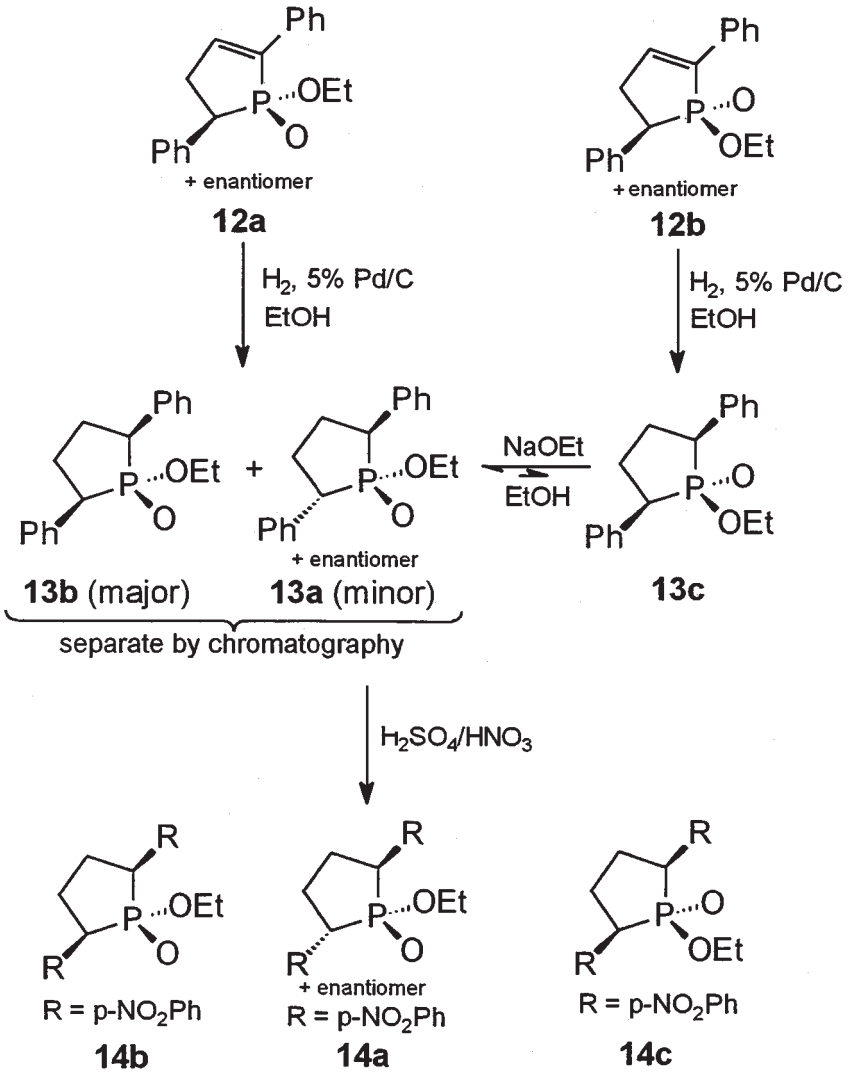
McCormack reactions are usually carried out neat or in an aprotic solvent, such as benzene, at room temperature or, more rarely, under reflux conditions (13). However, we were unable to detect any reaction between 2-chloroethyldichlorophosphite, **10**, and 1,4-diphenyl-1,3-butadiene, **11**, when performed neat (with heating) or in refluxing benzene. This is most probably due to both steric effects and the deactivating effect of the phenyl groups on the cycloaddition reaction

Scheme 2.



© 2000 NRC Canada

Scheme 3.



(14).[3] However, performing the reaction in a pressure tube at 170°C (neat) or 175°C (benzene as solvent) followed by reaction of the crude reaction mixture with excess ethanol in benzene and 1 equiv. of triethylamine, yielded the 2,3-dihydro cyclic phosphinate products **12a** and **12b** (Scheme 2) in an overall yield of 30–37%. Although a McCormack reaction of this type usually yields the 3,4-dihydro products, the formation of the 2,3-dihydro products **12a** and **12b** was not entirely unexpected since studies by other workers have shown that double bond migration sometimes occurs when McCormack reactions are conducted at high temperatures (13, 21). Isomers **12a** and **12b** could be separated using silica gel chromatography yielding the *trans* isomer, **12a**, (phenyl group and ethoxy group *trans* to one another) and *cis* isomer, **12b** (phenyl group and ethoxy group *cis*) in a 1:1 ratio if performed neat or 2:1 in favor of **12a** if performed in benzene.

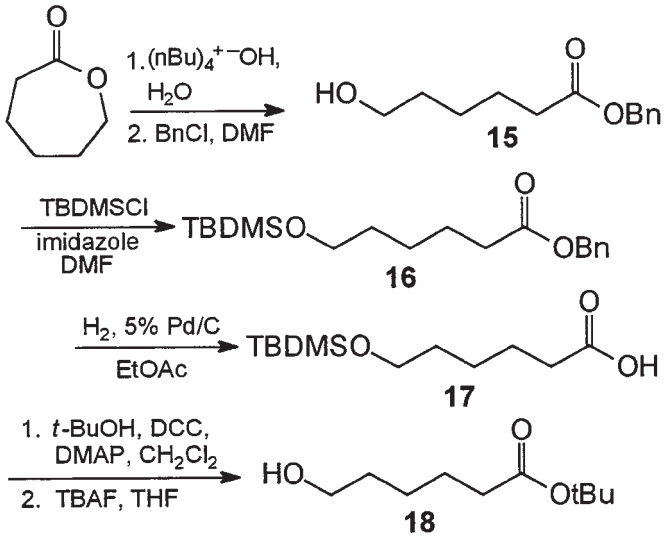
The *cis–trans* relationship of the ethoxy and phenyl groups in **12a** and **12b** was readily determined by conventional ^{1}H NMR spectroscopy. In the *trans* isomer, **12a**, the methyl and methylene protons of the ethoxy group appear as a triplet at δ 1.15–1.25 and as a complex multiplet at δ 3.9–4.3 respectively and these chemical shifts are typical of ethoxy groups in most simple ethoxy phosphinates. However, with the *cis* isomer, **12b**, the methyl protons appear as a triplet at δ 0.85–0.95, considerably further upfield than those of the *trans* isomer. In addition, the methylene protons appear as *two separate multiplets*, one proton at δ 3.7–3.95 ppm and the other at δ 3.4–3.65, again considerably further upfield than those of the *trans* isomer. The upfield shift of these protons in the *cis* isomers is a result of the shielding effect of the phenyl moiety that is located at the 5-position on the phospholene ring. This does not occur with the *trans* isomers since the ethoxy and phenyl ring are on opposite sides of the phospholene ring. A similar phenomenon has been reported with some 2-phenyl-2-phospholene-1-oxides (22).

Hydrogenation (5% Pd/C) of the *cis* phospholenate ester, **12b**, yielded the "all *cis*" phospholanate ester **13c** (both phenyl groups and the ethoxy group *cis* to one another) exclusively in 82% yield (Scheme 3). Hydrogenation of **12a**

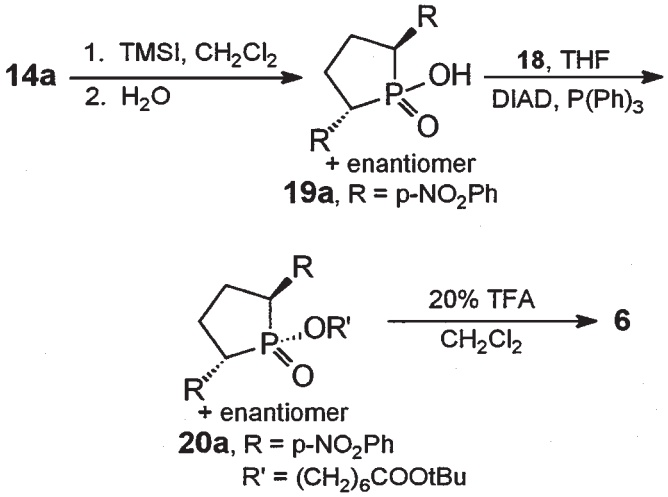
[3] U.S. Patents 2,663,736 and 3,663,737.

© 2000 NRC Canada

Scheme 4.



Scheme 5.



gave both the "phenyl *cis*" phospholanate ester, **13b**, (major product, the two phenyl groups *cis* to one another and the ethoxy group *trans* to the phenyl groups) and the "phenyl *trans*" phospholanate ester, **13a** as the minor product in an overall 99% yield. These two isomers could be readily separated from one another using conventional silica gel chromatography. We found that sufficient quantities of the phenyl *trans* isomer, **13a**, could be obtained by isomerization of either of the less stable *cis* esters, **13b** and **13c** in sodium ethoxide solutions. For example, a solution of pure **13b** was isomerized in a 0.5 M solution of sodium ethoxide in ethanol in just a few hours to yield mainly **13a**. This isomerization could be followed by ^{31}P NMR. After equilibrium is reached, the reaction was quenched with mild acid and two isomers were readily separated using conventional silica gel chromatography. Esters **13a**–**c** were bis-*para*-nitrated to form **14a**–**c** in moderate to good yields (55% for **14a**, 64% for **14b**, and 75% for **14c**, Scheme 3) employing classical nitration conditions (HNO_3/H_2SO_4).

The all *cis* isomers (**13c** and **14c**) and phenyl *cis* isomers (**13b** and **14b**) could be readily distinguished from the phenyl *trans* isomers (**13a** and **14a**) since the *cis* isomers are symmetrical meso compounds and their phospholane ring carbons appear as only two sets of doublets in the ^{13}C NMR as opposed to four sets of doublets for the unsymmetrical phenyl *trans* ester. The all *cis* and phenyl *cis* isomers were readily distinguished on the basis of their ^1H NMRs. For example, in the all *cis* isomer, **13c**, the methylene protons of the ethoxy group appear considerably more upfield (δ 3.19–3.35) than is normally found with a phosphorus ethyl ester (typically δ 3.9–4.4) due to the shielding effect of the phenyl rings and are even further upfield than the benzylic phospholane ring protons (δ 3.33–3.51). In the case of the phenyl *cis* isomer, **13b**, the ethyl group is on the opposite side of the phospholane ring as the phenyl groups. Thus, the methylene protons appear much further downfield and have chemical shifts that one would expect to have for a "normal" phosphinate ethyl ester (δ 3.94–4.12) and are much further downfield than the benzylic protons (δ 3.2–3.4). The stereochemical relationship between the ethoxy and phenyl groups in all subsequent phospholanate esters reported in this study were readily determined in the same manner simply by examining the chemical shift of the -CH_2-O-P protons and by ^{13}C NMR.

A *tert*-butyl-protected linker arm was prepared as shown in Scheme 4. Thus, caprolactone was reacted with tetrabutylammonium hydroxide in water to form the carboxylate salt, followed by reaction with benzyl chloride in DMF to give the hydroxyester **15** in an overall yield of 89%. Compound **15** was converted to a *tert*-butyl ester protected linker arm by first protecting the alcohol moiety as the TBDMS ether (**16**, 92%) followed by hydrogenolysis to obtain the acid **17** (87% from **15**). The acid was converted into the *tert*-butyl ester using DCC–DMAP and *t*-butanol and the silyl protecting group removed using TBAF to give the *tert*-butyl ester protected linker arm **18** (38% from **17**).

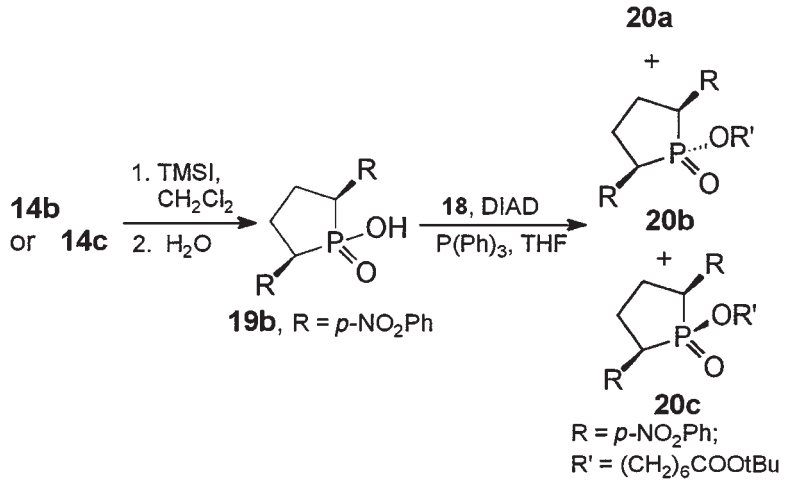
Trans ester, **14a**, was converted into the free acid, **19a**, using TMSI followed by hydrolysis of the resulting TMS ester in an overall yield of 90% (Scheme 5). The linker arm was attached via a Mitsonobu reaction (23) between **19a** and **18** to give the protected racemic TSA **20a** in an 80% yield. Removal of the *t*-butyl group using 20% TFA in CH_2Cl_2 proceeded smoothly to give the *trans* TSA, **6** (80% yield).

Compounds **14b** or **14c** were converted into the *cis* free acid **19b** using the same procedure described for the *trans* acid **19a** (Scheme 6). However, Mitsonobu coupling of **18** to **19b** proceeded very sluggishly. Partial purification of the reaction mixture revealed that approximately equal amounts of isomers **20a**–**c** were formed (Scheme 6) in an overall low yield (45% yield). The fact that all possible isomers (**20a**–**c**) were obtained suggested that not only was isomerization taking place, but that at least some of the all *cis* isomer **19c** was formed initially. This was confirmed by performing the Mitsonobu reaction with the unnitrated acid, **21**, which yielded *exclusively the all cis ester,* **22b** in a 60% yield (Scheme 7). It also appears that the presence of the nitro groups in **19b** are responsible for the isomerization (by increasing the acidity of the benzylic protons on the phospholane ring) and that this occurs fairly readily.

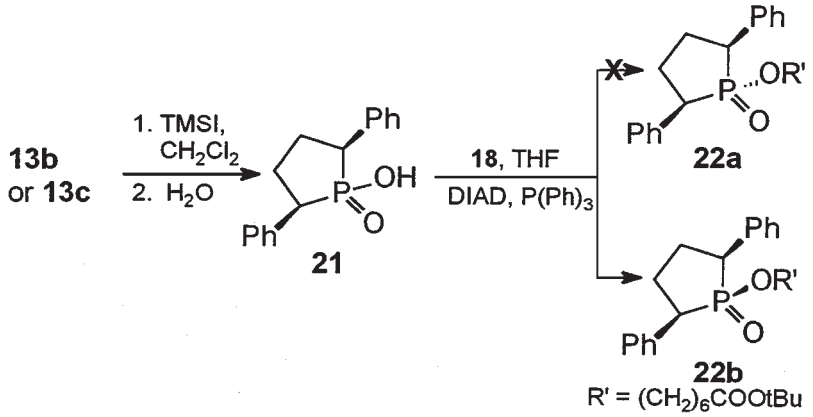
Since the Mitsonobu procedure with **19b** produces a mixture of isomeric products, an alternative method for attaching the linker arm was necessary. We attempted to synthesize

© 2000 NRC Canada

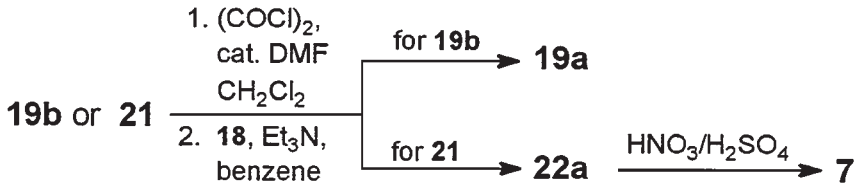
Scheme 6.



Scheme 7.



Scheme 8.

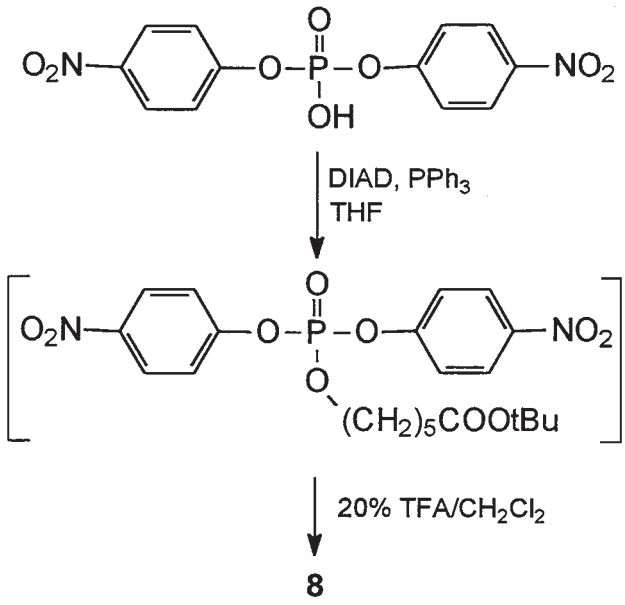


20b by converting **18b** into the acid chloride using oxalyl chloride and cat. DMF, followed by reaction with **18** in the presence of 1.0 equiv. amine base in benzene (Scheme 8). However, isomerization occurred during the reaction and the undesired "aryl *trans*" ester, **20a**, was the predominant product. However, this was not the case with the unnitrated acid **21** which yielded exclusively the desired phenyl *cis* ester **22a** in a 54% yield. To obtain the *cis* TSA **7**, we subjected **22a** to HNO_3–H_2SO_4 (Scheme 8) which we anticipated would result in both ring nitration and loss of the *tert*-butyl protecting group. This was successful, yielding TSA **7** in a 45% yield and no products resulting from isomerization were obtained.

Crucial to the success of our approach to obtaining phosphohydrolase antibodies is that the CPC bond angle in TSAs **6** and **7** is compressed towards the optimal TBP transition state angle of 90°. To our knowledge, the only report describing a crystal structure of a saturated phospholanate is that of phospholanic acid, obtained by Alver and Kjoge (9) in 1969. The CPC bond angle was reported to be 94.8°. Since it was possible that the CPC bond angles in TSAs **6** and **7** may differ significantly from that found in phospholanic acid due to the presence of the aryl groups at positions 2 and 5 in the phospholanate ring and the ester linkage, we obtained the crystal structures of the TSA precursors, **14a** and **14b**. The CPC bond angle for **14a** is 97.4° while that for **14b** is 94.0°. It is unlikely that replacing the ethyl group in **14a** or **14b** with the linker arm found in TSAs **6** and **7** would result in a significant change in the endocyclic CPC bond angles. Thus, it may be concluded that the CPC bond angles in **6** and **7** are significantly distorted or strained towards the optimal unstrained TBP transition state angle of 90°.

© 2000 NRC Canada

Scheme 9.



Synthesis of substrates 8 and 9

Phosphate ester substrate **8** was synthesized by coupling linker arm **18** to bis(*p*-nitrophenyl)phosphate using a Mitsonobu reaction followed by removal of the *tert*-butyl protecting group from the crude ester using TFA (73% overall yield, Scheme 9).

Phosphonate ester substrate **9** was synthesized as outlined in Scheme 10. Thus, hydrolysis of phosphonate **23** in aqueous NaOH followed by acidification gave the phosphonic acid **24** in 90% yield. EDC coupling of *p*-nitrophenol to **24** gave the ester **25** in 64% yield. Reaction of **25** with NaBr in refluxing butanone followed by acidification gave phosphonic acid **26** in 93% yield. The linker arm **18** was attached to phosphonic acid **26** using a Mitsonobu reaction. The resulting ester **27** was not isolated in pure form but instead the crude was reacted with TFA–CH_2Cl_2 to give substrate **9** (64% from **26**).

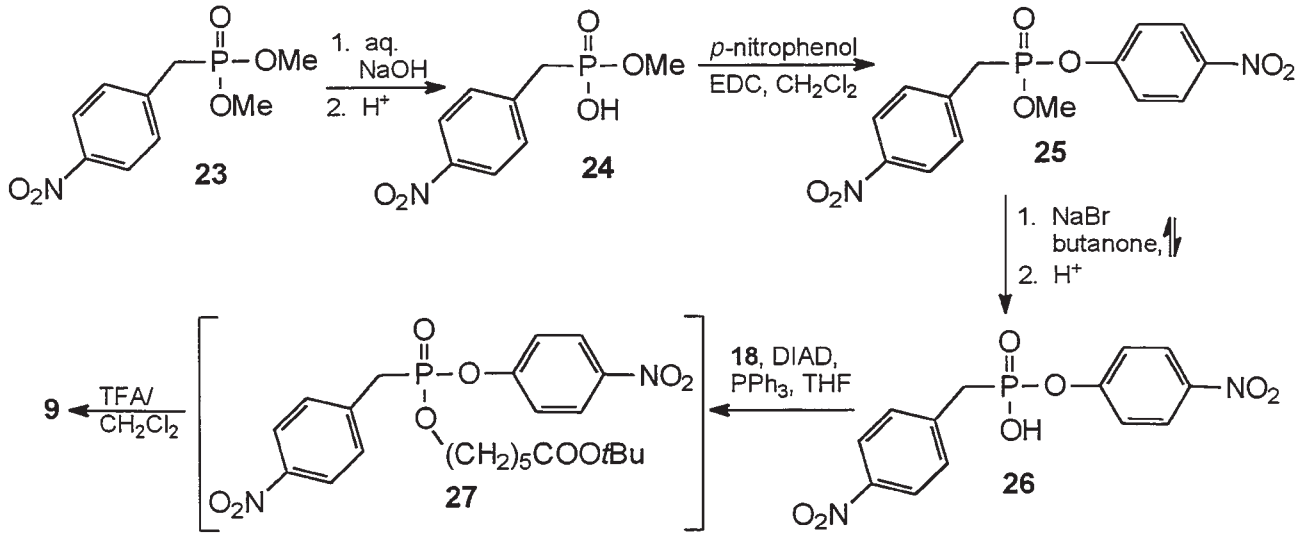
The half-lives of **8** and **9** in 10 mM CHES buffer, 50 mM NaCl at pH 9.0, were determined using spectrophotometry by measuring the increase in absorbance at 400 nm. Under these conditions, the half life of the phosphate **8** was 14 h while that of the phosphonate **9** was 29 h.

Antibody production and catalytic screening

Compounds **6** and **7** were coupled to carrier proteins BSA and KLH for monoclonal antibody production and screening by converting their carboxylic acid moieties to activated esters using *N*-hydroxy sulfosuccinimide and EDC as coupling agent followed by reaction of the resulting activated esters with BSA or KLH in 50 mM phosphate buffer. Monoclonal antibodies to each hapten (KLH conjugates) were raised using standard hybridoma technology (24). After propagation and subcloning of the hybridomas, seven hybridoma cell lines were obtained that produced antibody capable of binding the TSAs as determined by solid phase radio immune assays (SPRIA). Isotyping of the seven antibodies revealed that three were IgM's and four were IgG's. Only one of these antibodies, Jel 541, was able to distinguish, in terms of binding affinity, between the *trans* TSA and *cis* TSA, exhibiting a greater affinity for the *trans* hapten than the *cis* hapten. Surprisingly, Jel 541 was obtained from mice immunized with the *cis* hapten. To determine if this may have been due to isomerization of the *cis* hapten to the thermodynamically more stable *trans* hapten during the immunization process, *cis* hapten **7** was incubated in 50 mM phosphate buffer at pH 7.5, and then examined for the formation of the *cis* TSA **6** by HPLC over a period of one week. After 1 week, 8% of **7** had isomerized to **6**. These results suggest that some isomerization of the *cis* to the *trans* hapten occurred during the eight week immunization process.

The hybridomas clones were grown intraperitoneally in mice and the antibodies purified from ascitic fluid. Competitive SPRIA experiments with purified Jel 541 indicated that Jel 541 bound the *trans* TSA approximately 100 times more tightly than the *cis* TSA. All seven antibodies were screened for activity by incubating the antibodies (~5 μM) with substrates **8** or **9** (500 μM) in 10 mM HEPES buffer at pH 7.0

Scheme 10.



© 2000 NRC Canada

Fig. 1. Hydrolysis of phosphonate substrate **9** (0.5 mM) in 10 mM HEPES, 50 mM NaCl, pH 7.0 by buffer alone (●), 5 μM Jel 541 (○).

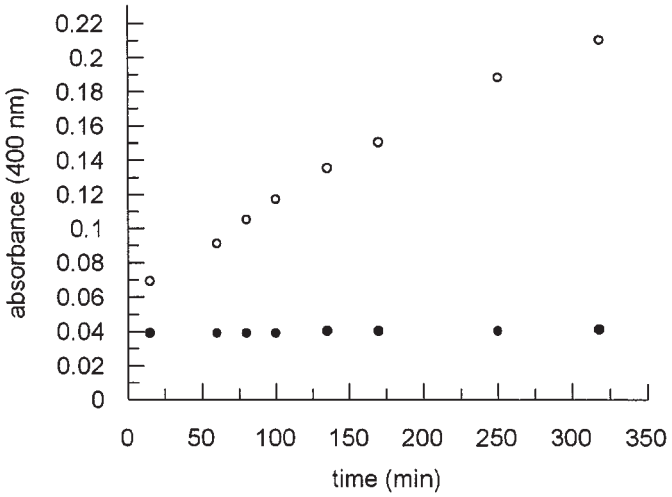
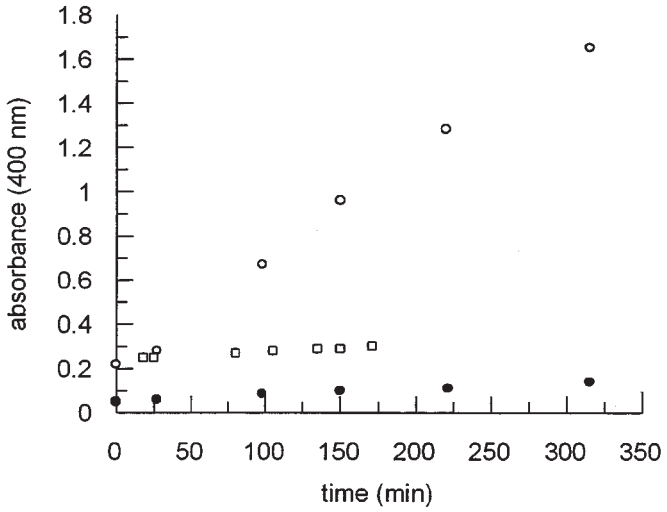


Fig. 2. Hydrolysis of phosphonate substrate **9** (0.5 mM) in 10 mM CHES, 50 mM NaCl, pH 9.0 by buffer alone (●), 5 μM Jel 541 (○), 5 μM Jel 541 + 0.5 mM TSA **6** (□).



and determining the absorbance of the reaction solution at 400 nm at various time intervals over a period of several hours. Only Jel 541, one of the IgM class antibodies, catalyzed the hydrolysis of phosphonate **9** (Fig. 1) This antibody was also capable of functioning at pH 9.0 (Fig. 2). Jel 541 also catalyzed the hydrolysis of the phosphate substrate **8** (data not shown) at pH 9.0 but to a much lesser extent than the phosphonate substrate. This result is consistent with the fact that the phosphonate substrate is structurally more similar to the hapten than the phosphate substrate. The possibility that the observed activity was due to contamination by an unknown murine phosphatase can be excluded for the following reasons. First, none of the other antibodies obtained in this study showed activity yet were prepared in an identical manner to Jel 541. Second, the catalytic activity of Jel 541 is completely inhibited by the presence of the *trans* TSA (Fig. 2). Although it is clear that Jel 541 is capable of catalyzing the hydrolysis of the substrates, the relative instability and poor solubility of Jel 541 has prevented us from performing an accurate and detailed kinetic analysis. Consequently, we have been unable to determine the basic kinetic parameters (k_{cat}/k_{uncat}, K_m etc.) of the abzyme. These are common problems when dealing with IgM class antibodies (25) which have molecular weights of approximately 10^3 kDa. To avoid some of the problems associated with IgM Mabs, we attempted to convert Jel 541 Mab into a more soluble Fab fragment by digesting the Mab with trypsin in the presence of a reducing agent such as cysteine followed by alkylation with iodoacetamide and purification (25). However, we were unable to obtain significant quantities of pure Fab using this procedure. It is clear that an IgG class abzyme will have to be obtained to fully assess the viability of our approach to phosphohydrolase abzymes.

Summary

In summary, two novel phospholanates **6** and **7** were prepared and used as TSAs for obtaining phosphohydrolase antibodies. One IgM class antibody, Jel 541, was obtained that catalyzed the hydrolysis of the phosphonate substrate **9** and to a much lesser extent the phosphate substrate **8**. Although it was not possible to characterize Jel 541 in detail, these results demonstrate that phosphohydrolase antibodies can indeed be obtained using haptens such as **6**. We are currently attempting to obtain more IgG class monoclonal antibodies to **6**, since this class of antibodies are much easier to characterize than IgM class antibodies and will allow for a more complete assessment of this approach to obtaining phosphohydrolase abzymes.

Experimental

General

All starting materials for organic synthesis were obtained from commercial suppliers (Sigma–Aldrich Canada, Oakville, Ontario, Canada or Lancaster Synthesis Inc., Windham, New Hampshire, U.S.A.) unless stated otherwise. Solvents were purchased from Caledon Laboratories (Georgetown, Ontario, Canada), Lancaster Synthesis Inc., or BDH Canada (Toronto, Canada). Reagents for hybridoma production were obtained from Gibco-BRL. Tetrahydrofuran (THF) and diethyl ether were distilled over sodium metal in the presence of benzophenone. Benzene and CH_2Cl_2 were distilled over calcium hydride. Ethanol was distilled over magnesium turnings. Dry chloroform was obtained by distillation over phosphorus pentoxide. All glassware was predried prior to use and all liquid transfers were performed using dry syringes and needles. Silica gel chromatography was performed on 40–60μ particle silica gel obtained from Toronto Research Chemicals (Toronto, Ontario, Canada). Melting points were obtained on a Electrothermal Inc. melting point apparatus and are uncorrected. ^1H and ^{31}P NMR spectra were recorded on a Varian 200-Gemini NMR machine at approximately 200 MHz, and 80 MHz respectively. ^{13}C NMR spectra were recorded on a Varian-500 NMR at 126 MHz or on a Varian 200-Gemini NMR machine at 50.3 MHz. The abbreviations s, d, t, q, qt, m, dd, and b are used for singlet, doublet, triplet, quartet, quintet, multiplet, doublet of doublets and broad respectively. Coupling constants are reported in Hertz (Hz). All NMRs were run using

© 2000 NRC Canada

$CDCl_3$ as solvent unless stated otherwise. Chemical shifts (δ) for ^1H NMR spectra run in $CDCl_3$ are reported in ppm relative to the internal standard tetramethylsilane (TMS). Chemical shifts (δ) for ^1H NMR spectra run in CD_3OD are reported in ppm relative to residual solvent protons (δ 4.87). Chemical shifts (δ) for ^1H NMR spectra run in $DMSO_{d-6}$ are reported in ppm relative to residual solvent protons (δ 2.50). For ^{13}C NMR spectra run in $CDCl_3$, chemical shifts are reported in ppm relative to the $CDCl_3$ residual carbons (δ 77.0 for the central peak). For ^{13}C NMR spectra run in $DMSO_{d-6}$, chemical shifts are reported in ppm relative to the DMSO residual carbons (δ 39.5 for the central peak). For ^{31}P NMR spectra, chemical shifts are reported in ppm relative to 85% phosphoric acid (external). Electron impact (EI) mass spectra were obtained on a Micromass 70-S-250 mass spectrometer. HPLC purifications and hapten isomerization studies were performed on a Waters LC 450 System equipped with an Waters 2487 absorbance detector using an Altech normal phase silica preparative HPLC column (250 mm × 22 mm i.d. with 10 μ Econosil silica, cat. no. 6259) or an Altech normal phase analytical HPLC column (10 μ Econosil silica, cat. no. 60090). All of the phospholanate esters reported here were analyzed by HPLC using the above system equipped with the above mentioned Altech normal phase analytical HPLC column and were found to exhibit a single peak in the HPLC chromatogram.

*(±)-*trans*-1-Ethoxy-2,5-diphenyl-2,3-dihydro-1*H*-1λ^5-phosphol-1-one (**12a**) and (±)-*cis*-1-ethoxy-2,5-diphenyl-2,3-dihydro-1*H*-1λ^5-phosphol-1-one (**12b**)*

Method A: 1,4 Diphenyl-1,3-butadiene (2.06 g, 10 mmol, 1 equiv.) was combined with 2,6-di-*tert*-butyl-4-methyl phenol (10 mg, 2 mol%) in a 15 mL ACE Glass pressure tube (cat. no. 8648–75) equipped with a stir bar and then flushed thoroughly with Ar. Phosphorous trichloride (0.545 mL, 6.33 mmol, 0.66 equiv.) and tris(2-chloroethyl) phosphite (0.635 mL, 3.33 mmol, 0.33 equiv.) was added to the tube under a stream of Ar. The glass bomb was rapidly sealed and the thick, mainly solid mixture was vigorously shaken by hand for about 30 s to mix the contents. The tube was immersed in an oil bath, stirred vigorously, and slowly heated to 170°C and maintained at this temperature for 19 h during which time the solid diene melted and the solution reaction became an orange colour. **CAUTION: This procedure must be performed in a fumehood behind a blast shield.** In addition to several broad beaks, the ^{31}P NMR of the crude reaction mixture exhibited two sharp peaks of approximately equal magnitude at 68.6 and 69.7 ppm. After removing the oil bath and allowing the tube to cool to room temperature, the tube was fitted with a septum and dry benzene (20 mL) was added to the crude reaction mixture under argon. The solution was transferred very slowly over a period of 30 min via syringe to an ice cold solution of dry ethanol (5.8 mL, 100 mmol, 10 equiv.) and triethylamine (1.7 mL, 10 mmol, 1 equiv.) in dry benzene (20 mL) and the reaction was stirred overnight at room temperature under Ar. The volume of the crude reaction mixture was reduced to one quarter by rotary evaporation and diluted with ether (75 mL) which resulted in the precipitation of triethylamine hydrochloride which was removed by suction filtration. The filter cake was washed with ether and the filtrate was washed with 0.1 N HCl (3 × 50 mL), 5% $NaHCO_3$ (3 × 50 mL), brine (3 × 50 mL), and then dried ($MgSO_4$) and concentrated in vacuo to yield a crude orange oil which was subjected to silica gel column chromatography. Flash chromatography (silica, 90% CH_2Cl_2 – 10% EtOAc, three columns required) of the crude reaction yielded **12a** as a pale yellow solid (577 mg, 19.2%). TLC (silica, 90% CH_2Cl_2 – 10% EtOAc): R_f = 0.4; mp 82–86°C. ^1H NMR δ: 1.23 (3 H, t, J = 6.9 Hz), 2.81–2.96 (1 H, m), 3.10–3.54 (2 H, m), 3.98–4.23 (2 H, m), 7.03 (1 H, t, J = 3.3 Hz), 7.42 (8 H, m), 7.65 (2 H, d, J = 6.2 Hz). ^{13}C NMR δ: 142.20 (d, J = 36.1),138.35 (br d), 136.95 (d, J = 4.6 Hz), 133.59 (d, J = 9.1 Hz), 128.70, 128.39 (d, J = 11.5 Hz), 126.96, 126.68 (d, J = 5.5 Hz), 61.58 (d, J = 6.4 Hz), 42.28 (d, J = 92.8 Hz), 35.57 (d, J = 17.8 Hz), 16.66 (d, J = 5 Hz). ^{31}P NMR δ: 60.41 (s). MS, *m*/*z* (relative intensity): 298 (64), 270 (36), 205 (100), 104 (31), 91 (41), 77 (30). HRMS calcd. for $C_{18}H_{19}O_2P$: 298.1123; found 298.1127. From the same column **12b** was obtained as a white solid (533 mg, 17.8%). TLC (silica, 90% CH_2Cl_2 – 10% EtOAc): R_f = 0.6; mp 102–104°C. ^1H NMR δ: 0.91 (3 H, t, J = 5.9 Hz), 2.84–3.93 (5.5 H, m), 7.08 (0.5 H, t, J = 3.75 Hz), 7.35 (8 H, m), 7.71 (2 H, d, J = 7 Hz). ^{13}C NMR δ: 142.23 (d, J = 35.7 Hz), 137.58, 136.12 (d, J = 6.5 Hz), 135.20, 133.14 (br d), 128.70 (d, J = 6.2 Hz), 128.34, 126.92, 126.66 (d, J = 3.7), 61.58 (d, J = 6.4), 43.44 (d, J = 90.6), 33.19 (d, J = 16.4) 16.16. ^{31}P NMR δ: 60.05 (s). MS, *m*/*z* (relative intensity) 298 (100), 270 (66), 254 (47), 205 (50), 194 (83), 91 (43), 77 (30). HRMS calcd. for $C_{18}H_{19}O_2P$: 298.1123; found 298.1134.

Method B: The above McCormack reaction can also be performed in a similar manner as described above using dry benzene as solvent (approximately 3 mL of benzene per gram of diene) and heating the reaction in the sealed tube for 72 h at 185°C. This procedure produces **12a** and **12b** in a 2:1 ratio in yields that are slightly higher that obtained by method A. **CAUTION: When performing the reaction using benzene as solvent, for safety reasons, the total volume of the reaction in the pressure tube must not be greater than half the total capacity of the pressure tube. The reaction must be performed in a fumehood behind a blast shield.**

*(±)-1-Ethoxy-*trans*-2,5-diphenyl-1λ^5-phospholan-1-one (**13a**) and (meso)-*trans*-1-ethyoxy-cis-2,5-diphenyl-1λ^5-phospholan-1-one (**13b**)*

A solution of **12a** (1.530 g, 5.03 mmol) in ethanol (20 mL) containing 10% Pd/C (100 mg) was hydrogenated overnight at 30 psi under a H_2 atmosphere using a Parr hydrogenation apparatus. The Pd catalyst was removed by filtration and the filtrate concentrated in vacuo leaving a pale yellow oil which was subjected to column chromatography (silica, 90% CH_2Cl_2 – 10% EtOAc) to give pure **13a** and **13b**. Overall yield was 99%. **13a** was obtained as a white solid (432 mg, 27%). TLC (silica, 90% CH_2Cl_2 – 10% EtOAc): R_f = 0.5; mp 103–105°C. ^1H NMR δ: 0.93 (3 H, t, J = 7.2 Hz), 2.07–2.60 (4 H, m), 3.09–3.52 (3 H, m), 3.66–3.85 (1 H, m), 7.35 (10 H, cm). ^{13}C NMR δ: 137.13 (d, J = 5.5 Hz), 128.70 (d, J = 5.5 Hz), 127.52, 126.68, 61.37 (d, J = 6.4 Hz), 43.59 (d, J = 85.1 Hz), 29.57 (d, J = 14.6 Hz), 16.69. ^{31}P NMR δ: 61.73 (s). MS, m/*z* (relative intensity): 300 (87), 206 (42), 196 (36), 104 (100), 91 (28), 78 (22).

© 2000 NRC Canada

HRMS calcd. for $C_{18}H_{21}O_2P$: 300.1279; found 300.1272. **13b** was obtained as a white solid (1.10 g, 72%). TLC (silica, 90% CH_2Cl_2 – 10% EtOAc): R_f = 0.3; mp 69–72°C. ^{1}H NMR δ: 1.24 (3 H, t, *J* = 7.1 Hz), 2.33–2.46 (4 H, m), 3.21–3.37 (2 H, m), 4.00 (2 H, m), 7.35 (10 H, m). ^{13}C NMR δ: 136.69 (bd), 136.22 (d, *J* = 2.7 Hz), 128.76, 128.56, 128.14 (d, *J* = 4.6 Hz), 126.81, 61.24 (d, *J* = 7.3 Hz), 46.68 (d, *J* = 84.1 Hz), 45.50 (d, *J* = 86.9 Hz), 30.40 (d, *J* = 12.8 Hz), 27.85 (d, *J* = 9.0 Hz), 16.26 (d, *J* = 4.6 Hz). ^{31}P NMR δ: 62.37 (s). MS, *m*/*z* (relative intensity): 300 (91), 206 (41), 196 (26), 104 (100), 91 (30), 78 (20). HRMS calcd. for $C_{18}H_{21}O_2P$: 300.1279; found 300.1294.

(meso)-cis-*1-Ethoxy*-cis-*2,5-diphenyl-1λ^5-phospholan-1-one (**13c**)*

A solution of **12b** (820 mg, 2.75 mmol) in ethanol (20 mL) containing 10% Pd/C (60 mg) was hydrogenated overnight at 30 psi under a H_2 atmosphere using a Parr hydrogenation apparatus. The Pd catalyst was removed by filtration and the filtrate concentrated in vacuo leaving a pale yellow solid. Column chromatography (silica, 100% EtOAc) yielded pure **13c** as a white solid (674 mg, 82%). TLC (silica, 100% EtOAc): R_f = 0.40; mp 133–137°C. ^{1}H NMR δ 0.64 (3 H, t, *J* = 7 Hz), 2.42 (4 H, m), 3.22–3.54 (4 H, m), 7.31 (10 H, m). ^{13}C NMR δ: 135.54 (d, *J* = 5.5 Hz), 128.41, 127.94 (d, *J* = 3.7 Hz), 126.63, 61.20 (d, *J* = 7.4 Hz), 43.96 (d, *J* = 82.4 Hz), 27.45 (d, *J* = 12.8 Hz), 15.90. ^{31}P NMR δ: 65.14 (s). MS, *m*/*z* (relative intensity): 300 (64), 206 (48), 196 (18), 104 (100), 91 (29), 78 (25)). HRMS calcd. for $C_{18}H_{21}O_2P$: 300.1279; found 300.1290.

*General procedure for the nitration of 2,5-diphenyl-1λ^5-phospholan-1-one esters **14a**,[44] **14b**,[4] and **14c***

To an ice cold solution of **13a**, **13b** or **13c** (100 mg, 0.33 mmol, 1 equiv.) in H_2SO_4 (1.5 mL) was added a solution of HNO_3:H_2SO_4 (1:1, 0.0180 mL, 0.86 mmol, 2.6 equiv. HNO_3) dropwise of a period of 1 min. The reaction was stirred at 0°C for 30 min and then poured into a beaker containing ice which upon melting left a suspension. $CHCl_3$ (20 mL) was added and the two layers were separated. The aqueous layer was further extracted with $CHCl_3$ (3 × 20 mL) and the combined organics were washed with brine (2 × 30 mL), dried ($MgSO_4$) and concentrated in vacuo leaving an oily solid residue. Pure nitrated esters (**14a**, **14b**, and **14c**) were obtained by either silica gel chromatography or recrystallization of the crude residue.

(±)-1-Ethoxy-trans-*2,5-di(4-nitrophenyl)-1λ^5-phospholan-1-one (**14a**)*: Obtained in 55% yield as a white solid from **13a** using the general procedure described above. Purification was achieved using flash chromatography (silica, 80% EtOAc – 20% hexane). TLC (80% EtOAc – 20% hexane): R_f = 0.70; mp 179–180°C. ^{1}H NMR δ: 0.98 (3 H, t, *J* = 7 Hz), 2.22 (2 H, m), 2.56 (2 H, m), 3.45 (3 H, m), 3.83 (1 H, m), 7.54 (4 H, dd, *J* = 8 Hz, *J* = 2.1 Hz), 9.24 (4 H, d, *J* = 8.4 Hz). ^{13}C NMR δ: 147.32, 144.00, 143.46 (br d, *J* = 13.8 Hz), 129.45 (d, *J* = 5.5 Hz), 128.90, 123.73, 62.10 (d, *J* = 5.4 Hz), 46.7 (d, *J* = 84.2 Hz), 45.5 (d, H = 86.1 Hz), 30.37, (d, *J* = 11 Hz), 27.73 (d, *J* = 11 Hz.), 16.30. ^{31}P NMR δ: 59.7 (s). MS, *m*/*z* (relative intensity): 390 (100), 362 (28), 296 (61), 149 (86), 119 (51), 103 (55), 77 (58). HRMS calcd. for $C_{18}H_{19}N_2O_6P$: 390.0981; found 390.0994.

(meso)-trans-*1-ethoxy-cis-2,5-di(4-nitrophenyl)-1λ^5-phospholan-1-one (**14b**)*: Obtained in 64% yield as a white solid from **13b** using the general procedure described above. Purification was achieved by recrystallization in EtOAc–hexane. mp 190–192°C. ^{1}H NMR δ: 1.24 (3 H, t, *J* = 7.2 Hz), 2.45 (6 H, m), 3.40 (2 H, m), 4.03 (2 H, m), 7.52 (4 H, dd, *J* = 2 Hz, *J* = 7 Hz), 8.22 (4 H, d, *J* = 8.7 Hz). ^{13}C NMR ($CDCl_3$) δ: 147.32, 144.16 (d, *J* = 5.4 Hz), 129.45, 123.73, 62.26 (d, *J* = 7.3 Hz), 43.66 (d, *J* = 86.1 Hz), 29.31 (d, *J* = 12.8 Hz), 16.60. ^{31}P NMR δ: 60.49 (s). MS, *m*/*z* (relative intensity): 390 (100), 362, (26), 296 (77), 148 (95), 119 (44), 103 (37), 77 (36). HRMS calcd. for $C_{18}H_{19}N_2O_6P$: 390.0981; found 390.0989.

(meso)-cis-*1-Ethoxy-cis-2,5-di(4-nitrophenyl)-1λ^5-phospholan-1-one (**14c**)*: Obtained in 75% yield as a white solid from **13c** using the general procedure described above. Purification was achieved using flash chromatography (silica, 100% EtOAc). TLC (silica): R_f = 0.3; white solid, mp 180–182°C. ^{1}H NMR δ: 0.65 (3 H, t, *J* = 7), 2.45 (4 H, m), 3.38 (2 H, m), 3.59 (2 H, m), 7.51 (4 H, dd, *J* = 2.2 Hz, *J* = 9.1 Hz), 8.21 (4 H, d, *J* = 8.8 Hz). ^{13}C NMR δ: 147.28, 143.54 (d, *J* = 8.2 Hz), 128.63 (d, *J* = 4.6 Hz), 123.62, 62.15 (d, *J* = 7.3 Hz), 44.10 (d, *J* = 81.5 Hz), 26.88 (d, *J* = 7.9 Hz), 15.94 (d, *J* = 3.7 Hz). ^{31}P NMR δ: 59.9 (s). MS, *m*/*z* (relative intensity): 390 (35), 362 (20), 296 (50), 149 (100), 119 (42), 103 (39), 77 (42). HRMS calcd. for $C_{18}H_{19}N_2O_6P$: 390.0981; found 390.0992.

*Benzyl 6-hydroxyhexanoate (**15**)*: To an aqueous solution of 20% tetrabutylammonium hydroxide (100 mL, 77.1 mmol, 1 equiv.) was added ε-caprolactone (8.79 g, 77.1 mmol, 1 equiv.) and the solution heated to 65°C for 2 h during which time the solution became homogeneous. The solution was concentrated by rotary evaporation leaving a white solid that was dried under high vacuum for several hours. The solid was dissolved in dry DMF (80 mL) and benzylchloride (10.7 g, 84.8 mmol, 1.1 equiv.) was added and the reaction stirred for 24 h. The reaction mixture was diluted with 80 mL water and the extracted with ether (4 × 150 mL). The ether layers were combined and dried (Na_2SO_4), then concentrated leaving a pale yellow oil. Flash chromatography (silica, 60% hexane – 40% EtOAc) of the oil yielded pure **15** as a colourless oil (15.2g, 89%). TLC (silica, 60% hexane – 40% EtOAc): R_f = 0.3. ^{1}H NMR δ: 1.33–1.71 (7 H, m), 1.91 (1 H, s), 2.37 (2 H, t, *J* = 7.3 Hz), 3.60 (2 H, t, *J* = 5.8 Hz), 5.10 (2 H, s), 7.34 (5 H, s). ^{13}C NMR δ: 173.43, 136.23, 128.50, 128.08, 66.05, 62.30, 34.25, 32.30, 25.34, 24.71. MS, *m*/*z* (relative intensity): 223 (3), 194 (12), 115 (59), 108

[4] Table of crystallographic details, atomic coordinates, anisotropic displacement parameters, and bond distances and angles have been deposited and may be purchased from: The Depository of Unpublished Data, Document Delivery, CISTI, National Research Council Canada, Ottawa, Ontario, Canada, K1A 0S2. Table of bond distances and angles and H coordinates have also been deposited with the Cambridge Crystallographic Data Centre and can be obtained on request from: The Director, Cambridge Crystallographic Data Centre, University Chemical Laboratory, 12 Union Road, Cambridge, CB2 1Ez, U.K.

© 2000 NRC Canada

(52), 91 (100). HRMS calcd. for $C_{13}H_{18}O_3$ *m/z*: 222.1256 (M^+); found 222.1252.

*Benzyl 6-(*tert*-butyldimethylsilyloxy)hexanoate (**16**)*: To a solution of **15** (7.0 g, 31.5 mmol) in dry DMF (15 mL) was added imidazole (5.14 g, 75.6 mmol, 2.4 equiv.) and the solution stirred until all of the imidazole dissolved. *tert*-Butyldimethylsilylchloride (5.69 g, 37.8 mmol, 1.2 equiv.) was added in portions over a period of approximately 4 min and the solution stirred under argon overnight. The reaction was diluted with ether (400 mL) and washed with water (2 × 200 mL), 10% $NaHCO_3$ (2 × 200 mL), saturated brine (2 × 200 mL), dried ($MgSO_4$), and concentrated leaving a pale yellow oil. Flash chromatography (silica, 90% hexane – 10% EtOAc) of the crude oil yielded pure **16** as a colourless oil (9.71 g, 92%). TLC (silica, 90% hexane – 10% EtOAc): R_f = 0.6. ^{1}H NMR δ: 0.044 (6 H, s); 0.89 (9 H, s); 1.36–1.71 (6 H, m); 2.37 (2 H, t, *J* = 7.3 Hz); 3.59 (2 H, t, *J* = 5.9 Hz); 5.12 (2 H, s); 7.36 (5 H, s). ^{13}C NMR δ: 173.17, 136.47, 136.38, 128.46, 128.04, 65.94, 62.90, 34.34, 32.48, 25.97, 25.53, 24.82, 18.29, –5.30. MS, *m/z* (relative intensity): 279 (13), 171 (4), 91 (100). HRMS calcd. for $C_{15}H_{23}O_3Si$ *m/z*: 279.1416 ($M^+ - C_4H_9$); found 279.1411.

*6-(*tert*-Butyldimethylsilyloxy)hexanoic acid (**17**)*: To a solution of **16** (9.71 g, 28.8 mmol) in EtOAc (100 mL) was added 5% Pd/C (400 mg). The flask was fitted with a balloon filled with H_2 and the reaction stirred for 16 h. The reaction was filtered through filter paper, concentrated, and diluted with 50 mL EtOAc. The solution was filtered again, concentrated and residual solvent removed under high vacuum leaving pure **17** as a colourless oil (6.79 g, 95%). ^{1}H NMR δ: 0.044 (6 H, s), 0.89 (9 H, s), 1.39–1.69 (6 H, m), 2.36 (2 H, t, *J* = 7.3 Hz), 3.61 (2 H, t, *J* = 5.9 Hz), 11.05 (1 H, bs). ^{13}C NMR δ: 179.18, 62.85, 33.97, 32.39, 25.89, 25.40, 24.51, 18.23, –5.39. MS, *m/z* (relative intensity): 231 (2), 229 (4), 213 (7), 189 (37), 171 (89), 75 (100). HRMS calcd. for $C_{11}H_{23}O_3Si$ *m/z*: 231.1416 ($M^+ - CH_3$); found 231.1416.

tert-*Butyl 6-hydroxyhexanoate (**18**)*: To a solution of **17** (4g, 16.2 mmol) in dry CH_2Cl_2 (15 mL) was added DMAP (396 mg, 20 mol%), *t*-BuOH (6.19 mL, 64.8 mmol, 4 equiv.) and the solution was cooled in an ice bath. DCC was added (3.52g, 17.0 mmol, 1.05 equiv.) in portions over a three min period. The solution was stirred for 1 h at 0°C and then allowed to warm to room temperature then stirred for a further 24 h. The reaction was filtered and the filtrate concentrated leaving a pale yellow oil. The oil was dissolved in ether (300 mL) and washed with water (2 × 150 mL), 10% $NaHCO_3$ (1 × 150 mL), saturated brine (1 × 150 mL), dried ($MgSO_4$) and concentrated to approximately 20 mL. The solution was filtered and the filtrate concentrated leaving a yellow oil. The oil was distilled (bp 65–68°C, 100 μm) to give 3.0 g of a colourless oil. In addition to the desired *tert*-butyl ester of **17**, the ^{1}H NMR of the distilled material indicated that small amounts (approximately 5%) of both DCC and DCU were present. 2.5 g (approximately 8.25 mmol) of the impure distilled oil was dissolved in dry THF (6 mL). To this was added TBAF (24 mL of a 1.0 M solution in THF, 24 mmol) and the solution stirred for 48 h. The solution was diluted with ether (300 mL) and then washed with water (7 × 200 mL), 10% $NaHCO_3$ (2 × 200 mL), saturated brine (1 × 200 mL), dried ($MgSO_4$) and concentrated leaving a yellow oil. Flash chromatography (silica, 70% hexane – 30% EtOAc) of the oil yielded pure **18** as a pale yellow oil (1.15 g, 38%). TLC (silica, 70% hexane – 30% EtOAc): R_f = 0.25. ^{1}H NMR δ: 1.36–1.63 (6 H, m), 1.41 (9 H, s), 1.86 (1 H, s), 2.20 (2 H, t, *J* = 7.3 Hz), 3.60 (2 H, bt). ^{13}C NMR δ: 173.14, 79.90, 61.99, 35.37, 32.17, 27.95, 25.17, 24.71. MS, *m/z* (relative intensity): 132 (8), 115 (48), 97 (34), 69 (35), 57 (100). HRMS calcd. for $C_{11}H_{23}O_3Si$ *m/z*: 132.0777 ($M^+ - C_4H_9$); found 132.0786.

*General procedure for the deprotection of esters **13b**, **13c**, **14a**, **14b**, and **14c***

Trimethyl silyl iodide (1.2 equiv.) was added dropwise to a solution of the ester (**13b**, **13c**, **14a**, **14b**, or **14c**) in dry CH_2Cl_2 (approx. 1 mmol ester/mL of solvent) and the reaction stirred for 2 h under an Ar atmosphere. Additional CH_2Cl_2 was added and the product was extracted into a 0.1 N sodium hydroxide solution. The two layers were immediately separated and the aqueous layer rapidly acidified to pH 2 (pH paper) with 6 N hydrochloric acid which resulted in the formation of the desired acid product as a precipitate. The product (**19a**, **19b**, or **21**) was recovered by suction filtration. In some instances, further purification by HPLC was necessary.

(±)-1-Hydroxy-trans-*2,5-di(4-nitrophenyl)-1λ^5-phospholan-1-one (**19a**)*: Obtained in a 90% yield as amorphous yellow solid from **14a** using the general procedure for ester deprotection described above; mp 271–273°C. ^{1}H NMR (DMSO-d_6) δ: 2.04–2.45 (4 H, m), 3.40–3.64 (2 H, m), 7.62 (4 H, d, *J* = 5.8 Hz), 8.27 (4 H, d, *J* = 5.8 Hz). ^{13}C (DMSO-d_6) δ: 146.26, 129.68 (d, *J* = 5.4 Hz), 123.17, 45.68 (d, *J* = 82.2 Hz), 28.54 (d, *J* = 10 Hz). ^{31}P NMR (DMSO-d_6) δ: 58.60 (s). MS, *m/z* (relative intensity): 362 (100), 298 (36), 149 (54), 119 (38), 103 (26), 77 (29). HRMS calcd. for $C_{16}H_{15}N_2O_6P$: 362.0668; found 362.0671.

1-Hydroxy-cis-*2,5-di(4-nitrophenyl)-1λ^5-phospholan-1-one (**19b**)*: Obtained in a 90% yield as an amorphous light yellow solid from **14b** or **14c** using the general procedure for ester deprotection described above. Purification was achieved via HPLC (isocratic, 99% $CHCl_3$ – 1% MeOH, retention time = 13 min); mp 278–281°C. ^{1}H NMR (DMSO-d_6) δ: 2.06–2.48 (4 H, m), 3.45–3.64 (2 H, m), 7.62 (4 H, d, *J* = 7.3 Hz), 8.22 (4 H, d, *J* = 8.8 Hz). ^{31}P NMR (DMSO-d_6) δ: 59.17 (s). ^{13}C (DMSO-d_6) δ: 146.24, 129.56 (d, *J* = 4.5 Hz), 123.15, 43.71 (d, *J* = 82.4 Hz), 28.52 (d, *J* = 3.3 Hz). MS, *m/z* (relative intensity): 362 (36), 298 (19), 149 (100), 133 (43), 119 (20), 103 (32), 77 (43). HRMS calcd. for $C_{16}H_{15}N_2O_6P$: 362.0668; found 362.0681.

1-Hydroxy-cis-*2,5-diphenyl-1λ^5-phospholan-1-one (**21**)*: Obtained in a 90% yield as a white solid from **13b** or **13c** using the general procedure for ester deprotection described above; mp 169–171°C. ^{1}H NMR (DMSO-d_6) δ: 2.13–2.44 (4 H, m), 3.20–3.37 (2 H, m), 7.16–7.39 (10 H, m). ^{13}C (DMSO-d_6) δ: 138 (δ, *J* = 6.5 Hz), 128.42 (d, *J* = 5.5 Hz), 128.08, 126.01, 43.23 (d, *J* = 84.2 Hz), 27.61 (d, *J* = 12.9 Hz). ^{31}P NMR (DMSO-d_6) δ 60.32 (s). MS, *m/z* (relative intensity):

© 2000 NRC Canada

272 (57), 168 (23), 104 (100), 91 (24), 78 (25). HRMS calcd. for $C_{16}H_{17}O_2P$: 272.0966; found 292.0976.

*(±)-*tert-*Butyl 6-{[*trans-*2,5-di(4-nitrophenyl)-1-oxo-1λ⁵-phospholan-1-yl]oxy}hexanoate (**20a**) from **19a** via the Mitsonobu procedure*: **18** (39 mg, 0.21 mmol, 1.5 eq), **19a** (50 mg, 1.4 mmol, 1.5 equiv.), triphenylphosphine (54.3 mg, 0.21 mmol, 1.5 equiv.), and diisopropylazidodicarboxylate (DIAD) (0.041 mL, 0.21 mmol, 1.5 equiv.) were dissolved in dry THF (1.5 mL). The solution was stirred for 30 min at room temperature followed by removal of the solvent by rotary evaporation. Flash chromatography (silica, 50% EtOAc – 50% hexane) of the crude residue yielded pure **20a** as a clear colourless oil (60.1 mg, 82%). TLC (silica, 50% EtOAc – 50% hexane): R_f = 0.5. ^{1}H NMR δ: 1.00–1.48 (15 H, m), 2.00–2.74 (6 H, m), 3.19–3.86 (4 H, m), 7.45–7.58 (4 H, m), 8.23 (4 H, dd, *J* = 0.9 Hz, *J* = 6.9 Hz). ^{13}C NMR δ: 172.42, 147.41, 143.84 (d, *J* = 3.7 Hz), 143.21 (d, *J* = 6.4 Hz), 129.50 (d, *J* = 5.5 Hz), 128.82 (d, *J* = 4.6 Hz), 123.80, 123.77, 80.08, 65.77 (d, *J* = 7.3 Hz), 46.83 (d, *J* = 83.3 Hz), 45.51 (d, *J* = 86 Hz), 35.17, 30.50, 30.24, 28.11, 27.77, 27.57, 24.89, 24.38. ^{31}P NMR δ: 59.77 (s). MS, *m/z* (relative intensity): 476 (12), 459 (65), 363 (89), 280 (48), 216 (54), 57 (100). HRMS calcd. for $C_{26}H_{34}N_20_8P$ (-C_4H_8): 476.1348; found 476.1351.

*(±)-6-{[*trans-*2,5-Di(4-nitrophenyl)-1-oxo-1λ⁵-phospholan-1-yl]oxy}hexanoic acid (**6**)*: **20a** (35 mg, 0.066 mmol) was dissolved in 20% TFA – CH_2Cl_2 (1.5 mL) and stirred overnight at room temperature. The CH_2Cl_2 and TFA was removed by rotary evaporation. Flash chromatography (silica, 80% EtOAc – 20% hexane) on the crude residue yielded pure **6** as a clear colourless oil (25 mg, 80%). TLC (silica, 80% EtOAc – 20% hexane): R_f = 0.5. ^{1}H NMR δ: 1.09–1.65 (6 H, m), 2.05–2.75 (6 H, m), 3.17–3.98 (4 H, m), 7.52 (4 H, m), 8.22 (4 H, m). ^{13}C NMR δ: 175.92, 147.44, 143.65 (d, *J* = 3.7 Hz), 143.11 (d, *J* = 6.4 Hz), 129.53 (d, *J* = 5.5 Hz), 128.87 (d, *J* = 3.7 Hz), 123.82, 65.83 (d, *J* = 7.3 Hz), 46.64 (d, *J* = 84.2 Hz), 45.50 (d, *J* = 85.1 Hz), 33.23, 30.33, 30.02, 24.80, 24.02. ^{31}P NMR δ: 60.17 (s). MS *m/z* (relative intensity): 477, 444 (8), 363 (83), 280 (84), 216 (53), 149 (54), 119 (56), 69 (82). HRMS calcd. for $C_{22}H_{25}N_2O_8P$ (-OH): 459.1321; found 459.1327.

*(meso)-*trans-tert-*Butyl 6-{[1-oxo-*cis-*2,5-diphenyl-1λ⁵-phospholan-1-yl]oxy}hexanoate (**22a**)*: To a solution of **21** (120 mg, 0.55 mmol, 1 equiv.) in dry CH_2Cl_2 (2 mL) was added oxalyl chloride (0.144 mL, 1.65 mmol, 3 equiv.) dropwise over a period of 1 min and the solution was stirred for 3 h. The solvent was removed by rotary evaporation and the crude acid chloride subjected to high vacuum for 12 h. The crude acid chloride was dissolved in dry benzene (1 mL) and a solution of **18** (125 mg, 0.66 mmol, 1.1 equiv.) and triethylamine (0.100 mL, 0.72 mmol, 1.2 equiv.) in dry benzene (1 mL) was added dropwise over a period of 2 min and the reaction was stirred for 24 h. Ether was added which resulted in the precipitation of triethylamine hydrochloride which was removed by vacuum filtration and the filtrate was concentrated by rotary evaporation. Flash chromatography (silica, 90% CH_2Cl2 – 10% EtOAc) on the crude residue yielded pure **22a** as a clear colourless oil (140 mg, 57%). TLC (silica, 90% CH_2Cl_2 – 10% EtOAc): R_f = 0.6. ^{1}H NMR δ: 1.23–1.65 (15 H, m), 2.18 (2 H, t, *J* = 7.3 Hz), 2.40 (4 H, m), 3.29 (2 H, m), 3.91 (2 H, q, *J* = 6.6 Hz), 7.35 (10 H, m). ^{13}C NMR δ: 172.66, 137.07 (d, *J* = 4.6 Hz), 128.75, 128.63, 128.50, 126.68, 79.92, 65.18 (d, *J* = 6.5), 43.51 (d, *J* = 86.0 Hz), 35.39, 30.49 (d, *J* = 5.5 Hz), 29.51 (d, *J* = 14.7 Hz), 28.15, 25.13, 24.62. ^{31}P NMR δ: 62.56 (s). MS, *m/z* (relative intensity): 442, 386 (99), 369 (33), 272 (60), 104 (100). HRMS calcd. for $C_{26}H_{35}O_4P$: 442.2297; found 442.2293.

*(meso)-*trans-*6-{[*cis-*2,5-Di(4-nitrophenyl)-1-oxo-1λ⁵-phospholan-1-yl]oxy}hexanoic acid (7)*: **22a** (120 mg, 0.27 mmol, 1 equiv.) was dissolved in 0.5 mL of H_2SO_4 at 0°C. A solution of HNO_3–H_2SO_4 (1:1, 0.062 mL, 2.6 equiv. HNO_3) was added and the reaction was stirred at 0°C for 30 min. The reaction was poured into a beaker containing ice which upon melting left a suspension. $CHCl_3$ (5 mL) was added and the two layers were separated. The aqueous layer was further extracted with $CHCl_3$ (4 × 10 mL) and the combined organics were washed with brine (2 × 15 mL), dried ($MgSO_4$), and concentrated in vacuo leaving an oily of solid residue. Attempts to obtain pure product by subjecting the crude residue to silica gel flash chromatography were unsuccessful. Final purification of the desired product was accomplished using HPLC (isocratic, 70% EtOAc – 30% hexane, retention time = 18 min) to give **7** as a clear colourless oil (51 mg, 44%). ^{1}H NMR δ: 1.23–1.68 (6H, m), 2.24 (2 H, t, *J* = 7 Hz), 2.35–2.60 (4 H, m), 3.35–3.57 (2 H, m), 3.87–4.03 (2 H, dd, *J* = 6.6 Hz, *J* = 7.7 Hz), 7.52 (4 H, dd, *J* = 1.8 Hz, *J* = 6.9 Hz), 8.19 (4 H, dd, *J* = 8.4 Hz). ^{13}C NMR δ: 176.79, 147.28, 143.97 (d, *J* = 7.3 Hz), 129.46 (d, *J* = 5.5 Hz), 123.84, 66.23 (d, *J* = 7.3 Hz), 43.56 (d, *J* = 84.2 Hz), 33.48, 30.30 (d, *J* = 5.5 Hz), 29.26 (d, *J* = 14.7 Hz), 24.96, 24.1. ^{31}P NMR ($CDCl_3$) δ: 61.11 (s). MS, *m/z* (relative intensity): 363(53), 280(57), 149(52). HRMS calcd. for $C_{22}H_{25}N_2O_8P$: 477.1427; found 477.1432.

*(meso)-*cis-tert-*Butyl 6-{[1-oxo-cis-2,5-diphenyl-1λ⁵-phospholan-1-yl]oxy}hexanoate (**22b**)*: **18** (60 mg, 0.33 mmol, 1.5 equiv.), triphenyl phosphine (87 mg, 0.33 mmol, 1.5 equiv.), **21** (60 mg, 0.22 mmol, 1 equiv.), and DIAD (65 uL, 67 mg, 0.33 mmol, 1.5 equiv.) were dissolved in dry THF (1.5 mL) and stirred at room temperature for 30 min. The solvent was removed under reduced pressure. Flash chromatography of the crude residue (silica, 60% EtOAc – 40% hexane) yielded **22b** as a clear colourless oil (58.5 mg, 60%). TLC (silica, 60% EtOAc – 40% hexane): R_f = 0.4. ^{1}H NMR δ: 0.65–0.85 (2 H, br m), 0.89–1.04 (2 H, br m), 1.20–1.26 (3 H, br m), 1.439, (7 H, s), 1.75 (1 H, s), 1.97 (3 H, t, *J* = 8.1 Hz), 2.35–2.48 (4 H, br m), 3.11–3.20 (2 H, br m), 3.38–3.54 (2 H, br m), 7.20–7.35 (10 H, br m). ^{13}C NMR δ: 172.94, 136.29 (d, *J* = 8.1 Hz), 128.43 (d, *J* = 2.2 Hz), 127.80 (d, *J* = 5.1 Hz), 126.65 (d, *J* = 3.0 Hz), 79.83, 64.69 (d, *J* = 7.4 Hz), 43.74 (d, *J* = 82.0 Hz), 35.24, 29.87 (d, *J* = 5.1 Hz), 28.05, 27.48 (d, *J* = 7.2 Hz), 24.44, 24.34. ^{31}P NMR δ: 61.75 (s). MS, *m/z* (relative intensity): 443 (18), 387 (58), 272 (49), 104 (100). HRMS calcd. for $C_{26}H_{35}O_4P$: 442.2273; found 442.2264.

Formation of bovine serum albumin (BSA)–TSA and keyhole lympet hemocyanin (KLH)–TSA conjugates

To a solution of TSAs **6** or **7** (~6 mg, ~0.013 mmol) in DMF:water (3:2, 3 mL) was added *N*-hydroxysulfosuccinimide

© 2000 NRC Canada

(3.5 mg, 0.016 mmol) and EDC (3.1 mg, 0.016 mmol). The reaction was stirred at rt for 3 h. The reaction mixture was divided into two equal aliquots (1.5 mL each). One aliquot was added to a solution of BSA (6.3 mg) in 50 mM phosphate buffer (pH 7.5, 3 mL) and the other aliquot was added to a solution of KLH (6.1 mg) in the same buffer. The reaction were shaken at 4°C for 16 h. Unconjugated hapten was removed by dialysis (6 × 1 L, 3 h each) in 50 mM phosphate buffer, pH 7.5 at 4°C. The number of haptens per BSA was determined using the method of Habeeb (27). The number of *trans* haptens **6** per BSA was 11 and the number of *cis* haptens **7** per BSA was 19. We were unable to determine the number of haptens per KLH due to the nonhomogeneous nature of the KLH solutions. The conjugates were stored at –20°C.

*6-{[*Di*(4-nitrophenoxy)phosphoryl]oxy}hexanoic acid (**8**)*: To a solution of **18** (125 mg, 0.66 mmol) in dry THF (4 mL) was added bis(4-nitrophenyl)phosphate (150 mg, 0.44. mmol), triphenyl phosphine (173 mg, 0.66 mmol), and DIAD (130 uL, 130 mg, 0.66 mmol). The solution was stirred under argon for 30 min, the solvent was then removed by rotary evaporation and the crude residue chromatographed (silica, 95% CH_2Cl_2 – 5% EtOAc). TLC (silica, 95% CH_2Cl_2 – 5% EtOAc): R_f = 0.7. Due to slow product breakdown, it was not possible to separate the *tert*-butyl-6-{[di(4-nitrophenoxy)phosphoryl]oxy}hexanoate product from trace amounts of 4-nitrophenol. Thus, the impure product was dissolved in a solution of TFA:CH_2Cl_2 (1:5) and stirred for 16 h. The solvent was removed by rotary evaporation and the product obtained by flash chromatography (silica, 50% hexane – 50% EtOAc) yielded **8** as a white solid (146 mg, 73% overall yield). TLC (silica, 50% hexane – 50% EtOAc): R_f = 0.2; mp 77–78°C. ^{1}H NMR δ: 1.20–1.90 (7 H, c m), 2.35 (2 H, t, *J* = 7 Hz), 4.34 (2 H, q, *J* = 6.6 Hz), 7.40 (4 H, d, *J* = 9.2 Hz), 8.26 (4 H, d, *J* = 7.3 Hz). ^{13}C NMR δ: 178.16, 154.74 (d, *J* = 6.4 Hz), 145.40, 125.81, 120.71 (d, *J* = 4.7 Hz), 70.49, 33.57, 29.81, 24.84, 24.02. ^{31}P NMR δ: –15.83 Hz (s). MS, *m*/*z* (relative intensity): 341 (80), 316 (51), 139 (100), 109 (82), 65 (70). HRMS calcd. for $C_{18}H_{19}0_{10},N_2P$: 455.08556; found 455.0830.

*Methyl hydrogen (4-nitrobenzyl)phosphonate (**24**)*: A mixture composed of dimethyl (4-nitrobenzyl)phosphonate (26) (2.5 g, 10.2 mmol) and sodium hydroxide (816 mg, 20.4 mmol) in water (60 mL) was heated at 75°C until homogeneous. The solution was acidified to pH 1 with concentrated hydrochloric acid (6 M), filtered, the precipitate washed with water giving **24** as a white solid (2.12 g, 90% yield); mp 132–134°C. ^{1}H NMR ($DMSO_{d6}$) δ: 3.19 (2 H, d, *J* = 22.8 Hz), 3.59 (3 H, d, *J* = 11.3 Hz), 7.44 (2 H, dd, *J* = 2.5 Hz, *J* = 8.8 Hz), 8.17 (2 H, d, *J* = 8 Hz). ^{13}C NMR δ: 146.28, 142.02 (d, *J* = 9.2 Hz), 130.90 (d, *J* = 5.5 Hz), 123.13, 51.72 (d, *J* = 6.4 Hz), 33.30 (d, *J* = 131.8). ^{31}P NMR δ: 25.48 (s). MS, *m*/*z* (relative intensity): 231 (50), 214 (100), 184 (31), 136 (31), 107 (62), 89 (52). HRMS calcd. for $C_8H_{10}O_5NP$: 231.0297; found 231.0314.

*Methyl (4-nitrophenyl) (4-nitrobenzyl) phosphonate (**25**)*: Compound **24** (1 g, 4.33 mmol) was suspended in dry methylene chloride (40 mL). To the suspension was added 4-nitrophenol (722 mg, 5.19 mmol) and EDC (995 mg, 5.19 mmol). The reaction was stirred under argon for 72 h. The solution was diluted with methylene chloride (20 mL), washed with 5% sodium bicarbonate (2 × 50 mL), 0.1 N HCl (2 × 50 mL), and saturated brine (1 × 50 mL), dried ($MgSO_4$) and concentrated leaving a solid residue. Recrystallization of the crude in hexane–ethyl acetate yielded pure **25** as a white solid (64% yield); mp 112–114°C. ^{1}H NMR δ: 3.48 (2 H, d, *J* = 22.7 Hz), 3.80 (3 H, d, *J* = 11 Hz), 7.29 (2 H, d, *J* = 8.8 Hz), 7.51 (2 H, dd, *J* = 2.9 Hz, *J* = 5.9 Hz), 8.22 (4 H, d, *J* = 8.8 Hz). ^{13}C NMR δ: 155.31 (d, *J* = 8.2 Hz), 147.48, 144.90, 138.09 (d, *J* = 9.1 Hz), 130.78 (d, *J* = 6.4 Hz), 125.61, 123.86, 120.85 (d, *J* = 4.6 Hz), 53.91 (d, *J* = 6.4 Hz), 33.55 (d, *J* = 139.1 Hz). ^{31}P NMR δ: 20.94. MS, *m*/*z* (relative intensity): 352 (100), 335 (41), 305 (27), 257 (34), 136 (49). HRMS calcd. for $C_{14}H_{13}O_7N_2P$: 352.0460; found 352.0450.

*4-nitrophenyl hydrogen (4-nitrobenzyl)-phosphonate (**26**)*: To a solution of **25** (1.83 g, 5.4 mmol) in dry butanone (40 mL) was added NaBr (833 mg, 8.10 mmol) and the resulting solution refluxed for 16 h. Upon cooling the solution to rt, a precipitate formed. The mixture was filtered and the precipitate washed with cold butanone. The solid was dissolved in water and the solution was acidified with 6 N HCl to pH 2 which resulted in the formation of a white precipitate. The mixture was filtered and the precipitate washed with cold water then dried under vacuum to give **26** as a white solid (535 mg, 93% yield). ^{1}H NMR ($DMSO_{d6}$) δ: 3.54 (2 H, dd, *J* = 8.1 Hz, *J* = 23 Hz), 7.38 (2 H, d, *J* = 8 Hz), 7.59 (2 H. d. *J* = 5.9 Hz), 8.19 (4 H, d, *J* = 9.5 Hz). ^{13}C NMR δ: 156.20, 146.44, 143.68, 141.11 (d, *J* = 9.1 Hz), 131.07 (d, *J* = 6.4 Hz), 125.48, 123.19, 121.07 (d, *J* = 4.6 Hz), 34.35 (d, *J* = 133.6 Hz). ^{31}P NMR δ: 21.66. MS, *m*/*z* (relative intensity): 338 (33), 228 (18), 210 (24), 139 (100), 109 (83). HRMS calcd. for $C_{13}H_{11}O_7N_2P$: 338.0304; found 338.0310.

*6-{[4-Nitrobenzyl)(4-nitrophenoxy)phosphoryl]oxy}hexanoic acid (**9**)*: To a solution of hydroxy ester **18** (156 mg, 0.83 mmol) in dry THF (1.5 mL) was added phosphonic acid **26** (180 mg, 0.55 mmol), triphenyl phosphine (218 mg, 0.83 mmol), and DIAD (180 ul, 180 mg, 0.83 mmol). The reaction was stirred for 1 h. The solvent was removed by rotary evaporation and the crude purified by chromatography (silica. 40% hexane – 60% EtOAc). We were unable to separate the phosphonate product **27** from small amounts of contaminating of *p*-nitrophenol. Consequently, the slightly impure phosphonate **27** was dissolved in a solution of 20% TFA–CH_2Cl_2 (1 mL) and stirred for 16 h. The solvent was removed by rotary evaporation and the crude residue chromatographed (silica, 20% hexane – 80% EtOAc) to yield pure **9** as a thick colourless oil (159 mg, 64% overall yield). TLC (silica, 20% hexane – 80% EtOAc): R_f = 0.6. ^{1}H NMR ($DMSO_{d6}$) δ: 0.75–1.75 (7 H, m), 2.30 (2 H, t, *J* = 7.2 Hz), 3.52 (2 H, *J* = 22.7 Hz), 4.15 (2 H, m), 7.29 (2 H, d, *J* = 9.6 Hz), 7.51 (2 H, dd, *J* = 2.6 Hz, 8.20 (4 H, d, *J* = 8.8 Hz). ^{13}C NMR δ: 177.47, 155.16 (d, *J* = 7.1 Hz), 147.50, 144.93, 138.07 (d, *J* = 9.1 Hz), 130.85 (d, *J* = 5.5 Hz), 125.63, 123.84, 121.00, 67.83 (d, *J* = 7.3 Hz), 33.80 (d, *J* = 138.1), 33.61, 29.92 (d, *J* = 4.6 Hz), 24.84, 24.07. ^{31}P NMR δ: 19.7. MS, *m*/*z* (relative intensity): 339 (64), 314 (58), 139

© 2000 NRC Canada

(77), 109 (51), 97 (66), 69 (100). HRMS calcd. for $C_{19}H_{21}0_9,N_2P$: 453.1063; found 453.1086.

Kinetic studies with substrates 8 and 9 in the absence of antibody

A 20 μL aliquot of a 1 mM stock solution of **8** or **9** in DMF was added to a cuvette containing 980 μL of 10 mM CHES, 50 mM NaCl, pH 9.0 preincubated at 25°C. The cuvette was incubated at 25°C and the hydrolysis reaction was followed by measuring the absorbance at 400 nm every 30 min using a Cary 1B UV–Vis spectrophotometer until the reaction had proceeded to approximately 3–4 half-lives. The data was fitted to the first-order rate equation using the GraFit program (28). Each reaction was performed in duplicate.

Isomerization studies with 7

A 500 μM solution of **7** (3.0 mL) in 20 mM phosphate buffer at pH 7.5 was incubated at 25°C. Aliquots (0.5 mL) were removed at various time intervals and quenched with 1 M HCl (40 μL) and then extracted with EtOAc (0.5 mL). The extent of isomerization to **6** was determined by normal phase HPLC analysis of the EtOAc solutions using EtOAc as eluant (1.0 mL/min for 5 min then switching to 2.0 mL for 6 min) and the detector set at 280 nm. Under these conditions, the retention time of the *cis* TSA **7** was 4.2 min and the *trans* TSA **6** was 6.2 min.

Antibody production

Balb/c mice were immunized IP five times at ten day intervals with 50 μg of the KLH conjugates. The first four injections were given intraperitoneally after emulsification of the conjugate with Freund's adjuvant while the final injection was given intravenously with just conjugate in PBS. Three days after the final injection, hybridoma production was initiated as described previously (29, 30). The fusion was screened by solid phase radio immune assays (SPRIA) (29, 30) using PVC plates coated with the BSA conjugates. Seven cell lines, two obtained from mice immunized with the *trans* TSA **6** and five obtained from mice immunized with the *trans* TSA **7**, were cloned. Isotyping of the antibodies obtained from mice immunized with the trans hapten **6** revealed that one was an IgM class and one an IgG class antibody, while those obtained from mice immunized with the *cis* hapten **7** revealed that three were IgG class antibodies and two were IgM class antibodies. Ascites fluid was prepared (29, 30) from these seven cell lines and the antibodies were purified by gel exclusion chromatography on a Sephracryl S-200 column as previous described (29, 30). SDS-PAGE (12%) analysis of Jel 541 revealed only a single band at the top of the gel (Coomassie Blue staining). Competitive SPRIAs (29, 30) were performed with plates coated with the BSA conjugate of the *cis* TSA **7**.

Antibody kinetics

Purified antibody was dialyzed overnight into 10 mM CHES, 50 mM NaCl, pH 9.0 or 10 mM HEPES, 50 mM NaCl, pH 7.0. A stock solution of the substrates in DMSO was added directly to the antibody solutions. The final volume was 0.300 mL and the total amount of DMSO in the assay mix was 1% (v/v). The change in absorbance at 400 nm was monitored at 25°C in a Gilford 260 spectrophotometer.

Acknowledgements

We would like to thank the Medical Research Council of Canada (MRC) for financial support. We thank Alan Lough for performing X-ray structure analyses.

References

1. J. S. Rosenblum, L.-C. Lo, T. Li, K.D. Janda, and R.A. Lerner. Angew. Chem. Int. Ed. Eng. **34**, 2275 (1995).
2. B.J. Lavey and K.D. Janda. Bioorg. Med. Chem. Lett. **6**, 1523 (1996).
3. B.J. Lavey and K.D. Janda. J. Org. Chem. **61**, 7633 (1996).
4. D.A. Spivak, T. Hoffman, A.H. Moore, M.J. Taylor, and K.D. Janda. Bioorg. Med. Chem. **7**, 1145 (1999).
5. G.R.J. Thatcher and R. Kluger. Adv. Phys. Org. Chem. **25**, 99 (1989).
6. F.H. Westheimer. Acc. Chem. Res. **1**, 70 (1968).
7. R. Kluger and S. Taylor. J. Am. Chem. Soc. **112**, 6669 (1990).
8. S. Taylor and R. Kluger. J. Am. Chem. Soc. **114**, 3067 (1992).
9. Y.H. Chiu and W.N. Lipscomb. J. Am. Chem. Soc. **91**, 4150 (1969).
10. E. Alver and H.M. Kjoge. Acta Chem. Scand. **23**, 1101 (1969).
11. V.V. Prezhdo, O.V. Prezdho, and E.V. Vaschenko. J. Mol. Struct. **385**, 137 (1996).
12. S.M. Kalinov, M.F. Rostovskaya, and V.I. Vysotskii. Zh. Obshch. Khim. **58**, 783 (1988).
13. L.D. Quin. The Heterocyclic Chemistry of Phosphorus. Wiley, New York. 1981. Chap. 2.
14. W.B. McCormack. Chem. Abstr. **49**, 7601 (1955).
15. A.H. Cowley, R.A. Kemp, J.G. Lasch, N.C. Norman, C.A. Stewart, B.R. Whittlesey, and T.C. Wright. Inorg. Chem. **25**, 740 (1986).
16. K. Moedritzer. Synth. React. Inorg. Met. Org. Chem. **5**, 45 (1975).
17. J.-C. Fiaud and J.-Y. Legros. Tetrahedron Lett. **32**, 5089 (1991).
18. I.G.M. Campbell, R.C. Cookson, M.B. Hocking, and A.N.J. Hughes. J. Chem. Soc. 2184 (1965).
19. B. Lukas, R.M.G. Roberts, J. Silver, and A.S. Wells. J. Organometal. Chem. **256**, 103 (1983).
20. J.M. Holland and D.W. Jones. J. Chem. Soc. Perkin Trans. 1, 927 (1973).
21. L.D. Quin, J.P. Gratz, and J. Barket. J. Org. Chem. **33**, 1034 (1968).
22. R. Bodalski, K.M. Pietrusiewicz, and J. Koszuk. Tetrahedron, **31**, 1907 (1975).
23. D.A. Campbell and J.C. Bermak. J. Org. Chem. **59**, 658 (1994).
24. G. Kohler and C. Milstein. Nature (London), **256**, 495 (1975).
25. J.M. Bidlack and P.C. Mabie. J. Immunol. Meth. **91**, 157 (1986).
26. S.D. Taylor, C.C. Kotoris, A.N. Dinaut, and M.-J. Chen. Tetrahedron, **5**4 1691 (1998).
27. A.F. Habeeb. Anal. Biochem. **14**, 328 (1966).
28. R.J. Leatherbarrow. GraFit Version 3.0, Erithacus Software Ltd., Staines, U.K. 1992.
29. J.S. Lee, M.L. Woodsworth, and L.J.P. Latimer. Biochemistry, **23**, 3277 (1984).
30. J.S. Lee, D.F. Dombrowski, and T.R. Mosmann. Biochemistry, **21**, 4940 (1982).

© 2000 NRC Canada

Efficient method for the preparation of pinacols derived from aromatic and aliphatic ketones by using low-valent titanium reagents in dichloromethane–pivalonitrile

Akifumi Kagayama, Koji Igarashi, and Teruaki Mukaiyama

Abstract: The reductive coupling reaction of aldehydes and ketones, including unsymmetrical aliphatic ketones, proceeded smoothly to give the corresponding pinacols in good to high yields under mild conditions by using combination of titanium(II) chloride and zinc or titanium(IV) chloride and zinc in dichloromethane–pivalonitrile. *Meso*-selective formation of the coupling products was observed in the cases of some aliphatic ketones. The diastereoselectivities of coupling products depend on both difference of bulkiness of 2-, and 2′-substituents of carbonyl group of the reactant, and overall steric effect around the carbonyl groups.

Key words: diastereoselective pinacol reaction, dichloromethane-pivalonitrile, titanium(II) chloride, titanium(IV) chloride, zinc.

Résumé : La réaction de couplage réducteur d'aldéhydes ou des cétones, y compris des cétones aliphatiques non symétriques, se produit facilement et elle conduit aux pinacols correspondants avec des rendements allant de bons à élevés, dans des conditions douces, en opérant dans un mélange de dichlorométhane et de pivalonitrile en présence de zinc et de chlorure de titane(II) ou de chlorure de titane(IV). On a observé une formation sélective de l'isomère *méso* dans les cas de quelques cétones aliphatiques. Les diastéréosélectivités des produits de couplage dépendent de la différence de taille des substituants en positions 2 et 2′ par rapport au groupe carbonyle qui réagit ainsi que de l'effet stérique global autour des groupes carbonyles.

Mots clés : réaction pinacolique diastéréosélective, dichlorométhane-pivalonitrile, chlorure de titane(II), chlorure de titane(IV), zinc.

[Traduit par la Rédaction]

Introduction

The reductive coupling of carbonyl compounds using low-valent metal species has been known as pinacol coupling reaction since last century. In 1973, two research groups, Mukaiyama (1*a*) and Tyrlik (1*b*), independently reported this coupling reaction and its subsequent deoxygenation reaction that afforded olefin with low-valent titanium species. In the above two methods, the former used either combination of $TiCl_4$ and Zn, or $TiCl_4$ and $LiAlH_4$, and the latter employed the combination of $TiCl_3$ and Mg for the generation of active low-valent species. McMurry and co-workers studied this coupling reaction in detail by using either $TiCl_3$ and $LiAlH_4$, or $TiCl_3$ and Zn-Cu from 1974 (1*c*). The coupling reactions using other transition metals as a reducing reagent have been extensively studied in this decade (2).

Concerning intermolecular type pinacol reactions, recent topics are directed to investigate the formation of C_2 or S_2 symmetric homocoupling products with high diastereoselectivities (*dl* or *meso*) under mild conditions. In the cases of aromatic aldehydes, for example, the corresponding homocoupling products were afforded with high *dl*-selectivities when several kinds of low-valent metals such as Ti (3), Sm (4), and Nb (5) were used.[2] Further, it was recently reported that *dl*-homocoupling product was preferentially formed from acetophenone by the combined use of a $TiCl_3$–Mg–catechol system (7).

This *dl*-selection was explained by assuming the generation of intermediate radical species as sketched in Scheme 1, in which oxygen atoms of two ketyl radicals are placed side by side and phenyl groups are arranged *anti* to each other to minimize the steric interaction when these ketyl radicals approach each other. The location of two oxygen atoms was controlled by the interaction between metal on the ketyl radical and oxygen atom of the other ketyl radical, and (or)

Received August 12, 1999. Published on the NRC Research Press website on May 19, 2000.

This paper is dedicated to Professor Stephan Hanessian on the occasion of his 65th birthday in recognition of his significant contributions to the art of organic synthesis.

A. Kagayama, K. Igarashi, and T. Mukaiyama.[1]
Department of Applied Chemistry, Faculty of Science, Science University of Tokyo, Kagurazaka, Shinjuku-ku, Tokyo 162–8601, Japan.

[1]Author to whom correspondence may be addressed. Telephone: +81-3-3260-4271. Fax: +81-3-3235-2214. e-mail: mukaiyam@rs.kagu.sut.ac.jp.

[2]Stereoselective pinacol coupling reactions using a catalytic amount of low-valent metal were recently reported; see ref 6.

© 2000 NRC Canada

bridged two metal atoms. However, there has been no systematic study on relationship between the diastereoselectivities of coupling products and the steric effects of substituents at 2- and 2′-positions of carbonyl group of the reactants.

To investigate this subject, it is appropriate to examine the coupling reaction of unsymmetrical aliphatic ketones; however, in this reductive coupling, the reactivities of aliphatic ketones are generally low and the required severe reaction conditions cause pinacol rearrangement or deoxygenation of the initially produced pinacol to form the corresponding olefins.

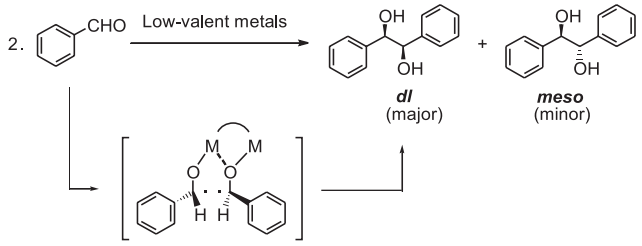
Recently, we found that pinacol coupling reaction of aliphatic ketones proceeded smoothly in dichloromethane–pivalonitrile by using the combination of titanium(II) chloride and zinc at room temperature (8). Further, usefulness of $TiCl_2$ was demonstrated in the following experiment, i.e., in our total synthesis of antitumor agent Taxol (9), construction of the A ring onto the BC ring system was performed by intramolecular pinacol coupling reaction using low-valent titanium species prepared in situ from $TiCl_2$–$LiAlH_4$. Though a similar reaction was observed by the combined use of $TiCl_3$–$LiAlH_4$, the generation of low-valent titanium species took place in less acidic media when the former combination was employed. The titanium(II) reagent, $TiCl_2$, is facilely prepared from $TiCl_4$ and hexamethyldisilane according to the reported procedure (10), and it can be stored under argon atmosphere for a long time.[3] In this article, we would like to describe the relationship between the diastereoselectivities of coupling products and the steric effects of substituents at 2-, and 2′-positions of carbonyl group of the reactants in the pinacol coupling reaction by using $TiCl_2$ and Zn. The results obtained by further examination of this type of coupling reaction using a combination of $TiCl_4$ and Zn are also discussed herein.

Results and discussion

Acetophenone was reductively coupled by using $TiCl_2$ and Zn in THF at 0°C to give 2,3-diphenyl-2,3-butanediol in 93% yield (*dl*:*meso* = 76:24) while 4-phenyl-2-butanone did not react under the same reaction conditions. Porta et al. reported that $TiCl_3$ could reduce benzaldehyde in dichloromethane to afford the corresponding pinacol though the same reaction did not proceed in THF which is commonly employed solvent in these reactions (3b). Actually, 4-phenyl-2-butanone was reductively coupled by using the combination of $TiCl_2$–Zn in dichloromethane and the desirable pinacol was obtained in 23% yield and 65% of the 4-phenyl-2-butanone was recovered.

Although several additives such as pyridine (12) and HMPA (13) used to be known effective in this coupling reaction, these two additives and 2-methyloxazoline were not effective for the present reaction when the combination of $TiCl_2$ and Zn system was used (0, 0, and 13% yields, respectively). On the other hand, it was found that nitriles, especially pivalonitrile, accelerated this reaction to give the pinacol in 63% yield by using 2 molar equivalents of $TiCl_2$ and Zn. Finally, it was found that the yield was improved up to 87% when 2 molar equivalents of $TiCl_2$ were gradually added to the reaction mixture for the duration of the 6 h period in the presence of Zn and pivalonitrile at room temperature. When acetonitrile or *o*-methoxybenzonitrile was used as a co-solvent in the above reaction, the corresponding pinacol was obtained in 78 or 52% yield, respectively. Fürstner and Hupperts demonstrated the beneficial effect of a cyano function tethered to a chlorosilane on the reductive coupling reaction using a catalytic amount of $TiCl_3$–Zn–chlorosilane system in their indole synthesis reaction (15).

Scheme 1.



These results indicate that nitriles moderately coordinate to the low-valent titanium species to form the active complexes, which helps both the solvation of the titanium particles and electron donation of the titanium complex to the carbonyl compounds.[4,5] On the other hand, other additives (pyridine, HMPA, and 2-methyloxazoline) coordinate too strongly to the low-valent titanium species, which result in the decreased reactivities.

Yields and diastereoselectivities of the pinacol coupling reactions using several ketones and aldehydes are summarized in Table 1. Aromatic ketones were transformed to the corresponding pinacols in high yields with *dl*-selectivies (Entries 1–5) though the selectivity in case of acetophenone was rather low in comparison with the reported one (7). This *dl*-selectivity increased either when electron-donating group substituted benzaldehyde derivatives or carbonyl compound with bulky group at the 2-position were used, that is, the diastereoselectivity came up kinetically. This consideration may be supported by the results that no diastereoselectivity was observed in the case of highly reactive benzaldehyde while moderate selectivity was observed in the reaction of less reactive 3-phenylpropanal (Entries 11 and 12).

In the reactions of aliphatic ketones (Entries 6–10), the corresponding pinacols were obtained in good to high yields except for 3,3-dimethyl-2-butanone. The diastereoselectivity was not observed when 4-phenyl-2-butanone was used as a substrate that has a set of methyl and methylene groups attached to 2- and 2′-positions of carbonyl group of the reactant (Entry 6). On the other hand, the *meso*-selective reaction took place when substrates that have two dimensionally different substituents, i.e., the respective combination of

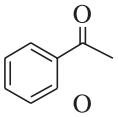
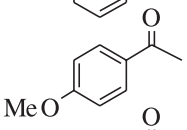
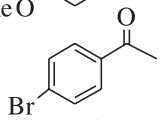
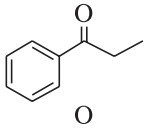
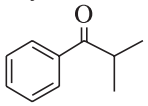
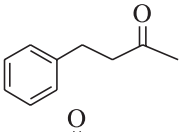
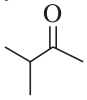
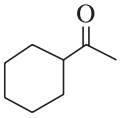
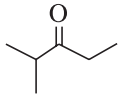
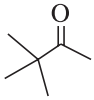
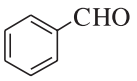
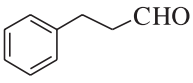
[3] A few types of titanium(II) chloride complexes were used for pinacol coupling reactions, which were carried out only in ethers such as $TiCl_2$·LiCl (11a) or $TiCl_2(thf)_2$·xLiCl (11b).

[4] Actually, on ^{13}C NMR spectra, signals of pivalonitrile (δ: 27.5, 27.8 and 125.3 ppm) shifted and broadened (δ: 24.8, 31.0 and 131.3 ppm) by addition of 1/3 molar equivalent of $TiCl_2$ in chloroform-*d* at room temperature. This result indicates the formation of coordinated complex.

[5] Structural data on the coordination of nitriles onto low-valent titanium are shown in ref 14. Fowles and Lester reported the structure of isolated polymeric titanium(II) complexes as TiX_2·$2CH_3CN$ (14*b*).

© 2000 NRC Canada

Table 1. Yields and selectivities of the formation of pinacols from various ketones and aldehydes.

Entry	Ketone	Method [a]	Yield / %	*dl* : *meso* [b]
1		A	93 (98) [c]	71:29 (72:28) [c]
2		A	93	79:21
3		A	90	66:34
4		A	94	68:32
5		A	83	98:2
6		B	87 (44) [d]	50:50 (50:50) [d]
7		B	90 (44) [d]	39:61 (36:64) [d]
8		B	87	35:65
9		B	61	23:77
10		B	trace	—
11		A	88	47:53
12		A	95	67:33

[a] A=ketone:$TiCl_2$:Zn=1:1:1. B=ketone:$TiCl_2$:Zn=1:2:2.

[b] Ratios determined by ^1H NMR analysis of crude reaction mixture

[c] Method B, $TiCl_2$ 1.2 equiv.

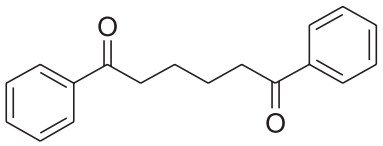
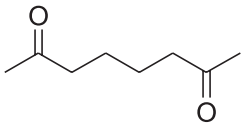
[d] Method A, $TiCl_2$ 1 equiv.

methyl and methyne (Entries 7 and 8), or methylene and methyne (Entry 9) groups, were used.

McMurry and Siemers studied intramolecular pinacol coupling reaction of several dialdehydes, in which the relationship between the diastereoselectivities and the ring number of products was examined in detail (16). In the present experiment, two types of diketones were examined (Table 2), and the selectivity decreased a little in the case of aliphatic diketone while aromatic diketone reacted in perfect *cis*-selective manner. It suggested that the interaction

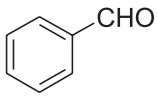
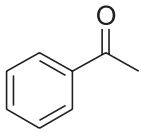
© 2000 NRC Canada

Table 2. Yields and selectivities of the formation of 1,2-cyclohexanediol derivatives from diketones.

Entry	Diketone	Method [a]	Yield / %	*cis:trans* [b]
1		A	71	>99:1
2		B	70	95:5

[a] A= ketone:$TiCl_2$:Zn=1:1:1, B=ketone:$TiCl_2$:Zn=1:2:2.
[b] Ratios determined by ^{1}H NMR analysis of crude reaction mixture.

Table 3. Yields and selectivities of pinacol coupling reactions without using zinc metal.[a]

Entry	Carbonyl compound	Yield / %	*dl:meso* [b]
1		36	90:10
2		47	>99:1

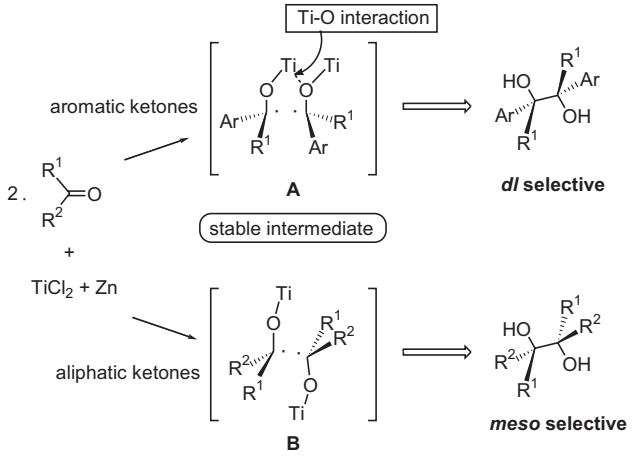
[a] Conditions: ketone:$TiCl_2$:pivalonitrile=1:1:4, rt., 12h.
[b] Ratios determined by ^{1}H NMR analysis of crude reaction mixture.

between Ti and oxygen would be rather weak in the case of aliphatic ketone than that of aromatic ketone.

Benzaldehyde and acetophenone were reductively coupled by using $TiCl_2$ in the absence of Zn (Table 3). Though the yields were rather low, *dl*-selectivities became very much higher than those of the reaction when a $TiCl_2$–Zn system was applied. These results may be explained by considering the kinetic effect and the Lewis acidity of titanium species which may also influence the above diastereoselectivities (see Scheme 1). The higher-valent metal behaved as a stronger Lewis acid compared with the lower-valent one, so that, in the absence of Zn, the Ti(III) atom on the ketyl radical (formed from $TiCl_2$ and the carbonyl compound) is coordinated more strongly to build a Ti-bridging intermediate (3b) (17) compared with Ti(I) (or Ti(II)) atom on the ketyl radical existed in the reaction using the $TiCl_2$–Zn system.

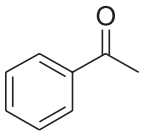
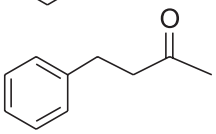
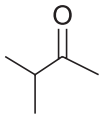
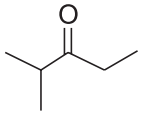
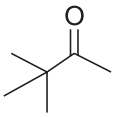
From these results, the mechanism of diastereoselection in the present reaction may be explained as shown in Scheme 2. When isobutyrophenone is used, the generated ketyl radical species form an intermediate Ti-bridging complex **A**, which is in turn connected to *dl*-products. When other aromatic ketones are used, more highly reactive ketyl radicals would be generated because these compounds are less hindered compared to isobutyrophenone. Therefore,

Scheme 2.



© 2000 NRC Canada

Table 4. Pinacol coupling reaction of ketones by using combinations of equimolar amounts of $TiCl_x$ and Zn.

Entry	Substrate	Yield (%) [*dl*:*meso*]	
		$TiCl_2 + Zn$	$TiCl_4 + 2{\cdot}Zn$
1		93 [71:29] [a]	97 [84:16] [a]
2		44 [50:50] (87 [50:50]) [b]	86 [50:50]
3		44 [36:64] (90 [39:61]) [b]	88 [35:65]
4		—— (61 [23:77]) [b]	59 [25:75] (78 [24:76]) [b]
5		trace [b]	trace [b]

[a] Carried out at 0°C.
[b] 2 equiv. of $TiCl_x$ was used for ketones.

other pathways to be connected to *meso*-products can be assumed to exist in addition to that mentioned above and relatively lower stereoselectivities were observed. On the other hand, in the cases of aliphatic ketones, the highly symmetrical intermediate **B**, a pair of two ketyl radicals, is formed to preferentially produce *meso*-pinacol because these radical species would be relatively unstable and the interaction between titanium and oxygen atoms in the intermediate would be rather weak.

It is noted that the selectivity depends on the difference of bulkiness of the 2- and 2′-substituents of the carbonyl group of the reactants and the overall steric interaction around the carbonyl group.

Application of $TiCl_4$ instead of $TiCl_2$ was studied in this type of reaction in dichloromethane–pivalonitrile. So far many kinds of low-valent titanium reagents have been generated from $TiCl_3$ rather than from $TiCl_4$ because the latter is coordinated so strongly by THF which has been generally considered as the most effective solvent for reductive coupling reaction. Concerning the reaction using low-valernt titanium reagent generated from $TiCl_4$ and Zn in THF, Mukaiyama et al. reported that aliphatic aldehydes or ketones were reduced to give the corresponding pinacols at rather high temperatures (1*a*). Therefore, it was considered that the highly active low-valent titanium species giving the corresponding olefin could only be generated from $TiCl_3$.

Since the present reaction proceeded at room temperature in dichloromethane–pivalonitrile by using the $TiCl_2$–Zn system, the similar reactions using $TiCl_3$ or $TiCl_4$ were also tried under the same reaction conditions. While a system ($TiCl_3$ and 1.5 equivalents Zn) in dichloromethane–pivalonitrile did not reduce the 4-phenyl-2-butanone, a system ($TiCl_4$ and 2 equivalents Zn) produced the desired coupling product in 86% yield.

Titanium(IV) chloride did not react with Zn in dichloromethane solvent; however, the addition of pivalonitrile to this mixture induced the generation of low-valent titanium species in which the gray suspension turned to dark blue, and then to dark brown. On the other hand, when acetonitrile was used as a co-solvent, the mixture of generated low-valent titanium species was not homogeneous and the yield of pinacol originated from 4-phenyl-2-butanone decreased to 24%. These results indicate that pivalonitorile would increase the solubility of generated low-valent titanium species by forming a soluble complex and the polarity of the reaction media to help both electron-transfer reaction.[6]

The yields and diastereoselectivities of the pinacols formed from several ketones by using $TiCl_4$–Zn are summarized in

[6] It is generally known that the nitriles are one of the most popular solvents for the electrochemical studies

© 2000 NRC Canada

Table 4, together with the results using $TiCl_2$–Zn. These reactions employing equimolar amount of $TiCl_4$ proceeded smoothly to give several coupling products of aliphatic ketones in high yields except 3,3-dimethyl-2-butanone. Since the generated low-valent titanium species from $TiCl_4$ was more soluble in the above solvent, results obtained here were better than those using $TiCl_2$.

Summary

The reductive coupling reactions of various ketones and aldehydes including aliphatic unsymmetrical ketones proceeded under mild conditions by using $TiCl_2$–Zn or $TiCl_4$–Zn in dichloromethane–pivalonitrile. It was also shown that the diastereoselectivities of coupling products depend not only on the difference of bulkiness of 2-, and 2′-substituents of carbonyl group of the reactants, but also on overall steric effect around the carbonyl groups.

Experimental Section

General

Melting points were recorded on a Yanaco MP-S3 micro melting point apparatus. Elemental analyses were performed by MC Research Center Inc. FT-IR spectra were recorded on a Horiba FT-300 infrared spectrometer. ^1H- and ^{13}C NMR spectra were recorded on a JEOL JNM-EX270L, a JEOL JNM-LA400, and a JEOL JNM-LA500 spectrometer using tetramethylsilane (TMS) or chloroform-*d* ($CDCl_3$) as internal standard. The following abbreviations are used: s = singlet, d = doublet, t = triplet, q = quartet, m = multiplet, and br = broad. High-resolution mass spectra were recorded on a JEOL JMS-SX102A instrument with 4-nitrobenzyl alcohol as a matrix. Thin layer chromatography used routinely for purification and separation of product mixtures was performed on Wakogel B5F. Analytical thin layer chromatography was performed using E. Merck 0.25 mm silica gel 60 F254 plates, and visualization was accomplished with ethanolic phosphomolybdic acid. All reactions were carried out under argon atmosphere in dried glassware. Dichloromethane and pivalonitrile were distilled from diphosphorus pentoxide, then calcium hydride, and dried over MS 4A. All substrates were purchased from Tokyo Kasei Kogyo, Kanto Chemical, Aldrich Chemical, or Merck. Ketones and aldehydes were used after purification by distillation. 1,4-Dibenzoylbutane and 2,6-octanedione were used as received.

Titanium(II) chloride was prepared by Nalura's procedure (9). Anal. calcd. for $TiCl_2$: Ti 40.31, Cl 59.69; found: Ti 39.89, Cl 59.28. Zinc powder (Kanto Chemical) was activated by 1 N HCl, washed with distilled water and ether successively, and dried in vacuo.

Typical procedure for the reductive titanium(II) chloride and zinc in dichloromethane with pivalonitrile:

Method A

To a suspension of $TiCl_2$ (59 mg, 0.5 mmol) and activated Zn powder (32 mg, 0.5 mmol) in CH_2Cl_2 (2.5 mL) was added ^{t}BuCN (0.22 mL, 2 mmol). After the resulting dark brown suspension was cooled to 0°C, a solution of acetophenone (60 mg, 0.5 mmol) in CH_2Cl_2 (1.3 mL) was added dropwise. Once TLC analysis indicated that all of the ketone had been consumed (<16 h), saturated aqueous NH_4Cl was added to the reaction mixture. The reaction mixture was filtered, and the filtrate was separated. The aqueous portion was extracted with CH_2Cl_2 (4 mL × 3), and combined organic layers were washed successively with a saturated aqueous $NaHCO_3$ and brine, and dried over Na_2SO_4, filtered, and concentrated. The crude product was subjected to thin-layer chromatography (hexane – ethyl acetate) to afford the desired pinacol (56 mg, 93%).

Method B

To a gray suspension of activated Zn powder (65 mg, 1 mmol) and ^{t}BuCN (0.44 mL, 4 mmol) in CH_2Cl_2 (2.5 mL) was added a solution of 4-phenyl-2-butanone (74 mg, 0.5 mmol) in CH_2Cl_2 (1.3 mL). After stirring for 30 min, $TiCl_2$ (119 mg, 1 mmol) was added gradually (divided in 6 times at interval of 1 h) under argon by powder inlet equipped to the reaction apparatus. The resulting mixture was stirred for an additional 1 h, and then saturated aqueous NH_4Cl was added. The same work up as method A gave the desired pinacol (65 mg, 87%).

Typical procedure for the reductive coupling reaction of ketones using titanium(IV) chloride and zinc in dichloromethane with pivalonitrile

To a gray suspension of $TiCl_4$ (95 mg, 0.5 mmol) and activated Zn powder (65 mg, 1 mmol) in CH_2Cl_2 (2.5 mL) was added ^{t}BuCN (0.22 mL, 2 mmol) dropwise. After the resulting dark brown suspension was stirred for 30 min, a solution of 4-phenyl-2-butanone (74 mg, 0.5 mmol) in CH_2Cl_2 (1.3 mL) was added. The reaction mixture was stirred for 16 h at room temperature and then saturated aqueous NH_4Cl was added. The same work up as above procedure gave the desired pinacol (64 mg, 86%).

Diastereoselectivities of pinacols

400 MHz ^1H NMR spectra assignments were used for the determination of the *dl*:*meso* ratio of the crude pinacols obtained.

meso- *and* dl-*2,3-Diphenyl-2,3-butanediol* (***18***): Colorless solid; ^1H NMR ($CDCl_3$) δ: 1.48 (6H, s, CH_3, *dl*), 1.57(6H, s, CH_3, *meso*), 2.36 (2H, br, OH, *meso*), 2.63 (2H, br, OH, *dl*), 7.24–7.15 (20H, m, Ph-H). Assignments were made by comparing the relative heights of methyl signals at δ 1.48 and δ 1.57, respectively.

meso- *and* dl-*2,3-Bis(4-methoxyphenyl)-2,3-butanediol* (***17***): Colorless solid; ^1H NMR ($CDCl_3$) δ: 1.45 (6H, s, CH_3, *dl*), 1.54 (6H, s, CH_3, *meso*), 2.35 (2H, br, OH, *meso*), 2.64 (2H, br, OH, *dl*), 3.78 (6H, s, OCH_3, *meso*), 3.79 (6H, s, OCH_3, *dl*), 6.75–7.11 (16H, m, Ph-H). Assignments were made by comparing the relative heights of methyl signals at δ 1.45 and δ 1.54, respectively.

meso- *and* dl-*2,3-Bis(4-bromophenyl)-2,3-butanediol* (***17***): Colorless solid; ^1H NMR ($CDCl_3$) δ: 1.45 (6H, s, CH_3, *dl*), 1.53 (6H, s, CH_3, *meso*), 2.28 (2H, br, OH, *meso*), 2.60 (2H, br, OH, *dl*), 7.02–7.36 (16H, m, Ph-H). Assignments were made by comparing the relative heights of methyl signals at δ 1.45 and δ 1.53, respectively.

© 2000 NRC Canada

meso- *and* dl-*3,4-Diphenyl-3,4-hexanediol (**19**)*: Colorless solid; ^{1}H NMR ($CDCl_3$) δ: 0.59 (6H, dd, *J* = 7.3, 7.3 Hz, CH_3, *meso*), 0.60 (6H, dd, *J* = 7.3, 7.3 Hz, CH_3), 1.59 (2H, dq, *J* = 7.3, 14.3 Hz, CH_2, *meso*), 1.71 (2H, dq, *J* = 7.3, 14.3Hz, CH_2), 2.07 (2H, dq, *J* = 7.3, 14.3Hz, CH_2), 2.13 (2H, br, OH, *meso*), 2.60 (2H, br, OH), 2.27 (2H, dq, *J* = 7.3, 14.3 Hz, CH_2, *meso*), 7.28–7.15 (20H, m, Ph-H). Assignments were made by comparing the relative areas of methylene signals at δ 1.71 and δ 1.59, respectively.

meso- *and* dl-*2,5-Dimethyl-3,4-diphenyl-3,4-hexanediol (**19**)*: Colorless solid; ^{1}H NMR ($CDCl_3$) δ: 0.39 (6H, d, *J* = 6.9 Hz, CH_3, *dl*), 0.67 (6H, d, *J* = 6.9 Hz, CH_3, *meso*), 0.75 (6H, d, *J* = 6.6 Hz, CH_3, *meso*), 1.22 (6H, d, *J* = 6.3 Hz, CH_3, *dl*), 1.78 (2H, sep, *J* = 6.6 Hz, CH, *dl*), 2.30 (2H, sep, *J* = 6.9 Hz, CH, *meso*), 2.84 (2H, s, OH, *dl*), 2.95 (2H, s, OH, *meso*), 7.45–7.23 (20H, m, Ph-H). Assignments were made by comparing the relative areas of methyl signals at δ 0.39 and δ 0.67, respectively.

meso- *and* dl-*3,4-Dimethyl-1,6-diphenyl-3,4-hexanediol (**6a**)*: Colorless oil; IR (neat) ν: 3432, 3024, 2954, 2924, 1604, 1496, 1450, 1373, 1111, 1056, 949, 748, 702 cm^{-1}; ^{1}H NMR ($CDCl_3$) δ: 1.25 (6H, s, CH_3), 1.28 (6H, s, CH_3), 1.64–1.74 (4H, m, CH_2), 1.87–1.98 (4H, m, CH_2), 2.05 (4H, br, OH), 2.64–2.72 (4H, m, CH_2), 2.76–2.85 (4h, m, CH_2), 7.15–7.30 (20H, m, Ph-H); ^{13}C NMR ($CDCl_3$) δ: 20.8, 21.1, 30.2, 30.3, 38.2, 38.5, 76.98, 125.7, 128.1, 128.37, 128.40, 142.6, 142.7; HRMS ([M + Na]$^+$): calcd for $C_{20}H_{26}O_2Na$: 321.1831; found: 321.1847. Diastereomeric ratio (50:50) was determined from the two equivalent methyl signals at 1.25 and δ 1.28 in the ^{1}H NMR spectrum of the crude product. It was supported that almost equivalent amounts of two isomers of 2,2-dimethyl-1,3-dioxolane derivatives were obtained from acetonide protection described below.

cis- *and* trans-*2,2-Dimethyl-4,5-bis(3-phenylethyl)-1,3-dioxolane*: To a solution of *meso*- and *dl*-3,4-Dimethyl-1,6-diphenyl-3,4-hexanediol (50 mg, 0.17 mmol) in CH_2Cl_2 (2 mL) and 2,2-dimethoxypropane (4 mL) at 0°C was added CSA (28 mg, 0.12 mmol). After the reaction mixture had been stirred for 16 h at room temperature, triethylamine (0.3 mL) was added. After evaporation of the solvent, the thin-layer chromatography to afford *cis*- and *trans*-2,2-dimethyl-4,5-*bis*(3-phenylethyl)-1,3-dioxolane. *cis*-Isomer (26 mg, 45%): colorless oil; IR (neat) ν: 3062, 2993, 2939, 2870, 1604, 1496, 1458, 1373, 1211, 1111, 1065, 1011, 895, 841, 748, 701, 517 cm^{-1}; ^{1}H NMR ($CDCl_3$) δ: 1.29 (6H, s, CH_3), 1.54 (6H, s, CH_3), 1.64 (2H, ddd, *J* = 4.9, 5.0, 13.1 Hz, CH_2), 2.11 (2H, ddd, *J* = 4.2, 4.2, 13.1 Hz, CH_2), 2.73 (2H, ddd, *J* = 4.2, 5.0, 13.2 Hz, CH_2), 2.87 (2H, ddd, *J* = 4.2, 4.9, 13.2 Hz, CH_2), 7.20–7.37 (10H, m, Ph-H); ^{13}C NMR ($CDCl_3$) δ: 19.5, 29.6, 30.2, 38.9, 84.7, 106.6, 125.8, 128.3, 128.4, 142.7; HRMS ([M + Na]$^+$): calcd for $C_{23}H_{30}O_2Na$: 361.2144; found: 361.2158. *trans*-Isomer (24 mg, 42%): colorless oil; IR (neat) ν: 3062, 2985, 2939, 2870, 1743, 1604, 1496, 1458, 1373, 1219, 1180, 1065, 1011, 895, 841, 748, 701, 525 cm^{-1}; ^{1}H NMR ($CDCl_3$) δ: 1.33 (6H, s, CH_3), 1.49 (3H, s, CH_3), 1.51 (3H, s, CH_3), 1.57 (ddd, *J* = 4.9, 5.1, 13.1 Hz, 2H, CH_2), 1.99 (ddd, *J* = 4.1, 4.4, 13.1 Hz, 2H, CH_2), 2.70 (ddd, *J* = 4.4, 5.1, 13.1 Hz, 2H, CH_2), 2.81 (ddd, *J* = 4.1, 4.9 Hz, 2H, CH_2), 7.07–7.35 (10H, m, Ph-H); ^{13}C NMR ($CDCl_3$) δ: 19.5, 29.6, 29.8, 30.4, 38.1, 38.9, 84.7, 106.7, 125.8, 128.3, 128.4, 142.5; HRMS ([M + Na]$^+$): calcd for $C_{23}H_{30}O_2Na$: 361.2144; found: 361.2113.

meso- *and* dl-*2,3,4,5-Tetramethyl-3,4-hexanediol (**20**)*: Colorless oil. Anal. calcd. for $C_{10}H_{22}O_2$: C 68.92, H 12.72; found: C 69.30, H 12.30. Assignments were made by comparing the relative heights of methyl signals at δ 1.14 and δ 1.15, respectively. Separation of the pure isomers from crude reaction mixture was achieved by benzylidene protection,[7] thin-layer chromatography (hexane – ethyl acetate), and cleavage of the protecting group as described below.

*(4*R,*5*RS*)- and (2*R,*4*RS,*5*SR*)-4,5-Diisopropyl-4,5-dimethy-2-phenyl-1,3-dioxolane*: To a solution of *meso*- and *dl*-2,3,4,5-tetramethyl-3,4-hexanediol (50 mg, 0.29 mmol) in CH_2Cl_2 (2 mL) and α,α-dimethoxytoluene (175 mg, 1.2 mmol) at 0°C was added CSA (35 mg, 0.15 mmol). After the reaction mixture had been stirred for 16 h at room temperature, triethylamine (0.5 mL) was added. After evaporation of the solvent, the crude product was purified by the thin-layer chromatography to afford (4*RS*,5*RS*)- and (2*R*,4*RS*,5*SR*)[8]-4,5-diisopropyl-4,5-dimethy-2-phenyl-1,3-dioxolane.

*(4*RS,*5*RS*)-Isomer (27 mg, 36%)*: Colorless oil; IR (neat) ν: 3062, 2970, 2877, 1466, 1381, 1219, 1095, 1026, 895, 702 cm^{-1}; ^{1}H NMR ($CDCl_3$) δ: 0.91 (3H, d, *J* = 7.0 Hz, CH_3) 0.93 (3H, d, *J* = 7.0 Hz, CH_3), 0.95 (3H, d, *J* = 6.6 Hz, CH_3), 1.07 (3H, d, *J* = 6.6 Hz, CH_3), 1.22 (3H, s, CH_3), 1.25 (3H, s, CH_3), 2.15 (1H, qq, *J* = 7.0, 6.6 Hz, CH), 2.26 (1H, qq, *J* = 7.0, 6.6 Hz, CH), 5.85 (1H, s, CHPh), 7.30–7.37 (3H, m, Ph-H), 7.46–7.49 (2H, m, Ph-H); ^{13}C NMR ($CDCl_3$) δ: 13.3, 15.9, 19.1, 19.2, 19.5, 19.8, 31.5, 32.9, 88.1, 88.2, 98.6, 126.5, 128.1, 128.5, 139.9; HRMS ([M + Na]$^+$): calcd for $C_{17}H_{26}O_2Na$: 285.1831; found: 285.1872.

*(2*R,*4*RS,*5*SR*)-Isomer (16 mg, 21%)*: Colorless oil; IR (neat) ν: 3060, 2978, 2877, 1458, 1381, 1219, 925, 864, 725 cm^{-1}; ^{1}H NMR ($CDCl_3$) δ: 0.90 (6H, d, *J* = 6.1 Hz, CH_3), 0.92 (6H, d, *J* = 6.2 Hz, CH_3), 1.22 (6H, s, CH_3), 2.17 (2H, qq, *J* = 6.1, 6.2 Hz, CH), 5.93 (1H, s, CHPh), 7.29–7.36 (3H, m, Ph-H), 7.48 (2H, m, Ph-H); ^{13}C NMR ($CDCl_3$) δ: 14.9, 19.1, 19.6, 31.3, 87.8, 98.6, 126.1, 128.0, 128.1, 140.0; HRMS ([M + Na]$^+$): calcd for $C_{17}H_{26}O_2Na$: 285.1831; found: 285.1799.

dl-*2,3,4,5-Tetramethyl-3,4-hexanediol*: To a solution of (4*RS*,5*RS*)-4,5-diisopropyl-4,5-dimethyl-2-phenyl-1,3-dioxolane (27 mg, 0.10 mmol) in EtOH (2 mL) was added $Pd(OH)_2$ (14 mg, 0.10 mmol) under an argon atmosphere. Hydrogen gas was purged through the mixture and stirred for 1 h. The reaction mixture was filtered and evaporated. Thin-layer chromatography afforded *dl*-2,3,4,5-tetramethyl-3,4-hexanediol (17 mg, 0.097 mmol, 97%). Colorless solid; mp 45–47°C; IR (neat) ν: 3471, 2993, 2962, 2915, 1466, 1381, 1173, 1118, 1072, 1018, 918, 887, 594 cm^{-1}; ^{1}H NMR ($CDCl_3$) δ: 0.99 (6H, d, *J* = 6.7 Hz, CH_3), 1.00 (6H, d, *J* = 6.4 Hz,

[7] The acetonide protection for 2,3,4,5-tetramethyl-3,4-hexanediol was tried, but the corresponding 2,2-dimethyl-1,3-dioxolane derivatives were not obtained at all.

© 2000 NRC Canada

CH_3), 1.15 (6H, s, CH_3), 1.75 (2H, br, OH), 2.09 (2H, qq, *J* = 6.7, 6.4 Hz, CH); ^{13}C NMR ($CDCl_3$) δ: 18.7, 19.1, 19.8, 33.7, 79.1. Anal. calcd. for $C_{10}H_{22}O_2$: C 68.92, H 12.72; found: C 68.88, H 12.71.

meso-*2,3,4,5-Tetramethyl-3,4-hexanediol*: This isomer was obtained from (2*R*,4*RS*,5*SR*)-4,5-diisopropyl-4,5-dimethy-2-phenyl-1,3-dioxolane by the same procedure as the case of *dl* -isomer in 92% yield. Colorless solid; mp 62–64°C; IR (neat) ν: 3417, 2969, 2908, 1466, 1389, 1165, 1103, 1033, 1003, 918, 895, 517 cm^{-1}; ^1H NMR ($CDCl_3$) δ: 0.96 (6h, d, *J* = 7.0 Hz, CH_3), 1.03 (6H, d, *J* = 6.7 Hz, CH_3), 1.14 (6H, s, CH_3), 2.02 (2H, qq, *J* = 6.7, 7.0 Hz, CH), 2.28 (2H, br, OH); ^{13}C NMR ($CDCl_3$) δ: 19.0, 19.7, 20.6, 33.2, 79.2. Anal. calcd. for $C_{10}H_{22}O_2$: C 68.92, H 12.72; found: C 68.96, H 12.59.

meso- *and* dl-*2,3-Dicyclohexyl-2,3-butanediol*: Colorless solid. Anal. calcd. for $C_{16}H_{30}O_2$: C 75.54, H 11.89; found: C 75.78, H 11.52. Assignments were made by comparing the relative heights of methyl signals at δ 1.14 and δ 1.15, respectively. Separation of the pure isomers from crude reaction mixture was achieved by the same method as the case of 2,3,4,5-tetramethyl-3,4-hexanediol.

*(4*RS,*5*RS*)- and (2*R,*4*RS,*5*SR*)-4,5-Dicyclohexyl-4,5-dimethy-2-phenyl-1,3-dioxolane*: These two isomers were obtained from *meso*- and *dl*-2,3-dicyclohexyl-2,3-butanediol:

*(4*RS,*5*RS*)-Isomer (29% yield)*: Colorless oil; IR (neat) ν: 3062, 2954, 2854, 1689, 1450, 1381, 1296, 1103, 1072, 1026, 926, 887, 764, 710 cm^{-1}; 1H NMR($CDCl_3$) δ: 0.96–1.33 (10H, m, CH_2) 1.24 (3H, s, CH_3), 1.27 (3H, s, CH_3), 1.69–1.88 (10H, m, CH_2), 1.99–2.02 (2H, m, CH), 5.82 (1H, s, CHPh), 7.30–7.37 (3H, m, Ph-H), 7.46–7.48 (2H, m, Ph-H); ^{13}C NMR($CDCl_3$) δ 14.7, 17.6, 26.67, 26.74, 26.9, 27.1, 28.6, 28.8, 29.9, 30.3, 42.9, 44.0, 87.9, 88.0, 98.7, 126.6, 128.1, 128.6, 139.8; HRMS ($[M + Na]^+$): calcd for $C_{23}H_{34}O_2Na$: 365.2457; found: 365.2440.

*(2*R,*4*RS,*5*SR*)-Isomer*[8] (19% yield): Colorless oil; IR (neat) ν: 3008, 2924, 2854, 1682, 1612, 1450, 1373, 1242, 1141, 1095, 1025, 926, 849, 756 cm^{-1}; ^1H NMR($CDCl_3$) δ: 1.01–1.34 (10H, m, CH_2) 1.21 (6H, s, CH_3), 1.61–1.96 (12H, m, CH_2+CH), 5.91 (1H, s, CHPh), 7.29–7.36 (3H, m, Ph-H), 7.47–7.49 (2H, m, Ph-H); ^{13}C NMR ($CDCl_3$) δ: 16.1, 25.9, 26.0, 26.1, 26.4, 26.5, 26.6, 26.8, 28.3, 28.7, 29.9, 31.5, 49.1, 51.8, 87.4, 99.0, 126.3, 128.0, 128.3, 139.8; HRMS ([M + Na]+): calcd for $C_{23}H_{34}O_2Na$: 365.2457; found: 365.2388.

dl-*2,3-Dicyclohexyl-2,3-butanediol*: This isomer was obtained from (4*RS*,5*RS*)-4,5-dicyclohexyl-4,5-dimethy-2-phenyl-1,3-dioxolane in 99% yield. Colorless solid; mp 99–101°C; IR (neat) ν: 3448, 2924, 2854, 1450, 1373, 1126, 1080, 1057, 995, 926, 903, 602 cm^{-1}; ^1H NMR ($CDCl_3$) δ: 1.02–1.31 (10H, m, CH_2), 1.15 (6H, s, CH_3), 1.65–1.83 (10H, m, CH_2), 1.90–1.96 (2H, m, CH), 1.93 (2H, br, OH); ^{13}C NMR ($CDCl_3$) δ: 19.6, 26.7, 27.0, 27.1, 28.0, 30.0, 44.5, 79.1; HRMS ($[M + Na]^+$): calcd for $C_{16}H_{30}O_2Na$: 277.2143; found: 277.2052. Anal. calcd. for $C_{16}H_{30}O_2$: C 75.54, H 11.89; found: C 75.45, H 11.91.

meso-*2,3-Dicyclohexyl-2,3-butanediol (**20**)*: This isomer was obtained from (2*R*,4*RS*,5*SR*)-4,5-dicyclohexyl-4,5-dimethy-2-phenyl-1,3-dioxolane in 99% yield. Colorless solid; mp 118–119°C (lit. 124°C); IR (KBr) ν: 3502, 2938, 2916, 2854, 1450, 1381, 1134, 1088, 1065, 995, 926, 895, 594, 532 cm^{-1}; ^1H NMR ($CDCl_3$) δ: 1.06–1.31 (10H, m, CH_2), 1.14 (6H, s, CH_3), 1.58–1.79 (10H, m, CH_2), 2.02- 2.05 (2H, m, CH), 2.28 (2H, br, OH); ^{13}C NMR ($CDCl_3$) δ: 21.4, 26.5, 26.9, 27.0, 28.2, 29.3, 44.0, 79.2; HRMS ($[M + Na]^+$): calcd for $C_{16}H_{30}O_2Na$: 277.2143; found: 277.2079.

meso- *and* dl-*3,4-diethyl-2,5-Dimethyl-3,4-hexanediol*: Colorless oil. Anal. calcd. for $C_{12}H_{26}O_2$: C 71.23, H 12.95; found: C 71.51, H 12.55. Assignments were made by comparing the relative areas of methylene signals at δ 1.59 and δ 1.67, respectively. Separation of the pure isomers from crude reaction mixture was achieved by the same method as the case of 2,3,4,5-tetramehtyl-3,4-hexanediol.

*(4*RS,*5*RS*)- and (2*R,*4*RS,*5*SR*)-4,5-diethyl-4,5-Diisopropyl-2-phenyl-1,3-dioxolane*: These two isomers were obtrained from *meso*- and *dl*-2,5-dimethyl-3,4-diethyl-3,4-hexanediol:

*(4*RS,*5*RS*)-Isomer (29% yield)*: Colorless oil; IR (neat) ν: 3062, 2978, 2877, 1458, 1381, 1219, 1095, 1026, 941, 764, 725, 702 cm^{-1}; ^1H NMR($CDCl_3$) δ: 0.84 (3H, dd, *J* = 7.3, 7.6 Hz, CH_3) 0.99 (3H, d, *J* = 7.0 Hz, CH_3), 1.02 (3H, d, *J* = 7.0 Hz, CH_3), 1.06 (3H, dd, *J* = 7.3, 7.6 Hz, CH_3), 1.06 (3H, d, *J* = 7.0 Hz, CH_3), 1.12 (3H, d, *J* = 7.0 Hz, CH_3), 1.62 (1H, dq, *J* = 7.6, 14.6 Hz, CH_2), 1.67 (1H, dq, *J* = 7.3, 14.6 Hz, CH_2), 1.72 (1H, dq, *J* = 7.3, 14.6 Hz, CH_2), 1.94 (1H, dq, *J* = 7.6, 14.6 Hz, CH_2), 2.21 (1H, qq, *J* = 7.0, 7.0 Hz, CH), 2.29 (1H, qq, *J* = 7.0, 7.0 Hz, CH), 5.88 (1H, s, PhCH), 7.28–7.36 (3H, m, Ph-H), 7.50–7.52 (2H, m, Ph-H); ^{13}C NMR ($CDCl_3$) δ: 9.7, 10.2, 19.31, 19.33, 20.3, 20.6, 22.8, 24.5, 31.0, 31.4, 90.0, 90.3, 98.7, 126.1, 127.91, 127.93, 140.6; HRMS ($[M + Na]^+$): calcd for $C_{19}H_{31}O_2Na$: 313.2144; found: 313.2093.

*(2*R,*4*RS,*5*SR*)-Isomer*[8] *(11% yield)*: Colorless oil; IR (neat) ν: 3062, 2962, 2870, 1458, 1381, 1219, 1095, 1018, 941, 764, 725, 702 cm^{-1}; ^1H NMR ($CDCl_3$) δ: 0.95 (6H, d, *J* = 7.0 Hz, CH_3), 0.96 (6H, d, *J* = 6.7 Hz, CH_3), 1.05 (6H, dd, *J* = 7.3, 7.6 Hz, CH_3), 1.71 (2H, dq, *J* = 7.3, 14.6 Hz, CH_2), 1.87 (2H, dq, *J* = 7.6 Hz, CH_2), 2.19 (2H, qq, J = 6.7, 7.0 Hz, CH), 5.89 (1H, s, CHPh), 7.29–7.36 (3H, m, Ph-H), 7.51–7.53 (2H, m, Ph-H); ^{13}C NMR ($CDCl_3$) δ: 10.2, 19.3, 20.2, 23.6, 31.5, 89.9, 98.8, 126.2, 127.9, 128.0, 140.2; HRMS ($[M + Na]^+$): calcd for $C_{19}H_{31}O_2Na$: 313.2144; found: 313.2199.

dl-*3,4-diethyl-2,5-Dimethyl-3,4-hexanediol*: This isomer was obtained from (4*RS*,5*RS*)-4,5-diisopropyl-4,5-diethy-2-phenyl-1,3-dioxolane in 96% yield. Colorless oil; IR (KBr) ν: 3417, 2978, 2939, 1473, 1389, 1149, 964, 586, 555 cm^{-1}; ^1H NMR ($CDCl_3$) δ: 0.96 (6H, dd, *J* = 7.6, 7.6 Hz, CH_3), 1.01 (6H, d, *J* = 7.0 Hz, CH_3), 1.03 (6H, d, *J* = 7.0 Hz, CH_3), 1.67 (2H,

[8] Only one C_s symmetric product was obtained. From *meso* diol, two isomers, i.e., (2*R*,4*RS*,5*SR*)-isomer and (2*S*,4*RS*,5*SR*)-isomer, are possible, but it was considered that the latter (all *cis*) would hardly be thermodynamically produced because of its steric hinderance.

© 2000 NRC Canada

dq, J = 7.6, 14.7 Hz, CH_2), 1.71 (2H, dq, J = 7.6, 14.7 Hz, CH_2), 2.08 (2H, qq, J = 7.0, 7.0 Hz, CH), 2.18 (2H, br, OH); ^{13}C NMR ($CDCl_3$) δ: 9.6, 18.9, 19.4, 27.1, 33.6, 80.7. Anal. calcd. for $C_{12}H_{26}O_2$: C 71.23, H 12.95; found: C 70.99, H 12.94.

meso-*3,4-diethyl-2,5-Dimethyl-3,4-hexanediol*: This isomer was obtained from (2*R*,4*RS*,5*SR*)-4,5-diisopropyl-4,5-diethyl-2-phenyl-1,3-dioxolane in 94% yield. Colorless solid; mp 50–51°C; IR (KBr) ν: 3471, 2970, 2939, 1466, 1389, 1103, 957, 532 cm^{-1}; ^{1}H NMR ($CDCl_3$) δ: 0.99 (6H, dd, J = 7.5, 7.3 Hz, CH_3), 0.99 (6H, d, J = 7.0 Hz, CH_3), 1.03 (6H, d, J = 7.0 Hz, CH_3), 1.59 (2H, dq, J = 7.3, 18.5 Hz, CH_2), 1.71 (2H, dq, J = 7.5, 18.5 Hz, CH_2), 2.07 (2H, qq, J = 7.0, 7.0 Hz, CH), 2.34 (2H, br, OH); ^{13}C NMR ($CDCl_3$) δ: 9.7, 18.9, 19.4, 26.4, 34.2, 80.9. Anal. calcd. for $C_{12}H_{26}O_2$: C 71.23, H 12.95; found: C 71.04, H 12.78.

meso-, *and* dl-*1,2-Diphenyl-1,2-ethanediol (**18**)*: Colorless solid; ^{1}H NMR ($CDCl_3$) δ: 2.38 (2H, br, OH, *meso*), 3.04 (2H, br, OH, *dl*), 4.65 (2H, s, CH, *dl*), 4.79 (2H, s, CH, *meso*), 7.07–7.30 (20H, m, Ph-H). Assignments were made by comparing the relative heights of carbinol proton signals at δ 4.67 and δ 4.79, respectively.

meso-, *and* dl-*1,6-Diphenyl-3,4-hexanediol (**6a,b,d**)*: Colorless solid; ^{1}H NMR ($CDCl_3$) δ: 1.76–1.87 (8H, m, CH_2), 2.65–2.90 (12H, m, CH_2 + OH), 3.50 (2H, m, CH, *dl*), 3.65 (2H, m, CH, *meso*), 7.22–7.36 (20H, m, Ph-H). Assignments were made by comparing the relative areas of carbinol proton signals at δ 3.50 and δ 3.65, respectively.

cis-*1,2-Diphenyl-1,2-cyclohexanediol (**15**)*: Colorless solid; ^{1}H NMR ($CDCl_3$) δ: 2.02–1.91 (6H, m, CH_2), 2.74–2.22 (2H, m, CH_2), 2.94 (2H, br, OH), 7.12–7.03 (10H, m,Ph-H). ^{13}C NMR ($CDCl_3$) δ: 21.9, 35.9, 77.2, 126.7, 126.9, 127.1, 144.1.

cis-, *and* trans-*1,2-Dimethyl-1,2-cyclohexanediol*: Assignments were made by comparing the relative hights of methyl signals at δ 1.27 and δ 1.21, respectively. Identification of each isomer was achieved as described below.

cis-*1,2-Dimethyl-1,2-cyclohexanediol (**21**)*: Repeated thin layer chromatography of the crude pinacol product gave pure *cis*-isomer: Colorless solid; mp 48–50°C (lit. 51°C); ^{1}H NMR ($CDCl_3$) δ: 1.21 (6H, s, CH_3), 1.36–1.51 (4H, m, CH_2), 1.57–1.64 (2H, m, CH_2), 1.71–1.77 (2H, m, CH_2), 2.20 (2H, br, OH); ^{13}C NMR ($CDCl_3$) δ: 22.4, 23.6, 36.7, 74.0.

trans-*1,2-Dimethyl-1,2-cyclohexanediol (**21**)*: Separation of the pure *trans*-isomer from crude reaction mixture was not achieved. It was prepared according to the litarature. Colorless solid, mp 90–92°C (lit. 93°C); ^{1}H NMR ($CDCl_3$) δ: 1.26 (6H, s, CH_3), 1.43–1.50 (2H, m, CH_2), 1.46 (2H, br, OH), 1.55–1.60 (4H, m, CH_2), 1.71–1.75 (2H, m, CH_2); ^{13}C NMR ($CDCl_3$) δ: 22.0, 23.3, 36.4, 74.3.

References

1. (*a*) T. Mukaiyama, T. Sato, and J. Hanna. Chem. Lett. 1041 (1973); (*b*) S. Tyrlik and I. Wolochowicz. Bull. Soc. Chim. Fr. 2147 (1973); (*c*) J.E. McMurry and M.P. Fleming. J. Am. Chem. Soc. **96**, 4708 (1974).
2. (*a*) A. Fürstner and B. Bogdanovic. Angew. Chem. Int. Ed. Engl. **35**, 2442(1996); (*b*) T. Wirth. Angew. Chem. Int. Ed. Engl. **35**, 61 (1996); (*c*) A. Fürstner. Angew. Chem. Int. Ed. Engl. **32**, 164 (1993); (*d*) G.M. Robertson. *In* Comprehensive organic synthesis. Vol. 3. *Edited by* B.M. Trost and I. Fleming. Pergamon Press, Oxford, 1991, p. 563.
3. (*a*) Y. Handa and J. Inanaga. Tetrahedron Lett. **28**, 5717 (1987); (*b*) A. Clerici, L. Clerici, and O. Porta. Tetrahedron Lett. **37**, 3035 (1996); (*c*) M.C. Barden and J. Schwartz. J. Am. Chem. Soc. **118**, 5484 (1996).
4. (*a*) J.L. Namy and H.B. Kagan. Tetrahedron Lett. **24**, 765 (1983); (*b*) G.A. Molander. Chem. Rev. **92**, 29 (1992); (*c*) N. Taniguchi, N. Kaneta, and M. Uemura. J. Org. Chem. **61**, 6088 (1996).
5. (*a*) J. Szymoniak, J. Besançon, and C. Moïse. Tetrahedron, **48**, 3867 (1992); (*b*) J. Szymoniak, J. Besançon, and C. Moïse. Tetrahedron, **50**, 2841 (1994).
6. (*a*) R. Nomura, T. Matsuno, and T. Endo. J. Am. Chem. Soc. **118**, 11666 (1996); (*b*) T.A. Lipski, M.A. Hilfiker, and S.G. Nelson. J. Org. Chem. **62**, 4566 (1997); (*c*) A. Gansäuer and D. Bauer. J. Org. Chem. **63**, 2070 (1998); (*d*) T. Hirao, M. Asahara, Y. Muguruma, and A. Ogawa. J. Org. Chem. **63**, 2812 (1998); (*e*) M. Bandini, P.G. Cozzi, S. Morganti, and A. Umani-Ronchi. Tetrahedron Lett. **40**, 1997 (1999).
7. N. Balu, S.K. Nayak, and A. Banerji. J. Am. Chem. Soc. **118**, 5932 (1996).
8. T. Mukaiyama, A. Kagayama, and I. Shiina. Chem. Lett. 1107 (1998).
9. (*a*) I. Shiina, H. Iwadare, H. Sakoh, M. Hasegawa, Y. Tani, and T. Mukaiyama. Chem. Lett. 1 (1998); (*b*) T. Mukaiyama, I. Shiina, H. Iwadare, M. Saitoh, T. Nishimura, N. Ohkawa, H. Sakoh, K. Nishimura, Y. Tani, M. Hasegawa, K. Yamada, and K. Saitoh. Chem. Eur. J. **5**, 121 (1999).
10. S.P. Narula and H.K. Sharma. Inorg. Synth. **24**, 181 (1987).
11. (*a*) B. Bogdanovic and A. Bolte. J. Organomet. Chem. **502**, 109 (1995); (*b*) J.J. Eisch, X. Shi, and J. Lasota. Z. Naturforsch. B: Chem. Sci. **50**, 342 (1995).
12. (*a*) A. Ishida and T. Mukaiyama. Chem. Lett. 1127 (1976); (*b*) C.S. Swindel, M.C. Chander, J.M. Heerding, P.G. Klimko, L.T. Rahman, J.V. Rahman, and H. Venkataraman. J. Org. Chem. **61**, 1101 (1996).
13. K. Otsubo, J. Inanaga, and M. Yamaguchi. Tetrahedron Lett. **27**, 5763 (1986).
14. (*a*) R.J.H. Clark, J. Lewis, D.J. Machin, and R.S. Nyholm. J. Chem. Soc. 379 (1963); (*b*) G.W.A. Fowles and T.E. Lester. Chem. Commun. 47 (1967).
15. A. Fürstner and A. Hupperts. J. Am. Chem. Soc. **117**, 4468 (1995).
16. J.E. McMurry and N.O. Siemers. Tetrahedron Lett. **34**, 7891 (1993).
17. A. Clerici and O. Porta. J. Org. Chem. **50**, 76 (1985).
18. A. Fürstner, R. Czuk, C. Rohrer, and H. Weidmann. J. Chem. Soc. Perkin Trans. 1, 1729 (1988).
19. T. Matsuura and Y. Kitaura. Bull. Chem. Soc. Jpn. **41**, 2483 (1968).
20. H. Birkhofer, H-D. Beckhaus, and C. Rüchardt. Chem. Ber. **126**, 1023 (1993).
21. E.S. Huyser and L.G. Rose. J. Org. Chem. **37**, 851 (1972).

© 2000 NRC Canada

Silver-catalyzed asymmetric amination of silyl enol ethers

Yasuhiro Yamashita, Haruro Ishitani, and Shū Kobayashi

Abstract: Catalytic amination of silyl enol ethers with azo diester compounds was investigated. It was shown that $Cu(OTf)_2$ or AgOTf had high catalytic activity and that AgOTf was the most efficient among the catalysts tested in the reactions. In asymmetric reactions, the $AgClO_4$–BINAP system showed high enantioselectivity. In a mixture of toluene or mesitylene and THF, silyl enol ethers reacted with dibenzyl azodicarboxylate (DBnAD) smoothly to afford the corresponding amination adducts in excellent yields with up to 86% ee.

Key words: amination, amino acid, asymmetric synthesis, chiral catalyst, silver.

Résumé : On a étudié l'amination catalytique d'éthers énoliques silylés par des composés azodiesters. Il a été démontré que le $Cu(OTf)_2$ et le AgOTf possèdent une activité catalytique élevée et que le AgOTf est l'un des catalyseurs les plus efficaces pour ces réactions. Dans les réactions asymétriques, le système $AgClO_4$·BINAP donne lieu à une énantiosélectivité élevée. Dans un mélange de toluène ou de mésitylène avec du THF, les éthers énoliques silylés réagissent facilement avec l'azodicarboxylate de dibenzyle (ADDBn) pour conduire à la formation des adduits d'amination correspondants, avec d'excellents rendements et un ee pouvant aller jusqu'à 86%.

Mots clés : amination, acide aminé, synthèse asymétrique, catalyseur chiral, argent.

[Traduit par la Rédaction]

Introduction

Amination at the α-position of carbonyls provides one of the most efficient methods for synthesis of α-amino acids and their derivatives (for a review see ref. (1)). Several electrophilic aminations have been reported (1) and among them, the reactions of silyl enol ethers with azo diesters are promising because the starting materials are stable and readily available, and the hydrazine groups produced are easily converted to amino groups by reductive N—N bond cleavage (Scheme 1) (2, 3). In the previous reports, however, thermal conditions (4) or stoichiometric amounts of Lewis acids (2*a*, *d*–*f*) were required for the reaction of silyl enol ethers with azo diesters. Quite recently, we have reported our preliminary results on silver and copper-catalyzed amination of silyl enol ethers (5). This was the first example of catalytic amination of silyl enol ethers, and we have since continued to investigate asymmetric versions of these reactions. As for asymmetric amination, although many diastereoselective approaches using lithium enolates or silyl enol ethers and azo compounds were reported, (2*a*–*d*, 6) examples of catalytic enantioselective reactions have been limited. In 1997, Evans and Nelson (7) reported enantioselective amination of *N*-acyloxazolines with an azodicarboxylate using a chiral magnesium bis(sulfonamide). In this paper, we report full details of our results on catalytic asymmetric amination, including the first finding of efficient achiral catalysts. (Quite recently, Evans and Johnson reported chiral copper-catalyzed enantioselective amination of enolsilanes with azodicarboxylate derivatives. See ref. (8)).

Results and discussion

Recently, we have found that metal trifluoromethanesulfonates (triflates) are excellent catalysts in several carbon–carbon bond-forming reactions. Based on these results, we first examined the reaction of the silyl enol ether derived from *S*-ethyl propanethioate with dibenzyl azodicarboxylate (DBnAD) using catalytic amounts of several metal triflates (Table 1) (for recent reports on reactions using metal triflates as catalysts see ref. (9)). When $Zn(OTf)_2$, $Fe(OTf)_3$, $Yb(OTf)_3$, $Zr(OTf)_4$, or $Hf(OTf)_4$ was used, little rate enhancement was observed. On the other hand, while the reaction proceeded moderately in the presence of $Sn(OTf)_2$ or $Sc(OTf)_3$, the desired products were obtained in high yields when AgOTf or $Cu(OTf)_2$ was employed as the catalyst.

We then investigated the effect of solvents using AgOTf as a catalyst (Table 2). While the amination reaction proceeded cleanly in dichloromethane, lower yields were obtained in toluene, THF, and propionitrile. For azo diester compounds, not only DBnAD but also diethyl azodicarboxylate and *tert*-butyl azodicarboxylate gave the corresponding amination

Received September 17, 1999. Published on the NRC Research Press website on May 19, 2000.

Dedicated to Professor Stephen Hanessian on the occasion of his 65th birthday.

Y. Yamashita, H. Ishitani, and S. Kobayashi.[1] Graduate School of Pharmaceutical Sciences, The University of Tokyo, CREST, Japan Science and Technology Corporation (JST), Hongo, Bunkyo-ku, Tokyo 113-0033, Japan.

[1]Author to whom correspondence may be addressed.

 © 2000 NRC Canada

Scheme 1.

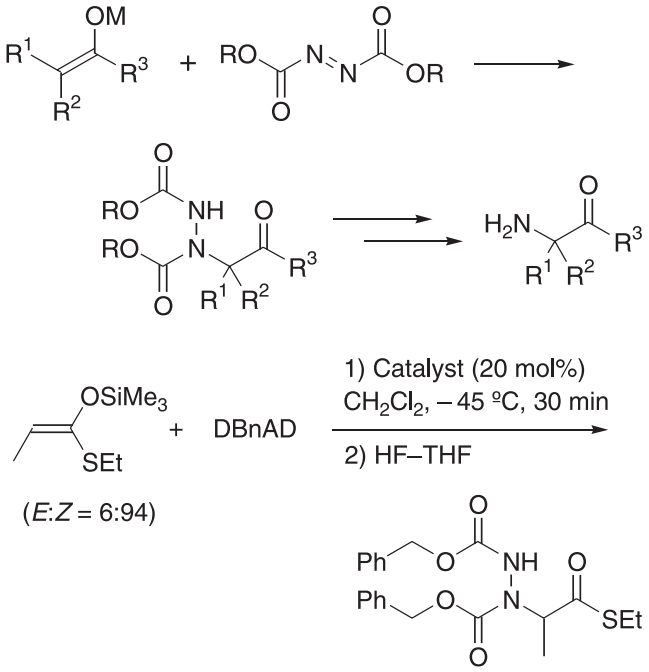
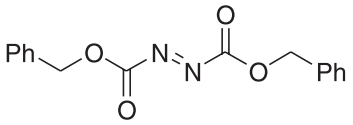


Table 1. Effect of Catalysts

Entry	Catalyst	Yield (%)
1	—	12
2	$Zn(OTf)_2$	13
3	$Zr(OTf)_4$	16
4	$Hf(OTf)_4$	14
5	$Yb(OTf)_3$	14
6	$Fe(OTf)_3$	29
7	$Sc(OTf)_3$	40
8	$Sn(OTf)_2$	58
9	$Cu(OTf)_2$	89
10	AgOTf	92



(DBnAD)

adducts in high yields (Table 3). The catalytic activities of AgOTf and $Cu(OTf)_2$ in the reactions of several silyl enol ethers with DBnAD were studied, and the results are summarized in Table 4. When the amount of AgOTf or $Cu(OTf)_2$ was decreased in the reaction with the trimethylsilyl enol ether derived from *S*-ethyl propanethioate, the catalytic activity was maintained and the adduct was

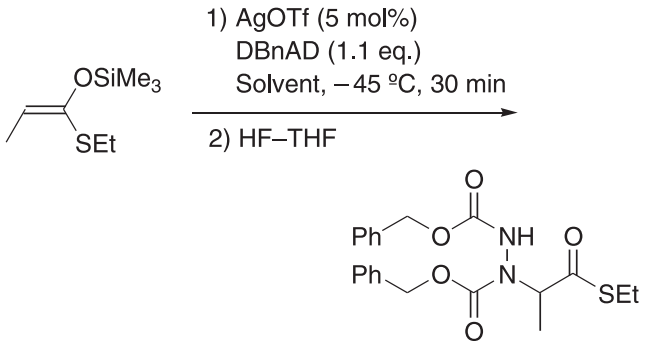


Table 2. Effect of Solvents

Solvent	Yield (%)
CH_2Cl_2	90
Toluene	83
THF	71
C_2H_5CN	46

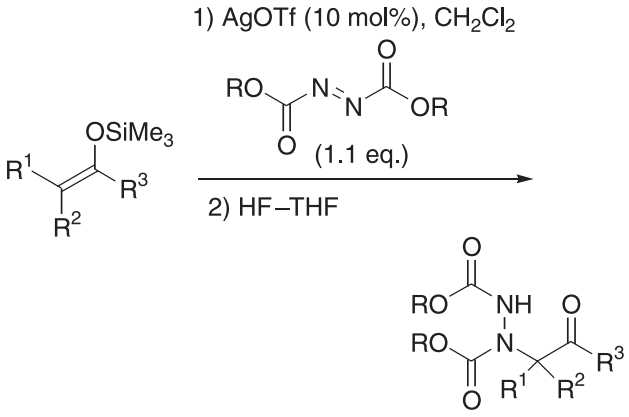
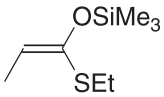
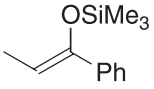


Table 3. Effect of Azo Compounds

Substrate	Azo Compound	Conditions (°C/h)	Yield (%)
	R = Bn	–45, 0.5	90[a]
	R = Et	–45, 0.5	90
	R = ^{t}Bu	–45, 1.5	91
	R = Bn	0, 0.5	84
	R = Et	0, 0.5	81
	R = ^{t}Bu	0, 3	92

[a]AgOTf: 5 mol%.

obtained in a high yield even when 1 mol% of AgOTf was used. In the reaction of the ketene silyl acetal derived from methyl isobutyrate, AgOTf gave a better yield of the desired adduct.[2] Moreover, the *tert*-butyldimethylsilyl group also

[2]Side reactions predominated when the amination was performed without the catalyst.

© 2000 NRC Canada

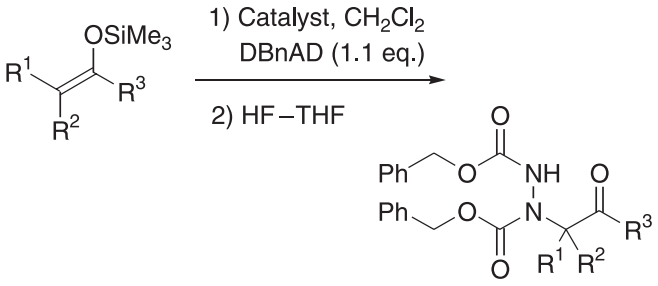
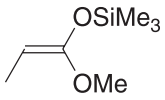
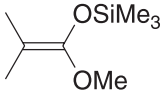
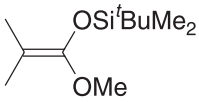
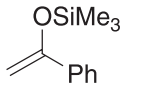
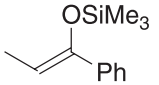
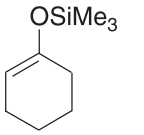


Table 4. Ag or Cu-Catalyzed Aminations

Entry	Substrate	Catalyst (mol%)	Conditions (°C/h)	Yield (%)
1		$Cu(OTf)_2$ (10)	–45, 0.5	90
2		$Cu(OTf)_2$ (5)	–45, 0.5	86
3	(*E*:*Z* = 94:6)	AgOTf (5)	–45, 0.5	90
4		AgOTf (1)	–45, 0.5	91
5		$Cu(OTf)_2$ (10)	–45, 0.5	48
6		AgOTf (10)	–45, 0.5	97
7		AgOTf (10)	0, 0.5	95
8		$Cu(OTf)_2$ (10)	0, 2.5	70
9		AgOTf (10)	0, 0.5	91
10		$Cu(OTf)_2$ (10)	0, 2.5	39
11		AgOTf (10)	0, 0.5	84
12		$Cu(OTf)_2$ (10)	0, 2.5	39
13		AgOTf (10)	0, 0.5	91

worked well as a silyl moiety instead of the trimethylsilyl group. When less reactive silyl enol ethers derived from ketones were examined, it was found that the reactions also proceeded smoothly in the presence of a catalytic amount of AgOTf or $Cu(OTf)_2$. Also in these cases, AgOTf showed higher activity than $Cu(OTf)_2$.

We then examined asymmetric versions of these aminations. In the presence of a catalytic amount of a AgOTf–BINAP system, (10) the silyl enol ether of propiophenone was treated with DBnAD in THF. The reaction proceeded smoothly at –45°C to afford the corresponding amination adduct in 83% yield with 29% ee. Several reaction conditions were then examined to improve the selectivity. The effect of silver salts is shown in Table 5. When $AgClO_4$ was used as a catalyst, the ee was improved to 68%. The effects of temperature, azo compounds, and solvents are summarised in Tables 6, 7, and 8, respectively. The ee obtained at –45°C was not improved even when the reaction was carried out at lower temperatures such as –60°C and –78°C. As for azo compounds, DBnAD gave the best result. We observed interesting effects of the solvents. When a single solvent of THF or toluene was used, 68% ee (THF) or 67% ee (toluene) was obtained. On the other hand, greater than 74% ee were observed when a mixture of THF and toluene, *m*-xylene, or mesitylene was used. The best ee (86%) was obtained when a 5:1 mixture of mesitylene and THF was employed as the solvent. It is interesting to note that no chiral induction was observed when dichloromethane was used as a solvent, albeit the reaction proceeded cleanly to give the desired adduct in 90% yield.

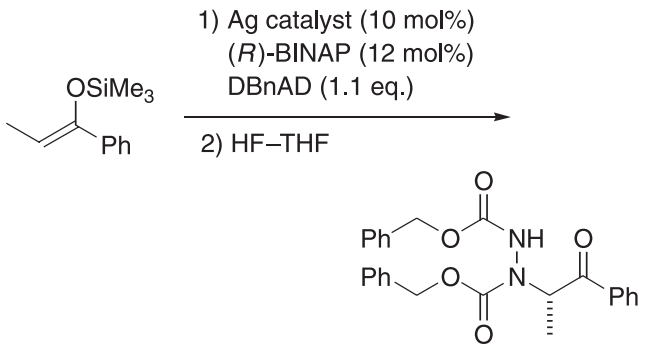


Table 5. Effect of Silver Salts[a]

Entry	Catalyst	Yield (%)	ee (%)
1	AgOTf	83	29
2	$AgBF_4$	87	41
3	$AgSbF_6$	92	46
4	$AgPF_6$	99	55
5	$AgClO_4$	99	68

[a] THF, –45 °C, 1 h.

Several examples of catalytic asymmetric amination are shown in Table 9. The silyl enol ethers derived from α-tetralone and phenyl propyl ketone reacted with DBnAD in the presence of a catalytic amount of $AgClO_4$–BINAP to afford the corresponding amination adducts in high yields with good ee. In the reaction of the silyl enolate of phenyl propionate, 51% ee of the amination adduct was obtained using the same system. As for the absolute configuration of the amination product, the product was converted to the literature known compound (**1**) (8)[3] according to standard procedures (Scheme 2).

[3] $[\alpha]_D^{31}$ = +8.9 (c 1.69, $CHCl_3$) (63% ee) (lit. (8) $[\alpha]_D^{24}$ = –17.9 (c 1.15, $CHCl_3$); $[\alpha]_D^{20}$ = –15.9 (c 0.38, $CHCl_3$) (4*R*,5*R*)) (11).

© 2000 NRC Canada

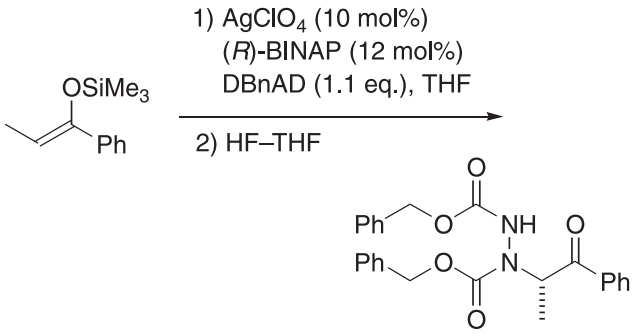


Table 6. Effect of Temperature

Entry	Conditions	Yield (%)	ee (%)
1	0°C, 1 h	86	30
2	–23°C, 1 h	90	55
3	–45°C, 1 h	99	68
4	–60°C, 1.5 h	96	66
5	–78°C, 7 h	95	63

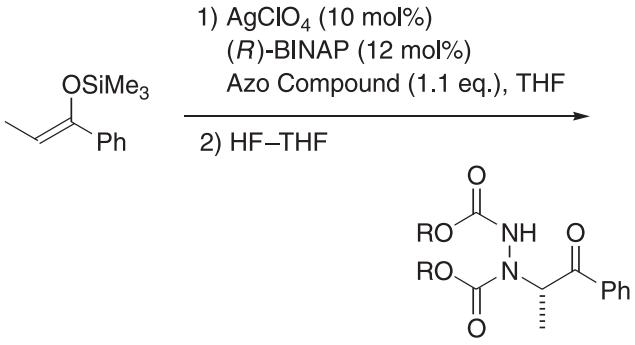


Table 7. Effect of Azo Compounds

Entry	R	Conditions	Yield (%)	ee (%)
1	Bn	–45°C, 1 h	99	68
2	Et	–45°C, 1 h	91	46
3	^{t}Bu	–45°C, 18 h	88	31

In summary, amination reactions of silyl enol ethers with azo diester compounds proceeded smoothly in the presence of a catalytic amount of AgOTf or $Cu(OTf)_2$. AgOTf gave better results than $Cu(OTf)_2$ in most cases. Various kinds of silyl enol ethers including those derived from esters, thioesters, and ketones worked well. It is noted that all the examined reactions proceeded cleanly using a small amount of the catalyst, and that the procedures are very simple. As for the catalytic asymmetric version of these aminations, $AgClO_4$–BINAP worked well to afford the corresponding adducts in excellent yields with moderate to high ee. Interesting solvent effects were observed, and these silver-catalyzed asymmetric aminations would provide one of the most efficient methods for the preparation of chiral and achiral α-amino carbonyl compounds.

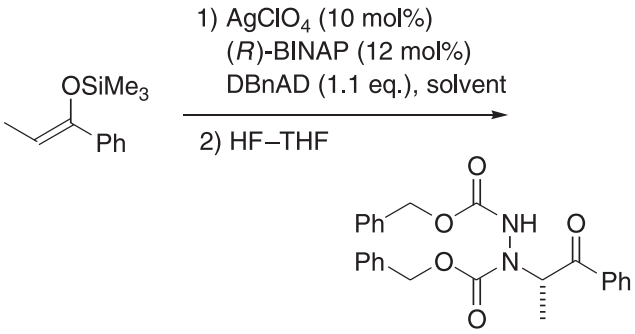


Table 8. Effect of Solvents

Entry	Solvent	Conditions (°C/h)	Yield (%)	ee (%)
1	THF	–45, 1	99	68
2	Toluene[a]	–45, 18	96	67
3	DME	–45, 1	90	58
4	CH_2Cl_2	–45, 1	90	0
5	THF + MS 5A	–45, 1	92	66
6	Toluene–THF[a] (1:1)	–45, 1	95	74
7	Toluene–THF[a] (5:1)	–45, 1	97	83
8	Toluene–THF[a] (20:1)	–45, 3	90	75
9	*m*-Xylene–THF[a] (5:1)	–45, 18	96	85
10	Mesitylene–THF[a] (5:1)	–45, 18	95	86

[a] The catalyst was prepared in THF and after removal of THF, new solvents were added.

Experimental

General

Melting points were uncorrected. ^{1}H and ^{13}C NMR spectra were recorded on a JEOL JNM-LA300, JNM-LA400, or JNM-LA500 spectrometer in $(CD_3)_2SO$. $(CD_3)_2SO$ was used as internal standard (δ = 2.49 for ^{1}H NMR and δ = 39.5 for ^{13}C NMR). IR spectra were measured with JASCO FT/IR-610 spectrometers. High-resolution mass spectra (HRMS) were measured with JEOL JMX-SX-102 mass spectrometer. High-performance liquid chromatography was carried out using the following apparatuses: SHIMADZU LC-10AT (liquid chromatograph), SHIMADZU SPD-10A (UV detector), and SHIMADZU C-R6A Chromatopac. Column chromatography was conducted on Silica gel 60 (Merck) and preparative thin-layer chromatography was carried out using Wakogel B-5F. All chemical compounds were purified based on standard procedures.

© 2000 NRC Canada

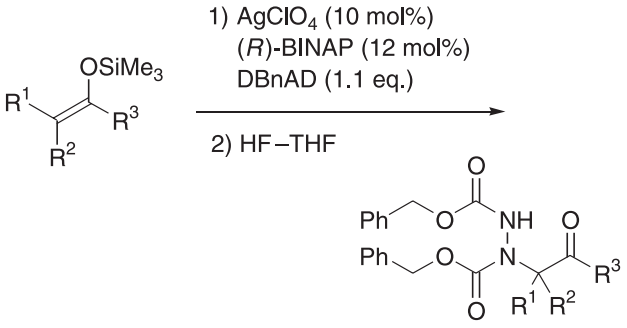
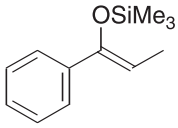
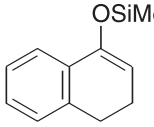
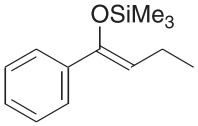
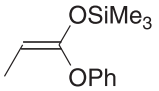


Table 9. Catalytic Asymmetric Amination

Entry	Silyl Enol Ether	Conditions (°C/h)	Yield (%)	ee (%)
1		–45, 1[a]	99	68
2		–45, 1[b]	97	86
3		–45, 5[a]	82	65
4		–45, 3[a]	93	59
5		–45, 18[a]	92	24
6	(*E*:*Z* = 93:7)	–45, 3[c]	73	51

[a] THF.
[b] Mesitylene–THF (5:1).
[c] Toluene–THF (5:1).

A general procedure of asymmetric reactions

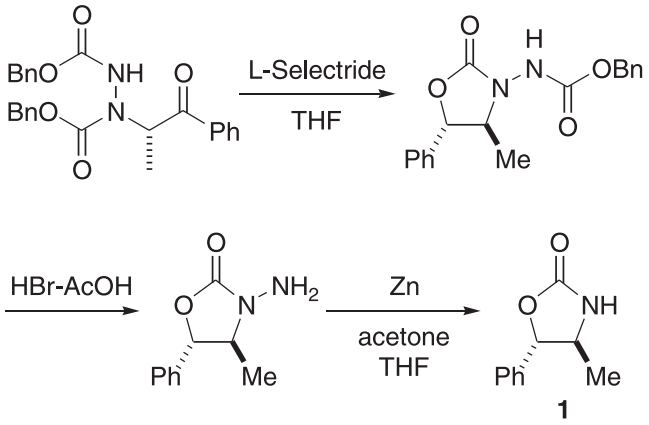
Achiral reactions

A typical experimental procedure is as follows: To a stirred suspension of AgOTf (0.040 mmol) in CH_2Cl_2 (1.0 mL) was added DBnAD (0.44 mmol) in CH_2Cl_2 (0.5 mL) at the temperature shown in Table 2. After stirring for 10 min, a silyl enol ether (0.40 mmol) in CH_2Cl_2 (0.5 mL) was added dropwise, and the mixture was stirred at the same temperature. A 20% HF(aq)–THF (1:1) solution was then added and the mixture was stirred for 1 h at room temperature. After being basified with saturated aq $NaHCO_3$, the aqueous layer was extracted with CH_2Cl_2. The organic layers were combined and dried over anhyd Na_2SO_4. After filtration and concentration, the residue was purified by preparative thin layer chromatography on silica gel to afford the desired amination adduct.

Asymmetric reactions

$AgClO_4$ (0.040 mmol, 10 mol%) and (*R*)-BINAP (0.048 mmol, 12 mol%) were dissolved in THF (1 mL). After stirring for 30 min at room temperature, the mixture was cooled to the desired temperatures. In cases of the reactions in toluene or toluene–THF, THF of the catalyst solution was removed under reduced pressure (1.0 mmHg, 30 min) first, and the desired solvent was added. To the cooled catalyst solution was added DBnAD (0.44 mmol) in the solvent (0.5 mL). After stirring for 10 min, a silyl enol ether (0.4 mmol) in the solvent (0.5 mL) was added dropwise, and the mixture was stirred at the same temperature. An aqueous 20% HF–THF (1:1) solution was then added and the mixture was stirred for 1h at room temperature. After basified with saturated $NaHCO_3$, the aqueous layer was extracted with dichloromethane. The organic layers were combined and dried over anhyd Na_2SO_4. After filtration and concentration, the residue was purified by preparative thin layer chromatography on silica gel to afford the desired adduct. The enantiomeric excess was determined by HPLC analysis (DAICEL CHIRALCEL OD or AS).

Scheme 2.



S-Ethyl 2-(N,N′-dibenzyloxycarbonylhydrazino)propanethioate: IR (neat) (cm^{-1}): 3304, 1759, 1724, 1687. ^1H NMR ($(CD_3)_2SO$, 70°C) δ: 1.16 (t, 3H, *J* = 7.0 Hz), 1.31 (d, 3H, *J* = 7.1 Hz), 2.81 (q, 2H, *J* = 7.0 Hz), 4.75 (m, 1H), 5.10 (s, 2H), 5.12 (s, 2H), 7.2–7.4 (m, 10H), 9.48 (br, 1H). ^{13}C NMR ($(CD_3)_2SO$, 70°C) δ: 13.6, 13.9, 22.2, 63.2, 66.0, 67.1, 127.0, 127.2, 127.6, 127.9, 128.0, 135.7, 136.0, 154.8, 156.1, 198.2. MS (*m*/*z*): 417 (M^++1). HRMS (*m*/*z*) calcd. for $C_{21}H_{25}N_2O_5S$ (M^++1): 417.1484; found: 417.1472.

Methyl 2-(N,N′-dibenzyloxycarbonylhydrazino)-2-methylpropionate: mp 104.0°C. IR (KBr) (cm^{-1}): 3317, 1739, 1696. ^1H NMR ($(CD_3)_2SO$, 70°C) δ: 1.09 (s, 3H), 1.30 (s, 3H), 3.54 (s, 3H), 4.9–5.2 (m, 4H), 7.2–7.4 (m, 10H), 9.59 (br, 1H). ^{13}C NMR ($(CD_3)_2SO$, 70°C) δ: 22.8, 23.6, 51.6, 63.3, 66.0, 66.7, 127.0, 127.2, 127.5, 127.6, 128.0, 128.0, 135.9, 136.2, 154.3, 156.2, 173.0. MS (*m*/*z*): 401 (M^++1). Anal. calcd for $C_{21}H_{24}N_2O_6$: C 62.99, H 6.04, N 7.00; found: C 63.06, H 5.96, N 6.90.

Dibenzyl N-(2-oxo-2-phenylethyl)-N,N′-hydrazinedicarboxylate: mp 103.5°C. IR (KBr) (cm^{-1}): 3285, 1739, 1708, 1679. ^1H NMR ($(CD_3)_2SO$, 70°C) δ: 4.98 (s, 2H), 5.11 (s, 2H), 5.13 (s, 2H), 7.2–7.5 (m, 10H), 7.52 (m, 2H), 7.65 (m, 1H), 7.96 (d, 2H, *J* = 7.7 Hz), 9.70 (br, 1H). ^{13}C NMR ($(CD_3)_2SO$, 70°C) δ: 56.7, 65.9, 66.9, 126.9, 127.2, 127.5, 127.5, 127.6,

© 2000 NRC Canada

127.9, 128.0, 128.4, 133.2, 134.6, 135.9, 136.1, 155.4, 193.5. MS (*m*/*z*): 418 (M^++1). Anal. calcd. for $C_{24}H_{22}N_2O_5$: C 68.89, H 5.30, N 6.69; found: C 69.03, H 5.46, N 6.55.

Dibenzyl N-(1-methyl-2-oxo-2-phenylethyl)-N,N′-hydrazinedicarboxylate: $[\alpha]_D^{30}$ = +27.8 (c 1.29, $CHCl_3$) (86% ee). IR (neat) (cm^{-1}): 3301, 1714. ^1H NMR ($(CD_3)_2SO$, 70°C) δ: 1.32 (d, 3H, *J* = 7.0 Hz), 5.08 (br, 4H), 5.62 (q, 1H, *J* = 7.0 Hz), 7.2–7.4 (m, 10H), 7.46 (t, 2H, *J* = 7.3 Hz), 7.60 (t, 1H, *J* = 7.3 Hz), 7.94 (d, 2H, *J* = 8.9 Hz), 9.49 (br, 1H). ^{13}C NMR ($(CD_3)_2SO$, 70°C) δ: 13.3, 57.7, 65.9, 67.0, 127.0, 127.2, 127.5, 127.5, 127.9, 128.0, 128.0, 128.2, 132.7, 135.0, 135.7, 136.1, 154.8, 156.1, 196.7. HRMS (*m*/*z*) calcd. for $C_{25}H_{24}N_2O_5$ (M^+): 432.1685; found: 432.1685.

Dibenzyl N-(2-oxocyclohexyl)-N,N′-hydrazinedicarboxylate: IR (neat) (cm^{-1}): 3303, 1729, 1713. ^1H NMR ($(CD_3)_2SO$, 70°C) δ: 1.4–1.6 (m, 1H), 1.7–1.9 (m, 3H), 1.9–2.0 (m, 1H), 2.17 (br, 1H), 2.3–2.4 (m, 1H), 2.4–2.5 (m, 1H), 4.70 (br, 1H), 5.0–5.2 (m, 4H), 7.3–7.5 (m, 10H), 9.14 (br, 1H). ^{13}C NMR ($(CD_3)_2SO$, 70°C) δ: 23.1, 25.7, 29.6, 40.1, 65.8, 65.9, 66.7, 126.9, 127.1, 127.4, 127.5, 127.9, 136.0, 136.2, 155.2, 156.2, 204.7. MS (*m*/*z*): 396 (M^+). HRMS (*m*/*z*) calcd. for $C_{22}H_{24}N_2O_5$ (M^+): 396.1685; found: 396.1690.

S-Ethyl 2-(N,N′-diethyloxycarbonylhydrazino)propanethioate: IR (neat) (cm^{-1}): 3304, 1748, 1724, 1691. ^1H NMR ($(CD_3)_2SO$, 70°C) δ: 1.1–1.2 (m, 9H), 1.29 (d, 3H, *J* = 7.1 Hz), 2.82 (q, 2H, *J* = 7.3 Hz), 4.0–4.2 (m, 4H), 4.69 (br, 1H), 9.14 (br, 1H). ^{13}C NMR ($(CD_3)_2SO$, 70°C) δ: 13.6, 13.9, 14.0, 22.2, 60.6, 61.7, 63.1, 154.9, 156.1, 198.5. MS (*m*/*z*): 293 (M^++1). HRMS (*m*/*z*) calcd. for $C_{11}H_{21}N_2O_5S$ (M^++1): 293.1171; found: 293.1161.

S-Ethyl 2-(N,N′-di-tert-butyloxycarbonylhydrazino)propanethioate: IR (neat) (cm^{-1}): 3330, 1714, 1691. ^1H NMR ($(CD_3)_2SO$, 70°C) δ: 1.18 (t, 3H, *J* = 7.3 Hz), 1.27 (d, 3H, *J* = 7.1 Hz), 1.40 (s, 9H), 1.41 (s, 9H), 2.81 (q, 2H, *J* = 7.3 Hz), 4.61 (br, 1H), 8.62 (br, 1H). ^{13}C NMR ($(CD_3)_2SO$, 70°C) δ: 13.7, 14.1, 22.1, 27.5, 27.6, 62.4, 79.3, 80.5, 153.5, 155.1, 198.9. MS (*m*/*z*): 349 (M^++1). HRMS (*m*/*z*) calcd. for $C_{15}H_{29}N_2O_5S$ (M^++1): 349.1797; found: 349.1810.

Diethyl N-(1-methyl-2-oxo-2-phenylethyl)-N,N′-hydrazinedicarboxylate: IR (neat) (cm^{-1}): 3304, 1734. ^1H NMR ($(CD_3)_2SO$, 70°C) δ: 1.11 (t, 6H, *J* = 7.1 Hz), 1.30 (d, 3H, *J* = 7.0 Hz), 3.8–4.3 (m, 4H), 5.56 (br, 1H), 7.4–7.8 (m, 3H), 7.96 (d, 2H, *J* = 8.6 Hz), 9.10 (br, 1H). ^{13}C NMR ($(CD_3)_2SO$, 70°C) δ: 13.3, 13.8, 13.8, 57.5, 60.4, 61.6, 128.0, 128.2, 132.6, 135.1, 155.0, 156.0, 196.8. MS (*m*/*z*): 308 (M^+). HRMS (*m*/*z*) calcd. for $C_{15}H_{20}N_2O_5$ (M^+): 308.1372; found: 308.1360.

Di-tert-butyl N-(1-methyl-2-oxo-2-phenylethyl)-N,N′-hydrazinedicarboxylate: IR (neat) (cm^{-1}): 3325, 1690. ^1H NMR ($(CD_3)_2SO$, 70°C) δ: 1.28 (d, 3H, *J* = 6.9 Hz), 1.32 (s, 9H), 1.37 (br, 9H), 5.44 (br, 1H), 7.48 (m, 2H), 7.59 (m, 1H), 7.96 (d, 2H, *J* = 7.3 Hz), 8.65 (br, 1H). ^{13}C NMR ($(CD_3)_2SO$, 70°C) δ: 13.3, 27.4, 27.6, 56.8, 79.1, 80.3, 128.0, 128.1, 132.5, 135.2, 153.8, 155.1, 197.1. MS (*m*/*z*): 364 (M^+). HRMS (*m*/*z*) calcd. for $C_{19}H_{28}N_2O_5$ (M^+): 364.1998; found: 364.1990.

Dibenzyl N-(1,2,3,4-tetrahydro-1-oxonaphthalen-2-yl)-N,N′-hydrazinedicarboxylate: mp 141.0°C. IR (KBr) (cm^{-1}): 3295, 1737, 1704, 1685. ^1H NMR ($(CD_3)_2SO$, 70°C) δ: 2.2–2.4 (m, 2H), 2.9–3.5 (m, 2H), 4.92 (br, 1H), 5.09 (s, 2H), 5.13 (s, 2H), 7.2–7.5 (m, 12H), 7.56 (t, 1H, *J* = 7.5 Hz), 7.89 (d, 1H, *J* = 7.9 Hz), 9.35 (br, 1H). ^{13}C NMR ($(CD_3)_2SO$, 70°C) δ: 26.7, 27.6, 64.7, 65.9, 66.8, 126.3, 126.6, 126.9, 127.2, 127.5, 127.5, 128.0, 128.0, 128.6, 131.3, 133.5, 136.0, 136.2, 143.8, 155.3, 156.3, 192.6. MS (*m*/*z*): 444 (M^+). Anal. calcd for $C_{26}H_{24}N_2O_5$: C 70.26, H 5.44, N 6.30; found: C 70.52, H 5.57, N 6.13.

Dibenzyl N-(1-ethyl-2-oxo-2-phenylethyl)-N,N′-hydrazinedicarboxylate: mp 119.5°C. ^1H NMR ($(CD_3)_2SO$, 70°C) δ: 0.89 (t, 3H, *J* = 7.3 Hz), 1.79 (dq, 2H, *J* = 7.3 Hz, 7.3 Hz), 4.8–5.2 (m, 4H), 5.50 (br, 1H), 7.2–7.7 (m, 13H), 9.35 (br, 1H). ^{13}C NMR ($(CD_3)_2SO$, 70°C) δ: 9.9, 20.5, 61.7, 65.8, 67.1, 127.1, 127.4, 127.9, 128.1, 132.7, 135.7, 136.0, 155.1, 155.8, 195.9. IR (KBr) (cm^{-1}): 3275, 1746, 1693, 1671. MS (*m*/*z*): 446 (M^+). Anal. calcd for $C_{26}H_{26}N_2O_5$: C 69.94, H 5.87, N 6.27; found: C 69.65, H 5.90, N, 6.25.

Phenyl 2-(N,N′-dibenzyloxycarbonylhydrazino)propionate: IR (neat) (cm^{-1}): 3299, 1758, 1716. ^1H NMR ($(CD_3)_2SO$, 70°C) δ: 1.48 (d, 3H, *J* = 7.1 Hz), 5.0 (m, 1H), 5.16 (s, 2H), 5.20 (s, 2H), 7.0–7.5 (m, 15H), 9.68 (br, 1H). ^{13}C NMR ($(CD_3)_2SO$, 70°C) δ: 13.6, 56.7, 66.1, 67.1, 121.2, 125.5, 127.1, 127.3, 127.6, 128.0, 128.0, 129.0, 135.8, 136.1, 150.3, 154.9, 156.2, 168.9. MS (*m*/*z*): 449 (M^++1). HRMS (*m*/*z*) calcd. for $C_{25}H_{25}N_2O_6$ (M^++1): 449.1713; found: 449.1725.

Acknowledgment

This work was partially supported by a Grant-in-Aid for Scientific Research from the Ministry of Education, Science, Sports, and Culture, Japan.

References

1. (*a*) O. Mitsunobu. *In* Comprehensive organic synthesis. Vol. 6. *Edited by* B.M. Trost. Pergamon Press, Oxford. 1991. p. 65; (*b*) R. Askani. *In* Comprehensive organic synthesis. Vol. 6. *Edited by* B.M. Trost. Pergamon Press, Oxford. 1991. p. 103; (*c*) T. Sheradsky. The chemistry of amino, nitroso, and nitro compounds and their derivertives. Part 1. *Edited by* S. Patai. John Wiley & Sons, New York. 1982. p. 395; (*d*) J.D. Bois, C.S. Tomooka, J. Hong, and E.M. Carreira. Acc. Chem. Res. **30**, (1997); (*e*) P. Phukan and A. Sudalai. Tetrahedron: Asymmetry, **9**, 1001 (1998); (*f*) S. Minakata, T. Ando, M. Nishimura, I. Ryu, and M. Komatsu. Angew. Chem. Int. Ed. Engl. **37**, 3392 (1998).
2. (*a*) C. Gennari, L. Colombo, and G. BertoLini. J. Am. Chem. Soc. **108**, 6394 (1986); (*b*) D.A. Evans, T.C. Britton, R.L. Dorow, J. F. Dellaria, Jr. Tetrahedron, **44**, 5525 (1988); (*c*) L.A. Trimble, and J.C. Vederas. J. Am. Chem. Soc. **108**, 6397 (1986); (*d*) W. Oppolzer, and R. Moretti. Tetrahedron **44**, 5541 (1988); (*e*) Y. Yamamoto, S. Hatsuya, and J. Yamada. Tetrahedron Lett. **30**, 3445 (1989); (*f*) Y. Yamamoto, M. Yumoto, and J. Yamada. Tetrahedron Lett. **32**, 3079 (1991).
3. T.L. Gilchrist. *In* Comprehensive organic synthesis. Vol. 8. *Edited by* B.M. Trost. Pergamon Press, Oxford. 1991. p. 381.

© 2000 NRC Canada

4. (*a*) R.M. Moriarty, and I. Prakash. Synth. Commun. **15**, 649 (1985); (*b*) P. Beslin, and P. Marion. Tetrahedron Lett. **33**, 935 (1992).
5. S. Kobayashi, Y. Yamashita, and H. Ishitani. Chem. Lett. 307 (1999).
6. (*a*) G. Guanti, L. Banfi, and E. Narisano. Tetrahedron, **44**, 5553 (1988); (*b*) C. Greck, L. Bischoff, F. Ferreira, C. Pinel, E. Piveteau, and J.P. Genêt. Synlett. 475 (1993); (*c*) P.C.B. Page, S.M. Allin, E.W. Collington, and R.A.E. Carr. Tetrahedron Lett. **35**, 2427 (1994); (*d*) A.R. Sting and D. SeeBach. Tetrahedron, **52**, 279 (1996); (*e*) J.M. Harris, R. McDonald, and J.C. Vederas. J. Chem. Soc. Perkin Trans. 1, 2669 (1996).
7. D.A. Evans and S.G. Nelson. J. Am. Chem. Soc. **119**, 6452 (1997).
8. D.A. Evans and D.S. Johnson. Org. Lett. **1**, 595 (1999).
9. (*a*) S. Kobayashi. Eur. J. Org. Chem. 15 (1999); (*b*) S. Kobayashi and S. Iwamoto. Tetrahedron Lett. **39**, 4697 (1998).
10. (*a*) A. Yanagisawa, H. Nakashima, A. Ishiba, and H. Yamamoto. J. Am. Chem. Soc. **118**, 4723 (1996); (*b*) A. Yanagisawa, Y. Matsumoto, H. Nakashima, K. Asakawa, and H. Yamamoto. J. Am. Chem. Soc. **119**, 9319 (1997); (*c*) A. Yanagisawa, Y. Matsumoto, K. Asakawa, and H. Yamamoto. J. Am. Chem. Soc. **121**, 892 (1999); (*d*) D. Ferraris, B. Young, T. Dudding, and T. Lectka. J. Am. Chem. Soc. **120**, 4548 (1998).
11. V.J. Jephcote, A.J. Pratt, and E.J. Thomas. J. Chem. Soc. Perkin Trans. 1, 1529 (1989).

© 2000 NRC Canada

Diastereoselective alkylations of chiral, phosphorus-stabilized carbanions: *N*-alkyl substituent effects in *P*-alkyl-1,3,2-diazaphosphorinane 2-oxides

Scott E. Denmark and Jung-Ho Kim

Abstract: A systematic study of the diastereoselective alkylation of anions derived from racemic *N*-substituted *P*-alkyl 1,3,2-diazaphosphorinane 2-oxides was carried out with variation of the *N*-substituent. High diastereoselectivity for the methylation of a *P*-benzyl anion has been achieved with *N*-neopentyl derivative **5d**. Similarly, a *P*-ethyl anion derived from *N*-neopentyl derivative **6d** showed high diastereoselectivity upon benzylation. The observed difference in alkylation diastereoselectivity between *P*-ethyl and *P*-benzyl anions for various *N*-alkyl substituents is discussed.

Key words: phosphonamide-stabilized carbanions, alkylation, asymmetric, stereoselective, organolitihium.

Résumé : On a réalisé une étude systématique de l'alkylation diastéréosélective d'anions dérivés de 2-oxydes de *P*-alkyl-1,3,2-diazaphosphorinanes *N*-substitués racémiques portant divers substituants sur l'azote. Avec l'anion **5d** qui porte des groupes *P*-benzyle et *N*-néopentyle, la méthylation se fait avec une diastéréosélectivité élevée. Il en est de même lors de la réaction de benzylation de l'anion **6d** qui porte des groupes *P*-éthyle et *N*-néopentyle. On discute des différences observées dans la diastéréosélectivité des anions *P*-éthyle et *P*-benzyle portant divers substituants *N*-alkyles.

Mots clés : carbanions phosphonamides stabilisés, alkylation, asymétrique, stéréosélective, organolithium.

[Traduit par la Rédaction]

Introduction and background

In recent years there has been considerable interest in carbon–carbon single-bond forming reactions involving heteroatom-stabilized carbanions (for reviews see ref. (1)). Among them, phosphorus-based reagents have great potential for auxiliary-based chiral modification (2). As part of an ongoing program on the chemistry of chiral, phosphorus-stabilized carbanions (3) we have been interested in developing general auxiliaries which give rise to highly selective transformations at the anionic carbon. The design criteria we formulated require that the auxiliary be capable of biasing the rotameric population about the C—P bond and also shield one of the anion faces to achieve a highly selective approach of the electrophilic reagents. In addition, other practical considerations were: (*i*) ease of synthesis in enantiomerically pure form, (*ii*) chemical stability under the attachment and recovery conditions, and (*iii*) structural simplicity while providing high stereochemical bias. Auxiliaries (4, 5) and controller groups (6) of C_2-symmetry have been utilized a great deal in asymmetric synthesis. In the chemistry of phosphorus-stabilized anions as well, Hanessian has pioneered the use of the 1,2-cyclohexanediamine based auxiliary for controlling the environment in a phosphonamide (7). Cyclic phosphonamides derived from C_2-symmetric diamines exist as a single pair of enantiomers because phosphorus is not a stereogenic center. Therefore, these auxiliaries can eliminate problems associated with amino alcohol auxiliaries in which the P-atom is stereogenic and contains a strong P—O bond (3*f*). As part of our examination of the relationship of anion structure and reaction stereoselectivity, we were interested in evaluating the various aspects of ring size, polycyclic structure, and nitrogen substituent in the design of phosphorus-based auxiliaries and the investigation of the anions derived therefrom. With this in mind we have chosen a collection of candidates in the C_2-diamine family to survey (Chart 1).

Our previously reported X-ray crystal structural analysis (8) of the lithio 2-benzyl-1,3-dimethyl-1,3,2-diazaphosphorinane 2-oxide showed that the anion is intrinsically chiral as the nitrogens are pyramidal and the *N*-methyl groups are oriented in equatorial and axial positions (Fig. 1). Furthermore, the key features of this structure are: (*i*) there is no C-Li contact, (*ii*) the carbanion is almost planar, and (*iii*) the phenyl group is oriented *anti* to the P=O bond (O–P–C–C dihedral angle = 168.9°). Further studies on the dynamic, solution behavior (8*a*, 9) of this and related anions and computational studies (10) have shown that the rotational

Received July 28, 1999. Published on the NRC Research Press website on May 19, 2000.

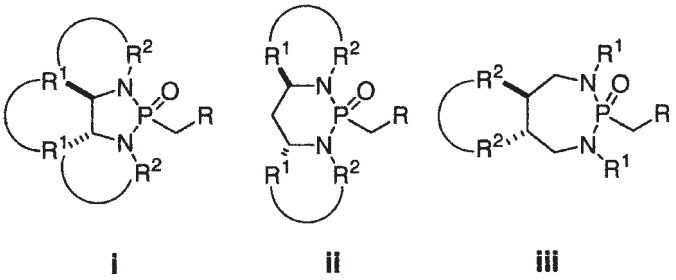
Dedicated to Professor Stephen Hanessian in recognition of his significant contributions to the art of organic synthesis

S.E. Denmark[1] and J.-H. Kim. Roger Adams Laboratory, Department of Chemistry, University of Illinois, Urbana, IL 61801, U.S.A.

[1]Author to whom correspondence may be addressed at: University of Illinois, Department of Chemistry, 245 Roger Adams Laboratory, Box 18, 600 S. Mathews Avenue, Urbana, IL 61801, U.S.A. Telephone: (217) 333-0066. Fax: (217) 333-3984. e-mail: denmark@scs.uiuc.edu

© 2000 NRC Canada

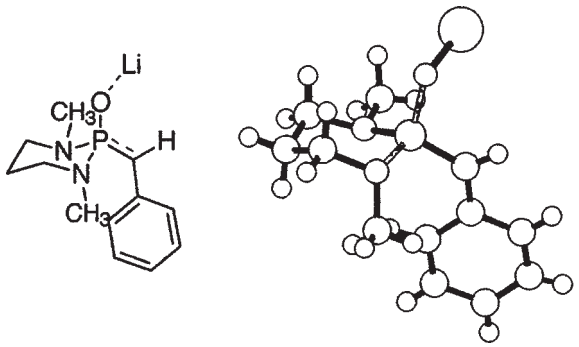
Chart 1.



barrier around the C—P bond in the benzyl anion is extremely low (ca. 6–8 kcal/mol). On the basis of the observations in the simple six-membered ring system, the chirally modified diazaphosphorinane **ii** was selected to investigate alkylation behavior of the derived *P*-alkyl anions. By comparison to five- and seven-membered analogs **i** and **iii**, system **ii** has the advantage of having the *N*-alkyl group closest to the anionic center due to ring angles[2].

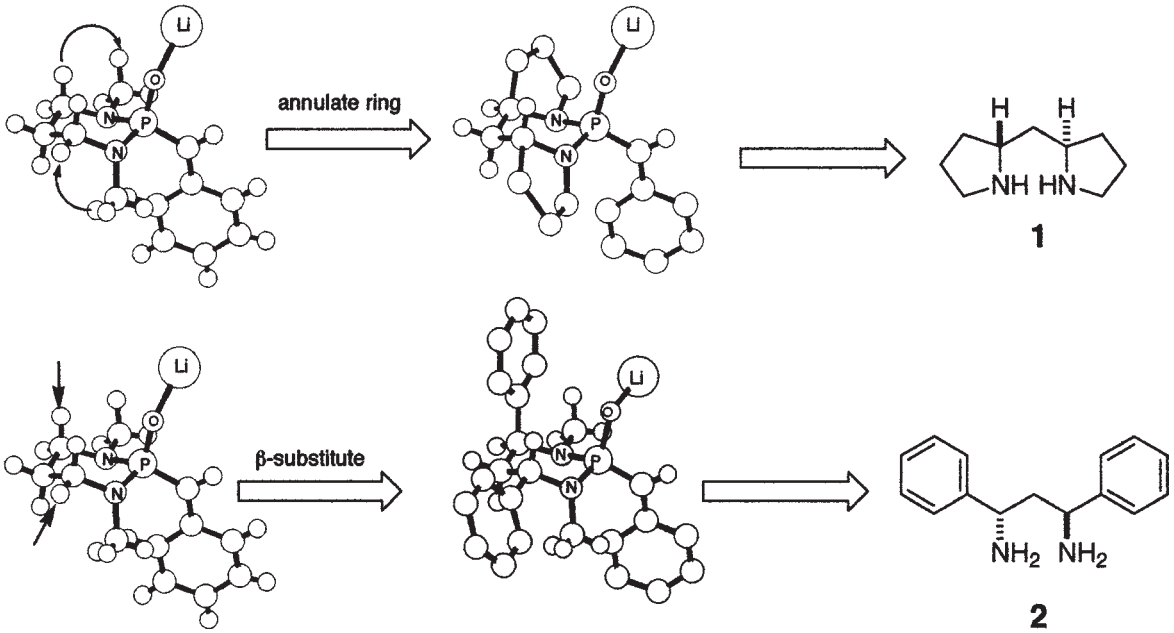
The key controlling attribute to obtaining high selectivity in alkylation was expected to be the ability to preordain the disposition of the N-substituents which in turn provide the chiral environment necessary for asymmetric reaction. On the basis of the assumption that chirally modified system **ii** would maintain the basic features of the parent system as elucidated in the X-ray crystal structure (8), diamines **1** and **2** were chosen as specific models to be investigated (Fig. 2). As shown in Fig. 2, the two proposed mechanisms for controlling the disposition of the N-substituents are: (*i*) annulating two five-membered rings to the central 1,3,2-diazaphospholidine ring thus leading to the dipyrrolidinomethane **1**, and (*ii*) placing substituents at the C(4) and C(6) positions to influence the hybridization of the nitrogen through torsional interactions. The *P*-alkyl anions derived from **1** and **2** provide six-membered ring phosphorus heterocycles which are expected to maintain a chair conformation, though the distortions due to the axially oriented phenyl group were not a priori obvious. Additionally, the *P*-benzyl-1,3,2-diazaphosphorinane 2-oxide anions generated from diamines **1** and **2** should adopt a conformation similar to the model in which the nitrogens are pyramidal. Thus, the disposition of the *N*-alkyl groups or the two *N*-methylenes of the fused rings distinguish the faces in the anions.

Fig. 1. Chem-3D presentation of lithio 2-benzyl-1,3-dimethyl-1,3,2-diazaphosphorinane 2-oxide (8).



In a preliminary study we prepared the tricyclic *P*-benzyl diazaphosphorinane **3** derived from **1** by simple condensation with benzylphosphonic dichloride[3] (11). The methylation diastereoselectivity of the lithio anion derived from **3**

Fig. 2. Chiral 1,3-diamine design to control nitrogen substituent pyramidality.

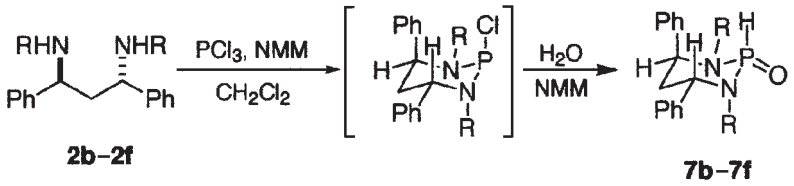


[2] In the five-membered-ring analog **i**, the N-substituents are pulled away from the anion due to the external bond angles. In the seven-membered analog **iii**, the ring is considerably more flexible allowing the N-substituents to avoid the anionic center.

[3] The diamine **3** was prepared in enantiomerically enriched form (96% ee) from L-proline in nine steps and convertd to **3** using benzylphosphonic dichloride.

© 2000 NRC Canada

Table 1. Preparation of the cyclic phosphoramides **7b**–**7f**.

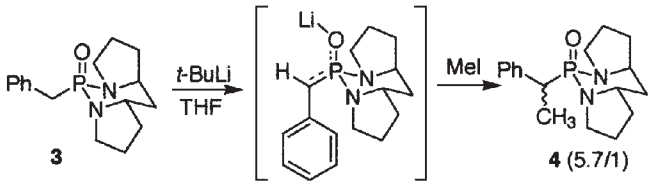


Entry	Diamine	R	Phosphite	Yield (%)[a]
1	**2b**	Et	**7b**	63[b]
2	**2c**	*i*-Pr	**7c**	82
3	**2d**	*t*-BuCH_2	**7d**	96
4	**2e**	PhCH_2	**7e**	92
5	**2f**	2,4,6-$(CH_3)_3C_6H_2CH_2$	**7f**	82[b]

[a]Yields are for isolated products after chromatography.

[b]Triethylamine was used.

Scheme 1.



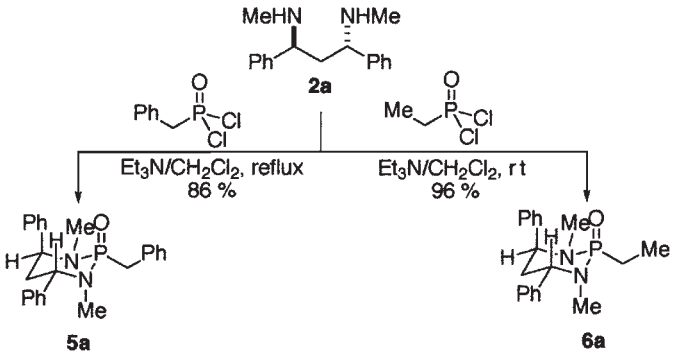
was 5.7/1 (Scheme 1). Since perhydropyrimidines normally exist in chair conformations (12), we expected the tricyclic system **3** to adopt a *cis*/*anti*/*cis* chair conformation thereby forcing the two different methylene units to orient in equatorial and axial positions. Thus, electrophiles approach away from the axial *N*-methylene unit. Unfortunately, the steric bulk of the methylene unit does not provide a sufficiently strong π-facial discrimination. Further variation was considered to be impractical since placing additional substituents in the five-membered rings would be synthetically challenging. Consequently, we chose to pursue the opportunities provided by the acyclic 1,3-diamine **2** which is much more amenable to variation in the size of the N-substituent. We describe herein a systematic examination of the effect of steric bulk of the N-substituent in the alkylation selectivity of anions derived from diamine **2**.

Results

Preparation of *P*-alkyl-1,3,2-diazaphosphorinanes

For the systematic study of the steric effect of *N*-alkyl substituents, six different *P*-benzyl-1,3,2-diazaphosphorinanes (*N*-methyl (**5a**), *N*-ethyl (**5b**), *N*-isopropyl (**5c**), *N*-neopentyl (**5d**), *N*-benzyl (**5e**), and *N*-mesitylmethyl (**5f**)) and three different *P*-ethyl-1,3,2-diazaphosphorinanes (*N*-methyl (**6a**), *N*-isopropyl (**6c**), and *N*-neopentyl (**6d**)) were chosen. All six requisite diamines (**2a**–**f)** were prepared by our previously reported procedures (13). Generally, the preparation of *P*-alkyl-1,3,2-diazaphosphorinanes was accomplished in a straightforward manner by combining the appropriate alkylphosphonic dichlorides (14) with the requisite diamines in the presence of triethylamine (2, 15). Sterically less demanding *N*,*N*′-dimethyl-1,3-diphenyl-1,3-propanediamine (**2a**) was amenable to these reaction conditions, providing *P*-benzyl- and *P*-ethyl diazaphosphorinane **5a** and **6a** in 86% and 96% yield, respectively (Scheme 2). Unfortunately, other higher alkyl diamines (**2b**–**f**) did not provide products in reasonable yield presumably due to the steric bulk of the diamines.

Scheme 2.



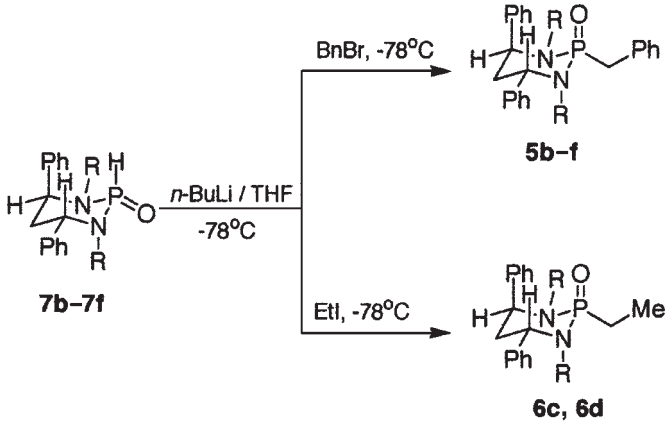
Fortunately, diamines **2b**–**f** did react with phosphorus trichloride (PCl_3) in the presence of *N*-methylmorpholine (NMM) or triethylamine (Et_3N) to afford *P*-chlorodiazaphosphorinanes which upon hydrolysis produced cyclic hydrogen phosphites **7b**–**f** in good yield (63–96%) (Table 1). Phosphites **7b**–**f** were unexpectedly stable and could be purified by silica gel column chromatography. It is important to note the buttressing effect of the 4 and 6-phenyl groups toward *N*-alkyl groups which will make the phosphorus center more sterically hindered and thus less sensitive to oxidation. The characteristic structural feature of phosphites **7b**–**f** is strong tautomeric preference for cyclic hydrogen phosphondiamide structure as evidenced by a strong infrared stretching band for the P=O group (1217–1246 cm^{-1}) and a diagnostic stretching band for the P—H unit (2211–2384 cm^{-1}) (16). The magnitude of the P—H coupling constant (J_{PH} = 595–629 Hz) is strongly suggestive of an axial P—H bond (17) The characteristic NMR spectral data are summarized in Table 2. Unlike trivalent trialkyl phosphites in which the phosphorus resonance appears in the neighborhood of 140 ppm (17), all resonances of the hydrogen phosphonamides **7b**–**f** appeared at –0.86–12.69 ppm.

© 2000 NRC Canada

Table 2. ^{31}P NMR data of phosphites **7b–f** and phosphorinanes **5a–f** and **6a**, **6c**, **6d**.

Entry	R	Phosphite, **7**, δ (ppm)	R′	Phosphorinane, **5**/**6**, δ (ppm)
1	Me		CH_2Ph	**5a**, 27.67
2	Me		Et	**6a**, 31.73
3	Et	**7b**, 3.61	CH_2Ph	**5b**, 24.96
4	*i*-Pr	**7c**, –0.86	CH_2Ph	**5c**, 21.64
5	*i*-Pr		Et	**6c**, 27.51
6	*t*-$BuCH_2$	**7d**, 12.69	CH_2Ph	**5d**, 24.45
7	*t*-$BuCH_2$		Et	**6d**, 30.99
8	$PhCH_2$	**7e**, 5.81	CH_2Ph	**5e**, 24.84
9	$(CH_3)_3C_6H_2CH_2$	**7f**, 3.09	CH_2Ph	**5f**, 26.87

Table 3. Preparation of *P*-alkyl 1,3,2-diazaphosphorinane 2-oxides.



Entry	Phosphite	R	Phosphonamide	Yield (%)[a]
1	**7b**	Et	**5b**	93
2	**7c**	*i*-Pr	**5c**	61
3	**7c**	*i*-Pr	**6c**	97
4	**7d**	*t*-$BuCH_2$	**5d**	81
5	**7d**	*t*-$BuCH_2$	**6d**	62
6	**7e**	$PhCH_2$	**5e**	83
7	**7f**	2,4,6-$(CH_3)_3C_6H_2CH_2$	**5f**	61

[a]Yields are for isolated products after chromatography.

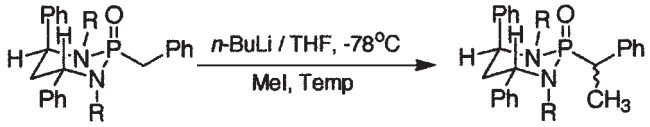
Though less acidic than the corresponding dioxa analogs,[4] the hydrogen phosphonamides **7b–f** are sufficiently acidic to be deprotonated by *n*-BuLi at low temperature (–78°C). Importantly, no nucleophilic addition products to the phosphorus center were observed in the diaza analogs, presumably due to a combination of steric hindrance coupled with electronic deactivation of phosphonamides versus phosphonates. The use of triethylamine led to a sluggish reaction even at elevated temperatures and hydride bases such as NaH and KH were not suitable, affording unidentified side products. However, treatment of hydrogen phosphites **7b–f** with *n*-BuLi followed by alkylation with ethyl iodide and benzyl bromide afforded *P*-alkyl-1,3,2-diazaphosphorinane 2-oxides **5b–f, 6c,** and **6d**, in reasonable yields (61–97%) (Table 3).

The structures of the *P*-alkyl-1,3,2-diazaphosphorinanes **5a–f** and **6a**, **6c**, **6d**, and were secured by spectroscopic methods. First, in the ^{13}C NMR spectra, the α-methylene carbons displayed resonances at 38.55–43.40 ppm ($^1J_{CP}$ = 102.7–121.6 Hz) for *P*-benzyl-1,3,2-diazaphosphorinane 2-oxides **5a–f** and 25.43–29.35 ppm ($^1J_{CP}$ = 121.8–129.7 Hz) for *P*-ethyl-1,3,2-diazaphosphorinanes **6a**, **6c**, and **6d**. Second, diagnostic α-methylene protons showed phosphorus-coupled eight-line patterns at 3.35–3.69 ppm for *P*-benzyl-1,3,2-diazaphosphorinanes **5a–f** and 1.88–2.38 ppm for *P*-ethyl-1,3,2-diazaphosphorinanes **6a**, **6c**, and **6d**. Finally, the observation of a strong, characteristic P=O stretch (1208–1271 cm^{-1}) obviously eliminated the possibility of the formation of regioisomeric *O*-alkylated products. It is noteworthy that the reaction of the lithiated phosphite with silylating agents provided *O*-silylated phosphite exclusively (18). Additional characteristic features were noted in the ^{31}P NMR as all *P*-alkyl 1,3,2-diazaphosphorinane 2-oxides displayed resonances in the region shifted downfield (21.64–31.73 ppm)

[4]Diethyl hydrogenphosphonate is easily deprotonated at 0°C using NaH or Et_3N.

© 2000 NRC Canada

Table 4. Methylations of *P*-benzyl-1,3,2-diazaphosphorinane 2-oxides **5a**–**f**.

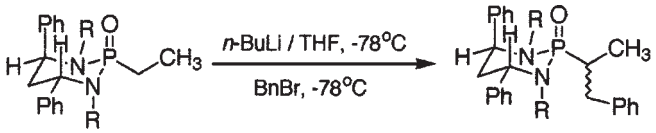


5a–5f **8a–8f**

Entry	5	R	Time (h)	Temp (°C)	d.s.	Yield (%)[a]
1	**5a**	Me	2.5	–78	7.7:1[b]	**8a**, 91
2	**5b**	Et	3.0	–78 to –60	1.6:1[b]	**8b**, 78[d]
3	**5c**	*i*-Pr	3.0	–78 to –60	1.4:1[c]	**8c**, 87
4	**5d**	*t*-BuCH_2	3.0	–78 to –60	11.5:1[c]	**8d**, 82[e]
5	**5e**	PhCH_2	2.0	–78	3.0:1[c]	**8e**, 96
6	**5f**	$(CH_3)_3C_6H_2CH_2$	2.0	–78	2.9:1[c]	**8f**, 94

[a]Yields are for isolated products after chromatography.
[b]Ratio determined by HPLC.
[c]Ratio determined by ^{31}P NMR.
[d]15% of **5b** recovered.
[e]11% of **5d** recovered.

Table 5. Diastereoselective benzylations of *P*-ethyl-1,3,2-diazaphosphorinane 2-oxide **6a**, **6c**, and **6d**.



6a, 6c, 6d **9a, 9c, 9d**

Entry	6	R	d.s.	Yield (%)[a]
1	**6a**	Me	1.3:1[b]	**9a**, 83
2	**6c**	*i*-Pr	3.6:1[c]	**9c**, 96
3	**6d**	*t*-BuCH_2	11.5:1[c]	**9d**, 98

[a]Yields are for isolated products after chromatography.
[b]Ratio determined by ^{31}P NMR.
[c]Ratio determined by HPLC.

compared to those of hydrogen phosphoramides **7b**–**f** (Table 2). The ring conformation is believed to adopt an axial P=O unit on the basis of X-ray crystallographic evidence (19) and the large difference in ^{1}H NMR resonances for HC(4) and HC(6) in **5** and **6** compared to **7**.

Diastereoselective methylation of *P*-benzyl-1,3,2-diazaphosphorinane 2-oxides 5a–f

The methylation of benzylic carbanions derived from **5a**–**f** was examined first. The sterically least demanding *N*-methyl analog **5a** and *N*-benzylic derivatives **5e**, and **5f** reacted rapidly and were completely methylated at –78°C within 2 to 2.5 h. However, in the case of sterically demanding substrates **5b**, **5c**, and **5d**, the reaction was sluggish at –78°C but proceeded at –60°C within 3 h. Clearly, the steric bulk of the *N*-alkyl group controlled the facility of the approach of the electrophile to the anionic center. *N*-Benzylic derivatives **5e** and **5f**, which are somewhat bulkier than methyl groups, may also benefit from contributions of the aromatic ring. As shown in Table 4, the methylation of the *P*-stabilized benzylic carbanions Li^+**5a**–**f**$^-$ proceeded with moderate to high diastereoselectivity. Interestingly, diastereoselectivity was not merely a function of the steric bulk of the alkyl group on the nitrogen as the *N*-methyl analog **5a** afforded remarkably high diastereoselectivity compared to the corresponding *N*-ethyl (**5b**) and *N*-isopropyl (**5c**) analogs. The most sterically demanding *N*-neopentyl analog **5d** showed the highest selectivity (entry 4). Moderate selectivities were found in the case of benzyl and mesityl analogs **5e** and **5f**.

Diastereoselective benzylations of *P*-ethyl-1,3,2-diazaphosphorinanes 6a, 6c, and 6d

P-Ethyl anions were much more reactive than the corresponding *P*-benzyl anions as evidenced by the consumption of educt which was complete at –78°C within 30 min. Moreover, in contrast to the alkylation behavior of the *P*-benzyl anions, the benzylation of the *P*-ethyl anions from **6a**, **6c**, and **6d** showed a qualitative linear dependency of diastereoselectivity as a function of steric bulk of the *N*-alkyl groups (Table 5). The most sterically demanding *N*-neopentyl

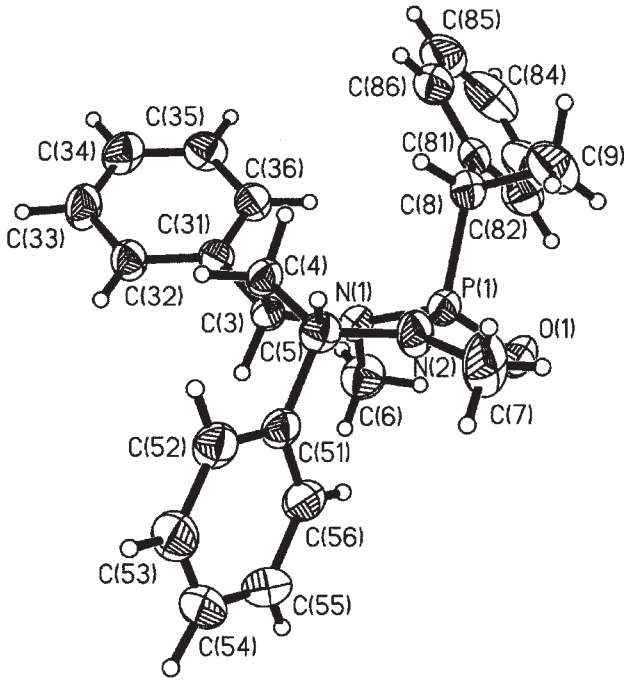
© 2000 NRC Canada

Table 6. Data for the methylation products **8a**–**8f**.

N-Substituent	**8**	ratio	^{31}P NMR (δ, ppm)		HPLC (t_R, min)[a]	
			major	minor	major	minor
Me	**8a**	7.7:1	31.80	29.82		
Et	**8b**	1.6:1	29.34	28.76	8.37	7.25
i-Pr	**8c**	1.4:1	29.16	28.13	8.57	7.30
t-BuCH_2	**8d**	11.5:1	28.47	29.55	8.30	9.62
PhCH_2	**8e**	3.4:1	29.54	29.54	19.15	16.39
$(CH_3)_3C_6H_2CH_2$	**8f**	2.4:1	30.42	32.15		

[a]Column: Supelco LC-NH_2.

Fig. 3. ORTEP (35% thermal ellipsoids) representation of (*S**,*S**,*S**)-**8a**.



analog **6d** gave the highest selectivity (entry 3) whereas the sterically least demanding *N*-methyl analog **6a** afforded the lowest selectivity (entry 1). The disparate behavior of the *P*-benzyl and *P*-ethyl series may ultimately relate to the differences in conformational composition and rotational barriers (vide infra). The discrepancy between *N*-isopropyl analogs **5c** and **6c** might also be explained by the size difference of the electrophiles (benzyl vs. methyl). An electrophile dependence in the alkylation of related *P*-benzyl 1,3,2-oxazaphosphorinane 2-oxides has been previously noted, however in this case, methylation proceeds with higher selectivity than benzylation (3*c*)[5].

Stereochemical course of the reaction

In the course of the routine characterization of the alkylation products we noticed an interesting trend which suggested that the sense of asymmetric induction may not be the same for all of the substrates **5a–5f.** The two diagnostic features are the ^{31}P NMR chemical shifts and the HPLC elution orders for the two diastereomeric methylation products (Table 6). For the *N*-methyl (**8a**), *N*-ethyl (**8b**), and *N*-isopropyl (**8c**) alklyation products, the major diastereomer displays a lower field ^{31}P NMR chemical shift and is more strongly retained on the HPLC (aminopropyl silica). The *N*-benzyl alkylation products (**8e**) display a single ^{31}P resonance, but have a similar behavior on HPLC. Curiously, the *N*-neopentyl (**8d**) and *N*-mesityl (**8f**) analogs exhibit the reverse trend, i.e., the major diastereomer appears at *higher field* and is *less retained* on the HPLC. We thus suspected that the sense of relative asymmetric induction for **5a–5c** and **5e** might be different from that for **5d** and **5f**. This is an intriguing hypothesis which would require a complex conformational/mechanistic analysis to explain the reversal. It would however, help clarify the "non-linear" dependence of alkylation selectivity on N-substituent. Thus, to verify this hypothesis we elected to independently establish the configurations of the major alkylation products from the most selective representatives in the series, **8a** and **8d**.

The sense of asymmetric induction in the major alkylation product **8a** was established by a single crystal X-ray analysis of the racemic compound. The ORTEP image is shown in Fig. 3. Simple inspection of the structure provides the answer that the (*S*,*S*)-diazaphosphorinane induced the *S* configuration at the newly created stereogenic center in the alkylation. Other implications of the structure and an interpretation of the origin of stereoselection are provided in the discussion section.

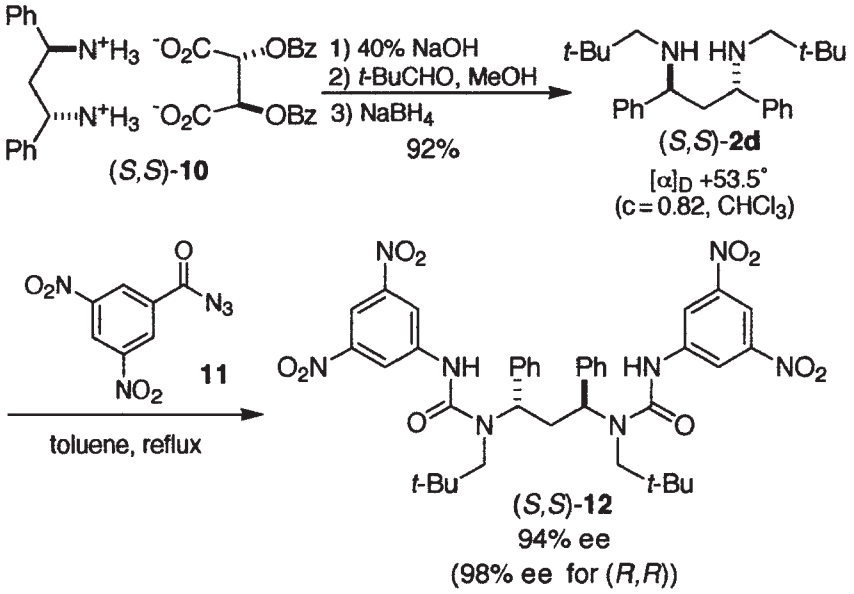
To establish the stereochemical course for the alkylation reaction of **5d**, diamine **2** was resolved with dibenzoyl-D-tartaric acid according to the literature procedure (20). The enantiomeric purity of the diamine was determined for the *N*,*N*-dineopentyldiamine derivative **2d** by analyzing the Pirkle derivative by chiral HPLC on an *N*-naphthyl-L-alanine column (21). The enantiomeric excesses were 94% for the (*S*,*S*)-enantiomer and 98% for (*R*,*R*)-enantiomer (Scheme 3).

Preparation of enantiomerically enriched (*S*,*S*)-**5d** was carried out following the procedure for the racemic material described previously (Scheme 4). Thus, treatment of diamine (*S*,*S*)-**2d** with PCl_3 and Et_3N followed by hydrolytic workup gave phosphite (*S*,*S*)-**7d** in 90% yield. Subsequent transformation of (*S*,*S*)-**7d** to (*S*,*S*)-**5d** was performed in 81% yield. The asymmetric methylation of (*S*,*S*)-**5d** was accomplished by treatment with *n*-BuLi followed by addition of an excess of methyl iodide to give a 15.7:1 ratio of mixture of diastereomers of (–)-**8d** and 21% of unreacted (*S*,*S*)-**5d**. The

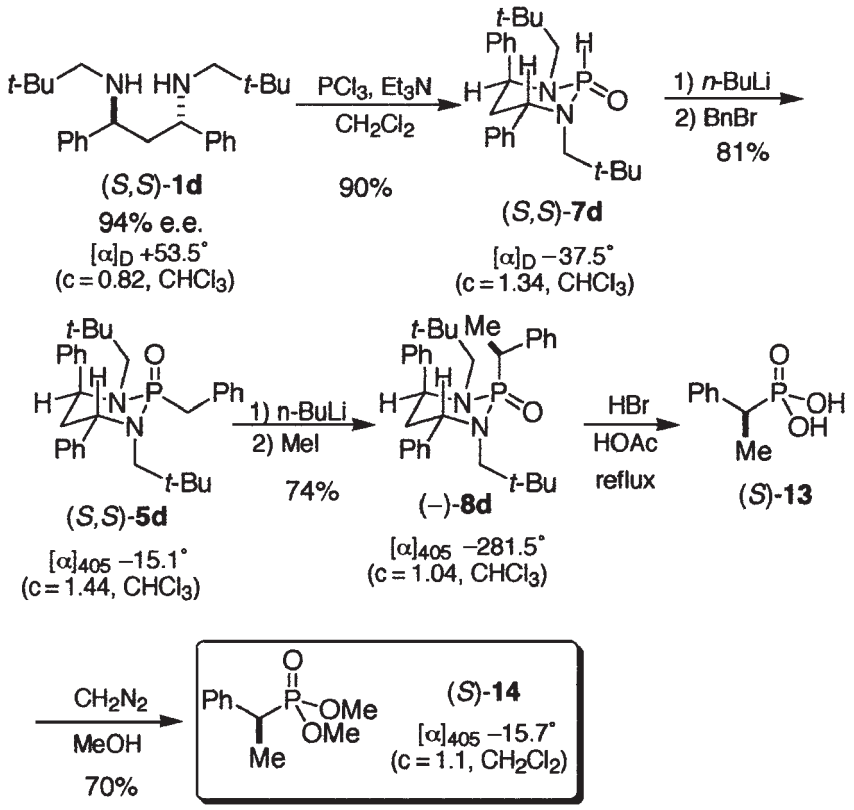
[5] Attempted benzylation of Li^+**5d**$^-$ at –60°C was unsuccessful. Warming to –20°C resulted in a diastereomeric mixture (2:1) of benzylated products.

© 2000 NRC Canada

Scheme 3.



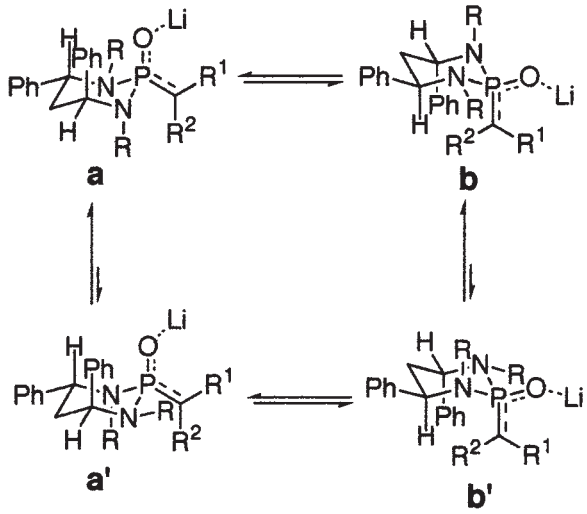
Scheme 4.



mixture of diastereomers was subjected to conventional hydrolysis conditions to give the phosphonic acid: 1 N HCl in THF, 6 N or 12 N HCl in dioxane. However, the very sterically hindered alkylation product (–)-**8d** was unaffected by these conditions. Eventually, (–)-**8d** was cleanly hydrolyzed with aqueous 48% HBr in refluxing acetic acid to give phosphonic acid (–)-**13**. The phosphonic acid (–)-**13** was purified by ion-exchange column chromatography and then was converted to the dimethyl phosphonate ester (–)-**14** by treatment with diazomethane (70% yield) followed by further purification by silica gel column chromatography. The absolute configuration of the dimethyl phosphonate (–)-**14** was confirmed to be *S* by comparison of its specific rotation with the literature value (3*c*, 3*f*). Therefore, net result of the

© 2000 NRC Canada

Fig. 4. Limiting chair-like conformations of the anions.



reaction is stereochemical conversion of 2-benzyl-1,3,2-diazaphosphorinane 2-oxide ((*S*,*S*)-**5d**) to dimethyl phosphonate (*S*)-**14**. *This fact then establishes unambiguously that the stereochemical course of alkylation of* ***5a*** *and* ***5d*** *proceeded in the same relative sense.*

Discussion

The central issue in all of our studies of phosphorus-stabilized anions is to create a structural model of reactivity which provides an understanding and ultimately a prediction of the stereochemical course of the reactions at the anionic centers. For the molecules examined in this study, the key question is the way in which the chirality of the 1,3,2-diazaphosphorinane skeleton (due to the phenyl substituents) is manifest in the dissymetry of the two faces of the benzylic anion.

To begin the analysis, we make recourse to the X-ray crystal structures of the achiral, unsubstituted lithio 1,3,2-oxazaphosphorinane 2- oxides, e.g., Fig. 1. The first point of consideration is the aggregation state of the anions. Even though the model anion crystallized as a dimer (8), the more sterically demanding 3,5-diphenyl substituted chiral anions might exist as *monomeric species*. Moreover, the aggregation state of these anions has been shown to be dependent on the nature of the substituents on nitrogen. For example, the anion derived from highly sterically demanding 1,3-bis(*tert*-butyl)-2-isopropyl-1,3,2-diazaphosphorinane has shown characteristic dynamic solution behavior of a monomer (10)[6]. That notwithstanding, Denmark et al. (8) have previously shown that aggregation effects for the oxaza-analog did not influence diastereoselectivity (21). Indeed, the anion derived from enantiomerically enriched (94% ee) diazaphosphorinane (*S*,*S*)-**5d** produced a diastereomeric mixture in a similar ratio compared to the anion derived from (±)-**5d**. Addition of the highly coordinating triamine, pentamethyldiethylentriamine, to the reaction in THF did not change the reaction selectivity. This implied that either the aggregate structure (homochiral vs. heterochiral dimers) is not responsible for the different alkylation selectivities or the reactive species are monomeric.

Fig. 5. Rationale for the diastereoselective methylation of *P*-benzyl-1,3,2-diazaphosphorinanes (**5**).

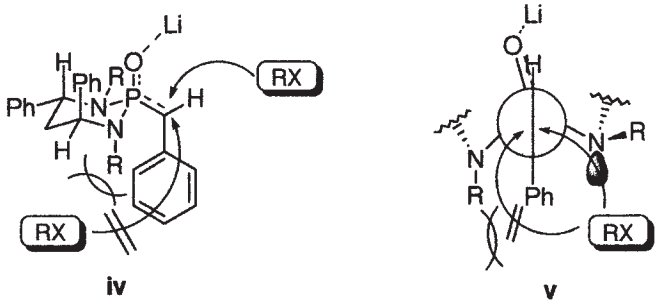
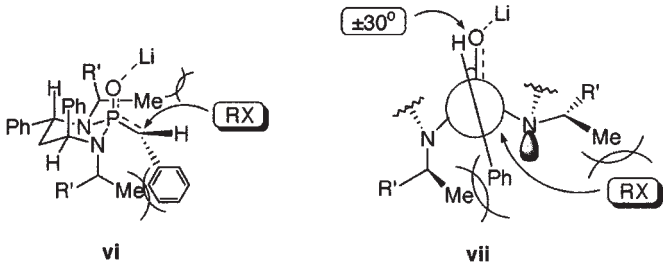


Fig. 6. Proposed skewed conformation of the anions.



The second critical issue is the conformation of the anion. Without direct spectroscopic information, we can only speculate about the ring conformation on the basis of the X-ray structures of unsubstituted anions and the neutral alkylation product (*S**,*S**,*S**)-**8a**. Close inspection of this structure reveals a surprising, albeit understandable deviation from the ideal chair conformation usually seen for these structures. The ring in (*S**,*S**,*S**)-**8a** is a flattened boat. The reason for this conformation most likely originates in a second unusual feature namely the axial positioning of the 1-phenylethyl group which itself results from an avoidance of non-bonding interactions of this phosphorus substituent with the neighboring *N*-methyl groups. Thus, to avert severe 1,3-diaxial interactions with one of the phenyl groups, the ring distorts to a boat. The flattening of the ring is due to the near planarity of the nitrogen atoms. It is however noteworthy that N(1) is slightly pyramidalized (Σangles = 356.3°) compared to N(2) (Σangles = 359.9°). Finally, the locations of the peripheral *N*-alkyl groups are determined by a combination of the ring conformation, gauche interactions with the phenyl groups at C(3) and C(5) and the hybridization of the nitrogen atoms.

Clearly, the proximal *N*-alkyl groups of the anions served as the chiral controlling elements during the course of the alkylation reaction. If we assume that the anion takes up a chair-like conformation, the limiting structures to consider at depicted in Fig. 4. We propose that the preferred anion is represented by structures **a**/**a′** in which the phosphonyl oxygen (and attendant lithium counterion with solvent) is in an axial position and the phenyl group is antiperiplanar to the P—O bond (R^1 = H, R^2 = Ph). The **a**/**a′** equilibrium relates

[6] P.C. Miller. Unpublished results from these laboratories.

© 2000 NRC Canada

to the alternative invertomers at the nitrogen atoms assuming, as is the case in all 1,3,2-diazaphosphorinane 2-oxide anions, that one substituent is axial and one is equatorial. Examination of the non-bonding interactions of the substituents around the ring shows that vicinally located pair of *N*-alkyl *C*-phenyl groups prefer invertomer **a** due to the elimination of one gauche interaction.

The high diastereoselectivity obtained from *N*-neopentyl analog **5d** results from a strong stereochemical bias between two π-faces of the derived planar anion Li^+**5d**$^-$ in which the phenyl ring might similarly orient anti to the P=O bond as shown in the model. The simplified structure of the antiperiplanar anion is depicted as **iv** and Newman projection **v** in Fig. 5. The electrophile would approach from the side away from the axially disposed *N*-alkyl group to avoid van der Waals interactions. For the neopentyl derivatives, the differentially disposed *N*-*tert*-butyl groups tethered by a methylene chain locate differently with respect to the anionic center.

The low diastereoselectivity observed from the *P*-benzyl anions derived from *N*-ethyl and *N*-isopropyl derivatives is believed to arise from a change in location of the phenyl ring. The phenyl group of the anion is believed to exist in a skew form and thus reside anticlinal (±150°) to the P=O bond to avoid non-bonding interaction with the substituent on the axially disposed *N*-alkyl group. The reactive conformation of this anion (**vi**) along with its Newman (**vii**) are shown in Fig. 6. Approach of the electrophile to either face of this anion experiences similar interactions with either of the N-substituents thus affording little bias in the alkylation event.

The direct relationship of the diastereoselectivity to steric bulkiness of the *N*-alkyl groups in the case of benzylation of the *P*-ethyl anion is explained by invoking the antiperiplanar anionic conformer **vii**. Since the α-methyl group of the anion is comparably small, the interaction with axially disposed *N*-alkyl group is insufficient to force the anion to be skewed. Thus, the diastereoselectivity directly reflects the steric bulkiness of *N*-alkyl groups. The erosion of selectivity for *P*-ethyl anions is mostly due to the low rotation barrier of the P—C bond and the lesser bias toward the antiperplanar vs. the synplanar conformation.[7]

It should also be recognized that the anions may exist in flattened boat-like conformations with an axially standing *P*-benzyl group. Here, the shielding of the anion faces is much less predictable. Moreover, the anion ring conformation may in fact be dependent on the ring substituents, making a consistent analysis impossible.

In summary, the methylation of Li^+**5a**$^-$–Li^+**5h**$^-$ proceeds with moderate to high diastereoselectivity and was highly conformation dependent due to the *N*-alkyl substituents. The benzylation selectivity of Li^+**6a**$^-$, Li^+**6c**$^-$, and Li^+**6d**$^-$ showed linear dependency on the *N*-alkyl steric bulk. *N*-Neopentyl analogs **5d** and **6d** afforded the highest selectivities (92:8) in both cases. From a systematic study of *N*-alkyl substituents and a comprehensive understanding of the structure of the anions, new C_2-symmetric diamine-based auxiliaries and their utilities in the reaction of the phosphorus-based alkyl anions can be developed in the future.

Experimental section

General Methods

See supporting information.[8]

Starting materials

The diamines **2a**–**f** were prepared in these laboratories and the procedures have been reported elsewhere (14). Ethylphosphonic dichloride is commercially available. Benzylphosphonic dichloride was prepared by a literature procedure and used after recrystallization from pentane (15).

*(*RS*)-(4*l*,6*l*)-2-Benzyl-1,3-dimethyl-4,6-diphenyl-1,3,2-diazaphosphorinane 2-oxide (**5a**)*: In a 25-mL, three-necked round bottom flask equipped with a reflux condenser, a N_2 inlet tube, a rubber septum, and a magnetic stirring bar was placed with 0.57 mL (4.13 mmol) of Et_3N in 5 mL of CH_2Cl_2. This solution was heated to reflux and then 420 mg (1.65 mmol) of diamine **2a** in 6 mL of CH_2Cl_2 and 362 mg (1.73 mmol) of benzylphosphonic dichloride in CH_2Cl_2 (6 mL) were simultaneously added over 1 h by syringe pump. After heating to reflux for 10 h, the oil bath was removed. The cooled reaction mixture was poured into water (20 mL) and extracted with CH_2Cl_2 (3 × 30 mL). The extracts were dried (Na_2SO_4), filtered, and concentrated to give 700 mg of yellow orange oil, which was purified by SiO_2 column chromatography (EtOAc/*i*-PrOH, 19:1) to give 552 mg (86%) of diazaphosphorinane **5a** as a colorless solid. An analytical sample was obtained by recrystallization from pentane/Et_2O: mp 147–148°C. IR (CCl_4): 3065 w, 1271 s. TLC: R_f 0.35 (EtOAc/*i*-PrOH, 19:1). ^{1}H NMR (300 MHz): 7.45–7.29 (m, 11 H), 7.18 (t, J = 3.0, 2 H), 6.79 (dd, J = 6.0, 3.0, 2 H), 4.23 (dt, J = 13.7, 3.8, 1 H), 3.75 (dd, J = 11.5, 3.5, 2 H), 3.51 (dd, J = 19.4, 4.8, 1 H), 3.36 (dd, J = 18.5, 4.8, 1 H), 2.66 (d, J = 8.2, 3 H), 2.48 (d, J = 9.0, 3 H), 1.80 (m, 2 H, 2 H). ^{13}C NMR (75.5 MHz): 142.38 (J_{CP} = 6.5), 140.15, 134.76 (J_{CP} = 8.9), 129.82, 129.74, 128.67, 128.34, 128.29, 128.24, 127.36, 127.15, 126.84, 126.48, 126.41, 62.65, 58.58, 41.43 (J_{CP} = 3.5), 38.55 (J_{CP} = 121.6), 34.07 (J_{CP} = 4.6), 32.28 (J_{CP} = 3.0). ^{31}P NMR (121.6 MHz): 27.67. MS (70 eV): 390 (M^+ < 0.1), 299 (100). Anal. calcd. for $C_{24}H_{27}N_2OP$ (390.46): C 73.83, H 6.97, N 7.17, P 7.93; found: C 73.79, H 6.98, N 7.11, P 7.84.

*(*RS*)-(4*l*,6*l*)-1,3-Dimethyl-4,6-diphenyl-2-ethyl-1,3,2-diazaphosphorinane 2-oxide (**6a**)*: In a 50-mL, three-necked round bottom flask equipped with a N_2 inlet tube, a septum and a magnetic stirring bar was placed 370 mg (1.45 mmol) of diamine **2a** and 0.51 mL (3.63 mmol) of Et_3N in 15 mL of CH_2Cl_2. Ethylphosphonic dichloride (170 μL, 1.60 mmol) was then added by a syringe over a time period of 5 min.

[7] S.E. Denmark, K.A. Swiss, R.L. Dorow, P.C. Miller, and S.R. Wilson. In a detailed NMR study, no decoalescence of the achiral parent of **6a** was detected down to –117°C (500 MHz, ^{1}H NMR observation). Manuscript in preparation.

[8] General experimental methods along with full spectroscopic data and assignments for **5a-f**, **6a**, **6c**, **6d**, **7b-f**, **8a-f**, **9a**, **9c**, **9d**, and **14** (15 pages). Copies of material on deposit may be purchased from the Depository of Unpublished Data, Document Delivery, CISTI, National Research Council of Canada, Ottawa, ON, K1A OS2, CANADA.

© 2000 NRC Canada

After stirring for 22 h at rt, the reaction mixture was concentrated under reduced pressure. The residue was treated with EtOAc (15 mL), filtered, and the filter cake was washed with EtOAc (2 × 10 mL). The combined filtrates were washed with brine (15 mL) and the aqueous layer was extracted with EtOAc (2 × 10 mL). The combined organic extracts were dried (Na_2SO_4), filtered, and concentrated to give a colorless oil, which was purified by SiO_2 column chromatography (hexane/EtOAc/*i*-PrOH, 35:62:3, then EtOAc/*i*-PrOH (9:1) to afford 457 mg (96%) of diazaphosphorinane **6a** as a foam. An analytical sample was obtained by recrystallization from pentane/TBME: mp 66–68°C. TLC: R_f 0.30 (EtOAc/*i*-PrOH, 9:1). IR (CCl_4): 3030 w, 1267 s. ^{1}H NMR (300 MHz): 7.50–7.11 (m, 10 H), 4.33 (dt, J = 13.4, 3.8, 1 H), 3.78 (dd, J = 10.1, 1.7, 1 H), 2.70 (d, J = 8.1, 3 H), 2.54 (d, J = 8.8, 3 H), 2.40 (ddd, J = 14.2, 12.4, 4.6, 1 H), 2.20–1.88 (m, 3 H), 1.31 (dt, J = 19.3, 7.5, 3 H). ^{13}C NMR (75.5 MHz): 142.01 (J_{CP} = 5.0), 140.06, 128.44, 128.33, 127.13, 126.93, 126.29, 126.11, 62.33, 59.42, 41.90 (J_{CP} = 5.2), 33.52 (J_{CP} = 4.7), 32.66 (J_{CP} = 3.1), 25.43 (J_{CP} = 129.7), 7.68 (J_{CP} = 6.3). ^{31}P NMR (121.6 MHz) 31.73. MS (70 eV): 329 (M^+ + 1, 22), 328 (M^+, 98), 299 (100). Anal. calcd. for $C_{19}H_{25}N_2OP$ (328.39): C 69.49, H 7.67, N 8.53, P 9.43; found: C 69.49, H 7.69, N 8.51, P 9.40.

*Representative procedure for the preparation of cyclic hydrogen phosphites **7b-f***

The detailed procedure for the preparation of **7b** is given. For all of the other phosphites only the amounts of reagents and methods of purification are provided along with the analytical data.

*(*RS*)-(4*l*,6*l*)-1,3-Diethyl-4,6-diphenyl-1,3,2-diazaphosphorinane 2-oxide (**7b**)*: In a 25-mL, three-necked, round bottom flask, equipped with a reflux condenser, a rubber septum, a N_2 inlet tube and a magnetic stirring bar was placed 109 μL (1.25 mmol) of PCl_3, and a solution of 0.35 mL (2.51 mmol) of Et_3N in 5 mL of CH_2Cl_2. The mixture was heated to reflux and a solution of 335 mg (1.19 mmol) of diamine **2b** in CH_2Cl_2 (5 mL) was added via syringe over a time period of 5 min. After heating to reflux for an additional 1.5 h, 0.18 mL (1.25 mmol) of Et_3N was added. The oil bath was removed and the reaction mixture was poured into 20 mL of water and extracted with CH_2Cl_2 (3 × 20 mL). The combined extracts were dried (Na_2SO_4) and concentrated to give a yellow oil which was purified by SiO_2 column chromatography eluting with EtOAc/*i*-PrOH (19:1) to give 247 mg (63%) of cyclic phosphite **7b** as a colorless oil which solidified at –20°C. An analytical sample was obtained by recrystallization from Et_2O: mp 111–112°C. IR (CCl_4): 3031 w, 1240 s. TLC: R_f 0.34 (EtOAc/*i*-PrOH, 19:1). ^{1}H NMR (300 MHz): 7.74 (d, J = 599.4, 1 H), 7.45–7.23 (m, 10 H), 4.27–4.14 (m, 2 H), 3.37–3.16 (m, 2 H), 2.91–2.81 (m, 2 H), 2.36 (m, 2 H), 1.03 (t, J = 7.1, 3 H), 0.97 (t, J = 7.1, 3 H). ^{13}C NMR (75.5 MHz): 141.39, 140.72, 128.49, 128.41, 127.30, 127.35, 126.72, 126.28, 57.67, 57.47, 42.42 (J_{CP} = 9.6), 40.45 (J_{CP} = 5.6), 40.25 (J_{CP} = 8.1), 14.08, 13.44. ^{31}P NMR (121.6 MHz): 3.61. MS (70 eV): 328 (M^+, 29), 134 (100). Anal. calcd. for $C_{19}H_{25}N_2OP$ (328.39): C 69.49, H 7.67, N 8.53, P 9.43; found: C 69.50, H 7.67, N 8.50, P 9.37.

*(*RS*)-(4*l*,6*l*)-1,3-Bis-(1-methylethyl)-4,6-diphenyl-1,3,2-diazaphosphorinane 2-oxide (**7c**)*: From 315 mg (1.02 mmol) of diamine **2c**, 95 μL (1.09 mmol) of PCl_3 and 0.36 mL (3.27 mmol) of *N*-methylmorpholine followed by purification by SiO_2 column chromatography (hexane/EtOAc/*i*-PrOH, 35:62:3) was obtained 288 mg (79%) of **7c** as a colorless solid. A lager scale reaction gave 82% of **7c**. An analytical sample was obtained by recrystallization from pentane/Et_2O: mp 126–127°C. IR (CCl_4): 3067 w, 1275 s. TLC: R_f 0.32 (hexane/EtOAc/*i*-PrOH, 35:62:3). ^{1}H NMR (300 MHz): 7.83 (d, J = 595.4, 1 H), 7.51 (d, J = 7.2, 2 H), 7.41–7.27 (m, 8 H), 4.24 (m, 1 H), 4.11 (ddd, J = 13.2, 8.5, 5.1, 1 H), 3.58 (heptet, J = 6.8, 1 H), 3.38 (heptet, J = 6.8, 1 H), 2.40 (m, 2 H), 1.32 (d, J = 6.8, 3 H), 1.22 (d, J = 6.8, 3 H), 1.08 (d, J = 6.8, 3 H), 0.96 (d, J = 6.8, 3 H). ^{13}C NMR (75.5 MHz): 142.58, 128.28, 127.01, 126.69, 126.15, 55.56, 55.37, 49.73 (J_{CP} = 5.1), 48.16 (J_{CP} = 8.2), 43.67 (J_{CP} = 10.6), 22.00 (J_{CP} = 2.8), 21.68, 21.05 (J_{CP} = 4.1), 20.86. ^{31}P NMR (121.6 MHz): –0.86. MS (70 eV): 356 (M^+, 16), 176 (100). Anal. calcd. for $C_{21}H_{29}N_2OP$ (356.45): C 70.76, H 8.20, N 7.86, P 8.69; found: C 70.91, H 8.20, N 7.83, P 8.53.

*(*RS*)-(4*l*,6*l*)-1,3-Bis(2,2-dimethylpropyl)-4,6-diphenyl-1,3,2-diazaphosphorinane 2-oxide (**7d**)*: From 410 mg (1.12 mmol) of diamine **2d**, 107 μL (1.23 mmol) of PCl_3, and 0.41 mL (3.73 mmol) of *N*-methylmorpholine followed by purification by SiO_2 column chromatography (hexane/EtOAc, 4:1) was obtained 379 mg (82%) of **7d** as a sticky oil. A larger scale reaction gave 96% yield of **7d**. A sample of (*S*,*S*)-**7d** was also prepared from (*S*,*S*)-**2d** (94% ee) in 90% yield. For (*S*,*S*)-**7d**: $[\alpha]_D$ –37.5 (c = 1.34, $CHCl_3$). IR (CCl_4): 3065 w, 1246 s. TLC: R_f 0.33 (hexane/EtOAc, 2:1). ^{1}H NMR (300 MHz): 7.77 (d, J = 608.9, 1 H), 7.42–7.20 (m, 10 H), 4.33 (ddd, J = 17.1, 7.6, 5.2, 1 H), 4.18 (quintet, J = 5.8, 1 H), 3.05 (dd, J = 15.2, 12.8, 1 H), 2.98 (dd, J = 14.8, 12.3, 1 H), 2.74 (dd, J = 14.8, 9.1, 1 H), 2.39 (m, 2 H), 2.34 (dd, J = 15.2, 12.8, 1 H), 0.76 (s, 9 H), 0.72 (s, 9 H). ^{13}C NMR (75.5 MHz): 141.35, 140.66, 128.55, 128.52, 127.18, 126.61, 62.09, 60.97, 58.89 (J_{CP} = 3.7), 56.95 (J_{CP} = 4.3), 42.10 (J_{CP} = 12.6), 34.26 (J_{CP} = 1.5), 33.62 (J_{CP} = 1.9), 28.14, 28.08. ^{31}P NMR (121.6 MHz): 12.69. MS (70 eV): 412 (M^+), 355 (100). Anal. calcd. for $C_{25}H_{37}N_2OP$ (412.55): C 72.78, H 9.04, N 6.79, P 7.51; found: C 72.56, H 9.01, N 6.65, P 7.42.

*(*RS*)-(4*l*,6*l*)-1,3-Dibenzyl-4,6-diphenyl-1,3,2-diazaphosphorinane 2-oxide (**7e**)*: From 84 μL (0.97 mmol) of PCl_3, 358 mg (0.88 mmol) of **2e**, and 0.39 mL (2.77 mmol) of *N*-methylmorpholine followed by purification by SiO_2 column chromatography (hexane/EtOAc, 2:1) was obtained 366 mg (92%) of **7e** as a colorless oil which solidified on standing at –20°C. An analytical sample was obtained by recrystallization from pentane/Et_2O: mp 59–60°C. IR (CCl_4): 3065 w, 1227 s. TLC: R_f 0.41 (hexane/EtOAc, 1:1). ^{1}H NMR (300 MHz): 8.14 (d, J = 628.9, 1 H), 7.36–7.11 (m, 20 H), 4.73 (dd, J = 14.6, 9.9), 4.66 (dd, J = 15.6, 10.9, 1 H), 4.12 (quintet, J = 5.5, 1 H), 3.93 (m, 1 H), 3.70 (dd, J = 15.6, 9.8, 1 H), 3.62 (dd, J = 14.6, 11.3, 1 H), 2.30 (ddd, J = 14.5, 9.3, 4.7, 1 H), 2.13 (ddd, J = 14.5, 6.0, 4.8, 1 H). ^{13}C NMR (75.5 MHz): 140.57 (J_{CP} = 1.4) 139.43, 136.89 (J_{CP} = 2.8), 136.74, 129.42, 128.67, 128.46, 128.40, 128.16, 128.08,

© 2000 NRC Canada

127.46, 127.36, 127.33, 127.27, 126.80, 126.59, 57.45, 56.50, 48.51 (J_{CP} = 6.9), 48.29 (J_{CP} = 5.6), 41.58 (J_{CP} = 12.6). ^{31}P NMR (121.6 MHz): 5.81. MS (70 eV): 452 (M^+, 3), 91 (100). Anal. calcd. for $C_{29}H_{29}N_2OP$ (452.53): C 76.97, H 6.46, N 6.19, P 6.84; found: C 76.94, H 6.48, N 6.18, P 6.82.

*(*RS*)-(4*l*,6*l*)-1,3-Bis-(2,4,6-trimethylphenylmethyl)-4,6-diphenyl-1,3,2-diaza-phosphorinane 2-oxide (**7f**)*: From 127 μL (1.45 mmol) of PCl_3, 0.62 mL (4.46 mmol) of NEt_3, and 680 mg (1.39 mmol) of **2f** followed by purification by SiO_2 column chromatography (hexane/EtOAc, 2:1) was obtained 612 mg (82%) of **7f** as a gummy solid. An analytical sample was obtained by recrystallization from pentane/TBME: mp 178–190°C. IR (CCl_4): 3029 w, 1217 s. TLC: R_f 0.36 (hexane/EtOAc, 2:1). ^{1}H NMR (300 MHz): 7.48–7.09 (m, 10 H), 7.22 (d, J = 616.0, 1 H), 6.78 (s, 2 H), 6.67 (s, 2 H), 4.36 (dd, J = 13.5, 3.3, 1 H), 4.27 (dd, J = 13.5, 7.2, 1 H), 4.06 (dd, J = 12.7, 5.1, 1 H), 4.01–3.92 (m, 2 H), 3.68 (t, J = 12.7, 1 H), 2.34 (m, 2 H), 2.24 (s, 3 H), 2.16 (s, 3 H), 2.13 (s, 6 H), 2.08 (s, 6 H). ^{13}C NMR (75.5 MHz): 141.46, 140.89, 138.34 (J_{CP} = 4.3), 137.33, 136.81, 128.93, 128.83, 128.60, 128.21, 127.98, 127.91, 127.24, 126.78, 125.82, 59.29, 55.88, 48.59 (J_{CP} = 6.9), 44.99 (J_{CP} = 6.6), 42.12 (J_{CP} = 9.0), 20.76, 20.60, 19.86, 19.61. ^{31}P NMR(121.6 MHz): 3.09. MS (70 eV): 536 (M^+, 2), 133 (100). Anal. calcd. for $C_{35}H_{41}N_2OP$ (412.55): C 78.33, H 7.70, N 5.22, P 5.77; found: C 78.31, H 7.79, N 5.14, P 5.56.

Representative procedure for the preparation of 2-alkyl-1,3,2-diaza-phosphorinane 2-oxides

The detailed procedure for the preparation of **5b** is given. For all of the other diazaphosphorinanes only the amounts of reagents and methods of purification are provided along with the analytical data.

*(*RS*)-(4*l*,6*l*)-2-Benzyl-1,3-diethyl-4,6-diphenyl-1,3,2-diazaphosphorinane 2-oxide (**5b**)*: To a flame-dried, 25-mL, three-necked, round bottom flask equipped with a thermometer, a rubber septum, a N_2 inlet, and a magnetic stirring bar was added a solution of 180 mg (0.55 mmol) of phosphite **7b** in THF (10 mL). The mixture was cooled to –78°C and 0.34 mL (0.58 mmol) of *n*-BuLi (1.71 M) was slowly added to give a yellow-orange solution which was stirred at –78°C for 15 min. Benzyl bromide (71 μL, 0.60 mmol) was then added via syringe and the color dissipated immediately. After being stirred for 1 h at –78°C, the reaction mixture was warmed to rt, poured into water (20 mL), extracted with EtOAc (3 × 15 mL), washed with brine (10 mL), and dried (Na_2SO_4). Filtration followed by concentration gave a yellow oil which was purified by SiO_2 column chromatography (hexane/EtOAc/*i*-PrOH, 35:62:3) to afford 140 mg (61%) of diazaphosphorinane **5b** as a foam. An analytical sample was obtained by recrystallization from pentane/Et_2O: mp 98–99°C. IR (CCl_4): 3031 w, 1239 s. TLC: R_f 0.22 (hexane/EtOAc/*i*-PrOH, 34:63:3). ^{1}H NMR (300 MHz): 7.52–7.16 (m, 13 H), 6.77 (m, 2 H), 4.49 (dt, J = 15.4, 3.7, 1 H), 3.93 (dd, J = 12.0, 3.0, 1 H), 3.45 (d, J = 18.9, 2 H), 3.51–3.35 (m, 1 H), 3.24 (heptet, J = 7.3, 1 H), 2.90 (heptet, J = 7.3, 1 H), 2.53–2.36 (m, 1 H), 2.07 (ddd, J = 14.0, 12.3, 4.3, 1 H), 1.91 (dt, J = 14.0, 3.2, 1 H), 1.01 (t, J = 7.1, 3 H), 0.96 (t, J = 6.9, 3 H). ^{13}C NMR (75.5 MHz): 141.35 (J_{CP} = 5.0), 140.55, 134.90 (J_{CP} = 8.4), 129.97, 129.89, 128.45, 128.34, 128.31, 128.21, 127.30, 127.12, 126.94, 126.78, 126.35, 126.31, 58.14, 54.58, 41.66 (J_{CP} = 4.7), 40.54 (J_{CP} = 121.3), 39.87 (J_{CP} = 4.6), 38.87 (J_{CP} = 3.6), 13.52 (J_{CP} = 2.4), 13.36. ^{31}P NMR (121.6 MHz): 24.96. MS (70 eV): 328 (M^+ + 1 – $PhCH_2$, 22), 327 (M^+ – $PhCH_2$, 100). Anal. calcd. for $C_{26}H_{31}N_2OP$ (418.52): C 74.62, H 7.47, N 6.69, P 7.40; found: C 74.49, H 7.57, N 6.63, P 7.25.

*(*RS*)-(4*l*,6*l*)-2-Benzyl-1,3-bis-(1-methylethyl)-4,6-diphenyl-1,3,2-diaza-phosphorinane 2-oxide (**5c**)*: From 195 mg (0.55 mmol) of diamine **7c**, 0.33 mL (0.61 mmol) of *n*-BuLi (1.84 M), and 78 μL (0.66 mmol) of benzyl bromide followed by purification by SiO_2 column chromatography (hexane/EtOAc/*i*-PrOH, 45:52:3) was obtained 198 mg (81%) of **5c** as a colorless solid. An analytical sample was obtained by recrystallization from Et_2O: mp 144–145°C. IR (CCl_4): 3065 w, 1240 s. TLC: R_f 0.54 (hexane/EtOAc/*i*-PrOH, 45:52:3). ^{1}H NMR (300 MHz): 7.63–7.07 (m, 15 H), 4.56 (dt, J = 14.9, 3.7, 1 H), 3.91–3.82 (m, 2 H, HC(4)), 3.59 (dd, J = 18.6, 14.6, 1 H), 3.50–3.33 (m, 1 H), 3.38 (dd, J = 17.6, 14.6, 1 H), 2.28 (ddd, J = 15.2, 14.3, 3.9, 1 H), 2.12 (dt, J = 14.2, 4.1, 1 H), 1.12 (d, J = 6.6, 3 H), 1.03 (d, J = 7.0, 3 H), 0.87 (d, J = 6.7, 3 H), 0.76 (d, J = 6.7, 3 H). ^{13}C NMR (75.5 MHz): 144.35 (J_{CP} = 3.0), 142.82, 134.80 (J_{CP} = 7.8), 130.28, 130.19, 128.25, 128.15, 128.13, 128.02, 127.11, 126.93, 126.60, 126.28, 126.25, 58.34, 53.40, 49.64 (J_{CP} = 2.7), 46.22 (J_{CP} = 5.4), 43.60 (J_{CP} = 7.2), 43.40 (J_{CP} = 117.6), 23.51, 22.23, 21.30, 20.13 (J_{CP} = 2.5). ^{31}P NMR (121.6 MHz) 21.64. MS (70 eV): 446 (M^+), 355 (100). Anal. calcd. for $C_{28}H_{35}N_2OP$ (446.57): C 75.31, H 7.90, N 6.27, P 6.94; found: C 75.26, H 7.94, N 6.24, P 6.86.

*(*RS*)-(4*l*,6*l*)-2-Benzyl-1,3-bis-(2,2-dimethylpropyl)-4,6-diphenyl-1,3,2-diaza-phosphorinane 2-oxide (**5d**)*: From 150 mg (0.36 mmol) of **7d**, 0.27 mL (0.40 mmol) of *n*-BuLi (1.48 M), and 87 μL (0.73 mmol) of benzyl bromide followed by purification by SiO_2 column chromatography (hexane/EtOAc, 4:1) was obtained 123 mg (67%) of **5d** as a viscous oil. A sample of (*S*,*S*)-**5d** was also prepared from (*S*,*S*)-**7d** in 81% yield. For (*S*,*S*)-**5d**: [α] = –2.1 (c = 1.44, $CHCl_3$), [α] = – 15.1 (c = 1.44, $CHCl_3$). IR (CCl_4): 3065 w, 1235 s. TLC: R_f 0.44 (hexane/EtOAc, 4:1). ^{1}H NMR (300 MHz): 7.65–7.05 (m, 15 H), 4.62 (dt, J = 15.3, 4.0, 1 H), 4.13 (ddd, J = 11.5, 7.2, 4.2, 1 H), 3.69 (dd, J = 18.4, 14.8, 1 H), 3.48 (dd, J = 17.4, 14.8, 1 H), 3.13 (dd, J = 14.8, 8.9, 1 H), 2.84 (dd, J = 14.9, 8.6, 1 H), 2.75 (dd, J = 14.9, 7.8, 1 H), 2.50 (ddd, J = 15.1, 12.0, 3.9, 1 H), 2.42 (dd, J = 14.8, 11.2, 1 H), 2.15 (dt, J = 13.9, 4.1, 1 H), 0.78 (s, 9 H), 0.72 (s, 9 H). ^{13}C NMR (75.5 MHz): 141.62, 140.46, 134.98 (J_{CP} = 7.4), 130.23, 130.14 128.35, 128.30, 128.12, 127.33, 127.31, 127.17, 127.03, 126.27, 126.24, 61.98, 59.32, 58.33 (J_{CP} = 2.3), 55.91 (J_{CP} = 2.8), 43.23 (J_{CP} = 115.2), 42.88 (J_{CP} = 9.3), 33.66, 33.02 (J_{CP} = 3.4), 28.98, 28.83. ^{31}P NMR (121.6 MHz): 24.45. MS (70 eV): 446 (M^+ + 1 – $(CH_3)_3C$, 16), 445 (M^+ – $(CH_3)_3C$, 51), 91 (100). Anal. calcd. for $C_{32}H_{43}N_2OP$ (502.68): C 76.46, H 8.62, N 5.57, P 6.16; found: C 76.32, H 8.62, N 5.53, P 6.20.

*(*RS*)-(4*l*,6*l*)-1,2,3-Tribenzyl-4,6-diphenyl-1,3,2-diazaphosphorinane 2-oxide (**5e**)*: From 288 mg (0.64 mmol) of **7e**, 0.45 mL (0.77 mmol) of *n*-BuLi (1.70 M), and 83 μL (0.70 mmol) of

© 2000 NRC Canada

benzyl bromide followed by purification by SiO_2 column chromatography (hexane/EtOAc, 2:1) afforded 285 mg (83%) of **5e** as a colorless solid. An analytical sample was obtained by recrystallization from pentane/Et_2O: mp 137–138°C. IR (CCl_4): 3065 w, 1219 s. TLC: R_f 0.35 (hexane/EtOAc, 2:1). ^{1}H NMR (300 MHz): 7.54–7.14 (m, 23 H) and 6.85–6.82 (m, 2 H), 4.76 (dd, *J* = 15.7, 8.6, 1 H), 4.48 (dd, *J* = 14.5, 8.6, 1 H), 4.35 (dt, *J* = 15.0, 3.7, 1 H), 3.85 (dd, *J* = 15.7, 5.8, 1 H), 3.68 (dd, *J* = 19.8, 14.6, 1 H), 3.70–3.62 (m, 1 H), 3.51 (dd, *J* = 17.9, 14.6, 1 H), 3.18 (t, *J* = 13.8, 1 H), 2.30 (ddd, *J* = 14.1, 12.6, 4.4, 1 H), 1.88 (dt, *J* = 14.4, 3.2, 1 H). ^{13}C NMR (75.5 MHz): 141.14 (J_{CP} = 4.4), 139.06, 137.26 (J_{CP} = 4.2), 136.63, 134.33 (J_{CP} = 8.3), 130.10, 130.05, 128.61, 128.40, 128.37, 127.67, 127.45, 127.30, 127.09, 127.06, 126.93, 126.53, 126.49, 58.53, 55.41, 48.88 (J_{CP} = 4.6), 47.85 (J_{CP} = 3.2), 42.90 (J_{CP} = 121.6), 41.82 (J_{CP} = 5.2). ^{31}P NMR (121.6 MHz): 24.84. MS (70 eV): 91 (100). Anal. calcd. for $C_{36}H_{35}N_2OP$ (542.66): C 79.68. H 6.50, N 5.16, P 5.71; found: C 79.62, H 6.53, N 5.07, P 5.65.

*(*RS*)-(4*l*,6*l*)-2-Benzyl-1,3-bis-(2,4,6-trimethylphenylmethyl)-4,6-diphenyl-1,3,2-diazaphosphorinane 2-oxide (**5f**)*: From 570 mg (1.06 mmol) of phosphite **7f**, 0.65 mL (1.11 mmol) of *n*-BuLi (1.71 M), and 138 μL (1.17 mmol) of benzyl bromide followed by purification by SiO_2 column chromatography (hexane/EtOAc, 4:1–2:1) afforded 402 mg (61%) of diazaphosphorinane **5f** as a foam. An analytical sample was obtained by recrystallization from pentane/Et_2O: mp 149–150°C. IR (CCl_4): 3063 w, 1223 s. TLC: R_f 0.54 (hexane/EtOAc, 2:1). ^{1}H NMR (300 MHz): 7.63 (d, *J* = 7.5, 1 H), 7.40–7.22 (m, 9 H), 6.99 (dd, *J* = 5.1, 1.6, 2 H), 6.74 (dd, *J* = 7.5, 3.7, 2 H), 6.64 (s, 2 H), 6.32 (s, 2 H), 4.33–4.24 (m, 4 H), 4.10 (dd, *J* = 13.5, 9.1, 1 H), 3.36 (quintet, *J* = 5.6), 3.48 (dd, *J* = 19.7, 14.4, 1 H), 3.35 (dd, *J* = 17.4, 14.4, 1 H), 2.46 (m, 1 H), 2.10 (m, 1 H), 2.19 (s, 6 H), 2.14 (s, 3 H), 2.00 (s, 3 H), 1.68 (s, 6 H, 2 X). ^{13}C NMR (75.5 MHz): 142.97 (J_{CP} = 2.7), 141.01, 138.21 (J_{CP} = 7.8), 136.72, 136.15, 134.26 (J_{CP} = 7.3), 130.25, 130.16, 129.60, 129.46 (J_{CP} = 5.5), 128.83, 128.19, 128.11, 127.38, 126.61, 126.39, 126.32, 126.29, 126.10, 125.67, 59.92, 57.14, 45.96 (J_{CP} = 2.4), 44.81 (J_{CP} = 2.0), 43.41 (J_{CP} = 6.4), 42.57 (J_{CP} = 102.7), 20.60, 20.40, 20.09, 19.55. ^{31}P NMR (121.6 MHz): 26.87. MS (70 eV): 626 (M^+, 1), 133 (100). Anal. calcd. for $C_{42}H_{47}N_2OP$ (626.82): C 80.48, H 7.56, N 4.47, P 4.94; found: C 80.60, H 7.62, N 4.40, P 4.86.

*(*RS*)-(4*l*,6*l*)-1,3-Bis-(1-methylethyl)-4,6-diphenyl-2-ethyl-1,3,2-diaza-phosphorinane 2-oxide (**6c**)*: From 310 mg (0.87 mmol) of phosphite **7c**, 0.56 mL (0.96 mmol) of *n*-BuLi, and 104 μL (1.31 mmol) of ethyl iodide followed by purification by SiO_2 column chromatography (hexane/EtOAc/*i*-PrOH, 35:62:3) afforded 310 mg (93%) of diazaphosphorinane **6c** as a colorless solid. An analytical sample was obtained by recrystallization from Et_2O/pentane: mp 141–142°C. IR (CCl_4): 3063 w, 1246 s. MS (70 eV): 384 (M^+, 22), 355 (100). TLC: R_f 0.31 (hexane/EtOAc/*i*-PrOH, 35:62:3). ^{1}H NMR (300 MHz): 7.60 (d, *J* = 7.4, 2 H), 7.38 (t, *J* = 7.5, 2 H), 7.30–7.17 (m, 4 H), 7.16 (d, *J* = 6.8, 2 H), 4.51 (dt, *J* = 10.9, 3.7, 1 H), 3.98 (dheptet, *J* = 15.9, 6.9, 1 H), 3.85 (dt, *J* = 11.4, 4.7, 1 H), 3.68 (dheptet, *J* = 15.9, 6.9, 1 H), 2.30–2.12 (m, 3 H), 1.96 (octet, *J* = 7.5, 1 H), 1.39 (dt, *J* = 19.1, 7.6), 1.19 (d, *J* = 6.5, 3 H), 1.17 (d, *J* = 6.8, 3 H), 0.93 (d, *J* = 7.2, 3 H), 0.90 (d, *J* = 7.2, 3 H). ^{13}C NMR (75.5 MHz): 144.76 (J_{CP} = 3.2), 142.67, 128.21, 127.79, 126.91, 126.71, 126.63, 126.24, 55.73, 52.90, 48.69 (J_{CP} = 3.2), 45.61 (J_{CP} = 6.0), 43.54 (J_{CP} = 7.3), 27.88 (J_{CP} = 123.7), 23.01 (J_{CP} = 2.5), 22.72, 21.19, 19.92, 8.31 (J_{CP} = 6.3). ^{31}P NMR (121.6 MHz): 27.51. Anal. calcd. for $C_{23}H_{33}N_2OP$ (384.50): C 71.85, H 8.65, N 7.29, P 8.06; found: C 71.93, H 8.64, N 7.30, P 8.08.

*(*RS*)-(4*l*,6*l*)-1,3-Bis-(2,2-dimethylpropyl)-4,6-diphenyl-2-ethyl-1,3,2-diaza-phosphorinane 2-oxide (**6d**)*: From 670 mg (1.52 mmol) of phosphite **7d**, 1.05 mL (1.79 mmol) of *n*-BuLi (1.70 M), and 195 μL (2.44 mmol) of ethyl iodide followed by purification by SiO_2 column chromatography (hexane/EtOAc, 3:1–2:1) afforded 697 mg (97%) of diazaphosphorinane **6d** as a foam. An analytical sample was obtained by recrystallization from pentane: mp 124–125°C. IR (CCl_4): 3031 w, 1246 m. TLC: R_f 0.34 (hexane/EtOAc, 2:1). ^{1}H NMR (300 MHz): 7.55 (d, *J* = 7.4, 2 H), 7.41 (t, *J* = 7.5, 2 H), 7.33–7.24 (m, 4 H), 7.12 (d, *J* = 7.1, 2 H), 4.62 (dt, *J* = 15.0, 4.0, 1 H), 4.10 (ddd, *J* = 11.8, 7.4, 4.5, 1 H), 3.30 (dd, *J* = 14.8, 9.2, 1 H), 3.05 (dd, *J* = 14.7, 8.0, 1 H), 2.70 (dd, *J* = 14.8, 9.2, 1 H), 2.64 (dd, *J* = 14.7, 10.9, 1 H), 2.52–2.28 (m, 2 H), 2.18–1.97 (m, 2 H), 1.38 (dt, *J* = 18.5, 7.6, 3 H), 0.88 (s, 9 H), 0.79 (s, 9 H). ^{13}C NMR (75.5 MHz): 142.03, 140.17, 128.41, 128.18, 127.26, 127.12, 127.09, 126.92, 61.44, 59.55, 57.35 (J_{CP} = 3.0), 56.50 (J_{CP} = 2.5), 42.29 (J_{CP} = 9.4), 33.79, 33.23 (J_{CP} = 2.9), 29.35 (J_{CP} = 121.8), 28.89, 28.85, 8.60 (J_{CP} = 6.0). ^{31}P NMR (121.6 MHz): 30.99. MS (70 eV): 425 ($M^+ - CH_3$, 2.7), 383 (100). Anal. calcd. for $C_{27}H_{41}N_2OP$ (440.61): C 73.60, H 9.38, N 6.36, P 7.03; found: C 73.65, H 9.42, N 6.34, P 6.98.

Representative procedure for the alkylation of 1,3,2-diazaphosphorinane 2-oxides

The detailed procedure for the methylation of **5a** to afford **8a** is given. For all of the other alkylations, only the amounts of reagents, methods of analysis of diastereomeric mixtures and purification of the products are provided, along with the analytical data.

*(*RS*)-(4*l*,6*l*,1′*x*)-1,3-Dimethyl-4,6-diphenyl-2-(1-phenylethyl)-1,3,2-diaza-phosphorinane 2-oxide (**8a**)*: A flame-dried, 25-mL, three-necked, round-bottomed flask was charged with 105 mg (0.27 mmol) of diazaphosphorinane **5a** and 4 mL of THF. The flask was cooled to –78°C using a dry ice-acetone bath. *n*-BuLi (0.16 mL, 0.27 mmol, 1.71 M) was added to give a pale-yellow solution which was stirred for 30 min. Methyl iodide (65 μL, 1.04 mmol) was added by a syringe and the color dissipated slowly. After stirring for 1.1 h at –78°C, the reaction mixture was quenched with water (0.2 mL), then poured into water (10 mL), extracted with EtOAc (3 × 10 mL), and dried (Na_2SO_4). Filtration followed by concentration gave a pale yellow oil, which was assayed by HPLC (Supelco LC-NH_2) and found to be a mixture of diastereomers (87:13). Purification by column chromatography (hexane/EtOAc/*i*-PrOH, 35:62:3) gave 19 mg (17.5%) of minor **8a′** and 79.8 mg (73.3%) of major **8a** as a colorless solids. Data for **8a**: mp 141–142°C (pentane/Et_2O). IR (CCl_4): 3065 w, 1267 s. TLC: R_f = 0.3 (hexane/EtOAc/*i*-PrOH, 35:62:3). ^{1}H NMR (300 MHz): 7.48–7.17 (m, 13 H),

© 2000 NRC Canada

6.91 (m, 2 H), 4.08 (ddd, *J* = 11.7, 4.7, 2.6, 1 H), 3.69 (dd, *J* = 11.9,3.1, 1 H), 3.51 (dq, *J* = 20.3, 7.3, 1 H), 2.78 (d, *J* = 7.8, 3 H), 2.45(d, *J* = 8.9, 1 H), 1.77 (dd, *J* = 17.1, 7.4, 3 H), 1.59 (m, 1 H), 1.47 (ddd, *J* = 14.3, 12.0, 4.8, 1 H). ^{13}C NMR (75.5 MHz): 141.56 (J_{CP} = 6.5), 140.43 (J_{CP} = 6.7), 140.35, 128.77, 128.69, 128.62, 128.12, 128.08, 128.04, 127.22, 127.14, 126.91, 126.64, 126.59, 126.53, 61.16, 59.12, 44.16 (J_{CP} = 121.3), 40.86 (J_{CP} = 3.3), 34.45 (J_{CP} = 4.4), 33.99 (J_{CP} = 1.7), 15.80 (J_{CP} = 4.2). ^{31}P NMR (121.6 MHz): 31.80. MS (70 eV): 300 (M^+ +1 – PhC_2H_4, 20), 626 (M^+ – PhC_2H_4, 100). Anal. calcd. for $C_{25}H_{29}N_2OP$ (404.49): C 74.24, H 7.23, N 6.93, P 7.66; found: C 74.31, H 7.26, N 6.94, P 7.76. Data for **8a′**: TLC: R_f = 0.42 (hexane/EtOAc/*i*-PrOH, 35:62:3). ^{1}H NMR (300 MHz): 7.51–7.09 (m, 15 H), 4.26 (dt, *J* = 11.3, 3.5, 1 H), 3.77 (dd, *J* = 12.2, 1.5, 1 H), 3.35 (dq, *J* = 17.8, 7.2, 1 H), 2.59 (d, *J* = 8.4, 3 H), 2.45 (m, 1 H), 2.07 (d, *J* = 7.4, 3 H), 2.03 (m, 1 H), 1.77 (dd, *J* = 117.6, 7.2, 3 H). ^{31}P NMR (121.6 MHz): 29.82. MS (70 eV): 313 (14), 300 (M^+ + 1 – PhC_2H_4, 20), 626 (M^+ – PhC_2H_4, 100).

*(*RS*)-(4*l*,6*l*,1′*x*)-1,3-Diethyl-4,6-diphenyl-2-(1-phenylethyl)-1,3,2-diaza-phosphorinane 2-oxide (**8b**)*: From 98 mg (0.23 mmol) of **5b**, 138 µL (0.23 mmol) of *n*-BuLi (1.70 M), and 44 µL (0.71 mmol) of methyl iodide followed by purification by SiO_2 column chromatography (hexane/EtOAc/*i*-PrOH, 31:62:7) was obtained 80 mg (78%) of a 61:39 (HPLC) diastereomeric mixture of **8b** as a sticky oil and 14.3 mg (13%) of recovered **5b**. An analytical sample was obtained by recrystallization from pentane/Et_2O at –78°C: mp 49–53°C. IR (CCl_4): 3029 w, 1239 s. TLC: R_f 0.44 (minor), 0.34 (major) (hexane/EtOAc/*i*-PrOH, 31:62:7). HPLC: t_R = 7.25 min (39%), 8.37 min (61%), (Supelco LC-NH_2, (hexane/EtOAc, 30:70), flow rate = 1.0 mL/min). ^{1}H NMR (300 MHz): 7.57–7.08 (m, 15 H), 4.50–4.45 (m, 1H), 4.02–3.95 (m, 1 H), 3.53–3.19 (m, 2.6 H), 3.04–2.90 (m, 1 H), 2.64–2.52 (m, 1 H), 2.42 (ddd, *J* = 14.0, 10.2, 4.1, 0.4 H), 2.31 (dheptet, *J* = 9.2, 6.9, 0.4 H), 2.07 (dt, *J* = 14.6, 3.1, 0.4 H), 1.95 (ddd, *J* = 16.8, 14.2, 4.3, 0.6 H), 1.83–1.78 (m, 0.6 H), 1.77 (dd, *J* = 9.6, 7.4, 1.8 H), 1.74 (dd, *J* = 10.0, 7.3, 1.2 H), 1.08 (t, *J* = 7.1, 1.8 H), 1.03 (t, *J* = 7.0, 1.2 H), 0.96 (t, *J* = 6.9, 1.8 H), 0.44 (t, *J* = 7.1, 1.2 H). ^{13}C NMR (75.5 MHz): 142.20 (J_{CP} = 4.8), 141.38 (J_{CP} = 5.3), 140.94 (J_{CP} = 5.7), 140.81 (J_{CP} = 6.2), 140.31, 140.05, 129.03, 128.99, 128.59, 128.44, 128.39, 128.29, 128.12, 128.06, 127.42, 127.38, 127.22, 127.20, 127.10, 126.99, 126.92, 126.67, 126.60, 126.58, 126.46, 57.87, 57.41, 55.05, 54.18, 48.46 (J_{CP} = 121.7), 45.86 (J_{CP} = 122.0), 41.61 (J_{CP} = 5.8), 41.27 (J_{CP} = 4.2), 39.93 (J_{CP} = 2.9), 39.85, 39.81, 39.64, 17.63 (J_{CP} = 3.2), 17.26 (J_{CP} = 3.7), 13.59, 13.33 (J_{CP} = 3.7), 13.28, 12.20 (J_{CP} = 3.6). ^{31}P NMR (121.6 MHz): 29.34 (major), 28.76 (minor). MS (70 eV): 328 (M^+ +1 – PhC_2H_4, 22), 327 (M^+ – PhC_2H_4, 100). Anal. calcd. for $C_{27}H_{33}N_2OP$ (432.54): C 74.97, H 7.69, N 6.48, P 7.16; found: C 74.88, H 7.87, N 6.36, P 6.94.

*(*RS*)-(4*l*,6*l*,1′*x*)-1,3-Bis(1-methylethyl)-4,6-diphenyl-2-(1-phenylethyl)-1,3,2-diazaphosphorinane 2-oxide (**8c**)*: From 170 mg (0.38 mmol) of **5c**, 224 µL (0.38 mmol) of *n*-BuLi (1.70 M), and 71 µL (1.14 mmol) of methyl iodide followed by purification by column chromatography (hexane/EtOAc/*i*-PrOH, 35:60:5) was obtained 153 mg (87%) of a 58:42 (^{31}P NMR) diastereomeric mixture of **8c** as a foam. An analytical sample was obtained by recrystallization from pentane/Et_2O: mp 114–117°C. IR (CCl_4): 2904 s, 1252 s. TLC: R_f 0.41 (hexane/EtOAc/*i*-PrOH, 35:60:5). HPLC: t_R = 7.30 min (42%), 8.57 min (58%), Supelco LC-NH_2, (hexane/EtOAc, 3:2), flow rate = 1.0 mL/min). ^{1}H NMR ($CDCl_3$, 300 MHz): 7.48–7.17 (m, 15 H), 4.55 (dt, *J* = 13.1, 3.7, 0.4 H), 4.46 (dt, *J* = 9.9, 3.8, 0.6 H), 4.14 (dt, *J* = 12.4, 3.0, 0.6 H), 4.04–3.77 (m, 1 H), 3.69–3.26 (m, 1.4 H), 2.62–2.52 (m, 0.6 H), 2.33–2.23 (m, 0.4 H), 1.98–1.80 (m, 1 H), 1.82 (dd, *J* = 17.5, 7.2, 1.8 H), 1.74 (dd, *J* = 17.4, 7.3, 1.2 H), 1.29 (d, *J* = 6.8, 1.8 H) 1.22 (d, *J* = 6.7, 1.2 H), 1.16 (d, *J* = 6.9, 1.2 H), 0.96 (d, *J* = 6.8 1.8 H), 0.86 (d, *J* = 6.6, 1.2 H), 0.72 (d, *J* = 6.7, 1.8 H), 0.54 (d, *J* = 6.8, 1.2 H), 0.48 (d, *J* = 6.7, 1.8 H). ^{13}C NMR (75.5 MHz): 145.30 (J_{CP} = 3.8), 144.33 (J_{CP} = 4.7), 143.47, 143.43, 141.50 (J_{CP} = 5.2), 141.12 (J_{CP} = 4.8), 129.25, 129.17, 129.06, 128.98, 128.42, 128.21, 128.19, 128.00, 127.97, 127.93, 127.91, 127.83, 127.26, 127.11, 127.07, 127.03, 126.95, 126.84, 126.49, 126.45, 126.30, 126.28, 55.20, 54.97, 54.47 (J_{CP} = 1.9), 54.25, 49.35, 48.57 (J_{CP} = 117.6), 47.54 (J_{CP} = 3.4), 47.01 (J_{CP} = 4.3), 46.85 (J_{CP} = 119.6), 43.10 (J_{CP} = 6.2), 43.00, 25.15, 24.74, 23.12 (J_{CP} = 3.3), 21.91 (J_{CP} = 2.6), 21.89, 21.36, 20.22 (J_{CP} = 4.2), 18.71 (J_{CP} = 3.4), 18.27 (J_{CP} = 4.1), 18.06 (J_{CP} = 3.4). ^{31}P NMR (121.6 MHz): 29.16 (major), 28.13 (minor). MS (70 eV): 445 (M^+ – CH_3), 355 (100). Anal. calcd. for $C_{29}H_{37}N_2OP$ (460.60): C 75.62, H 8.10, N 6.08, P 6.72; found: C 75.42, H 8.17, N, 5.99, P 6.74.

*(*RS*)-(4*l*,6*l*,1′*x*)-1,3-Bis-(2,2-dimethylpropyl)-4,6-diphenyl-2-(1-phenylethyl)-1,3,2-diazaphosphorinane 2-oxide (**8d**)*: From 180 mg (0.36 mmol) of **5d**, 211 µL (0.36 mmol) of *n*-BuLi (1.70 M), and 67 µL (1.07 mmol) of methyl iodide followed by purification by SiO_2 column chromatography (hexane/EtOAc, 2:1) was obtained 152 mg (82%) of a 92:8 (^{31}P NMR) diastereomeric mixture of **8d** as a foam and 19.5 mg (11%) of recovered **5d**. An analytical sample was obtained by recrystallization from TBME. Enantiomerically enriched (–)-**8d** was also prepared from (*S*,*S*)-**5d** in 74% yield with 94:6 ratio of diastereomers: mp 150–152°C. For (–)-**8d**: [α] = – 98.4 (c = 1.04, $CHCl_3$), [α] = – 281.5 (c = 1.04, $CHCl_3$). IR (CCl_4): 3065 w, 1244 s. TLC: R_f 0.54 (hexane/EtOAc, 2:1). HPLC: t_R = 8.30 min (92%), 9.62 min (8%), (Supelco LC-NH_2, (hexane/EtOAc, 85:15), flow rate = 1.0 mL/min). ^{1}H NMR (300 MHz): 7.60–7.14 (m, 15 H), 4.65–4.58 (m, 0.08 H), 4.39–4.33 (m, 1.84 H), 4.24–4.17 (m, 0.08 H), 3.46 (dq, *J* = 14.3, 7.3, 1 H), 3.29 (dd, *J* = 14.6, 8.0, 0.92 H), 3.22 (dd, *J* = 14.8, 8.4, 0.08 H), 3.12 (dd, *J* = 14.8, 5.9, 0.08 H), 2.96 (dd, *J* = 15.2, 8.5, 0.08 H), 2.73 (ddd, *J* = 16.5, 12.9, 4.2, 0.92 H), 2.55–2.44 (m, 1.92 H), 2.34–2.21 (m, 0.08 H), 2.15–1.93 (m, 2 H), 1.77 (dd, *J* = 17.6, 7.2, 0.24 H), 1.75 (dd, *J* = 16.8, 7.2, 2.76 H). ^{13}C NMR (75.5 MHz): 142.07, 141.86 (J_{CP} = 5.5), 141.67, 129.38, 129.29, 129.06, 128.99, 128.66, 128.28, 128.03, 127.62, 127.41, 127.33, 127.19, 127.10, 127.01, 126.85, 126.57, 126.54, 126.42, 63.44, 61.36 (J_{CP} = 1.7), 60.89, 58.75, 57.98, 57.70 (J_{CP} = 2.7), 56.11 (J_{CP} = 1.9), 55.19 (J_{CP} = 2.2), 49.64 (J_{CP} = 109.5), 47.11 (J_{CP} = 110.0), 42.78 (J_{CP} = 9.5), 42.49 (J_{CP} = 7.2), 34.27, 33.52, 32.46 (J_{CP} = 3.7), 31.68 (J_{CP} = 3.2), 29.34, 29.23, 29.09, 28.27, 20.19 (J_{CP} = 4.9), 18.66 (J_{CP} = 4.2). ^{31}P NMR (121.6 MHz): 29.55 (minor), 28.47 (major). MS (70 eV): 501 (M^+ – CH_3, 2.2), 411

© 2000 NRC Canada

(100). Anal. calcd. for $C_{29}H_{37}N_2OP$ (516.71): C 76.71, H 8.78, N 5.42, P 5.99; found: C 76.64, H 8.79, N 5.40, P 5.97.

*(*RS*)-(4*l*,6*l*,1′*x*)-1,3-Dibenzyl-4,6-diphenyl-2-(1-phenylethyl)-1,3,2-diaza-phosphorinane 2-oxide (**8e**)*: From 192 mg (0.35 mmol) of **5e**, 0.21 mL (0.35 mL) of *n*-BuLi (1.70 M), and 66 mL (1.06 mmol) of methyl iodide followed by purification by SiO_2 column chromatography (hexane/EtOAc, 4:1–2:1) was obtained 189 mg (96%) of a 75:25 (HPLC) diastereomeric mixture of **8e** as a colorless solid. An analytical sample was obtained by recrystallization from pentane/Et_2O: mp 175–179°C. IR (CCl_4): 3065 w, 1210 s. MS (70 eV): 451 (100). TLC: R_f 0.47 (hexane/EtOAc, 4:1). HPLC: t_R = 16.39 min (25%), 19.15 min (75%), (Supelco LC-NH_2, (hexane/EtOAc, 85:15), flow rate = 1.0 mL/min). ^{1}H NMR (300 MHz): 7.70–6.49 (m, 25 H), 4.90 (dd, *J* = 16.5, 8.1, 0.75 H), 4.86 (dd, *J* = 14.0, 7.0, 0.25 H), 4.40 (dd, *J* = 14.8, 7.8, 0.75 H), 4.36 (dt, *J* = 15.4, 3.5, 0.75 H), 4.11 (dt, *J* = 12.7, 3.6, 0.25 H), 4.03 (dd, *J* = 16.5, 4.0, 0.75 H), 3.88 (dd, *J* = 14.7, 7.3, 0.25 H), 3.79–3.75 (m, 0.25 H), 3.67 (dd, *J* = 14.7, 3.4, 0.25 H), 3.60–3.40 (m, 2 H), 2.89 (t, *J* = 14.2), 2.57–2.47 (m, 0.25 H), 2.29–2.19 (m, 0.75 H), 1.87 (dd, *J* = 17.9, 7.3, 0.75 H), 1.76 (dd, *J* = 17.4, 7.2, 2.25 H), 1.76 (dd, *J* = 17.4, 7.2, 2.25 H), 1.87–1.64 (m, 1 H). ^{13}C NMR (75.5 MHz): 141.81 (J_{CP} = 3.7), 141.04 (J_{CP} = 6.1), 140.61 (J_{CP} = 4.7), 138.88, 138.67, 137.32 (J_{CP} = 4.8), 136.73 (J_{CP} = 4.9), 136.60 (J_{CP} = 7.3), 130.52, 130.26, 129.15, 129.06, 128.98, 128.71, 128.47, 128.45, 128.32, 128.20, 128.18, 128.12, 128.06, 127.77, 127.51, 127.56, 127.43, 127.29, 127.18, 126.98, 126.89, 126.82, 126.61, 126.53, 59.30, 58.77, 55.34, 55.14, 50.48 (J_{CP} = 3.3), 49.43 (J_{CP} = 3.9), 48.98 (J_{CP} = 120.7), 48.72 (J_{CP} = 123.7), 48.39 (J_{CP} = 2.7), 48.08 (J_{CP} = 2.1), 41.61 (J_{CP} = 5.1), 18.76 (J_{CP} = 4.3), 18.06 (J_{CP} = 3.8). ^{31}P NMR (121.6 MHz): 29.54 (as a mixture). Anal calcd. for $C_{29}H_{37}N_2OP$ (556.69): C 75.62, H 8.10, N 6.08, P 6.72; found: C 75.42, H 8.17, N 5.99, P 6.74.

*(*RS*)-(4*l*,6*l*,1′*x*)-4,6-Diphenyl-1,3-bis-(2,4,6-trimethylphenylmethyl)-2-(1-phenylethyl)-1,3,2-diazaphosphorinane 2-oxide (**8f**)*: From 250 mg (0.40 mmol) of **5f**, 0.24 mL (0.40 mmol) of *n*-BuLi (1.70 M), and 75 μL (1.05 mmol) of methyl iodide followed by purification by SiO_2 column chromatography (hexane/EtOAc, 4:1) was obtained 240 mg (94%) of a 74:26 (^{31}P NMR) diastereomeric mixture of **8f** as a colorless solid. An analytical sample was obtained by recrystallization from Et_2O: mp 208–209°C. IR (CCl_4) 3063 m, 1229 s. TLC: R_f 0.42 (hexane/EtOAc, 4:1). ^{1}H NMR (300 MHz): 7.63 (d, *J* = 7.4, 2 H), 7.38 (t, *J* = 7.3, 2 H), 7.27–6.80 (m, 11.26 H), 6.85 (m, 1.48 H), 6.57 (s, 0.74 H), 6.53 (s, 0.26 H), 6.43 (d, *J* = 7.6, 0.26 H), 6.40 (s, 0.26 H), 6.27 (s, 0.74 H), 4.90 (dd, *J* = 13.8, 6.3, 0.76 H), 4.68 (dd, *J* = 13.4, 7.7, 0.26 H), 4.51 (dd, *J* = 13.8, 8.1, 0.26 H), 4.42 (dd, *J* = 13.8, 4.4, 0.76 H), 4.41–4.34 (m, 0.26 H), 4.12 (m, 0.74 H), 3.98 (dd, *J* = 13.5, 6.0, 0.74 H), 3.91–3.84 (m, 1.52 H), 3.71–3.65 (m, 0.26 H), 3.59 (dq, *J* = 14.1, 7.1, 0.74 H), 3.41 (dq, *J* = 16.3, 7.4, 0.26 H), 2.85–2.74 (m, 0.74 H), 2.62 (d, *J* = 13.5, 0.78 H), 2.49–2.38 (m, 0.26 H), 2.34 (s, 0.78 H), 2.13–1.79 (m, 20.44 H). ^{13}C NMR (75.5 MHz): 142.53 (J_{CP} = 4.5), 142.22 (J_{CP} = 2.1), 142.07 (J_{CP} = 1.7), 141.40 (J_{CP} = 5.1), 140.78 (J_{CP} = 5.4), 138.78, 138.01, 137.73, 136.62, 136.45, 136.18, 129.74, 129.67, 129.63, 129.55, 129.39, 129.31, 128.96, 128.88, 128.74, 128.66, 128.27, 128.20, 127.40, 126.96, 126.93, 126.81, 126.71, 126.64, 126.52, 126.41, 126.12, 126.07, 125.99, 125.60, 125.43, 60.87, 60.44, 56.61, 56.43, 49.40, 47.57 (J_{CP} = 113.4), 46.93 (J_{CP} = 2.9), 45.57, 44.41 (J_{CP} = 2.0), 43.31, 42.98 (J_{CP} = 10.6), 22.22, 20.87, 20.59, 20.51, 20.36, 20.07, 19.71, 19.43 (J_{CP} = 3.5), 17.60 (J_{CP} = 4.8), 14.08, 13.96. ^{31}P NMR (121.6 MHz): 32.15 (minor), 30.42 (major). MS (70 eV): 640 (M^+, 0.7), 133 (100). Anal. calcd. for $C_{43}H_{49}N_2OP$ (640.85): C 80.59, H 7.71, N 4.37, P 4.83; found: C 80.64, H 7.71, N 4.35, P 4.79.

*(*RS*)-(4*l*,6*l*,1′*x*)-1,3-Dimethyl-4,6-diphenyl-2-(1-methyl-2-phenylethyl)-1,3,2-diazaphosphorinane 2-oxide (**9a**)*: From 230 mg (0.70 mmol) of **6a**, 0.45 mL (0.70 mmol) of *n*-BuLi (1.55 M), and 125 μL (1.05 mmol) of benzyl bromide followed by purification by SiO_2 column chromatography (hexane/EtOAc/*i*-PrOH, 35:60:5) was obtained 243 mg (83%) of a 65:35 (^{31}P NMR) diastereomeric mixture of **9a** as a viscose oil. IR (CCl_4): 3067 w, 1267 s. TLC: R_f 0.51 (hexane/EtOAc/*i*-PrOH, 35:60:5). ^{1}H NMR (300 MHz): 7.47–7.12 (m, 15 H), 4.43–4.35 (m, 1 H), 3.82–3.79 (m, 1 H), 3.48 (ddd, *J* = 112.1, 8.1, 2.9, 0.35 H), 3.38 (ddd, *J* = 12.5, 9.0, 2.4, 0.65 H), 2.75 (d, *J* = 7.6, 3 H), 2.64 (d, *J* = 8.2, 1.95 H), 2.61 (d, *J* = 7.8, 1.05 H), 2.71–2.46 (m, 2 H), 2.43–2.24 (m, 1 H), 2.13–2.04 (m, 1 H), 1.22 (dd, *J* = 17.8, 7.3, 1.95 H), 1.19 (dd, *J* = 17.5, 7.2, 1.05 H). ^{13}C NMR (75.5 MHz): 142.00 (J_{CP} = 5.1), 140.17, 140.06, 139.93, 139.87, 139.84, 128.72, 128.67, 128.55, 128.40, 128.17, 128.13, 127.23, 127.09, 126.46, 126.33, 126.18, 126.00, 125.89, 125.85, 62.32, 62.20, 59.87, 59.80, 42.43 (J_{CP} = 126.6), 41.64 (J_{CP} = 4.4), 41.49 (J_{CP} = 5.3), 40.40 (J_{CP} = 126.9), 37.02, 36.59, 34.31, 34.26, 34.18, 33.59, 13.54 (J_{CP} = 3.7), 12.99 (J_{CP} = 3.3). ^{31}P NMR (121.6 MHz): 33.82 (minor), 33.76 (major). MS (70 eV): 418 (M^+, 5), 91 (100). Anal. calcd. for $C_{36}H_{31}N_2OP$ (418.52): C 74.62, H 7.47, N 6.69, P 7.40; found: C 74.47, H 7.53, N 6.62, P 7.28.

*(*RS*)-(4*l*,6*l*,1′*x*)-1,3-Bis-(1-methylethyl)-4,6-diphenyl-2-(1-methyl-2-phenylethyl)-1,3,2-diazaphosphorinane 2-oxide (**9c**)*: From 240 mg (0.62 mmol) of **6c**, 0.40 mL (0.62 mmol) of *n*-BuLi (1.56 M), and 111 μL (0.93 mmol) of benzyl bromide followed by purification by SiO_2 column chromatography (hexane/EtOAc/*i*-PrOH, 35:62:3) was obtained 286 mg (96%) of a 78:22 (HPLC) diastereomeric mixture of **9c** as a colorless solid. An analytical sample was obtained by recrystallization from pentane/TBME: mp 138–142°C. IR (CCl_4): 3029 w, 1231 s. TLC: R_f 0.56 (hexane/EtOAc/*i*-PrOH, 35:60:5). HPLC: t_R = 19.08 min (78%), 23.20 min (22%), (Supelco LC-NH_2, (hexane/EtOAc, 4:1), flow rate = 1.0 mL/min). ^{1}H NMR (300 MHz): 7.67–7.19 (m, 15 H), 4.59 (dt, *J* = 14.6, 3.6, 1 H), 4.08–3.95 (m, 2 H), 3.84–3.59 (m, 2 H), 2.65 (ddd, *J* = 12.9, 12.6, 3.9, 1 H), 2.63–2.33 (m, 2 H), 2.02 (dt, *J* = 14.3, 3.6, 1 H), 1.40–1.19 (m, 4 H), 1.38 (d, *J* = 6.8), 1.27 (d, *J* = 6.7), 0.98 (d, *J* = 6.8), 0.94 (d, *J* = 6.8, 12 H), 0.91 (d, *J* = 6.9), 0.87 (d, *J* = 6.9). ^{13}C NMR (75.5 MHz): 144.53 (J_{CP} = 4.7), 143.03, 140.71 (J_{CP} = 17.3), 128.75, 128.67, 128.19, 128.17, 127.78, 126.94, 126.80, 126.65, 126.42, 125.84, 125.79, 55.24, 54.74, 53.64, 53.58, 49.39 (J_{CP} = 1.9), 48.83 (J_{CP} = 2.8), 46.49 (J_{CP} = 7.4), 46.41 (J_{CP} = 5.3), 43.54 (J_{CP} = 7.4), 43.46 (J_{CP} = 5.7), 39.98 (J_{CP} = 124.1),

© 2000 NRC Canada

38.72 (J_{CP} = 125.4), 38.49, 37.52, 24.21, 23.89, 22.91 (J_{CP} = 3.2), 22.54 (J_{CP} = 2.2), 21.48, 21.39, 20.13 (J_{CP} = 4.0), 19.96 (J_{CP} = 3.5), 15.01 (J_{CP} = 3.6), 13.75 (J_{CP} = 2.8). ^{31}P NMR (121.6 MHz): 31.58 (minor), 31.23 (major). MS (70 eV): 355 (100). Anal. calcd for $C_{30}H_{39}N_2OP$ (474.62): C 75.92, H 8.28, N 5.90, P 6.53; found: C 75.86, H 8.34, N 5.85, P 6.42.

*(*RS*)-(4*l,6*l,*1′*x)-1,3-Bis-(2,2-dimethylpropyl)-4,6-diphenyl-2-(1-methyl-2-phenylethyl)-1,3,2-diazaphosphorinane 2-oxide (**9d**)*: From 265 mg (0.60 mmol) of **6d**, 0.38 mL (0.60 mmol) of *n*-BuLi, and 107 μL (0.90 mmol) of benzyl bromide followed by purification by SiO_2 column chromatography (hexane/EtOAc, 2:1) was obtained 314 mg (98%) of a 92:8 (HPLC) diastereomeric mixture of **9d** as a foam. An analytical sample was obtained by recrystallization from Et_2O: mp 208–209°C. IR (CCl_4): 3065 w, 1200 s. TLC: R_f 0.48 (hexane/EtOAc, 2:1). HPLC: t_R = 46.13 min (8%), 49.36 min (92%), (LC-Prep-Si (hexane/EtOAc/*i*-PrOH, 79.8:20:0.2), flow rate = 1.2 mL/min). ^{1}H NMR (300 MHz): 7.61–7.13 (m, 15 H), 4.70 (dt, *J* = 15.1, 3.6, 0.92 H), 4.69 (dt, *J* = 14.4, 3.6, 0.08 H), 4.36–4.20 (m, 1 H), 3.72–3.66 (m, 0.92 H), 3.56–3.47 (m, 0.08 H), 3.39–3.22 (m, 2 H), 3.04 (dd, *J* = 14.8, 6.1, 0.08 H), 2.93 (dd, *J* = 14.9, 5.6, 0.92 H), 2.81–2.43 (m, 4 H), 2.12 (dt, *J* = 14.5, 3.8, 1 H), 1.36 (dd, *J* = 17.3, 6.9, 0.06 H), 1.22 (dd, *J* = 18.0, 7.0, 2.7 H), 0.87 (s, 9 H), 0.85 (s, 9 H). ^{13}C NMR (75.5 MHz): 141.51, 140.68, 140.45, 139.80, 128.92, 128.79, 128.43, 128.30, 128.27, 127.50, 127.24, 127.16, 127.07, 126.06, 125.96, 61.42, 61.05, 58.35 (J_{CP} = 2.6), 58.28 (J_{CP} = 1.8), 58.04, 57.46, 55.98(J_{CP} = 1.7), 55.77 (J_{CP} = 1.9), 42.77 (J_{CP} = 7.0, 42.62 (J_{CP} = 2.9), 41.35 (J_{CP} = 120.6), 38.00, 37.77, 33.99, 33.04, 32.91 (J_{CP} = 3.9), 32.77 (J_{CP} = 3.6), 29.51, 29.38, 29.18, 29.11, 14.66 (J_{CP} = 2.0), 14.31 (J_{CP} = 3.1). ^{31}P NMR (121.6 MHz): 33.18 (as a mixture). MS (70 eV): 515 ($M^+ - CH_3$, 2.7), 473 (100). Anal. calcd. for $C_{34}H_{47}N_2OP$ (530.73): C 76.95, H 8.93, N 5.28, P 5.84; found: C 76.90, H 9.03, N 5.26, P 5.82.

*(*S*)-Dimethyl-1-phenylethylphosphonate (**14**)*: In a 25-mL, round-bottomed flask equipped with a reflux condenser was placed a solution of (–)-**8d** in 4 mL of HOAc acid and 48% HBr solution. The reaction mixture was heated to reflux for 15 h, then was concentrated under reduced pressure to give a yellow orange oil. The oil was passed through ion-exchange resin column (AG® 50W-X8) using water as eluent. The major fraction was collected and concentrated to give a white solid. The solid was dissolved in water and basified with 1 N NaOH solution (pH ~ 13), reacidified, concentrated, and the acidic residue dissolved in methanol. The methanolic solution of **13** was treated with excess etheneal diazomethane diluted with water (10mL) and extracted with diethyl ether (3 × 10 mL). The combined organic layers were dried (Na_2SO_4), filtered, and concentrated to give a yellow oil. The oil was purified by SiO_2 column chromatography (EtOAc/*i*-PrOH, 99:1) to give 53 mg (70%) of (*S*)-**14** as a colorless oil. An analytical sample was obtained by Kugelrohr distillation: bp 115°C (0.3 Torr (1 Torr = 133.322 Pa)). $[\alpha]_{405}$ –15.7 c = 1.1, CH_2Cl_2) ((*S*)-configuration, 87% ee). TLC: R_f 0.23 (EtOAc/*i*-PrOH, 99:1). ^{1}H NMR (300 MHz): 7.37–7.24 (m, 5 H), 3.69 (d, *J* = 10.0, 3 H), 3.53 (d, *J* = 10.0, 3 H), 3.21 (dq, *J* = 22.7, 7.7, 1 H), 1.58 (dd, *J* = 18.5, 7.5, 3 H). ^{31}P NMR (121.6 MHz): 32.75.

Acknowledgment

We wish to thank the National Institute of Health (PHS R01 GM45532) for financial support. We are grateful to Dr. Michael Kranz for obtaining the X-ray crystal structure of (*S**,*S**,*S**)-**8a**.

References

1. (*a*) J.-F. Biellmann and J.P. Ducep. Org. React. (N.Y.), **27**, 1 (1982); (*b*) D. Hoppe. Angew. Chem. Int. Ed. Engl. **23**, 932 (1984); (*c*) N.H. Werstiuk. Tetrahedron, **39**, 205 (1983); (*d*) S. Oae and Y. Uchida. *In* The chemistry of sulfones and sulfoxides. *Edited by* C.J.M. Sterling, S. Patai, and Z. Rappoport. Wiley–Interscience, New York. 1988. Chap. 12; (*e*) G. Solladie. Chimia, **38**, 233 (1984); (*f*) G. Solladie. Synthesis, 185 (1981); (*g*) A. Krief. Tetrahedron, **36**, 2531 (1980); (*h*) P. Beak, W.J. Zajdel, and D.B. Reitz. Chem. Rev. **84**, 47 (1984); (*i*) A.I. Meyers. Aldrichimica Acta, **18**, 59 (1985); (*j*) T. Kramer, J.-R. Schwork, and D. Hoppe. Tetrahedron Lett. **30**, 7037 (1989); (*k*) D. Seebach, R. Hassig, and J. Gebriel. Helv. Chim. Acta, **66**, 308 (1983); (*l*) H. Siegal. Top. Curr. Chem. **106**, 55 (1982); (*m*) J.I.G. Cadogan (*Editor*). Organophosphorus reagents in organic synthesis. Academic Press, New York. 1979; (*n*) J. Clayden and S. Warren. Angew. Chem. Int. Ed. Engl. **35**, 241 (1996); (*o*) C.R. Johnson. Aldrichimica Acta, **18**, 3 (1985); (*p*) B. Zwannenburg and A.J.H. Klunder (*Editors*). Perspectives in the organic chemistry of sulfur. Elsevier, Amsterdam. 1987; (*q*) S. Oae and Y. Uchida. *In* The chemistry of sulfones and sulfoxides. *Edited by* S. Patai, Z. Rappoport, and C.J.M. Stirling. Wiley, New York. 1988. Chap. 12; (*r*) H.J. Reich. *In* Organoselenium chemistry. *Edited by* D. Liotta. Wiley, New York. 1987. Chap. 5.
2. (*a*) H.J. Bestmann, E. Heid, W. Ryschka, and J. Lienert. Liebigs Ann. Chem. 1684 (1974); (*b*) C.R. Johnson, R.C. Elliott, and N.A. Meanwell. Tetrahedron Lett. **23**, 5005 (1982); (*c*) B.M. Trost and D.P. Curran. J. Am. Chem. Soc. **102**, 5699 (1980); (*d*) P.A. Bartlett and K.L. Mclaren. Phosphorus Sulfur Relat. Elem. **37**, 1 (1987); (*e*) D.H. Hua, R. Chan-Yu-King, J.A. Kakie, and L.J. Myer. Am. Chem. Soc. **109**, 5026 (1987); (*f*) M. Sting and W. Steglich. Synthesis, 132 (1990); (*g*) M. Sawamura, Y. Ito, and T. Hayashi. Tetrahedron Lett. **30**, 2247 (1989); (*h*) R. Jacquier, F. Ouazzani, M.L. Roumestant, and P. Villefont. Phosphorus Sulfur Relat. Elem. **36**, 73 (1988).
3. (*a*) S.E. Denmark and J.E. Marlin. J. Org. Chem. **52**, 5742 (1987); (*b*) S.E. Denmark, G. Rajendra, and J.E. Marlin. Tetrahedron Lett. **30**, 2469 (1989); (*c*) S.E. Denmark and R.L. Dorow. J. Org. Chem. **55**, 5926 (1990); (*d*) S.E. Denmark, H. Stadler, R.L. Dorow, and J.H. Kim. J. Org. Chem. **56**, 5063 (1991); (*e*) S.E. Denmark, N. Chatani, and S.V. Pansare. Tetrahedron, **48**, 2191 (1992); (*f*) S.E. Denmark and C.-T. Chen. J. Org. Chem. **59**, 2922 (1994); (*g*) S.E. Denmark and C.-T. Chen. Heteroat. Chem. **6**, 133 (1995); (*h*) S.E. Denmark and C.-T. Chen. J. Am. Chem. Soc. **117**, 11879 (1995); (*i*) S.E. Denmark and J.-H. Kim. J. Org. Chem. **60**, 7535 (1995).
4. (*a*) J.K. Whitesell. Chem. Rev. **89**, 1581 (1989); (*b*) K. Tomioka. Synthesis, 541 (1990).
5. (*a*) D. Cubinot, P. Mangeney, A. Alexakis, J.F. Normant, and J.P. Lellouche. J. Org. Chem. **54**, 2420 (1989); (*b*) P. Mangeney, A. Alexakis, and J.F. Normant. Tetrahedron Lett. **29**, 2677 (1988); (*c*) A. Alexakis, R. Sedrani, P. Mangeney, and J.F. Normant. Tetrahedron Lett. **29**, 4411 (1988); (*d*) E.J. Corey and S.S. Kim. J. Am. Chem. Soc. **112**, 4976 (1990);

© 2000 NRC Canada

(*e*) E.J. Corey and D.-H. Lee. J. Am. Chem. Soc. **113**, 4026 (1991); (*f*) E.J. Corey, C.-M. Yu, and D.-H. Lee. J. Am. Chem. Soc. **112**, 878 (1990).

6. (*a*) E.J. Corey, C.-M. Yu, and S.S. Kim. J. Am. Chem. Soc. **111**, 5495 (1989); (*b*) E.J. Corey, P.D. Jardine, S. Virgil, P.-W. Yuen, and R.P. Connell. J. Am. Chem. Soc. **111**, 9243 (1989); (*c*) K. Tomioka, M. Nakajima, and K. Koga. J. Am. Chem. Soc. **109**, 6213 (1989); (*d*) K. Tomioka, M. Shindo, and K. Koga. J. Am. Chem. Soc. **111**, 8266 (1989); (*e*) M. Tokles and J.K. Snyder. Tetrahedron Lett. **27**, 3951 (1986); (*f*) W. Zhang, J.L. Loebach, S.R. Wilson, and E.N. Jacobsen. J. Am. Chem. Soc. **112**, 2801 (1990); (*g*) T. Oishi and M. Hirama. J. Org. Chem. **54**, 5834 (1989); (*h*) M. Hirama, T. Oishi, and S. Ito. J. Chem. Soc. Chem. Commun. 665 (1989); (*i*) H. Nishiyama, H. Sakaguchi, T. Nakamura, M. Horihata, M. Kondo, and K. Itoh. Organometallics, **8**, 846 (1989); (*j*) H. Brunner and A. Kurzinger. J. Organomet. Chem. **346**, 413 (1988); (*k*) M. Yoshioka, T. Kawakita, and M. Ohno. Tetrahedron Lett. **30**, 1657 (1989); (*l*) K. Tomioka, M. Shindo, and K. Koga. J. Am. Chem. Soc. **111**, 8266 (1989); (*m*) K. Maruoka, T. Itoh, T. Shirasaka, and H. Yamamoto. J. Am. Chem. Soc. **110**, 310 (1988).
7. (*a*) S. Hanessian, D. Delorme, S. Beaudoin, and Y. LeBlanc. J. Am. Chem. Soc. **106**, 5754 (1984); (*b*) S. Hanessian, D. Delorme, S. Beaudoin, and Y. Leblanc. Chem. Scr. **25**, N55 (1985); (*c*) S. Hanessian, Y.L. Bennani, and D. Delome. Tetrahedron Lett. **31**, 6461 (1990.); (*d*) S. Hanessian and Y.L. Bennani. Tetrahedron Lett. **31**, 6465 (1990); (*e*) S. Hanessian and S. Beaudoin. Tetrahedron Lett. **33**, 7655 (1992); (*f*) S. Hanessian and S. Beaudoin. Tetrahedron Lett. **33**, 7659 (1992); (*g*) S. Hanessian, A. Gomtsyan, A. Payne, Y. Hervé, and S. Beaudoin. J. Org. Chem. **58**, 5032 (1993); (*h*) S. Hanessian, D. Andreotti, and A. Gomtsyan. J. Am. Chem. Soc. **117**, 10393 (1995); (*i*) Y.L. Bennani and S. Hanessian. Tetrahedron, **52**, 13837 (1966); (*j*) Y.L. Bennani, and S. Hanessian. Chem. Rev. **97**, 3161 (1997).
8. (*a*) S.E. Denmark and R.L. Dorow. J. Am. Chem. Soc. **112**, 864 (1990); (*b*) S.E. Denmark, K.A. Swiss, R.L. Dorow, P.C. Miller, and S.R. Wilson. J. Am. Chem. Soc. **116**, 2437 (1994).
9. S.E. Denmark, P.C. Miller, and S.R. Wilson. J. Am. Chem. Soc. **113**, 1468 (1991).
10. (*a*) S.E. Denmark and C.J. Cramer. J. Org. Chem. **55**, 1806 (1990); (*b*) S.E. Denmark and M. Kranz. J. Org. Chem. **60**, 5867 (1995); (*c*) S.E. Denmark, M. Kranz, K.A. Swiss, and S.R. Wilson. J. Org. Chem. **61**, 8551 (1996).
11. J.-H. Kim. Ph.D. thesis, Univerisity of Illinois, Urbana-Champaign. 1992.
12. (*a*) H. Booth and R.U. Lemieux. Can. J. Chem. **49**, 777 (1971); (*b*) R.O. Hutchins, L.D. Kopp, and E.L. Eliel. J. Am. Chem. Soc. **90**, 7174 (1968); (*c*) R.A.Y. Jones, A.R. Katritzky, and A.C. Richards. J. Chem. Soc. Chem. Commun. 708 (1969); (*d*) F.G. Riddel and D.A.R. William. Tetrahedron Lett. 2073 (1971).
13. S.E. Denmark and J.-H. Kim. Synthesis, 229 (1992).
14. (*a*) N.N. Bhongle, R.H. Notter, and J.G. Turcotte. Synth. Commun. **17**, 1071 (1987); (*b*) T. Morita, Y. Okamoto, and H. Sakurai. Chem. Lett. 435 (1980); (*c*) T. Morita, Y. Okamoto, and H. Sakurai. Tetrahedron Lett. 2523 (1978); (*d*) M.H.B. Stowell, J.M. Ueland, and R.W. McClard. Tetrahedron Lett. **31**, 3261 (1990).
15. (*a*) R.S. Edmundson. J. Chem. Soc. C, 2730 (1969); (*b*) J.H. Billman, J.L. Misenheimer, and R.A. Awl. J. Med. Chem. **7**, 366 (1964); (*c*) R. Kraemer and J. Navech. Bull. Soc. Chim. Fr. 3580 (1971).
16. (*a*) J.C. Tebby. *In* Organophosphorus chemistry, specialist periodical reports. *Edited by* S. Tripett. 1976. Chap. 12.; (*b*) E.N. Tsvetkov and M.I. Kabachnik. Russ. Chem. Rev. (Engl. Transl.), **40**, 97 (1971); (*c*) L.C. Thomas. The Interpretation of the infrared spectra of phosphorus compounds. Heydon, London. 1974.
17. (*a*) J.R. Van Wazer, J.H. Letcher, V. Mark, C.H. Dungan. Crutchfield, *In* Topics in phosphorus chemistry. *Edited by* M. Grason and E.J. Griffith. Interscience, New York. 1968. Vol. 5; (*b*) J.C. Tebby. Handbook of phosphorus-31 nuclear magnetic resonance data. CRC Press, Boca Raton. 1991.
18. L. Wozniak and J. Chojnowski. Tetrahedron, **45**, 2465 (1989).
19. R.L. Dorow. Ph.D. dissertation. University of Illinois, Urbana. 1990.
20. S. Arakawa, K. Kashiwabara, J. Fujita, and K. Saito. Bull. Chem. Soc. Jpn. **50**, 2108 (1977).
21. W.H. Pirkle, G. Mahler, and M.H. Hyun. J. Liq. Chromatogr. **9**, 443 (1986).

© 2000 NRC Canada

Delineating the possibilities for intramolecular interception of the squarate ester cascade through the use of metalated enecarbamates

Jinsung Tae and Leo A. Paquette

Abstract: Highly functionalized and annulated 2,4-cyclooctadienones are formed in a stereoselective manner by sequential treatment of squarate esters with a lithiated enecarbamate (six-membered ring or larger) and a cycloalkenyl- or 1-alkenyllithium reagent. The mechanistic details of this multistep process are presented. Particular attention is drawn to the step that involves intramolecular nucleophilic attack by a proximal oxido anion at the carbamate carbonyl and results in redirection of the cascade. This step is thwarted when five-membered cyclic enecarbamates are employed because of the excessive buildup of ring strain in the associated transition state.

Key words: squarate esters, enecarbamates, conrotatory ring opening, intramolecular acylation, alkenyllithium reagents.

Résumé : Des cyclooctadiène-2,4-ones à anneaux et hautement fonctionnalisées se forme de façon stéréosélective par un traitement séquentiel d'esters de l'acide squarique avec un ènecarbamate lithié (cycle à six chaînons ou plus) et un réactif cycloalcényl- ou 1-alcényllithium. On présente les détails mécanistiques de ce processus en plusieurs étapes. On porte une attention particulière à l'étape qui implique l'attaque nucléophile intramoléculaire d'un anion oxydo se trouvant à proximité sur le carbonyle du carbamate et qui conduit à une redirection de la cascade. En raison de l'augmentation excessive de la tension de cycle dans l'état de transition qui lui est associé, cette étape ne se produit pas lorsqu'on utilise des ènecarbamates cycliques à cinq chaînons.

Mots clés : esters de l'acide squarique, ènecarbamates, ouverture de cycle conrotatoire, acylation intramoléculaire, réactifs alcényllithium.

[Traduit par la Rédaction]

Introduction

The appreciable electrophilic character, highly functionalized nature, and inordinately strained features of squarate esters have the combined effect of rendering these reagents particularly susceptible to ring expansion following nucleophilic addition. The growing family of rearrangements that has been discovered is most impressive (1–4). Eguchi, Liebeskind, Moore, and their associates continue their efforts toward defining the regio- and (or) stereocontrol attainable in several of these multistep processes (5–7). Our laboratory has been engaged in elucidating the mechanistic features of the so-called "squarate ester cascade" that arises following the *twofold* addition of alkenyllithium reagents (8). Customarily, trans 1,2-addition of such organometallics (either the same or different) dominates, thereby setting the stage for the subsequent chemical events depicted in Scheme 1 (9). In those instances where the first nucleophile is chiral, diastereomeric 1:1 adducts arise at nearly equivalent levels. This initial lack of diastereoselection has no impact on the overall stereochemical outcome because the ensuing conrotatory ring opening and subsequent mechanistic developments result in a loss of the initial sense of chirality (10). In fact, only during ultimate conrotatory 8π closure to form the mesocyclic dienolates **3** and **4** is product configuration regulated. This uncommon series of chemical events is made possible because of helical equilibration that allows ready interconversion between **1** and **2**. The sterically least crowded transition state associated with formation of the eight-membered ring is kinetically favored (11). In the example shown, **5** is formed exclusively.

Under normal circumstances and in the absence of β-eliminatable substituents (8*b*, 11*c*, 12) dienolates such as **4** are the resting points of the cascade. Ensuing chemistry operates only following the addition of an electrophile. If those cases where water is involved, transannular aldol cyclization ensues after monoprotonation to deliver polycyclic products. An alternative synthetic ploy for utilizing the ease of assembly of reactive intermediates of type **4** is to intercept these species by some intramolecular means. Herein we disclose that recourse to metalated enecarbamates as one of the nucleophilic reagents can indeed result in redirection of the cascade under the proper circumstances (13).

Received June 16, 1999. Published on the NRC Research Press website on May 19, 2000.

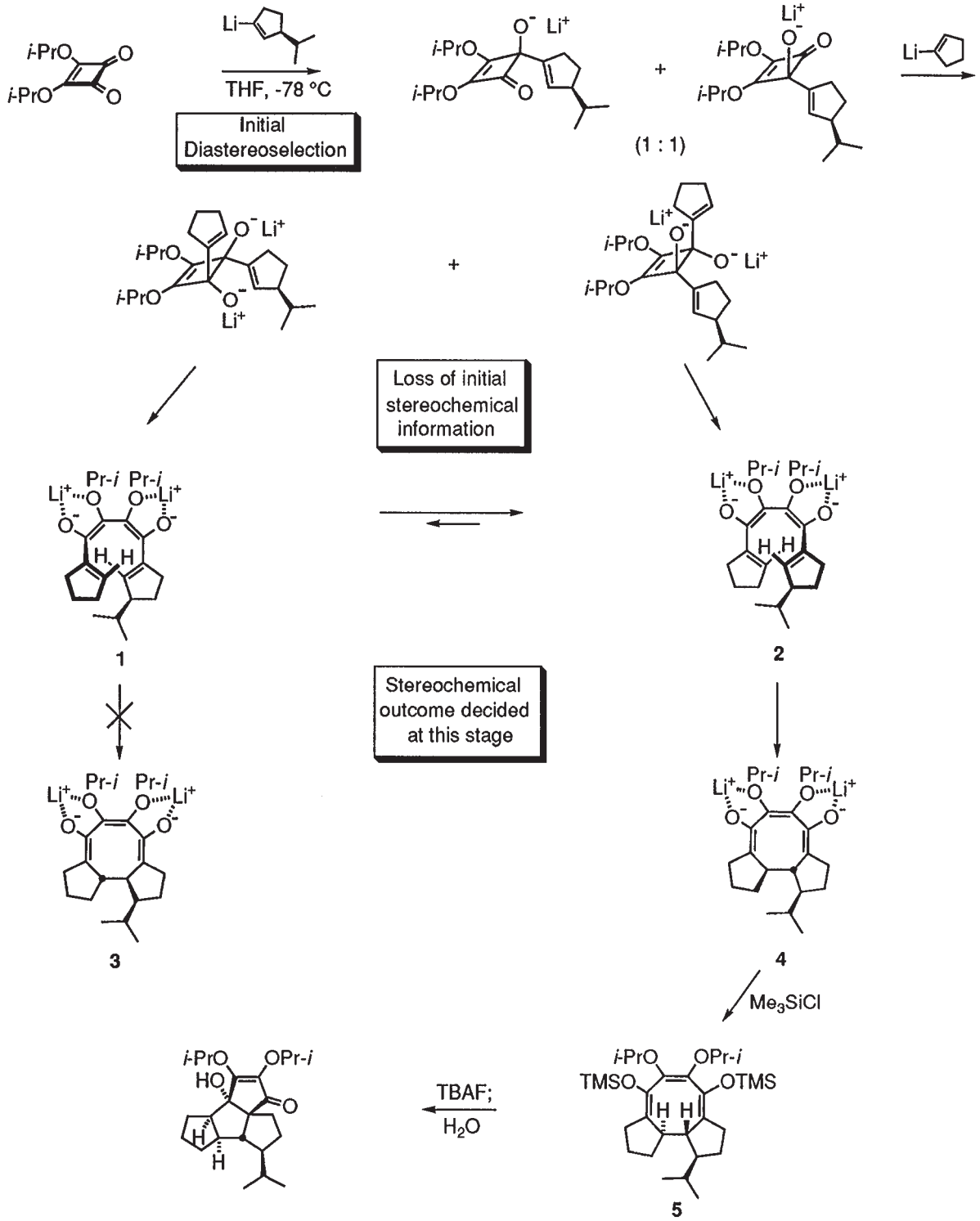
This paper is dedicated with warmth and admiration to Prof. Stephen Hanessian on the occasion of his 65th birthday.

J. Tae and L.A. Paquette.[1] Evans Chemical Laboratories, The Ohio State University, Columbus, OH 43210, U.S.A.

[1]Author to whom correspondence may be addressed. Telephone: (614) 292–2520.

© 2000 NRC Canada

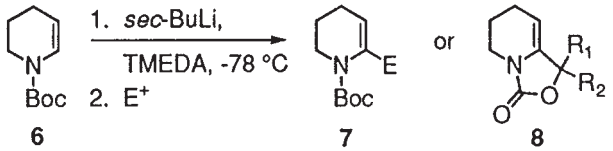
Scheme 1.



Results and discussion

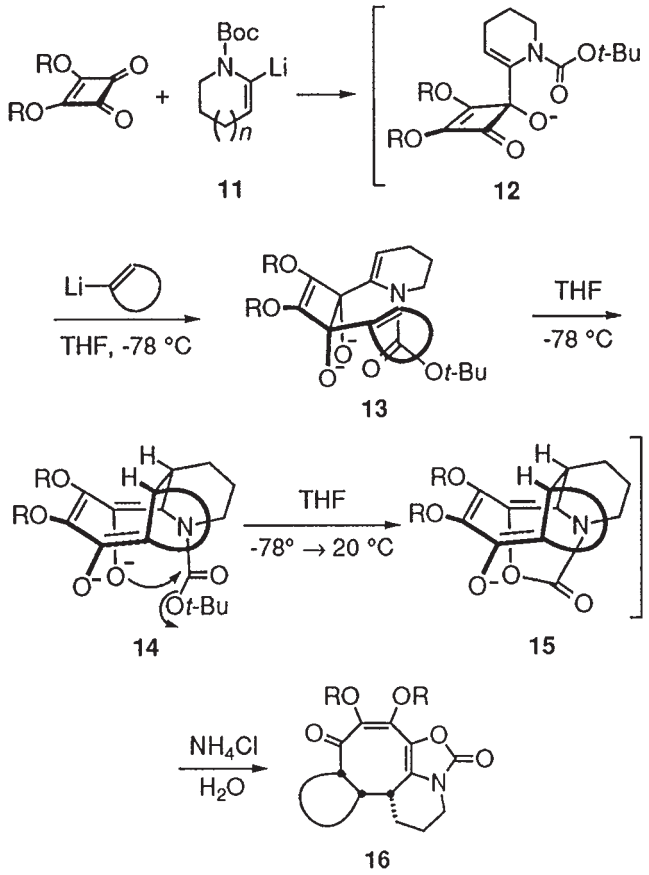
Intramolecular enolate interception

Although a wide range of α-heteroatom-substituted 1-alkenyllithium reagents is available (14), the direct application of metalated enecarbamates to synthetic endeavors has been undertaken only recently. Beak and Lee have demonstrated that **6** is amenable to α-lithiation with *sec*-butyllithium in the presence of TMEDA (15). This species is an effective reaction partner with electrophiles, giving

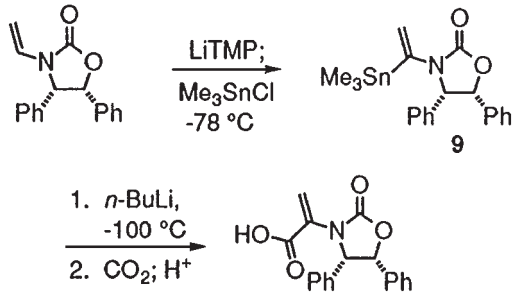


© 2000 NRC Canada

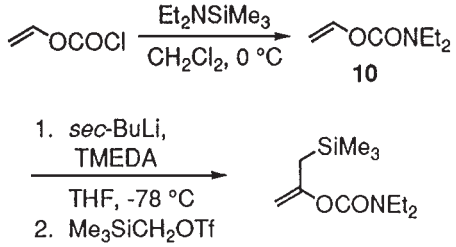
Scheme 2.



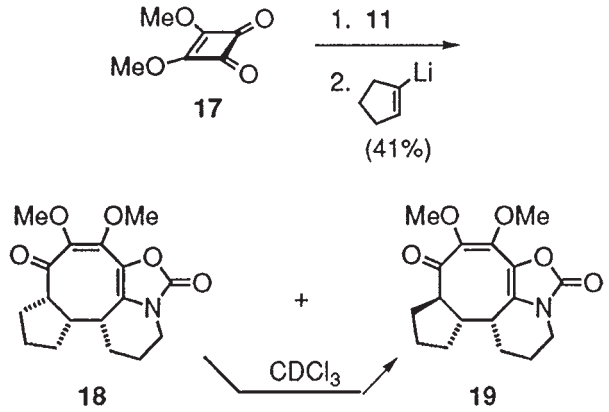
rise to **7** or **8** depending upon the chemical constitution of the co-reactant. Lander and Hegedus made recourse to vinylstannane precursors such as **9** in their quest of similar intermediates (16). Sengupta and Snieckus recognized that



the structurally simple building block **10** constitutes a versatile acyl anion equivalent (17). Other variants on this theme have been reported (18).



Scheme 3.



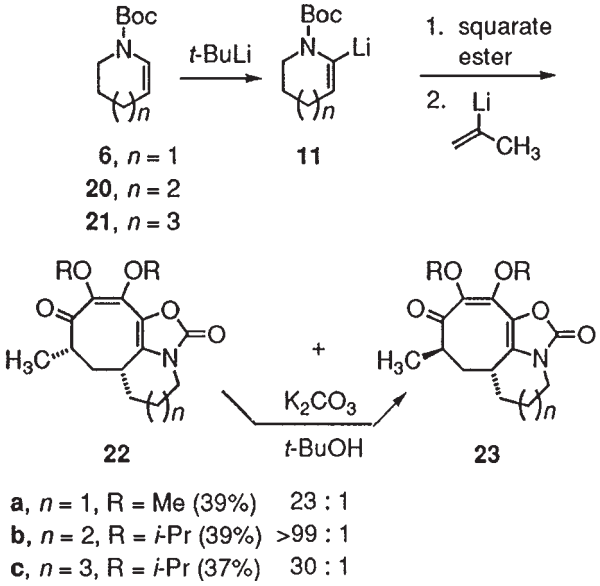
Our plan was to use the heterocyclic building block **11** as the lead nucleophile and to vary the structural specifications of the alkenyllithium as shown in Scheme 2. The expectation was that strong chelative interactions of the second anion to the carbamate functionality in monoadduct **12** would draw this reagent into kinetically favored *cis* addition and provide **13**. Should this reaction channel operate, charge-accelerated [3,3] sigmatropy was certain to ensue rapidly with formation of dienolate **14** via a boatlike transition state. With stereodirected arrival at **14**, two *cis* hydrogens will have been set, thereby making it possible for one of the oxido anions to attack the flanking ester group. The likelihood of this intramolecular acylation to generate **15** was suggested by prior discovery of the **6** → **8** conversion. The conformationally inflexible tub conformation held by **15** can be expected to be conducive to protonation from the exterior thereby delivering the all-*syn* stereoisomer **16**. The simplicity of this stereochemically distinctive route to polycondensed heterocyclic systems in one laboratory operation is emphasized.

Indeed, when dimethyl squarate (**17**) (19) was sequentially treated with **11** and cyclopentenyllithium, mixtures of **18** and **19** were produced in highly variable proportions (Scheme 3). The discovery was soon made that this product distribution was intimately linked to two time elements: the duration of the quenching process and the speed with which the stereoisomers were removed from the basic aqueous solution. The epimerization of **18** was subsequently discovered to be especially facile in acidic or alkaline environments. As an example, dissolution of pure **18** in $CDCl_3$ resulted in conversion to a 1:3 mixture of **18** and **19** within only 5 min. The *trans*, *cis* arrangement of the three contiguous stereogenic centers in **19** was readily deduced on the basis of NOE measurements. This finding requires that **18** have *cis*, *cis* stereochemistry, completely in agreement with expectations based on Scheme 2. The thermodynamic preference for *cis*, *trans* fusion of two five-membered rings to a cyclooctane core has been noted previously in a different context (20).

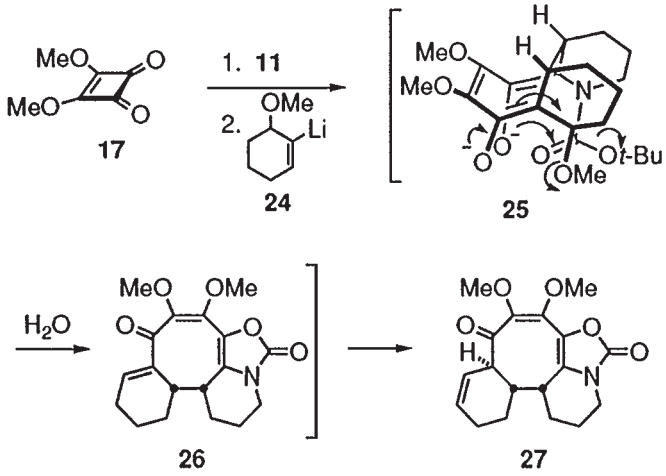
Pairing **11** with 2-lithiopropene had the effect of delivering a chromatographically inseparable 23:1 mixture of **22a** and **23a** (Scheme 4). As in the preceding example, the predominance of the *syn* isomer was clearly demonstrated to be the consequence of kinetic control. Thus, treating the **22a**–**23a** mixture with potassium carbonate in *tert*-butyl alcohol resulted in a pronounced increase in the proportion of **23a** to

© 2000 NRC Canada

Scheme 4.



Scheme 5.



ca. 90%. Advantage was taken of the high crystallinity of **23a** to confirm the stereochemical assignments by means of X-ray diffraction.

In order to expand on these observations, literature precedent was followed to prepare the homologous enecarbamates **20** and **21** (21). The cascade reactions involving their lithiated counterparts **11** (n = 2 and 3) were found to be equally diastereoselective, giving rise very predominantly to **22b** and **22c**, respectively. Comparative NOE studies of these cyclooctadienones established that they share in common a *syn*, *cis* α-methyl substituent.

The involvement of methoxy-substituted cyclohexenyllithium **24** as the second nucleophile was expected to result in the ultimate introduction of another degree of unsaturation in the product as a consequence of the β-elimination depicted in **25** (Scheme 5). If operative, this step would lead in combination with the ejection to *t*-butoxide ion to **26**. In actuality, the admixing of this triad of reagents led to the formation of **27** in modest yield. The migration of the cyclohexenyl double bond to the β,γ-position presumably operates in order to reduce the strain in **26**. It is reasonable to conclude that this ring strain is likewise contributory to the diminished efficiency with which **27** is formed.

The consequences of ring size

The issue of structural constraint surfaces in a more dramatic fashion when the ring size of the enecarbamate is reduced to the pyrrolidine level. In our hands, all experiments involving **28** resulted in an inability to intercept the bisenolate as in **14** or **25**. Apparently, a five-membered heterocycle is insufficiently flexible to allow further progression in the direction followed by the homologous enecarbamates. Azapolycyclics such as **29–31** are consequently formed instead (Scheme 6). These products bear a close resemblance to those formed in the non-intercepted squarate ester cascade.

Since the two isomers of **29** were chromatograhically inseparable, it proved inadvisable to distinguish the specific stereochemical features of the heterocyclic ring fusion. The near equitable proportion of these epimers significantly diminishes the importance of this distinction. In the 1-lithiocyclopentene example, **30** is formed with a fivefold greater preference than **31**. The major isomer was readily separated by crystallization and identified as the all-*syn* stereoisomer by NOE measurements (see Experimental section).

Although all of the yields reported are moderate, control experiments have shown that the lowered levels of product formation are due predominantly to the efficiency of the enecarbamate metalation step and are not intrinsic to the cascade. No attempt was made to enhance yields by making stoichiometric adjustments different from the above.

Selected chemical transformations of 22a

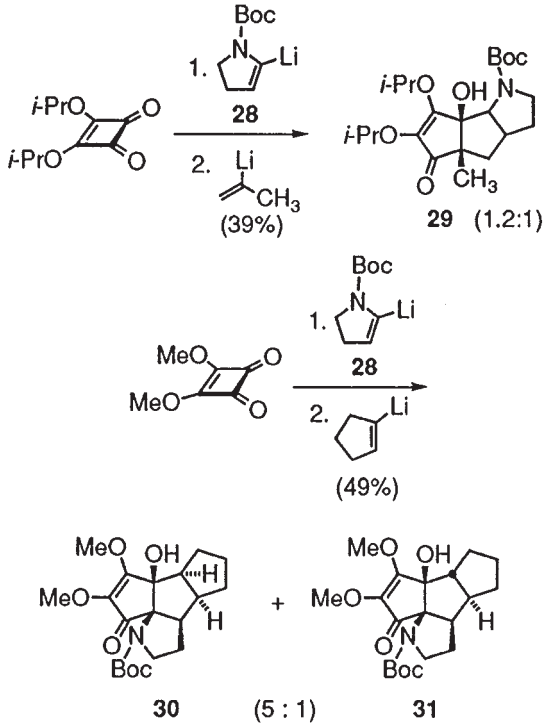
The structural features of the mesocyclic products resulting from the interrupted squarate cascade were considered to be sufficiently unusual to warrant modest exploration of their chemical reactivity. The readily available prototype **22a** was selected for further study. Enolate anion generation proved feasible provided that recourse was made to a hindered non-nucleophilic base. The use of potassium *tert*-butoxide in dimethyl sulfoxide is exemplary. As anticipated from precedent (22), this reagent combination was particularly conducive to *O*-methylation when coupled with the use of dimethyl sulfate. Triene **32** was isolated in 76% yield (Scheme 7).

When **22a** was dissolved instead in a 1:1 mixture of methanol and THF containing sodium methoxide, nucleophilic attack at the carbamate carbonyl and epimerization of the α-proton occurred to generate the alternative enolate anion **33**. As a consequence of proximity effects, transannular aldolization operates readily with formation of the *cis*-fused diquinane **34**. The generation of this alkoxide opens the way for ultimate ejection of methoxide ion with formation of the isomeric carbamate **35** in which five heteroatoms are bonded to the same cyclopentene ring.

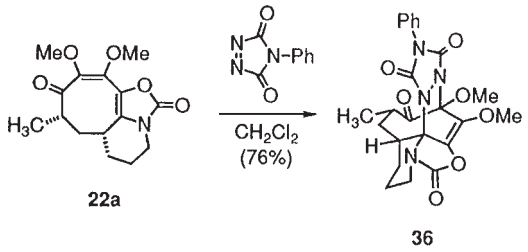
As a diene, **22a** proved unreactive to most dienophiles, a likely consequence of the nonplanarity of its two double bonds. Notwithstanding, [4+2] cycloaddition was realized in the presence of *N*-phenyltriazolinedione with formation of **36**. The direction of the overwhelming π-facial diastereoselectivity

© 2000 NRC Canada

Scheme 6.



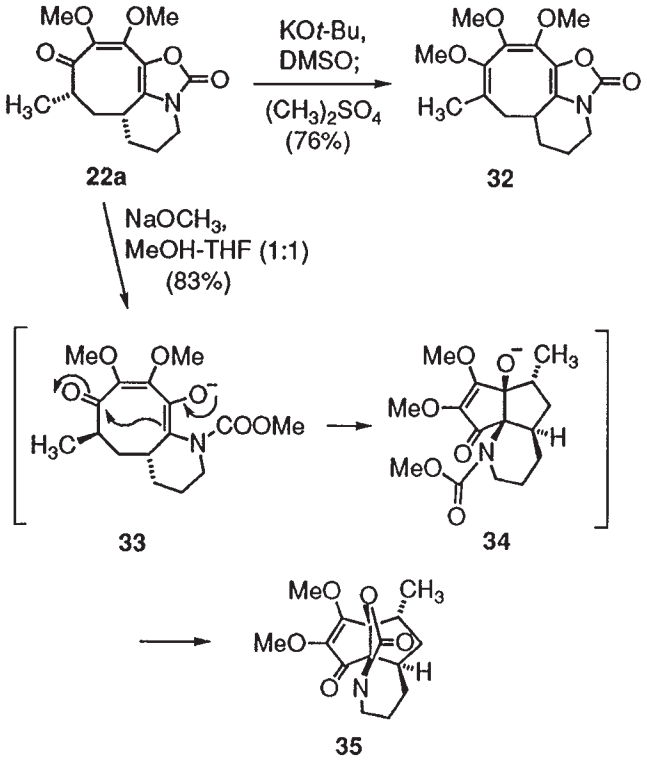
observed for this process was ascertained by X-ray crystallographic analysis of the only product.



Conclusions

A new method for accessing highly functionalized eight-membered ring ketones in a single laboratory step is described. The mechanistic requirements for this multistep transformation of squarate esters involve initial 1,2-addition of a metalated enecarbamate, chelation-controlled *cis* addition of an alkenyllithium co-reactant, dianionic oxy-Cope rearrangement of the resulting doubly charged intermediate via a boatlike transition state, and intramolecular nucleophilic capture of the carbamate functionality. The cyclic enecarbamates must be six-membered or larger in order to perform satisfactorily in the product-defining step. The excessive strain present when lower homologs are involved does not allow for rerouting of the cascade, and polycyclic nitrogen-containing products indicative of this fact make their appearance. Finally, adoption of the sigmatropic pathway necessarily provides all-*syn* stereoisomeric products as the end result of kinetic control. Since these isomers are often not the thermodynamically favored epimers, their exposure to mildly acidic or basic conditions suffices to make available a companion set of configurationally distinctive compounds for further investigation.

Scheme 7.



Experimental

General information

Tetrahydrofuran and ether were distilled from sodium benzophenone ketyl under nitrogen just prior to use. For dichloromethane and dimethyl sulfoxide, the drying agent was calcium hydride. All reactions were performed under a nitrogen atmosphere. Analytical thin-layer chromatography was carried out on E. Merck silica gel 60 F_{254} aluminum-backed plates. The 230–400 mesh size of the same absorbent was utilized for all chromatographic purifications. The organic extracts were dried over anhydrous $MgSO_4$. ^1H and ^{13}C NMR spectra were recorded on Bruker instruments at 300 and 75 MHz, respectively. Infrared spectra were recorded with a Perkin–Elmer 1320 spectrometer. The high-resolution mass spectra were recorded at The Ohio State University Campus Chemical Instrumentation Center.

Prototypical procedure for cascade rearrangements involving the enecarbamates

A. A cold (–78°C) solution of **6** (515 mg, 2.81 mmol) in dry THF (10 mL) was treated dropwise with *tert*-butyllithium (1.84 mL of 1.7 M). After 1 h of stirring at this temperature, a solution of dimethyl squarate (266 mg, 1.87 mmol) in THF (5 mL) was next introduced in dropwise fashion. One hour later, 1-lithiocyclopentene (prepared from the iodide (726 mg, 3.74 mmol) and *tert*-butyllithium (7.48 mmol) at –78°C during 30 min) was added rapidly. After an additional 2 h at –78°C, the reaction mixture was allowed to warm to room temperature overnight, recooled to

© 2000 NRC Canada

0°C, treated with deoxygenated saturated NH_4Cl solution (10 mL), stirred for 30 min, and warmed to room temperature. After 30 min, saturated $NaHCO_3$ solution was added and the separated aqueous layer was extracted with ether. The combined organic layers were dried and concentrated to leave a residue that was chromatographed on silica gel. Elution with 50% ethyl acetate in hexanes afforded 244 mg (41%) of a 1:5 mixture of **18** and **19**.

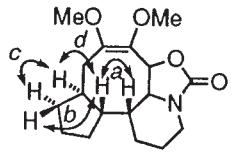
Upon crystallization from 5% CH_2Cl_2 in hexanes, it was possible to obtain samples of **18** having >99% isomeric purity. Dissolution of a pure sample of **18** in $CDCl_3$ resulted in conversion to a 1:3 mixture of **18** and **19** within 5 min.

For **18**: white crystals, mp 140–142°C; IR (film) ν: 1759, 1693, 1644, 1452, 1256 cm^{-1}; ^1H NMR (C_6D_6) δ: 3.51 (3H, s), 3.43 (3H, s), 3.30 (1H, m), 2.70 (1H, m), 2.50 (1H, m), 2.14–1.98 (2H, m), 1.77–1.64 (1H, m), 1.57–1.37 (3H, m), 1.37–1.17 (1H, m), 1.17–1.05 (1H, m), 0.95–0.70 (4H, m) ppm; ^{13}C NMR (C_6D_6) δ: 202.8, 154.8, 144.3, 129.1, 128.2, 127.9, 59.1, 58.9, 58.5, 53.0, 40.6, 34.9, 30.0, 27.1, 23.8, 23.0, 17.1 ppm; HRMS (EI) calcd. for $C_{17}H_{21}NO_5$, *M*: 319.1419; found: 319.1432. Anal. calcd. for $C_{17}H_{21}NO_5$: C 63.94, H 6.63; found: C 63.66, H 6.60.

For **19**: colorless oil; IR (film) ν: 1760, 1651, 1446, 1238 cm^{-1}; ^1H NMR ($CDCl_3$) δ: 3.87 (3H, s), 3.75 (1H, m), 3.65 (3H, s), 3.42 (1H, m), 2.99 (1H, m), 2.82 (1H, m), 2.63 (1H, m), 2.11 (1H, m), 2.05–1.55 (8H, series of m), 1.33 (1H, m); ^{13}C NMR ($CDCl_3$) δ 197.8, 154.2, 148.7, 142.0, 131.5, 129.2, 62.2, 61.1, 60.5, 52.3, 40.7, 30.8, 29.8, 25.3, 22.6, 21.9, 19.4; HRMS (EI) calcd. for $C_{17}H_{21}NO_5$, *M*: 319.1419; found: 319.1419.

The following NOE interactions were observed:

Structure 1.



a: 12.5% **c**: 5.8%
b: 3.0% **d**: 0%

B. Reaction of 573 mg (3.12 mmol) of **6** with dimethyl squarate (296 mg, 2.08 mmol), and 2-lithiopropene (4.17 mmol) in the predescribed manner furnished 235 mg (39%) of a 23:1 mixture of **22a** and **23a**. Treating a 50 mg sample of this mixture with potassium carbonate (50 mg) in *tert*-butyl alcohol (5 mL) at room temperature overnight gave a mixture rich in **23b** (now 1:10). Crystallization of this material from ether:CH_2Cl_2 (10:1) gave pure **23b**.

For **22a**: colorless oil; IR (film) ν: 1760, 1694, 1651, 1455, 1412, 1328, 1257 cm^{-1}; ^1H NMR ($CDCl_3$) δ: 3.80–3.60 (1H, m), 3.70 (3H, s), 3.69 (3H, s), 3.25 (1H, m), 3.02 (1H, m), 2.90 (1H, m), 1.95–1.65 (6H, m), 1.09 (3H, d, *J* = 6.7 Hz) ppm; ^{13}C NMR ($CDCl_3$) δ: 207.6, 154.8, 141.9, 129.4, 128.4, 128.3, 59.6, 58.8, 45.1 (2 C), 40.8, 29.8, 27.5, 17.3, 16.3 ppm; HRMS (EI) calcd. for $C_{15}H_{19}NO_5$, *M*: 293.1263; found: 293.1268.

For **23a**: yellowish crystals, mp 149–151°C; IR (film) ν: 1759, 1613, 1535, 1452, 1250 cm^{-1}; ^1H NMR ($CDCl_3$) δ: 3.90–3.80 (1H, m), 3.86 (3H, s), 3.61 (3H, s), 3.25 (1H, m), 3.05–2.80 (2H, m), 2.20–1.95 (2H, m), 1.95–1.80 (2H, m), 1.80–1.60 (2H, m), 1.03 (3H, d, *J* = 6.5 Hz) ppm; ^{13}C NMR ($CDCl_3$) δ: 202.2, 153.9, 148.1, 139.7, 132.1, 128.2, 60.8, 60.1, 48.1, 40.7, 40.1, 28.8, 23.6, 16.8, 16.0 ppm; HRMS (EI) calcd. for $C_{15}H_{19}NO_5$, *M*: 293.1263; found: 293.1264. Anal. calcd. for $C_{15}H_{19}NO_5$: C 61.42, H 6.53; found: C 61.34, H 6.50.

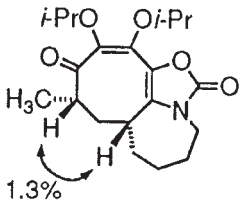
The structure of **23a** was corroborated by X-ray diffraction analysis.

C. From 373 mg (1.89 mmol) of **20**, 250 mg (1.26 mmol) of diisopropyl squarate, and 2-lithiopropene (2.52 mmol), there was isolated 180 mg (39% of a >99:1 mixture of **22b** and **23b**.

For **22b**: yellow crystals, mp 94–96°C; IR (film) ν: 1760, 1650, 1555, 1455, 1375, 1245 cm^{-1}; ^1H NMR ($CDCl_3$) δ 4.47 (1H, septet, *J* = 6.1 Hz), 4.26 (1H, m), 4.10 (1H, septet, *J* = 6.2 Hz), 3.29 (1H, m), 3.00 (1H, m), 2.81 (1H, septet, *J* = 6.5 Hz), 2.25–1.50 (6H, series of m), 1.33 (3H, d, *J* = 6.2 Hz), 1.23 (3H, d, *J* = 6.2 Hz) 1.17 (3H, d, *J* = 6.2 Hz), 1.14 (3H, d, *J* = 6.2 Hz), 1.05 (3H, d, *J* = 6.5 Hz), 1.90–1.70 (2H, m) ppm; ^{13}C NMR ($CDCl_3$) δ: 202.3, 154.4, 145.1, 141.5, 135.9, 128.8, 74.7, 74.3, 46.8, 45.2, 40.5, 33.9, 30.3, 27.6, 23.8, 22.7, 22.6, 22.5, 22.3, 16.0 ppm; HRMS (EI) calcd. for $C_{20}H_{29}NO_5$, *M*: 363.2045; found: 363.2055.

The following NOE interaction was observed:

Structure 2.

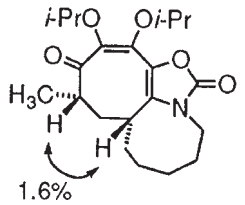


D. Parallel reaction of **21** (358 mg, 1.81 mmol) with diisopropyl squarate (239 mg, 1.20 mmol) and 2-lithiopropene (2.41 mmol) afforded 168 mg (37%) of a 30:1 mixture of **22c** and **23c**.

For **22c**: yellow solid, mp 131–133°C; IR (film), ν: 1765, 1658, 1452, 1371, 1211 cm^{-1}; ^1H NMR (C_6D_6) δ: 4.41–4.31 (2H, m), 3.97 (1H, m), 2.95 (1H, m), 2.71 (1H, septet, *J* = 6.1 Hz), 2.48 (1H, m), 1.80–1.50 (3H, m), 1.50–0.60 (7H, series of m), 1.34 (3H, d, *J* = 6.1 Hz), 1.25 (3H, d, *J* = 6.1 Hz), 1.24 (3H, d, *J* = 6.1 Hz), 1.09 (3H, d, *J* = 6.1 Hz), 1.02 (3H, d, *J* = 6.4 Hz) ppm; ^{13}C NMR (C_6D_6) δ: 200.5, 154.3, 141.7, 134.5, 128.6, 127.1, 74.1, 73.7, 50.4, 41.4, 39.8, 34.6, 29.2, 26.3, 26.0, 22.8, 22.5, 22.4, 22.2, 21.7, 16.0 ppm; HRMS (EI) calcd. for $C_{21}H_{32}NO_5$, *M*: 377.2202; found: 377.2211. Anal. calcd. for $C_{21}H_{32}NO_5$: C 66.82, H 8.28; found: C 66.87, H 8.29.

The following NOE interaction was observed:

Structure 3.



© 2000 NRC Canada

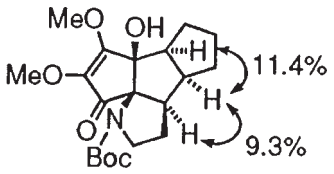
E. From 265 mg (1.87 mmol) of dimethyl squarate, 5.13 mg (2.80 mmol) of **6**, and 713 mg (3.73 mmol) of 1-bromo-6-methoxycyclohexene, there was isolated 99 mg (16%) of **27** as a colorless oil; ^{1}H NMR ($CDCl_3$) δ: 5.96 (1H, m), 5.44 (1H, m), 3.92 (3H, s), 3.84 (1H, m), 3.64 (3H, s), 3.56 (1H, m), 3.40 (1H, m), 2.50 (1H, m), 2.38–2.24 (2H, m), 2.17–1.95 (2H, m), 1.95–1.81 (3H, m), 1.78–1.58 (2H, m) ppm; ^{13}C NMR ($CDCl_3$) δ: 198.3, 154.1, 148.2, 140.5, 132.4, 130.4, 128.4, 123.9, 61.0 (2 C), 49.6, 46.3, 41.0, 33.9, 25.6, 22.6, 20.6, 16.7 ppm; HRMS (EI) calcd. for $C_{18}H_{21}NO_5$, *M*: 331.1420; found: 331.1403.

F. Reaction of *N*-(*tert*-butoxycarbonyl)-2-pyrroline (320 mg, 1.89 mmol), diisopropyl squarate (250 mg, 1.89 mmol), and 2-bromopropene (0.224 mL, 2.52 mmol) according to the general procedure gave 335 mg (39%) of **29** as a 1.2:1 mixture of isomers); colorless oil; IR (film) ν: 3462, 1698, 1620, 1393, 1298 cm^{-1}; ^{1}H NMR ($CDCl_3$) δ: 5.39 (0.45H, quintet, *J* = 6.2 Hz), 5.27 (0.55H, quintet, *J* = 6.2 Hz), 4.94 (1H, m), 4.32 (0.55H, d, *J* = 8.6 Hz), 4.27 (0.45H, d, *J* = 8.5 Hz), 3.35–3.15 (2H, m), 2.62 (1H, m), 2.19 (0.45H, d, *J* = 5.1 Hz), 2.14 (0.55H, d, *J* = 5.1 Hz), 1.90–1.70 (2H, m), 1.52 (4.05H, s), 1.47 (4.95H, s), 1.65–1.40 (1H, m), 1.40–1.15 (12H, series of d), 1.11 (1.65H, s), 1.10 (1.35H, s) ppm; ^{13}C NMR (C_6D_6) δ: (major isomer) 302.0, 167.6, 155.2, 131.0, 84.2, 78.9, 74.0, 73.2, 71.2, 56.7, 47.6, 40.9, 36.4, 29.8, 28.2 (3C), 22.9 (2C), 22.2 (2C), 20.1 ppm; δ: (minor isomer) 202.7, 166.9, 153.8, 131.0, 84.2, 79.1, 74.0, 73.6, 71.4, 56.5, 47.5, 41.9, 36.2, 29.8, 28.2 (3C), 22.7 (2C), 22.4 (2C), 20.3 ppm; HRMS (EI) calcd. for $C_{22}H_{35}NO_6$, *M*: 409.2464; found: 409.2469. Anal. calcd. for $C_{22}H_{35}NO_6$: C 64.52, H 8.61; found: C 64.61; H 8.66.

G. Reaction of *N*-(*tert*-butoxycarbonyl)-2-pyrroline (474 mg, 2.80 mmol) dimethyl squarate (265 mg, 1.87 mmol), and 1-iodocyclopentene (747 mg, 3.73 mmol) as described above gave 345 mg (49%) of a 5:1 mixture of **30** and **31**. Major product **30** was obtained as white crystals, mp 99–101°C; IR (film) ν: 3412, 1714, 1664, 1631, 1459, 1395; ^{1}H NMR ($CDCl_3$) δ: 4.45 (1H, s), 4.16 (3H, s), 3.79 (3H, s), 3.48–3.16 (2H, m), 2.73 (1H, m), 2.62 (1H, q, *J* = 9.0 Hz), 2.42 (1H, m), 2.00–1.30 (8H, series of m), 1.39 (9H, s); ^{13}C NMR ($CDCl_3$) δ: 199.0, 168.5, 157.1, 134.2, 83.0, 81.1, 80.1, 59.6 (2C), 51.9, 50.9, 50.0, 43.8, 28.2 (3C), 28.1, 27.4, 27.0, 26.5; HRMS (EI) calcd. for $C_{20}H_{29}NO_6$, *M*: 379.1995; found: 379.1991. Anal. calcd. for $C_{20}H_{29}NO_6$: C 63.31, H 7.70; found: C 63.34, H, 7.69.

The following NOE interactions were observed:

Structure 4.



*4,5,5a,6-Tetrahydro-8,9,10-trimethoxy-7-methyl-2*H,3H-*1-oxa-2a-azacyclooct[*cd*]inden-2-one (**32**)*: A solution of potassium *tert*-butoxide (230 mg, 2.05 mmol) in DMSO (7 mL) was cooled to 0°C and treated with a solution of **22a** (100 mg, 0.341 mmol) in DMSO (3 mL). After 30 min of stirring in the cold, dimethyl sulfate (0.20 mL, 2.1 mmol) was introduced and the reaction mixture was allowed to warm to room temperature over 15 h. After dilution with ether and brine the separated aqueous phase was extracted with ether and the combined organic layers were dried and concentrated. Flash chromatography of the residue on silica gel (elution with 20% ethyl acetate in hexanes) gave 80 mg (76%) of **32** as white crystals, mp 124–126°C (from hexanes:ether 1:5); IR (film) ν: 3495, 1755, 1633, 1454, 1410, 1292 cm^{-1}; ^{1}H NMR ($CDCl_3$) δ: 3.80 (1H, dd, *J* = 12.5, 5.7 Hz), 3.68 (3H, s), 3.57 (3H, s), 3.43 (3H, s), 3.24 (1H, dt, *J* = 12.5, 5.7 Hz), 2.90–2.78 (2H, m), 2.12–2.03 (2H, m), 1.90–1.63 (2H, m), 1.81 (3H, s), 1.53 (1H, m) ppm; ^{13}C NMR ($CDCl_3$) δ: 154.6, 145.4, 137.5, 132.8, 127.7, 126.9, 121.5, 59.2, 57.2, 56.5, 40.6, 36.0, 35.3, 27.6, 22.8, 17.9 ppm; HRMS (EI) calcd. for $C_{16}H_{21}NO_5$, *M*: 307.1419; found: 307.1448. Anal. calcd. for $C_{16}H_{21}NO_5$: C 62.53, H 6.89; found: C 62.60, H 6.88.

*(4a*R**,6*R**,6a*S**,12a*R**)-2,3,4,4a,5,6-Hexahydro-7,8-dimethoxy-6-methyl-9*H*-6a,1-(epoxymethano)-1H-pentaleno[6a,1-*b*]pyridine-9,11-dione (**35**)*: To an excess of sodium methoxide (from 50 mg of sodium metal) in methanol (5 mL) and THF (3 mL) was added 100 mg (0.34 mmol) of **22a** dissolved in THF (2 mL). After 1 h, the reaction mixture was quenched with saturated NH_4Cl solution (10 mL) and ether (10 mL). The separated aqueous phase was extracted with ether, and the combined organic layers were dried and concentrated. Flash chromatography of the residue on silica gel (elution with 20% ethyl acetate in hexanes) gave **35** (83 mg, 83%) as white crystals, mp 98–100°C (from ether:CH_2Cl_2 20:1); IR (film) ν: 1761, 1712, 1625, 1461, 1389, 1339 cm; ^{1}H NMR ($CDCl_3$) δ: 4.10 (3H, s), 3.86 (3H, s), 3.77 (1H, m), 3.15 (1H, m), 2.51 (1H, quintet, *J* = 6.4 Hz), 2.35–2.05 (3H, m), 1.72 (1H, m), 1.65–1.49 (3H, m), 0.96 (3H, d, *J* = 7.6 Hz) ppm; ^{13}C NMR ($CDCl_3$) δ: 193.9, 163.2, 156.4, 135.9, 90.7, 69.4, 59.3, 59.2, 40.5, 39.9, 36.2, 33.6, 22.3, 19.2, 15.6 ppm; HRMS (EI) calcd. for $C_{15}H_{19}NO_5$, *M*: 293.1263; found: 293.1268. Anal. calcd. for $C_{15}H_{19}NO_5$: C 61.42, H, 6.53; found: C 61.31, H 6.49.

The structural assignment to **35** was corroborated by X-ray diffraction analysis.

*(3*R**,5*S**,6a*R**,13a*S**)-3,4,5,6,6a,7,8,9-Octahydro-3,14-dimethoxy-5-methyl-4,11-dioxo-*N*-phenyl-3,13-metheno-11*H*,13*H*-oxazolo[3′,4′:1,2]pyrido[2,3-*c*]-1,2-diazoline-1,2-dicarboxylate (**36**)*: To a cold (–78°C) solution of 4-phenyl-1,2,4-triazoline-3,5-dione (30 mg, 0.17 mmol) in CH_2Cl_2 (5 mL) was added a solution of **22a** (33 mg, 0.11 mmol) in CH_2Cl_2 (2 mL). After 30 min of stirring, the reaction mixture was allowed to warm to room temperature over 2 h and concentrated under vacuum. Flash chromatography on silica gel (elution with 20% ethyl acetate in hexanes) afforded **36** as white crystals (40 mg, 76%) of mp 193–195°C dec (from ether:CH_2Cl_2 20:1); IR (film) ν: 1805, 1782, 1731, 1600, 1503, 1415, 1247 cm^{-1}; ^{1}H NMR ($CDCl_3$) δ: 7.56–7.38 (5H, m), 4.13–3.93 (2H, m), 3.99 (3H, s), 3.37 (3H, s), 2.70 (1H, m), 2.10–1.62 (6H, series of m), 1.20 (3H, d, *J* = 6.7 Hz), 1.07 (1H, m) ppm; ^{13}C NMR ($CDCl_3$) δ: 197.4, 154.5, 152.4, 147.0, 130.3, 129.3 (2C), 129.1, 128.8, 126.1, 125.1 (2C), 88.9, 82.5, 61.1, 52.3, 49.7, 45.1, 41.9, 40.3, 27.1, 20.9, 18.1 ppm; HRMS (EI) calcd. for $C_{23}H_{24}N_4O_9$, *M*: 468.1644,

© 2000 NRC Canada

observed: 468.1644. Anal. calcd. for $C_{23}H_{24}N_4O_9$: C 58.97, H 5.16; found: C 58.99, H 5.11.

The structural assignment to **36** was corroborated by X-ray diffraction analysis.

Acknowledgements

The financial support of the National Science Foundation is gratefully acknowledged. X-ray crystallographic results were recorded by Prof. Robin Rogers and Dr. Judith Gallucci whom we thank. These data were deposited with the Cambridge Crystallographic Data Centre at the time of submission of the preliminary report (ref. 13). Assistance with nomenclature was provided by Dr. Kurt Loening.

References

1. L.S. Liebeskind. Tetrahedron, **45**, 3053 (1989).
2. (*a*) H.W. Moore and B.R. Yerxa. Chemtracts — organic chemistry, **5**, 273 (1992); (*b*) H.W. Moore and B.B. Yerxa. Adv. Strain Org. Chem. **4**, 81 (1995).
3. M. Ohno, Y. Yamamoto, and S. Eguchi. Synlett. 1167 (1998).
4. L.A. Paquette. Eur. J. Org. Chem. 1709 (1998).
5. Y. Yamamoto, M. Noda, M. Ohno, and S. Eguchi. J. Org. Chem. **62**, 1292 (1997), and previous papers.
6. F. Liu and L.S. Liebeskind. J. Org. Chem. **63**, 2835 (1998), and previous papers.
7. J.M. MacDougal, V.J. Santora, S.K. Verma, P. Turnbull, C.R. Hernandez, and H.W. Moore. J. Org. Chem. **63**, 6905 (1998), and previous papers.
8. (*a*) L.A. Paquette and J. Tae. J. Org. Chem. **63**, 2022 (1998); (*b*) L.A. Paquette, L.H. Kuo, and J. Tae. J. Org. Chem. **63**, 2010 (1998), and previous papers.
9. This normal predilection can be overturned by appropriate oxy substitution. The resulting chelation to the second entering organolithium reagent can markedly augment its *syn* delivery: (*a*) L.A. Paquette, L.H. Kuo, and J. Doyon. J. Am. Chem. Soc., **119**, 3038 (1997); (*b*) L.A. Paquette, L.H. Kuo, and J. Doyon. Tetrahedron, **52**, 11625 (1996). (*c*) L.A. Paquette, T.M. Morwick, J.T. Negri, and R.D. Rogers. Tetrahedron, **52**, 3075 (1996).
10. For a recent theoretical analysis of this mechanistic pathway, consult M. Oliva, L.R. Domingo, V.S. Safont, J. Andrés, R. Castillo, and V. Moliner. J. Phys. Org. Chem., **12**, 1 (1999).
11. (*a*) L.A. Paquette, J. Doyon, and L.H. Kuo. Tetrahedron Lett., **37**, 3299 (1996); (*b*) L.A. Paquette, A.T. Hamme, II, L.H. Kuo, J. Doyon, and R. Kreuzholz. J. Am. Chem. Soc. **119**, 1242 (1997); (*c*) L.A. Paquette, L.H. Kuo, A.T. Hamme, II, R. Kreuzholz, and J. Doyon. J. Org. Chem. **62**, 1730 (1997).
12. L.A. Paquette and J. Doyon. J. Org. Chem. **62**, 1723 (1997).
13. For a preliminary disclosure of these results, see L.A. Paquette and J. Tae. Tetrahedron Lett. **38**, 3151 (1997).
14. M. Braun. Angew. Chem. Int. Ed. **37**, 430 (1998).
15. P. Beak and W.K. Lee. J. Org. Chem. **58**, 1109 (1993).
16. P.A. Lander and L.S. Hegedus. J. Am. Chem. Soc. **116**, 8126 (1994).
17. S. Sengupta and V. Snieckus. J. Org. Chem. **55**, 5680 (1990).
18. For example: G.A. Weisenburger and P. Beak. J. Am. Chem. Soc. **118**, 12218 (1996).
19. H. Liu, C.S. Tomooka, and H.W. Moore. Synth. Commun. **27**, 2177 (1997).
20. L.A. Paquette, L.-Q. Sun, D. Friedrich, and P.B. Savage. Tetrahedron Lett. **38**, 195 (1997); J. Am. Chem. Soc. **119**, 8438 (1997).
21. R.K. Dieter and R.R. Sharma. J. Org. Chem. **61**, 4180 (1996).
22. L.A. Paquette and M.J. Broadhurst. J. Org. Chem. **38**, 1886 (1973).

© 2000 NRC Canada

Efficient synthesis of optically active 2-amino-2′-diphenylphosphino-1,1′-binaphthyl and its derivatives

Kenzo Sumi, Takao Ikariya, and Ryoji Noyori

Abstract: Optically active 2-amino-2′-diphenylphosphino-1,1′-binaphthyls having various functional groups, such as amino, alkoxycarbonylamino, acylamino, mono- and dialkylamino, and sulfonylamino at C2 position were prepared. The key intermediate of the above aminophosphines was 2-carbamoyl-2′-diphenylphosphinyl-1,1′-binaphthyl synthesized from optically active 2-cyano-2′-diphenylphosphinyl-1,1′-binaphthyl. The transformation of the carbamoyl group to an amino group was effected by the Hofmann reaction.

Key words: aminophosphine ligand, Hofmann reaction, optically active phosphine ligand.

Résumé : On a préparé des 2-amino-2′-diphénylphosphino-1,1′-binaphtyles optiquement actifs portant divers groupes fonctionnels, tels que amino, alkoxycarbonylamino, acylamino, mono- et dialkylamino et sulfonylamino en position C-2. L'intermédiaire clé de ces aminophosphines est le 2-carbamoyl-2′-diphénylphosphinyl-1,1′-binaphtyle synthétisé à partir du 2-cyano-2′-diphénylphosphinyl-1,1′-binaphtyle optiquement actif. La transformation du groupe carbamoyle en groupe amino a été réalisée par le biais d'une réaction d'Hofmann.

Mots clés : ligand aminophosphine, réaction d'Hofmann, ligand phosphine optiquement actif.

[Traduit par la Rédaction]

1. Introduction

Asymmetric reactions catalyzed by transition metal complexes containing optically active phosphine ligands have attracted significant interest for their synthetic utility.[2] Recent catalytic asymmetric synthesis has utilized atropisomeric diphosphine ligands, among which BINAP (**2**) is preeminent (2). The 1,1′-binaphthyl ring system is a key component of a number of chiral ligands that have been used very successfully for asymmetric synthesis (3). Most notable are 2,2′-disubstituted systems such as dihydroxy derivative **1** (4) and diphosphine **2** (2), other heteroatom substituted systems such as **3** (and derivatives of thereof) (5), **4** (6), and **5** (7) have also been recently described. In this way, a great deal of attention has been focused on atropisomeric C_2 symmetry binaphthyl derivatives.

Received August 11, 1999. Published on the NRC Research Press website on May 19, 2000.

This paper has been dedicated to Professor Dr. Stephen Hanessian on the occasion of his 65th birthday.

K. Sumi.[1] Takasago International Corporation, 4-11, 1-Chome, Nishi-Yawata, Hiratsuka, Kanagawa 254-0073, Japan.
T. Ikariya. Graduate School of Science and Engineering, Tokyo Institute of Technology, 2-12-1, Ookayama, Meguro-ku, Tokyo 152-8552, Japan.
R. Noyori. Department of Chemistry, Nagoya University, Chikusa, Nagoya 464-8602, Japan.

[1]Author to whom correspondence may be addressed. Telephone: +81 463 25 2000. Fax: +81 463 25 2084. e-mail: ksumi@ja2.so-net.ne.jp

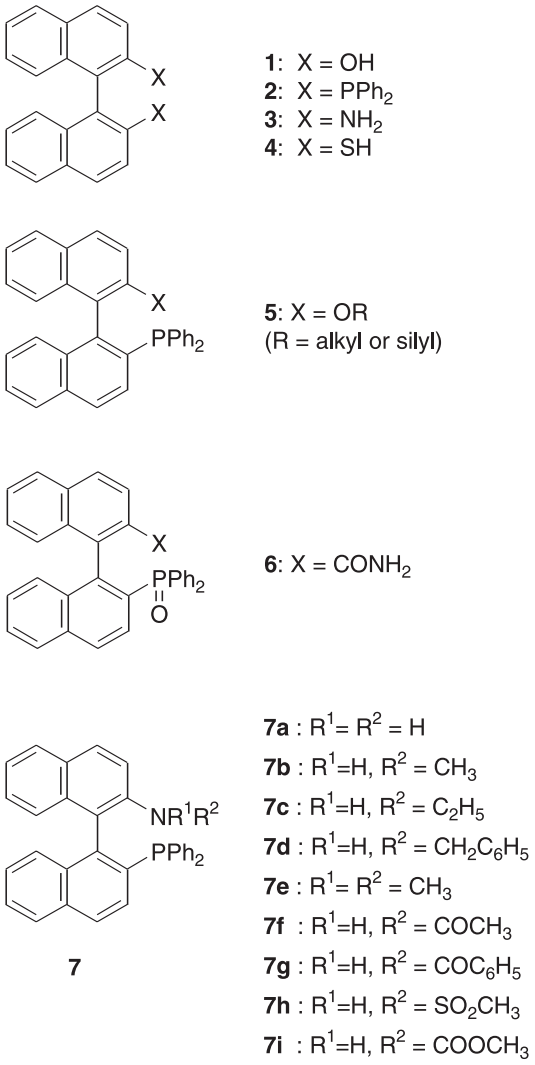
[2]For recent reviews on catalytic asymmetric reactions see ref. 1.

Chelating aminophosphines are often effective ligands for asymmetric homogeneous catalysis. Mixed *P,N*-ferrocenyl ligands have been shown by Cullen et al. (8) to give enantioselectivities as high as 84% in the rhodium-catalyzed hydrogenation of acetamidocinnamic acid (8*a*, *b*). The use of nitrogen-containing ligands in the coupling of secondary Grignard reagents with alkenyl halides has been pioneered by Hayashi and Kumada (9). The most successful ligands used for this reaction are chelating *P,N*-systems, derived from amino acids (10) or from chiral ferrocenyl systems (11). Some chiral pyridylphosphines bearing the chiral group bound to the phosphorus atom by an N—P linkage (12) and optically active pyridylphosphines without N—P bonds (13) have been described. Chiral aminophosphine derivatives bearing *N*-sulfonyl groups were efficient ligands for asymmetric Heck-type hydroarylation of norbornene with phenyl triflate (14). Furthermore, the activity of $RuCl_2[P(C_6H_5)_3]_3$ for hydrogenation of acetophenone was dramatically enhanced with an addition of ethylenediamine (15). Therefore, bidentate phosphine–nitrogen ligands containing soft phosphorus and hard nitrogen donors are expected to exhibit unique catalytic activities.

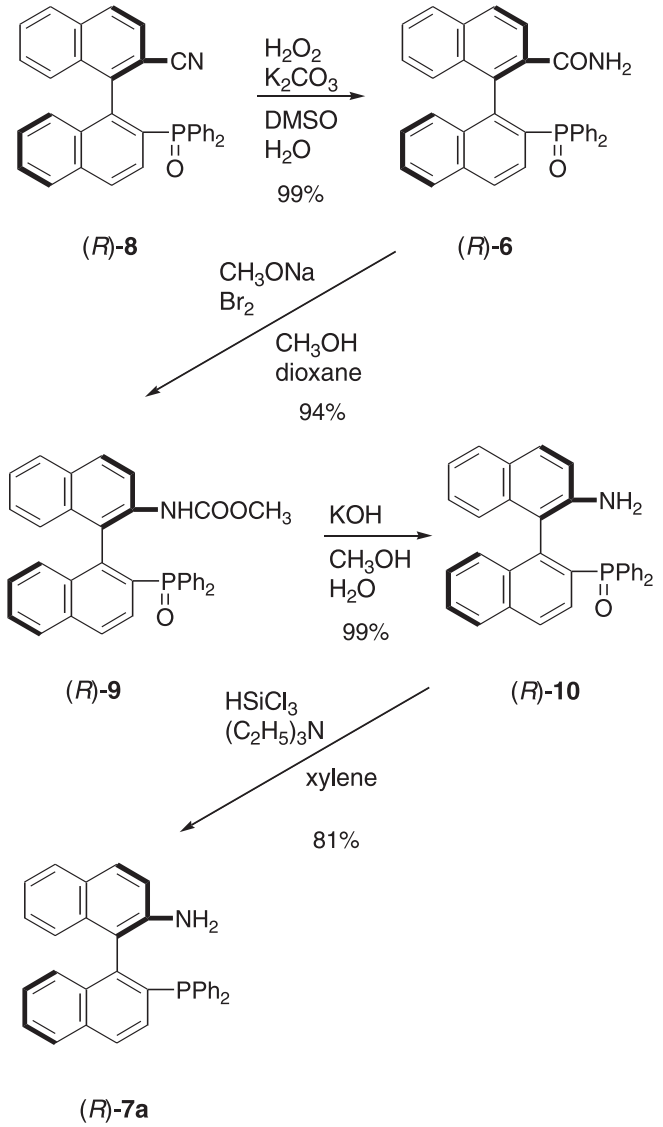
For these reasons, an alternative *P,N* chelate ligand was sought which might provide more tractable intermediates, and an atropisomerically chiral monoaminophosphine compound of type **7** (MAPs) is an attractive target. In order to increase the applicability of the axially chiral phosphine, we introduced several functional groups on the binaphthyl skeleton. We report here the preparation of 2-functionalized-2′-diphenylphosphino-1,1′-binaphthyls that contain amino,

 © 2000 NRC Canada

Chart 1.



Scheme 1.



alkoxycarbonylamino, acylamino, mono- and di-alkylamino, and sulfonylamino groups at the C2 position. These functional groups are expected to interact with transition metals or reacting substrates. Though ligands of this type have been made recently by Vyskocil et al. (16) and Ding et al. (17), during our study, carcinogenic 2-naphthylamine is indispensable to the method for the preparation of optically active *P,N*-type binaphthyl ligands from a binapthyl-type amino alcohol, NOBIN, available by Cu(II)-mediated oxidative coupling of 2-naphthol with 2-naphthylamine. Aranyos et al. (18) reported the preparation of racemic 2-dimethylamino-2′-di-*tert*-butylphosphino-1,1′-binaphthyl from racemic 2,2′-dibromo-1,1′-binaphthyl.

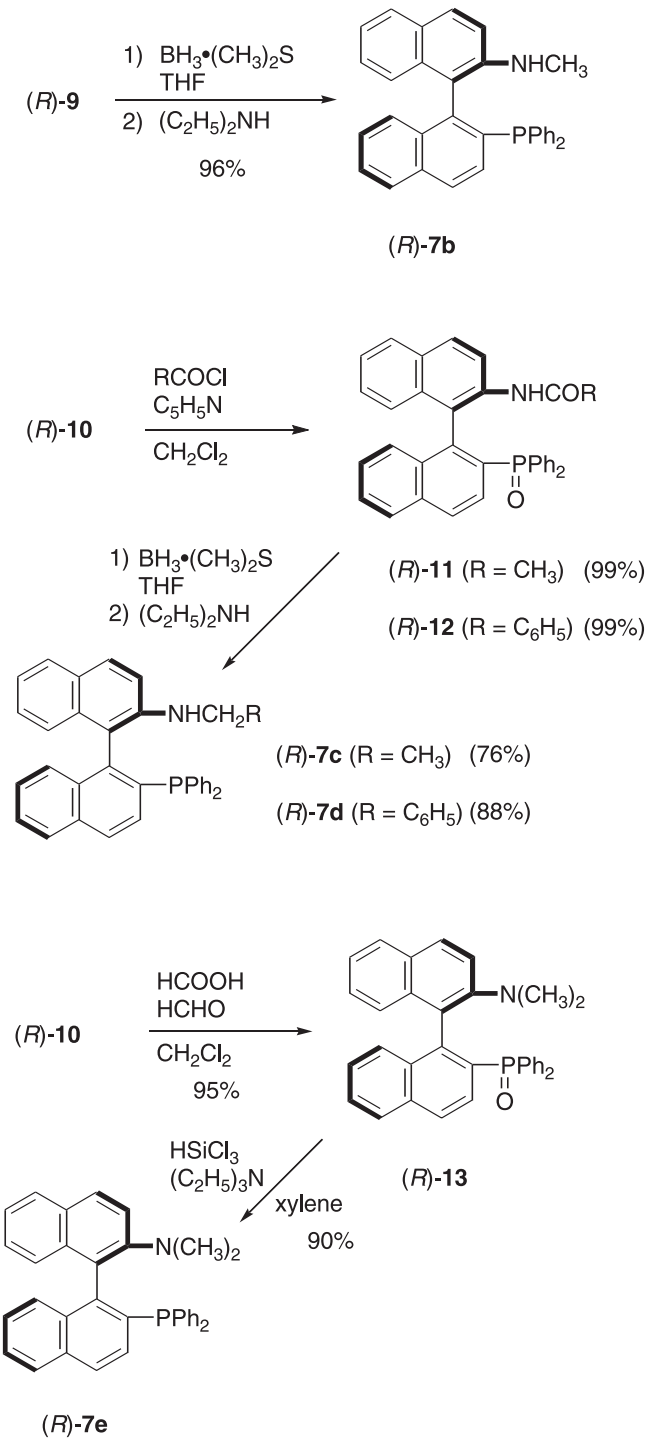
2. Results and discussion

As a part of our work aimed at the synthesis of chiral amino phosphine ligands, we undertook a study on methods to obtain chiral monodentate phosphine ligand, MOPs (**5**) (7), from optically active 1,1′-binaphthalene-2,2′-diol (**1**). This approach would access a series of binaphthyl-type phosphines, analogous to Hayashi's MOP, but having a nitrogen atom in place of oxygen. Wallis and Moyer (19) carried out the Hofmann reaction (20) on a chiral amide in a most convincing demonstration of the intramolecularity of the migration step. During rearrangement, the amide would lose chirality if the migrating bond simply stretched enough to allow rotation about the benzene—naphthalene bond. However, loss of chirality is not observed and the amide rearranges with retention of configuration. The result attracted our attention as a versatile starting compound for the preparation of chiral monoaminophosphine ligands **7**.

After optimization, a multistep synthesis resulting on good yield of the title compounds was succeeded based on the Hofmann reaction of a (*R*)-2-carbamoyl-2′-diphenylphosphinyl-1,1′-binaphthyl ((*R*)-**6**) with bromine in a basic methanol solution (21) to afford a (*R*)-2-methoxycarbonylamino-2′-diphenylphosphinyl-1,1′-binaphthyl ((*R*)-**9**). The amide (*R*)-**6** was obtained from (*R*)-2-cyano-2′-diphenylphosphinyl-1,1′-binaphthyl ((*R*)-**8**) whose preparation has been reported by Hayashi and coworkers (7*c*). Though the cyano group resisted acid or alkaline hydrolysis

© 2000 NRC Canada

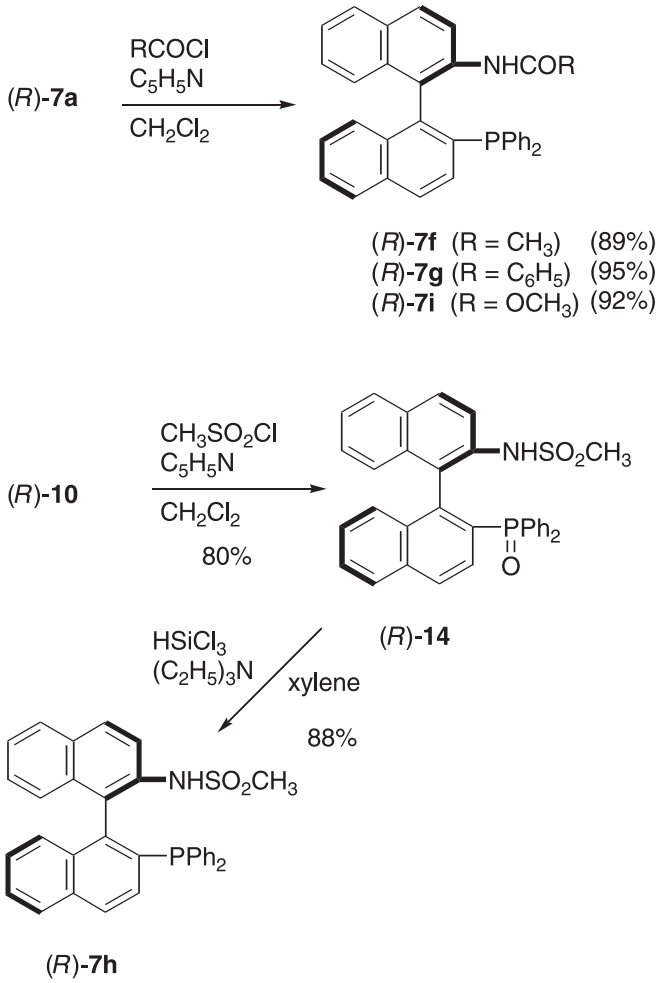
Scheme 2.



to a carbamoyl group, the amide (*R*)-**6** was prepared with alkaline hydrogen peroxide according to the procedures reported by Katritzky et al. (22).

The (*R*)-2-amino-2′-diphenylphosphinyl-1,1′-binaphthyl ((*R*)-**10**) was prepared by alkaline hydrolysis of the carbamate (*R*)-**9** with aqueous KOH in methanol upon heating. Subsequent reduction of (*R*)-**10** with trichlorosilane gave rise to the required (*R*)-2-amino-2′-diphenylphosphino-1,1′-binaphthyl ((*R*)-**7a**). For this simple class of *P,N*-type

Scheme 3.



ligand **7a**, we propose the acronym SMAP, standing for a simple monoaminophosphine, in analogy with MOP.

The carbamate (*R*)-**9** was reduced with borane to afford (*R*)-2-methylamino-2′-diphenylphosphino-1,1′-binaphthyl ((*R*)-**7b**). The reduction of the amido phosphine oxide, (*R*)-2-acetylamino-2′-diphenylphosphinyl-1,1′-binaphthyl ((*R*)-**11**) and (*R*)-2-benzoylamino-2′-diphenylphosphinyl-1,1′-binaphthyl ((*R*)-**12**), obtained from acylation of the aminophosphine oxide (*R*)-**10**, with borane gave (*R*)-2-ethylamino-2′-diphenylphosphino-1,1′-binaphthyl ((*R*)-**7c**) and (*R*)-2-benzylamino-2′-diphenylphosphino-1,1′-binaphthyl ((*R*)-**7d**), directly. Dimethylation of the primary amine in (*R*)-**10** with formaldehyde and formic acid (23) afforded (*R*)-2-dimethylamino-2′-diphenylphosphinyl-1,1′-binaphthyl ((*R*)-**13**), whose reduction with trichlorosilane produced (*R*)-2-dimethylamino-2′-diphenylphosphino-1,1′-binaphthyl ((*R*)-**7e**). (*R*)-2-acetylamino-2′-diphenylphosphino-1,1′-binaphthyl ((*R*)-**7f**) and (*R*)-2-benzoylamino-2′-diphenylphosphino-1,1′-binaphthyl ((*R*)-**7g**), or (*R*)-2-methoxycarbonylamino-2′-diphenylphosphino-1,1′-binaphthyl ((*R*)-**7i**) were derived from (*R*)-**7a** with the corresponding acyl chloride or methoxycarbonyl chloride. *N*-Sulfonylation of (*R*)-**10** with methanesulfonyl chloride gave (*R*)-2-methylsulfonylamino-2′-diphenylphosphinyl-1,1′-binaphthyl ((*R*)-**14**). Phosphine oxide (*R*)-**14** was reduced by trichlorosilane/triethylamine to

© 2000 NRC Canada

give (*R*)-2-methylsulfonylamino-2′-diphenylphosphino-1,1′-binaphthyl ((*R*)-**7h**).

In summary, a new practical method for the synthesis of optically active aminophosphine ligands, MAPs, was developed. SMAP (**7a**) was obtained from the nitrile **8** via the Hofmann rearrangement of the amide **6** under controlled conditions. The flexibility of the synthetic route realizes the fine tuning of the properties of the phosphine ligand. Work directed toward the extension of the series of different ligands of the aminophosphine ligand, and further applications in homogeneous asymmetric catalysis, including mechanistic studies, is in progress and will be reported in due course.

3. Experimental

General

All reactions were run under an atmosphere of dry nitrogen unless otherwise indicated. Anhydrous solvents were transferred by oven-dried syringe or canula. Acetonitrile, dichloromethane, methanol, dimethyl sulfoxide (DMSO), and pyridine were distilled from calcium hydride. Tetrahydrofuran (THF) was distilled from sodium benzophenone ketyl. Xylene was distilled from sodium.

Melting points were determined on a hot stage microscope (YANACO MP-500D) and were uncorrected. ^{1}H NMR spectra were measured on a Bruker DRX500 (500 MHz) or a Varian Gemini 200 (200 MHz) in $CDCl_3$. Chemical shifts of protons were reported in δ ppm referred to tetramethysilane as an internal standard. $^{31}P\{^1H\}$ NMR spectra were measured on a Bruker DRX500 (202 MHz) in $CDCl_3$ using H_3PO_4 as an external standard. Optical rotations were measured on a JASCO DIP-360 polarimeter. IR spectra were recorded on a Nocolet Avatar 360 spectrometer. EI mass spectra and high-resolution mass spectra were measured on a Hitachi M-2000A spectrometer at an ionization voltage of 70 eV. Silica gel column chromatography was carried out using Merck silica gel 60 (230–400 mesh ASTM). (*R*)-(+)-2-cyano-2′-diphenylphosphinyl-1,1′-binaphthyl ((*R*)-**8**) was prepared according to a literature procedure (7*c*).

*(*R*)-(+)-2-Carbamoyl-2′-diphenylphosphinyl-1,1′-binaphthyl ((*R*)-**6**)*

To a stirred solution of (*R*)-(+)-2-cyano-2′-diphenylphosphinyl-1,1′-binaphthyl ((*R*)-**8**) (7*c*) (9.99 g, 20.8 mmol) in DMSO (100 mL), cooled in an ice bath, were added 30% H_2O_2 (50 mL) and anhydrous K_2CO_3 (57.6 g). The mixture was allowed to warm up to room temperature (rt) (exothermic effect was observed). After 30 min, distilled water (43 mL) and DMSO (43 mL) were added, cooling applied, and the mixture was stirred at rt for 15 h. The reaction mixture was diluted with EtOAc and quenched with saturated NH_4Cl (100 mL). The organic phase was washed twice with H_2O and with brine, dried over Na_2SO_4, and concentrated under reduced pressure. The residue was purified by silica gel column chromatography (elution with EtOAc) giving 10.23 g of (*R*)-**6** (99%), mp 120–122°C, $[\alpha]_D^{24}$ 157 (*c* 1.0, $CHCl_3$). IR ($CHCl_3$) cm^{-1} ν: 1662, 1119. ^{1}H NMR δ: 9.44 (bs, 1H), 7.91 (d, *J* = 8.3 Hz, 1H), 7.86 (d, *J* = 8.8 Hz, 2H), 7.8–7.7 (m, 3H), 7.62 (d, *J* = 7.8 Hz, 1H), 7.6–7.4 (m, 5H), 7.3–7.2 (m, 1H), 7.2–7.0 (m, 5H), 7.0–6.9 (m, 2H), 6.64 (t, *J* = 7.0 Hz, 1H), 6.33 (d, *J* = 8.3 Hz, 1H), 5.52 (bs, 1H). $^{31}P\{^1H\}$ NMR δ: 30.9 (s). EIMS *m*/*z*: 497 (M^+, base peak). HRMS calcd for $C_{33}H_{24}NO_2P$: 497.1543; found: 497.1511.

*(*R*)-(–)-2-Methoxycarbonylamino-2′-diphenylphosphinyl-1,1′-binaphthyl ((*R*)-**9**)*

To a solution of 19.9 mL of 28% sodium methoxide in methanol (97.3 mmol) was added methanol (161 mL). The solution was cooled to –78°C and bromine (1.84 mL, 35.7 mmol) was added dropwise with vigorous stirring. After stirring at –78°C for 15 min, a solution of (*R*)-**6** (8.07 g, 16.2 mmol) in methanol (145 mL) and dioxane (145 mL) was added dropwise for 1 h. The reaction mixture was stirred at ambient temperature for 1 h and then stirred at 55°C for 1 h. After being cooled to rt, the mixture was diluted with EtOAc and quenched with saturated NH_4Cl. The organic layer was washed with brine and dried over Na_2SO_4. After removal of the solvent, the residue was chromatographed on silica gel (elution with *n*-hexane:EtOAc, 1:2) to give (*R*)-**9** (8.05 g, 94%), mp 127–128°C,$[\alpha]_D^{24}$ –155 (*c* 1.0, $CHCl_3$). IR ($CHCl_3$) cm^{-1} ν: 1723, 1507, 1238, 1171, 1115. ^{1}H NMR δ: 8.72 (bs, 1H), 7.9–7.6 (m, 5H), 7.65 (d, *J* = 8.8 Hz, 1H), 7.6–7.4 (m, 6H), 7.3–7.1 (m, 4H), 7.08 (d, *J* = 8.8 Hz, 1H), 6.94 (t, *J* = 7.1 Hz, 1H), 6.80 (t, *J* = 7.0 Hz, 1H), 6.7–6.6 (m, 2H), 6.50 (d, *J* = 6.8 Hz, 1H), 3.04 (bs, 3H). $^{31}P\{^1H\}$ NMR δ: 28.2 (s). EIMS *m*/*z*: 527 (M^+, base peak). HRMS calcd for $C_{34}H_{26}NO_3P$: 527.1648; found: 527.1592.

*(*R*)-(–)-2-Amino-2′-diphenylphosphinyl-1,1′-binaphthyl ((*R*)-**10**)*

To a solution of (*R*)-**9** (8.01 g, 15.2 mmol) in methanol (304 mL) was added 152 mL of 40% KOH solution and the mixture was refluxed for 2 h. After being cooled to rt, the mixture was diluted with EtOAc. The organic phase was washed with brine, dried over Na_2SO_4, and concentrated under reduced pressure. The crude material was purified by silica gel column chromatography (elution with EtOAc) giving 7.16 g (99%) of (*R*)-**10**, mp 133–134°C, $[\alpha]_D^{24}$ –199 (*c* 1.0, $CHCl_3$). IR ($CHCl_3$) cm^{-1} ν: 1622, 1172, 1115. ^{1}H NMR δ: 8.0–7.8 (m, 2H), 7.8–7.6 (m, 5H), 7.6–7.4 (m, 1H), 7.4–7.3 (m, 5H), 7.3–7.1 (m, 4H), 7.1–6.9 (m, 1H), 6.9–6.8 (m, 3H), 6.8–6.7 (m, 2H), 6.51 (d, *J* = 8.3 Hz, 1H), 3.94 (bs, 2H). $^{31}P\{^1H\}$ NMR δ: 27.1 (s). EIMS *m*/*z*: 469 (M^+, base peak). HRMS calcd for $C_{32}H_{24}NOP$: 469.1594; found: 469.1556.

*(*R*)-(–)-2-Amino-2′-diphenylphosphino-1,1′-binaphthyl ((*R*)-**7a**)*

Aminophosphine oxide (*R*)-**10** (7.16 g, 15.2 mmol) was placed in a pressure tube, then xylene (381 mL) added and stirred. Triethylamine (42.5 mL, 305.0 mmol) then trichlorosilane (7.70 mL, 76.3 mmol) were added at 0°C. After sealing the tube, the mixture was stirred at 150°C for 18 h. The reaction mixture was allowed to cool to rt, diluted with Et_2O, and quenched with saturated NH_4Cl. The organic layer was dried over Na_2SO_4 and concentrated under reduced pressure. The crude phosphine was purified by silica gel column chromatography (elution with *n*-hexane:EtOAc, 4:1) giving 5.60 g (81%) of (*R*)-**7a**, mp 104–106°C, $[\alpha]_D^{24}$ –27 (*c* 1.0, $CHCl_3$). IR ($CHCl_3$) cm^{-1} ν: 1622, 1514, 1433. ^{1}H NMR δ: 7.87 (d, *J* = 8.3 Hz, 2H), 7.77 (d, *J* = 8.7 Hz, 1H), 7.71 (d, *J* = 7.8 Hz, 1H), 7.5–7.4 (m, 2H), 7.4–7.2 (m, 7H), 7.2–7.0 (m, 6H), 7.0–6.9 (m, 2H), 6.67 (d, *J* = 8.8 Hz, 1H),

© 2000 NRC Canada

3.25 (bs, 2H). $^{31}P\{^{1}H\}$ NMR δ: –13.1 (s). EIMS *m/z*: 453 (M^+, base peak). HRMS calcd for $C_{32}H_{24}NP$: 453.1646; found: 453.1648.

*(*R*)-(–)-Methylamino-2′-diphenylphosphino-1,1′-binaphthyl ((*R*)-**7b**)*

To a solution of (*R*)-**9** (3.59 g, 6.81 mmol) in THF (170 mL) was added 2M borane – dimethyl sulfide complex in THF (27.2 mL, 54.4 mmol) at 0°C, the mixture was refluxed for 18 h. After being cooled to rt, the mixture was diluted with EtOAc and quenched with saturated NH_4Cl. The organic layer was washed with brine and dried over Na_2SO_4 and concentrated under reduced pressure. To the residue was added 272 mL of diethylamine and the reaction mixture was stirred at rt for 30 min. After removal of diethylamine, the residue was chromatographed on silica gel (elution with *n*-hexane:EtOAc, 16:1) to give (*R*)-**7b** (3.05 g, 96%), mp 100–101°C, $[\alpha]_D^{24}$ –27 (*c* 1.0, $CHCl_3$). IR ($CHCl_3$) cm^{-1} ν: 1599, 1555, 1345. ^1H NMR δ: 7.9–7.8 (m, 3H), 7.73 (d, *J* = 8.3 Hz, 1H), 7.5–7.4 (m, 2H), 7.3–6.9 (m, 15H), 6.70 (d, *J* = 8.3 Hz, 1H), 3.04 (bs, 1H), 2,37 (s, 3H). $^{31}P\{^{1}H\}$ NMR δ: –13.9 (s). EIMS *m/z*: 467 (M^+, base peak). HRMS calcd for $C_{33}H_{26}NP$: 467.1802; found: 467.1838.

*(*R*)-(–)-2-Acetylamino-2′-diphenylphosphinyl-1,1′-binaphthyl ((*R*)-**11**)*

To a solution of (*R*)-**10** (141 mg, 0.30 mmol) in 6 mL of CH_2Cl_2 were added pyridine (29 μL, 0.36 mmol) and acetyl chloride (24 μL, 0.33 mmol) at 0°C and the mixture was stirred at rt for 1 h. The mixture was diluted with CH_2Cl_2 and washed with saturated NH_4Cl and brine. The organic phase was dried over Na_2SO_4 and concentrated under reduced pressure. The residue was chromatographed on silica gel (elution with *n*-hexane:EtOAc, 4:1) giving 155 mg (99%) of (*R*)-**11**, mp 95–96°C, $[\alpha]_D^{24}$ –153 (*c* 1.0, $CHCl_3$). IR ($CHCl_3$) cm^{-1} ν: 1670, 1597, 1504, 1439, 1167. ^1H NMR δ: 9.73 (s, 1H), 8.0–7.9 (m, 4H), 7.8–7.6 (m, 2H), 7.6–7.4 (m, 6H), 7.3–7.1 (m, 5H), 7.0–6.9 (m, 1H), 6.8–6.7 (m, 1H), 6.7–6.6 (m, 1H), 6.53 (d, *J* = 8.3 Hz, 1H), 1.93 (s, 3H). $^{31}P\{^{1}H\}$ NMR δ: 29.6 (s). EIMS *m/z*: 511 (M^+, base peak). HRMS calcd for $C_{34}H_{26}NO_2P$: 511.1700; found: 511.1717.

*(*R*)-(–)-Ethylamino-2′-diphenylphosphino-1,1′-binaphthyl ((*R*)-**7c**)*

To a solution of (R)-**11** (127 mg, 0.25 mmol) in THF (6 mL) was added 2M borane – dimethyl sulfide complex in THF (620 μL, 1.24 mmol) at 0°C, the mixture was refluxed for 18 h. After being cooled to rt, the mixture was diluted with EtOAc and quenched with saturated NH_4Cl. The organic layer was washed with brine and dried over Na_2SO_4 and concentrated under reduced pressure. To the residue was added 8.2 mL of diethylamine and the reaction mixture was stirred at rt for 3 h. After removal of diethylamine, the residue was chromatographed on silica gel (elution with *n*-hexane:EtOAc, 50:1) to give (*R*)-**7c** (91 mg, 76%), mp 83–84°C, $[\alpha]_D^{24}$ –47 (*c* 1.0, $CHCl_3$). IR ($CHCl_3$) cm^{-1} ν: 1619, 1599, 1514, 1434, 1302, 1153. ^1H NMR δ: 8.0–7.8 (m, 3H), 7.74 (d, *J* = 8.5 Hz, 1H), 7.5–7.4 (m, 2H), 7.3–6.9 (m, 16H), 6.59 (d, *J* = 8.5 Hz, 1H), 3.07 (m, 2H), 2.9–2.7 (m, 1H), 0.78 (t, *J* = 7.0 Hz, 3H). $^{31}P\{^{1}H\}$ NMR δ: –13.3 (s). EIMS *m/z*: 481 (M^+, base peak). HRMS calcd for $C_{34}H_{28}NP$: 481.1958; found: 481.1996.

*(*R*)-(–)-2-Benzoylamino-2′-diphenylphosphinyl-1,1′-binaphthyl ((*R*)-**12**)*

To a solution of (*R*)-**10** (188 mg, 0.40 mmol) in 8 mL of CH_2Cl_2 were added pyridine (39 μL, 0.48 mmol) and benzoyl chloride (51 μL, 0.44 mmol) at 0°C and the mixture was stirred at rt for 1.5 h. The mixture was diluted with CH_2Cl_2 and washed with saturated NH_4Cl and brine. The organic phase was dried over Na_2SO_4 and concentrated under reduced pressure. The residue was chromatographed on silica gel (elution with *n*-hexane:EtOAc, 1:1) giving 228 mg (99%) of (*R*)-**12**, mp 247–249°C, $[\alpha]_D^{24}$ –98 (*c* 1.0, $CHCl_3$). IR ($CHCl_3$) ν: 1653, 1507, 1489, 1292, 1167. ^1H NMR δ: 10.62 (s, 1H), 8.0–7.8 (m, 7H), 7.72 (d, *J* = 8.0 Hz, 1H), 7.8–7.1 (m, 15H), 7.0–6.9 (m, 1H), 6.9–6.7 (m, 1H), 6.7–6.6 (m, 1H), 6.51 (d, *J* = 7.9 Hz, 1H). $^{31}P\{^{1}H\}$ NMR δ: 29.9 (s). EIMS *m/z*: 573 (M^+, base peak). HRMS calcd for $C_{39}H_{28}NO_2P$: 573.1857; found: 573.1895.

*(*R*)-(–)-Benzylamino-2′-diphenylphosphino-1,1′-binaphthyl ((*R*)-**7d**).*

To a solution of (R)-**12** (29 mg, 0.05 mmol) in THF (1.3 mL) was added 2M borane – dimethyl sulfide complex in THF (88 μL, 0.18 mmol) at 0°C, the mixture was refluxed for 18 h. After being cooled to rt, the mixture was diluted with EtOAc and quenched with saturated NH_4Cl. The organic layer was washed with brine and dried over Na_2SO_4 and concentrated under reduced pressure. To the residue was added 1.5 mL of diethylamine and the reaction mixture was stirred at rt for 5 h. After removal of diethylamine, the residue was chromatographed on silica gel (elution with *n*-hexane:EtOAc, 20:1) to give (*R*)-**7d** (24 mg, 88%), mp 70–71°C, $[\alpha]_D^{24}$ –34 (*c* 1.0, $CHCl_3$). IR ($CHCl_3$) cm^{-1} ν: 1599, 1496, 1342. ^1H NMR δ: 7.9–7.8 (m, 2H), 7.80 (d, *J* = 8.9 Hz, 1H), 7.69 (d, *J* = 8.8 Hz, 1H), 7.6–7.4 (m, 2H), 7.4–7.0 (m, 19H), 7.0–6.9 (m, 1H), 6.61 (d, *J* = 8.4Hz, 1H), 4.17 (d, *J* = 15.3 Hz, 1H), 3.99 (d, *J* = 15.3 Hz, 1H), 3,68 (bs, 1H). $^{31}P\{^{1}H\}$ NMR δ: –13.1 (s). EIMS *m/z*: 543 (M^+, base peak). HRMS calcd for $C_{39}H_{30}NP$: 543.2115; found: 543.2158.

*(*R*)-(–)-2-Dimethylamino-2′-diphenylphosphinyl-1,1′-binaphthyl ((*R*)-**13**)*

A mixture of (*R*)-**10** (3.18 g, 6.76 mmol), formic acid (67.6 mL, 1.79 mol), and 37% aqueous formaldehyde (67.6 mL, 0.89 mol) was refluxed for 20 h. The reaction mixture was made alkaline by the addition of saturated $NaHCO_3$ and extracted with Et_2O. The organic phase was dried over Na_2SO_4 and concentrated under reduced pressure. The residue was chromatographed on silica gel (elution with *n*-hexane:EtOAc, 1:1) giving 3.21 g (95%) of (*R*)-**13**, mp 82–83°C, $[\alpha]_D^{24}$ –17 (*c* 1.0, $CHCl_3$). IR ($CHCl_3$) cm^{-1} ν: 1597, 1506, 1438. ^1H NMR δ: 8.0–7.8 (m, 2H), 7.8–7.7 (m, 1H), 7.6–7.4 (m, 5H), 7.4–7.0 (m, 10H), 7.0–6.9 (m, 3H), 6.71 (d, *J* = 8.5 Hz, 1H), 2,37 (s, 6H). $^{31}P\{^{1}H\}$ NMR δ: 29.5 (s). EIMS *m/z*: 497 (M^+, base peak). HRMS calcd for $C_{34}H_{28}NOP$: 497.1907; found: 497.1927.

© 2000 NRC Canada

*(*R*)-(–)-2-Dimethyamino-2′-diphenylphosphino-1,1′-binaphthyl ((*R*)-**7e**)*

Aminophosphine oxide (*R*)-**13** (2.83 g, 5.68 mmol) was placed in a pressure tube, then xylene (142 mL) added and stirred. Triethylamine (15.8 mL, 113.6 mmol) then trichlorosilane (2.87 mL, 28.41 mmol) were added at 0°C. After sealing the tube, the mixture was stirred at 150°C for 18 h. The reaction mixture was allowed to cool to rt, diluted with Et_2O and quenched with saturated NH_4Cl. The organic layer was dried over Na_2SO_4 and concentrated under reduced pressure. The crude phosphine was purified by silica gel column chromatography (elution with *n*-hexane:EtOAc, 20:1) giving 2.47 g (90%) of (*R*)-**7e**, mp 90–92°C, $[\alpha]_D^{24}$ –32 (*c* 1.0, $CHCl_3$). IR ($CHCl_3$) cm^{-1} ν: 1594, 1506, 1480, 1434, 1352. ^1H NMR δ: 7.91 (d, *J* = 8.8 Hz, 1H), 7.9–7.7 (m, 3H), 7.5–7.3 (m, 4H), 7.3–7.1 (m, 7H), 7.1–6.9 (m, 6H), 6.77 (d, *J* = 8.3 Hz, 1H), 2.21 (s, 6H). $^{31}P\{^1H\}$ NMR δ: –12.6 (s). EIMS *m*/*z*: 481 (M^+, base peak). HRMS calcd for $C_{34}H_{28}NP$: 481.1958; found: 481.1961.

*(*R*)-(+)-2-Acetylamino-2′-diphenylphosphino-1,1′-binaphthyl ((*R*)-**7f**)*

To a solution of (*R*)-**7a** (1.15 g, 2.54 mmol) in 51 mL of CH_2Cl_2 were added pyridine (0.25 mL, 3.04 mmol) and acetyl chloride (0.20 mL, 2.78 mmol) at 0°C and the mixture was stirred at rt for 3 h. The mixture was diluted with CH_2Cl_2 and washed with saturated NH_4Cl and brine. The organic phase was dried over Na_2SO_4 and concentrated under reduced pressure. The residue was chromatographed on silica gel (elution with *n*-hexane:EtOAc, 3:1) giving 1.11 g (89%) of (*R*)-**7f**, mp 104–106°C, $[\alpha]_D^{24}$ 17 (*c* 1.0, $CHCl_3$). IR ($CHCl_3$) cm^{-1} ν: 1687, 1598, 1499. ^1H NMR δ: 8.47 (d, *J* = 9.1 Hz, 1H), 8.1–7.8 (m, 4H), 7.6–7.4 (m, 2H), 7.4–7.0 (m, 14H), 6.89 (d, *J* = 8.4 Hz, 1H), 6.26 (bs, 1H), 1.43 (bs, 3H). $^{31}P\{^1H\}$ NMR δ: –13.7 (s). EIMS *m*/*z*: 495 (M^+, base peak). HRMS calcd for $C_{34}H_{26}NOP$: 495.1750; found: 495.1728.

*(*R*)-(–)-2-Benzoylamino-2′-diphenylphosphino-1,1′-binaphthyl ((*R*)-**7g**)*

To a solution of (*R*)-**7a** (1.00 g, 2.21 mmol) in 44 mL of CH_2Cl_2 were added pyridine (0.21 mL, 2.65 mmol) and benzoyl chloride (0.28 mL, 2.43 mmol) at 0°C and the mixture was stirred at rt for 5 h. The mixture was diluted with CH_2Cl_2 and washed with saturated NH_4Cl and brine. The organic phase was dried over Na_2SO_4 and concentrated under reduced pressure. The residue was chromatographed on silica gel (elution with *n*-hexane:EtOAc, 6:1) giving 1.16 g (95%) of (*R*)-**7g**, mp 94–95°C, $[\alpha]_D^{24}$–20 (*c* 1.0, $CHCl_3$). IR ($CHCl_3$) cm^{-1} ν: 1673, 1597, 1503, 1428, 1286. ^1H NMR δ: 8.68 (d, *J* = 9.0 Hz, 1H), 8.06 (d, *J* = 9.0 Hz, 1H), 7.92 (d, *J* = 8.5 Hz, 1H), 7.9–7.8 (m, 2H), 7.6–7.4 (m, 2H), 7.4–6.9 (m, 21H). $^{31}P\{^1H\}$ NMR δ: –13.1 (s). EIMS *m*/*z*: 557 (M^+, base peak). HRMS calcd for $C_{39}H_{28}NOP$: 557.1907; found: 557.1877.

*(*R*)-(–)-2-Methylsulfonylamino-2′-diphenylphosphinyl-1,1′-binaphthyl ((*R*)-**14**)*

To a solution of (*R*)-**10** (6.62 g, 14.1 mmol) in 282 mL of CH_2Cl_2 were added pyridine (4.7 mL, 57.8 mmol) and methanesulfonyl chloride (4.1 mL, 53.6 mmol) at 0°C and the mixture was stirred at rt for 23 h. The mixture was diluted with CH_2Cl_2 and washed with saturated NH_4Cl and brine. The organic phase was dried over Na_2SO_4 and concentrated under reduced pressure. The residue was chromatographed on silica gel (elution with *n*-hexane:EtOAc, 3:2) giving 6.15 g (80%) of (*R*)-**14**, mp 281–283°C, $[\alpha]_D^{24}$ –71 (*c* 1.0, $CHCl_3$). IR ($CHCl_3$) cm^{-1} ν: 1324, 1151, 1115. ^1H NMR δ: 9.31 (bs, 1H), 8.0–7.9 (m, 4H), 7.80 (d, *J* = 8.2 Hz, 1H), 7.71 (d, *J* = 8.8 Hz, 1H), 7.6–7.4 (m, 6H), 7.3–7.1 (m, 4H), 7.01 (d, *J* = 8.8 Hz, 1H), 7.0–6.9 (m, 1H), 6.8–6.7 (m, 1H), 6.7–6.6 (m, 2H), 6.58 (d, *J* = 8.3 Hz, 1H), 2.26 (s, 3H). $^{31}P\{^1H\}$ NMR δ: 28.8 (s). EIMS *m*/*z*: 547 (M^+, base peak). HRMS calcd for $C_{33}H_{26}NO_3PS$: 547.1369; found: 547.1339.

*(*R*)-(+)-2-Methylsulfonylamino-2′-diphenylphosphino-1,1′-binaphtyl ((*R*)-**7h**)*

Aminophosphine oxide (*R*)-**14** (3.93 g, 7.17 mmol) was placed in a pressure tube, then xylene (179 mL) added and stirred. Triethylamine (20.0 mL, 143.4 mmol) then trichlorosilane (3.62 mL, 35.8 mmol) were added at 0°C. After sealing the tube, the mixture was stirred at 150°C for 18 h. The reaction mixture was allowed to cool to rt, diluted with Et_2O, and quenched with saturated NH_4Cl. The organic layer was dried over Na_2SO_4 and concentrated under reduced pressure. The crude phosphine was purified by silica gel column chromatography (elution with *n*-hexane:EtOAc, 6:1) giving 3.35 g (88%) of (*R*)-**7h**, mp 109–110°C, $[\alpha]_D^{24}$ 41 (*c* 1.0, $CHCl_3$). IR ($CHCl_3$) cm^{-1} ν: 1306, 1156. ^1H NMR δ: 8.1–7.9 (m, 4H), 7.83 (d, *J* = 8.3 Hz, 1H), 7.6–7.4 (m, 2H), 7.4–7.1 (m, 11H), 7.0–6.9 (m, 3H), 6.66 (d, *J* = 8.3 Hz, 1H), 6.01 (s, 1H), 2.59 (s, 3H). $^{31}P\{^1H\}$ NMR δ: –14.0 (s). EIMS *m*/*z*: 531 (M^+, base peak). HRMS calcd for $C_{33}H_{26}NO_2PS$: 531.1421; found: 531.1457.

*(*R*)-(+)-2-Methoxycarbonylamino-2′-diphenylphosphino-1,1′-binaphthyl ((*R*)-**7i**)*

To a solution of (*R*)-**7a** (1.20 g, 2.65 mmol) in 53 mL of CH_2Cl_2 were added pyridine (0.26 mL, 3.18 mmol) and methyl chloroformate (0.23 mL, 2.91 mmol) at 0°C and the mixture was stirred at rt for 21 h. The mixture was diluted with CH_2Cl_2 and washed with saturated NH_4Cl and brine. The organic phase was dried over Na_2SO_4 and concentrated under reduced pressure. The residue was chromatographed on silica gel (elution with *n*-hexane:EtOAc, 4:1) giving 1.25 g (92%) of (*R*)-**7i**, mp 92–93°C, $[\alpha]_D^{24}$ 46 (*c* 1.0, $CHCl_3$). IR ($CHCl_3$) cm^{-1} ν: 1736, 1599, 1506. ^1H NMR δ: 8.39 (bs, 1H), 8.0–7.8 (m, 4H), 7.6–7.4 (m, 2H), 7.4–6.9 (m, 14H), 6.81 (d, *J* = 8.6 Hz, 1H), 5.94 (bs, 1H), 3.45 (s, 3H). $^{31}P\{^1H\}$ NMR δ: –13.1 (s). EIMS *m*/*z*: 511 (M^+, base peak). HRMS calcd for $C_{34}H_{26}NO_2P$: 511.1700; found: 511.1729.

Acknowledgement

We are grateful to Takenobu Nishikawa and Naoki Isoda for their technical assistance.

References

1. (*a*) H. Brunner. Synthesis, 645 (1988); (*b*) G. Consiglio and R.M. Waymouth. Chem. Rev. **89**, 257 (1989); (*c*) R. Noyori and M. Kitamura. Modern synthetic methods. Vol. 5. (*Edited*

© 2000 NRC Canada

by) R. Scheffold. Springer, Berlin. 1989. p. 115; (*d*) I. Ojima, N. Clos, and C. Bastos. Tetrahedron, **45**, 6901 (1989); (*e*) C.G. Frost, J. Howarth, and J.M.J. Williams. Tetrahedron: Asymmetry, **3**, 1089 (1992); (*f*) R. Noyori. Asymmetric catalysis in organic synthesis. John Wiley & Sons, Inc., New York. 1994.
2. (*a*) A. Miyashita, A. Yasuda, H. Takaya, K. Toriumi, T. Ito, T. Souchi, and R. Noyori. J. Am. Chem. Soc. **102**, 7932 (1980); (*b*) R. Noyori. Chem. Soc. Rev. **18**, 187 (1989); (*c*) R. Noyori and H. Takaya. Acc. Chem. Res. **23**, 345 (1990).
3. (*a*) C. Rosini, L. Franzini, A. Raffaelli, and P. Salvadori. Synthesis, 503 (1992); (*b*) J.K. Whitesell. Chem. Rev. **89**, 1581 (1989).
4. (*a*) R. Noyori, I. Tomino, Y. Tanimoto, and M. Nishizawa. J. Am. Chem. Soc. **106**, 6709 (1984); (*b*) R. Noyori, I. Tomino, M. Yamada, and M. Nishizawa. J. Am. Chem. Soc. **106**, 6717 (1984); (*c*) N. Sakai, K. Nozaki, K. Mashima, and H. Takaya. Tetrahedron: Asymmetry, **3**, 583 (1992); (*d*) M. Smrcina, M. Lorenc, V. Hanus, P. Sedmera, and P. Kocovsky. J. Org. Chem. **57**, 1917 (1992); (*e*) M. Shibasaki, H. Sasai, and T. Arai. Angew. Chem. Int. Ed. Engl. **36**, 1236 (1997).
5. (*a*) S. Miyano, M. Nawa, A. Mori, and H. Hashimoto. Bull. Chem. Soc. Jpn. **57**, 2171 (1984); (*b*) K.J. Brown, M.S. Berry, K.C. Waterman, D. Lingenfelter, and J.R. Murdoch. J. Am. Chem. Soc. **106**, 4717 (1984); (*c*) M. Smrcina, M. Lorenc, V. Hanus, and P. Kocovsky. Synlett, 231 (1991); (*d*) C. Rosini, L. Franzini, A. Iuliano, D. Pini, and P. Salvadori. Tetrahedron: Asymmetry, **2**, 363 (1991).
6. (*a*) D.J. Cram, R.C. Helgeson, K. Koga, E.P. Kyba, K. Madan, L.R. Sousa, M.G. Siegel, P. Moreau, G.W. Gokel, J.M. Timko, and G.D.Y. Sogah. J. Org. Chem. **43**, 2758 (1978); (*b*) F. Di Furia, G. Licini, G. Modena, and O. De Lucchi. Tetrahedron Lett. **30**, 2575 (1989); (*c*) S. Cossu, G. Delogu, O. De Lucchi, D. Fabbri, and G. Licini. Angew. Chem. Int. Ed. Engl. **28**, 766 (1989); (*d*) A. Dore, S. Cossu, and O. De Lucchi. Tetrahedron Lett. **32**, 4771 (1991).
7. (*a*) Y. Uozumi and T. Hayashi. J. Am. Chem. Soc. **113**, 9887 (1991); (*b*) Y. Uozumi, A. Tanahashi, S.-Y. Lee, and T. Hayashi. J. Org. Chem. **58**, 1945 (1993); (*c*) Y. Uozumi, N. Suzuki, A. Ogiwara, and T. Hayashi. Tetrahedron, **50**, 4293 (1994).
8. (*a*) W.R. Cullen, F.W.B. Einstein, C.-H. Huang, A.C. Willis, and E.-S. Yeh. J. Am. Chem. Soc. **102**, 988 (1980); (*b*) W.R. Cullen and J.D. Woollins. Can. J. Chem. **60**, 1793 (1982); (*c*) T.D. Appleton, W.R. Cullen, S.V. Evans, T.-J. Kim, and J. Trotter. J. Organomet. Chem. **279**, 5 (1985).
9. T. Hayashi and M. Kumada. Asymmetric synthesis. Vol. 5. (*Edited by*) J.D. Morrison. Academic Press, New York. 1985. p. 147.
10. (*a*) T. Hayashi, M. Konishi, M. Fukushima, K. Kanehira, T. Hioki, and M. Kumada. J. Org. Chem. **48**, 2195 (1983); (*b*) T. Hayashi, M. Fukushima, M. Konishi, and M. Kumada. Tetrahedron Lett. **21**, 79 (1980).
11. (*a*) T. Hayashi, M. Konishi, M. Fukushima, T. Mise, M. Kagotani, M. Tajika, and M. Kumada. J. Am. Chem. Soc. **104**, 180 (1982); (*b*) T. Hayashi, M. Konishi, H. Ito, and M. Kumada. J. Am. Chem. Soc. **104**, 4962 (1982); (*c*) T. Hayashi, T. Hagihara, Y. Katsuro, and M. Kumada. Bull. Chem. Soc. Jpn. **56**, 363 (1983); (*d*) T. Hayashi, M. Konishi, Y. Okamoto, K. Kabeta, and M. Kumada. J. Org. Chem. **51**, 3772 (1986).
12. (*a*) H. Brunner, W. Li, and H. Weber. J. Organomet. Chem. **288**, 359 (1985); (*b*) H. Brunner and H. Weber. Chem. Ber. **118**, 3380 (1985).
13. (*a*) R. de Vaumas, A. Marinetti, L. Ricard, and F. Mathey. J. Am. Chem. Soc. **114**, 261 (1992); (*b*) N.W. Alock, J.M. Brown, and D.I. Hulmes. Tetrahedron: Asymmetry, **4**, 743 (1993); (*c*) G. Chelucci, M.A. Cabras, C. Botteghi, and M. Marchetti. Tetrahedron: Asymmetry, **5**, 299 (1994); (*d*) C.G. Arena, F. Nicolo, D. Drommi, G. Bruno, and F. Faraone. J. Chem. Soc. Chem. Commun. 2251 (1994).
14. S. Sakuraba, K. Awano, and K. Achiwa. Synlett, 291 (1994).
15. T. Ohkuma, H. Ooka, S. Hashiguchi, T. Ikariya, and R. Noyori. J. Am. Chem. Soc. **117**, 2675 (1995).
16. (*a*) S. Vyskocil, M. Smrcina, V. Hanus, M. Polasek, and P. Kocovsky. J. Org. Chem. **63**, 7738 (1998); (*b*) S. Vyskocil, M. Smrcina, and P. Kocovsky. Tetrahedron Lett. **39**, 9289 (1998).
17. K. Ding, Y. Wang, H. Yun, J. Liu, Y. Wu, M. Terada, Y. Okubo, and K. Mikami. Chem. Eur. J. **5**, 1734 (1999).
18. A. Aranyos, D.W. Old, A. Kiyomori, J.P. Wolfe, J.P. Sadighi, and S.L. Buchwald. J. Am. Chem. Soc. **121**, 4369 (1999).
19. E.S. Wallis and W.W. Moyer. J. Am. Chem. Soc. **55**, 2598 (1933).
20. E.S. Wallis and J.F. Lane. Org. React. N.Y. **3**, 267 (1946).
21. P. Radlick and L.R. Brown. Synthesis, 290 (1974).
22. A.R. Katritzky, B. Pilarski, and L. Urogdi. Synthesis, 949 (1989).
23. W.E. Parham, W.T. Hunter, R. Hanson, and T. Lahr. J. Am. Chem. Soc. **74**, 5646 (1952).

© 2000 NRC Canada

Preparation of homoallylic alcohols by reaction of aldehydes with η^3-allyl- and η^3-crotylmolybdenum complexes

Kevin P. Gable, M. Sundaram Shanmugham, and James D. White

Abstract: η^3-Allyl and η^3-methallyl complexes of molybdenum react with aldehydes to give homoallylic alcohols in preparative yields when water is used as a proton source, but the scope of the reaction is narrowed in the case of the η^3-crotylmolybdenum complex by the formation of both transposed and nontransposed products.

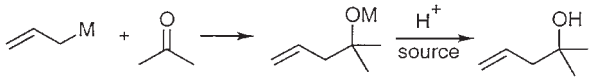
Key words: molybdenum, allylation, chelate model, transposition.

Résumé : Lorsqu'on utilise l'eau comme source de proton, les complexes η^3-allyle et η^3-méthallyle du molybdène réagissent avec les aldéhydes pour conduire aux alcools homoallyliques, avec des rendements préparatifs. Toutefois, dans le cas du complexe η^3-crotylmolybdène, la réaction est limitée par la formation de produits non transposés ainsi que de produits de transposition.

Mots clés : molybdène, allylation, modèle d'un chélate, transposition.

Introduction

The reaction of allylmetal reagents with carbonyl compounds provides a valuable method for the preparation of homoallylic alcohols (eq. [1]). A wide range of metals has been successfully employed in this process even though many allylmetal reagents are unstable and must generally be prepared and used in situ (1). In addition, allylboranes (2) and boronates (3) have found broad utility in applications where a homoallylic alcohol is needed in high enantiomeric excess.

[1] 

In 1989, Faller and co-workers (4) reported that η^3-allyl, η^3-methallyl, and η^3-crotyl complexes of bromo-(cyclopentadienyl)(nitroso)molybdenum react with aldehydes to give homoallylic alcohols. Faller et al. (5) further demonstrated that a chiral η^3-methallylmolybdenum complex could be resolved, and in a NMR experiment showed that its reaction with an aldehyde resulted in high asymmetric induction (6). Although the synthetic potential of these molybdenum compounds as reagents for the preparation of homoallylic alcohols is clear, the scope and limitations of their reactivity remain poorly defined. As part of a program designed to fabricate polyol substructures found in natural products, we were drawn to these π-allylmolybdenum reagents (7) by the fact that they are air and moisture stable substances which react with aldehydes under mild conditions (8).

Received September 27, 1999. Published on the NRC Research Press website on May 19, 2000.

This paper is dedicated to Professor Hanessian.

K.P. Gable, M.S. Shanmugham, and J.D. White.[1]
Department of Chemistry, Oregon State University, Gilbert Hall 153, Corvallis, OR 97331-4003, U.S.A.

[1]Author to whom correspondence may be addressed. Telephone: (503) 737-2173. Fax: (503) 737-2660. e-mail: james.white@orst.edu

Results and discussion

Molybdenum complexes **1**–**3** were prepared from tris(acetonitrile)molybdenum tricarbonyl (**4**) (9) via the dicarbonyl complex **5** using a variant of Faller's protocol (8) in which the bromine ligand was introduced with tetramethylammonium bromide. All three complexes are stable, yellow-orange solids that can be stored for many weeks with no special precautions. The η^3-crotyl complex **3** is a mixture of *syn* and *anti* stereoisomers, and there is evidence that these equilibrate during the reaction with aldehydes.

Since Faller had carried out all reactions of **2** in a mixture of dichloromethane and methanol, we first investigated the effect of varying the solvent on the reaction of **2** with benzaldehyde in the belief that the source of protons could play a pivotal role in this process. The results in Table 1 confirm that this is indeed the case, and that water is the most effective proton source. Optimized conditions for obtaining homoallylic alcohol **6** were realized with 3 equiv of water in dichloromethane; the absence of a proton source or the presence of a more acidic alcohol (CF_3CH_2OH) resulted in a significant proportion of the oxidized byproduct **7**.

The origin of the improved efficacy that the use of water imparts to these allylations bears comment. Faller et al. (5) have noted this effect and have attributed it in part to suppression of hemiacetal formation. However, this cannot be a significant factor. Intermolecular hemiacetal formation from aliphatic aldehydes and methanol is characterized by a small equilibrium constant, and at room temperature this process is

 © 2000 NRC Canada

Scheme 1.

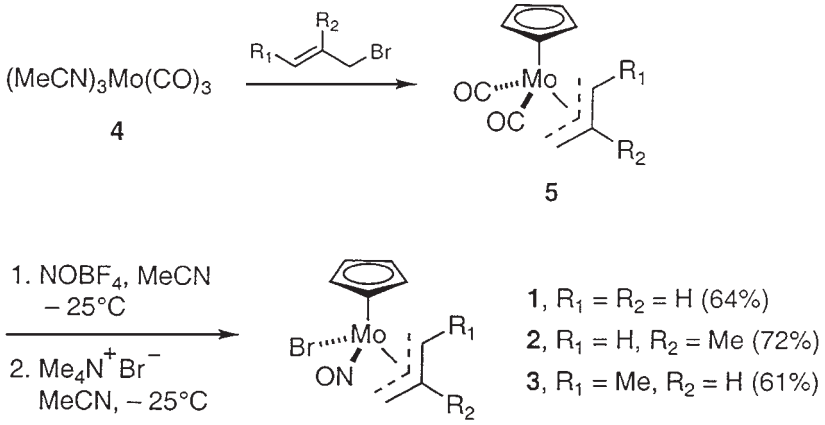
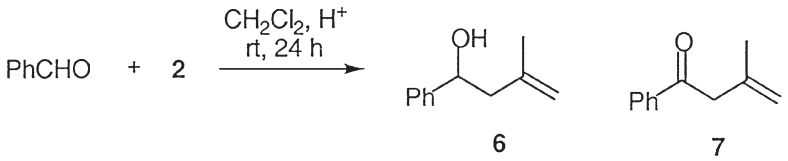


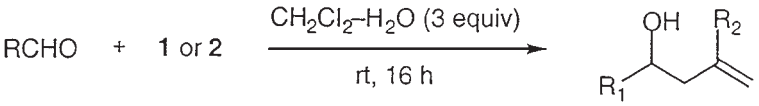
Table 1. Effect of proton source on the reaction of benzaldehyde with **2**.[a]



Solvent	Product(s)	Yield (%)
CH_2Cl_2 + MeOH (3 equiv)	**6**	64
CH_2Cl_2 + MeOH (1:1)	**6**	18
CH_2Cl_2	**6** + **7** (1:1)	52
CH_2Cl_2 + CF_3CH_2OH (3 equiv)	**6** + **7** (1:1)	74
CH_2Cl_2 + H_2O (3 equiv)	**6**	91

[a]Reactions were carried out using a 1.0:1.2 molar ratio of PhCHO:**2**. Increasing the proportion of **2** did not significantly alter yields.

Table 2. Reaction of aldehydes with **1** and **2**.



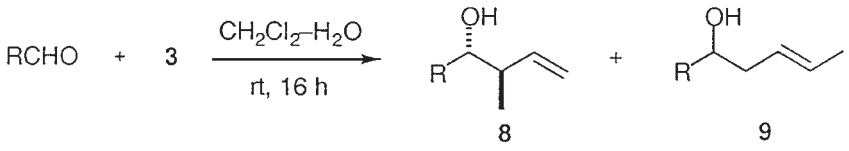
			Product		
Entry	Aldehyde	Reagent	R_1	R_2	Yield (%)
1	*n*-Heptanal	**1**	*n*-C_6H_{13}	H	85
		2	*n*-C_6H_{13}	CH_3	74
2	Cyclohexyl-carboxaldehdye	**1**	C_6H_{11}	H	90
		2	C_6H_{11}	CH_3	74
3	Pivaldehyde	**1**	Me_3C	H	70
			Me_3C	CH_3	76
4	Benzaldehyde	**1**	C_6H_5	H	88
			C_6H_5	CH_3	91
5	2-Heptenal	**1**	*n*-C_6H_{11}	H	89
6	2-Methyl-4-oxazole-carboxaldehyde[a]	**1**	C_4H_4NO	H	90

[a]A.S. Kende, B.E. Blass, and J.R. Henry. Tetrahedron Lett. **36**, 4741 (1995).

rapid compared to the allylation reaction (10). This literature also suggests that the equilibrium for hydration is actually more favored than that for hemiacetal formation. The possibility that pK_a of the proton source is the critical factor is ruled out by the fact that methanol and water have very similar acidities (11). Further, we see that trifluoroethanol leads to marginal improvement over running the reaction without a proton source prior to workup. The isolation of ketone **7**, presumably arising from a β-hydride elimination, suggests that timing of the proton transfer may be linked to binding of the conjugate base to the metal. A weakly Lewis basic species such as trifluoroethanol would not favour the

© 2000 NRC Canada

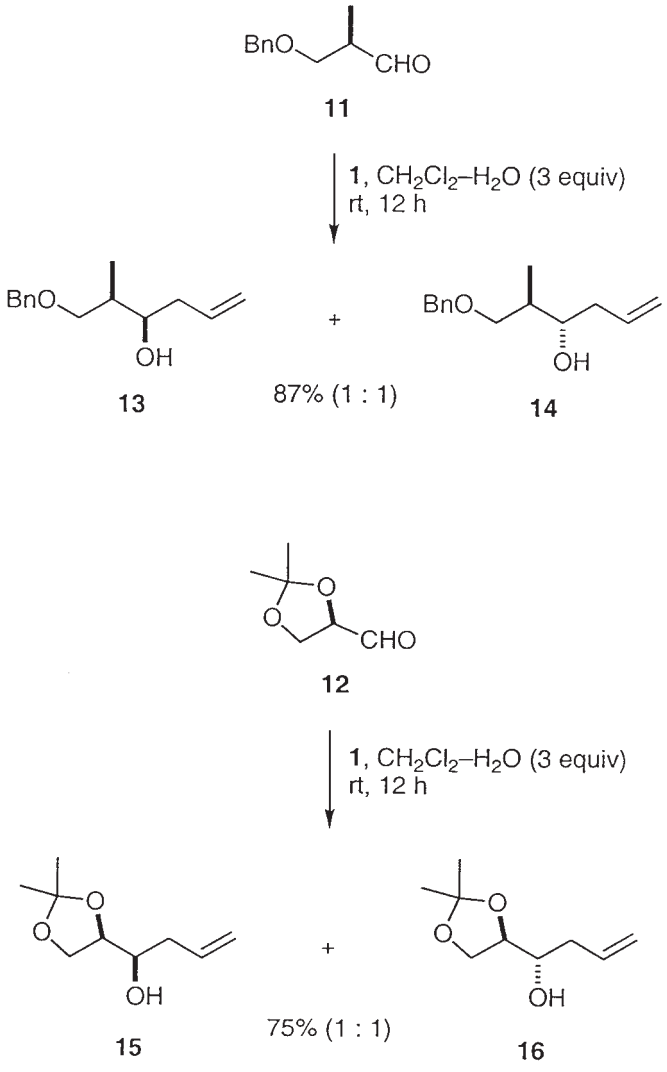
Table 3. Reaction of aldehydes with **3**.



Entry	Aldehyde	Product R	**8**[a]**:9**	Yield (%)
1	*n*-Heptaldehyde	*n*-C_6H_{13}	8:1	54
2	Cyclohexylcarboxaldehyde	C_6H_{11}	1:1	56
3	Pivaldehyde	Me_3C	1:1	64
4	Benzaldehyde	C_6H_5	23:1	87

[a]The *anti:syn* ratio was >98:2.

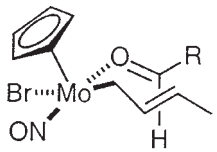
Scheme 2.



alkoxide exchange necessary to free the homoallylic alcohol, despite the enhanced proton availability. Methanol or other alcohols offer an improvement due to inductive donation by the alkyl group. Water, however, can engage in additional π-donation to the moderately oxophilic molybdenum centre, which encourages displacement of the product. Steric interference with other ligands is also minimized by this mechanism.

Application of the optimized conditions described above to the reaction of various aldehydes with 0.2–1 mmol of molybdenum complexes **1** and **2** afforded good to excellent yields of isolated and purified homoallylic alcohols (Table 2). The metal complexes react equally well with hindered (entry 3) and unhindered aldehydes (entry 1); however, they fail to react with ketones. Surprisingly, when the same aldehydes were exposed to molybdenum complex **3**, both transposed (**8**) and nontransposed (**9**) crotylation products were observed, the higher proportion of **9** being obtained with more sterically hindered aldehydes (entries 2 and 3). The configuration of the transposed homoallylic alcohol (**8**) in each case was found to be exclusively *anti* within the limits of detection, consistent with a six-centered, chelate transition state involving η^3-crotylmolybdenum complex **10**. However, the formation of **9** suggests that with **3** either a four-centre transition state or a non-chelate pathway must operate as well.

The question of facial (i.e., Felkin) selectivity in the reaction of molybdenum π-complexes with substrates bearing a



10

stereogenic center α to the aldehyde was addressed with (*R*)-3-benzyloxy-2-methylpropionaldehyde (**11**) and glyceraldehyde acetonide (**12**). In both cases, *syn* (**13**, **15**) and *anti* (**14**, **16**) products were formed in equal quantity, indicating complete absence of substrate stereocontrol in these reactions. This is consistent with an observation previously made by Faller et al. (6), and confirms that the overwhelming size of the metal complex dominates the stereochemical outcome with chiral aldehydes.

Conclusions

The reaction of η^3-allyl, η^3-methallyl, and η^3-crotyl complexes of bromo(cyclopentadienyl)(nitroso)molybdenum with aldehydes is shown to be a preparatively useful route to

© 2000 NRC Canada

homoallylic alcohols, supporting observations previously made by Faller and co-workers (4) on the basis of NMR experiments. The reactions are clean, and separation of the alcohol product from molybdenum byproducts presents no problems. The presence of water as a cosolvent is essential for optimum yields, but the role of water in these reactions is unclear. In reactions of η^3-crotyl molybdenum complexes with aldehydes, a complicating factor can be the formation of both transposed and nontransposed products. The latter are prevalent when a sterically hindered aldehyde is employed, indicating that these substrates interact with the bulky molybdenum reagent via a mechanism different from the conventional six-centered chelate model.

Experimental

In a typical procedure, *n*-heptanal (0.096 g, 0.84 mmol) and water (0.045 mL, 2.50 mmol) were added to a stirred solution of **1** (0.315 g, 1.00 mmol) in CH_2Cl_2 (4 mL). The biphasic mixture was stirred at room temperature for 12 h, after which the solvent was evaporated in vacuo. The crude residue was purified by column chromatography on silica gel, using ether–hexane (1:4) as eluent, to give 4-hydroxy-1-decene (0.111 g, 85%) as a colorless oil. The product was identified by comparison of its spectral properties with those described (12).

Acknowledgements

We thank the National Science Foundation (CHE-9619296 and 9711187-CHE) and Parke–Davis Pharmaceutical Research for their generous financial support.

References

1. Y. Yamamoto and N. Asao. Chem. Rev. **93**, 2207 (1993).
2. P.K. Jadhav, K.S. Bhat, P.T. Perumal, and H.C. Brown. J. Org. Chem. **51**, 432 (1986).
3. (*a*) R.W. Hoffmann. Angew. Chem. Int. Ed. Engl. **26**, 489 (1987); (*b*) W.R. Roush, A.D. Polkowitz, and K. Ando. J. Am. Chem. Soc. **112**, 6339 (1990).
4. (*a*) J.W. Faller, J.A. John, and M.R. Mazzieri. Tetrahedron Lett. **30**, 1769 (1989); (*b*) J.W. Faller and D.L. Linebarrier. J. Am. Chem. Soc. **111**, 1937 (1989).
5. J.W. Faller, K.J. Chase, and M. R. Mazzieri. Inorg. Chim. Acta, **229**, 39 (1995).
6. J.W. Faller, J.T. Nguyen, and M.R. Mazzieri. Appl. Organomet. Chem. **9**, 291 (1995).
7. (*a*) *Cf* W.-J. Vong, S.-H. Lin, R.-S. Liu, G.-H. Lee, and S.-M. Peng. Chem. Commun. 1285 (1990); (*b*) W.-J. Vong, S.-M. Peng, S.-H. Lin, W.-J. Lin, and R.-S. Liu. J. Am. Chem. Soc. **113**, 573 (1991).
8. J.W. Faller. *In* Reagents for organic synthesis. Vol. 1. *Edited by* L.A. Paquette. Wiley, Chichester. 1995. pp. 710–711.
9. D.P. Tate, W.R. Knipple, and J.M. Angl. Inorg. Chem. **1**, 433 (1962).
10. (*a*) E.G. Sander and W.P. Jencks. J. Am. Chem. Soc, **90**, 6154 (1968); (*b*) J.P. Guthrie. Can. J. Chem. **53**, 989 (1975).
11. (*a*) G.I. Mackay and D.K. Bohme. J. Am. Chem. Soc. **100**, 327 (1978); (*b*) W.N. Olmstead, Z. Margolin, and F.G. Bordwell. J. Org. Chem. **45**, 3295 (1980).
12. S.R. Wilson and M.E. Guazzaroni. J. Org. Chem. **54**, 3087 (1989).

© 2000 NRC Canada

Enantiomerically pure decalinic structures from carbohydrates using intramolecular Diels–Alder and Ferrier carbocyclization

Claude Taillefumier and Yves Chapleur

Abstract: The synthesis of enantiomerically pure decalinic structures, advanced intermediates for the synthesis of the hexahydronaphtalen part of mevinic acids, is described. The key steps are the intramolecular Diels–Alder cycloaddition of a suitably substituted sugar enone obtained via the Ferrier rearrangement of tri-*O*-acetyl-D-glucal with the appropriate alcohol representing the diene part of the system. Chemical manipulation of the resulting, diastereomerically pure, cycloadduct led to a 5,6-unsaturated carbohydrate which was submitted to the Ferrier carbocylization. This reaction proved difficult likely because of the embedding of the aglycon in a cycle, the hydration product of the double bond being the main product. This compound was in turn transformed into the decalinic structures by treatment in basic medium. The inverse strategy, Ferrier carbocyclization followed by IMDA of an enone and a diene linked via an ester bond was unsuccessful.

Key words: Intramolecular Diels–Alder reaction, enantiomerically pure decalin, Ferrier carbocyclization, carbohydrates.

Résumé : La synthèse de structures décaliniques énantiomériquement pures, intermédiaires avancés dans la synthèse de la partie hexahydronaphtalene des acides méviniques est décrite. Les étapes clés sont une cycloaddition de Diels–Alder sur une énone dérivée d'un sucre obtenu par réarrangement de Ferrier du tri-*O*-acetyl-D-glucal avec un alcool représentant la partie dièniique du système. Le cycloadduit obtenu, diastéréoisomériquement pur, est ensuite transformé en sucre 5,6 insaturé pouvant subir une carbocyclisation de Ferrier. Cette réaction donne, outre les décalones attendues, les produits d'hydratation de la double liaison, très probablement à cause de l'inclusion de l'aglycone dans un cycle. Un des produits d'hydratation a été carbocyclisé en milieu basique, sans l'aide de sels mercuriques, pour conduire aux structures décaliniques recherchées. La stratégie inverse, carbocyclisation de Ferrier suivie d'une cycloaddition intramoléculaire de l'énone résultante avec un diène lié par un pont ester s'est révèlée improductive.

Mots clés : Réaction de Diels–Alder intramoléculaire, décaline énantiomériquement pure, carbocyclisation de Ferrier, hydrates de carbone.

Introduction

Many naturally occuring compounds consist of a basic decalinic structure decorated with substituents and (or) functional groups. Among them, compounds such as mevinic acids mevinolin, pravastatin, and congeners (1) or diterpenoids like forskolin and representatives of the labdane series (2) are of interest as pharmaceuticals. Accordingly much synthetic work, devoted to the preparation of suitable functionalized decalinic structures, has been published in connection with the search for new drugs. The Diels–Alder cycloaddition played a prominent role in the synthesis of cyclohexane ring systems and the intramolecular version of this useful reaction (IMDA) (3–6) also led to major achievements in the field of mevinic acids synthesis (7). This reaction is also well precedented in carbohydrate chemistry (8).

In connection with a synthetic program originally dealing with the synthesis of the hexahydronaphthalene ring of mevinic acids using the Chiron approach (9), we have investigated the synthetic possibilities of two six-membered ring forming reactions namely IMDA and the Ferrier carbocyclization (10) This mercury-catalyzed intramolecular aldol reaction is a major breakthrough in carbohydrate chemistry which transforms a 5,6-unsaturated pyranoside into a chiral cyclohexanone. The high diastereoselection of the process led to numerous studies for the synthesis of highly functionalized cyclohexanes such as inositol (11), conduritols (12), and other natural products (13, 14). An elegant variant, using a 6-substituted 5,6-unsaturated pyranoside, allowed the synthesis of α-substituted cyclohexanone (15). In addition other conditions, which do not rely on a mercury catalysis, have led to interesting developments of this sugar to carbocycle transformation (16). However, if numerous examples of this basic transformation to form isolated cyclohexane rings are available, application of this reaction on annelated pyranose is very limited.

We have investigated such an approach with some success by combining an intramolecular Diels–Alder on a suitably

Received November 22, 1999. Published on the NRC Research Press website on May 19, 2000.

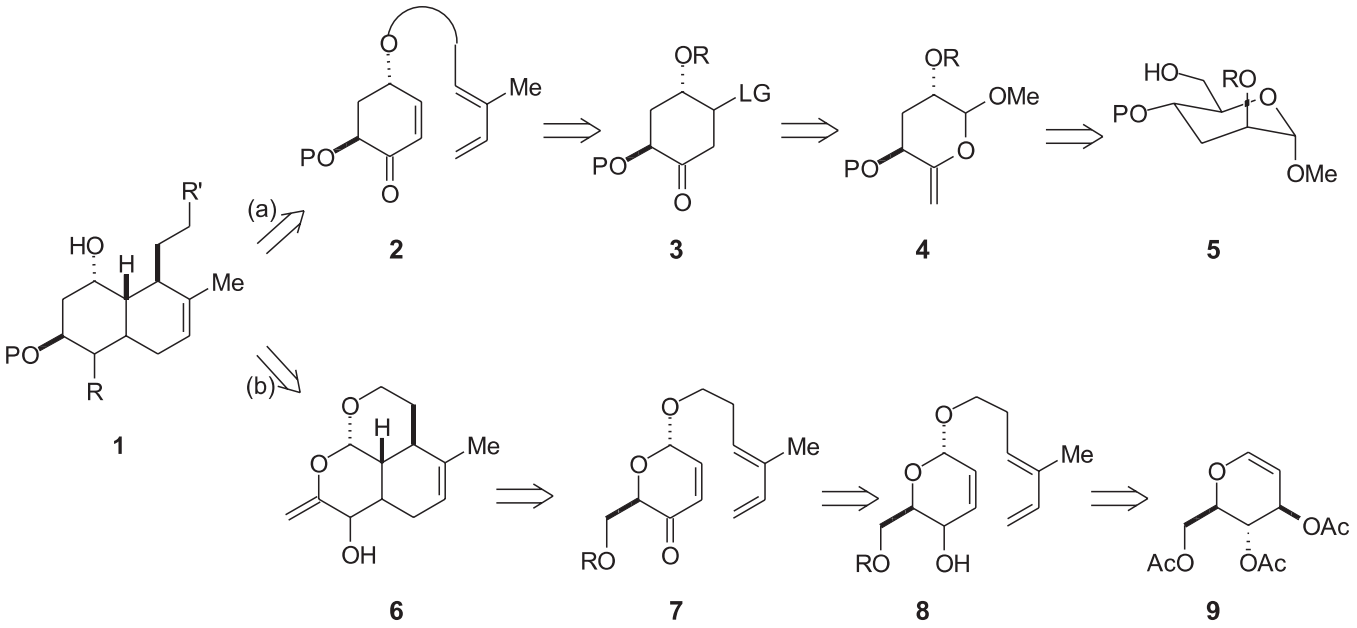
Warmly dedicated to Professor Stephen Hanessian in recognition of his visions and pioneering work in carbohydrate chemistry.

C. Taillefumier and Y. Chapleur.[1] Groupe SUCRES, Unité Mixte de Recherche 7565, CNRS-Université Henri Poincaré-Nancy I, BP 239, F-54506 Nancy-Vandoeuvre, France.

[1]Author to whom correspondence may be addressed. Fax: +33 383 91 24 79. e-mail: yves.chapleur@meseb.uhp-nancy.fr

© 2000 NRC Canada

Scheme 1. Two strategies for the synthesis of *cis* decalinic structures.



functionalized sugar followed by the Ferrier carbocyclization of the resulting annulated pyranoside. We have reported our preliminary results along this line (17). This paper describes the full details of our investigations together with another approach combining the Ferrier carbocyclization followed by IMDA on the resulting cyclohexenone which proved unsuccessful.

The dihydroxylated decalinic structure **1** seemed a particularly interesting target and the two retrosynthetic strategies toward this compound are depicted in Scheme 1. In the first approach (Route (a)) the IMDA was planned at the end of the synthesis. A chiral cyclohexenone would be the dienophile and the electron-rich diene was tethered to this first cyclohexane ring by an ester linkage on an hydroxyl group of the cyclohexenone **2**. The absolute configuration of the carbon bearing the tether was chosen to secure the required absolute stereochemistry of the ring junction by forcing the diene to interact preferentially with one face of the dienophile. The synthesis of cyclohexenone **2** was based on the Ferrier carbocyclization of an appropriate deoxy sugar **4** giving the aldol product **3** (10*b*). The starting sugar **5**, a precursor of the key intermediate **4** of the Ferrier carbocyclization, should be prepared from D-mannose by deoxygenation at C-3 (carbohydrate numbering) or from D-glucose by the same procedure and further inversion of configuration at C-2.

In the second approach (Route (b)) the Ferrier carbocyclization was now planned at the end of the synthesis on the annulated pyranoside **6**. The IMDA reaction could be also performed on a suitably activated double bond, i.e., the enone function of **7**. The advantage of this strategy relies on the fact that the tether between the diene and the dienophile does not have to be a detachable link because the Ferrier carbocyclization would cleave the glycosidic link. The trienic system **8** could came from the Ferrier rearrangement of tri-*O*-acetyl-D-glucal (**9**)with the corresponding dienic alcohol (18).

Results

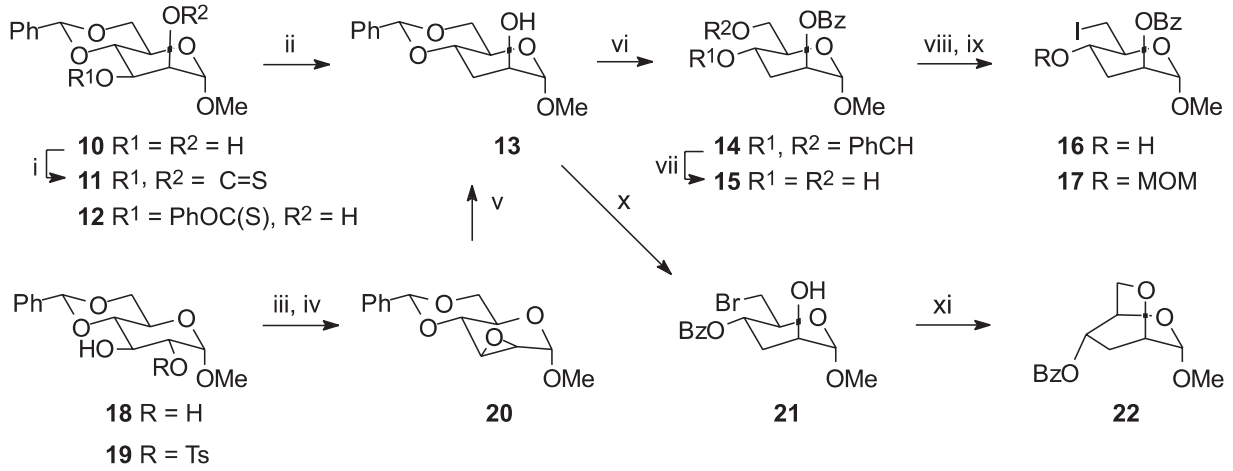
First approach

Two routes to the key intermediate **4** were explored, the first one involving selective protection at C-2 of the known mono-benzylidene derivative of D-mannose (**10**) (19). Assuming that subsequent deoxygenation should reasonably be carried out using a radical reaction, we attempted to introduce a phenylthionocarbonate group at C-3 by selective alkylation with phenylthionocarbonyl chloride (PTCCl) (20) using the stannylene approach as described by Nashed (21) for the synthesis of the 3-*O*-*para*-methoxybenzyl derivative of **10**. Thus treatment of **10** with dibutyltin oxide in refluxing methanol led to the intermediate stannylene which was treated with PTCCl in dimethylformamide at 100°C for 30 min. However, only the known cyclic thionocarbonate **11** was isolated (22). Gratifyingly the treatment of **10** with PTCCl, (1 molar equiv.) under standard conditions led to the expected monophenylthionocarbonate **12** in 54% yield and to the thionocarbonate **11** in 36% yield after chromatography on silica gel. Treatment of **12** with 1.3 equiv. of tris(trimethylsilyl)-silane (23, 24) and a catalytic amount of AIBN in refluxing toluene gave the deoxy-derivative **13** in 68% yield. The low overall yield of this sequence, prompted us to use a more efficient route from the known epoxide **20** (25) which was transformed into the alcohol **13** upon treatment with $LiAlH_4$.(26)

The next problem to address was the introduction of a leaving group at C-6 and to differentiate the two secondary hydroxyl groups at C-2 and C-4. We tried to take advantage of the presence of the benzylidene protecting group. Hanessian–Hullar opening of this acetal using our modified conditions (27), gave the corresponding 6-bromo derivative **21** but all attempts to eliminate hydrobromic acid using silver fluoride in hot pyridine led only to the unexpected 2,6-anhydro structure **22**. All other conditions, (AgF, pyridine, rt; DBU, rt) left the starting material unchanged.

© 2000 NRC Canada

Scheme 2. Reagents: (*i*) Phenyl thionocarbonyl chloride 1.1 equiv.; CH_2Cl_2–acetone–pyr 2 h, 54%; (*ii*) tris(trimethylsilyl) silane, 1.2 equiv.; AIBN, degassed toluene reflux, 68%; (*iii*) TsCl 1.4 equiv.; NaOH 5%; Bu_4NHSO_4, CH_2Cl_2, 93%; (*iv*) MeONa, MeOH reflux, quant.; (*v*) $LiAlH_4$, THF, 50°C, 100%; (*vii*) HCl 12 N; EtOH–H_2O (10:1), reflux, 67%; (*viii*) PPh_3, imidazole, I_2, toluene, 55°C, 82%; (*ix*) NaH, MOMCl; (*x*) NBS, 1.1 equiv.; $CaCO_3$, CCl_4, reflux, 98%; (*xi*) AgF, pyridine, 80°C.

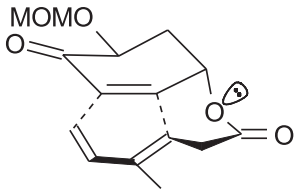


Hydrogenolysis of the benzylidene according to the Liptak procedure was also explored (28), but probably because of the absence of a chelating oxygen at C-3, a mixture of 4-*O*-benzyl and 6-*O*-benzyl derivatives in a 1:1 ratio was obtained. A multi-step sequence was then carried out which consisted first in the protection of the hydroxyl group at C-2 as a benzoate followed by acid hydrolysis of the benzylidene ring to give the diol **15** in 67% overall yield. This diol was treated with triphenylphosphine, imidazole, and I_2 to provide the iodo-derivative **16** in 82% yield. Treatment of **16** with silver fluoride in pyridine at room temperature gave the 5,6-unsaturated compound **23** (52%), which was treated with MOMCl to provide the fully protected derivative **24** in 85% yield. Alternately the alcohol **16** could be protected as the MOM ether **17** (71%) and subsequent elimination of iodohydric acid led to **24** in the same overall yield. Treatment of **24** with ammonia in methanol gave quantitatively the alcohol **25** which was esterified with the dienic acid **31**. The latter was prepared through a three-step sequence involving Wittig olefination of 2-methyl butenal (**29**) with carbethoxymethyl triphenylphosphorane followed by saponification of the resulting ester to provide **30**. Treatment with a base and trapping the kinetic enolate (29) gave the expected carboxylic acid **31**. Esterification of alcohol **25** using DCC activation gave the key intermediate **26** in 89% yield. In spite of the number of olefinic bonds and the presence of the MOM acetal, Ferrier carbocyclization catalyzed by mercuric sulfate proceeded uneventfully to give **27** and treatment of this compound with triflic anhydride at –10°C gave the expected enone **28** in modest yield.

Treatment of enone **28** in degassed toluene in the presence of hydroquinone failed to give any cyclized product. The only observable reaction was the splitting of the MOM protecting group. No reaction was observed using Lewis acid catalyst such as diethyl aluminium chloride which has been reported to have beneficial effects (30).

The presence of the ester function in the tether of the diene and the dienophile was likely responsible for the failure of this IMDA cyclization. One explanation should be that the preferred *transoid* form of the ester impedes the correct geometrical arrangement in the transition state. Another more likely reason is that the lone pair of the ester oxygen is almost perpendicular to the π orbital of the carbonyl in the transition state as shown on the approximate geometry of the transition state depicted on Fig. 1. Thus the absence of orbital overlap should destabilize the transition state of the cyclization. Such an explanation has already been invoked to explain the more drastic conditions needed to achieve intramolecular Diels–Alder reaction involving an ester junction (31).

Fig. 1. Approximate geometry of an *exo* transition state for the IMDA of **28**.



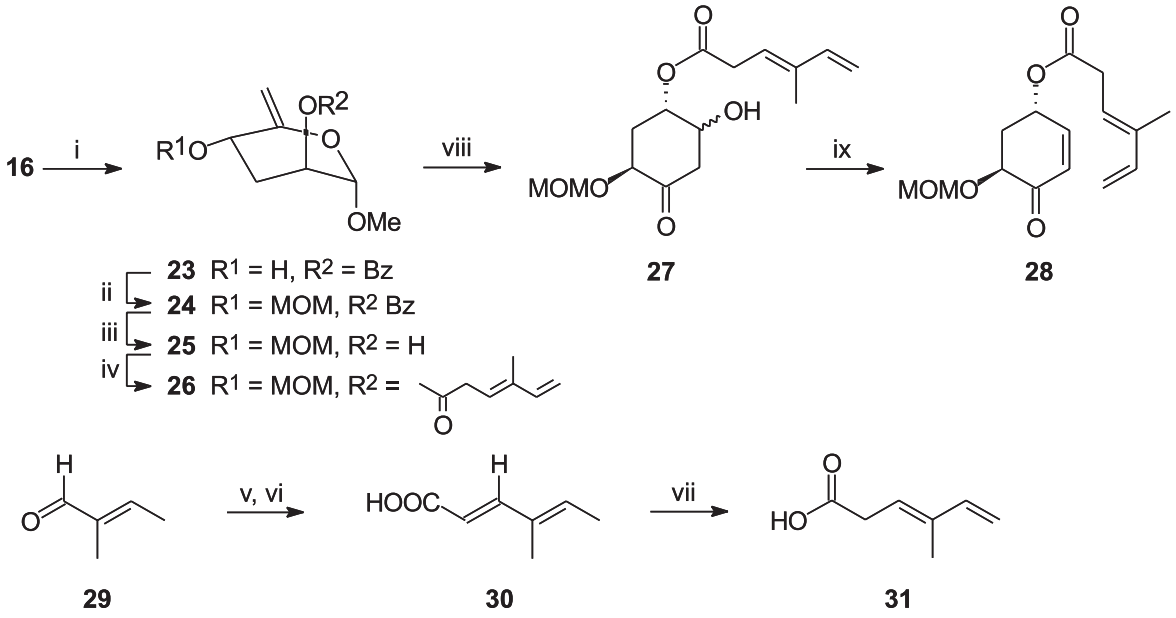
Second approach

The first crucial step of this second approach was the glycoside formation using Ferrier rearrangement of tri-*O*-acetyl-D-glucal with the dienic alcohol **33**. This homoallylic alcohol **33** was prepared in two steps from commercially available ocimen (**32**) by ozonolysis – sodium borohydride reduction according to patent literature (32). This alcohol was reacted with tri-*O*-acetyl-D-glucal (**9**) in the presence of boron trifluoride–etherate as the catalyst under carefully controlled conditions because compound **33** was prone to degradation in the presence of this catalyst. The unsaturated glycoside **34** was prepared in 84% as a α and β (80:20) mixture.

Saponification of the acetates under standard conditions led to the corresponding diols from which compound **35** was obtained as a pure product by column chromatography. Selective protection by selective pivaloylation was troublesome due to the high reactivity of the secondary allylic alcohol and gave **36** and the diester **37** as a 7:3 mixture. However the diester **37** could be recycled to the diol **35** by $LiAlH_4$ re-

© 2000 NRC Canada

Scheme 3. Reagents: (*i*) AgF, pyr. rt, 52%; (*ii*) MOMCl, iPr_2NEt, CH_2Cl_2, 85%; (*iii*) NH_3, MeOH, quant; (*iv*) **V**, DCC, CCl_4, DMAP, CH_2Cl_2, 89%; (*v*) $(Ph)_3PCHCOOEt$, THF reflux, 80%; (*vi*) NaOH 1 N, MeOH reflux; (*vii*) LDA, 2.2 equiv., –78°C then AcOH, 65%; (*viii*) $HgSO_4$ 0.02 equiv.;, H_2SO_4 5 mM; 1,4-dioxane, 50°C; (*ix*) Tf_2O, CH_2Cl_2–Pyr (10:1), –10°C, 30%, 2 steps.



duction. Oxidation of the alcohol **36** with pyridinium dichromate yielded the ketone **38** in 50–55% yield, and freshly prepared manganese dioxide cleanly oxidized the allylic alcohol in up to 90% yield. Ketone **38** proved very unstable and underwent decomposition, maybe by β-elimination of the ester group upon concentration, and was kept in solution.

The intramolecular Diels–Alder reaction proceeded uneventfully by simple treatment of **38** in degassed toluene at 155°C in a sealed tube in the presence of hydroquinone. The cycloadduct **40** was obtained in 75% overall yield. As seen from careful examination of the NMR spectrum, a single isomer was formed and the observed coupling constants $J_{1,2}$ 2.0 Hz and $J_{2,3}$ 3.5 Hz were in favour of an all *cis* arrangement of these three protons. This was in agreement with an attack of the enone double bond from the α face as expected. Determination of the configuration at C-3 (see Scheme 4), which reflects the attack from one face of the diene (i.e., *endo–exo* transition state) could not be determined on the basis of coupling constants due to signal overlaps. It was anticipated that an *exo* transition state would be favoured over the *endo* one to minimize steric interactions between the diene and the sugar ring.

Reduction of the keto group of **40** was achieved by lithium aluminium hydride, conditions which also removed the pivaloyl group. Low diastereoselection was observed for the ketone reduction and a 1.7:1 mixture of diols **42** and **43** was obtained.

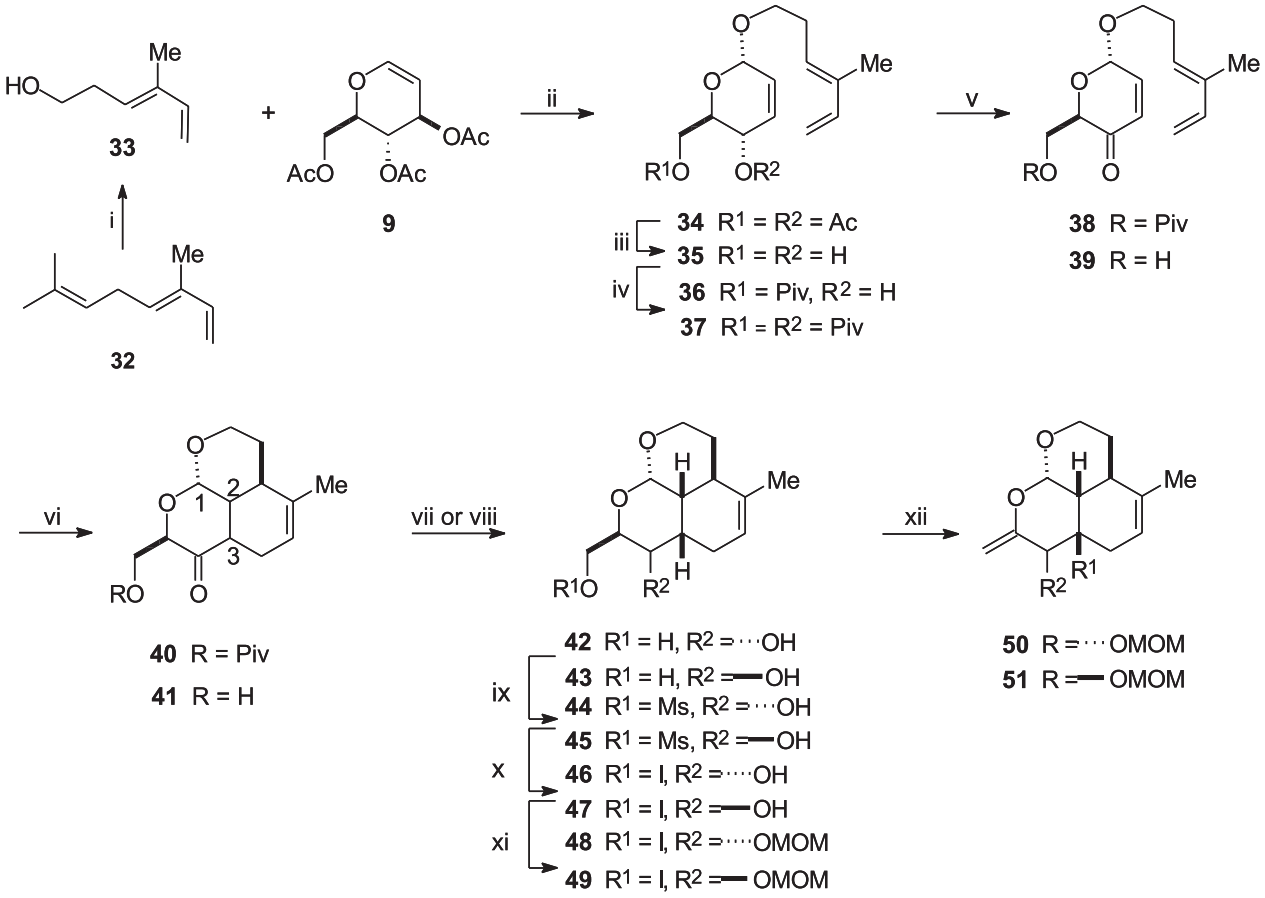
In the meantime, a shorter route to these compounds was sought which would avoid the formation of the bis-protected derivative **37**. Thus, selective oxidation of the allylic alcohol of the diol **35** by manganese dioxide was carried out to afford the ketone **39** in 83% yield. This unstable ketone was immediately engaged in the IMDA under our standard conditions to provide the adduct **41** in 66% yield as a single isomer. Formation of the diols **42** and **43** in almost equal amounts was achieved by sodium borohydride reduction of **41** in 88% yield.

The next problem to address was the chemical manipulation of the annulated pyranoside **40** to secure the formation of the 5,6-unsaturation required for the Ferrier carbocyclization. Selective mesylation of the primary alcohol of the **42** and **43** mixture gave the mesylates **44** and **45** respectively, easily separated by column chromatography. Substitution of the mesylate group by iodide was carried out separately on each compound giving **46** and **47** in 60 and 82% yield, respectively. If elimination of iodohydric acid can be performed cleanly on alcohol **46**, the same sequence cannot be applied to **47** without formation of an oxetane by intramolecular substitution of iodine by the hydroxyl group at C-4. Protection of the hydroxyl group of **46** and **47** was achieved and formation of the methoxy methyl ether proceeded in 60% yield to provide **48** and **49** respectively. Once again, treatment of each iodo-derivative with silver fluoride in pyridine cleanly gave **50** and **51** in 72% and 87% yield, respectively.

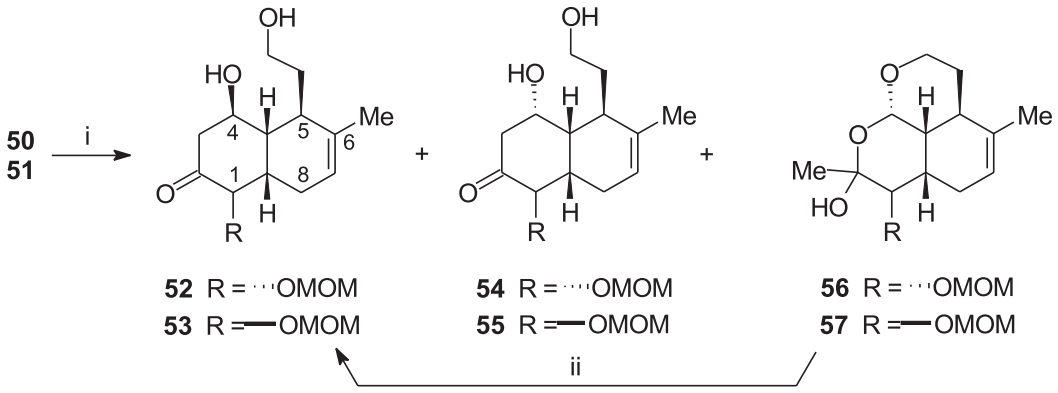
Only a few examples of the Ferrier carbocyclization on annulated pyranose have been reported in the literature (33). In addition, our substrates **50** and **51** bear two electron-rich double bonds which are susceptible to reaction with the mercury catalyst. Ferrier carbocyclization was investigated on these two key intermediates. A large panel of different catalysts and reaction conditions have been proposed in the literature for this reaction (10*b*). Mercuric trifluoroacetate, a catalyst we have introduced in 1984 for the carbocyclization of amino sugars (34), and which is efficient in a number of cases (35, 13), proved disappointing in our reaction. The catalytic method based on the use of mercury sulfate, introduced by Machado et al. (36), was more efficient. Thus, treatment of the unsaturated pyranoside **50** gave a mixture of three compounds **52**, **54,** and **56** in a 1:1:6 ratio in 95% overall yield. If compounds **52** and **54** where the expected

© 2000 NRC Canada

Scheme 4. Reagents: (*i*) O_3, MeOH, –50°C then $NaBH_4$, H_2O, 59%; (*ii*) BF_3–Et_2O, CH_2Cl_2, 84%; (*iii*) MeONa, MeOH; (*iv*) Pivaloyl chloride, CH_2Cl_2, Pyr, –5°C, **AI** 63%, **AH** 27%; (*v*) PDC, CH_2Cl_2, 55% from **AI**; MnO_2, CCl_4 90% from **AI**, 83% from **AG**; (*vi*) toluene, hydroquinone, 155°C, 75% from **AJ**, 66% from **JA**; (*vii*) $LiAlH_4$, THF, 87% from **AK**; (*viii*) $NaBH_4$, MeOH, 88%; (*ix*) MsCl, Pyr, 95%; (*x*) NaI, butanone reflux; (*xi*) MOMCl, iPr_2NEt, THF, 55°C, 62%; (*xii*) AgF, Pyr, 87%.



Scheme 5. Reagents: (*i*) Hg^{++}, H_2O see text; (*ii*) Na_2CO_3 1.8 equiv; DBU, THF–MEOH, rt, 50%.

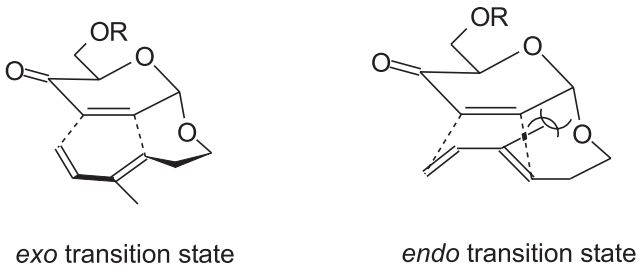


cyclohexanones, compound **56** was clearly the result of the hydroxy-mercuration of the 5,6-double bond. Suspecting an interruption of the catalytic cycle of mercury, we used a stoichiometric amount of mercury sulfate but **56** was still the major product of this reaction. The same results were obtained from olefin **51**. Three compounds **53**, **55**, and **57** were formed in a 1:1:2 ratio in 84% yield. The hydration product **57** again predominated. It should be emphasized that carbocyclization occurred without notable diastereoselection in contrast with other reported cases where one isomer is formed preferentially and even exclusively.

The formation of hydration products **56** and **57**, which are rarely observed in the Ferrier carbocyclization, may be due to the involvement of the aglycon into a tricyclic ring system. This arrangement should preclude the formation of the free aldehyde group needed for carbocyclization. The reaction is then considerably slowed down so that the intermediate mercury species did cyclize but was hydrolysed to the

© 2000 NRC Canada

Fig. 2. Transition states of the IMDA cyclization of **38** and **39**.



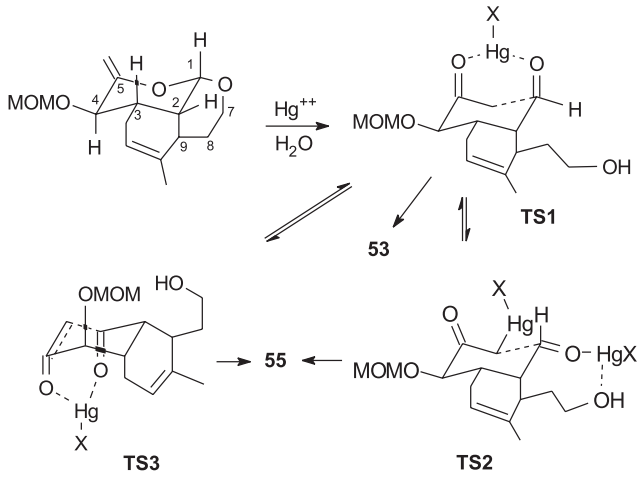
hydration products. Such hydration products have been observed by Blattner et al. (37) in the carbocyclization of 5,6-unsaturated pyranose having a benzoate group at the anomeric position. Hydration was believed to proceed by hydrolysis of the postulated intermediate 6-mercuriated species. This difficulty was overcome by using a stoichiometric amount of mercuric acetate to catalyse the carbocyclization. These conditions were tested on compounds **51** and a mixture of **53**, **55**, and **57** in a 2.5:1:1.7 ratio was obtained. It is worthy of note that the main product **53** has a "3,5-*trans*" (cyclohexanone numbering) relative stereochemistry which prevails in most of the reported Ferrier carbocyclizations (38).

Examination of the structure of compounds **56** and **57** shows that all requirements needed to perform an intramolecular aldol reaction, i.e., the keto group at C-5 and aldehyde at C-1, were present. We thus examined the possibility of going from compound **57** to carbocycles **53** or **55** without the use of mercury catalysis. After some experiments, we found that basic conditions in a protic medium, Na_2CO_3, DBU in THF/MeOH were well suited to transform compound **57** into aldol **53** *as a single isomer* in 50% yield and 50% recovered starting material. No attempt was made at this time for the cyclization of **56**. The structure of compound **53** was firmly established by single crystal X-ray diffraction (17). The absolute configurations at C-1, C-4, C-5, C-5a, and C-8a (See Scheme 5) which were tentatively assigned by NMR were thus confirmed. The complete stereocontrol of the IMDA reaction which occurred in the *exo* mode with attack of the diene from the bottom face of the dienophile was confirmed by the configuration of C-5. Moreover, this configuration was that of the mevinic acids (see Fig. 2).

It is worthy of note that the conformation of the decalone ring of **53** in the solid state as shown by X-ray crystal structure (17) is opposite to that determined on the basis of the ^{1}H NMR spectrum. The OH group was found to be in an equatorial orientation in solution as shown by the large $J_{2,3}$ = 10.3 Hz and $J_{3,4}$ = 9.5 Hz in benzene solution, which are typical of *trans* diaxial arrangement of these protons. The smaller values of these coupling constants in DMSO suggested that, in this solvent, a conformational equilibrium should take place. Molecular mechanics calculations performed on the two conformers have shown that the energy difference between these two conformers was less than 1.5 kcal/mol.

Formation of a single isomer in the carbocyclization of **57** to **53** deserves comments. Usually Ferrier carbocyclization gives high diastereoselection, the product having a 3,5 *trans* arrangement (cyclohexanone numbering) being formed preferentially (38). On the other hand, it has been shown that the stereochemistry at C-5 of the formed cyclohexanone can be correlated with the conformation of the starting sugar (36). Several mechanistic explanations for this phenomenon have been proposed. One explanation is based on a chelation by a mercury atom of the oxygen atoms of both the aldehyde and the ketone groups involved in this aldol-type reaction (39, 40). A chair transition state in which these carbonyl groups occupy two axial positions (see **TS1**, Fig. 3) should be favoured over a twisted transition state in which the two carbonyl groups are pseudo-equatorial. Another explanation involves a chelation between the mercury atom linked to C-6 and the substituent at C-3 (carbohydrate numbering) leading to a boat transition state in which the two carbonyl groups are located on the opposite side of the C-3 substituent. This explanation is supported by the absence of stereoselectivity in the Ferrier carbocyclization of 3-deoxy sugars (38).

Fig. 3. Possible transition states for the Ferrier carbocyclization of **51**.

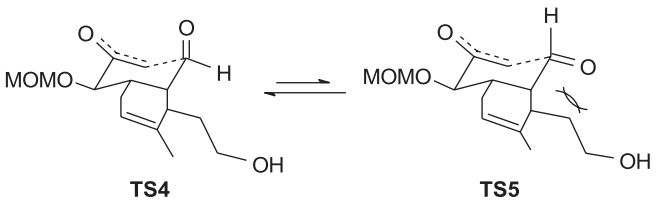


The C-2—C-3 and C-8—C-9 bonds in compounds **51** or **50** are in a *trans* relationship which forces these groups to be only in equatorial orientations. Thus, the conformation of the unsaturated pyranose ring is more or less fixed and should adopt only the $^1C_4$ conformation or the $^{2,5}B$ conformation. In compound **51**, the chair conformation places the C-4 OMOM substituent in an equatorial orientation and should be favoured over the boat conformation. This is confirmed by the coupling constant value in the ^{1}H NMR spectrum of **51** ($J_{3,4}$ = 10.5 Hz). On this basis, according to Machado et al. (36), it could be predicted that the major isomer would be compound **53**. The boat transition state involving chelation of the substituent at C-3 cannot be invoked in our case because of the absence of such a chelating group and because of the conformational bias. The transition state **TS1** leading to **53** should be a chair having the two oxygen chelated by mercury in an axial orientation.

To explain the substantial amount of the other isomer **55**, two possibilities can be envisioned. In the first one, the conformation of the intermediate resulting from the opening of the acetal function changes so that the orientation of the carbonyl groups are reversed and thus the aldehyde is then attacked from the other face via transition state **TS3** (Fig. 3). Another, maybe better, explanation takes into account the

© 2000 NRC Canada

Fig. 4. Possible transitions states for the ring closure of **57**.



presence of the hydroxyl group at C-7 which can be involved in a chelation with the aldehyde group and mercury so that again the *Si* face of the aldehyde is presented to the attacking carbon atom in **TS2** leading to **55**. In both hypotheses the presence of the bicyclic system or the hydroxyl group are responsible for the absence of selectivity. Support of this assumption is given by the fact that the aldol reaction conducted in basic medium in the absence of mercury is highly selective and probably involves a transition state in which the steric interactions rather than chelation govern the stereochemical course. As shown on Fig. 4, two transition states should be devised leading to both isomers but **TS4**, in which the carbonyl group points upwards is likely favoured over **TS5** in which strong 1,3-diaxial interactions between the carbonyl and the methylene groups may exist.

Experimental

All reactions were performed under nitrogen atmosphere. Melting points are uncorrected and recorded with a Büchi capillary tube melting-point apparatus. Optical rotations were measured on a Perkin Elmer 141 polarimeter in a 1 dm cell at 20°C. FTIR spectra were recorded on a Perkin–Elmer Spectrum 1000 on NaCl windows or KBr pellets. Unless otherwise stated ^{1}H NMR and ^{13}C spectra were recorded on a Bruker AC 250 spectrometer at 250 MHz and 62.5 MHz respectively. 400 MHz ^{1}H NMR were recorded on a Bruker AC 400 spectrometer. Chemical shifts are reported in ppm using the residual of chloroform as internal standard (7.27 ppm and 77.0 ppm respectively). Attribution of ^{13}C signals are based on the *J*-modulated spin-echo sequence. Analytical thin-layer chromatography were performed on Merck $60F_{254}$ precoated silica gel glass plates. Compounds were visualized on developed plates by UV light followed by charring with 10% H_2SO_4 in methanol. Preparative chromatography was performed on silica gel 60 (230–40 mesh ASTM) using ethyl acetate and hexane mixtures or by high pressure liquid chromatography using Merck silica gel 60H (45μM).

Methyl-4,6-*O*-phenylmethylene-2,3-thionocarbonyl-α-D-mannopyranoside (11)

To a solution of methyl-4,6-*O*-phenylmethylene-α-D-mannopyranoside (1,69 g, 6 mmol) in anhydrous methanol (200 mL) was added dibutyltin oxide (4.2 g, 16.8 mmol, 2.8 equiv.). The solution was heated at reflux for 4 h. Methanol was removed under vacuum, the residue was diluted with DMF (40 mL) and PTCCl (2.5 mL, 18 mmol, 3 equiv.) was added. The mixture was stirred at 100°C for 0.5 h then quenched with methanol and concentrated in vacuo. The residue was diluted with CH_2Cl_2, washed successively with 3 N aqueous NaOH, brine, dried over Na_2SO_4 and concentrated in vacuo. Chromatography on silica gel with *n*-hexane–EtOAc (9:1) yielded compound **11** (1,59 g, 0.51 mmol, 85%) as a white solid; mp 140–142°C (lit. (22) = 144–145°C). R_f 0.50 (hexane/EtOAc, 7:3). $[\alpha]_D^{22}$ –89.7° (c 1.0, $CHCl_3$) (lit. (22) = value $[\alpha]_D^{22}$ –85.7° (c 0.6, $CHCl_3$). ^{1}H NMR ($CDCl_3$) δ: 3.43 (s, 3 H, OCH_3), 3.72–3.90 (m, 3 H, H-4, H-6 and H-6′), 4.36 (m, 1 H, H-5), 4.78 (d, 1 H, $J_{2,3}$ 7.0 Hz, H-2), 5.07 (m, 1H, H-3), 5.10 (s, 1 H, H-1), 5.60 (s, 1 H, PhC*H*), 7.33–7.53 (m, 5 H, Ph). ^{13}C NMR ($CDCl_3$) δ: 55.75 (OCH_3), 59.52, 69.04, 77.97, 79.54, and 80.42 (C-2, C-3, C-4, C-5, and C-6), 96.62 (C-1), 102.11 (O*C*HPhO), 126.39 (Ph), 128.62 (Ph), 129.66 (Ph), 136.67 (Ph), 189.69 (C=S). Anal. calcd. for $C_{15}H_{16}O_6S$: C 55.54, H 4.97, S 9.88; found: C 55.71, H 5.05, S 9.77.

Methyl-4,6-*O*-phenylmethylene-3-*O*-phenylthionocarbonyl-α-D-mannopyranoside (12)

Methyl-4,6-*O*-phenylmethylene-α-D-mannopyranoside (980 g, 3.5 mmol) was dissolved in an anhydrous CH_2Cl_2–acetone–pyridine (4:2:1) mixture (35 mL) under nitrogen. To this solution cooled to 0°C was added dropwise phenyl chlorothionoformate (0.50 mL, 3.85 mmol, 1.1 equiv.). After being stirred for 2 h the reaction mixture was quenched with ethanol and solvents were evaporated under reduced pressure. The residue was diluted with CH_2Cl_2, washed with water until neutral, dried over Na_2SO_4, and concentrated in vacuo. At this stage, TLC revealed the presence of a single product (*Rf* 0.22 (hexane–EtOAc, 7:3)). The crude product was chromatographed on silica gel to afford the expected compound **12** (800 mg, 1.91 mmol, 54%) accompanied with the cyclic thionocarbonate **11** (400 mg, 1.28 mmol, 36%), the latter being formed during purification. R_f 0.22 (hexane–EtOAc, 7:3). ^{1}H NMR ($CDCl_3$) δ: 2.60 (br s, 1 H, OH), 3.43 (s, 3 H, OCH_3), 3.41–3.80 (m, 2 H, H-5 and H-6), 4.27–4.39 (m, 2 H, $J_{4,5}$ 9.5 Hz, H-4 and H-6′), 4.47 (br s, 1 H, H-2), 4.81 (d, 1 H, $J_{1,2}$ 1.5 Hz, H-1), 5.61 (s, 1 H, PhC*H*), 5.79 (dd, 1 H, $J_{2e,3a}$ 3.0; $J_{3a,4a}$ 10.0 Hz, H-3), 7.05–7.54 (m, 10 H, Ph).

Methyl 3-deoxy-4,6-*O*-phenylmethylene-α-D-arabino-hexopyranoside (13)

(*i*) By radical deoxygenation of **12**: To a solution of phenylthionocarbonate (**12**) (400 mg, 0.95 mmol) in degassed toluene (20 mL) under nitrogen was added in one portion AIBN (200 mg, 1.21 mmol, 1.2 equiv.). To the resulting mixture was added dropwise tris(trimethylsilyl)silane (0.38 mL, 1.23 mmol, 1.26 equiv.). The solution was then heated to reflux and after 40 min, TLC (hexane–EtOAc, 7:3) indicated complete reduction of the starting material. The solution was cooled and concentrated under reduced pressure. The residue was chromatographed on silica gel to give pure deoxy-compound **13** (170 mg, 0.64 mmol, 68%) as a white solid.

(*ii*) By epoxide opening: To 180 mg (4.7 mmol, 3.5 equiv.) of $LiAlH_4$ suspended in dry THF (20 mL) was added dropwise a solution of epoxide **20** (350 mg, 1.32 mmol) in dry THF. The resulting mixture was stirred for 18 h at 50°C and then treated successively with water (0.18 mL), aqueous 30% NaOH (0.54 mL), and water (0.54 mL). The salts were filtered off through a pad of Celite, washed with hot THF. The solvent was removed and the residue was chromatographed on silica gel with hexane/EtOAc (1:1) as eluent to give **13** in

© 2000 NRC Canada

nearly quantitative yield, mp 109°C (lit. (26) mp 111–112°C. R_f 0.31 (hexane–EtOAc, 3:2). $[\alpha]_D^{22}$ +95.5 (c 0.81, $CHCl_3$) (lit. (26) $[\alpha]_D^{22}$ +107.3° (c 0.94, $CHCl_3$)). IR (cm^{-1}): 3452 (OH). ^1H NMR ($CDCl_3$) δ: 1.99–2.18 (m, 2 H, 2 × H-3), 3.41 (s, 3 H, OCH_3), 3.73–4.04 (m, 4 H, H-2, H-5, and 2 × H-6), 4.25 (m, 1 H, H-4), 4.55 (s, 1 H, H-1), 5.58 (s, 1 H, PhC*H*), 7.31–7.52 (m, 5 H, Ph).

Methyl 2-*O*-benzoyl-3-deoxy-α-D-arabino-hexopyranoside (15)

To a solution of alcohol **13** (413 mg,1.55 mmol) in dry pyridine (15 mL) under argon was added dropwise benzoyl chloride (1.86 mmol, 1.2 equiv.). After being stirred overnight, pyridine was evaporated and the residue was codistillated three times with toluene to provide the expected crude benzoate as a crystalline solid. It was dissolved in a mixture of ethanol–water (10:1, 55 mL) and three drops of 12 N HCl were added. After 3 h at reflux the reaction was over. The pH was adjusted to 7 with aqueous 3 N NaOH, the solvent was evaporated under reduced pressure and the residue was taken up in CH_2Cl_2. The organic layer was washed with saturated aqueous $NaHCO_3$ and water, dried over Na_2SO_4, and concentrated in vacuo. Chromatography on silica gel with hexane–EtOAc as eluent yielded diol **15** (294 mg, 1.04 mmol 67%)as a white solid, mp 105°C (lit. (41) mp 109°C). R_f 0.39 (hexane–EtOAc, 1:4). $[\alpha]_D^{22}$ +49.4 (c 0.37, $CHCl_3$) (lit. (41)value $[\alpha]_D^{22}$ +52.2° (c 1.1, $CHCl_3$)). ^1H NMR ($CDCl_3$) δ: 2.05 (ddd, 1 H, J_{gem} 14.0, $J_{2,3a}$ 3.0, $J_{3a,4}$ 11.5 Hz, H-3a), 2.26 (ddd, 1 H, $J_{2,3e}$ 3.5, $J_{3e,4}$ 5.0 Hz, H-3e), 2.40–2.90 (m, 2 H, 2 × OH), 3.43 (s, 3 H, OCH3), 3.67 (ddd, 1 H, $J_{4,5}$ 10.0, $J_{5,6}$ 4.5, $J_{5,6'}$5.0 Hz, H-5), 3.83–3.97 (m, 2 H, H-6 and H-6′), 4.10 (ddd, 1 H, H-4), 4.71 (br s, 1 H, H-1), 5.16 (m, 1 H, $J_{1,2}$ 1.5 Hz, H-2), 7.40–8.12 (m, 5 H, Ph).

Methyl 2-*O*-benzoyl-3,6-dideoxy-6-iodo-α-D-arabino-hexopyranoside (16)

A mixture of diol **15** (483 mg, 1.71 mmol), triphenylphosphine (0.61 g, 2.32 mmol, 1.5 equiv.), imidazole (0.31 g, 4.65 mmol, 3 equiv.), and iodine (0.47 g, 1.86 mmol, 12 equiv.) in dry toluene (30 mL) was vigorously stirred at 55°C for 4 h. Toluene was evaporated and the residue was taken up in CH_2Cl_2, washed successively with aqueous 0.5 N HCl, aqueous 1 N $NaHCO_3$, and water. The organic layer was dried over $MgSO_4$ and concentrated in vacuo. Chromatography on silica gel eluting with hexane–EtOAc (4:1) gave the iodo-derivative **16** (503 mg, 1.28 mmol, 82%). R_f 0.27 (hexane–EtOAc, 4:1). $[\alpha]_D^{22}$ +77.5 (c 0.85, $CHCl_3$). IR (cm^{-1}): 3466, 1720. ^1H NMR ($CDCl_3$) δ: 2.06 (ddd, 1 H, J_{gem} 13.5, $J_{2,3a}$ 3.0, $J_{3a,4}$ 11.5 Hz H-3a), 2.25 (ddd, 1 H, $J_{2,3e}$ 4.0, $J_{3e,4}$ 5.0 Hz, H-3e), 3.37–3.55 (m, 5 H, OCH_3, H-5, H-6 and H-6′), 3.88 (m, 1 H, H-4), 4.73 (br s, 1 H, H-1), 5.15 (m, 1 H, H-2), 7.22–7.65 and 8.01–8.12 (m, 5 H, Ph). ^{13}C NMR ($CDCl_3$) δ: 8.06 (C-6), 32.51 (C-3), 55.30 (OCH_3), 66.75, 70.75, 72.36 (C-2, C-4 and C-5), 97.65 (C-1), 128.54 (Ph), 129.84 (Ph), 133.47 (Ph), 165.79 (C=O). Anal. calcd. for $C_{14}H_{17}O_5I$: C 42.87, H 4.36, I 32.35; found: C 42.36, H 4.43, I 32.52.

Methyl 2-*O*-benzoyl-3,6-dideoxy-6-iodo-4-*O*-methoxymethyl-α-D-arabino-hexopyranoside (17)

The alcohol **16** (4.0 g, 10.20 mmol) was protected as the methoxymethylether according to the procedure described for the preparation of **24** (3.16 g, 7.25 mmol, 71%). R_f 0.59 (hexane–EtOAc, 4:1). $[\alpha]_D^{22}$ +70.8 (c 0.70, $CHCl_3$). IR (cm^{-1}): 1722. ^1H NMR (250 MHz, $CDCl_3$) δ: 2.07 (ddd, 1 H, J_{gem} 13.5, $J_{2,3a}$ 3.0, $J_{3a,4}$ 11.0 Hz; H-3a), 2.35 (ddd, 1 H, $J_{2,3e}$ 3.5, $J_{3e,4}$ 4.5 Hz, H-3e), 3.28 (s, 3 H, CH_2OCH_3), 3.41 (dd, 1 H, J_{gem} 10.0, $J_{5,6}$ 6.5 Hz, H-6), 3.48 (s, 3 H, OCH_3), 3.52 (m, 1 H, H-5), 3.61 (dd, 1 H, $J_{5,6'}$ 2.5 Hz, H-6′), 3.80 (ddd, 1 H, $J_{4,5}$ 9.5 Hz, H-4), 4.69 (m, 2 H, J_{gem} 7.0 Hz, CH_2OCH_3), 4.72 (br s, 1 H, H-1), 5.15 (ddd, 1 H, $J_{1,2}$ 2.0 Hz, H-2), 7.40–8.12 (m, 5 H, Ph). ^{13}C NMR ($CDCl_3$) δ: 7.88 (C-6), 30.05 (C-3), 55.18, and 55.76 (2 × OCH_3) 70.05, 70.45, 72.43 (C-2, C-4, and C-5), 95.65, 97.59 (C-1 and OCH_2OCH_3), 128.37 (Ph), 129.79 (Ph), 133.20 (Ph), 165.46 (C=O). EIMS: 405 (M-OCH_3), 309 (M-I) 233 (100%), 221. Anal. calcd. for $C_{16}H_{21}IO_6$: C 44.05, H 4.85, I 29.06; found: C 44.36, H 4.95, I 28.54.

Methyl 4-*O*-benzoyl-6-bromo-3,6-dideoxy-α-D-arabino-hexopyranoside (21)

Compound **13** (350 mg, 1.31 mmol) was dissolved in dry CCl_4 (20 mL) under argon and N-bromosuccinimide (250 mg, 1.44 mmol, 1.1 equiv.) and calcium carbonate (140 mg, 1.44 mmol, 1.1 equiv.) were added successively. The mixture was refluxed for a few minutes. The resulting orange mixture was diluted with CH_2Cl_2, washed successively with aqueous 10% $NaHSO_3$ and water, dried over $MgSO_4$, and concentrated in vacuo. Chromatography on silica gel eluting with hexane–EtOAc (7:3) gave compound **21** (447 mg, 1.29 mmol, 98%) as a gum. R_f 0.47 (hexane–EtOAc, 3:2). $[\alpha]_D^{22}$ +87.6 (c 0.59, $CHCl_3$). IR (cm^{-1}): 3462 (OH), 1720 (C=O), 1601. ^1H NMR ($CDCl_3$) δ: 2.04 (ddd, 1 H, J_{gem} 13.0, $J_{2,3a}$ 3.0, $J_{3a,4}$ 12.0 Hz, H-3a), 2.33 (ddd, 1 H, $J_{2,3e}$ 4.0, $J_{3e,4}$ 4.5 Hz, H-3e), 3.40–3.54 (m, 4 H, $J_{5,6}$ 7.5 Hz, H-6 and OCH_3), 3.58 (dd, 1 H, J_{gem} 11.0, $J_{5,6'}$ 2.5 Hz, H-6′), 3.94 (m, 1 H, $J_{1,2}$ 2.0 Hz, H-2), 4.10 (m, 1 H, H-5), 4.67 (br s, 1 H, H-1), 5.26 (ddd, 1 H, $J_{4,5}$ 10.5 Hz, H-4), 7.40–8.10 (m, 5 H, Ph). Anal. calcd. for $C_{14}H_{17}BrO_5$: C 48.71, H 4.96, Br 23.14; found: C 48.92, H 5.03, Br 22.84.

Methyl 2,6-anhydro-4-*O*-benzoyl-3-deoxy-α-D-arabino-hexopyranoside (22)

Compound **21** (370 mg, 1.07 mmol) was suspended in dry pyridine (20 mL) with AgF (227 mg, 1.78 mmol, 1.7 equiv.) and the mixture was stirred overnight in the dark without any evolution. An additional amount of AgF (200 mg, 1.57 mmol) was added and the suspension was stirred at 80°C for 4 h. The mixture was then diluted with EtOAc, filtered off through Celite, and the solvent was evaporated. Chromatography of the brown residue with hexane–EtOAc (4:1) as eluent yielded **22** (80 mg, 0.30 mmol, 28%), mp 57–58°C, and starting material (129 mg, 0.37 mmol, 36%). R_f 0.54 (hexane–EtOAc, 3:2). $[\alpha]_D^{22}$ +20.0° (c 0.24, $CHCl_3$). IR (cm^{-1}): 1715 (C=O), 1602. ^1H NMR ($CDCl_3$) δ: 2.26 (m, 1 H, H-3e), 2.45 (ddd, 1 H, J_{gem} 14.5, $J_{2,3a}$ 3.5, $J_{3a,4}$ 10.0 Hz, H-3a), 3.51 (s, 3 H, OCH_3), 3.79–3.89 (m, 2 H, 2 × H-6), 4.07 (m, 1 H, $J_{5,6}$ 10.0, $J_{4,5}$ 3.0 Hz, H-5), 4.20 (m, 1 H, H-2), 5.06 (br d, 1 H, $J_{1,2}$ 3.0 Hz, H-1), 5.10 (ddd, 1 H, $J_{3e,4}$ 2.5 Hz, H-4), 7.40–7.43 and 8.06–8.15 (m, 5H, Ph). ^{13}C NMR ($CDCl_3$) δ: 28.57 (C-3), 54.93 (OCH_3), 65.33, 65.99, 67.31, 69.00 (C-2, C-4, C-5, and C-6), 99.76 (C-1), 128.41 (Ph), 129.79 (Ph), 130.25 (Ph), 133.12 (Ph), 166.27 (C=O). EIMS: 263 (M-H), 246, 233 (M-OCH_3), 204, 175, 142,

© 2000 NRC Canada

105. Anal. calcd. for $C_{14}H_{16}O_5$: C 63.62, H 6.10; found: C 63.51, H 6.15.

Methyl 2-*O*-benzoyl-3,6-dideoxy-α-D-*threo*-hex-5-enopyranoside (23)

Silver fluoride (0.45 g, 3.59 mmol, 1.5 equiv.) was suspended in dry pyridine (25 mL) containing the iodo-derivative **16** (940 mg, 2.39 mmol). Stirring was maintained overnight, in the dark and the mixture was poured in EtOAc (200 mL). After filtration of the salts, the solvent was evaporated and the brown residue was chromatographed with hexane–EtOAc (7:3) to yield derivative **23** (332 mg, 1.25 mmol, 52%). R_f 0.27 (hexane–EtOAc, 7:3). ^{1}H NMR ($CDCl_3$) δ: 2.13 (ddd, 1 H, J_{gem} 13.5, $J_{2,3a}$ 3.0, $J_{3a,4}$ 11.0 Hz, H-3a), 2.30 (ddd, 1 H, $J_{2,3e}$ 3.5, $J_{3e,4}$ 6.0 Hz, H-3e), 3.50 (s, 3 H, OCH_3), 4.55 (m, 1 H, H-4), 4.72 (br s, 1 H, H-1), 4.80 (br s, 1 H, H-6), 4.82 (br s, 1 H, H-6′), 5.24 (m, 1 H, $J_{1,2}$ 2.5 Hz, H-2), 7.40–8.12 (m, 5 H, Ph).

Methyl 2-*O*-benzoyl-3,6-dideoxy-4-*O*-methoxymethyl-α-D-*threo*-hex-5-enopyranoside (24)

To a solution of **23** (330 mg, 1.25 mmol) in anhydrous CH_2Cl_2 (15 mL) was added successively diisopropylethylamine (0.87 mL, 5 mmol, 4 equiv.) and MOMCl (0.19 mL, 2.5 mmol, 2 equiv.). The stirring was maintained for 12 h under argon and the mixture was diluted with CH_2Cl_2. The organic layer was washed with aqueous 3 N HCl, dried over $MgSO_4$, and concentrated in vacuo. Chromatography on silica gel gave **24** (328 mg, 1.06 mmol, 85%) as a gum. R_f 0.66 (hexane–EtOAc, 7:3). $[\alpha]_D^{22}$ –24.5 (c 0.36, $CHCl_3$). IR (cm^{-1}): 1722, 1662. ^{1}H NMR ($CDCl_3$) δ: 2.20–2.29 (m, 2 H, 2 × H-3), 3.40 (s, 3 H, CH_2OCH_3), 3.50 (s, 3 H, OCH_3), 4.45 (br dd, 1 H, H-4), 4.68–4.82 (m, 5 H, H-1, 2 × H-6 and CH_2OCH_3), 5.26 (br dd, 1 H, H-2), 7.40–8.12 (m, 5 H, Ph). ^{13}C NMR ($CDCl_3$) δ: 31.59 (C-3), 55.27, and 55.60 (2 × OCH_3), 68.44, 69.99 (C-2 and C-4), 95.40, 95.45, 99.67 (C-1, OCH_2O, and C-6), 128.39 (Ph), 129.75 (Ph), 133.27 (Ph), 155.63 (C-5), 165.47 (C=O). EIMS: 277 (M-OCH_3), 247, 233, 221, 215, 105 (100%), 77.

Methyl-3,6-dideoxy-4-*O*-methoxymethyl-α-D-*threo*-hex-5-enopyranoside (25)

Ammonia was bubbled through a solution of **24** (328 mg, 1.06 mmol) in MeOH (20 mL) for 5 h. The solvent was evaporated and the residue was chromatographed on silica gel with hexane–EtOAc (7:3) to give the alcohol **25** in quantitative yield. R_f 0.18 (hexane–EtOAc, 7:3). $[\alpha]_D^{22}$ +44.6 (c 1.82, $CHCl_3$). IR (cm^{-1}): 3436, 1660. ^{1}H NMR ($CDCl_3$) δ: 1.90 (ddd, 1 H, J_{gem} 13.5, $J_{2,3}$ 8.0, $J_{3,4}$ 4.5 Hz, H-3), 2.16 (ddd, 1 H, $J_{2,3'}$ 4.0, $J_{3',4}$ 6.5 Hz, H-3′), 2.35 (br d, 1 H, OH), 3.37 (s, 3 H, CH_2OCH_3), 3.53 (s, 3 H, OCH_3), 3.94 (ddd, 1 H, H-2), 4.28 (dd, 1 H, H-4), 4.39 (d, 1 H, $J_{1,2}$ 5.5 Hz, H-1), 4.56–4.62 (m, 2 H, J_{gem} 7.0, H-6 and $CHOCH_3$), 4.70–4.76 (m, 2 H, H-6′ and $CHOCH_3$). ^{13}C NMR ($CDCl_3$) δ: 34.36 (C-3), 55.49 and 56.23 (OCH_3 and OCH_2OCH3), 66.63 (C-2), 68.92 (C-4), 94.00 (OCH_2OCH_3), 97.65 (C-6), 105.08 (C-1), 155.02 (C-5).

4-Methyl-2,4-hexadienoic acid (30)

A mixture of carbethoxymethyl triphenylphosphorane (16.36 g, 46.95 mmol, 1.2 equiv.) and (*trans*) 2-methyl-2-butenal (3.78 mL, 39.13 mmol) in dry THF (225 mL) under argon was refluxed for 24 h. The solvent was evaporated and the residue was chromatographed with hexane–EtOAc (10:0.3) to afford the expected diene (4.77 g, 30.93 mmol, 80%) as an oil. Saponification of the ester function of the latter was carried out using one equiv. of aqueous 1 N NaOH in reflux methanol. The mixture was concentrated and the residue was acidified with 3 N aqueous HCl. The expected carboxylic acid was extracted with ether and then transformed into its carboxylate sodium salt with 1 N NaOH. The aqueous layer was acidified with 3 N HCl and extracted with ether. The organic layer was dried over $MgSO_4$ and concentrated in vacuo to provide the carboxylic acid **30** (3.11 g, 24.74 mmol, 80%) which was used in the next step without further purification.

4-Methyl-3,5-hexadienoic acid (31)

A solution of lithium diisopropylamide (2.2 equiv.) in THF was prepared by the slow addition of *n*-BuLi (46.80 mmol in hexane) to a solution of diisopropylamine (6.60 mL, 46.80 mmol) in dry THF (30 mL) under N_2. The solution was cooled to –80°C and dry hexamethyl phosphoramide (8.15 mL, 46.80 mmol) was added dropwise and the mixture allowed to stir for 0.5 h. Diene **30** (3.28 g, 21.28 mmol) was added to the cooled solution over 1h. Stirring was maintained an additional hour at –80°C and the mixture was transferred into a rapidly stirred solution of acetic acid (6.5 g) in water (130 mL). The resulting solution was adjusted to pH 1 with 3 N HCl and extracted with Et_2O. The organic layer was dried over $MgSO_4$ and concentrated under reduced pressure. Chromatography on silica gel with hexane–EtOAc (9:1) as eluent yielded compound **31** (2.13 g, 13.83 mmol, 65%) as an oil. ^{1}H NMR ($CDCl_3$) δ: 1.77 (s, 3 H, CH_3), 3.24 (d, 2 H, $J_{2,3}$ 7.5 Hz, 2 × H-2), 5.03 (d, 1 H, J_{cis} 10.5 Hz, H-6), 5.18 (d, 1 H, J_{trans} 17.5 Hz, H-6′), 5.64 (t, 1 H, H-3), 6.41 (dd, 1 H, H-5), 10–11 (br s, 1 H, COOH).

Methyl-3,6-dideoxy-2-*O*-[4′-methyl-3′,5′-hexadienoyl]-4-*O*-methoxymethyl-α-D-*threo*-hex-5-enopyranoside (26)

To a solution of alcohol **25** (200 mg, 0.98 mmol) in dry CH_2Cl_2 were added successively under argon, the carboxylic acid **31** (285 mg, 2.26 mmol, 2.3 equiv.), a catalytic amount of DMAP, and DCC (300 mg, 1.5 mmol, 1.5 equiv.) in solution in CCl_4. The mixture was stirred for 1 h and the salts were filtered off. After evaporation of the solvent, the brown residue was chromatographed on silica gel eluting with hexane–EtOAc (20:1) to give compound **26** (273 mg, 0.87 mmol, 89%). R_f 0.66 (hexane–EtOAc, 7:3). $[\alpha]_D^{22}$ –9.5 (c 1.09, $CHCl_3$). ^{1}H NMR ($CDCl_3$) δ: 1.77 (s, 3 H, CH_3 vinyl), 2.06–2.14 (m, 2 H, $J_{3,4} = J_{3',4}$ 8.0, H-3 and H-3′), 3.24 (m, 2 H, H-8 and H-8′), 3.39 (s, 3 H, CH_2OCH_3), 3.45 (s, 3 H, OCH_3), 4.33 (br dd, 1 H, 4-H), 4.64 (d, 1 H, $J_{1,2}$ 2.5 Hz, H-1), 4.65–4.76 (m, 4 H, H-6, H-6′ and CH_2OCH_3), 4.97–5.05 (m, 2 H, H-2 and H-12), 5.17 (d, 1 H, $J_{11,12'}$ 17.5 Hz, H-12′), 5.65 (dd, 1 H, $J_{8,9}$ 7.0, $J_{8',9}$ 7.5 Hz, H-9), 6.40 (dd, 1 H, $J_{11,12}$ 10.5 Hz, H-11).

(4*S*, 6*S*)-4-(4′-Methyl-3′,5′-hexadienoyl)oxy-6-methoxymethoxy-cycohex-2-enone (28)

To a solution of **26** (273 mg, 0.87 mmol) in dioxane (10 mL) was added $HgSO_4$ (5 mg, 0.017 mmol, 0.02 equiv.)

© 2000 NRC Canada

and 5 mM H_2SO_4 (2.6 mL). The mixture was stirred at 50°C for 4 h. The mixture was then cooled to room temperature, diluted with CH_2Cl_2, and washed with water until neutral. The organic layer was dried over $MgSO_4$, concentrated in vacuo to afford crude **27**. To a solution of the latter in CH_2Cl_2–pyridine (10:1, 11 mL) mixture under argon at –10°C was added triflic anhydride (0.15 mL, 0.97 mmol, 1.5 equiv.). The cooled mixture was stirred for 20 min and more triflic anhydride (0.15 mL) was added. The stirring was continued for 15 min and the mixture was diluted with CH_2Cl_2, washed with aqueous saturated $NaHCO_3$ and brine. The organic layer was dried over $MgSO_4$, concentrated in vacuo, and the residue was chromatographed on silica gel eluting with hexane–EtOAc (4:1) to afford **28** (69 mg, 0.25 mmol, 30%) as a gum. R_f 0.76 (hexane–EtOAc, 3:2). $[\alpha]_D^{22}$ –239.1 (c 0.32, $CHCl_3$). ^{1}H NMR ($CDCl_3$) δ: 1.79 (s, 3 H, CH_3 vinyl), 2.31 (ddd, 1 H, J_{gem} 13.5, $J_{4,5}$ 5.5, $J_{5,6}$ 5.0 Hz, H-5), 2.45 (ddd, 1 H, $J_{4,5'}$ 4.5, $J_{5',6}$ 8.5 Hz, H-5′), 3.24 (m, 2 H, H-2′a and H-2′b), 3.39 (s, 3 H, CH_2OCH_3), 4.36 (dd, 1 H, H-6), 4.71 (d, 1 H, J_{gem} 7.0 Hz, $CHHOCH_3$), 4.80 (d, 1 H, $CHHOCH_3$), 5.03 (d, 1 H, J_{cis} 10.5 Hz, H-6a′), 5.18 (d, 1 H, J_{trans} 17.5 Hz, H-6′b), 5.58–5.73 (m, 2 H, H-4 and H-3′), 6.07 (br d, 1 H, $J_{2,3}$ 10.5 Hz, H-2), 6.40 (dd, 1 H, H-5′), 6.84 (dd, 1 H, $J_{3,4}$ 4.0 Hz, H-3). Anal. calcd. for $C_{15}H_{20}O_5$: C 64.27, H 7.19; found: C 64.15, H 7.04.

Thermal cycloaddition of **28**: A solution of enone **28** (69 mg, 0.25 mmol) and hydroquinone (10 mg, 0.09 mmol, 0.37 equiv.) in degassed toluene (10 mL) was placed in a sealed tube and heated at 135°C for 6 h, 165°C for 12 h, and 220°C for 12 h. At the end of each period of heating, the crude mixture was analyzed by ^{1}H NMR spectroscopy, but no cycloadduct compound was detected. After concentration in vacuo, the residue was chromatographed on silica gel eluting with hexane–EtOAc (85:15) to afford the starting material (20 mg, 0.075 mmol, 30%) and a more polar product resulting from the splitting of the MOM protecting group (25 mg, 0.10 mmol, 44%).

(*E*)-(4′-Methyl-3′,5′-hexadien)yl 2,3-dideoxy-4,6-di-*O*-acetyl-α-D-*erythro*-hex-2-enopyranoside (34)

To a stirred solution of tri-*O*-acetyl-D-glucal (5.71 g, 21 mmol) and homoallylic alcohol **33** (2.7 g, 24 mmol, 1.15 equiv.) in anhydrous CH_2Cl_2 (200 mL) was added under argon boron trifluoride ethyl etherate (21 drops) over a period of 3.30 h. At the end of the addition the resulting brown mixture was quenched with pyridine (1 mL) and washed successively with aqueous saturated $NaHCO_3$ and brine. The organic layer was dried over $MgSO_4$, concentrated in vacuo, and chromatographed with hexane–EtOAc (4:1) to give an unseparable mixture of α and β-glycosides (**34**) in a 4:1 ratio (5.77 g, 17.8 mmol, 84%). R_f 0.35 (hexane–EtOAc, 4:1). $[\alpha]_D^{22}$ +69.6 (c 3.0, $CHCl_3$). IR (cm^{-1}): 1744, 1643, 1606, 1234. α *anomer*: ^{1}H NMR ($CDCl_3$) δ: 1.75 (s, 3 H, CH_3 vinyl), 2.07 (s, 6 H, 2 × $COCH_3$), 2.44 (t, 1 H, *J* 7.0, H-2′a), 2.47 (dd, 1 H, *J* 7.0, H-2′b), 3.55 (ddd, 1 H, *J* 9.5 Hz, H-1′a), 3.78 (ddd, 1 H, *J* 9.5 Hz, H-1′b), 4.10 (m, 1 H, H-5), 4.17–4.30 (m, 2 H, 2 × H-6), 4.96 (d, 1 H, J_{cis} 10.5 Hz, H-6′a), 5.11 (d, 1 H, J_{trans} 17.5 Hz, H-6′b), 5.03 (br s, 1 H, H-1), 5.31 (dd, 1 H, $J_{4,5}$ 10.0, $J_{3,4}$ 1,5 Hz, H-4), 5.50 (dd, 1 H, H-3′), 5.77–5.98 (m, 2 H, H-2 and H-3), 6.37 (dd, 1 H, H-5′). ^{13}C NMR ($CDCl_3$) δ: 14.05 (CH_3 vinyl), 20.69 and 20.75 (2 × $COCH_3$), 28.78 (C-2′), 62.96 (C-6), 65.24 (C-4), 66.92 (C-5), 68.05 (C-1′), 94.37 (C-1), 111.13 (C-6′), 127.79 (C-2 or C-3), 128.18 (C-3′), 129.05 (C-2 or C-3), 135.85 (C-4′), 141.12 (C-5′), 170.21 and 170.59 (2 × $COCH_3$).

(*E*)-(4′-Methyl-3′,5′-hexadien)yl 2,3-dideoxy-α-D-*erythro*-hex-2-enopyranoside (35)

Saponification of the acetates of **34** (5.77 g, 17.8 mmol, α and β mixture (4:1)) was achieved under Zemplen procedure to give the α-anomer **35** (3.53 g, 14.7 mmol, 82%) separated from its β-anomer (0.79 g, 3.30 mmol, 18%) by column chromatography over silica gel using hexane–EtOAc (1:1) as eluent. R_f 0.18 (hexane–EtOAc, 1:1). $[\alpha]_D^{22}$ +6.1 (c 0.47, $CHCl_3$). IR (cm^{-1}): 3350, 1719, 1601. ^{1}H NMR ($CDCl_3$) δ: 1.74 (s, 3 H, CH_3 vinyl), 2.10–2.14 (m, 2 H, 2 × OH), 2.45 (m, 2 H, 2 × H-2′), 3.53 (ddd, 1 H, J_{gem} 9.5, $J = J'$ 7.0 Hz, H-1′a), 3.70 (ddd, 1 H, $J_{4,5}$ 9.0, $J_{5,6} = J_{5,6'}$ 4.5 Hz, H-5), 3.74–3.92 (m, 3 H, H-6, H-6′ and H-1′b), 4.21 (dd, 1 H, $J_{2,4}$ 1.0 Hz, H-4), 4.90–5.01 (m, 2 H, H-1 and H-6′a), 5.10 (d, 1 H, J_{trans} 17.5 Hz, H-6′b), 5.48 (dd, 1 H, *J* 7.5, *J′* 8.0 Hz, H-3′), 5.74 (ddd, 1 H, $J_{2,3}$ 10.0, $J_{3,4}$ 2.5, $J_{1,3}$ 2.0 Hz, H-3), 5.95 (br d, 1 H, $J_{1,2}$ 1.5 Hz, H-2), 6.36 (dd, 1 H, J_{cis} 11.0 Hz, H-5′). ^{13}C NMR ($CDCl_3$) δ: 11.79 (CH_3 vinyl), 28.86 (C-2′), 62.27 (C-6), 63.70 (C-4), 67.96 (C-1′), 71.52 (C-5), 94.34 (C-1), 111.26 (C-6′), 125.93 (C-3), 128.30 (C-3′), 133.41 (C-2), 135.89 (C-4′), 141.14 (C-5′).

(*E*)-(4′-Methyl-3′,5′-hexadien)yl 2,3-dideoxy-6-(2,2-dimethylpropionyl)-α-D-*erythro*-hex-2-enopyranoside (36)

To a stirred solution of diol **35** (3.5 g, 14.5 mmol) in a CH_2Cl_2–pyridine (1:1.5, 25 mL) mixture was added dropwise, under argon at –5°C pivaloyl chloride (1.79 mL, 17.4 mmol, 1.2 equiv.). The solution was stirred for 1.30 h and a further amount of pivaloyl chloride (0.35 mL, 2.9 mmol, 0.2 equiv.) was added. Stirring for 2 additional h was followed by quenching with water and extractive work-up (CH_2Cl_2). The organic layer was dried over Na_2SO_4, concentrated in vacuo, and chromatographed with hexane–EtOAc (4:1) to give the ester **36** (2.96 g, 2.13 mmol, 63%) as a gum. R_f 0.25 (hexane–EtOAc, 4:1). $[\alpha]_D^{22}$ +3.5 (c 1.09, $CHCl_3$). IR (cm^{-1}): 3455, 1733, 1713, 1600. ^{1}H NMR ($CDCl_3$) δ: 1.25 (s, 9 H, $CO(CH_3)_3$), 1.75 (s, 3 H, CH_3 vinyl), 2.45 (m, 2 H, 2 × H-2′), 3.53 (ddd, 1 H, J_{gem} 14.0, $J = J'$ 7.0 Hz, H-1′a), 3.75–3.87 (m, 2 H, H-5 and H-1′b), 3.98 (m, 1 H, $J_{4,5}$ 9.5 Hz, H-4), 4.25 (dd, 1 H, $J_{5,6}$ 2.0, J_{gem} 12.5 Hz, H-6), 4.45 (dd, 1 H, $J_{5,6'}$ 5.0, H-6′), 4.92 –5.01 (m, 2 H, H-1 and H-6′a), 5.11 (d, 1 H, J_{trans} 17.5, H-6′b), 5.48 (t, 1 H, *J* 7.0 Hz, H-3′), 5.74 (m, 1 H, $J_{2,3}$ 10.0, $J_{3,4}$ 2.5 Hz, H-3), 5.95 (m, 1 H, H-2), 6.36 (dd, 1 H, J_{cis} 11.0 Hz, H-5′).

[2*R*-[2α,6β(*E*)]] 2,2-Dimethyl-[3,6-dihydro-6-[(4′-methyl-3′,5′-hexadienyl)oxy]-3-oxo-2*H*-pyran-2-yl]methyl ester propanoic acid (38)

(*i*) PDC oxidation: Freshly prepared pyridinium dichromate (1.57 g, 4.2 mmol, 1.38 equiv.) was suspended in dry CH_2Cl_2 (1.5 mL) containing the alcohol **36** (1.0 g, 3.08 mmol). The mixture was stirred for 20 h, a further amount of PDC (300 mg, 0.80 mmol, 0.26 equiv.) was added, and stirring was still maintained for 12 h. The mixture was diluted with hexane and the salts were filtered off through Celite, washed with a mixture of CH_2Cl_2 and hexane. After concentration of

© 2000 NRC Canada

the filtrate, the residue was chromatographed on silica gel eluting with hexane–EtOAc (9:1) to give the expected ketone **38** (545 mg, 1.69 mmol, 55%) as a gum.

(*ii*) Activated MnO_2 oxidation: Freshly prepared manganese dioxide (25 g) was suspended in dry carbon tetrachloride (350 mL) containing the alcohol **36** (3.0 g, 9.25 mmol). The resulting mixture was vigorously stirred for 3 h. Filtration over a pad of Celite and evaporation of the filtrate gave a residue which was chromatographed on silica gel eluting with hexane–EtOAc (9:1) to afford **38** (2.68 g, 8.32 mmol, 90%) as a gum. *Rf* 0.51 (hexane–EtOAc, 4:1). $[\alpha]_D^{22}$ –131.6 (c 0.58, $CHCl_3$). ^{1}H NMR ($CDCl_3$) δ: 1.17 (s, 9 H, $CO(CH_3)_3$), 1.75 (s, 3 H, CH_3 vinyl), 2.48 (m, 2 H, 2 × H-2′), 3.63 (ddd, 1 H, J_{gem} 9.5, *J* 6.5, *J′* 7.0, H-1′a), 3.86 (ddd, 1 H, *J* = *J′* 7.0 Hz, H-1′b), 4.42 (dd, 1 H, J_{gem} 12.0, *J* 5.5 Hz, C*H*HOCO$(CH_3)_3$), 4.52 (dd, 1 H, *J* 2.5 Hz, CH*H*OCO$(CH_3)_3$), 4.65 (dd, 1 H, H-2), 4.96 (d, 1 H, J_{cis} 11.0 Hz, H-6′a), 5.11 (d, 1 H, J_{trans} 17.5 Hz, H-6′b), 5.25 (d, 1 H, $J_{5,6}$ 3.5 Hz, H-6), 5.46 (m, 1 H, H-3′), 6.11 (d, 1 H, $J_{4,5}$ 10.5 Hz, H-4), 6.35 (dd, 1 H, H-5′), 6.87 (dd, 1 H, H-5).

[2*R*-[2α,6β(*E*)]] [3,6-Dihydro-6-[(4′-methyl-3′,5′-hexadienyl)oxy]-3-oxo-2*H*-pyran-2-yl]methanol (39)

Compound **39** was obtained in 83% yield from diol **35** according to the above mentioned procedure. *Rf* 0.29 (hexane–EtOAc, 1:1). ^{1}H NMR ($CDCl_3$) δ: 1.75 (s, 3 H, CH_3 vinyl), 2.30 (m, 1 H, $J_{2'a,3'}$ 7.0, J_{gem} 14.0 Hz, H-2′a), 2.50 (m, 1 H, $J_{2'b,3'}$ 7.5 Hz, H-2′b), 3.63 (ddd, 1 H, J_{gem} 13.0, *J* 6.5, *J′* 7.0, H-1′a), 3.80 (ddd, 1 H, *J* = *J′* 7.0 Hz, H-1′b), 3.90 (dd, 1 H, J_{gem} 12.0, *J* 4.5 Hz, C*H*HOH), 4.52 (dd, 1 H, *J* 2.5 Hz, CH*H*OH), 4.55 (dd, 1 H, H-2), 4.96 (d, 1 H, J_{cis} 11.0 Hz, H-6′a), 5.11 (d, 1 H, J_{trans} 17.5 Hz, H-6′b), 5.25 (d, 1 H, $J_{5,6}$ 3.5 Hz, H-6), 5.36 (m, 1 H, H-3′), 6.11 (d, 1 H, $J_{4,5}$ 10.5 Hz, H-4), 6.35 (dd, 1 H, H-5′), 6.87 (dd, 1 H, H-5).

[2*R*-(2α, 3aα, 6aβ, 9aα, 9bα)] 2,2-Dimethyl-(3, 3a, 4, 6a, 7, 8, 9a, 9b-octahydro-6-methyl-3-oxo-2*H*-pyrano[4, 3, 2-*ij*][2]benzopyran-2-yl)methyl ester propanoic acid (40)

A solution of enone **38** (2.5 g, 7.76 mmol) and hydroquinone (0.14 g, 1.39 mmol, 0.18 equiv.) in degassed toluene (150 mL) was placed in a sealed tube and heated at 155°C for 14 h. The resulting mixture was then cooled to room temperature, concentrated in vacuo, and purified by column chromatography with hexane–EtOAc (9:1) to provide the single cycloadduct **40** (1.87 g, 5.82 mmol, 75%) as a gum. R_f 0.44 (hexane–EtOAc, 1:1); $[\alpha]_D^{22}$ –343.4 (c 0.29, $CHCl_3$). IR (cm^{-1}): 1730. ^{1}H NMR (400 MHz; $CDCl_3$) δ: 1.20 (br s, 9 H, $CO(CH_3)_3$), 1.42 (m, 1 H, $J_{7,6a}$ 12.0 Hz, H-7), 1.61 (s, 3 H, CH_3 vinyl), 1.94 (m, 1 H, J_{gem} 13.0 Hz, H-7′), 2.08 (m, 1 H, H-4), 1.18–2.30 (m, 2 H, H-6a and H-9b), 2.80 (m, 1 H, $J_{4,4'}$ 18.5 Hz, H-4′), 2.91 (m, 1 H, $J_{3a,\ 9b}$ 3.5 Hz, H-3a), 3.83 (ddd, 1 H, $J_{7,\ 8'}$ 5.0, $J_{7',\ 8'}$ 2.0 Hz, H-8′), 4.05 (ddd, 1 H, $J_{8,\ 8'}$ 11.5, $J_{7,\ 8}$ 11.5, $J_{7',\ 8}$ 3.5 Hz, H-8), 4.35 (m, 2 H, CH_2OCO), 4.46 (t, 1 H, *J* = *J′* 4.0 Hz, H-2), 5.31 (m, 1 H, H-5), 5.64 (d, 1 H, $J_{9a,\ 9b}$ 2.0 Hz, H-9a).

[2*R*-(2α, 3aα, 6aβ, 9aα, 9bα)] (3, 3a, 4, 6a, 7, 8, 9a, 9b-Octahydro-6-methyl-3-oxo-2*H*-pyrano[4, 3, 2-*ij*][2]benzopyran-2-yl)methanol (41)

Adduct **41** was obtained as a gum in 66% yield from ketone **39** according to the above mentioned procedure and purification on silica gel eluting with hexane–EtOAc (3:1). R_f 0.29 (hexane–EtOAc, 1:1). IR (cm^{-1}): 3424, 1720. ^{1}H NMR ($CDCl_3$) δ: 1.42 (m, 1 H, $J_{6a,7}$ 12.5 Hz, H-7), 1.61 (s, 3 H, CH_3 vinyl), 1.94 (m, 1 H, J_{gem} 13 Hz, H-7′), 2.08 (m, 1 H, H-4), 1.18–2.30 (m, 2 H, H-6a and H-9b), 2.80 (m, 1 H, J_{gem} 18.5 Hz, H-4′), 2.91 (m, 1 H, $J_{3a,9b}$ 3.5 Hz, H-3a), 3.80 (ddd, 1 H, $J_{7,8'}$ 4.5, $J_{7',8'}$ 1.5 Hz, H-8′), 4.05 (ddd, 1H, J_{gem} 11.5, $J_{7,8}$ 11.5, $J_{7',8}$ 3.5 Hz, H-8).

Compound **42** and **43**: To a suspension of $LiAlH_4$ (430 mg, 11.3 mmol, 1.45 equiv.) in dry THF (90 mL) at 0°C under argon was added dropwise **40** (2.55 g, 7.75 mmol) in THF (2 mL). After the completion of the addition, the mixture was allowed to warm-up to room temperature and the stirring was continued for 4 h. To this mixture was then added at 0°C, water (0.45 mL), 30% aqueous NaOH (1.35 mL), and water (1.35 mL). Filtration over a pad of celite and washing the cake of salts with hot THF followed by concentration and purification on silica gel gave the diastereomeric mixture of **42** and **43** in a 1.7:1 ratio (1.62 g, 6.74 mmol, 87%). An analytical sample of this mixture was purified by preparative HPLC to separate the two diastereoisomers.

[2*R*-(2α, 3α, 3aα, 6aβ, 9aα, 9bα)] 3, 3a, 4, 6a, 7, 8, 9a, 9b-Octahydro-3-hydroxy-6-methyl-2*H*-pyrano[4, 3, 2-*ij*][2]benzopyran-2-methanol (42)

R_f 0.15 (hexane–EtOAc, 3:7); mp 168°C. $[\alpha]_D^{22}$ –91.0 (c 0.10, CH_3OH). ^{1}H NMR (400 MHz; CD_3OD) δ: 1.36 (m, 1 H, $J_{6a,7}$ 12.5, $J_{7,\ 8}$ 12.5 Hz, H-7), 1.65–1.77 (m, 4 H, H-9b and CH_3 vinyl), 1.97 (m, 1 H, J_{gem} 12.5 Hz, H-7′), 2.17 (m, 1 H, J_{gem} 18.5 Hz, H-4), 2.23 (m, 1 H, H-3a), 2.50 (m, 1 H, H-4′), 3.10 (m, 1 H, H-6a), 3.69 (d, 1 H, $J_{3,\ 3a}$ 3.5 Hz, H-3), 3.72 (dd, 1 H, *J* 6.5 Hz, C*H*HOH), 3.85 (ddd, 1 H, $J_{7',\ 8'}$ 1.5, $J_{7,\ 8'}$ 4.5, J_{gem} 11.5 Hz, H-8′), 3.88 (dd, 1 H, *J′* 7.0, J_{gem} 11.5 Hz, CH*H*OH), 4.05–4.20 (m, 2 H, H-2, H-8), 5.14 (d, 1 H, $J_{9a,\ 9b}$ 2.5 Hz, H-9a), 5.43 (m, 1H, H-5).

[2*R*-(2α, 3β, 3aα, 6aβ, 9aα, 9bα)] 3, 3a, 4, 6a, 7, 8, 9a, 9b-Octahydro-3-hydroxy-6-methyl-2*H*-pyrano[4, 3, 2-*ij*][2]benzopyran-2-methanol (43)

R_f 0.21 (hexane–EtOAc, 3:7); mp 128°C. $[\alpha]_D^{22}$ –6.3 (c 0.11, CH_3OH). ^{1}H NMR (CD_3OD) δ: 1.33 (m, 1 H, $J_{6a,7}$ 12.5, $J_{7,8}$ 12.5 Hz, H-7), 1.65 (s, 3 H, CH_3 vinyl), 1.77 (ddd, 1 H, $J_{9a,9b}$ 2.0, $J_{6a,9b}$ 11.5, $J_{3a,9b}$ 4.0 Hz, H-9b), 1.91 (m, 1 H, J_{gem} 12.5 Hz, H-7′), 2.02 (m, 1 H, H-3a), 2.13 (m, 1 H, H-4), 2.30 (m, 1 H, $J_{4,4'}$ 18.0 Hz, H-4′), 2.58 (m, 1 H, H-6a), 3.76 (ddd, 1 H, $J_{7',8'}$ 1.5, $J_{7,8'}$ 4.0, J_{gem} 11.5 Hz, H-8′), 3.81 (dd, 1 H, J_{gem} 10.5 Hz, C*H*HOH), 3.85–4.05 (m, 3 H, H-3, CH*H*OH and H-8), 4.15 (ddd, 1 H, *J* 3.5, *J′* 9.0, $J_{2,3}$ 6.0 Hz, H-2), 5.07 (d, 1 H, $J_{9a,9b}$ 2.0 Hz, H-9a), 5.21 (m, 1 H, H-5). Anal. calcd. for $C_{13}H_{20}O_4$: C 64.98, H 8.39; found: C 64.94, H 8.51.

Compounds **44** and **45**: To a solution of diols **42** and **43** (2.82 g, 11.7 mmol) in dry pyridine (120 mL) was added dropwise at 0°C under argon methanesulfonyl chloride (1.81 mL, 23.4 mmol, 1.2 equiv.). After the completion of the addition, the mixture was stirred for 5 h at room temperature, pyridine was removed in vacuo, and the resulting residue was diluted with methylene chloride. The solution was washed successively with 3 N aqueous HCl, water, 3 N aqueous NaOH, and water. The organic layer was dried over

© 2000 NRC Canada

Na_2SO_4 and concentrated in vacuo. Purification by column chromatography on silica gel gave the mesylates **44** (2.22 g, 7.02 mmol, 60%) as a solid and **45** (1.31 g, 4.09 mmol, 35%) as a foam.

[2*R*-(2α, 3α, 3aα, 6aβ, 9aα, 9bα)] 3, 3a, 4, 6a, 7, 8, 9a, 9b-Octahydro-3-hydroxy-6-methyl-2*H*-pyrano[4, 3, 2-*ij*][2]benzopyran-2-methanol α-methanesulfonate (44)

R_f 0.75 (EtOAc); mp 138°C. $[\alpha]_D^{22}$ –100.0 (c 0.11, $CHCl_3$). IR (KBr) (cm^{-1}): 3450, 1730, 1637. ^1H NMR ($CDCl_3$) δ: 1.35 (m, 1 H, $J_{6a,7}$ 12.5, $J_{7,8}$ 12.5, $J_{7,8'}$ 4.5 Hz, H-7), 1.67 (s, 3 H, CH_3 vinyl), 1.73 (ddd, 1 H, $J_{6a,9b}$ 11.0, $J_{3a,9b}$ 4.5 Hz, H-9b), 1.90 (m, 1 H, J_{gem} 12.5, $J_{6a,7'}$ 4.0 Hz, H-7′), 2.0–2.2 (m, 2 H, H-3a and H-4), 2.22 (d, 1 H, $J_{3,OH}$ 2.0 Hz, OH), 2.54 (m, 1 H, J_{gem} 19.0 Hz, H-4′), 3.00 (m, 1 H, H-6a), 3.10 (s, 3 H, $CH_2OSO_2CH_3$), 3.71 (br d, 1 H, $J_{3,3a}$ 3.5 Hz, H-3), 3.86 (ddd, 1 H, $J_{7',8'}$ 2.0, $J_{7,8'}$ 4.0 Hz, H-8′), 4.06 (ddd, 1 H, J_{gem} 11.5, $J_{7',8}$ 2.5, $J_{7,8}$ 13.0 Hz, H-8), 4.28 (dd, 1 H, *J* 5.0 Hz, C*H*$HOSO_2CH_3$), 4.40 (dd, 1 H, H-2), 4.51 (dd, 1 H, *J* 7.5, J_{gem} 10.0 Hz, CH*H*OSO_2CH_3), 5.10 (d, 1 H, $J_{9a,9b}$ 2.5 Hz, H-9a), 5.50 (m, 1 H, H-5). Anal. calcd. for $C_{14}H_{22}O_6S$: C 52.81, H 6.96 ; found: C 52.70, H 6.89.

[2*R*-(2α, 3β, 3aα, 6aβ, 9aα, 9bα)] 3, 3a, 4, 6a, 7, 8, 9a, 9b-Octahydro-3-hydroxy-6-methyl-2*H*-pyrano[4, 3, 2-*ij*][2]benzopyran-2-methanol α-methanesulfonate (45)

R_f 0.82 (EtOAc). $[\alpha]_D^{22}$ –17.2 (c 0.25, $CHCl_3$). ^1H NMR ($CDCl_3$) δ: 1.38 (m, 1 H, $J_{6a,7}$ 12.5, J_{gem} 12.5, H-7), 1.66 (s, 3 H, CH_3 vinyl), 1.84 (ddd, 1 H, $J_{6a,9b}$ 11.0, $J_{3a,9b}$ 4.5 Hz, H-9b), 1.89 (m, 1 H, H-7′), 1.92–2.28 (m, 3 H, H-3a, H-4 and H-4′), 2.51 (m, 1 H, H-6a), 3.11 (s, 3 H, $CH_2OSO_2CH_3$), 3.82 (ddd, 1 H, $J_{7',8'}$ 1.5, $J_{7,8'}$ 4.5, H-8′), 3.97 (ddd, 1 H, J_{gem} 11.5, $J_{7',8}$ 2.5, $J_{7,8}$ 12.5 Hz, H-8), 4.04 (dd, 1 H, $J_{3,3a}$ 11.5 Hz, H-3), 4.44 (ddd, 1 H, $J_{2,3}$ 6.5 Hz, H-2), 4.57 (dd, 1 H, *J* 3.0 Hz, C*H*$HOSO_2CH_3$), 4.74 (dd, 1 H, *J* 8.5, J_{gem} 11.5 Hz, CH*H*OSO_2CH_3), 5.24 (d, 1 H, $J_{9a,9b}$ 2.0 Hz, H-9a), 5.33 (m, 1 H, H-5).

[2*S*-(2α, 3α, 3aα, 6aβ, 9aα, 9bα)] 3, 3a, 4, 6a, 7, 8, 9a, 9b-Octahydro-2-(iodomethyl)-6-methyl-2*H*-pyrano[4, 3, 2-*ij*][2]benzopyran-3-ol (46)

To a solution of **44** (770 mg, 2.41 mmol) in butanone (100 mL) was added sodium iodide (10 g, 66.7 mmol, 27 equiv.) and the mixture was stirred at reflux for 36 h. Butanone was evaporated, the residue was diluted with CH_2Cl_2 and washed successively with water, 3 N aqueous NaOH, and brine. The organic layer was dried over Na_2SO_4 and concentrated in vacuo. The residue was chromatographed on silica gel to give **46** (506 mg, 1.44 mmol, 60%) as a white solid; mp 137–138°C. R_f 0.72 (hexane–EtOAc, 1:1). $[\alpha]_D^{22}$ –76.0 (c 0.25, $CHCl_3$). ^1H NMR ($CDCl_3$) δ: 1.34 (m, 1 H, $J_{6a,7}$ 12.5, J_{gem} 12.5 Hz, H-7), 1.62–1.73 (m, 4 H, H-9b and CH_3 vinyl), 1.89 (m, 1 H, H-7′), 1.58 (m, 1 H, OH), 2.00–2.20 (m, 2 H, H-3a and H-4), 2.55 (m, 1 H, H-4′), 2.98 (m, 1 H, H-6a), 3.22 (dd, 1 H, *J* 8.5 Hz, C*H*HI), 3.42 (dd, 1 H, *J* 7.0, J_{gem} 10.5, CH*H*I), 3.87 (ddd, 1 H, $J_{7',8'}$ 1.5, $J_{7,8'}$ 4.0, J_{gem} 11.5 Hz, H-8′), 3.94 (d, 1 H, $J_{3,3a}$ 3.5 Hz, H-3), 4.08 (ddd, 1 H, $J_{7,8}$ 12.5, $J_{7',8}$ 2.5 Hz, H-8), 4.32 (dd, 1 H, H-2), 5.01 (d, 1 H, $J_{9a,9b}$ 2.5 Hz, H-9a), 5.43 (1 m, 1 H, H-5). Anal. calcd. for $C_{13}H_{19}O_3I$: C 44.58, H 5.46, I 36.23; found: C 44.39, H 5.41, I 35.53.

[2*S*-(2α, 3β, 3aα, 6aβ, 9aα, 9bα)] 3, 3a, 4, 6a, 7, 8, 9a, 9b-Octahydro-2-(iodomethyl)-6-methyl-2*H*-pyrano[4, 3, 2-*ij*][2]benzopyran-3-ol (47)

Compound **47** was prepared from **45** (1.59 g, 5.0 mmol) according to the above mentioned procedure (1.44 g, 4.1 mmol, 82%); mp 152–153°C. R_f 0.73 (hexane–EtOAc, 1:1). $[\alpha]_D^{22}$ +9.7 (c 0.41, $CHCl_3$). ^1H NMR (CD_3OD) δ: 1.41 (m, 1 H, $J_{6a,7}$ 12.5, $J_{7,8}$ 12.5 Hz, H-7), 1.73 (s, 3 H, CH_3 vinyl), 1.86 (ddd, 1 H, $J_{6a,9b}$ 11.5, $J_{3a,9b}$ 4.5 Hz, H-9b), 2.01 (m, 1 H, J_{gem} 12.5 Hz, H-7′), 2.05–2.50 (m, 3 H, H-3a, H-4 and H-4′), 2.66 (m, 1 H, H-6a), 3.66 (dd, 1 H, *J* 4.0 Hz, C*H*HI), 3.76 (dd, 1 H, *J* 11.5, J_{gem} 11.5 Hz, CH*H*I), 3.86 (ddd, 1 H, $J_{7',8'}$ 1.5, $J_{7,8'}$ 4.5 Hz, H-8′), 3.91 (dd, 1 H, $J_{3,3a}$ 12.5, $J_{2,3}$ 6.5 Hz, 4-H), 4.06 (ddd, 1 H, J_{gem} 11.5, $J_{7',8}$ 2.5 Hz, H-8), 4.27 (ddd, 1 H, H-2), 5.11 (d, 1 H, $J_{9a,9b}$ 2.0 Hz, H-9a), 5.44 (m, 1 H, H-5). Anal. calcd. for $C_{13}H_{19}O_3I$: C 44.59, H 5.47, I 36.24; found: C 44.67, H 5.50, I 36.31.

[2*S*-(2α, 3β, 3aα, 6aβ, 9aα, 9bα)] 3, 3a, 4, 6a, 7, 8, 9a, 9b-Octahydro-2-(iodomethyl)-3-(methoxymethoxy)-6-methyl-2*H*-pyrano[4, 3, 2-*ij*][2]benzopyran (49)

To a solution of compound **47** (686 mg, 1.96 mmol) in dry CH_2Cl_2 (20 mL) was added dropwise at room temperature diisopropylethylamine (3.41 mL, 19.6 mmol, 10 equiv.) and chloromethylmethyl ether (1.2 mL, 15.7 mmol, 8 equiv.). The solution was stirred at 55°C for 12 h and further amounts of diisopropylethylamine (3.40 mL) and chloromethylmethyl ether (1.2 mL) were added. Stirring was maintained for 24 h and the solvents were evaporated. The residue was washed with water, 1 N aqueous HCl and brine. The organic layer was dried over $MgSO_4$ and concentrated in vacuo. Chromatography on silica gel eluting with hexane–EtOAc (20:1.5) afforded compound **49** (481 mg, 1.21 mmol, 62%). R_f 0.63 (hexane–EtOAc, 7:3). $[\alpha]_D^{22}$ +10.3 (c 1.76, $CHCl_3$). ^1H NMR ($CDCl_3$) δ: 1.36 (m, 1 H, $J_{6a,7}$ 12.5, $J_{7,8}$ 12.5 Hz, H-7), 1.64 (s, 3 H, CH_3 vinyl), 1.81 (ddd, 1 H, $J_{6a,9b}$ 11.0, $J_{3a,9b}$ 3.5 Hz, H-9b), 1.87 (m, 1 H, J_{gem} 12.5 Hz, H-7′), 2.00–2.20 (m, 3 H, H-3a, H-4 and H-4′), 2.55 (m, 1 H, H-6a), 3.39 (3 H, s, CH_2OCH_3), 3.45–3.60 (m, 2 H, CH_2I), 3.75 (dd, 1 H, $J_{3,3a}$ 11.5, $J_{2,3}$ 6.0 Hz, H-3), 3.81 (ddd, 1 H, $J_{7',8'}$ 1.5, $J_{7,8'}$ 4.0 Hz, H-8′), 4.00 (ddd, 1 H, J_{gem} 11.5, $J_{7',8}$ 2.5 Hz, H-8), 4.38 (m, 1 H, H-2), 4.50–4.70 (m, 2 H, CH_2OCH_3), 4.97 (d, 1 H, $J_{9a,9b}$ 2.0 Hz, H-9a), 5.30 (m, 1 H, H-5).

[3*R*-(3α, 3aα, 6aβ, 9aα, 9bα)] 3, 3a, 4, 6a, 7, 8, 9a, 9b-Octahydro-3-(methoxymethoxy)-6-methyl-2-methylene-2*H*-pyrano[4, 3, 2-*ij*][2]benzopyran (51)

To a solution of compound **49** (481 mg, 1.22 mmol) in dry pyridine (60 mL) was added AgF (450 mg, 3.5 mmol, 2.90 equiv.) and the resulting mixture was stirred at 85°C for 1 h in the dark and then poured into EtOAc (200 mL). After filtration of the salts, solvents were evaporated and the brown residue was chromatographed on silica gel eluting with hexane–EtOAc (9:1) to give compound **51** (284 mg, 1.06 mmol, 87%). R_f 0.71 (hexane–EtOAc, 7:3). $[\alpha]_D^{22}$ +54.1 (c 0.61, $CHCl_3$). ^1H NMR ($CDCl_3$) δ 1.42 (m, 1 H, H-7), 1.65 (s, 3 H, CH_3 vinyl), 1.80–2.35 (m, 5 H, $J_{6a,9b}$ 11.0 Hz, H-3a, H-4, H-4′, H-7′ and H-9b), 2.54 (m, 1 H, H-6a), 3.41 (s, 3 H, CH_2OCH_3), 3.88 (1 H, ddd, $J_{7',8'}$ 1.5, $J_{7,8'}$ 4.0, J_{gem} 11.5 Hz, H-8′), 3.92–4.07 (m, 2 H, $J_{7',8}$ 2.5, $J_{7,8}$

© 2000 NRC Canada

12.5, $J_{3,3a}$ 10.5 Hz, H-3 and H-8), 4.56 (d, 1 H, J_{gem} 1.0 Hz, C=C*H*H), 4.65 (d, 1 H, J_{gem} 7.0 Hz C*H*HOCH$_3$), 4.72 (d, 1 H, C=CH*H*), 4.74 (d, 1 H, CH*H*OCH$_3$), 5.01 (d, 1 H, $J_{9a,9b}$ 2.0 Hz, H-9a), 5.36 (m, 1 H, H-5). Anal. calcd. for $C_{15}H_{22}O_4$: C 67.65, H 8.33; found: C 67.74, H 8.43.

[3*S*-(3α, 3aβ, 6aα, 9aβ, 9bβ)] 3, 3a, 4, 6a, 7, 8, 9a, 9b-Octahydro-3-(methoxy methoxy)- 6-methyl-2-methylene-2*H*-pyrano[4, 3, 2-*ij*][2]benzopyran (50)

Compound **50** was prepared from **48** (154 mg, 0.39 mmol) according to the above mentioned procedure (75 mg, 0.28 mmol, 72%); mp 60°C. R_f 0.69 (hexane–EtOAc, 7:3). $[\alpha]_D^{22}$ –113.1 (c 0.32, $CHCl_3$). ^{1}H, NMR ($CDCl_3$) δ: 1.38 (m, 1 H, $J_{6a,7}$ 12.5, J_{gem} 12.5 Hz, H-7), 1.66 (s, 3 H, CH_3 vinyl), 1.70 (ddd, 1 H, $J_{6a,9b}$ 11.5, $J_{3a,9b}$ 4.5 Hz, H-9b), 1,89 (m, 1 H, $J_{6a,7'}$ 5.0 Hz, H-7′), 2.08 (m, 1 H, H-4), 2.15 (m, 1 H, H-3a), 2.40 (m, 1 H, H-4′), 2.95 (m, 1H, H-6a), 3.34 (s, 3 H, CH_2OCH_3), 3.86–3.96 (m, 2 H, $J_{3,3a}$ 4.5, $J_{7',8'}$ 1.5, $J_{7,8'}$ 4.0 Hz, H-3 and, H-8′), 4.06 (ddd, 1 H, J_{gem} 12.0, $J_{7',8}$ 2.5, $J_{7,8}$ 11.5 Hz, H-8), 4.45 (s, 1 H, C=C*H*H), 4.47 (d, 1 H, J_{gem} 6.5 Hz, CH*H*OCH$_3$), 4.75 (d, 1 H, CH*H*OCH$_3$), 4.78 (s, 1 H, C=CH*H*), 4.93 (d, 1 H, $J_{9a,9b}$ 2.5 Hz, H-9a), 5.35 (m, 1 H, H-5). Anal. calcd. for $C_{15}H_{22}O_4$: C 67.65, H 8.33; found: C 67.85, H 8.40.

*Ferrier carbocyclization of **50** using Lukacs method*

Compound **50** (100 mg, 0.37 mmol) was dissolved in 1,4-dioxane (10 mL) and $HgSO_4$ (6 mg, 0.02 mmol, 0.05 equiv.) and 5 mM aqueous H_2SO_4 (1.1 mL) were added successively. This mixture was then heated at 50°C for 1 h. At the end of this period TLC (hexane–EtOAc, 7:3) showed no more starting material and the formation of three products. The mixture was cooled to room temperature and diluted with CH_2Cl_2 (100 mL). The organic layer was washed with water and brine, dried over Na_2SO_4, and concentrated in vacuo. The residue was chromatographed on silica gel eluting with hexane–EtOAc (1:4) to give **52** (11.5 mg, 0.04 mmol, 12%), **54** (12 mg, 0.04 mmol, 12%), and **56** (76 mg, 0.26 mmol, 71%).

[1S-(1α,4aα,4aβ,5β,8aβ)] 3,4,4a,5,8,8a-Hexahydro-4-hydroxy-5-(2-hydroxyethyl)-1-(methoxymethoxy)-6-methyl-2(1*H*)-naphtalenone (52) (see numbering in Scheme 5)

R_f 0.49 (CH_2Cl_2–MeOH, 9:1). $[\alpha]_D^{22}$ + 4.6° (c 0.21, $CHCl_3$). ^{1}H NMR ($CDCl_3$) δ: 1.35–1.65 (m, 2 H, H-8 and C*H*HCH$_2$OH), 1.72 (s, 3 H, CH_3 vinyl), 1.94 (m, 1 H, J_{gem} 14.0 Hz, CH*H*CH$_2$OH), 2.06 (m, 1 H, $J_{4a,5}$ 10.5 Hz, H-4a), 2.14 (m, 1 H, J_{gem}.18.5 Hz, H-8′), 2.40–2.60 (m, 3-H, H-2, H-5 and H-8a), 2.80 (dd, 1 H, $J_{3',4}$ 5.5, J_{gem} 13.5 Hz, H-3′), 3.39 (s, 3 H, CH_2OCH_3), 3.74–3.87 (m, 3 H, H-4 and CH_2CH_2OH), 4.40 (d, 1 H, $J_{1,8a}$ 5.5 Hz, H-1), 4.71 (d, 1 H, J_{gem} 6.5 Hz, C*H*HOCH$_3$), 4.92 (d, 1 H, CH*H*OCH$_3$), 5.35 (m, 1 H, H-7). Anal. calcd. for $C_{15}H_{24}O_5$: C 63.36, H 8.51; found: C 63.12, H 8.47.

[1S-(1α,4β,4aβ,5β,8aβ)] 3,4,4a,5,8,8a-Hexahydro-4-hydroxy-5-(2-hydroxyethyl)-1-(methoxymethoxy)-6-methyl-2(1*H*)-naphtalenone (54)

R_f 0.47 (CH_2Cl_2–MeOH, 9:1). $[\alpha]_D^{22}$ + 20.2° (c 0.45, $CHCl_3$). ^{1}H NMR (400 MHz, C_6D_6) δ: 1.22 (m, 1 H, C*H*HCH$_2$OH), 1.50 (s, 3 H, CH_3 vinyl), 1.59 (m, 1 H, J_{gem} 14.3 Hz, CH*H*CH$_2$OH), 1.84 (m, 1 H, H-4a), 1.90 (m, 1H, $J_{4a,5}$ 9.5 Hz, H-5), 1.96 (dd, 1 H, J_{gem} 14.0, $J_{3,4}$ 3.9 Hz, H-3), 2.20–2.41 (m, 2 H, H-8 and H-8′), 2.50–2.64 (m, 2 H, $J_{3',4}$ 2.5 Hz, H-3′ and H-8a), 3.27 (s, 3 H, CH_2OCH_3), 3.31 (m, 2 H, CH_2CH_2OH), 3.93 (m, 1 H, H-4), 4.31 (d, 1 H, $J_{1,8a}$ 6.2 Hz, H-1), 4.71 (d, 1 H, J_{gem} 6.7 Hz, C*H*HOCH$_3$), 4.92 (d, 1 H, CH*H*OCH$_3$), 5.32 (m, 1 H, H-7). Anal. calcd. for $C_{15}H_{24}O_5$: C 63.36, H 8.51; found: C 64.01, H 8.50.

[2*S*-(2α, 3α, 3aα, 6aβ, 9aα, 9bα)]- and [2*R*-(2α, 3β, 3aβ, 6aα, 9aβ, 9bβ)]-3, 3a, 4, 6a, 7, 8, 9a, 9b-Octahydro-3-(methoxymethoxy)-2,6-dimethyl-2*H*-pyrano[4, 3, 2-*ij*][2]benzopyran-2-ol (56)

C-2 epimers mixture (1:1):. mp 92°C. R_f 0.15 (hexane–EtOAc, 7:3). $[\alpha]_D^{22}$ of the mixture –73.7° (c 1.23, $CHCl_3$). Anal. calcd. for $C_{15}H_{24}O_5$: C 63.36, H 8.51; found: C 63.95, H 8.42.

*Ferrier carbocyclization of **51** using Lukacs methodology*

Using the above mentioned procedure, compound **51** (100 mg, 0.37 mmol) was converted into cyclohexanones **53** and **55** and the hydration product **57** (1:1:2) in 84% overall yield.

[1R-(1α,4α,4aα,5α,8aα)] 3,4,4a,5,8,8a-Hexahydro-4-hydroxy-5-(2-hydroxyethyl)-1-(methoxymethoxy)-6-methyl-2(1*H*)-naphtalenone (53)

R_f 0.51 (CH_2Cl_2–MeOH, 9:1); mp 91°C. $[\alpha]_D^{22}$ +33.6° (c 0.12, $CHCl_3$). IR (cm^{-1}): 3416, 1711, 1661. ^{1}H NMR (400 MHz, C_6D_6) δ: 1.44 (m, 1 H, C*H*HCH$_2$OH), 1.58 (m, 1 H, H-8), 1.71 (m, 1 H, H-8′), 1.73 (s, 3 H, CH_3 vinyl), 1.83 (m, 1 H, CH*H*CH2OH), 2.38 (m, 2 H, H-4a and H-8a), 2.54 (m, 1 H, H-5), 2.61 (dd, 1 H, $J_{3,4}$ 4.8 Hz, H-3), 2.93 (dd, 1 H, $J_{3',4}$ 10.2, J_{gem} 12.7 Hz, H-3′), 3.19 (s, 3 H, CH_2OCH_3), 3.54 (ddd, 1 H, $J_{4,4a}$ 9.0 Hz, H-4), 3.61 (m, 1 H, CH_2CHHOH), 3.70 (m, 1 H, CH2CH*H*OH), 3.78 (d, 1 H, $J_{1,8a}$ 3.0 Hz, H-1), 4.50 (d, 1 H, J_{gem} 6.7 Hz, CH*H*OCH$_3$), 4.60 (d, 1 H, CH*H*OCH$_3$), 5.22 (m, 1 H, H-7). ^{1}H NMR (400 MHz, DMSO)δ 1.47 (m, 1 H, C*H*HCH$_2$OH), 1.52–1.75 (m, 5 H, CH_3, H-8 and CH*H*CH$_2$OH), 1.87 (m, 1 H, H-8′), 2.01 (ddd, 1 H, $J_{4,4a}$ 7.6, $J_{4a,8a}$ 4.0, $J_{4a,5}$ 4.0 Hz, H-4a), 2.29 (m, 2 H, H-5 and H-8a), 2,54 (m, 2 H, $J_{3,4}$ 8.0, $J_{3',4}$ 4.0 Hz, H-3 and H-3′), 3.25 (s, 3 H, CH_2OCH_3), 3.44 (m, 2 H, CH_2CH_2OH), 3.64 (m, 1 H, H-4), 3.68 (d, 1 H, $J_{1,8a}$ 5.9 Hz, H-1), 4.42 (t, 1 H, $J = J'$ 4.9 Hz, CH_2CH_2OH), 4.58 (m, 2 H, J_{gem} 6.7 Hz, CH_2OCH_3), 4.98 (d, 1 H, $J_{4,OH}$ 5.3 Hz, OH), 5.26 (m, 1 H, H-7). Anal. calcd. for $C_{15}H_{24}O_5$: C 63.36, H 8.51; found: C 63.62, H 8.42.

[1R-(1α,4β,4aα,5α,8aα)] 3,4,4a,5,8,8a-Hexahydro-4-hydroxy-5-(2-hydroxyethyl)-1-(methoxymethoxy)-6-methyl-2(1*H*)-naphtalenone (55)

R_f 0.54 (CH_2Cl_2–MeOH, 9:1). $[\alpha]_D^{22}$ +40.3° (c 0.33, $CHCl_3$). ^{1}H NMR ($CDCl_3$) 1.68–1.84 (m, 3 H, C*H*HCH$_2$OH, CH_3 vinyl), 1.92 (m, 1 H, CH*H*CH$_2$OH), 2.03–2.14 (m, 2 H, H-8 and H-8′), 2.20–2.34 (m, 2 H, H-5 and H-8a), 2.48 (ddd, 1 H, $J_{4,4a}$ 3.0, $J_{4a,8a}$ 5.0, $J_{4a,5}$ 6.0 Hz, H-4a), 2.57 (dd, 1 H, $J_{3,4}$ 6.5 Hz, H-3), 2.92 (dd, 1 H, J_{gem} 14.0, $J_{3',4}$ 4.5 Hz, H-3′), 3.35 (s, 3 H, CH_2OCH_3), 3.72–3.83 (m, 2 H, CH_2CH_2OH), 3.88 (d, 1 H, $J_{1,8a}$ 6.5 Hz, H-1), 4.26 (ddd, 1

© 2000 NRC Canada

H, H-4), 4.63 (d, 1 H, J_{gem} 13.5 Hz, C*H*HOCH$_3$), 4.66 (d, 1 H, CH*H*OCH$_3$), 5.49 (m, 1 H, H-7).

[2*S*-(2α, 3α, 3aα, 6aβ, 9aα, 9bα)] and [2*R*-(2α, 3β, 3aβ, 6aα, 9aβ, 9bβ)] 3, 3a, 4, 6a, 7, 8, 9a, 9b-Octahydro-3-(methoxymethoxy)-2,6-dimethyl-2*H*-pyrano[4, 3, 2-*ij*][2]benzopyran-2-ol (57)

C-2 epimers mixture (7:1): R_f 0.17 (hexane–EtOAc, 7:3). $[\alpha]_D^{22}$ +3.8 (c 0.28, $CHCl_3$). Major isomer: ^{1}H NMR ($CDCl_3$) δ: 1.36 (m, 1 H, $J_{7,8}$ 12.5, $J_{7,8'}$ 4.5, J_{gem} 12.5 Hz, H-7), 1.51 (s, 3 H, CH_3 vinyl), 1.64 (s, 3 H, C(OH)C*H*$_3$), 1.80 (ddd, 1 H, $J_{6a,9b}$ 11.5, $J_{9a,9b}$ 3.5, $J_{3a,9b}$ 4.0 Hz, H-9b), 1.86 (m, 1 H, H-7′), 2.13–2.34 (m, 3 H, H-3a, H-4 and H-4′), 2.42 (m, 1 H, H-6a), 2.71 (s, 1 H, OH), 3.40 (d, 1 H, $J_{3,3a}$ 10.5 Hz, H-3), 3.42 (s, 3 H, CH_2OCH_3), 3.83 (ddd, 1 H, $J_{7',8'}$ 1.5, $J_{7,8'}$ 5.0, J_{gem} 11.5 Hz, H-8′), 3.95 (ddd, 1 H, $J_{7',8}$ 2.5 Hz, H-8), 4.67 (d, 1 H, J_{gem} 7.0 Hz, C*H*HOCH$_3$), 4.73 (d, 1 H, CH*H*OCH$_3$), 5.30–5.40 (m, 2 H, H-5 and H-9a). ^{13}C NMR ($CDCl_3$) δ: 20.04 (C(OH)*C*H3), 25.09 (C-4), 27.30 (*C*H$_3$ vinyl), 29.09 (C-*7*), 30.65 (C-6a), 32.32 (C-3a), 41.72 (C-9b), 56.42 (CH_2OCH_3), 63.22 (C-8), 79.49 (C-3), 93.03 (C-9a), 98.13 (C-2 or C-6), 98.91 (*C*H$_2$OCH$_3$), 120.18 (C-5), 133.96 (C-2 or C-6).

*Ferrier carbocyclization of **51** using a stoichiometric amount of mercuric acetate*

To a solution of **51** (78 mg, 0.29 mmol) in a mixture of acetone (12 mL) and water (5 mL) was added $Hg(OAc)_2$ (160 mg, 0.52 mmol, 1.8 equiv.) and acetic acid (0.17 mL). The mixture was stirred at reflux for 12 h, solvents were evaporated under reduced pressure, and the residue was taken up with CH_2Cl_2. The organic layer was washed with saturated aqueous $NaHCO_3$, water, dried over $MgSO_4$, and concentrated in vacuo. Column chromatography on silica gel eluting with hexane–EtOAc afforded the cyclohexanones **53** (23 mg, 0.08 mmol, 28%) and **55** (9 mg, 0.03 mmol, 11%) and the hydration product **57** (14.5 mg, 0.05 mmol, 18%) [**53**:**55**:**57** (2.5:1:1.7)].

Conclusions

This work allowed the preparation of the bicyclic structures **55** and **54** which can be regarded as key compounds for the synthesis of the hexahydro-naphthalene ring of mevinic acids such as pravastatin and mevinolin, the keto group at C-1 being amenable to reduction or Wittig methylenation. This strategy is applicable for the synthesis of other complex decalinic structures present in a number of natural products. The IMDA reaction of cyclohexenone as the dienophile failed likely because of the ester link used in the tether. Other links like mixed acetals should be devised. This type of link was efficient in the IMDA of a sugar enone to provide bis-annulated pyranosides. However it is worth noting that the Ferrier carbocyclization on these bis-annulated pyranosides is less efficient than in the pyranoside series in terms of stereoselectivity and of yield. But one interesting consequence of this limitation was also the direct carbocyclization of **57** without mercury catalysis. It is likely that direct hydration of the double bond of **51** or **50** followed by base-catalyzed carbocyclization would be a good alternative and a good improvement of our synthetic sequence.

References

1. Y. Chapleur. The chemistry and total synthesis of mevinic acids. *In* Recent progress in the chemistry of antibiotics. Vol. 2. *Edited by* G. Lucaks and S. Ueno. Springer, New York. 1993. pp. 829–937.
2. M.I. Colombo, J. Zinezuk, and E.A. Ruveda. Tetrahedron, **48**, 963 (1992).
3. E. Ciganek. Org. React. (N.Y.) **32**, 1 (1984).
4. W.R. Roush. Intramolecular Diels–Alder reactions. *In* Comprehensive organic synthesis. Vol. 5. *Edited by* B.M. Trost and I. Fleming. Pergamon Press, Oxford. 1991. p. 513.
5. D. Craig. Chem. Soc. Rev. **16**, 187 (1987).
6. A.G. Fallis. Acc. Chem. Res. **32**, 464 (1999).
7. (*a*) E.A. Deutsch and B.B. Snider. J. Org. Chem. **47**, 2682 (1982); (*b*) G.E. Keck and D.F. Kachensky. J. Org. Chem. **51**, 2487 (1986); (*c*) K. Narasaka, M. Saito, and N. Iwasawa. Tetrahedron: Assymmetry. **2**, 1305 (1991); (*d*) S. Hanessian, P.J. Roy, M. Petrini, P.J. Hodges, R. Di Fabio, and G. Garganico. J. Org. Chem. **55**, 5766 (1990); (*e*) R.L. Funk and W.E. Zeller. J. Org. Chem. **47**, 180 (1982); (*f*) P.A. Grieco, R. Lis, R.E. Zelle, and J. Finn. J. Am. Chem. Soc. **108**, 5908 (1986); (*g*) A.H. Davidson, A.J. Jones, C.D. Floyd, C. Lewis, and P.L. Meyers. J. Chem. Soc. Chem. Commun. 1786 (1987); (*h*) J.S. Prasad, D.L.J. Clive, and G.V.J. da Silva. J. Org. Chem. **51**, 2717 (1986).
8. (*a*) R.M. Giuliano. Cycloaddition reactions in carbohydrate chemistry — an overview. Cycloaddition reactions in carbohydrate chemistry. Vol. 494. 1992. pp. 1–23; (*b*) J.C. Lopez, A.M. Gomez, and B. Fraser-Reid. J. Chem. Soc. Chem. Commun. 762 (1993); (*c*) R.V. Bonnert and P. Jenkins. J. Chem. Soc. Perkin Trans. 1, 413 (1989); (*d*) R.M. Giuliano, A.D. Jordan, A.D. Gauthier, and K. Hoogsteen. J. Org. Chem. **58**, 4979 (1993); (*e*) A.A. Ghini, C. Burnouf, J.C. Lopez, A. Olesker, and G. Lukacs. Tetrahedron Lett. **31**, 2301 (1990); (*f*) I. Hanna, J.-Y. Lallemand, and P. Wlodyka. Tetrahedron Lett. **35**, 6685 (1994); (*g*) J. Herscovici, S. Delatre, and K. Antonakis. Tetrahedron Lett. **32**, 1183 (1991); (*h*) R. Tsang and B. Fraser-Reid. J. Org. Chem. **57**, 1065 (1992); (*i*) S. Woo, S. Legoupy, S. Parra, and A.G. Fallis. Org. Lett. **1**, 1013 (1999); (*j*) J. Herscovici, S. Delatre, L. Boumaiza, and K. Antonakis. J. Org. Chem. **58**, 3928 (1993); (*k*) I. Hanna and P. Wlodyka. J. Org. Chem. **62**, 6985 (1997).
9. S. Hanessian. Total synthesis of natural products: the chiron approach. *Edited by* J.E. Baldwin. Pergamon Press, Oxford. 1983.
10. (*a*) R.J. Ferrier. J. Chem. Soc. Perkin Trans. 1, 1455 (1979); (*b*) R.J. Ferrier and S. Middleton. Chem. Rev. **93**, 2779 (1993).
11. (*a*) D.J. Jenkins, D. Dubreuil, and B.V.L. Potter. J. Chem. Soc. Perkin Trans. 1, 1365 (1996); (*b*) S. Augy-Dorey, D.H.R. Barton, S.D. Gero, B. Quiclet-Sire, and I. Sagnard. J. Chem. Soc. Chem. Commun. 960 (1993); (*c*) H.B. Mereyala and S. Guntha. J. Chem. Soc. Perkin Trans. 1, 841 (1993); (*d*) C. Jaramillo, J.-L. Chiara, and M. Martin-Lomas. J. Org. Chem. **59**, 3135 (1994); (*e*) E. Poirot, H. Bourdon, F. Chrétien, Y. Chapleur, B. Berton, M. Hilly, J.-P. Mauger, and G. Guillon. Biorg. Med. Chem. Lett. **5**, 569 (1995); (*f*) K. Sato, S. Sakuma, S. Muramatsu, and M. Bokura. Chem. Lett. 1473 (1991).
12. F. Chrétien, R. Wolf, and Y. Chapleur. Nat. Prod. Lett. **2**, 69 (1993).
13. (*a*) N. Chida, M. Ohtsuka, K. Nakazawa, and S. Ogawa. J. Org. Chem. **56**, 2976 (1991); (*b*) N. Chida, M. Ohtsuka, and S. Ogawa. J. Org. Chem. **58**, 4441 (1993).

© 2000 NRC Canada

14. F. Chrétien, S. Ibn Ahmed, A. Masion, and Y. Chapleur. Tetrahedron, **49**, 7463 (1993).
15. (*a*) Z.J. Jia, L. Olsson, and B. Fraser-Reid. J. Chem. Soc. Perkin Trans. 1, 631 (1998); (*b*) V.A. Estevez and G.D. Prestwich. J. Am. Chem. Soc. **113**, 9885 (1991); (*c*) S.L. Bender and R.J. Budhu. J. Am. Chem. Soc. **113**, 9883 (1991); (*d*) O. Thum, J. Chen, and G.D. Prestwich. Tetrahedron Lett. **37**, 9017 (1996); (*e*) G. Dorman, J. Chen, and G.D. Prestwich. Tetrahedron Lett. **36**, 8719 (1995); (*f*) J. Chen, G. Dorman, and G.D. Prestwich. J. Org. Chem. **61**, 393 (1996).
16. (*a*) S.K. Das, J.M. Mallet, and P. Sinaÿ. Angew. Chem. Int. Ed. Engl. **36**, 493 (1997); (*b*) M. Sollogoub, J.M. Mallet, and P. Sinaÿ. Tetrahedron Lett. **39**, 3471 (1998); (*c*) P.I. Dalko and P. Sinaÿ. Angew. Chem. Int. Ed. Engl. **38**, 773 (1999).
17. C. Taillefumier, Y. Chapleur, D. Bayeul, and A. Aubry. J. Chem. Soc. Chem. Commun. 937 (1995).
18. R.J. Ferrier and N. Prasad. J. Chem. Soc. Perkin Trans. 1, 570 (1969).
19. J.G. Buchanan and J.C.P. Schwarz. J. Chem. Soc. 4470 (1962).
20. M.J. Robins, J.S. Wilson, and F. Hansske. J. Am. Chem. Soc. **105**, 4059 (1983).
21. N.A. Nashed. Carbohydr. Res. **60**, 200 (1978).
22. K. Neumann. Acta Chem. Scand. **46**, 913 (1992).
23. C. Chatgilialoglu. Acc. Chem. Res. **25**, 188 (1992).
24. M. Ballestri, C. Chatgilialoglu, K.B. Clark, D. Griller, B. Giese, and B. Kopping. J. Org. Chem. **56**, 678 (1991).
25. H.R. Bollinger and D.A. Prins. Helv. Chim. Acta, **28**, 465 (1945).
26. D.A. Prins. J. Am. Chem. Soc. **70**, 3955 (1948).
27. F. Chrétien, M. Khaldi, and Y. Chapleur. Synth. Commun. **20**, 1589 (1990).
28. A. Liptak, P. Fügedi, and P. Nanasi. Carbohydr. Res. **68**, 151 (1979).
29. R.V. Stevens, R.E. Cherpeck, B.L. Harrison, J. Lai, and R. Lapalme. J. Am. Chem. Soc. **98**, 6317 (1976).
30. W.R. Roush, H.R. Gillis, and A.I. Ko. J. Am. Chem. Soc. **104**, 2269 (1982).
31. R.K. Boeckman, Jr. and D.M. Demko. J. Org. Chem. **47**, 1789 (1982).
32 E. Bertele and P. Schudel. FR 1572831, 1969.
33. I. Dyong, H.W. Hagedorn, and J. Thiem. Liebigs Ann. Chem. 551 (1986).
34. F. Chrétien and Y. Chapleur. J. Chem. Soc. Chem. Commun. 1268 (1984).
35. N. Chida, M. Ohtsuka, K. Ogura, and S. Ogawa. Bull. Chem. Soc. Jpn. **64**, 2118 (1991).
36. A.S. Machado, A. Olesker, and G. Lukacs. Carbohydr. Res. **135**, 231 (1985).
37. R. Blattner, R.J. Ferrier, and S.R. Haines. J. Chem. Soc. Perkin Trans. 1, 2413 (1985).
38. P. Laszlo, I.F. Pelyvas, and F. Sztaricskai. Carbohydr. Chem. **175**, 227 (1988).
39. A.S. Machado, D. Dubreuil, J. Cleophax, S.D. Gero, and N.F. Thomas. Carbohydr. Res. **233**, C5-C8 (1992).
40. T. Iimori, H. Takahashi, and S. Ikegami. Tetrahedron Lett. **37**, 649 (1996).
41. G. Rembarz. Chem. Ber. **95**, 825 (1962).

© 2000 NRC Canada

Hydrogen bonded supramolecular structures: a further insight into the diamine–diol recognition and self-assembly

Stefano Roelens, Paolo Dapporto, and Paola Paoli

Abstract: A new H-bonded supramolecular assembly of the diamine–diol family has been obtained from (1*R*,2*R*)-1,2-diaminocyclohexane (DAC) and (*S*)-1-phenyl-1,2-ethanediol (PED). The structure was characterized by single-crystal X-ray analysis and showed the typical architecture of DAC based assemblies, consisting of a three-stranded helicate coiling around a H-bonded core, with a predictable helicity sense determined by the configuration of DAC. The new assembly, while reconfirming the unique role of DAC as a powerful assembler of supramolecular structures, demonstrated that the C_2 symmetry of diol partners employed so far is not essential for assembling helicates, although chirality is. In the case of the adduct between (1*R*,2*R*)-1,2-diaminocyclohexane and (2*R*,3*R*)-2,3-butanediol, molecular recognition and self-assembly have been shown to take place even in the absence of solvent, in the gas phase, where long crystals were formed by spontaneous organized aggregation of diamine–diol units. A thorough analysis of the results from the present and previous investigations has lead to a deeper understanding of the key features of the diamine–diol molecular code and of the requirements for recognition and assembly.

Key words: supramolecular, hydrogen bonding, molecular recognition, self-assembly, diamines, diols.

Résumé : On a obtenu un nouvel assemblage supramoléculaire à liaisons hydrogènes de la famille diamine–diol à partir du (1*R*,2*R*)-1,2-diaminocyclohexane (DAC) et du (*S*)-1-phényléthane-1,2-diol (PED). On a caractérisé la structure par diffraction des rayons X et elle présente l'architecture typique des assemblages à base de DAC; elle est constituée d'une hélice à trois brins enroulée autour d'un noyau à liaisons hydrogènes avec un sens d'hélicité qui peut être prédit à partir de la configuration du DAC. Le nouvel assemblage reconfirme le rôle unique du DAC comme promoteur puissant de la formation de structures supramoléculaires et démontre que la symétrie C_2 des partenaires diols utilisés jusqu'à maintenant n'est pas essentielle pour la formation d'assemblages en hélice, même si la chiralité l'est. Dans le cas de l'adduit entre le (1*R*,2*R*)-1,2-diaminocyclohexane et le (2*R*,3*R*)-butane-2,3-diol, il a été démontré que la reconnaissance moléculaire et l'autoassemblage se produisent même en l'absence de solvant, en phase gazeuse, alors qu'il se forme de longs cristaux par l'agrégation organisée spontanée d'unités diamine–diol. Une analyse détaillée des résultats obtenus dans le présent travail et dans d'autres rapportés antérieurement permet de mieux comprendre les caractéristiques principales du code moléculaire diamine–diol et les impératifs pour la reconnaissance et l'assemblage.

Mots clés : supramoléculaire, liaison hydrogène, reconnaissance moléculaire, autoassemblage, diamines, diols.

Received August 4, 1999. Published on the NRC Research Press website on May 19, 2000.

Dedicated to Professor Stephen Hanessian on the occasion of his 65th birthday.

S. Roelens.[1] CNR, Centro di Studio sui Meccanismi di Reazione, Dipartimento di Chimica, Università La Sapienza, I-00185 Roma, Italy.

P. Dapporto and P. Paoli. Dipartimento di Energetica "Sergio Stecco", Università di Firenze, I-50139 Firenze, Italy.

[1]Author to whom correspondence may be addressed. Telephone: +39-055-275-7658. Fax: +39-055-247-6964. e-mail: roelens@chimorg.unifi.it

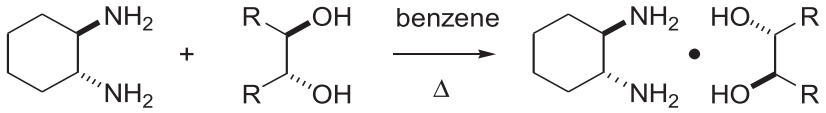
[2]A Chemical Abstract search for general reviews on hydrogen-bonded structures gave 957 references dating back from 1967, of which 47 references specifically dealing with supramolecular structures appeared from 1992–1999.

Introduction

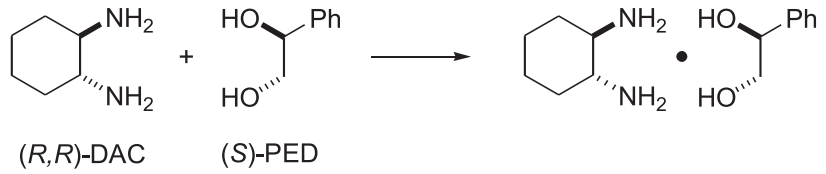
There is an overwhelming literature on hydrogen bonded supramolecular structures.[2] The vast majority of these are based on amidic type H-bonding, which is strong enough to ensure stability to the resulting entity. However, it has recently been shown that even much weaker H-bonding, such as that established between simple aromatic (1) and aliphatic (2) amino and hydroxy functionalities, is capable of generating supramolecular structures. Alcohols and primary amines are complementary H-bonding partners in that a single donor – double acceptor (oxygen) perfectly matches the coordination properties of a double donor – single acceptor (nitrogen). We (2*a*) and others (1*a*) have found that this complementarity constitutes a primary driving force for molecular recognition and self-assembly because saturation of the fourfold tetrahedral coordination capabilities of both heteroatoms provides the energetic advantage of the process through the establishment of additional H-bonds, overriding

© 2000 NRC Canada

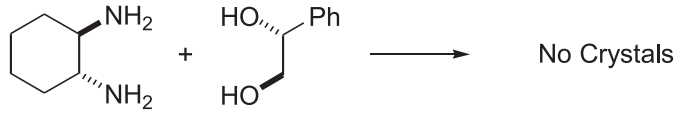
Scheme 1.



Scheme 2.



(*R,R*)-DAC (*S*)-PED



(*R,R*)-DAC (*R*)-PED

the natural donor–acceptor roles of oxygen and nitrogen (3). With chiral diamine and diol partners, such process determines not only molecular recognition and self-assembly into unique supramolecular architectures, but also the helical folding of the assembly, as the way to achieve full coordination of heteroatoms and the formation of the maximum number of H-bonds (2*a*); depending on the steric requirements of partners, in favorable cases this gives rise to a helical architecture of both the tertiary structure and the H-bonding network (2*b*, *c*). A number of examples of helicates based on *trans*-1,2-diaminocyclohexane (DAC) have been described (2), showing that the process relies on the remarkable assembling ability of DAC as well as on the information encoded in the two interacting partners. The helical motif is indeed a dominant feature of the architectural design of DAC; furthermore, the stereochemical information encoded in DAC drives the assembling process to select a specific chirality sense of the helicate, depending on the DAC enantiomer used. Such fascinating supramolecular architectures are thus the ultimate expression of a code imprinted in the partners' complementary structures and functionalities, which is read by the recognition process.

While several features of such H-bonded architectures have been unraveled, there is still a number of open issues concerning the rules that govern their molecular recognition and self-assembly. For example, is the diamine–diol the only perfect pair of partners or do other well-matched pairs exist? Is the C_2 symmetry of partners utilized so far essential for building helical superstructures? Is the assembling process a spontaneous build-up of diamine–diol units or rather a fit of the diol into the diamine crystal lattice? In an effort to gain a deeper insight into the many peculiar aspects of this phenomenon, we have explored in more detail the factors that are involved in the molecular recognition and self-assembly of the diamine–diol motif, in the belief that the understanding of the constitutional prerequisites and the elucidation of the molecular code may disclose unexpected chemical features and may open the way to a rational design of H-bonded supramolecular architectures. In a previous work (2*b*) it was noted that supramolecular structures could be obtained from DAC with several diols, but not vice versa. This led to the belief that DAC may possess specific recognition and assembling instructions that are not shared by other diamines or diols. Although another diamine, *trans*-2,3-diaminobutane, has been shown to be effective in some cases (2*c*), DAC was selected as the best suited *assembler* for the investigation.

Results and discussion

Diamine–diol supramolecular architectures were obtained by crystallization of the 1:1 mixture of the two partners from a nonpolar solvent that would not interfere with the forming H-bonds (2). In a typical procedure, equimolar amounts of DAC and of the selected diol, both enantiopure, were suspended in benzene and heated to complete solution (Scheme 1). Crystal needles normally separated upon standing at room temperature in a length of time ranging from few minutes to few hours. The crystalline form of needles is indicative of self-assembly into helicates, which typically grow monodirectionally around the core. Only one of the two diastereomeric pairs is well assorted: the well-matched pair diastereomer normally crystallizes faster, whereas the mismatched pair takes longer, if it crystallizes at all.

As mentioned, all the diols used so far were C_2 symmetry partners for the C_2 symmetrical DAC. A basic question is therefore what role symmetry and chirality are playing in the recognition and assembling process and how critical is the C_2 symmetry. To investigate this aspect, we treated (1*R*,2*R*)-DAC (Fluka, mp 43–45°C, $[\alpha]_D^{20}$ –25.5°, c = 5 in 1 N HCl) with both enantiomers of 1-phenyl-1,2-ethanediol ((*R*)-PED, Fluka, mp 66–68 °C, $[\alpha]_D^{20}$ –40°, c = 3 in acetone; (*S*)-PED, Fluka, mp 66–68 °C, $[\alpha]_D^{20}$ +40°, c = 3 in acetone), diols possessing C_1 symmetry, according to the general crystallization procedure (Scheme 2). Long needles (69%, mp 57–58°C)

© 2000 NRC Canada

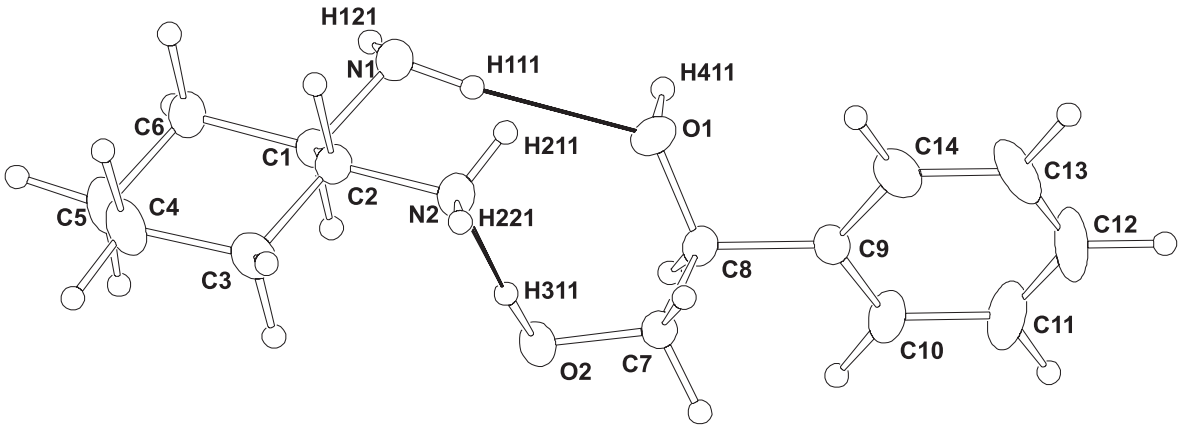
Table 1. Crystal data of the (*R*,*R*)-DAC–(*S*)-PED adduct.

Formula	$C_{14}H_{24}N_2O_2$
MW	252.35
Crystal Size (mm)	0.8 × 0.6 × 0.4
Crystal system	monoclinic
Space group	$P2_1$
a (Å)	10.084(2)
b (Å)	5.278(2)
c (Å)	13.622(2)
α (°)	90
β (°)	91.920(10)
γ (°)	90
V (Å^3)	724.6(3)
Z	2
D_C (g cm^{-3})	1.157
Radiation	MoKα graphite monochromated
F (000)	276
μ (mm^{-1})	0.077
T (K)	293
2θ range (°)	5–55
Scan mode	θ–2θ
Tot. Reflections Measured	1905
Unique Observed Reflections [$I > 2\sigma(I)$]	1834
Refined Parameters	188
R [obs. Reflections]	*R*1 = 0.056, *wR*2 = 0.132
Δρ max, min (e Å^{-3})	0.174, –0.190
Max Shift/esd	0.188

Table 2. Atomic coordinates (×10^4) and equivalent isotropic displacement parameters (Å^2 × 10^3) of the (*R*,*R*)-DAC–(*S*)-PED adduct.

	x	*y*	*z*	*U*(eq)
O(1)	1617(2)	1957(7)	5808(2)	63(1)
O(2)	3708(2)	1531(6)	4451(2)	55(1)
N(1)	–155(3)	5868(7)	6226(3)	54(1)
N(2)	–2208(4)	2163(8)	6064(2)	56(1)
C(1)	–983(3)	5314(7)	7070(2)	45(1)
C(2)	–1483(3)	2564(7)	7006(2)	46(1)
C(3)	–2355(4)	2017(9)	7859(3)	61(1)
C(4)	–1649(5)	2464(10)	8841(3)	74(1)
C(5)	–1088(5)	5136(9)	8901(3)	70(1)
C(6)	–228(4)	5712(8)	8039(2)	59(1)
C(7)	3901(3)	1350(8)	5484(2)	47(1)
C(8)	2908(3)	2941(7)	6022(2)	43(1)
C(9)	3241(3)	3034(7)	7115(2)	45(1)
C(10)	4038(4)	4945(9)	7489(3)	65(1)
C(11)	4335(6)	5063(14)	8481(4)	102(2)
C(12)	3866(7)	3329(17)	9102(4)	112(3)
C(13)	3086(6)	1354(16)	8742(4)	108(2)
C(14)	2779(4)	1229(11)	7742(3)	74(1)
H(111)	–654(36)	6074(90)	5623(29)	60(11)
H(121)	245(32)	7143(83)	6356(24)	33(10)
H(211)	–1655(41)	1898(104)	5544(29)	69(12)
H(221)	–2662(53)	732(136)	6118(40)	98(19)
H(311)	3216(55)	–188(144)	4240(40)	123(21)
H(411)	1020(55)	2927(136)	6001(42)	119(22)

Fig. 1. ORTEP drawing of the molecular structure of the 1:1 adduct between (1*R*,2*R*)-diaminocyclohexane (DAC) and (*S*)-1-phenyl-1,2-ethanediol (PED) with atom numbering scheme. H-bonds are represented as black lines.



crystallized soon from the diol of *S* configuration, whereas no crystalline material could be obtained from the *R* enantiomer even after long standing and concentration of the solution, which afforded glassy material. This evidence clearly indicated which was the well-matched pair of partners. The X-ray structure of the crystals (Tables 1–3)[3] showed a 1:1 adduct consisting of one molecule of (*R*,*R*)-DAC and one of (*S*)-PED, held together by two H-bonds linking a NH donor to an OH acceptor in the first and the reverse in the second (Fig. 1): the interchangeable H-bonding role of the two groups is clearly apparent. The supramolecular architecture of the adduct is displayed by crystal packing projections. From the top view (Fig. 2), the typical array of assemblies based on DAC is observed, consisting of a H-bonded

[3] Supplementary material available: anisotropic displacement parameters (Table S1), hydrogen coordinates and isotropic displacement parameters (Table S2), may be purchased from: The Depository of Unpublished Data, Document Delivery, CISTI, National Research Council of Canada, Ottawa, Canada K1A 0S2. The tables of crystal data and refinement, atomic coordinates, bond lengths and angles, and hydrogen atoms coordinates have also been deposited with the Cambridge Crystallographic Data Centre, and can be obtained on request from The Director, Cambridge Crystallographic Data Centre, University Chemical Laboratory, 12 Union Road, Cambridge, CB2 1EZ, U.K.

© 2000 NRC Canada

Table 3. Bond lengths (Å) and angles (°) of the (*R*,*R*)-DAC–(*S*)-PED adduct.

Bond lengths	(Å)
O(1)—C(8)	1.423(4)
O(2)—C(7)	1.418(4)
N(1)—C(1)	1.472(5)
N(2)—C(2)	1.471(4)
C(1)—C(6)	1.516(5)
C(1)—C(2)	1.538(5)
C(2)—C(3)	1.508(5)
C(3)—C(4)	1.512(6)
C(4)—C(5)	1.520(7)
C(5)—C(6)	1.515(6)
C(7)—C(8)	1.515(4)
C(8)—C(9)	1.516(4)
C(9)—C(14)	1.372(6)
C(9)—C(10)	1.377(5)
C(10)—C(11)	1.376(6)
C(11)—C(12)	1.342(10)
C(12)—C(13)	1.386(10)
C(13)—C(14)	1.388(7)
O(1)—H(411)	0.84(6)
O(2)—H(311)	1.07(7)
N(1)—H(111)	0.95(4)
N(1)—H(121)	0.80(4)
N(2)—H(211)	0.93(4)
N(2)—H(221)	0.89(7)
Angles	**(°)**
N(1)–C(1)–C(6)	111.8(3)
N(1)–C(1)–C(2)	109.7(3)
C(6)–C(1)–C(2)	109.5(3)
N(2)–C(2)–C(3)	111.0(3)
N(2)–C(2)–C(1)	109.7(3)
C(3)–C(2)–C(1)	109.6(3)
C(2)–C(3)–C(4)	112.5(3)
C(3)–C(4)–C(5)	110.8(4)
C(6)–C(5)–C(4)	111.5(4)
C(5)–C(6)–C(1)	111.3(3)
O(2)–C(7)–C(8)	111.8(3)
O(1)–C(8)–C(9)	112.6(3)
O(1)–C(8)–C(7)	108.3(3)
C(9)–C(8)–C(7)	111.4(2)
C(14)–C(9)–C(10)	118.9(4)
C(14)–C(9)–C(8)	121.4(4)
C(10)–C(9)–C(8)	119.7(3)
C(9)–C(10)–C(11)	120.1(5)
C(12)–C(11)–C(10)	121.2(6)
C(11)–C(12)–C(13)	119.8(5)
C(12)–C(13)–C(14)	119.2(6)
C(9)–C(14)–C(13)	120.6(6)
C(8)–O(1)–H(411)	112(4)
C(7)–O(2)–H(311)	105(3)
H(111)–N(1)–H(121)	110(3)
C(1)–N(1)–H(111)	113(2)
C(1)–N(1)–H(121)	107(2)
H(211)–N(2)–H(221)	105(4)
C(2)–N(2)–H(211)	113(2)
C(2)–N(2)–H(221)	107(3)

central core surrounded by four stacks of aliphatic and phenyl ring residues. Two side rows of additional H-bonds flank the assembly, engaging the second amino and hydroxy groups of each molecule not involved in the central core. The side view of the assembly (Fig. 3) shows instead the helicity of the central H-bonding network, reinforced by the two H-bonds side rows that run in the opposite direction of donation with respect to that of the core. Although NH···O bonds are longer than OH···N bonds, they are all well within the typical H-bonding distance (Table 4). All the heteroatoms in the structure are tricoordinated, with one NH and one oxygen lone pair apparently unemployed. However, in the central core these are engaged in a looser H-bonding interaction, showing an NH···O distance of 3.00 Å, slightly larger than the sum of their Van der Waals radii, and an angle of 152°. As a consequence, although the H-bonding network is not fully formed, the helicate shape of the assembly, typical of the family, is retained. The helical supramolecular structure of residues is better perceived from the spacefilling representation of the assembly, in which diamine and diol molecules linked by the row of H-bonds including the looser interaction are shown in different shades of gray (Fig. 4). Right-handed coiling of residues around the core, predictable from the configuration of DAC, is easily appreciated from Fig. 4, which also shows that three such rows of molecules run parallel giving rise to a trihelicate architecture.

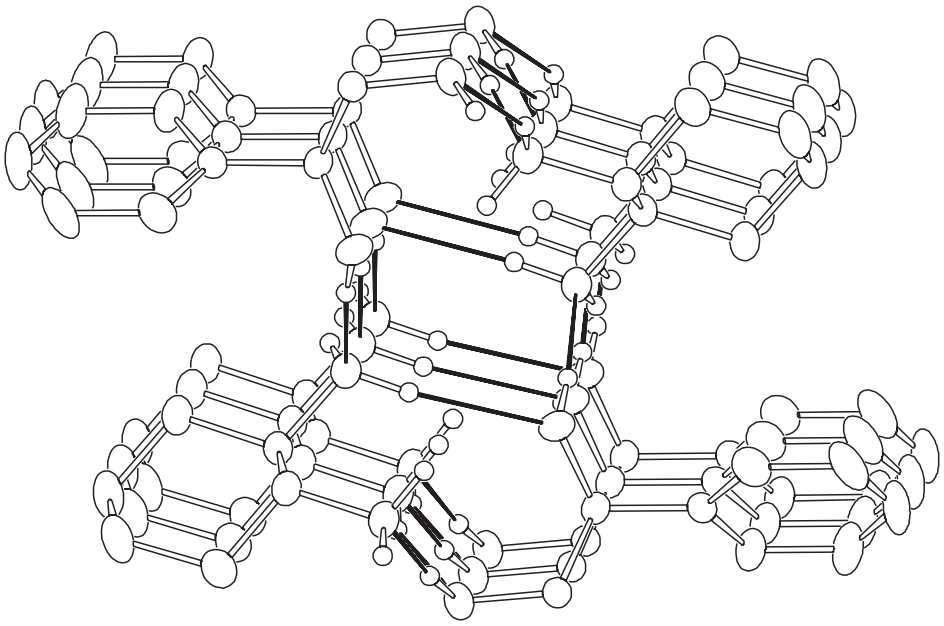
The supramolecular structure of the (*R*,*R*)-DAC–(*S*)-PED adduct presented here shed some light on the role of chirality and symmetry in the diamine–diol recognition. Indeed, the close analogy of the present assembly with those previously reported (2) demonstrate that the C_2 symmetry of the diol partner is not essential, although chirality certainly is. We were not able in fact to obtain crystals from unsubstituted ethylene glycol under the same conditions, while from a *cis* substituted diol (*meso*-1,2-cyclohexanediol) crystallization of a layered structure was reported (2*c*), evidence suggesting that a "chiral twist" (4) is somehow necessary for recognition and assembly with a chiral diamine. Analogously, ethylene diamine failed to give recognition with (2*R*,3*R*)-2,3-butanediol and with either enantiomer of *trans*-1,2-cyclohexanediol, which separated on standing from the diamine by evaporation of the solvent, whereas DAC was shown to give the strongest assemblies with these diols (2*b*). Adducts from planar, achiral aromatic diamines and diols have been reported to self-assemble, giving rise to achiral diamond-type structures (1*a*, *c*). However, we did not observe molecular recognition and self-assembly with nonplanar, achiral aliphatic diamine–diol pairs, such as ethylene diamine–ethylene glycol and *meso*-1,2-diaminocyclohexane–*meso*-1,2-cyclohexanediol. Further demonstration that chirality plays a crucial role in these architectures comes from a closer inspection of the assembly (Fig. 2). The hydroxy group engaged in the H-bonded core, responsible for the formation of the helicate, belongs to the phenyl-bearing stereogenic carbon, whereas the methylene hydroxyl group takes part in the flanking H-bonding side rows, although steric considerations would suggest the opposite arrangement. Correspondingly, the OH···N bonds in the side rows are shorter than those in the core; evidently, the need for a "chiral twist" overrides the steric congestion penalty imposed by the substituent. Such a compromise between chirality and steric requirements

© 2000 NRC Canada

Table 4. Selected hydrogen bonds (Å) with the angular value (°).

H-bond (symmetry operation)	H···X	O···N	Angle
O1-H411···N1 (*x*, *y*, *z*)	1.98 (7)	2.802(5)	164 (6)
N1-H111···O1 (–*x*, *y* + 0.5, –*z* + 1)	2.20 (4)	3.147(4)	172 (3)
O2-H331···N2 (–*x*, *y* – 0.5, –*z* + 1)	1.77 (7)	2.832(5)	172 (6)
N2-H221···O2 (–*x*, *y* – 0.5, –*z* + 1)	2.56 (7)	3.398(5)	157 (6)

Fig. 2. ORTEP drawing of the H-bonded assembly of the (*R*,*R*)-DAC–(*S*)-PED adduct (top view down the *a* axis). H-bonds are represented as black lines. H-atoms on carbon are omitted for clarity.



confirmed previous observations on the related C_2 symmetrical 1,2-diphenyl-1,2-ethanediol (DPED) (2*b*), from which two different supramolecular structures were obtained by the interaction of (*R*,*R*)-DAC with its two enantiomers: the *S*,*S* diol, the well-matched partner, gave the right-handed helicate showing the recurrent H-bonded core motif, whereas the *R*,*R* diol afforded lower melting crystals characterized by a layered structure, consisting of contiguous units of diamine and diol dimers. The result was ascribed to the sterically demanding phenyl groups in the mismatched diamine–diol pair, which caused disruption of the helicate architecture. Although the H-bonding network of the (*R*,*R*)-DAC–(*S*)-PED adduct is analogous to that of (*R*,*R*)-DAC–(*S*,*S*)-DPED, both featuring a spiral-shaped motif of the core, the relative position of diamine and diol molecules around the core resembles that exhibited by the adduct of DAC with cyclohexanediol, a more tightly bound assembly, probably a consequence of the steric relief for the missing phenyl substituent. The assembly of the monophenyl substituted diol represents the evidence that the compromise between chiral and steric requirements is still conducive to self-assembly with partners bearing a single stereocenter.

From the above discussion, *complementarity* emerges unambiguously as the fundamental requirement for recognition and assembly, in full agreement with the well known general principle (5). Besides the chirality requirement, functional, coordinative, symmetry, and steric complementarity have been demonstrated to be leading prerequisites in the diamine–diol structures described so far. An even subtle decrease in the complementarity of partners can induce degradation or loss of recognition and assembly. For example, it might be expected that a H-bonding group more acidic than the hydroxyl, such as the thiol group, would be an equally good or even better partner for DAC. Instead, while *trans*-1,2-cyclohexanediol was efficiently resolved by crystallization with enantiopure DAC because of the significantly different solubility of the two diastereomeric assemblies (6), resolution of *trans*-1,2-cyclohexanedithiol could not be obtained under the same conditions, which only gave the unaltered mixture of reagents as an oil. Analogous results were observed with 2,3-butanedithiol. This suggested that replacement of hydroxyl with thiol groups may disrupt the functional complementarity of partners to such an extent that recognition was prevented, despite the greater thiol acidity: matching of donating–accepting properties appears to take priority over acidity. Recognition was also suppressed by a variation as subtle as the replacement of the cyclohexane with the cyclopentane ring in the diol partner. Again, all attempts of resolution of *trans*-1,2-cyclopentanediol made by us and others (2*c*) met with disappointment. Thus geometric and conformational issues, likely related to the achievement of a perfectly staggered conformation as in the cyclohexane ring, appear to play a significant role in the process as well. All the described failures give an idea of how crucial the complementarity requirements can be in systems featuring weak H-bonding.

© 2000 NRC Canada

Fig. 3. ORTEP drawing of the H-bonded assembly of the (*R*,*R*)-DAC–(*S*)-PED adduct (side view along the *a* axis) with relevant H-bonding distances (Å). H-bonds are represented as black lines. H-atoms on carbon are omitted for clarity.

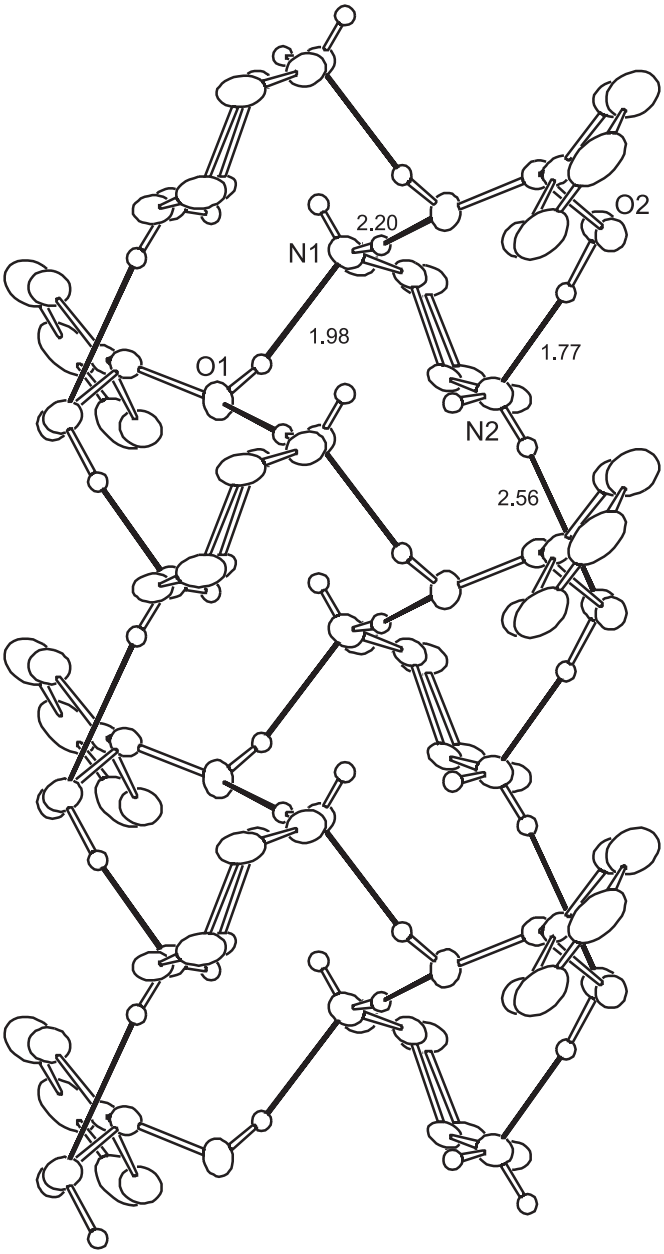
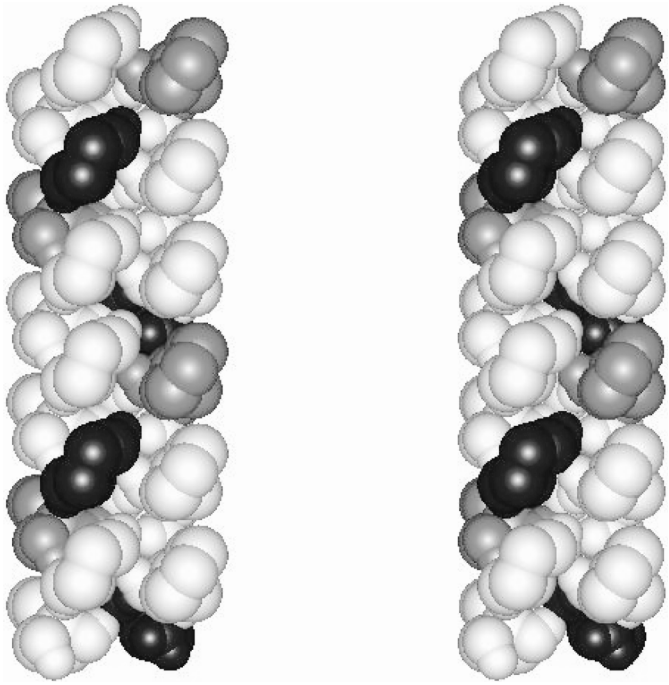


Fig. 4. Spacefilling (CPK) representation (stereoview) of the right-handed, triple-stranded helicate structure of the (*R*,*R*)-DAC–(*S*)-PED adduct (side view along the *a* axis). One of the three strands of diamines and diols linked by the same H-bonding row is represented in darker (DAC) and medium (PED) shades of gray, while the remaining two strands are in lighter shades of gray. H-atoms on carbon are omitted for clarity.



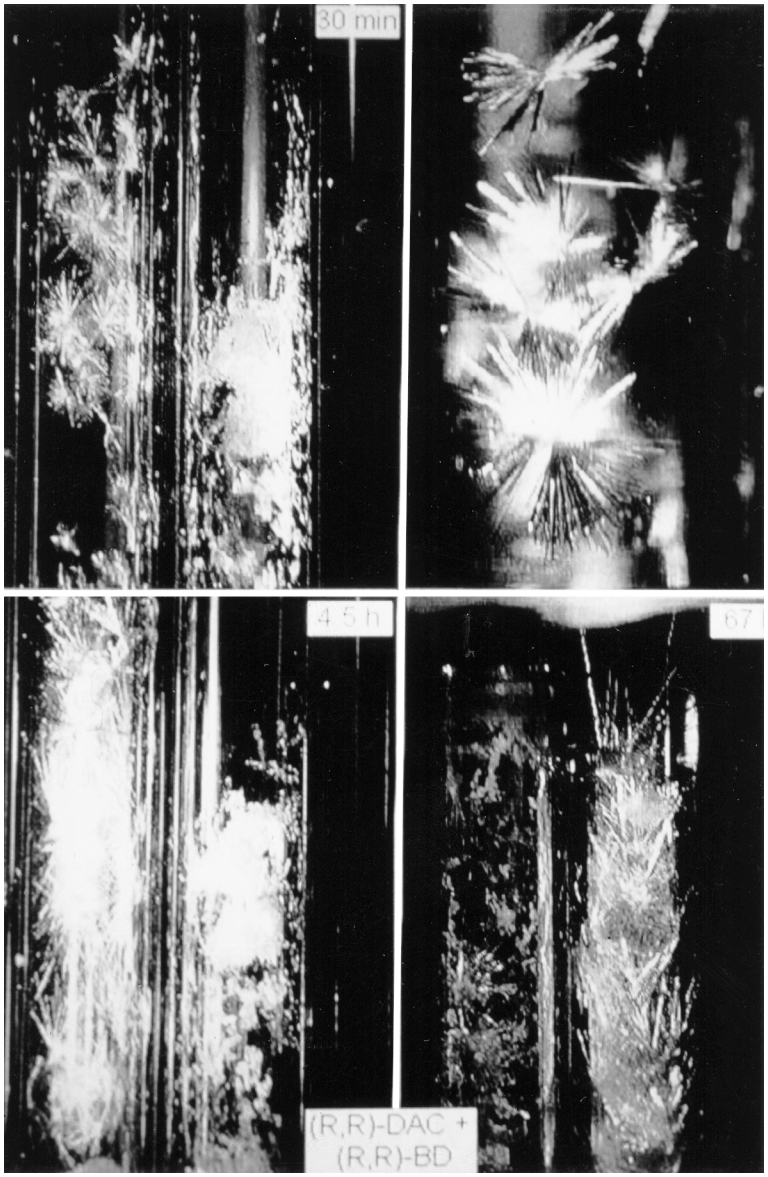
A clear-cut answer came from an experiment designed to ascertain whether self-assembly occurs by insertion of the diol partner in the crystal lattice of the diamine (inclusion) or by organized aggregation of diamine–diol units (build-up). (*R*,*R*)-DAC and (2*R*,3*R*)-2,3-butanediol (BD) have been shown to give the most largely H-bonded assembly observed, featuring full tetracoordination of *all* the heteroatoms and a helical arrangement of both the assembly *and* the H-bonding network. The two reagents (DAC, low melting solid; BD, liquid) were placed neat in two separate capillary tubes, which were introduced in a tube under moderate vacuum. Crystals in the shape of needles growing from nucleation points began to form shortly on the glass walls of the capillary containing the least volatile diol. After a few hours, crystals had filled the capillary and complete consumption of the solid diamine in a few days produced a bulky agglomerate of crystals several centimeters long (Fig. 5). The obtained crystals had the same physical and spectroscopic properties as those used for the structure solution. Molecular recognition and self-assembly of the two partners had taken place in the gas phase, in the absence of solvent, simply driven by H-bonding, unambiguously demonstrating a build-up process. The inclusion process, feasible in solution, can not occur in the gas phase; however, under both conditions, the organization of the assembly is dominated by the strong directing ability of the diamine.

Diamine–diol recognition and self-assembly: features and requirements

From the analysis of results presented here and of previously reported structures (2), which now constitute a significantly broad family of 13 members, several aspects of the interaction between diamines and diols have been understood. Even though from the available data it is not possible yet to predict if a diamine–diol pair will self-assemble into a supramolecular structure, it is nevertheless possible to infer the basic requirements and the key features characterizing the molecular recognition and self-assembling code of this family of H-bonding partners. We believe it useful to highlight them briefly.

© 2000 NRC Canada

Fig. 5. Top left: crystals of the 1:1 adduct between (1*R*,2*R*)-diaminocyclohexane (DAC) and (2*R*,3*R*)-2,3-butanediol (BD) growing under vacuum on the wall of the 5 mm capillary tube on the left containing neat BD, from neat DAC contained in the 5 mm capillary tube on the right, after 30 min. Top right: same as above, in a magnified representation. Bottom left: same as above, after 4.5 h. Bottom right: same as above, after 67 h. The capillary tube containing residual DAC is on the left side while that originally containing BD is on the right side.



Complementarity

Electronic as well as coordinative complementarity make the primary amino and the hydroxy groups the perfect matching functional groups for H-bonding. Aliphatic vicinal diamines and diols are constitutionally capable of exploiting such a H-bonding complementarity for giving rise to molecular recognition and for self-assembling into supramolecular architectures. Tendency to achieve full tetracoordination of both nitrogen and oxygen is the driving force, whereas acidity–basicity or donor–acceptor properties of partners do not appear to be determinant prerequisites.

Chirality

Chirality of both partners is essential for self-assembly into helicate architectures. C_2 has proved to be the optimum symmetry for best geometric complementarity, although C_1 symmetry is effective as well, but the "chiral twist" is a necessary feature. A well-matched combination of partners' enantiomers consistently gives rise to assemblies of higher symmetry and larger H-bonds number than does its diastereomeric counterpart. Achiral aliphatic species as the diamine and (or) the diol partners either give layered structures in special cases (only a single example at present) or, more commonly, do not assemble at all.

Steric and conformational prerequisites

Due to weak H-bonding, diamine–diol assemblies appear to be critically sensitive to the steric and conformational requirements. While methyl and cyclohexano substituents are accepted, the size of phenyl groups appear to be at the limit

© 2000 NRC Canada

for self-assembly. Even minimal changes in the size and geometry of partners induce drastic modifications of the architecture. Conformational flexibility is advantageous for partners to adapt to each other and for the assembly to fold in order to achieve the largest number of H-bonds, but the rigid and perfectly staggered conformation of cyclohexane, although preventing the assembly from folding, with well-matched complementary partners gives rise to thermodynamically more stable structures, most likely for entropic reasons related to the lack of conformational freedom loss. Again, minor conformational changes such as those resulting from replacing cyclohexane with cyclohexene or cyclopentane, produce dramatic consequences on the H-bonded network motif.

The assembler

trans-1,2-Diaminocyclohexane (DAC) is a superior assembler of supramolecular structures. It possesses optimal geometric, functional, symmetry, steric, and conformational properties to assemble a whole family of diols into organized architectures. The more flexible *trans*-2,3-diaminobutane is also effective with constrained cyclohexanediol partners, but it lacks the "preorganization" of DAC. Other chiral diamines failed to give self-assembly. Furthermore, the assembling properties of DAC are not shared by any of the diols investigated so far, unable to assemble diamines.

Supramolecular architecture

The helicate is the preferred structural motif. The backbones of diamine and diol molecules linked by H-bonding rows coil around the H-bonded core in a helical fashion. Typically, three strands of such rows run parallel in the assembly, generating a triple-stranded helicate. Whenever permitted by steric, geometric and complementarity requirements, the ribbon-shaped H-bonded core also folds over in a helical fashion, thus allowing full tetracoordination of all the heteroatoms involved. Degradation of the helical motif is caused by steric or symmetry reasons, first leading to unfolded ribbon (pleated sheet) and to incompletely bonded core still exhibiting a persistent helicate structure of the backbone, then to layered structures and eventually to suppression of self-assembly. The helicity sense of the assembly is determined by the diamine: a right-handed helicity is predicted for the diamine of (*R*,*R*) configuration; when *both* the backbone and the core are helical, they show opposite helicity and the sense of the core's helix takes priority over that of the backbone, folding in a right-handed way.

Solution and gas phase features

Diamine–diol assemblies are supramolecular solid-state architectures. In solution, NMR evidence unequivocally demonstrated that these are fast-exchanging aggregates, showing molecular recognition and chiral discrimination. While molecular recognition is exhibited by a much larger set of diamine–diol pairs than the described set of X-ray structures, not all give rise to self-assembly, demonstrating that the requirements for the latter process are more restrictive than those for the former. Formation of crystals from a diamine–diol solution is strongly indicative that, beyond molecular recognition, the self-assembling process has the energy gain required to take place. Sublimation of crystals into unaltered supramolecular structures guarantees the stability of the assembly. Needles growing in the gas-phase from neat reagents show that self-assembly is carried out by an organized build-up of diamine–diol units, and suggest the formation of a helicate occurring through the establishment of a monodirectional H-bonding network.

In conclusion, the body of data collected on the diamine–diol family has grown large enough to provide a basic understanding of the fundamental features and requirements that characterize their molecular recognition and self-assembling code. Hopefully, this knowledge will inspire the design of new and exciting architectures.

Experimental section

Crystal data and refinement

Crystal data and refinement details of the structure are reported in Table 1. Unit cell parameters and intensity data were obtained from crystals sealed in a capillary tube under Ar atmosphere on a Nonius CAD4 diffractometer. Cell dimensions were determined by least-squares fitting of 25 centered reflections. Intensity data were corrected for Lorentz and polarization effects, an absorption correction was applied once the structure was solved by using the Walker and Stuart method (7). The structure was solved by direct methods, using the SIR-92 program (8) and subsequently refined by the full-matrix least-squares program SHELXL-93.[4] The hydrogen atoms linked to nitrogen and oxygen atoms were localized in ΔF Fourier syntheses and individually refined. The hydrogen atoms of the carbon atoms, on the contrary, were introduced in calculated positions, and their coordinates refined in agreement with those of the linked atoms. The hydrogen atoms linked to carbon atoms were refined with an overall isotropic temperature factor [U = 0.082(3) Å^2], whereas the hydrogen atoms linked to N1, N2 O1 and O2 were refined with an individual isotropic temperature factor. All the non-hydrogen atoms were refined anisotropically. Atomic scattering factors and anomalous dispersion corrections for all the atoms were taken from International Tables for X-ray Crystallography (9). Geometrical calculations were performed by PARST93 (10). The molecular plots were produced by the ORTEP program (11). Table 2 reports the atomic coordinates of the non-hydrogen atoms and Table 3 bond lengths and angles.

Acknowledgements

We are grateful to Mr. Sandro Papaleo, Dipartimento di Chimica Organica, Università di Firenze, for the microscope pictures of the gas phase experiments.

References

1. (*a*) O. Ermer and A. Eling. J. Chem. Soc. Perkin Trans. 2, 925 (1994); (*b*) J.H. Loehlin, M.C. Etter, C. Gendreau, and E. Cervasio. Chem. Mater. **6**, 1218 (1994); (*c*) F. Toda, S. Hyoda, K. Okada, and K. Hirotsu. J. Chem. Soc. Chem. Commun.

[4] G.M. Sheldrick. SHELXL-93. Program for crystal structure refinement. University of Göttingen, Germany. 1993.

© 2000 NRC Canada

1531 (1995); (*d*) J.H. Loehlin, K.J. Franz, L. Gist, and R.H. Moore. Acta Crystallogr. Sect. B: Struct. Sci. **54**, 695 (1998).
2. (*a*) S. Hanessian, A. Gomtsyan, M. Simard, and S. Roelens. J. Am. Chem. Soc. **116**, 4495 (1994); (*b*) S. Hanessian, M. Simard, and S. Roelens. J. Am. Chem. Soc. **117**, 7630 (1995); (*c*) S. Hanessian, R. Saladino, R. Margarita, and M. Simard. Chem. Eur. J. **5**, 2169 (1999).
3. H.J. Bohm, S. Brode, U. Hesse, and G. Klebe. Chem. Eur. J. **2**, 1509 (1996).
4. Y. Dobashi, A. Dobashi, H. Ochiai, and S. Hara. J. Am. Chem. Soc. **112**, 6121 (1990).
5. J.-M. Lehn. Supramolecular chemistry. VCH, Weinheim. 1995. p. 11.
6. M. Kawashima and A. Hirayama. Chem. Lett. 763 (1991).
7. N. Walker and D.D. Stuart. Acta Crystallogr. Sect. A: Fundam. Crystallogr. **39**, 158 (1983).
8. A. Altomare, G. Cascarano, C. Giacovazzo, A. Guagliardi, M.C. Burla, G. Polidori, and M. Camalli. J. Appl. Crystallogr. **27**, 435 (1992).
9. International tables for X-ray crystallography. Vol. 4. Kynoch Press, Birmingham. UK. 1974.
10. M. Nardelli. Comput. Chem. **7**, 95 (1983).
11. C.K. Johnson. ORTEP II, Rep.-5138. Oak Ridge National Laboratory, Tenn. U.S.A. (1973).

© 2000 NRC Canada

A new strategy for synthesis of attached rings

Larry E. Overman and Lewis D. Pennington

Abstract: The first investigation of the use of pinacol-terminated Prins cyclizations to form attached rings is reported. Treatment of triisopropylsilyl ethers of (*Z*)- or (*E*)-[2-(6,6-dimethoxyhexylidene)cyclohexanol with $SnCl_4$ provides bicyclic products having attached rings. The approach is synthetically useful in the *Z* alkylidenecyclohexane series, proceeding selectively by a pathway involving carbon migration in the pinacol rearrangement step, to provide methoxy epimers of 1-(2-methoxycyclohexyl)cyclopentylcarboxaldehyde. Reaction of the corresponding *E* stereoisomer is more complex and yields a mixture of products resulting from both hydride and carbon migration in the pinacol rearrangement step.

Key words: Prins cyclization, pinacol rearrangement, attached rings.

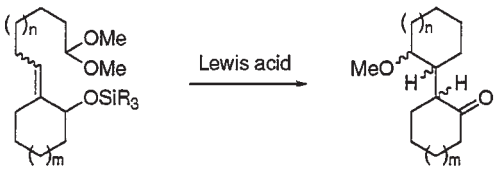
Résumé : On a réalisé la première étude de l'utilisation de cyclisations de Prins terminées par du pinacol dans le but de former produits auxquels des cycles sont attachés. Le traitement des éthers triisopropyliques des (*Z*)- et (*E*)-[2-(6,6-diméthoxyhexylidène)]-cyclohexanol avec du $SnCl_4$ conduit à la formation de produits bicycliques auxquels des cycles sont attachés. L'approche est utile en synthèse dans la série du *Z*-alkylidènecyclohexane puisque, par le biais d'une voie impliquant la migration d'un carbone dans l'étape du réarrangement pinacolique, elle conduit d'une façon sélective aux 1-(2-méthoxycyclohexyl)-cyclopentylcarboxaldéhydes épimères au niveau du méthoxy. La réaction du stéréoisomère *E* correspondant est plus complexe et elle conduit à un mélange de produits qui, dans l'étape du réarrangement pinacolique, résultent de migrations tant d'hydrure que de carbone.

Mots clés : cyclisation de Prins, réarrangement pinacolique, cycles attachés.

[Traduit par la Rédaction]

Introduction

Myriad opportunities in ring construction are realized by utilizing a pinacol rearrangement to terminate a Prins cyclization. One of the earliest examples is credited to Mousset and co-workers (1), who discovered serendipitously the synthesis of substituted tetrahydrofurans by acid-promoted reaction of allylic diols with aldehydes. Recent investigations in our laboratory (for brief reviews of our early work in this area, see ref. 2) (3), and elsewhere (for contributions from other laboratories, see ref. 4) have documented the utility of "Prins-pinacol" reactions for forming various oxacyclic and carbocyclic ring systems. We have highlighted the power of this ring construction method by employing it as the key strategic element in the synthesis of natural products having diverse architectures (5). Prins-pinacol reactions have been most widely employed to form fused polycyclic ring systems (2–5), while their use to form spirocyclic rings is less developed (3*i*). Herein we report the first use of a Prins-pinacol reaction to access attached rings, rings linked by a C—C σ-bond (eq. [1]). When the attachment centers are stereogenic,

[1] 

attached rings pose a notable challenge for stereocontrolled synthesis (the insect antifeedant azadirachtin is exemplary, see ref. 6).

Received September 25, 1999. Published on the NRC Research Press website on June 1, 2000.

Dedicated to Professor Stephen Hanessian in recognition of his many contributions to the science of organic synthesis.

L.E. Overman[1] and L.D. Pennington. Department of Chemistry, 516 Rowland Hall, University of California, Irvine, CA 92697-2025, U.S.A.

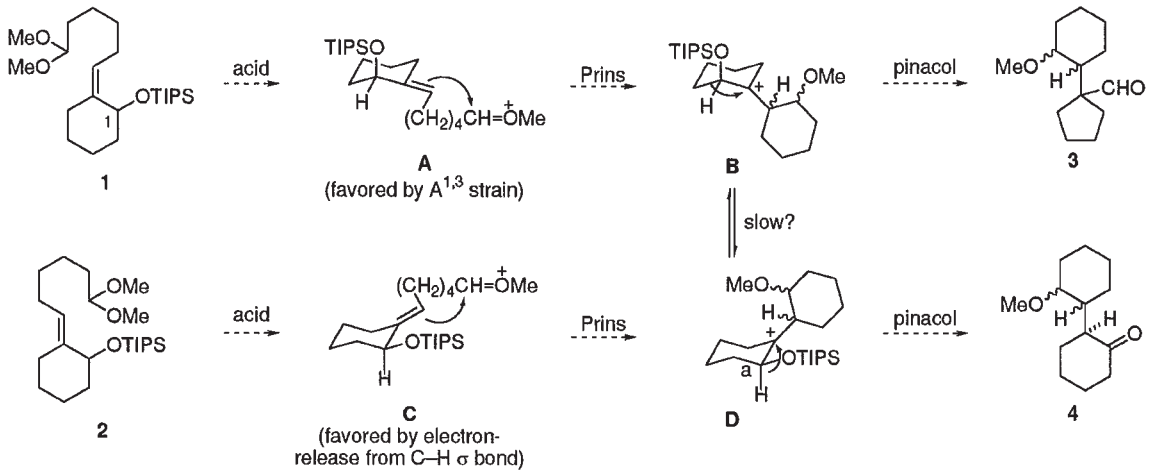
[1]Author to whom correspondence may be addressed. Fax: (949) 824-3866. e-mail: leoverma@uci.edu

Results

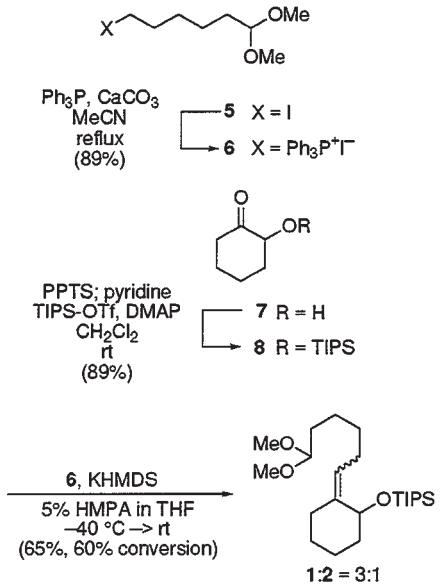
The *Z* and *E* alkylidenecyclohexanes **1** and **2** were chosen for this exploratory investigation (Scheme 1). The stereochemical outcome of the Prins-pinacol reactions studied in our laboratory is accommodated by a sequence in which stereochemistry is dictated in the Prins cyclization step, that is pinacol rearrangement occurs more rapidly than conformational changes of the putative carbocation generated upon Prins cyclization (3*i*). Thus, our initial expectation was that **1** and **2** would cyclize to give aldehyde **3** and ketone **4**, respectively. This prediction follows from the presumption that allylic interactions between the siloxy group and the alkylidene side chain ($A^{1,3}$ strain) would favor cyclization topography **A** for the *Z* substrate (7), while an electronic preference for having an electronegative oxygen substituent in the plane of the nucleophilic alkene π-system would favor topography **C** for the *E* substrate (8).

 © 2000 NRC Canada

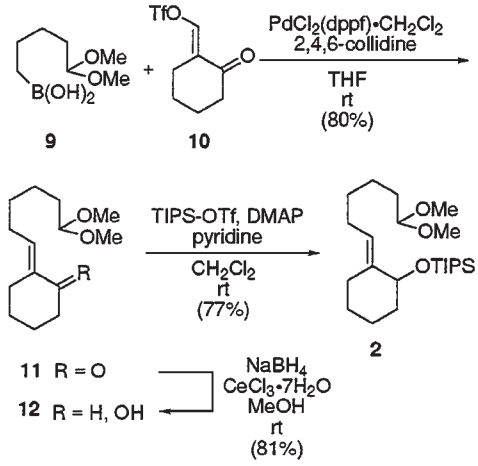
Scheme 1.



Scheme 2.



Scheme 3.



Pinacol rearrangement of carbocation **B** would occur by migration of a ring carbon to yield **3**, since the C_1—H σ-bond is orthogonal to the vacant *p*-orbital, preventing hydride migration. Pinacol rearrangement of carbenium ion **D** would produce **4** if hydride migration occurred in preference to migration of ring bond a (for reviews of the pinacol rearrangement, see ref. (9*a*)). The relative stereochemistry at the stereogenic attached carbons of **4** would be governed by which face of the alkene participated in the transformation of **C** → **D**. Additionally, the stereochemistry of the methoxy substituent in the products would be determined by the orientation of the alkene and the oxocarbenium ion during Prins cyclization. Although our exploratory investigations would be carried out with racemic substrates, one appeal of the route to **4** proposed in Scheme 1 was the expectation that **2** would also be readily available in enantioenriched form.

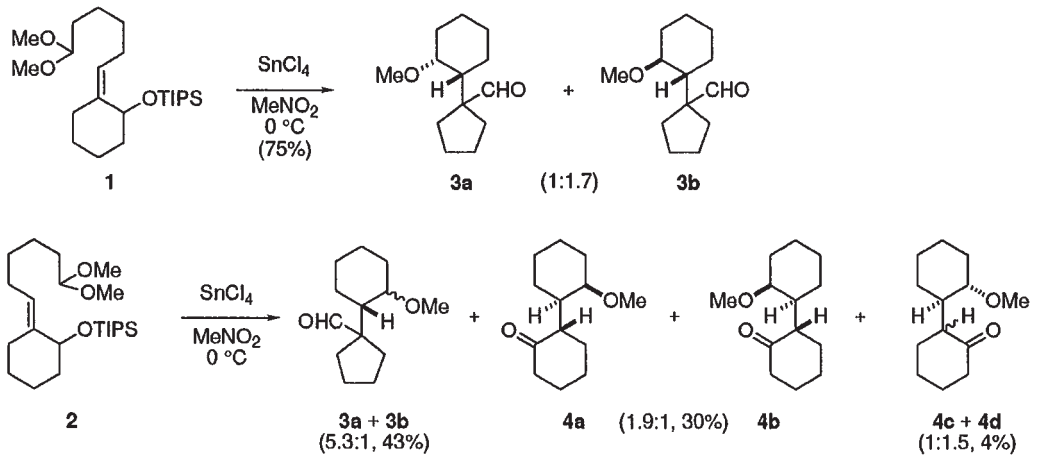
Alkylidenecyclohexyl ethers **1** and **2** were initially prepared by coupling phosphonium salt **6** (the known iodide **5** (10) was prepared in three steps and 72% yield from 6-bromohexan-1-ol: (*i*) PCC, CH_2Cl_2, rt; (*ii*) *p*-TsOH·H_2O, MeOH, rt; and (*iii*) NaI, acetone, rt) and α-siloxycyclohexanone **8**, utilizing "salt-free" Wittig conditions (11) (Scheme 2). The 3:1 mixture of **1** and **2** thus obtained could be separated by flash chromatography using $AgNO_3$-impregnated silica gel.

A route that would lend itself to obtaining enantioenriched **2** by enantioselective reduction of an enone precursor (12) was also developed (Scheme 3). The key step in this sequence was Suzuki coupling of boronic acid **9** generated in situ from the corresponding alkene (14) by a standard hydroboration–oxidation sequence (13), and enol triflate **10** (15) (although not mentioned in (15), triflate 10 decomposed rapidly at room temperature if 2,4,6-collidine was not present) to give enone **11**. Luche reduction (16) of **11** produced alcohol **12**, which was then silylated to furnish **2**.

^{1}H NMR nOe difference experiments readily confirmed stereochemical assignments for the alkylidene stereoisomers: **2** displayed reciprocal nOe enhancements between the vinylic and C1 hydrogens, while **1** did not. ^{1}H NMR spectra of **1** and **2** suggested somewhat different conformations for the two substrates. Diagnostic were signals for the C1

© 2000 NRC Canada

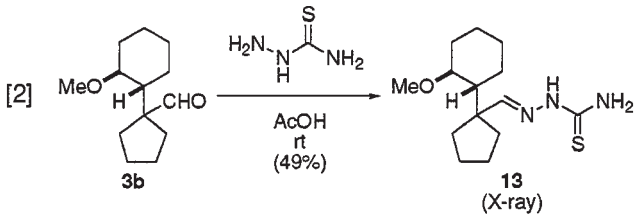
Scheme 4.



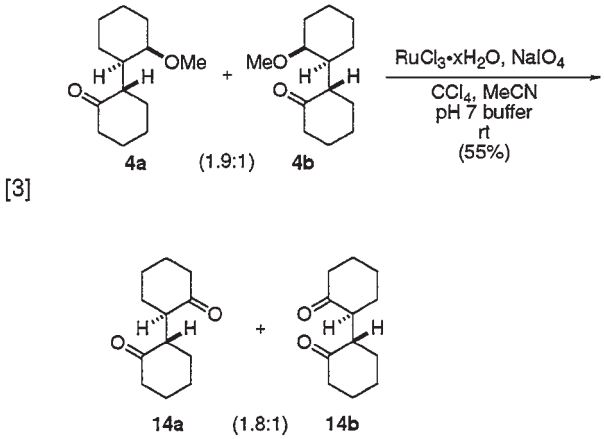
hydrogen, which for **1** appeared as a broad singlet ($w_{h/2}$ = 7.7 Hz) at δ 4.71, whereas the corresponding hydrogen of **2** appeared as a multiplet ($w_{h/2}$ = 15.4 Hz) at δ 4.10. These differences reflect the greater proportion of conformers having the siloxy substituent axial in **1**.

Exposure of **1** or **2** in $MeNO_2$ to 0.5 equiv. of $SnCl_4$ at 0°C for 2 h resulted in efficient Prins-pinacol reaction to give bicyclic products (Scheme 4). No reaction was observed under identical conditions at –23°C. The *Z* alkylidene substrate **1** provided exclusively aldehyde products **3a** and **3b** in a 1:1.7 ratio. In contrast, the *E* alkylidene substrate **2** delivered a complex mixture of six products, in which the ratio of cyclopentylcarboxyaldehyde to cyclohexanone products was 1.3:1. In this latter case, aldehyde stereoisomer **3a** was favored to the extent of 5.3:1, while two major ketone stereoisomers **4a** and **4b** were produced in a 1.9:1 ratio. With the exception of **4a** and **4b**, all products could be separated by medium pressure liquid chromatography (MPLC). The mixture of **4a** and **4b** was contaminated with triisopropylsiloxy residues, thus the yield and ratio of these products are estimates based on ^{1}H NMR analysis.

The stereochemistry of **3a** and **3b** were defined by single-crystal X-ray analysis of thiosemicarbazone derivative **13** prepared from **3b**[2] (eq. [2]). The relative stereochemistry of



the attached stereogenic carbons of **4a** and **4b** was determined by oxidizing (17) a 1.9:1 mixture of these stereoisomers with RuO_4 to yield a 1.8:1 mixture of the known diketones **14a** and **14b** (18) (eq. [3]). These diketones were readily separated by MPLC and characterized by their distinctive ^{1}H and ^{13}C NMR spectra (18). The



axial disposition of the methoxy substituent in **4a** and **4b** was readily apparent from ^{1}H NMR spectra: the ether methine hydrogens in the **4a**–**4b** mixture appear as partially overlapping broad singlets at δ 3.39 and δ 3.36, while the corresponding signals of **4c** and **4d** appear as diagnostic triplet of doublets at δ 3.30 (*J* = 10.3, 4.0 Hz) and δ 2.84 (*J* = 9.7, 4.0 Hz), respectively.

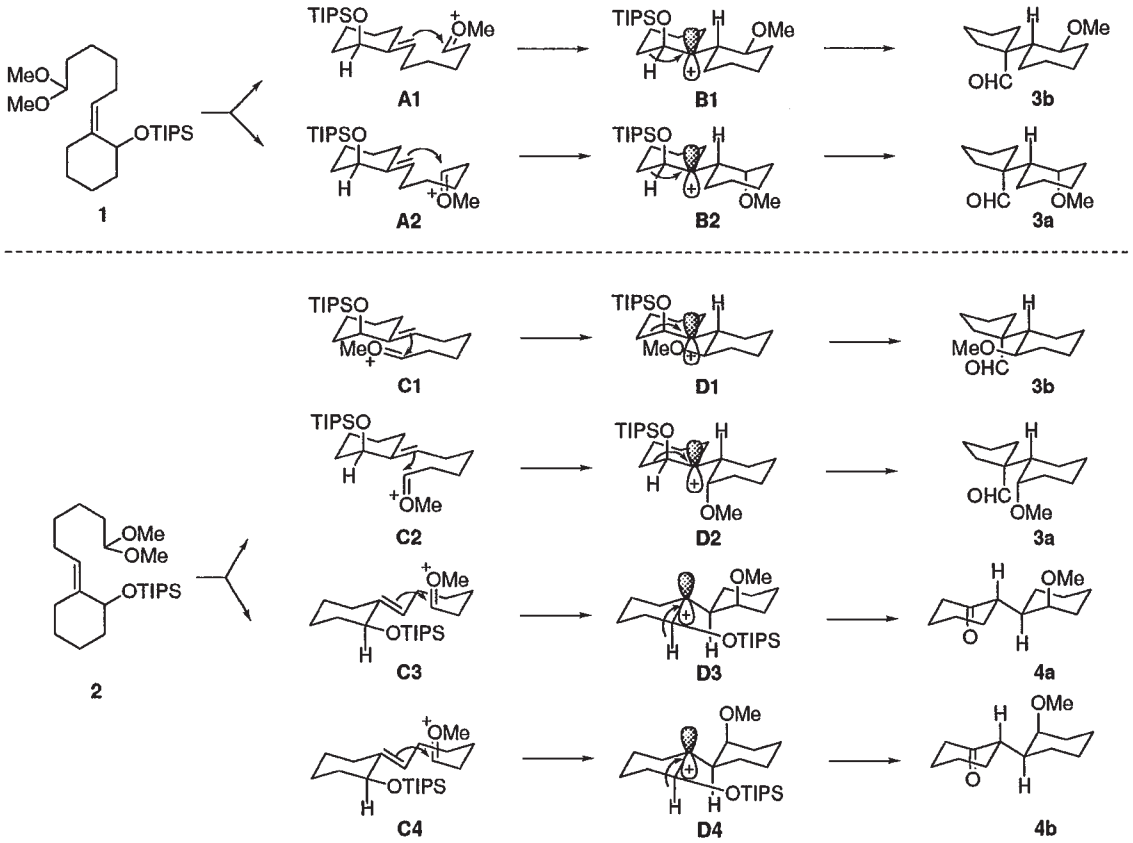
Discussion

The results summarized in Scheme 4 establish that Prins-pinacol reactions can be profitably employed to prepare attached ring systems. However, our initial expectations were realized to only a limited extent. As we had anticipated, the pinacol rearrangement step in the reaction of *Z* alkylidene stereoisomer **1** occurs exclusively by ring contraction (carbon migration) to form 1-(cyclohexyl)cyclopentylcarboxaldehyde products **3** (Scheme 5). Since hydride migration to form ketone products was not observed, conformational conversion of **B1** or **B2** to their pseudoequatorial siloxy counterparts apparently was not competitve with pinacol rearrangement. Attack of the alkene is depicted in Scheme 5

[2] The authors have deposited atomic coordinates for 13 with the Cambridge Crystallographic Data Centre. The coordinates can be obtained, on request, from the Director, Cambridge Crystallographic Data Centre, 12 Union Road, Cambridge, CB2, 1EZ, U.K.

© 2000 NRC Canada

Scheme 5.



to occur opposite the siloxy group in **A1** and **A2**, although there is no experimental support for this supposition. The stereochemical information necessary to define face selectivity is lost since C1 in **3** is not stereogenic.

The generation of both cyclopentylcarboxaldehyde and cyclohexanone products from Prins-pinacol reaction of *E* stereoisomer **2** is consistent with cyclization–rearrangement occurring through pathways of similar energy having the siloxy substituent either pseudoequatorial or pseudoaxial in the starting cyclohexane ring (Scheme 5). If this group is axial, cyclopentylcarboxaldehydes **3a** and **3b** would be formed (**C1** → **D1** → **3b** and **C2** → **D2** → **3a**). Alternatively, Prins cyclization of oxocarbenium ion conformers **C3** and **C4** having the siloxy substituent equatorial, would initially generate cyclohexyl cations **D3** and **D4**. Migration of either the ring bond to generate **3a**, or methine hydrogen to generate **4a** from **D3** (and **4b** from **D4**), is stereoelectronically feasible (the dihedral angle between both of these groups and the vacant *p*-orbital would be ca. 60°C; this analysis assumes that pinacol rearrangement occurs faster than conformational interconversion of the cyclohexylcarbenium ion (3*i*)). The typical preference for hydride migration in stereoelectronically unbiased systems suggest that **4a** and **4b** would be the major products of these latter pathways (for pinacol rearrangements of cyclohexylcarbenium ions, see ref. (9*b*)).

The stereochemistry of the methoxy substituent in aldehydes **3** and ketones **4** reflects the orientation of the alkene and the oxocarbenium ion in the Prins cyclization (Fig. 1). If

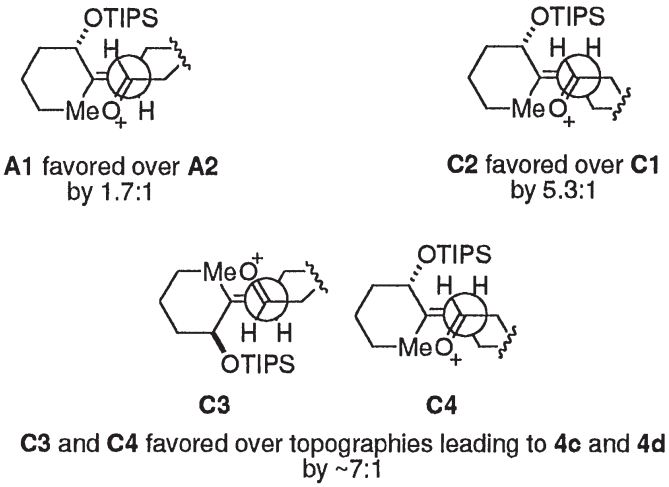


Fig. 1. Favored synclinal orientations in the Prins cyclization step of the exocyclic alkene and the α-alkoxycarbenium ion.

one assumes that the stereoisomeric products are generated by the sequences proposed in Scheme 5, a synclinal orientation (19) having the methoxy portion of the oxocarbenium ion oriented away from the siloxy group is favored in both reaction manifolds (Fig. 1).

© 2000 NRC Canada

Experimental section[3]

2-(Triisopropylsiloxy)cyclohexanone (8)

A mixture of pyridinium *p*-toluenesulfonate (PPTS, 0.22 g, 0.88 mmol), 2-hydroxycyclohexanone (1.0 g, 8.7 mmol), and CH_2Cl_2 (33 mL) was stirred at rt for 3 h. Pyridine (1.1 mL, 14 mmol), triisopropylsilyl triflate (TIPS-OTf, 3.3 mL, 12 mmol), and 4-(dimethylamino)pyridine (DMAP, 0.11 g, 0.92 mmol) were added sequentially and the resulting mixture was stirred at rt for 10 min. The mixture was partitioned between saturated aqueous $NaHCO_3$ (200 mL) and pentane (200 mL), the layers were separated and the organic layer was washed sequentially with H_2O (200 mL), and brine (200 mL), dried ($MgSO_4$), and concentrated. Purification of the residue by column chromatography on silica gel (18:1 hexane–ethyl acetate) gave 2.1 g (89%) of **8** as a clear pale yellow oil. FT-IR (neat): 1727 cm^{-1}. ^1H NMR (300 MHz, $CDCl_3$) δ: 4.21–4.16 (m, 1H), 2.68–2.59 (m, 1H), 2.26–2.17 (m, 1H), 2.08–1.58 (m, 6H), 1.15–0.96 (m, 21H). ^{13}C NMR (75 MHz, $CDCl_3$) δ: 210.4, 39.7, 37.3, 27.7, 22.2, 17.9, 17.7, 12.2. HRMS (FAB): *m*/*z* 271.2098 (MH, 271.2093 calcd. for $C_{15}H_{31}O_2Si$). Anal. calcd. for $C_{15}H_{30}O_2Si$: C 66.61, H 11.18; found: C 66.70, H 11.12.

***Z*-[2-(6,6-Dimethoxyhexylidene)cyclohexyloxy]triisopropylsilane (1)**

Calcium carbonate (0.81 g, 8.1 mmol), Ph_3P (5.1 g, 19 mmol), and CH_3CN (5.0 mL) were added sequentially to iodide **5** (10, 11, 24) (4.4 g, 16 mmol). After bubbling N_2 through the mixture for 5 min, the mixture was heated to reflux. After stirring for 2.5 h, the mixture was cooled to rt and concentrated. The crude product was purified by column chromatography on neutral alumina (sequential elution, 1:1 hexane–ethyl acetate, to isolate excess Ph_3P; 18:1 CH_2Cl2–MeOH, to isolate **6**) to give 7.7 g (89%) of slightly impure **6** as a hygroscopic and colorless waxy solid. ^1H NMR (300 MHz, $CDCl_3$) δ: 7.75–7.61 (m, 15H), 4.21 (t, *J* = 5.5 Hz, 1H), 3.57–3.48 (m, 2H), 3.19 (s, 6H), 1.59–1.23 (m, 8H). HRMS (CI): *m*/*z* 407.2131 (M–I, 407.2140 calcd. for $C_{26}H_{32}O_2P$).

Using a modified version of the general procedure of Koreeda et al. (12), potassium bis(trimethylsilyl)amide (KHMDS, 30 mL, 15 mmol, 0.5 M solution in toluene) was added to a solution of phosphonium salt **6** (7.4 g, 14 mmol) in THF (83 mL) and hexamethylphosphoramide (HMPA, 9.2 mL) at –40°C. After stirring the resulting mixture for 10 min, a cooled (–40°C) solution of **8** (1.9 g, 9.9 mmol) and THF (7.7 mL) was added, and the cooling bath was removed. After 1 h, saturated aqueous $NaHCO_3$ (100 mL) and hexanes (200 mL) were added and the layers were separated. The organic layer was washed sequentially with saturated aqueous $NaHCO_3$ (200 mL), 10% aqueous $Na_2S_2O_3$ (200 mL), H_2O (100 mL), brine (100 mL), dried ($MgSO_4$), and concentrated. The crude product was purified by column chromatography on $AgNO_3$-impregnated silica gel (9:1 CH_2Cl_2–benzene), yielding 0.92 g of a mixture of **1** and **8** and 0.13 g of a mixture of **1** and **2**.

Pure **1** was obtained from the mixture of **1** and **8** as follows. Sodium borohydride ($NaBH_4$, 41 mg, 1.1 mmol) was added to a solution of the **1**–**8** mixture (0.92 g) and MeOH (5.0 mL). After stirring for 20 min, saturated aqueous $NaHCO_3$ (5 mL) and hexanes (100 mL) were added, the organic layer was washed with saturated aqueous $NaHCO_3$ (3 × 50 mL) and brine (100 mL), dried ($MgSO_4$), and concentrated. The silyl ether protecting group of the diols derived from **8** was then selectively removed (to facilitate isolation of pure **1**) by maintaining a solution of this residue, tetra-*n*-butylammonium fluoride (TBAF, 0.86 mL, 0.86 mmol, 1.0 M solution in THF), and THF (5.0 mL) at rt for 12 h. Saturated aqueous $NaHCO_3$ (10 mL) and hexanes (70 mL) were added, the organic layer was washed with saturated aqueous $NaHCO_3$ (5 × 50 mL), brine (50 mL), dried ($MgSO_4$), and concentrated. The crude product was purified by column chromatography on silica gel (18:1 hexane–ethyl acetate) to give 0.70 g (42%, 3 steps, 60% conversion during Wittig coupling) of **1** as a clear yellow oil. ^1H NMR (300 MHz, $CDCl_3$) δ: 5.01 (t, *J* = 6.9 Hz, 1H), 4.71 (br s, 1H), 4.35 (t, *J* = 5.6 Hz, 1H), 3.31 (s, 6H), 2.50–2.45 (m, 1H), 2.03–1.22 (m, 15H), 1.04–0.93 (m, 21H). ^{13}C NMR (75 MHz, $CDCl_3$) δ: 141.8, 121.5, 104.4, 66.0, 52.6, 52.5, 36.1, 32.4, 30.0, 28.9, 27.0, 24.4, 20.5, 18.1, 18.0, 12.3. FT-IR (neat): 2938, 2864 cm^{-1}. HRMS (FAB): *m*/*z* 397.3148 (M–H, 397.3138 calcd. for $C_{23}H_{45}O_3Si$). Anal. calcd. for $C_{23}H_{46}O_3Si$: C 69.29, H 11.63; found: C 69.38, H 11.53.

***E*-[2-(6,6-Dimethoxyhexylidene)]cyclohexanone (11)**

A mixture of 9-borabicyclo[3.3.1]nonane (9-BBN, 2.5 g, 10 mmol) in THF (65 mL) was added to a solution of 1,1-dimethoxypent-4-ene (15) (2.4 mL, 16 mmol) and THF (21 mL) at 0°C, and the cooling bath was removed. After stirring for 6 h, 3 M aqueous NaOH (7.6 mL, 23 mmol) was added, and after stirring vigorously for an additional 15 min, the crude organoborane was added by cannula to a solution of triflate **10** (2.1 g, 8.3 mmol), 2,4,6-collidine (3.0 g, 25 mmol), $PdCl_2(dppf)\bullet CH_2Cl_2$ (0.93 g, 1.1 mmol), and THF (40 mL). After stirring for 30 min, the reaction mixture was partitioned between pentane (200 mL) and H_2O (200 mL) and the layers were separated. The organic layer was washed sequentially with saturated aqueous $CuSO_4$ (3 × 200 mL), saturated aqueous $NaHCO_3$ (200 mL), and brine (200 mL), dried ($MgSO_4$), and concentrated. The residue was triturated with pentane and the filtrate was concentrated. The crude product was purified by column chromatography on silica gel (5:1 hexane–ethyl acetate) to give 2.2 g (80%) of **11** as a clear pale yellow oil. ^1H NMR (300 MHz, $CDCl_3$) δ: 6.58 (t, *J* = 7.5 Hz, 1H), 4.32 (t, *J* = 5.7 Hz, 1H), 3.28 (s, 6H), 2.46–2.37 (m, 4H), 2.08 (q, *J* = 7.3 Hz, 2H), 1.86–1.30 (m, 10H). ^{13}C NMR (75 MHz, $CDCl_3$) δ: 201.1, 139.2, 136.2, 104.3, 52.6, 40.1, 32.2, 28.2, 27.6, 26.6, 24.3, 23.5, 23.3. FT-IR (neat): 1688, 1615 cm^{-1}. HRMS (FAB): *m*/*z* 263.1616 (M+Na, 263.1623 calcd. for $C_{14}H_{24}NaO_3$).

***E*-[2-(6,6-Dimethoxyhexylidene)]cyclohexanol (12)**

Cerium(III) chloride heptahydrate (3.4 g, 9.0 mmol) was added to a solution of **11** (2.2 g, 9.0 mmol) and MeOH

[3] Experimental details for preparation of **5** and correlation of the **4a**–**4b** mixture with diketones **14*a*** and **14*b*** are provided as Supplementary Material.

© 2000 NRC Canada

(49 mL). After stirring for 5 min, $NaBH_4$ (0.37 g, 9.7 mmol) was added portionwise, and after stirring for an additional 20 min, saturated aqueous $NaHCO_3$ (10 mL) and pentane (250 mL) were added. The organic layer was washed with saturated aqueous $NaHCO_3$ (2 × 150 mL), brine (2 × 150 mL), dried ($MgSO_4$), and concentrated. The crude product was purified by column chromatography on silica gel (5:1 hexane–ethyl acetate) to give 1.7 g (78%) of **12** as a clear pale yellow oil. ^{1}H NMR (300 MHz, $CDCl_3$) δ: 5.32 (t, *J* = 6.8 Hz, 1H), 4.33 (t, *J* = 5.7 Hz, 1H), 4.04 (br s, 1H), 3.28 (s, 6H), 2.41–2.33 (m, 1H), 2.01–1.33 (m, 16H). ^{13}C NMR (75 MHz, $CDCl_3$) δ: 141.1, 120.8, 104.4, 73.6, 52.5, 36.1, 32.2, 29.7, 27.2, 26.6, 25.9, 24.2, 22.8. FT-IR (neat): 3440 cm^{-1}. HRMS (FAB): *m*/*z* 265.1773 (M+Na, 265.1779 calcd. for $C_{14}H_{26}NaO_3$). Anal. calcd. for $C_{14}H_{26}O_3$: C 69.38, H 10.81; found: C 69.17, H 10.65.

_E_-[2-(6,6-Dimethoxyhexylidene)cyclohexyloxy]triisopropylsilane (2)

Pyridine (0.77 mL, 9.5 mmol), TIPS-OTf (2.6 mL, 9.5 mmol), and DMAP (0.083 g, 0.68 mmol) were added sequentially to a solution of **12** (1.7 g, 6.8 mmol) and CH_2Cl_2 (68 mL). After stirring for 20 min, the reaction mixture was partitioned between pentane (125 mL) and saturated aqueous $NaHCO_3$ (100 mL). The organic layer was washed sequentially with saturated aqueous $NaHCO_3$ (100 mL), H_2O (75 mL), saturated aqueous $CuSO_4$ (75 mL), H_2O (75 mL), and brine (2 × 75 mL), dried ($MgSO_4$), and concentrated. The crude product was purified by column chromatography on silica gel (18:1 hexane–ethyl acetate) to give 2.0 g (73%) of **2** as a clear pale yellow oil. ^{1}H NMR (300 MHz, $CDCl_3$) δ: 5.34 (t, *J* = 7.3 Hz, 1H), 4.35 (t, *J* = 5.7 Hz, 1H), 4.11–4.09 (m, 1H), 3.31 (s, 6H), 2.38–2.35 (m, 1H), 2.01–1.34 (m, 15H), 1.10–0.98 (m, 21H). ^{13}C NMR (75 MHz, $CDCl_3$) δ: 141.5, 120.4, 104.5, 74.5, 52.6, 37.5, 32.4, 29.8, 27.6, 26.6, 25.9, 24.3, 22.8, 18.1, 12.3. FT-IR (neat): 2939, 2863 cm^{-1}. HRMS (CI): *m*/*z* 398.3216 (M, 398.3216 calcd. for $C_{23}H_{46}O_3Si$). Anal. calcd. for $C_{23}H_{46}O_3Si$: C 69.29. H 11.63; found: C 69.39, H 11.69.

Prins-pinacol rearrangement of 2

Tin(IV) chloride ($SnCl_4$, 0.20 mL, 1.7 mmol) was added dropwise to a stirring suspension of **2** (1.4 g, 3.4 mmol) and $MeNO_2$ (34 mL) at 0°C. After stirring at 0°C for 2 h, Et_3N (15 mL) and MeOH (15 mL) were added sequentially, and the mixture was warmed to rt and was diluted with hexanes (250 mL). The organic layer was washed with saturated aqueous $NaHCO_3$ (3 × 200 mL) and brine (200 mL), dried ($MgSO_4$), and concentrated. The crude product was purified by medium pressure liquid chromatography (MPLC) (Lobar prepacked column, LiChroprep™ Si 60 silica gel; gradient elution, hexane → 18:1 hexane–ethyl acetate) to give the following fractions.

3a

0.27 g (37%) as a clear, pale yellow oil. FT-IR (neat): 1715 cm^{-1}. ^{1}H NMR (300 MHz, $CDCl_3$) δ: 9.56 (s, 1H), 3.39 (br s, 1H), 3.15 (s, 3H), 2.27–2.21 (m, 1H), 2.02–1.96 (m, 2H), 1.79–1.13 (m, 14H). ^{13}C NMR (75 MHz, $CDCl_3$) δ: 203.7, 60.4, 55.7, 53.0, 32.6, 31.4, 27.8, 26.7, 24.8, 24.1, 23.3, 19.9. HRMS (FAB): *m*/*z* 211.1703 (M+H, 211.1698 calcd. for $C_{13}H_{22}O_2$). This product was unstable and was converted immediately to the corresponding thiosemicarbazone **15** for additional characterization (vide infra).

3b

0.039 g (5%) as a clear colorless oil. FT-IR (neat): 1714 cm^{-1}. ^{1}H NMR (300 MHz, $CDCl_3$) δ: 9.28 (s, 1H), 3.11 (s, 3H), 2.67 (td, *J* = 9.7, 3.7 Hz, 1H), 2.14–2.03 (m, 2H), 1.85–1.04 (m, 15H). ^{13}C NMR (75 MHz, $CDCl_3$) δ: 201.3, 82.1, 58.8, 55.6, 47.5, 31.3, 30.9, 26.9, 25.8, 25.2, 25.1, 24.9, 24.5. HRMS (FAB): *m*/*z* 211.1696 (M+H, 211.1698 calcd. for $C_{13}H_{22}O_2$). This product was unstable and was converted immediately to thiosemicarbazone **13** (vide infra).

4a* + *4b

0.25 g (30%, contaminated with what is estimated by ^{1}H NMR analysis to be 40 mg of hydroxytriisopropylsilane, TIPS-OH) as a clear, pale yellow oil. Characterization data for this mixture, FT-IR (neat): 1707 cm^{-1}. ^{1}H NMR (300 MHz, $CDCl_3$) δ: 3.39 (br s, 1H), 3.36 (br s, 1H), 3.25 (s, 3H), 3.21 (s, 3H), 2.61–1.12 (m, 36H). ^{13}C NMR (75 MHz, $CDCl_3$) δ: 214.3, 77.6, 74.7, 56.2, 55.6, 53.5, 51.9, 42.8, 42.7, 39.5, 39.1, 31.2, 30.9, 29.1, 28.8, 27.8, 27.5, 26.5, 26.0, 25.9, 24.9, 24.8, 23.2, 19.9, 19.8. HRMS (CI): *m*/*z* 211.1696 (M+H, 211.1698 calcd. for $C_{13}H_{22}O_2$). This mixture was converted immediately to known diketones **14a** and **14b** (vide infra).

4c

10 mg (1.5%) as a clear, colorless oil. FT-IR (neat): 1707 cm^{-1}. ^{1}H NMR (300 MHz, $CDCl_3$) δ: 3.30 (td, *J* = 10.3, 4.0 Hz, 1H), 3.26 (s, 3H), 2.61–2.56 (m, 1H), 2.39–1.02 (m, 17H). ^{13}C NMR (75 MHz, $CDCl_3$) δ: 212.6, 80.4, 55.9, 50.0, 45.2, 42.2, 30.8, 30.0, 26.8, 26.5, 26.1, 24.9. HRMS (CI): *m*/*z* 211.1695 (M+H, 211.1698 calcd. for $C_{13}H_{22}O_2$).

4d

17 mg (2.3%) as a clear, colorless oil. FT-IR (neat): 1707 cm^{-1}. ^{1}H NMR (300 MHz, $CDCl_3$) δ: 3.24 (s, 3H), 2.84 (td, *J* = 9.7, 4.0 Hz, 1H), 2.62 (m, 1H), 2.46 (m, 1H), 2.29–1.61 (m, 12H), 1.29–0.87 (m, 4H). ^{13}C NMR (75 MHz, $CDCl_3$) δ: 212.9, 80.3, 55.7, 50.9, 41.7, 30.8, 27.7, 27.5, 27.1, 25.6, 24.7, 24.1. HRMS (FAB): *m*/*z* 211.1694 (M+H, 211.1698 calcd. for $C_{13}H_{22}O_2$).

Prins-pinacol rearrangement of 1

The procedure was identical to that described above for **2**; **1** gave 0.11 g (29%) of **3a** and 0.17 g (46%) of **3b** as clear, pale yellow oils.

(±)-*rel*-*R*,*S*-[1-(2-Methoxycyclohexyl)cyclopentylmethylene]thiosemicarbazone (15)

A solution of **3a** (0.049 g, 0.23 mmol), glacial acetic acid (2.3 mL), and thiosemicarbazide (0.043 g, 0.47 mmol) was maintained at rt for 4 h. The reaction mixture was diluted with toluene (5.0 mL), concentrated, and the residue was purified by column chromatography on silica gel (5:1 hexane–ethyl acetate) to give 66 mg (81%) of **15** as an off-white solid, mp 175–177°C. FT-IR (KBr): 3435, 3256, 3149, 3029,

© 2000 NRC Canada

1594, 1534 cm^{-1}. ^1H NMR (300 MHz, $CDCl_3$) δ: 8.99 (br s, 1H), 7.33 (s, 1H), 7.03 (br s, 1H), 6.26 (br s, 1H), 3.47 (br s, 1H), 3.19 (s, 3H), 2.13–1.92 (m, 3H), 1.76–1.13 (m, 14H). ^{13}C NMR (75 MHz, $CDCl_3$) δ: 177.8, 154.8, 77.2, 55.5, 53.3, 52.9, 34.8, 34.7, 28.1, 26.5, 23.7, 23.4, 19.8. HRMS (CI): *m*/*z* 283.1712 (M, 283.1718 calcd. for $C_{14}H_{25}N_3OS$). Anal. calcd. for $C_{14}H_{25}N_3OS$: C 59.33, H 8.89, N 14.83; found: C 59.45, H 8.86, N 14.71.

(±)-*rel*-*S*,*S*-[1-(2-Methoxycyclohexyl)cyclopentylmethylene]thiosemicarbazone (13)

The procedure followed was identical to that described for **3a**; **3b** gave 0.088 g (49%) of **13** as a colorless solid, mp 168–170°C. FT-IR (KBr): 3430, 3269, 3142, 1589, 1522 cm^{-1}. ^1H NMR (300 MHz, $CDCl_3$) δ: 10.03 (br s, 1H), 7.29 (s, 1H), 7.05 (d, *J* = 3.0 Hz, 1H), 6.68 (br s, 1H), 3.21 (s, 3H), 2.76 (td, *J* =10.0, 3.9 Hz, 1H), 2.13–1.93 (m, 3H), 1.84–0.91 (m, 14H). ^{13}C NMR (75 MHz, $CDCl_3$) δ: 177.4, 154.8, 82.1, 55.4, 52.7, 52.1, 36.4, 32.6, 31.2, 27.3, 25.8, 24.5, 24.2, 23.2. HRMS (CI): *m*/*z* 283.1719 (M, 283.1718 calcd. for $C_{14}H_{25}N_3OS$). Anal. calcd. for $C_{14}H_{25}N_3OS$: C 59.33, H 8.89, N 14.83; found: C 59.36, H 8.84, N 14.72.

Conclusions

This study constitutes the first investigation of the use of pinacol-terminated Prins cyclizations to form attached rings. In the *Z* alkylidenecyclohexane series, the approach is synthetically useful, proceeding selectively by a pathway involving carbon migration, to provide methoxy epimers of 1-(2-methoxycyclohexyl)cyclopentylcarboxaldehyde. Reaction of the corresponding *E* stereoisomer is more complex and yields a mixture of products resulting from both hydride and carbon migration. Future efforts to exploit this novel approach to the synthesis of attached rings should focus on *Z* alkylidene substrates.

Acknowledgements

This research was supported by NIH grant NS-12389. We are grateful to Dr. Joseph Ziller for X-ray analyses and Dr. John Greaves and Dr. John Mudd for mass spectrometric analyses. NMR and mass spectra were obtained at UCI using instrumentation acquired with the assistance of NSF and NIH Shared Instrumentation programs.

References

1. (*a*) P. Martinet, G. Mousset, and M.C.R. Colineau. Acad. Sci. Ser. C, **268**, 1303 (1969); (*b*) P. Martinet and G. Mousset. Bull. Soc. Chim. Fr. 1071 (1970); (*c*) P. Martinet and G. Mousset. Bull. Soc. Chim. Fr. 4093 (1971).
2. (*a*) L.E. Overman. Lect. Heterocycl. Chem. **8**, 59 (1985); (*b*) L.E. Overman. NATO ASI Ser. Ser. C, **289**, 1 (1989); (*c*) L.E. Overman. Acc. Chem. Res. **25**, 352 (1992); (*d*) L.E. Overman. Aldrichimica Acta, **28**, 107 (1995).
3. (*a*) P.M. Herrinton, M.H. Hopkins, P. Mishra, M.J. Brown, and L.E. Overman. J. Org. Chem. **52**, 3711 (1987); (*b*) M.H. Hopkins and L.E. Overman. J. Am. Chem. Soc. **109**, 4748 (1987); (*c*) G.C. Hirst, P.N. Howard, and L.E. Overman. J. Am. Chem. Soc. **111**, 1514 (1989); (*d*) T.O. Johnson, Jr. and L.E. Overman. Tetrahedron Lett. **32**, 7361 (1991); (*e*) M.H. Hopkins, L.E. Overman, and G.M. Rishton. J. Am. Chem. Soc. **113**, 5354 (1991); (*f*) M.J. Brown, T. Harrison, P.M. Herrinton, M.H. Hopkins, K.D. Hutchinson, P. Mishra, and L.E. Overman. J. Am. Chem. Soc. **113**, 5365 (1991); (*g*) L.E. Overman and G.M. Rishton. Org. Synth., **71**, 63 (1992); (*h*) S. Ando, K.P. Minor, and L.E. Overman. J. Org. Chem. **62**, 6379 (1997); (*i*) K.P. Minor and L.E. Overman. Tetrahedron, **53**, 8927 (1997); (*j*) M.J. Cloninger and L.E. Overman. J. Am. Chem. Soc. **121**, 1092 (1999).
4. (*a*) M. Sworin and W.L. Neumann. J. Org. Chem. **53**, 4894 (1988); (*b*) B.M. Trost and D.C. Lee. J. Am. Chem. Soc. **110**, 6556 (1988); (*c*) T. Nakamura, T. Matsui, K. Tanino, and I. Kuwajima. J. Org. Chem. **62**, 3032 (1997).
5. (*a*) M.J. Brown, T. Harrison, and L.E. Overman. J. Am. Chem. Soc. **113**, 5378 (1991); (*b*) G.C. Hirst, T.O. Johnson, and L.E. Overman. J. Am. Chem. Soc. **115**, 2992 (1993); (*c*) T.A. Grese, K.D. Hutchinson, and L.E. Overman. J. Org. Chem. **58**, 2468 (1993); (*d*) D.W.C. MacMillan and L.E. Overman. J. Am. Chem. Soc. **117**, 10391 (1995).
6. S.V. Ley, A.A. Denholm, and A. Wood. Nat. Prod. Rep. 109 (1993).
7. E.L. Eliel and S.H. Wilen. *In* Stereochemistry of organic compounds. John Wiley & Sons, New York. 1994, p. 738.
8. (*a*) K.N. Houk, S.R. Moses, W. Yun-Dong, R. Nelson, J. Volker, R. Schohe, and F.R. Fronczek. J. Am. Chem. Soc. **106**, 3880 (1984); (*b*) K.N. Houk, J. Haller, and T. Strassner. J. Am. Chem. Soc. **119**, 8031 (1997).
9. (*a*) M. Bartok and A. Molnar. *In* Chemistry of ethers, crown ethers, hydroxyl compounds and their sulfur analogs. Part 2. *Edited by* S. Patai. New York. 1980; and B. Rickborn. *In* Comprehensive organic synthesis. Vol. 3. *Edited by* B.M. Trost. Pergamon Press, Oxford, U.K. 1991; (*b*) P.L. Barili, G. Berti, B. Macchia, F. Macchia, and L. Monti. J. Chem. Soc. C, 1168 (1970).
10. B.G. Kovalev, R.N. Vaskan, and E.S. Lavrinenko. Zh. Org. Khim. **7**, 667 (1971).
11. M. Koreeda, P.D. Patel, and L. Brown. J. Org. Chem. **50**, 5910 (1985).
12. A.F. Simpson, D.C. Lathbury, and T. Gallagher. Tetrahedron: Asymmetry, **8**, 673 (1997).
13. N. Miyaura and A. Suzuki. Chem. Rev. **95**, 2457 (1995).
14. C.C. Price and R.B. Balsley. J. Org. Chem. **31**, 3406 (1966).
15. K. Brickmann, F. Hambloch, J. Suffert, and R. Bruckner. Liebigs Ann. Chem. 457 (1996).
16. A.L. Gemal and J.L. Luche. J. Am. Chem. Soc. **103**, 5454 (1981).
17. P.H.J. Carlsen, T. Katsuki, V.S. Martin, and K.B. Sharpless. J. Org. Chem. **46**, 3936 (1981).
18. S.E. Denmark, C.J. Cramer, and J.A. Sternberg. Tetrahedron Lett. **27**, 3693 (1986).
19. S.E. Denmark, E.J. Weber, T.M. Wilson, and T.M. Willson. Tetrahedron, **45**, 1053 (1989).

© 2000 NRC Canada

Stereoselective synthesis of renin inhibitor BILA 2157 BS

Bruno Simoneau, Pierre Lavallée, Murray Bailey, Jean-Simon Duceppe, Chantal Grand-Maître, Louis Grenier, William W. Ogilvie, Marc-André Poupart, and Bounkham Thavonekham

Abstract: We have developed a convergent and stereoselective synthesis of orally active renin inhibitor **BILA 2157 BS**. Three building blocks were used to generate the basic skeleton of the inhibitor. The key feature consisted of the late elaboration of the 2-amino-4-thiazolyl heterocycle from a vinylbromide precursor. The synthetic sequence, which required a total of 22 chemical steps, provided 0.6 kg of **BILA 2157 BS** in 7.3% overall yield.

Key words: renin, inhibitor, peptidomimetic, stereoselective synthesis.

Résumé: On a développé une synthèse convergente et stéréosélective de **BILA 2157 BS**, un inhibiteur de la rénine actif oralement. Trois synthons ont été utilisés pour assembler le squelette de base de l'inhibiteur. L'élaboration tardive de l'hétérocycle, le 2-amino-4-thiazolyl, à partir d'un précurseur bromovinyl a constitué l'étape clé de l'approche utilisée. La synthèse, qui a requis un total de 22 transformations chimiques, a fourni 0.6 kg de **BILA 2157 BS** avec 7.3% de rendement.

Mots clés : rénine, inhibiteur, peptido-mimétique, synthèse stereosélective.

Introduction

Renin, an aspartyl protease, catalyzes in the first and rate-limiting step of the renin–angiotensin cascade (1). Renin cleaves its substrate angiotensinogen to generate angiotensin I, a decapeptide, that is in turn processed to angiotensin II by the angiotensin converting enzyme (ACE). Angiotensin II is one of the most potent vasoconstrictors known. The success of ACE inhibitors in the treatment of hypertension has been an incentive for the search for other modes of intervention in the same cascade. Considerable efforts were invested in the search for orally active renin inhibitors (1) and angiotensin II antagonists (2). Our own efforts led to the identification of **BILA 2157 BS**, a potent and specific inhibitor of human renin (3). This inhibitor exhibited IC_{50} values of 1.4 and 2.7 nM in human plasma renin assays at pH 6.0 and 7.4 respectively. **BILA 2157 BS** was selected as a candidate for pre-development based on its high in vivo efficacy in a primate model of hypertension. This compound was orally active at a dose of 3 mg/kg in conscious sodium depleted cynomolgus monkeys and possessed an outstanding oral bioavailability of 40% in cynomolgus monkey. A large amount of **BILA 2157 BS** was required for toxicity studies. We report here an improved synthetic sequence for the preparation of **BILA 2157 BS** on a 0.6 kg scale.

Received March 12, 1999. Published on the NRC Research Press website on June 7, 2000.

This research article is dedicated with friendship and admiration to Professor Stephen Hanessian on the occasion of his 65th birthday.

B. Simoneau,[1] P. Lavallée, M. Bailey, J.-S. Duceppe, C. Grand-Maître, L. Grenier,[2] W.W. Ogilvie, M.-A. Poupart, and B. Thavonekham. Boehringer Ingelheim (Canada) Ltd., Bio-Méga Research Division, 2100 Cunard Street, Laval QC H7S 2G5, Canada.

[1]Author to whom correspondence may be addressed. Telephone: (450) 682-4640. Fax: (450) 682-4189. e-mail: bsimoneau@lav.boehringer-ingelheim.com

[2]Present address: ProScript, Inc., 38 Sidney Street, Cambridge, MA 02139, U.S.A.

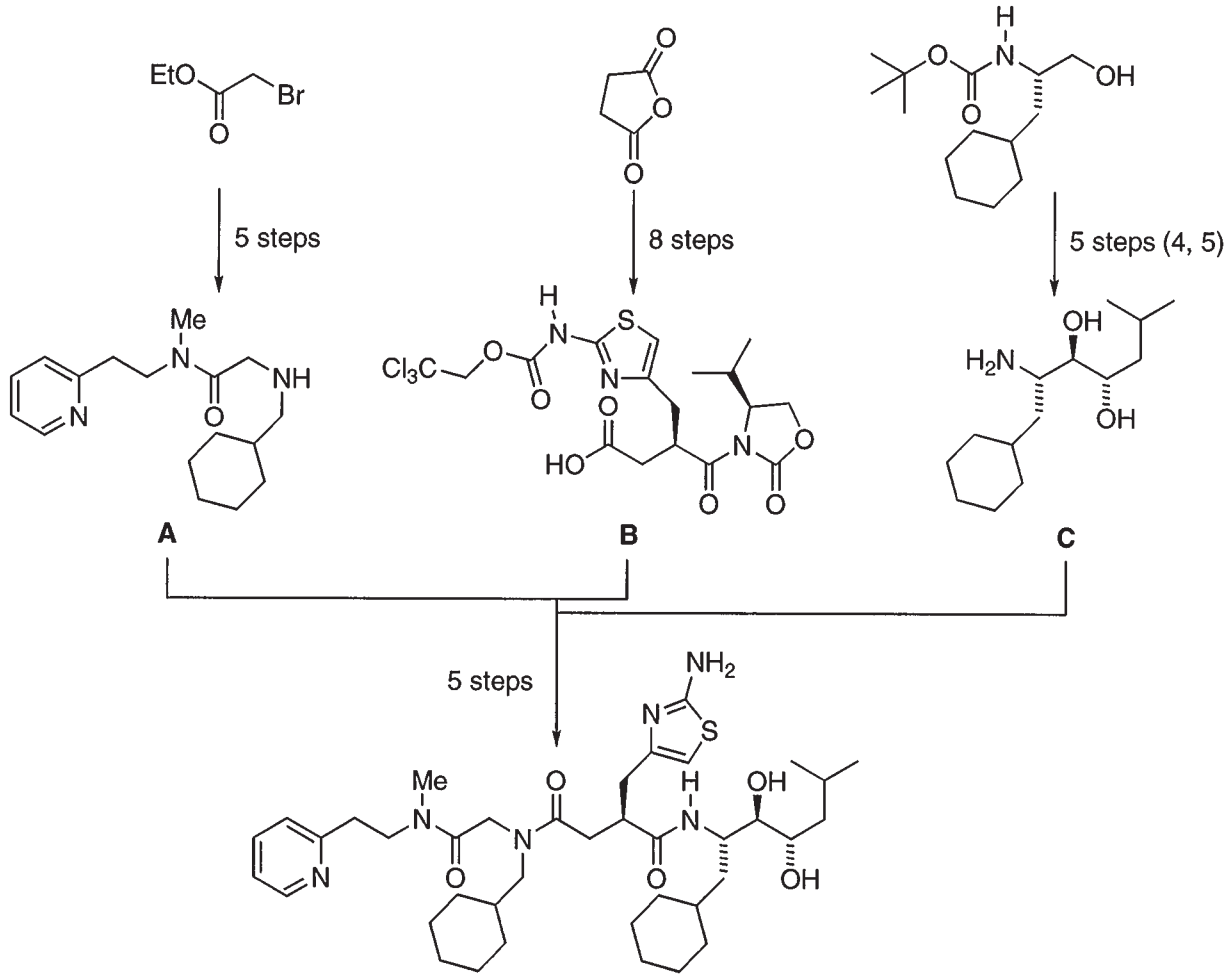
Discussion

BILA 2157 BS is a non-peptidic renin inhibitor that contains four stereogenic centers. Three of them are located in the transition state analog moiety (P_1-P_1') and one is located on the P_2-P_3 butanediamide segment. A convergent approach based on three key fragments was originally used in medicinal chemistry to provide the inhibitor in 23 steps and in about 6% yield overall (Scheme 1). This synthetic approach, developed for structure-activity relationship studies, was utilized for the preparation of inhibitors on a relatively small scale (from 100 mg to a few grams).

In the analysis of the original synthesis (3), we realized that some critical problems had to be considered and solved for the preparation of hundreds of grams of **BILA 2157 BS**. We considered that the fragments **A** and **C** (4, 5) could be amenable to kilogram scale preparation using the existing synthetic sequences. In contrast, the use of diazomethane in the preparation of fragment **B** should preferably be avoided on large scale. In addition, the use of the rather expensive chiral oxazolidinone was also a pertinent question although it provided high diastereoselectivity and could be recycled. The major drawback of this synthesis was the concomitant formation of the 2(*S*)-butanediamide epimer (5 to 10%) in the coupling of the **A**-**B** acid unit to **C**, which made purification of the trichloroethyl carbamate derivative, or **BILA**

 © 2000 NRC Canada

Scheme 1. Original synthesis of **BILA 2157 BS**.



2157 BS itself, extremely difficult. Since these two compounds were amorphous solids, chromatography was the only solution for removal of this undesired side product. The separation and purification could be achieved on a gram scale but was considered to be impractical on large amounts. The formation of salts of **BILA 2157 BS** did not produce any crystalline salt and was complicated by the presence of products resulting from *N*,*O*-acyl shift of the aminodiol portion (6).[3] A potential solution to the problem generated by the presence of the 2(*S*)-butanediamide epimer came from the observations made during the optimization of the P_2 side-chain of the inhibitors. During these studies, we realized that neutral side-chains such as cyclopropylmethyl or thienylmethyl produced very low levels of the undesired epimer at C-2 of the 4-oxo-4-substituted aminobutanoic acids. It was therefore decided to delay the introduction of the 2-amino-4-thiazolyl heterocycle until the end of the synthesis while maintaining a convergent approach.

As a result of this exercise, we selected synthon **B′** (Scheme 2), which had a 2-bromo-2-propenyl substituent in contrast to the synthon **B** utilized in the first approach. The bromovinyl moiety could be easily converted into the corresponding bromoketone with aqueous NBS (7) and finally into the 2-amino-4-thiazolyl heterocycle with thiourea (Hantzsch's synthesis). For reason of expediency, the Evans' alkylation method was retained for the control of the formation of the lone stereogenic center of **B′**. While this approach was sufficient for the short term and the scale of the sequence, alternative strategies were examined in parallel to address the long-term practicality and cost efficiency of installing this stereogenic center. The new global strategy used for the preparation of **BILA 2157 BS** is outlined in Scheme 2.

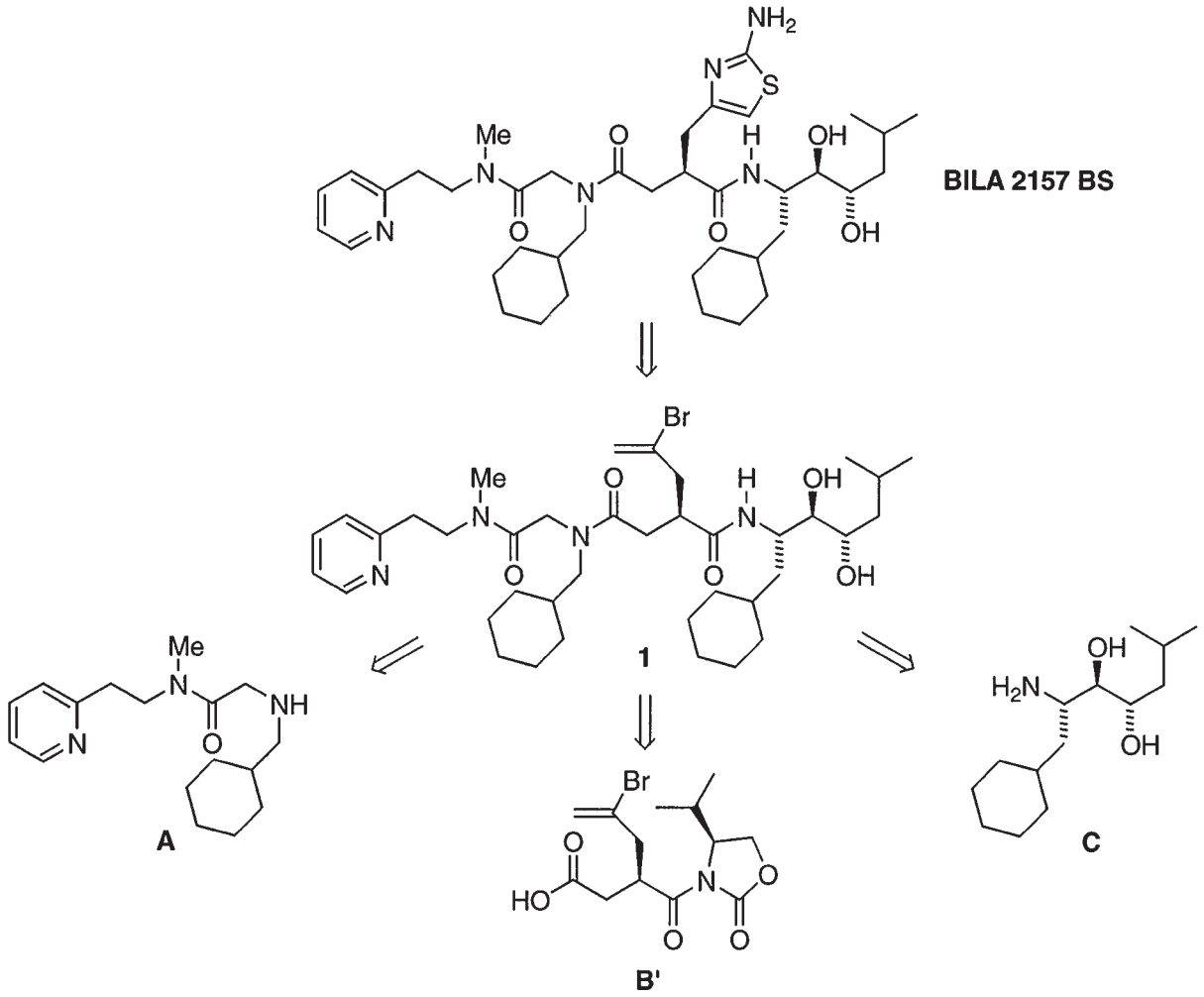
Results

Fragment **A** was prepared using basically the same five-step synthetic sequence that was used on small scale (Scheme 3). The first three chemical steps were combined into a one-pot procedure. Cyclohexanemethylamine was first alkylated with ethyl 2-bromoacetate in the presence of Et_3N in THF. On a kilogram scale, the reagents were mixed at

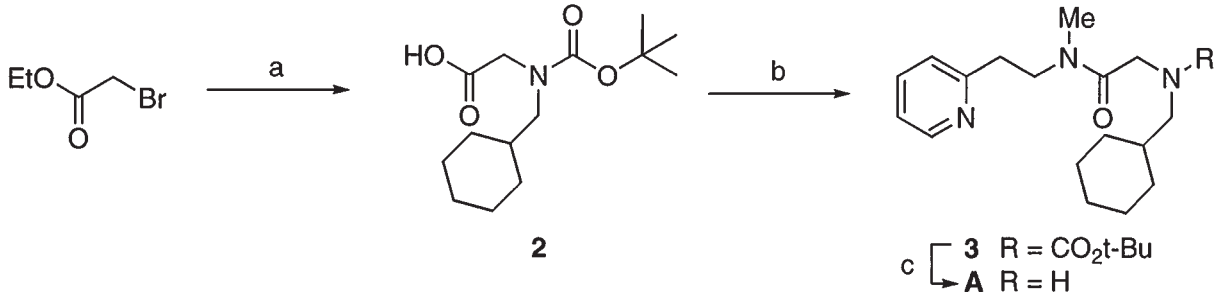
[3] For a detailed analysis of *N*,*O*-acyl transfer on a related compound, see reference 6.

© 2000 NRC Canada

Scheme 2. Retrosynthetic analysis of **BILA 2157 BS**.



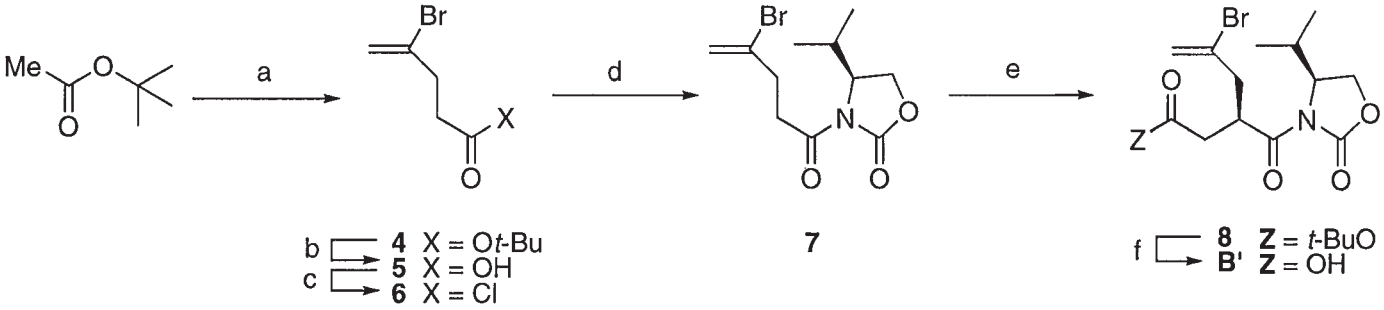
Scheme 3. Synthesis of amine **A**. Reagents and conditions: (*a*) (*c*-C_6H_{11})CH_2NH_2, Et_3N, THF, 25°C then $(BOC)_2O$, 25°C then aq. 2 N NaOH, 25°C, 70%; (*b*) $(CH_3)_3CCOCl$, Et_3N, THF then 2-pyr$(CH_2)_2$NHMe, 0 to 15°C; (*c*) 4 N HCl, dioxane, 25°C, 87% from **2**.



–50°C but the reaction occurred smoothly at 25°C. The resulting secondary amine was then transformed into the BOC derivative by simple addition of $(BOC)_2O$ to the reaction mixture. Finally, aqueous NaOH was introduced to saponify the ethyl ester. Acid **2** was isolated in 70% yield by a simple acid-base extraction procedure. The by-products generated in the course of the three-step sequence consisted of *N*-(cyclohexylmethyl)-*N*-(carboxymethyl)glycine (ca. 5%) and *tert*-butyl *N*-(cyclohexylmethyl)carbamate (ca. 5%). The former resulted from the double alkylation of cyclohexanemethylamine by ethyl 2-bromoacetate and subsequent ester hydrolysis while the second came from reaction of the remaining cyclohexanemethylamine with $(BOC)_2O$. Both of these by-products were easily eliminated in the extractive work-up. The coupling of commercially available 2-[2-(methylamino)ethyl]pyridine with the mixed anhydride derived from acid **2** and pivaloyl chloride gave amide **3**. After cleavage of the BOC protective group of **3** with 4 N HCl in dioxane and neutralization of the resulting hydrochloride salt, amine **A** was isolated in 87% yield from acid **2**. This

© 2000 NRC Canada

Scheme 4. Preparation of fragment **B′**. Reagents and conditions: (*a*) LDA, THF, –78°C then CH_2=$CBrCH_2Br$, 64%; (*b*) 4 N HCl, dioxane, 25°C, 82%; (*c*) $(COCl)_2$, DMF cat., CH_2Cl_2, 0 to 25°C, 99%; (*d*) Lithium 4(*S*)-$((CH_3)_2CH)$-2-oxazolidinone, THF, –78°C; (*e*) NaHMDS, THF, –78°C then $BrCH_2CO_2t$-Bu, 53% from **6**; (*f*) 4 N HCl, dioxane, 25°C, 100%.



sequence produced 1.16 kg of **A**, a viscous oil, in 60% yield overall. The crude product was of sufficient purity (>97% by HPLC) for direct use in the assembly sequence.

Fragment **B′** was prepared from *tert*-butyl acetate in six steps as described in Scheme 4. The lithium enolate of *tert*-butyl acetate was first alkylated with 2,3-dibromo-1-propene at –78°C to provide *tert*-butyl 4-bromo-4-pentenoate (**4**) in 64% yield after purification by distillation. Treatment of ester **4** with 4 N HCl in dioxane gave acid **5** in 82% yield. Although it was not used for this particular synthesis, we found that **5** could also be obtained in three steps (54% yield overall) from the alkylation of dimethyl malonate with 2,3-dibromo-1-propene in the presence of sodium methoxide in methanol, followed by the usual saponification and decarboxylation reactions. Acid **5** was then converted into acyl chloride **6** using oxalyl chloride.

Reaction of crude acyl chloride **6** with the lithium salt of 4(*S*)-(1-methylethyl)-2-oxazolidinone provided acyl oxazolidinone **7** which was used without any purification in the Evans' alkylation reaction (8). The sodium enolate of acyl oxazolidinone **7** was treated with *tert*-butyl 2-bromoacetate to give, after purification by crystallization, **8** in 53% yield (from acid **5**). The diastereomeric excess was greater than 99% as determined by HPLC. The high crystallinity of **8** (the compound crystallized from the reaction mixture as soon as it was formed) and its ease of preparation facilitated its use on a scale of hundreds of grams. Finally, the *tert*-butyl ester was cleaved using 4 N HCl in dioxane to give acid **B′** in quantitative yield. A total of 1.27 kg of acid **B′** was obtained in 28% yield overall from *tert*-butyl acetate.

Fragment **C** was prepared from *N*-BOC-cyclohexylalaninol using the five-step procedure described by Abbott scientists (4, 5). The required 0.7 kg of **C** was obtained in two batches in 25% overall yield. The cyanohydrin route was preferred to the one using an osmylation reaction.

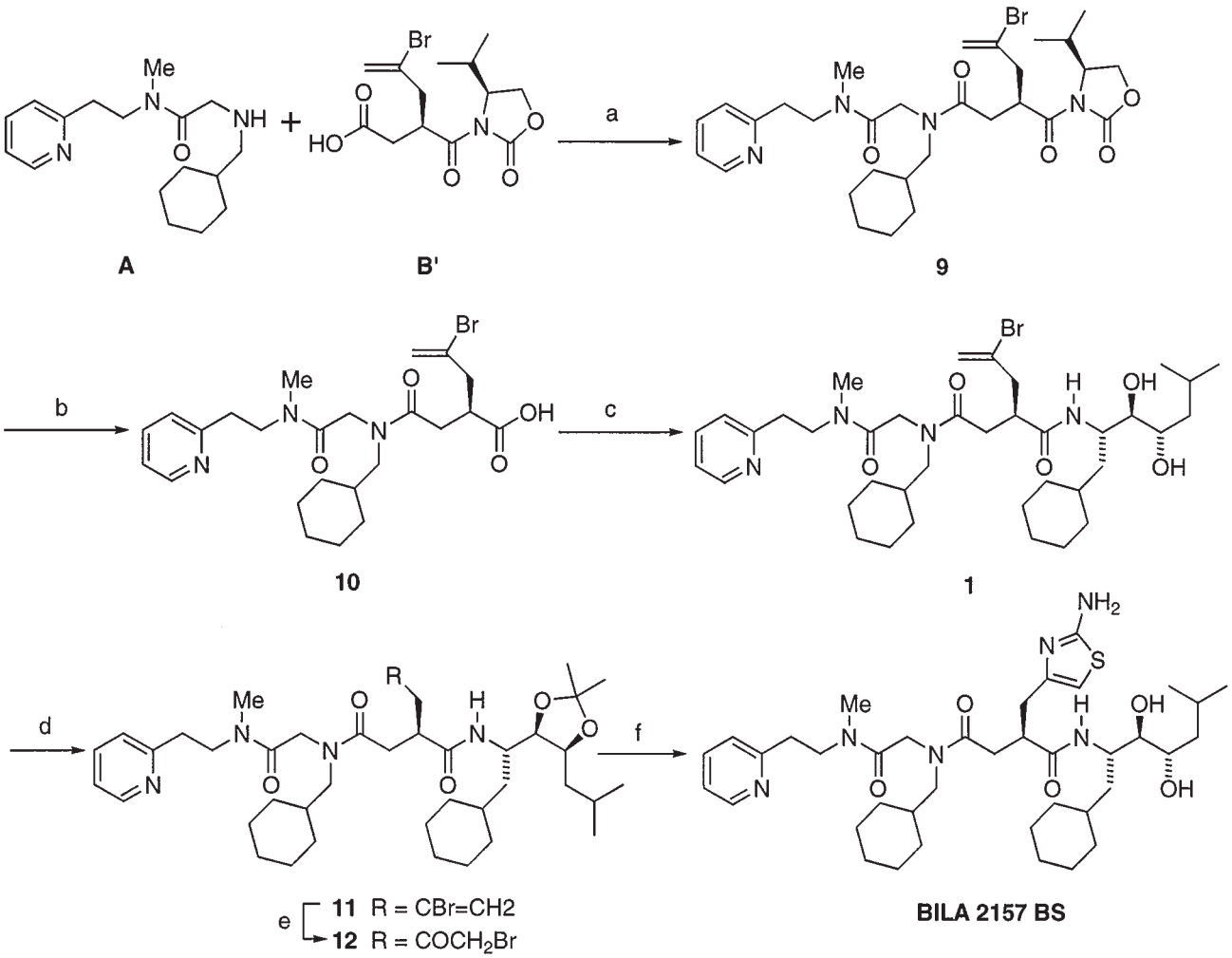
The assembly of the three fragments and the transformation of the bromovinyl moiety into the 2-amino-4-thiazolyl heterocycle required six steps (Scheme 5). The mixed anhydride generated by the treatment of acid **B′** with *iso*-butyl chloroformate at –40°C was treated with amine **A** to give **9**. Cleavage of the chiral auxiliary using LiOOH (9) at 0°C provided the corresponding acid **10** in 77% yield for the two steps. Acid **10** was contaminated with a small amount of the chiral auxiliary (2% w/w), which was not detrimental to the next step. The coupling of acid **10** and aminodiol **C** was the key step of our synthetic strategy. We had envisaged that having a 2-bromo-1-propenyl side-chain, the coupling of **10** and **C** should not produce large amounts of the 2(*R*)-butanediamide epimer as had been observed when a protected 2-amino-4-thiazolylmethyl group was used. In the original synthetic sequence (Scheme 1), the presence of this epimer made the purification difficult even on a small scale. We have therefore investigated many reagents for the coupling of **10** and **C** and found, as expected, only a small amount of the unwanted 2(*R*)-butanediamide epimer (<1%) in each case. For convenience, TBTU was selected as the coupling agent. Starting with 1.4 kg of **10** and 0.70 kg of **C**, the coupling occurred smoothly with TBTU to give **1**. In contrast to **BILA 2157 BS**, **1** was crystalline and was purified by recrystallization to give a 69% yield of highly pure material (>98%, HPLC). In the process, the small amount of the 2(*R*)-epimer (ca. 0.5%) was completely removed and the sole detectable impurity consisted of the corresponding pyridine *N*-oxide (0.3%, HPLC). This impurity was probably formed by oxidation with the peracid intermediate generated in situ during the cleavage of the chiral auxiliary. In addition to controlling the amount of the 2(*R*)-epimer, compound **1**, which had the basic skeleton of **BILA 2157 BS**, turned out to be a very valuable crystalline intermediate.

The last requirement for the completion of the synthesis was the transformation of the vinylbromide moiety present in **1** into the 2-amino-4-thiazolyl heterocycle. Attempts to generate the required bromoketone from **1** with aqueous NBS in the presence of the diol resulted in a complex mixture. The diol was therefore protected using 2-methoxypropene in the presence of PPTS to give acetonide **11** in quantitative yield.

Using acetonide **11**, transformation of the vinylbromide into bromoketone **12** occurred smoothly with NBS (7, 10) in aqueous acetonitrile. The rather unstable bromoketone **12** was not isolated. Instead, the small excess of remaining NBS in the reaction mixture was quenched by the addition of 2-methoxypropene followed by treatment with thiourea to generate the 2-amino-4-thiazolyl ring, which was produced as the hydrobromide salt. Upon heating to complete the heterocycle formation, the HBr catalyzed the concomitant hydrolysis of the acetonide to provide **BILA 2157 BS**. This final sequence, the formation of the bromoketone, the elaboration of the heterocycle, and finally the hydrolysis of the acetonide could be achieved efficiently in a one-pot operation. Using acid-base extraction procedures and precipitation, **BILA 2157 BS** was obtained in 93% homogeneity as determined

© 2000 NRC Canada

Scheme 5. Synthesis of **BILA 2157 BS**. Reagents and conditions: (*a*) $ClCO_2i$-Bu, Et_3N, THF, –40 to 25°C, 100%; (*b*) LiOOH, THF-H_2O, 0°C, 77%; (*c*) TBTU, *i*-Pr_2NEt, **C**, MeCN, 0 to 25°C, 70%; (*d*) CH_2=CMe(OMe), PPTS, CH_2Cl_2, 25°C; (*e*) NBS, aq. MeCN, 25°C; (*f*) thiourea, 25°C to Δ, 50% from **11**.



by HPLC. Since the compound could not be purified further by conventional extractive or crystallization procedures, **BILA 2157 BS** was filtered through a column of silica gel. A total of 0.59 kg of **BILA 2157 BS** of high purity (homogeneity >99% by HPLC) was obtained for a 50% yield from **1**.

Conclusions

The original synthetic sequence leading to **BILA 2157 BS** was improved in order to generate 0.6 kg of this renin inhibitor for preliminary toxicity studies. Three building blocks, readily accessible from commercially available starting materials, were used to generate the basic skeleton of the inhibitor. The key modification consisted in the late stage elaboration of the 2-amino-4-thiazolyl heterocycle from a vinylbromide precursor. This modification allowed us to eliminate the purification problems due to the formation of the undesired 2-substituted butanediamide epimer in the original sequence. A valuable advanced crystalline intermediate, compound **1**, was also generated as a result of this strategic decision. While the synthetic sequence required 22 distinct chemical steps, a few multi-step one-pot operations were implemented to generate **BILA 2157 BS** in 7.3% yield. Nevertheless, this convergent and stereoselective synthesis has to be further improved in a cost related fashion for multikilogram scale. The most important issue concerns the fragment **B′**. Alternatives for the use of an expensive chiral auxiliary and three low temperature operations for its preparation are needed. Optimization of the reactions transforming key crystalline intermediate **1** into **BILA 2157 BS** should also help to facilitate final purification and eliminate the sole chromatographic purification. Work is well underway to improve the 22-step sequence described here and the results will be described elsewhere.

Experimental section

All reactions were performed under a nitrogen atmosphere. Reagents and anhydrous solvents were obtained from commercial sources and were used without further purification or treatment. Melting points were determined on an electrothermal Büchi 510 apparatus and are uncorrected. NMR spectra were recorded on a Bruker AMX400 spectrometer.

© 2000 NRC Canada

Optical rotations were measured on a Perkin–Elmer 241 polarimeter. IR spectra were recorded on a Perkin–Elmer 781. Fast atom bombardment (FAB) mass spectra were determined on a VG AutoSpec-Q or Kratos M550 apparatus at the Université de Montréal mass spectrometry center. Microanalyses were performed on a Carlo Erba 1100 or Fisons EA 1108 instruments. Residual amounts of H_2O were quantified using the Karl Fisher method with a Metrohn 652 KF-coulometer. RP-HPLC analyses were performed on a Waters 600-MS system (A: Supelcosil™ LC-ABZ; MeCN + 0.1% TFA–H_2O + 0.1% TFA) and (or) a Waters 625 system (B: Nova-Pak™ C_8 column; MeCN–NaH_2PO_4 50 mM, pH 4.4) using a photodiode array detector.

1,1-Dimethylethyl N-*(carboxymethyl)*-N-*(cyclohexylmethyl)carbamate (**2**)*: To a cold (–50°C) solution of Et_3N (1398 g, 13.88 mol) and cyclohexanemethylamine (783 g, 6.91 mol) in THF (4 L) was added ethyl 2-bromoacetate (1.156 kg, 6.91 mol) over 5 min. The cold bath was removed and after 25 min the mixture was diluted with THF (4 L). Stirring was maintained for an additional 2.5 h at room temperature. After cooling to 10°C, $(BOC)_2O$ (1.52 kg, 6.98 mol) was added at such a rate so as to maintain the internal temperature below 25°C. After 2 h, a solution of NaOH (1.10 kg) in H_2O (4.5 L) was added slowly, followed by MeOH (800 mL), and the mixture was left stirring overnight. The volatiles were removed under reduced pressure, the oily residue was diluted with water (8 L), and the mixture washed with hexane (2 × 4 L). The aqueous solution was acidified with citric acid (1.27 kg) and extracted with EtOAc (3 × 2 L). The combined organic extracts were washed successively with 10% citric acid solution (1 L), water (3 L), and brine (2 L). The solution was then dried ($MgSO_4$) and concentrated under reduced pressure to give acid **2** (1.32 kg, 70%) as a yellow solid: mp 78.5–80.5°C; IR (KBr) ν_{max}: 3120–2540, 1730, 1690 cm^{-1}; ^1H NMR ($CDCl_3$) δ: (*1.3*:1.0 mixture of rotamers) *3.97*, 3.90 (2s, 2H), 3.11 (broad d, J = 6.4 Hz, 2H), 1.73–1.67 (m, 5H), 1.56–1.47 (m, 1H), *1.47*, 1.43 (2s, 9H), 1.27–1.14 (m, 3H), 0.94–0.89 (m, 2H); ^{13}C NMR ($CDCl_3$) δ: 175.6, 175.1, 156.5, 155.5, 80.5, 80.3, 54.7, 54.5, 49.8, 49.2, 37.1, 36.9, 30.8, 30.7, 28.3, 28.2, 26.4, 25.8; MS (CI) *m*/*z*: 272 (MH^+). Anal. calcd. for $C_{14}H_{25}NO_4$: C 61.99, H 9.20, N 5.16; found: C 61.99, H 9.45, N 5.26.

1,1-Dimethylethyl N-*[2-[methyl[2-(2-pyridinyl)ethyl]amino]-2-oxoethyl]*-N-*(cyclohexylmethyl)carbamate (**3**)*: To an ice-cold solution of acid **3** (1.31 kg, 4.84 mol) in THF (8 L) was added Et_3N (745 mL, 5.34 mol) over a period of 5 min. The mixture was stirred until the temperature reached 5°C and then, trimethylacetyl chloride (565 g, 4.69 mol) was added dropwise over 45 min. After stirring the pale yellow suspension at 5–10°C for 1 h, 2-[(2-methylamino)ethyl]pyridine (625 g, 4.58 mol) was added slowly over 45 min. The mixture was stirred at 15°C for 2.5 h, then diluted with H_2O (4 L) and extracted with EtOAc (7 × 1 L). The combined organic extracts were washed with saturated $NaHCO_3$ solution (2 × 1 L), H_2O (1 L), brine (2 × 1 L), dried ($MgSO_4$), filtered, and concentrated under reduced pressure. The residue was further dried under reduced pressure overnight to afford **3** as a viscous liquid (2.16 kg, 121% mass recovery) containing H_2O (1.74% w/w) and EtOAc (2% w/w, determined by ^1H NMR): ^1H NMR ($CDCl_3$) δ: (3:3:1:1 mixture of rotamers) 8.60–8.58, 8.54 (m and d, J = 4.5 Hz, 1H), 7.64–7.60 (m, 1H), 7.26–7.13 (m, 2H), 3.98, 3.90, 3.89, 3.80 (4s, 2H), 3.74–3.68 (m, 2H), 3.12–2.97, 2.93, 2.92 (m and 2s, 7H), 1.73–1.60 (m, 5H), 1.58–1.44 (m, 1H), 1.47, 1.45, 1.41, 1.40 (4s, 9H), 1.28–1.14 (m, 3H), 0.98–0.84 (m, 2H); MS (FAB) *m*/*z*: 390 (MH^+). The crude product was used directly in the next step.

2-[(Cyclohexylmethyl)amino]-N-*methyl*-N-*[2-(2-pyridinyl)ethyl]-acetamide (**A**)*: To an ice-cold solution of crude **3** (2.16 kg, 4.59 mol) in 1,4-dioxane (1.5 L) was slowly added over 75 min a 4 N solution of HCl in 1,4-dioxane (4 L). The light yellow suspension was stirred at ambient temperature for 3 h leaving a gummy precipitate at the bottom of the flask. The solvent was then removed and the precipitate solubilized in H_2O (7 L). The resulting solution was cooled to 0°C, rendered basic with NaOH (550 g), and extracted with ether (2 × 1.5 L) and EtOAc (3 × 1.5 L). The combined organic extracts were washed with H_2O (1 L), brine (1 L), dried (Na_2SO_4), filtered, and concentrated under reduced pressure. The residue was further dried under reduced pressure (0.5 mm Hg, 6 h) to afford the amine **A** as a brownish oil (1.16 kg, 84% from **2**) contaminated with 1,4-dioxane (0.3% w/w determined by ^1H NMR): IR (film) ν_{max}: 3520–3300, 1650, 1590 cm^{-1}; ^1H NMR ($CDCl_3$) δ: (*1.2*:1.0 mixture of rotamers) 8.46, *8.42* (2 broad d, J = 4.8 Hz, 1H), 7.54–7.49 (m, 1H), 7.12–7.02 (m, 2H), 3.67, 3.58 (2t, J = 7.0 Hz, 2H), *3.24*, 3.14 (2s, 2H), 2.93 (t, J = 7.0 Hz, 2H), 2.86, *2.77* (2s, 3H), 2.41 (broad s, 1H), *2.32*, 2.18 (2d, J = 6.7 Hz, 2H), 1.70–1.54 (m, 5H), 1.39–1.28 (m, 1H), 1.19–1.03 (m, 3H), 0.88–0.76 (m, 2H); MS (FAB) *m*/*z*: 290 (MH^+). Anal. calcd. for $C_{17}H_{27}N_3O$ + 4.0% (w/w) H_2O (and accounting for 1,4-dioxane content): C 67.79, H 9.47, N 13.92; found: C 67.69, H 9.50, N 13.77. RP-HPLC (A) indicated 98.4% homogeneity. The material was kept at 4°C, in darkness, and under an inert atmosphere.

*1,1-Dimethylethyl 4-bromo-4-pentenoate (**4**)*: A solution of *tert*-butyl acetate (581 g, 5.00 mol) in THF (350 mL) was added dropwise over 45 min to a cold (–78°C) solution of LDA — prepared at –30°C from *n*-BuLi (2.5 M in hexanes, 2.20 L, 5.50 mol) and *i*-Pr_2NH (771 mL, 5.50 mol) — in THF (2.2 L). After stirring at –78°C for 45 min, a solution of 2,3-dibromopropene (620 mL, 6.00 mol) (filtered on neutral alumina and dried over 4 Å molecular sieves) in THF (600 mL) was slowly added over 2 h while the temperature was maintained below –60°C. After 3.5 h, a saturated solution of NH_4Cl (1 L) was added and the mixture was allowed to warm to room temperature and stirred for an additional 12 h. The reaction mixture was partitioned between ether (500 mL) and H_2O (1.5 L) and the aqueous phase was extracted with Et_2O (2 × 250 mL). The combined organic extracts were washed with H_2O (3 × 100 mL), 2 N HCl solution (5 × 150 mL), brine (2 × 300 mL), dried ($MgSO_4$ and charcoal), filtered over a pad of Celite®, and concentrated under reduced pressure to give a red-brown oil. Distillation of the oily residue using a short Vigreux column afforded the expected ester **4** as a colorless oil (749 g, 64%), contaminated with 2% of 2,3-dibromopropene: bp 55–65°C at 0.5 mm Hg; IR (film) ν_{max}: 1735, 1635 cm^{-1}; ^1H NMR

© 2000 NRC Canada

(200 MHz, $CDCl_3$) δ: 5.63 (dt, *J* = 1.7, 1.1 Hz, 1H), 5.43 (d, *J* = 1.7 Hz, 1H), 2.72 (t, *J* = 7.4 Hz, 2H), 2.48 (td, *J* = 7.4, 1.1 Hz, 2H), 1.45 (s, 9H); MS (CI) *m*/*z*: 235/237 (MH^+). Similarly, starting with twice the amount of *tert*-butyl acetate (1.16 kg, 10.0 mol), 1.63 kg (69%) of **4** was obtained.

*4-Bromo-4-pentenoic acid (**5**)*: A 4 N HCl solution in 1,4-dioxane (4.8 L, 19.2 mol) was added to ester **4** (1.48 kg, 6.30 mol) while stirring under inert atmosphere. After 18 h an additional portion of 4 N HCl in 1,4-dioxane (800 mL, 3.20 mol) was introduced. After stirring for an additional 24 h, the solvent was removed under reduced pressure, the residue was dissolved in Et_2O (3 L), and the solution washed with 2 N NaOH (4 × 1 L). The combined aqueous washings were acidified with 6 N HCl (1.4 L, 8.4 mol) to pH 2 and extracted with a 5:1 mixture of Et_2O:EtOAc (3 × 1.2 L). The combined organic extracts were washed with brine (1 L), dried ($MgSO_4$), filtered, and the solvent evaporated under reduced pressure. The residue was co-evaporated with hexane and dried under reduced pressure to give acid **5** as a tan solid (919 g, 82%): IR (KBr) ν_{max}: 3130–2900 (broad), 1715, 1635 cm^{-1}; ^1H NMR ($CDCl_3$) δ: 10.57 (broad s, 1H), 5.67 (q, *J* = 1.0 Hz, 1H), 5.46 (d, *J* = 1.0 Hz, 1H), 2.78 (t, *J* = 7.3 Hz, 2H), 2.66 (td, *J* = 7.3, 1.0 Hz, 2H); MS (CI) *m*/*z*: 179/181 $(MH)^+$. The product was used directly in the next step. Alternatively, TFA (490 mL, 6.40 mol) was added over 60 min to an ice-cold solution of **4** (748 g, 3.18 mol) in CH_2Cl_2 (1 L). The mixture was stirred at 25°C for 48 h then was concentrated under reduced pressure. The residue was diluted with Et_2O (2 L) and the solution was extracted with aqueous 2 N NaOH (5 × 400 mL). The combined aqueous extracts were rendered acidic with 6 N HCl (500 mL) and extracted with Et_2O (4 × 500 mL). The combined ethereal extracts were washed with H_2O (3 × 300 mL) and brine (300 mL), dried (Na_2SO_4), filtered, and concentrated under reduced pressure. The residue was dissolved in toluene and concentrated under reduced pressure to give **5** (488 g, 86%) as a yellowish solid: analytical data identical to those described above.

*4-Bromo-4-pentenoyl chloride (**6**)*: To a cold (0°C) solution of the crude acid **5** (918 g, 5.13 mol) in CH_2Cl_2 (2.0 L) containing DMF (0.5 mL) was added oxalyl chloride (490 mL, 5.60 mol) over a period of 3 h. After stirring for 18 h at room temperature, the solvent was removed under reduced pressure and the residue dried under reduced pressure (0.5 mm Hg, 1.5 h) to afford crude acyl chloride **6** as a liquid (1003 g, 99%): ^1H NMR ($CDCl_3$) δ: 5.71 (broad d, *J* = 1.9 Hz, 1H), 5.51 (d, *J* = 1.9 Hz, 1H), 3.19 (t, *J* = 7.2 Hz, 2H), 2.82 (broad t, *J* = 7.2 Hz, 2H). The material was used directly in the next step. Similarly, a second run starting with about half the quantity of **5** (487 g, 2.72 mol) gave 533 g of **6** (99%), identical to the material obtained above.

*3-(4-Bromo-1-oxo-4-pentenyl)-4(*S*)-(1-methylethyl)-2-oxazolidinone (**7**)*: To a cold (–78°C) solution of 4(*S*)-(1-methylethyl)-2-oxazolidinone (642 g, 4.97 mol) and Ph_3CH (300 mg, as indicator) in dry THF (9 L) was added dropwise *n*-BuLi (2.5 M in hexanes, 2.05 L, 5.12 mol) until a pink color appeared. After stirring the suspension for 1 h, crude acyl chloride **6** (1001 g, 5.07 mol) was added via cannula over a 1.5 h period. Stirring was maintained for an additional 15 min at –78°C and for 2.5 h at room temperature. The mixture was diluted with H_2O (4 L) and saturated $NaHCO_3$ solution (2 L) and extracted with Et_2O (4 × 1.5 L). The combined organic extracts were washed with water (2 × 800 mL), brine (1.5 L), dried ($MgSO_4$), filtered, and the solvent evaporated under reduced pressure. The residue was further dried under reduced pressure (0.5 mm Hg, 15 h) to afford **7** as a yellow solid (1.42 kg, 98%). ^1H NMR ($CDCl_3$) δ: 5.66 (broad d, *J* = 1.7 Hz, 1H), 5.44 (d, *J* = 1.7 Hz, 1H), 4.42 (ddd, *J* = 8.3, 3.8, 3.2 Hz, 1H), 4.28 (dd, *J* = 9.1, 8.3 Hz, 1H), 4.21 (dd, *J* = 9.1, 3.2 Hz, 1H), 3.29–3.12 (m, 2H), 2.80 (broad t, *J* = 7.5 Hz, 2H), 2.36 (sept d, *J* = 7.0, 3.8 Hz, 1H), 0.91 (d, *J* = 7.0 Hz, 3H), 0.87 (d, *J* = 7.0 Hz, 3H). The material was used in the subsequent reaction without further purification. Similarly, a second run starting with 532 g of **6** (2.69 mol) produced 710 g of **7** (92%), identical to the material described above.

*3-[4-Bromo-2(*S*)-[2-(1,1-dimethylethoxy)-2-oxoethyl]-1-oxo-4-pentenyl]-4(*S*)-(1-methylethyl)-2-oxazolidinone (**8**)*: To a cold (–78°C) solution of crude acyl oxazolidinone **7** (1.42 kg, 4.90 mol) in dry THF (3 L) was added dropwise a 1 M solution of NaHMDS in THF (5.5 L, 5.50 mol) over a 2 h period. After stirring mechanically for 1.5 h at –78°C, a solution of *tert*-butyl 2-bromoacetate (900 mL, 5.57 mol) in THF (1 L) was added dropwise over 1.5 h. The mixture was stirred for an additional 1.5 h and a saturated $NaHCO_3$ solution (4 L) was introduced. After warming to room temperature, the THF extract was removed and the aqueous extract was extracted with EtOAc (2 × 2 L). The combined organic solutions (THF and EtOAc) were concentrated under reduced pressure to give a solid residue which was suspended in hexane (3 L) and filtered. The material was washed with H_2O (2 × 1 L), hexane (2 × 1.5 L), filtered, and dried under reduced pressure over P_2O_5. The solid was dissolved in CH_2Cl_2 (3.5 L), the solution was filtered through a microglass filter, and concentrated under reduced pressure to a semi-solid mass. After dilution with hexane (3.5 L), the resulting crystals were filtered and dried under reduced pressure to afford **8** as small white needles (1.02 kg, 53%): mp 121–122.5°C; $[\alpha]_D^{25}$ + 49.8° (*c* 1.28, $CHCl_3$); IR (KBr) ν_{max}: 1770, 1735, 1705, 1640 cm^{-1}; ^1H NMR ($CDCl_3$) δ: 5.67 (broad s, 1H), 5.50 (d, *J* = 1.6 Hz, 1H), 4.51–4.44 (m, 1H), 4.42 (ddd, *J* = 8.1, 3.8, 3.2 Hz, 1H), 4.27 (dd, *J* = 9.2, 8.1 Hz, 1H), 4.22 (dd, *J* = 9.2, 3.2 Hz, 1H), 2.87 (broad dd, *J* = 14.5, 6.4 Hz, 1H), 2.73 (dd, *J* = 16.5, 9.1 Hz, 1H), 2.56 (broad dd, *J* = 14.5, 7.6 Hz, 1H), 2.52 (dd, *J* = 16.5, 5.1 Hz, 1H), 2.38 (sept d, *J* = 7.0, 3.8 Hz, 1H), 1.42 (s, 9H), 0.93 (d, *J* = 7.0 Hz, 3H), 0.91 (d, *J* = 7.0 Hz, 3H); ^{13}C NMR ($CDCl_3$) δ: 173.9, 170.4, 153.5, 129.9, 119.8, 80.8, 63.3, 58.8, 42.4, 38.5, 36.5, 28.2, 28.0, 18.4, 14.6; MS (FAB) *m*/*z*: 404/406 (MH^+). Anal. calcd. for $C_{17}H_{26}NO_5Br$: C 50.50, H 6.48, N 3.46; found: C 50.20, H 6.50, N 3.49. The diastereomeric purity was found to be >99% when assessed by HPLC using a chiral column (CHIRALPAK® AS, Daicel Chem. Co.; 0.5% EtOH in hexane). A second run starting with 707 g (2.44 mol) of **7** yielded 514 g (52%) of **8**.

*3-[4-Bromo-2(*S*)-(carboxymethyl)-1-oxo-4-pentenyl]-4(*S*)-(1-methylethyl)-2-oxazolidinone (**B′**)*: Ester **8** (1.48 kg, 3.67 mol) was dissolved in 4 N HCl 1,4-dioxane (8.8 L, 35.2 mol) and the solution was stirred at room temperature for

© 2000 NRC Canada

20 h. The yellow solution was concentrated to half volume by partial evaporation of the solvent under reduced pressure and then poured into water (40 L). The white solid formed was filtered and re-dissolved in Et_2O (10 L). The solution was washed with brine (3 × 1 L), treated with anhydrous $MgSO_4$ and charcoal, and filtered through a pad of Celite®. The pale yellow filtrate was concentrated under reduced pressure to give a white solid which, after drying under reduced pressure for 3 h, afforded **B′** as an amorphous product (1.27 kg, 100% mass recovery, containing 2.47% w/w of 1,4-dioxane): mp 124–125°C; ^{1}H NMR ($CDCl_3$) δ: 5.70 (broad s, 1H), 5.54 (d, *J* = 1.6 Hz, 1H), 4.54–4.48 (m, 1H), 4.43 (ddd, *J* = 7.9, 3.5, 3.2 Hz, 1H), 4.30–4.22 (m, 2H), 2.89 (dd, *J* = 17.4, 10.2 Hz, 1H), 2.86 (dd, *J* = 14.1, 5.1 Hz, 1H), 2.64 (dd, *J* = 17.4, 4.3 Hz, 1H), 2.53 (dd, *J* = 14.1, 8.6 Hz, 1H), 2.37 (sept d, *J* = 7.0, 3.5 Hz, 1H), 0.91 (d, *J* = 7.0 Hz, 3H), 0.89 (d, *J* = 7.0 Hz, 3H); MS (FAB) *m*/*z*: 348/350 (M^+). Anal. calcd. for $C_{13}H_{18}NO_5Br$ (+ 2.47% w/w 1,4-dioxane): C 45.08, H 5.32, N 3.92; found: C 45.15, H 5.69, N 3.62.

*3-[4-Bromo-2(*S*)-[2-[(cyclohexylmethyl)[2-[methyl[2-(2-pyridinyl)ethyl]amino]-2-oxoethyl]amino]-2-oxoethyl]-1-oxo-4-pentenyl]-4(*S*)-(1-methylethyl)-2-oxazolidinone (**9**)*: Et_3N (1.02 L, 7.30 mol) was added in one portion to a solution of **B′** (1.27 kg, 3.65 mol) in dry THF (5 L). The mixture was cooled to –45°C and iso-butyl chloroformate (497 mL, 3.83 mol) was added dropwise over a 30 min period while maintaining the temperature below –40°C. After stirring for 30 min, a solution of amine **A** (1.16 kg, 3.99 mol, 1.1 equiv.) in dry THF (2 L) was added dropwise over 45 min and the resulting mixture was stirred at room temperature for 2.5 h. H_2O (7 L) was added and the mixture was extracted with EtOAc (6 × 1 L). The combined organic extracts were washed successively with a 10% citric acid solution (6 × 500 mL), H_2O (2 × 1 L), saturated $NaHCO_3$ solution (3 × 1 L), and brine (2 × 1 L). The solution was treated with anhydrous $MgSO_4$ and charcoal, filtered through a pad of Celite®, and concentrated under reduced pressure to give amide **9** as a yellow gum (2.27 kg, 100%): ^{1}H NMR ($CDCl_3$) δ: (3:3:1:1 mixture of rotamers) 8.61, 8.55, 8.51 (3d, *J* = 4.1, 4.8, 3.8 Hz, 1H), 7.68–7.58 (m, 1H), 7.24–7.11 (m, 2H), 5.72, 5.67, 5.64 (3s, 1H), 5.52, 5.51, 5.48, 5.46 (4d, *J* = 1.6, 1.3, 1.3, 1.6 Hz, 1H), 4.57–4.47 (m, 1H), 4.45–4.40 (m, 1H), 4.28–4.17 (m, 2H), 4.17–3.68 (m, 4H), 3.50–3.30 and 3.19–2.83 (m, 5H), 2.97, 2.95, 2.90, 2.87 (4s, 3H), 2.75–2.54 (m, 2H), 2.43–2.36 (m, 1H), 2.15–2.07 (m, 1H), 1.76–1.45 (m, 6H), 1.29–1.15 (m, 3H), 0.95–0.85 (m, 8H); MS (FAB) *m*/*z*: 619/621 (MH^+). The material was used directly in the subsequent reaction.

*2(*S*)-(2-Bromo-2-propenyl)-4-[(cyclohexylmethyl)[2-[methyl[2-(2-pyridinyl)ethyl]amino]-2-oxo-ethyl]amino]-4-oxobutanoic acid (**10**)*: To a mechanically stirred solution of the crude tertiary amide **9** (2269 g, 3.65 mol) in a 6:1 THF:H_2O mixture (16 L) cooled to 0°C, was added a 30% H_2O_2 solution (2042 mL, 18.31 mol). After 10 min, $LiOH•H_2O$ (384 g, 9.16 mol) was added and the mixture was stirred vigorously for 40 min. A Na_2SO_3 solution (2552 g in 5.7 L of H_2O) was slowly added over 40 min while keeping the temperature below 25°C. After stirring for an additional 15 min to ensure complete neutralization of the peroxide, the solution was concentrated under reduced pressure to remove the THF. The aqueous extract was extracted with EtOAc (6 × 1 L) and the combined organic extracts were extracted with saturated $NaHCO_3$ (8 × 500 mL). The combined aqueous extracts containing the carboxylic acid sodium salt were extracted manually with ether (7 × 750 mL) and then submitted to continuous extraction with Et_2O (4 L) for 17 h. All the organic extracts were combined and evaporated to dryness allowing recovery of the chiral auxiliary. The aqueous extracts were acidified with solid citric acid to pH 3 and extracted with EtOAc (4 × 1 L). The combined organic extracts were washed with brine (2 × 600 mL), treated with anhydrous $MgSO_4$ and charcoal, filtered through Celite®, and concentrated under reduced pressure. The resulting gummy residue was further dried at 45°C under reduced pressure for 8 h to afford acid **10** as a yellow glassy solid (1.51 kg, 77%) contaminated with EtOAc (2.5% w/w) and residual chiral auxiliary (2.5% w/w): ^{1}H NMR ($CDCl_3$) δ: 10.00 (broad s, 1H), 8.62, 8.58, 8.55, 8.53 (4d, *J* = 4.4, 4.8, 5.1, 5 Hz, 1H), 7.73–7.66 (m, 1H), 7.33–7.17 (m, 2H), 5.74, 5.69, 5.63 (3s, 1H), 5.50, 5.47, 5.45 (3 broad s, 1H), 4.09–3.85 (m, 2H), 3.77–3.60 (m, 2H), 3.25–3.04 (m, 5H), 2.98, 2.97, 2.94, 2.90 (4s, 3H), 2.99–2.88, 2.74–2.67 and 2.51–2.30 (m, 4H), 1.76–1.44 (m, 6H), 1.27–1.13 (m, 3H), 0.95–0.85 (m, 2H); MS (FAB) *m*/*z*: 508/510 (MH^+). Homogeneity was determined to be 97.8% (chiral auxiliary not detected by UV) by RP-HPLC (A). This acid (**10**) was used directly in the subsequent reaction.

N^4*-(Cyclohexylmethyl)*-N^4*-[2-[methyl[2-(2-pyridinyl)ethyl]amino]-2-oxoethyl]*-N^1*-[1(*S*)-(cyclohexylmethyl)-2(*R*),3(*S*)-dihydroxy-5-methylhexyl]-2(*S*)-(2-bromo-2-propenyl)butanediamide (**1**)*: A mixture of acid **10** (1394 g, 2.74 mol), aminodiol **C** (704.5 g, 2.89 mol), and TBTU (880.4 g, 2.74 mol, 1 equiv.) was dissolved in MeCN (7 L) and cooled to 0–5°C under an inert atmosphere before i-Pr_2NEt (1433 mL, 8.23 mol) was added portionwise over a 15 min period raising the temperature to 15°C. The bath was removed and the mixture was stirred at room temperature for 2 h. Water (8 L) was added and the mixture was extracted with EtOAc (6 × 650 mL). The combined organic extracts were washed successively with 10% citric acid solution (6 × 1 L), water (6 × 1 L), saturated $NaHCO_3$ solution (4 × 1 L), and brine (2 × 1 L). The organic solution was treated with anhydrous $MgSO_4$ and charcoal, and filtered through a pad of Celite®. The solution was filtered twice through a pad of silica gel and washed with EtOAc (2 × 5 L). The combined organic filtrates were concentrated under reduced pressure to give a 6 L solution which was left at room temperature overnight to allow crystallization. The solid was filtered, washed with hexane (3 × 1 L), and dried overnight under reduced pressure to afford a first crop of **1** as white micro-needles (1.20 kg, 59.9%): mp 139–141°C; ^{1}H NMR (DMSO-d_6) δ: (1.7:1.0:1.0 mixture of rotamers) 8.54–8.51, 8.48 (m and d, *J* = 4.8 Hz, 1H), 7.75–7.67 (m, 2H), 7.33–7.19 (m, 2H), 5.77, 5.71, 5.68 (3s, 1H), 5.42, 5.40, 5.38 (s and 2d, *J* = 1.5, 1.5 Hz, 1H), 4.61 (broad s, 1H), 4.51 (broad s, 1H), 4.21–3.88 (m, 3H), 3.70–3.54 (m, 2H), 3.10–2.85, 2.84, 2.80 (m and 2 s, 10H), 2.70–2.65 (1H), 2.52–2.05 (m, 3H), 1.76–1.10 (m, 23H), 0.92–0.70 (m, 4H), 0.86 (d, *J* = 6.6 Hz, 3H), 0.79 (d, *J* = 6.6 Hz, 3H); MS (FAB) *m*/*z*: 733/735 (MH^+). Anal. calcd. for

© 2000 NRC Canada

$C_{38}H_{61}N_4O_5Br$: C 62.20, H 8.38, N 7.63; found: C 61.54, H 8.48, N 7.66. Homogeneity was determined to be 98.6% by RP-HPLC (A), with 0.3% of the corresponding pyridine *N*-oxide derivative. This first crop of **1** was used directly in the subsequent reaction sequence leading to **BILA 2157 BS**.

Concentration of the mother liquors under reduced pressure gave a solid residue that was filtered and washed successively with a 1:1 EtOAc–hexane mixture (2 L) and then hexane (3 L). The solid was dissolved in hot EtOAc (1 L), the solution was filtered through Celite®, and stored at 0–5°C overnight. The crystalline white solid was filtered, washed with hexane, and dried under reduced pressure to afford an impure crop of intermediate **1** (281 g): mp 132–133°C. RP-HPLC (A) indicated 92% homogeneity. The solid was dissolved in EtOAc (3 L) and the resulting solution was filtered twice through a pad of silica gel and washed with EtOAc (2 × 600 mL). The combined organic filtrates were concentrated under reduced pressure to give a 1 L solution which was left at room temperature overnight to allow crystallization. The solid was filtered, washed with hexane, and dried over P_2O_5 under reduced pressure to afford a second crop of **1** as a white powder (189 g, 9.5%): mp 140–142°C; $[\alpha]_D^{25}$ –27.1° (*c* 1.03, MeOH); IR (KBr) ν_{max}: 3450, 3280, 1655, 1630 cm^{-1}; ^1H NMR and MS identical to those of first crop of **1**. Anal. calcd. for $C_{38}H_{61}N_4O_5Br$: C 61.82, H 8.38, N 7.63; found: C 61.82, H 8.44, N 7.63. RP-HPLC (A) indicated 99.2% homogeneity.

N^4*-(Cyclohexylmethyl)*-N^4*-[2-[methyl[2-(2-pyridinyl)ethyl]-amino]-2-oxoethyl]*-N^1*-[1(*S*)-(cyclohexylmethyl)-2(*R*),3(*S*)-dihydroxy-5-methylhexyl]-2(*R*)-[(2-amino-4-thiazolyl)methyl]butanediamide (**BILA 2157 BS**)*: To a solution of butanediamide intermediate **1** (1.20 kg, 1.63 mol) in CH_2Cl_2 (6.5 L), was added 2-methoxypropene (783 mL, 8.18 mol) followed by a catalytic amount of PPTS (41.0 g, 163 mmol). The mixture was stirred at room temperature for 15 h. The solvent was evaporated under reduced pressure and the residue was co-evaporated with Et_2O (3 × 1 L). The oily residue was dissolved in EtOAc (2.5 L) and washed successively with H_2O (2 × 500 mL) and saturated $NaHCO_3$ solution (2 × 500 mL). The solution was treated with anhydrous $MgSO_4$ and charcoal, and filtered through a pad of Celite®. The filtrate was concentrated under reduced pressure to afford the corresponding crude acetonide derivative **11** as a yellow gum (1.35 kg, 107% mass recovery). RP-HPLC (B) analysis indicated homogeneity of 94%. The crude product was used immediately in the subsequent reaction.

To a solution of crude acetonide **11** (1.35 kg, 1.63 mol) in a mixture of MeCN (12 L) and H_2O (3 L) protected from light, was added NBS (349 g, 1.96 mol) in two portions at 10 min intervals. The mixture was stirred for 50 min and treated with 2-methoxypropene (31.0 mL, 0.33 mol) to neutralize the excess NBS. After 5 min, thiourea (156 g, 2.04 mol) was added in one portion. After 15 min, the mixture was heated to 60–65°C under reduced pressure to distill off 5 L of MeCN while completing the hydrolysis of the acetonide (4.5 h). Water (4 L) was then added and the mixture was left stirring at room temperature overnight. The remaining MeCN was removed under reduced pressure and the solution was washed successively with TBME (8 × 2 L), EtOAc (8 × 2 L), and CH_2Cl_2 (8 × 2 L). The aqueous solution containing **BILA 2157 BS** as its HBr salt was treated with charcoal, filtered through a pad of Celite®, and brought to pH 9 by addition of solid NaOH (290 g). The mixture was extracted with $CHCl_3$ (3 × 2 L) and the combined organic extracts were washed with H_2O (3 × 1.5 L) and brine (2 × 1 L). The solution was filtered through a pad of silica gel (G-60, 500 g) and the pad was washed with $CHCl_3$ (500 mL). The combined filtrate and washing solutions were evaporated under reduced pressure to give 930 g of crude **BILA 2157 BS** (93% homogeneity by RP-HPLC, A). This crude product was purified in 6 portions by flash chromatography (silica gel G-60, 6 kg) using a gradient of MeOH in EtOAc (5 to 20%) as eluent. Following RP-HPLC analysis, fractions containing pure product were combined and the solvent was evaporated to dryness. The residue (603.6 g) was dissolved in EtOAc (2 L) and the solution was filtered through a microfiber filter. After evaporation of the solvent, the residue was co-evaporated with MeOH (2 × 1.5 L) and then dissolved in MeOH (700 mL). The brown solution was added dropwise over a 1 h period to a mixture of water (30 L) and ice (5 L) under vigorous mechanical stirring. The resulting precipitate was filtered, air dried overnight, and then dried under reduced pressure for 48 h to afford **BILA 2157 BS** as an off-white amorphous solid (518 g, 44%): mp 92–97°C; $[\alpha]_D^{25}$ –26.0° (*c* 1.02, MeOH); IR (KBr) ν_{max}: 3600–3040, 1645 (broad) cm^{-1}; ^1H NMR (DMSO-d_6) δ: (1:1:1:1 mixture of rotamers) 8.54–8.51, 8.48 (m and d, *J* = 4.8 Hz, 1H), 7.75–7.67 (m, 1H), 7.59, 7.56, 7.53 (3d, *J* = 9.0, 9.9, 9.6 Hz, 1H), 7.33–7.19 (m, 2H), 6.77, 6.73 (2s, 2H), 6.18, 6.17, 6.10, 6.06 (4s, 1H), 4.64–4.61, 4.59, 4.56 (m and 2d, *J* = 6.6, 6.6 Hz, 2H), 4.18, 4.17, 4.11, 4.09–4.01, 3.88, 3.85 (3d, m and 2d, *J* = 17.8, 16.2, 16.5, 17.8, 16.2 Hz, 3H), 3.69–3.51 (m, 2H), 3.10–2.80 (m, 7H), 2.90, 2.89, 2.83, 2.80 (4s, 3H), 2.74–2.62 (m, 1H), 2.51–2.32, 2.24, 2.14, 2.02 (m and 3dd, *J* = 15.8, 7.8 Hz, *J* = 16.1, 5.7 Hz, *J* = 15.8, 5.7 Hz, 3H), 1.78–1.05 (m, 23H), 0.90–0.69 (m, 4H), 0.86 (d, *J* = 6.9, 3H), 0.77 (d, *J* = 6.6 Hz, 3H); MS (FAB) *m*/*z*: 727 (MH^+). Anal. calcd. for $C_{39}H_{62}N_6O_5S$ + 1.53% (w/w) H_2O: C 63.45, H 8.63, N 11.39; found: C 63.03, H 8.64, N 11.31. RP-HPLC analysis indicated homogeneities of 99.9% (A) and 99.6% (B). An additional amount of **BILA 2157 BS** (73.0 g, 6%) was obtained after purification by flash chromatography of the mixed fractions: mp 88–94°C; $[\alpha]_D^{25}$ –25.5° (*c* 1.03, MeOH); IR, ^1H NMR and MS identical to those described above. Anal. calcd. for $C_{39}H_{62}N_6O_5S$ + 0.78% (w/w) H_2O: C 63.93, H 8.62, N 11.47; found: C 63.96, H 9.02, N 11.29. RP-HPLC analysis indicated homogeneities of 99.9% (A) and 99.6% (B).

Acknowledgements

The authors would like to thank Dr. Karl Grozinger and Dr. John Landi of Boehringer Ingelheim Pharmaceuticals Inc. for the preparation of the *N*-BOC derivative of amine **C**, and Colette Boucher, Sylvain Bordeleau and Serge Valois for analytical support.

References

1. S.H. Rosenberg. Renin inhibitors. *In* Progress in medicinal chemistry. *Edited by* G.P. Ellis and D.K. Luscombe. Elsevier, New York. 1995. Vol. 32, pp. 37–114.

© 2000 NRC Canada

2. M. Burnier and H.R. Brunner. Expert Opin. Invest. Drugs, **6**, 489 (1997).
3. B. Simoneau, P. Lavallée, P.C. Anderson, M. Bailey, G. Bantle, S. Berthiaume, C. Chabot, G. Fazal, T. Halmos, W.W. Ogilvie, M.-A. Poupart, B. Thavonekham, Z. Xin, D. Thibeault, G. Bolger, M. Panzenbeck, R. Winquist, and G.L. Jung. Bioorg. Med. Chem. **7**, 489 (1999).
4. J.R. Luly, C.-N. Hsiao, N. BaMaung, and J.J. Plattner. J. Org. Chem. **53**, 6109 (1988).
5. S.H. Rosenberg, K.P. Spina, K.W. Woods, J. Polakowski, D.L. Martin, Z. Yao, H.H. Stein, J. Cohen, J.L. Barlow, D.A. Egan, K.A. Tricarico, W.R. Baker, and H.D. Kleinert. J. Med. Chem. **36**, 449 (1993).
6. T.R. Hurley, C.E. Colson, G. Hicks, and M.J. Ryan. J. Med. Chem. **36**, 1496 (1993).
7. C.-N. Hsiao, M.R. Leanna, L. Bhagavatula, E. De Lara, T.M. Zydowsky, B.W. Horrom, and H.E. Morton. Synth. Commun. **20**, 3507 (1990).
8. D.A. Evans, M.D. Ennis, and D.J. Mathre. J. Am. Chem. Soc. **104**, 1737 (1982).
9. D.A. Evans, T.C. Britton, and J.A. Ellman. Tetrahedron Lett. **28**, 6141 (1987).
10. H.E. Morton and M.R. Leanna. Tetrahedron Lett. **34**, 4481 (1993).

© 2000 NRC Canada

Construction of bicyclic tetrahydroisoquinolinones by combination of an IMDAF-ring cleavage reaction of *N*-allyl-2-furan-2-yl-acetamides

Albert Padwa and Thomas S. Reger

Abstract: The intramolecular Diels–Alder reaction of furanyl amides derived from 2-furylacetic acid has been examined. Substrates containing either an imide or tertiary amide linkage between the furan and the dienophile underwent smooth cycloaddition upon thermolysis. By varying the reaction conditions, either the primary cycloadduct or the ring-opened and acetylated product could be isolated in excellent yield. The stereochemical outcome of the IMDAF cycloaddition has the side arm of the tethered alkenyl group oriented *syn* with respect to the oxygen bridge. Semi-empirical AM1 calculations show that the *exo*-cycloadduct is 11 kcal lower in energy than the corresponding *endo* adduct and, presumably, some of this energy difference is reflected in the transition state for the cycloaddition. The IMDAF reaction of *N*-allyl-[2-(3,4-dimethoxyphenethyl)]-2-furanyl-2-yl-acetamide proceeded in 90% yield upon heating in xylene. The 4+2-cycloadduct undergoes ring-opening on treatment with base and the resulting alcohol was converted into the corresponding benzyl ether. Raney nickel reduction followed by Bischler–Napieralski cyclization furnished the tetracyclic skeleton of the berberine alkaloids.

Key words: intramolecular, cycloaddition, Diels–Alder, furanylamide, heterocycle.

Résumé : On a étudié la réaction de Diels–Alder intramoléculaire de furanylamides (« IMDAF ») dérivés de l'acide furyl-2-acétique. Par thermolyse, les substrats comportant soit une liaison imide ou amide tertiaire entre le furane et le diénophile subissent une cycloaddition facile. En faisant varier les conditions réactionnelles, on peut isoler avec un excellent rendement soit le cycloadduit primaire ou le produit dérivant d'une ouverture de cycle et d'une acétylation. D'un point de vue stéréochimique, la cycloaddition « IMDAF » conduit à un produit dans lequel la chaîne latérale du groupe alcényle prend une orientation *syn* par rapport au pont oxygéné. Des calculs semi-empiriques AM1 montrent que l'énergie du cycloadduit *exo* est inférieure de 11 kcal par rapport à celle de l'adduit *endo* correspondant; il est vraisemblable qu'une partie de cette différence d'énergie se reflète dans l'état de transition de la cycloaddition. La réaction « IMDAF » du *N*-allyl-[2-(3,4-diméthoxyphénéthyl)]-2-furanyl-2-yl-acétamide se produit avec un rendement de 90% par chauffage dans le xylène. Le cycloadduit 4+2 subit une ouverture de cycle par traitement avec une base et l'alcool qui en résulte a été transformé en éther benzylique correspondant. Une réduction à l'aide de nickel de Raney, suivie d'une cyclisation de Bischler–Napieralski, conduit au squelette tétracyclique des alcaloïdes de la berbérine.

Mots clés : intramoléculaire, cycloaddition, Diels–Alder, furanylamide, hétérocycle.

Introduction

Furans are common substructures found in numerous natural products and are also present in many commercial products, including pharmaceuticals, fragrances, and dyes (1–4). Furans also play an important role as intermediates in many synthetic pathways, primarily because they react as a special class of vinyl ethers (5, 6) or as dienes in the Diels–Alder reaction (7). The resultant 7-oxabicyclo-[2.2.1]heptanes are valuable synthetic intermediates which have been further elaborated to substituted arenes, carbohydrate derivatives, and various natural products (8–17). A crucial synthetic transformation employing these oxabicyclic compounds involves cleavage of the oxygen bridge to produce functionalized cyclohexene derivatives (18–23). The intramolecular Diels–Alder reactions of furans, often designated as IMDAF, has proven to be an extremely valuable method for the construction of more complex oxygenated, bicyclic structures (7). The IMDAF generally proceeds at lower temperature than its bimolecular counterpart and, more importantly, often allows for the use of unactivated alkenes as dienophiles (24). Recent work in our laboratory has shown that the intramolecular Diels–Alder of 2-amido substituted furans such as **1** represents an effective route to indolines and tetrahydroquinolines (25). This methodology has also been utilized for the synthesis of the hexahydroindolinone skeleton found in numerous alkaloids (26). Intramolecular cycloaddition of the 2-amidofuran followed by ring opening gives a zwitterionic intermediate **3** that can be channeled to different products depending on the

Received June 22, 1999. Published on the NRC Research Press website on June 7, 2000.

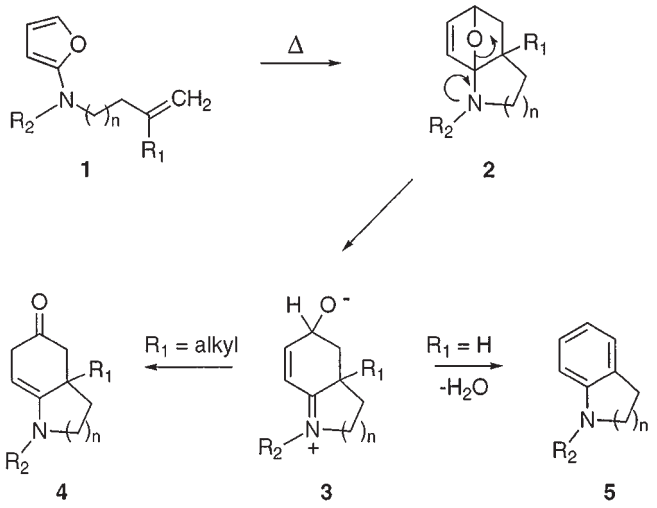
This paper is dedicated to Stephen Hanessian on the occasion of his 65th birthday and for his many significant contributions to the art of organic synthesis.

A. Padwa[1] and T.S. Reger. Department of Chemistry, Emory University, Atlanta, GA 30322, U.S.A.

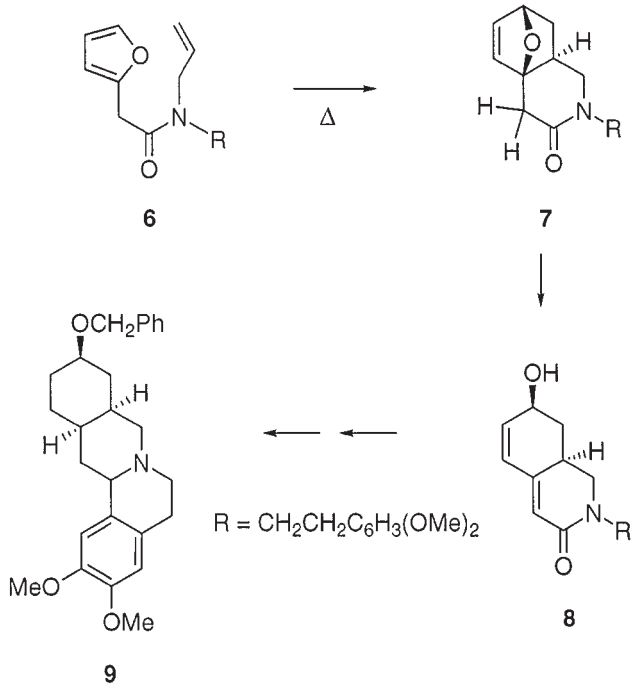
[1]Author to whom correspondence may be addressed. Telephone: (404) 727-0283. Fax: (404) 727-6629. e-mail: chemap@emory.edu

© 2000 NRC Canada

Scheme 1.



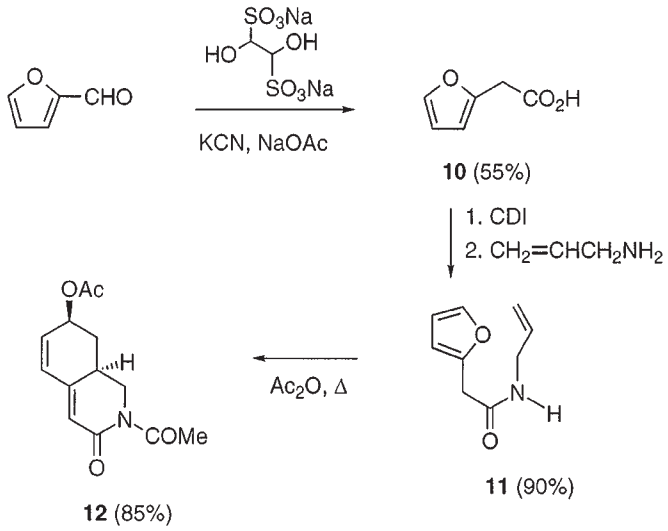
Scheme 2.



nature of the substituent group attached to the π-bond (i.e., R_1) (Scheme 1).

One of the most attractive features of this reaction sequence is the propensity for nitrogen assisted ring-opening and subsequent iminium ion formation of the oxabicyclic cycloadducts (i.e., **2** → **3**). The majority of work carried out by other investigators on the IMDAF reaction utilizing nitrogen containing tethers was done with furfurylamine derived substrates whose cycloadducts are not predisposed to spontaneous ring-opening (27–29). As an extension of our earlier work in this area, we believed that related furanyl amides such as **6** should also be excellent substrates for intramolecular Diels–Alder cycloaddition and oxabicyclic

Scheme 3.



ring-opening as a consequence of the acidic nature of the protons adjacent to the oxygen bridge (Scheme 2). To the best of our knowledge, amides derived from 2-furylacetic acid have not been utilized in Diels–Alder chemistry. A study to examine the synthesis of furans such as **6** and their subsequent cycloaddition and ring-opening chemistry was initiated with the intention of using this method as an entry into the berberine alkaloid family (30). The biological activity that these molecules display varies widely and includes anti-inflammatory, antimicrobial and antileukemic, as well as antitumor, properties (30). In the light of these properties and due to the general challenge that the construction of complex alkaloids offers, the development of new methods for the stereoselective synthesis of these nitrogen heterocycles is of considerable interest. In this paper we report the results of our IMDAF studies dealing with *N*-allyl 2-furan-2-yl-acetamides.

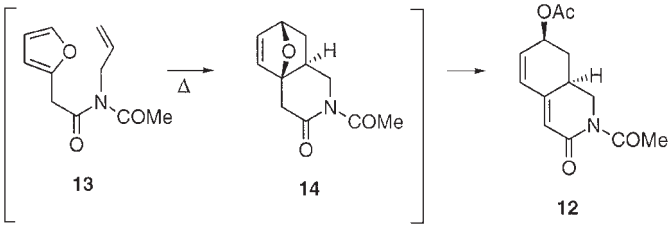
Results and discussion

As an entry into furanyl amides such as **6**, 2-furylacetic acid (**10**) was required as the key starting material. In our hands, the most reliable synthesis corresponds to the one-pot reaction between 2-furaldehyde and potassium cyanide (31). Reaction of these two reagents in the presence of sodium carbonate and glyoxal (sodium bisulfite addition compound hydrate) in a 20:1 water:dioxane solution reproducibly gave **10** in 55% yield. Carboxylic acid **10** was converted to the *N*-allyl amide **11** in 90% yield by reaction with 1,1-carbonyldiimidazole (CDI) followed by quenching with allylamine (Scheme 3). The attempted Diels–Alder cycloaddition of **11** in refluxing toluene or xylene led only to recovered starting material. This result is perfectly consistent with the earlier reports of Jung (27) and Parker (28) who found that related furans containing secondary amide tethers failed to undergo the Diels–Alder reaction. Cycloaddition could be effected, however, by heating **11** in refluxing acetic anhydride.[2] Under these conditions, the initial formation of imide **13** presumably

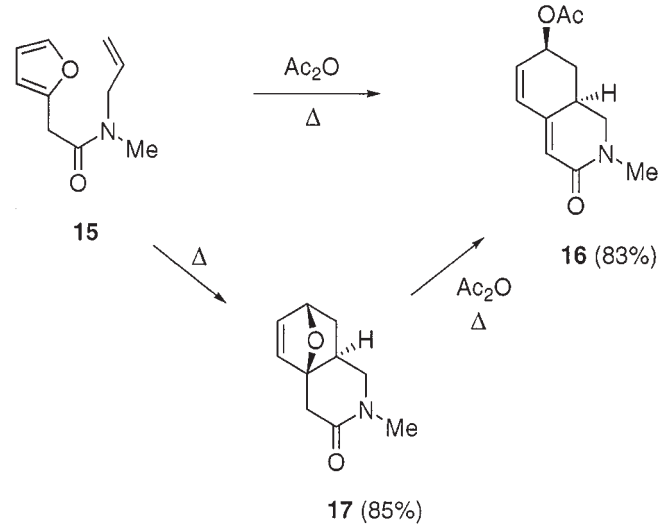
[2] The role of acetic anhydride in this reaction is to promote the [4+2]-cycloaddition by acylation at nitrogen as well as to assist in the subsequent oxa-bridge cleavage.

© 2000 NRC Canada

Scheme 4.



Scheme 5.

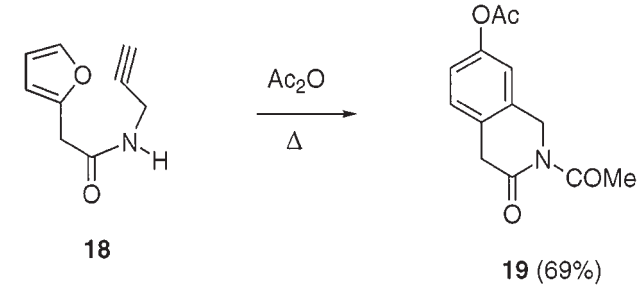


facilitates the Diels–Alder reaction to give the oxabicyclic intermediate **14**. The cycloadduct was not isolated as it undergoes spontaneous ring-opening and O-acetylation to furnish **12** as a single diastereomer in 85% yield (Scheme 4).

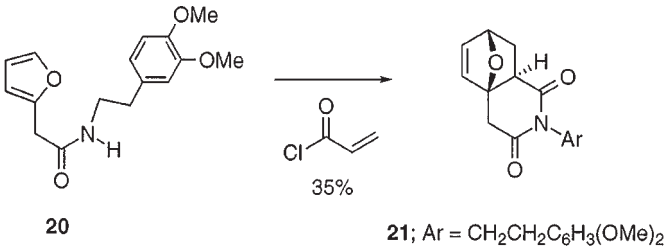
The *trans* relationship between the acetate and the bridgehead hydrogen is derived from the presumed cycloadduct **14** which results from *exo* orientation of the tether during the cycloaddition. This mode of cyclization for the IMDAF reaction of substrates containing nitrogen in the tether is analogous to that reported by others for related furanyl systems possessing short tethers (32, 33). The ring-opened acetate **12** is thus derived from an IMDAF cycloaddition where the side arm of the tethered alkenyl group is oriented *syn* (*exo*) with respect to the oxygen bridge. Products resulting from an *endo* side arm transition state were neither detected nor isolated. This result is not so surprising since, in these mobile cycloaddition equilibria, the *exo* adducts are expected to be thermodynamically more favored. Indeed, semi-empirical AM1 calculations show that the *exo*-cycloadduct is 11 kcal lower in energy than the corresponding *endo* (with respect to the tether) adduct and, presumably, some of this energy difference is reflected in the transition state for cycloaddition.

We next turned our attention to determining whether a tertiary amide linkage between the furan and alkene would allow the cycloaddition to proceed. Amide **15** was prepared in 94% yield by reaction of carboxylic acid **10** with CDI followed by quenching with *N*-methylallylamine. Upon thermolysis of **15** in acetic anhydride, the expected ring-opened and acetylated lactam **16** was isolated in 83% yield as a single diastereomer. The formation of **16** proceeds by a

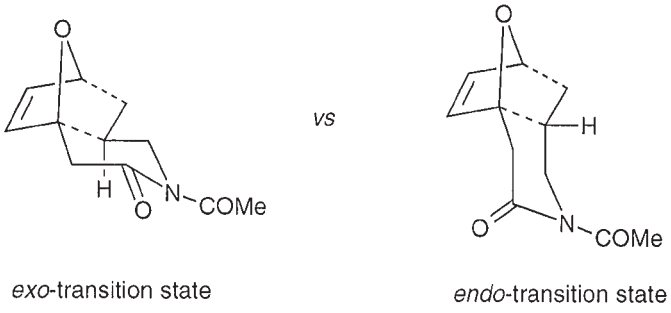
Scheme 6.



Scheme 7.



Structure 1.



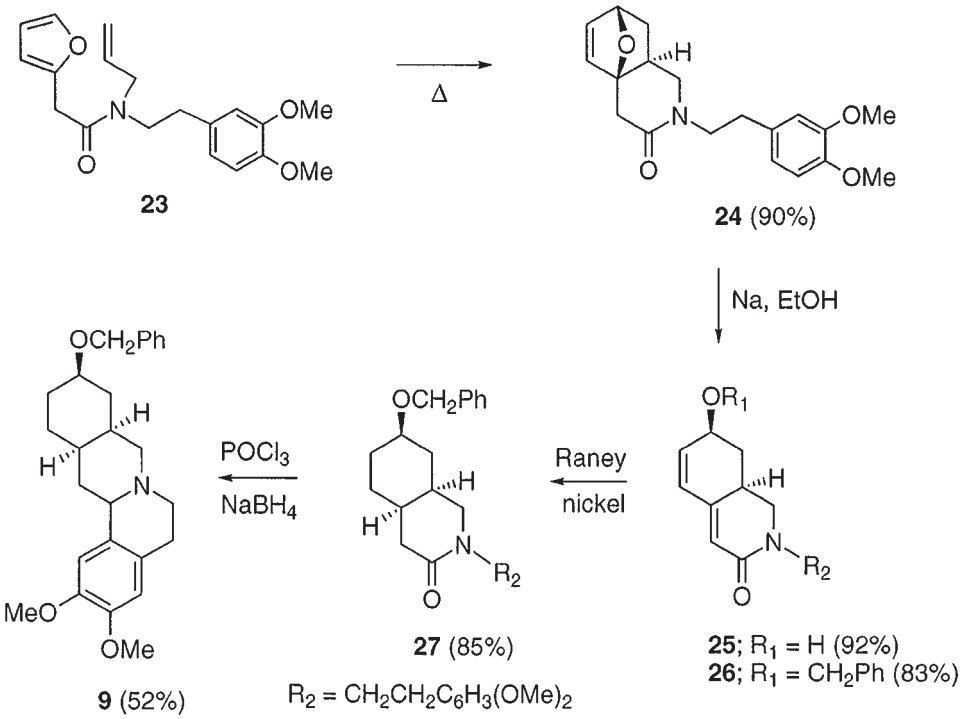
similar pathway to that described for **13**. Interestingly, when amide **15** was heated in refluxing toluene, the primary cycloadduct **17** was obtained in 85% yield, also as a single diastereomer, and could be quantitatively converted to **16** by heating in acetic anhydride (Scheme 5).

To further examine the scope of this cycloaddition with respect to the dienophile, furan **18** containing an alkyne tether was prepared in 86% yield. Heating a sample of **18** in acetic anhydride gave the isoquinoline derivative **19** in 69% yield (Scheme 6).

We next turned our attention to substrates bearing both a dienophile and an electron-rich aromatic group connected to the amide nitrogen (i.e., **23**). It was envisioned that a Bischler–Napieralski type cyclization (vide infra) could be effected on the Diels–Alder cycloaddition product. To this end, amide **20** was prepared in 87% yield by the usual reaction of 2-furylacetic acid with CDI and quenching with 3,4-dimethoxyphenethylamine. Unfortunately, all of our attempts to alkylate **20** with allyl bromide using a variety of bases (Cs_2CO_3 (DMF); NaH (THF); NaOH, K_2CO_3, Bu_4NHSO_4) failed to give any product. Imide formation with acryloyl chloride at room temperature in the presence of 4 Å molecular sieves did produce cycloadduct **21**, but only in 35% yield (Scheme 7).

© 2000 NRC Canada

Scheme 8.



As an alternative route to **23**, the known secondary amine allyl-[2-(3,4-dimethoxyphenethylamine)] (**22**) (34) was prepared and used to generate the desired tertiary amide directly. Thus, the reaction of carboxylic acid **10** with CDI followed by addition of amine **22** gave the desired cyclization precursor **23** in 77% yield. Upon heating **23** in refluxing xylene, cycloadduct **24** was isolated in 90% yield as a single diastereomer. A variety of bases were examined to induce ring-opening of **24** to the allylic alcohol **25**. Triethylamine, sodium hydride, and potassium *tert*-butoxide were all successful, but the use of the sodium in ethanol gave the highest yield (92%) and cleanest reaction. We then attempted a Bischler–Napieralski cyclization of the aromatic ring onto the amide carbonyl of **25** but this gave only a complex mixture of unidentifiable products. Instead, the alcohol was protected as its benzyl ether with sodium hydride and benzyl bromide in 83% yield. Compound **26** was then reduced to the decahydroisoquinoline **27** with Raney nickel in 85% yield. This compound was formed as a single diastereomer and there is literature precedence for a similar transformation in which Raney nickel reduction occurs from the *exo* face of a bicyclic structure to yield a *cis* ring junction (35). The Bischler–Napieralski cyclization of **27** was effected with $POCl_3$ followed by $NaBH_4$ and furnished **9** in 52% yield (Scheme 8). The appearance of two singlets in the aromatic region of the ^{1}H-NMR spectrum of **9** was indicative that the desired cyclization had taken place. This reaction proved to be very sensitive to the experimental conditions and, unfortunately, even the use of freshly distilled $POCl_3$ offered no advantage in terms of reaction yield. Nevertheless, the tetracyclic compound **9** containing the core skeleton of the berberine alkaloids was readily accessible in just five steps from relatively simple cyclization precursors.

In conclusion, the intramolecular Diels–Alder reaction of furanyl amides derived from 2-furylacetic acid proceeds smoothly and in high yield. The cyclization precursors are easily synthesized from readily available starting materials. The cycloaddition can be carried out under a variety of conditions to yield either the primary cycloadduct or the ring-opened and acetylated product. Consistent with previous studies, only compounds bearing imide or tertiary amide linkages between the furan and tethered dienophile were suitable substrates for cycloaddition. Overall, this methodology represents an efficient route to functionalized members of the tetrahydroisoquinolinone ring system in various oxidation states which could serve as intermediates to members of the berberine alkaloid family. Applications toward specific natural products and the further development of the IMDAF are currently underway and will be reported in due course.

Experimental section

Melting points are uncorrected. Mass spectra were determined at an ionizing voltage of 70 eV. Unless otherwise noted, all reactions were performed in flame-dried glassware under an atmosphere of dry argon. Solutions were evaporated under reduced pressure with a rotary evaporator, and the residue was chromatographed on a silica gel column using an ethyl acetate – hexane mixture as the eluent unless specified otherwise.

N-*Allyl-2-furan-2-yl-acetamide (**11**)*: To a solution containing 1.4 g (11 mmol) of furan-2-yl-acetic acid (**10**) (31) in 25 mL of CH_2Cl_2 was added 2.0 g (12.6 mmol) of 1,1′-carbonyldiimidazole. After stirring at room temperature for 1.5 h, 1.3 g (22 mmol) of allylamine was added and the mixture was stirred for an additional 1 h. The mixture was concentrated under reduced pressure and the crude product was purified by silica gel chromatography to give 1.6 g (90%) of

© 2000 NRC Canada

11 as a pale yellow liquid; IR (neat) ν: 3290, 1652, 1545, 1418, and 1246 cm^{-1}; ^{1}H-NMR (400 MHz, $CDCl_3$) δ: 3.64 (2H, s), 3.85–3.89 (2H, m), 5.08–5.14 (2H, m), 5.75–5.85 (1H, m), 5.95 (1H, brs), 6.24 (1H, d, *J* = 3.2 Hz), 6.36 (1H, dd, *J* = 3.2 and 1.6 Hz), and 7.39 (1H, d, *J* = 1.6 Hz) ppm; ^{13}C-NMR (100 MHz, $CDCl_3$) δ: 36.1, 41.8, 108.5, 110.7, 116.0, 133.8, 142.4, 148.6, and 168.4 ppm; HRMS calcd for $C_9H_{11}NO_2$: 165.0790; found: 165.0787.

*7-Acetoxy-2-acetyl-1,7,8,8a-tetrahydro-2*H-*isoquinoline-3-one (**12**)*: A solution containing 0.3 g (1.7 mmol) of **11** in 10 mL of acetic anhydride was heated at reflux for 20 h. The solution was concentrated under reduced pressure and the crude product was purified by silica gel chromatography to give 0.36 g (85%) of **12** as a white solid, mp 160–161°C; IR (neat): 1734, 1676, 1467, 1371, and 1289 cm^{-1}; ^{1}H-NMR (400 MHz, $CDCl_3$) δ: 1.46 (1H, dd, *J* = 12.8 and 11.6 Hz), 2.11 (3H, s), 2.30–2.35 (1H, m), 2.56 (3H, s), 2.69–2.76 (1H, m), 2.99 (1H, t, *J* = 12.8 Hz), 4.75 (1H, dd, *J* = 12.8 and 4.8 Hz), 5.55–5.59 (1H, m), 5.83 (1H, d, *J* = 2.0 Hz), 6.20 (1H, d, *J* = 10.0 Hz), and 6.35 (1H, dd, *J* = 10.0 and 2.0 Hz) ppm; ^{13}C-NMR (100 MHz, $CDCl_3$) δ: 21.0, 27.2, 31.9, 45.8, 68.6, 120.0, 127.3, 138.6, 151.0, 165.9, 170.2, and 172.8 ppm. Anal. calcd. for $C_{13}H_{15}NO_4$: C 62.64, H 6.07, N 5.62; found: C 62.52, H 6.09, N 5.54.

N-*Allyl-2-furan-2-yl*-N-*methyl-acetamide (**15**)*: To a solution of 0.6 g (4.8 mmol) of furan-2-yl-acetic acid (**10**) in 20 mL of CH_2Cl_2 was added 1.0 g (6.4 mmol) of 1,1′-carbonyldiimidazole. After stirring for 1 h at room temperature, 0.7 g (9.6 mmol) of *N*-methylallylamine was added and the mixture was stirred for an additional 1 h. The solution was concentrated under reduced pressure and the crude product was purified by silica gel chromatography to yield 0.8 g (94%) of **15** as a pale yellow oil which contained a mixture of amide rotamers in solution; IR (neat) ν: 1652, 1477, 1396, and 1147 cm^{-1}; ^{1}H-NMR (400 MHz, $CDCl_3$) δ: 2.94 (3H, s) and 3.00 (3H, s), 3.71 (2H, s) and 3.76 (2H, s), 3.97 (2H, m) and 4.01 (2H, m), 5.11–5.24 (2H, m), 5.68–5.79 (1H, m), 6.19–6.20 (1H, m), 6.31–6.33 (1H, m), and 7.34–7.35 (1H, m) ppm; ^{13}C-NMR (100 MHz, $CDCl_3$) δ: 33.5, 33.6, 34.0, 34.9, 50.0, 52.4, 107.4, 110.4, 116.7, 117.2, 132.2, 132.5, 141.5, 141.6, 148.6, 148.7, 168.3, and 168.7 ppm; HRMS calcd. for $C_{10}H_{13}NO_2$: 179.0946; found: 179.0939.

*7-Acetoxy-2-methyl-1,7,8,8a-tetrahydro-2*H-*isoquinoline-3-one (**16**)*: A solution containing 0.2 g (1.1 mmol) of furan **15** in 10 mL of acetic anhydride was heated at reflux for 20 h. The solution was concentrated under reduced pressure and the crude solid was purified by silica gel chromatography to give 0.21 g (83%) of **16** as a white solid, mp 104–105 °C; IR (neat) ν: 1730, 1652, 1590, and 1232 cm^{-1}; ^{1}H-NMR (400 MHz, $CDCl_3$) δ: 1.38–1.47 (1H, m), 2.10 (3H, s), 2.24–2.30 (1H, m), 2.82–2.85 (1H, m), 3.01 (3H, s), 3.26–3.36 (2H, m), 5.52–5.55 (1H, m), 5.77 (1H, d, *J* = 1.6 Hz), 6.02 (1H, d, *J* = 10.0 Hz), and 6.29 (1H, dd, *J* = 10.0 and 1.6 Hz) ppm; ^{13}C-NMR (100 MHz, $CDCl_3$) δ: 20.9, 31.2, 31.8, 34.2, 52.9, 68.6, 119.8, 127.9, 135.3, 145.4, 165.4, and 170.2 ppm. Anal. calcd. for $C_{12}H_{15}NO_3$: C 65.14, H 6.83, N 6.33; found: C 65.38, H 6.91, N 6.47.

*4-Methyl-11-oxa-4-aza-tricyclo[6.2.1.0^{1,6}]undec-9-en-3-one (**17**)*: A solution containing 1.6 g (8.8 mmol) of furan **15** in 15 mL of toluene was heated at reflux for 20 h. The solution was concentrated under reduced pressure and the crude solid was purified by silica gel chromatography to give 1.3 g (85%) of **17** as a white solid, mp 89–90°C; IR (neat) ν: 1646, 1495, 1394, and 1315 cm^{-1}; ^{1}H-NMR (400 MHz, $CDCl_3$) δ: 1.44–1.51 (2H, m), 1.85–1.91 (1H, m), 2.94 (1H, d, J = 18.8 Hz), 3.00 (3H, s), 3.14 (1H, d, *J* = 18.8 Hz), 3.31–3.34 (2H, m), 4.94 (1H, dd, *J* = 4.0 and 1.6 Hz), 6.14 (1H, d, *J* = 6.0 Hz), and 6.40 (1H, dd, *J* = 6.0 and 1.6 Hz) ppm; ^{13}C-NMR (100 MHz, $CDCl_3$) δ: 30.6, 35.0, 35.2, 35.5, 52.9, 78.1, 85.6, 137.3, 137.4, and 168.4 ppm. Anal. calcd. for $C_{10}H_{13}NO_2$: C 67.02, H 7.31, N 7.82; found: C 66.75, H 7.24, N 7.73.

2-Furan-2-yl-N-*prop-2-ynyl-acetamide (**18**)*: To a solution containing 0.8 g (6.4 mmol) of furan-2-yl-acetic acid (**10**) in 25 mL of CH_2Cl_2 was added 1.4 g (8.6 mmol) of 1,1′-carbonyldiimidazole. After stirring at room temperature for 1.5 h, 0.6 mL (8.7 mmol) of propargylamine was added and the mixture was stirred for an additional 1 h. The solution was concentrated under reduced pressure and the crude product was purified by silica gel chromatography to give 0.9 g (86%) of **18** as a white solid, mp 75–76°C; IR (neat) ν: 3286, 1648, 1552, 1424, and 1240 cm^{-1}; ^{1}H-NMR (400 MHz, $CDCl_3$) δ: 2.23 (1H, t, *J* = 2.4 Hz), 3.63 (2H, s), 4.02 (2H, dd, *J* = 2.8 and 2.4 Hz), 6.23 (1H, d, *J* = 2.8 Hz), 6.34–6.36 (1H, m), 6.50 (1H, brs), and 7.38 (1H, s) ppm; ^{13}C-NMR (100 MHz, $CDCl_3$) δ: 29.1, 35.7, 71.4, 79.2, 108.4, 110.6, 142.3, 148.2, and 168.4 ppm. Anal. calcd. for $C_9H_9NO_2$: C 66.25, H 5.56, N 8.58; found: C 66.16, H 5.49, N 8.61.

*2-Acetyl-7-acetoxy-1,4-dihydro-2*H-*isoquinolin-3-one (**19**)*: A solution containing 0.2 g (1.4 mmol) of furan **18** in 10 mL of acetic anhydride was heated at reflux for 24 h. The solution was concentrated under reduced pressure and the crude residue was purified by silica gel chromatography to give 0.24 g (69%) of **19** as a pale yellow oil; IR (neat) ν: 1760, 1705, 1498, 1367, and 1208 cm^{-1}; ^{1}H-NMR (300 MHz, $CDCl_3$) δ: 2.32 (3H, s), 2.58 (3H, s), 3.74 (2H, s), 4.92 (2H, s), 7.02–7.05 (1H, m), 7.05 (1H, s), and 7.22–7.26 (1H, m) ppm; ^{13}C-NMR (75 MHz, $CDCl_3$) δ: 21.0, 27.2, 40.8, 45.3, 119.2, 121.2, 127.5, 129.5, 133.5, 149.4, 169.2, 170.8, and 172.1 ppm; HRMS (FAB) calcd. for $C_{13}H_{13}NO_4Li$ (M + Li): 254.1005; found: 254.1006.

N-*[2-(3,4-Dimethoxyphenethyl)]-2-furan-2-yl-acetamide (**20**)*: To a solution containing 0.86 g (6.8 mmol) of furan-2-yl-acetic acid (**10**) in 25 mL of CH_2Cl_2 was added 1.5 g (9.0 mmol) of 1,1′-carbonyldiimidazole. After stirring for 1 h at room temperature, 1.9 g (10.3 mmol) of 3,4-dimethoxyphenethylamine was added and the mixture was stirred for an additional 1 h. The solution was concentrated under reduced pressure and the crude product was purified by silica gel chromatography to give 1.7 g (87%) of **20** as a white solid, mp 78–79°C; IR (neat) ν: 3293, 1648, 1511, and 1258 cm^{-1}; ^{1}H-NMR (400 MHz, $CDCl_3$) δ: 2.72 (3H, t, *J* = 6.8 Hz), 3.46 (2H, dt, *J* = 6.8 and 6.0 Hz), 3.57 (2H, s), 3.84 (3H, s), 3.85 (3H, s), 5.85 (1H, brs), 6.15–6.16 (1H, m), 6.31–6.33 (1H, m), 6.63–6.67 (2H, m), 6.76–6.78 (1H, m),

© 2000 NRC Canada

and 7.32–7.33 (1H, m) ppm; ^{13}C-NMR (100 MHz, $CDCl_3$) δ: 34.9, 36.1, 40.7, 55.6, 55.7, 108.3, 110.6, 111.1, 111.7, 120.4, 131.0, 142.2, 147.4, 148.6, 148.8, and 168.3 ppm; Anal. calcd. for $C_{16}H_{19}NO_4$: C 66.42, H 6.62, N 4.84; found: C 66.40, H 6.60, N 4.89.

*4-[2-(3,4-Dimethoxyphenethyl)]-11-oxa-4-aza-tricyclo[6.2.1.0^{1,6}] undec-9-ene-3,5-dione (**21**)*: To a solution containing 0.5 g (1.7 mmol) of amide **20** in 15 mL of CH_2Cl_2 was added 1.7 g of powdered molecular sieves (4 Å) followed by 0.46 g (5.1 mmol) of acryloyl chloride and the mixture was stirred at room temperature for 20 h. The solution was filtered through a pad of celite and concentrated under reduced pressure. The crude product was purified by silica gel chromatography to give 0.2 g (35%) of **21** as a pale yellow solid, mp 170–171°C; IR (neat) ν: 1730, 1680, 1515, and 1365 cm^{-1}; ^{1}H-NMR (400 MHz, $CDCl_3$) δ: 1.74 (1H, dd, *J* = 12.0 and 4.8 Hz), 2.26–2.32 (1H, m), 2.75–2.78 (3H, m), 3.24 (1H, d, *J* = 16.8 Hz), 3.46 (1H, d, *J* = 16.8 Hz), 3.86 (3H, s), 3.88 (3H, s), 3.91–4.06 (2H, m), 5.09 (1H, dd, *J* = 4.8 and 2.0 Hz), 5.78 (1H, d, *J* = 5.6 Hz), 6.56 (1H, d, *J* = 5.6 Hz), and 6.75–6.81 (3H, m) ppm; ^{13}C-NMR (100 MHz, $CDCl_3$) δ: 28.6, 33.4, 40.5, 41.5, 47.1, 55.7, 55.8, 80.3, 82.1, 111.0, 112.0, 120.9, 130.6, 131.6, 141.7, 147.6, 148.7, 170.0, and 171.0 ppm; Anal. calcd. for $C_{19}H_{21}NO_5$: C 66.46, H 6.16, N 4.08; found: C 66.39, H 6.14, N 4.06.

N-*Allyl-[2-(3,4-dimethoxyphenethyl)]-2-furan-2-yl-acetamide (**23**)*: To a solution containing 0.2 g (1.7 mmol) of furan-2-yl-acetic acid (**10**) in 8 mL of CH_2Cl_2 was added 0.4 g (2.5 mmol) of 1,1′-carbonyldiimidazole. After stirring at room temperature for 1 h, 0.5 g (2.4 mmol) of allyl-[2-(3,4-dimethoxyphenethyl)]amine (**22**) (34) was added and the mixture was stirred for an additional 2 h. The solution was concentrated under reduced pressure and the crude product was purified by silica gel chromatography to give 0.4 g (77%) of **23** as a clear oil which contained a mixture of amide rotamers in solution; IR (neat) ν: 1651, 1515, 1457, and 1260 cm^{-1}; ^{1}H-NMR (400 MHz, $CDCl_3$) δ: 2.74 (2H, t, *J* = 7.2 Hz) and 2.82 (2H, t, *J* = 7.2 Hz), 3.51–3.56 (2H, m), 3.70 (1H, s), 3.82–3.83 (2H, m), 3.84 (3H, s) and 3.85 (3H, s), 3.86 (3H, s) and 3.87 (3H, s), 4.02 (1H, d, *J* = 6.0 Hz), 5.13–5.21 (2H, m), 5.71 (1H, m) and 5.81 (1H, m), 6.14–6.18 (1H, m), 6.31–6.34 (1H, m), 6.65–6.83 (3H, m), and 7.33–7.36 (1H, m) ppm; ^{13}C-NMR (100 MHz, $CDCl_3$) δ: 33.4, 33.5, 33.7, 34.5, 48.0, 48.6, 49.2, 51.1, 55.7, 55.8, 55.9, 107.4, 107.5, 110.4, 110.5, 111.1, 111.4, 111.8, 111.9, 116.6, 117.1, 120.6, 120.7, 130.5, 131.6, 132.7, 133.1, 141.6, 141.7, 147.4, 147.8, 148.7, 148.8, 168.3, and 168.7 ppm; Anal. calcd. for $C_{19}H_{23}NO_4$: C 69.28, H 7.04, N 4.17; found: C 68.98, H 7.04, N 4.22.

*4-[2-(3,4-Dimethoxyphenethyl)]-11-oxa-4-aza-tricyclo[6.2.1.0^{1,6}] undec-9-en-3-one (**24**)*: A solution containing 0.17 g (5.2 mmol) of furan **23** in 10 mL of xylene was heated at reflux for 20 h. The solution was concentrated under reduced pressure and the crude solid was purified by silica gel chromatography to give 0.15 g (90%) of **24** as a white solid, mp 119–120°C; IR (neat) ν: 1644, 1513, 1449, and 1154 cm^{-1}; ^{1}H-NMR (400 MHz, $CDCl_3$) δ: 1.39–1.44 (2H, m), 1.71–1.75 (1H, m), 2.79–2.83 (2H, m), 2.92 (1H, d, *J* = 18.8 Hz), 3.15 (1H, d, *J* = 18.8 Hz), 3.18–3.22 (2H, m), 3.51–3.58 (1H, m), 3.66–3.73 (1H, m), 3.86 (3H, s), 3.88 (3H, s), 4.89 (1H, dd, *J* = 4.0 and 1.6 Hz), 6.14 (1H, d, *J* = 5.6 Hz), 6.37 (1H, dd, *J* = 5.6 and 1.6 Hz), and 6.75–6.81 (3H, m) ppm; ^{13}C-NMR (100 MHz, $CDCl_3$) δ: 30.3, 33.5, 35.9, 36.0, 50.0, 51.6, 55.7, 55.8, 78.1, 85.6, 111.1, 111.8, 120.6, 131.4, 137.3, 137.4, 147.4, 148.7, and 168.6 ppm; Anal. calcd. for $C_{19}H_{23}NO_4$: C 69.28, H 7.04, N 4.25; found: C 69.11, H 7.09, N 4.21.

*2-[2-(3,4-Dimethoxyphenethyl)]-7-hydroxy-1,7a,8,8a-tetrahydro-2*H*-isoquinoline-3-one (**25**)*: To a solution containing 0.24 g (10 mmol) of sodium metal in 25 mL of EtOH was added 1.0 g (3.0 mmol) of cycloadduct **24** at 0 °C. After stirring for 1 h at room temperature, 20 mL of water was added and the solution was extracted with CH_2Cl_2. The organic layer was dried over $MgSO_4$, concentrated under reduced pressure, and the crude product was purified by silica gel chromatography to give 0.9 g (92%) of **25** as a white solid, mp 137–139°C; IR (neat) ν: 3348, 1641, 1511, 1478, and 1244 cm^{-1}; ^{1}H-NMR (400 MHz, $CDCl_3$) δ: 1.21–1.30 (1H, m), 1.91 (1H, d, *J* = 6.6 Hz, exchangeable with D_2O), 2.08–2.13 (1H, m), 2.57–2.60 (1H, m), 2.80–2.85 (2H, m), 3.17 (1H, s), 3.20 (1H, d, *J* = 3.6 Hz), 3.51–3.73 (2H, m), 3.86 (3H, s), 3.87 (3H, s), 4.41 (1H, dd, *J* = 10.0 and 4.8 Hz), 5.71 (1H, d, *J* = 1.6 Hz), 6.17 (2H, dd, *J* = 18.8 and 10.0 Hz), and 6.76–6.83 (3H, m) ppm; ^{13}C-NMR (100 MHz, $CDCl_3$) δ: 31.8, 33.5, 35.4, 49.0, 51.9, 55.6, 55.7, 65.9, 111.2, 111.9, 118.3, 120.6, 126.0, 131.3, 141.1, 147.4, 148.7, and 165.8 ppm; Anal. calcd. for $C_{19}H_{23}NO_4$: C 69.28, H 7.04, N 4.25; found: C 69.14, H 7.05, N 4.20.

*7-Benzyloxy-2-[2-(3,4-dimethoxyphenethyl)]-1,7a,8,8a-tetrahydro-2*H*-isoquinolin-3-one (**26**)*: To a 5 mL solution of THF was added 0.04 g (1.0 mmol) of NaH (60% dispersion) which had been rinsed with hexane. After cooling to 0°C, 0.13 g (0.4 mmol) of alcohol **25** in 10 mL of THF was added and the mixture was warmed to room temperature. After stirring for 2 h, 0.24 g of benzyl bromide was added and the solution was heated at 60°C for 15 h. The reaction was cooled to 0°C and 10 mL of water was added slowly. The mixture was extracted with ethyl acetate and the organic layer was dried over $MgSO_4$ and concentrated under reduced pressure. Purification of the crude mixture by silica gel chromatography gave 0.12 g (83%) of **26** as a white solid, mp 118–119°C; IR (neat) ν: 1647, 1510, 1453, and 1260 cm^{-1}; ^{1}H-NMR (400 MHz, $CDCl_3$) δ: 1.25–1.38 (1H, m), 2.14–2.19 (1H, m), 2.50–2.58 (1H, m), 2.81–2.85 (2H, m), 3.11–3.21 (2H, m), 3.52–3.73 (2H, m), 3.85 (3H, s), 3.87 (3H, s), 4.21 (1H, dd, *J* = 10.4 and 5.2 Hz), 4.62 (2H, s), 5.74 (1H, d, *J* = 2.4 Hz), 6.22 (2H, s), 6.75–6.81 (3H, m), and 7.30–7.36 (5H, m) ppm; ^{13}C-NMR (100 MHz, $CDCl_3$) δ: 31.8, 32.7, 33.7, 49.0, 52.1, 55.7, 55.8, 70.5, 73.2, 111.1, 111.9, 119.4, 120.6, 126.9, 127.6, 127.8, 128.4, 131.6, 137.9, 146.6, 147.4, 148.8, and 165.2 ppm; Anal. calcd. for $C_{26}H_{29}NO_4$: C 74.44, H 6.97, N 3.34; found: C 74.28, H 6.90, N 3.31.

*7-Benzyloxy-2-[2-(3,4-dimethoxyphenethyl)]-octahydroisoquinolin-3-one (**27**)*: To a solution of 0.05 g (0.13 mmol) of **26** in 8 mL of EtOH was added a slight excess of Raney nickel. After stirring at room temperature for 15 h, the mixture was filtered through Celite with ethyl acetate. The

© 2000 NRC Canada

solution was concentrated under reduced pressure and the crude product was purified by silica gel chromatography to give 0.047 g (85%) of **27** as a clear oil; IR (neat) ν: 1636, 1511, 1452, and 1264 cm^{-1}; ^{1}H-NMR (400 MHz, $CDCl_3$) δ: 1.49–1.69 (5H, m), 1.83–1.91 (2H, m), 2.07–2.11 (2H, m), 2.27–2.47 (2H, m), 2.76–2.85 (2H, m), 3.07 (1H, dd, *J* = 12.0 and 2.8 Hz), 3.33–3.43 (3H, m), 3.68–3.75 (1H, m), 3.84 (3H, s), 3.87 (3H, s), 4.54 (2H, d, *J* = 2.4 Hz), 6.73–6.77 (3H, m), and 7.25–7.35 (5H, m) ppm; ^{13}C-NMR (100 MHz, $CDCl_3$) δ: 26.3, 26.7, 30.8, 31.4, 32.3, 32.6, 33.1, 49.1, 52.9, 55.7, 55.8, 69.8, 76.1, 111.1, 112.0, 120.7, 127.3, 127.4, 128.3, 131.6, 138.7, 147.4, 148.8, and 168.9 ppm; HRMS calcd. for $C_{26}H_{33}NO_4$: 423.2410; found: 423.2397.

*10-Benzyloxy-2,3-dimethoxy-5,8,8a,9,10,11,12,12a,13,13a-decahydro-6*H*-isoquino[3,2-a]isoquinoline (**9**)*: To a solution of 0.3 g (0.6 mmol) of **27** in 10 mL of benzene was added 0.2 g (1.3 mmol) of phosphorous oxychloride. After heating at reflux for 2 h, the solvent was removed under reduced pressure and the crude product was taken up in 10 mL of methanol. To this solution was added 0.05 g (1.3 mmol) of sodium borohydride and the mixture was stirred for an additional 2 h. The solvent was removed under reduced pressure and the crude material was purified by silica gel chromatography to give 0.15 g (52%) of **9** as a yellow foam; IR (neat) ν: 1601, 1510, and 1270 cm^{-1}; ^{1}H-NMR (400 MHz, $CDCl_3$) δ: 1.32–1.45 (1H, m), 1.56–2.04 (9H, m), 2.39 (1H, dt, *J* = 11.6 Hz and 3.6 Hz), 2.50–2.57 (2H, m), 2.72 (1H, dd, *J* = 11.6 and 1.6 Hz), 2.81–2.85 (1H, m), 3.02–3.11 (2H, m), 3.34–3.42 (1H, m), 3.84 (3H, s), 3.85 (3H, s), 4.55 (2H, dd, *J* = 23.6 and 12.4 Hz), 6.57 (1H, s), 6.68 (1H, s), and 7.24–7.33 (5H, m) ppm; ^{13}C-NMR (100 MHz, $CDCl_3$) δ: 27.0, 29.4, 29.5, 32.0, 32.3, 34.3, 35.1, 52.6, 55.7, 55.9, 62.0, 63.3, 69.3, 78.0, 108.0, 111.3, 127.0, 127.1, 127.3, 128.2, 130.5, 139.3, 147.0, and 147.1 ppm; HRMS calcd. for $C_{26}H_{33}NO_3$: 408.2539; found: 408.2526.

Acknowledgements

We gratefully acknowledge the National Science Foundation (CHE-9806331) for generous support of this work. High-field NMR spectrometers used in these studies were made possible through equipment grants from the NIH and NSF.

References

1. B. Lipshutz. Chem. Rev. **86**, 795 (1986).
2. B. Trost and J. Flygare. J. Org. Chem. **59**, 1078 (1994).
3. A.A. Look, M.T. Burch, W. Fenical, Z. Qi-tai, and J. Clardy. J. Org. Chem. **50**, 5741 (1985).
4. W. Fenical, R.K. Okeeda, M.M. Basnadurraga, P. Culver, and R.S. Jacobs. Science (Washington, D.C.), **212**, 1512 (1981).
5. K. Wiesner, T. Tsai, R. Kumar, and H. Sivaramakrishnon. Helv. Chim. Acta, **67**, 1128 (1984).
6. D.M.X. Donnelly and M.J. Meegan. *In* Comprehensive heterocyclic chemistry. *Edited by* A.R. Katritzky and C.W. Rees. Pergamon, Oxford. 1984. Vol. 4, pp. 657–712.
7. C.O. Kappe, S.S. Murphree, and A. Padwa. Tetrahedron, **53**, 14179 (1997).
8. (*a*) P. Vogel, D. Fattori, F. Gasparini, and C. Le Drian. Synlett, 173 (1990); (*b*) J.L. Reymond, A.A. Pinkerton, and P. Vogel. J. Org. Chem. **56**, 2128 (1991).
9. P. Renaud and J.P. Vionnet. J. Org. Chem. **58**, 5895 (1993).
10. T.A. Eggette, H. de Koning, and H.O. Huisman. J. Chem. Soc. Perkin Trans. 1, 980 (1978).
11. A. Ogawa, Y. Iwasawa, T. Nose, T. Suami, S. Ohba, M. Ito, and Y. Saito. J. Chem. Soc. Perkin Trans. 1, 903 (1985).
12. G. Just and S. Kim. Tetrahedron Lett. **17**, 1063 (1976).
13. A. Murai, K. Takahashi, H. Taketsuru, and T. Masamune. J. Chem. Soc. Chem. Commun. 221 (1981).
14. H. Kotsuki and H. Nishizawa. Heterocycles, **16**, 1287 (1981).
15. P.J. Cox and N.S. Simpkins. Synlett, 321 (1991).
16. L.A. Van Royen, R. Mijngheer, and P.J. De Clercq. Tetrahedron Lett. **24**, 3145 (1983).
17. (*a*) A.B. Smith, N.J. Liverton, N.J. Hrib, H. Sivaramakrishnan, and K. Winzenberg. J. Org. Chem. **50**, 3239 (1985); (*b*) A.B. Smith, N.J. Liverton, N.J. Hrib, H. Sivaramakrishnan, and K. Winzenberg. J. Am. Chem. Soc. **108**, 3040 (1986); (*c*) W.M. Best and D.Wege. Tetrahedron Lett. **22**, 4877 (1981).
18. (*a*) C. Le Drian, E. Vieira, and P. Vogel. Helv. Chim. Acta, **72**, 338 (1989); (*b*) T. Takahashi, A. Iyobe, Y. Arai, and T. Koizumi. Synthesis, 189 (1989); (*c*) A.J. Guilford and R.W. Turner. J. Chem. Soc. Chem. Commun. 466 (1983); (*d*) W. Yang and M. Koreeda. J. Org. Chem. **57**, 3836 (1992).
19. (*a*) T. Suami. Pure Appl. Chem. **59**, 1509 (1987); (*b*) L.M. Harwood, B. Jackson, K. Prout, and F.J. Witt. Tetrahedron Lett. **31**, 1885 (1990); (*c*) M. Koreeda, K.-Y. Jung, and M. Hirota. J. Am. Chem. Soc. **112**, 7413 (1990); (*d*) E. Reynard, J.-L. Reymond, and P. Vogel. Synlett, 469 (1991); (*e*) S. Ogawa, M. Yoshikawa, and T. Taki. J. Chem. Soc. Chem. Commun. 406 (1992). (*f*) S. Ogawa and H. Tsunoda. Liebigs Ann. Chem. 637 (1992).
20. (*a*) M.E. Jung and L. Street. J. Am. Chem. Soc. **106**, 8327 (1984); (*b*) S. Mirsadeghi and B. Rickborn. J. Org. Chem. **50**, 4340 (1985).
21. P.A. Grieco, R. Lis, R.E. Zelle, and J. Finn. J. Am. Chem. Soc. **108**, 5908 (1986).
22. (*a*) H. Takayama, K. Hayashi, and T. Koizumi. Tetrahedron Lett. **27**, 5509 (1986); (*b*) S. Hanessian, P. Beaulieu, and D. Dube. Tetrahedron Lett. **27**, 5071 (1986).
23. O. Arjona, A. Dios, R.F. Pradilla, J. Plumet, and A. Viso. J. Org. Chem. **59**, 3906 (1994).
24. (*a*) D.D. Sternbach, D.M. Rossana, and K.D. Onan. J. Org. Chem. **49**, 3427 (1984); (*b*) M.E. Jung and J. Gervey. J. Am. Chem. Soc. **111**, 5469 (1989); (*c*) L.L. Klein. J. Org. Chem. **50**, 1770 (1985).
25. (*a*) A. Padwa, M. Dimitroff, A.G. Waterson, and T. Wu. J. Org. Chem. **62**, 4088 (1997); (*b*) A. Padwa, M. Dimitroff, A.G. Waterson, and T. Wu. J. Org. Chem. **63**, 3986 (1998). (*c*) A. Padwa, M.A. Brodney, B. Liu, K. Satake, and T. Wu. J. Org. Chem. **64**, 3595 (1999).
26. A. Padwa, M.A. Brodney, and M. Dimitroff. J. Org. Chem. **63**, 5304 (1998).
27. (*a*) M.E. Jung and L.J. Street. J. Am. Chem. Soc. **106**, 8327 (1984); (*b*) M. E. Jung and L.J. Street. Tetrahedron Lett. **26**, 3639 (1985).
28. K.A. Parker and M.R. Adamchuk. Tetrahedron Lett. **19**, 1689 (1978).
29. (*a*) J.E. Hernandez, S. Fernandez, and G. Arias. Synth. Commun. **18**, 2055 (1988); (*b*) T. Hudlicky, G. Butora, S.P. Fearnley, A.G. Gum, P.J. Persichini, M.R. Stabile, and J.S. Merola. J. Chem. Soc. Perkin Trans. 1 2393 (1995); (*c*) T. Mukaiyama, T. Tsuji, and N. Iwasawa. Chem. Lett. 697 (1979).
30. (*a*) C.W.W. Beecher and W.J. Kelleher. *In* Alkaloids: chemical and biological perspectives. *Edited by* S.W. Pelletier. John Wiley and Sons, New York. 1988. Vol. 6, pp. 297–337;

© 2000 NRC Canada

(*b*) G. Memetzidis, J.F. Stambach, L. Jung, C. Schott, C. Heitz, J.C. Stoclet. Eur. J. Med. Chem. **26**, 605 (1991).
31. L. Breen, F.W. Eastwood, T. Ockman, I.D. Rae, and A.M. Redwood. Aust. J. Chem. **26**, 2221 (1973).
32. (*a*) S. Woo and B.A. Keay. Tetrahedron: asymmetry, **5**, 1411 (1994); (*b*) C. Rogers and B.A. Keay. Tetrahedron Lett. **32**, 6477 (1991); (*c*) C. Rogers and B.A. Keay. Synlett, 353 (1991); (*d*) C. Rogers and B.A. Keay. Can. J. Chem. **70**, 2929 (1992).
33. (*a*) P.J. De Clercq and L.A. Van Royen. Synth. Commun. **9**, 771 (1979); (*b*) L.A. Van Royen, R. Mijngheer, and P.J. De Clercq. Bull. Soc. Chim. Belg. **93**, 1019 (1984); (*c*) K. Fischer and S. Hunig. J. Org. Chem. **52**, 564 (1987).
34. M. Reiffen, W. Eberlein, P. Mueller, M. Psiorz, and K. Noll. J. Med. Chem. **33**, 1496 (1990).
35. Y. Tamura, H. Maeda, S. Akai, and H. Ishibashi. Tetrahedron Lett. **23**, 2209 (1982).

© 2000 NRC Canada

Studies on the synthesis of the decahydro-*as*-indacene ring system of (–)-spinosyn A via transannular Diels–Alder reactions of substituted (*E,E,E*)-cyclododeca-1,6,8-trienes

Scott A. Frank, Andrea B. Works, and William R. Roush

Abstract: Stereoselective syntheses of decahydro-*as*-indacenes **31** and **54** are reported. The key features of our syntheses of **31** and **54** are the tandem Ireland–Claisen ring contraction of lactones **29** and **38** followed by the transannular Diels–Alder cyclization of cyclododecatrienes **30** and **35**. Transition state modeling of both the transannular Diels–Alder reaction and the Ireland–Claisen ring contraction using PCModel is also described.

Key words: transannular Diels–Alder reactions, tandem reactions, Claisen ring contraction, Spinosyn A, synthetic study.

Résumé : On a réalisé la synthèse stéréosélective des décahydro-*as*-indacènes **31** et **54**. Les principales caractéristiques de nos synthèses de ces produits sont les contractions de cycle d'Ireland–Claisen en tandem des lactones **29** et **38**, suivies d'une cyclisation transannulaire de Diels–Alder des cyclodécatriènes **30** et **35**. On décrit aussi la modélisation moléculaire à l'aide d'un ordinateur des états de transition de la réaction de Diels–Alder transannulaire ainsi que de la réaction de contraction de cycle d'Ireland–Claisen.

Mots clés : réactions de Diels–Alder transannulaires, réactions en tandem, contraction de cycle de Claisen, Spinosyn A., étude synthétique.

[Traduit par la Rédaction]

Introduction

Spinosyn A (**1**) and D (**2**), ikarugamycin (**3**), and capsimycin (**4**) are natural products that possess perhydro-*as*-indacene subunits (Scheme 1). While ikarugamycin and capsimycin are relatively potent anti-bacterial agents (1, 2), the spinosyns display very potent insecticidal activity (3, 4) and are marketed for use against a wide variety of insects (5). Several total syntheses of these natural products have been developed (6–13). Many of the syntheses of **1** and **3** have utilized intramolecular Diels–Alder reactions of appropriately substituted (*E,E,E*)-dodeca-2,7,9-trienes to construct a trans-fused hexahydroindene subunit, with the third ring of the indacene nucleus being formed by a subsequent annulation sequence. We were intrigued with the notion that the tricyclic nucleus **6** of the spinosyns could be assembled in a single step by the transannular Diels–Alder reaction of an appropriately substituted (*E,E,E*)-cyclododeca-1,6,8-triene, such as **5**, as shown in Scheme 2. Hirata has suggested that a transannular Diels–Alder reaction may be involved in the biosynthesis of **3** (14), and Kirst has suggested that a similar transformation may occur in the biosynthetic pathway to **1** (15).

Transannular Diels–Alder reactions display significant advantages over conventional intramolecular Diels–Alder variants (16, 17) due to a lowered $\Delta G^{\ddagger}$ resulting from a decreased $\Delta S^{\ddagger}$. As a result, reactions which generally do not proceed intramolecularly work smoothly in the transannular version (18, 19). This process has also been used for the synthesis of strained, medium-sized rings via the transannular cyclization of macrocyclic trienes, a procedure representing an overall ring contraction, as we have demonstrated in our work on nargenicin A_1 (20). While the transannular Diels–Alder reaction is emerging as a powerful tool for the construction of fused, polycyclic ring systems (21), the factors that control the stereochemical outcome of these reactions are still being elucidated (22). Indeed, prior to the initiation of our studies, we were aware of only one other report detailing the preparation of an unsubstituted perhydro-*as*-indacene by a transannular Diels–Alder reaction (23).

From the outset, we realized that forming the requisite 12-membered triene **5** could be difficult. In general, the formation of 11, 12, and 13-membered macrocyclic dienes and trienes by direct cyclization of acyclic precursors can be troublesome as we and other groups have observed (24–27). Fortunately, access to strained, medium-sized rings can be achieved by other means. A particularly useful strategy involves the ring contraction of a larger and more accessible ring system. Although a number of ring contraction protocols exist, we were interested in using the Ireland–Claisen

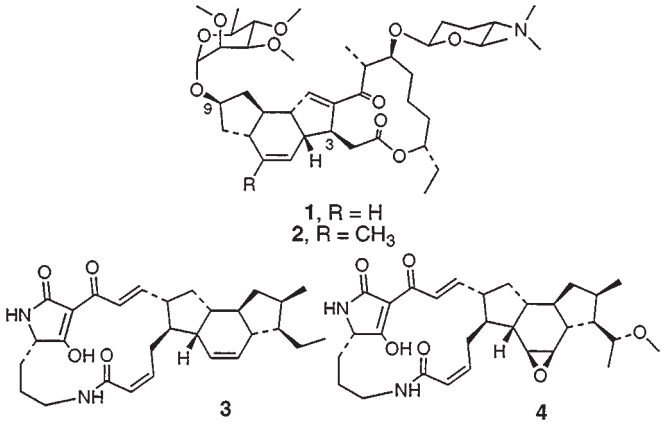
Received August 20, 1999. Published on the NRC Research Press website on June 7, 2000.

S.A. Frank, A.B. Works, and W.R. Roush.[1] Department of Chemistry, University of Michigan, 930 N. University, Ann Arbor, MI 48197, U.S.A. and Department of Chemistry, Indiana University, Bloomington, IN 47405, U.S.A.

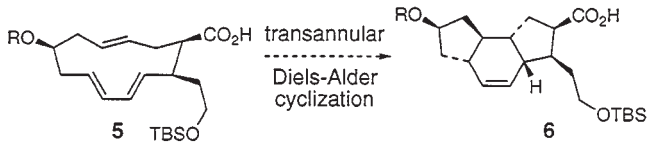
[1]Author to whom correspondence may be addressed (please send to University of Michigan address). Telephone: (734) 647-9278. Fax: (734) 647-9279. e-mail: roush@umich.edu

© 2000 NRC Canada

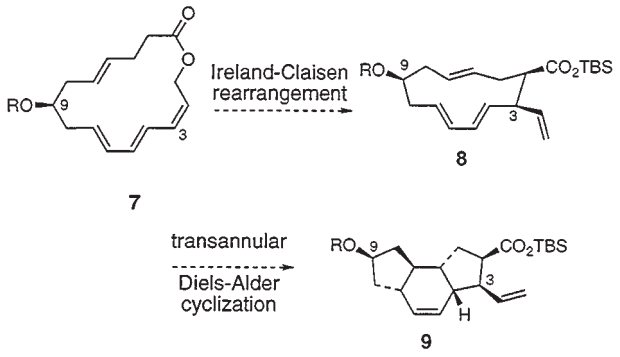
Scheme 1.



Scheme 2.



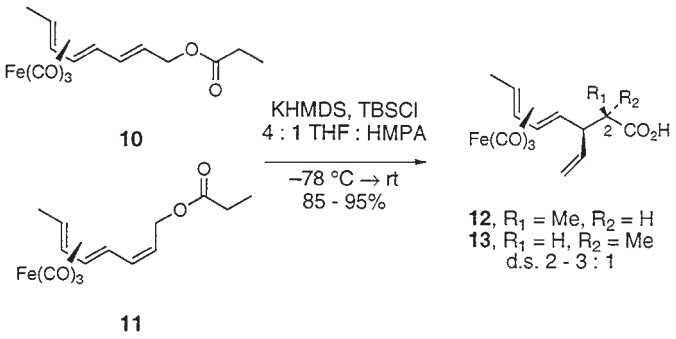
Scheme 3.



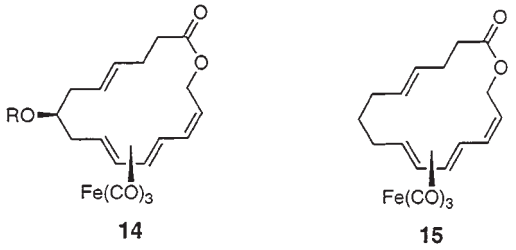
reaction (28–31) for these purposes since a product properly functionalized for further elaboration towards **1** would be produced. Extensive studies of the ring contractive Claisen rearrangement indicate that *cis*-disubstituted carbocycles (referring to the stereochemistry of the new vinyl and carboxylate stereocenters) generally are obtained with good diastereoselectivity (32–34). Accordingly, we targeted the synthesis of a macrocyclic lactone substrate such as **7**. Owing to the significant rate accelerations associated with Diels–Alder reactions performed in the transannular mode, we anticipated that the ring contraction and transannular Diels–Alder reaction could be performed as a single step (35, 36), thereby providing **9** directly from **7** via intermediate triene **8** (Scheme 3).

For this strategy to be applied successfully to the synthesis of **1**, two critical stereochemical issues needed to be resolved. First, a method for controlling the stereochemistry of the ring contraction of **7** would need to be devised such that the remote C(3)–C(9) stereochemical relationship of **8** could be controlled. Second, the stereochemical course of the transannular Diels–Alder reaction would also need to be regulated as four different tricycles can be generated from **8**.

Scheme 4.



Scheme 5.



With respect to the first issue, at the outset we anticipated that it might be possible to relay the stereochemical information at the C(9)-alkoxy group via a chiral diene(irontricarbonyl) complex which would serve as the stereochemical control element for the Claisen ring contraction step. Our previous studies on the Ireland–Claisen rearrangements of η^4-(1-acyloxy-2,4,6-octatrienyl)tricarbonyliron complexes **10** and **11** established that very high diasterofacial selectivity could be achieved with respect to the iron(tricarbonyl) group, as shown in Scheme 4 (37).

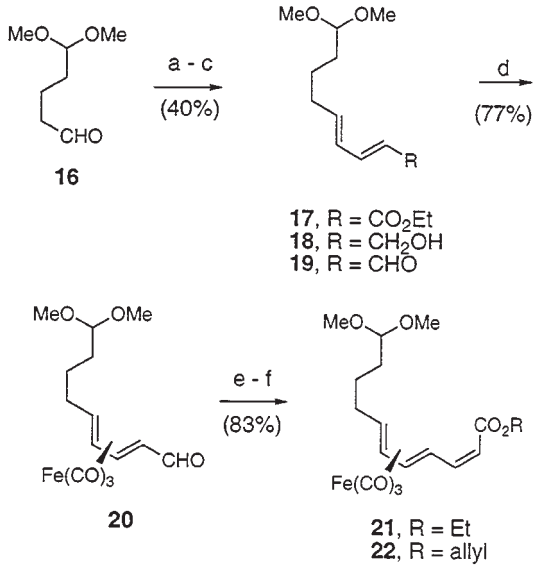
Although mixtures of **12** and **13** were obtained in these experiments, we established that the mixture of C(2)-epimers resulted from poor control of enolate geometry (38, 39). We hoped that constraints imposed by the macrocycle would facilitate greater stereochemical control in the Claisen ring contraction of **14** (Scheme 5). However, rather than embark immediately on the synthesis of **14**, we decided it was prudent to access the simplified substrate **15** in order to study both the stereochemistry of the Claisen ring contraction as well as the transannular Diels–Alder reaction.

Synthesis and attempted Ireland–Claisen ring contraction of 15

We began by treating 5,5-dimethoxypentanal **16** (40) with the lithium anion of triethylphosphonocrotonate (41) which provided the dienylic ester **17** in 61% yield (Scheme 6). DIBAL reduction of the ester (71%) followed by barium manganate (42) oxidation of allylic alcohol **18** gave diene aldehyde **19** (93%). Iron(tricarbonyl) complex **20** was obtained in 77% yield by portionwise addition of diiron nonacarbonyl to a heated solution of the diene in benzene over 5 h (43). A Still modified Horner–Wadsworth–Emmons olefination of **20** afforded the triene ester **21** in high yield (>95%) and as a single (*Z*)-olefin isomer (44). Transesterification of **21** was accomplished in 85% yield by treatment with the sodium salt of allyl alcohol in the presence of 3 Å sieves. Incorporation

© 2000 NRC Canada

Scheme 6. (*a*) triethylphosphonocrotonate, LHMDS, THF, –78°C (61%); (*b*) DIBAL, toluene, –78°C (71%); (*c*) $BaMnO_4$, CH_2Cl_2, 23°C (93%); (*d*) diiron nonacarbonyl (5 portions), benzene, 80°C (77%); (*e*) ethyl bis(2,2-trifluoroethyl)phosphonoacetate, 18-crown-6, KHMDS, THF, –78°C (98%); (*f*) allyl alcohol, Na^0 (sodium metal), 3 Å molecular sieves (85%).



of the allyl ester permits deprotection of the trienoate in the presence of a methyl ester at a later point in the synthesis.

Deprotection of the dimethyl acetal of **22** with 4:1 acetic acid:water gave aldehyde **23** which was treated with vinyl magnesium bromide to afford a mixture of allylic alcohols, **24** (Scheme 7). This mixture was then treated with trimethyl orthoacetate and catalytic propionic acid at 78°C for 48 h to afford **25** in 87% yield as a single olefin isomer (45). The allyl ester of **25** was deprotected in the presence of the methyl ester by using catalytic tetrakis(triphenylphosphine)palladium(0) and diethylamine, (46) yielding mono-acid **26** in 90% yield. Acid **26** was converted to a mixed anhydride and then reduced to alcohol **27** with sodium borohydride in ethanolic tetrahydrofuran (79%) (47). Hydrolysis of the methyl ester of **27** was accomplished using lithium hydroxide in 4:1 dimethoxyethane:water to give the very unstable seco-acid **28** (>95%). This intermediate was used immediately in the macrolactonization (48, 49), which could be carried out in one of two ways. One procedure (50) involved addition of a –78°C solution of **28** dropwise over 12 h to a suspension of 4-dimethylaminopyridine and bromotrispyrrollidino-phosphonium hexafluorophosphate (PyBroP) (51) in 12:1 toluene:dichloromethane. This method provided **15** in 48% yield. Alternatively, **28** could be converted to a mixed anhydride by using 2,4,6-trichlorobenzoyl chloride in the presence of triethylamine (52). Filtration of the amine hydrochloride salts, followed by slow addition of the mixed anhydride solution into a mixture of 4-dimethylaminopyridine and toluene at 63°C gave **15** (39%) and **29** (12%) (53, 54). Finally, complexed lactone **15** could be converted to **29** by treatment with ferric chloride in propionitrile at –50°C (67%).

With **15** now in hand we were ready to investigate the planned Ireland–Claisen ring contraction (Scheme 8). Unfortunately, all attempts at performing the Ireland–Claisen ring contraction on **15** were unsuccessful. For example, treatment of **15** with potassium hexamethyldisilazide in the presence of *tert*-butyldimethylsilyl triflate, conditions successfully employed in our studies of **10** and **11**, led to decomposition products. We were very pleased however to discover that the uncomplexed tetraene **29** underwent the desired ring contraction and transannular Diels–Alder reaction to give **31** after hydrolytic workup. A second isomer (**32**) was also obtained and separated from **31** (4:1 ratio of **31**:**32**) by recrystallization. Triene **30** was not detected during the course of the experiment. The stereochemistry of **31** was confirmed by X-ray crystallographic analysis,[2] but the stereostructure of **32** was not determined.

The stereochemistry of **31** requires that macrocyclic triene **30** is *cis*-disubstituted, and that **31** derives from transition state **A** (Scheme 9). Examination of transition states **A**–**C** indicates that **A** contains no serious nonbonded interactions, with C(14)-H and C(12)-H in a *cis*-relationship, and with C(5) of the diene unit *cis* to C(3)-H, thereby minimizing allylic interactions at this position (55). In contrast the carboxyl unit of **30** interacts with C(12)-H in transition state **B**, and an allylic interaction occurs between C(5) and the C(3)-vinyl substituent in **C**, thereby raising the energy of transition states **B** and **C** compared to **A**.

While we were encouraged by the ability to access macrocyclic triene **30** via the Claisen ring contraction of **29**, it was readily apparent that some means of altering the relative energetics of transition states **A** and **B** would be required if we hoped to apply this strategy towards a synthesis of spinosyn A: we required that vinyl and carboxyl substituents emerge on the *cis*-fused cyclopentane ring (as in **33**), and not in the *trans*-fused ring, as is the case with **31**. Coupled with the requirement that C(9) would need to be functionalized prior to the transannular reaction, we considered using macrocyclic triene **35** containing geminal carboalkoxy groups at C(9). Examination of transition states **D** and **E**, analogous to **A** and **B**, respectively, (Scheme 10), suggested that transition state **E** might be destabilized relative to **D** by virtue of the interaction between the axial carboalkoxy substituent and C(11)-H. Dreiding model analysis of **D** and **E** also indicated the presence of interactions involving the *gem*-carboalkoxy group in **E**, in principle further destabilizing this transition state. Use of the *gem*-carboalkoxy substituents would also allow for a very simple synthesis involving the dialkylation of a malonate ester with two allylic electrophiles, **39** and **40**, as suggested in Scheme 11 (56). Finally, we thought it likely that the *gem*-carboalkoxy substituents of **37** could serve as a predecessor of the oxygen functionality needed at this position (57, 58). Hence, substrate **38** was elected as the immediate precursor to the tandem Ireland–Claisen contraction and Diels–Alder cycloaddition.

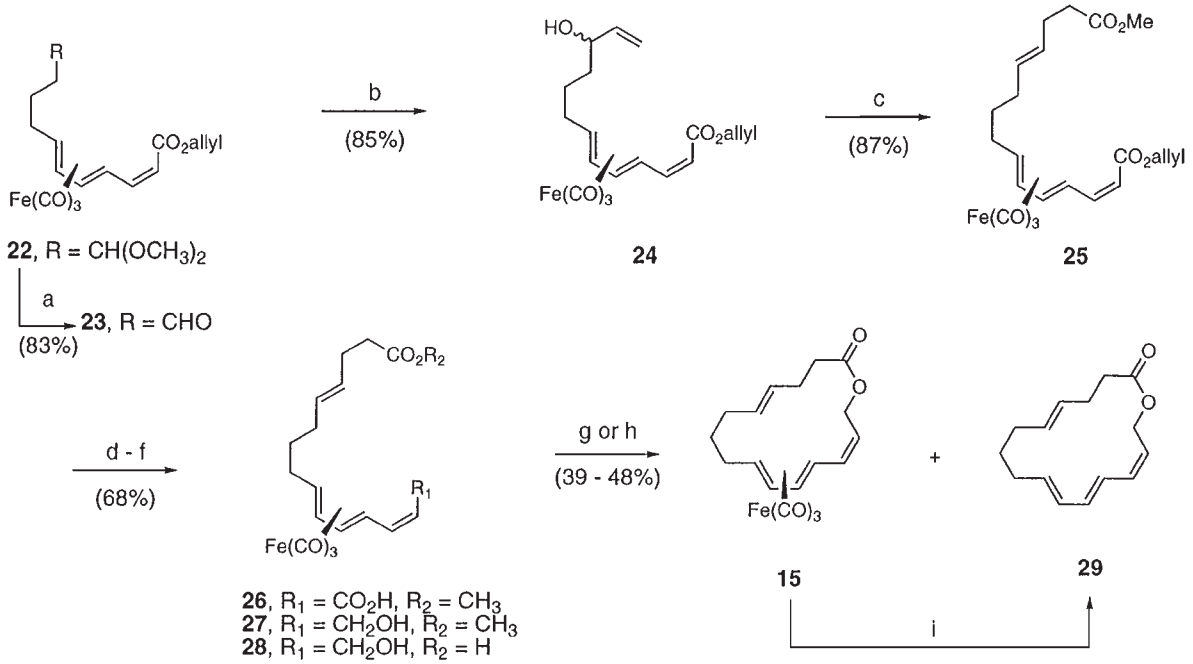
Synthesis and tandem Ireland–Claisen contraction and Diels–Alder reaction of 38

Di-*tert*-butyl malonate **41** was treated with butadiene monoepoxide **42** in the presence of 1 mole % tetrakis(triphenylphosphine)palladium(0) (59), giving allylic

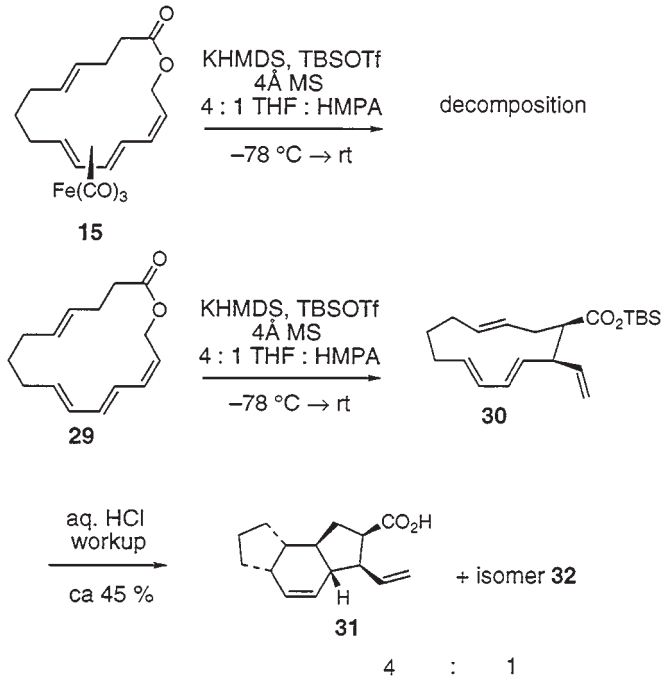
[2] We thank Dr. John Huffman for the X-ray structure determination of **31** (Indiana University Molecular Structure Center Report No. 95180).

© 2000 NRC Canada

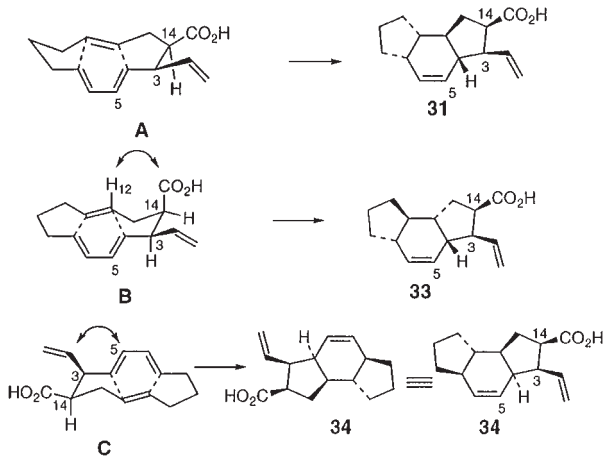
Scheme 7. (*a*) 4:1 HOAc:H_2O, rt (83%); (*b*) vinyl magnesium bromide, 4 Å molecular sieves, THF –78°C (85%); (*c*) trimethyl orthoacetate, propionic acid, 80°C (87%); (*d*) tetrakis(triphenylphosphine)palladium) (0), diethylamine, THF, rt (90%); (*e*) methyl chloroformate, triethylamine, THF, 0°C then 1:1 EtOH:THF, $NaBH_4$, –35°C → rt (79%); (*f*) lithium hydroxide, 4:1 DME:H_2O (>95%); (*g*) 2,4,6-trichlorobenzoyl chloride, 4 Å molecular sieves, THF, triethylamine, 0°C then 4-dimethylaminopyridine, toluene, 63°C (39% **15** + 12% **29**); (*h*) PyBrOP, 4-dimethylaminopyridine, 12:1 toluene:CH_2Cl_2, rt (48% **15**); (*i*) $FeCl_3$, propionitrile, –50°C (67%).



Scheme 8.



Scheme 9.

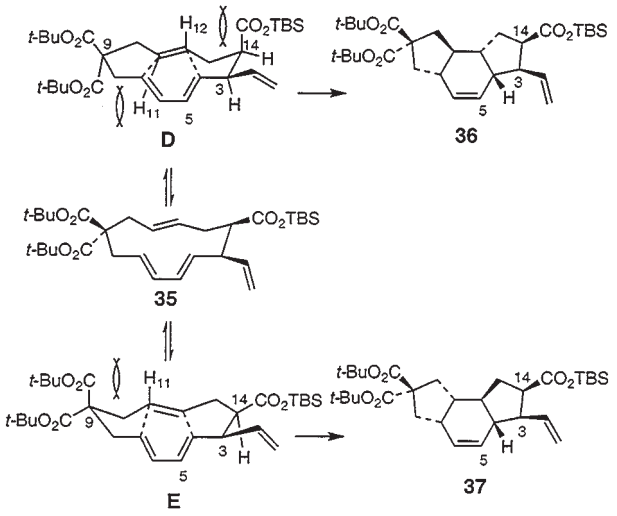


alcohol **43** in 79% yield as a 2:1 mixture of *E*:*Z* olefin isomers (Scheme 12). Preparation of the dienophilic portion of the macrocycle **38** was accomplished starting from bromohydrin **44**, which is readily available from butadiene and aqueous *N*-bromosuccinimide (60). Allylic alcohol **44** was subjected to the Johnson orthoester Claisen rearrangement (45), and methyl ester **45** was isolated in moderate yield (56%). The coupling of **43** and **45** was effected with sodium hydride in refluxing THF, and product **46** was isolated in good yield (78%). Allylic alcohol **46** was oxidized with PCC (61), and the resulting enal **47** was obtained in 93% yield as a single olefin isomer.

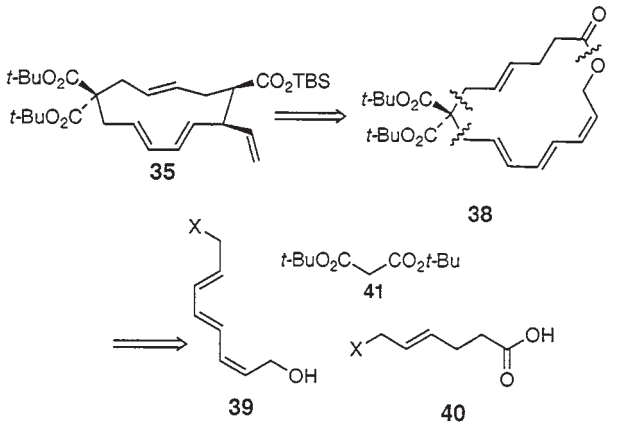
Exposure of **47** to chromous chloride and iodoform in tetrahydrofuran (62) followed by stirring the reaction mixture for 30 min with a 1 M aqueous sodium serinate solution (63) afforded dienyl iodide **48**, as summarized in Scheme 13. The isomeric purity of the newly formed olefin was 7:1 (*E*:*Z*). Use of Kishi's serinate workup procedure for the Takai olefination gave the best results, as omitting this step from the reaction workup provided **48** in lower yield. Crude **48** was dissolved in triethylamine and treated with

© 2000 NRC Canada

Scheme 10.



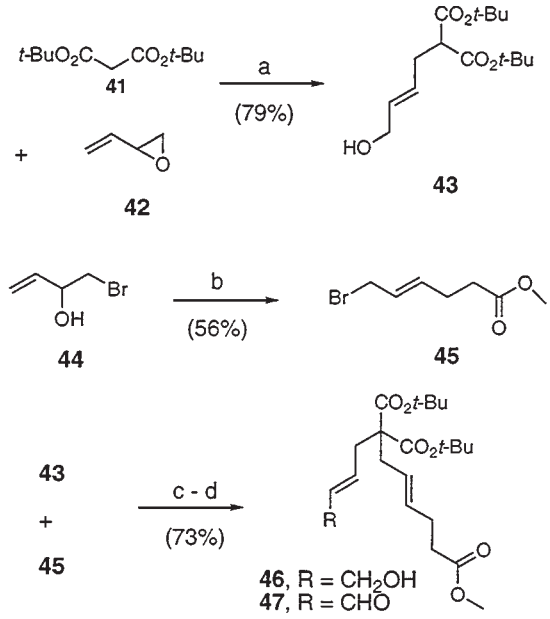
Scheme 11.



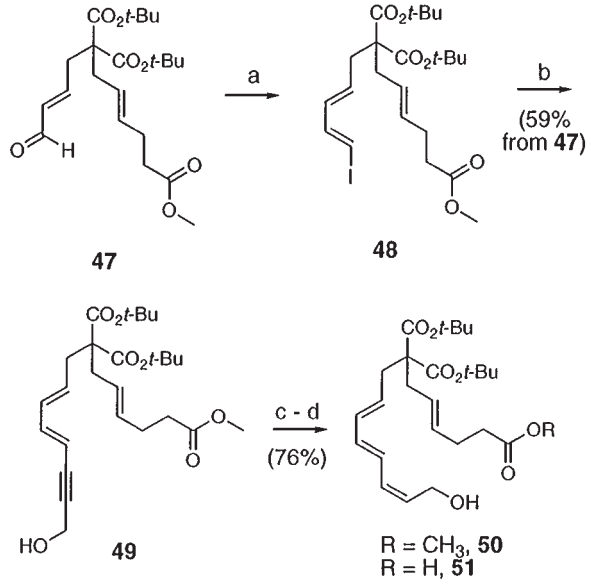
catalytic bis(triphenylphosphine)palladium(II) dichloride, cuprous iodide, and propargyl alcohol to give trienyne **49** in 59% overall yield from enal **47** (64). We now turned our attention to the *cis*-reduction of alkyne **49**. Studies on related systems had indicated that Lindlar hydrogenations yielded a mixture of products, including products of overreduction (65). However, use of an activated zinc species to reduce **49** afforded tetraene **50** in 93% yield (66). Hydrolysis of the methyl ester was effected with lithium hydroxide in a mixture of tetrahydrofuran, methanol, and water to give the very unstable seco acid **51** in 80% yield, which was best used immediately in the next step as the C(2)–C(3) (*Z*)–olefin would undergo isomerization if **51** was stored at ambient temperature.

Macrolactonization of **51** (see Scheme 14) was accomplished using the Mukaiyama procedure (43% yield) (67). Other macrolactonization methods (Yamaguchi (52) and Mitsunobu (68) protocols) gave reduced yields of **38**. The low yield of **38** may be due in part to its thermal instability, as purified samples of this lactone decomposed when heated overnight. When the Mukaiyama macrolactonization was performed at a lower temperature, diminished amounts of **38** were obtained. Interestingly, the macrolactonization of **52** proceeded in only ca. 5% yield, indicating that the *gem*-

Scheme 12. (*a*) tetrakis(triphenylphosphine)palladium (0), THF, 0°C → rt (79%); (*b*) propionic acid, trimethyl orthoacetate, toluene, 110°C (56%); (*c*) sodium hydride, THF, 67°C (78%); (*d*) pyridinium chlorochromate, Celite®, CH_2Cl_2, rt (93%).



Scheme 13. (*a*) $CrCl_2$, CHI_3, THF, 0°C → rt; (*b*) CuI (10 mol %), bis(triphenylphosphine)palladium (II) chloride (5 mol %), propargyl alcohol, triethylamine, rt (59% from **47**); (*c*) zinc, copper (II) acetate dihydrate, silver nitrate, MeOH, H_2O, rt (95%); (*d*) lithium hydroxide, THF, MeOH, H_2O (80%).

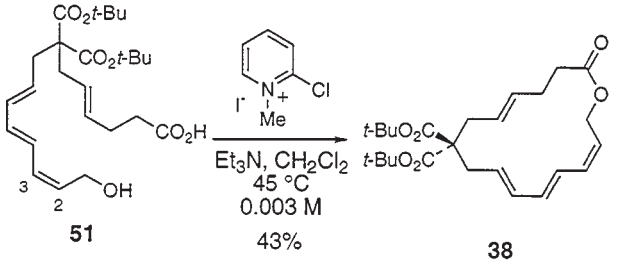


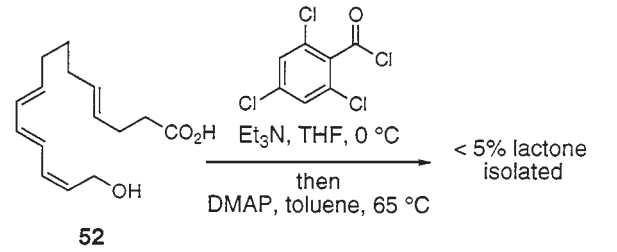
carboalkoxy substituent exerts a beneficial Thorpe–Ingold effect on this reaction (69).

In an effort to improve the efficiency of the macrocyclization step, we examined the intramolecular alkylation of **53**, shown below in Scheme 15. Unfortunately, we were unable to isolate any of the desired macrolactone from the attempted cyclization of **53**. Treatment of **53** with either cesium carbonate and 18-crown-6 in refluxing acetonitrile

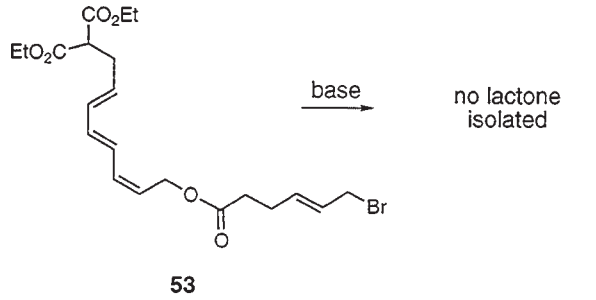
© 2000 NRC Canada

Scheme 14.





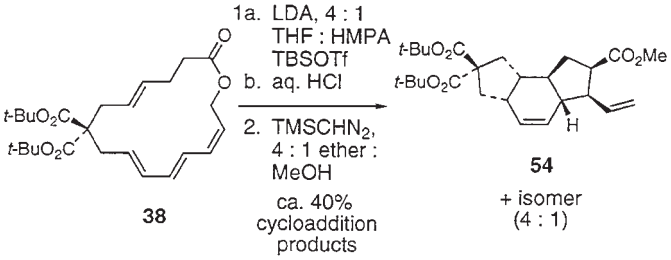
Scheme 15.



(0.005 M) (27), 1,8-diazabicyclo[5.4.0]undec-7-ene (DBU) at 0.003 M in dichloromethane, or finally potassium *tert*-butoxide in tetrahydrofuran (at 0.003 and at 0.0001 M), provided only decomposition, recovered starting material, or dimeric products.

Treatment of a solution of lactone **38** in 4:1 THF:HMPA at –78°C with *t*-butyldimethylsilyl triflate followed by addition of LDA and then warming this mixture to room temperature yielded two cycloadducts in a 4:1 product ratio (Scheme 16). Esterification of this mixture with trimethylsilyldiazomethane afforded the two cycloadducts in 40% yield. Although we were unable to separate this mixture by recrystallization or chromatography, we were successful in assigning the stereochemistry depicted in structure **54** to the major product using a combination of COSY and NOESY ^{1}H HMR techniques. While the ^{1}H NMR spectrum of **54** was complex in C_6D_6, in $CDCl_3$ a much more highly resolved spectrum was obtained. The *cis*-relationship of C(7)-H and C(11)-H, as well as the *cis*-relationship between C(3)-H and C(14)-H, was assigned based upon the NOE data. In addition, the 1,3- and 1,4-*syn* relationships of C(12)-H with C(14)-H and C(3)-H were assigned based upon the presence of observed NOEs. Unfortunately, **54** does not possess the correct stereochemistry for use in a synthesis of **1**.

Scheme 16.



As before, we were unable to determine the stereochemistry of the minor product.

Transition state modeling of the transannular Diels–Alder reaction

While we were successful in developing a tandem Claisen ring contraction and transannular Diels–Alder sequence, our goal of constructing the perhydro-*as*-indacene subunit of **1** remained unrealized. In an effort to define what interactions were controlling the outcome of the Diels–Alder reaction, and also to aid in the design of improved substrates for preparing **1**, we turned to molecular modeling to estimate the energies of the various transition states for the cyclizations of trienes **55**–**60** (Scheme 17). For this purpose, we used the transition state subroutine within PCModel.[3] The transition states are depicted as structures **F**–**I** with the values obtained from the modeling provided in Table 1 (kcal/mol).

We initially examined the transition states **H** and **I** for the Diels–Alder reaction of trienes **55** and **58** (entries 1 and 4). The defining interaction for these two transition states apparently is the interaction of the C(14)-carboxyl group with C(12)-H, thus **I** is favored by 0.8 to 1.4 kcal/mol (entries 1 and 4). For the cyclization of **58** (entry 4), the 1,3 interaction that R_1 experiences with C(11)-H in **H** also occurs with R_2 in **I**. Thus, these two interactions nullify each other and transition state **I** predominates both computationally and experimentally. Based upon these calculations, we believe that the minor isomer isolated from the transannular Diels–Alder reaction is most likely **61**. Clearly, the conformational bias which we had anticipated based upon the Dreiding model analysis of transition states **H** and **I** is not substantial enough to alter the product distribution.

We next analyzed transition states **F** and **G** for the cyclization of **55** and **58** (leading to products **63** and **64**), which are destabilized by *A*-1,3 strain between the diene and the vinyl group. These two transition states are predicted to be ca. 1.4 kcal/mol higher in energy than analogous transition states **H** and **I**. This prediction is consistent with our experimental results, as cycloadducts **63** and **64** were not observed.

To determine if we could favor transition state **H**, we examined the placement of a steric directing group upon the diene at C(6), trienes **56**, **57**, **59**, and **60** (entries 2–3 and 5–6) (70). This strategy has been successfully used in other intramolecular Diels–Alder reactions to alter the energetics of competing transition states. In all cases studied thus far,

[3] PCModel uses the MMX force field and is available from Serena Software, Bloomington, IN 47405. Bond orders of 0.3 were used for both the bond breaking and bond forming atoms in the MMXE subroutine within PCModel.

© 2000 NRC Canada

Scheme 17.

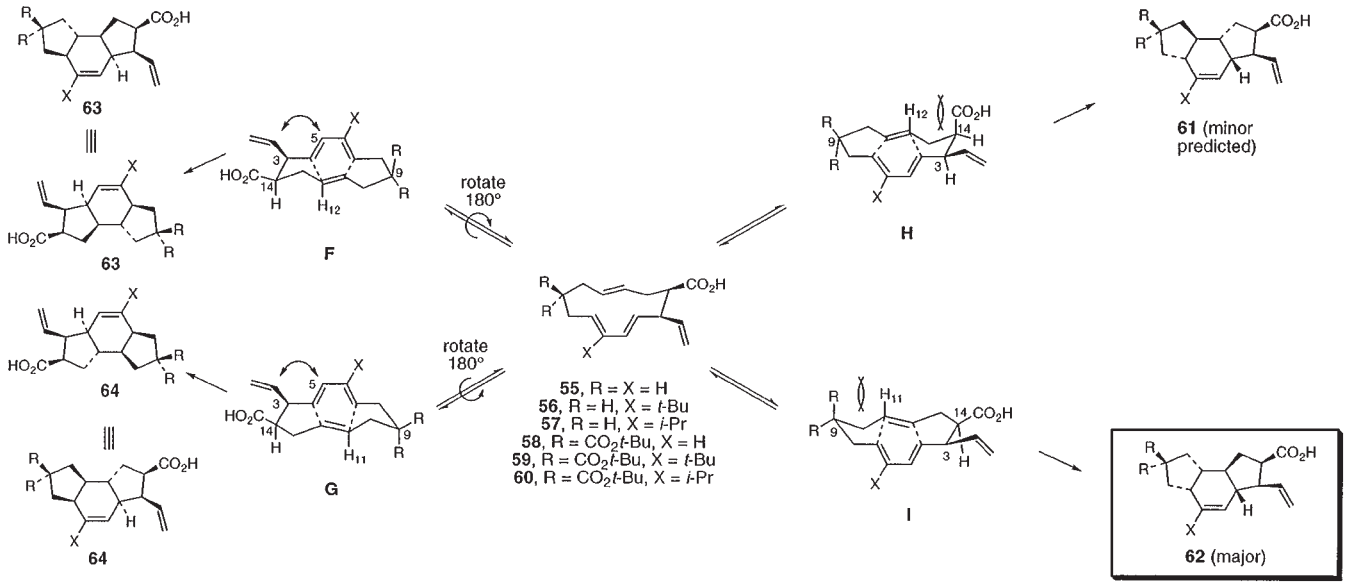


Table 1. MMX analysis of transition states F–I.

Entry	Triene	R	X	Transition state energies (kcal/mol)				Predicted product
				F	G	I	H	
1	55	H	H	18.66	18.39	17.00	17.82	62
2	56	H	*t*-Bu	30.86	33.04	31.81	29.84	61
3	57	H	*i*-Pr	25.78	26.14	25.00	24.76	61
4	58	CO_2t-Bu	H	27.83	27.18	25.73	27.15	62
5	59	CO_2t-Bu	*t*-Bu	38.76	44.36	41.92	38.96	63
6	60	CO_2t-Bu	*i*-Pr	33.22	35.31	33.97	33.90	63

the steric directing group enhances formation of a *trans*-ring fusion at the adjacent position (71). Trimethylsilyl and bromo substituents (X = TMS or Br) have been used for these purposes. Unfortunately, PCModel will not allow the attachment of halogen or silyl substituents to the atoms of the transition state that are undergoing rehybridization. Consequently, we chose to approximate the trimethylsilyl group as either a *tert*-butyl or an iso-propyl group. Based upon an *A*-value analysis, the iso-propyl group is a more accurate approximation of a trimethylsilyl group than is a *tert*-butyl group (72). Nonetheless, we incorporated both of these groups into our modeling efforts. While it appears that introduction of a *tert*-butyl group at C(6) significantly favors transition state **H** for the cyclization of triene **57**, the isopropyl substituted triene **58** seems only moderately biased to cyclize via transition state **H**. For trienes **59** and **60**, the transition states appear to be much closer in energy. However, the desired trans ring junction is predicted to appear on the side adjacent to the directing group. Efforts to test these predictions experimentally are in progress.

Transition state modeling of the Ireland–Claisen ring contraction

We also used molecular modeling to examine the transition states of the Ireland–Claisen rearrangement of the 16-membered lactone **29** (Scheme 18) (73, 74). We were interested to determine what influence the enolate geometry would have on the outcome of the rearrangement, and thus, if we could access the trans-disubstituted cyclododecatriene by altering the enolate geometry (38, 75). For this purpose, we again used the transition state subroutine present in PCModel.[3] The results of these studies are summarized below.

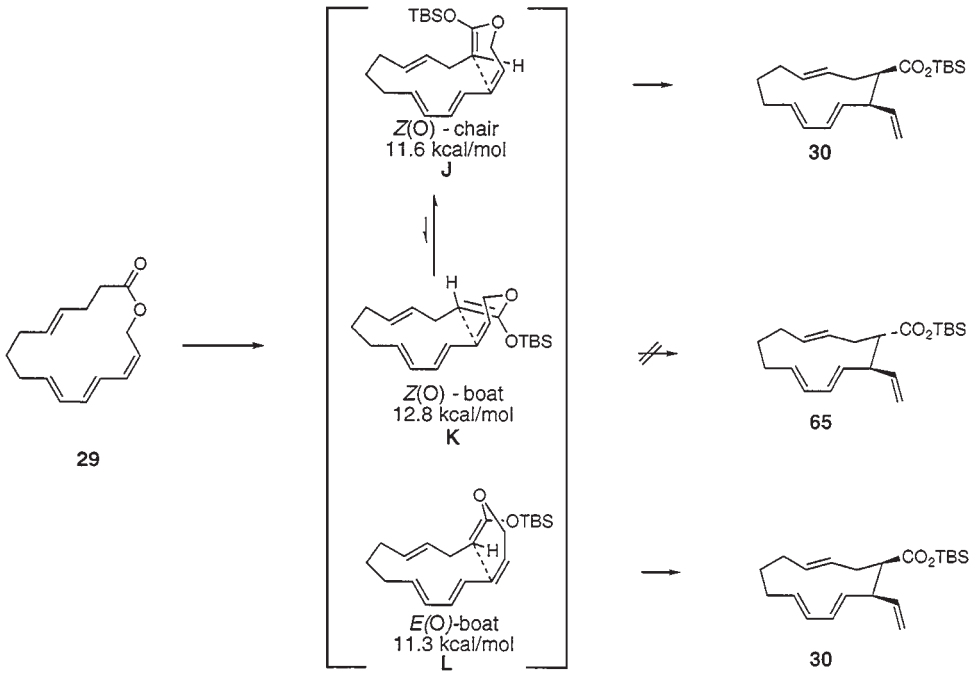
Our modeling predicts that regardless of what enolate geometry is generated from **29**, the cis-substituted product will be preferentially formed. The *E*(*O*)-silyl ketene acetal boat transition state **L** and *Z*(*O*)-silyl ketene acetal chair transition state **J**, which both lead to **30**, are of comparable energy. The *Z*(*O*)-silyl ketene acetal boat transition state **K**, which leads to **65**, is notably higher in energy than **J**. The *E*(*O*)-silyl ketene acetal chair transition state (which is not shown) is substantially higher energetically (>5 kcal) than **J**–**L**. From these modeling results, we fully expect that regardless of enolate geometry, *cis*-disubstituted product **29** will predominate in lieu of **65**.

Conclusions

We have demonstrated that the combination of an Ireland–Claisen ring contraction of a 16-membered lactone in tandem with a transannular Diels–Alder reaction of the newly formed cyclododecatriene is an effective protocol to prepare decahydro-*as*-indacenes with good diastereoselectivity. Although we were unsuccessful in developing a

© 2000 NRC Canada

Scheme 18.



system that would be applicable to **1**, we were encouraged that our after the fact transition state modeling was in good agreement with the experimental results. We are hopeful that the knowledge gained from the modeling exercise will aid in the development of substrates useful for the stereoselective synthesis of the *as*-indacene nucleus of **1**. Results of these efforts will be reported in due course.

Experimental section[4]

*Ethyl (2*E*,4*E*)-9,9-dimethoxy-nona-2,4-dienoate (**17**)*: To distilled hexamethyldisilazane (24.2 mL, 115 mmol) in THF (200 mL) at –78°C was added *n*-butyllithium (2.5 M in hexanes, 46 mL, 115 mmol). After 20 min at –78°C, the solution was warmed to –30°C and triethyl phosphonocrotonate (25 mL, 126 mmol) was added. The reaction was then cooled to –50°C and a solution of aldehyde **16** (40) (23.5 g, 161 mmol) in THF (50 mL) was added via cannula. The reaction mixture was warmed to 10°C over 2 h and was then diluted with ether (200 mL) and quenched with saturated aqueous $NaHCO_3$ (250 mL). The layers were separated and the organic phase was washed with saturated aqueous $NaHCO_3$ (250 mL). The combined aqueous phases were washed with ether (3 × 50 mL), and the combined organic phases were washed with saturated aqueous NaCl (5 mL), dried ($MgSO_4$), concentrated, and purified by flash chromatography. Ester **17** (17.2 g, 61%) was isolated as a clear oil: ^{1}H NMR (400 MHz, $CDCl_3$) δ: 7.28–7.21 (m, 1H), 6.21–6.06 (m, 2H), 5.78 (d, *J* = 15.4 Hz, 1H), 4.36 (t, *J* = 5.6 Hz, 1H), 4.19 (q, *J* = 7.1 Hz, 2H), 3.31 (s, 6H), 2.19 (q, *J* = 7.1 Hz, 2H), 1.64–1.57 (m, 2H), 1.53–1.45 (m, 2H), 1.29 (t, *J* = 7.1 Hz, 3H); ^{13}C NMR (100 MHz, $CDCl_3$) δ: 167.3, 144.8, 143.7, 128.7, 119.5, 104.2, 60.2, 52.7, 32.7, 31.9, 23.7, 14.3; IR (CCl_4) 3000, 2980, 1720, 1650, 1620, 1370, 1250, 1130, 1000, 950 cm^{-1}; HRMS calcd. for $C_{12}H_{19}O_3$ $[M–OCH_3]^+$: 211.1334, found: 211.1328 *m*/*z*.

*(2*E*,4*E*)-9,9-Dimethoxy-nona-2,4-dien-1-ol (**18**)*: To a solution of ester **17** (14.4 g, 59.5 mmol) in toluene (200 mL) at –78°C was added diisobutylaluminum hydride (1.5 M in toluene, 90 mL, 135 mmol). After 5 min, excess MeOH was slowly added to the vigorously stirred solution at –78°C. When hydrogen evolution had ceased, the solution was warmed to room temperature and stirred overnight with saturated aqueous sodium potassium tartrate (200 mL). The biphasic mixture was separated, and the organic phase was washed with aqueous sodium potassium tartrate (3 × 40 mL). The combined aqueous phases were washed with ether (3 × 25 mL), and the combined organic phases were washed with saturated aqueous NaCl (5 mL), dried ($MgSO_4$), concentrated, and purified by flash chromatography. Alcohol **18** (8.48 g, 71%) was isolated as a clear oil: ^{1}H NMR (400 MHz, $CDCl_3$) δ: 6.22–6.16 (m, 1H), 6.07–6.00 (m, 1H), 5.74–5.63 (m, 2H), 4.35 (t, *J* = 5.66 Hz, 1H), 4.14 (d, *J* = 5.50 Hz, 1H), 3.30 (s, 3H), 3.29 (s, 3H), 2.09 (q, *J* = 7.23 Hz, 2H), 1.62–1.56 (m, 2H), 1.47–1.40 (m, 4H); ^{13}C NMR (100 MHz, $CDCl_3$) δ: 134.8, 131.8, 129.8, 129.7, 104.3, 63.4, 52.6, 32.3, 31.9, 24.1; IR (CCl_4) 3620 (s), 3450 (br), 3000, 2960, 990 cm^{-1}; HRMS calcd. for $C_{10}H_{15}O$ $[M–OCH_3–H_2O]^+$: 151.1123, found: 151.1118 *m*/*z*. Anal. calcd. for $C_{11}H_{20}O_3$: C 65.97, H 10.07; found: C 65.96, H 10.32.

*(2*E*,4*E*)-9,9-Dimethoxy-nona-2,4-dienal (**19**) (43)*: To a solution of alcohol **18** (8.25 g, 41 mmol) in CH_2Cl_2 (150 mL) at 25°C was added $BaMnO_4$ (12 g, 46.9 mmol). After 1 h, more $BaMnO_4$ (12 g, 46.9 mmol) was added, and the

[4] General experimental procedures have been deposited as supplementary material and may be purchased from: The Depository of Unpublished Data, Document Delivery, CISTI, National Research Council Canada, Ottawa, Ontario, Canada, K1A 0S2.

© 2000 NRC Canada

mixture was stirred overnight. An additional portion of $BaMnO_4$ (3 g, 11.7 mmol) was then added, and the mixture was stirred for 3 h and then filtered through a short plug of Celite® and silica gel using copious amounts of ethyl acetate as eluant. Concentration of the filtrate afforded aldehyde **19** (7.62 g, 93%) as a clear oil which used without further purification: ^{1}H NMR (400 MHz, $CDCl_3$) δ: 9.53 (d, *J* = 8.0 Hz, 1H), 7.07 (dd, *J* = 15.3, 10.1 Hz, 1H), 6.36–6.21 (m, 2H), 6.07 (dd, *J* = 15.3, 8.0 Hz, 1H), 4.37 (t, *J* = 5.5 Hz, 1H), 3.32 (s, 6H), 2.25 (apparent q, *J* = 7.1 Hz, 2H), 1.66–1.59 (m, 2H), 1.57–1.49 (m, 2H); ^{13}C NMR (100 MHz, $CDCl_3$) δ:193.9, 152.6, 146.4, 130.3, 129.0, 104.2, 52.8, 32.9, 32.0, 23.5; IR (CCl_4) 2960, 2840, 1690, 1640, 1130, 1010, 990 cm^{-1}; HRMS calcd. for $C_{10}H_{15}O_2$ $[M–OCH_3]^+$: 167.1072, found: 167.1073 *m/z*.

*Tricarbonyl [(2*E*,4*E*)-(2–5-*η*^{4})-9,9-dimethoxy-nona-2,4-dienal]iron (**20**)*: To a degassed solution of aldehyde **19** (560 mg, 2.83 mmol) in benzene (100 mL) was added diiron nonacarbonyl (800 mg, 2.20 mmol) and the solution was brought to a gentle reflux. Additional diiron nonacarbonyl (4 × 800 mg) was added at intervals of 45 min–1 h, after which time ^{1}H NMR analysis indicated complete consumption of starting material. The solution was cooled to ambient temperature, filtered through Celite® using ether as eluant and concentrated to a final volume of 15 mL. The residue was purified by careful chromatography using a slow gradient of hexanes → 1:1 hexanes:ether. Complexed aldehyde **20** (783 mg, 77%) was isolated as an orange oil: ^{1}H NMR (400 MHz, $CDCl_3$) δ: 9.26 (d, *J* = 4Hz, 1H), 5.78 (ddd, *J* = 8.2, 5.0 Hz, 1.1 Hz, 1H), 5.29 (ddd, *J* = 8.9, 5.0 Hz, 0.4 Hz, 1H), 4.36 (t, *J* = 5.6 Hz, 1H), 1.81–1.46 (m, 7H), 1.13 (ddd, *J* = 8.4, 4.4 Hz, 1.2 Hz, 1H); ^{13}C NMR (100 MHz, $CDCl_3$) δ: 209.2 (broad), 196.1, 104.2, 88.5, 81.5, 66.2, 54.7, 52.9, 52.8, 33.9, 32.0, 27.0; IR (CCl_4) 2940, 2060 (vs), 1990, 1680, 1650, 1445, 1120 cm^{-1}; HRMS calcd. for $C_{13}H_{15}O_5Fe$ $[M–OCH_3]^+$: 307.0269, found 307.0254 *m/z*; HRMS calcd. for $C_{11}H_{15}O_3Fe$ $[M–OCH_3–2(CO)]^+$: 251.0371, found: 251.0372 *m/z*. Anal. calcd. for $C_{14}H_{18}O_6Fe$: C 49.73, H 5.37; found: C 49.83, H 5.37.

*Tricarbonyl [methyl (2*Z*,4*E*,6*E*)-(4–7-*η*^{4})-9,9-dimethoxy-undeca-(2,4,6)-trienoate]iron (**21**) (**44**)*: To a solution of 18-crown-6 (23 g, 86 mmol) and ethyl bis(2,2-trifluoroethyl)phosphonoacetate (4.1 mL, 19 mmol) in THF (380 mL) at –78°C was added potassium hexamethyldisilazide (0.5 M in toluene, 38 mL, 19 mmol). After 5 min, the solution was warmed to 0°C for 10 min, then was re-cooled to –78°C and aldehyde **20** (5.9 g, 17 mmol) in THF (50 mL) was added dropwise via cannula. The mixture was stirred for 1 h at –78°C, then saturated aqueous $NaHCO_3$ (150 mL) was added, and the layers were separated. The organic layer was washed with saturated aqueous $NaHCO_3$ (2 × 50 mL), and the combined aqueous layers were washed with ether (4 × 100 mL). The organic layers were washed with saturated aqueous NaCl (15 mL), dried ($MgSO_4$), concentrated, and purified by flash chromatography (5:1 → 3:1 hexanes:ether). Unsaturated ester **21** (6.2 g, 91%) was isolated as a yellow oil: ^{1}H NMR (400 MHz, $CDCl_3$) δ: 6.07 (t, *J* = 11.0 Hz, 1H), 5.57 (d, *J* = 11.2 Hz, 1H), 5.29 (dd, *J* = 8.9, 4.8 Hz, 1H), 5.10 (dd, *J* = 8.0, 4.8 Hz, 1H), 4.35 (t, *J* = 5.6 Hz, 1H), 3.71 (s, 3H), 3.32 (s, 3H), 3.31 (s, 3H), 3.06 (dd, *J* = 10.5, 9.5 Hz, 1H), 1.71–1.50 (m, 7H); ^{13}C NMR (100 MHz, $CDCl_3$) δ: 211.1 (broad), 166.9, 150.0, 115.0, 104.3, 86.1, 84.8, 64.7, 54.0, 52.9, 52.6, 51.1, 34.1, 32.1, 27.1; IR (CCl_4) 2940, 2810, 2025 (vs), 1990, 1970, 1710, 1610, 1200, 1180 cm^{-1}; HRMS calcd. for $C_{15}H_{22}O_5Fe$ $[M–2(CO)]^+$: 338.0725, found 338.0815 *m/z*; HRMS calcd. for $C_{14}H_{23}O_4Fe$ $[M–2(CO) + H]^+$: 311.0809, found: 311.0804 *m/z*. Anal. calcd. for $C_{17}H_{22}O_7Fe$: C 51.79, H 5.63; found: C 52.05, H 5.47.

*Tricarbonyl [(2*Z*,4*E*,6*E*)-(4–7-*η*^{4})-9,9-dimethoxy-undeca-(2,4,6)-trienoic acid allyl ester]iron (**22**) (**76**)*: Allyl alcohol (freshly distilled from CaH_2, 100 mL) was treated with Na^0 (sodium metal) (1.4 g, 60.9 mmol) at 0°C. To this solution was added 3 Å sieves (flame-dried in vacuo, 5.2 g). Methyl ester **21** (6.1 g, 15.5 mmol) in allyl alcohol (20 mL) was then added dropwise via cannula. The reaction mixture was stirred for 3 h, then was filtered and partitioned between ether and saturated. aqueous NaCl (100 mL each). The organic layer was washed with saturated. aqueous NaCl (3 × 100 mL), and the combined aqueous layers were washed with ether (4 × 50 mL). The organic layers were washed with saturated. aqueous NaCl (5 mL), dried ($MgSO_4$), concentrated, and purified by flash chromatography (slow gradient from hexanes → 5:1 hexanes:ether). Allyl ester **22** (5.56 g, 85%) was isolated as an orange oil: ^{1}H NMR (400 MHz, $CDCl_3$) δ: 6.08 (t, *J* = 11.1 Hz, 1H), 5.95 (ddt, *J* = 17.1, 10.4, 5.7 Hz, 1H), 5.60 (dd, *J* = 11.1, 0.8 Hz, 1H), 5.35 (q, *J* = 1.6 Hz, 1H), 5.31–5.22 (m, 3H), 5.10 (dd, *J* = 7.9, 5.2 Hz, 1H), 4.66–4.57 (m, 2H), 4.36 (t, *J* = 5.6 Hz, 1H), 3.32 (s, 3H), 3.31 (s, 3H), 3.10–3.05 (m, 1H), 1.74–1.46 (m, 7H); ^{13}C NMR (100 MHz, $CDCl_3$) δ: 211.1 (broad), 166.1, 150.3, 132.4, 118.2, 115.1, 104.3, 86.0, 84.8, 64.8, 54.1, 52.8, 52.7, 34.1, 32.1, 27.1; IR (CCl_4) 3070, 2970, 2850, 2040 (vs), 1980, 1710, 1610, 1170, 980, 930 cm^{-1}; HRMS calcd. for $C_{16}H_{24}O_4Fe$ $[M–3(CO)]^+$: 336.1024, found: 336.1037 *m/z*. Anal. calcd. for $C_{19}H_{24}O_7Fe$: C 54.30, H 5.76; found: C 54.50, H 5.87.

*Tricarbonyl [(2*Z*,4*E*,6*E*)-(4–7-*η*^{4})-11-oxo-undeca-2,4,6-trienoic acid allyl ester]iron (**23**)*: Allyl ester **22** (522 mg, 1.24 mmol) was suspended in a 4:1 mixture of acetic acid and water and stirred until acetal hydrolysis was complete by TLC analysis. The solvents were removed by lyophilization, and the residue was purified by flash chromatography (slow gradient from hexanes → 1:1 hexanes:ether). Aldehyde **23** (387 mg, 83%) was isolated as a viscous orange oil: ^{1}H NMR (400 MHz, $CDCl_3$) δ: 9.77 (s, 1H), 6.09 (apparent t, *J* = 11.1 Hz, 1H), 5.95 (dddd, *J* = 17.3, 10.4, 5.8, 5.7 Hz, 1H), 5.61 (dd, *J* = 11.2, 0.8 Hz, 1H), 5.35–5.23 (m, 3H), 5.10 (ddd, *J* = 4.9, 3.8, 1.1 Hz, 1H), 4.67–4.57 (m, 2H), 3.12–3.07 (m, 1H), 2.56–2.42 (m, 2H), 1.74–1.46 (m, 7H); ^{13}C NMR (100 MHz, $CDCl_3$) δ: 210.8 (broad), 201.8, 166.1, 150.1, 132.3, 118.2, 115.3, 85.9, 84.9, 64.7, 63.5, 54.2, 43.2, 33.6, 24.3; IR (CCl_4) 2055 (vs), 1990, 1970, 1730, 1710, 1610, 1170, 980, 930 cm^{-1}; HRMS calcd. for $C_{15}H_{18}O_4Fe$ $[M–2(CO)]^+$: 318.0555; found: 318.0537 *m/z*; HRMS calcd. for $C_{14}H_{18}O_3Fe$ $[M–3(CO)]^+$: 290.0606; found: 3290.0600 *m/z*. Anal. calcd. for $C_{17}H_{18}O_6Fe$: C 54.57, H 4.85; found: C 54.46, H 4.91.

*Tricarbonyl [allyl (2*Z*,4*E*,6*E*)-(4–7-*η*^{4})-11-hydroxy-trideca-(2,4,6,12)-trienoate]iron (**24**)*: A solution of aldehyde **23** (387 mg, 1.03 mmol) in THF (20 mL) was stirred with 4 Å

© 2000 NRC Canada

sieves (~75 mg) for 20 min. The solution was then cooled to –97°C and vinyl magnesium bromide (1 M in THF, 1.05 mL, 1.05 mmol) was added. The reaction temperature was maintained between –95 and –100°C for 20 min, then was warmed to –90°C for 10 min and –78°C for 2 h. The reaction was then quenched at this temperature with 1 M HCl in saturated aqueous NaCl (10 mL). After the mixture reached ambient temperature, ether (10 mL) was added and the layers were separated. The organic layer was washed with 1 M HCl in saturated aqueous NaCl (2 × 10 mL) and saturated aqueous NaCl (2 × 5 mL), and the combined aqueous layers were washed with ether (3 × 15 mL). The organic layers were washed with saturated aqueous NaCl (5 mL), dried ($MgSO_4$), concentrated, and purified by flash chromatography (slow gradient from 3:1 → 1:1 hexanes:ether). Allylic alcohol **24** (355 mg, 85%) was isolated as an orange oil: ^{1}H NMR (400 MHz, $CDCl_3$) δ: 6.08 (apparent t, *J* = 11.1 Hz, 1H), 5.91 (dddd, *J* = 17.3, 10.4, 5.8, 5.7 Hz, 1H), 5.86 (dddd, *J* = 17.1, 10.4, 6.5, 0.8 Hz, 1H), 5.60 (dd, *J* = 11.2, 0.8 Hz, 1H), 5.35 (q, *J* = 1.6 Hz, 1H), 5.31–5.21 (m, 3H), 5.15–5.08 (m, 2H), 4.68–4.58 (m, 2H), 4.14–4.06 (m, 1H), 3.07 (dt, *J* = 9.9, 1.0 Hz, 1H), 1.76–1.46 (m, 7H); ^{13}C NMR (100 MHz, $CDCl_3$) δ: 211.2 (broad), 166.2, 150.3, 140.9, 132.3, 118.2, 115.1, 86.1, 84.7, 73.1, 73.0, 64.9, 64.7, 54.0, 36.4, 34.2, 27.8, 27.8; IR (CCl_4) 3620, 3400 (br), 3080, 2940, 2025 (vs), 1990, 1970, 1710, 1610, 1170, 985, 920 cm^{-1}; HRMS calcd. for $C_{16}H_{22}O_3Fe$ [M–3(CO)]$^+$: 318.0919, found: 318.0915 *m*/*z*. Anal. calcd. for $C_{19}H_{22}O_6Fe$: C 56.74, H 5.51; found: C 57.02, H 5.58.

*Tricarbonyl [allyl (2*Z*,4*E*,6*E*,11*E*)-(4–7-*η^4*)-15-carbomethoxy-pentadeca-(2,4,6,11)-tetraenoate]iron (**25**) (45)*: Allylic alcohol **24** (355 mg, 0.88 mmol), trimethyl orthoacetate (5 mL, 39.3 mmol), and propionic acid (6.5 μL, 0.09 mmol) were heated at 80°C (oil bath temperature) under a steady stream of nitrogen until TLC analysis indicated complete consumption of starting alcohol. This process usually required 2–4 h, and trimethyl orthoacetate was replenished as it was depleted. The flask was sealed (for larger scale reactions, a reflux condenser is advised) and the reaction was heated at 78°C for 2 d. Concentration of the mixture in vacuo and purification of the crude product by flash chromatography (5:1 hexanes:ether) afforded methyl ester **25** (352 mg, 87%) as an orange oil: ^{1}H NMR (400 MHz, $CDCl_3$) δ: 6.08 (t, *J* = 11.0 Hz, 1H), 5.95 (ddt, *J* = 17.1, 10.4, 5.8 Hz, 1H), 5.59 (dd, *J* = 11.0, 0.8 Hz, 1H), 5.48–5.36 (m, 2H), 5.34 (dd, *J* = 3.1, 1.5 Hz, 1H), 5.31–3.21 (m, 2H), 5.08 (dd, *J* = 7.5, 4.8 Hz, 1H), 4.66–4.56 (m, 2H), 3.67 (s, 3H), 3.09–3.04 (m, 1H), 2.39–2.27 (m, 4H), 2.10–1.93 (m, 2H), 1.74–1.46 (m, 5H); ^{13}C NMR (100 MHz, $CDCl_3$) δ: 211.0 (very broad), 173.6, 166.1, 150.3, 132.2, 130.9, 128.7, 118.2, 115.0, 86.1, 84.6, 65.2, 64.7, 54.0, 51.5, 34.1, 33.7, 32.0, 31.7, 27.8; IR (CCl_4) 2940, 2045 (vs), 1980, 1965, 1740, 1710, 1610, 1170, 990, 970, 930 cm^{-1}; HRMS calcd. for $C_{19}H_{26}O_4Fe$ [M–3CO]$^+$: 374.1181, found: 374.1174 *m*/*z*; HRMS calcd. for $C_{16}H_{21}O_4Fe$ [M–3CO–C_3H_5]$^+$: 333.0789, found: 333.0758 *m*/*z*. Anal. calcd. for $C_{22}H_{26}O_7Fe$: C 57.66, H 5.72; found: C 57.90; H 5.83.

*Tricarbonyl [(2*Z*,4*E*,6*E*,11*E*)-(4–7-*η^4*)-15-carbomethoxy-pentadeca-(2,4,6,11)-tetraenoic acid]iron (**26**) (46)*: Allyl ester **25** (311 mg, 0.68 mmol) and $(Ph_3P)_4Pd$ (39 mg, 0.03 mmol) were degassed in vacuo and then dissolved in THF (freshly distilled, 14 mL). Diethylamine (350 μL, 3.4 mmol) was added and the mixture was stirred at ambient temperature for 6 h. The reaction mixture was concentrated and applied directly to a hexanes-packed silica gel column with benzene. Ordinary flash chromatography (slow gradient from hexanes → 1:1 hexanes:ether, all containing 2% acetic acid) afforded the unstable acid **26**, which contained 4% decomplexed acid: mp 54.5–56.5°C; ^{1}H NMR (400 MHz, $CDCl_3$) δ: 6.17 (t, *J* = 11.2 Hz, 1H), 5.57 (t, *J* = 11.2 Hz, 1H), 5.48–5.36 (m, 2H), 5.29 (dd, *J* = 8.7, 5.0 Hz, 1H), 5.10 (dd, *J* = 7.5, 5.0 Hz, 1H), 3.66 (s, 3H), 2.96 (apparent t, *J* = 9.8 Hz, 1H), 2.39–2.29 (m, 4H), 2.08–1.94 (m, 2H), 1.70–1.46 (m, 5H); ^{13}C NMR (100 MHz, $CDCl_3$) δ: 210.9 (very broad), 173.7, 171.8, 152.7, 130.9, 128.7, 114.4, 86.4, 84.9, 65.2, 53.7, 51.5, 34.0, 33.7, 32.0, 31.6, 27.8; IR (CCl_4) 3600–2400 (br), 2940, 2025 (vs), 1990, 1970, 1740, 1690, 1610, 1430, 1230, 970 cm^{-1}; HRMS calcd. for $C_{16}H_{22}O_4Fe$ [M–3CO]$^+$: 334.0868; found: 334.0856 *m*/*z*.

*Tricarbonyl [(4*E*,9*E*,11*E*,13*Z*)-(9–12-*η^4*)-15-hydroxy-pentadeca-(4,9,11,13)-tetraenoic acid methyl ester]iron (**27**) (47)*: To a solution of carboxylic acid **26** (236 mg, 0.56 mmol) and triethylamine (310 μL, 2.25 mmol) in THF (5 mL) at 0°C was added methyl chloroformate (90 μL, 1.13 mmol). This reaction was stirred at 0°C for 30 min. The solution was then diluted with hexanes (10 mL) and filtered through a plug of Celite®. The filtrate was concentrated and the residue was immediately dissolved in 5 mL of THF and 5 mL of absolute ethanol and cooled to –35°C. Sodium borohydride (31 mg) was added in one portion and the reaction was warmed to ambient temperature over a period of 30 min. Ether (10 mL) and 1 M HCl in saturated aqueous NaCl (15 mL) were then added, and the layers were separated. The organic layer was washed with 1 M HCl in saturated aqueous NaCl (3 × 5 mL), and the aqueous layers were back-extracted with ether (2 × 5 mL). The combined organic layers were washed with saturated aqueous NaCl (5 mL), dried ($MgSO_4$), filtered, and concentrated. Purification of the crude product by flash chromatography (1:1 hexanes:ether) afforded alcohol **27** (180 mg, 79%) as a yellow oil which was contaminated with 8% of decomplexed alcohol: ^{1}H NMR (400 MHz, $CDCl_3$) δ: 5.56–5.36 (m, 4H), 5.17 (ddd, *J* = 8.5, 4.9, 1.10 Hz, 1H), 5.04 (ddd, *J* = 9.0, 4.9, 0.8 Hz, 1H), 4.26 (t, *J* = 5.5 Hz, 2H), 3.66 (s, 3H), 2.39–2.27 (m, 4H), 2.10–1.93 (m, 2H), 1.84 (t, *J* = 8.8 Hz, 1H), 1.74–1.63 (m, 2H), 1.58–1.42 (m, 2H), 1.33–1.27 (m, 2H); ^{13}C NMR (100 MHz, $CDCl_3$) δ: 212.0 (very broad), 173.7, 133.3, 131.0, 128.7, 128.3, 84.8, 82.6, 64.0, 59.0, 55.0, 51.5, 34.1, 33.6, 32.0, 31.7, 27.8; IR (CCl_4) 3600–3100 (br), 2930, 2030 (vs), 1930 (br), 1740, 970, 790, 765 cm^{-1}; HRMS calcd. for $C_{16}H_{24}O_3Fe$ [M–3CO]$^+$: 320.1075, found: 320.0189 *m*/*z*. Anal. calcd. for $C_{19}H_{24}O_6Fe$: C 56.45, H 5.98; found: C 56.74, H 6.18.

*Tricarbonyl [(5*E*,10*E*,12*E*,14*Z*)-(10–13-*η^4*)-oxacyclohexadeca-(5,10,12,14)-tetraene-2-one]iron (**15**)*:

A. Via Yamaguchi lactonization (52). To a solution of ester **27** (101 mg, 0.25 mmol) in 4:1 dimethoxyethane:water (5 mL) was added LiOH (36 mg, 1.5 mmol). The resulting heterogeneous mixture was stirred for 5 h. The reaction was acidified to pH = 3 with 1 M HCl in saturated aqueous

© 2000 NRC Canada

NaCl, then ether (10 mL) was added and the layers were separated. The organic layer was washed with aqueous HCl (pH = 3, 3 × 5 mL), and the combined aqueous layers were washed with ether (2 × 5 mL). The combined organic layers were washed with saturated aqueous NaCl (5 mL), dried ($MgSO_4$), filtered through a plug of silica gel (ether as eluant), and concentrated. Seco-acid **28** (97 mg, >95%) was isolated as a highly unstable yellow oil: ^{1}H NMR (400 MHz, $CDCl_3$) δ: 5.53 (broad s), 5.45 (broad s), 5.18 (broad s), 5.05 (broad s), 4.27 (broad s), 2.42 (broad s), 2.33 (broad s), 2.02 (broad s), 1.86 (broad s), 1.68 (broad s), 1.51 (broad s), 1.33 (broad s), 1.25 (broad s); IR (thin film) 3670–2415 (v br), 2934, 2864, 2047 (vs), 1978, 1710, 1555, 1204 cm^{-1}; HRMS calcd. for $C_{15}H_{22}O_3Fe$ [M–3CO]$^+$: 306.0919, found: 306.0930 *m/z*.

The seco-acid **28** produced above was immediately used in the next reaction. A suspension of crude **28** (97 mg, 0.25 mmol) and 4 Å sieves (33 mg) in THF (10 mL) was cooled to 0°C. To this solution was added triethylamine (104 μL, 0.75 mmol) and trichlorobenzoyl chloride (47 μL, 0.30 mmol). The reaction was stirred at 0°C for 4.5 h, then was filtered, diluted with toluene (50 mL), and added over 6 h via cannula to a 63°C solution (oil bath temperature) of DMAP (915 mg, 29 mM) in toluene (200 mL). After being stirred for 9 h, the solution was cooled, concentrated, and partitioned between ether and saturated aqueous $NaHCO_3$ (30 mL each). The layers were separated, the organic layer was washed with saturated aqueous $NaHCO_3$ (3 × 15 mL), and the combined aqueous layers were washed with ether (3 × 10 mL). The combined organic layers were washed with saturated aqueous NaCl (5 mL), dried ($MgSO_4$), and concentrated. The residue was purified by flash chromatography using 5:1 hexanes:ether as eluant. Lactone **15** (37 mg, 39%) was isolated as a yellow oil, along with a small amount of decomplexed lactone **29** (3 mg, 12%). Analytical data is reported for lactone **15**: ^{1}H NMR (400 MHz, $CDCl_3$) δ: 5.67 (t, *J* = 10.9 Hz, 1H), 5.61–5.42 (m, 3H), 5.15–5.11 (m, 1H), 5.00–4.97 (m, 1H), 4.63 (dd, *J* = 5.8, 0.7 Hz, 2H), 2.59–2.52 (m, 1H), 2.44–2.32 (m, 3H), 2.30–2.21 (m, 1H), 2.16–2.07 (m, 1H), 1.78–1.66 (m, 4H), 1.64–1.56 (m, 2H); ^{13}C NMR (100 MHz, $CDCl_3$) δ: 212.1 (broad), 173.3, 137.8, 133.4, 128.5, 120.9, 84.6, 81.3, 64.6, 60.5, 56.4, 34.4, 33.8, 32.7, 28.3, 27.1; IR (CCl_4) 3030, 2930, 2030 (vs), 1990–1965, 1740, 1440, 1140, 975, 790 cm^{-1}; HRMS calcd. for $C_{16}H_{20}O_3Fe$ [M–2CO]$^+$: 316.0762, found: 316.0767 *m/z*. Anal. calcd. for $C_{18}H_{20}O_5Fe$: C 58.09, H 5.42; found: C 58.09, H 5.42.

B. Via PyBroP lactonization (46). Seco-acid **28** prepared as described above (38.5 mg, 0.10 mmol) was dissolved in toluene (15 mL) and dichloromethane (5 mL), and cooled to –78°C. This solution was added via cannula over 12 h to a solution of PyBroP (51) (550 mg, 1.18 mmol) and DMAP (488 mg, 25 mM) in toluene (125 mL) and dichloromethane (10 mL) at ambient temperature. After stirring for 4 h, the solution was worked up as described above for the Yamaguchi lactonization, and the residue was purified by flash chromatography (20:1 → 5:1 hexanes:ether). Lactone **15** (17.5 mg, 48%) was isolated as a yellow oil.

*(5*E*,10*E*,12*E*,14*Z*)-Oxacyclohexadeca-(5, 10, 12, 14)-tetraene-2-one (29)*: To a solution of iron(tricarbonyl)-complexed lactone **15** (39 mg, 0.10 mmol) in propionitrile (5 mL) maintained at –50°C was added $FeCl_3$ (170 mg, 1.05 mmol) portion wise over 45 min. The reaction was partitioned between ether and saturated aqueous $NaHCO_3$ (20 mL each). The layers were separated, the organic layer was washed with saturated aqueous $NaHCO_3$ (3 × 10 mL), and the combined aqueous layers were washed with ether (5 × 5 mL). The combined organic layers were washed with saturated aqueous NaCl (2 × 5 mL), dried ($MgSO_4$), and concentrated. The residue was purified by flash chromatography (slow gradient from hexanes → 7:1 hexanes:ether as eluant), giving lactone **29** (16.3 mg, 67%) as a clear oil: ^{1}H NMR (400 MHz, $CDCl_3$) δ: 6.48 (dd, *J* = 15.1, 10.9 Hz, 1H), 6.22 (dd, *J* = 10.9, 0.8 Hz, 1H), 6.12 (dd, *J* = 15.1, 9.3 Hz, 1H), 5.95 (ddd, *J* = 15.4, 9.3, 0.8 Hz, 1H), 5.74 (dt, *J* = 15.4, 6.9 Hz, 1H), 5.53 (dt, *J* = 10.9, 5.5 Hz, 1H), 5.44–5.28 (m, 2H), 4.79 (dd, *J* = 5.5, 1.3 Hz, 2H), 2.46–2.43 (m, 2H), 2.38–2.33 (m, 2H), 2.13 (q, *J* = 6.3 Hz, 2H), 2.07 (qd, *J* = 6.3, 1.1 Hz, 2H), 1.61–1.55 (m, 2H); ^{13}C NMR (100 MHz, $CDCl_3$) δ: 172.3, 132.9, 132.7, 132.6, 131.8, 131.4, 129.1, 126.3, 122.8, 61.0, 34.0, 32.5, 31.6, 27.1, 25.8; IR (CCl_4) 3020, 2960, 1740, 1440, 1150, 995, 970, 910, 725, 650 cm^{-1}; HRMS calcd. for $C_{15}H_{20}O_2$ [M]$^+$: 232.1463, found: 232.1469 *m/z*.; HRMS calcd. for $C_{15}H_{21}O_2$ [M + H]$^+$: 233.1541, found: 233.1538 *m/z*.

*3-Vinyl-1,2,3,3a,5a,6,7,8,8a,8b-decahydro-*as*-indacene-2-carboxylic acid (31)*: Lactone **29** (31.5 mg, 0.14 mmol) and activated, crushed 4 Å molecular sieves (16 mg) were stirred at room temperature in a mixture of dry THF (2.1 mL) and hexamethylphosphoramide (625 μL) for 30 min. The mixture was cooled to –78°C, then *tert*-butyldimethylsilyl triflate (35 μL) was added to the vigorously stirred solution, followed approximately 2 min later by potassium hexamethyldisilazide (315 μL, 0.47 M in toluene). The cooling bath was removed 1 min later, and the reaction mixture was allowed to warm to ambient temperature. The mixture was stirred overnight at 65°C, then 5 mL of a 1 M HCl in saturated aqueous NaCl and 3 mL of ether were added, and this heterogeneous mixture was stirred vigorously for 2 min. The layers were separated, and the organic layer was further washed with 1 M HCl in saturated aqueous NaCl (3 × 5 mL). The aqueous layers were washed with ether (3 × 5 mL), and the combined organic layers were washed with saturated aqueous NaCl, dried ($MgSO_4$), concentrated, and purified by flash chromatography (slow gradient from 5:1 hexanes:ether → 98% 1:1 hexanes:ether + 2% acetic acid). Lactone **29** (8.4 mg, 27%) was recovered, and acid **31** (13.8 mg, 44%) containing ca. 20% of diastereomer **32** was isolated as a white solid. A portion of this solid was recrystallized from an ether–hexanes mixture: mp 127–128°C; ^{1}H NMR (400 MHz, $CDCl_3$) δ: 5.80–5.66 (m, 3H), 5.15–5.10 (m, 2H), 3.10 (apparent q, *J* = 8.8 Hz, 1H), 2.52–2.44 (m, 1H), 2.44–2.36 (m, 1H), 2.13–1.96 (m, 3H), 1.91–1.83 (m, 2H), 1.72–1.63 (m, 2H), 1.56–1.37 (m, 2H), 1.28–1.17 (m, 3H); ^{13}C NMR (100 MHz, $CDCl_3$) δ: 180.1, 136.8, 132.3, 126.9, 117.3, 50.9, 46.8, 46.8, 42.4, 42.2, 33.0, 32.9, 31.0, 25.2; IR (CCl_4) 3600–2500 (br), 3030, 2900, 1700, 1640, 905 cm^{-1}; HRMS calcd. for $C_{15}H_{21}O_2$ [M + H]$^+$: 233.1541, found: 233.1534 *m/z*; HRMS calcd. for $C_{15}H_{20}O_2$ [M]$^+$: 232.1463, found 232.1469 *m/z*.

*(*E*)-6-Bromo-hex-4-enoic acid methyl ester (45) (45)*: To a solution of **44** (60) (6.2 g, 41.1 mmol) in toluene (65 mL)

© 2000 NRC Canada

was added trimethyl orthoacetate (26.0 mL, 205.4 mmol) and propionic acid (0.3 mL, 4.1 mmol). The reaction was refluxed for 72 h and then all of the solvents were removed in vacuo. The crude product was purified by column chromatography (3:1 hexanes:diethyl ether) to give 4.80 g of **45** (56%) as a light yellow oil: ^{1}H NMR (400 MHz, $CDCl_3$) δ: 5.79–5.67 (m, 2H), 3.94 (d, *J* = 6.6 Hz, 2H), 3.69 (s, 3H), 2.42–2.40 (m, 4H); ^{13}C NMR (100 MHz, $CDCl_3$) δ: 173.1, 133.9, 127.6, 51.6, 33.2, 32.8, 27.3; IR (thin film) 3020, 2980, 2960, 2870, 1750, 1660, 1500, 1200, 970; HRMS calcd. for $C_7H_{15}O_2BrN$ [M + NH_4]$^+$: 224.0286, found: 224.0289 *m*/*z*.

*(*E*)-2-(4′-Hydroxy-but-2′-enyl)-malonic acid di*-tert-*butyl ester (**43**) (59)*: To a 0°C solution of butadiene monoepoxide **42** (0.95 g, 13.6 mmol) in THF (15 mL) was added $(Ph_3P)_4Pd$ (0.16 g, 0.01 mmol). Di-*tert*-butyl malonate **41** (3.6 mL, 16.3 mmol) was dropwise by syringe over 5 min. The mixture was stirred at 0°C for 30 min and at ambient temperature for an additional 3 h. The mixture was concentrated, and the crude residue was directly chromatographed using 1.5:1 ether:hexanes as eluant, giving allylic alcohol **43** as a light yellow oil (3.54 g, 79%). The olefin ratio was determined to be 2:1 *E*:*Z* by ^{1}H NMR analysis. An analytical sample was prepared by HPLC (1:1 ethyl acetate:hexanes): ^{1}H NMR (400 MHz, $CDCl_3$) δ: 5.76–5.62 (m, 2H), 4.08 (d, *J* = 5.0 Hz, 2H), 3.20 (t, *J* = 7.5 Hz, 1H), 2.55 (t, *J* = 6.8 Hz, 1H), 1.45 (s, 18H); ^{13}C NMR (100 MHz, $CDCl_3$) δ: 168.3, 131.8, 128.3, 81.6, 63.4, 53.7, 31.7, 28.0; IR (thin film) 3444 (br s), 2979, 2934, 2872, 1728 (s), 1478, 1457, 1394, 1369, 1251, 1144 (s), 1007, 971, 848 cm^{-1}; HRMS calcd. for $C_{15}H_{27}O_5$ [M + H]$^+$: 287.1858, found: 287.1868 *m*/*z*. Anal. calcd. for $C_{15}H_{26}O_5$: C 62.91, H 9.15; found: C 62.63, H 9.25.

*(2′*E*,2″*E*)-2-(4′-Hydroxy-but-2′-enyl)-2-(5″-carbomethoxy-hex-2″-enyl)malonic acid di*-tert-*butyl ester (**46**)*: Sodium hydride (0.09 g, 3.62 mmol, rinsed with dry THF) was slurried in THF (5 mL) and cooled to 0°C. Alcohol **43** (1.00 g, 3.62 mmol) in THF (5 mL) was carefully added to the slurry via cannula to control hydrogen evolution. The solution was allowed to warm to ambient temperature and to stir for 30 min. Allylic bromide **45** (0.75 g, 3.62 mmol) in THF (5 mL) was added to the malonate anion solution via cannula. The resulting mixture was then heated in a 65°C oil bath overnight. The resulting suspension was cooled to room temperature and partitioned with ether (50 mL) and water (20 mL). The aqueous layer was separated and the organic layer was washed sequentially with saturated aqueous NH_4Cl and an aqueous saturated NaCl solution. The organic layer was dried over $MgSO_4$ and filtered. Concentration of the solution followed by column chromatography (2:1 ether:hexanes) of the crude product afforded 1.16 g (78%) of **46** as a 2:1 *E*:*Z* mixture of olefin isomers, as determined by ^{1}H NMR analysis. An analytical sample was prepared by HPLC (1:1 ethyl acetate:hexanes). Selected data is reported for the (*E*)–olefin isomer only: ^{1}H NMR (500 MHz, $CDCl_3$) δ: 5.70 (dt, *J* = 15.4, 5.9 Hz, 1H), 5.53–5.47 (m, 2H), 5.28 (dt, *J* = 15.1, 7.6 Hz, 1H), 4.06 (d, *J* = 5.6 Hz, 2H), 3.65 (s, 3H), 2.50 (d, *J* = 7.3 Hz, 2H), 2.46 (d, *J* = 7.6 Hz, 2H), 2.36–2.29 (m, 4H), 1.42 (s, 18H); ^{13}C NMR (100 MHz, $CDCl_3$) δ: 173.5, 170.0, 133.4, 132.6, 126.3, 125.1, 81.3, 63.4, 57.9, 51.6, 35.1, 34.8, 33.8, 28.0, 27.9; IR (thin film) 3457 (br s), 2978, 2932, 2857, 1727 (s), 1438, 1369, 1288, 1250, 1163 (s), 1147 (s), 972, 847 cm^{-1}; HRMS calcd. for $C_{22}H_{40}O_7N$ [M + NH_4]$^+$: calcd. 430.2805, found: 430.2792 *m*/*z*.

(2′E,2″E)-2-(4′-Oxo-but-2′-enyl)-2-(5″-carbomethoxy-hex-2″-enyl)malonic acid di-tert-*butyl ester (**47**) (61)*: To a solution of alcohol **46** (1.0 g, 2.42 mmol) in CH_2Cl_2 (8 mL) was added Celite® (2 g) and pyridinium chlorochromate (0.65 g, 3.03 mmol). The solids were rinsed into the flask with an additional amount of CH_2Cl_2 (2 mL). The mixture was stirred at room temperature for 4 h. The dark brown mixture was then diluted with a 1:1 mixture of ether:hexanes (100 mL). The solution was filtered and concentrated and the crude dark brown residue was redissolved in ether (10 mL). The suspension was then filtered through a plug of 1:1 Celite®:Florisil® and rinsed with ether (100 mL). The solution was concentrated to afford 0.92 g (93%) of enal **47** as a light yellow oil. An analytical sample was prepared by HPLC (2:1 hexanes:ethyl acetate): ^{1}H NMR (400 MHz, $CDCl_3$) δ: 9.48 (d, *J* = 7.7 Hz, 1H), 6.72 (dt, *J* = 15.4, 7.3 Hz, 1H), 6.10 (ddt, *J* = 15.4, 8.1, 1.1 Hz, 1H), 5.52 (dt, *J* = 15.4, 6.2 Hz, 1H), 5.27 (dt, *J* = 15.0, 7.3 Hz, 1H), 3.65 (s, 3H), 2.73 (dd, *J* = 7.3, 1.1 Hz, 2H), 2.50 (d, *J* = 7.7 Hz, 2H), 2.35–2.30 (m, 4H), 1.42 (s, 18H); ^{13}C NMR (100 MHz, $CDCl_3$) δ: 193.5, 173.3, 169.3, 152.9, 135.6, 133.5, 124.5, 82.0, 57.7, 51.6, 36.2, 35.7, 33.7, 27.9, 27.8; IR (thin film) 2979, 2743, 1732 (s), 1694 (s), 1641, 1438, 1369, 1290 (s), 1256 (s), 1148 (s), 976, 846 cm^{-1}; HRMS calcd. for $C_{22}H_{38}O_7N$ [M + NH_4]$^+$: 428.2648, found 428.2633 *m*/*z*. Anal. calcd. for $C_{22}H_{37}O_7$: C 64.37, H 8.35; found: C 64.35, H 8.49.

*(2′*E*,4′*E*,2″*E*)-2-(5′-Iodo-penta-2′,4′-dienyl)-2-(5″-carbomethoxy-hex-2″-enyl)-malonic acid di*-tert-*butyl ester (**48**) (62)*: A 250 mL round bottom single necked flask containing $CrCl_2$ (11.5 g, 93.6 mmol) was cooled to 0°C and the solid was suspended in THF (100 mL). To the purple mixture was added a solution of CHI_3 (16.3 g, 41.4 mmol) and enal **47** (6.8 g, 16.6 mmol) in THF (20 mL) via cannula. The reaction was allowed to warm to room temperature and to stir for 1 h. The dark brown mixture was diluted a 1 M sodium serinate solution and the resulting biphasic mixture was stirred for 15 min. The organic layer was separated and the aqueous layer was washed twice with a 1:1 hexanes:ethyl acetate mixture and the combined organics dried over $MgSO_4$. The mixture was filtered and the solution was concentrated affording vinyl iodide **48** (>10 g) as a crude yellow oil contaminated with residual iodoform. The vinyl iodide was used immediately in the subsequent step. ^{1}H NMR analysis indicated the iodoolefin to consist of a 6.5:1 *E*:*Z* isomer mixture. Analytical data is reported for the mixture and for the ^{1}H NMR, only selected data for **48** is reported: ^{1}H NMR (400 MHz, $CDCl_3$) δ: 6.97 (ddd, *J* = 14.3, 10.6, 0.7 Hz, 1H), 6.23 (d, *J* = 14.3 Hz, 1H), 6.00 (dd, *J* = 15.0, 10.6 Hz, 1H), 5.58–5.46 (m, 2H), 5.32–5.24 (m, 1H), 3.67 (s, 3H), 2.49 (d, *J* = 7.7 Hz, 2H), 2.46 (d, *J* = 7.7 Hz, 2H), 2.37–2.31 (m, 4H), 1.43 (s, 18H); IR (thin film) 2977, 2927, 1726 (s), 1368, 1290, 1250, 1145, 1161, 980, 847 cm^{-1}; HRMS calcd. for $C_{23}H_{39}O_6IN$ [M + NH_4]$^+$: 552.1824, found: 552.1817 *m*/*z*.

© 2000 NRC Canada

*(2′*E*,4′*E*,2″* E*)-2-(8′-Hydroxy-octa-2′,4′-dien-6′-ynyl)-2-(5″-carbomethoxy-hex-2″-enyl)-malonic acid di*-tert-*butyl ester (**49**) (64)*: The crude vinyl iodide **48** (>10 g, 16.6 mmol) was dissolved in triethylamine (160 mL) and nitrogen was vigorously bubbled through the solution for 15 min. Propargyl alcohol (1.20 mL, 19.9 mmol) and $(Ph_3P)_2PdCl_2$ (0.58 g, 0.83 mmol) were then added. The flask was covered with aluminum foil and CuI (0.32 g, 1.66 mmol) was added. The reaction mixture was vigorously stirred for 3 h and then diluted with 200 mL of ether. Saturated aqueous ammonium chloride was added and this mixture was stirred for 30 min. The organic layer was separated, washed twice with 1 M HCl, and dried over $MgSO_4$. Filtration followed by concentration of the filtrate afforded a crude oil which was purified by column chromatography (1:1 ether:hexanes → 3:1 ether:hexanes), giving dienyne **49** (4.50 g, 59% from enal **47**). An analytical sample was prepared by HPLC (1.2:1 ethyl acetate:hexanes): ^{1}H NMR (400 MHz, $CDCl_3$) δ: 6.52 (dd, *J* = 15.7, 11.0 Hz, 1H), 6.09 (dd, *J* = 15.0, 11.0 Hz, 1H), 5.62 (dt, *J* = 15.0, 8.1 Hz, 1H), 5.54–5.46 (m, 2H), 5.28 (dt, *J* = 15.4, 7.3 Hz, 1H), 4.39 (br s, 2H), 3.66 (s, 3H), 2.54 (d, *J* = 7.7 Hz, 2H), 2.26 (d, *J* = 7.3 Hz, 2H), 2.37–2.30 (m, 4H), 1.42 (s, 18H); ^{13}C NMR (100 MHz, $CDCl_3$) δ: 173.3, 169.9, 142.0, 133.0, 132.7, 131.7, 125.1, 109.3, 89.4, 84.9, 81.4, 58.1, 51.7, 51.6, 35.7, 35.6, 33.8, 28.0, 27.9; IR (thin film) 3515 (br s), 2978, 2932, 1727 (s), 1438, 1394, 1369, 1289, 1251, 1165, 1023, 987, 846 cm^{-1}; HRMS calcd. for $C_{26}H_{42}O_7N$ $[M + NH_4]^+$: 480.2961, found: 480.2957 *m*/*z*.

*(2′*E*,4′*E*,6′*Z*,2″* E*)-2-(8′-Hydroxy-octa-2′,4′,6′-trienyl)-2-(5″- carbomethoxy-hex-2″-enyl)-malonic acid di*-tert-*butyl ester (**50**) (66)*: Zinc (32.0 g, 496 mmol) which had been prewashed with 1 M HCl was suspended in water (150 mL). Nitrogen was bubbled through the vigorously stirred mixture for 30 min, then $Cu(OAc)_2 \times 2H_2O$ (3.30 g, 16.5 mmol) was added. This mixture was stirred for 30 min, and then $AgNO_3$ (3.21 g, 19.5 mmol) was added. The mixture was stirred for 1 h (exotherm), at which time it was filtered. The filter cake was washed twice successively with water, methanol, acetone, and ether (75 mL each). The filter cake was then resuspended in 1:1 methanol:water (100 mL) and then **49** (4.50 g, 9.73 mmol) was added to the mixture in methanol (20 mL). The reaction mixture was stirred overnight at ambient temperature, then was filtered through Celite®. The solids were washed twice with ether (200 mL each) and the organic layer was separated. The aqueous layer was washed with ether (50 mL) and then combined organics were dried over $MgSO_4$, filtered, and concentrated. The crude residue was redissolved in ether (100 mL) and washed with a saturated aqueous NaCl solution. The organic layer was dried over $MgSO_4$, filtered, and concentrated to afford 4.20 g of tetraene **50** (93%) as a light yellow oil. An analytical sample was prepared by HPLC (1.2:1 ethyl acetate:hexanes): ^{1}H NMR (400 MHz, C_6D_6) δ: 6.37 (dd, *J* = 14.4, 11.5 Hz, 1H), 6.18 (dd, *J* = 14.6, 10.7 Hz, 1H), 6.08 (dd, *J* = 14.6, 11.0 Hz, 1H), 5.95 (apparent t, *J* = 11.2 Hz, 1H), 5.75 (dt, *J* = 14.9, 7.6 Hz, 1H), 5.52–5.43 (m, 3H), 4.04 (d, *J* = 6.6 Hz, 2H), 3.37 (s, 3H), 2.87 (d, *J* = 7.6 Hz, 2H), 2.78 (d, *J* = 5.6 Hz, 2H), 2.22–2.19 (m, 2H), 2.12 (dd, *J* = 7.8, 7.1 Hz, 2H), 1.36 (s, 18H); ^{13}C NMR (100 MHz, $CDCl_3$) δ: 173.4, 170.0, 134.4, 133.9, 132.6, 130.7, 129.6, 129.5, 126.0, 125.1, 81.3, 58.8, 58.1, 51.6, 35.6, 35.4, 33.9, 27.9, 27.9; IR (thin film) 3449 (s br), 2978, 2932, 2953, 1726 (s), 1438, 1369, 1289, 1252, 1163 (s), 1146 (s), 997, 846 cm^{-1}; HRMS calcd. for $C_{25}H_{38}O_7$ $[M + H]^+$: 465.2852, found: 465.2848 *m*/*z*.

*(2′*E*,4′*E*,6′*Z*,2″* E*)-2-(8′-Hydroxy-octa-2′,4′,6′-trienyl)-(5″-carboxy-hex-2″-enyl)-malonic acid di*-tert-*butyl ester (**51**)*: Tetraene **50** (0.22 g, 0.47 mmol) was dissolved in 1:1 methanol:THF (2 mL), then a solution of LiOH (0.04 g, 0.98 mmol) in water (1 mL) was added. The mixture was stirred at room temperature for 3 h, diluted with ether (25 mL), and then acidified with 1 M HCl. The organic layer was separated and dried over $MgSO_4$. The crude product was purified by rapid column chromatography (12:1 dichloromethane:methanol), giving 0.17 g (80%) of seco acid **51**. Partial analytical data reported is for a mixture of **51** and the all *E* tetraene, which was generated upon concentration of the sample. For the ^{1}H NMR, selected data for **51** is reported: ^{1}H NMR (400 MHz, C_6D_6) δ: 6.48 (dd, *J* = 14.6, 11.7 Hz, 1H), 6.19 (dd, *J* = 14.9, 10.7 Hz, 1H), 6.08 (dd, *J* = 10.7, 7.1 Hz, 1H), 5.98 (apparent t, *J* = 10.7 Hz, 1H), 5.70 (dt, *J* = 14.9, 7.6 Hz, 1H), 5.50–5.41 (m, 3H), 4.09 (d, *J* = 6.8 Hz, 2H), 2.86 (d, *J* = 7.6 Hz, 2H), 2.75 (d, *J* = 6.3 Hz, 2H), 2.18–2.12 (m, 4H), 1.34 (s, 18H); IR (thin film) 3449 (br s), 2978, 2932, 1724 (s), 1394, 1369, 1291, 1251, 1160 (s), 1146 (s), 998, 846 cm^{-1}; HRMS calcd. for $C_{25}H_{42}O_7N$ $[M + NH_4]^+$: 468.2961, found: 468.2961 *m*/*z*.

*(5*E*, 10*E*, 12*E*, 14*Z*)-Oxacyclohexadeca-(5, 10, 12, 14)-tetraene-8-bis(carbo-*tert-*butoxy)-2-one (**38**) (67)*: To a 70°C solution of 2-chloro-1-methylpyridinium iodide (0.23 g, 0.89 mmol) in acetonitrile (65 mL) was added a solution of seco-acid **51** (0.10 g, 0.22 mmol) and Et_3N (0.25 mL, 1.76 mmol) in acetonitrile (10 mL). The addition was performed using a Hamilton syringe pump over 5 h. Upon completion of the addition of the triethylamine–seco-acid mixture, the reaction was allowed to stir at 70°C for an additional 2 h. The solution was allowed to cool to room temperature and concentrated. The residue was dissolved with ether (50 mL) and washed with a 1 M aqueous $NaHSO_4$ solution and than a saturated aqueous NaCl solution. The organic layer was dried over $MgSO_4$, filtered, and concentrated. Purification of the crude residue by column chromatography (CH_2Cl_2 → 9:1 CH_2Cl_2:MeOH) yielded 0.04 g (40%) of lactone **38** as an off white solid. A portion was recrystallized from a ca. 15:1 hexanes:ether mixture: mp 130–132°C; ^{1}H NMR (400 MHz, C_6D_6) δ: 6.75 (dd, *J* = 14.9, 11.2 Hz, 1H), 6.04–5.88 (m, 3H), 5.66 (dt, *J* = 15.1, 7.6 Hz, 1H), 5.53–5.47 (m, 1H), 5.44–5.38 (m, 1H), 5.04 (dt, *J* = 11.5, 4.2 Hz, 1H), 4.57 (d, *J* = 2.7 Hz, 2H), 2.92 (d, *J* = 7.6 Hz, 2H), 2.77 (d, *J* = 6.8 Hz, 2H), 2.19–2.08 (m, 4H), 1.35 (s, 18H); ^{13}C NMR (100 MHz, $CDCl_3$) δ: 172.3, 170.6, 136.7, 133.4, 131.7, 129.9, 128.6, 126.0, 124.3, 123.9, 81.3, 77.3, 62.5, 56.8, 36.9, 36.0, 33.9, 27.9, 27.1; IR (thin film) 2978, 2931, 1724 (s), 1432, 1393, 1369, 1282, 1253, 1163 (s), 1000, 847 cm^{-1}; HRMS calcd. for $C_{25}H_{40}O_6N$ $[M + NH_4]^+$: 450.2856, found: 450.2846 *m*/*z*. Anal. calcd. for $C_{25}H_{36}O_6$: C 69.42, H 8.39; found: C 69.43, H 8.65.

*2-Carbomethoxy-3-vinyl-7-bis(carbo-*tert-*butoxy)-1,2,3,3a,5a,6,7,8,8a,8b-decahydro-as-indacene (**54**)*: Powdered 4 Å molecular sieves (15 mgs) were flame dried under high

© 2000 NRC Canada

vacuum. The dried sieves were allowed to cool to room temperature, then a solution of lactone **38** (0.10 g, 0.24 mmol) in THF (3.0 mL) was added via cannula. Hexamethylphosphoramide (0.8 mL) was added then the suspension was cooled to –78°C and *t*-butyldimethylsilyl triflate (68 µL, 0.30 mmol) was added by syringe. A slurry immediately formed. To the slurry was added lithium diisopropylamide (0.50 mL of a 0.5 M solution, 0.25 mmol) and the reaction was allowed to stir at –78°C for 15 min. An initial yellow color which developed upon addition of the lithium diisopropylamide dissipated upon prolonged stirring. After 15 min, the reaction was allowed to warm to room temperature and to stir overnight. The mixture was diluted with ether (10 mL) and stirred with 1 M HCl (3 mL) for 30 min. The organic layer was separated, washed twice with 1:1 aqueous saturated NaCl:1 M HCl, and dried over $MgSO_4$. The crude product was purified by column chromatography (20:1 CH_2Cl_2:methanol). A small amount of lactone **38** was recovered (0.02 g, 20%) along with 0.06 g of tricyclic carboxylic acids. The acid was dissolved in 4:1 ether:methanol (5 mL) and treated with trimethylsilyldiazomethane (0.50 mL of 2 M solution, 1.00 mmol). The resulting yellow solution was stirred for 1 h, and then concentrated. HPLC purification of a portion (ca. 0.04 g) of the crude methyl ester (6:1 hexanes:ethyl acetate) afforded 0.02 g (ca. 40%) of the tricyclic adduct **54** and an inseparable diastereomer. Analytical data reported is for the mixture of **54** and the inseparable isomer. For the ^1H and ^{13}C NMR, selected data for **54** is reported: ^1H NMR (400 MHz, $CDCl_3$) δ: 5.69–5.58 (m, 3H), 5.10–5.05 (m, 2H), 3.63 (s, 3H), 3.10 (dt, *J* = 10.6, 8.1 Hz, 1H), 2.67–2.62 (m, 1H), 2.50 (ddd, *J* = 13.9, 8.8, 0.7 Hz, 1H), 2.42–2.33 (m, 2H), 2.23–2.15 (m, 1H), 2.09 (ddd, *J* = 12.5, 8.4, 6.6 Hz, 1H), 1.98 (apparent t, *J* = 11.5 Hz, 1H), 1.90 (dd, *J* = 14.3, 4.4 Hz, 1H), 1.77 (t, *J* = 12.8 Hz, 1H), 1.67 (dt, *J* = 12.1, 7.7 Hz, 1H), 1.45 (s, 9H), 1.43 (s, 9H), 1.27–1.21 (m, 1H); ^{13}C NMR (125 MHz, $CDCl_3$) δ: 175.5, 171.6, 137.0, 130.4, 127.9, 117.1, 81.1, 81.0, 61.5, 51.4, 50.8, 46.9, 46.9, 46.6, 42.0, 41.0, 40.0, 38.2, 32.5, 27.9; IR (thin film) 2977, 1725 (s), 1458, 1393, 1368, 1281, 1170, 1144, 849 cm^{-1}; HRMS calcd. for $C_{26}H_{39}O_6$ $[M + H]^+$: 447.2746, found: 447.2743 *m*/*z*. Anal. calcd. for $C_{26}H_{38}O_6$: C 69.93, H 8.58; found: C 69.83, H 8.57.

Acknowledgement

Financial support provided by the National Institute of General Medical Sciences (GM 26782) is gratefully acknowledged.

References

1. S. Ito and Y. Hirata. Tetrahedron Lett. 2557 (1972).
2. S. Aizawa, H. Akutsu, T. Satomi, T. Nagatsu, R. Taguchi, and A. Seino. J. Antibiot. **32**, 193 (1979).
3. H.A. Kirst, K.H Michel, J.W. Martin, L.C. Creemer, E.H. Chio, R.C. Yao, W.M. Nakatsukasa, L.D. Boeck, J.L. Occolowitz, J.W. Paschal, J.B. Deeter, N.D. Jones, and G.D. Thompson. Tetrahedron Lett. **32**, 4839 (1991).
4. T.C. Sparks, G.D. Thompson, H.A. Kirst, M.B. Hertlein, L.L. Larson, T.V. Worden, and S.T. Thibault. J. Econ. Entomol. **91**, 1277 (1998).
5. R. Dagani. Chem. Eng. News, **77**, July 5, 31 (1999).
6. D.A. Evans and W.C. Black. J. Am. Chem. Soc. **115**, 4497 (1993).
7. L.A. Paquette, Z. Gao, Z. Ni, and G.F. Smith. J. Am. Chem. Soc. **120**, 2543 (1998).
8. L.A. Paquette, I. Collado, and M. Purdie. J. Am. Chem. Soc. **120**, 2553 (1998).
9. R.K. Boeckman, Jr., C.H. Weidner, R.B. Perni, and J.J. Napier. J. Am. Chem. Soc. **111**, 8036 (1989).
10. J.K. Whitesell and M.A. Minton. J. Am. Chem. Soc. **109**, 6403 (1987).
11. L.A. Paquette, D. Macdonald, and L.G. Anderson. J. Am. Chem. Soc. **112**, 9292 (1990).
12. L.A. Paquette, J.L. Romine, H.-S. Lin, and J. Wright. J. Am. Chem. Soc. **112**, 9284 (1990).
13. W.R. Roush and C.K. Wada. J. Am. Chem. Soc. **116**, 2151 (1994).
14. S. Ito and Y. Hirata. Bull. Chem. Soc. Jpn. **50**, 1813 (1977).
15. H.A. Kirst, K.H. Michel, E.H. Chio, R.C. Yao, W.M. Nakatsukasa, L.D. Boeck, J.L. Occolowitz, J.W. Paschal, J.B. Deeter, and G.D. Thompson. *In* Microbial metabolites. Vol. 32. *Edited by* C. Nash. Dubuque: Wm. C. Brown, p. 109.
16. W.R. Roush. *In* Comprehensive organic synthesis. *Edited by* L.A. Paquette. Pergamon Press, Oxford. 1991. Vol. 5, p. 513.
17. E. Ciganek. Org. React. (N.Y.) **32**, 1 (1984).
18. P. Deslongchamps. Aldrichimica Acta, **24**, 43 (1991).
19. J.A. Porco, Jr., F.J. Schoenen, T.J. Stout, J. Clardy, and S.L. Schreiber. J. Am. Chem. Soc. **112**, 7410 (1990).
20. W.R. Roush, K. Koyama, M.L. Curtin, and K.J. Moriarty. J. Am. Chem. Soc. **118**, 7502 (1996).
21. P. Deslongchamps. Pure Appl. Chem. **64**, 1831 (1992).
22. Y.L. Dory, P. Soucy, M. Drouin, and P. Deslongchamps. J. Am. Chem. Soc. **117**, 518 (1995).
23. F. Turecek, V. Hanus, P. Sedmera, H. Antropiusová, and K. Mach. Tetrahedron, **35**, 1463 (1979).
24. W.R. Roush, J.S. Warmus, and A.B. Works. Tetrahedron Lett. **34**, 4427 (1993).
25. A.B. Works. Ph.D. thesis. Indiana University, Bloomington, IN. 1995.
26. S.H. Jung, Y.S. Lee, H. Park, and D.-S. Kwon. Tetrahedron Lett. **36**, 1051 (1995).
27. D. Brillon, and P. Deslongchamps. Tetrahedron Lett. **27**, 1131 (1986).
28. M.M. Abelman, R.L. Funk, and J.D. Munger, Jr. J. Am. Chem. Soc. **104**, 4030 (1982).
29. S. Pereira, and M. Srebnik. Aldrichimica Acta, **26**, 17 (1993).
30. R.E. Ireland, R.H. Mueller, and A.K.Willard. J. Am. Chem. Soc. **98**, 2868 (1976).
31. R.L. Funk, T.A. Olmstead, and M. Parvez. J. Am. Chem. Soc. **110**, 3298 (1988).
32. R.L. Funk, M.M. Abelman, and J.D. Munger. Tetrahedron, **42**, 2831 (1986).
33. K.M. Khan and D.W. Knight. J. Chem. Soc. Chem. Commun. 1699 (1991).
34. E.J. Corey and R.S. Kania. J. Am. Chem. Soc. **118**, 1229 (1996).
35. K. Neuschütz, J. Velker, and R. Neier. Synthesis, 227 (1998).
36. J.D. Winkler. Chem. Rev. **96**, 167 (1996).
37. W.R. Roush and A.B. Works. Tetrahedron Lett. **38**, 351 (1997).
38. R.E. Ireland, P. Wipf, and J.D. Armstrong, III. J. Org. Chem. **56**, 650 (1991).
39. M. Kobayashi, K. Masumoto, E. Nakai, and T. Nakai. Tetrahedron Lett. **37**, 3005 (1996).
40. S.L. Schreiber, R.E. Claus, and J. Reagan. Tetrahedron Lett. **23**, 3867 (1982).

© 2000 NRC Canada

41. W.S.J. Wadsworth. Org. React. **25**, 73 (1978).
42. H. Firouzabadi and E. Ghaderi. Tetrahedron Lett. 839 (1978).
43. R. Grèe. Synthesis, 341 (1989).
44. W.C. Still and C. Gennari. Tetrahedron Lett. **24**, 4405 (1983).
45. W.S. Johnson, L. Werthemann, W.R. Bartlett, T.J. Brocksom, T.-T. Li, D.J. Faulkner, and M.R. Petersen. J. Am. Chem. Soc. **92**, 741 (1970).
46. S. Freidrich-Bochnitschek, H. Waldmann, and H. Kunz. J. Org. Chem. **54**, 751 (1989).
47. T. Itaya, T. Fujii, A. Evidente, G. Randazzo, G. Surico, and N.S. Iacobellis. Tetrahedron Lett. **27**, 6349 (1986).
48. Q. Meng and M. Hesse. Top. Curr. Chem. **161**, 107 (1991).
49. G. Rousseau. Tetrahedron, **51**, 2777 (1995).
50. J.L. Wood, J.A. Porco, Jr., J. Taunton, A.Y. Lee, J. Clardy, and S.L. Schreiber. J. Am. Chem. Soc. **114**, 5898 (1992).
51. J. Coste, E. Frérot, P. Jouin, and B. Castro. Tetrahedron Lett. **32**, 1967 (1991).
52. J. Inanaga, K. Hirata, H. Saeki, T. Katsuki, and M. Yamaguchi. Bull. Chem. Soc. Jpn. **52**, 1989 (1979).
53. H. Tone, T. Nishi, Y. Oikawa, M. Hikota, and O. Yonemitsu. Tetrahedron Lett. **28**, 4569 (1987).
54. M. Hikota, H. Tone, K. Horita, and O. Yonemitsu. J. Org. Chem. **55**, 7 (1990).
55. R.W. Hoffmann. Chem. Rev. **89**, 1841 (1989).
56. D. Brillon and P. Deslongchamps. Can. J. Chem. **65**, 43 (1987).
57. For review of the use of malonates as carbonyl precursors: T.A. Hase and J.K. Koskimies. Aldrichimica Acta, **14**, 73 (1981).
58. R. Bonjouklian and R.A. Ruden. J. Org. Chem. **42**, 4095 (1977).
59. T. Tsuda, M. Tokai, T. Ishida, and T. Saegusa. J. Org. Chem. **51**, 5216 (1986).
60. A.T. Bottini and D. Dev. J. Org. Chem. **27**, 968 (1962).
61. E.J. Corey and J.W. Suggs. Tetrahedron Lett. 2647 (1975).
62. K. Takai, K. Nitta, and K. Utimoto. J. Am. Chem. Soc. **108**, 7408 (1986).
63. D.P. Stamos, X.C. Sheng, S.S. Chen, and Y. Kishi. Tetrahedron Lett. **38**, 6355 (1997).
64. K. Sonogashira, Y. Tohda, and N. Hagihara. Tetrahedron Lett. 4467 (1975).
65. E.N. Marvell and T. Li. Synthesis, 457 (1973).
66. W. Boland, N. Schroer, C. Sieler, and M. Feigel. Helv. Chim. Acta, **70**, 1025 (1987).
67. T. Mukaiyama, M. Usui, and K. Saigo. Chem. Lett. 49 (1976).
68. D.L. Hughes. Org. Prep. Proced. Int. **28**, 129 (1996).
69. (*a*) M.E. Jung and J. Gervay. J. Am. Chem. Soc. **113**, 224 (1991); (*b*) M.E. Jung and B.T. Vu. Tetrahedron Lett. **37**, 451 (1996).
70. R.K. Boeckman, Jr. and T.E. Barta. J. Org. Chem. **50**, 3421 (1985).
71. W.R. Roush, M. Kageyama, R. Riva, B.B. Brown, J.S. Warmus, and K.J. Moriarity. J. Org. Chem. **56**, 1192 (1991).
72. W. Kitching, H.A. Olszowy, G.M. Drew, and W. Adcock. J. Org. Chem. **47**, 5153 (1982).
73. J.J. Gajewski and J. Emrani. J. Am. Chem. Soc. **106**, 5733 (1984).
74. J.J. Gajewski. Acc. Chem. Res. **30**, 219 (1997).
75. P.A. Magriotis and K.D. Kim. J. Am. Chem. Soc. **115**, 2972 (1993).
76. N. Engel, B. Kübel, and W. Steglich. Angew. Chem. Int. Ed. Engl. **16**, 394 (1977).

© 2000 NRC Canada

Synthesis of novel pentacyclic β-lactam antibacterial agents

Daniele Andreotti, Stefano Biondi, Daniele Donati, Sergio Lociuro, and Gilles Pain

Abstract: The search for new antibacterial agents still represents an active area of research. In this paper the synthesis of a new class of β-lactam agents characterized by an interesting antibacterial profile is reported; together with a description of the most significant synthetic aspects encountered during this work.

Key words: β-lactams, pentacyclic, O-alkylation, trinem.

Résumé : La recherche de nouveaux agents antibactériens constitue toujours un champ de recherche actif. Cet article rapporte la synthèse d'une nouvelle classe de β-lactames caractérisés par un intéressant profil antibactérien, ainsi que la description des aspects synthétiques les plus importants rencontrés au cours de ces travaux.

Mots clés : β-lactames, pentacyclique, O-alkylation, trinème.

Introduction

The search for new β-lactam motifs able to address problems both in clinical practice and in community acquired infection has seen the involvement of both pharmaceutical companies and research groups (1). One of the most significant problems in clinical practice is the constant occurrence in the isolation of methicillin resistant *Staphylococcus aureus* (MRSA) against which most of the β-lactams, acting through irreversible inhibition of Penicillin Binding Proteins (PBPs), are ineffective. In these strains the expression of an additional high molecular weight PBP, known as PBP2a (PBP2′), with extremely low affinity for all β-lactam antibiotics, has been recognized as the cause of resistance (2). Consequently the search for new antibacterial agents able to effectively treat infections caused by MRSA represents an active area of investigation.

Recently in our laboratories we identified a class of trinem derivatives (**1)** endowed with high affinity for both PBP2a and other essential PBPs. These compounds are characterized by the presence of an unsaturated side chain bearing a (hetero)aromatic substitution at position 4 of the trinem nucleus (3), and showed a broad spectrum of activity including MRSA.

Received October 12, 1999. Published on the NRC Research Press website on June 9, 2000.

Dedicated to Professor Stephen Hanessian in recognition of his significant contributions to the art of organic synthesis.

D. Andreotti,[1] S. Biondi, D. Donati, S. Lociuro, and G. Pain. GlaxoWellcome, S.p.A. Medicine Research Centre, Via A. Fleming 4, 37100 Verona, Italy.

[1]Author to whom correspondence may be addressed. Telephone: +39-045-9218767. Fax: +39-045-9218196. e-mail: DGA9946@glaxowellcome.co.uk

As an extension of this class we decided to investigate whether conformationally more constrained pentacyclic β-lactams of general formula **2** would further improve the antimicrobial potency (Fig. 1). This paper describes the synthesis of these compounds.

Results and discussion

According to the retrosynthetic analysis, the azetidinone derivatives **9**–**12** (see Scheme 1) were identified as key intermediates in the synthesis of β-lactams **2**. Such intermediates have then been obtained by direct condensation of the corresponding aromatic ketones **4**–**8** (Fig. 2), with the commercially available azetidinone **3**.

Ketones **4**–**8** whose synthesis has been already reported in the literature (4) were selected to investigate the effect of chemical modification of rings D or E on the microbiological profile of this new class of β-lactams.

The nitrogen atom in the aromatic ring D of **2** was chosen to offer potential advantage in terms of both chemical feasibility and water-solubility of the final molecule.

With respect to the stereochemistry at position 16 of β-lactams **2**, we expected, on the basis of our previous experience (1*i*, 5) in the field, that compounds with the *R* configuration [16β] would posses a better microbiological profile than the corresponding epimer.

The validity of such a hypothesis has then been taken into consideration by preparing and testing a number of different isomers.

Treatment of the 4-acetoxyazetidinone **3** with 2.5 equivalents of the enolate derived from **4** furnished in 33% yield a diastereomeric mixture **9** (2′α:2′β = 1:1) which was then submitted to a cyclization protocol (6) leading to the formation of pentacyclic β-lactams **13a** and **13b**. At this stage the diastereoisomers were separated by flash chromatography to afford the β isomer **13b** in 23% yield and the α isomer **13a** in 12% yield. A subsequent deprotection of the secondary

© 2000 NRC Canada

Scheme 1. (*i*) 2.5 equiv. of **4**, **5**, **6**, **7**, or **8**, 2.5 eq of LHMDS, THF, –78°C; (*ii*) $ClCOCO_2All$, TEA, CH_2Cl_2; (*iii*) MeP(OEt)2, toluene, reflux; (*iv*) TBAF, AcOH, THF; (*v*) $Pd(Ph_3P)_4$, Na 2-ethylhexanoate, THF.

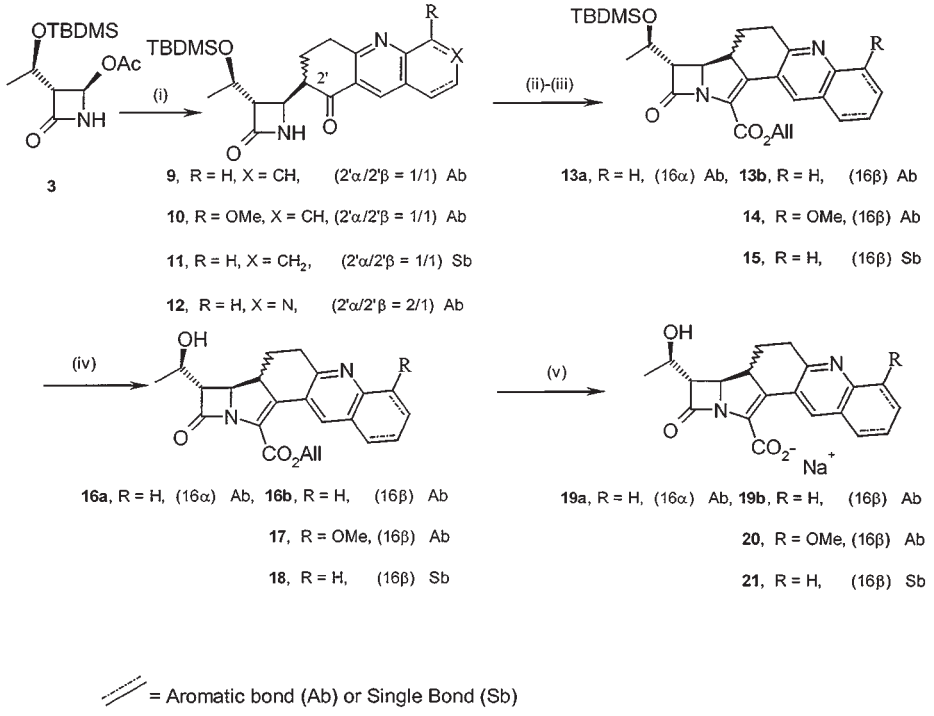


Figure 1.

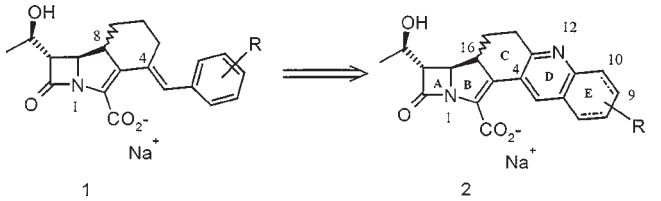
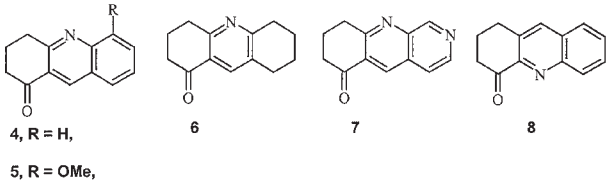


Figure 2.



hydroxyl group of **13a** by means of TBAF in acetic acid led in 40% yield to **16a** which was then transformed, using $Pd(Ph_3P)_4$ and sodium 2-ethylhexanoate (7), to the corresponding sodium salt **19a**[2] (70% yield). Repeating the same procedure on diastereoisomer **13b**, the pentacyclic β-lactam **19b**[3] was obtained in 31% overall yield from **13b**.

Similarly, condensation between **5** and **3** gave a mixture of compounds containing the desired mixture of azetidinones **10** in a diastereoisomeric ratio 2′α:2′β = 1:1 (32%) and the O-alkylated adduct **22** (22% yield) as side product (Fig. 3). The formation of this kind of O-alkylated side product occurs mainly when the oxygen of the enolate is poorly associated with the cation, as the case of Na- and K-enolates. In the case of Li-enolate where there is a strong interaction between oxygen and Li^+, the C-alkylation is normally preferred. Although in this case we are using the Li enolate, it is possible that the cation is chelated intermolecularly by both the nitrogen and oxygen present in the electron rich enolate of 8-methoxy-quinoline system, giving rise to a poorly associated Li-enolate.

A similar result was obtained during the condensation of ketone **7** with **3**. The desired 2′β isomers of **12** (2′α = 14%, 2′β = 6%) were obtained in a very low yield, discouraging any further effort to prepare the corresponding pentacyclic β-lactam derivative, while the product of O-alkylation (**23**, Fig 3) was obtained in 30% yield.

Intriguingly, after cyclization of the diastereoisomeric mixture **10** using the standard procedure, only the β isomer **14** was isolated (22% yield), while no significant traces of the corresponding α isomer were detected. Preliminary indications suggested that the α isomer gave rise to a reduction product such as **24** (Fig. 3); however, further studies would be required to fully characterize this product. Deprotection of compound **14** at the hydroxyethyl moiety following standard procedure gave the intermediate **17**, which was in turn

[2] ^{1}H NMR and IR assignment of pentacyclic β-lactam **19a**. ^{1}H NMR (400 MHz, D_2O) δ: 1.22 (3H, d), 1.88 (1H, m), 2.31 (1H, m), 3.18–3.20 (2H, m), 3.40–3.48 (2H, m), 3.85 (1H, m), 4.16 (1H, m), 7.46 (1H, t), 7.65 (1H, t), 7.75 (1H, d), 7.80 (1H, d), 8.87 (1H, s); IR (nujol, cm^{-1}): 1752.

[3] ^{1}H NMR and IR assignment of pentacyclic β-lactam **19b**. ^{1}H-NMR (400 MHz, D_2O) δ: 1.20 (3H, d), 1.92 (1H, m), 2.15 (1H, m), 3.10–3.40 (3H, m), 3.54 (1H, dd), 4.19 (1H, m), 4.35 (1H, dd), 7.46 (1H, m), 7.63 (1H, m), 7.75 (1H, d), 7.78 (1H, d), 8.27 (1H, s); IR (nujol, cm^{-1}): 1756.

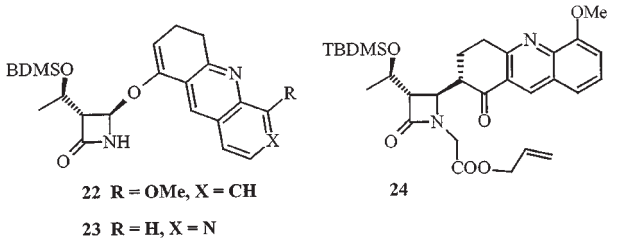
© 2000 NRC Canada

Table 1. Minimum inhibitory concentration (MIC) (μg/mL).

	Gram-positive				Gram-negative	
Compound	*S. aur.* pen-r	*S. aur.* COL[a]	*S. pne.* pen-s	*E. faecalis*	*E. coli*	*H. influenzae* 49247ATCC
19a	0.5	>32	0.5	>32	>32	32
19b	0.25	4	0.25	1	1	0.5
20	0.25	2	0.25	2	8	2
21	0.25	4	0.25	2	0.5	8
1 R = H, (8β)	1	4	0.03	4	8	2
Vancomycin	0.25	2	0.5	1	>32	>32

[a]MRSA constitutive strain.

Figure 3.



converted to the deallylated desired compound **20**[4] in 21% yield from **14**.

Starting from **3** and using the ketone **6**, the compound **21**[5] was eventually obtained in approximately 6% overall yield using the procedures already described in Scheme 1.

Although **11** was obtained as an equimolar mixture of diastereomers (2′α:2′β = 1:1), after the cyclization procedure, only the isomer **15** [16β] was isolated and progressed.

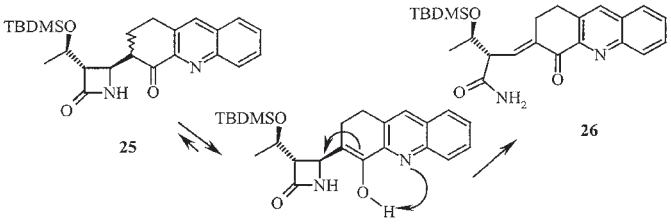
By reacting the lithium enolate of the ketone **8** with the 4-acetoxyazetidinone **3**, only **26** was isolated (25% yield). Such an unexpected result could be explained assuming that a desired product **25** is converted to **26**, by a nitrogen-assisted retro-Michael reaction as depicted in Fig. 4.

In conclusion, a new class of β-lactam antibacterial agent has been disclosed. Clearly, the procedures used to obtain the final β-lactams were extrapolated from our previous experience on the chemistry of β-lactam trinems and have not yet been optimized. In a few cases it has been possible to recover the starting ketone, however, all the reported yields are based on the amount of reagent **3** used during the reaction of condensation with the corresponding ketone.

All the final target molecules were shown to possess good water solubility.

The microbiological activities of **19a**, **19b**, **20**, and **21** (Table 1) were assayed against a panel of Gram-positive and Gram-negative strains including methicillin resistant staphylococci, in comparison with trinem **1** (R = H, 8β) and the glycopeptide vancomycin. The latter is a pure anti-Gram-positive agent and it is considered the last resort for the treatment of infection caused by drug resistant Gram-positive bacteria. Similarly to what was observed in other trinem classes, the α stereochemistry at the corresponding position 16 (e.g. **19a** compared to **19b**) has a detrimental effect on the antibacterial activity of these compounds. Compounds **19b**, **20**, and **21** showed comparable anti-MRSA activity to vancomycin with the advantage of possessing a broader antibacterial spectrum including relevant Gram-negative strains. The presence of ring D gives rise to a more conformationally constrained pentacyclic β-lactam ring which retains a comparable, and in same cases better, in vitro antimicrobial profile to the corresponding 4-*exo* methylene trinem derivative (e.g. **19b** compared to **1**). Aromaticity of ring E does not seem to be an essential requirement for retaining good antibacterial activity (e.g. **21** compared to **1**) within this new class of pentacyclic β-lactams.

Figure 4.



References

1. (*a*) R.R. Wilkening, R.W. Ratcliffe, K.J. Wildonger, L.D. Cama, K.D. Dykstra, F.P. DiNinno, T.A. Blizzard, M.L. Hammond, J.V. Heck, K.L. Dorso, E. St. Rose, J. Kohler, and G.G. Hammond. Bioorg. Med. Chem. Lett. **9**, 673 (1999); (*b*) S. Hanessian and G.B. Reddy. Tetrahedron, **55**, 3427 (1999); (*c*) S. Hanessian, A.M. Griffin, and M.J. Rozema. Bioorg. Med. Chem. Lett. **7**, 1857 (1997); (*d*) Y. Narukawa, K. Nishi, and H. Onoue. Tetrahedron, **53**, 539 (1997); (*e*) H.W. Lee, E.N. Kim, H.J. Son, S.K. Ahn, K.H. Chung, J.W. Kim, and C.R. Lee. Chem. Pharm. Bull. **44**, 2326 (1996); (*f*) G. Burton, N.J.C. Clear, A.J.G.T. Eglington, W. Angela, E. Hunt, A. Naylor, M.J. Pearson, and A.K. Takle. J. Antibiot. **49**, 1258 (1996); (*g*) S. Hanessian and G.B. Reddy. Bioorg. Med. Chem. Lett. **4**, 2285 (1994); (*h*) S. Hanessian and M.J. Rozema. Bioorg. Med. Chem. Lett. **4**, 2279 (1994); (*i*) B. Tamburini, A.

[4] ^{1}H NMR and IR assignment of pentacyclic β-lactam **20**. ^{1}H-NMR (400 MHz, D_2O) δ: 1.22 (3H, d), 1.95 (1H, m), 2.10 (1H, m), 3.11–3.48 (3H, m), 3.44 (1H, dd), 4.06 (3H,s), 4.20 (1H, m), 4.35 (1H, dd), 6.91 (1H, d), 7.11 (1H, d), 7.30 (1H, m), 8.20 (1H, s); IR (nujol, cm^{-1}): 1750.

[5] ^{1}H NMR and IR assignment of pentacyclic β-lactam **21**. ^{1}H NMR (400 MHz, D_2O) δ: 1.18 (3H, d), 1.60–1.80 (5H, m), 2.04 (1H, m), 2.50–2.70 (4H, m), 2.80–2.92 (2H, m), 3.09 (1H, m), 3.46 (1H, dd), 4.15 (1H, m), 4.26 (1H, dd), 7.46 (1H, s); IR (nujol, cm^{-1}): 1753.

© 2000 NRC Canada

Perboni, T. Rossi, D. Donati, D. Andreotti, G. Gaviraghi, R. Carlesso, and C. Bismara. European Patent Application EP416953 A2 19910313, (1991); (*l*) G. Franceschi, E. Perrone, M. Alpegiani, A. Bedeschi, C. Della Bruna, and F. Zarini. Spec. Publ. R. Soc. Chem. **70** (Recent Adv. Chem. β-lactam Antibiot.), 222, (1989); (*m*) C. Battistini, M. Alpegiani, A. Bedeschi, E. Perrone, C. Scarafile, and G. Franceschi. Spec. Publ.-R. Soc. Chem. **52** (Recent Adv. Chem. β-lactam Antibiot.), 357, (1985); (*n*) W.J. Leanza, K.J. Wildonger, T.W. Miller, and B.G. Christensen. J. Med. Chem. **22**, 1435 (1979).

2. (*a*) H.F. Chambers and M. Sachdeva. J. Infect. Dis. **161**, 1170 (1990); (*b*) H.F. Chambers, M. Sachdeva, and S. Kennedy. J. Infect. Dis. **162**, 705 (1990).
3. T. Rossi, D. Andreotti, G. Tedesco, L. Tarsi, E. Ratti, A. Feriani, D.A Pizzi, G. Gaviraghi, S. Biondi, and G. Finizia. PCT Int. Appl. WO 9821210 (1998).
4. (*a*) D.E. O'Brien, L.T. Weinstock, and C.C. Cheng. J. Heterocycl. Chem. **7**, 99 (1970); (*b*) G.M. Shutske and J.D. Tomer. J. Heterocycl. Chem. **30**, 23 (1993); (*c*) C. Ruangsiyanand, H.J. Rimek, and F. Zymalkowski. Chem. Ber. **103**, 2403, (1970); (*d*) M.G. Vetelino and J.W. Coe. Tetrahedron Lett. **35**, 219 (1994); (*e*) A.D. Batcho and W. Leimgruber. U.S. Patent 3-976-639 (Chem. Abstr. 86:29624, (1977)); (*f*) R. Pappo, D.S. Allen, Jr., R.U. Lemieux, and W.S. Johnson. J. Org. Chem. **21**, 478, (1956); (*g*) L.J. Dolby. J. Am. Chem. Soc. **88**, 1049 (1966); (*h*) S.V. Sunthankar and S.D. Mehendale. Indian J. Chem. Sect. B: Org. Chem. Incl. Med. Chem. **14B**, 94 (1976).
5. (*a*) D. Andreotti, T. Rossi, G. Gaviraghi, D. Donati, C. Marchioro, E. Di Modugno, and A. Perboni. Bioorg. Med. Chem. Lett. **6**, 91 (1996); (*b*) S. Biondi. Spec. Publ.-R. Soc. Chem. **198** (Anti-Infectives), 86, (1997).
6. A. Yoshida, T. Hayashi, N. Takeda, and S. Oida. Chem. Pharm. Bull. **31**, 768 (1983).
7. P.D. Jeffrey and S.W. McCombie. J. Org. Chem. **47**, 587, (1982).

© 2000 NRC Canada

Synthesis of 8-*epi*-castanospermine and 6,7,8-tri-*epi*-castanospermine

Yves St-Denis and Tak Hang Chan

Abstract: 8-*epi*-Castanospermine (**11**) and 6,7,8-tri-*epi*-castanospermine (**12**) were synthesized from the hydroxyproline precursor **13** which was obtained enantioselectively via an enzymatic process.

Key words: castanospermine, synthesis of, enzymatic reduction, enzymatic resolution, asymmetric synthesis.

Résumé : On a synthétisé les 8-*épi*-castanospermine (**11**) et 6,7,8-tri-*épi*-castanospermine (**12**) à partir du précurseur hydroxyproline (**13**) obtenu de façon énantiosélective par le biais d'un processus enzymatique.

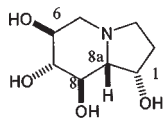
Mots clés : castanospermine, synthèse, réduction enzymatique, résolution enzymatique, synthèse asymétrique.

Introduction

Castanospermine (**1**) is a polyhydroxylated indolizidine alkaloid which has elicited much biological and chemical interest (1). It was isolated from the Australian legume *Castanospermum australe* (Moreton Bay chestnut) and has been shown to be a potent inhibitor of various glycosidases (2). It also inhibits the processing of *N*-linked glycoproteins (3). Castanospermine and its analogs have been examined as potential therapeutic agents (4) in the treatment of cancer (5) and HIV-I (6). Epimers of castanospermine, including 6-*epi*-castanospermine (**2**) (7) and 6,7-di-*epi*-castanospermine (**3**) (8), have been isolated as well. Comparison of their inhibitory activities toward different glycosidases showed that the change of stereochemistry at a single hydroxy group could alter the inhibitory properties.

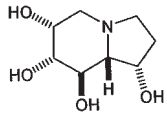
Many syntheses of **1** and its modifications have been reported (9). A commonly used synthetic approach is to start with the appropriate carbohydrate precursor. Depending on the carbohydrate precursor used, epimers of castanospermine have also been synthesized. Thus, the syntheses of 6-*epi*- (**2**), 1,6-di-*epi*- (**4**), 1-*epi*- (**5**), 1,6,8-tri-*epi*- (**6**), 1,7,8-tri-*epi*- (**7**), and 1,6,7,8-tetra-*epi*-castanospermine (**8**) have all been reported (10). We recently reported on the use of the amino acid derivative (*S*)-prolinol (**9**) as the precursor for the synthesis of various isomers of 1-deoxycastanospermine (**10**) (11, 12, footnote 2). We have now extended the approach by starting with an amino acid precursor with the incorporation of the 1-hydroxy function. The results gave rise to a synthesis of 8-*epi*- (**11**) and 6,7,8-tri-*epi*-castanospermine (**12**) (13).

Structure 1.



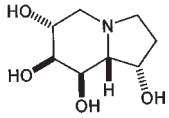
1

Structure 2.



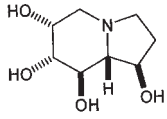
2

Structure 3.



3

Structure 4.



4

Received August 30, 1999. Published on the NRC Research Press website on June 9, 2000.

Dedicated to Professor Stephen Hanessian on the occasion of his 65th birthday in recognition of his significant contributions to the art of organic synthesis.

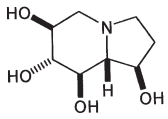
Y. St-Denis and T.H. Chan.[1] Department of Chemistry, McGill University, Montreal, QC H3A 2K6, Canada.

[1]Author to whom correspondence may be addressed. e-mail: thchan@chemistry.mcgill.ca

[2]Recent work by Martin et al. (12) has led to reassignment of the stereochemistry of the compounds reported by us in reference 11. The revised stereochemistries should be: compound **22aa**: 6*R*, 7*S*, 8*R*, 8a*S*; **22ab**: 6*S*, 7*R*, 8*R*, 8a*S*; **22ba**: 6*S*, 7*R*, 8*S*, 8a*S*; **22bb**:

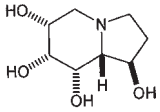
© 2000 NRC Canada

Structure 5.



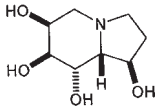
5

Structure 6.



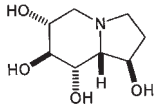
6

Structure 7.



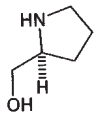
7

Structure 8.



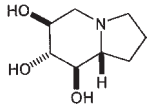
8

Structure 9.



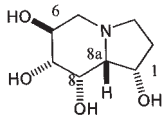
9

Structure 10.



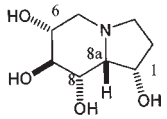
10

Structure 11.



11

Structure 12.



12

Results and discussion

Preparation of (2*R*,3*S*)-*N*-benzyloxycarbonyl-3-methoxymethyloxypyrrolidine-2-carboxaldehyde (13)

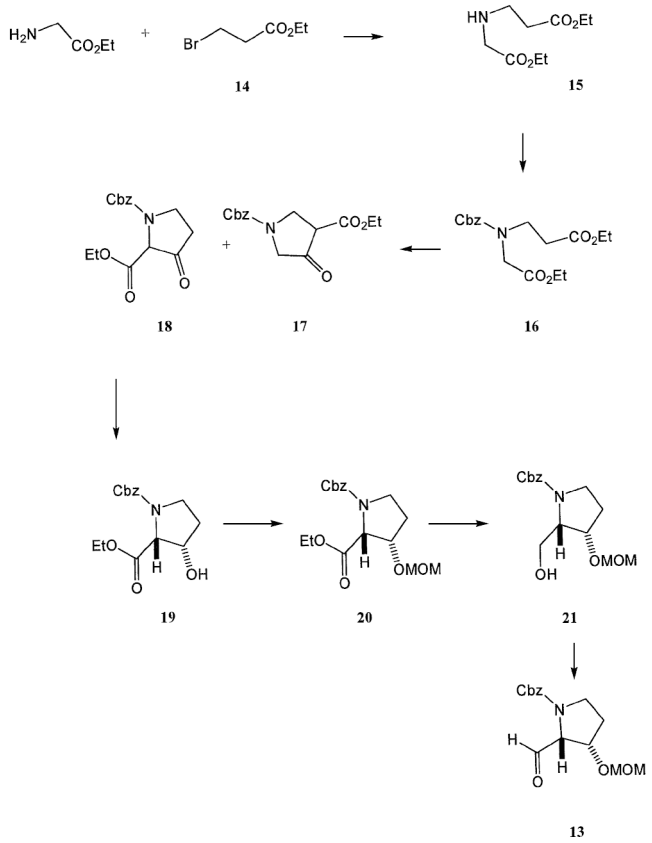
Since the stereochemistry of the 8a position of castanospermine itself corresponds to the unnatural *R*-configuration of proline, the requisite 3-hydroxylated proline precursor **13** cannot be prepared from the natural amino acids. In the literature, Sih and coworkers have used microbial enzymatic reduction or hydrolysis to prepare (2*R*,3*S*)-3-hydroxyproline derivatives (3*b*). Alternatively, Sibi and Christensen improved an already known baker's yeast reduction method to give the (2*R*,3*S*)-Boc-protected proline ester in good chemical and optical yields (14). Since the baker's yeast reduction is easy to perform, we adopted this method with modification (15) to prepare the Cbz protected compound **13** according to Scheme 1. Thus, condensation of ethyl 3-bromopropionate (**14**) with freshly prepared ethyl glycinate was accomplished in refluxing benzene to give a good yield of the *N*,*N*-disubstituted aminodiester **15**. Protection of the free amine with the Cbz group was performed to provide the carbamate **16** in good yield (16). Dieckmann cyclization of **16** using potassium *t*-butoxide in toluene afforded a 1.3:1 mixture of regioisomers **17** and **18** which could be separated by distillation and chromatography. Even though the required **18** was the minor isomer, the sequence for its preparation was nevertheless quite short and utilized cheap and readily available starting materials. Baker's yeast reduction of **18** gave the (2*R*,3*S*)-β-hydroxyester **19** in good enantioselectivity (>99% ee). For comparison purpose, sodium borohydride reduction of **18** in ethanol gave the racemic **19** as the sole diastereomer, spectroscopically identical to the enantiomerically pure compound. Many of the subsequent reactions could therefore be explored with the racemic compound first. Protection of the secondary alcohol of (+)-**19** with the MOM protecting group gave compound **20**. Reduction of **20** with lithium borohydride in ether gave a good yield of the primary alcohol **21**, which was oxidized by the Swern oxidation to the aldehyde **13** in quantitative yield.

Synthesis of 8-*epi*- (11) and 6,7,8-tri-*epi*-castanospermine (12) (Scheme 2)

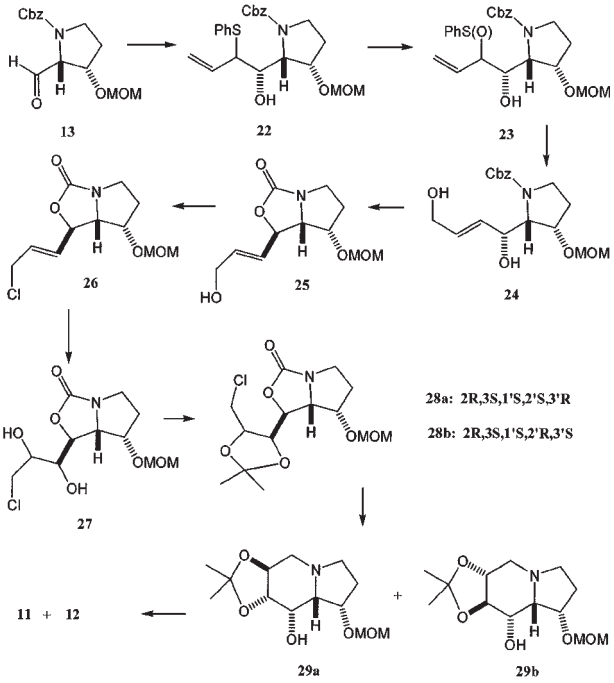
Coupling of **13** with the titanium reagent derived from the anion of allyl phenyl sulfide gave only one stereoisomer, **22** (17). It is interesting to compare the stereoselectivity in the present coupling with our previously reported coupling of *N*-Cbz-pyrrolidine-2-carboxaldehyde where the 3-MOM substituent was missing (11). The stereoselectivity is much higher in the present case, presumably due to the influence of the MOM group. Since it was established by Yamamoto and co-workers that the coupling reaction gave excellent erythro selectivity (17), the two newly created stereogenic centers could have either the 1′*S*, 2′*S* or the 1′*R*, 2′*R* configurations. Definitive assignment could not be made at this point. Furthermore, the stereochemistry at the carbon 2 position is of no real interest to us since it will be destroyed in the subsequent reactions. In any case, oxidation of the

© 2000 NRC Canada

Scheme 1.



Scheme 2.



sulfide **22** to the corresponding sulfoxide **23** followed by trimethyl phosphite treatment (18) gave the rearranged diol **24**. In conformity with similar rearrangements observed previously (11), the double bond in **24** was expected to have the *trans* stereochemistry. This was confirmed through the coupling constants of the olefinic protons in the bicyclic compound **25** prepared by intramolecular cyclization of **24** under basic conditions. The primary allylic alcohol function in **25** was transformed to the chloride **26** with triphenylphosphine in carbon tetrachloride (19). Hydroxylation of the double bond of **26** with osmium tetroxide and *N*-methylmorpholine *N*-oxide (20) led to an inseparable mixture of diols **27a** and **27b**. Conversion of the diols to the corresponding acetonides allowed separation into individual compounds **28a** and **28b** in a ratio of about 5:3. Base hydrolysis of compound **28a,** the major isomer, followed by spontaneous intramolecular cyclization gave the protected indolizidine **29a**. Removal of the MOM and the isopropylidene protecting groups of **29a** under aqueous acidic conditions gave in quantitative yield the product **11** which we subsequently assigned the structure as (+)-8-*epi*-castanospermine (vide infra). Base hydrolysis of **28b**, the minor isomer, led not only to cyclization but deprotection as well to give product **12** to which the structure 6,7,8-tri-*epi*-castanospermine was assigned.

Assignment of stereochemistry

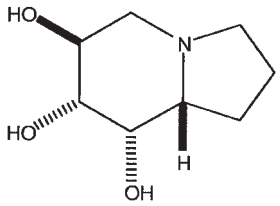
Castanospermine (**1**) itself has the 1*S*, 6*S*, 7*R*, 8*R*, and 8a*R* configurations. From the ^{1}H and ^{13}C NMR spectra of compounds **11** and **12**, it is clear that they are not identical to that of castanospermine (9*f*). In starting from the known pyrrolidinecarboxaldehyde **13**, the stereochemistries of carbons 1 and 8a (corresponding to carbons 2 and 3 of **13**) are secured as 1*S* and 8a*R* in the final products **11** and **12**. Since the dihydroxylation of double bond with osmium tetroxide has been well established to give the *cis* diol (20), the relative stereochemistry of carbons 6 and 7 in compounds **11** and **12** must be *trans*. There were two reactions in Scheme 2 which could give rise to uncertain stereochemical outcomes. The first was the conversion of **13** to **22**, which created the stereogenic carbon 8 in the final products. The stereochemistry could be either 8*S* or 8*R*. The second was that, in the hydroxylation step, the relative stereochemistry of the *cis* diol with respect to the existing stereogenic carbon 8 could be *syn* or *anti* (21). Consequently, there could be four stereochemical outcomes from Scheme 2. If, in the conversion of **13** to **22** the stereochemistry was 8*R*, then the final two products must have either 1*S*, 6*S*, 7*R*, 8*R*, 8a*R* (castanospermine **1**) or 1*S*, 6*R*, 7*S*, 8*R*, 8a*R* (6,7-di-*epi*-castanospermine **3**) stereochemistry. These two possibilities can be ruled out because the NMR spectra of neither **11** nor **12** correspond to the known **1** (9*f*) and **3** (8). If, on the other hand, in the conversion of **13** to **22** the stereochemistry was 8*S*, then the final two products must have either 1*S*, 6*S*, 7*R*, 8*S*, 8a*R* (8-*epi*-castanospermine) or 1*S*, 6*R*, 7*S*, 8*S*, 8a*R* (6,7,8-tri-*epi*-castanospermine) stereochemistry. We were able to assign compound **11** to the 8-*epi*-castanospermine structure based on comparison of the coupling constants in the ^{1}H NMR spectrum of **11** with those reported for the various stereoisomers of castanospermine (Table 1). In particular, the H6 proton has a *trans*-diaxial coupling with H7 (J = 9.5 Hz), which has a gauche coupling with H8 (J = 3.0 Hz), fully compatible with the 6*S*, 7*R*, 8*S* relative configurations of *trans*-diaxial/gauche relationship between the three protons. Martin et al. recently reported on the synthesis of 1-deoxy-8-*epi*-castanospermine (**30**) (22). The three protons

© 2000 NRC Canada

Table 1. Partial ^{1}H NMR spectra of castanospermine and epimers.

	Castanospermine (**1**)[a]	6,7-*epi*- (**3**)[b]	Compound **11**[c]	1-Deoxy-8-*epi*- (**30**)[d]
H6	3.41–3.47 (m) for H6 and H8	3.98 (dd, *J* = 1.5, 2) for H6 and H7	3.43 (ddd, *J* = 5.5, 9.5, 11.2)	3.72 (ddd, *J* = 5.2, 9.6, 10.7)
H7	3.15 (t, *J* = 9.0)	see H6	2.96 (dd, *J* = 3.0, 9.5)	3.34 (dd, *J* = 3.5, 9.6)
H8	see H6	4.08 (dd, *J* = 2, 10)	3.89 (dd, *J* = 1.0, 3.0)	3.84 (dd, *J* = 1.4, 3.5)

[a]Reference 9f.
[b]Reference 3.
[c]This work.
[d]Reference 12.



30

H6, H7, and H8 in compound **30** have the same relative configurations of 6*S*, 7*R*, and 8*S* and similar coupling constants of $J_{H6–H7}$ = 9.6 Hz and $J_{H7–H8}$ = 3.5 Hz.

Experimental[3]

The assignment of the peaks for some ^{1}H and ^{13}C NMR spectra were complicated because of the geometric isomers produced by the Cbz group in compounds **16**, **18**, **19**, **20**, **21**, **13**, **22**, and **24**.

Ethyl *N*-(2-ethoxycarbonylethyl)-glycinate (15)

To a solution of freshly prepared ethyl glycinate (10.2 g, 98.4 mmol: from ethyl glycinate hydrochloride neutralized with 10 M NaOH: pH 9.5 and extracted with chloroform) in dry benzene (10 mL) was added ethyl 3-bromopropionate (**14**. 6.3 mL, 0.5 equiv.) in benzene (5 mL). A white solid formed immediately upon addition. The suspension was heated at 60°C for 5 h and poured into saturated aqueous sodium carbonate solution. The aqueous phase was extracted with chloroform (3×) and the combined organic extracts were dried ($MgSO_4$) and evaporated. The residue was distilled (95°C, 0.25 mm Hg) to yield **15** as a colorless oil (6.3 g, 63%). IR (neat): 3348, 2985, 1721, and 1121 cm^{-1}. ^{1}H NMR ($CDCl_3$): 4.05 (q, 2H, *J* = 7.2), 4.01 (q, 2H, *J* = 7.2), 3.27 (s, 2H), 2.76 (t, 2H, *J* = 6.6), 2.36 (t, 2H, *J* = 6.6), 1.72 (s, 1H), 1.14 (t, 3H, *J* = 7.2), 1.12 (t, 3H, *J* = 7.2). ^{13}C NMR ($CDCl_3$): 172.8, 172.6, 61.1, 60.8, 51.2, 45.1, 35.2, 14.6. MS: 204 (5), 203 (7), 174 (2), 158 (4), 130 (100), 116 (49), 84 (76), 56 (14), 42 (38).

Ethyl *N*-benzoxycarbonyl-*N*-(2-ethoxycarbonylethyl)-glycinate (16)

To a solution of **15** (3.88 g, 20.2 mmol) in dry acetonitrile (40 mL) at 0°C, under argon, was added slowly benzyl chloroformate (3.17 mL, 1.1 equiv.). The solution was stirred at 0°C for 1 h after which it was poured into water (50 mL). The phases were separated and the aqueous layer was extracted with methylene chloride (3×). The combined organic extracts were washed with 5% HCl, water, brine, and dried ($MgSO_4$). Evaporation of the solvents was followed by distillation (198°C, 0.25 mm Hg) to afford **16** as a colorless oil (5.4 g, 80%). IR (neat): 2978, 1722, and 1693 cm^{-1}. ^{1}H NMR ($CDCl_3$): 7.40–7.18 (m, 5H), 5.13 + 5.07 (2s, 2H), 4.14 + 4.11 (2q, 2H, *J* = 7.1), 4.06 (2q, 2H, *J* = 7.1), 3.59 + 3.58 (2t, 2H, *J* = 6.4), 2.64 + 2.58 (2t, 2H, *J* = 6.4), 1.22 + 1.15 (2t, 3H, *J* = 7.1), 1.21 + 1.20 (2t, 3H, *J* = 7.1). ^{13}C NMR ($CDCl_3$): 172.7 + 172.4, 170.4 + 170.3, 156.7 + 156.2, 136.8, 129.0 + 128.9, 128.5 + 128.4, 128.3 + 128.2, 68.0 + 67.8, 61.6, 61.1 + 61.0, 50.9, 45.8 + 45.0, 34.6 + 34.0, 14.6. MS: 337 (4), 229 (2), 264 (2), 220 (12), 202 (28), 91 (100).

Ethyl *N*-benzoxycarbonyl-3-oxopyrrolidine-2-carboxylate (18)

To a suspension of potassium *t*-butoxide (2.52 g, 1.4 eq) in dry toluene (54 mL) at 0°C, under argon, was added **16** (5.41 g, 16.0 mmol) in toluene (10 mL) over a period of 10 min. The suspension was stirred at 0°C for 30 min after which 2 mL of glacial acetic acid were added, immediately followed by a solution of sodium dihydrogen phosphate hydrate (9.1 g) in water (91 mL). The heterogeneous mixture was extracted with chloroform (3×), and the combined organic extracts were dried ($MgSO_4$) and concentrated. The residue was dissolved in cold toluene (100 mL) and washed with cold, pH 9.5 carbonate buffer (3×). The toluene solution was washed with water, dried ($MgSO_4$), and concentrated. The residue was distilled (Kugelrohr: oven temperature 160°C, 0.03 mm Hg) and the distillate was purified by flash chromatography over silica gel with hexanes:ethyl acetate (2:1) as eluent. Compound **18** was obtained as a colorless oil (slightly contaminated with compound **17**). IR (neat): 2978, 1741, 1712, and 1695 cm^{-1}. ^{1}H NMR ($CDCl_3$): 7.41–7.23 (m, 5H), 5.22 + 5.15 and 5.20 + 5.07 (2 AB, 2H, *J* = 8.2), 4.58 + 4.54 (2s, 1H), 4.24 (q, 2H, *J* = 4.7), 4.08 (m, 1H), 3.96 (m, 1H), 3.85 (m, 1H), 2.67 (t, 2H, *J* = 4.9), 1.28 + 1.14 (2t, 3H, *J* = 4.7). ^{13}C NMR ($CDCl_3$): 204.6, 166.4, 154.9, 136.6 + 136.4, 128.9, 128.7,

[3]For general experimental conditions, see reference 11.

© 2000 NRC Canada

128.5 + 128.4, 68.03, 65.9 + 65.8, 62.8, 42.6, 37.3 + 36.7, 14.5 + 14.4. MS: 292 (100), 248 (80), 176 (32), 158 (23).

Ethyl (2*R*,3*S*)-*N*-benzoxycarbonyl-3-hydroxypyrrolidine-2-carboxylate (19)

To a solution of sucrose (300 mg) in distilled water (4.1 mL) was added baker's yeast (200 mg). The flask was equipped with a bubble counter and the suspension was heated at 32°C for 1 h. The content of the flask was then poured into a 15 mL flask containing the keto ester **18** (0.12 g, 0.42 mmol). Stirring was continued for 24 h after which additional sucrose (300 mg) in warm (40°C) distilled water (1 mL) was added. After 48 h, celite (500 mg) was added to the mixture and the suspension was filtered through a sintered glass funnel (medium porosity). After the filtrate was washed with water, the aqueous layer was extracted with ether (3×) and the combined organic extracts were dried ($MgSO_4$). After filtration, the solvent was evaporated and the residue was purified by flash chromatography (silica gel, 3:7 hexanes:ethyl acetate) to give the optically active compound **19** (55 mg, 45%). $[\alpha]_D^{20}$ = +22.8° (*c*: 2.7 in CH_2Cl_2); lit. $[\alpha]_D^{20}$ = +21.9° (*c*: 2.0 in CH_2Cl_2)(15). IR (neat): 3378, 2978, 1741, 1701 cm^{-1}. ^1H NMR ($CDCl_3$): 7.40–7.22 (m, 5H), (5.13 + 5.00) + 5.11 (1 AB and 1s, 2H, J_{AB} = 12.5), 4.56 (q, 1H, *J* = 6.4), 4.39 (t, 1H, *J* = 6.4), 4.19–4.06 (m, 2H), 3.66 (m, 1H), 3.49 (m, 1H), 2.02 (m, 1H), 1.23 + 1.11 (2t, 3H, *J* = 7.1). ^{13}C NMR ($CDCl_3$): 170.7 + 170.5, 155.4 + 154.9, 136.9 + 136.8, 128.9 + 128.8, 128.5, 128.4 + 128.2, 72.7 + 71.8, 67.6, 64.4 + 64.1, 61.8 + 61.7, 44.9 + 44.7, 33.2 + 32.4, 14.6 + 14.5. Exact mass calcd. for $C_{15}H_{19}NO_5$ ($M^{\cdot+}$ + H): 294.1342, found: 284.1341.

Racemic **19** was prepared by the reduction of **18** with sodium borohydride. To a solution of **18** (0.29 g, 0.72 mmol) in absolute ethanol (3.6 mL) at 0°C, under argon, was added sodium borohydride (29.8 mg, 1.1 equiv.). The solution was stirred at 0°C for 60 min after which a few drops of acetic acid were added. The solution was poured in saturated aqueous sodium bicarbonate and the aqueous layer was extracted with ether (3×). The combined organic extracts were washed with brine and dried ($MgSO_4$). After fitration, the solvents were evaporated and the residue was purified by flash chromatography to give racemic **19** (0.14 g, 66%), identical in all spectroscopic aspects with those of (+)-**19**.

Ethyl (2*R*,3*S*)-*N*-benzoxycarbonyl-3-methoxymethyloxypyrrolidine-2-carboxylate (20)

To a solution of the alcohol (+)-19 (0.14 g, 0.48 mmol) in methylene chloride (4.8 mL) at 0°C, under argon, was successively added diisopropylethylamine (0.25 mL, 3 equiv.) and chloromethyl methyl ether (0.11 mL, 3 equiv.). The solution was stirred at rt for 24 h after which it was poured into 5% HCl. The aqueous phase was extracted with methylene chloride (3×) and the combined organic extracts were washed with saturated aqueous sodium bicarbonate and dried ($MgSO_4$). After evaporation of the solvent, the residue was purified by flash chromatography on silica gel with 1:1 hexanes:ethyl acetate as eluent to give compound **20** as a colorless oil (0.15 g, 92%). $[\alpha]_D^{20}$ = –18.4° (*c*: 1.1 in $CHCl_3$). IR (neat) : 2957, 1746, 1701 cm^{-1}. ^1H NMR ($CDCl_3$): 7.42–7.20 (m, 5H), (5.14 + 5.02) + 5.11 (AB + s, 2H, J_{AB} = 12.2), (4.68 + 4.60) + (4.66 + 4.58) (2 AB, 2H, *J* = 6.9), 4.21–4.07 (2q, 2H, *J* = 7.1), 3.70 (m, 1H), 3.49 (m. 1H), 3.34 + 3.33 (2s, 3H), 2.10 (m, 2H), 1.25 + 1.14 (2t, 3H, *J* = 7.1). ^{13}C NMR ($CDCl_3$): 170.0 + 169.9, 155.2 + 154.8, 136.9, 128.9 + 128.8, 128.5 + 128.4, 128.2, 96.1, 76.7 + 76.0, 67.6, 62.6 + 62.3, 61.5 + 61.4, 56.2, 44.8 + 44.6, 31.0 + 30.2, 14.7 + 14.6. Exact mass calcd. for $C_{17}H_{23}NO_6$ ($M^{\cdot+}$ + H): 338.1605, found: 338.1604.

(2*S*,3*S*)-*N*-Benzoxycarbonyl-2-hydroxymethyl-3-methoxymethyloxypyrrolidine (21)

To a solution of the ester **20** (0.84 g, 2.48 mmol) in ether (25 mL) at 0°C, under argon, was added lithium borohydride (0.12 g, 2.2 eq) and the suspension was stirred at 0° for 4 h. Acetic acid (1 mL) was then added to destroy the excess hydride and the solution was poured in saturated aqueous sodium bicarbonate solution. The phases were separated and the aqueous phase was extracted with ether (2×). The combined organic phase was washed with brine and dried ($MgSO_4$). Filtration and evaporation of the solvent was followed by flash chromatography (silica gel, 4:6 hexanes:ethyl acetate) of the residue to give alcohol **21** as a colorless oil (0.53 g, 72%). $[\alpha]_D^{20}$ = +44.7° (*c*: 1.1 in $CHCl_3$). IR (neat): 3450, 2948, 2888, 1704 cm^{-1}. ^1H NMR ($CDCl_3$): 7.40–7.22 (m, 5H), 5.12 (s, 2H), 4.71–4.58 (m, 2H), 4.32 (q, 1H, *J* = 5.3), 3.96 (m. 1H), 3.89–3.75 (m, 2H), 3.51 (t, 2H, *J* = 6.8), 3.36 (s, 3H), 3.27 (bs, 1H), 1.98 (t, 2H, *J* = 6.8). ^{13}C NMR ($CDCl_3$): 156.9, 136.9, 129.0, 128.6, 128.4, 96.2, 77.8, 67.7, 63.4, 63.2, 56.3, 45.1, 30.6. Exact mass calcd. for $C_{15}H_{21}NO_5$ ($M^{\cdot+}$ + H): 296.1499, found: 296.1498.

(2*R*,3*S*)-*N*-Benzoxycarbonyl-3-methoxymethyloxypyrrolidine-2-carboxaldehyde (13)

Dimethyl sulfoxide (49.3 µl, 2.84 equiv.) was slowly added to a solution of oxalyl chloride (30.1 µl, 1.41 equiv.) in methylene chloride (2 mL) under argon at –78°C. The colorless solution was stirred for 15 min after which a solution of the alcohol **21** (72.2 mg, 0.24 mmol) in methylene chloride (1 mL) was added dropwise over a period of 5 min. A white precipitate was formed and the suspension was stirred for 1 h. Triethylamine (0.17 mL, 5 equiv.) in methylene chloride was added and the solution was allowed to slowly warm to room temperature. The mixture was diluted with methylene chloride (10 mL) and washed successively with 5% HCl, water, brine, and dried ($MgSO_4$). Evaporation of the solvent under vacuum gave a pale brown oil which was purified by flash chromatography (silica gel, 1:1 hexanes:ethyl acetate) to give the aldehyde **13** as a pale yellow oil (70.0 mg, 98%). $[\alpha]_D^{20}$ = +70.4° (*c*: 1.1 in $CHCl_3$). IR (neat): 2958, 2888, 1736, 1701 cm^{-1}. ^1H NMR ($CDCl_3$): 9.53 + 9.44 (2d, 1H, *J* = 2.5), 7.42–7.21 (m, 5H), 5.14 + 5.09 (2s, 2H), 4.72–4.51 (m, 3H), 4.27 + 4.21 (2dd, 1H, *J* = 2.5, 5.7), 2.75–3.60 (m, 2H), 3.29 (s, 3H), 2.16–1.80 (m, 2H). ^{13}C NMR ($CDCl_3$): 200.2 + 200.1, 155.7 + 154.8, 136.8 + 136.6, 129.0, 128.6, 128.5 + 128.4, 95.8, 79.4 + 78.3, 68.4 + 68.0, 67.8, 56.3, 45.7 + 45.1, 31.5 + 30.9. Exact mass calcd. for $C_{15}H_{19}NO_5$ ($M^{\cdot+}$ + H): 294.1342, found: 294.1341.

(2*R*,3*S*,1′*S*,2′*S*)-*N*-Benzoxycarbonyl-2-(1′-hydroxy-2′thiophenyl-3′-butenyl)-3-methoxymethyloxypyrrolidine (22)

To a solution of allyl phenyl sulfide (0.35 g, 15 equiv.) in dry THF (10.5 mL) at –78°C, under argon, was added

© 2000 NRC Canada

n-butyllithium (2.0 M in pentane, 1.16 mL, 1.5 equiv.) and the solution was stirred at 0°C for 30 min. It was then brought back to –78°C and titanium (IV) isopropoxide (0.69 mL, 1.5 equiv.) was added slowly. After 10 min, aldehyde **13** (0.45 g, 1.55 mmol) in THF (5 mL) was added over a period of 10 min. The solution was stirred for 10 min and warmed up at 0°C for 30 min. It was then poured into 5% HCl and extracted with ether (3×). The combined organic extracts were washed with brine, dried ($MgSO_4$), and filtered. Evaporation of the solvent followed by flash chromatography (silica gel, 1:1 hexanes:ethyl acetate) gave the product **22** as a colorless oil (0.49 g, 72%). $[\alpha]_D^{20}$ = +50.2° (*c*: 1.1 in $CHCl_3$). IR (neat): 3424, 2948, 2893, 1693 cm^{-1}. ^1H NMR ($CDCl_3$): 7.54–7.09 (m, 10H), 6.06 (m, 1H), 5.12 (s, 2H), 5.06 (d, 1H, *J* = 10.7), 4.90 (d, 1H, *J* = 17.2), 4.63 (s, 2H), 4.60 (m, 1H), 4.26 (q, 1H, *J* = 6.0), 4.14 (bs, 1H), 3.95 (d, 1H, *J* = 9.6), 3.66–3.42 (m, 2H), 3.33 (s, 3H), 2.15–1.84 (m, 2H). ^{13}C NMR ($CDCl_3$): 158.2, 136.7, 134.9, 133.4, 129.1, 128.7, 128.6, 127.6, 126.0, 118.5, 96.4, 77.1, 72.8, 68.0, 63.1, 56.8, 56.5, 45.3, 30.8. Exact mass calcd. for $C_{24}H_{29}NO_5S$ ($M^{\cdot+}$ + H): 444.1846, found: 444.1845.

(2*R*,3*S*,1′*R*)-*N*-Benzoxycarbonyl-2-(1′,4′-dihydroxy-2′-butenyl)-3-methoxymethyloxypyrrolidine (24)

To a solution of the hydroxysulfide **22** (0.49 g, 1.11 mmol) in methylene chloride (11.1 mL) at 0°C under argon was added *m*-chloroperoxybenzoic acid (0.27 g, 1.4 equiv.) and the solution was stirred for 60 min. It was then dissolved in ether, washed with saturated aqueous sodium bicarbonate solution (2×), dried ($MgSO_4$), filtered, and the solvent was evaporated. The residue was dissolved in dry methanol (11.1 mL) and trimethyl phosphite (0.65 mL, 5 equiv.) was added slowly. After 2 h of stirring at 60°C, the methanol was evaporated and the thick residual oil was purified by flash chromatography (silica gel, 2:8 hexanes:ethyl acetate, then ethyl acetate as eluents) to give the allylic alcohol **24** (0.28 g, 71%). $[\alpha]_D^{20}$ = +31.2° (*c*: 1.5 in $CHCl_3$). IR (neat): 3450, 2948, 2888, 1704, 1671 cm^{-1}. ^1H NMR ($CDCl_3$): 7.42–7.21 (m, 5H), 5.96–5.70 (m, 2H), 5.12 (s, 2H), 4.67 (s, 2H), 4.51 (m, 1H), 4.29 (m, 1H), 4.21–3.88 (m. 3H), 3.62–3.43 (m, 2H), 3.37 (s, 3H), 3.29 (m, 1H), 3.16 (bs, 1H), 2.20–1.91 (m, 2H). ^{13}C NMR ($CDCl_3$): 157.3, 136.9, 131.8, 131.0, 129.0, 128.6, 128.4, 97.0, 78.2, 72.1, 67.8, 63.2, 56.4, 45.5, 30.9. Exact mass calcd. for $C_{18}H_{25}NO_6$ ($M^{\cdot+}$ + H): 352.1761, found: 352.1760.

(2*R*,3*S*,1′*R*)-1,1′-*N*,*O*-Carbonyl-2-(1′,4′-dihydroxy-2′-butenyl)-3-methoxymethyloxypyrridine (25)

To a solution of the allylic diol **24** (0.21 g, 0.61 mmol) in 2-propanol:water (2:1, 6.1 mL) was added finely powdered potassium carbonate (0.17 g, 2 equiv.) and the solution was heated at 65°C for 15 h. The solvent was evaporated and the residue purified by flash chromatography (silica gel, ethyl acetate) to give the product **25** as a colorless oil (0.11 g, 77%). $[\alpha]_D^{20}$ = +99.6° (*c*: 1.1 in $CHCl_3$). IR (neat): 3436, 2946, 2895, 1751, 1674 cm^{-1}. ^1H NMR ($CDCl_3$): 5.96 (dt, 1H, *J* = 4.0, 15.5), 5.83 (dd, 1H, *J* = 6.5, 15.5), 5.04 (dd, 1H, *J* = 3.6, 6.5), 4.63 (AB, 2H, *J* = 7.0), 4.13 (d, 2H, *J* = 4.0), 4.08 (td, 1H, *J* = 0.9, 3.6), 3.62 (t, 1H, *J* = 3.6), 3.54 (ddd, 1H, *J* = 7.8, 9.5, 10.8), 3.32 (s, 3H), 3.19 (ddd, 1H, *J* = 2.1, 9.6, 10.8), 2.83 (bs, 1H), 2.25 (dddd, 1H, *J* = 0.9, 2.1, 7.8, 14.1), 1.92 (dddd, 1H, *J* = 3.6, 9.5, 9.6, 14.1). ^{13}C NMR ($CDCl_3$): 162.2, 134.5, 127.6, 95.5, 75.5, 75.4, 69.4, 62.3, 56.3, 44.2, 32.6. Exact mass calcd. for $C_{11}H_{17}NO_5$ ($M^{\cdot+}$ + H): 244.1186, found: 244.1185.

(2*R*,3*S*,1′*R*)-1,1′-*N*,*O*-Carbonyl-2-(1′hydroxy-4′-chloro-2′-butenyl)-3-methoxymethyloxypyrrolidine (26)

To a solution of the allylic alcohol **25** (0.11 g, 0.47 mmol) in a mixture of carbon tetrachloride:methylene chloride (4:1, 6.0 mL) were added successively finely powdered potassium carbonate (0.13 g, 2 equiv.) and triphenylphosphine (0.31 g, 2.5 equiv.) and the solution was stirred at 60°C for 8 h. The solvent was evaporated and the residue was purified by flash chromatography (silica gel, 2:8 hexanes:ethyl acetate) affording the chloride **26** (83.9 mg, 70%) as a pale yellow oil. $[\alpha]_D^{20}$ = +87.7° (*c*: 1.5 in $CHCl_3$). IR (neat): 2965, 2895, 1751 cm^{-1}. ^1H NMR ($CDCl_3$): 6.06–5.84 (m, 2H), 5.06 (dd, 1H, *J* = 3.6, 5.1), 4.65 (AB, 2H, *J* = 7.0), 4.11 (td, 1H, *J* = 1.1, 3.6), 4.05 (d, 2H, *J* = 6.2), 3.62 (t, 1H, *J* = 3.6), 3.58 (ddd, 1H, *J* = 7.9, 9.5, 11.0), 3.33 (s, 3H), 3.22 (ddd, 1H, *J* = 2.2, 9.7, 11.0), 2.28 (dddd, 1H, *J* = 1.1, 2.2, 7.9, 14.1), 1.93 (dddd, 1H, *J* = 3.6, 9.5, 9.7, 14.1). ^{13}C NMR ($CDCl_3$): 161.8, 131.7, 129.9, 95.5, 75.6, 74.4, 69.1, 56.4, 44.3, 43.9, 32.5. Exact mass calcd. for $C_{11}H_{16}NO_4Cl$ ($M^{\cdot+}$ + H): 262.0847, found: 262.0846.

(2*R*,3*S*,1′*S*,2′*S*,3′*R*)- and (2*R*,3*S*,1′*S*,2′*R*,3′*R*)-1,1′-*N*,*O*-Carbonyl-2-(1′,2′,3′-trihydroxy-4′-chlorobutanyl)-3methoxymethyloxypyrrolidine (27a and 27b)

To a solution of the chloride **26** (83.9 mg, 0.32 mmol) in a mixture of acetone:water:*t*-butanol (6:3:1, 2.0 mL) were added successively *N*-methylmorpholine-*N*-oxide (45.1 mg, 1.2 equiv.) and osmium tetroxide (15.0 mg, 0.05 equiv.). The orange solution was stirred at room temperature for 3 h, after which 2 mL of a solution-suspension of magnesium silicate and sodium hydrosulfite (1.2 g and 0.1 g respectively in 8 mL of water) was added. The slurry was filtered through celite and the cake was rinsed with acetone. The solvents were evaporated and the dark residual oil was purified by flash chromatography (silica gel, ethyl acetate) to provide a mixture of the products **27a** and **27b** (2:1 by NMR, 94.8 mg, 99%). IR (neat): 3335, 2952, 1751 cm^{-1}. ^1H NMR ($CDCl_3$): 4.83–4.59 (m, 3H), 4.09 (m, 2H), 3.95 (m, 1H), 3.86 (m, 1H), 3.77–3.46 (m, 5H), 3.32 (s, 3H), 3.27 (m, 1H), 2.29 (m, 1H), 2.01 (m, 1H). ^{13}C NMR ($CDCl_3$): **27a**: 162.1, 95.7, 76.1, 75.5, 71.1, 70.8, 66.1, 56.3, 45.8, 44.0, 33.0; **27b**: 162.0, 95.5, 76.4, 75.3, 72.1, 71.6, 66.0, 56.3, 45.8, 44.0, 32.8. Exact mass calcd. for $C_{11}H_{18}NO_6Cl$ ($M^{\cdot+}$ + H): 296.0902, found: 296.0901.

(2*R*,3*S*,1′*S*,2′*S*,3′*R*)- and (2*R*,3*S*,1′*S*,2′*R*,3′*S*)-1,1′-*N*,*O*-Carbonyl-2-(1′hydroxy-2′,3′-*O*-isopropylidene-4′-chlorobutanyl)-3-methoxymethyloxypyrrolidine (28a and 28b)

To a solution of the diol mixture **27a** and **27b** (94.8 mg, 0.32 mmol) in dry acetone (3.2 mL) at room temperature under argon were added 2,2-dimethoxypropane (0.20 mL, 5 equiv.) and camphorsulfonic acid (5.2 mg, 0.05 equiv.). The solution was stirred for 15 h at room temperature and heated at 40°C for 1 h after which a few drops of conc. ammonium hydroxide were added. The solvent was evaporated and the residue was taken up in ethyl acetate. The organic solution

© 2000 NRC Canada

was washed with brine and dried ($MgSO_4$). Evaporation of the solvent followed by flash chromatography (silica gel, 6:4 hexanes:ethyl acetate) purification gave **28a** (51.0 mg, 48%) and **28b** (31.7 mg, 29%) separately, for a combined yield of 77%. Compound **28a** (white solids): mp 74–76°C. $[\alpha]_D^{20}$ = +50.8° (*c*: 1.0 in $CHCl_3$). IR ($CHCl_3$): 2980, 1751 cm^{-1}. ^1H NMR ($CDCl_3$): 4.70 + 4.62 (AB, 2H, *J* = 7.0), 4.60 (dd, 1H, *J* = 3.2, 8.3), 4.21 (ddd, 1H, *J* = 3.8, 5.2, 7.0), 4.13 (td, 1H, *J* = 0.9, 3.2), 4.05 (dd, 1H, *J* = 7.0, 8.3), 3.88 (t, 1H, *J* = 3.2), 3.80 (dd, 1H, *J* = 3.8, 11.8), 3.65 (dd, 1H, *J* = 5.2, 11.8), 3.59 (ddd, 1H, *J* = 7.8, 9.5, 10.8), 3.34 (s, 3H), 3.26 (ddd, 1H, *J* = 2.1, 9.8, 10.8), 2.32 (dddd, 1H, *J* = 0.9, 2.1, 7.8, 14.1), 1.98 (dddd, 1H, *J* = 3.2, 9.5, 9.8, 14.1), 1.44 (s, 3H), 1.40 (s, 3H). ^{13}C NMR ($CDCl_3$): 162.0, 112.1, 96.3, 80.8, 79.4, 76.5, 76.4, 67.7, 57.2, 45.7, 45.1, 33.5, 28.6, 28.4. Exact mass calcd. for $C_{14}H_{22}NO_6Cl$ ($M^{\cdot+}$ + H): 336.1215, found: 336.1214.

Compound **28b** (white solids): mp 153–155°C. $[\alpha]_D^{20}$ = +66.1° (*c*: 1.6 in $CHCl_3$). IR ($CHCl_3$): 2997, 1751 cm^{-1}. ^1H NMR ($CDCl_3$): 4.77 (dd, 1H, *J* = 1.8, 3.4), 4.71 + 4.63 (AB, 2H, *J* = 7.0), 4.40 (ddd, 1H, *J* = 4.4, 6.6, 7.5), 4.11 (td, 1H, *J* = 0.9, 3.4), 4.08 (dd, 1H, *J* = 1.8, 7.5), 3.91 (t, 1H, *J* = 3.4), 3.73 (dd, 1H, *J* = 4.4, 11.4), 3.62 (dd, 1H, *J* = 6.6, 11.4), 3.40 (ddd, 1H, *J* = 8.0, 9.5, 10.9), 3.34 (s, 3H), 3.31 (ddd, 1H, *J* = 2.1, 9.8, 10.9), 2.32 (dddd, 1H, *J* = 0.9, 2.1, 8.0, 14.3), 1.97 (dddd, 1H, *J* = 3.4, 9.5, 9.8, 14.3), 1.43 (s, 6H). ^{13}C NMR ($CDCl_3$): 171.1, 112.1, 96.4, 81.8, 76.7, 76.5, 74.1, 67.1, 57.3, 45.4, 45.3, 33.5, 28.6, 27.9. Exact mass calcd. for $C_{14}H_{22}NO_6Cl$ ($M^{\cdot+}$ + H): 336.1215, found: 336.1214.

(1*S*,6*S*,7*R*,8*S*,8a*R*)-1-Methoxymethyloxy-6,7-*O*-isopropylidene-8-hydroxyindolizidine (29a)

To a solution of the chloride **28a** (51.0 mg, 0.15 mmol) in a mixture of methanol:water (1:1, 2 mL) was added sodium hydroxide (18.3 mg, 3 equiv.) and the solution was stirred at 85°C for 18 h. The solvents were evaporated and the solid residue was extracted with chloroform. The chloroform solution was evaporated to give the aminoalcohol **29a** as a waxy solid (41.0 mg, 98%). $[\alpha]_D^{20}$ = +50.6° (*c*: 0.83 in $CHCl_3$). IR ($CHCl_3$): 3450, 2986 cm^{-1}. ^1H NMR ($CDCl_3$): 4.67 + 4.59 (AB, 2H, *J* = 7.1), 4.54 (bs, 1H), 4.46 (m, 1H), 4.35 (td, 1H, *J* = 4.2, 10.2), 3.49 (dd, 1H, *J* = 4.2, 9.3), 3.36 (s, 3H), 3.33 (m, 1H), 3.19 (t, 1H, *J* = 8.4), 2.25–2.12 (m, 4H), 1.95 (m, 1H), 1.46 (s, 3H), 1.42 (s, 3H). ^{13}C NMR ($CDCl_3$): 111.5, 95.1, 83.2, 77.9, 77.7, 71.3, 68.4, 66.4, 54.0, 51.7, 32.5, 27.4, 27.1. Exact mass calcd. for $C_{13}H_{23}NO_5$ ($M^{\cdot+}$ + H): 274.1655, found: 274.1654.

(1*S*,6*S*,7*R*,8*S*,8a*R*)-1,6,7,8,-Tetrahydroxyindolidine (8-*epi*-castanospermine, 11)

A solution of compound **29a** (41.0 mg, 0.15 mmol) in a 4:4:2 mixture of 6 M HCl:water:tetrahydrofuran was stirred for 15 h after which the solvents were evaporated. The residue was dissolved in methanol and stirred for 1 h with Amberlyst A-26 ion exchange resin (OH^- form). Filtration followed by evaporation of the methanol gave a brownish solid which was purified by flash chromatography (silica gel, 70:20:5:5 chloroform:methanol:water:NH_4OH; spray reagent: $KMnO_4$–NaOH in water) affording the tetraol **11** as an off white solid in quantitative yield (28.4 mg). It had a melting point of 190–192°C. $[\alpha]_D^{20}$ = +44.4° (*c*: 1.3 in H_2O). IR (KBr): 3450 cm^{-1}. ^1H NMR (D_2O): 4.07 (ddd, 1H, *J* = 2.1, 4.5, 6.5), 3.89 (dd, 1H, *J* = 1.2, 3.0), 3.43 (ddd, 1H, *J* = 5.5, 9.5, 11.2), 3.09 (ddd, 1H, *J* = 4.4, 9.0, 10.0), 3.07 (dd, 1H, *J* = 5.5, 11.2), 2.96 (dd, 1H, *J* = 3.0, 9.5), 2.70 (d, 1H, *J* = 4.5), 2.45 (ddd, 1H, *J* = 7.9, 10.0, 10.1), 2.23 (t, 1H, *J* = 11.2), 1.87 (dddd, 1H, *J* = 4.4, 6.5, 10.1, 14.3), 1.31 (dddd, 1H, *J* = 2.1, 7.9, 9.0, 14.3). ^{13}C NMR (D_2O): 76.2, 73.1, 71.8, 69.8, 67.9, 56.0, 53.8, 35.4. Exact mass calcd. for $C_8H_{15}NO_4$ ($M^{\cdot+}$ + H): 190.1080, found: 190.1079.

(1*S*,6*R*,7*S*,8*R*,8a*R*)-1,5,7,8-Tetrahydroxyindolizidine (6,7,8-tri-*epi*-castanospermine, 12)

The same experimental procedures for the conversion of compound **28a** to **29a** were followed by starting with compound **28b**. The deprotection of the MOM ether group as well as the isopropylidene occurred during the cyclization. The reaction time was 36 h. The purification procedures for **11** were followed but with 70:24:3:3 chloroform:methanol:water:NH_4OH as eluent for the flash chromatography (silica gel) to give compound **12** in 65% yield. $[\alpha]_D^{20}$ = –7.3° (*c*: 1.0 in H_2O). IR (KBr): 3500 cm^{-1}. ^1H NMR (D_2O): 4.00 (ddd, 1H, *J* = 2.4, 4.8, 7.1), 3.55 (t, 1H, *J* = 4.3), 3.27 (t, 1H, *J* = 4.8), 3.14 (q, 1H, *J* = 4.2), 2.79–2.59 (m, 2H), 2.46–2.31 (m, 2H), 2.17 (m, 1H), 1.71 (dddd, 1H, *J* = 3.8, 7.1, 9.5, 14.0), 1.21 (dddd, 1H, *J* = 2.4, 8.8, 8.8, 14.0). ^{13}C NMR (D_2O): 74.5, 72.7, 72.6, 71.2, 68.07, 56.9, 55.0, 34.7. Exact mass calcd. for $C_8H_{15}NO_4$ ($M^{\cdot+}$ + H): 190.1080, found: 190.1079.

Acknowledgements

We thank NSERC of Canada for financial support of this research. THC acknowledges the Department of Applied Biology and Chemical Technology, Hong Kong Polytechnic University for their hospitality during his sabbatic leave.

References

1. (*a*) L.D. Hobenschutz, E.A. Bell, P.J. Jewess, D.P. Leworthy, R.J. Pryce, E. Arnold, and J. Clardy. Phytochemistry, **20**, 811 (1981); (*b*) J.P. Michael. Nat. Prod. Rep. **7(6)**, 485 (1990).
2. (*a*) R. Saul, J.P. Chambers, R.J. Molyneux, and A.D. Elbein. Arch. Biochem. Biophys. **221**, 593 (1983); (*b*) R. Saul, R.J. Molyneux, and A.D. Elbein. Arch. Biochem. Biophys. **230**, 668 (1984).
3. Y.T. Pan, H. Hori, R. Saul, B.A. Sanford, R.J. Molyneux, and A.D. Elbein. Biochemistry,, **22**, 3975 (1983).
4. A.D. Elbein. Crit. Rev. Biochem. **16**, 21 (1984).
5. (*a*) M.J. Humphries, K. Matsumoto, S.L. White, and K. Olden. Cancer Res. **46**, 5215 (1986); (*b*) J.W. Dennis. Cancer Res. **46**, 5131 (1986).
6. B.D. Walker, M. Kowalski, W.C. Goh, K. Kozarsky, M. Krieger, C. Rosen, L. Rohrschneider, W.A. Haseltine, and J. Sodroski. Proc. Natl. Acad. Sci. U.S.A. **262**, 7575 (1987).
7. R.J. Molyneux, J.N. Roitman, G. Dunnheim, T. Szumilo, and A.D. Elbein. Arch. Biochem. Biophys. **251**, 450 (1986).
8. R.J. Molyneux, Y.T. Pan, J.E. Tropea, M. Benson, G.P. Kaushal, and A.D. Elbein. Biochemistry, **30**, 9981 (1991).
9. (*a*) S.A. Miller and A.R. Chemberlain. J. Am. Chem. Soc. **112**, 8100 (1990); (*b*) R. Bhide, R. Mortezaei, A. Scilimatii, and C.J. Sih. Tetrahedron Lett. **31**, 4827 (1990); (*c*) J.L. Reymond,

© 2000 NRC Canada

and P. Vogel. Tetrahedron Lett. **30**, 705 (1989); (*d*) J.L. Reymond, A.A. Pinketon, and P. Vogel. J. Org. Chem. **56**, 2128 (1991); (*e*) Y. Chen and P. Vogel. J. Org. Chem. **59**, 2487 (1994); (*f*) G. Casiraghi, F. Zanardi, G. Rassu, and P. Spanu. Chem. Rev. **95**, 1677 (1995); (*g*) N.-S. Kim, J.-R. Choi, and J.K. Cha. J. Org. Chem. **58**, 7096 (1993); (*h*) H. Zhao and D.R. Mootoo. J. Org. Chem. **61**, 6762 (1996); (*i*) S.E. Denmark and E.A. Martinborough. J. Am. Chem. Soc. **121**, 3046 (1999).

10. (*a*) G.W.J. Fleet, N.G. Ramsden, R.J. Molyneux, and G.S. Jacob. Tetrahedron Lett. **29**, 3603 (1988); (*b*) M. Gerspacher and H. Rapoport. J. Org. Chem. **56**, 3700 (1991); (*c*) J. Mulzer and H. Dehmlow. J. Org. Chem. **57**, 3194 (1992); (*d*) K. Burgess, D.A. Chaplin, and I. Henderson. J. Org. Chem. **57**, 1103 (1992); (*e*) H. Ina and C. Kibayashi. J. Org. Chem. **58**, 52 (1993).
11. Y. St-Denis and T.H. Chan. J. Org. Chem. **57**, 3078 (1992).
12. S.F. Martin, H.-J. Chen, and V.M. Lynch. J. Org. Chem. **60**, 276 (1995).
13. Taken in part from the Ph. D. thesis of Y. St-Denis, McGill University.
14. M.P. Sibi and J.W. Christensen. Tetrahedron Lett. **31**, 5692 (1990).
15. J. Blake, C.D. Wilson, and H. Rapoport. J. Am. Chem. Soc. **86**, 5293 (1964).
16. P.D. Feil and J.R. Vercellotti. Carbohydr. Res. 311 (1973).
17. (*a*) Y. Ikeda, K. Furuta, N. Meguriya, N. Ikeda, and H. Yamamoto. J. Am. Chem. Soc. **104**, 7663 (1982); (*b*) Y. Ikeda, K. Furuta, N. Meguriya, N. Ikeda, and H. Yamamoto. Bull. Chem. Soc. Jpn. **57**, 2781 (1984).
18. D.A. Evans and G.C. Andrews. Acc. Chem. Res. **7**, 147 (1974).
19. J.B. Lee and T.J. Nolan. Can. J. Chem. **44**, 1331 (1966). For a review, see: R. Appel. Angew. Chem. Int. Engl. **14**, 801 (1975).
20. For a review on osmium tetroxide catalyzed oxidation, see: M. Schroder. Chem. Rev. **80**, 187 (1980).
21. The stereochemical outcome of the hydroxylation of a double bond which has an adjacent chiral center at the allylic position has been studied. See: J.K. Cha, W.J. Christ, and Y. Kishi. Tetrahedron Lett. **24**, 3943, 3947 (1983).
22. S.F. Martin, H.-J. Chen, and C.-P. Yang. J. Org. Chem. **58**, 2867 (1993). For stereochemical assignment of **30**, see reference 12.

© 2000 NRC Canada

Dimerization of conjugated 1-indanones

Yves Leblanc, Claude Dufresne, Rajiv Dhawan, Jason Ollerenshaw, Adam Littke, Laird A. Trimble, and Nancy N. Tsou

Abstract: Conjugated 1-indanones dimerize under basic conditions to provide spirodimers. For example when 2-(*E*)-carbomethoxymethylene-1-indanone (**5**) was treated with Cs_2CO_3 in CH_3CN, two spirodimers, **6** and **7**, were produced via two modes of reaction (mode A and mode B). With 2-(*E*)-cyanomethylene-1-indanone (**9**) only mode A dimerized spiro products (**10** and **11**) were observed whereas with 2-chloromethylidene-1-indanone (**12**) a 1,2-dimer (**13**) was obtained instead of the expected spirodimer.

Key words: dimerization, conjugated 1-indanones, spirodimers.

Résumé : Les 1-indanones dimérisent en présence d'une base pour donner des spirodimères. Par exemple, lorsqu'on traite le 2-(*E*)-carbomethoxymethylène-1-indanone (**5**) avec Cs_2CO_3 dans CH_3CN on obtient les spirodimères **6** et **7**. Ces deux dimères sont produits par deux modes de dimérisation (mode A et mode B). Dans le cas du 2-(*E*)-cyanomethylène-1-indanone (**9**) uniquement la dimérization de type A a lieu pour produire les produits spiros **10** et **11** tandis qu'avec le 2-chloromethylidène-1-indanone (**12**) comme produit de départ on obtient un dimère de type 1,2 (**13**).

Mots clés : dimérisation, 1-indanones conjugués, spirodimères.

Introduction

In a previous report we presented our study on the dimerization of 2-benzylidene-1-indanone (**1a**, Scheme 1) (1). The structure and the stereochemistry of the major spirodimer (**3a**) obtained from this reaction had initially been established by COSY, HMQC, HMBC, and NOESY NMR correlation techniques. The structure was then confirmed by X-ray crystallography (1). The stereochemistry assigned for dimer **3a** (Scheme 1) differs from previous reports (2, 3) where X-ray crystallographic analysis was not used to prove the stereochemistry. To the best of our knowledge no examples of this dimerization other than the benzylidene case (**1a**) have been published. Herein we describe new results on the dimerization of substituted benzylidene-1-indanones and other conjugated 1-indanones to assess the generality of the reaction.

Results and discussion

For the benzylidene cases, the monomers **1b** (X = SMe) and **1c** (X = SO_2Me) were chosen as substrates to verify the effect of the electronic nature of the aromatic substituents on the outcome of the reaction. The monomer **1b** was readily prepared by condensation of 1-indanone with 4-thiomethylbenzaldehyde in EtOH under acidic conditions. The monomer **1c** derives from oxidation of **1b** with Oxone® in CH_2Cl_2–MeOH. With monomers **1b** and **1c** (Table 1), the reactions proceeded smoothly to provide the corresponding dimers (Scheme 1). Moderate yields (60%) of the spirodimers were obtained with Cs_2CO_3 as the base (entry 3 and 5, Table 1). In addition, it has been observed that in the case where KHMDS was used as the base for substrate **1b,** the reaction took place very rapidly (5 min) at –78°C to provide the corresponding spirodimers **3b** and **4b** in high yields (85%) (Table 1). The relative stereochemistry of the predominant dimers (**3b** and **3c**) is the same as that observed for the unsubstituted case (**3a**). In all cases the dimerization gave, as the major product, the spirodimers with the phenyl substituents on the convex face of the molecule.

The preceding results suggest that the electronic nature of the substituents on the aromatic ring have little influence on the outcome of the reaction. Following these results, we turned our attention to other conjugated 1-indanones without a phenyl ring. With 2-(*E*)-carbomethoxy-methylene-1-indanone (**5**) as the substrate (Scheme 2), rapid dimerization (0.5 h) was observed with Cs_2CO_3 in CH_3CN (entry 1, Table 2) providing two spirodimers, **6** and **7**, in a 1:1 ratio. The KHMDS reaction conditions (entry 2, Table 2) were also applied to indanone **5** to afford dimers **6** and **7**, also in a 1:1

Received May 6, 1999. Published on the NRC Research Press website on June 9, 2000.

This manuscript is dedicated to Professor Hanessian to underline his major achievements in organic chemistry.
Ce manuscrit est dédié au Professeur Hanessian dans le but de souligner son apport à la chimie organique.

Y. Leblanc,[1] C. Dufresne, R. Dhawan, J. Ollerenshaw, A. Littke, and L.A. Trimble. Merck Frosst Centre for Therapeutic Research, P.O. Box 1005, Pointe-Claire – Dorval, QC H9R 4P8, Canada.
N.N. Tsou. Merck & Co. Inc., 126 E. Lincoln Avenue, P.O. Box 2000, Rahway, NJ 07065–0900, U.S.A.

[1]Author to whom correspondence may be addressed. Telephone: (514) 428-3096. Fax: (514) 428-4900.
e-mail: yves_leblanc@merck.com

 © 2000 NRC Canada

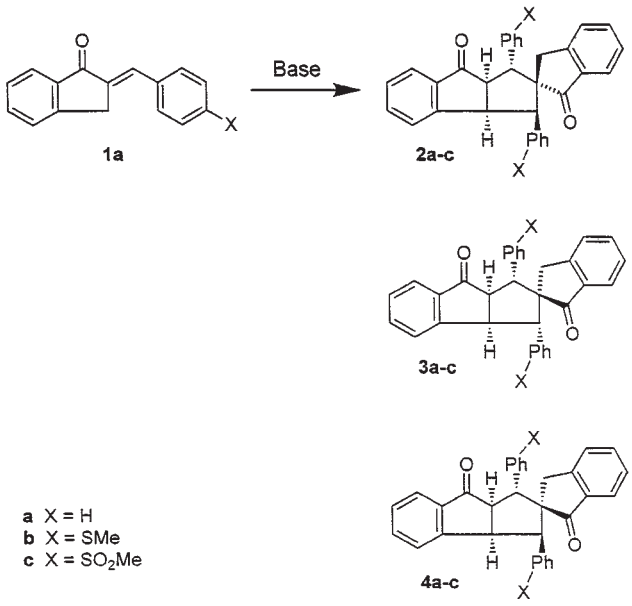
Table 1. Reaction conditions and isolated yields for the dimerization of **1a–c** to produce various spirodimers.

Entry	X	Indanone	Time	Condition	% Yield of Dimer **2**	% Yield of Dimer **3**	% Yield of Dimer **4**
1	H	**1a**	18 h	Cs_2CO_3, CH_3CN, rt	0	93	4
2	H	**1a**	5 min	KHMDS, THF, –78°C	0	81	6
3	SMe	**1b**	50 h	Cs_2CO_3, CH_3CN, rt	0	52	8
4	SMe	**1b**	5 min	KHMDS, THF, –78°C	0	80	5
5	SO_2Me	**1c**	16 h	Cs_2CO_3, CH_3CN, rt	0	57	3

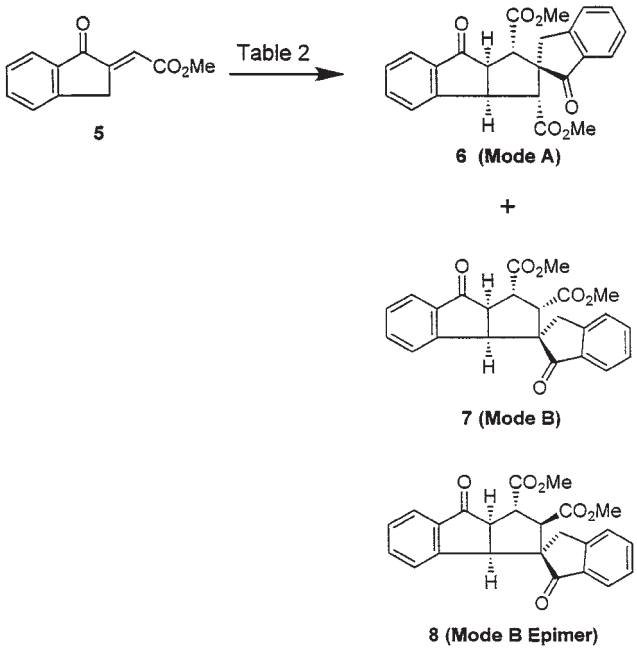
Table 2. Reaction conditions for dimerization of compound **5**.

Entry	Conditions	Yield (%)	Ratios Dimer **6**	Ratios Dimer **7**	Ratios Dimer **8**
1	Cs_2CO_3, CH_3CN, rt/30 minutes	85	1	1	—
2	KHMDS, THF, –78°C/4 minutes	80	1	1	—
3	(–)-spartine, THF, rt/18 h	83	1	2.2	—
4	DBU, THF, rt/18 h	60	3.6	2.8	1

Scheme 1.



Scheme 2.

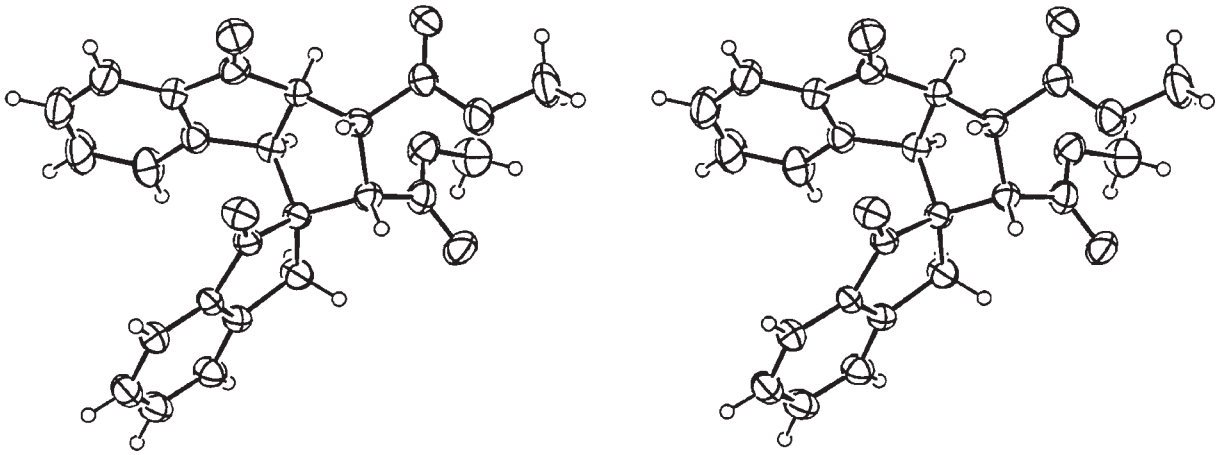


ratio. In the case where the dimerization was achieved with DBU as a base (entry 4, Table 2), a third dimer (**8**) was produced late in the reaction. This dimer is also formed from dimer **7** using DBU which suggests that compound **8** is derived by epimerization of **7**. The dimerization of **5** can also be achieved with (–)-spartine in THF to provide dimers **6** and **7** in a 1:2 ratio (entry 3, Table 2). Under these conditions no enantioselectivity was observed for this dimerization using chiral HPLC column for analysis. The spirodimers **6** and **7** are easily separable by TLC. The more mobile dimer **6** is produced by the same mode of dimerization (mode A, see Scheme 3) as observed in the benzylidene cases **1**. The second dimer originates from a different mode of dimerization (mode B) providing the vicinal diester **7**. As described in Scheme 3, the latter dimer results from the addition of the enolate **5a** onto the β carbon of the ester of a second monomer (**5**), followed by an intramolecular addition to the β carbon of the ketone. Initially, the structure and the stereochemistry of dimer **6** and of dimer **7** were established by the same NMR techniques used for the spirodimer **3a**. To prove the structure of dimer **7,** it was submitted for X-ray crystallographic analysis. As depicted in Fig. 1, the X-ray structure is identical to the structure derived from NMR.

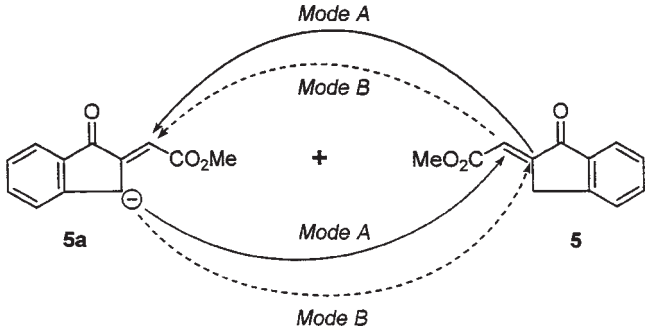
When the dimerization of the cyano compound **9** was studied, a similar reaction pattern to that obtained with the corresponding ester **5** was expected. Using Cs_2CO_3 as a base, the dimerization of **9** was completed within a few minutes and, in contrast to ester **5**, two dimers **10** and **11** were isolated that arose from a mode A type addition. No

© 2000 NRC Canada

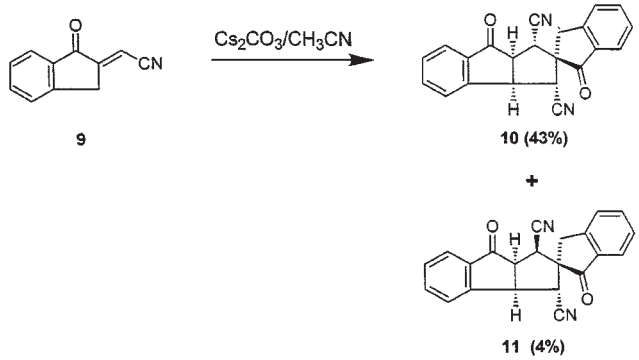
Fig. 1. Stereoview of the ORTEP representation of **7**.[3] Non-hydrogen atoms are represented by ellipsoids corresponding to 30% probability.



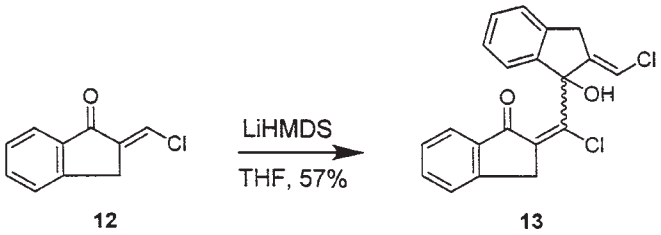
Scheme 3.



Scheme 4.



Scheme 5.



formation of a mode B type dimer was observed (Scheme 4). Presumably, the cyano compound undergoes only mode A dimerization because the addition onto the β carbon of the nitrile would lead to an intermediate with a negative charge α to the nitrile, and would thus make it less stable than in the ester case. As was the case for ester **7**, treatment of dimer **10** under basic conditions (Cs_2CO_3–CH_3CN) resulted in the production of its epimer **11**.

The last case studied was the chloromethylene analog **12** which was prepared according to a literature procedure (4). Interestingly, when this monomer was subjected to basic conditions (LiHMDS, THF, –78°C), none of the expected spirodimer was produced; however, the 1,2-dimer **13**[2] was formed exclusively (Scheme 5). It appears that the electronic nature of the substituent on the double bond has an effect on the site of reactivity of both the cross conjugated enolate and the monomer.

In conclusion, conjugated 1-indanones provide spirodimers when exposed to basic conditions. This allows the preparation of molecules containing five stereogenic centers from achiral monomers in a single step. The only exception to this statement so far is the chloromethylene analog **12**. The formation of the spirodimers is probably the result of either a double Michael reaction as already proposed (1) or of an ionic cycloaddition (Scheme 6) which could explain the high degree of diastereoselectivity observed in these reactions.

Experimental

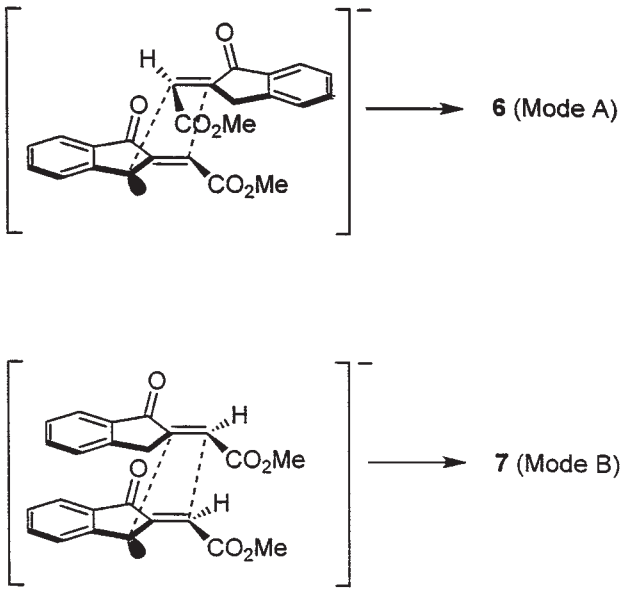
2-(*E*)-*p*-thiomethylbenzylidene-1-indanone (1b)

To a mixture of 1-indanone (4.97 g, 37.6 mmol) and 4-thiomethylbenzaldehyde (4.60 mL, 34.6 mmol) in EtOH (50 mL) was added 25 drops of concentrated HCl. The resulting mixture was refluxed at 80°C for 19 h and then allowed to cool to room temperature to give a yellow solid. The solid was filtered and washed with EtOH to provide 8.16 g (89%) of the title compound **1b**: mp 130–133°C (EtOH); ^{1}H NMR

[2] The stereochemistry of the double bond has not been established.
[3] N.N. Tsou, R.G. Ball, C. Dufresne, and Y. Leblanc. Acta Cryst. C. (2000). In preparation.

© 2000 NRC Canada

Scheme 6.



(300 MHz, acetone-d_6, 27°C) δ: 7.79 (d, *J* = 7.5 Hz, 1H), 7.72 (d, *J* = 8.5 Hz, 2H), 7.69–7.66 (m, 2H), 7.52 (t, *J* = 2.1 Hz, 1H), 7.49–7.44 (m, 1H), 7.38 (d, *J* = 8.5 Hz, 2H), 4.11 (d, *J* = 2.0 Hz, 2H), 2.56 (s, 3H). ^{13}C NMR (125 MHz, acetone-d_6, 27°C) δ: 193.9, 150.7, 142.5, 138.9, 135.3, 133.2, 132.7, 132.0, 128.4, 127.4, 126.7, 124.4, 33.0, 14.8. HRMS calcd. for $C_{17}H_{15}OS$ [M + H]$^+$: 267.0842, found: 267.0843. Elemental analysis calcd. for $C_{17}H_{14}OS$: C 76.66, H 5.30, S 12.04; found: C 76.69, H 5.38, S 12.11.

2-(*E*)-*p*-methylsulfonebenzylidene-1-indanone (1c)

To a solution of **1b** (1.00 g, 3.75 mmol) in a mixture of MeOH (53 mL) and CH_2Cl_2 (5 mL) was added dropwise a suspension of OXONE® (10 g, 16.3 mmol) in water (37 mL). The resulting mixture was stirred for 28 h and then partitioned between H_2O and CH_2Cl_2. The organic phase was separated, dried over Na_2SO_4, filtered, and evaporated under reduced pressure to yield a white solid. The crude solid was stirred vigourously with Et_2O for about 5 min, filtered, and dried under vacuum for several hours to provide 0.97 g (87%) of the title compound **1c**: mp 211–214°C (EtOH); ^{1}H NMR (300 MHz, acetone-d_6, 27°C) δ: 8.06–8.04 (m, 4H), 7.83 (d, *J* = 7.8 Hz, 1H),7.75–7.68 (m, 2H), 7.62 (t, *J* = 2.3 Hz, 1H), 7.50 (t, *J* = 8.0 Hz, 1H), 4.21 (d, *J* = 2.1 Hz, 2H), 3.17 (s, 3H). ^{13}C NMR (125 MHz, acetone-d_6, 27°C) δ: 193.9, 151.0, 142.5, 141.3, 139.4, 138.4, 135.9, 132.0, 131.4, 128.7, 128.6, 127.5, 124.7, 44.2, 32.8. HRMS calcd. for $C_{17}H_{15}O_3S$ [M + H]$^+$: 299.0740, found: 299.0741.

Dimerization of 2-(*E*)-*p*-thiomethylbenzylidene-1-indanone (1b) using CS_2CO_3 as a base to yield 3b and 4b

To a stirring solution of **1b** (0.65 g, 2.00 mmol) in CH_3CN (9.5 mL) was added Cs_2CO_3 (0.65 g, 2.00 mmol). The resulting mixture was stirred for 50 h at room temperature and was then quenched by the addition of aqueous NH_4OAc (10 mL), followed by addition of ethyl acetate (50 mL). The organic phase was separated and the aqueous phase was extracted twice more with ethyl acetate (2 × 50 mL). The organic portions were combined, dried over Na_2SO_4, filtered, and evaporated under reduced pressure. The crude mixture was then purified by column chromatography with 5% EtOAc in toluene followed by a preparative plate purification (5% EtOAc in toluene) to yield 0.25 g (52%) of pure dimer **3b** and 0.040 g (8%) of isomer **4b**.

*Isomer **3b***: mp 181–183°C (EtOH); ^{1}H NMR (500 MHz, benzene-d_6, 27°C) δ: 7.78 (d, *J* = 7.1 Hz, 1H), 7.60 (d, *J* = 7.4 Hz, 1H), 7.23 (d, *J* = 8.3 Hz, 2H), 7.09 (d, *J* = 8.6 Hz, 2H), 7.01–6.91 (m, 3H), 6.89 (d, *J* = 1.6 Hz, 2H), 6.88 (d, *J* = 1.6 Hz, 2H), 6.68 (t, *J* = 7.3 Hz, 1H), 6.60 (app. q, 2H), 4.31 (d, *J* = 11.0 Hz, 1H), 4.06 (dd, *J* = 9.0 Hz, 1H), 3.90 (d, *J* = 11.0 Hz, 1H), 3.60 (dd, *J* = 9.0, 11.0 Hz, 1H), 2.79 (s, 2H), 1.80 (s, 3H), 1.79 (s, 3H). HRMS calcd. for $C_{34}H_{29}O_2S_2$ [M + H]$^+$: 533.1608, found: 533.1609. Elemental analysis calcd. for $C_{34}H_{28}O_2S_2$: C 76.60, H 5.30, S 12.05; found: C 76.21, H 5.34, S 12.28.

*Isomer **4b** (oil)*: ^{1}H NMR (500 MHz, benzene-d_6, 70°C) δ: 8.00 (d, *J* = 7.5 Hz, 1H), 7.42 (d, *J* = 7.9 Hz, 1H), 7.13 (d, *J* = 8.4 Hz, 2H), 7.06 (t, *J* = 7.7 Hz, 1H), 6.99 (d, *J* = 8.0 Hz, 2H), 6.97 (app. s, 1H), 6.92 (t, *J* = 7.7 Hz, 1H), 6.78–6.73 (m, 3H), 6.71 (d, *J* = 7.9 Hz, 1H), 6.60 (d, *J* = 8.3 Hz, 2H), 6.50 (d, *J* = 7.6 Hz, 1H), 4.20 (d, *J* = 4.4 Hz, 1H), 4.05 (app. t, *J* = 9.3 Hz, 1H), 3.67 (d, *J* = 10.3 Hz, 1H), 3.46 (dd, *J* = 4.2, 8.1 Hz, 1H), 2.79 (d, *J* = 17.6 Hz, 1H), 2.47 (d, *J* = 17.5 Hz, 1H), 2.07 (s, 3H), 1.84 (s, 3H). ^{13}C NMR (125 MHz, 27°C, acetone-d_6) δ: 207.2, 205.9, 154.3, 152.5, 139.8, 139.5, 137.9, 137.8, 137.2 135.3, 134.0, 133.6, 132.2, 130.1, 129.2, 128.1, 128.0, 127.1, 126.9, 125.5, 123.9, 123.6, 68.1, 58.8, 58.7, 51.9, 49.1, 37.6, 15.2, 14.9. HRMS calcd. for $C_{34}H_{29}O_2S_2$ [M + H]$^+$: 533.1608, found: 533.1609.

Dimerization of 2-(*E*)-*p*-methylsulfonebenzylidene-1-indanone (1c) using Cs_2CO_3–CH_3CN to afford 3c and 4c

To a stirring solution of **1c** (0.10g, 0.35 mmol) in CH_3CN (1.8 mL) was added Cs_2CO_3 (0.13 g, 0.39 mmol). The resulting mixture was stirred for 16 h at room temperature and was then quenched by the addition of aqueous NH_4OAc (2 mL), followed by addition of ethyl acetate (10 mL). The organic phase was separated and the aqueous phase was extracted twice more with ethyl acetate (2 × 10 mL). The organic portions were combined, dried over Na_2SO_4, filtered, and evaporated under reduced pressure. Addition of a 70% EtOAc in hexane solution to the crude mixture resulted in the precipitation of the major isomer **3c** as a white solid, which was filtered and dried under vacuum for several hours; to afford 0.05 g (51%). Purification of the filtrate by preparative plate (7% EtOAc–hexane) yielded a further 0.006 g of isomer **3c** (total mass obtained: 0.060 g, 57%), and 0.002 g (3%) of isomer **4c**.

*Isomer **3c***: mp 249–251°C (EtOH); ^{1}H NMR (500 MHz, benzene-d_6, 27°C) δ: 7.75 (d, *J* = 7.3 Hz, 1H), 7.56 (d, *J* = 8.4 Hz, 2H), 7.54 (d, *J* = 8.4 Hz, 2H), 7.46 (d, *J* = 7.6 Hz, 1H), 7.24 (d, *J* = 8.4 Hz, 2H), 7.08 (d, *J* = 7.9 Hz, 2H), 7.00 (t, *J* = 7.6 Hz, 1H), 6.96 (t, *J* = 7.6 Hz, 1H), 6.72 (d, *J* = 7.2 Hz, 1H), 6.59 (t, *J* = 7.6 Hz, 1H), 6.53 (t, *J* = 6.9 Hz, 1H), 6.38 (d, *J* = 7.6 Hz, 1H), 4.18 (d, *J* = 10.8 Hz, 1H), 3.95 (t, *J* = 9.4 Hz, 1H), 3.76 (d, *J* = 10.5 Hz, 1H), 3.47 (dd, *J* = 8.9, 10.7 Hz, 1H), 2.52 (d, *J* = 17.5 Hz, 1H), 2.47 (d,

© 2000 NRC Canada

J = 17.5 Hz, 1H), 2.10 (s, 3H), 2.07 (s, 3H). HRMS calcd. for $C_{34}H_{29}O_6S_2$ $[M + H]^+$: 597.1408, found: 597.1405. Elemental analysis calcd. for $C_{34}H_{28}O_6S_2$: C 68.44, H 4.73, S 10.75; found: C 68.42, H 4.77, S 10.81.

Isomer ***4c*** *(oil)*: ^{1}H NMR (500 MHz, benzene-d_6, 70°C) δ: 7.91 (d, J = 7.7 Hz, 1H), 7.73 (d, J = 8.4 Hz, 2H), 7.39 (d, J = 7.9 Hz, 2H), 7.34 (d, J = 8.1 Hz, 1H), 7.07 (d, J = 8.3 Hz, 2H), 6.99 (t, J = 7.6 Hz, 1H), 6.92 (t, J = 7.6 Hz, 1H), 6.87 (t, J = 7.6 Hz, 1H), 6.74 (t, J = 7.4 Hz, 1H), 6.71 (d, J = 8.5 Hz, 1H), 6.56 (d, J = 8.5 Hz, 2H), 6.26 (d, J = 7.8 Hz, 1H), 4.23 (d, J = 5.6 Hz, 1H), 3.96 (t, J = 9.3 Hz, 1H), 3.44 (d, J = 10.3 Hz, 1H), 3.36 (dd, J = 5.4, 8.7 Hz, 1H), 2.56 (d, J = 17.0 Hz, 1H), 2.34 (s, 3H), 2.31 (d, J = 17.0 Hz, 1H), 2.14 (s, 3H). HRMS calcd. for $C_{34}H_{29}O_6S_2$ $[M + H]^+$: 597.1408, found: 597.1405.

Dimerization of 2-(*E*)-*p*-thiomethylbenzylidene-1-indanone (1b) using $KN(SiMe_3)_2$ to yield 3b and 4b

To a solution of **1b** (0.15 g, 0.56 mmol) in THF (1.6 mL) at –78°C was added dropwise via syringe a 0.5 M toluene solution of $KN(SiMe_3)_2$ (1.2 mL, 0.60 mmol). The solution was allowed to stir for one hour at –78°C and was then quenched by addition of 3 mL of aqueous NH_4OAc via syringe followed by immediate warming to room temperature. The workup and purification procedure followed was the same as that described for the dimerization of **1b** using Cs_2CO_3–CH_3CN and yielded 0.12 g (80%) of isomer **3b** and 0.005 g (5%) of isomer **4b**.

Dimerization of 2-(*E*)-benzylidene-1-indanone (1a) using $KN(SiMe_3)_2$ to yield 3a and 4a

The experimental procedure and workup followed was that as described above for the dimerization of **1b** using $KN(SiMe_3)_2$. Quantities of reagents and solvents used: 2-(*E*)-benzylidene-1-indanone (0.10 g, 0.45 mmol); THF 1.1 mL; $KN(SiMe_3)_2$ (0.5 M, 0.92 mL, 0.460 mmol). Purification was achieved by flash column chromatography (6% EtOAc in toluene), which separated most of isomer **3a** from **4a**, followed by a preparative plate purification (6% EtOAc in toluene) to separate the remaining fractions from the previous column. This procedure yielded 0.08 g (81%) of isomer **3a** and 0.006 g (6%) of isomer **4a**. The isomers were identified on the basis of their ^{1}H NMR spectra, which were identical to those reported previously (1).

Dimerization of 2-carbomethoxymethylene-1-indanone (5) using Cs_2CO_3–CH_3CN to afford 6 and 7

To a solution of 2-carbomethoxymethylene-1-indanone (**5**) (5) (0.50 g, 2.30 mmol) in CH_3CN (22 mL) was added Cs_2CO_3 (0.75 g, 2.30 mmol). The resulting mixture was stirred at room temperature for 0.5 h. The reaction mixture was partitioned between 25% aqueous NH_4OAc and ethyl acetate. The organic phase was separated, dried over Na_2SO_4, and evaporated. The crude mixture was purified by flash chromatography to afford dimer **6** (0.19 g, 43%) and dimer **7** (0.19 g, 42%).

Dimer ***6***: mp 163–164°C. ^{1}H NMR (500 MHz, benzene-d_6, 22°C) δ: 7.79 (d, J = 7.7 Hz, 1H), 7.69 (d, J = 7.7 Hz, 1H), 7.51 (d, J = 7.7 Hz, 1H), 7.10 (t, J = 7.5 Hz, 1H), 7.04 (t, J = 7.3 Hz, 1H), 6.95 (d, J = 8.0 Hz, 2H), 6.92 (t, J = 7.3 Hz, 1H), 6.84 (t, J = 7.3 Hz, 1H), 4.16 (t, J = 9.9 Hz, 1H), 3.78 (t, J = 9.4 Hz, 1H), 3.67 (d, J = 9.5 Hz, 1H), 3.30 (d, J = 10.1 Hz, 1H), 3.07 (d, J = 17.6 Hz, 1H), 2.83 (s, 3H), 2.79 (s, 3H), 2.77 (d, J = 16.6 Hz, 1H). ^{13}C NMR (125.6 MHz, acetone-d_6, 22°C) δ: 203.8, 202.0, 171.0, 170.4, 154.5, 151.0, 137.0, 136.0, 135.0, 127.7, 127.6, 126.3, 126.0, 124.6, 124.4, 124.1, 63.4, 58.0, 53.5, 52.1, 51.1, 51.0, 45.0, 32.4. Elemental analysis calcd. for $C_{24}H_{20}O_6$: C 71.28, H 4.98; found: C 71.30, H 4.87. Mass spectrum m/z = 405.

Dimer ***7***: mp 170–171°C ^{1}H NMR (500 MHz, benzene-d_6, 22°C) δ: 7.68 (d, J = 6.7 Hz, 1H), 7.45 (d, J = 8.0 Hz, 1H), 7.10 (t, J = 7.8 Hz, 1H), 6.99 (d, J = 7.4 Hz, 1H), 6.82 (m, 3H), 6.48 (d, J = 7.4 Hz, 1H), 4.30 (dd, J = 4.4, 7.3 Hz, 1H), 3.77 (dd, J = 4.4, 7.9 Hz, 1H), 3.70 (d, J = 7.9 Hz, 1H), 3.63 (d, J = 17.0 Hz, 1H), 3.46 (d, J = 7.4 Hz, 1H), 3.35 (s, 3H), 3.22 (s, 3H), 2.97 (d, J = 17.0 Hz, 1H). ^{13}C NMR (125.6 MHz, acetone-d_6), 298 K) δ: 204.7, 204.7, 173.0, 171.3, 151.7, 151.2, 137.7, 136.7, 134.8, 133.9, 127.0, 127.2, 126.6, 126.3, 124.2, 123.8, 60.4, 55.3, 55.2, 53.9, 51.9, 51.2, 47.7, 39.3. Elemental analysis calcd. for $C_{24}H_{20}O_6$: C 71.28, H 4.98; found: C 71.26, H 5.08. Mass spectrum m/z = 405.

Dimerization of 2-carbomethoxymethylene-1-indanones (5) using $KN(SiMe_3)_2$ to yield 6 and 7

The indanone **5** (0.05 g, 0.25 mmol) was dissolved in THF (1.5 mL) and cooled to –78°C for 5 min. This was followed by the addition of a 0.05 M solution of $KN(SiMe_3)_2$ in toluene (0.10 eq, 50 μL). The crude deep purple mixture was partitioned between ethyl acetate and 25% aqueous NH_4OAc. The organic layer was separated, dried over $MgSO_4$, and filtered through silica gel to provide the title products **6** and **7** (0.04 g, 80% yield) in a 1:1 ratio.

Dimerization of 2-carbomethoxymethylene-1-indanones (5) using DBU to yield 6,7 and 8

To a solution of the indanone **5** (0.25 g, 1.24 mmol) in THF (5 mL) was added DBU (0.18 mL, 6.20 mmol). The resulting dark purple solution was allowed to react overnight and this resulted in an additional dimeric product that was more polar than those seen previously (**6** and **7**). The mixture of dimers was purified to afford: 0.07 g (28.4%) of **6**, 0.06 g (22.4%) of **7** and 0.008 g (8.0%) of **8**: Dimer **8** mp 198–200°C. ^{1}H NMR (500 MHz, acetone-d_6, 22°C) δ: 7.66 (t, J = 7.3 Hz, 1H), 7.62 (d, J = 7.7 Hz, 1H), 7.56 (d, J = 7.3 Hz, 1H), 7.30 (t, J = 7.5 Hz, 1H), 7.27 (t, J = 7.5 Hz, 1H), 7.23 (t, J = 7.5 Hz, 1H), 7.13 (d, J = 7.1 Hz, 1H), 6.91 (d, J = 7.5 Hz, 1H), 4.43 (d, J = 8.7 Hz, 1H), 4.02 (dd, J = 6.0, 11.5 Hz, 1H), 3.98 (d, J = 11.5 Hz, 1H), 3.89 (d, J = 17.5 Hz, 1H), 3.82 (d, J = 17.5 Hz, 1H), 3.77 (s, 3H), 3.50 (dd, J = 6.2, 9.0 Hz, 1H), 3.35 (s, 3H). ^{13}C NMR (125.6 MHz, acetone-d_6, 22°C) δ: 206.4, 206.1, 175.2, 171.4, 153.5, 150.8, 138.4, 138.1, 135.9, 134.9, 129.3, 128.3, 127.2, 126.5, 124.0, 123.8, 60.1, 59.4, 55.8, 54.3, 52.6, 52.1, 46.5, 40.1. HRMS calcd. for $C_{24}H_{21}O_6$ $[M + H]^+$: 405.1339, found: 405.1338.

Preparation of spirodimer 8 from dimer 7

To a solution of dimer **7** (0.02 g, 0.04 mmol) in THF (0.40 mL) was added DBU (0.06 mL, 0.39 mmol). After a

© 2000 NRC Canada

period of 72 h at room temperature, the reaction mixture was partitioned between ethyl acetate and 25% aqueous NH_4OAc. The organic layer was separated, dried over Na_2SO_4, filtered, and evaporated. After purification by flash chromatography, dimer **8** was obtained (0.012 g, 75%).

Preparation of 2-(1-oxo-1,3-dihydro-2*H*-inden-2-ylidene)acetonitrile (9)

To a mixture of 2-carboxymethylene-1-indanone (6) (0.50 g, 2.66 mmol) in dichloromethane (5.0 mL) was added an excess of oxalyl chloride (1.0 mL, 11.5 mmol) and a catalytic amount of dry DMF. This resulting mixture was allowed to react for 1.5 h at room temperature. At this point, the solvent was evaporated in vacuo and the excess of oxalyl chloride co-evaporated with dichloromethane (3 × 5 mL). The acid chloride was then dissolved in THF (10 mL) and added to a cold solution of saturated NH_4OAc (50 mL). The ice cooled reaction mixture was then stirred for 30 min. The aqueous phase was extracted with ethyl acetate and the organic layer was dried over $MgSO_4$, filtered, and the solvent evaporated under reduced pressure to provide 0.38 g (77%) of a white solid. The acetamide was used to synthesize the nitrile without further purification. To a 0°C solution of the acetamide (0.16 g, 0.85 mmol) and pyridine (0.13 g, 1.70 mmol) in 1,4-dioxane was then added trifluoroacetic anhydride (0.19 g, 0.94 mmol) over a period of 1 hour. The slurry was kept at 0°C during the addition of the trifluoroacetic anhydride. The reaction was stirred for an additional 5 min and was then poured onto a cold NH_4OAc buffer solution. The aqueous layer was extracted with ethyl acetate, dried over $MgSO_4$, and the solvent evaporated in vacuo to provide a crude brown solid. The compound was purified by flash chromatography (20% ethyl acetate – hexanes) to provide **9** as a white crystalline material (0.10 g, 69%), mp 138–140°C. ^{1}H NMR (500 MHz, acetone-d_6, 22°C) δ: 7.83 (d, J = 7.8 Hz, 1H), 7.80 (t, J = 7.5 Hz, 1H), 7.71 (d, J = 7.7 Hz, 1H), 7.54 (t, J = 7.4 Hz, 1H), 6.50 (t, J = 2.5 Hz, 1H), 4.10 (d, J = 2.3 Hz, 2H).^{13}C NMR (500 MHz, acetone-d_6, 295 K) δ: 190.5, 156.6, 149.6, 137.5, 136.8, 129.0, 127.2, 124.8, 116.5, 101.0, 32.0. calcd. for $C_{11}H_7NO$: C 78.09, H 4.17, N 8.28; found: C 78.18, H 4.02, N 8.19. Mass spectrum m/z = 168 (M – 1).

Dimerization of 2-(1-oxo-1,3-dihydro-2*H*-inden-2-ylidene)acetonitrile (9) with Cs_2CO_3–CH_3CN to yield 10 and 11

To a solution of the nitrile **9** (0.14 g, 0.89 mmol) in acetonitrile (8 mL) was added Cs_2CO_3 (0.75 g, 2.30 mmol). After a period of 10 min, followed by standard work up procedure, the crude mixture was purified on silica gel using flash chromatography (40% ethyl acetate – hexanes followed by 60% ethyl acetate – hexanes for the more polar compound). This afforded one major dimer **10** (0.06 g, 43%) mp >230°C and a minor dimer **11** (0.006 g, 4%) mp >230°C.

*Dimer **10***: ^{1}H NMR (500 MHz, chloroform-d_3, 22°C) δ: 7.86 (d, J = 7.8 Hz, 2H), 7.79 (t, J = 7.4 Hz, 1H), 7.78 (t, J = 6.8 Hz, 1H), 7.68 (d, J = 7.9 Hz, 1H), 7.66 (d, J = 8.0 Hz, 1H), 7.60 (t, J = 7.7 Hz, 1H), 7.52 (t, J = 7.7 Hz, 1H), 4.35 (t, J = 9.7 Hz, 1H), 3.69 (d, J = 17.5 Hz, 1H), 3.67 (t, J = 8.8 Hz, 1H), 3.65 (d, J = 17.5 Hz, 1H), 3.35 (d, J = 9.2 Hz, 1H), 3.07 (d, J = 10.1 Hz, 1H). ^{13}C NMR (125.6 MHz, acetone-d_6, 22°C) δ: 201.9, 200.9, 153.0, 152.5, 137.9, 137.1, 136.4, 135.6, 130.5, 129.6, 128.0, 126.6, 125.3, 125.3, 117.9, 117.8, 64.5, 54.2, 48.1, 42.4, 37.8, 34.7. Calcd. for $C_{22}H_{14}N_2O_2$: C 78.09, H 4.17, N 8.28; found: C 77.87, H 4.21, N 8.02. Mass spectrum m/z = 339 $(M - H)^-$.

*Dimer **11***: ^{1}H NMR (500 MHz, chloroform-d_3, 22°C) δ: 7.90 (d, J = 7.7 Hz, 1H), 7.86 (d, J = 7.7 Hz, 1H), 7.79 (t, J = 7.6 Hz, 1H), 7.75 (t, J = 7.9 Hz, 1H), 7.71 (d, J = 7.6 Hz, 1H), 7.59 (t, J = 7.5 Hz, 1H), 7.56 (d, J = 7.7 Hz, 1H), 7.51 (t, J = 7.4 Hz, 1H), 4.37 (t, J = 8.7 Hz, 1H), 3.77 (t, J = 9.8 Hz, 1H), 3.74 (d, J = 17.1 Hz, 1H), 3.62 (d, J = 8.7 Hz, 1H), 3.40 (d, J = 9.2 Hz, 1H), 3.25 (d, J = 17.3 Hz, 1H). ^{13}C NMR (125.6 MHz, CD_3CN, 22°C) δ: 202.6, 201.3, 153.7, 152.4, 137.9, 137.6, 135.7, 130.7, 129.8, 128.0, 127.2, 125.4, 125.1, 119.1, 117.8, 118.6, 63.6, 53.8, 48.4, 41.6, 39.6, 37.9. HRMS calcd. for $C_{22}H_{14}N_2O_2$ $[M + H]^+$: 339.1332, found: 339.1333.

Preparation of spirodimer 11 from dimer 10

To a solution of the dimer **10** (0.02 g, 0.06 mmol) in THF (0.40 mL) was added DBU (0.03 mL, 0.19 mmol). After a period of 72 h at room temperature, the reaction mixture was partitioned between EtOAc and saturated NH_4OAc. The organic layer was separated, dried over Na_2SO_4, filtered, and evaporated. After purification by flash chromatography, dimer **11** was obtained (0.006 g, 30%), with no trace of **10** in the reaction.

Dimerization of 2-chloromethylidene-1-indanone (12) using LiHMDS to yield 13

To a solution of 2-chloromethylidene-1-indanone (**12**) (4) (0.15 g, 0.84 mmol) in THF (4 mL) at –78°C was added LiHMDS 500 μL of 1.0 M solution in THF, 0.50 mmol). After a period of 5 min, followed by standard workup procedure, the crude mixture was purified by flash chromatography (20% ethyl acetate – hexanes). White crystalline, air sensitive material was isolated in 57% yield (0.08 g). Compound **13** mp 90–110°C (decomposes). ^{1}H NMR (500 MHz, acetone-d_6, 22°C) δ: 8.66 (s, 1H), 7.88 (d, J = 7.5 Hz, 1H), 7.80 (td, J = 7.5, 0.9 Hz, 1H), 7.66 (d, J = 7.7 Hz, 1H), 7.56 (td, J = 7.2, 0.7 Hz, 1H), 7.41 (d, J = 7.4 Hz, 1H), 7.39 (dd, J = 6.9, 0.5 Hz, 1H), 7.36 (td, J = 7.1, 1.0 Hz, 1H), 7.29 (t, J = 7.8 Hz, 1H), 6.71 (t, J = 2.7 Hz, 1H), 4.03 (d, J = 21.1 Hz, 1H), 3.98 (d, J = 21.1 Hz, 1H), 3.89 (dd, J = 21.1, 2.2 Hz, 1H), 3.79 (dd, J = 21.1, 2.2 Hz, 1H). ^{13}C NMR (125.6 MHz, acetone-d_6, 22°C) δ: 194.1, 155.8, 150.8, 150.5, 149.5, 147.1, 140.3, 139.7, 137.3, 135.8, 130.3, 129.1, 128.5, 127.2, 125.8, 125.2, 118.5, 89.6, 37.5, 36.6. HRMS calcd. for $C_{20}H_{15}Cl_2O_2$ $[M + H]^+$: 357.0448, found: 357.0449.

Acknowledgements

The authors would like to thank Renata Oballa and Patrick Roy for helpful discussions in the preparation of the manuscript.

© 2000 NRC Canada

References

1. C. Berthellette, C. McCooye, Y. Leblanc, and L.A. Trimble. J. Org. Chem. **62**, 4339 (1997).
2. W. Wendelin, K. Schermanz, and K. Britmaier. Monatsh. Chem. **119**, 355 (1988).
3. W.J. Houlihan, M.J. Shapiro, and J.A. Chin. J. Org. Chem. **62**, 1529 (1997).
4. G.P. Newsoroff and S. Sternhell. Aust. J. Chem. **25**, 1669 (1972).
5. A. Padwa and A. Ku. J. Am. Chem. Soc. **100**, 2181 (1978).
6. Y. Tanaka, S. Niwa, H. Nishioka, T. Yamanaka, M. Torizuka, K. Yoshinaga, N. Kobayashi, Y. Ikeda, and H. Arai. J. Med. Chem. **37**, 2071 (1994).

© 2000 NRC Canada

On the reduction of tertiary radicals by samarium diiodide (SmI_2)

Tadamichi Nagashima, Alexey Rivkin, and Dennis P. Curran

Abstract: Reduction of *o*-iodophenyl 3-methylbut-2-enyl ether with samarium diiodide generates mixtures of 3-isopropyl-2,3-dihydrobenzofuran and 3-(2-propenyl)-2,3-dihydrobenzofuran along with a small amount of dimer. If a source of deuterium is present during the reduction, then the 3-isopropyl product predominates and this product is labeled with one deuterium. However, attempts to quench the putative tertiary organosamarium reagent by adding a deuterium source after the reduction were not very successful at room temperature. But at 0°C, the organosamarium reagent was generated (at least to the extent of about 50%, as measured by deuterium quenching), and its decomposition was followed over time by a series of quenching experiments. The results suggest that tertiary radicals are reduced to a significant extent by SmI_2 to form an anionic (presumably alkylsamarium) species. This species is thermally unstable and decomposes to the corresponding reduced and eliminated products. The reduced product is consistently formed in slight excess over the eliminated one, and the mechanism of formation of these products is not yet clear.

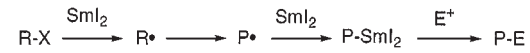
Key words: samarium diiodide, SmI_2, reduction, alkyl samarium.

Résumé : La réduction de l'oxyde d'*o*-iodophényle et de 3-méthylbut-2-ényle par le diiodure de samarium conduit à un mélange de 3-isopropyl-2,3-dihydrobenzofurane et de 3-(prop-2-ényl)-2,3-dihydrobenzofurane en plus de faibles quantités de dimères. Si la réduction se fait en présence d'une source de deutérium. Le produit 3-isopropyle est alors prédominant et il est marqué par un deutérium. Toutefois, tous les essais effectués à la température ambiante en vue de piéger le réactif organosamarium tertiaire putatif par addition d'une source de deutérium après la réduction ont été infructueux. Toutefois, à 0°C, on a généré le réactif organosamarium (au moins jusqu'à un niveau de 50% si l'on se base sur le produit piégé au deutérium) et on a étudié sa décomposition en fonction du temps en faisant appel à des expériences de piégeage. Les résultats suggèrent que le SmI_2 provoque une importante réduction des radicaux tertiaires avec formation d'espèces anioniques (probablement de l'alkylsamarium). Cette espèce est thermiquement instable et elle se décompose pour donner les produits correspondants de réduction et d'élimination. Il y a toujours formation d'une quantité légèrement supérieure de produit réduit par rapport au produit d'élimination et le mécanisme de formation de ces produits n'est toujours pas clair.

Mots clés : diiodure de samarium, SmI_2, réduction, alkylsamarium.

Introduction

Samarium diiodide (SmI_2) is a powerful and soluble reducing agent whose popularity in organic synthesis is continually increasing (1). The use of samarium diiodide to control sophisticated sequences of radical and ionic reactions (2) rests on the understanding of how SmI_2 reacts with functional groups, radicals, and radical ions. It is well demonstrated that the reductions of halides by SmI_2 initially produce radicals (1), and it is now generally accepted that these radicals often can be reduced by another equivalent of SmI_2 to give putative organosamarium intermediates (eq. [1]) (3, 4). Little is known about the structure of these intermediates, and they sometimes have limited stability (4*a*, 5). But they often behave like "carbanions" and combine with reactive electrophiles to give trapped products (1–4).



Reduction by SmI_2 occurs readily for radicals bearing electron withdrawing groups as well as primary alkyl radicals. In contrast, most vinyl and aryl radicals appear to undergo radical–solvent reactions (H-abstraction, addition) faster than they are reduced by SmI_2 (however, when electron withdrawing groups are present, vinyl radicals may be reduced to vinylsamarium reagents. See ref. (6)). The situation with secondary and especially tertiary radicals is less clear. Labeling studies (4*a*, *b*) with electrophiles show that secondary radicals can be reduced to organosamarium reagents, but the trapped products are frequently accompanied by small amounts of products of (apparent) radical disproportionation. Tertiary radicals frequently do not give trapped products at all (4–6). (Qualitatively similar behavior is seen in solid phase reactions. See ref. (7)).

Received September 14, 1999. Published on the NRC Research Press website on June 2, 2000.

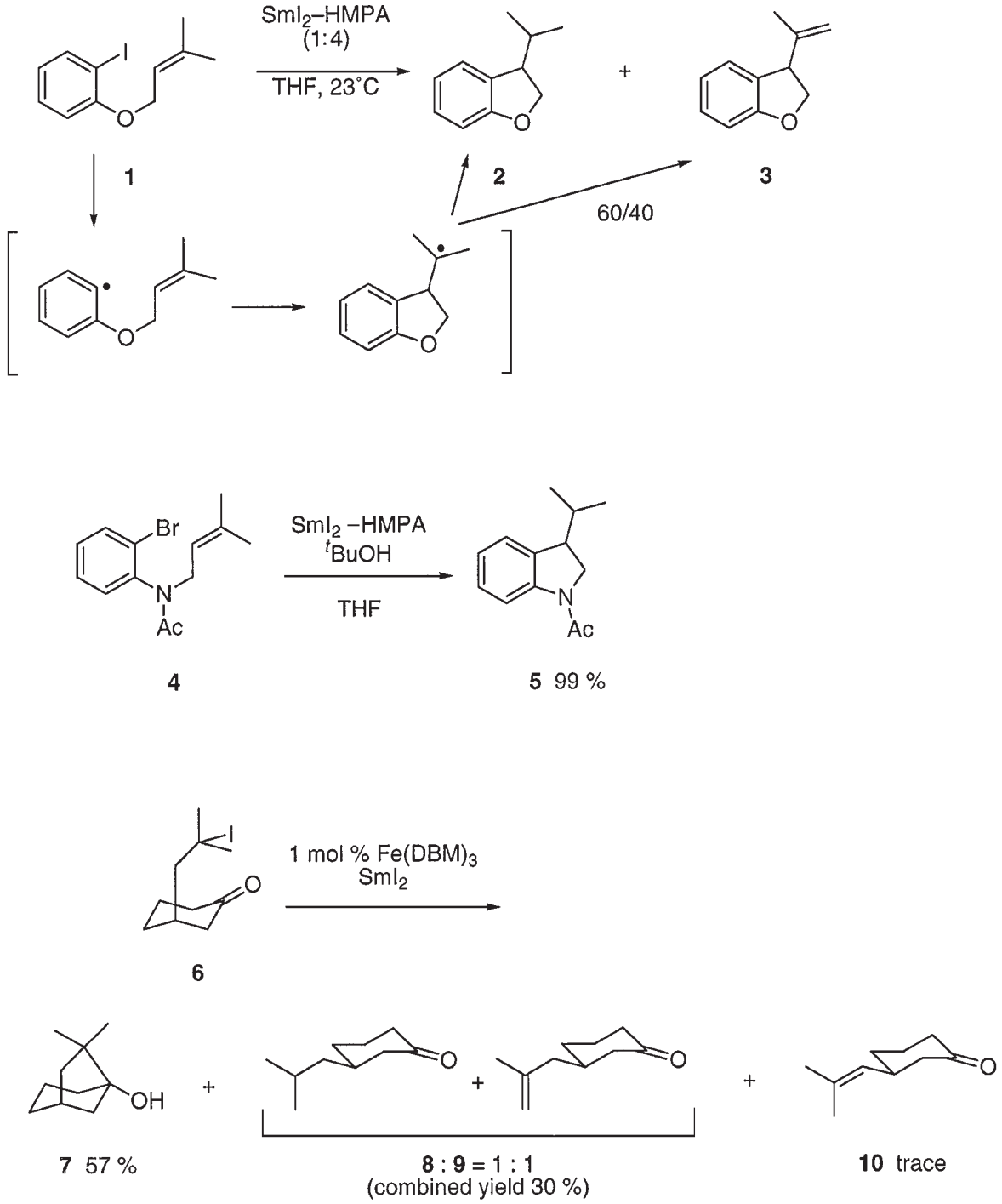
We dedicate this paper to Prof. Stephen Hanessian on the occasion of his 65th birthday.

T. Nagashima, A. Rivkin, and D.P. Curran.[1] Department of Chemistry, University of Pittsburgh, Pittsburgh PA 15260, U.S.A.

[1]Author to whom correspondence may be addressed. Telephone: (412) 624-8240. Fax: (412) 624-9861. e-mail: curran+@pitt.edu

© 2000 NRC Canada

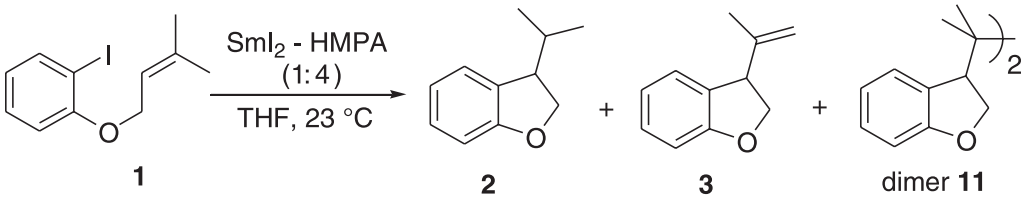
Fig. 1. Generation and reaction of 3°-radicals by SmI_2. (*a*) See Curran and Totleben (4*b*); (*b*) See Inanaga et al. (8); (*c*) See Molander and McKie (4*c*).



Three key reactions of precursors of tertiary radicals in the presence of SmI_2 are shown in Fig. 1. We reported (4*b*) that the reduction of aryl iodide **1** by SmI_2 in THF/HMPA without a proton source provided products **2** and **3** in a 60:40 ratio and concluded that these products probably resulted from radical disproportionation. This result is typical of other related systems (7). However, Inanaga (8) reported that a very similar reduction of **4** with SmI_2/HMPA in the presence of *tert*-butanol provided **5** in 99% yield. In an intramolecular example, Molander and McKie (4*c*) reported that the reduction of **6** with SmI_2/HMPA in the presence of 1% $Fe(DBM)_3$ gave the cyclized product **7** in 57% yield along with 30% yield of a 1:1 mixture of **8** and **9** (and a trace of **10**). These divergent results are difficult to compare directly due to the different reaction conditions and because the presence of the ketone in **6** may alter the reduction pathway (9), so we decided to undertake a series of experiments designed to probe how tertiary radicals

© 2000 NRC Canada

Table 1. Reduction of **1**. Product study.



Entry	SmI_2/1	Ratio[a] 2:3:11	Combined yield[b]
1	2.2	54 : 43 : 3	85%
2[c]	1.1	53 : 44 : 3	79%

[a]Based on the ^{1}H NMR spectrum of the crude misture.

[b]Based on the weight of the crude mixture.

[c]7% of the iodine **1** was recovered.

react with SmI_2. We show that both in the presence and absence of proton sources, tertiary radicals can be reduced by SmI_2. These resulting anionic species are unstable and decompose to reduced and eliminated products.

Results and discussion

We initially chose to repeat the reduction of **1**. If the products from this reaction are formed exclusively by radical–radical reactions, then **2** and **3** should be formed in a 50:50 (not 60:40) ratio, and there should also be some dimer **11** from radical recombination and perhaps the other possible regioisomeric alkene (not shown) from disproportionation. Formation of products by radical–radical reactions also only requires 1 equiv. of SmI_2, whereas electrophile-trapped products generally consume 2 equiv. of SmI_2. It is known that 4 equiv. of HMPA are required to generate SmI_2 with maximum reducing power (3, 10), and for consistency all reactions in this work employed those conditions. In addition, aqueous quenches were not used in any reactions, since it is also known that SmI_2 does not react rapidly with water and that water increases the reduction potential of SmI_2 (in other words, addition of water tends to promote reductions rather than stopping them (11)). Reactions were quenched by bubbling dry air through the mixture until the color of SmI_2 had dissipated (a few seconds). Data for the initial reductions of **1** are shown in Table 1.

Reduction of **1** with 2.2 equiv. of SmI_2 (Table 1, entry 1) gave results very similar to those reported (4*b*), except that we were now able to carefully separate and characterize a small amount of dimer **11** (as a *meso–d,l*-mixture). The starting iodide **1** was completely consumed in this reaction, even though the characteristic purple color of the SmI_2 never dissipated. Products **2**, **3**, and **11** were formed in 85% combined (isolated) yield in a ratio of 53:44:3. Thus, dimer **11** is formed, but the regioisomeric alkene of **3** (not shown) is not, and there is somewhat more **2** than **3**. The reaction was repeated with 1.1 equiv. of SmI_2 (entry 2), and this time the SmI_2 rapidly decolorized. The same three products were isolated in the same ratio in 79% yield. The starting iodide **1** was recovered in 7% yield, thus accounting for the marginally lower yield.

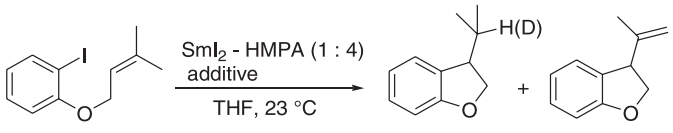
These results seem reasonably consistent with formation of products by radical reactions, if one hypothesizes that the excess of **2** over **3** can be accounted for by a small amount of two electron reduction followed by protonation (proton source unknown). If about 10% of **2** is formed by two electron reduction, then this could even account for the observation that 1.1 equiv. of SmI_2 was not quite sufficient to consume all of **1**. However, the authentic product ratios of radical–radical reactions are not known, and the results in Table 1 might also be explained by reduction of the tertiary radical to an organosamarium reagent, followed by decomposition to the observed products with regeneration of Sm(II). This decomposition must be quite rapid, otherwise more starting material should have been recovered from experiment 2. This possibility is not unreasonable, since many organometallic species decompose by disproportionation and coupling reactions that do not involve free radicals.

To investigate the effect of proton sources, we next conducted the reduction of **1** in the presence of alcohols, and the results of these experiments are reported in Table 2. Consistent with the results of Inanaga (8), reduction of **1** with 2.2 equiv. SmI_2 in the presence of *tert*-butanol now provided only protonated product **2** in 79% yield (Table 2, entry 1). Neither the alkene **3** nor the dimer **11** was detected. The use of methanol-d_4 provided mostly the reduced product **2** along with a trace of the alkene **3** (ratio 97:3). The yield was somewhat diminished (54%), but **2** contained 89% deuterium at the methine position based on GC–MS analysis (Table 2, entry 2). In two related experiments, **1** was reduced in the absence of methanol, and then methanol-d_4 was added (prior to oxygen quenching) after 30 s and 5 min, respectively, (Table 2, entries 3 and 4). As expected, this gave results similar to entries 1 and 2 of Table 1, although the yields were not quite as high (we did not analyze for the dimer in these experiments). Interestingly, the reduced product **2** contained 7–8% deuterium.

We next ran a series of experiments at 0°C in an effort to see if a more long-lived organosamarium species could be generated. Blank experiments using a slight deficiency of SmI_2 (1.8 equiv.) showed that at 0°C the color dissipated about 30–40 s after the end of the addition of the iodide. Thus, we choose 1 min as the shortest quench to ensure that the deuterium source was not introduced prior to the consumption of the starting material. In a series of experiments, the time between completion of addition of **1** and addition of the quench was extended from 1 min to 180 min, as shown

© 2000 NRC Canada

Table 2. Reduction of **1** with alcohol additives.

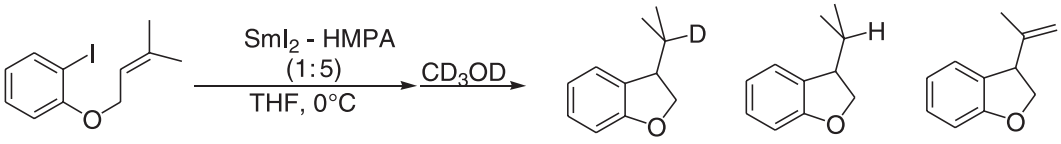


1 (**1** : SmI_2 = 1 : 2.2) **2** **3**

Entry	Additive	Ratio 2:3[b]	Combined yield	%D in **2**
1	^{t}BuOH	**2** only	79%	—
2	CD_3OD	97:3	54%	89[a]
3	After 5 min, CD_3OD	56:44	52%	8[a]
4	After 30 sec, CD_3OD	58:42	68%[c]	7[b]

[a]Based on the ^{1}H NMR spectrum of the crude mixture.
[b]Based on the GC–MS of the crude mixture.
[c]Based on the weight of crude mixture.

Table 3. Reduction of **1** at 0°C with CD_3OD quenching.



1 (**1**:SmI_2 = 1:2.2) **2D** **2H** **3**

Entry	Rxn time (min)[a]	Ratio 2D:2H:3[b]	% Yield (2H+2D+3)[d]
1	0	91:06:03	91
2	1	59:27:14	91
3	2	52:30:18	91
4	4	45:33:22	91
5	5	41:35:24	90
6	10	35:37:28	90
7	20	27:43:30	89
8	30	21:48:31	90
9	40	17:51:32	88
10	50	14:53:33	89
11	60	11:54:35	90
12	180	00:58:42	89

[a]Time between the addition of **1** and CD_3OD.
[b]Based on ^{1}H NMR spectrum.
[c]The CD_3OD was present when **1** was added.
[d]Combined isolated yield.

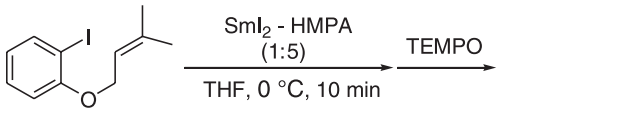
in Table 3, entries 2–12. The Table shows the %D incorporation of **2**D as well as the ratio of **2**D:**2**H:**3**. Accepting that product **2**D is a marker for the formation of an anionic (organosamarium) species, these data show that at least about 60% of **1** is reduced to an anionic species in the absence of an added proton source. Over 3 h, the evolution of this species is revealed by tracing the decrease in the yield of **2**D (to 0%) and the increases in the yield of both **2**H and **3**. Over this time, the combined isolated yield of the three products remains constant (about 90%). Accordingly, the initial 59% of anionic species (reflected by the amount of **2**D in entry 2) decomposed over 3 h to 31% **2**H and 28% **3**.

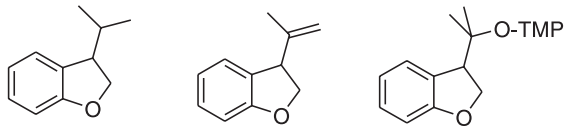
We have recently shown that organosamarium reagents react with TEMPO (12), so we tried duplicate quenching experiments with TEMPO in place of methanol, as shown in Table 4. In addition to **2** and **3**, these experiments also provided the TEMPO quenched product **12**, although the efficiency of the TEMPO quenching (21–23%) at 10 min is considerably less than that of the MeOD quenching (35°C, see Table 3, entry 6). The experiments also prove that reactions were complete when the alcohol or TEMPO quench was added. A separate experiment showed that addition of **1** and SmI_2 to TEMPO provided recovered starting material **1**; presumably, the TEMPO was reduced by SmI_2.

To complement the quenching studies with deuterated methanol, we next prepared hexa-deutero substrates **13a**, **b** shown in Table 5 (see the Experimental section for their synthesis). These substrates were reduced as usual with 1.1

© 2000 NRC Canada

Table 4. Reduction of **1** at 0°C with TEMPO quenching.



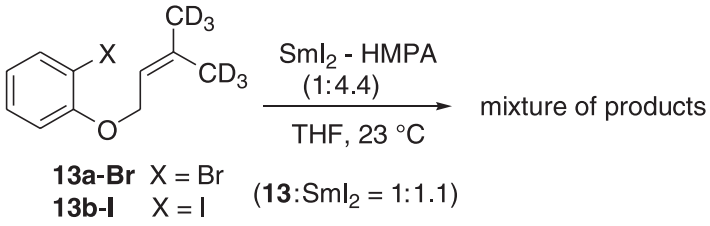


2 **3** **12**

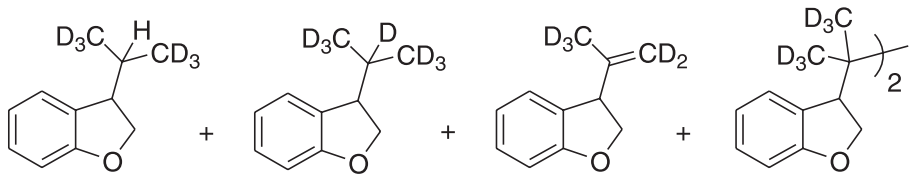
Run	Ratio 1:2:12[a]	Yield of **12**[b]
1	45:32:23	16
2	49:30:21	19

[a]Based on the ^{1}H NMR spectrum of the crude mixture.
[b]Isolated yield.

Table 5. Reduction of deuterated analogs of **1**.



Products



14 **15** **16** **17**

Entry	X	Ratio **14**:**15**:**16**:**17**:**13** (**15**:**16**)[a]
1	I	16:44:34:04:02 (56:44)
2	Br	48:29:23:02:20 (56:44)

[a]Based on ^{1}H NMR spectrum of the product mixture.

equiv. of SmI_2, and then the product ratios were assessed by recording and integrating the crude ^{1}H NMR spectra of the reaction mixtures. The results of these two experiments are shown in Table 5, entries 1,2. While the reduction of the iodide **13b** was instantaneous, the bromide **13a** required 2 h for decolorization of the SmI_2, and 20% unreacted bromide was still recovered after workup. The formation of substantial amounts of d_7 product **15** in both cases clearly shows that protonation cannot account for formation of all the reduced products and that some form of disproportionation is occurring. Interestingly, the reduction of the (less reactive) bromide **13b** gave considerably more of the d_6 (protonated) product **14**. If the increased amount of **14** in the case of bromide was a result of more efficient reduction to the 3°-alkylsamarium reagent, then this could explain why 20% of bromide remained after the samarium was consumed. However, the bromide and iodide must yield the same radical after reduction, so it is unclear how the nature of the original radical precursor can affect the fate of the cyclized radical. Due caution should be exercised in interpreting these experiments due to possible experimental error; in each experiment, the recorded yield of the d_7 product **15** somewhat exceeded that of the d_5 alkene product **16**. This is not possible according to any mechanism, since the average total of deuteria per molecule must be six.

Finally, to gauge the effect of an added ketone, we conducted reduction of **13a** in the presence of ketone **18** (Fig. 2). This experiment is complicated because the ketone

© 2000 NRC Canada

Fig. 2. Coreduction of **13a** and a ketone.

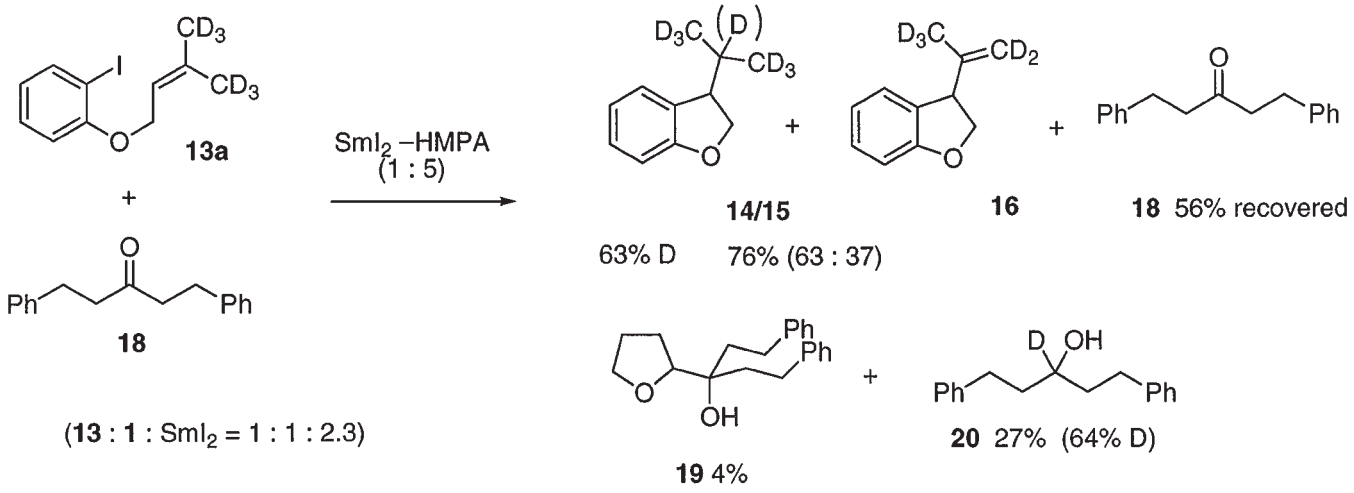
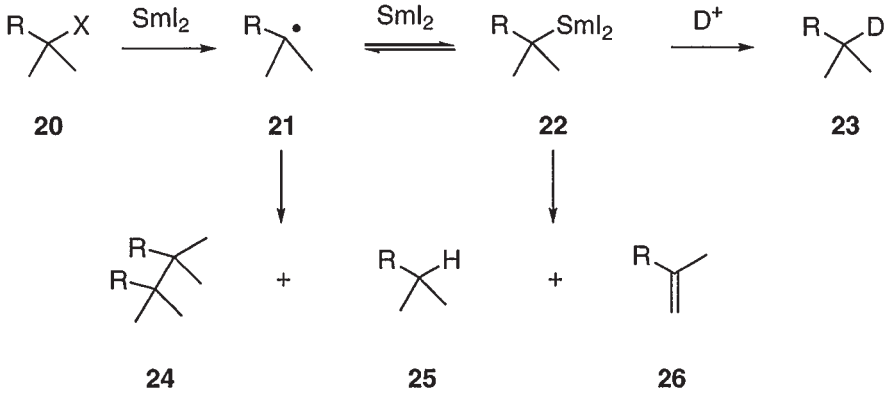


Fig. 3. Pathways for product formation reduction of 3°-halides by SmI_2.



can be reduced in competition with the iodide. As before, disproportionation products **14**/**15**/**16** were produced and the reduction product **14**/**15** contains a significant amount (63%) of deuterium in the methine position. The ratio of reduced product **14**/**15** to alkene **16** is also higher than in the experiments without the ketone. As for the fate of the ketone **16** itself, 56% is recovered unchanged while 4% is trapped as the THF adduct **19** (this product is thought to result from H-abstraction from the THF followed by reduction to an organosamarium reagent and addition to the ketone) (4). About 27% of ketone **18** is reduced to alcohol **20**. In turn, this alcohol also contains 64% D, showing that there is a significant pathway for transfer of allyl hydrogen from **13a**.

Conclusions

The results in this paper provide new insights into the behavior of tertiary radicals in the presence of SmI_2. Some of the possible reaction pathways are illustrated in Fig. 3. Tertiary radical **21** could directly recombine and disproportionate to give the observed products **24**–**26**. Alternatively, it could be reduced to a tertiary alkylsamarium species **22**, which in turn provides the final products either by protonation (to give **23**) in competition with bimolecular disproportionation (to give **24**–**26**) and (or) homolysis back to the radical **21** (that is, the reduction step is reversible). In either case, an equivalent of Sm(II) must be regenerated in tandem with disproportionation.

When the reduction is carried out in the presence of a proton source at either 25°C or 0°C, a good yield of the labeled, reduced product **23** is formed. This strongly suggests that the tertiary organosamarium species **22** is formed. Whether or not the organosamarium species **22** is formed when the reduction is conducted in the absence of proton source is less clear. While proton sources are known to boost the reduction potential of SmI_2 in the absence of HMPA (11), the strong ligating capabilities of HMPA for Sm (10) suggest that it would dampen or eliminate any effect of added proton sources. If this is correct, then the reductions in the absence of the proton source should also provide the tertiary alkyl samarium reagent **22**, and we interpret our inability to efficiently trap this intermediate by subsequent addition of a proton source as due to its instability with respect to disproportionation. Supporting this analysis are the results of the study at 0°C (Table 3), in which a significant amount of the organosamarium reagent was generated and its decomposition to the disproportionation products was followed over time.

While the results support the postulate that a substantial amount of the products derive from alkylsamarium reagents,

© 2000 NRC Canada

they certainly do not exclude the formation of some products through radical reactions. For example, the dimer **24** may form through a radical recombination (although we cannot exclude the possibility of coupling of organosamarium reagents), and the inability to ever observe quantitative deuterium incorporation in the reduced product **23** may point to the occurrence of radical hydrogen transfer reactions from the solvent. In addition, the mechanism of the decomposition of the intermediate organosamarium reagent **22** is also not clear. This reagent could return to the radical **21** by the reverse of the reduction or it could decompose by a number of ionic pathways. At this point, the radical pathway seems less likely since the ratio of disproportionation products to recombination products is higher than that for typical tertiary radicals.

In summary, tertiary halides are not very cooperative partners in a number of C—C bond forming processes mediated by SmI_2. In the past, this has been interpreted by us and others as due to the inability of SmI_2 to reduce 3°-radicals to samarium reagents. Our new results suggest that SmI_2 is more efficient at reducing 3°-radicals than previously thought, and that the problems with subsequent bond forming reactions arise due to the instability of the samarium reagents, which disproportionate over a period of minutes or less at room temperature.

Experimental

Typical procedure for the reduction of *O*-prenyl-2-iodophenol (1) by SmI_2–HMPA in the absence of electrophile

HMPA (0.60 mL, 3.45 mmol) was added to SmI_2 (0.10 M in THF, 8.8 mL, 0.88 mmol) at 23°C. After 1 h, *O*-prenyl-2-iodophenol **1** (0.116 g, 0.402 mmol) in THF (0.7 mL) was added. After 21 h, dry air was bubbled through the mixture until the color changed to light brown and then 0.1 N HCl (20 mL) was added. The mixture was extracted with Et_2O (3 × 20 mL). The combined ether layers were washed with 5% $Na_2S_2O_3$ (1 × 20 mL), sat. NH_4Cl (1 × 20 mL), and brine (1 × 20 mL), and were dried over $MgSO_4$. The ratio of the products (**2**, **3**, and **11**) was determined by recording the ^1H NMR spectrum of the crude mixture. The products were purified by flash chromatography (SiO_2, hexanes/EtOAc = 15:1) to give the dimer **11** (1.6 mg, 2% yield) and a mixture (34.4 mg) of 3-(2-propyl)-2,3-dihydrobenzofuran (**1**) and 3-(propen-2-yl)-2,3-dihydrobenzofuran (**2**). The ratio of these products was determined by ^1H NMR spectrum of the mixture.

(*dl*,*meso*)-2,3-Bis(2,3-dihydrobenzofuran-3-yl)-2,3-dimethylbutane (11)

^1H NMR (300 MHz, $CDCl_3$) (mixture of *dl* and *meso*) δ: 7.23 (2 H, d, *J* = 7.5 Hz), 7.19–7.09 (2 H, m), 6.91–6.77 (8 H, m), 4.78–4.66 (2 H, m), 4.42 (2 H, q, *J* = 9.4 Hz), 3.55 (1 H, dd, *J* = 8.6, 1.6 Hz), 3.48 (1 H, dd, *J* = 9.0, 3.1 Hz), 1.05 (3 H, s), 1.00 (3 H, s), 0.95 (3 H, s), 0.84 (3 H, s). MS (EI) *m*/*z*: 322, 238, 161, 119. HRMS (EI) *m*/*z*: Anal. calcd. for $C_{22}H_{26}O_2$ 322.1933; found: 322.1923.

Typical procedure for the reduction of *O*-prenyl-2-iodophenol (1) in the presence of a proton source

HMPA (0.25 mL, 1.44 mmol) was added to SmI_2 (0.10 M in THF, 3.3 mL, 0.33 mmol) at 23°C. After 30 min, ^{t}BuOH (16 μL, 0.17 mmol) was added, and 5 min later, *O*-prenyl-2-iodophenol (**1**) (42.7 mg, 0.148 mmol) in THF (0.5 mL) was added in one portion at 23°C. After 30 min, dry air was bubbled for 1 min, and then 0.1 N HCl (10 mL) was added. The mixture was extracted with Et_2O (3 × 10 mL). The combined ether layers were washed with 5% $Na_2S_2O_3$ (1 × 10 mL), sat. NH_4Cl (1 × 15 mL), and brine (1 × 15 mL), and were dried over $MgSO_4$. The mixture was passed through a SiO_2 column (eluent: hexanes/Et_2O = 2:1) to give 3-(2-propyl)-2,3-dihydrobenzofuran (**2**) (19.0 mg, 0.117 mmol, 79% yield).

General procedure for the reduction of *O*-prenyl-2-iodophenol (1) by SmI_2–HMPA with CD_3OD quenching

To SmI_2 (0.10 M in THF, 40.0 mL, 4.00 mmol) was added HMPA (3.5 mL, 20 mmol) at 23°C. After 1 h, 3.82 mL of the mixture was transferred to another flask, and cooled to 0°C. A solution of *O*-prenyl-2-iodophenol (**1**) (50 mg, 0.17 mmol) in THF (0.3 mL) was added dropwise over the period of 20 s, and 5 min later, CD_3OD (0.2 mL, 4.9 mmol) was added. After 2 min, air was bubbled through the mixture until the color turned to yellow. After the addition of 0.1 N HCl (5 mL), the mixture was extracted with Et_2O (3 × 5 mL). The combined ether layers were concentrated and the mixture was passed through a short SiO_2 column (eluent: dichloromethane) to give a mixture of products (25.3 mg). The product ratio was determined by ^1H NMR spectrum of the mixture.

Ethyl 3-trideuteriomethyl-4,4,4-trideuterio-2-butenoate

Triethyl phosphonoacetate (20.5 mL, 10.3 mmol) was added dropwise into a suspension of NaH (2.15 g, 89.6 mmol) in THF 100 mL at 0°C. After 5 min, the cooling bath was removed. After 1.5 h, acetone-d_6 (8.0 mL, 0.11 mol) was added. After 2 h, the mixture was poured into 10% NH_4Cl (500 mL), and was extracted with Et_2O (1 × 100 mL and 2 × 50 mL). The combined ether layers were washed with sat. NH_4Cl (1 × 50 mL) and brine (1 × 50 mL), and were dried over $MgSO_4$. The product was purified by distillation (bp = 76.0–76.5°C at 54 mmHg) to give the product (7.57 g, 56.4 mmol, 62% based on NaH). IR (film)(cm^{-1}): 1694, 1144. ^1H NMR (300 MHz, $CDCl_3$) δ: 5.66 (1 H, s), 4.13 (2 H, q, *J* = 7.1 Hz), 1.26 (3 H, t, *J* = 7.1 Hz). ^{13}C NMR (75 MHz, $CDCl_3$) δ: 166.21 (s), 155.72 (s), 115.95 (d), 58.97 (t), 26.0 (m), 18.8 (m), 13.97 (q). MS (EI) *m*/*z*: 134, 106, 89, 83. HRMS (EI) m/*z*: Anal. calcd. for $C_7H_6D_6O_2$ 134.1214; found: 134.1254.

3-Trideuteriomethyl-4,4,4-trideuterio-2-buten-1-ol

DIBALH (1.0 M in hexane, 100 mL, 0.10 mol) was added dropwise to a solution of the above ester (6.76 g, 50.4 mmol) in CH_2Cl_2 (50 mL) at 0°C. After 1.5 h, MeOD (6 mL) was added dropwise. After the mixture became cloudy, sat. potassium sodium tartrate (25 mL) was added. The mixture was poured into Et_2O (150 mL), and 2 N HCl (150 mL) was added. After the separation, the aqueous layer was extracted with Et_2O (1 × 100 mL). The combined organic

© 2000 NRC Canada

layers were washed with 1 N HCl (1 × 50 mL) and brine (2 × 25 mL), and were dried over $MgSO_4$. The product was purified by distillation at normal pressure (bp = 129–139°C) to give alcohol (3.12 g, 33.9 mmol, 67%). IR (film) (cm^{-1}): 3322, 1101, 1070. ^1H NMR (300 MHz, $CDCl_3$) δ: 5.41 (1 H, t, *J* = 7.1 Hz), 4.20–4.08 (2 H, m), 1.20 (1 H, m). ^{13}C NMR (75 MHz, $CDCl_3$) δ: 135.37 (s), 123.76 (d), 58.88 (t), 24.5 (m), 17.0 (m). MS (EI) *m/z*: 92, 74. HRMS (EI) *m/z*: Anal. calcd. for $C_5H_4D_6O$ 92.1108; found: 92.1114.

O-(3-Trideuteriomethyl-4,4,4-trideuterio-2-buten-1-yl)-2-iodophenol (13b)

Diethyl azodicarboxylate (2.96 g, 17.0 mmol) in THF (2 mL) was added into a mixture of 2-iodophenol (3.52 g, 16.0 mmol), PPh_3 (4.20 g, 16.0 mmol), and the above prenyl alcohol-d_6 (1.39 g, 15.1 mmol) in THF (35 mL) at 0°C. The temperature was gradually raised to 23°C. After 16 h, most of the solvent was removed under reduced pressure, and pentane (100 mL) was added to give a precipitate. After the removal of the precipitate by filtration, the product was purified by flash chromatography (SiO_2, hexanes/Et_2O = 30:1) to give **13b** (3.05 g, 10.4 mmol, 69% yield). IR (film) (cm^{-1}): 1469, 1275, 1239, 1016, 748. ^1H NMR (300 MHz, $CDCl_3$) δ: 7.77 (1 H, dd, *J* = 7.7, 1.6 Hz), 7.28 (1 H, dt, *J* = 8.5, 1.6 Hz), 6.82 (1 H, dd, *J* = 8.2, 0.9 Hz), 6.70 (1 H, dt, *J* = 1.1, 7.6 Hz), 5.51 (1 H, t, *J* = 6.5 Hz), 4.58 (2 H, d, *J* = 6.5 Hz). ^{13}C NMR (75 MHz, $CDCl_3$) δ: 157.38, 139.68, 137.68, 129.30, 122.38, 119.52, 112.57, 86.89, 66.16, (two CD_3 carbons were not detected). MS (EI) *m/z*: 294, 221, 75. HRMS (EI) *m/z*: Anal. calcd. for $C_{11}H_7D_6IO$ 294.0388; found: 294.0382.

1-[2-(2,3-Dihydrobenzofuran-3-yl)propyl-2-oxy]-2,2,6,6-tetra-methylpiperidine (12)

HMPA (4.0 mL, 23 mmol) was added to SmI_2 (0.1 M in THF, 44.0 mL, 4.40 mmol) at 23°C. After 14 min, the mixture was cooled to 0°C, and *O*-prenyl-2-iodophenol (**1**) (0.576 g, 2.00 mmol) in THF (2 mL) was added dropwise over the period of 2 min. After 10 min, TEMPO (0.943 g, 6.04 mmol) in THF (1 mL) was added in one portion. After 1 min, a mixture of sat. potassium sodium tartrate (10 mL), sat. $NaHCO_3$ (5 mL), and 5% $Na_2S_2O_3$ (5 mL) was added, and the mixture was extracted with Et_2O (3 × 15 mL). The combined ether layers were washed with 5% $Na_2S_2O_3$ (1 × 15 mL), a mixture of sat. potassium sodium tartrate and sat. $NaHCO_3$ (5 mL each, 1 ×), H_2O (2 × 15 mL), and brine (1 × 15 mL), and were dried over $MgSO_4$. The product was purified by flash chromatography (SiO_2, hexanes/Et_2O = 10:1) to give **12** (0.122 g, 0.385 mmol, 19% yield). IR (film) (cm^{-1}): 1483, 1460, 1375, 1364, 1234, 1132, 748.; ^1H NMR (300 MHz, $CDCl_3$) δ: 7.33 (1 H, d, *J* = 7.3 Hz), 7.13 (1 H, t, *J* = 7.4 Hz), 6.83 (1 H, t, *J* = 7.0 Hz), 6.78 (1 H, d, *J* = 8.0 Hz), 4.73 (1 H, dd, *J* = 9.5, 5.5 Hz), 4.54 (1 H, t, *J* = 9.6 Hz), 3.94 (1 H, dd, *J* = 9.5, 5.4 Hz), 1.68–1.45 (4 H, m), 1.38 (3 H, s), 1.37–1.26 (2 H, m), 1.16 (3 H, s), 1.154 (3 H, s), 1.146 (3 H, s), 1.12 (3 H, s), 1.11 (3 H, s). ^{13}C NMR (75 MHz, $CDCl_3$) δ: 161.10 (s), 128.75 (s), 128.36 (d), 125.72 (d), 119.99 (d), 109.54 (d), 80.90 (s), 73.34 (t), 59.56 (s), 59.43 (s), 53.25 (d), 40.96 (t), 35.23 (q), 35.13 (q), 23.71 (q), 23.32 (q), 23.71 (q), 23.32 (q), 21.03 (q), 20.90 (q), 17.18 (t). MS (CI) *m/z*: 318 [M + H], 157, 142.

O-(3-Trideuteriomethyl-4,4,4-trideuterio-2-buten-1-yl)-2-bromo-phenol (13a)

Diethyl azodicarboxylate (2.96 g, 17.0 mmol) in THF (2 mL) was added into a mixture of 2-bromophenol (2.78 g, 16.1 mmol), PPh_3 (4.20 g, 16.0 mmol), and the above alcohol (1.38 g, 15.0 mmol) in THF (40 mL) at 0°C. The temperature was gradually raised to 23°C. After 17.5 h, most of the solvent was removed under reduced pressure, and pentane (100 mL) was added to give a precipitate. After the removal of the precipitate by filtration, the product was purified by flash chromatography (SiO_2, hexanes/Et_2O = 10:1) followed by distillation (bp = 90–98°C at 0.2 mmHg) to give **13a** (2.64 g, 10.7 mmol, 71% yield). IR (film) (cm^{-1}): 1476, 1276, 1030, 744 ^1H NMR (300 MHz, $CDCl_3$) δ: 7.54 (1 H, dd, *J* = 7.7, 1.6 Hz), 7.24 (1 H, dt, *J* = 1.6, 7.4 Hz), 6.90 (1 H, dd, *J* = 8.3, 1.1 Hz), 6.82 (1 H, dt, *J* = 1.5, 7.7 Hz), 5.51 (1 H, t, *J* = 6.6 Hz), 4.60 (2 H, d, *J* = 6.6 Hz). ^{13}C NMR (75 MHz, $CDCl_3$) δ: 155.11, 137.21, 128.26, 121.60, 119.40, 113.52, 112.19, 65.93, (two CD_3 carbons were not detected). MS (EI) *m/z*: 248, 246, 228, 188, 186, 175, 173. HRMS (EI) *m/z*: Anal. calcd. for $C_{11}H_7D_6BrO$ 246.0526; found: 246.0490.

General procedure for the reduction of *O*-prenyl(d_6)-2-halophenol 13a, b by SmI_2–HMPA

To SmI_2 (0.10 M in THF, 11.0 mL, 1.10 mmol) was added HMPA (0.85 mL, 4.89 mmol) at 23°C. After 20 min, *O*-prenyl(d_6)-2-iodophenol (**13a**) (0.299 g, 1.02 mmol) in THF (1 mL) was added. After 8 h, dry air was bubbled until the mixture turned to yellow, and then 0.1 N HCl (15 mL) was added. After the extraction with Et_2O (3 × 10 mL), the combined ether layers were washed with 5% $Na_2S_2O_3$ (1 × 10 mL), 0.1 N HCl (1 × 10 mL), and brine (1 × 10 mL), and were dried over $MgSO_4$. The crude mixture was passed through a SiO_2 column (eluent: hexanes/Et_2O = 10:1) to give a mixture of products (0.130 g). The products ratio was determined by ^1H NMR spectrum of the mixture.

SmI_2 reduction of *O*-prenyl(d_6)-2-iodophenol (13a) in the presence of the ketone 18

HMPA (0.95 mL, 5.5 mmol) was added to SmI_2 (0.1 M in THF, 11.0 mL, 1.10 mmol) at 23°C. After 50 min, a mixture of *O*-prenyl(d_6)-2-iodophenol (**13a**) (0.142 g, 0.483 mmol) and 1,5-diphenylpentan-3-one (**18**) (0.120 g, 0.504 mmol) in THF (1 mL) was added in one portion. After 1 h, dry air was bubbled through the mixture, and then 0.1 N HCl (15 mL) and brine (5 mL) were added. After the extraction with Et_2O (3 × 10 mL), the combined ether layers were washed with 5% $Na_2S_2O_3$ (1 × 10 mL), 0.1 N HCl (1 × 10 mL), and brine (1 × 10 mL), and were dried over $MgSO_4$. The products were separated by flash chromatography (SiO_2, hexanes/EtOAc = 10:1 – 5:1) to give a mixture of 3-(2-propyl)-2,3-dihydrobenzofuran (d_6 and d_7) (**14** and **15**) and 3-(propen-2-yl)-2,3-dihydrobenzofuran (d_5) (**16**) (61.1 mg), a mixture of 1,5-diphenyl-3-pentanol (**20**) and 1,5-diphenyl-3-(2-tetrahydrofuranyl)-3-pentanol (**19**) (39.1 mg), and 1,5-diphenyl-3-pentanone (**18**) (67.0 mg, 56% recovery).

1,5-Diphenyl-3-(tetrahydrofuran-2-yl)pentan-3-ol (19)

The authentic sample of **19** was prepared as follows: HMPA (0.95 mL, 5.46 mmol) was added to SmI_2 (0.1 M in

© 2000 NRC Canada

THF, 11 mL, 1.1 mmol) at 23°C. After 40 min, a mixture of iodobenzene (0.334 g, 1.64 mmol) and 1,5-diphenylpentan-3-one (**18**) (113.9 mg, 0.478 mmol) in THF (1 mL) was added. After 21 h, 0.1 N HCl (15 mL) was added. The mixture was extracted with Et_2O (3 × 10 mL). The combined ether layers were washed with 5% $Na_2S_2O_3$ (1 × 10 mL), 0.1 N HCl (1 × 10 mL), and brine (1 × 10 mL), and dried over $MgSO_4$. The product was purified by flash chromatography (SiO_2, hexanes/EtOAc = 5:1 – 3:1) to give **19** (0.124 g, 0.398 mmol, 83% yield). IR (film) (cm^{-1}): 3461, 1495, 1453, 1066, 749, 699.; ^1H NMR (300 MHz, $CDCl_3$) δ: 7.37–7.13 (10 H, m), 3.94–3.77 (3 H, m), 2.83–2.57 (4 H, m), 2.08 (1 H, s), 2.07–1.82 (7 H, m), 1.73 (1 H, dt, J = 5.3, 12.6 Hz). ^{13}C NMR (75 MHz, $CDCl_3$) δ: 142.56 (s), 142.44 (s), 128.49 (d), 128.42 (d), 125.94 (d), 125.81 (d), 83.32 (d), 74.47 (s), 68.58 (t), 38.89 (t), 36.59 (t), 30.27 (t), 29.79 (t), 26.27 (t), 25.59 (t). MS (EI) *m*/*z*: 239, 91. HRMS (EI) *m*/*z*: Anal. calcd. for $C_{17}H_{19}O$ [M – C_4H_7O] 239.1436; found: 239.1437.

Acknowledgments

We thank the National Institutes of Health for funding this work.

References

1. (*a*) A. Krief and A.M. Laval. Chem. Rev. **99**, 745 (1999); (*b*) R. Nomura and T. Endo. Chem. Eur. J. **4**, 1605 (1998); (*c*) G.A. Molander. *In* Comprehensive organic synthesis. Vol. 1. *Edited by* B.M. Trost and I. Fleming. Pergamon, Oxford. 1991. p. 251. (*d*) F.A. Khan and R. Zimmer. J. Prakt. Chem. Chem. Ztg. **339**, 101 (1997); (*e*) M. Murakami and Y. Ito. J. Organometal. Chem. **473**, 93 (1994); (*f*) G.A. Molander. *In* Organic reactions. Vol. 46. *Edited by* L.A. Paquette. Wiley, N.Y. 1994. p. 211. (*g*) G.A. Molander. Chem. Rev. **92**, 29 (1992); (*h*) J.A. Soderquist. Aldrichimica Acta, **24**, 15 (1991).
2. (*a*) G.A. Molander amd C.R. Harris. Tetrahedron, **54**, 3321 (1998); (*b*) T. Skrydstrup. Angew. Chem. Int. Ed. Eng. **36**, 345 (1997); (*c*) G.A. Molander and C.R. Harris. Chem. Rev. **96**, 307 (1996); (*d*) D.P. Curran and R.L. Wolin. Synlett. 317 (1991); (*e*) T.L. Fevig, R.L. Elliott, and D.P. Curran. J. Am. Chem. Soc. **110**, 5064 (1988).
3. E. Hasegawa and D.P. Curran. Tetrahedron Lett. **34**, 1717 (1993).
4. (*a*) D.P. Curran, T.L. Fevig, C.P. Jasperse, and M.J. Totleben. Synlett. 943 (1992); (*b*) D.P. Curran and M.J. Totleben. J. Am. Chem. Soc. **114**, 6050 (1992); (*c*) G.A. Molander and J.A. McKie. J. Org. Chem. **56**, 4112 (1991).
5. G.A. Molander and J.A. McKie. J. Org. Chem. **58**, 7216 (1993).
6. M. Hojo, H. Harada, J. Yoshizawa, and A. Hosomi. J. Org. Chem. **58**, 6541 (1993).
7. (*a*) X.H. Du and R.W. Armstrong. J. Org. Chem. 62, 5678 (1997); (*b*) X.H. Du and R.W. Armstrong. Tetrahedron Lett. **39**, 2281 (1998).
8. J. Inanaga, O. Ujikawa, and M. Yamaguchi. Tetrahedron Lett. **32**, 1737 (1991).
9. D.P. Curran, X. Gu, W. Zhang, and P. Dowd. Tetrahedron, **53**, 9023 (1997).
10. (*a*) M. Shabangi and R.A. Flowers. Tetrahedron Lett. **38**, 1137 (1997); (*b*) M. Shabangi, J.M. Sealy, J.R. Fuchs, and R.A. Flowers. Tetrahedron Lett. **39**, 4429 (1998).
11. E. Hasegawa and D.P. Curran. J. Org. Chem. **58**, 5008 (1993).
12. T. Nagashima and D.P. Curran. Synlett. 330 (1996).

© 2000 NRC Canada

Trifluoroacetic acid-mediated intramolecular formal N-H insertion reactions with amino-α-diazoketones: a facile and efficient synthesis of optically pure pyrrolidinones and piperidinones

Hua Yang, Valdas Jurkauskas, Nicole Mackintosh, Tobias Mogren, Corey R. J. Stephenson, Katherine Foster, William Brown, and Edward Roberts

Abstract: Trifluoroacetic acid (TFA) was found to promote intramolecular formal N-H insertion reactions. Upon treatment with TFA, optically pure *N*-Boc-β′-amino-α-diazoketones (**5a**–**c**) and *N*-Boc-γ′-amino-α-diazoketones (**10a**–**d**) can be converted, with retention of chirality, into pyrrolidinones (**11a**–**c**) and piperidinones (**12a**–**d**), respectively, with concomitant removal of the Boc group, in good to excellent yields.

Key words: α-diazoketone, amino acid, pyrrolidinone, piperidinone, N-H insertion.

Résumé : Le TFA induit des réactions d'insertion formelle de N-H intramoléculaires. Par traitement avec du TFA, les *N*-Boc-β′-amino-α-diazocétones (**5a**–**c**) et les *N*-Boc-γ′-amino-α-diazocétones (**10a**–**d**) optiquement pures peuvent être converties avec rétention de chiralité en pyrrolidinones (**11a**–**c**) et pipéridinones (**12a**–**d**) avec déprotection simultanée de l'amine dans de bons à excellents rendements.

Mots clés : α-diazocétone, acide aminé, pyrrolidinone, pipéridinone, insertion de N-H.

Introduction

C—N bond forming reactions are one of the most interesting research areas in synthetic organic and medicinal chemistry (for recent reviews on the synthesis of C—N bond containing heterocycles see ref. (1)). N-H insertion reactions with α-diazoketones are one of the frequently utilized techniques to form C—N bonds (for recent reviews on the applications of N-H insertion reactions with α-diazoketones in organic synthesis, see ref. (2)). These N-H insertion reactions can be performed either in an intermolecular or intramolecular fashion (2). The intramolecular N-H insertion reactions give access to a variety of heterocyclic molecules, including azetidinones (for selected examples of N-H insertion reactions to generate azetidinone derivatives, see ref. (3)), pyrrolidinones (for selected examples of N-H insertion reactions to form pyrrolidinone derivatives, see ref. (4) and also refs. (3*e*) and (5*b*)), and piperidinones (for selected examples of N-H insertion reactions to form piperidinone derivatives see ref. (5) and also ref. (4*a*), (4*c*)), which have been widely used in drug discovery processes (for selected examples, see ref. (6)). These reactions with α-diazoketones commonly employ metal catalysts, such as rhodium(II) and copper(I). However, Rh(II) and Cu(I) catalyzed N-H insertion reactions are sometimes accompanied with a significant level of C-H insertion or other side reactions (2, 3*d*, 4*a*), depending upon the structures of the α-diazoketones.

As part of the ongoing research program exploiting the chemistry of α-diazoketones and its applications in medicinal chemistry at our laboratory, we have found that upon treatment with trifluoroacetic acid (TFA), *N*-Boc-α-amino α′-diazoketones can be converted into 1,3-oxazine-2,5-diones via an intramolecular oxygen insertion pathway with good to excellent yields (Scheme 1).[2] It is of interest to investigate if the oxygen insertion reaction could also be conducted with homolagated *N*-Boc-amino-α-diazoketones. Surprisingly,

Received November 30, 1999. Accepted March 11, 2000. Published on the NRC Research Press website on June 7, 2000.

This paper is dedicated to Professor Stephen Hanessian on the occasion of his 65th birthday.

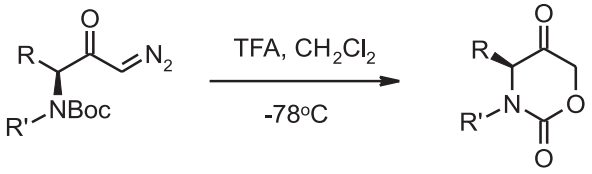
H. Yang,[1] V. Jurkauskas, N. Mackintosh, T. Mogren, C.R.J. Stephenson, K. Foster, W. Brown, and E. Roberts. Chemistry Department, AstraZeneca R&D Montreal, 7171 Frederick-Banting, Ville St. Laurent, Quebec, Canada, H4S 1Z9

[1]Author to whom correspondence may be addressed. Telephone: (514) 832-3200 ext. 2404. Fax: (514) 832-3232. e-mail: hua.yang@astrazeneca.com

[2]H. Yang, T. Mogren, C.R.J. Stephenson, V. Jurkauskas, W. Brown, and E. Roberts. Unpublished results. Upon treatment of the *N*-Boc-α-amino-α′-diazoketones with TFA, *1,3*-oxazine-*2,5*-diones were produced with good to excellent yields. Presumably the reactions proceed through a six-membered ring oxonium intermediate, which was generated from an intramolecular oxygen addition. In situ FTIR studies of the reactions suggested the presence of the oxonium intermediate before it cleaved the *tert*-butyl to the final product.

 © 2000 NRC Canada

Scheme 1.



treatment of the *N*-Boc-β-amino-α′-diazoketones and *N*-Boc-γ-amino-α′-diazoketones with TFA, respectively, results in the isolation of the corresponding pyrrolidinones and piperidinones, presumably via an intramolecular formal N-H insertion pathway. It has been documented in the literature that protic acid and Lewis acid can also promote other intramolecular reactions, such as C—C bond formation from α-diazoketones (*2a*). Thus, the results we found would further extend the utility of acid-mediated intramolecular cyclization with α-diazoketones. In this paper, we would like to report our research efforts on the synthesis of pyrrolidinones and piperidinones using TFA-mediated formal N-H insertion reactions with amino-α-diazoketones.

Results and discussion

Synthesis of the β′-amino-α-diazoketones

Synthesis of the precursors of the *N*-Boc-β′-amino-α-diazoketones can be accomplished starting from commercially available α-amino acids, as depicted in Scheme 2. The commercially available *N*-Boc-α-amino acids (**1a**–**c**) were treated with *i*-BuOCOCl followed by diazomethane (*3b*) to afford α-diazoketones (**2a**–**c**). Silver benzoate-catalyzed Wolff rearrangement reactions (7) with compounds **2a**–**c** followed by hydrolysis resulted in the formation of homologated β′-amino-acids (**4a**–**c**). Repetition of steps 1 and 2 with **4a**–**c** furnished the desired precursors *N*-Boc-β′-amino-α-diazoketones (**5a**–**c**).

Synthesis of the γ′-amino-α-diazoketones

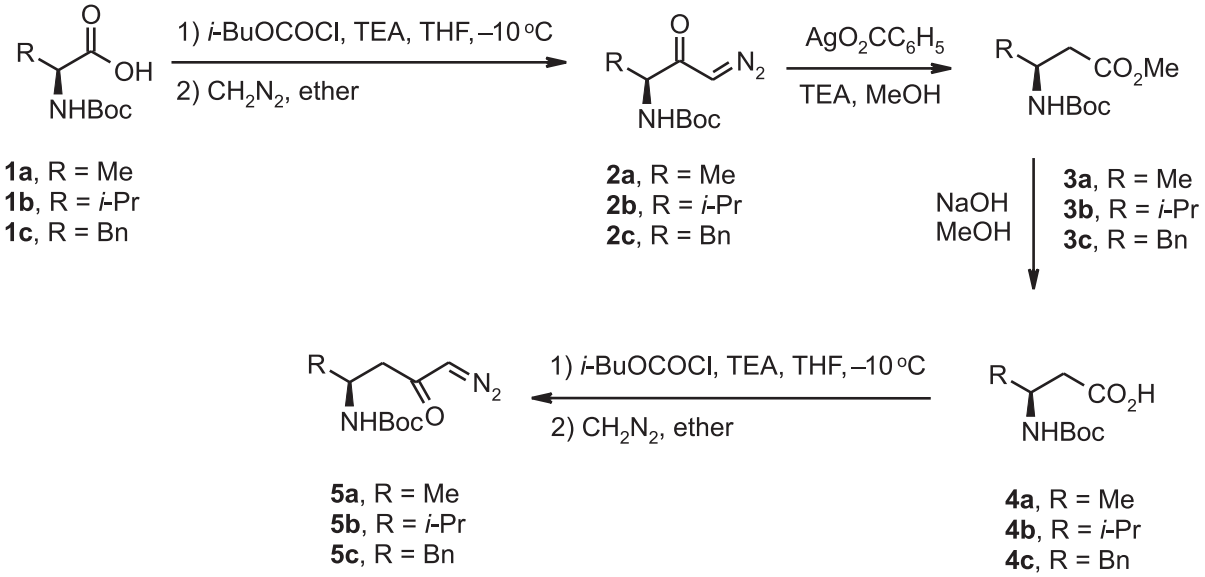
The synthesis of the *N*-Boc-γ′-amino-α-diazoketones can also be efficiently achieved starting from commercially available *N*-Boc-α-amino-acids, as shown in Scheme 3. DIBAL-H reduction of methyl esters **6a**–**d** followed by in situ Wittig reaction (8) gave the α, β-unsaturated methyl esters **7a**–**d**. Treatment of the esters **7a**–**d** with a sequence of reactions, involving hydrolysis, hydrogenation, mixed anhydride generation, and diazomethane coupling, resulted in the isolation of the desired precursors *N*-Boc-γ′-amino-α-diazoketones (**10a**–**d**). With both types of the precursors in hand, we set the stage to examine the TFA mediated intramolecular formal N-H insertion reactions with **5a**–**c** and **10a**–**d**.

Results and discussion

First, we examined the TFA-mediated reactions with the corresponding *N*-Boc-β′-amino-α-diazoketones. Thus, these *N*-Boc-β′-amino-α-diazoketones (**5a**–**c**) were treated with TFA in dichloromethane at –78°C. Interestingly, an intramolecular formal N-H insertion reaction was observed with concomitant removal of the Boc group, instead of the oxygen insertion, resulting in the generation of five-membered-ring pyrrolidinones **11a**–**c** in good to excellent yields (84–93%), as shown in Table 1.

All these reactions had gone to completion in less than 5 min. These reactions were very clean, and usually required no further purification after evaporation and washing with ether prior to subsequent chemical manipulations, such as reductive amination. However, a low concentration is essential to ensure a clean and high-yielding formal intramolecular N-H insertion. It is noted that concentrations of 0.005 M were sufficient for most of the reactions tested thus far. We reasoned that a low concentration might prevent side reactions related to intermolecular couplings with the diazo moiety. In contrast, *N*-Boc-α′-amino-α-diazoketones can undergo TFA-mediated intramolecular oxygen insertion reactions at concentrations as high as 0.5 M, without compromising the quality of the reaction.[2] This difference implies that the six-

Scheme 2.



© 2000 NRC Canada

Scheme 3.

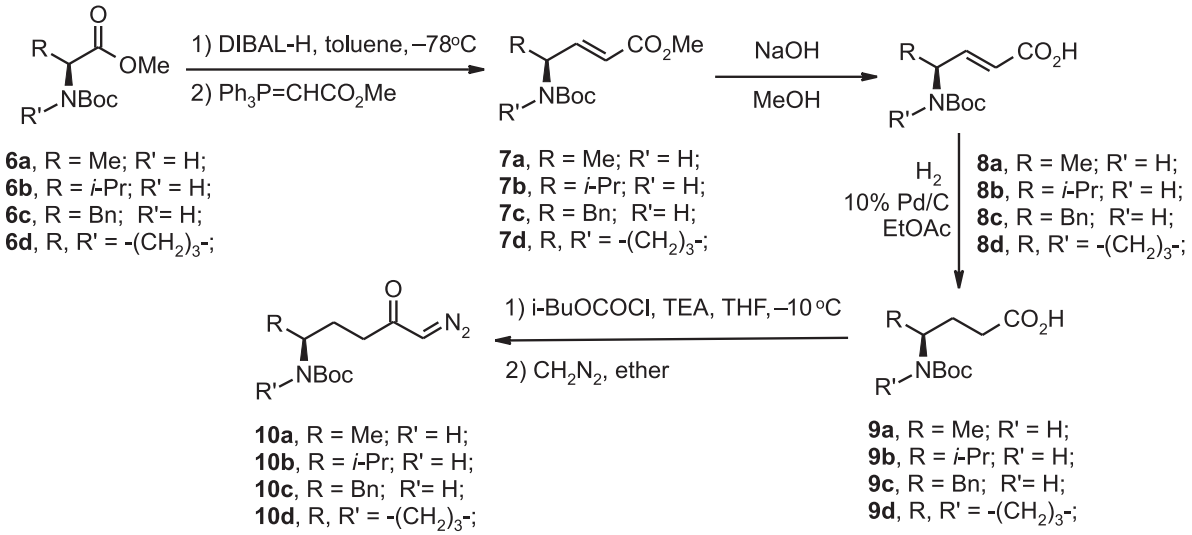
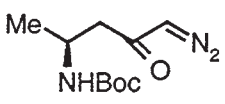
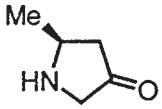
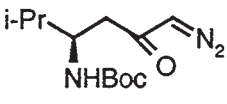
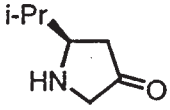
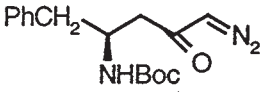
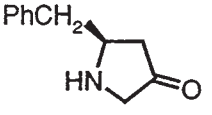


Table 1.[a] TFA mediated reactions with *N*-Boc-β′-amino-α-diazoketones.

Entry	Diazoketone	Product[b]	Yield[c]	$[\alpha]_D$[d]
1	 **5a**	 **11a**	86%	+162.5° (c 0.20)
2	 **5b**	 **11b**	93%	+84.4° (c 0.25)
3	 **5c**	 **11c**	84%	+41.6° (c 0.25)

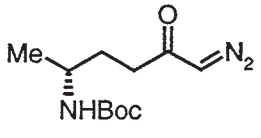
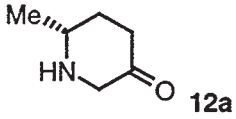
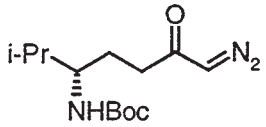
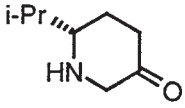
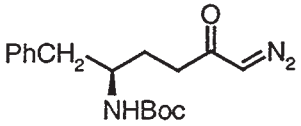
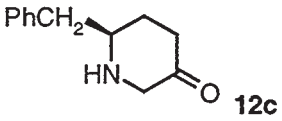
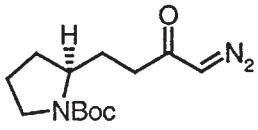
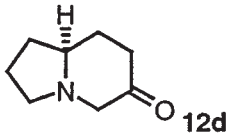
[a] All reactions were run using the procedures as described in the experimental section (average of two runs for each reaction).
[b] TFA salt.
[c] Isolated yield.
[d] $[\alpha]_D$s were measured as a TFA salt in methanol.

membered ring oxygen insertion may be a much more efficient process than the five-membered ring nitrogen insertion in the cases we have studied thus far. Presumably, the nucleophilicity of the nitrogen atom was markedly reduced by the Boc group.

Next, the *N*-Boc-γ′-amino-α-diazoketones **10a**–**c** were treated with TFA in dichloromethane at –78°C. Not surprisingly, six-membered ring piperidinones **12a**–**c** were isolated with good to excellent yields (62–88%), after removal of the solvent and the excess TFA (entries 1–3, Table 2). Presumably, a formal N-H insertion with concomitant cleavage of the Boc group is involved, an observation similar to the five-membered ring pyrrolidinone generation reactions. Interestingly, the construction of the six-membered ring piperidinones is as efficient as that of the five-membered ring pyrrolidinones. They are all very clean, and no further purification is required after removal of the solvent and the excess TFA, provided that low concentrations are applied while running the reactions. The fact that high concentrations may increase the level of potential side reactions also

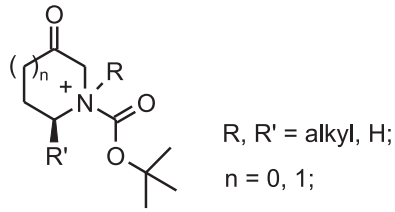
© 2000 NRC Canada

Table 2.[a] TFA mediated reactions with *N*-Boc-γ′-amino-α-diazoketones.

Entry	Diazoketone	Product[b]	Yield[c]	$[\alpha]_D$[d]
1	 **10a**	 **12a**	69%	-57.1° (c 0.21)[e]
2	 **10b**	 **12b**	79%	-30.7° (c 0.37)[e]
3	 **10c**	 **12c**	62%	+19.6° (c 0.24)[f]
4	 **10d**	 **12d**	88%	+172.9° (c 0.36)

[a]All reactions were run using the procedures as described in the experimental section (average of two runs for each reaction).
[b]TFA salt.
[c]Isolated yield.
[d]$[\alpha]_D$s were measured as a TFA salt in dichloromethane.
[e]Prepared from the corresponding *D*-α-amino acid.
[f]$[\alpha]_D$ was measured as a TFA salt in methanol.

Scheme 4.



suggests that a six-membered ring formal N-H insertion reaction is not as efficient as the six-membered ring oxygen insertion in the cases we have studied thus far.[2]

We also examined the chemistry of *N*-Boc-γ′-amino-α-diazoketone **10d**, derived from *N*-Boc-proline (Scheme 3) under the reaction condition described above. Interestingly, α-diazoketone **10d** (entry 4, Table 2) underwent a formal intramolecular N-H insertion reaction with concomitant Boc removal to afford the expected azobicyclic molecule **12d**. This reaction continues to have enjoyed the characteristics of the TFA-mediated intramolecular formal N-H insertion reaction, being fast (<5 min) and clean at low concentrations.

We believe that all the intramolecular formal N-H insertion reactions in Tables 1 and 2 may proceed through the same type of intermediate: nitronium species, as depicted in Scheme 4. The neutralization of the cation intermediate may constitute the driving force in the subsequent step of cleaving the Boc group. In situ FTIR studies of the intramolecular formal N-H insertion reactions with these amino-α′-diazoketones support this hypothesis. The poor nucleophilicity of the TFA counteranion together with low concentration may have suppressed the possible undesired intermolecular reactions. The detailed results of the mechanistic studies of the TFA-mediated intramolecular formal N-H insertion will be reported in due course.

Conclusions

We have demonstrated that TFA is an efficient reagent to promote intramolecular formal N-H insertion reactions with *N*-Boc-β′- and γ′-amino-α-diazoketones. A nitronium species might be involved in this transformation. Pyrrolidinones, piperidinones, and azabicyclic molecules have been readily prepared using this method. This method will find a variety of applications in synthetic organic and medicinal chemistry (9), complementary to the existing synthetic methodology (2).

© 2000 NRC Canada

Experimental part

General

Specific optical rotations ($[\alpha]_D$) were measured on a Perkin–Elmer 243B Polarimeter using a 1 dm path length micro cell and are reported in deg dm^{-1}. The concentration (*c*) is given in 10 mg mL^{-1} in the specified solvent. NMR spectra were recorded on a Varian 400GX Fourier Transform Spectrometer. The chemical shifts (δ) are expressed in parts per million (ppm) and coupling constants (*J*) are reported in Hertz (Hz). Infrared spectra were recorded on a Perkin–Elmer FTIR Spectrometer Paragon 1000 (ν in cm^{-1}). Mass spectroscopy data were obtained using either a Micromass Quattro LC (LC–MS–MS) or a Micromass LCT (time of flight) spectrometer; HRMS data were obtained by the University of Montreal mass spec. facility. Thin layer chromatography was performed on Silica Gel 60 F_{254} precoated plates and visualized with ultraviolet light and developed by staining with either basic potassium permanganate solution or acidic ammonium molybdate (IV). Column chromatography was carried out using Silica Gel 60 (70–230 mesh).

Organic solvents were used as purchased in sure sealed bottles and stored on molecular sieves. All reagents were used as received from commercial suppliers unless otherwise stated.

Diazomethane was prepared by dissolving Diazald® in diethyl ether and the resulting solution was added dropwise to a stirring solution of KOH in ethanol and water at 65°C. Diazomethane solution in diethyl ether obtained by distillation from the reaction's mixture is used without further purification (10).

N-Boc-α-amino-α′-diazoketones

General procedure A

The α-amino acid was dissolved in THF and cooled to –10°C. Triethylamine was added followed by the dropwise addition of isobutylchloroformate. The reaction was stirred at –10°C, under a nitrogen atmosphere, for 20 min then the white precipitate was filtered through celite. The filtrate was cooled to –10°C and freshly prepared diazomethane was added dropwise. The reaction was allowed to warm to room temperature and stirred for 18 h. The reaction was quenched with saturated aqueous NH_4Cl and the resulting layers were separated. The aqueous layer was extracted with EtOAc (3×) and the combined organic layers were washed with H_2O (1×) and saturated aqueous NaCl (1×), dried over Na_2SO_4, filtered, and concentrated.

(3S)-tert-*Butyl 3-diazo-1-methyl-2-oxopropylcarbamate (**2a**)*: Following the general procedure A. (2*S*)-*N*-Boc-alanine **1a** (3.0 g, 15.8 mmol) in THF (100 mL) with triethylamine (6.6 mL, 47.0 mmol) and isobutylchloroformate (2.5 mL, 19.0 mmol). Approximately 2 equiv. of diazomethane in ether solution. MPLC (Silica gel 60, EtOAc–Heptane (50:50)) gave **2a** as a yellow solid (2.84 g, 84%). IR (NaCl disc) υ: 3334, 2978, 2106, 1701, 1636, 1517, 1453, 1366, 1166 cm^{-1}. ^1H NMR (400 MHz, $CDCl_3$) δ: 1.33 (3H, d, *J* = 6.6 Hz), 1.44 (9H, s), 4.22 (1H, brs), 5.11 (1H, brs), 5.43 (1H, brs).

(3S)-tert-*Butyl 3-diazo-1-isopropyl-2-oxopropylcarbamate (**2b**)*: Following the general procedure A. (2*S*)-*N*-Boc-valine **1b** (3.0 g, 13.8 mmol) in THF (100 mL) with triethylamine (5.8 mL, 41.4 mmol) and isobutylchloroformate (2.2 mL, 16.5 mmol). Approximately 2 equiv. of diazomethane in ether solution. MPLC (Silica gel 60, EtOAc–Heptane (50:50)) gave **2b** as a yellow oil (3.08 g, 92%). IR (NaCl disc) υ: 3334, 2967, 2105, 1716, 1698, 1650, 1634, 1519, 1504, 1367, 1172 cm^{-1}. ^1H NMR (400 MHz, $CDCl_3$) δ: 0.89 (3H, d, *J* = 7.3 Hz), 0.98 (3H, d, *J* = 6.6 Hz), 1.44 (9H, s), 2.08 (1H, q, *J* = 6.3 Hz), 4.06 (1H, brs), 5.13 (1H, brs), 5.42 (1H, brs).

(3S)-tert-*Butyl 1-benzyl-3-diazo-2-oxopropylcarbamate (**2c**)*: Following the general procedure A. (2*S*)-*N*-Boc-phenylalanine **1c** (3.0 g, 11.3 mmol) in THF (100 mL) with triethylamine (4.7 mL, 34.0 mmol) and isobutylchloroformate (1.8 mL, 13.5 mmol). Approximately 2 equiv. of diazomethane in ether solution. MPLC (Silica gel 60, EtOAc–Heptane (50:50)) gave **2c** as a brown solid (3.30 g, 100%). IR (NaCl disc) υ: 3334, 2976, 2359, 2106, 1706, 1698, 1635, 1496, 1366, 1166 cm^{-1}; ^1H NMR (400 MHz, $CDCl_3$) δ: 1.41 (9H, s), 3.03 (2H, d, *J* = 6.6 Hz), 4.42 (1H, brs), 5.09 (1H, brs), 5.22 (1H, brs), 7.17–7.34 (5H, m).

N-Boc-β-amino acid methyl esters

General procedure B

A solution of silver benzoate in triethylamine was added dropwise to a solution of α-diazoketone in MeOH at room temperature under a nitrogen atmosphere. Upon addition of the silver benzoate, bubbles were observed, the reaction darkened in color. It was noted that the reaction was exothermic. The resulting mixture was allowed to stir for 18 h and filtered through Celite® and concentrated to give a crude sample which was purified by MPLC.

*Methyl (3S)-3-[(*tert-*butoxycarbonyl)amino]butanoate (**3a**)*: Following the general procedure B. α-Diazoketone **2a** (2.84 g, 13.3 mmol) in MeOH (100 mL) and silver benzoate (0.31 g, 1.33 mmol) in triethylamine (10 mL). MPLC (Silica gel 60, EtOAc–Heptane (50:50)) gave **3a** as a yellow solid (2.77 g, 96%). ^1H NMR (400 MHz, $CDCl_3$) δ: 1.21 (3H, d, *J* = 6.6 Hz), 1.44 (9H, s), 2.45–2.57 (2H, m), 3.69 (3H, s), 4.04 (1H, brs), 4.94 (1H, brs). MS (*m*/*z*): 218.16 (M + H).

*Methyl (3R)-3-[(*tert-*butoxycarbonyl)amino]-4-methylpentanoate (**3b**)*: Following the general procedure B. α-Diazoketone **2b** (3.07 g, 12.7 mmol) in MeOH (100 mL) and silver benzoate (0.29 g, 1.27 mmol) in triethylamine (10 mL). MPLC (Silica gel 60, EtOAc–Heptane (50:50)) gave **3b** as a yellow oil (2.92 g, 93%). ^1H NMR (400 MHz, $CDCl_3$) δ: 0.92 (6H, d, *J* = 6.6 Hz), 1.45 (9H, s), 1.72–1.86 (1H, m), 2.41–2.57 (2H, m), 3.68 (3H, s), 3.69–3.80 (1H, m), 4.86 (1H, brs). MS (*m*/*z*): 246.15 (M + H).

*Methyl (3S)-3-[(*tert-*butoxycarbonyl)amino]-4-phenylbutanoate (**3c**)*: Following the general procedure B. α-Diazoketone **2c** (3.20 g, 11.0 mmol) in MeOH (100 mL) and silver benzoate (0.259 g, 1.10 mmol) in triethylamine (10 mL). MPLC (Silica gel 60, EtOAc–Heptane (50:50)) gave **3c** as a yellow oil (3.25 g, 100%). ^1H NMR (400 MHz, $CDCl_3$) δ: 1.41 (9H, s), 2.40–2.55 (2H, m), 2.75–2.98 (2H, m), 3.69 (3H, s),

© 2000 NRC Canada

4.06–4.21 (1H, m), 5.04 (1H, brs), 7.10–7.32 (5H, m). MS (*m*/*z*): 294.14 (M + H).

N-Boc-γ-amino-α,β-unsaturated methyl esters

General procedure C

0.5 M solution of DIBAL-H (2 equiv.) in toluene at –78°C was added dropwise over 2 h to a solution of *N*-Boc-α-amino acid methyl ester in toluene (0.1 M) at –78°C. The reaction was monitored by TLC. Methanol was added at this temperature and the resulting mixture stirred for additional 30 min. Then methyl (triphenylphosphoranylidene) acetate (1.15 equiv.) was added at –78°C and the resulting mixture stirred for 12 h allowing it to warm to room temperature. The mixture was filtered over Celite®, washed with warm ethyl acetate, concentrated in vacuo, and purified by chromatography.

*Methyl (E,4R)-4-[(*tert-*butoxycarbonyl)amino]-2-pentenoate (**7a**)*: Following the general procedure C. (2*R*)-*N*-Boc-alanine methyl ester **6a** (1.00 g, 4.92 mmol) in toluene (100 mL) at –78°C and DIBAL-H (9.64 mL, 9.64 mmol, 1 M in toluene). Reaction was quenched with MeOH (1 mL). Added methyl (triphenylphosphoranylidene) acetate (1.90 g, 5.69 mmol). Chromatography (Silica gel 60, EtOAc–Heptane (30:70)) gave unsaturated ester **7a** as a colorless oil (0.812 g, 72%). ^{1}H NMR (400 MHz, $CDCl_3$) δ: 1.25 (3H, d, *J* = 6.6 Hz), 1.44 (9H, s), 3.77 (3H, s), 4.40 (1H, brs), 4.58 (1H, brs), 5.91 (1H, dd, *J* = 15.4, 1.5 Hz), 6.88 (1H, dd, *J* = 15.4, 4.4 Hz). ^{13}C NMR (100 MHz, $CDCl_3$) δ: 20.97, 29.02, 47.71, 52.31, 120.38, 150.39, 155.56, 167.51.

*Methyl (*E,4R*)-4-[(*tert-*butoxycarbonyl)amino]-5-methyl-2-hexenoate (**7b**)*: Following the general procedure C. (2*R*)-*N*-Boc-valine methyl ester **6b** (2.11 g, 91.1 mmol) in toluene (100 mL) at –78°C and DIBAL-H (18.22 mL, 18.22 mmol, 1 M in toluene). The reaction was quenched with MeOH (2 mL). Added methyl (triphenylphosphoranylidene) acetate (3.66 g, 11.0 mmol). Chromatography (Silica gel 60, EtOAc–Heptane (30:70)) gave unsaturated ester **7b** as a white solid (2.17 g, 93%). ^{1}H NMR (400 MHz, $CDCl_3$) δ: 0.83 (6H, t, *J* = 6.6 Hz), 1.35 (9H, s), 1.72–1.81 (1H, m), 3.64 (3H, s), 4.07 (1H, brs), 4.71 (1H, d, *J* = 8.8 Hz), 5.84 (1H, d, *J* = 16.1 Hz), 6.78 (1H, dd, *J* = 15.4, 5.1 Hz).

*Methyl (*E,4S*)-4-[(*tert-*butoxycarbonyl)amino]-5-phenyl-2-pentenoate (**7c**)*: Following the general procedure C. (2*S*)-*N*-Boc-phenylalanine methyl ester **6c** (4.59 g, 16.4 mmol) in toluene (250 mL) at –78°C and DIBAL-H (33.0 mL, 33.0 mmol, 1 M in toluene). The reaction was quenched with MeOH (2 mL). Added methyl (triphenylphosphoranylidene) acetate (6.30 g, 18.86 mmol). Usual work-up gave unsaturated ester **7c** as a crude sample that was used directly in the next step.

tert-*Butyl (2S)-2-[(*E*)-3-methoxy-3-oxo-1-propenyl]-1-pyrrolidinecarboxylate (**7d**)*: Following the general procedure C. (2*S*)-*N*-Boc-proline methyl ester **6d** (3.36 g, 14.65 mmol) in toluene (120 mL) at –78°C and DIBAL-H (15.0 mL, 15.0 mmol, 1 M in toluene). Reaction was quenched with MeOH (2 mL). Added methyl (triphenylphosphoranylidene) acetate (5.63 g, 16.85 mmol). Chromatography (Silica gel 60, EtOAc–Heptane (30:70)) gave unsaturated ester **7d** which was used immediately in the next step. ^{1}H NMR (400 MHz, $CDCl_3$) δ: 1.41 (9H, s), 1.60–2.00 (4H, m), 3.34–3.59 (2H, m), 3.73 (3H, s), 4.37 (1H, brs), 5.83 (1H, d, *J* = 14.6 Hz), 6.78–6.90 (1H, m).

N-Boc-amino acids

General procedure D

The *N*-Boc-amino acid methyl ester was dissolved in MeOH and treated with 10% aqueous NaOH. The reaction was stirred for 18 h at room temperature. The MeOH was removed in vacuo and the remaining mixture was diluted with H_2O. The aqueous layer was washed with EtOAc (2×) and acidified to pH 2 with 10% aqueous HCl. The aqueous layer was extracted with EtOAc (3×) and the combined organic layers washed with saturated aqueous NaCl (1×), dried over Na_2SO_4, filtered, and concentrated.

*(3S)-3-[(*tert*-Butoxycarbonyl)amino]butanoic acid (**4a**)*: Following the general procedure D. The β-amino acid methyl ester **3a** (2.73 g, 12.6 mmol) in MeOH (50 mL) and 10% aqueous NaOH (50 mL). Flash chromatography (silica gel 60, 100% EtOAc) gave β-amino acid **4a** as a pale yellow viscous oil (2.60 g, 100%). ^{1}H NMR (400 MHz, $CDCl_3$) δ: 1.24 (3H, d, *J* = 6.6 Hz), 1.45 (9H, s), 2.46–2.62 (2H, m), 4.05 (1H, brs), 4.95 (1H, brs). MS (*m*/*z*): 204.10 (M + H).

*(3*R*)-3-[(*tert-*Butoxycarbonyl)amino]-4-methylpentanoic acid (**4b**)*: Following the general procedure D. The β-amino acid methyl ester **3b** (2.90 g, 11.8 mmol) in MeOH (50 mL) and 10% aqueous NaOH (50 mL). Flash chromatography (Silica gel 60, 100% EtOAc) gave β-amino acid **4b** as a pale yellow viscous oil (2.80 g, 100%). ^{1}H NMR (400 MHz, $CDCl_3$) δ: 0.93 (3H, d, *J* = 6.6 Hz), 1.44 (9H, s), 1.76–1.91 (1H, m), 2.40–2.65 (2H, m), 3.70–3.82 (1H, m), 4.92 (1H, d, *J* = 9.5 Hz). MS (*m*/*z*): 232.09 (M + H).

*(3*S*)-3-[(*tert-*Butoxycarbonyl)amino]-4-phenylbutanoic acid (**4c**)*: Following the general procedure D. The β-amino acid methyl ester **3c** (3.26 g, 11.1 mmol) in MeOH (50 mL) and 10% aqueous NaOH (50 mL). Flash chromatography (Silica gel 60, 100% EtOAc) gave β-amino acid **4c** as a pale yellow solid (0.56 g, 19%). ^{1}H NMR (400 MHz, $CDCl_3$) δ: 1.40 (9H, s), 2.45–2.61 (2H, m), 2.80–3.00 (2H, m), 4.18 (1H, brs), 5.06 (1H, brs), 7.17–7.33 (5H, m). MS (*m*/*z*) 280.21 (M + H).

*(*E,4R*)-4-[(*tert-*Butoxycarbonyl)amino]-2-pentenoic acid (**8a**)*: Following the general procedure D. The unsaturated γ-amino acid methyl ester **7a** (0.65 g, 2.83 mmol) in MeOH (5 mL) and 10% aqueous solution NaOH (5 mL). MPLC (Silica gel 60, EtOAc–Heptane (40:60 – 60:40)) gave unsaturated acid **8a** (367 mg, 61%). IR (NaCl disc) υ: 3330 (br), 2976, 1703, 1646 cm^{-1}. ^{1}H NMR (400 MHz, $CDCl_3$) δ: 1.28 (3H, d, *J* = 6.6 Hz), 1.45 (9H, s), 4.44 (1H, brs), 4.56 (1H, brs), 5.91 (1H, d, *J* = 15.4 Hz), 6.98 (1H, dd, *J* = 15.4, 4.4 Hz). ^{13}C NMR (100 MHz, $CDCl_3$) δ: 14.1, 20.1, 28.1, 28.2, 119.3, 151.8.

*(*E,4R*)-4-[(*tert-*Butoxycarbonyl)amino]-5-methyl-2-hexenoic acid (**8b**)*: Following the general procedure D. The unsaturated γ-amino acid methyl ester **7b** (1.98 g, 7.73 mmol) in MeOH (2 mL) and 10% aqueous NaOH (2 mL). MPLC

© 2000 NRC Canada

(Silica gel 60, EtOAc–Heptane (40:60 – 60:40)) gave unsaturated acid **8b** (1.56 g, 83%) as a white foam. ^{1}H NMR (400 MHz, $CDCl_3$) δ: 0.94 (6H, m), 1.45 (9H, s), 1.84–1.92 (1H, m), 4.23 (1H, brs), 4.60 (1H, brs), 5.94 (1H, d, *J* = 16.1 Hz), 6.96 (1H, dd, *J* = 15.4, 5.1 Hz).

*(*E*,4*S*)-4-[(*tert*-Butoxycarbonyl)amino]-5-phenyl-2-pentenoic acid (**8c**)*: Following the general procedure D. The unsaturated γ-amino acid methyl ester **7c** in MeOH (30 mL) and 10% aqueous NaOH (30 mL). MPLC (Silica gel 60, EtOAc–Heptane (40:60 – 60:40)) gave unsaturated acid **8c** (1.40 g, 29% over 2 steps) as a white solid. ^{1}H NMR (400 MHz, $CDCl_3$) δ: 1.40 (9H, s), 2.90 (2H, brs), 4.12 (1H, q, *J* = 7.3 Hz), 4.60 (1H, m), 5.85 (1H, d, *J* = 15.4 Hz), 6.99 (1H, dd, *J* = 16.1, 5.1 Hz), 7.15–7.39 (5H, m).

*(*E*)-3-[(2*S*)-1-(*tert*-Butoxycarbonyl)pyrrolidinyl]-2-propenoic acid (**8d**)*: Following the general procedure D. The unsaturated γ-amino acid methyl ester **7d** in MeOH (30 mL) and 10% aqueous NaOH (30 mL). MPLC (Silica gel 60, EtOAc–Heptane (40:60 – 60:40)) gave unsaturated acid **8d** (3.24 g, 92% over 2 steps) as a colourless oil. ^{1}H NMR (400 MHz, $CDCl_3$) δ: 1.39 (9H, s), 1.70–1.93 (4H, m), 3.22–3.48 (2H, m), 4.34 (3H, brs), 5.80 (1H, d, *J* = 16.1 Hz), 6.80–6.96 (1H, m), 9.80 (1H, brs).

N-Boc-γ-amino acids (9)

General procedure E

The *N*-Boc-γ-amino-α,β-unsaturated acid was dissolved in ethyl acetate followed by addition of 10% Pd/C (10% in weight). The resulting mixture was shaken under the hydrogen atmosphere (45 psi) for 3 h. The catalyst was filtered over Celite®, and the filtrate washed with ethyl acetate and concentrated in vacuo to give the γ-amino acid which was used in the next step without further purification.

*(4*R*)-4-[(*tert*-Butoxycarbonyl)amino]pentanoic acid (**9a**)*: Following the general procedure E. The unsaturated γ-amino acid **8a** (0.36 g, 1.7 mmol) in EtOAc (20 mL) and cat. 10% Pd/C with H_2. Washed with EtOAc (120 mL) to give γ-amino acid **9a** (0.37 g, 100%) as a white solid. ^{1}H NMR (400 MHz, $CDCl_3$) δ: 1.14 (3H, d, *J* = 3.6 Hz), 1.41 (9H, s), 1.60–1.71 (1H, m), 1.72–1.82 (1H, m), 2.39 (2H, t, *J* = 2.8 Hz), 3.69 (1H, brs), 4.40 (1H, brs).

*(4*S*)-4-[(*tert*-Butoxycarbonyl)amino]-5-methylhexanoic acid (**9b**)*: Following the general procedure E. The unsaturated γ-amino acid **8b** (1.28 g, 5.26 mmol) in EtOAc (10 mL) and cat. 10% Pd/C with H_2. Washed with EtOAc (120 mL) to give γ-amino acid **9b** (1.22 g, 95%) as a white solid. ^{1}H NMR (400 MHz, $CDCl_3$) δ: 0.86 (6H, t, *J* = 6.6 Hz), 1.39 (9H, s), 1.50–1.58 (1H, m), 1.60–1.72 (1H, m), 1.74–1.87 (1H, m), 2.31–2.40 (2H, m), 3.30–4.46 (1H, m), 4.37 (1H, d, *J* = 10.2 Hz). MS (*m*/*z*): 246.23 (M + H).

*(4*R*)-4-[(*tert*-Butoxycarbonyl)amino]-5-phenylpentanoic acid (**9c**)*: Following the general procedure E. The unsaturated γ-amino acid **8c** (1.39 g, 4.77 mmol) in EtOAc (10 mL) and cat. 10% Pd/C with H_2. Washed with EtOAc (120 mL) to give γ-amino acid **9c** (1.24 g, 87%) as a white solid. ^{1}H NMR (400 MHz, $CDCl_3$) δ: 1.38 (9H, s), 1.82–1.91 (2H, m), 2.33–2.46 (2H, m), 2.70–2.82 (2H, m), 3.80–3.90 (1H, m), 4.39 (1H, d, *J* = 10.2 Hz), 7.13–7.33 (5H, m).

*3-[(2*S*)-1-(*tert*-Butoxycarbonyl)pyrrolidinyl]propanoic acid (**9d**)*: Following the general procedure E. The unsaturated γ-amino acid **8d** (3.24 g, 13.4 mmol) in EtOAc (40 mL) and cat. 10% Pd/C with H_2. Washed with EtOAc (120 mL) to give γ-amino acid **9d** as a white solid (2.45 g, 74%). $[\alpha]_D$ + 85.6° (MeOH, c 0.74).

N-Boc-β-amino-α′-diazoketones

*tert-Butyl (1*S*)-1-methyl-4-diazo-3-oxobutylcarbamate (**5a**)*: Following the general procedure A. β-Amino acid **4a** (2.70 g, 13.3 mmol) in THF (100 mL) with triethylamine (5.5 mL, 39.8 mmol) and isobutylchloroformate (2.07 mL, 15.9 mmol). Approximately 2 equiv. of diazomethane in ether solution. MPLC (Silica gel 60, EtOAc–Heptane (20 – 50:80 – 50)) gave diazoketone **5a** as a yellow solid (0.33 g, 10%). $[\alpha]_D$ + 19.03° (MeOH, c 0.77). IR (NaCl disc) υ: 3370, 2976, 2100, 1710, 1694, 1681, 1633, 1519, 1371, 1163 cm^{-1}. ^{1}H NMR (400 MHz, $CDCl_3$) δ: 1.23 (3H, d, *J* = 6.6 Hz), 1.44 (9H, s), 2.52 (2H, brs), 3.98 (1H, brs), 4.99 (1H, brs), 5.32 (1H, brs). MS (*m*/*z*): 228.2 (M + H). HRMS calcd. for $C_{10}H_{17}N_3O_3$ + H: 228.1348; found: 228.1346.

*tert-Butyl (1*R*)-1-isopropyl-4-diazo-3-oxobutylcarbamate (**5b**)*: Following the general procedure A. β-Amino acid **4b** (2.80 g, 12.1 mmol) in THF (100 mL) with triethylamine (5.1 mL, 36.3 mmol) and isobutylchloroformate (1.88 mL, 14.5 mmol). Approximately 2 equiv. of diazomethane in ether solution. MPLC (Silica gel 60, EtOAc–Heptane (20 – 50:80 – 50)) gave diazoketone **5b** as a yellow solid (0.26 g, 9%). $[\alpha]_D$ + 28.23° (MeOH, c 0.58). IR (NaCl disc) υ: 3376, 3074, 2964, 2102, 1688, 1631, 1519, 1386, 1366, 1248, 1173 cm^{-1}. ^{1}H NMR (400 MHz, $CDCl_3$) δ: 0.91 (6H, d, *J* = 6.6 Hz), 1.43 (9H, s), 1.86 (1H, brs), 2.51 (2H, brs), 3.68 (1H, brs), 4.92 (1H, brs). MS (*m*/*z*): 256.2 (M + H). HRMS calcd. for $C_{12}H_{21}N_3O_3$ + H: 256.1661; found: 256.1649.

*tert-Butyl (1*S*)-1-benzyl-4-diazo-3-oxobutylcarbamate (**5c**)*: Following the general procedure A. β-Amino acid **4c** (0.58 g, 2.07 mmol) in THF (25 mL) with triethylamine (0.87 mL, 6.22 mmol) and isobutylchloroformate (0.32 mL, 2.49 mmol). Approximately 2 equiv. of diazomethane in ether solution. MPLC (Silica gel 60, EtOAc–Heptane (20 – 50:80 – 50)) gave α-diazoketone **5c** as a yellow solid (80.1 mg, 13%). IR (NaCl disc) υ: 3364, 3076, 2979, 2102, 1691, 1633, 1523, 1386, 1366, 1249, 1171 cm^{-1}. ^{1}H NMR (400 MHz, $CDCl_3$) δ: 1.41 (9H, s), 2.48 (2H, brs), 2.78–3.04 (2H, m), 4.04–4.15 (1H, m), 5.14–5.30 (2H, m), 7.17–7.32 (5H, m). MS (*m*/*z*): 304.2 (M + H). HRMS calcd. for $C_{16}H_{21}N_3O_3$ + H: 304.1661; found: 304.1673.

N-Boc-γ-amino-α′-diazoketones

*tert-Butyl (1R)-5-diazo-1-methyl-4-oxopentylcarbamate (**10a**):* Following the general procedure A. To a solution of γ-amino acid **9a** (0.373 g, 1.728 mmol) in 15 mL of THF was added *i*BuOCOCl (0.27 mL, 2.07 mmol), triethylamine (0.73 mL, 5.18 mmol), followed by about 10-fold excess of diazomethane solution in ether. Compound **10a** was obtained

© 2000 NRC Canada

(0.135 g, 32%) as a yellow solid. $[\alpha]_D$ –13.7° (MeOH, c 0.68). R_f = 0.30 in 30% of EtOAc in heptane. IR (NaCl disc) ν: 3358, 3082, 2975, 2101, 1682, 1633, 1531, 1455, 1389 cm^{-1}. ^1H NMR (400 MHz, $CDCl_3$) δ: 1.05 (3H, d, J = 6.5 Hz), 1.45 (9H, s), 1.6–1.8 (2H, m), 2.40 (2H, brs), 3.70 (1H, brs), 4.20 (1H, brs), 5.25 (1H, brs). HRMS (FAB) calcd. for $C_{11}H_{20}O_3N_3$ + H: 242.1505; found: 242.1498.

tert-*Butyl (1*S*)- 5-diazo-1-isopropyl-4-oxopentylcarbamate (**10b**)*: Following the general procedure A. To a solution of γ-amino acid **9b** (1.22 g, 4.97 mmol) in 40 mL of THF, was added *i*BuOCOCl (0.78 mL, 5.96 mmol) and triethylamine (2.10 mL, 14.9 mmol), followed by 10-fold excess of diazomethane in ether. Compound **10b** (0.74 g, 55%) was obtained as a yellow crystal. $[\alpha]_D$ –20.1° (CH_2Cl_2, c 0.74). R_f = 0.30 in 30% of EtOAc in heptane. IR (NaCl disc) ν: 3347, 2963, 2104, 1703, 1633, 1519, 1366, 1248, 1172, 1067 cm^{-1}. ^1H NMR (400 MHz, $CDCl_3$) δ: 0.90 (6H, d, J = 6.5 Hz), 1.25 (9H, s), 1.6–1.8 (2H, m), 1.85 (1H, m), 2.40 (2H, brs), 3.40 (1H, m), 4.17 (1H, d, J = 6.5 Hz), 5.15 (1H, brs). HRMS (FAB) calcd. for $C_{13}H_{24}O_3N_3$ + H: 270.1817; found: 270.1824.

tert-*Butyl (1*R*)-5-diazo-1-benzyl-4-oxopentylcarbamate (**10c**)*: Following the general procedure A. To a solution of γ-amino acid **9c** (1.20 g, 4.09 mmol) in 40 mL of THF, was added *i*BuOCOCl (0.64 mL, 4.90 mmol) and triethylamine (1.73 mL, 12.26 mmol) followed by 10-fold excess of diazomethane in ether. Compound **10c** (0.35 g, 27%) was obtained as a yellow solid. $[\alpha]_D$ + 14.44° (MeOH, c 0.45). R_f = 0.30 in 35% of EtOAc in heptane. IR (NaCl disc) ν: 3352, 3083, 2979, 2357, 2101, 1682, 1633, 1524, 1447, 1385, 1348 cm^{-1}. ^1H NMR (400 MHz, $CDCl_3$) δ: 1.45 (9H, s), 1.70–1.60 (1H, brs), 1.90–1.80 (1H, brs), 2.40 (2H, brs), 2.90–2.80 (2H, ddd), 3.80 (1H, brs), 4.40 (1H, brs), 5.15 (1H, brs), 7.40–7.20 (5H, m). HRMS (FAB) calcd. for $C_{17}H_{24}O_3N_3$ + H: 318.1818; found: 318.1832.

tert-*Butyl (2*S*)-2-(4-diazo-3-oxobutyl)-1-pyrrolidinecarboxylate (**10d**)*: Following the general procedure A. To a solution of γ-amino acid **9d** (2.45 g, 10.2 mmol) in 80 mL of THF, was added *i*BuOCOCl (1.72 mL, 13.2 mmol) and triethylamine (4.65 mL, 32.9 mmol) followed by 10-fold excess of diazomethane in ether. Compound **10d** (1.54 g, 56%) was obtained as a yellow oil. $[\alpha]_D$ + 91.80° (MeOH, c 0.74). R_f = 0.30 in 30% of EtOAc in heptane. IR (NaCl disc) ν: 2974, 2103, 1692, 1392, 1165 cm^{-1}. ^1H NMR (400 MHz, $CDCl_3$) δ: 1.40 (9H, d), 2.0–1.60 (6H, m), 2.30 (1H, brs), 3.30 (2H, brs), 3.40 (2H, brs), 3.70 (1H, brs), 4.20 (1H, m), 5.20 (1H, m). HRMS (FAB) calcd. for $C_{13}H_{22}O_3N_3$ + H: 268.1661; found: 268.1666.

Intramolecular formal N-H insertion reactions

General procedure F

The α′-diazoketone was dissolved in CH_2Cl_2 and cooled to –78°C. Trifluoroacetic acid was added dropwise and the reaction stirred under a nitrogen atmosphere for 5 min and then concentrated in vacuo to give the desired product as a TFA salt. The excess TFA could also be removed by washing with ether (2×).

3-Pyrrolidinones

*(5*S*)-5-Methyl-3-pyrrolidinone trifluoroacetate (**11a**)*: Following the general procedure F. α-Diazoketone **5a** (5.1 mg, 0.022 mmol) in CH_2Cl_2 (10 mL) with trifluoroacetic acid (1 mL) gave cyclized product **11a** as a yellow solid (4.1 mg, 86%). $[\alpha]_D$ + 162.5° (MeOH, c 0.20). IR (NaCl disc) υ: 3391, 1694, 1446, 1318, 1179 cm^{-1}. ^1H NMR (400 MHz, $CDCl_3$) δ: 1.38 (3H, d, J = 6.6 Hz), 2.86–3.03 (2H, m), 3.88–3.98 (1H, m), 4.54 (1H, d, J = 16.9 Hz), 4.80 (1H, d, J = 16.9 Hz), 6.99 (1H, s). HRMS calcd. for C_5H_9NO: 99.0685; found: 99.0709.

*(5*R*)-5-Isopropyl-3-pyrrolidinone trifluoroacetate (**11b**)*: Following the general procedure F. α-Diazoketone **5b** (4.9 mg, 0.019 mmol) in CH_2Cl_2 (10 mL) with trifluoroacetic acid (1 mL) gave cyclized product **11b** as a yellow viscous oil (4.3 mg, 93%). $[\alpha]_D$ + 84.40° (MeOH, c 0.25). IR (NaCl disc) υ: 3417, 1766, 1682, 1201 cm^{-1}. ^1H NMR (400 MHz, $CDCl_3$) δ: 1.00 (3H, d, J = 6.0 Hz), 1.01 (3H, d, J = 6.0 Hz), 1.83–1.94 (1H, m), 2.73–3.08 (2H, m), 3.63–3.88 (1H, m), 4.50 (1H, d, J = 16.8 Hz), 4.70 (1H, d, J = 16.8 Hz), 6.74 (1H, s). HRMS calcd. for $C_7H_{13}NO$ + H: 128.1076; found: 128.0322.

*(5*S*)-5-Benzyl-3-pyrrolidinone trifluoroacetate (**11c**)*: Following the general procedure F. α-Diazoketone **5c** (5.9 mg, 0.019 mmol) in CH_2Cl_2 (10 mL) with trifluoroacetic acid (1 mL) gave cyclized product **11c** as an off-white solid (4.7 mg, 84%). $[\alpha]_D$ + 41.60° (MeOH, c 0.25). IR (NaCl disc) υ: 3390, 2931, 1770, 1682, 1455, 1319, 1172 cm^{-1}. ^1H NMR (400 MHz, $CDCl_3$) δ: 2.84–3.05 (4H, m), 3.90–3.99 (1H, m), 4.53 (1H, d, J = 16.8 Hz), 4.72 (1H, d, J = 16.8 Hz), 6.53 (s, 1H), 7.14–7.40 (m, 5H). MS (*m*/*z*): 176.2 (M + H). HRMS calcd. for $C_{11}H_{13}NO$ + H: 176.1075; found: 176.1079.

3-Piperidinoes

*(6*R*)-6-Methyl-3-piperidinone trifluoroacetate (**12a**)*: Following the general procedure F. To a solution of γ-amino-α′-diazoketone **10a** (9 mg, 0.037 mmol) in CH_2Cl_2 (6 mL) was added TFA (2 mL). Compound **12a** (69%) was obtained. $[\alpha]_D$ –57.1° (CH_2Cl_2, c 0.21). IR (NaCl disc) ν: 3365, 2976, 1736, 1676, 1424, 1202, 1179, 1134 cm^{-1}. ^1H NMR (400 MHz, $CDCl_3$) δ: 1.5 (3H, d, J = 6.6 Hz), 2.0–1.9 (1H, m), 2.70–2.60 (1H, m), 3.20–3.10 (2H, m), 4.55 (1H, m), 4.80 (2H, brs). MS (*m*/*z*): 114.1 (M + 1). HRMS calcd. for $C_6H_{11}NO$ + H: 114.0919; found: 114.0916.

*(6*S*)-6-Isopropyl-3-piperidinone trifluoroacetate (**12b**)*: Following the general procedure F. To a solution of γ-amino-α′-diazoketone **10b** (8.0 mg, 0.030 mmol) in CH_2Cl_2 (10 mL) was added TFA (1 mL). Compound **12b** (6.0 mg, 79%) was obtained. $[\alpha]_D$ –30.68° (CH_2Cl_2, c 0.37). IR (NaCl disc) ν: 2967, 1770, 1673, 1504, 1192, 1080, 1014 cm^{-1}. ^1H NMR (400 MHz, $CDCl_3$) δ: 0.9 (3H, d, J = 6.6 Hz), 1.1 (3H, d), 2.2–2.0 (2H, m), 2.4 (1H, m), 3.1 (2H, m), 4.3 (1H, m), 4.8 (2H, m). HRMS (FAB) calcd. for $C_8H_{16}ON$ + H: 142.1232; found: 142.1229.

*(6*R*)-6-Benzyl-3-piperidinone trifluoroacetate (**12c**)*: Following the general procedure F. To a solution of γ-amino-

© 2000 NRC Canada

α′-diazoketone **10a** (9.8 mg, 0.031 mmol) in CH_2Cl_2 (10 mL) was added TFA (1 mL). Compound **12c** (5.8 mg, 62%) was obtained. $[\alpha]_D$ + 19.58° (MeOH, c 0.24). IR (NaCl disc) ν: 2969, 2358, 1770, 1681, 1504, 1417, 1139, 1163, 1081 cm^{-1}. ^1H NMR (400 MHz, $CDCl_3$) δ: 2.2 (1H, m), 2.5–2.4 (1H, m), 2.8–2.6 (1H, m), 2.9 (1H, m), 3.0 (1H, m), 3.2 (1H, m), 4.70–4.80 (3H, m), 7.4–7.2 (5H, m). HRMS (FAB) calcd. for $C_{12}H_{16}ON$ + H: 190.1232; found: 190.1226.

*(8a*S*)-Hexahydro-6(5*H*)-indolizinone trifluoroacetate (**12d**)*: Following the general procedure F. To a solution of γ-amino-α′-diazoketone **10d** (11.8 mg, 0.044 mmol) in CH_2Cl_2 (10 mL) was added TFA (1 mL). Compound **12d** (9.4 mg, 88%) was obtained. $[\alpha]_D$ + 172.9° (CH_2Cl_2, c 0.36). IR (NaCl disc) ν: 3417, 2988, 2555, 1782, 1673, 1446, 1326, 1177 cm^{-1}. ^1H NMR (400 MHz, $CDCl_3$) δ: 1.3 (1H, m), 2.1–1.8 (4H, m), 2.4 (1H, m), 2.6 (1H, m), 3.4 (1H, m), 3.7 (2H, m), 4.1 (1H, m), 4.8–4.5 (2H, m). HRMS (FAB) calcd. for $C_8H_{14}ON$ + H: 140.1075; found: 140.1072.

Acknowledgments

We thank Dr. M. Evans for HRMS analysis, Dr. Chris Walpole for helpful discussion.

References

1. (*a*) R.R. Gupta, M. Kumar, and V. Gupta. *In* Heterocyclic chemistry. Vol. I, II, and III. Springer, Berlin. 1998; (*b*) G. Kettschau, A. Podwa, and L.F. Tietze. *In* Stereoselective heterocyclic synthesis I. *Edited by* P. Metz. Springer, Berlin. 1997.
2. (*a*) M.P. Doyle, M.A. McKervey, and T. Ye. *In* Modern catalytic methods for organic synthesis with diazo compounds. John Wiley & Son, Toronto. 1998; (*b*) M.P. Doyle. Chem. Rev. **86**, 919 (1986).
3. (*a*) J. Poldech and D. Seebach. Helv. Chim. Acta, **78**, 1238 (1995); (*b*) S. Hanessian, J.-M. Fu, J.-L. Chiara, and R. Di Fabio. Tetrahedron Lett. **34**, 4157 (1993); (*c*) G. Emmer. Tetrahedron, **48**, 7165 (1992); (*d*) M.P. Moyer, P.L. Feldman, and H. Rapoport. J. Org. Chem. **50**, 5223 (1985); (*e*) O.V. Isakova, A.M. Sipyagin, and V.V. Kartsev. Zh. Org. Khim. **17**, 1522 (1980).
4. (*a*) C.F. Garcia, M.A. McKervey, and T. Ye. J. Chem. Soc. Chem. Commun. 1465 (1996); (*b*) E. Beausoleil, B. L'Archeveque, L. Belec, M. Atfani, and W. Lubell. J. Org. Chem. **61**, 9447 (1996); (*c*) J.S. Clark and P.B. Hodgson. J. Chem. Soc. Chem. Commun. 2701 (1994); (*d*) G. Bouthillier, H. Mastalerz, and M. Menard. Tetrahedron Lett. **35**, 4689 (1994); (*e*) K. Burger, M. Rudolph, and S. Fehn. Angew. Chem. Int. Ed. Engl., **32**, 285 (1993); (*f*) J.V. Heck, M.J. Szymonifka, and B.G. Christensen. Tetrahedron Lett. **23**, 1519 (1982); (*g*) J.V. Heck and B.G. Christensen. Tetrahedron Lett. **22**, 5027 (1981).
5. (*a*) C.F. Garcia, M.A. McKervey, and T. Ye. J. Chem. Soc. Chem. Commun. 1465 (1996); (*b*) F.G. West and B.N. Naidu. J. Am. Chem. Soc. **116**, 8420 (1994); (*c*) F.G. West and B.N. Naidu. J. Am. Chem. Soc. **115**, 1177 (1993); (*d*) K.-Y. Ko, K.-I. Lee, and W.-J. Kim. Tetrahedron Lett. **33**, 6651 (1992).
6. (*a*) P. Conti, M. De Amici, G. De Sarro, M. Rizzo, T.B. Stensbol, M. Brauner-Osborne, U. Madsen, L. Toma, and C. De Micheli. J. Med. Chem. **42**, 4099 (1999); (*b*) M. Gerasimov, D. Marona-Lewicka, D.M. Kurrasch-Orbaugh, A.M. Qandil, and D.E. Nichols. J. Med. Chem. **42**, 4257 (1999); (*c*) K.E. Andersen, J.L. Sorensen, P.O. Huusfeldt, L.J.S. Knutsen, J. Lau, B.F. Lundt, H. Petersen, P.D. Suzdak, and M.D.B. Swedberg. J. Med. Chem. **42**, 4281 (1999).
7. D. Cole. Tetrahedron, **50**, 9517 (1994).
8. S. Hanessian and R. Schaum. Tetrahedron Lett. **38**, 163 (1997).
9. J. Bergman, H.C. Van der Plas, and M. Simonyi (*Editors*). Heterocycles in bio-organic chemistry. Bookcraft Ltd., Bath. 1991.
10. T.H. Black. Aldrichim. Acta, **16**, 3 (1983).

© 2000 NRC Canada

Straightforward synthesis of new tetrahydroquinoline derivatives

Romano Di Fabio, Giuseppe Alvaro, Barbara Bertani, and Simone Giacobbe

Abstract: To identify novel classes of glycine antagonists, compounds potentially useful as neuroprotective after stroke, novel substituted tetrahydroquinoline derivatives, satisfying the key pharmacophoric requirements for glycine antagonists, were designed. To explore the SAR of these compounds an efficient synthetic route was set up exploiting the outstanding reactivity of suitable *N*-aryl imine derivatives. In particular an allylmetalation reaction or the addition of bis(trimethyldisilyl)ketene acetals allowed the preparation of versatile intermediates which were smoothly transformed into the desired bicycle tetrahydroquinoline derivatives by a Heck-type cyclization reaction.

Key words: glycine antagonists, neuroprotection, tetrahydroquinolines, synthesis, allylmetalation.

Résumé : Pour identifier de nouvelles classes d'antagonistes du récepteur de la glycine, composées potentiellement utiles en tant qu'agents neuroprotectifs après l'ischémie cérébrale, une nouvelle classe de dérivés de la tétrahydroquinoline substituée, satisfaisant les prérequis pharmacophorique pour les antagonistes du récepteur de la glycine, fut proposée. Afin d'explorer la relation structure-activité (SAR) de ces composés, une route synthétique efficace fut développée exploitant la haute réactivité des dérivés des *N*-aryl imines. En particulier, la réaction d'allylmétalation ou l'addition des bis(triméthyldisilyl)cétènes acétals permirent la préparation d'intermédiaires facilement transformables en dérivés bicycliques de la tétrahydroquinoline utilisant une réaction de cyclisation du type Heck.

Mots clés : antagonistes de la glycine, neuroprotection, tétrahydroquinoléines, synthèse, allylmétallation.

The modulation of the NMDA receptor (1) is considered as one of the most promising biological strategies to identify effective neuroprotective agents able to block the dynamic progression of the brain damage after stroke (for a review on different neuroprotective approaches potentially useful to control the progression of the brain damage after stroke see ref. (2)). In this event, noncompetitive NMDA antagonists acting at the glycine binding site (3), have been proven to counteract efficaciously the excitotoxic cascade triggered by glutamate in animal model of cerebral ischemia, after permanent occlusion of the middle cerebral artery (MCA) (4).

The extensive exploration performed by GlaxoWellcome of the indole-2-carboxylate template allowed identification of several compounds exhibiting outstanding neuroprotective activity in rats and a clean safety profile (5). Among those, the indole-2-carboxylate derivative GV150526 shown in Fig. 1, is undergoing Phase III clinical trails to prove the glycinergic hypothesis in man. To discover a novel series of glycine antagonists the tetrahydroquinoline (THQ) derivatives of general structure A as depicted in Fig. 1, were proposed as potential ligands of the glycine binding site satisfying the key pharmacophoric requirements (5*g*). To explore in detail the SAR of these new compounds, and in particular of the *N*-aryl moiety belonging to the α,β-unsaturated chain, an efficient synthetic route was needed (for an alternative synthesis of THQ derivatives see ref. (6)). In this event, Scheme 1 is shows the first retrosynthetic analysis proposed. Considering the possibility of performing a sequential Wittig-type olefination reaction to introduce the α,β-unsaturated side chain followed by a Heck-type cyclization reaction (7), the dissection of the *exendo* bond and the allylic double bond, respectively, seemed to be the most appropriate. To test this working hypothesis, identification of an efficient synthesis to prepare in large scale the *N*-aryl allyl glycine derivative, was perceived as the most urgent problem to solve. Among the different potential synthetic approaches (i.e., disconnection of C—N or N—C bond or, alternatively, of the C—C allylic bond), it was speculated that, as shown in Scheme 2, the addition of an allyl metal derivative **2** to the *N*-aryl aldimine **1**, generated in situ from a substituted aniline and a suitable glyoxylic ester in the presence of a Lewis acid, could afford the desired key intermediate **3**. To our surprise this allylmetalation reaction, although widely explored with different imines (for a review on the addition of different organometallic reagents to imines see ref. (8)), was unknown for the aldimine derivative of type **1**.

Following this preliminary analysis, the synthetic route shown in Scheme 3 was performed. In particular, as far as the key allylmetalation reaction is concerned, when the aryl

Received October 14, 1999. Published on the NRC Research Press website on June 7, 2000.

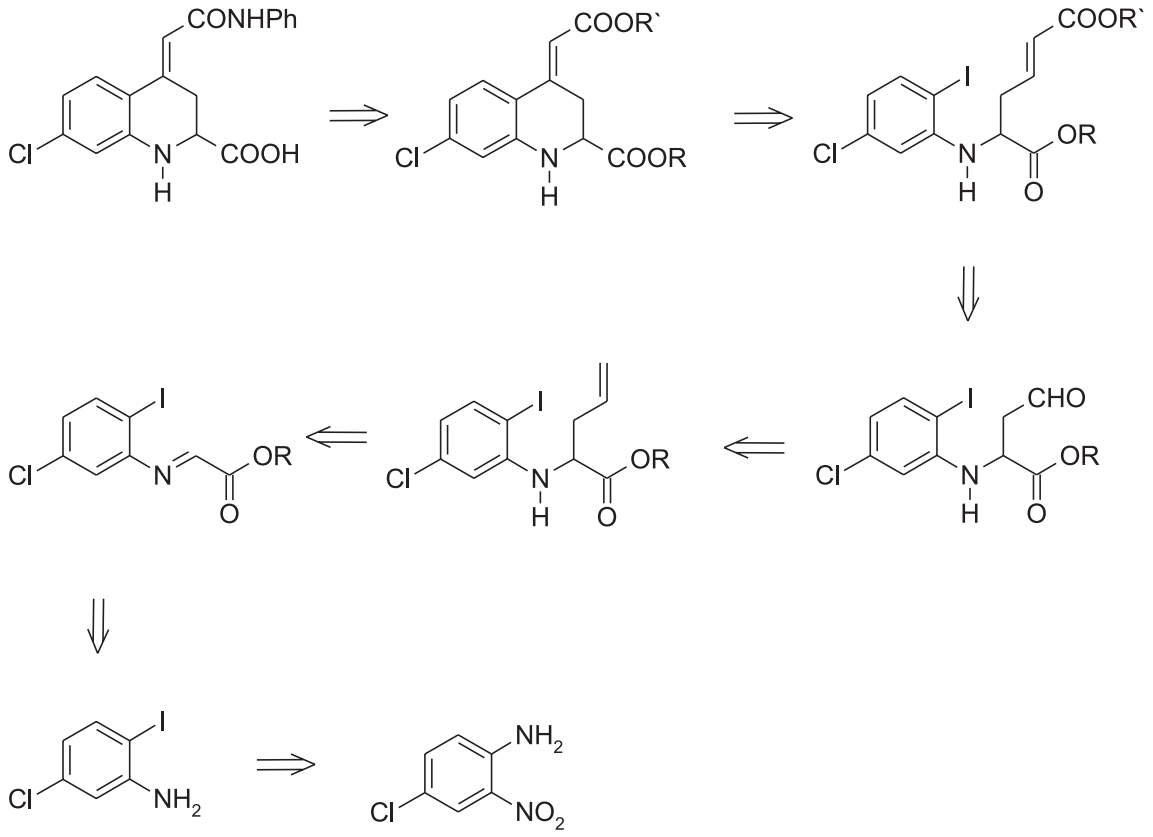
Dedicated to Professor Steve Hanessian on the occasion of his 65th birthday.

R. Di Fabio,[1] G. Alvaro, B. Bertani, and S. Giacobbe. Department of Medicinal Chemistry, Medicines Research Centre, Glaxo Wellcome S.p.A, Via Fleming 4, 37100 Verona, Italy.

[1]Author to whom correspondence may be addressed. Fax: 39 45 9218196. e-mail: rdf26781@GlaxoWellcome.co.uk

 © 2000 NRC Canada

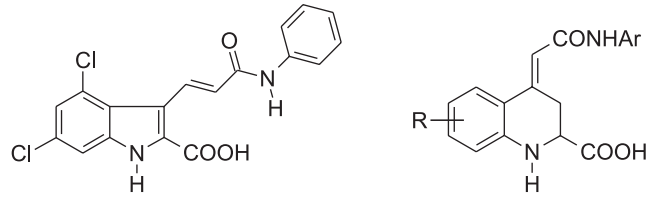
Scheme 1.



amine **6**, smoothly prepared in two steps and high total yield from the commercially available 3-chloro-2-nitroaniline **4**, was treated with ethyl glyoxylate overnight in refluxing toluene continuously removing H_2O from the reaction mixture by a Dean–Stark apparatus, the desired aldimine **7** was obtained. After evaporation of the solvent, without any purification, the crude intermediate **7** was dissolved in dry CH_2Cl_2 and treated at –78°C with $TiCl_4$ (1.1 equiv.). Then allyltributyltin (1.2 equiv.) was dropped into the reaction mixture resulting in a smooth addition reaction to give the desired *N*-aryl α amino ester derivative **8** in 88% yield from **6**, after purification by flash chromatography. As highlighted above, the addition of allyl metal derivatives to aldimines of this type has not been reported. Because of the synthetic versatility of the allyl double bond, this reaction represents a straightforward method to prepare substituted *N*-aryl amino acids.

After the identification of an efficient route to introduce a formal allyl glycine residue on the aromatic moiety, the allyl derivative **8** was transformed into the α,β-unsaturated compound **10** in two steps in high overall yield. The aldehyde derivative **9**, easily generated by ozonolysis, was submitted to a Wittig-type reaction with (*tert*-butylcarbonylmethylene)triphenylphosphorane in dry toluene at reflux to afford the olefinic compound **10** with high stereocontrol in the formation of the expected *E* isomer (ratio *E*/*Z* = 98:2), which was isolated, as pure compound, by flash chromatography in 90% yield. The following Heck-type cyclization reaction was performed in DMF at 120°C for 2 h with Et_3N in the presence of catalytic amount of $Pd(PPh_3)_4$, to give the desired *exo* compound **11** in 85% yield. As expected, the *E*

Fig. 1.

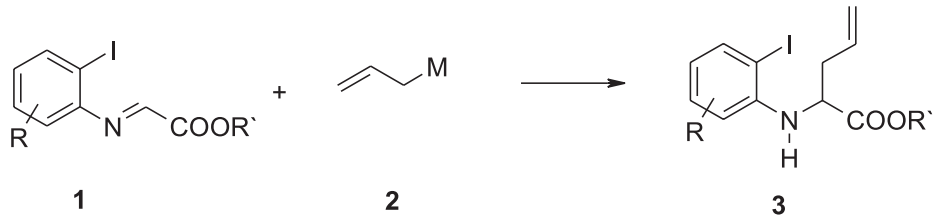


stereochemistry of the double bond was completely controlled. Chemoselective removal of the *tert*-butyl protecting group with HCOOH yielded quantitatively the free carboxyl derivative **12**, the key intermediate for the exploration of the SAR of the northeastern region of the THQ template. As an example, **12** was transformed into the corresponding *N*-phenyl amide derivative **14**. Among the different amidation methods available, excellent results were obtained when the carboxyl group was activated via the corresponding 2-pyridyl thiolester (9). When compound **12** was treated with 2,2′-dipyridyldisulfide and PPh_3 in THF at room temperature for 3 h, the intermediate **13** was isolated in 67% yield after purification by flash chromatography. Subsequent reaction with aniline in toluene at reflux for 2 h gave the amido derivative **14** in high yield. Finally, the ester group of this compound was hydrolized with NaOH in EtOH–MeOH (95:5) to furnish the desired sodium carboxylate **15**.

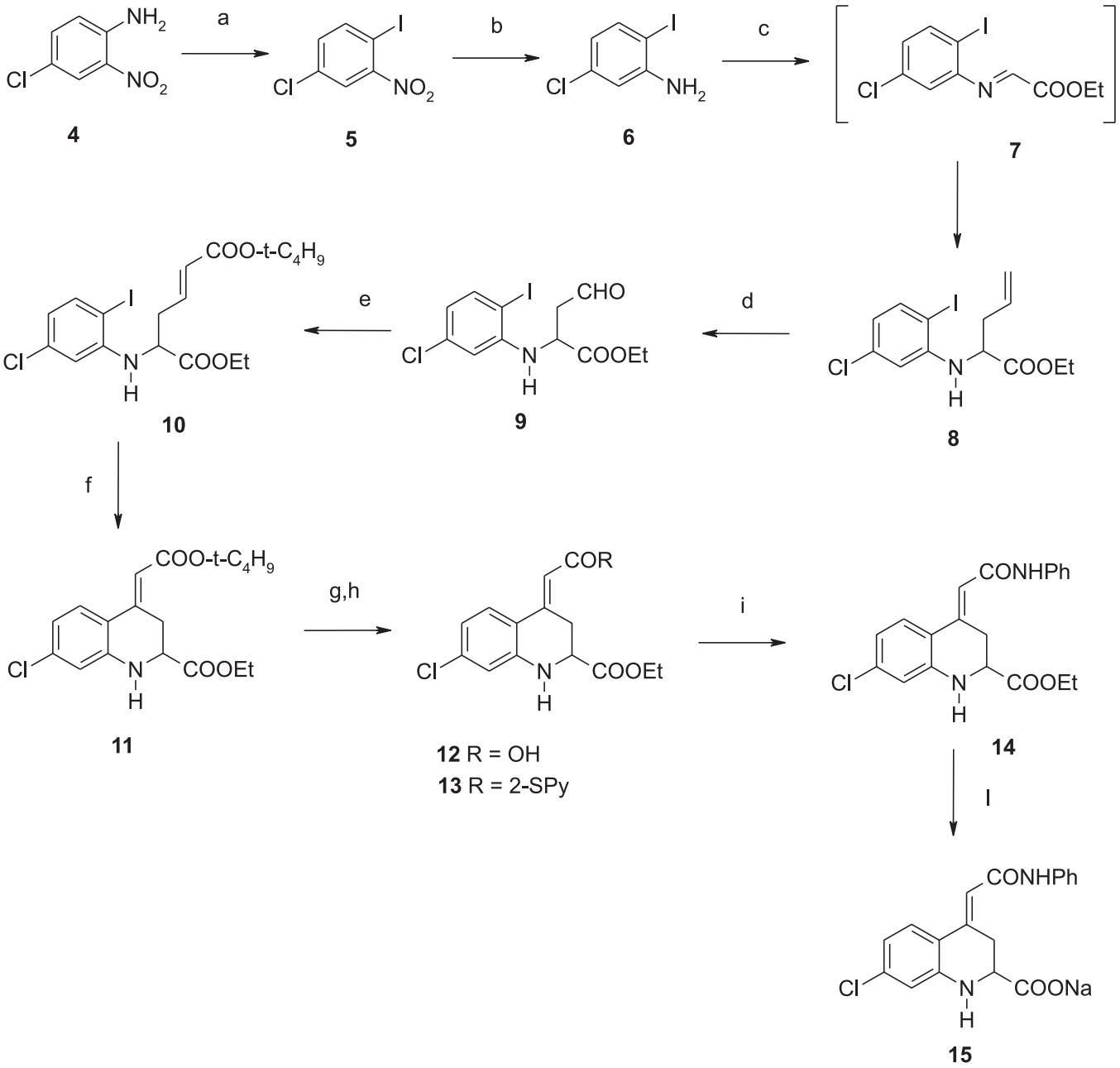
In summary, this synthetic approach allowed efficient preparation of the desired compound **15**, as the first member

© 2000 NRC Canada

Scheme 2.

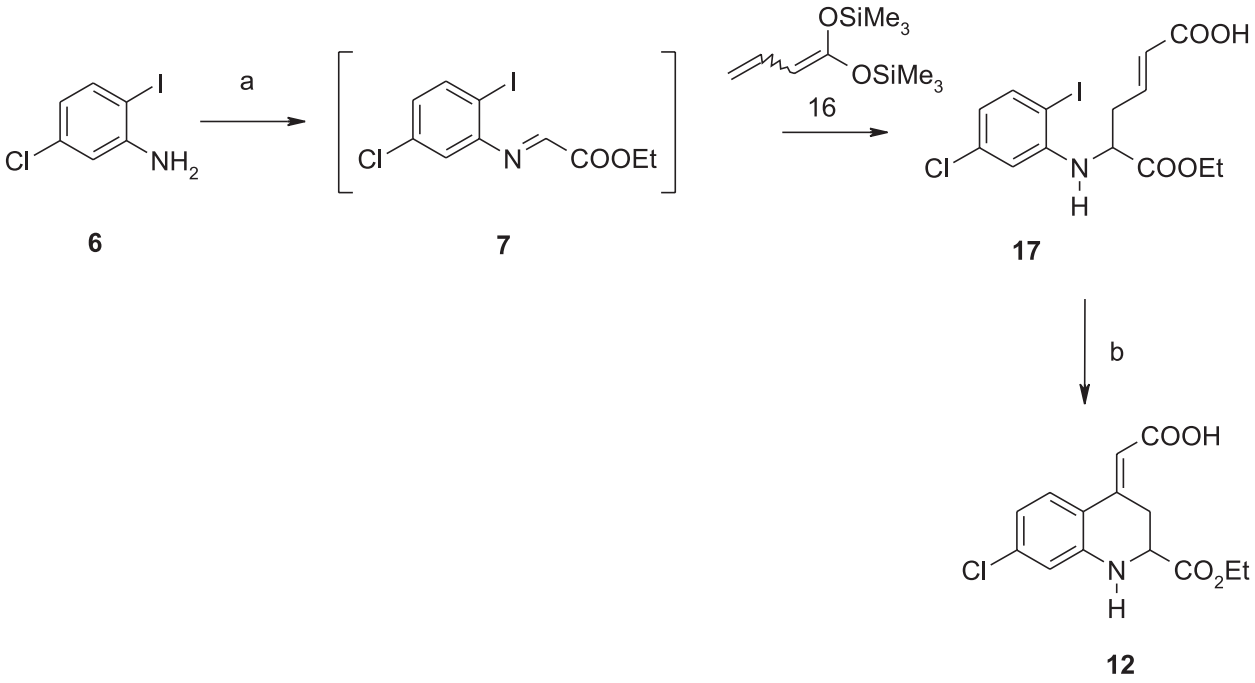


Scheme 3. (*a*) $NaNO_2$, H_2SO_4, KI, 3 h, 82%; (*b*) Fe, AcOH, EtOH, 100°C, 1 h, 82%; (*c*) (*i*) $CHOCO_2Et$, toluene, reflux; and (*ii*) CH_2Cl_2, $TiCl_4$, allyltributltin, –78°C, 88%; (*d*) O_3, CH_2Cl_2, –78°C, 2 h, 69%; (*e*) $Ph_3P{=}CHCO_2tBu$, toluene, 1 h, reflux, 90%; (*f*) $Pd(PPh_3)_4$, Et_3N, DMF, 120°C, 2 h, 85%; (*g*) HCO_2H, rt, 24 h, 100%; (*h*) 2,2′-dipyridyl disulphide, PPh_3, THF, rt, 3 h, 67%; (*i*) $C_6H_5NH_2$, toluene, 2 h, reflux, 78%; (*j*) NaOH, EtOH–MeOH, 95:5, 30 min, 90%.



© 2000 NRC Canada

Scheme 4. (*a*) $CHOCO_2Et$, toluene, 1,1-bis(trimethylsilyloxy)buta-1,3-diene, $TiCl_4$, CH_2Cl_2, –78°C; (*b*) $Pd(PPh_3)_4$, Et_3N, DMF, 120°C, 3 h, 70% from **7**.



of a novel and promising class of glycine antagonists. However, this synthesis was affected by two main drawbacks: the presence of Bu_3SnCl formed during the allylmetalation reaction, resulting in a more difficult purification of intermediate **8** in case of scale up, and the following hazardous ozonolysis of the allylic double bond. Therefore, to further increase the efficiency of this synthesis, in view of the observed outstanding reactivity of the *N*-aryl imine **7**, the synthetic sequence shown in Scheme 4 was carried out. This novel route, avoiding both the allylmetalation of the aldimine **7** and the following ozonolysis reaction, could result in a straightforward preparation of intermediate **12**. Thus, the 1,1-bis(trimethylsilyloxy)buta-1,3-diene **16**, prepared from crotonic acid as previously described (10), was treated with aldimine **7** in the presence of $TiCl_4$ in CH_2Cl_2 at –78°C, to give a smooth addition reaction to afford the free carboxyl derivative **17**. Remarkably, complete regio- and stereocontrol was observed in the formation of the linear derivative (for some examples of the addition of ketene bis(timethylsilyl) acetals to aldimines see ref. (11)) **17**. The following Heck-type cyclization reaction, performed this time without protecting the carboxyl group, afforded the target intermediate **12** in 70% yield from **7**, which was then transformed into the final *N*-aryl amide derivatives as previously described.

In conclusion an efficient preparation of THQ derivatives, in six-steps from the commercially available aniline derivative **4**, was developed. Following this versatile synthetic approach an in depth and rapid exploration of the SAR of this class of glycine antagonists was performed.[2]

Experimental section

All the reactions were performed in oven-dried glassware under a positive pressure of nitrogen. Unless otherwise noted, materials were obtained from commercial suppliers and used without further purification. THF was distilled from Na–benzophenone ketyl; CH_2Cl_2 was distilled from P_2O_5; anhydrous DMF and CH_3CN were purchased from Aldrich. ^{1}H NMR spectra were recorded on Bruker AC 200F (200 MHz), Varian VXR5000S (300 MHz), and Varian Unity (400 MHz) spectrometers. The data are reported as follows: chemical shift in ppm from the internal standard Me_4Si on δ scale, multiplicity (b = broad, s = singlet, d = doublet, t = triplet, q = quartet, m = multiplet), and coupling constants (Hertz). IR spectra were recorded on a Bruker IFS48 instrument. Mass spectra were recorded on a Fisons VG-4 instrument in FAB mode. Melting points (mp) are uncorrected and were determined on a Buchi 510 apparatus. Analytical thin layer chromatography (TLC) was performed on Merck silica gel 60 F254 plates (0.25mm); all R_f values are determined visualizing all spots with UV light (254 nm) and (or) phosphomolybdic acid solution. Flash chromatography was performed on Merck silica gel 60 (230–400 mesh).

4-Chloro-1-iodo-2-nitrobenzene (5)

To a suspension of 5-chloro-2-nitroaniline (10 g, 58 mmol) in H_2SO_4 (100 mL, 37% soln) at 0°C, a solution of $NaNO_2$ (5.2 g, 75 mmol) in H_2SO_4 (40 mL, 37% soln) was carefully added. To the resulting mixture, PPA (80 mL) was added and the reaction mixture was allowed to warm at room

[2] (*a*) R. Di Fabio, A. Pasquarello, and F.M. Sabbatini. International Patent WO9807704 A1 19980226; (*b*) R. Di Fabio, S. Giacobbe, B. Bertani, and F. Micheli. International Patent WO9712870 A1 19970410.

© 2000 NRC Canada

temperature and stirred for 3 h. The solution was poured into crushed ice and urea was added until gas evolution ceased. The resulting solution was treated with an aqueous solution of KI (13.5 g, 81.2 mmol) and heated at 70°C for 2 h. To the red solution, brine (100 mL) was added followed by AcOEt (300 mL). The organic layer was separated, washed with brine, dried over anhydrous Na_2SO_4 and concentrated in vacuo. The crude mixture was purified by flash chromatography (eluant cyclohexane–AcOEt, 98:2) to afford the title compound as a yellow solid (13.5g, 82%), mp 55–57°C. IR (Nujol): 1535, 1354 cm^{-1}. ^1H NMR ($CDCl_3$, 300MHz) δ: 7.98 (d, 1H), 7.80 (d, 1H), 7.28 (dd, 1H). MS *m*/*e*: 283 (M + 1), 237, 110. Anal. calcd. for $C_6H_3ClINO_2$: C 25.42, H 1.07, Cl 12.51, I 44.77, N 4.94; found: C 25.38, H 1.05, Cl 12.49, I 44.69, N 4.91.

5-Chloro-2-iodoaniline (6)

To a solution of intermediate **5** (13 g, 45.8 mmol) in 95% EtOH (80 mL) and glacial AcOH (80 mL), Fe powdered (11 g, 196 mmol) was added. The reaction mixture was heated at 100°C for 1 h then diluted with a saturated solution of $NaHCO_3$ and extracted with AcOEt. The organic layer was washed with brine, dried over anhydrous Na_2SO_4 and evaporated in vacuo to give a crude residue which was purified by flash chromatography (cyclohexane–AcOEt, 90:10) to afford the title compound as a pale yellow solid (9.5g, 82%), mp 75–77°C. IR (Nujol): 3468, 3371, 1592 cm^{-1}. ^1H NMR ($CDCl_3$, 300MHz) δ: 7.5 (d, 1H), 6.70 (d, 1H), 6.5 (dd, 1H), 4.20 (bs, 2H). MS *m*/*e*: 253, 126. HRMS calcd. for C_6H_5ClIN: 252.915529; found: 252.915582.

Ethyl-(5-chloro-2-iodophenylimino)acetate (7)

A solution of ethyl glyoxylate (4.78 mL, 23.67 mmol) in dry toluene (20 mL) was refluxed for 30 min in the presence of a Dean–Stark apparatus. Then, a solution of 5-chloro-2-iodoaniline (5 g, 19.7 mmol) in dry toluene (40 mL) and anhydrous $MgSO_4$ (15 g) was added. The resulting mixture was heated at 120°C for 2 h. After filtration, the solvent was evaporated in vacuo to afford the title compound as an yellow oil (6.4 g, 100%). IR (Nujol): 1744 cm^{-1}. ^1H NMR (DMSO, 300 MHz) δ: 7.92 (d, 1H), 7.89 (s,1H), 7.33 (d, 1H), 7.15 (dd, 1H), 4.33 (m, 2H), 1.31 (t, 3H). MS *m*/*e*: 338 (M + 1).

(±)-Ethyl-2-(5-chloro-2-iodo-phenylamino)-pent-4-enoate (8)

To intermediate **7** (3 g, 8.9 mmol) dissolved in dry CH_2Cl_2 (50 mL)) was added $TiCl_4$ (1.07 mL, 9.79 mmol) at –78°C. Then, tributylallyltin (3.3 mL, 10.7 mmol) was dropped into the reaction mixture and the resulting suspension was stirred for 1 h. A saturated solution of NH_4Cl was added and the mixture was extracted with AcOEt. The organic layer was washed with brine, dried over anhydrous Na_2SO_4, and evaporated in vacuo. The crude residue was purified by flash chromatography (cyclohexane–AcOEt, 95:5) to afford the title compound as a colourless oil (2.97g, 88%). IR (neat): 3373, 1739, 1572 cm^{-1}. ^1H NMR (DMSO, 300 MHz) δ: 7.57 (1H, d), 6.49 (1H, dd), 6.45 (1H, dd), 5.79 (1H, m), 5.24 (1H, dd), 5.25 (1H, dd), 4.83 (1H, d), 4.25 (2H, q), 4.13 (1H, m), 2.66 (2H, m), 1.3 (3H, t). MS *m*/*e*: 380 (M + 1), 379, 338. Anal. calcd. for $C_{14}H_{17}ClINO_2$: C 42.72, H 4.35, Cl 9.01, I 32.24, N 3.56; found C 42.61, H 4.28, Cl 8.95, I 32.15, N 3.48.

(±)-Ethyl-2-(5-chloro-2-iodo-phenylamino)-4-oxo-butyrrate (9)

Ozone was bubbled through a solution of intermediate **8** (2 g, 5.3 mmol) in dry CH_2Cl_2 (50 mL) at –78°C until a brick-red color appeared (20 min). PPh_3 (1.5 g, 5.7 mmol) was added and the mixture stirred at room temperature for 2 h. The solvent was evaporated in vacuo and the crude residue was purified by flash chromatography (cyclohexane–AcOEt, 80:20) to afford the title compound as a white foam (1.4 g, 69%). IR (Nujol): 3372, 1738, 1732cm^{-1}. ^1H NMR ($CDCl_3$, 300 MHz) δ: 9.80 (t, 1H), 7.57 (d, 1H), 6.55 (d, 2H), 6.51 (dd, 1H), 4.99 (d, 1H), 4.46 (m, 1H), 4.24 (q, 2H), 3.08 (m, 2H), 1.28 (t, 3H). MS *m*/*e*: 382 (M + 1). Anal. calcd. for $C_{13}H_{15}ClINO_3$: C 39.47, H 3.82, Cl 8.96, I 32.08, N 3.54; found: C 39.41, H 3.79, Cl 8.91, I 32.01, N 3.49.

(±)-Ethyl-6-(*E*)-5-(5-chloro-2-iodo-phenylamino)-hex-2-enoate-1-*tert*-butylester (10)

(*tert*-Butoxycarbonylmethylene)triphenyl phosphorane (1.38 g, 3.67 mmol) was added to a solution of intermediate **9** (1.4 g, 3.67 mmol) in dry toluene (30 mL). The mixture was refluxed for 1 h, then the solvent was evaporated in vacuo and the crude residue was purified by flash cromatography (cyclohexane–AcOEt, 90:10) to afford the title compound as a yellow oil (1.58 g, 90%). IR (Nujol): 3371, 1732, 1628 cm^{-1}. ^1H NMR (DMSO, 300 MHz) δ: 7.65 (d, 1H), 6.73 (m, 1H), 6.70 (d, 1H), 6.53 (dd, 1H), 5.8 (d, 1H), 5.21 (d, 1H), 4.59 (m, 1H), 4.19 (m, 2H), 2.78 (m, 2H), 1.43 (s, 9H), 1.19 (t, 3H). HRMS calcd. for $C_{18}H_{23}ClINO_4$: 479.036038; found: 479.036030.

(±)-Ethyl-(*E*)-7-chloro-4-*tert*-butoxycarbonylmethylene-1,2,3,4-tetrahydro-quinoline-2-carboxylate (11)

$Pd(PPh_3)_4$ (0.12 g, 0.10 mmol) and TEA (0.35 mL, 2.50 mmol) were added to a solution of compound **10** (1 g, 2.08 mmol) in dry DMF (50 mL). The mixture was heated to 120°C for 2 h. A saturated solution of NH_4Cl was added and the resulting mixture was extracted with AcOEt. The organic layer was washed with brine, dried over anhydrous Na_2SO_4 and the solvent was evaporated in vacuo. The crude residue was purified by flash chromatography (cyclohexane–AcOEt, 90:10) to afford the title compound as a yellow oil (0.62 g, 85%). IR (Nujol): 3371, 1724, 1707 cm^{-1}. ^1H NMR (DMSO, 300 MHz) δ: 7.65 (d, 1H), 7.26 (d, 1H), 6.69 (m, 2H), 6.29 (d, 1H), 4.29 (m, 1H), 4.12–3.94 (m, 2H), 4.01 (m, 1H), 2.68 (m, 1H), 1.44 (s, 9H), 1.14 (t, 3H). Anal. calcd. for $C_{18}H_{22}ClNO_4$: C 61.45, H 6.30, Cl 10.08, N 3.98, O 18.19; found: C 61.42, H 6.28, Cl 10.01, N 3.95.

(±)-Ethyl-(*E*)-7-chloro-4-carboxymethylene-1,2,3,4-tetrahydro-quinoline-2-carboxylate (12)

Intermediate **11** (0.6 g, 1.7 mmol) was dissolved in HCOOH (10 mL, 96%) and stirred at room temperature for 24 h. The reaction mixture was then evaporated in vacuo to give the title compound (0.5 g, 100%) as a yellow solid, mp 172–174°C. IR (Nujol): 3379, 1715, 1685cm^{-1}. ^1H NMR (DMSO, 300 MHz) δ: 12.1 (s, 1H), 7.45 (d, 1H), 6.94 (d, 1H), 6.77 (d, 1H), 6.53 (dd, 1H), 6.16 (s, 1H), 4.18 (m, 1H), 4.12–3.8 (m, 2H), 3.86 (dd, 1H), 2.96 (m, 1H), 1.17 (t, 3H).

© 2000 NRC Canada

MS *m*/*e*: 296 (M + 1), 278. Anal. calcd. for $C_{14}H_{14}ClNO_4.H_2O$: C 53.60, H 5.14, Cl 11.30, N 4.46; found: C 53.57, H 5.11, Cl 11.25, N 4.46.

(±)-Ethyl-(*E*)-7-chloro-4-(pyridin-2-ylsulfanylcarbonyl-methylene)-1,2,3,4-tetrahydro quinoline-2-carboxylate (13)

PPh_3 (1 g, 3.81 mmol) and 2,2′-dipyridyldisulphide (0.84 mg, 3.81 mmol) were added to a solution of intermediate **12** (0.45 g, 1.52 mmol) in dry THF (25 mL). The resulting solution was stirred at room temperature for 3 h, then diluted with a 0.5 M NaOH. The mixture was extracted with AcOEt. The organic layer was washed with brine, dried over anhydrous Na_2SO_4 and the solvent was evaporated in vacuo. The crude residue was purified by flash chromatography (cyclohexane–AcOEt, 70:30) to afford the title compound as a yellow solid (0.4 g, 67%), mp 163–165°C. IR (Nujol): 3380, 1716, 1677cm^{-1}. ^{1}H NMR (DMSO, 300 MHz) δ: 8.60 (m, 1H), 7.90 (m, 1H), 7.67 (d, 1H), 7.64 (m, 1H), 7.44 (d, 1H), 7.15 (d, 1H), 6.83 (d, 1H), 6.71 (s, 1H), 6.58 (dd, 1H), 4.21–4.00 (m, 3H), 3.70 (dd, 1H), 3.03 (m, 1H), 1.10 (t, 3H). MS *m*/*e*: 389 (M + 1), 411. Anal. calcd. for $C_{19}H_{17}ClN_2O_3S$: C 58.69, H 4.41, Cl 9.12, N 7.20, S 8.25; found: C 58.61, H 4.38, Cl 9.08, N 7.18, S 8.22.

(±)-Ethyl-(*E*)-7-chloro-4-(phenylcarbamoylmethylene)-1,2,3,4-tetrahydroquinoline-2-carboxylate (14)

Aniline (0.134 mL, 1.465 mmol) was added to a solution of intermediate **13** (0.38 g, 0.977 mmol) in dry toluene (10 mL) and the mixture was refluxed for 2 h. The yellow solution was allowed to warm to room temperature and the solid formed was filtered and washed with Et_2O to afford the title compound as a pale yellow solid (0.28 g, 78%), mp 198–200°C. IR (Nujol): 3386, 3316, 1723, 1651cm^{-1}. ^{1}H NMR (DMSO, 300 MHz) δ: 10.02 (bs, 1H), 7.63 (d, 1H), 7.38–7.30 (m, 4H), 7.03 (d, 1H), 6.89 (d, 1H), 6.79 (s, 1H), 6.62 (dd, 1H), 6.48 (s, 1H), 4.18 (m, 1H), 4.14–3.89 (m, 2H), 3.95 (dd, 1H), 3.08 (m, 1H), 1.08 (t, 3H). MS *m*/*e*: 371 (M + 1), 341, 297, 278, 204. Anal. calcd. for $C_{20}H_{19}ClN_2O_3$: C 64.78, H 5.16, Cl 9.56, N 7.55; found: C 64.75, H 5.18, Cl 9.55, N 7.55.

(±)-(*E*)-7-chloro-4-(phenylcarbamoylmethylene)-1,2,3,4-tetrahydroquinoline-2-carboxylic acid, sodium salt (15)

NaOH (1 M, 0.57 mL, 0.57 mmol) was added to a solution of intermediate **14** (0.2 g, 0.5476 mmol) dissolved in EtOH–MeOH (95:5) (5 mL). After 4 h at room temperature, the solvent was evaporated and the solid treated with Et_2O (5 mL) to give a pale yellow solid (0.175 g, 90%), mp 198–200°C. IR (Nujol): 3180–3500, 1651, 1599 cm^{-1}. ^{1}H NMR (DMSO, 300MHz) δ: 10.89 (bs, 1H), 7.70 (d, 2H), 7.30 (d, 1H), 7.27 (t, 2H), 6.99 (t, 1H), 6.77 (d, 1H), 6.42 (dd, 1H), 6.37 (s, 1H), 6.25 (s, 1H), 3.42–3.25 (m, 2H), 2.69 (dd, 1H). MS *m*/*e*: 365 (M + 1), 343. HRMS calcd. for $C_{18}H_{14}ClN_2O_3Na$: 365.066890; found: 365.066950.

6-Ethyl-(±)-(*E*)-5-(5-chloro-2-iodo-phenylamino)-hex-2-endioic acid (17)

$TiCl_4$ (0.22 mL, 2 mmol) was added dropwise at –78°C to a solution of intermediate **7** (3.4 g, 10 mmol) in dry CH_2Cl_2 (50 mL). Then, a solution of 1,1-bis(trimethylsilyloxy)-buta-1,3-diene (2.5 g, 12 mmol) in dry CH_2Cl_2 (10 mL) was slowly added and the resulting solution was stirred for 1 h. A saturated solution of NH_4Cl was added and the mixture was extracted with AcOEt. The organic layer was washed with brine, dried over Na_2SO_4, and evaporated in vacuo to give crude intermediate **17** (4 g) used without any purification in the next step. IR (Nujol): 3371, 3400–2500, 1732–1698 cm^{-1}. ^{1}H NMR (DMSO, 300 MHz) δ: 12.27 (bs, 1H), 7.65 (d, 1H), 6.76 (d, 1H), 6.68 (d, 2H), 6.53 (dd, 1H), 6.16 (s, 1H), 5.88 (dd,1H), 4.98 (d, 1H), 4.57 (m, 1H), 4.15 (m, 2H), 2.75 (m, 2H), 1.19 (t, 3H). MS *m*/*e*: 424 (M + 1), 338.

Ethyl-(±)-(*E*)-7-chloro-4-carboxymethylene-1,2,3,4-tetrahydro-quinoline-2-carboxylate (12)

$Pd(PPh_3)_4$ (2.3 g, 2 mmol) and TEA (4.18 mL, 30 mmol) were added to a solution of intermediate **17** in DMF (100 mL). The mixture was heated to 120°C for 2 h. Then, a saturated solution of NH_4Cl was added and the resulting mixture was extracted with AcOEt. The organic layer was washed with brine, dried over anhydrous Na_2SO_4, and the solvent was evaporated in vacuo. The crude residue was purified by flash chromatography (cyclohexane–AcOEt, 50:50) to afford the title compound **12** as a yellow oil (2.06 g, 70% from intermediate **7**).

References

1. G.L. Collingridge and J.C. Watkins (*Editors*). The NMDA receptor. 2nd Ed. IRL Press, Oxford. 1994.
2. J.A. Zivin. Drugs, **54**, 83 (1997).
3. (*a*) R. Di Fabio, G. Gaviraghi, and A. Reggiani. Chim. Ind. (Milan), **78**, 283 (1996); (*b*) P.D. Leeson and L.L. Iversen. J. Med. Chem. **37**, 4053 (1994); (*c*) L.L. Iversen, J.A. Kemp, and P.D. Leeson. Trends Pharmacol. Sci. **14**, 20 (1993).
4. A. Tamura, D.I. Graham, J. McCullogh, and G.M. Teasdale. J. Cereb. Blood Flow Metab. **1**, 53 (1981).
5. (*a*) R. Di Fabio, N. Conti, E. De Magistris, A. Feriani, S. Provera, F.M. Sabbatini, A. Reggiani, and L. Rovatti. J. Med. Chem. **42**, 3486 (1999); (*b*) S.A. Giacobbe, R. Di Fabio, D. Baraldi, A. Cugola, and D. Donati. Synth. Commun. **29**, 3125 (1999); (*c*) F. Micheli, R. Di Fabio, A.M. Capelli, A. Cugola, O. Curcuruto, A. Feriani, P. Gastaldi, G. Gaviraghi, C. Marchioro, A. Orlandi, A. Pozzan, A.M. Quaglia, A. Reggiani, and F. van Amsterdam. Arch. Pharm. Pharm. Med. Chem. **332**, 73 (1999); (*d*) C.T. Hewkin, R. Di Fabio, N. Conti, A. Cugola, P. Gastaldi, F. Micheli, and A.M. Quaglia. Arch. Pharm. Med. Chem. **332**, 55 (1999); (*e*) R. Di Fabio, A. Cugola, D. Donati, A. Feriani, G. Gaviraghi, E. Ratti, D.G. Trist, and A. Reggiani. Drugs Future, **23**, 61 (1998); (*f*) S.A. Giacobbe, D. Baraldi, and R. Di Fabio. Bioorg. Med. Chem. Lett. **8**, 1689 (1998); (*g*) R. Di Fabio, A.M. Capelli, N. Conti, A. Cugola, D. Donati, A. Feriani, P. Gastaldi, G. Gaviraghi, C.T. Hewkin, F. Micheli, A. Missio, M. Mugnaini, A. Pecunioso, A.M. Quaglia, E. Ratti, L. Rossi, G. Tedesco, D.G. Trist, and A. Reggiani. J. Med. Chem. **40**, 841 (1997).
6. R.W. Carling, P.D. Leeson, A.M. Moseley, R. Baker, A.C. Foster, S. Grimwood, J.A. Kemp, and G.R. Marshall. J. Med. Chem. **35**, 1942 (1992).
7. (*a*) J. Tsuji. Palladium reagents and catalysts. John Wiley & Sons Ltd., Chichester. 1995; (*b*) R.F. Heck. Palladium reagents in organic synthesis. Academic Press, London. 1985.
8. R. Bloch. Chem. Rev. **98**, 1407 (1998).
9. R. Di Fabio, V. Summa, and T. Rossi. Tetrahedron, **49**, 2239 (1993), and refs. therein.

© 2000 NRC Canada

10. G.S. Welmaker. Org. Prep. Proced. Int. **25**, 595 (1993).
11. (*a*) R. Bellassoued, R. Ennigrou, R. Gil, and N. Lensen. Synth. Commun. **28**, 3955 (1998); (*b*) M. Mladenova and M. Bellassoued. Synth. Commun. **23**, 725 (1993); (*c*) S.H. Brandstadter and I. Ojima. Tetrahedron Lett. **28**, 613 (1987).

© 2000 NRC Canada

On diastereomeric perturbations

Christian Girard and Henri B. Kagan

Abstract: For more than a century, organic chemists have been playing in Nature's laboratory. Their first goal was to understand the organization of atoms in the living matter and then to reproduce it by synthesis. This quest gave rise to several efficient techniques to synthesise molecules; many of them still in use nowadays, as such or with little modifications. Even at the beginning of this journey, the chemists discovered that their methods were far from being as efficient as the ones used by Nature to produce substances. The natural molecules were chiral and there was even an enantiomer that was produced over the other;a lesson of perfection. This was another challenge for the chemists and they succeeded by first developing techniques to separate enantiomers and more recently reagents and reactions to produce only the desired stereoisomer. Asymmetric synthesis uses chiral auxiliaries, reagents or catalysts to create chirality into the desired compound. The common perception, as a minimum condition, was that the chiral substance used to perform such a transformation has to be of the highest enantiomeric purity to obtain a very high selectivity. The relation between the enantiomeric excesses of the chiral substance and the product was suggested to be linear. But there were a lot of surprises left in the laboratory. Who would have thought that an impure substance could give an enantiomeric excess in the product higher than its own purity? The molecules are acting in different ways in solution. Self-organization and aggregation can arise depending on the structure of the substance or its environment. Such phenomenon can generate deviations to the awaited behaviour of the molecules that can be observed in many cases. This article tries to present some examples of the historical reports of such peculiar behaviours, their influence on physico-chemical properties and the final discovery of the now well-known nonlinear effects in asymmetric synthesis.

Key words: asymmetric synthesis, diastereomeric interactions, nonlinear effects.

Résumé : Depuis plus d'un siècle, les chimistes organiciens ont investi le laboratoire de Mère Nature. Leur objectif initial était de déterminer la structure des molécules isolées d'organismes vivants et de la reproduire par voie de synthèse. Ils ont donc dû développer nombre de techniques pour réaliser la synthèse de molécules, plusieurs d'entre elles très efficaces et étant encore utilisées de nos jours sous leur forme originelle ou d'une variante. Cependant les chimistes ont rapidement découvert que la Nature leur donnait une leçon de perfection. Les molécules isolées étaient chirales et, qui plus est, un énantiomère était produit préférentiellement. Les chimistes ont donc dû relever un autre défi qui fut dans un premier temps la mise au point des techniques permettant de séparer les deux énantiomères produits par leurs méthodes. Ils surent par la suite développer des réactions et des réactifs sélectifs permettant de n'obtenir que le stéréoisomère désiré. La synthèse asymétrique était née utilisant auxiliaires, réactifs ou catalyseurs chiraux pour induire la chiralité dans la substance à synthétiser. On croyait alors que la pureté énantiomérique de la substance utilisée pour effectuer une transformation de ce type était un gage minimum d'obtention d'une haute énantio sélectivité. La relation entre les excès énantiomériques de la substance chirale et du produit de la réaction était considérée linéaire et personne ne remettait en question ces hypothèses. Mais c'était sans compter sur les surprises que réserve le laboratoire. Qui eut cru qu'une substance chirale énantiomériquement impure puisse donner naissance à un produit dont la pureté énantiomérique est supérieure à la sienne? Les molécules peuvent se comporter de différentes façons en solution. Des phénomènes d'autoassociation et d'agrégation, qui sont fonction de la structure de la molécule et de son environnement, sont monnaie courante. Ils produisent en général des perturbations du système qui font en sorte que les molécules sont loin de se comporter de façon idéale. Cet article essaie de retracer quelques-uns des rapports historiques ayant mis à jour de tels phénomènes, leur influence sur des propriétés physico-chimiques et la découverte plus récente de ce nous connaissons maintenant sous le nom d'effets non-linéaires en synthèse asymétrique.

Mots clés : synthèse asymétrique, interactions diastéréoisomériques, effets non-linéaires.

Received October 5, 1999. Accepted April 13, 2000. Published on the NRC Research Press Website on June 13, 2000.

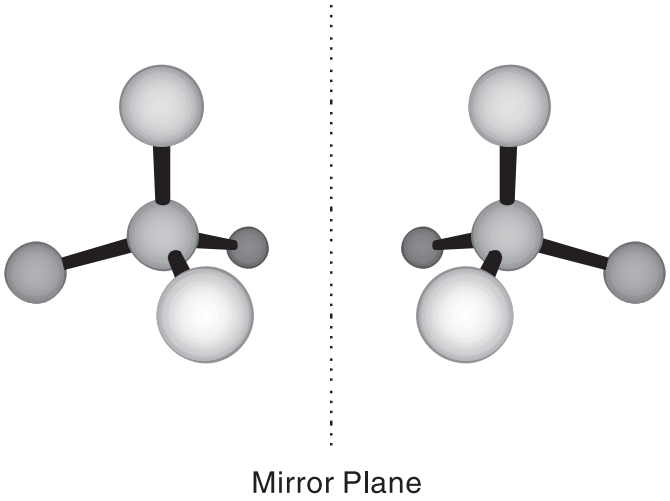
Dedicated to Professor Stephen Hanessian in recognition of his significant contributions to the art of organic synthesis.

C. Girard.[1] Laboratoire de Chimie Bioorganique et de Biotechnologie Moléculaire & Cellulaire UMR 7001, Ecole Nationale Supérieure de Chimie de Paris, 11, rue Pierre et Marie Curie, 75005 Paris, France.
H.B. Kagan.[1] Laboratoire de Catalyse Moléculaire UPRESA 8075, Université Paris-Sud, Institut de Chimie Moléculaire d'Orsay, Bâtiment 420, 91405 Orsay CEDEX, France.

[1]Author to whom correspondence may be addressed. e-mail (CG): cgirard@ext.jussieu.fr; (HBK): kagan@u-psud.fr

 © 2000 NRC Canada

Fig. 1. Enantiomers; mirror images of the same spatial arrangement in a molecule.



1. Introduction

Organic chemistry; the Art of Synthesis of molecules issued from and for the living. The organic chemist is an artist playing with atoms, reagents, molecules… a never-ending quest to find the perfect transformation that will ultimately lead to "gold" from carbon, hydrogen, oxygen, nitrogen and other simple elements… he is an alchemist.

Historically, organic chemistry started by the synthesis of simple molecules, natural or artificial, to try to reproduce Nature's perfection. Urea, dyes, salicylic acid and its derivatives, sugars, antibiotics, perfumes, and poisons; the molecular complexity was increasing and with it the tools to synthesise molecules. And this journey was creating fields that were to become independent sciences: pharmacology, biochemistry, molecular biology to name a few.

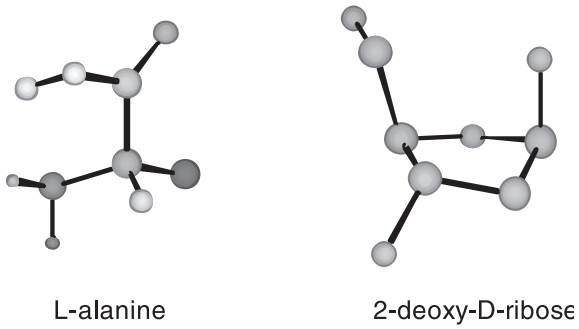
Nowadays, these sciences reach the conclusion that all the knowledge on molecules, their structure, synthesis, behaviour and activity are all intimately linked; expressions of the subtle ways the organic substances exist and interact.

This paper does not intend to be an history of organic chemistry or of asymmetric synthesis. It will try to present only a few historical hints of unexpected molecular behaviours chemists encountered while developing organic synthesis and moreover the field dealing with enantiomers and generation of chirality. The observation of these perturbations ultimately led to the discovery of non-linear effects in asymmetric synthesis.

2. The mirror image

Since the work of Biot (1), the organic chemist found out that some molecules can rotate the plane of polarized light. Furthermore, molecules having the same composition but different spatial arrangements of the constituents have different properties. Some are only geometrical isomers. But what if the substituents are arranged in a way that two molecules have the same spatial distribution differing only by the fact that they are the exact mirror image one to another? They become what we call *enantiomers*; mirror replicas of the same compound that are not superimposable (Fig. 1).

Fig. 2. Nature and her selection of L-amino acids and D-sugars.



They are therefore defined as *chiral* molecules. Each enantiomer has the exact same influence on polarized light but in the exact opposite direction. They are optically active substances (2). One of the enantiomers rotates the plane of polarized light to the right and is called the *dextro isomer* (+) (or *d*) the other one rotating the light to the left being called the *lævo isomer* (–) (or *l*).[2] That is the only difference in their physico-chemical properties. Mix them together in equal amounts and the rotation becomes equal to zero, the effect of each enantiomer being cancelled by the other. This mixture was called *racemic* and could not be separated by classical methods based on the differences of physico-chemical properties.

With the help of polarimetry, chemists found out that living systems were quite selective in their production of chiral substances. The products were enantiomerically pure and some classes of compounds has the same sense of chirality. Proteins are all constituted of L-amino acids and nucleic acids of D-sugars. Life is based on a twist in chirality that selected only one (3) (Fig. 2).

While Nature was producing only one enantiomer, the first syntheses were giving racemic mixtures. Following Pasteur's discoveries, organic chemists found the possibility to separate the two produced enantiomers by using a now well-known technique; the resolution of racemic mixtures (4). This method is based on the use of a chiral molecule, enantiopure, which can form complexes or salts with the product to resolve (2, 5). The chirality of the resolving agent gave the opportunity to form preferentially an association with only one enantiomer of the racemic mixture, one of the *diastereomeric* complexes being then separated by crystallization (Fig. 3).

The diastereomeric complexes, $d\cdot X^*$ vs. $l\cdot X^*$ for example, are not mirror images. They thus possess different physico-chemical properties which allowed the chemists to effect the separation of enantiomers. This method of separation is therefore based on the difference in properties between the complex and the remaining enantiomer and the preference of a diastereomeric complex with the resolving agent over the other.

[2] Remember that the old notation *d* and *l* refers to the sense of deviation of polarized light by the molecule (to the right or the left) in specific rotation while D and L refer only to the configuration of the last carbon in the Fischer projection by comparison with glyceraldehyde (D on the right side, L on the left side). There is no direct relationship between the two descriptors since, for example, a L product can be dextrorotatory (*d*).

© 2000 NRC Canada

Fig. 3. Resolution of a racemic (*d* + *l*) mixture using a chiral resolving agent (X*).

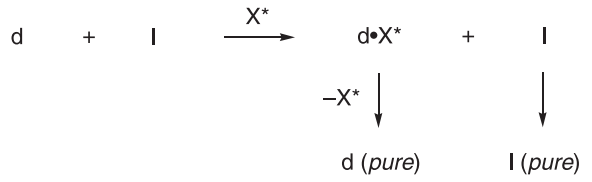
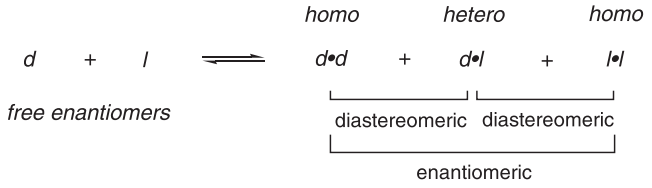


Fig. 4. Association of enantiomers to form two homodimers and a heterodimer.



But what happens if the enantiomers can interact together, without any external influence, if they can form pairs or higher associated species. Lets consider the case of enantiomers able to form dimers by association through weak interactions; like hydrogen bonding for example. If we consider all the possible permutations in a racemic mixture, we should expect the formation of three different couples (Fig. 4).

The two homodimers (*d*·*d* and *l*·*l*) are in fact enantiomers and will not differ in properties. However, the heterodimer (*d*·*l* or *l*·*d* which is the same) is in a diastereomeric relationship with the homo ones. The properties of this hetero combination will therefore be quite different to the properties of the homo associations.

In regard to these associations of enantiomers, the chemists became interested in studying the behaviour of such diastereomeric species. As we will see in the following sections, the evaluation of the properties of enantiomeric relations gave rise to numerous interesting observations.

3. Pasteur and tartaric acid

One of the most widely studied natural products, thanks to the French wine industry, was tartaric acid and its derivatives (Fig. 5). Pasteur first discovered, by studying the optical rotation of solutions of tartaric acid, that the natural acid was dextrorotatory while the synthetic one was not deviating the light having thus a zero value of rotation (6). The natural substance was optically active, the artificial one was racemic.

But this was only the beginning of Pasteur's work that laid the foundations of stereochemistry (2, 7, 8) and later the elucidation of the geometry of the carbon atom (9). The most important discovery was done by a combination of observation and serendipity. From a solution of the sodium ammonium salt of racemic tartaric acid, Pasteur was able to manually separate enantiomorphous crystals according to their hemihedral morphology (Fig. 6).

The separated acid salt crystals were then hydrolyzed back to the acid and gave two samples of tartaric acid; one which had the same rotation as the natural acid (+) and the other one with the exact opposite rotation (–). The sodium ammonium tartrate is a rare example of those crystals in which the enantiomers prefer to crystallize separately by forming conglomerate, allowing a spontaneous resolution (for a recent highlight on this still up to date subject, see ref. (10)).

This discovery triggered the examination of enantiopure substances and racemic mixtures to evaluate the possibilities of stereoselective associations of enantiomers in solid, liquid state and solution.

Pasteur observed in 1850 that the mixing of two concentrated solutions of both enantiomers of tartaric acid was somewhat exothermic (11). This was later confirmed by measurement by Berthelot and Jungfleisch (12). The heat evolved was calculated to be of 4.4 kcal mol^{-1} and was suggested to be the consequence of the formation of a "solid racemate" (13).[3]

Several other properties of the solutions of tartaric acid were then measured. Small differences were found for the densities of pure and racemic acids (5×10^{-4} for 25%

Fig. 5. The tartaric acid under its natural configuration (L-**1**) and the nonnatural enantiomericform (D-**1**).

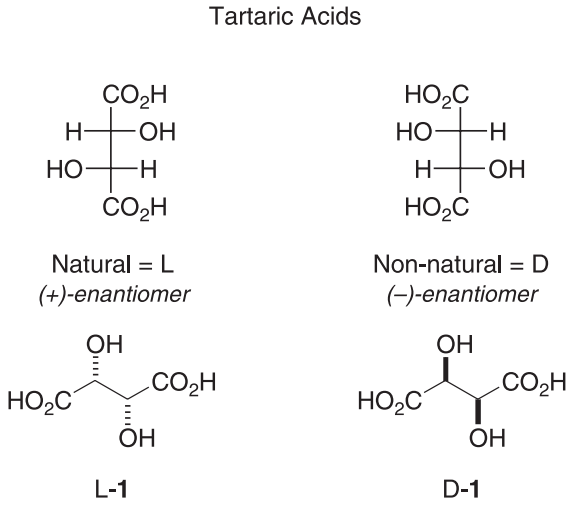
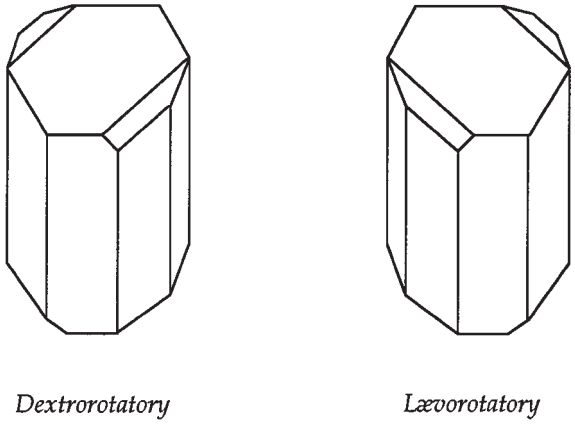


Fig. 6. The two enantiomorphous crystals of sodium ammonium tartrate.



[3] A much smaller value was later found by Amaya and co-workers (13). Measurements made at the end of the 19th century were very dependent on the sensitivity and the efficiency of the instrument and sometimes even on the purity of the substances.

© 2000 NRC Canada

Table 1. Melting point and solubility in water of the pure tartaric acid enantiomers (L and D) and the racemate (DL).

Tartaric acid	Melting point (°C)	Water solubility (g/100 mL at 20°C)
L	168–170	139
DL	206	20.6
D	168–170	139

aqueous solutions) by Perkin and Marchlewski (14*a*, *b*) that were said to be the consequence of a stronger association between the D·L pair, thus more stable, than for the homochiral associations (D·D, L·L). The same conclusion was reached by Raoult (15) while evaluating the molecular masses by cryoscopy and by Stewart (16) by ultraviolet spectroscopy.

The most spectacular experiment in this series is the one by Cotton (17) who mixed two light-blue solutions of D- and L-copper potassium tartrate to give a deep-blue one. The explanation was that there was formation of racemates in solution. Wilkinson (18) for whom the colour change could be attributed to the polymerization degree of the diasteromeric complexes, confirmed the idea that there was diastereomeric associations.

There are also huge differences in the melting points and solubilities (19) of the pure and racemic tartaric acids (Table 1). These values can suggest that the DL pair is much more stable than the LL or DD ones, by its higher fusion temperature and sparing solubility in water.

Many other substances were studied to evaluate their behaviour as pure enantiomers and racemates. Molecules from natural sources like terpenes, hydroxy acids, amines, and alcohols were examined similarly, but unfortunately the differences were very small or the measurements difficult to reproduce (20; only a few studies of enthalpic properties of diastereomeric salts were conducted but the subject is still of interest, see ref. (21*a*, *b*)).

During the last century, the study of racemic and enantiopure substances continued. This gave rise to a better understanding of their properties but also ultimately led to modern stereochemistry, the relationships between isomers, the ways to separate or produce them, and to wonderful total syntheses of natural products. But much later, more than one century after the first studies of Pasteur and others, a new field of organic chemistry emerged as mature, the enantioselective synthesis.

Since enantioselective reactions were not and are not always totally selective, the organic chemists developed methods to assess the enantiomeric purity of the synthesised substances. But the question rose once again: what if the substance is not racemic nor enantiomerically pure; what if there was interactions in solution? Would these associations have any influence on the analysis technique that was used?

4. The enantiomerically impure

One of the first exhaustive studies of the influence of the enantiomeric purity on the characterization of a substance is the one of 1-ethyl-1-methylsuccinic acid **2** (20, 22). Horeau et al. studied in great details the behaviour of this compound starting by the investigation of the observed variation of specific rotation of the enantiopure diacid **2** as a function of its concentration (Fig. 7).

Fig. 7. The two enantiomers of 1-ethyl-1-methylsuccinic acid (**2**).

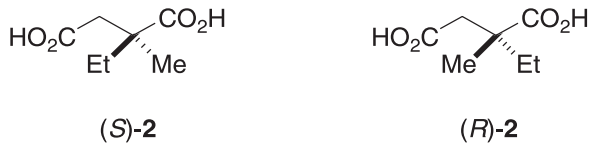
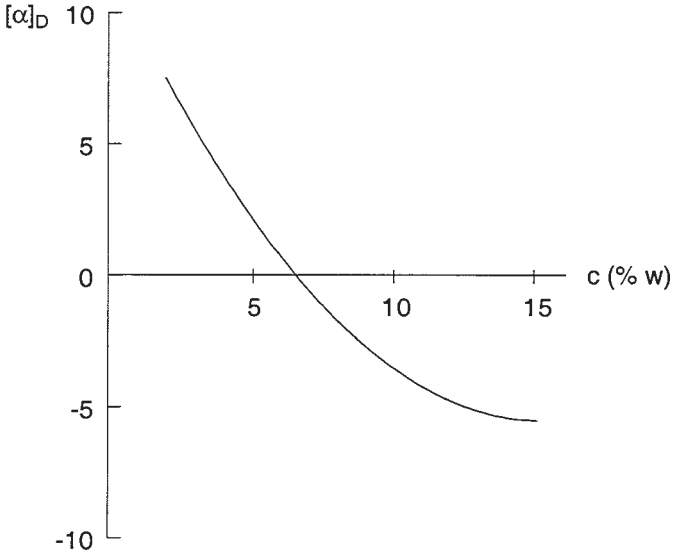


Fig. 8. Variations of specific rotation ($[\alpha]_D$) of (*S*)-1-ethyl-1-methylsuccinic acid (*S*)-**2** as a function of its concentration (*c*, % $^{w}/_{w}$) in chloroform.



This was true in chloroform as it can be seen in Fig. 8. At low concentration, the acid (*S*)-**2** is dextrorotatory while at high concentration it is lævorotatory. The specific rotation of the enantiomerically pure substance even becomes equal to zero at 6.3% w, as if it was racemic!

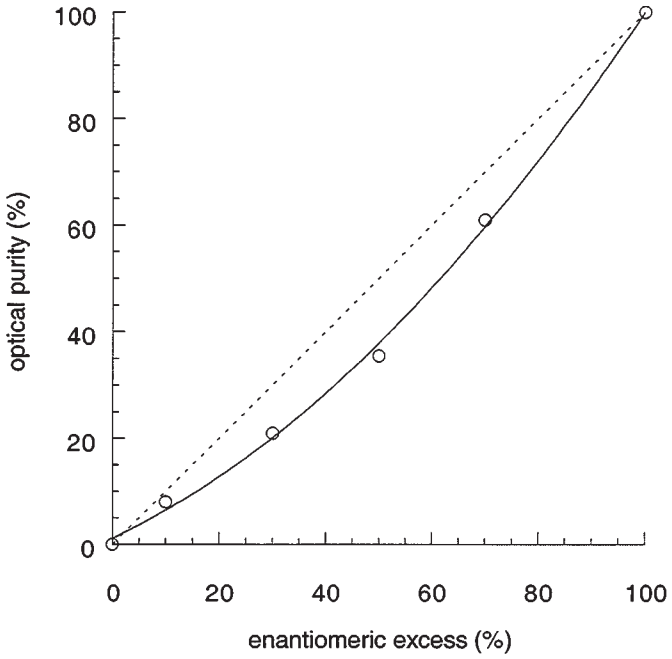
The same behaviour was observed in dichloromethane and for the corresponding α-isopropyl-α-methyl diacid. However, when the rotation was measured in polar solvents like ethyl and methyl alcohol, pyridine, diglyme, or acetonitrile, the phenomenon just disappeared. This first observation was suggestive of association of the molecules of the diacid **2** in solution, probably by hydrogen bonding, which had a striking influence on the specific rotation. The use of polar solvents was breaking down the oligomeric structures and giving a perfectly normal reading.

If there were interactions between the molecules of an enantiopure substance in solution, Horeau et al. (20, 22) were then interested in studying the cases where the enantiomeric excess (ee)[4] of that substance was different from 0% (racemic) and 100% (enantiomerically pure). The first thing they discovered was that the relation between the

[4] The enantiomeric excess being defined as the difference between the quantities of each enantiomer on their sum, for a *R*-rich substance ee = $(R - S)/(R + S)$.

© 2000 NRC Canada

Fig. 9. Optical purity of 1-ethyl-1-methylsuccinic acid (**2**) as a function of its enantiomeric excess (ee). Dotted line: the awaited linear relationship. Plain line and open circles: experimental curve.



enantiomeric excess and the optical purity[5] of 1-ethyl-1-methylsuccinic acid (**2**) was not a linear one (Fig. 9).

If no interactions between the molecules in chloroform were taking place, there would not have been any difference between the optical purities and enantiomeric excesses and their relation should have been linear. In the present case, the measured optical purity is always lower than the ee. The molecules in solution are interacting and lowering the specific rotation of the sample.

Horeau and Guetté (20) interpreted the phenomenon in the following way: "Les écarts à la linéarité dans les variations du pouvoir rotatoire en fonction de la composition énantiomérique seraient dus aux différences de stabilité des associations diastéréoisomères des antipodes en solution."[6]

Furthermore, they were able to determine the heat generated while mixing two solutions of both enantiomers of **2** to be of 140 J mol^{-1} at 25°C for a concentration of 0.8% in chloroform. The explanation becomes more precise with the hypothesis that since the mixing of the two enantiomers was exothermic, the stability of the D–L interactions was greater than those of D–D and L–L. Vapour pressure osmometry indicated that the molecules exist as dimers, even in very dilute solutions and readily forms oligomeric species as the concentration increases.

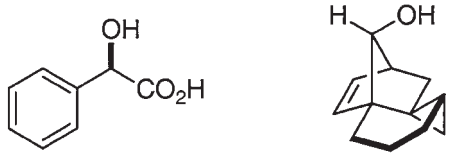
Their study was completed by recording the proton nuclear magnetic resonance spectra (NMR) of 1-ethyl-1-methylsuccinic acid (**2**) at three different enantiomeric purities in deuteriochloroform (Table 2).

They analyzed the α-methylene AB signal and discovered that there were only small differences between the enantiomerically pure and the racemic ($\Delta\delta$). The spectrum of the sample of 50% ee gave however two different sets of signals. Once again the differences were explained by the stability of the diastereomeric species in solution.

Table 2. ^{1}H-NMR of 1-ethyl-1-methylsuccinic acid (**2**) in $CDCl_3$ at 100 MHz at various enantiomeric excess (ee) showing the chemical shift of the 2-methylene hydrogens (δ_1, δ_2), difference between the values ($\Delta\delta$), and the coupling constant (J_{AB}).

Diacid **2**	δ_1 (ppm)	$\Delta\delta_1$ (ppm)	δ_2 (ppm)	$\Delta\delta_2$ (ppm)	J_{AB} (Hz)
100% ee	2.514	0	2.349	0	16.5
50% ee	2.504	0.010	2.335	0.014	16.9
	2.477	0.037	2.305	0.044	17.2
0% ee	2.489	0.025	2.319	0.030	17.0

Fig. 10. Mandelic acid (**3**) and the borneol (**4**) exhibit spontaneous resolution during sublimation when partially resolved.



(*R*)-(–)-isomer **3** (–)-isomer **4**

Similar differences in NMR spectra was already observed by Uskokovic and co-workers (23) while analyzing samples of racemic and natural (enantiomerically pure) dihydroquinine. In this case, the phenomenon was called self-induced nonequivalence (24) and was also encountered sometimes while working molecules capable of autoassociation like amino acids, ureas and stannoxanes, to name a few (25).

The surprises uncovered by these different groups were not the last. While the racemic mixtures were inseparable, reports of enhancement of enantiomeric excesses of partially resolved chiral compounds began to appear. Nowadays, it is well known that the ee of a compound could sometimes be increased by fractional crystallization.

Enantiomeric enrichment can also occur using other purification methods. One of the first examples was the use of sublimation which was then exemplified in several other cases (26). Compounds like mandelic acid (**3**) and the borneol **4** (27) exhibit such a partial resolution when subjected to sublimation (Fig. 10).

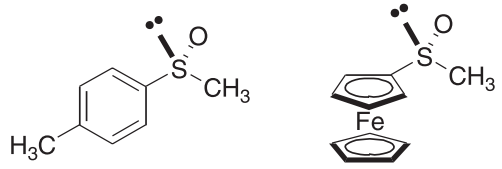
The associations herein existing gave rise to the preferential sublimation of an enantiomerically enriched solid while the one left is sometimes racemic.

This type of associations can also lead to a enantiomeric fractionation during chromatographic separation on an achiral stationary phase (like silica or alumina of an enantiomerically impure compound). Several examples have been published for compounds like amino acid derivatives, peptides, natural and biologically active substances (28), and more recently (Fig. 11) for many sulphoxides like (*R*)-methyl

[5] The optical purity is evaluated by the ratio of the measured $[\alpha]_D$ of the sample on the $[\alpha]_D$ of the enantiomerically pure substance.
[6] Differences to the linearity as a function of the ee are due to diastereomeric associations of the enantiomers in solution.

© 2000 NRC Canada

Fig. 11. (*R*)-methyl *p*-tolyl sulphoxide (**5**) and (*R*)-ferrocenyl methyl suphoxide (**6**) can be enantiomerically enriched on achiral stationary phases.



5 **6**

p-tolyl sulphoxide (**5**) and (*R*)-ferrocenyl methyl sulphoxide (**6**) (29).

In the case of the sulphoxides **5** and **6**, the first fractions being eluted are always enriched (10–20% ee higher) and the last ones of lower ee than the initial ee of the injected sulphoxide. In those cases, the explanation can be that either there is stronger association of the racemate on the stationary phase or that the sulfoxides are associated in the mobile phase, thus giving rise to the formation of diastereomeric species of different mobilities.

The last, but not the least example of resolution occurred during the distillation of a trifluorolactate (30*a*). There are striking differences in the boiling point of isopropyl trifluorolactate (**7**) depending on its enantiomeric excess. Under atmospheric pressure, the racemate boiled at 93°C while the enantiomerically pure compound (*S*)-**7** had a boiling point of 136°C, a difference of 43°C! (Fig. 12).

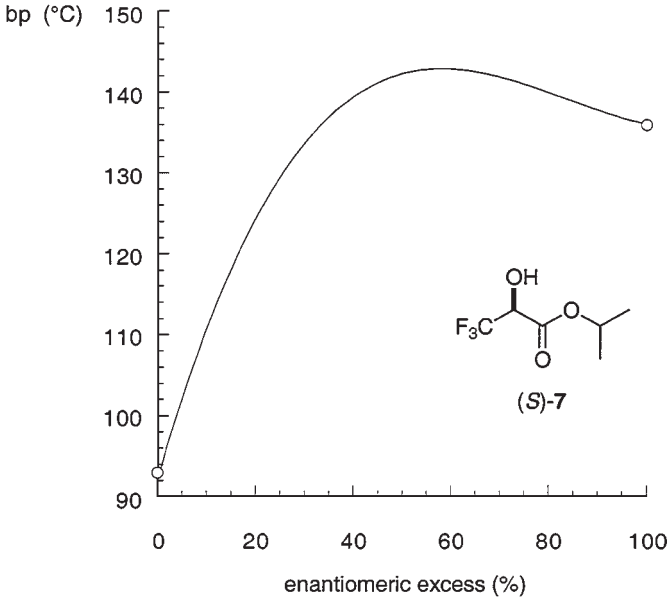
The resolution in this particular case is surprising and hardly understood. The possibility of fractionation by distillation of a mixture of enantiomers has already been discussed, but all attempts had thus so far failed (20).

The authors suggested that the origins of the phenomenon was based on the presence of hydrogen bonding and a possible participation of fluorine atoms in the discrimination process, since the nonfluorinated ethyl lactate has a constant boiling point (154°C). But the exact origin by which the effect is taking place is not quite clear and could also be attributed to resolution through a sublimation and (or) crystallization process (30*b*).

Selective associations between enantiomers were thus once again the cause of this phenomenon and all those discussed before. The interest of Pasteur for enantiomers and their interactions was the focal point where started all the investigations on their behaviour. The study of racemate and enantiomers is still going on today, but during more than a century a lot was discovered. Nowadays, we know more about the ways they interact between them or with chiral molecules. We know how to resolve them. We also developed techniques for the analysis and separation of enantiomers using chiral stationary phases. We know how to evaluate enantiomeric purity by chiral chromatography or numerous other methods.

But all the knowledge we were able to obtain from the study of the molecules themselves was the result of a simple goal. The organic chemist was looking to synthesise chiral molecules. He wanted to be able to effect a transformation and to obtain only the desired stereoisomer with the highest

Fig. 12. Boiling point (bp) of isopropyl trifluorolactate (**7**) as a function of its enantiomeric excess (ee).



selectivity. This never ending quest gave rise to the Art of asymmetric synthesis.

Asymmetric synthesis is giving access to chiral molecules using the principle of stereoselection. This is possible by the use of another chiral molecule which is readily available from natural sources or simple transformations on natural or chiral synthetic products. Resolution is still in use for the preparation of such synthetic precursors but we can also take advantage of the chirality found in Nature to prepare precursors for our tools and even for natural products synthesis itself (31).

These chiral compounds and their chirality were and are used in enantioselective transformations as, for example, auxiliaries grafted on the molecule to transform, chiral additives to protonate selectively, or catalysts to form transient species, and ligands to chelate organometallic reagents or metals to catalyze a reaction. They are the source of the stereoselectivity, the molecules having the stereochemistry dictated by the chiral compound used in such a transformation.

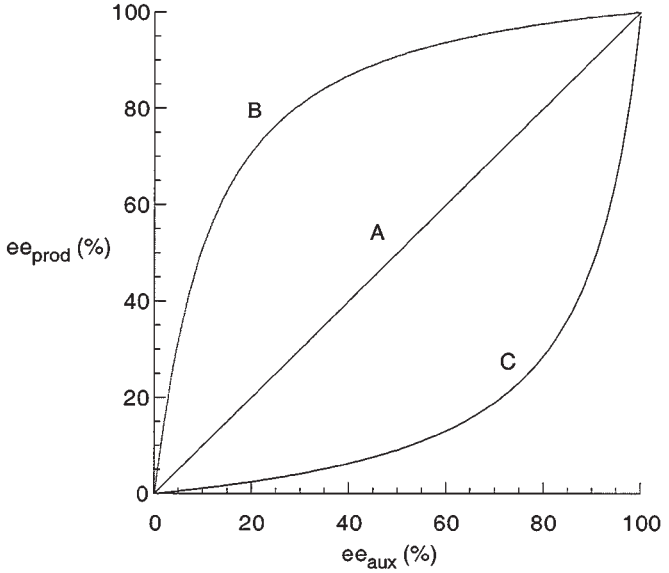
But what are those chiral auxiliaries used in asymmetric synthesis? There are mainly natural products like amino acids and their derivatives, amino alcohols, tartaric acid or esters, alkaloids, as well as artificial compounds like atropoisomeric biphenyls and binaphthyls and other related structures. Almost all the chiral molecules used are capable of interactions between themselves as such or when chelating ions or metals.

5. Nonlinear effects

In 1986, Kagan and co-workers (32) started to study asymmetric synthesis using a nonenantiomerically pure chiral catalyst or auxiliary. They questioned the well accepted hypothesis that the ee of an asymmetric synthesis product (ee_{prod}) was proportional to the ee of the chiral auxiliary (ee_{aux}) used, according to a linear relationship. The

© 2000 NRC Canada

Fig. 13. Enantiomeric excess of the product of an asymmetric reaction (ee_{prod}) as a function of the enantiomeric excess of the chiral auxiliary (ee_{aux}) showing the linear relationship (**A**) and positive (**B**) and negative (**C**) nonlinear effects.



usual way to obtain an approximation of the experimental ee (ee_{prod}) when using a nonenantiopure auxiliary was to used the simple formulæ: $ee_{prod} = ee_o \times ee_{aux}$ with the term ee_o being the ee_{prod} reached using the enantiopure chiral auxiliary under the same reaction conditions.

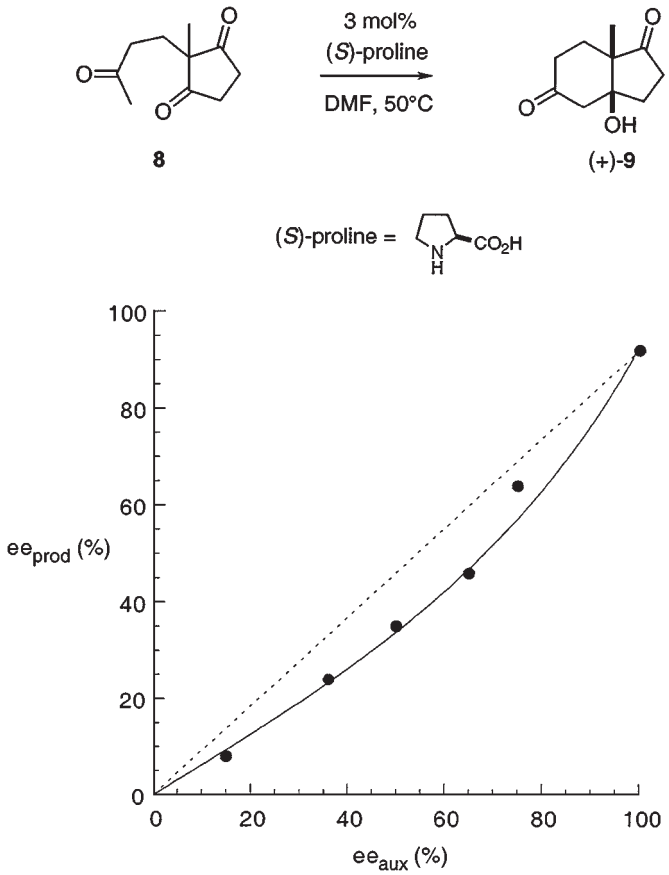
But this simple equation was to be used with caution. A caveat was that this approximation was based on the fact that each enantiomer of the chiral auxiliary was acting independently. But what if there was the type of interactions we previously encountered? There will be an influence on the outcome of the asymmetric synthesis and the results obtained to be different from the linear prediction; the relationship between the enantiomeric excesses will then behave nonlinearly.

The nonlinearities should be the result of interaction between the enantiomers of the chiral catalyst, generating diastereomeric perturbations of the system. This may occur by autoassociation, or association around a matrix, of the chiral species. The perturbations will then add a multiplication factor to the previous equation, a quantification of the deviation from linearity of the relation between ee_{prod} and ee_{aux}.

The graphical representation in Fig. 13 gives a better way to see the effects and influence of such associations during asymmetric reactions. The theoretical linear relationship, for an ee_o = 100%, is given by curve A. Since the linearity should not be followed in systems when interactions between the catalytic species occurs, there are two possibilities. The multiplication factor can increase the awaited ee_{prod} and a plain curve above the line (curve B) called positive nonlinear effect or (+)-NLE should be obtained. If the effect is giving a product with an ee_{prod} lower than expected, a curve below the line (curve C), a negative nonlinear effect or (–)-NLE, will then be drawn.

To test their hypothesis, Kagan et al. (32) studied three different systems. The first reaction was the asymmetric

Fig. 14. Hajos–Parrish–Wiechert reaction of the triketone **8** catalyzed by (*S*)-proline. A slight (–)-NLE between the ee of proline (ee_{aux}) and the ee of bicyclic product **9** (ee_{prod}) is observed.



Robinson annulation, or Hajos–Parrish–Wiechert reaction (33), of the triketone **8** using catalytic amounts of (*S*)-proline (Fig. 14). The ee of (*S*)-proline (ee_{aux}) was plotted as a function of the ee of the produced *cis*-ketol **9** (ee_{prod}), and a slight (–)-NLE was observed in this case.

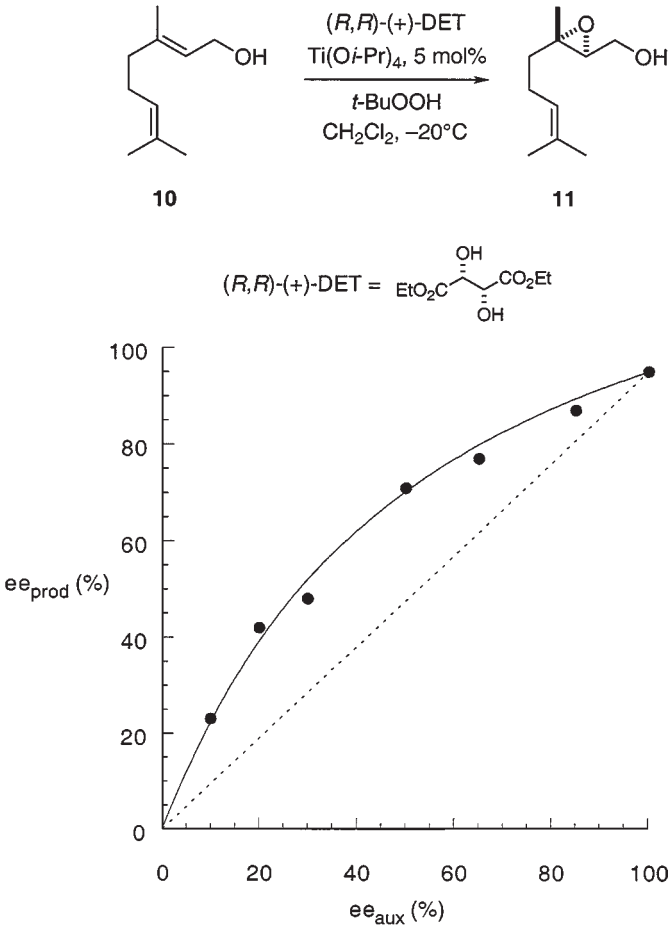
Investigations of the mechanism of this reaction by Agami (34*a*, *b*) demonstrated that two steps took place before cyclization can occur: chiral enamine formation followed by complexation of the intermediate with a molecule of catalyst. This was confirmed by a kinetic model based on a second-order reaction dependence on proline. The (–)-NLE was explained by the fact that heterochiral complexes reacted twice as fast as the homochiral complexes.

For the second reaction, another behaviour was recorded during Katsuki-Sharpless' (35) epoxidation of geraniol (**10**). A positive nonlinear effect is taking place when varying the ee of (*R*,*R*)-(+)-diethyl tartrate {(*R*,*R*)-(+)-DET} used as the catalyst (Fig. 15). The enantiomeric excess of the resulting epoxide **11** (ee_{prod}) was indeed greater than expected when plotted as a function of the ee of (+)-DET (ee_{aux}). A less reactive dimeric heterochiral species, thus more stable, than its homochiral counterparts was suggested to be the cause of the (+)-NLE, since some racemic DET will be retained in the inactive meso complex.

This hypothesis was compatible with the Sharpless mechanism of asymmetric epoxidation, which indicates the

© 2000 NRC Canada

Fig. 15. Sharpless' epoxidation of geraniol **10** catalyzed by (*R*,*R*)-(+)-DET. The reaction shows a (+)-NLE between the ee of DET (ee_{aux}) and the ee of epoxide **11** (ee_{prod}).



intervention of a dimeric complex, introducing two tartrate units in the active species.

For the last reaction, the authors tested their water-modified Sharpless reagent for asymmetric oxidation of sulphides by hydroperoxides (36). Oxidation of methyl *p*-tolyl sulphide **12** into sulphoxide **13** gave a NLE which was quite different from the previous results (Fig. 16).

The relation between the ee's is clearly a (–)-NLE but this effect is taking place up to a value of 70% ee of diethyl tartrate. The linear relationship is then prevailing until 100% ee. This perturbed behaviour is indicative of a complicated structure for the water-modified reagent.

These first experiments were a revelation in the behaviour of mixtures of enantiomeric reagents or catalysts. They were an indication of subtle interactions taking place in their solutions with participation of diastereomeric species. Furthermore, the analysis of the perturbations generated by mixing various amounts of enantiomers on the enantioselectivity of the reaction was also giving information about the reaction itself.

Mathematical models were developed by Kagan and coworkers (37) that helped to understand and to quantify the nonlinear effect phenomenon. Most of the NLEs to be reported could be explained based on the "ML_2 model" (Fig. 17). The chiral substance (L) used for an asymmetric

Fig. 16. Kagan's asymmetric oxidation of sulphide **12** into sulphoxide **13**. A (–)-NLE between the ee of DET (ee_{aux}) and the one of sulphoxide **13** (ee_{prod}) is observed up to 70% ee DET.

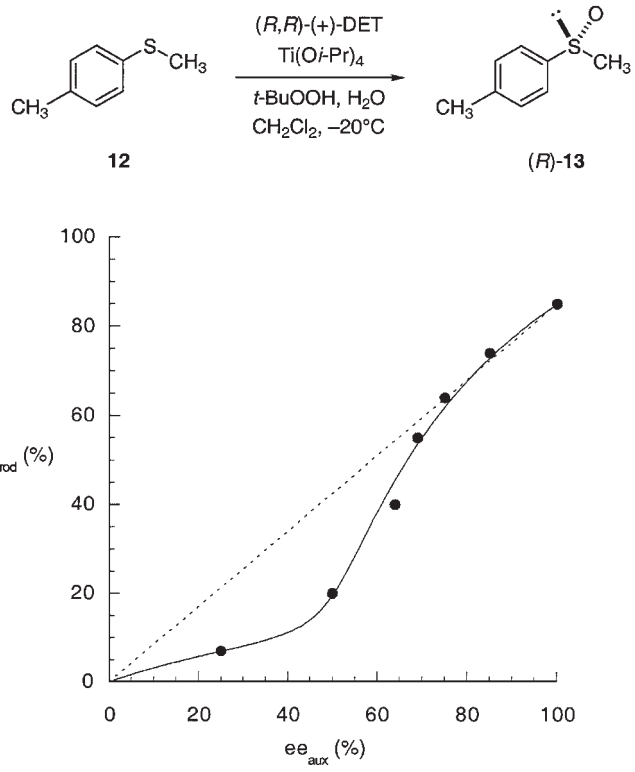
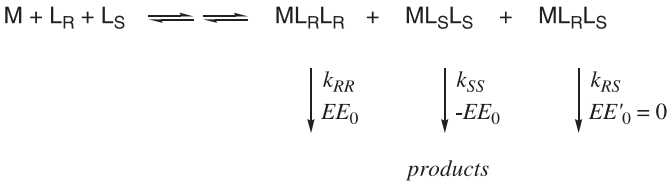


Fig. 17. Kagan's ML_2 model for nonlinear effects.



transformation is usually interacting with a metallic centre (M) to form the reagent or catalyst. If both enantiomers are present (L_R and L_S), the species formed will be constituted of homo (ML_RL_R and ML_SL_S) and hetero (ML_RL_S) complexes.

These complexes will then react to give the desired product, the homo complexes giving the products with opposite configuration while the hetero one will give the racemate. If there is one of the complex type which is more stable than the other, a NLE will be observed. If the meso ML_RL_S species is more reactive, there will more racemate produced and the ee lower than expected, generating a (–)-NLE. If however this meso complex is more stable, the homo species will enter the reaction cycle giving rise to a (+)-NLE since the minor enantiomer of the chiral ligand will be trapped inside the less reactive ML_RL_S species. The discussion is exactly the same if one assumes the formation of dimeric species of $(ML)_2$ type, this case being similar to diastereomeric interactions that were reported for the chiral substances alone (vide supra).

© 2000 NRC Canada

Fig. 18. Asymmetric diethylzinc (curve ●) reaction on benzaldehyde (**14**) catalyzed by DAIB leading to the alcohol **15** showing a strong (+)-NLE. A smaller effect was also observed when using Me_2Zn (curve ■).

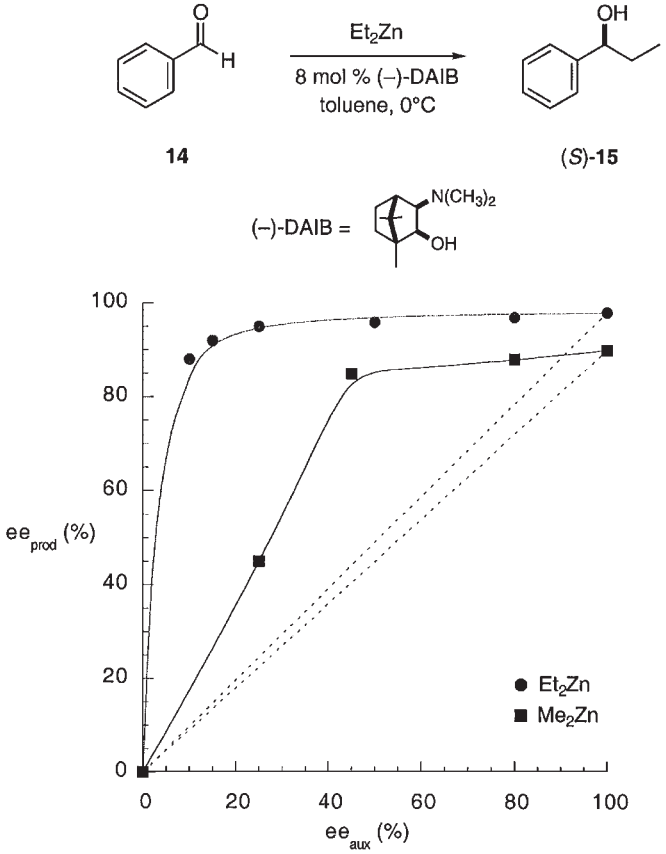
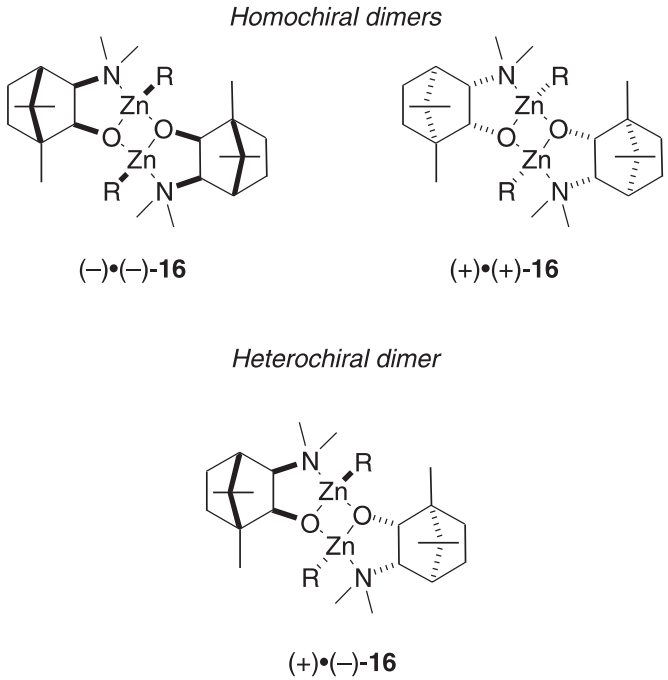


Fig. 19. Mixtures of (–)- and (+)-DAIB and dialkylzinc form enantiomeric DAIB-ZnR organometallics. The active reagent then forms homodimers (–)·(–)-**16** and (+)·(+)-**16** and the heterochiral one (–)·(+)-**16**.



It became clear that looking for non-linear effects in a given system is a probe for analysing the nature of the catalytic species involved in an asymmetric synthesis. Results emerging from the data collected were clear indications that such nonlinear effects were to be encountered in many cases. The following section will present only a few examples of nonlinear effects that were published after their initial discovery in 1986. Exhaustive recollection of NLE in asymmetric synthesis can be found in highlights and reviews on the subject (38, 39).

6. NLE, an ubiquitous phenomenon

One useful method of alkylating carbonyl compounds is the use of organozincs coupled with a catalyst which is needed to observe any reaction. During their work on alkylation of benzaldehyde (**14**) by diethylzinc, Oguni et al. (40) discovered in 1988 that a positive nonlinear effect (called *asymmetric amplification* by the authors) was present when chiral β-amino alcohols were used as catalysts.

The following year, Noyori and co-workers (41) published a detailed mechanistic study on catalysed addition of organozincs on aldehydes. They observed as well a strong (+)-NLE when using (–)-3-*exo*-(dimethylamino)isoborneol, or (–)-DAIB, in various ee's as a catalyst (Fig. 18). This effect was very impressive, the maximum enantioselectivity of the reaction being reached at very low *ee* of DAIB (curve ●). The 1-phenylpropanol (*S*)-**9** can thus be prepared with very high enantioselectivity (95% *ee*) with a very impure catalyst (15% ee). A similar but less pronounced effect was also observed when using dimethylzinc (curve ■) for the alkylation.

Noyori et al. (41) suggested that this strong (+)-NLE was due to autoassociation of the chiral reagent. The organometallic DAIB-zinc formed is undergoing dimerisation as depicted in Fig. 19. When the mixture of (–) and (+)-DAIB is used, there is formation of two types of dimeric species: the usual homochiral complexes (–)·(–)-**16** and (+)·(+)-**16** and the heterochiral one (–)·(+)-**16**.[7] The enantiomeric monomers of DAIB-ZnR (*R* = Me or Et) are herein the active reagents and each one will produce one enantiomer of the alcohol **15**.

The existence of dimeric species was confirmed by several experiments. Cryoscopic molecular weight measurements demonstrated that DAIB-ZnR was dimeric in solution. Nuclear magnetic resonance (NMR) of homochiral and heterochiral reagents gave insights on the relative stability of the dimeric organozincs. Upon addition of benzaldehyde, noticeable changes were observed in the NMR spectrum of the homochiral dimer, whereas the spectrum of the heterochiral complex remained unchanged, revealing a lower reactivity.

The differences were understood by X-ray diffraction analysis of each of the dimers obtained by reaction of dimethylzinc with the chiral ligand. The homochiral species (–)·(–)-**16** (*R* = CH_3) possess a C_2 symmetry with a Zn_2O_2 four-membered ring showing a *syn* relationship between the

[7] The signs on each side of the dot refer to the enantiomer of the chiral ligand included in the complex.

© 2000 NRC Canada

Fig. 20. Nonlinear effects during Ipc_2BCl reduction of the ketone **17**. The ee of the alcohol **18** (ee_{prod}) is higher than the ee of pinene (ee_{aux}) used to prepare the reagent at the beginning (curve ●) and the end of the reaction (curve ■). Calculated ees of **18**, based on a statistical distribution of the pinene in the reagent, are also included (curve ○).

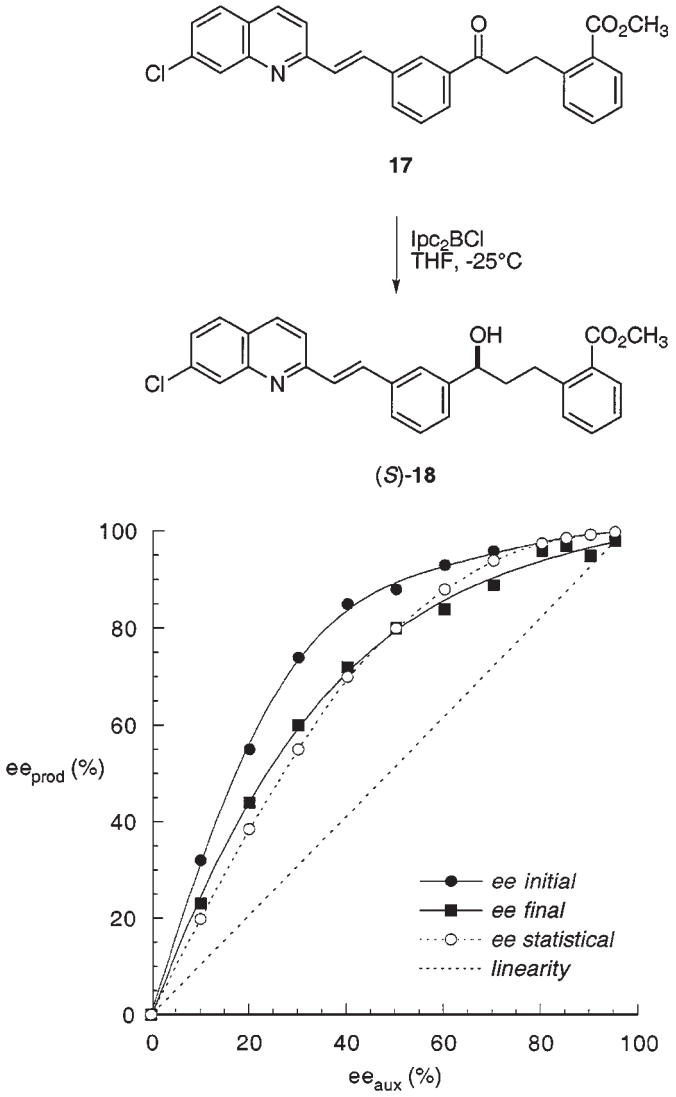
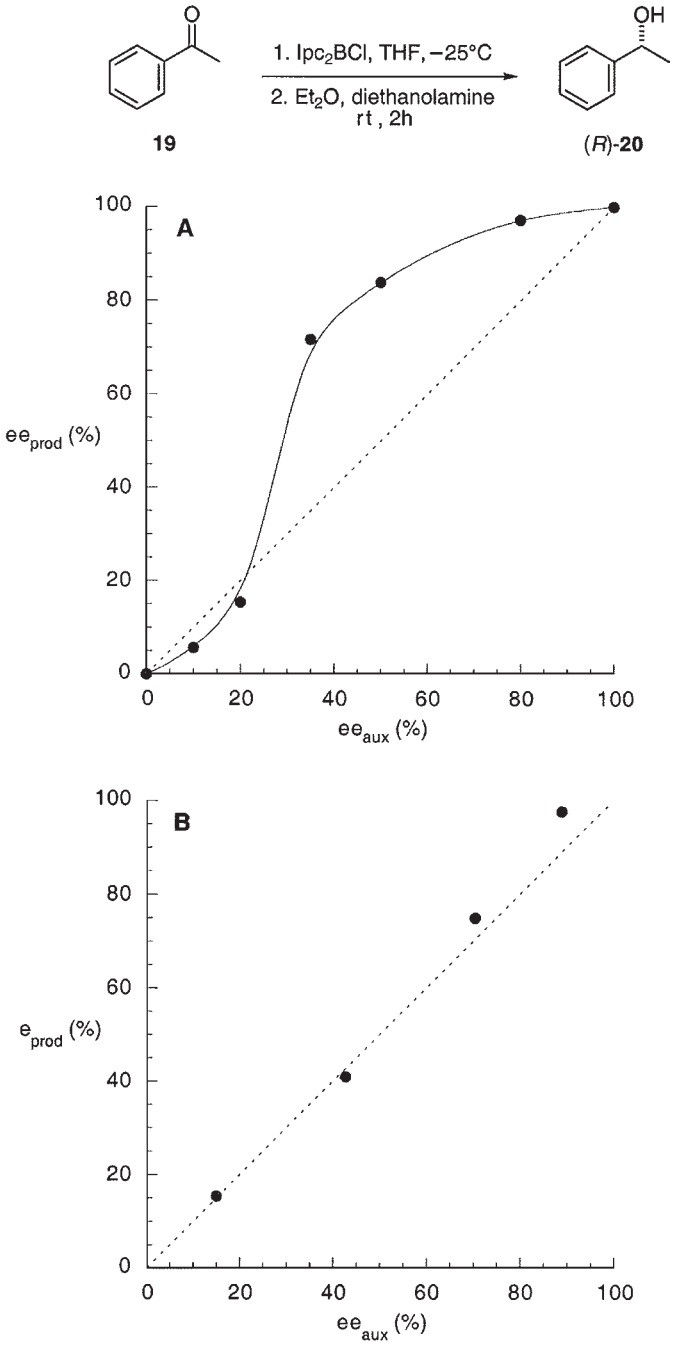


Fig. 21. Reduction of acetophenone (**19**) into chiral alcohol **20** with Ipc_2BCl. Curve **A** was obtained with the reagent prepared from pinene of various enantiomeric purity. Curve **B** was drawn from reactions using Ipc_2BCl in variable enantiomeric excesses prepared by mixing enantiomers of the reagent itself.



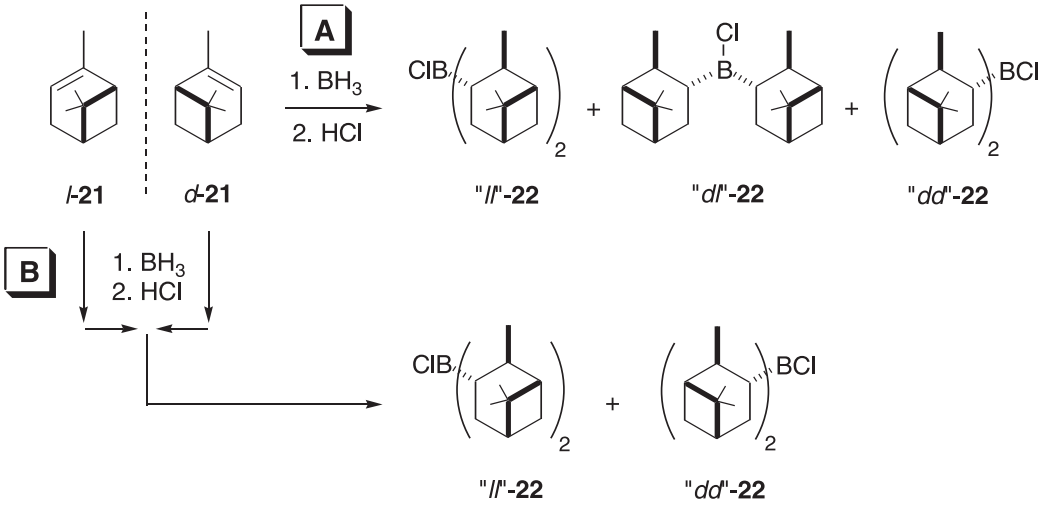
methyls borne by the zinc atoms. This ring is "*endo*-fused" relative to the DAIB-Zn system. The heterochiral dimer (+)·(–)-**16** ($R = CH_3$) also have a Zn_2O_2 cycle *endo*-fused but the methyls on metallic centres, as well as the DAIB fragments, are oriented in an *anti* fashion one to another; this feature being responsible for the greater thermodynamical stability of this dimer. This was later complemented by energetic calculations on simpler models.

Nonlinear effects were not only found in catalytic asymmetric reactions. The use of chiral reagents incorporating nonenantiopure material can also give rise to a very similar phenomenon.

One of the first examples was published in 1994 by Merck researchers (42) and regarding the asymmetric production of an alcohol, which is a useful intermediate in synthesis of a LTD_4 antagonist. The use of Brown's diisopinocampheyl chloroborane (Ipc_2BCl), prepared from (–)-α-pinene and BH_2Cl, to reduce ketone **17** into alcohol **18**, showed a nonlinear behaviour. Starting from pinene of 98% or 70% ee gave the alcohol **18** with an enantiomeric purity of 97% ee and 95% ee respectively (Fig. 20). It was hypothesized that three reagents (two homochiral and one *meso*) were present and statistically distributed, the *meso* borane being very

© 2000 NRC Canada

Fig. 22. Different methods for the preparation of Ipc_2BCl. Method **A**: from pinene (**21**) of various ee; and Method **B**: by mixing boranes of different ee. The two methods produce homoboranes *ll*–**22** and *dd*–**22**, while the heteroborane *dl*–**22** is present only in Method **A**.



sluggish to react, thus being the cause of the observed (+)-NLE.

The same system was studied in 1995 by Kagan et al. in the asymmetric reduction of acetophenone (**19**) by Ipc_2BCl (4 equiv.) using the reagent derived from (–)-α-pinene (43) and prepared accordingly to H. C. Brown procedure (44). It was shown that the way the reagent was synthesized had a great influence on the outcome of the reduction (Fig. 21). As a matter of fact, when Ipc_2BCl was prepared with pinene of various ee, a strong (+)-NLE between the ee of the alcohol **20** and the pinene one took place (curve **A**). If however the reducing agent was obtained by mixing Ipc_2BCl of different enantiomeric purities, the relation became perfectly linear (curve **B**).

The linear relationship suggested that each of the enantiomeric reagents was acting independently in the reduction process. The separate preparation of Ipc_2BCl (**22**), from enantiopure α-pinenes (**21**) gave both enantiomers *"ll"*–**22** and *"dd"*–**22**, which were then mixed in various amounts to reach the desired ee_{aux} (Method **B**, Fig. 22). Such a mixture should behave linearly since each enantiomer of the reagent is acting independently and producing an enantiomer of the alcohol **20**. In the other procedure, the reagent was obtained starting from mixtures of (–)- and (+)-α-pinene in various ees (*l*- and *d*-**21**). This method (**A**) was suggested to generate three boranes: *"ll"*–**22**, *"dd"*–**22**, and *"dl"*–**22** (Fig. 22). The (+)-NLE is in agreement with a very low reactivity of the *meso* reagent *"dl"*–**22** formed in this case which was trapping the minor enantiomer of pinene, thus increasing the effective ee of the reagent.

As an added proof, studies by the Merck group demonstrated that the ee of their reduction product was time-dependent (**18**, Fig. 20). The NLE was indeed more important at lower conversion than after completion of the reaction (45). The curves however keep the same shape during the course of the reduction; which is close to the calculated curve based on a statistical distribution of the pinene on the boron atom. Girard and Kagan (46) also published another study where the stoichiometry of Ipc_2BCl was varied. The curves had the same shape but the NLE was increasing with the amount of reductant used. These complementary results suggest that the more reactive homochiral species is giving better ee at the beginning of the reaction or by the use of a larger quantity of reagent. But as soon as the amount of this species drops the less reactive heterochiral borane becomes involved in the reduction, thus lowering slightly the ee of the product.

Apart from mechanistic interests (47), the possibility of creating a strong (+)-NLE in Ipc_2BCl reductions, allows one to avoid the use of expensive enantiopure α-pinene and to replace it with the one of ees lower than 90%.

The few reports discussed in the last sections highlighted the fact that diastereomeric interactions could lead to perturbations in the behaviour of chiral substances. The discovery of nonlinear effects while using chiral reagents, auxiliaries and catalysts was of a great importance for the understanding of enantioselective systems. They often gave the opportunity to clarify mechanisms or the nature of species involved in some enantioselective reactions.

7. Conclusion and perspectives

The examples presented in this article show how important the influence of diastereomeric perturbations may be on the properties of a chiral material or the outcome of an asymmetric synthesis. They highlight the fact that chiral molecules sometimes present a behaviour which is not the predicted one. The impact of diastereomeric associations may be beneficial, allowing resolution of enantiomers or highly selective asymmetric synthesis using a nonenantiopure chiral substance if a (+)-nonlinear effect is present. On the other hand, the same interactions can lead to the opposite phenomenon where the reaction will not be as selective as it should be, even if the chiral auxiliary is quite pure, if a (–)-NLE rules the system. The effect can be much more complex if higher aggregated species are present and a caveat should be made about empirical predictions of the selectivity of a reaction.

© 2000 NRC Canada

But the study of nonlinear effects also provides a simple and additional probe to detect and explain aggregation or self-assemblies that may arise. Furthermore, the presence of a strong asymmetric amplification could be a very useful property which allows the use of enantiomerically impure chiral auxiliaries, thus giving the opportunity to produce chiral compounds in a faster and cheaper way. It also paves the way to the possibility to build some autocatalytic systems with autoinduction (48*a–c*; for a mathematical model of autoinduction, see ref. (48*d*)). These systems could be synthetically useful or can suggest additional models for prebiotic generation of optical activity on earth (49).

The basic concepts which are the roots of the nonlinear effects in enantioselective reactions should apply as well to kinetic resolution (50), diastereoselective reactions, the use of pseudo-enantiomeric (51) and diastereomeric (52) catalysts in enantioselective synthesis.

The diastereomeric perturbations are thus a long time companion of the organic chemist. Sometimes hidden, a few being uncovered during the short history of organic chemistry, these effects are nowadays coming out in many cases using chiral substances (during the preparation of this manuscript, a short historical review on "NLE" has been published, see ref. (53)). Reports on the interactions between hetero and homo species formed by the mirror images will for sure continue to exert a delightful fascination in the future.

Acknowledgements

C. Girard wants to thank Steve for the great opportunity to learn with him, complete a Ph.D. in his laboratory, and most of all for his friendship. Funds provided by Ministère de l'Education Nationale, de la Recherche et de la Technologie, by Centre National de la Recherche Scientifique (UMR 7001 and UPRESA 8075 CNRS) and by Aventis (Rhône–Poulenc–Rorer) are greatly acknowledged.

References

1. J.B. Biot. Mem. Acad. Sci. Inst. Fr. **15**, 93 (1838).
2. (*a*) E.L. Eliel, S.H. Wilen, and L.N. Mander. Stereochemistry of organic compounds. Wiley, New York. 1994; (*b*) M. Nógrádi. Stereochemistry. Pergamon, New York. 1981; (*c*) H.B. Kagan. Organic stereochemistry. Wiley, New York. 1979.
3. S.F. Mason. Nature (London), **311**, 19 (1984).
4. J. Jacques, A. Collet, and S.H. Wilen. Enantiomers, racemates and resolutions. Wiley, New York. 1981.
5. M. de Min, G. Levy, and J.C. Michaud. J. Chim. Phys. **85**, 603 (1988).
6. L. Pasteur. C. R. Acad. Sci. Paris, **26**, 535 (1848).
7. L. Pasteur. Ann. Chim. Phys. **24**, 442 (1848).
8. L. Pasteur. Ann. Chim. Phys. **38**, 437 (1853).
9. (*a*) J.A. LeBel. Bull. Soc. Chim. Fr. **22**, 337 (1874); (*b*) J.H. van't Hoff. Arch. Neerl. Sci. Ex. Nat. **9** 445 (1874).
10. M. Lahav and L. Leiserowitz. Angew. Chem. Int. Ed. **38**, 2533 (1999).
11. L. Pasteur. Ann. Chim. Phys. **28**, 56 (1850).
12. M. Berthelot and K. Jungfleisch. Ann. Chim. Phys. **4**, 147 (1875).
13. S. Takagi, R. Fujishiro, and K. Amaya. Chem. Comm. 480 (1968).
14. (*a*) W.H. Perkin. J. Chem. Soc. **51**, 362 (1887); (*b*) L. Marchlewski. Ber. Dtsch. Chem. Ges. **25**, 1556 (1892).
15. F.M. Raoult. Z. Phys. Chem. Stoechiom. Vewandtschaftsl. **1**, 186 (1887).
16. A.W. Stewart. J. Chem. Soc. **91**, 1537 (1907).
17. (*a*) A. Cotton. Ann. Chim. Phys. **8**, 347 (1896); (*b*) A. Cotton. C. R. Acad. Sci. Paris, **189**, 1211 (1929); (*c*) A. Byk. Z. Phys. Chem. **49**, 682 (1904).
18. J.H. Dunlop, D.F. Evans, R.D. Gillard, and G. Wilkinson. J. Chem. Soc. 1260 (1966).
19. (*a*) Merck Index, 11th Ed. *Edited by* S. Budavari. Merck, Rahway. 1989; (*b*) CRC Handbook of Chemistry and Physics, 62nd Ed. *Edited by* R.C. Weast. CRC Press, Boca Raton. 1981.
20. A. Horeau and J. P. Guetté. Tetrahedron, **30**, 1923 (1974).
21. (*a*) M. Leclercq and J. Jacques. Bull. Soc. Chim. Fr. 2052 (1975); (*b*) Z. Buday, A.K. Rappe, and T.G. Lenz. Chirality, **9**, 325 (1997) and refs. therein.
22. (*a*) G. Krow and R.K. Hill. Chem. Comm. 431 (1968); (*b*) A. Horeau. Tetrahedron Lett. 3121 (1969).
23. T. Williams, R.G. Pitcher, P. Bommer, J. Gutzwiller, and M. Uskokovic. J. Am. Chem. Soc. **91**, 1871 (1969).
24. W.H. Pirkle and D.J. Hoover. Top. Stereochem. **13**, 263 (1982).
25. (*a*) A. Dobashi, N. Saito, Y. Motoyama, and S. Hara. J. Am. Chem. Soc. **108**, 307 (1986); (*b*) C.Y. Hong and Y. Kishi. J. Am. Chem. Soc. **114**, 7001 (1992); (*c*) A. Shanzer, J. Libman, and H.E. Gottlied. J. Org. Chem. **48**, 4612 (1983).
26. (*a*) H. Kwart and D.P. Hoster. J. Org. Chem. **32**, 1867 (1967); (*b*) U.I. Zahorsky and H. Musso. Chem. Ber. **106**, 3608 (1973); (*c*) H.M. Fales and G.J. Wright. J. Am. Chem. Soc. **99**, 2339 (1977).
27. (*a*) D.L. Garin, D.J. Cooke Greco, and L. Kelley. J. Org. Chem. **42**, 1249 (1977); (*b*) L.A. Paquette and C.L. Jau. J. Org. Chem. **52**, 1634 (1987).
28. (*a*) K.C. Cundy and P.A. Crooks. J. Chromatogr. **281**, 17 (1983); (*b*) R. Charles and E. Gil-Av. J. Chromatogr. **298**, 516 (1984); (*c*) W.L. Tsai, K. Hermann, E. Hug, B. Rohde, and A.S. Dreiding. Helv. Chim. Acta, **68**, 2238 (1985); (*d*) A. Dobashi, Y. Motoyama, K. Kinoshita, S. Hara, and N. Fukasaku. Anal. Chem. **59**, 2209 (1987); (*e*) R. Matusch and C. Coors. Angew. Chem. Int. Ed. Engl. **21**, 626 (1989); (*f*) R.M. Carman and K.D. Klika. Aust. J. Chem. **44**, 895 (1989).
29. P. Diter, S. Taudien. O. Samuel, and H.B. Kagan. J. Am. Chem. Soc. **59**, 370 (1994).
30. (*a*) T. Katagiri, C. Yoda, K. Furuhashi, K. Ueki, and T. Kobuta. Chem. Lett. 115 (1996); (*b*) K. Mikami, T. Yajima, M. Tereda, Y. Suzuki, and J. Kobayashi. J. Chem. Soc. Chem. Commun. 57 (1997).
31. S. Hanessian. Total synthesis of natural products: the "chiron" approach. *Edited by* J.E. Baldwin. Pergamon, New York. 1983.
32. C. Puchot, O. Samuel, E. Duñach, S. Zhao, C. Agami, and H.B. Kagan. J. Am. Chem. Soc. **108**, 2353 (1986).
33. (*a*) U. Eder, G. Sauer, and P. Wiechert. Angew. Chem. Int. Ed. Engl. **10**, 496 (1971); (*b*) Z.G. Hajos and D. Parrish. J. Org. Chem. **39**, 1615 (1974).
34. (*a*) C. Agami and C. Puchot. J. Mol. Catal. **38**, 341 (1986); (*b*) C. Agami. Bull. Soc. Chim. Fr. 499 (1988).
35. (*a*) K. Katsuki and K.B. Sharpless. J. Am. Chem. Soc. **102**, 5974 (1980); (*b*) M.G. Finn and K.B. Sharpless. J. Am. Chem. Soc. **113**, 113 (1991).
36. P. Pitchen, E. Duñach, M.N. Deshmukh, and H.B. Kagan. J. Am. Chem. Soc. **106**, 8188 (1984).
37. D. Guillaneux, S.H. Zhao, O. Samuel, D. Rainford, and H.B. Kagan. J. Am. Chem. Soc. **116**, 9430 (1994).

© 2000 NRC Canada

38. C. Girard and H.B. Kagan. Angew. Chem. Int. Ed. Engl. **37**, 2923 (1998).
39. (*a*) R. Noyori and M. Kitamura. Angew. Chem. Int. Ed. Engl. **30**, 49 (1990); *(b)* R. Noyori. Asymmetric catalysis in organic synthesis. Wiley, New York. 1994. pp. 273–297; (*c*) C. Bolm. *In* Advanced asymmetric synthesis. *Edited by* G.R. Stephenson. Blackie Academic and Professional, New York. 1996. pp. 9–26; (*d*) H.B. Kagan, C. Girard, D. Guillaneux, D. Rainford, O. Samuel, S.Y. Zhang, and S.H. Zhao. Acta Chem. Scand. **50**, 345 (1996); (*e*) M. Reggelin. Nachr. Chem. Tech. Lab. **45**, 392 (1997); **45**, 622 (1997); (*f*) M. Avalos, R. Babiano, P. Cintas, J.L. Jiménez, and J.C. Palacios. Tetrahedron: Asymmetry, **8**, 2997 (1997).
40. N. Oguni, Y. Matsuda, and T. Kaneko. J. Am. Chem. Soc. **110**, 7877 (1988).
41. (*a*) M. Kitamura, S. Okada, and R. Noyori. J. Am. Chem. Soc. **111**, 4028 (1989); (*b*) M. Yamakawa and R. Noyori. J. Am. Chem. Soc. **117**, 6327 (1995).
42. (*a*) A.O. King, E.G. Corley, R.K. Anderson, R.D. Larsen, T.R. Verhoeven, P.J. Reider, Y.B. Xiang, M. Belley, Y. Leblanc, M. Labelle, P. Prasit, and R.J. Zamboni. J. Org. Chem. **58**, 3731 (1993); (*b*) I. Shinkai, A.O. King, and R.D. Larsen. Pure Appl. Chem. **66**, 7551 (1994).
43. C. Girard and H.B. Kagan. Tetrahedron: Asymmetry, **6**, 1881 (1995).
44. H.C. Brown and N.N. Joshi. J. Org. Chem. **53**, 4059 (1988).
45. M. Zhao, A.O. King, R.D. Larsen, T.R. Verhoeven, and P.J. Reider. Tetrahedron Lett. **38**, 2641 (1997).
46. C. Girard and H.B. Kagan. Tetrahedron: Asymmetry, **8**, 3851 (1997).
47. D.G. Blackmond. J. Am. Chem. Soc. **119**, 12934 (1997); **120**, 13349 (1998).
48. (*a*) T. Shibata, H. Morioka, T. Hayase, K. Choji, and K. Soai. J. Am. Chem. Soc. **118**, 471 (1996); (*b*) T. Shibata, T. Takahashi, T. Konishi, and K. Soai. Angew. Chem. Int. Ed. Engl. **36**, 2458 (1997); (*c*) T. Shibata, S. Yonekubo, and K. Soai. Angew. Chem. Int. Ed. **38**, 659 (1999); (*d*) P.D. Bailey. J. Chem. Soc. Chem. Commun. 1707 (1995).
49. (*a*) T. Shibata, J. Yamamoto, N. Matsumoto, S. Yonekubo, S. Osanai, and K Soai. J. Am. Chem. Soc. **120**, 12157 (1998); (*b*) K. Soai, S. Osanai, K. Kadowaki, S. Yonekubo, T. Shibata, and I. Sato. J. Am. Chem. Soc. **121**, 11235 (1999); (*c*) B.L. Feringa and R.A. van Delden. Angew. Chem. Int. Ed. **38**, 3418 (1999).
50. (*a*) T.O. Luukas, C. Girard, D.R. Fenwick, and H.B. Kagan. J. Am. Chem. Soc. **121**, 9299 (1999); (*b*) D.W. Johnson, Jr. and D.A. Singleton. J. Am. Chem. Soc. **121**, 9307 (1999).
51. S.Y. Zhang, C. Girard, and H.B. Kagan. Tetrahedron: Asymmetry, **6**, 2637 (1995).
52. (*a*) M. Kitamura, S. Suga, M. Niwa, and R. Noyori. J. Am. Chem. Soc. **117**, 4832 (1995); (*b*) M. Kitamura, M. Yamakawa, H. Oka, S. Suga, M. Niwa, and R. Noyori. Chem. Eur. J. **2**, 1173 (1997).
53. D. Heller, H.-J. Drexler, C. Fischer, H. Buschmann, W. Baumann, and B. Heller. Angew. Chem. Int. Ed. **39**, 495 (2000).

© 2000 NRC Canada

Solid phase assisted synthesis of HIV-1 protease inhibitors. Expedient entry to unsymmetrical substitution of a C_2 symmetric template

Karin Oscarsson, Björn Classon, Ingemar Kvarnström, Anders Hallberg, and Bertil Samuelsson

Abstract: A solid phase synthesis has been developed leading up to unsymmetrical HIV-1 protease inhibitors that are not readily available by conventional solution phase chemistry (**18a–g)**. To prepare these compounds the hydroxyl group of (1*S*,2*R*)-(–)-*cis*-1-phthalimido-2-indanol (**3**) was coupled to a Merrifield resin via a dihydropyrane linker. Cleavage of the phthalimido protecting group and reaction of the liberated amine with the bis-activated symmetrical diacid **15** resulted in the resin bound amide **16**. Coupling of **16** with amino acids and amines followed by hydrolysis produced the desired unsymmetrical products **18a–g** from which potent HIV-1 protease inhibitors were identified, e.g., **18e** (k_i = 0.1 nM), **18a** (k_i = 0.2 nM) and **18c** (k_i = 2 nM).

Key words: HIV, inhibitor, protease, solid phase.

Résumé : On a mis au point une synthèse en phase solide qui permet d'obtenir des inhibiteurs non symétriques de protéase HIV-1 (**18a–g**) qu'il est difficile d'obtenir par la chimie conventionnelle en solution. Dans cette synthèse, on couple le groupement hydroxyle du (1*S*,2*R*)-(–)-*cis*-1-phtalimido-indan-2-ol (**3**) à une résine de Merrifield à l'aide d'une liaison avec un dihydropyrane. Après clivage du groupe phtalimido protecteur et réaction de l'amine libérée avec le diacide symétrique **15** doublement activé, on obtient l'amide **16** lié à la résine. Le couplage de **16** avec des acides aminés ou avec des amines suivi d'une hydrolyse permet d'obtenir les produits non symétriques désirés **18a–g** à partir desquels il a été possible d'identifier de puissants inhibiteurs de protéase de l'HIV-1, par exemple **18e** (k_i = 0,1 nM), **18a** (k_i = 0,2 nM) et **18c** (k_i = 2 nM).

Mots clés : HIV, inhibiteur, protéase, phase solide.

[Traduit par la Rédaction]

Introduction

The human immunodeficiency virus (HIV) has been identified as the etiologic agent of AIDS (1, 2). The HIV-1 protease is a member of the aspartic protease family of enzymes (3–5), producing essential structural and functional viral proteins by proteolytic processing of the *gag*- and *gag-pol* viral gene products (6, 7). Inhibition of the HIV-1 PR have been shown to lead to the inactivation of HIV-1 (4, 8–10). Notably, protease inhibitors have shown clinical efficacy and there are presently five protease inhibitors approved by the FDA for the treatment of HIV-1 infection: saquinavir, ritonavir, indinavir, nelfinavir, and amprenavir (11, 12). Whereas these inhibitors effectively reduce the plasma viral load in infected individuals (11), the rapid turnover of HIV-1 and the high frequency of mutations in the HIV genome eventually results in the selection of mutant strains and in development of clinical resistance (5, 13–15). Moreover, the high cost of therapy precludes the widespread use of the currently approved HIV-1 protease inhibitors. Not withstanding the progress achieved to date there is thus a pressing need for the development of new and cost-effective HIV-1 protease inhibitors.

We recently reported on the design, synthesis, and antiviral activity of new carbohydrate based C_2-symmetrical protease inhibitors e.g., compounds **1** and **2** (Table 1) (16) which are readily prepared in three steps from commercially available starting materials. However, to prepare unsymmetrical inhibitors based on the C_2-symmetric core template (Fig. 1), a new synthetic procedure had to be developed, as treatment

Received June 29, 1999. Published on the NRC Research Press Website on June 13, 2000.

Dedicated to Professor Stephen Hanessian in recognition of his outstanding contribution to the art and logic of organic synthesis.

K. Oscarsson, B. Classon, and B. Samuelsson.[1] Dept. of Organic Chemistry, Arrhenius Laboratory, Stockholm University, SE-106 91 Stockholm, Sweden.
I. Kvarnström. Dept. of Chemistry, Linköping University, S-581 83 Linköping, Sweden.
A. Hallberg. Dept. of Organic Pharmaceutical Chemistry, Uppsala University, BMC, S-751 23 Uppsala, Sweden.

[1]Author to whom correspondence may be addressed. Telephone: +46 8 6083100. Fax: +46 8 6083199.
e-mail: bertil.samuelsson@medivir.se
[1]Additional address: Medivir AB, Lunastigen 7, SE-14144 Hudding, Sweden.

© 2000 NRC Canada

Scheme 1. Synthesis of protected (1*S*,2*R*)-(–)-*cis*-1-amino-2-indanol.

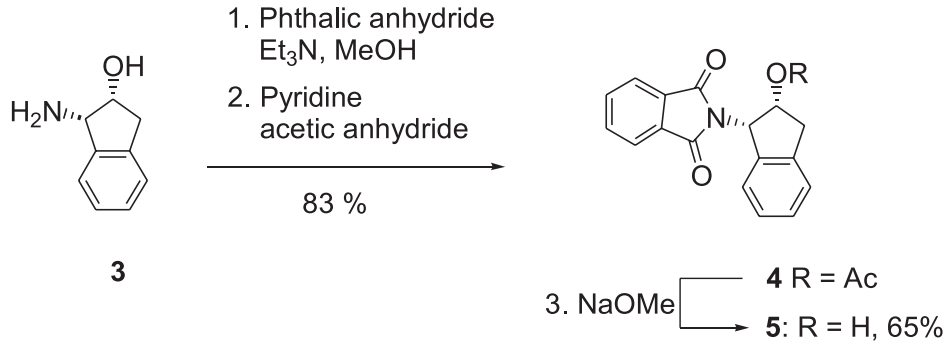
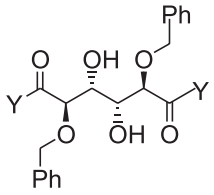
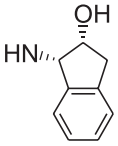
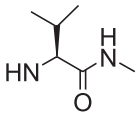


Table 1. C_2-symmetrical protease inhibitors.



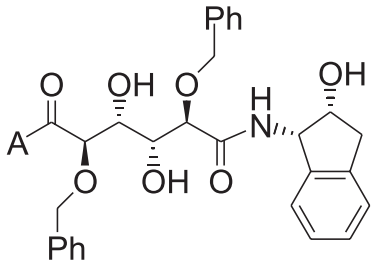
Y	Cmpd. no.	K_i [a] (nM)	ED_{50} [b] (μM)
	**1**	0.4	0.1
	**2**	0.6	1

[a] Standard error 20 %

[b] ED_{50} for reference substances tested in the same assay: ritnonavir (ED_{50}, 0.06 μM), indinavir (ED_{50}, 0.06 μM), saquinavir (ED_{50}, 0.01 μM), nelfinavir (ED_{50}, 0.04 μM).

of either the bislactone (**10**) or the activated L-mannaric acid (**15**) with amines at various conditions preferentially gives the symmetrical products with only minor amounts of the monosubstituted product being present in the reaction mixture at any given time. We now report on the use of solid phase synthesis to prepare unsymmetrical protease inhibitors based on the previously disclosed C_2-symmetric core template (16). The amino indanol **3** has been shown by others (17–19) and us (16) to be an excellent *P*2/*P*2′ ligand for the *S*2/*S*2′ pockets of the HIV-1 protease. Thus in the present work the amino indanol *P*2 residue (**3**) has been kept constant while the *P*2′ residue has been varied using parallel synthesis (Fig. 1). The protected amino indanol **5** was coupled to a THP linker (20) on a Merrifield resin (21), followed by deprotection of the phthalimido group liberating

Figure 1. Unsymmetrical inhibitors, A = Amines.



the free amino function which was reacted with the bis-activated L-mannaric acid (**15**) resulting in the resin bound monoactivated amide **16**. Coupling of **16** with a selection of amines, followed by hydrolysis gave the desired products **18a**–**g** and **1**. Not withstanding this selectivity, a minor amount of the symmetrical inhibitor **1** was formed from "in-land" cross- coupling as evidenced by analysis of the products formed in the reaction. Notably the present solid phase chemistry methodology opens up for further developments of this class of compounds using combinatorial chemistry (22, 23). The compounds produced were screened for HIV-1 protease inhibition and for anti HIV-1 activity in a cell culture assay.

Results and discussion

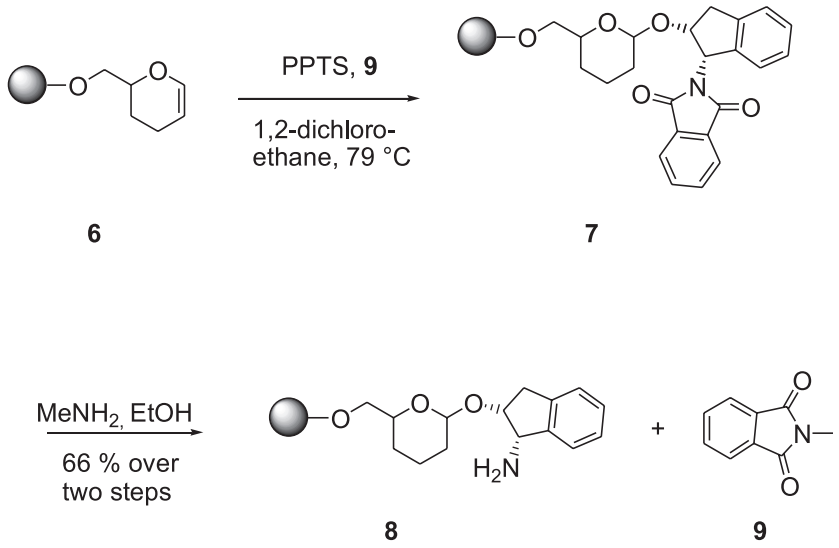
Chemistry

The phthalimido derivative **5** was prepared in two steps by reacting compound **3** with phthalic anhydride in the presence of triethylamine in methanol followed by pyridine – acetic anhydride to give **4** in 83% yield. Deacetylation with sodium methoxide in methanol–dichloromethane gave **5** in 65% yield (Scheme 1). The protected amino indanol **5** was coupled to the solid support 3,4-dihydro-2*H*-2-ylmethoxymethyl polystyrene (**6**) in 1,2-dichloroethane using pyridinium *p*-toluenesulfonate (PPTS) (24) as a catalyst to give **7** (Scheme 2) (22). The phthalimido protecting-group was thereafter cleaved off using methylamine in ethanol for 16 h to give the free amine **8** and the liberated *N*-methyl phthalimide (**9**) in solution. The loading onto the solid support was calculated to be 66% based on the recovery of **9**.

Initial attempts to react the bislactone (**10**) (16) (lactone ring opening) with the free amino group on the solid support **8** failed to give satisfactory results due to unexpected low reactivity under standard reaction conditions (dichloromethane, reflux). Instead an alternative route was investigated

© 2000 NRC Canada

Scheme 2. Coupling of protected (1*S*,2*R*)-(–)-*cis*-1-amino-2-indanol to Merrifield resin.



employing the bissuccinimidyl ester (**15**) (16) for which a new and improved synthetic route was developed. Benzylated bislactone (**10**) (16) was thus reacted with methylamine catalyzed by 2-hydroxypyridine to give bisamide (**11**) in 87% yield (Scheme 3). Use of 2-hydroxypyridine (25) as a catalyst for this reaction gave the highest yields due to suppression of a β-elimination side reaction. The diol in compound **11** was protected using 2,2-dimethoxypropane in acetone containing camphorsulfonic acid to give **12** in 85% yield (16). The corresponding dicarboxylic acid (**14**) was prepared in essentially quantitative yield by reacting compound **12** with dinitrogen tetraoxide (26) and anhydrous sodium acetate in dichloromethane (27, 28) to provide the bis-[*N*-nitrosoamide] (**13**), which was hydrolyzed with lithium hydroxide and hydrogen peroxide (29, 30) to furnish the dicarboxylic acid (**14**). Activation of **14** with *N*,*N*-disuccinimidyl carbonate delivered the corresponding activated bissuccinimidyl ester (**15**) in 95% yield (16).

The amino indanol on the solid support (**8**), was reacted with compound **15** to give the monoamide **16** (Scheme 4) and subsequent coupling of **16** with a series of amines (A = amine, Table 2) gave the unsymmetrical products **17a**–**g** as well as the symmetrical product **17h** linked to solid support. Hydrolysis with 2.3 M HCl in methanol produced compounds **18a**–**g** together with the symmetrical inhibitor **1**. The yields of pure products (**18a**–**g**) over the three steps, based on the loading of the solid support, ranged from 17–47%. Approximately 4% yield of symmetrical inhibitor **1** isolated by chromatography, was formed in each reaction (Table 2).

HIV-1 protease inhibition

(Table 1 and 2) HIV-1 protease was cloned and heterologously expressed in *Escherichia coli* (31). K_i-values were determined in a fluorometric assay (32).

In vitro anti-HIV activity

(Table 1 and 2) The anti-HIV activity was assayed by a HIV cytopathic assay in MT-4 cells where the effects were quantified using vital dye XTT (33). The 50% inhibitory concentrations (ED_{50}) were calculated from the percent cytoprotection for individual compounds.

Structure activity relationship

From Table 2 it is evident that unsymmetrical L-mannaric amides of simple structures can be potent HIV-1 protease inhibitors. The potency of inhibitor **18e** (K_i = 0.1 nM) is somewhat surprising. The *P*2′ benzyl group of inhibitor **18e** can be viewed as a truncated *P*2′ amino indanol of **1** lacking the conformational rigidity of the amino indanol and lacking the hydrogen bond of the corresponding amino indanol hydroxyl group to the Asp 29 of the HIV-1 protease (16). Indeed, the X-ray crystal structure of **18e** complexed with HIV-1 protease shows that the phenyl group is superimposed onto the aryl part of the corresponding amino indanol in inhibitor **1**.[2] However, substitution of the benzyl *P*2′ residue with hydrogen bond accepting or electron donating groups as in the inhibitors **18f** and **18g** leads to less active compounds. These results correlate well with earlier observations, that aromatic substitutions lead to less active inhibitors (15).

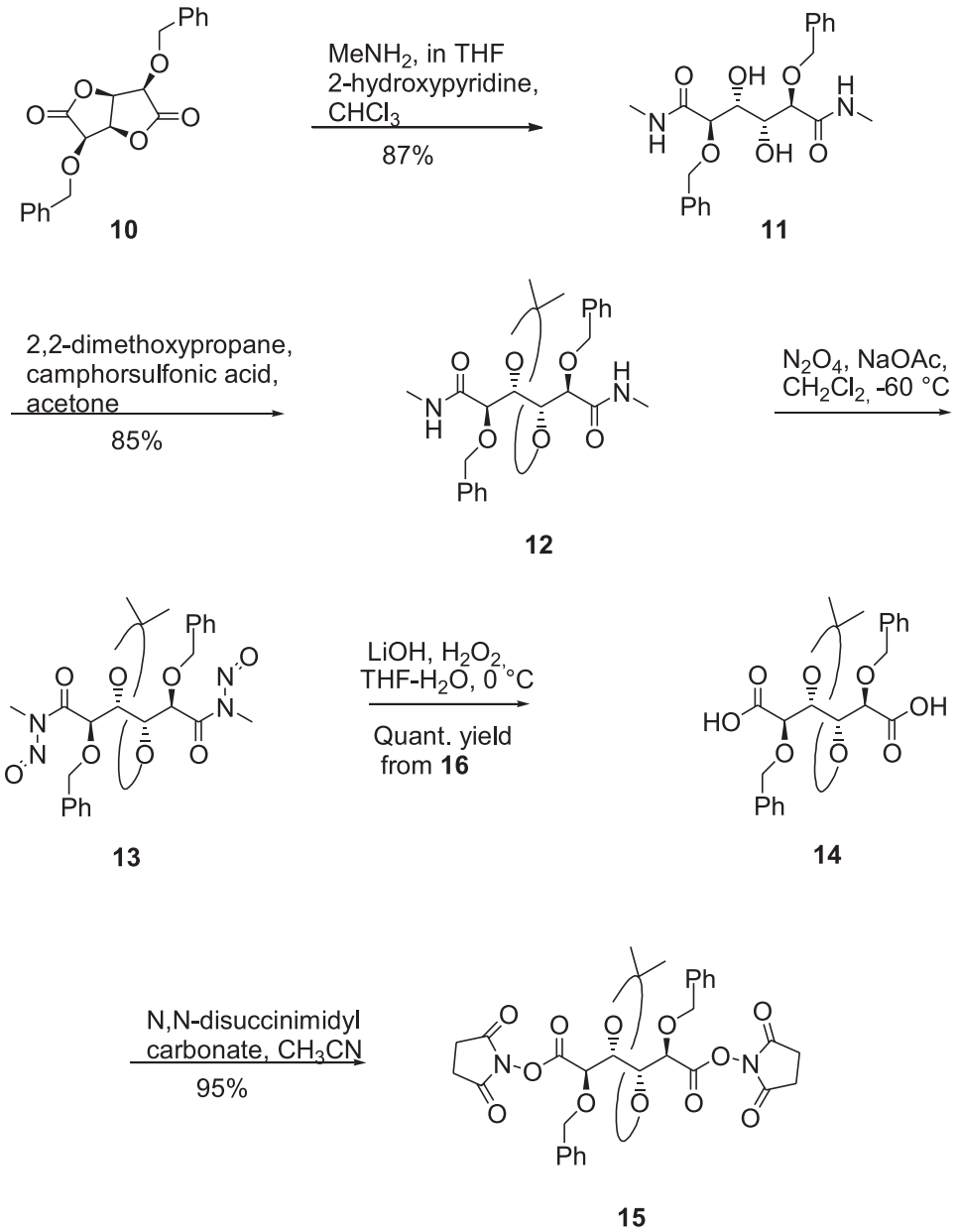
Inhibitor **18a** has similar potency (k_i = 0.2 nM) as the potent corresponding symmetrical inhibitors **1** (k_i = 0.4 nM) and **2** (k_i = 0.6 nM) (16). Inhibitors **18b**, **18c**, and **18d** are *P*2′ truncated simplified analogues of **18a**. Both **18b** and **18d** are considerably less potent, while the methyl amide **18c** (k_i = 2 nM) is notably potent. This inhibitor effectively lacks a *P*2′ residue and the high potency presumably results from an energetically more favorable hydrogen bond interaction between the methyl amide carboxyl oxygen and the structural water that is tetra- coordinated to the inhibitor carbonyls and the Ile 50/150 residues of the HIV-1 protease.

In spite of the promising HIV-1 protease inhibition activities obtained for some of these inhibitors, the antiviral activities in cell culture (ED_{50}) were not improved over inhibitor **1** although inhibitor **18a** was equipotent (Table 2). Further studies are necessary to rationalize the SAR for antiviral activity in cell culture for this class of compounds (34, 35).

[2] Unpublished results.

© 2000 NRC Canada

Scheme 3. Synthesis of bissuccinimidyl ester.



Experimental section

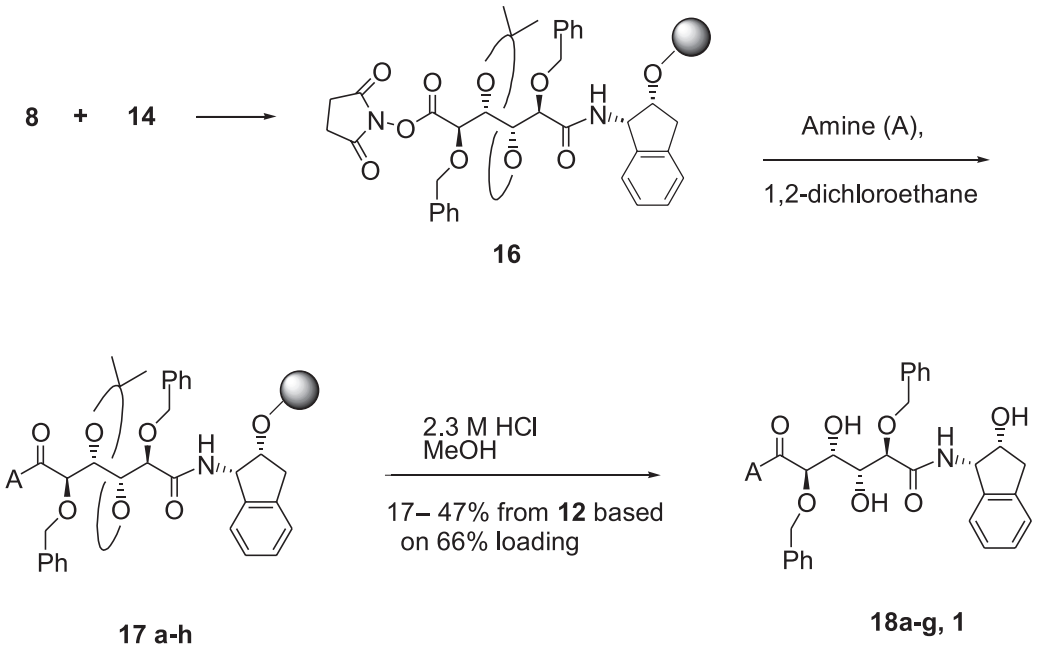
Thin layer chromatography was performed using silica gel 60 F-254 (Merck) plates with detection by UV and (or) charring with 8% sulphuric acid or by charring with ammonium molybdate (100 g):Cer(IV)sulfate (2 g):sulfuric acid (10%, 2 L). Column chromatography was performed on silica gel (Matrix Silica Si 60A, 35–70m, Amicon). Organic phases were dried over anhydrous sodium sulfate or magnesium sulphate. Concentrations were performed under reduced pressure. NMR spectra were recorded on a JEOL GSX-270 instrument (^{13}C NMR 67 MHz and ^{1}H NMR 270 MHz). Chemical shifts are reported in ppm (δ) downfield from tetramethylsilane in $CDCl_3$, unless otherwise stated. Accurate mass measurements were recorded on a Finnigan MAT 900S Electrospray. Mass spectra were recorded on a Hewlett–Packard 1100MSD.

(1*S*,2*R*)-(–)-*cis*-1-Phthalimido-2-*O*-acetoxy (4)

A mixture of **3** (3.0 g, 20 mmol), phthalic anhydride (3.6 g, 24.3 mmol), and triethylamine (2.8 mL, 20.0 mmol) in MeOH (50 mL) was stirred at room temperature for 70 min under an argon atmosphere. After concentration the oily residue was dissolved in pyridine (40 mL) and acetic anhydride (20 mL) and stirred at room temperature for 16 h. The mixture was worked-up by adding CH_2Cl_2 (100 mL) extracted with cold 10% HCl (2 × 40 mL). The combined aqueous phases were washed with CH_2Cl_2 (2 × 50 mL) and the organic layer was washed with saturated $NaHCO_3$ (2 × 100 mL) and saturated NaCl (2 × 100 mL). The combined aqueous phases were washed with CH_2Cl_2 (2 × 75 mL), dried and concentrated. The crude product was purified using column chromatography (toluene – ethyl acetate, 15:1) to give **4** (5.3 g 83%) as a yellow solid. ^{1}H NMR ($CDCl_3$) δ: 1.86 (s, 3H, 1 CH_3), 3.46–3.49 (t, 2H, 1 CH_2), 5.64–5.72 (q,

© 2000 NRC Canada

Scheme 4. Synthesis of L-mannaric diamides.



1H, 1 CH), 5.96–5.99 (d, 1H, 1 CH), 7.20–7.32 (m, 4H, Ar), 7.71–7.86 (m, 4H, Ar). ^{13}C NMR (67MHz, $CDCl_3$) δ: 20.3 (CH_3), 37.7 (CH_2), 54.4 (*C*H-N), 72.6 (*C*H-O), 123.0, 124.3, 124.5, 126.9, 128.7, 131.4, 133.8, 136.4, and 140.6 (aromatic C), 167.4 and 168.9 (C=O). MS (API-ES) calcd. for 321.10; found: 321.1.

(1*S*,2*R*)-(–)-*cis*-1-Phthalimido-2-indanol (5)

To a stirred solution of **4** (5.3 g, 16 mmol) in MeOH (250 mL) and CH_2Cl_2 (100 mL), sodium methoxide in MeOH (0.1 M) was added dropwise until pH reached 7.5. After 5 h Dowex® HCR-W2 (H^+) ion exchange resin was added to neutralize the solution. The product was purified using column chromatography (toluene – ethyl acetate, 5:1). Concentration gave pure **5** (2.98 g, 65%) as a white solid. ^{1}H NMR ($CDCl_3$) δ: 2.84 (s, 1H, 1 OH), 3.20–3.38 (m, 2H, 1 CH_2), 4.75–4.77 (q, 1H, CHOH), 5.77–5.80 (d, 1H, CHN), 7.09–7.33 (m, 4H, Ar), 7.67–7.83 (m, 4H, Ar). ^{13}C NMR (67MHz, $CDCl_3$) δ: 41.2 (CH_2), 57.7 (*C*H-N), 74.0 (*C*H-OH), 123.4, 124.2, 125.5, 126.9, 128.5, 131.8, 134.1, 137.1, and 140.2 (aromatic C), 169.0 (C=O). Anal. calcd. ($C_{17}H_{13}NO_3$): C 73.11, H 4.69, N 5.02; found: C 72.98, H 4.55, N 4.98.

(1*S*,2*R*)-(–)-*cis*-1-Phthalimido-2-indanol on solid support (7)

Dry Merrifield resin with a dihydropyran linker (**6**) (400 mg, 0.51 mmol/g, 0.20 mmol linker) was swollen in dry 1,2-dichloroethane (5.5 mL) under an argon atmosphere. Anhydrous PPTS (100 mg, 0.40 mmol) and **5** (200 mg, 0.72 mmol) were added and the mixture was heated to 79°C. After 16 h the mixture was cooled to room temperature and the solid support was rinsed with CH_2Cl_2 (20 mL) and MeOH (20 mL) to give **7**. The filtrate was concentrated and the solid residue was purified using column chromatography (toluene – ethyl acetate, 5:1) to recover unreacted **3** (104 mg, 0.47 mmol). All the solid phase was used in the subsequent step.

(1*S*,2*R*)-(–)-*cis*-1-Amino-2-indanol on solid support (8)

Methylamine in ethanol (4.5 mL, 33%) was added to the solid phase from the previous step (**7**) and stirred for 16 h. The solid phase was rinsed with CH_2Cl_2 (10 mL), MeOH (10 mL), and then $CHCl_3$ (10 mL) to give **8**. All the solid phase will be used in the subsequent step.

The combined organic phases were concentrated and the formed *N*-methylphthalimide (**9**) was purified using column chromatography (chloroform–methanol, 20:1) which gave pure **9** as a white solid (21 mg, loading 66%). ^{1}H NMR (270 MHz, $CDCl_3$) δ: 2.94 (s, 3H, 1 CH_3), 7.01–7.67 (m, 4H, Ar). ^{13}C NMR (67MHz, $CDCl_3$) δ: 26.8 (CH_3), 125.7, 128.3, 129.0, 130.1, 134.6, and 140.7 (aromatic C), 170.0 (C=O).

***N*1,*N*6-Dimethyl-(2*R*,3*R*,4*R*,5*R*)-2,5-dibenzyloxy-3,4-dihydroxy hexanediamide (11)**

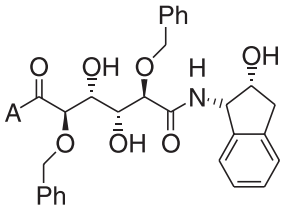
A mixture of benzylated bislactone (**10**) (7.64 g, 21.6 mmol), 2-hydroxypyridine (2.06 g, 21.7 mmol), and methylamine in THF (2 M, 23 mL, 46 mmol) in $CHCl_3$ (60 mL) was stirred at ambient temperature for 15 min. The organic phase was washed with saturated $NaHCO_3$ (3x), dried, concentrated, and the residue purified by column chromatography ($CHCl_3$–MeOH, 20:1) to give pure **11** (7.83 g, 18.8 mmol, 87%) as a white solid. ^{13}C NMR ($CDCl_3$) δ: 25.8 (2 *C*H_3-NH), 71.1, 73.8, 79.6 (2 O*C*H_2Ph, C2, C3, C4, and C5), 128.1, 128.2, 128.6, 136.7 (aromatic C), 172.7 (2 C=O). MS (API-ES) calcd. for 416.1; found: 416.1.

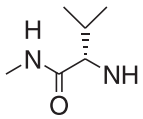
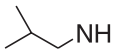
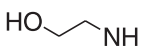
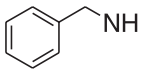
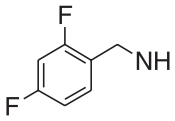
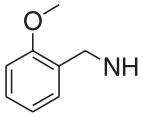
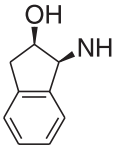
***N*1,*N*6-Dimethyl-(2*R*,3*R*,4*R*,5*R*)-2,5-dibenzyloxy-3,4-dihydroxy-3,4-*O*-isopropylidenehexanediamide (12)**

Dimethoxypropane (15 mL, 123 mmol) and camphorsulfonic acid (2.66 g, 11.5 mmol) were added to a stirred mixture of **11** (6.0 g, 14.4 mmol) in dry acetone (70 mL). The precipitated product was filtered off after 15 min to give pure **12**. The solution was concentrated, CH_2Cl_2 was added

© 2000 NRC Canada

Table 2. Structure, yields, and HIV-1 protease inhibitory acitivity and in vitro antiHIV-1 acitvity of unsymmetrical L-mannaric diamides with 2*R*, 3*R*, 4*R*, 5*R* configuration.



A	Cmpd. no.	Yield (%)[a]	K_i[b] (nM)	ED_{50}[c] (μM)
	**18 a**	23	0.2	0.1
	**18 b**	28	70	> 100
CH_3NH	**18 c**	35	2	2
	**18 d**	26	200	60
	**18 e**	21	0.1	3
	**18 f**	17	20	>100
	**18 g**	47	2	4
	**1**	17	0.4	0.1

[a] from **12** based on 66% loading

[b] Standard error 20 %

[c] ED_{50} for reference substances tested in the same assay: ritnonavir (ED_{50}, 0.06 μM), indinavir (ED_{50}, 0.06 μM), saquinavir (ED_{50}, 0.01 μM), nelfinavir (ED_{50}, 0.04 μM).

to the residue, and the organic phase was washed with saturated $NaHCO_3$ (3x), dried and concentrated. The solid was washed with a small amount of dry, cold acetone to give pure **12** (5.58 g, 12.2 mmol, 85%). ^{13}C NMR ($CDCl_3$) δ: 25.6, 26.9 (4 *C*H_3), 73.5, 77.5, 79.3 (2 O*C*H_2Ph, C2, C3, C4, and C5), 110.0 (O-*C*-O), 128.0, 128.1, 128.5, 136.8 (aromatic C), 169.3 (C=O). Anal. calcd. ($C_{25}H_{32}N_2O_6$): C 65.77, H 7.06. N 6.14; found: C 65.65, H 6.83, N 6.01.

***N*1,*N*6-Dimethyl-*N*1,*N*6-dinitroso-(2*R*,3*R*,4*R*,5*R*)-2,5-dibenzyloxy-3,4-dihydroxy-3,4-*O*-isopropylidenehexanediamide (13)**

To produced N_2O_4, $Pb(NO_3)_2$ (20 g, 60 mmol) was heated over an open flame and the gas was led down into CH_2Cl_2 at –10°C. The solution was cooled to –60°C under an argon atmosphere and anhydrous sodium acetate (4.2 g, 51.2 mmol) was added followed by **12** (3.25 g, 7.12 mmol). The –60°C

© 2000 NRC Canada

bath was replaced with an ice salt bath after 30 min and the mixture was stirred at –10°C until the substrate was consumed (1 h). The solution was poured into ice and water and the phases were separated. The organic phase was washed with ice cold 5% sodium bicarbonate. The organic phase was washed with ice cold 5% sodium bicarbonate, dried briefly at 0°C, and concentrated to give **13** as a yellow oil. The nitrosoamide solution was never allowed to warm above 0°C. All the product was used immediately in the next step.

2,5-Di-*O*-benzyl-3,4-*O*-isopropylidene-L-mannaric acid (14)

Hydrogen peroxide (12.5 g 30%) and LiOH (1.26 g, 52.7 mmol) were added to a stirred solution of **13** from the previous step in THF–H_2O (3:1) (100 mL) at 0°C. The mixture was stirred for 20 min at 0°C. The reaction was quenched with Na_2SO_3 (15 mL, 1.5 M). The THF was evaporated and the water phase was acidified with Dowex® HCR-W2 (H^+) ion exchange resin, and extracted with EtOAc. The phases were separated and the organic phase was dried and concentrated to give **14** (3.05 g, 7.08 mmol, 100%) as a white solid. ^{13}C NMR (CD_3OD) δ: 27.5 (2 CH_3), 73.6, 80.0, 80.3 (2 OCH_2Ph, C2, C3, C4, and C5), 112 (O-*C*-O), 129.0, 129.3, 129.4, 138.5 (aromatic C), 173.1 (C=O).

***N*1-[(2*R*)-Hydroxy-1(*S*)indanyl]-*N*6-succinimidyl-(2*R*,3*R*,4*R*,5*R*)-2,5-dibenzyloxy-3,4-dihydroxy-3,4-*O*-isopropylidenehexanediamide on solid support (16)**

The solid phase from the previous step (**8**) was swollen in dry 1,2-dichloroethane (4.5 mL) for 40 min under an argon atmosphere. The bissuccinimidyl diester (**15**) (900 mg, 1.44 mmol) was added and the mixture was stirred for 16 h under an argon atmosphere at 60°C. The solid phase was rinsed with $CHCl_3$ (20 mL), THF (10 mL), and then 1,2-dichloroethane (10 mL) to give **16**. All the solid phase was used in the subsequent step.

General procedure for preparation of compounds 17a–h

The solid phase from the previous step (**16**) was swollen in dry 1,2-dichloroethane (4 mL) for 40 min under an argon atmosphere. The amine (2.0 mmol) was added and the mixture was stirred for 16 h under argon at 60°C. The solid phase was rinsed with $CHCl_3$ (20 mL), THF (10 mL), and then 1,2-dichloroethane (10 mL) to give **17a–h**. All the solid phase was used in the subsequent step.

***N*1-[(1*R*,2*S*)-2-Hydroxy-2,3-dihydro-1*H*-indenyl]-*N*6-(isobutyl)-(2*R*,3*R*,4*R*,5*R*)-2,5-dibenzyloxy-3,4-dihydroxy-3,4-*O*-isopropylidenehexanediamide on solid support (17a)**

The solid phase **16** was reacted according to the general procedure, vide supra, using the amine isobutylamine (200 μL, 2.01 mmol) to give **17a**.

***N*1-[(1*R*,2S)-2-Hydroxy-2,3-dihydro-1*H*-indenyl]-*N*6-(methyl)-(2*R*,3*R*,4*R*,5*R*)-2,5-dibenzyloxy-3,4-dihydroxy-3,4-*O*-isopropylidenehexanediamide on solid support (17b)**

The solid phase **16** was reacted according to the general procedure, vide supra, using the amine methylamine in THF (2 mL, 2 M) to give **17b**.

***N*1-[(1*R*,2*S*)-2-Hydroxy-2,3-dihydro-1*H*-indenyl]-*N*6-(2-hydroxyethyl)-(2*R*,3*R*,4*R*,5*R*)-2,5-dibenzyloxy-3,4-dihydroxy-3,4-*O*-isopropylidenehexanediamide on solid support (17c)**

The solid phase **16** was reacted according to the general procedure, vide supra, using the amine ethanolamine (120 μL, 2 mmol) to give **17c**.

***N*1-[(1*R*,2*S*)-2-Hydroxy-2,3-dihydro-1*H*-indenyl]-*N*6-[(1*S*)-2-methyl-1-(methylcarbamoyl)propyl]-(2*R*,3*R*,4*R*,5*R*)-2,5-dibenzyloxy-3,4-dihydroxy-3,4-*O*-isopropylidenehexanediamide on solid support (17d)**

The solid phase **16** was reacted according to the general procedure, vide supra, using the amine valine methylamide (195 mg, 1.5 mmol) to give **17d**.

***N*1-[(1*R*,2*S*)-2-Hydroxy-2,3-dihydro-1*H*-indenyl]-*N*6-(2,4-difluorobenzyl)-(2*R*,3*R*,4*R*,5*R*)-2,5-dibenzyloxy-3,4-dihydroxy-3,4-*O*-isopropylidenehexanediamide on solid support (17e)**

The solid phase **16** was reacted according to the general procedure, vide supra, using the amine 2,4-difluorobenzylamine (240 μL, 2.02 mmol) to give **17e**.

***N*1-[(1*R*,2*S*)-2-Hydroxy-2,3-dihydro-1*H*-indenyl]-*N*6-(benzyl)-(2*R*,3*R*,4*R*,5*R*)-2,5-dibenzyloxy-3,4-dihydroxy-3,4-*O*-isopropylidenehexanediamide on solid support (17f)**

The solid phase **16** was reacted according to the general procedure, vide supra, using the amine benzylamine (220 μL, 2.01 mmol) to give **17f**.

***N*1-[(1*R*,2*S*)-2-Hydroxy-2,3-dihydro-1*H*-indenyl]-*N*6-(2-methoxybenzyl)-(2*R*,3*R*,4*R*,5*R*)-2,5-dibenzyloxy-3,4-dihydroxy-3,4-*O*-isopropylidenehexanediamide on solid support (17h)**

The solid phase **16** was reacted according to the general procedure, vide supra, using the amine 2-methoxybenzylamine (250 μL, 1.92 mmol) to give **17h**.

***N*1,*N*6-Di[(2*R*)-hydroxy-1(*S*)-indenyl]-(2*R*,3*R*,4*R*,5*R*)-2,5-di(benzyloxy-3,4-dihydroxy-3,4-dihydroxyhexanediamide on solid support (17g)**

The solid phase **16** was reacted according to the general procedure, vide supra, using the amine (1*S*,2*R*)-(–)-cis-1-amino-2-indanol (301 mg, 2.03 mmol) to give **17g**.

General procedure for the preparation of compounds 18a–h and 1

2.3 M HCl in methanol (5.5 mL) was added to the solid phase from the previous step (**17a–h**). After stirring for 4 h at room temperature under an argon atmosphere, the solid phase was rinsed with $CHCl_3$ (20 mL) and MeOH (10 mL). The combined organic layer was diluted by 20 mL $CHCl_3$ and extracted with saturated $NaHCO_3$ (2 × 30 mL). The combined aqueous phases were washed with $CHCl_3$ (2 × 40 mL). The combined organic layer was dried, concentrated, and purified by column chromatography to give **18a–h** and **1**.

© 2000 NRC Canada

***N*1-[(1*R*,2*S*)-2-Hydroxy-2,3-dihydro-1*H*-indenyl]-*N*6-(isobutyl)-(2*R*,3*R*,4*R*,5*R*)-2,5-dibenzyloxy-3,4-*O*-isopropylidenehexanediamide (18a)**

The solid phase **17a** was reacted according to the general procedure, vide supra, to give pure **18a** (21 mg, 0.036 mmol, 28% based on loading) after purification with column chromatography (chloroform–methanol, 40:1). ^{13}C NMR ($CDCl_3$) δ: 20.0 (2 CH_3), 28.4 (CH), 39.3 (*C*H_2-Ar), 46.4 (*C*H_2-NH), 58.0 (*C*H-NH), 71.6, 71.9, 72.6, 73.6, 74.1, 80.5, 81.4 (*C*H-OH, 2 O*C*H_2Ph, C2, C3, C4, and C5), 124.0, 125.4, 127.0, 128.2, 128.3, 128.5, 128.7, 128.8, 136.7, 139.8, 140.8 (aromatic C), 171.5, 172.3 (2 C=O). HRMS calcd. for 576.2835; found 576.2829.

***N*1-[(1*R*,2*S*)-2-Hydroxy-2,3-dihydro-1*H*-indenyl]-*N*6-(methyl)-(2*R*,3*R*,4*R*,5*R*)-2,5-dibenzyloxy-3,4-*O*-isopropylidenehexanediamide (18b)**

The solid phase **17b** was reacted according to the general procedure, vide supra, to give pure **18b** (24 mg, 0.045 mmol, 35% based on loading) after purification with column chromatography (chloroform–methanol, 40:1). ^{13}C NMR ($CDCl_3$) δ: 25.9 (CH_3), 39.3 (*C*H_2-Ar), 58.0 (*C*H-NH), 71.5, 71.9, 72.6, 73.6, 74.0, 80.7, 81.5 (*C*H-OH, 2 O*C*H_2Ph, C2, C3, C4, and C5), 124, 125.4, 127.1, 128.2, 128.4, 128.4, 128.7, 136.6, 139.7, 140.8 (aromatic C), 172.0, 172.3, (2 C=O). HRMS calcd. for 534.2366, found 534.2359.

***N*1-(1*R*,2*S*)-2-Hydroxy-2,3-dihydro-1*H*-indenyl]-*N*6-(2-hydroxyethyl)-(2*R*,3*R*,4*R*,5*R*)-2,5-dibenzyloxy-3,4-*O*-dihydroxyhexanediamide (18c)**

The solid phase **17c** was reacted according to the general procedure, vide supra, to give pure **18c** (19 mg, 0.034 mmol, 26% based on loading) after purification with column chromatography (chloroform–methanol, 20:1). ^{13}C NMR ($CDCl_3$) δ: 39.3 (*C*H_2-Ar), 41.9 (*C*H_2-NH), 57.6 (*C*H-NH), 61.1 (*C*H_2-OH), 71.5, 71.6, 72.5, 73.2, 73.3 (*C*H-OH, 2 O*C*H_2Ph, C2, C3, C4, and C5), 124.0, 125.3, 127.0, 128.1, 128.2, 128.3, 128.6, 136.6, 136.8, 139.8, 140.7 (aromatic C),171.6 (C=O). HRMS calcd. for 564.2472; found 564.2460.

***N*1-[(1*R*,2*S*)-2-Hydroxy-2,3-dihydro-1*H*-indenyl]-*N*6-[(1*S*)-2-methyl-1-(methylcarbamoyl)propyl]-(2*R*,3*R*,4*R*,5*R*)-2,5-dibenzyloxy-3,4-*O*-isopropylidenehexanediamide (18d)**

The solid phase **17d** was reacted according to the general procedure, vide supra, to give pure **18d** (17 mg, 0.029 mmol, 23% based on loading) after purification with column chromatography (chloroform–methanol, 40:1). ^{13}C NMR ($CDCl_3$) δ: 17.1, 19.6 (*C*H_3-CH); 26.1 (*C*H_3-NH), 29.1 (CH), 39.3 (*C*H_2-Ar); 58.0, 58.4 (*C*H-NH and O=C-*C*H-NH), 72.2, 72.4, 72.8, 73.4, 81.3, 81.8 (*C*H-OH, 2 O*C*H_2Ph, C2, C3, C4, and C5), 123.9, 125.4, 127.0, 128.1, 128.2, 128.4, 128.5, 128.7, 128.7, 136.4, 139.6, 140.8 (aromatic C), 170.9, 172.0 (2 C=O). HRMS calcd. for 610.2679; found 610.2673.

***N*1-[(1*R*,2*S*)-2-Hydroxy-2,3-dihydro-1*H*-indenyl]-*N*6-(2,4-difluorobenzyl)-(2*R*,3*R*,4*R*,5*R*)-2,5-dibenzyloxy-3,4-*O*-isopropylidenehexanediamide (18e)**

The solid phase **17e** was reacted according to the general procedure, vide supra, to give pure **18e** (14 mg, 0.020 mmol 17% based on loading) after purification with column chromatography (chloroform–methanol, 40:1). ^{13}C NMR ($CDCl_3$) δ: 36.6 (*C*H_2-NH), 39.3 (*C*H_2-Ar), 58.0 (*C*H-NH), 71.6, 71.8, 72.5, 73.6, 74.0, 80.4, 81.3 (*C*H-OH, 2 O*C*H_2Ph, C2, C3, C4, and C5), 103.9, 111.6, 124.0, 125.4, 127.1, 128.2, 128.3, 128.5, 128.7, 130.9, 136.5, 136.6, 139.7, 140.8 (aromatic C), 171.6, 172.3 (2 C=O). HRMS calcd. for 646.2491; found 646.2493.

***N*1-[(1*R*,2*S*)-2-Hydroxy-2,3-dihydro-1*H*-indenyl]-*N*6-(benzyl)-(2*R*,3*R*,4*R*,5*R*)-2,5-dibenzyloxy-3,4-*O*-isopropylidenehexanediamide (18f)**

The solid phase **17f** was reacted according to the general procedure, vide supra, to give pure **18f** (17 mg, 0.028 mmol, 21% based on loading) after purification with column chromatography (chloroform–methanol, 40:1). ^{13}C NMR ($CDCl_3$) δ: 39.3 (*C*H_2-Ar), 43.1 (*C*H_2-NH), 57.9 (*C*H-NH), 71.7, 71.8, 72.5, 73.6, 74.0, 80.4, 81.4 (*C*H-OH, 2 O*C*H_2Ph, C2, C3, C4, and C5), 124.1, 125.4, 127.1, 127.6, 128.2, 128.4, 128.7, 130.9, 136.5, 137.5, 139.7, 140.8 (aromatic C), 171 5, 172.3 (2 C=O). HRMS calcd. for 633.3050; found 633.3056.

***N*1-[(1*R*,2*S*)-2-Hydroxy-2,3-dihydro-1*H*-indenyl]-*N*6-(2-methoxybenzyl)-(2*R*,3*R*,4*R*,5*R*)-2,5-dibenzyloxy-3,4-*O*-isopropylidenehexanediamide (18g)**

The solid phase **17g** was reacted according to the general procedure, vide supra, to give pure **18g** (38 mg, 0.06 mmol, 47% based on loading) after purification with column chromatography (chloroform–methanol, 40:1). ^{13}C NMR ($CDCl_3$) δ: 39.2, 39.2 (*C*H_2-Ar and *C*H_2-NH), 55.1 (*C*H_3-O), 57.9 (*C*H-NH), 71.4, 71.8, 72.5, 73.4, 73.8, 80.4, 81.1 (*C*H-OH, 2 O*C*H_2Ph, C2, C3, C4, and C5), 110.2, 120.6, 124.0, 125.3, 125.5, 126.9, 128.1, 128.2, 128.5, 129.0, 129.5, 136.7, 136.7, 139.9, 140.7, 157.5 (aromatic C), 171.0, 172.2 (2 C=O). HRMS calcd. for 640.2785; found 640.2783.

***N*1,*N*6-Di[(2*R*)-hydroxy-1(*S*)-indanyl]-(2*R*,3*R*,4*R*,5*R*)-2,5-di(benzyloxy-3,4-dihydroxyhexanediamide (1)**

The solid phase **17h** was reacted according to the general procedure, vide supra, to give pure **1** (14 mg, 0.021 mmol, 17% based on loading) after purification with column chromatography (chloroform–methanol, 40:1). ^{13}C NMR ($CDCl_3$) δ: 39.1 (2 *C*H_2-Ar), 57.7 (2 *C*H-NH), 71.6, 72.5, 73.4, 81.3 (*C*H-OH, 2 O*C*H_2Ph, C2, C3, C4, and C5), 124.0, 125.3, 126.9, 128.1, 128.2, 128.6, 136.7, 139.8, 140.8 (aromatic C), 171.5 (C=O).

Conclusions

A solid phase parallel synthesis of unsymmetrical inhibitors has been developed which will aid further development and combinatorial amplification. A number of new potent inhibitors were discovered.

Acknowledgment

We gratefully acknowledge support from the Swedish National Board for Technical Development (NUTEK) and from Medivir AB, Huddinge, Sweden and Dr. Karl-Erik Karlsson Hässle AB for HRMS.

© 2000 NRC Canada

References

1. R.C. Gallo, P.S. Sarin, E.P. Gelmann, M. Robert-Guroff, E. Richardson, V.S. Kalyanaraman, D. Mann, G.D. Sidhu, R.E. Stahl, S. Zolla-Pazner, J. Leibowitch, and M. Popovic. Science (Washington, D.C.), **220**, 865 (1983).
2. F. Barrè-Sinoussi, J.C. Chermann, F. Rey, M.T. Nugeyre, S. Chamaret, J. Gruest, C. Dauguet, C. Axler-Blin, F. Vèzinet-Brun, C. Rouzioux, W. Rozenbaum, and L. Montagnier. Science (Washington, D.C.), **220**, 868 (1983).
3. J. Erickson, D.J. Neidhart, J. VanDrie, D.J. Kempf, X.C. Wang, D.W. Norbeck, J.J. Plattner, J.W. Rittenhouse, M. Turon, N. Wideburg, W.E Kohlbrenner, R. Simmer, R. Helfrich, D.A. Paul, and M. Knigge. Science (Washington, D.C.), **249**, 527 (1990).
4. L.H. Pearl and W.R. Taylor. Nature (London), **329**, 351 (1987).
5. De Clercq. J. Med. Chem. **38**, 2491 (1995).
6. C. Peng, B.K. Ho, T.W. Chang, and N.T. Chang. J. Virol. **63**, 2550 (1989).
7. T.J. Mcquade, A.G. Tomasselli, L. Liu, V. Karacostas, B. Moss, T.K. Sawyer, R.L. Heinrikson, and W.G. Tarpley. Science (Washington, D.C.), **247**, 454 (1990).
8. D.J. Kempf and H.L. Sham. Curr. Pharm. Des. **2**, 225 (1996).
9. J.S. Mills. Antiviral Chem. Chemother. **7**, 281 (1996).
10. J.R. Huff. J. Med. Chem. **34**, 2305 (1991).
11. S.G. Deeks and P.A. Volberding. Aids Clinical Review 1997/1998. *Edited by* P.A. Volberding and A.M Jacobson. Marcel Dekker, Inc., San Fransisco. 1997. pp. 145–185.
12. J.P. Vacca and J.H. Condra. Drug Discovery Today, **2**, 261 (1997).
13. R.D. Tung et al. (*Editors*). 39th Interscience Conference on Antimicrobial Agents and Chemotherapy Paper no. 913. San Francisco.
14. J.H. Condra, W.A Schleif, O.M Blahy, L.J. Gabryelski, D.J. Graham, J.C. Quintero, A. Rhodes, H.L. Robbins, E. Roth, M. Shivaprakash, D. Titus, T. Yang, H. Teppler, K.E. Squires, P.J. Deutsch, and E. Emini. Nature (London), **374**, 569 (1995).
15. J.M Coffin. Science (Washington, D.C.), **267**, 483 (1995).
16. M. Alterman, M. Björsne, A. Mühlman, B. Classon, I. Kvarnström, H. Danielson, P.-O. Markgren, U. Nillroth, T. Unge, A. Hallberg, and B. Samuelsson. J. Med. Chem. **41**, 3782 (1998).
17. A.K. Ghosh, S. Fidanze, and C.H. Senanayake. Synthesis, 937 (1998).
18. T.A. Lyle, C.M. Wiscount, J.P. Guare, W.J. Thompson, P.S. Anderson, P.L Darke, J.A. Zugay, E.A. Emini, W.A. Schleif, J.C. Quintero, R.A.F. Dixon, I.S. Sigal and J.R. Huff. J. Med. Chem. **34**, 1228 (1991).
19. B.D. Dorsey, R.B. Levin, S.L. McDaniel, J.P. Vacca, J.P. Guare, P.L. Darke, J.A. Zugay, E.A. Emini, W.A. Schleif, J.C. Quintero, J.H. Lin, I.-W. Chen, M.K. Holloway, P.M.D. Fitzgerald, M.G. Axel, D. Ostovic, P.S. Anderson and J.R. Huff. J. Med. Chem. **37**, 3443 (1994)
20. L.A. Thompson and J.A.S Ellman. Tetrahedron. **35**, 9333 (1994).
21. R.B. Merrifield. J. Am. Chem. Soc. **85**, 2149 (1963).
22. P.H.H. Hermkens, H.C.J. Ottenheijm, and D. Rees. Tetrahedron, **52**, 4527 (1996).
23. N.K. Terret, M. Gardner, D.W. Gordon.,R.J Kobylecki and J. Steele. Tetrahedron, **51**, 8135 (1995).
24. M. Miyashita, A. Yoshikoshi and P.A. Grieco. J. Org. Chem. 42, 3772 (1977).
25. H.T. Openshaw and N. Whittaker. J. Chem. Soc. C: 89. (1969).
26. CD Römpp Chemie Lexikon. Version 1.0. Georg Thieme Verlag, Stuttgart, New York. (1995).
27. E.H. White and J.C.A. Aufderdermarsh. J. Am. Chem. Soc. **83**, 1179 (1961).
28. E.H. White. J. Am. Chem. Soc. **77**, 6008 (1955).
29. D.A. Evans, T.C. Britton, and J.A. Ellman. Tetrahedron, **28**, 6141 (1987).
30. D.A. Evans, P.H. Carter, C.J. Dinsmore, J.C. Barrow, J.L. Katz, and D.W. Kung. Tetrahedron Lett. **38**, 4535 (1997).
31. U.H. Danielson, M. Lindgren, P.-O. Markgren, and U. Nillroth. Investigation of an allosteric site of HIV-1 proteinase involved in inhibition by Cu^{2+}. *In* Aspartic proteinas. *Edited by* James, Plenum Press, New York. 1998. pp. 99–103.
32. U. Nillroth, L. Vrang, P.-O. Markgren, J. Hultèn, A. Hallberg, and U.H. Danielsson, Antimicrob. Agents and Chemother. **41**, 2383 (1997).
33. O.S. Weislow, R. Kiser, D.L. Fine, J. Bader, R.H. Shoemaker, and M.R. Boyd. J. Nat. Cancer Inst. **81**, 577 (1989).
34. C.A. Lipinski, F. Lombardo, B.W. Dominy, and P. Feeney. J. Advanced Drug Delivery Reviews, **23**, 3 (1987).
35. M.A. Navia and P.R. Chaturvedi. DDT, **1**, 179 (1996).

© 2000 NRC Canada

A facile new procedure for the deprotection of allyl ethers under mild conditions

Yun-Jin Hu, Romyr Dominique, Sanjoy Kumar Das, and René Roy

Abstract: A novel isomerization of *O*-allyl glycosides into prop-1-enyl glycosides was observed instead of cross-metathesis during an olefin metathesis reaction using Grubbs' ruthenium benzylidene catalyst $(Cy_3P)_2RuCl_2$=CHPh (**1**), *N*-allyltritylamine, and *N*,*N*-diisopropylethylamine as necessary auxiliary reagents. In the search for a better catalytic system, it has been found that dichlorotris(triphenylphosphine)ruthenium(II), $[(C_6H_5)_3P]_3RuCl_2$, (**2**) was much more efficient for the isomerization of allylic ethers. The labile prop-1-enyl group was easily hydrolyzed using $HgCl_2$–HgO and the hemiacetals (**25**–**32**) were isolated in excellent yields (ca. 90%).

Key words: allyl ether, carbohydrate, Grubbs' catalyst, isomerization, metathesis, deprotection.

Résumé : Au cours d'une réaction de métathèse d'oléfine impliquant du catalyseur de Grubbs, le benzylidène de ruthénium, $(Cy_3P)_2RuCl_2$=CHPh (**1**), de la *N*-allyltritylamine et du *N*,*N*-diisopropyléthylamine comme réactifs auxiliaires nécessaires, on a observé une nouvelle isomérisation des glycosides de *O*-allyle en glycosides de prop-2-ényle. Au cours de nos travaux en vue développer un meilleur système catalytique, on a trouvé que le dichlorotris(triphénylphosphine)ruthénium(II), $[(C_6H_5)_3P]_3RuCl_2$ (**2**), est beaucoup plus efficace pour l'isomérisation des éthers allyliques. Le groupe prop-1-ényle labile est hydrolysé facilement à l'aide de $HgCl_2$–H_2O et on a isolé les hémiacétals (**25**–**32**) avec d'excellents rendements (environ 90%).

Mots clés : éther allylique, catalyseur de Grubbs, isomérisation, métathèse, déprotection.

[Traduit par la Rédaction]

Introduction

The use of allyl ether protecting groups is of great importance in carbohydrate chemistry and other natural product syntheses (1) because of their ready availability and stability under reasonably strong acidic and basic conditions. Several methods for the deprotection of allyl ethers have already been described in the literature (2–11). Most methods involve initial isomerization of allyl to prop-1-enyl ethers with either a base such as $[(CH_3)_3COK]$ (2) or transition metals: Ti(0) (3), Rh(I) (4), Ir(I) (5), Pd-C (6), $Pd(PPh_3)_4$ (7), $Pd(OAc)_2$ (7), $H_2Ru(PPh_3)_4$ (8), $Fe(CO)_5$ (9). The labile prop-1-enyl ethers can then be cleaved to the corresponding alcohols by mineral acids or $HgCl_2$–HgO (10) (Scheme 1). Direct cleavage of allyl ethers is generally carried out using stoichiometric amounts of palladium salts or complexes such as $PdCl_2(PhCN)_2$, $PdCl_2$ (11). However, some of these methods are still less than satisfactory for practical use and sometimes are found to be capricious (12). Herein, we wish to report a new method for the deprotection of the allyl group from carbohydrate derivatives using Grubbs' ruthenium benzylidene catalyst $(Cy_3P)_2RuCl_2$=CHPh **1** or dichlorotris(triphenylphosphine)ruthenium(II) (**2**) in excellent yields (ca. 90%).

Received November 8, 1999. Accepted April 4, 2000. Published on the NRC Research Press website on June 13, 2000.

Y.-J. Hu, R. Dominique, S.K. Das, and R. Roy.[1]
Department of Chemistry, University of Ottawa, Ottawa, ON K1N 6N5, Canada.

[1]Author to whom correspondence may be addressed.
Telephone: (613) 562-5800, ext 6055. Fax: (613) 562-5170.
e-mail: rroy@science.uottawa.ca

Results and discussion

Recently we have been interested in the metathesis reaction of *O*-allyl glycosides using Grubbs' catalyst **(**$Cy_3P)_2Cl_2Ru$=CHPh (**1**) (13, 14). However, when the cross-metathesis reaction between *N*-allyltritylamine **3** (15) and allyl 2,3,4,6-tetra-*O*-acetyl-α-D-galactopyranoside **9** (16) was carried out with **1**, an unexpected isomerization product **17** was isolated in 30% yield instead of the anticipated cross metathesis compound. Furthermore, neither sugar nor *N*-allyltritylamine dimer could be detected. Treatment of **9** with 1,4-diazabicyclo[2,2,2]octane (DABCO) in the presence of Grubbs' catalyst **1** afforded only 4% of the isomerized product **17** together with 40% of allyl α-D-galactopyranoside homodimer (14). Similar results were obtained when triethylamine was used as base. Neither isomerization nor metathesis products were detected when diethylamine or pyridine were used (Table 1, entries 6 and 7). The isomerized product **17** was obtained with the highest yield when **9** was treated with diisopropylethylamine (DIPEA) in the presence of Grubbs' catalyst **1**. However, all the isomerization yields of those reactions were still very low in the absence of *N*-allyltritylamine **3** (Scheme 2). When both **3** and 1 equiv. of DIPEA were simultaneously used in the reaction, the isomerization yield was improved dramatically to 80% (Table 1, entry 8). Furthermore, there was no self-metathesis product that could be detected.

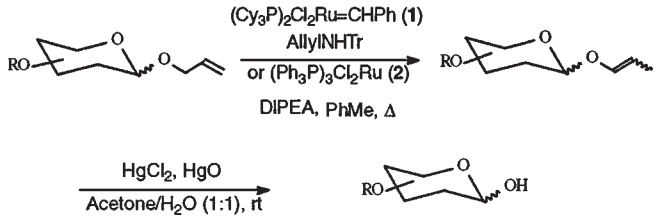
© 2000 NRC Canada

Table 1. Isomerization of allyl α-D-galactopyranoside **9** with different bases or additives in the presence of Grubbs' catalyst (**1**).

Entry	Base or additive	Recycled glycosides (%)	Self metathesis sugar dimer (%)	Isomerization (%)
1	**3**	67	—	30
2	DABCO	55	40	4
3	Et_3N	45	45	3
4	NMM[a]	80	12	6
5	DIPEA	35	50	10
6	Diethylamine	100	—	—
7	Pyridine	100	—	—
8	**3** and DIPEA	16	—	80
9	**4**	78	20	—
10	**5**	65	30	—

[a]NMM: *N*-methylmorpholine.

Scheme 1.



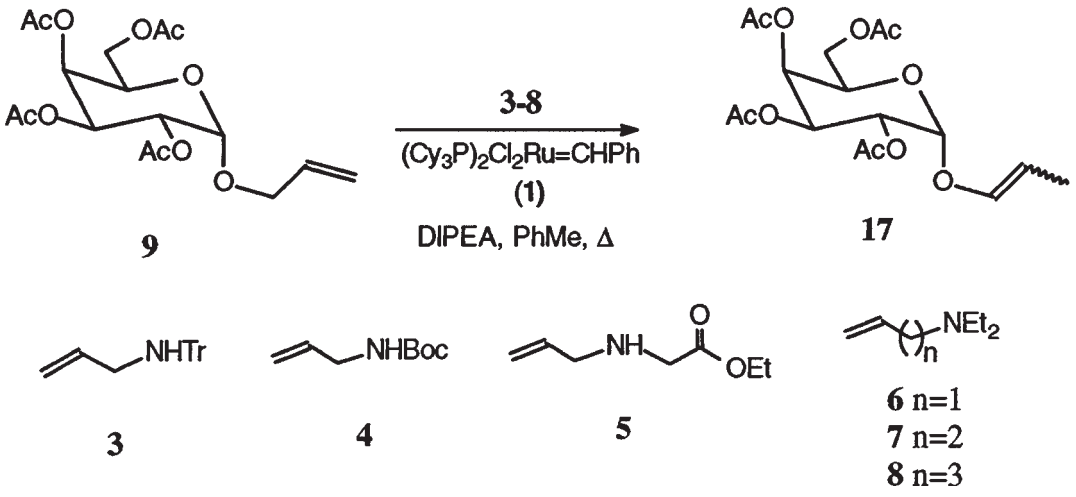
Bearing in mind the above observations, alternative bases which could provide both basicity and olefinic functionality were explored. To this end, several *N*-allylated amine derivatives (**4**–**8**) that could mimic the structure of amine **3** were synthesized to test the reaction. It was found that Boc-allyl carbamate **4** and amine **5** did not catalyze this reaction at all. Several tertiary amines **6**–**8** with increasing chain length also failed to afford the desired isomerization products with **3** and catalyst **1** when they were subjected to the optimum conditions. This demonstrates that the strong steric hindrance of *N*-allyltritylamine also had an important influence on the isomerization of **9** as well as its basicity. At this stage, we believed the presence of the secondary amine **3** as an auxiliary reagent was crucial for the isomerization to occur.

More detailed studies showed that the isomerization of allyl ethers to propenyl ethers with Grubbs' catalyst proceeded smoothly in the presence of amine **3** and a stoichiometric amount of base such as diisopropylethylamine (DIPEA). To improve the yield of the isomerization and suppress the formation of metathesis products, 1.0 equiv. of DIPEA and 2.0 equiv. of **3** were treated with different glycosides in the presence of 0.1 equiv. of **1** (toluene, reflux, 4 h). Good yields were obtained without any metathesis product being detected in any of these experiments (Table 2).

The ratios of the unseparated *E* and *Z* stereoisomers in the pro-1-enyl glycosides were determined from the analysis of the ^1H NMR spectra of the crude mixtures by observation of the $^3J_{H,H}$ coupling constants of the alkenyl protons (17). Interestingly, the *cis* stereoisomers predominated. Isomerization of partially protected glycosides **12** and **15** proceeded in lower yields, presumably because some of the remaining free hydroxyl groups of the substrates coordinated to some extent with the catalyst and reduced or prevented its activity. When control experiments were performed in the absence of **3** and DIPEA, only the expected self-metathesis products were obtained in high yields (14).

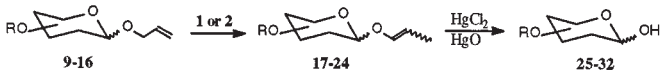
We noticed that olefin isomerization of allylic ether and allyl alcohol can be catalyzed by $Ru(II)(H_2O)_6(tos)_2$ (tos = *p*-toluenesulfonate) (18) in aqueous solution and

Scheme 2.

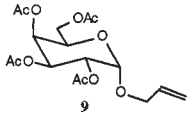
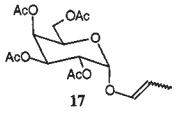
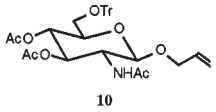
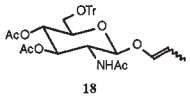
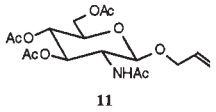
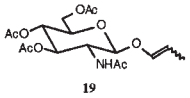
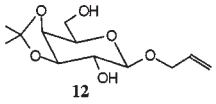
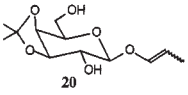
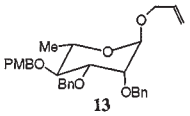
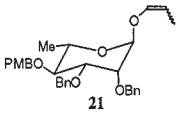
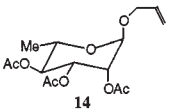
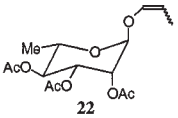
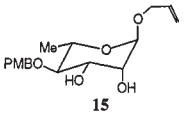
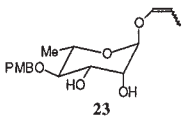
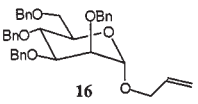
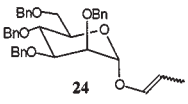


© 2000 NRC Canada

Table 2. Results from the isomerization and hemiacetal transformations (**25–32**) ($HgCl_2$–HgO) of various allyl glycosides (**9–16**) into prop-1-enyl glycosides (**17–24**) in the presence of Grubbs' catalyst **1** and amine **3,** or catalyst **2** $(Ph_3P)_3Cl_2Ru$(II) and DIPEA ($PhCH_3$, reflux, 4 h).



9-16 17-24 25-32

Entry	Starting material	Products	Yield (%)/ catalyst	Hemiacetal formation	Yield (%)
1	 **9**	 **17**	80/1 96/2	**25**	92
2	 **10**	 **18**	85/1 95/2	**26**	92
3	 **11**	 **19**	70/1 92/2	**27**	92
4	 **12**	 **20**	20/1 92/2	**28**	90
5	 **13**	 **21**	75/1 94/2	**29**	91
6	 **14**	 **22**	77/1 95/2	**30**	92
7	 **15**	 **23**	21/1 96/2	**31**	93
8	 **16**	 **24**	nd 84/2	**32**	78

$(PPh_3)_2X_2Ru$=CH-CH=CPh_2 (X = Cl or CF_3COO) (19) in dichloromethane. When compared to existing methodologies, however, Ru(II)$(H_2O)_6(tos)_2$, $(PPh_3)_2X_2Ru$=CH-CH=CPh_2, or Grubbs' catalyst are relatively expensive and the isomerization yields are not competitive. We therefore initiated a search for a better catalyst by screening a family of ruthenium complexes for activity in this reaction. From this investigation, it was found that the commercially available, dichlorotris(triphenylphosphine)ruthenium(II) [$(PPh_3)_3RuCl_2$ (**2**)] can be used as an efficient catalyst for the deprotection of allyl group from the glycosides **9–16** following a two-step procedure.

We began with the isomerization reaction of peracetylated allyl α-D-galactopyranoside (**9**) in different aprotic solvents

© 2000 NRC Canada

Scheme 3.

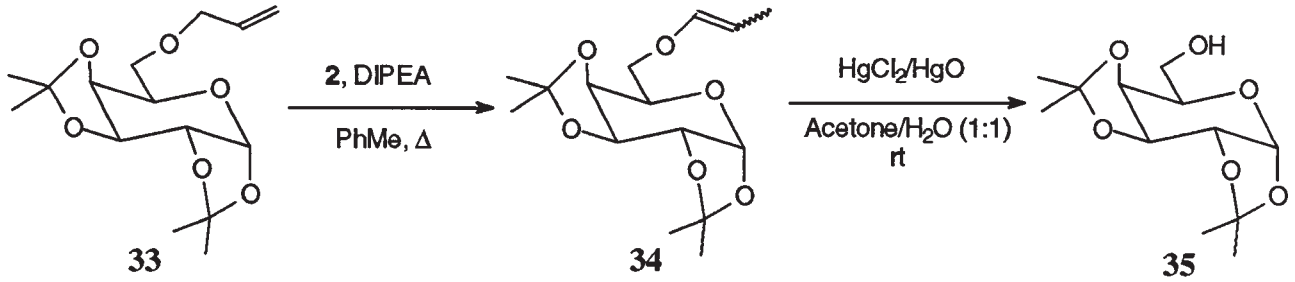


Table 3. [$(Ph_3P)_3RuCl_2$]-catalyzed isomerization of *O*-allyl glycosides (**9, 11**).

Entry	Glycoside	Base	Solvent	Time (h)	Product	Yield (%)
1	**9**	DIPEA	THF	2	**17**	0
2	**9**	DIPEA	CH_3CN	2	**17**	0
3	**9**	DIPEA	CH_2Cl_2	2	**17**	80
4	**9**	DIPEA	Toluene	1	**17**	96
5	**9**	DIPEA	Ethanol:H_2O (9:1)	2	**17**	-[a]
6	**9**	DIPEA	Methanol	2	**17**	-[a]
7	**9**	—	Toluene	6	**17**	0
8	**11**	Pyridine	Toluene	6	**19**	0
9	**11**	NMO[b]	Toluene	6	**19**	54
10	**11**	DABCO[c]	Toluene	2	**19**	85
11	**11**	Et_3N	Toluene	3	**19**	82
12	**11**	DIPEA	Toluene	2	**19**	94

[a]Deacetylation was detected during the isomerization.
[b]NMO: *N*-methylmorpholine oxide.
[c]1,4-Diazabicyclo[2.2.2]octane.

such as tetrahydrofuran, acetonitrile, dichloromethane, and toluene in the presence of **2** and DIPEA (Table 3). No isomerization was detected when THF and acetonitrile were used as solvents. When the reaction was carried out in refluxing dichloromethane, the isomerized product (**17)** was obtained in 80% yield. The best result was obtained when the reaction was performed in toluene under refluxing conditions. Lower yields were obtained when the reactions were performed in anhydrous methanol or aqueous ethanol due to competing de-*O*-acetylation. It is noteworthy that no isomerized product was detected in the absence of catalyst or base, even under forcing conditions such as prolonged reaction time, higher reaction temperature, and the use of up to 20 mol% of catalyst. Several common organic bases were examined for activity in the isomerization of **11**. No isomerization product was formed in pyridine. Upon treatment with triethylamine or 1,4-diazabicyclo[2,2,2]octane, the isomerization reactions proceeded smoothly. It was found that diisopropylethylamine (DIPEA) was the most suitable base for the system in terms of the high yields obtained for both **9** and **11** (Table 3). This novel isomerization reaction most likely follows the metal hydride addition-elimination mechanism (18).

Various allyl glycosides were subjected to the following standard conditions: a catalytic amount of **2** (10 mol%) was utilized as catalyst and a stoichiometric amount of DIPEA as base and the reactions were performed in refluxing toluene. Isomerized products were obtained in excellent yields (Table 2). It is also noteworthy that even those *O*-allyl glycosides (**12, 15**) with free hydroxyl groups, which were not suitable for the metathesis reaction because of the coordination to the metal in the Grubbs' catalyst, were still good substrates for these isomerization conditions.

As expected, hydrolysis of the enol ethers proceeded rapidly under acidic conditions (pH = 2) to provide hemiacetals (4). Alternatively, treatment of prop-1-enyl ethers with $HgCl_2$–HgO in aqueous acetone at room temperature for 1 h gave deprotected products in high yields. The whole procedure could be simplified as a two-step one-pot reaction: after isomerization of allyl ether, toluene and DIPEA were removed under reduced pressure and the resulting residue was then subjected to 0.5 equiv. of HgO and 1.0 equiv. of $HgCl_2$ in aqueous acetone (water:acetone – v/v 1:1) at room temperature for 1 h.

The excellent results described above provide a new route towards the deprotection of *O*-allyl glycosides in the field of carbohydrate chemistry. Up to now, there were several methods reported for the deprotection of *O*-allyl ethers (2–10, 20–22), however, these methods have been limited by severe reaction conditions such as: using strong base (2) or strong acid (20) as catalyst, performing reactions in aqueous alcohol (4) or alkaline solution (9), using oxidizing (21) or reducing (22) conditions, and operating under severe oxygen-free and anhydrous conditions (5). Compared to Wilkinson's catalyst (4), which is commonly used for deprotection of *O*-allyl ether in carbohydrate chemistry, ruthenium (II) complexes have two advantages with similarly effective performance with respect to promoting the

© 2000 NRC Canada

isomerization of *O*-allyl glycosides. First, the ruthenium (II) complex is more than two times cheaper than Wilkinson's catalyst; second, the ruthenium (II) complex does not reduce the alkene as is sometimes observed when using $(Ph_3P)_3RhCl$ (23). As for Felkin's Ir (I) catalyst, which is not commercially available, the procedure must be performed under strictly oxygen-free and anhydrous conditions (5). Our method for the isomerization of allyl groups by dichlorotris(triphenylphosphine)ruthenium(II) (**2**) is widely applicable and easy to perform under mild reaction conditions (Table 2). The isomerization of *O*-allyl ethers proceeds readily at refluxing temperature without affecting free hydroxyl, *O*-isopropylidene, trityl, acetyl, benzyl, or *p*-methoxylbenzyl groups.

Saloman and coworkers (24) reported the selective rearrangement of diallyl ethers catalyzed by dichlorotris(triphenylphosphine)ruthenium(II) (**2**) involving a preliminary rearrangement to allyl vinyl ethers followed by a Claisen rearrangement. However, high temperature (200°C) instead of an organic base was used in their experiments. A recent report showed that isomerization of *O*-allyl ethers using **2** at 130°C led to the formation of many byproducts (9), so it would appear that its use has not been exploited until now. To the best of our knowledge, there are no other reports of the application of this catalyst for the deprotection of *O*-allyl groups.

The simplicity and mildness of this methodology led us to explore this procedure for the deprotection of allyl ether from 6-*O*-allyl-1,2:3,4-di-*O*-isopropylidene-α-D-galactopyranose (**33**). Treatment of **33** with catalyst **2** and DIPEA under the same reaction conditions gave the isomerized product **34** in 95% yield (Scheme 3).

Conclusions

In conclusion, an efficient isomerization of *O*-allyl glycosides has been achieved in the presence of a catalytic amount of dichlorotris(triphenylphosphine)ruthenium(II) (**2**), from which we have developed a facile method for the deprotection of *O*-allyl acetals and ethers. This is preparatively a very useful method, which is performed under mild conditions and is compatible with the presence of various protecting groups. It is also worth noting that the commercially available polystyrene-anchored $(PPh_3)_2RuCl_2$ should show similar activity towards the isomerization of *O*-allyl glycosides, which would make the actual procedure even more attractive (25).

Experimental section

Materials

^1H and ^{13}C NMR spectra were recorded at 500 or 200 MHz and 125 or 50 MHz respectively, with tetramethylsilane (0.00 ppm) as an internal reference. Thin-layer chromatography (TLC) was performed using silica gel 60 F_{254} aluminum sheets purchased from E. Merck. Reagents used for developing plates include ceric sulfate (1% w/v) and ammonium sulfate (2.5% w/v) in 10% (v/v) aqueous sulfuric acid, iodine, dilute aqueous potassium permanganate, and UV light. TLC plates were heated to approximately 150°C when necessary. Purifications were performed by gravity or flash chromatography on silica gel 60 (230–400 mesh; E. Merck No. 9385). Solvents were evaporated under reduced pressure using a rotary evaporator connected to a water aspirator. All chemicals used in experiments were of reagent grade. Solvents were purified by published procedures. Compounds **10** and **11** were synthesized by the reported procedure (26). Compound **12** was prepared by the method reported by Fraser–Reid et al. (27). Allyl α-L-rhamnopyranosides (**13**–**15**) were prepared according to the method reported by Luckas et al. (28). Allyl glycoside **16** was synthesized by the published procedure (16).

Typical procedure for isomerization of glycosides by Grubbs' catalyst (1); procedure A

To a solution of glycoside (0.1 mmol) in toluene (2 mL), *N*-allyltritylamine (**3**) (0.2 mmol), Grubbs' catalyst **1** (8.2 mg, 0.01 mmol) and DIPEA (0.1 mmol) were added under a nitrogen atmosphere. The reaction mixture was stirred under reflux conditions for 4 h. The resulting red solution was concentrated using a rotary evaporator and the residue was partitioned between water and dichloromethane. The organic layer was dried (Na_2SO_4), concentrated, and purified by column chromatography.

Typical procedure for isomerization using $(Ph_3P)_3Cl_2Ru$ (2); procedure B

To a solution of glycosides (0.1 mmol) in toluene (2 mL), dichlorotris(triphenylphosphine)ruthenium(II) (9.6 mg, 0.01 mmol) and DIPEA (0.2 mmol) were added under a nitrogen atmosphere. The resulting solution was stirred under reflux conditions for 2 h and then toluene and DIPEA were removed under reduced pressure. The residue was purified by silica gel column chromatography to obtain the appropriate isomerized product.

Procedure for the deprotection of prop-1-enyl group

The purified isomerization product (0.1 mmol) was dissolved in 2 mL of acetone:water (1:1). To the solution, HgO (10.8 mg, 0.05 mmol) and $HgCl_2$ (27.2 mg, 0.1 mmol) were added. After stirring for 1 h at room temperature, with monitoring by TLC, the deprotected product was extracted with ethyl acetate and washed with potassium iodide solution to remove mercuric compounds. Following a usual work-up, colorless oil was obtained and purified by silica gel column chromatography to obtain the appropriate product as an α and β mixture.

Prop-1-enyl 2,3,4,6-tetra-O-*acetyl*-α-D-*galactopyranoside* (***17***): After silica gel column chromatography with ethyl acetate and hexane as eluent (1:2), compound **17** (as a mixture of *E* and *Z* isomers in 1:2 ratio) was isolated as a syrup, R_f (hexane:EtOAc = 2:1): 0.38. For *E* isomer: ^1H NMR (200 MHz, $CDCl_3$), δ: 6.13 (dq, 1H, J = 12.3, 1.6 Hz), 5.50–5.35 (m, 2H), 5.36–5.29 (m, 1H), 5.25–5.09 (m, 2H), 4.27–4.15 (m, 1H), 4.12–3.98 (m, 2H), 2.14 (s, 3H), 2.07 (s, 3H), 2.02 (s, 3H), 2.00 (s, 3H), 1.55 (dd, 3H, J = 7.0, 1.6 Hz). For *Z* isomer: ^1H NMR (200 MHz, $CDCl_3$), δ: 6.05 (dq, 1H, J = 6.1, 1.6 Hz), 5.50–5.35 (m, 2H), 5.36–5.29 (m, 1H), 5.25–5.09 (m, 1H), 4.70–4.59 (m, 1H), 4.27–4.15 (m, 1H), 4.12–3.98 (m, 2H), 2.14 (s, 3H), 2.07 (s, 3H), 2.02 (s, 3H), 2.00 (s,

© 2000 NRC Canada

3H), 1.62 (dd, 3H, *J* = 6.9, 1.6 Hz). HRMS(FAB), calcd. for $C_{17}H_{24}O_{10}K$ (M + K^+): 427.1007, found: 427.1456.

Prop-1-enyl 2-acetamido-3,4-di-O-*acetyl-2-deoxy-6*-O-*trityl*-β-*D-glucopyranoside (**18**)*: Compound **18** (as a *Z* isomer) was obtained from **10** as a syrup in 85% yield using Grubbs' catalyst. The expected product was obtained in 95% yield using catalyst **2**. R_f (hexane:EtOAc = 1:1): 0.23. For *Z* isomer: ^{1}H NMR (200 MHz, $CDCl_3$), δ (ppm): 7.60–7.00 (m, 15H), 6.29 (dq, 1H, *J* = 6.2, 1.7 Hz), 5.54 (d, 1H, *J* = 9.2 Hz), 5.26–5.23 (m, 2H), 4.83 (d, 1H, *J* = 8.2 Hz), 4.75–4.68 (m, 1H), 4.20–4.15 (m, 1H), 3.61–3.52 (m, 1H), 3.31–3.12 (m, 2H), 2.07 (s, 3H), 2.02 (s, 3H), 1.78 (s, 3H), 1.68–1.65 (m, 3H). HRMS (FAB), calcd. for $C_{34}H_{37}N_1O_8K$ (M + K^+): 626.2156, found: 626.2150.

Prop-1-enyl 2-acetamido-3,4,6-tri-O-*acetyl-2-deoxy*-β-D-*glucopyranoside (**19**)*: Known compound **19** (29) (*E*:*Z* = 1:3) was obtained as a colorless oil in 70% yield using Grubbs' catalyst and 92% yield using catalyst **2**. R_f (hexane:EtOAc = 1:6): 0.34. For *E* isomer: ^{1}H NMR (500 MHz, $CDCl_3$), δ (ppm): 6.19 (m, 1H), 5.62 (d, 1H, *J* = 8.8 Hz), 5.31 (dd, 1H, *J* = 10.2, 9.2 Hz), 5.15–5.05 (m, 2H), 4.83 (d, 1H, *J* = 8.3 Hz), 4.26 (dd, 1H, *J* = 12.2, 4.5 Hz), 4.13 (dd, 1H, *J* = 10.0, 2.3 Hz), 4.03 (m, 1H), 3.78 (m, 1H), 2.08 (s, 3H), 2.04 (s, 3H), 2.02 (s, 3H), 1.95 (s, 3H), 1.55 (dd, 3H, *J* = 6.8, 1.7 Hz). For *Z* isomer: ^{1}H NMR (500 MHz, $CDCl_3$), δ (ppm): 6.15 (dq, 1H, *J* = 4.5, 1.7 Hz), 5.62 (d, 1H, *J* = 8.8 Hz), 5.31 (dd, 1H, *J* = 10.2, 9.2 Hz), 5.10 (m, 1H), 4.83 (d, 1H, *J* = 8.3 Hz), 4.61 (m, 1H), 4.26 (dd, 1H, *J* = 12.2, 4.5 Hz), 4.13 (dd, 1H, *J* = 10.0, 2.3 Hz), 4.03 (m, 1H), 3.78 (m, 1H), 2.08 (s, 3H), 2.04 (s, 3H), 2.02 (s, 3H), 1.95 (s, 3H), 1.56 (dd, 3H, *J* = 6.9, 1.7 Hz).^{13}C NMR (125 MHz, $CDCl_3$), δ (ppm): 170.5, 170.4, 170.3, 142.4 (*E*), 141.2 (*Z*), 105.7 (*E*), 105.6 (*Z*), 95.9 (*E*), 95.3 (*Z*), 67.9, 67.7, 67.5, 66.8, 61.4, 20.6, 12.3 (*E*), 9.2 (*Z*). HRMS (FAB), calcd. for $C_{17}H_{26}NO_9$ (M + 1): 388.1608, found: 388.1877.

Prop-1-enyl 3,4-O-*isopropylidene*-β-*D-galactopyranoside (**20**)*: Compound **20** (*E*:*Z* = 1:1) was obtained as colorless oil in 20% yield using Grubbs' catalyst. The expected product **20** was obtained in 92% yield using catalyst **2**. R_f (hexane:EtOAc = 1:3): 0.32. For *E* isomer: ^{1}H NMR (200 MHz, $CDCl_3$), δ (ppm): 6.24 (dq, 1H, *J* = 12.3, 1.7 Hz), 5.23–5.10 (m, 1H), 4.41 (d, 1H, *J* = 8.3 Hz), 4.30–4.07 (m, 2H), 4.06–3.58 (m, 4H), 2.38 (d, 1H, *J* = 2.4 Hz), 1.62–1.36 (m, 9H). For *Z* isomer: ^{1}H NMR (200 MHz, $CDCl_3$), δ (ppm): 6.17 (dq, 1H, *J* = 6.4, 1.6 Hz), 5.23–5.10 (m, 1H), 4.70–4.57 (m, 1H), 4.41 (d, 1H, *J* = 8.3 Hz), 4.30–4.07 (m, 2H), 4.06–3.58 (m, 4H), 2.38 (d, 1H, *J* = 2.4 Hz), 1.62–1.36 (m, 9H). ^{13}C NMR (50 MHz, $CDCl_3$), δ (ppm): 143.6 (*E*), 142.6 (*Z*), 110.5, 105.0 (*E*), 104.5 (*Z*), 101.9 (*Z*), 101.3 (*E*), 78.7, 73.8, 73.7, 73.1, 62.2, 28.0, 26.2, 12.2 (*E*), 9.4 (*Z*). MS (FAB) *m*/*z*: 260 (M^+).

Prop-1-enyl 2,3-di-O-benzyl-4-O-(p-*methoxybenzyl*)-α-*L-rhamnopyranoside (**21**)*: Compound **21** (*E*:*Z* = 1:1) was isolated from **13** as a syrup in 77% and 94% yield using Grubbs' catalyst (**1**) and catalyst **2**, respectively. R_f (hexane:EtOAc = 10:1): 0.40. For *E* isomer: ^{1}H NMR (500 MHz, $CDCl_3$), δ (ppm): 7.40–6.86 (m, 14H), 6.12 (dq, 1H, *J* = 12.4, 1.6 Hz), 5.05–4.95 (m, 1H), 4.96 (d, 1H, *J* = 1.0 Hz), 4.89–4.56 (m, 6H), 3.91–3.59 (m, 4H), 3.80 (s, 3H), 1.53–1.51 (m, 3H), 1.32 (d, 3H, *J* = 5.7 Hz*)*. For *Z* isomer: ^{1}H NMR (500 MHz, $CDCl_3$), δ (ppm): 7.40–6.86 (m, 14H), 6.10 (dq, 1H, *J* = 6.9, 1.6 Hz), 4.96 (d, 1H, *J* = 1.0 Hz), 4.89–4.56 (m, 6H), 4.55–4.46 (m, 1H), 3.91–3.59 (m, 4H), 3.80 (s, 3H), 1.53–1.51 (m, 3H), 1.32 (d, 3H, *J* = 5.7 Hz*)*. MS (FAB) *m*/*z*: 504 (M^+).

Prop-1-enyl 2,3,4-tri-O-*acetyl*-α-*L-rhamnopyranoside (**22**)*: Compound (*E*:*Z* = 1:2) was obtained as a syrup in 95% yield using procedure B, R_f (hexane:EtOAc = 1:4): 0.27. For *E* isomer: ^{1}H NMR (200 MHz, $CDCl_3$), δ (ppm): 6.13 (dq, 1H, *J* = 12.3, 1.7 Hz), 5.40–5.00 (m, 4H), 4.94 (s, 1H), 3.84 (dq, 1H, *J* = 9.7, 6.2 Hz), 2.15 (s, 3H), 2.05 (s, 3H), 1.99 (s, 3H), 1.55 (dd, 3H, *J* = 7.0, 1.7 Hz), 1.21 (d, 3H, *J* = 6.2 Hz). For *Z* isomer: ^{1}H NMR (200 MHz, $CDCl_3$), δ (ppm): 6.07 (dq, 1H, *J* = 6.2, 1.7 Hz), 5.40–5.00 (m, 3H), 4.94 (s, 1H), 4.73–4.55 (m, 1H), 3.84 (dq, 1H, *J* = 9.7, 6.2 Hz), 2.15 (s, 3H), 2.05 (s, 3H), 1.99 (s, 3H), 1.63 (dd, 3H, *J* = 7.0, 1.7 Hz), 1.21 (d, 3H, *J* = 6.2 Hz).^{13}C NMR (50 MHz, $CDCl_3$), δ (ppm): 169.9, 169.9, 169.8, 141.6 (*E*), 140.7 (*Z*), 105.3 (*E*), 105.0 (*Z*), 97.1 (*Z*), 96.5 (*E*), 70.9, 70.8, 69.2, 68.8, 66.8, 20.9, 17.4, 12.4 (*E*), 9.3 (*Z*). HRMS (FAB), calcd. for $C_{15}H_{23}O_8$ (M + 1): 331.1733, found: 331.1749.

Prop-1-enyl 4-O-*(*p-*methoxybenzyl)*-α-*L-rhamnopyranoside (**23**)*: Compound **23** (*E*:*Z* = 1:2) was obtained from **15** as colorless oil in 96% yield using catalyst **2**. For *E* isomer: ^{1}H NMR (500 MHz, $CDCl_3$), δ (ppm): 7.28 (d, 2H, *J* = 7.7 Hz), 6.87 (d, 2H, *J* = 7.7 Hz), 6.16 (dq, 1H, *J* = 12.2, 1.6 Hz), 5.03 (m, 1H), 4.96 (d, 1H, *J* = 1.5 Hz), 4.65–4.48 (m, 2H), 3.98–3.63 (m, 3H), 3.75 (s, 3H), 3.32 (dq, 1H, *J* = 9.4, 4.4 Hz), 2.57 (bs, 1H), 1.54–1.50 (m, 3H), 1.32 (d, 3H, *J* = 4.4 Hz). For *Z* isomer: 7.28 (d, 2H, *J* = 7.7 Hz), 6.87 (d, 2H, *J* = 7.7 Hz), 6.08 (dq, 1H, *J* = 6.1, 1.9 Hz), 4.96 (d, 1H, *J* = 1.5 Hz), 4.65–4.48 (m, 3H), 3.98–3.63 (m, 3H), 3.75 (s, 3H), 3.32 (dq, 1H, *J* = 9.4, 4.4 Hz), 2.37 (bs, 1H), 1.54–1.50 (m, 3H), 1.32 (d, 3H, *J* = 4.4 Hz). ^{13}C NMR (125 MHz, $CDCl_3$), δ (ppm): 142.4 (*E*), 141.3 (*Z*), 129.7, 114.1, 104.5 (*E*), 103.8 (*Z*), 99.0 (*Z*), 98.5 (*E*), 81.0, 74.7, 71.3, 70.4, 67.9, 55.3, 17.9, 12.4 (*E*), 9.2 (*Z*). HRMS (FAB), calcd. for $C_{17}H_{24}O_6$ (M + 1): 324.1573, found: 324.1708.

Prop-1-enyl 2,3,4,6-tetra-O-*benzyl*-α-*D-mannopyranoside (**24**)*: Compound **24** (*E*:*Z* = 1:1) was obtained as colorless syrup in 84%, R_f (hexane:EtOAc = 4:1): 0.30, *E*:*Z* = 1:1. For *E* isomer: ^{1}H NMR (500 MHz, $CDCl_3$), δ (ppm): 7.46–7.24 (m, 20H), 6.25 (dq, 1H, *J* = 12.3, 1.6 Hz), 5.18 (br, 1H), 5.16 (m, 1H), 4.98–4.58 (m, 8H), 4.16 (t, 1H, *J* = 8.6 Hz), 4.06 (dd, 1H, *J* = 8.6, 1.0 Hz), 3.95–3.78 (m, 4H), 1.61 (m, 3H). For *Z* isomer: ^{1}H NMR (500 MHz, $CDCl_3$), δ (ppm): 7.46–7.24 (m, 20H), 6.21 (dq, 1H, *J* = 6.7, 1.6 Hz), 5.18 (br, 1H), 4.98–4.58 (m, 8H), 4.60 (m, 1H), 4.16 (t, 1H, *J* = 8.6 Hz), 4.06 (dd, 1H, *J* = 8.6, 1.0 Hz), 3.95–3.78 (m, 4H), 1.61 (m, 3H). ^{13}C NMR (125 MHz, $CDCl_3$), δ (ppm): 142.5 (*E*), 141.5 (*Z*), 138.5, 128.4, 128.3, 128.1, 128.0, 127.8, 127.7, 127.6, 127.5, 104.6 (*E*), 103.8 (*Z*), 98.0 (*Z*), 97.8 (*E*), 80.1, 75.3, 75.1, 74.7, 73.4, 73.3, 72.4, 72.3, 69.0, 12.5 (*E*), 9.3 (*Z*). HRMS (FAB), calcd. for $C_{37}H_{40}O_6K$ (M + K^+): 619.2462, found: 619.2437.

© 2000 NRC Canada

2,3,4,6-Tetra-O-*acetyl*-α,β-*D-galactopyranose (**25**) (30)*: The purified isomerized product **17** (38.8 mg, 0.1 mmol) was dissolved in 2 mL of acetone:water (1:1), then HgO (10.8 mg, 0.05 mmol) and $HgCl_2$ (27.2 mg, 0.1 mmol) were added. The reaction mixture was stirred for 20 min at room temperature, monitored by TLC, the deprotected product was extracted with ethyl acetate and washed with potassium iodide solution to remove mercuric compounds. Following a usual work-up, known compound **25** (30) was obtained in 92% yield, α:β = 3:1. For α anomer: ^{1}H NMR (500 MHz, $CDCl_3$), δ (ppm): 5.47 (dd, 1H, *J* = 3.4, 3.3 Hz), 5.43 (m, 1H), 5.37 (dd, 1H, *J* = 10.9, 3.3 Hz), 5.11 (dd, 1H, *J* = 10.7, 3.4 Hz), 4.43 (t, 1H, *J* = 6.7 Hz), 4.06 (m, 1H), 4.05 (m, 1H), 3.68 (bs, 1H), 2.11 (s, 3H), 2.05 (s, 3H), 2.01 (s, 3H), 1.95 (s, 3H). For β anomer: ^{1}H NMR (500 MHz, $CDCl_3$), δ (ppm): 5.43 (m, 1H), 5.37 (dd, 1H, *J* = 10.9, 3.3 Hz), 5.04 (m, 1H), 4.67 (dd, 1H, *J* = 7.8, 7.4 Hz), 4.11 (d, 1H,. *J* = 7.4 Hz), 4.06 (m, 1H), 4.05 (m, 1H), 3.93 (t, 1H, *J* = 6.7 Hz), 2.11 (s, 3H), 2.05 (s, 3H), 2.01 (s, 3H), 1.95 (s, 3H). ^{13}C NMR (125 MHz, $CDCl_3$), δ (ppm): 171.0, 170.6, 170.5, 170.4, 170.2, 170.1, 170.0, 95.9, 90.6, 71.0, 70.4, 68.3, 68.2, 67.2, 66.1, 61.8, 61.5, 42.4, 20.6. MS (FAB) *m*/*z*: 349 (M + 1).

2-Acetamido-3,4-di-O-*acetyl-2-deoxy-6*-O-*trityl*-α,β-*D-glucopyranose (**26**)*: Compound **26** (as an α and β mixture) was obtained from **18** in 92% yield as colorless oil, R_f (hexane:EtOAc = 1:1): 0.20. For α anomer: ^{1}H NMR (200 MHz, $CDCl_3$), δ (ppm): 7.33 (m, 15H), 5.79 (d, 1H, *J* = 9.3 Hz), 5.30–5.18 (m, 3H), 4.33–4.12 (m, 2H), 3.55 (d, 1H, *J* = 2.5Hz), 3.20 (dd, 1H, *J* = 10.4, 2.1 Hz), 3.04 (dd, 1H, *J* = 10.4, 4.6 Hz), 1.98 (s, 3H), 1.91 (s, 3H), 1.70 (s, 3H). For β anomer: ^{1}H NMR (200 MHz, $CDCl_3$), δ (ppm): 7.33 (m, 15H), 5.79 (d, 1H, *J* = 9.3 Hz), 5.30–5.18 (m, 2H), 4.33–4.12 (m, 3H), 4.12 (m, 1H), 3.55 (d, 1H, *J* = 2.5Hz), 3.20 (dd, 1H, *J* = 10.4, 2.1 Hz), 3.04 (dd, 1H, *J* = 10.4, 4.6 Hz), 1.98 (s, 3H), 1.91 (s, 3H), 1.70 (s, 3H). MS (FAB) *m*/*z*: 471 (M + 1).

3,4-O-*Isopropylidene*-α,β-*D-galactopyranose (**28**)*: Compound **28** (α:β = 2:1) was obtained as a syrup in 90% yield from **20,** R_f (EtOAc): 0.23. For α anomer: ^{1}H NMR (500 MHz, $CDCl_3$), δ (ppm): 5.61 (bs, 1H), 5.23 (bs, 1H), 4.30–3.5 (m, 6H), 1.49 (s, 3H), 1.30 (s, 3H). For β anomer: ^{1}H NMR (500 MHz, $CDCl_3$), δ (ppm): 6.32 (bs, 1H), 4.65 (bs, 1H), 4.30–3.5 (m, 6H), 1.49 (s, 3H), 1.30 (s, 3H). ^{13}C NMR (125 MHz, $CDCl_3$), δ (ppm): 110.4 (β), 109.8 (α), 95.9 (β isomer), 91.3 (α), 79.1, 75.6, 74.3, 74.1, 73.8, 73.4, 69.2, 68.9, 62.5, 62.2, 28.0, 27.4, 26.3, 25.7. HRMS (FAB), calcd. for $C_9H_{17}O_6$ (M + 1): 221.1025, found: 221.1289.

2,3-Di-O-*benzyl-4*-O-*(p-methoxybenzyl)*-α,β-*L-rhamnopyranose (**29**)*: Compound **29** (α:β = 5:1) was obtained as syrup in 91% yield, R_f (hexane:EtOAc = 4:1): 0.25. For α anomer: ^{1}H NMR (500 MHz, CD_3COCD_3), δ (ppm): 7.43–7.24 (m, 12H), 6.86 (d, 2H, *J* = 8.6 Hz), 5.17 (s, 1H), 4.84–4.57 (m, 6H), 3.89 (m, 2H), 3.82 (m, 1H), 3.77 (s, 3H), 3.52 (t, 1H, *J* = 9.1 Hz), 1.18 (d, 3H, *J* = 6.2 Hz). For β anomer: ^{1}H NMR (500 MHz, CD_3COCD_3), δ (ppm): 7.43–7.24 (m, 12H), 6.86 (d, 2H, *J* = 8.6 Hz), 4.84–4.57 (m, 7H), 3.89 (m, 2H), 3.82 (m, 1H), 3.77 (s, 3H), 3.52 (t, 1H, *J* = 9.1 Hz), 1.18 (d, 3H, *J* = 6.2 Hz). ^{13}C NMR (125 MHz, CD_3COCD_3), δ (ppm): 140.2, 132.2, 130.4, 129.1, 129.0, 128.9, 128.7, 128.5, 128.4, 128.2, 128.1, 114.3, 93.0 (β), 92.9 (α), 83.9, 81.2, 77.2, 75.4, 73.3, 72.4, 68.2, 55.5, 18. HRMS (FAB), calcd. for $C_{28}H_{33}O_6$ (M + 1): 465.2277, found: 465.2224.

2,3,4-Tri-O-*acetyl*-α,β-*L-rhamnopyranose (**30**)*: Known compound **30** (31) was obtained from **22** as a syrup in 92% yield, α:β = 13:1. For α anomer: ^{1}H NMR (500 MHz, CD_3COCD_3), δ (ppm): 6.02 (d, 1H, *J* = 4.4 Hz), 5.29 (dd, 1H, *J* = 10.1, 3.5 Hz), 5.17 (dd, 1H, *J* = 3.5, 1.8 Hz), 5.09 (dd, 1H, *J* = 4.4, 1.8 Hz), 4.99 (t, 1H, *J* = 10.1 Hz), 4.05 (m, 1H), 2.07 (s, 3H), 2.01 (s, 3H), 1.95 (s, 3H), 1.91 (s, 3H), 1.12 (d, 3H, *J* = 6.3 Hz). ^{13}C NMR (125 MHz, CD_3COCD_3), δ (ppm): 170.5, 170.4, 170.3, 92.6, 71.7, 71.4, 69.8, 66.6, 20.7, 17.9. HRMS (FAB), cacld. for $C_{12}H_{19}O_8$ (M + 1): 291.0180, found: 291.0216.

4-O-*(*p-*Methoxybenzyl)*-α,β-*L-rhamnopyranose (**31**)*: Compound **31** (α:β = 9:1) was obtained as colorless oil in 93%. For α anomer: ^{1}H NMR (500 MHz, CD_3COCD_3), δ (ppm): 7.29 (d, 2H, *J* = 8.7 Hz), 6.87 (d, 2H, *J* = 8.7 Hz), 5.31 (d, 1H, *J* = 4.0 Hz), 5.05 (bs, 1H), 4.83 (d, 1H, *J* = 10.9 Hz), 4.58 (d, 1H, *J* = 11.0 Hz), 4.00–3.80 (m, 3H), 3.76 (s, 3H), 3.32 (dd, 1H, *J* = 9.3, 9.0 Hz), 1.16 (d, 3H, *J* = 6.3 Hz). For β anomer: ^{1}H NMR (500 MHz, CD_3COCD_3), δ (ppm): 7.29 (d, 2H, *J* = 8.7 Hz), 6.87 (d, 2H, *J* = 8.7 Hz), 5.16 (d, 1H, *J* = 9.3 Hz), 4.68 (d, 1H, *J* = 9.3 Hz), 4.83 (d, 1H, *J* = 10.9 Hz), 4.58 (d, 1H, *J* = 11.0 Hz), 4.00–3.80 (m, 3H), 3.76 (s, 3H), 3.32 (dd, 1H, *J* = 9.3, 9.0 Hz), 1.19 (d, 3H, *J* = 5.8 Hz). ^{13}C NMR (125 MHz, CD_3COCD_3), δ (ppm): 160.0, 132.4, 130.3, 114.3, 95.0, 82.2, 74.8, 73.2, 72.4, 67.6, 55.5, 14.5. HRMS (FAB), calcd. for $C_{14}H_{20}O_6K$ (M + K^+): 323.0897, found: 323.1397.

2,3,4,6-Tetra-O-*benzyl*-α,β-*D-mannopyranose (**32**)*: Compound **32** (α:β = 3:1) was obtained as colorless oil in 78% yield, R_f (hexane:EtOAc = 4:1): 0.20. For α anomer: ^{1}H NMR (500 MHz, $CDCl_3$), δ (ppm): 7.60–7.00 (m, 20H), 5.25 (d, 1H, *J* = 1.6Hz), 5.05–4.49 (m, 8H), 4.04 (m, 1H), 3.96 (dd, 1H, *J* = 9.6, 2.8 Hz), 3.86 (t, 1H, *J* = 9.6 Hz), 3.79 (dd, 1H, *J* = 2.8, 1.6 Hz), 3.73–3.67 (m, 2H). For β anomer: ^{1}H NMR (500 MHz, $CDCl_3$), δ (ppm): 7.60–7.00 (m, 20H), 5.05–4.49 (m, 9H), 4.04 (m, 1H), 3.96 (dd, 1H, *J* = 9.6, 2.8 Hz), 3.86 (t, 1H, *J* = 9.6 Hz), 3.79 (dd, 1H, *J* = 2.8, 1.6 Hz), 3.73–3.67 (m, 2H). ^{13}C NMR (125 MHz, $CDCl_3$), δ (ppm): 138.4, 138.4, 138.3, 138.0, 128.5, 128.5, 128.3, 128.3, 128.1, 128.0, 127.9, 127.9, 127.8, 127.8, 127.7, 127.6, 127.6, 127.5, 127.5, 93.7 (β isomer), 92.7 (α isomer), 79.7, 74.6, 73.3, 72.7, 72.6, 72.2, 71.5, 69.6. MS (FAB) *m*/*z*: 541 (M + 1).

1,2:3,4-Di-O-*isopropylidene-6*-O-*(prop-1-enyl)*-α-*D-galactopyranose (**34**)*: Compound **34** was obtained from **33** (32) in 95% yield as a syrup, R_f (hexane:EtOAc = 1:6): 0.40. *E*:*Z* = 5:1. For *E*-isomer, ^{1}H NMR (500 MHz, $CDCl_3$), δ (ppm): 6.20 (dq, 1H, *J* = 12.6, 1.6 Hz), 5.50 (d, 1H, *J* = 5.0 Hz), 4.77 (m, 1H), 4.57 (dd, 1H, *J* = 7.9, 2.5 Hz), 4.28 (dd, 1H, *J* = 5.0, 2.5 Hz), 4.22 (dd, 1H, *J* = 7.9, 2.0 Hz), 3.99 (m, 1H), 3.80 (dd, 1H, *J* = 10.3, 5.9 Hz), 3.74 (dd, 1H, *J* = 10.3, 6.8 Hz), 1.54 (dd, 3H, *J* = 6.8, 1.7 Hz), 1.41 (s, 3H), 1.30 (s, 3H), 1.29 (s, 6H). ^{13}C NMR (125 MHz, $CDCl_3$), δ (ppm): 146.2, 109.3, 108.6, 98.9, 96.3, 70.6, 70.5, 67.4, 66.1, 25.9,

© 2000 NRC Canada

24.9, 24.4, 12.4. HRMS (FAB), calcd. for $C_{15}H_{25}O_6$ (M + 1): 301.1691, found: 301.1624.

1,2:3,4-Di-O-*isopropylidene*-α-*D*-*galactopyranose (35)*: Known compound **35**[2] was obtained from **34** in 91% yield as colorless oil, R_f (hexane:EtOAc = 1:3): 0.30. ^{1}H NMR (200 MHz, $CDCl_3$), δ (ppm): 5.55 (d, 1H, J = 5.0 Hz), 4.60 (dd, 1H, J = 7.9, 2.2 Hz), 4.32 (dd, 1H, J = 5.0, 2.2 Hz), 4.25 (dd, 1H, J = 7.9, 1.2 Hz), 3.86–3.80 (m, 4H), 1.51 (s, 3H), 1.44 (s, 3H), 1.32 (s, 6H).

Acknowledgements

Support of this work by the Natural Sciences and Engineering Research Council of Canada (NSERC) is gratefully acknowledged.

References

1. (*a*) T.W. Greene and P.G.M. Wuts. *In* Protective groups in organic synthesis. John Wiley and Sons, New York. 1991. p. 42; (*b*) R. Gigg and C.D. Warren. J. Chem. Soc. 2205 (1965); (*c*) P.A. Gent, R. Gigg, and A.A.E. Penglis. J. Chem. Soc. Perkin Trans. 1, 1395 (1976).
2. (*a*) T.J. Prosser. J. Am. Chem. Soc. **83**, 1701 (1961); (*b*) C.C. Price and W.H. Snyder. J. Am. Chem. Soc. **83**, 1773 (1961).
3. S.M. Kadam, S.K. Nayak, and A. Banerji. Tetrahedron Lett. **33**, 5129 (1992).
4. (*a*) E.J. Corey and J.W. Suggs. J. Org. Chem. **38**, 3223 (1973); (*b*) G.-J. Boons, A. Burton, and S. Isles. Chem. Commun. 141 (1996).
5. (*a*) D. Baudry, M. Ephritikhine, and H. Felkin. Chem. Commun. 694 (1978); (*b*) J.J. Oltvoort, C.A.A. van Boeckel, J.H. DeKoning, and J.H. van Boom. Synthesis, 305 (1981).
6. R. Boss and R. Scheffold. Angew. Chem. Int. Ed. Engl. **15**, 588 (1976).
7. M. Honda, H. Morita, and I. Nagakura. J. Org. Chem. **62,** 8932 (1997).
8. K.C. Nicolaou, C.W. Hummel, N.J. Bockovich, and C.-H. Wong. Chem. Commun. 870 (1991).
9. J.V. Crivello and S. Kong. J. Org. Chem. **63**, 6745 (1998).
10. R. Gigg and C.D. Warren. J. Chem. Soc. C, 1903 (1968).
11. (*a*) M. Bruce and Y. Roshan-Ali. J. Chem. Res. Synop., 193 (1981); (*b*) T. Ogawa, T. Kitajima, and T. Nukada. Carbohydr. Res. **123**, C5 (1983); (*c*) T. Ogawa and S. Nakabayasi. Carbohydr. Res. **93**, C1 (1981); (*d*) H.B. Mereyala and S. Guntha. Tetrahedron Lett. **34**, 6929 (1993).
12. (*a*) K. Nakayama, K. Uoto, K. Higashi, T. Soga, and T. Kusama. Chem. Pharm. Bull. **40**, 1718 (1992); (*b*) J. Luning, U. Moller, N. Debski, and P. Welzel. Tetrahedron Lett. **34**, 5871 (1993); (*c*) B. Yu, B. Li, J. Zhang, and Y. Hui. Tetrahedron Lett. **39**, 4871 (1998).
13. (*a*) S.T. Nguyen, L.K. Johnson, and R.H. Grubbs. J. Am. Chem. Soc. **114**, 3974 (1992); (*b*) M. Schuster and S. Blechert. Angew. Chem. Int. Ed. Engl. **36**, 2036 (1997); (*c*) S.K. Armstrong. J. Chem. Soc. Perkin Trans. 1, 371 (1998); (g) S.C.G. Biagini, S.E. Gibson, and S.P.J. Keen. J. Chem. Soc. Perkin Trans. 1, 2485 (1998).
14. For a review see: R. Roy and S. Das. Chem. Commun. 519 (2000).
15. H.E. Applegate, C.M. Cimarusti, J.E. Dolfini, P.T. Funke, W.H. Koster, M.S. Puar, W.A. Slusarchyk, and M.G. Young. J. Org. Chem. **44**, 811 (1979).
16. F.M. Winnik, J.P. Carver, and J.J. Krepinski. J. Org. Chem. **47**, 2701 (1982).
17. D.L. Pavia, G.M. Lampman, and G.S. Kriz. *In* Introduction to spectroscopy. Harcourt Brace College Publishers, Washington. 1996.
18. D.V. McGrath and R.H. Grubbs. Organometallics, **13**, 224 (1994).
19. Z. Wu, S.T. Nguyen, R.H. Grubbs, and J.W. Ziller. J. Am. Chem. Soc. **117,** 5503 (1995).
20. S.P. Chavan, P.K. Zubaidha, S.W. Dantale, A. Keshavaraja, A. Ramaswamy, and T. Ravindranathan. Tetrahedron Lett. **36**, 237 (1995).
21. M. Ochiai, T. Ito, H. Takahashi, A. Nakanishi, M. Toyonari, T. Sueda, S. Goto, and M. Shiro. J. Am. Chem. Soc. **118**, 7716 (1996).
22. R. Beugelmans, S. Bourdet, A. Bigot, and J. Zhu. Tetrahedron Lett. **35,** 4349 (1994).
23. (*a*) C.D. Warren and R.W. Jeanloz. Carbohydr. Res. **53**, 67 (1977); (*b*) T. Nishiguchi, K. Tachi, and K. Fukuzumi. J. Org. Chem. **40**, 237 (1975); (*c*) C.A.A. van Boeckel and J.H. van Boom. Tetrahedron, 3561 (1979).
24. J.M. Reuter and R.G. Salomon. J. Org. Chem. **42**, 3360 (1977).
25. A. Zoran and Y. Sasson. J. Org. Chem. **46**, 255 (1981).
26. R.T. Lee and Y.C. Lee. Carbohydr. Res. **37**, 193 (1974).
27. B. Fraser-Reid, U.E. Udodong, Z. Wu, H. Ottosson, J.R. Merritt, C.S. Rao, C. Roberts, and R. Madsen. Synlett, 927 (1992).
28. L. Valente, A. Olesker, R. Rabanal, L.E.S. Barata, G. Lukacs, and T.T. Thang. Tetrahedron Lett. **13**, 1153 (1979).
29. M.A. Nashed, C.W. Slife, M. Kiso, and L. Anderson. Carbohydr. Res. **82**, 237 (1980).
30. M. Mikamo. Carbohydr. Res. **191**, 150 (1989).
31. V. Pozsgay and A. Neszmelyi. Carbohydr. Res. **80**, 196 (1980).
32. T. Bieg and W. Szeja. J. Carbohyd. Chem. **4**, 441 (1985).

[2] The spectral data of **35** were identical with the product from Aldrich Chemical Co.

© 2000 NRC Canada

Synthetic applications of the ruthenium-catalyzed hydrogenation via dynamic kinetic resolution

Virginie Ratovelomanana-Vidal and Jean-Pierre Genêt

Abstract: This review summarizes some recent work in the field of homogeneous ruthenium-catalyzed hydrogenation via dynamic kinetic resolution. The hydrogenation reaction of various α-substituted β-oxo esters using chiral ruthenium(II) catalysts is presented as well as the synthesis of some key intermediates of pharmaceutical interest.

Key words: dynamic kinetic resolution, ruthenium, hydrogenation, α-substituted β-keto ester.

Résumé : Cette revue résume quelques resultats récents dans le domaine de l'hydrogénation asymétrique, catalysée par des complexes du ruthénium en utilisant le principe du dédoublement cinétique dynamique appliquée aux β-céto esters α-substitués. L'hydrogénation stéréosélective de β-céto esters α-substitués variés ainsi que la préparation de quelques intermédiaires clefs d'intérêt thérapeutique sont présentés.

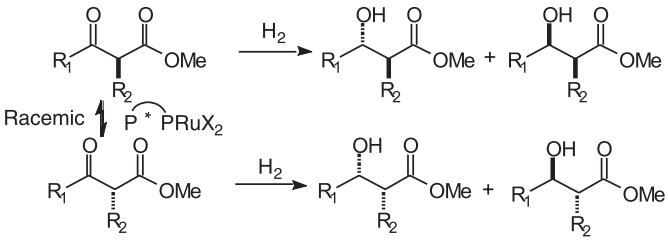
Mots clés : dédoublement cinétique dynamique, ruthénium, hydrogénation, β-céto esters α-substitués.

Introduction

In contrast with kinetic resolution processes where the maximum theoretical yield of one enantiomer is limited to 50%, the dynamic kinetic resolution involving in situ racemization of the substrates can afford the desired isomer in a yield approaching 100%. This process is thus much more efficient. A racemic starting material such as α-substituted β-keto esters bearing a configurationally labile stereogenic center and a prochiral unsaturated moiety, can be converted to one major *syn* or *anti* stereoisomer, among the four stereoisomers, through enantioselective hydrogenation via dynamic kinetic resolution (for general reviews on dynamic kinetic resolution, see ref. (1*a*–*f*); for a mathematical treatment of the kinetics in the DKR, see ref. (1*g*, *h*)). In this process, the slower reacting isomer is converted into the other one in situ (Scheme 1). In this paper, we detail how both *syn* and *anti* α-substituted β-hydroxy esters were synthesized using some selective ruthenium-catalyzed hydrogenation reactions based on this principle.

Because asymmetric catalysis is widely used in organic synthesis (2–14), it is important to expand this area of research to find new catalytic routes to obtain optically pure compounds. One of the easiest way to introduce an hydrogen atom in an appropriate prochiral center is to use asymmetric hydrogenation. The first homogeneous asymmetric hydrogenation has been reported independently by Horner and Knowles and co-workers (15, 16). The breakthrough in this topic was the discovery of the DIOP, a C_2 symmetric

Scheme 1.



chiral diphosphine obtained from tartaric acid, by Kagan coworkers (17). Today, a large number of amino acids are readily synthesized in ee up to 99% with chiral phosphine rhodium catalysts. However, the scope of Rh-catalyzed hydrogenations is not wide in comparison with Ru-catalyzed hydrogenation reactions. The first chiral Ru(II)-catalyst was reported by James et al. (18) in 1975 to catalyze the hydrogenation of unsaturated carboxylic acids in 60% ee. Since the discovery of the $[RuCl_2(Binap)]_2NEt_3$ complex by Ikariya et al. (19) and the subsequent discovery of $Ru(OAc)_2$[(*R*) or (*S*)-Binap] by Noyori et al. (20), the use of these catalysts in many enantioselective hydrogenations has drawn considerable

Received August 11, 1999. Published on the NRC Research Press website on June 15, 2000.

Dedicated to Professor S. Hanessian in recognition of his significant contributions to the art of organic synthesis.

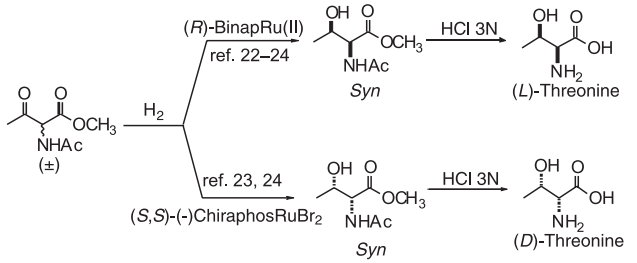
V. Ratovelomanana-Vidal[1] and J.-P. Genêt. Laboratoire de Synthèse Sélective Organique et Produits Naturels associé au CNRS (UMR 7573), 11 rue P. et M. Curie, F-75231 Paris CEDEX 05, France.

[1]Author to whom correspondence may be addressed. Fax: (33)1 44 07 10 62. e-mail: gvidal@ext.jussieu.fr and genet@ext.jussieu.fr

 © 2000 NRC Canada

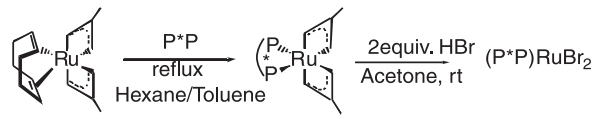
attention to homogeneous hydrogenations catalyzed by Ru(II)-complexes (for some reviews see ref. (21)). The simultaneous work of Noyori and co-workers (22) and Genêt and co-workers(23)[2] led to the first examples of enantioselective ruthenium-promoted hydrogenations of racemic α-acetamido β-keto esters via dynamic kinetic resolution. Noyori et al. reported the hydrogenation of 2-acetamido derivative (Scheme 2) in dichloromethane leading to the protected *syn L*-threonine (98% ee) and *anti* allothreonine with 99:1 selectivity. This remarkable *syn* stereoselectivity was also observed for some threonine type products which were synthesized with excellent ees and in high yields using the BINAP-Ru catalyzed hydrogenation (22). We achieved simultaneously the synthesis of *L* and *D*-threonine via asymmetric hydrogenation of racemic 2-acylamino-3-oxobutyrates, prepared in a two-step sequence from the corresponding β-keto ester (23)[2] (Scheme 2).

Scheme 2.



An ideal dynamic kinetic resolution was obtained by using the BINAP-Ru(II) complex. The ruthenium dihalide catalysts containing CHIRAPHOS, prepared as shown in Scheme 3, catalyzed the hydrogenation of methyl 2-acetamido-3-oxobutanoate affording the corresponding *syn* α-amino β-hydroxy ester in dichloromethane with high enantio (85% ee) and diastereomeric excesses. The use of methanol as solvent instead of dichloromethane resulted in a decreased diastereoselectivity. In the last few years, we have been interested in the ruthenium-promoted hydrogenation reactions and we have developed a general strategy for the synthesis of chiral Ru(II)-catalysts (24) (Scheme 3). This method can be applied to a whole set of chiral diphosphines such as the atropoisomeric ligands BINAP, BIPHEMP, and

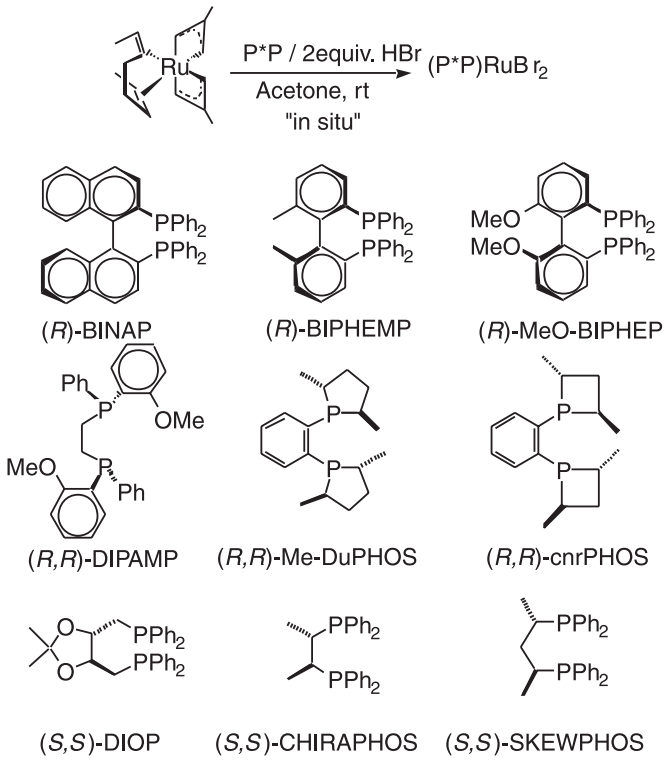
Scheme 3.



MeO-BIPHEP, but also DIPAMP, DIOP, CHIRAPHOS, Me-DuPHOS (24), SKEWPHOS (25), Cnr-PHOS (26) etc. The corresponding halogen-containing ruthenium complexes with the empirical formula $(P^*P)RuBr_2$ are efficient for the asymmetric hydrogenations of olefins and carbonyl groups, which lead to functionalized alcohols with high levels of enantioselectivity (27).

The catalyst synthesis was improved (24); the halogen-containing catalysts were more conveniently prepared in situ under milder conditions, in a one-step sequence from a commercially available starting material, $(COD)Ru(\eta^3\text{-}(CH_2)_2CCH_3)_2$ (24) (Scheme 4). This technique is advantageous for several reasons: (*i*) wide scope; (*ii*) predictable absolute configurations of the chiral functionalized alcohols;

Scheme 4.



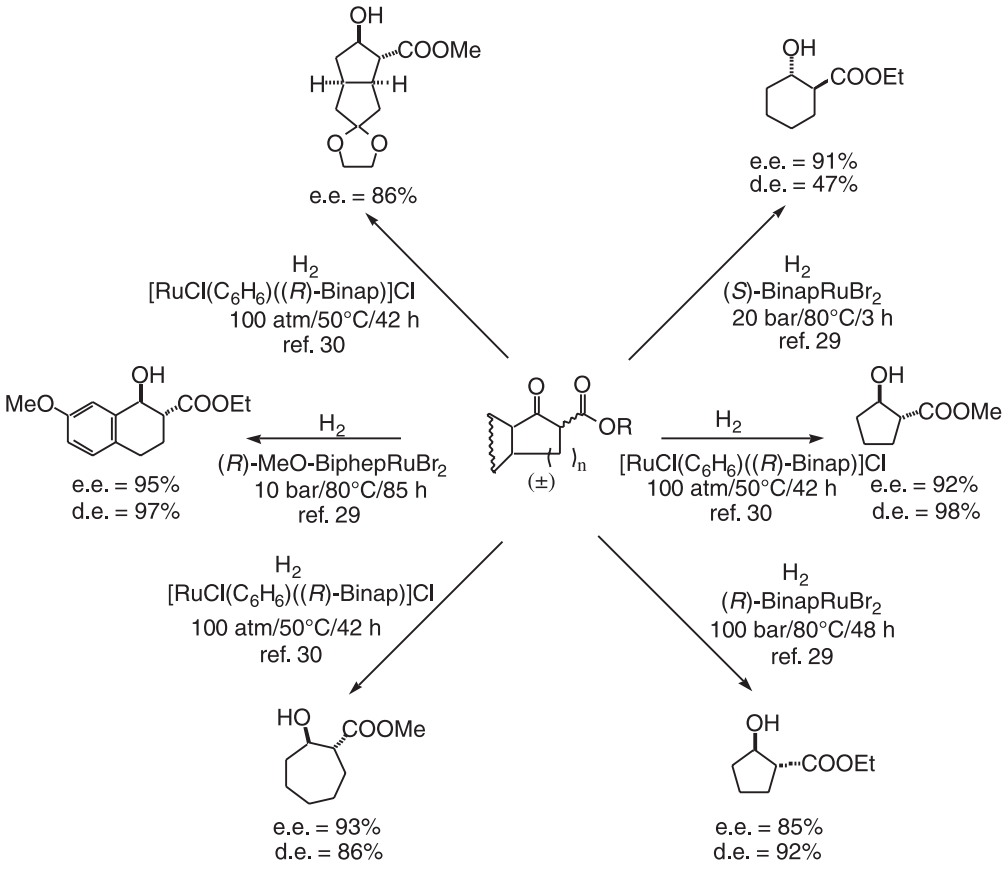
(*iii*) and ready availability of the chiral Ru(II)-catalysts in either enantiomeric forms. Furthermore, this process gives high yields and is easy to perform on large scale.

The ruthenium-promoted hydrogenation reaction of cyclic 2-substituted 3-oxo carboxylic esters has been examined (Scheme 5) by Noyori et al. and our group using the in situ generated ruthenium(II) catalysts. The stereochemical course of the reaction was highly influenced by substrate structures and reactions conditions (28, 29). When comparing the asymmetric hydrogenation of the five-membered ring to those obtained with cyclic six-membered rings, the following comment can be made: in the case of 2-(ethoxycarbonyl)cyclopentanone or (methoxycarbonyl)cyclopentanone, the hydrogenation reaction proceeded with high diastereo- and enantioselectivity (respectively, de = 92%, ee = 85% and de = 98%, ee = 92%) by using (*R*)-BINAP as chiral auxiliary, leading to the corresponding (2*R*,3*R*) *trans* product. However, in increasing the ring size to a six-membered ring with (*S*)-BinapRu(II) catalyst, the diastereoselectivity decreased to some extent (de = 47%). Nevertheless, significant enantiomeric excess was reached for the ruthenium-promoted hydrogenation reaction of 2-(ethoxycarbonyl)cyclohexanone (28) in dichloromethane affording the (2*S*,3*S*) *trans* product

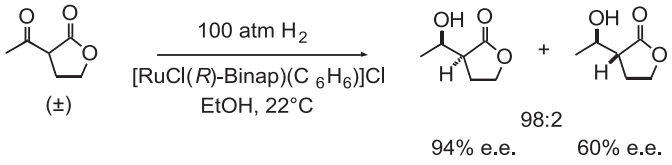
[2] J.P. Genêt, S. Mallart, and S. Jugé. French Patent, 8911159 (1989).

© 2000 NRC Canada

Scheme 5.



Scheme 6.



(ee = 91%). A relevant dynamic kinetic resolution was achieved for cyclic β-keto esters containing a tetralone moiety i.e., 7-methoxy-2(ethoxycarbonyl)tetralone. The *trans* cyclic β-hydroxy ester was synthesized in methanol using (*R*)-MeO-BIPHEP as chiral auxiliary with excellent enantio- and diastereofacial discrimination (de = 97%, ee = 95%) under 10 bar of hydrogen pressure and 80°C. The absolute configuration of the hydroxyl-substituted carbon was determined by the configuration of the chiral auxiliary (BINAP or MeO-BIPHEP) although the configuration of the α stereogenic center was dependent on the nature of the substrate and reaction conditions. The ruthenium-promoted hydrogenation reaction of a bicyclic substrate that contained one chirally labile and two stable stereogenic centers (29) has been reported using 0.36 mol% of [RuCl(C_6H_6)(*R*)-Binap]Cl and the alcohol was obtained in 86% ee and in 32% yield.

Hydrogenation of racemic 2-acetyl-4-butanolide (Scheme 6) proceeded with 96% *syn* diastereoselectivity and good enantiomeric excesses (29).

The hydrogenation reaction of α-chloro β-keto esters has been studied (30) (Scheme 7). Behavior of the open chain α-chloro β-keto esters was different from the cyclic substrates. We succeeded in the hydrogenation by using a simple catalytic system prepared by mixing (COD)Ru(η^3-$(CH_2)_2CCH_3)_2$ and the chiral diphosphine (BINAP or MeO-BIPHEP). Under optimized conditions (80 bar and 80°C) in dichloromethane, the corresponding *anti* α-chloro β-hydroxy esters bearing an alkyl or an aromatic substituent were synthesized with high levels of enantio- and diastereoselection varying from 70 to 99%. Indeed, the use of methanol as solvent resulted in the formation of the *syn* chlorhydrins with moderate de (30). A *syn* diastereoselectivity was also reported using a (*R*)-BinapRu(II) catalyst (31).

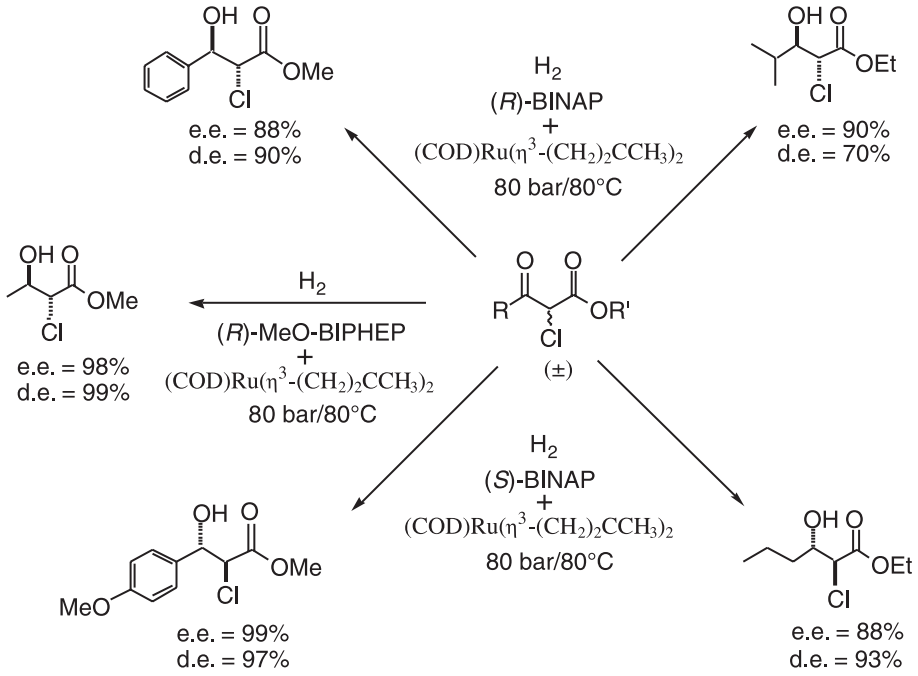
These enantiomerically enriched α-chloro β-hydroxy esters were used to synthesize optically active glycidates (30) (Scheme 8) such as (2*R*,3*S*)-3-(4-methoxyphenyl) glycidate which was a practical key intermediate for the synthesis of diltiazem®, a potent channel blocker. The *trans* (2*S*,3*R*)-methyl-3-phenylglycidate was obtained under similar conditions and provided an efficient route to taxotere® side chain.

The dynamic kinetic resolution of α-acetamido β-keto ester was successfully applied to produce an important intermediate (Scheme 9) for the synthesis of carbapenems (32).

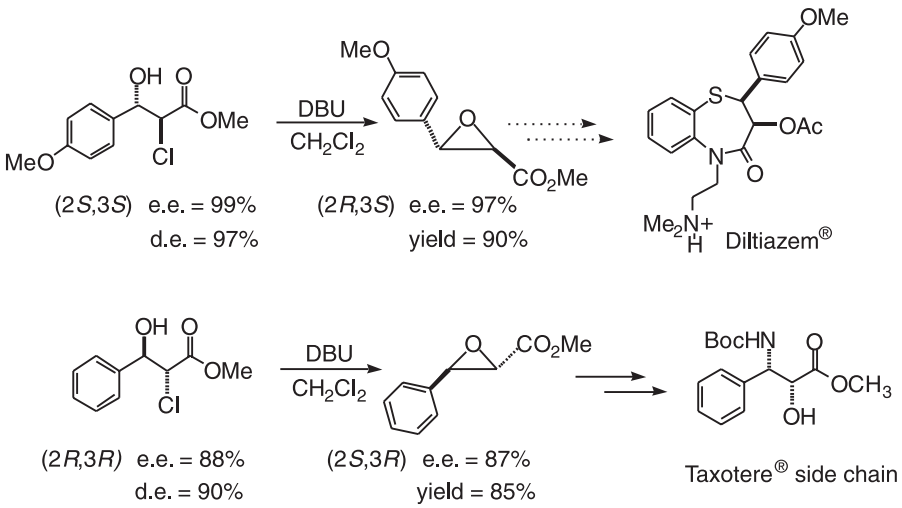
The synthesis of (2*S*,3*R*) methyl *p*-chloro-3-hydroxytyrosinate, a component of Vancomycin, was achieved using the dynamic kinetic resolution of an α-acetamido β-keto ester prepared from *m*-chloro-*p*-hydroxybenzoic acid

© 2000 NRC Canada

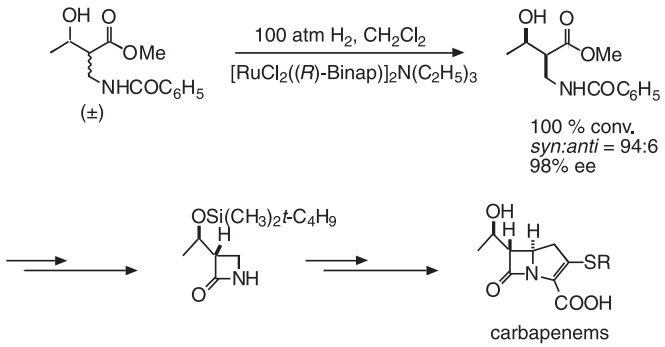
Scheme 7.



Scheme 8.



Scheme 9.

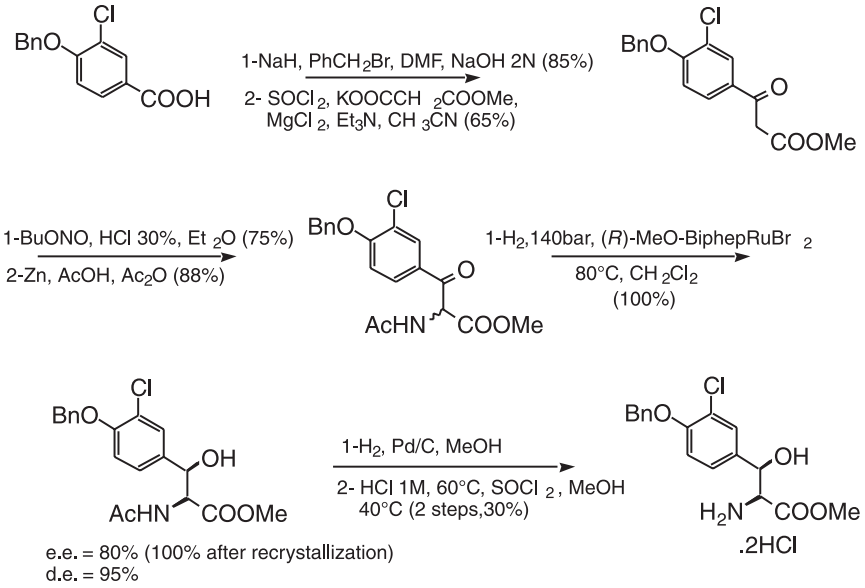


(Scheme 10) (33). The *syn* β-hydroxy α-amino ester was quantitatively synthesized and isolated as optically pure after two recrystallizations in ethanol.

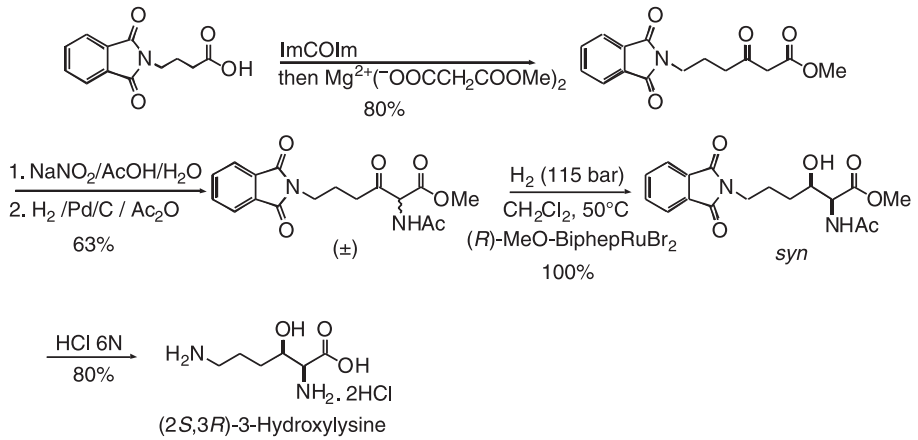
The reactions using dynamic kinetic resolution of α-substituted β-keto esters have been used for the total synthesis of statine and analogues (34), HMG-CoA synthase inhibitor 1233 A (35), a chiral diphosphine (36), Biphenomycin A (37), and roxaticin (38). Genêt and co-workers (39) recently achieved an efficient synthesis of (2*S*,3*R*)-3-hydroxylysine from the commercially available 4-phtalimidobutyric acid (Scheme 11); an ideal dynamic kinetic resolution of racemic methyl-2-acetamido-3-keto-6-phtalimidohexanoate was obtained under 115 bar of hydrogen pressure at 50°C in dichloromethane affording the desired optically pure *syn* α-acetamido β-hydroxy ester in quantitative yield. This key step allowed the formation of both stereogenic centers

© 2000 NRC Canada

Scheme 10.



Scheme 11.

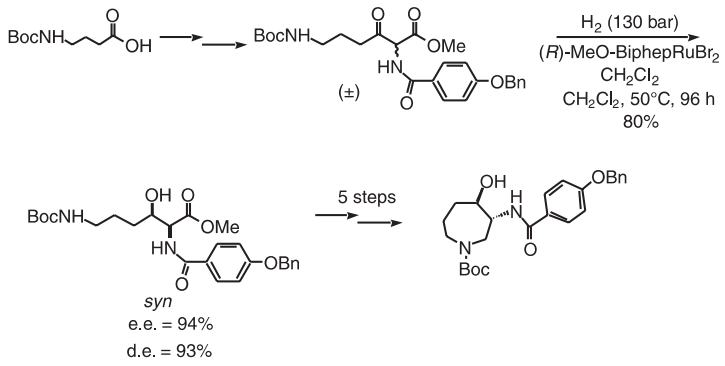


of (2*S*,3*R*)-3-hydroxylysine in a single stereocontrolled catalytic step using (*R*)-MeO-BIPHEP as the chiral auxiliary.

The same strategy has been used for an expeditive synthesis of the hexahydroazepine unit (40) of (–)-balanol (proteine kinase C inhibitor) (Scheme 12).

The dynamic kinetic resolution through ruthenium-promoted hydrogenation of chirally labile racemic α-substituted β-keto ester is a method of choice to synthesize chiral compounds of high enantiomeric purity. In ideal situations, it is possible in one single step to obtain the desired

Scheme 12.



© 2000 NRC Canada

optically pure compound with two contiguous stereogenic centers having relative *syn* or *anti* configurations, in both acyclic and cyclic skeletons.

Acknowledgements

We would like to thank Dr R. Schmidt (Hoffman La Roche) for samples of (*R*) and (*S*)-MeO-BIPHEP.

References

1. (*a*) B.A. Persson, A.L.E. Larsson, M. Le Ray, and J.E. Bäckvall. J. Am. Chem. Soc. **121**, 1645 (1999); (*b*)R.N. Ben and T. Durst. J. Org. Chem. **64**, 7700 (1999); (*c*) R. Stürmer. Angew. Chem. Int. Ed. Engl. **36**, 1173 (1997); (*d*) S. Caddick and K. Jenkins. Chem. Soc. Rev. 447 (1996); (*e*) H. Stecher and K. Faber. Synthesis, 1 (1997); (*f*) R.S. Ward. Tetrahedron: Asymmetry, 6 1475 (1995). (*g*) M. Kitamura, M. Tokunaga, and R. Noyori. J. Am. Chem. Soc. **115**, 144 (1993); (*h*) M. Kitamura, M. Tokunaga, and R. Noyori. Tetrahedron, **49**, 1853 (1993).
2. (*a*) H.B. Kagan. Asymmetric synthesis using organometallic catalysts. *In* Comprehensive organometallic chemistry. Vol. 8. *Edited by* G. Wilkinson, F.G.A. Stone, and E.W. Abel. Pergamon Press, Oxford. 1982. Chap. 53. p. 463; (*b*) H.B. Kagan. Bull. Soc. Chim. Fr. 846 (1988).
3. G. Consiglio and R.M. Waymouth. Chem. Rev. **89**, 257 (1989).
4. J.W. ApSimon and T.L. Collier. Tetrahedron, **42**, 5157 (1986).
5. S.L. Blystone. Chem. Rev. **89**, 1664 (1989).
6. I. Ojima, N. Clos, and C. Bastos. Tetrahedron, **45**, 6901 (1989).
7. J.K. Whitesell. Chem. Rev. **89**, 1581 (1989).
8. B. James, A.M. Joshi, P. Kvintovics, and R.M. Morris. *Edited by* D.W. Thorburn-Blackburn. Catalysis of organic reactions. Marcel Dekker, New York. 1990. p. 11.
9. R. Noyori. Tetrahedron, **50**, 4259 (1994).
10. A.N. Collins, G.N. Sheldrake, and J. Crosby (*Editors*). Chirality in industry. J. Wiley, New York. 1992.
11. R. Noyori. Asymmetric Catalysis. J. Wiley, New York. 1994.
12. S. Akutagawa. Appl. Catal. A, **128**, 171 (1995).
13. H.B. Kagan. Asymmetric synthesis. *Edited by* J.D. Morrison. Academic Press, 1985. p. 5.
14. H. Brunner. Top. Stereochem. **18**, 541 (1988).
15. L. Horner, H. Siegel, and H. Büthe. Angew. Chem. Int. Ed. Engl. **7**, 942 (1968).
16. (*a*) W.S. Knowles and M.J. Sabacky. J. Chem. Soc. Chem. Commun. 1445 (1968); (*b*) W.S. Knowles, M.J. Sabacky, and B.D. Vineyard. J. Chem. Soc. Chem. Commun. 10 (1972).
17. (*a*) T.P. Dang and H.B. Kagan. J. Chem. Soc. Chem. Commun. 481 (1971); (*b*) W. Dumont, J.C. Poulin, T.P. Dang, and H.B. Kagan. J. Am. Chem. Soc. **95**, 8285 (1973).
18. B.R. James, D. Wang, and R.F. Voigt. J. Chem. Soc. Chem. Commun. 574 (1975).
19. T. Ikariya, Y. Ischii, H. Kawano, T. Arai, M. Saburi, S. Yoshikawa, and S. Akutagawa. J. Chem. Soc. Chem. Commun. 922 (1985).
20. (*a*) R. Noyori, M. Ohta, Y. Hsiao, M. Kitamura, T. Ohta, and H. Takaya. J. Am. Chem. Soc. **108**, 7117 (1986); (*b*) M. Kitamura, T. Ohkuma, S. Inoue, N. Sayo, H. Kumobayashi, S. Akutagawa, T. Ohta, H. Takaya, R. Noyori, and K. Takaya. J. Am. Chem. Soc. **110**, 629 (1988); (*c*) T. Ohta, H. Takaya, and R. Noyori. Inorg. Chem. **27**, 566 (1988).
21. (*a*) R. Noyori and S. Hashiguchi. Acc. Chem. Res. **3**0 97 (1997); (*b*) J.P. Genêt. *In* Reductions in organic synthesis in A.C.S. symposium series, **641**, 31 (1996); (*c*) J.P. Genêt. *In* Advances in asymmetric synthesis. *Edited by* G.R. Stephenson. Chapman and Hall, London. 1996. p. 60; (*d*) J.P. Genêt. Acros Chim. Acta, **1**, 4 (1995); (*e*) H. Takaya, T. Ohta, and R. Noyori. Catalytic asymmetric synthesis. I. Ojima, New York. 1993; (*f*) R. Noyori and H. Takaya. Acc. Chem. Res. **23**, 345 (1990).
22. (*a*) R. Noyori, T. Ikeda, T. Ohkuma, M. Widhalm, M. Kitamura, H. Takaya, S. Akutagawa, N. Sayo, T. Saito, T. Taketomi, and H. Kumobayashi. J. Am. Chem. Soc. **111**, 9134 (1989); (*b*) R. Noyori, M. Tokunaga, and M. Kitamura. Bull. Chem. Soc. Jpn. **68**, 36 (1995), and refs. therein.
23. J.P. Genêt, C. Pinel, S. Mallart, S. Jugé, S. Thorimbert, and J.A. Laffitte. Tetrahedron: Asymmetry, **2**, 555 (1991).
24. (*a*) J.P. Genêt, C. Pinel, V. Ratovelomanana-Vidal, S. Mallart, X. Pfister, M.C. Caño de Andrade, and J.A. Laffitte. Tetrahedron: Asymmetry, **5**, 665 (1994); (*b*) J.P. Genêt, C. Pinel, V. Ratovelomanana-Vidal, S. Mallart, X. Pfister, L. Bischoff, M.C. Caño de Andrade, and J.A. Laffitte. Tetrahedron: Asymmetry, **5**, 675 (1994); (*c*) J.P. Genêt, V. Ratovelomanana-Vidal, M.C. Caño de Andrade, X. Pfister, P. Guerreiro, and J.Y. Lenoir. Tetrahedron Lett. **36**, 4801 (1995).
25. D. Blanc, J.C. Henry, V. Ratovelomanana-Vidal, and J.P. Genêt. Tetrahedron Lett. **38**, 6603 (1997).
26. A. Marinetti, J.P. Genêt, S. Jus, D. Blanc, and V. Ratovelomanana-Vidal. Chem. Eur. J. **5**, 1160 (1999).
27. V. Ratovelomanana-Vidal and J.P. Genêt. J. Organomet. Chem. **567**, 163 (1998).
28. (*a*) J.P. Genêt, X. Pfister, V. Ratovelomanana-Vidal, C. Pinel, and J.A. Laffitte. Tetrahedron Lett. **35**, 4559 (1994); (*b*) M.J. Burk, T.G.P. Harper, and C.S. Kalberg. J. Am. Chem. Soc. **117**, 4423 (1995).
29. (*a*) M. Kitamura, T. Ohkuma, M. Tokunaga, and R. Noyori. Tetrahedron: Asymmetry, **1**, 1 (1990). (*b*)R. Noyori. Asymmetric catalytic synthesis. J. Wiley, New York. 1994.
30. J.P. Genêt, M.C. Caño de Andrade, and V. Ratovelomanana-Vidal. Tetrahedron Lett. **36**, 2063 (1995).
31. S. Akutagawa. Chirality in industry. *Edited by* A.N. Collins, G.N. Sheldrake, and J. Crosby. J. Wiley, New York. 1992. Chap. 17. N. Sayo, N. Sano, H. Kumobayachi EP 519763A2 (1992).
32. K. Mashima, Y. Matsumura, K. Kusano, H. Kumobayashi, N. Sayo, Y. Hori, T. Ishizaki, S. Akutagawa, and H. Takaya. J. Chem. Soc. Chem. Commun. 609 (1991).
33. A. Girard, C. Greck, D. Ferroud, and J.P. Genêt. Tetrahedron Lett. **37**, 7967 (1996).
34. T. Nishi, M. Kitamura, T. Ohkuma, and R. Noyori. Tetrahedron Lett. **29**, 6327 (1988).
35. P.M. Wovkulich, K. Shankaran, J. Kiegiel, and M.R. Uskokovic. J. Org. Chem. **58**, 832 (1993).
36. K. Inoguchi and K. Achiwa. Synlett. **49**, xxx (1991).
37. U. Schmidt, V. Leitenberger, H. Griesser, J. Schmidt, and R. Meyer. Synthesis, **12**, 1248 (1992).
38. S.D. Rychnovsky and R.C. Hoye. J. Am. Chem. Soc. **116**, 1753 (1994).
39. E. Coulon, M.C. Cano de Andrade, V. Ratovelomanana-Vidal, and J.P. Genêt. Tetrahedron Lett. **39**, 6467 (1998).
40. P. Phannarath, S. Duprat de Paule, V. Ratovelomanana-Vidal, and J.P. Genêt. In press.

© 2000 NRC Canada

Free radicals and Lewis acid. Chelation-controlled radical allylations of substituted α-halo- or α-phenylseleno-β-alkoxy esters. The endocyclic effect.

B. Guérin, C. Chabot, N. Mackintosh, W.W. Ogilvie, and Y. Guindon

Abstract: The radical allylation of a series of α-halo or α-phenylseleno-β-alkoxy esters in the presence of $MgBr_2 \cdot OEt_2$ is reported and compared with analogous reactions under non-chelating conditions. The addition of $MgBr_2 \cdot OEt_2$ gives excellent selectivity favoring *anti* products; in some cases ratios >100:1 are obtained. Varying the substrate substituents reveals that these reactions are quite tolerant of alkyl functionalities at the β-position. Changes to the alkoxy function indicate that a chelate is involved in the reaction. The reactions are successful with secondary iodides, bromides, and phenylselenides, as well as tertiary iodides, which all give very high ratios under chelation control. Performing less well under the same conditions are substrates with a radical exocyclic to a tetrahydrofuran ring. EDTA titration is used to determine the amount of Mg^{2+} dissolved in the allylation reaction mixture, and ^{13}C NMR is employed to better define the nature of the complex formed (chelate or monodentate) prior to the reaction. Competition experiments suggest that the chelate and monodentate pathways are in competition for the radical allylation with allyltributyltin.

Key words: allylation, radicals, Lewis acid, stereoselectivity, 1,2-induction.

Résumé : Les allylations radicalaires, pour une série d'esters α-halo or phenylseleno-β-alkoxylés, en présence de $MgBr_2 \cdot OEt_2$, sont rapportées et comparées aux réactions analogues sans acide de Lewis. L'addition de $MgBr_2 \cdot OEt_2$ conduit à une excellente sélectivité en faveur des produits *anti*, pour certains cas, des ratios >100:1 ont été obtenus. Les variations des substituants sur les substrats montrent que ces réactions tolèrent une variété de fonctions alkyles en position β. Les changements de la fonction alkoxy suggèrent qu'un chelate est impliqué lors de la réaction. Les allylations fonctionnent bien avec les iodures, les bromures ainsi qu'avec les phénylsélenures secondaires. Les iodures tertiaires donnent des ratios très élevés en présence d'acide de Lewis. Les substrats générant un radical exocyclique à un cycle tetrahydrofurane donnent de moins bons résultats sous ces conditions. Le titrage à l'EDTA a été utilisé pour déterminer la quantité de Mg^{2+} dissous dans le mélange réactionnel lors de l'allylation, et les données RMN ^{13}C ont été utilisées pour mieux définir la nature des complexes formés (chelate ou monodentate) avant la réaction. Les expériences de compétition suggèrent que les deux chemins réactionnels, chelate et monodentate, sont en compétition pour l'allylation radicalaire avec l'allyle d'étain.

Mots clés : allylation, radicaux, acide de Lewis, stéréoselectivité, induction-1,2.

1. Introduction

This decade (1) has shown that free radical based reactions could be useful synthetic approaches for making acyclic molecules with high levels of diastereoselectivity and enantioselectivity. Significant levels of stereocontrol have been achieved in strategies involving pre-existing chiral centers (2, 3) or chiral auxiliaries (4). The scope of these reactions has been expanded by using mono (5) or bidentate Lewis acids (6, 7), solvent complexation (8), and intramolecular hydrogen bonding (9). Additionally, reagent control approaches employing chiral Lewis acid or chiral tin hydride have been recently devised (10).

We have been particularly interested in studying the reactivity of radicals flanked by an ester and a stereogenic center bearing a heteroatom in reactions involving hydrogen-atom

Received December 6, 1999. Accepted March 28, 2000. Published on the NRC Research Press Website on June 13, 2000.

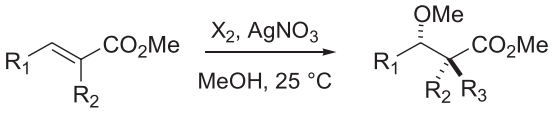
This article is dedicated to Professor Stephen Hanessian on the occasion of his 65th birthday. It is an accolade to my mentor, colleague, and friend, written in celebration of his many years of scientific achievement and the many more to come.

B. Guérin and Y. Guindon.[1,2] Institut de recherches cliniques de Montréal (IRCM), Bio-organic Chemistry Laboratory, 110, avenue des Pins Ouest, Montréal, QC H2W 1R7, Canada.
C. Chabot, N. Mackintosh, and W.W. Ogilvie. Bio-Méga/Boehringer Ingelheim Research, Inc., 2100 rue Cunard, Laval, QC H7S 2G5, Canada.

[1]Also at: Department of Pharmacology and Department of Chemistry, Université de Montréal, Montréal, QC H3C 3J7, Canada.
[2]Author to whom correspondence may be addressed. Telephone: (514) 987–5785. Fax: (514) 987–5789.
e-mail: guindoy@ircm.qc.ca.

 © 2000 NRC Canada

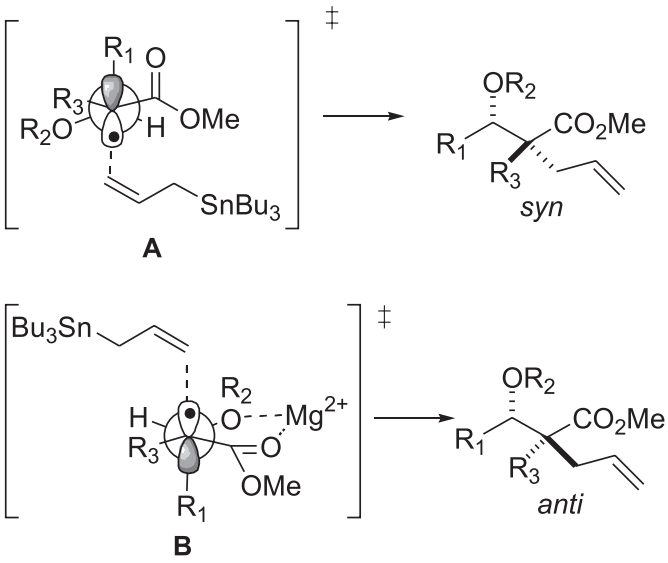
Table 1. Preparation of substrates **9**–**21** by alkoxy-etherification.



Entry	olefin	R_1	X_2	R_2	R_3	Substrate	Yield (%)
1	**1**	Me	I_2	H	I	**9**	60
2	**2**	i-Pr	I_2	H	I	**10**	38
3	**3**	c-C_6H_{11}	I_2	H	I	**11**	45
4	**4**	Ph	I_2	H	I	**12**	78
5	**4**	Ph	I_2	H	I	**13**[a]	61
6	**4**	Ph	Br_2	H	Br	**14**	70
7	**4**	Ph	PhSeBr[b]	H	PhSe	**15**	90
8	**5**[c]	Ph	I_2	I	H	**16**	77
9	**5**[c]	Ph	Br_2	Br	H	**17**	78
10	**5**[c]	Ph	PhSeBr[b]	PhSe	H	**18**	93
11	**6**	Ph	I_2	Me	I	**19**	66
12	**7**	Me	I_2	Me	I	**20**[d]	81
13	**8**	Et	I_2	Me	I	**21**[d]	42

[a]Benzylalcohol was used to give the β-benzyloxy-α-iodo-ester.
[b]PhSeBr was used with AgOTf.
[c]Methyl-*Z*-cinnamate was used to give *syn* substrate.
[d]Ethyl ester was used.

Scheme 1. (*a*) In absence of $MgBr_2 \cdot OEt_2$; (*b*) In presence of $MgBr_2 \cdot OEt_2$.



transfer (3), additions to olefins (7*e*), cyclizations (3*f*), and allylation reactions (3*b*, 3*g*, 7*b*). Our first studies dealing with the induction of new chiral centers on acyclic molecules, using free radical chemistry, spawned from unexpected experimental results. The realization that the planarity of radicals adjacent to an ester or amide group might resemble *Z*-enolates led to the hypothesis that allylic 1,3-strain (1*a*, 2*c*) could be one of the factors controlling stereoselectivity. The stereochemical outcome of the allylation reaction has been best rationalized by transition state **A** (Scheme 1*a*) (1, 2, 3, 4), which takes into account allylic 1,3-strain and electronic factors such as dipole–dipole repulsion (3) and hyperconjugative stabilization (3*e*). Thus, the *syn* isomer is the major compound obtained when such a radical intermediate, originating from the homolytic extrusion of a phenylseleno ether or a halogen, is reacted with allyltributyltin.

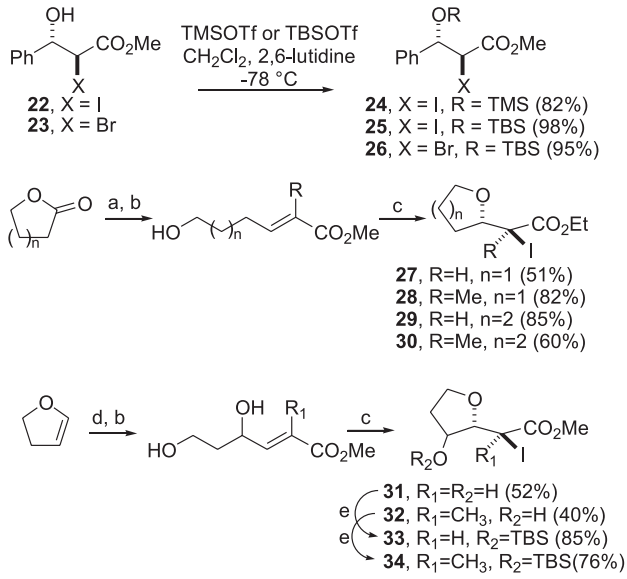
In response to this finding, our group hypothesized that a bidentate Lewis acid could, through complexation with the oxygen of the stereogenic center and the carbonyl of the ester, reposition the R_1 group onto the opposite face of the radical, thus allowing for a preferred attack on the top side leading to the *anti* product (Scheme 1*b*, transition state **B**). Our previous work in hydrogen-atom transfer reactions (7*a*, *e*) had shown that this approach could be feasible. Those findings inspired studies to show that the facial selectivity of a radical based allylation could be inverted (from *syn* to *anti*) through the simple expedient of adding $MgBr_2 \cdot OEt_2$ to the reaction mixture (7*b*). This strategy was further shown by both our group (7*c*) and Porter's group (11) to be successful in atom transfer reactions. Reported now are the full experimental details of chelation-controlled allylations of β-alkoxy esters, including studies on the importance of the stereochemistry of the starting material in such radical processes and on the possible formation of bidentate intermediates. Preliminary experiments that explain the need for an excess of $MgBr_2 \cdot OEt_2$ in the reaction and that elucidate further mechanistic details will also be presented.

2. Preparation of materials and standards

Secondary and tertiary iodides **9**–**13**, **16**, **19**–**21**, and bromides **14** and **17**, were prepared, by halo-etherification reaction, from the corresponding olefins **1**–**8** as shown in Table 1 (12, 13). Phenylselenides **15** and **18** were synthesized using a modification of the same method wherein AgOTf, a soluble silver salt, was used in place of $AgNO_3$. *Syn* substrates **16**–**18** were prepared from the appropriate *Z* olefin using

© 2000 NRC Canada

Scheme 2. (*a*) DIBAL-H, CH_2Cl_2, –78°C; (*b*) $Ph_3{=}C(R)CO_2Me$ (ethyl ester was used when R=Me), $PhCO_2H$, THF, reflux; (*c*) I_2, $NaHCO_3$, THF, 25°C; (*d*) *m*-CPBA, Et_2O, H_2O, 0 to 25°C; (*e*) TBSOTf, CH_2Cl_2, 2,6-lutidine, 0°C.



procedures analogous to those of the corresponding *anti* substrate (12). Silyl ethers **24**–**26** were readily derivated from the secondary alcohols (14) as described previously (Scheme 2) (15). Tetrahydrofurans **27**–**28** and tetrahydropyrans **29**–**30** were prepared in three steps as outlined in Scheme 2 (3*d*, 7*c*). DIBAL reduction of γ-butyrolatone or δ-valerolactone followed by Wittig olefination of the resultant lactols afforded the corresponding α,β-unsaturated esters. Cyclization of the olefins under kinetic conditions (I_2, $NaHCO_3$, THF, 25°C) (16) produced the expected iodoesters. Tetrahydrofurans **31** and **32** (17) were prepared by treating dihydrofuran with *m*-CPBA (H_2O–Et_2O, 82%) to give the hemiacetal that was then subjected to $Ph_3P{=}C(R)CO_2Et$ (THF, reflux). An iodocyclization reaction was done on the resulting compound. Protection of alcohols **31** and **32** (*t*-$BuMe_2SiOTf$, CH_2Cl_2, 2,6-lutidine, 0°C) gave either **33** or **34** (Scheme 2).

The relative configurations of the allylated products were established by independent synthesis and correlation of the NMR spectra (7*c*). In every case, the difference in chemical shift between the NMR resonances of the methylene protons in the allyl side chain (Δυ) for the *anti* diastereoisomers was greater than the Δυ values for the *syn* diastereoisomers. The chemical shifts of the resonances of the same hydrogens in the *anti* series were also consistently upfield to the resonances of the corresponding *syn* counterparts (18).

3. The radical-mediated allylations of α-halo- or α-phenylseleno-β-alkoxy esters

Treating a solution of 3-methyl-3-methoxy-2-iodopropionate **9** with allyltributyltin and 3 equivalents of $MgBr_2{\cdot}OEt_2$ gave a mixture of adducts in a 51:1 ratio favoring the *anti* product (Table 2, entry 1). Achieving interesting diastereoselectivity has been shown (vide infra) to require the presence of an excess of $MgBr_2{\cdot}OEt_2$. In the absence of $MgBr_2{\cdot}OEt_2$, substrate **9** showed a preference for the *syn* product, but poor selectivity was observed (entry 2). Other acyclic secondary iodides performed well under chelation-controlled conditions, affording *anti* isomers with excellent diastereofacial selectivity (entries 3, 5, 7). These substrates displayed a preference for the *syn* adduct in the absence of $MgBr_2{\cdot}OEt_2$ (entries 4, 6, 8). A greater selectivity was observed for substrate **12** when the reaction was conducted in toluene at –78°C (entry 8 versus 9).

Modifications to the β-alkoxy group (X) and their effects on the allylation reactions are shown in entries 7–15. Replacement of the methoxy group by a benzyloxy ether led to an erosion of *anti* diastereoselectivity under chelation-controlled conditions (entries 7 and 10). When the methoxy group was replaced by a silyl ether, the Lewis acid lost its influence in controlling the stereochemical outcome (entries 7, 8, 12–15). Generally, the steric congestion offered by the larger silyl groups (relative to Me) should preclude chelation of the oxygen with Lewis acid (19). As was hypothesized at the onset of this study, these results strongly suggest that the formation of cyclic intermediates, through $MgBr_2{\cdot}OEt_2$ complexation with the oxygens of the alkoxy and the carbonyl functions, is required in order to obtain *anti* adducts in this series of molecules.

In addition to *anti* iodide **12**, *anti* bromide **14** and *anti* phenylselenide **15** were also transformed into their corresponding allyl derivatives with excellent selectivity and yield when $MgBr_2{\cdot}OEt_2$ was present (entries 7, 16, and 18). For each substrate, the *anti* isomer was formed preferentially to the extent of 38:1, 19:1, and 65:1, respectively. Under the same conditions, *syn* iodide **16** led to reduced levels of diastereoselectivity and gave a 5:1 ratio in favor of the *anti* product (entry 20). By contrast, ratios greater than 20:1 were observed for *syn* bromide **17** and *syn* phenylselenide **18** (entries 22 and 24). Without Lewis acid, the allylation reactions favored the *syn* isomer (entries 8, 17, 19, 21, 23, and 25) in a consistent ratio of approximately 5:1. One should note that the presence of Lewis acid usually reverses the facial bias and is accompanied by a significant increase in diastereoselectivity (entries 7, 16, and 18 versus 8, 17, and 19, respectively).

Tertiary iodides displayed excellent diastereoselectivity in chelation-controlled allylations (entries 26, 28, and 30). Since asymmetric quaternary centers are difficult to form, these reactions clearly have interesting synthetic utility (20). Compared to the secondary iodides, the tertiary iodides in the absence of $MgBr_2{\cdot}OEt_2$ showed lower reactivity[3] but slightly higher diastereoselectivity favoring the *syn* product (entries 2, 4, 6, and 8 versus 27, 29, and 31).

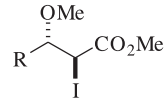
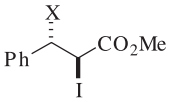
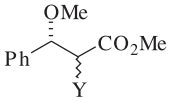
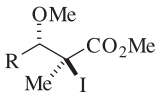
Assuming that the cyclic intermediate bearing a carbon-based radical was at the origin of the *anti* diastereoselectivity noted for the chelation-controlled allylation (the endocyclic effect) (Scheme 1*b*), we were anxious to evaluate the effect of a ring adjacent to the radical. Indeed, a bicyclic intermediate had to then be considered in this scenario.

Table 3 lists some preliminary results from this study. Note that entries 1 and 3 indicate a lower preference for the

[3] The lower reactivity is reflected by longer reaction times, even when conducted in hexanes at reflux.

© 2000 NRC Canada

Table 2. Radical allylation of various substrates under chelation and non-chelation control.

Entry	Substrate	Conditions[a]	Products		Ratio			Yield
			anti	*syn*	*anti*	:	*syn*	(%)
								
1	**9** : R=Me	A	**35**	**36**	51	:	1	79
2	**9** : R=Me	B	**35**	**36**	1	:	3	73
3	**10** : R=*i*Pr	A	**37**	**38**	>100	:	1	51
4	**10** : R=*i*Pr	B	**37**	**38**	1	:	3.3	82
5	**11** : R=c-C_6H_{11}	A	**39**	**40**	>100	:	1	95
6	**11** : R=c-C_6H_{11}	B	**39**	**40**	1	:	3.5	84
								
7	**12** : X=OMe	A	**41**	**42**	38	:	1	80
8	**12** : X=OMe	B[b]	**41**	**42**	1	:	5	82
9	**12** : X=OMe	B[c]	**41**	**42**	1	:	17	75
10	**13** : X=OBn	A	**43**	**44**	5	:	1	52
11	**13** : X=OBn	B[b]	**43**	**44**	1	:	10	60
12	**24** : X=OTMS	A	**45**	**46**	1	:	4	78
13	**24** : X=OTMS	B	**45**	**46**	1	:	3	84
14	**25** : X=OTBS	A	**47**	**48**	1	:	8	90
15	**25** : X=OTBS	B[b]	**47**	**48**	1	:	13	86
								
16	**14** : Y=Br (*anti*)	A	**41**	**42**	19	:	1	78
17	**14** : Y=Br (*anti*)	B[b]	**41**	**42**	1	:	5	73
18	**15** : Y=SePh (*anti*)	A	**41**	**42**	65	:	1	90
19	**15** : Y=SePh (*anti*)	B[b]	**41**	**42**	1	:	5	63
20	**16** : Y=I (*syn*)	A	**41**	**42**	5	:	1	69
21	**16** : Y=I (*syn*)	B[b]	**41**	**42**	1	:	6	84
22	**17** : Y=Br (*syn*)	A	**41**	**42**	20	:	1	80
23	**17** : Y=Br (*syn*)	B[b]	**41**	**42**	1	:	6	82
24	**18** : Y=SePh (*syn*)	A	**41**	**42**	38	:	1	76
25	**18** : Y=SePh (*syn*)	B[b]	**41**	**42**	1	:	6	86
								
26	**19** : R=Ph	A	**49**	**50**	>100	:	1	76
27	**19** : R=Ph	B	**49**	**50**	1	:	16	75
28	**20** : R=Me[d]	A	**51**	**52**	>100	:	1	65
29	**20** : R=Me[d]	B	**51**	**52**	1	:	4.5	44
30	**21** : R=Et[d]	A	**53**	**54**	90	:	1	80
31	**21** : R=Et[d]	B	**53**	**54**	1	:	4.8	45

[a]A:2.0 equiv of allylSnBu$_3$, 3.0 equiv of MgBr$_2$·OEt$_2$, 0.2 equiv of Et$_3$B, CH$_2$Cl$_2$, –78°C. B:2.0 equiv of allylSnBu$_3$, 0.2 equiv of AIBN, hexanes, reflux.

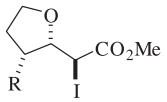
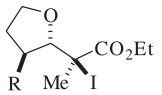
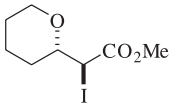
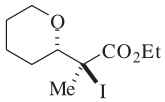
[b]2.0 equiv of allylSnBu$_3$, 0.2 equiv of Et$_3$B, CH$_2$Cl$_2$, –78°C.

[c]2.0 equiv of allylSnBu$_3$, 0.2 equiv of Et$_3$B, toluene, –78°C.

[d]Ethyl ester was used.

© 2000 NRC Canada

Table 3. Radical allylation of tetrahydrofuran and tetrahydropyran derivatives under chelation and non-chelation control.

Entry	Substrate	Conditions[a]	Products *anti*	Products *syn*	Ratio *anti* : *syn*	Yield (%)
						
1	**27** : R = H	A	**55**	**56**	5 : 1	91
2	**27** : R = H	B	**55**	**56**	1 : 6	90
3	**33** : R = OTBS	A	**57**	**58**	6 : 1	80
4	**33** : R = OTBS	B	**57**	**58**	1 : 51	74
						
5	**28** : R = H	A	**59**	**60**	1 : 1	82
6	**28** : R = H	B	**59**	**60**	1 : 10	81
7	**34** : R = OTBS	A	**61**	**62**	7 : 1	70
8	**34** : R = OTBS	B	**61**	**62**	1 : 16	65
						
9	**29**	A	**63**	**64**	18 : 1	84
10	**29**	B	**63**	**64**	1 : 10	89
						
11	**30**	A	**65**	**66**	27 : 1	54
12	**30**	B	**65**	**66**	1 : 18	77

[a]A:2.0 equiv of allylSnBu$_3$, 3.0 equiv of MgBr$_2$·OEt$_2$, 0.2 equiv of Et$_3$B, CH$_2$Cl$_2$, –78°C. B:2.0 equiv of allylSnBu$_3$, 0.2 equiv of AIBN, hexanes, reflux.

anti product when the carbon bearing the radical was adjacent to a tetrahydrofuran (THF) ring and when MgBr$_2$·OEt$_2$ was present. This trend is magnified in the tertiary iodide series (entries 1 and 3 versus 5 and 7), where a 7:1 ratio favoring the *anti* isomer was the best selectivity obtained. In contrast, substrates bearing a tetrahydropyran (THP) ring α to the radical gave excellent diastereoselectivity under chelation-controlled conditions (entries 9 and 11). From the THF and THP substrates, *syn* isomers were obtained in good ratios in the absence of Lewis acid, considering that the reactions were performed in hexanes at reflux (entries 2, 4, 6, 8, 10, and 12). The bicyclic intermediate chelate with two 6-membered rings was clearly more efficient in inducing *anti* diastereoselectivity than the bicyclic intermediate with one 5- and one 6-membered ring.

4. The role of MgBr$_2$·OEt$_2$. Determination of the amount of Mg^{2+} present in the allylation reaction by EDTA titration

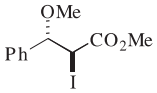
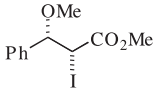
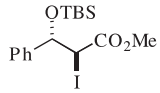
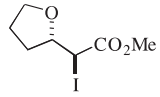
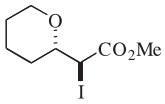
With conditions for the chelation-controlled allylation optimized, we turned our attention to the problem of why an excess of MgBr$_2$·OEt$_2$ (3 equivalents) was needed to maximize diastereoselectivity. Table 4 (entries 1–3) shows that 0.25, 1, and 3 equivalents of MgBr$_2$·OEt$_2$, complexed with iodide **12,** gave ratios of 1.6:1, 7:1, and 38:1, respectively; however, no increase in ratio was noted with 5 equivalents of MgBr$_2$·OEt$_2$ (see entry 4). The results were surprising because the subequimolar amount of MgBr$_2$·OEt$_2$ was accompanied by insoluble material in the reaction medium. We had, of course, expected that one equimolar amount of Lewis acid would be sufficient for the chelation (vide infra), but our assumption had not taken into account the possibility of other competing intermediates.

To shed some light on the above results, we decided to determine the amount of Mg^{2+} actually present in the reaction mixture. The first step in doing so was to allow the Lewis acid to equilibrate at –78°C in the presence of iodide **12** (5 mL of 0.1 M solution) and allyltributyltin. After 10 min, 3 mL of the solution was filtered and analyzed for magnesium content by EDTA titration (21). Et$_3$B was added to the remaining solution to measure allylation efficacy and diastereoselectivity.

The amount of Mg^{2+} dissolved in solution increased concomitantly with the amount of MgBr$_2$·OEt$_2$ introduced at the beginning of the reaction (entries 1, 2, and 3). A maximum of 1.6 equivalents of dissolved Mg^{2+} was reached in the reaction containing 3 equivalents of MgBr$_2$·OEt$_2$ (entry 3). Concurrently, the *anti*:*syn* ratio of the allylated products steadily increased, giving a maximum selectivity of 38:1

© 2000 NRC Canada

Table 4. Determination of the amount of magnesium dissolved in allylation reaction mixtures by filtration and EDTA titration.

Entry	Substrate	Equivalents $MgBr_2 \cdot OEt_2$ added[a]	Equivalents Mg^{2+} in solution[b]	Ratio *anti* : *syn*
				
1	**12**	0.25	0.18	1.6 : 1
2	**12**	1.0	0.72	7 : 1
3	**12**	3.0	1.63	38 : 1
4	**12**	5.0	1.57	30 : 1
5	none	3.0	0.25[c]	
				
6	**16**	3.0	1.64	5 : 1
				
7	**25**	3.0	0.99	1 : 8
				
8	**27**	3.0	0.88	4.6 : 1
				
9	**29**	3.0	1.85	18 : 1

[a]Equivalents of $MgBr_2 \cdot OEt_2$ relative to the amount of substrate.

[b]Equivalents of Mg^{2+} measured relative to the amount of substrate.

[c]Experiment run under identical conditions relative to reactions with substrate present.

when the 3 equivalents of $MgBr_2 \cdot OEt_2$ were used. More than 3 equivalents of $MgBr_2 \cdot OEt_2$ did not increase further either the amount of Mg^{2+} in solution or the allylation ratio (entry 4).

In the absence of the substrate, the solubility of Mg^{2+} in CH_2Cl_2 at –78°C, relative to the amount of substrate normally used, was found to be 0.25 equivalent (entry 5). Note that the number of equivalents reported is always relative to the number of mmoles of substrate normally used. From the above results can be concluded that the intrinsic solubility of $MgBr_2 \cdot OEt_2$ in CH_2Cl_2 is low and that the substrate brings into solution an additional equivalent of Mg^{2+}, suggesting a strong interaction between the substrate and the Lewis acid. Note that there is a ca 30% excess of the added $MgBr_2 \cdot OEt_2$ that does not go into solution (entries 1 and 2), and that this amount in suspension can vary depending on the source of Lewis acid.[4] However, the ratio being the same with or without filtration strongly indicates that the insoluble materials have no effect on the outcome of the reactions.

This experimental protocol was repeated for *syn* isomer **16**, which gave the same amount of Mg^{2+} dissolved in solution but much less impressive diastereoselectivity, as already noted (entry 6).

One equivalent of Mg^{2+} was found for silyl compound derivative **25** in the presence of $MgBr_2 \cdot OEt_2$ compared to 0.25 equivalent without the substrate (entry 7 versus 1). Therefore, around 0.7 equivalent was brought in solution by the substrate. Qualitatively, this result is not so surprising. The Lewis acid can easily form a monodentate complex with substrate **25** since the latter presents a Lewis base functionality, the ester.

Similarly, THF derivative **27** (entry 8) and silyl compound **25** (entry 7), which formed a monodentate complex, extracted almost the same amount of Mg^{2+}. This contrasts the result for THP **29**, which brought into solution 1.85 equivalents of Mg^{2+} (entry 9). This is as much as methyl ether **12**, the bidentate chelate, brought. One has to remember that THF derivative **27** gave a much poorer ratio in favor of the *anti* product than THP derivative **29** afforded (entries 8 versus 9).

These measurements of Mg^{2+} dissolved in solution indicate that an equimolar complex with $MgBr_2 \cdot OEt_2$ is formed

[4]The material in suspension could be less soluble magnesium salts.

© 2000 NRC Canada

Table 5. ^1H and ^{13}C data of $MgBr_2 \cdot OEt_2$ in CD_2Cl_2 at –23 and 23°C in the presence and absence of **12**.

Entry	Mixture	Temperature (°C)	δ CH_2CH_3 (ppm)		δ CH_2CH_3 (ppm)	
			^1H	^{13}C	^1H	^{13}C
1	**12** + $MgBr_2 \cdot OEt_2$	–23	3.97	66.1	1.30	14.0
2	$MgBr_2 \cdot OEt_2$	–23	3.90	66.4	1.29	14.2
3	OEt_2	–23	3.40	65.9	1.12	15.3
4	**12** + $MgBr_2 \cdot OEt_2$	23	3.89	66.7	1.31	14.8
5	$MgBr_2 \cdot OEt_2$	23	3.80	66.7	1.29	14.8
6	OEt_2	23	3.44	66.1	1.15	15.5

with iodides **12** and **29,** which suggests a chelation. Such a condition seems to be essential for achieving good *anti* diastereoselection in this series of substrates. However, it may not be a sufficient condition, considering the modest diastereoselectivity noted for *syn* iodide **16**. This realization led us to another set of experiments, but this time using ^1H and ^{13}C NMR studies.

5. NMR studies of $MgBr_2 \cdot OEt_2$ complexes

The first consideration for this study was whether or not diethyl ether was present as a ligand on magnesium. Table 5 shows the ^1H and ^{13}C chemical shifts of diethyl ether measured alone (entries 3 and 6), in solution as part of the $MgBr_2 \cdot OEt_2$ (entries 2 and 5), or in chelate form using iodide **12** (entries 1 and 4). The latter two results being the same indicates that most if not all of the diethyl ether is still attached to the magnesium following the formation of complexes with **12**, regardless of temperature (entries 1–2, 4–5).

Previous studies done by Eliel (22), on chelates as intermediates in nucleophilic additions to α- and β-alkoxy ketones, have suggested that a strong chelation is consistent with a greater extent of change in the ^{13}C chemical shift of the carbonyl. Table 6 presents comparable NMR studies that consider various substrates in the presence of 3 equivalents of $MgBr_2 \cdot OEt_2$.

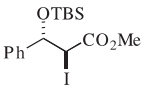
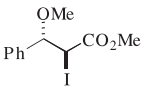
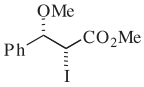
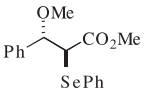
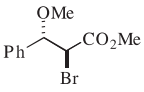
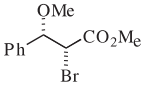
As seen in entry 1, the carbonyl signal of the ester for silyl ether **25** shifted only slightly downfield (2.7 ppm) when Lewis acid was present in the reaction, suggesting a preference for the formation of a monodentate complex with the ester. The difference in carbonyl chemical shift was significantly higher for methyl ether **12** (7.5 ppm), which is consistent with chelation (entry 2). The magnitude of these shifts concurs with Eliel's results (22).

Syn iodide **16** gave a shift of 4.8 ppm. As already shown by the solubility experiments, s*yn* iodide **16** formed a complex with $MgBr_2 \cdot OEt_2$ strong enough to bring into solution an amount of Lewis acid equivalent to that obtained from *anti* iodide **12** (Table 4, entry 6 versus 3). Yet, the ^{13}C data suggests that the *syn* iodide chelate should be qualitatively less strong than the one formed by the *anti* iodide (4.8 versus 7.5, Table 6, entries 2–3).[5] This would be consistent with the lower stereocontrol observed for **16** in chelation-controlled radical allylations.

Anti phenylselenide **15**, as well as bromides **14** and **17**, showed large displacements of the carbonyl signal upon the addition of $MgBr_2 \cdot OEt_2$ (entries 4–6) that correlate with strong chelation and high selectivity in the allylation. It would seem that the greater the carbonyl signal shift, the greater the *anti* preference; but this statement would need to be validated by additional experiments.

So far, the solubility experiments have shown that both monodentate and bidentate species bring Mg^{2+} in solution. The NMR studies have facilitated the ability to differentiate

Table 6. ^{13}C data of β-alkoxyesters in presence of saturating amount of $MgBr_2 \cdot OEt_2$ in CD_2Cl_2 at –23°C.

Entry	Substrate	Dd[a] C=O	Ratio[b] *anti* : *syn*
1	 **25**	2.7	1 : 8
2	 **12**	7.5	38 : 1
3	 **16**	4.8	5 : 1
4	 **15**	8.4	65 : 1
5	 **14**	6.4	19 : 1
6	 **17**	5.7	20 : 1

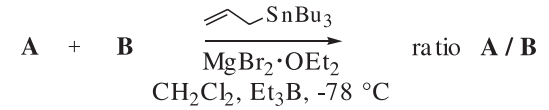
[a]Chemical shift of substrate with 3 equiv of $MgBr_2 \cdot OEt_2$ – chemical shift of substrate.

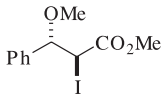
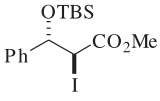
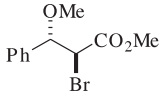
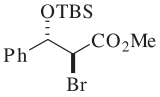
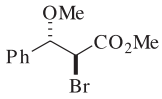
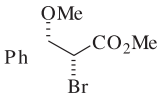
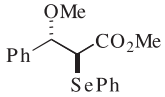
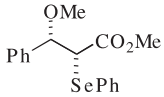
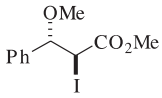
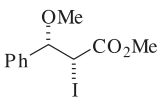
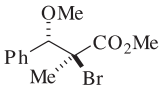
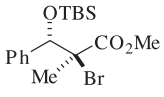
[b]See Table 1.

[5] The study of the THF derivative **27** and the THP derivative **29** under the same conditions did not give spectra of sufficient quality to be used in this study.

© 2000 NRC Canada

Table 7. Competition experiments.



Entry	Substrate **A**	Substrate **B**	Equivalents $MgBr_2 \cdot OEt_2$	Ratio[a] **A** : **B**
				
1	**12**	**25**	0	1 : 1.8
2	**12**	**25**	3	1 : 2
				
3	**14**	**26**	0	1 : 1
4	**14**	**26**	3	1 : 2
				
5	**14**	**17**	0	1 : 1
6	**14**	**17**	3	1 : 1
				
7	**15**	**18**	0	3 : 1
8	**15**	**18**	3	1 : 1
				
9	**12**	**16**	0	5 : 1
10	**12**	**16**	3	2 : 1
				
11	**67**	**68**	0[b]	1 : 1
12	**67**	**68**	5[b]	8 : 1

[a]0.5 equiv of $allylSnBu_3$, 0.5 equiv of substrates **A** and **B**.

[b]reaction was performed with Bu_3SnH, see ref 7e.

between these species prior to the reaction. Remaining to be determined is whether or not the species participate competitively in the establishment of the final product distribution resulting from the allylation reaction. Preliminary experiments involving competition reactions have been designed to shed some light in this regard. (Vide infra.)

6. Competition reactions

All of the competition experiments were performed with two substrates of equimolar amounts, which were dissolved in CH_2Cl_2 together with allyltributyltin in either the absence or presence of $MgBr_2 \cdot OEt_2$ (3 equivalents). Only half an equivalent of allyltributyltin was used to obtain 50% conversion to the allylated products. NMR spectra of the crude reaction isolates were recorded to determine the relative conversion of each reactant. The results of these experiments are summarized in Table 7.

As seen in entry 1, a 1:1.8 ratio of unreacted methyl ether **12** to unreacted silyl ether **25** was noted, indicating that the methyl ether reacted faster than the silyl ether in the absence of Lewis acid. Similar results were obtained when $MgBr_2 \cdot OEt_2$ was present in the reaction mixture (entry 2). For the analogous bromide series, the consumption of methyl ether **14** (bidentate) was found to be slightly higher than that of silyl ether **26** (monodentate) in the presence of

© 2000 NRC Canada

$MgBr_2 \cdot OEt_2$ (entry 4). In the control experiment (entry 3), performed in the absence of Lewis acid, species **14** and **26** reacted at the same rate.

Next, the relative stereochemistry of bromides, selenides, and iodides was examined. In the presence of Lewis acid, *anti* and *syn* bromides **14** and **17** reacted at the same rate, as did the corresponding selenides **15** and **18** (entries 6 and 8). *Syn* iodide **16** reacted faster than *anti* iodide **12** both in the presence and absence of Lewis acid (entries 9 and 10). Notably, both *syn* selenide **18** and *syn* iodide **16**[6] reacted faster than their *anti* counterparts in the control experiments (entries 7 and 9). This result is without explanation at this time.

Two reactions were then done in parallel with *anti* silyloxy iodide **25** under standard conditions. The sole variable was $MgBr_2 \cdot OEt_2$, which was present in only one of the reactions. Comparable yields of allylated products (80%) were repeatedly obtained; however, the time to complete the reaction was shorter when Lewis acid was present.

Apparent from these studies is that the chelate intermediate, proposed in the case of the methyl ethers, does not have a significant advantage from a reactivity standpoint over the silyl ethers, which reacted only as monodentate complexes or free substrates. As demonstrated by entries 4 and 12, under chelation-controlled conditions, the allylation reaction differs from the hydrogen-atom transfer reactions (7*e*) with the bromide substrates. In the latter case, silyl ether **68** was consumed eight times faster than methyl ether **67**, indicating that the bidentate pathway was at a strong disadvantage.

7. Discussion

The chelation of the Lewis acid to the β-alkoxy ester is envisioned as the initial step of the allylation process (Scheme 3).[7] Subsequent homolytic cleavage of the α-halide or α-phenylselenide by attack of the tin radical ($Bu_3Sn\cdot$) gives a cyclic free-radical intermediate, which may benefit from the endocyclic (chelated) effect. Note that variations in the alkoxy function, and their ultimate effect on the ratio, support strongly the involvement of an endocyclic radical (Table 2, entries 7–15). The presence of the chelate prior to the generation of the radical is also supported by our ^{13}C NMR studies. The chelate is strong enough to bring into solution an equimolar amount of magnesium.

Once formed, the chelated radical may exist in two conformers, **75** and **76**, that lead to transition states **E** and **F**, respectively. The *anti* predictive transition state **E** should be favored over the *syn* predictive **F** on both electronic and steric grounds. Electronically, the electron-poor radical should be better stabilized, through hyperconjugation, by the overlap of the C—R (R = alkyl) bond in **E** than by that of the C—H bond in **F** (3*e*). From a steric standpoint, when R_2 is a methyl group, an additional allylic 1,2-strain between R and R_2 should increase the energy of transition state **F** relative to that of **E**.

Two other transition states should also be examined. Transition state **C** considers the radical in the absence of Lewis acid, while transition state **D** reflects the radical in a monodentate complex form. Both **C** and **D** are *syn* predictive transition states.

The rate of halogen abstraction by an electropositive tin radical should be enhanced by the presence of an adjacent electron-withdrawing group, such as an ester. A more electrophilic ester, obtained via coordination with a Lewis acid, should further facilitate the abstraction rate. The rate of addition should also be improved by the reaction of a more electrophilic radical with an electron rich double bond, such as the one on the allyltributyltin. Therefore, transition state **E** should be of lower energy than **C**. Indeed, allylation was apparently faster with $MgBr_2 \cdot OEt_2$ in the parallel reactions performed for the competition experiments.

One should note that transition states **D** and **E** both benefit from activation by the Lewis acid. The fact that the methoxy and silyloxy derivatives reacted at comparable rates in competitive experiments suggests the possibility that the monodentate acyclic pathway could actually be as rapid as, and therefore an alternative to, the cyclic pathway. As depicted in Scheme 3, a potential equilibrium could exist between **74** and **75** (or **70** and **71**). After all, these species differ by only a simple folding of the substrate molecule. If such equilibrium were to exist, the difference in energy between transition states **D** and **E** would likely dictate the outcome of the reaction.

The comparable reaction rates of the silyloxy and methoxy derivatives suggest that transition states **D** and **E** are of similar energy in the allylation. This result contrasts that of competition experiments involving hydrogen-atom transfer reactions, which showed the monodentate pathway to be favored over the bidentate (7*e*), indicating that a transition state similar to **D** would be lower in energy than a transition state analogous to **E** when tributyltin hydride is involved. It should be noted that the major product obtained originated, in both cases, from the attack on the top face of the radical (transition state **E**) in the presence of $MgBr_2 \cdot OEt_2$.

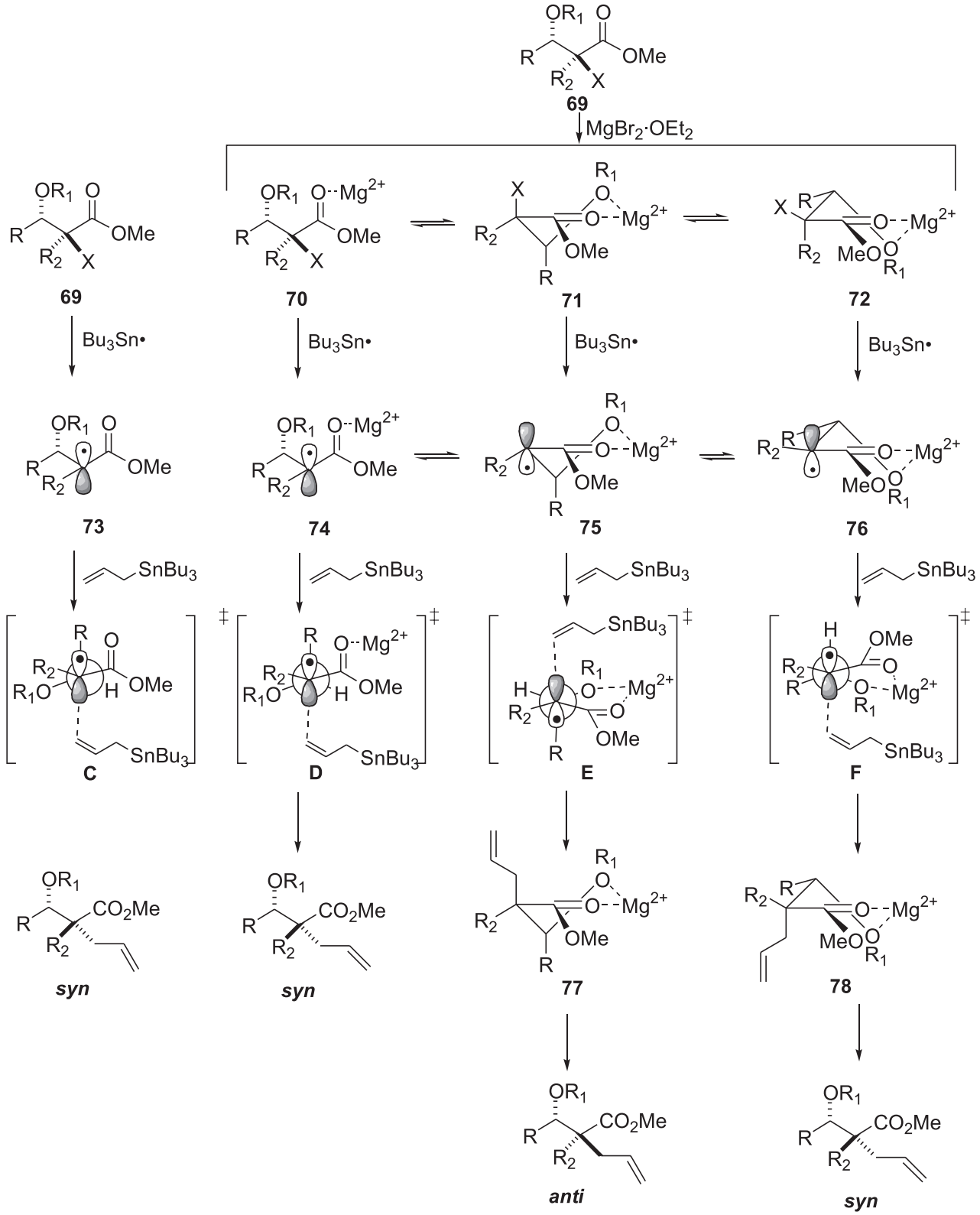
It should be remembered that significant levels of selectivity and differences in ratios, depending upon the stereochemistry of the halides and selenides (precursors to the same radical), were noted for the allylation reactions (vide supra). These results, along with those obtained from competition experiments, are more consistent with the equilibrium between **74** and **75** being rather slow, which suggests that the reactions are dependent upon the pre-existing mixture of complexes **70**, **71**, and **72**.

This dependency can explain the low selectivity obtained for the THF derivatives. A potential rationale illustrated by Scheme 4 shows that, for these substrates, the formation of a bicyclic intermediate may be impaired by the development of eclipsing interactions between the C–O bond and an Mg–Br bond in the *cis* bicyclo complex. An additional eclipsing interaction could be observed between the C–I bond and the Mg–Br (or $Mg–OEt_2$) bond if the geometry of the magnesium is either square planar pyramidal or bipyramidal trigonal. Such interaction implies that the preexisting complex mixture could have contained monodentate complexes or uncomplexed substrates. The smaller amount of Mg^{2+} found in solution supports this argument. By contrast, less

[6] The ratios were also verified by ^1H NMR prior to the allylation.
[7] The ligands on Mg^{2+} have been excluded for simplicity.

© 2000 NRC Canada

Scheme 3.

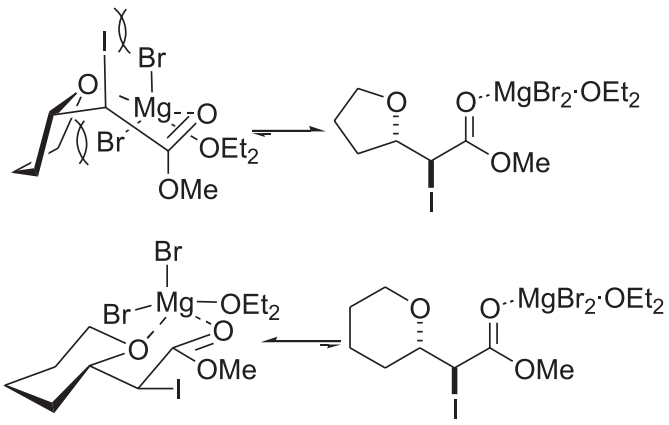


steric interaction is present for the bicyclo complex with THP. The pre-equilibrium for the THP substrates seems to favor the chelate formation. This conclusion is further supported by the high level of selectivity obtained for this series and by the amount of Mg^{2+} found in solution.

This discussion may not have sufficiently appreciated an important contributor: the $MgBr_2 \cdot OEt_2$. What is the nature of the complexes formed with the alkoxy esters and the $MgBr_2 \cdot OEt_2$? For instance, could there be two alkoxy esters serving as ligands on a magnesium (23) for the monodentate

© 2000 NRC Canada

Scheme 4.



complex (**70′**, Scheme 5)?[7] If so, an excess of $MgBr_2 \cdot OEt_2$ could then be important in the pre-equilibrium phase for assuring the formation of another species involving one alkoxy ester as a ligand, depicted as bidentate complex **71** (Scheme 3). This would explain why the equilibrium between **74** and **75** is slow. Indeed, a ligand (another substrate) might have to be displaced in order for **74′** to reach **75**; a process that may not be fast enough to allow for kinetic selection between the two pathways (Scheme 4).

Only recently has the structure of $MgBr_2 \cdot OEt_2$ been resolved (24). The structure of complexes generated by alkoxy esters and $MgBr_2 \cdot OEt_2$ remain to be better defined. This is the topic of ongoing research.

8. Conclusion

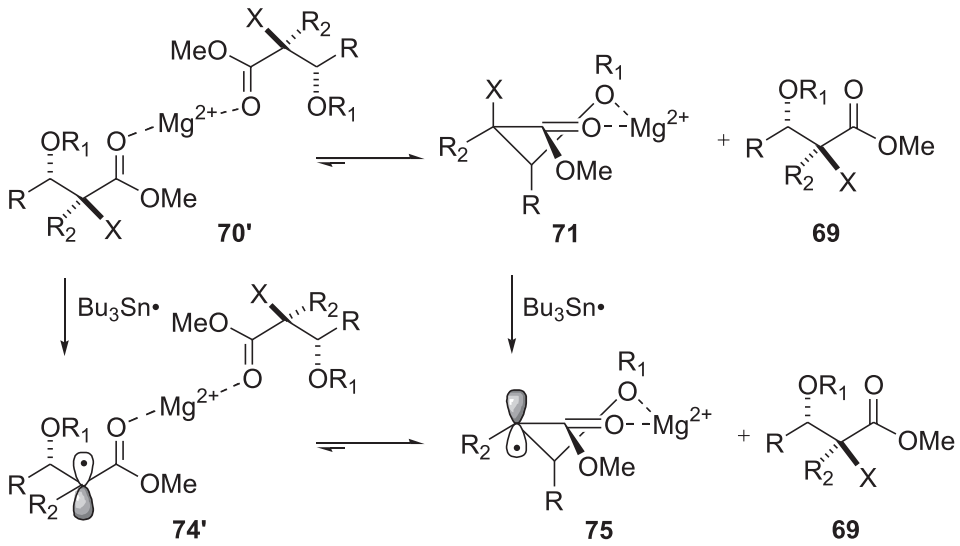
The described chemistry represents a significant advance in the field of stereocontrol in radical reactions. Our studies of substituent effects clearly establish the scope and limitations of the chelation-controlled radical allylation of α-halo or α-phenylseleno-β-alkoxy esters. This reaction tolerates a wide variety of substitutions and, except for THF and *syn* iodide substrates, gives a high level of diastereoselectivity favoring *anti* products. This is true even for secondary iodides, bromides, and phenylselenides, as well as tertiary iodides. The requirement of radical initiation and the fact that the reaction can be inhibited are indicative of a free radical process. Other types of acyclic radical-based reactions are presently being evaluated. The influence of Lewis acid on the outcome of these reactions will also be studied.

9. Experimental section

General methods

All reactions requiring anhydrous conditions were conducted under a positive nitrogen atmosphere in oven-dried glassware using standard syringe techniques. The anhydrous solvents were purchased from Aldrich and were used as received. i-Pr_2NH and Et_3N were freshly distilled from CaH_2 under N_2 atmosphere. Allyltributyltin and triethylborane (1 M solution in hexane) were also purchased from Aldrich and used as received. Flash chromatography was performed on Merck silica gel 60 (0.040–0.063 mm) using nitrogen pressure. Analytical thin-layer chromatography (TLC) was carried out on precoated (0.25 mm) Merck silica gel F-254 plates. The uncorrected melting points were determined on an electrothermal melting point apparatus. NMR spectra were recorded via Bruker AC200, AMX300, ARX400, or Varian VXR-400S spectrometers, with chemical shifts reported relative to residual chloroform at 7.26 ppm. IR spectra were recorded on a Perkin-Elmer 781 spectrophotometer. CI and EI mass spectra were recorded on an MF 50 TATC instrument operating at 70 eV. FAB mass spectra were performed on a VG AutospecQ. Capillary GC analyses were performed on a Shimadzu GC-9AM instrument or a HP 6890 instrument using 0.25 mm × 30 m Supelcowax™10 and SE-30 columns.

Scheme 5.



© 2000 NRC Canada

Preparation of starting materials

The preparation and characterization data of **9**–**12** (7*d*), **14**–**21** (7*d*), **25** (7*d*), **27**–**30** (3*d*, 7*d*), and **34** (7*a*) have been reported previously.

*Methyl (±)-(2*S**,3*S**)-2-iodo-3-benzyloxy-3-phenylpropanoate (**13**)*: To a solution of methyl cinnamate (381 mg, 2.35 mmol) in benzylalcohol (3.5 mL) were added successively $AgNO_3$ (305 mg, 2.82 mmol) and iodine (710 mg, 2.82 mmol). The reaction mixture was stirred at room temperature in the dark for 24h, then filtered through celite and concentrated. The residue was taken up in EtOAc and washed with 10% $Na_2S_2O_3$, water, and brine. The organic layer was dried ($MgSO_4$), filtered, and concentrated to afford a residue, which was then purified by flash chromatography (CH_2Cl_2) to afford pure iodide **13** as a white solid (568 mg, 61%); mp 50–51°C; ^{1}H NMR (400 MHz, $CDCl_3$) δ 3.77 (s, 3H), 4.31 (d, *J* = 10.6 Hz, 1H), 4.40 (d, *J* = 10.6 Hz, 1H), 4.45 (d, *J* = 11.3 Hz, 1H), 4.80 (d, *J* = 11.3 Hz, 1H), 7.18–7.41 (m, 10H); ^{13}C NMR (100 MHz, $CDCl_3$) δ 24.80, 52.99, 71.89, 82.89, 127.85, 127.97, 128.33, 128.49, 129.08, 137.46, 137.58, 170.80; IR ($CHCl_3$) 3030, 2950, 1740, 1455 cm^{-1}; MS (FAB) 397 (MH, 8), 289 (35), 154 (49), 91 (100); HRMS calcd. for $C_{17}H_{18}O_3I$ (MH): 397.0301, found: 397.0290 (2.7 ppm). Anal. calcd. for $C_{17}H_{17}IO_3$: C 51.53, H 4.32; found: C 51.36, H 4.26.

*Methyl (±)-(2*S**,3*S**)-2-iodo-3-[(trimethylsilyl)oxy]-3-phenylpropanoate (**24**)*: To a solution of iodohydrin **22** (7*d*) (713 mg, 2.32 mmol) and 2,6-lutidine (540 μL, 4.64 mmol) in CH_2Cl_2 (25 mL) at –78°C was added slowly trimethylsilyl trifluoromethanesulfonate (670 μL, 3.48 mmol). After the reaction was judged complete by TLC, the mixture was diluted with ether and washed with water, saturated NH_4Cl, and brine. Drying over $MgSO_4$ followed by flash chromatography (4% EtOAc in hexanes) afforded silyl ether **24** as a colorless oil (720 mg, 82%). ^{1}H NMR (300 MHz, $CDCl_3$) δ –0.05 (s, 9H), 3.81 (s, 3H), 4.37 (d, *J* = 10.2 Hz, 1H), 5.05 (d, *J* = 10.1 Hz, 1H) 7.34–7.38 (m, 5H); ^{13}C NMR (100 MHz, $CDCl_3$) δ –0.26, 27.44, 52.66, 77.21, 127.50, 128.03, 128.44, 140.32, 170.73; IR (neat) 2955, 1742, 1495, 1435, 1252, 1166, 1070, 873 cm^{-1}; MS (FAB) 379 (MH, 11), 363 (24), 289 (77), 179 (100), 121 (42); HRMS calcd. for $C_{13}H_{20}IO_3Si$ (MH) 379.0226, found: 379.0209 (4.6 ppm). Anal. calcd. for $C_{13}H_{19}IO_3Si$: C 41.28, H 5.06; found: C 41.11, H 4.80.

*Methyl (±)-(2*S**,3*S**)-2-bromo-3-[((1,1-dimethylethyl)dimethylsilyl)oxy]-3-phenylpropanoate (**26**)*: Compound **26** was prepared with bromohydrin **23** (14) (1.20 g, 4.62 mmol) and *t*-butyldimethylsilyl trifluoromethanesulfonate (1.60 mL, 6.92 mmol) following the procedure described above for **24**. Purification by flash chromatography (CH_2Cl_2) afforded silyl ether **26** as a white solid (1.64 g, 95%). Mp 38°C; ^{1}H NMR (400 MHz, $CDCl_3$) δ –0.30 (s, 3H), 0.01 (s, 3H), 0.78 (s, 9H), 3.82 (s, 3H), 4.21 (d, *J* = 10.0 Hz, 1H), 4.98 (d, *J* = 10.0 Hz, 1H) 7.33–7.37 (m, 5H); ^{13}C NMR (50.3 MHz, $CDCl_3$) δ –5.42, –4.75, 17.95, 25.49, 49.29, 52.85, 76.61, 127.62, 128.21, 128.63, 140.02, 169.53; IR ($CDCl_3$) 2850, 1745, 1590, 1450, 1355, 1315, 1080, cm^{-1}; MS (FAB) 373 (MH, 12), 317 (17), 221 (15), 131 (13), 73 (100); HRMS calcd. for $C_{16}H_{25}{}^{79}BrO_3Si$ (MH) 372.0756, found: 372.0746 (2.7 ppm). Anal. calcd. for $C_{16}H_{25}BrO_3Si$: C 51.47, H 6.75; found: C 51.55, H 6.92.

*Ethyl (±)-(2*S**)-2-[(2*S**,3*R**)-3-((1,1-dimethylethyl)dimethylsilyl)oxytetrahydrofuran-2-yl]-2-iodopropanoate (**33**)*: Compound **33** was prepared with iodoester **31** (17) (775 mg, 2.58 mmol) and *t*-butyldimethylsilyl trifluoromethanesulfonate (0.90 mL, 3.87 mmol) following the procedure described above for **24**. Purification by flash chromatography (5% EtOAc in hexanes) afforded silyl ether **33** (908 mg, 85%) as a colorless oil. ^{1}H NMR (300 MHz, $CDCl_3$) δ 0.15 (s, 3H), 0.22 (s, 3H), 0.95 (s, 9H), 1.30 (t, *J* = 7.1 Hz, 3H), 1.91–2.09 (m, 1H), 4.04–4.12 (m, 2H), 4.23 (q, *J* = 7.1 Hz, 2H), 4.35–4.36 (m, 2H), 4.53–4.55 (m, 1H); ^{13}C NMR (100 MHz, $CDCl_3$) δ –4.46, –4.09, 13.69, 18.01, 18.22, 25.92, 35.96, 61.79, 68.69, 72.64, 84.41, 170.54; IR (neat) 2960, 1740, 1470, 1260 cm^{-1}; MS (CI, CH_4) *m*/*z* 415 (MH^+, 95), 399 (37), 369 (100), 357 (27), 283 (39), 155 (9). Anal. calcd. for $C_{14}H_{27}IO_4Si$: C 40.58, H 6.57; found: C 40.93, H 6.43.

Allylation products

The preparation and characterization data of **35**–**42**, **47**–**56**, **63**, and **64** have been reported previously (7*d*).

General procedure for the allylation of α-iodoesters under chelation-controlled conditions (Conditions A)

To a stirred solution of α-iodoester (1 equiv) in dry CH_2Cl_2 (0.1 M) at –78°C was added $MgBr_2{\cdot}OEt_2$ (3 equiv). The mixture was stirred for 15 min at the same temperature before allyltributyltin (2 equiv) and Et_3B (0.2 equiv of a 1.0 M solution in hexanes) were added. The resulting suspension was stirred at –78°C, and 0.2 equivalent of Et_3B was added each 30 min until the reaction was judged complete by TLC. 1,3-Dinitrobenzene (0.2 equiv) was then added to the solution and the mixture was stirred an additional 15 min at –78°C. The reaction mixture was poured into a saturated $NaHCO_3$ solution and extracted with CH_2Cl_2. The combined organic extracts were washed with brine, dried over $MgSO_4$, filtered, and concentrated under reduced pressure.

*Methyl (±)-(2*S**,3*S**)-2-[propen-3-yl]-3-benzyloxy-3-phenylpropanoate (**43**)*: Compound **43** was prepared with iodoester **13** (97 mg, 0.24 mmol) following the general procedure described above. A 5:1 ratio of *anti*:*syn* products was determined by GC and ^{1}H NMR analyses of the crude isolate. Purification by flash chromatography (5% EtOAc in hexanes) afforded allylated products **43** and **44** (40 mg, 52%). **43**: Colorless oil; ^{1}H NMR (400 MHz, $CDCl_3$) δ 1.77–1.83 (m, 1H), 2.05–2.18 (m, 1H), 2.81–2.94 (m, 1H), 3.73 (s, 3H), 4.21 (d, *J* = 11.8 Hz, 1H), 4.39 (d, *J* = 11.8 Hz, 1H), 4.47 (d, *J* = 9.9 Hz, 1H), 4.87–4.98 (m, 2H), 5.47–5.59 (m, 1H), 7.17–7.45 (m, 10H); ^{13}C NMR (100 MHz, $CDCl_3$) δ 33.22, 51.45, 53.07, 70.45, 82.58, 116.80, 127.43, 127.62, 127.75, 128.12, 128.40, 128.56, 134.43, 138.89, 137.97, 174.17; IR (neat) 2980, 1738, 1642, 1434, 1195 cm^{-1}; MS (FAB) 311 (MH, 100), 203 (22), 171 (25), 143 (87), 133 (83); HRMS calcd. for $C_{20}H_{23}O_3$ (MH) 311.1647, found: 311.1659 (–3.7 ppm).

© 2000 NRC Canada

*Methyl (±)-2-[propen-3-yl]-3-[(trimethylsilyl)oxy]-3-phenylpropanoate (**45** and **46**)*: Compounds **45** and **46** were prepared with iodoester **24** (63 mg, 0.17 mmol) following the general procedure described above. A 1:4 ratio of *anti*:*syn* products was determined by GC and ^{1}H NMR analyses of the crude isolate. Purification by flash chromatography (4% EtOAc in hexanes) afforded a mixture of allylated products **45** and **46** as a colorless oil (38 mg, 78%). ^{1}H NMR (300 MHz, $CDCl_3$) δ **45 (2*S**,3*S**)**: –0.05 (s, 9H), 1.77–1.84 (m, 1H), 2.11–2.19 (m, 1H), 3.72 (s, 3H), 4.72 (d, *J* = 9.6 Hz, 1H), 4.92–5.00 (m, 2H), 5.54–5.60 (m, 1H), 7.20–7.35 (m, 5H), **46 (2*R**,3*S**)**: 0.01 (s, 9H), 2.47–2.54 (m, 2H), 2.71–2.76 (m, 1H), 3.44 (s, 3H), 4.81 (d, *J* = 7.9 Hz, 1H), 5.01–5.08 (m, 2H), 5.68–5.82 (m, 1H), 7.20–7.35 (m, 5H); ^{13}C NMR (100 MHz, $CDCl_3$) δ **45**: 0.04, 33.11, 51.27, 55.10, 76.76, 116.52, 126.91, 127.44, 127.83, 128.18, 134.64, 141.92, 174.82, **46**: 0.05, 32.76, 51.07, 55.19, 76.59, 116.30, 126.29, 127.44, 127.94, 135.59, 142.58, 173.31; IR (neat) 3065, 2953, 1736, 1641, 1495, 1454, 1250, 1194, 1087, 995 cm^{-1}; MS (FAB) 293.5 (MH, 58), 277.4 (30), 179 (100), 143 (55), 120 (12), 104 (20); HRMS calcd. for $C_{16}H_{25}SiO_3$ (MH) 293.1573, found: 293.1584 (–3.8 ppm).

*Ethyl (±)-(2*S*)-2-[(2S*,3R*)-3-((1,1-dimethylethyl)dimethylsilyl)oxytetrahydrofuran-2-yl]-2-[propen-3-yl]-propanoate (**57**)*: Compound **57** was prepared with iodoester **33** (30 mg, 0.08 mmol) following the general procedure described above. A 6:1 ratio of *anti*:*syn* products was determined by GC and ^{1}H NMR analyses of the crude isolate. Purification by flash chromatography (5% EtOAc in hexanes) afforded allylated products **57** and **58** (19 mg, 80%). **57**: Colorless oil; ^{1}H NMR (400 MHz, $CDCl_3$) δ 0.11 (s, 6H), 0.92 (s, 9H), 1.27 (t, *J* = 7.0 Hz, 3H), 1.72–1.87 (m, 1H), 2.00–2.08 (m, 1H), 2.26–2.31 (m, 2H), 2.92–2.96 (m, 1H), 3.80–3.85 (m, 2H), 3.95–4.00 (m, 1H), 4.15–4.22 (m, 2H), 4.32–4.38 (m, 1H), 4.99–5.10 (m, 2H), 5.70–5.82 (m, 1H); ^{13}C NMR (100 MHz, $CDCl_3$) δ –4.61, –4.82, 14.23, 17.79, 25.66, 33.24, 35.77, 45.62, 60.23, 66.18, 71.50, 83.63, 116.64, 134.47, 174.38; IR (neat) 2930, 2850, 1735, 1460, 1170, 1040 cm^{-1}; MS (FAB) 329 (MH, 85), 283 (85), 169 (27). Anal. calcd. for $C_{17}H_{32}O_4Si$: C 62.15, H 9.82; found: C 61.72, H 9.61.

*Ethyl (±)-(2*S*)-2-[(2S*)-tetrahydrofuran-2-yl]-2-[propen-3-yl]-2-methylpropanoate (**59**)*: Compound **59** was prepared with iodoester **28** (135 mg, 0.45 mmol) following the general procedure described above. A 1:1 ratio of *anti*:*syn* products was determined by GC and ^{1}H NMR analyses of the crude isolate. Purification by flash chromatography (10% EtOAc in hexanes) afforded allylated products **59** and **60** (79 mg, 82%). **59**: Colorless oil; ^{1}H NMR (400 MHz, $CDCl_3$) δ 1.12 (s, 3H), 1.27 (t, *J* = 7.1 Hz, 3H), 1.69–1.92 (m, 4H), 2.08 (dd, *J* = 7.7, 13.5 Hz, 1H), 2.49 (dd, *J* = 7.1, 13.5 Hz, 1H), 3.75–3.86 (m, 2H), 4.07–4.11 (m, 1H), 4.17 (q, *J* = 7.1 Hz, 2H), 5.03–5.10 (m, 2H), 5.65–5.77 (m, 1H); ^{13}C NMR (100 MHz, $CDCl_3$) δ 14.15, 15.97, 25.92, 26.28, 40.42, 49.96, 60.04, 68.47, 83.43, 117.84, 133.64, 175.09; IR (neat) 2990, 1730, 1640, 1460, 1380, 1140, 1060 cm^{-1}; MS (FAB) m/z 213 (MH^+, 100), 167 (22), 155 (26), 137 (74), 123 (30), 109 (40); HRMS calcd. for $C_{12}H_{21}O_3$ *m*/*z* (MH^+) 213.1491, found: 213.1484 (3.1 ppm). Anal. calcd. for $C_{12}H_{20}O_3$: C 67.89, H 9.50; found: C 67.92, H 9.36.

*Ethyl (±)-(2*S*)-2-[(2S*,3R*)-3-((1,1-dimethylethyl)dimethylsilyl)oxytetrahydrofuran-2-yl]-2-[propen-3-yl]-2-methylpropanoate (**61**)*: Compound **61** was prepared with iodoester **34** (77 mg, 0.18 mmol) following the general procedure described above. A 7:1 ratio of *anti*:*syn* products was determined by GC and ^{1}H NMR analyses of the crude isolate. Purification by flash chromatography (5% EtOAc in hexanes) afforded allylated products **61** and **62** (43 mg, 70%). **61**: Colorless oil; ^{1}H NMR (400 MHz, $CDCl_3$) δ 0.08 (s, 6H), 0.89 (s, 9H), 1.11 (s, 3H), 1.26 (t, *J* = 7.1 Hz, 3H), 1.74–1.80 (m, 1H), 1.85–1.94 (m, 1H), 2.14 (dd, *J* = 7.9, 13.5 Hz, 1H), 2.60 (dd, *J* = 6.6, 13.5 Hz, 1H), 3.82–3.95 (m, 3H), 4.11–4.19 (m, 2H); 4.29–4.32 (m, 1H), 5.04–5.10 (m, 2H), 5.67–5.77 (m, 1H); ^{13}C NMR (100 MHz, $CDCl_3$) δ –4.82, –4.61, 14.13, 16.73, 17.68, 25.59, 36.40, 40.37, 48.82, 60.45, 66.91, 72.85, 91.26, 118.04, 133.53, 174.76; IR (neat) 2980, 1735, 1460, 1110, 830 cm^{-1}; MS (FAB) *m*/*z* 343 (MH^+, 13), 327 (16), 285 (100), 211 (29), 201 (18), 171 (12); HRMS calcd. for $C_{18}H_{35}O_4Si$ (MH^+) *m*/*z* 343.2305, found: 343.2290 (4.3 ppm).

*Ethyl (±)-(2*S*)-2-[(2S*)-tetrahydropyran-2-yl]-2-[propen-3-yl]-2-methylpropanoate (**65**)*: Compound **65** (59 mg, 54%) was prepared with iodoester **30** (148 mg, 0.48 mmol) following the general procedure described above. A 27:1 ratio of *anti*:*syn* products was determined by GC and ^{1}H NMR analyses of the crude isolate. Purification by flash chromatography (10% EtOAc in hexanes) afforded allylated product **65** as a colorless oil. ^{1}H NMR (400 MHz, $CDCl_3$) δ 1.11 (s, 3H), 1.24 (t, *J* = 7.1 Hz, 3H), 1.27–1.57 (m, 5H), 1.85–1.89 (m, 1H), 2.07 (dd, *J* = 7.8, 13.5 Hz, 1H), 2.38 (dd, *J* = 7.2, 13.5 Hz, 1H), 3.33–3.41 (m, 1H), 3.48–3.52 (m, 1H), 3.93–3.97 (m, 1H), 4.07–4.22 (m, 2H), 5.01–5.07 (m, 2H), 5.63–5.69 (m, 1H); ^{13}C NMR (100 MHz, $CDCl_3$) δ 14.11, 15.90, 23.58, 25.31, 25.97, 40.01, 50.29, 60.07, 68.86, 82.51, 117.76, 133.67, 176.03; IR (neat) 2930, 2870, 1725, 1640, 1435, 1080, 920 cm^{-1}; MS (FAB) *m*/*z* 227 (MH^+, 100), 199 (13), 185 (33), 151 (38), 135 (28); HRMS calcd. for $C_{13}H_{23}O_3$ (MH^+) *m*/*z* 227.1647, found: 227.1654 (–3.0 ppm).

General procedure for the allylation of α-iodoesters in the absence of Lewis acid (Conditions B)

To a solution of α-iodoester (1 equiv.) in hexanes (0.1 M) at 23°C were added allyltributyltin (2 equiv) and AIBN (0.2 equiv). After being allowed to reflux, the mixture was stirred until the reaction was judged complete by TLC.

Methyl (±)-(2R,3S*)-2-[propen-3-yl]-3-benzyloxy-3-phenylpropanoate (**44**)*: To a solution of iodoester **13** (175 mg, 0.44 mmol) in CH_2Cl_2 (4.5 mL) at –78°C were added allyltributyltin (275 μL, 0.88 mmol) and Et_3B (90 μL of a 1.0 M solution in hexanes, 0.09 mmol). The reaction mixture was stirred at –78°C with 0.2 equivalent of Et_3B added each 30 min until the reaction was judged complete by TLC. A 1:10 ratio of *anti*:*syn* products was determined by GC and ^{1}H NMR analyses of the crude isolate. Purification by flash chromatography (5% EtOAc in hexanes) afforded allylated products **43** and **44** (82 mg, 60%). **44**: Colorless oil; ^{1}H NMR (400 MHz, $CDCl_3$) δ 2.41–2.57 (m, 1H), 2.66–2.78 (m, 1H), 2.86–2.92 (m, 1H), 3.41 (s, 3H), 4.22 (d, *J* = 11.6 Hz, 1H), 4.44 (d, *J* = 11.6 Hz, 1H), 4.47 (d, *J* = 8.8 Hz, 2H), 4.95–5.09 (m, 2H), 5.78–5.81 (m, 1H), 7.25–7.43 (m,

© 2000 NRC Canada

10H); ^{13}C NMR (100 MHz, $CDCl_3$) δ 33.31, 51.12, 53.71, 70.57, 81.30, 116.64, 127.36, 127.62, 127.84, 128.08, 128.31, 128.32, 135.33, 137.94, 139.50, 172.93; IR (neat) 3030, 2949, 1736, 1641, 1454, 1356, 1166, 1067, 920 cm^{-1}; MS (FAB) *m/z* 311 (MH^+, 26), 233 (13), 143 (58), 133 (100), 121 (20), 105 (15), 91 (100). Anal. calcd. for $C_{20}H_{22}O_3$: C 77.39, H 7.14; found: C 77.19, H 7.30.

*Ethyl (±)-(2*R*)-2-[(2*S*,3*R*)-3-((1,1-dimethylethyl)dimethylsilyl)oxytetrahydrofuran-2-yl]-2-[propen-3-yl]-propanoate (**58**)*: Compound **58** was prepared with iodoester **33** (52.5 mg, 0.13 mmol) following the general procedure described above. A 1:51 ratio of *anti*:*syn* products was determined by GC and ^{1}H NMR analyses of the crude isolate. Purification by flash chromatography (5% EtOAc in hexanes) afforded allylated product **58** as a colorless oil (30.5 mg, 74%). ^{1}H NMR (400 MHz, $CDCl_3$) δ 0.00 (s, 3H), 0.06 (s, 3H), 0.88 (s, 9H), 1.25 (t, *J* = 7.1 Hz, 3H), 1.78–1.91 (m, 1H), 2.00–2.18 (m, 1H), 2.44–2.52 (m, 1H), 2.60–2.67 (m, 1H), 2.81–2.92 (m, 1H), 3.73–4.25 (m, 5H), 4.38–4.43 (m, 1H), 4.97–5.11 (m, 2H), 5.69–5.90 (m, 1H); ^{13}C NMR (100 MHz, $CDCl_3$) δ –5.40, –4.49, 14.19, 17.87, 25.62, 34.26, 36.14, 44.33, 59.82, 65.82, 72.27, 81.66, 116.74, 134.83, 173.38; IR (neat) 2910, 1730, 1645, 1460, 1370, 1240, 1175, 1070, 820 cm^{-1}; MS (FAB) *m/z* 329 (MH^+, 12), 283 (16), 271 (82), 149 (100); HRMS calcd. for $C_{17}H_{33}O_4Si$ *m/z* (MH^+) 329.2148, found: 329.2130 (5.5 ppm).

*Ethyl (±)-(2*R*)-2-[(2*S*)-tetrahydrofuran-2-yl]-2-[propen-3-yl]-2-methylpropanoate (**60**)*: Compound **60** was prepared with iodoester **28** (163 mg, 0.55 mmol) following the general procedure described above. A 1:10 ratio of *anti*:*syn* products was determined by GC and ^{1}H NMR analyses of the crude isolate. Purification by flash chromatography (10% EtOAc in hexanes) afforded allylated products **59** and **60** (94 mg, 81%). **60**: Colorless oil; ^{1}H NMR (400 MHz, $CDCl_3$) δ 1.11 (s, 3H), 1.25 (t, *J* = 7.1 Hz, 3H), 1.68–1.91 (m, 4H), 2.32 (dd, *J* = 7.9, 13.6 Hz, 1H), 2.54 (dd, *J* = 6.8, 13.6 Hz, 1H), 3.73–3.85 (m, 2H), 4.02–4.07 (m, 1H), 4.14 (q, *J* = 7.1 Hz, 2H), 5.03–5.10 (m, 2H), 5.67–5.79 (m, 1H); ^{13}C NMR (100 MHz, $CDCl_3$) δ 14.12, 15.86, 26.01, 26.87, 41.59, 49.83, 60.17, 68.49, 82.85, 117.62, 134.05, 174.94; IR (neat) 2990, 1730, 1645, 1465, 1380, 1140, 1065 cm^{-1}; MS (EI) *m/z* 213 (MH^+, 14), 171 (10), 142 (21), 69.5 (100); HRMS cacld for $C_{12}H_{21}O_3$ *m/z* (MH^+) 213.1491, found: 213.1499 (–3.9 ppm). Anal. calcd. for $C_{12}H_{20}O_3$: C 67.89, H 9.50; found: C 67.96, H 9.35.

*Ethyl (±)-(2*R*)-2-[(2*S*,3*R*)-3-((1,1-dimethylethyl)dimethylsilyl)oxytetrahydrofuran-2-yl]-2-[propen-3-yl]-2-methylpropanoate (**62**)*: Compound **62** was prepared with iodoester **34** (33.5 mg, 0.08 mmol) following the general procedure described above. A 1:16 ratio of *anti*:*syn* products was determined by GC and ^{1}H NMR analyses of the crude isolate. Purification by flash chromatography (5% EtOAc in hexanes) afforded allylated products **61** and **62** (17.5 mg, 65%). **62**: Colorless oil; ^{1}H NMR (200 MHz, $CDCl_3$) δ 0.05 (s, 6H), 0.86 (s, 9H), 1.25 (t, *J* = 7.1 Hz, 3H), 1.67–1.97 (m, 2H), 2.19 (dd, *J* = 7.7, 13.6 Hz, 1H), 2.57 (dd, *J* = 6.9, 13.6 Hz, 1H), 3.77–3.98 (m, 3H), 4.02–4.22 (m, 2H), 4.30–4.36 (m, 1H), 5.01–5.09 (m, 2H), 5.60–5.78 (m, 1H); ^{13}C NMR (50.3 MHz, $CDCl_3$) δ –4.86, –4.33, 14.19, 17.43, 17.75, 25.68, 36.59, 40.93, 48.90, 60.47, 67.03, 73.37, 91.81, 117.98, 133.93, 174.66; IR (neat) 2950, 1725, 1645, 1460, 1375, 1250, 1070, 910, 830, 770 cm^{-1}; MS (CI, CH_4) *m/z* 343 (MH^+, 25), 327 (19), 285 (9), 269 (8), 257 (12), 210 (100), 169 (10).

*Ethyl (±)-(2*R*)-2-[(2*S*)-tetrahydropyran-2-yl]-2-[propen-3-yl]-2-methylpropanoate (**66**)*: Compound **66** was prepared with iodoester **30** (187 mg, 0.60 mmol) following the general procedure described above. A 1:18 ratio of *anti*:*syn* products was determined by GC and ^{1}H NMR analyses of the crude isolate. Purification by flash chromatography (10% EtOAc in hexanes) afforded allylated product **66** as a colorless oil (105 mg, 77%). ^{1}H NMR (400 MHz, $CDCl_3$) δ 1.01 (s, 3H), 1.24 (t, *J* = 7.1 Hz, 3H), 1.36–1.53 (m, 5H), 1.82–1.86 (m, 1H), 2.30 (dd, *J* = 7.9, 13.6 Hz, 1H), 2.50 (dd, *J* = 6.9, 13.6 Hz, 1H), 3.36–3.46 (m, 2H), 3.97–4.02 (m, 1H), 4.13 (q, *J* = 7.1 Hz, 2H), 5.01–5.08 (m, 2H), 5.65–5.79 (m, 1H); ^{13}C NMR (100 MHz, $CDCl_3$) δ 14.12, 15.98, 23.60, 26.01, 26.32, 40.88, 50.26, 60.12, 68.99, 81.77, 117.50, 134.33, 174.98; IR (neat) 2920, 1725, 1450, 1300, 1210, 1085, 910 cm^{-1}; MS (FAB) *m/z* 227 (MH^+, 100), 199 (13), 185 (27), 151 (31), 143 (15), 135 (25); HRMS cacld for $C_{13}H_{23}O_3$ *m/z* (MH^+) 227.1647, found: 227.1656 (–3.9 ppm). Anal. calcd. for $C_{13}H_{22}O_3$: C 68.99, H 9.80; found: C 68.58, H 10.17.

Determination of magnesium concentrations in allylation reaction mixtures by filtration and EDTA titration

Preparation of the sample: To a stirred solution of α-iodoester (0.5 mmol) in dry CH_2Cl_2 (5 mL) at –78°C was added $MgBr_2{\cdot}OEt_2$. The mixture was stirred for 15 min at this temperature before allyltributyltin (1.0 mmol) was added. A 3 mL aliquot of the solution was removed from the flask using a syringe equipped with a filter (Millex HV 0.45 mm). This 3 mL aliquot was then concentrated under reduced pressure.

Titration of magnesium by EDTA: Deionized water (5 mL) and CH_2Cl_2 (5 mL) were added to the sample. The mixture was then shaken and poured into a 125 mL erlenmeyer flask. Deionized water (10 mL), NH_3–NH_4Cl buffer solution at pH = 10 (4 mL), and six drops of Calmagite indicator were added successively to the stirred solution, which was then titrated with a standardized EDTA solution (0.099 M, Aldrich) until the color changed completely from red to blue. The amount of Mg (mmol) in the total sample = 0.099 mmol/mL × V_{EDTA} added (mL) × (5/3).

The buffer pH = 10 was prepared from concentrated NH_4OH solution (57 mL) and 7 g of NH_4Cl in sufficient deionized water to give 100 mL of solution.

The calmagite indicator solution was prepared by adding 0.05 g of calmagite to 50 mL of deionized water.

^{13}C observations of β-alkoxyesters in the presence of a saturating amount of $MgBr_2{\cdot}OEt_2$ in CD_2Cl_2 at –23°C.

To a stirred solution of α-iodoester (1 equiv) in CD_2Cl_2 (0.1 M) at –23°C was added $MgBr_2{\cdot}OEt_2$ (3 equiv). The solution was then stirred for 15 min at the same temperature. A 1.5 mL aliquot of solution was removed from the flask using a syringe equipped with a filter (Millex HV 0.45 mm). The aliquot was placed in an NMR tube and kept at –23°C

© 2000 NRC Canada

until the ^{13}C NMR spectrum was recorded on a Bruker ARX400 spectrometer at that temperature.

Competition experiments

Substrates **A** (0.5 equiv) and **B** (0.5 equiv) were dissolved in $CDCl_3$ and the mixture was analyzed by NMR ^1H integration to determine the exact **A**:**B** ratio before the allylation reaction. The solution was concentrated and redissolved in dry CH_2Cl_2 (0.1 M) at –78°C before $MgBr_2 \cdot OEt_2$ (3 equiv) was added. The mixture was then stirred for 15 min at the same temperature, and allyltributyltin (0.5 equiv) as well as Et_3B (0.2 equiv of a 1.0 M solution in hexanes) were subsequently added. The resulting suspension was stirred at –78°C, and 0.2 equivalent of Et_3B was added each 30 min until the reaction was judged complete by TLC. The reaction mixture was then poured into a saturated $NaHCO_3$ solution and extracted with CH_2Cl_2. The combined organic extracts were washed with brine, dried over $MgSO_4$, filtered, and concentrated under reduced pressure. Another ^1H NMR analysis was done on the crude mixture to determine the exact **A**:**B** ratio after the allylation reaction.

10. Acknowledgement

We would like to thank Ms. LaVonne Dlouhy for her assistance in the preparation of this manuscript.

11. Supplementary material available

^{13}C NMR spectra for compounds **23**, **43**, **45**–**46**, **58**, **61**, **62**, and **65**. Tables of NMR chemical shift correlations for allylated products (11 pages) have been deposited as supplementary material and may be purchased from: The Depository of Unpublished Data, Document Delivery, CISTI, National Research Council Canada, Ottawa, Ontario, Canada, K1A 0S2.

References

1. For reviews see: (*a*) N.A. Porter, B. Giese, and D.P. Curran. Acc. Chem. Res. **24**, 296 (1991); (*b*) D.C. Liotta, K.A. Durkin, and J.J. Soria. Chemtracts: Org. Chem. **5**, 197 (1992); (*c*) G.S. Miracle, S.M. Cannizzaro, and N.A. Porter. Chemtracts: Org. Chem. **6**, 147 (1993); (*d*) W. Smadja. Synlett, **2**, 154 (1994); (*e*) B. Giese, W. Damm, and R. Batra. Chemtracts: Org. Chem. **7**, 355 (1994); (*f*) D.P. Curran, N.A. Porter, and B. Giese. *In* Stereochemistry of radical reactions—concepts, guidelines and synthetic applications. VCH, New York. 1996; (*g*) P. Renaud and M. Gerster. Angew. Chem. Int. Ed. Engl. **37**, 2562 (1998).
2. Selected examples: (*a*) P.A. Bartlett and J.L. Adams. J. Am. Chem. Soc. **102**, 337 (1980); (*b*) D.J. Hart and H.-C. Huang. Tetrahedron Lett. **26**, 3749 (1985); (*c*) D.J. Hart and R. Krishnamurthy. J. Org. Chem. **57**, 4457 (1992); (*d*) B. Giese, W. Damm, F. Wetterich, and H.-G. Zeitz. Tetrahedron Lett. **33**, 1863 (1992); (*e*) D.P. Curran and P.S. Ramamoorthy. Tetrahedron, **49**, 4841 (1993); (*f*) T. Morikawa, Y. Washio, S. Harada, R. Hanai, T. Kayashita, H. Nemoto, M. Shiro, and T. Taguchi. J. Chem. Soc. Perkin Trans. 1, **3**, 271 (1995); (*g*) C.J. Easton and M.C. Merrett. Tetrahedron, **53**, 1151, (1997); (*h*) H. Suzuki, S. Aoyagi, and C. Kibayashi. J. Org. Chem. **60**, 6114 (1995).
3. (*a*) Y. Guindon, C. Yoakim, R. Lemieux, L. Boisvert, D. Delorme, and J.-F. Lavallée. Tetrahedron Lett. **31**, 2845 (1990); (*b*) Y. Guindon, J.-F. Lavallée, L. Boisvert, C. Chabot, D. Delorme, C. Yoakim, D. Hall, R. Lemieux, and B. Simoneau. Tetrahedron Lett. **32**, 27 (1991); (*c*) K. Durkin, D. Liotta, J. Rancourt, J.-F. Lavallée, L. Boisvert, and Y. Guindon. J. Am. Chem. Soc. **114**, 4912 (1992); (*d*) Y. Guindon, C. Yoakim, V. Gorys, W.W. Ogilvie, D. Delorme, J. Renaud, G. Robinson, J.-F. Lavallée, A. Slassi, G. Jung, J. Rancourt, K. Durkin, and D. Liotta. J. Org. Chem. **59**, 1166 (1994); (*e*) Y. Guindon, A. Slassi, J. Rancourt, G. Bantle, M. Bencheqroun, L. Murtagh, E. Ghiro, and G. Jung. J. Org. Chem. **60**, 288 (1995); (*f*) Y. Guindon and R.C. Denis. Tetrahedron Lett. **39**, 339 (1998); (*g*) Y. Guindon, G. Jung, B. Guérin, and W.W. Ogilvie. Synlett, **3**, 213 (1998).
4. Selected examples: (*a*) D. Crich and J.W. Davies. Tetrahedron Lett. **28**, 4205 (1987); (*b*) N.A. Porter, D.M. Scott, B. Lacher, B. Giese, H.G. Zeitz, and H.J. Lindner. J. Am. Chem. Soc. **111**, 8311 (1989); (*c*) D.P. Curran, H. Qi, S.J. Geib, and N.C. DeMello. J. Am. Chem. Soc. **116**, 3131 (1994); (*d*) N.A. Porter, R.L. Carter, C.L. Mero, M.G. Roepel, and D.P. Curran. Tetrahedron, **52**, 4181 (1996), and refs. therein; (*e*) C. Andrés, J.P. Duque-Soladana, J.M. Iglesias, and R. Pedrosa. Tetrahedron Lett. **37**, 9085 (1996); (*f*) I.J. Rosenstein and T.A. Tynan. Tetrahedron Lett. **39**, 8429 (1998); (*g*) D.P. Curran, S. Geib, and N. DeMello. Tetrahedron, **55**, 5681 (1999).
5. (*a*) P. Renaud and Ribezzo. J. Am. Chem. Soc. **113**, 7803 (1991); (*b*) P. Renaud, N. Moufid, L.H. Kuo, and D.P. Curran. J. Org. Chem. **59**, 3547 (1994); (*c*) D.P. Curran and L.H. Kuo. J. Org. Chem. **59**, 3259 (1994); (*d*) M. Nishida, E. Ueyama, H. Hayashi, Y. Ohtake, Y. Yamaura, E. Yanaginuma, O. Yonemitsu, A. Nishida, and N. Kawahara. J. Am. Chem. Soc. **116**, 6455 (1994); (*e*) P. Renaud, T. Bourquard, M. Gerster, and N. Moufid. Angew. Chem. Int. Ed. Engl. **33**, 1601 (1994); (*f*) M. Nishida, H. Hayashi, Y. Yamaura, E. Yanaginuma, O. Yonemitsu, A. Nishida, and N. Kawahara. Tetrahedron Lett. **36**, 269 (1995); (*g*) M. Murakata, H. Tsutsui, and O. Hoshino. J. Chem. Soc. Chem. Commun. **4**, 481 (1995); (*h*) H. Urabe, K. Kobayashi, and F. Sato. J. Chem. Soc. Chem. Commun. **10**, 1043 (1995); (*i*) N. Moufid, P. Renaud, C. Hassler, and B. Giese. Helv. Chim. Acta. **78**, 1006 (1995).
6. (*a*) T. Toru, Y. Watanabe, M. Tsusaka, and Y. Ueno. J. Am. Chem. Soc. **115**, 10464 (1993); (*b*) K. Rück and H. Kunz. Synthesis, 1018 (1993); (*c*) H. Nagano and Y. Kuno. J. Chem. Soc. Chem. Commun. **8**, 987 (1994); (*d*) Y. Yamamoto, S. Onuki, M. Yumoto, and N. Asao. J. Am. Chem. Soc. **116**, 421 (1994); (*e*) H. Urabe, K. Yamashita, K. Suzuki, K. Kobayashi, and F. Sato. J. Org. Chem. **60**, 3576 (1995); (*f*) M. Gerster, L. Audergon, N. Moufid, and P. Renaud. Tetrahedron Lett. **37**, 6335 (1996); (*g*) M.P. Sibi, C.P. Jasperse, and J.G. Ji. J. Am. Chem. Soc. **117**, 10779 (1995); (*h*) M.P. Sibi and J.G. Ji. Angew. Chem. **2**, 190 (1996); (*i*) M.P. Sibi, J.J. Shay, and J.G. Ji. Tetrahedron Lett. **38**, 5955 (1997); (*j*) C. Ha, O.M. Musa, F.N. Martinez, and M. Newcomb. J. Org. Chem. **62**, 2704 (1997).
7. (*a*) Y. Guindon, J.-F. Lavallée, M. Linas-Brunet, G. Horner, and J. Rancourt. J. Am. Chem. Soc. **113**, 9701 (1991); (*b*) Y. Guindon, B. Guérin, C. Chabot, N. Mackintosh, and W.W. Ogilvie. Synlett, **5**, 449 (1995); (*c*) Y. Guindon, B. Guérin, C. Chabot, and W.W. Ogilvie. J. Am. Chem. Soc. **118**, 12528 (1996); (*d*) Y. Guindon, Z. Liu, and G. Jung. J. Am. Chem. Soc. **119**, 9289 (1997); (*e*) Y. Guindon and J. Rancourt. J. Org. Chem. **63**, 6554 (1998).
8. (*a*) A. Waldner, A. De Mesmaeker, P. Hoffmann, T. Mindt, and T. Winkler. Synlett, **2**, 101 (1991); (*b*) A. De Mesmaeker, A. Waldner, P. Hoffmann, and T. Mindt. Synlett, **11**, 871 (1993).

© 2000 NRC Canada

9. (*a*) D.P. Curran, A.C. Abraham, and H.-T. Liu. J. Org. Chem. **56**, 4335 (1991); (*b*) E.P. Kündig, L.-H. Xu, and P. Romanens. Tetrahedron Lett. **36**, 4047 (1995); (*c*) S. Hanessian, H. Yang, and R. Schaum. J. Am. Chem. Soc. **118**, 2507 (1996).
10. (*a*) M.P. Sibi, C.P. Jasperse, and J.G. Ji. J. Am. Chem. Soc. **117**, 10779 (1995); (*b*) J.H. Wu, R. Radinov, and N.A. Porter. J. Am. Chem. Soc. **117**, 11029 (1995); (*c*) M.P. Sibi and J.G. Ji. J. Am. Chem. Soc. **118**, 3063 (1996); (*d*) M.P. Sibi and J.G. Ji. Angew. Chem. Int. Ed. Engl. **2**, 190 (1996); (*e*) M.P. Sibi, J.G. Ji, J.H. Wu, S. Gurtler, and N.A. Porter. J. Am. Chem. Soc. **118**, 9200 (1996); (*f*) A.-R. Fhal and P. Renaud. Tetrahedron Lett. **38**, 2661 (1997); (*g*) M.P. Sibi and J.G. Ji. J. Org. Chem. **62**, 3800 (1997); (*h*) M. Blumenstein, K. Schwarzkopf, and J.O. Metzer. Angew. Chem. **3**, 235 (1994).
11. C.L. Mero and N.A. Porter. J. Am. Chem. Soc. **121**, 5155 (1999).
12. L.C. Vishwakarma and J.S. Walia. J. Indian Chem. Soc. **53**, 156 (1976).
13. The olefins were either purchased or prepared from the corresponding acids, which were commercially available. The olefin 5 was prepared by an esterification of phenylpropiolic acid (MeOH, H_2SO_4, reflux) followed by hydrogenation with modified Lindlar catalyst. See J. Rajaram, A.P.S. Narula, H.P.S. Chawla, and S. Dev. Tetrahedron, **39**, 2315 (1983).
14. For **22** see reference 7*c*, and for **23** see: J. Read and A. Andrews. J. Chem. Soc. **119**, 1774 (1921).
15. R.C. Cambie, D. Chambers, P.S. Rutledge, and P.D. Woodgate. J. Chem. Soc. Perkin Trans. 1, **20**, 2231 (1977).
16. G. Cardillo and M. Orena. Tetrahedron, **46**, 3321 (1990), and refs. therein.
17. Y. Guindon and M. Labelle. J. Am. Chem. Soc. **111**, 2204 (1989). See also reference 7*a*.
18. A similar observation has been observed in the case of reduction. See reference 4 and: F.H. Gouzoules and R.A. Whitney. J. Org. Chem. **51**, 2024 (1986).
19. Silyl ether is known to be less efficient in complexation with Lewis acid. See X. Chen, E.R. Hortelano, E.L. Eliel, and S.V. Frye. J. Am. Chem. Soc. **114**, 1778 (1992), and refs. therein.
20. K. Fuji. Chem. Rev. **93**, 2037 (1993).
21. (*a*) D.G. Christian. *In* Analytical chemistry. John Wiley & Sons Ed., New York. 1986. pp. 586–587; (*b*) D.A. Skoog, D.M. West, and F.J. Holler. *In* Fundamentals of analytical chemistry. Saunders College Publishing Ed., New York. 1988; (*c*) R.A. Day and A.L. Underwood. *In* Quantitative analysis. Prentice-Hall Ed., New York. 1986.
22. X. Chen, E.R. Hortelano, E.L. Eliel, and S.V. Frye. J. Am. Chem. Soc. **114**, 1778 (1992).
23. Under varying conditions, magnesium has been isolated with coordination numbers from two to ten, with six being the most frequent. C.E. Holloway and M. Melnik. J. Organomet. Chem. **465**, 1 (1994).
24. A. Ecker, C. Üffing, and H. Schnöckel. Chem. Eur. J. **2**, 1112 (1996).

© 2000 NRC Canada

Diastereoselective double ring closing metathesis reactions as an approach to symmetrical bicyclodienes

Mark Lautens, Gregory Hughes, and Valentin Zunic

Abstract: A new class of bicyclic dienes which contain a σ plane of symmetry are efficiently prepared in a diastereoselective fashion using ring closing metathesis reactions. These molecules have potential as starting materials for a wide range of organic targets.

Key words: metathesis, catalysis, stereoselective, decalin, desymmetrization.

Résumé : Faisant appel à des réactions de métathèse de fermeture de cycle, on a développé une méthode efficace de préparer de façon diastéréosélective une nouvelle classe de dienes bicycliques qui contiennent un plan de symétrie σ. Ces molécules pourraient éventuellement servir de produit de départ pour une grande variété de cibles organiques.

Mots clés : métathèse, catalyse, stéréosélective, décaline, désymétrisation.

Introduction

In recent years there has been tremendous interest in ring closing olefin metathesis (RCM) chemistry due largely to the development of well defined transition metal alkylidenes such as $[Cl_2(Cy_3P)_2Ru{=}CHPh]$ (**1**) and $[PhMe_2CCH{=}Mo{=}N\{2,6\text{-}(i\text{Pr})_2C_6H_3\}\{OCMe(CF_3)_2\}_2]$ (**2**) which display tolerance to a significant range of functional groups (for recent reviews of olefin metathesis see ref. (1)). We became interested in using RCM methodology as a key step in the projected total synthesis of the HMG CoA reductase inhibitor (+)-mevinolin (Scheme 1). We reasoned that a diastereoselective double ring closing metathesis strategy involving **A**, followed by an alkene selective sigmatropic rearrangement of a substrate such as **B**, would provide convenient access to the carbon skeleton of the hexahydronaphthalene portion of the target (for other examples of diastereoselective RCM reactions see ref. (2)); (for other examples of double RCM reactions see ref. (3)). A preliminary report on these investigations has appeared (4).

Received March 7, 2000. Published on the NRC Research Press website on June 15, 2000.

Dedicated to Professor Stephen Hanessian on the occasion of his 65th birthday.

M. Lautens,[1] G. Hughes, and V. Zunic. University of Toronto, Department of Chemistry, 80 St. George St., Toronto, ON M5S 3H6, Canada.

[1]Author to whom correspondence may be addressed. Telephone: (416) 978-6083. Fax: (416) 978-6083. e-mail: mlautens@alchemy.chem.utoronto.ca

[2]4-Bromo-1-butene: $1088.91/mol; 3-buten-1-ol: $432.44/mol; 1,4-dichlorobut-2-ene (mixture of *cis* and *trans*): $20.70/mol. Prices in Canadian dollars listed in Aldrich's 1999 catalogue for the largest available denomination.

We opted to use unsubstituted tetraenes **C** for our initial studies. This simplified system is particularly attractive since the product of double ring closing metathesis, **D**, is a useful starting material for subsequent investigations in the area of enantioselective alkene differentiation reactions.

Results

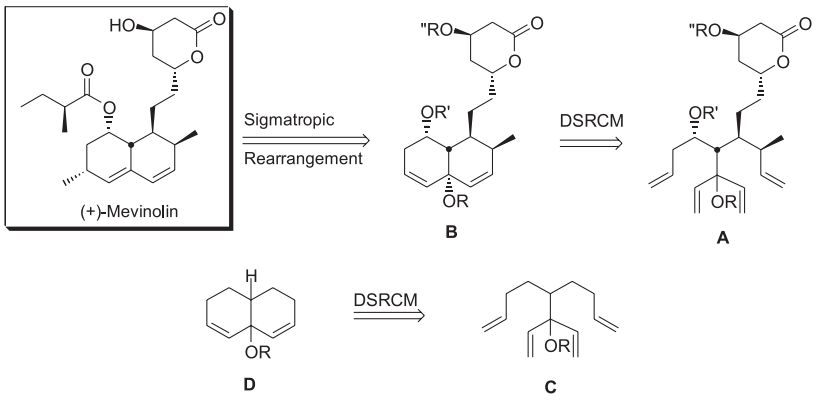
We envisioned a general approach to a variety of tertiary diallylic alcohols involving dialkylation of malonate, Krapcho decarboxylation and addition of two equivalents of a vinyl organometallic reagent (Scheme 2).

For our first investigations we wanted to prepare a tetraene derived from double alkylation of malonate with a butenyl electrophile. The most obvious butenyl source would be commercially available 4-bromo-1-butene, or a derivative of 3-buten-1-ol (e.g., $CH_2{=}CH(CH_2)_2OTs$, $CH_2{=}CH(CH_2)_2OTf$, $CH_2{=}CH(CH_2)_2I$). However, the expense of both 4-bromo-1-butene and 3-buten-1-ol,[2] as well as the need to use these electrophiles in moderate excess due to their tendency to undergo elimination under basic conditions made this approach less attractive for the large scale preparation of materials needed for our investigations. We examined an alternative approach involving sequential additions of malonate to acrolein, followed by Wittig olefination. While the route furnished the desired dibutenylated malonate, the procedure was laborious, and the yields were low to moderate. In addition, the large quantities of triphenyl phosphine oxide produced on scaling up the reaction made this approach unattractive.

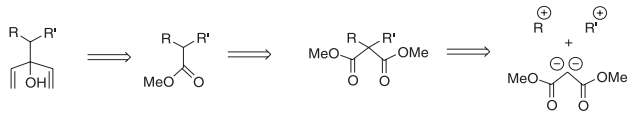
Inspired by the work of Tsuji and co-workers (5) and Shimizu and co-workers (5), we developed an alternative strategy for the butenylation of malonates, as well as a variety of other nucleophiles (6). In this approach, the appropriate nucleophile is alkylated with 1,4-dichlorobutene, which is a fraction of the cost of either 4-bromo-1-butene or 3-buten-1-ol,[2] to afford an allyl chloride. Formate reduction

 © 2000 NRC Canada

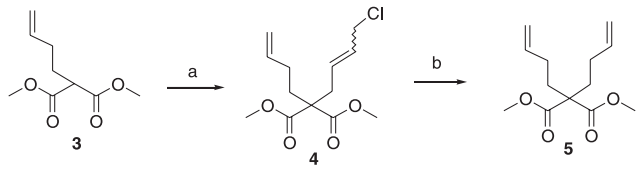
Scheme 1. Potential retrosynthetic approach to (+)-Mevinolin.



Scheme 2. Synthetic approach to model systems.



Scheme 3. Preparation of a dibutenylated malonate: (*a*) MeO^-Na^+ (1.5 equiv.), $ClCH_2CH{=}CHCH_2Cl$ (4.0 equiv., mixture of *cis* and *trans*), MeOH, 23°C→reflux, 57%; (*b*) HCO_2NH_4 (2.2 equiv.), Pd_2dba_3 (0.25 mol%), nBu_3P (2 mol%), toluene, 100°C, 16 h, 90%.



under Pd catalysis affords the desired butenylated compound as a single regioisomer within the detection limits of ^1H NMR. Dimethyl monobutenylated malonate **3** was prepared from dimethyl malonate and *trans*-1,4-dichloro-2-butene according to a two step procedure described by Shimizu and Aida (6*a*). This product was then converted to allyl chloride **4** using standard alkylation chemistry and finally to **5** by a Pd catalyzed formate reduction (Scheme 3). In this manner, **5** could be easily prepared in good overall yield in batches of 50 g.

Decarboxylation of **5** and its diallyl analogue **6** proceeded in good yield to give the desired methyl esters **7** and **8**. The addition of 2 equiv. of vinyl lithium or magnesium reagents to **7** and **8** proved troublesome as the second equivalent strongly preferred to undergo conjugate addition, to afford less than 10% of the desired tertiary alcohols **9** and **10** (7). It had been reported that the addition of two equivalents of a vinyl cerium reagent to an ester could generate a tertiary alcohol in 35% yield (8). The literature conditions called for the use of 3 equiv. each of vinylmagnesium bromide and predried $CeCl_3$ at 0°C. We found that more extensive drying of the $CeCl_3{\cdot}7H_2O$ (6–12 h at 140°C, <0.1 mmHg), lower reaction temperatures (–78°C), and the use of 3.5 equiv. of vinylmagnesium bromide and 4.0 equiv. of $CeCl_3$ gave **9** and **10** in 86 and 90% respectively. The alcohols were then converted to ethers **11** and **12** under standard conditions (Scheme 4).

With the desired tetraenes in hand we initiated the diastereoselective RCM (DSRCM) studies. Treating **11** with 3 mol% of **1** for 3 h gave the cycloheptene **13** in 70% yield. Ring closing metathesis via sequential reaction of the two less hindered alkenes occurs, in spite of the fact that this leads to seven-membered ring formation rather than the cyclohexene. However, by increasing the catalyst loading to 10–12mol%, increasing the reaction time to 22 h, and conducting the reaction in the presence of ethylene, it was possible to isolate *cis*- and *trans*-**14** in 80% as an 8:1 mixture of diastereomers with the *syn* product predominating (Scheme 5). Similar results were realized using **2** as a catalyst. The successful conversion of **13** to **14** suggested a more efficient route to **14** using **16**. Fortunately, this methyl ester can be prepared on large scale in good yield from inexpensive materials as outlined in Scheme 6 (9).

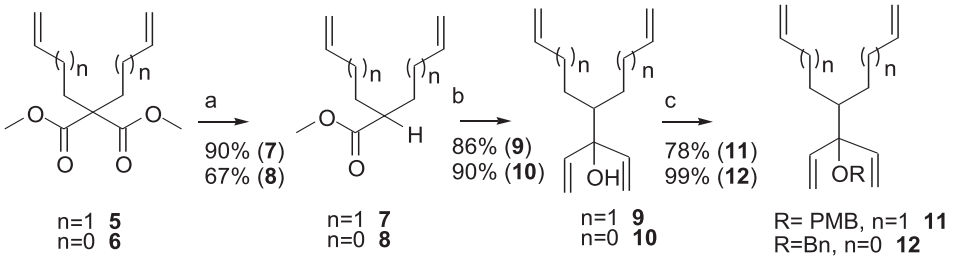
In contrast to the reactions of ethers **10** or **12** which give *cis*-fused bicyclic compounds, treating free alcohol **9** with **1** for 30 min gave a 2.7:1 mixture of diastereomers where the *trans*-fused isomer of **15** is favored (Scheme 5).

We could also form *cis*-fused diquinane **19** from tetraene **12** by treating it with 4 mol% of **1** for 18 h (Scheme 7). A 6.5:1 ratio was observed between **19** and cyclopentene **20** which fails to undergo further RCM reactions as this would result in the formation of a highly strained *trans* bicyclo[3.3.0]octadiene system. Again, cyclization with the less hindered olefin appears to occur initially to give symmetrical cyclopentene **18**, but upon prolonged reaction times this intermediate then ring opens and recyclizes to give the desired bicyclic product.

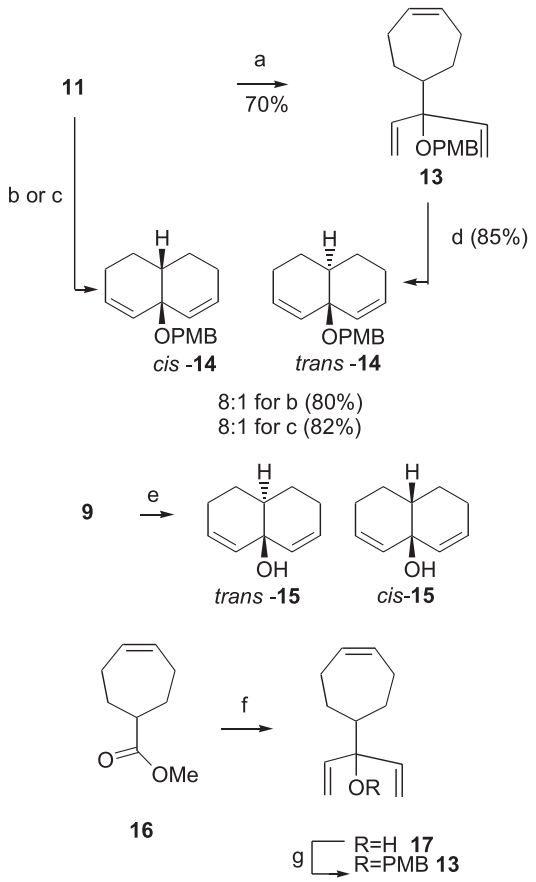
To examine the diastereoselectivity in the first step of the cyclization and its reversibility, trienes **22**, **23**, **26**, and **27** were prepared as outlined in Scheme 8. Six-membered ring precursors were prepared by alkylation of **3** with $TBDPSO(CH_2)_3Br$, followed by Krapcho decarboxylation and vinylcerium addition to give **22**. Protection of the free

© 2000 NRC Canada

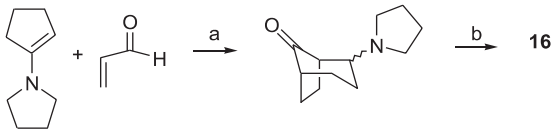
Scheme 4. Synthesis of tetraene 3° diallylic alcohols and ethers: (*a*) NaCl (2.4 equiv.), H_2O, DMSO, 180°C, 4 h; (*b*) CH_2=CHMgBr (3.5 equiv.), $CeCl_3$ (4.0 equiv., anhydrous), THF, –78°C; (*c*) **9**→**11**: NaH (2.0 equiv.), PMBBr (2.0 equiv.), DMF, 23°C; **10**→**12**: THF, 60°C, KH (2.0 equiv.), BnBr (1.5 equiv.); PMB = *p*-methoxybenzyl.



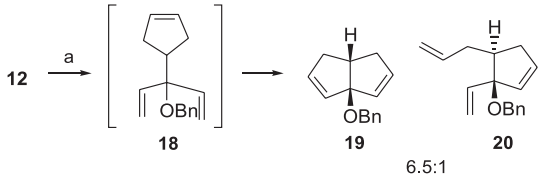
Scheme 5. DSRCM as an approach to *cis*- and *trans*-fused decalin systems: (*a*) $(PCy)_2Cl_2Ru$=CHPh (3 mol%), CH_2Cl_2, 3 h; (*b*) $(PCy_3)_2Cl_2Ru$=CHPh (12 mol%), CH_2Cl_2, ethylene atm, 18 h; (*c*) $((CF_3)_2CH_3CO)_2Mo(=NAr)(=CHC(CH_3)_2Ph)$ (Ar = 2,6-diisopropylphenyl) (12 mol%), C_6H_6, 30 min; (*d*) $(PCy_3)_2Cl_2Ru$=CHPh (10 mol%), CH_2Cl_2, ethylene atm, 18 h; (*e*) $(PCy_3)_2Cl_2Ru$=CHPh (10 mol%), CH_2Cl_2, closed system, 30 min; (*f*) CH_2=CHMgBr (3.5 equiv.), $CeCl_3$ (4.0 equiv., anhydrous), THF, –78°C; (*g*) NaH (2.0 equiv.), PMBBr (2.0 equiv.), DMF, 23°C.



Scheme 6. Alternative approach to cycloheptenoates: (*a*) THF, 0°C; (*b*) (*i*) MeI, THF; (*ii*) NaOH; (*iii*) H_2SO_4 (cat.), MeOH.



Scheme 7. DSRCM as an approach to diquinane systems: **1** (4 mol%), CH_2Cl_2, 18 h.



alcohol gave **23**. Five-membered ring precursors were prepared by alkylation of dimethylmalonate with $TBSO(CH_2)_3Br$, followed by allylation. Krapcho decarboxylation and vinyl cerium addition then gave **26** and protection of the free alcohol gave **27**.

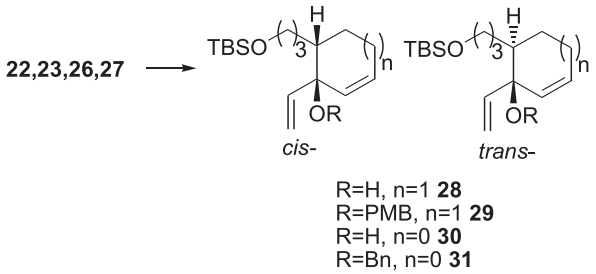
Results from treating these trienes with **1** and **2** are summarized in Table 1. Treating **22** with **1** gave a 1:2.8 mixture of diastereomers favoring *trans*-**28** (CH_2=CH ↔ $(CH_2)_3OSiR_3$) (entry 1),[3] whereas treating **23** with **1** gave a 6.1:1 mixture of diastereomers favoring the *cis* (CH_2=CH↔$(CH_2)_3OSiR_3$) isomer (entry 2), and switching to **2** gave slightly higher levels of stereoselectivity (7.8:1, entry 3). Cyclopentenol **30** was formed as a 1:1 mixture of diastereomers upon treatment with **1** (entry 4), whereas the benzyl ether gave rise to cyclopentene **31** in an 8.0:1 mixture of diastereomers, favoring *cis*-**31** (entry 5). The use of **2** gave the same sense of selectivity in forming **31**, but with significantly lower levels of stereoselectivity (1.7:1, entry 6).

These results parallel the observations made in bicycle formation suggesting that although RCM transformations are potentially reversible we did not observe that process in this series. In fact submitting the minor isomers isolated from the reaction mixtures to the original reaction conditions failed to show any equilibration.

[3] While somewhat unorthodox, the nomenclature used here to designate relative stereochemistry was chosen for the sake of clarity. In using (*R**,*S**) vs. (*R**,*R**) nomenclature, the designation reverses when ring size is changed from five to six without changing the relative orientations of the vinyl and alkyl substiuents. The *cis* and *trans* designations were chosen on the basis of whether a *cis*- or *trans*-fused bicyclic system would be formed were a second RCM reaction possible. For proof of stereochemistry, see supporting information of ref. (2).

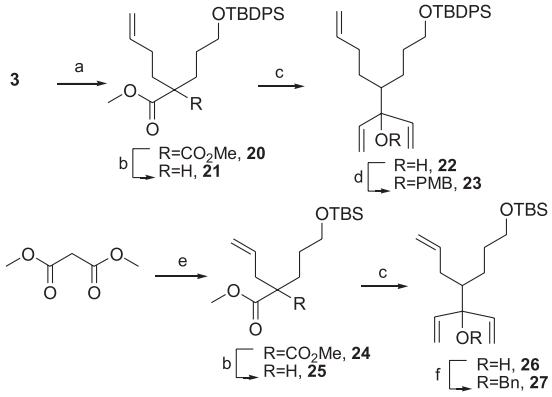
© 2000 NRC Canada

Table 1. DSRCM from monocycloalkene formation.

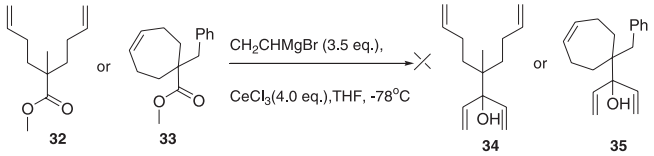


Entry	Starting material	Product	Catalyst	Mol%/Time (h)	Yield (%)	*cis:trans* CH_2=CH↔$(CH_2)_3$OP
1	**22**	**28**	1	12/5	80	1:2.8
2	**23**	**29**	1	3/3	96	6.1:1
3	**23**	**29**	2	6/1.5	86	7.8:1
4	**26**	**30**	1	6/1.5	65	1:1
5	**27**	**31**	1	3/1	99	8.0:1
6	**27**	**29**	2	6/0.5	94	1.7:1

Scheme 8. Synthesis of triene tertiary diallylic alcohols and ethers: (*a*) NaH (5.0 equiv.), $Br(CH_2)_3OTBDPS$ (1.5 equiv.), THF, 60°C, 48%; (*b*) NaCl (2.4 equiv.), H_2O, DMSO, 180°C, 4 h, 58%; (*c*) CH_2=CHMgBr (3.5 equiv.), $CeCl_3$ (4.0 equiv., anhydrous), THF, –78°C, 57% (**22**), 32% (**26**); (*d*) NaH (2.0 equiv.), PMBBr (2.0 equiv.), DMF, 23°C, 67%; (*e*) (*i*) NaH (1.0 equiv.), $Br(CH_2)_3OTBS$ (0.3 equiv.), THF, 60°C, 31%; (*ii*) NaH (2.0 equiv.), allyl bromide (1.5 equiv.) THF, 60°C, 83%; (*f*) KH (1.5 equiv.), BnBr (1.5 equiv.), THF, 60°C, 89%.



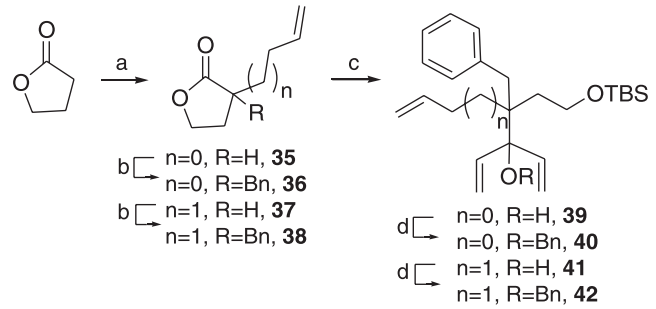
Scheme 9. Failure of esters having an α tertiary center to undergo reaction with vinyl cerium.



To probe the effect of bridgehead substituents on the efficiency and diastereoselectivity of the DRCM, substrates **32** and **33** were treated with the vinylcerium reagent but both failed to give the desired products. Steric effects at the α position may be responsible. (Scheme 9).

This problem was overcome by the use of lactones, where the third substituent is incorporated into the ring. For example, double alkylation to give lactones **36** and **38** followed by reaction with vinylcerium gave tertiary alcohols **39** and **41** in good overall yields as outlined in Scheme 10. Selective protection of the primary alcohols followed by benzylation of the tertiary alcohols furnished ethers **40** and **42**.

Scheme 10. Preparation of 3° alcohols from α,α-disubstituted lactones: (*a*) *n* = 0: LDA, allyl bromide, THF, –78°C, 80%; *n* = 1: (*i*) LDA, 1,4-dichlorobut-2-ene, THF– HMPA (7:1), –78°C; (*ii*) HCO_2NH_4, Pd_2dba_3, nBu_3P, toluene, 100°C, 3 h, 45% (2 steps); (*b*) LDA, BnBr, THF, 77% (**36**), 74% (**38**); (*c*) (*i*) CH_2=CHMgBr (3.5 equiv.), $CeCl_3$ (4.0 equiv., anhydrous), THF, –78°C; (*ii*) TBSCl (1.05 equiv.), imidazole (1.5 equiv.), DMF, 23°C, 57% (**39**), 48% (**41**); (*d*) KH (3.0 equiv.), BnBr (1.5 equiv.), THF, 23°C, 12 h, 85% (**40**), 90% (**42**).

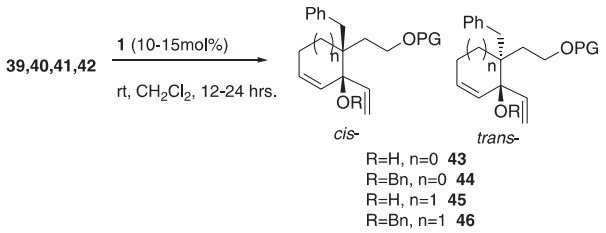


The butenylation of butyrolactone with conventional methodologies gave only low yields of **37** (<10%), but the two step approach mentioned above for the butenylation of a variety of nucleophiles proved to be more successful (6). Thus, alkylation with 1,4-dichlorobut-2-ene, followed by Pd catalyzed formate reduction furnished **37** in 45% yield over two steps.

The results from treating these trienes with Grubbs' catalyst are summarized in Table 2. Reaction of **39** with **1** (24-hour portion-wise addition) gave cyclopentene **43** as essentially a single diastereomer in 60% isolated yield. This diastereomer was shown to be *trans*-**43** (CH_2=CH↔$(CH_2)_2OSiR_3$) by ROSEY experiments (10). Treatment of **40** with the same catalyst gave a 2:1 mixture with *cis*-**44** (CH_2=CH↔$(CH_2)_3OSiR_3$) now being favored.

© 2000 NRC Canada

Table 2. DSRCM for 3° diallylic systems having an α tertiary center.

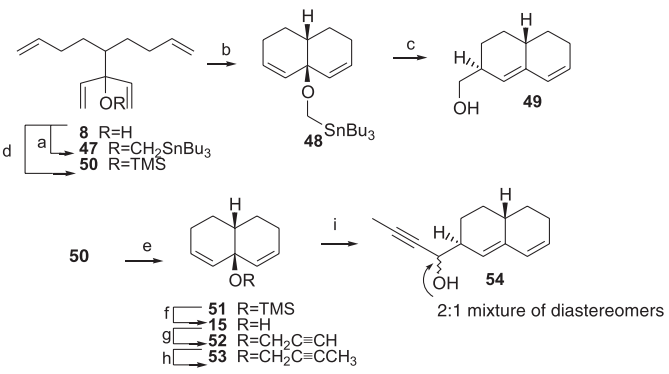


Entry	Starting Material	Product	Mol%/ Time (h)	Yield (%)	*cis*:*trans* CH_2=CH↔$(CH_2)_3$OP
1	**39**	**43**	15/24	60[a]	<1:>20
2	**40**	**44**	15/24	100[b]	2:1
3	**41**	**45**	8/12	100[b]	1:1
4	**42**	**46**	8/12	100[b]	4.5:1

[a]Isolated yield.

[b]Based on 100% conversion by ^{1}H NMR (400 MHz) analysis.

Scheme 11. [2,3] Wittig rearrangements as an approach to the hexahydronaphthalene portion (+)–melvinolin: (*a*) KH (3.0 equiv.), 18-crown-6 (cat.), ICH_2SnBu_3 (1.5 equiv.), THF, reflux, 93%; (*b*) **1** (12 mol%), CH_2=CH_2, CH_2Cl_2, reflux, 86%; (*c*) MeLi (1.05 equiv.), HMPA (4.0 equiv.), THF, –78°C, 67%; (*d*) KH (2.0 equiv.), TMSCl (1.05 equiv.), THF, 90%; (*e*) **2** (10 mol%), C_6H_6, 99%, dr = 5:1; (*f*) TBAF (3.0 equiv.), THF, 23°C, 86%; (*g*) NaH (5.0 equiv.), $BrCH_2C{\equiv}CH$ (5.0 equiv.), THF, 46%; (*h*) *n*-BuLi (1.1 equiv.), MeI (1.5 equiv.), THF, –78°C, 90%; (*i*) *t*-BuLi (4.0 equiv.), THF,–78°C, 63% (dr = 2:1).



Cyclohexenes having a bridgehead substituent were also formed in good yields. Treatment of the free alcohol **41** with **1** provided **45** as a 1:1 mixture of diastereomers. The analogous benzyl protected ethers were formed in a 4.5:1 mixture of diastereomers, favoring *cis*-**46**.

We have investigated potentially useful derivatizations of the bicyclic compounds. Deprotonation of **8** with KH, followed by alkylation with an iodomethyl stannane proceeds in good yield. DSRCM occurred in high yield to give the desired bicycle **48**. Treating this stannyl methyl ether with MeLi at –78°C afforded a 67% yield of the [2,3]-Wittig rearrangement product **49** (Scheme 11) (11).

A variation of the Wittig rearrangement was also investigated involving methyl propargyl ether **53**, prepared as outlined in Scheme 11 (12). DSRCM of **50** with **2** (12 mol%, 0.5 h) gave a 5:1 mixture of diastereomers. Desilylation afforded a separable mixture of free alcohols. The *cis*-fused free alcohol *cis*-**15** was converted to propargyl ether **53** in two steps. Treatment with *t*-BuLi at –78°C gave the [2,3]-Wittig rearrangement product in 63% yield as a 2:1 mixture of diastereomeric alcohols.

Discussion

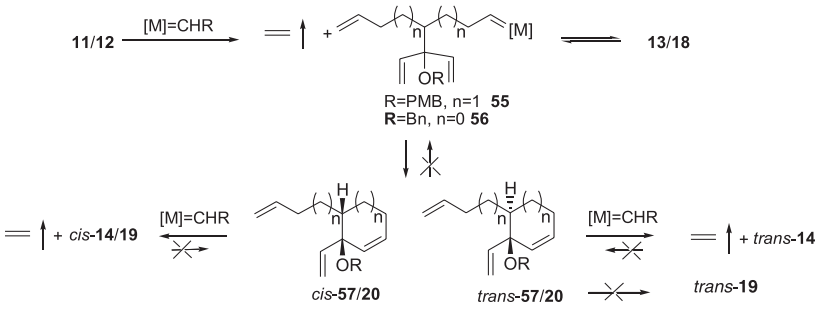
Based on our studies and previous work outlining the reactivity patterns of various olefins (13), we propose the following reaction pathway for decalin formation from **11** and **12**.

Transalkylidenation in **11** or **12** occurs at one of the two olefins lacking an α substituent to give **55**/**56** (Scheme 12). These intermediates then cyclizes initially to give cycloalkenes **13** or **18**. The formation of both **13** and **18** is reversible, as demonstrated by the observation that **13** and **18** are alternative entries into the catalytic cycle. A second less favorable but irreversible pathway involves cyclization onto one of the two more sterically hindered diastereotopic olefins to give either *cis*-**57**/**20** or *trans*-**57**/**20**. The formation of these cycloalkenes has been proven to be irreversible under all conditions examined to date. RCM between the two remaining acyclic olefins then affords bicyclic products, a process which should also be initiated by reaction at the less hindered alkene. While both *cis*- and *trans*-**57** will go on to give the corresponding *cis*- and *trans*-fused hexahydronaphthalenes, only *cis*-**20** goes onto to *cis*-fused diquinane as further cyclization of *trans*-**20** would give rise to a highly unstable *trans*-fused bicyclo[3.3.0] compound.

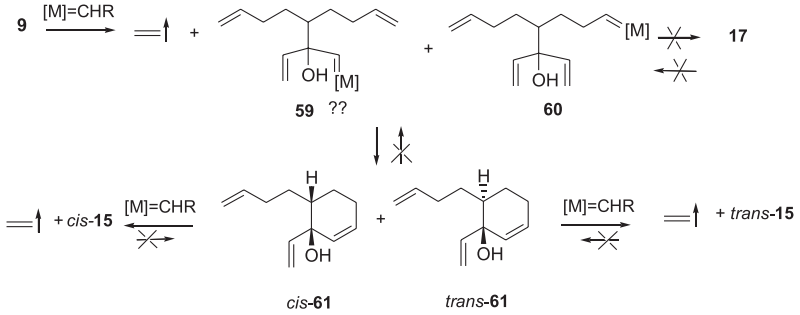
Double cyclization of free alcohols display interesting differences in diastereoselectivity compared to their protected analogues. As others have previously noted (14), free alcohols appear to cyclize at accelerated rates relative to the analogous ethers. For example whereas the *p*-methoxybenzyl ether **11** reacts to give the cycloheptene **13** faster than to form a cyclohexene **57**, we have been unable to observe the formation of cycloheptene **17** when free alcohol **9** is used as starting material. In fact, when **17** is used as starting material, no conversion to decalin is observed, suggesting that alkylidene formation may be taking place at the more hindered olefin (Scheme 13). The implications of these observations with regard to stereoselectivity issues are intriguing and are currently under investigation.

© 2000 NRC Canada

Scheme 12. Reaction pathway of decalin and diquinane formation.



Scheme 13. DSRCM reactions involving free alcohols.



The effect of added ethylene depends on the structure of the tetraene (for examples of other systems where added ethylene was found to enhance RCM see ref. (15)), enhancing the conversion with some substrates and hindering the cyclization of others. For example, when cyclizing free alcohol **9**, the use of an ethylene atmosphere resulted in incomplete conversion (~50%) before the catalyst decomposed. If the reaction was repeated but using a stream of Ar, the reaction also failed to go to completion. However when the reaction was conducted in a sealed system so that the ethylene produced upon cyclization was retained, complete consumption of starting material was observed. The cause of these effects are somewhat puzzling and warrant further study.

The relative sensitivities of the *cis*- and *trans*-fused decalins also warrants further mention. As one might expect, the tertiary diallylic alcohols and ethers are susceptible to solvolysis under acidic conditions. While most of the RCM precursors and the monocyclic intermediates could be isolated without difficulty, bicyclic materials were found to decompose upon chromatography unless the silica gel was neutralized with triethyl amine. The *trans*-fused decalins were found to be particularly acid sensitive, decomposing during TLC development, while the *cis*-fused analogues did not. Geometry optimization calculations (3–21G*) of *cis*-**15** and *trans*-**15** revealed that the dihedral angles between the olefin planes and the allylic C—O bond are 130° and 97° for *cis*-**15**, whereas both dihedral angles in *trans*-**15** are 90°, leaving the C—O bond in an antiperiplanar orientation with both double bonds, which would be expected to lower the energy barrier to carbenium ion formation.

Experimental

Toluene and THF were distilled from sodium–benzophenone. DMF was dried by prolonged standing over molecular sieves. HMPA was distilled under reduced pressure from CaH_2. CH_2Cl_2 was distilled from CaH_2. Grubbs' catalyst was prepared according to a literature procedure (16) and triturated for 12–18 h in a 1:1 mixture of acetone and methanol. The absence of free tricyclohexyl phosphine and tricyclohexyl phosphine oxide was confirmed by ^{31}P NMR, and was crucial in order for the double metathesis reactions to proceed. Schrock's catalyst was used as received from Strem. Computational work was done using MacSpartan Plus©, version 1.1.7 (Wavefunction Int. Irvine, Calif. 1996–1997).

General procedure for the decarboxylation of dimethyl malonates

To a 23°C solution of malonate in DMSO (1.0 M) was added NaCl (1.5 equiv.) and water (1 drop/1 mL DMSO). The resulting mixture was heated to 180°C for 5–10 h. The mixture was cooled to 23°C, diluted with ether and washed with water. The aqueous layer was extracted three times with ether. The organic layers were combined, washed with brine, dried over magnesium sulfate, and filtered. The filtrate was concentrated in vacuo and purified by flash chromatography on silica gel.

General procedure for the conversion of methyl esters to diallylic tertiary alcohols

$CeCl_3 \cdot 7H_20$ (4.0 equiv.) was ground with a mortar and pestle, placed under vacuum (<0.1 mmHg) and warmed to 140°C for 2 h. A stir bar was added and heating under vacuum continued for a further 4–10 h. The resulting powder was cooled to 0°C and THF (3 mL/mmol of $CeCl_3$) was added via cannula under vacuum. The remaining vacuum was displaced with N_2 and the resulting suspension stirred for 24 h, then cooled to –78°C. Vinylmagnesium bromide (~1 M in THF, 3.5 equiv.) was added via syringe at a rate such that the internal temperature was kept below –65°C.

© 2000 NRC Canada

After 1 h a solution of ester (1.0 equiv.) in THF (~1 M) was added via cannula at a rate such that the internal temperature did not exceed –65°C. After 30 min, the mixture was diluted with ethyl acetate and water was added. The organic layer was decanted off and the aqueous slurry extracted three times with ethyl acetate. The organic layers were combined, washed with brine, dried over sodium sulfate, and filtered. The filtrate was concentrated in vacuo and purified by flash chromatography on triethyl amine washed silica gel.

General procedure for the p-methoxy benzylation of tertiary diallylic alcohols

NaH (60% suspension in oil, 5.0 equiv.) was washed three times with pentane, dried under a stream of N_2 and suspended in DMF (0.3 M). A solution of alcohol in DMF (1.0 M) was added via cannula at a rate such the H_2 evolution is controlled. After 5 min, PMBBr was added via syringe and the resulting mixture was stirred at 23°C for 16 h. The mixture was diluted with ether and the reaction carefully quenched by drop-wise addition of saturated ammonium chloride. The aqueous layer was extracted three times with ether; the organic layers were combined, washed with brine, dried over sodium sulfate, and filtered. The filtrate was concentrated in vacuo and purified by flash chromatography on triethyl amine washed silica gel.

General procedure for the benzylation of tertiary diallylic alcohols

Potassium hydride (35% suspension in oil, 1.5 equiv.) was washed three times with pentane, dried under a stream of argon, and suspended in THF (half of total reaction volume). A solution of alcohol in THF (half of reaction volume, reaction concentration of 0.2 M) was added via cannula. The resulting suspension was warmed to 60°C and after 10 min benzyl bromide (1.5 equiv.) was added via syringe and the resulting mixture was stirred for an hour, cooled to 23°C, diluted with ether, and quenched carefully by drop-wise addition of water. The aqueous layer was extracted two times with ether, the organic layers were combined, washed with brine, dried over sodium sulfate, filtered and concentrated in vacuo. The residue was purified by flash chromatography on triethyl amine washed silica gel.

*Methyl 2-(but-3-enyl) hex-5-enoate (**7**)*

2,2 Di-(2-but-3-enyl) malonic acid dimethyl ester **5** (6.70 g, 27.9 mmol) was reacted according to the general procedure for decarboxylation. The crude product was purified by flash chromatography (3% ether–hexanes) to yield the title compound as a colorless oil (3.62 g, 71%). ^{1}H NMR (400 MHz, $CDCl_3$) δ: 1.48–1.57 (m, 2H), 1.64–1.76 (m, 2H), 1.94–2.08 (m, 4H), 2.35–2.43 (m, 1H), 4.94 (dq, J = 9, 1 Hz, 2H), 4.98 (dm, J = 17, 2 Hz, 2H), 5.69–5.79 (m, 2H). ^{13}C NMR (100 MHz, $CDCl_3$) δ: 31.52, 44.35, 51.36, 114.89, 137.70, 176.00.

*2-But-3-enyl-1-vinyl-octa-1,7-dien-3-ol (**9**)*

Methyl ester **7** (1.00 g, 5.49 mmol) was reacted according to the general procedure for the conversion of methyl esters to tertiary diallylic alcohols. The crude mixture was purified by flash chromatography (3% ether–hexanes) on triethyl amine washed silica gel to yield the title compound as a colorless oil (606 mg, 53%). IR (neat): 3478, 3078, 2934, 2978, 1640, 1456, 1414, 1300, 996, 912, 735. ^{1}H NMR (400 MHz, $CDCl_3$) δ: 1.18–1.28 (m, 2H), 1.41–1.49 (m, 2H), 1.59–1.69 (m 2H), 1.97–2.08 (m, 2H), 2.09–2.20 (m, 2H), 4.92 (dm, J = 10 Hz, 2H), 4.98 (dq, J = 17, 2 Hz, 2H), 5.14(dd, J = 11, 1 Hz, 2H), 5.25 (dd, J = 17, 1 Hz, 2H), 5.71–5.82 (m, 2H), 5.94 (dd, J = 17, 11 Hz, 2H). ^{13}C NMR (100 MHz, $CDCl_3$) δ: 29.39, 32.99, 45.78, 79.05, 113.42, 114.41, 138.97, 142.07.

*4-Allyl-3-vinyl-hepta-1,5-dien-3-ol (**10**)*

Methyl 2-propenylpent-4-enoate **8** (600 mg, 3.89 mmol) was reacted according to the general procedure for the formation of a tertiary diallylic alcohol. Purification by flash chromatography (5% ether–hexanes) on triethyl amine washed silica gel yielded the title compound as a colorless oil (460 mg, 66%). R_f = 0.19 (5% ether). IR (neat): 3072, 2933, 2859, 1738, 1642, 1473, 1428, 1390, 1195, 1164, 1112, 998, 917, 824, 741, 703, 614. ^{1}NMR (400 MHz, $CDCl_3$) δ: 1.70 (sept., J = 4 Hz, 1H), 1.87 (s, 1H), 2.07 (quint, J = 8 Hz, 2H), 2.28–2.36 (m, 2H), 5.00 (d, J = 9 Hz, 2H), 5.03 (d, J = 17 Hz, 2H), 5.79–5.91 (m, 2H), 5.95 (dd, J = 17 Hz, 11 Hz, 2H). ^{13}C NMR (100 MHz, $CDCl_3$) δ: 19.20, 23.65, 26.85, 31.60, 32.38, 36.42, 45.32, 51.33, 63.60, 116.62, 127.57, 129.49, 134.05, 135.50, 135.54, 176.04. HRMS calcd. for $(M\text{-}H)^+$: 177.1279; found: 177.1287.

*[2-But-3-enyl-1,1-divinyl-hex-5-enyloxymethyl]-4-methoxybenzene (**11**)*

Alcohol **9** (200 mg, 0.969 mmol), was reacted according to the general procedure for the *p*-methoxy benzylation of tertiary diallylic alcohols. The crude mixture was purified by flash chromatography (5% ether–hexanes) on triethyl amine washed silica gel to yield the title compound as a pale green oil (240 mg, 76%). IR (neat): 3478, 3078, 2934, 2978, 1640, 1456, 1414, 1300, 996, 912, 735. ^{1}H NMR (400 MHz, $CDCl_3$) δ: 1.11–1.22 (m, 2H), 1.60 (hept, J = 4 Hz, 1H), 1.67–1.77 (m, 2H), 2.02–2.21 (m, 4H), 3.81 (s, 3H), 4.31 (s, 2H), 4.94 (dm, J = 10 Hz, 2H), 5.01 (dq, J = 17, 2 Hz, 2H), 5.31 (dd, J = 18, 1.5 Hz, 2H), 5.37 (dd, J = 11, 2 Hz, 2H), 5.76–5.86 (m, 2H), 5.88 (dd, J = 18, 11 Hz, 2H), 6.88 (AB, J = 9 Hz, 2H), 7.26 (AB, J = 9 Hz, 2H). ^{13}C NMR (100 MHz, $CDCl_3$) δ: 30.05, 33.37, 47.30, 55.24, 64.82, 83.96, 113.57, 114.18, 117.39.

*[2-Allyl-1,1-divinyl-pent-4-enyloxymethyl] benzene (**12**)*

Tertiary alcohol **10** (500 mg, 2.80 mmol) was reacted according to the general procedure for the benzylation of tertiary diallylic alcohols. The crude product was purified by flash chromatography (100% hexanes –> 2% ether–hexanes) on triethyl amine washed silica gel to yield the title compound as a colorless oil (590 mg, 78%). R_f = 0.29 (2% ether–hexanes). IR (neat): 3074, 2920, 1639, 1497, 1453, 1414, 1377, 1096, 1064, 1000, 910, 729. ^{1}H NMR (400 MHz, $CDCl_3$) δ: 1.84 (sept., J = 4 Hz, 1H), 1.96 (dt, J = 14, 8 Hz, 2H), 2.44 (dm, J = 14.5 Hz, 2H), 4.38 (s, 2H), 4.94 (d, J = 11 Hz, 2H), 4.98 (d, J = 18 Hz, 2H), 5.79–5.90 (m, 2H), 5.90 (dd, J = 18, 11 Hz, 2H), 7.21–7.26 (m, 1H), 7.29–7.36 (m, 4H). ^{13}C NMR (100 MHz, $CDCl_3$) δ: 34.41, 48.07, 65.15, 83.53, 115.12, 117.63, 126.79, 126.85, 128.15,

© 2000 NRC Canada

137.87, 138.73, 139.88. HRMS calcd. for $(M-H)^+$: 267.1749; found: 267.1734.

*4a-(4-Methoxy-benzyloxy)-1,2,4a,7,8,8a-hexahydronaphthalene (**14**) (Ru Cat.)*

To a solution of **11** (200 mg, 0.613 mmol) in dichloromethane (12 mL) at 23°C was added **1** (61 mg, 0.073 mmol) and the mixture was placed under an atmosphere of ethylene. After 18 h, the mixture was concentrated in vacuo. The residue was purified by flash chromatography (3% ether–hexanes) on triethyl amine washed silica gel to yield the title compound as a colorless oil (115 mg, 70%). R_f = 0.15 (4% ether–hexanes). IR (neat): 3019, 2826, 1653, 1613, 1586, 1559, 1513, 1456, 1374, 1301, 1248, 1172, 1034, 947, 821. ^{1}H NMR (400 MHz, $CDCl_3$) δ: 1.50–1.61 (m, 2H), 1.85 (quintd, *J* = 6.5, 3.5 Hz, 2H), 1.98–2.14 (m, 4H), 2.19 (hept, *J* = 4 Hz, 1H), 3.79 (s, 3H), 4.38 (s, 2H), 5.61 (dt, *J* = 10, 2 Hz, 2H), 5.87 (dt, *J* = 10, 4 Hz, 2H), 6.85 (AB, *J* = 9 Hz, 2H), 7.25 (AB, *J* = 9 Hz, 2H). ^{13}C NMR (100 MHz, $CDCl_3$) δ: 23.32, 24.29, 34.43, 55.25, 64.10, 74.14, 113.70, 129.05, 129.64, 130.27, 132.18, 158.87. HRMS calcd. form M^+: 270.1620; found: 270.1611.

Cycloheptene intermediate: 5-(penta-1,4-dien-3-ol, *p*-methoxy benzyl ether)-cyclohept-1-ene (**13**): R_f = 0.37 (4% ether–hexanes). IR (neat): 2919, 1612, 1585, 1512, 1450, 1300, 1247, 1108, 1037, 927, 820, 737, 697. ^{1}H NMR (400 MHz, $CDCl_3$) δ: 1.05 (q, *J* = 11 Hz, 2H)1.77 (tt, *J* = 11, 3 Hz, 1H), 1.92–2.06 (m, 4H), 2.21–2.33 (m, 2H), 3.79 (s, 3H), 4.29 (s, 2H), 5.28 (dd, *J* = 18, 6 Hz, 2H), 5.35 (dd, *J* = 11, 2 Hz, 2H), 5.72–5.80 (m, 2H), 5.86 (dd, *J* = 18, 11 Hz, 2H), 6.87 (AB, *J* = 9 Hz, 2H), 7.26 (AB, *J* = 9 Hz, 2H). ^{13}C NMR (100 MHz, $CDCl_3$) δ: 27.98, 28.02, 52.62, 55.24, 64.72, 83.36, 117.25, 128.21, 131.87, 132.06, 138.16, 158.65.

*4a-(4-Methoxy-benzyloxy)-1,2,4a,7,8,8a-hexahydronaphthalene (**14**) (Mo Cat.)*

To a solution of **11** (47 mg, 0.142 mmol) in C_6H_6 (0.5 mL) at 23°C was added a solution of **2** (12 mg, 0.016 mmol) in C_6H_6 (1.5 mL). After 20 h the mixture was concentrated in vacuo and the residue purified by flash chromatography (3% ether–hexanes) on triethyl amine washed silica gel to yield the title compound as a colorless oil (28 mg, 73%).

cis- *and* trans-*2,7,8,8a-Tetrahydro-1*H-*naphthalen-4-ol (**15**)*

To a solution of **9** (100 mg, 0.242 mmol) in dichloromethane (4.5 mL) at 23°C was added **1** (40 mg, 0.049 mmol). After 1 hour PPh_3 (17 mg, 0.065 mmol) was added and the mixture was concentrated in vacuo and the residue was purified by flash chromatography (30% ether–hexanes) on triethyl amine washed silica gel to yield the title compounds as a white solid and a colorless oil (45 mg, 62% (*trans*)), (16 mg, 22% (*cis*)). Due to the sensitivity of the *trans* compound, it was immediately hydrogenated and characterized. The structure of the resulting decahydronaphthalenol was confirmed by comparison to spectral data reported in the literature (17).

cis-: IR (neat): 3351, 3023, 2908, 1429, 1383, 1326, 1204, 1021, 960. ^{1}H NMR (400 Mhz, $CDCl_3$) δ: 1.49–1.60 (m, 2H), 1.76–1.84 (m, 2H), 1.87–1.94 (m, 1H), 2.01–2.07 (m, 4H), 5.58 (dt, *J* = 10, 2 Hz, 2H), 5.77 (dt, *J* = 10, 3.7 Hz, 2H). ^{13}C NMR δ: 23.11, 24.27, 39.70, 38.34, 128.19, 131.34. HRMS calcd. for $C_{10}H_{14}O^+$ (M^+): 150.1045; found: 150.1044.

cis-*3a-Benzyloxy-1,3a,6,6a-tetrahydro-pentalene (**19**) (Ru Cat.)*

To a solution of benzyl ether **12** (100 mg, 0.372 mmol) in dichloromethane (4 mL) at 23°C was added **1** (12 mg, 0.04 equiv.). The resulting solution was stirred under an ethylene atmosphere for 20 h before PPh_3 (14 mg, 0.053 mmol) was added and the mixture concentrated in vacuo. The residue was purified by flash chromatography (2% ether–hexanes) on triethyl amine washed silica gel to yield the title compound as a colorless oil along with cyclopentene **20** (63 mg, 80%) and (12 mg, 13%), respectively. R_f = 0.11 and 0.34 (2% ether–hexanes) respectively. IR (neat) 3053, 2919, 2848, 1497, 1448, 1378, 1349, 1216, 1139, 1099, 1028, 991, 733, 697. ^{1}H NMR (400 MHz, $CDCl_3$) δ: 2.06–2.15 (m, 2H), 2.81–2.91 (m, 3H), 4.42 (s, 2H), 5.83 (dt, *J* = 6, 2 Hz, 2H), 5.92 (dt, *J* = 6, 2 Hz, 2H), 7.21–7.26 (m, 1H), 7.28–7.35 (m, 4H). ^{13}C NMR δ: 40.72, 43.03, 65.58, 105.70, 127.16, 127.55, 128.25, 132.54, 134.27, 139.56. HRMS calcd. for $C_{15}H_{16}O$ (M^+): 212.1201; found: 212.1196.

*Cyclopentene intermediate **11***: ^{1}H NMR (400 MHz, $CDCl_3$) δ: 2.38 (d, *J* = 6 Hz, 4H), 2.74 (quint, *J* = 8Hz, 1H), 4.43 (s, 2H), 5.32 (AB, *J* = 1.5 Hz, 2H), 5.35 (q, *J* = 1.5 Hz, 2H), 5.62 (s, 2H), 5.90 (dd, *J* = 18, 10.5 Hz, 2H), 7.22–7.26 (m, 1H), 7.30–7.37 (m, 4H). ^{13}C NMR δ: 34.27, 45.33, 65.089, 82.77, 117.11, 126.82, 126.87, 128.15, 129.74, 138.04.

2-But-3-enyl-2-(3-tert-*butyldiphenylsiloxy-propyl) malonic acid dimethyl ester (**20**)*

Sodium hydride (1.10 g, 32.2 mmol) was washed three times with pentane, dried under a stream of nitrogen, and suspended in DMF (40 mL). A solution of dimethyl but-3-enyl malonate **3** (4.00 g, 21.5 mmol) in DMF (10 mL) was added via cannula at a rate such that hydrogen evolution was controlled. After 30 min, a solution $TBDPSO(CH_2)_3Br$ in DMF (10 mL) was added via cannula. After 20 h, the mixture diluted with ether and quenched by careful addition of water. The aqueous layer was extracted with ether, the organic layers were combined, washed with brine, dried over magnesium sulfate, filtered and concentrated in vacuo. The residue was purified by flash chromatography (5% ether–hexanes) to yield the title compound as a colorless oil (5.00 g, 48%). IR (neat): 2954, 2858, 1732, 1434, 1257, 1104, 837, 776. ^{1}H NMR (400 MHz, $CDCl_3$) δ: 1.05 (s, 9H), 1.36–1.46 (m, 3H), 1.89–2.05 (m, 7H) 3.65 (t, *J* = 6 Hz, 2H), 3.70 (s, 6H), 4.97 (dd, *J* = 10, 1.5 Hz, 1H), 5.03 (dd, *J* = 17, 1.5 Hz, 1H), 5.72–5.83 (m, 1H), 7.36–7.45 (m, 6H), 7.64–7.67 (m, 4H). ^{13}C NMR (100 MHz, $CDCl_3$) δ: 19.17, 26.81, 27.28, 28.30, 28.91, 31.60, 52.29, 57.04, 63.57, 115.00, 127.60, 129.56, 133.79, 135.52, 137.46, 172.02. HRMS calcd. for $C_{24}H_{29}O_5Si$ ($M-C_4H_9$): 425.1784; found: 425.1793.

2-(3-tert-*Butyldiphenylsiloxy-propyl)-hex-5-enoic acid methyl ester (**21**)*

Malonate **20** (5.00 g, 10.4 mmol) was reacted according to the general procedure for decarboxylation. The crude mixture was purified by flash chromatography (5% ether–hexanes) to yield title compound as a colorless oil (2.58 g,

© 2000 NRC Canada

58%). IR (neat): 2930, 1734, 1428, 1111. ^{1}H NMR ($CDCl_3$) δ: 1.05 (s, 9H), 1.49–1.79 (m, 6H), 2.00–2.08 (m, 2H), 2.35–2.44 (m, 1H), 3.63–3.68 (m, 5H), 4.97 (dm, *J* = 10 Hz, 1H), 5.02 (dq, *J* = 17, 2 Hz, 1H), 5.72–5.83 (m, 1H), 7.36–7.46 (m, 6H), 7.65–7.69 (m, 4H). ^{13}C NMR (100 MHz, $CDCl_3$) δ: 19.20, 26.84, 28.59, 30.22, 31.47, 31.54, 44.62, 51.33, 63.51, 115.02, 127.59, 129.53, 133.94, 135.54, 137.85, 176.51. HRMS calcd. for $C_{22}H_{25}O_3Si$ (M-$C_4H_9^+$): 367.1729; found: 367.1725.

4-(3-tert-*Butyldiphenylsiloxy-propyl)-3-vinyl-hepta-1,6-dien-3-ol (**22**)*

Methyl ester **26** (1.25 g, 2.94 mmol) was reacted according to the general procedure for the conversion of a methyl ester to a tertiary diallylic alcohol. The crude product was purified by flash chromatography (8% ether–hexanes) on triethyl amine washed silica gel to yield the title compound as a pale green oil (754 mg, 57%). R_f = 0.25 (10% ether–hexanes). IR (neat): 3475, 2930, 1636, 1472, 1427, 1111. ^{1}H NMR (400 MHz, $CDCl_3$) δ: 1.05 (s, 9H), 1.14–1.26 (m, 2H), 1.38–1.44 (m, 1H), 1.46–1.69 (m, 5H), 1.94–2.06 (m, 1H), 2.09–2.20 (m, 1H), 3.63 (t, *J* = 6 Hz, 2H), 4.93 (dm, *J* = 10 Hz, 1H), 4.98 (dq, *J* = 17, 2 Hz, 1H), 5.14 (ddd, *J* = 11, 3.5, 1 Hz, 2H), 5.25 (ddd, *J* = 17, 4, 1 Hz, 2H), 5.71–5.82 (m, 1H), 5.94 (ddd, *J* = 17, 11, 2 Hz, 2H), 7.35–7.45 (m, 6H), 7.65–7.69 (m, 4H). ^{13}C NMR (100 MHz, $CDCl_3$) δ: 19.19, 26.09, 26.87, 29.38, 31.86, 32.86, 46.18, 64.14, 79.10, 113.37, 114.39, 127.56, 129.50, 134.05, 135.57, 139.02, 142.06, 142.15. HRMS calcd. for $C_{25}H_{31}O_2Si$ (M-$C_4H_9^+$): 391.2093; found: 391.2098.

[2-(3-tert-*Butyldiphenylsiloxy-propyl)-1,1-divinyl-hex-5-enyloxymethyl]-4-methoxy-benzene (**23**)*

Alcohol **22** (400 mg, 0.891 mmol) was reacted according to the general procedure for the *p*-methoxy benzylation of tertiary diallylic alcohols. The crude material was purified by flash chromatography (2% ether–hexanes) on triethyl amine washed silica gel to yield the title compound as a colorless oil (325 mg, 65%). R_f = 0.22 (5% ether–hexanes). IR (neat): 2930, 1615, 1513, 1428, 1247, 1111. ^{1}H NMR (400 MHz, $CDCl_3$) δ: 1.08 (s, 9H), 1.12–1.24 (m, 2H), 1.55–1.80 (m, 5H), 2.02–2.23 (m, 2H), 3.66 (t, *J* = 6 Hz, 2H), 3.81 (s, 3H), 4.32 (s, 2H), 4.95 (dm, *J* = 10 Hz, 1H), 5.01 (dq, *J* = 17, 2 Hz, 1H), 5.31 (dt, *J* = 18, 1.5 Hz, 2H), 5.37 (ddd, *J* = 11, 4, 1.5 Hz, 2H), 5.78–5.87 (m 1H), 5.88 (ddd, *J* = 18, 11, 1 Hz, 2H), 6.87 (AB, *J* = 9 Hz, 2H), 7.27 (AB, *J* = 9 Hz, 2H), 7.37–7.47 (m, 6H), 7.68–7.72 (m, 4H). ^{13}C NMR (100 MHz, $CDCl_3$) δ: 19.20, 26.81, 26.88, 30.01, 32.29, 33.28, 47.70, 55.22, 64.37, 64.82, 84.01, 113.58, 114.13, 117.28, 127.54, 128.13, 129.45, 132.14, 134.16, 135.57, 138.15, 138.23, 139.35, 158.54. HRMS calcd. for $C_{33}H_{39}O_3Si$ (M-$C_4H_9^+$): 511.2668; found: 511.2689.

2-Allyl-(3-tert-*Butyldimethylsiloxy-propyl)-malonic acid dimethyl ester (**24**)*

Sodium hydride (4.16 g, 104.1 mmol) and potassium hydride (cat.) were washed three times with pentane, suspended in DMF (75 mL) and cooled to 0°C. A solution of dimethyl malonate (11.9 mL, 104.1 mmol) in DMF (50 mL) was added via addition funnel at a rate such that the evolution of H_2 was controlled. The mixture was warmed to room temperature. After 30 min, a solution of TBDPSO$(CH_2)_3$Br (8.80 g, 34.7 mmol) in DMF (10 mL) was added via cannula. After 14 h, the mixture was diluted with ether and quenched carefully with water. The aqueous layer was washed three times with ether; the organic layers were combined, washed with brine, dried over magnesium sulfate, and filtered. The filtrate was concentrated in vacuo and the residue purified by fractional distillation. Collection of the fraction boiling between 100–110°C (0.1 mmHg) yielded the monoalkylated malonate as a colorless liquid (3.26 g, 31%). R_f = 0.23 (15% ether–hexanes). IR (neat): 2955, 2858, 1768, 1436, 1389, 1255, 1155, 1099, 1009, 837, 777. ^{1}H NMR (400 MHz, $CDCl_3$) δ: 0.03 (s, 6H), 0.88 (s, 9H), 1.49–1.57 (m, 2H), 1.91–2.00 (m, 2H), 3.41 (t, *J* = 8 Hz, 1H), 3.62 (t, *J* = 6 Hz, 2H), 3.73 (s, 6H). ^{13}C NMR (100 MHz, $CDCl_3$) δ: –5.41, 18.26, 25.47, 25.87, 30.27, 51.35, 52.39, 62.40, 169.86. HRMS calcd. for (M-CH_3)$^+$: 289.1471; found: 289.1474.

Sodium hydride (0.509 g, 21.2 mmol) was washed three times with pentane and suspended in THF (20 mL). A solution of the monoalkylated malonate prepared as described above (3.00 g, 9.85 mmol) in THF (20 mL) was added via cannula at a rate such that H_2 evolution is controlled. After 15 min, allyl bromide (1.86 mL, 21.2 mmol) was added via syringe. After 1 h the mixture was diluted with ether, quenched carefully with water, and the aqueous layer was extracted two times with ether. The organic layers were combined, washed with brine, dried over magnesium sulfate and filtered. The filtrate was concentrated in vacuo and purified by flash chromatography (10% ether–hexanes) on silica gel to yield the title compound as a colorless oil (2.80 g, 83%). R_f = 0.32 (15% ether–hexanes). IR (neat): 2954, 2858, 1737, 1435, 1388, 1361, 1256, 1210, 1099, 1034, 921, 837, 776. ^{1}H NMR (400 MHz, $CDCl_3$) δ: 0.03 (s, 6H), 0.87 (s, 9H), 1.35–1.44 (m, 2H), 1.87–1.95 (m, 2H), 2.64 (d, *J* = 7 Hz, 2H), 3.58 (t, *J* = 6 Hz, 2H), 3.70 (s, 6H), 5.05–5.13 (m, 2H), 5.57–5.69 (m, 1H). ^{13}C NMR (100 MHz, $CDCl_3$) δ: –5.36, 18.26, 25.89, 27.45, 28.84, 37.09, 52.29, 57.38, 62.86, 118.91, 132.38, 171.68. HRMS calcd. for (M-CH_3)$^+$: 329.1784; found: 329.1801.

2-(3-tert-*Butyldimethylsiloxy-propyl)-pentenoic acid methyl ester (**25**)*

Malonate **24** (2.61 g, 7.58 mmol) was reacted according to the general decarboxylation procedure. The crude mixture was purified by flash chromatography (7% ether–hexanes) to yield the title compound as a colorless oil (960 mg, 44%). R_f = 0.20 (5% ether–hexanes). IR (neat): 2952, 2858, 1740, 1361, 1256, 1167, 1102, 1006, 915, 837, 776. ^{1}H NMR (400 MHz, $CDCl_3$) δ: 0.02 (s, 6H), 0.87 (s, 9H), 1.44–1.66 (m, 4H), 2.18–2.26 (m, 1H), 2.30–2.40 (m, 1H), 2.41–2.49 (m, 1H), 3.58 (td, *J* = 6, *J* = 2 Hz, 2H), 3.65 (s, 3H), 4.97–5.08 (m, 2H), 5.66–5.78 (m, 1H). ^{13}C NMR (100 MHz, $CDCl_3$) δ: –5.36, 18.27, 25.89, 28.07, 30.40, 36.45, 44.97, 51.34, 62.72, 116.68, 135.41, 175.97. HRMS calcd. for (M-CH_3)$^+$: 271.1729; found: 271.1742.

4-(3-tert-*Butyldimethylsiloxy-propyl)-3-vinyl-hepta-1,6-dien-3-ol (**26**)*

Methyl ester **25** (0.900 g, 3.13 mmol) was reacted under standard condition for the conversion of methyl esters to

© 2000 NRC Canada

diallylic tertiary alcohols. The crude product was purified by flash chromatography (7% ether–hexanes) on triethyl amine washed silica gel to yield the title compound as a pale green oil (314 mg, 32%). R_f = 0.25 (10% ether–hexanes). IR (neat): 3475, 3079, 2929, 2858, 1639, 1472, 4109, 1361, 1256, 1100, 999, 921, 836, 775, 735. ^{1}H NMR (400 MHz, $CDCl_3$) δ: 0.04 (s, 6H), 0.88 (s, 9H), 1.16–1.26 (m, 1H), 1.42–1.52 (m, 1H), 1.53–1.70 (m, 3H), 1.83 (s, 1H), 2.02 (quint, *J* = 7 Hz, 1H), 2.30–2.38 (m, 1H), 3.56 (t, *J* = 6 Hz, 2H), 4.98 (dquint, *J* = 10, 0.5 Hz, 1H), 5.02 (dq, *J* = 17, 0.5 Hz, 1H), 5.16 (dd, *J* = 11, 1 Hz, 2H), 5.28 (dt, *J* = 17, 1 Hz, 2H), 5.81–6.00 (m, 3H). ^{13}C NMR (100 MHz, $CDCl_3$) δ: –5.29, 18.31, 25.32, 25.94, 31.75, 34.34, 46.51, 63.31, 79.23, 113.48, 115.80, 138.37, 141.79, 142.20. HRMS calcd. for $C_{17}H_{31}O_2Si$ $(M\text{-}CH_3)^+$: 295.2091; found: 295.2091.

2-(3-tert-*Butyldimethylsiloxy-propyl)-1,1-divinyl-pent-4-enyloxymethyl)-benzene (**27**)*

Alcohol **26** (288 mg, 0.927 mmol) was reacted according to the general benzylation procedure to yield the title compound as a colorless oil (329 mg, 89%). R_f = 0.21 (2% ether–hexanes). IR (neat): 3086, 2929, 2858, 1639, 1497, 1472, 1408, 1380, 1255, 1099, 1027, 1004, 929, 836, 775, 728, 695, 661. ^{1}H NMR (400 MHz, $CDCl_3$) δ: 0.03 (s, 6H), 0.88 (s, 9H), 1.10–1.20 (m, 1H), 1.46–1.57 (m, 1H), 1.58–1.74 (m, 3H), 1.82–1.94 (m, 1H), 2.46–2.54 (m, 1H), 3.55 (t, *J* = 6 Hz, 2H), 4.37 (s, 2H), 4.93 (d, *J* = 10 Hz, 1H), 4.99 (dq *J* = 17, 1 Hz, 1H), 5.30 (dd, *J* = 17, 1.5 Hz, 2H), 5.36 (dd, *J* = 11, 1.5 Hz, 2H), 5.80–5.90 (m, 1H), 5.89 (dd, *J* = 18, 11 Hz, 2H), 7.21–7.26 (m, 1H), 7.29–7.36 (m, 4H). ^{13}C NMR (100 MHz, $CDCl_3$) δ: –5.26, 18.33, 25.97, 26.36, 32.30, 35.13, 48.00, 63.56, 65.12, 83.79, 114.92, 117.48, 117.55, 126.75, 126.81, 128.14, 137.81, 138.16, 139.06, 139.98. HRMS calcd. for $(M\text{-}CH_3)^+$: 385.2563; found: 385.2581.

cis- *and* trans-*6-(3*-tert-*Butyldiphenylsiloxy-propyl)-1-vinyl-cyclohex-2-enol (**28**)*

To a 23°C solution of triene **22** (200 mg, 0.446 mmol) in dichloromethane (4.5 mL) was added **1** (44 mg, 0.053 mmol). After 5 h PPh_3 (28 mg, 0.107 mmol) was added and the mixture concentrated in vacuo. A crude ^{1}H NMR showed a 2.8:1 mixture of diastereomers in favor of the product having the methine proton and OH substituent *trans* to one another. The residue was purified by flash chromatography (15% ether–hexanes) on triethyl amine washed silica gel to yield the title product as a colorless oil (151 mg, 80%).

cis-: IR (neat): 3441, 3071, 2931, 1651, 1590, 1472, 1428, 1390, 1361, 1175, 1111, 998, 822. ^{1}H NMR (400 MHz, $CDCl_3$) δ: 0.94–1.08 (m, 1H), 1.05 (s, 9H), 1.20–1.33 (m, 1H), 1.47–1.59 (m, 2H), 1.62–1.78 (m, 3H), 2.01–2.07 (m, 2H), 3.62–3.71 (m, 2H), 5.14 (dd, *J* = 11, 2 Hz, 1H), 5.18 (dd, *J* = 17, 2 Hz, 1H), 5.41 (dt, *J* = 10, 2 Hz, 1H), 5.87 (dt, *J* = 10, 4 Hz, 1H), 5.87 (dd, *J* = 17, 11 Hz, 1H), 7.35–7.45 (m, 6H), 7.65–7.69 (m, 4H). ^{13}C NMR (100 MHz, $CDCl_3$) δ: 19.22, 24.78, 25.21, 25.92, 26.91, 30.79, 45.21, 64.30, 75.31, 114.38, 127.58, 128.44, 129.50, 132.63, 134.15, 135.60, 140.37.

trans-: IR (neat): 3471, 3071, 3020, 2931, 1649, 1589, 1472, 1428, 1390, 1361, 1304, 1111, 997, 954, 921, 823, 937, 701, 614. ^{1}H NMR (400 MHz, $CDCl_3$) δ: 1.07 (s, 9H), 1.10–1.21 (m, 1H), 1.34–1.54 (m, 4H), 1.60–1.78 (m, 3H), 1.92–2.04 (m, 1H), 2.07–2.16 (m, 1H), 3.68 (t, *J* = 6 Hz, 2H), 5.14 (dd, *J* = 11, 1.5 Hz, 1H), 5.32 (dd, *J* = 17, 1.5 Hz, 1H), 5.52 (dt, *J* = 10, 2 Hz, 1H), 5.83 (dd, *J* = 17, 11 Hz, 1H), 5.87 (dq, *J* = 10, 2.5 Hz, 1H), 7.36–7.46 (m, 6H), 7.66–7.71 (m, 4H). ^{13}C NMR (100 MHz, $CDCl_3$) δ: 19.19, 22.85, 24.67, 25.43, 26.89, 30.75, 42.84, 64.18, 72.71, 113.14, 127.54, 129.47, 130.35, 131.78, 134.15, 135.58, 144.45. HRMS calcd. for $(M\text{-}C_4H_9)^+$: 363.1780; found: 363.1887.

cis- *and* trans-*[6-(3*-tert-*Butyldiphenylsiloxy-propyl)-1-vinyl-cyclohex-2-enyloxymethyl]-4-methoxy-benzene (**29**) (Mo Cat.)*

To a solution of triene **23** (51 mg, 0.089 mmol) in C_6H_6 (0.5 mL) at 23°C was added a solution of **2** (4 mg, 0.006 mmol) in C_6H_6 (0.5 mL). The resulting solution was stirred for 90 min before the mixture was concentrated in vacuo. A crude ^{1}H NMR showed a 7.8:1 mixture favoring the *cis*-diastereomer. The ratio was determined by comparing the integration of the doublets of triplets appearing at δ 5.61 (*cis*-) and δ 5.75 (*trans*-) in the crude ^{1}H NMR. The residue was purified by flash chromatography (2% ether–hexanes) on triethyl amine washed silica gel to yield the title compounds as colorless oils (42 mg, 86%).

cis-: R_f = 0.20, (5% ether–hexanes). IR (neat) 2931, 1613, 1513, 1472, 1428, 1301, 1247, 1171, 1111, 998, 822, 702. ^{1}H NMR (400 MHz, $CDCl_3$) δ: 0.92–1.10 (m, 1H), 1.05 (s, 9H), 1.26–1.38 (m, 1H), 1.44–1.55 (m, 1H), 1.63–1.89 (m, 4H), 2.03–2.09 (m, 2H), 3.66 (td, *J* = 6, 1.5 Hz, 2H), 3.79 (s, 3H), 4.38 (s, 2H), 5.18 (dd, *J* = 17, 2 Hz, 1H), 5.22 (dd, *J* = 11, 2 Hz, 1H), 5.61 (dt, *J* = 10, 2 Hz, 1H), 5.88 (dd, *J* = 17, 11 Hz, 1H), 5.99 (dt, *J* = 10, 3.5 Hz, 1H) 6.84 (AB, *J* = 9 Hz, 2H), 7.24 (AB, *J* = 9 Hz, 2H), 7.35–7.45 (m, 6H), 7.66–7.70 (m, 4H). ^{13}C NMR (100 MHz, $CDCl_3$) δ: 19.00, 23.86, 25.03, 25.19, 26.68, 30.58, 40.43, 55.06, 65.93, 64.27, 76.48, 30.58, 40.43, 55.06, 65.93, 64.27, 76.48, 80.56, 113.44, 116.25, 127.35, 128.469, 129.22, 129.26, 131.08, 132.87, 134.96, 135.37, 140.89, 158.53. HRMS calcd. for $C_{31}H_{35}O_3Si$ $(M\text{-}C_4H_9)^+$: 483.2355; found: 483.2363.

trans-: R_f = 0.29, (5% ether–hexanes). ^{1}H NMR (400 MHz, $CDCl_3$) δ: 1.04 (s, 9H), 1.26–1.50 (m, 3H), 1.56–1.76 (m, 3H), 1.76–1.86 (m, 1H), 1.92–2.04 (m, 1H), 2.07–2.17 (m, 1H), 3.64 (t, *J* = 6.5 Hz, 2H), 3.78 (s, 3H), 4.39 (AB, *J* = 11 Hz, 1H), 4.42 (AB, *J* = 11 Hz, 1H), 5.18 (dd, *J* = 6, 1.5 Hz, 1H), 5.22 (s, 1H), 5.75 (dt, *J* = 10, 2 Hz, 1H), 5.88–5.96 (m, 1H), 6.01 (dq, *J* = 10, 2 Hz, 1H), 6.84 (AB, *J* = 9 Hz, 2H), 7.24 (AB, *J* = 9 Hz, 2H), 7.34–7.44 (m, 6H), 7.65–7.70 (m, 4H). ^{13}C NMR (100 MHz, $CDCl_3$) δ: 19.21, 22.73, 24.08, 25.30, 26.88, 31.03, 43.83, 55.26, 64.36, 64.58, 110.39, 113.56, 115.25, 127.53, 128.16, 128.49, 129.42, 132.05, 132.49, 134.21, 135.58, 143.14, 158.50.

cis- *and* trans-*[6-(3*-tert-*Butyldiphenylsiloxy-propyl)-1-vinyl-cyclohex-2-enyloxymethyl]-4-methoxy-benzene (**29**) (Ru Cat.)*

To a solution of triene **23** (200 mg, 0.351 mmol) in dichloromethane (3.5 mL) at 23°C was added **1** (12 mg, 0.014 mmol). After 3 h, PPh_3 (7 mg, 0.029 mmol) was

© 2000 NRC Canada

added and the mixture was concentrated in vacuo. A crude ^{1}H NMR showed a 6.1:1 mixture favoring the *cis*-diastereomer. The ratio was determined by comparing the integration of the doublets of triplets appearing at δ 5.61 (*cis*-) and δ 5.75 (*trans*-) in the crude ^{1}H NMR. The residue was purified by flash chromatography (5% ether–hexanes) on triethyl amine washed silica gel to yield the title compounds as colorless oils (181 mg, 96%).

cis- *and* trans-*5-(3*-tert-*Butyldimethylsiloxy-propyl)-1-vinyl-cyclopent-2-enol (**30**)*

To a solution of triene **26** (29 mg, 0.093 mmol) in C_6H_6 (1.0 mL) at 23°C was added **1** (4.6 mg, 0.0056 mmol). The resulting solution was stirred for 90 min before PPh_3 (6 mg, 0.0075 mmol) was added and the mixture concentrated in vacuo. A crude ^{1}H NMR showed a 1:1 mixture of diastereomers. The ratio was determined by comparing the integration of the doublets of quartets appearing at δ 5.59 and δ 5.69 in the crude ^{1}H NMR. The mixture was purified by flash chromatography (10% ether–hexanes) on triethyl amine washed silica gel to yield the title compounds as a colorless oil (17 mg, 65%).

cis- *and* trans-*mixture*: IR (neat): 3418, 2929, 1472, 1255, 1097, 995, 922, 836, 775, 663. ^{1}H NMR (400 MHz, $CDCl_3$) δ: 0.04 (s, 6H), 0.88 (s, 9H), 1.20–1.32 (m, 1H), 1.34–1.44 (m, 1H), 1.50–1.64 (m, 2H), 1.87 (s, 1H), 1.86–2.18 (m, 2 H), 2.54 (tdq, *J* = 16.5, 7.5, 1.5 Hz, 1H), 3.62 (m, 2H), 5.06–5.31 (series of doublets, 2H), 5.59, (dq, *J* = 6, 1 Hz, 0.5 H), 5.69 (dq, *J* = 6, 1 Hz, 0.5H), 5.82 (dd, *J* = 17, 11 Hz, 0.5 H), 5.98 (dd, *J* = 17, 11 Hz, 0.5 H), 5.91 (quint., *J* = 2 Hz, 0.5H), 5.99–6.03 (m, 0.5H). ^{13}NMR (100 MHz, $CDCl_3$) δ: –5.26, 18.37, 25.99, 26.70, 31.65, 37.59, 37.64, 47.66, 51.96, 63.39, 63.48, 84.77, 87.21, 112.31, 113.05, 132.32, 134.19, 136.12, 136.79, 143.43.

cis- *and* trans-*5-(3*-tert-*Butyldimethylsiloxy-propyl)-1-vinyl-cyclopent-2-enyloxy benzyl ether (**31**) (Mo Cat.)*

To a solution of triene **27** (20 mg, 0.050 mmol) in C_6H_6 (0.5 mL) at 23°C was added a solution of **2** (2.5 mg, 0.003 mmol) in C_6H_6 (0.5 mL). The resulting solution was stirred for 30 min before PPh_3 (10 mg, 0.038 mmol) was added and the mixture concentrated in vacuo. A crude ^{1}H NMR showed a 1.7:1 mixture favoring the (*R**,*S**) diastereomer. The ratio was determined by comparing the integration of the doublets of triplets appearing at δ 5.81 (*cis*-) and δ 6.17 (*trans*-) in the crude ^{1}H NMR. The mixture was purified by flash chromatography (1% ether–hexanes) on triethyl amine washed silica gel to yield the title compounds as colorless oils (35 mg, 94%).

cis-: R_f = 0.15, (2% ether–hexanes). IR (neat): 3062, 2929, 2856, 1497, 1472, 1406, 1381, 1360, 1255, 1096, 1064, 1028, 1005, 924, 836, 775, 733, 696, 667. ^{1}H NMR (400 MHz, $CDCl_3$) δ: 0.04 (s, 6H), 0.89 (s, 9H), 1.17–1.28 (m, 1H), 1.50–1.66 (m, 3H), 1.87 (qt, *J* = 8, 2 Hz, 1H), 2.31–2.41 (m, 1H), 2.56 (qq, *J* = 8, 1.5, 1H), 3.55–3.64 (m, 2H), 4.49, 4.53 (AB, 12 Hz, 2H), 5.12 (dd, *J* = 18, 2 Hz, 1H), 5.19 (dd *J* = 11, 2 Hz, 1H), 5.81 (dt, *J* = 6, 2 Hz, 1H), 5.89 (dd, *J* = 18, 11 Hz, 1H), 6.05 (dt, *J* = 6, 1.5 Hz, 1H), 7.21–7.26 (m, 1H), 7.28–7.36 (m, 4H). ^{13}C NMR (100 MHz, $CDCl_3$) δ: –5.27, 18.33, 25.97, 26.81, 31.78, 37.06, 47.79, 63.44, 65.64, 93.08, 115.19, 127.01, 127.11, 128.19, 132.74, 134.44, 138.85, 139.90. HRMS calcd. for $C_{23}H_{36}O_2Si$ (M^+): 372.2453; found: 372.2469.

trans-: R_f = 0.10, (2% ether–hexanes). IR (neat): 3056, 2929, 2857, 1741, 1608, 1472, 1434, 1380, 1255, 1094, 996, 924, 835, 775, 742, 695. ^{1}H NMR (400 MHz, $CDCl_3$) δ: 0.05 (s, 6H), 0.90 (s, 9H), 1.51–1.68 (m, 3H), 1.68–1.80 (m, 1H), 2.22 (ddt, *J* = 16.5, 8, 2 Hz, 1H), 2.52 (dddd, *J* = 16.5, 9, 3, 1.5 Hz, 1H), 3.59–3.68 (m, 2H), 4.36, 4.48 (AB, 12 Hz, 2H), 5.14 (dd, *J* = 11, 2 Hz, 1H), 5.24 (dd, *J* = 18, 2 Hz, 1H), 5.81 (dq, *J* = 6, 1.5 Hz, 1H), 6.04 (dd, *J* = 18, 11 Hz, 1H), 6.17 (dt, *J* = 6 Hz, 2 Hz, 1H), 7.20–7.26 (m, 1H), 7.28–7.36 (m, 4H). ^{13}C NMR (100 MHz, $CDCl_3$) δ: –5.25, 18.37, 24.36, 25.99, 31.96, 38.32, 50.08, 63.59, 65.26, 77.31, 89.21, 113.84, 126.65, 126.76, 128.06, 132.63, 137.06, 140.30, 142.13. HRMS calcd. for $C_{19}H_{27}O_2Si$ ($M\text{-}C_4H_9$): 315.1780; found: 315.1781.

cis- *and* trans-*5-(3*-tert-*Butyldimethylsiloxy-propyl)-1-vinyl-cyclopent-2-enyloxy benzyl ether (**31**) (Ru Cat.)*

To a solution of triene **27** (39 mg, 0.097 mmol) in dichloromethane (1.0 mL) at 23°C was added **1** (2.4 mg, 0.003 mmol). The resulting solution was stirred for 1 h before PPh_3 (3 mg, 0.014 mmol) was added and the mixture concentrated in vacuo. A crude ^{1}H NMR showed an 8:1 mixture favoring the (*cis*-). The ratio was determined by comparing the integration of the doublets of triplets appearing at δ 5.81 (*cis*-) and δ 6.17 (*trans*-) in the crude ^{1}H NMR. The mixture was purified by flash chromatography (1% ether–hexanes) on triethyl amine washed silica gel to yield the title compounds as colorless oils (36 mg, 99%).

*3-Allyl-3-benzyl-dihydro-furan-2-one (**36**)*

Diisopropylamine (10.98 mmol, 1.32 mL) is added to THF (13 mL) and the resulting solution is cooled to –78°C. *n*-BuLi (10.98 mmol, 2.5 M in hexanes, 4.39 mL) is then added dropwise. The solution is stirred for an additional 30 min at –78°C at which time 3-allyl-dihydro-furan-2-one (18) in THF (13mL) is added dropwise by cannula addition. The solution is stirred for an additional 30 min at –78°C followed by dropwise addition of benzyl bromide (11.98 mmol, 1.42 mL) in HMPA(2.2 mL). The solution is stirred for an additional 3 h at –78°C. The reaction is quenched with aq. sat'd. ammonium chloride solution and the mixture is diluted with ether. The layers are separated and the aqueous layer is extracted with ether (three times). The combined organic layers are dried over $MgSO_4$, filtered, and concentrated. The crude product is purified by flash chromatography (20% Et_2O–hexanes) to yield the title compound as a colorless oil (1.39 g, 77%). IR (neat): 2915 (m), 1757 (s), 1212 (w), 1166 (s), 1029 (s), 920 (m), 702 (m). ^{1}H NMR (400 MHz, $CDCl_3$) δ: 2.15 (t, *J* = 8 Hz, 2H), 2.33 (dd, *J* = 13.8 Hz, 8 Hz, 1H), 2.51 (dd, *J* = 14 Hz, 6.4 Hz, 1H), 2.74 (d, *J* = 13.2 Hz, 1H), 3.07 (d, *J* = 13.2 Hz, 1H), 3.46 (q, *J* = 8.8 Hz, 1H), 4.02 (q, *J* = 6.4 Hz, 1H), 5.17 (dd, *J* = 9.2 Hz, 1.2 Hz, 1H), 5.21 (s, 1H), 5.79 (qt, *J* = 8.4 Hz, 2 Hz, 1H), 7.19–7.32 (m, 5H). ^{13}C NMR (100MHz, $CDCl_3$) δ: 29.87, 42.15, 42.88, 48.07, 65.43, 119.98, 127.23, 128.68, 130.08, 132.80, 136.63, 180.96. HRMS calcd. (M^+): 216.1150; found: 216.1152.

© 2000 NRC Canada

*4-Benzyl-4-(2-*tert*-butyldimethylsiloxy-ethyl)-3-vinyl-hepta-1,6-diene-3-ol (**39**)*

3-Allyl-3-benzyl-dihydro-furan-2-one (1.0 g, 4.6 mmol) was reacted under standard conditions for the conversion of methyl esters to diallylic tertiary alcohols. The crude product was dissolved in DMF (40 mL) and imidazole (0.469 g, 6.9 mmol) and *tert*-butyldimethylsilyl chloride (0.69 g, 4.6 mmol) were added. The solution is stirred at room temperature for 12 h. The reaction volume is doubled with water and extract with ether (three times). Wash the organic layers with water, dry over Na_2SO_4, filter, and concentrate. Flash chromatography (5% Et_2O–hexanes) provided the title compound as a colourless oil (1.0 g, 57% over two steps). IR (neat): 3359 (s), 2936 (s), 2838 (w), 2309 (w), 1254 (m), 1081 (s), 997 (m), 916 (m), 839 (m), 772 (w). ^{1}H NMR (400 MHz, $CDCl_3$) δ: 0.08 (s, 6H), 0.91 (s, 9H), 1.72 (t, *J* = 6 Hz, 2H), 2.20 (dd, *J* = 15 Hz, 6.4 Hz, 1H), 2.41 (dd, *J* = 15 Hz, 6.4 Hz, 1H), 2.80 (d, *J* = 14 Hz, 1H), 2.88 (d, *J* = 14 Hz, 1H), 3.77 (t, *J* = 6 Hz, 2H), 4.10 (brs, 1H), 4.93–5.01 (m, 2H), 5.19 (ddd, *J* = 10.8 Hz, 4.8 Hz, 1.6 Hz, 2H), 5.35 (ddd, *J* = 18.5 Hz, 3 Hz, 1.6 Hz, 2H), 5.59–5.70 (m, 1H), 6.15 (dd, *J* = 14.8 Hz, 10.8 Hz, 1H), 6.20 (dd, 14.8 Hz, 10.8 Hz, 1H), 7.16–2.27 (m, 5H). ^{13}C NMR (100 MHz, $CDCl_3$) δ: –5.23, –5.18, 18.57, 26.17, 36.33, 38.99, 40.49, 47.62, 60.35, 80.24, 114.73, 114.76, 116.98, 126.23, 128.11, 131.21, 1136.70, 139.36, 140.55, 140.58. HRMS calcd. $(M\text{-}CH_3)^+$: 371.2406; found: 371.2414.

trans-*5-Benzyl-5-(2-*tert*-butyldimethylsiloxy-ethyl)-1-vinyl-cyclopent-2-enol (**43**)*

To a solution of triene (240 mg, 0.6217 mmol) in dichloromethane (25 mL) at 23°C was added **1** (25.5 mg, 0.03 mmol). The solution is stirred for 6 h at room temperature at which time **1** (25.5 mg, 0.03 mmol) is again added. The solution is stirred for an additional 12 h at room temperature, when **1** (25.5 mg, 0.03 mmol) is added for the final time. After stirring at room temperature for an additional 6 h, the reaction is opened to air and the solvent is removed in vacuo. Flash chromatography(5% Et_2O– hexanes) provides the title compound (134 mg, 60%) as a single diastereomer, as a colourless oil. The stereochemistry was determined by ROESY experiment. R_f = 0.10 (5% Et_2O–hexanes). IR (neat): 3397 (s), 2928 (s), 1495 (m), 1257(s), 1079 (s), 1023 (m), 836 (m), 720 (m). ^{1}H NMR (400 MHz, $CDCl_3$) δ: 0.55 (s, 6H), 0.90 (s, 9H), 1.26 (m, 2H), 1.86 (ddd, *J* = 15.2 Hz, 10.4 Hz, 2.4 Hz, 1H), 1.20 (dd, *J* = 16.2 Hz, 1.6 Hz, 1H), 2.55 (d, *J* = 16.4 Hz, 1H), 2.64 (d, *J* = 13.6 Hz, 1H), 2.80 (d, *J* = 13.6 Hz, 1H), 3.54 (td, *J* = 10.4 Hz, 1.2 Hz, 1H), 3.65 (ddd, *J* = 10.5 Hz, 5.8 Hz, 2.8 Hz, 1H), 5.16 (dd, *J* = 10.6 Hz, 2 Hz, 1H), 5.21 (s, 1H), 5.25 (dd, *J* = 17.4 Hz, 2 Hz, 1H), 5.64–5.66 (m, 1H), 5.84–5.87 (m, 1H), 5.97 (dd, *J* = 17.4 Hz, 10.8 Hz, 1H), 7.11–7.26 (m, 5H). ^{13}C NMR (100 MHz, $CDCl_3$) δ: –5.57, –5.38, 18.38, 26.05, 37.81, 41.81, 43.20, 52.59, 59.92, 87.75, 112.91, 126.03, 128.06, 129.32, 130.46, 138.24, 140.22, 140.72. HRMS calcd. $(M\text{-}C_4H_9)^+$: 301.1623; found: 301.1618.

*[2-Allyl-3-benzyloxy-2-(2-*tert*-butyldimethylsiloxy-ethyl)-3-vinyl-pent-4-enyl]-benzene (**40**)*

4-Benzyl-4-(2-*tert*-butyldimethylsiloxy-ethyl)-3-vinyl-hepta-1,6-diene-3-ol (300 mg, 0.77 mmol) was reacted acccording to the general benzylation procedure to yield the title compound as a colorless oil (314 mg, 85%) after flash chromatography(100% hexanes). R_f = 0.6 (5% Et_2O–hexanes). IR (neat): 2950 (s), 2852 (m), 1634 (w), 1461 (w), 1254 (m), 1085 (s), 1064 (s), 930 (m), 835 (m), 772 (w). ^{1}H NMR (400 MHz, $CDCl_3$) δ: 0.01 (s, 6H), 0.87 (s, 9H), 1.745 (m, 2H), 2.21 (dd, *J* = 14.8 Hz, 6.8 Hz, 1H), 2.37 (dd, *J* = 14.8 Hz, 7.6 Hz, 1H), 2.87 (d, *J* = 13.6 Hz, 1H), 2.97 (d, *J* = 13.6 Hz, 1H), 3.68 (m, 1H), 3.87 (m, 1H), 4.32 (s, 2H), 4.92 (dd, *J* = 10 Hz, 2 Hz, 1H), 4.95 (dd, *J* = 17.2 Hz, 2 Hz, 1H), 5.30 (dd, *J* = 4 Hz, 1.6 Hz, 1H), 5.35 (dd, *J* = 4 Hz, 1.6 Hz, 1H), 5.44 (dd, *J* = 8 Hz, 1.6 Hz, 1H), 5.47 (dd, *J* = 6.8 Hz, 1.6 Hz, 1H), 5.794 (m, 1H), 6.04 (dd, *J* = 16 Hz, 11.2 Hz, 1H), 6.09 (dd, *J* = 16 Hz, 11.2 Hz, 1H), 7.21–7.37 (m, 10H). ^{13}C NMR (100 MHz, $CDCl_3$) δ: –5.01, 18.50, 26.18, 27.06, 37.81, 39.39, 47.79, 60.71, 65.67, 86.48, 116.00, 118.42, 118.60, 126.06, 127.05, 127.12, 127.94, 128.35, 131.36, 136.26, 136.52, 136.89, 139.56, 139.66. HRMS calcd. $(M\text{-}C_4H_9)$: 419.2406; found: 419.2392.

*[2-Benzyloxy-1-(2-*tert*-butyldimethylsiloxy-ethyl)-2-vinyl-cyclopent-3-enylmethyl]-benzene (**44**)*

To a solution of triene **40** (30 mg, 0.063 mmol) in dichloromethane(1 mL) at 23°C was added **1** (5.168 mg, 0.0063 mmol). After 12 h at room temperature, the reaction is opened to air and the solvent is removed in vacuo. A crude ^{1}H NMR showed a 2:1 mixture of diastereomers, favouring the *cis*-diastereomer. The two diastereomers were inseparable by flash chromatography. To confirm the stereochemistry of the diastereomers, alcohol *trans*-**43** (30 mg, 0.083 mmol) was reacted under the general benzylation procedure to yield *trans*-**44** (35 mg, 95%) as a colourless oil after flash chromatography (100% hexanes).

trans-: IR (neat): 2950 (m), 2852 (m), 1602 (w), 1451 (m), 1254 (m), 1081 (s), 906 (m), 737 (s), 691 (s). ^{1}H NMR (400 MHz, $CDCl_3$) δ: –0.04 (s, 3H), –0.03 (s, 3H), 0.84 (s, 9H), 1.86 (t, 7.6 Hz, 2H), 2.10 (dt, *J* = 16.8 Hz, 2 Hz, 1H), 2.33 (ddd, *J* = 16.6 Hz, 2.8 Hz, 1.6 Hz, 1H), 2.45 (d, *J* = 13.6 Hz, 1H), 2.69 (d, *J* = 13.6 Hz, 1H), 3.69–3.76 (m, 1H), 3.84–3.91 (m, 1H), 4.39 (d, *J* = 11.6 Hz, 1H), 4.50 (d, *J* = 11.6 Hz, 1H), 5.26 (dd, *J* = 17.6 Hz, 1.6 Hz, 1H), 5.34 (dd, *J* = 10.8 Hz, 1.6 Hz, 1H), 5.94 (dd, *J* = 17.6 Hz, 10.8 Hz, 1H), 5.99 (dt, *J* = 6 Hz, 1.6 Hz, 1H), 6.08 (dt, *J* = 6 Hz, 2.4 Hz, 1H), 7.15–7.39 (m, 10H). HRMS calcd. (M^+): 448.2797; found: 448.2802.

cis-: IR (neat): 2950 (m), 2852 (m), 1602 (w), 1451 (m), 1254 (m), 1081 (s), 906 (m), 737 (s), 691 (s). ^{1}H NMR (400 MHz, $CDCl_3$) δ: –0.02 (s, 3H), –0.01 (s, 3H), 0.84 (s, 9H), 1.53 (t, *J* = 7.6 Hz, 2H), 2.08 (d, *J* = 16.4 Hz, 1H), 2.58 (d, *J* = 16.4 Hz, 1H), 2.97 (d, *J* = 13.6 Hz, 1H), 3.06 (d, *J* = 13.6 Hz, 1H), 3.38–3.45 (m, 1H), 3.55–3.61 (m, 1H), 4.37 (d, *J* = 11.6 Hz, 1H), 4.47 (d, *J* = 11.6 Hz, 1H), 5.25 (s, 1H), 5.28 (dd, *J* = 5.2 Hz, 1.6 Hz, 1H), 5.79 (dd, *J* = 18 Hz, 10.4 Hz, 1H), 6.04 (s, 2H), 7.15–7.34 (m, 10H). HRMS calcd. (M^+): 448.2797; found: 448.2802.

^{13}C NMR (100 MHz, $CDCl_3$) mixture of diastereomers δ: –5.10, –5.06, 18.41, 26.12, 33.68, 36.57, 41.00, 41.72, 52.65, 61.41, 65.84, 93.07, 117.10, 125.99, 127.04, 127.10,

© 2000 NRC Canada

127.88, 128.25, 128.54, 128.92, 129.15, 130.98, 131.44, 135.52, 137.92, 139.09, 139.81, 140.07.

*3-Benzyl-3-but-3-enyl-dihydro-furan-2-one (**38**)*

3-But-3-enyl-hihydrofuran-2-one (**37**) (1.1 g, 7.857 mmol) was reacted according to the same procedure for the synthesis of 3-allyl-3-benzyl-dihydro-furan-2-one (**36**). Flash chromatography (20% Et_2O–hexanes) provides 1.32 g (74%) of the title compound as a colourless oil. R_f = 0.5 (50% Et_2O–hexanes). IR (neat): 2910 (m), 1760 (s), 1634 (w), 1447 (m), 1173 (s), 1029 (s), 913 (m). ^{1}H NMR (400 MHz, $CDCl_3$) δ: 1.68–1.81 (m, 2H), 2.06–2.25 (m, 4H), 2.75 (d, *J* = 13.6 Hz, 1H), 3.05 (d, *J* = 13.6 Hz), 3.45–3.51 (m, 1H), 4.00–4.06 (m, 1H), 4.98 (d, *J* = 10.4 Hz, 1H), 5.05 (dt, *J* = 17.2 Hz, 1.6 Hz, 1H), 5.75–5.85 (m, 1H), 7.18–7.30 (m, 5H). ^{13}C NMR (100 MHz, $CDCl_3$) δ: 28.82, 30.60, 36.74, 42.76, 47.91, 65.26, 115.41, 127.22, 128.67, 130.06, 136.65, 137.52, 181.07. HRMS calcd. (M^+): 230.1306; found: 230.1259.

*4-Benzyloxy-4-(2-*tert*-butyldimethylsiloxy-ethyl)-3-vinyl-octa-1,7-dien-3-ol (**41**)*

3-Benzyl-3-but-3-enyl-dihydro-furan-2-one **38** (1.0 g, 4.37 mmol) was reacted under standard conditions for the conversion of methyl esters to tertiary diallylic alcohols. The crude product was dissolved in DMF (50 mL) and imidazole (0.469 g, 6.9 mmol) and *tert*-butyldimethylsilyl chloride (0.69 g, 4.6 mmol) were added. After stirring at room temperature for 12 h, water (50 mL) is added. Extract with ether (three times) and wash with water. Dry over Na_2SO_4, filter, and concentrate. Flash chromatography (5% Et_2O–hexanes) provides 0.825 g (48% over two steps) of the title compound as a colourless oil. R_f = 0.3 (5% Et_2O–hexanes). IR (neat): 3371 (s), 2929 (s), 1639 (w), 1471 (m), 1255 (m), 1079 (s), 910 (s), 836 (m), 733 (m). ^{1}H NMR (400 MHz, $CDCl_3$) δ: 0.12 (s, 6H), 0.94 (s, 9H), 1.50–1.96 (m, 6H), 2.81 (d, *J* = 14 Hz, 1H), 2.86 (d, *J* = 14 Hz, 1H), 3.76–3.84 (m, 2H), 3.98 (br s, 1H), 4.88 (s, 1H), 4.91 (d, *J* = 6.8 Hz, 1H), 5.20 (dd, *J* = 12 Hz, 1.6 Hz, 1H), 5.23 (dd, *J* = 12 Hz, 1.6 Hz, 1H), 5.38 (dd, *J* = 17.2 Hz, 2 Hz, 1H), 5.39 (dd, *J* = 17.2 Hz, 2 Hz, 1H), 5.66–5.76 (m, 1H), 6.20 (dd, *J* = 17.2 Hz, 10.8 Hz, 1H), 6.20 (dd, *J* = 17.2 Hz, 10.8 Hz, 1H), 7.17–7.29 (m, 5H). ^{13}C NMR (100 MHz, $CDCl_3$) δ: –5.21, –5.17, 18.55, 26.16, 29.30, 33.00, 36.30, 40.78, 47.17, 60.39, 80.19, 114.02, 114.02, 114.73, 114.84, 126.20, 128.11, 130.97, 139.40, 139.54, 140.59, 140.76. HRMS calcd. $(M\text{-}C_4H_9)^+$: 343.0183; found: 343.0187.

*[2-(1-Benzyloxy-1-vinyl-allyl)-2-(2-*tert*-butyldimethylsiloxy-ethyl)-hex-5-enyl]-benzene (**42**)*

Alcohol **41** (150 mg, 0.375 mmol) was reacted according to the general benzylation procedure to yield the title compound as a colourless oil (165 mg, 90%) after flash chromatography (100% hexanes). R_f = 0.7 (5% Et_2O–hexanes). IR (neat): 2950 (m), 2859 (m), 1641 (m), 1451 (m), 1254 (m), 1081 (s), 930 (m), 835 (s). ^{1}H NMR (400 MHz, $CDCl_3$) δ: 0.01 (s, 6H), 0.87 (s, 9H), 1.42–2.11 (m, 6H), 2.86 (d, *J* = 14 Hz, 1H), 2.92 (d, *J* = 13.6 Hz, 1H), 3.60–3.67 (m, 1H), 3.82–3.88 (m, 1H), 4.33 (s, 2H), 4.87 (s, 1H), 4.90 (d, *J* = 7.8 Hz, 1H), 5.34 (dd, *J* = 19.4 Hz, 2 Hz, 1H), 5.34 (dd, *J* = 17.6 Hz, 1.6 Hz, 1H), 5.46 (dd, *J* = 11 Hz, 2 Hz, 1H), 5.46 (dd, *J* = 11.2 Hz, 1.2 Hz, 1H), 5.65–5.75 (m, 1H), 6.02 (dd, *J* = 17.8 Hz, 11 Hz, 1H), 6.07 (dd, *J* = 17.8 Hz, 11 Hz, 1H), 7.19–7.36 (m, 10H). ^{13}C NMR (100 MHz, $CDCl_3$) δ: –5.00, 18.49, 26.19, 29.45, 33.58, 37.54, 40.03, 47.45, 60.83, 65.77, 86.63, 113.85, 118.47, 118.70, 126.06, 127.07, 127.10, 128.00, 128.37, 131.11, 136.16, 136.52, 139.65, 139.76, 139.81. HRMS calcd. $(M\text{-}C_4H_9)^+$: 433.2562; found: 433.2576.

*6-Benzyl-6-(2-*tert*-butyldimethylsiloxy-ethyl)-1-vinyl-cyclohex-2-en-1-ol (**45**)*

To a solution of triene **41** (100 mg, 0.25 mmol) id dichloromethane(20 mL) is added **1** (24 mg, 0.03 mmol). The solution is stirred for 12 h at room temperature at which time the reaction is opened to air and the solvent is removed in vacuo. A crude ^{1}H NMR showed a 1:1 mixture of diastereomers at 100% conversion. The residue is purified by flash chromatography (5% Et_2O–hexanes) to provide the R*,S* diastereomer (37.6 mg, 40%) and the R*,R* diastereomer (30 mg, 32%) as colourless oils. The stereochemistry of the R*,S* diastereomer was proven by ROESY experiment.

trans-: IR (neat): 3388 (s), 2929 (m), 1471 (w), 1255 (m), 1078 (s), 1003 (m), 836 (s), 777 (m), 702 (w). ^{1}H NMR (400 MHz, $CDCl_{3)}$) δ: 0.08 (s, 6H), 0.91 (s, 9H), 1.43–1.53 (m, 2H), 1.58–1.66 (m, 1H), 1.73 (ddd, *J* = 17.6 Hz, 8.4 Hz, 2.4 Hz, 1H), 1.93–2.13 (m, 2H), 2.59 (d, *J* = 13.6 Hz, 1H), 3.04 (d, *J* = 13.6 Hz, 1H), 3.68–3.73 (m, 1H), 4.01 (ddd, *J* = 11 Hz, 8.8 Hz, 2.4 Hz, 1H), 4.89 (s, 1H), 5.22 (dd, *J* = 10.8 Hz, 2 Hz, 1H), 5.29 (dd, *J* = 17.4 Hz, 2 Hz, 1H), 5.48 (dt, *J* = 10 Hz, 2.4 Hz, 1H), 5.69 (dt, *J* = 10 Hz, 2.4 Hz, 1H), 6.10 (ddd, *J* = 17.2 Hz, 10.8 Hz, 0.8 Hz, 1H), 7.07–7.27 (m, 5H). ^{13}C NMR (100 MHz, $CDCl_3$) δ: –5.29, –5.18, 18.33, 22.69, 26.00, 26.21, 29.10, 35.18, 39.38, 43.31, 60.20, 76.49, 114.46, 125.98, 126.13, 127.98, 131.23, 134.02, 139.08, 142.19. HRMS calcd. (M^+): 372.2482; found: 372.2483.

cis-: IR (neat): 3388 (s), 2929 (m), 1471 (w), 1255 (m), 1078 (s), 1003 (m), 836 (s), 777 (m), 702 (w). ^{1}H NMR ($CDCl_3$) δ: 0.13 (d, *J* = 0.8 Hz, 6H), 0.94 (s, 9H), 1.23–1.49 (m, 3H), 1.62–1.69 (m, 1H), 2.20–2.30 (m, 1H), 2.79 (d, *J* = 14.8 Hz, 1H), 3.19 (d, *J* = 14.8 Hz, 1H), 3.48 (dt, *J* = 11.2 Hz, 4.4 Hz, 1H), 4.11 (td, *J* = 10.88 Hz, 3.2 Hz, 1H), 4.31 (br s, 1H), 5.12 (dd, *J* = 10.6 Hz, 1.6 Hz, 1H), 5.19 (*J* = 16 Hz, 2 Hz, 1H), 5.43 (dt, *J* = 9.6 Hz, 2.4 Hz, 1H), 5.81 (dt, *J* = 10 Hz, 3.6 Hz, 1H), 6.14 (dd, *J* = 17.2 Hz, 10.4 Hz, 1H), 7.16–7.28 (m, 5H). ^{13}C NMR δ: –0.53, –5.15, 0.14, 22.92, 26.22, 28.90, 37.39, 43.38, 60.60, 95.61, 114.31, 125.96, 128.12, 130.77, 131.99, 142.65. HRMS calcd. (M^+): 372.2482; found: 372.2483.

*[2-Benzyloxy-1-(2-*tert*-butyldimethylsiloxy-ethyl)-2-vinyl-cyclohex-3-enylmethyl]-benzene (**46**)*

A solution of triene **42** (100 mg, 0.204 mmol) in dichloromethane (10 mL) is added **1** (16 mg, 0.02 mmol). The solution is stirred for 12 h at room temperature at which time the reaction is opened to air and the solvent removed in vacuo. A crude ^{1}H NMR showed a 4.5:1 mixture of diastereomers, favouring the R*,R* *cis*-diastereomer. Unable to separate the diastereomers by flash chromatography, the diastereomeric

© 2000 NRC Canada

alcohols **45** reacted under the general benzylation procedure to yield the title compounds as colourless oils.

cis- *and* trans-*mixture*: IR (neat): 2927 (m), 1495 (w), 1254 (m), 1067 (s), 929 (w), 835 (m), 774 (w), 731 (w), 701 (m). ^{1}H NMR (400 MHz, $CDCl_3$) δ: –0.11 (s, 6H), 0.77 (s, 9H), 1.32–1.45 (m, 2H), 1.75–1.85 (m, 3H), 2.08–2.23 (m, 2H), 2.54 (d, *J* = 13.6 Hz, 1H), 2.71 (d, *J* = 13.6 Hz, 1H), 3.35–3.46 (m, 1H), 3.62–3.69 (m, 1H), 4.38 (d, *J* = 11.6 Hz, 1H), 4.46 (d, *J* = 11.6 Hz, 1H), 5.23 (dd, *J* = 17.6 Hz, l.6 Hz, 1H), 5.41 (dd, *J* = 10.8 Hz, 1.6 Hz, 1H), 5.79 (dt, *J* = 10.4 Hz, 2 Hz, 1H), 6.00 (dt, *J* = 10.4 Hz, 3.6 Hz, 1H), 6.05 (dd, *J* = 17.8 Hz, 11.2 Hz, 1H), 7.14–7.28 (m, 10H). ^{13}C NMR (100 MHz, $CDCl_3$) δ: –5.08, 18.43, 23.47, 25.47, 26.15, 36.98, 40.12, 43.53, 61.19, 64.88, 118.69, 125.99, 126.95, 126.99, 127.18, 127.98, 128.24, 131.09, 131.18, 139.41, 140.21, 140.79.

*5-(1-Tributylstannylmethoxy-1-vinyl-allyl)-nona-1,8-diene (**47**)*

Potassium hydride (729 mg, 7.27 mmol) was washed three times with pentane, dried under a stream of argon and suspended in THF (5 mL). A solution of alcohol **8** (500 mg, 2.42 mmol) in THF (3 mL) was added via cannula. After 5 min, a solution of ICH_2SnBu_3 in THF (2 mL) was added via cannula followed by a small crystal of dry 18-crown-6. The resulting mixture was heated to reflux for 1 h, cooled to 23°C, diluted with ether, and quenched carefully by dropwise addition of water. The aqueous layer was extracted two times with ether, the organic layers were combined, washed with brine, dried over sodium sulfate, filtered and concentrated in vacuo. The residue was purified by flash chromatography (100% hexanes) on triethyl amine washed silica gel to yield the title compound as a colorless oil (1.15 g, 93%). R_f = 0.55 (100% hexanes). IR (neat): 3079, 2926, 1640, 1456, 1416, 1017, 909. ^{1}H NMR (400 MHz, $CDCl_3$) δ: 0.89 (t, *J* = 7 Hz, 9H), 0.89 (tt, $J^{(H\text{-}Sn)}$ = 25 Hz, $J^{(H\text{-}H)}$ = 8 Hz, 6H), 1.04–1.14 (m, 2H), 1.30 (hex., *J* = 7 Hz, 6H), 1.40–1.82 (m, 11H), 1.86–2.18 (m, 5H), 3.40 (t, $J^{(H\text{-}Sn)}$ = 10 Hz, 2H), 4.92 (dm, *J* = 10 Hz, 2H), 4.97 (dq, *J* = 17, 2 Hz, 2H), 5.17 (dd, *J* = 18, 2 Hz, 2H), 5.34 (dd, 11, 2 Hz, 2H), 5.74 (dd, *J* = 18, 11 Hz, 2H), 5.72–5.86 (m, 2H). ^{13}C NMR (100 MHz, $CDCl_3$) δ: 8.84 (t, $J^{(C\text{-}Sn)}$ = 61 Hz), 13.73, 27.36 (t, $J^{(C\text{-}Sn)}$ = 26 Hz), 29.21 (t, $J^{(C\text{-}Sn)}$ = 10 Hz), 30.12, 33.46, 47.02, 52.46, 85.45, 114.03, 117.42, 137.92, 139.40. HRMS calcd. for $C_{23}H_{41}OSn$ ($M\text{-}C_4H_9^+$): 453.2179; found: 453.2181.

cis-*4a-Tributylstannylmethoxy-1,2,4a,7,8,8a-hexahydrohaphthalene (**48**)*

To a solution of **47** (1.00 g, 1.96 mmol) in dichloromethane (20 mL) at 23°C was added **1** (194 mg, 0.240 mmol). The reaction mixture was placed under an atmosphere of ethylene and heated to reflux. After 7 h the reaction was concentrated in vacuo and the residue purified by flash chromatography (100% hexanes → 0.5% → 1% → 2% ether–hexanes) on triethyl amine washed silica gel to yield the title compound as a colorless oil (760 mg, 86%). R_f = 0.19 (1% ether–hexanes). IR (neat) 3051, 2924, 1464, 1348, 1040, 758. ^{1}H NMR (400 MHz, $CDCl_3$) δ: 0.88 (t, *J* = 7 Hz, 9H), 0.88 (tt, $J^{(H\text{-}Sn)}$ = 25 Hz, $J^{(H\text{-}H)}$ = 8 Hz, 6H), 1.25–1.34 (m, 6H), 1.43–1.54 (m, 6H), 1.70–1.79 (m, 2H), 1.98–2.05 (m, 4H), 2.13 (hept., *J* = 3.5 Hz, 1H), 2.71–2.84 (m, 3H), 3.53 (t, $J^{(H\text{-}Sn)}$ = 10 Hz, 2H), 5.51 (dt, *J* = 10, 2 Hz, 2H), 5.80 (dt, *J* = 10, 4 Hz, 2H). ^{13}C NMR (100 MHz, $CDCl_3$) δ: 8.93 (t, $J^{(C\text{-}Sn)}$ = 61 Hz), 13.74, 23.41, 24.30, 27.31 (t, $J^{(C\text{-}Sn)}$ = 26 Hz), 29.17 (t, $J^{(C\text{-}Sn)}$ = 10 Hz), 32.99, 50.86, 74.69, 129.02, 130.49.

cis-*(2,3,4,4a,5,6-Hexahydronaphthalen-2-yl)-methanol (**49**)*

MeLi (1.08 M, 214 μL): To a solution of stannyl methyl ether **48** (100 mg, 0.221 mmol) and HMPA (154 μL, 0.882 mmol) was added MeLi (1.08 M, 214 μL). After 15 min the reaction was quenched by adding MeOH (2 drops). The mixture was purified by adding the crude reaction directly to column of triethyl amine washed silica gel and eluting with 30% ether–hexanes to yield the title compound as a colorless oil (25 mg, 67%). R_f = 0.17 (30% ether–hexanes). ^{1}H NMR (400 MHz, $CDCl_3$) δ: 1.21–1.36 (m, 3H), 1.36–1.47 (m, 1H), 1.77–1.94 (m, 3H), 2.08–2.26 (m, 3H), 2.39–2.49 (bs, 1H), 3.50–3.61 (m, 2H), 5.37 (s, 1H), 5.72–5.78 (m, 1H), 6.02 (dm, *J* = 10 Hz, 1H). ^{13}C NMR (100 MHz, $CDCl_3$) δ: 25.97, 26.07, 30.10, 30.21, 35.76, 39.71, 67.50, 123.77, 128.62, 129.12, 139.59.

*5-(1-Trimethylsiloxy-1-vinyl-allyl)-nona-1,8-diene (**50**)*

A 23°C suspension of KH (161 mg, 1.27 mmol, 35% suspension in oil, washed three times with pentane) in THF (5 mL) was added to **9** (250.09, 1.21 mmol). After 15 min, TMSCl (161 μL, 1.27 mmol) was added via syringe. After 30 min, water was added, and the mixture extracted three times with Et_2O. The organic layers were washed with brine, dried over Na_2SO_4, filtered and concentrated to dryness. The residue was purified by flash chromatography (100% hexanes) on triethyl amine washed silica gel to yield the title compound as a colorless oil (310 mg, 92%). ^{1}H NMR (400 MHz, $CDCl_3$) δ: 0.88 (s, 9H), 1.05 (m, 2H), 1.39 (septet, *J* = 3.5, 1H), 1.58–1.65 (m, 2H), 1.99–2.19 (m, 4H), 4.92 (dm, *J* = 10 Hz, 2H), 4.99 (dq, *J* = 17, 1.7 Hz, 2H), 5.21 (dd, *J* = 10.5, 2 Hz, 2H), 5.25 (dd, *J* = 17.5, 2 Hz, 2H), 5.73–5.84 (m, 2H), 5.92 (dd, *J* = 17.5, 10.5 Hz, 2H). ^{13}C NMR (100 MHz, $CDCl_3$) δ: 2.59, 30.09, 33.50, 48.05, 81.60, 114.14, 115.81, 139.38, 141.03. HRMS calcd. for $C_{15}H_{27}OSi$ ($M\text{-}C_2H_3$)$^+$: 251.1831; found: 251.1824.

cis-*4a-Trimethylsiloxy-1, 2, 4a, 7, 8, 8a-hexahydronaphthalene (**51**)*

A solution of **2** (174 mg, 0.23 mmol) in C_6H_6 (5 mL) was added to a flask containing **50** (603 mg, 2.30 mmol). After 30 min, 600 mg of PPh_3 was added and the mixture concentrated to dryness. The residue was purified by flash chromatography (2% Et_2O on triethylamine washed silica gel) to yield to title compound as a colorless oil consisting of a 5:1 mixture of diastereomers favoring the *cis*-isomer (64 mg, 99%). ^{1}H NMR (400 MHz, $CDCl_3$) δ: 0.12 (s, 9H), 1.44–1.53 (m, 2H), 1.76–1.84 (m, 2H), 1.91–1.98 (m, 1H), 1.99–2.12 (m, 4H), 5.57 (dt, *J* = 10, 2Hz, 2H), 5.71 (dt, *J* = 10, 3.7 Hz, 2H). ^{13}C NMR δ: 2.66, 23.23, 24.24, 39.85, 71.25, 127.38, 132.35.

cis-*4a-(Prop-2-enyloxy)-1, 2, 4a, 7, 8, 8a-hexahydronaphthalene (**52**)*

A THF (1 mL) solution of **15** (100 mg, 0.67 mmol) was added to a 23°C suspension of sodium hydride (133 mg,

© 2000 NRC Canada

3.33 mmol, 60% suspension in oil) which had been washed three times with pentane. After five minutes, propargyl bromide (375 μL, 3.33 mmol, 70% solution in toluene) was added via syringe. After 16 h, the reaction was quenched by the careful addition of water. The mixture was extracted three times with Et_2O, the organic layers were combined, washed with brine, dried over Na_2SO_4, filtered and concentrated to dryness. The residue was purified by flash chromatography (5% Et_2O– hexanes) on triethylamine washed silica gel to yield the title compound as a colorless liquid (58 mg, 46%). IR (neat, cm^{-1}): 3298, 3025, 2919, 1436, 1052. ^1H NMR (400 MHz, $CDCl_3$) δ: 1.46–1.56 (m, 2H), 1.78–1.87 (m, 2H), 1.96–2.15 (m, 5H), 2.36 (t, *J* = 2.5 Hz, 1H), 4.07 (d, *J* = 2.5 Hz, 2H), 5.54 (dt, *J* = 10, 2Hz, 2H), 5.88 (dt, *J* = 10, 3.7 Hz, 2H). ^{13}C NMR δ: 23.26, 24.17, 34.25, 50.53, 72.90, 75.24, 81.89, 129.35, 130.53. HRMS calcd. for M^+: 187.1123; found: 187.1126.

cis-*4a-(But-2-yloxy), 1, 2, 4a, 7, 8, 8a, hexahydronaphthalene (**53**)*

A solution of *n*-BuLi (90 μL, 0.233 mmol, 2.5 M solution in hexanes) was added via syringe to a –78°C solution of **52** (40 mg, 0.212 mmol) in THF (2 mL). After 15 min, methyl iodide (20 μL, 0.318 mmol) was added via syringe and the mixture was allowed to warm to 23°C. After 2 h, water was added and the mixture was extracted three times with Et_2O, the organic layers were combined, washed with brine, dried over Na_2SO_4, filtered and concentrated to dryness. The residue was purified by flash chromatography (5% Et_2O–hexanes) on triethyl amine washed silica gel to yield the title compound as a colorless liquid (39 mg, 65%). ^1H NMR (400 MHz, $CDCl_3$) δ: 1.49 (sextet, *J* = 7 Hz, 2H), 1.75–1.88 (m, 4H), 1.94–2.12 (m, 5H), 3.98–4.05 (m 2H), 5.56 (d, *J* = 10 Hz, 2H), 5.87 (dt, *J* = 10, 3.7 Hz, 2H). ^{13}C NMR δ: 3.70, 23.23, 24.18, 34.07, 50.89, 74.67, 76.86, 80.97, 129.54, 130.13.

1S/R*,1aS*, 4aS*-1-(2, 3, 4, 4a, 5,6-Hexahydronaphthalen-2-yl)-but-2yn-1-ol (**54**)*

^{t}BuLi (233 μL, 0.396 mmol, 1.7 M solution in pentane) was added to a –78°C solution of **53** (20 mg, 0.099 mmol) in THF (1 mL). After 30 min, water is added and the mixture extracted three times with Et_2O, the organic layers were combined, washed with brine, dried over $MgSO_4$, filtered and concentrated to dryness. The residue was purified by flash chromatography (10% Et_2O–hexanes) to yield the title compound as a colorless liquid (12 mg, 63%). IR (neat): 3400, 6064, 2922, 2858, 1716, 1668, 1448, 1377, 1261, 1052. ^1H NMR (400 MHz, $CDCl_3$) δ: 1.2–2.24 (m, 10H), 2.5 (bs, 1H), 4.15 (bs, 1H (minor isomer), 4.24 (bs, 1H (major isomer), 5.44 (s, 1H (major isomer)), 5.58 (s, 1H (minor isomer), 5.72–5.80 (m, 1H), 6.00–6.10 (m, 1H). ^{13}C NMR δ: –0.03, 3.61, 14.11, 22.67, 24.46, 24.86, 25.41, 25.97, 26.90, 29.69, 30.04, 30.08, 30.23, 35.72, 43.91, 66.32, 66.58, 79.05, 81.83, 122.12, 123.02, 128.69, 128.76, 129.23, 140.08. HRMS calcd. for M^+: 202.1358; found: 202.1351.

Conclusions

In conclusion, we have demonstrated a novel diastereoselective double ring closing metathesis reaction as an approach to the synthesis of bicyclo[4.4.0]decadienes and bicyclo[3.3.0]octadienes. The new bicyclic compounds allow for further synthetic transformations enabling the construction of valuable intermediates such as that found in the HMG CoA Reductase inhibitor (+)-Mevinolin. Present efforts are directed towards enantioselective alkene differentiation reactions that would allow the synthesis of enantioenriched bicyclic compounds. The methodology and concepts outlined in this paper should prove useful in the synthesis of complex natural products.

Acknowledgements

M.L. thanks the Merck Frosst Center for Therapeutic Research and Natural Sciences and Engineering Research Council of Canada (NSERC) for support of this work. G.H. and V.Z. both thank NSERC for predoctoral fellowships. G.H. thanks the Walter C. Sumner Foundation for a predoctoral fellowship. We thank Professor Ian Flemming, Cambridge, for bringing the synthesis outlined in Scheme 6 to our attention.

References

1. (*a*) K.J. Ivin. J. Mol. Catal. A Chem. **133**, 1 (1998); (*b*) R.H. Grubbs and S. Chang. Tetrahedron, **54**, 4413 (1998); (*c*) M.S. Schuster and S. Blechert. Angew. Chem. Int. Ed. Engl. **36**, 2036 (1997); (*d*) M.L. Randall and M.L. Snapper. J. Mol. Catal. A-Chem. **133**, 29 (1998); (*e*) S.K. Armstrong. J. Chem. Soc. Perkin Trans. 1, 371 (1998); (*f*) A. Fürstner. Top. Catal. **4**, 285 (1997); (*g*) A. Fürstner. Topics in organometallic chemistry. Vol. 1. Springer, Berlin. 1998.
2. (*a*) C.M. Huwe, J. Velder, and S. Blechert. Angew. Chem. Int. Ed. Engl. **35**, 2376 (1996); (*b*) H. Oguri, S. Sasaki, T. Oishi, and M. Hirama. Tetrahedron Lett. **40**, 5405 (1999); (*c*) B. Schmidt and H. Wildemann. Synlett. 1591 (1999).
3. (*a*) C. Baylon, M.-P. Heck, and C. Mioskowski. J. Org. Chem. **64**, 3354 (1999); (*b*) M.J. Bassindale, P. Hamley, A. Leitner, and J.P.A. Harrity. Tetrahedron Lett. **40**, 3247 (1999); (*c*) J.S. Clark and O. Hamelin. Angew. Chem. Int. Ed. Engl. **39**, 372 (2000).
4. M. Lautens and G. Hughes. Angew. Chem. Int. Ed. Engl. **38**, 129 (1999).
5. (*a*) I. Shimizu and F. Aida. Chem. Lett. 601 (1988); (*b*) J. Tsuji and T. Mandai. Synthesis, 1 (1996); (*c*) J. Tsuji, I. Minami, and I. Shimizu. Synthesis, 623 (1986).
6. G. Hughes, M. Lautens, and J. Wu. Synlett. 835 (2000).
7. S. Watanbe, K. Suga, T. Fujita, and N. Saito. Aust. J. Chem. **30**, 427 (1977).
8. T. Imamoto, N. Takiyama, K. Nakamura, T. Hatajima, and Y. Kamiya. J. Am. Chem. Soc. **111**, 4392 (1989).
9. D.F. Murray, M.W. Baum, and M. Jones. J. Org. Chem. **51**, 1 (1985).
10. (*a*) A.J. Shaka and R. Freeman. J. Magn. Reson. **51**, 169 (1983); (*b*) H. Kessler, C. Griesinger, R. Kerssebaum, K. Wagner, and R.R. Ernst. J. Am. Chem. Soc. **109**, 607 (1987); (*c*) A. Bax and D.G. Davis. J. Magn. Reson. **107**, 207 (1985).
11. (*a*) H. Priepke and R. Brückner. Chem. Ber. **123**, 153 (1990); (*b*) W.C. Still. J. Am. Chem. Soc. **100**, 1481 (1978); (*c*) W.C. Still and A. Mitra. J. Am. Chem. Soc. **100**, 1927 (1978).
12. K. Tomooka, N. Komine, and T. Nakai. Tetrahedron Lett. **39**, 5513 (1998), and refs. therein.

© 2000 NRC Canada

13. T.A. Kirkland and R.H. Grubbs. J. Org. Chem. **62,** 7310 (1997).
14. T.R. Hoye and H. Zhao. Org. Lett. **1**, 1123 (1999).
15. (*a*) J.P.A. Harrity, M.S. Visser, J.D. Gleason, and A.H. Hoveyda. J. Am. Chem. Soc. **119**, 1488 (1997); (*b*) G.S. Weatherhead, J.G. Ford, E.J. Alexanian, R.R. Schrock, and A.H. Hoveyda. J. Am. Chem. Soc. **122**, 1828 (2000), and refs. therein.
16. P. Schwab, R.H. Grubbs, and J.W. Ziller. J. Am. Chem. Soc. **118**, 100 (1996).
17. (*a*) W.A. Ayer, L.M. Browne, S. Fung, and J.B. Stothers. Org. Magn. Reson. **11**, 73 (1978); (*b*) L.M. Brown, R.E. Klinck, and J.B. Stothers. Org. Magn. Reson. **12**, 561 (1979).
18. G.A. Molander and C.R. Harris. J. Am. Chem. Soc. **117**, 3705 (1995).

© 2000 NRC Canada

Synthesis of aspartic acid derivatives useful for the preparation of misacylated transfer RNAs

Michiel Lodder, Curtis F. Crasto, Andrei L. Laikhter, Haoyun An, Tuncer Arslan, Vladimir A. Karginov, Glenn F. Short, III, and Sidney M. Hecht

Abstract: Several derivatives of aspartic acid were protected on N^{α} as their NVOC derivatives, and on the side chain carboxylates as nitroveratryl esters. Following activation as the cyanomethyl esters, these fully protected aspartate derivatives were converted to the respective pdCpA esters. The protected aspartyl-pdCpA esters were then utilized as substrates for T4 RNA ligase in the presence of in vitro transcripts of tRNA lacking the pCpA dinucleotide normally found at the 3′-end. In this fashion, several misacylated tRNAs were prepared; following photolytic deprotection, these were employed successfully for incorporation into proteins at predetermined positions.

Key words: aminoacylated nucleotides, amino acid protection, protein synthesis, tRNA activation.

Résumé : On a préparé plusieurs dérivés de l'acide aspartique dans lesquels le N^{α} est protégé par un groupe "NVOC" et les groupes carboxyles de la chaîne latérale sont protégés par des esters nitrovératryles. Ces dérivés de l'acide aspartique totalement protégés, activés sous la forme d'esters cyanométhyles, ont été transformés en esters "pdCpA." Les esters aspartyl-pdCpA protégés ont alors été utilisés comme substrats pour la ligase d'ARN T4, en présence de produits de transcriptions in vitro de *t*-ARN ne portant pas le dinucléotide pCpA que l'on retrouve normalement à l'extrémité 3′. De cette façon, on a pu préparer plusieurs tARN anormalement aminoacétylés; après déprotection photolytique, ces produits ont été incorporés avec succès dans des protéines à des positions prédéterminées.

Mots clés : nucléotides aminoacétylés, protection d'acides aminés, synthèse de protéines, activation de la tARN.

[Traduit par la Rédaction]

Introduction

In 1962, Chapeville et al. (1) demonstrated that a cysteine-specific transfer RNA (tRNA) misactivated with alanine could be used to direct the incorporation of alanine into protein at sites intended for cysteine. While the lack of a general method for elaborating misacylated tRNAs initially limited the strategy to misacylated tRNAs accessible by chemical modification of enzymatically activated tRNAs (2), the Hecht laboratory discovered that virtually any misacylated tRNA could be prepared via the T4 RNA ligase-mediated condensation of a chemically synthesized aminoacylated pCpA derivative with a tRNA from which the last two nucleotides had been removed (3). Technical modifications, including the use of aminoacylated pdCpA derivatives (4) and in vitro RNA transcripts lacking the terminal CpA moiety (5) have facilitated the preparation of misacylated tRNAs by the use of this strategy, as have the development of methods for reversible *N*-protection of the aminoacyl moiety, resulting in aminoacylated dinucleotides and tRNAs of enhanced stability (3, 6).

The availability of misacylated tRNAs of diverse structure has permitted the elaboration of modified peptides (3, 7, 8) and proteins (9). That the elaborated species can include peptide and protein analogues of altered connectivity (8, 10) underscores the potential of this strategy for creating novel biomaterials, and for defining the chemistry that the ribosome is actually capable of mediating in the presence of suitable aminoacyl-tRNA analogues.

While the synthesis of aminoacylated dinucleotides for the preparation of misacylated tRNAs has been described (3, 6–9), modifications of the chemistry are required when the amino acid of interest has side-chain functionality. Presently, we describe the chemistry employed for the synthesis of pdCpA derivatives esterified with aspartate analogues, and the use of the derived dinucleotides for the elaboration of misacylated aspartyl-tRNAs. We have previously described the use of such species for the preparation of structurally modified analogues of dihydrofolate reductase (11) and HIV-1 protease (12).

Results and discussion

The aspartic acid derivatives shown in Fig. 1 were commercially available with the exception of the carboxyproline

Received July 22, 1999. Published on the NRC Research Press website on June13, 2000.

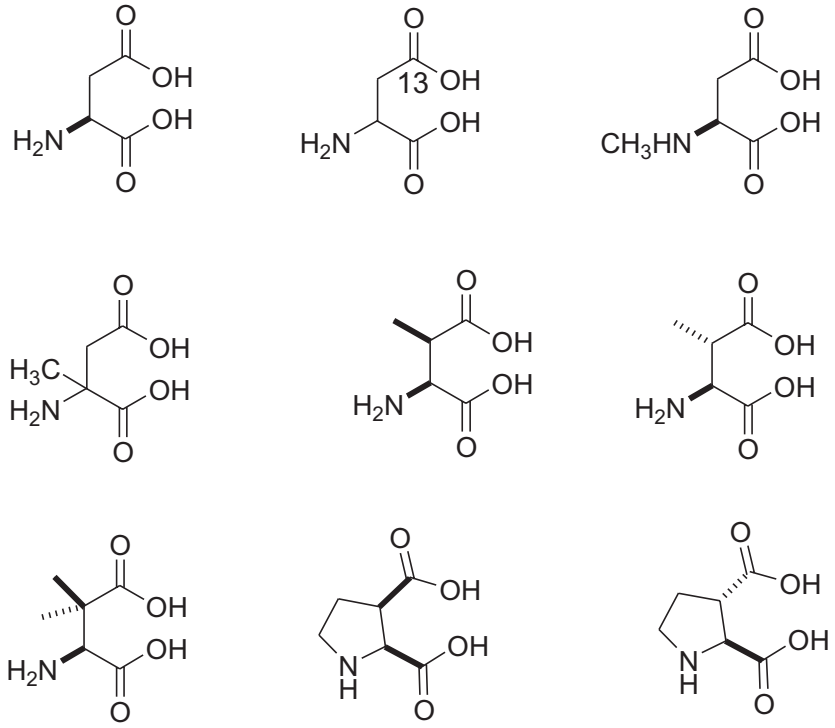
This manuscript is dedicated to Professor Stephen Hanessian on the occasion of his 65th birthday, in appreciation of his many contributions to organic chemistry and to the chemical community.

M. Lodder, C.F. Crasto, A.L. Laikhter, H. An, T. Arslan, V.A. Karginov, G.F. Short, III, and S.M. Hecht.[1]
Departments of Chemistry and Biology, University of Virginia, Charlottesville, VA 22901, U.S.A.

[1]Author to whom correspondence may be addressed. Telephone: (804) 924-3906. Fax: (804) 924-7856. e-mail: sidhecht@virginia.edu

© 2000 NRC Canada

Fig. 1. Aspartic acid derivatives used for the preparation of misacylated tRNAs.



derivatives and β,β-dimethylaspartic acid. *Threo*- and *erythro*-carboxyproline were prepared as described (13).

With the exception of β,β-dimethylaspartic acid, all of the aspartic acid derivatives shown in Fig. 1 were converted to suitably protected cyanomethyl esters as exemplified in Scheme 1 for [α-^{13}C]aspartic acid. In all cases, N^{α} was protected with the NVOC group, while the side-chain carboxylate was protected as the nitroveratryl ester. As shown in Scheme 1, treatment of [α-^{13}C]aspartic acid (**1**) with 6-nitroveratryl chloroformate (14), followed by treatment with 6-nitroveratryl bromide (15) provided fully protected **3** in good yield. Selective hydrolysis of the substituted benzyl ester with 1 equiv. of LiOH (16) gave β-monoester **4** in nearly quantitative yield. This intermediate was converted to cyanomethyl ester **5** (17) in 70% yield by treatment with chloroacetonitrile and triethylamine. It may be noted that this method has been utilized previously for the synthesis of **5** lacking ^{13}C enrichment (4). The other aspartic derivatives shown in Fig. 1 were converted to their fully protected cyanomethyl esters analogously, and in reasonable yields.

The strategy used for the synthesis and protection of β,β-dimethylaspartic acid is shown in Scheme 2. Known compound **6** (18) was treated with potassium bis(trimethylsilyl)amide and methyl iodide to provide the respective dimethylated derivative **7**. Removal of the 9-phenylfluorenyl group by hydrogenation, followed by treatment with 6-nitroveratryl chloroformate gave NVOC protected **8** in 98% yield. Hydrolysis of the methyl esters and treatment with 6-nitroveratryl bromide then provided bis-nitroveratryl ester **9**. Finally, in analogy with the transformations described for compound **3**, compound **9** was converted to cyanomethyl ester **11** by selective hydrolysis and treatment with chloroacetonitrile.

Table 1. Yields of incorporation of aspartic acid analogues into position 25 of HIV-1 protease.

Aspartic acid derivative	Yield (%)
Aspartic acid	22
erythro-β-Methylaspartic acid	33
threo-β-Methylaspartic acid	17
β,β-Dimethylaspartic acid	17

Scheme 3 shows an example of the attachment of an aspartic acid analogue to the dinucleotide pdCpA (4) and the subsequent ligation of the aminoacylated pdCpA derivative to a tRNA transcript lacking the 3′-terminal pCpA moiety. The cyanomethyl ester of (*2S, 3R*)-carboxyproline (**12**) was treated with the tetrabutylammonium salt of pdCpA as described (4). The protected aminoacylated dinucleotide **13** was then ligated to a truncated tRNA (tRNA-C_{OH}) via the agency of T4 ligase (3, 8–11). Removal of the protecting groups was accomplished by irradiation with a 500 W mercury–xenon lamp for 5 min. The deblocked misacylated tRNAs (e.g., **II**) were used promptly in an in vitro protein biosynthesizing system, yielding proteins containing the unnatural aspartic acid derivatives at predetermined sites (11, 12). The incorporation yields for several aspartic derivatives are illustrated in Table 1 using an optimized bacterial protein synthesizing system (19) programmed to elaborate analogues of HIV-1 protease.

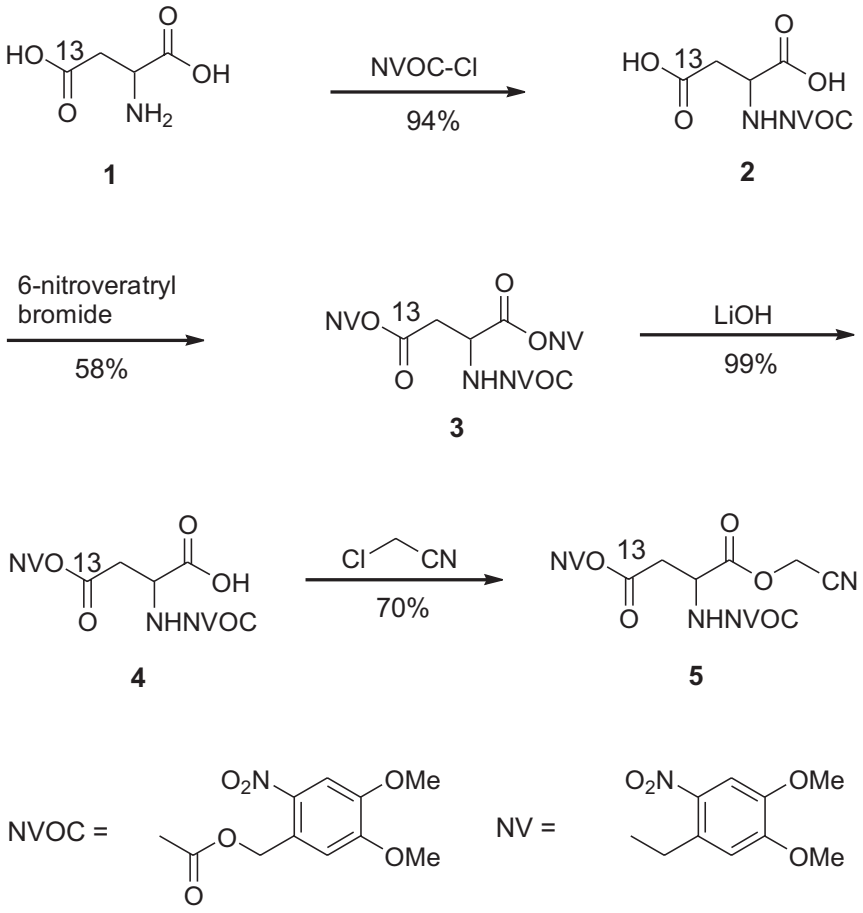
Experimental

General information

Melting points were taken on a capillary melting point apparatus and are uncorrected. Moisture sensitive reactions were conducted under argon in oven-dried glassware.

© 2000 NRC Canada

Scheme 1.



Acetonitrile and dichloromethane were distilled from CaH_2, and DMF was distilled from CaH_2 under diminished pressure. THF was distilled from $LiAlH_4$. Triethylamine was distilled from P_2O_5. All other chemicals were purchased from Aldrich Chemicals or Sigma Chemicals and were used without further purification. Analytical thin layer chromatography was performed on 60 F_{254} (E. Merck) plates. Flash chromatography was performed using 230–400 mesh silica gel. High resolution mass spectra were recorded at the Michigan State University-NIH Mass Spectrometry Facility in East Lansing, MI. T4 RNA ligase was purchased from Amersham Pharmacia Biotech.

N-*(6-Nitroveratryloxycarbonyl)-4-*^{13}*C-(*RS*)-aspartate (**2**)*

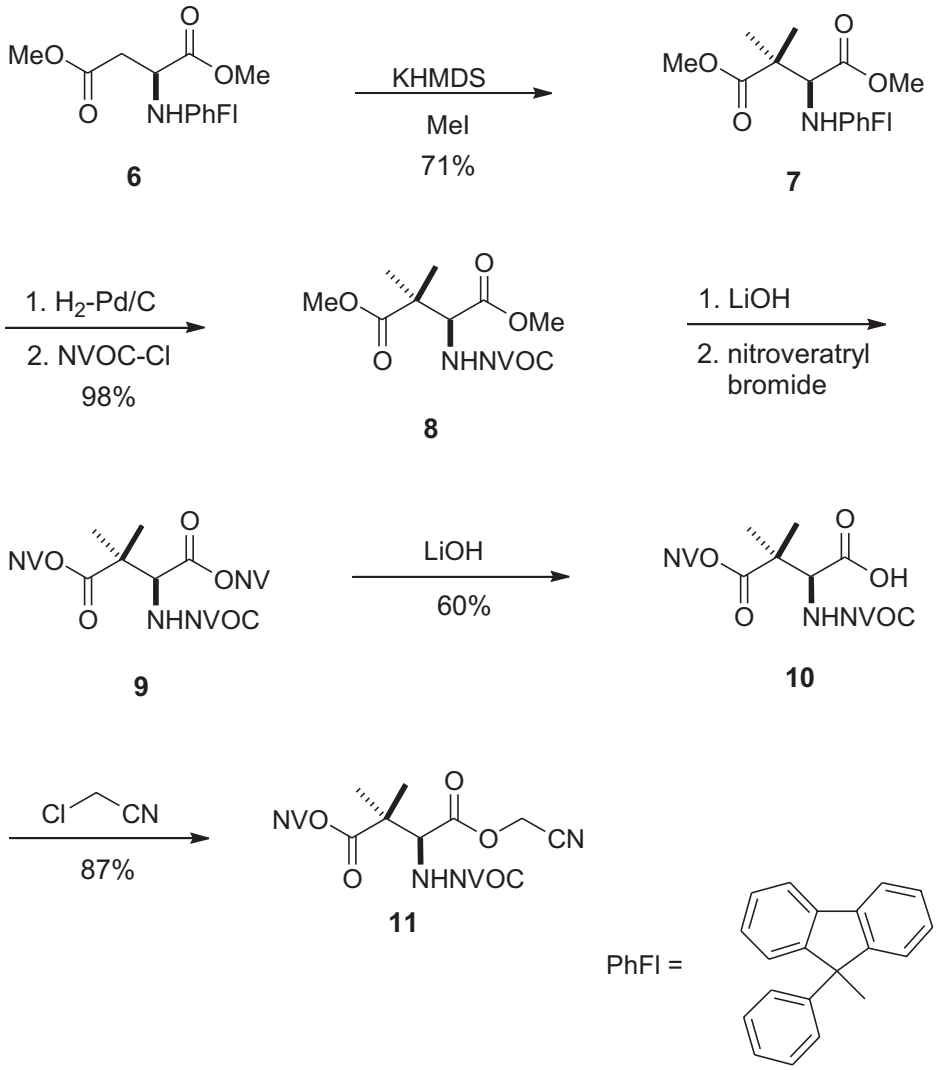
To a solution containing 50 mg (0.37 mmol) of 4-^{13}C-(*RS*)-aspartic acid (**1**) and 157 mg (1.87 mmol) of $NaHCO_3$ in 5 mL of dioxane and 2 mL of H_2O was added a solution of 184 mg (0.67 mmol) of 6-nitroveratryl chloroformate. After stirring at room temperature for 5 h the reaction mixture was diluted with 10 mL of 1 N $NaHSO_4$ and extracted with four 6-mL portions of ethyl acetate. The combined extract was dried (Na_2SO_4) and concentrated under diminished pressure. The crude product was applied to a silica gel column (25 × 2 cm); elution with 5:1:4 ethyl acetate – acetic acid – hexanes provided *N*-(6-nitroveratryloxycarbonyl)-4-^{13}C-(*RS*)-aspartate (**2**) as an orange solid: yield 131 mg (94%), mp 168–172°C. Silica gel TLC R_f: 0.31 (5:1:4 ethyl acetate – acetic acid – hexanes). ^{1}H NMR ($CDCl_3$) δ: 2.73–2.83 (m, 1H), 2.90–2.98 (m, 1H), 3.87 (s, 3H), 3.92 (s, 3H), 4.47–4.53 (m, 1H), 5.43–5.53 (m, 3H), 6.99 (s, 1H), 7.64 (s, 1H). ^{13}C NMR ($CDCl_3$) δ: 30.0, 56.6, 64.1, 108.5, 109.8, 139.6, 148.3, 154.4, 156.5, 173.6. Mass spectrum (chemical ionization) *m/z*: 374.090 $(M+H)^+$ ($C_{13}{}^{13}CH_{17}N_2O_{10}$ requires 374.0917).

Dinitroveratryl N-*(6-nitroveratryloxycarbonyl)-4-*^{13}*C-(*RS*)-aspartate (**3**)*

To a solution containing 131 mg (0.35 mmol) of *N*-(6-nitroveratryloxycarbonyl)-4-^{13}C-(*RS*)-aspartate (**2**) and 292 mg (1.06 mmol) of 6-nitroveratryl bromide in 5 mL of DMF was added 161 mg (1.06 mmol) of CsF. After stirring at room temperature for 24 h the reaction mixture was diluted with 10 mL of ethyl acetate and washed with 10 mL of saturated aqueous $NaHCO_3$ and with 10 mL of brine. The organic layer was dried (Na_2SO_4) and concentrated under diminished pressure. The crude product was applied to a silica gel column (27 × 2 cm); elution with 10–50% ethyl acetate in hexanes provided dinitroveratryl *N*-(6-nitroveratryloxycarbonyl)-4-^{13}C-(*RS*)-aspartate (**3**) as a yellow solid: yield 160 mg (58%), mp 126–134°C. Silica gel TLC R_f: 0.17 (1:1 ethyl acetate–hexanes). ^{1}H NMR ($CDCl_3$) δ: 2.90–3.15 (m, 2H), 3.88 (m, 18H), 4.71 (m, 1H), 5.37–5.45 (m, 6H), 5.50 (br, 1H), 6.89 (s, 1H), 6.98 (s, 2H), 7.62 (s, 3H). ^{13}C NMR ($CDCl_3$) δ: 30.1, 36.3, 37.9, 50.9, 56.7, 64.4, 64.5, 108.6,

© 2000 NRC Canada

Scheme 2.



111.0, 111.2, 126.2, 128.2, 140.1, 148.9, 154.1, 156.7, 170.7. Mass spectrum (electron impact) *m*/*z*: 763.192 ($C_{31}{}^{13}CH_{34}N_4O_{18}$ requires 763.1902).

β-*Nitroveratryl* N-*(6-nitroveratryloxycarbonyl)-4-*^{13}*C-(*RS*)-aspartate (4)*

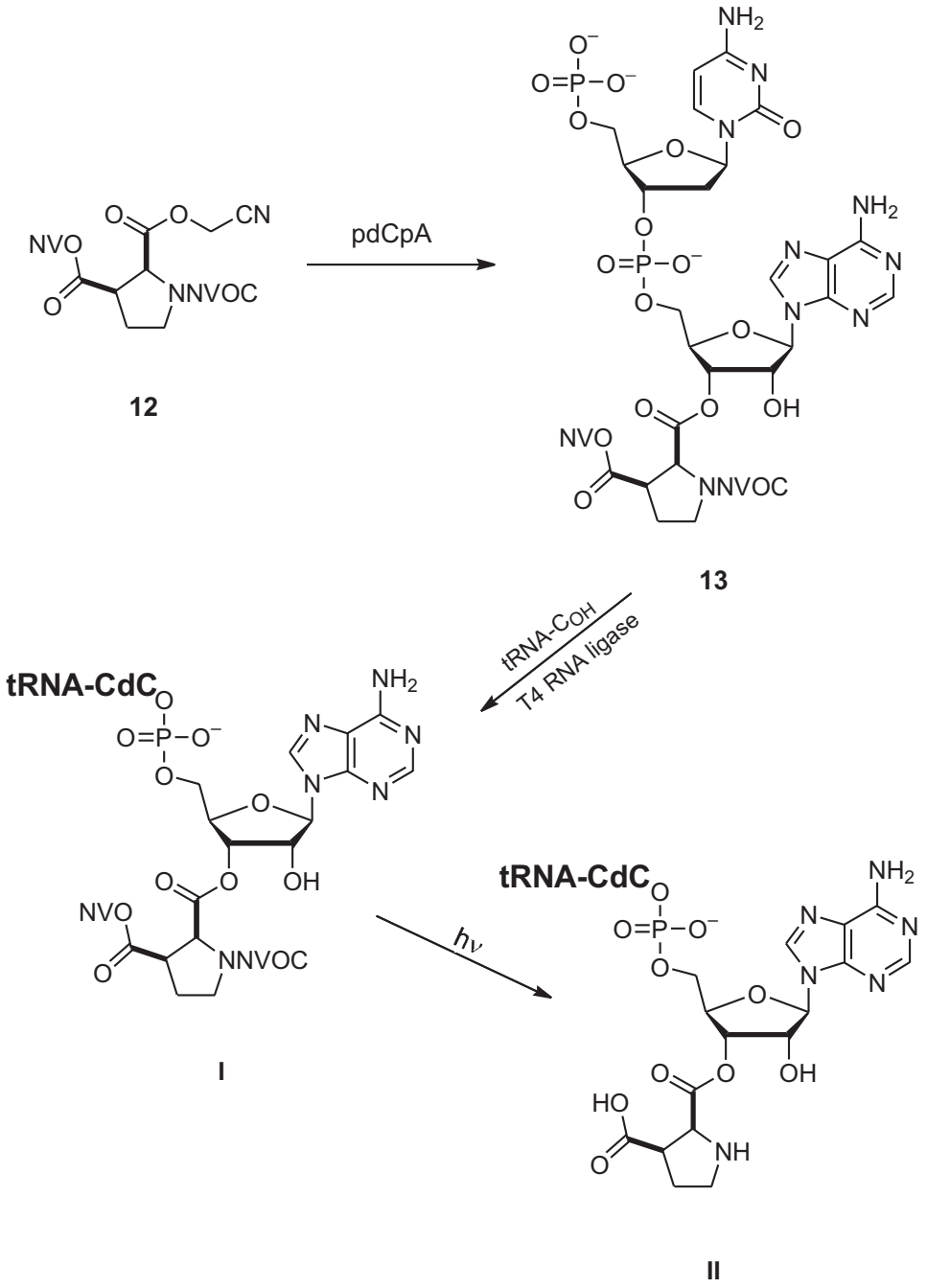
To a cooled (0–5°C) solution containing 89 mg (0.12 mmol) of dinitroveratryl *N*-(6-nitroveratryloxycarbonyl)-4-^{13}C-(*RS*)-aspartate (**3**) in 13 mL of acetone and 2 mL of H_2O was added 12 mL of a 0.1 N solution of LiOH in H_2O. After stirring at room temperature for 16 h, the reaction mixture was diluted with 20 mL of 1 N $NaHSO_4$ and extracted with five 10-mL portions of CH_2Cl_2. The combined organic extract was washed with 10 mL of brine, dried ($MgSO_4$), and concentrated under diminished pressure. The crude product was applied to a silica gel column (26 × 2 cm); elution with 10:1:1:8 ethyl acetate – acetic acid – MeOH – hexanes provided β-nitroveratryl *N*-(6-nitroveratryloxycarbonyl)-4-^{13}C-(*RS*)-aspartate (**4**) as a yellow solid: yield 65 mg (99%). Silica gel TLC R_f: 0.18 (10:1:1:8 ethyl acetate – acetic acid – MeOH – hexanes). ^{1}H NMR ($CDCl_3$) δ: 2.95–3.04 (m, 1H), 3.16–3.24 (m, 1H), 3.93–3.97 (m, 12H), 4.78 (m, 1H), 5.48–5.56 (m, 4H), 5.97 (br, 1H), 6.94 (m, 2H), 7.02 (s, 1H), 7.68–7.70 (m, 2H). Mass spectrum (electron impact) *m*/*z*: 569.142 $(M+H)^+$ ($C_{22}{}^{13}CH_{26}N_3O_{14}$ requires 569.1448).

Cyanomethyl β-*nitroveratryl* N-*(6-nitroveratryloxycarbonyl)-4-*^{13}*C-(*RS*)-aspartate (5)*

To a solution containing 66 mg (0.12 mmol) of β-nitroveratryl *N*-(6-nitroveratryloxycarbonyl)-4-^{13}C-(*RS*)-aspartate (**4**) in 2 mL of acetonitrile was added 100 μL (0.72 mmol) of Et_3N, followed by 0.5 mL (7.90 mmol) of chloroacetonitrile. After stirring at room temperature for 24 h, the reaction mixture was diluted with 10 mL of 1 N HCl and extracted with five 4-mL portions of CH_2Cl_2. The combined organic extract was washed with 5 mL of brine, dried (Na_2SO_4), and concentrated under diminished pressure. The crude product was applied to a silica gel column (12 × 2 cm); elution with 10–50% ethyl acetate in hexanes provided cyanomethyl β-nitroveratryl *N*-(6-nitroveratryloxycarbonyl)-4-^{13}C-(*RS*)-aspartate (**5**) as a yellow solid: yield 50 mg (70%), mp 129–134°C. Silica gel TLC R_f: 0.51 (1:4 ethyl acetate–CH_2Cl_2). ^{1}H

© 2000 NRC Canada

Scheme 3.



NMR ($CDCl_3$) δ: 3.00 (m, 1H), 3.21 (m, 1H), 3.96–4.02 (m, 12H), 4.78 (m, 3H), 5.43–5.59 (m, 4H), 5.80 (br, 1H), 6.95 (s, 1H), 7.05 (s, 1H), 7.73 (s, 2H). ^{13}C NMR (acetone-d_6) δ: 35.0, 35.8, 48.5, 50.2, 55.2, 55.4, 63.24, 63.39, 107.6, 109.3, 110.2, 124.7, 125.8, 127.4, 127.6, 128.4, 139.0, 147.8, 148.1, 153.5, 155.1, 169.0, 169.2. Mass spectrum (chemical ionization) *m/z*: 608.152 $(M+H)^+$ ($C_{24}{}^{13}CH_{27}N_4O_{14}$ requires 608.1557).

Dimethyl N-*(9-phenylfluorenyl)*-β,β-*dimethyl-(*S*)-aspartate (7)*

To a cooled (–78°C) solution containing 5.17 mL of a 0.5 M solution of potassium bis(trimethylsilyl)amide in toluene (2.58 mmol) in 30 mL of THF was added dropwise a solution of 683 mg (1.70 mmol) of dimethyl *N*-(9-phenylfluorenyl)-(*S*)-aspartate (**6**) in 20 mL of THF. After stirring for 1 h, a solution containing 0.45 mL (7.18 mmol) of methyl iodide in 1 mL of THF was added. After stirring for an additional 1 h, another 5.20 mL portion of the 0.5 M potassium bis(trimethylsilyl)amide solution was added. After 2 h the reaction mixture was quenched with 2 mL of MeOH, diluted with 30 mL of 1 N H_3PO_4, and extracted with three 15-mL portions of ethyl acetate. The organic extract was washed with 10 mL of brine, dried ($MgSO_4$), and concentrated under diminished pressure. The crude product was applied to a silica gel column (20 × 2 cm); elution with 4:1 hexanes–ethyl acetate provided dimethyl *N*-(9-phenylfluorenyl)-β,β-dimethyl-(*S*)-aspartate (**7**) as a pale yellow oil: yield 522 mg

© 2000 NRC Canada

(71%). Silica gel TLC R_f: 0.24 (1:1 ethyl acetate–hexanes). ^{1}H NMR ($CDCl_3$) δ: 1.12 (s, 3H), 1.28 (s, 3H), 2.93 (d, 1H, J = 11 Hz), 3.19 (s, 3H), 3.55 (s, 3H), 5.20 (s, 1H), 7.20–7.75 (m, 13H). ^{13}C NMR ($CDCl_3$) δ: 21.4, 22.7, 46.9, 51.7, 52.4, 54.0, 61.5, 73.1, 120.4, 127.3, 127.7, 127.8, 128.1, 148.4, 148.7, 174.6, 176.4. Mass spectrum (electron impact) *m*/*z*: 429.194 ($C_{27}H_{27}NO_4$ requires 429.1940).

Dimethyl N-*(6-nitroveratryloxycarbonyl)*-β,β-*dimethyl-(*S*)-aspartate (**8**)*

To a solution containing 250 mg (0.58 mmol) of dimethyl *N*-(9-phenylfluorenyl)-β,β-dimethyl-(*S*)-aspartate (**7**) in MeOH was added 125 mg of 10% Pd/C. The reaction mixture was shaken under H_2 at 50 psi for 24 h. The reaction mixture was filtered through Celite and the filtrate was concentrated under diminished pressure. The residue was dissolved in 5 mL of H_2O and washed with three 5-mL portions of CH_2Cl_2. The aqueous layer was diluted with 6 mL of dioxane and 122 mg (1.45 mmol) of $NaHCO_3$ was added, followed by a solution containing 289 mg (1.05 mmol) of 6-nitroveratryl chloroformate in 4 mL of dioxane. After stirring at room temperature for 16 h, the reaction mixture was diluted with 20 mL of 1 N $NaHSO_4$ and extracted with four 25-mL portions of ethyl acetate. The combined extract was washed with 15 mL of brine, dried ($MgSO_4$), and concentrated under diminished pressure. The crude product was applied to a silica gel column (20 × 2 cm); elution with 10–50% ethyl acetate in hexanes gave dimethyl *N*-(6-nitroveratryloxycarbonyl)-β,β-dimethyl-(*S*)-aspartate (**8**) as a yellow solid: yield 244 mg (98%). Silica gel TLC R_f: 0.24 (2:3 ethyl acetate–hexanes). ^{1}H NMR ($CDCl_3$) δ: 1.14 (s, 3H), 1.24 (s, 3H), 3.64 (s, 3H), 3.65 (s, 3H) 3.87 (s, 3H), 3.91 (s, 3H), 4.55 (d, 1H, J = 10 Hz), 4.88 (s, 2H), 5.44 (br, 1H), 6.92 (s, 1H), 7.61 (s, 1H). ^{13}C NMR ($CDCl_3$) δ: 22.3, 23.3, 52.9, 56.7, 56.8, 60.5, 62.8, 64.4, 108.4, 108.5, 110.1, 110.9, 133.1, 139.8, 148.1, 154.3, 156.4, 171.2, 176.2. Mass spectrum (electron impact) *m*/*z*: 428.142 ($C_{18}H_{24}N_2O_{10}$ requires 428.1431).

Dinitroveratryl N-*(6-nitroveratryloxycarbonyl)*-β,β-*dimethyl-(*S*)-aspartate (**9**)*

To a solution containing 249 mg (0.58 mmol) of dimethyl *N*-(6-nitroveratryloxycarbonyl)-β,β-dimethyl-(*S*)-aspartate (**8**) in 12 mL of acetone and 6 mL of H_2O was added 14.6 mL of a 0.1 N solution of LiOH in H_2O. After stirring at 40°C for 2 days the reaction mixture was diluted with 10 mL of ethyl acetate and the layers were separated. The aqueous layer was acidified with 1 N $NaHSO_4$ and extracted with four 10-mL portions of ethyl acetate. The combined extract was washed with 10 mL of brine, dried ($MgSO_4$), and concentrated under diminished pressure. The crude diacid was dissolved in 2 mL of DMF and 155 mg (0.56 mmol) of 6-nitroveratryl bromide was added, followed by 85 mg (0.56 mmol) of CsF. After stirring at room temperature for 2 days, the reaction mixture was diluted with 10 mL of ethyl acetate and washed with 10 mL of saturated aqueous $NaHCO_3$ and 10 mL of brine. The organic layer was dried (Na_2SO_4) and concentrated under diminished pressure. The crude product was applied to a silica gel column (18 × 2 cm); elution with 10–50% ethyl acetate in hexanes gave dinitroveratryl *N*-(6-nitroveratryloxycarbonyl)-β,β-dimethyl-(*S*)-aspartate (**9**) as a yellow syrup: yield 124 mg (27%). Silica gel TLC R_f: 0.50 (3:2 ethyl acetate–hexanes). ^{1}H NMR ($CDCl_3$) δ: 1.29 (s, 3H), 1.41 (s, 3H), 3.90–3.93 (m, 18H), 4.71 (d, 1H, J = 10 Hz), 5.39–5.50 (m, 6H), 6.02 (br, 1H), 6.91 (s, 1H), 6.97 (s, 2H), 7.62–7.66 (m, 3H). ^{13}C NMR ($CDCl_3$) δ: 22.8, 23.8, 45.8, 60.7, 64.5, 64.9, 108.5, 110.0, 110.9, 111.3, 126.2, 126.6, 128.2, 140.0, 140.3, 148.6, 148.8, 154.0, 154.2, 156.4, 170.3, 175.3. Mass spectrum (FAB) *m*/*z*: 791.226 $(M+H)^+$ ($C_{34}H_{39}N_4O_{18}$ requires 791.2259).

β-*Nitroveratryl* N-*(6-nitroveratryloxycarbonyl)*-β,β-*dimethyl-(*S*)-aspartate (**10**)*

To a cooled (0–5°C) solution containing 119 mg (0.15 mmol) of dinitroveratryl *N*-(6-nitroveratryloxycarbonyl)-β,β-dimethyl-(*S*)-aspartate (**9**) in 5 mL of acetone and 2 mL of H_2O was added 1.6 mL (0.16 mmol) of a 0.1 N solution of LiOH in H_2O. After stirring at room temperature for 24 h, the reaction mixture was concentrated under diminished pressure. The residue was dissolved in 4 mL of saturated aqueous $NaHCO_3$ and washed with three 5-mL portions of ethyl acetate. The aqueous layer was acidified with 1 N $NaHSO_4$ and extracted with three 6-mL portions of ethyl acetate. The combined extract was washed with 6 mL of brine, dried ($MgSO_4$), and concentrated under diminished pressure. The crude product was applied to a silica gel column (13 × 2 cm); elution with 10:1:1:8 ethyl acetate – MeOH – acetic acid – hexanes gave β-nitroveratryl *N*-(6-nitroveratryloxycarbonyl)-β,β-dimethyl-(*S*)-aspartate (**10**) as a pale yellow syrup: yield 54 mg (60%). Silica gel TLC R_f: 0.48 (10:1:9 ethyl acetate – MeOH – hexanes). ^{1}H NMR ($CDCl_3$) δ: 1.23 (s, 3H), 1.41 (s, 3H), 3.94–3.97 (m, 12H), 4.65 (d, 1H, J = 10 Hz), 5.51 (m, 4H), 6.02 (br, 1H), 7.02 (s, 2H), 7.67 (s, 2H), 11.0 (br, 1H). Mass spectrum (FAB) *m*/*z*: 596.170 $(M + H)^+$ ($C_{25}H_{30}N_3O_{14}$ requires 596.1728).

Cyanomethyl β-*nitroveratryl* N-*(6-nitroveratryloxycarbonyl)*-β,β-*dimethyl-(*S*)-aspartate (**11**)*

To a solution containing 52 mg (0.087 mmol) of β-nitroveratryl *N*-(6-nitroveratryloxycarbonyl)-β,β-dimethyl-(*S*)-aspartate (**10**) in 2 mL of acetonitrile was added 61 μL (0.44 mmol) of Et_3N, followed by 100 μL (1.58 mmol) of chloroacetonitrile. After stirring at room temperature for 24 h the reaction mixture was diluted with 5 mL of CH_2Cl_2 and washed successively with 4 mL of 1 N HCl, two 4-mL portions of saturated aqueous $NaHCO_3$, and 5 mL of brine. The organic layer was dried (Na_2SO_4) and concentrated under diminished pressure. The crude product was applied to a silica gel column (15 × 2 cm); elution with 10–50% ethyl acetate in hexanes provided cyanomethyl β-nitroveratryl *N*-(6-nitroveratryloxycarbonyl)-β,β-dimethyl-(*S*)-aspartate (**11**) as a pale yellow solid: yield 48 mg (87%), mp 69–72°C. Silica gel TLC R_f: 0.24 (1:1 ethyl acetate–hexanes). ^{1}H NMR ($CDCl_3$) δ: 1.33 (s, 3H), 1.44 (s, 3H), 3.96 (s, 6H), 4.00 (s, 6H), 4.65 (m, 1H), 4.71 (m, 2H), 5.51 (m, 2H), 5.56 (m, 2H), 5.92, (br, 1H), 7.03 (s, 2H), 7.72 (s, 2H). Mass spectrum (FAB) *m*/*z*: 634.172 ($C_{27}H_{30}N_4O_{14}$ requires 634.1759).

β-*Nitroveratryl* N-*(6-nitroveratryloxycarbonyl)-(2*S*,3*R*)-carboxyproline pdCpA ester (**13**)*

A solution of 4 mg (2.94 μmol) of the tris(tetrabutylammonium) salt of pdCpA and 9.8 mg (13.7 μmol) of β-nitroveratryl *N*-(6-nitroveratryloxycarbonyl)-(*2S,3R*)-carboxy-

© 2000 NRC Canada

proline cyanomethyl ester (**12**) in 50 μL of DMF was stirred at room temperature for 4 h. A 10-μL aliquot of the mixture was diluted with 90 μL of 1:1 CH_3CN – 50 mM NH_4OAc, pH 4.5. Ten μL of the diluted aliquot was analyzed by HPLC on a C_{18} reversed phase column (250 × 10 mm). The column was washed with 1→63% CH_3CN in 50 mM NH_4OAc, pH 4.5, over a period of 45 min at a flow rate of 3.5 mL/min (monitoring at 260 nm). The reaction mixture was diluted to a total volume of 400 μL of 1:1 CH_3CN – 50 mM NH_4OAc, pH 4.5, and purified using the same semipreparative C_{18} reversed phase column, affording β-nitroveratryl *N*-(6-nitroveratryloxycarbonyl)-(*2S*,*3R*)-carboxyproline pdCpA ester (**13**) as a pale yellow foam: yield 0.5 mg (14%). Mass spectrum (FAB) *m/z*: 1212.257 $(M+H)^+$ ($C_{44}H_{52}N_{11}O_{26}P_2$ requires 1212.2560).

Synthesis of misacylated tRNAs

Ligation reactions were carried out in 50 μL of 50 mM Na Hepes buffer, pH 7.5, containing 5 μL (~0.2 nmol) of $tRNA_{(CUA)}C_{OH}$, 0.5 A_{260} unit (~20 nmol) of an aminoacyl-pdCpA, 0.5 mM ATP, 15 mM $MgCl_2$, 10% dimethylsulfoxide, and 100 units of T4 RNA ligase. Reaction mixtures were incubated at 37°C for 25 min and then quenched by the addition of 5 μL of 3 M Na acetate, pH 4.5. The aminoacylated tRNA (**I**) was precipitated with 2.5 volumes of ethanol, collected by centrifugation, washed with 70% ethanol, and dried. The product was redissolved in 1 mM KOAc to a final concentration of 1 μg/μL and then irradiated with a 500 W mercury–xenon lamp using Pyrex and water filters. The protected aminoacyl tRNA (**I**) was cooled in an ice bath during irradiation, which was typically carried out for 5 min for amino acid derivatives containing an NVOC group and a nitroveratryl ester. The deprotected aminoacyl-tRNAs (**II**) were used in in vitro suppression experiments soon after deprotection.

Acknowledgment

This work was supported by Research Grant CA77359 from the National Cancer Institute.

References

1. F. Chapeville, F. Lipmann, G. von Ehrenstein, B. Weisblum, W.J. Roy, and S. Benzer. Proc. Natl. Acad. Sci. U.S.A. **48**, 1086 (1962).
2. (*a*) S. Fahnestock and A. Rich. Nature New Biol. **229**, 8 (1971); (*b*) S. Fahnestock and A. Rich. Science (Washington, D.C.), **173**, 340 (1971); (*c*) A.E. Johnson, W.R. Woodward, E. Herbert, and J.R. Menninger. Biochemistry, **15**, 569 (1976).
3. (*a*) S.M. Hecht, B.L. Alford, Y. Kuroda, and S. Kitano. J. Biol. Chem. **253**, 4517 (1978); (*b*) T.G. Heckler, Y. Zama, T. Naka, and S.M. Hecht. J. Biol. Chem. **258**, 4492 (1983); (*c*) T.G. Heckler, L.-H. Chang, Y. Zama, T. Naka, and S.M. Hecht. Tetrahedron, **40**, 87 (1984); (*d*) T.G. Heckler, L.-H. Chang, Y. Zama, T. Naka, M.S. Chorghade, and S.M. Hecht. Biochemistry, **23**, 1468 (1984); (*e*) T.G. Heckler, J.R. Roesser, X. Cheng, P.-I. Chang, and S.M. Hecht. Biochemistry, **27**, 7254 (1988).
4. (*a*) S.A. Robertson, C.J. Noren, S.J. Anthony-Cahill, M.C. Griffith, and P.G. Schultz. Nucleic Acids Res. **17**, 9649 (1989); (*b*) S.A. Robertson, J.A. Ellman and P.G. Schultz. J. Am. Chem. Soc. **113**, 2722 (1991).
5. C.J. Noren, S.J. Anthony-Cahill, D.J. Suich, K.A. Noren, M.C. Griffith, and P.G. Schultz. Nucleic Acids Res. **18**, 83 (1990).
6. (*a*) J.R. Roesser, C. Xu, R.C. Payne, C.K. Surratt, and S.M. Hecht. Biochemistry, **28**, 5185 (1989); (*b*) C.J. Noren, S.J. Anthony-Cahill, M.C. Griffith, and P.G. Schultz. Science (Washington, D.C.), **244**, 182 (1989); (*c*) D. Mendel, J.A. Ellman, and P.G. Schultz. J. Am. Chem. Soc. **113**, 2758 (1991); (*d*) M. Lodder, S. Golovine, and S.M. Hecht. J. Org. Chem. **62**, 778 (1997); (*e*) M. Lodder, S. Golovine, A.L. Laikhter, V.A. Karginov, and S.M. Hecht. J. Org. Chem. **63**, 794 (1998).
7. (*a*) J.D. Bain, C.G. Glabe, T.A. Dix, A.R. Chamberlin, and E.S. Diala. J. Am. Chem. Soc. **111**, 8013 (1989); (*b*) J.D. Bain, A. Dean, D.A. Wacker, E.E. Kuo, and A.R. Chamberlin. Tetrahedron **47**, 2389 (1991); (*c*) J.D. Bain, C. Switzer, S.A. Benner, and A.R. Chamberlin. Nature (London), **356**, 537 (1992); (*d*) S.M. Hecht. Acc. Chem. Res. **25**, 545 (1992).
8. J.A. Killian, M.D. Van Cleve, Y.F. Shayo, and S.M. Hecht. J. Am. Chem. Soc. **120**, 3032 (1998).
9. (*a*) C.J. Noren, J. Spencer, S.J. Anthony-Cahill, M.C. Griffith, and P.G. Schultz. Science (Washington, D.C.), **244**, 182 (1989); (*b*) J. Ellman, D. Mendel, S. Anthony-Cahill, C.J. Noren, and P.G. Schultz. Methods Enzymol. **202**, 301 (1991); (*c*) J.A. Ellman, D. Mendel, and P.G. Schultz. Science (Washington, D.C.), **255**, 197 (1992); (*d*) J.A. Ellman, B.F. Volkman, D. Mendel, P.G. Schultz, and D.E. Wemmer. J. Am. Chem. Soc. **114**, 7959 (1992); (*e*) D. Mendel, J.A. Ellman, Z. Chang, D.L. Veenstra, P.A. Kollman, and P.G. Schultz. Science (Washington, D.C.), **256**, 1798 (1993); (*f*) J.K. Judice, T.R. Gamble, E.C. Murphy, A.M. deVos, and P.G. Schultz. Science (Washington, D.C.), **261**, 1578 (1993); (*g*) H.-H. Chang, D.R. Benson, and P.G. Schultz. Science (Washington, D.C.), **259**, 806 (1993); (*h*) D. Mendel, J.A. Ellman, and P.G. Schultz. J. Am. Chem. Soc. **115**, 4359 (1993); (*i*) V.W. Cornish, D.R. Benson, C.A. Altenbach, K. Hideg, W.L. Hubbell, and P.G. Schultz. Proc. Natl. Acad. Sci. U.S.A. **91**, 2910 (1994); (*j*) J.S. Thorson, E. Chapman, E.C. Murphy, P.G. Schultz, and J.K. Judice. J. Am. Chem. Soc. **117**, 1157 (1995); (*k*) V.W. Cornish, D. Mendel, and P.G. Schultz. Angew. Chem. Int. Ed. Engl. **34**, 621 (1995); (*l*) M.W. Nowak, P.C. Kearney, J.R. Sampson, M.E. Saks, C.G. Labarca, S.K. Silverman, W. Zhong, J. Thorson, J.N. Abelson, N. Davidson, P.G. Schultz, D.A. Dougherty, and H.A. Lester. Science (Washington, D.C.), **268**, 439 (1995); (*m*) S.V. Mamaev, A.L. Laikhter, T. Arslan, and S.M. Hecht. J. Am. Chem. Soc. **118**, 7243 (1996); (*n*) M.E. Saks, J.R. Sampson, M.W. Nowak, P.C. Kearney, F. Du, J.N. Abelson, H.A. Lester, and D.A. Dougherty. J. Biol. Chem. **271**, 23169 (1996); (*o*) L.E. Steward, C.S. Collins, M.A. Gilmore, J.E. Carlson, J.B.A. Ross, and A.R. Chamberlin. J. Am. Chem. Soc. **119**, 6 (1997); (*p*) T. Arslan, S.V. Mamaev, N.V. Mamaeva, and S.M. Hecht. J. Am. Chem. Soc. **119**, 10877 (1997); (*q*) P.M. England, H.A. Lester, N. Davison, and D.A. Dougherty. Proc. Natl. Acad. Sci. U.S.A. **94**, 11025 (1997).
10. J.R. Roesser, M.S. Chorghade, and S.M. Hecht. Biochemistry, **25**, 6361 (1986).
11. V.A. Karginov, S.V. Mamaev, H. An, M.D. Van Cleve, S.M. Hecht, G.A. Komatsoulis, and J.N. Abelson. J. Am. Chem. Soc. **119**, 8166 (1997).
12. (*a*) G.F. Short, III, M. Lodder, A.L. Laikhter, T. Arslan, and S.M. Hecht. J. Am. Chem. Soc. **121**, 478 (1999); (*b*) G.F. Short, III, A.L. Laikhter, M. Lodder, Y. Shayo, T. Arslan, and S.M. Hecht. Biochemistry. In press.
13. J.M. Humphrey, R.J. Bridges, J.A. Hart, and A.R. Chamberlin. J. Org. Chem. **59**, 2467 (1994).

© 2000 NRC Canada

14. A. Patchornik, B. Amit, and U. Zehavi. J. Org. Chem. **39**, 192 (1974).
15. M. Wilcox, R.W. Viola, K.W. Johnson, A.P. Billington, B.K. Carpenter, J.A. McCray, A.P. Guzikowski, and G.P. Hess. J. Org. Chem. **55**, 1585 (1990).
16. (*a*) P.M. Bryant, R.H. More, P.J. Pimlott, and G.T. Young. J. Chem. Soc. 3868 (1959); (*b*) J.M. Davey, A.H. Laird, and J.S. Morley. J. Chem. Soc. (C) 555 (1966).
17. M. Bodanszky and A. Bodanszky. In the practice of peptide synthesis. 2nd ed. Springer–Verlag, Berlin, Heidelberg, New York. 1994. p. 96.
18. P. Gmeiner, P.L. Feldman, M.Y. Chu-Moyer, and H. Rapoport. J. Org. Chem. **55**, 3068 (1990).
19. G.F. Short, III, S.Y. Golovine, and S.M. Hecht. Biochemistry, **38**, 8808 (1999).

© 2000 NRC Canada

Substrate specificity of fucosyl transferase III: An efficient synthesis of sialyl Lewis^x-, sialyl Lewis^a-derivatives and mimetics thereof

Beat Ernst, Bea Wagner, Gabi Baisch, Andreas Katopodis, Tammo Winkler, and Reinhold Öhrlein

Abstract: Fucosyl transferase III (FucT III) has previously been characterized as the most general enzyme of the FucT family, as judged from its ability to catalyze the transfer of fucose to both Galβ(1–3)Glc*N*Ac and Galβ(1–4)Glc*N*Ac. In order to explore the synthetic potential of FucT III for the enzymatic synthesis of sialyl Lewis^x and sialyl Lewis^a derivatives, its substrate specificity has been probed using a number of natural substrate mimetics. A remarkable range of acceptor substrates was found when *N*-acetyl glucosamine was replaced by D-glucal, (*R*,*R*)-1,2-cyclohexanediol and (*R*,*R*)-butan-2,3-diol. Although the reaction rates were low compared to the reaction with the natural substrates, they proved to be sufficient for the synthesis of preparative amounts.

Key words: fucosyl transferase III, sialyl Lewis^a, sialyl Lewis^x, carbohydrate mimetics.

Résumé : La fucosyle transférase III (FucT III) a déjà été caractérisée comme étant l'enzyme le plus général de la famille des FucT, tel que le prouve sa capacité à catalyser le transfert du fucose aux deux Gal 1–3 Glc*N*Ac et Gal 1–4 GlcVAc. Dans le but d'explorer le potentiel synthétique du FucT III pour la synthèse enzymatique des dérivés du sialyl Lewis^x et du sialyl Lewis^a, on a mis en évidence la spécificité de son substrat en utilisant divers analogues de substrats naturels. On trouvé un remarquable échantillonnage de substrats accepteurs lorsqu'on remplace la *N*-Acétyl glucosamine par le D-glucal, le (*R*,*R*)-1,2-cyclohexanediol et le (*R*,*R*)-butan-2,3-diol. Bien que les vitesses de réaction soient plus lentes que celles des produits naturels, elles se révèlent acceptables pour la synthèse à grande échelle.

Mots clés : fucosyle transférase III, sialyl Lewis^x et du sialyl Lewis^a, analogues d'hydrates de carbone.

[Traduit par la Rédaction]

Introduction

Numerous diseases and pathological situations are associated with excessive influx of leukocytes into tissues. Although this influx normally represents an essential defense mechanism against infection, excessive, or inappropriate leukocyte accumulation results in injury to host tissues as observed in ischemia-reperfusion injury, respiratory disease, dermatitis, or gastro-intestinal inflammation (1).

Early in the inflammatory response leukocytes adhere to and roll along endothelial cells on the inner surface of blood vessels. It has been clearly shown that an inducible set of calcium dependent adhesion molecules, the selectins, mediates this initial event (2). Since leukocyte rolling is a prerequisite for later inflammatory events, inhibition of selectins is a valuable strategy for preventing the deleterious consequences of excessive leukocyte influx.

Studies of the carbohydrate specificity of E- and P-selectin uncovered a recognition motif common to both receptors, the sialylated and fucosylated tetrasaccharide antigens sialyl Lewis^x (**1**) (3) and sialyl Lewis^a (**2**) (4). Later, L-selectin was also shown to bind sLe^x and sLe^a containing oligosaccharides (5). These two tetrasaccharides have therefore served as lead structures in our search for selectin antagonists with increased biological activity, simplified structure and improved bioavailability (6). For the discovery of their structure-activity relationship, numerous derivatives of **1** and **2** have been synthesized. It is worth mentioning that these derivatives have not only been obtained by chemical (7) but also by enzymatic synthesis (Scheme 1); e.g., sialyl Lewis^x and sialyl Lewis^a derivatives with a modified *N*-acyl group of the D-glucosamine nitrogen (e.g., **3**, **4**) (8) or compounds where fucose is replaced by other L-sugars (e.g., **5**, **6**) (9).

Although a number of studies showed that non-natural substrates are accepted by glycosyl transferases (10), only a limited number of structurally more distant compouds have been probed to date (11). To further explore the synthetic potential of the enzymatic approach for the synthesis of sialyl Lewis^x and sialyl Lewis^a derivatives and to widen the synthetic value of these biocatalysts, we decided to

Received September 17, 1999. Published on the NRC Research Press Website on June 16, 2000.

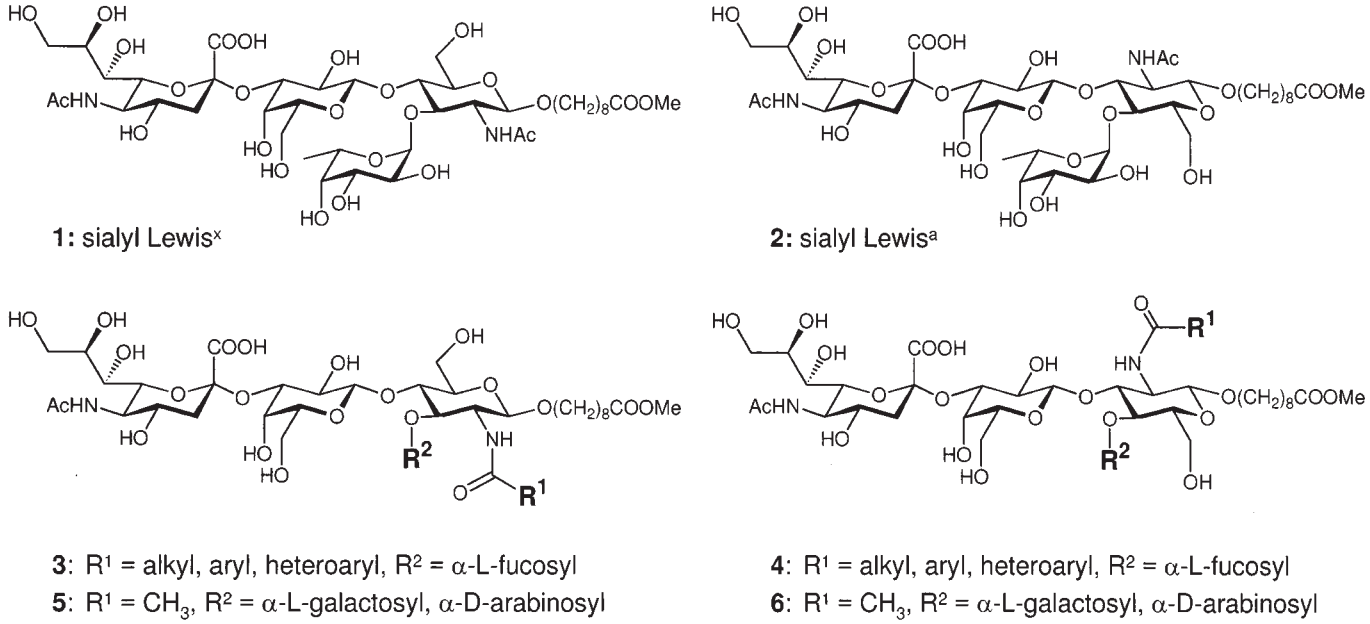
This paper is dedicated to Professor Hanessian.

B. Ernst[1] and B. Wagner. Institute of Molecular Pharmacy, Pharmacenter, University of Basel, CH-4056 Basel, Switzerland.
G. Baisch, A. Katopodis, and R. Öhrlein. Novartis Pharma AG, CH-4002 Basel, Switzerland.
T. Winkler. Novartis Crop Protection AG, CH-4002 Basel, Switzerland.

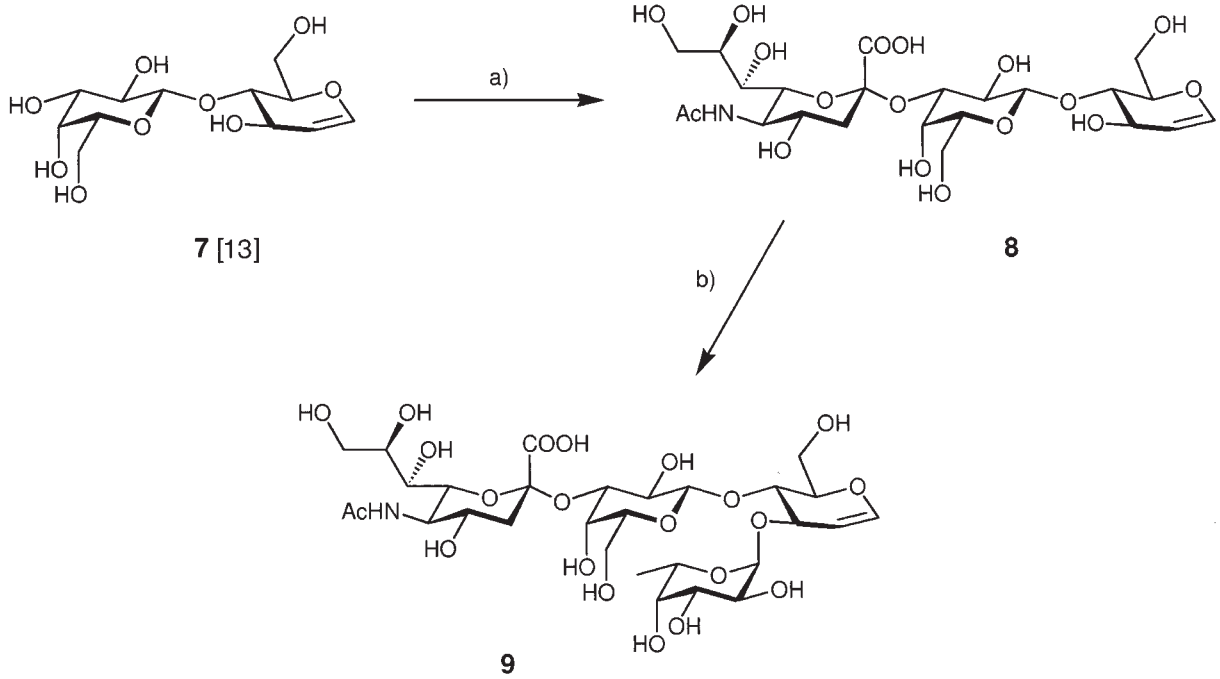
[1]Author to whom correspondence may be addressed (e-mail: beat.ernst@unibas.ch).

© 2000 NRC Canada

Scheme 1. sLe^x and sLe^a and enzymatically synthesized derivatives thereof (8, 9).



Scheme 2. (*a*) CMP-Neu-5-*N*Ac, α(2–3)sialyl transferase (65%); (*b*) GDP-fucose, FucT III (83%).



investigate the substrate specificity of the enzymatic fucosylation reaction. As judged from its ability to catalyze the transfer of fucose to both α1,3 and α1,4 linkages FucT III has previously been characterized as the most general enzyme of the FucT III family (12). We therefore concentrated our investigation on the substrate specificity of FucT III.

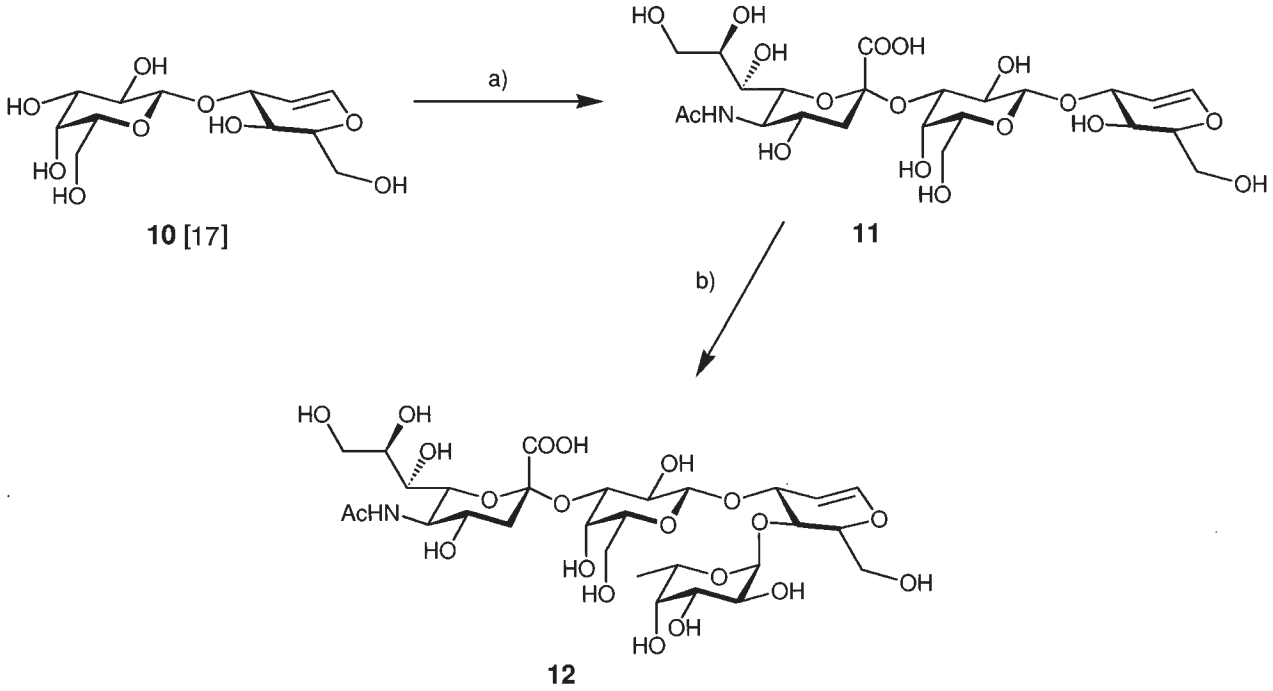
Results and discussion

Since the chemical approach to sialyl Lewis^x and sialyl Lewis^a analogs requires multi-step syntheses, the chemoenzymatic approach was considered as an alternative. The advantages of using glycosyl transferases for the construction of glycosidic bonds include mild reaction conditions, the lack of requirement for protection and deprotection steps and the regio- and stereospecificity of the glycosylation.

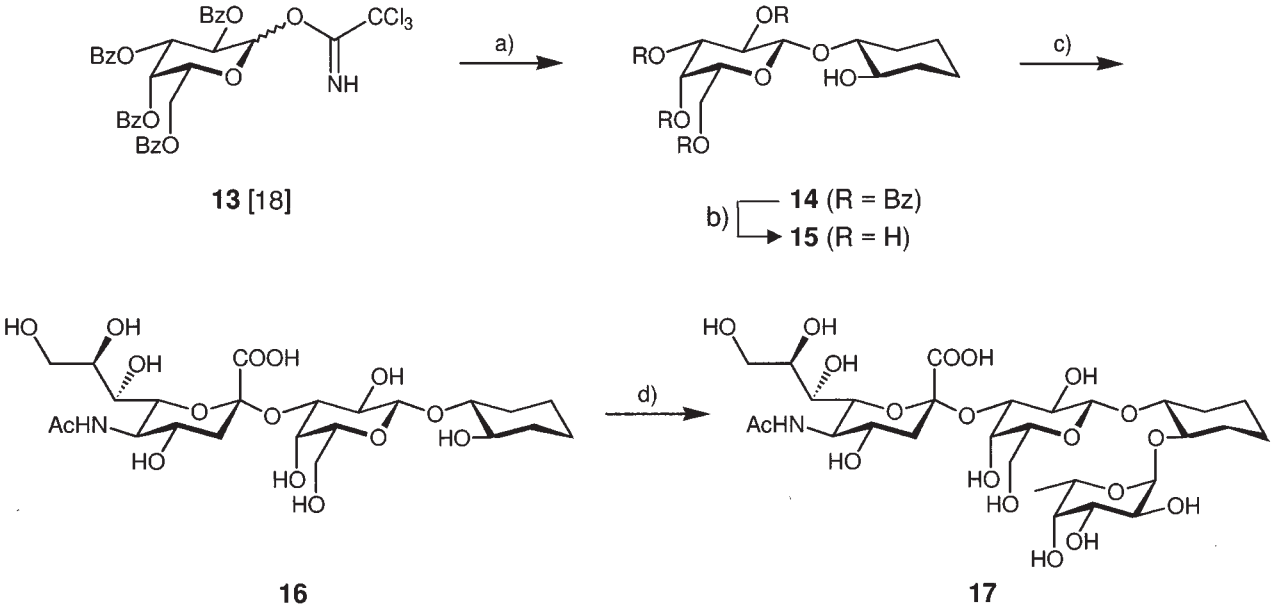
In a first attempt, lactal **7**, which can easily be obtained from D-lactose (13) served as a mimic of *N*-acetyllactosamine (Scheme 2). It was first incubated with recombinant α(2–3)sialyl transferase (14) and subsequently with recombinant fucosyl transferase FucT III (15). As expected, α-sialylation occurred at the 3-OH of galactose. Surprisingly, the allylic OH-group of the glucal moiety was fucosylated exclusively, generating the desired sLe^x derivative **9**. A

© 2000 NRC Canada

Scheme 3. (*a*) CMP-Neu-5-*N*Ac, α(2–3)sialyl transferase (92%); (*b*) GDP-fucose, FucT III (82%).



Scheme 4. (*a*) (*R*,*R*)-cyclohexan-1,2-diol, TESOTf, CH_3CN, 1 h (74%); (*b*) cat. NaOMe, MeOH, rt, 6 h (75%); (*c*) CMP-Neu-5-*N*Ac, α(2–3)sialyl transferase (64%); (*d*) GDP-fucose, FucT III (71%).



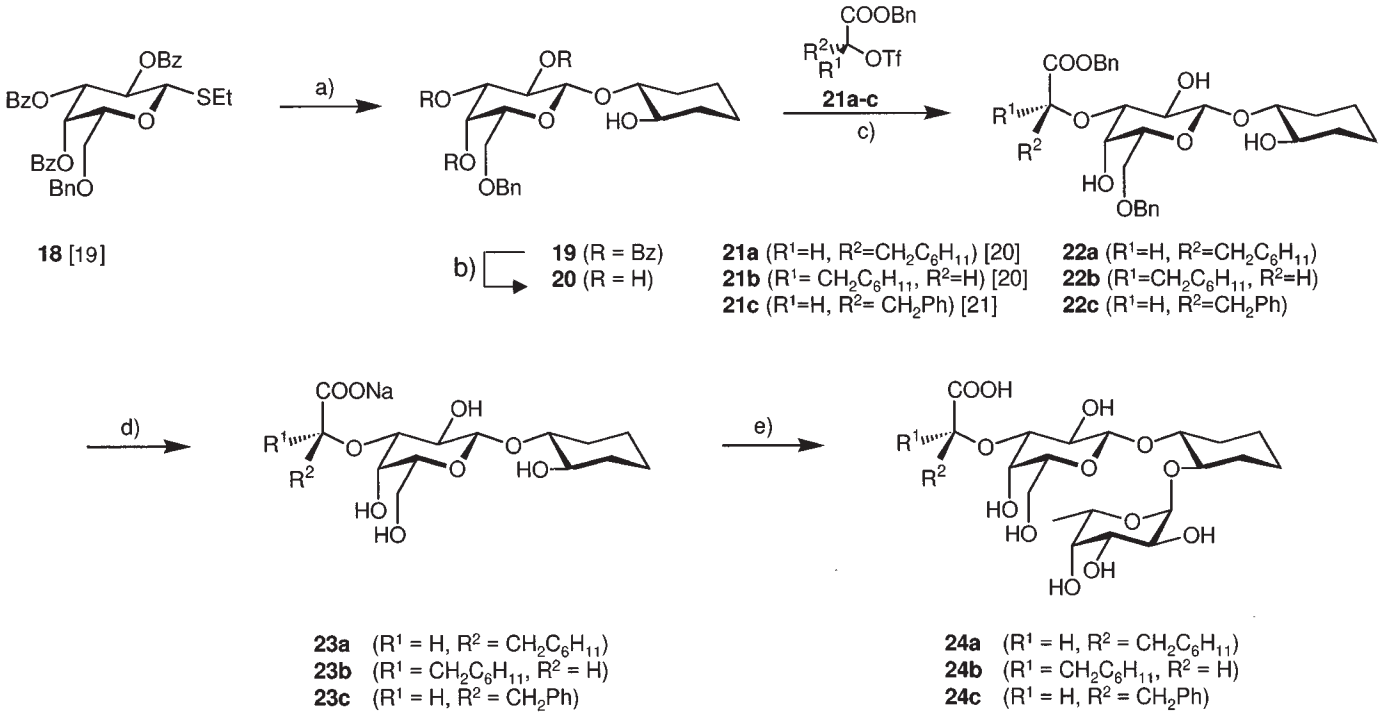
similar reaction sequence starting from **7** had previously been carried out successfully by Wong et al. (16) using FucT V instead of FucT III.

Galactosyl-β(1–3)glucal **10** (17), a type I congener of lactal **7**, could equally well be sialylated (→ **11**) (Scheme 3). Also in this case, FucT III accepted a glucal derivative as substrate. Therefore, the *N*-acetyl group of the natural glucosamine substrate is not a prerequisite for a successful fucosylation.

In a further step (see Scheme 4), the glucal ring system was replaced by (*R*,*R*)-cyclohexan-1,2-diol. The precursor pseudodisaccharide **15** was obtained in a two step procedure by galactosylation of commercially available (*R*,*R*)-1,2-cyclohexanediol using the trichloroacetimidate **13** (18) as the galactosyl donor and TESOTf as the promotor (→ **14**) followed by removal of the benzoate protecting groups by transesterification. In the first enzymatic step, **15** was incubated with CMP-Neu-5-NAc and recombinant α(2–3)sialyl transferase (14) to yield **16**. As observed for **7** and **10,** the activity of the α(2–3)sialyl transferase was not affected by the character of the aglycon at the reducing end of the galactose moiety. In the subsequent fucosylation step, incubation

© 2000 NRC Canada

Scheme 5. (*a*) (*R*,*R*)-cyclohexan-1,2-diol, DMTST (20), CH_2Cl_2, 4 Å molecular sieves, 3 h (59%); (*b*) cat. NaOMe, MeOH, rt, 3 h (96%); (*c*) $^nBu_2SnO$, MeOH, rfl., 2 h; CsF, DMF, rt, 3 h, with benzyl (*R*)-3-cyclohexyl-2-trifluoromethansulfonyloxy-propionate **21a** (→ **22a**, 76%), with benzyl (*S*)-3-cyclohexyl-2-trifluoromethansulfonyloxy-propionate **21b** (→ **22b**, 66%), with benzyl (*R*)-3-phenyl-2-trifluoromethansulfonyloxy-proprionate **21c** (→ **22c**, 82%); (*d*) 20% $Pd(OH)_2$, H_2, dioxane–H_2O–AcOH; Dowex 50 (Na^+ form) (**23a**, 66%; **23b**, 72%; **23c**, 68%); (*e*) GDP-fucose, FucT III (**24a**, 54%; **24b**, 61%; **24c**, 96%).



of the trisaccharide **16** with GDP-fucose and recombinant FucT III (15) gave **17**, which can be regarded as mimic of either sLe^x or a sLe^a. The connectivity pattern in **17** was confirmed by ROESY.

Next, the enzymatic fucosylations of the pseudotrisaccharides **23a**–**c** were examined. In these compounds the D-glucosamine and the *N*-acetylneuraminic acid moiety of the natural substrate are replaced by (*R*,*R*)-cyclohexan-1,2-diol and *R*- and *S*-lactic acid derivatives, respectively. The glycosyl acceptors **23a**–**c** were obtained by galactosylation of (*R*,*R*)-cyclohexan-1,2-diol with ethyl 6-*O*-benzyl-2,3,4-tri-*O*-benzoyl-1-thio-β-D-galactopyranoside **18** (19) using dimethylmethylthiosulfonium triflate (DMTST) (20) as promoter (→ **19**) followed by the removal of the benzoate protecting groups by transesterification (→ **20**). Finally, alkylation of **20** with the lactic acid derivatives **21a,b** (21) and **21c** (22), respectively, (→ **22a**–**c**) and final deprotection by hydrogenolysis gave the substrates **23a**–**c**. As observed for **16**, the hydroxy group of the cyclohexane moiety was fucosylated with good to excellent yield using FucT III. The replacement of neuraminic acid by lactic acid derivatives does not influence proper fucosylation. Furthermore, the stereochemical orientation of the lactic acid substituents – with *S*-configuration in **23a** and *R*-configuration in **23b** – did not affect the outcome of the fucosylation.

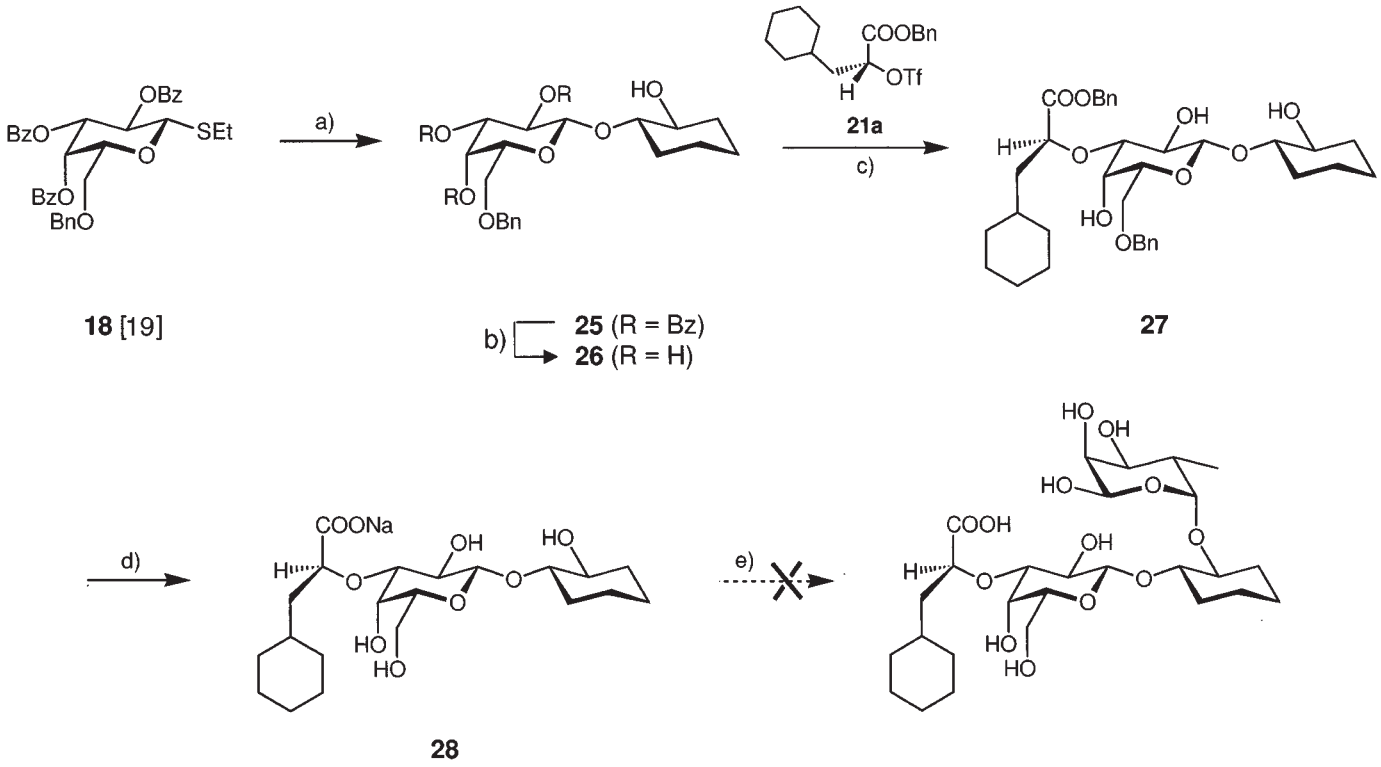
D-Galactose carrying a substituent with the acceptor OH group in the proper stereochemical arrangement at the reducing end is therefore the only structural motif critical for recognition by FucT III. (*R*,*R*)-cyclohexan-1,2-diol can be considered as a perfect mimic for the 3- and 4-hydroxy groups of a D-glucose/D-glucosamine in the $^4C_1$ conformation.

We further investigated (*S*,*S*)-cyclohexan-1,2-diol, which represents a mimic of *N*-acetyl-L-glucosamine. The pseudotrisaccharide **28** was obtained in analogy to **23a** (see Scheme 6): β-Galactosylation of (*S*,*S*)-cyclohexan-1,2-diol gave the pseudodisaccharide **25** in moderate yield. After removal of the benzoates, **26** was regioselectively alkylated with benzyl (*R*)-3-cyclohexyl-2-trifluoromethansulfonyloxy-propionate. Finally, the benzyl protective groups were removed by hydrogenation to yield **28**, which however did not act as a substrate for FucT III as well as for FucT VI (23).

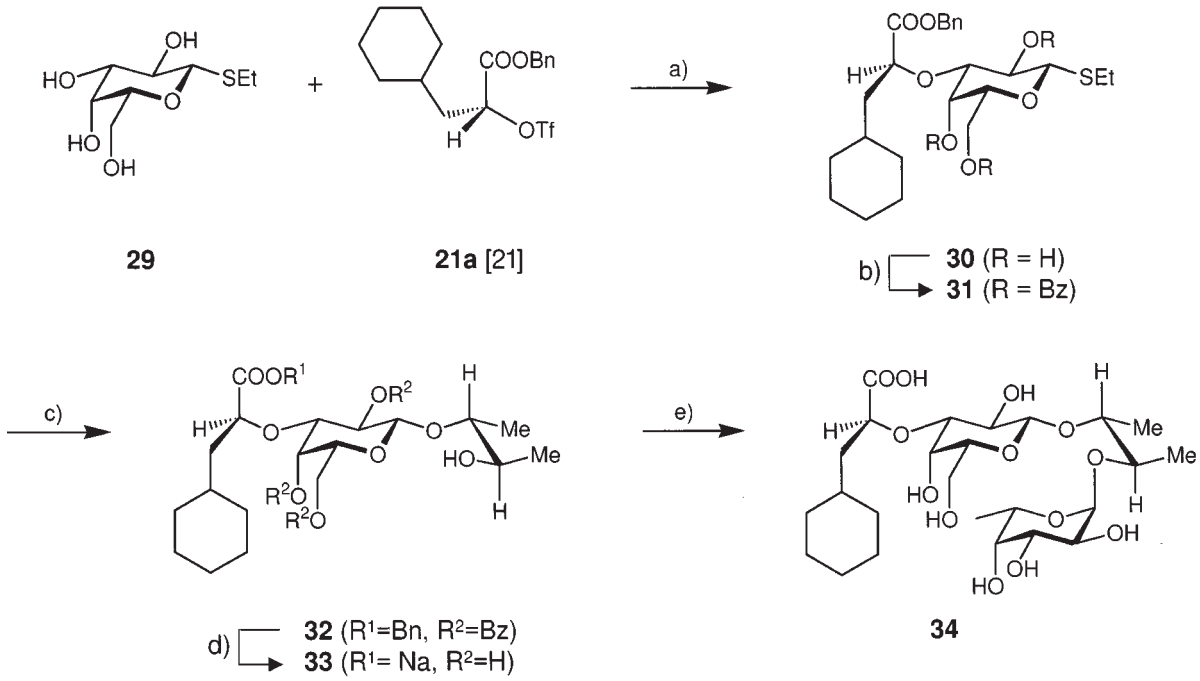
Finally, we examined (*R*,*R*)-butan-2,3-diol as a mimic of the 3- and 4-hydroxy groups of a D-glucose/D-glucosamine. For the synthesis of the corresponding substrate **33,** the 3-hydroxy group of ethyl 1-thio-β-D-galactopyranoside **29**, was regioselectively alkylated. For this purpose, the stannylene acetal (24) of the two trans hydroxy groups (2- and 3-position) of ethyl 1-thio-β-D-galactopyranoside **29** was formed in situ and treated with benzyl (*R*)-3-cyclohexyl-2-trifluoromethansulfonyloxy-propionate **21a** in DME at room temperature in the presence of caesium fluoride. The resulting thiogalactoside **30** was then perbenzoylated (BzCl, pyridine, DMAP) to yield the glycosyl donor **31**, which was used for the galactosylation of (*R*,*R*)-2,3-butandiol with DMTST (19) as promotor. After deprotecton by saponification, the substrate for the enzymatic step was obtained in excellent yield. The trisaccharide mimic **33** was then incubated with FucT III and GDP-fucose. To our surprise, this highly flexible compound proved to be an excellent substrate

© 2000 NRC Canada

Scheme 6. (*a*) (*S*,*S*)-cyclohexan-1,2-diol, DMTST (20), CH_2Cl_2, 4 Å molecular sieves, 3 h (59%); (*b*) cat. NaOMe, MeOH, rt, 3 h (82%); (*c*) $^nBu_2SnO$, MeOH, rfl., 2 h; CsF, DMF, rt, 3 h, with benzyl (*R*)-3-cyclohexyl-2-trifuoromethansulfonyloxy-propionate **21a** (→ **26a**, 69%); (*d*) 20% $Pd(OH)_2$, H_2, dioxane–H_2O–AcOH; Dowex 50 (Na^+ form) (78%); (*e*) GDP-fucose, FucT III or FucT VI: no reaction.



Scheme 7. (*a*) $^nBu_2SnO$, MeOH, rfl., 2 h; benzyl (*R*)-3-cyclohexyl-2-trifuoromethansulfonyloxy-propionate (**21a**), CsF, DME, rt, 2 h (67%); (*b*) benzoyl chloride, pyridine, DMAP (91%); (*c*) (*R*,*R*)-2,3-butandiol, CH_2Cl_2, 4 Å molecular sieves, DMTST (20), rt, 2 h (70%); (*d*) LiOH, H_2O–MeOH, 60°C, 5 h; Dowex 50 (Na^+ form) (94%); (*e*) GDP-fucose, FucT III (47%).



© 2000 NRC Canada

of FucT III yielding the α-fucosylated product **34**. This structure was confirmed based on the ^{1}H and ^{13}C chemical shift of H-1 and C-1 of the fucose moiety (4.99 ppm (J = 3.3 Hz) and 96.4 ppm, respectively). In addition, the ^{13}C signals of both CHO carbons of the butandiol moiety which are shifted upfield by approximately 2 ppm proving the site of the fucosylation.

In the examples shown, the FucT III was found to have a remarkable flexibility in the recognition of acceptor substrates. Further modifications are under current investigation. However, in many cases the reaction rates were very low compared to the reaction with the natural substrate sialylα(2–3)lacNAc. Such rates, however, proved to be sufficient for the synthesis of preparative amounts of oligosaccharide derivatives and mimics.

A severe drawback for the feasibility of the enzymatic synthesis of oligosaccharides and derivatives thereof stems from the availability of glycosyl transferases. Although an increasing number of transferases are commercially available, they are still prohibitively expensive, particularly for synthesis on a preparative scale. For this reason, we have initiated programs to clone and overexpress our own transferases for mechanistic and synthetic studies.

The sugar nucleotides CMP-NeuNAc and GDP-Fuc are commericially available (footnotes 2, 3) and numerous chemical and chemo-enzymatic approaches for their syntheses have been developed in recent years (25). This has decisively improved the availability of activated sugars in preparative amounts and therefore the feasibility of the enzymatic synthesis of oligosaccharides and derivatives thereof.

Experimental

General methods

Chemicals used were reagent grade and were used as supplied except where noted. Solvents were either dried by standard procedures or used as purchased. Unless otherwise stated, all reactions were performed under an argon atmosphere. All chemical glycosylation reactions were performed using molecular sieves, which were flame-dried under high vacuum immediately before the reaction. Analytical thin-layer-chromatography (TLC) was performed using silica gel 60 F_{254} glass plates (MERCK); compound spots were visualized by UV light (254 nm) and by staining with a solution containing *p*-anisaldehyde (25 mL), conc. sulfuric acid (15 mL), glacial acidic acid (5 mL) in EtOH (900 mL). Flash column chromatography was performed on silica gel 60 (0.040–0.063 mm, MERCK).

Bovine serum albumine (BSA) was obtained from BOEHRINGER (no. 28031). Calf intestine alkaline phosphatase (CIAP) (E.C.3.1.3.1) was purchased from BOEHRINGER (no. 108146, 7500 U / 498 µl). Recombinant α (2,3)sialyl transferase (~100 U/l, from transfected insect cells) (14) (EMBL accession no. M97754), recombinant fucosyl transferase III (~10 U/l, baculovirus transfected insect cells) (15) (EMBL accession no. X53578), and recombinant fucosyl transferase VI (~16 U/l, from transfected CHO-cells) (23) (EMBL accession no. LO1698) were used. GDP-fucose was donated by YAMASA–corp.[2] CPM-Neu-5-*N*Ac was purchased from Forschungszentrum Jülich GmbH.[3]

^{1}H NMR and ^{13}C NMR spectra were recorded on a BRUKER AC 400 and (or) a VARIAN Unity 500 spectrometer. COSY, TOCSY, HMBC, and HSQC experiments were performed using the manufacturer's software. ^{1}H NMR-shifts and ^{13}C NMR-shifts are referenced to the solvent line (given in ppm) unless otherwise stated. Chemical shifts marked with an asterisk (*) may be interchanged. ESI-MS were recorded on VG Platform II (MicroMass, Manchester U.K.) equipped with a HP 1050 and a CTC PAL autosampler. Flow injection mass spectrometry was done with 100 µL/min in H_2O:CH_3CN, 1:4 over a mass range of (+) 100–1500 Da / 1.5 s, (–) 120–1500 Da / 1.5 s.

*5-Acetamido-3,5-dideoxy-*D*-glycero-*α*-*D*-galacto-2-nonulopyranosylonic acid-(2–3)*-O-β-*D*-*galactopyranosyl-(1–4)-glucal (**8**)*: In a buffered solution containing sodium cacodylate buffer (75 µL, 0.5 M), $MnCl_2$-solution (100 µL, 0.5 m) and bidistilled water (2.1 mL), *O*-β-D-galactopyranosyl(1–4)-1,5-anhydro-D-arabino-hex-1-enitol (D-lactal) **7** (20.0 mg, 64.9 µmol) (13), CMP-sialic acid (23.2 mg, 79.8 µmol), and bovine serum albumine (1.5 mg) were dissolved. The clear solution was incubated for 24 h with α(2–3)sialyl transferase (20 µL, 160 µU) and calf intestine alkaline phosphatase (2 µL, 30 U) at 37°C. A second portion of CMP-sialic acid (24.9 mg, 85,6 µmol) α(2–3)sialyl transferase (20 µL, 160 mU) was added and the incubation continued for 2 days. The reaction mixture was then lyophilized and passed over sephadex G-10. The sugar containing fractions were combined and chromatographed on silica (CH_2Cl_2:MeOH:H_2O, 10:4:0.1 to 6:4:1) to yield **8** (24.5 mg, 65%): ^{1}H NMR (D_2O, 250.13 MHz) δ: 1.78 (1H, t, J = 12.8 Hz, H-3_{sia}), 2.00 (3H, s, Ac), 2.73 (1H, dd, J = 4.2 Hz, 12.8 Hz, H-3_{sia}), 3.51–4.06 (17H, m), 4.10 (1H, dd, J = 2.8 Hz, 9.8 Hz, H-3_{gal}), 4.59 (1H, d, J = 8.3 Hz, H-1_{gal}), 6.41 (1H, dd, J = 1.4 Hz, 6.2 Hz, H_{vinyl}); ^{13}C (D_2O, 62.89 MHz) δ: 24.00, 41.57, 53.63, 61.54, 62.92, 64.51, 69.17, 69.37, 70.03, 70.34, 71.34, 73.73, 74.82, 77.05, 77.47, 78.74, 79.21, 101.79, 103.76, 104.57, 145.92, 175.88, 176.96; m/z = 598 [M^+ – H]; Anal. calcd. for $C_{23}H_{37}NO_{17}$: C 46.1, H 6.2; found: C 45.6, H 6.0.

*5-Acetamido-3,5-dideoxy-*D*-glycero-*α*-*D*-galacto-2-nonulopyranosylonic acid-(2–3)*-O-β-*D*-*galactopyranosyl-(1–3)*-O-[α-*L*-fucopysanosyl]-(1–4)-glucal (**9**)*: GDP-fucose (25.1 mg, 39.5 µmol) and bovine serum albumine (1.6 mg) were added to a mixture of sodium cacodylate buffer (450 µL, 250 mM, pH 6.5), of $MnCl_2$-solution (150 µL, 250 mM) and bidistilled water (600 µl) **8** (20.0 mg, 33.4 µmol). The clear solution was incubated at 37°C with a solution of recombinant FucT III (83 µL, 498 µU) and calf intestine alkaline phosphatase (2 µL, 30 U) for one day. After 2 h a second portion of GDP-fucose (10.0 mg, 15.7 µmol) and transferase (16.6 µL, 99.6 mU) were added and the incubation continued, until TLC control (EtOAc:iso-propanol:water, 2:2:1) indicated the complete consumption of the substrate **8**. For the work-up, the reaction mixture was centrifugated, lyophilized and chromatographed on silica (ethyl acetate:iso-propanol: water, 2:2:1). The product containing fractions were

[2] H. Kusakabe, YAMASA–corp., 1–23–8, Nihonbashi-Kakigaracho, Chou-ku, Tokyo 103, Japan. e-mail: kusakabe@yamasa.com.
[3] U. Kragl and C. Wandrey, Forschungszentrum Jülich GmbH, P.O. Box 1913, D-5170 Jülich.

© 2000 NRC Canada

combined, passed over a sephadex G-10 column and lyophilized to yield **9** (20.6 mg, 83%): ^{1}H NMR (D_2O, 500.13 MHz) δ: 1.12 (3H, d, *J* = 6.5 Hz, H-6_{fuc}), 1.82 (1H, t, *J* = 13.0 Hz, H-3_{sia}), 2.03 (3H, s, Ac), 2.74 (1H, dd, *J* = 4.8 Hz, 13.0 Hz, H-3_{sia}), 3.53 (1H, dd, *J* = 7.0 Hz, 9.5 Hz, H-2_{gal}), 3.55–3.70 (7H, m, H-6_{gal}, H-4,6,7,8, 9_{sia}, H-6_{cycl}), 3.78 (1H, dd, *J* = 3.6 Hz, 8.3 Hz, H-2_{fuc}), 3.79 (1H, d, *J* = 3.0 Hz, H-4_{fuc}), 3.82–3.92 (5H, m, H-6′$_{gal}$, H-5,9′$_{sia}$, H-3_{fuc}, H-6′$_{cycl}$), 3.93 – 4.00 (2H, m, H-5_{gal}, H-5_{cycl}), 4.09 (1H, dd, *J* = 2.4 Hz, 10.0 Hz, H-3_{gal}), 4.14–4.19 (2H, m, H-4_{gal}, H-4_{cycl}), 4.32 (1H, broad s, H-3_{cycl}), 4.47 (1H, q, *J* = 6.5 Hz, H-5_{fuc}), 4.62 (1H, d, *J* = 8.0 Hz, H-1_{gal}), 4.98 (1H, dd, *J* = 2.8 Hz, 6.0 Hz, H-2_{cycl}), 5.04 (1H, d, *J* = 3.6 Hz, H-1_{fuc}), 6.26 (1H, d, *J* = 6.0 Hz, H-1_{cycl}); ^{13}C (D_2O, 62.9 MHz) δ: 18.74, 25.52, 43.14, 55.17, 62.58, 64.68, 66.08, 70.26, 70.80, 71.25, 71.58, 71.85, 72.94 (2 × C), 73.41, 75.37, 75.87, 76.37, 78.44, 79.15, 80.91, 99.52, 102.34, 103.26, 105.33, 147.85, 177.41, 178.50. The connections of the carbohydrate residues were confirmed by a ROESY experiment. In detail, sialylation of the 3-OH of the galactosyl moiety is shown by a strong crosspeak between the axial H-3_{sia} and H-3_{gal}. Fucosylation at H-3_{cycl} is similarily shown by a strong crosspeak between H-1_{fuc} and H-3_{cycl}. A further strong crosspeak between H-4_{cycl} and H-1_{gal} corroborates the attachment of the galactose at O-C(4) of the glucal moiety. The fucosyl residue occupies the usual preferred position below the galactosyl residue as evidenced by a weak crosspeak between H-5_{fuc} and H-2_{gal}; *m*/*z* = 768 [M^+ + Na]; Anal. calcd. for $C_{29}H_{47}NO_{21}$: C 46.7, H 6.3; found: C 46.9, H 6.3.

*5-Acetamido-3,5-dideoxy-*D*-glycero-*α*-*D*-galacto-2-nonulopyranosylonic acid-(2–3)*-O-β-*D*-*galactopyranosyl-(1–3)-glucal **(11)***: D-galβ(1–3)glucal **10** (28.8 mg, 93.4 μmol) (16), CMP-sialic acid (30.0 mg, 113.8 μmol) and bovine serum albumine (2.1 mg) were dissolved in a buffered solution containing sodium cacodylate buffer (75 μL, 0.5 M), $MnCl_2$-solution (100 μL, 0.5 m) and bidistilled water (2.1 mL). The clear solution was then incubated at 37°C with α(2–3)sialyl 30 U transferase (200 μL, 700 μU) and calf intestine alkaline phosphatase (2 μL, 30 U) for 3 days. A second portion of CMP-sialic acid (45.0 mg, 167 μmol) and sialyl transferase (100 μL, 350 μU) were added and the incubation continued. After 3 days the reaction mixture was lyophilized and chromatographed on silica (CH_2Cl_2:MeOH:H_2O, 10:4:0.1 to 6:4:1). The product containing fractions were passed over sephadex G-10 to yield **11** (51.2 mg, 92%): ^{1}H NMR (D_2O, 250.13 MHz) δ: 1.81 (1H, t, *J* = 12.8 Hz, H-3_{sia}), 2.04 (3H, s, Ac), 2.78 (1H, dd, *J* = 4.2 Hz, 12.8 Hz, H-3_{sia}), 3.51–4.06 (17H, m), 4.14 (1H, dd, *J* = 2.8 Hz, 9.8 Hz, H-3_{gal}), 4.41 (1H, m), 4.41 (1H, m), 4.99 (1H, d, *J* = 8.3 Hz, H-1_{gal}), 6.49 (1H, dd, *J* = 1.4 Hz, 6.2 Hz, H_{vinyl}); ^{13}C (D_2O, 62.89 MHz) δ: 24.18, 41.73, 53.81, 62.15, 63.14, 64.71, 69.07 (2 × C), 69.61, 70.22, 70.49, 71.26, 73.89, 74.96, 77.20, 77.93, 78.83, 80.08, 101.85, 102.00, 103.29, 146.92, 175.99, 177.15; *m*/*z* = 598 [M^+ – H].

*5-Acetamido-3,5-dideoxy-*D*-glycero-*α*-*D*-galacto-2-nonulopyranosylonic acid-(2–3)*-O-β-*D*-*galactopyranosyl-(1–4)*-O-[α-*L*-fucopysanosyl]-(1–3)-glucal **(12)***: Trisaccharide **11** (18.0 mg, 30.0 μmol), GDP-fucose (26.3 mg, 41.4 μmol) and bovine serum albumine (1.6 mg) were added to a mixture of sodium cacodylate buffer (450 μL, 250 mM, pH 6.5), $MnCl_2$-solution (150 μL, 250 mM) and bidistilled water (600 μL). The clear mixture was incubated at 37°C with recombinant FucT III (100 μL, 600 μU/mL) and calf intestine alkaline phosphatase (2 μL, 30 U). After three days TLC control (EtOAc:iso-propanol:water, 2:2:1) indicated that all the starting material had been consumed. For the work-up, the reaction mixture was centrifugated, lyophilized, and chromatographed on silica. The product was finally passed over a sephadex G-10 column and lyophilized to yield **12** (18.1 mg, 82%). ^{1}H NMR (D_2O, 500.13 MHz) δ: 1.21 (3H, d, *J* = 6.5 Hz, H-6_{fuc}), 1.81 (1H, t, *J* = 13.0 Hz, H-3_{sia}), 2.04 (3H, s, Ac), 2.79 (1H, dd, *J* = 4.8 Hz, 13.0 Hz, H-3_{sia}), 3.58 (1H, dd, *J* = 7.0 Hz, 9.5 Hz, H-2_{gal}), 3.60–3.76 (7H, m, H-5,6_{gal}, H-4,6,7,8, 9_{sia}), 3.78 (1H, dd, *J* = 3.6 Hz, 8.3 Hz, H-2_{fuc}), 3.79 (1H, d, *J* = 3.0 Hz, H-4_{fuc}), 3.83–3.93 (5H, m, H-6′$_{gal}$, H-5,9′$_{sia}$, H-3_{fuc}, H-6′$_{cycl}$), 3.93–4.00 (2H, m, H-5_{gal}, H-5_{cycl}), 4.05 (1H, broad t, *J* = 6.0 Hz, H-4_{cycl}), 4.10 (1H, dd, *J* = 2.4 Hz, 10.0 Hz, H-3_{gal}), 4.15 (1H, m, H-5_{cycl}), 4.46 (1H, q, *J* = 6.5 Hz, H-5_{fuc}), 4.53 (1H, broad t, *J* = 4 Hz, H-3_{cycl}), 4.61 (1H, d, *J* = 8.0 Hz, H-1_{gal}), 5.07 (1H, dd, *J* = 2.8 Hz, 6.0 Hz, H-2_{cycl}), 5.10 (1H, d, *J* = 3.6 Hz, H-1_{fuc}), 6.51 (1H, d, *J* = 6.0 Hz, H-1_{cycl}); ^{13}C (D_2O, 125 MHz) δ: 17.00, 23.57, 41.18, 53.23, 60.78, 62.77, 64.11, 68.57, 69.00, 69.53, 69.65, 69.96, 70.58, 70.82, 73.21, 73.33, 73.43, 73.70, 74.37, 76.35, 77.38, 78.96, 100.03, 100.59, 101.38, 101.72, 146.28, 175.55, 176.59; Structure confirmed by a ROESY experiment as detailed for **9**; *m*/*z* = 768 [M^+ + Na]; Anal. calcd. for $C_{29}H_{47}NO_{21}$: C 46.7, H 6.3; found: C 46.9, H 6.4.

(1R,2R) 2-Hydroxy-cyclohexyl β-*D*-*galactopyranoside **(15)***: At room temperature the imidate **13** (640 mg, 1.0 mmol) and (*R*,*R*)-cyclohexan-1,2-diol (174 mg, 1.50 mmol) were dissolved in CH_3CN (5 mL) and treated with trimetylsilyl triflate (20 μL). After 1 h the solvent was rotovaped off and the residue chromatographed on silica (petrolether 40/60:EtOAc, 2:3) to yield (1*R*,2*R*) 2-hydroxy-cyclohexyl 2,3,4,6-tetra-*O*-benzoyl-β-D-galactopyranoside (**14**) (506 mg, 73%). **14** was dissolved in MeOH (5 mL) containing catalytic amounts of NaOMe and stirred for 6 h. Then the reaction mixture was neutalized with AcOH, evaporated and chromatographed on silica (toluene:EtOH, 1:1) to give **15** (152 mg, 75%): ^{1}H NMR (CD_3OD, 400.13 MHz) δ: 1.19 (4H, m), 1.62 (2H, m), 1.98 (2H, m), 3.35 (2H, m, 2 × C*H*O$_{cycl}$), 3.44 (3H, m, H-2,3,5$_{gal}$), 3.63 (1H, dd, *J* = 6.6 Hz, 9.8 Hz, H-6), 3.71 (1H, dd, *J* = 7.4 Hz, 11.5 Hz, H-6′), 3.76 (1H, broad d, *J* = 4.1 Hz, H-4), 4.28 (1H, d, *J* = 7.4 Hz, H-1).

*(1*R,*2*R*) 2-Hydroxy-cyclohexyl 3*-O-*[2*-O-*(5-acetamido-3,5-dideoxy-*D*-glycero-α-*D*-galacto-2-nonulopyranosonate)]*-β-*D*-*galactopyranoside **(16)***: The cyclohexane derivative **15** (23.5 mg, 84.4 μmol), CMP-sialic acid (68.5 mg, 104.0 μmol) and bovine serum albumine (1.8 mg) were dissolved in a buffered solution containing sodium cacodylate buffer (2 mL, 0.05 M), $MnCl_2$-solution (2 mL, 0.06 m) and bidistilled water (1.3 mL). The clear solution was incubated at 37°C with α(2–3)sialyl transferase (100 μL, 700 μU) and calf intestine alkaline phosphatase (2 μL, 30 U) for 24 h. After the addition of a second portion of CMP-sialic acid (10 mg, 15.2 μmol) the incubation was continued for 5 h. The reaction mixture was then lyophilized and

© 2000 NRC Canada

chromatographed on silica (CH_2Cl_2:MeOH:H_2O, 10:4:0.5) to yield **16** (31.2 mg, 64%): ^{1}H NMR (D_2O, 250.13 MHz) δ: 1.30 (4H, m), 1.73 (2H, m), 1.85 (1H, t, *J* = 12.8 Hz, H-3_{sia}), 2.08 (3H, s, Ac), 2.11 (2H, m), 2.80 (1H, dd, *J* = 4.2 Hz, 12.8 Hz, H-3_{sia}), 3.51–3.96 (13H, m), 4.00 (1H, d, *J* = 2.8 Hz, H-4_{gal}), 4.14 (1H, dd, *J* = 2.8 Hz, 8.3 Hz, H-3_{gal}), 4.61 (1H, d, *J* = 8.3 Hz, H-1_{gal}); ^{13}C (D_2O, 100.03 MHz) δ: 20.43, 21.76, 21.93, 28.15, 30.44, 37.94, 50.07, 59.48, 60.95, 65.97, 66.48, 66.80, 67.55, 70.14, 71.22, 71.30, 73.26, 74.19, 81.25, 98.27, 98.78, 172.34, 173.40.

2-O-*{1*-O-*[(1*R,*2*R*) 2*-O-*(*α-L-*fucopyranosyl)cyclohexyl]*β-D-*galactopyranos-3-yl} 5-acetamido-3,5-dideoxy-D*-glycero-α-D-galacto-*2-nonulopyranosylonic acid (17)*: The sialic acid derivative **16 (**17.5 mg, 29.3 μmol), GDP-fucose (33.9 mg, 53.4 μmol) and bovine serum albumine (1.9 mg) were added to a mixture of sodium cacodylate buffer (450 μL, 250 mM, pH 6.5), $MnCl_2$-solution (150 μL, 250 mM) and bidistilled water (600 μL). The clear mixture was incubated at 37°C with recombinant FucT III solution (83 μL, 498 μU/mL) and calf intestine alkaline phosphatase (2 μL, 30 U) for one day, until TLC control (CH_2Cl_2:MeOH, 6:4) of the turbid incubation mixture indicated that **16** was consumed. After lyophilization the residue was chromatographed on silica (CH_2Cl_2:MeOH, 6:4). The product containing fractions were combined and finally passed over a sephadex G-10 column and lyophilized to yield **17** (15.6 mg, 71%): $[\alpha]_{589}$ –17.8° (*c* = 1.25, H_2O); ^{1}H NMR (D_2O, 500.13 MHz) δ: 1.24 (3H, d, *J* = 6.5 Hz, H-6_{fuc}), 1.30 (4H, m), 1.76 (2H, m), 1.87 (1H, t, *J* = 13.0 Hz, H-3_{sia}), 2.09 (3H, s, Ac), 2.14 (1H, m), 2.19 (1H, m), 2.81 (1H, dd, *J* = 4.8 Hz, 13.0 Hz, H-3_{sia}), 3.56 (1H, dd, *J* = 7.7 Hz, 9.5 Hz, H-2_{gal}), 3.58 (1H, m, CHO_{cycl}), 3.63–3.69 (4H, m, H-5_{gal}, H-6,7,9_{sia}), 3.70–3.79 (3H, m, H-6_{gal}, H-4,8_{sia}), 3.80–3.86 (3H, m, H-2,4_{fuc}, CHO_{cycl}), 3.90 (1H, t, *J* = 10.0 Hz, H-5_{sia}), 3.92–3.96 (2H, m, H-6_{gal}, H-8_{sia}), 3.97 (1H, dd, *J* = 3.5 Hz, 10.0 Hz, H-3_{fuc}), 3.98 (1H, d, *J* = 3.2 Hz, H-4_{gal}), 4.13 (1H, dd, *J* = 3.2 Hz, 9.5 Hz, H-3_{gal}), 4.63 (1H, d, *J* = 7.7 Hz, H-1_{gal}), 4.68 (q, 1 H, *J* = 6.5 Hz, H-5_{fuc}), 5.04 (1H, d, *J* = 5.5 Hz, H-1_{fuc}); ^{13}C (D_2O, 100.03 MHz) δ: 15.55, 17.73, 22.36, 23.49, 29.54, 29.91, 39.90, 52.01, 61.75, 62.89, 66.78, 67.86, 68.25, 68.42, 68.74, 69.69, 69.87, 72.07, 72.34, 73.13, 74.92, 76.26, 77.45, 78.37, 95.77, 99.75, 100.17, 174.35, 175.34; Structure confirmed by a ROESY experiment as detailed for **9**; Anal. calcd. for $C_{29}H_{49}NO_{19}$: C 48.7, H 6.9; found: C 48.2, H 6.6.

*(1*R,*2*R*)-2-Hydroxy-cyclohexyl 6*-O-*benzyl-2,3,4-tri*-O-*benzoyl*-β-D-*galactopyranoside (19)*: Under argon 23.0 g of finely ground 4 Å molecular sieves were added to a mixture of ethyl 6-*O*-benzyl-2,3,4-tri-*O*-benzoyl-thio-β-D-galactopyranoside **18** (11.41 g, 18.0 mmol) (19) and (*R,R*)-*trans*-1,2-cyclohexandiol (1.76 g, 15.2 mmol) in 100 mL dry CH_2Cl_2. After stirring for 2 h at room temperature, dimethylmethylthiosulfonium triflate (DMTST) (7.83 g, 30.0 mmol) (20) dissolved in dry CH_2Cl_2 (70 mL) was added portionwise over 1 h. The slurry was stirred for 3 h and then diluted with CH_2Cl_2. After filtration over celite, the organic phase was washed with 10% $NaHCO_3$ and brine, dried over $NaSO_4$ and concentrated. The residue was chromatographed on silica (toluene:EtOAc, 95:1 to 85:15) to yield **19** (6.85 g, 67%): $[\alpha]_{589}$ +105.2° (*c* = 0.79, $CHCl_3$); ^{1}H NMR ($CDCl_3$, 400.13 MHz) δ: 1.22 (4H, m), 1.69 (3H, m), 2.08 (1H, m), 3.39 (1H, m), 3.50 (1H, m), 3.68 (2H, m, H-6,6′), 3.93 (1H, s, OH), 4.23 (1H, broad t, *J* = 4.4 Hz, H-5), 4.46 (1H, d, *J* = 12.1 Hz, C*H*$_2$Bn), 4.57 (1H, d, *J* = 12.1 Hz, C*H*$_2$Bn), 4.87 (1H, d, *J* = 8.8 Hz, H-1), 5.59 (1H, dd, *J* = 7.7 Hz, 4.4 Hz, H-3), 5.76 (1H, dd, *J* = 8.8 Hz, 7.7 Hz, H-2), 5.97 (1H, dd, *J* = 4.4 Hz, 4.4 Hz, H-4), 7.24 (7H, m), 7.48 (6H, m), 7.64 (1H, m), 7.80 (2H, m), 7.98 (2H, m), 8.06 (2H, m); ^{13}C ($CDCl_3$, 100.03 MHz) δ: 23.65, 24.18, 30.75, 31.99, 67.62, 68.24, 70.00, 71.76, 72.87, 72.96, 73.64, 87.87, 101.90, 127.76–137.26 aromatics, 165.21, 165.51, 165.55; Anal. calcd. for $C_{40}H_{40}O_{10}$: C 70.6, H 5.9; found: C 70.4, H 6.0.

*(1*R,*2*R*) 2-Hydroxy-cyclohexyl 6*-O-*benzyl*-β-D-*galactopyranoside (20)*: The pseudodisaccharide **19** (2.0 g, 2.9 mmol) was suspended in dry methanol (40 mL), a catalytic amount of sodium methanolate was added and the reaction mixture stirred at room temperature for 3 h until TLC control (CH_2Cl_2:MeOH, 9:1) indicated complete consumption of the starting material. Then the mixture was neutralized with amberlyste 15 and filtered over celite. Evaporation leaves an oil which is chromatographed on silica (CH_2Cl_2:MeOH, 19:1 to 9:1) to yield **20** (1.01 g, 94%): $[\alpha]_{589}$ –33.2° (*c* = 0.94, CH_2Cl_2); ^{1}H NMR ($CDCl_3$, 400.13 MHz) δ: 1.28 (4H, m), 1.73 (2H, m), 2.06 (2H, m), 3.40 (4H, m), 3.61 (1H, dd, *J* = 4.4 Hz, 8.8 Hz), 3.74 (4H, m), 4.01 (1H, t, *J* = 3.3 Hz), 4.34 (1H, d, *J* = 8.8 Hz, H-1), 4.60 (2H, q, 2 H, *J* = 12.1 Hz, C*H*$_2$Bn), 7.43 (5H, m); ^{13}C ($CDCl_3$, 100.03 MHz) δ: 23.84, 24.31, 30.98, 32.46, 69.00, 69.07, 71.34, 73.10, 73.48, 73.61, 73.66, 85.63, 102.43, 127.82, 128.46, 137.67; Anal. calcd. for $C_{19}H_{28}O_7$: C 61.9, H 7.7; found: C 61.7, H 7.7.

*Benzyl (2*R*) 3-cyclohexyl-2*-O-*{1*-O-*[(1*R,*2*R*) cyclohexyl]-6*-O-*benzyl*-β-D-*galactopyranos-3-yl}propanoate (22a):*
Glycoside **20** (0.98 g, 2.66 mmol) and dibutyltin oxide (995 mg, 3.99 mmol) in MeOH (40 mL) were refluxed for 2.5 h to give a clear, colourless solution. After removal of the solvent, the residue (white foam) was dissolved in dry CH_2Cl_2 (29 mL), CsF (2.02 g,13.3 mmol) and the triflate **21a** (5.25 g, 13.3 mmol) were added and the resulting solution stirred vigorously for 3 h. The reaction mixture was then diluted with CH_2Cl_2 and washed with 10% KF–KH_2PO_4 and brine. After drying the combined organic layers with Na_2SO_4, the solvent was evaporated and the resulting oil chromatographed on silica (hexane:EtOAc, 6:4) to yield **22a** (1.25 g, 76%): $[\alpha]_{589}$ –40.7° (*c* = 0.59, $CHCl_3$); ^{1}H NMR ($CDCl_3$–D_2O, 400.13 MHz) δ: 0.91 (2H, m), 1.28 (8H, m), 1.70 (9H, m), 2.04 (2H, m), 3.29 (1H, dd, *J* = 3.3 Hz, 8.8 Hz, H-2), 3.37 (1H, m, C*H*O-cyclohexanol), 3.44 (1H, m, C*H*O-cyclohexanol), 3.70 (3H, m, H-5, 6, 6′), 3.79 (1H, t, *J* = 3.3 Hz, H-4), 3.83 (dd, *J* = 3.3 Hz, 9.9 Hz, H-2), 4.28 (1H, dd, *J* = 2.3 Hz, 10.0 Hz), 4.31 (1H, d, *J* = 9.9 Hz, H-1), 4.60 (2H, q, *J* = 12.1 Hz, C*H*$_2$Bn), 5.19 (2H, q, *J* = 12.1 Hz, C*H*$_2$Bn), 7.43 (10H, m); ^{13}C ($CDCl_3$, 100.03 MHz) δ: 23.80, 24.34, 26.01, 26.21, 26.40, 31.21, 32.12, 32.20, 33.53, 33.92, 40.92, 66.83, 67.15, 68.95, 70.72, 73.05, 73.61, 73.66, 82.87, 86.78, 103.03, 127.72, 127.92, 128.40, 128.51, 128.62, 128.66, 135.12, 137.92, 174.72; Anal. calcd. for $C_{35}H_{48}O_9$: C 68.6, H 7.9; found: C 68.4, H 7.8.

© 2000 NRC Canada

*Benzyl (2S) 3-cyclohexyl-2-*O*-{1-*O*-[(1R,2R) cyclohexyl]-6-O-benzyl-β-D-galactopyranos-3-yl}propanoate (**22b**)*: According the protocol for the preparation of **22a**, **22b** (270 mg, 46%) was obtained starting from **20** (350 mg, 0.95 mmol) and the triflate **21b** (922 mg, 2.375 mmol): $[\alpha]_{589}$ –24.4° (*c* = 2.0, $CHCl_3$); ^{1}H NMR ($CDCl_3$–D_2O, 400.13 MHz) δ: 0.94 (2H, m), 1.26 (8H, m), 1.72 (9H, m), 2.06 (2H, m), 3.35 (2H, m), 3.48 (1H, m, C*H*O-cyclohexanol), 3.78 (4H, m), 3.83 (dd, *J* = 3.3 Hz, 9.9 Hz, H-2), 4.28 (1H, dd, *J* = 2.3 Hz, 10.0 Hz), 4.31 (1H, d, *J* = 9.9 Hz, H-1), 4.60 (2H, q, *J* = 12.1 Hz, CH_2Bn), 5.18 (2H, q, *J* = 12.1 Hz, CH_2Bn), 7.43 (10H, m); ^{13}C ($CDCl_3$, 100.03 MHz) δ: 23.79, 24.27, 25.98, 26.25, 26.36, 30.84, 32.18, 32.25, 33.83, 33.98, 40.13, 67.11, 68.55, 69.81, 71.29, 73.16, 73.67, 73.76, 82.32, 87.35, 100.31, 127.86, 127.91, 128.41, 128.52, 128.58, 128.66, 134.98, 137.44, 169.06.

*Benzyl (2R) 3-phenyl-2-*O*-{1-*O*-[(1R,2R) cyclohexyl]-6-O-benzyl-β-D-galactopyranos-3-yl}propanoate (**22c**)*: According the protocol for the preparation of **22a**, **22c** (437 mg, 82%) was obtained starting from **20** (320 mg, 0.87 mmol) and *R*-phenyl lactic acid dervivative **21c** (1.68 g, 4.343 mmol): $[\alpha]_{589}$ –26.4° (*c* = 2.0, $CHCl_3$); ^{1}H NMR ($CDCl_3$, 400.13 MHz) δ: 1.28 (4H, m), 1.72 (3H, m), 2.00 (2H, m), 2.99 (1H, dd, *J* = 9.5 Hz, 14.4 Hz, CH_2Ph), 3.11 (1H, dd, *J* = 3.2 Hz, 9.5 Hz, H-3), 3.20 (1H, dd, *J* = 3.2 Hz, 14.4 Hz, CH_2Ph), 3.29 (2H, m, H-5, C*H*O-cyclohexanol), 3.41 (1H, m, C*H*O-cyclohexanol), 3.58 (1H, dd, *J* = 5.7 Hz, 6.4 Hz, H-6), 3.68 (3H, m, H-2, 6′, OH), 3.76 (1H, m, H-4), 4.06 (1H, broad s, OH), 4.20 (1H, d, *J* = 8.0 Hz, H-1), 4.32 (dd, *J* = 3.2 Hz, 9.5 Hz, BnC*H*O), 4.51 (1H, d, *J* = 11.1 Hz, OCH_2Ph), 4.61 (1H, d, *J* = 11.1 Hz, OCH_2Ph), 5.16 (1H, d, *J* = 11.1 Hz, OCH_2Ph), 5.22 (1H, d, *J* = 11.1 Hz, OCH_2Ph), 7.43 (15H, m); ^{13}C ($CDCl_3$, 100.03 MHz) δ: 23.80, 24.32, 31.05, 32.24, 39.54, 66.54, 67.49, 68.82, 70.34, 73.00, 73.40, 73.65, 80.22, 84.19, 86.52, 105.48, 127.19, 127.69, 127.88, 128.37, 128.63, 128.70, 128.76, 129.20, 134.83, 136.66, 137.91, 173.17; *m*/*z* = 624 [$M^+ + NH_4$].

*Sodium (2R) 3-cyclohexyl-2-*O*-{1-*O*-[(1R,2R) cyclohexyl]β-D-galactopyranos-3-yl}propanoate (**23a**)*: The benzyl protected **22a** (287 mg, 0.46 mmol) was dissolved in a mixture of dioxane (9 mL), water (4.5 mL) and acetic acid (2.3 mL). After addition of 300 mg (20%) of Pd $(OH)_2$, the resulting slurry was vigorously stirred for 22 h at room temperature in an atmosphere of hydrogen. The reaction mixture was then filtered and evaporated three times with water. The residue was dissolved in H_2O–MeOH and treated with Dowex 50 (Na^+ form). Filtration and lyophilization gave a white powder which was chromatographed on RP-18 silica (H_2O–MeOH, 7:3) to yield **23a** (141 mg, 66%): $[\alpha]_{589}$ –43.2° (*c* = 0.21, $CHCl_3$); ^{1}H NMR (D_2O, 400.13 MHz) δ: 0.92 (2H, m), 1.23 (7H, m), 1.62 (10H, m), 2.04 (2H, m), 3.41 (1H, dd, *J* = 3.7 Hz, 12.8 Hz, H-3), 3.55 (3H, m, H-2, 2xC*H*O-cyclohexanol), 3.66 (1H, ddd, *J* = 0.9 Hz, 4.6 Hz, 8.2 Hz, H-5), 3.74 (1H, q, *J* = 11.9 Hz, H-6), 3.76 (q, *J* = 11.9 Hz, H-6′), 3.92 (1H, dd, *J* = 3.5 Hz, 3.7 Hz, H-4), 4.49 (1H, d, *J* = 8.3 Hz, H-1); ^{13}C (D_2O, 100.03 MHz) δ: 22.12; 22.29, 24.67, 24.93, 28.60, 30.62, 30.80, 32.03, 32.38, 39.97, 59.96, 65.06, 68.68, 71.70, 73.30, 78.18, 81.59, 81.97, 99.62, 181.41; m/*z* = 432 [M^+ – Na].

*Sodium (2S) 3-phenyl-2-*O*-{1-*O*-[(1R,2R) cyclohexyl]β-D-galactopyranos-3-yl}propanoate (**23b**):* Following the protocol for **23a**, the pseudotrisaccharide **23b** (235 mg, 72%) was obtained from **22b** (438 mg, 0.71 mmol) as a white solid: $[\alpha]_{589}$ +21.6° (*c* = 2.1, H_2O); ^{1}H NMR (D_2O, 400.13 MHz) δ: 1.01 (2H, m), 1.29 (7H, m), 1.69 (10H, m), 2.08 (2H, m), 3.46 (1H, dd, *J* = 3.5 Hz, 12.9 Hz, H-3), 3.55 (4H, m, H-2, 5, 2 × C*H*O-cyclohexanol), 3.77 (1H, dd, *J* = 4.0 Hz, 12.1 Hz, H-6), 3.83 (1H, dd, *J* = 8.7 Hz, 12.1 Hz, H-6′), 4.07 (broad d, *J* = 3.1 Hz, H-4), 4.11 (1H, dd, *J* = 4.3 Hz, 7.8 Hz), 4.55 (1H, d, *J* = 7.8 Hz, H-1); ^{13}C (D_2O, 100.03 MHz) δ: 25.54; 25.72, 27.89, 28.08, 28.34, 32.00, 33.83, 34.20, 35.82, 35.84, 42.74, 63.36, 68.25, 71.66, 75.14, 77.50, 80.34, 83.31, 85.16, 103.03, 184.16; *m*/*z* = 431.2 [M^+ – Na].

*Sodium (2R) 3-phenyl-2-*O*-{1-*O*-[(1R,2R) cyclohexyl]β-D-galactopyranos-3-yl}propanoate (**23c**)*: Following the protocol for **23a**, the pseudotrisaccharide **23c** was obtained (155 mg, 50%) from **22c** (420 mg, 0.69 mmol) as a white solid: $[\alpha]_{589}$ –34.9° (*c* = 2.1, H_2O); ^{1}H NMR (D_2O, 400.13 MHz) δ: 1.23 (4H, m), 1.69 (2H, m), 2.00 (2H, m), 2.99 (1H, dd, *J* = 12.0 Hz, 13.2 Hz, CH_2Ph), 3.13 (1H, dd, *J* = 4.4 Hz, 13.2 Hz, CH_2Ph), 3.30 (1H, dd, *J* = 4.4 Hz, 7.7 Hz, H-3), 3.51 (3H, m, H-2, 2 × C*H*O-cyclohexanol), 3.51 (1H, m, H-5), 3.70 (1H, dd, *J* = 8.7 Hz, 12.1 Hz, H-6′), 4.88 (1H, dd, *J* = 9.9 Hz, 12.1 Hz, H-6), 3.92 (broad d, *J* = 3.1 Hz, H-4), 4.14 (1H, dd, *J* = 4.4 Hz, 12.0 Hz, C*H*Bn), 4.39 (1H, d, *J* = 8.8 Hz, H-1), 7.32 (5H, m, phenyl); ^{13}C (D_2O, 100.03 MHz) δ: 23.67, 23.83, 30.10, 32.34, 39.62, 61.48, 66.42, 70.18, 73.23, 74.86, 82.40, 82.89, 83.41, 100.82, 127.00, 128.87, 129.81, 138.41, 180.90; *m*/*z* = 425 [M^+ – Na].

*(2R) 3-cyclohexyl-2-*O*-{1-*O*-[(1R,2R) 2-O-(α-L-fucopyranosyl)cyclohexyl]β-D-galactopyranos-3-yl}propionic acid (**24a**)*: The pseudotrisaccharide **23a** (42.5 mg, 93.5 μmol), GDP-fucose (79.1 mg, 124.5 μmol) and bovine serum albumine (1.5 mg) were added to a mixture of sodium cacodylate buffer (450 μL, 250 mM, pH 6.5), $MnCl_2$-solution (150 μL, 250 mM) and bidistilled water (600 μL). The clear mixture was incubated at 37°C with recombinant FucT III (100 μL, 200 mU) and calf intestine alkaline phosphatase (3 μL, 45 U) for two days. The turbid incubation mixture was absorbed on a C-18 reversed phase column. After washing with H_2O, the product was eluted with MeOH. MeOH was then evaported and the residue chromatographed on silica (CH_2Cl_2:MeOH:H_2O, 10:3:0.3). The product containing fractions were combined and finally passed over a sephadex G-10 column to yield **24a** (30.2 mg, 54%). An analogous incubation with recombinant FucT VI gave no detectable amounts of **24a**: $[\alpha]_{589}$ –42.4° (*c* = 0.4, H_2O); ^{1}H NMR (CD_3OD, 400.13 MHz) δ: 0.77–0.95 (2H, m); 1.12 (3H, d, *J* = 6.6 Hz, H-6_{fuc}); 1.12–1.38 (7H, m); 1.45–1.74 (9H, m); 1.84 (1H, broad d, *J* = 12.5 Hz,); 1.94–2.05 (2H, m); 3.13 (1H, dd, *J* = 2.3, 7.7 Hz, H-3_{gal}); 3.41 (1H, broad t, *J* = 4.4 Hz, H-5_{gal}); 3.43–3.52 (2H, m, H-2_{gal}, C*H*O_{cycl}); 3.57–3.74 (5H, m, H-6,6′$_{gal}$, H-2,3_{fuc}, C*H*O_{cycl}); 3.59–3.86 (3H, m, H-4_{gal}, H-4_{fuc}, C*H*(O)O); 4.25 (1H, d, *J* = 8.6 Hz, H-1_{gal}); 4.50 (1H, q, *J* = 6.6 Hz, H-5_{fuc}); fucose H-1 beyond water (DHO) at 4.80 ppm; ^{13}C (CD_3OD, 100.03 MHz, shifts in

© 2000 NRC Canada

ppm relative to solvent) δ: 16.56; 24.49; 27.26; 27.56; 27.83; 29.91; 30.95; 33.49; 34.74; 35.50; 43.32; 63.15; 67.43; 67.72; 69.89; 71.45; 71.68; 73.78; 75.87; 77.04; 79.24; 80.76; 85.53; 96.84; 102.60; 183.40; *m*/*z* = 623 [M^+ + Na]; Anal. calcd. for $C_{27}H_{46}O_{13}$: C 56.0, H 8.0; found: C 55.8, H 7.8.

*(2*S*) 3-cyclohexyl-2-*O*-{1-*O*-[(1*R*,2*R*) 2-*O*-(α-L-fucopyranosyl)cyclohexyl]*β-D*-galactopyranos-3-yl}propionic acid (**24b**)*: Following the protocol for **24a**, **24b** (34.1 mg, 61%) was obtained from the pseudotrisaccharide **23b** (42.5 mg, 93.5 μmol) and GDP-fucose (81.8 mg, 128.7 μmol): ^{1}H NMR (CD_3OD, 400.13 MHz) δ: 0.78–0.92 (2H, m); 1.09 (d, 3-H, *J* = 6.6 Hz, H-6_{fuc}); 1.10–1.37 (7H, m); 1.48–1.70 (9H, m); 1.80 (1H, broad d, *J* = 12.6 Hz); 1.91–2.00 (2H, m); 3.23 (1H, dd, *J* = 2.6 Hz, 7.8 Hz, H-3_{gal}); 3.32 (1H, broad t, J 6.0 Hz, H-5_{gal}); 3.42–3.70 (7H, m, H-2,6,6′$_{gal}$, H-$2,4_{fuc}$, 2 × C*H*O_{cycl}); 3.80 (1H, dd, *J* = 4.2 Hz, 10.8 Hz, H-3_{fuc}); 3.88 (1H, d, *J* = 4.8 Hz, H-4_{gal}); 3.98 (1H, m, C*H*(O)O); 4.23 (1H, d, *J* = 7.2 Hz, H-1_{gal}); 4.47 (1H, q, *J* = 6.6 Hz, H-5_{fuc}); fucose H-1 beyond water (DHO) at 4.80 ppm; ^{13}C (CD_3OD, 100.03 MHz) δ: 16.58; 24.37; 27.28; 27.46; 27.76; 29.85; 30.87; 33.64; 35.17; 35.35; 43.22; 62.79; 67.39; 67.59; 70.00; 70.19; 70.55; 73.81; 76.36; 76.93; 79.29; 82.45; 85.53; 96.85; 102.91; C=O not resolved; *m*/*z* = 623 [M^+ + Na]; Anal. calcd. for $C_{27}H_{46}O_{13}$: C 56.0, H 8.0; found: C 55.6, H 7.9.

*(2*R*) 3-phenyl-2-*O*-{1-*O*-[(1*R*,2*R*) 2-*O*-(α-L-fucopyranosyl)cyclohexyl]*β-D*-galactopyranos-3-yl}propionic acid (**24c**)*: Following the protocol for **24a**, **24c** (16.0 mg, 96%) was obtained from the pseudotrisaccharide **23c** (12.5 mg, 29.3 μmol) and GDP-fucose (28.1 mg, 44.2 μmol): $[\alpha]_{589}$ –84.4° (*c* = 0.8, H_2O); ^{1}H NMR (CD_3OD, 400.13 MHz) δ: 1.18 (3H, d, *J* = 6.6 Hz, H-6fuc); 1.18–1.29 (4H, m); 1.62–1.74 (2H, m); 2.00–2.11 (2H, m); 2.97 (1H, dd, *J* = 8.4 Hz, 12.0 Hz, C*H*2Ph); 3.14 (1H, dd, *J* = 5.4, 12.6 Hz, C*H*2Ph); 3.28 (1H, dd, *J* = 3.0, 9.6 Hz, H-3_{gal}); 3.44–3.56 (3H, m, H-$2,5_{gal}$, C*H*O_{cycl}); 3.65–3.80 (5H, m, H-6,6′$_{gal}$, H-$2,3_{fuc}$, C*H*O_{cycl}); 3.88–3.93 (2H, m, H-4_{gal}, H-4_{fuc}); 4.17 (1H, dd, *J* = 5.4 Hz, 9.6 Hz, C*H*(O)O); 4.28 (1H, d, *J* = 7.2 Hz, H-1_{gal}); 4.60 (1H, q, *J* = 6.6 Hz, H-5_{fuc}); 4.96 (1H, d, *J* = 3.2 Hz, H-1_{fuc}); 7.31 (1H, m, Ph); 7.39 (4H, m, Ph);^{13}C (CD_3OD, 100.03 MHz) δ: 16.54; 24.43; 24.48; 29.91; 30.87; 41.44; 47.92; 63.05; 67.40; 69.91; 71.46; 71.60; 73.79; 75.89; 77.00; 79.13; 83.94; 85.94; 85.58; 96.85; 102.13; 127.23; 129.23 (2 × C); 130.62 (2 × C); 140.61; 181.49; *m*/*z* = 617 [M^+ + Na]; Anal. calcd. for $C_{27}H_{40}O_{13}$: C 56.6, H 7.0; found: C 56.2, H 6.8.

*(1*S*,2*S*)-2-Hydroxy-cyclohexyl 6-*O*-Benzyl-2,3,4-tri-*O*-benzoyl-β-D-galactopyranoside (**25**)*: According the protocol for the preparation of compound **14**, **25** (265 mg, 59%) is obtained from ethyl 6-*O*-benzyl-2,3,4-tri-*O*-benzoyl-1-thio-β-D-galactopyranoside (500 mg, 0.80 mmol) and (*S*,*S*) cyclohexan-1,2-diol (77 mg, 0.66 mmol): ^{1}H NMR ($CDCl_3$, 400.13 MHz) δ: 1.24 (3H, m), 1.46 (1H, m), 1.70 (2H, m), 1.97 (1H, m), 2.14 (1H, m), 3.45 (2H, m, 2 × C*H*O_{cycl}), 3.71 (2H, m, H-6, 6′), 4.19 (dt, 1 H, *J* = 0.7, 5.9 Hz, H-5), 4.46 (1H, d, *J* = 12.1 Hz, C*H*$_2$Bn), 4.54 (1H, d, *J* = 12.1 Hz, C*H*$_2$Bn), 4.98 (1H, d, *J* = 7.3 Hz, H-1), 5.60 (1H, dd, *J* = 3.7 Hz, 11.4 Hz, H-3), 5.76 (1H, dd, *J* = 7.3,11.4 Hz, H-2), 5.94 (1H, dd, *J* = 0.7, 3.7 Hz, H-4), 7.19–8.09 (20H, m, aromatics); ^{13}C ($CDCl_3$, 100.03 MHz) δ: 25.02, 25.30, 32.42, 32.97, 68.13, 68.54, 71.05, 71.51, 72.89, 74.52, 74.98, 85.11, 101.00, 127.76–135.61 aromatics, 165.21, 165.51, 165.55.

*(1*S*,2*S*) 2-Hydroxy-cyclohexyl 6-*O*-benzyl-β-D-galactopyranoside (**26**)*: According the protocol for the preparation of compound **15**, **26** (115 mg, 82%) was obtained from glycoside **25** (262 mg, 0.39 mmol): $[\alpha]_{589}$ +5.6° (*c* = 1.5, $CHCl_3$); ^{1}H NMR (CD_3OD, 400.13 MHz) δ: 1.21 (4H, m), 1.61 (2H, m), 1.87 (1H, m), 2.12 (1H, m), 3.29 (1H, m, C*H*O-cyclohexanol), 3.38 (1H, m, C*H*O-cyclohexanol), 3.40 (1H, dd, *J* = 3.7 Hz, 10.3 Hz, H-3), 3.48 (1H, dd, *J* = 7.8 Hz, 10.3 Hz, H-2), 3.52 (3H, m, H-5, 6, 6′), 3.73 (1H, d, *J* = 3.5 Hz, H-4), 4.34 (1H, d, *J* = 7.8 Hz, H-1), 4.50 (2H, m, C*H*$_2$Bn), 7.23 (5H, m); ^{13}C (CD_3OD, 100.03 MHz) δ: 24.28, 24.37, 32.49, 32.93, 69.61, 69.78, 72.14, 73.19, 73.87, 73.97, 74.06, 86.38, 105.24, 127.60, 127.86, 137.67; *m*/*z* = 391 [M^+ + Na].

*Benzyl (2*R*) 3-cyclohexyl-2-*O*-{1-*O*-[(1*S*,2*S*) cyclohexyl]-6-O-benzyl-β-D-galactopyranos-3-yl}propanoate (**27**)*: According the protocol for the preparation of compound **22a**, **27** (94 mg, 59%) was obtained from **26** (96 mg, 0.26 mmol) and the *R*-cyclohexyl lactic acid derivative **21a** (514 mg, 1.30 mmol): $[\alpha]_{589}$ –4.5° (*c* = 1.5, chloroform); ^{1}H NMR ($CDCl_3$, 400.13 MHz) δ: 0.92 (2H, m), 1.22 (6H, m), 1.46 (2H, m), 1.69 (9H, m), 2.00, (1H, m), 2.11 (1H, m), 3.25 (1H, dd, *J* = 3.7 Hz, 9.2 Hz, H-3), 3.38 (2H, m, C*H*O_{cycl}, OH), 3.51 (1H, m, C*H*O_{cycl}), 3.59 (1H, t, *J* = 6.1 Hz, H-5), 3.75 (3H, m, H-4, 6, 6′), 3.89 (dd, *J* = 7.9 Hz, 9.2 Hz, H-2), 4.16 (1H, dd, *J* = 4.3 Hz, 9.2 Hz, C*H*C(O)O), 4.49 (1H, d, *J* = 7.9 Hz, H-1), 4.57 (1H, d, *J* = 11.9 Hz, C*H*$_2$Bn), 4.60 (1H, d, *J* = 11.9 Hz, C*H*$_2$Bn), 5.14 (1H, d, *J* = 12.2 Hz, C*H*$_2$Bn), 5.19 (1H, d, *J* = 12.2 Hz, C*H*$_2$Bn), 7.35 (10H, m); ^{13}C ($CDCl_3$, 100.03 MHz) δ: 25.67, 24.47, 25.95, 26.12, 26.32, 32.03, 32.21, 32.43, 33.61, 33.75, 40.84, 66.63, 67.17, 69.39, 71.09, 73.48, 73.58, 74.33, 77.34, 83.91, 86.92, 104.39, 127.61, 127.67, 128.34, 128.48, 128.62, 135.05, 138.19, 174.77; *m*/*z* = 657 [M^+ + HCOO].

*Sodium (2*R*) 3-cyclohexyl-2-*O*-{1-*O*-[(1*S*,2*S*) cyclohexyl]β-D-galactopyranos-3-yl}propanoate (**28**)*: According the protocol for the preparation of compound **23a, 28** (40 mg, 58%) is obtained from **27** (93 mg, 0.15 mmol): $[\alpha]_{589}$ –3.1° (*c* = 1.5, H_2O); ^{1}H NMR (D_2O, 400.13 MHz) δ: 0.92 (2H, m), 1.22 (7H, m), 1.62 (9H, m), 1.79 (1H, m), 1.97 (1H, m), 2.12 (1H, m), 3.41 (1H, dd, *J* = 3.9 Hz, 9.8 Hz, H-3), 3.55 (2H, m, 2 × C*H*O_{cycl}), 3.61 (1H, dd, *J* = 8.2 Hz, 9.8 Hz, H-2), 3.66 (1H, broad dd, *J* = 3.1, 5.5 Hz, H-5), 3.74 (2H, m, H-6, 6′), 3.91 (1H, d, *J* = 3.1 Hz, H-4), 3.96 (1H, m, C*H*C(O)O), 4.56 (1H, d, *J* = 8.2 Hz, H-1); ^{13}C (D_2O, 100.03 MHz) δ: 21.45, 21.71, 23.79, 24.06, 24.24, 29.73, 29.96, 30.25, 31.36, 31.70, 39.32, 59.01, 64.23, 68.56, 71.70, 72.56, 77.49, 80.79, 83.52, 101.58, 180.76; *m*/*z* = 432 [M^+].

*Benzyl (2*R*) 3-cyclohexyl-2-*O*-[1-*O*-ethyl-β-D-thio-galactopyranos-3-yl]propanoate (**30**)*: Thioglycoside **29** **(**5.0 g, 22.29 mmol) and di-^{n}butyl tinoxide (6.7 g, 26.8 mmol) were refluxed in methanol (150 mL) for 2 h. The methanol was then evaporated and the residue thoroughly dried. The

© 2000 NRC Canada

resulting foam was dissolved in dimethoxyethane (40 mL) and treated with triflate **21a** (13.2 g, 33.4 mmol) (20) and cesium fluoride (4.1 g, 26.8 mmol) in dimethoxyethane (20 mL) at room temperature for 90 min. The turbid mixture was diluted with EtOAc and then washed with 2N potassium dihydrogenphosphate containing 15 g KF (200 mL), 10% potassium fluoride solution and brine. The organic phase was dried with sodium sulfate and evaporated. The residue was purified on silica (acetone:hexane, 1:4 to 1:2) yielding **30** (7.0 g, 67%): ^{1}H NMR ($CDCI_3$, 400. 13 MHz) δ: 0.92 (2H, m, cycl), 1.23 (4H, m, cycl), 1.32 (3H, t, *J* = 8.8 Hz, C*H*$_3$), 1.68 (7H, m), 2.29 (broad, OH), 2.41 (broad, OH), 2.78 (2H, m, C*H*$_2$S), 3.30 (1H, dd, *J* = 2.2 Hz, 9.9 Hz, H-3), 3.41 (broad, OH), 3.49 (1H, m), 3.73 (1H, m), 3.86 (2H, m), 3.93 (1H, m), 4.30 (2H, m), 5. 8 (1H, d, *J* = 13.2 Hz, C*H*$_2$O), 5.12 (1H, d, *J* = 13,2 Hz, C*H*$_2$O), 7.38 (5H, m, aromatic).

*Benzyl (2*R*) 3-cyclohexyl-2-*O-*[1-*O*-ethyl-2,4,6-tri-*O*-benzoyl-*β-*D-thio-galactopyranos-3-yl]propanoate (**31**)*: 30 (7.0 g, 14.9 mmol) was dissolved in pyridine (75 mL), cooled to 0°C, and treated with benzoyl chloride (18.88 g,134.4 mmol) and a catalytic amount of DMAP (0.5 g). The mixture was stirred for 6 h at room temperature and then evaporated. The resulting residue was dissolved in EtOAc and subsequently washed with 0.1 N HCl, sat. $NaHCO_3$, and finally with brine. The combined organic layers were dried with Na_2SO_4 and evaporated. The residue was chromatographed on silica (EtOAc:hexane, 1:6) to give **31** (10.7 g, 91%): ^{1}H NMR ($CDCI_3$, 400. 13 MHz) δ: 0.50 (2H, m, cycl), 0.71 (1H, m, cycl) 0.84 (2H, m, cycl), 1.07 (1H, m, cycl), 1.29 (6H, m, cycl, 3H, C*H*$_3$), 2.78 (2H, m, C*H*$_2$S), 3.91 (1H, dd, *J* = 2.2, 9.9 Hz, H-3), 4.01 (broad t, 1H; *J* = 6.6 Hz, H-5), 4.20 (1H, m, C*H*O), 4.43 (1H, dd, *J* = 6.6, 12.1 Hz, H-6), 4.49 (dd,1 H, *J* = 8.8, 12.1 Hz, H-6′), 4.62 (1H, d, *J* = 9.9 Hz, H 1), 5.08 (1H, d, *J* = 13.2 Hz, C*H*$_2$O), 5.21 (1H, d, *J* = 13.2 Hz, C*H*$_2$O), 5.68 (1H, t, *J* = 9.9 Hz, H-2), 6.00 (1H, d, *J* = 2.2 Hz, H-4), 7.33 (5H, m, aromatic), 7.47 (6H, m, aromatic), 7.59 (3H, m, aromatic), 8.10 (6H, m, aromatic).

*Benzyl (2*R*) 3-cyclohexyl-2-*O-*{2-*O-*[(2*R*,3*R*)butyl]2,4,6-tri-O-benzoyl-β-*D-thio-galactopyranos-3-yl}propanoate (**32**)*: The thioglycoside **31** (500 mg, 0.64 mmol) and (*R*,*R*)-2,3-butandiol (0.29 g, 3.20 mmol) were dissolved in CH_2Cl_2 (5 mL). After the addition of molecular sieves 4 Å (0.25 g), the mixture was stirred for 1 h at room temperaure. Within 1 h, three portions of DMTST (0.5 eq each) (19) were added. After strring for an additional hour, the suspension was filtered on celite, diluted with CH_2Cl_2 and washed with sat. $NaHCO_3$, brine, and water. The residue obtained after evaporation of the organic phase was chromatographed on silica (EtOAc:hexane, 1:4 to 1:2) yielding **32** (367 mg, 70%): $[\alpha]_{589}$ +20.1° (*c* = 2.1, $CHCl_3$); ^{1}H NMR ($CDCl_3$, 400.13 MHz) δ: 0.53 (2H, m), 0.71 (1H, m), 0.89 (2H, m), 0.95 (3H, d, *J* = 8.8 Hz, CH_3), 1.09 (3H, d, *J* = 8.8 Hz, CH_3), 1.34 (8H, m), 3.41 (1H, broad s, OH), 3.43 (1H, dq, *J* = 2.2 Hz, 8.8 Hz, C*H*CH_3), 3.60 (1H, dq, *J* = 2.2 Hz, 8.8 Hz, C*H*CH3) 3.91 (1H, dd, *J* = 3.3 Hz, 9.9 Hz, H-3), 3.99 (1H, broad t, *J* = 8.8 Hz, H-5), 4.19 (1H, dd, *J* = 3.3 Hz, 8.9 Hz, OC*H*C(O)OBn), 4.40 (1H, dd, *J* = 12.1, 14.8 Hz, H-6), 4.52 (1H, dd, *J* = 7.6, 14.8 Hz, H-6′), 4.59 (1H, d, *J* = 12.0 Hz, H-1), 5.06 (1H, d, *J* = 17.6 Hz, OC*H*$_2$Ph), 5.19 (1H, d, *J* = 17.6 Hz, OC*H*$_2$Ph), 5.62 (1H, t, *J* = 12.0 Hz, H-2), 5.92 (1H, d, *J* = 3.3 Hz, H-4), 7.58 (14H, m, aromatics), 8.15 (6H, m, aromatics); ^{13}C ($CDCl_3$, 100.03 MHz) δ: 16.71, 18.23, 25.30, 25.56, 25.87, 32.35, 33.14, 33.21, 40.17, 62.53, 66.46, 69.52, 70.34, 71.88, 72.54, 78.02, 84.29, 101.29, 128.10, 128.20, 128.23, 128.32, 128.35, 128.38, 129.31, 129.40, 129.70, 129.91, 132.88, 132.98, 133.13, 135.25, 164.70, 165.53, 165.95, 172.20; *m*/*z* = 831 [M^+ + Na].

*Sodium (2*R*) 3-cyclohexyl-2-*O-*{2-*O-*[(2*R*,3*R*)butyl]β-*D-thio-galactopyranos-3-yl}propanoate (**33**)*: The protected glycoside **32** (500 mg, 0.62 mmol) and 10 eq. of LiOH × H_2O (0.26 g) in a mixture of water (15 mL) and methanol (5 mL) were dissolved and stirred for 5 h at 60°C. After evaporation of the solvent the residue was chromatographed on a P-2 gel, passed over Dowex 50 (Na^+ form) and finally chromatographed on RP-18 silica (H_2O:MeOH, 9.5:0.5 to 1:1) to yield **33** (250 mg, 94%) as a white solid: $[\alpha]_{589}$ –35.1° (*c* = 1.9, water); ^{1}H NMR (D_2O, 400.13 MHz) δ: 0.96 (2H, m), 1.19 (8H, m), 1.64 (7H, m), 1.81 (1H, m), 3.41 (1H, dd, *J* = 2.3, 9.4 Hz, H-3), 3.58 (1H, t, *J* = 9.4 Hz, H-2), 3.66 (1H, m, H-5), 3.74 (4H, m, H-6,6′, 2 × C*H*CH_3), 3.91 (1H, broad t, *J* = 2.3 Hz, H-4), 3.97 (1H, m, OC*H*C(O)ONa), 4.45 (1H, d, *J* = 9.4 Hz, H-1); ^{13}C (D_2O, 100.03 MHz) δ: 17.00, 19.16, 27.45, 27.71, 27.90, 33.59, 35.01, 35.36, 42.96, 62.93, 68.03, 71.72, 72.24, 76.22, 81.17, 81.56, 102.52, 184.46; MS found: 405.3 [M^+ – Na].

*(2*R*) 3-cyclohexyl-2-*O-*{2-*O-*[(2*R*,3*R*) 3-*O-*(α-*L-fucopyanosyl)butyl]β-*D-thio-galactopyranos-3-yl}propionic acid (**34**)*: The pseudotrisaccharide **33** (20.9 mg, 51.5 μmol), GDP-fucose (47.0 mg, 74.0 μmol) and bovine serum albumine (2.8 mg) was treated with sodium cacodylate buffer (450 μL, 250 mM, pH 6.5), $MnCl_2$-solution (150 μL, 250 mM) and bidistilled water (600 μL). The clear mixture was incubated at 37°C with recombinant FucT III solution (210 μL, 410 mU) and calf intestine alkaline phosphatase (3 μL, 45 U) for two days until TLC control (CH_2Cl_2:MeOH, 6:4) indicated that the starting material was completely consumed. After lyophilization the residue was chromatographed on silica (CH_2Cl_2:MeOH, 6:4). The product containing fractions were combined, passed over a sephdex G-10 column and lyophilized to yield **34** (13.3 mg, 47%):$[\alpha]_{589}$ –88.1° (*c* = 1.19, water); ^{1}H NMR (D_2O, 400.13 MHz) δ: 0.91 (2H, m), 1.19 (12H, m), 1.59 (7H, m), 1.78 (1H, m), 3.40 (1H, dd, *J* = 3.3 Hz, 9.9 Hz, H-3$_{gal}$), 3.51–3.81 (6H, m, 1 × C*H*CH_3, H-2$_{gal}$, H-6,6′$_{gal}$, H-2,3,4$_{fuc}$), 3.89, (2H, m, H-4,5$_{gal}$), 3.98 (2H, m, 1 × C*H*CH_3, C*H*C(O)O), 4.35 (1H, q, *J* = 6.5 Hz, H-5$_{fuc}$), 4.46 (1H, d, *J* = 9.8 Hz, H-1$_{gal}$), 4.99 (1H, d, *J* = 3.3 Hz, H-1$_{fuc}$); ^{13}C (D_2O, 100.03 MHz) δ: 14.26, 16.10, 16.52, 26.26, 26.35, 26.52, 32.17, 33.48, 34.91, 41.74, 61.30, 65.22, 67.39, 68.28, 69.91, 70.00, 72.35, 74.84, 75.22, 77.74, 79.57, 82.97, 96.35, 101.30, C=O not resolved; Anal. calcd. for $C_{25}H_{44}O_{13}$: C 54.3, H 8.0; found: C 54.8, H 7.8.

Acknowledgement

We thank Dr. Hitoshi Kusakabe, YAMASA Corp., Tokyo, Japan for the generous gift of GDP-fucose.

© 2000 NRC Canada

References

1. S.R. Sharar, R.K. Winn, and J.M. Harlan. Springer Semin. Immunopathol. **16**, 359 (1995); Physiology and pathophysiology of leukocyte adhesion. *Edited by* D.N. Granger and G.W. Schmid-Schönbein. New York, Oxford University Press. 1995.
2. J. Bischoff. Trends Glycosci. Glycotechnol. **6**, 351 (1994); R.P. McEver. Curr. Opin. Immunol. **6**, 75 (1994); L.A. Lasky. Annu. Rev. Biochem. **64**, 113 (1995); S.A. Mousa and D.A. Cheresh. TDD (Trends in Drug Design) **2**, 187 (1997); G.S. Kansas. Blood, **88**, 3259 (1996).
3. L. Phillips, E. Nudelman, F.C.A. Gaeta, M. Perez, A.K. Singhal, S.-I. Hakomori, and J.C. Paulson. Science (Washington, D.C.), **250**, 1130 (1990); G. Walz, A. Aruffo, W. Kolanus, M. Bevilacqua, and B. Seed. Science (Washington, D.C.), **250**, 1132 (1990); M.J. Polley, M.L. Phillips, E. Wayner, E. Nudelman, A.K. Singhal, S.-I. Hakomori, and J.C. Paulson. Proc. Natl. Acad. Sci. U.S.A. **88**, 6224 (1991).
4. J.L. Magnani. Science (Washington, D.C.), **250**,1132 (1990); E.L. Berg, M.K. Robinson, O. Mansson, E.C. Butcher, and J.L. Magnani. J. Biol. Chem. **266**,14869 (1991).
5. E.L. Berg, J.L. Magnani, R.A. Warnock, M.K. Robinson, and E.C. Butcher. Biochem. Biophys. Res. Commun. **184**, 1048 (1992).
6. *Determination of the bioactive conformation*: K. Scheffler, B. Ernst, A. Katopodis, J.L. Magnani, W.T. Wang, R. Weisemann, and T. Peters. Angew. Chem. Int. Ed. Engl. **34,** 1841 (1995); K. Scheffler, J.-R. Brisson, R. Weisemann, J.L. Magnani, B. Ernst, and T. Peters. J. Biomol. NMR, **9**, 423 (1997); D. Henrichsen, B. Ernst, J.L. Magnani, W.-T. Wang, B. Meyer, and T. Peters. Angew. Chem. Int. Ed. Engl. **38**, 98 (1999); R. Harris, G.R. Kiddle, R.A. Field, B. Ernst, J.L. Magnani, and S. Homans. J. Am. Chem. Soc. **121**, 2546 (1999); W. Jahnke, H.C. Kolb, M.J.J. Blommers, J.L. Magnani, and B. Ernst. Angew. Chem. Int. Ed. Engl. **36**, 2603 (1997); *Design of sialyl Lewis^x mimics*: H.C. Kolb and B. Ernst. Pure Appl. Chem. **69**, 1879 (1997); H.C. Kolb and B. Ernst. Chem. Eur. J. **3**, 1571 (1997); S. Hanessian, G.V. Reddy, H.K. Huynh, J. Pan, S. Pedatella, H.C. Kolb, and B. Ernst. Bioorg. Med. Chem. Lett. **7**, 2729 (1997); R. Bänteli and B. Ernst. Tetrahedron Lett. **38**, 4059 (1997); D. Roche, R. Bänteli, T. Winkler, F. Casset, and B. Ernst. Tetrahedron Lett. **39**, 2545 (1998); S. Hanessian, H.K. Huynh, G.V. Reddy, G. McNaughton-Smith, B. Ernst, H.C. Kolb, J.L. Magnani, and C. Sweeley. Bioorg. Med. Chem. Lett. **8**, 2803 (1998); C.-Y. Tsai, W.K.C. Park, G. Weitz-Schmidt, B. Ernst, and C.-H. Wong. Bioorg. Med. Chem. Lett. **8**, 2333 (1998); *Biological evaluation of selectin antagonists*: K.E. Norman, G.P. Anderson, H.C. Kolb, K. Ley, and B. Ernst. Blood, **91**, 475 (1998).
7. The pharmacophores of sialyl Lewis^x have been determined by: M. Yoshida, A. Uchimura, M. Kiso, and A. Hasegawa. Glycoconjugate J. **10**, 3 (1993); B.K. Brandley, M. Kiso, S. Abbas, P. Nikrad, O. Srivastava, C. Foxall, Y. Oda, and A. Hasegawa. Glycobiology, **3**, 633 (1993); R.M. Nelson, S. Dolich, A. Aruffo, O. Cecconi, and M.P. Bevilacqua. J. Clin. Invest. **91**, 1157 (1993); W. Stahl, U. Sprengard, G. Kretzschmar, and H. Kunz. Angew. Chem. **106**, 2186 (1994); A. Hasegawa, T. Ando, M. Kato, H. Ishida, and M. Kiso. Carbohydr. Res. **257**, 67 (1994); J.Y. Ramphal, Z.-I. Zheng, C. Perez, L.E. Walker, S.A. Defrees, and F.C.A. Gaeta. J. Med. Chem. **37**, 3459 (1994); S. Komba, H. Ishida, M. Kiso, and A. Hasegawa. Glycoconjugate J. **13**, 241 (1996); G. Kuznik, B. Hörsch, G. Kretzschmar, and C. Unverzagt. Bioorg. Med. Chem. Lett. **7**, 577 (1997); H.C. Kolb and B. Ernst. Chem. Eur. J. **3**, 1571 (1997); H.C. Kolb and B. Ernst. Pure Appl. Chem. **69**, 1879 (1997).
8. G. Baisch, R. Öhrlein, A. Katopodis, and B. Ernst. Bioorg. Med. Chem. Lett. **6**, 759 (1996); R. Öhrlein, G. Baisch, A. Katopodis, M. Streiff, and F. Kolbinger. J. Mol. Catal. B: Enzym. **5**, 125 (1998); G. Baisch, R. Öhrlein, and M. Streiff. Bioorg. Med. Chem. Lett. **8**, 161 (1998).
9. R. Öhrlein, G. Baisch, A. Katopodis, M. Streiff, and F. Kolbinger. Bioorg. Med. Chem. Lett. **7**, 2447 (1997); R. Öhrlein, G. Baisch, and A. Katopodis. Bioorg. Med. Chem. Lett. **7**, 2431 (1997); G. Baisch, R. Öhrlein, M. Streiff, and F. Kolbinger. Bioorg. Med. Chem. Lett. **8**, 755 (1998).
10. B. Ernst and R. Öhrlein. Glycoconjugate J. **16**, 161 (1999), and refs. therein; R. Öhrlein. Top. Curr. Chem. **200**, 227 (1999), and refs. therein; S. Ogawa, N. Matsunaga, H. Li, and M.M. Palcic. Eur. J. Org. Chem. 631 (1999); P.-P. Lu, O. Hindsgaul, H. Li, and M.M. Palcic. Can. J. Chem. **75**, 790 (1997); J.A.L.M. van Dorst, J.P. Kamerling, and J.F.G. Vliegenthart. Pure Appl. Chem. **69**, 537 (1997); M.M. Palcic and O. Hindsgaul. Trends Glycosci. Glycotechnol. **8**, 37 (1996), and refs therein; Y. Nishida, T. Wiemann, and J. Thiem. Tetrahedron Lett. **34**, 2905 (1993); C.-H. Wong, Y. Ichikawa, T. Krach, C. Gautheron-Le Narvor, D.P. Dumas, and G.C. Look. J. Am. Chem. Soc. **113**, 8137 (1991).
11. X. Qian, O. Hindsgaul, H. Li, and M.M. Palcic. J. Am. Chem. Soc. **120**, 2184 (1998); S. Ogawa, T. Furuya, H. Tsunoda, O. Hindsgaul, K. Stangier, and M.M. Palcic. Carbohydr. Res. **271**, 197 (1995); C. Hällgren and O. Hindsgaul. J. Carbohydr. Chem. **14**, 453 (1995).
12. D.J. Legault, R.J. Kelly, Y. Natsuka, and J.B. Lowe. J. Biol. Chem. **270**, 20987 (1995); T. de Vries, C.A. Srnka, M.M. Palcic, S.J. Swiedler, D.H. van den Eijnden, and B.A. Macher. J. Biol. Chem. **270**, 8712 (1995); O. Zöllner and D. Vestweber. J. Biol. Chem. **271**, 33002 (1996).
13. P.W. Kent and S.D. Dimitrijevich. J. Fluorine Chem. **10**, 455 (1977).
14. Cloning and expression of α(2–3)sialyl transferase: D.X. Wen, B.D. Livingston, K.F. Medziharaszky, S. Kelm, A.L. Burlingame, and J.C. Paulson. J. Biol. Chem. **267**, 21011 (1992).
15. Cloning and expression of FucT III: K. Sasaki, K. Kurata, K. Funayama, M. Nagata, E. Watanabe, S. Ohta, N. Hanai, and T. Nishi. J. Biol. Chem. **269**, 14730 (1994).
16. D.P. Dumas, Y. Ichikawa, C.-H. Wong, J.B. Lowe, and R.P. Nair. Bioorg. Med. Chem. Lett. **1**, 425 (1991); S.A. DeFrees, F.C.A. Gaeta, Y.-C. Lin, Y. Ichikawa, and C.-H. Wong. J. Am. Chem. Soc. **115**, 7549 (1993).
17. G.C. Look, Y. Ichikawa, G.-J. Shen, P.-W. Cheng, and C.-H. Wong. J. Org. Chem. **58**, 4326 (1993).
18. R.R. Schmidt, J. Michel, and M. Roos. Liebigs Ann. Chem. **86**, 1343 (1984).
19. **18** was obtained in quantitative yield by benzoylation of ethyl 6-*O*-benzyl-1-thio-β-D-galactopyranoside; S. Sato, Y. Ito, and T.A. Ogawa. Carbohydr. Res. **155**, C1 (1986).
20. H. Meerwein, K.F. Zenner, and R. Gipp. Liebigs Ann. Chem. **67**, 688 (1965).
21. M.N. Qabar, J.P. Meara, C. Lum, H.-K. Kim, and M. Kahn. Tetrahedron Lett. **39**, 5895 (1998).
22. F. Degerbeck, B. Fransson, L. Grehn, and U. Ragnarsson. J. Chem. Soc. Perkin Trans 1, 11 (1993).
23. Cloning and expression of FucT VI: K.L. Koszdin and B.R. Bowen. Biochem. Biophys. Res. Commun. **187**, 152 (1992).
24. D.J. Jenkins and B.V.L. Potter. Carbohydr. Res. **265**, 145 (1994); H. Qin and T.B. Grindley. J. Carbohydr. Chem. **15**, 95 (1996).

© 2000 NRC Canada

25. **CMP-Neu-5-NAc:** M.D. Chappell and R.L. Halcomb. Tetrahedron, **53**, 109 (1997); Y. Kajihara, T. Ebata, K. Koseki, H. Kodama, H. Matsushita, and H. Hashimoto. J. Org. Chem. **60**, 5732 (1995); M. Kittelmann, T. Klein, U. Kragl, C. Wandrey, and O. Ghisalba. Appl. Microbiol. Biotechnol. **44**, 59 (1995); **GDP-Fuc:** K. Adelhorst and G.M. Whitesides. Carbohydr. Res. **242**, 69 (1993); V. Wittmann and C.-H. Wong. J. Org. Chem. **62**, 2144 (1997); G. Baisch and R. Öhrlein. Bioorg. Med. Chem. **5**, 383 (1997).

© 2000 NRC Canada

The directed *ortho* metalation – palladium catalyzed cross coupling connection. A general regiospecific route to 9-phenanthrols and phenanthrenes. Exploratory further metalation

Jian-min Fu and Victor Snieckus

Abstract: A new general and regiospecific synthesis of 9-phenanthrols (**1** + **2** → **3** → **4**, Scheme 1, Table 1) proceeding by a Directed *ortho* Metalation (DoM), Suzuki–Miyaura cross coupling, and a new LDA-mediated Directed remote Metalation sequence is described. The facile Pd-catalyzed hydrogenolysis of the phenanthrols **4** into the corresponding phenanthrenes **5** via their triflates **18** translates the original DoM regioselectivity also into a general synthesis of phenanthrenes (Table 2). Further DoM (**19** → **20, 21; 24** → **25**), cross coupling (**20c** → **23**), as well as oxidation – ring contraction (**4b, 4f** → **28a, 28b**) chemistry of phenanthrene derivatives is reported.

Key words: 9-phenanthrols, directed ortho metalation, Suzuki cross coupling, synthesis.

Résumé : On décrit une nouvelle synthèse, générale et régiospécifique, des 9-phénanthrols (**1** + **2** → **3** → **4** du tableau 1) par une séquence impliquant une réaction de métallation orientée vers la position *ortho* (DoM), un couplage croisé de Suzuki–Miyaura et une nouvelle métallation à distance orientée à l'aide de LDA. La transformation des phénanthrols (**4**) en phénanthrènes correspondants (**5**) qui se fait facilement par hydrogénolyse catalysée par le palladium des triflates (**18**) reflète la régiosélectivité de la réaction de DoM initiale en une synthèse générale des phénanthrènes (Tableau 2). On rapporte aussi d'autres réactions de DoM (**19** → **20; 21; 24** → **25**), de couplages croisés (**20c** → **23**) ainsi que la chimie de l'oxydation et de la contraction de cycle (**4b**, **4f** → **28a, 28b**) de dérivés du phénanthrène.

Mots clés : 9-phénanthrols, métallation orientée en ortho, couplage croisé de Suzuki, synthèse.

Introduction

Within the last decade, rapid and regioselective access of polysubstituted aromatics, an endeavor of special significance in the pharmaceutical industry, has been facilitated by the development of the Directed *ortho* Metalation (DoM) reaction (1). This strategy, which oftimes overcomes issues of harsh conditions and lack of regiocontrol inherent in the classical aromatic electrophilic subsitution reactions, has been extensively pursued for a variety of Directed Metalation Group (DMG) – bearing benzenes; significantly less attention has been given to exploration of DoM in more highly condensed aromatics. To take the simple step to greater complexity, naphthalene DoM chemistry has been scantily studied (2) and only sporadic reports have appeared in more highly fused aromatic systems (3). In the course of work aimed to generalize the synthetic link between DoM and the Suzuki–Miyaura Pd-catalyzed cross coupling reaction (4), the 2-carboxamido-2′-methyl biaryls **3** (Scheme 1) were prepared from partners **1** and **2** (5). At this point, stimulated by the delineation of the Complex Induced Proximity Effect (CIPE) concept (6), which was rewarded by the discovery of the LDA-mediated conversion of biaryl amides **6** into fluorenones **7** (7), we tested the conjecture that deprotonation of the vinylogously acidic 2′-methyl hydrogen in **3** would result in cyclization to 9-phenanthrols **4**, a process which, as for the conversion **6** → **7**, may be termed Directed remote Metalation (DreM).

Herein we report full details (8) of the successful verification and generalization of this reaction for the regiospecific construction of 9-phenanthrols **4**, their facile conversion into the corresponding phenanthrenes **5**, and selected further DoM, Suzuki–Miyaura cross coupling, and oxidation – ring contraction reactions of phenanthrene derivatives. Phenanthrenes

Received November 19, 1999. Accepted March 9, 2000. Published on the NRC Research Press website on June 14, 2000.

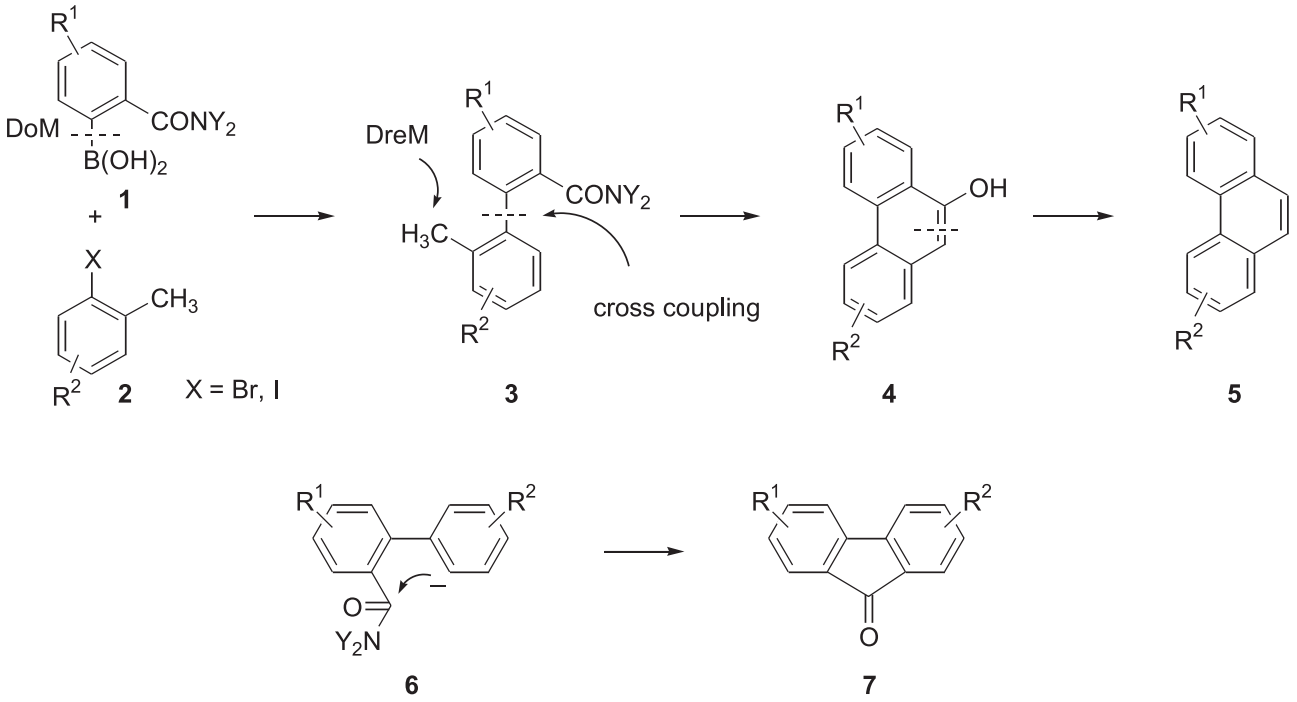
This paper is dedicated to Professor Stephen Hanessian, our lifetime friend, in celebration of his 65th birthday and with appreciation of his lasting and purposeful contributions to chemical synthesis.

J.-m. Fu[1] and V. Snieckus.[2, 3] Guelph–Waterloo Centre for Graduate Work in Chemistry, University of Waterloo, Waterloo, ON N2L 3G1, Canada.

[1]Current address: Pharmacia Corp., Structural, Analytical and Medicinal Chemistry, 7255–209–706, 301 Henrietta St., Kalamazoo, MI 49007, U.S.A.
[2]Current address: Department of Chemistry, Queen's University, Kingston, ON K7L 3N6, Canada.
[3]Author to whom correspondence may be addressed (e-mail: snieckus@chem.queensu.ca).

© 2000 NRC Canada

Scheme 1.



(9) represent an ambivalent class of substances which, on the one hand, are carcinogens found in the environment (10) and, on the other, natural products exhibiting potential for treatment of carcinomas and other disease states (11). Classical syntheses for phenanthrenes (12), e.g., ring annulations (13); carbocyclic ring expansion (14); intramolecular cyclization (15); and intermolecular cycloaddition (16), normally are long and laborious; inherently limited by availability of starting materials for more than trivial substitution patterns; and lack well-defined regiocontrol elements. The new carbanionic protocol (**3** → **4** → **5**) reported herein enjoys the advantages of the regiospecificity of DoM for the construction of benzamide boronic acids **1**, the ready availability of both **1** and **2** from materials of commerce, and the efficacy of the Suzuki–Miyaura reaction.

Synthesis of 2′-methylbiaryl-2-carboxamides 3 and conversion into 9-pheanthrols 4 (Table 1)

The requisite benzamide boronic acids **1** for the coupling reaction were prepared by standard *ortho*-lithiation (*s*-BuLi/TMEDA/–78°C/THF/1h) of the corresponding *N*,*N*-diethyl or *N*,*N*-diisopropyl benzamides followed by quenching with trimethyl borate and acidic workup. The boronic acids, usually obtained as fluffy solids, were not purified but directly subjected, as the excessive reactant (1.4 equiv) to the Suzuki–Miyaura cross coupling reaction (17*a*) with mainly bromo toluenes **2,** using a slightly modified procedure (DME as solvent) (17*b*, *c*). Ethanol was added as cosolvent as required for some insoluble boronic acids. Product biaryls **3** were obtained in good to excellent yields (Table 1) from coupling of unsubstituted (most entries) and methoxy (entries 3–5, 7) benzamide boronic acids **1** with 2-bromotoluenes **2** containing Cl (entries 5, 6) and electron withdrawing carboxamido (entries 8–10) and nitro (entries 11–15) groups.

The advantage of the greater reactivity of 2-iodotoluenes and choice of solvent is evident in sterically demanding cross coupling reactions. Thus, while coupling of **1e** with 2-bromotoluene (**2a**) (Scheme 2) gave **3g** in 23% (DME) and 5% (PhH) yields respectively, the corresponding iodotoluene **2c** afforded the product **3g** in 78% yield, optimized in DME.

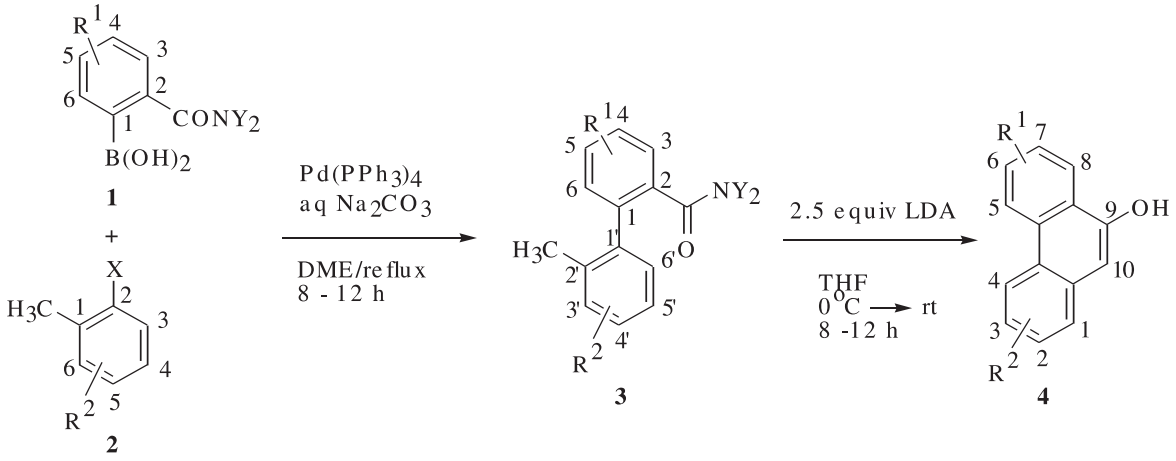
Consideration of pK_a data (LDA pK_a = 36 (18), 4-methylbiphenyl pK_a > 40.2 (18, 19)) and the admittedly minor vinylogous acidity effect on the methyl hydrogens in the twisted biaryl **3a** provided the expectation that equilibrium concentrations of anion **8** will be formed (Scheme 3), triggered by a CIPE from amide – LDA coordination. Subsequent cyclization to the tetrahedral intermediate **9** is ultimately driven by aromatization to **11** which could occur indirectly, via elimination to the ketone **10** or, more likely, by direct elimination. Both paths would require a second equivalent of LDA to drive the equilibrium to completion. In congruence with this hypothesis in practice, treatment of the substrate **3a** with 1 equiv. of LDA at –78°C or at 0°C followed by warming to rt overnight gave 9-phenanthrol (**4a**) in only 50–58% yield, together with recovered starting material **3a** (~40%). However, using 2.5 equiv of LDA afforded 9-phenanthrol (**4a**) in 92% isolated yield.

With these general conditions established, the directed remote metalation – cyclization reaction to 9-phenanthrols was then extended to other biaryl substrates (Table 1). The absence of an amide steric effect is apparent from the fact that the *N*,*N*-diisopropyl amide **3b** underwent cyclization to give 9-phenanthrol (**4a**) in comparable high yield (entry 2) to that achieved starting with the *N*,*N*-diethyl amide **3a**. Methoxy, chloro, and carboxamido substituted phenanthrols were

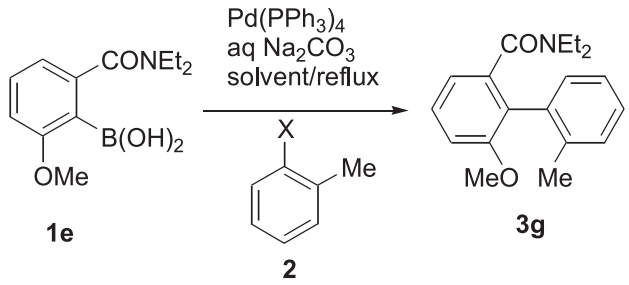
© 2000 NRC Canada

Table 1. Synthesis of 9-phenanthrols **4**.

	$ArB(OH)_2$ **1**			AR′X **2**			Ar – Ar′ **3**		Phenanthrols **4**			
Entry		R^1	Y		R^2	X	(Yield (%))			R^1	R^2	Yield (%)
1	**1a**	H	Et	**2a**	H	Br	**3a**	(87)	**4a**	H	H	(92)
2	**1b**	H	Pr^i	**2a**	H	Br	**3b**	(81)	**4a**	H	H	(98)
3	**1c**	3-OMe	Et	**2a**	H	Br	**3c**	(85)	**4b**	8-OMe	H	(92)
4	**1d**	5-OMe	Et	**2a**	H	Br	**3d**	(83)	**4c**	6-OMe	H	(88)
5	**1d**	5-OMe	Et	**2b**	5-Cl	Br	**3e**	(98)	**4d**	6-OMe	2-Cl	(93)
6	**1a**	H	Et	**2b**	5-Cl	Br	**3f**	(85)	**4e**	H	2-Cl	(96)
7	**1e**	6-OMe	Et	**2c**	H	I	**3g**	(78)	**4f**	5-OMe	H	(92)
8	**1a**	H	Et	**2d**	$5\text{-}CONEt_2$	Br	**3h**	(77)	**4g**	H	$2\text{-}CONEt_2$	(78)
9	**1a**	H	Et	**2e**	$4\text{-}CONEt_2$	Br	**3i**	(82)	**4h**	H	$3\text{-}CONEt_2$	(92)
10	**1b**	H	Pr^i	**2e**	$4\text{-}CONEt_2$	Br	**3j**	(79)	**4h**	H	$3\text{-}CONEt_2$	(94)
11	**1b**	H	Pr^i	**2f**	$6\text{-}NO_2$	Br	**3k**	(96)	**4i**	H	$1\text{-}NO_2$	NR
12	**1a**	H	Et	**2g**	$5\text{-}NO_2$	Br	**3l**	(82)	**4j**	H	$2\text{-}NO_2$	NR
13	**1b**	H	Pr^i	**2g**	$5\text{-}NO_2$	Br	**3m**	(98)	**4j**	H	$2\text{-}NO_2$	NR
14	**1a**	H	Et	**2h**	$4\text{-}NO_2$	Br	**3n**	(99)	**4k**	H	$3\text{-}NO_2$	NR
15	**1b**	H	Pr^i	**2h**	$4\text{-}NO_2$	Br	**3o**	(99)	**4k**	H	$3\text{-}NO_2$	NR



Scheme 2.



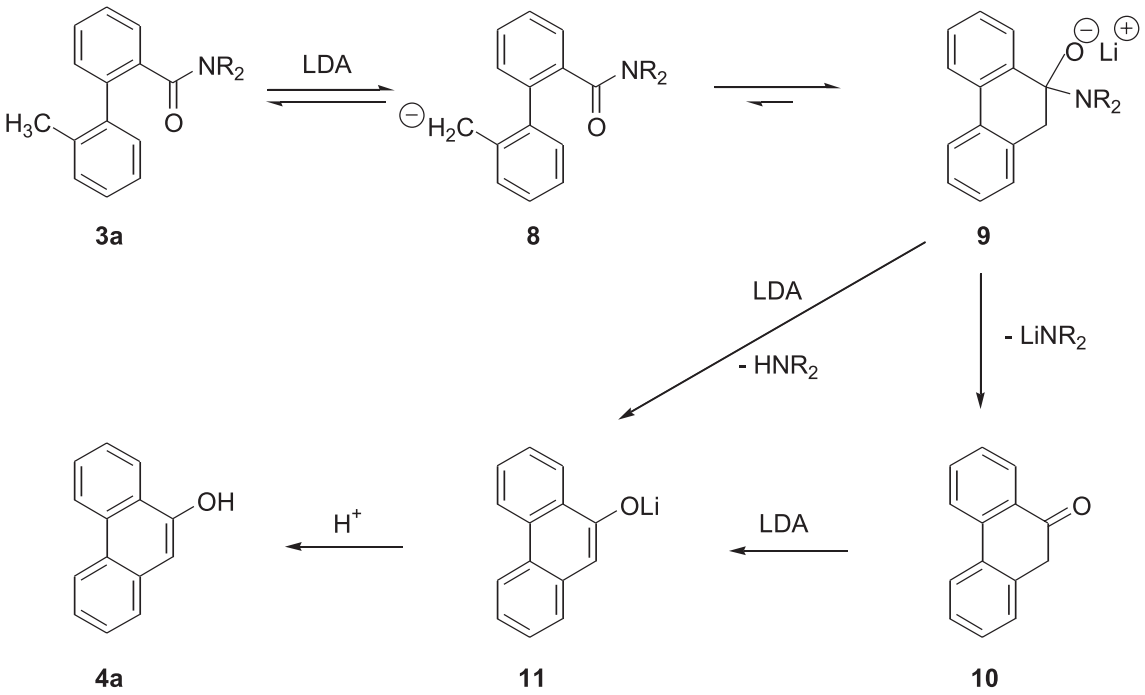
2	X	Solvent	**3g**, Yield%
2a	Br	DME	23
2a	Br	PhH	5
2c	I	PhH	29
2c	I	DME	78

prepared in good yields (entries 3–10). The requirement of 2 equiv. of LDA for optimum yields was also ascertained in the case of 8-methoxy-9-phenanthrol (**4b**) (entry 3), formed in 92% yield compared to 63% when 1 equiv. of LDA was used. Nitro substituted biaryls failed to cyclize (entries 11–15). Although LDA addition to the THF solutions of these biaryls resulted in color changes from yellow to purple, aqueous workup led to decoloration and recovery of starting materials or decomposed products. These results may be due to the onset of single electron transfer processes between the nitrobiaryl (electron acceptor) (20) and LDA (electron donor) (21) partners. Use of bases which are successful in the Reissert indole synthesis involving 2-nitrotoluene deprotonation (e.g., NaH, KO*t*-Bu) (22) also failed to give nitro-substituted 9-phenanthrols. The characterization of some 9-phenanthrols required derivatization to acetate and (or) triflate due to their instability, as evidenced by brown discoloration after flash chromatography.

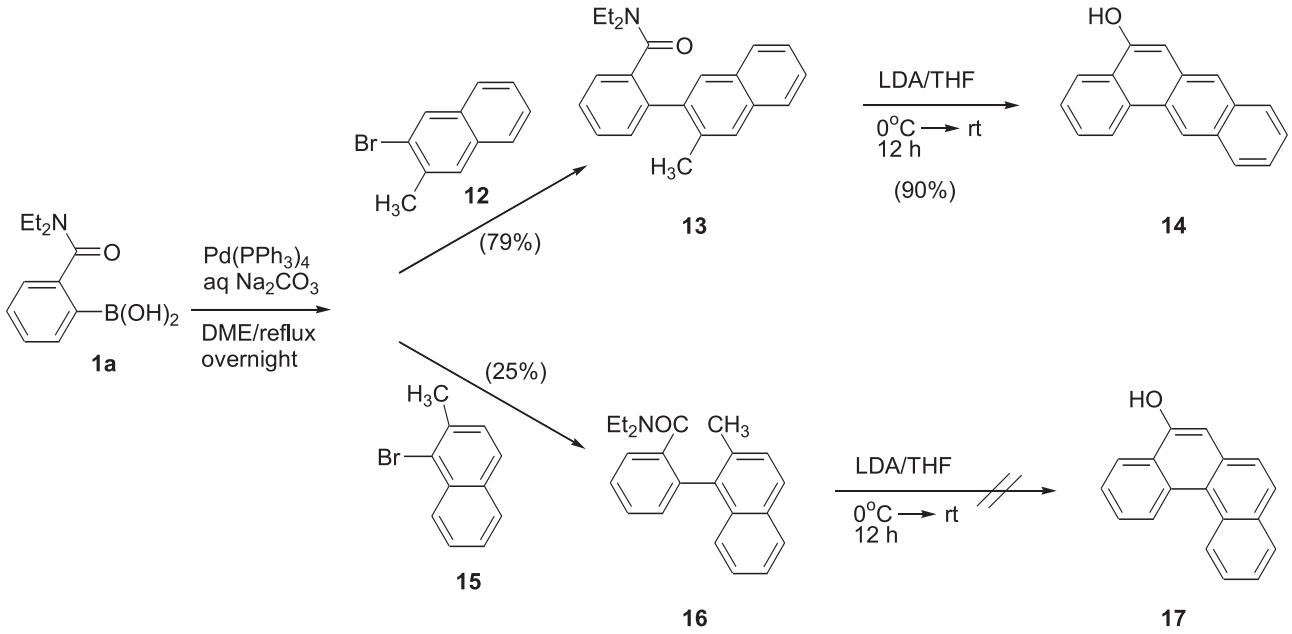
The potential value of the DreM-based 9-phenanthrol synthesis for the construction of more highly condensed polycyclic aromatics was tested on two selected cases **13** and **16** (Scheme 4) which were prepared from the cross coupling of **1a** with isomeric methyl bromonapthalenes **12** and **15** respectively. While **13** underwent LDA-mediated

© 2000 NRC Canada

Scheme 3.



Scheme 4.



cyclization to 5-hydroxy benz[*c*]anthracene (**14**) in excellent yield, **16** failed to give the expected 10-hydroxy benz[*c*]phenanthrene (**17**) even under vigorous conditions (4 equiv of LDA in refluxing THF; quantitative recovery of **16**). The latter result, already foreshadowed by low yield in the cross coupling reaction to **16**, may be rationalized by a peri-hydrogen effect which inhibits achievement of the angle required for the non-linear (23) approach of carbanion to amide carbonyl or in the planarization needed for the tetrahedral intermediate corresponding to **9**.

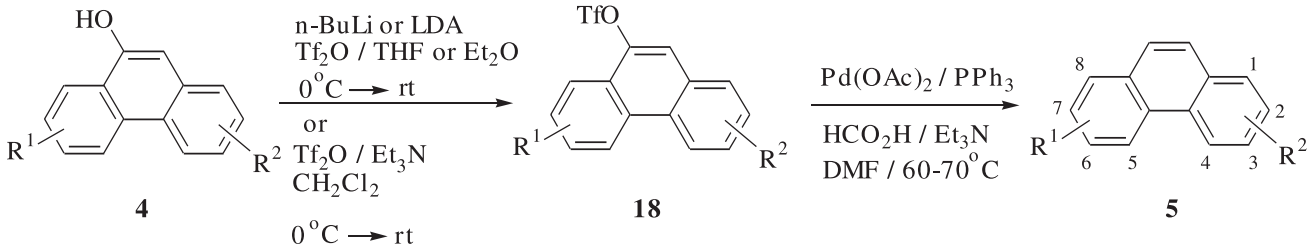
The 9-phenanthrol to phenanthrene conversion (4 → 18 → 5)

To establish a general regiospecific phenanthrene synthesis based on the DreM protocol, the Pd-catalyzed hydrogenolysis of aryl triflates, independently discovered by three groups (24, 25) was adapted. Thus remarkably stable phenanthryl triflates **18** (Table 2), obtained by treatment of the corresponding phenanthrols **4** with *n*-BuLi or LDA

© 2000 NRC Canada

Table 2. Synthesis of phenanthrenes.

Entry	R^1	R^2	Triflate	Yield (%)	Phenanthrene	Yield (%)
1	H	H	**18a**	80	**5a**	67
2	8-OMe	H	**18b**	75	**5b**	97
3	6-OMe	H	**18c**	65	**5c**	73
4	H	2-Cl	**18d**	90	**5d**	68
5	5-OMe	H	**18e**	71	**5e**	93
6	H	2-$CONEt_2$	**18f**	59	**5f**	90
7	H	3-$CONEt_2$	**18g**	69	**5g**	69



followed by triflic anhydride (24*a*) or by triethyl amine – triflic anhydride, (26) were subjected to reaction with $Pd(OAc)_2$ and PPh_3 in DMF followed by addition of Et_3N and formic acid to afford phenanthrenes **5** in good to excellent yields. The overall route to phenanthrenes, **1 + 2** → **3** → **4** → **18** → **5** constitutes a general, efficient, regiospecific, and convenient process which is expected to compete favorably with known methods for the preparation of this class of aromatic hydrocarbons. For example, the phenanthrene **5b** and **5e** were obtained in 57% and 47% overall yield respectively compared to ~10% overall yield for both compounds by the Stobbe condensation involving the intramolecular cyclization reaction as the key step (27).

DoM and other reactions of 9-phenanthrols

To explore phenanthrene C_{10} – DoM paths, the *N*,*N*-diethyl 9-phenanthryl *O*-carbamate **19** (Scheme 5) was prepared from the corresponding phenanthrol (**4a**) ($ClCONEt_2$/pyridine/reflux). When subjected to the standard metalation (*s*-BuLi/TMEDA/THF/–78°C/1 h) – silylation sequence, **19** afforded product **20a** in <44% yields; however, under *t*-BuLi metalation conditions, **20a** was obtained in 88% yield. Using these conditions, the 10-methyl phenanthrene **20b** was also prepared and exclusion of electrophile allowed the anionic Fries rearrangement (28) to proceed smoothly to give compound **21** in excellent yield. Treatment of the 9-TMS phenanthrene **20a** with BBr_3 resulted in ipso borodesilylation (29) to cleanly produce the corresponding boronic acid **20c** which underwent smooth palladium catalyzed cross coupling with 4-nitrobromobenzene (**22**) to furnish the biaryl **23** in good yield (80%). This sequence of potential generality presents an alternate route to Suzuki–Miyaura cross coupling partners which allows a C-H site *ortho* to a DMG to remain in a holding pattern as the TMS masked derivative and to be subsequently exposed by an regioselective ipso process.

In further examination of DoM chemistry of the phenanthrene nucleus (3), the available *N*,*N*-diethyl amides **5f** and **5g** (Table 2) were subjected to the standard metalation conditions followed by quenching with TMSCl. In each case, an inseparable mixture of the TMS isomers was obtained thus rendering this reaction of limited synthetic value. On the other hand, the phenanthryl-4-*O*-carbamate **24**, prepared from 4-methoxyphenanthrene (**5e**) by demethylation with BBr_3 and carbamoylation (Scheme 6), gave, upon metalation with either *s*-BuLi and TMEDA, or *t*-BuLi in THF at –78°C and warming to rt, the anionic Fries rearrangement (28) product **25** in quantitative yield. Attempts to trap the incipient *ortho* lithiated species with electrophiles such as TMSCl led also mainly to the formation of **25** (80%), thus suggesting a rapid migration presumably resulting from steric relief of the carbamate – C_5- peri – hydrogen interaction. These restricted observations suggest that phenanthrenes are substrates for profitable DoM and cross coupling chemistry, e.g., after phenol protection in **25**, further metalation may be contemplated.

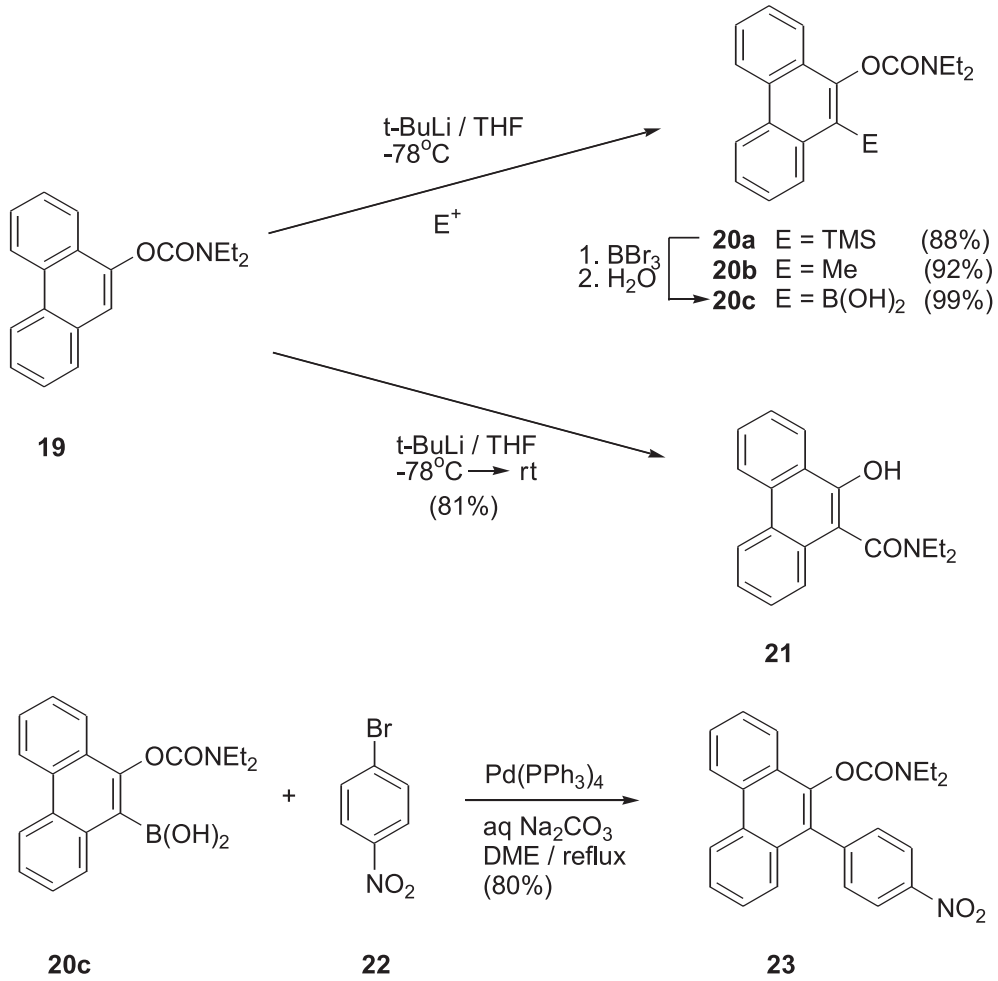
The known facile oxidation of 9-phenanthrols into 9,10-phenanthroquinones (30) and the potential for a benzil-benzilic acid rearrangement (31) in the latter invited the development of a ring-contraction route to fluorenones (32). In this pursuit, 9-phenanthrols **4b** and **4f** (Scheme 7) were oxidized by bubbling oxygen into a DMF solution containing a catalytic amount of salcomine (33) to give the methoxy phenanthroquinones **26a** and **26b** in quantitative yields. Treatment with 2 M potassium hydroxide at 90°C provided mixtures of the benzil – benzilic acid rearrangement products **27** (major) together with fluorenones **28** (minor) which, without separation, were treated with lead tetraacetate (34), to afford the fluorenones **28** in excellent overall yields. Through this simple sequence, a synthetic conduit from phenanthrene to fluorenone aromatics is established.

Conclusions

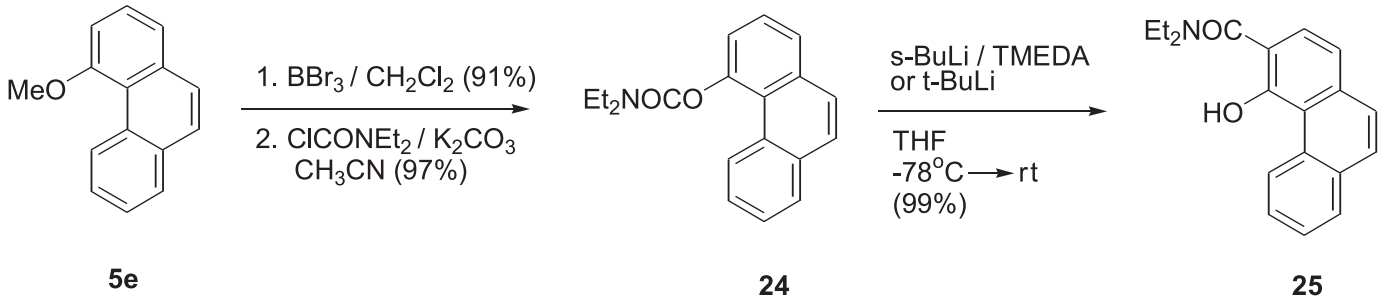
A new general 9-phenanthrol synthesis proceeding by a Directed *ortho* Metalation (DoM) – Suzuki–Miyaura – Directed remote Metalation (DreM) sequence (**1 + 2** → **3** → **4**, Table 1) has been demonstrated. It posits advantages of inherent regiospecificity (DoM), brevity, mild conditions, and starting material availability. Furthermore, it serves as a relay for a regioselective synthesis of the corresponding

© 2000 NRC Canada

Scheme 5.



Scheme 6.



phenanthrenes by a Pd-catalyzed hydrogenolysis of the intermediate triflates (**4** → **18** → **5**, Table 2). These results together with additional exploratory DoM, cross coupling, and oxidation-rearrangement chemistry (Schemes 5–7) suggest considerable opportunity for the regiospecific construction of polysubstituted phenanthrene derivatives according to protocols elaborated herein which will compete favorably with or supercede classical methodologies.

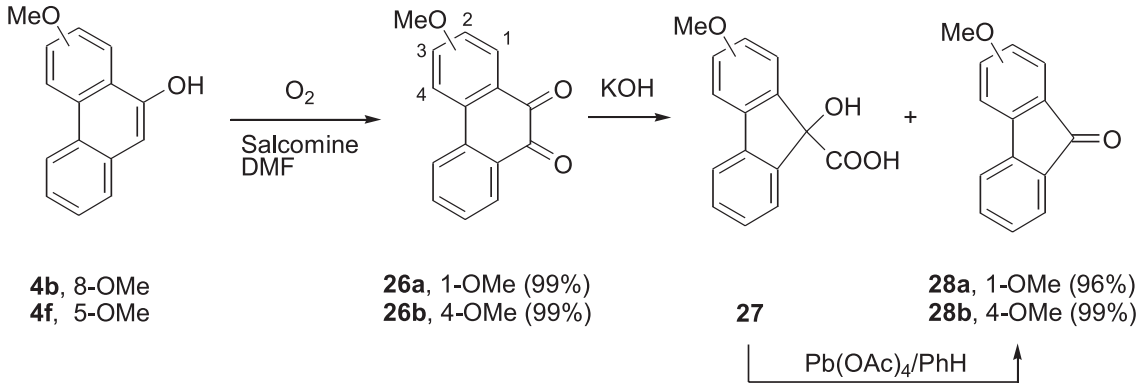
Experimental section

General

Flash chromatography was carried out using Merck silica gel 60 (0.04–0.06 mm) purchased from BDH Chem. Co. Canada with EtOAc–hexane as eluent unless otherwise specified. Analytical thin layer chromatography (TLC) was performed using Merck precoated silica gel 60F-254 sheets. Melting points were determined using a Buchi model SMP-20 instrument and are uncorrected. IR spectra were recorded

© 2000 NRC Canada

Scheme 7.



on a Perkin-Elmer 983 IR spectrophotometer neat between NaCl plates, in $CHCl_3$ solution, Nujol, or KBr plate form. ^{1}H NMR and ^{13}C NMR spectra were recorded on AC-200 or AM-250 spectrometers in $CDCl_3$ solution using tetramethylsilane as internal standard unless otherwise specified. Mass spectra and HRMS were determined by Dr. R. Smith, McMaster University, Hamilton, Ontario, Canada, using VG 7070F or Varian spectrometers in EI mode unless otherwise specified. Elemental analysis were performed by Galbraith Laboratories, Knoxville, Tennessee. All dry solvents used were purified according to Perrin (35). Tetrahydrofuran, dimethoxyethane and diethyl ether were distilled from sodium-benzophenone ketyl under nitrogen immediately prior to use. Solutions of *n*-BuLi (hexane), *s*-BuLi (cyclohexane), and *t*-BuLi (pentane) were purchased from Aldrich Chemical Co. They were stored in resealable containers, and titrated periodically against 2,5-dimethoxybenzyl alcohol. *N*,*N*,*N′*,*N′*-Tetramethylethylenediamine (TMEDA) was dried over and distilled from CaH_2 before use. Lithium diisopropylamide (LDA) was always prepared before reactions by stirring a 1:1 mixture of diisopropylamine and *n*-BuLi at 0°C for 10 min (36). All commercial materials were purchased from Aldrich Chemical Co. or Lancaster Synthesis Ltd. Tetrakis(triphenylphosphine)palladium (0) was prepared following a literature procedure (37). All reactions were carried out under N_2 or Ar atmosphere unless otherwise specified. The –78°C temperature designated is approximate as achieved by a dry ice – acetone bath. The phrase "normal workup" means the addition of saturated aqueous NH_4Cl solution to the reaction mixture followed by CH_2Cl_2 extraction, drying over Na_2SO_4, filtration, and evaporation of the filtrate in vacuo to afford the crude product.

Synthesis of tertiary benzamides

The tertiary benzamides were prepared using the procedure described by Hall (38) from the reactions of corresponding carboxylic acids with $SOCl_2$ followed by treatment with an excess of the appropriate amines.

N,N-*Diethyl 3-methyl-4-bromobenzamide* (***2d***): bp: 120–122°C (0.02 mm). Lit. (39): bp 154°C (0.05 mm).

N,N-*Diethyl 3-bromo-4-methylbenzamide* (***2e***): mp 53–55°C (hexane); IR (KBr) 1617 cm^{-1}; ^{1}H NMR δ 1.05–1.30 (br, 6 H), 2.41 (s, 3 H), 3.20–3.60 (2 br, 4 H), 7.18–7.27 (m, 2 H), 7.54 (s, 1 H); MS *m*/*e* (rel intensity) 270 (M^+ + 2 – 1, 16), 268 (M^+ – 1, 14), 199 (34), 197 (35). Anal. calcd. for $C_{12}H_{16}BrNO$: C 53.35, H 5.97, N 5.19; found: C 53.55, H 5.96, N 5.14.

General procedure for the preparation of benzamide boronic acids (1) (method A)

A solution of the benzamide (1.00 mmol), dissolved in anhydrous THF (2 mL) was added dropwise to a stirred solution of a 1:1 *s*-BuLi–TMEDA complex or *t*-BuLi (1.10 mmol) in anhydrous THF (3 mL) at –78°C. The resulting mixture was stirred at –78°C for 1 h (unless otherwise specified), treated with an excess (4.0 mmol) of $B(OMe)_3$ and the whole was allowed to warm to room temperature overnight (8–12 h). A few drops of saturated aqueous NH_4Cl solution were added and the mixture was acidified with 2 M HCl until pH 5–6. After THF was removed in vacuo, the aqueous mixture was subjected to normal workup to afford the crude product.

*2-(*N,N-*Diethylcarboxamido)phenylboronic acid* (***1a***): According to method A, to a solution of *N*,*N*-diethyl benzamide (9.91 g, 56.74 mmol), *s*-BuLi (48.4 mL of 1.27 M solution, 61.5 mmol), and TMEDA (9.3 mL, 7.15 g, 61.5 mmol) in THF, was added $B(OMe)_3$ (25.4 mL, 23.25 g, 223.7 mmol). Acidification with 2 M HCl to pH 5–6 followed by normal workup afforded 11.63 g (94%) of **1a** as a fluffy solid which was used in cross coupling reactions without further purification.

*2-(*N,N-*Diisopropylcarboxamido)phenylboronic acid* (***1b***): According to method A, to a solution of *N*,*N*-diisopropyl benzamide (12.32 g, 60.0 mmol), *s*-BuLi (52.8 mL of 1.25 M solution, 66.0 mmol), and TMEDA (9.96 mL, 7.67 g, 66.0 mmol) in THF was added $B(OMe)_3$ (27.3 mL, 24.94 g, 240.0 mmol). Acidification with 2 M HCl to pH 5–6 followed by normal workup afforded 14.65 g (98%) of **1b** which was used in cross coupling reactions without further purification.

*3-Methoxy-2-(*N,N-*diethylcarboxamido)phenylboronic acid* (***1c***): According to method A, to a solution of *N*,*N*-diethyl 2-methoxybenzamide (6.22 g, 30.0 mmol), *s*-BuLi (25.4 mL of 1.30 M solution, 33.0 mmol), and TMEDA (5.0 mL, 3.85 g, 33.0 mmol) in THF, was added $B(OMe)_3$ (10.2 mL, 9.35 g, 90.0 mmol). Acidification with 2 M HCl to pH 5–6 followed

© 2000 NRC Canada

by normal workup afforded 7.31 g (97%) of **1c** which was used in cross coupling reactions without further purification.

*5-Methoxy-2-(*N,N-*diethylcarboxamido)phenylboronic acid (**1d**)*: According to method A, to a solution of *N*,*N*-diethyl 4-methoxybenzamide (3.40 g, 16.4 mmol), *s*-BuLi (14.0 mL of 1.29 M solution, 18.1 mmol), and TMEDA (2.7 mL, 2.01 g, 18.1 mmol) was added $B(OMe)_3$ (7.5 mL, 6.85 g, 65.7 mmol). Acidification with 2 M HCI to pH 5–6 followed by normal workup afforded 4.08 g (99%) of **1d**, which was used in cross coupling reactions without further purification.

*6-Methoxy-2-(*N,N-*diethylcarboxamido)phenylboronic acid (**1e**)*: According to method A, to a solution of *N*,*N*-diethyl 3-methoxybenzamide (2.07 g, 10.0 mmol), *s*-BuLi (8.7 mL of 1.27 M solution, 11.0 mmol), and TMEDA (1.66 mL, 1.28 g, 11.0 mmol) was added $B(OMe)_3$ (4.5 mL, 4.16 g, 40.0 mmol) at –78°C. The resulting mixture was stirred at –40°C for 4 h, quenched with saturated aqueous NH_4Cl solution at –40°C, and allowed to warm to rt over 1 h. Acidification with 2 M HCl to pH 5–6 and normal workup afforded 2.34 g (96%) of **1e** which was used in cross coupling reactions without further purification.

General procedure for the preparation of 2-methylbiaryl-2-carboxamides (3) (method B)

A mixture of $Pd(PPh_3)_4$ (0.04 mmol) and aryl halide or aryl triflate (1 mmol) in DME (3 mL) was stirred at rt for 10 min. The solution of benzamide boronic acid (**1**) (1.4 mmol) in DME (2 mL) was added. For insoluble boronic acids, a mixture of DME and a minimum amount of EtOH was used. 2 M aqueous Na_2CO_3 solution (3 mL) was added and the resulting mixture was refluxed overnight (8–12 h), cooled to rt and subjected to filtration. The filtrate was treated according to normal workup to afford the crude product.

N,N-*Diethyl 2′-methylbiphenyl-2-carboxamide (**3a**)*: According to method B, 2-bromotoluene (1.71 g, 10.0 mmol) was coupled with 2-(*N*,*N*-diethylcarboxamido)phenylboronic acid (3.01 g, 14.0 mmol) in the presence of $Pd(PPh_3)_4$ (0.462 g, 0.40 mmol). Normal workup followed by flash chromatography (1:2) afforded 2.31 g (87%) of **3a**: mp 67–68°C (hexane), (lit. (40) bp 130–135°C (0.05 mm)); IR ($CHCl_3$) 1620 cm^{-1}; ^1H NMR δ 0.65–0.71 (t, *J* = 7.1 Hz, 3 H), 0.90 (br, 3 H), 2.20 (s, 3 H), 2.60–3.90 (m, 4 H), 7.10–7.50 (m, 8 H).

N,N-*diisopropyl 2′-methylbiphenyl-2-carboxamide (**3b**)*: According to method B, 2-bromotoluene (1.04 g, 6.12 mmol) was coupled with 2-(*N*,*N*-diisopropylcarboxamido)phenylboronic acid (2.13 g, 8.56 mmol) in the presence of $Pd(PPh_3)_4$ (0.353 g, 0.31 mmol). Normal workup followed by flash chromatography (1:2) afforded 1.46 g (81%) of **3b**: mp 93–94°C (hexane); IR ($CHCl_3$) 1618 cm^{-1}; ^1H NMR δ 0.40–0.80 (br, 3 H), 0.97–1.00 (d, *J* = 6.3 Hz, 3 H), 1.04–1.07 (d, *J* = 6.8 Hz, 3 H), 1.46–1.49 (d, *J* = 6.8 Hz, 3 H), 2.23 (s, 3 H), 3.40–3.70 (br, 2 H), 7.12–7.41 (m, 8 H); MS *m*/*e* (rel intensity) 295 (M^+, 7), 252 (17), 195 (100), 165 (25). Anal. calcd. for $C_{20}H_{25}NO$: C 81.31, H 8.53, N 4.74; found: C 80.98, H 8.61, N 4.66.

N,N-*Diethyl 3-methoxy-2′-methylbiphenyl-2-carboxamide (**3c**)*: According to method B, 2-bromotoluene (2.05 g, 12.0 mmol) was coupled with 3-methoxy-2-(*N*,*N*-diethylcarboxamido)phenylboronic acid (4.23 g, 17.0 mmol) in the presence of $Pd(PPh_3)_4$ (0.555 g, 0.48 mmol). Normal workup followed by flash chromatography (1:1) afforded 3.02 g (85%) of **3c**: mp 90–91°C (cyclohexane); IR ($CHC1_3$) 1616 cm^{-1}; ^1H NMR δ 0.58–0.63 (t, *J* = 7.1 Hz, 3 H), 0.80–1.10 (br, 3 H), 2.20 (s, 3 H), 2.70–3.83 (m, 4 H), 3.86 (s, 3 H), 6.89–6.93 (dd, *J* = 7.6, 0.7 Hz, 1 H), 7.18–7.36 (m, 6 H); MS *m*/*e* (rel intensity) 297 (M^+, 1), 225 (100), 224 (32). Anal. calcd. for $C_{19}H_{23}NO_2$: C 76.74, H 7.80, N 4.71; found: C 76.71, H 7.84, N 4.95.

N,N-*Diethyl 5-methoxy-2′-methylbiphenyl-2-carboxamide (**3d**)*: According to method B, 2-bromotoluene (0.99 g, 5.77 mmol) was coupled with 5-methoxy-2-(*N*,*N*-diethylcarboxamido)phenylboronic acid (2.03 g, 8.08 mmol) in the presence of $Pd(PPh_3)_4$ (0.334 g, 0.29 mmol). Normal workup followed by flash chromatography (1:1) afforded 1.43 g (83%) of **3d**: bp 145–150°C (0.02 mm); IR (neat) 1637 cm^{-1}; ^1H NMR δ 0.65–0.72 (t, *J* = 7.1 Hz, 3 H), 0.86–0.93 (t, *J* = 7.0 Hz, 3 H), 2.24 (s, 3 H), 2.80–3.80 (2 br, 4 H), 3.83 (s, 3 H), 6.78–6.79 (d, *J* = 2.5 Hz, 1 H), 6.88–6.95 (m, 2 H), 7.16–7.37 (m, 4 H); MS *m*/*e* (rel intensity) EI 296 (M^+–1, 3), 225 (37), 135 (100); CI (NH_3) 299 (M^+, 20), 298 (M^++1, 100), 208 (92); HRMS (EI) calcd. for $C_{19}H_{23}NO_2$-H: 296.1652; found: 296.1649.

N,N-*Diethyl 5-methoxy-2′-methyl-4′-chlorobiphenyl-2-carboxamide (**3e**)*: According to method B, 2-bromo-5-chlorotoluene (1.22 g, 5.95 mmol) was coupled with 5-methoxy-2- (*N*,*N*-diethylcarboxamido)phenylboronic acid (2.09 g, 8.33 mmol) in the presence of $Pd(PPh_3)_4$ (0.344 g, 0.30 mmol). Normal workup followed by flash chromatography (1:3) afforded 1.94 g (98%) of **3e**: mp 95–97°C (hexane); IR ($CHC1_3$) 1628 cm^{-1}; ^1H NMR δ 0.73–0.80 (t, *J* = 7.1 Hz, 3 H), 0.90–0.97 (t, *J* = 7.1 Hz, 3 H), 2.22 (s, 3 H), 2.97–3.80 (m, 4 H), 3.83 (s, 3 H), 6.73–6.74 (d, *J* = 2.6 Hz, 1 H). 6.90–6.95 (dd, *J* = 8.5, 2.6 Hz, 1 H), 7.13–7.31 (m, 4 H); MS *m*/*e* (rel intensity) 333 (M^+, 1), 331 (M^+, 2), 261 (34), 260 (20), 259 (100). Anal. calcd. for $C_{19}H_{22}ClNO_2$: C 68.77, H 6.68, N 4.22; found: C 69.03, H 6.98, N 4.19.

N,N-*Diethyl 2′-methyl-4′-chlorobiphenyl-2-carboxamide (**3f**)*: According to method B, 2-bromo-5-chlorotoluene (1.03 g, 5.0 mmol) was coupled with 2-(*N*,*N*-diethylcarboxamido)phenylboronic acid (1.55 g, 7.0 mmol) in the presence of $Pd(PPh_3)_4$ (0.231 g, 0.20 mmol). Normal workup followed by flash chromatography (1:1) afforded 1.28 g (85%) of **3f**: mp 83–85°C (hexane); IR ($CHC1_3$) 1615 cm^{-1}; ^1H NMR δ 0.74–0.80 (t, *J* = 7.1 Hz, 3 H), 0.94 (br, 3 H), 2.19 (s, 3 H), 2.70–3.90 (br, 4 H), 7.12–7.23 (m, 3H), 7.36–7.42 (m, 4 H); MS *m*/*e* (rel intensity) 303 (M^+, 1), 301 (M^+, 5), 231 (16), 229 (51), 166 (34), 165 (40), 58 (100). Anal. calcd. for $C_{18}H_{20}ClNO$: C 71.63, H 6.68, N 4.64; found: C 71.34, H 6.89, N 4.50.

N,N-*Diethyl 6-methoxy-2′-methylbiphenyl-2-carboxamide (**3g**)*: According to method B, 2-iodotoluene (1.73 g, 8.0 mmol) was coupled with 6-methoxy-2-(*N*,*N*-diethylcarboxamido)phenylboronic acid (2.80 g, 11.2 mmol) in the presence of

© 2000 NRC Canada

$Pd(PPh_3)_4$ (0.390 g, 0.34 mmol). Normal workup followed by flash chromatography (1:1) afforded 1.80 g (78%) of **3g**: mp 105–107°C (hexane); IR ($CHC1_3$) 1630 cm^{-1}; ^1H NMR δ 0.65–0.71 (t, *J* = 7.1 Hz, 3 H), 0.85–1.00 (br, 3 H), 2.24 (s, 3 H), 2.80–3.15 (br, 2 H), 3.80–3.85 (m, 5 H), 6.90–6.94 (dd, *J* = 8.4, 2.5 Hz, 1 H), 7.10–7.31 (m, 6 H); MS *m*/*e* (rel intensity) 297 (M^+, 11), 225 (39), 224 (28), 135 (49), 71 (100); HRMS calcd. for $C_{19}H_{23}NO_2$-H: 296.1652; found: 296.1650.

N,N-*Diethyl 2′-methyl-4′-(*N,N-*diethylcarboxamido)biphenyl-2-carboxamide (**3h**)*: According to method B, *N*,*N*-diethyl 3-methyl-4-bromobenzamide (2.07 g, 7.7 mmol) was coupled with 2-(*N*,*N*-diethylcarboxamido)phenylboronic acid (2.37 g, 10.7 mmol) in the presence of $Pd(PPh_3)_4$ (0.358 g, 0.31 mmol). Normal workup followed by flash chromatography (1:1) afforded 2.19 g (77%) of **3h**: bp 182–186°C (0.005 mm); IR (neat) 1635 cm^{-1}; ^1H NMR δ 0.70–0.76 (t, *J* = 7.1 Hz, 3 H), 0.93–1.05 (2 br, 3 H), 1.10–1.40 (2 br, 6 H), 2.23 (s, 3 H), 2.80–3.80 (m, 8 H), 7.14–7.71 (m, 7 H); MS *m*/*e* (rel intensity) 366 (M^+, 24), 294 (100), 266 (22), 221 (22), 165 (20), 100 (23); HRMS calcd. for $C_{23}H_{30}N_2O_2$: 366.2309; found: 366.2310.

N,N-*Diethyl 2′-methyl-5′-(*N,N-*diethylcarboxamido)biphenyl-2-carboxamide (**3i**)*: According to method B, *N*,*N*-diethyl 3-bromo-4-methylbenzamide (2.97 g, 11.0 mmol) was coupled with 2-(*N*,*N*-diethylcarboxamido)phenyl boronic acid (3.40 g, 15.4 mmol) in the presence of $Pd(PPh_3)_4$ (0.635 g, 0.55 mmol). Normal workup followed by flash chromatography (1:1) afforded 3.30 g (82%) of **3i**: bp 196–200°C (0. 1 mm); IR (neat) 1640, 1621 cm^{-1}; ^1H NMR δ 0.73–0.78 (t, *J* = 7.1 Hz, 3 H), 0.93–0.99 (t, *J* = 7.0 Hz, 3 H), 1.02–1.17 (br, 6 H), 2.21 (s, 3 H), 2.90–3.70 (br, 8 H), 7.21–7.47 (m, 7 H); MS *m*/*e* (rel intensity) 366 (M^+, 7), 209 (19), 193 (40), 192 (29), 121 (100), 105 (27); HRMS calcd. for $C_{23}H_{30}N_2O_2$: 366.2309; found: 366.2300.

N,N-*Diisopropyl 2′-methyl-5′-(*N,N-*diethylcarboxamido)biphenyl-2-carboxamide (**3j**)*: According to method B, *N*,*N*-diethyl 3-bromo-4-methylbenzamide (2.83 g, 10.6 mmol) was coupled with 2-(*N*,*N*-diisopropylcarboxamido)phenylboronic acid (3.65 g, 14.7 mmol) in the presence of $Pd(PPh_3)_4$ (0.611 g, 0.53 mmol). Normal workup followed by flash chromatography (1:1) afforded 3.27 g (79%) of **3j**: mp 105–107°C (hexane); IR ($CHC1_3$) 1618, 1612 cm^{-1}; ^1H NMR δ 0.60–1.19 (m, 15 H), 1.44–1.47 (d, *J* = 6.8 Hz, 3 H), 2.23 (s, 3 H), 3.20–3.80 (2 br, 4 H), 7.21–7.42 (m, 7 H); MS *m*/*e* (rel intensity) 394 (M^+, 12), 393 (20), 322 (37), 294 (16), 266 (24), 221 (100), 207 (25), 195 (21), 165 (50). Anal. calcd. for $C_{25}H_{34}N_2O_2$: C 76.10, H 8.69, N 7.10; found: C 76.23, H 8.70, N 7.08.

N,N-*Diisopropyl 2′-methyl-3′-nitrobiphenyl-2-carboxamide (**3k**)*: According to method B, 2-bromo-6-nitrotoluene (0.65 g, 3.0 mmol) was coupled with 2-(*N*,*N*-diisopropylcarboxamido)phenylboronic acid (1.05 g, 4.2 mmol) in the presence of $Pd(PPh_3)_4$ (0.139 g, 0. 12 rnmol). Normal workup followed by flash chromatography (1:1) afforded 0.98 g (96%) of **3k**: mp 97–98.5°C (hexane); IR ($CHC1_3$) 1621, 1527, 1340 cm^{-1}; ^1H NMR δ 0.59–0.62 (d, *J* = 6.7 Hz, 3 H), 0.88–1.13 (m, 6 H), 1.43–1.49 (m, 3 H), 2.36 (s, 3 H), 3.19–3.79 (m, 2 H), 7.24–7.46 (m, 6 H), 7.78–7.81 (d, *J* = 7.5 Hz, 1 H); MS *m*/*e* (rel intensity) 340 (M^+, 25), 297 (31), 240 (89), 194 (65), 165 (100). Anal. calcd. for $C_{20}H_{24}N_2O_3$: C 70.57, H 7.11, N 8.23; found: C 70.61, H 7.01, N 8.19.

N,N-*Diethyl 2′-methyl-4′-nitrobiphenyl-2-carboxamide (**3l**)*: According to method B, 2-bromo-5-nitrotoluene (1.08 g, 5.0 mmol) was coupled with 2-(*N*,*N*-diethylcarboxamido)phenylboronic acid (1.55 g, 7.0 mmol) in the presence of $Pd(PPh_3)_4$ (0.231 g, 0.20 mmol). Normal workup followed by flash chromatography (1:1) afforded 1.27 g (82%) of **3l**: mp 94–95°C (hexane–CH_2Cl_2); IR ($CHC1_3$) 1621, 1518, 1348 cm^{-1}; ^1H NMR δ 0.73–0.78 (t, *J* = 7.1 Hz, 3 H), 0.96–1.02 (t, *J* = 7.1 Hz, 3 H), 2.31 (s, 3 H), 2.90–3.10 (br, 2 H), 3.20–3.50 (br, 2 H), 7.21–7.48 (m, 5 H), 7.99–8.04 (dd, *J* = 8.4, 2.3 Hz, 1 H), 8.12–8.13 (d, *J* = 2.3 Hz, 1 H); MS *m*/*e* (rel intensity) 312 (M^+, 11), 311 (36), 240 (56), 194 (100), 165 (96); HRMS calcd. for $C_{18}H_{20}N_2O_3$-H: 311.1397; found: 311.1393.

N,N-*Diisopropyl 2′-methyl-4′-nitrobiphenyl-2-carboxamide (**3m**)*: According to method B, 2-bromo-5-nitrotoluene (0.65 g, 3.0 mmol) was coupled with 2-(*N*,*N*-diisopropylcarboxamido)phenylboronic acid (1.05 g, 4.2 mmol) in the presence of $Pd(PPh_3)_4$ (0.139 g, 0. 12 mmol). Normal workup followed by flash chromatography (1:1) afforded 1.00 g (98%) of **3m**: mp 139–141°C (hexane–CH_2Cl_2); IR ($CHC1_3$) 1622, 1516, 1346 cm^{-1}; ^1H NMR δ 0.60–1.20 (m, 9 H), 1.45–1.48 (d, *J* = 6.6 Hz, 3 H), 2.33 (s, 3 H), 3.20–3.90 (2 br, 2 H), 7.23–7.45 (m, 5 H), 8.00–8.05 (dd, *J* = 8.4, 2.2 Hz, 1 H), 8.12–8.13 (d, *J* = 2.2 Hz, 1 H); MS *m*/*e* (rel intensity) 340 (M^+, 10), 297 (26), 240 (27), 194 (36), 165 (100). Anal. calcd. for $C_{20}H_{24}N_2O_3$: C 70.57, H 7.11, N 8.23; found: C 70.60, H 6.82, N 7.99.

N,N-*Diethyl 2′-methyl-5′-nitrobiphenyl-2-carboxamide (**3n**)*: According to method B, 2-bromo-4-nitrotoluene (1.08 g, 5.0 mmol) was coupled with 2-(*N*,*N*-diethylcarboxamido)phenylboronic acid (1.55 g, 7.0 mmol) in the presence of $Pd(PPh_3)_4$ (0.231 g, 0.20 mmol). Normal workup followed by flash chromatography (1:2) afforded 1.55 g (99%) of **3n**: mp 124–125°C (hexane); IR ($CHC1_3$) 1618, 1517, 1348 cm^{-l}; ^1H NMR δ 0.66–0.73 (t, *J* = 7.1 Hz, 3 H), 1.03–1.10 (t, *J* = 7.1 Hz, 3 H), 2.30 (s, 3 H), 2.90–3.70 (2 br, 4 H), 7.22–7.51 (m, 5 H), 7.99 (br, 1 H), 8.07–8.13 (dd, *J* = 8.4, 2.5 Hz, 1 H); MS *m*/*e* (rel intensity) 312 (M^+, 18), 295 (61), 240 (69), 165 (100). Anal. calcd. for $C_{18}H_{20}N_2O_3$: C 69.21, H 6.45, N 8.97; found: C 68.99, H 6.36, N 8.96.

N,N-*Diisopropyl 2′-methyl-5′-nitrobiphenyl-2-carboxamide (**3o**)*: According to method B, 2-bromo-4-nitrotoluene (1.08 g, 5.0 mmol) was coupled with 2-(*N*,*N*-diisopropylcarboxamido)phenylboronic acid (1.74 g, 7.0 mmol) in the presence of $Pd(PPh_3)_4$ (0.231 g, 0.20 mmol). Normal workup followed by flash chromatography (1:1) afforded 1.68 g (99%) of **3o**: mp 143.5–145°C (hexane–CH_2Cl_2); IR ($CHC1_3$) 1624, 1519, 1348 cm^{-1}; ^1H NMR δ 0.96–0.99 (d, *J* = 6.8 Hz, 3 H), 1.12 (br, 6 H), 1.43–1.46 (d, *J* = 6.6 Hz, 3 H), 2.32 (s, 3 H), 3.20–3.40 (br, 1 H), 3.80–4.00 (br, 1 H), 7.26–7.45 (m, 5 H), 7.95 (br, 1 H), 8.08–8.12 (dd, *J* = 8.4, 2.5 Hz, 1 H); MS *m*/*e* (rel intensity) 340 (M^+, 18), 240 (100), 165 (27). Anal. calcd. for $C_{20}H_{24}N_2O_3$: C 70.57, H 7.11, N 8.23; found: C 70.35, H 7.01, N 8.25.

© 2000 NRC Canada

General procedure for the synthesis of 9-phenanthrols (4) (method C)

To a freshly prepared solution of LDA (2.50 mmol) in THF (8 mL) at 0°C was added a solution of 2′-methylbiaryl-2-carboxamide (1.00 mmol) in THF (2 mL). The resulting mixture was stirred at rt for 3–12 h to give a brown or black solution that went colorless upon quenching with a few drops of aqueous NH_4Cl solution. This reaction mixture was acidified (2 M HCl) to pH 5–6 and the whole was evaporated to dryness in vacuo. Normal workup followed by flash chromatography afforded the desired product.

When, due to instability, 9-phenanthrol products required conversion into their acetate derivatives, these were prepared by stirring the 9-phenanthrols in acetic anhydride at rt overnight followed by evaporation to dryness in vacuo, normal workup, and flash chromatography.

*9-Phenanthrol (**4a**)*: According to method C treatment of *N,N*-diethyl 2′-methylbiphenyl-2-carboxamide (1.01 g, 4.1 mmol) with LDA (9.03 mmol) for 3 h followed by acidification, normal workup and flash chromatography (1:1) afforded 0.74 g (92%) of **4a**: mp 151–152°C (PhH) (lit. (41) mp 149–152°C); ^{1}H NMR spectrum was identical with that of authentic material (Aldrich Chem. Co.). Under similar conditions, treatment of the diisopropyl amide **3b,** (0.74 g, 2.5 mmol) with LDA (6.25 mmol) for 3 h followed by acidification, normal workup and flash chromatography (1:1) afforded 0.48 g (98%) of **4a** whose physical and spectroscopic properties were identical with those of the material obtained above.

*8-Methoxy-9-phenanthrol (**4b**)*: According to method C treatment of *N,N*-diethyl 3-methoxy-2′-methylbiphenyl-2-carboxamide (1.49 g, 5.0 mmol) with LDA (12.50 mmol) for 3 h followed by acidification, normal workup and flash chromatography (1:1) afforded 1.03 g (92%) of **4b**: mp 133–134°C (cyclohexane); IR ($CHC1_3$) 3387 cm^{-1}; ^{1}H NMR (DMSO-d_6) δ 4.08 (s, 3 H), 7.05 (s, 1 H), 7.24–7.27 (d, *J* = 7.9 Hz, 1 H), 7.39–7.46 (m, 1 H), 7.49–7.55 (ddd, *J* = 8.0, 7.0, 1.1 Hz, 1 H), 7.60–7.66 (dd, *J* = 8.2, 8.2 Hz, 1 H), 7.71–7.75 (dd, *J* = 8.0, 1.2 Hz, 1 H), 8.43–8.46 (d, *J* = 8.2 Hz, 1 H), 8.61–8.64 (d, *J* = 8.2 Hz, 1 H), 9.60 (s, 1 H); MS *m*/*e* (rel intensity) 224 (M^+, 74), 181 (100), 152 (43). Anal. calcd. for $C_{15}H_{12}O_2$: C 80.34, H 5.39; found: C 80.32, H 5.50.

*6-Methoxy-9-phenanthrol (**4c**)*: According to method C treatment of *N,N*-diethyl 5-methoxy-2′-methylbiphenyl-2-carboxamide (1.81 g, 6.1 mmol) with LDA (15.25 mmol) for 6 h followed by acidification, normal workup and flash chromatography (1:1) afforded 1.21 g (88%) of **4c** which was characterized as its *triflate* **18c** (see below).

*2-Chloro-6-methoxy-9-phenanthrol (**4d**)*: According to method C treatment of *N,N*-diethyl 5-methoxy-2′-methyl- 4′-chlorobiphenyl-2-carboxamide (0.84 g, 2.5 mmol) with LDA (6.30 mmol) for 3 h followed by acidification, normal workup and flash chromatography (1:2) afforded 0.60 g (93%) of **4d**: mp 164–167°C (hexane–CH_2Cl_2); IR ($CHC1_3$) 3333 cm^{-1}; ^{1}H NMR (DMSO-d_6) δ 3.98 (s, 3 H), 6.91 (s, 1 H), 7.25–7.30 (dd, *J* = 9.0, 2.4 Hz, 1 H), 7.35–7.39 (dd, *J* = 8.9, 2.2 Hz, 1 H), 7.80–7.81 (d, *J* = 2.2 Hz, 1 H), 8.11–8.12 (d, *J* = 2.4 Hz, 1 H), 8.15–8.18 (d, *J* = 9.0 Hz, 1 H), 8.67–8.71 (d, *J* = 8.9 Hz, 1 H), 10.46 (s, 1 H); MS m/*e* (rel intensity) 260 (M^+, 35), 258 (M^+, 100), 217 (14), 215 (41), 195 (13) which, due to instability, was converted into its *acetate*: mp 151–152°C (hexane); IR (KBr) 1747 cm^{-1}; ^{1}H NMR δ 2.48 (s, 3 H), 4.01 (s, 3 H), 7.25–7.29 (dd, *J* = 9.0, 2.3 Hz, 1 H), 7.30 (s, 1 H), 7.51–7.55 (dd, *J* = 8.9, 2.0 Hz, 1 H), 7.78–7.79 (d, *J* = 2.0 Hz, 1 H), 7.84–7.88 (d, *J* = 9.0 Hz, 1 H), 7.96–7.97 (d, *J* = 2.3 Hz, 1 H), 8.45–8.49 (d, *J* = 8.9 Hz, 1 H); MS *m*/*e* (rel intensity) 302 (M^+, 5), 300 (M^+, 16), 260 (34), 259 (17), 258 (100), 215 (31), 186 (16), 152 (26). Anal. calcd. for $C_{17}H_{l3}ClO_3$: C 67.90, H 4.36; found: C 67.97, H 4.34.

*2-Chloro-9-phenanthrol (**4e**)*: According to method C treatment of *N,N*-diethyl 2′-methyl-4′-chlorobiphenyl-2-carboxamide (0.60 g, 2.0 mmol) with LDA (5.00 mmol) for 1 h followed by acidification, normal workup and flash chromatography (1:1) afforded 0.44 g (96%) of **4e**: ^{1}H NMR (DMSO-d_6) δ 7.06 (s, 1 H), 7.40–7.44 (dd, *J* = 8.8, 2.3 Hz, 1 H), 7.62–7.75 (m, 2 H), 7.85–7.86 (d, *J* = 2.3 Hz, 1 H), 8.24–8.27 (m, 1 H), 8.66–8.70 (d, *J* = 8.8 Hz, 1 H), 8.73–8.76 (m, 1 H) which, due to instability, was converted into its *triflate* **18d** (see below).

*5-Methoxy-9-phenanthrol (**4f**)*: According to method C treatment of *N,N*-diethyl 6-methoxy-2′-methylbiphenyl-2-carboxamide (0.69 g, 2.3 mmol) with LDA (5.75 mmol) overnight followed by acidification, normal workup and flash chromatography (1:1) afforded 0.47 g (92%) of **4f** which was characterized as its *acetate*: mp 75–77°C (hexane–CH_2Cl_2); IR ($CHC1_3$) 1759 cm^{-1}; ^{1}H NMR δ 2.49 (s, 3 H), 4.14 (s, 3 H), 7.19–7.26 (m, 2 H), 7.54–7.66 (m, 4 H), 7.82–7.85 (m, 1 H), 9.62–9.65 (m, 1 H); MS *m*/*e* (rel intensity) 266 (M^+, 24), 224 (100) and its *triflate* **18e** (see below).

*2-(*N,N-*Diethylcarboxamido)-9-phenanthrol (**4g**)*: According to method C treatment of *N,N*-diethyl 2′-methyl-4′-(*N,N*-diethylcarboxamido)biphenyl-2-carboxamide (1.46 g, 4.0 mmol) with LDA (10.0 mmol) for 3 h followed by acidification, normal workup and flash chromatography (EtOAc) afforded 0.92 g (78%) of **4g**: mp 217–219°C (EtOAc); IR ($CHC1_3$) 1626 cm^{-1}; ^{1}H NMR (DMSO-d_6) δ 1.10–1.20 (br, 6 H), 3.20–3.70 (br, 4 H), 7.13 (s, 1 H), 7.34–7.39 (dd, *J* = 8.5, 1.6 Hz, 1 H), 7.62–7.76 (m, 3 H), 8.23–8.30 (dd, *J* = 8.1, 1.0 Hz, 1 H), 8.68–8.72 (d, *J* = 8.5 Hz, 1 H), 8.76–8.83 (m, 1 H), 10.46 (s, 1 H); MS *m*/*e* (rel intensity) 293 (M^+, 27), 221 (53); HRMS calcd. for $C_{19}H_{19}NO_2$: 293.1417; found: 293.1409.

*3-(*N,N-*Diethylcarboxamido)-9-phenanthrol (**4h**)*: According to method C treatment of *N,N*-diethyl 2′-methyl-5′- (*N,N*-diethylcarboxamido)biphenyl-2-carboxamide (3.11 g, 8.5 mmol) with LDA (21.2 mmol) for 10 min at 0°C resulted in a gray yellow turbid mixture which was quenched with saturated NH_4Cl solution at 0°C. Acidification to pH 5–6, removal of THF in vacuo, and filtration afforded 1.67 g of a **4h** as a colorless solid. Normal workup of the aqueous filtrate followed by flash chromatography (EtOAc) afforded additional product (0.63 g) for a combined yield 2.30 g (92%) of **4h**: mp 255–257°C (MeOH); IR (KBr) 3390, 1623 cm^{-1}; ^{1}H NMR (DMSO-d_6) δ 1.00–1.30 (br, 6 H),

© 2000 NRC Canada

3.20–3.60 (br, 4 H), 7.10 (s, 1 H), 7.43–7.47 (dd, J = 8.2, 1.3 Hz, 1 H), 7.63–7.73 (m, 2 H), 7.76–7.79 (d, J = 8.2 Hz, 1 H), 8.25–8.29 (m, 1 H), 8.59–8.60 (d, J = 1.3 Hz, 1 H), 8.78–8.82 (m, 1 H), 10.49 (s, 1 H); MS *m*/*e* (rel intensity) 293 (M^+, 40), 221 (100), 193 (20), 165 (22); HRMS calcd. for $C_{19}H_{19}NO_2$: 293.1417; found: 293.1412.

Similarly, treatment of *N*,*N*-diisopropyl 2′-methyl-5′-(*N*,*N*-diethylcarboxamido)biphenyl-2-carboxamide (0.40 g, 1.0 mmol) with LDA (2.50 mmol) for 5 min at 0°C afforded 0.276 g (94%) of **4h** whose physical and spectroscopic properties were shown to be identical with those of product obtained above.

N,N-*Diethyl 2-(3′-methylnaphthyl-2′)benzamide (**13**)*: According to method B, 2-bromo-3-methylnaphthalene (1.11 g, 5.0 mmol) was coupled with 2-(*N*,*N*-diethylcarboxamido)-phenylboronic acid (1.44 g, 6.5 mmol) in the presence of $Pd(PPh_3)_4$ (0.231 g, 0.20 mmol). Normal workup followed by flash chromatography (1:1) afforded 1.25 g (79%) of **13**: mp 85.5–87°C (hexane); IR ($CHC1_3$) 1617 cm^{-1}; ^1H NMR δ 0.44–0.51 (t, J = 7.1 Hz, 3 H), 0.7–1.1 (br, 3 H), 2.37 (s, 3 H), 2.60–3.80 (br, 4 H), 7.27–7.46 (m, 6 H), 7.69–7.78 (m, 4 H); MS *m*/*e* (rel intensity) 317 (M^+, 12), 245 (89), 244 (100), 215 (29), 202 (28). Anal. calcd. for $C_{22}H_{23}NO$: C 83.24, H 7.30, N 4.41; found: C 82.94, H 7.33, N 4.27.

*5-Hydroxy-benz[a]anthracene (**14**)*: According to method C treatment of *N*,*N*-diethyl 2-(3′-methylnaphthyl-2′)benzamide (0.461 g, 1.4 mmol) with LDA (3.64 mmol) for 3 h followed by acidification, normal workup and flash chromatography (1:1) afforded 0.32 g (90%) of **14** which was characterized as its acetate: mp 124–127°C (hexane–CH_2Cl_2) (lit. (42) mp 127–128°C); IR ($CHC1_3$) 1758 cm^{-1}; ^1H NMR δ 2.52 (s, 3 H), 7.52–7.77 (m, 5 H), 7.90–7.94 (m, 1 H), 7.99–8.14 (m, 2 H), 8.33 (s, 1 H), 8.84–8.88 (m, 1 H), 9.15 (s, 1 H); MS *m*/*e* (rel intensity) 286 (M^+, 22), 245 (20), 244 (100), 215 (48).

N,N-*Diethyl 2-(2′-methylnaphthyl-1′)benzamide (**16**)*: According to method B, 1-bromo-2-methylnaphthylene (0.88 g, 4.0 mmol) was coupled with 2-(*N*,*N*-diethylcarboxamido)phenylboronic acid (1.24 g, 5.6 mmol) in the presence of $Pd(PPh_3)_4$ (0.185 g, 0.16 mmol). Normal workup followed by flash chromatography (1:1) afforded 0.352 g (25%) of **16**: mp 137–139°C (hexane); IR (KBr) 1619 cm^{-1}; ^1H NMR δ 0.23–0.29 (t, J = 7.1 Hz, 3 H), 0.83–0.88 (t, J = 6.9 Hz, 3 H), 2.30 (s, 3 H), 2.40–3.60 (br, 4 H), 7.27–7.55 (m, 8 H), 7.72–7.80 (m, 2 H); MS *m*/*e* (rel intensity) 318 (M^++1, 49), 316 (M^+–1, 35), 246 (25), 245 (100), 244 (58), 215 (31), 202 (39). Anal. calcd. for $C_{22}H_{23}NO$: C 83.24, H 7.30, N 4.41; found: C 82.95, H 7.25, N 4.41.

General procedure for the synthesis of 9-phenanthrol triflates (18) (method D)

A solution of the 9-phenanthrol (1.0 mmol) at <0°C in Et_2O (10 mL) or THF (5 mL) was treated with *n*-BuLi or LDA (1.10 mmol), the mixture was stirred for 5 min and treated with triflic anhydride (1.1 mmol). The resulting mixture was allowed to warm to rt overnight, treated with a few drops of aqueous NH_4Cl solution and the whole was evaporated to dryness in vacuo. Normal workup followed by flash chromatography afforded the product.

*Phenanthren-9-yl trifluoromethanesulfonate (**18a**)*: According to method D, to a solution of 9-phenanthrol (1.17 g, 6.0 mmol) and *n*-BuLi (4.7 mL of 1.55 M solution, 7.2 mmol) in Et_2O at 0°C was added triflic anhydride (1.21 mL, 2.03 g, 7.2 mmol). Normal workup followed by flash chromatography (1:1) afforded 1.45 g (80%) of **18a**: bp 114–116°C (0.01 mm); IR (neat) 1412, 1211, 1135 cm^{-1}; ^1H NMR δ 7.60–7.79 (m, 5 H), 7.86–7.90 (dd, J = 7.7, 1.4 Hz, 1 H), 8.11–8.16 (m, 1 H), 8.62–8.71 (m, 2 H); MS *m*/*e* (rel intensity) 326 (M^+, 28), 193 (47), 165 (100); HRMS calcd. for $C_{15}H_9F_3O_3S$: 326.0225; found: 326.0227.

*8-Methoxyphenanthren-9-yl trifluoromethanesulfonate (**18b**)*: According to method D, to a solution of 8-methoxy- 9-phenanthrol (0.46 g, 2.1 mmol) and *n*-BuLi (1.65 mL of 1.50 M solution, 2.5 mmol) in Et_2O was added at 0°C triflic anhydride (0.42 mL, 0.70 g, 2.5 mmol). Normal workup followed by flash chromatography (1:2) afforded 0.55 g (75%) of **18b**: mp 149–151°C (hexane); IR (KBr) 1418, 1219, 1142 cm^{-1}; ^1H NMR δ 4.05 (s, 3 H), 7.13–7.16 (d, J = 8.5 Hz, 1 H), 7.56 (s, 1 H), 7.61–7.73 (m, 3 H), 7.84–7.88 (dd, J = 7.3, 1.8 Hz, 1 H), 8.32–8.35 (d, J = 8.5 Hz, 1 H), 8.62–8.65 (d, J = 8.0 Hz, 1 H); MS *m*/*e* (rel intensity), 356 (M^+, 31), 223 (29), 195 (47), 165 (100), 152 (32), 149 (27); HRMS calcd. for $C_{16}H_{11}F_3O_4S$: 356.0330; found: 356.0342.

*6-Methoxyphenanthren-9-yl trifluoromethanesulfonate (**18c**)*: According to method D, to a solution of 6-methoxy-9-phenanthrol (1.21 g, 5.4 mmol) and LDA (6.50 mmol) in THF was added triflic anhydride (1.09 mL, 1.83 g, 6.5 mmol) at 0°C. Normal workup followed by flash chromatography (1:2) afforded 1.26 g (65%) of **18c**: mp 68–70°C (hexane); IR ($CHC1_3$) 1406, 1224, 1135 cm^{-1}; ^1H NMR δ 4.04 (s, 3 H), 7.34–7.39 (dd, J = 9.0, 2.4 Hz, 1 H), 7.59 (s, 1 H), 7.61–7.74 (m, 2 H), 7.86–7.91 (m, 1 H), 8.05–8.09 (m, 2 H), 8.65–8.61 (m, 1 H); MS *m*/*e* (rel intensity) 356 (M^+, 28), 195 (100), 152 (32); HRMS calcd. for $C_{16}H_{11}F_3O_4S$: 356.0330; found: 356.0330.

*2-Chlorophenanthren-9-yl trifluoromethanesultonate (**18d**)*: According to method D, to a solution of 2-chloro-9-phenanthrol (0.457 g, 2.0 mmol) and *n*-Buli (1.63 mL of 1.55 M solution, 2.4 mmol) in THF was added at 0°C triflic anhydride (0.42 mL, 0.712 g, 2.40 mmol). Normal workup followed by flash chromatography (1:1) afforded 0.65 g (90%) of **18d**: mp 119.5–121°C (hexane); IR ($CHC1_3$) 1423, 1229, 1140 cm^{-1}; ^1H NMR δ 7.66–7.86 (m, 4 H), 7.91–7.92 (d, J = 2.2 Hz, 1 H), 8.13–8.19 (m, 1 H), 8.59–8.63 (d, J = 8.0 Hz, 1 H), 8.65–8.75 (dd, J = 8.0, 2.2 Hz, 1 H); MS *m*/*e* (rel intensity) 362 (M^+, 12), 360 (M^+, 32), 229 (17), 227 (47), 201 (34), 199 (100), 163 (26), 149 (29); HRMS calcd. for $C_{15}H_8F_3ClO_3S$: 359.9835; found: 359.9835.

*5-Methoxyphenanthren-9-yl trifluoromethanesulfonate (**18e**)*: According to method D, to a solution of 5-methoxy-9-phenanthrol (0.72 g, 3.2 mmol) and *n*-BuLi (2.36 mL of 1.50 M solution, 3.54 mmol) in THF was added triflic anhydride (0.65 mL, 1.09 g, 3.9 mmol) at –40°C. The resulting solution was warmed to –20°C, quenched with a saturated aqueous NH_4Cl solution, and the reaction mixture was allowed to warm to rt. Normal workup followed by flash chromatography (1:2) afforded 0.82 g (71%) of **18e**: mp

© 2000 NRC Canada

106–107°C (hexane); IR ($CHC1_3$) 1418, 1226, 1138 cm^{-1}; ^1H NMR δ 4.17 (s, 3 H), 7.27–7.30 (d, *J* = 7.9 Hz, 1 H). 7.60–7.83 (m, 5 H), 7.88–7.91 (dd, *J* = 7.6, 1.5 Hz, 1 H), 9.65–9.68 (d, *J* = 8.4 Hz, 1 H); MS *m*/*e* (rel intensity) 356 (M^+, 39), 223 (54), 195 (100), 152 (57); HRMS calcd. for $C_{16}H_{11}F_3O_4S$: 356.0330; found: 356.0342.

*2-(*N,N-*Diethylcarboxamido)phenanthren-9-yl trifluoromethanesulfonate (**18f**)*: To a solution of 2-(*N*,*N*-diethylcarboxamido)-9-phenanthrol (2.44 g, 8.3 mmol) and Et_3N (3.47 mL, 2.52 g, 24.9 mmol) in CH_2Cl_2 (250 mL) was added triflic anhydride (4.19 mL, 7.03 g, 24. mmol) slowly at 0°C. The resulting solution was stirred at rt overnight. Normal workup followed by flash chromatography (1:3) afforded 2.10 g (59%) of **18f**: mp 76–78°C (hexanes); IR (KBr) 1618, 1427, 1223, 1140 cm^{-1}; ^1H NMR δ 1.00–1.50 (br, 6 H), 3.20–3.80 (2 br, 4 H), 7.71–7.86 (m, 4 H), 7.94–7.95 (d, *J* = 1.7 Hz, 1 H), 8.16–8.20 (m, 1 H), 8.69–8.76 (m, 2 H); MS *m*/*e* (rel intensity) 425 (M^+, 14), 353 (30), 292 (66), 221 (31), 220 (36), 164 (36), 69 (100); HRMS calcd. for $C_{20}H_{l8}F_3NO_4S$: 425.0909; found: 425.0900.

*3-(*N,N-*diethylcarboxamido)phenanthren-9-yl trifluoromethanesulfonate (**18g**)*: To a suspension of 3-(*N*,*N*-diethylcarboxamido)-9-phenanthrol (1.47 g, 5.0 mmol) and Et_3N (2.09 mL, 1.52 g, 15.0 mmol) in CH_2Cl_2 (250 mL) at 0°C was added slowly triflic anhydride (2.52 mL, 4.23 g, 15.0 mmol). The resulting mixture was stirred and allowed to warm to rt. Normal workup followed by flash chromatography (1:1) afforded 1.46 g (69%) of **18g**: mp 89–90°C (hexanes); IR (KBr) 1629, 1413, 1215, 1137 cm^{-1}; ^1H NMR δ 1.05–1.48 (br, 6 H), 3.20–3.80 (2 br, 4 H), 7.63–7.68 (dd, *J* = 8.1, 1.5 Hz, 1 H), 7.73–7.86 (m, 3 H), 7.94–7.98 (d, *J* = 8.1 Hz, 1 H), 8.16–8.21 (m, 1 H), 8.71 (s, 1 H), 8.73–8.75 (m, 1 H); MS *m*/*e* (rel intensity) 425 (M^+, 75), 423 (41), 353 (82), 292 (69), 221 (24), 220 (100), 192 (51), 165 (32), 164 (90), 163 (48); HRMS calcd. for $C_{20}H_{l8}F_3NO_4S$: 425.0909; found: 425.0908.

General procedure for the synthesis of phenanthrenes (5) (method E):

*Phenanthrene (**5a**)*: A stirred mixture of phenanthren-9-yl trifluoromethane sulfonate (0.61 g, 2.0 mmol), $Pd(OAc)_2$ (0.018 g, 0.08 mmol), PPh_3 (0.042 g, 0.16 mmol), Et_3N (1.67 mL, 1.21 g, 12.0 mmol) and HCO_2H (0.31 mL of a 97% aqueous solution, 0.37 g, 8.00 mmol) in DMF (10 mL) was heated at 60–70°C overnight. After cooling to rt, the mixture was poured onto crushed ice (~20 mL) and the resulting solution was extracted with EtOAc (3 × 30 mL). The combined organic layer was dried (Na_2SO_4), filtered and concentrated to dryness in vacuo. Preparative TLC (hexane) afforded 0.239 g (67%) of **5a** which was shown to be identical to authentic material (Aldrich Chem. Co) by mp and spectroscopic comparison.

*1-Methoxyphenanthrene (**5b**)*: According to method E, treatment of 8-methoxy-phenanthren-9-yl trifluoromethanesulfonate (0.071 g, 0.20 mmol) with $Pd(OAc)_2$ (0.001 g, 0.004 mmol), PPh_3 (0.002 g, 0.008 mmol), Et_3N (0.084 mL, 0.06 g, 0.60 mmol) and HCO_2H (0.015 mL of a 97% aqueous solution, 0.018 g, 0.40 mmol) in DMF (1.5 mL) followed by flash chromatography (1:5) afforded 0.041 g (97%) of **5b**: mp 105–106°C (hexanes) (lit. (27) mp 105–106°C); ^1H NMR δ 4.03 (s, 3 H), 6.98–7.02 (d, *J* = 7.8 Hz, 1 H), 7.53–7.67 (m, 3 H), 7.72–7.76 (d, *J* = 9.1 Hz, 1 H), 7.87–7.91 (m, 1 H), 8.21–8.29 (m, 2 H), 8.64–8.68 (m, 1 H); MS *m*/*e* (rel intensity) 208 (M^+, 100), 193 (40), 165 (96).

*3-Methoxyphenanthrene (**5c**)*: According to method E, treatment of 6-methoxy-phenanthren-9-yl trifluoromethanesulfonate (0.178 g, 0.50 mmol) with $Pd(OAc)_2$ (0.002 g, 0.01 mmol), PPh_3 (0.005 g, 0.02 mmol), Et_3N (0.21 mL, 0.152 g, 1.50 mmol) and HCO_2H (0.04 mL of a 97% aqueous solution, 0.046 g, 1.0 mmol) in DMF (2 mL) followed by flash chromatography (hexanes) afforded 0.076 g (73%) of **5c**: mp 56–57°C (hexanes) (lit. (43) mp 57°C); ^1H NMR δ 4.03 (s, 3 H), 7.22–7.28 (dd, *J* = 8.7, 2.5 Hz, 1 H), 7.54–7.72 (m, 4 H), 7.79–7.83 (d, *J* = 8.7 Hz, 1 H), 7.85–7.90 (m, 1 H), 8.05–8.06 (d, *J* = 2.5 Hz, 1 H), 8.59–8.64 (m, 1 H); MS *m*/*e* (rel intensity) 208 (M^+, 76), 193 (19), 165 (100).

*2-Chlorophenanthrene (**5d**)*: According to method E, treatment of 2-chloro-phenanthren-9-yl trifluoromethanesulfonate (0.074 g, 0.21 mmol) with $Pd(OAc)_2$ (0.001 g, 0.004 mmol), PPh_3 (0.002 g, 0.008 mmol), Et_3N (0.09 mL, 0.062 g, 0.62 mmol) and HCO_2H (0.02 mL of a 97% aqueous solution, 0.019 g, 0.41 mmol) in DMF (2 mL) followed by preparative TLC (hexanes) afforded 0.030 g (68%) of **5d**: mp 82–83°C (lit. (44) mp 85.5–86°C); ^1H NMR δ 7.46–8.03 (m, 7 H), 8.46–8.87 (m, 2 H).

*4-Methoxyphenanthrene (**5e**)*: According to method E, treatment of 4-methoxy-phenanthren-9-yl trifluoromethanesulfonate (0.178 g, 0.50 mmol) with $Pd(OAc)_2$ (0.002 g, 0.01 mmol), PPh_3 (0.005 g, 0.02 mmol), Et_3N (0.21 mL, 0.152 g, 1.5 mmol) and HCO_2H (0.04 mL of a 97% aqueous solution, 0.046 g, 1.0 mmol) in DMF (2 mL) followed by flash chromatography (1:10) afforded 0.097 g (93%) of **5e**: mp 67–68°C (lit. (27) mp 69°C); ^1H NMR δ 4.14 (s, 3 H), 7.14–7.18 (m, 1 H), 7.50–7.76 (m, 6 H), 7.86–7.90 (dd, *J* = 7.5, 2.0 Hz, 1 H), 9.64- 9.68 (dd, *J* = 8.0, 1.4 Hz, 1 H); MS m/*e* (rel intensity) 208 (M^+, 100), 193 (35), 165 (66).

N,N-*Diethyl phenanthren-2-yl-carboxamide (**5f**)*: According to method E, treatment of 2-(*N*,*N*-diethylcarboxamido)phenanthren-9-yl trifluoromethanesulfonate (1.27 g, 3.0 mmol) with $Pd(OAc)_2$ (0.014 g, 0.06 mmol), PPh_3 (0.032 g, 0.12 mmol), Et_3N (1.25 mL, 0.911 g, 9.00 mmol) and HCO_2H (0.21 mL of a 97% aqueous solution, 0.258 g, 6.00 mmol) in DMF (15 mL) followed by flash chromatography (1:1) afforded 0.747 g (90%) of **5f**: mp 130–131°C (hexane–CH_2Cl_2); IR (KBr) 1613 cm^{-1}; ^1H NMR δ 1.23 (br, 6 H), 3.20–3.80 (2 br, 4 H), 7.58–7.82 (m, 5 H), 7.89–7.93 (m, 2 H), 8.66–8.73 (m, 2 H); MS *m*/*e* (rel intensity) 277 (M^+, 34), 276 (28), 205 (100), 177 (52), 176 (33). Anal. calcd. for $C_{19}H_{19}NO$: C 82.28, H 6.91, N, 5.05; found: C 82.13, H 6.89, N 5.04.

N,N-*Diethyl phenanthren-3-yl-carboxamide (**5g**)*: According to method E, treatment of 3-(*N*,*N*-diethylcarboxamido)phenanthren-9-yl trifluoromethane sulfonate (0.851 g, 2.00 mmol) with $Pd(OAc)_2$ (0.009 g, 0.04 mmol), PPh_3 (0.021 g, 0.08 mmol), Et_3N (0.84 mL, 0.607 g, 6.0 mmol) and HCO_2H (0.15 mL of a 97% aqueous solution, 0. 184 g, 4.00 mmol)

© 2000 NRC Canada

in DMF (10 mL) followed by flash chromatography (1:1) afforded 0.381 g (69%) of **5g**: mp 60–62°C (hexane–PhH); IR (KBr) 1604 cm^{-1}; ^1H NMR δ 1.00–1.50 (2 br, 6 H), 3.20–3.80 (2 br, 4 H), 7.58–7.81 (m, 5 H), 7.89–7.93 (m, 2 H), 8.65–8.70 (m, 2 H); MS *m*/*e* (rel intensity) 277 (M^+, 49), 276 (40), 206 (25), 205 (100), 177 (61), 176 (46), 170 (33), 152 (35); HRMS calcd. for $C_{19}H_{19}NO$: 277.1468; found: 277.1469.

N,N-*Diethyl phenanthren-9-yl*-O-*carbamate (**19**)*: A solution of 9-phenanthrol (1.94 g, 10.0 mmol) and *N*,*N*-diethylcarbamylchloride (1.77 mL, 1.90 g, 14.0 mmol) in pyridine (15 mL) was refluxed overnight, cooled, and poured onto crushed ice. The resulting solution was extracted with CH_2Cl_2 (3 x) and the organic layer was washed sequentially with saturated aqueous $NaHCO_3$ solution (2 x), aqueous HCl (2 x), brine and dried (Na_2SO_4) and filtered. The filtrate was concentrated *in vacuo* to dryness. Flash chromatography (1:2) afforded 2.50 g (85%) of **19**: mp 67–68°C (hexane–CH_2Cl_2); IR ($CHC1_3$) 1707 cm^{-1}; ^1H NMR δ 1.24–1.30 (t, *J* = 7.0 Hz, 3 H), 1.38–1.44 (t, *J* = 7.0 Hz, 3 H), 3.43–3.52 (q, *J* = 7.0 Hz, 2 H), 3.61–3.69 (q, *J* = 7.0 Hz, 2 H), 7.53–7.71 (m, 5 H), 7.82–7.85 (m, 1 H), 7.98–8.02 (m, 1 H), 8.63–8.72 (m, 2 H); MS *m*/*e* (rel intensity) 293 (M^+, 18), 165 (15), 100 (100). Anal. calcd. for $C_{19}H_{19}NO_2$: C 77.79, H 6.53, N 4.78; found: C 77.82, H 6.80, N 4.77.

N,N-*Diethyl 10-trimethylsilylphenanthren-9-yl*-O-*carbamate (**20a**)*: According to method A, to a solution of *t*-BuLi (0.75 mL of 1.60 M solution, 1.20 mmol) and *N*,*N*-diethyl phenanthren-9-yl-O-carbamate (0.29 g, 1.0 mmol) in THF (5 mL) was added TMSCl (0.51 mL, 0.44 g, 4.0 mmol). Normal workup followed by flash chromatography (1:3) afforded 0.32 g (88%) of **20a**: mp 136–137°C (hexane); IR ($CHC1_3$) 1695 cm^{-1}; ^1H NMR (CH_2Cl_2 was used as an internal standard) δ 1.25–1.30 (t, *J* = 7.1 Hz, 3 H), 1.43–1.49 (t, *J* = 7.1 Hz, 3 H), 3.35–4.00 (br, 4 H), 7.55–7.70 (m, 4 H), 7.81–7.85 (m, 1 H), 8.24–8.27 (m, 1 H), 8.67–8.74 (m, 2 H); MS *m*/*e* (rel intensity) 365 (M^+, 3), 350 (12), 250 (13), 165 (17), 100 (100). Anal. calcd. for $C_{22}H_{27}NO_2Si$: C 72.29, H 7.45, N 3.83; found: C 72.65, H 7.50, N 3.85.

N,N-*Diethyl 10-methylphenanthren-9-yl*-O-*carbamate (**20b**)*: According to method A, to a solution of *t*-BuLi **(**0.51 mL of a 1.64 M solution, 0.84 mmol) and *N*,*N*-diethyl phenanthren-9-yl-carbamate (0.21 g, 0.70 mmol) in THF (5 mL) was added iodomethane (0.18 mL, 0.40 g, 2.8 mmol). Normal workup followed by flash chromatography (1:1) afforded 0.198 g (92%) of **20b**: mp 82–84°C (hexane); IR ($CHC1_3$) 1711 cm^{-1}; ^1H NMR δ 1.25–1.30 (t, *J* = 7.1 Hz, 3 H), 1.42–1.48 (t, *J* = 7.1 Hz, 3 H), 2.58 (s, 3 H), 3.44–3.53 (q, *J* = 7.1 Hz, 2 H), 3.66–3.75 (q, *J* = 7.1 Hz, 2 H), 7.59–7.67 (m, 4 H), 7.85–7.89 (m, 1 H), 8.04–8.08 (m, 1 H), 8.65–8.71 (m, 2 H); MS *m*/*e* (rel intensity) 307 (M^+, 10), 178 (9), 100 (100); HRMS calcd. for $C_{20}H_{21}NO_2$: 307.1573; found: 307.1568.

*9-(*N,N-*Diethyl*-O-*carbamato)-phenanthren-10-yl-boronic acid (**20c**)*: To a solution of *N*,*N*-diethyl 10-trimethylsilylphenanthren-9-yl-*O*-carbamate (0.300 g, 0.82 mmol) in CH_2Cl_2 (5 mL) at –78°C was added BBr_3 (1.64 mL of 1.0 M solution in CH_2Cl_2, 1.64 mmol). The resulting mixture was stirred at rt overnight and MeOH (0.07 mL, 0.05 g, 1.64 mmol) was added. Normal workup afforded 0.273 g (99%) of **20c**, which was used without further purification in the cross coupling reaction described below.

*10-(*N,N-*Diethylcarboxamido)-9-phenanthrol (**21**)*: To a solution of *t*-BuLi (0.55 mL of a 1.70 M solution, 0.93 mmol) in THF (3 mL**)** at –78°C was added a solution of *N*,*N*-diethyl phenanthren-9-yl-O-carbamate (0.227 g, 0.77 mmol) in THF (2 mL). The reaction mixture was stirred at –78°C for 1 h and allowed to warm to rt overnight. Acidification (2 M HCl) to pH 5–6 followed by normal workup and flash chromatography (1:2) afforded 0.183 g (81%) **21**: mp 171–172°C (cyclohexane); IR ($CHC1_3$) 1598 cm^{-1}; ^1H NMR (DMSO-d_6) δ 0.82–1.34 (2 br, 6 H), 3.02–3.78 (br, 4 H), 7.48–7.62 (m, 3 H), 7.65–7.77 (m, 2 H), 8.31–8.35 (m, 1 H), 8.74–8.85 (m, 2 H), 9.78 (s, 1 H); MS *m*/*e* (rel intensity) 326 (M^+, 3), 293 (52), 221 (30), 165 (48), 164 (37), 149 (23). Anal. calcd. for $C_{19}H_{19}NO_2$: C 77.82, H 6.80, N 4.77; found: C 77.54, H 6.62, N 4.69.

N,N-*Diethyl 10-(4′-nitrophenyl)phenanthren-9-yl*-O-*carbamate (**23**)*: According to method B, 4-bromonitrobenzene (0.135 g, 0.67 mmol) was coupled with 9-(*N*,*N*-diethyl-*O*-carbamato)phenanthren-10-yl-boronic acid (0.273 g, 0.81 mmol) in the presence of $Pd(PPh_3)_4$ (0.039 g, 0.03 mmol). Normal workup followed by flash chromatography (1:5) afforded 0.219 g (80%) of **23**: mp 176–178°C (cyclohexane); IR ($CHC1_3$) 1713, 1518, 1348 cm^{-1}; ^1H NMR δ 0.95–1.07 (m, 6 H), 3.10–3.40 (br, 4 H), 7.37–7.79 (m, 7 H), 7.93–7.98 (m, 1 H), 8.34–8.39 (m, 2 H), 8.74–8.79 (d, *J* = 8.7 Hz, 2 H); MS *m*/*e* (rel intensity) 415 (25), 414 (M^+, 28), 315 (23), 268 (30), 239 (54), 100 (100); HRMS calcd. for $C_{25}H_{22}N_2O_4$: 414.1581; found: 414.1577.

N,N-*Diethyl phenanthren-4-yl*-O-*carbamate (**24**)*: To a solution of 4-methoxyphenanthrene (2.47 g, 11.8 mmol) in CH_2Cl_2 (60 mL) at –78°C was added BBr_3 (2.24 mL, 5.93 g, 23.7 mmol). The resulting mixture was stirred and allowed to warm to rt overnight. Normal workup followed by flash chromatography (1:6) afforded 2.08 g (91%) of 4-phenanthrol: mp 111–113°C (hexane) (lit. (45) mp 113–115°C); IR (KBr) 3514 cm^{-1}; ^1H NMR δ 5.71 (s, 1 H), 6.94–6.98 (dd, *J* = 7.5, 1.3 Hz, 1 H), 7.37–7.74 (m, 6 H), 7.85–7.89 (dd, *J* = 7.5, 1.9 Hz, 1 H), 9.61–9.65 (m, 1 H). A solution of the 4-phenanthrol (1.63 g, 8.4 mmol) in MeCN (50 mL) was treated with K_2CO_3 (1.62 g, 11.7 mmol) and *N*,*N*-diethylcarbamylchloride (1.49 mL, 1.59 g, 11.7 mmol) and the resulting mixture was refluxed overnight, cooled, and subjected to filtration. The filtrate was evaporated to dryness in vacuo. Normal workup followed by flash chromatography (1:5) afforded 2.39 g (97%) of **24**: mp 113–115°C (hexane); IR (KBr) 1705 cm^{-1}; ^1H NMR δ 1.23–1.29 (t, *J* = 7.1 Hz, 3 H), 1.41–1.47 (t, *J* = 7.1 Hz, 3 H), 3.43–3.52 (q, *J* = 7.1 Hz, 2 H), 3.71–3.80 (q, *J* = 7.1 Hz, 2 H), 7.31–7.34 (dd, *J* = 7.7, 1.3 Hz, 1 H), 7.53–7.61 (m, 3 H), 7.68–7.78 (m, 3 H), 7.84–7.91 (m, 1 H), 9.00–9.06 (m, 1 H); MS *m*/*e* (rel intensity) 293 (M^+, 12), 165 (13), 100 (100). Anal. calcd. for $C_{19}H_{19}NO_2$: C 77.79, H 6.53, N 4.78; found: C 77.77, H 6.53, N 4.69.

© 2000 NRC Canada

*3-(*N,N-*Diethylcarboxamido)-4-phenanthrol (**25**)*: To a yellow stirred solution of *s*-BuLi (4.01 mL of 1.15 M solution, 4.6 mmol) and TMEDA (0.70 mL, 0.54 g, 4.6 mmol) in THF (20 mL) at –78°C was added a solution of *N*,*N*-diethyl phenanthren-4-yl-*O*-carbamate (1.23 g, 4.2 mmol) in THF (5 mL). The resulting brown solution was allowed to warm to rt overnight. Normal workup followed by flash chromatography (1:1) afforded 1.22 g (99%) of **25**: oil; IR (neat) 3130 (br), 1589 cm^{-1}; ^1H NMR δ 1.30–1.36 (t, *J* = 7.1 Hz, 6 H), 3.55–3.64 (q, *J* = 7.1 Hz, 4 H), 7.33–7.37 (d, *J* = 8.3 Hz, 1 H), 7.44–7.48 (d, *J* = 8.3 Hz, 1 H), 7.56–7.72 (m, 3 H), 7.78–7.82 (d, *J* = 8.8 Hz, 1 H), 7.86–7.90 (dd, *J* = 7.7, 1.6 Hz, 1 H), 9.10 (br, 1 H), 9.81–9.84 (d, *J* = 8.7 Hz, 1 H); MS *m*/*e* (rel intensity) 293 (M^+, 59), 221 (26), 220 (100), 165 (20); HRMS calcd. for $C_{19}H_{19}NO_2$: 293.1417; found: 293.1433.

*1-Methoxy-9,10-phenanthraquinone (**26a**):* A solution of 8-methoxy-9-phenanthrol (0.173 g, 0.77 mmol) and salcomine (0.025 g, 0.077 mmol) in DMF (5 mL) at rt was subjected to a stream of O_2 via a bubbler for 4 h. The mixture was diluted with water (5 mL) and the resulting solution was extracted with EtOAc (3×). The organic layer was dried (Na_2SO_4), subjected to filtration and the filtrate was concentrated to dryness in vacuo. The resulting residue was recrystallized to afford 0.182 g (99%) of **26a**: mp 181–183°C (EtOAc); IR (KBr) 1688, 1670 cm^{-l}; ^1H NMR (DMSO-d_6) δ 3.90 (s, 3 H), 7.22–7.26 (d, *J* = 8.5 Hz, 1 H), 7.49–7.57 (ddd, *J* = 7.6, 7.5, 1.0 Hz, 1 H), 7.70–7.82 (m, 2 H), 7.86–7.90 (d, *J* = 7.9 Hz, 1 H), 7.94–7.99 (dd, *J* = 7.6, 1.5 Hz, 1 H), 8.26–8.30 (d, *J* = 8.2 Hz, 1 H); MS *m*/*e* (rel intensity) 238 (M^+, 42), 210 (46), 181 (100), 180 (30), 152 (54), 151 (25). Anal. calcd. for $C_{15}H_{10}O_3$: C 75.62, H 4.23; found: C 75.66, H 4.30.

*4-Methoxy-9,10-phenanthraquinone (**26b**)*: Following the above procedure, treatment of 5-methoxy-9-phenanthrol (0.276 g, 1.23 mmol) with O_2 in the presence of salcomine (0.04 g, 0.123 mmol) afforded 0.289 g (99%) of **26b**: mp 196–197°C (EtOAc); IR (KBr) 1689, 1661 cm^{-1}; ^1H NMR (DMSO-d_6) δ 4.01 (s, 3 H), 7.44–7.58 (m, 3 H), 7.67–7.78 (m, 2 H), 8.00–8.05 (dd, *J* = 7.7, 1.6 Hz, 1 H), 8.87–8.91 (d, *J* = 8.3 Hz, 1 H); MS *m*/*e* (rel intensity) 238 (M+, 25), 210 (79), 195 (23), 167 (28), 139 (100). Anal. calcd. for $C_{15}H_{10}O_3$: C 75.62, H 4.23; found: C 75.48, H 4.27.

*1-Methoxy-9-fluorenone (**28a**)*: A suspension of 1-methoxy-9,10-phenanthraquinone (0.165 g, 0.69 mmol) in aqueous KOH (2 M, 10 mL**)** was heated at 90°C for 1 h, cooled, and treated with conc. H_2SO_4 to pH 5–6. Normal workup gave a crude solid which was treated with $Pb(OAc)_4$ (0.841 g, 2.19 mmol) in benzene (10 mL) and the resulting mixture was stirred at rt overnight. The reaction mixture was diluted with water (10 mL), and subjected to filtration. Normal workup and flash chromatography (1:10) afforded 0.140 g (96%) of **28a**: mp 140–142°C (EtOAc) (lit. (46) mp 140–141°C); IR (nujol) 1699 cm^{-1}; ^1H NMR δ 3.98 (s, 3 H), 6.81–6.86 (d, *J* = 8.5 Hz, 1 H), 7.11–7.14 (d, *J* = 7.4 Hz, 1 H), 7.25–7.32 (ddd, *J* = 7.2, 7.2, 1.6 Hz, 1 H), 7.41–7.51 (m, 3 H), 7.63- 7.66 (dd, *J* = 7.2, 0.7 Hz); MS *m*/*e* (rel intensity) 210 (M^+, 86), 181 (100), 153 (20), 152 (44), 151 (24).

*4-Methoxy-9-fluorenone (**28b**)*: Following the above procedure, 4-methoxy-9,10-phenanthraquinone (0.098 g, 0.41 mmol) was sequentially treated with aqueous KOH (2 M, 10 mL) and $Pb(OAc)_4$ (0.549 g, 1.24 mmol) in benzene to furnish 0.086 g (99%) of **28b**: mp 114–115°C (EtOAc) (lit. (46) mp 114.5–115.5°C); IR (KBr) 1708 cm^{-1}; ^1H NMR δ 3.98 (s, 3 H), 7.03–7.06 (dd, *J* = 7.4, 1.7 Hz, 1 H), 7.19–7.31 (m, 3 H), 7.41–7.48 (ddd, *J* = 7.5, 7.5, 1.2 Hz, 1 H), 7.61–7.64 (d, *J* = 7.3 Hz, 1 H), 7.80–7.83 (d, *J* = 7.5 Hz, 1 H); MS *m*/*e* (rel intensity) 210 (M^+, 100), 195 (21),167 (20),139 (55).

Acknowledgements

We are grateful to NSERC Canada and the Ontario Ministry of the Environment for financial support of this work. We are grateful to Dr. Juerg Faessler for his meticulous help in the preparation of this manuscript.

References

1. (*a*) V. Snieckus. NATO ASI Ser. Ser. E, 320 (Chemical Synthesis), 191 (1996); (*b*) V. Snieckus. Chem. Rev. **90**, 847 (1990); (*c*) H.W. Gschwend and H.R. Rodriguez. Org. React. (N.Y.) **26**, 1 (1979).
2. (*a*) R.J. Mills. Ph.D. thesis. University of Waterloo. 1985; (*b*) K. Puumala. M.Sc. thesis. University of Waterloo. 1997. For other naphthalene metalation work, see: (*c*) J. Clayden. Synlett, 810 (1998); (*d*) R.D. Bindal and J.A. Katzenellenbogen. J. Org. Chem. **52**, 3182 (1987); (*e*) C.-W. Chen and P. Beak. J. Org. Chem. **51**, 3325 (1986).
3. M. Iwao, K.K. Mahalanabis, M. Watanabe, S.O. de Silva, and V. Snieckus. Tetrahedron, **39**, 1955 (1983).
4. (*a*) N. Miyaura and A. Suzuki. Chem. Rev. **95**, 2457 (1995); (*b*) C. James. Ph. D. thesis. University of Waterloo. 1998; (*c*) A. Suzuki. *In* Metal-catalyzed cross-coupling reactions. *Edited by* F. Diederich and P.J. Stang. Wiley-VCH, Weinheim. 1998, p. 49.
5. M.J. Sharp and V. Snieckus. Tetrahedron Lett. **26**, 5997 (1985).
6. (*a*) P. Beak and A.I. Meyers. Acc. Chem. Res. **19**, 356 (1986); (*b*) G.W. Klumpp. Recl. Trav. Chim. Pays-Bas, **105**, 1 (1986).
7. J.-m. Fu, B.-p. Zhao, M.J. Sharp, and V. Snieckus. J. Org. Chem. **56**, 1683 (1991).
8. For a preliminary communication, see J.-m. Fu, M.J. Sharp, and V. Snieckus. Tetrahedron Lett. **43**, 5459 (1988). For a similar approach for phenanthrene synthesis, see C.B. de Koning, J.P. Michael, and A.L. Rousseau. Tetrahedron Lett. **53**, 8725 (1998). For a McMurry condensation approach, see A.E. Gies and M. Pfeffer. J. Org. Chem. **64**, 3650 (1999).
9. (*a*) K. Naoji. Kagaku to Kogyo (Osaka), **60**, 274 (1986); Chem. Abs. **106**, 86571 (1987); (*b*) M. Sainsbury. *In* Rodd's chemistry of carbon compounds. Elsevier, Amsterdam. 1979. Vol III, Part H, p. 1.
10. R.G. Harvey (*Editor*). Polycyclic aromatic hydrocarbons, chemistry and carcinogenicity. Cambridge University Press, Cambridge. 1991.
11. (*a*) A.A. De'la Cruz, D.H. Miles, and K.D. Chapatwala. Life Sci. **30**, 1805 (1982); (*b*) K.D. Chapatwala, A.A. De'la Cruz, and D.H. Miles. Life Sci. **29**, 1977 (1981); (*c*) C. Luis and T. Gabriel. The Alkaloids, **39**, 99 (1990).
12. A.J. Floyd, S.F. Dyke, and S.E. Ward. Chem. Rev. **76**, 509 (1976).
13. C.K. Bradsher. Chem. Rev. **87**, 1277 (1987).

© 2000 NRC Canada

14. L.R.C. Barclay. *In* Friedel-crafts and related reactions. *Edited by* G.A. Olah. Interscience, New York. 1964. Vol. 2, Part 2, p. 785.
15. For the Pschorr reaction, see (*a*) P. Hanson, P.W. Lovenich, S.C. Rowell, P.H. Walton, and A.W. Timms. J. Chem. Soc. Perkin Trans. 2, 49 (1999); (*b*) D.F. DeTar. Org. React. **9**, 409 (1957); for photocyclization, see (*c*) F.B. Mallory, and C.W. Mallory. Org. React. **30**, 1 (1984); for recent work, see F.B. Mallory, M.J. Rudolph, and S.M. Oh. J. Org. Chem. **54**, 4619 (1989), and N.J. Lawrence, F.A. Ghani, L.A. Hepworth, J.A. Hadfield, A.T. McGown, and R.G. Pritchard. Synthesis, 1656 (1999); for Pd-catalyzed intramolecular reaction, see (*d*) A. de Meijere, Z.Z. Song, A. Lansky, S. Hyuda, K. Rauch, M. Noltemeyer, B. Konig, and B. Knieriem. Eur. J. Org. Chem. 2289 (1998).
16. (*a*) K.-y. Jung and M. Koreeda. J. Org. Chem. **54**, 5667 (1989); (*b*) H.L. Holmes. Org. React. **4**, 60 (1948).
17. (*a*) N. Miyaura, T. Yanagi, and A. Suzuki. Synth. Commun. **11**, 513 (1981); (*b*) S. Gronowitz, V. Bobosik, and K. Lawitz. Chem. Scr. **23**, 120 (1984); (*c*) B.I. Alo, A. Kandil, P.A. Patil, M.J. Sharp, M.A. Siddiqui, and V. Snieckus. J. Org. Chem. **56**, 3763 (1991).
18. R.R. Fraser and T.S. Mansour. J. Org. Chem. **49**, 3442 (1984).
19. A. Streitwieser, Jr. and F. Guibe. J. Am. Chem. Soc. **100**, 4532 (1978).
20. G. Bartoli, E. Marcantoni, M. Bosco, and R. Dalpozzo. Tetrahedron Lett. **29**, 2251 (1988).
21. (*a*) C.S.V. Houge-Frydrych, W.B. Motherwell, and D.M. O'Shea. J. Chem. Soc. Chem. Commun. 1819 (1987); (*b*) G.R. Newkome and D.C. Hager. J. Org. Chem. **47**, 599 (1982).
22. (*a*) A. Reissert. Ber. **30**, 1030 (1897); (*b*) W.E. Noland and F.J. Baude. Org. Syn. Coll. **5**, 567 (1973).
23. H.B. Buergi, J.D. Dunitz, and E. Shefter. J. Am. Chem. Soc. **95**, 5065 (1973).
24. (*a*) G.A. Peterson, F.-A. Kunng, J.S. McCallum, and W.D. Wulff. Tetrahedron Lett. **28**, 1381 (1987); (*b*) Q.Y. Chen, Y.B. He, and Z.Y. Yang. J. Chem. Soc. Chem. Commun. 1452 (1986); (*c*) S. Cacchi, P.G. Ciattini, E. Morere, and G. Ortar. Tetrahedron Lett. **27**, 5541 (1986).
25. For a recent dehydroxylation using similar method, see B.H. Lipshutz, D.J. Buzard, and R.W. Vivian. Tetrahedron Lett. **40**, 6871 (1999).
26. W.D. Wulff, J.S. McCallum, and F.-A. Kunng. J. Am. Chem. Soc. **110**, 7419 (1988).
27. S.M. Abdel-Wahhab, L.S. El-Assal, N. Ramses, and A.H. Shehab. J. Chem. Soc. C, 863 (1968).
28. M.P. Sibi and V. Snieckus. J. Org. Chem. **48**, 1935 (1983).
29. D. Kauffmann. Chem. Ber. **120**, 901 (1987).
30. M. Yao and X. Wang. Huaxue Shiji, **14**, 367 (1992); Chem. Abs. **118**, 191255 (1993).
31. K. Auwers and V. Meyer. Chem. Ber. **22**, 1985 (1889).
32. For DreM approaches to fluorenones, including natural products and environmental pollutants, see (*a*) J.-M. Fu, B.-P. Zhao, M.J. Sharp, and V. Snieckus. Can. J. Chem. **72**, 227 (1994); (*b*) W. Wang, and V. Snieckus. J. Org. Chem. **57**, 424 (1992); (*c*) T. Iihama, J.-M. Fu, M. Bourguignon, and V. Snieckus. Synthesis, 184 (1989).
33. T. Kamikawa, and K. Isao. Synthesis, 431 (1986).
34. G.M. Rubottom. *In* Oxidation in organic chemistry. *Edited by* W.S. Trahanovsky. Academic, New York. 1982. Part D, pp. 1–145.
35. D.D. Perrin, W.L. Armarego, and D.R. Perrin. Purification of laboratory chemicals. 2nd ed. Pergamon Press, Oxford. 1980.
36. K.F. Podraza and R.L. Bassfield. J. Org. Chem. **53**, 2643 (1988).
37. R.F. Heck. Palladium reagents in organic synthesis. Academic, New York. 1985.
38. E.T. McCabe, W.F. Barthel, S.I. Gertler, and S.A. Hall. J. Org. Chem. **19**, 493 (1954).
39. G. Pagani, G. Caccialanza, and P. Borgna. Farmaco, Ed. Sc. **28**, 835 (1973).
40. M.J. Sharp. M.Sc. thesis. University of Waterloo. 1986.
41. I.M. Hunsberger, R. Ketcham, and H.S. Gutowsky. J. Am. Chem. Soc. **74**, 4839 (1952).
42. R.G. Harvey, S.H. Goh, and C. Cortez. J. Am. Chem. Soc. **97**, 3468 (1975).
43. C. Brown, B.J. Sikkel, C.F. Carvalho, and M.V. Sargent. J. Chem. Soc. Perkin Trans. 1, 3007 (1982).
44. W.E. Bechmann and C.H. Boatner. J. Am. Chem. Soc. **58**, 2194 (1936).
45. E. Mosettig and H.M. Durall. J. Am. Chem. Soc. **59**, 367 (1937).
46. R. Huisgen and H. Rist. Ann. **594**, 137 (1955).

© 2000 NRC Canada

Heck reaction using palladium complexed to dendrimers on silica

Howard Alper, Prabhat Arya, S. Christine Bourque, Gary. R. Jefferson, and Leo E. Manzer

Abstract: Polyamidoamine dendrimers, constructed on the surface of silica, were phosphonated using diphenylphosphinomethanol (prepared in situ) and complexed to form a palladium–dimethyl TMEDA complex. This catalyst was found to be effective in the Heck reaction of aryl bromides with both butyl acrylate and styrene, affording coupling products in moderate to good yields. The heterogeneous palladium catalyst can also be recycled and reused with only moderate reduction in activity.

Key words: dendrimer, Heck, palladium, silica.

Résumé : Utilisant du diphénylphosphinométhanol (préparé in situ), on a réalisé la phosphonation de dendrimères de polyamidoamines synthétisés sur une surface de silice et en a fait un complexe de palladium–« TMEDA » de diméthyle. On a trouvé que ce catalyseur est efficace dans la réaction de Heck des bromures d'aryles avec aussi bien l'acrylate de butyle que le styrène et que ces réactions fournissent des produits de couplage avec des rendements allant de modérés à bons. On peut aussi régénérer le catalyseur hétérogène et le réutiliser avec une perte mineure d'activité.

Mots clés : dendrimère, Heck, palladium, silce.

[Traduit par la Rédaction]

Introduction

The demand for cleaner, environmentally friendly chemistry is coming from many quarters. Legislative, public, and corporate pressure has led to the rapid development of new innovations in green technology. While the majority of new chemical processes developed in the last 50 years are catalytic, there are still problems associated with catalyst recovery, both in terms of reusing the catalyst or at least recovery of the precious metals often used, with the added advantage of easier purification of products.

Over the past 20 years the Heck reaction, used in the coupling of aryl halides with vinylic substrates, has been shown to be a versatile tool which allows easy access to often complex products from relatively simple substrates (1). Despite the practical ease of reaction and the reliably good yields, the Heck reaction has not developed past a laboratory method, bar a few examples (2).

The lack of transfer to an industrial scale is primarily due to the expense of the palladium catalyst, as high loadings of palladium (e.g., 10 mol%) (3) and, as with homogeneously catalyzed systems, costly removal of the catalyst residues are required. Only when the reaction products are of high commercial value (e.g., pharmaceutical products) can this catalytic system be used viably because the cost of the catalyst is appreciably a smaller percentage of the final product than in the bulk chemical case. Hence in the large scale synthesis of bulk chemicals, the Heck reaction has made little impact.

Over approximately the last 10 years, in an attempt to extend the Heck reaction to the bulk chemical sector, several groups have worked on developing heterogeneous catalytic systems (4). Such systems could, in principle, reduce the cost and technical problems associated with removal of the catalyst and also increase the lifetime of the palladium catalyst. The use of lower concentrations of palladium might also be a consequence of heterogenizing the catalyst. Many groups have attacked this problem and have made considerable headway in some cases. Of particular note is the work of Ying et al. (5), who have developed a palladium [0] complex on silica which shows very high turnover rates especially for activated bromoarene systems. However it should be noted that the catalyst preparation requires specialized techniques.

Most of the other examples in the literature utilize iodoarenes (6), the most reactive of the haloarene family in the Heck reaction, but unfortunately the most expensive and

Received July 7, 1999. Published on the NRC Research Press website on June 14, 2000.

Dedicated to Steve Hanessian – a trailblazer in research; a first class supervisor of some of our leaders of tomorrow; a genuine friend.

H. Alper,[1] S.C. Bourque, and G.R. Jefferson. Department of Chemistry, University of Ottawa, 10 Marie Curie, Ottawa, ON K1N 6N5, Canada.
P. Arya. Steacie Institute for Molecular Sciences, National Research Council Canada, 100 Sussex Dr. Ottawa, ON K1A 0R6, Canada.
L.E. Manzer. DuPont Central Research & Development, Experimental Station, Wilmington, DE 19880–0262, U.S.A.

[1]Author to whom correspondence may be addressed. Telephone: (613) 562-5189. Fax: (613) 562-5871. e-mail: halper@science.uottawa.ca

© 2000 NRC Canada

also generally less readily available than its bromo and chloro counterparts. One of the main goals of the Heck reaction in both a heterogeneous and homogenous sense is to utilize the cheaper bromo- and chloroarenes.

Polymer supported metal complexes have attracted considerable interest over the last few years. Terasawa et al. (7) have studied the Heck reaction of styrene with iodobenzene comparing a variety of heterogeneous catalysts. A phosphinated polystyrene complex was compared to palladium with the analogous free palladium complex, palladium salts, Pd/C in terms of catalytic activity and selectivity, and it was found that the polymer supported palladium complex is highly active but noticeable deactivation was observed during repeated use. Zhang et al. reported a polymer supported phenanthroline palladium catalyzed arylation of acrylamide (8); however, when tributylamine was used the catalyst activity declined significantly on recycling, and preparation of the catalyst is complicated. Although there have been several advances in the Heck reaction in terms of increased turnovers and catalyst stability for both heterogeneous and homogenous systems, the catalyst lifetimes and turnovers still preclude industrial use.

We recently developed a dendritic silica supported bidentate phosphine ligand (9). It was postulated that this ligand could be utilized in the Heck reaction with a suitable palladium catalyst. The dendritic support is thought to work with many facets, one of which is to give the reaction a degree of homogenous character, as the dendritic support would be highly solvated in a suitable solvent system. It is also speculated that the ligand increases the stability of the catalytic system.

In recent years, major efforts have been directed toward the development of new catalytic systems that effectively combine the advantages of both heterogeneous and homogeneous catalysis (10). Such a catalyst would ideally be easily recoverable and potentially recyclable while maintaining high catalytic efficiency. Dendrimer–metal complexes are particularly attractive in this regard.

Dendrimers are highly branched macromolecules, which are capable of having multiple sites for metal coordination (11). In 1994, van Koten and coworkers demonstrated that soluble polycarbosilane dendrimer complexes of nickel (II) catalyze the addition of polyhaloalkenes to double bonds (12). Three years later, Reetz and coworkers synthesized a polyaminodiphosphine dendrimer to coordinate to rhodium and palladium catalysts (13). Our research has led to the development of heterogeneous polyaminoamidodiphosphonated dendrimers built on a silica gel core support (PPh_2–PAMAM–SiO_2). This article describes the use of these dendrimers, when complexed to palladium, as effective catalysts for the Heck reaction.

Results and discussion

(*a*) Preparation of PAMAM–SiO_2 dendrimers

Commercial aminopropyl silica gel was used to prepare generation 0–4 polyaminoamido (PAMAM) dendrimers (9). Propagation of the dendrimers was achieved by standard dendrimer building methods pioneered by Tomalia and coworkers (14). Amino propionate esters were obtained by Michael type addition of the preexisting amino group to methyl acrylate. Amidation of the ester units with ethylenediamine completes the generation, with repetition of the two steps affording the desired generation of the dendrimer.

Scheme 1.

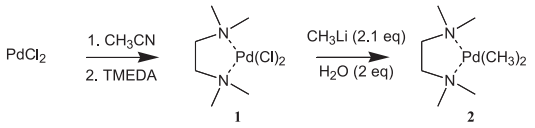


Table 1. Palladium content of the various PPh_2–PAMAM–SiO_2 dendrimers.

Generation	Percentage palladium (%)[a]	g Pd/g Si	mμ mol Pd/25 mg SiO_2
G-0	2.93	0.0293	6.91
G-1	1.34	0.0134	3.16
G-2	1.13	0.0113	2.66

[a]Determined by ICP analysis

Coordination of the dendrimers to palladium was effected first by phosphonation. Diphenylphosphinomethanol, prepared in situ from paraformaldehyde and diphenylphosphine, was excellent for the double phosphinomethylation of each terminal amine group.

The complex **2** is easily synthesized starting from palladium chloride, in situ formation of the bis(acetonitrile)palladium dichloride (15), followed by displacement of the acetonitrile ligands with TMEDA forming complex **1**. Reaction of complex **1** with methyl lithium gives complex **2** in 65% overall yield (Scheme 1).

The palladium complex is coordinated to the dendrimer on silica by simply stirring the dendrimer in degassed benzene with one equivalent of palladium complex **2**, relative to the theoretical number of end phosphine groups for the respective dendrimer. The dendrimer complexes are easily isolated by microporous membrane filtration. The resulting complexed dendrimers (see Fig. 1) were characterized by ^{31}P solid state NMR (complexed δ = 6 ppm, uncomplexed δ = –27 ppm) (13*a*).

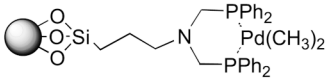
The palladium complexed PPh_2–PAMAM–SiO_2 dendrimers were digested with hydrofluoric acid or aqua regia (nitrohydrochloric acid) by microwave heating and analyzed for Pd content by ICP analysis. The palladium content of the various generations is summarized in Table 1. The degree of complexation decreases significantly with dendrimer generation from G-0 to G-2, and was so low for G-3 and G-4 as to preclude further studies with the latter generations of dendrimers. This is believed to be due to incomplete phosphonation reactions arising from steric crowding and ultimately resulting in the threshold of dendrimer growth being reached.

(*b*) Catalytic heck reaction of aryl bromides using palladium complexed silica supported dendrimers

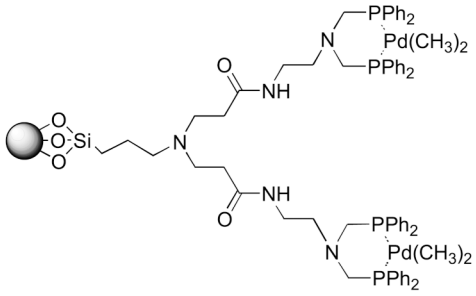
As a model reaction for assessing the utility of these Heck catalysts, the reaction of bromobenzene with styrene in DMF at 120°C was investigated in the presence of sodium acetate as base, primarily because these were the conditions

© 2000 NRC Canada

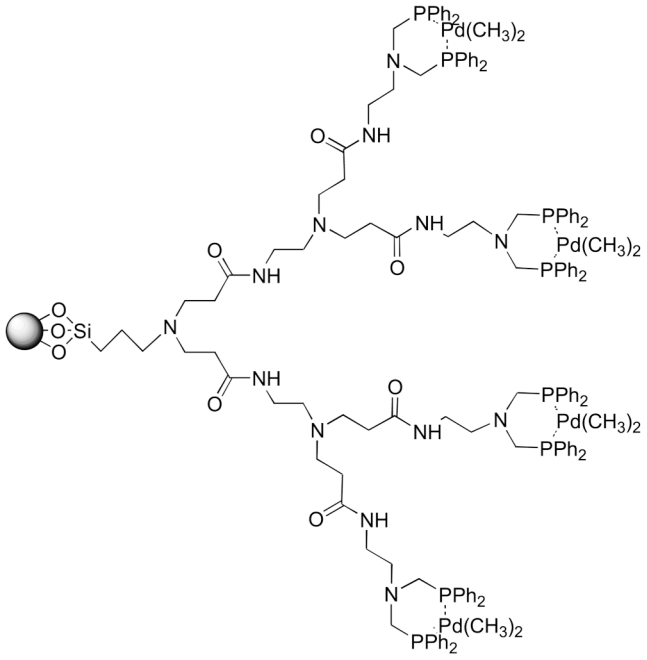
Fig. 1. Dendrimer generations $(CH_3)_2Pd\text{-}PPh_2$–PAMAM–SiO_2.



G-0 $Pd(CH_3)_2$

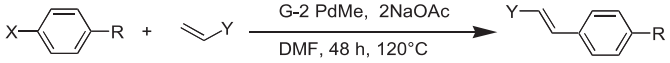


G-1 $Pd(CH_3)_2$



G-2 $Pd(CH_3)_2$

employed by Reetz and co-workers for their dendritic Heck system. The catalytic activity of the palladium complexed PPh_2–PAMAM–SiO_2 dendrimers was investigated with re-



gards to the Heck reaction (Reaction [1]) and the results are summarized in Table 2. Treatment of styrene and bromobenzene in dimethylformamide, with Pd complexed PPh_2–PAMAM–SiO_2 dendrimer, and sodium acetate affords *trans* stilbene in good yield and regioselectivity for generations 0, 1, and 2. The yields of stilbene was significantly less when generation 3 and 4 dendrimer complexes are used as catalysts.

The best turnovers in terms of molecules of *trans*-stilbene formed per mol of palladium was achieved with the generation 2 catalyst, as may be expected as this catalyst would have the greatest homogenousity factor (Table 3).

The effect of temperature on the Heck reaction was studied with the generation 2 catalyst and it was found that the best yields were obtained when the temperature was in the 110 to 140°C range (Table 4). At lower temperatures the yields were low due to either poor conversion of the catalyst precursor to the catalyst via reductive elimination of the methyls, or just a factor of low turnovers at low temperatures. At temperatures above 140°C the yield was reduced by catalyst deactivation with noticeable palladium black formation.

The effect of the base on the reaction was studied in terms of yield and recoverability of the catalyst (Table 5). The inorganic bases; potassium carbonate and sodium acetate were used as well as the organic base, triethylamine. Potassium carbonate and sodium acetate gave the best yields, and low product yield was found using triethylamine (13*a*). This triethylamine effect was also observed by Reetz and coworkers using their dendritic Heck catalyst system.

As some loss in activity of the catalyst was noticed we examined the possibility of leaching of the catalyst into the reaction mixture. The reaction was carried out with styrene and bromobenzene using the G-2 catalyst, and after 16 h, the reaction was filtered under nitrogen. A further 2 mmol of

Table 2. Conversions in the Heck reaction of styrene and bromobenzene using the Pd–PPh_2–PAMAM–SiO_2 catalysts.[a]

Time	G-0	G-1	G-2
6 h	67%[b]	10%	17%
24 h	76%	37%	49%
48 h	79%	47%	59%

[a]6.0 mmol each of styrene and bromobenzene, 6.6 mmol of NaOAc, and 50 mL of DMF.

[b]Yields determined by GC and NMR analysis.

Table 3. Turnovers for generations 0, 1, and 2 of the Pd–PPh_2–PAMAM–SiO_2 dendrimers.[a]

Dendrimer generation	Turnovers (h after 6 h)	Turnovers (h after 24 h)
0	72	21
1	31	30
2	81	58

[a]6.0 mmol each of styrene and bromobenzene, 6.6 mmol of NaOAc, 50 mL of DMF.

© 2000 NRC Canada

Table 4. Conversions in the Heck reaction of styrene and bromobenzene using the Pd–PPh_2–G2–PAMAM–SiO_2 dendrimer at different temperatures.[a]

Temperature (°C)	25	50	80	110	140	170
Yield[b] (%)	NR	NR	5	69	44	NR

[a]2.0 mmol each of styrene and bromobenzene, 2.2 mmol of NaOAc, and 50 mL of DMF.

[b]NR = No reaction, Yields were determined by NMR analysis.

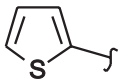
Table 5. Conversions in the Heck reaction of styrene and bromobenzene using the Pd–PPh_2–G2–PAMAM–SiO_2 dendrimer with different bases.[a]

Base	Cycle 1 (%)	Cycle 2 (%)
K_2CO_3	53[b]	43
NEt_3	5	—
NaOAc	39–69	20–45

[a]2.0 mmol each of styrene and bromobenzene, 2.2 mmol of NaOAc, 50 mL of DMF.

[b]Yields were determined by NMR analysis.

Table 6. Catalytic activity of the G-2 complex catalyst for the reaction of a variety of haloarenes with styrene and butyl acrylate.[a]

R group	X group	Y = C(O)O^{n}Bu	Y = Ph
		Isolated yield[b] (%)	Isolated yield[b] (%)
H	I	—	68
H	Br	85	69
H	Cl	—	0
p-Me	Br	76	81
p-OMe	Br	75	85
p-C(O)OMe	Br	61	59
p-NO_2	Br	45	31
	Br	67	76

[a]2.0 mmol each of styrene and haloarene, 2.2 mmol of NaOAc, 50 mL of DMF.

[b]Yields were determined by NMR analysis.

styrene and bromobenzene was added and sample was taken for GC analysis. The reaction was run for a further 48 h and no further reaction of the mixture took place.

The generality of the catalytic system was investigated for a variety of haloarenes, and the results are presented in Table 6. Initially the nature of the halogen used was studied. It was found that the reaction of bromo and iodobenzene gave similar yields with no detectable product using chlorobenzene. We then examined the effect of *para* substituents on the haloarenes. It was surprising to find that electron withdrawing substituents (nitro, ester) gave relatively low yields and conversions, while electron donating groups (methoxy, methyl) gave moderate to good yields of coupled products. This observation suggests that the oxidative addition step of the Heck reaction is relatively facile whereas the alkene insertion or reductive elimination is the rate determining step. This reactivity may be a function of the nitrogen in the ligand donating into the metal center leading to facile oxidative addition. The catalyst system was also found to be active for thiophenes with no catalyst poisoning resulting from the sulfur atom.

Summary

The dendrimer supported complexes, Pd–PPh_2–PAMAM–SiO_2, are new and highly active catalysts for the Heck reaction of a variety of bromoarenes with styrene and butyl acrylate, affording *para* substituted stilbenes and cinnamate esters in good yields. This dendritic system shows comparable activity to the Reetz dendrimer system (13) and can be easily recycled.

Experimental

General

Dimethylformamide (Aldrich) was used in anhydrous form. All the aryl bromides, iodobenzene and alkene substrates were purified before use. Aminopropyl silica gel was purchased from Fluka.

General procedure for the complexation of PPh_2–PAMAM–SiO_2 with palladium

The PPh_2–PAMAM–SiO_2 (1.0 mmol with respect to PPh_2) was added to a solution of Pd $(Me_2NCH_2CH_2NMe_2)(Me)_2$ (0.5 mmol) in freshly distilled benzene (20 mL). The mixture was stirred at room temperature overnight under nitrogen. The product was filtered through a 0.45 mm membrane filter under a stream of nitrogen and washed with ether (50 mL). Residual ether was removed in vacuo.

General procedure for the Heck reaction

The substrates, base, and solvent (dimethylformamide 20 mL) were placed in a 50 mL round bottom-flask equipped with a magnetic stirring bar and condenser connected to a vacuum line. The solution was flushed five times with nitrogen using a vacuum nitrogen cycle. The catalyst was then added. The autoclave was placed in an oil bath and the desired temperature was reached by stirring on a hot plate. After the appropriate reaction time, the reaction was allowed to cool to room temperature. The resulting solution was filtered to remove the catalyst. The filtrate was extracted with diethyl ether (4 × 40 mL), and the ether extracts were washed with brine and distilled water, followed by drying over magnesium sulfate. The product was analyzed by ^{1}H NMR spectroscopy and (or) gas chromatography, and identified by comparison of spectral results with literature data (6).

Acknowledgements

We are grateful to DuPont Canada and to the NSERC/NRC Research Partnership Program for support of this research.

References

1. (*a*) R.F. Heck. Comprehensive organic synthesis. *Edited by* B.M. Trost and I. Fleming. Pergamon, Oxford, 4, 883. 1991. (*b*) A. de Meijer and F.E. Meyer. Angew. Chem. Int. Ed Engl. **33**, 2379 (1994).

© 2000 NRC Canada

2. B. Cornils and W.A. Herrmann. Applied homogenous catalysis with organometallic compounds. VCH Publishers Inc., Weinheim. 1996.
3. R.F. Heck. Acc. Chem. Res. **12**, 146 (1979).
4. (*a*) M.T. Reetz and G. Lohmer. Chem. Commun. (Cambridge), 1921 (1996); (*b*) M. Beller, H. Fischer, K. Kuhlein, C.P. Reisinger, and W.A. Herrmann. J. Organomet. Chem. **520**, 257 (1996).
5. (*a*) C.P. Mehnert and J.Y. Ying. Chem. Commun. (Cambridge), 2215 (1997); (*b*) C.P. Mehnert and J.Y. Ying. J. Am. Chem. Soc. **120**, 12288 (1998).
6. (*a*) J. Kiviaho, T. Hanoka, Y. Kubota, and Y. Sugi. J. Mol. Catal. A: Chem. **101**, 25 (1995); (*b*) R.L. Augustine and S.T. O'Leary. J. Mol. Catal. A: Chem. **99**, 277 (1995); (*c*) M.Z. Cai, C.S. Song, and X. Huang. Synthesis, 521 (1997); (*d*) R.L. Augustine and S.T.J. O'Leary. J. Mol. Catal. **72**, 229 (1992); (*e*) D. Villemin, P. Jaffres, B. Nechab, and F. Courivaud. Tetrahedron Lett. **38**, 6581 (1997); (*f*) P. Yi, Z. Zhuangyu, and H. Hongwen. J. Mol. Catal. **62**, 297 (1990); (*g*) P.E. Wang and M.A. Fox. J. Org. Chem. **59**, 5358 (1994).
7. M.K. Terasawa, T. Kanda, Y. Imanaka, and S. Ternashi. J. Organomet. Chem. **162**, 403 (1978).
8. Z. Zhang, Y. Pan, H.W. Hu, and T.Y. Kao. Synthesis, 539 (1991).
9. S.C. Bourque, F. Maltais, W.-J. Xiao, O. Tardif, H. Alper, P. Arya, and L.E. Manzer. J. Am. Chem. Soc. **121**, 3035 (1999).
10. (*a*) S.J. Shuttleworth, M. Allin, and P.K. Sharma. Synthesis, 1217 (1997); (*b*) K. Nozaki, Y. Itoi, F. Shibahara, E. Shirakawa, T. Ohta, H. Takaya, and T. Hiyama. J. Am. Chem. Soc. **120**, 4051 (1998); (*c*) J. Chen and H. Alper. J. Am. Chem. Soc. **119**, 895 (1997); (*d*) A. Nait Ajjou and H. Alper. J. Am. Chem. Soc. 120, 1466 (1998); (*e*) J.Y. Ying, C.P. Mehnert, and M.S. Wng. Angew. Chem. Int. Ed. Engl. **38**, 56 (1999).
11. (*a*) O.A. Matthews, A.N. Shipway, and J.F. Stoddart. Prog. Polym. Sci. **23**, 56 (1998); (*b*) J.M.J. Frechet, C.J. Hawker, I. Gitsov, and J.W. Leon. Pure Appl. Chem. **10**, 1399 (1996); (*c*) N. Ardoin and D. Astruc. Bull. Soc. Chim. Fr. **132**, 875 (1995).
12. (*a*) J.W.J. Knapen, A.W. van der Made, J.C. de Wilde, P.W.N.M. van Leeuwen, P. Wijkens, D.M. Grove, and G. van Koten. Nature (London), **372**, 659 (1994); (*b*) J.L. Hoare, K. Lorenz, N.J. Hovestad, W.J.J. Smeets, A.L. Spek, A.J. Canty, H. Frey, and G. van Koten. Organometallics, **16**, 4167 (1997); (*c*) A.W. Kleijn, H. Kleijn, J.T.B.H. Jastrzebski, A.L. Spek, and G. van Koten. Organometallics, **18**, 277 (1999).
13. (*a*) M.T. Reetz, G. Lohmer, and R. Schwickardi. Angew. Chem. Int. Ed. Engl. **36**, 1526 (1997); (*b*) M.T. Reetz. Top. Catal. **4**, 187 (1997).
14. (*a*) D.A. Tomalia, H. Baker, M. Hall, G. Kallos, S. Martin, J. Roeck, J. Ryder, and P. Smith. Polym. J. (Tokyo), **17**, 117 (1995); (*b*) D.A. Tomalia, H. Baker, J. Dewald, M. Hall, G. Kallos, S. Martin, J. Roeck, J. Ryder, and P. Smith. Macromolecules, **19**, 2466 (1986); (*c*) D.A. Tomalia, M. Hall, and D. Hedstrand. J. Am. Chem. Soc. **109**, 1061 (1987); (*d*) D.A. Tomalia, V. Berry, M. Hall, and D. Hedstrand. Macromolecules, **20**, 1164 (1987).
15. W. de Graff, J. Boersma, J.J. Smeets, A.L. Spek, and G. van Koten. Organometallics, **8**, 2907 (1989).

© 2000 NRC Canada

Synthesis of dimeric and tetrameric macrolactams with cytotoxic activity[1]

Gabriella Gentile, Daniela Fattori, Maurizio Botta, Federico Corelli, Domenico Fusar-Bassini, and Doriano Lamba

Abstract: Cyclization of amino acid **14**, in turn prepared from 4,4-dimethylcyclohex-2-en-1-one by standard chemistry, yielded the dimeric and tetrameric macrolactams **15** and **16**, respectively, representing the first examples of "taxoid-like" compounds with heterocyclic B rings. Compounds **15** and **16** exhibited moderate antiproliferative activity in an in vitro cytotoxicity assay. Consequently, an orthogonally diprotected, dimeric macrolactam **19** was synthesized and, after selective deprotection of the hydroxy group, was coupled with the docetaxel side chain to give the final compound **2**, showing three-dimensional shape similarity to paclitaxel. Contrary to our expectations, **2** proved to be as active as the parent compound **15**. The structure of **15** has been confirmed by X-ray crystallographic analysis and is also reported.

Key words: macrolactams, macrocyclic compounds, taxane analogs, cytotoxic activity.

Résumé: La cyclisation de l'acide aminé **14,** préparé à partir de la 4,4-diméthylcyclohex-2-én-1-one donne des macrolactames dimère **15** et tétramère **16** qui sont les premiers exemples de composés de type taxoïde avec un noyau B hétérocyclique. Les composés **15** et **16** exhibent une activité antiprolifère modérée lors d'un essai de cytotoxicité in vitro. En conséquence, on a synthétisé un macrolactame dimère **19**, ayant orthogonalement deux groupes protecteurs, et après une déprotection sélective du groupe hydroxyle, on l'a couplé avec la chaîne latérale du docétaxel pour obtenir le produit final **2,** dont la forme tridimensionnelle est semblable à celle du paclitaxel. Contrairement à nos attentes, le composé **2** s'est révélé aussi actif que le composé parent **15**. On rapporte la structure du composé **15** que l'on a confirmée par cristallographie de rayons X.

Mots clés: macrolactames, composés macrocycliques, analogues du taxane, activité cytotoxique.

[Traduit par la Rédaction]

Introduction

In the last years paclitaxel (1) (Fig. 1) has proven to be a major achievement in the field of cancer chemotherapy, particularly for the treatment of advanced ovarian and breast cancer (for several reviews on paclitaxel see ref. (1)). Due to the novelty of its mode of action (2) as well as to its unique structural complexity (3), it has been the objective of total synthetic (4) and structure–activity relationship studies (for selected recent contributions see ref. (5)). Intense efforts have been directed toward structural modifications of paclitaxel aimed at defining its pharmacophore (6) and developing analogues with better therapeutic profile and improved water-solubility (7*a*) (for a review see ref. (7*b*)). It has been recently reported in the literature that several macrocyclic compounds, such as taxuspines, sarcodictyins (and related eleutherobin and eleuthosides), epothilones, discodermolide, and rhazinilam (and related nine-membered macrolactams), though belonging to different chemical families, exert antitumor activity through a paclitaxel-like mechanism (for taxuspines see ref. (8*a*); sarcodictyins, eleutherobin, eleuthosides see ref. (8*b*); epothilones see ref. (8*c*); discodermolide see ref. (8*d*); rhazinilam and analogs thereof see ref. (8*e*)). In the course of our investigations on taxane systems (9) and on new analogues of paclitaxel and docetaxel (10), we conceived the possibility of preparing heterocyclic analogs which are expected to be more water-soluble (11).

Received June 9, 1999. Published on the NRC Research Press website on June 15, 2000.

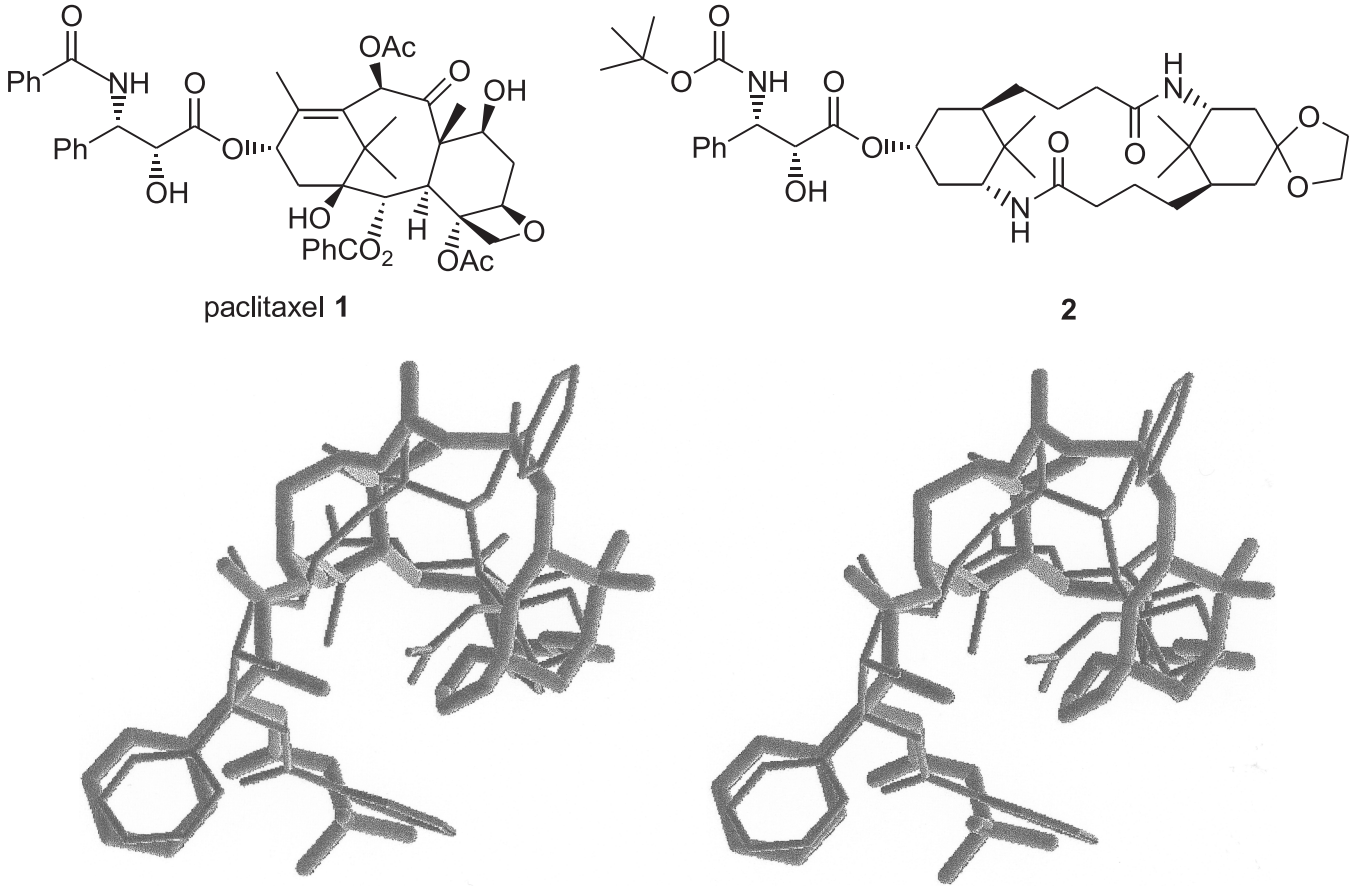
Dedicated to Professor Stephen Hanessian in recognition of his significant contribution to the art of organic synthesis

G. Gentile,[2] D. Fattori,[3] M. Botta,[4] and F. Corelli.[4] Dipartimento Farmaco Chimico Tecnologico, Università degli Studi di Siena, Banchi di Sotto 55, 53100 Siena, Italy.
D. Fusar-Bassini. Chemistry Department, Pharmacia & Upjohn, Via Giovanni XXIII, 20014 Nerviano, Milano, Italy.
D. Lamba. International Centre for Genetic Engineering and Biotechnology, Area Science Park, Padriciano 99, I-34012 Trieste, Italy and Istituto di Strutturistica Chimica "G. Giacomello" C.N.R, Sezione di Trieste, Area Science Park, SS 14, Km 163.5, Basovizza, I-34012 Trieste, Italy.

[1]Taken in part from: Gentile, G. Ph.D. Thesis, University of Siena, February 1998.
[2]Present address: GlaxoWellcome, Via Fleming 4, 37135 Verona, Italy.
[3]Present address: IRBM, Via Pontina km 30,600, 00040 Pomezia, Roma, Italy.
[4]Authors to whom correspondence may be addressed. Telephone: +39 0577 45393. Fax: +39 0577 232183. e-mail: botta@unisi.it; corelli@unisi.it

 © 2000 NRC Canada

Fig. 1. Top: Structure of paclitaxel (1) and macrolactam **2**. Bottom: stereoview of the superimposition between lowest-energy conformations of **2** (thick) and paclitaxel (thin).



In particular, the superimposition between the lowest-energy conformation of the dimeric macrolactam **2** and the lowest-energy conformation of **1** (10) highlighted good shape similarity between the partners (Fig. 1) and led us to identify **2** as an interesting heterocyclic mimic of paclitaxel. We wish to describe herein our synthetic efforts in this direction.

Results and discussion

Enone **3** (12) (Scheme 1) was subjected to hydrocyanation (13) followed by ketalization and partial hydrolysis of the nitrile to give the primary amide **4** in 60% overall yield. Hofmann rearrangement of this amide was best accomplished by treatment with bromine and sodium hydroxide. The resulting amine was protected as the corresponding Cbz derivative and treated with HCl in THF to give **5**. The transformation of **5** into **6** could be efficiently[5] performed following the Saegusa procedure (14). Reaction of **5** with TMSCl in the presence of triethylamine afforded a silyl enol ether mixture, which was treated with palladium(II) acetate in refluxing acetonitrile in the presence of $CaCO_3$. Chromatographic purification on silica gel led to the enone **6** as the sole reaction product in an overall yield of 70% from **5**. Insertion of a side chain at C-5 was realized through $TiCl_4$-catalyzed reaction of allyltrimethylsilane with the enone system of **6** to give the allyl derivative **7** as the only isomer. The *trans* relative stereochemistry was assigned according to the usual stereochemical outcome of the Sakurai reaction (15*a*, *b*) (for a discussion of the stereochemistry of conjugate addition reactions to 5-substituted cyclohex-2-ene-1-one derivatives, see ref. (15*c*). Oxidative cleavage of the double bond afforded the aldehyde **8**, which was in turn subjected to Wadsworth–Emmons olefination with methyl (triphenylphosphoranylidene)acetate to give in 72% yield the unsaturated esters **9** as a 9:1 *E*:*Z* mixture.[6] Subsequent ketalization of **9** under standard conditions afforded compound **10**. This key intermediate (Scheme 2) was hydrogenated to give the saturated amine **11** and hydrolyzed to the free acid **12** in 92% and 93% yield, respectively. These two synthons were coupled to afford the amide **13**, which was in turn advanced to the amino acid **14**.

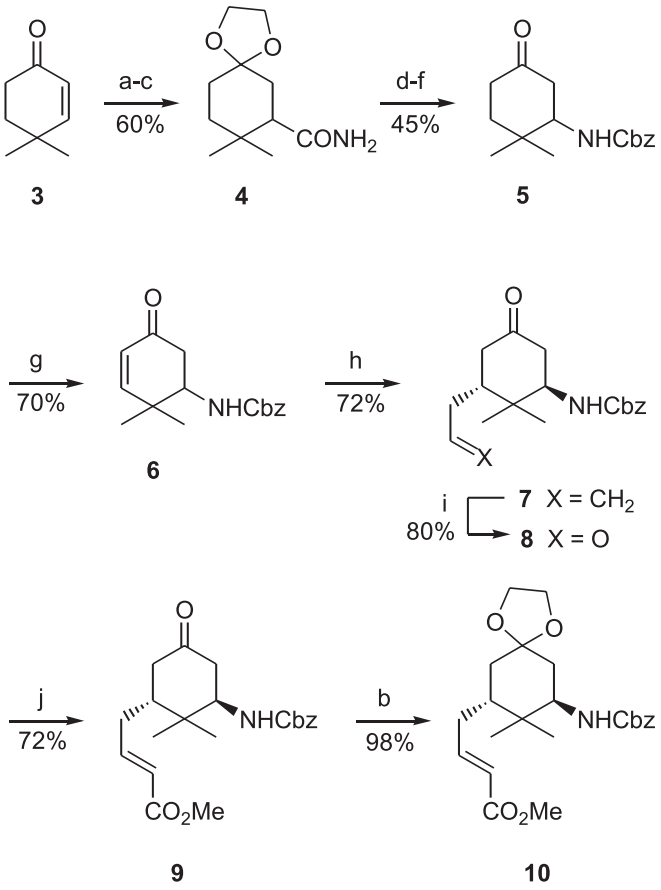
Having secured an access to **14**, several procedures based on the condensing reagents for peptide synthesis were investigated to accomplish its cyclization to the 16-membered lactam **15** (Scheme 3). DPPA-mediated cyclization of **14** provided the macrolactam **15** as a colorless solid in a most

[5] Attempts to convert **5** to **6** by regioselective bromination-dehydrobromination sequence afforded unsatisfactory results as a complex mixture of compounds was obtained. On the other hand, direct reaction of **5** with PhSeCl showed little regioselectivity providing, after selenoxide elimination, a mixture of the enone **6** and its regioisomer.

[6] For simplicity, only the predominant (*E*)-isomer of compounds **9**, **10**, **12**, **13**, **17**, and **18** are shown in the Schemes.

© 2000 NRC Canada

Scheme 1. Key: (a) KCN, EtOH, H_2O, AcOH, 40°C; (*b*) $HOCH_2CH_2OH$, CSA, toluene, reflux; (*c*) NaOH, 30% H_2O_2, EtOH, 50°C; (*d*) Br_2, NaOH, 0–80°C; (*e*) CbzCl, $NaHCO_3$, EtOH, H_2O; (*f*) Hcl, THF; (g) (*i*) LiHMDS, TMSCl, Et_3N, THF, –78°C; (*ii*) $Pd(OAc)_2$, CaCo3, CH_3CN, reflux; (h) allyltrimethylsilane, $TiCl_4$, CH_2Cl_2, –78 to –30°C; (*i*) OsO_4, $NaIO_4$, Et_2O, H_2O, rt; (j) methyl (triphenylphosphoranylidene)acetate, toluene, reflux.



satisfactory yield of 28%, along with the tetramer **16** (10%). 500 MHz ^{1}H NMR spectroscopy revealed that compound **15** was indeed a mixture of two isomers in the ratio 3:1, as evidenced by the presence of two doublets at 7.16 and 7.02 ppm relative to the NH groups and integrating for 1.5 and 0.5 protons, respectively.[7] Although attempts to separate these isomers by HPLC were unsuccessful, the major isomer was obtained in pure form by two successive recrystallizations from methanol–water.

X-ray crystallographic analysis of this sample (Fig. 2) showed that the structure is centrosymmetric, with an *R*-relative configuration of both the chiral centers at C-2 and C-6 and a *trans* conformation of the N-1—C-9 amide bond. In terms of the conformational descriptors (16) (P = 56.5° and τ = 24.0°), an *envelope* conformation can be assigned to the dioxolane ring. The C-4, O-2, O-3, and C-10 atoms define a nearly perfect plane, with C-11, in the *flap* position, displaced out of the plane by 0.337 Å. The cyclohexane moiety exhibits a *chair* conformation, with C-3 and C-6 atoms displaced out of the plane defined by C-1, C-2, C-4, and C-5 by 0.647 Å and 0.643 Å, respectively, at opposite sites, the Cremer and Pople (17) puckering parameters being Q = 0.547 Å, θ = 3.4°, and ϕ = 42.4°.

Compounds **15** and **16** were evaluated in an in vitro cytotoxicity assay on a B16-F10 murine melanoma cell line and in a tubulin polymerization assay (18) performed spectrophotometrically. While no activity against tubulin assembly was observed, **15** and **16** displayed an IC_{50} value of 45 μM and 37 μM, respectively, in the cytotoxicity test. Although no attempt has been made to establish the mechanism of the antiproliferative activity of the tested compounds, the preliminary biological results indicated that **15**[8] might have been of interest as a lead compound in the search of new antitumor agents in spite of its modest cytotoxic activity (to the best of our knowledge, the tested compounds constitute the first example of "taxoid-like" compounds with heterocyclic B rings. For an example of analogs oxygenated in the C ring, see ref. (19)). In fact, it should be kept in mind that baccatin (i.e., paclitaxel without a C-13 side chain) itself shows a comparable cytotoxicity, which increases by four orders of magnitude after esterification at C-13 with the appropriate *N*-acylphenylisoserine side chain (20).

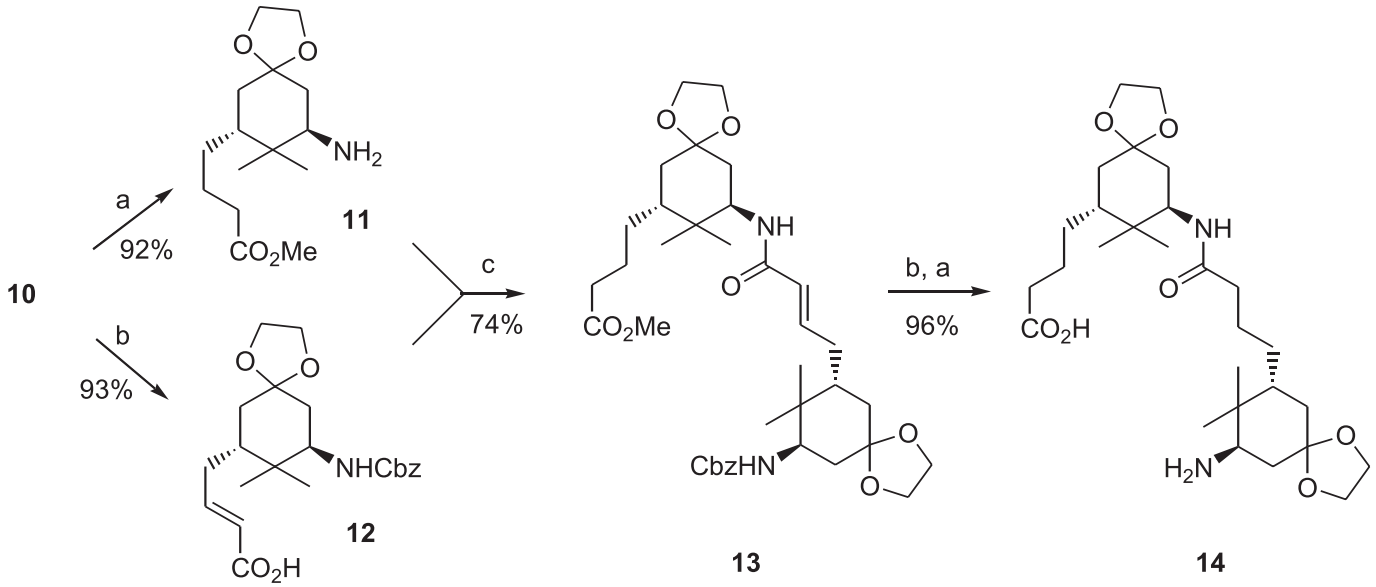
It now remained to elaborate the dimeric macrolactam **15** by introducing an *N*-acylphenylisoserine chain to enhance its cytotoxic activity. Since an attempt to selectively cleave only one ketal group in **15** proved to be unpractical because of the formation of mixtures, we turned our attention to ketone **9**. Reduction with $NaBH_4$ (Scheme 4) provided two isomers (in the ratio 7:1)[9] of the expected alcohol, whose structures were assigned on the basis of their ^{1}H NMR spectrum, which revealed an intramolecular hydrogen bonding between the OH and NH groups (which must be therefore *cis*) in the minor, less polar, isomer (δ_{NH} 6.23 vs. 4.88 ppm). Silylation of the hydroxy group of the major isomer followed by hydrolysis of methyl ester gave the acid **17** in 78% overall yield from **9**. Acylation of amine **11** with **17** under mixed anhydride conditions led to the amide **18**, which was advanced to the orthogonally protected macrolactam **19**. TBAF-mediated desilylation of **19** provided the hydroxy derivative **20**, which by reaction with (4*S*,5*R*)-*N*-(*tert*-butoxycarbonyl)-2-(2,4-dimethoxyphenyl)-4-phenyloxazolidine-5-carboxylic acid (**21**) as one (unspecified) stereoisomer (21) in the presence of *N*-cyclohexyl-*N*′-(2-morpholinoethyl)carbodiimide methyl *p*-toluenesulfonate (CMC) and 4-dimethylaminopyridine (DMAP), followed by selective cleavage of the aminoacetal group, was converted to the intended target **2** (an inseparable mixture of stereoisomers) in 32% overall yield from **19**.

In the cytotoxicity and tubulin polymerization assays **2** showed approximately the same biological profile as **15**. This result, though discouraging, is not completely surprising, since it is well known that neither an intact taxane

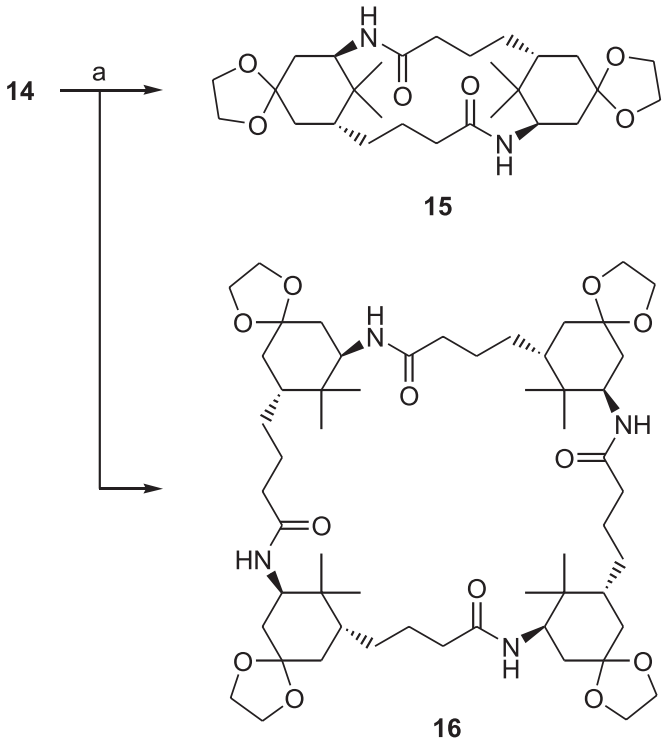
[7] No coalescence of these signals was observed by raising temperature until 80°C.
[8] Although **16** has proven to be the most active compound, it was not further considered as a possible lead owing to its molecular weight > 1000.
[9] Attempts to improve the stereoselectivity of the reduction by using bulkier reagents (L-selectride) or lower reaction temperature (–30 to –60°C) were unsuccessful.

© 2000 NRC Canada

Scheme 2. Key: (a) H_2, 60 psi, 10% Pd/C, EtOH; (b) LiOH, MeOH–H_2O, 45°C; (c) *i*-BuOCOCl, *N*-methylmorpholine, CH_2Cl_2, 0°C; (d) DPPA, $NaHCO_3$, DMF.

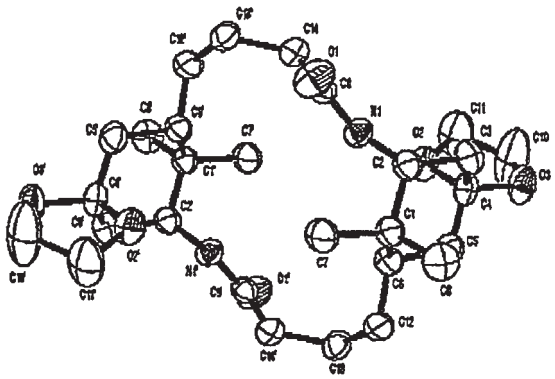


Scheme 3. Key: (a) DPPA, $NaHCO_3$, DMF.



skeleton nor a phenylisoserine side chain are structural elements per se sufficient for cytotoxic and in vitro microtubule assembly activity. Thus, even if the inactive baccatin III becomes the fully active paclitaxel by esterification at C-13 with the appropriate chain, esterification of simpler cyclic alcohols with *N*-acylphenylisoserine does not lead to compounds with paclitaxel-like activities. Although the role of the paclitaxel side chain in affecting biological activity has not yet been fully determined, it is thought that the principal recognition partner is the taxane skeleton itself. The

Fig. 2. Perspective view and arbitrary atom labelling of compound **15**. Thermal ellipsoids are drawn at the 50% probability level; symmetry transformation used to generate equivalent atoms (′) is (–x + 1, –y + 1, –z + 1).



paclitaxel side chain may be preorganized through hydrogen bonding and may fit into a hydrophobic cleft on the taxane binding site, which stabilizes the drug–tubulin interaction (5*b*). Therefore, the moderate cytotoxicity of compounds **2** and **15** is likely to be due to mechanism(s) not involving microtubule stabilization.

Experimental

Materials

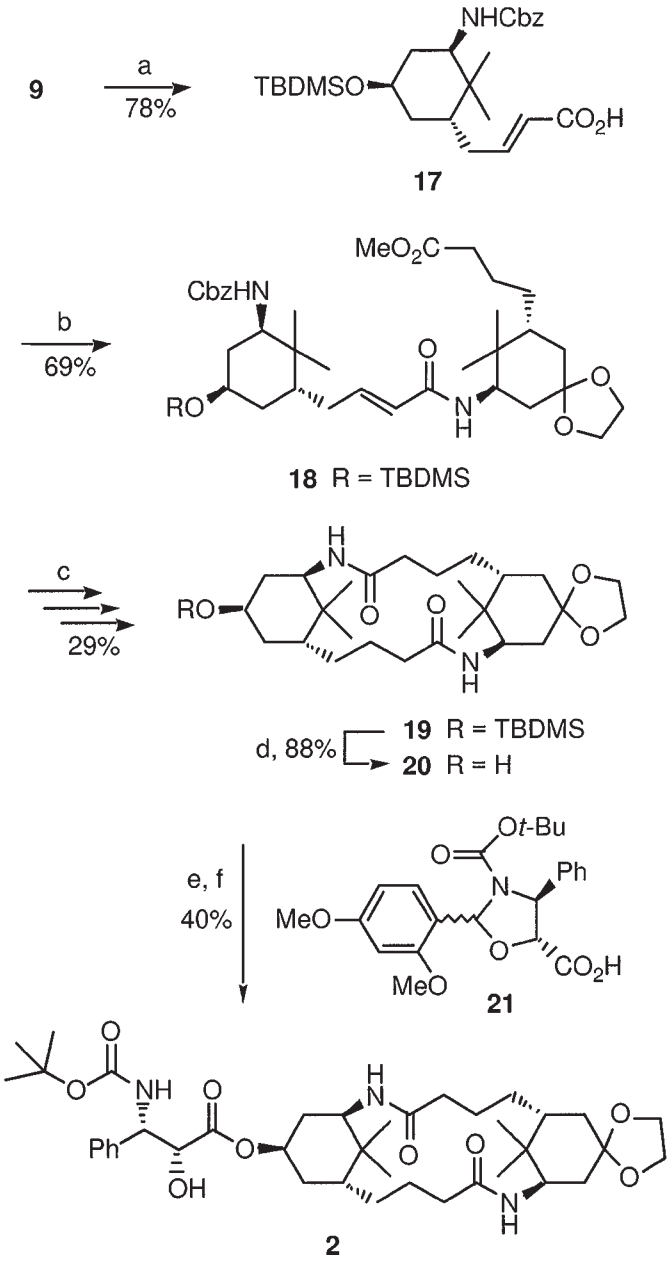
Reagents were from commercial suppliers and used without further purification. All solvents were dried over standard drying agents (22) and freshly distilled prior to use.

Instrumentation and techniques

Merck silica gel 60 was used for chromatography (70–230 mesh) and flash chromatography (230–400 mesh) columns. Analytical and preparative TLC were performed with Merck silica gel 60 F_{254} (0.2 mm and 2 mm thickness, respectively) precoated aluminum sheets with visualization by UV light,

© 2000 NRC Canada

Scheme 4. Key: (a) (*i*) $NaBH_4$, MeOH; (*ii*) TBMDSCl, imidazole, DMF, 70°C; (*iii*) LiOH, MeOH, H_2O, 40°C; (b) **11**, I-BuOCOCl, *N*-methylmorpholine, CH_2Cl_2, 0°C; (c) see (b), (a) in Scheme 2 and (a) in Scheme 3; (d) TBAF, THF; (e) CMC, DMAP, toluene; (f) 0.1 N HCl, MeOH.



charring with H_2SO_4 (10% in water), or charring with anisaldehyde in ethanolic sulfuric acid (23). Melting points are uncorrected. ^1H and ^{13}C NMR spectra were measured in $CDCl_3$ at 200 and 50 MHz, respectively, unless otherwise stated. Mass spectra were obtained at low and high resolution. Elemental analyses (C, H, N) were performed in house.

*2,2-Dimethyl-5-ethylenedioxycyclohexane-1-carboxamide (**4**)*

A solution of KCN (7.88 g, 121 mmol) in water (20 mL) was added slowly to a solution of **3** (7.51 g, 60 mmol) and AcOH (3.45 mL) in 95% EtOH (150 mL) warmed to 40°C. After stirring at 40°C for 4 h, the mixture was cooled to rt and filtered through a short plug of silica gel. The solution was evaporated and the residue was chromatographed on silica gel (toluene) to give 6.50 g (71%) of an oil, which crystallized on standing; mp 78–79°C. This compound was dissolved in a mixture of toluene (200 mL) and ethylene glycol (20 mL) containing camphorsulfonic acid (CSA, 400 mg). After stirring for 8 h under reflux with azeotropical removal of water, the mixture was cooled to rt and washed with 5% aqueous $NaHCO_3$ and brine, then evaporated under reduced pressure. The oily residue was dissolved in 95% EtOH (15 mL) and treated with 6 N NaOH (15 mL) and 30% H_2O_2 (15 mL). The mixture was heated at 50°C for 6 h, cooled to rt, and diluted with CH_2Cl_2 and 5% aqueous $Na_2S_2O_3$. The organic layer was extracted twice with CH_2Cl_2 and the combined organic solution was washed with brine, dried, and evaporated to afford **4** (6.42 g, 60% overall yield from **3**) as a white solid, which was purified by trituration with hexanes–Et_2O, mp 178–182°C. IR (KCl): 3628, 3395, 1662, 1546 cm^{-1}. ^1H NMR δ: 5.65 (d, 2H), 3.91 (s, 4H), 2.31 (dd, *J* = 3.5, 13.0 Hz, 1H), 2.00 (dd, *J* = 3.5, 13.0 Hz, 1H), 1.85–1.25 (m, 5H), 1.17 (s, 3H), 1.02 (s, 3H). ^{13}C NMR δ: 175.6, 108.7, 64.3, 64.1, 51.2, 38.8, 34.0, 32.1, 31.0, 30.3, 19.9. EIMS (*m*/*z*): 213 (M^+, 7), 169 (25), 99 (100), 86 (55). Anal. calcd. for $C_{11}H_{19}NO_3$: C 61.94, H 8.98, N 6.57; found: C 62.19, H 9.09, N 6.40.

*3-[(Benzyloxycarbonyl)amino]-4,4-dimethylcyclohexanone (**5**)*

Bromine (0.8 mL) was added to 2.5 N NaOH (30 mL) cooled in an ice bath, followed after 15 min by amide **4** (2.0 g, 9.75 mmol) in small portions. The mixture was stirred at 0–5°C for 45 min, then at rt for a further 30 min, and finally heated at 80°C for 1 h. After cooling, the reaction mixture was extracted with Et_2O (6 × 20 mL) and the combined organic solution was washed with brine and evaporated. The oily residue was dissolved in 95% EtOH (15 mL) and 5% aqueous Na_2CO_3 (10 mL) and benzyl chloroformate (1.08 mL, 7.55 mmol) was added dropwise. After stirring at rt for 3 h, the reaction mixture was diluted with water and extracted with Et_2O (4 × 50 mL). The organic layer was washed with brine, dried and evaporated to give an oil, which was purified by flash chromatography on silica gel (hexanes–EtOAc, 4:1). The yellow oil (1.58 g, 4.96 mmol) was dissolved in 30 mL of 1 N HCl–THF (1:1) and the solution was stirred at rt for two days. After removal of THF under reduced pressure, the aqueous phase was neutralized with solid $NaHCO_3$ and extracted with Et_2O (4 × 50 mL). The organic layer was washed with brine, dried, and evaporated. Flash chromatography of the residue on silica gel (hexanes–EtOAc, 4:1) gave **5** (1.26 g, 45% overall yield from **4**) as a white solid, which was recrystallized from hexanes–EtOAc (4:1), mp 106–107°C. IR (KCl): 3450, 3060, 2980, 1730, 1520 cm^{-1}. ^1H NMR δ: 7.35 (m, 5H), 5.11 (s, 2H), 4.88 (d, *J* = 10.0 Hz, 1H), 3.83 (ddd, *J* = 5.0, 10.0, 10.0 Hz, 1H), 2.61 (dd, *J* = 5.0, 15.0 Hz, 1H), 2.33 (m, 2H), 2.27 (dd, *J* = 10.0, 15.0 Hz, 1H), 1.67 (m, 2H), 1.09 (s, 3H), 1.00 (s, 3H). ^{13}C NMR δ: 208.59, 155.74, 136.27, 128.54, 127.55, 126.93, 66.95, 56.76, 44.64, 37.61, 36.17, 34.14, 27.25, 19.90. EIMS (*m*/*z*): 275 (M^+, 10), 219 (22), 184 (20), 91 (100). Anal. calcd. for $C_{16}H_{21}NO_3$: C 69.79, H 7.69, N 5.09; found: C 69.58, H 7.83, N 5.25.

© 2000 NRC Canada

*5-[(Benzyloxycarbony)lamino]-4,4-dimethylcyclohex-2-en-1-one (**6**)*

To a solution of LHMDS in THF (10.89 mL, 1 M, 10.89 mmol) was added a solution of **5** (1.0 g, 3.36 mmol) in THF (10 mL) dropwise at –78°C. The solution was stirred at this temperature for 1.5 h, and then freshly distilled Et_3N (2.50 mL, 18.15 mmol) and TMSCl (1.38 mL, 10.89 mmol) were added and the reaction was allowed to warm to rt. After filtration and evaporation of volatiles, the residual oil was dissolved in acetonitrile (30 mL) and $Pd(OAc)_2$ (896.4 mg, 3.99 mmol) and $CaCO_3$ (363.3 mg, 3.63 mmol, previously dried at 120°C overnight) were added. The mixture was refluxed for 2 h, then evaporated under reduced pressure. Flash chromatography of the crude residue on silica gel (hexanes–EtOAc, 3:1) provided **6** (694.9 mg, 70%) as a white solid, which was recrystallized from hexanes–EtOAc (4:1), mp 120°C. IR (KCl): 3437, 2969, 1721, 1679, 1512, 1466 cm^{-1}. ^1H NMR δ: 7.33 (m, 5H), 6.65 (d, *J* = 10.0 Hz, 1H), 5.89 (d, *J* = 10.0 Hz, 1H), 5.09 (s, 2H), 5.01 (br d *J* = 9 Hz, 1H), 4.11 (m, 1H), 2.65 (dd, *J* = 4.5, 16.5 Hz, 1H), 2.42 (dd, *J* = 10.0, 16.5 Hz, 1H), 1.20 (s, 3H), 1.08 (s, 3H). ^{13}C NMR δ: 208.43, 155.57, 136.09, 128.07, 66.08, 44.49, 37.47, 36.02, 33.99, 27.10, 19.73. EIMS (*m*/*z*): 273 (M^+, 5), 167 (19), 139 (10), 96 (100). Anal. calcd. for $C_{16}H_{19}NO_3$: C 70.31, H 7.01, N 5.13; found: C 70.51, H 6.96, N 5.03.

*3β-[(Benzyloxycarbonyl)amino]-4,4-dimethyl-5α-(2-propenyl)cyclohexanone (**7**)*

Titanium tetrachloride (1.2 mL, 10.97 mmol) was added dropwise to a solution of **6** (1.50 g, 5.49 mmol) in dry CH_2Cl_2 (112 mL) at –78°C. The solution was stirred at this temperature for 5 min, then a solution of freshly distilled allyltrimethylsilane (3.49 mL, 21.96 mmol) in dry CH_2Cl_2 (27 mL) was added slowly. The dark red mixture was kept at –78°C for 5 h, then warmed to –30°C. After 2 h the reaction was quenched with water (50 mL) and allowed to warm to rt. The organic layer was separated and the aqueous phase was extracted with Et_2O (4 × 100 mL). The combined organic solution was washed with brine, dried, and concentrated to a yellowish oil, which was purified by flash chromatography on silica gel (hexanes–EtOAc, 4:1) to give **7** (1.25 g, 72%) as white crystals, mp 79–80°C. IR (KCl): 3065, 1708, 1640, 1586, 1370 cm^{-1}. ^1H NMR δ: 7.33 (m, 5H), 5.61 (m, 1H), 5.07 (s, 2H), 5.00 (m, 2H), 4.70 (br d, *J* = 9.0 Hz, 1H), 4.01 (m, 1H), 2.73 (dd, *J* = 4.5, 16.5 Hz, 1H), 2.47–2.08 (m, 4H), 1.71 (m, 2H), 1.12 (s, 3H), 1.08 (s, 3H). ^{13}C NMR δ: 208.43, 155.62, 136.09, 128.05, 117.09, 66.83, 57.81, 44.46, 42.46, 42.09, 36.78, 36.35, 34.35, 23.69, 21.49. EIMS (*m*/*z*): 315 (M^+, 5), 272 (12), 224 (22), 180 (15), 114 (33), 91 (100). Anal. calcd. for $C_{19}H_{25}NO_3$: C 72.35, H 7.99, N 4.44; found: C 72.46, H 7.88, N 4.56.

*3β-[(Benzyloxycarbonyl)amino]-4,4-dimethyl-5α-(2-oxoethyl)cyclohexanone (**8**)*

OsO_4 (catalytic amount) was added as a single portion to a stirring solution of **7** (1.10 g, 3.50 mmol) in 70 mL of Et_2O–H_2O (1:1). After stirring for 5 min, the solution turned black and $NaIO_4$ (1.49 g, 7.0 mmol) was added in small portions. Stirring was continued for 8 h until TLC analysis indicated the absence of the starting material. The pale yellow organic layer was separated and the aqueous phase was extracted with Et_2O (4 × 100 mL). The combined organic solution was washed with brine, dried, and concentrated. Flash chromatography of the resulting oil on silica gel (hexanes–EtOAc, 7:3) gave the expected aldehyde **8** (0.89 g, 80%) as a colorless oil. IR ($CHCl_3$): 3064, 1711, 1585, 1468 cm^{-1}. ^1H NMR δ: 9.73 (s, 1H), 7.33 (m, 5H), 5.08 (s, 2H), 4.85 (br d, *J* = 9.0 Hz, 1H), 3.97 (m, 1H), 2.77–2.12 (m, 7H), 1.09 (s, 3H), 1.07 (s, 3H). ^{13}C NMR δ: 207.86, 200.16, 155.74, 136.05, 128.05, 66.83, 57.18, 44.48, 43.15, 36.21, 34.35, 36.21, 25.41, 23.35, 21.73. EIMS (*m*/*z*): 317 (M^+, 2), 182 (15), 108 (23), 91 (100). HRMS calcd. for $C_{18}H_{23}NO_4$: 317.16271; found 317.16180. Anal. calcd. for $C_{18}H_{23}NO_4$: C 68.12, H 7.30, N 4.41; found: C 68.36, H 7.26, N 4.29.

*4-[3β-[(Benzyloxycarbonyl)amino]-2,2-dimethyl-5-oxocyclohex-1α-yl]-2-butenoic acid methyl ester (**9**)*

To a solution of aldehyde **8** (102 mg, 0.32 mmol) in dry toluene (10 mL) at rt was added methyl (triphenylphosphoranylidene)acetate (131 mg, 0.32 mmol). The reaction mixture was stirred for 8 h at rt. Evaporation of the solvent followed by flash chromatography on silica gel (hexanes–EtOAc, 4:1) gave **9** (86 mg, 72%) as a 9:1 mixture of (*E*–*Z*)-isomers. A sample of the pure (*E*)-isomer was obtained by TLC, mp 104–105°C. IR ($CHCl_3$): 1658 cm^{-1}. ^1H NMR δ: 7.32 (m, 5H), 6.75 (ddd, *J* = 16.0, 9.0, 7.0 Hz, 1H), 5.80 (d, *J* = 16.0 Hz, 1H), 5.06 (s, 2H), 4.84 (br d, *J* = 9.0 Hz, 1H), 4.01 (m, 1H), 3.62 (s, 3H), 2.80–1.80 (m, 7H), 1.10 (s, 3H), 1.08 (s, 3H). EIMS (*m*/*z*): 355 (M^+–H_2O, 70), 281 (2), 223 (12), 95 (100), 81 (42), 67 (95). HRMS calcd. for $C_{21}H_{27}NO_5$: 373.18892; found: 373.18800. Anal. calcd. for $C_{21}H_{27}NO_5$: C 67.54, H 7.29, N 3.75; found: C 67.70, H 7.36, N 3.57.

*4-[3β-[(Benzyloxycarbonyl)amino]-5-ethylenedioxy-2,2-dimethylcyclohex-1α-yl]-2-butenoic acid methyl ester (**10**)*

A solution of **9** (267 mg, 0.72 mmol), camphorsulphonic acid (catalytic amount), and ethylene glycol (0.4 mL, 7.2 mmol) in toluene (30 mL) was stirred at 130°C for 4 h with azeotropical removal of water. The cooled solution was washed with 5% aqueous $NaHCO_3$ and brine, then evaporated under reduced pressure. The oily residue was flash chromatographed on silica gel (hexanes–EtOAc, 7:3) to give **10** (289 mg, 98%) as a colorless oil. ^1H NMR δ: 7.34 (m, 5H), 6.87 (ddd, *J* = 15.0, 8.0, 5.8 Hz, 1H), 6.05 (br d, *J* = 9.8 Hz, 1H), 5.70 (d, *J* = 15.0 Hz, 1H), 5.07 (s, 2H), 3.90 (m, 4H), 3.77 (m, 1H), 3.70 (s, 3H), 2.37–1.20 (m, 7H), 0.99 (s, 3H), 0.91 (s, 3H). HRMS calcd. for $C_{23}H_{31}NO_6$: 417.21514; found: 417.21610. Anal. calcd. for $C_{23}H_{31}NO_6$: C 66.16, H 7.49, N 3.36; found: C 65.80, H 7.59, N 3.11.

*4-(3β-Amino-5-ethylenedioxy-2,2-dimethylcyclohex-1α-yl)-butanoic acid methyl ester (**11**)*

A mixture of **10** (200 mg, 0.20 mmol) and Pd/C (20 mg, 10%) in EtOH (10 mL) was shaken in a Parr apparatus under 4 atm (1 atm = 101.325 kPa) of pressure of hydrogen for 8 h. Filtration of the mixture through Celite followed by solvent removal under reduced pressure gave **10** (137 mg, 92%) as a TLC-homogeneous colorless oil. IR ($CHCl_3$): 3155, 1731, 1580 cm^{-1}. ^1H NMR δ: 3.79 (m, 4H), 3.35 (m, 5H), 2.70 (br s, 2H), 2.16–1.02 (m, 10H), 0.80 (s, 3H), 0.70 (s, 3H). ^{13}C NMR δ: 173.78, 155.67, 108.53, 64.29, 64.18, 63.79, 63.72, 58.15, 56.00, 51.30, 37.05, 34.85, 34.02,

© 2000 NRC Canada

29.48, 28.78, 28.27, 25.28, 23.11, 19.82. FABMS (*m*/*z*): 286 (M^+ + H) (100), 269 (449), 215 (22). HRMS calcd. for $C_{15}H_{27}NO_4$: 285.19401; found: 285.19500. Anal. calcd. for $C_{15}H_{27}NO_4$: C 63.13, H 9.54, N 4.91; found: C 63.32, H 9.60, N 4.83.

*4-[3β-[(Benzyloxycarbonyl)amino]-5-ethylenedioxy-2,2-dimethylcyclohex-1α-yl]-2-butenoic acid (**12**)*

To a stirring solution of **10** (58.7 mg, 0.14 mmol) in MeOH–H_2O (3:2, 0.8 mL) was added LiOH (7.0 mg, 0.17 mmol) in one portion at rt. Stirring was continued for 1.5 h at 60°C, then the mixture was cooled to 0–5°C, acidified to pH ~ 4 by adding 6 N HCl, and repeatedly extracted with EtOAc. The combined organic phase was dried, and the solvent was removed under reduced pressure. The residue was purified by flash chromatography on silica gel (EtOAc) to afford **12** (52.8 mg, 93%) as a white foam. A sample of the pure (*E*)-isomer was obtained by TLC. IR ($CHCl_3$): 3500, 2946, 1698, 1287 cm^{-1}. ^1H NMR δ: 9.11 (br s, 1H), 7.34 (m, 5H), 6.97 (ddd, *J* = 15.0, 8.0, 5.8 Hz, 1H), 6.05 (br d, *J* = 9.8 Hz, 1H), 5.70 (d, *J* = 15.0 Hz, 1H), 5.07 (s, 2H), 3.90 (m, 4H), 3.77 (m, 1H), 3.70 (s, 3H), 2.47–1.20 (m, 5H), 1.00 (s, 3H), 0.91 (s, 3H). ^{13}C NMR δ: 156.21, 136.64, 128.31, 108.47, 66.38, 64.30, 63.90, 56.74, 38.07, 37.12, 36.05, 32.72, 24.61, 19.84. FABMS (*m*/*z*): 402 (M^+ – H), 294 (95), 255 (100), 149, (80). HRMS calcd. for $C_{22}H_{29}NO_6$: 403.19949; found: 403.20185. Anal. calcd. for $C_{22}H_{29}NO_6$: C 65.49, H 7.24, N 3.47; found: C 65.29, H 7.29, N 3.38.

*Synthesis of compound **13***

To a solution of **12** (282.1 mg, 0.70 mmol) in dry CH_2Cl_2 (14 mL) were added (at –15°C) *N*-methylmorpholine (85 μL, 0.78 mmol) and *i*-butyl chloroformate (90 μL, 0.70 mmol). After stirring at –15°C for 1 h, a solution of **11** (201 mg, 0.70 mmol) in dry CH_2Cl_2 (14 mL) was added slowly. The reaction was allowed to warm to rt, then was quenched with water and extracted with CH_2Cl_2 (4 × 15 mL). The combined organic phase was washed with brine, dried, and evaporated to give an oily residue, which after flash chromatography (SiO_2; hexanes–EtOAc, 4:1) afforded **13** (347.1 mg, 74%) as a colorless oil. A sample of the pure (*E*)-isomer was obtained by TLC. ^1H NMR δ: 7.33 (m, 5H), 6.78 (d, *J* = 9.0 Hz, 1H), 6.74 (m, *J* = 10.0, 7.0, 3.0 Hz, 1H), 6.05 (d, *J* = 8.5 Hz, 1H), 5.70 (d, *J* = 10.0 Hz, 1H), 5.08 (q, 2H), 4.01 (m, 1H), 3.93 (m, 10H), 3.87 (m, 1H), 3.63 (s, 3H), 2.35–1.19 (m, 16H), 0.98 (s, 3H), 0.9 (s, 9H). ^{13}C NMR δ: 186.22, 173.78, 164.66, 156.16, 136.73, 128.28, 127.81, 124.09, 108.56, 63.81, 56.92, 54.33, 37.19, 36.96, 35.82, 34.68, 32.38, 28.72, 24.37, 19.85, 14.02. FABMS (*m*/*z*): 671 (M^+ + H) (15), 269 (100), 225 (20), 165 (12), 147 (10). HRMS calcd. for $C_{37}H_{54}N_2O_9$: 670.38293; found: 670.38460. Anal. calcd. for $C_{37}H_{54}N_2O_9$: C 66.24, H 8.11, N 4.18; found: C 66.50, H 8.00, N 3.93.

*Synthesis of amino acid **14***

Prepared in 96% overall yield from **13** by hydrolysis followed by hydrogenation according to the procedures described for the synthesis of **12** and **11**, respectively. Colorless foam. ^1H NMR δ: 7.24 (d, *J* = 9.0 Hz, 1H), 5.05 (br s, 1H), 3.88 (m, 8H), 3.20 (s, 2H), 2.35–1.19 (m, 24H), 0.85 (s, 3H), 0.83 (s, 9H). ^{13}C NMR δ: 171.72, 109.08, 107.96, 64.29, 63.77, 54.23, 53.22, 37.39, 35.82, 29.15, 28.56, 27.80, 25.09, 24.89, 23.56, 20.49, 19.71, 19.47. FABMS (*m*/*z*): 525 (M^+ + H). HRMS calcd. for $C_{28}H_{48}N_2O_7$: 524.34615; found: 524.34790. Anal. calcd. for $C_{28}H_{48}N_2O_7$: C 64.09, H 9.22, N 5.34; found: C 63.88, H 9.30, N 5.50.

*Preparation of macrolactams **15** and **16***

To a 5×10^{-4} M solution of **14** (58 mg, 0.11 mmol) in dry DMF (220 mL) was added $NaHCO_3$ (46 mg, 0.55 mmol) followed by DPPA (0.24 mL, 1.10 mmol). The reaction mixture was stirred at rt for five days, then the solvent was removed under reduced pressure and the residue was taken up in EtOAc (50 mL). The solution was washed with water and brine, dried, and evaporated. Flash chromatography of the residue on silica gel ($CHCl_3$–MeOH, 19:1) gave **15** (15.7 mg, 28%), followed by **16** (10.8 mg, 10%), as colorless foams.

15: IR ($CHCl_3$): 2421, 1652, 1593, 840 cm^{-1}. ^1H NMR (500 MHz) δ: 7.16 (d, 1.5H), 7.02 (d, 0.5H), 4.02 (m, 10H), 2.46 (m, 4H), 2.36 (m, 4H), 2.20 (m, 8H), 1.56 (m, 12H), 1.03 (m, 6H). ^{13}C NMR (75 MHz) δ: 172.66, 171.16, 109.99, 108.99, 64.42, 64.36, 64.20, 63.92, 55.06, 54.81, 37.83, 37.72, 37.23, 36.96, 34.94, 34.14, 33.63, 33.49, 30.50, 29.69, 25.69, 25.60, 22.98, 22.35, 20.48, 19.64, 19.56. HRMS calcd. for $C_{28}H_{46}N_2O_6$: 506.33559; found: 506.33390. Anal. calcd. for $C_{28}H_{46}N_2O_6$: C 66.37, H 9.15, N 5.53; found: C 66.52, H 9.06, N 5.38.

16: FD MS (*m*/*z*): 1014 (M^+ + H). Anal. calcd. for $C_{56}H_{92}N_4O_{12}$: C 66.37, H 9.15, N 5.53; found: C 66.57, H 9.21, N 5.33.

*4-[3β-[(Benzyloxycarbonyl)amino]-5β-[(tert-butyldimethylsilyl)oxy]-2,2-dimethylcyclohex-1α-yl]-2-butenoic acid (**17**)*

To a solution of **9** (100 mg, 0.27 mmol) in MeOH (10 mL) was added $NaBH_4$ (41 mg, 1.08 mmol) in one portion. After stirring at rt for 1 h, the solvent was removed under reduced pressure and the residue was taken up in EtOAc. Usual workup of the organic solution gave an oily mixture, which was separated by flash chromatography (SiO_2; hexanes–EtOAc, 3:2) to provide two isomers of the expected alcohol as colorless oils. Minor isomer (11 mg, 11%). R_f = 0.4. HRMS calcd. for $C_{21}H_{29}NO_5$: 375.20457; found: 375.20299. Major isomer (81 mg, 81%). R_f = 0.2. HRMS calcd. for $C_{21}H_{29}NO_5$: 375.20457; found: 375.20310.

TBDMSCl (165 mg, 1.10 mmol) was added to a solution of the above product (major isomer, 75 mg, 0.20 mmol) and imidazole (163 mg, 2.40 mmol) in dry DMF (1.5 mL). The reaction mixture was stirred at 70°C for 1 h, then cooled to rt, diluted with Et_2O (100 mL) and washed with water (5 × 2 mL). Solvent removal followed by flash chromatography (SiO_2; hexanes–EtOAc, 9:1) gave in quantitative yield the silylated compound, which was then hydrolyzed with LiOH using the same procedure described for the preparation of **12**. Flash chromatography of the crude product (SiO_2, EtOAc) afforded the expected acid **17** in 98% yield (94 mg, 78% overall yield from **9**) as a white foam. ^1H NMR δ: 7.35 (m, 5H), 6.93 (m, 1H), 5.85 (d, *J* = 10 Hz, 1H), 5.09 (overlapping m, 3H), 3.70 (m, 2H), 2.62–0.91 (m, 13H),

© 2000 NRC Canada

0.85 (s, 9H), 0.01 (s, 6H). ^{13}C NMR δ: 171.72, 109.08, 107.96, 64.29, 63.77, 54.23, 53.22, 37.39, 35.82, 29.15, 28.56, 27.80, 25.09, 24.89, 23.56, 20.49, 19.71, 19.47. FABMS (*m*/*z*): 498 (M^+ + Na). HRMS calcd. for $C_{26}H_{41}NO_5SiNa$: 498.26517; found: 498.26655. Anal. calcd. for $C_{26}H_{41}NO_5Si$: C 65.64, H 8.69, N 2.95; found: C 65.90, H 8.77, N 3.14.

*Synthesis of amide **18***

Starting from **17** and following the same procedure described for the preparation of **13**, the title compound was prepared in 69% yield after chromatographic purification (SiO_2; hexanes–EtOAc, 7:3). Separation by TLC gave a sample of the pure geometric isomers.

*(E)-**18***: R_f = 0.3. ^{1}H NMR δ: 7.32 (m, 5H), 6.75 (superimposed signals, 2H), 5.75 (d, *J* = 15 Hz, 1H), 5.20 (m, 2H), 4.83 (br d, 1H), 4.09 (m, 1H), 3.92 (m, 4H), 3.63 (overlapping signals, 5H), 2.32 (m, 2H), 2.04–1.05 (m, 16H), 0.94 (s, 6H), 0.90 (s, 6H), 0.88 (s, 9H), 0.01 (s, 6H). ES MS (*m*/*z*): 743 (M^+ + H). HRMS calcd. for $C_{41}H_{66}N_2O_8Si$: 742.45885; found: 742.46555. Anal. calcd. for $C_{41}H_{66}N_2O_8Si$: C 66.36, H 8.95, N 3.77; found: C 66.70, H 8.81, N 3.47.

*(Z)-**18***: R_f = 0.2. ^{1}H NMR δ: 7.32 (m, 5H), 6.75 (superimposed signals, 2H), 5.75 (d, *J* = 9.0 Hz, 1H), 5.26 (m, 2H), 4.83 (br d, 1H), 4.06 (m, 1H), 3.91 (m, 4H), 3.63 (overlapping signals, 5H), 2.28 (m, 2H), 2.03–1.05 (m, 16H), 0.93 (s, 6H), 0.90 (s, 6H), 0.88 (s, 9H), 0.01 (s, 6H). ES MS (*m*/*z*): 743 (M^+ + H). HRMS calcd. for $C_{41}H_{66}N_2O_8Si$: 742.45885; found: 742.45690. Anal. calcd. for $C_{41}H_{66}N_2O_8Si$: C 66.36, H 8.95, N 3.77; found: C 66.01, H 8.77, N 3.52.

*Synthesis of macrolactam **19***

Prepared in 29% overall yield (after chromatography on SiO_2; $CHCl_3$–MeOH, 19:1) from **18** through a sequence of hydrolysis-, hydrogenation-, DPPA-mediated macrolactamization as described for the conversion of **13** into **15**. ^{1}H NMR δ: 6.98 (br d, 2H), 3.98 (superimposed signals, 5H), 3.71 (m, 2H), 2.17–1.22 (m, 22H), 0.83 (s, 21H), 0.01 (s, 6H). HRMS calcd. for $C_{32}H_{58}N_2O_5Si$: 578.41150; found: 578.41312. Anal. calcd. for $C_{32}H_{58}N_2O_5Si$: C 66.39, H 10.10, N 4.84; found: C 66.58, H 10.22, N 4.56.

Preparation of 2

To a solution of **19** (17.3 mg, 0.03 mmol) in THF (1.0 mL) at 0°C was added a solution of *n*-Bu_4NF (0.12 mL, 1.0 M, 0.12 mmol) in THF, and the mixture was stirred for 3 h at rt, then quenched with saturated aqueous NH_4Cl, and diluted with Et_2O and the organic layer was washed with water and brine and dried. Filtration and evaporation of the solvent followed by column chromatography (SiO_2; $CHCl_3$–MeOH, 19:1) gave the expected alcohol **20** (12.2 mg, 88%) as a colorless oil. HRMS calcd. for $C_{26}H_{44}N_2O_5$: 464.32502; found: 464.32622.

To a solution of (4*S*,5*R*)-*N*-(*tert*-butoxycarbonyl)-2(2,4-dimethoxyphenyl)-4-phenyloxazolidine-5-carboxylic acid (**21**) (12.0 mg, 0.028 mmol), CMC (20.3 mg, 0.026 mmol) and DMAP (3.2 mg, 0.026 mmol) in dry toluene (2.0 mL) was added alcohol **20** (11.1 mg, 0.024 mmol) and the mixture was stirred at rt for 20 h. The filtered solution was concentrated to yield the crude product, which was redissolved in MeOH (3.0 mL) and 0.1 N HCl (1.5 mL). After stirring at rt for 2 h, the reaction was neutralized by adding 5% aqueous $NaHCO_3$ and concentrated to a small volume. Extraction with EtOAc followed by the usual workup of the organic solution afforded a residue, which was purified by column chromatography (SiO_2; $CHCl_3$–MeOH, 19:1) to give the final compound **2** (7.0 mg, 40% overall yield) as a colorless foam. ^{1}H NMR δ: 7.48 (m, 5H), 6.78 (br d, 2H), 5.59 (deformed d, *J* = 9.5 Hz, 1H), 5.40 (deformed d, *J* = 9.0 Hz, 1H), 5.03 (m, 1H), 3.98 (superimposed signals, 5H), 3.61 (m, 2H), 2.20–1.24 (m, 22H), 1.12 (s, 9H), 0.90 (s, 6H), 0.84 (s, 6H). HRMS calcd. for $C_{40}H_{61}N_3O_9$: 727.44078; found: 727.43811. Anal. calcd. for $C_{40}H_{61}N_3O_9$: C 66.00, H 8.45, N 5.77; found: C 59.73, H 8.58, N 5.95.

Single-crystal X-ray diffraction study of 15

Colourless prismatic crystals of **12** were grown from H_2O–MeOH at 277 K. Crystal data: $C_{28}H_{46}N_2O_6$; Mr = 506.67; space group, triclinic *P*1; *a* = 9.176(2) Å, *b* = 9.692(2) Å, γ = 8.530(2) Å, α = 107.47(2)°, β = 109.82(2)°, γ = 89.38(2)°; *V* = 677.3(3) Å^3; *Z* = 1; *F*(000) = 276; D_x = 1.242 g cm^{-3}; Cu K_α = 1.5418 Å; μ = 0.697 mm^{-1}. X-ray data were collected on a Rigaku AFC5R automated diffractometer (graphite-monochromated Cu K_α radiation). Intensity data were collected, the experimental conditions being $(\sin\theta/\lambda)_{max}$ = 0.57 Å^{-1}; 2θ – ω scan mode; scan range 1.0°, scan rate 1.0°–16.0° min^{-1} (depending on reflection intensity), background count time a quarter of the scan time. There was no significant intensity variation for 3 standard measured every 200 (1.3%). Lorentz, polarization, absorption (min and max transmission factors 0.91 and 1.00) but no extinction corrections were applied. Of the 2342 reflections measured, 2144 were unique (R_{int} = 0.067 based on F^2) and 1626 with $I > 2.0\sigma(I)$ were considered as observed. The structure was solved by direct methods and refined based on F^2, using the SHELXL-97 package (24). Difference Fourier syntheses, using only data with $(\sin\theta/\lambda)$ = 0.50 Å^{-1}, computed at the end of the anisotropic least-squares refinement, showed all H-atoms in configurationally feasible positions. The final refinements were carried out by full-matrix with the H-atoms allowed to ride on the corresponding C and N atoms (165 parameters). The final *R* values are 0.061 for 1626 $I > 2\sigma(I)$ and of 0.087 for all 2144 data; the *wR* are 0.156 and 0.173 respectively. The goodness of fit *S* is 1.072 for all 2144 data, based on F^2. Heights in final difference Fourier map ρ_{max} = 0.32 e Å^{-3} and ρ_{min} = –0.40 e Å^{-3}. A perspective view of the molecular structure of **15**[10] was prepared using ORTEP-3 (25).

Superimposition of macrolactam 2 with paclitaxel

Calculations and graphic manipulations were performed on a SiliconGraphics workstation Indigo R4000. The PCMODEL software package (26) equipped with the MMX force field

[10]Supplementary material has been deposited and may be purchased from: The Depository of Unpublished Data, Document Delivery, CISTI, National Rsearch Council of Canada, Ottawa, Ontario, Canada, K1A 0S2. Tables of bond lengths and angles and hydrogen coordinates have also been deposited with the Cambridge Crystallographic Data Centre and can be obtained on request from: The Director, Cambridge Crystallographic Data Centre, 12 Union Road, Cambridge, CB2 1EZ, U.K.

© 2000 NRC Canada

was used in this study to perform all the calculations. Solvent effects were not taken into account. All the graphic manipulations were accomplished using the program InsightII.[11] The lowest-energy conformation of paclitaxel, already determined in a previous study by some of us (10), was used here as the reference geometry. The lowest-energy conformation of **2** was secured by a conformational search performed following the protocol already applied to paclitaxel (10) to perform a reliable structural comparison.

Acknowledgments

Thanks are due to Dr. N. Mongelli, Pharmacia & Upjohn, Milano (Italy) for helpful discussions. Financial support from Pharmacia & Upjohn and the program P.O.P. Regione Calabria 1994–1998 — Misura 4.4 — "Ricerca Scientifica e Tecnologica" is gratefully acknowledged. M.B. wishes to thank the NATO International Scientific Exchange Programme "Bioactive Conformation and Design Mimics for the Anticancer Agent Taxol," 1996, for a collaborative research grant as well as the Merck Research Laboratories for the 1998 Academic Development Program (ADP) Chemistry Award.

References

1. Taxane anticancer agents: basic science and current status. *Edited by* G.I. Georg, T.C. Chen, I. Ojima, and D.M. Vyas. ACS Symposium Series no. 583, Washington, D.C. 1995.
2. (*a*) S.B. Horwitz. Trends Pharmacol. Sci. **13**, 134 (1992); (*b*) M.L. Rothenberg. Curr. Opin. Invest. Drugs, **2**, 1269 (1993).
3. M.C. Wani, H.L. Taylor, M.E. Wall, P. Coggon, and A. Mcphail. J. Am. Chem. Soc. **93**, 2325 (1971).
4. (*a*) R.A. Holton, C. Somoza, H.B. Kim, F. Liang, R.J. Biediger, P.D. Boatman, M. Shido, C.C. Smith, S. Kim, H. Nadizadeh, Y. Suzuki, C. Tao, P. Vu, S. Tang, P. Zhang, K.K. Murthi, L.N. Gentile, and J.H. Liu. J. Am. Chem. Soc. **116**, 1597 (1994); (*b*) R.A. Holton, C. Somoza, H.B. Kim, F. Liang, R.J. Biediger, P.D. Boatman, M. Shido, C.C. Smith, S. Kim, H. Nadizadeh, Y. Suzuki, C. Tao, P. Vu, S. Tang, P. Zhang, K.K. Murthi, L.N. Gentile, and J.H. Liu. J. Am. Chem. Soc. **116**, 1599 (1994); (*c*) K.C. Nicolaou, Z. Yang, J.J. Liu, H. Ueno, P.G. Nantermet, R.K. Guy, C.F. Claiborne, J. Renaud, E.A. Couladouros, K. Paulvannan, and E.J. Sorensen. Nature (London), **367**, 630 (1994); (*d*) K.C. Nicolaou, P.G. Nantermet, H. Ueno, R.K. Guy, E.A. Couladouros, and E.J. Sorensen. J. Am. Chem. Soc. **117**, 624 (1995); (*e*) K.C. Nicolaou, J.J. Liu, Z. Yang, H. Ueno, E.J. Sorensen, C.F. Claireborne, R.K. Guy, C.K. Hwang, M. Nakada, and P.G. Nantermet. J. Am. Chem. Soc. **117**, 634 (1995); (*f*) K.C. Nicolaou, Z. Yang, J.J. Liu, P.G. Nantermet, C.F. Claireborne, J. Renaud, R.K. Guy, and K. Shibayama. J. Am. Chem. Soc. **117**, 645 (1995); (*g*) K.C. Nicolaou, H. Ueno, J.J. Liu, P.G. Nantermet, Z. Yang, J. Renaud, K. Paulvannan, and R. Chadha. J. Am. Chem. Soc. **117**, 653 (1995); (*h*) J.J. Masters, J.T. Link, L.B. Snyder, W.B. Young, and S.J. Danishefsky. Angew. Chem. Int. Ed. Engl. **34**, 1723 (1995); (*i*) S.J. Danishefsky, J.J. Masters, W.B. Young, J.T. Link, L.B. Snyder, T.V. Magee, B.K. Yung, R.C.A. Isaacs, W.G. Bornmann, C.A. Alaimo, C.A. Coburn, and M.J. Di Grandi. J. Am. Chem. Soc. **118**, 2843 (1996); (*j*) P.A. Wender, N.F. Badham, S.P. Conway, P.E. Floreancig, T.E. Glass, C. Gränicher, J.B. Houze, J. Jänichen, D. Lee, D.G., Marquess, P.L. McGrane, W. Meng, T.P. Mucciaro, M. Mühlebach, M.G. Natchus, H. Paulsen, D.B. Rawlins, J. Satkofsky, A.J. Shuker, J.C. Sutton, R.E. Taylor, and K. Tomooka. J. Am. Chem. Soc. **119**, 2755 (1997); (*k*) P.A. Wender, N.F. Badham, S.P. Conway, P.E. Floreancig, T.E. Glass, J.B. Houze, N.E. Krauss, D. Lee, D.G., Marquess, P.L. McGrane, W. Meng, M.G. Natchus, A.J. Shuker, J.C. Sutton, and R.E. Taylor. J. Am. Chem. Soc. **119**, 2757 (1997).
5. (*a*) D. Guénard, F. Guéritte-Voegelein, and P. Potier. Acc. Chem. Res. **26**, 160 (1993); (*b*) K.C. Nicolaou, W.-M. Dai, and R.K. Guy. Angew. Chem. Int. Ed. Engl. **33**, 15 (1994); (*c*) A.N. Boa, P.R. Jenkins, and N.J. Lawrence. Contemp. Org. Synth. **1**, 47 (1994).
6. I. Ogima, S. Chakravarty, T. Inoue, S. Lin, L. He, S.B. Horwitz, S.D. Kuduk, and S.J. Danishefsky. Proc. Natl. Acad. Sci. U.S.A. **96**, 4256 (1999).
7. (*a*) R.B. Greenwald, C.W. Gilbert, A. Pendri, C.D. Conover, J. Xia, and A. Martinez. J. Med. Chem. **39**, 424 (1996), and refs. therein; (*b*) M. Suffness. Annu. Rep. Med. Chem. **28**, 305 (1993).
8. (*a*) J. Kobayashi, H. Hosoyama, X. Wang, H. Shigemori, Y. Koiso, S. Iwasaki, T. Sasaki, M. Naito, and T. Tsuruo. Bioorg. Med. Chem. Lett. **7**, 393 (1997), and refs. therein; (*b*) K.C. Nicolaou, S. Kim, J. Pfefferkorn, J. Xu, T. Ohshima, S. Hosokawa, D. Vourloumis, and T. Li. Angew. Chem. Int. Ed. Engl. **37**, 1418 (1998), and refs. therein; (*c*) D.M. Bollag, P.A. McQueney, J. Zhu, O. Hensens, L. Koupal, J. Liesch, M. Goetz, E. Lazarides, and C.M. Woods. Cancer Res. **55**, 2325 (1995); (*d*) E. Ter Haar, R.J. Kowalski, E. Hamel, C.M. Lin, R.E. Longley, S.P. Gunasekera, H.S. Rosenkranz, and B.W. Day. Biochemistry, **35**, 243 (1996); (*e*) C. Pascal, J. Dubois, D. Guénard, and F. Guéritte. J. Org. Chem. **63**, 6414 (1998), and refs. therein.
9. (*a*) F. Corelli, D. Dei, M. Menichincheri, J.P. Snyder, and M. Botta. Tetrahedron Lett. **38**, 2759 (1997); (*b*) A. Gambacorta, S. Turchetta, S. Stefanelli, and M. Botta. Tetrahedron Lett. **32**, 6805 (1991); (*c*) A. Gambacorta, S. Turchetta, P. Bovicelli, and M. Botta. Tetrahedron Lett. **32**, 9097 (1991).
10. M. Menichincheri, M. Botta, W. Ceccarelli, M. Ciomei, F. Corelli, M. D'Anello, D. Fusar-Bassini, N. Mongelli, E. Pesenti, V. Pinciroli, A. Tafi, and E. Vanotti. Med. Chem. Res. **5**, 534 (1995).
11. F. Orvieto, M. Botta, F. Corelli, and S. Harper. Synth. Commun. **29**, 3635 (1999).
12. C.F.H. Allen and R.K. Kimball. Organic Syntheses, Coll. Vol. II. Wiley, New York. 1943. p. 498.
13. M.E. Flaugh, T.A. Crowell, and D.S. Farlow. J. Org. Chem. **45**, 5399 (1980).
14. Y. Ito, T. Hirao, and T. Saegusa. J. Org. Chem. **43**, 1011 (1978).
15. (*a*) A. Hosomi and H. Sakurai. J. Am. Chem. Soc. **99**, 1673 (1977); (*b*) T.A. Blumenkupf and C.H. Heathcock. J. Am. Chem. Soc. **105**, 2354 (1983); (*c*) M.E. Jung. *In* Comprehensive organic synthesis. Vol. 4. *Edited by* B.M. Trost and I. Fleming. Pergamon Press, Oxford. 1991. pp. 1–67.
16. S.T. Rao, E. Westhof, and M. Sandaralingam. Acta Crystallogr. **A37**, 421 (1981).
17. D. Cremer and J.A. Pople. J. Am. Chem. Soc. **97**, 1354 (1975).
18. C.S. Swindell, N.E. Krauss, S.B. Horwitz, and I. Ringel. J. Med. Chem. **34**, 1176 (1991).

[11]Molecular Simulations Inc., 9685 Scranton Road, San Diego, Calif.

© 2000 NRC Canada

19. S. Blechert, R. Jansen, and J. Velder. Tetrahedron, **32**, 9649 (1994).
20. J. Parness, D.G.I. Kingston, R.G. Powell, C. Harracksingh, and S.B. Horwitz. Biochem. Biophys. Res. Commun. **105**, 1082 (1982).
21. M. Menichincheri, W. Ceccarelli, D. Fusar-Bassini, E. Vanotti, M. Ciomei, N. Mongelli, V. Pinciroli, and A. Vulpetti. Med. Chem. Res. **6**, 264 (1996).
22. D.D. Perrin and W.L.F. Armarego. Purification of laboratory chemicals. 3rd ed. Pergamon Press, Oxford. 1988.
23. M. Casey, J. Leonard, B. Lygo, and G. Procter. Advanced practical organic chemistry. 1st ed. Chapman & Hall, New York. 1990.
24. G.M. Sheldrick. SHELXL-97. A program for the refinement of crystal structures from diffraction data. Institut fuer Anorg. Chemie, Goettingen, Germany. 1997.
25. (*a*) C.K. Johnson and M.N. Burnett. ORTEP-3 for Windows. ORTEP-III, Version 1.0.2; (*b*) J.L. Farrugia. Windows 32-bit version 1.0.4β (February 1998). Dept. of Chemistry, University of Glasgow, U.K.
26. PCMODEL (version 4.0). Molecular Modeling Software, available from Serena Software, Box 3076, Bloomington, Ind.

© 2000 NRC Canada

Conformational effects in the diastereoselective protonation of chiral enolates derived from 2,4-dimethyl-1-tetralone using carbonyl chelating proton donors

Gregory S. Coumbarides, Jason Eames, and Neluka Weerasooriya

Abstract: The synthesis of *syn*-2,4-dimethyl-1-tetralone **6** via a reprotonation strategy using chelating proton donors is discussed. We comment on the comformational effects associated with these acids, and discuss the differences between direct protonation and deprotonation-reprotonation of chiral enolates in the presence of diisopropylamine and LiBr.

Key words: conformation, chelating proton donors, deprotonation-reprotonation strategy, diastereoselective protonation and solvent effects.

Résumé : On discute de la synthèse de la *syn*-2,4-diméthyl-1-tétralone **6** via une stratégie de reprotonation qui utilise des donneurs de protons chélateurs. Nous examinons les effets conformationnels associés à ces acides, et nous discutons des différences entre la protonation directe et la déprotonation-reprotonation des énolates chiraux en présence de la diisopropylamine et du LiBr.

Mots clés : conformation, donneurs de protons chélateurs, stratégie de déprotonation-reprotonation, protonation diastéréosélective, effets de solvant.

[Traduit par la Rédaction]

Diastereoselective protonation of chiral enolates is well documented (1). Of these reports, the majority deal with direct protonation of chiral enolates under either kinetic (2) or thermodynamic substrate control (3). There are fewer cases where the diastereoselective stereochemical determining protonation step is under reagent control (4), the most notable examples being the use of *chelating proton donors* (CPD's) (5) such as salicylic esters **1**, (5) and β-amino alcohols **2** (6). The behaviour of such acids are characterised by their ability to chelate to lithium of an enolate, and thus kinetically direct protonation, regioselectively on carbon of an enolate, like **3**, rather than the preferred kinetic O-protonation for non-coordinating acids to give enols (Scheme 1) (7).

We now wish to report our study into the use of carbonyl based chelating proton donors (like **4**) for regioselective and kinetic C-protonation of enolates by using a similar diastereoselective protonation approach. We also comment on factors (such as the acidity and conformation of the proton donor, solvent, and salt effects) which affect the outcome of the stereoselective protonation step, all of which help to elucidate the mechanism of protonation.

Received January 6, 2000. Published on the NRC Research Press website on June 23, 2000.

G.S. Coumbarides, J. Eames,[1] and N. Weerasooriya. Department of Chemistry, Queen Mary and Westfield College, London E1 4NS, U.K.

[1]Author to whom correspondence may be addressed. Telephone: +44-0171-795-5251. Fax: +44-020-7882-7794. e-mail: J.Eames@qmw.ac.uk

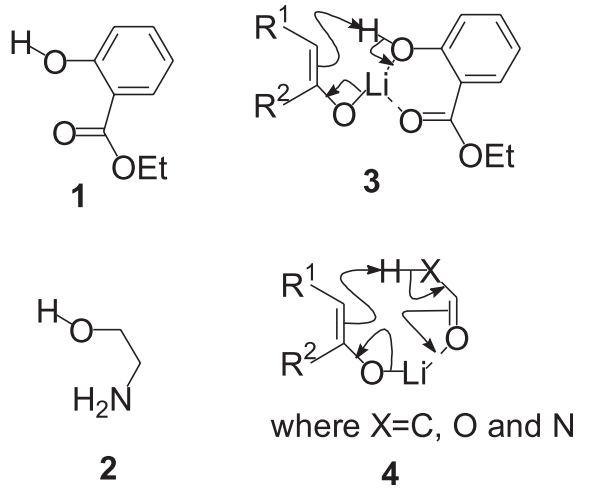
We chose the tetralone framework as our model system because there was no ambiguity with the formation and configuration of the *endo*-cyclic enolate geometry. The 2,4-dimethyl tetralone **6** required for this study was synthesised by deprotonation of the commercially available 4-methyl tetralone **5** with LDA in THF at –78°C, and subsequent alkylation with methyl iodide gave the *syn* and *anti*-2,4-dimethyl tetralone **6** as a partially separable mixture (50:50) of diastereoisomers in excellent yield (Scheme 2). Evidently, methylation of this intermediate chiral enolate occurs equally on both diastereotopic faces and shows that there was no substrate control from the resident stereocentre.

We first studied the diastereoselective protonation of the chiral enolate **8a** in the presence of the diisopropylamine (derived from the LDA), which has previously been documented to cause enolate deaggregation (4) and also act as a competitive base to cause internal proton return (8). Treatment of the diastereoisomeric mixture of 2,4-dimethyl tetralone **6** with LDA in THF at –78°C and re-protonation with a series of carbonyl-based acids gave the diastereoisomeric tetralones *syn*- and *anti*-**6** (Scheme 3).

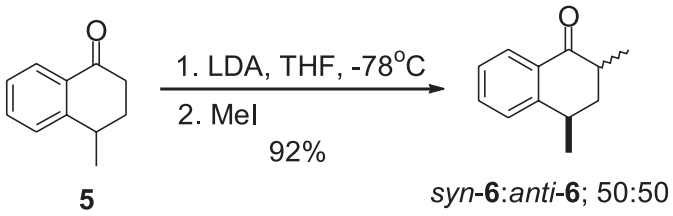
The choice of proton donor (HA) used in this reprotonation step did give rather markedly different results. Conformationally restricted sp^2 nitrogen based amides, such as urea (Scheme 3, entry 1), thiourea (entry 2), and the 2-oxazolidinone (entry 3) gave poor diastereoisomeric control, slightly in favour of the *syn*-diastereoisomer. The ratio was substantially improved by using the more acidic (glacial) acetic acid (entry 4). But, greater diastereoselective control came from mildly acidic carbon-based acids like pentane-2,4-dione and ethyl acetoacetate (entry 5 and 6), whereas

© 2000 NRC Canada

Scheme 1.



Scheme 2.



further addition of an ethyl ester linkage in the form of diethyl malonate (entry 7) caused the selectivity to be reduced dramatically. To attempt to assess whether this control was due to the difference in their coordination ability, conformation, or acidity; we chose to quench the enolate **8a** with conformationally restricted carbon-based acids like dimedone (entry 8) and Meldrum's acid (entry 9). The more acidic dimedone gave substantially lower diastereocontrol with respect to their parent acyclic acid (from 96:4 to 74:26), whereas Meldrum's acid gave an increase (from 52:48 to 79:21). The preferred conformer of such acids are clearly different than that of their near acyclic relatives. Both carbonyl groups are clearly in an fixed eclipsing conformation due to their cyclic framework, and since both gave very similar selectivity it does appear that their relative acidity plays a minor role. Protonation must occur via the conformation (e.g., **9**) leading to the *syn*-tetralone **6** as the major diastereoisomer (Scheme 4). For conformationally mobile acyclic 1,3-dicarbonyl-based acids, such as **10**, their preferred conformation (9) (where both carbonyl groups oppose each other to minimize the molecule's overall dipole moment) must be responsible for the higher diastereoselectivity. We would have imagined that the better the chelator, the tighter the transition state on protonation and therefore the better the selectivity. Because the chelating abilities of such acyclic proton donors are as: diethyl malonate > acetoacetate > pentane-2,4-dione, it does seem rather surprising that the better chelator, diethyl malonate, does not obey this trend. However, it does appear that there is a fine balance between these acids behaving as a coordinating acid like **11a** and as a chelating acid **11b**. When such acids do chelate to the lithium cation of the enolate in the form of **11b**, no stereocontrol was observed and this was presumably due to protonation occurring via the enol acid **11c** (9). The conformers that are responsible for the observed diastereocontrol is illustrated in Scheme 5.

By comparison, direct protonation with MeOH gave a ratio of 60:40 in favour of the *syn*-tetralone **6** (93%). Whereas, under thermodynamic control by treatment of the *syn*-diastereoisomer **6** with *t*-BuOK in THF overnight favoured the equilibrium ratio (50:50). Clearly, the *syn*-diastereoisomer **6** is the kinetic product (relative stereochemistry determined by a 600 MHz NOESY) and thus protonation on the less hindered face of the enolate **8a** is preferred.

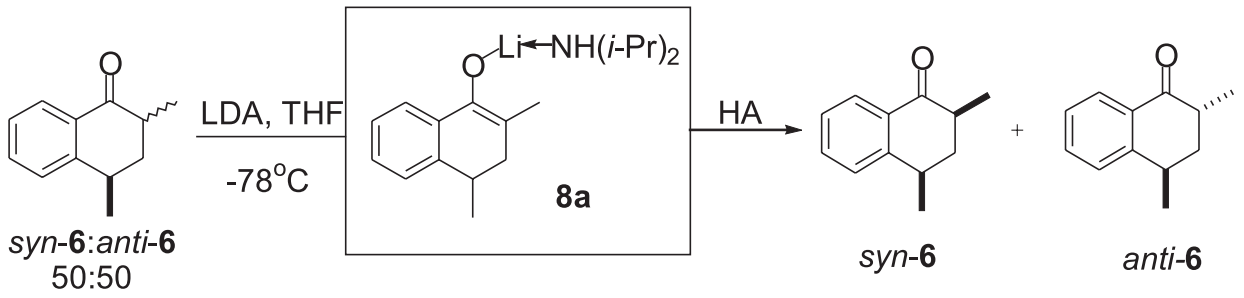
We next probed the effect of the residual diisopropylamine in **8a** on the stereochemistry determining protonation step. We chose to generate the enolate under "base free" conditions using Koga's silyl enol ether procedure (10). Treatment of the 2,4-dimethyl tetralone **6** with LDA at –78°C and quenching with Me_3SiCl gave the required silyl enol ether **12** in near quantitative yield (Scheme 6), and the addition of MeLi at 0°C generated the "base free" chiral enolate **8b**. Direct protonation of this lithium enolate at –78°C with a series of carbonyl chelating proton donors (as shown in Scheme 7) gave the diastereoisomeric tetralone **6** in good yield.

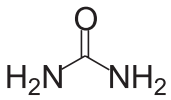
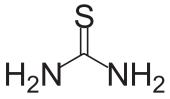
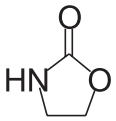
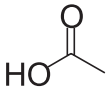
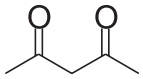
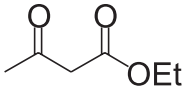
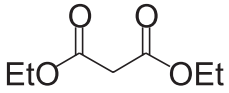
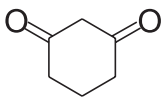
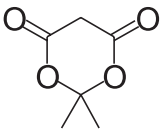
By comparison, in the absence of diisopropylamine, the diastereoselectivity of protonation was substantially reduced for the carbon-based acids, but a slight increase for acetic acid was observed; in all cases the *syn*-diastereoisomer was favoured (Scheme 7: entries 1–5). In the case of glacial acetic acid it appears that diisopropylammonium acetate (by in situ-reaction of acetic acid with diisopropylamine) does act as an additional acid (7) since the presence of the diisopropylamine (Scheme 7: entry 4) did have a detrimental effect on the diastereoselectivity. To determine the degree to which this diisopropylammonium salt behaved as an additional acid, we quenched the enolates **8a** (derived from **6**) and **8b** with diisopropylammonium chloride. A much lower diastereoselectivity was observed giving the *syn*- and *anti*-tetralone **6** in a ratio of 75:25 (85%) and 70:30 (80%) and clearly in these cases the diastereoselectivity was being compromised by competitive protonation from the ammonium salt.

However, in the case of the carbon-based acids, such as the more acidic pentane-2,4-dione, full deprotonation by diisopropylamine is not favoured and proton transfer is known to be much slower, by at least four orders of magnitude (9). Even more surprising, the presence of this amine in the enolate **8a** and not **8b**, clearly makes the enolates different; since the diastereoselectivity of protonation with a better chelator, such as ethyl acetoacetate falls substantially (95:5 to 70:30) in the absence of amine. The enolate **8b** can be converted into **8a** (by the simple addition of diisopropylamine) and quenching with ethyl acetoacetate gives identical diastereoselectivity (95:5) in 83% yield. An attempt to increase the diastereoselectivity by protonation in a non polar solvent like toluene, to promote chelation, only lowered the diastereoselectivity (62:38; 82%) in favour of *syn*-**6**. This results in a much lower diastereoselectivity, and thus a reversal of coordination ability dominants – the poorer the donor, the better the control. As expected, for the conformationally restricted cyclic carbon-based acids no real change occurred.

© 2000 NRC Canada

Scheme 3.

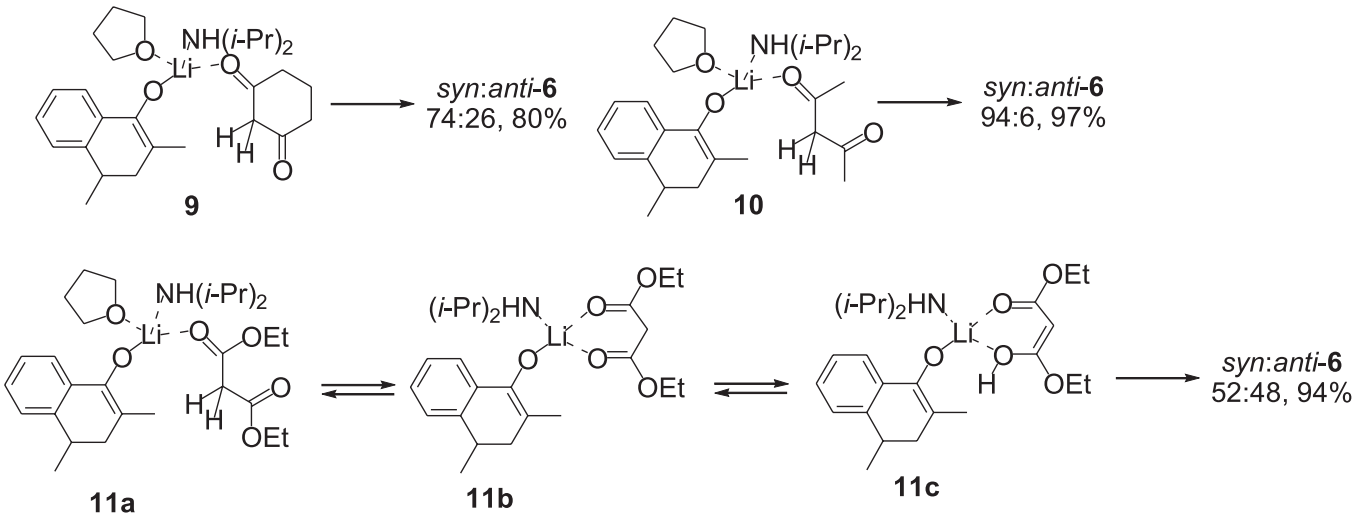


Entry	Acid (HA)	*syn*-**6**:*anti*-**6**	Yield (%)
1		60:40	92
2		62:38	96
3		55:45	93
4		85:15	92
5		94:6	97
6		**95:5**	**98**
7		52:48	94
8		74:29	80
9		79:21	74

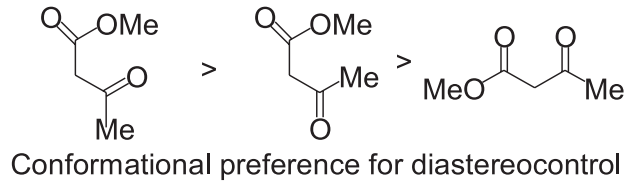
By the simple addition of LiBr to the enolate (by treatment of **7** with a MeLi·LiBr complex) the diastereoselectivity of protonation improved even further (Scheme 7: entries 6–10), giving exclusively the *syn*-tetralone **6** (>98:2 by ^{1}H NMR) by using ethyl acetoacetate as the proton source. The effect of diisopropylamine and LiBr on the behaviour of the lithium enolate is dramatic and appears to create the optimum environment for simple donation from these carbonyl chelating proton donors. This is presumably due to a fine balance between the electronic properties of the lithium enolate aggregate and the ability for direct coordination. Under these conditions, is it surprisingly advantageous to use weakly coordinating 1,3-dicarbonyl acids. It has previously been reported that such proton donors like acetoacetate act as genuine carbon-based acids like **13**, rather than the kinetically preferred oxygen-based enol acids such as **14**. We are currently investigating the degree to which this is true under our reaction conditions.

© 2000 NRC Canada

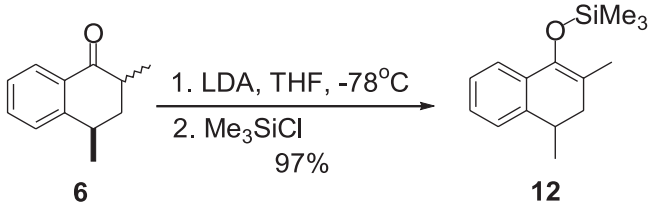
Scheme 4.



Scheme 5.



Scheme 6.



In conclusion, we have shown that carbonyl based acids (like acetic acid, pentane-2,4-dione and acetoactetate) can act as potential *chelating proton donors* for kinetic C-protonation of enolates. Subtle changes in the enolate substructure, conformation of the acid, change in the solvent, and the presence of amine and LiBr, does have a dramatic effect on the observed diastereoselectivity of protonation of these chiral enolates. High diastereoselectivity (up to >98:2) is generally observed in the presence of diisopropylamine and LiBr when using acyclic 1,3-dicarbonyl acids under reagent control.

Experimental

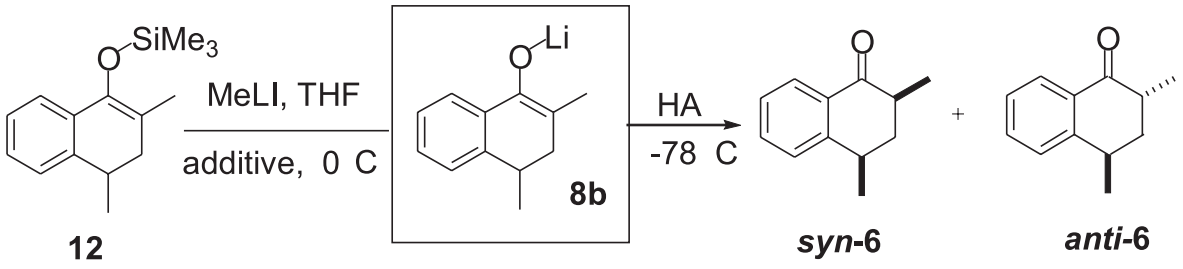
All solvents were distilled before use. Tetrahydrofuran (THF) and ether were freshly distilled from $LiAlH_4$. Triphenylmethane was used as the indicator for THF. All reactions were carried out under nitrogen using oven-dried glassware. Flash column chromatography was carried out using Merck Kieselgel 60 (230–400 mesh). Thin layer chromatography (TLC) was carried out on commercially available pre-coated plates (Merck Kieselgel $60F_{254}$ silica). Proton and carbon NMR spectra were recorded on a Bruker AM 250 Fourier transform spectrometers using an internal deuterium lock. Chemical shifts are quoted in parts per million downfield from tetramethylsilane. Carbon NMR spectra were recorded with broad proton decoupling. Infrared spectra were recorded on a Shimadzu 8300 FTIR machine and mass spectra were recorded on a Kratos 50MSTC machine using a DS503 data system for high resolution analysis.

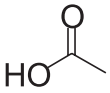
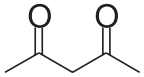
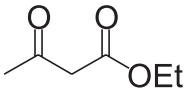
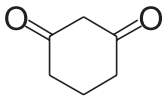
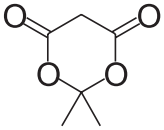
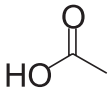
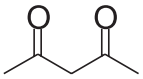
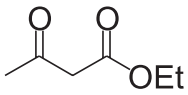
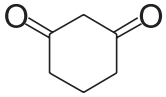
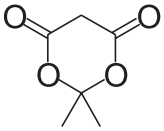
***syn*-(2*RS*,4*SR*)-Dimethyl tetralone 6 and *anti*-(2*RS*,4*RS*)-dimethyl tetralone 6**

4-Methyl tetralone **5** (1.86 g, 1.7 mL, 11.6 mmol) was slowly added dropwise to a stirred solution of LDA (6.38 mL, 2 M in THF, 11.6 mmol) in THF (100 mL) at –78°C and stirred for 20 min. MeI (1.64 g, 0.72 mL, 11.6 mmol) was added and this solution was stirred for 12 h. A solution of NH_4Cl (50 mL) was added and the mixture was extracted with ether (3 × 50 mL). The combined organic layers were dried ($MgSO_4$) and evaporated under reduced pressure. The residue was purified by flash column chromatography on silica gel eluting with light petroleum (bp 40–60°C) – ether (19:1) to give the *syn*- and *anti*-2,4-dimethyl tetralone **6** (1.86 g, 92%) as a colourless oil; R_f (light petroleum (bp 40–60°C):ether (9:1)) 0.5; $\nu_{max}(CHCl_3)$ (cm^{-1}): 2962, 2927 and 2807 (CH), 1685 (CO) and 1600 (br, Ar); δ_H (250 MHz; $CDCl_3$) 8.04 (1H, d, J = 7.0, CH; Ar), 7.51 (3H, t, J = 7.0, CH; Ar), 7.35 (1H. d, J = 7.0, CH; Ar), 7.30 (1H, t, J = 7.0, CH; Ar), 3.20 (1H, m, *CH*Me[a]) 3.06 (1H, septet, J = 7.1, C*H*Me), 2.62 (2H, m, $CH_AH_B{}^s$ and $CH_AH_B{}^a$), 2.20 (2H, m, J = 13.9 and 7.1, $CH_AH_B{}^s$ and $CH_AH_B{}^a$), 1.59 (1H, q, J = 13.9, $CH_AH_B{}^s$), 1.50 (1H, m, $CH_AH_B{}^a$), 1.41 (3H, d, J = 7.1, *Me*CH[s]), 1.40 (3H, d, J = 7.2, *Me*CH[a]), 1.25 (3H, d, J = 7.2, *Me*CH[s]), and 1.23 (3H, d, J = 7.2, *Me*CH[a]); δ_C (67.5 MHz; $CDCl_3$) 200.9[a], 200.8[s], 148.9[a], 148.2[s], 133.3[a], 133.2[s], 132.2[s], 128.3[a], 127.5[a], 127.3[s], 126.5[a], 126.3[s], 126.4[a], 43.0[a], 42.9[s], 41.0[s], 37.94[a], 37.3[a], 31.1[s], 31.7[a], 21.7[a], 20.3[s], 15.7[a], 15.4[s] (Found M^+, 174.1054. $C_{12}H_{14}O$ requires M^+, 174.1044); *m*/*z* 174.1 (5%, M), 173.9 (30, M – CH_2), 130.9 (100, M – COMe), and 117.9 (20, M – COCHMe).

© 2000 NRC Canada

Scheme 7.



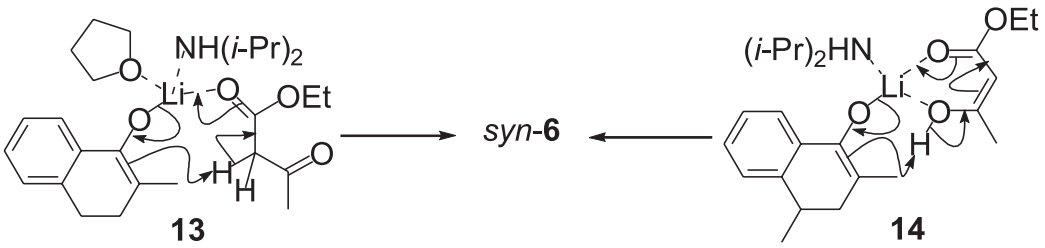
Entry	Acid (HA)	Additive	*syn*-6:*anti*-6	yield (%)
1		none	**95:5**	**87**
2		none	80:20	85
3		none	70:30	78
4		none	90:10	80
5		none	87:13	74
6		LiBr	95:5	88
7		LiBr	**>98:<2**	**84**
8		LiBr	90:10	81
9		LiBr	74:26	80
10		LiBr	70:30	79

2-Trimethylsiloxy-4-methyltetral-2-ene 12

2,4-Methyl tetralone **6** (2.2 g, 12.6 mmol) was slowly added dropwise to a stirred solution of LDA (7.6 mL, 2 M in THF, 15.2 mmol) in THF (100 mL) at –78°C and stirred for 20 min. Me_3SiCl (1.92 g, 2.3 mL, 17.7 mmol) was added and this solution was stirred for 3 h. A solution of NH_4Cl (50 mL) was added and the mixture was extracted with ether (3 × 50 mL). The combined organic layers were dried

© 2000 NRC Canada

Scheme 8.



($MgSO_4$) and evaporated under reduced pressure. The residue was purified by flash column chromatography on silica gel eluting with light petroleum (bp 40–60°C) – ether (19:1) to give the 2-trimethylsiloxy-4-methyltetral-2-ene **12** (3.05 g, 97%) as a colourless oil; R_f (light petroleum (bp 40–60°C):ether (9:1)) 0.9; $\nu_{max}(CHCl_3)$ (cm^{-1}): 2958, 2908 and 2827 (CH), 1654 (br, Ar); δ_H (250 MHz; $CDCl_3$) 7.30–7.1 (4H, m, Ar), 2.89 (1H, sextet, J = 6.9, C*H*Me), 2.45 (1H, dd, J = 15.0 and 6.9, CH_AH_B), 2.10 (1H, dd, J = 15.0 and 6.9, CH_AH_B), 1.80 (3H, s, Me), 1.25 (3H, d, J = 6.9, Me), and 0.2 (9H, s, $SiMe_3$); δ_C (67.5 MHz; $CDCl_3$) 141.8, 140.8, 133.5, 126.5, 125.9, 125.4, 121.75, 114.9, 37.0, 32.2, 20.0, 17.6, 0.6 (Found M^+, 246.0634. $C_{12}H_{22}OSi$ requires M^+, 246.1439); *m*/*z* 246.1 (100%, M) and 74.6 (45, $SiMe_3$).

Typical deprotonation–reprotonation procedure using LDA: 2,4-Methyl tetralone **6** (0.29 g, 1.67 mmol) was slowly added dropwise to a stirred solution of LDA (1 mL, 2 M in THF, 2 mmol) in THF (5 mL) at –78°C and stirred for 20 min. The chosen proton source (2 mmol) was added and this solution was stirred for 30 min. A solution of NH_4Cl (10 mL) was added and the mixture was extracted with ether (3 × 20 mL). The combined organic layers were dried ($MgSO_4$) and evaporated under reduced pressure. The residue was purified by flash column chromatography on silica gel eluting with light petroleum (bp 40–60°C) – ether (19:1) gave the 2,4-dimethyl tetralone **6** as a mixture of diastereoisomers. The *syn*:*anti* ratio of 2,4-dimethyl tetralone **6** was measured by ^1H NMR spectroscopy.

*Typical deprotonation–reprotonation procedure using a "base" free enolate **8b***: A solution of MeLi (0.8 mL, 1 M in ether, 0.8 mmol) was added dropwise to the silyl enol ether **12** (0.2 g, 0.81 mmol) at room temperature. The resulting solution was stirred for 1 h. THF (3 mL) was then added and the solution cooled to –78°C. The chosen proton source (1 mmol) was then added and the solution stirred for 30 min. A solution of NH_4Cl (10 mL) was added and the mixture was extracted with ether (3 × 20 mL). The combined organic layers were dried ($MgSO_4$) and evaporated under reduced pressure. The residue was purified by flash column chromatography on silica gel eluting with light petroleum (bp 40–60°C) – ether (19:1) gave the 2,4-dimethyl tetralone **6** as a mixture of diastereoisomers.

*Typical deprotonation–reprotonation procedure using a "base" free enolate **8b** in the presence of LiBr*: A solution of MeLi–LiBr (0.65 mL, 1.54 M in ether, 1 mmol) was added dropwise to the silyl enol ether **12** (0.25 g, 1 mmol) at room temperature. The resulting solution was stirred for 1 h. THF (3 mL) was then added and the solution cooled to –78°C. The chosen proton source (1 mmol) was then added and the solution stirred for 30 min. A solution of NH_4Cl (10 mL) was added and the mixture was extracted with ether (3 × 20 mL). The combined organic layers were dried ($MgSO_4$) and evaporated under reduced pressure. The residue was purified by flash column chromatography on silica gel eluting with light petroleum (bp 40–60°C) – ether (19:1) gave the 2,4-dimethyl tetralone **6** as a mixture of diastereoisomers.

Acknowledgements

We thank both the Faculty of Natural Science at Queen Mary and Westfield College (University of London), London University Central Research Fund and the Nuffield Foundation (NUF-NAF 99) for grants.

References

1. S. Yanagisawa, T. Watanabe, T. Kikuchi, T. Kuribayahi, and H. Yamamoto. Synlett, 956 (1997).
2. (*a*) U. Gerlach, T. Haubenrich, S. Hunigs, and Y. Keita. Chem. Ber. **126**, 1205 (1993); (*b*) W.R. Baker and J.K. Pratt. Tetrahedron, **49**, 8757 (1993); (*c*) S. Takano, J. Kudo, M. Takahashi, and K. Ogasawara. Tetrahedron Lett. **27**, 2405 (1986); (*d*) S.G. Davies, O. Ichihara, I. Lenoir, and I.A.S. Walters. J. Chem. Soc. Perkin Trans. 1, 1411 (1994); (*e*) S. Takano, W. Uchida, S. Hatakeyama, and K. Ogasawara. Chem. Lett. 733 (1982); (*f*) S. Berrada and P. Metzner. Tetrahedron Lett. **28**, 409 (1987); (*h*) O. Piva. J. Org. Chem. **60**, 7879 (1995).
3. (*a*) H.E. Zimmerman. Acc. Chem. Res. **20**, 263 (1987); (*b*) L. Duhamel, P. Duhamel, J.-C. Launay, and J.-C. Plaquevent. Bull. Soc. Chim. Fr. Pt II 421, (1984); (*c*) M. Tabchen, C. Guibourdenche, L. Pappalardo, M.-L. Roumestant, and P. Viallefont. Tetrahedron: Asymmetry, **9**, 1493 (1998).
4. (*a*) D. Seebach. Angew Chem. Int. Ed. Engl. **27**, 1624 (1988); (*b*) N. Krause, S. Ebert, and A. Haubrich. Liebigs Ann./Recl. 2409 (1997); and refs. therein.
5. N. Krause. Angew. Chem. Int. Ed. Engl. **33**, 1764 (1994).
6. D. Awandi, F. Henin, J. Muzart, and J.-P. Pete. Tetrahedron: Asymmetry, **2**, 1101 (1991**)**.
7. M. Eigen. Angew. Chem. Int. Ed. Engl. **3**, 1 (1964), and refs. therein.
8. T. Laube, J.D. Dunitz, and D. Seebach. Helv. Chim. Acta, **68**, 1371 (1985).
9. (*a*) K. Kalsbeek. Acta Crystallogr. Sect. C: Cryst. Struct. Commun. **48**, 878 (1992); (*b*) D. Adhikesavalu and K. Venkatesan. Acta Crystallogr. Sect. C: Cryst. Struct. Commun. **39**, 1044 (1983); (*c*) J. Emsley, D.J. Jones, and R. Kuroda. J. Chem. Soc. Dalton Trans. 1179 (1982); (*d*) G. Lundgren and B. Aurivillius. Acta Chem. Scand. **18**, 1642 (1964); (*e*) M.A.M. Meester, H. Schenk, and C.H. MacGillavry. Acta

© 2000 NRC Canada

Crystallogr. Sect. B: Struct. Crystallogr. Cryst. Chem. **27**, 630 (1971); (*f*) J.A. Kanters and J. Kroon. Acta Crystallogr. Sect. B: Struct. Crystallogr. Cryst. Chem. **28**, 1345 (1972).

10. T. Yasukata and K. Koga. Tetrahedron: Asymmetry, **4**, 35 (1993).

© 2000 NRC Canada

Benzyloxy(4-substituted benzyloxy)carbenes. Generation from oxadiazolines and fragmentation to radical pairs in solution

Nadine Merkley and John Warkentin

Abstract: Thermolysis of 2,2-dibenzyloxy-5,5-dimethyl-Δ^3-1,3,4-oxadiazoline in benzene at 110°C leads to dibenzyloxycarbene. The carbene was trapped with *tert*-butyl alcohol to afford dibenzyl-*tert*-butyl orthoformate. In the absence of a trapping agent for the carbene, it fragmented to benzyloxycarbonyl and benzyl radicals, as shown by trapping the latter with TEMPO. In the absence of both TEMPO and *tert*-butyl alcohol, the radicals were partitioned between coupling to benzyl phenylacetate and decarboxylation, with subsequent formation of bibenzyl. The preferred sense of fragmentation of the analogous carbenes from benzyloxy-(*p*-substituted-benzyloxy)carbenes was determined by comparing the yields of the two possible esters, $ArCH_2O(CO)CH_2Ph$ and $PhCH_2O(CO)CH_2Ar$. It was found that an electron-withdrawing group in the *para* position favoured fragmentation to the benzylic radical containing that group. A Hammett plot of the data gave a best fit with σ^- substituent constants (r = 0.994, $\rho_{(PhH,\ 110°C)}$ = 0.7) suggesting that the fragmentation involves charge separation in the sense that increases electron density on the group that is becoming a benzylic radical and decreases electron density on the carbonyl group that is becoming the benzyloxycarbonyl radical.

Key words: carbene, dibenzyloxycarbene, fragmentation, substituent effect, radical pair, TEMPO.

Résumé : La thermolyse du 2,2-dibenzyloxy-5,5-diméthyl-Δ^3-1,3,4-oxadiazoline, dans le benzène à 100°C, conduit à la formation de dibenzyloxycarbène. On a piégé le carbène à l'aide d'alcool *tert*-butylique, avec formation d'orthoformiate de dibenzyle et de *tert*-butyle. En absence d'agent pour piéger le carbène, il se fragmente pour conduire à la formation de radicaux benzyloxycarbonyle et benzyle dont l'existence à été démontrée en piégeant le dernier à l'aide de « TEMPO ». En absence d'alcool *tert*-butylique ainsi que de « TEMPO », les radicaux se répartissent entre un couplage conduisant au phénylacétate de benzyle et une décarboxylation avec formation subséquente de dibenzyle. En se basant sur une comparaison des rendements des deux esters possibles, $ArCH_2O(CO)CH_2Ph$ et $PhCH_2O(CO)CH_2Ar$, on a déterminé la voie préférée de fragmentation de carbènes analogues provenant de carbènes portant des groupes benzyloxyles différents, l'un substitué en para et l'autre non substitué. On a trouvé qu'un groupe électroaffinitaire en position para favorise la fragmentation conduisant aux radical benzylique contenant ce groupe. Le meilleur ajustement de la courbe d'Hammett des données est obtenu avec des constantes de substituants σ^- (r = 0,994, $\rho_{(PhH,\ 110°C)}$ = 0,7), ce qui suggère que l'état de transition pour la fragmentation implique une séparation de charge dans le sens qui augmente la densité électronique sur le groupe qui devient un radical benzylique et qui diminue la densité électronique sur le groupe carbonyle qui devient le radical benzyloxycarbonyle.

Mots clés : carbène, dibenzyloxycarbène, fragmentation, effet de substituant, paire de radicaux, « TEMPO ».

[Traduit par la Rédaction]

Introduction

Most reactions of carbenes increase the co-ordination number of the carbene carbon from two to four, as expected for a species having a pair of electrons in a σ–orbital and a virtual *p*-orbital (singlet) or an unpaired electron in each of two singly occupied orbitals (triplet). It may be surprising that stabilized carbenes can break a bond to the carbene carbon, instead of forming new ones, but such a fragmentation has been observed with oxycarbenes and dioxycarbenes. Presumably it is the formation of the strong carbonyl double bond that drives those fragmentations, which can be heterolytic or homolytic. Heterolytic fragmentations, to ion pairs, have been reported when alkoxy(halo)carbenes are generated in a polar solvent such as acetonitrile, Scheme 1 (1–5). Homolytic fragmentations of dioxycarbenes can occur in the gas phase or in non-polar solvents, particularly if one of the oxy groups is allylic or benzylic, Scheme 1 (6–10).

Recently it was reported that methoxy(cinnamyloxy)carbene and its isomer, generated by thermolysis of oxadiazolines **1a** and **1b** in benzene at 110°C (10) fragment to radical pairs. The carbene from **1a** could be trapped with *tert*-butyl alcohol and the radicals could be trapped with TEMPO. Moreover, the sequence oxadiazoline → carbene → radical pair was supported, Scheme 2, by showing that the yield of orthoformate increased, at the expense of esters, with

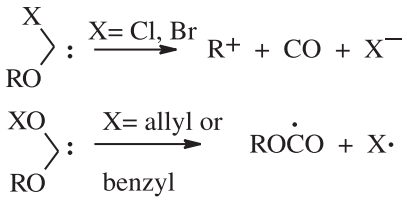
Received January 10, 2000. Published on the NRC Research Press website on July 6, 2000.

N. Merkley and J. Warkentin.[1] Department of Chemistry, McMaster University, Hamilton, ON L8S 4M1, Canada.

[1]Author to whom correspondence may be addressed. Fax: (905) 522-2509. e-mail: warkent@mcmaster.ca

© 2000 NRC Canada

Scheme 1.

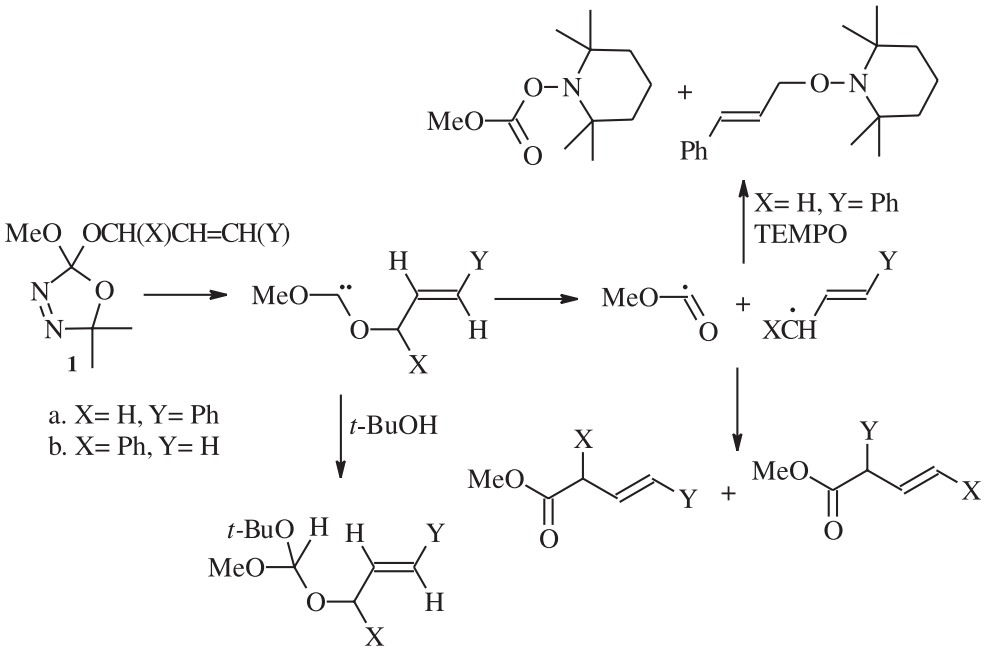


increasing concentration of carbene trap. More recently benzyloxymethoxycarbene was shown to fragment similarly, to methoxycarbonyl and benzyl radicals, and again both the carbene and the radicals were trapped (11). Although *p*-substituted benzyloxy oxadiazolines were studied also, it was not possible to make strong inferences about the effects of *p*-substituents on the ease of carbene fragmentation from the yields of esters, which were below 50%. In those circumstances a dependence of yields on substituents could possibly be attributed to a substituent effect on a competing reaction, such as the observed alternative fragmentation of the oxadiazolines to carbonates and diazopropane (11). For that reason we prepared unsymmetric bis-benzyloxy oxadiazolines in order to have internal competition in a carbene that could fragment to either the benzyl radical and a *p*-substituted benzyloxycarbonyl radical or to a *p*-substituted benzyl radical and the benzyloxycarbonyl radical. We now report the results of that study.

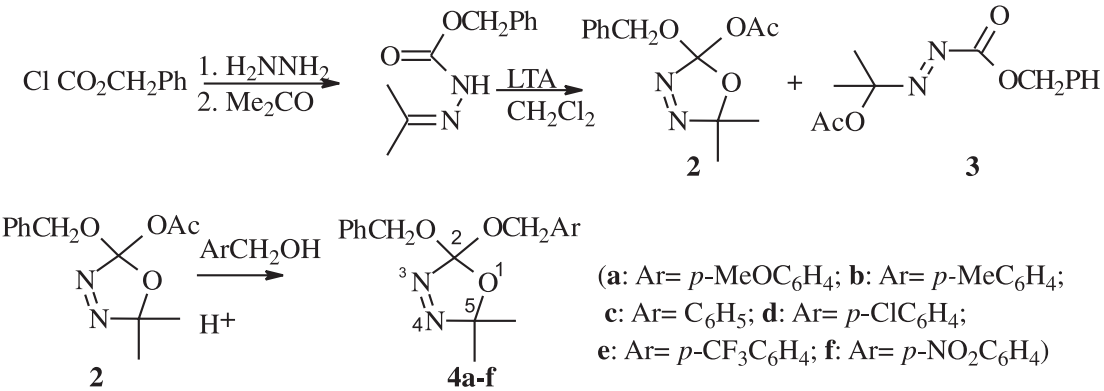
Methods results and discussion

The oxadiazoline substrates (**4a**–**f**) were prepared from a common precursor, namely 2-acetoxy-2-benzyloxy oxadiazoline (**2**), by means of the substitution reaction in Scheme 3. Precursor **2** was obtained by oxidative cyclization of the benzyloxycarbonyl hydrazone of acetone with lead tetraacetate in dichloromethane, which afforded **2** and **3** in the ratio 60:40. Although that mixture could be used directly for the substitution, substantial purification was achieved by washing with base and subsequent chromatography on silica. The oxadiazoline produced in this way did contain a small amount (ca. 5%) of dibenzyl carbonate and the final yield of that product from the thermolysis was corrected for the

Scheme 2.

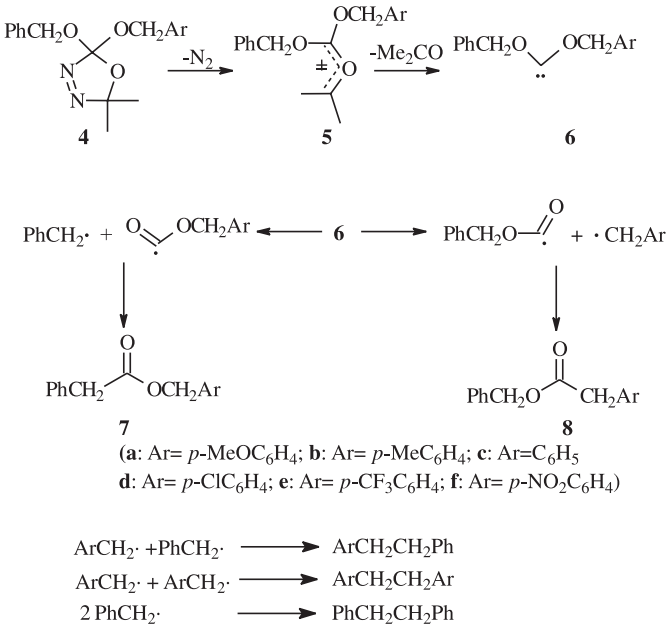


Scheme 3.



© 2000 NRC Canada

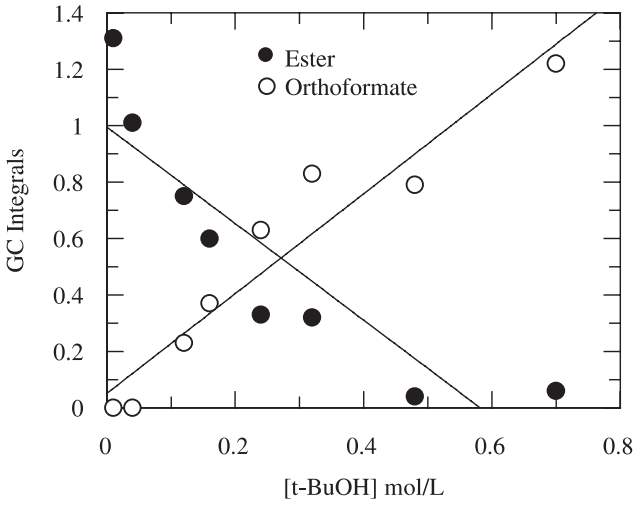
Scheme 4.



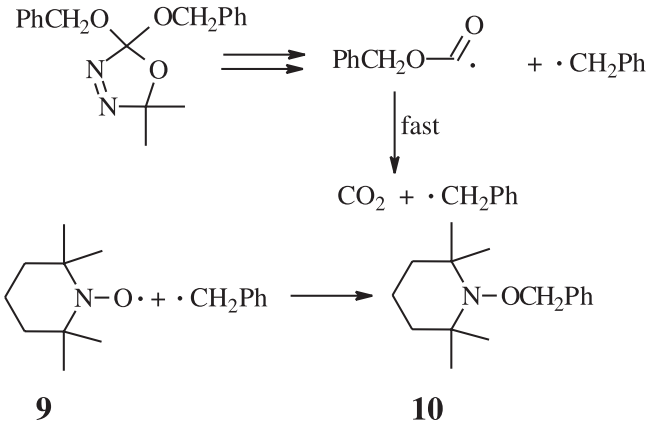
quantity initially present. Thermolyses were done in evacuated, sealed glass tubes that were heated for 24 h at 110.0 ± 0.1°C with an oil bath.

The mechanism of thermolysis of oxadiazolines analogous to **4** generally involves 1,3-dipolar cycloreversion in the first step, to afford a carbonyl ylide intermediate (12–14). The latter then fragments to acetone and a dialkoxycarbene, Scheme 4. An alternative mechanism, proposed by Smith (15) on the basis of computation, involving concerted fragmentation to N_2, acetone, and dialkoxycarbenes, cannot be ruled out for an oxadiazoline with new substituents. In the present case, knowledge of the mechanism by which the carbene intermediate is generated is not critical, nor does the carbene have to be formed in essentially quantitative yield. In Scheme 4, stepwise fragmentation is illustrated with the important feature being the intramolecular competition in the fragmentation of carbene **6**. Formation of a carbene intermediate was established by trapping **6c** with *tert*-butyl alcohol (Fig. 1). It was assumed that the other oxadiazolines formed analogous carbenes, albeit not necessarily with the same efficiency. Products from thermolysis of **4c** in the absence of a trap included acetone (88%),[2] bibenzyl (14%), benzyl phenylacetate (29%), dibenzyl carbonate (6%), a trace of benzyl alcohol, benzyl formate (22%), and tribenzyl orthoformate (19%). The latter two are presumably derived from adventitious water, which traps the carbene intermediate to form benzyl formate and benzyl alcohol via the hemi orthoformate. Benzyl alcohol then traps the carbene to generate the orthoformate. Products from **4a**, **b**, and **d**–**f** were more complex, containing three bibenzyls (primarily $ArCH_2CH_2Ph$, with smaller amounts of $PhCH_2CH_2Ph$ and $ArCH_2CH_2Ar$), two orthoformates, ($HC(OPh)_2OAr$ and

Fig. 1. GC integrals, on an arbitrary scale, vs. concentration of *tert*-BuOH. The scatter is believed to be caused by the various concentrations of adventitious water.



Scheme 5.



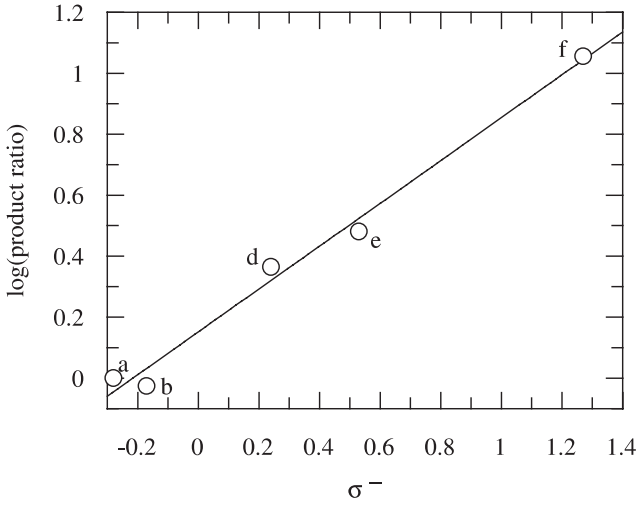
$HCOPh(OAr)_2$), an unsymmetric carbonate ($ArOCO_2Ph$) (all indicated by GC/MS), and two esters. The product composition was not determined in detail but it was possible to determine the relative yields of esters **7** and **8** in each case, although the C_6D_6 had to be evaporated and replaced with CCl_4 in the case of products from **4a** because the ^1H NMR signals of interest were not resolved in benzene solution. Identities of the isomers **7** and **8** in each of the reaction mixtures were secured through comparison with the ^1H NMR spectra of authentic compounds.

The bibenzyls are strong indicators of radical chemistry and radical intermediates were confirmed by capturing benzyl radicals from **4c** with TEMPO, Scheme 5. Trapping of benzyloxycarbonyl radicals with TEMPO was not to be expected because the rate constant for decarboxylation of benzyloxycarbonyl radicals has the value $k_{110°C} \approx 10^9\ s^{-1}$ (extrapolated from published data) (16). In the case of benzyloxymethoxycarbene, both the methoxycarbonyl and benzyl radicals were trapped with TEMPO (**9**) (11).

[2] We have not always used an adequate pulse delay when examining oxygen-free solutions by ^1H NMR spectroscopy. The yield of acetone, in particular, comes out too low if an inadequate pulse delay is used.

© 2000 NRC Canada

Fig. 2. Logarithms of the ratios of esters (**8**/**7**) versus σ^- substituent constants.



The sense and magnitude of the selectivity in the carbene fragmentation step should be reflected in the relative yields of esters **7a**, **b**, **d**–**f** and **8a**, **b**, **d**–**f** from the corresponding precursors (**4a**, **b**, **d**–**f**). The results show clearly that there is selectivity in the sense favouring fragmentation to afford the benzylic radical with an electron-withdrawing group in the *para* position. The ratios (**8**:**7**) were: **a**, 1.0; **b**, 0.94; **d**, 2.3; **e**, 3.0; **f**, 11.4. A good correlation of logarithms of product ratios (assumed to reflect the ratios of fragmentation rate constants well) with σ^- substituent constants was found, with $\rho_{(PhH,\ 110°C)} = 0.7$, (Fig. 2), indicating that the fragmentation of the carbenes is lower in energy if electron density is allowed to increase at the carbon atom that is becoming the benzylic radical fragment. A corollary is that the electron density at the other developing fragment must decrease correspondingly. The correlation with σ^- suggests that the fragmentation has more polar character (benzyl anion-like and benzyloxycarbonyl cation-like) than radical character. Whether or not there is a transition state for the homolysis is not known. For homolysis of a model system there is a transition state only for the conformation with the departing group *syn* to the carben's lone pair (9).

The benzyloxycarbonyl–benzyl radical pair is formed in the singlet state (9, 10, 17) in a solvent cage. Coupling in the cage must be very fast, given that it can compete with both decarboxylation of the benzyloxycarbonyl radical and diffusive separation of that pair. Very fast coupling of such pairs is reasonable, given that the rate constant for cage coupling is not limited by diffusion but only by a very small kinetic barrier, if any. An alternative explanation would have the esters originating from 1,2-rearrangement of the carbenes rather than from radical coupling. Carbene rearrangement is very unlikely, given that computation shows the barrier to fragmentation to be much lower than that for 1,2-rearrangement in allyloxyhydroxycarbene, a model for **6** (17).

Experimental

General

Although some of the compounds encountered in this work have been reported previously, NMR and spectra were generally not included. We report NMR spectra for both $CDCl_3$ and C_6D_6; the latter because reactions were run in C_6D_6. Chemical shifts (ppm) for $CDCl_3$ are referenced to TMS, while those for C_6D_6 are referenced to *p*-xylene (2.10 ppm) or 1,4-dimethoxybenzene (6.80 ppm). The numbers in brackets in the MS data are relative signal intensities.

Synthesis of oxadiazolines (4)

A solution of benzyl chloroformate (10.0 mL, 0.071 mol) in ether (72 mL) was added slowly (ca. 1 h) to a cooled solution (–5°C) of hydrazine monohydrate (16.8 mL, 0.33 mol) in ether (10.0 mL) (18). After addition, the ice bath was removed and stirring was continued for 1 h. The white precipitate formed during the reaction dissolved upon the addition of water. The ether layer was separated and washed three times with water (25 mL) before it was dried with magnesium sulphate. After filtering, the ether was removed with a rotary evaporator to leave benzyl hydrazinocarboxylate as a white solid (7.55 g, 0.045 mol), 82% yield, mp 65–66°C; ^{1}H NMR (200 MHz, $CDCl_3$) δ: 3.74 (s, 2H, NH_2), 5.12 (s, 2H, CH_2O), 6.12 (s, 1H, NH), 7.3 (m, 5H); ^{13}C NMR (50 MHz, $CDCl_3$) δ: 67.34 (CH_2), 128.21, 128.34, 128.57, 136.03, 155.55 (C=O); MS (EI) *m*/*z*: 122 (9), 91 (100), 65 (9); MS (CI, NH_3) *m*/*z*: 184 ($(M + NH_4)^+$, 33), 167 ($(M + H)^+$, 100), 123 (12), 108 (21), 91 (62).

Magnesium sulphate (5g) was added to a solution of benzyl hydrazinocarboxylate (7.55 g, 0.045 mol) in 40 mL of acetone and the reaction mixture was stirred overnight. The magnesium sulphate was removed by vacuum filtration and the solvent was removed with a rotary evaporator. The resultant white solid (**1**) (7.15 g, 82%) melted at 75–77°C, lit (19) mp 85°C; ^{1}H NMR (200 MHz, $CDCl_3$) δ: 1.76 (s, 3H), 2.00 (s, 3H), 5.21 (s, 2H), 7.34 (m, 5H); ^{13}C NMR (50 MHz, $CDCl_3$) δ: 16.08 (CH_3), 25.28 (CH_3), 67.33 (CH_2), 128.31, 128.41, 128.52, 135.98, 151.14 (C=N), 154.80 (C=O); MS (EI) *m*/*z*: 206 (M^+, 1), 91 (100), 65 (10), 49 (22); MS (CI, NH_3) *m*/*z*: 207 ($(M + H)^+$, 100), 91 (32).

Acetone benzyloxycarbonyl hydrazone (7.15 g, 0.037 mol) in dichloromethane (70 mL) was added dropwise to a solution of lead (IV) acetate (28.0 g, 0.106 mol) in ice-cold dichloromethane (60 mL) under nitrogen. After the addition the ice bath was removed and the solution was stirred for two hours. The mixture was filtered through Celite and washed once with water and twice with 5% sodium bicarbonate. After filtration through a layer of Celite to remove additional lead salts, the dichloromethane layer was dried over magnesium sulphate. Fitration and evaporation of the solvent left a yellow oil (5.43 g, 58%) which was a mixture of the oxadiazoline **2** (60 parts) and the acyclic by-product **3** (40 parts). ^{1}H NMR of **2** (200 MHz, $CDCl_3$) δ: 1.52 (s, 3H, CCH_3), 1.67 (s, 3H, CCH_3, 2.10 (s, OAc, overlapping with OAc signal from **3**), 4.91 (d, ^2J = 8.6 Hz, 1H), 4.99 (d, ^2J = 8.6 Hz, 1H), 7.2–7.5 (m, overlapping with m from **3**, the overlapping signals integrated satisfactorily; ^{1}H NMR of **3** (200 MHz, $CDCl_3$) δ: 1.63 (s, 6H, $C(CH_3)_2$, 2.10 (s, OAc, overlapping with OAc signal from **2**), 5.40 (s, 2H, CH_2), 7.2–7.5 (m, overlapping with m from **2**), the overlapping signals integrated satisfactorily; ^{13}C NMR (composite spectrum, 50 MHz, $CDCl_3$) δ: 20.51 (H_3CC=O), 21.39 (H_3C-C=O), 22.45 (CH_3), 24.12 (CH_3), 24.47 (CH_3), 25.27 (CH_3), 67.51 (CH_2), 69.96 (CH_2), 122.47 (C5), 127.89, 128.10,

© 2000 NRC Canada

128.45, 128.66, 128.71, 128.79, 133.18, 134.14, 136.08 (C2), 166.45 (O(C=O) 169.17 (N-C=O-O).

Benzyl alcohol (0.48 g, 4.4 mmol) and a mixture of **2** and **3** (above, 0.10 g, 3.7 mmol) were dissolved in dichloromethane (30 mL) before trifluoroacetic acid (0.096 mL, 1.25 mmol) was added to the reaction mixture. After stirring for approximately 1 h, progress was monitored by ^{1}H NMR spectroscopy, revealing that the pair of doublets at 4.93 ppm had been replaced with a new pair of doublets at 4.85 ppm (200 MHz, $CDCl_3$). Aqueous NaOH (35 mL) was added and the mixture was stirred for another hour. The dichloromethane layer was separated, washed twice with water (15 mL), and dried over magnesium sulphate. After filtration and removal of the dichloromethane the components of the reaction mixture were separated by means of centrifugal chromatography (Chromatotron, 100% hexanes). The pale yellow oil obtained (0.29 g, 41%) was **4c** containing about 4.5% of dibenzylcarbonate. ^{1}H NMR (300 MHz, C_6D_6) δ: 1.30 (s, 6H), 4.80 (d, ^2J = –11.6 Hz, 2H, CH_2Ph), 4.91 (d, ^2J = –11.6 Hz, 2H, CH_2Ph), 7.06–7.41 (m, 10H); ^{1}H NMR (200 MHz, $CDCl_3$) δ: 1.50 (s, 6H), 4.76 (d, ^2J = –11.4 Hz, 2H, CH_2Ph), 4.86 (d, ^2J = –11.4 Hz, 2H, CH_2Ph), 7.30–7.35 (m, 10H); ^{13}C NMR (50 MHz, $CDCl_3$) δ: 24.1 (CH_3), 66.9 (CH_2), 119.6 (C5), 127.8, 127.9, 128.4, 136.2 (C2), 136.7.

Oxadiazolines **4a**, **b**, and **d**–**f** were prepared by the above procedure for **4c**, with substituted benzyl alcohols instead of benzyl alcohol

4a: Yellow oil, yield 53%; ^{1}H NMR (200 MHz, $CDCl_3$) δ: 1.59 (s, 6H), 3.79 (s, 3H), 4.72 (d, ^2J = –11.2 Hz, 1H), 4.78 (d, ^2J = –11.5 Hz, 1H), 4.83 (d, ^2J = –11.2 Hz, 1H), 4.88 (d, ^2J = –11.5 Hz, 1H), 6.86 (d, ^3J = 8.62 Hz, 2H) 7.29–7.33 (m, 7H); ^{1}H NMR (200 MHz, C_6D_6) δ: 1.23 (s, 3H), 1.25 (s, 3H), 3.27 (s, 3H), 4.72–4.92 (m, 4H), 6.69 (d, ^3J = 6.6 Hz, 2H), 6.71–7.25 (m, 7H); ^{13}C NMR (50 MHz, $CDCl_3$) δ: 24.01, 55.14, 66.56, 66.69, 113.71, 119.32 (C5), 127.67, 128.27, 128.67, 129.45, 136.66 (C2, PhC1), 159.31(ArC4) MS (EI) *m*/*z*: 191 (3), 163 (51), 121 (100), 91 (87), 84 (24), 43 (24); MS (CI, NH_3) *m*/*z*: 260 (4), 163 (20), 121 (100), 108 (23), 65 (8), 43 (12).

4b: Clear oil, yield 41%; ^{1}H NMR (200 MHz, $CDCl_3$) δ: 1.59 (s, 6H), 2.35 (s, 3H), 4.74 (d, ^2J = –11.0 Hz, 1H), 4.83 (d, ^2J = –11.0 Hz, 2H), 4.89 (d, ^2J = –11.4 Hz, 1H), 7.14–7.35 (m, 9H); ^{1}H NMR (300 MHz, C_6D_6) δ: 1.24 (s, 2H), 1.25 (s, 3H), 2.09 (s, 3H), 4.73–4.94 (m, 4H), 6.90–7.28 (m, 9H); ^{13}C NMR (75 MHz, $CDCl_3$) δ: 21.09, 24.04, 66.72, 119.37 (C5), 127.71. 127.84, 128.29, 128.99, 133.56, 136.55 (C2), 136.67; MS (EI) *m*/*z*: 181 (3), 105 (95), 91 (100), 43 (10); MS (CI, NH_3) *m*/*z*: 274 (3), 147 (8), 122 (18), 105 (100), 91 (53).

4d: Pale yellow oil, yield 80%; ^{1}H NMR (200 MHz, $CDCl_3$) δ: 6.56 (s, 6H), 4.74 (d, ^2J = –11.6 Hz, 2H), 4.84 (d, ^2J = –11.6 Hz, 2H), 7.24–7.34 (m, 9H); ^{1}H NMR (300 MHz, C_6D_6) δ: 1.21 (s, 3H), 1.22 (s, 3H), 4.57 (d, ^2J = –11.8 Hz, 1H), 4.66 (d, ^2J = –11.8 Hz, 1H), 4.68 (d, ^2J = –11.6 Hz, 1H), 4.78 (d, ^2J = –11.6 Hz, 1H), 6.88 (d, ^3J = 8.6 Hz, 2H), 7.00–7.12 (m, 5H), 7.21 (d, ^3J = 8.6 Hz, 2H); ^{13}C NMR (75 MHz, $CDCl_3$) δ: 24.00, 24.07, 66.02, 66.78, 119.63 (C5), 127.69, 127.8, 128.36, 128.48, 129.03, 133.61, 135.19, 136.47 (C5); MS (EI) *m*/*z*: 237 (3), 203 (3), 195 (4), 167 (10), 125 (44), 105 (12), 91 (100); MS (CI, NH_3) *m*/*z*: 294 (5), 142 (12), 125 (33), 91 (100).

4e: Clear oil, yield 68%; ^{1}H NMR (200 MHz, $CDCl_3$) δ: 1.48 (s, 3H), 1.49 (s, 3H), 4.64 (d, ^2J = –11.5 Hz, 1H), 4.71 (d, ^2J = –13.9 Hz, 1H), 4.75 (d, ^2J = –13.9 Hz, 1H), 4.84 (d, ^2J = –11.5 Hz, 1H), 7.15–7.24 (m, 5H), 7.35 (d, ^3J = 8.0 Hz, 2H), 7.50 (d, ^3J = 8.0 Hz, 2H); ^{1}H NMR (300 MHz, C_6D_6) δ:1.26 (s, 6H), 4.60–4.82 (m, 4H), 6.97–7.26 (m, 9H); ^{13}C NMR (75 MHz, $CDCl_3$) δ: 24.00, 24.12, 65.96, 66.87, 119.33 (C5), 125.33, 127.61, 127.72, 127.97, 128.40, 136.43 (C2), 136.64; ^{19}F NMR (282 MHz, $CDCl_3$, ref. CCl_3F) δ: –62.80 (s); MS (EI) *m*/*z*: 249 (2), 229 (2), 159 (56), 133 (57), 91 (100); MS (CI, NH_3) *m*/*z*: 328 (2), 176 (9), 159 (18), 108 (42), 91 (100).

4f: Yellow oil, yield 56%; ^{1}H NMR (200 MHz, $CDCl_3$) δ: 1.57 (s, 3H), 1.59 (s, 3H), 4.71 (d, ^2J = –11.4 Hz, 1H), 4.79 (d, ^2J = –11.4 Hz, 1H), 4.88 (d, ^2J = –13.1 Hz, 1H), 4.97 (d, ^2J = –13.1 Hz, 1H), 7.24–7.32 (m, 5H), 7.47 (d, ^3J = 8.6 Hz, 2H), 8.16 (d, ^3J = 8.6 Hz, 2H); ^{1}H NMR (300 MHz, C_6D_6) δ: 1.23 (s, 6H), 4.53–4.72 (m, 4H), 6.82 (d, ^3J = 8.8 Hz, 2H), 7.00–7.21 (m, 5H), 7.74 (d, ^3J = 8.8 Hz, 2H); ^{13}C NMR (75 MHz, $CDCl_3$) δ: 23.89, 24.11, 65.46, 66.85, 119.96 (C5), 123.48, 127.64, 127.73, 127.96, 128.36, 136.24, 136.48 (C2), 144.19, 147.36; MS (EI) *m*/*z*: 137 (13), 136 (95), 91 (100), 49 (24), 43 (16); MS (CI, NH_3) *m*/*z*: 254 (2), 153 (13), 136 (24), 107 (60), 91 (100), 60 (16).

Typical thermolysis of an oxadiazoline

The following procedure for **4c** was also followed for the others except that *p*-xylene was the reference. Signals from 1,4-dimethoxybenxene interfered in those cases. Neither internal standard reacted to afford any products detectable by GC/MS.

A solution of dibenzyloxy oxadiazoline (**4c**, 15.9 mg, 0.05mmol) containing 4.6% of dibenzyl carbonate and 1,4-dimethoxybenzene (1.0 mg, 0.0072 mmol) as internal standard, in 0.52 mL of benzene-d_6 in an NMR tube was degassed three times (freeze-pump-thaw sequence) before sealing. The NMR tube was then kept for 24 h in an oil bath at 110 ± 0.1°C. Product yields were determined by ^{1}H NMR spectroscopy, with a pulse delay time of 3 min for products from **4c** and 5 min for the other mixtures, to ensure reliable integral ratios for **7** and **8** (average of 5 intergrations). Chemical shifts (CH_2CO) in C_6D_6 (those of **7a** and **8a** in CCl_4) used for measurement of those relative yields were: *p*-xylene, 2.10; 1,4-dimethoxybenzene, 6.80; **7a**, 3.52; **8a**, 3.48; **7b**, 3.32; **8b**, 3.34; **7d**, 3.29; **8d**, 3.12; **7e**, 3.31; **8e**, 3.14; **7f**, 3.31; **8f**, 3.06.

Products from **4c** were: acetone, 88%, ^{1}H NMR (200 MHz, C_6D_6) δ: 1.606 (s). Bibenzyl, 14%, ^{1}H NMR (200 MHz, C_6D_6) δ: 2.78 (s, 4H), 7.02–7.20 (m, overlap with other signals); GC/MS (EI) *m*/*z*: 182 (M^+, 26), 91 (100), 65 (13). Benzyl phenylacetate, 29%, ^{1}H NMR (200 MHz, C_6D_6) δ: 3.38 (s, 2H), 4.96 (s, 2H), 7.02–7.20 (m, overlap with other signals); GC/MS (EI) *m*/*z*: 226 (M^+, 1), 91 (100), 65 (10). Dibenzyl carbonate, 6%, ^{1}H NMR (200 MHz, C_6D_6) δ: 4.98 (s, 4H), 7.02–7.20 (m, overlap with other signals), GC/MS (EI) *m*/*z*: 180 (33), 151 (26), 107 (60), 91 (100), 79 (48), 65 (29). Tribenzyl orthoformate,

© 2000 NRC Canada

19%, ^{1}H NMR (200 MHz, C_6D_6) δ: 4.66 (6H), 5.46 (s, 1H), 7.02–7.20 (overlap with other signals); GC/MS (EI), *m/z*: 197 (9), 181 (10), 107 (10), 91 (100). Benzyl formate, 22%, ^{1}H NMR (200 MHz, C_6D_6) δ: 4.91 (2H), 7.02–7.20 (m, overlap with other signals), 7.60 (1H).

Synthesis of benzyl arylacetate reference compounds

The required arylacetyl chloride **8a**, **b**, **d–f** (0.061 g, 6.4 mmol) was dissolved in benzene (5 mL) and added slowly to a solution of benzyl alcohol (0.16 g, 0.8 mmol) in pyridine (0.2 mL, 2.3 mmol) which was cooled in an ice bath. After addition the stirring was continued for one hour. The benzene layer was washed twice with water (5 mL), and dried with magnesium sulphate. After filtration and evaporation of the benzene, the ^{1}H NMR spectrum in C_6D_6, referenced to *p*-xylene at 2.10 ppm, was recorded.

8c: (20) pale yellow oil; ^{1}H NMR (200 MHz, $CDCl_3$) δ: 3.60 (s, 2H), 5.03 (s, 2H), 7.08–7.29 (m, 10H); ^{1}H NMR (300 MHz, C_6D_6) δ: 3.40 (s, 2H), 4.97 (s, 2H), 7.09–7.22 (m, 10H); ^{13}C NMR (50 MHz, $CDCl_3$) δ: 41.33, 66.61, 128.18, 128.54, 129.27, 135.83, 171.39 (C=O); ^{13}C NMR (75 MHz, C_6D_6) δ: 41.35, 66.42, 128.2, 128.3, 128.7, 129.6, 134.5, 170.92 (C=O). GC/MS (EI) *m/z*: 226 (M^+, 1), 91 (100), 65 (10).

8a: (21–23) Oil; ^{1}H NMR (200 MHz, $CDCl_3$) δ: 3.59 (s, 2H), 3.78 (s, 3H), 5.10 (s, 2H), 6.84 (d, ^3J = 8.6 Hz, 2H), 7.16–7.30 (m, 7H); ^{1}H NMR (300 MHz, C_6D_6) δ: 3.23 (s, 3H), 3.32 (s, 2H), 4.92 (s, 2H), 6.68 (d, ^3J = 8.7 Hz, 2H), 7.00–7.08 (m, 7H); ^{13}C NMR (50 MHz, $CDCl_3$) δ: 40.43, 55.26, 66.55, 114.00, 128.10, 128.51, 130.30, 132.29, 172.93 (C=O).

8b: (24) Oil; ^{1}H NMR (200 MHz, $CDCl_3$) δ: 2.33 (s, 3H), 3.63 (s, 2H), 5.13 (s, 2H), 7.10–1.33 (m, 9H); ^{1}H NMR (300 MHz, C_6D_6) δ: 2.02 (s, 3H), 3.34 (s, 2H), 4.90 (s, 2H), 6.87–7.12 (m, 9H); ^{13}C NMR (50 MHz, $CDCl_3$) δ: 21.03, 40.91, 66.53, 128.09, 128.49, 129.24, 130.83, 135.92, 136.70, 171.57 (C=O); MS (EI) *m/z*: 240 (M^+, 25), 193 (13), 181 (16), 105 (100), 91 (76); MS (CI, NH_3) *m/z*: 258 (($M + NH_4$)$^+$, 13), 241 (($M + H$)$^+$, 5), 216 (79), 108 (51), 91 (100).

8d: (23) oil; ^{1}H NMR (300 MHz, $CDCl_3$) δ: 3.60 (s, 2H), 5.10 (s, 2H), 7.16–7.32 (m, 9H); ^{1}H NMR (300 MHz, C_6D_6) δ: 3.13 (s, 2H), 4.88 (s, 2H), 6.76 (d, ^3J = 8.4 Hz, 2H), 6.79–7.15 (m, 7H); ^{13}C NMR (75 MHz, $CDCl_3$) δ: 40.52, 66.69, 128.09, 128.24, 128.49, 130.60, 132.25, 133.04, 170.91 (C=O); MS (EI) *m/z*: 260 (M^+, 10), 181 (10), 127 (24), 125 (60), 91 (100), 65 (16), 63 (10); MS (CI, NH_3) *m/z*: 278 (($M + NH_4$)$^+$, 55), 125 (44), 108 (49), 91 (100), 80 (42); HRMS calculated for $C_{15}H_{13}O_2Cl$: 260.0604, found: 260.0603.

8e: Oil; ^{1}H NMR (300 MHz, $CDCl_3$) δ: 3.71 (s, 2H), 5.13 (s, 2H), 7.28–7.35 (m, 5H) 7.38 (d, ^3J = 8.1 Hz, 2H), 7.56 (d, ^3J = 8.1 Hz, 2H); ^{1}H NMR (300 MHz, C_6D_6) δ: 3.13 (s, 2H), 4.88 (s, 2H), 6.76 (d, ^3J = 8.0 Hz, 2H), 6.79–7.15 (m, 7H); ^{13}C NMR (75 MHz, $CDCl_3$) δ: 29.69, 66.95, 125.48, 125.55, 128.24, 128.38, 128.54, 128.61, 129.37, 129.71, 135.61, 137.84, 170.55 (C=O); ^{19}F NMR (282 MHz, $CDCl_3$, ref. CCl_3F) δ: –62.82 (s); MS (EI) *m/z*: 294 (M^+, 3), 181 (8), 159 (5), 108 (21), 91 (100), 65 (10); MS (CI, NH_3) *m/z*: (($M + NH_4$)$^+$, 5), 159 (5), 108 (21), 91 (100); HRMS calculated for $C_{16}H_{13}O_2F_3$: 294.0867, found: 294.0872.

8f: pale yellow solid, mp 80–84°C, lit. (25) mp 90–92°C; ^{1}H NMR (300 MHz, $CDCl_3$) δ: 3.76 (s, 2H), 5.14 (s, 2H), 7.29–7.35 (m, 5H), 7.43 (d, ^3J = 8.7 Hz, 2H), 8.16 (d, ^3J = 6.6 Hz, 2H); ^{1}H NMR (300 MHz, C_6D_6) δ: 3.03 (s, 2H), 4.27 (s, 2H), 4.86 (s, 2H), 6.66 (d, ^3J = 8.7 Hz, 2H), 6.93–7.07 (m, 5H), 7.69 (d, ^3J = 8.7 Hz, 2H); ^{13}C NMR (75 MHz, $CDCl_3$) δ: 40.96, 67.14, 123.73, 126.97, 128.61, 130.29, 135.35, 141.12, 169.98; MS (EI) *m/z*: 271 (M^+, 8), 136 (8), 91 (100), 65 (9); MS (CI, NH_3) *m/z*: 289 (($M + NH_4$)$^+$, 6), 271 (M^+, 3), 135 (10), 108 (9), 91 (100); HRMS calculated for $C_{15}H_{13}NO_4$: 271.0845; found: 271.0827.

Synthesis of 4-substituted-benzyl phenylacetates (7a–f)

A solution of phenylacetyl chloride (0.51 g, 3.0 mmol) in benzene (5 mL) was added slowly to a cooled solution of the appropriate arylmethanol (0.4 g, 3.0 mmol) in pyridine (0.5 mL, 9.0 mmol). After one hour the benzene solution was washed twice with water and dried with magnesium sulphate. Benzene was removed with a rotary evaporator. Some of the esters were purified by radial chromatography (Chromatotron, 10% EtOAc in hexanes).

7a: (21,22) Oil; ^{1}H NMR (300 MHz, $CDCl_3$) δ: 3.61 (s, 2H), 3.77 (s, 2H), 5.04 (s, 2H), 6.83–6.87 (m, 2H), 7.20–7.28 (m, 7H); ^{1}H NMR (300 MHz, C_6D_6) δ: 3.20 (s, 3H), 3.32 (s, 2H), 4.89 (s, 2H), 6.65 (d, ^3J = 8.7 Hz, 2H), 7.00–7.10 (m, 7H); ^{13}C NMR (75 MHz, $CDCl_3$) δ: 41.28, 55.17, 66.37, 113.56 (C2), 126.97, 127.93, 128.46, 129.19, 129.89, 133.90, 159.55, 171.39 (C=O); MS (EI) *m/z*: 256 (M^+, 21), 121 (100), 91 (37); MS (CI, NH_3) *m/z*: 256 (M^+, 8), 138 (8), 121 (100).

7b: (24) Oil; ^{1}H NMR (300 MHz, $CDCl_3$) δ: 2.34 (s, 3H), 6.65 (s, 2H), 5.08 (s, 2H), 7.13–7.31 (m, 9H); ^{1}H NMR (300 MHz, C_6D_6) δ: 2.00 (s, 3H), 3.32 (s, 2H), 4.91 (s, 2H) 6.85–7.12 (m, 9H); ^{13}C NMR (75 MHz, $CDCl_3$) δ: 21.16, 41.36, 66.57, 127.06, 128.27, 128.55, 129.21, 129.27, 132.89, 133.95, 138.03, 171.41(C=O); MS (EI) *m/z*: 240 (M^+, 16), 209 (5), 105 (100), 91 (46), 65 (12); MS (CI, NH_3) *m/z*: (($M + NH_4$)$^+$, 26), 154 (16), 105 (100), 91 (34), 65 (5).

7d: Oil; ^{1}H NMR (300 MHz, $CDCl_3$) δ: 3.63(s, 2H), 5.05 (s, 2H), 7.17–7.29 (m, 9H); ^{1}H NMR (300 MHz, C_6D_6) δ: 3.29 (s, 2H), 4.69 (s, 2H), 6.73 (d, ^3J = 8.4 Hz, 2H), 6.93–7.12 (m, 7H); ^{13}C NMR (75 MHz, $CDCl_3$) δ: 41.23, 65.64, 127.10, 128.52, 128.62, 129.17, 133.67, 134.29 (C2), 171.19 (C=O); MS (EI) *m/z*: 260 (M^+, 8), 125 (87), 91 (100), 65 (18), 51 (5); MS (CI, NH_3) *m/z*: 278 (($M + NH_4$)$^+$, 55), 260 (M^+, 5), 184 (42), 125 (100), 108 (19), 91 (39); HRMS calculated for $C_{15}H_{13}O_2Cl$: 260.0604 found: 260.0603.

7e: Yellow solid, ^{1}H NMR (300 MHz, $CDCl_3$) δ: 3.66 (s, 2H), 5.14 (s, 2H), 7.22–7.29 (m, 5H), 7.35 (d, ^3J = 8.0 Hz, 2H), 7.55 (d, ^3J = 8.1 Hz, 2H); ^{1}H NMR (300 MHz, C_6D_6) δ: 3.31 (s, 2H), 4.69 (s, 2H), 6.80 (d, ^3J = 8.0 Hz, 2H), 7.00–7.12 (m, 5H), 7.20 (d, ^3J = 8.1 Hz, 2H); ^{13}C NMR (75 MHz, $CDCl_3$) δ: 4.21, 65.45, 125.40, 127.17, 127.87, 128.53, 129.17, 133.53 (C2), 139.76, 171.06 (C=O); ^{19}F NMR

© 2000 NRC Canada

(282 MHz, $CDCl_3$) δ: –62.89 (s); MS (EI) *m/z*: 294 (M^+, 8), 159 (60), 109 (18), 91 (100), 65 (33), 49 (82); MS (CI, NH_3) *m/z*: 312 ($(M + NH_4)^+$, 90), 272 (8), 176 (16), 159 (18), 108 (71), 91 (100); HRMS calculated for $C_{16}H_{13}O_2F_3$: 294.0868, found: 294.0858.

7f: White solid mp 59–61°C; ^1H NMR (300 MHz, $CDCl_3$) δ: 3.67 (s, 2H), 5.18 (s, 2H), 7.22–7.32 (m, 5H), 7.37 (d, ^3J = 8.6 Hz, 2H), 8.13 (d, ^3J = 8.1 Hz, 2H); ^1H NMR (300 MHz, C_6D_6) δ: 3.31 (s, 2H), 4.60 (s, 2H), 6.63 (d, ^3J = 8.7 Hz, 2H), 7.01–7.12 (m, 5H), 7.68 (d, ^3J = 8.8 Hz, 2H); ^{13}C NMR (75 MHz, $CDCl_3$) δ: 41.18, 64.90, 123.65, 127.26, 128.06, 129.16, 133.38, 143.03, 147.59, 170.93 (C=O); MS (EI) *m/z*: 271 (M^+, 5), 136 (5), 106 (3), 91 (100), 65 (10); MS (CI, NH_3) *m/z*: 289 ($(M + NH_4)^+$, 8), 271 (M^+, 2) 135 (11), 108 (10), 91 (100), 65 (6). HRMS calculated for $C_{15}H_{13}NO_4$: 271.0845, found: 271.0861.

Dibenzylcarbonate

To benzyl alcohol (1.5 g, 13 mmol) and pyridine (0.98 g, 12.3 mmol) in 60 mL of dichloromethane under nitrogen, 1,1-carbonyldiimidazole (1 g, 6.1 mmol) in 20 mL of dichloromethane was added during 1 h. The solution was stirred overnight, washed once with water, twice with 5% HCl, once with water, and then with brine. Drying with magnesium sulphate, filtration, and removal of the solvent left crude dibenzyl carbonate that was purified by centrifugal chromatography, mp 28–29°C (lit. (26) mp 27.3–29.1°C); ^1H NMR (200 MHz $CDCl_3$) δ: 5.09 (s, 4H), 7.13–7.37 (m, 10H); ^1H NMR (200 MHz, C_6D_6) δ: 4.94 (s, 4H), 7.04–7.17 (m, 10H); ^{13}C NMR (50 MHz, $CDCl_3$) δ: 69.58 (CH_2), 128.21, 128.47, 135.13, 154.99 (C=O); MS (EI) *m/z*: 180 (4), 151 (5), 107 (32), 91 (100), 79 (32), 65 (14), 51 (11); MS (CI) *m/z*: 260 ($(M + NH_4)^+$, 100), 243 $(M + H)^+$, 10), 198 (26), 181 (32), 108 (73), 91 (72).

Tribenzylorthoformate

To **4c** (30.3 mg, 0.106 mmol, containing 9% carbonate) in benzene (1 mL) was added dimethoxybenzene (3.6 mg, 0.026 mmol, internal standard) and benzyl alcohol (60.6 mg, 0.56 mmol). The solution was flame sealed into an NMR tube after three freeze-pump-thaw cycles and heated at 110°C for 24 h. Column chromatography with 10% EtOAc in hexanes yielded tribenzylorthoformate (27). ^1H NMR (200 MHz, $CDCl_3$) δ: 4.66 (s, 6H), 5.43 (s, 1H), 7.24–7.35 (m, 15H); ^{13}C NMR (50 MHz, $CDCl_3$) δ: 66.33, 111.51 (orthoformyl), 127.71, 127.88, 128.41, 128.58, 137.46.

Benzyl formate

Benzyl alcohol (2.16 g, 0.02 mol), ethyl formate (1 g, 0.013 mol) and a catalytic amount of H_2SO_4 were dissolved in 10 mL of benzene and heated at 50°C for 24 h. After cooling the solution was washed with 10 mL of 10% NaOH and then with 10 mL of saturated NaCl. Evaporation of the solvent and unreacted ethyl formate left benzyl formate (28) that was purified by means of centrifugal chromatography (Chromatotron, 10% EtOAc in hexanes). ^1H NMR (200 MHz, $CDCl_3$) δ: 4.60 (s, 2H), 7.23–7.43 (m, 5H), 8.13 (s, 1H); ^1H NMR (200 MHz, C_6D_6) δ: 4.91 (s, 2H), 7.12–7.15 (m. 5H), 7.63 (s, 1H); ^{13}C NMR (50 MHz, $CDCl_3$) δ: 65.64, 128.32, 128.48, 128.62, 135.19, 160.71 (C=O).

Ratios of non-ester products

The thermolysis mixtures from the substituted dibenzyloxy oxadiazolines **4a**, **b**, **d**, and **e** were analyzed by means of GC/MS (DB-5 capillary column, i.d. 0.25 mm) and GC/FID (DB-1 megabore column, 0.53 mm i.d., flow rate 15 mL/min) equipped with an integrator. Both separated all of the products except the isomeric esters. Correction factors were used to correct the responses from the FID (29). Thermolysis of each of the substrates **4a**, **b**, and **d**–**f** gave 2 benzyl formates and 3 bibenzyls, which were identified from their mass spectra, as well as two orthoformates. Ratios were estimated from GC/FID data. Identification of benzyl formate, bibenzyl and tribenzyl orthoformate was confirmed by comparison with the GC trace of authentic samples.

The following are some product ratios. Benzyl formates, HCO_2CH_2Ph:HCO_2CH_2Ar from **4a**, 1.0:0.79; **4b**, 1.0:0.42; **4d**, 1.0:1.5; **4e**, 1.0:1.6. Bibenzyls, $PhCH_2CH_2Ph$:$PhCH_2CH_2Ar$:$ArCH_2CH_2Ar$ from **4a**, 1.0:1.7:0.40; **4b**, 1.0:1.8:0.85; **4d**, 1.0:1.7:0.70; **4e**, 1.0:1.9:0.74. Orthoformates, $HC(OCH_2Ph)_2OCH_2Ar$:$HCOCH_2Ph(OCH_2Ar)_2$ from **4a**, 0.39:1.0; **4b**, 1.15:1.0; **4d**, 1.06:1.0

Thermolysis of 4c in the presence of *tert*-butyl alcohol

A solution of **4c** (224 mg, 0.72 mmol), containing 4.6% dibenzyl carbonate, *tert*-butyl alcohol (1.69 g, 22.9 mmol) and 1,4 dimethoxybenzene (10.1 mg, internal standard) in dry benzene (28 mL) was sealed into a resealable thermolysis tube after three cycles of freeze-pump-thaw degassing. The sealed tube was kept at 110 ± 0.1°C in an oil bath for 24 h. Removal of the solvent and unreacted *tert*-butyl alcohol with a rotary evaporator left dibenzyl *tert*-butyl orthoformate in 43% yield. ^1H NMR (200 MHz, C_6D_6) δ: 1.19 (s, 9H), 4.74 (s, 4H), 5.62 (s, 1H), 7.13–7.43 (m, 10H); ^{13}C NMR (50 MHz, C_6D_6) δ: 28.8 (CH_3), 65.1 (CH_2), 74.2 (CMe_3), 108.8 (orthoformyl), 127.5, 127.9, 128.5, 138.9. Dibenzyl carbonate (3%) was also formed; spectra above.

Thermolysis of 4c in the presence of TEMPO (9)

A solution of **4c** (30.6 mg, 0.098 mmol), **9** (131.4 mg, 0.84 mmol), and 1,4-dimethoxy benzene (2.3 mg, internal standard) in 0.8 mL of dry benzene was degassed as described above before it was sealed into a thermolysis tube for 24 h of heating at 110°C. The products from the thermolysis, listed below, were identified by means of GC/FID (DB-1 column, 30m × 0.53 mm, flow rate 15 mL min^{-1}), by coinjection of authentic samples. A correction factor was applied to the GC integrals for the yield calculations (29).

Benzyl formate, 18%, retention time 10.0 min; **10**, 18%, retention time 26.6 min; benzyl phenylacetate, 13%, retention time 28.1 min; dibenzyl carbonate, 18%, retention time 30.4 min; tribenzylorthoformate, 42%, retention time 41.2 min.

Synthesis of authentic 10

Adduct **10** was prepared from TEMPO, toluene, and di-*tert*-butylperoxide as described previously (11).

Thermolysis rate constant for 4c

The rate of fragmentation of **4c** was monitored by ^1H NMR spectroscopy (200 MHz). A solution of **4c** (16.9 mg, 0.05 mmol) and *p*-xylene (1 μL, 0.008 mmol) in benzene-d_6 (0.54 mL) was sealed into an NMR tube after three sequences

© 2000 NRC Canada

of freeze-pump-thaw degassing. The tube was removed at intervals from an oil bath at 110°C and cooled to room temperature before the ^{1}H NMR spectrum was obtained. Corrections to the time scale were not made for cooling and reheating of the contents of the tube.

A plot of ln (I_t/I_0) vs. time, where I_t and I_0 are the normalized integrals for the oxadiazoline CH_3 hydrogens at time t and time zero, was linear (12 data points, r = 0.9963). The first order decomposition rate constant ($k_{110°C} = 8.7 \times 10^{-5}$ s^{-1}) was obtained from the slope of the least squares line through the origin. The fragmentation of **4f**, followed by the above procedure, gave $k_{110°C} = 7.9 \times 10^{-5}$ s^{-1} (r = 0.9985).

Dependence of product yields on concentration of *tert*-BuOH

Solutions of dibenzyloxy oxadiazoline (**4c**, 0.023 M), 1,4-dimethoxybenzene (0.009 M) and *tert*-BuOH (0.01, 0.04, 0.08, 0.12, 0.16, 0.24, 0.32, 0.18, and 0.70 M) in one mL of benzene were heated at 110°C for 24 h after being flame sealed into an NMR tube following degassing by means of the freeze-pump-thaw cycle. Plots of the normalized GC integrals, for the ester and for dibenzyl *tert*-butyl orthoformate, against the *tert*-BuOH concentration, are in Fig. 1.

Acknowledgements

Financial support from NSERC and helpful discussions with Darren L. Reid are gratefully acknowledged.

References

1. R.A. Moss, C.-S. Ge, and L. Maksimovic. J. Am. Chem. Soc. **118**, 9792 (1996).
2. R.A. Moss, L.A. Johnson, D.C. Merrer, and G.E. Lee, Jr. J. Am. Chem. Soc. **121**, 5940 (1999).
3. R.A. Moss and T. Zdrojewski. Tetrahedron Lett. **32**, 5667 (1991).
4. R.A. Moss, B.K. Wilk, and L.M. Hadel. Tetrahedron Lett. **28**, 1969 (1987).
5. R.A. Moss and H.-R. Kim. Tetrahedron Lett. **31**, 4715 (1990).
6. R.J. Crawford and R. Raap. Proc. Chem. Soc. London, 370 (1963).
7. R.W. Hoffmann, R. Hirsch, R. Fleming, and M.T. Reetz. Chem. Ber. **105**, 3532 (1972).
8. P.C. Oele and R. Louw. Tetrahedron Lett. **48**, 4941 (1972).
9. D.L. Reid, J. Hernández-Trujillo, and J. Warkentin. J. Phys. Chem. A, **104**, 3398 (2000).
10. P.C. Venneri and J. Warkentin. J. Am. Chem. Soc. **120**, 11182 (1998).
11. N. Merkley, M. El-Saidi, and J. Warkentin. Can. J. Chem. **78**, 356 (2000).
12. R.W. Hoffmann and H.J. Luthardt. Chem. Ber. **101**, 3861 (1968).
13. P. Sharma and J. Warkentin. Tetrahedron Lett. **36**, 7591 (1995).
14. P. Couture, M. El-Saidi, and J. Warkentin. Can. J. Chem. **75**, 326 (1997).
15. W.B. Smith. J. Org. Chem. **60**, 7456 (1995).
16. P.A. Simakov, F.N. Martinez, J.H. Horner, and M. Newcomb. J. Org. Chem. **63**, 1226 (1998).
17. D.L. Reid and J. Warkentin. J. Chem. Soc. Perkin Trans. 2, (2000). In press.
18. E. Wünsch. Chem. Ber. **98**, 797 (1965).
19. R. Calabretta, C. Gallina, and C. Giordano. Synthesis, 536 (1991).
20. M. Selva, C.A. Marques, and P. Tundo. J. Chem. Soc. Perkin Trans. 1, 1889 (1995).
21. A.A.M. Roof, H.T. VanWoerden, and H. Cerfontain. J. Chem. Soc. Perkin Trans. 2, 838 (1980).
22. B.M. Bhawal, S.D. Khanapure, and E.R. Biehl. Synthesis, 112 (1991).
23. T. Aoyama and T. Shiori. Chem. Pharm. Bull. **29**, 3249 (1981).
24. T.O. Mieggs, L.I. Grossweiner, and S.I. Miller. J. Am. Chem. Soc. **9**4 7986 (1972).
25. J.H. Bowic and B. Nussey. Org. Mass Spectrom. **1**, 310 (1974).
26. T. Mizano, F. Nakamura, Y. Egashira, I. Nishiguchi, T. Hirashima, A. Ogawa, N. Kambe, and N. Sonoda. Synthesis, 636 (1989).
27. H.R. El-Seedi, H.M. Jensen, N. Kure, I. Thomsen, and K.B.G. Torssell. Acta Chem. Scand. **47**, 1004 (1993).
28. (*a*) ^{1}H NMR (CCl_4) Sadtler Standard NMR Spectra, Vol. 11 # 6694; (*b*) J. Barluenga, P.J. Campos, E. Gonzalez, and G. Asensio. Synthesis, 426 (1985).
29. M.J. O'Brien. *In* Modern practice of gas chromatography. *Edited by* R.L. Grob. 2nd ed. John Wiley and Sons, Toronto. 1985. pp. 247–248.

© 2000 NRC Canada

Methylamination of some 3,6-dinitro-1,8-naphthyridines with liquid methylamine – potassium permanganate

Marian Woźniak, Maria Grzegożek, and Piotr Suryło

Abstract: 3,6-Dinitro-1,8-naphthyridine and its 2-substituted derivatives are dehydro-methylaminated with the solution of potassium permanganate in liquid methylamine (LMA–PP) to the corresponding mono- or mono- and bis(methylamino)-3,6-dinitro-1,8-naphthyridines. In the case of 2-chloro- and 2-methoxy-3,6-dinitro-1,8-naphthyridine the replacement of chloro and methoxy substituents by the $NHCH_3$ group occurs as well. Quantum-chemical calculations indicate the reactions to be controlled by the interaction of the frontal molecular orbitals (FMO) of the reagents. Moreover the heats of formation of intermediary methylamino-σ-adducts and transition states are calculated for the reaction studied. The calculations show satisfactory agreement between calculated and observed results. A convenient synthesis of some 2-substituted-3,6-dinitro-1,8-naphthyridines is reported.

Key words: methylaminations, calculations PM3, nitro-1,8-naphthyridines, oxidation.

Résumé : Sous l'influence d'une solution de permanganate de potassium en solution dans de la méthylamine liquide (PP–MAL), la 3,6-dinitro-1,8-naphtyridine et ses dérivés substitués en position 2 subissent une réaction de déhydro-méthylamination pour conduire aux mono- ou mono- et bis(méthylamino)-3,6-dinitro-1,8-naphtyridines. Dans les cas des 2-chloro- et 2-méthoxy-3,6-dinitro-1,8-naphtyridines, on observe aussi un remplacement des substituants chloro ou méthoxy par le groupe $NHCH_3$. Des calculs de chimie quantique indiquent que les réactions sont contrôlées par l'interaction entre les orbitales moléculaires frontales des réactifs. On a calculé de plus les chaleurs de formation des adduits-σ-méthylamino intermédiaires et des états de transition de la réaction étudiée. Les calculs conduisent à un accord satisfaisant entre les résultats observés et calculés. On a mis au point une méthode pratique de synthèse pour quelques 3,6-dinitro-1,8-naphtyridines substituées en position 2.

Mots clés : méthylaminations, calculs PM3, nitro-1,8-naphtyridines, oxydation.

In a previous paper we reported that 3-nitro-1,8-naphthyridine and some of its 2-substituted derivatives are dehydro-methylaminated in the solution of potassium permanganate in liquid methylamine (LMA–PP) to the corresponding 4-(methylamino)-3-nitro-1,8-naphthyridines (1). The reactions proceed through intermediates 4-methylamino-σ-adducts which in the next stage are oxidized by $KMnO_4$ to the 4-methylamino products.

The methylamination reactions of the 3-nitro-1,8-naphthyridines occur selectively in a good yield. Extending our investigations on the dehydro-methylamination of nitronaphthyridines we studied recently, analogous methylamination with LMA–PP of some 3,6-dinitro-1,8-naphthyridines. The presence of the second nitro group at the 1,8-naphthyridine ring with its strongly π-electron withdrawing properties causes considerable increase of π-electron deficiency of 1,8-naphthyridine ring. Therefore, it was interesting to compare the results of both methylaminations i.e., of 3-nitro- and of 3,6-dinitro-1,8-naphthyridines. Moreover, new methylamino derivatives of 3,6-dinitro-1,8-naphthyridine synthesized in this manner can show interesting biological and useful properties (on the application of methylamino nitroaromatics see ref. (2)).[2 3 4]

The methylamination of the 3,6-dinitro-1,8-naphthyridines was carried out under the same conditions as previously i.e., at the boiling point (ca. –7°C) of liquid methylamine. The results obtained are compiled in Scheme 1. The structure of the obtained methylamino products has been established on the basis of spectroscopic data, in particular ^{1}H NMR data, and in a few cases also by a comparison of their properties with those of authentic compounds, synthesized independently (see Experimental part).

Amination of unsubstituted 3,6-dinitro-1,8-naphthyridine, **1a**, with LMA–PP affords three products of dehydro-methylamination: 2,4-bis(methylamino)-3,6-dinitro-1,8-naphthyridine, **2a**, 3,5-bis(methylamino)-3,6-dinitro-1.8-naphthyridine,

Received November 2, 1999. Published on the NRC Research Press website on June 23, 2000.

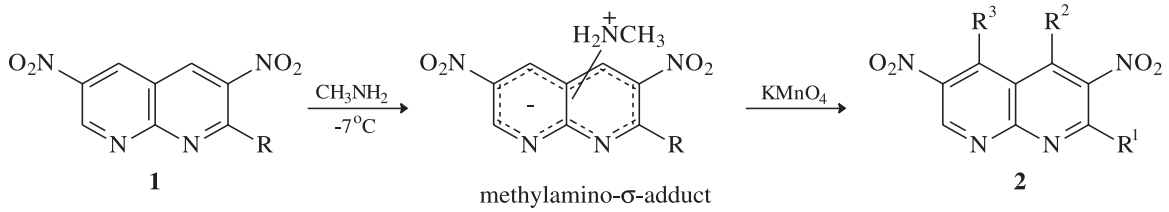
M. Woźniak,[1] M. Grzegożek, and P. Suryło. Institute of Organic Chemistry and Technology, Cracow University of Technology, ul. Warszawska 24, PL-31155 Kraków, Poland.

[1]Author to whom correspondence may be addressed. Telephone–Fax: 048–12–6325352. e-mail: Wozn@indy.chemia.pk.edu.pl

[2]F. Konno, N. Umehara, K. Isomae, and T. Katori. Jpn Kokai Tokuo Koho J.P. 6354, 363 [8854, 363], (1986).
[3]Rose, D. Ger. Offen. 2,441, 599, (1974).
[4]P.B. Merkel, D. Hoke. U.S. Patent 4923791.

 © 2000 NRC Canada

Scheme 1.



	Starting compound **1**				Product **2**	
1	R	**2**	R^1	R^2	R^3	Yield (%)
a	H	**a**	$NHCH_3$	$NHCH_3$	H	44
a	H	**b**	H	$NHCH_3$	$NHCH_3$	12
a	H	**c**	$NHCH_3$	H	H	9
b	$NHCH_3$	**a**	$NHCH_3$	$NHCH_3$	H	62
c	NH_2	**d**	NH_2	$NHCH_3$	H	50
d	NHC_6H_5	**e**	NHC_6H_5	$NHCH_3$	H	46
e	Cl	**a**	$NHCH_3$	$NHCH_3$	H	65
f	OCH_3	**f**	OCH_3	$NHCH_3$	$NHCH_3$	22
f	OCH_3	**a**	$NHCH_3$	$NHCH_3$	H	40
g	OH	**g**	OH	$NHCH_3$	H	27
g	OH	**h**	OH	H	$NHCH_3$	14

2b, and 2-(methylamino)-3,6-dinitro-1,8-naphthyridine, **2c**. The bis(methylamino) product **2b** showed in the aromatic region of its ^{1}H NMR only one singlet, δ (DMSO) = 9.20. This ^{1}H NMR pattern can be assigned to the structure of 2,7- or 4,5-bis(methylamino)-1,8-naphthyridine. On the basis of our quantum-chemical calculations (see further) the structure of **2b** was determined tentatively as 4,5-bis(methylamino)-3,6-dinitro-1,8-naphthyridine. Additional suggestion for this structure is the fact that in analogous amination of 3,6-dinitro- (3) and of 2-substituted 3,6-dinitro-1,8-naphthyridines (4) with liquid ammonia – potassium permanganate no amino substitution in position 7 was observed.

2-(Methylamino)-3,6-dinitro-1,8-naphthyridine, **1b**, is aminated with LMA–PP to 2,4-bis(methylamino)-3,6-dinitro-1,8-naphthyridine, **2a**, with fair yield. Similarly from 2-amino-3,6-dinitro-1,8-naphthyridine, **1c**, and from 2-(phenylamino)-3,6-dinitro-1,8-naphthyridine, **1d**, only mono 4-methylamino derivatives **2d** and **2e**, respectively, were obtained.

2-Chloro-3,6-dinitro-1,8-naphthyridine, **1e**, undergoes with LMA–PP simultaneously dehydro-methylamination in position 4 and dechloro-methylamination to give 2,4-bis(methylamino)-3,6-dinitro-1,8-naphthyridine, **2a**. No indications for the presence of 2-chloro-4-(methylamino)-3,6-dinitro-1,8-naphthyridine was found.

Treatment of 2-methoxy-3,6-dinitro-1,8-naphthyridine, **1f,** with LMA–PP gives 2-methoxy-4,5-bis(methylamino)-3,6-dinitro-1,8-naphthyridine, **2f**, and 2,4-bis(methylamino)-3,6-dinitro-1,8-naphthyridine, **2a**. In this reaction **1f** undergoes partly demethoxy-methylamination to form **2a**. The amination of 2-chloro-3,6-dinitro-, **1e**, and 2-methoxy-3,6-dinitro-1,8-naphthyridine, **1f**, probably does not proceed via rate-limiting formation of the σ-adduct, i.e., once formed the adduct loses chloride or methoxide anion. In the case of addition at the position where oxidation by permanganate is required to give the substituted product, is it not possible that the addition is highly reversible. Therefore it seems that at first replacement of 2-chloro or 2-methoxy substituent in **1e** or **1f** occurs and then oxidative amination in position 4.

Amination of 2-hydroxy-3,6-dinitro-1,8-naphthyridine [3,6-dinitro-1,8-naphthyridin-2(1*H*)-one], **1g**, with LMA–PP gives a nonseparable mixture of two isomeric products of dehydro-methylamination: 2-hydroxy-4-(methylamino)-3,6-dinitro-1,8-naphthyridine [4-(methylamino)-3,6-dinitro-1,8-naphthyridin-2(1H)-one], **2g**, and 2-hydroxy-5-(methylamino)-3,6-dinitro-1,8-naphthyridine [5-(methylamino)-3,6-dinitro-1,8-naphthyridin-2(1H)-one, **2h**. Both **2g** and **2h** have very similar R_f values in various eluent systems. They were identified by mass spectrometry and ^{1}H NMR spectroscopy. Based on the peak areas of the ^{1}H NMR resonance signals for 7H in **2g** and **2h** the ratio of **2g**:**2h** could be established as ca. 2:1.

In comparison with the methylamination of the 3-nitro-1,8-naphthyridines by LMA–PP the reactions of the 3,6-dinitro-1,8-naphthyridines with LMA–PP occur less selectively and with lower yield. In the reactions form many tarry substances and small amounts of unidentified products. In all cases the reaction products had to be purified or separated by column chromatography. It is reasonable to suppose that intermediary methylamino-σ-adducts of the 3,6-dinitro-1,8-naphthyridines possessing nonaromatic structure are not stable and give with potassium permanganate, besides methylamino products, also products of decomposition. During the reactions manganese dioxide is formed as a result of the reduction of potassium permanganate. On the other hand, liquid methylamine at low reaction temperature (–7°C) is stable and we do not observe detectable amounts of its oxidation products.

We tried to determine, as previously (1), the structure of intermediate methylamino-σ-adducts of some of the 3,6-dinitro-1,8-naphthyridines by ^{1}H NMR technique. However due to the very low solubility of these intermediates in liquid methylamine, it was not possible to assign the proton signals

© 2000 NRC Canada

Table 1. π-Electron stabilization energy calculated according to the eq. [1] for the 3,6-dinitronaphthyridines **1a**–**1g**.[a]

Compound	Values of ΔE when a molecule of CH_3NH_2 attacks position:								Preferable positions for CH_3NH_2 attack under	
	N-1	C-2	C-3	C-4	C-5	C-6	C-7	N-8	Orbital control FMO	Experimental conditions
1a	0.016	0.054	0.063	0.069	0.069	0.063	0054	0.016	C-4	C-2, C-4
1b	0.020	0.051	0.042	0.086	0.075	0.045	0.040	0.018	C-4	C-4
1c	0.020	0.053	0.042	0.087	0.075	0.045	0.041	0.018	C-4	C-4
1d	0.020	0.055	0.043	0.086	0.074	0.044	0.039	0.019	C-4	C-4
1e	0.034	0.061	0.065	0.072	0.065	0.059	0.052	0.031	C-4	C-2, C-4
1f	0.027	0.054	0.059	0.073	0.068	0.059	0.054	0.029	C-4	C-2, C-4
1g	0.028	0.056	0.059	0.075	0.067	0.059	0.055	0.028	C-4	C-4, C-5

[a]The quantum-chemical calculations were done by the PM3 method.

for σ-adducts. It should be noted that 3,6-dinitro-1,8-naphthyridines containing amino substituents in position 2 (the compounds **1b**, **1c**, and **1d**), in contrary to other studied 3,6-dinitro-1,8-naphthyridines, react with LMA–PP exclusively to the mono 4-methylamino products. It is probably due to the strongly electron-donating properties of the amino groups' deactivating naphthyridine ring for the further nucleophilic attack. Contrary to 2-methoxy-3-nitro-1,8-naphthyridine, 2-methoxy-3,6-dinitro-1,8-naphthyridine, **1f,** partly undergoes demethoxy-methylaminaton with LMA–PP.

2,4-Bis(methylamino)-3,6-dinitro-1,8-naphthyridine, **2a**, obtained in the reactions of **1a**, **1b**, and **1c** with LMA–PP undergoes acid hydrolysis only in position 4 to give with high yield, isomeric to **2g** and **2h**, 4-hydroxy-2-(methylamino)-3,6-dinitro-1,8-naphthyridine [2-(methylamino)-3,6-dinitro-1,8-naphthyridin-4(1H)-one], **2i** (R^1 = $NHCH_3$, R^2 = OH, R^3 = H). That is a convenient manner to prepare **2i**.

To understand better the nature of regioselectivity of the methylamination reactions studied, we applied the perturbation theory of molecular orbitals (PMO). The calculations of the π-electron energy (ΔE_π) for all positions in the studied dinitronaphthyridines were carried out according to a simplified second-order perturbation (eq. [1]), as in a previous work (5) by the PM3 method.

$$[1] \qquad \Delta E_\pi \approx 2\left[\frac{C_S^2(\mathrm{LUMO})}{\left|E^{\mathrm{N}}_{\mathrm{HOMO}} - E^{\mathrm{A}}_{\mathrm{LUMO}}\right|} + \frac{C_S^2(\mathrm{LUMO}+1)}{\left|E^{\mathrm{N}}_{\mathrm{HOMO}} - E^{\mathrm{A}}_{\mathrm{LUMO+1}}\right|}\right]$$

The value of the LUMO and LUMO +1 energy levels (E^A) and respective coefficient C_A for the starting dinitronaphthyridines were calculated by PM3 method. They are available upon request. For the methylamine the value $E^{\mathrm{N}}_{\mathrm{HOMO}}$ = –9.40 eV was found.

The results of these calculations are given in Table 1 and they indicate that the methylamination of 3,6-dinitronaphthyridines (**1a**–**g)** ought to occur mainly in the C-4 position for which, in fact, the highest values of ΔE_π have been found. Thus it seems that the methylamination of **1b**–**d** and **1g** is controlled by the interaction of the frontal molecular orbital (FMO) of the reagents because these data correlate well with experimentally observed substitution products (Scheme 1). In **1a** the calculations predict the methylamination at C-4 but it has not been confirmed experimentally. In this case, the formation of the 2,4-(**3a**) and 4,5-(**3b**)-bis(methylamino) and 2-(**3c**)-(methylamino) products were observed. The same conclusion can be reached for reactions of methylamination of 2-chloro-(**1e**) and 2-methoxy-(**1f**)-3,6-dinitro-(**1a**)1,8-naphthyridines where first of all the nucleophilic displacement of chloro and methoxy group and then the methylamination in position C-4 respectively was observed.

In addition, we wished to explain regioselectivity of the attack of methylamine on the 3,6-dinitro-1,8-naphthyridine ring system. First, we calculated heats of formation (ΔH) of the ground state of the reaction system and of the intermediate σ-adducts **2a**–**g** and transition structures (TS) for all the unsubstituted positions in **1a**–**g** and additionally for position C-2 substituted by chloro and methoxy group in **1e**–**f**, using the PM3 method (see Table 2).[5]

The results of calculations indicate that the heats of formation of intermediary σ-adducts **2a**–**g** at the position C-4 have, in comparison with other positions in dinitronaphthyridines, the lowest energy values just as the values for the energy of activation ($\Delta E^{\#}$) at the same C-4 position in **1a**–**g.** It indicates that the C-4 positions in studied dinitronaphthyridines are favored for nucleophilic attack. Fig. 1 shows the reaction profile obtained by calculations with the PM3 method and the structures of the ground state, transition states, and intermediates for the reactions studied.

In conclusion, FMO perturbation theory correctly predicts the observed course of the most of the reactions studied. Additionally, the results of calculations of reaction pathways for the nucleophilic attack of methylamine confirm the regioselectivity of methylamination **1b**–**d** and **1g**. For compounds **1e**–**f** the substitution of chloro and methoxy groups occurs faster than dehydro-methylamination and this effect suggests the multistep addition–elimination process. However, the calculations of the reaction pathways do not con-

[5]The PM3 method was used for the semiempirical MO calculations using the MOPAC (version 6) molecular orbital package. The starting geometries and intermediary structures were obtained from the corresponding molecular models, fully optimized using keywords PRECISE. Transitions states (TS) were calculated using a SADDLE subroutine. An NLLSQ procedure was used for gradient optimization (<0.1 kcal/mol/Å). Calculations were performed until at least one negative Hessian was obtained. The THERMO procedure was used to correct the results of calculations for temperature 266 K.

© 2000 NRC Canada

Table 2. Results of PM3 calculations: geometry[a] and heats of formation of the ground-state of the reaction system (**1** + CH_3NH_2), transition state (TS), intermediary structures (σ-adduct) of **2**.[b]

Structure	**1** + CH_3NH_2		r_1	Transition state (TS)	r_2	σ-Adduct (**2**)	r_3	Energy of activation
		ΔH (kcal mol^{-1})	Å	ΔH (kcal mol^{-1})	Å	ΔH (kcal mol^{-1})	Å	$\Delta H^{\#}$ (kcal mol^{-1})
1a	C-2	30.70	5.25	46.17	2.00	43.34	1.62	15.47
	C-4	30.70	2.94	44.29	2.07	39.76	1.62	13.59
1b	C-4	25.96	4.18	37.85	2.09	32.58	1.61	11.89
	C-5	25.96	4.20	38.63	2.07	33.96	1.62	12.67
	C-7	25.96	6.48	41.26	1.96	39.27	1.62	15.30
1c	C-4	26.40	4.17	37.74	2.10	32.91	1.62	11.34
	C-5	26.52	2.95	40.10	2.04	36.18	1.61	13.58
	C-7	26.52	5.24	41.47	1.97	39.36	1.62	14.95
1d	C-4	57.85	3.51	69.02	2.09	63.72	1.61	11.17
	C-5	58.00	3.70	69.37	2.07	65.38	1.63	11.37
1e	C-2	27.10	5.24	42.40	2.05	34.85	1.57	15.30
	C-4	27.10	2.94	40.22	2.09	35.40	1.62	13.12
	C-5	27.10	3.80	40.41	2.07	36.25	1.63	13.31
	C-7	27.10	6.19	42.77	2.00	39.87	1.62	15.67
1f	C-2	–9.41	5.23	7.00	2.01	6.04	1.68	16.41
	C-4	–9.41	3.85	4.23	2.09	–1.11	1.61	13.64
	C-5	–9.41	2.94	4.35	2.07	0.40	1.63	13.76
	C-7	–9.41	6.24	6.94	1.98	4.65	1.62	16.35
1g	C-4	–16.98	2.94	–3.62	2.10	–9.60	1.61	13.36
	C-5	–16.98	3.84	–3.27	2.07	–7.46	1.63	13.71
	C-7	–16.98	6.24	–0.80	2.00	–3.44	1.62	16.18

[a] r_1, r_2, r_3 — the distances between the unsubstituted carbon atoms in **1**, TS, and **2** respectively and N in CH_3NH_2.
[b] The results of calculations were corrected for temperature 266 K.

firm this process. In the case of **1a** the calculations predict C-4 as the favorable site for nucleophilic attack but on the base of results of study reaction it is difficult to predict which positions (C-2 or C-4) are attacked by nucleophilic reagents at first.

Experimental

Melting points (uncorrected) were determined on a Kofler plate. The ^{1}H NMR spectra were recorded on Tesla BS-587A (80 MHz) spectrometer. The infrared spectra were recorded on UR-20 or Bio-Rad FTS-175C spectrometer (in potassium bromide pellets). The mass spectra were recorded on LKB GC–MS 9000 spectrometer. Silica gel (Merck, 230–400 mesh) was used for column chromatography. Quantum-chemical calculations were carried out with PM3 method using MOPAC program (version 6.0) available from Research Laboratory, US Air Force Academy, Colorado Springs, U.S.A.

1. Synthesis of starting and references compounds

3,6-Dinitro-, **1a** (3), 2-chloro-3,6-dinitro-, **1e** (6), and 2-amino-1,8-naphthyridine (7) were prepared according to the literature procedures. 2-Hydroxy-3,6-dinitro-1,8-naphthyridine, **1g**, was prepared by the procedure described earlier (6), however by using 65% oleum the reaction time could be shortened from 30 h to 3 h. Attempts to obtain 2-amino-3,6-dinitro-1,8-naphthyridine, **1c**, by nitration of 2-amino-1,8-naphthyridine under various conditions gave 2-hydroxy-3,6-dinitro-, **2g** or 2-hydroxy-3-nitro-1,8-naphthyridine. Nitration of 2-amino-1,8-naphthyridine at 0°C yielded 2-nitramino-1,8-naphthyridine which, however, could not be rearranged to an amino nitro-1,8-naphthyridine.

*2-(Methylamino)-3,6-dinitro-1,8-naphthyridine (**1b**)*

2-Chloro-3,6-dinitro-1,8-naphthyridine (0.2 g, 0.8 mmol) in 20 mL of saturated methanol solution of methylamine was stirred at r t for 10 min. Precipitated yellow crystals were filtered off and washed with methanol to yield 0.12 g (60%) of **1b**, mp 234–236°C. MS (70 eV), *m*/*z* (%): 249 (18) [M^+], 165 (100). IR ν_{max}: 3424 (NH), 1557 (NO_2, as), 1339 (NO_2, s) cm^{-1}. ^{1}H NMR ($CDCl_3$) δ: 9.74 (7H, d), 9.09 (4H. s), 8.95 (5H, d), 8.38 (NH, br.s), 3.38 (CH_3, d), $J_{5,7}$ = 2.9 Hz, $J_{NH,CH}$ = 4.9 Hz. Anal. calcd. for $C_9H_7N_5O_4$: C 43.38, H 2.38, N 28.11; found: C 43.61, H 2.71, N 28.01.

*2-Amino-3,6-dinitro-1,8-naphthyridine (**1c**)*

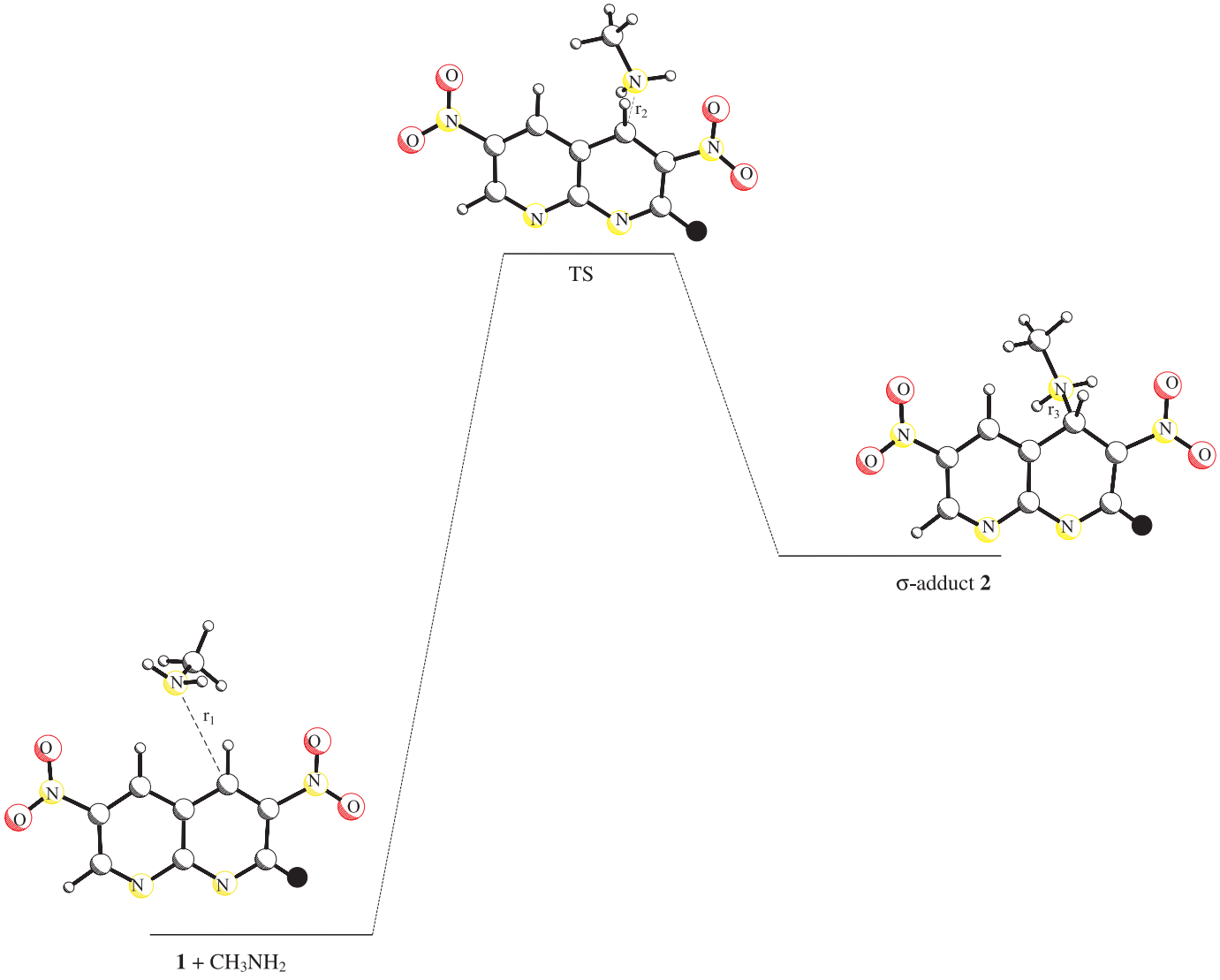
2-Chloro-3,6-dinitro-1,8-naphthyridine (0.1 g, 0.4 mmol) in 25 mL of saturated methanol solution of ammonia was stirred at r t for 15 h. Methanol and ammonia were removed under vacuum and the residue obtained was crystallized from nitromethane to yield 75 mg (75%) of **1c**; yellow needles with mp >350°C. [Lit. (6) mp >350°C]. MS (70 eV), *m*/*z* (%): 235 (100) [M^+]. IR ν_{max}: 3459 (NH), 1538 (NO_2, as), 1325 (NO_2, s) cm^{-1}. ^{1}H NMR (DMSO) δ: 9.57 (7H, d), 9.46 (4H, s), 9.35 (5H, d), 8.44 (NH, br. s), $J_{5,7}$ = 2.9 Hz. Anal. calcd. for $C_8H_5N_5O_4$: C 40.86, H 2.14, N 29.78; found: C 40.82, H 2.09, N 26.69.

*2-(Phenylamino)-3,6-dinitro-1,8-naphthyridine (**1d**)*

2-Chloro-3,6-dinitro-1,8-naphthyridine (0.15 g, 0.6 mmol) and 0.1 mL (1.1 mmol) of fresh distilled aniline in 25 mL of

© 2000 NRC Canada

Fig. 1. PM3 results for the pathway from **1** →**2**; details are given in Table 2 ; ● = R (R = H, $NHCH_3$, NH_2, NHPh, Cl, OCH_3, OH).



methanol was heated on a water bath for 10 h. Methanol and the excess of aniline were removed and to the residue 15 mL of 15% water solution of sodium hydroxide was added. The solid was filtered off and crystallized from a mixture of water and dioxane to afford 0.13 g (70%) of **1f**; red prisms with mp 300–303°C. MS (70 eV), *m*/*z* (%): 311 (54) [M^+], 310 (100) [M^+– H]$^+$. IR ν_{max}: 3330 (NH), 1571 (NO_2, as), 1341 (NO_2, s) cm^{-1}. ^1H NMR (CF_3COOD) δ: 9.77 (7H, d), 9.69 (5H, d), 9.60 (4H, s), 7.71–7.61 (phenyl, m), $J_{5,7}$ = 2.7 Hz. Anal. calcd. for $C_{14}H_9N_5O_4$: C 54.02, H 2.91, N 22.50; found: C 53.91, H 2.89, N 22.11.

*2-Methoxy-3,6-dinitro-1,8-naphthyridine (**1f**)*

To a solution of 0.1 g (0.4 mmol) of 2-chloro-3,6-dinitro-1,8-naphthyridine ca. 5 mg of sodium hydroxide was added and then heated on a water bath for 7.5 h. The excess of methanol was distilled off and the residue was twice crystallized from *n*-octane (charcoal) to give 40 mg (40%) of **1f**; white needles with mp 172–173°C. MS (70 eV), *m*/*z* (%): 250 (35) [M^+], 230 (100) [M^+– NO]$^+$. IR ν_{max}: 1549 (NO_2, as), 1336 (NO_2, s) cm^{-1}. ^1H NMR ($CDCl_3$) δ: 9.86 (7H, d), 9.11 (5H, d), 8.83 (4H, s), 4.38 (CH_3, s), $J_{5,7}$ = 2.7 Hz. Anal. calcd. for $C_9H_6N_4O_5$: C 43.21, H 2.42, N 22.11; found: C 43.24, H 2.38, N 22.11.

*2-Hydroxy-3,6-dinitro-1,8-naphthyridine (**1g**)*

A solution of 2.0 g (13.7 mmol) of 2-hydroxy-1,8-naphthyridine in 20 mL of fuming nitric acid (*d* = 1.51) and 20 mL of fuming sulfuric acid containing 65% sulfur trioxide, was heated at 100–110°C on an oil bath for 3 h. The solution was cooled and poured on 150 g of crushed ice and the mixture was neutralized to pH ~ 6 with water solution of ammonia. The precipitate obtained was filtered off, washed with water, and crystallized from water to give 1.8 g (56%) of **1g**; yellow crystals with mp 302–310°C (decomp.) The compound was identical to the reference sample.

Nitration of 2-amino-1,8-naphthyridine

(*a*) A mixture of 2-amino-1,8-naphthyridine (0.1 g, 0.7 mmol), 2 mL of sulfuric acid, and 0.4 mL of nitric acid

© 2000 NRC Canada

(d = 1.42) was heated on a water bath for 3 h. The solution was poured on ca. 50 mL of cold water. The precipitate was filtered off, washed with water, and dried to yield 50 mg (39%) of 2-hydroxy-3-nitro-1,8-naphthyridine; light-yellow crystals with mp 265–320°C (subl.), (Lit (7) 265–320°C (subl.)). The compound was identical (IR and ^{1}H NMR) to the reference sample (7). The water filtrate was neutralized with water ammonia, acidified with acetic acid to pH 5, and extracted continuously with chloroform for 5 h. Chloroform was removed from the extract, the solid was dried under vacuum, washed with hexane to give 55 mg of 2-hydroxy-1,8-naphthyridine with mp 197–203°C, (Lit. (7) 198–199°C). ^{1}H NMR spectroscopy showed that the product contained ca. 5% of 2-hydroxy-3-nitro-1,8-naphthyridine and no amount of starting material.

(*b*) 2-Amino-1,8-naphthyridine (0.2 g, 0.14 mmol) was nitrated with 2 mL of fuming nitric acid and 2 mL of 65% oleum in the same manner as that described for nitration of 2-hydroxy-1,8-naphthyridine. After crystallization from water 0.15 g (50%) of 2-hydroxy-3,6-dinitro-1,8-naphthyridine, **1g**, was obtained. The compound was identified by comparison properties (mp, IR, and ^{1}H NMR) with those of the reference sample.

(*c*) To the stirred solution of 2-amino-1,8-naphthyridine (50 mg, 0.035 mmol) in 1 mL of sulfuric acid, 0.2 mL of nitric acid (d = 1.42) was added at 0°C. The solution was kept at 0°C for 0.5 h and then at r t for 20 h. The solution was neutralized with water ammonia, acidified to pH ~ 5 with acetic acid, and extracted continuously with chloroform for 5 h. Chloroform was stripped off and the residue was purified by column chromatography (2.5 × 50 cm) using 500 mL of chloroform–methanol (10 : 1) as the eluent. The eluent was removed and the residue was crystallized from methanol to yield 40 mg (61%) of 2-nitramino-1,8-naphthyridine; light-yellow needles which above 140°C are transformed into plates with mp 210–211°C. MS (70 eV), *m*/*z* (%): 190 (12) [M^+], 144 (100) [M^+–NO_2]$^+$. IR ν_{max}: 3450 (NH), 1545 (NO_2), 1370 (NO_2, s) cm^{-1}. ^{1}H NMR ($CDCl_3$) δ: 8.74 (7H, dd), 8.16 (5H, dd), 8.12 (4H, d), 7.56 (6, dd), 7.12 (3H, d), $J_{3,4}$ = 9.0 Hz, $J_{5,6}$ = 8.5 Hz, $J_{5,7}$ = 2.0 Hz, $J_{6,7}$ = 5.0 Hz. Anal. calcd. for $C_8H_6N_4O_2$: C 50.53, H 3.18, N 29.46; found: C 50.44, H 3.16, N 29.30.

2. General procedure: amination of 3,6-dinitro-1,8-naphthyridines with methylamine – potassium permanganate

0.2–0.3 g of potassium permanganate was added to 25–30 mL of liquid methylamine and 0.1–0.2 g of dinitronaphthyridine and the resulting mixture stirred at –7°C for 0.5 h. After evaporation of methylamine ca. 30 mL of water was added to the residue and the mixture was extracted continuously with chloroform for 15 h. The residue obtained after evaporation of the solvent from the extract was worked up in the manner described below.

*Methylamination of 3,6-dinitro-1,8-naphthyridine (**1a**)*

0.1 g (0.45 mmol) of **1a** was treated according to the general procedure. The residue was separated by column chromatography (2.5 × 70 cm). The first fraction was eluted with 2 L of dichloromethane and after stripping off the eluent was washed with methanol to give 10 mg (9%) of 2-methylamino-3,6-dinitro-1,8-naphthyridine, **2c** (**1b**). The compound had the same properties as **1b** synthesized from **1e** (see section 1). The second fraction was eluted with 500 mL of chloroform–methanol (10 : 1) and crystallized from toluene to yield 55 mg (44%) of 2,4-bis(methylamino)-3,6-dinitro-1,8-naphthyridine, **2a**; yellow needles with mp 268–270°C (decomp.). MS (70 eV), *m*/*z* (%): 278 (53) [M^+], 261 (100). IR ν_{max}: 2365 (NH), 1560 (NO_2, as), 1295 (NO_2, s) cm^{-1}. ^{1}H NMR (DMSO) δ: 9.48 (7H, d), 9.37 (5H, d), 8.19 (NH, br.s), 2.99 (CH_3, d), 2.87 (CH_3, s), $J_{5,7}$ = 2.5 Hz, $J_{CH,NH}$ = 4.0 Hz. Anal. calcd. for $C_{10}H_{10}N_6O_4$: C 43.17, H 3.62, N 30.21; found: C 43.15, H 3.62, N 30.03.

The third fraction (500 mL, chloroform–methanol (10:1)) was crystallized from methanol to give 15 mg (12%) of 4,5-bis(methylamino)-3,6-dinitro-1,8-naphthyridine; dark yellow needles with mp 261–263°C (decomp). MS (70 eV), *m*/*z* (%): 278 (10) [M^+], 261 (100) [M^+–OH]$^+$. IR ν_{max}: 3288 (NH), 1569 (NO_2, as), 1385 (NO_2,s) cm^{-1}. ^{1}H NMR (DMSO) δ: 9.20 (2H, 7H, s), 8.69 (NH, br.s), 2.72 (CH_3, s). Anal. calcd. for $C_{10}H_{10}N_6O$: C 43.17, H 3.62, N 30.21; found: C 43.09, H 3.52, N 30.35.

*Methylamination of 2-(methylamino)-3,6-dinitro-1,8-naphthyridine (**1b**)*

0.1 g (0.4 mmol) of **1b** was treated according to the general procedure. The residue was dissolved in the mixture of chloroform–methanol (10 : 1) and purified by column chromatography using 150 mL of the same solvent as eluent. The eluent was removed and the residue was crystallized from toluene to yield 70 mg (62%) of 2,4-bis(methylamino)-3,6-dinitro-1,8-naphthyridine, **2a**. The compound showed identical properties (mp, ^{1}H NMR, IR) with those of **2a** obtained from **1a**.

*Methylamination of 2-amino-3,6-dinitro-1,8-naphthyridine (**1c**)*

0.1 g (0.43 mmol) of **1c** was treated according to the general procedure. The residue was purified by column chromatography (2.5 × 50 cm), using 1 L of chloroform–methanol (5:0.25) as eluent, and crystallized from methanol to afford 55 mg (50%) of 2-amino-4-(methylamino)-3,6-dinitro-1,8-naphthyridine, **2d**; yellow needles with mp >280^o C (decomp.). MS (70 eV), *m*/*z* (%): 264 (100) [M^+], 247 (30) [M^+– OH]$^+$. IR ν_{max}: 3425, 3250, 3105 (NH), 1535 (NO_2, as), 1345 (NO_2, s) cm^{-1}. ^{1}H NMR (DMSO) δ: 9.46 (7H, d), 9.36 (5H, d), 2.87 (CH_3, s), $J_{5,7}$ = 2.5 Hz. Anal. calcd. for $C_9H_8N_6O_4$: C 40.91, H 3.08, N 31.81; found: C 40.75, H 3.12, N 31.62.

*Methylamination of 2-(phenylamino)-3,6-dinitro-1,8-naphthyridine (**1d**)*

0.16 g (0.52 mmol) of **1d** was treated according to the general procedure. The residue was purified by column chromatography (2.5 × 50 cm) using 500 mL of chloroform–methanol (5:0.25) as the eluent. The eluent was removed and the residue was crystallized from methanol to give 80 mg (46%) of 4-(methylamino)-2-(phenylamino)-3,6-dinitro-1,8-naphthyridine, **2e**; orange plates with mp 254–256°C (decomp.). MS (70 eV), *m*/*z* (%): 340 (35) [M]$^+$, 339 (100) [M^+–1]. IR ν_{max}: 3440, 3330 (NH), 1540 (NO_2, as), 1320 (NO_2, s) cm^{-1}. ^{1}H NMR (DMSO) δ: 9.54 (7H, d), 9.41 (5H,

© 2000 NRC Canada

d), 7.87–7.16 (phenyl, m), 2.91 (CH_3, s), $J_{5,7}$ = 2.5 Hz. Anal. calcd. for $C_{15}H_{12}N_6O_4$: C 52.94, H 3.55, N 24.70; found: C 52.80, H 3.68, N 24.51.

*Methylamination of 2-chloro-3,6-dinitro-1,8-naphthyridine (**1e**)*

0.2 g (0.78 mmol) of **1e** was treated according to the general procedure. The residue was purified by column chromatography (2.5 × 50 cm) using 500 mL of chloroform–methanol (5:0.2) as the eluent and crystallized from toluene to yield 0.14 g (65%) of 2,4-bis(methylamino)-3,6-dinitro-1,8-naphthyridine, **1a**. The compound was identical (mp, IR, ^{1}H NMR) with **2a** obtained by methylamination of **1a**.

*Methylamination of 2-methoxy-3,6-dinitro-1,8-naphthyridine (**1f**)*

0.1 g (0.4 mmol) of **1f** was treated according to the general procedure. The residue was separated by column chromatography (2.5 × 70 cm) using chloroform as the eluent. The first fraction (500 mL) was crystallized from methanol to give 30 mg (22%) of 2-methoxy-4,5-bis(methylamino)-3,6-dinitro-1,8-naphthyridine, **2f**; orange needles with mp 245–247°C. MS (70 eV), *m*/*z* (%): 308 (35) [M^+], 290 (100). IR ν_{max}: 3425, 3366 (NH), 1545 (NO_2, as), 1330 (NO_2,s) cm^{-1}. ^{1}H NMR (DMSO) δ: 9.33 (7H, s), 8.45 (NH, br.s), 4.09 (OCH_3, s), 3.05 (NCH_3, d), 2.98 (NCH_3, s), $J_{CH,NH}$ = 4.0 Hz. Anal. calcd. for $C_{11}H_{12}N_6O_5$: C 42.86, H 3.92, N 27.26; found C 43.07, H 3.91, N 27.00.

The second fraction (700 mL) was crystallized from toluene to yield 45 mg (44%) of 2,4-bis(methylamino)-3,6-dinitro-1,8-naphthyridine, **2a**. The compound showed identical properties (mp, IR, ^{1}H NMR) with those of **2a** obtained from **1a** (or **1b**).

*Methylamination of 2-hydroxy-3,6-dinitro-1,8-naphthyridine (**1g**)*

0.13 g (0.55 mmol) of **1g** was treated according to the general procedure. The residue was purified by column chromatography (2.4 × 30 cm) using chloroform–methanol (10:1) as the eluent.

The eluent was removed and the remaining solid was washed with methanol to give 60 mg (41%) of the mixture of 2-hydroxy-4-(methylamino)-3,6-dinitro-1,8-naphthyridine, **2g** and of 2-hydroxy-5-(methylamino)-3,6-dinitro-1,8-naphthyridine, **2h**; yellow plates with mp >290°C. MS (70 eV), *m*/*z* (%): 265 (100) [M^+], 247 (74). IR ν_{max} : 3371 (NH), 1674 (CO), 1566 (NO_2, as), 1332 (NO_2, s) cm^{-1}. ^{1}H NMR (DMSO) δ of **2g**: 9.53 (7H, d), 9.39 (5H, d), 3.02 (CH_3, s), $J_{5,7}$ = 2.5 Hz. ^{1}H NMR (DMSO) δ of **2h**: 8.87 (7H, s), 4.83 (4H, s), 2.84 (CH_3, s). Anal. calcd. for $C_9H_7N_5O_5$: C 40.76, H 2.66, N 26.41; found: 40.85, H 2.71, N 26.53.

3. Hydrolysis of 2,4-bis(methylamino)-3,6-dnitro-1,8-naphthyridine (2a)

60 mg (0.22 mmol) of **2a**, 4 mL of hydrochloric acid (*d* = 1.18), and 4 mL of water were heated at boiling point for 8 h. The solution was neutralized with water ammonia. The solid was filtered off, washed with water and then with methanol, and dried to give 55 mg (95%) of 2-(methylamino)-4-hydroxy-3,6-dinitro-1,8-naphthyridine [2-(methylamino)-3,6-dinitro-1,8-naphthyridin-4-(1H)-one], **2j**; yellow needles with mp >280°C (decomp.). MS (70 eV), *m*/*z* (%): 265 (33) [M^+], 247 (100). IR ν_{max}: 3355 (NH), 1630 (CO), 1530 (NO_2, as), 1335 (NO_2,s) cm^{-1}. ^{1}H NMR (DMSO) δ: 9.22 (7H, d), 8.81 (5H, d), 7.22 (NH, br.s), 3.06 (CH_3, s), $J_{5,7}$ = 2.5 Hz. Anal. calcd. for $C_9H_7N_5O_5$: C 40.76, H 2.66, N 26.41; found: C 40.98, H 2.80, N 26.25.

Acknowledgments

The authors wish to thank Dr. P. Kowalski for his help with the quantum-chemical calculations and Dr. E. Cholewka for measuring the ^{1}H NMR and IR spectra.

References

1. M. Woźniak, M. Grzegożek, and P. Suryło. Liebigs Ann. / Recueil, 2601 (1997).
2. (*a*) F. Konno, N. Umehara, K. Isomae, and T. Katori. Chem. Abstr. **109**, 93064f (1988); (*b*) D. Rose. Chem. Abstr. **84**, 166265z (1976); (*c*) P.B. Merkel and D. Hoke. Chem. Abstr. **113**, 123764m (1990).
3. M. Woźniak and M. Tomula. Liebigs Ann. Chem. 471 (1993).
4. M. Woźniak and H.C. van der Plas. J. Heterocycl. Chem. **23**, 473 (1986).
5. (*a*) J. Fleming. *In* Frontier orbitals and organic chemical reactions. *Edited by* J. Wiley. Chichester, England. 1976; (*b*) M. Woźniak and M. Grzegożek. Liebigs Ann. Chem. 823 (1993).
6. M. Woźniak, H.C. van der Plas, M. Tomula, and A. van Veldhuizen. J. Heterocycl. Chem. **22**, 761 (1985).
7. W. Roszkiewicz and M. Woźniak. Synthesis, 691 (1976).

© 2000 NRC Canada

The Suzuki, the Heck, and the Stille reaction — three versatile methods for the introduction of new C—C bonds on solid support

Robert Franzén

Abstract: Metal-catalyzed coupling reactions are very efficient and reliable methods for the introduction of new carbon–carbon bonds onto molecules attached to a solid support. This review summarizes recent advances in utilizing the three most used methods, the Suzuki reaction, the Heck reaction, and the Stille reaction, in the field of solid phase organic synthesis resulting in small organic molecule libraries.

Key words: metal-catalyzed coupling reactions, carbon—carbon bonds, solid phase synthesis, combinatorial chemistry, drug discovery.

Résumé : Les réactions de couplage catalysées par les métaux sont des méthodes efficaces et fiables pour l'introduction de nouvelles liaisons carbone-carbone dans des molécules attachées à un support solide. Cette revue résume les développements récents dans l'utilisation des trois méthodes les plus courantes, la réaction de Suzuki, la réaction de Heck et la réaction de Stille, dans le domaine de la synthèse organique en phase solide conduisant à l'élaboration de librairies de petites molécules organiques.

Mots clés : réactions de couplage à catalyse métallique, liasons carbone—carbone, synthèse en phase solide, chimie combinatoire, découverte de médicaments.

[Traduit par la Rédaction]

Introduction

Over the past 10 years, small molecule solid phase synthesis has become an important part in the discovery of new drugs (1, 2). In fact, most of the organic chemical libraries synthesized to date have been constructed using solid-phase methods. In the development of organic chemistry, the carbon–carbon bond formation has always been one of the most useful and fundamental reactions, (3–5) and numerous papers and reviews have detailed the progress of several reactions in solution phase since the end of the 19th century. The literature for new synthetic methods of carbon–carbon bond formation on solid-support has not been extensively reviewed. Recently, a short review by Andres et al. (6) on the utilization of some metal-catalyzed coupling reactions on solid phase was published. The current paper summarizes recent developments in metal-catalyzed coupling reactions performed on a polymeric material. The three following methods are investigated in detail: (*i*) the cross-coupling of aryl halides with aryl boronic acids (*the Suzuki coupling*); (*ii*) the palladium-catalyzed reaction between an aryl and (or)alkyl halide and a vinyl functionality (*the Heck reaction*); and (*iii*) the palladium-catalyzed cross-coupling reaction of organotin reagents with a variety of organic electrophiles (*the Stille reaction*) on solid support. Only one remarkable preparation of compound libraries on solid phase utilizing the Stille reaction in the synthesis of hundreds of 1,4-benzodiazepine derivatives was reported by Plunkett and Ellman (7). The Suzuki reaction and the Heck reaction have not been applied for the preparation of compound libraries consisting of more than 20 compounds.

Received November 26, 1999. Published on the NRC Research Press website on July 6, 2000.

R. Franzén.[1] University of Helsinki, Division of Pharmaceutical Chemistry, Department of Pharmacy, P.O. Box 56, FIN-00014 Helsinki, Finland.

[1]Address for correspondence: Dr. Robert Franzén, Graduate School of Pharmaceutical Sciences, University of Tokyo, 7-3-1 Hongo, Bunkyo-ku, Tokyo 113-0033, Japan. Telephone–Fax: +81 3 5689.3522. e–mail: rfranzen@mol.f.u-tokyo.ac.jp

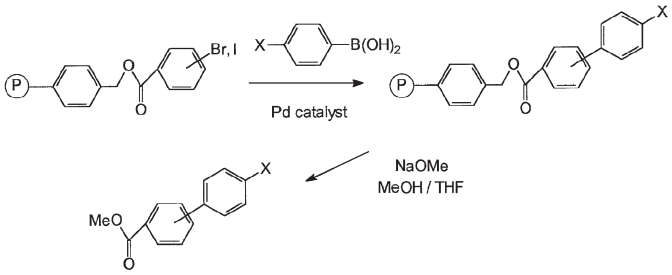
The Suzuki coupling

Palladium-catalyzed coupling via Suzuki reactions are powerful methods for C—C bond formation (8–10). The reaction generally results in an excellent yield when performed at temperatures of 60–80°C. Therefore, it is of high interest to adapt this reaction to a resin mounted procedure.

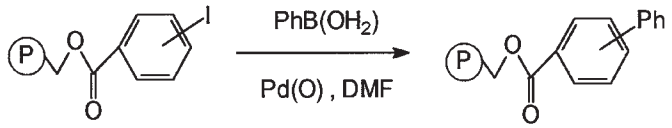
Solid-phase Suzuki coupling was first utilized in the preparation of biaryls. In the work by Frenette and Friesen (11) the cross-coupling reaction between aryl boronic acids and aryl bromides and iodides catalyzed by palladium on Merrifield resin was studied (Scheme 1). The biaryl products were released from the solid support by simple transesterification. A similar reaction was demonstrated by Guiles et al. (Scheme 2) (12). Han et al. (13) reacted several polymer bound arylhalides with a wide range of functionalized boronic acids under the Suzuki cross-coupling reaction conditions (Scheme 3) and produced several *ipso*-substitution products in good yields. Finally the Suzuki coupling for the production of biaryls has also been assisted by microwave irradiation as demonstrated by Larhed et al. (14) (Scheme 4).

© 2000 NRC Canada

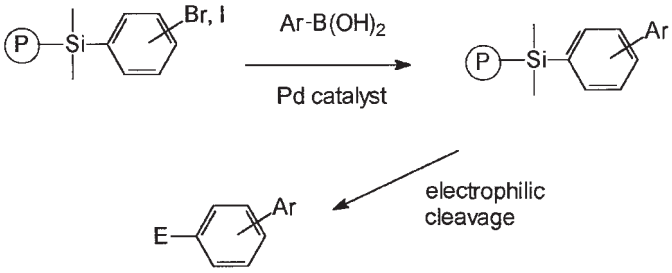
Scheme 1.



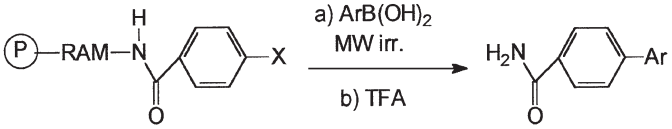
Scheme 2.



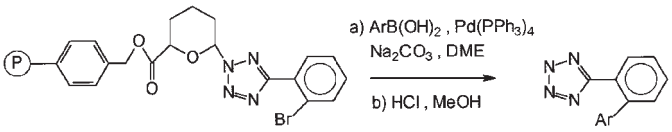
Scheme 3.



Scheme 4.

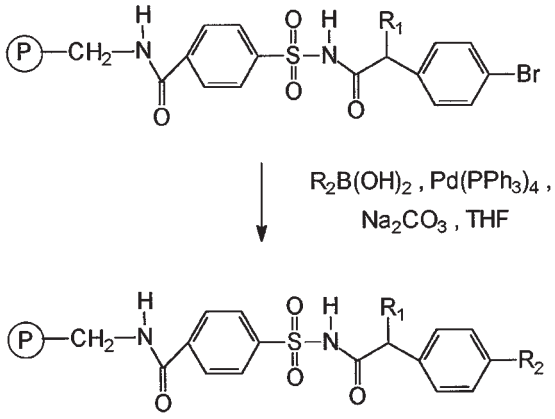


Scheme 5.

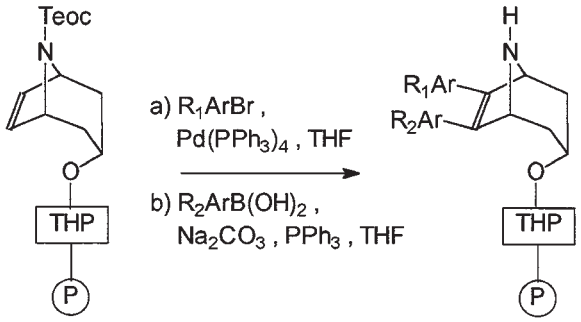


A Suzuki type solid-phase aryl–aryl coupling reaction for the preparation of various biphenyltetrazole derivatives was demonstrated by Yoo et al. (15) (Scheme 5). Marquis and Arlt (16) and Rottlander and Knochel (17) have also demonstrated that several biphenyls can be prepared from palladium-catalyzed reactions of aryl zinc bromides instead of phenyl boronic acids. Backes and Ellman (18) used the Suzuki reaction on solid support starting from a polymer supported acyl sulfonamide (Scheme 6) and in another paper Koh and Ellman (19) reported a palladium-mediated three component coupling (Scheme 7). In the work, several aryl boronic acids were used as coupling partners according to standard Suzuki coupling conditions. Ellman and co-workers (20) has also demonstrated that a Suzuki cross-coupling can

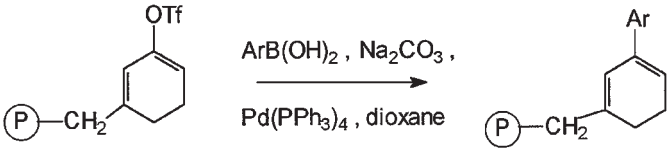
Scheme 6.



Scheme 7.



Scheme 8.

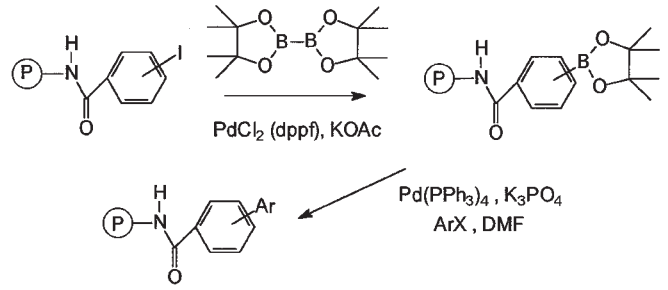


be performed in the synthesis of a 1,4-benzodiazepine-2,5-dione on solid support. Fraley and Rubino (21) utilized a Suzuki cross-coupling reaction between a vinyl triflate resin and boronic acid catalyzed by $Pd(PPh_3)_4$ (Scheme 8). Also a variety of other boronic coupling agents (heteroaryl, alkyl, alkenyl, and alkynyl) have been optimized under conditions similar to those used for the phenyl boronic acid coupling (12). Commonly, it has been concluded that the optimal Pd catalyst varies strongly depending upon the boronic coupling partner (22). In this paper, the importance of resin type and solvent composition for Suzuki reactions wherein the boronic acid moiety is either in solution or attached to the resin, was noticed.

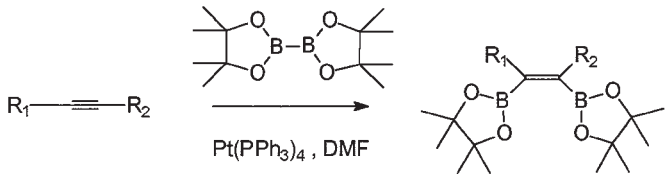
Piettre and Baltzer (23) modified the solid-phase reaction and treated polymer-bound aryl halides with pinacol ester of diboron under palladium (0) catalysis and produced polymer-bound boronates that could be used for Suzuki coupling reaction with a variety of aryl halides (Scheme 9). A coupling of a resin bound aryl iodide with phenyl boronic acid produced the biaryl compound in different yield depending on the catalysis system used in the reaction. When using the $PdCl_2$(dccf) as catalyst in the presence of triethylamine in DMF the best yield could be obtained. Ishiyama et al. (24)

© 2000 NRC Canada

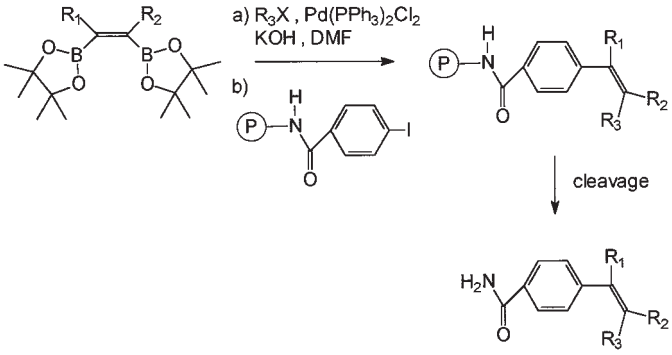
Scheme 9.



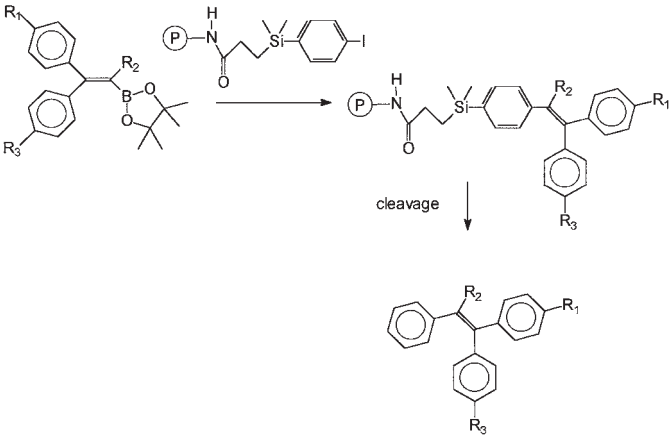
Scheme 10.



Scheme 11.

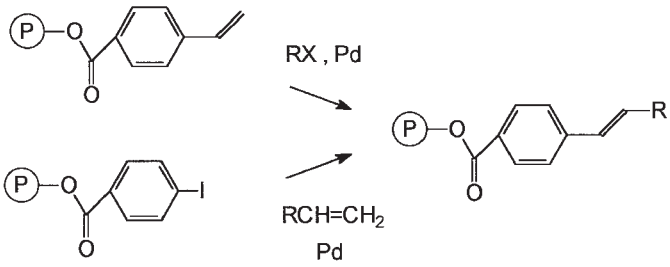


Scheme 12.

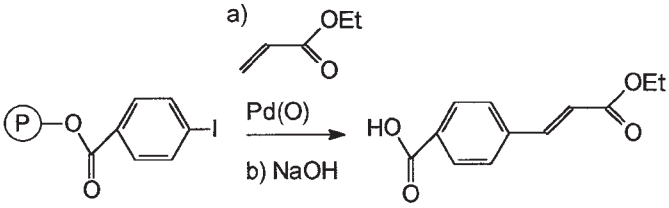


described the platinum-catalyzed diboration of alkynes to give bis(boryl)alkenes with very high *cis* selectivity (Scheme 10). Brown and Armstrong (25, 26) have utilized this approach in the preparation of tetra-substituted ethylenes (Scheme 11) and Tamoxifen derivatives (Scheme 12) on solid support via resin capture. The Suzuki coupling reaction has also been utilized in the preparation of new linkers and resins to be used in combinatorial chemistry (27–29). Due to the high yield in the cross-coupling on solid-support, the reaction has been used for reaction monitoring in Spin Echo Magic Angle Spinning ^{1}H NMR experiments (30).

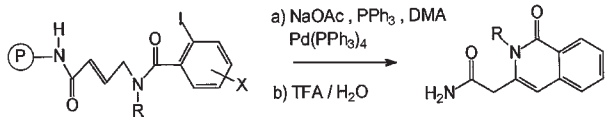
Scheme 13.



Scheme 14.



Scheme 15.



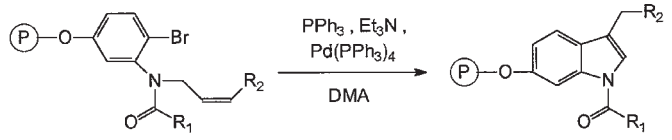
The Heck reaction

The Heck reaction (31, 32) has shown to be very useful for the preparation of especially disubstituted olefins. In the palladium catalyzed reaction the carbon–carbon bond is formed from a vinyl functionality and an aryl and (or) alkyl halide. The reaction is well adapted for automation due to the fact that it does not require inert atmosphere conditions. The intramolecular Heck reaction has been well-established as a powerful tool for the construction of complex polycyclic ring systems in the context of natural product synthesis. This process has been adapted in the solid-phase synthesis of several different types of molecules.

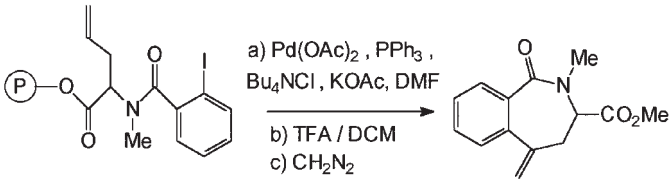
Yu et al. (33) used the reaction of polymer bound aryl iodide or styrene with olefins or arylhalides in the generation of 1,2-disubstituted olefin libraries (Scheme 13). Hiroshige et al. (34) studied the formation of a C—C bond in the palladium-promoted vinylation of aryl iodide bound to a solid support (Scheme 14). The solvent effect of Pd-catalyzed vinylation using different vinylic reagents was examined. The same group demonstrated also later that a macrocyclic molecule could efficiently be generated on solid support using a modified Heck reaction (35). This palladium-catalyzed intramolecular Heck reaction was also used by Goff and Zuckermann (36) (Scheme 15) for the solid-phase synthesis of substituted peptoid 1(2*H*)-isoquinolinones and by Yun

© 2000 NRC Canada

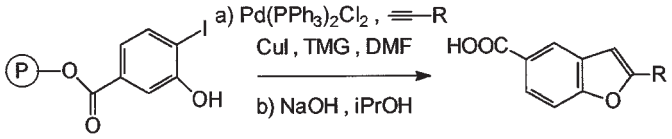
Scheme 16.



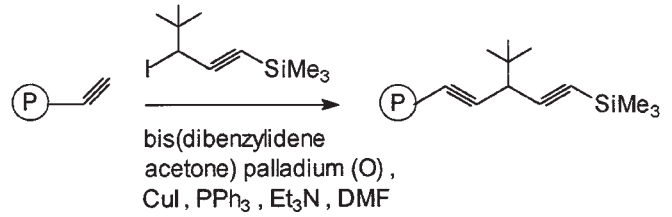
Scheme 17.



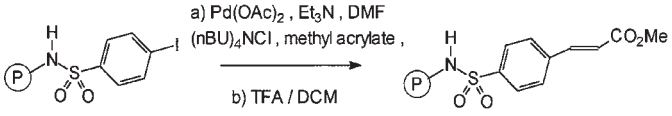
Scheme 18.



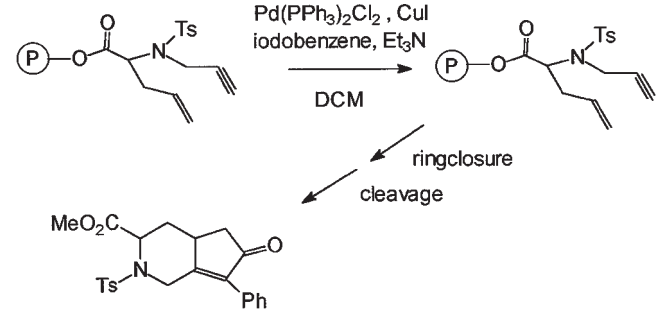
Scheme 19.



Scheme 20.

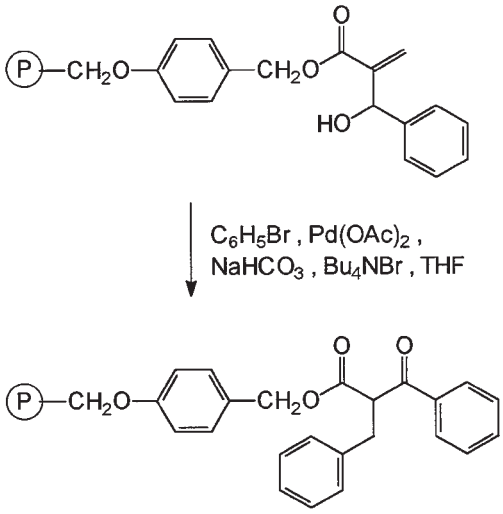


Scheme 21.

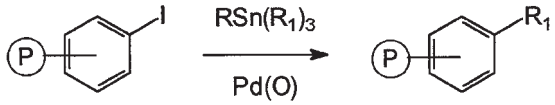


and Mohan (37) (Scheme 16) for the synthesis of indole analogues. A macrocyclization on solid-support using the Heck reaction has also been utilized by Akaji and Kiso (38) when a cyclic tetrapeptide derivative was synthesized. Lately, Bolton and Hodges (39) (Scheme 17) have prepared substituted benzazepines via intramolecular Heck cyclization on solid-phase.

Scheme 22.



Scheme 23.



Fancelli et al. (40) utilized the solid-phase Heck-coupling in the preparation of 2-substituted benzofuran carboxylic acids (Scheme 18). The reaction between the resin-bound hydroxy iodide and several acetylenes was examined. In the synthesis of phenyl acetylene oligomers, the Heck reaction was employed between a resin-bound aryl iodide and a terminal acetylene (41) (Scheme 19).

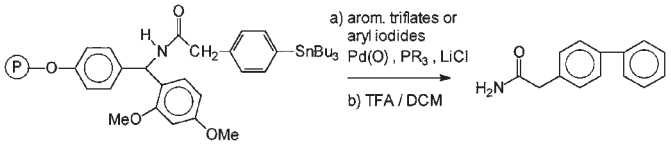
Beaver et al. (42) (Scheme 20) have performed Heck reactions with sulfonamide resins. The resin bound aryliodide reacted with methyl acrylate in the presence of $Pd(OAc)_2$. Following cleavage the α,β-unsaturated methyl ester phenyl sulfonide was obtained in high yield. The Heck reaction has also been used in the solid-phase synthesis of fused bicyclic amino acid derivatives (Scheme 21) (43) and in the monitoring of a solid-phase reaction by MAS NMR spectroscopy. Recently, β-keto esters have been prepared on solid support via a sequential Baylis–Hillman and Heck reaction (Scheme 22) (44).

The Stille reaction

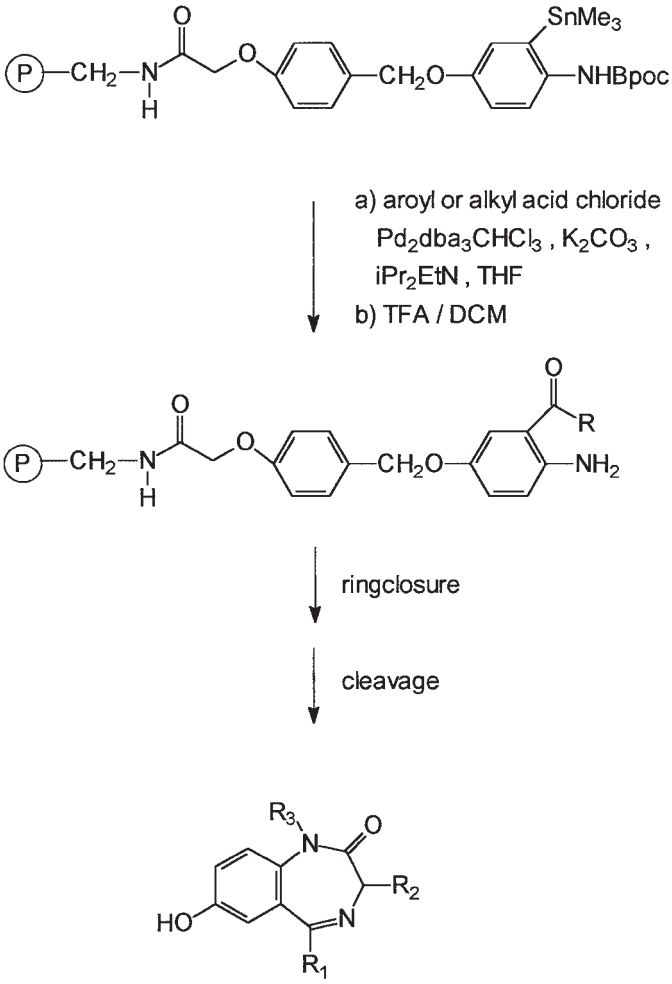
Palladium-catalyzed substitution and addition involving organotin compounds (45–47) have been used by many research groups throughout the world for synthetic purposes. Several applications of the Stille reaction for efficient carbon–carbon bond formation on solid-support have been reported: (*i*) Desphande (48) used the Stille coupling reaction on solid support for the preparation of biaryls. In his report, he coupled vinyl and (or) aryl stannanes with polymer bound aryl iodides (Scheme 23). The cross-coupled products were obtained following cleavage from the support in high yield. A year later, Forman and Sucholeiki (49) used the reaction for the preparation of biaryl derivatives and studied the reaction of polymer-bound aryl stannanes with aryl iodides

© 2000 NRC Canada

Scheme 24.



Scheme 25.

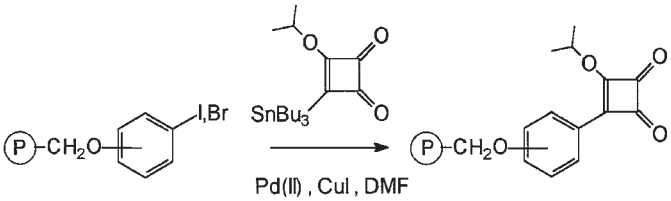


or triflates (Scheme 24). Tributylphenyltin was attached by an amide bond to the Rink amide resin and a palladium-mediated coupling with aryl triflates and aryl iodides was investigated.

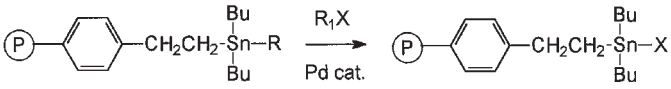
Ellman and co-workers (7, 50, 51) have demonstrated in several papers how the Stille coupling can be utilized in the preparation of small molecule libraries. His group discovered an excellent method (52) for the preparation of 1,4-benzodiazepine derivatives on solid-support and using the Stille coupling he could produce structurally diverse derivatives a few years later (7, 50, 51) (Scheme 25). Recently (53), the group has utilized the Stille coupling in the preparation of new traceless linkers to be used in solid-phase synthesis.

In the preparation of cyclobutenedione derivatives on solid-support, Tempest and Armstrong (54) used a Mitsonobu reaction (55) coupled with a tributyltin isopropyl squarate under Stille conditions (Scheme 26). The reaction

Scheme 26.



Scheme 27.



proceeded well and after TFA cleavage only the expected product was obtained in high yield. Finally, Kuhn and Neumann (56) (Scheme 27) investigated the Stille reaction carried out with polymer-supported organotin reagents. This work showed that organitin by-products could easily be separated by filtration and that the target molecule was free of toxic organotin materials.

Concluding remarks

Carbon–carbon bond formation reactions on solid-support are highly useful and versatile methods needed for the development of modern drug discovery. This review encompasses most of the metal-catalyzed coupling reactions performed on solid-support starting from 1980. The review focuses on the investigation of the solid-phase adaption of the Suzuki, the Heck, and the Stille coupling reactions due to the fact that these have proven to be both reliable and efficient methods.

References

1. E.M. Gordon, R.W. Barret, W.J. Dower, S.P.A. Fodor, and M.A. Gallop. J. Med. Chem. **37**, 1233 (1994).
2. N.K. Terrett, M. Gardner, D.W. Gordon, and R.J. Kobylecki. Tetrahedron, **51**, 8135 (1995).
3. C. Friedel and J.M. Crafts. C. R. Hebd. Seances Acad. Sci. **84**, 1392 (1877).
4. V. Grignard. Compt. Rend. **130**, 1322 (1900).
5. O. Diels and K. Alder. Justus Liebigs Ann. Chem. **460**, 98 (1928).
6. C.J. Andres, D.L. Whitehouse, and M.S. Desphande. Curr. Opin. Chem. Biol. **2**, 353 (1998).
7. M.J. Plunkett and J.A. Ellman. J. Am. Chem. Soc. **117**, 3306 (1995).
8. N. Miyaura, T. Yanagi, and A. Suzuki. Synth. Commun. **11**, 513 (1981).
9. A. Suzuki. Pure Appl. Chem. **57**, 1749 (1985).
10. M. Sato, N. Miyaura, and A. Suzuki. Chem. Lett. 1405 (1989).
11. R. Frenette and R.W. Friesen. Tetrahedron Lett. **35**, 9177 (1994).
12. J.W. Guiles, S.G. Johnson, and W.V. Murray. J. Org. Chem. **61**, 5169 (1996).
13. Y. Han, S.D. Walker, and R.N. Young. Tetrahedron Lett. **37**, 2703 (1996).
14. M. Larhed, G. Lindeberg, and A. Hallberg. Tetrahedron Lett. **37**, 8219 (1996).

© 2000 NRC Canada

15. S. Yoo, J. Seo, K. Yi, and Y. Gong. Tetrahedron Lett. **38**, 1203 (1997).
16. S. Marquais and M. Arlt. Tetrahedron Lett. **37**, 5491 (1996).
17. M. Rottlander and P. Knochel. Synlett. 1084 (1997).
18. B.J. Backes and J.A. Ellman. J. Am. Chem. Soc. **116**, 11171 (1994).
19. J.S. Koh and J.A. Ellman. J. Org. Chem. **61**, 4494 (1996).
20. C.G. Boojamra, K.M. Burow, and J.A. Ellman. J. Org. Chem. **60**, 5742 (1995).
21. M.E. Fraley and R.S. Rubino. Tetrahedron Lett. **38**, 3365 (1997).
22. B. Ruhland, A. Bombrun, and M.A. Gallop. J. Org. Chem. **62**, 7820 (1997).
23. S.R. Piettre and S. Baltzer. Tetrahedron Lett. **38**, 1197 (1997).
24. T. Ishiyama, N. Matsuda, N. Miyaura, and A. Suzuki. J. Am. Chem. Soc. **115**, 11018 (1993).
25. S.D. Brown and R.W. Armstrong. J. Am. Chem. Soc. **118**, 6331 (1996).
26. S.D. Brown and R.W. Armstrong. J. Org. Chem. **62**, 7076 (1997).
27. B. Chenera, J.A. Finkelstein, and D.F. Veber. J. Am. Chem. Soc. **117**, 11999 (1995).
28. N.D. Hone, S.G. Davies, N.J. Deverreux, S.L. Taylor, and A.D. Baxter. Tetrahedron Lett. **39**, 897 (1998).
29. R.S. Garigipati. Tetrahedron Lett. **38**, 6807 (1997).
30. R.S. Garigipati, B. Adams, J.L. Adams, and S.K. Sarkar. J. Org. Chem. **61**, 2911 (1996).
31. R.F. Heck. Org. React. N.Y. **27**, 345 (1982).
32. J.E. Plevyak and R.F. Heck. J. Org. Chem. **43**, 2454 (1978).
33. K.-L. Yu, M.S. Desphande, D.M. Vyas. Tetrahedron Lett. **35**, 8919 (1994).
34. M. Hiroshige, J.R. Hauske, P. Zhou. Tetrahedron Lett. **36**, 4567 (1995).
35. M. Hiroshige, J.R. Hauske, P. Zhou. J. Am. Chem. Soc. **117**, 11590 (1995).
36. D.A. Goff and R.N. Zuckermann. J. Org. Chem. **60**, 5748 (1995).
37. W. Yun and R. Mohan. Tetrahedron Lett. **37**, 7189 (1996).
38. K. Akaji and Y. Kiso. Tetrahedron Lett. **38**, 5185 (1997).
39. G.L. Bolton, and J.C. Hodges. J. Comb. Chem. **1**, 130 (1999).
40. D. Fancelli, M.C. Fagnola, D. Severino, A. Bedeschi. Tetrahedron Lett. **38**, 2311 (1997).
41. J.K. Young, J.C. Nelson, and J.S. Moore. J. Am. Chem. Soc. **116**, 10841 (1994).
42. K. Beaver, A.C. Siegmund, and K.L. Spear. Tetrahedron Lett. **37**, 1145 (1996).
43. G.L. Bolton. Tetrahedron Lett. **37**, 3433 (1996).
44. B.A. Kulkarni and A. Ganesan. J. Comb. Chem. **1**, 373 (1999).
45. J.W. Labadie, D Tueting, and J.K. Stille. J. Org. Chem. **48**, 4634 (1983).
46. A.M. Echavarren and J.K. Stille. J. Am. Chem. Soc. **110**, 1557 (1988).
47. T.N. Mitchell. Synthesis, 803 (1992).
48. M.S. Desphande. Tetrahedron Lett. **35**, 5613 (1994).
49. F.W. Forman and I. Sucholeiki. J. Org. Chem. **60**, 523 (1995).
50. B.A. Bunin, M.J. Plunkett, and J.A. Ellman. Proc. Natl. Acad. Sci. U.S.A. **91**, 4708 (1994).
51. M.J. Plunkett and J.A. Ellman. J. Org. Chem. **60**, 6006 (1995).
52. B.A. Bunin and J.A. Ellman. J. Am. Chem. Soc. **114**, 10997 (1992).
53. M.J. Plunkett and J.A. Ellman. J. Org. Chem. **62**, 2885 (1997).
54. P.A. Tempest and R.W. Armstrong. J. Am. Chem. Soc. **119**, 7607 (1997).
55. O. Mitsunobu and M. Yamada. Bull. Chem. Soc. Jpn. **40**, 2380 (1967).
56. H. Kuhn and W.P. Neumann. Synlett. 123 (1994).

© 2000 NRC Canada

Synthesis and photophysical properties of fluorophore-labeled abscisic acid

X. Hou, S.R. Abrams, J.J. Balsevich, N. Irvine, T. Norstrom, M. Sikorski, H.K. Sinha, and R.P. Steer

Abstract: The 8′-benzophenone, 8′-dansylhydrazone, 3′-*S*-(2-ethyldansylamide), and 3′-*S*-acetamidofluorescein derivatives of the plant hormone abscisic acid (ABA) have been synthesized for use in photoaffinity labeling (the benzophenone derivative) or fluorescence probe experiments and have been spectroscopically characterized. One of the three fluorescent compounds, the 3′-tethered fluorescein derivative, exhibits spectroscopic and photophysical properties which indicate that it could be an excellent fluorescent probe of ABA interactions in vivo. The 3′-tethered fluorescein and ABA moieties do not interact strongly, so that the fluorescence properties of the fluorescein-labelled hormone are very similar to those of fluorescein itself. Measurements of the absorption, emission, and fluorescence excitation spectra, fluorescence quantum yields, and fluorescence decay parameters of this derivative as a function of pH indicate that the photophysics is dominated by ground and excited state prototropic equilibria involving only the fluorescein moiety. The fluorescein dianion is the only significant absorber and emitter at pH > 6.7, whereas only the cation absorbs and emits at pH < 0. In the intervening pH range, strong emission from the monoanion and weak emission from two neutral species, tentatively assigned to the zwitterion and the lactone of the fluorescein moiety, is observed.

Key words: abscisic acid, fluorescein, synthesis, photophysics.

Résumé : On a effectué la synthèse de dérivés 8′-benzophénone, 8′-dansylhydrazone, 3′-*S*-(2-éthyldanzylamide) et 3′-*S*-acétamidofluorescéine de l'acide abscisique (« ABA »), une hormone végétale. Ces dérivés, préparés pour utilisation comme sonde de fluorescence ou dans des expériences de marquage par photoaffinité (le dérivé benzophénone), ont été caractérisés par spectroscopie. L'un des trois composés fluorescents, le dérivé de la fluorescéine attaché en position 3′, possède des propriétés spectroscopiques et photophysiques qui suggèrent qu'il pourrait très bien agir comme sonde fluorescente des interactions « ABA » in vivo. Les portions « ABA » et fluorescéine attachée en position 3′ n'interagissent pas très fortement ce qui fait que les propriétés de fluorescence de l'hormone marquée à la fluorescéine sont très semblables à celles de la fluorescéine seule. Des mesures des spectres d'absorption, d'émission et d'excitation de fluorescence, des rendements quantiques de fluorescence et des paramètres de décroissance de la fluorescence en fonction du pH indiquent que la photophysique est dominée par les équilibres protoniques des états excité et fondamental n'impliquant que la portion fluorescéine. Le dianion de la fluorescéine est la seule entité absorbante et émettrice significative à des pH > 6,7 alors que seul de cation absorbe et émet à des pH < 0. Dans la zone des pH intermédiaires, on observe une émission forte de la part du monoanion et une faible émission provenant de deux entités neutres que l'on attribue provisoirement au zwitterion et à la lactone de la portion fluorescéine.

Mots clés : acide abscisique, fluorescéine, synthèse, photophysique.

[Traduit par la Rédaction]

Introduction

The plant hormone abscisic acid (**1**, ABA) is a signaling compound found in all higher plants (1). ABA is involved in mediating numerous aspects of plant growth and development including plants' responses to environmental stress and processes in seed development such as deposition of storage reserves, induction of desiccation tolerance, and control of germination (2). The plant biomolecules that interact with ABA as receptors and carriers and the enzymes that act on the hormone are targets of biotechnology research for improving environmental stress tolerance and plant productivity. The present study is directed towards developing photochemical and photophysical tools for probing the interactions of ABA with plant biomolecules that bind the hormone.

The ABA signal transduction pathway is a subject of intense investigation but, although progress has been made, a clear understanding of how the hormone is initially perceived has not emerged (3). In particular, the location of receptors in plant tissues or cells has not been clearly

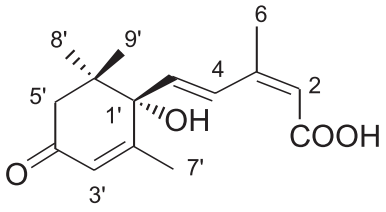
Received January 31, 2000. Published on the NRC Research Press website on July 5, 2000.

X. Hou, M. Sikorski,[1] H.K. Sinha, and R.P. Steer.[2] Department of Chemistry, University of Saskatchewan, 110 Science Place, Saskatoon, SK S7N 5C9, Canada.
S.R. Abrams, J.J. Balsevich, N. Irvine, and T. Norstrom. National Research Council, Plant Biotechnology Institute, 110 Gymnasium Place, Saskatoon, SK S7N 0W9, Canada.

[1]Faculty of Chemistry, A. Mickiewicz University, 60-780 Poznan, Poland.
[2]Author to whom correspondence may be addressed. Fax: (306) 966-4730. e-mail: ron.steer@usask.ca

© 2000 NRC Canada

Fig. 1. Structure and conventional numbering system of natural (+)-*S*-2-*cis*, 4-*trans*-abscisic acid, ABA (**1**).



1

determined (4). In addition, the nature and multiplicity of ABA receptors are unknown, although evidence from experiments with chiral analogs indicate that there may be more than one receptor for ABA in a given plant (5). Attempts to identify ABA receptors by photoaffinity labeling have met with little success (6). There are several reports of the isolation of ABA binding proteins using affinity chromatography techniques, but the function of the isolated proteins is unclear. Carrier proteins that transport ABA across membranes have been partially characterized, and structural variants of ABA have been useful for probing the structural requirements of the active sites (see for example ref. (7)). Nevertheless, the nature and locations of the receptors remain unclear, and this has motivated us to consider developing fluorescent probes and photoaffinity labels for elucidating these aspects of ABA's function.

Photochemical or photophysical probes for studying the binding of ABA in a biological matrix must incorporate an ABA-like molecular structure that can bind in the active site(s). The ABA moiety needs to be linked through a tether to a molecular fragment that has the desired photochemical or photophysical properties (reactivity or fluorescence, respectively) while maintaining its biological activity. Changes to the structure of ABA generally reduce its biological activity and also are likely to affect its binding to receptors. In particular, the activity of ABA is generally reduced when the carbonyl group of the ring or the carboxyl group of the sidechain is modified (8). Thus, other sites on the ABA molecule are required for attaching a photochemically reactive fragment or fluorophore. In the present studies, two different points of connection were considered. Modification of the molecule by substitution at the 3′-carbon (for the conventional numbering system see the ABA structure, Fig. 1) had previously been shown to afford molecules with biological activity; the 3′-modified ABA had been used for affinity chromatography in purifying anti-ABA monoclonal antibodies (9). Alteration of the ABA molecule by substitution at the 8′-carbon atom has also afforded analogs with high biological activity, due in part, to their reduced metabolism by enzymes that degrade the hormone (10). To increase the probability that the ABA derivatives would have biological activity, tethers of different length and structure were incorporated at the 3′- or 8′-carbon atom.

In an effort to expand our knowledge of ABA's in vivo molecular function, we have synthesized several derivatives, one for photoaffinity labeling and three fluorescence probes, and have characterized them using spectroscopic and photophysical measurements. For the present work on the initial development of a method for synthesis and material for photophysical characterization, racemic compounds have been employed. For studies with ABA-binding proteins, probes having the ABA portion in optically pure form will be required. One derivative substituted at the 3′ position by a tethered fluorescein moiety has been found to exhibit promise as a fluorescence probe.

Results

Four ABA derivatives were synthesized: (*i*) an 8′-tethered benzophenone derivative **10** for possible photoaffinity labelling experiments; and (*ii*) an 8′-tethered dansyl derivative **6**; (*iii*) a similar 3′-tethered dansyl derivative **14**; (*iv*) and a 3′-tethered fluorescein derivative **12** for possible fluorescence labeling studies.

The 8′-tethered ABA derivatives were synthesized as shown in Scheme 1, starting with cyclohexadienone **2** (11). Conjugate addition of vinyl magnesium bromide gave the known 8′-methylene ABA methyl ester **3** (10). Ozonolysis afforded the aldehyde **4**, which on reaction with dansyl chloride led to the dansyl derivative **5** which was converted to the abscisic acid derivative **6** by alkaline hydrolysis. The benzophenone derivative **10** was synthesized in four steps from **2**, by conjugate addition of the Grignard reagent derived from the THP ether of 6-bromohexanol, deprotection of the primary alcohol and the carboxylic acid, and coupling of the benzophenone with the activated derivative affording the tethered 8′-benzophenone ABA analog.

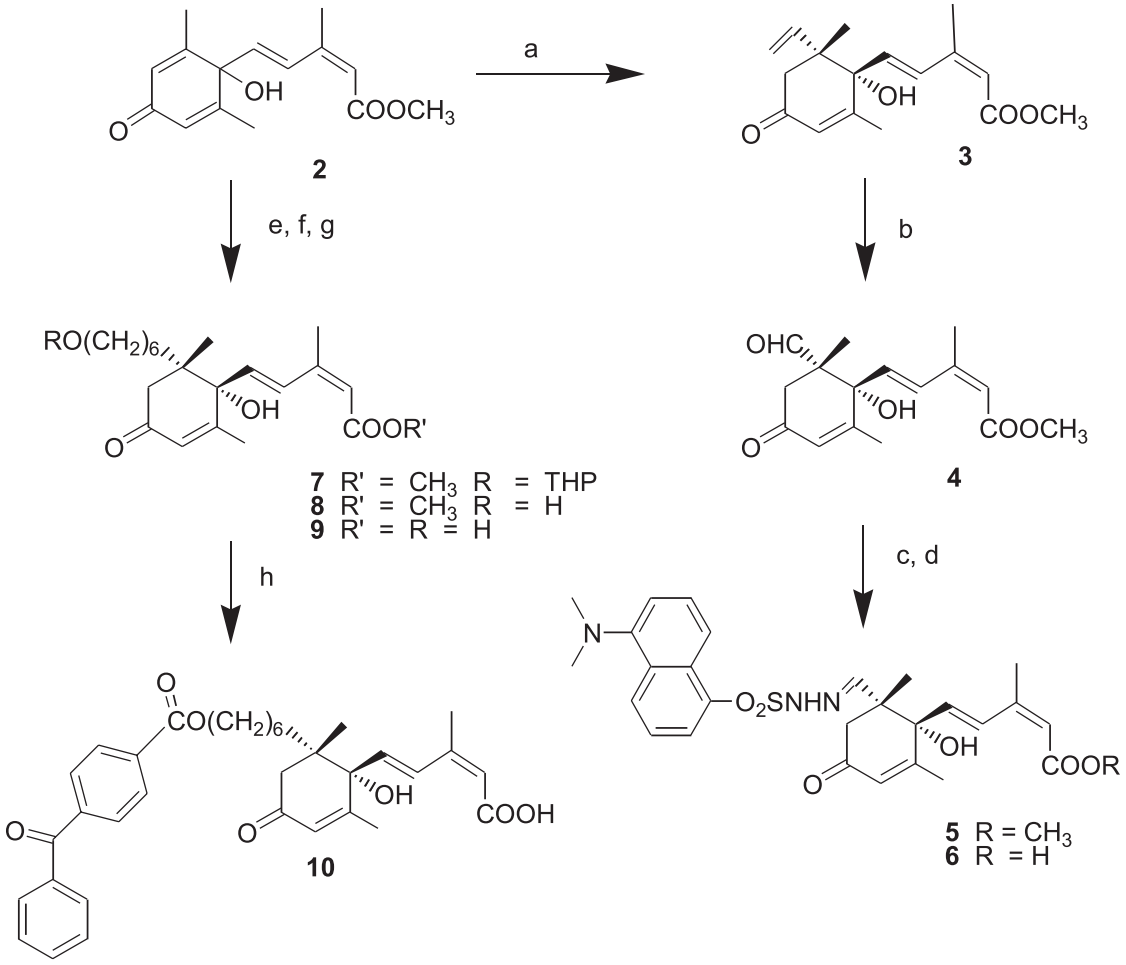
The fluorescent derivatives of ABA altered at the 3′-carbon were prepared as shown in Scheme 2, starting with the known 2′,3′-epoxide of ABA (**11**) (12). The fluorescein group was added to the 3′-carbon by first making the thiol derivative (**12**) which was further reacted with the iodoacetamide derivative of fluorescein affording the tethered ABA analog **13**. The 3′-dansyl derivative of ABA **14** was synthesized from the ABA epoxide **11** and the thioacetate dansyl derivative.

The benzophenone derivative of ABA behaves like many such compounds prepared for photoaffinity labeling (13). It exhibits a weak $n \rightarrow \pi^*$ transition in the near UV and a strong $\pi \rightarrow \pi^*$ transition further to the blue with λ_{max} = 256 nm and $\varepsilon_{max} = 3.0 \times 10^4$ M^{-1} cm^{-1} in 50% v/v water–methanol. It is almost nonfluorescent in solution. It is therefore suitable from a spectroscopic perspective for photoaffinity labelling since it can be excited in the $\lambda >$ 320 nm range where damage to proteins is minimized, and in the free form it will not contribute significant intensity to a fluorescent signal developed by photoreaction of the benzophenone moiety in the active site. The only drawback is the poor solubility of this ABA derivative in pure water.

The dansyl-ABA derivatives exhibit a moderately strong absorption band (shoulder) in the near UV with a maximum near 327 nm and a strongly Stokes-shifted fluorescence emission band with a maximum near 575 nm in neutral aqueous solution. As is typical of dansyl derivatives in polar solvents (14, 15), the quantum yields of emission, ϕ_f, are low in aqueous solution. For the 3′-derivative for example, ϕ_f increases from 3.9×10^{-3} to 6.9×10^{-3} as the pH decreases from 10.6 to 8.3, and then falls monotonically with further decreases in pH to $<10^{-5}$ at pH = 2. These quantum yields of fluorescence are independent of the concentration

© 2000 NRC Canada

Scheme 1. a, vinyl magnesium bromide; **b**, ozone; **c,** dansyl hydrazine and trichloroacetic acid; **d**, 10% potassium hydroxide in methanol; **e**, magnesium and 2-(6-bromohexoxy)-tetrahydro-2*H*-pyran; **f**, pyridinium *p*-toluenesulfonate; **g**, 10% potassium hydroxide in methanol; **h**, 3′-*O*-(4-benzoyl)-benzoyl imidazolide.



of the 3′-dansyl-ABA compound in the 10^{-6} – 2×10^{-6} M range. Although the dependence of the spectra and emission quantum yields on the polarity of the surrounding medium might be exploited to educe some information about the nature of the ABA binding site, the temporal fluorescence behaviour of both the 3′- and the 8′-derivatives proved to be complex, with the excited state fluorescence decays exhibiting multiple-exponential character. This behaviour is unlike those of other dansyl derivatives which are known to exhibit single-exponential fluorescence decay functions. The reasons for this behaviour were not explored, but it was concluded that these derivatives were not altogether suitable for use as fluorescent probes and they were not further investigated.

Preliminary experiments showed that the 3′-substituted fluorescein derivative suffered from none of the shortcomings of the dansyl derivatives, and this compound was therefore subjected to a detailed photophysical examination. The emission and fluorescence excitation spectra of the 3′-substituted fluorescein derivative as a function of pH are shown in Fig. 2. These spectra suggest that this compound behaves much like fluorescein itself which is known to exhibit multiple prototropic equilibria in aqueous solution. To aid in the analysis, the spectroscopy and photophysics of the fluorescein-ABA derivative were examined in several different pH ranges.

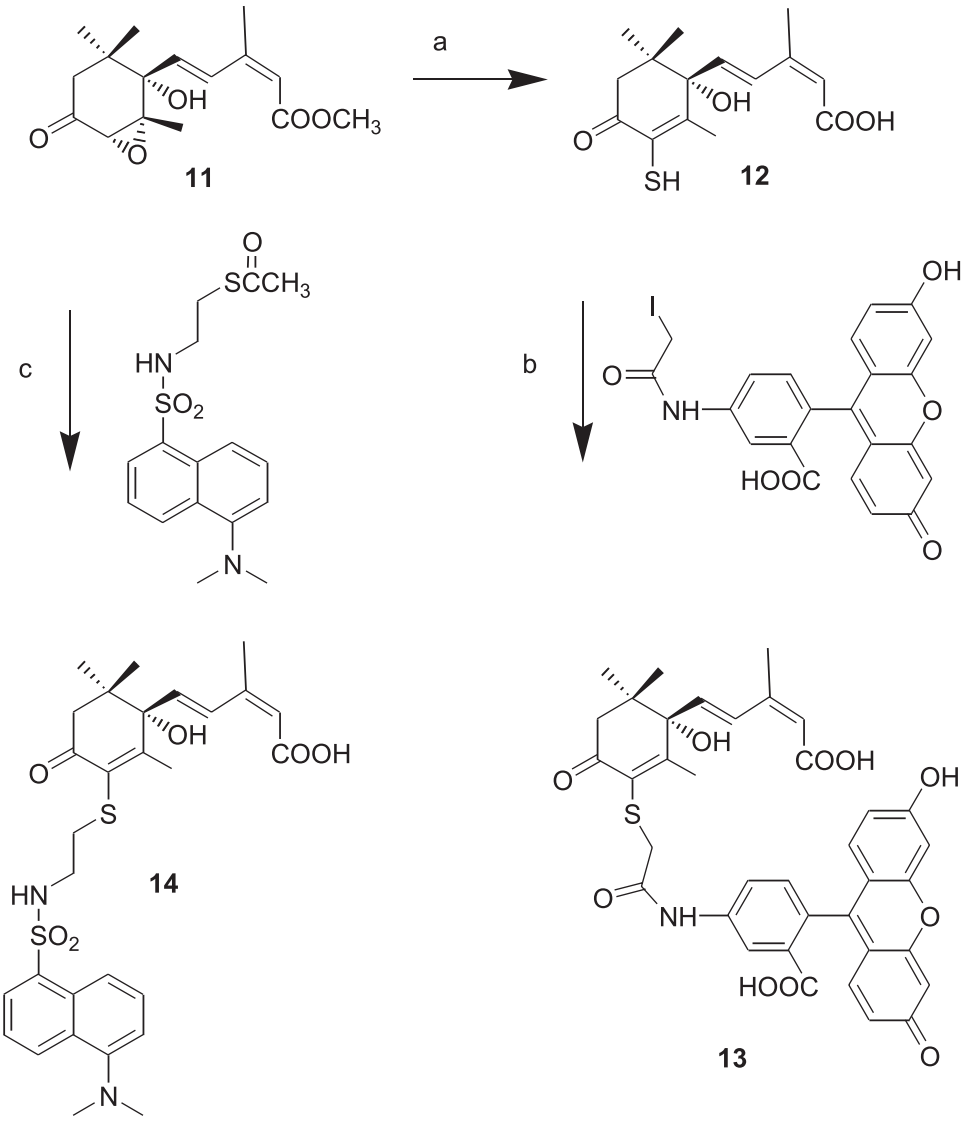
(*i*) 11.7 = pH = 6.7

In this pH range, the absorption, corrected fluorescence excitation, and emission spectra of the fluorescein-labelled compound (Fig. 2A) are all independent of pH. In addition, the corrected fluorescence excitation spectra are identical with the absorption spectra (λ_{max} = 492 nm) throughout the near UV-vis range, the emission spectra (λ_{max} = 517 nm) are independent of excitation wavelength, and the excitation spectra are independent of emission wavelength. The temporal fluorescence decay profiles (Fig. 3A) are well-represented by a single exponential decay function with an average lifetime of $\tau = 4.30 \pm 0.04$ ns, independent of pH in this range. The quantum yield of fluorescence is $\phi_f = 0.89 \pm 0.04$, also independent of pH in this range. The compound is stable in aqueous base up to at least pH 12.

These observations all lead to the conclusion that, in this pH range, a single chemical species is responsible for the absorption and that its excitation yields a single emitting species. By analogy with the spectra, lifetimes and quantum yields (Tables 1 and 2) of fluorescein itself (16, 17), the

© 2000 NRC Canada

Scheme 2. a, sodium hydride, thiol acetic acid; **b**, iodoacetamidofluorescein; **c**, 1 M sodium hydroxide.



absorber and emitter in this pH range are assigned to the ground (S_0) and lowest excited singlet (S_1) states of the dianion of the fluorophore. Fluorescein itself has ground state pK_a values (16) of 2.08, 4.31, and 6.43, corresponding to the equilibria shown in Scheme 3, and therefore exists as the dianion in this pH range. ABA itself, with pK_a = 4.8 (carboxyl dissociation (1)), exists as the monoanion in this pH range, but the state of ionization of the ABA moiety has no significant effect on the spectra and photophysical properties of the fluorophor. These observations suggest that there is little interaction between the ABA and fluorescein moieties in the 3′-tethered compound.

The above photophysical data may be used to calculate the radiative rate constant, k_r, and the sum of the rate constants, Σk_{nr}, of all nonradiative processes by which the fluorescent S_1 state of the dianion of the fluorophore relaxes to the ground state. Using the well-known (18) relationships $k_r = \phi_f/\tau$ and $\Sigma k_{nr} = (1 - \phi_f)/\tau$, values of $k_r = (2.1 \pm 0.1) \times 10^8$ s^{-1} and $\Sigma k_{nr} = (2.6 \pm 0.1) \times 10^7$ s^{-1} are calculated when the average values of ϕ_f and τ in the range $11.7 \geq pH \geq 6.7$ are employed. These values are very similar to $k_r = 2.3 \times 10^8$ s^{-1} and $\Sigma k_{nr} = 1.7 \times 10^7$ s^{-1} which may be calculated for the S_1 state of the dianion of fluorescein itself using the reported values (14) of $\phi_f = 0.93$ and $\tau = 4.1$ ns.

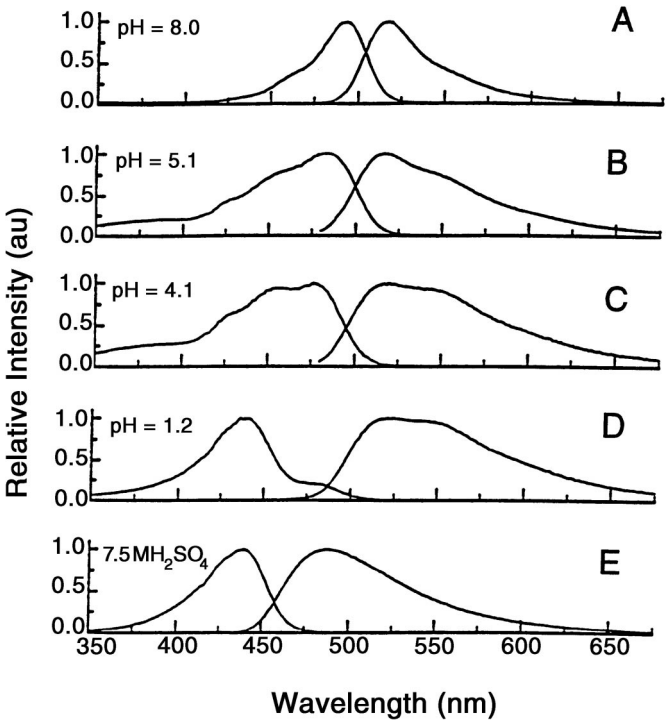
(*ii*) 6 ≥ pH ≥ 5

In fluorescein itself, pK_3 = 6.43 for the ground state prototropic equilibrium between the monoanion and the dianion in aqueous solution at room temperature, and the monoanion reaches its maximum concentration at pH ≈ 5 (16). For the 3′-tethered fluorescein derivative of ABA, evidence of significant amounts of fluorescent monoanion is found at pH < 6, and changes in both the spectra and excited state decay parameters are readily observed in the 6 ≥ pH ≥ 5 range (cf. Fig. 1). The absorption and corrected fluorescence excitation spectra decrease in intensity with decreasing pH at constant solute concentration and their λ_{max} shift to lower wavelengths, whereas the emission spectra broaden and a shoulder at ca. 560 nm becomes more prominent. The overall quantum yield of fluorescence drops from 0.89 at higher pH to ca. 0.3 in this range.

In this pH range, the temporal fluorescence profiles are best described by double exponential decay functions

© 2000 NRC Canada

Fig. 2. Corrected emission and emission–excitation spectra of the 3′-tethered fluorescein derivative of ABA as a function of pH. A, region (*i*) pH = 8.0; B, region (*ii*) pH = 5.1; C, region (*iii*) pH = 4.2; D, region (*iv*), pH = 1.2; E, region (*v*), 7.5 M H_2SO_4.



(Fig. 3B), $I(t) = a_1 \exp(-t/\tau_1) + a_2 \exp(-t/\tau_2)$, in which the two emitters have average lifetimes of 4.32 ± 0.04 ns and 2.19 ± 0.02 ns. The fraction of the emission due to the jth emitter can be obtained from the relationship $F_j = a_j\tau_j/\Sigma a_i\tau_i$. Analysis of the temporal fluorescence data shows that the fraction of the emission due to the longer-lived emitter decreases and the fraction due to the shorter-lived emitter increases with decreasing pH, Table 2. The fraction of the emission from the shorter-lived species also increases slightly with increasing emission wavelength at fixed pH (Table 2), consistent with the shorter-lived species having a red-shifted emission spectrum compared with that of the longer-lived species.

It is reasonable to assign the longer-lived species which has an emission spectrum shaded more to the blue to the dianion of the fluorescein moiety in its S_1 state, and to assign the shorter-lived species to the monoanion of the fluorophore, consistent with its more red-shaded emission spectrum. The lifetime of the longer-lived species is identical to that measured for the excited dianion in the higher pH region. A lifetime of approximately 3 ns has been measured for the monoanion of fluorescein itself using a modulated fluorescence excitation technique (16). The lifetime of the monoanion of the fluorescein–ABA compound obtained in the 6 ≥ pH ≥ 5 range is 2.19 ns, which is similar to the lifetime of the monoanion of fluorescein itself at similar pH.

(*iii*) 4.1 ≥ pH ≥ 2.7

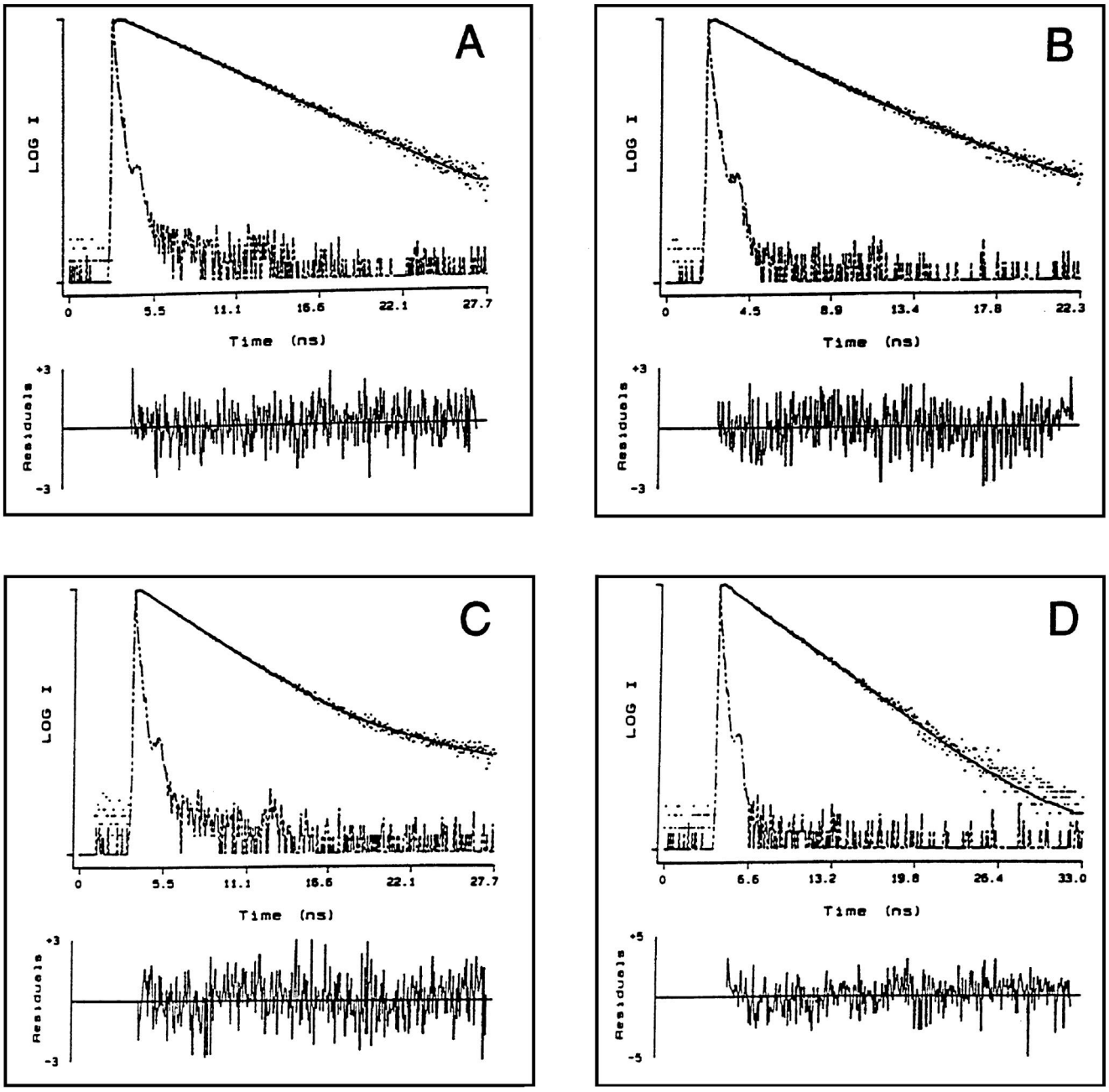
In this region the absorption and corrected emission–excitation spectra are pH sensitive but the emission spectra are not (Fig. 2C). Two features, one at ca. 475 nm and another, some 25–35 nm further to the blue, are prominent in the visible portion of the absorption and emission–excitation spectra. The feature at ca. 475 nm does not change position with decreasing pH, but the feature immediately to the blue increases in relative intensity and shifts to shorter wavelengths in this pH range. The emission spectrum exhibits two features, a maximum at 519 nm and a shoulder at ca. 550 nm whose relative intensities are independent of pH and excitation wavelength at pH = 3.4 (vide infra). The temporal fluorescence decay profile is complex, but is adequately modeled by a triple exponential function, as exemplified by Fig. 3C. The component of intermediate lifetime dominates the distribution of emitting species ($F \geq 0.85$, independent of pH), as shown in Table 2.

Fluorescein itself exhibits $pK_2 = 4.31$ and $pK_1 = 2.08$, and neutral species dominate the ground state equilibria in the 4 ≥ pH ≥ 3 region (16). The neutral species can exist in *p*-quinoid, lactone, and zwitterionic forms, with their total reaching a maximum mol fraction at ca. pH = 3.5. A similar distribution of species is expected in the 3′-tethered fluorescein derivative of ABA, so that in the ground state at pH = 3.4 the total mol fraction of the neutral species is expected to be at least 0.7 (16). The change in the ground state distribution with pH thus accounts for the changes in the absorption and fluorescence excitation spectra of the 3′-tethered derivative in this region. In contrast, the emission spectrum is not pH sensitive for excitation at a fixed wavelength and is similar to the emission spectrum of the monoanion. This observation suggests that the dominant emitting species, the monoanion, is obtained by fast protolytic dissociation of one or more of the excited neutral species, as is found in fluorescein itself (16). This interpretation is consistent with the fluorescence lifetime data, in which the dominant emitting species ($F = 0.89$, independent of pH) has a lifetime of ca. 2.6 ns, a value which is not significantly different from the lifetime of the anion measured at higher pH where the decay is less complex.

Fluorescence decay measurements using excitation modulation and phase sensitive detection revealed only a single emitter with a lifetime of ca. 3 ns in aqueous fluorescein itself in this pH range (16). Thus, earlier work on fluorescein provides no clue to the assignment of the minor components in the three-component decay of the emission from the 3′-tethered fluorescein derivative of ABA. Nevertheless, it is reasonable to assign these minor components to emission from the excited states of two of the three forms of the neutral species which dominate the ground state equilibria in this pH range. Note that the minor components contribute no more than 15% of the total emission, according to the analysis of the lifetime data. Provided that the neutral species do not exhibit large quantum yields of fluorescence, and their emission spectra are not completely different from that of the dominant monoanionic emitter, emission from the minor species would be difficult to detect by spectroscopic means alone. Detailed studies of the photophysics of several rhodamine dyes in polar solvents (19, 20) suggest that the electrically neutral lactone and zwitterionic forms of those compounds, which are structurally similar to fluorescein, are both either weakly fluorescent or nonfluorescent. For example, in butyronitrile the excited state lifetimes of the zwitterion of rhodamine B are typically

© 2000 NRC Canada

Fig. 3. Temporal fluorescence decay profiles of the 3′-tethered fluorescein derivative of ABA as a function of pH. λ_{ex} = 310 nm. In each case the $\log_{10}$ of the total number of counts in each channel minus background (log *I*) is plotted against time in ns. The maximum number of counts in the peak channel is ca. 10^4 for the monoexponential decays and ca. 2×10^4 for the multiexponential decays. The dashed line is the instrument response function; the dots are the TCSPC data points; the solid line is the best fit of the trial decay function convoluted with the instrument response function. The bottom panel gives the distribution of weighted residuals between the data and the computed fit. A, region (*i*) pH = 11.7, τ = 4.26 ns, χ^2 = 1.00. B, region (*ii*), pH = 5.1, a_1 = 0.31, τ_1 = 4.49 ns, a_2 = 0.69, τ_2 = 2.30 ns, F_1 = 0.46, F_2 = 0.54, χ^2 = 1.05. C, region (*iii*), pH = 4.1, a_1 = 0.85, τ_1 = 2.58 ns, a_2 = 0.12, τ_2 = 0.74 ns, a_3 = 0.03, τ_3 = 8.00 ns, F_1 = 0.89, F_2 = 0.0.04, F_3 = 0.0.08, χ^2 = 1.16. D, region (*v*), 7.5 M H_2SO_4, τ = 3.35 ns, χ^2 = 1.08.



in the range of 0.1–0.7 ns, and are 5–10 ns for the lactone (19). If the neutral forms of fluorescein and rhodamine are similar, one might reasonably assign the shortest-lived ($\tau \approx$ 0.7 ns), least abundant (F = 0.04) component in the triple-exponential decay of the fluorescein–ABA compound at pH = 3.4 to the excited state of the zwitterion, and the longest-lived ($\tau \approx$ 8–10 ns) component (with F = 0.08) to the excited lactone.

(*iv*) 2.2 ≥ pH ≥ ca. 0

The absorption and emission–excitation spectra are pH sensitive in this region with the feature at ca. 475 nm

© 2000 NRC Canada

Table 1. Spectroscopic data for the 3′-tethered fluorescein derivative of ABA as a function of pH.

pH	$\lambda_{max, abs}$ (nm)	$\lambda_{max, em}$ (nm)	ϕ_f	Literature for fluorescein[a]
11.7–6.7	492	517	0.89	490, 520, 0.93
6.0–5.0	475	519	~ 0.3	473, 520, 0.25–0.35
	450 (sh)	550 (sh)		
4.1–2.7	450	520	—	435, 473, 0.20–0.25
	475 (sh)	550 (sh)		
2.1–ca. 0	440	520	—	—
		550 (sh)		
7.5 M H_2SO_4	439	488	0.18	435, 520?, 0.18

[a]Given as $\lambda_{max, abs}$ (nm), $\lambda_{max, em}$ (nm), ϕ_f ; from ref. (16).

Table 2. Temporal fluorescence decay data for 3′-tethered fluorescein derivative of ABA as a function of pH.

pH	a_1	τ_1 (ns)	F_1	a_2	τ_2 (ns)	F_2	a_3	τ_3 (ns)	F_3
11.7–6.7	1.00	4.30[a]	1.00		—			—	
5.8	0.75	4.13	0.86	0.25	1.95	0.14		—	
5.1 λ_{em} = 520 nm	0.31	4.49	0.46	0.69	2.30	0.54		—	
λ_{em} = 560 nm	0.28	4.35	0.43	0.72	2.21	0.57		—	
λ_{em} = 600 nm	0.25	4.29	0.40	0.75	2.25	0.60		—	
4.1	0.85	2.58	0.89	0.12	0.74	0.04	0.02	8.00	0.08
2.7	0.89	2.64	0.90	0.09	0.70	0.03	0.02	9.54	0.07
2.2–ca. 0	multiexponential decay								
7.5 M H_2SO_4	1.00	3.36	1.00		—			—	

[a]For fluorescein itself, τ = 4.1 ns in 0.1 M NaOH (16).

disappearing at pH ≤ 1.2 (Fig. 2), but the emission spectrum remains approximately independent of pH and similar to those seen in the intermediate pH ranges and attributed to the excited monoanion. The temporal fluorescence profiles are very complex in this region and can only be modeled if four or more components are summed in the fitting function. We did not attempt to extract information from the spectra and decay curves obtained in this pH range, and can only state that multiple ground and excited state prototropic equilibria are the sources of the complexity.

(*v*) 7.5 M aqueous H_2SO_4

The spectra and temporal decays of the 3′-tethered fluorescein ABA derivative are very simple in strongly acid media. The absorption and corrected fluorescence excitation spectra are identical in the visible region of the spectrum and consist of a single, unstructured feature with a maximum at 439 nm. The emission spectrum is a good mirror image of the absorption spectrum and exhibits a maximum at 488 nm (Fig. 2E). The fluorescence decay profile is well-described by a single-exponential decay function with τ = 3.36 ± 0.03 ns, independent of emission wavelength (Fig. 3D and Table 2). The fluorescence quantum yield is 0.18 ± 0.09, a value which is identical with that obtained for fluorescein itself in 10 M HCl (17).

The simplest interpretation of these data is that the absorption in the visible is due exclusively to the ground state of the cation of the fluorophore, and that the emission is exclusively from the corresponding excited cation. The most likely structure of such a cation is one in which the keto group of the fluorescein moiety is protonated and the molecule exists primarily in a resonance form in which the positive charge is centered on C-9 (cf. Scheme 3). Using the measured quantum yield and lifetime data allows the calculation of values of $k_r = (5.4 \pm 0.3) \times 10^7$ s^{-1} and $\Sigma k_{nr} = (2.4 \pm 0.1) \times 10^8$ s^{-1}, the decay constants of the excited cation.

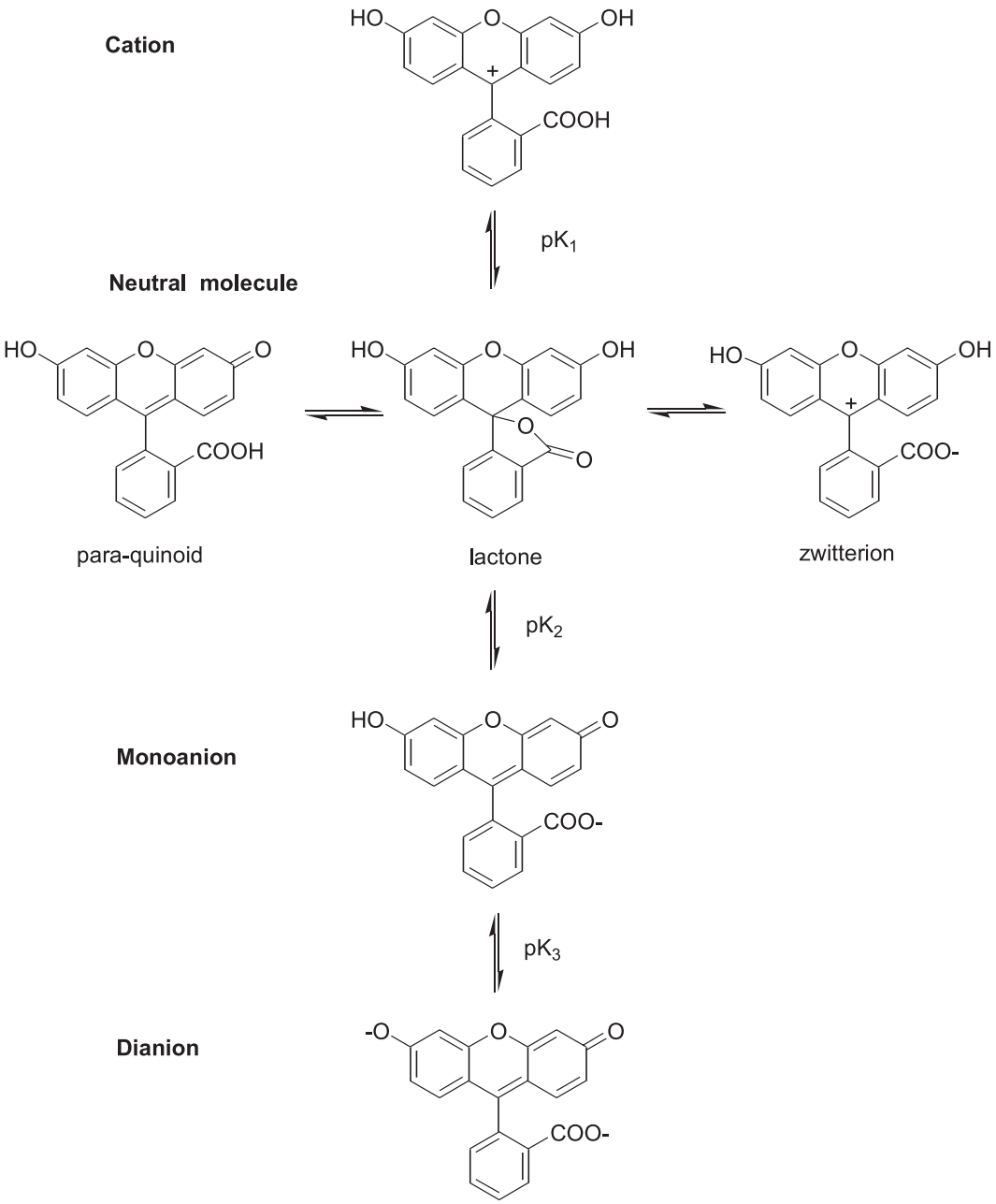
To ensure that the emitting species was the tethered fluorescein–ABA compound and not protonated fluorescein resulting from its hydrolysis, the spectra of fluorescein itself were measured in 7.5 M aqueous H_2SO_4 and compared with those reported above. The spectra of fluorescein and the ABA–fluorecein derivative are similar in this medium, but not identical; both the emission and excitation spectra are shifted about 4 nm to the red in the tethered compound relative to that of fluorescein itself. In addition, the spectra of the monoanion of the tethered compound could be recovered by neutralizing the sulfuric acid solution with base to pH 3–4, demonstrating that significant hydrolysis did not occur over the course of an experiment (ca. 30 min).

Conclusions

Several potentially useful derivatives of ABA have been prepared and spectroscopically characterized. One of them, a 3′-tethered fluorescein derivative, has been subjected to a full photophysical examination and exhibits properties which make it suitable for binding studies. The compound is soluble in aqueous solution over a wide range of pH. Little interaction between the ABA and the fluorescein moieties is observed spectroscopically in the tethered compound. At pH > 6.7 the system behaves in a particularly simple fashion, with only one species, the dianion, present in significant quantity in both the ground and excited states. The quantum yield of fluorescence is high (0.89) and the fluorescence follows a monoexponential

© 2000 NRC Canada

Scheme 3. Prototropic equilibria of fluorescein in aqueous solution.



temporal decay profile with τ = 4.30 ns. This compound and perhaps others with fluorophores tethered at the 3′ position of ABA would appear to be suitable for hormone binding studies using both time resolved and steady state fluorescence and fluorescence depolarization methods. The fluorescein derivative may be particularly useful because its spectroscopic and temporal decay characteristics vary with pH, and in principle it can therefore be employed to determine the local pH at the ABA binding site in vivo (21).

The 8′-tethered dansyl derivative of ABA could possibly serve as an indicator of binding site polarity, but is not well-suited to quantitatve photophysical studies based on its complex fluorescence decay. The 8′-tethered benzophenone derivative might be useful for photoaffinity labelling if its poor solubility in aqueous media is not a limiting factor.

Experimental section

Synthesis

General

Mps are uncorrected. IR spectra were recorded using KBr pellets on a Perkin–Elmer Paragon 1000. Proton nuclear magnetic resonance (^{1}H NMR) were recorded on a Bruker AMX 500 MHz spectrometer. Unless otherwise stated, $CDCl_3$ was used as solvent in all NMR experiments with $CHCl_3$ as a reference. Chemical shifts (δ) and coupling constants (J) are reported as if they are first order. Low (LRMS) and high (HRMS) resolution mass spectra were recorded in either the electron impact (EI) mode, the chemical ionization (CI) mode, or fast atom bombardment (FAB) mode on a VG

© 2000 NRC Canada

70–250SEQ double-focusing hybrid spectrometer with a Digital PDP 11/73 data system. Mass spectral data are reported in mass to charge units (*m*/*z*).

Flash column chromatography was performed using Merck silica gel 60 (230–400 mesh). Merck silica gel 60 F254 plates (0.2 mm) with aluminum sheet backing were used in analytical TLC. UV active materials were detected under a UV lamp. The plates were then dipped into a solution of phosphomolybdic acid and heated on a hot plate to visualize the spots.

The solvent tetrahydrofuran (THF) was dried by distillation from sodium and benzophenone. Unless otherwise indicated, all reactions were conducted under an atmosphere of dry argon.

Preparation of the 8′-Dansylhydrazone Derivative of ABA (6)

8′-Aldehyde ABA Me ester (4)

Ozone was passed through a solution of Sudan Red 7B (1.4 mL, 0.03% in ethanol) and 8′-methylene ABA Me ester **3** (994 mg, 3.43 mmol, ref. (10)) in ethanol (20 mL) cooled to –78°C for 5 min. Argon was then bubbled through the solution to remove the excess ozone and dimethyl sulphide (2.5 mL) was added. The cooling bath was removed and the mixture was allowed to stir at room temperature for 2 h. The solution was concentrated, and the residue was purified by column chromatography (20% EtOAc in hexane) to provide 434 mg (44%) recovered olefin **3** and 321 mg (32%) of aldehyde **4** (57% based on recovered starting material), mp 159–161.5°C (EtOAc–hexane). IR ν_{max} (cm^{-1}): 3393 (OH), 1715 (CO), 1653 (C=C). ^{1}H NMR δ: 9.58 (s, CHO, 1H), 7.86 (d, *J* = 16.0 Hz, H-4, 1H), 5.95 (br.s, H-3′, 1H), 5.91 (d, *J* = 16.0 Hz, H-5, 1H), 5.76 (br.s, H-2, 1H), 3.68 (s, COOMe, 3H), 2.73 (d, *J* = 18.0 Hz, H-5′, 1H), 2.53 (d, *J* = 18.0 Hz, H-5′, 1H), 1.98 (d, *J* = 1.1 Hz, 6-CH_3 or 7′-CH_3, 3H), 1.98 (d, *J* = 1.3 Hz, 6-CH_3 or 7′-CH_3, 3H), 1.19 (s, 9′-CH_3, 3H). LRFABMS (*m*/*z*) (rel. int.): 293 $[M+1]^+$ (23), 134 (100). HRFABMS (*m*/*z*) $C_{16}H_{20+1}O_5$ requires: 293.1389 $[M+1]^+$; found: 293.1394 $[M+1]^+$.

8′-Dansylhydrazone ABA Me ester (5)

A solution of dansylhydrazine (49 mg, 0.184 mmol) and aldehyde **4** (54 mg, 0.184 mmol) in ethanol and trichloroacetic acid (95:5, 1.5 mL) was heated at 75°C for 10 min. The mixture was cooled, concentrated, and the residue was purified by column chromatography (50% EtOAc in hexane) to provide 89 mg (90%) of hydrazone **5**, mp 94–98°C (EtOAc–hexane). IR ν_{max} (cm^{-1}): 3486 (OH), 3201, 1712 (CO), 1659 (C=C). ^{1}H NMR δ: 8.59 (d, *J* = 8.5 Hz, 1H), 8.28 (dd, *J* = 7.3, 1.2 Hz, 1H), 8.17 (d, *J* = 8.7 Hz, 1H), 7.94 (s, NH, 1H), 7.69 (d, *J* = 16.0 Hz, H-4, 1H), 7.56 (m, 2H), 7.18 (d, *J* = 7.5 Hz, 1H), 7.05 (s, H-8′, 1H), 5.82 (d, *J* = 16.0 Hz, H-5, 1H), 5.69 (br.s, H-3′, 1H), 5.37 (d, *J* = 0.9 Hz, H-2, 1H), 3.66 (s, COOMe, 3H), 2.89 (s, NMe_2, 6H), 2.35 (br.s, H-5′, 2H), 1.91 (d, *J* = 1.2 Hz, 6-CH_3, 3H), 1.53 (d, *J* = 1.3 Hz, 7′-CH_3, 3H), 1.01 (s, 9′-CH_3, 3H). LRFABMS (*m*/*z*) (rel. int.): 540 $[M+1]^+$ (32), 171 (100). HRFABMS (*m*/*z*) $C_{28}H_{33+1}N_3O_6S$ requires: 540.2168 $[M+1]^+$; found: 540.2204 $[M+1]^+$.

8′-Dansylhydrazone ABA (6)

10% KOH (16 mL) was added to a solution of hydrazone **3** (42 mg, 0.078 mmol) in methanol (4 mL) at room temperature and the mixture was stirred overnight. The solution was extracted with EtOAc and discarded, and the remaining aqueous layer was carefully acidified with 10% HCl to pH 3. After stirring for half an hour, the aqueous mixture was extracted several times with Et_2O. The organic layers were combined, washed once with brine, and were dried (Na_2SO_4). The mixture was concentrated to provide 26 mg (64%) of dansylhydrazone **6**, mp 118–121°C (EtOAc–hexane). IR ν_{max} (cm^{-1}): 3462, 3201, 1706 (CO), 1651 (C=C), 1162. ^{1}H NMR δ: 8.56 (d, *J* = 8.6 Hz, 1H), 8.23 (m, 2H), 7.69 (d, *J* = 16.1 Hz, H-4, 1H), 7.42 (m, 2H), 7.19 (s, H-8′, 1H), 7.13 (d, *J* = 7.5 Hz, 1H), 5.89 (d, *J* = 16.1 Hz, H-5, 1H), 5.71 (br.s, H-3′, 1H), 5.41 (br.s, H-2, 1H), 2.87 (s, NMe_2, 6H), 2.41 (d, *J* = 17.6 Hz, H-5′, 1H), 2.33 (d, *J* = 17.6 Hz, H-5′, 1H), 1.97 (s, 6-CH_3, 3H), 1.54 (s, 7′-CH_3, 3H), 1.03 (s, 9′-CH_3, 3H). LRFABMS (*m*/*z*) (rel. int.): 526 $[M+1]^+$ (92), 171 (100). HRFABMS (*m*/*z*) $C_{27}H_{31+1}N_3O_6S$ requires: 526.2011 $[M+1]^+$; found: 526.2012 $[M+1]^+$.

Preparation of the 8′-benzophenone derivative of ABA (10)

THP ABA derivative 7

The Grignard reagent was prepared in situ by reacting magnesium (316 mg, 15.0 mmol) and 2-(6-bromohexoxy)tetrahydro-2*H*-pyran (1.76 mL, 8.0 mmol) in THF (15 mL) at room temperature for 2 h. The mixture was then cooled to –78°C and a solution of dienoic ester **2** (417 mg, 1.6 mmol) in THF (40 mL) was added via syringe. After stirring at –78°C for 10 min, the reaction vessel was put in the freezer (–20°C) overnight. The mixture was quenched with saturated NH_4Cl and extracted with ether (×3). The organic layers were combined, washed once with brine, were dried (Na_2SO_4), concentrated, and the residue was purified by column chromatography (25% EtOAc in hexane) to provide 494 mg (69%) of compound **7**, mp 87–89°C (hexane). IR ν_{max} (cm^{-1}): 3481 (OH), 1717 (CO), 1653 (C=C). ^{1}H NMR δ: 7.85 (d, *J* = 16.1 Hz, H-4, 1H), 6.14 (d, *J* = 16.1 Hz, H-5, 1H), 5.94 (br.s, H-2 or H-3′, 1H), 5.74 (br.s, H-2 or H-3′, 1H), 4.54 (m, 1H), 3.84 (m, 1H), 3.70 (m, 1H), 3.68 (s, COOMe, 3H), 3.49 (m, 1H), 3.34 (m,1H), 2.43 (d, *J* = 17.3 Hz, H-5′, 1H), 2.32 (d, *J* = 17.3 Hz, H-5′, 1H), 1.99 (d, *J* = 0.9 Hz, 6-CH_3, 3H), 1.90 (d, *J* = 7′-CH_3, 3H), 1.80 (m, 1H), 1.69 (m, 1H), 1.56–1.20 (m, 14H), 0.95 (s, 9′-CH_3, 3H). LRESMS (*m*/*z*) (rel. int.): 449 $[M+1]^+$ (90), 366 (78), 365 (100). HRFABMS (*m*/*z*)$C_{26}H_{40}O_6$ requires: 448.2825 $[M]^+$; found: 448.2826 $[M]^+$.

Alcohol 8

A solution of THP ether **7** (235 mg, 0.524 mmol) and pyridinium *p*-toluenesulfonate (13 mg, 0.052 mmol) in EtOH (15 mL) was heated at 60°C for 3 h. The solvent was removed and the residue was purified by column chromatography (33% hexane in EtOAc) to provide 190 mg (99%) of alcohol **8**, mp 126–129°C (hexane). IR ν_{max} (cm^{-1}): 3480 (OH), 1716 (CO), 1653 (C=C). ^{1}H NMR δ: 7.84 (d, *J* = 16.0 Hz, H-4, 1H), 6.14 (d, *J* = 16.0 Hz, H-5, 1H), 5.93

© 2000 NRC Canada

(br.s, H-2 or H-3′, 1H), 5.73 (br.s, H-2 or H-3′), 3.67 (s, COOMe, 3H), 3.60 (t, J = 6.6 Hz, 2H), 2.43 (d, J = 17.1 Hz, H-5′, 1H), 2.32 (d, J = 17.1 Hz, H-5′, 1H), 1.99 (d, J = 1.1 Hz, 6-CH_3, 3H), 1.90 (d, J = 1.3 Hz, 7′-CH_3, 3H), 1.57–1.19 (m, 10H), 0.94 (s, 9′-CH_3). LRFABMS (*m*/*z*) (rel. int.): 365 $[M+1]^+$ (100), 85 (93). HRFABMS (*m*/*z*) $C_{21}H_{32}O_5$ requires: 365.2328 $[M+1]^+$; found: 365.2325 $[M+1]^+$.

*Hydroxy acid **9***

A solution of ester **8** (100 mg, 0.274 mmol) in MeOH (2 mL) and 10% KOH (2 mL) was stirred at 50°C for 1 h. Water was added and the mixture was extracted with EtOAc and discarded. The remaining aqueous layer was then acidified with 10% HCl to pH 3 and was extracted several times with EtOAc. The organic layers were combined, washed with water, brine, and were dried (Na_2SO_4). The solvent was removed and the residue was purified by column chromatography (50% acetone in hexane) to give 66 mg (69%) of the acid **9**. IR ν_{max} (cm^{-1}): 3308 (OH), 1704 (CO). ^1H NMR δ: 7.77 (d, J = 16.1 Hz, H-4, 1H), 6.15 (d, J = 16.1 Hz, H-5, 1H), 5.96 (br.s, H-2 or H-3′, 1H), 5.75 (br.s, H-2 or H-3′), 3.60 (t, J = 6.5 Hz, 2H), 2.44 (d, J = 17.2 Hz, H-5′, 1H), 2.34 (d, J = 17.2 Hz, H-5′, 1H), 2.03 (d, J = 1.2 Hz, 6-CH_3, 3H), 1.90 (d, J = 1.0 Hz, 7′-CH_3, 3H), 1.58–1.17 (m, 10H), 0.96 (s, 9′-CH_3). LRFABMS (*m*/*z*) (rel. int.): 351 $[M+1]^+$ (100), 102 (64). HRFABMS (*m*/*z*) $C_{20}H_{30}O_5$ requires: 351.2171 $[M+1]^+$; found: 351.2150 $[M+1]^+$.

*Benzophenone coupling (**10**)*

A solution of acid **9** (16.0 mg, 0.046 mmol), Et_3N (0.13 mL, 0.914 mmol), and 3′-*O*-(4-benzoyl)benzoyl imidazolide (22) (44.0 mg, 0.138 mmol) in CH_2Cl_2 (1 mL) was stirred at room temperature overnight. The mixture was then quenched with 5% HCl. The organic layer was then separated, and washed with brine, was dried (Na_2SO_4) and was concentrated. Purification of the residue by preparative thin layer chromatography (5% MeOH in CH_2Cl_2) provided 9.6 mg (38%) of the 8′-benzophenone ABA derivative **10**, mp 141–143°C (hexane). ^1H NMR δ: 8.12 (m, 2H), 7.80 (m, 5H), 7.60 (m, 1H), 7.48 (m, 2H), 6.16 (d, J = 16.0 Hz, H-5, 1H), 5.95 (br.s, H-2 or H-3′, 1H), 5.76 (br.s, H-2 or H-3′), 4.31 (t, J = 6.6 Hz, 2H), 2.44 (d, J = 17.3 Hz, H-5′, 1H), 2.34 (d, J = 17.3 Hz, H-5′, 1H), 2.03 (d, J = 0.9 Hz, 6-CH_3, 3H), 1.90 (d, J = 1.0 Hz, 7′-CH_3, 3H), 1.77–1.18 (m, 10H), 0.96 (s, 9′-CH_3). LRFABMS (*m*/*z*) (rel. int.): 558 $[M+1]^+$ (100), 102 (64). HRFABMS (*m*/*z*) $C_{34}H_{38}O_7$ requires: 559.2696 $[M+1]^+$; found: 559.2660 $[M+1]^+$.

Preparation of the 3′-*S*-acetamidofluorescein derivative of ABA (13)

NaH (60% in oil, 20 mg, 0.5 mmol) was added to a solution of 2′,3′-epoxy ABA **11** (100 mg, 0.357 mmol, ref. (12)) in THF (6 mL) at 0°C under nitrogen. Thiol acetic acid (5 drops, ca. 55 mg, 0.7 mmol) and a further portion of sodium hydride (60% in oil, 15 mg, 0.38 mmol) were then added and the reaction mixture was allowed to warm to room temperature. After stirring for an hour, a solution of 0.25 M NaOH (15 mL) was added and stirring continued under nitrogen for another hour. The resultant mixture was concentrated in vacuo to ca. 10 mL, water (25 mL) was added, and was washed with ether (2 × 15 mL). The ether washings were discarded and the aqueous layer was acidified with 1 M citric acid and extracted with EtOAc (3 × 20 mL). The organic extracts were combined, washed with brine, dried (Na_2SO_4), and were concentrated to afford 100 mg (95%) of 3′-thiol ABA **12**, which was used immediately in the next step. IR ν_{max} (cm^{-1}): 3369, 2924, 1671, 1599, 1246. ^1H NMR δ: 7.77 (d, J = 16 Hz, 1H), 6.11 (d, J = 16 Hz, 1H), 5.74 (s, 1H), 4.67 (s, 1H), 2.55 (d, J = 17 Hz, 1H), 2.50 (d, J = 17 Hz, 1H), 2.02 (s, 3H), 1.96 (s, 3H), 1.07 (s, 3H), 1.01 (s, 3H).

A solution of the crude thiol ABA **12** (100 mg, 0.33 mmol) and (iodoacetamido)-fluorescein (200 mg, 0.40 mmol) in MeOH (30 mL) was treated with 1 M NaOH (3 mL) at room temperature under nitrogen. After 2 days the mixture was concentrated in vacuo, and the residue was dissolved in water (100 mL), acidified with 1 M HCl, and was extracted with ethyl acetate (3 × 20 mL). The organic extracts were dried (Na_2SO_4), concentrated in vacuo, and the residue chromatographed (toluene–EtOAc–HOAc, 50:30:2) to afford 3′-*S*-acetamidofluorescein ABA **13** (113 mg, 50%) as a yellow glass. IR ν_{max} (cm^{-1}): 3417, 2922, 1734, 1384, 1113. ^1H NMR (CD_3OD) δ: 7.93 (d, J = 8.5 Hz, 1H), 7.85 (dd, J = 8.5, 1.7 Hz, 1H), 7.54 (d, J = 16.3 Hz, 1H), 7.45 (d, J = 1.7 Hz, 1H), 6.75 (m, 2H), 6.66 (m, 2H), 6.57 (m, 2H), 5.87 (d, J = 16.3 Hz, 1H), 4.89 (s, 1H), 3.57 (d, J = 14.4 Hz, 1H), 3.42 (d, J = 14.4 Hz, 1H), 2.48 (d, J = 16.6 Hz, 1H), 2.18 (d, J = 16.6 Hz, 1H), 2.17 (s, 3H), 1.76 (s, 3H), 0.95 (s, 3H), 0.93 (s, 3H). ESMS *m*/*z*: 301 (100), 684 $[M+1]^+$ (10). HREIMS (*m*/*z*) $C_{37}H_{34}NO_{10}S$ requires: 684.1903 $[M+1]^+$; found: 684.1885 $[M+1]^+$.

Preparation of the 3′-*S*-(2-ethyldansylamide) derivative of ABA

*5-(*N,N-*Dimethylamino)naphthalene-1-sulfon(2-hydroxyethyl)amide*

A solution of pyridine (3 mL) and ethanolamine (281 mg, 4.6 mmol) under N_2 was treated with dansyl chloride (500 mg, 1.9 mmol) and stirred for 17 h. Water (15 mL) was added and stirring continued for a further 1 h followed by extraction of the mixture with EtOAc (3 × 25 mL). The combined organic extract was washed with brine (2 × 75 mL), dried (Na_2SO_4), and concentrated in vacuo to afford the dansyl ethanolamide as a light green oil (545 mg, 100% based on dansyl chloride). The product was homogeneous by TLC (toluene–EtOAc–HOAc, 25:15:2), R_f ca. 0.30 and used without further purification. UV λ_{max} (nm): 217, 250, 335. IR ν_{max} (cm^{-1}): 3509, 3301, 2944, 2871, 2788, 1575, 1456, 1312, 1143, 1060, 940, 790. ^1H NMR ($CDCl_3$) δ: 8.51 (1H, d, J = 8.5 Hz), 8.24 (1H, d, J = 8.6 Hz), 8.21 (1H, d, J = 7.2 Hz), 7.52 (1H, t, J = 8.0 Hz), 7.49 (1H, t, J = 7.8 Hz), 7.15 (1H, d, J = 7.5 Hz), 5.68 (1H, bs), 3.59 (2H, t, J = 4.9 Hz), 3.00 (2H, t, J = 4.9 Hz), 2.86 (6H, s). MS (FIB) (*m*/*z*) (rel. int.): 295 $[MH]^+$ (100), 294 $[M]^+$ (70), 252 (5), 218 (7), 184 (10), 170 (70), 157 (11), 128 (7), 88 (15). HRMS (FIB) calcd. for $C_{14}H_{19}N_2O_3S_1$ $[MH]^+$: 295.1116; found: 295.1113.

*5-(*N,N-*Dimethylamino)naphthalene-1-sulfon(2-mesyloxyethyl)amide*

A solution of dansyl ethanolamide (320 mg, 1.1 mmol) in pyridine (5 mL) was treated with methanesulfonyl chloride

© 2000 NRC Canada

(450 μL, 5.9 mmol). After stirring for 45 min, water (15 mL) was added and stirring continued. After 30 min the mixture was extracted with EtOAc (3 × 25 mL) and the combined organic extract washed with brine (1 × 75 mL), dried (Na_2SO_4), and concentrated in vacuo to give the mesyate (409 mg, 100%) as a moss green oil, homogeneous by TLC (toluene–EtOAc–HOAc, 25:15:2), R_f ca 0.40. UV λ_{max} (nm): 217, 251, 336. IR ν_{max} (cm^{-1}): 3303, 2943, 2849, 2788, 1575, 1456, 1330, 1174, 1144, 917, 791. ^1H NMR ($CDCl_3$) δ: 8.54 (1H, d, *J* = 8.5 Hz), 8.24 (1H, d, *J* = 8.5 Hz), 8.22 (1H, d, *J* = 7.2 Hz), 7.55 (1H, t, *J* = 8.0 Hz), 7.51 (1H, t, *J* = 7.8 Hz), 7.17 (1H, d, *J* = 7.5 Hz), 5.43 (1H, bs), 4.15 (2H, t, *J* = 5.0 Hz), 3.35 (2H, d, *J* = 3.9 Hz), 2.87 (6H, s), 2.84 (3H, s). MS (FIB) (*m*/*z*) (rel. int.): 373 $[MH]^+$ (80), 272 $[M]^+$ (70), 256 (55), 313 (7), 234 (8), 184 (16), 170 (100), 157 (12), 127 (10), 115 (11). HRMS (FIB) calcd. for $C_{15}H_{21}N_2O_5S_2$ $[MH]^+$: 373.0892; found: 373.0922.

*5-(*N,N-*Dimethylamino)naphthalene-1-sulfon(2-acetothioethyl)amide*

A solution of the dansyl mesyloxyethylamide (149 mg, 0.40 mmol) and thiolacetic acid (57 μL, 0.80 mmol) in freshly distilled THF (5 mL) under N_2, was treated portionwise with sodium hydride mineral oil suspension (60%, 20 mg, 0.80 mmol). The reaction mixture was stirred for 22 h then treated with water (5 mL), made approximately neutral with 0.1 M HCl, and extracted with EtOAc (3 × 25 mL). The extract was dried (Na_2SO_4), concentrated in vacuo, and the residue purified by TLC on silica gel using toluene–EtOAc (90:10) to give the dansyl acetothioethylamide as a yellow oil (55.2 mg, 39%). UV λ_{max} (nm): 212, 328. IR ν_{max} (cm^{-1}): 3293, 2920, 2853, 1740, 1699, 1575, 1456, 1144, 946, 790. ^1H NMR ($CDCl_3$) δ: 8.52 (1H, d, *J* = 8.5 Hz), 8.22 (2H, d, *J* = 8.1 Hz), 7.55 (1H, t, *J* = 8.0 Hz), 7.50 (1H, t, *J* = 7.9 Hz), 7.17 (1H, d, *J* = 7.5 Hz), 4.98 (1H, t, *J* = 6 Hz), 3.08 (2H, q, *J* = 6.3 Hz), 2.87 (6H, s), 2.86 (2H, t, *J* = 6.6 Hz), 2.17 (3H, s). MS (FIB) *m*/*z* (rel. int.): 353 $[MH]^+$ (86), 252 $[M]^+$ (55), 321 (25), 311 (12), 301 (14), 295 (27), 285 (17), 177 (100). HRMS (FIB) calcd. for $C_{16}H_{21}N_2O_3S_2$ $[MH]^+$: 353.0994; found: 353.1002.

3′-ABA-thio(2-ethyldansylamide)

A solution of dansyl acetothioethylamide (59 mg, 0.17 mmol) in methanol (3 mL) under N_2 was treated with N_2-purged 1 M NaOH (1.5 mL). After 45 min ABA 3′-(-epoxide) (23) (50 mg, 0.17 mmol) dissolved in methanol (1 mL) was added dropwise over 2 h. The reaction was heated at 45°C for 1 h followed by stirring at ambient temperature for a further 19 h. Tartaric acid (225 mg) was added and stirring continued for a further 30 min. The resultant suspension was filtered to remove precipitated sodium bitartrate and the filtrate was concentrated in vacuo. The residue was purified via TLC on silica gel using EtOAc–hexane–HOAc (1:1:.025) to give the 3′-dansyl-linked ABA **14** (33 mg, 34%) as a yellow-green film. UV λ_{max} (nm): 216, 250, 327 (sh). IR ν_{max} (cm^{-1}): 3502, 3269, 2952, 1683, 1575, 1456, 1234, 1145. ^1H NMR ($CDCl_3$) δ: 8.49 (1H, d, *J* = 8 Hz), 8.26 (1H, d, *J* = 8.6 Hz), 8.17 (1H, d, *J* = 7.2 Hz), 7.62 (1H, d, *J* = 16 Hz, C-5), 7.51 (1H, t, *J* = 8.1 Hz), 7.46 (1H, t, *J* = 7.6 Hz), 7.14 (1H, d, *J* = 7.5 Hz), 6.08 (1H, d, *J* = 16 Hz, C-4), 6.01 (1H, bs), 5.73 (1H, s, C-2) 3.00 (2H, m), 2.84 (6H, s), 2.75 (2H, m), 2.46 (1H, d, *J* = 16 Hz, C-5′α or C-5′β), 2.32 (1H, d, *J* = 16 Hz, C-5′α or C-5′β), 2.09 (3H, s, C-6), 1.99 (3H, s). MS (FIB) (*m*/*z*) (rel. int.): 573 $[MH]^+$ (47), 572 $[M]^+$ (15), 555 (11), 340 (14), 263 (13), 236 (17), 219 (17), 203 (16), 181 (46), 170 (89), 156 (29), 133 (31), 111 (64), 89 (100). HRMS (FIB) calcd. for $C_{29}H_{37}N_2O_6S_2$ $[M]^+$: 573.2093; found: 573.2095.

Spectroscopy and photophysics

Materials

Water was purified by distillation and use of a Millipore filtration system and exhibited negligible fluorescence when excited at the excitation wavelengths used in this study. Fluorescein-labelled ABA dissolves well in water, but the dansyl and benzophenone derivatives are poorly soluble in pure water and were dissolved in either methanol or methanol–water solutions. The pH of aqueous solutions of the fluorescein-labelled derivative was adjusted using either sulfuric acid or aqueous NaOH.

Instrumentation

Absorption spectra were measured with either a Cary 118 or a Cary 1A UV-vis spectrophotometer. Emission and emission excitation spectra and fluorescence quantum yields were measured with a Spex Fluorolog 222 spectrofluorometer at a spectral resolution of 1.8 nm. All spectra were corrected for background and variations of the instrument response with wavelength.

Fluorescence lifetimes were measured by time correlated single photon counting (TCSPC) using a mode-locked, synchronously pumped, cavity-dumped argon ion-dye laser for excitation and a fast microchannel plate detection system both of which have been previously described (23, 24). In these experiments ca. 850 mW of average power in the mode-locked argon ion green line at 514.5 nm was used to synchronously pump either R6G or DCM in an extended-cavity dye-laser, the output of which was tuned with a three-plate Lyot filter and was cavity-dumped with an acousto-optic Bragg cell. For the fluorescein-labeled compound, the fundamental of the cavity-dumped R6G dye laser was frequency-doubled in KDP to obtain between 100–300 μW of cw average power for excitation at ca. 310 nm. For the dansyl derivative the DCM fundamental was frequency doubled to provide excitation wavelengths near 340 nm. The cavity dumper was operated at a repetition rate of 4 MHz and the excitation pulses in the fundamental had widths of 12 ps as measured by autocorrelation. The instrument response function of the detection system has a width of ca. 40 ps FWHM.

Methods

Fluorescence quantum yields were determined by the standard relative method using quinine sulfate in 0.5 M aqueous H_2SO_4 as a standard (ϕ_f = 0.55 in the excitation wavelength range employed (25)) and right angle excitation–emission geometry. In all quantum yield experiments the absorbances of both the sample and standard solutions were matched at a value of ca. 0.05, so that errors due to inner filter effects and spatially nonlinear absorption would be minimized. Because the sample and standard were both prepared

© 2000 NRC Canada

in aqueous solution, corrections for refractive index were unnecessary.

Excited state lifetimes were obtained by an iterative reconvolution process in which trial fluorescence decay functions were convoluted with the measured instrument response function and errors between the resulting synthesized temporal fluorescence decay profile and the measured one were minimized using a least-squares fitting procedure. The distribution of weighted residuals and the value of χ^2 were used as "goodness-of-fit" criteria. These procedures have been described in detail elsewhere (23).

All experiments were carried out at room temperature.

Acknowledgements

The authors gratefully acknowledge the continuing financial support of this research by the Natural Sciences and Engineering Research Council of Canada. X.H. thanks the University of Saskatchewan for the award of a Teaching Assistantship.

References

1. W.J. Davies and H.G. Jones. Abscisic acid: physiology and biochemistry. Bios Scientific Publishers, Oxford, U.K. 1991.
2. J.A.D. Zeevaart and R.A. Creelman. Annu. Rev. Plant Physiol. Plant Mol. Biol. **39**, 439 (1988).
3. J. Leung and J. Giraudat. Annu. Rev. Plant Physiol. Plant Mol. Biol. **49**, 199 (1998).
4. S.M. Assman. Plant Cell, **6**, 1187 (1994).
5. M.K. Walker-Simmons, R.J. Anderburg, P.A. Rose, and S.R. Abrams. Plant Physiol. **99**, 501 (1992).
6. C. Hornberg and E.W. Weiler. Nature (London), **310**, 321 (1984).
7. M. Perras, P.A. Rose, E.W. Pass, K.B. Chatson, J.J. Balsevich, and S.R. Abrams. Phytochemistry, **46**, 215 (1997).
8. D.C.R. Hite, W.H. Outlaw, and M.A. Seavy. Physiol. Plant. **92**, 79 (1994).
9. J.J. Balsevich, G.G. Bishop, and G.M. Banowetz. Phytochemistry, **44**, 215 (1997).
10. S.R. Abrams, P.A. Rose, A.J. Cutler, J.J. Balsevich, B. Lei, and M.K. Walker-Simmons. Plant Physiol. **114**, 89 (1997).
11. B. Lei, S.R. Abrams, B. Ewan, and L.V. Gusta. Phytochemistry, **37**, 289 (1994).
12. Y. Todoroki, N. Hirai, and H. Ohigashi. Tetrahedron, **51**, 6911 (1995).
13. G. Dorman and G.D. Prestwich. Biochemistry, **33**, 5661 (1994).
14. Y.-H. Li, L.-M. Chan, L. Tyer, R.T. Moody, C.M. Himel, and D.M. Hercules. J. Am. Chem. Soc. **97**, 3118 (1975).
15. J. Slavik. Fluorescent probes in cellular and molecular biology. CRC Press, Boca Raton. 1994. p. 133 ff.
16. R. Sjoback, J. Nygren, and M. Kubista. Spectrochim. Acta, A, **51**, L7 (1995).
17. H. Leonhardt, L. Gordon, and R. Livingstone. J. Phys. Chem. **75**, 245 (1971).
18. N.J. Turro. Modern molecular photochemistry. Benjamin–Cummings, Menlo Park. 1978. p. 176 ff.
19. J. Karpiuk. Photophysical and photochemical processes in lactones of some rhodamines. Ph.D. thesis, University of Warsaw. 1996.
20. J.E.T. Corrie and D.R. Trentham. J. Chem. Soc. Perkin Trans. 1, 1993 (1995).
21. J. Slavik. J. Lumin. **72–74**, 575 (1997).
22. N. Williams, S.H. Ackerman, and P.S. Coleman. Methods Enzymol. **126,** 667 (1986).
23. D.R. James, D.R.M. Demmer, R.E. Verrall, and R.P. Steer. Rev. Sci. Instrum. **54**, 1121 (1983).
24. M. Szymanski, M. Maciejewski, and R.P. Steer. Chem. Phys. **175**, 413 (1993).
25. S. Meech and D. Phillips. J. Photochem. **23**, 193 (1983).

© 2000 NRC Canada

A solid-state ^{133}Cs nuclear magnetic resonance and X-ray crystallographic study of cesium complexes with macrocyclic ligands

Alan Wong, Simon Sham, Suning Wang, and Gang Wu

Abstract: We report solid-state NMR determination of the ^{133}Cs chemical shift anisotropy (CSA) for a series of cesium complexes with macrocyclic ligands. It was found that the isotropic ^{133}Cs chemical shifts are related to the number of oxygen atoms to which the Cs^+ ion is coordinated. The ^{133}Cs chemical shifts were found to correlate with average Cs—O distances. We also attempt to use the established correlation to deduce Cs^+ coordination environment for compounds with unknown structures. We also report the X-ray determination of the crystal structure for $Cs(DB18C6)_2SCN•1/2CH_3OH•1/2H_2O$. The compound crystallizes in monoclinic, a = 14.503(2), b = 15.152(3), c = 39.989(6) Å, β = 90.796(8)°, space group $P2_1/c$, Z = 8. There are two independent molecules in the asymmetric unit cell where each of the two Cs^+ ions is coordinated to two DB18C6 ligand molecules forming a sandwich-type structure.

Key words: solid state NMR, alkali metal, ^{133}Cs chemical shift, macrocyclic ligand, crystal structure.

Résumé : On a mesuré l'anisotropie du déplacement chimique du ^{133}Cs dans les spectres RMN à l'état solide d'une série de complexes du césium avec des ligands macrocycliques. On a trouvé que les déplacements chimiques isotropes du ^{133}Cs sont reliés au nombre d'atomes d'oxygène formant une coordination avec le Cs^+. On a trouvé qu'il existe une corrélation entre les déplacements chimiques du ^{133}Cs et les distances moyennes Cs—O. On a aussi essayé d'établir une corrélation qui permettrait de déduire l'environnement de coordination du Cs^+ dans des composés de structures inconnues. On a aussi déterminé la structure du $Cs(DB18C6)_2SCN•1/2CH_3OH•1/2H_2O$ par diffraction des rayons X. Les cristaux sont monocliniques, groupe d'espace $P2_1/c$, avec a = 14,503(2), b = 15,152(3) et c = 39,989(6) Å, β = 90,796(8)° et Z = 8. Il y a deux molécules indépendantes dans la maille élémentaire asymétrique dans laquelle chacun des deux ions Cs^+ est coordiné à deux molécules de ligand DB18C6 formant une structure de type sandwiche.

Mots clés : RMN à l'état solide, métal alcalin, déplacement chimique du ^{133}Cs, ligand macrocyclique, structure cristalline.

Introduction

Since Pedersen's (1) first synthesis of macrocyclic polyethers, a large number of acyclic, cyclic, and bicyclic crown ethers containing oxygen, nitrogen, and sulfur donor atoms have been prepared and extensively investigated (2). In the past 20 years, alkali metal nuclear magnetic resonance (NMR) spectroscopy has served as a major technique for studying the cation-binding properties of these macrocyclic complexes in solutions; however, relatively few solid-state alkali metal NMR studies were reported in the literature (3, 4). The advantage of solid-state metal NMR is that the alkali metal ions under observation are usually located in a well-defined coordination environment. In contrast, alkali metal ions often undergo rapid exchange between bound and free states in the liquid phase, resulting in averaged NMR parameters. Since a large number of alkali metal complexes have been characterized by X-ray diffraction studies, it is desirable to document NMR parameters for alkali metal ions in various ion-binding environments. In addition, solid-state NMR is capable of yielding the orientation dependence of NMR parameters. This information is usually unavailable from the solution NMR spectra because of the molecular tumbling motion.

Cesium-133 is perhaps the easiest alkali metal nuclide for NMR measurements because of its favorable nuclear properties: 100% natural abundance, I = 7/2, and a small quadrupole moment of $Q = -3 \times 10^{-31}$ m^2. There have been several recent reports on the determination of ^{133}Cs chemical shift anisotropy (CSA) in simple inorganic salts (5–10); however, relatively little is known about solid-state ^{133}Cs NMR data for cesium macrocyclic complexes, except for solid alkalides and electrides studied by Dye and co-workers (11–14). In this contribution, we report the determination of ^{133}Cs CSAs in a number of cesium macrocyclic compounds (Scheme 1). These complexes are used as models for establishing correlation between solid-state ^{133}Cs NMR parameters and Cs^+

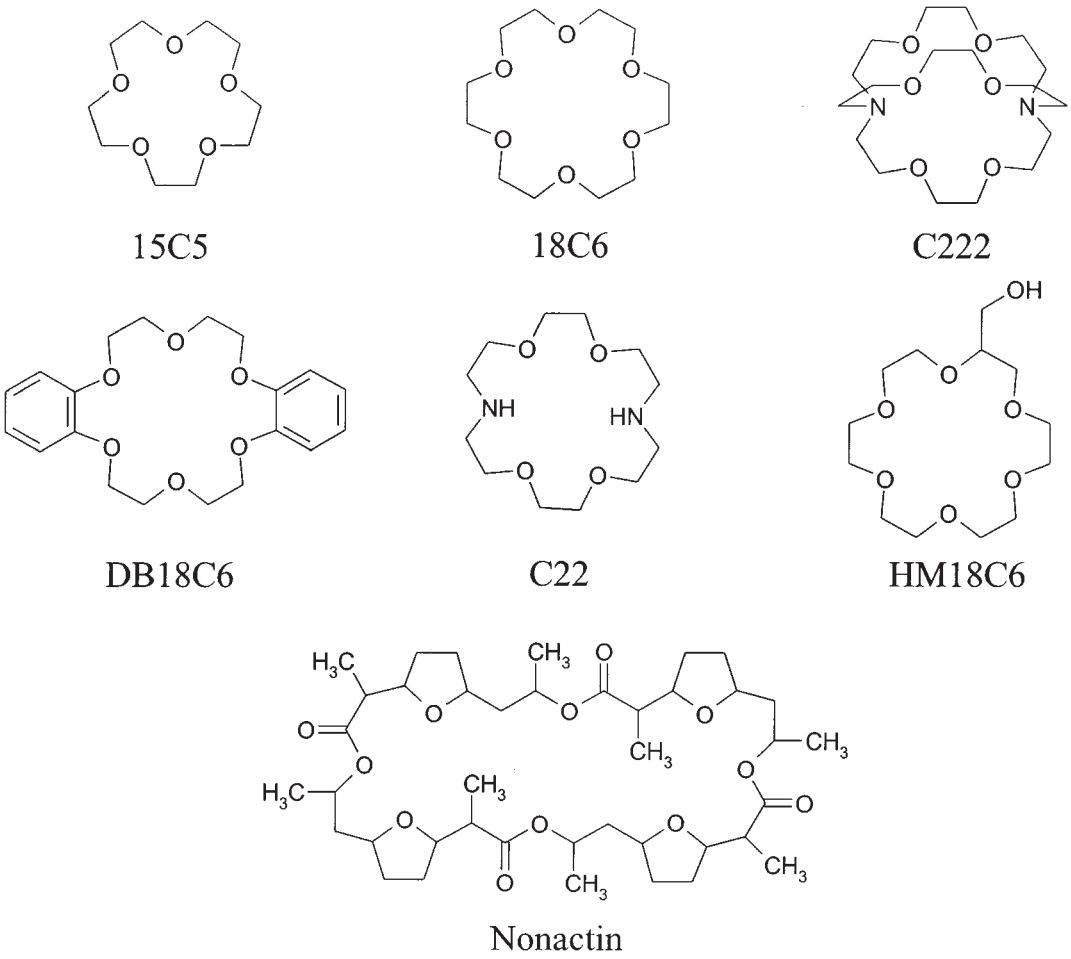
Received January 14, 2000. Published on the NRC Research Press website on July 7, 2000.

A. Wong, S. Sham, S. Wang, and G. Wu.[1] Department of Chemistry, Queen's University, Kingston, ON K7L 3N6, Canada.

[1]Author to whom correspondence may be addressed. Telephone: (613) 533-2644. Fax: (613) 533-6669. e-mail: gangwu@chem.queensu.ca

© 2000 NRC Canada

Scheme 1.



binding environment. We also report the crystal structure for $Cs(DB18C6)_2SCN$.

Experimental

Materials

Cesium thiocyanate, cesium chloride, and macrocyclic ligands were purchased from Aldrich and used without further purification. All complexes were prepared according to the literature methods (15). In general, ligand and cesium salt are mixed in a suitable molar ratio in various solvents (methanol, ethanol, or acetone) and crystallized at either room temperature or 5°C. The melting points of the compounds were consistent with the literature values: mp: 201–202°C for Cs(18C6)SCN, 191–193°C for $Cs(18C6)_2SCN$, 152–153°C for $Cs(DB18C6)_2SCN$, 99–100°C for Cs(C222)SCN, and 146–148°C for Cs(C22)SCN. Nonactin (purchased from Sigma) was mixed with CsSCN in a molar ratio of 1:1.5 in methanol. Gramicidin D [Dubos] was purchased from Sigma (80% gramicidin A, 6% gramicidin B, and 14% gramicidin C). Gramicidin A (25 mg/mL) was crystallized at 5°C from 50 mM solution of CsCl in methanol.

X-ray diffraction analyses

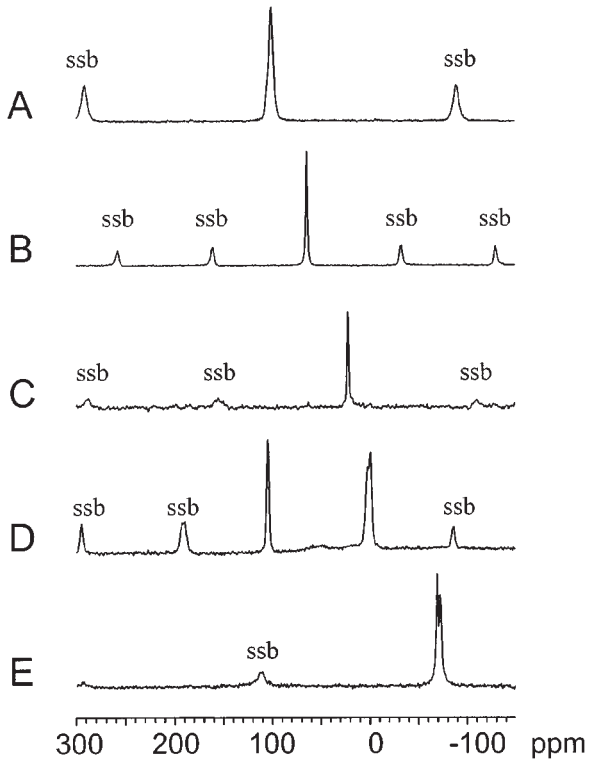
Large colorless crystals of $Cs(DB18C6)_2SCN$ were prepared according to the procedure of Pederson (15) and recrystallized twice from methanol. A crystal of size 0.2 × 0.5 × 0.4 mm was sealed in a glass capillary. The X-ray data were collected on a Siemens P4 single-crystal diffractometer with graphite-monochromated Mo Kα radiation, operated at 50 kV and 40 mA at 296 K. The data were collected over θ = 1.94–22.51°. Data were processed on a Pentium PC using Siemens SHELXTL software package (16) and corrected for Lorentz and polarization effects.

Solid-state ^{133}Cs NMR

Solid-state ^{133}Cs NMR spectra were obtained on two spectrometers: Tecmag Apollo-200 (4.7 T, 26.32 MHz for ^{133}Cs) and Bruker Avance – 500 (11.7 T, 65.59 MHz for ^{133}Cs). Typical MAS frequencies were 5–12.5 kHz with Bruker 4 mm MAS probes. In MAS and central-transition static experiments, a single pulse sequence was used with pulse width of 1 μs (approx. 30° for the central transition). For the satellite-transition static experiments, a Hahn echo sequence was used to avoid acoustic ringing from the probe. Recycle times of 10–30 s were used. All ^{133}Cs chemical shifts were referenced to 0.5 M CsCl (aq.), δ = 0 ppm, by setting the ^{133}Cs NMR signal of solid CsCl to δ = 223.2 ppm. Spectral simulation was performed with the WSOLIDS program provided by Drs. Klaus Eichele and Rod Wasylishen (Dalhousie University, Halifax, Nova Scotia, Canada).

© 2000 NRC Canada

Fig. 1. Experimental ^{133}Cs MAS NMR spectra (11.75 T) of (*a*) Cs(C22)SCN, (*b*) Cs(18C6)SCN, (*c*) Cs(15C5)$_2$SCN, (*d*) Cs(nonactin)SCN, (*e*) Cs(DB18C6)$_2$SCN.



Results and discussion

A. MAS ^{133}Cs NMR spectra

Solid-state ^{133}Cs NMR spectra obtained under the MAS condition are shown in Fig. 1. Since the ^{133}Cs nucleus has a very small quadrupole moment, no second-order quadrupolar broadening was observed at 11.75 T for the compounds studied in the present work. As shown in Fig. 1, each of the ^{133}Cs MAS spectra exhibits sharp isotropic peaks flanked by a large number of spinning side-bands due to the first-order quadrupole interaction. The Cs^+ ion in Cs(C22)SCN exhibits the least chemical shielding, δ_{iso} = 100 ppm. The isotropic ^{133}Cs chemical shift for Cs(18C6)SCN is 64 ppm, which is quite different from the value of 73 ppm reported by Dye and coworkers (11). The reason for this discrepancy is unclear at this time. For the sandwich-type complex, Cs(15C5)$_2$SCN, the Cs^+ ion shows more shielded environment, δ_{iso} = 22 ppm. This chemical shift value is very similar to those found in alkalides, Cs(15C5)$_2M^-$ (M = Na, K, Rb) (12), suggesting that the Cs^+ cation is well shielded by the two 15C5 ligands. For the Cs^+–nonactin complex, the isotropic peak appears at 4 ppm and exhibits some broadening or splitting. Note that the sharp signal at 110 ppm is due to the excessive CsSCN in the sample. The ^{133}Cs NMR experiments performed at a different magnetic field (4.7 T) indicated that the broadening or splitting arises from a chemical shift distribution rather than from the second-order quadrupole interaction. Since the sample was prepared by lyophilizing a mixture containing excessive CsSCN ligand, it is of poorly crystalline nature. Consequently, the observed broadening or slitting may be attributed to either lack of crystallinity or presence of polymorphs. The ^{133}Cs MAS spectrum of Cs(18C6)$_2$SCN exhibits a sharp peak at –72 ppm, which is dramatically different from that for Cs(18C6)SCN, 64 ppm. The structure of Cs(18C6)$_2$SCN was speculated by Pedersen (15) to have a sandwich-type structure. The observation of a ^{133}Cs chemical shift of –72 ppm strongly supports the sandwich structure. Two sharp peaks were observed in the multiple-field ^{133}Cs MAS spectra of Cs(DB18C6)$_2$SCN, δ_{iso} = –70 and –72 ppm, indicating the presence of two crystallographically distinct Cs sites. Since the crystal structure of Cs(DB18C6)$_2$SCN has not been reported in the literature, we decided to carry out an X-ray single crystal diffraction study for this compound.

B. Crystal structure of Cs(DB18C6)$_2$SCN

The crystal structure of Cs(DB18C6)$_2$SCN indicated the presence of two solvent molecules, thus the complete formula is Cs(DB18C6)$_2$SCN•1/2CH_3OH•1/2H_2O. The crystal data are summarized in Table 1. The atomic coordinates with their estimated standard deviations are given in Table 2. Selected bond lengths and bond angles are listed in Table 3. As shown in Fig. 2, there are two molecules in the asymmetric unit cell, giving rise to two crystallographically inequivalent Cs sites. This finding is consistent with the observation of two chemical shifts in the ^{133}Cs MAS spectra. Each cesium ion is coordinated to twelve ether oxygen atoms from the two DB18C6 molecules, forming a hexagonal *anti*-prism coordination geometry around the Cs^+ ion. The Cs—O distances range from 3.188 to 3.586 Å for one site and from 3.206 to 3.787 Å for the other. The planes of the sandwiched cesium complex are approximately perpendicular to one another. The disordered counter ion (SCN^-), and both of the solvent molecules are not in direct contact with the central cesium ion. Interestingly, the crystal structure of Cs(DB18C6)$_2$SCN is very different from that of a closely related compound, Cs(tetramethyl-DB18C6)$_2$SCN. The crystals of Cs(tetramethyl-DB18C6)$_2$SCN are tetragonal with space group of $P4_2/n$ (17). The asymmetric unit cell contains only one dimeric complex. Therefore, one isotropic ^{133}Cs chemical shift would be observed for this complex. The two ligand molecules lie on crystallographic two-fold axis giving rise to the $\bar{4}$ symmetry at the Cs^+ site. The three independent Cs—O distances in Cs(tetramethyl-DB18C6)$_2$SCN, 3.12, 3.27, and 3.36 Å, are much shorter than those in Cs(DB18C6)$_2$SCN.

C. Stationary ^{133}Cs NMR spectra

In order to obtain ^{133}Cs CSAs for the macrocyclic Cs complexes, it is necessary to obtain NMR spectra for stationary powder samples. The stationary ^{133}Cs NMR spectra are shown in Fig. 3. Since the ^{133}Cs second-order quadrupolar broadening is expected to be negligible (vide infra), it is straightforward to analyze the stationary ^{133}Cs NMR line shapes. In general, the ^{133}Cs CSAs for the macrocyclic polyether compounds are quite small, ranging from 50 to 90 ppm. However, a cryptand complex, Cs(C22)SCN exhibits a uniquely large CSA, 208 ppm. It is noted that similarly large ^{133}Cs CSAs have been previously observed in simple inorganic Cs salts. For example, the ^{133}Cs CSAs for the two

© 2000 NRC Canada

Table 1. Crystal data and structure refinement.

Empirical formula	$C_{41}H_{48}CsNO_{12}S$ / $0.5CH_3OH$ / $0.5H_2O$
Formula weight	936.3
Temperature	296(2) K
Wavelength	0.71073 Å
Crystal system	Monoclinic
Space group	$P2_1/c$
Unit cell dimensions	a = 14.503(2) Å α = 90°
	b = 15.152(3) Å β = 90.796(8)°
	c = 39.989(6) Å γ = 90°
Volume, Z	8787(2) Å^3, 8
Density (calculated)	1.416 g/cm^3
Absorption coefficient	9.53 cm^{-1}
F(000)	3852
Crystal size	0.2 × 0.5 × 0.4 mm
θ range for data collection	1.94 to 22.51°
Limiting indices	$0 \le h \le 14$, $-16 \le k \le 0$, $-43 \le l \le 43$
Reflections collected	11516
Independent reflections	10999 [R(int) = 0.0344]
Absorption correction	None
Refinement method	Full-matrix least-squares on F^2
Data / restraints / parameters	10656 / 0 / 1060
Goodness-of-fit on F^2	1.129
Final R indices [$I > 2\sigma(I)$]	$R_1{}^a$ = 0.0771, $wR_2{}^b$ = 0.1981
R indices (all data)	$R_1{}^a$ = 0.1198, $wR_2{}^b$ = 0.4128
Largest diff. peak and hole	0.855 and –1.180 eÅ^{-3}

$^a R_1 = \Sigma||F_o| - |F_c||/\Sigma|F_o|$

$^b wR_2 = [\Sigma w[(F_o^2 - F_c^2)^2]/\Sigma[w(F_o^2)^2]]^{0.5}$ where $w = 1/[\sigma^2(F_o^2) + (0.075P)^2]$, where $P = [\max(F_o^2, 0) + 2F_c^2]/3$

Table 2. Atomic coordinates (× 10^4) and equivalent isotropic displacement parameters (Å^2 × 10^3). U(eq) is defined as one third of the trace of the orthogonalized U_{ij} tensor.

	x	y	z	U(eq)
N(1)	–1658(13)	4539(18)	–2496(5)	175(9)
S(1)	3358(12)	6030(7)	116(3)	195(6)
Cs(1)	2147(1)	1050(1)	576(1)	61(1)
C(1)	895(8)	–758(7)	1143(3)	64(3)
O(1)	37(5)	167(5)	790(2)	68(2)
Cs(2)	3438(1)	4007(1)	–1777(1)	64(1)
S(2)	–2355(4)	4008(3)	–3078(2)	123(2)
N(2)	1660(35)	6556(26)	–57(14)	154(19)
C(2)	1077(9)	–1114(9)	1467(3)	76(4)
O(2)	72(5)	1341(5)	241(2)	74(2)
N(2A)	2266(31)	5959(29)	772(20)	241(39)
O(3)	1535(6)	1222(5)	–227(2)	73(2)
C(3)	557(11)	–849(11)	1727(4)	94(5)
O(4)	2890(5)	149(5)	–134(2)	64(2)
C(4)	–137(10)	–251(10)	1686(4)	83(4)
O(5)	2906(5)	–981(5)	436(2)	64(2)
C(5)	–328(8)	100(8)	1387(4)	75(4)
O(6)	1354(5)	–956(5)	862(2)	68(2)
C(6)	169(7)	–152(8)	1099(3)	59(3)
O(7)	3001(6)	676(6)	1311(3)	81(3)
C(7)	–663(9)	818(9)	740(4)	83(4)
O(8)	1647(5)	1992(5)	1310(2)	67(2)
C(8)	–750(9)	994(9)	383(4)	88(4)
O(9)	1521(5)	3049(5)	810(2)	73(2)
C(9)	–66(10)	1435(11)	–106(4)	95(5)
C(10)	768(11)	1820(10)	–261(4)	102(5)

Table 2 (*Continued*).

	x	y	z	U(eq)
O(10)	2793(6)	2929(6)	295(2)	85(3)
O(11)	4513(7)	2040(6)	447(3)	87(3)
C(11)	2315(9)	1427(8)	–402(3)	69(3)
C(12)	2420(11)	2124(9)	–609(4)	83(4)
O(12)	4476(7)	720(6)	840(3)	99(3)
C(13)	3218(15)	2256(10)	–772(4)	106(5)
O(13)	2676(6)	4702(6)	–1004(3)	94(3)
O(14)	4579(6)	4440(7)	–1109(3)	93(3)
C(14)	3954(12)	1703(10)	–725(4)	100(5)
C(15)	3874(10)	991(8)	–515(3)	78(4)
O(15)	5147(6)	2829(5)	–1366(2)	77(2)
O(16)	3942(6)	1836(6)	–1633(3)	87(3)
C(16)	3053(9)	838(7)	–356(3)	60(3)
C(17)	3662(8)	–379(8)	–38(4)	76(4)
O(17)	2113(6)	2292(6)	–1622(3)	94(3)
O(18)	1442(7)	3928(6)	–1365(3)	94(3)
C(18)	3332(9)	–1186(7)	130(3)	68(3)
C(19)	2504(9)	–1765(8)	573(4)	76(4)
O(19)	3004(6)	3173(6)	–2542(2)	89(3)
C(20)	2098(8)	–1586(7)	897(4)	74(4)
O(20)	1835(7)	4392(9)	–2452(3)	123(4)
O(21)	2273(6)	5787(7)	–2020(3)	112(4)
C(21)	809(8)	2413(8)	1273(3)	64(3)
O(22)	4118(6)	6108(5)	–1853(2)	81(3)
C(22)	75(10)	2330(9)	1483(4)	88(4)
O(23)	5383(5)	5048(5)	–2044(3)	82(3)

© 2000 NRC Canada

Table 2 (*Continued*).

	x	*y*	*z*	*U*(eq)
C(23)	–745(11)	2787(12)	1413(5)	109(6)
O(24)	4874(5)	3488(5)	–2388(2)	70(2)
C(24)	–802(11)	3330(11)	1155(5)	107(6)
C(25)	–54(11)	3451(9)	947(5)	98(5)
O(25)	891(17)	–5302(22)	1691(8)	303(14)
C(26)	764(9)	2992(8)	1005(4)	77(4)
C(27)	1537(10)	3666(9)	540(4)	86(4)
C(28)	2494(10)	3740(8)	428(4)	79(4)
C(29)	3607(12)	2922(11)	94(4)	106(5)
C(30)	4430(11)	2863(12)	260(5)	118(6)
O(30)	1842(11)	6419(11)	1316(5)	187(7)
C(31)	5290(10)	1929(8)	632(3)	71(3)
C(32)	6058(10)	2441(10)	610(4)	85(4)
C(33)	6803(12)	2283(13)	808(5)	103(5)
C(34)	6792(13)	1583(16)	1035(5)	116(6)
C(35)	6024(14)	1059(12)	1060(5)	112(6)
C(36)	5272(11)	1211(9)	849(4)	82(4)
C(37)	4291(13)	38(10)	1075(5)	114(6)
C(38)	3899(13)	321(15)	1363(6)	154(10)
C(39)	2729(10)	1123(10)	1613(4)	90(4)
C(40)	1764(9)	1405(8)	1585(3)	70(3)
C(41)	1228(10)	4081(9)	–1037(4)	77(4)
C(42)	379(11)	3832(10)	–905(5)	105(5)
C(43)	218(13)	4050(13)	–563(6)	120(7)
C(44)	872(15)	4440(14)	–379(5)	119(7)
C(45)	1706(12)	4675(11)	–510(5)	104(5)
C(46)	1880(11)	4484(9)	–841(4)	83(4)
C(47)	3426(14)	5033(16)	–800(6)	170(12)
C(48)	4181(14)	5110(15)	–911(7)	172(11)
C(49)	5275(11)	3955(10)	–948(4)	89(4)
C(50)	5771(9)	3417(9)	–1202(4)	80(4)
C(51)	5476(9)	2290(8)	–1602(3)	70(3)
C(52)	6383(9)	2250(9)	–1707(4)	77(4)
C(53)	6631(11)	1674(11)	–1954(4)	93(4)
C(54)	5989(12)	1160(10)	–2108(4)	94(5)
C(55)	5063(11)	1174(8)	–2004(4)	83(4)
C(56)	4821(9)	1740(8)	–1765(3)	68(3)
C(57)	3265(11)	1235(9)	–1745(4)	94(5)
C(58)	2407(11)	1408(10)	–1567(5)	112(6)
C(59)	1198(12)	2410(13)	–1496(6)	132(7)
C(60)	935(11)	3325(14)	–1577(6)	130(7)
C(61)	4946(8)	6225(7)	–1694(3)	58(3)
C(62)	5149(8)	6855(7)	–1447(3)	67(3)
C(63)	6029(10)	6891(9)	–1307(3)	79(4)
C(64)	6697(10)	6319(9)	–1404(4)	89(4)
C(65)	6507(8)	5691(8)	–1651(4)	73(4)
C(66)	5624(8)	5643(7)	–1790(3)	65(3)
C(67)	6047(8)	4444(9)	–2154(4)	76(4)
C(68)	5687(9)	3964(9)	–2442(4)	82(4)
C(69)	4561(9)	3029(10)	–2680(3)	79(4)
C(70)	3679(10)	2566(9)	–2618(4)	87(4)
C(71)	2098(9)	2907(11)	–2534(3)	81(4)
C(72)	1828(12)	2039(13)	–2566(4)	115(6)
C(73)	881(16)	1859(18)	–2545(6)	146(8)
C(74)	243(16)	2523(22)	–2515(7)	156(9)
C(75)	537(12)	3361(17)	–2490(4)	120(7)
C(76)	1480(10)	3585(13)	–2487(4)	95(5)

Table 2 (*Concluded*).

	x	*y*	*z*	*U*(eq)
C(77)	1290(14)	5183(18)	–2380(5)	165(11)
C(78)	1540(20)	5700(20)	–2216(12)	364(37)
C(79)	2699(11)	6612(10)	–2048(4)	92(5)
C(80)	3411(8)	6750(8)	–1785(3)	69(3)
C(81)	1218(19)	–4550(14)	1815(5)	157(9)
C(82A)	2501(41)	6013(22)	479(14)	156(35)
C(84)	–1959(13)	4301(13)	–2745(6)	109(6)
C(83A)	2284(46)	6304(27)	53(14)	138(20)
C(85)	5000	5000	0	312(40)

Table 3. Selected Cs—O bond lengths (Å) and O-Cs-O bond angles (°).

Cs(1)—O(10)	3.206(8)
Cs(1)—O(7)	3.225(9)
Cs(1)—O(9)	3.303(8)
Cs(1)—O(2)	3.307(8)
Cs(1)—O(5)	3.317(7)
Cs(1)—O(3)	3.330(9)
Cs(1)—O(4)	3.341(8)
Cs(1)—O(8)	3.352(8)
Cs(1)—O(6)	3.449(8)
Cs(1)—O(1)	3.459(8)
Cs(1)—O(12)	3.559(11)
Cs(1)—O(11)	3.787(9)
Cs(2)—O(14)	3.188(10)
Cs(2)—O(17)	3.295(9)
Cs(2)—O(21)	3.321(10)
Cs(2)—O(24)	3.326(8)
Cs(2)—O(22)	3.348(8)
Cs(2)—O(19)	3.361(9)
Cs(2)—O(18)	3.351(11)
Cs(2)—O(23)	3.417(8)
Cs(2)—O(16)	3.416(9)
Cs(2)—O(15)	3.452(9)
Cs(2)—O(13)	3.458(10)
Cs(2)—O(20)	3.586(12)
O(10)-Cs(1)-O(7)	111.4(2)
O(10)-Cs(1)-O(9)	50.7(2)
O(7)-Cs(1)-O(9)	90.3(2)
O(10)-Cs(1)-O(2)	90.5(2)
O(7)-Cs(1)-O(2)	136.8(2)
O(9)-Cs(1)-O(2)	74.9(2)
O(10)-Cs(1)-O(5)	131.7(2)
O(7)-Cs(1)-O(5)	82.4(2)
O(9)-Cs(1)-O(5)	172.7(2)
O(2)-Cs(1)-O(5)	110.9(2)
O(10)-Cs(1)-O(3)	70.6(2)
O(7)-Cs(1)-O(3)	170.7(2)
O(9)-Cs(1)-O(3)	97.5(2)
O(2)-Cs(1)-O(3)	50.9(2)
O(5)-Cs(1)-O(3)	89.7(2)
O(10)-Cs(1)-O(4)	88.1(2)
O(7)-Cs(1)-O(4)	125.3(2)
O(9)-Cs(1)-O(4)	135.2(2)

© 2000 NRC Canada

Table 3 (*Continued*).

O(2)-Cs(1)-O(4)	90.7(2)
O(5)-Cs(1)-O(4)	50.7(2)
O(3)-Cs(1)-O(4)	45.4(2)
O(10)-Cs(1)-O(8)	89.8(2)
O(7)-Cs(1)-O(8)	50.3(2)
O(9)-Cs(1)-O(8)	45.3(2)
O(2)-Cs(1)-O(8)	95.2(2)
O(5)-Cs(1)-O(8)	128.2(2)
O(3)-Cs(1)-O(8)	138.8(2)
O(4)-Cs(1)-O(8)	173.7(2)
O(10)-Cs(1)-O(6)	177.4(2)
O(7)-Cs(1)-O(6)	70.7(2)
O(9)-Cs(1)-O(6)	128.3(2)
O(2)-Cs(1)-O(6)	86.9(2)
O(5)-Cs(1)-O(6)	49.6(2)
O(3)-Cs(1)-O(6)	107.6(2)
O(4)-Cs(1)-O(6)	92.0(2)
O(8)-Cs(1)-O(6)	90.5(2)
O(10)-Cs(1)-O(1)	134.0(2)
O(7)-Cs(1)-O(1)	92.1(2)
O(9)-Cs(1)-O(1)	92.1(2)
O(2)-Cs(1)-O(1)	49.4(2)
O(5)-Cs(1)-O(1)	88.8(2)
O(3)-Cs(1)-O(1)	92.5(2)
O(4)-Cs(1)-O(1)	110.4(2)
O(8)-Cs(1)-O(1)	75.2(2)
O(6)-Cs(1)-O(1)	43.7(2)
O(10)-Cs(1)-O(12)	87.0(2)
O(7)-Cs(1)-O(12)	49.8(2)
O(9)-Cs(1)-O(12)	107.9(2)
O(2)-Cs(1)-O(12)	173.3(2)
O(5)-Cs(1)-O(12)	66.7(2)
O(3)-Cs(1)-O(12)	122.4(2)
O(4)-Cs(1)-O(12)	83.0(2)
O(8)-Cs(1)-O(12)	90.9(2)
O(6)-Cs(1)-O(12)	95.6(2)
O(1)-Cs(1)-O(12)	135.4(2)
O(10)-Cs(1)-O(11)	48.0(2)
O(7)-Cs(1)-O(11)	81.8(2)
O(9)-Cs(1)-O(11)	85.9(2)
O(2)-Cs(1)-O(11)	135.4(2)
O(5)-Cs(1)-O(11)	92.4(2)
O(3)-Cs(1)-O(11)	93.8(2)
O(4)-Cs(1)-O(11)	75.1(2)
O(8)-Cs(1)-O(11)	99.1(2)
O(6)-Cs(1)-O(11)	134.5(2)
O(1)-Cs(1)-O(11)	173.5(2)
O(12)-Cs(1)-O(11)	40.4(2)
O(14)-Cs(2)-O(17)	107.6(3)
O(14)-Cs(2)-O(21)	109.5(3)
O(17)-Cs(2)-O(21)	113.6(3)
O(14)-Cs(2)-O(24)	109.9(2)
O(17)-Cs(2)-O(24)	108.9(2)
O(21)-Cs(2)-O(24)	107.3(3)
O(14)-Cs(2)-O(22)	74.4(2)
O(17)-Cs(2)-O(22)	160.1(2)
O(21)-Cs(2)-O(22)	49.5(2)

Table 3 (*Concluded*).

O(24)-Cs(2)-O(22)	88.3(2)
O(14)-Cs(2)-O(19)	158.1(2)
O(17)-Cs(2)-O(19)	76.8(3)
O(21)-Cs(2)-O(19)	87.2(3)
O(24)-Cs(2)-O(19)	49.7(2)
O(22)-Cs(2)-O(19)	109.0(2)
O(14)-Cs(2)-O(18)	92.2(2)
O(17)-Cs(2)-O(18)	50.9(2)
O(21)-Cs(2)-O(18)	74.5(3)
O(24)-Cs(2)-O(18)	154.9(2)
O(22)-Cs(2)-O(18)	109.6(2)
O(19)-Cs(2)-O(18)	106.3(2)
O(14)-Cs(2)-O(23)	75.3(2)
O(17)-Cs(2)-O(23)	155.4(2)
O(21)-Cs(2)-O(23)	87.2(2)
O(24)-Cs(2)-O(23)	49.6(2)
O(22)-Cs(2)-O(23)	44.5(2)
O(19)-Cs(2)-O(23)	91.9(2)
O(18)-Cs(2)-O(23)	153.2(2)
O(14)-Cs(2)-O(16)	87.1(2)
O(17)-Cs(2)-O(16)	48.2(2)
O(21)-Cs(2)-O(16)	159.7(2)
O(24)-Cs(2)-O(16)	76.2(2)
O(22)-Cs(2)-O(16)	150.2(2)
O(19)-Cs(2)-O(16)	80.1(2)
O(18)-Cs(2)-O(16)	93.9(2)
O(23)-Cs(2)-O(16)	108.8(2)
O(14)-Cs(2)-O(15)	49.2(2)
O(17)-Cs(2)-O(15)	85.4(2)
O(21)-Cs(2)-O(15)	156.7(2)
O(24)-Cs(2)-O(15)	77.0(2)
O(22)-Cs(2)-O(15)	108.9(2)
O(19)-Cs(2)-O(15)	111.3(2)
O(18)-Cs(2)-O(15)	111.6(2)
O(23)-Cs(2)-O(15)	78.3(2)
O(16)-Cs(2)-O(15)	43.3(2)
O(14)-Cs(2)-O(13)	50.1(2)
O(17)-Cs(2)-O(13)	83.0(2)
O(21)-Cs(2)-O(13)	81.2(3)
O(24)-Cs(2)-O(13)	159.9(2)
O(22)-Cs(2)-O(13)	83.7(2)
O(19)-Cs(2)-O(13)	150.4(2)
O(18)-Cs(2)-O(13)	44.3(2)
O(23)-Cs(2)-O(13)	114.5(2)
O(16)-Cs(2)-O(13)	102.3(2)
O(15)-Cs(2)-O(13)	88.2(2)
O(14)-Cs(2)-O(20)	156.9(3)
O(17)-Cs(2)-O(20)	84.0(3)
O(21)-Cs(2)-O(20)	47.6(3)
O(24)-Cs(2)-O(20)	83.8(2)
O(22)-Cs(2)-O(20)	88.0(3)
O(19)-Cs(2)-O(20)	42.7(2)
O(18)-Cs(2)-O(20)	79.6(3)
O(23)-Cs(2)-O(20)	102.6(3)
O(16)-Cs(2)-O(20)	114.7(2)
O(15)-Cs(2)-O(20)	153.7(2)
O(13)-Cs(2)-O(20)	114.3(2)

© 2000 NRC Canada

Fig. 2. Diagram illustrating the two crystallographically inequivalent Cs sites in $Cs(DB18C6)_2SCN \cdot 1/2CH_3OH \cdot 1/2H_2O$.

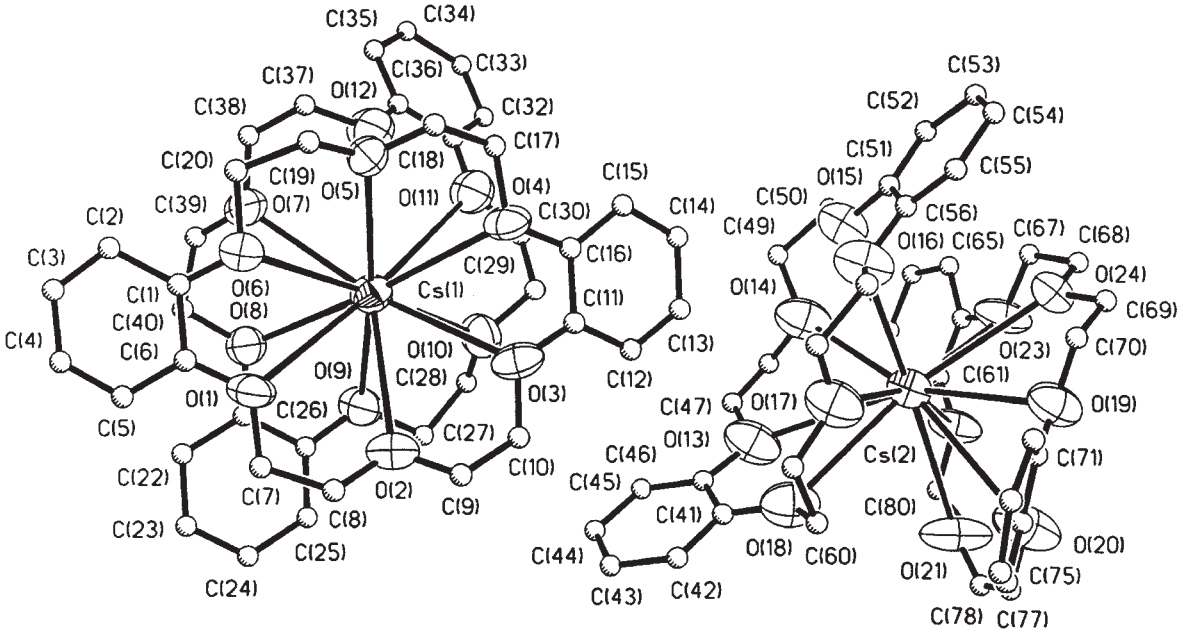
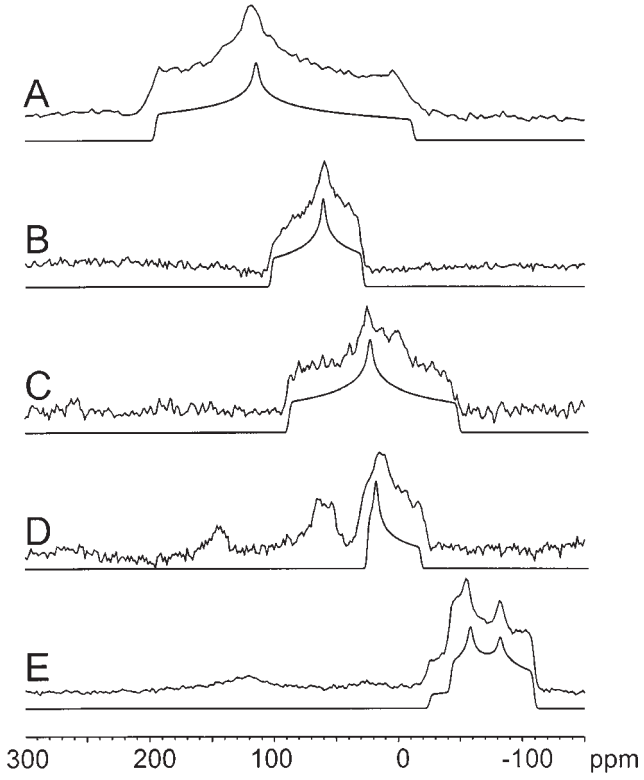


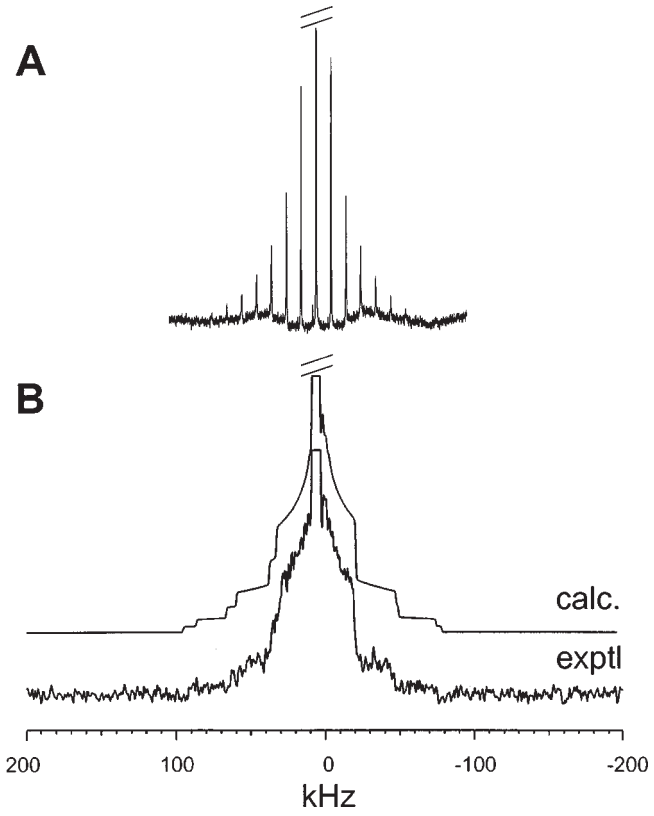
Fig. 3. Experimental (upper trace) and simulated (lower trace) central-transition ^{133}Cs stationary NMR spectra (11.75 T) of (*a*) Cs(C22)SCN, (*b*) Cs(18C6)SCN, (*c*) $Cs(15C5)_2SCN$, (*d*) Cs(Nonactin)SCN, and (*e*) $Cs(DB18C6)_2SCN$.



Cs sites in Cs_2CrO_4 are 337 and 226 ppm (8). We also obtained the ^{133}Cs CSA for another cryptand complex, C222: δ_{11} = 251, δ_{22} = 224, and δ_{33} = 200 ppm. The ^{133}Cs CSA for the Cs^+–nonactin complex is also small. This is consistent with the crystal structure of CsSCN/nonactin where the Cs^+ ion is located approximately at the center of a cube whose eight corners are formed by oxygen donor atoms from the nonactin molecule (18). The stationary ^{133}Cs NMR spectrum of $Cs(DB18C6)_2SCN$ exhibits a complex line shape due to the presence of two Cs sites. Since the isotropic chemical shifts have been determined from analysis of the MAS spectrum of $Cs(DB18C6)_2SCN$, it is straightforward to analyze the stationary spectrum and obtain the principal components of the two ^{133}Cs CS tensors. The ^{133}Cs CSA results for the

© 2000 NRC Canada

Fig. 4. All-transition 10 kHz-MAS (*a*) and stationary (*b*) ^{133}Cs NMR spectra (11.75 T) of Cs(18C6)SCN. The following parameters were used in the simulation shown in (b): δ_{11} = 103, δ_{22} = 61, and δ_{33} = 29 ppm; QCC = 0.41 MHz; η = 0.85; α = 0; β = 80; and γ = 0°.

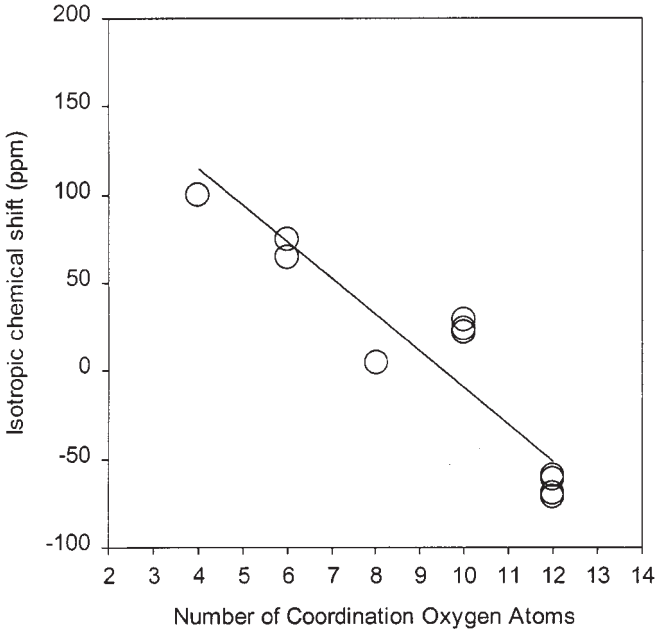


macrocyclic complexes are summarized in Table 4. However, it is also evident from Fig. 3 that some additional features are present in the ^{133}Cs stationary spectra. For example, a broad hump at 120 ppm was observed in the stationary spectrum of Cs(DB18C6)$_2$SCN (Fig. 3d). Since the ^{133}Cs MAS spectra of these complexes did not indicate any impurity, the low-intensity spectral features must arise from the satellite transitions. To obtain an estimate of the ^{133}Cs quadrupole coupling constant (QCC) for Cs-macrocyclic complexes, we recorded a complete stationary spectrum for Cs(18C6)SCN, i.e., both central- and satellite transitions. As shown in Fig. 4, the all-transition ^{133}Cs NMR spectrum covers a range of approximately 200 kHz. Simulation yields that the ^{133}Cs QCC is 0.41 MHz and the asymmetry parameter is 0.85 for Cs(18C6)SCN. At 11.75 T, the second-order ^{133}Cs quadrupolar interaction contributes less than 1 ppm to the stationary central-transition ^{133}Cs spectra and, consequently, can safely be ignored in the spectral analysis, confirming our previous assumptions. The ^{133}Cs MAS spectra of other Cs macrocyclic complexes exhibited similar spinning sideband manifold, suggesting that the QCCs are of similar magnitude as that for Cs(18C6)SCN.

D. ^{133}Cs chemical shifts and ion-binding environment

The origin of ^{133}Cs chemical shielding (σ) can be written as a sum of two contributions (19):

Fig. 5. Correlation between the experimental ^{133}Cs isotropic chemical shift and the number of coordination oxygen atoms for cesium-macrocyclic compounds.



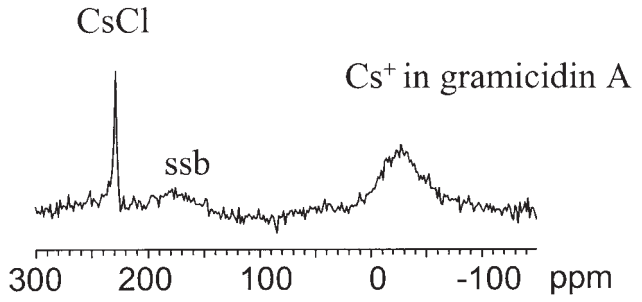
$$\sigma = \sigma_d + \sigma_p$$

where σ_d is the diamagnetic shielding term arising from the induced motion of a spherically symmetric electron cloud at a nucleus, and σ_p is the paramagnetic term caused by mixing of the electronic ground state with excited states in the presence of a strong external magnetic field. To a very crude approximation the paramagnetic shielding (σ_p) is proportional to $-(1/\Delta E) < 1/r^3 > (\rho_e)$, where ΔE is the average energy separation between the ground and excited states of the molecule, $< 1/r^3 >$ is the average distance between electrons and the nucleus of interest, and ρ_e is the relative electron densities in the various *p* orbitals involved in bonding (20-22). In the case of ^{133}Cs NMR, the paramagnetic term is usually a dominant contributor to variations of ^{133}Cs chemical shifts because of the relatively low energy gap (ΔE) and the availability of the outer *p* and *d* orbitals (23).

As shown in Fig. 5, the isotropic ^{133}Cs chemical shifts in macrocyclic compounds exhibit a clear correlation with the number of the oxygen atoms to which the Cs^+ ion is coordinated. It should be pointed out that for complexes with unknown crystal structures, all oxygen atoms in the macrocyclic ligand molecule were assumed to participate the interaction to the Cs^+ ion. Figure 5 suggests that, as the coordination number is increased, the chemical shielded at the Cs center is also increased. A similar correlation has also been observed between the Gutmann donor number (24) of the solvent and NMR chemical shifts of ^{23}Na (25, 26), ^{133}Cs (27), and ^{39}K (28) nuclei. The range of the ^{133}Cs chemical shifts plotted in Fig. 5, 100 ppm to –71 ppm, covers approximately the entire ^{133}Cs chemical shift range for Cs compounds containing oxygen ligands. However, one notable exception is the isotropic ^{133}Cs chemical shift for Cs(C222)SCN, δ_{iso} = 225 ppm. The cage structure of the C222 molecule forces very close contacts between the Cs^+

© 2000 NRC Canada

Fig. 6. Central-transition ^{133}Cs MAS spectrum (11.75 T) of gramicidin A/CsCl.

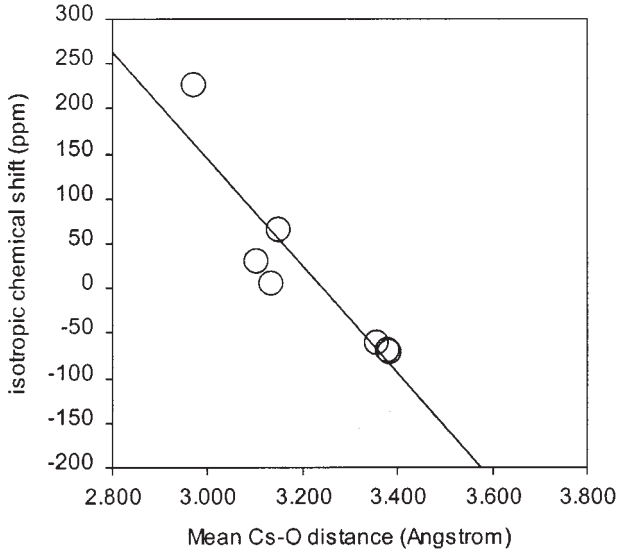


ion and the six oxygen donor atoms, with the average Cs—O distance of 2.970 Å (29). This strong Cs–O overlap is responsible for the unusually large chemical shift in Cs(C222)SCN (vide infra).

Ideally, one would use such a linear correlation to predict Cs^+ binding environments for compounds whose crystal structures are unknown. To test this idea, we obtained the solid-state ^{133}Cs NMR spectra for Cs(HM18C6)SCN•xH$_2$O. The isotropic ^{133}Cs chemical shift for this compound was found to be 0 ppm. Using the correlation curve shown in Fig. 5, we may predict that the Cs^+ ion in Cs(HM18C6)SCN•xH$_2$O is probably coordinated to approximately nine or ten oxygen atoms. This indicates that, in addition to the six oxygen atoms from the 18C6 ring, the hydroxyl side-arm must also be bound to the Cs^+ ion, presumably in a similar fashion as those in sodium and potassium complexes of 16-(2-hydroxyethyl)-1,4,7,10,13-pentaoxa-16-azacyclooctadecane (30). The additional oxygen donors may come from water molecules. It is known that hydration water molecules are also commonly found in metal macrocyclic complexes (30). Therefore, the observed ^{133}Cs isotropic chemical shift of Cs(HM18C6)SCN•xH$_2$O can be rationalized by a Cs^+ ion-binding environment containing nine or ten Cs–O interactions.

A crystalline sample of gramicidin A/CsCl complex was also prepared with the expectation that solid-state ^{133}Cs NMR may shed some light on the Cs^+ binding geometry inside the ion channel. The unit cell dimensions determined for our crystals are 35.565, 35.565, and 62.086 Å with the space group of *P*4222. However, these crystal data are different from all available crystal structures for gramicidin A/CsCl system (31–35). Clearly, our gramicidin A/CsCl crystals represented a new polymorph. Unfortunately, attempts to find the solution of the crystal structure for our gramicidin A/CsCl crystals were unsuccessful. Nevertheless, we obtained the ^{133}Cs MAS NMR spectrum for this crystalline sample. As shown in Fig. 6, a broad peak at 17 ppm is observed in the ^{133}Cs MAS spectrum. The line width of the broad peak is approximately 3.3 kHz. The broadening may be due to the presence of multiple Cs sites in the gramicidin A channel formed by a gramicidin dimer and likely the presence of two independent dimers in the asymmetric unit cell (31–35). In addition, it is also likely that, for each Cs^+ site, there exists a distribution of ^{133}Cs chemical shifts due to the presence of disorder. According to the correlation shown in Fig. 5, the ^{133}Cs chemical shift value of 17 ppm indicates the number of oxygen coordination at the binding sites is approximately 8. This type of binding environment is consistent with those reported for other forms of gramicidin A crystals (31–36). For example, a recent X-ray study of gramicidin A/CsCl (36) revealed that two dimers are present in the asymmetric unit cell and that each gramicidin channel (dimer) contains three Cs^+ binding sites. On average, each Cs^+ ion has eight closest contacts arising from six carbonyl oxygens (3.6–4.5 Å) and two water oxygens (2.8–3.1 Å). Therefore, our solid-state ^{133}Cs NMR observation is in agreement with the crystallographic studies in the Cs^+ binding environment, despite the difference in overall crystal structures. It would be of interest to extend the alkali metal NMR to other gramicidin-cation complexes (Na and K).

Fig. 7. Correlation between the ^{133}Cs chemical shifts and the average Cs—O distance for cesium-macrocyclic compounds.



In the above discussion, we have focused only on the isotropic ^{133}Cs chemical shifts. In the discussion that follows, we briefly comment on the observed tensor components for the Cs complexes with macrocyclic ligands. As seen from Table 4, the span of the chemical shift tensor varied from 26 ppm in Cs(18C6)$_2$SCN to 208 ppm in Cs(C22)SCN. This large difference may be interpreted as due to the structural difference between the two complexes. Clearly, the Cs^+ coordination environment in Cs(18C6)$_2$SCN is more "spherical" than that in Cs(C22)SCN. In principle, the tensor components are more informative than the isotropic value alone. However, for the ^{133}Cs NMR data presented in Table 4, there does not exist any clear trend between δ_{11} and δ_{33} components and ion-binding environment. Interestingly, the δ_{22} components show a nice correlation to the isotropic values. More studies are clearly required to unravel the relationship between individual chemical shift tensor components and ion coordination geometry.

In general, increasing the number of metal-ligand coordination also leads to an increase in the average metal-ligand distance. This is also true in the systems studied here. For example, the average Cs—O distance in Cs(18C6)SCN is 3.150 Å, which compares to 3.382 Å in Cs(DB18C6)$_2$SCN. Dye and coworkers (12) suggested an inverse correlation between ^{133}Cs chemical shifts and the mean Cs—O distance. Figure 7 shows the ^{133}Cs isotropic chemical shift versus the

© 2000 NRC Canada

Table 4. Experimental ^{133}Cs NMR chemical shift tensors and structural data for the Cs macrocyclic complexes.

Compound	δ_{iso} (ppm)	δ_{11} (ppm)	δ_{22} (ppm)	δ_{33} (ppm)	Ω^a (ppm)	Coordination oxygen atom	Average d(Cs…O) (Å)	Range d(Cs…O) (Å)	NMR ref.
Cs(18C6)SCN	64	103	61	29	74	6	3.150[b]	3.040–3.270	This work
$Cs(18C6)_2SCN$	–72	–61	–68	–87	26	12	—	—	This work
$Cs(DB18C6)_2SCN$ (1)	–70	–42	–58	–109	67	12	3.386	3.206–3.787	This work
$Cs(DB18C6)_2SCN$ (2)	–72	–25	–82	–109	84	12	3.377	3.188–3.586	This work
Cs(C22)SCN	100	196	115	–12	208	4	—	—	This work
Cs(Nonactin)SCN	4	27	10	–26	53	8	3.136[c]	3.069–3.181	This work
$Cs(15C5)_2SCN$	22	90	25	–46	136	10	—	—	This work
$Cs(HM18C6)SCN•xH_2O$	0	38	–12	–26	64		—	—	This work
Cs(C222)SCN	225	251	224	200	51		2.970[d]	2.960–2.970	This work
$Cs(18C6)_2Na^-$	–61	—	—	—	—	12	3.357[e]	3.287–3.468	12
$Cs(18C6)_2Cs^-$	–61	—	—	—	—	12	3.31[f]	3.113–3.516	11
$Cs(15C5)_2Na^-$	24	—	—	—	—	10	—	—	12
$Cs(15C5)_2Rb^-$	24	—	—	—	—	10	—	—	12
$Cs(15C5)_2K^-$	29	—	—	—	—	10	3.088[g]	3.056–3.171	12
Cs(18C6)SCN	73	—	—	—	—	6	—	—	11
$Cs(18C6)_2SCN$	–59	—	—	—	—	12	—	—	11

[a]Span, = $\delta_{11} - \delta_{33}$.
[b]From ref. 38.
[c]From ref. 18.
[d]From ref. 29.
[e]From ref. 39.
[f]From ref. 12.
[g]From ref. 40.

average Cs—O distance for compounds with known crystal structures. Clearly, large ^{133}Cs chemical shifts are observed at short Cs—O distances. There also exist several examples in the literature where large ^{133}Cs chemical shift values were found for Cs sites exhibiting short Cs—O distances. Skibsted et al. (7) have observed a large ^{133}Cs chemical shift, 178 ppm, in Cs_2CO_3 for a site that is associated with a very short average Cs—O distance, 2.69 Å. Such a short Cs—O distance may allow an efficient electron transfer to occur from the donor oxygen atom in the ligand molecule to a 3*p* orbital of the metal ion (37), thus increasing the paramagnetic shielding contribution.

Conclusions

We have reported the determination of ^{133}Cs CSAs for a series of Cs complexes with macrocyclic molecules. The ^{133}Cs isotropic chemical shifts were found to exhibit a linear dependence on the number of oxygen atoms to which the Cs^+ ion is coordinated. In addition, the ^{133}Cs chemical shifts were also found to correlate with the average Cs—O distances. It would be of interest to find a general bonding parameter that can unify the two aforementioned dependencies. The established correlation may be useful in predicting Cs^+ ion-binding environment for unknown systems based on solid-state ^{133}Cs NMR data alone. We have also determined the crystal structure for $Cs(DB18C6)_2SCN•1/2CH_3OH•1/2H_2O$.

Acknowledgments

This research was financially supported by grants from the Natural Sciences and Engineering Research Council (NSERC) of Canada. We wish to thank Mr. Chris Freure and Dr. Shuan Dong for assistance in sample preparation and Dr. Zongchao Jia for the X-ray measurement of gramicidin A/CsCl crystals.

Supplementary material available

Anisotropic displacement parameters and hydrogen coordinates for $Cs(DB18C6)_2SCN•1/2CH_3OH•1/2H_2O$ (5 pages) have been deposited as supplementary material and may be purchased from: The Depository of Unpublished Data, Document Delivery, CISTI, National Research Council Canada, Ottawa, Ontario, Canada, K1A 0S2.

References

1. C.J. Pedersen. J. Am. Chem. Soc. **89**, 7017 (1967).
2. (*a*) J.J. Christensen, D.J. Eatough, and R.M. Izatt. Chem. Rev. **74**, 351 (1974); (*b*) N.S. Poonia and A.V. Bajaj. Chem. Rev. **79**, 389 (1979).
3. C. Detellier, H.P. Graves, and K.M. Brière. *In* Isotopes in physical and biomedical science. *Edited by* E. Buncel and J.R. Jones. Elsevier Science Publications B.V., Amsterdam, 1991. Vol. 2, Chap. 4.
4. G.W. Buchanan. Prog. Nucl. Magn. Reson. Spectrosc. **34**, 327 (1999).
5. S. Mooibroek, R.E. Wasylishen, R. Dickson, and G. Facey. J. Magn. Reson. **66**, 542 (1986).
6. W.P. Power, R.E. Wasylishen, S. Mooibroek, B.A. Pettitt, and W. Danchura. J. Phys. Chem. **94**, 591 (1990).
7. S. Kroeker, K. Eichele, R.E. Wasylishen, and J.F. Britten. J. Phys. Chem. B, **101**, 3727 (1997).
8. W.P. Power, S. Mooibroek, R.E. Wasylishen, and T.S. Cameron. J. Phys. Chem. **98**, 1552 (1994).
9. J. Skibsted, T. Vosegaard, H. Bildsφe, and H.J. Jakobsen. J. Phys. Chem. **100**, 14872 (1996).

© 2000 NRC Canada

10. H. Honda, M. Kenmotsu, N.O. Yamamuro, H. Ohki, S. Ishimaru, R. Ikeda, and Y. Furukawa. Z. Naturforsch. A: Phys. Sci. **51a**, 761 (1996).
11. A. Ellaboudy, J.L. Dye, and P.B. Smith. J. Am. Chem. Soc. **105**, 6490 (1983).
12. R.H. Huang, D.L. Ward, M.E. Kuchenmeister, and J.L. Dye. J. Am. Chem. Soc. **109**, 5561 (1987).
13. M.J. Wagner, L.E.H. McMills, A. Ellaboudy, J.L. Eglin, J.L. Dye, P.P. Edwards, and N.C. Pyper. J. Phys. Chem. **96**, 9656 (1992).
14. A. Ellaboudy, M.L. Tinkham, B.V. Eck, and J.L. Dye. J. Phys. Chem. **88**, 3852 (1984).
15. C.J. Pedersen. J. Am. Chem. Soc. **92**, 386 (1970).
16. SHELXTL Crystal Structure Analysis Package; Version 5. Bruker Analytical X-ray System, Siemens, Madison, Wis. 1995.
17. P.R. Mallinson. J. Chem. Soc. Perkin Trans. 2, 261 (1975).
18. T. Sakamaki and Y. Iitaka. Acta Crystallogr. Sect B: Struct. Crystallogr. Cryst. Chem. **B33**, 52 (1977).
19. (*a*) N.F. Ramsey. Phys. Rev. **78**, 699 (1950); (*b*) **83**, 540 (1951); (*c*) **86**, 243 (1952).
20. M. Karplus and J.A. Pople. J. Chem. Phys. **38**, 2803 (1963).
21. C.J. Jameson and H.S. Gutowsky. J. Chem. Phys. **40**, 1714 (1964).
22. J.A. Pople. Mol. Phys. **7**, 301 (1964).
23. D.W. Hafemeister and W.A. Flygare. J. Chem. Phys. **44**, 3584 (1966).
24. V. Gutmann and W. Wychera. Inorg. Nucl. Chem. Lett. **2**, 257 (1966).
25. E.G. Bloor and R.G. Kidd. Can. J. Chem. **46**, 3425 (1968).
26. R.H. Erlich, E. Roach, and A.I. Popov. J. Am. Chem. Soc. **92**, 4989 (1970).
27. W.J. DeWitte, L. Liu, E. Mei, J.L. Dye, and A.I. Popov. J. Solution. Chem. **6**, 337 (1977).
28. J.S. Shih and A.I. Popov. Inorg. Nucl. Chem. Lett. **13**, 105 (1977).
29. P.D. Moras, B. Metz, and R. Weiss. Acta Crystallogr. Sect B: Struct. Crystallogr. Cryst. Chem. **B29**, 388 (1973).
30. F.R. Fronczek and R.D. Gandour. *In* Cation binding by macrocycles. Marcel New Dekker Inc., New York. 1990.
31. R.E. Koeppe, J.M. Berg, K.O. Hodgson, and L. Stryer. Nature (London), **279**, 723 (1979).
32. B.A. Wallace and K. Ravikumar. Science (Washington, D.C.), **241**, 182 (1988).
33. B.A. Wallace, W.A. Hendrickson, and K. Ravikumar. Acta Crystallogr. Sect B: Struct. Crystallogr. Cryst. Chem. **B46**, 440 (1990).
34. B.A. Wallace. Progr. Biophys. Mol. Biol. **57**, 59 (1992).
35. D.A. Doyle and B.A. Wallace. J. Mol. Biol. **266**, 963 (1997).
36. B.M. Burhart, N. Li, D.A. Langs, W.A. Pangborn, and W.L. Duax. Proc. Natl. Acad. Sci. U.S.A. **95**, 12950 (1998).
37. R. Tabeta, M. Aida, and H. Saito. Bull. Chem. Soc. Jpn. **59**, 1957 (1986).
38. M. Dobler and R.P. Phizackerley. Acta Crystallogr. Sect B: Struct. Crystallogr. Cryst. Chem. **B30**, 2748 (1974).
39. S.B. Dawes, D.L. Ward, O. Fussa-Rydel, R.H. Huang, and J.L. Dye. Inorg. Chem. **28**, 2132 (1989).
40. D.L. Ward, R.H. Huang, and J.L. Dye. Acta Crystallogr. Sect C: Cryst. Struct. Commun. **C46**, 1838 (1990).

© 2000 NRC Canada

Isolation of bioactive 5α,8α-epidioxy sterols from the marine sponge *Luffariella cf. variabilis*

Anne Gauvin, Jacqueline Smadja, Maurice Aknin, Robert Faure, and Emile-Marcel Gaydou

Abstract: The lipid extract of the marine sponge *Luffariella cf. variabilis* from Mayotte (Indian Ocean) has proven to be an extraordinarily rich source of a wide variety of unusual steroids belonging to the 5α,8α-epidioxy sterol family. Ten epidioxy sterols have been identified: 5α,8α-epidioxycholesta-6,22-dien-3β-ol, 5α,8α-epidioxycholest-6-en-3β-ol, 5α,8α-epidioxy-24(ξ)-methylcholesta-6,22-dien-3β-ol, 5α,8α-epidioxy-24(*S*)-methylcholest-6-en-3β-ol and its epimer (24*R*), 5α,8α-epidioxy-24(*S*)-ethylcholesta-6,22-dien-3β-ol and its epimer (24*R*), 5α,8α-epidioxy-24(*S*)-ethylcholest-6-en-3β-ol and its epimer (24*R*), along with 5α,8α-epidioxy-24(ξ)-methylcholesta-6,9(11),22-trien-3β-ol. Their structures were determined by nuclear magnetic resonance (^{1}H, ^{13}C) and electron impact mass spectrometry. The mixture of the 10 steroids showed inhibitive activity against the human T-cell leukemia/lymphotropic virus type I (HTLV-I) and also displayed cytotoxic activity against the human breast cancer cell line (MCF_7WT).

Key words: *Luffariella cf. variabilis*, marine sponge, 5α,8α-epidioxy sterols, antitumor and antiviral activities.

Résumé : L'extrait lipidique de l'éponge marine *Luffariella cf. variabilis* de Mayotte (Océan Indien) s'est révélé être une source extraordinairement riche d'une grande variété de stéroïdes particuliers appartenant à la famille des 5α,8α-épidioxy stérols. Dix épidioxy stérols ont été identifiés: 5α,8α-épidioxycholesta-6,22-dien-3β-ol, 5α,8α-épidioxycholest-6-en-3β-ol, 5α,8α-épidioxy-24(ξ)-methylcholesta-6,22-dien-3β-ol, 5α,8α-épidioxy-24(*S*)-methylcholest-6-en-3β-ol et son épimère (24*R*), 5α,8α-épidioxy-24(*S*)-ethylcholesta-6,22-dien-3β-ol et son épimère (24*R*), 5α,8α-épidioxy-24(*S*)-ethylcholest-6-en-3β-ol et son épimère (24*R*), ainsi que le 5α,8α-épidioxy-24(ξ)-methylcholesta-6,9(11),22-trien-3β-ol. Leurs structures ont été déterminées par résonance magnétique nucléaire (^{1}H, ^{13}C) et par spectrométrie de masse en impact électronique. Le mélange des 10 stéroïdes a montré une activité inhibitrice sur le virus de la leucémie–lymphome à cellules-T humain de type I (HTLV-I) et possède également une activité cytotoxique sur les cellules cancéreuses humaines du sein (MCF_7WT).

Mots clés : *Luffariella cf. variabilis*, éponge marine, 5α,8α-épidioxy stérols, activités antitumorale et antivirale.

Marine organisms are an established source of a great diversity of unconventional sterols with unusual functionalization, unique side chains, and nuclei. Several of these steroids, notably those with multiple oxygen functionalities, exhibited a broad range of activities (1, 2). During our ongoing program to isolate novel antiviral and antitumor marine natural products, the lipidic fraction of the sponge *Luffariella cf. variabilis* (family: Thorectidae, order: Dictyoceratida) collected on the coasts of Mayotte Island (Indian Ocean) has been investigated. Although the conventional 3β-hydroxysteroids were totally absent, the crude lipidic extract contained a mixture of 10 bioactive 5α,8α-epidioxy sterols (Fig. 1). In the present paper, we report the isolation and the structure elucidation of these 5α,8α-epidioxy sterols which contain a variety of side chains. This group of steroids with oxygenated functionalities in the nucleus, constitutes a long-recognized class of metabolites isolated from marine organisms such as sponges (3–10), tunicates (6, 11, 12), sea hares (6, 13), gorgonians (14), sea anemones (15), mussels (11, 16), and other marine specimens (12, 16, 17, 18). However, this is the first time that they have been isolated from a sponge of the genus *Luffariella*, and that attention is called to their potential antiviral and antitumor activities.

The crude lipidic extract (2.5%, dry weight of the sponge) of *L. cf. variabilis* collected by SCUBA off the coasts of Mayotte, Indian Ocean, was subjected to the purification procedure as outlined in the Experimental section. The final separation using high-pressure liquid chromatography (HPLC) yielded five fractions (Fig. 2) containing 10 5α,8α-epidioxy sterols (**1**–**10**) (Fig. 1). They were readily identified

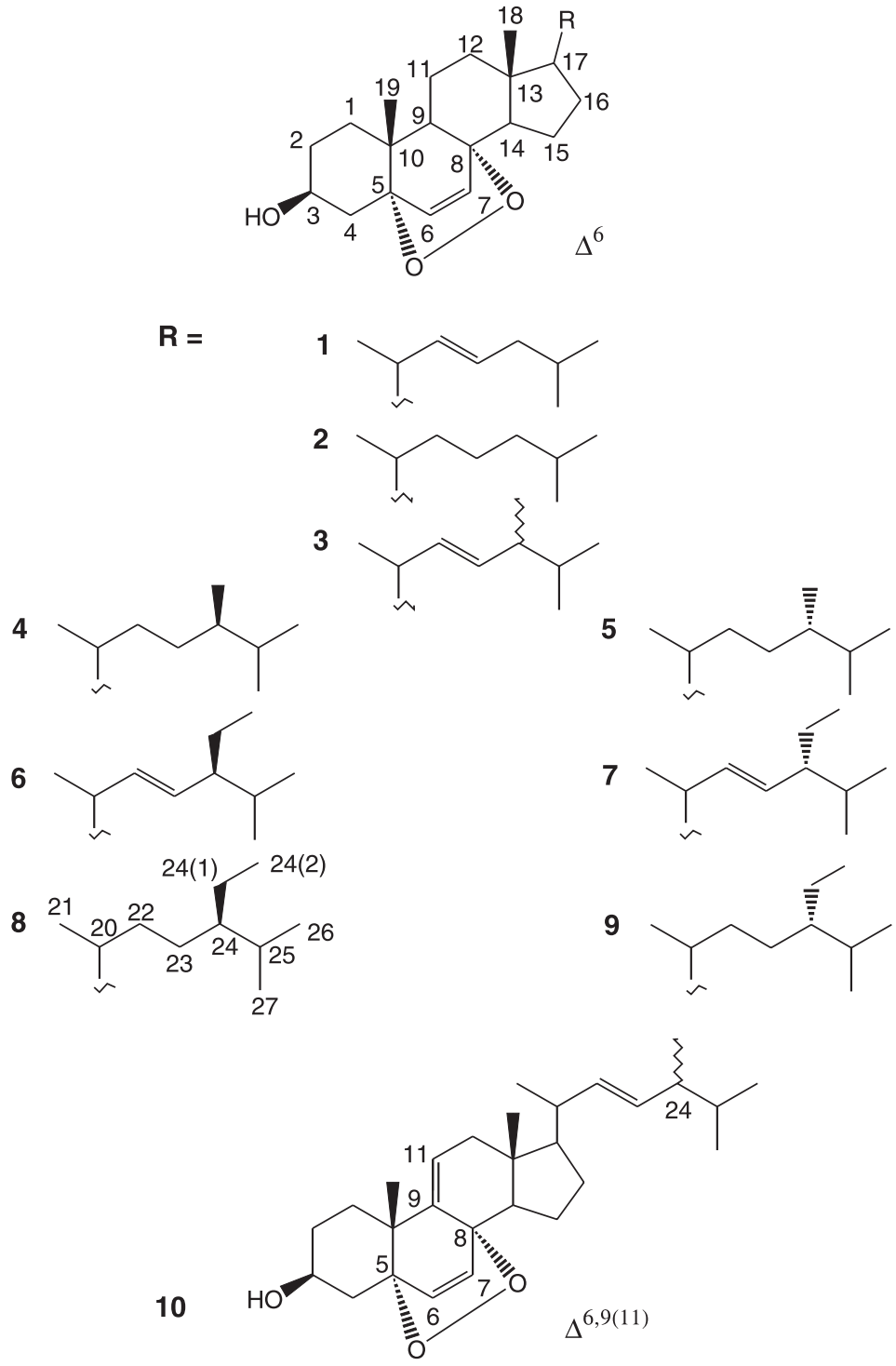
Received December 22, 1999. Published on the NRC Research Press website on July 6, 2000.

A. Gauvin[1], J. Smadja, and M. Aknin. Laboratoire de Chimie des Substances Naturelles et des Sciences des Aliments, Faculté des Sciences et Technologies, Université de La Réunion, 15, Avenue René Cassin, B.P. 7151, 97715 Saint-Denis Messag. CEDEX 9, Reunion, D.O.M. France.
R. Faure and E.-M. Gaydou. Laboratoire de Phytochimie, Faculté des Sciences et Techniques de Saint-Jérôme, Université d'Aix-Marseille III, Avenue Escadrille Normandie-Niémen, 13397 Marseille CEDEX 20, France.

[1]Author to whom correspondence may be addressed. Telephone: 33–262 93 81 85 or 33–262 93 81 97. Fax: 33–2 62 93 81 83. e-mail: gauvin@iremia.univ-reunion.fr

 © 2000 NRC Canada

Fig. 1. 5α,8α-Epidoxy sterols isolated from *L. cf. variabilis.*

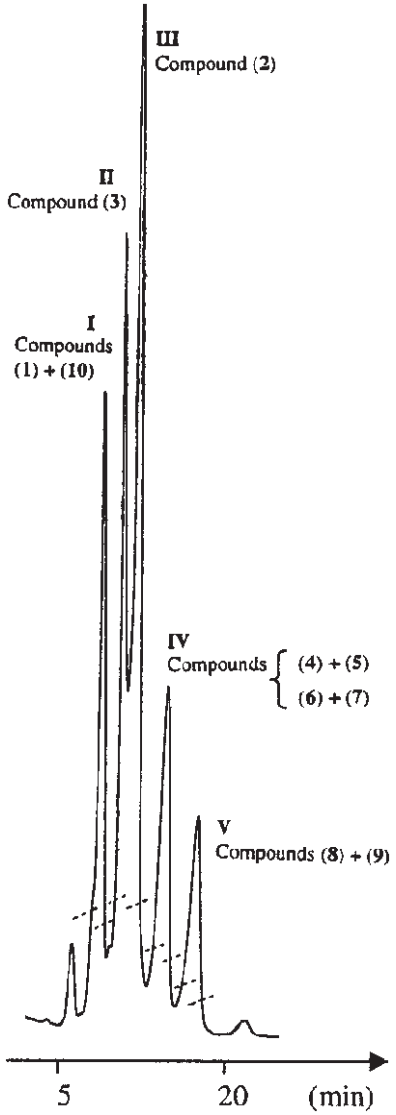


in fractions I–V by chromatographic and spectroscopic methods and by comparison with spectral data given in the literature (6, 18, 19). Chemical shifts of proton and carbon resonances of **1**–**10** are respectively given in Table 1 and Table 2; their mass spectra are summarized in Table 3.

Compounds **1**–**9** are characterized by having a steroid nucleus (19 carbon atoms) possessing an endocyclic double bond between the carbons C-6 and C-7, and a peroxy group between the carbons C-5 and C-8. Only the differences in the side chain structures enable the nine compounds to be distinguishable. Two of them (**1**, **2**) have a cholestane skeleton, three others (**3**, **4**, **5**) possess an ergostane skeleton and the last four (**6**, **7**, **8**, **9**) have a stigmastane skeleton. Components **1**, **3**, **6**, and **7** possess a double bond between the carbons C-22 and C-23. The molecular formulas of the epidioxy sterols were determined from the electron impact mass spectra (EIMS) of the five fractions isolated by HPLC. Each of their spectra also displayed an intense ion (M^+-O_2)

© 2000 NRC Canada

Fig. 2. High-performance liquid chromatography of the 5α,8α-epidoxy sterols mixture isolated from the marine sponge *L. cf. variabilis* on a Merck LiChrospher RP-18 column (Darmstadt, Germany; 25 cm × 4 mm i.d.) with 3% aqueous methanol as mobile phase. Elution conditions are given in the Experimental section. Fractions I–V were retrieved as indicated by the dotted lines.



due to the loss of O_2 from the molecular ion, presumably by a retro Diels–Alder fragmentation (6) providing support for the presence of the peroxy group. The presence of this group was also suggested by ^{13}C NMR signals around δ 79.5 (C-8) and 82.2 (C-5) due to quaternary carbons each bearing an oxygen atom. The Δ^6 unsaturation was determined by the ^1H NMR and ^{13}C NMR spectra: H-6 and H-7 were found as a doublet (J = 8.5 Hz) around δ 6.2 and 6.4, respectively, and the chemical shifts of C-6 and C-7 were observed around δ 135.6 and 130.9, respectively. The chemical shifts and AB coupling patterns of the olefinic protons are also indicative of a 5α,8α-epidioxy orientation. The H-6 and H-7 protons are usually found at around δ 6.5 and 6.3, respectively in 5α,8α-epidioxy systems and at δ 5.9 and 5.6 in 5β,8β-epidioxy systems (18). The ^1H NMR signal at δ 3.95 was assigned to H-3, indicating that an hydroxyl group is attached to the C-3 position. The NMR spectra were also useful in characterizing the side chains present in these epidioxy sterols. The Δ^{22} unsaturation in particular was determined for compounds **1**, **3**, **6**, and **7**, by the olefinic proton signals between δ 5.10–5.29 and 5.00–5.17 assigned to H-22 and H-23, respectively. It was also confirmed by ^{13}C NMR signals between δ 137.72–135.52 and 127.03–132.56 due to C-22 and C-23, respectively. Moreover, differences in the chemical shifts of the side chain carbons permitted the determination of the absolute configuration at C-24 for steroids **4**–**9**. Wright et al. (19) have shown indeed that the chemical shift data obtained for the side chain carbons of diastereoisomeric model steroids epimeric at C-24 are insensitive to structural changes remote from the asymetric centre. Thus, the absolute configuration at C-24 for **4**–**9** was deduced by comparing the chemical shifts of their side chain carbons with those given by Wright et al. (19) for several C-24 alkyl 3β-hydroxysterols. Also, as the spin-lattice relaxation times of corresponding carbons in the two epimeric side chains are very similar (19), the composition of mixtures of stereoisomers was obtained from the relative intensities of corresponding carbon signals. So, we found a mixture of 90:10 for the C-24 epimers **4** and **5**, 50:50 for **6** and **7**, and 50:50 for **8** and **9**. ^1H NMR and ^{13}C NMR spectra of fraction II revealed the presence of only one C-24 epimer of the 24-methylepidioxysterol (**3**). However, the absolute configuration at C-24 could not be determined without ambiguity because the chemical shifts of the side chain carbons were not similar enough to those given in the literature (19) for the epimers 24(*R*) or 24(*S*). Therefore, because of these only slight chemical shift differences, we preferred not to assign the stereochemistry at C-24 for compound **3**.

Another minor steroid, 5α,8α-epidioxy-(24ξ)-methylcholesta-6,9(11),22-trien-3β-ol (**10**), (Fig. 1) was also detected along with **1** in fraction I (Fig. 2). This steroid is characterized by a diunsaturated nucleus $\Delta^{6,9(11)}$ and an ergostane side chain having a Δ^{22} unsaturation. As with the nine previously described epidioxy sterols, the Δ^6 unsaturation of **10** was detected by the presence of the two mutually coupled ^1H signals at δ 6.27 (d, J = 8.5 Hz) and δ 6.58 (d, J = 8.5 Hz) due to the olefinic protons H-6 and H-7 respectively. However, the ^{13}C signals of C-6 and C-7, probably concealed by those of compound **1** were not detected. The presence of $\Delta^{9(11)}$ unsaturation was assumed from the ^1H NMR; a doublet of doublet at δ 5.40 was assigned to H-11. In the ^{13}C NMR spectrum, the chemical shifts of C-11 and C-9 at δ 119.80 and 142.60, respectively, was consistent with the presence of a $\Delta^{9(11)}$ unsaturation. Location of the double bond at position 22 was achieved by ^{13}C NMR signals at δ 135.50 (C-22) and 134.40 (C-23). Also, the methyl region of the ^1H NMR spectrum showed a doublet (J = 6.7 Hz) at δ 0.90 suggesting a 24-methyl side chain. However, further investigations are necessary for complete structure elucidation. Indeed, the weak intensity of ^1H and ^{13}C NMR signals prevented the determination of the C-24 stereochemistry.

The determination of relative retention times by HPLC (Table 4) allowed us to confirm NMR and EIMS results by comparison with those given by the literature (6).

© 2000 NRC Canada

Table 1. ^{1}H (400 MHz) NMR chemical shifts[a] ($CDCl_3$) of the 5α,8α-epidioy sterols **1**–**10** isolated from *L. cf. variabilis*.

Position	1	2	3	4/5	6/7	8/9	10
3	3.95 (m)	3.94 (m)	3.95 (m)	3.95 (m)	3.95 (m)	3.95 (m)	
6	6.22 (d, 8.5)	6.22 (d, 8.5)	6.22 (d, 8.5)	6.22 (d, 8.5)	6.22 (d, 8.5)	6.22 (d, 8.5)	6.27 (d, 8.5)
7	6.48 (d, 8.5)	6.45 (d, 8.5)	6.48 (d, 8.5)	6.48 (d, 8.5)	6.48 (d, 8.5)	6.48 (d, 8.5)	6.58 (d, 8.5)
11							5.40 (dd, 2.0, 6.0)
18	0.79 (s)	0.77 (s)	0.79 (s)	0.78 (s)	0.78 (s)	0.78 (s)	0.79 (s)
19	0.86 (s)	0.85 (s)	0.86 (s)	0.86 (s)	0.86 (s)	0.86 (s)	1.07 (s)
21	0.97 (d, 6.5)	0.87 (d, 6.5)	0.97 (d, 6.6)	0.99 (d, 6.1)	0.99 (d, 6.1)	0.89 (d, 6.5)	0.97 (d, 6.6)
22	5.29 (dd, 7.0, 15.1)		5.17 (dd, 7.5, 15.2)		5.10 (dd, 8.4, 15.2)		
23	5.17 (dt, 8.4, 15.1)		5.11 (dd, 7.8, 15.2)		5.00 (dd, 8.6, 15.2)		
24(1)			0.89 (d, 6.8)	0.89 (d, 6.6)			0.90 (d, 6.7)
24(2)					0.80 (m)	0.83 (t, 7.4)	
26	0.83 (d, 6.6)	0.83 (d, 6.6)	0.79 (d, 7.0)	0.82 (d, 6.2)	0.75 (d, 6.2)	0.80 (d, 6.7)	0.88 (d, 6.4)
27	0.84 (d, 6.6)	0.84 (d, 6.6)	0.81 (d, 7.2)	0.83 (d, 7.2)	0.76 (d, 6.8)	0.81 (d, 6.8)	0.89 (d, 6.8)

[a]Multiplicities and *J* values (Hz) are given in parenthesis.

Discussion

Many sponges belonging to the order Dictyoceratida (20) are characterized by a very low sterol content. This usually coincides with high content of terpenes indicative of a metabolic shift in this group which favours the continued head-to-tail fusion of isoprene units rather than an enzymatic mechanism for converting two farnesyl pyrophosphate units tail-to-tail to form a sterol precursor. It is nevertheless noteworthy that in *L. cf. variabilis*, the lack of 3β-hydroxysterols seems to be compensated by a high amount of 5α,8α-epidioxy sterols. The precise origin of 5α,8α-epidioxy sterols in marine organisms has not yet been identified. Because of the easy conversion of $\Delta^{5,7}$-sterols into their epidioxides, naturally isolated sterol peroxydes could first be suspected to be artifacts. The conjugated diene system in $\Delta^{5,7}$-sterols is unstable and can easily be oxidized during storage and (or) experiments. Elenkov and co-workers (10) investigated the autooxidation of native $\Delta^{5,7}$-sterols to 5α,8α-epidioxy sterols in the Black Sea sponge *Dysidea fragilis*. They showed that after a rapid extraction and analysis, $\Delta^{5,7}$-sterols are the main constituents of *D. fragilis* sterols and only traces of 5α,8α-epidioxy sterols are present. The crude extract was then stored. After a month, only a low concentration of $\Delta^{5,7}$-sterols remained with a higher concentration of 5α,8α-epidioxy sterols being found, and after three months, no $\Delta^{5,7}$-sterols were detected.

In the present study, we think that the artifactual origin of epidioxides in *L. cf. variabilis* can be excluded. The sponge was indeed rapidly extracted and immediately analyzed by thin layer chromatography showing without ambiguity, the presence of 5α,8α-epidioxy sterols. Moreover, no corresponding $\Delta^{5,7}$-sterols were encountered. In agreement with the findings of others (6, 21) it is felt that the 5α,8α-epidioxy sterols could also be native metabolites. This was confirmed by Serebryakov et al. (21) who isolated these steroids from fungi in the absence of oxygen. Several hypotheses were suggested concerning their biological function in marine organisms and notably that they may act as substrates for various enzyme systems. For example, the cooccurence of epidioxy sterols and $\Delta^{4,7}$-3,6-diketones in the marine sponge *Raphidostila incisa* has led to the proposal that epidioxy sterols may be biosynthetic precursors for the latter group of compounds (5). 5α,8α-Epidioxy sterols could also be biogenetic precursors of polyhydroxylated sterols in *Dysidea* species (10). The isolation of polyketide peroxides from a number of marine sponges of the genus *Plakortis* suggests the possible occurrence of peroxydase enzymes in these organisms (22). The above-mentioned metabolic transformations of epidioxides however are postulated on the basis of the feasibility of certain reactions that proceed well in vitro and on the coexistence in the same animal of epidioxides with those end products. There is no evidence to confirm the suggested hypotheses. Undoubtedly, epidioxy sterols remain an unusual and biosynthetically intriguing group of marine sterols which merits additional biosynthetic investigation.

On the assumption that sponges, which include 5α,8α-epidioxy sterols in their lipid content, have a common (or similar) and specific enzyme system(s), it would have been possible to use these steroids for a chemotaxonomic study. However, this taxonomic consideration turned out to be difficult because it has been found that, in addition to *L. cf. variabilis*, 5α,8α-epidioxy sterols were isolated from seven sponges of completely different genera, families and orders: *(i) Axinella cannabina* (3); (*ii*) *Tethya aurantia* (4); *(iii) Raphidostila incisa* (5); (*iv*) *Thalysias juniperina* (6); (*v*) *Haliclona rubens* (7); (*vi*) *Hyrtios* sp. (8); (*vii*) *Axinissa* sp. (9); and (*viii*) *D. fragilis* (10), and we therefore concluded that contrary to the 3β-hydroxysterols, 5α,8α-epidioxy sterols are not of some chemotaxonomic value. Thus, we were led to think that the metabolites may rather be produced by common symbiotic microorganisms. However, this is one further hypothesis which also requires further investigations as well.

Biological assays

Since the crude lipidic extract of *L. cf. variabilis* was found in a preliminary test (23), to be toxic for the brine shrimp *Artemia salina* (LD_{50} = 50 μg mL^{-1}), the mixture of the 10 5α,8α-epidioxy sterols was submitted to a series of antiviral and antitumoral assays. The metabolites displayed a significant and selective activity against the human T-cell leukemia–lymphotropic virus type I (HTLV-I) which is the cause of both a hematopoietic malignancy and adult T-cell leukemia–lymphoma (24). The reduction until 50% of

© 2000 NRC Canada

Table 2. ^{13}C (100 MHz) NMR chemical shifts ($CDCl_3$) of the 5α,8α-epidioy sterols **1**–**10** isolated from *L. cf. variabilis*.

Position	1	2	3	4	5	6	7	8	9	10
1	34.89 (CH_2)	34.74 (CH_2)	34.83 (CH_2)	34.76 (CH_2)	34.76 (CH_2)	34.76 (CH_2)	34.76 (CH_2)	34.75 (CH_2)	34.75 (CH_2)	
2	30.31 (CH_2)	30.16 (CH_2)	30.26 (CH_2)	30.19 (CH_2)	30.19 (CH_2)	30.19 (CH_2)	30.19 (CH_2)	30.16 (CH_2)	30.16 (CH_2)	
3	66.56 (CH)	66.52 (CH)	66.58 (CH)	66.54 (CH)	66.54 (CH)	66.54 (CH)	66.54 (CH)	66.52 (CH)	66.52 (CH)	
4	37.12 (CH_2)	37.00 (CH_2)	37.08 (CH_2)	37.01 (CH_2)	37.01 (CH_2)	37.01 (CH_2)	37.01 (CH_2)	37.00 (CH_2)	37.00 (CH_2)	
5	82.25 (C)	82.24 (C)	82.25 (C)	82.22 (C)	82.22 (C)	82.22 (C)	82.22 (C)	82.24 (C)	82.24 (C)	82.80 (C)
6	135.62 (CH)	135.46 (CH)	135.52 (CH)	135.46 (CH)	135.46 (CH)	135.46 (CH)	135.46 (CH)	135.46 (CH)	135.46 (CH)	
7	130.94 (CH)	130.83 (CH)	130.86 (CH)	130.83 (CH)	130.83 (CH)	130.83 (CH)	130.83 (CH)	130.83 (CH)	130.83 (CH)	
8	79.52 (C)	79.54 (C)	79.52 (C)	79.52 (C)	79.52 (C)	79.49 (C)	79.49 (C)	79.54 (C)	79.54 (C)	79.52 (C)
9	51.27 (CH)	51.10 (CH)	51.25 (CH)	51.14 (CH)	51.14 (CH)	51.14 (CH)	51.14 (CH)	51.10 (CH)	51.10 (CH)	142.60 (CH)
10	37.12 (C)	37.00 (C)	37.08 (C)	37.01 (C)	37.01 (C)	37.01 (C)	37.01 (C)	37.00 (C)	37.00 (C)	
11	23.60 (CH_2)	23.46 (CH_2)	23.52 (CH_2)	23.48 (CH_2)	23.48 (CH_2)	23.48 (CH_2)	23.48 (CH_2)	23.48 (CH_2)	23.48 (CH_2)	119.80 (CH_2)
12	39.53 (CH_2)	39.49 (CH_2)	39.56 (CH_2)	39.49 (CH_2)	39.49 (CH_2)	39.42 (CH_2)	39.42 (CH_2)	39.49 (CH_2)	39.49 (CH_2)	
13	44.66 (C)	44.80 (C)	44.68 (C)	44.61 (C)	44.61 (C)	44.79 (C)	44.79 (C)	44.80 (C)	44.80 (C)	
14	51.88 (CH)	51.63 (CH)	51.84 (CH)	51.64 (CH)	51.64 (CH)	51.76 (CH)	51.76 (CH)	51.63 (CH)	51.63 (CH)	
15	20.84 (CH_2)	20.68 (CH_2)	20.78 (CH_2)	20.69 (CH_2)	20.69 (CH_2)	20.77 (CH_2)	20.77 (CH_2)	20.68 (CH_2)	20.68 (CH_2)	
16	28.95 (CH_2)	28.32 (CH_2)	28.98 (CH_2)	28.27 (CH_2)	28.27 (CH_2)	29.05 (CH_2)	28.95 (CH_2)	28.32 (CH_2)	28.32 (CH_2)	
17	56.30 (CH)	56.46 (CH)	56.31 (CH)	56.34 (CH)	56.34 (CH)	56.21 (CH)	56.21 (CH)	56.36 (CH)	56.36 (CH)	
18	13.05 (CH_3)	12.69 (CH_3)	12.96 (CH_3)	12.69 (CH_3)	12.69 (CH_3)	12.51 (CH_3)	12.30 (CH_3)	12.69 (CH_3)	12.69 (CH_3)	
19	18.38 (CH_3)	18.24 (CH_3)	18.27 (CH_3)	18.23 (CH_3)	18.23 (CH_3)	18.23 (CH_3)	18.23 (CH_3)	18.24 (CH_3)	18.24 (CH_3)	
20	39.87 (CH)	35.29 (CH)	39.87 (CH)	35.40 (CH)	35.70 (CH)	40.09 (CH)	40.03 (CH)	36.01 (CH)	36.01 (CH)	
21	20.96 (CH_3)	18.64 (CH_3)	21.02 (CH_3)	18.63 (CH_3)	18.82 (CH_3)	21.16 (CH_3)	20.98 (CH_3)	18.71 (CH_3)	18.71 (CH_3)	
22	137.65 (CH)	36.00 (CH_2)	135.52 (CH)	33.57 (CH_2)	33.57 (CH_2)	137.72 (CH)	137.67 (CH)	34.75 (CH_2)	34.75 (CH_2)	135.50 (CH_2)
23	127.03 (CH)	23.86 (CH_2)	132.56 (CH)	30.34 (CH_2)	30.62 (CH_2)	129.97 (CH)	130.02 (CH)	26.11 (CH_2)	26.13 (CH_2)	134.40 (CH_2)
24	42.11 (CH_2)	39.49 (CH_2)	43.15 (CH)	38.87 (CH)	39.10 (CH)	51.29 (CH)	51.24 (CH)	45.86 (CH)	46.10 (CH)	
24(1)			18.27 (CH_3)	15.43 (CH_3)	15.51 (CH_3)	25.42 (CH_2)	25.42 (CH_2)	23.11[a] (CH_2)	23.05[a] (CH_2)	
24(2)						12.92 (CH_3)	12.92 (CH_3)	12.38[b] (CH_3)	12.04[b] (CH_3)	
25	28.74 (CH)	28.06 (CH)	33.31 (CH)	32.47 (CH)	31.51 (CH)	31.92 (CH)	31.86 (CH)	29.20 (CH)	28.99 (CH)	
26	22.48 (CH_3)	22.62 (CH_3)	20.22 (CH_3)	20.26 (CH_3)	17.66 (CH_3)	21.22 (CH_3)	18.76 (CH_3)	19.89 (CH_3)	19.03[c] (CH_3)	
27	22.54 (CH_3)	22.89 (CH_3)	19.75 (CH_3)	18.28 (CH_3)	20.56 (CH_3)	19.00 (CH_3)	21.18 (CH_3)	18.76[c] (CH_3)	19.66 (CH_3)	

[a]Assignments may be interchanged.

[b]Assignments may be interchanged.

[c]Assignments may be interchanged.

© 2000 NRC Canada

Table 3. Mass spectral data of the 5α,8α-epidioxy sterols **1**–**10** isolated from *L. cf. variabilis*.

Compound	Major fragment ions (*m*/*z*) (% relative abundance)
1	414 (M^+, 38), 396 (M-H_2O, 22), 382 (M-O_2, 100), 349 (M-H_2O-O_2-CH_3, 25), 323 (M-O_2-C_3H_7O, 10), 303 (M-side chain, 10), 301 (M-side chain-2H, 12)
2	416 (M^+, 37), 398 (M-H_2O, 46), 384 (M-O_2, 97), 351 (M-H_2O-O_2-CH_3, 26), 325 (M-O_2-C_3H_7O, 12), 303 (M-side chain, 6), 301 (M-side chain-2H, 5)
3	428 (M^+, 37), 410 (M-H_2O, 35), 396 (M-O_2, 100), 363 (M-H_2O-O_2-CH_3, 24), 337 (M-O_2-C_3H_7O, 8), 303 (M-side chain, 17), 301 (M-side chain-2H, 19)
4/**5**	430 (M^+, 24), 412 (M-H_2O, 60), 396 (M-O_2, 100), 365 (M-H_2O-O_2-CH_3, 28), 339 (M-O_2-C_3H_7O, 12), 303 (M-side chain, 17), 301 (M-side chain-2H, 18)
6/**7**	442 (M^+, 30), 424 (M-H_2O, 33), 410 (M-O_2, 100), 377 (M-H_2O-O_2-CH_3, 41), 351 (M-O_2-C_3H_7O, 12), 303 (M-side chain, 18), 301 (M-side chain-2H, 19)
8/**9**	444 (M^+, 35), 426 (M-H_2O, 63), 412 (M-O_2, 67), 379 (M-H_2O-O_2-CH_3, 22), 353 (M-O_2-C_3H_7O, 9), 303 (M-side chain, 7), 301 (M-side chain-2H, 4)
10	426 (M^+)

Table 4. Composition and HPLC relative retention times of 5α,8α-epidioxy sterols from *L. cf. variabilis*.

Compound	Composition[a] (%)	Relative retention times[b]	
		Exp.[c]	Lit. (6)[d]
(**10**)	18.0	0.74	0.71
(**1**)			0.77
(**3**)	19.5	0.89	0.89
(**2**)	36.6	1.00	1.00
(**4**) + (**5**)	13.3	1.15	1.14
(**6**) + (**7**)			1.16
(**8**) + (**9**)	9.4	1.37	1.36

[a]Quantification of the 5α,8α-epidioxy sterols was based on the area of the HPLC peaks.

[b]Compound **2** has been used as standard for relative retention times.

[c]Obtained on a Merck LiChrospher RP-18 column (25 cm × 4 mm i.d.) with 3% aqueous methanol as mobile phase.

[d]Obtained on a Whatmann Partisil M9 10/50 ODS-2 column (50 cm × 9 mm i.d.) with 8% aqueous methanol as mobile phase.

β-galactosidase whose production is directly related to HTLV-I activity, was observed for a concentration of 0.3 mg mL^{-1}. As far as is known, 5α,8α-epidioxy sterols are the first natural products showing in vitro potency against the HTLV-I virus. Thus, they could be promising agents in the research on natural compounds for therapeutical interventions. These steroids were also assayed on the human imunodeficiency virus (HIV). However, no inhibitory activity was observed. Finally, the mixture was screened for in vitro cytotoxicity against the human breast cancer cell line (MCF_7WT) and 87% inhibition was observed at a concentration of 80 μg mL^{-1}. Other assays are in progress to precisely acscertain the antiviral and antitumor activity of each individual epidioxy sterol isolated in useful quantities. The antiviral (HTLV-I, HIV) and antitumoral assays were performed as described previously (25).

Experimental section

General experimental procedures

All solvents were redistilled before use. Column chromatographic separations were performed on silica gel (Merck, Darmstadt, Germany; type 60, 70–230 or 230–400 Mesh) as the adsorbent. Nuclear magnetic resonance spectra were recorded on a Brucker AMX-400 (Karlsruhe, Germany) in $CDCl_3$, at 400.13 MHz for ^1H NMR spectra and at 100.11 MHz for ^{13}C NMR spectra. Chemical shifts are given in ppm relative to tetramethylsilane as internal standard. Electron impact mass spectra were obtained on a Jeol AX-500 mass spectrometer (Tokyo, Japan) with a source temperature of 200°C and ionization energy of 70 eV. High-pressure liquid chromatography was performed on a Spectraseries P100 (California, U.S.A.) equipped with a Rheodyne injector, a differential refractometer (California, U.S.A.; Thermoseparation products) and a Merck LiChrospher RP-18 column (Darmstadt, Germany ; 25 cm × 4 mm i.d., 5 μm).

Animal material

The sponge sample was collected by SCUBA at a depth between 10–40 m in Passe Longogori (Mayotte Island, northwest of Madagascar, Indian Ocean). The sample was immediately frozen at –20°C and kept in a freezer until extraction. The sponge was identified as *L. cf. variabilis* (Family: Thorectidae, order: Dictyoceratida) by Dr. N. Boury-Esnault (Station Marine d'Endoume, Marseille, France) and Pr. Dr. P. Bergquist (School of Biological Sciences, Auckland, New Zealand). A voucher specimen has been deposited at the Laboratoire de Chimie des Substances Naturelles et des Sciences des Aliments of the Reunion University (Reunion Island, D.O.M, France) under the reference AGL-2–97M.

Extraction and isolation

Frozen sponge tissue (1343 g, dry weight) was cut up and homogenized in a Waring blender in methanol–chloroform (1:2, v/v). After filtration, the solvent was removed under reduced pressure to give the crude material (33.4 g). This lipidic extract was then partitioned between *n*-hexane and 10% aqueous methanol to yield after evaporation of the solvent, 17.1 g of *n*-hexane residue. A part of the *n*-hexane residue (4.8 g) was chromatographed on silica gel (70–230 Mesh) column eluted with a gradient of *n*-hexane–ethyl acetate (5% stepwise elution from *n*-hexane to ethyl acetate). The mixture of 5α,8α-epidioxy sterols eluted with *n*-hexane–ethyl acetate (9:1, v/v) was further purified by chromatography with *n*-hexane–ethyl acetate (9:1, v/v) on silica gel (230–400 Mesh) and isolated as white crystals (59 mg) after

© 2000 NRC Canada

precipitation in *n*-hexane. This fraction was separated by reverse-phase HPLC (1 mL min^{-1} elution with 3% aqueous methanol) to give five fractions I–V (Fig. 2) which respectively contained 5 mg of a mixture of **1** + **10**, 16 mg of **3**, 5 mg of **2**, 4 mg of a mixture of **4** + **5** (90:10, relative % of the epimeric pair) and **6** + **7** (50:50) and 5 mg of a mixture of **8** + **9** (50:50).

Acknowledgements

The authors are grateful to Dr. N. Boury-Esnault and to Pr. Dr. P. Bergquist for the identification of the sponge. The authors also thank the Laboratoire de Chimie Bio-organique de l'Université de Bordeaux II (Bordeaux, France), the Institut National de la Santé et de la Recherche Médicale (INSERM), Fondation Bergognié (Bordeaux, France), the Laboratoire de Virologie, Hôpital Pellegrin (Bordeaux, France) and the Laboratoire de Pharmacologie des médicaments anticancéreux, Fondation Bergonié (Bordeaux, France) for biological assays.

References

1. D.J. Faulkner. Nat. Prod. Rep. **15**, 113 (1998) and preceding papers in the series.
2. R.G. Kerr and B.J. Baker. Nat. Prod. Rep. **8**, 465 (1991).
3. E. Fattorusso, S. Magno, C. Santacroce, and D. Sica. Gazz. Chim. Ital. **104**, 409 (1974).
4. Y.M. Sheikh and C. Djerassi. Tetrahedron, **30**, 4095 (1974).
5. A. Malorni, L. Minale, and R. Riccio. Nouv. J. Chim. **2**, 351 (1978).
6. A.A.L. Gunatilaka, Y. Gopichand, F.J. Schmitz, and C. Djerassi. J. Org. Chem. **46**, 3860 (1981).
7. J.S. Calderon, L. Quijano, F. Gomez, F. Acosta, and T. Rios. Rev. Latinoam. Quim. **13**, 49 (1982).
8. P. Koch, C. Djerassi, V. Lakshmi, and F.J. Schmitz. Helv. Chim. Acta, **66**, 2431 (1983).
9. K. Iguchi, H. Shimura, Z. Yang, and Y. Yamada. Steroids, **58**, 410 (1993).
10. I. Elenkov, T. Milkova, S. Andreev, and S. Popov. Comp. Biochem. Physiol. **107B**, 547 (1994).
11. I. Stoilov, S. Popov, N. Marekov, and St. Andreev. Comp. Biochem. Physiol. **79B**, 225 (1984).
12. C. Jimenez, E. Quinoa, L. Castedo, and R. Riguera. J. Nat. Prod. **49**, 905 (1986).
13. T. Miyamoto, M. Honda, S. Sugiyama, R. Higuchi, and T. Komori. Liebigs Ann. Chem. 589 (1988).
14. S. Pantoja, M. Hoeneisen, J. Becerra, M. Silva, and D.J. Faulkner. J. Nat. Prod. **49**, 357 (1986).
15. J.A. Findlay and A.D. Patil. Steroids, **44**, 261 (1984).
16. I. Stoilov, S. Popov, and St. Andreev. Comp. Biochem. Physiol. **79B**, 493 (1984).
17. C. Jimenez, E. Quinoa, R. Riguera, R. Vilalta, and J.M. Quintela. J. Nat. Prod. **52**, 619 (1989).
18. Y. Seo, J.-R. Rho, and J. Shin. Ocean Res. **18**, 83 (1996).
19. J.L.C. Wright, A.G. McInnes, S. Shimizu, D.G. Smith, J.A. Walter, D. Idler, and W. Khalil. Can. J. Chem. **56**, 1898 (1978).
20. P.R. Bergquist, W. Hofheinz, and G. Oesterhelt. Biochem. Syst. Ecol. **8**, 423 (1978).
21. E. Serebryakov, A. Simolon, V. Kucherov, and B. Rusinov. Tetrahedron, **26**, 5215 (1970).
22. D.B. Stierle and D.J. Faulkner. J. Org. Chem. **45**, 3396 (1980).
23. B.N. Meyer, N.R. Ferrigni, J.E. Putnam, L.B. Jacobsen, D.E. Nichols, and J.L. McLaughlin. Planta Med. **45**, 31 (1982).
24. F. Genoveffa. Blood, **86**, 3619 (1995).
25. A. Gauvin. *In* Etude de Cinq Eponges de l'Océan Indien. Contribution Chimiotaxonomique – Recherche de Molécules Bioactives. Ph.D. Thesis. Reunion University, France. 1998. pp. 243–264; 308–311.

© 2000 NRC Canada

Distribution of microamounts of some M^{2+} ions during $ZnSO_4 \cdot 7H_2O$ crystallization

Marek Smolik

Abstract: Distribution coefficients (*D*) of trace amounts of Ni^{2+}, Co^{2+}, Mg^{2+}, Cd^{2+}, Cu^{2+}, Mn^{2+}, Ca^{2+}, and Fe^{2+} have been determined during crystallization of $ZnSO_4 \cdot 7H_2O$. Their dependencies on the ionic radii of M^{2+} ions, solubilities and structures of the corresponding sulfates as well as their abilities to form solid solutions with $ZnSO_4 \cdot 7H_2O$ have been analyzed. The *D* values are in the range <0.006 (D_{Ca}) – 1.61 (D_{Ni}) and depend mainly on similarity of the structures of the corresponding sulfates and the ability of $MSO_4 \cdot nH_2O$ to form solid solutions with $ZnSO_4 \cdot 7H_2O$. The order of lowering some of the determined distribution coefficients ($D_{Ni} > D_{Mg} > D_{Co} > D_{Fe} > D_{cu}$) exactly agrees with increase of the deformation trend of octahedral coordination of corresponding ions resulting from their electronic configuration. The *D* coefficients do not depend on similarity of size of *ionic radii* of microcomponent ($r_{M^{2+}}$) to macrocomponent ($r_{Zn^{2+}}$), however for ions forming monoclinic sulfate hydrates at 20°C (Co^{2+}, Fe^{2+}, Cd^{2+}, Ca^{2+}) this dependence of distribution coefficients on $r_{M^{2+}}$ is linear in a plot of log *D* against ionic radius. The effect of solubilities of corresponding sulfates in water on the *D* coefficients is complex and clouded by crystal-chemical factors.

Key words: crystallization, zinc(II) sulfate heptahydrate, cocrystallization, distribution coefficients *D* (Henderson-Kraček, Khlopin), distribution of trace impurities.

Résumé : On a déterminé les coefficients de distribution (*D*) de quantités à l'état de traces de Ni^{2+}, Co^{2+}, Mg^{2+}, Cd^{2+}, Cu^{2+}, Mn^{2+}, Ca^{2+} et Fe^{2+} au cours de la cristallisation du $ZnSO_4 \cdot 7H_2O$. On a analysé leurs dépendances sur les rayons ioniques des ions M^{2+}, les solubilités et les structures des sulfates correspondants ainsi que leurs habilités à former des solutions solides avec le $ZnSO_4 \cdot 7H_2O$. Les valeurs de *D* sont comprises entre <0,006 (D_{Ca}) et 1,61 (D_{Ni}) et elles dépendent principalement de la similarité des structures des sulfates correspondants et de l'habilité du $MSO_4 \cdot nH_2O$ à former des solutions solides avec le $ZnSO_4 \cdot 7H_2O$. L'ordre de décroissance de quelques-uns des coefficients de distribution $D_{Ni} > D_{Mg} > D_{Co} > D_{Fe} > D_{Cu}$ est en parfait accord avec une augmentation dans la tendance à la déformation de la coordination tétraédrique des ions correspondants qui résultent de leur configuration électronique. Les coefficients *D* ne dépendent pas de la similarité des tailles des rayons ioniques des microcomposants ($r_{M^{2+}}$) par rapport au macrocomposant ($r_{Zn^{2+}}$); toutefois, pour les ions qui forment des sulfates monocliniques hydratés à 20°C (Co^{2+}, Fe^{2+}, Cd^{2+}, Ca^{2+}) cette dépendance des coefficients de distribution sur $r_{M^{2+}}$ est linéaire lorsqu'on fait une courbe de logD en fonction du rayon ionique. L'effet de la solubilité des sulfates correspondants dans l'eau sur les coefficients D est complexe et il est rendu plus difficile à comprendre en raison de facteurs cristallins et chimiques.

Mots clés : cristallisation, sulfate de zinc(II) heptahydraté, cocristallisation, coefficients de distribution, *D*, (Henderson-Kraček, Khlopin), distribution d'impuretés à l'état de traces.

[Traduit par la Rédaction]

Introduction

Distribution coefficients *D* of microcomponents during crystallization are important indicators of its effectiveness as a purification process. However, the literature data concerning these coefficients are rather scarce. Hence, it seems reasonable to determine the dependence of distribution coefficients on various physicochemical and crystal-chemical factors (such as: ionic charges and radii, similarity of crystal structure and unit cell dimensions, ability to form solid solutions as well as solubilities of corresponding salts), which would allow to predict the values of *D* coefficients for various crystallization systems which have not been investigated so far.

The effect of each of these factors on the *D* coefficients may be predominant for various crystallization systems and as shown by investigations on cocrystallization of microcomponents in several sulfate systems (triclinic: $CuSO_4 \cdot 5H_2O$ (1) and $MnSO_4 \cdot 5H_2O$ at 20°C (2); monoclinic: $FeSO_4 \cdot 7H_2O$ at 20°C (3), at 5°C and 50°C (4), as well as $MnSO_4 \cdot 7H_2O$ at 2°C (2)) very often these influences overlap. There is a lack of data concerning the effect of these factors on *D* coefficients for crystallization of $ZnSO_4 \cdot 7H_2O$, which is one of orthorhombic sulfate hydrates. Cocrystallization of hydrates of M(II) sulfates with zinc(II) sulfate heptahydrate has been recognized to some extent ($FeSO_4 \cdot 7H_2O$ (5–7), $CoSO_4 \cdot 7H_2O$ (8–9), $NiSO_4 \cdot 7H_2O$ (8, 10–11), $CuSO_4 \cdot 5H_2O$ (5, 10, 13), $MgSO_4 \cdot 7H_2O$ (6, 12),

Received February 22, 1999. Published on the NRC Research Press website on July 6, 2000.

M. Smolik.[1] Institute of Chemistry, Inorganic Technology and Electrochemistry, Silesian Technical University, 44-100 Gliwice, Poland.

[1]Telephone: 048 32 2372815. Fax: 048 32 2372277. e-mail: msmolik@zeus.polsl.gliwice.pl

© 2000 NRC Canada

Table 1. Standard conditions of determination of microcomponents by AAS.

Microcomponent	Lamp	Continuous operating current of lamp (mA)	Wavelength (nm)	Slit (nm)	Flame
Ca	HCL[a]	20	422.7	0.7	C_2H_2–N_2O
Cd	EDL[b]	6 watts (power)	228.8	0.7	C_2H_2–air
Co	HCL	30	240.7	0.2	C_2H_2–air
Cu	HCL	30	324.8	0.7	C_2H_2–air
Fe	HCL	30	248.3	0.2	C_2H_2–air
Mg	HCL	20	285.2	0.7	C_2H_2–air
Mn	HCL	30	279.5	0.2	C_2H_2–air
Ni	HCL	30	232.0	0.2	C_2H_2–air

[a]Hollow cathode lamp.

[b]Electrodeless discharge lamp.

$MnSO_4 \cdot 5H_2O$ (14)). However, these investigations concerned mainly macroamounts (>1%) of the mentioned sulfates. Cocrystallization of microamounts of M^{2+} ions was investigated only in a few cases: (*i*) Co^{2+} (D_{Co} = 1.20 at 20°C) (9); (*ii*) Cu^{2+} (D_{Cu} = 0.16 at 20°C)(13); and *(iii)* Mn^{2+} (D_{Mn} = 0.13 at 20°C)(14)).

The purpose of the present study was to determine distribution coefficients, *D*, of trace amounts (10^{-3}–10^{-1}%) of M^{2+} ions {Fe^{2+}, Co^{2+}, Mn^{2+}, Cu^{2+}, Cd^{2+}, Ni^{2+}, Mg^{2+}, Ca^{2+}} during the crystallization of $ZnSO_4 \cdot 7H_2O$ as well as to identify relations between these coefficients and the mentioned physicochemical and crystal-chemical factors.

Experimental

Reagents and solutions

Zinc(II) sulfate heptahydrate, p.a. was additionally purified by crystallization in the presence of H_2O_2. High-purity zinc(II) sulfate heptahydrate, containing less than 1 ppm of each investigated element obtained in the Institute of Chemistry, Inorganic Technology and Electrochemistry Silesian Technical University (Gliwice). Solutions of Fe(II), Co(II), Mn(II), Cu(II), Cd(II), Ni(II), Mg(II) sulfates, and Ca(II) nitrate of determined concentration were used. Ammonia solution (14 mol/dm^3) was obtained by saturating distilled water with ammonia gas. Sodium versenate p.a. (POCh-Gliwice) – 0.1mole/dm^3 water solution, hydrazine sulfate p.a. (POCh-Gliwice), and eriochrome black T ind. (POCh-Gliwice) were used.

Apparatus

Atomic absorption spectrometer model 3300 manufactured by Perkin–Elmer was applied.

Analytical methods

Determination of the macrocomponent

Zinc(II) was determined by complexometric titration with sodium versenate at pH 10 in the presence of eriochrome black T (15).

Determination of microcomponents

Initial concentrations of microcomponents ([ppm] in relation to $ZnSO_4 \cdot 7H_2O$): (*i*) in supersaturated $ZnSO_4$·solution before crystallization (a'_o) (series 1); (*ii*) in saturated solution "purified" (a'_{ro}) and "contaminated" (a''_{ro}) as well as in $ZnSO_4 \cdot 7H_2O$ crystal "purified" (a''_{ko}) and "contaminated" (a'_{ko}) before long-time stirring (series 2); (*iii*) in samples of crystals (a'_k) and mother solutions (a'_r) after crystallization as well as in actually applied washing solution were determined by means of direct atomic absorption spectrometry (AAS) from solutions containing 1.000 g (or less) of $ZnSO_4 \cdot 7H_2O$ in 25 cm^3. All mentioned samples and sets of standards (prepared on the basis of high-purity zinc(II) sulfate), whose $ZnSO_4$ concentrations were the same, were excited in flame and their absorbance measured under the same conditions, which are presented in Table 1.

Method for determination of coefficients D

After crystallization, the crystals were separated from the mother solution by means of filtration through a Büchner funnel with a sintered glass disk, washed with saturated, purified $ZnSO_4 \cdot 7H_2O$ solution, weighed, and dissolved in water. From the zinc(II) content in both solutions, the degree of $ZnSO_4 \cdot 7H_2O$ crystallization α was found from the following formula

$$\alpha = \frac{m_{Ms}}{m_{Mk} + m_{Mr}}$$

where

m_{Ms} = mass of the macrocomponent ($ZnSO_4 \cdot 7H_2O$) in the solid phase

m_{Mk} = mass of the macrocomponent in the crystal

m_{Mr} = mass of the macrocomponent in the mother solution;

$$m_{Ms} = m_k \frac{C_k - C_r}{100 - C_r}$$

m_k = mass of the crystal

C_k = % of the macrocomponent in the crystal; $(100 - C_k)$ – crystal humidity (%)

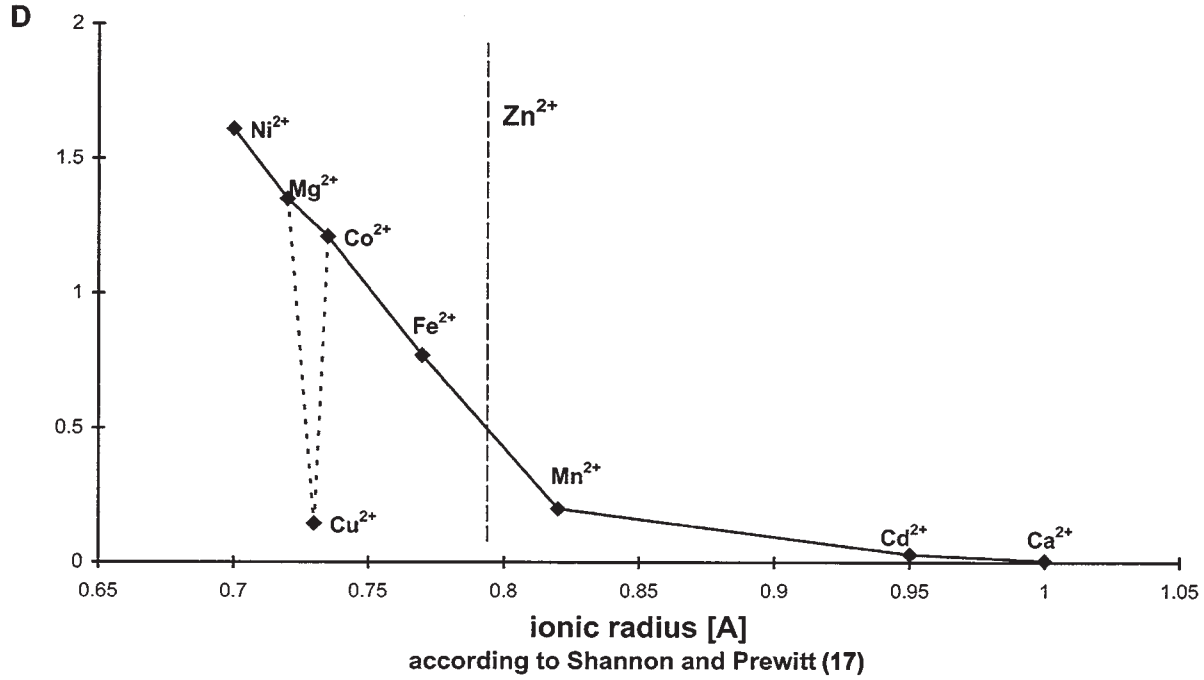
C_r = % of the macrocomponent in the mother solution

and the volumes of the samples necessary to determine the microcomponents were calculated. The concentration was equal to 1.00 g (or less) of $ZnSO_4 \cdot 7H_2O$ in 25 cm^3.

Relative concentrations of microcomponents ([ppm] in relation to $ZnSO_4 \cdot 7H_2O$) in the mother solution (a'_r) and in the washed crystal (a'_k) determined by direct atomic absorption permitted the calculation of homogeneous distribution coefficient (D) (Henderson-Kraček, Khlopin)) from the following relation

© 2000 NRC Canada

Fig. 1. Dependence of distribution coefficients, *D*, of microcomponents, M^{2+}, during $ZnSO_4 \cdot 7H_2O$ crystallization at 20°C on their ionic radii.



$$D = \frac{a'_k}{a'_r}$$

Conditions of crystallization

1. Establishing the effect of initial concentration of microcomponents on their distribution coefficients, (D) during $ZnSO_4 \cdot 7H_2O$ crystallization at 20°C

The 31–33.5% zinc(II) sulfate solutions of different initial concentrations of microcomponents (a'_o) were cooled to temperatures close to 20°C and then poured into several beakers with water jackets and evaporated while stirring with a magnetic stirrer (~250 rpm) at 20 ± 1°C over 16–25 h. In another series the supersaturated (38–42%) zinc(II) sulfate solutions of different initial concentrations of microcomponents (a'_o) containing hydrazine sulfate were cooled to temperatures close to 20°C and poured into several beakers with water jackets. Having been covered with watch glasses, the solutions were stirred (or evaporated while stirring) with a magnetic stirrer (~250rpm) at 20 ± 1°C over 5–25 h. The applied conditions and obtained results are presented in Tables 2 and 3.

2. Determination of equilibrium distribution coefficients (D) of the microcomponents (M^{2+})

To determine the equilibrium distribution coefficients the method of long-time stirring of crushed crystals in saturated solution was applied (16). The equilibrium was reached starting either from initial concentration ratio of a microcomponent in crystal and in solution exceeding expected value of its equilibrium coefficient (D°_{max}) or from this ratio lower than expected value (D°_{min}). When selecting values D°_{max} and D°_{min} the highest and the lowest values of *D* obtained during crystallization of $ZnSO_4 \cdot 7H_2O$ at 20°C (series 1) were taken into consideration. The experiments were carried out in the following way: "contaminated" $ZnSO_4 \cdot 7H_2O$ crystals (a'_{ko}), crushed to pass a 0.1 mm sieve, were introduced into several beakers together with saturated, "purified" zinc(II) sulfate solution (a'_{ro}). Crystals of purified $ZnSO_4 \cdot 7H_2O$ (a''_{ko}) crushed to pass a 0.1 mm sieve and contaminated saturated solution of zinc(II) sulfate (a''_{ro}) were introduced to some other beakers. Each beaker, covered with watch glass, was placed on the water bath in a closed room. Their contents were stirred for ~360 h with magnetic stirrers. Fluctuations of temperature (which happened) facilitated recrystallization of $ZnSO_4 \cdot 7H_2O$ and helped attain equilibrium and homogeneous partition of microcomponents in crystal. These fluctuations were recorded. Mean value of temperature was equal to 23 ± 1°C. The results are presented in Table 4.

Results and discussion

The data presented in Tables 2 and 3 show that distribution coefficients, *D*, of most microcomponents do not depend essentially on their initial concentration (in the given investigated range).

The distribution coefficients of each of the ions M^{2+} {Co^{2+}, Mn^{2+}, Cu^{2+}, Fe^{2+}, Mg^{2+}, Ni^{2+}, and Cd^{2+}} for two series (D°_{max} and D°_{min}) do not differ from each other considerably, which means that the equilibrium condition was reached for them, and average values for both series are equilibrium values (Table 4). For most microcomponents, those values do not differ essentially from *D* values obtained during isothermal lowering supersaturation or isothermal evaporation at 20 ± 1°C (Table 2 and 3).

The determined partition coefficients, *D*, are diverse: from <0.006 for Ca^{2+} to 1.61 for Ni^{2+}. The determined values of

© 2000 NRC Canada

Table 2. Effect of Ni^{2+}, Co^{2+}, Mn^{2+}, and Cu^{2+} initial concentration (a'_o [ppm]) on their distribution coefficients, D during $ZnSO_4 \cdot 7H_2O$ crystallization at 20 ± 1°C. ($\omega \approx 250$ rpm).

Initial concentration of $ZnSO_4$ (wt %)	Time of crystallization (h)	α	Ni^{2+} a'_o	a'_k	a'_r	D_i	$\overline{D} \pm t_{0.05}\frac{s}{\sqrt{n}}$	$\overline{D} \pm t_{0.05}\frac{s}{\sqrt{n}}$	Co^{2+} a'_o	a'_k	a'_r	D_i	$\overline{D} \pm t_{0.05}\frac{s}{\sqrt{n}}$	$\overline{D} \pm t_{0.05}\frac{s}{\sqrt{n}}$
33.5	16	0.095	400	6.00	360	1.67	1.67 ± 0.08		300	360	290	1.24	1.20 ± 0.09	
	16	0.112		610	380	1.61				340	270	1.26		
	25	0.385		520	310	1.68				330	290	1.14		
	25	0.417		500	290	1.72				330	280	1.18		
33.5	16	0.104	200	290	180	1.61	1.61 ± 0.15		150	180	145	1.24	1.24 ± 0.11	
	20	0.228		280	175	1.60				160	140	1.14		
	25	0.435		240	160	1.50				170	130	1.31		
	25	0.452		260	150	1.73				170	135	1.26		
33.5	16	0.114	100	160	95	1.68	1.61 ± 0.18	1.61 ± 0.04	75	87	75	1.21	1.17 ± 0.12	1.21 ± 0.03
	16	0.147		140	95	1.47				80	74	1.08		
	25	0.484		125	80	1.56				78	62	1.26		
	25	0.568		120	70	1.71				80	70	1.14		
31	16	0.072	40	58	39	1.49	1.56 ± 0.08		30	32	28	1.14	1.22 ± 0.10	
	16	0.074		60	38	1.58				35	27	1.30		
	16	0.088		58	36	1.61				36	30	1.20		
	25	0.226		53	34	1.56				35	28	1.25		
			Cu^{2+}						Mn^{2+}					
33.5	16	0.095	300	50	305	0.164	0.159 ± 0.021		90	22	97	0.23	0.21 ± 0.05	
	16	0.112		48	300	0.160				23	100	0.23		
	25	0.385		63	450	0.140				23	130	0.18		
	25	0.417		80	470	0.170				29	135	0.21		
33.5	16	0.104	150	22	160	0.138	0.134 ± 0.014		45	11	48	0.23	0.20 ± 0.04	
	20	0.228		22	165	0.133				11	55	0.20		
	25	0.435		34	280	0.121				12	69	0.17		
	25	0.452		37	260	0.142		0.144 ± 0.010		13	72	0.18		0.20 ± 0.02
33.5	16	0.114	75	13	90	0.144	0.146 ± 0.041		22	6.4	23	0.28	0.21 ± 0.08	
	16	0.147		16	90	0.178				5.4	24	0.23		
	25	0.484		15	130	0.115				6.3	37	0.17		
	25	0.568		19	130	0.146				7.2	41	0.18		
31	16	0.072	30	3.8	32	0.119	0.139 ± 0.033		9	2.0	9.6	0.21	0.20 ± 0.03	
	16	0.074		5.5	33	0.167				1.9	8.8	0.22		
	16	0.088		4.3	30	0.143				2.2	11.0	0.20		
	25	0.226		4.9	38	0.129				1.9	11.0	0.17		

Note: Other definitions: $\overline{D}$, mean value of D; *sd*, standard deviation; *n*, number of determinations; $t_{0.05}$, value of Student *t*-test for n – 1 degrees of freedom and for the confidence level of $1 - \alpha = 0.95$.

© 2000 NRC Canada

Table 3. Effect of Fe^{2+}, Mg^{2+}, Cd^{2+}, and Ca^{2+} initial concentration (a'_o[ppm]) *on their distribution coefficients, D,* during $ZnSO_4 \cdot 7H_2O$ crystallization at 20 ± 1°C. (ω ≈ 250 rpm).

Initial concentration of $ZnSO_4$ (wt %)	Time of crystallization (h)	α	a'_o	a'_k	a'_r	D_i	$\bar{D} \pm t_{0.05}\frac{s}{\sqrt{n}}$	$\bar{D} \pm t_{0.05}\frac{s}{\sqrt{n}}$
			Fe^{2+}					
42	5	0.270	120	93	130	0.72	0.76 ± 0.04	
	5	0.220		97	125	0.78		
	5	0.260		100	130	0.77		
	5	0.250		96	128	0.75		
39	5	0.123	50	37	51	0.73	0.72 ± 0.15	
	5	0.167		37	53	0.70		0.75 ± 0.03
	5	0.136		33	52	0.63		
	5	0.136		41	50	0.82		
39[a]	25	0.410	13	11	14	0.79	0.79 ± 0.08	
	25	0.420		10	13	0.77		
	25	0.482		11	15	0.73		
	25	0.467		12	14	0.86		
			Cd^{2+}					
33.5	16	0.095	40	1.3	50	0.026	0.028 ± 0.003	0.030 ± 0.004
	16	0.112		1.4	46	0.030		
	25	0.385		1.6	62	0.026		
	25	0.417		1.7	60	0.028		
33.5	16	0.104	20	0.7	22	0.032	0.032 ± 0.008	
	20	0.228		0.8	26	0.031		
	25	0.435		1.4	36	0.039		
	25	0.452		1.0	38	0.026		

Initial concentration of $ZnSO_4$ [wt.%]	Time of crystallization [h]	α	a'_o	a'_k	a'_r	D_i	$\bar{D} \pm t_{0.05}\frac{s}{\sqrt{n}}$	$\bar{D} \pm t_{0.05}\frac{s}{\sqrt{n}}$
			Mg^{2+}					
38	5	0.073	23	28	23	1.22	1.31 ± 0.12	
	5	0.116		30	23	1.30		
	5	0.119		29	22	1.32		
	5	0.119		31	22	1.41		
39	5	0.123	7.8	9.9	7.6	1.30	1.35 ± 0.08	
	5	0.136		10.0	7.6	1.32		1.33 ± 0.04
	5	0.136		10.5	7.4	1.42		
	5	0.167		9.8	7.2	1.36		
39[a]	25	0.410	2.6	3.1	2.4	1.29	1.33 ± 0.07	
	25	0.420		2.9	2.2	1.32		
	25	0.467		2.9	2.2	1.32		
	25	0.482		3.2	2.3	1.39		
			Ca^{2+}					
38	5	0.073	50	<0.3	56	<0.006	<0.006	<0.006
	5	0.116		<0.3	53	<0.006		
	5	0.119		<0.3	54	<0.006		
	5	0.119		<0.3	60	<0.005		

Note: Other definitions: $\bar{D}$, mean value of *D*; *sd*, standard deviation; *n*, number of determinations; $t_{0.05}$, value of Student *t*-test for n – 1 degrees of freedom and for the confidence level of 1 – α = 0.95.
[a]Evaporation.

© 2000 NRC Canada

Table 4. Distribution coefficients, D, of microcomponents M^{2+} during long-time (~360 h) stirring of crushed $ZnSO_4 \cdot 7H_2O$ crystals in their saturated solution at average temperature (23 ± 1°C).

Micro-component	Initial concentration of microcomponent		$D^{o}_{min} = \frac{a''_{ko}}{a''_{ro}}$	Concentration of microcomponent after stirring		D_{min}	$\overline{D} \pm t_{0.05}\frac{s}{\sqrt{n}}$	Initial concentration of microcomponent		$D^{o}_{max} = \frac{a'_{ko}}{a'_{ro}}$	Concentration of microcomponent after stirring		D_{max}	$\overline{D} \pm t_{0.05}\frac{s}{\sqrt{n}}$	Average equilibrium distribution coefficient, D
	a''_{ko}	a''_{ro}		a'_{k}	a'_{r}			a''_{ko}	a''_{ro}		a'_{k}	a'_{r}			
Ni^{2+}	280	230	1.22	335	225	1.49	1.52 ± 0.06	270	145	1.86	260	170	1.53	1.62 ± 0.09	1.57 ± 0.06
				330	230	1.43					225	140	1.61		
				300	200	1.50					285	160	1.78		
				320	210	1.52					260	160	1.63		
				340	220	1.55					250	160	1.56		
				340	210	1.62					240	150	1.60		
Cu^{2+}	21	250	0.084	24	200	0.120	0.136 ± 0.018	31	140	0.22	23	140	0.164	0.152 ± 0.009	0.144 ± 0.010
				27	200	0.135					21	140	0.150		
				36	250	0.144					23	160	0.144		
				29	260	0.112					22	140	0.157		
				28	180	0.156					23	150	0.153		
				28	190	0.147					24	170	0.141		
Co^{2+}	200	260	0.77	250	230	1.09	1.18 ± 0.09	340	180	1.89	280	240	1.17	1.20 ± 0.05	1.19 ± 0.04
				260	230	1.13					280	240	1.17		
				220	190	1.16					270	220	1.23		
				230	200	1.15					290	230	1.26		
				280	230	1.22					260	230	1.13		
				240	180	1.33					270	220	1.23		
Fe^{2+}	110	260	0.42	150	210	0.71	0.72 ± 0.05	260	180	1.44	170	240	0.71	0.79 ± 0.06	0.76 ± 0.04
				160	210	0.76					190	250	0.76		
				150	210	0.71					220	250	0.88		
				160	210	0.76					200	240	0.83		
				120	190	0.63					180	230	0.78		
				160	210	0.76					170	220	0.77		
Mg^{2+}	11	67	0.16	41	33	1.24	1.33 ± 0.12	52	15	3.47	37	28	1.32	1.40 ± 0.09	1.36 ± 0.07
				43	33	1.30					38	27	1.41		
				47	38	1.29					41	27	1.52		
				48	39	1.23					37	27	1.37		
				45	30	1.50					41	28	1.46		
				46	32	1.44					34	26	1.31		
Mn^{2+}	20	160	0.13	22	130	0.17	0.17 ± 0.02	18	65	0.28	13	62	0.21	0.20 ± 0.02	0.19 ± 0.02
				26	140	0.19					15	67	0.22		
				25	140	0.18					16	72	0.22		
				28	170	0.16					12	62	0.19		
				14	110	0.13					12	62	0.19		
				24	130	0.18					15	88	0.17		

© 2000 NRC Canada

Table 4. (*concluded*).

Micro-component	Initial concentration of microcomponent a''_{ko}	a''_{ro}	$D^{o}_{min} = \frac{a''_{ko}}{a''_{ro}}$	Concentration of microcomponent after stirring a'_k	a'_r	D_{min}	$\overline{D} \pm t_{0,05}\frac{s}{\sqrt{n}}$	Initial concentration of microcomponent a''_{ko}	a''_{ro}	$D^{o}_{max} = \frac{a'_{ko}}{a'_{ro}}$	Concentration of microcomponent after stirring a'_k	a'_r	D_{max}	$\overline{D} \pm t_{0,05}\frac{s}{\sqrt{n}}$	Average equilibrium distribution coefficient, D
Cd^{2+}	2.5	190	0.013	4.8	150	0.032	0.026 ± 0.004	4	76	0.053	2.5	76	0.033	0.030 ± 0.008	0.028 ± 0.002
				4.2	165	0.025					2.7	86	0.031		
				3.8	170	0.022					2.4	80	0.030		
				5.0	190	0.026					2.5	83	0.030		
				2.7	120	0.023					2.2	75	0.029		
				4.0	150	0.027					2.3	94	0.024		

Note: Other definitions: $\overline{D}$, mean value of D, *sd*, standard deviation; n, number of determinations, $t_{0,05}$, value of Student *t*-test for n – 1 degrees of freedom and for the confidence level of 1 – α = 0.95.

D_{Fe} are lower than those obtained for macroamounts of $FeSO_4 \cdot 7H_2O$ by Balarev and Karaivanova (5) at 25°C and Gorstein (7) at 0°C. In the case of cocrystallization of Co^{2+} ion the determined coefficient D_{Co} is close to that obtained by Gorshtein and Silant'eva (9), but differs considerably from that given by Aslanian et al. (8). The coefficient D_{Ni} is very close to that determined for macroamounts of $NiSO_4 \cdot 7H_2O$ by Oikova et al. (11) and Jangg and Gregori (10), but is slightly lower than that obtained by Aslanian et al. (8) for macroamounts of nickel(II) sulfate heptahydrate. In the case of Mg^{2+} the values of D_{Mg} are slightly smaller than those given by Balarev and co-workers (6, 12) during cocrystallization of macroamounts of $MgSO_4 \cdot 7H_2O$ with $ZnSO_4 \cdot 7H_2O$. The coefficient D_{Cu} differs slightly from that determined by Purkayastha and Das (13) for microamounts of Cu^{2+}, but is considerably lower than that obtained by Jangg and Gregori (10) for macroamounts of Cu^{2+}. In the case of Mn^{2+}, the determined coefficients are slightly lower than those obtained by Purkayastha and Das (14).

The values of determined distribution coefficients D of the microcomponents M^{2+} are a measure of the ability to include ions of guest (M^{2+}) into the crystal lattice of the host ($ZnSO_4 \cdot 7H_2O$) or reciprocal solubility of both sulfate hydrates in the solid phase. According to the generally known principle "similar dissolves in the similar" this ability may be greater, the greater the similarity of radii of substituting ions, their coordination environment in crystal, or crystal structures and unit cell dimensions.

The dependence of D coefficients of the microcomponent on the ionic radius has been presented in Fig. 1. The D coefficients decrease with the increase of the ionic radius $r_{M^{2+}}$. For the most distant ion Ca^{2+}, its value is close to zero ($D <$ 0.006). But there is some irregularity in monotonic run of the $D = f(r_{M^{2+}})$ curve (for Cu^{2+}). It is caused by a considerable difference between the structures of triclinic $CuSO_4 \cdot 5H_2O$ and orthorhombic $ZnSO_4 \cdot 7H_2O$ as well as by a difference in coordination environments of both metal ions in the crystal resulting from their electron configurations. The open-cell Cu^{2+} ions yield highly distorted octahedra due to the Jahn–Teller effect and they can only in slight degree substitute Zn^{2+} ion, on account of the difficulty of acceptance of the coordination environment of the more regular octahedron of Zn^{2+} (18). Furthermore in the run of $D = f(r_{M^{2+}})$ dependence there is not any maximum of D for values of $r_{M^{2+}}$, the most close to the ionic radius of macrocomponent ($r_{Zn^{2+}}$) which often occurred in other crystallization systems (1–4). It means that in this crystallization system similarity of radii of the substituting ions does not influence D coefficients, although their dependence on the $r_{M^{2+}}$ for ions, which form at 20–23°C, (monoclinic sulfate hydrates (Co^{2+}, Fe^{2+}, Cd^{2+}, Ca^{2+})) is linear in a plot of log D against ionic radius with a coefficient of linear correlation $r_{xy} = -0.9941$ (Fig. 2).

The data presented in Table 5 indicate that values of coefficient D are essentially influenced by the similarity of the crystal structure of corresponding sulfate hydrates. The highest distribution coefficients occur for Ni^{2+} and Mg^{2+}, whose s**ulfate hydrates belong to the same orthorhombic crystal system as $ZnSO_4 \cdot 7H_2O$**, have almost the same unit cell dimensions, andcan also form continuous solid solutions ($Zn(Ni)SO_4 \cdot 7H_2O$ and $Zn(Mg)SO_4 \cdot 7H_2O$) without a

© 2000 NRC Canada

Fig. 2. Dependence of distribution coefficients, *D*, of microcomponents, M^{2+}, forming at 20°C of monoclinic sulfate hydrates on their ionic radii.

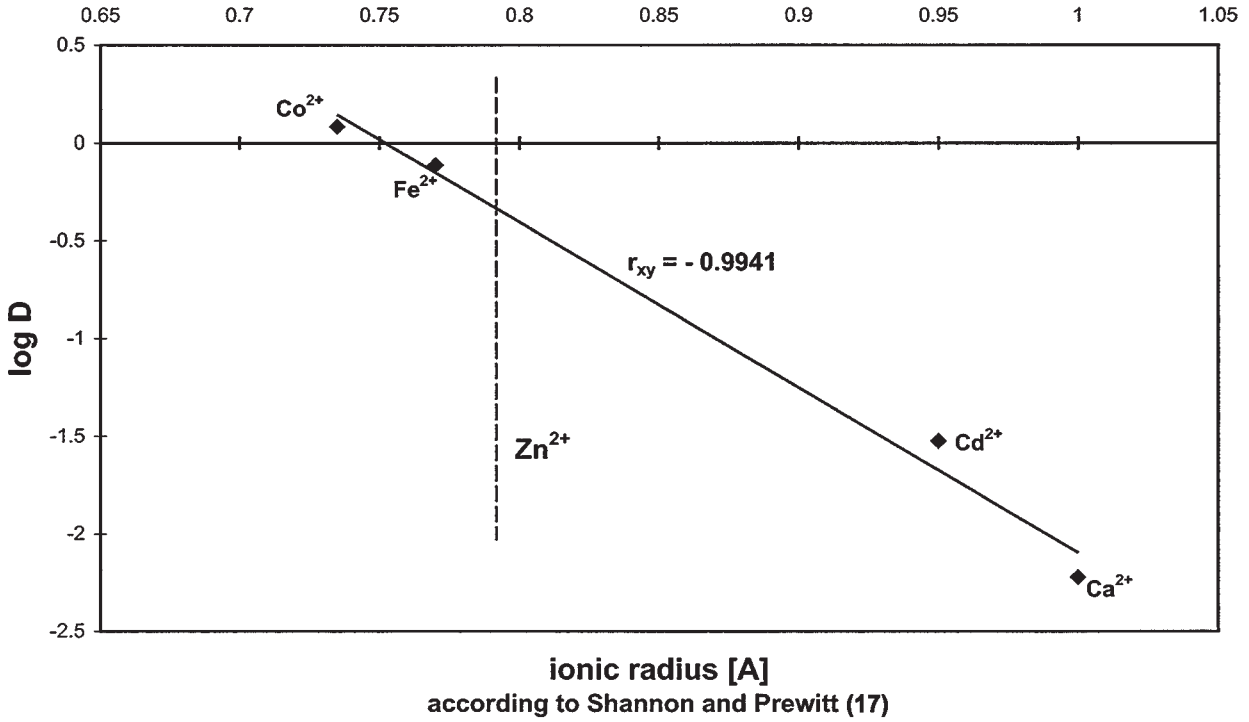
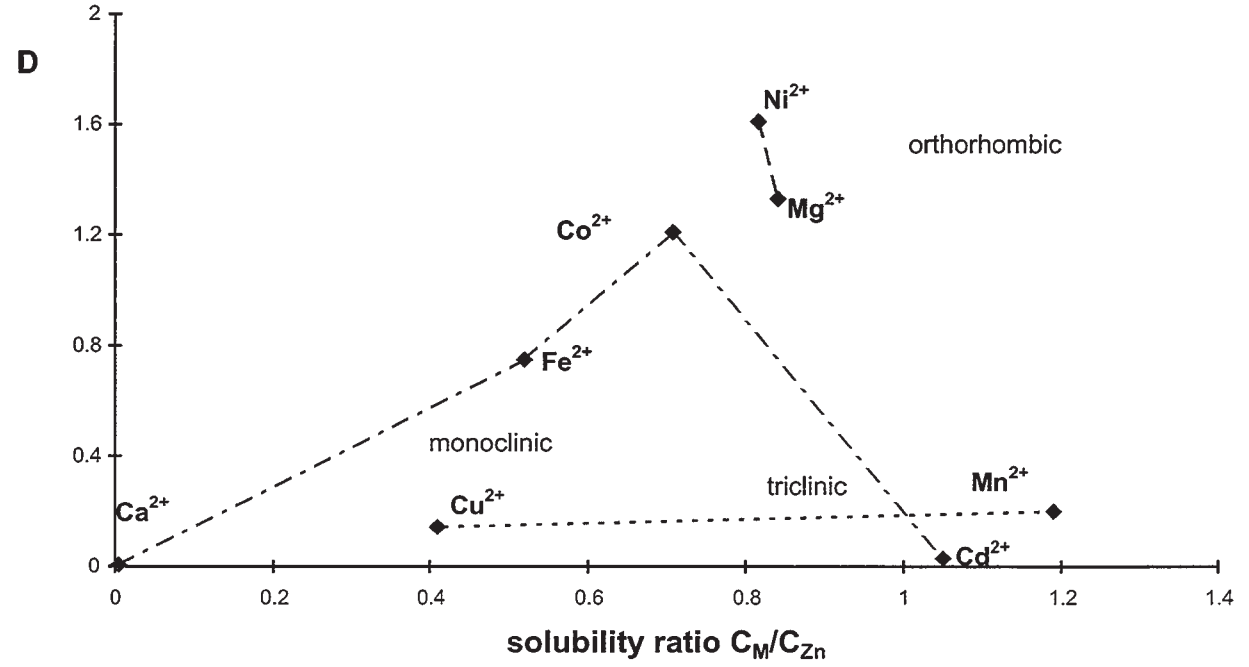


Fig. 3. Relationship between distribution coefficients, *D*, of M^{2+} ions forming at 20°C of sulfate hydrates belonging to the same crystal system and solubility ratio C_M/C_{Zn}.



miscibility gap (6, 8). The coefficients D_{Co} and D_{Fe} are lower, but the similarity of crystal structure of monoclinic $CoSO_4 \cdot 7H_2O$ and $FeSO_4 \cdot 7H_2O$ to $ZnSO_4 \cdot 7H_2O$ is lower as well. Though these monoclinic sulfate hydrates form solid solutions with zinc(II) sulfate heptahydrate ($Zn(Co)SO_4 \cdot 7H_2O$ and $Zn(Fe)SO_4 \cdot 7H_2O$), they are discontinuous. There is a miscibility gap from about 27% $CoSO_4 \cdot 7H_2O$ in the solid to about 46% $CoSO_4 \cdot 7H_2O$ (8) (as well as from about 55% $FeSO_4 \cdot 7H_2O$ in the solid to about 63% $FeSO_4 \cdot 7H_2O$ (6)). In this case, lowering similarity of crystal structure causes lowering reciprocal solubility sulfate hydrates in solid phase. This is accompanied with lowering distribution coefficients of *D*. The smallest *D* coefficients occur for Cd^{2+}, Ca^{2+}, Cu^{2+}, and Mn^{2+}. The first two ions

© 2000 NRC Canada

Table 5. Effect of crystal structure of $MSO_4 \cdot nH_2O$ and their solubility in solid $ZnSO_4 \cdot 7H_2O$ on distribution coefficients, D, of M^{2+} ions during crystallization of zinc(II) sulfate heptahydrate at 20°C.

		Crystal structure of $MSO_4 \cdot nH_2O$						Solubility of $MSO_4 \cdot nH_2O$ in solid		
	Stable sulfate hydrate at	Crystal	Space	Unit cell dimensions						
Microcomponent	20–23°C	system	group	a (Å)	b (Å)	c (Å)	angles (°)	References	$ZnSO_4 \cdot 7H_2O$	References	D
Ca^{2+}	$CaSO_4 \cdot 2H_2O$	monoclinic	$C2/c$	6.28	15.15	5.67	114.20	(22)	[a]		<0.005
Cd^{2+}	$3CdSO_4 \cdot 8H_2O$	monoclinic	$C2/c$	14.82	11.90	9.47	97.65	(23)	[b]	(25)	0.030
Cu^{2+}	$CuSO_4 \cdot 5H_2O$	triclinic	$P1$	6.11	10.71	5.96	97.57 107.28 77.43	(22)	6.7%[c]	(26)	0.144
Mn^{2+}	$MnSO_4 \cdot 5H_2O$	triclinic	$P1$	6.37	10.77	6.13	98.77 109.95 75.03	(24)	6.5%[c]	(26)	0.20
Fe^{2+}	$FeSO_4 \cdot 7H_2O$	monoclinic	$P2_1/C$	14.07	6.50	11.04	105.60	(22)	55%	(6)	0.75
Co^{2+}	$CoSO_4 \cdot 7H_2O$	monoclinic	$P2_1/C$	14.13	6.55	11.00	105.08	(22)	27%	(8)	1.21
Mg^{2+}	$MgSO_4 \cdot 7H_2O$	orthorhombic	$P2_12_12_1$	11.87	12.00	6.86		(22)	→100%	(6)	1.33
Ni^{2+}	$NiSO_4 \cdot 7H_2O$	orthorhombic	$P2_12_12_1$	11.86	12.08	6.81		(22)	→100%	(8)	1.61
Zn^{2+}	$ZnSO_4 \cdot 7H_2O$	orthorhombic	$P2_12_12_1$	11.85	12.09	6.83		(22)			

[a] No literature data.
[b] Forms isodimorphic mixed crystals.
[c] The highest concentration occurred in goslarite ($ZnSO_4 \cdot 7H_2O$).

have the greatest ionic radii, which hinder their inclusion into the crystal lattice of zinc(II) sulfate heptahydrate. However though Mn^{2+} and Cu^{2+} radii are close to $r_{Zn^{2+}}$, their triclinic sulfate pentahydrates show the lowest symmetry and their crystal structures differ most considerably from structure of $ZnSO_4 \cdot 7H_2O$.

According to Aslanian and Balarev (18) the differences in the crystal structure of the heptahydrate as well as the existence or nonexistence of crystal hydrates of some ions (Co^{2+}, Cu^{2+}, Fe^{2+}, Mg^{2+}, and Ni^{2+}) may be explained with their electron configuration. The deformation trend of octahedral coordination of mentioned ions increases in the following order: $Ni^{2+} < Zn^{2+} < Mg^{2+} < Co^{2+} < Fe^{2+} < Cu^{2+}$. Determined D cocrystallization coefficients of microamounts of these ions with $ZnSO_4 \cdot 7H_2O$ decrease in the same order.

The relationship between D coefficients of M^{2+} ions and solubility ratio C_M/C_{Zn} (where C_M and C_{Zn} are molar solubilities in water of $MSO_4 \cdot nH_2O$ and $ZnSO_4 \cdot 7H_2O$ respectively (19–20)) is very complex (Fig. 3). According to general thermodynamic prediction, D coefficients should decrease with the increasing solubility ratio C_M/C_{Zn}, assuming that activity coefficients ratio of ions in solution as well as activity coefficients ratio of both sulfate hydrates in crystal are unity (21). However they are the lowest in the case of Ca^{2+} for which the solubility ratio is the lowest. Then partition coefficients increase monotonically with the increase of C_M/C_{Zn} ratio (from D_{Ca} to D_{Ni}), and next, they decrease in an irregular way. Based on this dependence for specified groups of M^{2+} ions, which form sulfate hydrates belonging to the same crystal system, we may state that in the case of orthorhombic sulfate hydrates, distribution coefficients, D, obey this thermodynamic prediction, but in the case of monoclinic as well as triclinic sulfate hydrates dependence, $D = f(C_M/C_{Zn})$ does not agree with this prediction. It may result from the great difference between ionic radii of macrocomponent (Zn^{2+}) and microcomponents (Ca^{2+} and Cd^{2+}), causing activity coefficients ratios in solution ($\gamma_{Zn^{2+}}/\gamma_{Ca^{2+}}$ and $\gamma_{Zn^{2+}}/\gamma_{Cd^{2+}}$) are different from unity as well as from the great difference between crystal structure of microcomponents sulfate hydrates ($MnSO_4 \cdot 5H_2O$, $CuSO_4 \cdot 5H_2O$, $CaSO_4 \cdot 2H_2O$, $3CdSO_4 \cdot 8H_2O$) and macrocomponent ($ZnSO_4 \cdot 7H_2O$) causing activity coefficients ratios of corresponding sulfate hydrates in the solid phase to differ from unity.

Conclusions

The coefficients of cocrystallization, D, of investigated microcomponents M^{2+} with zinc(II) sulfate heptahydrate are in the range <0.006 (D_{Ca}) – 1.61 (D_{Ni}). In the case of Ni^{2+}, Mg^{2+} and Co^{2+}, whose D coefficients are greater than 1, crystallization of $ZnSO_4 \cdot 7H_2O$ does not lead to its purification.

The values of D distribution coefficients first of all depend on similarity of the *crystal structure of M(II) sulfate hydrates.* They are the highest for Ni^{2+} and Mg^{2+} (their orthorhombic sulfate heptahydrates are isomorphous with $ZnSO_4 \cdot 7H_2O$, have almost the same unit cell dimensions, and form continuous solid solutions with it). For Co^{2+} and Fe^{2+} they are lower (their sulfate heptahydrates are monoclinic, have different unit cell dimensions, and form solid solutions of limited reciprocal solubility (with miscibility

© 2000 NRC Canada

gap)). The lowest values of D occur for Mn^{2+}, Cu^{2+}, Cd^{2+}, and Ca^{2+} (they do not form sulfate heptahydrates and the structures of their hydrates differ considerably from the structure of $ZnSO_4 \cdot 7H_2O$).

The order of lowering some of the determined distribution coefficients ($D_{Ni} > D_{Mg} > D_{Co} > D_{Fe} > D_{cu}$) exactly agrees with increase of the deformation trend of octahedral coordination of corresponding ions resulting from their electronic configuration.

The D coefficients do not depend on the similarity of ionic radii of microcomponent ($r_{M^{2+}}$) to macrocomponent ($r_{Zn^{2+}}$) since there is no maximum of D for values of $r_{M^{2+}}$ the closest to $r_{Zn^{2+}}$. However, this dependence of D for microcomponents forming at 20°C monoclinic sulfate hydrates (Co, Fe, Cd, Ca) is linear in a plot of log D against ionic radius.

The dependence of D coefficients of M^{2+} ions on the *solubility ratio* C_M/C_{Zn} is very complex. For Ni^{2+} and Mg^{2+} forming isomorphous sulfate hydrates with $ZnSO_4 \cdot 7H_2O$, they get smaller with increasing C_M/C_{Zn} according to general thermodynamic prediction. In the case of the remaining microcomponents, this dependence is disturbed by the influence of ionic radii as well the structure of corresponding sulfate hydrates. They cause activity coefficients ratio of respective ions in solution or activity coefficients ratio of corresponding sulfates in crystal to be different from unity.

References

1. M. Smolik and M. Zołotajkin. Pol. J. Chem. **67**(3), 383 (1993).
2. M. Smolik and B. Lipowska. Indian J. Chem. Sect. A: Inorg. Bio-inorg. Phys. Theor. Anal. **34A**, 230 (1995).
3. M. Smolik and B. Lipowska. Pol. J. Appl. Chem. **1**(39), 143 (1995).
4. M. Smolik, M. Zołotajkin, and J. Kluczka. Pol. J. Chem. **69**, 1322 (1995).
5. Kh. Balarev, and V. Karaivanova. Krist. Tech. **10**(11), 1101 (1975).
6. Kh. Balarev, V. Karaivanova, and S. Aslanian. Krist. Tech. **8**(1–3), 115 (1973).
7. G.I. Gorshtein and N.I. Silant'eva. Tr. Vses. Nauchno. Issled. Inst. Khim. Reakt. Osobo Chist. Khim. Veshchestv. **22**, 12(1958).
8. S. Aslanian, Kh. Balarev, and T. Oikova. Krist. Tech. **7**(5), 513 (1972).
9. G.I. Gorshtein and N.I. Silant'eva. *In* Isotopy i isluchenie v khimii. *Edited by* Nauka. Moskva. 1958. p. 203.
10. G. Jangg and H. Gregori. Z. Anorg. Allg. Chem. **351**, 81 (1967).
11. T. Oikova, L. Makarov, Kh. Balarev, and M. Miloshova. Z. Phys. Chem. (Leipzig), **255**, 453 (1974).
12. Kh. Balarev, P. Dobreva, and T. Oikova. God. Vissh. Khim. Tekhnol. Inst. Burgas, **10**, 523 (1972).
13. B.C. Purkayastha and N. Das. J. Radioanal. Chem. **25**, 35 (1975).
14. B.C. Purkayastha, and N. Das. Aust. J. Chem. **26**(6), 1243 (1973).
15. W.J. Welcher. *In* The analytical uses of EDTA. *Edited by* van Nostrand Comp. Inc., New Jersey, London, Toronto. 1958. p. 149.
16. V.G. Khlopin. *In* Izbr. trudy. Vol. 6. *Edited by* Izd. AN SSSR, Moskva 1957. p.173.
17. R.D. Shannon and Ch.T. Prewitt. Acta Cryst. **B25**, 925 (1969).
18. S. Aslanian and Kh. Balarev. Krist. Tech. **12**(5), 435 (1977).
19. A. Seidel and W.F. Linke. Solubilities of inorganic and metal organic compounds. *Edited by* Van Nostrand. New York. 1958.
20. M. Broul, J. Nyvlt, and O. Sohnel. Solubility in inorganic two-component system. *Edited by* Prague Academia, Prague. 1981.
21. H.A. Laitinen. *In* Chemical analysis. *Edited by* McGraw-Hill Book Comp. Inc. New York, Toronto, London. 1960. pp 171–174.
22. Crystal data. Determinative tables. Vol.2. *Edited by* U.S. Department of Commerce. National Bureau of Standards and the Joint Commitee on Powder Diffraction Standards. (1972).
23. R. Camimiti and G. Johanson. Acta Chem. Scand. **A35**(6), 451 (1981).
24. M. Nambu, K. Tamida, C.Kitamura, and E. Kato. Mineral. J. **9**, 28 (1978).
25. Kh. Balarev, V. Karaivanova, and P. Dobreva. God. Vissh. Khim. Tekhnol. Inst. Burgas, **9**(9), 251 (1973).
26. A.S. Povrenykh. *In* Kristalokhimicheskaya Klassifikacya Mineralnykh Vidov. *Edited by* Naukova Dumka. Kiev. 1966. p. 459.

© 2000 NRC Canada

Synthesis, characterization, and reactivity of scandium chloro, alkyl, aryl, and borohydride complexes, $Sc(\eta^5\text{-}C_5H_5)R[N(SiMe_2CH_2P^iPr_2)_2]$ (R = Cl, Me, Ph, and BH_4)

Michael D. Fryzuk, Garth R. Giesbrecht, and Steven J. Rettig

Abstract: Reaction of $ScCl_2(THF)[N(SiMe_2CH_2P^iPr_2)_2]$ with NaCp(DME) leads to $Sc(\eta^5\text{-}C_5H_5)Cl[N(SiMe_2CH_2P^iPr_2)_2]$ (**1**). The X-ray crystal structure shows the scandium centre to reside in a square pyramidal environment with the $[N(SiMe_2CH_2P^iPr_2)_2]$ – ligand bound in a pseudo-meridional fashion. The ^1H NMR spectrum is consistent with a C_s symmetric structure in solution. Metathesis of the chloride ligand with RLi (R = Me, Ph, BH_4) yields the five-coordinate species $Sc(\eta^5\text{-}C_5H_5)R[N(SiMe_2CH_2P^iPr_2)_2]$. Phenyl **3** and borohydride **4** are isolated as crystalline solids, while methyl **2** resisted crystallization. **2**–**4** exhibit ^1H NMR spectra consistent with C_s symmetric solution structures. $Sc(\eta^5\text{-}C_5H_5)Ph[N(SiMe_2CH_2P^iPr_2)_2]$ (**3**) was characterized in the solid state and found to have a similar geometry to that of the parent chloride. Reaction of $Sc(\eta^5\text{-}C_5H_5)Me[N(SiMe_2CH_2P^iPr_2)_2]$ (**2**) with NH_2R (R = Ph, ^{t}Bu) yields the amides $Sc(\eta^5\text{-}C_5H_5)NHPh[N(SiMe_2CH_2P^iPr_2)_2]$ (**5**) and $Sc(\eta^5\text{-}C_5H_5)NH^tBu[N(SiMe_2CH_2P^iPr_2)_2]$ (**6**) via σ-bond metathesis routes; these reactions are accompanied by a competing reaction at the scandium-amide bond to produce the protonated ligand, $HN(SiMe_2CH_2P^iPr_2)_2$. **5** and **6** are also produced by salt-elimination from the chloride **1** and LiNHR (R = Ph, ^{t}Bu). $Sc(\eta^5\text{-}C_5H_5)(BH_4)[N(SiMe_2CH_2P^iPr_2)_2]$ (**4**) reacts with PMe_3 to produce the putative hydride, $Sc(\eta^5\text{-}C_5H_5)H[N(SiMe_2CH_2P^iPr_2)_2]$ (**7**); this species was identified in solution. An equilibrium between **4**, PMe_3, **7**, and $PMe_3{\cdot}BH_3$ exists which greatly favors the starting scandium-borohydride. Crystals of $Sc(\eta^5\text{-}C_5H_5)Cl[N(SiMe_2CH_2P^iPr_2)_2]$ (**1**) are monoclinic, a = 17.409(2), b = 10.0803(7), c = 17.688(2) Å, β = 94.606(8)°, Z = 4, space group $P2_1/c$; and those of $Sc(\eta^5\text{-}C_5H_5)Ph[N(SiMe_2CH_2P^iPr_2)_2]$ (**3**) are triclinic, a = 10.5129(15), b = 19.124(2), c = 9.114(2) Å, α = 95.582(13), β = 107.047(12), γ = 90.042(11)°, Z = 2, space group P. The structures were solved by Patterson (**1**) and direct (**3**) methods and refined by full-matrix least-squares procedures to R = 0.047 and 0.054 (R_w = 0.042 and 0.049) for 2414 and 2844 reflections with $I \geq 3\sigma(I)$, respectively.

Key words: scandium, σ-bond metathesis, borohydride.

Résumé : La réaction du $ScCl_2(THF)[N(SiMe_2CH_2CH_2P^iPr_2)_2]$ avec le NaCp(DME) conduit à la formation du $Sc(\eta^5\text{-}C_5H_5)Cl[N(SiMe_2CH_2CH_2P^iPr_2)_2]$ (**1**). La structure cristalline obtenue par diffraction des rayons X montre que le centre scandium se trouve dans un environnement pyramidal carré où le ligand $[N(SiMe_2CH_2CH_2P^iPr_2)_2]$ est lié d'une façon pseudoméridionale. Le spectre RMN du ^1H est en accord avec une structure symétrique $\mathbf{C_s}$, en solution. La métathèse du ligand chlorure avec du RLi (R = Me, Ph, BH_4) fournit des espèces pentacoordinées $Sc(\eta^5\text{-}C_5H_5)R[N(SiMe_2CH_2CH_2P^iPr_2)_2]$. Les dérivés phényle (**3**) et borohydrure (**4**) ont été isolés sous forme de solides cristallins alors que le dérivé méthyle (**2**) n'a pu être cristallisé. Les spectres RMN du ^1H des dérivés **2**–**4** sont en accord avec des structures symétriques $\mathbf{C_s}$ en solution. Le composé $Sc(\eta^5\text{-}C_5H_5)Ph[N(SiMe_2CH_2CH_2P^iPr_2)_2]$ (**3**) a été caractérisé à l'état solide et on a trouvé qu'il possède une géométrie similaire à celle du dérivé chloré qui lui a donné naissance. La réaction du $Sc(\eta^5\text{-}C_5H_5)Me[N(SiMe_2CH_2CH_2P^iPr_2)_2]$ (**2**) avec le NH_2R (R = Ph, *t*-Bu) conduit aux amides $Sc(\eta^5\text{-}C_5H_5)NHPh[N(SiMe_2CH_2CH_2P^iPr_2)_2]$ (**5**) et $Sc(\eta^5\text{-}C_5H_5)NH^tBu[N(SiMe_2CH_2CH_2P^iPr_2)_2]$ (**6**) par le biais de réactions de métathèses impliquant la liaison σ; ces réactions sont accompagnées par une réaction parallèle au niveau de la liaison scandium-amide qui produit le ligand protoné $HN(SiMe_2CH_2CH_2P^iPr_2)_2$. Les composés **5** et **6** se produisent aussi par une élimination de sel à partir du chlorure **1** et du LiNHR (R = Ph, *t*-Bu). Le $Sc(\eta^5\text{-}C_5H_5)BH_4[N(SiMe_2CH_2CH_2P^iPr_2)_2]$ (**4**) réagit avec le PMe_3 et donne lieu à la formation de l'hydrure putatif $Sc(\eta^5\text{-}C_5H_5)H[N(SiMe_2CH_2CH_2P^iPr_2)_2]$ (**7**) qui a été identifié en solution. Il existe un équilibre entre les produits **4**, PMe_3, **7** et $PMe_3{\cdot}BH_3$ qui favorise fortement le borohydrure de scandium de départ. Les cristaux de $Sc(\eta^5\text{-}C_5H_5)Cl[N(SiMe_2CH_2CH_2P^iPr_2)_2]$ (**1**) sont monocliniques, groupe d'espace $P2_1/c$, avec a = 17,409(2), b = 10,803(7) et c = 17,688(2) Å, β = 94,606(8)° et Z = 4; ceux du $Sc(\eta^5\text{-}C_5H_5)Ph[N(SiMe_2CH_2CH_2P^iPr_2)_2]$ (**3**) sont tricliniques, groupe d'espace P, avec a = 10,5129(15), b = 19,124(2) et

Received January 12, 2000. Published on the NRC Research Press website on July 11, 2000.

M.D. Fryzuk,[1] G.R. Giesbrecht, and S.J. Rettig. Department of Chemistry, University of British Columbia, 2036 Main Mall, Vancouver, BC V6T 1Z1, Canada.

[1]Author to whom correspondence may be addressed. Telephone: (604) 822-2897. Fax: (604) 822-2847. e-mail: fryzuk@chem.ubc.ca

© 2000 NRC Canada

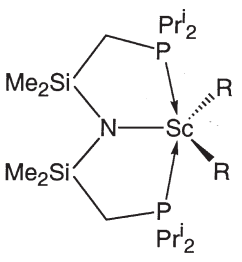
c = 9,114(2) Å, α = 95,582(13), β = 107,047(12) et γ = 90,042(11)° et Z = 2. On a résolu les structures par les méthodes de Patterson et directes et on les a affinées par la méthode des moindres carrés (matrice entière) jusqu'à des valeurs de R = 0,047 et 0,054 (R_w = 0,042 et 0,049) pour respectivement 2414 et 2844 réflexions avec $I \geq 3\sigma(I)$.

Mots clés : scandium, métathèse par liaison-σ, borohydrure.

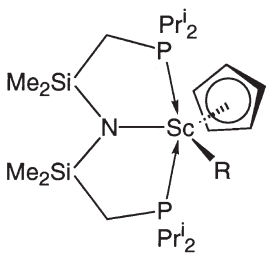
Introduction

Until recently, the chemistry of scandium was largely unexplored, in part due to the general assumption that the Lewis acidic scandium centre offered little in the way of useful reactivity (1). Although early work with scandium utilized large alkyl (2, 3) or cyclopentadienyl ligands, (4–6) complexes of the general type Cp^*_2ScR (Cp^* = pentamethylcyclopentadienyl, R = hydride, alkyl, aryl) were found to participate in many useful transformations, including olefin polymerization (7–9) and C-H activation (or σ-bond metathesis) (7, 8, 10). Although organoscandium chemistry, and organolanthanide chemistry in general, has been dominated by pentamethylcyclopentadienyl-based ligands, (11) recent work has been directed towards generating reactive scandium alkyl complexes by incorporating nitrogen-containing ligands (12) such as porphyrins, (13–16) amidinates (17), or trispyrazolylborates (18). However, these ligand sets have yet to surpass the unique stabilization provided to the metal centre by either two Cp^* ligands (7, 19, 20) or the combination of a Cp^* ligand and an amide (7, 21–23).

We recently reported the synthesis, characterization, and reactivity of a series of five-coordinate scandium dialkyls, $ScR_2[N(SiMe_2CH_2P^iPr_2)_2]$ (R = Me, Et, CH_2SiMe_3) (**A**) (24). Unfortunately, these scandium dialkyls suffer a similar fate to many lanthanide dialkyls stabilized by a single ancillary ligand (25–27). Although these complexes are stable enough to be isolated, they decompose to multiple, unidentifiable products when reacted with small molecules. One approach to this problem is to replace a chloride with a larger, unreactive ligand, which will result in a more coordinatively saturated complex. Additionally, if the ligand can be chosen to donate more than two electrons to the metal, the compound will have greater electronic stability. This leaves a site at the metal at which to pursue reaction chemistry. In an effort to generate more stable derivatives, and better defined reaction pathways, we metathesized a chloride with NaCp(DME) to generate compounds of the type $Sc(\eta^5\text{-}C_5H_5)R[N(SiMe_2CH_2P^iPr_2)_2]$ (**B**), which have added steric bulk and an additional four electrons, as compared to the $ScR_2[N(SiMe_2CH_2P^iPr_2)_2]$ series. Herein we describe the synthesis, characterization, and reactivity of $Sc(\eta^5\text{-}C_5H_5)R[N(SiMe_2CH_2P^iPr_2)_2]$ (R = Cl, Me, Ph, BH_4).



A



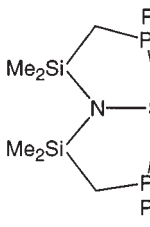
B

Results and discussion

Synthesis of $Sc(\eta^5\text{-}C_5H_5)Cl[N(SiMe_2CH_2P^iPr_2)_2]$ (1)

The addition of a THF solution of NaCp(DME) to a solution of $ScCl_2(THF)[N(SiMe_2CH_2P^iPr_2)_2]$ (24) in THF maintained at –78°C results in $Sc(\eta^5\text{-}C_5H_5)Cl[N(SiMe_2CH_2P^iPr_2)_2]$ (**1**) (eq. [1]). Additionally, the same metathesis can be effected by the addition of solid NaCp(DME) to a toluene solution of the starting dichloride, although this route requires a longer reaction time (1 week).

$$ScCl_2(THF)[N(SiMe_2CH_2PPr^i_2)_2] + NaCp(DME) \xrightarrow[(-\ NaCl)]{THF,\ -78\ ^\circ C} \quad [1]$$



1

Compound **1** is isolated as a slightly yellow, waxy solid and forms colorless crystals upon slow evaporation of a saturated toluene solution. The ^{1}H NMR spectrum of **1** shows a doubling of the ligand resonances, due to the presence of a chloride and a cyclopentadienide ligand. Heating a d_8-toluene solution of **1** to 100°C does not result in the averaging of the diastereotopic ligand resonances, indicating that the positions of the Cp and Cl moieties are fixed, and not subject to exchange via a process such as phosphine dissociation, followed by rotation about the scandium-amide bond and re-coordination. The $^{31}P\{^1H\}$ NMR spectrum of **1** exhibits a broad singlet (δ –1.2 ppm, $\Delta_{1/2}$ = 425 Hz) at all temperatures, due to the interaction with the quadrupolar scandium nucleus (^{45}Sc, I = 7/2, 100% natural abundance) (28). As well, the five equivalent Cp protons couple to two equivalent phosphorous-31 nuclei, exhibiting a triplet in the ^{1}H NMR spectrum at 6.51 ppm ($^3J_{H\text{-}P}$ = 1.3 Hz). The identity of the compound was confirmed by mass spectral, microanalytical and X-ray crystallographic studies.

Synthesis of scandium alkyls $Sc(\eta^5\text{-}C_5H_5)R[N(SiMe_2CH_2P^iPr_2)_2]$ (R = Me (2), Ph (3), BH_4 (4))

Metathesis of the chloride ligand of $Sc(\eta^5\text{-}C_5H_5)Cl[N(SiMe_2CH_2P^iPr_2)_2]$ (**1**) is undertaken by a number of alkyl, aryl, or borohydride lithium reagents (eq. [2]).

$$\underset{\mathbf{1}}{Sc(\eta^5\text{-}C_5H_5)Cl[N(SiMe_2CH_2PPr^i_2)_2]} + RLi \xrightarrow[(-\ LiCl)]{toluene} Sc(\eta^5\text{-}C_5H_5)R[N(SiMe_2CH_2PPr^i_2)_2] \quad [2]$$

2 : R = Me
3 : R = Ph
4 : R = BH_4

© 2000 NRC Canada

Fig. 1. Molecular structure of $Sc(\eta^5\text{-}C_5H_5)Cl[N(SiMe_2CH_2P^iPr_2)_2]$ (**1**); 33% probability thermal ellipsoids are shown. Hydrogen atoms are omitted for clarity.

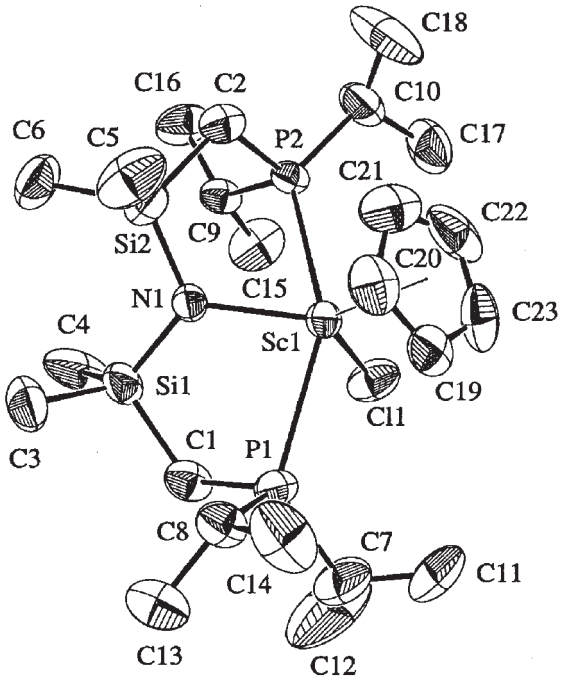
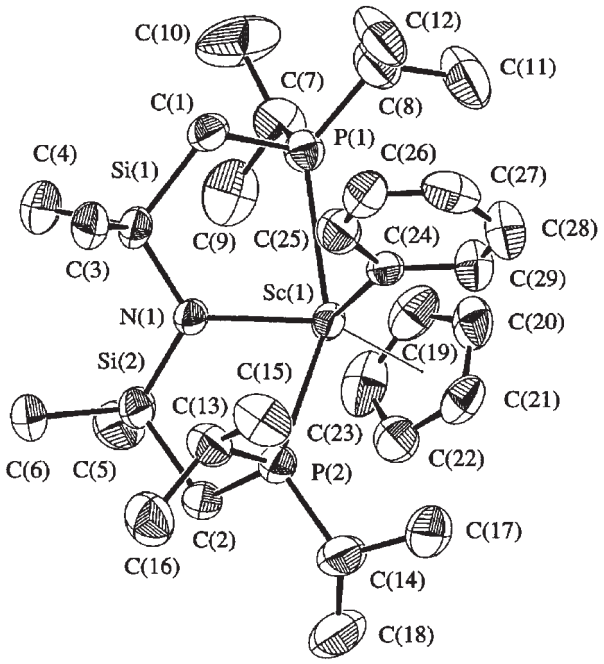


Fig. 2. Molecular structure of $Sc(\eta^5\text{-}C_5H_5)Ph[N(SiMe_2CH_2P^iPr_2)_2]$ (**3**); 33% probability thermal ellipsoids are shown. Hydrogen atoms are omitted for clarity.



The presence of the Cp ring reduces the tendency for these complexes to incorporate LiCl, which was found to occur in the dialkyl species, $ScR_2[N(SiMe_2CH_2P^iPr_2)_2]$ (R = Et, CH_2SiMe_3) (24). The phenyl complex **3** and the borohydride complex **4** were isolated as thermally-stable, off-white solids, which were subsequently obtained as air- and moisture-sensitive colorless crystals from hexamethyldisiloxane solutions. However, methyl **2** resisted crystallization and was used as a yellow, sticky solid. The ^1H NMR spectrum of each complex shows a doubling of the ligand backbone resonances, due to the presence of an alkyl, aryl, or borohydride ligand, and a Cp ligand. In the case of methyl **2**, the methyl protons ($ScCH_3$) resonate as a triplet at –0.19 ppm ($^3J_{H\text{-}P}$ = 4.3 Hz) due to coupling to two equivalent phosphorus-31 nuclei. For all three derivatives, the five Cp protons are equivalent, appearing as a triplet around 6.5 ppm. The $^{31}P\{^1H\}$ NMR spectra of **2**–**4** show broad, temperature invariant singlets at about 0 ppm ($\Delta_{1/2}$ = 100–200 Hz). The structure of the phenyl derivative **3** was investigated by X-ray crystallography.

Structure of $Sc(\eta^5\text{-}C_5H_5)Cl[N(SiMe_2CH_2P^iPr_2)_2]$ (1) and $Sc(\eta^5\text{-}C_5H_5)Ph[N(SiMe_2CH_2P^iPr_2)_2]$ (3)

The evaporation of a saturated toluene solution of **1** yielded large colorless crystals for X-ray analysis. The molecular structure and numbering scheme are presented in Fig. 1. Complete details of the structural analyses of **1** and **3** are presented in Table 1. Final atomic coordinates and B_{eq} for **1** and **3** are available in Table 2. The scandium centre has a geometry intermediate between trigonal bipyramidal and square pyramidal; if the Cp ligand occupies the apical position, the square pyramidal geometry is completed by the amide, the two phosphines and the chloride.

The angles defined by the Cp—scandium bond, and the four members of the base of the pyramid range from 105.4 to 127.9° (Cp = cyclopentadienyl centroid). The P(1)-Sc(1)-P(2) angle of 147.08(6)° is similar to that in $Sc(CH_2SiMe_3)_2[N(SiMe_2CH_2P^iPr_2)_2]$ (154.92(6)°) (24). The phosphorus-scandium bond lengths (2.804(2) and 2.822(2) Å) are slightly longer than those found for $ScCl_2(THF)[N(SiMe_2CH_2P^iPr_2)_2]$, as is the scandium-amide bond length of 2.116(4) Å (compared to 2.101(7) Å in $ScCl_2(THF)[N(SiMe_2CH_2P^iPr_2)_2]$) (24). The scandium centre is equidistant from all five Cp carbons (2.480(9)–2.511(7) Å), consistent with an η^5-bound cyclopentadienyl ligand. The scandium—Cp bond length (2.21 Å) is similar to that found for $(Cp_2ScCl)_2$ [5] and $(OEP)Sc(\eta^5\text{-}C_5H_5)$ [14] (2.19 and 2.20 Å, respectively) (OEP = octaethylporphyrin). Bond lengths and angles for **1** and **3** are presented in Tables 3 and 4, respectively.

Colorless crystals suitable for X-ray crystallographic analysis were grown from a saturated hexamethyldisiloxane solution of phenyl **3**. Figure 2 shows the numbering scheme and solid state structure. As for the chloride derivative **1**, the scandium centre has a distorted square pyramidal geometry.

In this case, the four angles involving the Cp ring, the scandium centre and the bases of the pyramid range from 104.0 to 130.2°. The P(1)-Sc(1)-P(2) bond angle (149.77(6)°) is in the same range as that determined for **1** and the bis(trimethylsilylmethyl) complex, $Sc(CH_2SiMe_3)_2[N(SiMe_2CH_2P^iPr_2)_2]$ (24). All of the bond lengths involving scandium are normal and show little variation from the parent chloride. The 2.229(6) Å spacing between the scandium centre and the ipso-carbon of the phenyl ring may be compared with distances of 2.242(3) Å for $ScEt_2[N(SiMe_2CH_2P^iPr_2)_2]$ and 2.204(5) and 2.126(4) Å for $Sc(CH_2SiMe_3)_2[N(SiMe_2CH_2P^iPr_2)_2]$. (24)

© 2000 NRC Canada

Table 1. Crystallographic data.[a]

Compound	**1**	3
Formula	$C_{23}H_{49}ClNP_2ScSi_2$	$C_{29}H_{54}NP_2ScSi_2$
fw	538.17	579.83
Crystal system	Monoclinic	Triclinic
Space group	$P2_1/c$ (No. 14)	P
a (Å)	17.409(2)	10.5129(15)
b (Å)	10.0803(7)	19.124(2)
c (Å)	17.688(2)	9.114(2)
α (°)	90	95.582(13)
β (°)	94.606(8)	107.047(12)
γ (°)	90	90.042(11)
V (Å^3)	3094.0(4)	1742.8(5)
Z	4	2
ρ_{calc}, (g/cm^3)	1.155	1.105
F(000)	1160	628
Radiation	Cu	Mo
μ (cm^{-1})	46.10	3.85
Crystal size (mm)	0.05 × 0.25 × 0.50	0.25 × 0.35 × 0.40
Transmission factors	0.44–1.00	0.91–1.00
Scan type	ω – 2θ	ω – 2θ
Scan range (° in ω)	0.94 + 0.20 tan θ	1.25 + 0.35 tan θ
Scan speed (°/min)	16 (up to 9 scans)	16 (up to 9 scans)
Data collected	—	+ h, ± k, ± l
$2\theta_{max}$ (°)	155	50
Crystal decay (%)	negligible	13.4
Total reflections	6949	6485
Total unique reflections	6758	6107
R_{merge}	0.038	0.045
Reflections with $I \epsilon 3\sigma(I)$	2414	2844
No. of variables	272	316
R	0.047	0.054
R_w	0.042	0.049
gof	1.98	2.77
Max Δ/σ (final cycle)	0.002	0.0005
Residual density (e/Å^3)	–0.21 to 0.25	–0.27 to 0.33

[a]Temperature 294 K, Rigaku AFC6S diffractometer, Cu K_α (λ = 1.54178 Å) or Mo K_α (λ = 0.71069 Å) radiation, graphite monochromator, takeoff angle 6.0°, aperture 6.0 × 6.0 mm at a distance of 285 mm from the crystal, stationary background counts at each end of the scan (scan/background time ratio 2:1), $\sigma^2(F^2) = [S^2(C + 4B)]/Lp^2$ (S = scan rate, C = scan count, B = normalized background count), function minimized $\Sigma w(|F_o| - |F_c|)^2$ where $w = 4F_o^2/\sigma^2(F_o^2)$, $R = \Sigma||F_o| - |F_c||/\Sigma|F_o|$, $R_w = (\Sigma w(|F_o| - |F_c|)^2/\Sigma w|F_o|^2)^{1/2}$, and gof = $[\Sigma w(|F_o| - |F_c|)^2/(m - n)]^{1/2}$. Values given for R, R_w, and gof are based on those reflections with $I \geq 3\sigma(I)$.

Structure of $Sc(\eta^5\text{-}C_5H_5)(BH_4)[N(SiMe_2CH_2P^iPr_2)_2]$ (4)

Colorless crystals of the borohydride complex **4** remained after the evaporation of a saturated hexamethyldisiloxane solution. Although the basic structural features of the complex were confirmed, a refined structure was not obtained due to disorder. The labile nature of the $[BH_4]^-$ unit, and its proximity to the quadrupolar scandium nucleus, prevented these resonances from being observed in the ^{1}H NMR spectrum. The absence of peaks assignable to BH_4 protons is a characteristic of the ^{1}H NMR spectrum of $[\eta^5\text{-}C_5H_3(SiMe_3)_2]_2Sc(BH_4)$ as well (29). The fluxionality of the $[BH_4]^-$ moiety is readily demonstrated by ^{11}B NMR spectroscopy: at ambient temperature, the spectrum consists of a 1:4:6:4:1 quintet at –27.6 ppm, consistent with coupling to 4 equivalent protons ($^1J_{B\text{-}H}$ = 85 Hz, $\Delta_{1/2}$ = 32 Hz). When a d_8-toluene solution of **4** is cooled to –80°C, the fluxional exchange process between bridge (H_b) and terminal (H_t) hydrogens is retarded; thus, a single broad peak at –27.0 ppm is observed ($\Delta_{1/2}$ = 160 Hz). This is faster than the exchange in $[\eta^5\text{-}C_5H_3(SiMe_3)_2]_2Sc(BH_4)$ which must be heated to 100°C before a quintet is observed ($^1J_{B\text{-}H}$ = 75 Hz) (29).

The solid state infrared spectrum of **4** consists of a sharp, strong band at 2478 cm^{-1} and a broader, weaker signal at 2211 cm^{-1}. These data are consistent with a BH_4 ligand bound in a tridentate fashion (30). These numbers compare favorably with a series of lanthanide tetrahydroborates $[\eta^5\text{-}C_5H_3(SiMe_3)_2]_2M(BH_4)$ (M = La, Pr, Nd, Sm) (29) which feature IR peaks diagnostic of tridentate coordination at 2420 and 2240 cm^{-1}. The band at 2478 cm^{-1} is assigned to the B—H_t stretch (A_1) and the broad band at 2211 cm^{-1} to the B—H_b stretching modes (A_1 and E) (30) In contrast to **4**, the previously characterized scandium tetrahydroborates $[\eta^5\text{-}C_5H_3(SiMe_3)_2]_2Sc(BH_4)$, (29) $[TolC(NSiMe_3)_2]_2Sc(BH_4)(THF)$ (17), and $Sc(BH_4)_3\cdot THF$ (31) bind BH_4 in a bidentate manner. The solution IR spectrum of **4** (hexanes) is identical to that of the solid state.

© 2000 NRC Canada

Table 2. Final atomic coordinates (fractional) and B_{eq} (10^3 Å^2)[a] for Sc(η^5-C_5H_5)Cl[N($SiMe_2CH_2P^iPr_2$)$_2$] (**1**) and Sc(η^5-C_5H_5)Ph[N($SiMe_2CH_2P^iPr_2$)$_2$] (**3**).

Atom	*x*	*y*	*z*	B_{eq}
1				
Sc(1)	0.24886(6)	0.1811(1)	0.21131(6)	4.26(3)
Cl(1)	0.15861(10)	0.1129(2)	0.29803(10)	7.45(5)
P(1)	0.11514(9)	0.2238(2)	0.11506(10)	5.03(4)
P(2)	0.35370(9)	–0.0050(2)	0.28002(9)	4.47(4)
Si(1)	0.1941(1)	–0.0342(2)	0.0744(1)	6.56(6)
Si(2)	0.3628(1)	–0.0004(2)	0.1104(1)	5.96(5)
N(1)	0.2695(3)	0.0423(4)	0.1256(2)	4.3(1)
C(1)	0.1013(4)	0.0480(6)	0.0969(3)	6.0(2)
C(2)	0.4198(3)	–0.0019(5)	0.2055(3)	5.6(2)
C(3)	0.2033(5)	–0.0246(8)	–0.0318(4)	11.6(3)
C(4)	0.1791(5)	–0.2116(6)	0.0991(6)	12.3(3)
C(5)	0.4088(5)	0.1192(8)	0.0471(4)	10.2(3)
C(6)	0.3766(5)	–0.1685(7)	0.0673(4)	9.2(2)
C(7)	0.0242(5)	0.2920(10)	0.1460(5)	9.7(3)
C(8)	0.1198(4)	0.2941(6)	0.0191(4)	6.4(2)
C(9)	0.3201(3)	–0.1790(6)	0.2759(3)	5.0(2)
C(10)	0.4105(4)	0.0062(8)	0.3718(4)	8.0(2)
C(11)	0.0344(5)	0.406(1)	0.1972(6)	14.1(4)
C(12)	–0.0295(6)	0.201(1)	0.1709(8)	19.6(5)
C(13)	0.0558(4)	0.2537(7)	–0.0400(4)	8.5(2)
C(14)	0.1321(6)	0.4383(8)	0.0160(5)	11.3(3)
C(15)	0.2569(5)	–0.2065(7)	0.3267(4)	9.2(3)
C(16)	0.3832(4)	–0.2841(6)	0.2882(4)	8.4(2)
C(17)	0.3594(5)	0.0391(8)	0.4353(4)	9.9(3)
C(18)	0.4815(6)	0.069(1)	0.3767(5)	14.8(4)
C(19)	0.2511(5)	0.4291(6)	0.2011(6)	6.8(2)
C(20)	0.3137(7)	0.3856(8)	0.1676(5)	7.4(3)
C(21)	0.3643(6)	0.3277(9)	0.2246(9)	9.6(3)
C(22)	0.3291(9)	0.3401(10)	0.2900(7)	10.2(4)
C(23)	0.2600(7)	0.4018(8)	0.2770(6)	8.9(3)
3				
Sc(1)	0.33795(10)	0.26039(6)	0.42077(12)	4.39(3)
P(1)	0.3591(2)	0.37187(9)	0.6543(2)	5.22(5)
P(2)	0.23580(15)	0.12485(9)	0.2814(2)	5.05(4)
Si(1)	0.1031(2)	0.28231(10)	0.6107(2)	5.05(5)
Si(2)	0.0107(2)	0.22527(10)	0.2816(2)	5.66(5)
N(1)	0.1370(4)	0.2579(2)	0.4407(5)	4.30(12)
C(1)	0.2487(5)	0.3353(3)	0.7485(6)	5.5(2)
C(2)	0.0801(5)	0.1578(3)	0.1620(6)	5.4(2)
C(3)	0.0788(6)	0.2066(4)	0.7170(7)	6.6(2)
C(4)	–0.0519(6)	0.3357(4)	0.5895(8)	7.7(2)
C(5)	–0.0654(6)	0.2933(4)	0.1539(8)	8.6(2)
C(6)	–0.1306(6)	0.1790(4)	0.3253(8)	8.3(2)
C(7)	0.2928(7)	0.4606(4)	0.6000(10)	7.9(2)
C(8)	0.5136(7)	0.3999(4)	0.8087(9)	8.0(2)
C(9)	0.1746(8)	0.4531(4)	0.4584(11)	10.2(3)
C(10)	0.2628(11)	0.5069(5)	0.7264(11)	14.8(4)
C(11)	0.6218(7)	0.4239(5)	0.7432(9)	11.1(3)
C(12)	0.5613(7)	0.3572(5)	0.9280(10)	10.6(3)
C(13)	0.1795(6)	0.0668(3)	0.4033(8)	6.4(2)
C(14)	0.3022(7)	0.0626(4)	0.1576(9)	8.6(2)
C(15)	0.2959(7)	0.0294(4)	0.5053(8)	8.4(2)
C(16)	0.0678(7)	0.0129(4)	0.3134(9)	8.7(2)
C(17)	0.4509(7)	0.0585(4)	0.2129(8)	8.0(2)

© 2000 NRC Canada

Table 2 *(Concluded)*.

Atom	*x*	*y*	*z*	B_{eq}
C(18)	0.2446(8)	0.0555(5)	–0.0080(9)	11.6(3)
C(19)	0.4158(13)	0.3602(4)	0.3043(12)	8.0(3)
C(20)	0.5196(8)	0.3177(6)	0.3346(9)	7.3(3)
C(21)	0.4838(10)	0.2567(5)	0.2423(11)	6.9(3)
C(22)	0.3556(10)	0.2610(6)	0.1517(8)	7.7(3)
C(23)	0.3105(9)	0.3272(7)	0.1893(12)	8.8(3)
C(24)	0.4879(6)	0.2099(3)	0.6037(7)	4.6(2)
C(25)	0.4587(6)	0.1834(4)	0.7233(9)	6.7(2)
C(26)	0.5404(8)	0.1527(4)	0.8435(9)	6.6(2)
C(27)	0.6734(9)	0.1446(4)	0.8553(9)	8.0(3)
C(28)	0.7145(7)	0.1680(4)	0.7375(11)	8.1(3)
C(29)	0.6273(7)	0.1991(4)	0.6203(9)	6.8(2)

[a] $B_{eq} = (8/3)\pi^2 \Sigma\Sigma(U_{ij} a_i \times a_j \times (\mathbf{a}_i \cdot \mathbf{a}_j))$.

Table 3. Selected bond lengths (Å) for Sc(η^5-C_5H_5)Cl[N($SiMe_2CH_2P^iPr_2$)$_2$] (**1**) (left) and Sc(η^5-C_5H_5)Ph[N($SiMe_2CH_2P^iPr_2$)$_2$] (**3**) (right).

P(1)–Sc(1)	2.804(2)	P(1)–Sc(1)	2.822(2)
P(2)–Sc(1)	2.822(2)	P(2)–Sc(1)	2.836(2)
N(1)–Sc(1)	2.116(4)	N(1)–Sc(1)	2.174(4)
Cp–Sc(1)	2.21	Cp–Sc(1)	2.24
Cl(1)–Sc(1)	2.383(2)	C(24)–Sc(1)	2.229(6)

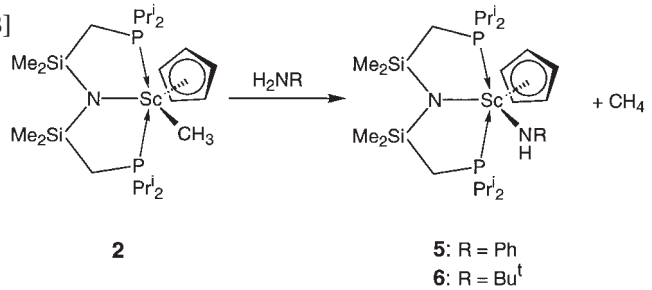
Table 4. Selected bond angles (°) for Sc(η^5-C_5H_5)Cl[N($SiMe_2CH_2P^iPr_2$)$_2$] (**1**) (left) and Sc(η^5-C_5H_5)Ph[N($SiMe_2CH_2P^iPr_2$)$_2$] (**3**) (right).

P(1)-Sc(1)-P(2)	147.08(6)	P(1)-Sc(1)-P(2)	149.77(6)
P(1)-Sc(1)-Cp	106.9	P(1)-Sc(1)-Cp	105.5
P(2)-Sc(1)-Cp	105.4	P(2)-Sc(1)-Cp	104.0
N(1)-Sc(1)-Cp	127.9	N(1)-Sc(1)-Cp	130.2
Cl(1)-Sc(1)-Cp	116.6	C(24)-Sc(1)-Cp	115.3

Reactivity of Sc(η^5-C_5H_5)Me[N($SiMe_2CH_2P^iPr_2$)$_2$] (2)

In contrast to the facile decomposition of dialkyls $ScR_2[N(SiMe_2CH_2P^iPr_2)_2]$ (R = Me, Et, CH_2SiMe_3) with H_2, (24) the scandium methyl complex **2** is inert to H_2 (4 atm, 5 days). However, exposure of methyl **2** to H_2NPh or H_2N^tBu (toluene solution, 1 equiv) yields the amides Sc(η^5-C_5H_5)NHPh[N($SiMe_2CH_2P^iPr_2$)$_2$] (**5**) and Sc(η^5-C_5H_5)NH^{t}Bu[N($SiMe_2CH_2P^iPr_2$)$_2$] (**6**) with the elimination of methane (eq. [3]).

[3]

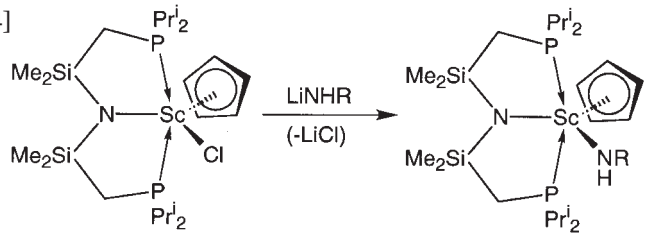


2 **5**: R = Ph; **6**: R = Bu^t

These reactions proceed analogously to those between Cp^*_2ScMe and H_2NR (R = H, Me, Ph, CH_2CMe_3) (32). The syntheses of **5** and **6** are accompanied by a competing decomposition to produce $HN(SiMe_2CH_2P^iPr_2)_2$ and an insoluble scandium-containing precipitate; thus the yields are quite low. (The amides Cp^*_2ScNHR are also produced in low yields (32)). The similar solubility of $HN(SiMe_2CH_2P^iPr_2)_2$ to amides **5** and **6** hindered our attempts to isolate them as pure solids. If a large excess of amine is used (4 equiv), only the protonated ligand is observed. We assume the amine proteolytically attacks the scandium-amide bond, resulting in decomposition accompanied by loss of $HN(SiMe_2CH_2P^iPr_2)_2$.

Cp^*_2ScMe reacts similarly with hydrazine; with 1 equiv, $Cp^*_2ScN(H)NH_2$ is formed although excess NH_2NH_2 results in decomposition to Cp^*H (33). To ensure the identity of the products, **5** and **6** were also synthesized by a salt-elimination route between the chloro species Sc(η^5-C_5H_5)Cl[N($SiMe_2CH_2P^iPr_2$)$_2$] (**1**) and LiNHR (R = Ph, ^{t}Bu) (eq. [4]).

[4]

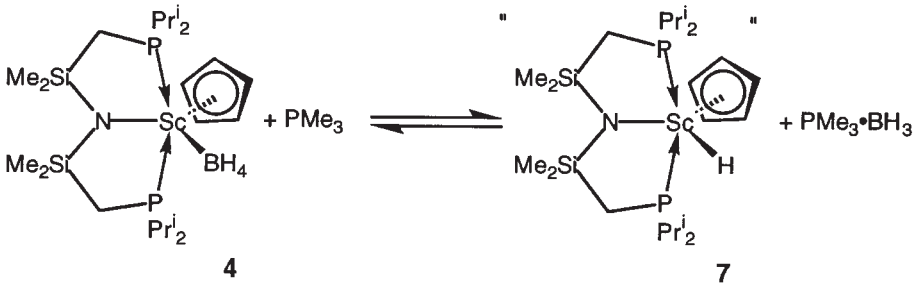


1 **5**: R = Ph; **6**: R = Bu^t

The ligand backbone and Cp resonances are shifted from the starting methyl complex, and peaks due to the phenyl ring are visible. The N*H* proton resides at 5.55 ppm (br s); by comparison, the N*H* resonance in $[PhC(NSiMe_3)_2]_2Sc(NHC_6H_3$-2,6-^{i}Pr$_2$) is located at 5.86 ppm (17). Even when synthesized from the lithium amides, **5** and **6** are contaminated with $HN(SiMe_2CH_2P^iPr_2)_2$, suggesting that intermolecular cleavage of Sc—N bonds by Sc(η^5-C_5H_5)NHR[N($SiMe_2CH_2P^iPr_2$)$_2$] may also occur. The related hydrazido complex $Cp^*_2ScN(H)NH_2$ also undergoes a concentration dependent decomposition to eliminate Cp^*H (33). The ^{1}H NMR spectrum of *tert*-butylamide **6** contains a NC*Me*$_3$ resonance at 1.37 ppm (s) and a broad peak which integrates for a single

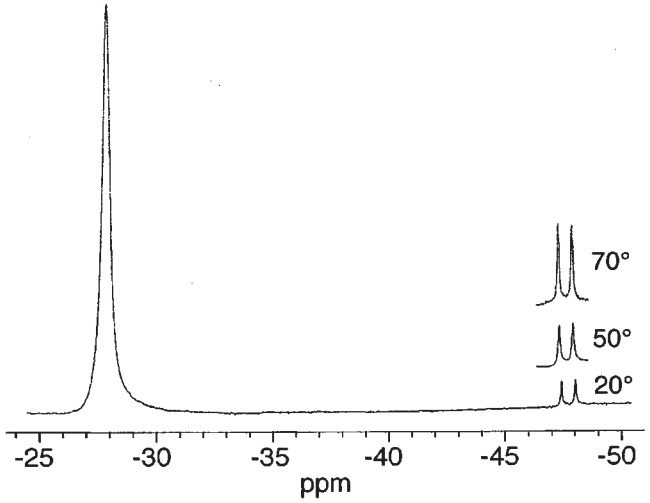
© 2000 NRC Canada

Scheme 1.



4 7

Fig. 3. Variable temperature 96.3 MHz $^{11}B\{^1H\}$ NMR spectra for the reaction between $Sc(\eta^5\text{-}C_5H_5)(BH_4)[N(SiMe_2CH_2P^iPr_2)_2]$ (**4**) and PMe_3 (~100 equiv).



proton at 4.70 ppm. The N*H* peak for the related compound $Cp^*_2Sc(NHCH_2CMe_3)$ resides at 4.75 ppm (32). Phenylamide **5** and *tert*-butylamide **6** exhibit broad peaks ($\Delta_{1/2}$ = 80 and 90 Hz, respectively) around 0 ppm in the $^{31}P\{^1H\}$ NMR spectra.

Reactions between methyl **2** and more acidic substrates such as primary and secondary phosphines were much less well behaved. The reaction of $Sc(\eta^5\text{-}C_5H_5)Me[N(SiMe_2CH_2P^iPr_2)_2]$ with H_2PPh or $HPPh_2$ (1 equiv in THF) results in protonation of the ancillary ligand to yield $HN(SiMe_2CH_2P^iPr_2)_2$ and an insoluble white precipitate. Attempts to generate scandium phosphides of the general formula $Sc(\eta^5\text{-}C_5H_5)(PR_2)[N(SiMe_2CH_2P^iPr_2)_2]$ (R = Ph, ^{i}Pr) via salt metathesis routes from chloride **1** and $LiPPh_2$ or LiP^iPr_2 resulted in unidentifiable mixtures. We also examined the potential of these systems as ethylene polymerization catalysts. Although phenyl **3** and borohydride **4** show no activity towards ethylene, methyl **2** polymerizes ethylene slowly either with or without methylalumoxane present as a co-catalyst.

Reactivity of $Sc(\eta^5\text{-}C_5H_5)(BH_4)[N(SiMe_2CH_2P^iPr_2)_2]$ (4)

Compounds that contain direct metal-hydrogen bonds are important due to their implication in a large number of stoichiometric and catalytic processes (34). In certain cases, transition-metal tetrahydroborate complexes serve as precursors to metal hydride derivatives if BH_3 can be cleaved from the $[BH_4]^-$ unit (35–38). Typically, strong σ-donors such as tertiary phosphines or amines are effective in this regard. The reaction of $Sc(\eta^5\text{-}C_5H_5)(BH_4)[N(SiMe_2CH_2P^iPr_2)_2]$ (**4**) with PMe_3 (~100 equiv) was followed by $^{11}B\{^1H\}$ NMR spectroscopy (Fig. 3).

The spectra consist of a large singlet due to the borohydride complex **4** at –27.6 ppm and a doublet at –47.8 ppm ($^1J_{B\text{-}P}$ = 48 Hz). If the spectrum is collected with proton coupling, this doublet appears as a quartet of doublets ($^3J_{B\text{-}H}$ = 86 Hz). This pattern is due to $PMe_3{\cdot}BH_3$. As the temperature is increased, the relative area of the peak due to $PMe_3{\cdot}BH_3$ increases. This indicates that an equilibrium is present between $Sc(\eta^5\text{-}C_5H_5)(BH_4)[N(SiMe_2CH_2P^iPr_2)_2]$ (**4**), PMe_3, $PMe_3{\cdot}BH_3$, and the putative hydride $Sc(\eta^5\text{-}C_5H_5)H[N(SiMe_2CH_2P^iPr_2)_2]$ (**7**) (Scheme 1).

From the van't Hoff plot, the following thermodynamic parameters were obtained: ΔH° = 8.8 ± 2 kcal mol^{-1} and ΔS° = 10.1 ± 8 cal K^{-1} mol^{-1}. From the equilibrium data, it appears unlikely that a scandium hydride can be isolated via this route. Even with a 100-fold excess of PMe_3 at 68°C, the equilibrium still favors the starting borohydride complex. We should also note that by studying the equilibrium by $^{11}B\{^1H\}$ NMR spectroscopy, we only have indirect evidence for the formation of the scandium hydride **7**. Although the observation of $PMe_3{\cdot}BH_3$ implies the existence of this species, we were not able to observe the scandium-hydride signal in the ^1H spectrum due to quadrupolar broadening; however new ligand and Cp resonances were evident (see Experimental Section). The positive entropy term indicates a monomeric species, as opposed to a dimeric or base-stabilized complex, which would be reflected in a significantly negative value of ΔS°.

Conclusions

In an attempt to generate more stable scandium-alkyls, a chloride in the starting complex $ScCl_2(THF)[N(SiMe_2CH_2P^iPr_2)_2]$ was replaced with a cyclopentadienyl ligand, to generate a more sterically and electronically saturated metal centre. The rationale for this was that the resulting alkyl complexes $Sc(\eta^5\text{-}C_5H_5)R[N(SiMe_2CH_2P^iPr_2)_2]$ should exhibit more controlled reactivity patterns as compared to the previously reported series $ScR_2[N(SiMe_2CH_2P^iPr_2)_2]$ (R = Me, Et, CH_2SiMe_3). Metathesis of the remaining chloride ligand in $Sc(\eta^5\text{-}C_5H_5)Cl[N(SiMe_2CH_2P^iPr_2)_2]$ (**1**) was easily undertaken. The methyl complex **2** was inert to H_2, but found to react with amines via C-H activation to yield phenylamide **5** and *tert*-butylamide **6** although a competing decomposition to $HN(SiMe_2CH_2P^iPr_2)_2$ was observed. The borohydride complex **4** reacts with PMe_3 to form a putative scandium-hydride complex **7**, as studied by $^{11}B\{^1H\}$ NMR spectroscopy. The presence of a single Cp ligand results in more

© 2000 NRC Canada

stable scandium alkyls, although reaction at the scandium-amide bond, as well as the scandium-alkyl bond, is still observed.

Experimental section

Procedures

Unless otherwise stated all manipulations were performed under an atmosphere of dry, oxygen-free dinitrogen or argon by means of standard Schlenk or glovebox techniques. The glovebox used was a Vacuum Atmospheres HE-553-2 model equipped with a MO-40-2H purification system and a –40°C freezer. ^{1}H, ^{31}P{^{1}H}, and ^{11}B{^{1}H} NMR spectroscopy were performed on a Varian XL-300 instrument operating at 299.9, 121.4, and 96.3 MHz, respectively. ^{1}H NMR spectra were referenced to internal C_6D_5H (7.15 ppm) or $C_6D_5CD_2H$ (2.09 ppm). ^{31}P{^{1}H} NMR spectra were referenced to external $P(OMe)_3$ (141.0 ppm with respect to 85% H_3PO_4 at 0.0 ppm). ^{11}B{^{1}H} NMR spectra were referenced to neat BEt_3 (0.0 ppm). Mass spectral studies were carried out on a Kratos MS 50 using an EI source. Infrared spectra were recorded on a BOMEM MB-100 spectrometer. Solution samples were recorded on a 0.1 mm KBr cell and solid samples were recorded as KBr pellets. Microanalyses (C, H, N) were performed by Mr. P. Borda of this department.

Materials

$ScCl_2(THF)[N(SiMe_2CH_2P^iPr_2)_2]$ was prepared by a published procedure (24). MeLi (1.4 M solution in ether) was purchased from Aldrich and used as received. $LiBH_4$ and $NaBH_4$ were purchased from Strem and used as received. H_2NPh and H_2N^tBu were purchased from Aldrich and distilled over sodium benzophenone. PMe_3 was purchased from Aldrich and vacuum transferred over sodium benzophenone. LiNHPh and $LiNH^tBu$ were prepared by the addition of BuLi to an ether solution of the amine. NaCp(DME) (39) and PhLi (40) were prepared according to published procedures.

Toluene, Et_2O, THF, and hexamethyldisiloxane were refluxed over CaH_2 prior to a final distillation from either sodium metal or sodium benzophenone ketyl under an argon atmosphere. Deuterated solvents were dried by distillation from sodium benzophenone ketyl; oxygen was removed by 3 freeze-pump-thaw cycles.

Syntheses

*Sc(η^5-C_5H_5)Cl[N(SiMe$_2$CH$_2$P^{i}Pr$_2$)$_2$] (**1**). Method 1*: To a solution of $ScCl_2(THF)[N(SiMe_2CH_2P^iPr_2)_2]$ (572 mg; 0.985 mmol) in toluene (10 mL) was added solid NaCp(DME) (176 mg; 0.985 mmol). The reaction mixture was stirred at room temperature for 1 week. The reaction mixture was then passed through a frit lined with Celite to remove NaCl. The solvent was removed in vacuo to yield a yellow waxy solid. The residue was taken up in a minimum amount of toluene (approx. 5 mL). Slow evaporation of the solvent afforded large colorless plates (358 mg; 68% yield). *Method 2*: 10 mL of a THF solution of NaCp(DME) (400 mg, 2.25 mmol) was added dropwise to a THF solution (10 mL) of $ScCl_2$ $(THF)[N(SiMe_2CH_2P^iPr_2)_2]$ (1.270 g; 2.19 mmol) maintained at –78°C. This was stirred overnight and left to warm to room temperature. The THF was then removed in vacuo and the residue extracted with toluene (3 × 10 mL) and passed through a frit lined with Celite to remove NaCl. The solvent was removed in vacuo to yield a white waxy solid, which resulted in colorless plates upon crystallization from toluene (655 mg; 56% yield). ^{1}H NMR (C_6D_6) δ: 6.51 (t, 5H, C_5H_5, $^{3}J_{H\text{-}P}$ = 1.3 Hz), 2.15 and 1.78 (d of sept, 4H, C*H*Me$_2$, $^{3}J_{H\text{-}H}$ = 7.7 Hz, $^{2}J_{H\text{-}P}$ = 3.4 Hz), 1.34, 1.14, 1.11, and 1.06 (dd, 24H, CH*MeMe′*, $^{3}J_{H\text{-}H}$ = 7.7 Hz, $^{3}J_{H\text{-}P}$ = 6.5 Hz), 0.88 and 0.65 (dd, 4H, C*H*$_2$P, $^{2}J_{H\text{-}H}$ = 14.5 Hz, $^{2}J_{H\text{-}P}$ = 7.8 Hz), 0.28 and 0.24 (s, 12H, Si*Me*$_2$). ^{31}P{^{1}H} NMR (C_6D_6) δ: –1.2 (425 Hz peak width at half height). MS: *m/e* 538 (M^+). Anal. calcd. for $C_{23}H_{49}ClNP_2ScSi_2$: C 51.33, H 9.18, N 2.60; found: C 51.40, H 8.98, N 2.83.

*Sc(η^5-C_5H_5)Me[N(SiMe$_2$CH$_2$P^{i}Pr$_2$)$_2$] (**2**).* To a toluene solution (5 mL) of $Sc(\eta^5\text{-}C_5H_5)Cl[N(SiMe_2CH_2P^iPr_2)_2]$ (**1**) (302 mg; 0.561 mmol) was added MeLi (0.40 mL of a 1.4 M Et_2O solution, 0.560 mmol), dropwise. The reaction mixture became cloudy and was stirred overnight, after which time it was filtered through a frit lined with Celite to remove LiCl. The solvent was removed in vacuo to yield an orange-yellow waxy solid (187 mg; 65% yield). Because the product was low melting, elemental analysis was not possible. ^{1}H NMR (C_6D_6) δ: 6.49 (t, 5H, C_5H_5, $^{3}J_{H\text{-}P}$ = 1.1 Hz), 2.04 and 1.79 (d of sept, 4H, C*H*Me$_2$, $^{3}J_{H\text{-}H}$ = 7.4 Hz, $^{2}J_{H\text{-}P}$ = 4.1 Hz), 1.22, 1.15, 1.13 and 1.06 (dd, 24H, CH*MeMe′*, $^{3}J_{H\text{-}H}$ = 7.4 Hz, $^{3}J_{H\text{-}P}$ = 7.0 Hz), 0.83 and 0.69 (dd, 4H, C*H*$_2$P, $^{2}J_{H\text{-}H}$ = 14.0 Hz, $^{2}J_{H\text{-}P}$ = 4.0 Hz), 0.31 and 0.28 (s, 12H, Si*Me*$_2$), –0.19 (t, 3H, ScC*H*$_3$, $^{3}J_{H\text{-}P}$ = 4.3 Hz). ^{31}P{^{1}H} NMR (C_6D_6) δ: –2.0 (135 Hz peak width at half height). MS: *m/e* 502 (M^+ – Me).

*Sc(η^5-C_5H_5)Ph[N(SiMe$_2$CH$_2$P^{i}Pr$_2$)$_2$] (**3**).* To a toluene solution (10 mL) of $Sc(\eta^5\text{-}C_5H_5)Cl[N(SiMe_2CH_2P^iPr_2)_2]$ (**1**) (300 mg; 0.558 mmol) maintained at –60°C was added an ethereal solution of PhLi (1.2 mL of a 0.57 M solution; 0.684 mmol). The reaction mixture was left to warm up and stir overnight, and then filtered through a frit lined with Celite to remove LiCl, followed by solvent removal in vacuo. The residue was taken up in a minimum amount of hexamethyldisiloxane (approx. 5 mL). Subsequent slow evaporation resulted in the formation of colorless prisms (104 mg; 32% yield). ^{1}H NMR (C_6D_6) δ: 7.93 (d, 2H, *o*-Ph, $^{3}J_{H\text{-}H}$ = 8.2 Hz), 7.23 (t, 1H, *p*-Ph, $^{3}J_{H\text{-}H}$ = 8.0 Hz), 7.15 (m, 2H, *m*-Ph), 6.62 (t, 5H, C_5H_5, $^{3}J_{H\text{-}P}$ = 1.3 Hz), 1.71 (d of sept, 4H, C*H*Me$_2$, $^{3}J_{H\text{-}H}$ = 7.3 Hz, $^{2}J_{H\text{-}P}$ = 2.3 Hz), 1.05, 1.03, 0.85, and 0.55 (dd, 24H, CH*MeMe′*, $^{3}J_{H\text{-}H}$ = 7.3 Hz, $^{3}J_{H\text{-}P}$ = 7.0 Hz), 1.00 and 0.67 (dd, 4H, C*H*$_2$P, $^{2}J_{H\text{-}H}$ = 13.5 Hz, $^{2}J_{H\text{-}P}$ = 5.0 Hz), 0.42 and 0.32 (s, 12H, Si*Me*$_2$). ^{31}P{^{1}H} NMR (C_6D_6) δ: –2.8 (100 Hz peak width at half height). MS: *m/e* 580 (M^+). Anal. calcd. for $C_{29}H_{54}NP_2ScSi_2$: C 60.07, H 9.39, N 2.42; found: C 59.62, H 9.17, N 2.08.

*Sc(η^5-C_5H_5)(BH$_4$)[N(SiMe$_2$CH$_2$P^{i}Pr$_2$)$_2$] (**4**). Method 1*: Solid $LiBH_4$ (37 mg; 1.70 mmol) was added to a solution of $Sc(\eta^5\text{-}C_5H_5)Cl[N(SiMe_2CH_2P^iPr_2)_2]$ (**1**) (200 mg; 0.372 mmol) in toluene (10 mL). The reaction mixture was stirred at room temperature for 1 week and then passed through a frit lined with Celite to remove LiCl and excess $LiBH_4$. The solvent was removed in vacuo to yield a yellow waxy solid. The residue was taken up in a minimum amount of hexamethyldisiloxane (approx. 5 mL). Slow evaporation of the solvent

© 2000 NRC Canada

yielded large colorless plates (45 mg; 23% yield). *Method 2*: Sc(η^5-C_5H_5)Cl[N($SiMe_2CH_2P^iPr_2$)$_2$] (**1**) (130 mg; 0.242 mmol) and $NaBH_4$ (90 mg; 2.38 mmol) were placed in a bomb. 10 mL THF was distilled onto the mixture and left to stir overnight. The solvent was removed under vacuum and the residue extracted into toluene (3 × 5 mL). The reaction mixture was then passed through a frit lined with Celite to remove NaCl and excess $NaBH_4$. The solvent was then removed in vacuo to yield a white solid. The residue was taken up in a minimum amount of hexamethyldisiloxane (approx. 2 mL). Slow evaporation of the solvent gave large colorless plates (83 mg; 66% yield). ^{1}H NMR (C_6D_6) δ: 6.41 (t, 5H, C_5H_5, $^3J_{H-P}$ = 1.3 Hz), 1.99 and 1.80 (d of sept, 4H, C*H*Me$_2$, $^3J_{H-H}$ = 7.0 Hz, $^2J_{H-P}$ = 5.1 Hz), 1.23, 1.11, 1.08, and 1.03 (dd, 24H, CH*MeMe′*, $^3J_{H-H}$ = 7.0 Hz, $^3J_{H-P}$ = 6.0 Hz), 0.90 and 0.65 (dd, 4H, CH_2P, $^2J_{H-H}$ = 14.5 Hz, $^2J_{H-P}$ = 4.8 Hz), 0.31 and 0.28 (s, 12H, SiMe_2). ^{31}P{^{1}H} NMR (C_6D_6) δ: 0.5 (200 Hz peak width at half height). ^{11}B NMR (C_6D_6, 20°C) δ: –27.6, quint, BH_4, $^1J_{B-H}$ = 85 Hz, 32 Hz peak width at half height), (C_7D_8, –80°C) δ: –27.0 (br s, BH_4, 160 Hz peak width at half height). ^{11}B{^{1}H} NMR (C_6D_6, 20°C) δ: –27.6 (s, BH_4, 32 Hz peak width at half height). IR (KBr disc): ν_{B-H} = 2478 (H_t), 2211 cm^{-1} (H_b), (hexanes solution): ν_{B-H} = 2476 (H_t), 2212 cm^{-1} (H_b). MS: *m/e* 516 (M^+ – H). Anal. calcd. for $C_{23}H_{53}BNP_2ScSi_2$: C 53.38, H 10.32, N 2.71; found: C 53.79, H 10.40, N 2.86.

*Sc(η^5-C_5H_5)NHPh[N($SiMe_2CH_2P^iPr_2$)$_2$] (**5**). Method 1*: To Sc(η^5-C_5H_5)Me[N($SiMe_2CH_2P^iPr_2$)$_2$] (**2**) (92 mg; 0.178 mmol) in toluene (10 mL) was added a toluene solution (10 mL) of aniline (23 mg, 0.247 mmol). The yellow color of the solution gradually dissipated and the solution became cloudy. The reaction mixture was stirred overnight, and the contents of the flask filtered through Celite to remove a white precipitate, followed by solvent removal. **5** was isolated as an oil; the presence of HN($SiMe_2CH_2P^iPr_2$)$_2$ (by NMR spectroscopy) did not allow for a pure sample to be obtained (30 mg; 28% yield (estimated)). *Method 2*: An ethereal solution (5 mL) of LiNHPh (14 mg, 0.141 mmol) was slowly added by cannula to a toluene solution (10 mL) of Sc(η^5-C_5H_5)Cl[N($SiMe_2CH_2P^iPr_2$)$_2$] (**1**) (75 mg, 0.139 mmol) maintained at –78°C. The solution was allowed to warm to room temperature, during which time it became cloudy. The solution was filtered to remove LiCl and the solvent removed in vacuo to yield a yellow oil (25 mg; 30% yield (estimated)). ^{1}H NMR (C_6D_6) δ: 7.20 (t, 2H, *m*-Ph, $^3J_{H-H}$ = 6.0 Hz), 6.78 (d, 2H, *o*-Ph, $^3J_{H-H}$ = 6.0 Hz), 6.66 (t, 1H, *o*-Ph, $^3J_{H-H}$ = 6.0 Hz), 5.55 (br s, 1H, N*H*), 6.48 (t, 5H, C_5H_5, $^3J_{H-P}$ = 1.5 Hz), 1.87 and 1.73 (d of sept, 4H, C*H*Me$_2$, $^3J_{H-H}$ = 6.8 Hz, $^2J_{H-P}$ = 1.5 Hz), 1.13, 1.09, 0.99 and 0.92 (dd, 24H, CH*MeMe′*, $^3J_{H-H}$ = 6.8 Hz, $^3J_{H-P}$ = 6.5 Hz), 0.75 and 0.68 (dd, 4H, CH_2P, $^2J_{H-H}$ = 13.4 Hz, $^2J_{H-P}$ = 4.3 Hz), 0.30 and 0.28 (s, 12H, SiMe_2). ^{31}P{^{1}H} NMR (C_6D_6) δ: –1.0 (80 Hz peak width at half height).

*Sc(η^5-C_5H_5)NH^{t}Bu [N($SiMe_2CH_2P^iPr_2$)$_2$] (**6**). Method 1*: To Sc(η^5-C_5H_5)Me[N($SiMe_2CH_2P^iPr_2$)$_2$] (**2**) (90 mg; 0.174 mmol) in toluene (10 mL) was added a toluene solution (10 mL) of *tert*-butylamine (17 mg, 0.232 mmol). The yellow color of the solution dissipated and the solution became cloudy. The reaction mixture was stirred overnight, the contents of the flask filtered through Celite to remove a white precipitate, and the solvent removed. **6** was isolated as an oil; the presence of HN($SiMe_2CH_2P^iPr_2$)$_2$ (by NMR spectroscopy) did not allow for a pure sample to be obtained (41 mg; 41% yield (estimated)). *Method 2*: An ethereal solution (5 mL) of LiNH^{t}Bu (11 mg, 0.149 mmol) was slowly added by cannula to a toluene solution (10 mL) of Sc(η^5-C_5H_5)Cl[N($SiMe_2CH_2P^iPr_2$)$_2$] (**2**) (75 mg, 0.139 mmol) maintained at –78°C. The solution was allowed to warm to room temperature, during which time it became cloudy. The solution was filtered to remove LiCl and the solvent removed in vacuo to yield a yellow oil (20 mg; 25% yield (estimated)). ^{1}H NMR (C_6D_6) δ: 6.48 (s, 5H, C_5H_5), 4.70 (br s, 1H, N*H*), 1.80 and 1.71 (d of sept, 4H, C*H*Me$_2$, $^3J_{H-H}$ = 7.4 Hz, $^2J_{H-P}$ = 3.4 Hz), 1.37 (s, 9H, NMe_3), 1.15, 1.06, 1.04 and 1.00 (dd, 24H, CH*MeMe′*, $^3J_{H-H}$ = 14.8 Hz, $^3J_{H-P}$ = 7.4 Hz), 0.67 (other peak obscurred, dd, 4H, CH_2P, $^2J_{H-H}$ = 10.2 Hz, $^2J_{H-P}$ = 4.8 Hz), 0.42 and 0.35 (s, 12H, SiMe_2). ^{31}P{^{1}H} NMR (C_6D_6) δ: 1.0 (90 Hz peak width at half height).

*Sc(η^5-C_5H_5)H[N($SiMe_2CH_2P^iPr_2$)$_2$] (**7**).* A sealable NMR tube equipped with a Kontes valve was loaded with a 1 mL d_8-toluene solution of Sc(η^5-C_5H_5)(BH_4)[N($SiMe_2CH_2P^iPr_2$)$_2$] (**4**) (approx. 0.1 M). The NMR tube was attached via a glass bridge to a bomb containing PMe_3. The contents of the NMR tube were frozen and the head space evacuated. The head space was then opened to the bomb of PMe_3 and allowed to fill with vapour. The bomb was closed, and the vapour condensed into the NMR tube. The NMR tube was flame-sealed and carefully allowed to warm to room temperature. This method resulted in the exposure of Sc(η^5-C_5H_5)(BH_4)[N($SiMe_2CH_2P^iPr_2$)$_2$] to ~1 mL PMe_3 (approx. 100 equiv). Due to the large excess of PMe_3, the reaction was followed by ^{11}B{^{1}H} NMR spectroscopy. ^{1}H NMR (C_6D_6) δ: 6.30 (t, 5H, C_5H_5, $^3J_{H-P}$ = 1.1 Hz), 1.95 and 1.85 (d of sept, 4H, C*H*Me$_2$, $^3J_{H-H}$ = 7.1 Hz, $^2J_{H-P}$ = 4.5 Hz), 1.15, 1.13, 1.12 and 1.03 (dd, 24H, CH*MeMe′*, $^3J_{H-H}$ = 7.2 Hz, $^3J_{H-P}$ = 10.5 Hz), 0.22 and 0.16 (s, 12H, SiMe_2), methylene protons obscured by PMe_3. ^{31}P{^{1}H} NMR (C_6D_6) δ: 0.3 (430 Hz peak width at half height). ^{11}B{^{1}H} NMR (C_6D_6) δ: –27.6 (s, Sc(η^5-C_5H_5)(BH_4)[N($SiMe_2CH_2P^iPr_2$)$_2$]), –47.8 (d, PMe_3·*B*H_3, $^1J_{B-P}$ = 48 Hz). ^{11}B NMR (C_6D_6) δ: –27.6 (quint, Sc(η^5-C_5H_5)(BH_4)[N($SiMe_2CH_2P^iPr_2$)$_2$]), –47.8 (q of d, PMe_3·*B*H_3, $^1J_{B-P}$ = 48 Hz, $^3J_{B-H}$ = 86 Hz). The peak at –47.8 ppm increased in area as the temperature was elevated.

X-ray crystallographic analyses of Sc(η^5-C_5H_5)Cl[N($SiMe_2CH_2P^iPr_2$)$_2$] (1) and Sc(η^5-C_5H_5)Ph[N($SiMe_2CH_2P^iPr_2$)$_2$] (3)

Crystallographic data appear in Table 1. The final unit-cell parameters were obtained by least-squares on the setting angles for 25 reflections with 2θ = 31.3–47.0° for **1** and 20.1–27.4° for **3.** The intensities of three standard reflections, measured every 200 reflections throughout the data collection, showed only small random fluctuations for **1** and decayed linearly by 13.4% for **3**. The data were processed (41), corrected for Lorentz and polarization effects, decay (for **3**), and absorption (based on azimuthal scans).

The structure of **1** was solved by the Patterson method and that of **3** by direct methods. The structure analysis of **3** was initiated in the centrosymmetric space group *P* on the basis of the *E*-statistics, this choice being validated by subsequent

© 2000 NRC Canada

calculations. All nonhydrogen atoms were refined with anisotropic thermal parameters. Hydrogen atoms were fixed in calculated positions with C—H = 0.98 Å and B_H = 1.2 $B_{\text{bonded atom}}$. A correction for secondary extinction was applied for **1** (Zachariasen type, isotropic, gaussian), the final value of the extinction coefficient being 7.1(7) × 10^{-7}. No correction for secondary extinction was necessary for **3**. Neutral atom scattering factors for all atoms and anomalous dispersion corrections for the non-hydrogen atoms were taken from the International Tables for X-Ray Crystallography (42). Final atomic coordinates and equivalent isotropic thermal parameters, selected bond lengths, and selected bond angles appear in Tables 2–4, respectively. Tables of full crystallographic data, final atomic coordinates, bond lengths, bond angles, anisotropic thermal parameters, and torsion angles are available as supplementary material.[2]

Acknowledgements

Financial support was generously provided by NSERC of Canada in the form of grants to M.D.F. and a postgraduate scholarship to G.R.G.

References

1. G. Wilkinson and J.M. Birmingham. J. Am. Chem. Soc. **78**, 42 (1956).
2. M.F. Lappert and R. Pearce. J. Chem. Soc. Chem. Commun. 126 (1973).
3. F.A. Hart, A.G. Massey, and M.S. Saran. J. Organomet. Chem. **21**, 147 (1970).
4. R.S.P. Coutts and P.C. Wailes. J. Organomet. Chem. **25**, 117 (1970).
5. J.L. Atwood and K.D. Smith. J. Chem. Soc. Dalton Trans. 2487 (1973).
6. J. Holton, M.F. Lappert, G.R. Scollary, D.G.H. Ballard, R. Pearce, J.L. Atwood, and W.E. Hunter. J. Chem. Soc. Chem. Commun. 425 (1976).
7. W.E. Piers, P.J. Shapiro, E.E. Bunel, and J.E. Bercaw. Synlett. 74 (1990).
8. M.E. Thompson, S.M. Baxter, A.R. Bulls, B.J. Burger, M.C. Nolan, B.D. Santarsiero, W.P. Schaefer, and J.E. Bercaw. J. Am. Chem. Soc. **109**, 203 (1987).
9. B.J. Burger, M.E. Thompson, W.D. Cotter, and J.E. Bercaw. J. Am. Chem. Soc. **112**, 1566 (1990).
10. M.E. Thompson and J.E. Bercaw. Pure Appl. Chem. **56**, 1 (1984).
11. P.R. Meehan, D.R. Aris, and G.R. Willey. Coord. Chem. Rev. **181**, 121 (1999).
12. F.T. Edelmann. Angew. Chem. Int. Ed. Engl. **34**, 2466 (1995).
13. D. Dolphin. The porphyrins. Academic Press, New York. 1978.
14. J. Arnold and C.G. Hoffman. J. Am. Chem. Soc. **112**, 8620 (1990).
15. J. Arnold, C.G. Hoffman, D.Y. Dawson, and F.J. Hollander. Organometallics, **12**, 3645 (1993).
16. M.G. Sewchok, R.C. Haushalter, and J.S. Merola. Inorg. Chim. Acta. **144**, 47 (1988).
17. J.R. Hagadorn and J. Arnold. Organometallics, **15**, 984 (1996).
18. J. Blackwell, C. Lehr, Y. Sun, W.E. Piers, S. D. Pearce-Batchilder, M.J. Zaworotko, and V.G. Young, Jr. Can. J. Chem. **75**, 702 (1997).
19. W.E. Piers and J.E. Bercaw. J. Am. Chem. Soc. **112**, 9406 (1990).
20. S. Hajela and J.E. Bercaw. Organometallics, **13**, 1147 (1994).
21. P.J. Shapiro, E. Bunel, W.P. Schaefer, and J.E. Bercaw. Organometallics, **9**, 867 (1990).
22. P.J. Shapiro, W.D. Cotter, W.P. Shaefer, J.A. Labinger, and J.E. Bercaw. J. Am. Chem. Soc. **116**, 4623 (1994).
23. Y. Mu, W.E. Piers, D.C. MacQuarrie, M.J. Zawarotko, and V.G. Young, Jr. Organometallics, **15**, 2720 (1996).
24. M.D. Fryzuk, G.R. Giesbrecht, and S.J. Rettig. Organometallics, **15**, 3329 (1996).
25. H.J. Heeres, A. Meetsma, and J.H. Teuben. J. Chem. Soc. Chem. Commun. 962 (1988).
26. H. van der Heijden, C.J. Schaverien, and A.G. Orpen. Organometallics, **8**, 255 (1989).
27. H. van der Heijden, P. Pasman, E.J.M. de Boer, C.J. Schaverien, and A.G. Orpen. Organometallics, **8**, 1459 (1989).
28. E.D. Becker. High resolution NMR. Academic Press, New York. 1980.
29. M.F. Lappert, A. Singh, J.L. Atwood, and W.E. Hunter. J. Chem. Soc. Chem. Commun. 206 (1983).
30. T.J. Marks and J.R. Kolb. Chem. Rev. **77**, 263 (1977).
31. J.H. Morris and W.E. Smith. J. Chem. Soc. Chem. Commun. 245 (1970).
32. J.E. Bercaw, D.L. Davies, and P.T. Wolczanski. Organometallics, **5**, 443 (1986).
33. P.J. Shapiro, L.M. Henling, R.E. Marsh, and J.E. Bercaw. Inorg. Chem. **29**, 4560 (1990).
34. J.P. Collman, L.S. Hegedus, J.R. Norton, and R.G. Finke. Principles and applications of organotransition metal chemistry. University Science Books, Mill Valley. 1987.
35. M.D. Fryzuk and H.D. Williams. Organometallics, **2**, 162 (1983).
36. M.D. Fryzuk, S.J. Rettig, A. Westerhaus, and H.D. Williams. Inorg. Chem. **24**, 4316 (1985).
37. P.T. Wolczanski and J.E. Bercaw. Organometallics, **1**, 793 (1982).
38. J.D. James, R.K. Nauda, and M.G.H. Wallbridge. Inorg. Chem. **6**, 1979 (1967).
39. J.C. Smart and C.J. Curtis. Inorg. Chem. **16**, 1788 (1977).
40. M. Schlosser and V. Ladenburger. J. Organomet. Chem. **8**, 193 (1967).
41. (*a*) *teXsan*: Crystal Structure Analysis Package. Version 1.7. Molecular Structure Corp., The Woodlands, Tex. 1995; (*b*) *d*TREK*: Area Detector Software. Molecular Structure Corp., The Woodlands, Tex. 1997.
42. (*a*) International Tables for X-Ray Crystallography. Vol. IV. Kynoch Press. Birmingham, U.K. (present distributor Kluwer Academic Publishers: Boston, Mass., U.S.A.) 1974; (*b*) International Tables for Crystallography. Vol. C. Kluwer Academic Publishers. Boston, Mass., U.S.A. 1992.

[2] Copies of material on deposit may be purchased from: The Depository of Unpublished Data, Document Delivery, CISTI, National Research Council Canada, Ottawa, Canada, K1A 0S2. Full details of the crystallographic analyses have also been deposited with the Cambridge Crystallographic Data Centre and can be obtained on request from: The Director, Cambridge Crystallographic Data Centre, University Chemical Laboratory, 12 Union Road, Cambridge, U.K., CB2 1EZ.

© 2000 NRC Canada

Influence of the temperature on the viscosity measurements of solutions of a soil fulvic acid

Francisco Rey and Adelio A.S.C. Machado

Abstract: The influence of the concentration (ca. 45 to 300 mg L^{-1}), the pH (3.0 to 8.0), the ionic strength (0.005 to 0.10 M), and the temperature (283 to 303 K) on the viscosimetric behaviour of solutions of a soil fulvic acid has been analysed, and their molecular parameters (length, thickness, and molecular volume) calculated. The results indicate that the polyelectrolytic behaviour of the fulvic acid is similar at all the temperatures, i.e., increasing the viscosity when reducing the ionic strength and to increase the temperature. With respect to the pH an initial decrease in the viscosity is obtained followed by a rise to the highest pH values. These variations have been interpreted by their molecular parameters as due to modifications of the structure of the molecules of the fulvic acid.

Key words: fulvic acid, viscosity, temperature.

Résumé : L'influence de la concentration (ca. 45 à 300 mg L^{-1}), du pH (3.0 à 8.0), de la force ionique (0.005 á 0.10 M) et de la température (283 à 303 K) sur le comportement viscosimétrique de solutions d'acides fulviques de sol a été analysée, et leurs paramètres moléculaires (longueur, épaisseur et volume moléculaire) ont été calculés. Les résultats montrent que le comportement polyélectrolytique des acides fulviques est semblable à toutes les températures; plus précisément, la viscosité augment avec la diminution de la force ionique et l'augmentation de la température. L'influence du pH se traduit par une diminution initiale de la viscosité suivie ensuite par une augmentation celle-ci dans les valeurs de pH les plus élevées. Ces variations ont été interprétées, en fonction de leurs paramétres moléculaires, comme dues aux modifications de la structure des molécules d'acides fulviques.

Mots clés : acides fulviques, viscosité, température.

Introduction

Humic substances play a very important role in the environment because of their interaction with the particles of soils, trace metals and nutrients, their biological effects on plants and micro-organisms, and their influence on the quality of superficial and underground waters. It is well known that the pH, the concentration, and the presence of inert inorganic species, which alter the ionic strength, influence the behaviour of humic substances to a large extent (1). However, although temperature varies markedly in natural systems, its influence has been rarely considered in the study of the properties of these substances.

The measurement of the viscosity of fulvic or humic acid solutions can provide information about of the size and the shape of their molecules in solution, and the literature contains several studies in which the behavior of this type of substances is analysed by viscosimetric techniques (2 and references therein). However, in most of these cases the results are either incomplete or not comparable, due to differences in the extraction or purification methods or to the fact that values of the pH and of the ionic strength of the solutions studied were not the same or were not controlled.

Moreover, in spite of its importance, the analysis of the influence of the temperature on the viscosity of the humic material solutions (and consequently on the size and shape of their molecules) has not been approached in a systematic way. As far as the authors know, only Adhikari et al. (3) have measured the viscosities of humic acid solutions between 30 and 50°C, explaining the differences obtained in the reduced viscosity by the decrease of the viscous drag or by high-temperature coiling. These results are in agreement with those in Orlov's book (4). Finally, Stevenson (5) points out the influence of the temperature on the viscosimetric behavior of the humic substances when dissolved, but neither present nor refer to any published data.

In conclusion, the data in the literature do not clarify the influence of the temperature on the viscosity of humic materials in solution. Therefore, it was decided to include the viscosimetric measurements in a project in progress in our departments to study the behavior of the fulvic acids in solution (6–10). In a previous work (2), the influence of the concentration, the pH, and the background electrolyte concentration on the viscosimetric solution properties of a soil fulvic acid at low concentrations and constant temperature of 298 K were analysed. In the present work, the influence of temperature (283–303 K) on this behavior is reported. The dimensions of the molecules of the fulvic acid

Received April 22, 1999. Published on the NRC Research Press website on July 14, 2000.

F. Rey[1] and A.A.S.C. Machado.[2] Universidad de Vigo, Area de Química Física, Torrecedeira 86, E-36208 Vigo, Spain.

[1]Author to whom correspondence may be addressed. Telephone: 34-86-813688. Fax: 34-86-813663. e-mail: frey@correo.uvigo.es

[2]Permanent address: LAQUIPAI, Faculdade de Ciencias, Rua Campo Alegre 687, P-4150 Porto, Portugal.

© 2000 NRC Canada

were calculated, and their temperature-induced variations are discussed.

Experimental

Reagents and materials

All the reagents were for analysis quality and were used without further purification. For the preparation of the solutions deionised water Millipore Alpha Q was employed.

The fulvic acid sample used in the present work was isolated from a Portuguese soil of forest, collected in Famalicao (near Porto, 30 km to the Northeast), by the standard procedure proposed by the IHSS (11). For this purpose, portions of the soil dried in air were treated with hydrochloric acid (2 M, pH ≈ 2) by shaking during 15 days. The solid was separated by filtration and the liquid was concentrated in a column filled with Amberlite XAD-8 resin. The column was washed with water until free of chloride ions and then eluted with 0.1 M NaOH. The fulvic acid in the eluate was converted to its acidic form in a column with a cationic exchange resin (Merck Ion Exchanger I) and then freeze-dried to obtain a powder. The yield of the process was of the order of 0.5% of the fulvic acid – soil weights. Characterization parameters: elemental analysis: C 43.0, H 3.8, and N 1.7%; S and heavy metals not detected, O (51.5%) obtained by difference; Total acidity 11.9 meq g^{-1}, carboxylic acidity 5.3 meq g^{-1}; ash content lower than 0.5%.

To adjust the pH of the solutions, 0.1 M HCl and (or) 0.1 M NaOH solutions were used. $NaNO_3$ was used as support electrolyte to adjust the total ionic strength to desired values (see below).

Equipment

Free H^+ values (expressed as pH) were measured with a Crison μ-pH 2002 pH-meter (±0.1 mV) and an Ingold combined electrode, calibrated at each ionic strength by standard HCl–NaOH titrations (12). The viscosity measures were made with an Ostwald type viscosimeter (the flow time with deionised water at 298 K was 345.4 ± 0.2 s) at constant temperatures between 283 and 303 K, in 5 K steps (Tectron 4373200 thermostat, ±0.1 K). The density was measured with a glass picnometer calibrated with water at each temperature studied.

To obtain the average molecular weight (*M*) of the samples (used here as the average value of the heterogeneous mixture named fulvic acid), the semi-empirical equation obtained by Chin (13)

$$[1] \qquad M = 3.99\ \varepsilon + 490$$

where ε is the molar absorbtivity at 280 nm, was used. For this purpose, plots of the absorbance vs. concentration of the sample (in mg L^{-1}) buffered with 0.1 M sodium hydrogen carbonate were obtained at constant temperature using a Kontron Uvikon 930 UV–V spectrophotometer.

Procedure

The samples for the viscosimetric measurements were prepared by diluting aliquots of a 1000 mg L^{-1} stock solution of fulvic acid, and adjusting the pH and the total ionic strength to the required values. The experiments were done at twelve values of fulvic acid concentration, six pH values, and five temperatures (Table 1). The measurements of flow time were repeated at least twenty times and their mean values (after rejecting outlier values by a standard statistical technique (14)) were used to calculate the values of the absolute viscosities (standard deviations were always found to be less than 0.5%).

Table 1. Composition parameters for the experimental solutions.

Fulvic acid concentration (mg L^{-1})	pH	Ionic strength (M)
47.0	3.0	0.005
62.0	4.0	0.010
71.0	5.0	0.030
82.0	6.0	0.070
94.0	7.0	0.100
107.0	8.0	
118.0		
131.0		
163.0		
189.0		
236.0		
289.0		

Theory

The values of the relative (η_r), specific (η_{sp}), and reduced (η_z) viscosities were obtained from the experimental values of the absolute viscosity (η) by their respective definitions (eqs. [2]–[4]) (15)

$$[2] \qquad \eta_r = \frac{\eta}{\eta_0}$$

$$[3] \qquad \eta_{sp} = \frac{\eta - \eta_0}{\eta_0}$$

$$[4] \qquad \eta_z = \frac{\eta_{sp}}{c}$$

where η_0 is the absolute viscosity of the water and *c* the concentration of the solute in the solution. As intrinsic viscosities ([η]) are the base for molecular parameters calculation two different approaches were used to obtain their values, namely the extrapolation to zero concentration of the linear part of the plots of the reduced viscosity against concentration and the Fuoss and Cathers equation (16)

$$[5] \qquad \frac{c}{\eta_{sp}} = \frac{1}{A} + \frac{B}{A}\sqrt{c}$$

The results obtained by two methods are very similar (differences less than 2%) and mean values were used in calculations.

As the intrinsic viscosity can be related to the molecular weight (*M*) by Staundinger's equation of

$$[6] \qquad [\eta] = KM^{\alpha}$$

where *K* and α are coefficients depending on the temperature, the solvent and the polyelectrolyte, but are independent of the pH and of the ionic strength (15), values of the molecular weight at each pH and ionic strength are required for

© 2000 NRC Canada

Fig. 1. Variation of the specific viscosity with the fulvic acid concentration for the following experimental conditions: (■) pH = 5.0, I = 0.005 M, T = 283 K; (▲) pH = 4.0, I = 0.01 M, T = 288K; (+) pH = 5.0, I = 0.03 M, T = 293K; (*) pH = 6.0, I = 0.01, T = 298K; (□) pH = 4.0, I = 0.005, T = 303 K.

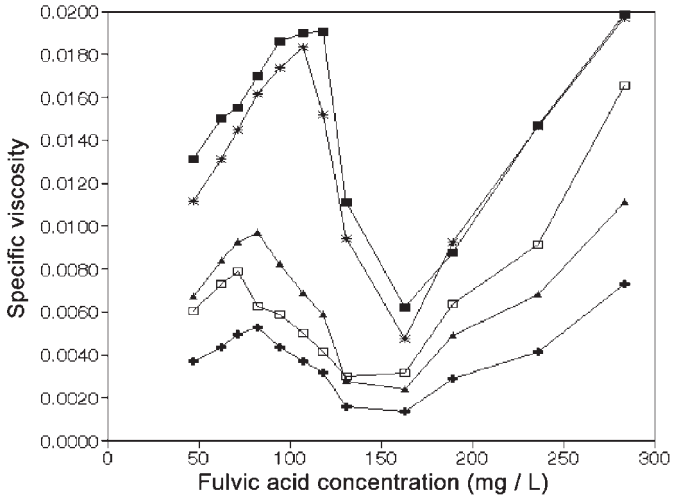
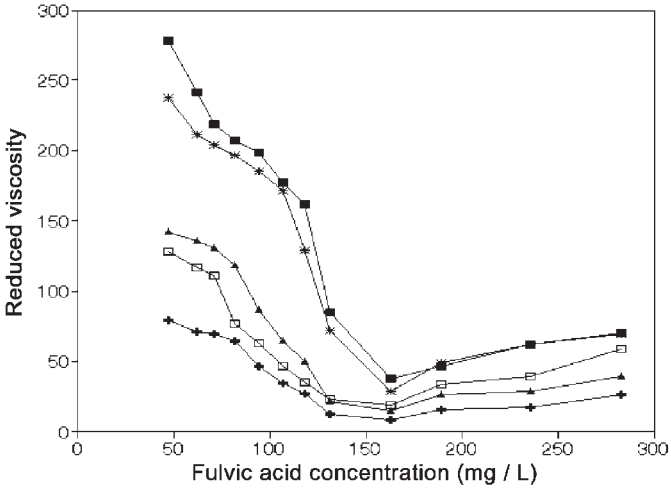


Fig. 2. Variation of the reduced viscosity with the fulvic acid concentration (same conditions as Fig. 1).



calculation of K and α. To estimate these values, absorbances at 280 nm were measured at the five temperatures used in the work (see eq. [1]), but were found to be constant within 2% maximum error. This shows that, under the present experimental conditions, M at each pH and ionic strength can be considered as constant over the whole temperature range. Therefore, values of molecular weights at 298 K, obtained in previous work at the same pH and ionic strength conditions (2), were used for the calculations of K and α, using the plots of the reduced viscosity against the molecular weight (see Fig. 4 below in "Results and Discussion").

The mean shape and the dimensions of the acid fulvic particles are important magnitudes when the physicochemical behaviour of these substances is analysed. The viscosity values can be used for their calculation, provided a model for such particles is used. In the bibliography, different shapes have been used, especially spheres, disks, and rods (15). In the analysis of the data obtained at 298 K it was concluded that from these three only the rod model, corresponding to a flexible linear colloid, was compatible with the experimental data (17). Therefore, this model was used in the present work, from which two relevant parameters were calculated, the length (a) and the thickness (b) of the rod, which are related to a function [k] through the equation (15)

$$[7] \qquad [k] = \frac{(a/b)^2}{15(\ln 2ab - 3/2)} + \frac{3(a/b)^2}{15(\ln 2ab - 1/2)} + \frac{14}{15}$$

This equation can be solved by numerical iteration to calculate the a/b ratio. The individual values of a and b can be determined from this ratio and the expression for the molecular volume given by

$$[8] \qquad V = \frac{\pi b^2 a}{4}$$

Results and discussion

Viscosimetric data for humic substances obtained at different temperatures can not be compared if the existence of a common general behaviour is not demonstrated. As it was stated at 298 K (2), the shape of the variation of the specific and reduced viscosity with the fulvic acid concentration are practically the same, despite of the composition of the solutions. Consequently, these plots can be used for an adequate verification of the constancy of this behaviour. So, in the figures 1 and 2 several examples of that type of plots are shown. As it can be seen, the shape of the curves is practically unalterable, and the range of values is similar to the reported for 298 K (2), which strongly suggest that the viscosimetric structure of this fulvic acid molecules is independent of the temperature, and, therefore, the same model can be applied to the data obtained at the five temperatures studied here. Moreover, this assumption is also confirmed when the variations of the intrinsic viscosity with the pH at constant ionic strength (Fig. 3) are analysed. A decrease of the intrinsic viscosity of the solutions of the fulvic acid when the pH is increased until about 5.0, followed by an increase in the neutral and alkaline pH ranges, is observed. This variation (also found at 298 K (2)) is a common fact for weak acid polyelectrolytes of the fulvic acid type, and it has been explained as a consequence of the existence of weaker binding forces at lower pH values [3] and the occurrence of aggregation due to cationic bridges and intermolecular interactions above pH 6 [4]. However, in absence of a more

© 2000 NRC Canada

Table 2. Variation of the intrinsic viscosity with pH, ionic strength, and temperature (298 K data obtained from reference (2)).

I	pH	*M*	283 K	288 K	293 K	298 K	303 K
0.005	3.0	91561	511	420	365	264	224
	4.0	57810	390	335	290	194	159
	5.0	42154	325	275	245	157	130
	6.0	34022	310	240	198	136	110
	7.0	37052	320	270	223	144	117
	8.0	41754	330	281	240	156	132
0.010	3.0	86433	498	415	350	254	218
	4.0	48304	361	295	262	172	127
	5.0	34022	312	249	225	136	110
	6.0	25125	256	210	180	111	88
	7.0	32540	287	250	211	132	112
	8.0	38599	328	260	229	148	120
0.030	3.0	54289	380	321	260	186	144
	4.0	28577	270	235	198	121	97
	5.0	22740	248	185	155	103	87
	6.0	16870	210	171	145	85	65
	7.0	19604	225	185	153	94	69
	8.0	22146	232	205	170	102	81
0.050	3.0	24452	252	215	180	109	87
	4.0	21501	235	190	162	100	81
	5.0	14275	187	150	135	76	55
	6.0	4110	97	81	55	33	27
	7.0	12091	175	142	105	68	47
	8.0	15124	199	161	138	79	60
0.070	3.0	11827	171	139	119	67	56
	4.0	11304	162	125	111	65	48
	5.0	5073	111	90	75	38	25
	6.0	1023	49	36	30	13	9
	7.0	5274	113	92	65	39	31
	8.0	7641	136	111	88	50	37

Fig. 3. Variation of the intrinsic viscosity with pH at different temperatures (I = 0.005): (■) 283 K; (*) 288 K; (▲) 293 K; (+) 298 K; (□) 303 K.

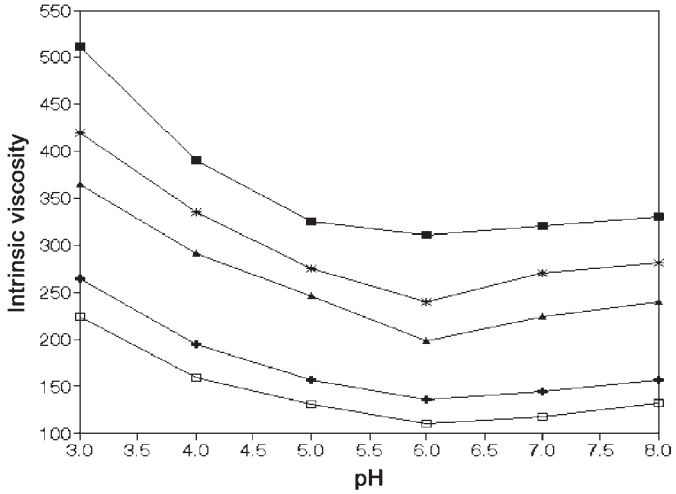


Table 3. Values of α and K at different temperatures obtained from the data of Table 2.

	283 K	288 K	293 K	298 K	303 K
α	0.53	0.55	0.58	0.67	0.71
K	1.25	0.84	0.51	0.13	0.06
r^2	0.998	0.997	0.995	0.998	0.994

complete characterisation of the sample, it must be considered only hypothetical for the present fulvic acid.

When data of intrinsic viscosity are compared at different temperatures (at constant pH), an important decrease when temperature rises was obtained. Because the size and shape of fulvic acid rods are the main factors that control the movement of these molecules in solution (and, hence, the viscosity) further discussion requires numerical values of length and thickness (see comments about Table 4) below.

In Table 2 the results for the intrinsic viscosity of the solutions of the fulvic acid at the values of pH, ionic strength and temperature studied in the present work are collected. Because the values of the absolute viscosity for the total ionic strength 0.1 M do not differ significantly from the viscosities of pure water at all temperatures, they were excluded from the table.

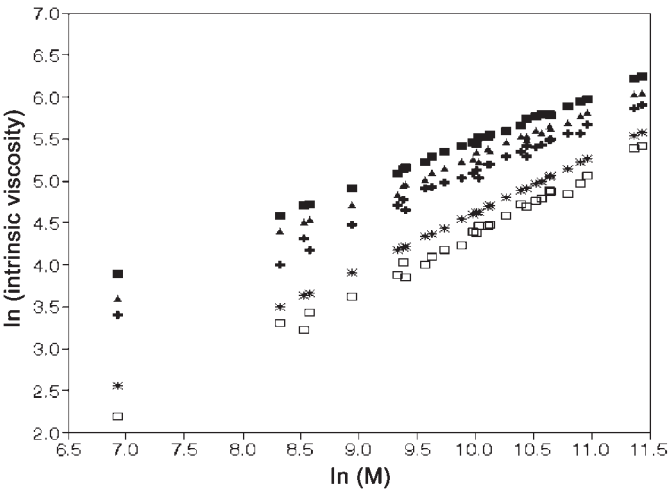
In Fig. 4, plots of ln ([η]) vs. ln M are presented. As shown, the plots are practically linear (r > 0.995 for all the

© 2000 NRC Canada

Table 4. Variation of molecular parameters with ionic strength, pH, and temperature.

I	pH	*V* (× 10^4)				*a*				*b*			
		283 K	288 K	293 K	303 K	283 K	288 K	293 K	303 K	283 K	288 K	293 K	303 K
0.005	3.0	9.4	9.4	9.4	9.4	1203	1118	1061	883	10.0	10.4	10.6	11.7
	4.0	5.9	5.9	5.9	5.9	933	881	834	665	9.0	9.3	9.5	10.7
	5.0	4.3	4.3	4.3	4.4	784	737	705	555	8.4	8.7	8.9	10.0
	6.0	3.5	3.5	3.5	3.5	718	651	606	483	7.9	8.3	8.6	9.6
	7.0	3.8	3.8	3.8	3.8	747	701	652	509	8.1	8.3	8.6	9.8
	8.0	4.3	4.3	4.3	4.3	786	740	697	556	8.3	8.6	8.9	10.0
0.010	3.0	8.9	8.9	8.9	8.9	1169	1092	1025	858	9.8	10.2	10.5	11.5
	4.0	5.0	5.0	5.0	5.0	854	791	757	575	8.6	8.9	9.1	10.5
	5.0	3.5	3.5	3.5	3.5	719	660	636	483	7.9	8.2	8.4	9.6
	6.0	2.6	2.6	2.6	2.6	603	560	529	403	7.4	7.7	7.9	9.1
	7.0	3.3	3.3	3.3	3.5	686	652	612	481	7.9	8.1	8.3	9.4
	8.0	4.0	4.0	4.0	4.0	764	700	667	522	8.1	8.5	8.7	9.9
0.030	3.0	5.6	5.6	5.6	5.6	905	849	784	627	8.9	9.	9.6	10.7
	4.0	2.9	2.9	2.9	3.0	643	610	572	435	7.6	7.8	8.1	9.3
	5.0	2.3	2.3	2.3	2.4	576	516	482	388	7.2	7.6	7.9	8.8
	6.0	1.7	1.7	1.7	1.7	491	453	426	313	6.7	7.0	7.2	8.4
	7.0	2.0	2.0	2.0	2.0	529	491	458	338	7.0	7.2	7.5	8.8
	8.0	2.3	2.3	2.3	2.3	557	532	495	372	7.2	7.4	7.7	8.9
0.050	3.0	2.5	2.5	2.5	2.5	595	560	524	396	7.3	7.6	7.8	9.0
	4.0	2.2	2.2	2.2	2.2	554	512	482	370	7.1	7.4	7.7	8.8
	5.0	1.5	1.5	1.5	1.5	293	408	392	277	4.3	6.8	6.9	8.2
	6.0	0.42	0.42	0.42	0.43	228	213	184	139	4.9	5.0	5.4	6.3
	7.0	1.2	1.2	1.2	1.3	409	378	337	246	6.2	6.5	6.9	8.1
	8.0	1.6	1.6	1.6	1.6	463	427	403	293	6.5	6.8	7.0	8.3
0.070	3.0	1.2	1.2	1.2	1.2	403	372	351	263	6.2	6.5	6.6	7.7
	4.0	1.2	1.2	1.2	1.2	389	352	336	243	6.2	6.5	6.6	7.8
	5.0	0.52	0.52	0.52	0,53	582	238	222	145	5.1	5.3	5.5	6.8
	6.0	0.11	0.11	0.11	0.11	110	97	91	56	3.5	3.7	3.8	4.9
	7.0	0.54	0.54	0.54	0.55	263	243	212	160	5.1	5.3	5.7	6.6
	8.0	0.78	0.79	0.79	0.79	319	296	270	193	5.6	5.8	6.1	7.2

Fig. 4. Plot of ln (intrinsic viscosity) vs. ln (molecular weight) at different temperatures: (■) 283 K; (*) 288 K; (▲) 293 K; (+) 298 K; (□) 303 K.



temperatures) which also confirm the assumption of the existence of an unique general behaviour, and allow the calculation of the parameters *K* and α; the values obtained are collected in Table 3. The results indicate an increase of the value of α and a decrease of *K* upon increasing the temperature, which can be attributed to the relative poorness of the solvent (18). Moreover, values of α fall in the range between 0.5 and 0.8, as for most of the polyelectrolyte–solvent systems (19).

In Table 4 the molecular parameters (i.e., molecular volume (*V*), length (*a*) and thickness (*b*)) for the molecules of the fulvic acid obtained at the different temperatures are collected (for values at 298 K, see reference 2). Although the values of *b* are of the same order of magnitude as those published (15), the values of *a* are larger. This is perhaps due to the different origin of the fulvic acids and to the lower concentrations range used (2). As shown by the data tables, these values depend markedly on the ionic strength, the pH, and the temperature, and therefore these three factors will be analysed separately.

As a rule, upon increasing the ionic strength a decrease in the molecular weight is observed as described before (2, 20), as well as a decrease of the size of the molecules of the fulvic acid due to the decrease in the values of both *a* and *b*. This can be attributed to further coiling of the fulvic acid

© 2000 NRC Canada

molecules (widely illustrated in the bibliography (5), due to the repulsion by the counterions or to the neutralisation of the superficial charges by the added salt (3).

With reference to the influence of the pH, an initial decrease of the values of both *a* and *b* upon increasing the pH is observed, until minima at pH ≈ 6 are reached, followed by a growth at higher pH values. This result is similar to others in the literature (15). The variation decreases when the ionic strength decreases (two to four times), and suggests that the presence of the counterions plays a very important role in the modifications of the structure of the molecules of fulvic acids.

A different variation is obtained when the temperature changes. In this case, at constant pH and ionic strength, a decrease of the length of the acid fulvic rods, probably due to coiling accompanied by increase of their thickness, is observed. As far as we know, this behaviour has not been described previously, though it has been suggested (3) that a decrease of the viscosity of solutions of humic substances upon increasing of the temperature is expected, due to the more extensive ionisation of these substances at higher temperatures. Since the length of the particles is the main variable responsible for the viscosity, its decrease explains why the viscosity decreases upon increasing the temperature and the consequent decrease of the viscous drainage.

As shown by the results of the present work, the external factors of the solutions (pH, ionic strength and, in particular, the temperature) can influence markedly the size of the molecules of fulvic acids in solution, and, consequently, their viscosimetric behaviour. However, the molecular weight, although changing with the ionic strength and the pH, keeps its value when the temperature is varied.

Acknowledgements

The authors acknowledge an Acción Integrada Hispano Portuguesa No. 1996 B-15 from the Conselho de Reitores das Universidades Portuguesas (Portugal) and the Ministerio de Educación y Ciencia (Spain). The authors also acknowledge the reviewer's comments, which have been very useful.

References

1. C.E. Clapp, W.W. Emerson, and A.E. Olness. Humic substances II. In search of structure. *Edited by* M.H.B. Hayes, P. MacCarthy, R.L. Malcolm, and R.S. Swift. Wiley, New York. 1989. pp. 498–514.
2. F. Rey, M.A. Ferreira, P. Facal, and A.A.S.C. Machado. Can. J. Chem. **74**, 295 (1996).
3. M. Adhikari, B. Mandal, and P. Sen. Proc. Ind. Nat. Sci. Acad. **46A**, 387 (1980).
4. D.S. Orlov. Humus acids of soils. A.A. Balkema, Rotterdam. 1985.
5. F.J. Stevenson. Humus chemistry: genesis, composition and reactions. Wiley. 1994.
6. J.C.G. Esteves, A.A.S.C. Machado, M.A. Ramos, F. Arce, and F. Rey. Environ. Sci. Technol. **30**, 3155 (1996).
7. F. Rey, A.A.S.C. Machado, F. Arce, M.A. Ferreira, and A. Toja. Anal. Chim. Acta, **304**, 375 (1995).
8. F. Rey, M. Pérez-Asenjo, A.A.S.C. Machado, P. Facal, M.A. Ferreira, and A. Toja. Talanta, **42**, 1919 (1995).
9. M.T.S.D. Vasconcelos, A.A.S.C. Machado, and F. Rey. An. Quim. Int. Ed. **92**, 243 (1996).
10. F. Rey, M. Pérez-Asenjo, A.A.S.C. Machado, P. Facal, and M.A. Ferreira. J. Electroanal. Chem. **431**, 77 (1997).
11. A. Kuwatsuka, A. Watanabe, K. Itoh, and S. Arai. Soil Sci. Plant. Nutr. (Tokyo) **38**, 23 (1992).
12. P.W. Linder, R.G. Torrington, and D.R. Williams. Analysis using glass electrodes. Open University Press. 1984.
13. Y-P. Chin, G. Aiken, and E. O'Loughline. Environ. Sci. Technol. **28**, 1853 (1994).
14. C. Miller and J.N. Millers. Statistics for analytical chemistry. Ellis Horwood. 1988.
15. Y. Chen and S. Schnitzer. Soil Sci. Soc. Am. J. **40**, 866, (1976).
16. R.M. Fuoss and G.I. Cathers. J. Polymer Sci. **4**, 97 (1949).
17. W. Flaig, H. Beutelspacher, and E. Rietz. Soil components. Springer-Verlag. 1975.
18. R. Simha and F.S. Chan. J. Phys. Chem. **75**, 256 (1971).
19. P. Munk. Introduction to macromolecular science. Wiley. 1986.
20. B. Ceccanti, M. Calcinai, M. Bonmati-Pont, C. Ciardi, and R. Tarsitano. Sci. Total Environ. **81/82**, 471 (1989).

© 2000 NRC Canada

The photoequilibration of the *ortho*-, *meta*-, and *para*-isomers of substituted benzenes in acetonitrile and the photoaddition of 2,2,2-trifluoroethanol (TFE) to the same isomers: a survey

J. Foster, A.L. Pincock, J.A. Pincock, S. Rifai, and K.A. Thompson

Abstract: The phototransposition (*ortho, meta, para*) in acetonitrile of a number (25) of disubstituted benzenes have been examined. For some cases (methylbenzonitriles, trifluoromethyltoluenes, and trifluoromethylbenzonitriles) photostationary states could be reached but others (methylanisoles, methoxybenzonitriles, dicyanobenzenes, and methy 4-toluyl sulfone) were unreactive. The photoaddition of 2,2,2-trifluoroethanol (TFE) to the same compounds as well as 5 monosubstituted cases was also examined. The products obtained for reactive compounds were all TFE ethers of bicyclo[3.1.0]hex-3-en-2-ol derivatives. For benzene and alkylbenzenes (toluene, *ortho*-xylene) these photoadducts are formed by ground state addition of TFE to benzvalene derivatives. For others (methylbenzonitriles), bicyclic diradicals or carbenes are likely intermediates. Many substituted compounds (anisole, fluorobenzene, methyl benzoate, methylanisoles, methoxybenzonitriles, dicyanobenzenes, trifluoromethylbenzonitriles, and fluorotoluenes) did not react with TFE. The trifluoromethylbenzonitriles did however undergo phototransposition in TFE, the only compounds to do so.

Key words: substituted benzenes, phototransposition, photoaddition.

Résumé : On a étudié la phototransposition (*ortho, méta, para*), réalisée dans l'acétonitrile, d'un certain nombre (environ 25) benzènes disubstitués. Dans certains cas (méthylbenzonitriles, trifluorométhyltoluènes et trifluorométhylbenzonitriles), il a été possible d'atteindre des états stationnaires, mais les autres méthylanisoles, méthoxybenzonitriles, dicyanobenzènes et méthyl(4-méthylphényl)sulfone] ne sont pas réactifs. On a aussi étudié la photoaddition du 2,2,2-trifluoroéthanol (TFE) à ces mêmes composés ainsi qu'aux cinq produits monosubstitués. Avec chacun des composés réactifs, les produits obtenus sont les éthers TFE des dérivés bicyclo[3.1.0]hex-3-én-ols. Pour le benzène et les alkylbenzènes (toluène, *ortho*-xylène), ces photoproduits se forment par une addition à l'état fondamental du TFE aux dérivés benzvalènes. Pour les autres composés (méthylbenzonitriles), les intermédiaires sont vraisemblablement des radicaux ou des carbènes bicycliques. Plusieurs composés substitués (anisole, fluorobenzène, benzoate de méthyle, méthylanisoles, méthoxybenzonitriles, dicyanobenzènes, trifluorométhylbenzonitriles et fluorotoluènes) ne réagissent pas avec le TFE. Toutefois, dans le TFE, les trifluorométhylbenzonitriles subissent une phototransposition; ce sont les seuls composés à le faire.

Mots clés : benzènes substitués, phototransposition, photoaddition.

Introduction

Recently, we reported on both the phototransposition reactions of *para*-, *meta*-, and *ortho*-methylbenzonitrile, **1**, **2**, and **3**, in acetonitrile (1) and the photoaddition reactions of the same isomers upon irradiation in 2,2,2-trifluoroethanol (TFE) (2). The photolysis of benzonitrile (**4**), 2,4,6-trideuteriobenzonitrile (**4(*d*$_3$)**), and 2,6-dideuterio-4-methylbenzonitrile (**1(*d*$_2$)**) in both acetonitrile and TFE proved to be very helpful in understanding the major pathway(s) for both phototranspositions and alcohol photoadditions. These pathways are shown for **1(*d*$_2$)** in Scheme 1.

In acetonitrile, the results can be summarized as follows: first, the phototransposition reaction converting **1**, **2**, and **3** leads to a steady state mixture of *para*:*meta*:*ortho* = 3:20:77 for irradiation of both **1** and **2**. For the *ortho* isomer, **3**, the phototransposition is considerably slower and the steady state composition is not reached; second, both 1,2- and 1,3-transpositions occur in the primary photochemical step; third, the relative reactivity of the three isomers in the phototransposition reaction is *para*:*meta*:*ortho* = 32:4:1; fourth, the quantum yield (at low conversion) of phototransposition for the *para* isomer is 0.025; fifth, quenching studies with 2,3-dimethyl-1,3-butadiene have shown the reactions to occur from the excited singlet state for both the *para* and *ortho* isomers; sixth, ^{13}C NMR analysis of the phototransposition products **2(*d*$_2$)** and **3(*d*$_2$)** from **1(*d*$_2$)** demonstrated that the cyano-substituted carbon was always involved in the phototransposition step. These six observations can be rationalized by the left-hand part of Scheme 1. For instance, the

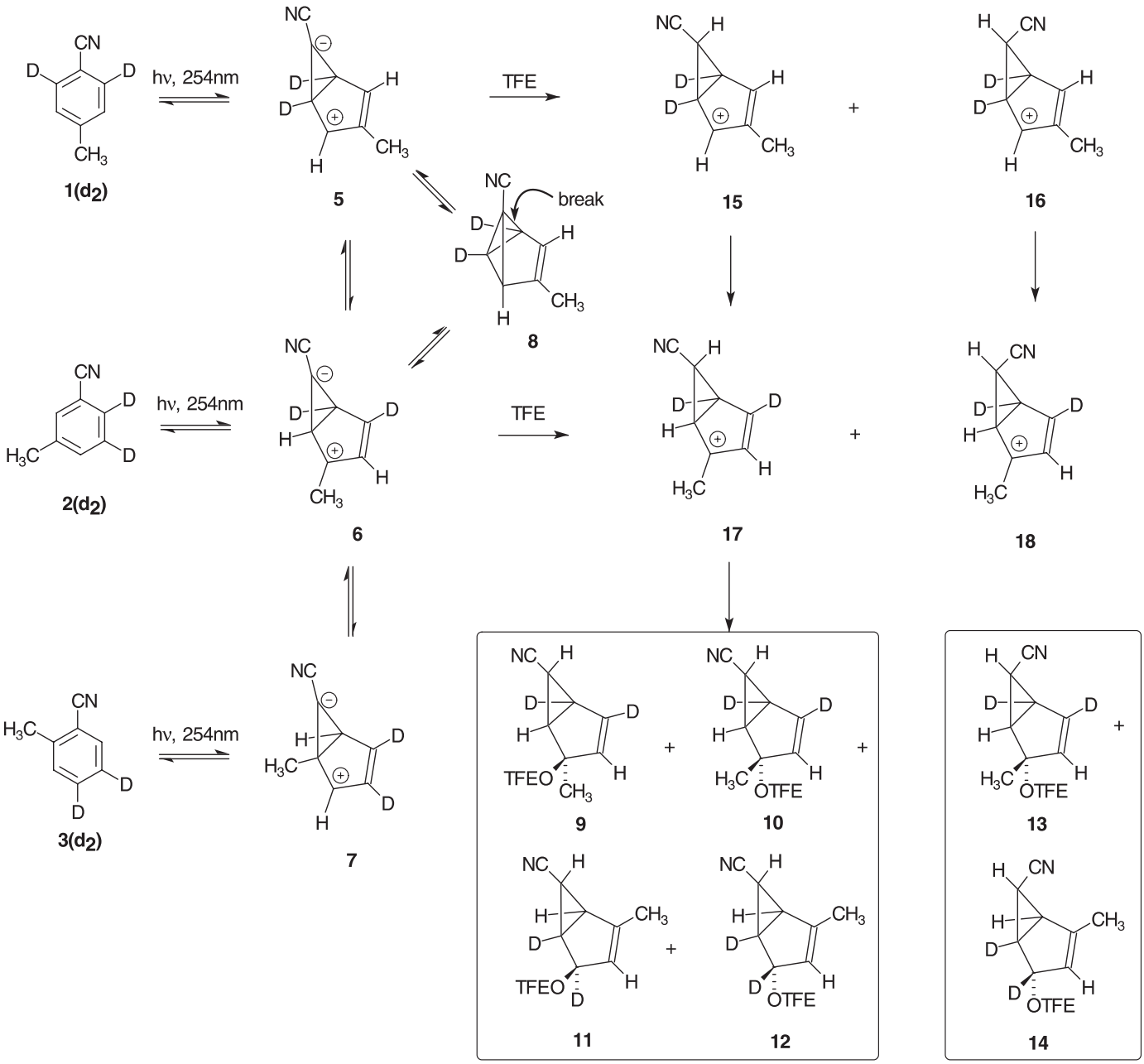
Received January 23, 2000. Published on the NRC Research Press website on July 13, 2000.

J. Foster, A.L. Pincock, J.A. Pincock,[1] S. Rifai, and K.A. Thompson. Department of Chemistry, Dalhousie University, Halifax, NS B3H 4J3, Canada.

[1]Author to whom correspondence may be addressed. Telephone: (902) 494–3324. Fax: (902) 494–1310. e-mail: PINCOCK@CHEM1.CHEM.DAL.CA

© 2000 NRC Canada

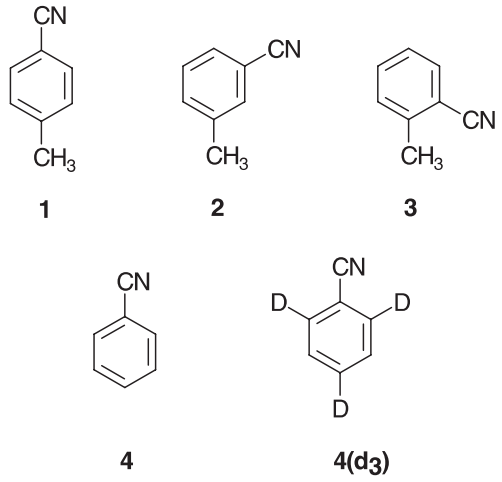
Scheme 1. Mechanistic scheme for the phototransposition and the photoaddition of TFE for the methylbenzonitriles, **1**, **2**, **3** using **1(d_2)** as the example.



excited singlet state of **1(d_2)** gives the bicyclo[3.1.0] intermediate **5** by *meta* bridging between C2 and C6. This intermediate singlet state is written as a zwitterion with the negative charge on the cyano-substituted carbon and the delocalized positive charge shown on only one of the two ends of the allylic part. Migration of the cyano-substituted carbon around the other five results in formation of the isomeric intermediates, **6** and **7**, which can return to **2(d_2)** and **3(d_2)**, respectively.

The potential energy surface connecting the three intermediates, **5**, **6**, and **7**, may not be as simple as implied in Scheme 1. First, as mentioned above and for convenience in describing the next results in TFE, the intermediates are shown as zwitterions but clearly, and depending on the substituents, they could have considerable biradical character. More important, for the unsubstituted derivative, e.g., C_6H_6, high level MO calculations (3) have shown that species other than these biradicals, such as the carbene structure 5-methylene-1,3-cyclopentadiene, are important. In fact, the carbene structures are of considerably lower energy than the biradicals. We are in the process of doing similar calculations for several substituted cases. Second, because we have no evidence that would require them, the corresponding benzvalene structures that would result from exergonic closure of the intermediate **5**, such as **8**, are not included in Scheme 1. Benzvalene itself can be prepared by photolysis of benzene (4) and, as will be discussed in more detail below, has been strongly implicated in phototranspositions of

© 2000 NRC Canada



deuterium substituted benzenes (5) and in the photoadditions of alcohols (6, 7, 8) and acids (7) to benzene. For the methyl benzonitriles, **8** could proceed thermally or perhaps, photochemically, to **6**, and hence to **2(d_2)**, by breaking the bond indicated in Scheme 1.

Photolysis of both the *para* and *meta* isomers, **1** (and the deuterated compound, **1(d_2)**) and **2**, in TFE resulted in six major addition products, **9**–**14**; the *ortho* isomer was unreactive. These six products are separated into two groups, the four that have a proton *endo* at C6 and the two that have the same proton *exo*; the ratios of the yields of the two groups are 79:21 from **1** and 64:36 from **2**, respectively. As shown in Scheme 1, these products can all be rationalized by nucleophilic trapping of the bicyclo[3.1.0]hexenyl cations, **17** and **18**. These cations are formed directly from the *meta* isomer (**2**) by *endo* and *exo* protonation, respectively, on C6 of **6** but indirectly via rearrangement of the cations **15** and **16** first formed from the *para* isomer. The driving force for the rapid rearrangement of **15** to **17** and **16** to **18** was ascribed to the enhanced stability of **17** and **18** as a result of methyl substitution at the terminal carbon, rather than at the node, of the allylic system. Very rapid rearrangements of bicyclo[3.1.0]hexenyl cations have been observed previously (7, 9).

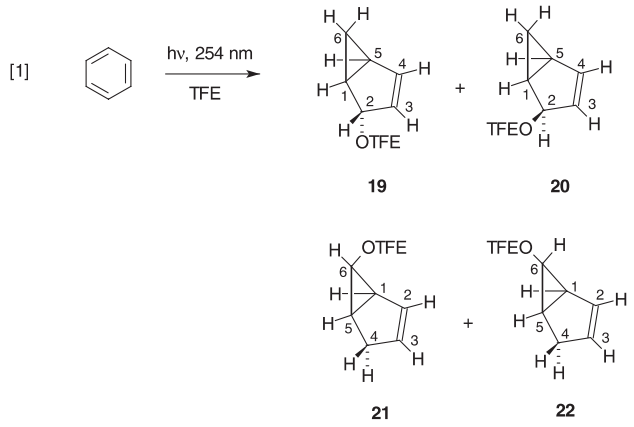
These phototranspositions and photoaddition reactions of nitrile-substituted benzenes indicate that the electron withdrawing substituent is critical in determining the efficiency of the reactions as well as the structures of the addition products. Clearly, the effect of other substituents is of interest. We now report a more general study of these reactions for a variety of substituted benzenes.

Results and discussion

Photolysis of benzene

The unimolecular photoreactivity of benzene was first discovered in 1957 for its conversion to fulvene. This observation stimulated considerable interest in benzene photochemistry which resulted in the observation of other photoisomerizations to benzvalene, Dewar benzene, and prismane as well as the photoaddition reactions of acids, alcohols, and water. This material has been reviewed a number of times (10–12). Particularly relevant to the present work is the observation that irradiation at 254 nm of 1,3,5-trideuteriobenzene gave the 1,2,4-d_3 isomer both in solution (hexadecane) and in the gas phase with quantum yields of 0.025 and 0.012, respectively, (5). The proposed intermediate was a deuterated benzvalene. In addition, irradiation of benzene in TFE gave the addition products **19**–**22**, eq. [1]. The initial publication (6) reported only formation of **19** and **21** in a ratio of 2:1. These compounds were isolated by preparative GC; ^{1}H NMR spectra were used to assign the structures. No information was provided to assign the stereochemistry given for the TFE group at C2 in **19** but, for **21**, the *endo* stereochemistry was assigned by the appearance of H6 as a pseudo triplet with J = ~7 Hz, typical of the *cis* H-H coupling constant in cyclopropanes. In a later publication (8), **19** and **20** were demonstrated to be the primary photoproducts and **21** and **22** were formed from them by benzene sensitization. In addition, **21** was converted to **22** as the photolysis of either **19** or **20** proceeded. These results were rationalized by formation of benzvalene in the primary photochemical event followed by ground state addition of TFE to give **19** and **20**. Confirmation of this was obtained by reacting benzene solutions of independently synthesized benzvalene with TFE and observing, as products, only **19** and **20**. Another important clue for the intermediacy of benzvalene was the observation, using deuterium incorporation, of exclusive *endo* protonation at C6 (7), as expected for addition to the strained cyclopropyl sigma bond in benzvalene.

We have repeated the photolysis of benzene in TFE to confirm these results and to obtain higher field ^{1}H and ^{13}C NMR spectra. Photolysis of benzene (2.81×10^{-2} M) in TFE for 4 h resulted in 53% conversion of the benzene to three addition products (GC and GC-MS) in the ratio of 3.6:1:1 and a total yield of 45%. At 10% conversion, this ratio was 6.1:1.7:1. The structures of these three compounds (**19**–**21** respectively, in eq. [1]) were confirmed by ^{1}H NMR (normal



and COSY) and ^{13}C NMR (normal and HMQC) of the mixture at 400 MHz. Chemical shifts and coupling constants are given in the Experimental Section. At these conversions, no evidence was obtained for the presence of **22**. The distinction between **21** and the other two isomers is easily made because there are only two signals, H2 and H3, above δ 4.4 in the ^{1}H NMR for **21**. Moreover, **19** and **20** both have two signals at δ 1.0 or less (H6 *endo* and *exo*) whereas **21** has none. The stereochemistry at C2 of the major product, **19**, was established by coupling because H2 appears as a

© 2000 NRC Canada

broadened singlet indicating a small coupling between H2 and H1 as is typical for the *endo* hydrogen at C2 in this ring system (2); in contrast, H2 in **20** appears as a doublet with splitting equal to 6.7 Hz. The stereochemistry at C6 in **21** was confirmed, as before, by the appearance of H6 as a pseudo triplet with splitting equal to 6.3 Hz, as expected for a cyclopropane hydrogen *cis* to the two hydrogens, H1 and H5 (6, 8).

A comparable photolysis of benzene-d_6 in TFE gave the same three products but with very simple ^{1}H NMR spectra because now only one diagnostic hydrogen (and the CH_2 from TFE) is observable. This hydrogen is clearly H6 *endo* (H6 *endo* : H6 *exo* > 50:1) in the major product, **19**, and in **20**. The situation is not so clear for the minor product **21** because of overlap of signals but the ratio of H4 *exo* to H4 *endo* is approximately 2:1.

All of these results are in agreement with the previously proposed mechanism (6–8) which suggested that the primary photoproducts (**19** and **20**) are formed by *endo* protonation of benzvalene followed by *exo* (major) and *endo* (minor) trapping of the allylic cation by TFE. The third product (**21**) results from benzene sensitized isomerization of the primary products. This observation of highly selective *endo* protonation contrasts with our results for benzonitrile derivatives where products resulting from *exo* and *endo* protonation at C6 are formed in almost equal amounts (2). The conclusion is that photochemical addition of TFE to benzene proceeds through benzvalene but that substituted benzvalenes are not involved in the photoaddition of TFE to benzonitriles.

A general comment about the TFE addition reactions to benzene and other aromatics would be useful at this point. The addition products that we obtained from the benzonitriles were stable and could be separated by silica gel chromatography, presumably because the nitrile functional group provides enough polarity to create differing R_f values. For benzene and the other aromatics discussed below, separation on silica gel was not achieved. Moreover, the addition products were not consistently stable so that the composition of mixtures would sometimes change on standing or on evaporation of the TFE solvent. At times, ^{1}H NMR spectra revealed that removal of the solvent left no characterizable products even though GC analysis had given well defined peaks. Most NMR spectra reported are therefore of crude reaction mixtures which always contained a broad, unidentified cluster of signals between δ 1 and 2 in the ^{1}H NMR (probably oligomers or polymers). As a consequence, well-defined NMR spectra for pure compounds could not be obtained. However, in the ^{1}H NMR spectra of the addition products, the high field region of the cyclopropyl hydrogens and the low field region of the hydrogens on the alkene and oxygen-substituted carbons could usually be analyzed. Fortunately, these two regions provide enough information about the structure of the addition products so that assignments can be made with considerable confidence.

Photolysis of monosubstituted benzenes in TFE

Because photolysis of benzonitriles in TFE gave four well characterized addition products, other mono substituted benzenes were also examined in TFE as described above for benzene. These included toluene, anisole, fluorobenzene, trifluoromethylbenzene, and methyl benzoate. Of these, only toluene and trifluoromethylbenzene reacted to any significant extent.

For toluene, after 4 h, 59% had reacted to give at least 12 addition products (23% total by GC), with two being the major (40% of the mixture) products. The ^{1}H NMR of the crude reaction mixture revealed that the major products were like that for benzene because of the observation of two *endo* protons at C6 ("quartet" at δ –0.05 and –0.12, respectively) of the bicyclo[3.1.0]hexene ring system; also the methyl group must be at C4 (lack of olefin doublet of doublets and no signal typical of H4 at ~ δ 6). Attempts to purify this compound by silica gel chromatography were unsuccessful. Photolysis of toluene-d_8 in TFE resulted in the same products (GC) and the ^{1}H NMR revealed again that protonation by TFE was highly preferred at C6 *endo*. These observations suggest that the major pathway for photoaddition of TFE is by protonation at C1 or C6 (identical by symmetry) of an intermediate methylbenzvalene (*x*-methyltricyclo[3.1.0.0^{2,6}]-3-hexene) that is not methyl substituted at C1 or C6. As observed previously, rapid isomerization of this bicyclo[3.1.0]-3-hexen-2-yl cation will result in the methyl substituent being at the terminal end of the allylic moiety (C2 or C4) so that, after *exo* and *endo* nucleophilic trapping by TFE, the major products will be 4-methyl-2-(2,2,2-trifluoroethyl) derivatives.

For trifluoromethylbenzene, 4 h photolysis gave 57% conversion of starting material to six additions products (GC and GC-MS) with one of them accounting for 53% of the mixture. At this point, the mass balance was still 72%. Again, silica gel chromatography gave no characterizable products from this mixture. Moreover, the ^{1}H NMR of the crude reaction mixture did not provide clear signals for any one compound. There were, however, no high field signals around δ 0 indicative of a cyclopropyl -CH_2-. Therefore, the photoaddition products are probably similar in structure to those of the benzonitriles, i.e., resulting from protonation at the CF_3 substituted carbon.

Photolysis of disubstituted benzenes

Xylenes

Alkyl substituted benzenes have been important in the understanding of aromatic phototransposition reactions. The gas phase isomerization of *o*-xylene to *m*-xylene and of *m*-xylene to both *o*- and *p*-xylene (ratio 1:4) and the isomerization of *m*-xylene in the pure liquid and in isohexane solvent were first reported in 1964 (13). In the same year, a study appeared on the photoequilibration of the di-*t*-butylbenzenes in ether (14). Later, for the solution (isohexane) photochemistry of *o*-xylene, the primary photochemistry was reported to give both *m*- and *p*-xylene in a ratio of 14:1 (15). Thus, both 1,2- and 1,3-transpositions are occurring simultaneously in solution for *o*-xylene.

More extensive results on the solution transposition photochemistry of the xylenes were reported by Anderson in 1970 (16). The phototranspositions were found to be independent of solvent (hexane and EPA (5:5:2 mixture of ether, isopentane, and ethanol)) and wavelength of excitation. Irradiation in the 230–280 nm range gave disappearance quantum yields in hexane of 0.00775, 0.0111, and 0.00274 for

© 2000 NRC Canada

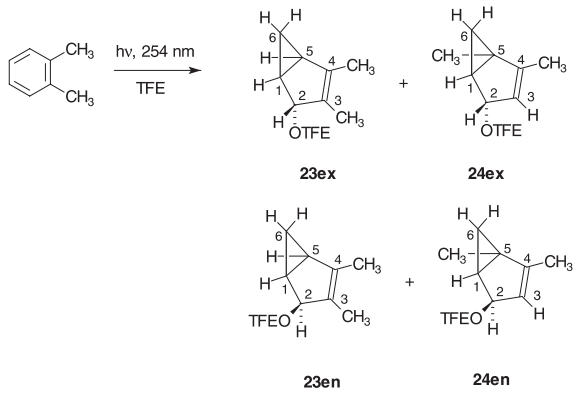
o-, *m*-, and *p*-xylene, respectively. At very low conversions, the ratio of *meta*:*para* from *ortho* was 8.8:1 indicated that again both 1,2- and 1,3-transpositions were occurring as a primary photochemical event. The ratio of *para* to *ortho* from *m*-xylene was 4.1 but no ratio of *ortho* to *meta* was reported for the very unreactive *para* isomer.

We have examined the xylene isomers in acetonitrile and observed similar results. By taking samples as a function of time under 1.5% conversion, primary product ratios were obtained by extrapolation to zero time. The values obtained are: *meta*:*para* = 11:1 for *ortho*; *ortho*:*para* = 6.0:1 for *meta*; and *meta*:*ortho* > 25:1 for *para*. The last value was difficult to obtain reliably because the *para* and *meta* isomers have very similar GC retention times on the column used. They can be resolved to the baseline when they are present in comparable amounts, but not when the ratio is greater than 100 to 1. Therefore, the *meta* isomer appears as a shoulder on the tail of the large *p*-xylene signal and quantifying its intensity is difficult. In agreement with the previous results, the *meta* isomer is the most reactive in the phototranspositions in acetonitrile and the *para* isomer, the least. Relative reactivities are approximately 1:1.4:0.3 for *ortho*:*meta*:*para*.

Irradiation of the xylenes in TFE gave characterizable products only for *o*-xylene. For both the *meta* and the *para* isomers, the starting material disappeared but no significant signals at the appropriate retention times appeared. In contrast, irradiation of a 2.52×10^{-2} M solution of *o*-xylene in TFE for 5 h resulted in 83% conversion to eight addition products in a total yield of 50%. Two of these eight accounted for 65% of the products formed, and two others, 21%. An important observation is that the photoaddition reaction in TFE is about 25 times more efficient than the phototransposition reaction in acetonitrile. Not surprisingly, therefore, no phototransposition was observed in TFE. The reported quantum yield of *o*- to *m*-xylene in hexane of ~0.007 suggests that the quantum yield for photoaddition is about 0.18.

Removal of the solvent allowed the identification of these major products, **23ex** and **24ex**, by ^{1}H NMR (normal and COSY) at 400MHz, eq. [2]. These assignments are made

[2]



with considerable confidence even though the cyclopropyl hydrogen at C1 and C5 were not observable as they fall underneath the broad, uncharacterizable signal between δ 1 and 2.5 (see above). Both clearly have a cyclopropyl CH_2 at C6 on the basis of the high field signal for H6 *endo* at δ –0.40 for **23ex** and δ 0.14 for **24ex**. Moreover for **23ex**, this signal is a pseudo-quartet (~3.6 Hz) as expected if there are hydrogens at both C1 and C5; in contrast, this signal is a pseudo-triplet (~4.0 Hz) for **24ex**, indicating methyl substitution at C1, C5, or C6 (It is actually at C5.). Neither compound has the expected doublet of doublets for hydrogens at both C3 and C4. For **23ex** there is only one signal in the low field region (δ 4.32) corresponding to H2 and it is a broad singlet indicating that the TFE group is *exo*. Moreover, the two methyl groups (δ 1.78 and 1.56) are broadened by the expected homoallylic coupling. For **24ex**, these are two low field signals at δ 4.38 (H2) and 5.02 (H3); again the TFE group is *exo*. The methyl groups are now more separated in chemical shift, δ 1.82 for 4-CH_3 and 1.28 for 5-CH_3, indicating cyclopropyl substitution for the latter. Finally, the other two major products in the mixture are very likely the corresponding *endo* isomers **23en** and **24en**, eq. [1], on the basis of the similarities in their ^{1}H NMR spectra to those for the *exo* isomers: δ 0.05, "q" and –0.19, "t," respectively, for H6 *endo* and the splitting of the signals for H2 into doublets (~8 Hz) by coupling to H1.

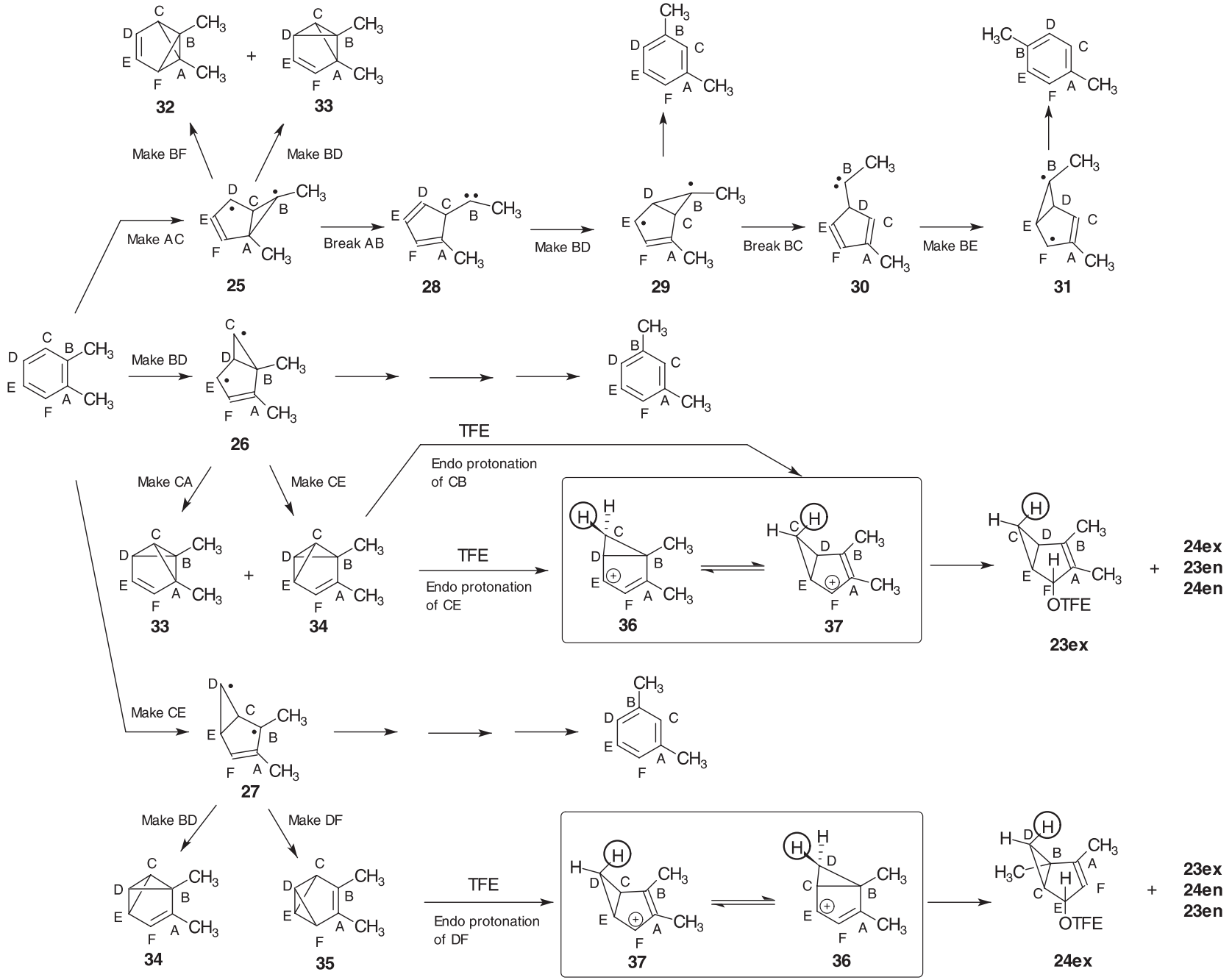
A similar photolysis of *o*-xylene-d_{10} in TFE gave the same products and the ratio of *endo*:*exo* protonation at C6 by TFE could easily be determined by ^{1}H NMR integrals of the corresponding hydrogens. For both **23** and **24**, the ratio was ~9:1.

The results for the *o*-xylene photochemistry in both acetonitrile and TFE can be rationalized by the mechanism outlined in Scheme 2. Photochemical excitation to S_1 leads to the pre-fulvene biradicals **25**, **26**, and **27**. For benzene itself, by MO calculations (17), this process proceeds over a small activation barrier to a conical intersection so that the biradical is on the ground state surface. For benzene there is only one such biradical but for *o*-xylene, three are possible. Each of these biradicals can collapse to one pair of the four possible benzvalene structures, **32**–**35**. A previously proposed and possible mechanism for *ortho* to *meta* phototransposition is then the return of the dimethylbenzvalene to xylene either thermally or, as has been suggested, by photochemical sensitization (13, 15). These dimethylbenzvalenes allow for phototransposition because two carbons of the original *o*-xylene can now switch positions on the return pathway. For instance, **33** was formed by AC plus BD bond formation. By next breaking bonds AB and CD, carbons B and C have been interchanged so that *o*-xylene has isomerized to *meta*. For *o*-xylene only one of the four dimethylbenzvalenes, i.e., **33**, leads to isomerization; the other three lead to undetectable carbon-carbon transpositions.

This mechanism for phototransposition cannot be the exclusive one for *o*-xylene because both 1,2- and 1,3-transpositions, in a ratio of 10.5:1, are observed in the primary photochemical process. Our preference is therefore for the pathway of migration in the biradicals. Thus **25**, rather than collapsing to benzvalenes **32** and **33**, ring-opens by AB bond cleavage to the cyclopentadienylcarbene, **28**. MO calculations (3) for benzene itself have shown that structures like **25** are not as stable as structures like **28**. We are in the process of doing similar calculations for substituted benzenes. This pathway of migration of a single carbon around the cycle formed by the other five has been strongly implicated in our previous study (1) on the phototransposition reactions of the

© 2000 NRC Canada

Scheme 2. Mechanism for the phototransposition and the photoaddition of TFE for *o*-xylene.



© 2000 NRC Canada

methylbenzonitriles in acetonitrile. Thus, **25** proceeds to **28** and then to **29** which can ring-open to *m*-xylene or proceed to **30** and finally to *p*-xylene. Similar pathways for the initially formed biradicals **26** and **27** (intermediates not shown in Scheme 2) can lead only to *m*-xylene. Because the efficiency of phototransposition for *o*-xylene is low, the major fate of the first-formed biradicals must be return to *o*-xylene or collapse to benzvalene.

The photoaddition reaction of *o*-xylene in TFE provides additional information about benzvalene formation. In contrast to the photoadditions to benzonitriles where both *exo* and *endo* protonation at C6 of the bicyclo[3.1.0] derivatives was observed, the products, like those from both benzene and *o*-xylene, exhibit a marked preference for *endo* protonation. Because the products formed from *o*-xylene are not methyl substituted at C6, benzvalene **32** cannot be a major intermediate and **33** is also unlikely because protonation at the methyl substituted carbon of the bonds AB or BD would be expected to occur some of the time. Therefore, **34** and **35** are the major benzvalenes most likely formed. By symmetry, **34** has only two observable modes of *endo* protonation: at CE, giving the bicyclic cation **36** and at CB, giving **37**. It is not possible to determine which of these is preferred because these cations will again equilibrate rapidly by thermally allowed 1,4-sigmatropic rearrangement, with retention of configuration of the migrating carbon (2). Thus, the *endo* H (circled) remains *endo*, as demonstrated by the results using deuterated *o*-xylene. In a similar way, *endo* protonation of the benzvalene **35** can only lead to the bicyclic cation **37** but again it should rapidly equilibrate with **36**.

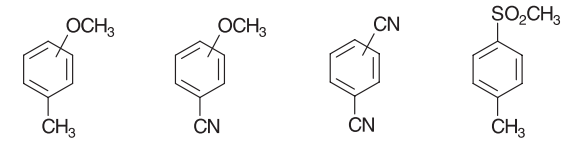
The products **23** and **24**, eq. [2], are clearly derived from *exo* (major) and *endo* (minor) trapping of the cations by TFE. The *exo* attack is presumably preferred for steric reasons. In principle, three such cations are possible (symmetry reduces the total from five to three) with the CH_2 group bridging any one of the five bonds in the dimethylcyclopentyl ring. However, only **36** and **37** have the allyl cation methyl substituted at the end. Therefore, these two are expected to be more stable; products from the other one are formed, if at all, in minor amounts. A similar observation was made in the photochemical TFE addition to *m*- and *p*-methylbenzonitrile (2). Finally, the TFE quenching of the cations **36** and **37** occurs mainly at the hydrogen substituted end. This may reflect the increased stability of the methyl substituted alkene in **23** and **24**.

The conclusion from this section on xylene photochemistry is that *o*-xylene most likely undergoes phototransposition through the biradical/carbene pathway and photoaddition through a much more efficient benzvalene pathway. *m*-Xylene undergoes phototransposition with comparable efficiency to both *o*- and *p*-xylene (ratio 6.0:1) but, for reasons that are unknown, the photoaddition products with TFE are not stable. Finally, *p*-xylene is very unreactive for either process and only very slow phototransposition is observe with a high preference for 1,2-transposition to *m*-xylene.

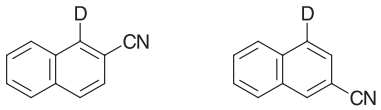
Other disubstituted benzenes

As a consequence of the observation of phototransposition and photoaddition of TFE to the methyl benzonitriles and xylenes, a survey of other disubstituted compounds was made. The compounds **38**–**42** were all found to be unreactive. Compound **42** was made from 2-aminonaphthalene by exchange at C1 with D_2O followed by Sandmeyer reaction to the nitrile. The idea was that if isomerization occurred by cyano-substituted carbon migration, as is the case of the methylbenzonitriles by bridging between C1 and C3, then 1-deuterio-2-cyanonaphthalene would be converted to 4-deuterio-2-cyanonaphthalene, **43**, a rearrangement that would be invisible without deuterium substitution. No reaction was observed by ^1H NMR analysis.

In contrast to these unreactive compounds, the substituted derivatives, **44**–**46**, showed photoreactivity but in ways that were different from the previously examined cases. The structures of **38**–**46** suggest that electron-withdrawing groups facilitate this type of aromatic photochemistry.



38 (*o, m, p*) **39** (*o, m, p*) **40** (*o, m, p*) **41**



42 **43**

*Trifluoromethyltoluenes, **44** (*o, m, p*)*

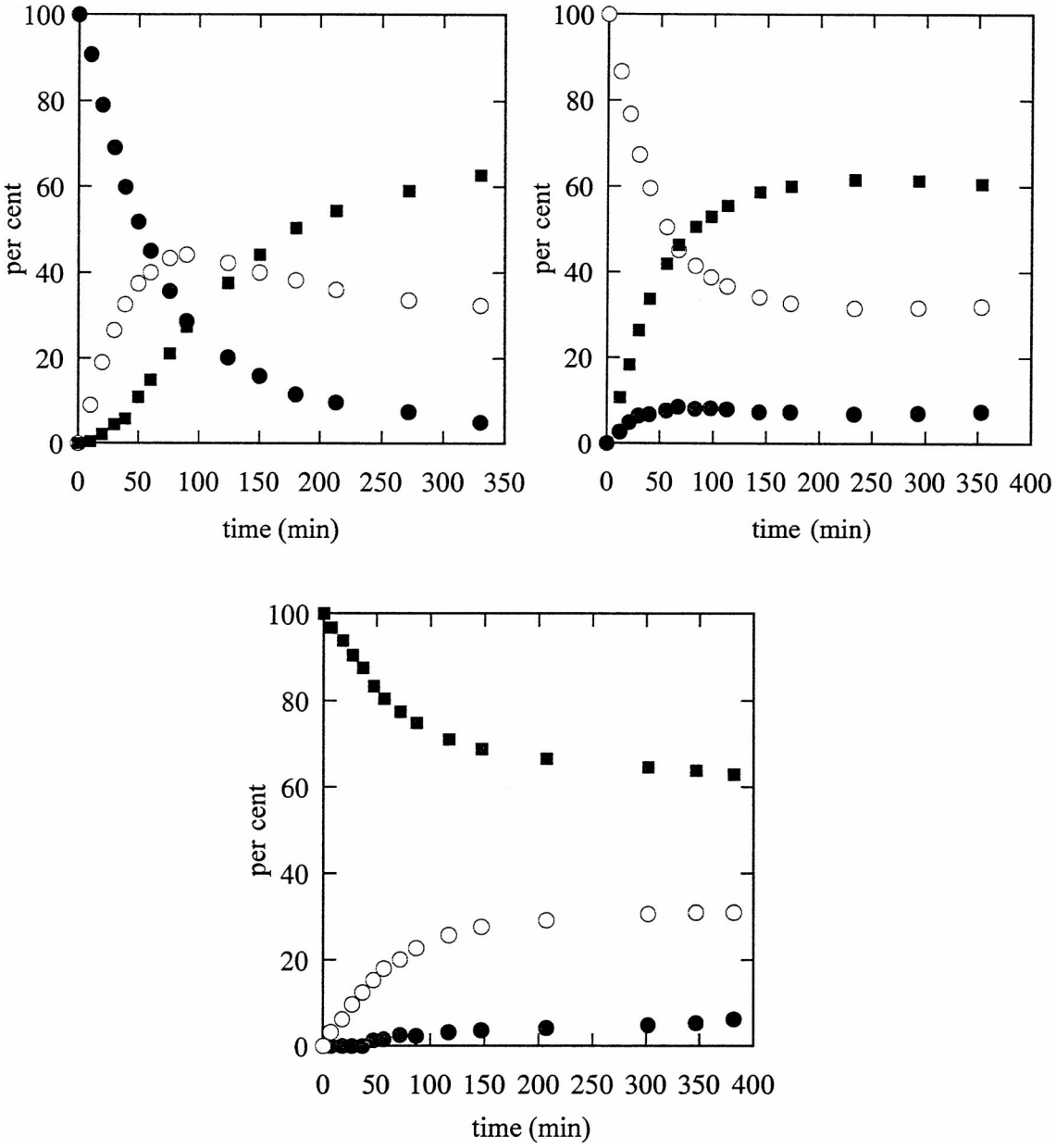
The plots for the photochemical interconversion of these three isomers are shown in Figs. 1*a*, *b*, and *c*. The reactions are considerably more efficient than the corresponding methylbenzonitriles, the steady state for photoequilibration being reached in about 200 min, about 10 times faster than for 4-methylbenzonitrile. More interesting is the observation that the steady state composition of *o*:*m*:*p* = 7:32:61 is essentially reversed from that observed for the methylbenzonitriles, *o*:*m*:*p* = 77:20:3. This occurs because for the CF_3 compounds, **44**, the *para* isomer is the least reactive and the *ortho* isomer is the most; the reverse order of reactivity holds for the methyl benzonitriles, **1**, **2**, and **3**.

The second major difference can be seen most clearly from Fig. 1*a* for the reactivity of the *ortho* isomer. At low conversions, as the *ortho* isomer disappears and the *meta* grows, the *para* is seen to have an induction period. The ratio of *para* to *meta* for the first sample taken at 10 minutes is greater than 10:1 but has dropped to 3:1 by 50 min. This implies that 1,2-transpositions are preferred to 1,3-transpositions in contrast to the observation for 4-methylbenzonitrile where the yields of the 3- and 2-substituted isomers increased simultaneously. The same is true for the *para* isomer, the ratio of *m*:*o* being greater than 20:1, Fig. 1*c*.

Photolysis of either **44*o*** or **44*m*** in TFE resulted in rapid formation of a complex mixture of at least 9 addition products (GC-MS); the major product accounted for 41% of the mixture. As in the case of the *m*- and *p*-methylbenzonitriles the product composition was essentially independent of the starting material. The mass balance was again good; 90%

© 2000 NRC Canada

Fig. 1. Plots of the phototransposition in acetonitrile of *o*-, *m*-, and *p*-trifluoromethyltoluenes, **44*o*** (●), **44*m*** (○), and **44*p*** (■): 1*a*, starting with **44o**; 1*b*, starting with **44*m***; and 1*c*, starting with **44*p***.

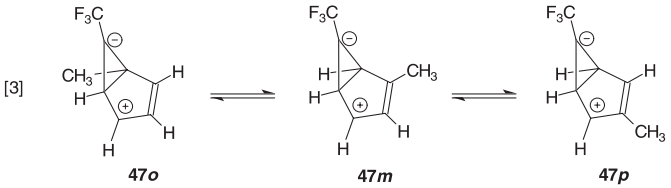


after 86% conversion for the *ortho* isomer and 81% after 85% conversion for the *meta* isomer. Unfortunately, evaporation of the solvent gave a residue whose ^{1}H NMR spectrum showed only a broad, unstructured signal covering the range of δ 2.5 to 0.5 ppm.

In contrast to the *ortho* and *meta* isomers, the *para* compound did not form any addition products in TFE. Moreover, the isomerization reaction occurred at a rate that was approximately 10 times slower than in acetonitrile, Fig. 1*a*. We conclude that some intermediate in the photochemistry of the *para* isomer is quenched by TFE (probably by protonation) but that this unknown species returns to starting material rather than leading to photoaddition products.

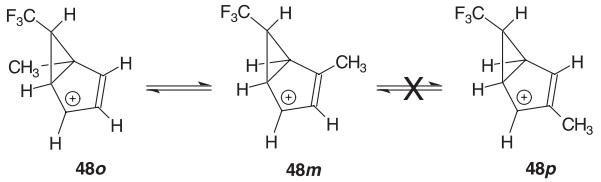
By analogy with the methylbenzonitriles, Scheme 1, we would expect the first formed intermediates to be bicyclic biradicals, perhaps **47o**, **47*m***, and **47*p*** from **44*o***, **44*m***, and **44*p***, respectively, eq. [3], and that these would form the

[3]



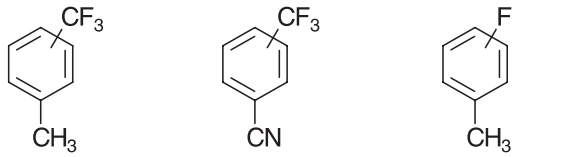
protonated species **48*o***, **48*m***, and **48*p*** in TFE, eq. [4]. The phototransposition in acetonitrile is explained by eq. [3] and the photoaddition in TFE by trapping of the cations, **48**. Surprisingly, **48*p***, if formed, does not lead to photoadducts.

© 2000 NRC Canada

[4] 

Moreover, **48*o*** and **48*m*** must again rapidly equilibrate because the product mixture obtained in TFE is identical for both **44*o*** and **44*m***; most of the products may be formed from the more stable cation, **48*m***.

Finally, for the methylbenzonitriles, we demonstrated by deuterium labelling and TFE trapping, that the cyano group was attached at C6 in the bicyclic intermediates. We have no evidence that the same is true for the trifluoromethyltoluenes (**44**) because we were unable to observe the ^{1}H NMR spectra of the photoadducts with TFE and have not attempted, nor thought of a convenient way, to synthesize specifically deuterated substrates.



44 (*o, m, p*) **45 (*o, m, p*)** **46 (*o, m, p*)**

*Trifluoromethylbenzonitriles, **45** (*o, m, p*)*

Photolysis in acetonitrile of both **45*m*** and **45*p*** resulted in photoequilibration to all three isomers, with the steady-state composition being similar for both; *o*:*m*:*p* = 40:20:40. The *meta* isomer was slightly more as reactive than the *para*. In contrast, the *ortho* isomer was considerably less reactive and a photostationary state was not reached. For the *para* isomer, product ratios for the *meta* and *ortho* isomers indicated that both 1,2- and 1,3-tranpositions were occurring simultaneously.

Surprisingly, irradiation in TFE gave essentially the same results as in acetonitrile. The plot is shown for the *para* isomer in Fig. 2. No products resulting from the addition of TFE were observed. These compounds are the only examples where we have observed efficient phototransposition reactions rather than photoadditions in TFE.

*Fluorotoluenes, **46** (*o, m, p*)*

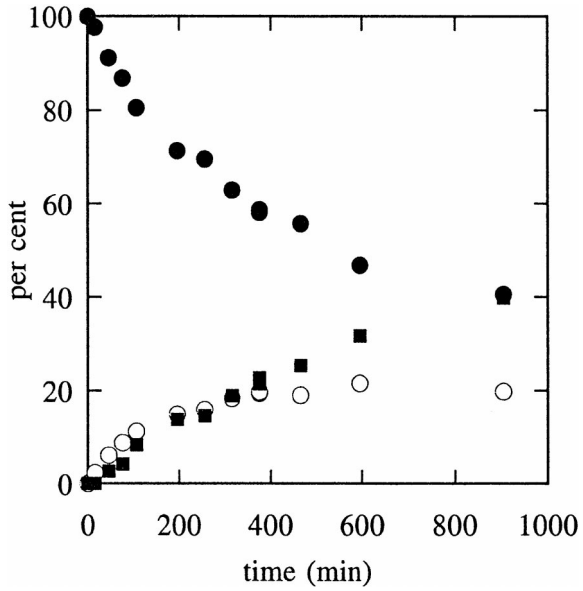
These compounds showed very low reactivity in either acetonitrile or TFE. However, **46*m*** did slowly react to form the *ortho* and *para* isomers in a ratio of 5:1 at low conversion but a steady-state mixture was not reached.

Summary

The results for the photochemistry reported in this work and for previously reported methylbenzonitriles (1, 2) and benzene-1,3,5-d_3 (5) are given in Table 1.

For benzene and alkyl benzenes (toluene, xylene) benzvalenes are probably the important intermediates, certainly for the TFE additions on the basis of the preference for *endo* protonation at C6 and probably for the phototranspositions

Fig. 2. Plot for the phototransposition in TFE of 4-trifluoromethylbenzonitrile, **45*p*** (●) to **45*m*** (○), and **45*p*** (■).



in acetonitrile because of the preference for 1,2-versus 1,3-transpositions.

For the disubstituted compounds that do react efficiently, namely the methylbenzonitriles (**1**, **2**, and **3**), the trifluoromethyltoluenes (**44(*o*, *m*, *p*)**), and the trifluorobenzonitriles (**45(*o*, *m*, *p*)**), three very different kinds of reactivity are observed. For the methylbenzonitriles in acetonitrile, clearly simultaneous 1,2- and 1,3-transpositions are occurring; in TFE both *endo* and *exo* protonation at C6 are observed. Therefore, bicyclic intermediate radicals (like **5**, **6**, and **7** in Scheme 1) and (or) carbenes (like **28** and **30** in Scheme 2) are the critical intermediates. Benzvalenes (like **8**b in Scheme 1) are of minor importance. For the trifluoromethyltoluenes, (**44(*o*, *m*, *p*)**), 1,2-transpositions dominate 1,3-transpositions (most clearly seen in Fig. 1*a*). Unfortunately, the structures of the photoaddition products in TFE could not be determined. For the trifluoromethylbenzonitriles (**45(*o*, *m*, *p*)**), essentially identical phototransposition results (but no photoadditions) were observed in both acetonitrile and TFE.

The other major observation to be made from the results in Table 1 is that many compounds, both mono- and disubstituted are photochemically very unreactive to either process, with the indication that electron withdrawing groups, either by inductive (CF_3) or resonance (CN) effects, are important.

Finally, even after completing the survey of compounds given in Table 1, no clear trends are obvious that would allow reliable prediction of the results for a new compound. Perhaps MO calculations for a variety of substituents will help to clarify these obviously complicated potential energy surfaces. Such calculations are in progress.

Experimental

Chemicals

The following compounds were obtained from Aldrich and were distilled before use: anisole; 2-, 3- and 4-methylanisole;

© 2000 NRC Canada

Table 1. Summary of phototranspositions (PT) in acetonitrile and photoadditions (PA) of TFE of substituted benzenes, C_6H_4XY

Compound	X	Y	Isomer	PT	PA
Benzene	H	H	-	Yes, with 1,3,5-d_3[a]	Yes, *endo*[b] [eq. 1]
Toluene	CH_3	H	-	-	Yes, *endo*[b]
Anisole	CH_3O	H	-	-	No
Fluorobenzene	F	H	-	-	No
Trifluoromethylbenzene	CF_3	H	-	-	Yes, GC/MS only
Methyl benzoate	CO_2CH_3	H	-	-	No
Xylene	CH_3	CH_3	*ortho*	*meta*:*para* = 11:1[c]	Yes, *endo*[b] (Scheme 2)
			meta	*ortho*:*para* = 6.0:1[c]	No stable products
			para	*meta*:*ortho* > 25:1[c]	No stable products
				ortho:*meta*:*para* = 1:1.4:0.3[d]	
Methylbenzonitrile (**1**, **2**, **3**) (Scheme 1)	CH_3	CN	*ortho*	*meta*:*para* = 7.1:1[c, e]	No[f]
			meta	*ortho*:*para* = 1.7:1[c, e]	Yes: same products as for *para*[f]
			para	*meta*:*ortho* = 4.2:1[c, e]	Yes: same products as for *meta*[f]
				ortho:*meta*:*para* = 1:4:32[d, e]	
				PSS[g] = 77:20:3	
Methylanisole (**38**)	CH_3	OCH_3	*o, m, p*	No	No
Methoxybenzonitrile (**39**)	OCH_3	CN	*o, m, p*	No	No
Dicyanobenzene (**40**)	CN	CN	*o, m, p*	No	No
Methyl 4-toluyl sulfone (**41**)	CH_3	SO_2CH_3	*para*	No	No
Trifluoromethyltoluene (**44**)	CH_3	CF_3	*ortho*	*meta*:*para* > 10:1[c] (Fig. 1*a*)	Yes, GC/MS only
			meta	*ortho*:*para* = 0.25[c] (Fig, 1*b*)	Yes, GC/MS only
			para	*meta*:*ortho* > 20:1[c] (Fig. 1*c*)	No
				ortho:*meta*:*para* = 1:0.67:0.16[d]	
				PSS[g] = 7:32:61	
Trifluoromethylbenzonitrile (**45**)	CF_3	CN	*ortho*	*meta*:*para* = 1.7:1[c]	No
			meta	*ortho*:*para* = 0.81:1[c]	No
			para	*meta*:*ortho* = 7.2:1[c] (Fig. 2)	No
				ortho:*meta*:*para* = 1:2.7:3.1[d]	
				In both acetonitrile and TFE	
				PSS[g] = 40:20:20	
Fluorotoluene (**46**)	CH_3	F	*ortho*	Very slow	No
			meta	*ortho*:*para* = 5.0:1[c]	No
			para	Very slow	No

[a]Ref. 5.

[b]Stereochemisty of the proton at C6 of the bicylo[3.1.0]hexene products – implies a benzvalene intermediate.

[c]Product ratio at very low conversion. High values from the *ortho* or *para* starting material suggest that 1,2-transpositions dominate.

[d]Relative reactivity.

[e]Ref. 1.

[f]Ref. 2.

[g]Photostationary state *ortho*:*meta*:*para*.

1,2-, 1,3-, and 1,4-dimethoxybenzene; methylbenzoate; α,α,α-trifluorotoluene; *o*-, *m*-, and *p*-xylene; 4-trifluoromethyltoluene; *o*-, *m*-, and *p*-trifluoromethylbenzonitrile; and 4-biphenylcarbonitrile. Both 2-trifluoromethyl and 3-trifluoromethyltoluene were synthesized by the Huang-Minlon (18) modification of the Wolff–Kishner reduction from the corresponding aldehydes, available from Aldrich. The deuterated substrates, benzene-d_6, toluene-d_8, and *o*-xylene-d_{10} were also obtained from Aldrich.

Photolysis

All photolysis were carried out in a Rayonet reactor, using 254 nm lamps, as described previously. The GC column used was also described previously (2). Because pure compounds could not be obtained for the addition of TFE, product yields were estimated by GC/FID peak areas without calibration.

Spectra of photoproducts from the addition of TFE to benzene

exo-*2-(2,2,2-trifluoroethoxy)bicyclo[3.1.0]hex-3-ene* (***19***): ^{1}H NMR (400 MHz, $CDCl_3$) δ 6.37 (d, *J* = 5.5 Hz, H4), 5.47 (d of t, *J* = 5.5, 1.7 Hz, H3), 4.51 (s, H2), 3.82 (q, *J* = 8.8 Hz, CH_2), 1.99 (m, H5), 1.80 (m, H1), 1.03 (m, *J* = 4.1, 7.7, 7.7 Hz, H6 *exo*), –0.05 ("q," "*J*" = 4.1 Hz, H6 *endo*);

© 2000 NRC Canada

^{13}C NMR (400 MHz, $CDCl_3$) δ 142.4 (C4), 126.1 (C3), 85.2 (C2), 63.7 (CH_2), 23.1 (C5), 22.4 (C1), 21.2 (C6).

endo-*2-(2,2,2-trifluoroethoxy)bicyclo[3.1.0]hex-3-ene (**20**)*: ^{1}H NMR (400 MHz, $CDCl_3$) δ 6.07 (d, *J* = 5.3 Hz, H4), 5.27 (d, *J* = 5.3, Hz, H3), 5.07 (d, *J* = 6.7 Hz, H2), 3.96 (q, *J* = 8.9 Hz, CH_2), 1.91 (m, H5), 1.65 (m, H1), 0.75 (m, H6 *exo*), 0.64 ("q," "*J*" = 4.0 Hz, H6 *endo*); ^{13}C NMR (400 MHz, $CDCl_3$) δ 138.7 (C4), 127.8 (C3), 86.8 (C2), 66.7 (CH_2), 24.5 (C5), 21.2 (C6), 15.0 (C2).

endo-*6-(2,2,2-trifluoroethoxy)bicyclo[3.1.0]hex-2-ene (**21**)*: ^{1}H NMR (400 MHz, $CDCl_3$) δ 5.64 (m, H4), 5.55 (m, H3), 3.64 (q, *J* = 8.8 Hz, CH_2), 3.59 (t, *J* = 6.3 Hz, H6 *exo*), 2.57 (dd, *J* = 18.0, 7.7 Hz, H4 *endo*), 2.41 (d, *J* = 18.0 Hz, H4 *exo)*, 2.06 (m, H5), 1.76 ("q," "*J*" = 7 Hz, H1); ^{13}C NMR (400 MHz, $CDCl_3$) δ 132.5 (C4), 123.3 (C3), 68.6 (CH_2), 59.7 (C6), 32.5 (C4), 30.6 (C5), 23.2 (C1).

Acknowledgements

We thank NSERC of Canada for financial support for this work and the Department of Chemistry, Dalhousie University, for Summer Research Awards to JF and KAT. We also thank Sepracor, Windsor, Nova Scotia, for their generous gift of chemicals.

References

1. P.J. MacLeod, A.L. Pincock, J.A. Pincock, and K.A. Thompson. J. Am. Chem. Soc. **120**, 6443 (1998).
2. J. Foster, A.L. Pincock, J.A. Pincock, and K.A. Thompson. J. Am. Chem. Soc. **120**, 13354 (1998).
3. H.F. Bettinger, P.R. Schreiner, H.F. Schaefer, III, and P.v.R. Schleyer. J. Am. Chem. Soc. **120**, 5741 (1998).
4. K. Wilzbach, J.S. Ritscher, and L. Kaplan. J. Am. Chem. Soc. **89**, 1032 (1966).
5. K.E. Wilzbach, A.L. Harkness, and L. Kaplan. J. Am. Chem. Soc. **90**, 1116 (1968).
6. L. Kaplan, J.S. Ritscher, and K.E. Wilbach. J. Am. Chem. Soc. **88**, 2881 (1966).
7. J.A. Berson and N.M Hasty. J. Am. Chem. Soc. **93**, 1549 (1971).
8. L. Kaplan, D.J. Rausch, and K.E. Wilzbach. J. Am. Chem. Soc. **94**, 8638 (1972).
9. P. Vogel, M. Saunders, N.M. Hasty, and J.A. Berson. J. Am. Chem. Soc. **93**, 1549 (1972).
10. D. Bryce-Smith and A. Gilbert. Tetrahedron, **32**, 1309 (1976).
11. D. Bryce-Smith and A. Gilbert. *In* Rearrangements in ground and excited states. Vol. 3. *Edited by* P. DeMayo. Academic Press, New York. 1980. pp. 349–379.
12. A. Gilbert. *In* CRC handbook of organic photochemistry and photobiology. *Edited by* W.M. Horspool and P.-S. Song. CRC Press, New York. 1995. pp 229–236.
13. K.E. Wilbach and L. Kaplan. J. Am. Chem. Soc. **86**, 2307 (1964).
14. A.W. Burgstahler, P.-L. Chien, and M.O. Abdel-Rahman. J. Am. Chem. Soc. **86**, 5281 (1964).
15. L. Kaplan, K.E. Wilzbach, W.G. Brown, and S.S. Yang. J. Am. Chem. Soc. **87**, 675 (1965).
16. D. Anderson. J. Phys. Chem. **74**, 1686 (1970).
17. I.J. Palmer, I.N. Ragazos, F. Bernardi, M. Olivucci, and M.A. Robb. J. Am. Chem. Soc. **115**, 673 (1993).
18. Huang-Minlon. J. Am. Chem. Soc. **68**, 2487 (1946).

© 2000 NRC Canada

An expeditious synthesis of (±)-decahydro-5*H*-dipyrrolo [1,2-*a*:1′,2′-*c*]pyrimidine-5-carbonitrile: a formal synthesis of (±)-tetraponerines-1, -2, -5, and -6

M. Plehiers, S. Heilporn, D. Ekelmans, S. Leclercq, M. Sangermano, J.C. Braekman, and D. Daloze

Abstract: A short and practical synthesis of (±)-decahydro-5*H*-dipyrrolo[1,2-*a*:1′,2′-*c*]pyrimidine-5-carbonitrile (**17**), a pivotal intermediate in the synthesis of (±)-tetraponerines-1 (**5**), -2 (**6**), -5 (**7**), and -6 (**8**), in three steps and 24% overall yield, from simple and inexpensive starting materials, is reported. The key step of our synthesis is a one pot stereoselective multistep process, whereupon two molecules of Δ^1-pyrroline (**9**) react with diethyl malonate (**10**) to afford the tricyclic lactam ester **13**, possessing the tetraponerine skeleton. Hydrolysis of the carboethoxy group of **13** followed by decarboxylation yields lactam **15**, which is converted into α-aminonitrile **17**. Our fruitless efforts to transform lactam **15** into the tetraponerines through reductive alkylation are also discussed.

Key words: alkaloids, tetraponerines, stereoselective synthesis, Robinson–Schöpf reaction, lactams, ants.

Résumé : Opérant à partir de produits de départ peu coûteux et facilement disponibles, on a mis au point une synthèse courte et pratique, en trois étapes et un rendement global de 24%, du (±)-décahydro-5*H*-dipyrrolo[1,2-*a*-:1′,2′-*c*]pyrimidine-5-carbonitrile (**17**), un intermédiaire dans la synthèse des (±)-tétraponérines-1 (**5**), -2 (**6**), -5 (**7**) et -6 (**8**). L'étape clé de notre synthèse est une réaction unipot stéréosélective à plusieurs étapes par laquelle deux molécules de la Δ^1-pyrroline (**9**) réagissent avec du malonate d'éthyle (**10**) pour conduire à la formation de l'ester lactame tricyclique **13** qui possède le squelette de la tétraponérine. L'hydrolyse du groupe carboéthoxy du composé **13**, suivie d'une décarboxylation, conduit au lactame **15** qui est finalement transformée en α-aminonitrile **17**. On discute aussi de nos vains efforts pour transformer le lactame **15** en tétraponérines par le biais d'une alkylation réductrice.

Mots clés : alcaloïdes, tétraponérines, synthèse stéréosélective, réaction de Robinson–Schöpf, lactames, fourmis.

Introduction

The tetraponerines are a group of eight tricyclic alkaloids isolated from the poison gland of the Neo Guinean ant *Tetraponera* sp. (1). These compounds are distributed into two families, which are based either on the 5-alkyldecahydro-5*H*-pyrido[1,2-*c*]pyrrolo[1′,2′-*a*]pyrimidine[3] skeleton ("6–6–5" skeleton) [T-3 (**1**), T-4 (**2**), T-7 (**3**), and T-8 (**4**)] or on the 5-alkyldecahydro-5*H*-dipyrrolo[1,2-*a*:1′,2′-*c*]pyrimidine[3] skeleton ("5–6–5" skeleton) [T-1 (**5**), T-2 (**6**), T-5 (**7**), and T-6 (**8**)] (Fig. 1) (2). In each family, the compounds differ from each other by the length of the alkyl chain (*n*-propyl or *n*-pentyl) and (or) by the configuration of the carbon atom to which it is attached.

Whereas several syntheses of tetraponerines **1**–**4** have been described (for a recent review see ref. (3)), only one synthesis of (±)-**7** and (±)-**8** (2), and one asymmetric synthesis of (+)-**5** to (+)-**8** (4) have been reported up to now. In the course of our work on the biosynthesis of the tetraponerines (5, 6), we needed a practical way to synthesize the tetraponerines **5**–**8** belonging to the "5–6–5" skeleton. In this context, we envisioned that a modified Robinson–Schöpf condensation between Δ^1-pyrroline (**9**) and diethyl malonate (**10**) could lead to the diester intermediate **11** which, through reaction with a second Δ^1-pyrroline unit, would afford **12**. Finally, the latter could lactamize into compound **13** having the required tricyclic skeleton (Scheme 1). This scheme is only a working hypothesis, since the order of the steps could

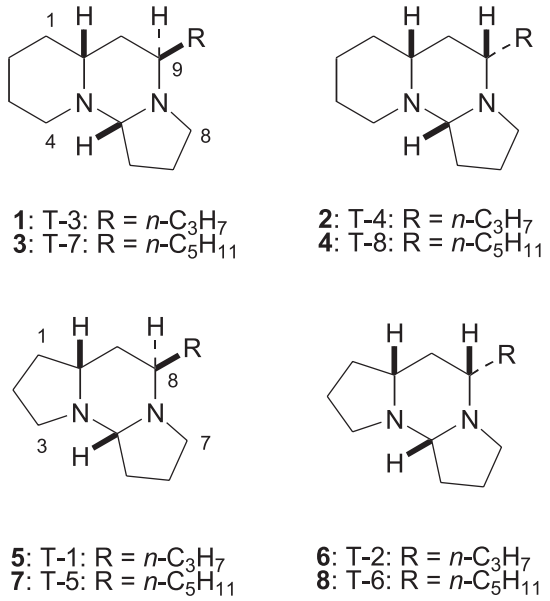
Received March 28, 2000. Published on the NRC Research Press website on July 13, 2000.

M. Plehiers, S. Heilporn, D. Ekelmans, S. Leclercq, M. Sangermano,[1] J.C. Braekman,[2] and D. Daloze.[2] Laboratory of Bioorganic Chemistry CP 160/07, Department of Organic Chemistry, University of Brussels, Av. F. D. Roosevelt, 50-1050 Brussels, Belgium.

[1]Present address: Dipartimento di Scienza dei Materiali e Ingegneria Chimica, Politecnico di Torino, C.so Duca degli Abruzzi 24, 10129, Torino, Italy.
[2]Authors to whom correspondence may be addressed. Telephone: 32 2 650 35 37. Fax: 32 2 650 27 98. e-mail: ddaloze@ulb.ac.be or braekman@ulb.ac.be
[3]IUPAC numbering. For convenience, we will use the numbering of earlier publications.

 © 2000 NRC Canada

Fig. 1. Structures of the eight tetraponerines.



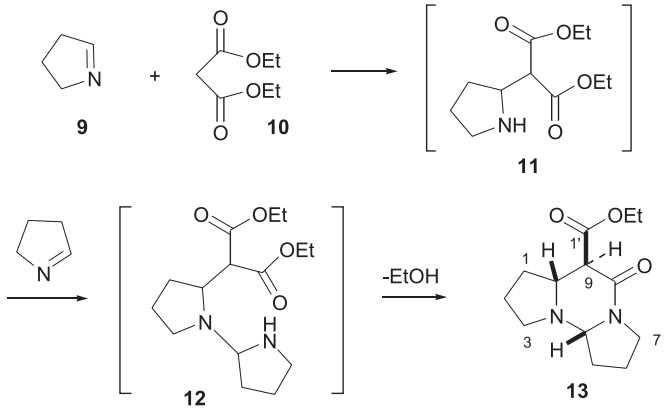
be reversed or several competitive processes could take place.

Results and discussion

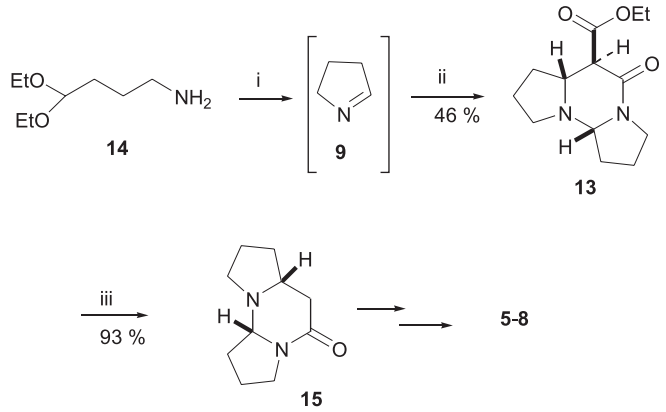
Our initial attempts along these lines, however, were disappointing. When Δ^1-pyrroline (**9**), generated through treatment of 4-aminobutanal diethylacetal (**14**) with an excess of 10% HCl (7), was reacted with 0.5–4 equiv of **10** in a citrate–phosphate buffer (pH 5.4) at 20°C for 24 h, as described by Stevens and Lee (8) for the synthesis of coccinelline, the reaction mixture showed only traces of the desired compound **13**. Instead, large amounts of **9** and **10** were still present, accompanied by polar compounds which were not investigated. The influence of different parameters, such as temperature, proportions of reactants, and pH, on the outcome of the reaction was studied. It turned out that an increase of pH had a beneficial effect because the yield of compound **13** reached 20% at pH 8 and 27% at pH 10, after work-up and silica gel chromatography. The optimum conditions we have found (2:1 ratio of **10** and **14**, pH 12, 20°C for 14 h, vigorous stirring) furnished **13** in a reproducible 46% yield (based on **14**) (Scheme 2). The structure of **13** was assigned on the basis of its spectral properties, particularly 1D and 2D NMR spectra at 600 MHz. The *trans*-relationship between H-9 and H-10 was based on the coupling constant $J_{9,10}$ = 10 Hz, whereas we assumed a *cis*-relationship between H-4 and H-10 based on the results of previous cyclization reactions in this series (2–4). This assignment was later confirmed by the conversion of **13** into **17**. Next, lactam ester **13** was decarboxylated into lactam **15** in a 93% yield, by treatment with 5% KOH–MeOH at 20°C for 2 h, followed by addition of 10% HCl to pH 4–5, and heating the resulting mixture for 2 h at 70°C (Scheme 2).

With compound **15** easily available in two steps, we turned our attention to the conversion of its lactam group

Scheme 1. Synthetic strategy towards tricyclic lactam **13**.



Scheme 2. Synthesis of tricyclic lactam **15**. Reagents and conditions: (*i*) 10% HCl, 20°C, 30 min; (*ii*) (*a*) 1 M KOH → pH 12; (*b*) **10** (2 equiv), 0°C → 20°C, 14 h; (*iii*) (*a*) 5% KOH–MeOH, 20°C, 2 h; (*b*) 10% HCl → pH 4–5, 0°C; (*c*) 70°C, 2 h.



into an α-alkylamine. Compounds bearing this functionality are important synthetic targets (3, see for example ref. (9)). One way to synthesize them is through reductive alkylation of lactams, which involves the addition of an alkyl organometallic reagent onto the lactam carbonyl, followed by iminium ion formation and reduction of the latter by an hydride reagent. Despite the well-known lack of reactivity of lactam carbonyls towards nucleophilic reagents, several examples of this process are nevertheless described in the literature (10–16). In this context, it is interesting to note that all our efforts to repeat the reductive alkylation described by Jones (13) as a key step in his short synthesis of tetraponerine-8 (**4**) failed. Indeed, when the conditions described by Jones (13) (pentylmagnesium chloride or bromide, TMEDA, followed by $LiAlH_4$ or $LiAl(Ot\text{-}Bu)_3H$) were applied to his bicyclic lactam, we observed only the reduction of the carbonyl group.[4] Other conditions were subsequently tried, such as *n*-BuLi, with or without TMEDA, pentylmagnesium chloride in the presence of Ce(III) salts (17), or preformed *n*-$BuCeCl_2$ (17), again without success.[4] Despite these negative results, we submitted lactam **15** to a reductive alkylation using *n*-$BuCeCl_2$ but, again, the results

[4] F. Broeders, C. Devijver, G. Daugimont, J.C. Braekman, and D. Daloze. Unpublished results.

© 2000 NRC Canada

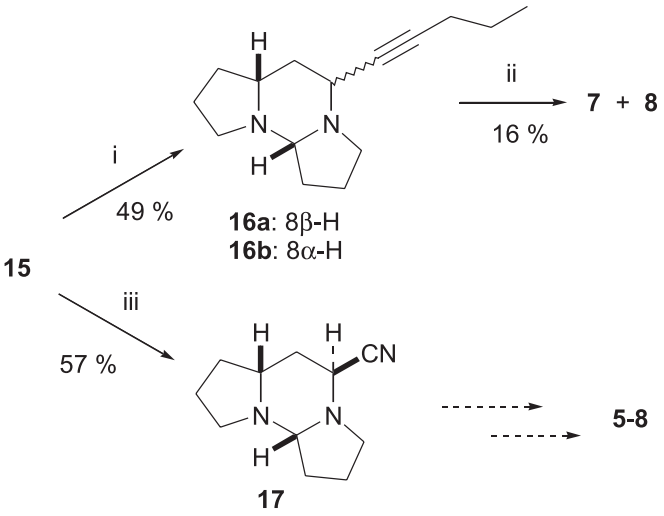
were disappointing. When the reducing step was performed with $NaBH_4$, most of starting **15** was recovered unchanged whereas with $LiAlH_4$ complex mixtures were obtained. Several authors have already reported that the addition of alkyl organometallic reagents to lactam carbonyls is fraught with difficulties (11, 12, 15, 16). This problem seems to be attributable to competitive enolate formation (15). Indeed, a close look at successful examples reported in the literature showed either that the lactam carbonyl is not sterically hindered (10), that it is activated towards nucleophilic attack (11, 14, 16), or still, that the organometallic reagents used [aryllithium (11), furyllithium (12), and alkylcerium (15) reagents] are less basic than alkylmagnesium or alkyllithium reagents. In agreement with this interpretation, Yamaguchi and Hirao (18) have described the successful synthesis of α-alkynylamines through the addition of alkynyllithium reagents to the carbonyl group of lactams in the presence of $BF_3{\cdot}Et_2O$, followed by $LiAlH_4$ reduction.

We thus submitted **15** to these conditions, using 1-pentynyllithium (Scheme 3). This procedure indeed furnished a 70:30 ratio of the two diastereomers **16a** and **16b** in a 49% yield. Unfortunately, the last step, namely, the reduction of the triple bond of **16** to afford T-5 (**7**) and T-6 (**8**) proved unsatisfactory. Several hydrogenation catalysts and various conditions of temperature and pressure were tried but with limited success. Either the reaction was not complete and stopped at the alkene stage (W_2 grade RaNi, with or without KOH), or overreduction was observed (Pd-C, PtO_2), leading to complex mixtures containing small amounts of **7** and **8**. The latter were accompanied by secondary products arising from hydrogenolysis of the aminal (5), or of the propargyl amine (19) functionalities of **16**. The best results (ca. 16% of a 54:46 mixture of T-5 (**7**) and T-6 (**8**)) were obtained with Wilkinson's catalyst (20) (Scheme 3), but the yield could not be improved. Thus, to circumvent this problem, we turned to an indirect alkylation method, namely the α-aminonitrile methodology of Stevens (21, 22). Accordingly, the iminium ion, resulting from partial reduction of **15** with DIBAL-H at –78°C followed by acid treatment, was trapped with cyanide ion to furnish in a 56% yield the α-aminonitrile **17** (Scheme 3), identical in all respects (except rotation power) with the pivotal intermediate described by Yue et al. (4) in their tetraponerine synthesis.

Conclusions

In conclusion, the results reported here constitute a short and convenient procedure to synthesize the four tetraponerines **5–8**. The key intermediate **15** was obtained from readily available and inexpensive starting materials in three steps and 24% overall yield. Through its simplicity and conciseness, this approach compares favourably with our previous one (2). On the other hand, the synthesis of Yue et al. (4) leads to enantiomerically pure compounds and good overall yields, but requires seven steps. It is noteworthy that all our attempts to directly transform lactam **15** into the tetraponerines through reductive alkylation failed, whatever the conditions used.

Scheme 3. Conversion of **15** into the tetraponerines. Reagents and conditions: (*i*) (*a*) 1-pentynyllithium (3 equiv), $BF_3{\cdot}Et_2O$ (3 equiv), –40°C, 4 h; (*b*) EtOH (3 equiv), then $LiAlH_4$ (excess), –40°C, 1 h; (*ii*) H_2, Wilkinson catalyst, atm. pressure, 20°C, 41 h; (*iii*) (*a*) DIBAL-H (1.2 equiv), –78°C, THF, 2 h; (*b*) $HClO_4$–EtOH → pH 3; (*c*) KCN (5.5 equiv), 14 h.



Experimental section

General

EIMS and EIHRMS were performed with a Fisons VG Micromass Autospec instrument (70 eV) and GC–EIMS analyses with the same instrument coupled to a Carlo Erba 8065 MS gas chromatograph equipped with a capillary column (carrier gas He). In all cases, peak intensities are expressed as % relative to the base peak. The ^1H NMR spectra were recorded in $CDCl_3$ at 250 MHz with a Bruker WM 250 spectrometer or at 600 MHz with a Varian UNITY 600 spectrometer and are reported in ppm from internal TMS on the scale. Data are reported as follows: chemical shift [multiplicity (s, singlet; bs, broad singlet; d, doublet; bd, broad doublet; t, triplet; q, quartet; sex, sextet; dd, double doublet; td, double triplet; m, multiplet; ms, massif), coupling constants in Hz, integration]. The IR spectra were recorded with a Bruker IFS 25 instrument. GLC analyses were performed with a Varian 3400 apparatus equipped with capillary columns (column 1, 25 m × 0.32 mm fused-silica column coated with OV1; column 2, 30 m × 0.53 mm fused-silica column coated with OV1701), carrier gas N_2. Thin layer chromatography analyses (TLC) were performed on 0.25 mm Polygram silica gel SILG–UV_{254} precoated plates (Macherey–Nagel). Column chromatographies were performed over silica gel (MN Kieselgel 60 0.04–0.063 mm) using the flash technique. Melting points are uncorrected.

Synthesis of 13

Compound **14** (0.52 g, 3.25 mmol) was dissolved with gentle heating in 10% HCl (10 mL) and left at 0°C for 20 min. Then, a 1 M KOH solution was added until the pH reached 12, and **10** (1.05 g, 6.5 mmol) was added in one portion. The mixture was vigorously stirred for 14 h and progressively allowed to warm from 0 to 20°C. After

© 2000 NRC Canada

addition of 50 mL of 10% NH_4OH solution, the mixture was extracted three times with CH_2Cl_2 (25 mL). The combined organic layers were filtered on a WA filter paper and evaporated in vacuo to give a residue which was purified by flash chromatography on a silica gel column (CH_2Cl_2–MeOH, 98:2) to afford **13** as an oil which crystallized on standing. Recrystallization in acetone–pentane (1:1) yielded 0.380 g of white crystals (1.5 mmol, 46%).

13: mp 100–102°C. EIHRMS (*m/z*): 252.1474 (25, $C_{13}H_{20}N_2O_3$), (calcd. for $C_{13}H_{20}N_2O_3$: 252.1474); 179.1187 (100, $C_{10}H_{15}N_2O$), (calcd. for $C_{10}H_{15}N_2O$: 179.1184); 155.0947 (70, $C_8H_{13}NO_2$), (calcd. for $C_8H_{13}NO_2$: 155.0946). EIMS (*m/z*): 252 (25, $M^{+\cdot}$), 251 (33), 224 (5), 209 (5), 207 (5), 183 (18), 179 (100), 155 (70), 138 (21), 110 (19). IR (KBr) (cm^{-1}): 2966, 2882, 2812, 1732, 1640, 1448, 1376, 1294, 1246, 1152. ^1H NMR ($CDCl_3$, 600 MHz): 1.30 (t, *J* = 7.8, 3 H, 3′-H_3), 1.60 and 2.05 (m, 1 H each, 1-H_2), 1.70 and 2.15 (m, 1 H each, 5-H_2), 1.82 and 2.0 (m, 1 H each, 6-H_2), 1.85 and 1.95 (m, 1 H each, 2-H_2), 2.35 (ddd, *J* = 8.5, 8.5, 8.5, 1 H, 3-H), 2.85 (m, 1 H, 10-H), 3.08 (ddd, *J* = 8.5, 8.5, 3.0, 1 H, 3-H), 3.20 (d, *J* = 10.0, 1 H, 9-H), 3.54 (dt, *J* = 10.0, <2.0, 1 H, 7-H), 3.64 (m, 1 H, 7-H), 3.90 (dd, *J* = 9.0, 5.0, 1 H, 4-H), 4.25 (m, 2 H, 2′-H_2). ^{13}C NMR ($CDCl_3$, 152.87 MHz): 14.1 (3′-C), 21.0 (6-C), 22.0 (2-C), 29.9 (1-C), 32.3 (5-C), 44.9 (7-C), 49.1 (3-C), 55.6 (9-C), 61.2 (2′-C), 64.1 (10-C), 77.9 (4-C), 163.8 (8-C), 169.5 (1′-C).

Hydrolysis and decarboxylation of 13 into 15

Compound **13** (150 mg, 0.6 mmol) was stirred in 5 mL of 5% aqueous KOH solution for 2 h at 20°C. Then, an aqueous 10% HCl solution was added dropwise at 0°C till pH 4–5, and the resulting mixture was heated at 70°C for 2 h. After basification with NH_4OH, the mixture was extracted three times with CH_2Cl_2 (25 mL). The combined organic layers were filtered on a WA filter paper and evaporated in vacuo to give 100 mg of **15** (0.56 mmol, 93%). Compound **15** is hygroscopic and must be carefully dried before being engaged in the next reaction.

15: EIHRMS (*m/z*): (180.1257, $C_{10}H_{16}N_2O$), (calcd. for $C_{10}H_{16}N_2O$: 180.1263); 179.1189 (100, $C_{10}H_{15}N_2O$), (calcd. for $C_{10}H_{15}N_2O$: 179.1184). EIMS (*m/z*): 180 (85, $M^{+\cdot}$), 179 (100), 152 (52), 150 (25), 137 (40), 135 (32), 124 (62), 110 (42), 96 (29), 83 (70), 70 (92), 55 (37), 41 (50). IR (film) (cm^{-1}): 2947, 1656, 1450. ^1H NMR ($CDCl_3$, 600 MHz): 1.50 and 2.05 (m, 1 H each, 1-H_2), 1.70 and 2.12 (m, 1 H each, 5-H_2), 1.80 and 2.0 (m, 1 H each, 6-H_2), 1.95 and 2.05 (m, 1 H each, 2-H_2), 2.20 (dd, *J* = 16.5, 10.0, 1 H, 9-Hax), 2.25 (ddd, *J* = 8.5, 8.5, 8.5, 1 H, 3-H), 2.50 (m, 1 H, 10-H), 2.58 (dd, *J* = 16.5, 4.8, 1 H, 9-He), 3.07 (ddd, *J* = 8.5, 8.5, 3.2, 1 H, 3-H), 3.47 (m, 1 H, 7-H), 3.60 (m, 1 H, 7-H), 3.68 (dd, *J* = 9.5, 5.0, 1 H, 4-H). ^{13}C NMR ($CDCl_3$, 152.87 MHz): 21.4 (6-C), 22.5 (2-C), 31.1 (1-C), 32.8 (5-C), 38.4 (9-C), 45.0 (7-C), 50.1 (3-C), 61.5 (10-C), 78.3 (4-C), 168.2 (8-C).

Reductive alkynylation of 15: compounds 16a and 16b

To 1-pentyne (82 μL, 0.83 mmol) in 1 mL of anhydrous THF was added under a nitrogen atmosphere at –78°C, *n*-BuLi (0.55 mL, 0.84 mmol) followed by $BF_3{\cdot}Et_2O$ (105 μL, 0.83 mmol). After stirring at –78°C for 1 h, lactam **15** (51 mg, 0.28 mmol) in 1 mL of THF was added dropwise and the stirring maintained at –40°C for 4 h. The reaction mixture turned progressively red. Then, EtOH (50 μL, 0.86 mmol) and $LiAlH_4$ (50 mg, 1.32 mmol) were added at –40°C and the mixture was stirred for 1 h. After addition of water, the mixture was extracted three times with CH_2Cl_2 (25 mL). The combined organic layers were dried over $MgSO_4$ and evaporated in vacuo. The residue was chromatographed on an alumina column (hexane:EtOAc, 98:2 – 95:5) to afford **16a** (22.5 mg, 0.097 mmol) and **16b** (9.5 mg, 0.041 mmol) (70:30 ratio, total yield 49%).

16a: EIMS (*m/z*): 232 (19, $M^{+\cdot}$), 231 (40), 217 (9), 203 (26), 189 (13), 163 (15), 151 (13), 137 (15), 125 (22), 123 (25), 111 (40), 109 (33), 97 (62), 95 (48), 83 (62), 81 (46), 71 (61), 70 (78), 69 (70), 57 (100), 55 (75). IR (film) (cm^{-1}): 2962, 2935, 2872, 2784, 1460, 1388, 1362, 1340, 1189, 1180. ^1H NMR ($CDCl_3$, 600 MHz) = 0.97 (t, *J* = 7.5, 3 H, 5′-H_3), 1.50 (sex, *J* = 7.5, 2 H, 4′-H_2), 1.45 and 1.70 (m, 1 H each, 1-H_2), 1.65 and 1.85 (m, 1 H each, 9-H_2), 1.75 and 1.85 (m, 1 H each, 5-H_2), 1.80 (m, 2 H, 6-H_2), 1.70 and 1.80 (m, 1 H each, 2-H_2), 2.10 (m, 1 H, 10-H), 2.15 (m, 2 H, 3′-H_2), 2.15 (m, 1 H, 7-H), 2.32 (ddd, *J* = 8.5, 8.5, 8.5, 1 H, 3-H), 2.66 (dd, *J* = 7.5, 6.2, 1 H, 4-H), 3.0 (dt, *J* = 3.2, 8.5, 1 H, 7-H), 3.02 (bdd, *J* = 11.0, 2.3, 1 H, 8-H), 3.32 (dt, *J* = 2.8, 8.5, 1 H, 3-H). ^{13}C NMR ($CDCl_3$, 152.87 MHz): 13.5 (5′-C), 19.8 (6-C), 20.7 (3′-C), 21.2 (2-C), 22.2 (4′-C), 28.8 (5-C), 29.6 (1-C), 35.9 (9-C), 48.0 (7-C), 49.2 (3-C), 52.5 (8-C), 63.1 (10-C), 80.2 (1′-C or 2′-C), 82.6 (4-C), 83.1 (2′-C or 1′-C).

16b: EIMS (*m/z*): 232 (8, $M^{+\cdot}$), 231 (15), 203 (7), 191 (7), 179 (8), 165 (10), 163 (9), 150 (18), 137 (20), 125 (30), 123 (25), 111 (50), 109 (36), 97 (70), 95 (53), 85 (48), 83 (70), 81 (48), 71 (70), 70 (40), 69 (75), 57 (100), 55 (70). IR (film) (cm^{-1}): 2962, 2933, 2873, 2810, 1653, 1460, 1390, 1346, 1173, 1162. ^1H NMR ($CDCl_3$, 600 MHz): 1.0 (t, *J* = 7.2, 3 H, 5′-H_3), 1.54 (sex, *J* = 7.2, 2 H, 4′-H_2), 1.45 and 1.75 (m, 1 H each, 1-H_2), 1.68 and 1.85 (m, 1 H each, 5-H_2), 1.70 and 1.80 (m, 1 H each, 6-H_2), 1.70 and 1.90 (m, 1 H each, 2-H_2), 1.75 and 1.80 (m, 1 H each, 9-H_2), 2.15 (ddd, *J* = 8.6, 8.6, 8.6, 1 H, 7-H), 2.19 (dt, *J* = 2.2, 7.0, 2 H, 3′-H_2), 2.39 (m, 1 H, 10-H), 2.65 (ddd, *J* = 8.4, 8.4, 8.4, 1 H, 3-H), 2.86 (m, 1 H, 3-H); 3.0 (m, 1 H, 7-H), 3.02 (m, 1 H, 4-H), 3.95 (bdd, *J* = 4.5, 2.0, 1 H, 8-H). ^{13}C NMR ($CDCl_3$, 152.87 MHz): 13.6 (5′-C), 21.2 (6-C), 20.7 (3′-C), 20.1 (2-C), 22.6 (4′-C), 28.7 (5-C), 29.6 (1-C), 34.7 (9-C), 48.9 (7-C), 48.1 (3-C), 48.0 (8-C), 59.4 (10-C), 77.0 (4-C), 86.4 (1′-C or 2′-C). One *sp* carbon signal was not detected.

Catalytic hydrogenation of 16a and 16b: synthesis of T-5 (7) and T-6 (8)

To a mixture of **16a** and **16b** (6.0 mg, 0.026 mmol) in toluene (10 mL) was added Wilkinson's catalyst (11.6 mg, 0.012 mmol) and the mixture was left under stirring for 41 h under an atmospheric pressure of hydrogen. After 23 h, a GC (column 2, from 180 to 260°C, programmed at 5°C/min) of the crude reaction mixture showed the presence of T-5 (**7**) and T-6 (**8**) in an approximately 70:30 ratio, along with 25% of starting material. After 41 h, the latter had disappeared, but secondary compounds were found besides a 54:46 mixture of T-5 (**7**) and T-6 (**8**). The reaction mixture was then evaporated in vacuo and the residue chromatographed on an

© 2000 NRC Canada

alumina column (hexane:AcOEt, 50:50), yielding T-5 and T-6 as a mixture (1 mg, 0.0042 mmol, 16%). The two compounds were identical in ^{1}H NMR and capillary GC with reference compounds (2).

Formation of 17

To lactam **15** (59.3 mg, 0.33 mmol) in anhydrous diethyl ether (4.0 mL) was added a 1 M solution of DIBAL-H in hexane (0.40 mL, 0.4 mmol), and the mixture stirred under a nitrogen atmosphere at –78°C for 2 h. Then, the mixture was acidified using a 10% ethanolic perchloric acid solution, till the pH reached about 3. Finally, KCN (118 mg, 2.15 mmol) in 1 mL of H_2O was added and the mixture left overnight at 20°C. After addition of a saturated $NaHCO_3$ solution to pH 8, the mixture was extracted three times with CH_2Cl_2. The combined organic phases were dried on $MgSO_4$, filtered, and evaporated in vacuo. Chromatography on a silica gel column (eluent hexane:AcOEt, from 8:2 to 7:3) yielded nitrile **17** (35 mg, 0.18 mmol, 56%). Compound **17** displayed MS, IR, ^{1}H, and ^{13}C NMR spectra identical with those reported by Yue et al. (4).

17: HRCIMS (*m*/*z*): 192.1491 (100, [M + H^+], $C_{11}H_{18}N_3$), (calcd. for $C_{11}H_{18}N_3$: 192.1500); 191.1416 (12, [M^+], $C_{11}H_{17}N_3$), (calcd. for $C_{11}H_{17}N_3$: 191.1422); 165.1399 (20, $C_{10}H_{17}N_2$), (calcd. for $C_{10}H_{17}N_2$: 165.1392); 138.1154 (20, $C_{10}H_{17}N_2$), (calcd. for $C_{10}H_{17}N_2$: 138.1157).

Acknowledgements

We thank Dr M. Luhmer for the NMR spectra and Mr C. Moulard for the mass spectra. S. L. thanks the Fonds National de la Recherche Scientifique de Belgique for financial support.

References

1. J.C. Braekman, D. Daloze, J.M. Pasteels, P. Vanhecke, J.P. Declercq, V. Sinnwell, and W. Francke. Z. Naturforsch. C: J. Biosci. **42c**, 627 (1987).
2. C. Devijver, P. Macours, J.C. Braekman, D. Daloze, and J.M. Pasteels. Tetrahedron, **51**, 10913 (1995).
3. S. Leclercq, J.C. Braekman, D. Daloze, and J.M. Pasteels. Prog. Chem. Org. Nat. Prod. **79**, part II, 115 (2000).
4. Ch. Yue, I. Gauthier, J. Royer, and H.P. Husson. J. Org. Chem. **61**, 4949 (1996).
5. B. Renson, P. Merlin, D. Daloze, J.C. Braekman, Y. Roisin, and J.M. Pasteels. Can. J. Chem. **72**, 105 (1994).
6. C. Devijver, J.C. Braekman, D. Daloze, and J.M. Pasteels. J. Chem. Soc. Chem. Comm. 661 (1997).
7. C. Schöpf and F. Oechler. Justus Liebigs Ann. Chem. **523**, 1 (1936).
8. R.V. Stevens and A.W.M. Lee. J. Am. Chem. Soc. **101**, 7032 (1979).
9. J.W. Daly. *In* The alkaloids: chemistry and pharmacology. Vol. 50. *Edited by* G.A. Cordell. Academic Press, San Diego. 1998. p. 141.
10. R. Adams and J.E. Mahan. J. Am. Chem. Soc. **64**, 2588 (1942).
11. H.W. Gschwend and A. Hamdan. J. Org. Chem. **47**, 3652 (1982).
12. Y.C. Hwang, M. Chu, and F.W. Fowler. J. Org. Chem. **50**, 3885 (1985).
13. T.H. Jones. Tetrahedron Lett. **31**, 4543 (1990).
14. Y. Shishido and C. Kibayashi. J. Org. Chem. **57**, 2876 (1992).
15. S. Nukui, M. Sodeoka, and M. Shibasaki. J. Org. Chem. **60**, 398 (1995).
16. L. Micouin, J.-C. Quirion, and H.-P. Husson. Tetrahedron Lett. **37**, 849 (1996).
17. T. Imamoto. *In* Comprehensive organic synthesis. Vol 1. *Edited by* B.M. Trost and I. Fleming. Pergamon Press, London. 1991. p. 231.
18. M. Yamaguchi, and I. Hirao. Tetrahedron Lett. **24**, 1719 (1983).
19. I.E. Kopka, Z.A. Fataftah, and M.W. Rathke. J. Org. Chem. **45**, 4616 (1980).
20. J.A. Osborn, F.H. Jardine, J.F. Young, and G. Wilkinson. J. Chem. Soc. 1711 (1966).
21. R.V. Stevens, and A.W.M. Lee. J. Chem. Soc. Chem. Comm. 103 (1982).
22. T.H. Jones, A. Laddago, A.W. Don, and M.S. Blum. J. Nat. Prod. **53**, 375 (1990).

© 2000 NRC Canada

Ab initio analysis of C—H and C—C stretching intensities in Raman spectra of hydrocarbons

Kathleen M. Gough, Jason R. Dwyer, and Richard Dawes

Abstract: Molecular polarizability and changes in the polarizability associated with the stretch of C—C and C—H bonds have been calculated for thirty-four saturated hydrocarbons, including the series of *n*-alkanes to C15, as well as several cyclo- and bicycloalkanes, propellanes, prismanes, and hedranes. The ab initio results (HF/D95(d,p)) are compared to experimental Raman trace scattering intensities where such information is available. Possible factors governing trends in the magnitude of the derivatives are considered. For the C—C stretches, chain length and position along the chain are the most important factors for the *n*-alkanes, whereas strain appears to be significant for the ring and caged structures. For the C—H stretches, the most significant factors are the same as those found in our earlier work: location, type, and orientation relative to the carbon skeleton.

Key words: hydrocarbons, Raman scattering intensities, molecular polarizability, polarizability derivatives, theory of atoms in molecules.

Résumé : On a calculé la polarisabilité moléculaire ainsi que les changements de polarisabilité associés à l'élongation des liaisons C—C et C—H de trente-quatre hydrocarbures saturés comprenant les alcanes normaux jusqu'en C15 ainsi que plusieurs cyclo- et bicycloalcanes, propellanes, prismanes et hédranes. Dans les cas où de telles données étaient disponibles, on a comparé les résultats des calculs ab initio (HF/D95(d,p)) avec les intensités de dispersion des spectres Raman expérimentaux. On a considéré les facteurs qui peuvent influencer les tendances dans l'amplitude des dérivées. Pour les élongations C—C, la longueur de la chaîne ainsi que la position le long de la chaîne sont les facteurs les plus importants des alcanes linéaires alors que, pour les structures cycliques ou en cage, la tension semble le facteur le plus important. Pour les élongations C—H, les facteurs les plus importants sont les mêmes que ceux observés dans notre travail antérieur: position, type et orientation relative par rapport au squelette carboné.

Mots clés : hydrocarbures, intensités de dispersion Raman, polarisabilité moléculaire, dérivées de polarisabilité, théorie des atomes dans les molécules.

Introduction

In the course of our study on Raman trace scattering intensities in hydrocarbons (1–4), we have shown that the polarizability derivative associated with the C—H bond stretching motion is not a readily transferable parameter. The principal geometric factors that correlate with the magnitude of the derivative are type and location of the bond, alignment relative to the carbon skeleton and local steric hindrance (1). To date, our theoretical study has been confined to C—H stretching vibrations which can be readily compared to experimental Raman scattering intensities (1–5). We have now extended the theoretical study to include symmetric C—C stretching vibrations in straight chain hydrocarbons, as well as in some ring and caged molecules exhibiting various degrees of strain (Fig. 1). The goals are

(1) to identify suitable molecules for in-depth experimental and theoretical study (preferably small molecules with high symmetry, only one or two different types of C—H and C—C bonds, and unusually high or low predicted intensities)

(2) to obtain theoretical data on molecules which are not amenable to experimental analysis, but which may provide us with more insight into the factors governing scattering intensities.

Experimental data for absolute Raman trace scattering intensities are quite limited, particularly for molecules with more than about 10 atoms. This is not surprising, given the requirements for obtaining reasonably accurate results. Nonresonant Raman trace scattering spectra must be acquired for the relatively isolated system, hence molecules should be in the gas phase. A force field analysis is required to convert the measured band intensities, first to derivatives of the polarizability with respect to normal coordinates, and then to derivatives with respect to internal coordinates. Experimental intensities are subject to considerable error margins, especially for the very weak modes. Thus, it is also important to obtain spectra for several isotopomers, on the

Received February 25, 2000. Published on the NRC Research Press website on July 13, 2000.

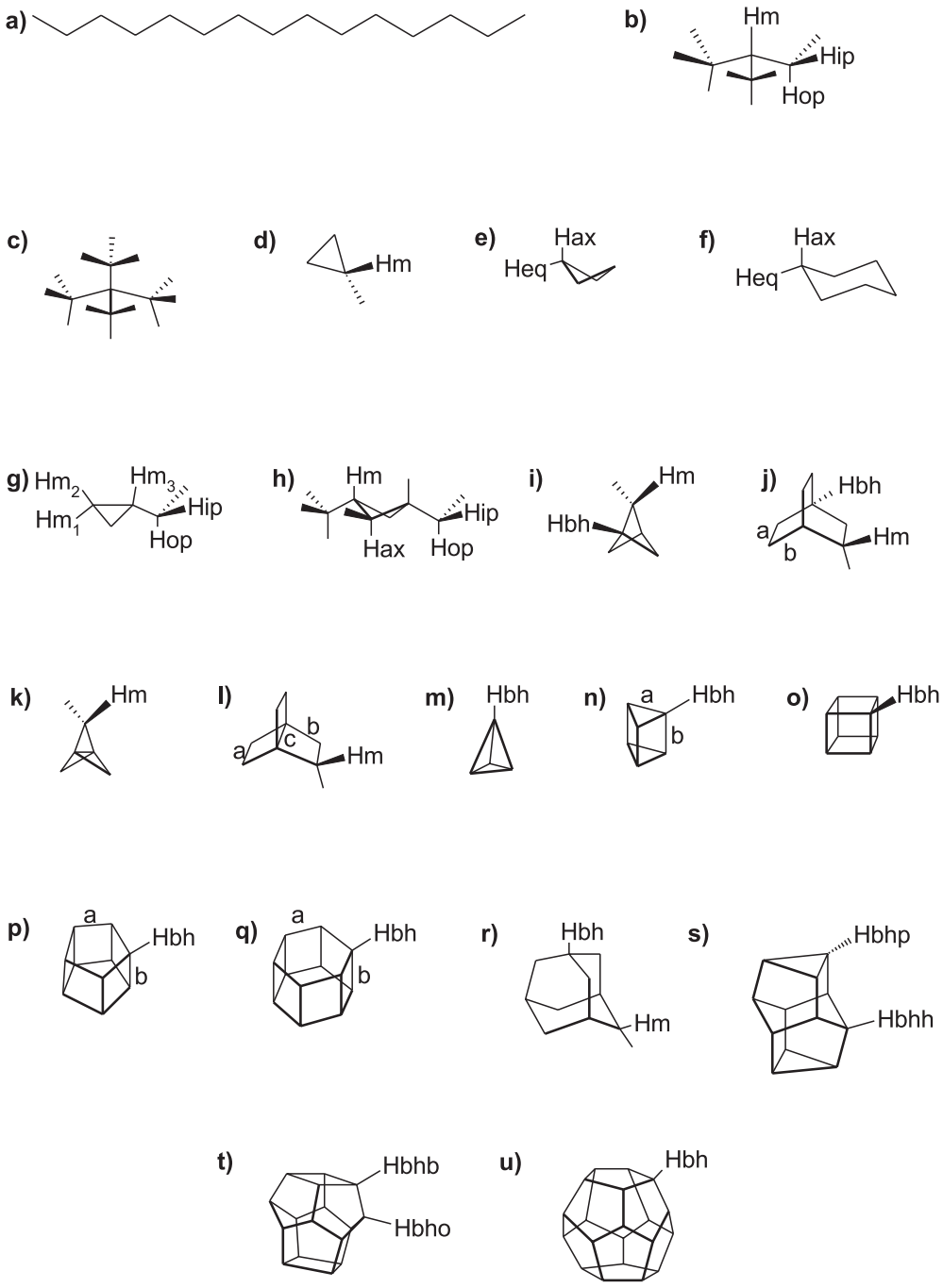
This paper is dedicated to Professor Ted Schaefer in recognition of his outstanding contributions to Canadian chemistry.

K.M. Gough[1] and R. Dawes. Department of Chemistry, University of Manitoba, Winnipeg MB R3T 2N2, Canada.
J.R. Dwyer. Department of Chemistry, University of Toronto, Toronto ON M5S 3H6, Canada.

[1]Author to whom correspondence may be addressed. Telephone: (204) 474-6262. Fax: (204) 474-7608.
e-mail: kmgough@ms.umanitoba.ca

© 2000 NRC Canada

Fig. 1. Structures of molecules in this study, showing unique bonds. Straight chain (**a**) is representative of the *n*-alkane series from ethane to penticosane, see Table 1.



assumption that the derivatives with respect to internal coordinates will be unchanged by isotopic substitution, while the composition of the normal modes will be different. This is achieved by recording the Raman spectra for the parent molecule and for several different deuterated species (2, 5–8). The problem is thus over-determined, with more items of independent data than there are parameters to be fit. This approach reduces the error in the final results, but limits the molecules for study to those with sufficient vapor pressure for gas phase work, and necessitates synthesis of specifically deuterated species.

More recently, we have focussed on the use of ab initio quantum chemistry calculations for the prediction of polarizability derivatives. The molecules we have chosen to investigate here include a homologous series of *n*-alkanes, small branched and ring alkanes as well as several strained ring systems. The latter have unusual structures such as the inverted tetrahedral geometry about the bridgehead carbon at-

© 2000 NRC Canada

oms in the propellanes and the curved bonds in small rings (9). Recent studies have shown that the C—H bond in tetrahedrane can act as a hydrogen donor (10), while the C—C bonds can function as proton acceptors (11). Detailed analyses (9) using the theory of atoms in molecules (AIM) developed by Bader (12) to characterize bond order, bond ellipticity, and charge concentrations of strained ring systems have underscored the unusual electronic character of these systems.

Observed trends in the intensities of hydrocarbon C—H stretching modes led to our present interpretations of intensity dependence (1). We now report the results of calculations on the C—C stretches and on those C—H stretches not previously reported, for these candidate molecules. The most significant variations and trends in this expanded set are discussed in relation to geometrical features of the molecules.

Calculation method

The procedures followed were identical to those used in our earlier work (1–4, 13) and are only briefly summarized here. The geometry of each molecule was optimized at the HF/D95(d,p) level with Gaussian 94 (14). This basis set provides a reasonable core size and balanced polarization functions necessary for good results (9, 13). The molecular polarizability was calculated at the optimized geometry with the coupled perturbed Hartree–Fock (CPHF) option in Gaussian 94 (14). The equations are solved analytically for this basis set. The polarizability was then recalculated for geometries in which symmetrically equivalent bonds were extended or compressed by $\Delta r = 0.010$ Å. The derivative was determined by finite difference

$$[1] \qquad \frac{\partial\bar{\alpha}}{\partial \mathrm{r}} \cong \frac{\Delta\alpha}{\Delta r} = \frac{1}{\mathrm{n}}\left(\frac{\bar{\alpha}' - \bar{\alpha}}{\Delta r}\right)$$

where $\bar{\alpha} = 1/3$ (trace of the polarizability tensor) = mean molecular polarizability, and n = number of symmetrically equivalent bonds stretched. The derivative reported is the average of those for $\pm\Delta r$; individual values differed from the average by 2% at most. This process was repeated for each unique bond type in the molecule.

We tested several variables with which the variations in C—C stretch derivatives might be correlated, including optimized bond length, strain energy and several AIM parameters reported by Wiberg et al. (9): charge density at bond critical point, bond ellipticity, and average electron population. The most useful descriptor was the strain energy, estimated in the manner described by Wiberg et al. (9). The molecular energy was calculated, after optimization with the *very tight* convergence criterion, for a set of standard molecules and for all the molecules in the study. The "strain-free" energy of individual components was determined from the standard reference set

(*i*) CH_3 = 1/2 E (ethane) = –39.6246205 au
(*ii*) CH_2 = 1/2 {[E (propane) – 2 × E (CH_3)] + [E (cyclohexane)/6]} = –39.0431489 au
(*iii*) CH = E (isobutane) – [3 × E (CH_3)] = –38.4623977 au
(*iv*) quaternary C = E (neopentane) – [4 × E (CH_3)] = –37.8810579 au

These values are quite similar to those calculated in the same way with a larger basis set (15). The strain energy of any molecule was then found as the difference between the energy of the given molecule and the sum of the energies of its strain-free components. The total strain energy was partitioned equally among the carbons in the molecule, in most cases. For the methylcycloalkanes, it was assumed that all the strain was located in the ring, hence strain energy for the methyl carbons was set to zero. The calculated strain energy was then divided equally among the ring carbons. The sum of strain energies for both carbons in a bond was compared to the magnitude of the polarizability derivative for the stretch of that bond. The equipartition is not strictly valid for the bicycloalkanes, propellanes, prismanes, and adamantane, but is regarded as a useful first approximation. Individual cases are discussed below.

Results

The structures of all the molecules in this study are presented in Fig. 1. The experimental molecular polarizability values are available for only some of the molecules: straight chain alkanes to C15 (16, 17), as well as isobutane (**b**) (16), neopentane (**c**) (18), cyclopropane (**d**) (19), and cyclohexane (**f**) (16). These experimental values are compared to the calculated equilibrium molecular polarizability in Fig. 2. As expected from previous work (1–4, 13, 15, 20–22), the calculated values are lower than those from experiment, but the correlation here is excellent ($r^2 = 0.9997$ for $n = 19$), giving us confidence in the level of theory.

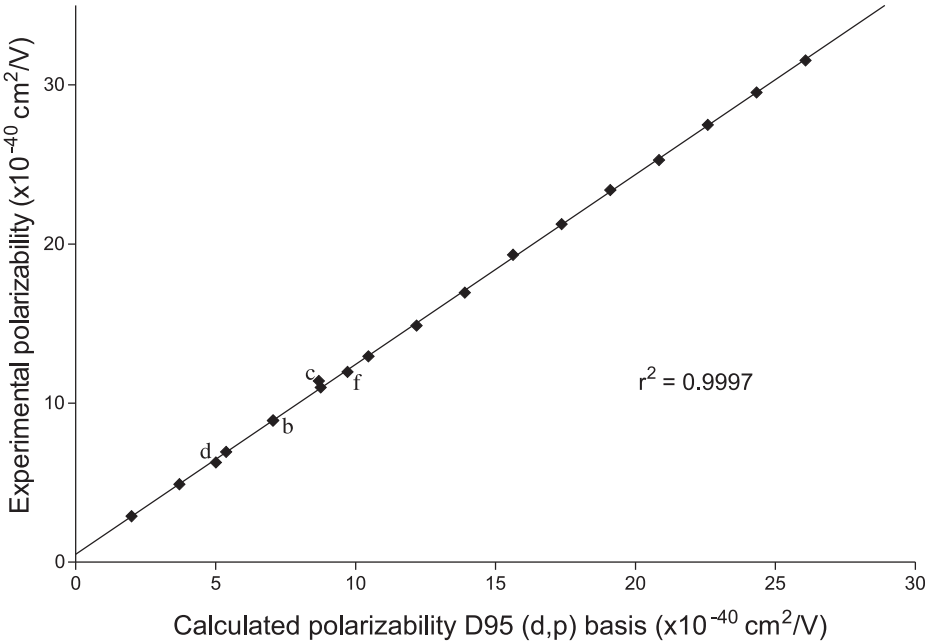
The derivatives of the mean molecular polarizability ($\partial\bar{\alpha}/\partial \mathrm{r}_{CC}$) with respect to the stretch of the C—C bonds have been calculated for the straight chain alkanes C2 to C15, and all the molecules in Fig. 1 except octahedrane (**s**) and decahedrane (**t**). The data for the straight chains are listed in Table 1. The derivatives calculated for the straight chain C—C stretches exhibit marked trends that are illustrated graphically in Fig. 3. The derivatives for the remaining molecules are shown in Table 2. The propellanes (**k** and **l**) represent special cases, since the variables cannot be strictly separated. For [1.1.1] propellane, all C—C bonds were stretched simultaneously, and the mixed result is reported. For the [2.2.2] propellane, shown below, the angle β is very nearly a right angle, at 91°. The 0.01 Å stretch of the nearly independent C—C bonds, labelled *b*, resulted in an increase of only about 0.0002 Å in the bonds labelled *a*. The derivative obtained is thus, to a very good approximation, the isolated stretch of bond *b*. The remaining bonds, *a* and *c*, cannot be disassociated, thus the derivative reported is for their simultaneous stretch.

The average strain energy per carbon is given in the last column of Table 2. The strain energy for each bond has been plotted against the derivative of each bond (Fig. 4). A moderate correlation is observed (see Discussion).

The C—H stretch polarizability derivatives for many of these molecules have been presented in an earlier paper (1). The calculated derivatives of the mean molecular polarizability expressed relative to the internal coordinate for CH stretch ($\partial\bar{\alpha}/\partial \mathrm{r}_{CH}$) are presented in Table 3 for the 10 new molecules. All of the derivatives have been calculated as described above, according to eq. [1].

© 2000 NRC Canada

Fig. 2. Correlation between experimental and calculated (HF/ D95(d,p), this work) mean molecular polarizability for the *n*-alkanes and molecules **b**, **c**, **d**, and **f**. See also Fig. 1 and Tables 1 and 2.



Discussion

Our previous work (1–4) has focused exclusively on C—H stretches. The current work addresses the C—C stretches in the same series of molecules and engenders some fundamental differences in our discussion. The C—H bonds are exterior to the carbon framework, consequently our correlations involved descriptors of their relation to that framework (e.g., axial–equatorial, endo–exo, bridgehead, etc.). We now turn our attention to the nature of the framework, to the location of the bond within the framework and their roles in determining the magnitude of the polarizability derivative for stretching C—C bonds.

The calculated equilibrium molecular polarizabilities are somewhat lower than the experimental values. This was not considered surprising, given that these are Hartree–Fock calculations, with neither configuration interaction nor electron correlation, and are static, not dynamic, polarizabilities (13, 20, 21). Nevertheless the excellent correlation between calculated and experimental mean molecular polarizability (Fig. 2) gives us confidence in the results. For discussion purposes, we group the C—C and C—H stretches separately. In the C—C stretch category, we consider first the unstrained hydrocarbons: straight and branched alkanes, and cyclohexane; and then the strained cyclic systems.

C—C bond stretches

Straight chain

Of the homologous series studied here, the experimental polarizability derivatives for the C—C stretch are available only for ethane (23), propane (8), and *trans*-butane (5) (Table 1). The level of calculation is sufficient to capture the relative magnitudes of the derivatives, though not the absolute values. This was also the case for the C—H stretches studied previously, and again, the ab initio results are convincingly parallel to those obtained experimentally.

In each molecule, the derivative of the terminal C—C bond is always greater than that for the first interior bond (Table 1, any individual row). The derivatives then *increase* for bonds that are located closer to the centre of the chain, reaching a maximum at the central bond. When chains of different length are compared (Table 1, any column) the magnitude of the derivative increases with chain length for any given position. The pattern that emerges (Fig. 3) is somewhat different from that observed for the C—H stretches. For the latter, it has been shown both by experiment and theory that the derivative for the terminal in-plane methyl C—H stretch increases monotonically with chain length. The derivatives for the methylene C—H bonds along the length of the chain are much smaller and decrease slightly with chain length and with position along the chain. Thus, there are two features to be explained for the C—C stretches: (a) the overall increase in the derivative with chain length; and (b) the relative ordering of the derivatives according to position within a single chain. Some factors are considered below.

Our interpretations of the CH-stretching intensities have been based on an analysis of the charge density with AIMPAC (11, 24). This software yields an atom by atom analysis of electron populations, both in the presence and absence of an applied field. The polarizability may be determined from these data. It is not possible to repeat the full AIMPAC analysis for C—C stretches in the longest chain molecules where the greatest differences are predicted. Not only is this time-consuming but the accumulated integration error can be at least as great as the small differences that are sought. In some cases, the calculations fail to converge due to problems with correct identification of the distorted interatomic surfaces when a field is applied.

© 2000 NRC Canada

Table 1. Values of $\partial\bar{\alpha}/\partial r_{CC}$ for straight-chain alkanes calculated with HF/D95(d,p) basis set.

Molecule	$\partial\bar{\alpha}/\partial r_{CC}$ (10^{-30} cm/V)											
	CH_3-CH_3	1,2	2,3	3,4	4,5	5,6	6,7	7,8	8,9	9,10	10,11	11,12	12,13
Ethane	1.388												
	1.32 ± 0.04[a, b]												
Propane		1.329											
		1.21 ± 0.02[a, c]											
Butane		1.461	1.280										
		1.47 ± 0.06[a, d]	*1.27 ± 0.06*[a, d]										
Pentane		1.514	1.423										
Hexane		1.558	1.470	1.576									
Heptane		1.581	1.512	1.622									
Octane		1.604	1.533	1.670	1.670								
Nonane		1.614	1.553	1.691	1.713								
Decane		1.626	1.563	1.713	1.738	1.758							
Undecane		1.632	1.575	1.723	1.760	1.779							
Tridecane		1.643	1.587	1.741	1.781	1.816	1.823						
Pentadecane		1.649	1.595	1.752	1.794	1.832	1.850	1.857					
Penticosane		1.660	1.607	1.769	1.814	1.857	1.879	1.899	1.909	1.919	1.924	1.929	1.927

[a]Experimental values are shown in italics below the calculated value.

[b]Ref (23).

[c]Ref. (8).

[d]Ref. (5).

© 2000 NRC Canada

Fig. 3. Variation of calculated polarizability derivative for the C—C stretch in *n*-alkanes, from ethane to penticosane. Numbering in legend identifies the two carbons in the bond, starting from the end of the chain (1, 2).

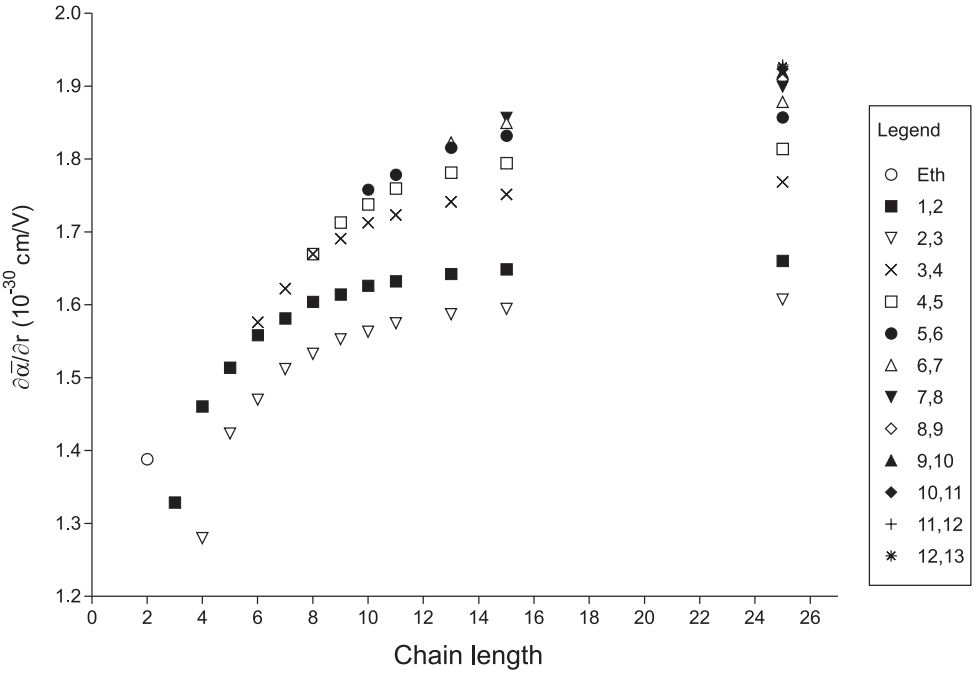


Table 2. Values of $\partial\bar{\alpha}/\partial r_{CC}$ and strain energies for cyclic alkanes calculated with the HF/D95 (d,p) basis set.

Molecule[a]	Stretch	$\partial\bar{\alpha}/\partial r_{CC}$[b]	Strain energy[c]
Isobutane (**b**)		1.280	0.00
Neopentane (**c**)		1.271	0.00
Cyclopropane (**d**)		1.196	18.76
Cyclobutane (**e**)		1.261	12.82
Cyclohexane (**f**)		1.217 (*1.03 ±.02*)[d]	0.12
Methylcyclopropane (**g**)	methyl ring	1.200	9.12
Methylcyclopropane (**g**)	ring	1.221	18.22
Dimethylcyclobutane (**h**)	methyl ring	1.370	5.84
Dimethylcyclobutane (**h**)	ring	1.293	11.70
Bicyclo[1.1.1]pentane (**i**)		1.218	27.30
Bicyclo[2.2.2]octane (**j**)	bonds labeled a	1.276	2.54
Bicyclo[2.2.2]octane (**j**)	bonds labeled b	1.145	2.54
[1.1.1]Propellane (**k**)	mixed symmetric stretch	1.157	40.90
[2.2.2]Propellane (**l**)	bonds labeled b	1.288	23.46
[2.2.2]Propellane (**l**)	mixed[e] stretch bonds a + c	1.092	23.46
Tetrahedrane (**m**)		0.981	69.92
Prismane (**n**)	bonds labeled a	0.978	47.60
Prismane (**n**)	bonds labeled b	1.085	47.61
Cubane (**o**)		1.053	38.72
Pentaprismane (**p**)	bonds labeled a	1.051	26.60
Pentaprismane (**p**)	bonds labeled b	1.007	26.60
Hexaprismane (**q**)	bonds labeled a	1.172	27.00
Hexaprismane (**q**)	bonds labeled b	0.904	27.00
Adamantane (**r**)		1.141	0.62
Octahedrane (**s**)	all bonds	1.037	12.96
Decahedrane (**t**)	all bonds	1.058	8.50
Dodecahedrane (**u**)		1.079	4.04

[a]Units: 10^{-30} cm/V.

[b]Letter in parentheses following name corresponds to structure in Fig. 1.

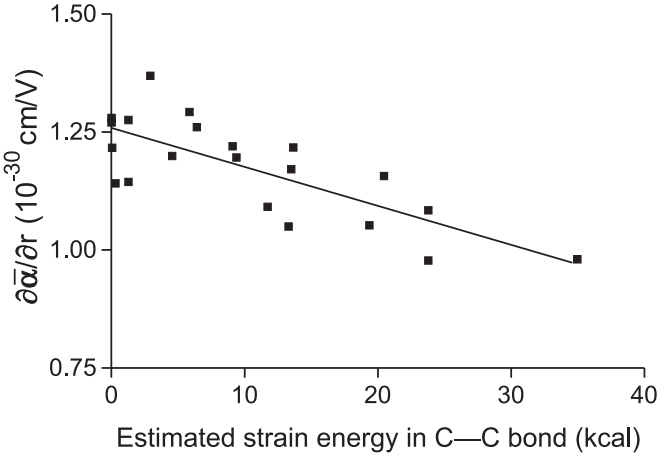
[c]Units: kcal/carbon atom.

[d]Ref. (7).

[e]See results for details on [2.2.2]propellane stretches.

© 2000 NRC Canada

Fig. 4. Variation of calculated polarizability derivative for the C—C stretch with estimated strain energy in some cyclic and caged molecules. See Table 2 for data.



The important results from the AIM analysis of the C—H stretches provide a guide for the C—C stretch intensities and are reviewed here (1–4, 13). For a straight chain molecule placed in an electric field, analysis of the charge distribution revealed that there was an end-to-end transfer of charge between terminal methyl hydrogen atoms (1–4, 13, 15). This dipole, induced along the molecule, was opposed by the atomic dipoles of the carbon atoms. The charge transfer term increased dramatically with chain length, and was the principal factor governing the magnitude of the unusually large derivative for the in-plane methyl C—H bond (1). For the stretch of the methylene C—H bonds, the charge transfer term remained fairly constant, in accord with the similar structure of the methylenes and their alignment relative to the molecular framework. Those derivatives were all quite similar, regardless of chain length or position along the chain.

We note that when any C—C bond is stretched, the overall chain length is being increased. We suspect that the charge transfer term, which was the most important factor in the large in-plane methyl CH derivative, above, is again playing the crucial role. This would also account for the overall increase in $\partial\bar{\alpha}/\partial r_{CC}$ with chain length. The ordering within any given chain is more puzzling. The stretch of the central C—C bond results in the separation of two equivalent halves of the molecule, with increased charge separation and increased polarizability. When bonds to either side of the centre are stretched, there is always a central portion that remains unchanged and may dampen the charge transfer effect. Certainly, the derivative decreases for bonds located further from the centre. It is only at the end of the chain that this effect is reversed, where the terminal methyl groups are stretched away from the methylene chain. The C1-C2 derivative is consistently larger than that for C2-C3. There is no immediately obvious reason for this difference. We are now attempting a complete AIM analysis of intermediate chains (*n*-heptane and *n*-nonane) that may provide some explanation.

Branched hydrocarbons and simple unstrained rings

The derivatives for the branched hydrocarbons isobutane and neopentane are shown in Table 2 along with those for the cyclic molecules. The two, branched hydrocarbons provide references for unstrained methine and quaternary carbons, respectively. Both derivatives are slightly smaller than but comparable to that of propane, and much smaller than those for the *n*-butane to *n*-hexane series. We conclude that the derivative is on the order of the longest chain segment in cases of branched connectivity.

Table 3. Values of $\partial\bar{\alpha}/\partial r_{CH}$ for branched and cyclic alkanes calculated with HF/D95 (d,p) basis set.

Molecule[a]	Bond[b]	$\partial\bar{\alpha}/\partial r_{CH}$[a] ($10^{-30}$ cm/V)
Neopentane (**c**)		1.032
Tetrahedrane (**m**)		1.161
Prismane (**n**)		1.328
Cubane (**o**)		1.365
Pentaprismane (**p**)		1.317
Hexaprismane (**q**)		1.306
Adamantane (**r**)	H_{bh}	1.287
Adamantane (**r**)	H_{m}	1.106
Octahedrane (**s**)	H_{bhb}	1.308
Octahedrane (**s**)	H_{bhh}	1.202
Decahedrane (**t**)	H_{bhb}	1.291
Decahedrane (**t**)	H_{bho}	1.218
Dodecahedrane (**u**)		1.220

[a]Bold letter in parentheses identifies structure in Fig. 1.
[b]Labels follow codes in Fig. 1.

It is anticipated that dimension should also have some effect on the derivatives in ring systems. In the simple, unstrained cyclohexane ring, the AIM analysis of the C—H stretch derivatives (3) showed the typical dependence of the derivative on end-to-end charge transfer cross the ring, giving rise to a much larger derivative for the equatorial C—H stretch compared to axial. The molecule lacks the open chain character that is associated with monotonic increase of $\partial\bar{\alpha}/\partial r_{CC}$ with chain length, but it is likely that charge transfer continues to play an important role. While the derivative is much smaller than those in *n*-hexane, it is the same as that of the interior C—C bond in *n*-butane, which it does resemble in projection.

Strained hydrocarbons

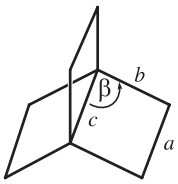
Both dimension and strain, which is determined by the local and global molecular and electronic structure, are anticipated to be significant qualifiers for the prediction of the polarizability derivatives for these molecules. The importance of strain seems apparent upon examination of the propyl series (units: 10^{-30} cm/V):

Propane	1.329
Cyclopropane	(d)1.196
Cyclopropyl ring in tetrahedrane (m)	0.981
Cyclopropyl ring in prismane (n)	0.978

Similarly, the derivative for cyclobutane is much smaller than derivatives for the C—C bonds in ethane, propane or *n*-butane. In Fig. 4, we have plotted strain energy, against C—C stretch derivative for most of the molecules in Table 2. Data were omitted where assignment of strain energy was ambiguous. Dimension and location of a bond within a molecule are thereby excluded, however the fact that the smallest derivative is found in the largest molecule indicates that

© 2000 NRC Canada

Scheme 1.



dimension is not the predominant factor here. While the correlation is not large, it is still significant, given the varied group. We conclude that there is a large reduction in intensity primarily associated with increased strain.

One of the problems with the strain energy correlation is that it is calculated for the entire molecule. The amount of strain associated with one bond or its stretch cannot be assigned in a straightforward manner. For example, in bicyclo[2.2.2]octane, there is surely more strain at the bridgehead carbons than at the methylene carbons. The derivative for the methylene–methylene bond (labelled a) is larger than for the bridgehead–methylene bond (labelled b), but the same strain energy term is used. It is possible that separate parameters could be obtained from an AIM analysis, but further restrictions occur in the prismane series (**n**–**q**). Each molecule may be described as a sandwich of two identical rings of 3, 4, 5. or 6 bonds (a) connected by vertical bonds (b). In each case, all carbon atoms are identical, and all the vertical bonds are very similar in length. If strain and size are the principal factors, then it is not surprising that the derivatives for the ring bonds increase with ring size, from 0.978 to 1.172 × 10^{-30} cm/V. However we are then unable to explain why the derivatives for the vertical bonds decrease, from 1.085 to 0.904 × 10^{-30} cm/V. Since all carbons are identical, the strain energy term is of no use here.

Previous studies on the C—H bonds have proven that the changes in the molecular polarizability cannot be attributed solely to changes in the bonds being stretched. Equilibrium structure dictates the measurable equilibrium properties but the polarizability and the derivative are dynamic responses of the entire molecule. The response cannot be thought of as something localized within a single structural alteration: the entire molecule and charge redistribution must be considered. Thus, while strain may be considered to be a useful general predictor, it cannot be considered as an analytical probe. Without a proper analysis of the total molecular charge distribution, we cannot attempt a more definitive explanation. This work is now in progress on those molecules amenable to the AIM analysis.

C—H stretch

The magnitude of $\partial\bar{\alpha}/\partial r_{CH}$ has been shown to be dependent on the location of the bond within the molecule, the alignment relative to the structure and the strain in the system (1). The derivatives calculated here (Table 3) continue to exhibit this behavior. Apart from the C—H bonds in neopentane (**c**) and methylene C—H in adamantane (**r**), all are classified as bridgehead. In (**c**), the derivative is small, and comparable to that of the methylene C—H in straight chain alkanes. This fits within the general pattern of the larger derivative being associated with a methyl C—H bond

Scheme 2.



lying in the plane of the carbon chain, for the *n*-alkanes. In propane, $\partial\bar{\alpha}/\partial r_{CH}$ is 1.18 (units: 10^{-30} cm/V) for the in-plane methyl C—H, and only 1.05 for the out-of-plane C—H (1). These values drop, and the difference is reduced, in isobutane (1): C—H (in-plane) 1.107; C—H (out-of-plane) 1.00. The value for the unique C—H bond in neopentane (**c**) fits nicely into this pattern, at 1.032. As the shape of the molecule becomes more spherical, the distinction between the C—H bonds vanishes, and the magnitude of the derivative falls to that of a typical methylene. At 1.106 × 10^{-30} cm/V, the derivative for the methylene C—H in (**r**) is similar to those in unstrained cycloalkanes with no axial–equatorial distinctions (1).

It was previously observed that $\partial\bar{\alpha}/\partial r_{CH}$ was unusually large for any bridgehead C—H (1). All the values for bridgehead C—H bonds studied here are large, with derivatives ranging from 20% to 30% higher than that of a methylene. The hedranes may be visualized as being formed by bonding three stacked rings: octahedrane (**s**) (3:6:3), decahedrane (**t**) (4:8:4), and dodecahedrane (**u**): (5:10:5). We now have two different types of bridgehead C—H: one attached to the carbon of the smaller ring, and one attached to the carbon of the larger, middle ring. In (**s**) and (**t**), the derivative is about 10% greater for the C—H attached to the smaller ring, perhaps reflecting the greater strain in that portion. In (**u**), all the C—H bonds are actually equivalent, there is much less strain in this larger system, and the derivative is only moderately elevated.

Conclusions

The C—C and C—H stretch polarizability derivatives have been calculated for straight chain and branched hydrocarbons as well as for a number of cyclic hydrocarbons exhibiting varying degrees of strain. In the straight chain hydrocarbons, the derivatives for the C—C stretch exhibit distinct and in some ways unexpected trends. There is an overall increase in magnitude of the derivative with increasing chain length. The derivatives, $\partial\bar{\alpha}/\partial r_{CC}$, are predicted to be larger for the bonds located closer to the centre of the chain, reaching a maximum with the central bond. The C—C stretch derivatives for the cyclic hydrocarbons are slightly smaller than those in comparable straight chain molecules, and decrease with increasing ring strain. The magnitudes of $\partial\bar{\alpha}/\partial r_{CH}$ calculated here follow the patterns already observed in our previous study. In cyclic molecules, the ordering of the derivatives is always axial << equatorial and endo << exo. Derivatives for undifferentiated methylene C—H bonds are quite similar, regardless of the molecule in which they are found. Derivatives for bridgehead C—H are 20–30% larger than for methylene C—H. It is interesting that strain is associated with a decrease in $\partial\bar{\alpha}/\partial r_{CC}$ and yet an increase in $\partial\bar{\alpha}/\partial r_{CH}$.

Calculations indicate that the derivatives for the bridgehead C—H bonds in bicyclo[1.1.1]pentane should be much larger than for the methylene CH, while $\partial\bar{\alpha}/\partial r_{CC}$ should be much smaller than that in either *n*-pentane or neopentane. This molecule exhibits many other useful characteristics: it

© 2000 NRC Canada

is small, has high symmetry, and is gas phase at room temperature. Work has begun on acquisition of the experimental absolute Raman trace scattering intensities along with complete AIM analysis of the charge distribution.

Acknowledgement

Funding for the research has been provided by the Natural Sciences and Engineering Research Council of Canada.

References

1. K.M. Gough and J.R. Dwyer. J. Phys. Chem. A **102**, 2723 (1998).
2. K.M. Gough and H.K. Srivastava. J. Phys. Chem. **100**, 5210 (1996).
3. K.M Gough, H.K. Srivastava, and K. Belohorcova. J. Phys. Chem. **98**, 771 (1994).
4. K.M Gough, H.K. Srivastava, and K. Belohorcova. J. Chem. Phys. **98**, 9669 (1993).
5. W.F. Murphy, J.M. Fernandez-Sanchez, and K. Raghavachari. J. Chem. Phys. **95**, 1124 (1991).
6. K.M Gough and W.F. Murphy. J. Mol. Struct. **224**, 73 (1990).
7. K.M Gough and W.F. Murphy. J. Chem. Phys. **87**, 1509 (1987).
8. K.M Gough, W.F. Murphy, T. Stroyer-Hansen, and E. Nørby-Svendsen. J. Chem. Phys. **87**, 341 (1987).
9. K.B. Wiberg, R.F.W. Bader, and C.D.H. Lau. J. Am. Chem. Soc. **109**, 985; **109**, 1001 (1987).
10. I. Alkorta, N. Campillo, I. Rozas, and J. Elguero. J. Org. Chem. **63**, 7759 (1998).
11. I. Rozas, I. Alkorta, and J. Elguero. J. Phys. Chem. A **101**, 9457 (1997).
12. R.F.W. Bader. Atoms in molecules: a quantum theory. Clarendon Press, Oxford. 1990.
13. K.M. Gough. J. Chem. Phys. **91**, 2424 (1989).
14. M.J. Frisch, G.W. Trucks, H.B. Schlegel, P.M.W. Gill, B.G. Johnson, M.A. Robb, J.R. Cheeseman, T. Keith, G.A. Petersson, J.A. Montgomery, K. Raghavachari, M.A. Al-Laham, V.G. Zakrzewski, J.V. Ortiz, J.B. Foresman, C.Y. Peng, P.Y. Ayala, W. Chen, M.W. Wong, J.L. Andres, E.S. Replogle, R. Gomperts, R.L. Martin, D.J. Fox, J.S. Binkley, D.J. Defrees, J. Baker, J.P. Stewart, M. Head-Gordon, C. Gonzalez, and J.A. Pople. Gaussian 94. Revision B.2. Gaussian, Inc., Pittsburgh. 1995.
15. R.F.W. Bader, T.A. Keith, K.M. Gough, and K.E. Laidig. Mol. Phys. **75**, 1167 (1992).
16. Landolt-Bornstein. Zahlenwerte und funktionen aus Physik, Chemie, Astronomie, Geophysik und technik. VI auflage, I band, 3 teil. Springer, Berlin. 1951.
17. D.R. Beck and D.H. Gay. J. Chem. Phys. **93**, 7264 (1990).
18. K.J. Miller. J. Am. Chem. Soc. **112**, 8543 (1990).
19. M.P Bogaard and B.J. Orr. Molecular structure and properties, international review of science, physics and chemistry. Vol. 2. Series II. Butterworth, London. 1965.
20. H.-J. Werner and W. Meyer. Mol. Phys. **31**, 855 (1976).
21. R.D. Amos. Mol. Phys. **38**, 33 (1979).
22. K.E. Laidig and R.F.W. Bader. J. Chem. Phys. **93**, 7213 (1990).
23. K.M. Gough and W.F. Murphy. J. Chem. Phys. **85**, 4290 (1986).
24. AIMPAC, McMaster University, 1990. F.W. Beigler-Konig, R.W.F. Bader, and T.H. Tang. J. Comput. Chem. **3**, 317 (1982).

© 2000 NRC Canada

Hydrogen bonding interaction of diphenylbarbituric acid and 9-ethyladenine. Crystal structure of a 1:1 complex

Arthur Camerman, Donald Mastropaolo, Andrew Hempel, and Norman Camerman

Abstract: There are several different types of adenosine receptors found in the brain and molecules capable of interacting with the adenine ring system may have an effect on brain activity. Phenobarbital and diphenylhydantoin, two commonly used antiepileptic drugs have been shown to form hydrogen bonded complexes with adenine derivatives. Although 5,5-diphenylbarbituric acid has anticonvulsant properties equivalent to phenobarbital, neither its structure nor possible interactions with adenine have been investigated. 5,5-Diphenylbarbituric acid and 9-ethyladenine were, therefore, cocrystallized and the three-dimensional 1:1 hydrogen bonded complex was determined by X-ray diffraction. The crystals are monoclinic, *C*2/*c*, a = 28.457(9), b = 10.633(3), c = 13.995(4) Å, β = 100.20(2)°, Z = 8, R = 0.067 for 1680 reflections with $I > 3\sigma(I)$. The molecules propagate along the b crystallographic axis in an alternating fashion in which adjacent adenine and barbiturate molecules interact through a pair of hydrogen bonds. Two-fold symmetry related barbiturate carbonyl groups in neighboring planes of hydrogen bonded ribbons are involved in dipole–dipole attractive interactions. This hydrogen bonding pattern is compared to patterns found in other barbiturate–adenine complexes.

Key words: hydrogen bonding, crystal structure, barbiturates, adenine, anticonvulsants.

Résumé : On connaît plusieurs types différents de récepteurs de l'adénosine et de molécules capables d'interagir avec le système cyclique de l'adénine qui peuvent avoir un effet sur l'activité cérébrale. On a démontré que deux médicaments fréquemment utilisés contre l'épilepsie, le phénobarbital et la diphénylhydantoïne, forment des complexes avec les dérivés de l'adénine par le biais de liaisons hydrogènes. Même si l'acide 5,5-diphénylbarbiturique possède des propriétés anticonvulsantes équivalentes à celles du phénobarbital, aucune étude n'a été faite sur sa structure ou sur ses interactions possibles avec l'adénine. On a donc cocristallisé de l'acide 5,5-diphénylbarbiturique et de la 9-éthyladénine et, faisant appel à la diffraction des rayons X, on a déterminé la nature tridimensionnelle du complexe 1:1 lié par liaisons hydrogènes. Les cristaux sont monocliniques, groupe d'espace *C*2/*c*, avec a = 28,457(9), b = 10633(3) et c = 13,995(4) Å, β = 100,20(2)°, Z = 8, R = 0,067 pour 1680 réflexions avec $I > 3\sigma(I)$. Les molécules se propagent le long de l'axe cristallographique d'une façon alternée dans laquelle les molécules adjacentes d'adénine et de barbiturate interagissent par le biais d'une paire de liaisons hydrogènes. La symétrie binaire apparentée aux groupes carbonyles du barbiturate de plans voisins des rubans de liaisons hydrogènes est impliquée dans les interactions d'attraction dipôle–dipôle. Ce patron de liaison hydrogène se compare à ceux retrouvés dans d'autres complexes barbiturate–adénine.

Mots clés : liaison hydrogène, structure cristalline, barbiturates, adénine, anticonvulsant.

[Traduit par la Rédaction]

Introduction

5,5-Diphenylbarbituric acid (DPB) is chemically very similar to diphenylhydantoin (DPH) and phenobarbital (PB), two of the drugs most widely used for the control of epileptic seizures. All three compounds possess two hydrophobic (phenyl, ethyl) groups attached to the tetrahedral carbon of a heterocyclic ring which contains at least two hydrogen bond acceptor atoms (see Fig. 1). Placement of these atoms with respect to each other in three-dimensional space is considered an important stereochemical factor in determining anticonvulsant activity (1). Despite its similarities with DPH and PB, early pharmacological studies of DPB (2–4) reported only weak anticonvulsant activity and dismissed DPB as a potentially new agent for the treatment of epilepsy. However, more than 25 years later another study (5) compared the anticonvulsant activity of DPB, DPH, and PB in the mouse by gavage administration of the drugs in conjunction with two standard laboratory tests most commonly used for the measurement of anticonvulsant efficacy, pentylenetetrazol (PTZ), and maximal electroshock (MES) induced seizures. The results showed that DPB when administered

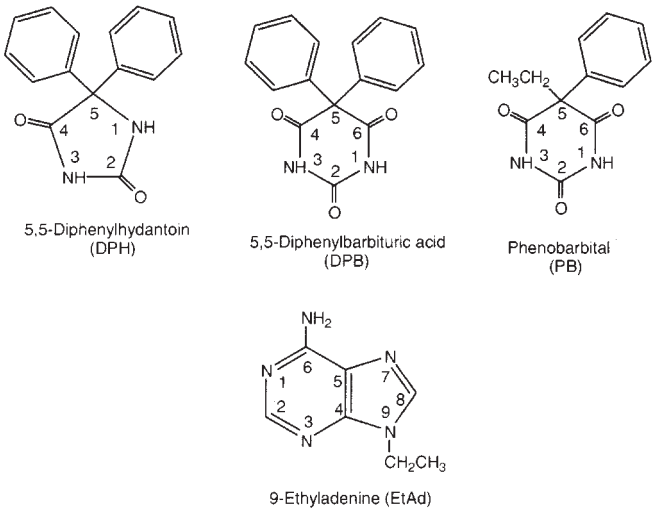
Received April 3, 2000. Published on the NRC Research Press website on July 28, 2000.

A. Camerman[1] and D. Mastropaolo. ARDONO Research, 8515-C 35th Ave. N.E., Seattle, WA 98115, U.S.A.
A. Hempel and N. Camerman. Biochemistry Department, University of Toronto, Toronto, ON M5S 1A8, Canada.

[1]Author to whom correspondence may be addressed. Telephone (206) 529–9421.
e-mail: ardonoresearch@hotmail.com

© 2000 NRC Canada

Fig. 1. Chemical drawings and numbering scheme of the heterocyclic rings of 5-5-diphenylhydantoin, 5,5-diphenylbarbituric acid, phenobarbital, and 9-ethyladenine.



by gavage has anticonvulsant properties comparable to PB. Experiments with intraperitoneally administered DPB also concluded that poor solubility of DPB in the gastrointestinal lumen was a major factor in limiting potency. These results suggest that solubility problems were most likely responsible for the weak anticonvulsant activity reported for DBP in the early trials.

At present the mechanisms of action of the antiepileptic drugs PB and DPH are not completely understood. Although the inhibition of membrane sodium channels has been shown to be a basic action of DPH (6) there is no single action of DPH that can account for all its effects on both neuronal and nonneuronal tissue. Other mechanisms of action could include regulation and inhibition of voltage-dependent neurotransmitter release at synapses and regulation of calmodulin and cyclic nucleotide second messenger systems (7). PB shows similar but less potent effects on Na^+ channels and also interacts with GABA-mediated receptors (8). Early on, the similarity of barbiturates to uracil was recognized and prompted several investigations into whether and how barbiturates and similar drugs might associate with adenine in an attempt to explain their pharmacological effects. Such studies have observed selective hydrogen bond interactions between barbiturates and adenine derivatives (9–14) and between substituted hydantoins and 9-ethyladenine (EtAd) (15, 16) in the solid state and in solution. As yet it is still unclear whether these specific hydrogen bond interactions can be correlated with any pharmacologic activity. However, these interactions have gained added significance with the more recent discovery of adenosine receptors in brain membranes (17) and the evidence of the anticonvulsant action of endogenous adenosine (18, 19). Thus it has been suggested that modification or modulation of this purinergic system might also provide a basis for a possible antiepileptic drug mechanism. For example, barbiturates and benzodiazepines have been shown (20, 21) to inhibit adenosine uptake in rodent brain synaptosomes which results in elevated synaptic adenosine levels. Similarly, DPH has been shown to inhibit adenosine uptake in rat cerebral cortical neurons (22). These increased levels of adenosine could be correlated with some of the depressant effects these compounds have on neuronal tissue. The complementarity that DPH and PB have shown to the purine ring system through hydrogen-bond formation might well be an indicator of their ability to effect changes in the purinergic system that has been postulated to be linked to antiepileptic drug action.

In light of the role adenosine may play in regulation of seizure activity, the more recent results showing DPB to be a better anticonvulsant than previously thought and the fact that DPH and PB form hydrogen-bonded complexes with adenine derivatives, we decided to investigate DPB's three-dimensional structure and its hydrogen bonding capabilities with adenine molecules. We successfully cocrystallized DPB and EtAd with the aim of elucidating the structure of the intermolecular complex which can then be compared to the structures of adenine complexes with DPH, with PB, and with other barbiturates. In addition, DPB's three-dimensional stereochemistry obtained from the crystal structure determination can be used for comparisons with known structures of the other anticonvulsants. Such information may prove helpful in understanding some modes of action of this important class of drugs.

Experimental

Equimolar amounts of DPB and EtAd were dissolved in a 50:50 acetone–water mixture. Slow solvent evaporation yielded colorless, thin, plate-like crystals. Weissenberg photographic methods revealed the monoclinic space group *C*2/*c* which was confirmed by structural analysis.

The crystal data including data collection and refinement parameters are summarized in Table 1. The data were corrected for Lorentz and polarization factors; no absorption correction was applied.

MULTAN 80 (23) was used to solve the structure. An E-map calculated with the phases from the solution with the best combined figure of merit revealed all 33 non-hydrogen atoms of the asymmetric unit. Hydrogen atoms were located from subsequent difference Fourier electron density maps and their positional parameters were refined along with nonhydrogen positional and anisotropic temperature factors. Hydrogen atoms were given fixed isotropic temperature factors equal to $B = 3.6$ Å^2. The refinement converged to a final residual of $R = 0.067$. The program used in the refinement was from the XRAY76 System (24). Table 2 lists the atom fractional coordinates.[2]

[2] Anisotropic temperature factors, hydrogen atom coordinates, interatomic distances, and angles and equations of selected least-square planes have been deposited as supplementary material and may by purchased from: The Depository of Unpublished Data, Document Delivery, CISTI, National Research Council Canada, Ottawa, Ontario, Canada, K1A 0S2. Crystallographic data for the structure(s) reported in this paper have been deposited with the Cambridge Crystallographic Data Centre (CDCC). Copies of the data can be obtained, free of charge on application to : The Director, Cambridge Crystallographic Data Centre, 12 Union Road, Cambridge, CB2 1EZ, U.K. (Fax: 44 1223 336033 or e-mail: deposit@ccdc.cam.ac.uk).

© 2000 NRC Canada

Table 1. Crystal data, data collection parameters, solution and refinement.

Crystal data	
Chemical formula	$(C_{16}H_{12}N_2O_3)\bullet(C_7H_9N_5)$
Molecular weight	443.47
Crystal system	Monoclinic
Space group	*C*2/*c*
a (Å)	28.457(9)
b (Å)	10.633(3)
c (Å)	13.995(4)
β (°)	100.20(2)
V (Å^3)	4168(1)
Z	8
*D*x(g cm^{-3})	1.368
No. of reflections for cell measurements	15
Range of cell parameters	$45 < \theta < 65$
Absorption μ (cm^{-1})	7.85
Temperature (K)	295
Crystal shape	plate
Crystal size (mm)	0.46 × 0.18 × 0.11
Crystal color	clear
Data collection	
Diffractometer	Picker FACS I
Radiation	Cu Kα
Wavelength (Å)	1.5418
Scan type	ω/2θ
θmax	65
Range of *h*, *k*, *l*	0→30 0→12 –16→16
No. of measured reflections	3510
No. of independent reflections	3510
No. of observed reflections	1680, $I > 3\sigma(I)$
No. of standard reflections	3 every 200 reflections
Intensity variation (%)	< 5
Data Reduction	
Corrections	Lorentz and polarization corrections
Solution and Refinement	
Solution	Direct methods (23)
Refinement	full-matrix refinement (24)
Atomic scattering	XRAY76
No. parameters used	361
Treatment of hydrogens	positions refined with fixed isotropic factors
R	0.067
wR	0.074
S	1.85
Weighting	$1/\sigma^2$ (*F*o)
Δ/σ_{max}	0.316
$\Delta\rho_{max}$ (e Å^{-3})	0.223
$\Delta\rho_{min}$ (e Å^{-3})	–0.317

Results and discussion

The crystal asymmetric unit contains one molecule of DPB and one molecule of EtAd. The adenine and barbiturate molecules are highly planar. The standard deviation of the nine atoms of the purine group from the least-squares plane defined by these atoms is 0.02 Å with the amino nitrogen situated only 0.01 Å from this plane. The standard deviation of the barbiturate atoms N(1), C(2), N(3), C(4), and C(6) from their least-squares plane is 0.05 Å with atoms O(4), C(5), and O(6) exhibiting the maximum deviations of –0.11, 0.06, and 0.09 Å, respectively. The phenyl groups are planar to within 0.01 Å. Bond distances and angles for DPB and EtAd are all within the normal range and are typical of barbiturate and adenine derivatives.

The pyrimidine ring of DPB is decidedly more planar than those of other barbiturates in which one of the C(5) substituents is a phenyl ring (11, 25 and refs. therein). Those

© 2000 NRC Canada

Table 2. Atomic coordinates ($\times 10^4$) and equivalent isotropic displacement parameters ($Å^2 \times 10^3$).

Atom	*X*	*Y*	*Z*	U_{eq}[a]
AN(1)	4808(2)	7104(5)	1232(4)	35(1)
AC(2)	5246(2)	6848(7)	1059(6)	43(1)
AN(3)	5594(2)	7637(5)	950(4)	38(1)
AC(4)	5454(2)	8832(6)	1066(5)	30(1)
AC(5)	5015(2)	9241(6)	1227(5)	30(1)
AC(6)	4682(2)	8318(6)	1319(5)	36(1)
AN(7)	5009(2)	10545(5)	1292(4)	33(1)
AC(8)	5441(3)	10866(6)	1175(6)	40(1)
AN(9)	5729(2)	9893(5)	1035(4)	34(1)
AN(6)	4237(2)	8562(6)	1475(5)	44(1)
AC(10)	6232(3)	9891(8)	921(7)	46(1)
AC(11)	6552(3)	9375(9)	1792(7)	51(1)
BN(1)	4390(2)	2614(5)	1505(4)	37(1)
BC(2)	4622(2)	3749(6)	1452(5)	30(1)
BO(2)	5033(2)	3792(4)	1327(4)	47(1)
BN(3)	4360(2)	4808(5)	1547(4)	35(1)
BC(4)	3914(2)	4856(6)	1755(4)	29(1)
BO(4)	3732(1)	5863(4)	1907(3)	39(1)
BC(5)	3627(2)	3631(6)	1704(4)	29(1)
BC(6)	3924(2)	2445(6)	1568(4)	28(1)
BO(6)	3752(2)	1391(4)	1530(3)	40(1)
BC(7)	3237(2)	3800(6)	804(5)	32(1)
BC(8)	3320(3)	3441(7)	–106(6)	40(1)
BC(9)	2987(3)	3696(8)	–928(6)	54(1)
BC(10)	2569(3)	4302(7)	–852(7)	54(1)
BC(11)	2483(3)	4662(8)	38(7)	52(1)
BC(12)	2813(2)	4432(7)	863(6)	41(1)
BC(13)	3453(2)	3416(6)	2672(5)	32(1)
BC(14)	3025(2)	2820(7)	2723(6)	38(1)
BC(15)	2899(3)	2578(7)	3615(6)	48(1)
BC(16)	3192(3)	2898(8)	4461(7)	57(1)
BC(17)	3628(3)	3452(7)	4426(6)	50(1)
BC(18)	3755(2)	3726(7)	3535(6)	42(1)

Note. Prefixes A and B refer to EtAd and DPB, respectively.

[a] $U_{eq} = (1/3)\sum_i\sum_j U_{ij} a_i^* a_j^* \mathbf{a}_i \mathbf{a}_j$.

structures contain pyrimidine rings described as envelope-shaped with C(5) 0.30–0.43 Å out of the plane in the direction of the phenyl group and atoms O(4) and O(6) displaced by more than 0.10 Å from the plane in the direction away from the phenyl group. It is not known whether the more planar conformation of the barbiturate ring observed in the crystal structure of DPB is a chemical effect related to the presence of two phenyl rings attached to C(5) or is a consequence of the crystal packing forces. It should be pointed out that others (26) have found no correlation between the chemical nature of the C(5) substituent and the extent of barbiturate ring puckering. Furthermore, the variation in barbiturate ring puckering reported in crystal structures all containing 5,5-diethylbarbituric acid (12, 27–30) indicates that the puckering in the solid state is dominated by crystal packing forces. Other than these small differences in the barbiturate ring planarity, DPB and PB are very similar in overall structural geometry and stereochemistry. In the reported three-dimensional structures of DPH (16,31) the hydantoin rings are planar to within experimental error.

DPB and EtAd form a 1:1 complex organized into infinite ribbons of alternating adenine and barbiturate residues in which adjacent adenine and barbiturate molecules interact through pairs of hydrogen bonds. The dihedral angle between the adenine and barbiturate planes is only 1.2°. DPB donates its N(1) hydrogen to N(7) of EtAd and the DPB carbonyl oxygen O(6) accepts a hydrogen from the EtAd amino group forming a Hoogsteen type pair of hydrogen bonds. The second pair of hydrogen bonds is of the Watson–Crick type and involves the N(3) hydrogen and O(4) carbonyl of DPB with N(1) and the other amino hydrogen of EtAd. The hydrogen bonding scheme is illustrated in Fig. 2 and Table 3 gives the hydrogen bonding geometry. The basic structural pattern is very similar to those of the crystalline complexes EtAd–5-isopropyl-5-bromoallylbarbiturate (I) (11) and EtAd–5,5-diethylbarbituric acid (II) (12). Figure 3 (Top) is a schematic drawing which summarizes the hydrogen bonding features of I, II, and the current structure. A unique feature of these structures is the positioning of two symmetry related barbiturate carbonyl groups, C(2)-O(2), which lie in neighboring planes of the hydrogen bonded ribbons with their bond vectors pointing in opposite directions as is shown in Fig. 2. The C(2)— O(2)′ intermolecular contact of 3.090(9) Å found in the present study is shorter than the same contact found in I (3.165(20) Å) and longer than that found in II (2.983(4) Å). Such an arrangement of carbonyl groups has also been observed in crystal structures of hydrated barbiturate derivatives (25). These noncovalent contacts which are less than or approximately equal to the normal van der Waals distance of 3.1 Å appear to be due to an attractive dipole–dipole interaction. The differences in the contact distances observed in these structures are most likely due to crystal packing requirements of the different sized barbiturate C(5) substituents which fill the spaces between the planar hydrogen-bonded layers. One other significant difference between the current structure and structures I and II is the dihedral angle between the hydrogen-bonded barbiturate and adenine ring planes. In I and II this angle is 10.5 and 10.2° respectively compared with just 1.2° found for the DPB–EtAd structure.

In all three structures the carbonyl oxygens adjacent to the C(5) atom of the barbiturates form extremely weak hydrogen bonds and the N(3) of EtAd and O(2) of the barbiturates are not involved in any hydrogen bonds. As previously suggested (11), the long contacts involving the adenine N(6) hydrogens and barbiturate O(4) and O(6) carbonyls might be explained by geometrical constraints placed on the molecular arrangement due to translational symmetry which propagates the 1:1 complex and forms the infinite hydrogen-bonded ribbon. Since there is one independent molecule of EtAd and one of DPB, any change in the contact on one side of N(6) will effect a change in the opposite direction on the other side. The observed distances are thus a result of a compromise between crystal packing symmetry and hydrogen bond forces. As we will see below, when there is a greater degree of freedom with two crystallographically independent molecules involved in forming the adenine–barbiturate hydrogen bonded pair, the N(6)—carbonyl oxygen hydrogen bond distances are less than 3.2 Å and in the more normal range. In structures I and II there was some speculation about hydrogen bond formation between adenine C2

© 2000 NRC Canada

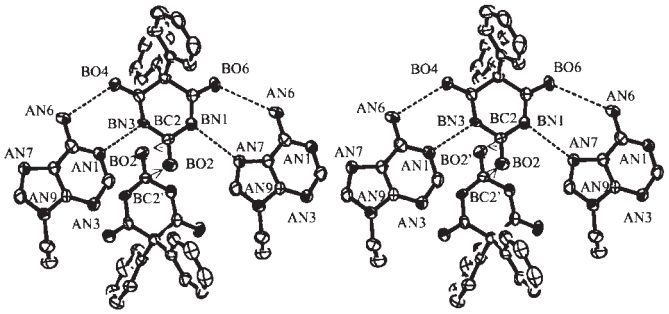
Table 3. Hydrogen bond distances (Å) and angles (°).

	H···O (or N)[a]	N···O (or N)[a]	< N-H···O (or N) [a]
BN(1)-H···AN(7)	2.03(7)	2.867(8)	170(6)
	1.89(3)	2.827(3)	171(3)
BN(3)-H···AN(1)	2.00(6)	2.825(8)	175(6)
	1.91(4)	2.832(3)	176(3)
AN(6)-H(1)···BO(6)	2.45(7)	3.316(6)	169(5)
	2.47(4)	3.387(4)	176(3)
AN(6)-H(2)···BO(4)	2.51(7)	3.312(7)	158(6)
	2.35(4)	3.218(4)	172(3)

Note. The prefixes A and B refer to EtAd and DPB, respectively.

[a]The second row of numbers per hydrogen bond are equivalent parameters reported in the 9-ethyladenine-5,5-diethylbarbituric acid 1:1 complex referred to as Structure II in the text.

Fig. 2. Stereoscopic drawing showing hydrogen bonding and bond–dipole interactions in the 1:1 EtAd–DPB crystal. Hydrogen bonds are represented by dashed lines and the C(2)—O(2) dipole interaction is indicated by arrows. Hydrogen atoms have been omitted for clarity.



and C8 hydrogens with the barbiturate O2. In the DPB–EtAd complex we find these C—O distances to be 3.34 Å with the C-H-O(2) angles less than 140° suggesting only normal van der Waals contacts. In I the adenine C8 and C2 distances to the barbiturate O2 are 3.28 and 3.31 Å, respectively which also indicate relatively weak interactions. In II the adenine C8 and barbiturate O2 distance is 3.18 Å indicating a stronger hydrogen bond-like interaction but the C-H-O(2) angle is only 129°. The adenine C2—barbiturate O2 distance of 3.37 Å found in II is more typical of a normal van der Waals contact.

In the structures of the complexes 8-bromo-9-ethyladenine–phenobarbital (III) (10) and 8-bromo-9-ethyladenine–5-allyl-5-isobutylbarbituric acid (IV) (13) a different hydrogen bonding scheme is found with no evidence of carbonyl dipole interactions (see Fig. 3 (Bottom)). In III and IV the barbiturate molecules form separate Watson–Crick-type hydrogen-bonded pairs with each of two crystallographically independent adenine derivatives utilizing the barbiturate hydrogen bond donors N(1) and N(3) and acceptors O(2) and O(4). In structure IV there is a second barbiturate molecule which hydrogen bonds to two independent adenine derivatives as depicted in Fig. 3. Also in IV there is no hydrogen-bonded dimer formed between the second of the two independent adenine molecules.

It should be pointed out that structure III is the only 2:1 adenine to barbiturate complex observed which might account for its different hydrogen bonding pattern. However the major factor in determining the two different hydrogen bonding schemes shown in Fig. 3 is the presence of the 8-bromo-substituent on the adenine molecules in the III and IV structures. This bulky substituent prevents the formation of the Hoogsteen-type pair that is observed in structures I, II, and the DPB–EtAd structure due to a sterically forbidden contact it would make with the barbiturate O(2) carbonyl oxygen. Since adenine moieties of nucleic acids and coenzymes are not usually substituted at the 8-position (especially with a bromine atom), it seems reasonable to suggest that if barbiturates complex with adenine bases or interact with similar receptors in vivo, the likely hydrogen bonding scheme is that found between DPB and EtAd

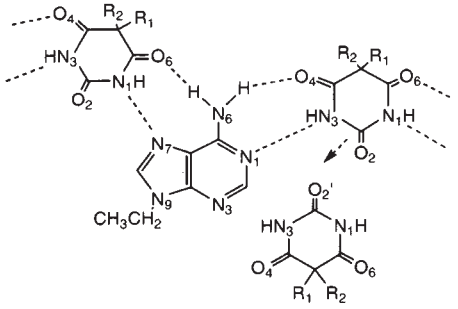
The comparisons made between the present structure and the others cited above thus indicate that the presence of the C(2)-O(2) dipole interaction is dependent on the adenine derivative and its hydrogen bonding requirements while the strength of the interaction appears to be balanced against the packing requirements of the different sized C(5) barbiturate substituents.

Unlike DPH (16), barbiturate molecules do not form self-associated hydrogen-bonded dimers when a complementary alternative molecule is available in the structure even if in some cases the other molecule happens to be water (25). Given an unrestricted choice of hydrogen bond pair formation with adenine molecules, barbiturates seem to prefer a mixed Watson–Crick, Hoogsteen-type pairing leaving the C(2)-O(2) available for dipole–dipole type interactions. Our crystal structure results along with the others discussed above suggest that in addition to hydrogen bonding these nonbonded carbonyl associations may also be important in determining molecular packing. Whether such dipole interactions might be involved in barbiturate–receptor binding or pharmacological signal transmission is not known.

It is of interest to note that primidone, the phenobarbital congener with the C(2)=O(2) replaced by CH2, is also a useful antiepileptic agent. Its spectrum of anticonvulsant effects resembles that of phenobarbital except that it is much less potent in antagonizing PTZ induced seizures. As barbiturate C(2)=O(2) carbonyls do not hydrogen bond to EtAd, it is likely that primidone could interact with adenine by forming the same pairs of hydrogen bonds as observed in the DPB–EtAd complex. Thus if some barbiturate anticonvulsant or other pharmacologic actions are mediated through this type of interaction they are likely to be those actions common to both phenobarbital and primidone.

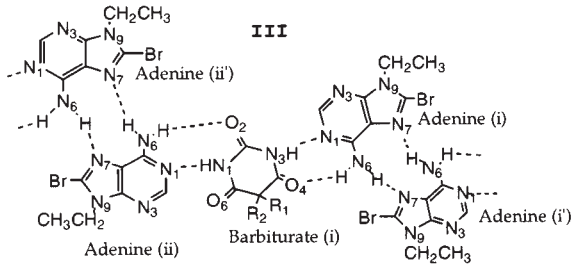
© 2000 NRC Canada

Fig. 3. Schematic drawing illustrating the different hydrogen bonding arrangements observed in crystal structures of adenine–barbiturate complexes.



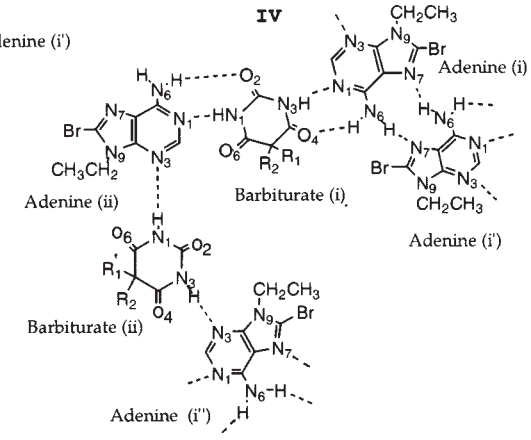
Distances (Å)

	I	II	This Work
AN6-BO6	3.12	3.39	3.32
AN7-BN1	2.81	2.83	2.87
AN6-BO4	3.34	3.22	3.31
AN1-BN3	2.79	2.83	2.83
BC2-BO2'	3.17	2.98	3.09



Distances (Å)

	III	IV
A(i)N6-B(i)O4	3.19	2.96
A(i)N1-B(i)N3	2.78	2.79
A(ii)N6-B(i)O2	2.97	3.07
A(ii)N1-B(i)N1	2.80	2.94
A(ii)N3-B(ii)N1	----	2.97
A(i'')N3-B(ii)N3	----	3.03
A(i)N6-A(i')N7	3.09	2.97
A(ii)N6-A(ii')N7	3.02	----



References

1. A. Camerman and N. Camerman. *In* Molecular and quantum pharmacology. *Edited by* E. Bergman and B. Pullman. D. Reidel, Dordrecht, Holland. 1975. pp. 213–228.
2. P.K. Knoefel and G. Lehman. J. Pharmacol. Exp. Ther. **76**, 194 (1942).
3. H.H. Merrit and T.J. Putnam. Epilepsia, **3**, 51 (1945).
4. G.C.H. Alles, G. A. Ellis, and M.A. Redmann. J. Pharmacol. Exp. Ther. **89**, 346 (1947).
5. A. Raines, J.M. Niner, and D.G. Pace. J. Pharmacol. Exp. Ther. **186**, 315 (1973).
6. J. Francis and W.M. Burnham. Mol. Pharmacol. **42**, 1097 (1992).
7. R. Levy, F.E. Dreifuss, R.H. Mattson, B.S. Meldrum, and J.K. Penry. (*Editors*). Antiepileptic drugs. Raven Press, New York. 1989. p. 155.
8. R.L Macdonald. Epilepsia, **34**(Suppl. 5), S1 (1993).
9. Y. Kyogoku, R.C. Lord, and A. Rich. Nature (London), **218**, 69 (1968).
10. S.H. Kim and A. Rich. Proc. Natl. Acad. Sci. U.S.A. **60**, 402 (1968).
11. D. Voet and A. Rich. J. Am. Chem. Soc. **94**, 5888 (1972).
12. D. Voet. J. Am. Chem. Soc. **94**, 8213 (1972).
13. R.H. Epstein, A.V. Zeiger, C. Crocker, and D. Voet. Acta Crystallogr. Sect. B: Struct. Crystallogr. Crys. Chem. **B32**, 2180 (1976).
14. E. Gentric, J.F. Meney, J. Lauransan, L.G. Bardou, and P. Saumagne. Chem. Biol. Interact. **54**, 117 (1985).
15. G.L. Jones and J.W. Kemp. Mol. Pharmacol. **10**, 48 (1974).
16. D. Mastropaolo, A. Camerman, and N. Camerman. Mol. Pharmacol. **23**, 273 (1983).
17. R.F. Bruns, J.W. Daly, and S.H. Snyder. Proc. Natl. Acad. Sci. U.S.A. **77**, 5547 (1980).
18. M. Dragunow. Prog. Neurobiol. (Oxford), **31**, 85 (1988).
19. G. Zhang, P.H. Franklin, and T.F. Murray. J. Pharmacol. Exp. Ther. **264**, 1415 (1993).
20. R.A. Gonzalez and S.W. Leslie. Biochem. Pharmacol. **34**, 1619 (1985).
21. J.W. Phillis, P.H. Wu, and A.S. Bender. Gen. Pharmacol. **12**, 67 (1981).
22. J.W. Phillis. Epilepsia, **25**, 765 (1984).
23. P. Main, S.J. Fiske, S.E. Hull, L. Lessinger, G. Germain, J.P. DeClercq, and M.M. Woolfson. MULTAN 80. A system of

© 2000 NRC Canada

computer programs for the automatic solution of crystal structures from x-ray diffraction data. Univs. of York, England and Louvain, Belgium. (1980).
24. J.M. Stewart. The Xray System. University of Maryland, College Park, Maryland. (1976).
25. P.P. Williams. Acta Crystallogr. Sect. B: Struct. Crystallogr. Crys. Chem. **B29**, 1572 (1973).
26. B.M. Gatehouse and B.M. Craven. Acta Crystallogr. Sect. B: Struct. Crystallogr. Crys. Chem. **B27**, 337 (1971).
27. B.M. Craven, E.A. Vizzini, and M.M. Rodrigues. Acta Crystallogr. Sect. B: Struct. Crystallogr. Crys. Chem. **B25,** 1978 (1969).
28. B.M. Craven and E.A. Vizzini. Acta Crystallogr. Sect. B: Struct. Crystallogr. Crys. Chem. **B27**, 1917 (1971).
29. B.M. Craven and G.L. Gartland. J. Pharm. Sci. **59**, 1666 (1970).
30. S. Kiryu. J. Pharm. Sci. **60**, 699 (1971).
31. A. Camerman and N. Camerman. Acta Crystallogr. Sect. B: Struct. Crystallogr. Crys. Chem. **B27**, 2205 (1971).

© 2000 NRC Canada

Reactions of the radical cation derived from 2,2′-azinobis(3-ethylbenzothiazoline-6-sulfonic acid) ($ABTS^{\cdot+}$) with amino acids. Kinetics and mechanism

C. Aliaga and E.A. Lissi

Abstract: Stable free radicals derived from 2,2′-azinobis(3-ethylbenzothiazoline-6-sulfonic acid) ($ABTS^{\cdot+}$) have been extensively employed to monitor the antioxidant capacity of biological fluids and beverages. Besides reacting with typical antioxidants (such as phenols or thiols) these radicals react with a variety of hydrogen or electron donors. The present work reports on the kinetics and mechanism of these radical reactions with several amino acids. Reaction rates notably increase when the pH of the media increases and, when measured under similar conditions, follows the order

cysteine > > tryptophan > tyrosine > histidine > cystine

The kinetics of the process is interpreted in terms of a mechanism comprising an initial pH dependent reversible step, followed by secondary reactions of the substrate derived radical with itself or with another $ABTS^{\cdot+}$; this simple three-step mechanism leads to very complex kinetic expressions. The specific rate constants of several of the elementary steps were determined by working under a wide range of substrate, radical, and ABTS concentrations. The values obtained for the initial interaction between the ABTS derived radical and the substrate range from 0.5 M^{-1} s^{-1} to 1.9×10^6 M^{-1} s^{-1} for histidine and cysteine, respectively.

Key words: ABTS radical cation, 2,2′-azinobis(3-ethylbenzothiazoline-6-sulfonic acid), amino acids, kinetics.

Résumé : On a fait appel à des radicaux libres stables dérivés de l'acide 2,2′-azinobis(3-éthylbenzothiazoline-3-sulfonique) ($ATBS^{\cdot+}$) pour de déterminer la capacité antioxydante de boissons et de fluides biologiques. En plus de réagir avec les antioxydants typiques (tels que les phénols et les thiols), ces radicaux réagissent avec un certain nombre de donneurs d'hydrogène ou d'électron. Dans le présent travail, on a déterminé la cinétique et le mécanisme de ces réactions radicalaires avec plusieurs acides aminés. Les vitesses de réaction augmentent beaucoup avec une augmentation du pH du milieu et, lorsqu'on les mesure dans des conditions identiques, elles suivent l'ordre suivant

cystéine > > tryptophane > tyrosine > histidine > cystine

On interprète la cinétique du processus en fonction d'un mécanisme impliquant une étape initiale réversible qui dépend du pH et qui est suivie par des réactions secondaires du radical dérivé du substrat soit avec lui-même soit avec une autre molécule de $ATBS^{\cdot+}$; ce mécanisme simple en trois étapes conduit à des expressions cinétiques très complexes. On a déterminé les constantes de vitesse spécifique de plusieurs étapes élémentaires en utilisant une grande variété de concentrations de substrats, de radicaux et d'ABTS. Les valeurs obtenues pour l'interaction initiale entre le radical provenant de l'ABTS et le substrat vont de 0,05 M^{-1} s^{-1} à $1{,}9 \times 10^6$ M^{-1} s^{-1} pour l'histidine et la cystéine respectivement.

Mots clés : cation radical ABTS, acide 2,2′-azinobis(3-éthylbenzothiazoline-3-sulfonique), acides aminés, cinétique.

Introduction

The capacity of additives to diminish the formation of the 2,2′-azinobis(3-ethylbenzothiazoline-6-sulfonic acid) (ABTS) derived radical cation ($ABTS^{\cdot+}$), when the parent compound is incubated in presence of a free radical source, has been extensively studied to evaluate the free radical trapping capacity of pure compounds and complex mixtures (1–4). Interpretation of the data in these systems is not straightforward, since the decrease in radical cation concentration observed in the presence of the additives can be due to trapping of the primary radicals and (or) to the bleaching of the formed radical cations by the additives. In this regard, it is interesting to evaluate the capacity of compounds of

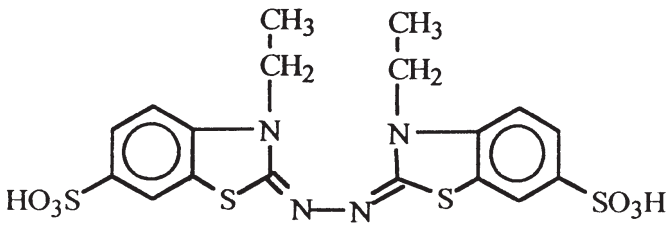
Received January 10, 2000. Published on the NRC Research Press website on July 31, 2000.

C. Aliaga. Facultad de Ciencias, Universidad de Chile, Casilla 653, Santiago, Chile.
E.A. Lissi.[1] Facultad de Química y Biología, Universidad de Santiago de Chile, Casilla 40-correo 33, Santiago, Chile.

[1]Author to whom correspondence may be addressed. Fax: 56 2 6812108. e-mail: caliaga@lauca.usach.cl

 © 2000 NRC Canada

biological interest to react with this stable free radical. Furthermore, methods have been proposed to evaluate the total antioxidant capacity of complex samples, from the bleaching extent of preformed radical cations (5, 6), and hence it is interesting to know which compounds, and at which rates, are able to react with the ABTS radical cation. This radical cation can be easily formed by the one electron oxidation of the colourless parent compound ABTS (**1**).



MnO_2, potassium persulfate, HRP, or any free radical source (i.e., azo compounds) under aerobic conditions can be employed as oxidant. The resulting radical cation is a long-living species with high extinction coefficients at 416, 650, and 734 nm. The concentration of the radical cation can be readily monitored by its absorbance at these long wavelengths (6, 7).

It has been reported that small molecules such as phenols, hydroperoxides, bilirubin, thiols, amines, and uric and ascorbic acids are capable of reducing this radical cation (5, 6), but a thorough kinetic study has been carried out only with a family of monophenols (7) and hydroperoxides (8) as substrates. The mechanism of the process was rationalized in terms of a first preequilibrium between $ABTS^{\cdot+}$ and the substrate, involving a reversible pH-dependent back reaction. Secondary reactions of the produced radicals lead to the final products.

Amino acids and serum albumin give positive responses when their antioxidant capacity is assayed by monitoring the extent of ABTS radical cation formation in the H_2O_2–Peroxidase–ABTS system (4, 6). Furthermore, it has been shown that proteins, such as albumin, are able to bleach ABTS preformed radical cations (5), but it has not been established which amino acids are reactive and (or) the kinetics, mechanism, and stoichiometry of the process. In the present work, we address this problem by studying the reaction between ABTS radical cations and several amino acids, which have a labile hydrogen atom in the side-chain group. The selected amino acids were cysteine (-SH), tryptophan (-NH), histidine (-NH), and tyrosine (-OH). Their reactivity was compared to that of amino acids that do not possess a reactive hydrogen atom.

Materials and methods

ABTS was purchased from Sigma and used as received. The radical cation was prepared by the reaction of ABTS (150 M) with MnO_2 (25 mg/mL) at room temperature. In this system, formation of the radical is almost instantaneous. After centrifugation and filtration to remove unreacted MnO_2, the $ABTS^{\cdot+}$ solution was stable for several hours at room temperature. The radical cation derived from it was prepared by the reaction of ABTS (150 μM) with 1.5 mM potassium peroxodisulphate (Merck). The reaction was carried out at 50°C during 2 h. After cooling to room temperature, the absorbance of the solution remains stable for several hours. The concentration of $ABTS^{\cdot+}$ was evaluated from the absorbance at 734 nm ($\varepsilon = 0.015\ M^{-1}\ cm^{-1}$). Along the kinetic runs the concentration of the parent compound was deduced from its absorbance at 340 nm ($\varepsilon = 0.039\ M^{-1}\ cm^{-1}$). The results obtained were independent of the method employed to produce the radical cations.

The amino acids L-tyrosine and L-tryptophan were purchased from Merck, L-cysteine from Sigma, and L-histidine from Eastman. This latter compound was purified prior to its use by recrystallization from methanol.

Each solution was prepared in buffer phosphate (Merck) at the desired pH and the kinetics of the reactions measured at 23 ± 1°C by monitoring absorbance changes in an UV–vis Chem Station Hewlett–Packard (diode array) spectrometer. The components of the reaction mixture were added to the reaction cell in the order $ABTS^{\cdot+}$, ABTS, and substrate. The additions were carried out under strong mixing to minimize mixing times. The mixing was maintained during all the reaction. The concentration ranges employed were: (*i*) $ABTS^{\cdot+}$ (9–60 M); (*ii*) ABTS (10–450 M), and (*iii*) amino acid (2 M–0.2 mM).

The pH was controlled with 100 mM phosphate (pH 6 and 7) and citrate (100 mM, pH 5). Some experiments were carried out employing water pretreated with Chellex-100 to remove metals from the medium.

Results

The addition of micromolar amino acid concentrations to an ABTS radical cation solution readily bleaches the sample absorbance at 734 nm. The effect of the additive depends upon the experimental conditions and the amino acid considered. Results obtained for several amino acids under similar conditions are shown in Fig. 1. The data given in Fig. 1 show that, under similar conditions, the reactivity follows the order

$$Cys >>> Trp > Tyr > His >>> Cystine$$

This different reactivity indicates that the rate is determined by the characteristics of the pendant group, with the aliphatic backbone totally unreactive. Relative reactivities are in close agreement with those reported by Lissi et al. (9) regarding the ability of amino acids to trap peroxyl radicals. Furthermore, they are also in fair agreement with the data reported by Meucci and Mele (4) on amino acid antioxidant capacity. These authors concluded, from experiments carried out in the ABTS/HRP system, that the best antioxidant was cysteine, with tyrosine and tryptophan showing rather similar antioxidant patterns.

To obtain kinetic information on the reaction between the amino acids and the ABTS radical cation, the rate of the reaction employing Cys, Trp, Tyr, and His was measured over a wide range of experimental conditions. In particular, we examined the effect of pH, $ABTS^{\cdot+}$, ABTS, and amino acid concentration on the rate of the process.

© 2000 NRC Canada

Fig. 1. Reaction profiles obtained for the bleaching of $ABTS^{\cdot+}$ elicited by Cys (□), Trp (○), Tyr (△), and His (*) under similar conditions: [$ABTS^{\cdot+}$] ≈ 22 M, [ABTS] = 50 M, [amino acid] = 30 M, pH 7.

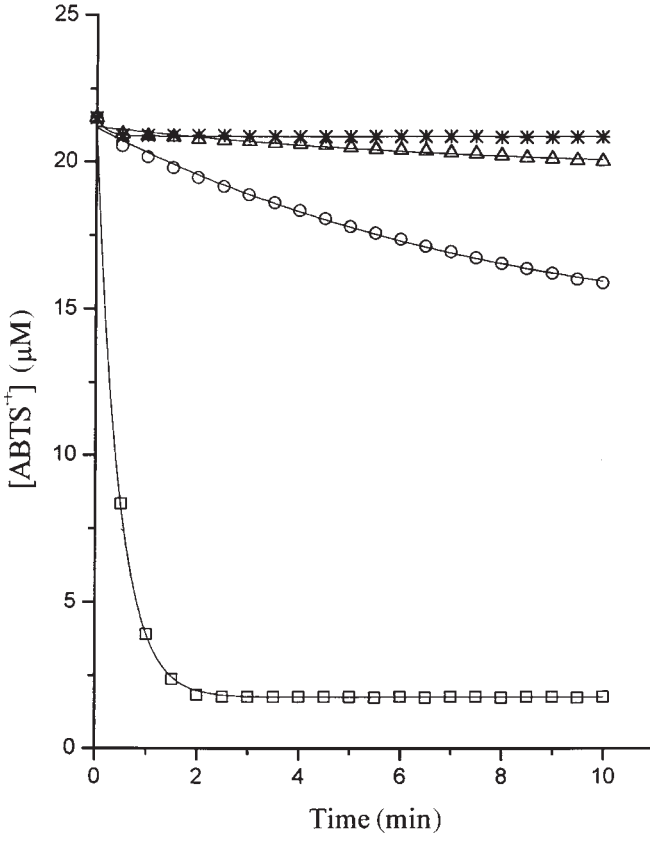
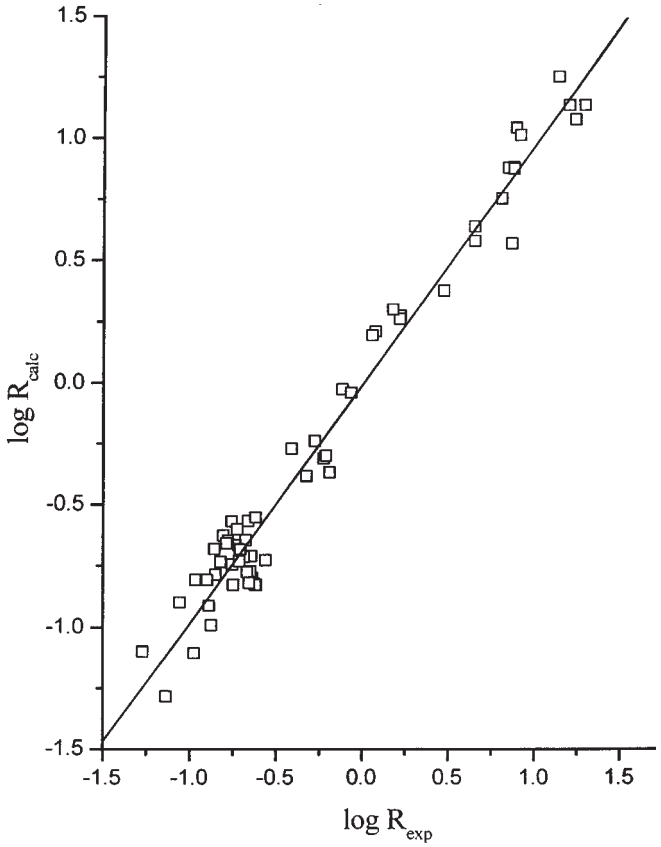


Fig. 2. Data obtained in the Cys–$ABTS^{\cdot+}$ system at pH 5. Correlation between experimental and calculated reaction rate obtained from eq. [3] with the parameters included in Table 1. Slope = 0.97, R = 0.985, N = 61, and P < 0.0001.



Cysteine

The reaction of cysteine with ABTS radical cations presents features similar to those previously reported for *tert*-butylhydroperoxide: the reaction rate increases with pH, increases both with cysteine and $ABTS^{\cdot+}$ concentrations, and is partially inhibited by ABTS. When initial rates (Ro) at different pH are measured employing a constant set of concentrations of ABTS, $ABTS^{\cdot+}$, and cysteine, the measurements can be fitted to an equation such as

$$[1] \qquad \log R_0 = k - \delta \text{ pH}$$

where k includes the contribution of all the reactants and products to the rate of the process. A plot of log R_0 vs. pH allows then an evaluation of the reaction order in protons (δ). The value obtained was ca. 0.22. This value, measured between pH 5 and 7, is bound to a rather large uncertainty because the high rate of the process hinders a precise evaluation of the initial rate, particularly at the higher pH.

Reaction rates over a wide range of conditions can be only measured at pH 5, due to the occurrence of a very fast reaction at higher pH. The values of Ro, were fitted to a kinetic law such as

$$[2] \qquad R_0 = k\,[\text{ABTS}]^{\alpha}\,[\text{ABTS}^{\cdot+}]^{\beta}\,[\text{Cys}]^{\chi}$$

The pseudo rate constant and apparent reaction orders were obtained by the best fit of the data to a lineal multiparametric equation

$$[3] \qquad \log Ro = \log k + \alpha \log [\text{ABTS}] + \beta \log [\text{ABTS}^{\cdot+}] + \chi \log [\text{Cys}]$$

The best values of the reaction orders obtained by this procedure are given in Table 1. The indicated values of k are those obtained when the concentrations are expressed in μM and the time in seconds.

The agreement between R_0 values calculated with this set of parameters and those experimentally determined is shown in Fig. 2. This figure shows that eq. [3] reproduces the data within a factor ca. 1.5 over all the conditions employed. The fractional orders and the dispersion of the data beyond that expected from the experimental errors, implies that the mechanism is complex and not completely represented by a simple rate law such as that given in eq. [3].

To test if air and (or) traces of metals influence the rate of the process, experiments were carried out under nitrogen. No significant differences were observed (data not shown). Similarly, no differences in reaction rates were observed when water was pretreated with chelex-100 (data not shown).

Formation of ABTS (as measured by the increase in absorbance at 340 nm, Fig. 3) is almost quantitative to the radical cation consumption over all the reaction process, both in presence of excess radical cation or cysteine.

The stoichiometry of the reaction between the radical cation and cysteine was measured only with excess radical

© 2000 NRC Canada

Table 1. Summary of the values for the reaction orders in ABTS (α), $ABTS^{\cdot+}$ (β), amino acid (χ), and protons (δ) obtained by eq. [3].

Fig. 3. Time course of the Cys + $ABTS^{\cdot+}$ reaction, followed by the growth of ABTS (from the sample absorbance at 340 nm) (□) and the consumption of $ABTS^{\cdot+}$ (from the decrease in absorbance at 734 nm) (○).

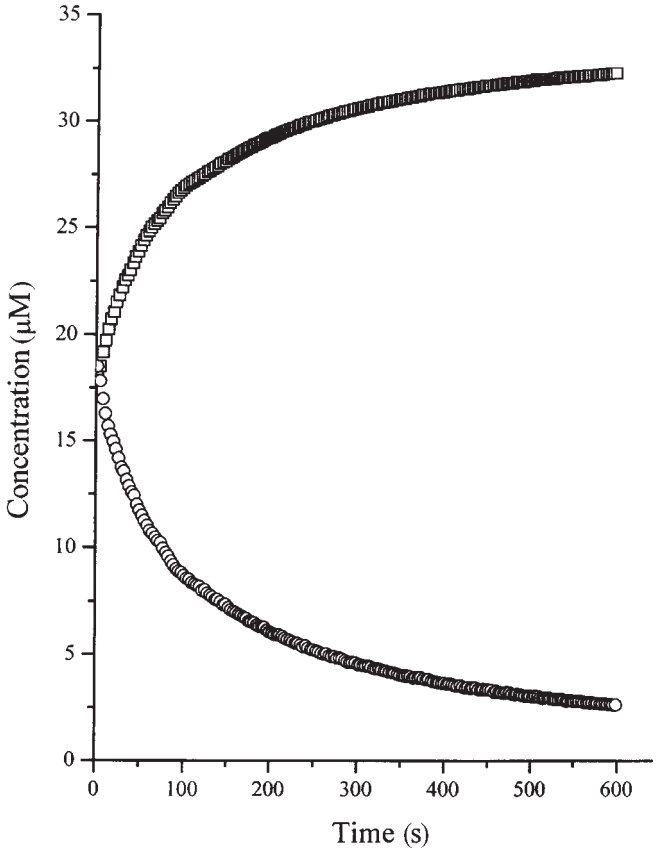
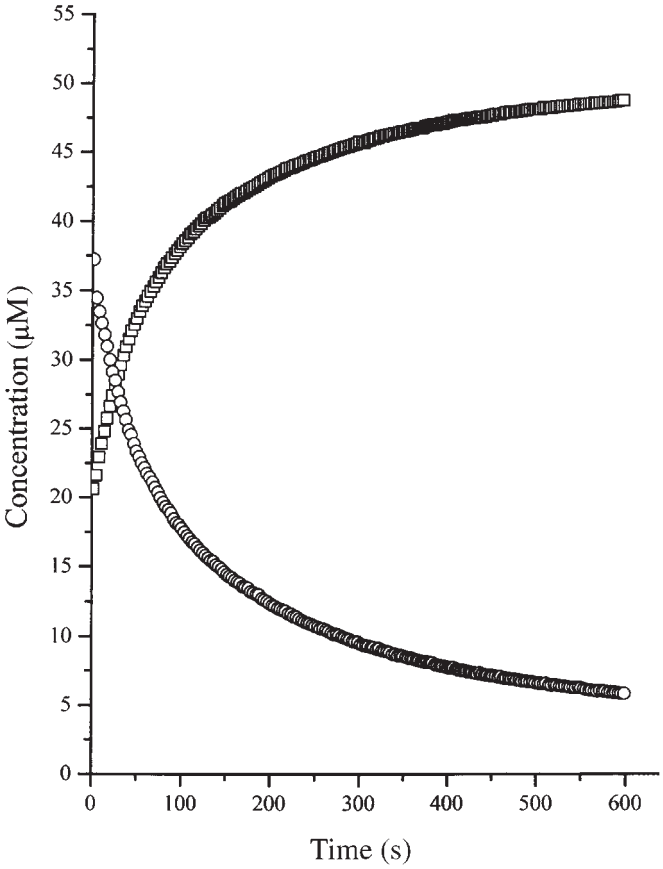


Fig. 4. Time course of the Trp + $ABTS^{\cdot+}$ reaction, followed by the growth of ABTS (from the sample absorbance at 340 nm) (□) and the consumption of $ABTS^{\cdot+}$ (followed by decrease in absorbance at 734 nm) (○).



cation. Nearly 1.8 radical cations were consumed by each cysteine introduced into the system. The overall reaction, in excess of radical cation, can be then represented by

[4] $2\ ABTS^{\cdot+} + Cys \rightarrow 2\ ABTS + products$

Tryptophan

The data obtained employing Trp conform to the same pattern than that of Cys. However, since the rate of the process is considerably slower, initial rates can be obtained over a wider range of conditions. The kinetic data obtained at pH 5 and 7, fitted to eq. [3], provide the pseudo-reaction orders included in Table 1. As with the other amino acids, the rate of the process is not influenced by traces of metals.

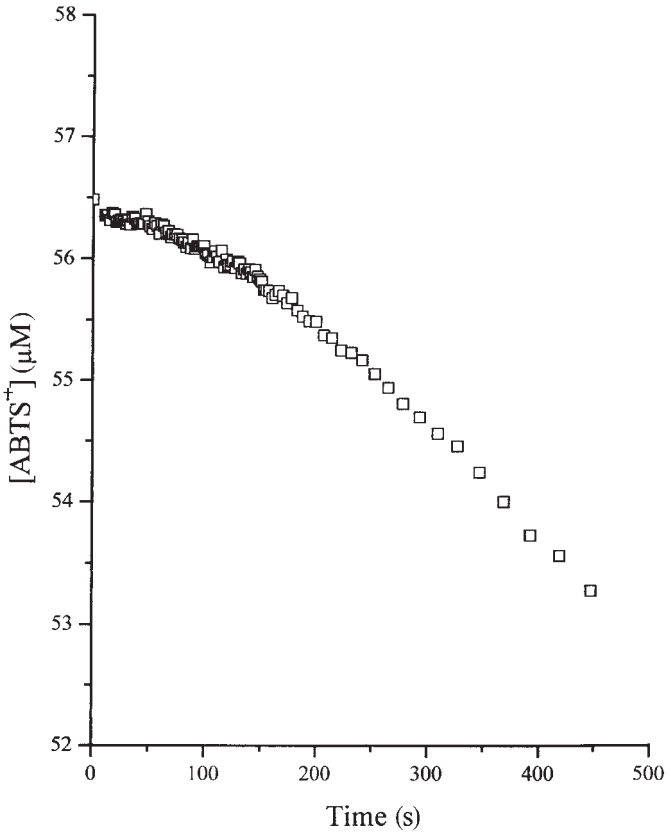
The consumption of the radical cation is accompanied by noticeable oxygen consumption (as measured with the selective oxygen electrode). In fact, nearly 0.33 mol of oxygen are consumed per each reacted mole of radicals. Since formation of ABTS, evaluated from the increase in absorbance at 340 nm, is almost quantitative (Fig. 4) and, in excess of radical cation, nearly three radicals are consumed by each Trp molecule introduced into the system, the overall stoichiometry of the process can be represented by

[5] $3\ ABTS^{\cdot+} + Trp + O_2 \rightarrow 3\ ABTS + \text{oxidation products}$

The fluorescence of the reacted sample (Excitation = 340 nm, Emission = 450 nm) would suggest the presence of kynurenine and formylkynurenine) among the products. These are the normal products associated to the free radical mediated oxidation of tryptophan (10).

© 2000 NRC Canada

Fig. 5. Kinetic profile of $ABTS^{\cdot+}$ bleaching by His at pH 7.0. This profile corresponds to a complex kinetic behaviour, with noticeable autoacceleration at long reaction times.



In spite of the relatively high oxygen uptake associated to the process (indicative of Trp oxidation), the rate of ABTS radical consumption induced by Trp measured at pH 7 is nearly independent of the presence of oxygen. Reactions carried out under nitrogen give the same initial rate than when the runs are carried out under air. This would indicate that oxygen is only involved in fast (not rate-limiting) secondary reactions of Trp derived radical intermediates.

Tyrosine and histidine

Tyrosine and histidine induced ABTS radical cation consumption present similar characteristics to those previously mentioned for Cys and Trp. Pseudo-reaction orders obtained when the data (measured at pH 5.0 for tyrosine and pH 7.0 for histidine) are fitted to eq. [1] are included in Table 1. When Tyr and His are employed, back formation of ABTS is also almost quantitative. However, the consumption of ABTS with His does not follow a simple pattern, presenting a very small fast initial reaction, followed by a slow process with significant autoacceleration at longer times (Fig. 5). No attempts were carried out to elucidate the origin of this complex reaction profile. Furthermore, and due to the slow rate of the process, the reaction can only be measured at pH 7.0. At lower pH, the reaction is extremely slow, while at higher pH, the ABTS radical cation becomes unstable even in the absence of additives. The rates measured correspond to the slow phase of the reaction.

Cystine (0.2 mM) and methionine (0.2 mM) did not produce any consumption of the ABTS radical cation (50 μM) during 1 h at pH 7.0. Complete lack of reaction was also observed when *N*-methyltryptophan (0.1 mM) and *O*-methyltyrosine (0.1 mM) were employed.

Discussion

The main features of the reaction between ABTS radical cations and phenols (7) and hydroperoxides (8) have been explained in terms of the following simplified mechanism where XH is a compound bearing a labile hydrogen atom.

[6] $ABTS^{\cdot+} + XH \rightleftharpoons ABTS + X\cdot + H^+$

[7] $ABTS^{\cdot+} + X\cdot \longrightarrow$ non–radical products

[8] $X\cdot + X\cdot \longrightarrow$ non–radical products

This simple scheme also explains the main features of the results obtained in the present work, at least when Cys, Trp, and Tyr are considered. The requirement of a labile hydrogen atom for the reaction is compatible with the lack of reactivity of cystine, methionine, *N*-methyltryptophan, and *O*-methyltyrosine. Reactions of the amino acid derived radical ($X\cdot$) with O_2 would provide an extra reaction channel for $X\cdot$ consumption, particularly when Trp and Cys are employed. However, the fact that the kinetic of $ABTS^{\cdot+}$ bleaching by the amino acid is nearly independent of oxygen pressure would suggest that oxygen/radical reactions are not kinetically relevant.

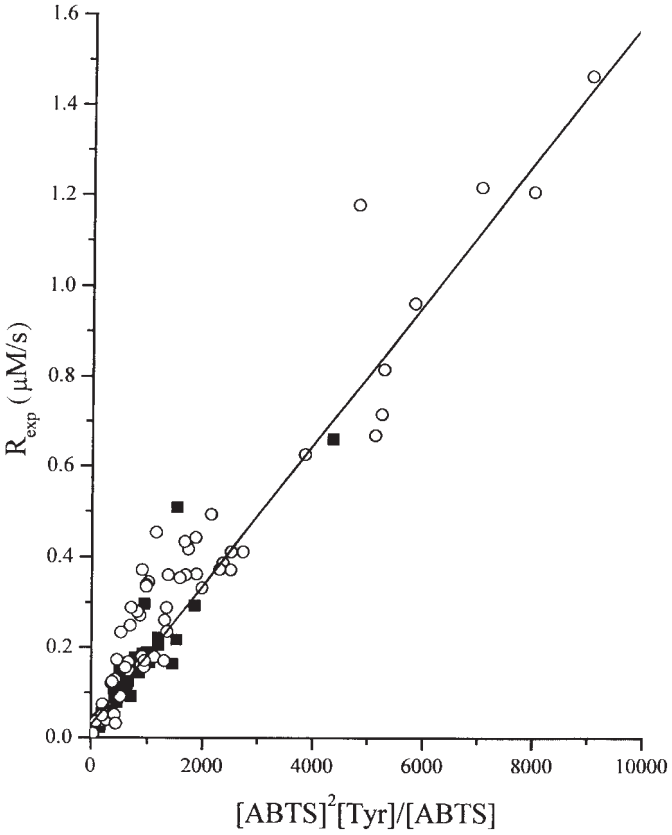
This simple mechanism predicts that the order of the inhibition by protons and ABTS must be similar. Furthermore, the magnitude of these orders must be related to the extent of reversibility of the initial step, ranging from zero (lack of reversibility) to two (complete reversibility and rxn. [8] as main reaction channel for removal of the $X\cdot$ radicals). The higher apparent reaction orders in ABTS and $ABTS^{\cdot+}$ obtained in the reaction of Trp at pH 5 than at pH 7 are compatible with a higher contribution of the back reaction when the proton concentration increases. Regarding cysteine, the low reaction orders obtained for protons and ABTS, as well as their similarity, would imply that the initial step is far from equilibrium. This is compatible with the fast rate of the total process measured for this amino acid, and could be related to the relative lability of the S—H bond. These criteria would indicate that in the reactions of the other amino acids, the initial hydrogen transfer is more reversible. However, the fact that both orders are significantly different implies that a simple mechanism, such as that depicted by eqs. [6]–[8], must be considered only as a first approximation.

The orders obtained employing tyrosine are close to those expected if the initial step were totally reversible, as reported for other phenols (7). To test this possibility, the experimental rates are plotted against $[ABTS^+]^2$ [Tyr]/[ABTS] in Fig. 6. The results show that, over all the conditions employed, the data conform to the kinetic law expected if rxn. [6] reaches equilibrium and rxn. [7] is the main step in the removal of Tyr derived radicals. For this compound the rate law can then be considered to be

[9] $\text{Rate} = k_{exp}\,[ABTS^+]^2\,[\text{Tyr}]/[\text{ABTS}]$

© 2000 NRC Canada

Fig. 6. Fit of Tyr data to a completely reversible mechanism. Following eq. [3], experimental rates are plotted against $[ABTS^{\cdot+}]^2[Tyr]/[ABTS]$. Correlation: $R = 0.9$. (O) $ABTS^{\cdot+}$ prepared with persulfate, (■) $ABTS^{\cdot+}$ prepared with MnO_2.



with

$$[10] \quad k_{exp} = K_6\, k_7$$

At pH 7, the best value of the k_{exp}, obtained from the slope of the plot shown in Fig. 6, is $1.65 \times 10^2\ M^{-1}\ s^{-1}$.

If the initial step is partially reversible, the kinetic law (and the stoichiometry of the process) will be determined by the relative rates of rxns. [7] and [8]. If it is assumed that the radical X· reaches a steady state condition, the two limiting situations above mentioned lead to the following rate laws (8)

Mechanism I (rate of rxn. [7] > > than rate of rxn [8])

$$[11] \quad R_{exp} = 2R_7 = 2k_7 \frac{k_6[XH][ABTS^{\cdot+}]^2}{k_{-6}[ABTS] + [ABTS^{\cdot+}]}$$

Mechanism II (rate of rxn. [7] < < than rate of rxn. [8])

$$[12] \quad R_{exp} = R_8 = k_8[X^{\cdot}]^2 = k_8\left(\frac{-k_{-6}[ABTS] + ((k_6[ABTS])^2 + 4k_8k_6)^{1/2}}{2k_8}\right)^2$$

Equation [11] can be arranged to

Table 2. Parameters derived from eq. [15].

$$[13] \quad \frac{[ABTS^{\cdot+}][XH]}{R_{exp}} = \frac{1}{k_6} + \frac{k_{-6}[ABTS]}{k_7k_6[ABTS^{\cdot+}]}$$

A plot of the left-hand side of this equation against $[ABTS]/[ABTS^{\cdot+}]$ can be employed to test if the data conform to this mechanism.

To fit the data to Mechanism II, eq. [12] can be arranged to

$$[14] \quad \frac{R_{exp}}{[ABTS^{\cdot+}][XH]} = k_6 - \frac{k_{-6}}{k_8} \quad \frac{k_{-6}\, R_{exp}^{1/2}[ABTS]}{k_8[ABTS^{\cdot+}][XH]}$$

and a plot of the left-hand side of this equation against $R_{exp}^{1/2}$ $[ABTS]/[ABTS^{\cdot+}][XH]$ can be employed as a mechanistic test (8).

The data obtained with Cys, Trp, and His do not conform to eq. [13] or eq. [14], implying that the whole mechanism must be considered to interpret the kinetic data. In spite of the apparent simplicity of this mechanism, it can not be reduced to a simple rate law and must be numerically solved. Applying the steady state hypothesis, the rate law can be expressed by a five-parameter eq. [8]

$$[15] \quad R = Ak_6^2\left[\frac{[ABTS^{\cdot+}]^2[XH]^2}{[ABTS]^2}\right] - Ak_6\left[\frac{2[ABTS^{\cdot+}][XH]R}{[ABTS]^2}\right] + A\left[\frac{R^2}{[ABTS]^2}\right] + Bk_6\left[\frac{[ABTS^{\cdot+}]^2[XH]}{[ABTS]}\right] - B\left[\frac{[ABTS^{\cdot+}]R}{[ABTS]}\right]$$

where:

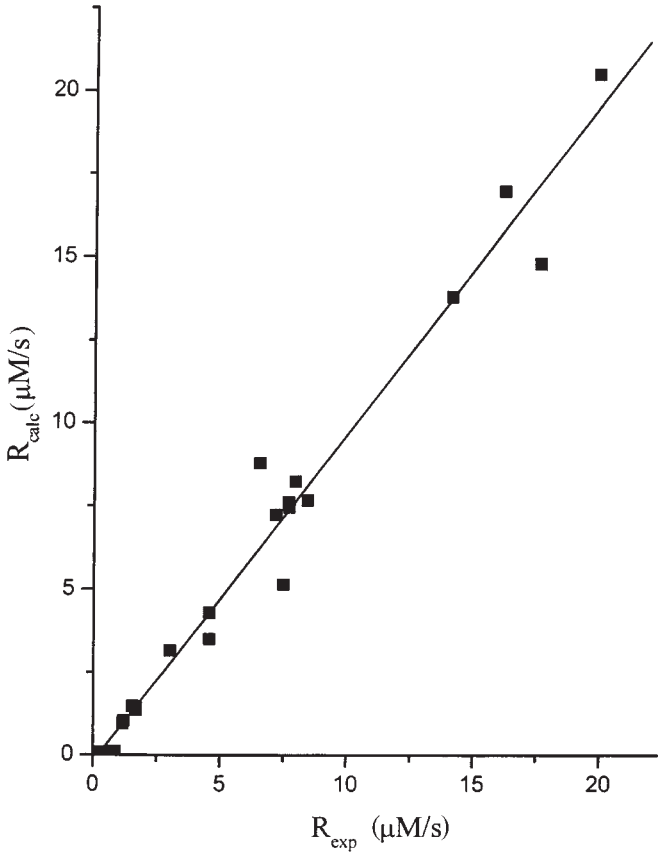
$$[16] \quad A = \frac{k_8}{k_{-6}^2} \quad \text{and} \quad \frac{k_8}{k_{-6}}$$

The best values of the five parameters (Ak_6^2, Ak_6, A, Bk_6, and B) of eq. [15] were obtained numerically by a minimum square methodology using a MAPLE-V software. This procedure allows an estimation of k_6, A, and B. The values obtained are collected in Table 2. Although these values, and particularly the A and B ratios, are subject to rather high uncertainties, some conclusions can be derived from the data collected in Table 2.

The derived values show that the reactivity of a given compound is directly related to the value of the specific rate constant of the initial step. In fact, this rate constant is highest for cysteine (the most reactive amino acid) and lowest for

© 2000 NRC Canada

Fig. 7. Correlation between measured and calculated reaction rates. Rates were calculated according to eq. [15] with the parameters given in Table 2. Data obtained employing (*a*) Cys, pH 5 (R = 0.99), (*b*) Trp, pH 5 (R = 0.97), and (*c*) His, pH 7 (R = 0.85).



the less reactive compound (histidine). Furthermore, relative values of k_6 are in agreement with the expected trend for a free radical hydrogen abstraction. In fact, two possible extreme mechanisms can be proposed for the postulated first step (rxn. [6]. In the first one, an initial hydrogen transfer

[17] $ABTS^{\cdot+} + XH \rightarrow ABTSH^{+} + X\cdot$

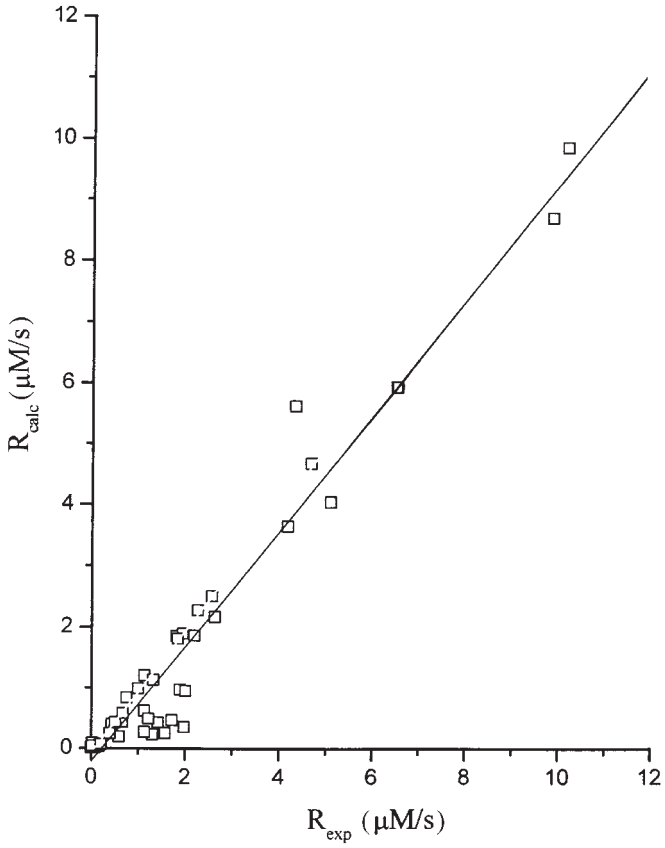
is followed by deprotonation of the $ABTSH^{+}$. If this is the limiting process, the relative rates could be expected to parallel those of other radical processes (9), in agreement with the relative values of k_6 found in the present work

Cys > Trp > Tyr

and the lack of reactivity of *N*-methyltryptophan, *O*-methyltyrosine, and cystine.

The other extreme mechanism involves an electron transfer followed by deprotonation of the substrate derived radical, followed by deprotonation of the amino acid. This first step would inversely correlate with the amino acid ionization potentials. However, semiempirical calculations (AM1 methodology (11)) and applying Koopman's theorem (12) gives lower *IP*, for Trp (8.38 eV) than for Cys (9.35 eV, in fair agreement with reported data (13)), suggesting that an initial limiting step mediated by an electron transfer could not be operative, at least for cysteine.

Fig. 7 (*Continued*).



The values of A and B given in Table 2 are compatible with those expected from the proposed mechanism and the characteristics of processes [6]–[8]. In fact, since the concentrations of ABTS and its radical cation are of the same order of magnitude, values of k_7/k_{-6} between 0.2 and 1.0 are consistent with a partial reversibility of step [6].

The data obtained for Trp show that the decrease in reaction rate when the pH decreases can be mostly ascribed to a decrease in k_{-6}, in agreement with the proposed mechanism. This would imply that ABTS radical cations are reacting with the neutral molecule and not with a small fraction of deprotonated compound in equilibrium. In this sense, the initial step can be represented by

[18] $ABTS^{\cdot+} + TrpH \leftrightarrow ABTS + TrpH^{+} \leftrightarrow ABTS + Trp\cdot + H^{+}$

and not by deprotonation of the amino acid

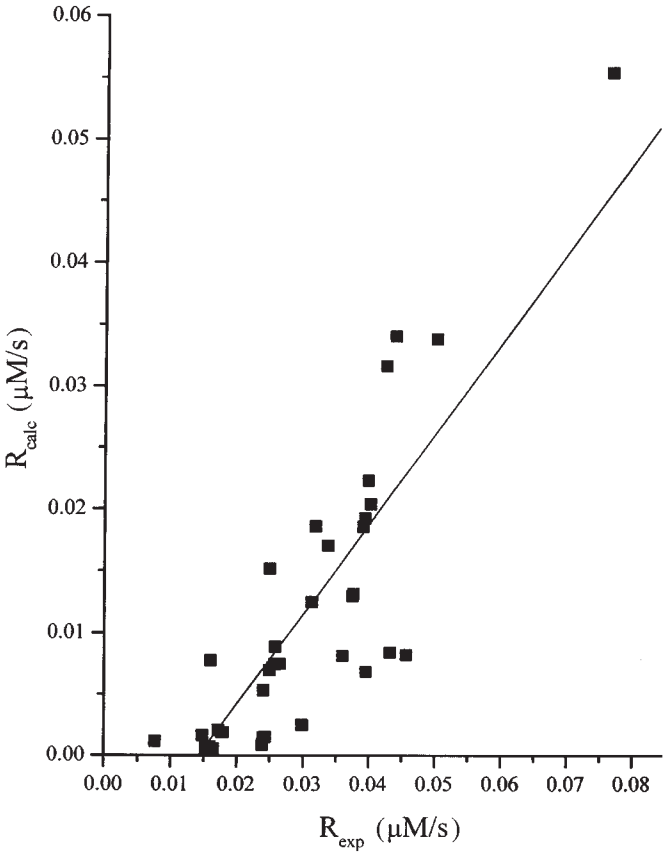
[19] $TrpH \rightarrow Trp^{-} + H^{+}$

followed by a reaction of the deprotonated compound with the ABTS radical cation.

The suitability of the parameters given in Table 2 to reproduce the experimental data under all the conditions employed can be assessed by plotting the calculated rates against the experimentally determined values. The data obtained employing Cys, Trp, and His are given in Fig. 7. These data show that the proposed equation reasonably fits experimental data obtained over a wide range of conditions.

© 2000 NRC Canada

Fig. 7 (*Concluded*).



This would indicate that the complete mechanism is able to interpret the main features of the kinetic process.

In conclusion, our data show that amino acids are able to bleach preformed ABTS radical cations with almost quantitative back formation of the parent ABTS. The rate of the process is mainly determined by the presence of labile hydrogen atoms in the amino acid side chain. The main features of the kinetic law can be explained in terms of a mechanism involving a partially reversible initial step. The relevance of the back reaction depends on the solution pH.

Several puzzling aspects are evidenced from a close examination of the data: (*i*) the lack of oxygen effect on the rate; (*ii*) the almost total recovery of the parent ABTS irrespective of the relevance of eq. [7]; and (*iii*) the dispersion of the data even when the whole mechanism is considered. Also, the lack of the relationship between the rate law and stoichiometric factors (related to the relative importance of process [7] and [8]) previously reported for a series of phenols (7). All these factors suggest that the mechanism depicted by eqs. [6]–[8] is an oversimplification and that some of the products (most likely those resulting from eq. [7]) are not stable. The decomposition of these initial products could consume oxygen, increase the ABTS yield, and modify the stoichiometry without altering the initial rates evaluated in the present work. Interestingly, in some compounds such as Trolox and Catechin, it was observed an overshoot in $ABTS^{\cdot+}$ consumption with a significant recovery after a few minutes (to be published). This could be explained by a transformation of the cross-adducts from rxn. [7] into the products of the type produced in rxn. [8].

The results obtained in the present work show that the mechanism of $ABTS^{\cdot+}$ reactions are extremely complex. This implies that extreme care must be exercised in the evolution of antioxidant capacities by procedures based on its bleaching (5, 14) or lack of formation (3), particularly when the information is derived from measurements carried out of a single reaction time (3, 14).

Acknowledgements

Financial support from projects FONDECYT no. 2980002 and no. 4990029 is acknowledged. Thanks are given to the reviewers for helpful suggestions.

References

1. C. Rice-Evans, N.J. Miller, P.G. Bolwell, P.M. Bramley, and J.B. Pridham. Free Radical Res. Commun. **22**, 375 (1995).
2. C. Rice-Evans and N.J. Miller. Methods Enzymol. **234**, 279 (1994).
3. N.J. Miller and C. Rice-Evans. Clin. Sci. **84**, 407 (1993).
4. E. Meucci and M.C. Mele. Amino Acids, **12**, 373 (1997).
5. C. Romay, C. Pascual, and E.A. Lissi. Braz. J. Med. Biol. Res. **29**, 175 (1996).
6. R. Re, N. Pellegrini, A. Proteggente, A. Pannala, M. Tang, and C. Rice-Evans. Free Radical Biol. Med. **9**/**10**, 1231 (1999).
7. A.M. Campos and E.A. Lissi. Int. J. Chem. Kinet. **29**, 219 (1997).
8. C. Aliaga and E.A. Lissi. Int. J. Chem. Kinet. **30**, 565 (1998).
9. E.A. Lissi, M. Faure, and N.Clavero. Free Radical Res. Commun. **14**, 373 (1991).
10. M. Friedman and J.L. Cuq. J. Agric. Food Chem. **36**, 1079 (1988).
11. M.J.S. Dewar, E.G. Zoebisch, and E.F. Healy. J. Am. Chem. Soc. **107**, 3902 (1985).
12. T. Koopmans. Physica, **1**, 104 (1934).
13. P.H. Cannington and N.S. Ham. J. Electron Spectrosc. Relat. Phenom. **32**, 139 (1983).
14. R. Re, N. Pellegrini, A. Proteggente, A. Pannala, M. Yang, and C. Rice-Evans. Free Radical Biol. Med. **26**, 1231 (1999).

© 2000 NRC Canada

The use of the Ramberg–Bäcklund rearrangement for the formation of aza-macrocycles: a total synthesis of manzamine C

David I. MaGee and Ellen J. Beck

Abstract: A total synthesis of the marine alkaloid manzamine C has been accomplished. A Ramberg–Bäcklund reaction was used as a key step to construct the required azacycloundecene ring.

Key words: alkaloid, macrocycle, Ramberg–Bäcklund, manzamine C.

Résumé : On a effectué une synthèse totale de la manzamine C, un alcaloïde marin. L'étape clé implique une réaction de Ramberg–Bäcklund qui permet de fabriquer le cycle azacycloundécène requis.

Mots clés : alcaloïde, macrocycle, Ramberg–Bäcklung, manzamine C.

[Traduit par la Rédaction]

Introduction

Manzamines are a growing family of novel oncolytic marine alkaloids isolated from several different genera of sponge off the coast of Okinawa, Japan. Manzamines A (**1**), B (**2**), and C (**3**) were first isolated and characterized by Higa and coworkers from *Haliclona* sp. (Scheme 1) (1, 2). Structurally, the manzamines consist of a β-carboline unit, at least one aza-macrocycle, several additional nitrogen atoms, and usually a complex array of rings of various sizes. The exception to this is manzamine C (**3)**, which contains only the β-carboline unit and an azacycloundecene ring. Despite the contrast in structures, manzamine C is just as potent as the other members, having an IC_{50} value of 3 μg/mL on P388 mouse leukemia cells (2). In comparison, manzamine B has an IC_{50} value of 6 μg/mL on the same cell line (2). Their challenging structural features as well as their potent biological activity have made the manzamines very attractive targets for synthesis (3, 4).

Our group is particularly interested in the development of novel methods for forming medium and large heterocycles and their application to natural product synthesis. This desire, as well as the potent biological activity of the manzamines, made them ideal targets. Due to the relative simplicity of manzamine C our investigations began there, because the knowledge gained from the construction of this alkaloid could then be applied to the synthesis of the more complex congeners.

Received November 22, 1999. Published on the NRC Research Press website on August 11, 2000.

D.I. MaGee[1] and E.J. Beck. Department of Chemistry, Bag Service #45222, University of New Brunswick, Fredericton, NB E3B 6E2, Canada.

[1]Author to whom correspondence may be addressed. Telephone: (506) 453-4870. Fax: (506) 453-4981. e-mail: dmagee@unb.ca

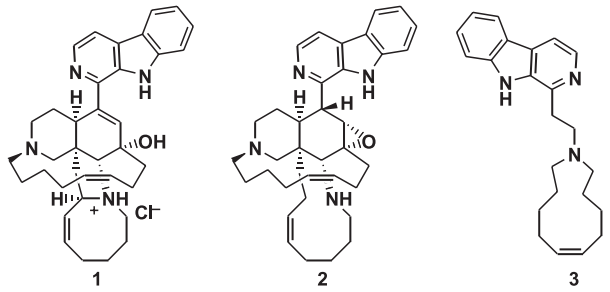
Manzamine C **3** was seen to arise from two basic fragments, the β-carboline unit **4** and azacycloundec-6-ene **7**, as shown in Scheme 2. In contrast to previous syntheses (5, 6), our route to β-carboline **4** began with the known alkaloid harmane **5** (7). This strategy was very appealing since the starting alkaloid could be efficiently prepared in gram quantities from cheap starting materials, and, in principle, only one other synthetic step would be needed to generate **4**. To construct the azacycloundecene ring we envisaged the use of an efficient procedure developed in our laboratories (8, 9) which involved the in situ formation and trapping of a ketene. With this methodology in mind, azacycloundecene **7** could be formed from alkynyl ether **8**, which in turn could be generated by a Wittig reaction between hydroxy phosphonium salt **10** and aldehyde **9**. Although this route appeared inviting, it was not without concern because preparation of aldehyde **9** was seen to arise from the oxidation of alcohol **14** (see Scheme 3) and, due to lack of literature precedent, it was not known whether the alkynyl ether would survive. Regardless, it was felt that suitable conditions could be found.

Results and discussion

There have been several reports of the formation and reaction of the dianion of harmane **5** with simple aldehyde and ketone electrophiles (10, 11). Following one of these protocols (11), the dianion was formed with *n*BuLi at room temperature and then subjected to several electrophiles including: *p*-formaldehyde, methylchloroformate, CO_2, ethyl isocyanate, and dimethylcarbonate. Regardless of the electrophile used to quench the dianion, a significant amount of starting material was always recovered, as well as a by-product that appeared to have an incorporated butyl group. To try and solve this problem we turned to the use of strong amide bases, and after much experimentation, it was found that the dianion could be efficiently generated by the use of 4 equivalents of LDA at –78°C for 1 hour. When the dianion

 © 2000 NRC Canada

Scheme 1. Manzamine A (**1**), Manzamine B (**2**), Manzamine C (**3**).



formed under these conditions was reacted with excess dimethylcarbonate (3 equiv) for 50 min, ester **4** (5) was obtained in 78% (Scheme 2). Significant amounts of the malonate was formed if longer reaction times were used.

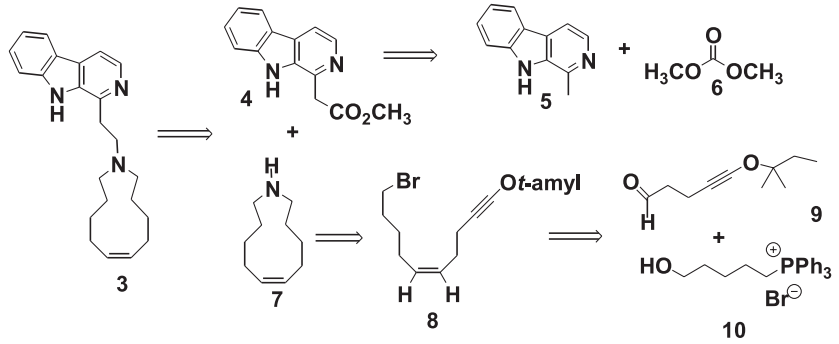
Construction of ketene precursor **8** began with the addition of lithium (2-methyl-2-butoxy) acetylide **11** to 3-bromo-1-(*tert*-butyldimethylsilyloxy)propane **12** to generate **13** in 70% yield (Scheme 3) (12). Deprotection of the silyl group with tetrabutylammonium fluoride proceeded uneventfully to give alcohol **14** in 75% yield. A variety of oxidizing agents were then analyzed for their effectiveness to achieve the desired transformation; these included PDC (13), Swern (14), DMS-NCS (15), Dess–Martin periodinane (DMP) (16), and SO_3·pyridine complex (17). While PDC and Swern led only to complete destruction of the starting material, presumably due to the acid lability of the alkynyl ether, DMS-NCS and DMP gave small amounts of aldehyde contaminated by a significant amount of an unknown byproduct. Fortunately, reaction with SO_3·pyridine complex in DMSO gave what appeared by ^{1}H NMR spectroscopy to be predominantly the desired aldehyde which, due to its sensitivity to purification by SiO_2 chromatography, was directly reacted with phosphorane **10** (18) to give alkene **8** in a disappointing 15–25% overall yield. Extensive experimentation proved that the low yield was a result of inefficient production of the aldehyde; however, attempts to try and improve this have thus far proved fruitless.

A new strategy

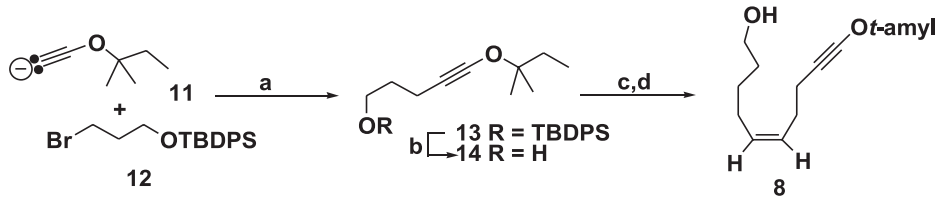
With our failure to secure the ketene precursor in useful yield, an alternative cyclization strategy was sought.[2] Ever mindful of our ultimate goal of a general aza-macrocyclization strategy that could be applied to the synthesis of the other manzamines, one method which appeared viable was the Ramberg–Bäcklund rearrangement (19–21). This option was inviting because synthesis of the requisite macrocycle should be straightforward and, more importantly, the site of the newly created olefin would be fixed by the position of the sulfone group and would not isomerize under the reaction conditions (22). Although the stereospecificity of the Ramberg–Bäcklund reaction was of concern, it was known that in acyclic systems the reaction leads to predominantly *cis*-olefins (22) and that in certain ring systems only *cis*-alkenes are produced (23–27). Surprisingly, we have not found any examples that address this stereospecificity question in flexible macrocyclic arrays.

With this strategy in mind, synthesis of the azacycloundecene ring began with condensation of 5-amino-1-pentanol **15** with δ-valerolactone **16** to afford amide-diol **17** quantitatively (Scheme 4). The amide **17** was directly reduced to the amine using BH_3–DMS (28) and isolated as the amine hydrochloride salt **18**, again in quantitative yield. Subsequent protection of the amino functionality as its *t*BOC-carbamate, followed by conversion of diol **19** to dibromide **21** via dimesylate **20**, generated the analogue

Scheme 2. Retrosynthetic analysis of manzamine C.



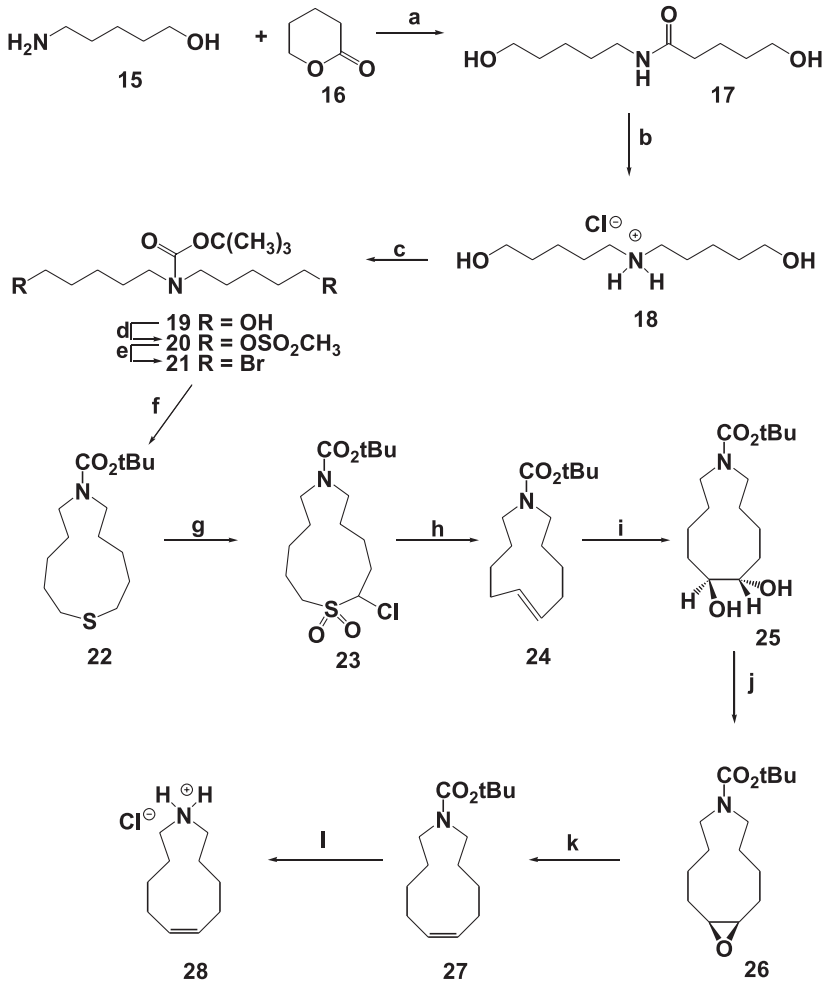
Scheme 3. (**a**) bromide **12**, HMPA, THF, 0°C – RT, 2 h; (**b**) TBAF, THF, RT, 1hr; (**c**) SO_3-pyridine complex, DMSO, RT, 20 min.; (**d**) ylide of phosphonium salt **10**, RT, 30 min.



[2] Many other routes were investigated in an attempt to arrive at ketene precursor **8**. These were either lengthy and prone to low yields or completely unsuccessful.

© 2000 NRC Canada

Scheme 4. (**a**) xylenes, reflux (92%); (**b**) (*i*) BH_3·DMS, THF, reflux, (*ii*) MeOH, anhyd. HCl, RT (100%); (**c**) Boc_2O, TEA, MeOH, reflux (83%); (**d**) methanesulfonyl chloride, pyridine, CH_2Cl_2, RT (94%); (**e**) LiBr, acetone, reflux (90%); (**f**) $Na_2S·9H_2O$, EtOH, reflux (86%); (**g**) (*i*) NCS, CCl_4, reflux, (*ii*) mCPBA, CH_2Cl_2, RT (58%); (**h**) KO*t*Bu, DMSO, RT (97%); (**i**) OsO_4, NMO, THF-*t*BuOH-H_2O, RT (84%); (**j**) (*i*) KO*t*Bu, THF, 0°C, (*ii*) 2,4,6-triisopropylbenzenesulfonyl chloride, 0°C–RT, (*iii*) KOtBu, RT (65%); (**k**) Rh(II) octanoate dimer, dimethyl diazomalonate, benzene, reflux (65%); (**l**) HCl(g), EtOAc, 0°C (100%).



required for cyclization in 71% overall yield. Attempts to effect cyclization of dibromide **21** with $Na_2S·9H_2O$ at high concentrations (29) only led to loss of starting material and little product formation. Fortunately refluxing **21** with $Na_2S·9H_2O$ in ethanol at high dilution (1.5×10^{-4} M) gave sulfide **22** in excellent yield (86%). Using these conditions, no dimer was observed, however, significant dimer formation was observed if the concentration was increased (e.g., 1.5×10^{-3} M) or if the diiodide was used in place of the dibromide. Sulfide **22** was then converted in a standard fashion to α-chlorosulfone **23** in 58% overall yield (30).

With **23** now in hand, investigations into the stereospecificity of the rearrangement began. Treatment of α-chlorosulfone **23** with potassium *t*-butoxide produced *trans*-olefin **24** with high stereospecificity (98:2 *trans*:*cis* ratio) and in a 97% yield! Although it had been noted in several acyclic examples that the use of strong bases, such as KOtBu, in the Ramberg–Bäcklund reaction predominantly gave *E*-olefins (22), it was nevertheless a surprise to get the *trans*-alkene almost exclusively in this cyclic system. Several milder, less bulky bases (2 M KOH, DBU, TEA, urea) were used in an attempt to predominantly form the *cis*-olefin, however, the results were not encouraging.

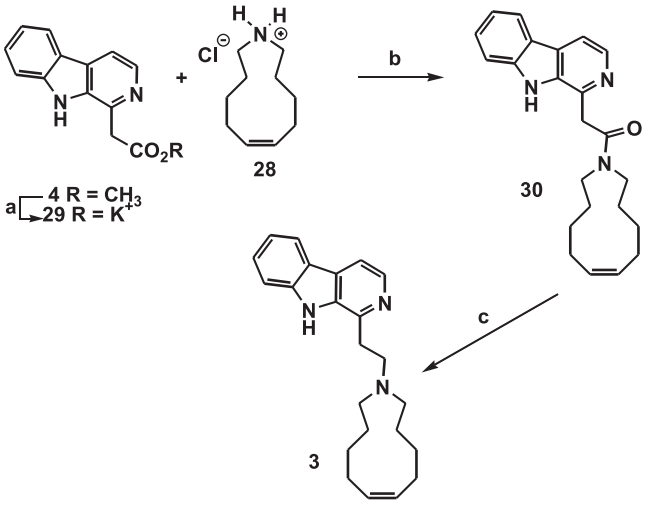
Table 1. Results of Ramberg–Bäcklund rearrangement using a variety of bases. The *E*:*Z* ratios were determined by GC analysis.

Reaction conditions	Yield (%)	% *Trans*	% *Cis*
KO*t*Bu, DMSO, RT, 10 min	97	98	2
aq. KOH, H_2O, 100°C, 1 h	57	61	39
DBU, toluene, 110°C, 1 h	56	57	43
TEA, toluene, 110°C, 1 h	NR	—	—
urea, H_2O, 100°C, 1 h	NR	—	—
NBu_3, toluene, 110°C, 1 h	NR	—	—

In acyclic systems it is known that aqueous hydroxide gives predominantly *cis*-olefins (22), therefore it was somewhat surprising to get principally *trans* in this case. In these systems, the *cis*-alkene is favored because of lower gauche interactions in the *cis*-episulfone formation when compared to the *trans*-episulfone formation (22). Presumably, it appears in the cyclic version that these gauche interactions are

© 2000 NRC Canada

Scheme 5. (*a*) KOH, EtOH, RT; (*b*) DPPA, TEA, amine **28**, RT (70% over 2 steps); (*c*) $LiAlH_4$, THF, 0°C–RT (42%).



not the only major contributor to determining the geometry, but also the transannular interactions that arise as a result of the ring trying to adopt the proper conformation for episulfone formation. These two factors appear to oppose one another because the degree of *trans*-episulfone formation in our example, as inferred from the amount of *trans*-alkene formed, is unusually high. This suggests that there are less unfavorable transannular interactions during the formation of the *trans*-episulfone, therefore it is the *trans*-alkene which is formed as the major product.

Although conditions were not found that would generate stereochemically pure *Z*-alkene, we were able to produce the *E*-alkene stereospecifically and in high yield. For our synthetic endeavours this was almost as good because a simple olefin inversion would furnish the required *Z*-azacycloundecene. To pursue this, a *trans*-epoxide was initially formed and then attempts were made to open the epoxide to a *cis*-diol. Unfortunately, endeavours to effect epoxide opening either under aqueous acidic (pTSA, $HClO_4$, H_2SO_4, HOAc) or basic conditions (NaOH or KOH in DMSO, RT–150°C) only led to recovered starting material or complete destruction. Replacement of the carbamate with a benzenesulfonamide group produced no better results. From molecular models it appears that the lack of reactivity is undoubtedly due to the conformation of the ring; that is for a nucleophile to add in an S_N2 manner, as it would in an epoxide opening, it would have to essentially add from "inside" the ring. Coupled with this, it appears that the nitrogen, although far less nucleophilic, may still be participating in assisted opening of the epoxide and hence leading to significant loss of material.

To alleviate this problem, an approach that did not involve epoxide opening was developed. Olefin **24** was oxidized to *trans*-diol **25** with OsO_4 in excellent yield, 84% (31). A monosulfonate was then generated from diol **25** under anionic conditions using 2,4,6-triisopropylbenzenesulfonyl chloride and KOtBu (32, 33). This intermediate was then treated in situ with an additional equivalent of KO*t*Bu, to obtain *cis*-epoxide **26** in 65% overall yield. Interestingly, no disulfonate was observed, presumably due to the bulkiness of the electrophile. Finally, deoxygenation (34) of *cis*-epoxide **26** with Rh(II) octanoate dimer and dimethyl diazomalonate furnished *cis*-olefin **27** in 65%. A solution of carbamate **27** in ethyl acetate was then treated with HCl gas to remove the *t*BOC protecting group and generate the amine hydrochloride salt **28** (5) in 100% yield.

With both segments (ester **4**, amine **28**) in hand, completion of the synthesis was straightforward. Following the procedure of Hino (5), ester **4** was first hydrolyzed with KOH in EtOH to obtain the potassium salt **29** (Scheme 5) which was then combined with amine hydrochloride **28** in DMF in the presence of diphenylphosphoryl azide and triethylamine to give the corresponding amide **30** (5) in 70% yield. Direct reduction of amide **30** with LAH afforded the natural product, which was identical to all spectral data reported by Higa (2), in 42% yield.

In conclusion, a straightforward and concise synthesis of manzamine C has been accomplished. The requisite *Z*-azacycloundecene was produced in a stereospecific manner by utilizing a Ramberg–Bäcklund rearrangement followed by olefin inversion. The generality of this approach for synthesizing other flexible macro-heterocycles found in the manzamines and other natural products is currently being investigated.

Experimental[3]

All reactions were carried out in flame-dried glassware under argon atmosphere using dry, freshly distilled solvents. Reagents were purchased from Aldrich Chemicals and used without further purification.

Melting points were obtained using a Gallenkamp melting point apparatus and are uncorrected. Infrared spectra were recorded on a Perkin–Elmer 598 infrared spectrophotometer, with all spectra run in NaCl cells with $CHCl_3$ as solvent or on a 3M polyethylene type 61 IR card with 19 mm aperture. Mass Spectra were recorded on a KRATOS MS50TC. ^1H NMR and ^{13}C NMR were recorded using a Varian Unity 400 (400 MHz) spectrometer. All NMR samples were run in $CDCl_3$ with 0.05% Me_4Si as internal reference, or methanol-d_4 at room temperature, or in DMSO-d_6 at higher temperatures (50°C, 90°C, or 100°C), as indicated. Purification of compounds by flash column chromatography was done using E. Merck silica gel 60 (particle size 0.040–0.062 mm). Preparative thin-layer chromatography was carried out on 0.25, 0.50, or 1 mm E. Merck silica gel plates.

N-*(5′-hydroxypentyl)-5-hydroxypentanamide (**17**)*: To a solution of δ-valerolactone **16** (1.7 mL, 18.3 mmol) in xylenes (50 mL) at 30°C was added 5-amino-1-pentanol **15** (2 mL, 18.3 mmol). The resulting mixture was refluxed for 18 h, followed by evaporation of the solvent in vacuo and recrystallization (hexane – ethyl acetate) to yield amide-diol **17** (3.61 g, 92%) as a colourless solid (mp 38.5–41.3°C). IR (IR Card): 3300, 3100, 2910, 2850, 1640, 1550, 1050 cm^{-1};

[3] Spectra have been deposited as supplementary material and may be purchased from the Depository of Unpublished Data, Document Delivery, CISTI, National Research Council Canada, Ottawa, ON, Canada K1A 0S2 (http://www.nrc.ca/cisti/irm/unpub_e.shtml).

© 2000 NRC Canada

^{1}H NMR (CD_3OD): 1.38 (m, 2 H), 1.52 (m, 6 H), 1.65 (m, 2 H), 2.19 (t, J = 7.5 Hz, 2 H), 3.16 (t, J = 7.0 Hz, 2 H), 3.54 (t, J = 6.7 Hz, 2 H), 3.55 (t, J = 6.5 Hz, 2 H); ^{13}C NMR (CD_3OD): 22.0, 22.8, 28.8, 31.6, 31.8, 35.4, 38.9, 61.1, 61.3, 174.5; HRMS (EI): $C_{10}H_{21}NO_3$(calc) = 203.15214, $C_{10}H_{21}NO_3$(obs) = 203.1526 (m^+).

*Bis(5-hydroxypentyl)amine hydrochloride (**18**)*: A 2.0 M borane – dimethyl sulfide solution in THF (57.1 mL, 0.114 mol) was added dropwise to a refluxing solution of amide-diol **17** (5.95 g, 29.3 mmol) in THF (100 mL). After addition of the BH_3–DMS was complete, the reaction mixture was refluxed for one hour. After cooling to room temperature, methanol (13.9 mL, 0.342 mol) was added dropwise over 15 min and the reaction mixture was then stirred until all the precipitate had dissolved. Anhydrous HCl in diethyl ether (24.8 mL, 0.117 mol, 4.72 M) was added and the reaction was stirred for 10 min at room temperature. Finally, the solvent was evaporated in vacuo, the residue was washed three times with Et_2O, and then dried under vacuum to furnish amine-diol-hydrochloride **18** (6.60 g, 100%) as a colourless solid (mp 60.1–61.0°C). IR (IR Card): 3330, 2920, 1450, 1040 cm^{-1}; ^{1}H NMR (CD_3OD): 1.46 (m, 4 H), 1.56 (m, 4 H), 1.73 (m, 4 H), 3.00 (t, J = 7.9 Hz, 4 H), 3.57 (t, J = 6.3 Hz, 4 H); ^{13}C NMR (DMSO-d_6, 90°C): 23.2, 25.9, 32.3, 47.5, 60.9; HRMS (EI): $C_{10}H_{24}NO_2Cl$(calc) = 225.1496, m^+/z-Cl(calc) = 190.1807, $C_{10}H_{24}NO_2$(obs) = 190.1808 (m^+-Cl).

N-*(*t-*butyloxycarbonyl)-bis(5-hydroxypentyl)amine (**19**)*: To a solution of amine-diol **18** (6.4 g, 28.3 mmol) in methanol (100 mL) was added triethylamine (15.8 mL, 113.0 mmol), followed by di-*tert*-butyl dicarbonate (7.4 g, 33.9 mmol). The reaction was then heated to reflux for 2 h and the solvent was then evaporated in vacuo. The residue was taken up in dichloromethane (100 mL), washed quickly with cold 1 M HCl and then brine, dried over $MgSO_4$, filtered, and the solvent evaporated. The residue was purified by SiO_2 chromatography (ethyl acetate) to yield carbamate-diol **19** (6.82 g, 83%) as a clear, colourless oil. IR (NaCl cells): 3610, 3440, 2930, 1670, 1160 cm^{-1}; ^{1}H NMR ($CDCl_3$): 1.32 (m, 4 H), 1.42 (s, 9 H), 1.54 (m, 8 H), 2.30 (s, 1 H), 2.51 (s, 1 H), 3.14 (m, 4 H), 3.60 (t, J = 6.5 Hz, 4 H); ^{13}C NMR (DMSO-d_6, 100°C): 23.3, 28.4, 28.6, 32.7, 47.1, 61.3, 78.5, 155.2; HRMS (EI): $C_{15}H_{31}NO_4$(calc) = 289.2252, m^+/z-$C_5H_9O_2$(calc) = 188.1650, $C_{10}H_{22}NO$(obs) = 188.1652.

N-*(*t-*butyloxycarbonyl)-bis(5-methanesulfonyloxypentyl)amine (**20**)*: Pyridine (2.6 mL, 31.6 mmol) was added to a solution of carbamate-diol **19** (2.3 g, 7.9 mmol) in dichloromethane (50 mL). This mixture was then cooled in an ice bath and methanesulfonyl chloride (2.5 mL, 31.6 mmol) was added. The reaction was stirred at room temperature for 18 h. The reaction mixture was then diluted with ether (75 mL); washed with cold 10% HCl, 10% NaOH (×2), H_2O, and brine; dried over $MgSO_4$; filtered; the solvent evaporated in vacuo; and the residue was purified by SiO_2 chromatography (2:1 hexane : ethyl acetate) to provide dimesylate **20** (3.31 g, 94%) as a colourless oil. IR (NaCl cells): 2940, 1675, 1350, 1160, 950 cm^{-1}; ^{1}H NMR ($CDCl_3$): 1.42 (m, 4 H), 1.46 (s, 9 H), 1.57 (m, 4 H), 1.79 (m, 4 H), 3.02 (s, 6 H), 3.19 (m, 4 H), 4.24 (t, J = 6.5 Hz, 4 H); ^{13}C NMR (DMSO-d_6, 70°C): 22.7, 27.9, 28.6, 28.7, 37.2, 46.6, 70.7, 78.7, 155.2; HRMS (EI): $C_{17}H_{35}NO_8S_2$(calc) = 445.1804, m^+/z-C_4H_9O(calc) = 372.1151, $C_{13}H_{26}NO_7S_2$(obs) = 372.1151.

N-*(*t-*butyloxycarbonyl)-bis(5-bromopentyl)amine (**21**)*: Dimesylate **20** (8.1 g, 18.1 mmol) was combined with lithium bromide (15.8 g, 0.181 mol) in acetone (150 mL) and refluxed for 18 h. The solvent was then removed in vacuo. The residue was taken up in diethyl ether (100 mL), washed with H_2O and brine, dried over $MgSO_4$, filtered, and then concentrated and purified by silica gel chromatography (10:1 hexane:ethyl actetate) to furnish dibromide **21** (6.74 g, 90%) as a clear, pale yellow oil. IR (NaCl cells): 2930, 1670, 1300, 1155, 555 cm^{-1}; ^{1}H NMR ($CDCl_3$): 1.44 (m, 4 H), 1.46 (s, 9 H), 1.54 (m, 4 H), 1.88 (m, 4 H), 3.17 (m, 4 H), 3.41 (t, J = 6.8 Hz, 4 H); ^{13}C NMR (DMSO-d_6, 90°C): 25.4, 27.6, 28.6, 32.4, 35.0, 46.7, 78.7, 155.2; HRMS (EI): $C_{15}H_{29}NO_2Br_2$(calc) = 413.0565, m^+/z-C_4H_9O(calc) = 339.9912, $C_{11}H_{20}NOBr_2$(obs) = 339.9917, 312 (m^+/z-$C_5H_9O_2$).

N-*(*t-*butyloxycarbonyl)-1-thia-7-azacyclododecane (**22**)*: Dibromide **21** (50 mg, 0.12 mmol) was combined with sodium sulfide nonahydrate (30 mg, 0.12 mmol) in absolute ethanol (500 mL) and refluxed for 18 h. The ethanol was then evaporated in vacuo. The residue was taken up with diethyl ether (50 mL) and washed with 5% sodium hydroxide (×3) and then water, dried with $CaCl_2$, filtered and then concentrated. Purification on a 1 mm preparatory plate (10:1 hexane : ethyl acetate) furnished the monomer sulfide **22** (30 mg, 86%) as a clear colourless oil. IR (NaCl cells): 2930, 1675, 1455, 1410, 1365, 1285, 1150, 990 cm^{-1}; ^{1}H NMR ($CDCl_3$): 1.47 (s, 9 H), 1.59 (m, 8 H), 1.67 (m, 4 H), 2.58 (t, J = 6.0 Hz, 4 H), 3.29 (m, 4 H); ^{13}C NMR (DMSO-d_6, 90°C): 22.9, 27.6, 27.7, 28.6, 30.9, 48.0, 78.6, 156.1; HRMS (EI): $C_{15}H_{29}NO_2S$(calc) = 287.1919, m^+/z -$C_5H_9O_2$(calc) = 186.1316, $C_{10}H_{20}NS$(obs) = 186.1320.

N-*(*t-*butyloxycarbonyl)-2-chloro-1,1-dioxo-1-thia-7-azacyclododecane (**23**)*: Sulfide **22** (0.22 g, 0.76 mmol) and *N*-chlorosuccinimide (0.10 g, 0.76 mmol) were combined in carbon tetrachloride (20 mL) and refluxed for 3 h. The reaction mixture was then cooled in an ice bath, the precipitate was filtered and the solvent was removed from the filtrate in vacuo. The residue was taken up in dichloromethane (20 mL) and cooled in an ice bath. *m*-Chloroperbenzoic acid (85%, 0.34 g, 1.99 mmol) was then added and the reaction was stirred for 18 h at room temperature. The reaction mixture was then cooled in an ice bath and the precipitate was filtered off. The filtrate was washed with 1 M NaOH (×2) and then brine, dried over $MgSO_4$, filtered, and the solvent removed. The crude product was purified by column chromatography (2:1 hexane : ethyl acetate) to supply chlorosulfone **23** (0.156 g, 58%) as a colourless solid (mp 147.8–149.5°C). IR (NaCl cells): 2930, 1680, 1450, 1410, 1365, 1310, 1150, 900 cm^{-1}; ^{1}H NMR ($CDCl_3$) 1.48 (s, 9 H), 1.50–1.85 (m, 7 H), 1.86–2.10 (m, 2 H), 2.10–2.30 (m, 2 H), 2.99 (m, 1 H), 3.19 (m, 1 H), 3.28 (m, 2 H), 3.47 (m, 2 H), 4.76 (dd, J = 4.1, 7.5 Hz, 1 H); ^{13}C NMR ($CDCl_3$): 21.3, 21.6, 23.1, 25.5, 25.8, 28.4, 31.6, 47.0, 47.2, 48.9, 73.1, 79.9, 156.5; HRMS (EI): $C_{15}H_{28}NO_4SCl$(calc) = 353.1428, m^+/z-$C_5H_9O_2$(calc) = 252.0825, $C_{10}H_{19}NO_2SCl$(obs) = 252.0830.

© 2000 NRC Canada

N-*(*t-*butyloxycarbonyl)-6-(*E*)-azacycloundecene (**24**)*: To a solution of chlorosulfone **23** (0.156 g, 0.44 mmol) dissolved in methyl sulfoxide (10 mL) was added potassium *tert*-butoxide (2.2 mL, 1.0 M solution in THF, 2.2 mmol). The reaction was then stirred at room temperature for 10 min. The reaction was diluted with diethyl ether (10 mL) and then poured into water (10 mL). The aqueous phase was extracted twice with diethyl ether. The combined organic phase was washed twice with water and then brine, dried over $MgSO_4$, filtered, and the solvent removed in vacuo. The residue was purified by silica gel chromatography (10:1 hexane : ethyl acetate) to provide *trans*-olefin **24** (0.108 g, 97%) as a clear, colourless oil. IR (NaCl cells): 2930, 1665, 1455, 1365, 1300, 1165, 1125, 980, 890 cm^{-1}; ^1H NMR ($CDCl_3$): 1.32 (m, 4 H), 1.42 (s, 9 H), 1.50 (m, 4 H), 2.15 (m, 4 H), 3.15 (m, 2 H), 3.25 (m, 2 H), 5.44 (t-like, J = 4.3 Hz, 2 H); ^{13}C NMR (DMSO-d_6, 90°C): 23.6, 25.7, 28.6, 33.8, 44.3, 78.4, 131.0, 154.7; HRMS (EI): $C_{15}H_{27}NO_2$(calc) = 253.2042, m^+/z -$C_5H_9O_2$(calc) = 152.1439, $C_{10}H_{18}NO_2$(obs) = 152.1451.

N-*(*t-*butyloxycarbonyl)-6,7-*trans-*azacycloundecandiol (**25**)*: To a stirred solution of *t*-butanol (32 mL), water (4 mL), THF (12 mL), 4-methylmorpholine-*N*-oxide (0.43 mL, 2.5 mmol), and *trans*–olefin **24** (0.52 g, 2.1 mmol) was added 2–3 crystals of osmium tetraoxide. The reaction was allowed to stir at room temperature for 18 h, then 2 g of florisil and 2 g sodium dithionite were added. This mixture was stirred for 5 min and then filtered through a pad of Celite. The solvent was removed in vacuo, the residue was taken up in ethyl acetate (20 mL); washed with 10% HCl, H_2O, and brine; dried over $MgSO_4$; filtered; and the solvent evaporated. The crude diol was purified by column chromatography (ethyl acetate) to furnish *trans*–diol **25** (0.498 g, 84%) as an off-white solid (mp 110.1–112.2°C). IR (NaCl cells): 3580, 2920, 1670, 1365, 1155 cm^{-1}; ^1H NMR ($CDCl_3$): 1.47 (s, 9 H), 1.5–1.7 (m, 8 H), 1.70 (s, 2 H), 1.84 (m, 2 H), 2.37 (m, 2 H), 3.25 (m, 4 H), 3.66 (s, 2 H); ^{13}C NMR (DMSO-d_6, 90°C): 20.5, 26.6, 27.8, 30.6, 49.0, 72.1, 77.8, 155.1; HRMS (EI): $C_{15}H_{29}NO_4$(calc) = 287.2097, m^+/z -$C_5H_9O_2$(calc) = 186.1494, $C_{10}H_{20}NO_2$(obs) = 186.1489.

N-*(*t-*butyloxycarbonyl)-6,7-*cis-*epoxyazacycloundecane (**26**)*: To a cooled solution of *trans*–diol **25** (0.087 g, 0.30 mmol) in THF (7 mL) was added potassium *tert*-butoxide (0.30 mL, 1.0M solution in THF, 0.30 mmol). After the reaction mixture was stirred for 15 min in an ice bath, 2,4,6-triisopropylbenzenesulfonyl chloride (0.092 g, 0.30 mmol) was added in THF (3 mL) and the reaction was allowed to stir at room temperature for 15 min. A second aliquot of potassium *tert*-butoxide (0.30 mL, 1.0 M solution in THF, 0.30 mmol) was added and the reaction was stirred for 10 min at room temperature. The reaction was diluted with diethyl ether (10 mL); washed with 1 M HCl, 10% NaOH, H_2O, and then brine; dried over $MgSO_4$; filtered; and the solvent evaporated. The crude product was purified by column chromatography (10:1 hexane : ethyl acetate to 2:1 ethyl acetate : hexane) to furnish *cis*–epoxide **26** (0.045 g, 65%) as a white solid (mp 81.4–83.8°C) and recovered *trans*–diol **25** (0.013 g). IR (NaCl cells): 2960, 2930, 1670, 1450, 1410, 1365, 1150, 900 cm^{-1}; ^1H NMR ($CDCl_3$): 1.36 (m, 2 H), 1.46 (s, 9 H), 1.58 (m, 4 H), 1.74 (m, 4 H), 1.92 (m, 2 H), 2.75 (m, 2 H), 2.92 (d, J = 10.3 Hz, 2 H), 3.66 (m, 2 H); ^{13}C NMR (DMSO-d_6, 90°C): 22.0, 23.9, 26.5, 28.6, 49.9, 57.2, 78.7, 155.6; HRMS (EI): $C_{15}H_{27}NO_3$(calc) = 269.1991, m^+/z -$C_5H_9O_2$(calc) = 168.1389, $C_{10}H_{18}NO$(obs) = 168.1388.

N-*(*t-*butyloxycarbonyl)-6-(*Z*)-azacycloundecene (**27**)*: To a refluxing solution of *cis*-epoxide **26** (0.054 g, 0.20 mmol) and 5 mg of Rh (II) octanoate dimer in benzene (3 mL) was added dimethyl diazomalonate (0.063 g, 0.40 mmol) in benzene (2 mL) slowly over ten minutes. After the addition was complete the reaction was refluxed for 30 min more, then cooled to room temperature, filtered through silica, and the solvent removed in vacuo. The crude product was purified by column chromatography (10:1 hexane : ethyl acetate) to furnish *cis*-olefin **27** as a clear, colourless oil (0.033 g, 65%). IR (NaCl cells): 2955, 1665, 1450, 1410, 1360, 1290, 1150, 1110, 885 cm^{-1}; ^1H NMR ($CDCl_3$): 1.47 (s, 9 H), 1.50 (m, 4 H), 1.68 (m, 4 H), 2.19 (m, 4 H), 3.27 (m, 4 H), 5.40 (m, 2 H); ^{13}C NMR (DMSO-d_6, 90°C): 24.4, 26.0, 26.1, 28.6, 48.9, 78.6, 130.7, 155.4; HRMS (EI): $C_{15}H_{27}NO_2$(calc) = 253.2042, m^+/z -$C_5H_9O_2$(calc) = 152.1439, $C_{10}H_{18}N$(obs) = 152.1447.

*6-(*E*)-azacycloundecene hydrochloride (**28**)*: HCl gas was bubbled into a cooled solution of *cis*-olefin **27** (0.1 g, 0.41 mmol) in ethyl acetate (10 mL) for 10 min. The reaction mixture was then stirred for 5 min more at room temperature before the solvent was evaporated in vacuo. The residue was washed with Et_2O (3×) and then dried under vacuum to provide the amine-hydrochloride salt **28** (0.078 g, 100%) as a white solid (mp 132.0–135.1°C). IR (IR card): 2890, 1590, 1435 cm^{-1}; ^1H NMR (CD_3OD): 1.60 (m, 4 H), 1.77 (m, 4 H), 2.32 (m, 4 H), 3.10 (t, J = 7.7 Hz, 4 H), 5.48 (t, J = 5.3 Hz, 2 H); ^{13}C NMR (CD_3OD): 22.4, 23.7, 25.0, 41.4, 130.8; HRMS (EI): $C_{10}H_{20}NCl$(calc) = 189.1284, m^+/z -Cl(calc) = 154.1596, $C_{10}H_{20}N$(obs) = 154.1580.

*1-methoxycarbonylmethyl-β-carboline (**4**)*: To a solution of LDA (4.4 mmol) in THF (20 mL) at –78°C was added harmane **5** (0.2 g, 1.1 mmol) in THF (10 mL). After stirring the resulting solution for 15 min at –78°C, dimethylcarbonate (0.28 mL, 3.3 mmol) was added and the solution was stirred at –78°C for 50 min. The cold bath was then removed and the reaction allowed to stir for 10 min, before quenching with a saturated solution of NH_4Cl. The aqueous phase was then extracted twice with dichloromethane. The combined organic phase was washed with brine, dried over $MgSO_4$, filtered, and the solvent evaporated in vacuo. Purification by flash chromatography (ethyl acetate) followed by crystallization (hexane – ethyl acetate) furnished harmane ester **4** (0.207 g, 78%) as an amorphous yellow solid (mp 109–111°C). IR (NaCl cells): 3420, 2950, 1720, 1630, 1430, 1380, 1310, 1120, 1005 cm^{-1}; ^1H NMR ($CDCl_3$): 3.76 (s, 3 H), 4.26 (s, 2 H), 7.31 (m, 1 H), 7.56 (m, 2 H), 7.92 (d, J = 5.3 Hz, 1 H), 8.13 (d, J = 7.7 Hz, 1 H), 8.41 (d, J = 5.3 Hz, 1 H), 9.17 (s, 1 H); ^{13}C NMR ($CDCl_3$): 42.5, 52.6, 111.9, 114.3, 120.2, 121.7, 121.7, 128.5, 129.7, 135.1, 137.2, 138.9, 140.6, 171.6; HRMS (EI): $C_{13}H_{12}N_2O_2$(calc) = 240.0899, $C_{13}H_{12}N_2O_2$(obs) = 240.0894.

*Manzamine amide (**30**)*: A 1.5 M aqueous solution of potassium hydroxide (0.26 mL, 0.39 mmol) was added to a solution of harmane ester **4** (0.049 g, 0.21 mmol) in ethanol

© 2000 NRC Canada

(2 mL) and the resulting solution was stirred for 2 h at room temperature. The solvent was then removed in vacuo and the residue was dried under vacuum for several hours. The residue was then dissolved in *N*,*N*-dimethylformamide (2 mL) and to this solution was added amine-olefin **28** (0.04 g, 0.21 mmol) in DMF (1 mL), diphenylphosphoryl azide (0.09 mL, 0.41 mmol), and triethylamine (0.06 mL, 0.41 mmol). The reaction mixture was stirred for 18 h at room temperature and then 10% aqueous NaOH solution was added until the reaction mixture was alkaline. The reaction mixture was extracted twice with dichloromethane. The combined organic phase was washed with H_2O (×5), dried over $MgSO_4$, filtered, and the solvent was evaporated in vacuo. Purification by flash chromatography (1:1 hexane : ethyl acetate) provided manzamine amide **30** (0.052 g, 70%) as an amorphous yellow solid (mp 138–140°C). IR (NaCl cells): 3450, 2930, 1610, 1430, 1365, 1315 cm^{-1}; ^1H NMR ($CDCl_3$): 1.46 (m, 4 H), 1.69 (m, 4 H), 2.18 (t-like, J = 5.6 Hz, 4 H), 3.32 (m, 2 H), 3.55 (m, 2 H), 4.25 (s, 2 H), 5.34 (t-like, J = 5.8 Hz, 2 H), 7.25 (m, 1 H), 7.52 (m, 2 H), 7.85 (d, J = 5.3 Hz, 1 H), 8.08 (d, J = 7.7 Hz, 1 H), 8.33 (d, J = 5.3 Hz, 1 H), 10.16 (s, 1 H); ^{13}C NMR ($CDCl_3$): 24.2, 24.5, 24.9, 25.1, 25.3, 26.1, 43.3, 46.3, 48.6, 112.2, 113.9, 119.8, 121.4, 121.6, 128.3, 129.0, 130.7, 130.7, 135.8, 138.2, 138.7, 140.6, 169.8; HRMS (EI): $C_{23}H_{27}N_3O$(calc) = 361.2154, $C_{23}H_{27}N_3O$(obs) = 361.2153, 181 (m^+-$C_{11}H_{18}NO$), 152 (m^+-$C_{13}H_9N_2O$), 209 (m^+-$C_{10}H_{18}N$).

*Manzamine C (**3**)*: To a cooled solution of $LiAlH_4$ (0.08 g, 2.15 mmol) in THF (10 mL) was added manzamine amide **30** (0.155 g, 0.43 mmol) in THF (5 mL). The reaction was stirred for 3 h at room temperature and then quenched by the addition of 10% aqueous NaOH (1–2 mL) until the organic layer was clear. The reaction mixture was then extracted with dichloromethane twice, dried over K_2CO_3, and the solvent evaporated in vacuo. Purification by flash chromatography (40:1 diethyl ether:methanol to 10:1 diethyl ether:methanol) furnished manzamine C **3** (0.055 g, 42%) as a pale yellow solid (88.5–90.5°C). IR (NaCl cells): 2920, 2850, 1615, 1450, 1370, 1315 cm^{-1}; ^1H NMR ($CDCl_3$): 1.54 (m, 4 H), 1.80 (m, 4 H), 2.31 (m, 4 H), 2.92 (t, J = 7.7 Hz, 4 H), 3.00 (t, J = 5.9 Hz, 2 H), 3.43, (t, J = 5.9 Hz, 2 H), 5.48 (t-like, J = 5.4 Hz, 2 H), 7.25 (m, 1 H), 7.53 (m, 2H), 7.84 (d, J = 5.4 Hz, 1 H), 8.13 (d, J = 7.9 Hz, 1 H), 8.29 (d, J = 5.4 Hz, 1 H), 12.54 (s, 1 H); ^{13}C NMR ($CDCl_3$): 22.9, 24.6, 26.0, 33.9, 48.6, 52.5, 112.0, 113.3, 119.2, 121.6, 121.8, 127.8, 128.4, 131.0, 135.4, 137.5, 140.7, 144.6; HRMS (EI): $C_{23}H_{29}N_3$(calc) = 347.2361, $C_{23}H_{29}N_3$(obs) = 347.2345, 166 (m^+-$C_{12}H_9N_2$).

Acknowledgments

We thank NSERC Canada (operating grant for D.M. and a PGS-A and PGS-B for E.B.) and the University of New Brunswick for financial support, Dr. Larry Calhoun for NMR assistance and Gilles Vautour for mass spectral service.

References

1. R. Sakai, T. Higa, C.W. Jefford, and G. Bernardinelli. J. Am. Chem. Soc. **108**, 6404 (1986).
2. R. Sakai, S. Kohmoto, T. Higa, C.W. Jefford, and G. Bernardinelli. Tetrahedron Lett. **28**, 5493 (1987).
3. For a review see: E. Magnier and Y. Langlois. Tetrahedron, **54**, 6201 (1996).
4. J.D. Winkler and J.M. Axten. J. Am. Chem. Soc. **120**, 6425 (1998).
5. Y. Torisawa, A. Hasimoto, M. Nakagawa, H. Seki, R. Hara, and T. Hino. Tetrahedron, **47**, 8067 (1991).
6. W. Nowak and H. Gerlach. Liebigs Ann. Chem. 153 (1993).
7. D.G. Harvey and W. Robson. J. Chem. Soc. 97 (1938).
8. L. Liang, M. Ramaseshan, and D.I. MaGee. Tetrahedron, **49**, 2159 (1993).
9. D. I. MaGee and M. Ramaseshan. Synlett. 743 (1994).
10. E.M. Kaiser and P.L.A. Knutson. Tetrahedron Lett. 3583 (1975).
11. E.M. Kaiser. Tetrahedron, **39**, 2055 (1983).
12. Anion **11** was synthesized according to the procedure given by: M.A. Pericas, F. Serratosa, and E. Valenti. Tetrahedron, **43**, 2311 (1987).
13. E.J. Corey and G. Schmidt. Tetrahedron Lett. 399 (1979).
14. D. Swern. J. Org. Chem. **43**, 2480 (1978).
15. E.J. Corey and C.U. Kim. J. Am. Chem. Soc. **94**, 7586 (1972).
16. D.B. Dess and J.C. Martin. J. Org. Chem. **48**, 4156 (1983).
17. J.R. Parikh and W. von E. Doering. J. Am. Chem. Soc. **89**, 5505 (1967).
18. B.E. Maryanoff, A.B. Reitz, and B.A. Duhl-Emswiler. J. Am. Chem. Soc. **107**, 217 (1985).
19. L. Ramberg and B. Bäcklund. Arkiv. Kemi. Mineral. Geol. **13A**, No. 27 (1940); Chem. Abstr. **34**, 4725 (1940).
20. L.A. Paquette. Acc. Chem. Res. **1**, 209 (1968).
21. L.A. Paquette. Org. React. (N.Y.) **25**, 1 (1977).
22. L.A. Paquette and L.S. Wittenbrook. J. Am. Chem. Soc. **90**, 6783 (1968).
23. For a review see: R.J.K. Taylor. J. Chem. Soc. Chem. Commun. 217 (1999).
24. K.C. Nicolaou, G. Zuccarello, Y. Ogawa, E.J. Schweiger, and T. Kumazawa. J. Am. Chem. Soc. **110**, 4866 (1988).
25. R.K. Boeckman, Jr., S.K. Yoon, and D.K. Heckendorn. J. Am. Chem. Soc. **113**, 9682 (1991).
26. K. Mlinariæ-Majerski, D. Pavloviæ, and Z. Mariniæ. Tetrahedron Lett. **37**, 4829 (1996).
27. E. Alverez, M.T. Diaz, L. Hanxing, and J.D. Martin. J. Am. Chem. Soc. **117**, 1437 (1995).
28. H.C. Brown, Y.M. Choi, and S. Narasimhan. J. Org. Chem. **47**, 3153 (1982).
29. A. Singh, A. Mehrotra, and S.L. Regen. Synth. Commun. **11**, 409 (1981).
30. P.G. Gassman, S.M. Bosner, and K. Mlinariæ-Majerski. J. Am. Chem. Soc. **111**, 2652 (1989).
31. V. VanReehan, R.C. Kelly, and D.Y. Chu. Tetrahedron Lett. 1973 (1976).
32. J.A. Marshall, L.J. Karas, and M.J. Coghlan. J. Org. Chem. **47**, 699 (1982).
33. J.A. Marshall, R.C. Andrews, and L. Lebioda. J. Org. Chem. **52**, 2378 (1987).
34. M.G. Martin and B. Ganem. Tetrahedron Lett. **25**, 251 (1984).

© 2000 NRC Canada

An unusually large secondary α-deuterium kinetic isotope effect in hydride ion S_N2 reactions

Terry Koerner, Kenneth Charles Westaway, Raymond A. Poirier, and Y. Wang

Abstract: Theoretical calculations at the HF/6–31+G* level suggest the secondary α-deuterium kinetic isotope effects for hydride ion S_N2 reactions are much larger than expected for the structure of the transition state. The secondary α-deuterium kinetic isotope effects for the S_N2 reactions between sodium borohydride (hydride ion) and *para*-methyl- and *para*-chlorobenzyl chlorides are much larger than expected as the theoretical calculations suggest. It appears the secondary α-deuterium isotope effects are larger than expected for the structure of the S_N2 transition state because the hydride ion is too small to affect the C_α—H(D) out-of-plane bending vibrations in the transition state.

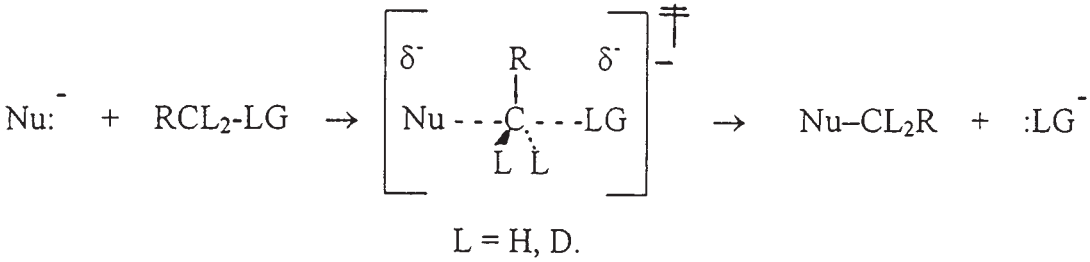
Key words: secondary α-deuterium kinetic isotope effects, S_N2, nucleophilic substitution, transition state, substituent effects.

Résumé : Des calculs théoriques au niveau HF/6–31+G* suggèrent que les effets isotopiques cinétiques secondaires des atomes deutérium en α dans les réactions S_N2 des ions hydrures sont beaucoup plus importants que ceux auxquels on pourrait s'attendre à partir de la structure de l'état de transition. Les effets isotopiques cinétiques secondaires des atomes deutérium en α dans les réactions S_N2 entre le borohydrure de sodium (ion hydrure) et les chlorures de *para*-méthyl- et *para*-chlorobenzyles sont beaucoup plus élevés que ceux auxquels on pourrait s'attendre sur la base des calculs théoriques. Il semble que les effets isotopiques cinétiques secondaires des atomes deutérium en α sont beaucoup plus élevés que ceux auxquels on pourrait s'attendre sur la base de l'état de transition S_N2 en raison du fait que l'ion hydrure est beaucoup trop petit pour affecter les vibrations de déformation hors-plan C_α—H(D) dans l'état de transition.

Mots clés : effets isotopiques cinétiques secondaires des atomes deutérium en α, S_N2, substitution nucléophile, état de transition, effets de substituant.

Introduction

In a theoretical study of the secondary α-deuterium kinetic isotope effects (KIEs) for S_N2 reactions, eq. [1], by Poirier et al., (1) the KIE was expressed as the

[1] 

product of a translational, a rotational, a vibrational, and a tunneling term (eq. [2]).

[2] $(k_H/k_D)_\alpha = (k_H/k_D)_{trans}\ (k_H/k_D)_{rot}\ (k_H/k_D)_{vib}\ (k_H/k_D)_{tunnelling}$

Received November 10, 1999. Published on the NRC Research Press website on July 31, 2000.

T. Koerner and K.C. Westaway.[1] Department of Chemistry and Biochemistry, Laurentian University, Sudbury, ON P3E 2C6, Canada.
R.A. Poirier[1] **and Y. Wang.** Department of Chemistry, Memorial University of Newfoundland, St. John's, NF A1B 3X7, Canada.

[1]Authors to whom correspondence may be addressed. KCW: Fax: (705) 675–4844. e-mail: Kwestawa@Nickel.Laurentian.Ca; RAP: Fax: (709) 737–3702. e-mail: Rpoirier@morgan.ucs.mun.ca

 © 2000 NRC Canada

Table 1. A comparison of the bending and stretching contributions to the secondary α-deuterium KIE for hydride ion and other nucleophiles with a similar nucleophile-leaving group distance in the transition state.

	Methyl chloride			Methyl fluoride		
	OH^-	H^-	% Difference	F^-	H^-	% Difference
$(k_H/k_D)_\alpha$	0.907	0.983	8.4	0.846	1.013	20.0
Nu···LG distance (Å)	4.37	4.32	1.1	3.69	3.65	1.1
$(k_H/k_D)_{stretching}$	0.714	0.707	1.0	0.677	0.653	3.5
$(k_H/k_D)_{bending}$	1.112	1.288	15.9	0.978	1.389	42.0

The vibrational term was factored into three terms (eq. [3]),

$$[3] \quad (k_H/k_D)_{vib} = (k_H/k_D)_{stretching}\,(k_H/k_D)_{bending}\,(k_H/k_D)_{other}$$

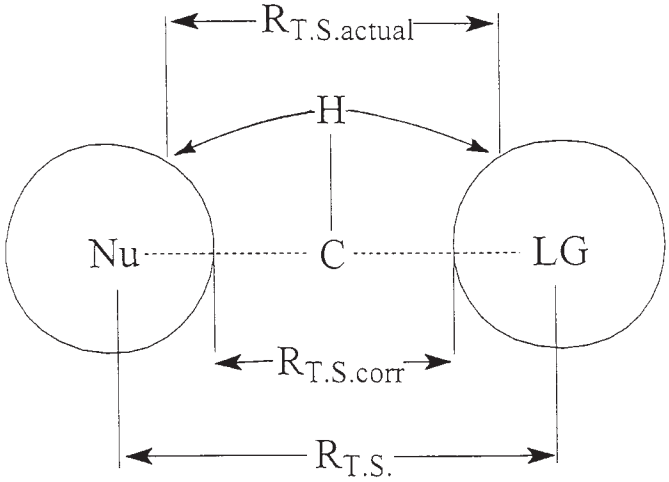
where $(k_H/k_D)_{stretching}$ is due to the changes that occur in the three C_α—H(D)stretching vibrations, $(k_H/k_D)_{bending}$ is the contribution due to the changes that occur in the seven C_α—H(D) bending (primarily the out-of-plane bending) vibrations, and $(k_H/k_D)_{other}$ is due to the changes that occur in the other vibrations, when the reactant is converted into the S_N2 transition state (1). The $(k_H/k_D)_{stretching}$ and $(k_H/k_D)_{bending}$ contributions to the KIE were calculated to determine how these vibrations affected the magnitude of the secondary α-deuterium KIE and to determine how the $(k_H/k_D)_{stretching}$ and $(k_H/k_D)_{bending}$ contributions to the KIE were related to the structure of the S_N2 transition state. The initial study (1) showed that the large and inverse stretching component of the KIEs was constant, but different, for each leaving group. For example, the stretching component of the secondary α-deuterium KIE for the S_N2 reactions between several nucleophiles and methyl chloride or methyl fluoride, were $(k_H/k_D)_{stretching}$ = 0.701 ± 0.014 and 0.677 ± 0.013, respectively. The bending contributions to the KIE on the other hand, varied markedly with the nucleophile and the nucleophile-leaving group (Nu···LG) distance ($R_{T.S.}$) in the transition state[2]. For instance, the $(k_H/k_D)_{bending}$ varied from 1.098 to 1.221 in the methyl chloride reactions and from 0.978 to 1.215 in the methyl fluoride reactions.

Since the $(k_H/k_D)_{stretching}$ contribution to the KIE is constant for a particular leaving group, the magnitude of both the total KIE and the bending contribution to the KIE were related to the Nu···LG distance in the S_N2 transition state (1) (Fig. 2).

Results and discussion

When the calculations described above were extended to the secondary α-deuterium KIEs for both the methyl chloride and methyl fluoride S_N2 reactions with hydride ion, the results showed that the hydride ion KIEs were significantly larger than expected, i.e., the KIE was much larger than expected given the Nu···LG distance in the transition state (Fig. 3).

Fig. 1. The relationship between $R_{T.S}$, $R_{T.S.corr}$, and $R_{T.S.actual}$ for the C_α—H(D) bending vibrations in the S_N2 transition state.

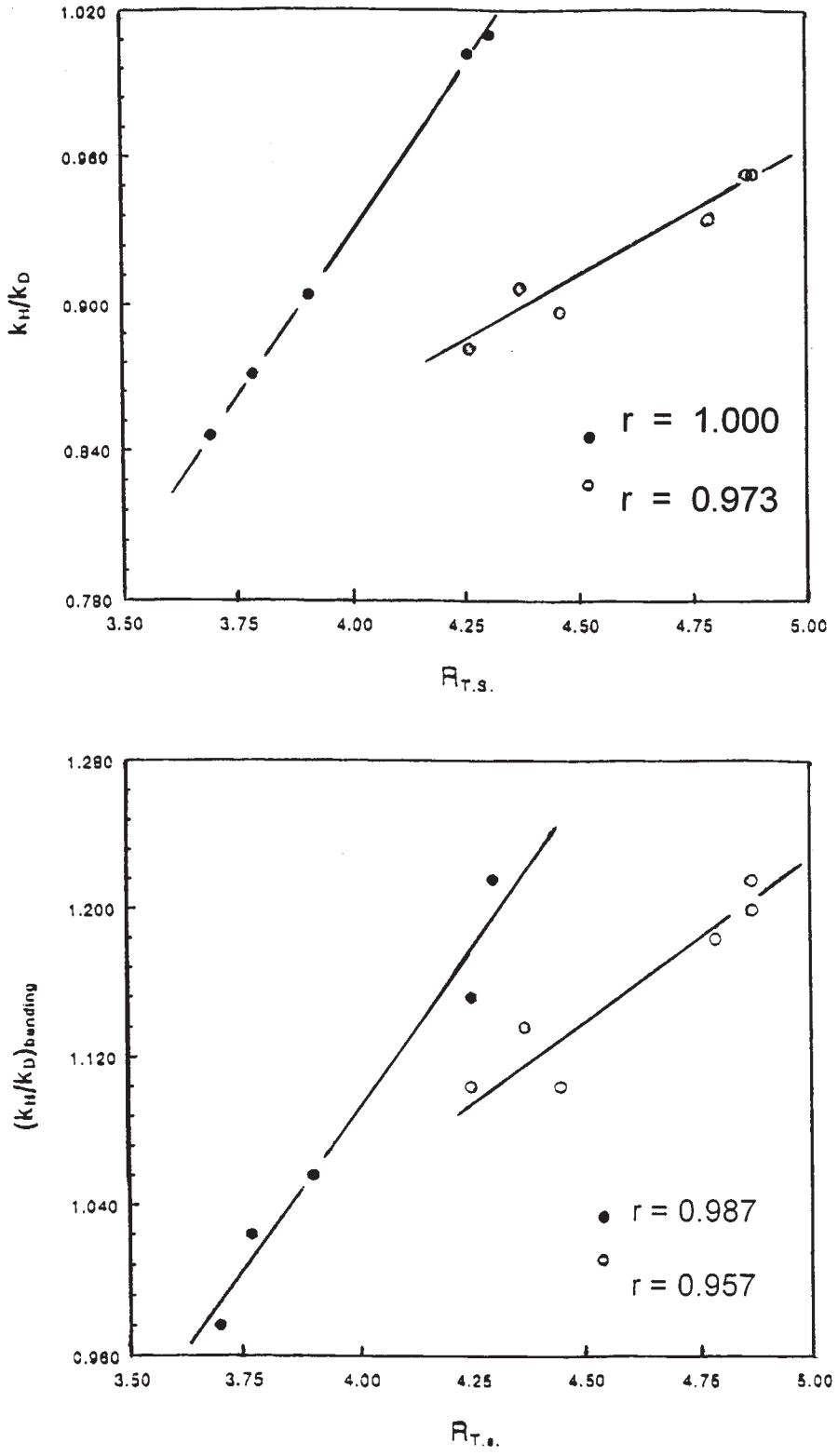


The results (Table 1) show that the KIE for the methyl chloride reaction with hydride ion is 8.4% larger (less inverse) than the hydroxide ion reaction that has an almost identical (4.37 rather than 4.32 Å) Nu···LG distance. In the methyl fluoride S_N2 reactions, the KIE for the hydride ion reaction is 20% larger than the KIE for the fluoride ion (identity reaction) even though both reactions have almost identical (3.65 vs. 3.69 Å) Nu···LG distances in the transition state. The stretching and bending contributions to the KIEs for the methyl chloride and methyl fluoride reactions with hydride ion were calculated in an effort to understand why the hydride ion reaction KIEs were so large. The stretching contribution to the methyl chloride and methyl fluoride reactions with hydride ion are virtually identical to those found for the reactions with other nucleophiles, i.e., the stretching vibration contribution to the KIEs for the H^- and OH^- reactions with methyl chloride and for the H^- and F^- reactions with methyl fluoride only differ by 1.0 and

[2] Glad and Jensen (2) suggested that the Nu···LG (internuclear) distance ($R_{T.S.}$) is not the correct parameter to use but that the Nu···LG distance minus the radius of both the nucleophile and the leaving group atoms ($R_{T.S.corr}$) should be used for determining the energy of the bending vibrations (the magnitude of the secondary α-deuterium KIE). We tried correlating the calculated KIE with $R_{T.S.corr}$ before publishing our first paper (1) but found the relationship between the $(k_H/k_D)_\alpha$ and $R_{T.S.corr}$ was worse than the correlation between $(k_H/k_D)_\alpha$ and $R_{T.S.}$ A possible explanation for this is that the α-hydrogen only approaches the nucleophile and the leaving group in the C_α—H(D) bending vibration approximately 0.8 Å above the internuclear axis joining the nucleophile, the α-carbon and the leaving group in the S_N2 transition state (Fig. 1). The curvature of the surfaces of the spherical nucleophile and leaving group nucleophilic atoms means $R_{T.S.actual}$ (the space available for the C_α—H(D) out-of-plane bending vibrations in the transition state) is greater than $R_{T.S.corr}$ and the higher correlation with $R_{T.S.}$ suggests $R_{T.S.actual}$ is closer to $R_{T.S.}$ than to $R_{T.S.corr}$.

© 2000 NRC Canada

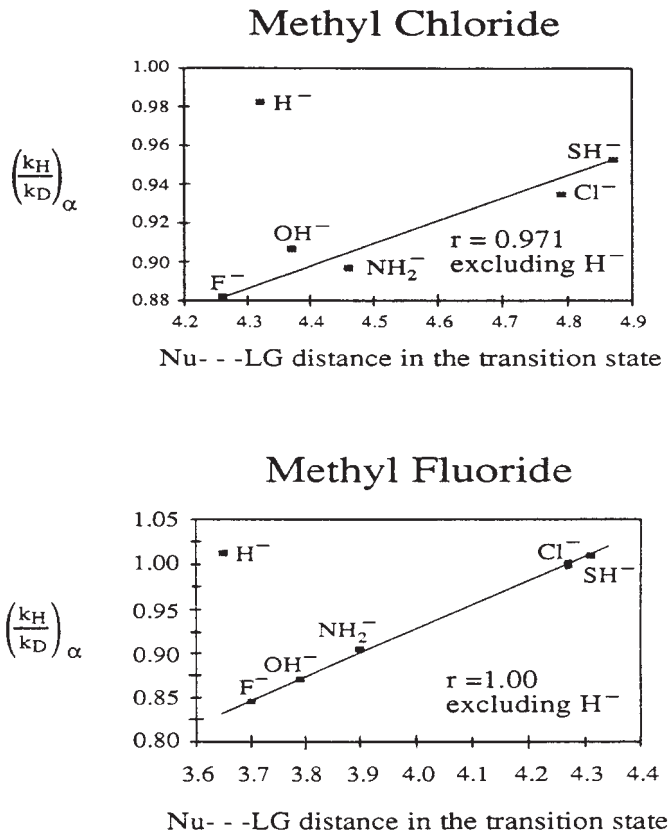
Fig. 2. The total KIE (curve a) and the bending vibration contribution to the KIE (curve b) vs. $R_{T.S.}$ for the S_N2 reactions of methyl chloride and methyl fluoride with various nucleophiles. The open circles are for the methyl chloride reactions and the solid circles are for the methyl fluoride reactions.



3.5%, respectively (Table 1). The major difference between the KIEs with the almost identical Nu···LG distances in the transition state, is due to the bending contribution to the KIE, i.e., the bending contribution to the H^- KIE is 15.9% larger than the bending contribution to the OH^- KIE when the substrate is methyl chloride. The effect is even more

© 2000 NRC Canada

Fig. 3. The secondary α-deuterium KIE as a function of the Nu···LG distance in the transition states for the S_N2 reactions of methyl chloride and methyl fluoride with various nucleophiles.



dramatic for the methyl fluoride reactions. Here, the bending contribution to the H^- KIE is 42.0% larger than the bending contribution to the F^- KIE.

The larger bending vibration contribution to the H^- KIEs obviously occurs because the zero-point energy difference in the C_α—H(D) out-of-plane bending vibrations is lower than expected in the S_N2 transition state (Fig. 4). The unusually large $(k_H/k_D)_{bending}$ contribution to the KIE means the C_α—H(D) bending vibrations in the transition state are low energy. One possible explanation for this is that the hydride ion is too small to affect the C_α—H(D) vibrations in the transition state (Fig. 5), i.e., the hydride ion is too small to sterically hinder the C_α—H(D) out-of-plane bending vibrations. This means the bending vibrations are low energy, the ZPE difference in the transition state is smaller than expected, and the KIE is larger than expected. It is interesting to note that the effect of the small hydride ion is greater in the methyl fluoride reactions which have a shorter Nu···LG distance in the transition state. Removing the effect of the hydride in a tighter transition state would be expected to have a greater effect on the C_α—H(D) out-of-plane bending vibrations and, therefore, on the KIE.

Fig. 4. A reaction coordinate diagram for an S_N2 reaction with low energy out-of-plane bending vibrations in the transition state.

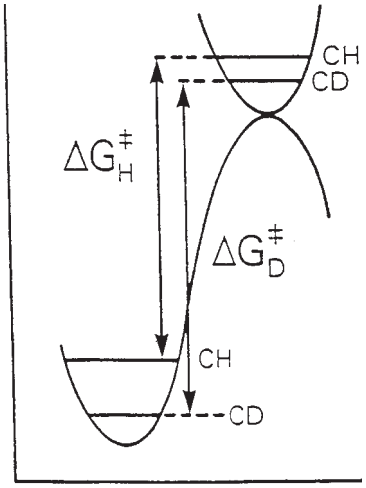
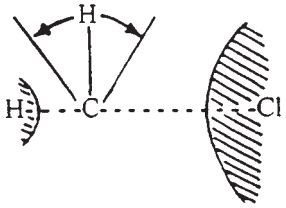


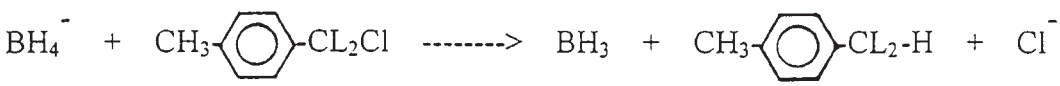
Fig. 5. The transition state for the hydride ion S_N2 reactions showing that the hydride ion is too small to affect the C_α—H(D) out-of-plane bending vibrations.



Although the above rationale for the larger secondary α-deuterium KIEs in the hydride ion reactions seems reasonable, experimental confirmation of this phenomenon is needed. The secondary α-deuterium KIE for the S_N2 reaction between sodium borohydride (hydride ion) and *para*-methylbenzyl chloride (eq. [4]), was determined to learn whether the KIE for the hydride ion reaction was, indeed, larger than expected.

Three labelled and three unlabelled reactions were done simultaneously. The three rate constants (3) for the unlabelled (k_H) and labelled (k_D) substrates were averaged and divided to obtain the secondary α-deuterium KIE. Each KIE was determined twice and all the second order (first order in $BH4^-$ and in substrate) kinetic plots were linear to at least 90% of completion and had correlation coefficients ≥0.998.

The average secondary α-deuterium KIE at 30.000 ± 0.002°C (Table 2), is 1.091 ± 0.002 or approximately 1.044/$_{\alpha\text{-D}}$. The $(k_H/k_D)_\alpha$ per α-deuterium for a carbenium ion S_N reaction of an alkyl chloride where the first step is fully rate-determining, is 1.11 (4–6). If dissociation of the intimate ion pair or formation of the free carbocation is rate-determining, the $(k_H/k_D)_\alpha$ would be approximately 1.15 per α-deuterium (5). The much smaller secondary α-deuterium KIE of



[4]

L = H, D

© 2000 NRC Canada

Table 2. The average rate constants and secondary α-deuterium KIEs for the sodium borohydride S_N2 reactions with *p*-methylbenzyl chloride in DMSO at 30.000 ± 0.002°C.

$k_H \times 10^3$	$k_D \times 10^3$	$(k_H/k_D)_\alpha$	$(k_H/k_D)/_{\alpha\text{-D}}$
1.735 ± 0.015[a]	1.595 ± 0.004[a]	1.088 ± 0.010[b]	1.043
1.698 ± 0.003	1.553 ± 0.017	1.093 ± 0.012	1.045
	Average	1.091 ± 0.002[c]	1.044

[a]Standard deviation for three separate kinetic runs.

[b]The error is $1/k_D[(\Delta k_H)^2 + (k_H/k_D)^2 \times (\Delta k_D)^2]^{1/2}$, where Δk_H and Δk_D are the standard deviations for the average rate constants for the reactions of the undeuterated and deuterated nucleophiles, respectively.

[c]Standard deviation.

Table 3. The average rate constants and secondary α-deuterium KIEs for the sodium borohydride S_N2 reactions with *p*-chlorobenzyl chloride in DMSO at 30.000 ± 0.002°C.

$k_H \times 10^3$	$k_D \times 10^3$	$(k_H/k_D)_\alpha$	$(k_H/k_D)/_{\alpha\text{-D}}$
1.806 ± 0.012[a]	1.655 ± 0.009[a]	1.091 ± 0.009[b]	1.045
1.640 ± 0.009	1.502 ± 0.002	1.092 ± 0.006	1.045
	Average	1.092 ± 0.001[c]	1.045

[a]Standard deviation for three separate kinetic runs.

[b]The error is $1/k_D[(\Delta k_H)^2 + (k_H/k_D)^2 \times (\Delta k_D)^2]^{1/2}$, where Δk_H and Δk_D are the standard deviations for the average rate constants for the reactions of the undeuterated and deuterated nucleophiles, respectively.

[c]Standard deviation.

$1.044/_{\alpha\text{-D}}$ found in this study, confirms that the reaction is an S_N2 process.

The secondary α-deuterium KIE = 1.091 or $1.044/_{\alpha\text{-D}}$ found for this reaction is near the maximum secondary α-deuterium KIE = $1.06/_{\alpha\text{-D}}$ found for an S_N2 reaction of an alkyl chloride (7–11). Thus, the hydride ion KIE is large. However, interpreting the KIE is difficult. Two explanations are possible. One possibility is that the large secondary α-deuterium KIE of 1.091 means that the transition state is loose, and symmetric, with long nucleophile—α- carbon *and* α-carbon—leaving group bonds. A large KIE would be observed in this case because the C_α—H(D) out-of-plane bending vibrations will be low energy in the transition state.

The second possibility is that the hydride ion – *p*-methylbenzyl chloride reaction has an unsymmetric transition state and an unusually large secondary α-deuterium KIE. Westaway et al. (12) suggested that some benzyl substrates react via an unsymmetric S_N2 transition state. In all the reactions where unsymmetric S_N2 transition states have been characterized in enough detail so that one knows the relative lengths of the nucleophile—α-carbon and the α- carbon—leaving group bonds in the transition state, the stronger reacting bond has always been short and the weaker reacting bond has been long. Since the H—C bond is much stronger than the C_α—Cl bond (the stretching frequencies are 2960 and 650 cm^{-1}, respectively), (13) an unsymmetric transition state should have a short H—C_α and a long C_α—Cl bond. If this is the case, one would expect a very small secondary α-deuterium KIE because the out-of-plane bending vibrations in the transition state will be determined by only the out-of-plane bending vibrations to the short reacting bond (12). In fact, the secondary α-deuterium KIEs in reactions with unsymmetric S_N2 transition states are all small because the out-of-plane bending vibrations in the reactant or the product and in the transition state are similar (12). In fact, this behaviour has been found experimentally. For instance, in the *p*-substituted benzyl chloride – cyanide ion reactions and in the cyanide ion – *m*-chlorobenzyl-*p*-substituted benzyl benzenesulphonate reactions which are believed to have unsymmetric S_N2 transition states, the secondary α-deuterium KIEs are small, i.e., they range from 1.008 to 1.011 and from 1.009 to 1.028, respectively (12, 14). Therefore, if the hydride ion – *p*-methylbenzyl chloride transition state is unsymmetric with a short H—C_α bond, one would expect a small secondary α-deuterium KIE to be found. The observed KIE of 1.091, which is near the maximum possible secondary α-deuterium KIE for an alkyl chloride, would be unusually large as the theoretical calculations suggest.

The problem then, is to determine whether the KIE is large because the S_N2 transition state is loose but symmetric or unsymmetric with a short H—C_α bond in the transition state. Westaway et al. (12) proposed that one could determine the symmetry of the S_N2 transition state if one varied a substituent on the benzene ring of the substrate. If the transition state is symmetric, the structure of the transition state and therefore, the KIE, would change with a change in substituent. If, on the other hand, the transition state was unsymmetric with a short H—C_α bond, changing the substituent on the benzene ring of the substrate would not alter the stronger H—C_α transition state bond significantly (the Bond Strength Hypothesis (15)) and therefore, the KIE, which is determined by the short H—C_α bond, will not change with substituent, i.e., the change in the long C_α—Cl transition state bond will occur too far away to affect the C_α—H(D) out-of-plane bending vibrations in the transition state (the KIE).

The secondary α-deuterium KIE for the S_N2 reaction between *p*-chlorobenzyl chloride and sodium borohydride was determined to learn if the S_N2 transition state was symmetric or unsymmetric. The secondary α-deuterium KIE of 1.092 ± 0.001 (Table 3), for the *p*-chlorobenzyl chloride hydride ion reaction at 30.000 ± 0.002°C is identical to the KIE = 1.091 ± 0.002 for the reaction with *p*-methylbenzyl chloride. Therefore, these S_N2 transition states must be unsymmetric with short H—C_α and long C_α—Cl transition state bonds.

Since the H—C_α bond is short in the S_N2 transition states of hydride ion reactions, one would expect the secondary α-deuterium KIE to be small (vide supra). However, the secondary α-deuterium KIE is large. The experimental KIEs, therefore, are larger than expected, presumably because the hydride ion in the transition state is too small to affect the C_α—H(D) out-of-plane bending vibrations (Fig. 5). This means the C_α—H(D) out-of-plane bending vibrations will be very low energy in the transition state of any hydride ion S_N2 reaction and therefore, the KIE will be much larger than one would expect given the H—C_α or Nu···LG distance in the S_N2 transition state.

Experimental

The *p*-methylbenzyl- and *p*-chlorobenzyl chlorides (Aldrich) were distilled before use. The preparation of the *p*-methyl- and *p*-chloro-1,1-d_2-benzyl chlorides has been described

© 2000 NRC Canada

previously (9). The description of the kinetic method used to measure the rate constants is described in ref. (3). The details of the theoretical calculations are given in ref. (1).

Acknowledgement

The authors wish to thank the Natural Sciences and Engineering Research Council of Canada (NSERC) for the funding that allowed this work to be completed.

References

1. R.A. Poirier, Y. Wang, and K.C. Westaway. J. Am. Chem. Soc. **116**, 2526 (1994).
2. S.S. Glad and F. Jensen. J. Am. Chem. Soc. **119**, 227 (1997).
3. K.C. Westaway, T. Koerner, Y.-R. Fang, J. Rudzinski, and P. Paneth. Anal. Chem. **70**, 3548 (1998).
4. V.J. Shiner, Jr. *In* Isotope effects in chemical reactions.. A.C.S. Publication 167. *Edited by* C.J. Collins and N.S. Bowman. Van Nostrand Rheinhold, New York. 1970. pp. 90–159.
5. V.J. Shiner, Jr., M.W. Rapp, E.A. Halevi, and M. Wolfsberg. J. Am. Chem. Soc. **90**, 7171 (1968).
6. K.C. Westaway. *In* Isotopes in organic chemistry. *Edited by* E. Buncel and C.C. Lee. Elsevier Science Publishing Comp. Inc., New York. 1987. p. 312.
7. K.M. Koshy and R.E. Robertson. J. Am. Chem. Soc. **96**, 914 (1974).
8. H. Strecker and H. Elias. Chem. Ber. **102**, 1270 (1969).
9. K.C. Westaway and Z. Waszczylo. Can. J. Chem. **60**, 2500 (1982).
10. K.C. Westaway and Z. Lai. Can. J. Chem. **66**, 1263 (1988).
11. K.C. Westaway. *In* Isotopes in organic chemistry. *Edited by* E. Buncel and C.C. Lee. Elsevier Science Publishing Comp. Inc., New York. 1987. pp. 313–319.
12. K.C. Westaway, T.V. Pham, and Y. Fang. J. Am. Chem. Soc. **119**, 3670 (1997).
13. J. Dyer. *In* Application of absorption spectroscopy of organic compounds. Prentice–Hall, Englewood Cliffs, N.J. 1965. pp. 25–36.
14. K.C. Westaway, Y.-R. Fang, J. Persson, and O. Matsson. J. Am. Chem. Soc. **120**, 3440 (1998).
15. K.C. Westaway. Can. J. Chem. **71**, 2084 (1993).

© 2000 NRC Canada

CP/MAS NMR and X-ray crystallographic characterization of *trans*-$PdX_2(PPh_2vinyl)_2$ (X = Cl, I); UV and $Et_2O{\cdot}BF_3$ reaction studies, including the formation of $[Pd(\mu\text{-}Cl)(PPh_2vinyl)_2]_2[BF_4]_2$

Michael B. Hursthouse, David G. Kelly, Mark E. Light, and Andrew J. Toner

Abstract: The complexes $PdCl_2(PPh_2vinyl)_2$ and $PdI_2(PPh_2vinyl)_2$ have been prepared and crystallographically characterized as their *trans* square planar isomers. *Trans*-$PdCl_2(PPh_2vinyl)_2$ exists in a centrosymmetric structure with a planar $PdCl_2P_2$ core whereas *trans*-$PdI_2(PPh_2vinyl)_2$ shows no local Pd-centred symmetry and significant distortion of the PdI_2P_2 core from planarity. Crystallographic data is in accord with the $^{31}P\{^1H\}$ CP/MAS NMR spectra of the two complexes, which display a single resonance for the chloro-complex and two resonances for the iodo-complex. UV irradiation of CH_2Cl_2 solutions of $PdCl_2(PPh_2vinyl)_2$ followed by re-dissolution in $CDCl_3$ indicates no permanent chemical change. However, post-irradiation CP/MAS $^{31}P\{^1H\}$ NMR spectroscopy demonstrates the presence of *trans*-$PdCl_2(PPh_2vinyl)_2$ in two solid state structures, plus *cis*-$PdCl_2(PPh_2vinyl)_2$. $PdI_2(PPh_2vinyl)_2$ exists only in its *trans* form in both solid state and solution. Irradiation results in phosphine displacement and the formation of *sym*-$[PdI_2(PPh_2vinyl)]_2$ and free phosphine, the latter being characterized as $Ph_2P(O)$vinyl following aerobic oxidation. $PdCl_2(PPh_2vinyl)_2$ reacts in the presence of $Et_2O{\cdot}BF_3$ to afford $[Pd(\mu\text{-}Cl)(PPh_2vinyl)_2]_2[BF_4]_2$ whereas $PdI_2(PPh_2vinyl)_2$ is recovered in 95% yield, with the remaining material undergoing phosphine abstraction to form *sym*-$[PdI_2(PPh_2vinyl)]_2$.

Key words: palladium, phosphine, alkene, isomerization, CP/MAS.

Résumé : On a préparé les complexes $PdCl_2(PPh_2vinyl)_2$ et $PdI_2(PPh_2vinyl)_2$ et sur la base de la cristallographie, on a établi qu'il s'agit des isomères plans carrés *trans*. Le *trans*-$PdCl_2(PPh_2vinyl)_2$ existe dans une structure centrosymétrique comportant une unité centrale $PdCl_2P_2$ plane alors que le *trans*-$PdI_2(PPh_2vinyl)_2$ est fortement déformé par rapport à la planéité. Les données cristallographiques sont en accord avec le spectre RMN CP/MAS du $^{31}P\{^1H\}$ des deux complexes qui ne présentent qu'une seule résonance pour le complexe chloré et deux résonances pour le complexe iodé. L'irradiation UV de solutions de CH_2Cl_2 du complexe $PdCl_2(PPh_2vinyl)_2$ suivie d'une redissolution dans le $CDCl_3$ indique qu'il n'y a pas de changement chimique permanent. Toutefois, la spectroscopie RMN CP/MAS du $^{31}P\{^1H\}$ démontre la présence de *trans*-$PdI_2(PPh_2vinyl)_2$ dans deux structures à l'état solide en plus de *cis*-$PdI_2(PPh_2vinyl)_2$. Le $PdI_2(PPh_2vinyl)_2$ n'existe que dans sa forme *trans* tant à l'état solide qu'en solution. L'irradiation provoque un déplacement de la phosphine et la formation de *sym*-$[PdI_2(PPh_2vinyl)]_2$ et de phosphine libre; cette dernière est caractérisée sous la forme de $Ph_2P(O)$vinyl après une oxydation aérobique. Le *trans*-$PdCl_2(PPh_2vinyl)_2$ réagit en présence de $Et_2O{\cdot}BF_5$ pour conduire à la formation de $[Pd(\mu\text{-}Cl)(PPh_2vinyl)_2]_2[BF_4]_2$ alors que le $PdI_2(PPh_2vinyl)_2$ est récupéré avec un rendement de 95%, le reste du produit subissant une abstraction de phosphine avec formation de la *sym*-$[PdI_2(PPh_2vinyl)]_2$.

Mots clés : palladium, phosphine, alcène, isomérisation, CP/MAS.

[Traduit par la Rédaction]

Introduction

Increasing interest exists in the formation of high molecular weight materials from metal complexes and the incorporation of such complexes into organic polymers. Pendant alkene moieties incorporated into phosphine ligands and their complexes have demonstrated polymerization in the presence of UV radiation and Lewis acids (1, 2). The potential for similar polymerization or alternative metal-centred reaction pathways is assessed in the present work for palladium(II) complexed diphenylvinylphosphine. Palladium(II) readily forms PdX_2P_2 (X = halide, *P* = tertiary phosphine) complexes with monodentate and bidentate phosphines. These complexes have formed the focus of numerous studies as a vehicle for probing *cis*/*trans* isomerization (3) and

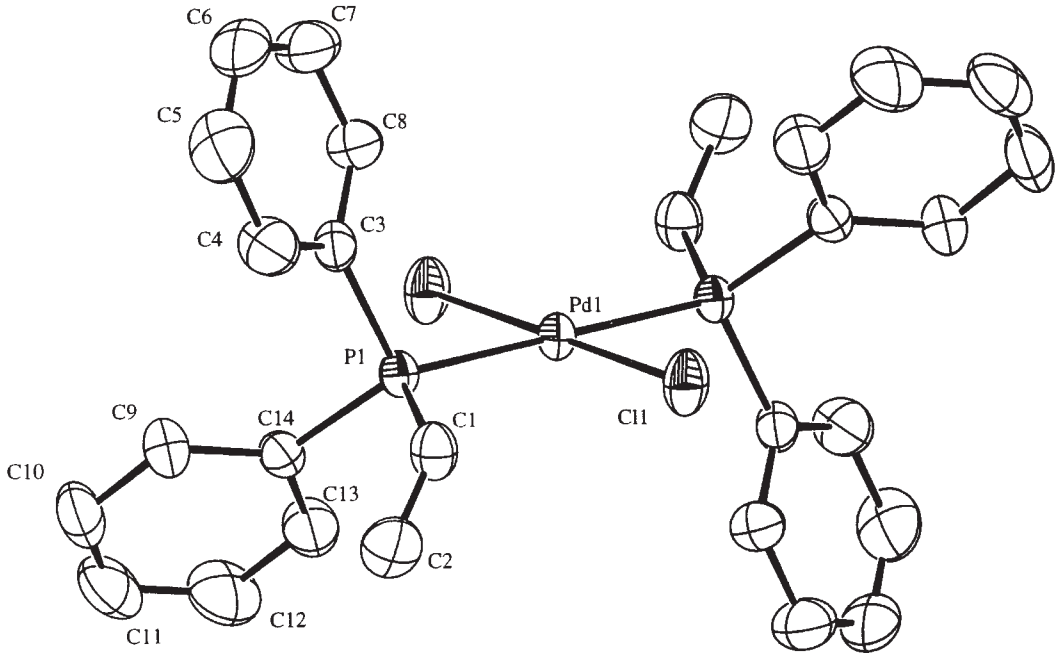
Received February 7, 2000. Published on the NRC Research Press website on August 11, 2000.

M.B. Hursthouse and M.E. Light. Department of Chemistry, University of Southampton, Highfield, Southampton, SO17 1BJ, U.K.
D.G. Kelly[1] and A.J. Toner. Department of Chemistry and Materials, The Manchester Metropolitan University, Chester Street, Manchester M1 5GD, U.K.

[1]Author to whom correspondence may be addressed. Telephone: (+44) 161 247 1425. Fax: (+44) 161 247 6357. e-mail: d.g.kelly@mmu.ac.uk

© 2000 NRC Canada

Fig. 1. Single crystal X-ray diffraction structure of *trans*-$PdCl_2(PPh_2vinyl)_2$.



ligand/anion exchange processes (4), and as potential stoichiometric and catalytic reagents in synthesis (5). The principal modes of characterization have been solution $^{31}P\{^1H\}$ NMR spectroscopy and single crystal X-ray diffraction studies. The former technique demonstrates that monodentate phosphine complexes generally exist as *cis*/*trans* mixtures in solution, although modification of P and X can lead to the *trans* isomer being overwhelmingly thermodynamically favored (6). Crystallization generally leads to the isolation of *trans* complexes; indeed 45 of the 55 reported PdX_2P_2 single crystal X-ray diffraction structures of monodentate phosphine complexes are of the *trans* isomer.[2] Solid state distortion from square planar geometries in these crystallographic studies is known but is not universal. In contrast, such distortion is not observed by solution $^{31}P\{^1H\}$ NMR spectroscopy.

Cross-polarization magic-angle-spinning (CP/MAS) NMR spectroscopy offers an increasingly available and complementary characterization technique that probes the solid state structure of non-crystalline materials. The study of solid samples by conventional NMR apparatus and experiments yields at best broad signals or a rolling baseline. Two principal factors contribute to this uninformative data; dipole-dipole nucleur interactions and chemical shift anisotropy (CSA). The former is removed in solution by molecular motion, which is sufficiently rapid to afford an averaged molecular orientation and thus zero local field. The effect of CSA, the directional influence of chemical bonds on nucleur shielding, is reduced to zero by the same motion in solution. Both factors vary in magnitude as a function of $3\cos^2\theta - 1$, where θ is the orientation to the applied field. Thus, spinning samples at a frequency larger than the CSA linewidth (usually a few kilohertz), and at an angle where the term $3\cos^2\theta - 1$ becomes zero (54° 44′) allows the observation of sharp solid state spectra. Such 'magic angle spinning' when coupled with the sensitivity enhancement of cross polarization provides effective and informative solid state NMR data. In the present study we have investigated the solid state and solution chemistry of the PdX_2P_2 complexes (X = Cl, I; *P* = PPh_2vinyl) as part of our recent studies of bifunctional phosphine/alkene ligands (7, 8). The reported solution NMR data for these complexes are supplemented here by crystallographic characterization, and by CP/MAS NMR spectroscopy (9). Reactivity initiated by UV irradiation and in the presence of Lewis acids has also been considered.

Results and discussion

Synthesis and characterization of $PdX_2(PPh_2vinyl)_2$ (X = Cl, I)

Synthesis of $PdCl_2P_2$ complexes (*P* = tertiary phosphine) is well established and readily achieved by the reaction of $PdCl_2(PhCN)_2$ with two equivalents of tertiary phosphine. Iodide complexes may be isolated in high yield by metathesis of the respective chloride with excess aqueous NaI (9). The utilization of such synthetic routes and subsequent recrystallization from diethylether–dichloromethane affords crystalline $PdCl_2(PPh_2vinyl)_2$ and $PdI_2(PPh_2vinyl)_2$ in high yield. Crystals of both $PdCl_2(PPh_2vinyl)_2$ and $PdI_2(PPh_2vinyl)_2$ proved suitable for single crystal X-ray diffraction studies, with structure elucidation demonstrating the formation of *trans* square planar $PdCl_2(PPh_2vinyl)_2$ and $PdI_2(PPh_2vinyl)_2$ (Figs. 1 and 2, respectively).

Metal-centred bond lengths and angles for $PdCl_2(PPh_2vinyl)_2$ indicate a centrosymmetric and therefore planar $PdCl_2P_2$ core, with Cl-Pd-Cl and P-Pd-P vectors being almost orthogonal (Table 1). In contrast, no local Pd-centred

[2] CCDC Data Base Search. Cambridge, U.K. December 1999.

© 2000 NRC Canada

Fig. 2. Single crystal X-ray diffraction structure of *trans*-$PdI_2(PPh_2vinyl)_2$.

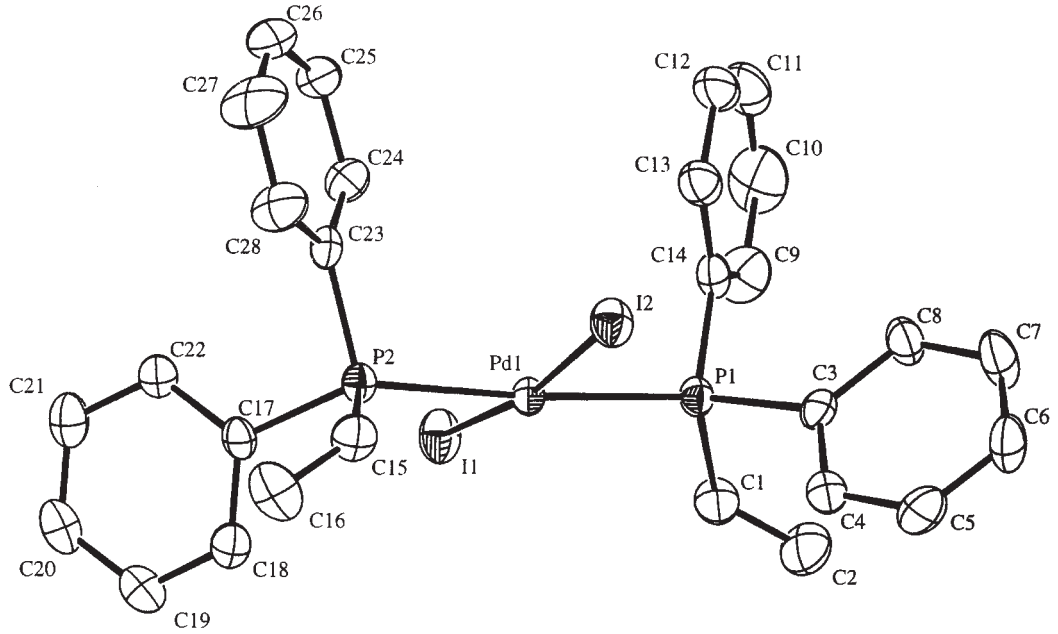


Table 1. Bond lengths and angles for *trans*-$PdCl_2(PPh_2vinyl)_2$ and *trans*-$PdI_2(PPh_2vinyl)_2$.

Bond lengths (Å) and angles (°)[a]	*trans*-$PdCl_2$-$(PPh_2vinyl)_2$	*trans*-PdI_2-$(PPh_2vinyl)_2$	$[Pd(\mu\text{-}Cl)(PPh_2$-$vinyl)_2]_2[BF_4]_2$
Pd—X(1)	2.2979(5)	2.5938(4)	2.3882(11)
Pd—X(2)	—	2.5959(4)	2.3927(10)
Pd—P(1)	2.3284(5)	2.3336(13)	2.2742(11)
Pd—P(2)	—	2.3324(13)	2.2599(12)
C(1)—C(2)	1.303(4)	1.287(8)	1.306(7)
C(15)—C(16)	—	1.294(8)	1.303(6)
X-Pd-X	180.0	169.78(2)	84.27(4)
P-Pd-P	180.0	175.80(5)	93.02(4)
X(1)-Pd-P(1)	90.967(19)	88.39(3)	90.79(4)
X(1)-Pd-P(2)	—	91.75(3)	175.14(4)
P(1)-C(1)-C(2)	126.0(2)	126.7(5)	125.6(4)
P(2)-C(15)-C(16)	—	126.6(5)	122.1(4)

[a]X = Cl, I.

symmetry is observed for $PdI_2(PPh_2vinyl)_2$. Moreover, there are significant distortions from planarity for the PdI_2P_2 core and non-equivalence of both iodide and phosphine moieties. The presence and absence of local symmetry between the chloride and iodide complexes may be attributed to the relative ligand field splitting contributions of the respective anions. Solution $^{31}P\{^1H\}$ NMR spectroscopy is not representative of either *trans* solid state structure. For the former complex, this is due to the rapid establishment of *cis-trans* equilibria. Whilst for the latter thermal energy is sufficient to allow rapid exchange on the NMR time-scale between inequivalent phosphines resulting in the observation of a single solution resonance for the two ligands, Table 2. However, CP/MAS $^{31}P\{^1H\}$ NMR spectroscopy does readily characterize the two solid state structures affording a single resonance for the centrosymmetric *trans*-$PdCl_2(PPh_2vinyl)_2$ and two resonances for the asymmetric *trans*-$PdI_2(PPh_2vinyl)_2$. In both cases, the observed chemical shifts are similar to those assigned to the solution resonances of the *trans*-$PdX_2(PPh_2vinyl)_2$ complexes, Table 2. $^{13}C\{^1H\}$ CP/MAS NMR spectroscopy has been successfully employed in the characterization of other palladium(II) phosphines (10). Such spectra were recorded here for both *trans* complexes. However, it is apparent from solution $^{13}C\{^1H\}$ NMR spectroscopy that phenyl and vinyl $^{13}C\{^1H\}$ resonances lie within the same region and display significant ^{13}C–^{31}P coupling. This feature, along with the additional complications of solid state line broadening, plus non-equivalence for the phosphine ligands of $PdI_2(PPh_2vinyl)_2$, results in extensively overlaid resonances for which deconvolution and assignment are unreliable.

UV irradiation of $PdX_2(PPh_2vinyl)_2$ (X = Cl, I)

The solution irradiation of $PdX_2(PPh_2vinyl)_2$ complexes offers three principal routes of reactivity. UV absorbance followed by relaxation to the kinetically favored *cis* isomer may occur to afford *trans-cis* isomerization (11). Alternatively, short wavelength UV activation of alkene moieties

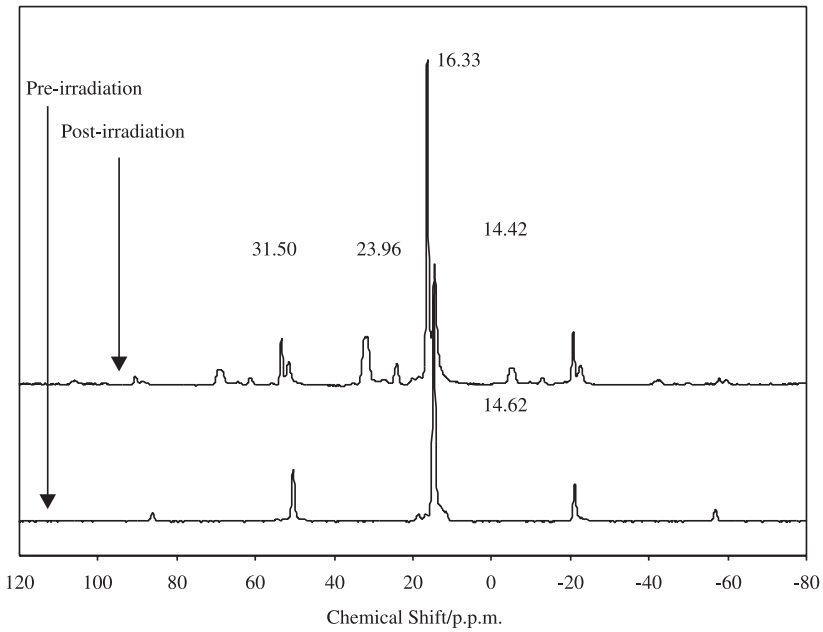
© 2000 NRC Canada

Table 2. CP/MAS $^{31}P\{^1H\}$ NMR data for *trans*-$PdCl_2(PPh_2vinyl)_2$, and *trans*-$PdI_2(PPh_2vinyl)_2$ and for the same complexes after UV irradiation.

Complex	Treatment	δ ^{31}P CP/MAS	Assignment[a]	δ ^{31}P $CDCl_3$	Assignment[a]
trans-$PdCl_2(PPh_2vinyl)_2$	Pre-irradiation	14.6	Symmetrical *trans*-$PdCl_2L_2$ $P\bar{1}$	13.6	*trans*-$PdCl_2L_2$
				21.8	*cis*-$PdCl_2L_2$
trans-$PdCl_2(PPh_2vinyl)_2$	Post-irradiation	14.5	Symmetrical *trans*-$PdCl_2L_2$ $P\bar{1}$	13.6	*trans*-$PdCl_2L_2$
		16.3	Symmetrical *trans*-$PdCl_2L_2$		
		24.2, 31.6	Asymmetric *cis*-$PdCl_2L_2$	21.8	*cis*-$PdCl_2L_2$
trans-$PdI_2(PPh_2vinyl)_2$	Pre-irradiation	5.4, 7.8	Asymmetric *trans*-PdI_2L_2 $P\bar{1}$	4.2	*trans*-PdI_2L_2
trans-$PdI_2(PPh_2vinyl)_2$	Post-irradiation	5.4, 7.6	Asymmetric *trans*-PdI_2L_2 $P\bar{1}$	4.2	*trans*-PdI_2L_2
		22.9	$Ph_2P(O)$vinyl	22.9	$Ph_2P(O)$vinyl
		28.1, 30.3	Asymmetric $[PdI_2L]_2$	26.9	$[PdI_2L]_2$

[a] L = PPh_2vinyl

Fig. 3. CP/MAS $^{31}P\{^1H\}$ NMR spectra of *trans*-$PdCl_2(PPh_2vinyl)_2$ before and after UV irradiation.



can produce oligomerization or polymerization (1), while homolytic or heterolytic bond cleavage may result in generalized or specific bond cleavage.[3] The significance of these various factors can be elucidated by comparison of pre- and post-irradiation solution and solid state NMR data (Table 2).

Irradiation of ca. 10^{-1} M CH_2Cl_2 solutions of $PdCl_2(PPh_2vinyl)_2$ and $PdI_2(PPh_2vinyl)_2$ using wavelengths of $\lambda \geq 200$nm results in the rapid precipitation of palladium containing materials. Precipitation results from the rapid solvent heating associated with the relaxation of excited states through vibrational processes. Where appropriate the formation of *cis*-$[PdCl_2P_2]$ and *sym*-$[PdI_2P]_2$, which are recognized to be of lower solubility than the corresponding *trans*-$[PdX_2P_2]$, may also be significant (6, 10, 11). Decanting residual solvent after ca. 2 min irradiation followed by drying in vacuo affords a 95% yield (wt/wt) of materials slightly darkened from the respective yellow and red colors of the initial complexes. Consideration of the post-irradiation NMR spectrum of $PdCl_2(PPh_2vinyl)_2$ affords the following observations. Solution ^1H NMR spectroscopy indicates no change in the extensively coupled vinylic protons associated with *cis* and *trans* $PdCl_2(PPh_2vinyl)_2$. Moreover, no upfield resonances are observed which might be assigned to polyvinyl moieties. Solution $^{31}P\{^1H\}$ NMR spectroscopy also displays resonances that can be assigned to *cis* and *trans* $PdCl_2(PPh_2vinyl)_2$, with no additional features (Table 2). Thus, it may be concluded that any new solid state feature observed in the post-irradiation CP/MAS $^{31}P\{^1H\}$ NMR spectrum of $PdCl_2(PPh_2vinyl)_2$ corresponds to *cis* and *trans* isomers of this complex (Fig. 3). Three new peaks are observed in the CP/MAS $^{31}P\{^1H\}$ NMR spectrum at 16.3, 24.0, and 31.5 ppm. The former may be assigned to a crystallization of *trans*-$PdCl_2(PPh_2vinyl)_2$ in an alternative space group to that crystallographically characterized here; a feature which has been observed for other palladium(II) and platinum(II) complexes (12, 13). Consideration of the resonances at 24.0 and 31.5 ppm in isolation is problematic because, in addition to *cis*-$[PdCl_2P_2]$ complexes, other species such as phosphine oxides afford similar chemical shifts. However, because only *cis* and *trans* $PdCl_2(PPh_2vinyl)_2$ are

[3] M. Edge, P. Faulds, D.G. Kelly, A. McMahon, G.C. Ranger, and D. Turner. Eur. Polym. J. manuscript 214/99, in press.

© 2000 NRC Canada

Fig. 4. CP/MAS $^{31}P\{^{1}H\}$ NMR spectra of *trans*-$PdI_2(PPh_2vinyl)_2$ before and after UV irradiation.

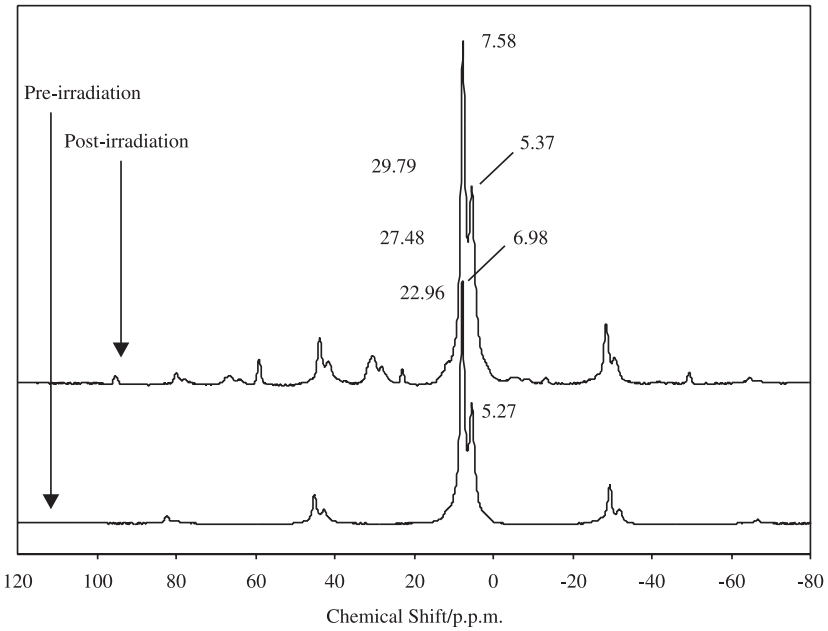


Table 3. $^{31}P\{^{1}H\}$, $^{13}C\{^{1}H\}$, and ^{1}H NMR data for $Ph_2P(O)vinyl$.

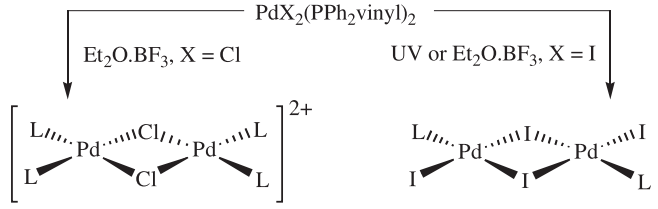
NMR nucleus	Position[a]	δ (ppm)	Coupling(Hz)
$^{31}P\{^{1}H\}$		23.3	
^{1}H	H_a	6.68	12.5,[b] 18.7,[c] 24.5[e]
	H_b	6.31	12.5,[b] 1.8,[c] 41.0[e]
	H_c	6.27	18.7,[c] 1.8,[d] 22.3[e]
	Ph	7.20–7.55	multiplet
$^{13}C\{^{1}H\}$	α	131.65	96.5[f]
	β	135.04	singlet
	i (ipso)	132.80	106.2[f]
	o (ortho)	131.75	9.7*f*
	m (meta)	128.97	12.2*f*
	p (para)	132.26	2.5[f]

[a] Ph_2P H_a >C=C< H_b H_c
[b] $^{3}J_{ab}$.
[c] $^{3}J_{ac}$.
[d] $^{3}J_{bc}$.
[e] $^{n}J_{PH}$.
[f] $^{n}J_{CP}$.

observed on re-dissolution these solid state resonances must be assigned to an unsymmetrical *cis*-$PdCl_2(PPh_2vinyl)_2$ species. While these solid state chemical shifts lie downfield by as much as 10 ppm from solution values, similar movements have been observed in comparable palladium(II) systems (11). Because conventional concentration and crystallization processes yield *trans*-$PdCl_2(PPh_2vinyl)_2$, irradiation may be viewed as enhancing the solid-state concentration of *cis*-$PdCl_2(PPh_2vinyl)_2$.

Irradiation of *trans*-$PdI_2(PPh_2vinyl)_2$ affords a material for which CP/MAS $^{31}P\{^{1}H\}$ resonances at 7.0 and 5.3 ppm are observed which are representative of the original complex. New resonances occur at 23.0, 27.5, and 29.8 ppm (Fig. 4). Unlike the additional post-irradiation resonances of $PdCl_2(PPh_2vinyl)_2$ these new peaks are not lost on re-dissolution. Instead, two peaks of approximately equal intensity are recorded at 22.9 and 26.9 ppm in the solution

Scheme 1. Reactivity of $PdX_2(PPh_2vinyl)_2$ on irradiation and in the presence of $Et_2O{\cdot}BF_3$.



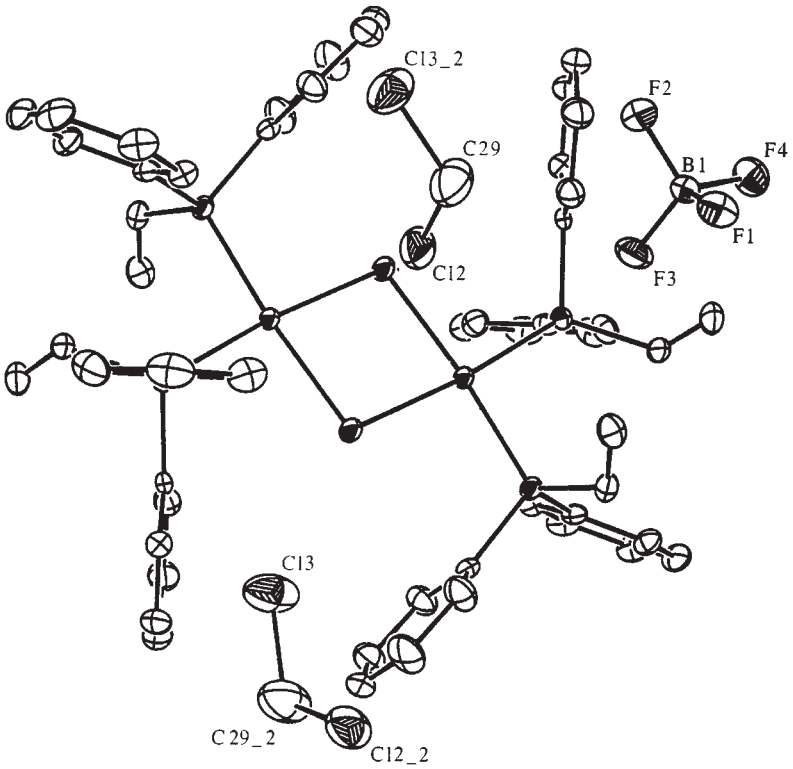
$^{31}P\{^{1}H\}$ NMR spectrum. Formation of *cis*-$PdI_2(PPh_2vinyl)_2$ is unlikely due to the relative instability of this isomer, which does not form by the solution equilibration of *trans*-$PdI_2(PPh_2vinyl)_2$. Moreover, kinetically slow isomerization of such an apparently thermodynamically unstable *cis* species may also be excluded by the static intensities of $^{31}P\{^{1}H\}$ solution NMR resonances over ca. 7 d. Thus, these new resonances may be assigned to reaction, rather than isomerization products. ^{1}H NMR spectroscopy again excludes polymerization products by the absence of upfield resonances. However, extraction of irradiated material with hexane affords identical $^{31}P\{^{1}H\}$ and ^{1}H NMR data to $Ph_2P(O)vinyl$ samples obtained by direct PPh_2vinyl oxidation (Table 3). Thus, it may be suggested that the relaxation of excited species can result in Pd—P cleavage and the subsequent aerobic oxidation of free phosphine (14). Extraction of $Ph_2P(O)vinyl$, followed by recrystallization of the remaining material from Et_2O–CH_2Cl_2 results in the preferential precipitation of deep red *sym*-$[PdI_2(PPh_2vinyl)]_2$. The latter may be manually separated from traces of the paler *trans*-$PdI_2(PPh_2vinyl)_2$. Elemental analysis and comparison with published NMR data confirm the formation of *sym*-$[PdI_2(PPh_2vinyl)]_2$ (15) (Scheme 1).

Reaction of $PdX_2(PPh_2vinyl)_2$ (X = Cl, I) and $Et_2O{\cdot}BF_3$

The addition of $Et_2O{\cdot}BF_3$ to a CH_2Cl_2 solution of $PdCl_2(PPh_2vinyl)_2$ results in an immediate yellow to orange

© 2000 NRC Canada

Fig. 5. Single crystal X-ray diffraction structure of $[Pd(\mu\text{-}Cl)(PPh_2vinyl)_2]_2[BF_4]_2$.



color change. Removal of solvent in vacuo after 12 h and recrystallization from Et_2O–CH_2Cl_2 yields the crystallographically characterized $[Pd(\mu\text{-}Cl)(PPh_2vinyl)_2]_2[BF_4]_2$, formed by a combination of halide abstraction and exchange (Fig. 5). Solution NMR spectroscopy indicates that this air stable complex is the sole palladium containing product. The complex is stable in CH_2Cl_2, but appears to be reduced to palladium metal in $CHCl_3$. Whilst reports exist of BF_3 extraction in palladium phosphine systems (16), it is notable that the reaction of $PdCl_2(PPh_2vinyl)_2$ with $AgBF_4$ results in palladium reduction to the phosphallyl complex $[Pd(\eta^1\text{-}PPh_2vinyl)(\eta^3\text{-}PPh_2vinyl)]_2[BF_4]_2$ (17) (Scheme 1).

The reactivity of $PdI_2(PPh_2vinyl)_2$ with $Et_2O{\cdot}BF_3$ differs markedly from that of the chloride analogue. Under identical conditions halide abstraction does not occur. The majority of the complex is recovered unchanged, with the remaining material undergoing phosphine abstraction to *sym*-$[PdI_2(PPh_2vinyl)]_2$. Abstraction occurs by virtue of the Lewis acid–base interaction with BF_3; a reaction that is confirmed by the observation of a comparable $^{31}P\{^1H\}$ NMR resonance from binary phosphine–BF_3 mixtures. The latter adduct is air sensitive, being hydrolyzed and oxidized in air to $Ph_2P(O)$vinyl. Separation and characterization of $PdI_2(PPh_2vinyl)_2$, $Ph_2P(O)$vinyl, and *sym*-$[PdI_2(PPh_2vinyl)]_2$ are thus accomplished by similar methods to those employed in UV initiated reaction studies.

The respective centrosymmetric and distorted square planar structures that have been crystallographically observed for *trans*-$PdCl_2(PPh_2vinyl)_2$ and *trans*-$PdI_2(PPh_2vinyl)_2$ have been confirmed using CP/MAS NMR spectroscopy. The latter technique, in conjunction with solution NMR spectroscopy, indicates that UV irradiation of $PdCl_2(PPh_2vinyl)_2$ affords *cis* and *trans*- $PdCl_2(PPh_2vinyl)_2$. Similar treatment of $PdI_2(PPh_2vinyl)_2$ results in phosphine dissociation and the formation of *sym*-$[PdI_2(PPh_2vinyl)]_2$. $PdCl_2(PPh_2vinyl)_2$ reacts in the presence of the Lewis acid $Et_2O{\cdot}BF_3$ to yield $[Pd(\mu\text{-}Cl)(PPh_2vinyl)_2]_2[BF_4]_2$, whilst the corresponding iodide again undergoes phosphine dissociation forming *sym*-$[PdI_2(PPh_2vinyl)]_2$. Although UV irradiation and Lewis acids have been reported to initiate vinyl phosphine polymerization, no evidence suggesting such reactivity is recorded in the present study.

Experimental

Crystallographic characterization

Data collection and structure solution for *trans*-$PdCl_2(PPh_2vinyl)_2$, *trans*-$PdI_2(PPh_2vinyl)_2$, and $[Pd(\mu\text{-}Cl)(PPh_2vinyl)_2]_2[BF_4]_2$ were performed using published methods (18), Table 4.[4]

[4] Complete X-ray data have been deposited as supplementary material and may be purchased from the Depository of Unpublished Data, Document Delivery, CISTI, National Research Council Canada, Ottawa, ON K1A 0S2. Crystallographic data for the structures reported in this paper have been deposited with the Cambridge Crystallographic Data Centre (CCDC Nos. 134114, 134115, and 136137, respectively). Copies of the data can be obtained, free of charge, on application to the Director, CCDC, 12 Union Road, Cambridge CB2 1EZ, U.K. (Fax: 44-1223-336033 or e-mail: deposit@ccdc.cam.ac.uk).

© 2000 NRC Canada

Table 4. Crystal data for *trans*-$PdCl_2(PPh_2vinyl)_2$, *trans*-$PdI_2(PPh_2vinyl)_2$, and $[Pd(\mu\text{-}Cl)(PPh_2vinyl)_2]_2[BF_4]_2$.

	trans- $PdCl_2$-$(PPh_2vinyl)_2$	*trans*- PdI_2-$(PPh_2vinyl)_2$	$[Pd(\mu\text{-}Cl)(PPh_2\text{-}vinyl)_2]_2[BF_4]_2$
Color and habit	yellow block	red block	yellow block
Size (mm)	0.30 × 0.20 × 0.20	0.30 × 0.20 × 0.20	0.10 × 0.10 × 0.05
Empirical formula	$C_{14}H_{13}ClPPd$	$C_{28}H_{26}I_2P_2Pd$	$C_{29}H_{28}BCl_3F_4P_2Pd$
Formula weight	300.86	784.63	738.01
a (Å)	8.0956(2)	9.6628(3)	13.3531(3)
b (Å)	9.3183(4)	11.8875(5)	13.5800(5)
c (Å)	10.2254(4)	14.1588(5)	17.4792(5)
α (°)	67.3560(14)	68.7735(17)	—
β (°)	88.185(2)	77.089(2)	103.4594(17)
γ (°)	68.614(2)	68.184(2)	—
V (Å^3)	657.57(4)	1400.02(9)	3082.54(16)
Mo-K_α, λ (nm)	0.71073	0.71073	0.71073
System	triclinic	triclinic	monoclinic
Space group	$P\bar{1}$	$P\bar{1}$	$P2_1/n$
Z	2	2	4
Temperature (K)	293(2)	293(2)	150(2)
Collection	Enraf Nonius KappaCCD	Enraf Nonius KappaCCD	Enraf Nonius KappaCCD
Total reflections	8104	19234	18038
Observed data ($I > 2\sigma(I)$)	2313	5713	4415
2θ	2.94 < 2θ < 25.03	2.28 < 2θ < 26.38	2.95 < 2θ < 23.25
Absorption correction	SORTAV	SORTAV	SORTAV
Solution	SHELXS-97	SHELXS-97	SHELXS-97
Refinement	SHELXL-97 Full matrix F^2	SHELXL-97 Full matrix F^2	SHELXL-97 Full matrix F^2
Hydrogen atoms	Detected & riding	Riding	Riding
R	0.0226	0.0409	0.0359
*w*R	0.0598	0.1014	0.0830
Difference (eÅ^{-3})	0.233, –0.556	0.878, –1.018	1.246, –0.850

Synthesis and spectroscopy

Solvents were dried and distilled under nitrogen by conventional methods (19). Palladium chloride, diphenylvinylphosphine, and Oxone® (potassium peroxymonosulfate, $2KHSO_5{\cdot}KHSO_4{\cdot}K_2SO_4$) were obtained from Aldrich and used as received. $Pd(PhCN)_2Cl_2$ was prepared by published methods (20). Solution NMR were recorded in $CDCl_3$ at 270.1, 67.9, 81.0 MHz for ^1H, $^{13}C\{^1H\}$, and $^{31}P\{^1H\}$, respectively, using a JEOL GSX-270 spectrometer. CP/MAS $^{31}P\{^1H\}$ NMR was recorded using a 7mm bore Varian UNITYplus spectrometer at 121 MHz. Acquisition parameters were; spectral width 100 kHz, relaxation delay 20.0 s, spin-rate 4500 Hz.

$PdCl_2(PPh_2vinyl)_2$: The complex was prepared on a 5 g scale using published methods; typical yields of 79–88% being obtained. Elemental analysis for $C_{28}H_{26}Cl_2P_2Pd$, expected: C 55.9, H 4.4; found: C 56.1, H 4.4. ^1H and $^{31}P\{^1H\}$ NMR spectra were recorded and found to correspond to published data (9).

$PdI_2(PPh_2vinyl)_2$: The complex was prepared by halide metathesis of $PdCl_2(PPh_2vinyl)_2$. Thus, $PdCl_2(PPh_2vinyl)_2$ (4.05 g; 6.8 mmol) was dissolved in CH_2Cl_2 (25 cm^3) and stirred with 10 cm^3 aqueous saturated NaI. After 0.5 h the aqueous solution was separated. The process was repeated with two further portions of aq. NaI. Finally the organic layer was separated and $PdI_2(PPh_2vinyl)_2$ precipitated by the addition of Et_2O. Yield (4.85 g, 91%). Elemental analysis for $C_{28}H_{26}I_2P_2Pd$, expected: C 42.8, H 3.3; found: C 42.8, H 3.3. ^1H and $^{31}P\{^1H\}$ NMR spectra were recorded and correspond to published data (9).

UV irradiation

The following is typical of the treatment of chloro- and iodo- complexes. $PdCl_2(PPh_2vinyl)_2$ (0.70 g; 1.16 mmol) was dissolved in 10 cm^3 of dry CH_2Cl_2. The solution was placed in a ca. 5 cm diameter petri dish, and exposed to UV radiation (λ ≥ 200 nm, 200 W) for 2 min. Remaining solvent was decanted from the precipitated material and the solid dried in vacuo. Yield 0.65 g (93% wt/wt).

BF_3 reactivity

The following is typical of the treatment of chloro- and iodo- complexes. $PdCl_2(PPh_2vinyl)_2$ (0.087 g; 0.14 mmol) was dissolved in 10cm^3 of dry CH_2Cl_2 under nitrogen. The addition of 100 μL $Et_2O{\cdot}BF_3$ (0.79 mmol) produced no visual change. The solution was stirred for ca. 12 h and concentrated to dryness before further study. Yield 0.67 g (96% wt/wt).

$Ph_2P(O)vinyl$: PPh_2vinyl (1.08 g; 5.1 mmol) was dissolved in CH_2Cl_2 (25 cm^3) and slurried with Oxone® for 1 d, after which the solution was filtered and concentrated to dryness affording $Ph_2P(O)vinyl$ in quantitative yield. Elemental analysis for $C_{14}H_{13}OP$, expected: C 64.5, H 5.7; found: C 64.7, H 6.0. NMR (see Table 3). IR (KBr); ν(O=P) 1148 cm^{-1}; MS (EI) *m*/*e* = 228 (100%).

© 2000 NRC Canada

[$PdI_2(PPh_2vinyl)]_2$: Complex was formed in ca. 5% yield along with $Ph_2P(O)$vinyl by the irradiation of $PdI_2(PPh_2vinyl)_2$. A ca. 12% yield, along with $F_3B{\cdot}PPh_2$vinyl, was observed from the reaction of $PdI_2(PPh_2vinyl)_2$ and $Et_2O{\cdot}BF_3$. In the latter reaction $F_3B{\cdot}PPh_2$vinyl was identified by comparison with $^{31}P\{^1H\}$ NMR data obtained from binary $Et_2O{\cdot}BF_3$ and PPh_2vinyl solutions (δ = 1.7 ppm, $CDCl_3$), and undergoes hydrolysis and oxidation in air to $Ph_2P(O)$vinyl. *sym*-$[PdI_2(PPh_2vinyl)]_2$ was readily separated from $Ph_2P(O)$vinyl by hexane extraction of the latter. The complex was then recrystallized from CH_2Cl_2–Et_2O from which this comparatively insoluble complex preferentially precipitates. Manual separation from traces of the visually distinct $PdI_2(PPh_2vinyl)_2$ affords spectroscopically and analytically pure *sym*-$[PdI_2(PPh_2vinyl)]_2{\cdot}Et_2O$. Elemental analysis for $C_{28}H_{26}I_4P_2Pd_2{\cdot}Et_2O$, expected: C 31.5, H 3.0; found: C 31.4, H 2.7. ^1H (for proton notation see Table 3) δ = 5.58 (H_b dd $^3J(PH)$ = 20.7 Hz, $^3J(H_aH_c)$ = 18.2 Hz, 2H, H_c), 6.10 (H_c dd $^3J(PH)$ = 42.4 Hz, $^3J(H_aH_b)$ = 12.0 Hz, 2H, H_b), 7.10 (H_a ddd $^2J(PH)$ = 24.1 Hz, $^3J(H_aH_c)$ = 18.2 Hz, $^3J(H_aH_b)$ = 12.0 Hz, 2H, H_a), 7.36–7.75 (m, 20H, Ph). $^{31}P\{^1H\}$ δ = 26.9.

[Pd(μ-Cl)($PPh_2vinyl)_2]_2[BF_4]_2$: Product formed by the method outlined above was crystallized from dichloromethane–diethylether to afford an orange microcrystalline solid. There is evidence of decomposition in air and over several hours in chloroform to afford palladium metal. However, the complex is sufficiently stable in $CDCl_3$ to obtain NMR spectra. Elemental analysis for $C_{28}H_{26}BClF_4PPd{\cdot}CH_2Cl_2$, expected: C 47.1, H 3.8; found: C 47.3, H 3.6. ^1H (for proton notation see Table 3) δ = 5.70 (H_b t, br), 6.06 (H_c t, br), 6.22 (H_a m, br), 7.38–7.58 (m, 20H, Ph). $^{31}P\{^1H\}$–$^{31}P\{^1H\}$ δ = 28.6.

Acknowledgements

CP/MAS NMR spectra were recorded by the EPSRC Solid State NMR Service, Durham U.K. Mr P. Warren (MMU) is thanked for obtaining solution NMR data. A.J.T. acknowledges funding from an MMU Faculty Studentship.

References

1. C. Wu and F.J. Welch. J. Org. Chem. **30**, 1229 (1965).
2. D.M. Paisley and C.S. Marvel. J. Polym. Sci. **56**, 533 (1962).
3. A.W. Verstuyft, L.W. Cary, and J.H. Nelson. Inorg. Chem. **15**, 3161 (1976).
4. A.W. Verstuyft, D.A. Redfield, L.W. Cary, and J.H. Nelson. Inorg. Chem. **15**, 1128 (1976); J.A. Rahn, M.S. Holt, and J.H. Nelson. Polyhedron, **8**, 897 (1989).
5. Palladium reagents and catalysts innovations in organic synthesis. T. Jiro, John Wiley and Sons, Chichester, 1995.
6. S.O. Grim and R.L. Keiter. Inorg. Chim. Acta, **4**, 56 (1970).
7. S.J. Coles, P. Faulds, M.B. Hursthouse, D.G. Kelly, G.C. Ranger, and N.M. Walker. J. Chem. Res. 418 (S) 1811 (M) (1999).
8. S.J. Coles, P. Faulds, M.B. Hursthouse, D.G. Kelly, G.C. Ranger, A.J. Toner, and N.M. Walker. J. Organomet. Chem. **586**, 234 (1999).
9. J.A. Rahn, M.S. Holt, M. O'Neil-Johnson, and J.H. Nelson. Inorg. Chem. **27**, 1316 (1988).
10. J.A. Rahn, D.J. O'Donnell, A. R. Palmer, and J.H. Nelson. Inorg. Chem. **28**, 2631 (1989).
11. N. Alcock, T.J. Kemp, F.L. Wimmer, and O. Traverso. Inorg. Chim. Acta, **44**, L245 (1980); N. Alcock, T.J. Kemp, and F.L. Wimmer. J. Chem. Soc. Dalton Trans. 635 (1981).
12. N.A. Bailey and R.A. Mason. J. Chem. Soc. A, 2594 (1968).
13. H. Kin-Chee, G.M. McLaughlin, M. McPartlin, and G.B. Robertson. Acta Crystallogr. Sect. B: Struct. Crystallogr. Cryst. Chem. **B38**, 421 (1982).
14. M. Cusumano, G. Guglielmo, V. Ricevuto, S. Sostero, O. Traverso, and T.J. Kemp. J. Chem. Soc. Chem. Commun. 775 (1979); M. Cusumano, G. Guglielmo, V. Ricevuto, S. Sostero, O. Traverso, and T.J. Kemp. J. Chem. Soc. Dalton Trans. 302 (1981).
15. N.W. Alcock, W.L. Wilson, and J.H. Nelson. Inorg. Chem. **32**, 3193 (1993).
16. H.C. Clark and K.R. Dixon. J. Am. Chem. Soc. **91**, 596 (1969).
17. W.L. Wilson, J.H. Nelson, and N.W. Alcock. Organometallics, **9**, 1699 (1990).
18. R.H. Blessing. J. Appl. Crystallogr. **30**, 421 (1997); G.M. Sheldrick. Acta. Crystallogr. Sect. A: Fundam. Crystallogr. **A46**, 467 (1990); G.M. Sheldrick. SHELX97. University of Göttingen, Germany.
19. S.J. Coles, M.B. Hursthouse, D.G. Kelly, A.J. Toner, and N.M. Walker. J. Organomet. Chem. **580**, 304 (1999).
20. G.K. Anderson and M. Lin. Inorg. Synth. **28**, 61 (1990).

© 2000 NRC Canada

Syntheses of 4-[1-(2-deoxy-β-D-ribofuranosyl)]-derivatives of 2-substituted-5-fluoroaniline: "cytosine replacement" analogs of deoxycytidine for evaluation as anticancer and antihuman immunodeficiency virus (anti-HIV) agents

Zhi-Xian Wang, Leonard I. Wiebe, Erik De Clercq, Jan Balzarini, and Edward E. Knaus

Abstract: A group of 4-[1-(2-deoxy-β-D-ribofuranosyl)]-derivatives of 5-fluoroaniline possessing a variety of aryl C-2 substituents (**6a** R = H, **6b** R = F, **6c** R = Me) were synthesized. Accordingly, a Heck-type coupling reaction of the 4-iodoaniline derivatives (**13a**–**c**) with the bis(*tert*-butyldimethylsilyl)glycal (**11**) in the presence of $Pd(OAc)_2$ and Ph_3As, followed by removal of the *tert*-butyldimethylsilyl protection groups using *n*-$Bu_4N^+F^-$, yielded the corresponding 4-(β-D-glycero-pentofuran-3-ulos-1-yl)aniline derivatives (**14a**–**c**) having a C-3 C=O in the sugar ring. Reduction of the C-3 C=O compounds (**14a**–**c**) using $NaB(OAc)_3H$ afforded the target 4-[1-(2-deoxy-β-D-ribofuranosyl)]-derivatives of the respective 2-substituted-5-fluoroaniline (**6a**–**c**). The deoxycytidine mimic, 3-fluoro-4-[1-(2-deoxy-β-D-ribofuranosyl)]aniline (**6a**), in which the cytosine ring of deoxycytidine is replaced by a 4-(3-fluoroaniline) ring system, was inactive as an anticancer agent against a variety of tumor cell lines, and as an antihuman immunodeficiency virus (HIV-1, HIV-2) agent. The failure of this unnatural deoxycytidine mimic (**6a**) to exhibit anticancer–antiviral activity may be due to its inability to undergo phosphorylation by host cell- and virus-induced kinases.

Key words: fluoroanilines, deoxycytidine mimics, anticancer–antihuman immunodeficiency virus (HIV) evaluation.

Résumé : On a synthétisé une série de dérivés 4-[1-(2-désoxy-β-D-ribofuranosyl)]- de la 5-fluoroaniline portant divers substituants en position C-2 du groupe aryle (**6a** R = H, **6b** R = F, **6c** R = Me). À cette fin, on a effectué une réaction de couplage de type Heck des dérivés 4-iodoaniline (**13a**–**c**) avec le bis(*tert*-butyldiméthylsilyl)glycal (**11**) en présence de $Pd(OAc)_2$ et de Ph_3As, suivie de l'élimination des groupes protecteurs *tert*-butyldiméthylsilyle à l'aide de $Bu_4N^+F^-$, conduit aux dérivés 4-(β-D-glycéro-pentofuran-3-ulos-1-yl)anilines correspondants (**14a**–**c**) comportant un C=O en position C-3. La réduction de ces composés carbonylés en C-3 (**14a**–**c**) à l'aide de $NaB(OAc)_3H$ conduit aux dérivés 4-[1-(2-désoxy-β-D-ribofuranosyl)]- recherchés des 5-fluoroanilines substituées en position C-2 (**6a**–**c**). La 3-fluoro-4-[1-(2-désoxy-β-D-ribofuranosyl)]aniline (**6a**) qui est une imitation de la désoxycytidine dans laquelle le cycle cytosine de la désoxycytidine a été remplacé par un système cyclique 4-(3-fluoroaniline) est inactive comme agent anticancéreux contre un grand nombre de familles de cellules tumorales ainsi que contre le virus d'immunodéficience humaine (HIV-1 et HIV-2). Ce manque d'activité anticancéreuse–antivirale de cette imitation non naturelle de la désoxycytidine (**6a**) peut découler de son inaptitude à subir une phosphorylation les kinases de la cellule réceptrice et celles induites par le virus.

Mots clés : fluoroanilines, imitation de la désoxycytidine, évaluation comme anticancéreux–antivirus de l'immunodéficience humaine.

Introduction

Modified nucleosides often exert important biological activities (for a review see ref. (1)), and when incorporated into nucleic acids by normal enzymatic processes, can further alter the structure and (or) function of these biopolymers. In this respect, a number of C-nucleosides have been shown to exhibit anticancer and antiviral activities, presumably due to their structural resemblance to natural *N*-nucleosides (2). Nonpolar hydrophobic isosteres of pyrimidine nucleosides which retain the closest possible structural, steric, and isoelectronic relationships to the natural base that

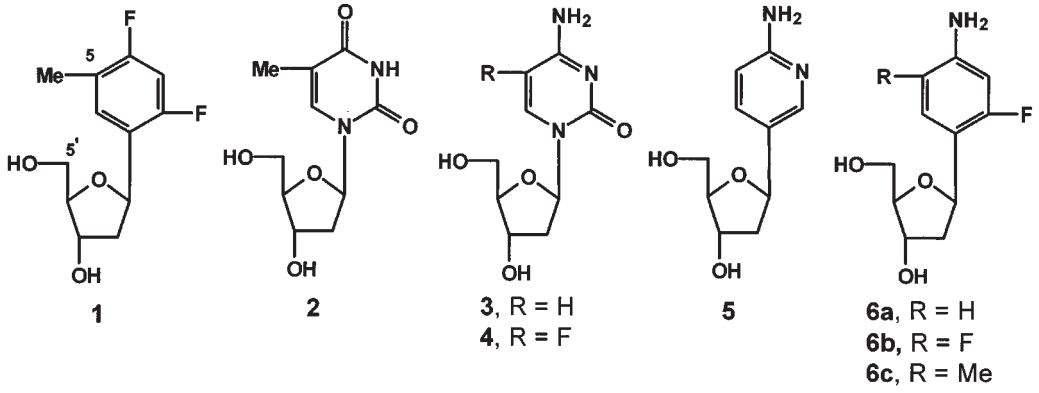
Received March 21, 2000. Published on the NRC Research Press website on August 3, 2000.

Z.-X. Wang, L.I. Wiebe, and E.E. Knaus.[1] Faculty of Pharmacy and Pharmaceutical Sciences, University of Alberta, Edmonton, AB T6G 2N8, Canada.
E. De Clercq and J. Balzarini. Rega Institute for Medical Research, Minderbroedersstraat 10, Leuven B-3000, Belgium.

[1]Author to whom correspondence may be addressed. Telephone: (780) 492-5993. Fax: (780) 492-1217.
e-mail: eknaus@pharmacy.ualberta.ca

 © 2000 NRC Canada

Fig. 1. The structures of the thymidine mimic (**1**), thymidine (**2**), 2′-deoxycytidine (**3**), 5-fluoro-2′-deoxycytidine (**4**), the deletion-modified 2′-deoxycytidine mimic (**5**), and the proposed cytosine replacement 2′-deoxycytidine mimics (**6a**–**c**).



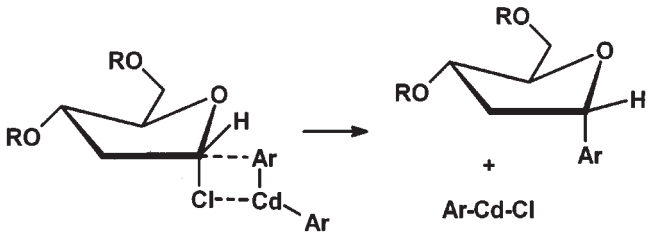
are not likely to form hydrogen bonds were recently designed by Kool and co-worker (3). Thus, the 2,4-difluoro-5-methylphenyl isostere (**1**) was designed as an unnatural mimic of thymidine (**2**). The 5′-triphosphate of **1** (**1**-TP) was inserted into replicating DNA strands by the Klenow fragment (KF, *exo*$^-$ mutant) of *E. coli* DNA polymerase 1 (4). Steady-state measurements indicated that **1**-TP was inserted opposite adenine (A) with an efficacy (V_{max}/K_m) only 40-fold lower than the triphosphate of thymidine (dTTP). Furthermore, it was inserted opposite A, relative to C, G, or T, with a selectivity nearly as high as that for dTTP. Therefore, the 2,4-difluoro-5-methylphenyl moiety of **1** is a shape mimic handled by KF polymerase similar to the natural thymine base which it replaces (5–7).

2′-Deoxycytidine (**3**) and 5-fluoro-2′-deoxycytidine (**4**) have been the subject of numerous chemical and pharmacological studies due to the inherent anticancer and antiviral activities exhibited by 5-fluoro-2′-deoxycytidine (8). Hsieh and McLaughlin (9) reported that the 5-(2-aminopyridyl) "deletion-modified" analog **5** of deoxycytidine (dC) may function as a dC mimic which would provide information regarding the role of the O^2-carbonyl in a variety of recognition and enzymatic processes. Although **5** has the potential to exhibit anticancer or antiviral properties, no biological activities were reported. It was therefore anticipated that structurally related 4-(2-substituted-5-fluoroaniline) nucleoside mimics (**6a**–**c**), which are hybrids of the C-aryl (**1**), C-pyridyl (**5**), and deoxycytidine (**3**–**4**) nucleosides, may be cytotoxic to rapidly multiplying cancer cells (inhibit tumor cell growth) and (or) act as antiviral agents due to their selective phosphorylation in virus-infected cells (10). We now report the synthesis, antiviral and anticancer activities for a group of 4-[1-(2-deoxy-β-D-ribofuranosyl)]- derivatives of 2-substituted-5-fluoroanilines (**6a**–**c**) that were designed as unnatural C-aryl deoxycytidine mimics.

Chemistry

A number of methodologies have been reported for the synthesis of 2′-deoxy-ribo-C-nucleosides (11). Synthesis of the thymidine mimic (**1**), and some related analogs, have been performed by reaction of an arylcadmium reagent with the well known Hoffer (12) α-chlorosugar synthon [2-deoxy-3,5-di-*O*-(*p*-toluoyl)-α-D-ribofuranosyl chloride] by Kool and co-workers (13–15). The resulting α-nucleoside mimic 3′,5′-di-*O*-toluoyl ester was then epimerized (α-epimer → β-epimer) using benzenesulfonic acid in xylene at reflux temperature to afford the desired β-anomeric product.

Fig. 2. Four-center transition state leading to the formation of the α-**8** anomer.

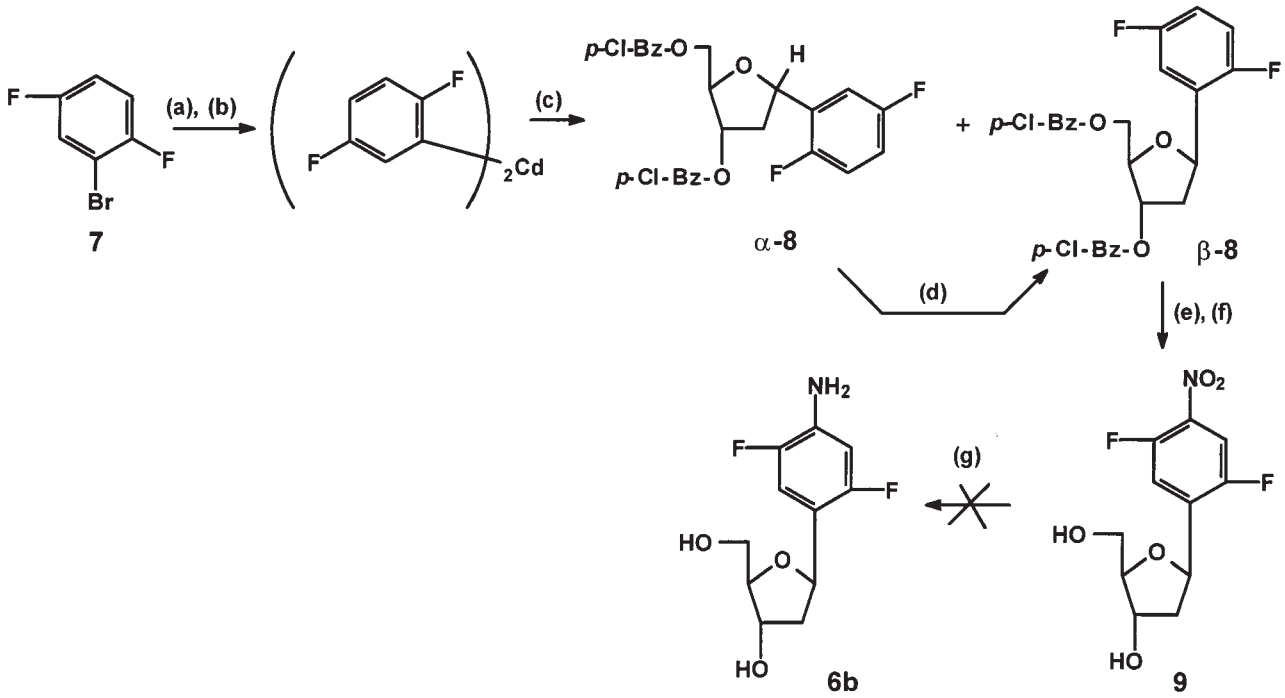


Hoffer's (12) original procedure for the preparation of 2-deoxy-3,5-di-*O*-(*p*-toluoyl)-α-D-ribofuranosyl chloride requires delicate and tedious handling of anhydrous HCl gas. We, and others (a 35% yield was obtained, see ref. (16*a*); for a modified method to prepare the Hoffer α-chlorosugar synthon see ref. (16*b*)), have experienced difficulties in obtaining acceptable yields using this method. Accordingly, 2-deoxy-3,5-di-*O*-(*p*-chlorobenzoyl)-α-D-ribofuranosyl chloride was used in place of the Hoffer α-chlorosugar synthon since it is more stable and readily crystallizes from the solvent. The coupling of 2-deoxy-3,5-di-*O*-(*p*-chlorobenzoyl)-α-D-ribofuranosyl chloride with the organocadmium reagent, generated by reaction of the Grignard reagent with $CdCl_2$, afforded a mixture of α-**8** and β-**8** anomers with an α:β ratio of 7.3 that could be separated by silica gel flash chromatography. The major isomer was formed with retention of configuration to produce the α-anomeric C-nucleoside (α-**8**) (Scheme 1). The predominant formation of the α-**8** anomer may be the result of a four-center transition state at C-1 of the chlorosugar (Fig. 2), as proposed by Hurd and Miles (17) for reactions involving related pyranose systems with Grignard reagents, or by a dissociative mechanism involving predominant α-face attack (18). The configuration at the C-1′carbon of α-**8** and β-**8** was determined from ^{1}H NMR analysis of the $H_{1'}$—$H_{2'}$ coupling constants and comparison to ^{1}H NMR spectral data reported by Kool and co-workers (13–15).

Based on the premise that α-anomer → β-anomer epimerization reactions may involve an acid-catalyzed reversible ring opening at the C-1 position of the sugar ring, we found that α-**8** could be epimerized in the presence of

© 2000 NRC Canada

Scheme 1. Reagents and conditions: (*a*) THF, Mg, I_2 catalyst, 40°C, 1 h; (*b*) $CdCl_2$, reflux, 1 h; (*c*) 2-deoxy-3,5-di-*O*-(*p*-chlorobenzoyl)-α-D-ribofuranosyl chloride, 25°C, 12 h; (*d*) $EtNO_2$, BF_3–Et_2O, 110–120°C, 2 h; (*e*) NH_4NO_3, $(CF_3CO)_2O$, 25°C, 30 min; (*f*) 2 N NaOH, THF, 25°C, 6 h; (*g*) 10% Pd-C, EtOH, H_2 gas.



$BF_3 \cdot Et_2O$ in nitroethane at 110–120°C during 2 h to afford a mixture of the α-**8** and β-**8** anomers with an α:β ratio of 3.3. Nitration of the β-anomer (β-**8**) with NH_4NO_3 in $(CF_3CO)_2O$ afforded the 4-nitro derivative (65%), which, on deprotection with NaOH in THF, yielded β-**9** (91%). However, hydrogenation of the 4-nitro compound (β-**9**), using 10% Pd-C and hydrogen gas, produced a complex mixture of products containing only a trace amount of the desired amino derivative (**6b**). Therefore, an alternative method for the synthesis of the deoxycytidine mimics (**6a**–**c**) was developed.

The Heck-type coupling reaction is a simple, but direct, method to form the C—C bond between a suitably protected glycal and an activated iodo- or trifluoromethanesulfonate-substituted heterocycle, to prepare the β-anomer of C-nucleosides in reasonable yields (9, 19). It was expected that the highly activated *p*-iodoanilines (**13a**–**c**) used in this study would undergo efficient coupling using the sequence of reactions illustrated in Scheme 2. The protected bis(*tert*-butyldimethylsilyl)ether ribofuranoid glycal **11** was readily prepared by known procedures (20). Accordingly, oxidation of 2-deoxy-D-ribose using bromine water followed by lactonization afforded 2-deoxy-D-ribonolactone (21). The crude lactone was treated immediately with *tert*-butyldimethylsilyl chloride in the presence of imidazole to give **10** in 80% yield from 2-deoxy-D-ribose. Reduction of the lactone **10** using diisobutylaluminum hydride (DIBAL-H) at –78°C gave the requisite 2-deoxy-D-pentofuranose derivative, which was sufficiently pure for direct mesylation in the presence of triethylamine in CH_2Cl_2 at –78°C. The intermediate mesylate was not isolated since the elimination reaction occurred readily at reflux temperature during 15 h to afford the glycal **11** in 82% yield after flash chromatography purification.

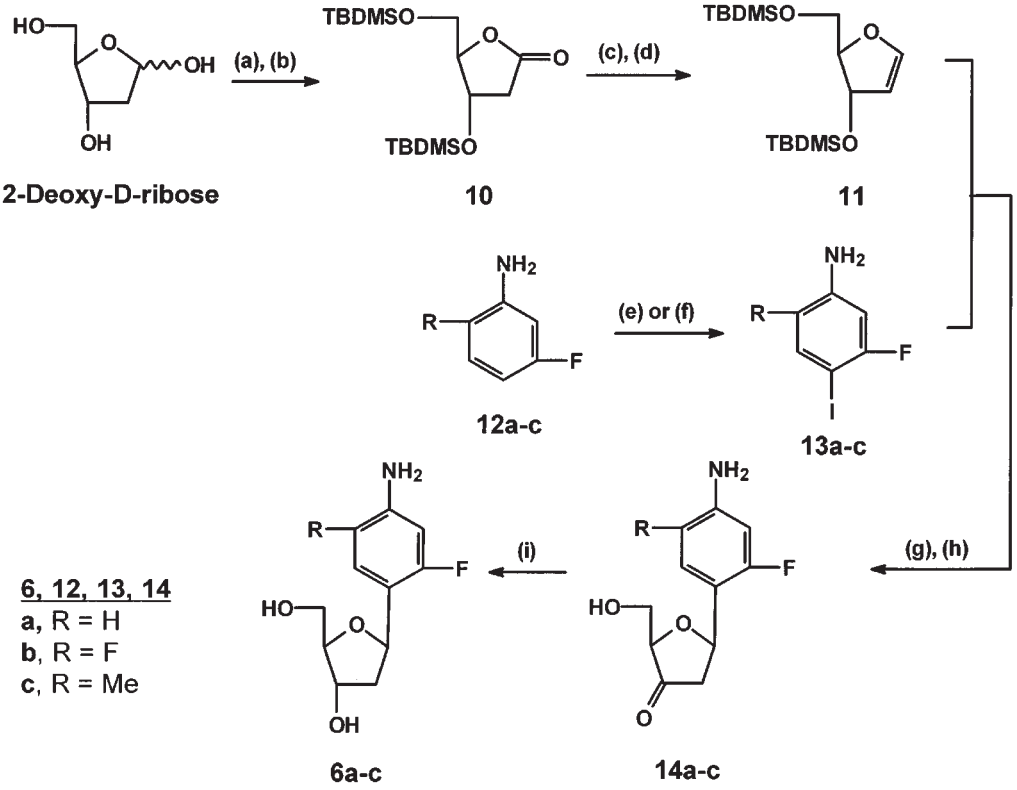
The *p*-iodoaniline derivatives (**13a**–**c**) were synthesized using two different methods. *m*-Fluoroaniline (**12a**) was treated with iodine and sodium periodate in the presence of H_2SO_4 in acetic acid to afford **13a** (Method A) (9). Compounds **13b**–**c** were prepared in good yield via treatment of **12b**–**c** with *N*-iodosuccinimide in trifluoroacetic acid using a method developed by Olah and co-workers (22) (Method B). Direct coupling of *p*-iodoanilines (**13a**–**c**) with the glycal (**11**) was carried out using palladium (II) acetate, triphenylarsine, and triethylamine in dry acetonitrile at 60–70°C (6 h). It was observed that the initially formed 3-silyl enol ether adduct was unstable under these weakly basic reaction conditions, and that a prolonged reaction time resulted in the formation of the 3-keto derivative. Therefore, the reaction mixture was treated with an excess of tetra-*n*-butylammonium fluoride (TBAF) to perform complete desilylation, which afforded the hydroxy ketone derivatives (**14a**–**c**) in 31–39% isolated yields. This procedure provided compounds **14a**–**c** having the β-configuration, since the α-product was produced in only trace amounts allowing its facile removal via simple recrystallization. Reduction of the hydroxy ketones (**14a**–**c**) with $NaB(OAc)_3H$ (6h) in CH_3CN selectively produced the target deoxycytidine C-nucleoside mimics (**6a**–**c**) in 52–75% isolated yields.

Biological evaluation of 4-[1-(2-deoxy-β-D-ribofuranosyl)]- derivatives of 2-substituted-5-fluoroaniline as anticancer and antihuman immunodeficiency virus (anti-HIV) agents

Replacement of the natural cytosine base moiety in deoxycytidine (**3**), or 5-fluorodeoxycytidine (**4**), by an unnatural aryl isostere such as a 2-substituted-5-fluoroaniline ring system attracted our attention since it could confer new

© 2000 NRC Canada

Scheme 2. Reagents and conditions: (*a*) Br_2, H_2O, 25°C, five days; (*b*) imidazole, CH_2Cl_2, 0°C, 30 min; and then *tert*-butyldimethylsilyl chloride, 25°C, 12 h; (*c*) diisobutylaluminum hydride (DIBAL-H), toluene, Et_2O, –78°C, 3.5 h; (*d*) $MeSO_2Cl$, Et_3N, CH_2Cl_2, –78°C for 2 h, –10 – –20°C for 2 h, and then at reflux for 15 h; (*e*) $NaIO_4$, I_2, conc. H_2SO_4, H_2O, CH_3CO_2H, 80°C, 4 h (Method A); (*f*) CF_3CO_2H, *N*-iodosuccinimide (NIS), 25°C, 3 h (Method B); (*g*) $Pd(OAc)_2$, Ph_3As, Et_3N, MeCN, 60°C, 20 h (**14a**), or 48 h (**14b**), or 15 h (**14c**); (*h*) *n*-$Bu_4N^+F^-$, 25°C, 2 h; (*i*) $NaB(OAc)_3H$, MeCN, 0°C, 2 h.



properties that may be useful in the design of a novel class of third generation C-aryl deoxycytidine mimics (**6**) for use as anticancer and (or) antiviral agents. C-aryl nucleoside mimics offer a number of potential advantages relative to classical 5-substituted-2′-deoxyuridines. In this respect, increased stability to pyrimidine phosphorylases (no glycosidic bond) would not require the presence of a 2′-ribo-F (23), or 2′-arabino-OH (24), substituent to provide in vivo stability. Compounds of this type may elicit decreased host cell toxicity due to their inability to inhibit thymidylate synthase, and they maybe resistant to deamination by deoxycytidine deaminase (10). Finally, their greater lipophilicity may alter tissue biodistribution, particularly to treat brain viral infections and brain tumors due to an enhanced ability to cross the blood-brain-barrier (BBB). This latter advantage offers an attractive alternative to making lipophilic prodrugs of nucleosides (25).

The ability of the 2-fluoro-4-aminophenyl compound having a C-3 C=O group in the sugar ring (**14a**), and the 2-fluoro-4-aminophenyl deoxycytidine mimic (**6a**), to inhibit the proliferation of murine leukemia cells (L1210/0), murine mammary carcinoma cells (FM3A/0), and human T-lymphocytes cells (Molt4/C8, CEM/O) in cell cultures by 50% (IC_{50} ± SEM) were evaluated using a previously reported procedure (26). In these assays, **6a** and **14a** provided negligible inhibition of L1210/0 proliferation (IC_{50} = 222 ± 219 μM (**6a**), IC_{50} = 478 ± 31 μM (**14a**)). Both **6a** and **14a** were inactive (IC_{50} > 500 μM) inhibitors of FM3A/0, Molt4/C8, and CEM/0 cell proliferation. In addition, **6a** and **14a** did not protect (IC_{50} > 250 μM) human T-lymphocytes (CEM cells) against the cytopathogenicity induced by human immunodeficiency viruses (HIV-1, HIV-2) (27).

The reason(s) why this novel class of deoxycytidine mimics (**6**) lack anticancer and (or) antiviral activity has not been elucidated. In the event that the failure of these compounds to undergo phosphorylation to the 5′-monophosphate is responsible for the lack of anticancer and (or) anti-HIV activities observed, it is possible that 5′-cycloSal-pronucleotide derivatives of **6** and **14** according to the kinase-bypass concept (28, 29) may result in the transformation of these inactive unnatural deoxycytidine mimics to a class of effective anticancer and (or) antiviral agents.

Experimental

Melting points were determined with a Thomas Hoover capillary apparatus and are uncorrected. Nuclear magnetic resonance spectra (^1H NMR, ^{13}C NMR, ^{19}F NMR) were measured on a Bruker AM-300 spectrometer. The assignment of exchangeable protons (O*H*) was confirmed by the addition of D_2O. Proton chemical shifts (δ) are given relative to internal TMS (δ 0). ^{13}C NMR spectra were acquired using the *J* modulated spin echo technique where methyl and methine carbon resonances appear as positive peaks and

© 2000 NRC Canada

methylene and quaternary carbons appear as negative peaks, and carbon chemical shifts (δ) are given relative to $CDCl_3$ (δ 77), or DMSO-d_6 (δ 39.5). Fluorine chemical shifts (δ) are given relative to external C_6F_6 (δ 0). The "prime numbers" in the ^{1}H NMR spectral data refer to the protons in the sugar ring system. Infrared spectra were recorded on a Nicolet Magna 550 IR spectrometer using air as the reference. Elemental analyses were performed by the MicroAnalysis Service Laboratory, Department of Chemistry, University of Alberta. Silica gel 60 (E. Merck Co.) was employed for all silica gel column flash chromatography separations. All reagents were purchased from the Aldrich Chemical Co.

2,5-Difluoro-1-[1-[2-deoxy-3,5-di-*O*-(*p*-chlorobenzoyl)-α-D-ribofuranosyl]]benzene (α-8) and 2,5-Difluoro-1-[1-[2-deoxy-3,5-di-*O*-(*p*-chlorobenzoyl)-β-D-ribofuranosyl]]benzene (β-8)

1-Bromo-2,5-difluorobenzene (**7**, 3.9 g, 20 mmol) was added drop wise with stirring to a mixture of Mg turnings (0.48 g, 20 mmol) and one crystal of iodine in dry THF (30 mL) under argon. This mixture was stirred at 40°C for 1 h, at which time formation of the Grignard reagent was complete, and a pale brown solution was obtained. Powdered $CdCl_2$ (1.84 g, 10 mmol) (dried in vacuo at 130°C for 2 h) was added, and the mixture was stirred at reflux temperature for 1 h. After cooling to 25°C, 2-deoxy-3,5-di-*O*-(*p*-chlorobenzoyl)-α-D-ribofuranosyl chloride (4.29 g, 10 mmol) was added in aliquots during 1 h, and the reaction mixture was stirred at 25°C for 12 h. The reaction was quenched with saturated aqueous NH_4Cl, and extracted with ether (3 × 20 mL). The combined organic extracts were washed with water, and brine, prior to drying (Na_2SO_4). After filtration, and removal of the solvent in vacuo, the residue obtained was purified via flash chromatography (hexane–ethyl acetate, 17.5:1, v/v) to afford β-**8** (0.32 g, 6.1% yield) and α-**8** (2.57 g, 51% yield).

$BF_3{\cdot}Et_2O$ (1.2 mL) was added to a solution of the α-**8** (1.2 g, 2.35 mmol) in nitroethane (12 mL) under argon, and the resulting solution was stirred at 110–120°C under argon for 2 h. After cooling to 25°C, the reaction mixture was poured onto cold water (20 mL), neutralized with saturated aqueous $NaHCO_3$, and extracted with ether (3 × 20 mL). The combined organic extracts were washed with water, and brine, prior to drying (Na_2SO_4). After filtration, and removal of the solvent in vacuo, the residue obtained was purified via flash chromatography (hexane–ethyl acetate, 17.5:1, v/v) to give the β-**8** anomer (0.226 g, 19%) as a colorless syrup, and the α-**8** anomer (0.75 g, 62%) as white crystals.

α-Anomer (α-8)

White crystals (recrystallized from hexane), mp 119–120°C. ^{1}H NMR ($CDCl_3$) δ: 8.06, 7.73, 7.48 and 7.39 (d, *J* = 8.5 Hz, 2H each), 7.37 (m, 1H), 7.1–6.9 (m, 2H), 5.65 (ddd, *J* = 6.4, 3.4, 2.1 Hz, 1H, H-3′), 5.60 (dd, *J* = 7.9, 4.9 Hz, 1H, H-1′), 4.78 (td, *J* = 5.2, 2.1 Hz, 1H, H-4′), 4.64 (dd, *J* = 11.7, 5.2 Hz, 1H, H-5′a), 4.58 (dd, *J* = 11.7, 5.2 Hz, 1H, H-5′b), 3.02 (ddd, *J* = 14.0, 7.9, 6.4 Hz, 1H, H-2′α), 2.35 (br d, *J* = 14.0 Hz, 1H, H-2′β). ^{13}C NMR ($CDCl_3$) δ: 165.72, 165.27, 159.32 (d, *J* = 241.7 Hz), 155.62 (dd, *J* = 241.7, 2.2 Hz), 140.30, 140.16, 132.42 (dd, *J* = 15.4, 7.7 Hz), 131.41, 131.28, 129.24, 129.14, 128.55, 128.19, 116.76 (dd, *J* = 24.2, 8.8 Hz), 115.37 (dd, *J* = 25.3, 8.8 Hz), 113.97 (dd, *J* = 25.3, 4.4 Hz), 82.85, 76.87, 75.30, 65.06, 39.58. ^{19}F NMR ($CDCl_3$) δ: 43.21 (m), 37.70 (m).

β-Anomer (β-8)

Colorless syrup. ^{1}H NMR ($CDCl_3$) δ: 8.06, 8.01, 7.50 and 7.43 (d, *J* = 8.5 Hz, 2H each), 7.31 (m, 1H), 7.1–6.9 (m, 2H), 5.64 (br d, *J* = 6.1 Hz, 1H, H-3′), 5.49 (dd, *J* = 10.7, 5.5 Hz, 1H, H-1′), 4.75 (dd, *J* = 11.7, 4.3 Hz, 1H, H-5′a), 4.69 (dd, *J* = 11.7, 3.7 Hz, 1H, H-5′b), 4.58 (ddd, *J* = 4.3, 3.7, 2.1 Hz, 1H, H-4′), 2.73 (br d, *J* = 13.7, 5.5 Hz, 1H, H-2′α), 2.17 (ddd, *J* = 13.7, 10.7, 6.1 Hz, 1H, H-2′β). ^{13}C NMR ($CDCl_3$) δ: 165.26, 165.07, 158.90 (dd, *J* = 241.7, 2.2 Hz), 155.44 (dd, *J* = 241.7, 2.2 Hz), 139.94, 139.34, 131.03, 130.94, 129.97 (dd, *J* = 16.5, 7.7 Hz), 128.83, 128.76, 128.13, 127.96, 116.24 (dd, *J* = 24.2, 8.8 Hz), 115.27 (dd, *J* = 24.2, 8.8 Hz), 113.36 (dd, *J* = 26.4, 4.4 Hz), 82.72, 77.24, 74.67, 64.65, 39.98. ^{19}F NMR ($CDCl_3$) δ: 43.89 (m), 36.96 (m).

2,5-Difluoro-4-nitro-1-[1-(2-deoxy-β-D-ribofuranosyl)]benzene (9)

Powdered NH_4NO_3 (0.32 g, 5 mmol) was added in aliquots to a solution of β-**8** (0.6 g, 1.18 mmol) in dry CH_2Cl_2 (5 mL) and trifluoroacetic anhydride (5 mL), and the reaction mixture was stirred at 25°C for 30 min. The resulting yellow solution was poured onto cold water, neutralized with $NaHCO_3$, and extracted with CH_2Cl_2 (3 × 30 mL). The combined organic extracts were washed with water, and brine, prior to drying (Na_2SO_4). Removal of the solvent in vacuo gave a residue that was purified via flash chromatography (hexane–ethyl acetate, 10:1 v/v) to give a yellow syrup (0.5 g), which was recrystallized from hexane–ether to give yellow crystals (0.42 g, 65%), mp 112–113°C. ^{1}H NMR ($CDCl_3$) δ: 8.04 (d, *J* = 8.8 Hz, 2H), 7.97 (d, *J* = 8.8 Hz, 2H), 7.80 (dd, *J* = 9.2, 5.8 Hz, 1H), 7.56 (dd, *J* = 11.0, 5.8 Hz, 1H), 7.48 (d, *J* = 8.8 Hz, 2H), 7.42 (d, *J* = 8.8 Hz, 2H), 5.64 (d, *J* = 6.1 Hz, 1H, H-3′), 5.47 (dd, *J* = 10.7, 5.2 Hz, 1H, H-1′), 4.79 (dd, *J* = 11.6, 4.0 Hz, 1H, H-5′a), 4.66 (dd, *J* = 11.6, 4.0 Hz, 1H, H-5′b), 4.60 (m, 1H, H-4′), 2.80 (dd, *J* = 14.0, 5.2 Hz, 1H, H-2′α), 2.11 (ddd, *J* = 14.0, 10.7, 6.1 Hz, 1H, H-2′β). ^{13}C NMR ($CDCl_3$) δ: 165.09, 164.93, 153.71 (dd, *J* = 247.2, 2.2 Hz), 151.93 (dd, *J* = 261.5, 2.2 Hz), 140.05, 139.79, 137.39 (dd, *J* = 16.5, 7.1 Hz), 135.99 (t, *J* = 8.8 Hz), 130.95, 130.77, 128.78, 127.88, 127.67, 116.48 (dd, *J* = 25.3, 4.4 Hz), 112.77 (dd, *J* = 28.6, 2.2 Hz), 83.08, 76.82, 74.15, 64.25, 39.69. ^{19}F NMR ($CDCl_3$) δ: 41.85 (m), 41.06 (m). Anal. calcd. for $C_{25}H_{17}Cl_2F_2O_7N$: C 54.37, H 3.10, N 2.54; found: C 54.09, H 3.11, N 2.54.

Aqueous NaOH (2 mL of 2 N, 4 mmol) was added to a solution of the product obtained above (0.33 g, 0.6 mmol) in THF (10 mL). After stirring at 25°C for 6 h, the reaction was quenched with solid NH_4Cl, and the solvent was removed in vacuo. The residue obtained was extracted with acetone (10 mL), filtered, and the solid was washed with acetone. Removal of the solvent from the filtrate gave a residue that was purified via flash chromatography (hexane–ethyl acetate, 1:2 – 1:5 v/v) to give a yellow solid, which was recrystallized from hexane–ether to afford **9** (0.151 g, 91%) as pale yellow crystals, mp 177–179°C. ^{1}H NMR

© 2000 NRC Canada

(CD_3OD) δ: 7.86 (dd, *J* = 9.5, 6.1 Hz, 1H), 7.72 (dd, *J* = 11.6, 5.8 Hz, 1H), 5.36 (dd, *J* = 10.1, 5.8 Hz, 1H, H-1′), 4.32 (m, 1H, H-3′), 3.98 (td, *J* = 4.6, 2.4 Hz, 1H, H-4′), 3.67 (m, 2H, H-5′), 2.37 (dd, *J* = 12.8, 5.8 Hz, 1H, H-2′α), 1.87 (ddd, *J* = 12.8, 10.1, 5.8 Hz, 1H, H-2′β). ^{13}C NMR (CD_3OD) δ: 155.11 (dd, *J* = 246.1, 2.2 Hz), 153.0 (dd, *J* = 259.3, 2.2 Hz), 140.55 (dd, *J* = 16.5, 7.7 Hz), 136.9 (t, *J* = 8.5 Hz), 117.66 (dd, *J* = 24.2, 4.4 Hz), 113.55 (d, *J* = 27.5 Hz), 89.07, 74.48, 73.82, 63.49, 43.31. Anal. calcd. for $C_{11}H_{11}F_2NO_5$: C 48.01, H 4.03, N 5.09; found: C 47.66, H 3.99, N 4.97.

3,5-Bis(*tert*-butyldimethylsilyl)-2-deoxy-D-ribonolactone (10)

Bromine (20 mL) was added to a solution of 2-deoxy-D-ribose (10 g, 74.4 mmol) in water (60 mL), and the brown solution was stirred at 25°C for five days. The excess bromine was extracted with ether, and treated with a saturated solution of NaOH. The solvent from the aqueous fraction was evaporated to give a pale brown syrup, which was heated at 75°C under reduced pressure (30 mmHg) for 4 h. Toluene (100 mL) was added, and the solvent was repeatedly evaporated after each addition of toluene. Methylene chloride (100 mL), and then imidazole (14 g, 206 mmol), were added at 0°C to the syrup obtained above. After stirring at 0°C for 30 min, the reaction mixture turned to a clear solution, to which *tert*-butyldimethylsilyl chloride (23 g, 153 mmol) was added. After stirring at 25°C overnight, the reaction mixture was diluted with ether (200 mL), and the solid was removed by filtration. Removal of the solvent from the filtrate gave a residue that was purified using a short silica gel column (hexane–ether, 10:1 v/v) to give the lactone **10** (21.5 g, 80%) as white crystals, mp 79–80.5°C. ^1H NMR ($CDCl_3$) δ: 4.50 (ddd, *J* = 6.7, 2.4, 2.1 Hz, 1H, H-3), 4.33 (ddd, *J* = 3.4, 2.7, 2.1 Hz, 1H, H-4), 3.81 (dd, *J* = 11.6, 3.4 Hz, 1H, H-5a), 3.76 (dd, *J* = 11.6, 2.7 Hz, 1H, H-5b), 2.82 (dd, *J* = 17.7, 6.7 Hz, 1H, H-2a), 2.39 (dd, *J* = 17.7, 2.4 Hz, 1H, H-2b), 0.89 (s, 18H), 0.09 (s, 6H), 0.08 (s, 3H), 0.06 (s, 3H). ^{13}C NMR ($CDCl_3$) δ: 175.47, 87.99, 69.56, 62.44, 38.97, 25.78, 25.63, 18.22, 17.90, –4.75, –4.82, –5.52, –5.64.

1,4-Anhydro-3,5-*O*-bis(*tert*-butyldimethylsilyl)-2-deoxy-D-erythro-pent-1-enitol (11)

DIBAL-H (1.5 M in toluene, 60 mL, 90 mmol) was added drop wise during 30 min to a cold suspension of the lactone **10** (21.5 g, 59.7 mmol) in dry ether (250 mL) at –78°C under argon. The resulting clear solution was stirred at –78°C for 3.5 h, and the reaction was quenched by slow addition of methanol (60 mL). After warming to 0°C, the reaction solution was washed with 10% aqueous disodium tartrate (2 × 200 mL), and the aqueous fraction was extracted with ether (2 × 100 mL). The combined organic extracts were washed with brine, and the organic fraction was dried (Na_2SO_4). Removal of the solvent gave a colorless oil (21.5 g), which was dissolved in CH_2Cl_2 (300 mL), and the resulting solution was cooled to –78°C under argon. Et_3N (31.5 mL), followed by the drop wise addition of methanesulfonyl chloride (6 mL, 77.5 mmol) were added under argon. The resulting solution was stirred at –78°C for 2 h, and then at –10 – –20°C for an additional 2 h. The reaction mixture was allowed to warm to 25°C prior to heating at reflux under argon for 15 h. After cooling to 25°C, the reaction mixture was diluted with hexane (200 mL), filtered through a silica gel pad, and washed with hexane–ether (1:1 v/v). Removal of the solvent from the filtrate gave a residue that was purified via flash chromatography (hexane–ether, 10:1 v/v) to give **11** (16.8 g, 82%) as a colorless liquid. ^1H NMR ($CDCl_3$) δ: 6.48 (d, *J* = 2.4 Hz, 1H, H-1), 5.02 (dd, *J* = 2.7, 2.4 Hz, 1H, H-2), 4.87 (t, *J* = 2.7 Hz, 1H, H-3), 4.29 (ddd, *J* = 6.4, 5.8, 2.7 Hz, 1H, H-4), 3.70 (dd, *J* = 10.7, 5.8 Hz, 1H, H-5a), 3.52 (dd, *J* = 10.7, 5.8 Hz, 1H, H-5b), 0.90 (s, 9H), 0.90 (s, 9H), 0.10 (s, 6H), 0.08 (s, 3H), 0.07 (s, 3H). ^{13}C NMR ($CDCl_3$) δ: 148.88, 103.35, 88.95, 76.01, 62.83, 25.93 (6C), 18.40, 18.09, –4.20, –4.34, –5.29, –5.32.

3-Fluoro-4-iodoaniline (13a) (Method A)

A mixture of *m*-fluoroaniline (**12a**, 2.22 g, 20 mmol), $NaIO_4$ (0.92 g, 4.3 mmol), iodine (2.04 g, 8.0 mmol), concentrated H_2SO_4 (0.4 mL), and water (4.4 mL) in acetic acid (14 mL) was stirred at 80°C for 4 h. After cooling to 25°C, the black reaction mixture was poured onto a cooled solution of sodium hydrosulfite, and extracted with ether (3 × 50 mL). The combined organic extracts were washed with a 10% solution of NaOH in water, and water, prior to drying (K_2CO_3). Removal of the solvent in vacuo gave a residue that was purified via flash chromatography (hexane–ethyl acetate, 4:1 v/v) and recrystallized from hexane–ether to afford **13a** (2.1 g, 50%) as brown crystals, mp 67–68.5°C. ^1H NMR ($CDCl_3$) δ: 7.42 (dd, *J* = 8.2, 7.6 Hz, 1H), 6.43 (dd, *J* = 10.1, 2.5 Hz, 1H), 6.28 (dd, *J* = 8.2, 2.5 Hz, 1H), 3.82 (br s, 2H, NH_2). ^{13}C NMR ($CDCl_3$) δ: 162.14 (d, *J* = 242.8 Hz), 148.52 (d, *J* = 9.9 Hz), 139.0 (d, *J* = 3.3 Hz), 112.86 (d, *J* = 2.2 Hz), 102.4 (d, *J* = 27.5 Hz), 65.39 (d, *J* = 25.3 Hz).

2,5-Difluoro-4-iodoaniline (13b) (Method B)

N-Iodosuccinimide (7.9 g, 35 mmol) was added in aliquots to an ice-cold solution of 2,5-difluoroaniline (**12b**, 3.9 g, 30 mmol) in trifluoroacetic acid (10 mL), and the resulting solution was stirred at 25°C for 3 h. The reaction mixture was poured onto ice water and neutralized with sodium hydroxide. Extraction with ether (2 × 50 mL), washing the combined organic extracts with a saturated solution of sodium hydrosulfite, and brine, prior to drying (Na_2SO_4). Removal of the solvent gave a residue that was purified via flash chromatography (hexane–ethyl acetate, 5:1 v/v) and recrystallization from hexane–ether to give **13b** (6.8 g, 89%) as pale brown crystals, mp 61–62°C. ^1H NMR ($CDCl_3$) δ: 7.27 (dd, *J* = 9.8, 5.6 Hz, 1H), 6.51 (dd, *J* = 8.5, 7.5 Hz, 1H), 3.87 (br s, 2H, NH_2). ^{13}C NMR ($CDCl_3$) δ: 158.29 (dd, *J* = 238.3, 2.2 Hz), 147.71 (dd, J = 239.5, 2.2 Hz), 136.03 (dd, *J* = 14.3, 9.9 Hz), 124.13 (dd, *J* = 23.1, 3.3 Hz), 103.03 (dd, *J* = 29.7, 3.3 Hz), 63.08 (dd, *J* = 37.3, 2.2 Hz).

2-Methyl-5-fluoro-4-iodoaniline (13c) (Method B)

Yield 65%, pale brown crystals, mp 75–77°C. ^1H NMR ($CDCl_3$) δ: 7.33 (d, *J* = 7.0 Hz, 1H), 6.41 (d, *J* = 9.5 Hz), 3.70 (br s, 2H, NH_2), 2.09 (s, 3H). ^{13}C NMR ($CDCl_3$) δ: 160.56 (d, *J* = 240.6 Hz), 146.28 (d, *J* = 9.9 Hz), 139.23 (d, *J* = 3.3 Hz), 120.21 (d, *J* = 2.2 Hz), 101.81 (d, *J* = 27.5 Hz), 64.99 (d, *J* = 26.4 Hz), 16.23.

© 2000 NRC Canada

3-Fluoro-4-(β-D-glycero-pentofuran-3-ulos-1-yl)aniline (14a)

A freshly dried 100 mL round-bottom flask was charged with palladium acetate (0.135 g, 0.6 mmol) and triphenylarsine (0.54 g, 1.8 mmol) under argon. Dry CH_3CN (20 mL) was added and the yellow suspension was stirred at 25°C for 30 min. A solution of the glycal (**11**, 1.38 g, 4 mmol), 3-fluoro-4-iodoaniline (**13a**, 0.95 g, 4 mmol) and triethylamine (1.2 mL) in CH_3CN (30 mL) was added to this suspension, and the resulting solution was stirred at 60°C for 20 h. After cooling to 25°C, *n*-$Bu_4N^+F^-$ (3.2 g, mmol) was added, and the mixture was stirred at 25°C for 2 h. The reaction was quenched with methanol (4 mL), the solvent was removed in vacuo, and the residue obtained was purified twice in succession via flash chromatography (hexane–ethyl acetate, 1:1 to 1:2 v/v) followed by recrystallization from ether to give **14a** (0.35 g, 39%) as pale yellow crystals, mp 132–133°C. IR (NaCl): 3446, 3364, 3220, 1752, 1635 cm^{-1}. ^1H NMR ($CDCl_3$) δ: 7.20 (dd, *J* = 8.5, 8.2 Hz, 1H), 6.39 (dd, *J* = 8.5, 2.14 Hz, 1H), 6.30 (dd, *J* = 12.5, 2.1 Hz, 1H), 5.22 (dd, *J* = 11.0, 6.0 Hz, 1H), 3.90 (t, *J* = 3.0 Hz, 1H), 3.78 (d, *J* = 3.0 Hz, 2H), 3.62 (br s, 3H, NH_2, OH), 2.70 (dd, *J* = 18.1, 6.0 Hz, 1H), 2.48 (dd, *J* = 18.1, 11.0 Hz, 1H). ^{13}C NMR ($CDCl_3$) δ: 214.2, 161.26 (d, *J* = 243.9 Hz), 148.61 (d, *J* = 9.9 Hz), 128.39 (d, *J* = 6.6 Hz), 115.4 (d, *J* = 14.5 Hz), 110.74 (d, *J* = 2.2 Hz), 101.68 (d, *J* = 25.3 Hz), 82.32, 72.1, 61.05, 43.87. Anal. calcd. for $C_{11}H_{12}FNO_3$: C 58.66, H 5.37, N 6.22; found: C 58.29, H 5.30, N 6.15.

2,5-Difluoro-4-(β-D-glycero-pentofuran-3-ulos-1-yl)aniline (14b)

Compound **14b** was prepared, using a procedure similar to that used for the preparation of **14a**, except that 2,5-difluoro-4-iodoaniline (**13b**) was used in place of 3-fluoro-4-iodoaniline (**13a**). The crude product was purified twice in succession via flash chromatography (hexane–ethyl acetate, 2:1 v/v) followed by recrystallization from ether to give **14b** (31%) as a pale brown syrup. IR (NaCl): 3465, 3368, 3231, 1758, 1649, 1522 cm–1. ^1H NMR ($CDCl_3$) δ: 7.14 (dd, *J* = 11.3, 6.4 Hz, 1H), 6.48 (dd, *J* = 11.3, 7.3 Hz, 1H), 5.29 (dd, *J* = 11.0, 5.8 Hz, 1H), 4.0 (t, *J* = 3.3 Hz, 1H), 3.95 (d, *J* = 3.3 Hz, 2H), 3.92 (br s, 2H, NH_2), 2.84 (dd, *J* = 18.0, 5.8 Hz, 1H), 2.49 (dd, *J* = 18.0, 11.0 Hz, 1H), 2.47 (br s, 1H, OH). ^{13}C NMR ($CDCl_3$) δ: 213.41, 156.45 (dd, *J* = 240.6, 2.2 Hz), 147.47 (dd, *J* = 235.1, 2.2 Hz), 135.83 (dd, *J* = 15.4, 12.1 Hz), 115.41 (dd, *J* = 16.0, 5.5 Hz), 113.5 (dd, *J* = 22.0, 5.5 Hz), 103.3 (dd, *J* = 27.5, 4.4 Hz), 82.0, 71.76, 61.40, 44.10. Anal. calcd. for $C_{11}H_{11}F_2NO_3$: C 54.32, H 4.56, N 5.76; found: C 54.61, H 5.05, N 5.51.

5-Fluoro-4-(β-D-glycero-pentofuran-3-ulos-1-yl)-2-methylaniline (14c)

Compound **14c** was prepared, using a procedure similar to that used for the preparation of **14a**, except that 2-methyl-5-fluoro-4-iodoaniline (**13c**) was used in place of 3-fluoro-4-iodoaniline (**13a**). The crude product was purified twice in succession via flash chromatography (hexane–ethyl acetate, 1:1 – 1:1.2 v/v) followed by recrystallization from ether to give **14c** (38%) as pale yellow crystals, mp 105–107°C. ^1H NMR ($CDCl_3$) δ: 7.11 (d, *J* = 8.2 Hz, 1H), 6.38 (d, *J* = 12.2 Hz, 1H), 5.29 (dd, *J* = 11.0, 6.1 Hz, 1H), 3.99 (t, *J* = 3.4 Hz, 1H), 3.91 (d, *J* = 3.4 Hz, 2H), 2.79 (ddd, *J* = 18.0, 6.1, 0.9 Hz, 1H), 2.60 (dd, *J* = 18.0, 11.0 Hz, 1H), 2.11 (s, 3H). ^{13}C NMR ($CDCl_3$) δ: 213.83, 159.81 (d, *J* = 242.9 Hz), 146.25 (d, *J* = 11.0 Hz), 129.01 (d, *J* = 5.5 Hz), 117.81 (d, *J* = 2.2 Hz), 115.14 (d, *J* = 13.2 Hz), 101.67 (d, *J* = 25.3 Hz), 82.04, 72.69 (d, *J* = 2.2 Hz), 61.52, 43.96, 16.52.

3-Fluoro-4-[1-(2-deoxy-β-D-ribofuranosyl)]aniline (6a)

$NaB(OAc)_3H$ was added in one portion to an ice cold solution of **14a** (0.225 g, 1 mmol) in dry CH_3CN (10 mL) with stirring under argon. After stirring at 0°C for 2 h, the reaction was quenched with methanol (10 mL), and the solvents were removed in vacuo. The residue obtained was purified via flash chromatography (hexane–ethyl acetate, 1:2 – 0:1 v/v) to give **6a** (0.17 g, 75%) as a pale yellow solid, which was recrystallized from ethanol to give white crystals (0.13 g, 58%), mp 183–184.5°C. ^1H NMR (DMSO-d_6) δ: 7.10 (dd, *J* = 8.8, 8.5 Hz, 1H), 6.34 (d, *J* = 8.5 Hz, 1H), 6.25 (d, *J* = 13.2 Hz, 1H), 5.31 (s, 2H, NH_2), 5.06 (dd, *J* = 10.4, 5.5 Hz, 1H), 5.0 (d, *J* = 4.0 Hz, 1H, 3′-OH), 4.69 (t, *J* = 5.5 Hz, 1H, 5′-OH), 4.14 (m, 1H), 3.69 (m, 1H), 3.41 (m, 2H), 1.94 (dd, *J* = 12.6, 5.5 Hz, 1H), 1.78 (ddd, *J* = 12.6, 10.4, 5.5 Hz, 1H). ^{13}C NMR (DMSO-d_6) δ: 160.52 (d, *J* = 241.7 Hz), 149.74 (d, *J* = 12.1 Hz), 128.12, 114.91 (d, *J* = 14.3 Hz), 109.73, 99.62 (d, *J* = 27.5 Hz), 87.05, 72.83, 72.30 (d, *J* = 8.8 Hz), 62.41 (d, *J* = 8.8 Hz), 41.76 (d, *J* = 3.3 Hz). ^{19}F NMR (DMSO-d_6) δ: 46.03 (dd, *J* = 12.2, 9.2 Hz). Anal. calcd. for $C_{11}H_{14}FNO_3$: C 58.14, H 6.21, N 6.16; found: C 58.08, H 6.41, N 6.10.

2,5-Difluoro-4-[1-(2-deoxy-β-D-ribofuranosyl)]aniline (6b)

A similar reduction of **14b**, using the procedure described for reduction of **14a** above, and purification of the product afforded **6b** (73%) as a pale yellow solid, which was recrystallized from ether to give pale yellow crystals (65%), mp 163–164.5°C. ^1H NMR (DMSO-d_6) δ: 7.09 (dd, *J* = 12.2, 6.71 Hz, 1H), 6.47 (dd, *J* = 11.9, 7.6 Hz, 1H), 5.35 (s, 2H, NH_2), 5.07 (dd, *J* = 10.4, 5.2 Hz, 1H), 5.02 (d, *J* = 3.7 Hz, 1H, 3′-OH), 4.74 (t, *J* = 5.5 Hz, 1H, 5′-OH), 4.15 (m, 1H), 3.72 (m, 1H), 3.43 (m, 2H), 1.98 (dd, *J* = 12.5, 5.2 Hz, 1H), 1.76 (ddd, *J* = 12.5, 10.4, 5.5 Hz, 1H). ^{13}C NMR (DMSO-d_6) δ: 155.53 (d, *J* = 238.4 Hz), 146.61 (d, *J* = 232.9 Hz), 136.58 (dd, *J* = 15.4, 12.1 Hz), 115.26 (dd, *J* = 16.5, 5.5 Hz), 112.95 (dd, *J* = 20.9, 6.6 Hz), 101.69 (dd, *J* = 27.5, 4.4 Hz), 87.17, 72.22, 72.14, 62.20, 42.02. Anal. calcd. for $C_{11}H_{12}F_2NO_3$: C 53.88, H 5.34, N 5.71; found: C 53.70, H 5.42, N 5.54.

5-Fluoro-4-[1-(2-deoxy-β-D-ribofuranosyl)]-2-methylaniline (6c)

$NaB(OAc)_3H$ (2.54 g, 12 mmol) was added in one aliquot to an ice cold solution of **14c** (0.72 g, 3 mmol) in dry CH_3CN (30 mL) with stirring under argon. After stirring at 0°C for 2 h, the reaction was quenched with methanol (20 mL), and the solvent was removed in vacuo. The residue obtained was purified via flash chromatography (hexane–ethyl acetate, 1:2 – 1:5 v/v) to give **6c** (0.37 g, 52%) as a pale yellow syrup. ^1H NMR (DMSO-d_6) δ: 6.99 (d, *J* = 8.5 Hz, 1H), 6.31 (d, *J* = 12.8 Hz, 1H), 5.05 (s, 2H, NH_2), 5.05 (m, 1H), 4.99 (d, *J* = 3.0 Hz, 1H, 3′-OH), 4.70 (t, *J* = 5.4 Hz, 1H, 5′-OH), 4.14 (m, 1H), 3.69 (m, 1H), 3.42 (m,

© 2000 NRC Canada

2H), 1.99 (s, 3H), 1.93 (dd, J = 11.9, 5.2 Hz, 1H), 1.80 (ddd, J = 11.9, 11.6, 5.8 Hz, 1H). ^{13}C NMR (DMSO-d_6) δ: 158.73 (d, J = 239.5 Hz), 147.14 (d, J = 11.0 Hz), 128.57 (d, J = 5.5 Hz), 116.69 (d, J = 2.2 Hz), 114.71 (d, J = 14.3 Hz), 99.54 (d, J = 25.3 Hz), 87.12, 72.74 (d, J = 2.2 Hz), 72.29, 62.43, 41.83, 16.67. Anal. calcd. for $C_{12}H_{16}FNO_3$: C 59.74, H 6.68, N 5.81; found: C 59.11, H 6.41, N 5.64.

Acknowledgments

We are grateful to the Medical Research Council of Canada (Grant no. MT-14480) for financial support of this research, and to the Alberta Heritage Foundation for Medical Research for a fellowship to one of us (Z.-X.W.). Work done at the Rega Institute was supported by the Fonds voor Wetenschappelijk Onderzoek (FWO)-Vlaanderen (Krediet no. 9.0104.98), and the Geconcerteerde Onderzoeksacties (GOA)-Vlaamse Gemeenschap contract no. 2000/12. We thank Ann Absillis, Anita Camps, Frieda De Meyer, Lizette van Berckelaer, Lies Vandenheurck, and Anita Van Lierde for excellent technical assistance.

References

1. C. Perigaud, G. Gosselin, and J.L. Imbach. Nucleosides Nucleotides, **11**, 903 (1992).
2. (*a*) U. Hacksell and G.D. Daves. Prog. Med. Chem. **22**, 1 (1985); (*b*) J.A. Montgomery. Antiviral Res. **12**, 113 (1989); (*c*) M.M. Mansuri and J.C. Martin. Annu. Rep. Med. Chem. **23**, 161 (1988).
3. B.A. Schweitzer and E.T. Kool. J. Org. Chem. **59**, 7238 (1994).
4. S. Moran, R.R.-X. Ren, and E.T. Kool. Proc. Natl. Acad. Sci. U.S.A. **94**, 10506 (1997).
5. S. Moran, R.R.-X. Ren, S. Rumney, and E.T. Kool. J. Am. Chem. Soc. **119**, 2056 (1997).
6. J. Morales and E.T. Kool. Nature Struct. Biol. **5**, 950 (1998).
7. K.M. Guckian, T.R. Krugh, and E.T. Kool. Nature Struct. Biol. **5**, 954 (1998).
8. (*a*) M. Yoshida, A. Hoshi, K. Kuretani, and M. Saneyoshi. Chem. Pharm. Bull. **30**, 1018 (1982); (*b*) M. Bretner, M. Balinska, K. Krawiec, B. Kierdaszuk, D. Shugar, and Y. Kulikowski. Nucleosides Nucleotides, **14**, 657 (1995).
9. H.-P. Hsieh and L.W. McLaughlin. J. Org. Chem. **60**, 5356 (1995).
10. E. De Clercq. Biochem. Pharmacol. **33**, 2159 (1984).
11. L.J. Knutsen. Nucleosides Nucleotides, **11**, 961 (1992) and refs. therein.
12. M. Hoffer. Chem. Ber. **93**, 2777 (1960).
13. (*a*) N.C. Chaudhuri and E.T. Kool. Tetrahedron Lett. **36**, 1795 (1995); and its corrigendum: **36**, 4910 (1995).
14. N.C. Chaudhuri, R.R.-X. Ren, and E.T. Kool. Synlett. 347 (1997).
15. R.R.-X. Ren, N.C. Chaudhuri, P.L. Paris, S. Rumney, and E.T. Kool. J. Am. Chem. Soc. **118**, 7671 (1996).
16. (*a*) H. Vorbruggen, K. Krolikiewicz, and B. Bennua. Chem. Ber. **114**, 1234 (1981); (*b*) V. Rolland, M. Kotera, and J. Lhomme. Synth. Commun. **27**, 3505 (1997).
17. C.D. Hurd and H.T. Miles. J. Org. Chem. **29**, 2976 (1964).
18. N.C. Chaudhuri, R.R.-X. Ren, and E.T. Kool. Synlett. 341 (1997).
19. (*a*) G.D. Daves. Acc. Chem. Res. **23**, 210 (1990); (*b*) U. Hacksell and G.D. Daves. J. Org. Chem. **48**, 2870 (1983); (*c*) R.A. Outten and G.D. Daves. J. Org. Chem. **54**, *29* (1989); (*d*) R.N. Farr and G.D. Daves. J. Carbohydr. Chem. **23**, 201 (1990); (*e*) R.N. Farr, D.-I. Kwok, J.C.-Y. Cheng, and G.D. Daves. J. Org. Chem. **57**, 2093 (1992); (*f*) H.C. Zhang and G.D. Daves. J. Org. Chem. **57**, 4690 (1992); (*g*) R.S. Coleman and M.L. Madaras. J. Org. Chem. **63**, 5700 (1998); (*h*) J.A. Walker, J.J. Chen, J.M. Hinkley, D.S. Wise, and L.B. Townsend. Nucleosides Nucleotides, **16**, 1999 (1997).
20. J.A. Walker, J.J. Chen, J.M. Hinkley, D.S. Wise, and L.B. Townsend. J. Org. Chem. **61**, 2219 (1996).
21. R.E. Deriaz, W.G. Overend, M. Stacey, E.G. Teece, and L.F. Wiggins. J. Chem. Soc. 1879 (1949).
22. G.A. Olah, Q. Wang, G. Sandford, and G.K.S. Prakash. J. Org. Chem. **58**, 3194 (1993).
23. J.R. Mercer, L.-H. Xu, E.E. Knaus, and L.I. Wiebe. J. Med. Chem. **32**, 1289 (1989).
24. M.J. Robins, S. Manfredini, S.G. Wood, R.J. Wanklin, B.A. Rennie, and S.L. Sacks. J. Med. Chem. **34**, 2275 (1991).
25. L.I. Wiebe and E.E. Knaus. Adv. Drug Del. Rev. **39**, 63 (1999).
26. E. De Clercq, J. Balzarini, P.F. Torrence, M.P. Mertes, C.L. Schmidt, D. Shugar, P.J. Barr, A.S. Jones, G. Verhelst, and R.T. Walker. Mol. Pharmacol. **19**, 321 (1981).
27. J. Balzarini, L. Naesens, J. Slachmuylders, H. Niphuis, I. Rosenberg, A. Holý, H. Schellekens, and E. De Clercq. AIDS, **5**, 21 (1991).
28. C. Meier, T. Knispel, E. De Clercq, and J. Balzarini. J. Med. Chem. **43**, 1604 (1999) and refs. therein.
29. C. Meier, M. Lorey, E. De Clercq, and J. Balzarini. J. Med. Chem. **41**, 1417 (1998).

© 2000 NRC Canada

Medium-sized cyclophanes. Part 53.[1] Synthesis and conformational studies, and photoinduced cyclization of *syn*-[n.2]metacyclophanenes

Takehiko Yamato, Koji Fujita, Keigo Futatsuki, and Hirohisa Tsuzuki

Abstract: A series of [n.2]metacyclophanenes (**3**) and (**6**) were prepared in good yields by a McMurry cyclization of 1,n-bis(3-acetyl-4-methoxyphenyl)alkanes (**2**) and 1,3-bis(3-formyl-4-methoxyphenyl)propane (**5**), respectively. Compounds **3b**, **3c** exist in the *syn*-conformation due to the steric repulsion between the methyl groups at the ethano bridge and the methoxy groups at the aromatic rings while compound **6** prefers the *anti*-conformation typical of [3.2]metacyclophanes. The assignment of *syn*-conformations has been confirmed by ^{1}H NMR analyses and X-ray diffraction studies. Photoinduced transannular cyclization of [n.2]metacyclophanenes (**3**) and (**6**) in the presence of iodine as an oxidant afforded phenanthrene-anellated polycyclic aromatic hydrocarbons. Apparently, the rate of the photocyclization of *anti*-**6** was found to be much faster than that of *syn*-**3b** and almost completed within 1 h. Thus, the different reactivities for the irradiation of *syn*- and *anti*-conformer were observed. The reason for the present preference for the formation of *trans*-dihydrophenanthrene rather than *cis*-dihydrophenanthrene as the intermediate might be attributable to the more stable chair form transition state than boat one and the conformational fixation to the chair form in the ground and transition state is possible in the *anti*-conformer.

Key words: cyclophanes, strained molecule, McMurry reaction, C—C coupling, conformation analysis, cyclizations, photolysis, transannular reactions, transition states.

Résumé : Faisant appel à une réaction de cyclisation de McMurry des 1,n-bis(3-acétyl-4-méthoxyphényl)alcanes (**2**) et 1,3-bis(3-formyl-4-méthoxyphényl)propane (**5**) respectivement, on a préparé une série de [n,2]métacyclophanènes (**3**) et (**6**). Les composés **3b** et **3c** existent dans la conformation syn en raison de la répulsion stérique entre les groupes méthyles du pont éthano et les groupes méthoxy des noyaux aromatiques alors que le composé **6** adopte la conformation anti des [3,2]métacyclophanes. L'attribution des conformations *syn* a été confirmée par des analyses de RMN du ^{1}H et des études de diffraction des rayons X. La cyclisation transannulaire photoinduite des [n,2]métacyclophanènes (**3**) et (**6**) en présence d'iode, utilisé comme antioxydant, conduit à des hydrocarbures aromatiques polycycliques du type phénanthrène avec annellation. Apparemment, la vitesse de photocyclisation du produit *anti*-**6** est beaucoup plus rapide que celle du *syn*-**3b** et elle est pratiquement complète en une heure. Ainsi, on a pu observer des réactivités différentes pour l'irradiation des conformères *syn* et *anti*. La raison de la formation observée d'une préférence pour la formation comme intermédiaire du *trans*-dihydrophénanthrène plutôt que du *cis*-dihydrophénanthrène pourrait être attribuée à l'état de transition en forme chaise qui est plus stable que celui en forme bateau ainsi que le fait que la conformation des états tant fondamental que de transition du conformère *anti* peut être fixée à la forme chaise.

Mots clés : cyclophanes, molécule tendue, réaction de McMurry, couplage C—C, analyse conformationnelle, photolyse, réactions transannulaires, états de transition.

[Traduit par la Rédaction]

Introduction

Although the parent [2.2]metacyclophane (MCP = metacyclophane) was first reported as early as 1899 by Pelligrin (2), the synthesis of *syn*-[2.2]MCP was not realized until 85 years later. Mitchell et al. (3) have successfully prepared *syn*-[2.2]MCP at low temperature by using (arene)chromiumcarbonyl complexation to control the stereochemistry. Later, Itô and co-workers (4) also isolated and characterized *syn*-[2.2]MCP without complexation. However, *syn*-[2.2]MCP isomerizes readily to the *anti*-isomer above 0°C. On the other hand, Mitchell and Boekelheide (5) and Staab

Received March 21, 2000. Published on the NRC Research Press website on August 4, 2000.

T. Yamato[2], K. Fujita, and K. Futatsuki. Department of Applied Chemistry, Faculty of Science and Engineering, Saga University, Honjo-machi 1, Saga-shi, Saga 840-8502, Japan.
H. Tsuzuki. Center of Environmental Analysis, Tohwa Institute for Science, Tohwa University, 1-1-1 Chikushigaoka, Minami-ku, Fukuoka-shi, Fukuoka 815-8510, Japan.

[1]Part 52. See Ref. 1.

[2]Author to whom correspondence may be addressed. Telephone: (0952)28-8679. Fax: (0952)28-8591.
e-mail: yamatot@cc.saga-u.ac.jp

© 2000 NRC Canada

et al. (6) succeeded in synthesizing intraannularly substituted *syn*-[2.2]MCPs, respectively. However, reports on synthesis and reactions of *syn*-[n.2]MCP-ene have not been published so far.

In cyclophane chemistry, the reductive coupling of carbonyl compounds by low-valent titanium, the McMurry reaction (7), has been used before by Mitchell and Weerawana (8) to synthesize cyclophanes with glycol units as bridges, by Tanner and Wennerström (9), and recently by Hopf and Mlynek (10) and Grützmacher et al. (11) for a cyclization of suitable dialdehydes to yield unsaturated cyclophanes.

In this paper, we report on the syntheses of *syn*- and *anti*-[n.2]MCP-enes using the low-valent titanium induced McMurry reaction and photoinduced transannular cyclization reaction to afford phenanthrene-anellated polycyclic aromatic hydrocarbons.

Results and discussion

1,2-Bis(4-methoxyphenyl)ethane (**1a**) has been prepared according our previous paper (12). The cross coupling reactions (13) of 4-methoxyphenylmagnesium bromide with 1,3-dibromopropane and 1,4-dibromobutane have been carried out in the presence of cuprous bromide as a catalyst in a mixture of hexamethylphosphoric triamide (HMPA) and tetrahydrofuran at reflux temperature to give the desired 1,3-bis(4-methoxyphenyl)propane (**1b**) and 1,4-bis(4-methoxyphenyl)butane (**1c)** in satisfactory yields. Although the $AlCl_3$–$MeNO_2$-catalyzed acetylation of compound **1a** with acetyl chloride at 20°C led to complete diacylation, a mixture of the desired 1,2-bis(3-acetyl-4-methoxyphenyl)ethane (**2a)** and other isomers was obtained. The desired product **2a** was isolated in pure by the fractional recrystallization from hexane–benzene (1:1) in 29% yield. In contrast, the $AlCl_3$–$MeNO_2$-catalyzed acetylation of compounds **1b** and **1c** with acetic anhydride or acetyl chloride at 20°C led to regioselective acylation at the meta positions of the 1,n-diphenylalkanes affording the desired 1,n-bis(3-acetyl-4-methoxyphenyl)alkanes (**2b**) and (**2c**) in good yields.

1,2-Bis(3-acetyl-4-methoxyphenyl)ethane **(2a**) was subjected to reductive coupling by the McMurry reaction (7) following the Grützmacher's procedure (11) (Scheme 1). Although none of the desired [2.2]MCP-1-ene (**3a**) was observed, the dimer **4a** was obtained in 19% yield. This finding seems to be due to the much more strained structure of **3a** than dimer **4a** during the formation of the unsaturated C=C linkage. Although several cyclizations of **2a** were attempted under the various reaction conditions, no formation of the desired **3a** was observed, with only dimer **4a** being obtained. Thus, during the McMurry reaction the intramolecular cyclization to afford **3a** might be quite difficult.

The structure of product dimer **4a** was determined on the basis of its elemental analysis and spectral data. The mass spectral data for dimer **4a** (M^+ m/z = 588) strongly supports cyclic dimeric structure. In the ^1H NMR spectrum of tetramethoxyMCP **4a**, methyl protons, methoxy protons, ArCH_2CH_2Ar methylene protons, and the ArC*H*=C*H*Ar olefinic protons each appear as a singlet at 27°C. This behavior indicates that the rate of conformational ring flipping of macrocycle **4a** is faster than the NMR time scale above this temperature. However, in dimer **4a** even at –60°C in

Scheme 1.

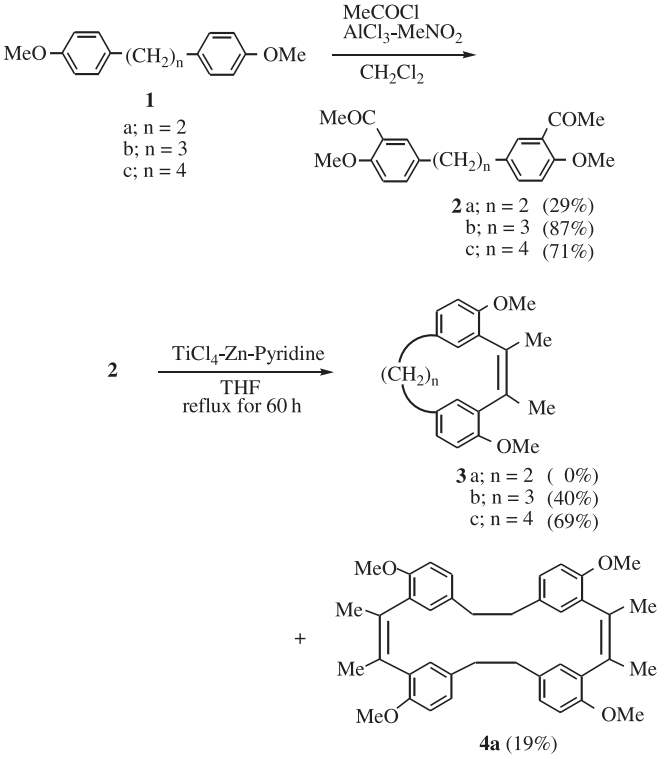
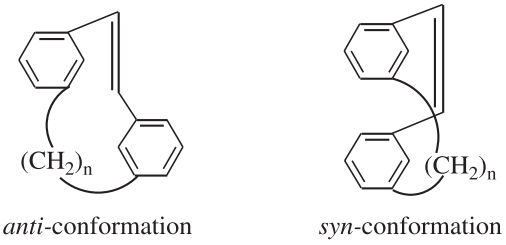


Fig. 1. Possible conformations of [n.2]metacyclophan-1-enes.



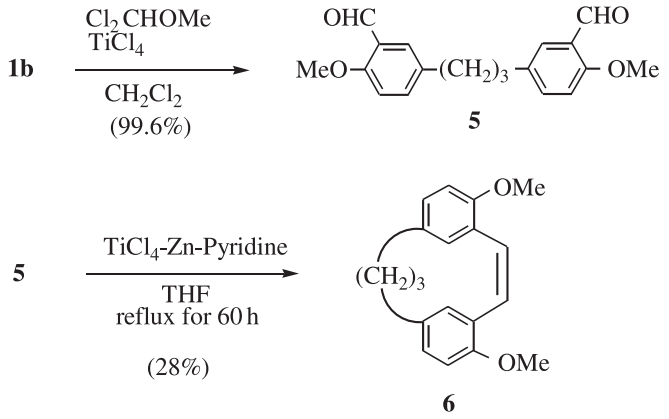
$CDCl_3$–CS_2 (1:3) the singlet signal of the ArCH_2CH_2Ar ethylene protons and the ArC*H*=C*H*Ar olefinic protons both remain unsplit. These observations indicate the flexible structure of **4a** similar to that of the saturated [2_4]MCP (14) in spite of the introduction of two additional double bonds of the ethylene bridge.

Similarly, 1,n-bis(3-acetyl-4-methoxyphenyl)alkanes (**2b**) and **2c** were subjected to reductive coupling by the McMurry reaction (Scheme 1). Novel [n.2]MCP-enes (**3b**) and (**3c**) have been prepared in 40% and 69% yields.

[n.2]MCP-enes adopt either a "staircase" *anti*-conformation or a *syn*-conformation with overlaying aromatic rings (15) (Fig. 1). Depending on the size of the bridges (16) and on the presence of intraannular substituents (17), the interconversion between the *syn*- and *anti*-conformers occur by ring flipping. ^1H NMR spectrum of **3b** showed the doublet of the intraannular proton H_i at δ = 6.95 (J = 2.0 Hz) apart from at δ = 6.33 and 6.60 of the other two protons at the aromatic rings. The methyl protons at the bridged double bond and methoxy protons were observed as a singlet at δ = 2.18 and 3.59, and the protons of the trimethylene bridge generate a complicated signal pattern as expected for a rigid

© 2000 NRC Canada

Scheme 2.



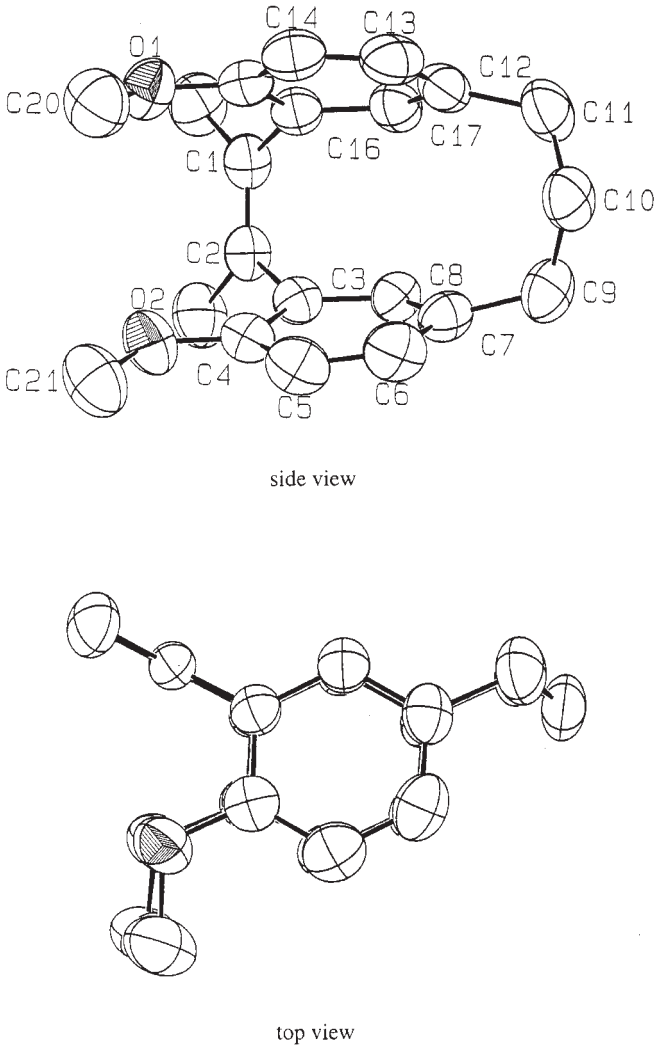
syn-[3.2]MCP-10-ene. The protons of the benzylic CH_2 group were observed as two multiplets centered at $\delta = 2.58$ and 2.91 which are further split by coupling with the protons of the central CH_2 group. This central CH_2 group was also observed as two multiplets centered at $\delta = 1.28$ and 2.18. This peak pattern ascribed to six chemically distinct protons of the propano bridge proves the absence of a *syn–syn* interconversion which would exchange H_A and H_B of each CH_2 group. Interestingly, similar findings were also observed in *syn*-[4.2]MCP-11-ene (*syn*-**3c**) in spite of being expected to be more flexible structure attributable to the larger cyclophane ring size. These observations suggest that the introduction of a double dond of the ethylene bridge as well as the substituents such as methyl groups and methoxy groups might control the *syn*- and *anti*-conformation of [n.2]MCP-enes (**3**).

To study the conformation of [n.2]MCP-enes **3** in more detail, we have investigated the conformation of the corresponding [3.2]MCP-10-ene **6**, which was prepared in 28% yield by the McMurry cyclization of 1,3-bis(3-formyl-4-methoxyphenyl)propane (**5**) under the same reaction conditions like *syn*-**3b** (Scheme 2).

Interestingly, in contrast to **3**, the doublet of H_i at $\delta = 6.05$ ($J = 2.4$ Hz) in the ^{1}H NMR spectrum of **6** shows clearly that **6** adopts a staircase *anti*-conformation as known for other [3.2]MCP-10-enes (11*a*, 11*b*) and [3.2]MCPs (13*c*, 15, 16). In addition, the protons of the trimethylene bridge give rise to two multiplets centered at $\delta = 2.35$ and 1.84, respectively, providing a fast interconversion of the two anti conformations of **6** by ring flipping. However, as the temperature of the solution in $CDCl_3$–CS_2 (1:3) is decreased, a single peak of the benzyl protons splits into a pair of doublets below 0°C. The energy barrier to the conformational ring flipping estimated from the coalescence temperature (T_c) is 12.4 kcal mol^{-1}. This finding indicates more flexible structure of **6** than that of *syn*-**3b** in spite of the same ring size.

Usually, the parent [3.2]MCPs in which intraannular substituents are absent, preferably adopt an *anti*-conformation (15, 16). However, in the case of the MCP **3b** the *syn*-conformation is induced by substituents at the ethano bridge. The substituent effect on the preferred conformation (18) and the different molecule flexibility of **3b** and **6** can be attributed to the van der Waals repulsion between the four methyl groups in **3b**. In the *anti*-conformation of [3.2]MCP-10-ene (**6**) the twisted ethano bridge tends to flatten the staircase structure to release the local strain. However, this flattening is especially opposed by the two methoxy groups in the extraannular position 7 and 13 and the two methyl groups in the bridge position 10 and 11 of **3b**. This effect is absent in the *syn*-conformation and, as a consequence, **3b** favors this *syn*-conformation. The conformation of *syn*-**3b** and *syn*-**3c** has also been confirmed by X-ray crystallographic analysis.

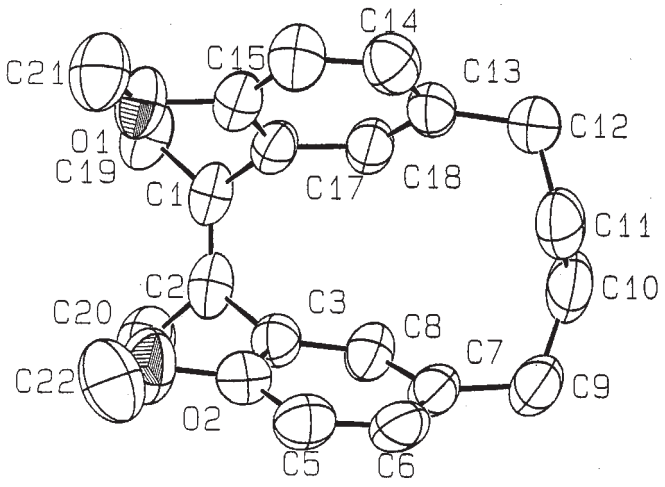
Fig. 2. ORTEP drawing of *syn*-7,13-dimethoxy-10,11-dimethyl-[3.2]MCP-10-ene (*syn*-**3b**). Thermal ellipsoids are drawn at the 50% probability level. All hydrogen atoms are omitted for clarity.



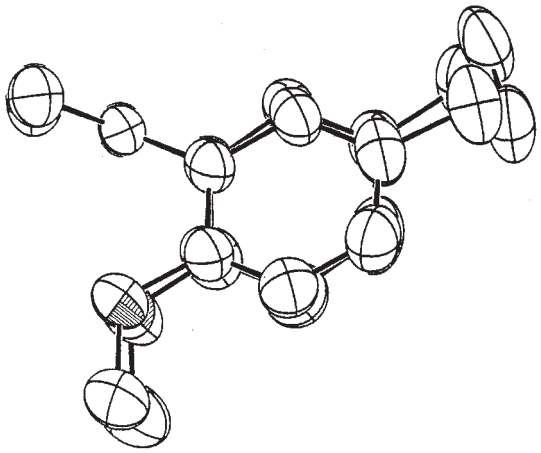
Single colorless crystals of the *syn*-**3b** and *syn*-**3c** suitable for X-ray crystallography were both obtained by recrystallization from methanol–chloroform (1:1). The perspective ORTEP drawings of the *syn*-**3b** and *syn*-**3c** are illustrated in Figs. 2 and 3, with the atom numbering system. Both compounds crystallized in the same monoclinic space group $P2_1/a$. The X-ray crystallography clearly reveals that both conformations of the *syn*-**3b** and *syn*-**3c** adopt the *syn*-form in which two aromatic rings face each other. Two aromatic rings of the *syn*-**3b** and *syn*-**3c**, which deviate from planarity to some extent, locate like an half-open bivalve

© 2000 NRC Canada

Fig. 3. ORTEP drawing of *syn*-8,14-dimethoxy-11,12-dimethyl-[4.2]MCP-11-ene (*syn*-**3c**). Thermal ellipsoids are drawn at the 50% probability level. All hydrogen atoms are omitted for clarity.



side view



top view

using the C(3), C(7), C(12), and C(16) and C(3), C(7), C(13), and C(17) carbons as roots, respectively, to avoid π-electronic repulsion as shown in the side view of the ORTEP drawing. Although the double bond lengths between C(1)-C(2) in the *syn*-**3b** and *syn*-**3c** are reasonable, 1.332 and 1.354 Å, respectively, these compounds have quite different conformations of the two aromatic rings due to the different methylene chain length.

In the *syn*-**3b**, two aromatic rings distort like a boat shape and deviate from planarity to some extent. The C(4), C(7), C(12), and C(15) carbons are out of the C(3)-C(5)-C(6)-C(8) and C(13)-C(14)-C(16)-C(17) planes. The dihedral angles of the C(3)-C(5)-C(6)-C(8) plane between the C(3)-C(4)-C(5) and C(6)-C(7)-C(8) planes, and those of the C(13)-C(14)-C(16)-C(17) plane between the C(14)-C(15)-C(16) and C(12)-C(13)-C(17) planes are 1.77°, 4.52°, 1.53°, and 5.54°, respectively, showing that the aromatic rings in the *syn*-**3b** adopts unsymmetrically strained structure and the rigid ethylene chain against the flexible methylene chains might loose the strain. Furthermore, the intramolecular distances of C(3)-C(16), C(4)-C(15), C(5)-C(14), C(6)-C(13), C(7)-C(12), C(8)-C(17) are 2.745, 3.688, 4.493, 4.229, 3.318, and 2.764 Å, and the dihedral angle between the C(3)-C(5)-C(6)-C(8) and C(13)-C(14)-C(16)-C(17) planes is 39.88°. These clearly show that two aromatic rings in the *syn*-**3b** do not adopt parallel conformation to avoid an electrostatic interaction.

Two aromatic rings in the *syn*-**3c** also strain like a boat shape as well as those in the *syn*-**3b** and the carbons, C(4), C(7), C(13), and C(16) are remote from the C(3)-C(5)-C(6)-C(8) and C(14)-C(15)-C(17)-C(18) planes. The dihedral angles of the C(3)-C(5)-C(6)-C(8) plane between the C(3)-C(4)-C(5) and C(6)-C(7)-C(8) planes, and those of the C(14)-C(15)-C(17)-C(18) plane between the C(15)-C(16)-C(17) and C(13)-C(14)-C(18) planes are 1.76°, 3.85°, 1.65°, and 3.99°, respectively. The fact that the dihedral angles on the side of the methylene chains are somewhat smaller than the corresponding ones in the *syn*-**3b** might be attributed to the cancel of strain to some extent because of lengthening the methylene chains.

Interestingly, the intramolecular distances of C(3)-C(17), C(4)-C(16), C(5)-C(15), C(6)-C(14), C(7)-C(13), and C(8)-C(18) in the *syn*-**3c** are 2.842, 4.060, 5.336, 5.323, 4.135, and 3.038 Å, which are much longer than those of the corresponding carbons in the *syn*-**3b**. The dihedral angle between the C(3)-C(5)-C(6)-C(8) and C(14)-C(15)-C(17)-C(18) planes is 59.53°, which is ca. 20° larger than the appropriate dihedral angle in the *syn*-**3b**. These indicate that two aromatic rings in the *syn*-**3c** might tilt to a greater extent than those in the *syn*-**3b**, since the methylene chain length of the *syn*-**3c** is longer than that of the *syn*-**3b** and the rings are easy to avoid an electronic repulsion.

The substituents effect on the conformation was observed, for example, in 10,15-dihydro-5*H*-tribenzo[*a*,*d*,*g*]cyclononene and its congeners which adopt their stable crown conformation, evidenced, in ^{1}H NMR spectra, by the characteristic AX quartet of the methylene bridges (19). Destabilization of the crown may arise from steric hindrance created either by geminal substitution of one methylene group (20) or by the presence of bulky substituents (21) such as a bromine atom or an allyl group at the aromatic positions *ortho* to the nine-membered ring except a methoxy group (21*d*, 21*e*).

In the present system, the similar substituents effect like 10,15-dihydro-5*H*-tribenzo[*a*,*d*,*g*]cyclononene might be also observed. To elucidate this, we have converted the methoxy group in *syn*-**3b** to hydroxy group by demethylation of *syn*-**3b** with boron tribromide (22). The desired diol **7b** was obtained in 44% yield. Similarly, dihydroxy[4.2]MCP-11-ene (**7c**) was obtained in 53% yield. Interestingly, the bridged double bond was stable in the acidic media quite differnt from the results obtained from the *anti*-[2.2]MCP-enes, in which the transannular cyclization reactions occur to afford the corresponding 4,5-dihydropyrenes under the acidic conditions (23). Furthermore, no *syn*- to *anti*-ring inversion occurred during the demethylation. The ^{1}H NMR spectra for *syn*-**7b** and *syn*-**7c** (in $CDCl_3$) show signals for the hydroxy groups at δ 5.29 and 5.15, respectively. It is well known that the stretching vibration of the OH groups at low frequency

© 2000 NRC Canada

Table 1. Conformational analysis of [n.2]MCP-enes **3**, **6**, and [n.2]MCPs **8**.

Compd	Number of methylene units (n)	Temp (°C)	^{1}H NMR (δ)[a] aromatic protons		Assignment
			H_i[b]	H_o[c]	
3b	3	27	6.95	6.33, 6.60	*syn*
3c	4	–40	6.93	6.41, 6.64	*syn*
6	3	–40	6.05	6.77, 6.97	*anti*
8b	3	27	4.87, 5.24	6.78, 6.97	*anti*
8c	4	–30	5.61, 5.92	6.77, 6.90	*anti*

[a]Determined in $CDCl_3$ at room temp by using $SiMe_4$ as a reference and expressed in ppm.

[b]H_i refers to internal protons.

[c]H_o refers to outer protons.

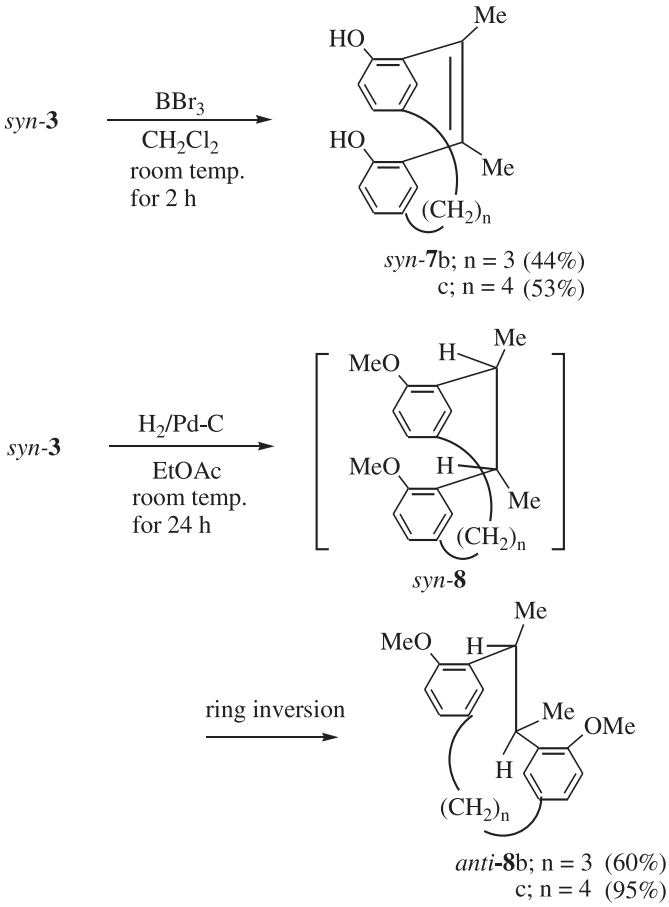
and the resonance for the protons of the OH groups at low field can be attributed to the intramolecular hydrogen bonding (13*c*, 22*d*, 24; for the circular intramolecular hydrogen bonding, see ref. (24*b*–*e*)). The υ_{OH} (3272 cm^{-1} for *syn*-**7b** and 3344 cm^{-1} for *syn*-**7c**) and δ_{OH} values in *syn*-**7b** and *syn*-**7c** in which two hydroxy groups are located in neighbouring positions, show slightly lower frequency IR vibrations and down-field NMR shifts, which imply that a weak hydrogen bond might exist. Therefore, it seems to assume that the *syn*-conformation of **7** might be due to the intramolecular hydrogen bonding. However, in DMSO-d_6 or pyridine-d_5 solution, which can disrupt the intramolecular hydrogen bonding, the ^{1}H NMR spectrum of *syn*-**7b** at room temperature is almost identical with that in $CDCl_3$ and no *anti*-conformer is observed. These findings might be attributable to the similar destabilization of the *anti*-conformation in *syn*-**7b** arising from steric hindrance between the hydroxy groups at the 7,13-positions and the methyl groups on the bridged double bond at 10,11-positions like *syn*-**3b**, but not the intramolecular hydrogen bonding among the two hydroxy groups.

An attempted hydrogenation of *syn*-**3b** in the presence of Pd-C in ethyl acetate at room temperature led to afford *anti*-**8b** in 60% yield. The desired product *syn*-**8b** has not been obtained. Thus, *syn*- to *anti*-ring inversion occurred during the hydrogenation (22). The same result was obtained in the case of the hydrogenation of *syn*-**3c** to afford *anti*-**8c**.

The structures of *anti*-**8b**, **8c** were assigned on the basis of elemental analyses and spectral data. The ^{1}H NMR spectral data of [n.2]MCP-enes **3**, **6** and [n.2]MCPs **8** are summarized in Table 1.

Griffin et al. (25) reported the structure of 1,2-dimethyl[2.2]MCP and assigned the *exo*-*endo*-arrangement (26). We have assigned the ^{1}H NMR signals of **8** in a similar fashion. In the ^{1}H NMR spectrum of *anti*-**8b** in $CDCl_3$ upfield shifts and the different chemical shifts for internal aromatic protons at δ 4.87 and 5.24 due to the ring current of the opposite aromatic ring were observed (27). These data strongly suggest that the structure of **8b** is the *anti*-conformer. Furthermore, the two methyl groups show different chemical shifts at δ 0.95 and 1.68 as a doublet with coupling constant J = 7.3 Hz. The higher field absorption is attributed to the *exo* methyl group and the lower field absorption is attributed to the *endo* methyl group which is in a strongly deshielding region of the oxygen atom of the methoxy group on the aromatic ring. These data strongly support that the two methyl groups are *exo*- and *endo*-arrangement and therefore, *anti*-**8b** is found to be *cis*-hydrogen adduct to the bridged double bond. This assignment is also applied to the hydrogenation product *anti*-**8c**.

Scheme 3.



The conformations of *syn*- and *anti*-[n.2]MCP-enes **3**, **6**, and *anti*-[n.2]MCP **8**, which have been prepared in the present work, in solution are studied by using variable temperature ^{1}H NMR spectroscopy and the results are compiled in Table 2.

The ^{1}H NMR spectrum of *syn*-**3b** and *anti*-**8b** in $CDCl_3$ at room temperature exhibits the split pattern of the protons at the methylene bridge. In spite of an increase of the temperature to 130°C in $CDBr_3$, no change of the spectrum is observed for saturated [3.2]-system *anti*-**8b**. However, in the case of the unsaturated [3.2]-system *syn*-**3b**, as the temperature

© 2000 NRC Canada

Table 2. The coalescence temperatures and energy barriers of *syn*- and *anti*-[n.2]MCP-enes **3**, **6**, and *anti*-[n.2]MCP **8**.[a]

Compd	Number of methylene units (n)	Solvent	T_c (°C)	$\Delta G^{\neq}$ (kcal mol^{-1})
syn-**3b**	3	$CDBr_3$	120	19.0
syn-**3c**	4	$CDCl_3$–CS_2	0	13.0
anti-**6**	3	$CDCl_3$–CS_2	0	12.4
anti-**8b**	3	$CDBr_3$	>130	—
anti-**8c**	4	$CDCl_3$–CS_2	35	14.4

[a]T_c and $\Delta G_c^{\neq}$ were determined in $CDCl_3$–CS_2 (1:3) or $CDBr_3$ using $SiMe_4$ as reference.

of the solution of the respective compound in $CDBr_3$, is increased, the individual peaks of the benzyl protons merge and eventually a single peak is observed above 120°C. This observation indicates that the rate of conformational ring flipping of *syn*-**3b** is faster than the NMR time scale at this temperature. The energy barrier to the conformational ring flipping estimated from the coalescence temperature (T_c) is 19.0 kcal mol^{-1}. The energy barriers for [4.2]-systems *syn*-**3c** and *anti*-**8c** were also estimated to be 13.0 (T_c = 0°C) and 14.4 (T_c = 35°C) kcal mol^{-1}, respectively. The unsaturated [3.2]-system *syn*-**3b** found to be about 6.0 kcal mol^{-1} larger than that for the corresponding [4.2]-system *syn*-**3c**. Thus, the solution conformation of [n.2]MCP-enes is sensitive to the chain length of the bridges. The ring inversion barriers determined by variable temperature ^{1}H NMR dramatically decrease with increasing length of the bridge by one unit.

Lower ring inversion barriers were observed for the unsaturated systems than those for saturated systems in spite of the smaller ring size due to the introduction of an additional double bond of the ethylene bridge. For example the barrier for ring inversion in the [4.2]-system decreases the rigidity of the system by about 1.4 kcal mol^{-1} in $CDCl_3$. The decreased rigidity of *syn*-[n.2]MCP-enes (**3**) may be attributed to the expanded bond angles of the bridged double bond.

Tetracyanoethylene (TCNE) complexes have often been used in studies on the relative π-base strength of various methyl-substituted benzenes (28). The π-basicity of the donor molecules increases with an increase in the number of substituted methyl groups and (or) stacking benzene rings and an increase in the face-to-face overlapping between aromatic nuclei (29). A solution of *anti*-[3.2]MCP-10-ene (*anti*-**6**) and TCNE in CH_2Cl_2 present a reddish brown colour and the charge-transfer band at 508 nm (log ε = 2.329) was observed in its UV spectrum. This absorption is due to the formation of 1:1 charge-transfer complex among the electron donor, [3.2]MCP, and the electron acceptor, TCNE. The position of absorption maximum and the shape of absorption curve remain unchanged when a 4–12-fold excess of TCNE was added. However, the charge transfer absorption band of the reference compound, 2,4-dimethylanisole (**9**) with TCNE was observed at 414 nm (log ε = 2.073). Such a red shift could be due to the through space electronic interaction of the opposite uncomplexed benzene ring, which tends to work as a π-electron donor.

In contrast to *anti*-[3.2]MCP-10-ene (*anti*-**6**), which exhibits the charge-transfer absorption band with TCNE at 508 nm (log ε = 2.329), a mixture of TCNE and *syn*-[3.2[MCP-10-ene (*syn*-**3b**) exhibits an absorption peak at 525 nm (log ε = 2.334), that of *syn*-[4.2[MCP-11-ene (*syn*-**3c**) is shifted to 466 nm (log ε = 2.001). Introduction of the one methylene to propane bridge of *syn*-**3b** causes a larger blue shift as indicated by the 60 nm shift for the CT-band of *syn*-**3c** due to the decreased transannular π-electron donation from the noncomplexed benzene ring to the complexed benzene ring. This finding is fairly consistent with the fact that the distance between two aromatic rings increased by one methylene bridge increased as previously described in the X-ray structures of *syn*-**3b** and *syn*-**3c**.

In the present [3.2]MCPs there are two possible conformers, *anti*- and *syn*-conformer. The through-space electronic interaction could be performed through the intraannular positions in the former conformer, but through face-to-face overlapping among the two benzene rings in the latter conformer (30). Thus, the charge-transfer complex would be stabilized by two types of the through-space electronic interaction, i.e., face-to-face overlapping and intraannular interaction with the opposing benzene ring, thus shifting the charge-transfer absorption band to the red region. The higher red shift of [3.2]MCP-10-ene (17 nm) are obtained in *syn*-conformer rather than in *anti*-conformer. Therefore, face-to-face overlapping might be much more favorable to stabilize the charge-transfer than the intraannular interaction.

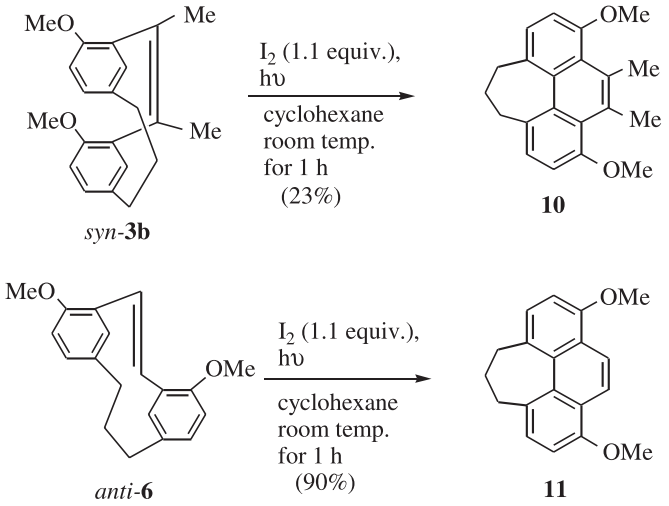
In spite of two routes for the photocyclization of stilbenes such as staircase *anti*-conformation and "face-to-face overlapping" *syn*-conformation are possible (31), the latter reaction pathway has not been established due to the lack of the model compounds. Most investigations of the photoconversion of stilbene derivatives to 9,10-dihydrophenanthrenes have used *anti*-[2.2]MCP-1-enes (32) and *anti*-[2.2]MCP-1,9-dienes (5*a*). Boekelheide et al. (32) reported the photocyclization of *anti*-[2.2]MCP-1-enes in the presence of oxidants to afford the corresponding phenanthrenes, but limited to *anti*-conformation. Later, Mitchell et al. (33) also reported the synthesis of *syn*-[2.2]MCP-1,9-diene, which valence isomerized to *cis*-dihydropyrene, but readily isomerized to *anti*-cyclophane systems. Thus, there is substantial interest in investigating the photocyclization of present *syn*-[n.2]MCP-enes to explore the above reaction pathways.

Actually, when *syn*-**3b** was irradiated in the presence of iodine as an oxidant at room temperature for 1 h, the desired phenanthrene **10** was obtained only in 23% yield along with recovery of the starting compound. In contrast, similar reaction of *anti*-**6** carried out under the same reaction conditions afforded the cyclization product **11** in 90% yield.

The rate of the photocyclization of *anti*-**6** was found to be much faster than that of *syn*-**3b** and almost completed within 1 h. The different reactivities for the irradiation of *syn*-**3b** and *anti*-**6** were observed. In the present photocyclization reaction of *syn*-**3b**, the photoinduced *syn*–*anti*-isomerization might be possible to afford the corresponding *anti*-conformer *anti*-**3b**, which is cyclized to the cyclization product

© 2000 NRC Canada

Scheme 4.



10. In fact, the irradiation of *syn*-**3b** in the absence of iodine as an oxidant at room temperature was attempted, but none of the formation of *anti*-conformer *anti*-**3b** was observed under the present reaction conditions. This result indicates that the cyclization product **10** might be directly formed via the *syn*-**3b**, but not the corresponding *anti*-**3b** as an intermediate.

Examination of molecular models led us to believe that the transformation of *anti*-**6** into phenanthrene **11** should be straightforward, since in the conformationally rigid stilbene moiety of *anti*-**6**, the π orbitals involved in the required photochemically produced disrotatory cyclization leading eventually to the phenanthrene **11** are apparently very close in space. The reason for the present preference for the formation of *trans*-dihydrophenanthrene rather than *cis*-dihydrophenanthrene as the intermediate might be attributable to the more stable chair form transition state than boat one and the conformational fixation to the chair form in the ground and transition state is possible in the *anti*-conformer.

In conclusion, a new synthesis of *syn*- and *anti*-[n.2]MCPenes by a McMurry cyclization has been developed and applied to the synthesis of phenanthrene-anellated polycyclic aromatic hydrocarbons substituted at positions 4 and 5 by the successive photoinduced transannular cyclization reaction. Further studies on the present novel photoinduced transannular cyclization reaction of **3** and **6** are now in progress.

Experimental

All melting points (Yanagimoto MP-S1) were uncorrected. Proton nuclear magnetic resonance (^{1}H NMR) spectra were recorded on a Nippon Denshi JEOL FT-270 spectrometer. Chemical shifts are reported as δ values (ppm) relative to internal Me_4Si. Mass spectra were obtained on a Nippon Denshi JMS-01SG-2 mass spectrometer at an ionization energy of 70 eV (*m*/*z* values reported include the parent ion peak). Infrared (IR) spectra were obtained on a Nippon Denshi JIR-AQ2OM spectrophotometer as KBr disks. Elemental analyses were performed by Yanaco MT-5. GLC analyses were performed by Shimadzu gas chromatograph GC-14A (Silicone OV-1, 2 m, programmed temperature rise, 12°C/min, carrier gas nitrogen, 25 mL/min).

Materials

1,n-Bis(4-methoxyphenyl)alkanes **1** were prepared following previous reports (12, 13).

Preparation of 1,n-bis(3-acetyl-4-methoxyphenyl)alkane (2) — typical procedure

To a solution of 1,3-bis(4-methoxyphenyl)propane (**1b**) (3.84 g, 15 mmol) and acetyl chloride (3.15 mL, 45 mmol) in methylene dichloride (60 mL) was added a solution of aluminum chloride (8.91 g, 67.5 mmol) in nitromethane (15 mL) at 0°C. After the reaction mixture had been stirred at room temperature for 3 h, it was poured into ice water (100 mL). The organic layer was extracted with CH_2Cl_2 (2 × 50 mL). The extract was washed with water (2 × 50 mL), dried (Na_2SO_4), and concentrated. The residue was chromatographed over silica gel (Wako C-300, 300 g) with $CHCl_3$ as eluent to give crude **2b** as a colorless solid. Recrystallization from hexane–benzene (1:1) gave 1,3-bis(3-acetyl-4-methoxyphenyl)propane (**2b**) (4.42 g, 87%) as colorless prisms, mp 46–48°C. IR (KBr) υ_{max}: 1667 (C=O) cm^{-1}. ^{1}H NMR ($CDCl_3$) δ: 1.85–1.95 (2 H, m), 2.55–2.62 (4 H, m), 2.60 (6 H, s), 3.89 (6 H, s), 6.90 (2 H, d, *J* = 8.0), 7.27 (2 H, dd, *J* = 8.0, 2.0), 7.52 (2 H, d, *J* = 2.0). MS *m*/*z*: M^+ 340. Anal. calcd. for $C_{21}H_{24}O_4$ (340.42): C 74.09, H 7.11; found: C 74.20, H 7.15.

Compounds **2a** and **2c** were similarly prepared in 29 and 71% yields, respectively.

*1,2-Bis(3-acetyl-4-methoxyphenyl)ethane (**2a**)*

Colorless prisms (hexane–benzene (1:1)), mp 114–115°C. IR (KBr) υ_{max}: 1664 (C=O) cm^{-1}. ^{1}H NMR ($CDCl_3$) δ: 2.60 (6 H, s), 2.84 (4 H, s), 3.89 (6 H, s), 6.87 (2 H, d, *J* = 8.7), 7.23 (2 H, dd, *J* = 8.7, 2.4), 7.54 (2 H, d, *J* = 2.4). MS *m*/*z*: M^+ 326. Anal. calcd. for $C_{20}H_{22}O_4$ (326.4): C 73.6, H 6.79; found: C 73.45, H 6.89.

*1,4-Bis(3-acetyl-4-methoxyphenyl)butane (**2c**)*

Colorless prisms (hexane–benzene (1:1)), mp 74–76°C. IR (KBr) υ_{max}: 1669 (C=O) cm^{-1}. ^{1}H NMR ($CDCl_3$) δ: 1.60 (4 H, m), 2.57 (4 H, m), 2.60 (6 H, s), 3.88 (6 H, s), 6.87 (2 H, d, *J* = 8.3), 7.25 (2 H, dd, *J* = 8.7, 2.4), 7.52 (2 H, d, *J* = 2.4). MS *m*/*z*: M^+ 354. Anal. calcd. for $C_{22}H_{26}O_4$ (354.5): C 74.55, H 7.39; found: C 74.26, H 7.18.

McMurry coupling reaction of 2 — typical procedure

The McMurry reagent was prepared from $TiCl_4$ [23.8 g (13.8 mL), 125 mmol] and 18 g (275 mmol) of Zn powder in 500 mL of dry THF, under nitrogen. A solution of **2b** (3.06 g, 9 mmol) and pyridine (22.5 mL, 200 mmol) in dry THF (250 mL) was added within 60 h from two Hershberg funnels to the black mixture of the McMurry reagent by using a high-dilution technique (34) with continuous refluxing and stirring. The reaction mixture was refluxed for an additional 8 h, cooled to room temp., and hydrized with aqueous 10% K_2CO_3 (200 mL) at 0°C. The reaction mixture was extracted with CH_2Cl_2 (3 × 200 mL). The combined extracts were washed with water, dried with Na_2SO_4 and concentrated.

© 2000 NRC Canada

The residue was chromatographed over silica gel (Wako C-300, 300 g) with benzene as eluents to give crude **3b** as a colorless solid. Recrystallization from benzene gave *syn*-7,13-dimethoxy-10,11-dimethyl[3.2]metacyclophan-10-ene (*syn*-**3b**) (1.10 g, 40%) as colorless prisms, mp 162–163°C. ^{1}H NMR ($CDCl_3$) δ: 1.20–1.45 (1 H, m), 2.10–2.25 (1 H, m), 2.18 (6 H, s), 2.50–2.65 (2 H, m), 2.85–2.98 (2 H, m), 3.59 (6 H, s), 6.33 (2 H, d, *J* = 8.0), 6.60 (2 H, dd, *J* = 2.0, 8.0), 6.95 (2 H, d, *J* = 2.0). MS *m/z*: M^+ 308. Anal. calcd. for $C_{21}H_{24}O_2$ (308.42): C 81.78, H 7.84; found: C 81.71, H 7.78.

Similarly, the McMurry coupling reaction was carried out for compounds **2a** and **2c** in the same manner as described above.

For **2a** the residue was chromatographed over silica gel (Wako C-300, 300 g) with benzene–$CHCl_3$ (1:1) as eluents to give crude **4a** as a colorless solid. Recrystallization from $CHCl_3$ gave **4a** (500 mg, 19%) as colorless prisms.

For **2c** the residue was chromatographed over silica gel (Wako C-300, 300 g) with hexane–benzene (1:1) as eluents to give crude *syn*-**3c** as a colorless solid. Recrystallization from hexane gave *syn*-**3c** (2.01 g, 69%) as colorless prisms.

*4,14,20,30-Tetramethoxy-1,2,17,18-tetramethyl[2.2.2.2]-metacyclophane-1,17-diene (**4a**)*

Colorless prisms ($CHCl_3$), mp 280–282°C. IR (KBr) υ_{max}: 2930, 1497, 1456, 1262, 1253, 1229, 1133, 1050, 1031, 810 cm^{-1}. ^{1}H NMR ($CDCl_3$) δ: 2.15 (12 H, s), 2.50 (8 H, broad s), 3.58 (12 H, s), 6.56 (4 H, d, *J* = 8.3), 6.71–6.80 (4 H, broad s), 6.83 (4 H, dd, *J* = 8.3, 2.0). MS *m/z*: M^+ 588. Anal. calcd. for $C_{40}H_{44}O_4$ (588.79): C 81.6, H 7.53; found: C 81.81, H 7.68.

syn-*8,14-Dimethoxy-11,12-dimethyl[4.2]metacyclophan-11-ene (*syn-***3c**)

Colorless prisms (hexane), mp 160–161°C. IR (KBr) υ_{max}: 2923, 1493, 1442, 1252, 1226, 1032, 805, 797 cm^{-1}. ^{1}H NMR ($CDCl_3$) (27°C) δ: 1.55 (4 H, broad s), 2.14 (6 H, s), 2.36 (4 H, broad s), 3.63 (6 H, s), 6.41 (2 H, d, *J* = 8.3), 6.59 (2 H, dd, *J* = 2.4, 8.3), 6.90 (2 H, d, *J* = 2.4). ^{1}H NMR ($CDCl_3$) (–40°C) δ: 1.1–1.4 (2 H, broad s), 1.72–1.92 (2 H, broad s), 2.17 (6 H, s), 2.1–2.3 (2 H, broad s), 2.4–2.6 (2 H, broad s), 3.67 (6 H, s), 6.41 (2 H, d, *J* = 8.3), 6.64 (2 H, dd, *J* = 2.4, 8.3), 6.93 (2 H, d, *J* = 2.4). MS *m/z*: M^+ 322. Anal. calcd. for $C_{22}H_{26}O_2$ (322.45): C 81.95, H 8.13; found: C 82.07, H 8.15.

Preparation of 1,3-bis(3-formyl-4-methoxyphenyl)-propane (5)

To a solution of 1,3-bis(4-methoxyphenyl)propane (**1b**) (2.24 g, 8.75 mmol) and Cl_2CHOCH_3 (2.28 mL, 25.2 mmol) in CH_2Cl_2 (20 mL) was added a solution of $TiCl_4$ (6.0 mL, 54.5 mmol) in CH_2Cl_2 (20 mL) at 0°C. After the reaction mixture was stirred at room temp for 3 h, it was poured into a large amount of ice water (400 mL) and extracted with CH_2Cl_2 (2 × 200 mL). The combined extracts were washed with water, dried with Na_2SO_4, and concentrated. The residue was chromatographed over silica gel (Wako C-300, 500 g) with $CHCl_3$ as eluent to give crude **5**. Recrystallization from hexane gave 2.81 g (99.6%) of 1,3-bis(3-formyl-4-methoxyphenyl)propane (**5**) as colorless prisms, mp 93–94°C. IR (KBr) υ_{max}: 1682 (C=O) cm^{-1}. ^{1}H NMR ($CDCl_3$) δ: 1.88–2.00 (2 H, m), 2.60–2.67 (4 H, m), 3.95 (6 H, s), 6.95 (2 H, d, *J* = 8.8), 7.39 (2 H, dd, *J* = 8.8, 2.4), 7.66 (2 H, d, *J* = 2.4), 10.48 (2 H, s). MS *m/z*: M^+ 312. Anal. calcd. for $C_{19}H_{20}O_4$ (312.37): C 73.06, H 6.45; found: C 73.19, H 6.32.

McMurry coupling reaction of 5

The McMurry reagent was prepared from $TiCl_4$ [23.8 g (13.8 mL), 125 mmol] and 18 g (275 mmol) of Zn powder in 500 mL of dry THF, under nitrogen. A solution of **5** (3.21 g, 9 mmol) and pyridine (22.5 mL, 200 mmol) in dry THF (250 mL) was added within 60 h to the black mixture of the McMurry reagent by using a high-dilution technique with continuous refluxing and stirring. The reaction mixture was refluxed for additional 8 h, cooled to room temp, and hydrized with aqueous 10% K_2CO_3 (200 mL) at 0°C. The reaction mixture was extracted with CH_2Cl_2 (3 × 200 mL). The combined extracts were washed with water, dried with Na_2SO_4, and concentrated. The residue was chromatographed over silica gel (Wako C-300, 300 g) with hexane–benzene (1:1) as eluents to give crude **6** as a colorless solid. Recrystallization from methanol gave *anti*-7,13-dimethoxy[3.2]metacyclophan-10-ene (*anti*-**6**) (711 mg, 28%) as colorless prisms, mp 94–95°C. IR (KBr) υ_{max}: 1593, 1485, 1461, 1276, 1255, 1242, 1114, 1027, 797, 753 cm^{-1}. ^{1}H NMR ($CDCl_3$) δ: 1.78–1.89 (2 H, m), 2.20–2.50 (4 H, broad s), 3.85 (6 H, s), 6.05 (2 H, d, *J* = 2.4), 6.77 (2 H, d, *J* = 8.3 Hz), 6.88 (2 H, s), 6.97 (2 H, dd, *J* = 8.3, 2.44). MS *m/z*: M^+ 308. Anal. calcd. for $C_{19}H_{20}O_2$ (280.37): C 81.4, H 7.19; found: C 81.62, H 7.26.

Demethylation of syn-3b

To a solution of *syn*-**3b** (32.2 mg, 0.105 mmol) in CH_2Cl_2 (5 mL) at 0°C was gradually added a solution of BBr_3 (0.03 mL, 0.3 mmol) in CH_2Cl_2 (1 mL) over a period of 15 min. After the reaction mixture has been stirred at room temperature for 2 h, it was poured into ice water (50 mL), extracted with CH_2Cl_2 (3 × 20 mL). The combined extracts were washed with water (2 × 20 mL), dried over Na_2SO_4, and concentrated in vacuo to leave a residue. The residue was recrystallized from hexane–ethyl acetate (1:1) gave *syn*-7,13-dihydroxy-10,11-dimethyl[3.2]metacyclophan-10-ene (*syn*-**7b**) (14.1 mg, 44%) as colorless prisms, mp 189–189.5°C. IR (KBr) υ_{max}: 3272 (OH) cm^{-1}. ^{1}H NMR ($CDCl_3$) δ: 2.23 (6 H, s), 2.05–2.28 (2 H, broad s), 2.45–2.62 (2 H, broad s), 2.78–2.98 (2 H, broad s), 5.29 (2 H, s, replaced by D_2O), 6.33 (2 H, d, *J* = 8.30), 6.56 (2 H, dd, *J* = 8.30, 2.44), 6.85 (2 H, d, *J* = 2.44). MS *m/z*: M^+ 306. Anal. calcd. for $C_{19}H_{20}O_2$ (280.37): C 81.4, H 7.19; found: C 81.62, H 7.28.

Compound *syn*-**7c** was similarly prepared in 53% yield.

syn-*8,14-Dihydroxy-11,12-dimethyl[4.2]metacyclophan-11-ene (*syn-***7c**)

Colorless prisms (hexane–ethyl acetate (1:1)), mp 194–194.5°C. IR (KBr) υ_{max}: 3344 (OH) cm^{-1}. ^{1}H NMR ($CDCl_3$) δ: 1.40–1.75 (4 H, broad s), 2.19 (6 H, s), 2.20–2.42 (4 H, broad s), 5.15 (2 H, broad s, replaced by D_2O), 6.38 (2 H, d, *J* = 8.3), 6.52 (2 H, dd, *J* = 2.4, 8.3), 6.80 (2 H, d, *J* = 2.4). MS *m/z*: M^+ 294. Anal. calcd. for $C_{20}H_{22}O_2$ (294.38): C 81.6, H 7.53; found: C 81.91, H 7.50.

© 2000 NRC Canada

Table 3. Crystallographic data and data collection details for *syn*-10,11-dimethyl-7,13-dimethoxy[3.2]MCP-10-ene (*syn*-**3b**) and *syn*-11,12-dimethyl-8,14-dimethoxy[4.2]MCP-11-ene (*syn*-**3c**).

	syn-**3b**	*syn*-**3c**
Formula	$C_{21}H_{24}O_2$	$C_{22}H_{26}O_2$
Mol. mass	308.42	322.45
Crystal size (mm)	0.4 × 0.25 × 0.25	0.30 × 0.25 × 0.25
	monoclinic	monoclinic
Space group	$P2_1/a$ (no. 14)	$P2_1/a$ (no. 14)
Z	4	4
a (pm)	1924.58 (26)	1983.78 (19)
b (pm)	759.26 (6)	819.66 (6)
c (pm)	1225. 00 (17)	1155.81 (13)
β (°)	102.80 (1)	98.9677 (85)
V (m^3)	1745.5 (4) × 10^{-30}	1856.4 (3) × 10^{-30}
D_c (gm^{-3})	1.154	1.174
Radiation	Cu-K_α	Cu-K_α
μ (Cu-K_α) (cm^{-1})	5.4	5.29
Total no. of unique reflections	3142	3365
R	0.117	0.067
R_w	0.091	0.107

Reduction of *syn*-3 with H_2 in the presence of Pd-C — typical procedure

To a solution of *syn*-**3b** (30 mg, 0.097 mmol) in ethyl acetate (40 mL) was added Pd-C (5%, 15 mg) and stirred for 24 h under the hydrogen atomosphere at room temp. The reaction mixture was concentrated. The residue was chromatographed over silica gel (Wako C-300, 100 g) with hexane–benzene (1:1) as eluents to give *anti*-**8b** (18.1 mg, 60%) as a colorless solid. Recrystallization from methanol gave *anti*-10-*exo*,11-*endo*-dimethyl-7,13-dimethoxy[3.2]metacyclophane (*anti*-**8b**) as colorless prisms, mp 84–85°C. ^{1}H NMR ($CDCl_3$) δ: 0.95 (3 H, d, J = 7.3), 1.68 (3 H, d, J = 7.3), 1.80–2.00 (2 H, m), 2.00–2.15 (1 H, m), 2.17–2.34 (1 H, m), 2.33–2.46 (1 H, m), 2.68–2.80 (2 H, m), 3.61–3.76 (1 H, m), 3.78 (3 H, s), 3.85 (3 H, s), 4.87 (1 H, d, J = 2.4), 5.24 (1 H, d, J = 2.4), 6.78 (2 H, d, J = 8.3), 6.93–7.01 (2 H, m). MS m/z: M^+ 310. Anal. calcd. for $C_{21}H_{26}O_2$ (310.44): C 81.25, H 8.44; found: C 81.12, H 8.28.

Compound *anti*-**8c** was similarly prepared in 95% yield.

anti-*11*-exo,*12*-endo-*Dimethyl-8,14-dimethoxy[4.2]metacyclophane (*anti-***8c***)*

Colorless prisms (methanol), mp 93–94°C. ^{1}H NMR ($CDCl_3$) (27°C), δ: 0.70–2.89 (16 H, broad m), 3.81 (6 H, s), 5.52–6.00 (2 H, s), 6.75 (2 H, d, J = 8.3), 6.86 (2 H, dd, J = 8.3, 2.4). ^{1}H NMR ($CDCl_3$–CS_2 (1:3)) (–30°C) δ: 0.82–1.08 (2 H, broad s), 0.98 (3 H, d, J = 7.3), 1.45–1.62 (2 H, broad s), 1.68 (3 H, d, J = 7.3), 2.09–2.28 (2 H, m), 2.55 (1 H, d, J = 7.3), 2.60–2.78 (2 H, m), 3.66 (1 H, d, J = 7.3), 3.80 (3 H, s), 3.87 (3 H, s), 5.61 (1 H, d, J = 2.4), 5.92 (1 H, d, J = 2.4), 6.77 (2 H, d, J = 8.3), 6.86–6.96 (2 H, m). MS m/z: M^+ 306. Anal. calcd. for $C_{22}H_{28}O_2$ (324.47): C 81.44, H 8.7; found: C 81.45, H 8.63.

Photoinduced cyclization of *anti*-6 in the presence of iodine

The mixture of *anti*-**6** (112 mg, 0.4 mmol) and iodine (112.0 mg, 0.44 mmol) was dissolved in cyclohexane (200 mL) in a Pyrex flask and then irradiated by a 400 W high-pressure mercury lamp while being monitored by GLC. Irradiation was continued until the disappearance of the reactant *anti*-**6** (1 h). The reaction mixture was washed with 10% sodium thiosulfate and water, dried with Na_2SO_4, and concentrated. The residue was chromatographed over silica gel (Wako C-300, 100 g) with hexane–benzene (1:1) as eluents to give **11** (100 mg, 90%) as a colorless solid. Recrystallization from hexane gave 1,8-dimethoxy-4,5-propanophenanthrene (**11**) as colorless prisms, mp 86–87°C. IR (KBr) υ_{max}: 2937, 1587, 1498, 1426, 1270, 1241, 1144, 1029, 810 cm^{-1}. ^{1}H NMR ($CDCl_3$) δ: 2.44–2.55 (2 H, m), 2.76–2.81 (4 H, m), 4.02 (6 H, s), 6.92 (2 H, d, J = 7.8), 7.32 (2 H, d, J = 7.8), 8.11 (2 H, s). MS m/z: M^+ 278. Anal. calcd. for $C_{19}H_{18}O_2$ (278.35): C 81.99, H 6.52; found: C 81.73, H 6.33.

Compound **10** was similarly prepared in 23% yield.

*3,6-Dimethoxy-9,10-dimethyl-4,5-propanophenanthrene (**10**)*

Colorless prisms (methanol), mp 51–53°C. IR (KBr) υ_{max}: 2925, 1577, 1159, 1029, 803, 667 cm^{-1}. ^{1}H NMR ($CDCl_3$) δ: 2.34–2.47 (2 H, m), 2.6–2.7 (4 H, m), 2.77 (6 H, s), 3.93 (6 H, s), 6.94 (2 H, d, J = 7.82), 7.18 (2 H, d, J = 7.82). MS m/z: M^+ 306. Anal. calcd. for $C_{21}H_{22}O_2$ (306.41): C 82.32, H 7.24; found: C 82.21, H 7.18.

Crystal data and refinement details for *syn*-3b and *syn*-3c

The unit cell constants were derived from least-squares analysis of the settings, on an Enraf–Nonius CAD4 FR 586 diffractometer, for 16 reflections for *syn*-**3b** and 25 reflections for *syn*-**3c** in the range 23.9° < θ < 24.6° for *syn*-**3b** and 22.0° < θ < 32.0° for *syn*-**3c**. The intensities of all independent reflections with 4° < 2θ < 140° for *syn*-**3b** and 4° < 2θ < 144° for *syn*-**3c** were measured with ω-2θ scan (ω scan width = 0.8 + 0.14 tan θ), Ni-filtered Cu–K_α radiation (λ = 1.54184 Å) was used. The structure was solved uneventfully by direct method (SIR88)[3] and difference Fourier syntheses, and refined in full-matrix least-squares method.

© 2000 NRC Canada

Table 4. Fractional atomic coordinates for the nonhydrogen atoms, with estimated standard deviations in parentheses, for *syn*-10,11-dimethyl-7,13-dimethoxy[3.2]metacyclophan-10-ene *(syn*-**3b**) and the isotropic equivalent displacement parameter defined as $B_{eq} = 4/3[a^2B_{11} + b^2B_{22} + c^2B_{33} + ab(\cos\gamma)B_{12} + ac(\cos\beta)B_{13} + bc(\cos\alpha)B_{23}]$.

Atom	*x*	*y*	*z*	B_{eq}
O1	0.58744(8)	–0.3100(2)	0.1709(1)	5.70(4)
O2	0.58885(9)	0.1258(3)	0.0417(1)	5.76(4)
C1	0.5922(1)	–0.0376(3)	0.3212(2)	4.24(4)
C2	0.5935(1)	0.1181(3)	0.2716(2)	4.02(4)
C3	0.6570(1)	0.1609(3)	0.2246(2)	3.79(4)
C4	0.6552(1)	0.1503(3)	0.1103(2)	4.45(4)
C5	0.7184(1)	0.1598(4)	0.0735(2)	5.60(5)
C6	0.7827(1)	0.1715(4)	0.1508(2)	5.68(5)
C7	0.7865(1)	0.1857(3)	0.2636(2)	4.57(5)
C8	0.7221(1)	0.1915(3)	0.2973(2)	4.04(4)
C9	0.8556(1)	0.1796(4)	0.3506(2)	5.61(6)
C10	0.8882(1)	–0.0039(4)	0.3781(2)	5.90(6)
C11	0.8532(1)	–0.1260(4)	0.4492(2)	6.24(6)
C12	0.7824(1)	–0.2014(3)	0.3877(2)	4.86(5)
C13	0.7784(1)	–0.3265(3)	0.3038(2)	5.77(6)
C14	0.7144(1)	–0.3711(3)	0.2340(2)	5.53(6)
C15	0.6526(1)	–0.2848(3)	0.2433(2)	4.62(5)
C16	0.6539(1)	–0.1597(3)	0.3269(2)	4.17(4)
C17	0.7188(1)	–0.1296(3)	0.4022(2)	4.64(5)
C18	0.5314(1)	–0.1036(4)	0.3690(2)	6.07(6)
C19	0.5353(1)	0.2551(4)	0.2568(2)	5.62(6)
C20	0.5874(2)	–0.3650(5)	0.0623(3)	7.40(8)
C21	0.5836(2)	0.1146(5)	–0.0745(2)	7.27(8)

Table 5. Fractional atomic coordinates for the nonhydrogen atoms, with estimated standard deviations in parentheses, for *syn*-11,12-dimethyl-8,14-dimethoxy[4.2]metacyclophan-11-ene *(syn*-**3c**) and the isotropic equivalent displacement parameter defined as $B_{eq} = 4/3[a^2B_{11} + b^2B_{22} + c^2B_{33} + ab(\cos\gamma)B_{12} + ac(\cos\beta)B_{13} + bc(\cos\alpha)B_{23}]$.

Atom	*x*	*y*	*z*	B_{eq}
O1	0.4222(1)	0.3732(4)	0.9651(2)	6.25(7)
O2	0.4134(2)	0.8045(4)	0.8287(3)	7.66(8)
C1	0.4001(2)	0.4031(5)	0.7251(3)	4.76(8)
C2	0.3997(2)	0.5510(6)	0.6729(3)	5.19(9)
C3	0.3421(2)	0.6681(5)	0.6799(3)	4.64(8)
C4	0.3497(2)	0.7917(5)	0.7625(3)	5.4(1)
C5	0.2953(2)	0.8913(5)	0.7764(4)	6.2(1)
C6	0.2324(2)	0.8633(5)	0.7075(4)	6.3(1)
C7	0.2231(2)	0.7419(5)	0.6239(3)	5.12(9)
C8	0.2799(2)	0.6516(5)	0.6083(3)	5.11(9)
C9	0.1534(2)	0.6992(7)	0.5598(4)	6.8(1)
C10	0.1347(2)	0.5164(7)	0.5720(4)	7.6(1)
C11	0.1267(2)	0.4716(7)	0.6951(4)	7.4(1)
C12	0.1514(2)	0.2948(6)	0.7300(4)	6.9(1)
C13	0.2236(2)	0.2972(5)	0.7929(4)	5.6(1)
C14	0.2387(2)	0.2821(6)	0.9144(4)	6.3(1)
C15	0.3039(2)	0.3013(7)	0.9732(4)	6.3(1)
C16	0.3563(2)	0.3432(5)	0.9129(3)	5.19(9)
C17	0.3441(2)	0.3575(5)	0.7896(3)	4.55(8)
C18	0.2786(2)	0.3266(5)	0.7343(3)	5.04(9)
C19	0.4561(2)	0.2791(6)	0.7226(4)	6.3(1)
C20	0.4550(2)	0.6146(7)	0.6101(4)	7.2(1)
C21	0.4353(2)	0.3887(7)	1.0876(4)	7.6(1)
C22	0.4220(3)	0.8954(8)	0.9299(5)	9.0(2)

All calculations were performed on a Micro VAX 3100 computer using a MolEN program package.[4]

Crystallographic data for *syn*-**3b** and *syn*-**3c** are given in Table 3.

The refined non-hydrogen atomic coordinates for *syn*-**3b** and *syn*-**3c** are listed in Tables 4 and 5, respectively, while the hydrogen coordinates, temperature factors (anisotropic for carbon atoms), scale factor, and secondary estimation coefficient for *syn*-**3b** and *syn*-**3c** are available on request.[5]

References

1. T. Yamato, K. Fujita, K. Okuyama, and H. Tsuzuki. New J. Chem. **24**, 221 (2000).
2. M. Pelligrin. Recl. Trav. Chim. Pays-Bas Belg. **18**, 458 (1899).
3. R.H. Mitchell, T.K. Vinod, and G.W. Bushnell. J. Am. Chem. Soc. **107**, 3340 (1985).
4. Y. Fujise, Y. Nakasato, and S. Itô. Tetrahedron Lett. **27**, 2907 (1986).
5. (*a*) R.H. Mitchell and V. Boekelheide. J. Am. Chem. Soc. **96**, 1547 (1974); (*b*) Y.-H. Lai and H.-L. Eu. J. Chem. Soc. Perkin Trans. 1, 233 (1993).
6. H.A. Staab, W.R.K. Riebel, and C. Krieger. Chem. Ber. **118**, 1230 (1985).
7. (*a*) J.E. McMurry, M.P. Fleming, K.L. Kees, and L.R. Krepski. J. Org. Chem. **43**, 3255 (1978); (*b*) J.E. McMurry. Acc. Chem. Res. **16**, 405 (1983); (*c*) J.E. McMurry, G.J. Haley, J.R. Matz, J.C. Clardy, and G.V. Duyne. J. Am. Chem. Soc. **106**, 5018 (1984); (*d*) J.E. McMurry. Chem. Rev. **89**, 1513 (1989).
8. R.H. Mitchell and S.A. Weerawana. Tetrahedron Lett. **27**, 453 (1986).
9. D. Tanner and O. Wennerström. Acta Chem. Scand. Ser. B, **37**, 693 (1983).
10. H. Hopf and C. Mlynek. J. Org. Chem. **55**, 1361 (1990).
11. (*a*) H.-F. Grützmacher, E. Neumann, F. Ebmeyer, K. Albrecht, and P. Schelenz. Chem. Ber. **122**, 2291 (1989); (*b*) H.-F. Grützmacher and E. Neumann. Chem. Ber. **126**, 1495 (1993); (*c*) H.-F. Grützmacher and G. Nolte. Chem. Ber. **127**, 1157 (1994); (*d*) H.-F. Grützmacher, A. Mehdizadeh, and A. Mülverstedt. Chem. Ber. **127**, 1163 (1994).

[4] MolEN, an interactive structure solution procedure. Enraf–Nonius, Delft, The Netherlands. 1990.

[5] Hydrogen coordinates, temperature factors (anisotropic for carbon atoms), scale factors, and secondary estimation coefficients have been deposited as supplementary material and may be purchased from The Depository of Unpublished Data, Document Delivery, CISTI, National Research Council Canada, Ottawa, Ontario, Canada, K1A 0S2 (for information on ordering electronically). Crystallographic data for the structure(s) reported in this paper havebeen deposited with the Cambridge Crystallographic Data Centre (CCDC). Copies of the data can be obtained, free of charge, on application to The Director, (CCDC), 12 Union Road, Cambridge CB2 1EZ, U.K. (Fax: 44-1223-336033 or e-mail: deposit@ccdc.cam.ac.uk).

© 2000 NRC Canada

12. M. Tashiro and T. Yamato. J. Org. Chem. **43**, 1413 (1978).
13. (*a*) T. Yamato, J. Matsumoto, M. Kajihara, and M. Tashiro. Chem. Express, **5**, 769 (1990); (*b*) T. Yamato, J. Matsumoto, S. Ide, K. Tokuhisa, K. Suehiro, and M. Tashiro. J. Org. Chem. **57**, 5243 (1992); (*c*) T. Yamato, J. Matsumoto, K. Tokuhisa, M. Kajihara, K. Suehiro, and M. Tashiro. Chem. Ber. **125**, 2443 (1992).
14. M. Tashiro, A. Tsuge, T. Sawada, T. Makishima, S. Horie, T. Arimura, S. Mataka, and T. Yamato. J. Org. Chem. **55**, 2404 (1990).
15. (*a*) Cyclophanes. Vol. 1. P.M. Keehn and S.M. Rosenfield (*Editors*). Academic Press, New York, 1983. Chap. 6, p. 428; (*b*) F. Vögtle. Cyclophane-Chemistry, Wiley, Chichester, 1993.
16. D. Krois and H. Lehner. Tetrahedron, **38**, 3319 (1982).
17. (*a*) H. Förster and F. Vögtle. Angew. Chem. **89**, 443 (1977); Angew. Chem. Int. Ed. Engl. **16**, 429 (1977); (*b*) R.H. Mitchell, K.S. Weerawana, and G.W. Bushnell. Tetrahedron Lett. **25**, 907 (1984). (*c*) K. Böckman and F. Vögtle. Chem. Ber. **114**, 1065 (1981); (*d*) M.F. Semmelhack, J.J. Harrisson, D.C. Young, Y. Guitierrez, S. Rafii, and J. Clardy. J. Am. Chem. Soc. **107**, 7508 (1985).
18. R.W. Hoffmann. Angew. Chem. **104**, 1147 (1992); Angew. Chem. Int. Ed. Engl. **31**, 1124 (1992).
19. (*a*) S. Cerrini, E. Giglio, F. Mazza, and N.V. Pavel. Acta Crystallogr. Sect. B: Struct. Crystallogr. Cryst. Chem. **B35**, 2605 (1979); (*b*) J.A. Hyatt, E.N. Duesler, D.Y. Curtin, and I.C. Paul. J. Org. Chem. **45**, 5074 (1980); (*c*) A. Collet and J. Gabard. J. Org. Chem. **45**, 5400 (1980); (*d*) A. Collet. Tetrahedron, **43**, 5725 (1987).
20. (*a*) R.C. Cookson, B. Halton, and I.D.R. Stevens. J. Chem. Soc. B, 767 (1968); (*b*) J.E. Baldwin and D.P. Kelly. J. Chem. Soc. Chem. Commun. 1664 (1968).
21. (*a*) J.F. Manville and G.E. Troughton. J. Org. Chem. **38**, 4278 (1973); (*b*) J. Canceil, J. Gabard, and A. Collet. J. Chem. Soc. Chem. Commun. 122 (1983); (*c*) G. Combaut, J.-M. Chantraine, J. Teste, J. Soulier, and K.-W. Glombitza. Tetrahedron Lett. 1699 (1978); (*d*) J. Bosch, J. Canals, and R. Granados. Anal. Quim. **72**, 709 (1976); (*e*) T. Yamato, N. Sakaue, L.K. Doamekpor, and M. Tashiro. J. Chem. Res. Synop. 176 (1994).
22. (*a*) T. Yamato, H. Sakamoto, K. Kobayashi, and M. Tashiro. J. Chem. Res. Synop. 352 (1986); J. Chem. Res. Miniprint, 2866 (1986); (*b*) T. Yamato, J. Matsumoto, M. Kajihara, K. Tokuhisa, K. Suehiro, and M. Tashiro. J. Org. Chem. **57**, 5154 (1992); (*c*) T. Yamato, J. Matsumoto, K. Tokuhisa, K. Suehiro, and M. Tashiro. J. Chem. Soc. Chem. Commun. 865 (1992); (*d*) T. Yamato, J. Matsumoto, M. Sato, K. Noda, and M. Tashiro. J. Chem. Soc. Perkin Trans 1, 1299 (1995).
23. (*a*) M. Tashiro and T. Yamato. J. Am. Chem. Soc. **104**, 3701 (1982); (*b*) M. Tashiro, K. Kobayashi, and T. Yamato. Chem. Lett. 327 (1985).
24. (*a*) T. Yamato, J. Matsumoto, M. Sato, K. Noda, T. Moriguchi, and M. Tashiro. Liebigs Ann. 995 (1995); (*b*) C.D. Gutsche. Calixarenes. Royal Society of Chemistry, Cambridge, 1989; (*c*) J. Vicens and V. Böhmer. Calixarenes: A Versatile Class of Macrocyclic Compounds. Kluwer Academic Publishers, Cambridge, 1990; (*d*) C.D. Gutsche. Acc. Chem. Res. **16**, 161 (1983); (*e*) J.A. Kanters, A. Schouten, E. Steinwender, J.H. van der Maas, L.C. Groenen, and D.N. Reinhoudt. J. Mol. Struct. **269**, 49 (1992).
25. R.W. Griffin, Jr., R.W. Baugman, and C.E. Ramey. Tetrahedron Lett. 5419 (1968).
26. (*a*) T. Yamato, J. Matsumoto, S. Ide, K. Suehiro, K. Kobayashi, and M. Tashiro. Chem. Ber. **126**, 447 (1993); (*b*) T. Yamato, M. Sato, K. Noda, J. Matsumoto, and M. Tashiro. J. Chem. Res. Synop. 394 (1993); J. Chem. Res. Miniprint, 2601 (1993); (*c*) T. Yamato, K. Fujita, T. Ando, S. Ide, Y. Nagano, and M. Tashiro. J. Chem. Res. Synop. 264 (1996); J. Chem. Res. Miniprint, 1434 (1996); (*d*) T. Yamato, K. Fujita, S. Ide, and Y. Nagano. J. Chem. Res. Synop. 190 (1997); J. Chem. Res. Miniprint, 1301 (1997).
27. (*a*) M. Tashiro and T. Yamato. J. Org. Chem. **46**, 4556 (1981); (*b*) M. Tashiro and T. Yamato. J. Org. Chem. **48**, 1461 (1983).
28. R.E. Merrifield and W.D. Phillips. J. Am. Chem. Soc. **80**, 2778 (1958).
29. (*a*) R. Boschi and W. Schmidt. Angew. Chem. Int. Ed. Engl. **12**, 402 (1973); (*b*) T. Sato and T. Takemura. J. Chem. Soc. Perkin Trans. 2, 1195 (1976); (*c*) S. Hayashi and T. Sato. Nippon Kagaku Zasshi, **91**, 950 (1970); (*d*) D.J. Cram and R.H. Bauer. J. Am. Chem. Soc. **81**, 5971 (1959); (*e*) L.A. Singer and D.J. Cram. J. Am. Chem. Soc. **85**, 1080 (1963); (*f*) M. Sheehan and D.J. Cram. J. Am. Chem. Soc. **91**, 3553 (1969); (*g*) T. Sato and K. Nishiyama. J. Chem. Soc. Chem. Commun. 220 (1973); (*h*) T. Sato and K. Nishiyama. J. Org. Chem. **37**, 3254 (1972); (*i*) M. Tashiro, T. Yamato, K. Kobayashi, and T. Arimura. J. Org. Chem. **52**, 3196 (1987); (*j*) T. Yamato, S. Ide, K. Tokuhisa, and M. Tashiro. J. Org. Chem. **57**, 271 (1992).
30. (*a*) T. Yamato, J. Matsumoto, N. Shinoda, S. Ide, M. Shigekuni, and M. Tashiro. J. Chem. Res. Synop. 178 (1994); (*b*) T. Yamato, H. Kamimura, F. Zhang, and H. Tsuzuki. Can. J. Chem. **76**, 997 (1998).
31. (*a*) F.B. Mallory, C.S. Wood, and J.T. Gordon. J. Am. Chem. Soc. **86**, 3094 (1964); (*b*) R. Srinivasan and J.N.C. Hsu. J. Am. Chem. Soc. **93**, 2816 (1971); (*c*) M.V. Sargent and C.J. Timmons. J. Am. Chem. Soc. **85**, 2186 (1963); (*d*) P.H.G. Op Het Veld and W.H. Laarhoven. J. Am. Chem. Soc. **99**, 7221 (1977); (*e*) R. Srinivasan, V.Y. Merrit, J.N.C. Hsu, P.H.G. Op Het Veld, and W.H. Laarhoven. J. Org. Chem. **43**, 980 (1978); (*f*) C.S. Wood and F.B. Mallory. J. Org. Chem. **29**, 3373 (1964); (*g*) K.A. Muszkat and E. Fischer. J. Chem. Soc. B, 662 (1967).
32. (*a*) H. Blaschke, C.E. Ramey, I. Calder, and V. Boekelheide. J. Am. Chem. Soc. **92**, 3675 (1970); (*b*) C.E. Ramey and V. Boekelheide. J. Am. Chem. Soc. **92**, 3681 (1970).
33. (*a*) R.H. Mitchell, T.K. Vinod, G.J. Bodwell, K.S. Weerawarna, W. Anker, R.V. Williams, and G.W. Bushnell. Pure Appl. Chem. **58**, 15 (1986); (*b*) Y.-H. Lai and S.-M. Lee. J. Org. Chem. **53**, 4472 (1988); (*c*) Y.-H. Lai and H.-L. Eu. J. Chem. Soc. Perkin Trans. 1, 233 (1993).
34. (*a*) M. Tashiro and T. Yamato. J. Org. Chem. **46**, 1543 (1981); (*b*) M. Tashiro, K. Koya, and T. Yamato. J. Am. Chem. Soc. **104**, 3707 (1982); (*c*) M. Tashiro and T. Yamato. J. Org. Chem. **50**, 2939 (1985); (*d*) T. Yamato, T. Arimura, and M. Tashiro. J. Chem. Soc. Perkin Trans. 1, 1 (1987).

© 2000 NRC Canada

Transition state stabilization by micelles: thiolysis of *p*-nitrophenyl alkanoates in cetyltrimethylammonium bromide micelles

Oswald S. Tee and Ogaritte J. Yazbeck

Abstract: Thiolysis of *p*-nitrophenyl esters (acetate to decanoate) by the anion of 2-mercaptoethanol (ME) is catalyzed by micelles of cetyltrimethylammonium bromide (CTAB) in aqueous solution. At fixed [ME], the observed rate constants (k_{obs}) show saturation with respect to added [CTAB], consistent with ester binding in the micelles. Plots of k_{obs} vs. [ME] are linear in the absence and in the presence of the CTAB, and analysis of the slopes of the plots afford rates constants for thiolate ion attack on the esters in the aqueous phase (k_N) and in the micellar phase (k_{cN}). The strengths of substrate binding and transition state binding to the micelles are strongly correlated, with a slope of *unity,* because they have the same dependence on the ester chain. Consequently, the catalytic ratios (k_{cN}/k_N) are independent of the length of the ester. Similar behaviour is found for thiolysis by the dianions of mercaptoacetic acid, 3-mercaptopropionic acid, and cysteine, and also for ester cleavage by the anions of glycine and 2,2,2-trifluoroethanol, as earlier for cleavage by hydroxide ion. The results are consistent with Kirby's dissection of transition state binding into "passive" and "dynamic" components. The passive component involves hydrophobic binding of the ester chain which is more or less the same as in the substrate binding. The dynamic component is associated with reaction in the Stern layer of the micelle, and its magnitude varies with the nucleophiles because of differences in their ease of exchange between the aqueous medium and the Stern layer.

Key words: catalysis, esters, thiolysis, micelles.

Résumé : La thiolyse des esters (acétate à décanoate) de *p*-nitrophényle, par l'anion 2-mercaptoéthanol (ME) en solution aqueuse, est catalysée par les micelles de bromure de cétyltriméthylammonium (« CTAB »). À des valeurs fixes de [ME], les constantes de vitesse observées (k_{obs}) présentent une saturation par rapport à la [CTAB] ajoutée et cette observation est en accord avec une fixation dans les micelles. Les courbes de k_{obs} en fonction de [ME] sont linéaires tant en absence qu'en présence de CTAB et une analyse des pentes de ces courbes permet de déterminer les constantes de vitesse pour l'attaque de l'ion thiolate sur les esters en phase aqueuse (k_N) et en phase micellaire (k_{cN}). Il existe une grande corrélation entre les forces de fixation des micelles avec le substrat ou de l'état de transition; la pente est égale à l'unité en raison du fait qu'elles dépendent toutes les deux de la même chaîne ester. En conséquence, les rapports catalytiques (k_{cN}/k_N) sont indépendants de la longueur de l'ester. On observe un comportement semblable lors de la thiolyse par les anions de l'acide mercaptoacétique, de l'acide 3-mercaptopropionique et de la cystéine ainsi que lors du clivage des esters par les anions de la glycine et du 2,2,2-trifluoroéthanol; antérieurement, on avait observé le même résultat avec l'ion hydroxyde. Les résultats sont en accord avec la dissection de Kirby de la fixation de l'état de transition en des composantes « passive » et « dynamique ». La composante passive implique une fixation hydrophobe de la chaîne de l'ester qui est à peu près semblable à la fixation du substrat; la composante dynamique est associée à la réaction dans la couche de Stern de la micelle et son amplitude varie avec les nucléophiles en raison des différences dans leur facilité d'échange entre le milieu aqueux et la couche de Stern.

Mots clés: catalyse, esters, thiolyse, micelles.

[Traduit par la Rédaction]

Introduction

Over the last forty years, the effects of micelles on organic reactions have been studied extensively (1). One of the first reactions to be studied in detail was the cleavage of aryl esters by hydroxide ion, which is retarded by anionic micelles but catalyzed by cationic ones (for example see ref. (2)). Since the catalytic effects of cationic micelles are more evident for esters with long chains, it was reasonable for authors to conclude that the acceleration is chain length

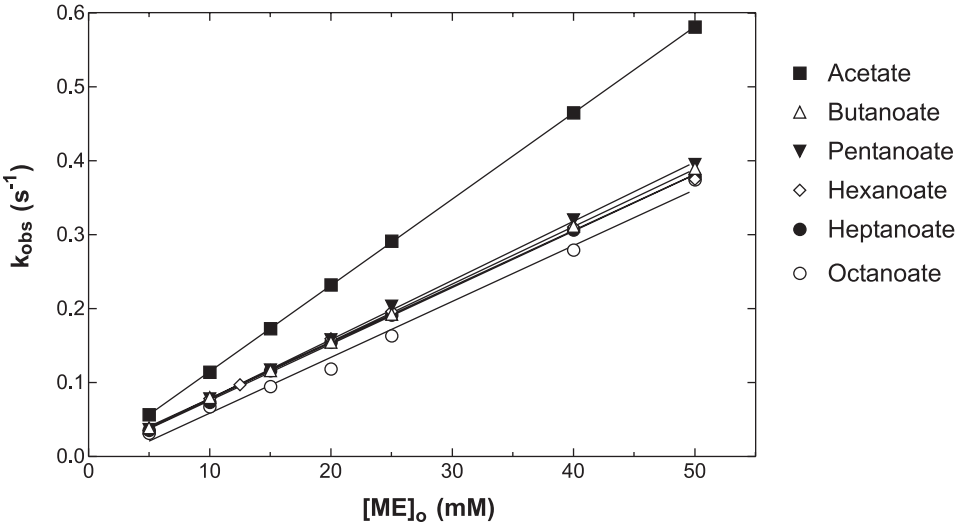
Received November 25, 1999. Published on the NRC Research Press website on August 3, 2000.

O.S. Tee[1] and O.J. Yazbeck. Department of Chemistry and Biochemistry, Concordia University, 1455 de Maisonneuve Blvd., Montreal, QC H3G 1M8, Canada.

[1]Author to whom correspondence may be addressed. Telephone: (514) 848-3348. Fax: (514) 848-2868.
e-mail: ostee@vax2.concordia.ca

© 2000 NRC Canada

Fig. 1. Variation of k_{obs} for ester cleavage with [ME] in the presence of 5.00 mM NaBr, but no CTAB, at pH 10.60. The data are for the esters acetate, butanoate, pentanoate, hexanoate, heptanoate, and octanoate, as indicated. The slopes of the plots provide k_N values (Table 1).



dependent, presumably because an ester with a longer acyl chain is more readily incorporated into the micelle.

The origin of the micellar catalysis of ester cleavage was ascribed to concentration of the reactants in the restricted volume of the micelle: hydroxide ion in the Stern layer, and the ester in the hydrophobic core but with its carbonyl group accessible to the aqueous environment of the Stern layer (1, 2). Consistent with this interpretation, Al-Awadi and Williams (3) found that the Hammett ρ value for basic cleavage of substituted phenyl dodecanoate esters in CTAB micelles is the same as the value for reaction in aqueous solution. Subsequently, one of us pointed out (4) that this finding means that the transition state stabilization by CTAB micelles is independent of the aryloxy leaving group of the ester, and so, presumably, it depends on the acyl chain length of the ester.

Recently, we tested this suggestion by studying the basic hydrolysis of *p*-nitrophenyl alkanoates (acetate to octanoate) in CTAB micelles (5). Remarkably, we found that the chain length dependence of the transition state binding, and thus of the transition state stabilization, is exactly the same as that for the substrate binding. As a result, the limiting acceleration is independent of the ester chain length, although it is more evident for longer esters because they bind to the micelles more strongly. The work described below was carried out to see if these features carry over to reactions of aryl esters with thiolate anion nucleophiles. There have been a few previous studies of the effect of cationic surfactants on ester thiolysis (6) but none of them focussed on a series of alkanoates, which is the case here.

Results

We have studied the effect of CTAB micelles on the thiolysis of *p*-nitrophenyl alkanoate esters: acetate, butanoate, pentanoate, hexanoate, heptanoate, octanoate, and in some cases the decanoate. The reaction medium was an aqueous 0.10 M carbonate buffer of pH 10.60. To be consistent with previous work (3, 5), and to avoid the complications arising from variable bromide ion exchange into the micelles (2*c*, 2*d*, 2*h*, 3, 7), the total bromide ion concentration was kept constant at 5.0 mM.

Our first series of experiments involved the anion of 2-mercaptoethanol (ME) as the thiolate nucleophile (Nuc). In the aqueous buffer with no CTAB, the dependence of k_{obs} on added nucleophile is strictly linear (Fig. 1), as expected from previous work (8). For reaction in the presence of a fixed concentration of CTAB, the dependence of k_{obs} on [Nuc] is also linear (Fig. 2), which indicates that even though thiolate ions exchange into the Stern layers of micelles, the effect does not approach saturation. At a fixed concentration of the nucleophile, the variation of k_{obs} with [CTAB] shows saturation behaviour (Fig. 3) due to binding of the ester substrates in the micelles.

Following the approach developed previously for bimolecular reactions mediated by cyclodextrins (8, 9), analysis of the data is based on consideration of four competing processes: (*i*) basic hydrolysis of the ester (Es) in the medium (eq. [1]); (*ii*) basic hydrolysis within the micelles (eq. [2]); (*iii*) nucleophilic attack in the medium (eq. [3]); and (*iv*) nucleophilic attack within the micelles (eq. [4]). Together, these four processes require the variation of the rate constant for ester cleavage with surfactant concentration, [Surf], which is given in eq. [5], assuming that the concentration of ester is low enough not to affect micellization. Note that binding of the ester to the micelle is characterized by a dissociation constant, K_S = [Es][Surf]/[Es/Surf].

[1] $$\mathrm{Es} \xrightarrow{k_u} \text{products}$$

[2] $$\mathrm{Es} + \mathrm{Surf} \underset{K_S}{\rightleftharpoons} \mathrm{Es{\cdot}Surf} \xrightarrow{k_c} \text{products}$$

[3] $$\mathrm{Es} + \mathrm{Nuc} \xrightarrow{k_N} \text{products}$$

[4] $$\mathrm{Es{\cdot}Surf} + \mathrm{Nuc} \xrightarrow{k_{cN}} \text{products}$$

[5] $$k_{obs} = \frac{(k_u K_S + k_c[\mathrm{Surf}]) + (k_N K_S + k_{cN}[\mathrm{Surf}])[\mathrm{Nuc}]}{(K_S + [\mathrm{Surf}])}$$

© 2000 NRC Canada

Fig. 2. Variation of k_{obs} for ester cleavage with [ME] in the presence of 5.00 mM of CTAB, but no NaBr, at pH 10.60. The data are for the esters indicated on the graph. Analysis of the slopes (see text) gives values of k_{cN}. Note that, because of micellar catalysis, the vertical scale here is 10 times that in Fig. 1.

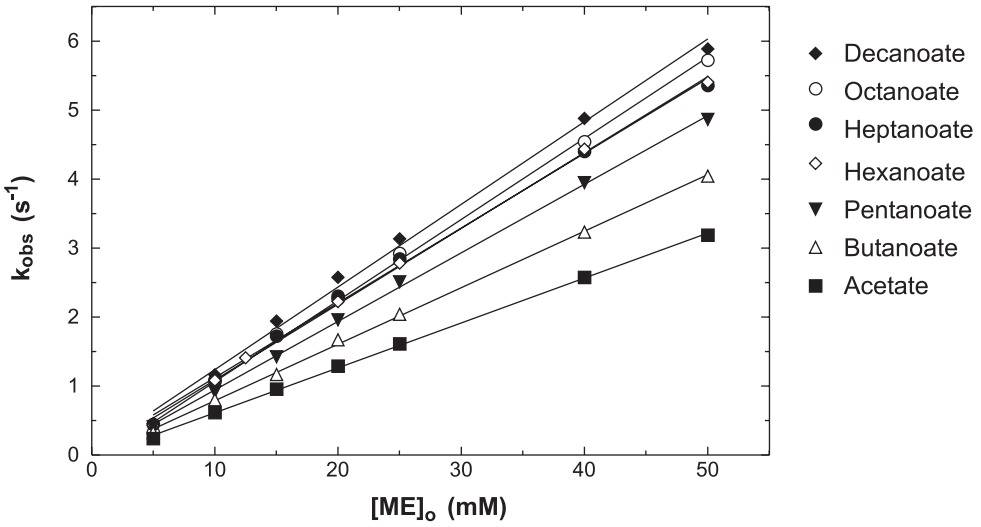
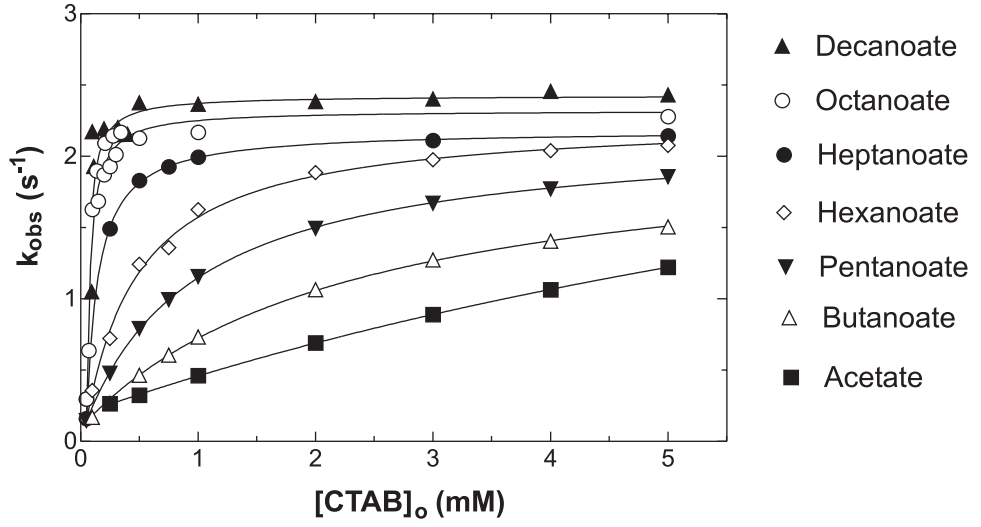


Fig. 3. Variation of k_{obs} for ester cleavage with [CTAB] in the presence of 20 mM mercaptoethanol, and total bromide ion = 5.00 mM, at pH 10.60. The data are for the esters indicated. Fitting eq. [6] to the data, with [Surf] = ([Surf]$_o$- cmc), provide values of K_S for the esters. See Experimental section.



Values of k_N are obtained from the linear plots found for experiments with no added surfactant, when $k_{obs} = k_u + k_N[Nuc]$ (e.g., Fig. 1). With varying [Surf], but constant [Nuc], and assuming that the added nucleophile does not alter K_S or [Surf], eq. [5] simplifies to eq. [6], where $k_u' = (k_u + k_N[Nuc])$ and $k_c' = (k_c + k_{cN}[Nuc])$. Equation [6] corresponds to simple saturation kinetics, as is observed (Fig. 3), and nonlinear regression of the data affords estimates of K_S, as well as of k_u' and k_c'.[2]

$$[6] \qquad k_{obs} = \frac{(k_u' K_S + k_c'[Surf])}{(K_S + [Surf])}$$

For the experiments with constant [Surf], eq. [5] requires a linear dependence of k_{obs} on [Nuc], as observed for ME (Fig. 2), with a slope of $(k_N K_S + k_{cN}[Surf])/(K_S + [Surf])$. Knowing k_N and K_S from the analyses of the other experiments, values of k_{cN} can be estimated from such slopes. Table 1 collects the values of k_N, k_{cN}, and K_S for reaction between the anion of ME and the series of esters, deduced from the kinetic data shown in Figs. 1, 2, and 3.

Analogous experiments with the dianion of mercaptoacetic acid (MAA) gave results similar to those found for the anion of ME. The slopes of the linear plots of k_{obs} vs. [Nuc] in the absence of CTAB provided k_N, and the saturation behaviour of k_{obs} with [CTAB], at fixed [Nuc],

[2] As explained in the Experimental Section, we have taken [Surf] = [Surf]$_o$ – cmc, with the critical micellar concentration (cmc) fixed at 0.05 mM.

© 2000 NRC Canada

Table 1. Constants for the reaction of thiolate ions and other nucleophiles with *p*-nitrophenyl alkanoates in the presence of CTAB micelles.[a]

Ester	k_N (M^{-1} s^{-1})	k_{cN} (M^{-1} s^{-1})	K_S (mM)	k_{cN}/k_N	K_{TS} (mM)
(*a*) Anion of 2-mercaptoethanol (ME)					
Acetate	11.7 ± 0.02	202 ± 3	12.7 ± 0.5	17.3	0.736
Butanoate	7.77 ± 0.04	117 ± 2	2.34 ± 0.10	15.1	0.155
Pentanoate	7.99 ± 0.08	118 ± 2	0.975 ± 0.015	14.8	0.0660
Hexanoate	7.59 ± 0.13	120 ± 2	0.465 ± 0.030	15.8	0.0294
Heptanoate	7.64 ± 0.06	110 ± 3	0.0995 ± 0.0040	14.4	0.00691
Octanoate	7.56 ± 0.31	118 ± 3	0.0323 ± 0.0065	15.6	0.00207
Decanoate	7.56[b]	120 ± 4	0.00585[c]	15.9	0.000369
(*b*) Dianion of mercaptoacetic acid (MAA)					
Acetate	15.6 ± 0.2	1780 ± 100	24.6 ± 4.0	114	0.216
Butanoate	10.4 ± 0.2	774 ± 26	2.60 ± 0.23	74.4	0.0349
Pentanoate	10.9 ± 0.2	776 ± 39	1.06 ± 0.07	71.2	0.0149
Hexanoate	11.0 ± 0.2	776 ± 24	0.374 ± 0.009	70.5	0.00530
Heptanoate	11.2 ± 0.2	915 ± 20	0.141 ± 0.009	81.7	0.00173
Octanoate	10.1 ± 0.1	886 ± 7	0.0539 ± 0.0032	87.7	0.000614
Decanoate	10.1[b]	867 ± 14	0.00664[c]	85.8	0.0000774
(*c*) Dianion of 3-mercaptopropionic acid (MPA)[d]					
Acetate	11.8 ± 0.2	786 ± 96	24.6	66.8	0.368
Butanoate	8.64 ± 0.07	453 ± 25	2.60	52.4	0.0497
Pentanoate	8.44 ± 0.19	435 ± 24	1.08	51.5	0.0205
Hexanoate	8.08 ± 0.25	462 ± 16	0.374	57.2	0.00654
Heptanoate	8.11 ± 0.11	421 ± 18	0.141	51.9	0.00271
Octanoate	7.62 ± 0.39	395 ± 25	0.0539	51.8	0.00104
(*d*) Dianion of cysteine (CYST)[d]					
Acetate	9.78 ± 0.08	812 ± 17	24.6	83.0	0.296
Butanoate	6.01 ± 0.07	362 ± 16	2.60	60.3	0.0431
Hexanoate	5.70 ± 0.03	364 ± 16	0.374	63.8	0.00586
Octanoate	6.91 ± 0.01	370 ± 9	0.0539	53.5	0.00101
(*e*) Anion of glycine (GLY)[d]					
Acetate	1.51 ± 0.03	2.55 ± 0.05	24.6	1.69	14.6
Butanoate	0.561 ± 0.025	0.711 ± 0.12	2.60	1.27	2.05
Hexanoate	0.573 ± 0.007	0.856 ± 0.068	0.374	1.49	0.250
Octanoate	0.477 ± 0.041	0.639 ± 0.055	0.0539	1.34	0.0402
(*f*) Anion of 2,2,2-trifluoroethanol (TFE)[e]					
Acetate	13.1 ± 0.08	531 ± 19	11.4	40.5	0.282
Butanoate	7.25 ± 0.09	196 ± 3	1.96	27.1	0.0723
Hexanoate	7.67 ± 0.02	178 ± 5	0.257	23.2	0.0111
Octanoate	7.00 ± 0.21	176 ± 2	0.0423	25.4	0.00167

[a]At 25°C, in an aqueous carbonate buffer of pH 10.60, with the total bromide concentration ([CTAB] + [NaBr]) kept at 5.00 mM. The actual data for ME are shown in Figs. 1, 2, and 3.

[b]Difficult to determine accurately and so assumed to be the same as for the octanoate.

[c]Obtained by extrapolation of the linear plot of pK_S vs. *N*.

[d]For the experiments with the anions of MPA, CYST, and GLY the values of K_S were to be taken to be the same as those found with the mercaptoacetate dianion.[4]

[e]For the experiments with the anion of TFE, the values of K_S were to be taken to be the same as those found earlier with hydroxide ion (5), under the same conditions.

was analyzed in terms of eq. [6] to find K_S. Plots of k_{obs} vs. [MAA] at fixed [CTAB] show very slight downward curvature[3] at the high end of the range of [MAA] = 0–25.0 mM, and to minimize its effect values of k_{cN} were estimated from the data points in the concentration range 0–15.0 mM, where the variation in k_{obs} is essentially linear.

[3]This curvature may indicate the onset of saturation of the micelles with the thiolate dianions which probably bind stronger than the monoanion of ME — see Discussion. Alternatively, high thiolate concentrations may start to alter the micellization parameters.

[4]The K_S values found with the anions of ME and MAA (Table 1) differ little from those found earlier with hydroxide ion (5), despite differences in pH, buffer, and ionic strength.

© 2000 NRC Canada

Experiments were also carried out with the dianions of 3-mercaptopropionic acid (MPA) and cysteine (CYST), and, for comparison, with the anion of glycine (GLY), an amine nucleophile, and the anion of 2,2,2-trifluoroethanol (TFE), an oxyanion. For the experiments with TFE, the medium was a 0.20 M phosphate buffer of pH 11.60, as used for previous studies of ester cleavage by hydroxide ion (5). Again, the plots of k_{obs} against [Nuc], at constant [CTAB], showed slight curvature at the high [Nuc], and so k_{cN} values were estimated from the linear dependence in the range [Nuc] = 0–15.0 mM. Since the values of K_S do not appear to be significantly sensitive to the nucleophile,[4] the values found from the experiments with MAA were used in the analyses to find k_{cN} values for the anions of MPA, CYST, and GLY. For the anion of TFE, the values of K_S that were found from reaction with hydroxide ion in the same phosphate buffer (5) were used.

Values of k_N and k_{cN} obtained for the anions of MAA, MPA, CYST, GLY, and TFE are also collected in Table 1, along with apparent "equilibrium constants," K_{TS}. Such constants are useful measures of transition state stabilization in catalyzed reactions (4). For the present purposes, K_{TS} is defined in eq. [7] to be the dissociation constant of the transition state for the micelle-catalyzed cleavage (TS·Surf) into the transition state of normal cleavage (TS) and the micellized surfactant (Surf). We have used analogous constants extensively in work on the effects of cyclodextrins on reactions (4, 8, 9, and references therein), as have other authors for various catalysts (10), including enzymes (11), enzyme mimics (12), and micelles (13).

$$[7] \qquad K_{TS} = [TS][Surf]/[TS\cdot Surf] = k_N/k_3 = k_N K_S/k_{cN}$$

Note that in eq. [7], k_3 is the third order rate constant corresponding to the overall process shown below in eq. [8] which is kinetically equivalent to that shown in eq. [4]. Hence, $k_3 = k_{cN}/K_S$.

$$[8] \qquad Es + Surf + Nuc \xrightarrow{k_3} products$$

Discussion

Two features of the rate and equilibrium constants in Table 1 are immediately apparent. First, beyond the acetate, the rate constants k_N and k_{cN} both show almost no variation with ester chain length and so the limiting accelerations, k_{cN}/k_N, are virtually constant for each nucleophile. Second, and in sharp contrast, the equilibrium constants K_S and K_{TS} vary appreciably with chain length. Consequently, the third order rate constants, $k_3 = k_{cN}/K_S$ (eq. [8]), increase substantially: (*i*) 1300-fold for the anion of ME and 1800 for the dianion of MAA (going from the acetate to the decanoate ester); (*ii*) 200-fold for the dianions of MPA and CYST, and (*iii*) 100-fold for the anions of GLY and TFE (going from the acetate to the octanoate). Similar behaviour was found earlier for cleavage of the same series of esters by hydroxide ion (5).

According to eq. [7], the "catalytic" ratio, $k_{cN}/k_N = K_S/K_{TS}$, is determined by the relative strengths of transition state binding and substrate binding (4, 12). Seen from this point of view, the nearly constant k_{cN}/k_N ratios for each nucleophile (Table 1) arise because the substrate binding and transition state binding have exactly the same sensitivity to elongation of the ester chain. This is precisely the case, as shown by the correlations summarised in Table 2, some of which are plotted in Fig. 4. For each thiolate nucleophile, the slopes of the plots of pK_{TS} vs. chain length (N) and pK_S vs. N, are all essentially the same ($\approx 0.43 \pm 0.02$),[5] and they are barely different for the other three nucleophiles: glycinate ion, the TFE anion, and hydroxide ion. Even more to the point, pK_{TS} values (for transition state binding) are very strongly correlated with pK_S values (for substrate binding), and the slopes are very close to *unity* (Table 2), suggesting that transition state binding and substrate binding are governed by the same structural feature(s) of the esters.

Kirby (12) has proposed that transition state binding can be divided into two, conceptually distinct components: (*i*) *passive binding*, which arises from noncovalent interactions, such as those involved in host–guest complexation; (*ii*) *dynamic binding*, which is due to interactions between the catalyst and the substrate(s) at the reaction centre. At first sight, this division may seem artificial or even naive, especially for catalysts as complex as enzymes and catalytic antibodies (12), but it does provide a useful framework for discussion. Moreover, the division seems entirely appropriate for the present results for micelles.

For micellar catalysis of ester cleavage by nucleophiles, transition state binding closely parallels substrate binding (Fig. 4 and Table 2). This behaviour suggests that the passive binding component is more or less totally hydrophobic in origin, since the slopes of the plots of pK_{TS} vs. N, and pK_S vs. N, of 0.4 (Table 2) are perfectly consistent with dominant hydrophobic interactions (5). Conceivably, then, the passive component of the transition state binding is little different from the initial state binding of the esters. The dynamic component, of course, is associated with nucleophilic attack on the micelle-bound ester and it will be greatly influenced by the exchange of nucleophiles into the micelles. The nearly constant ratios, k_{cN}/k_N, for each nucleophile (Table 1 and ref. (5)) are quite understandable if they are determined almost solely by the accessibility of the nucleophile to the micelle-bound ester.

A key feature of current models of the effects of micelles on reactivity is the exchange of ions between the Stern layer of the micelle and the bulk aqueous medium (1, 7). To quote Bunton et al. (1*f*), for cationic micelles, "large, weakly hydrated polarizable anions displace hydrophilic anions." Among other things, this factor explains why added bromide ion depresses the rate of CTAB-catalyzed hydroxide ion attack on esters (and other substrates) and why high concentrations of CTAB are less catalytic than moderate ones (2, 7). Also, it explains why cetyltrimethylammonium chloride micelles are better catalysts for hydroxide ion attack on esters than are CTAB micelles (for example see ref.(2)). With

[5] The cleavage of *p*-nitrophenyl alkanoates by hydroxide ion is strongly retarded by sodium dodecylsulfate (SDS) micelles (1, 2). Analysis of inhibition curves gives K_S values for binding of the esters to SDS micelles, and the slope of the plot of pK_S vs. N is 0.40 ± 0.01 ($r = 0.9986$, 5 points, for acetate to hexanoate) (A.A. Fedortchenko and O.S. Tee. Unpublished work).

© 2000 NRC Canada

Table 2. Least-squares correlations of substrate binding ($pK_S = -\log K_S$) and transition state binding ($pK_{TS} = -\log K_{TS}$) with acyl chain length (*N*), and with each other, for the reaction of nucleophiles with *p*-nitrophenyl alkanoates in the presence of CTAB micelles.[a]

Nucleophile	Plot	Slope	*r*	*n*
Anion of ME	pK_S vs. *N*	0.43 ± 0.03	0.9924	6
	pK_{TS} vs. *N*	0.43 ± 0.02	0.9950	7
	pK_{TS} vs. pK_S	0.99 ± 0.01	0.9998	7
Dianion of MAA	pK_S vs. *N*	0.44 ± 0.01	0.9994	6
	pK_{TS} vs. *N*	0.43 ± 0.01	0.9990	7
	pK_{TS} vs. pK_S	0.98 ± 0.03	0.9981	7
Dianion of MPA	pK_S vs. *N*	0.44 ± 0.01	0.9994	6[b]
	pK_{TS} vs. *N*	0.43 ± 0.01	0.9996	6
	pK_{TS} vs. pK_S	0.97 ± 0.02	0.9995	6[b]
Dianion of CYST	pK_S vs. *N*	0.44 ± 0.01	0.9993	4[b]
	pK_{TS} vs. *N*	0.41 ± 0.01	0.9997	4
	pK_{TS} vs. pK_S	0.94 ± 0.02	0.9994	4[b]
Anion of GLY	pK_S vs. *N*	0.44 ± 0.01	0.9993	4[b]
	pK_{TS} vs. *N*	0.43 ± 0.01	0.9997	4
	pK_{TS} vs. pK_S	0.97 ± 0.03	0.9992	4[b]
Anion of TFE	pK_S vs. *N*	0.41 ± 0.01	0.9996	4[c]
	pK_{TS} vs. *N*	0.38 ± 0.02	0.9972	4
	pK_{TS} vs. pK_S	0.92 ± 0.04	0.9980	4[c]
Hydroxide ion[d]	pK_S vs. *N*	0.42 ± 0.01	0.9983	7
	pK_{TS} vs. *N*	0.42 ± 0.02	0.9963	7
	pK_{TS} vs. pK_S	1.00 ± 0.02	0.9994	7

[a]Using the values of K_S and K_{TS} presented in Table 1, except for hydroxide ion where they are taken from ref. (5). "Slope" is the slope of the least squares line, "*r*" is the correlation coefficient, and *n* is the number of data points in the analysis.

[b]The values of K_S were taken to be the same as those found with the mercaptoacetate dianion.[4]

[c]The values of K_S were taken to be the same as those found with hydroxide ion under the same conditions (5).

[d]From previous experiments carried out in an aqueous phosphate buffer of pH 11.60 (5).

respect to the present results, replacement of bromide ions, as well as of hydroxide ion and buffer anions, in the Stern layer by less hydrophilic thiolate anions can explain the catalysis of thiolysis, and also the observation that the catalytic ratios k_{cN}/k_N are independent of the ester.

Hydroxide ion is a small, "hard" anion that is strongly solvated in water, and for its CTAB-catalyzed reaction with *p*-nitrophenyl esters the catalytic ratio k_{cN}/k_N is only 2.4 ± 0.3, when the total bromide ion is kept at 5.0 mM (5). This ratio is low because the heavily hydrated hydroxide ion does not compete well with bromide ion in the Stern layer (7). Thiolate ions, which are "softer," more polarizable, and less strongly solvated, interact more strongly with CTAB micelles, and so they exchange much more readily with bromide ions (6*d*). Consequently, CTAB catalysis of ester thiolysis is appreciably stronger. For the anion of 2-mercaptoethanol, the catalytic ratio is larger than for hydroxide ion and remarkably constant at 15.3 ± 0.6, for esters beyond the acetate (Table 1). For the mercaptoacetate dianion this ratio is larger still, at 79 ± 7, presumably because the double negative charge on the nucleophile enhances its ion exchange. The catalytic ratio is not quite as big for the 3-mercaptopropionate dianion (53 ± 2) or the cysteine dianion (59 ± 4), perhaps because in these larger ions the double negative charge is more spread-out or because they are hydrated slightly more strongly than the dianion of MAA.

By contrast to the high ratios found for the thiolate dianions, for the glycinate anion, which is an amine nucleophile, the catalytic ratio is barely greater than one, at ~1.4 (Table 2). This much lower value is presumably due to a combination of factors: (*i*) the lower overall charge, *(ii)* the harder, nitrogen nucleophile, and (*iii*) stronger hydration in the bulk aqueous medium. Interestingly, the TFE anion has a much higher catalytic ratio (~25) than hydroxide ion (~2.4), even though both are oxyanions. Almost certainly, the TFE anion is appreciably more hydrophobic and less strongly hydrated than hydroxide ion, so that it exchanges into the CTAB micelles more readily.

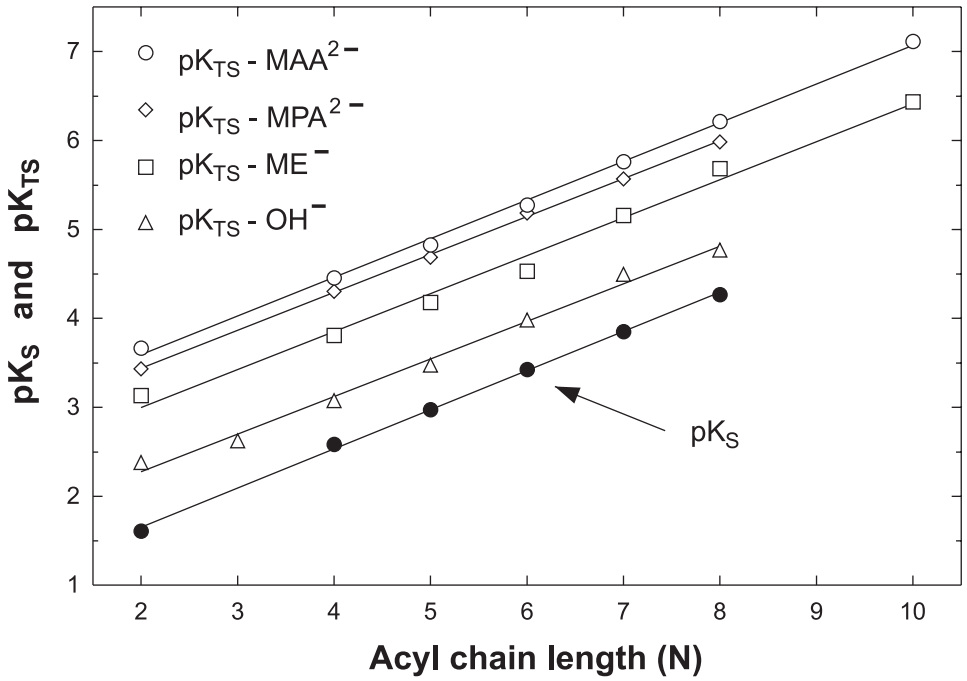
Catalysis of thiolate attack by cationic micelles has been observed before (6, 14, 15). Moreover, spectral measurements have shown that there are very strong interactions between thiophenoxide ions and CTAB micelles (14). Correspondingly, CTAB micelles catalyze the reaction of thiophenoxide ion with *p*-nitrophenyl acetate by 50-fold (15) and its reaction with 2,4-dinitrofluorobenzene even more so (14). Obviously in this latter case there are additional factors, besides ion exchange, contributing to the dynamic component of transition state stabilization.

Conclusions

On the face of it, Kirby's (12) dissection of transition state binding into passive binding and dynamic binding seems simplistic, and yet it appears to be particularly suitable for the cleavage of *p*-nitrophenyl alkanoates by thiolate ions and other nucleophilic anions in CTAB micelles. From the results discussed above, it is concluded that: (*i*) the passive component of the transition state binding involves hydrophobic binding of the acyl chain of the esters in the micelles that is more or less the same as that involved in the substrate

© 2000 NRC Canada

Fig. 4. The dependence of transition state binding (pK_{TS}) and substrate binding (pK_S) to CTAB micelles on the ester chain length (N) of *p*-nitrophenyl alkanoates. The values of pK_{TS} (open symbols) are for various nucleophiles, as indicated; the values of pK_S (●) are those found with MAA. The pK_{TS} points for CYST and TFE (not shown) are close to those for MPA, and those for GLY are barely different from pK_S because k_{cN}/k_N values are almost one (Table 1). The slopes of the graphs are all about 0.43 (Table 2). The corresponding plots of pK_{TS} against pK_S are linear, with slopes very close to one (Table 2).



binding (Fig. 4); (*ii*) the dynamic component is essentially constant for a given nucleophile because it is primarily determined by the interactions associated with acyl transfer in the Stern layer of the micelle; (*iii*) it varies with the nucleophiles because of differences in their ease of exchange into the Stern Layer, due to their hard and (or) soft character, solvation, and charge.

Support for our first conclusion, (*i*) above, is provided by a recent paper from Buurma et al. (13*c*). These authors probed the nature of the Stern region of micelles (cationic, anionic, and non-ionic) using the kinetics of two pH-independent hydrolysis reactions. From their findings they concluded "…. that the stabilisation by the hydrophobic parts of the micelle is similar for the reactant state and for the activated complex." Obviously, this conclusion is essentially the same as the one we have arrived at from the data in Table 2 and Fig. 4.

Experimental

The *p*-nitrophenyl esters were purchased from Sigma Chemical Co., except for the heptanoate which was synthesized as previously (16). Cetyltrimethylammonium bromide (hexadecyltrimethyl-ammonium bromide, CTAB) was obtained from ICN Biochemicals and purified by extraction with diethyl ether in a Soxhlet apparatus for 4 h to remove any residual amines (17), followed by drying overnight. The other chemicals were the best grades available from the Aldrich Chemical Co.mpany, except for standard NaOH solutions which were obtained from A & C Chemicals (Montreal).

The kinetics of the ester cleavage were followed by monitoring the pseudo-first order appearance of the *p*-nitrophenolate ion at 405 nm, using an Applied Photophysics Ltd. SX17MV Stopped-flow Spectrophotometer, with the cell temperature kept at 25.0 ± 0.1°C. From five to 10 absorbance traces were acquired and computer averaged before estimation of k_{obs} by nonlinear least-squares fitting of an exponential growth curve.

As outlined in the main text, three basic types of kinetics experiments were carried out: (*i*) to find k_N, determine k_{obs} vs. [Nuc], with no CTAB (Fig. 1); (*ii*) to find K_S, determine k_{obs} vs. [CTAB], with fixed [Nuc] (Fig. 2); (*iii*) to find k_{cN}, determine k_{obs} vs. [Nuc], with fixed [CTAB] (Fig. 3). Aliquots of stock ester solutions (0.1 M in spectral grade acetonitrile) were added to solutions of NaBr + requisite amount of CTAB in distilled water to give ester solutions of twice the desired final concentrations. The ester + CTAB solutions were sonicated for 10–20 min to facilitate complete solubilization of the ester and dispersal of the surfactant. The dilute substrate solution was mixed 1:1 with a solution containing carbonate buffer + Nuc, brought to pH 10.60. The final reacting solutions, after mixing in the stopped-flow machine, contained 0.10 M carbonate buffer, CTAB (0–5.00 mM), NaBr (5.00 mM – $[CTAB]_o$), and ester concentrations as follows: (*i*) acetate to pentanoate, 50 μM; (*ii*) hexanoate, 25 μM; (*iii*) heptanoate, 5 μM; (*iv*) octanoate, 2.5 μM; and (*v*) decanoate, 1.5 μM. Note that generally [ester] << $[CTAB]_o$, so the micelles would not be significantly affected by the presence of the esters (1). Experiments with TFE were carried out with a 0.20 M phosphate buffer, at pH 11.60, in place of the carbonate buffer.

© 2000 NRC Canada

Nonlinear fitting of eq. [6] was carried out with GraphPad Prism software. When using eqs. [5] and [6] in data analysis, one has to decide how to handle the concentration of surfactant [Surf] involved in micelles. This quantity is reduced from the total surfactant by the amount of the critical micellar concentration (cmc): [Surf] = ([Surf]$_o$ – cmc) (1). For CTAB, cmc is 0.92 mM at *zero* ionic strength, but it is appreciably lower at high salt concentrations (18) and the lowering effect is greater still for less hydrophilic anions like thiolate ions (19). For example, the addition of only 40 μM thiophenolate ion, in a 0.010 M borate buffer at pH 10, lowers the cmc of CTAB to 0.08 mM (14). In the present work, taking [Surf] = ([Surf]$_o$ – cmc), and treating cmc as a fitting parameter in eq. [6] for the data obtained for each of the seven esters reacting with 20 mM ME in 0.10 M carbonate buffer, gave values of cmc that were close to an average of 0.05 mM. Accordingly, for consistency we have taken the cmc to be equal to this value throughout.

According to the literature, the pK_as of the thiols at zero ionic strength are: (*i*) cysteine, 8.39 (20); (*ii*) 2-mercaptoethanol, 9.72 (21); (*iii*) mercaptoacetic acid, 10.56 (20);[6] (*iv*) 3-mercaptopropionic acid, 10.84 (21), but they are lower at high ionic strength. For example, at μ = 1.0 M, the pK_a of ME is 9.61 (22), and at μ = 0.2 M, the second pK_a of MAA drops from 10.56 to 9.84 (20). Thus, at the working pH of 10.60, in the 0.10 M carbonate buffer, the thiols will exist to a considerable extent as their reactive thiolate anions. The exact fractions of the anions are not important to the discussion above because they are the same for all the esters in the series, and they cancel out in the ratios k_{cN}/k_N and in $K_{TS} = k_N K_S/k_{cN}$ (eq. [7]). The relevant pK_a of glycine is 9.78 (23), and that of TFE is 12.4 (22, 24).

Acknowledgements

We thank the Natural Sciences and Engineering Research Council of Canada for operating grants and an equipment grant, and Mr. A.A Fedortchenko for technical advice. We have also benefited from correspondence with Prof. A. Williams, University of Kent, Canterbury (U.K.). OST is particularly grateful to Dr. Chris Easton and the Research School of Chemistry at the Australian National University for their hospitality during a sabbatical leave spent in Canberra.

References

1. (*a*) I.V. Berezin, K. Martinek, and A.K. Yatsimirski. Russ. Chem. Rev. Eng. Transla. **42**, 787 (1973); (*b*) J.H. Fendler and E.J. Fendler. Catalysis in micellar and macromolecular systems. Academic Press, New York, 1975; (*c*) C.A. Bunton. Pure Appl. Chem. **49**, 969 (1977); (*d*) E.J.R. Südholter, G.B. van de Langkruis, and J.B.F.N. Engberts. Recl. Trav. Chim. Pays-Bas Belg. **99**, 73 (1980); (*e*) C.A. Bunton and G. Savelli. Adv. Phys. Org. Chem. **22**, 21 (1986); (*f*) C.A. Bunton, F. Nome, F.H. Quina, and L.S. Romsted. Acc. Chem. Res. **24**, 357 (1991); (*g*) J.B.F.N. Engberts. Pure Appl. Chem. **64**, 1653 (1992); (*h*) S. Tascioglu. Tetrahedron, **52**, 11113 (1996); (*i*) M.-F. Ruasse. Pure Appl. Chem. **69**, 1923 (1997).
2. (*a*) M.T.A. Behme, J.G. Fullington, R. Noel, and E.H. Cordes. J. Am. Chem. Soc. **87**, 265 (1965); (*b*) F.M. Menger and C.E. Portnoy. J. Am. Chem. Soc. **89**, 4698 (1967); (*c*) L.R. Romsted and E.H. Cordes. J. Am. Chem. Soc. **90**, 4404 (1968); (*d*) M. Almgren and R. Rydholm. J. Phys.Chem. **83**, 360 (1979); (*e*) N. Funasaki. J. Phys. Chem. **83**, 237 (1979); (*f*) N. Funasaki and A. Murata. Chem. Pharm. Bull. **28**, 805 (1980); (*g*) T.J. Broxton. Aust. J. Chem. **35**, 1357 (1982); (*h*) E. Rodenas and S. Vera. J. Phys. Chem. **89**, 513 (1985).
3. N. Al-Awadi and A. Williams. J. Org. Chem. **55**, 2001 (1990).
4. O.S. Tee. Adv. Phys. Org. Chem. **29**, 1 (1994).
5. O.S. Tee and A.A. Fedortchenko. Can. J. Chem. **75**, 1434 (1997).
6. (*a*) W. Tagaki, T. Amada, Y. Yamashita, and Y. Yano. J. Chem. Soc. Chem. Commun. 1131 (1972); (*b*) I.M. Cuccovia, E.M. Schroter, P.M. Monteiro, and H. Chaimovich. J. Org. Chem. **43**, 2248 (1978); (*c*) M.K. Kawamuro, H. Chaimovich, E.B. Aubin, E.A. Lissi, and I.M. Cuccovia. J. Phys. Chem. **95**, 1458 (1991); (*d*) V.R Correia, I.M. Cuccovia, and H. Chaimovich. J. Phys. Org. Chem. **6**, 7 (1993).
7. (*a*) N. Funasaki. J. Phys. Chem. **83**, 1998 (1979); (*b*) H. Chaimovich, J.B.S. Bonihla, M.J. Politi, and F.H. Quina. J. Phys. Chem. **83**, 1851 (1979); (*c*) D. Bartet, C. Gamboa, and L. Sepulveda. J. Phys. Chem. **84**, 272 (1980); (*d*) F.H. Quina, M.J. Politi, I.M. Cuccovia, E. Baumgarten, S.M. Martins-Frachetti, and H. Chaimovich. J. Phys. Chem. **84**, 361 (1980); (*e*) C.A. Bunton and J.R. Moffat. J. Phys. Chem. **92**, 2896 (1988).
8. (*a*) O.S. Tee and T.A. Gadosy. J. Chem. Soc. Perkin Trans. 2, 2307 (1994); (*b*) T.A. Gadosy and O.S. Tee. J. Chem. Soc. Perkin Trans. 2, 71 (1995).
9. (*a*) O.S. Tee, T.A. Gadosy, and J.B. Giorgi. Can. J. Chem. **75**, 83 (1997); (*b*) O.S. Tee and M.J. Boyd. Can. J. Chem. **77**, 950 (1999).
10. For example: (*a*) M.J. Pregel, E.J.Dunn, and E.J. Buncel. J. Am. Chem. Soc. **113**, 3545 (1991); (*b*) R. Cacciapaglia and L. Mandolini. Chem. Soc. Rev. **22**, 221 (1993); (*c*) D.M. Davies, G.A. Garner, and J.R. Savage. J. Chem. Soc., Perkin Trans. 2, 1525 (1994); (*d*) D.R.J. Palmer, E. Buncel, and G.R.J. Thatcher. J. Org. Chem. **59**, 5286 (1994); (*e*) M.J. Pregel, E.J. Dunn, R. Nagelkerke, G.R.J. Thatcher, and E. Buncel. Chem. Soc. Rev. **24**, 449 (1995); (*f*) N. Pirrinccioiglu and A. Williams. J. Chem. Soc. Perkin Trans. 2, 37 (1998); (*g*) D.M. Davies, S.J. Foggo, and P.M. Paradis. J. Chem. Soc. Perkin Trans. 2, 1597 (1998); (*h*) D.M. Davies and M.E. Dreary. J. Chem. Soc. Perkin Trans. 2, 1027 (1999).
11. (*a*) R. Wolfenden. Acc. Chem. Res. **5**, 10 (1972); (*b*) G.E. Leinhard. Science (Washington, D.C.), **180**, 149 (1973); (*c*) W.P. Jencks. Adv. Enzymol. **43**, 219 (1975); (*d*) R.L. Schowen. *In* Transition states in biochemical processes. *Edited by* R.D. Gandour and R.L. Schowen. Plenum, New York, 1978; (*e*) J. Kraut. Science (Washington, D.C.), **242**, 533 (1988); (*f*) R. Wolfenden and W.M. Kati. Acc. Chem. Res. **24**, 209 (1991).
12. A.J. Kirby. Acta Chem. Scand. **50**, 203 (1996); Angew. Chem. Int. Ed. Engl. **35**, 707 (1996).
13. (*a*) D.M. Davies, N.D. Gillitt, and P.M. Paradis. J. Chem. Soc. Perkin Trans. 2, 659 (1996); (*b*) D.M. Davies and S.J. Foggo. J. Chem. Soc. Perkin Trans. 2, 247 (1998); (*c*) N.J. Buurma, A.M. Herranz, and J.F.B.N. Engberts. J. Chem. Soc. Perkin Trans. 2, 113 (1999); (*d*) N. Pirrinccioglu, F. Zuman, and A. Williams. J. Org. Chem. **65**, 2537 (2000).
14. H. Chaimovich, A. Blanco, L. Chayet, L.M. Costa, P.M. Monteiro, C.A. Bunton, and C. Paik. Tetrahedron, **31**, 1139 (1975).

[6] Irving et al. (21) determined a value of 10.68.

© 2000 NRC Canada

15. I.M. Cuccovia, E.H. Shroter, P.M. Monteiro, and H. Chaimovich. J. Org. Chem. **43**, 2248 (1978).
16. O.S. Tee and T.A. Gadosy. J. Chem. Soc. Perkin Trans. 2, 715 (1994).
17. D.D. Perrin, W.L.F. Armarego, and D.R. Perrin. Purification of laboratory chemicals. 2nd ed. Pergamon Press, Oxford. 1980.
18. M.J. Rosen. Surfactants and interfacial phenomena. 2nd ed., John Wiley and Sons, New York. 1989.
19. E.J.R. Südholter and J.B.F.N. Engberts. J. Phys. Chem. **83**, 1854 (1979).
20. D.P. Wrathall, R.M. Izatt, and J.J. Christiansen. J. Am. Chem. Soc. **86**, 4779 (1964).
21. R.J. Irving, L. Nelander, and I. Wadso. Acta Chem. Scand. **18**, 769 (1964).
22. D.J. Hupe and W.P. Jencks. J. Am. Chem. Soc. **99**, 454 (1977).
23. E.J. King. J. Am. Chem. Soc. **73**, 155 (1951).
24. C.H. Arrowsmith, A.J. Kresge, and Y.C. Tang. J. Am. Chem. Soc. **113**, 179 (1991).

© 2000 NRC Canada

The reaction between hydrazines and β-dicarbonyl compounds: proposal for a mechanism

Shiv P. Singh, Dalip Kumar, Hitesh Batra, Rajesh Naithani, Isabel Rozas, and José Elguero

Abstract: The reaction between aryl or heteroarylhydrazines with fluorinated β-diketones (CF_3COCH_2COR) yields a variety of 3-, 5-, and 3,5-trifluoromethylpyrazoles and 5-trifluoromethyl-5-hydroxy-Δ^2-pyrazolines. Twenty-one of such compounds have been isolated and identified by ^{13}C and ^{19}F NMR. Together with the results from the literature they provide a comprehensive overview of the reaction. Semi-empirical calculations at the PM3 level have been used to rationalize these results. The outcome that emerges seems to be that the dehydration of a pair of 3,5-dihydroxypyrazolidines kinetically controls the isomer formed.

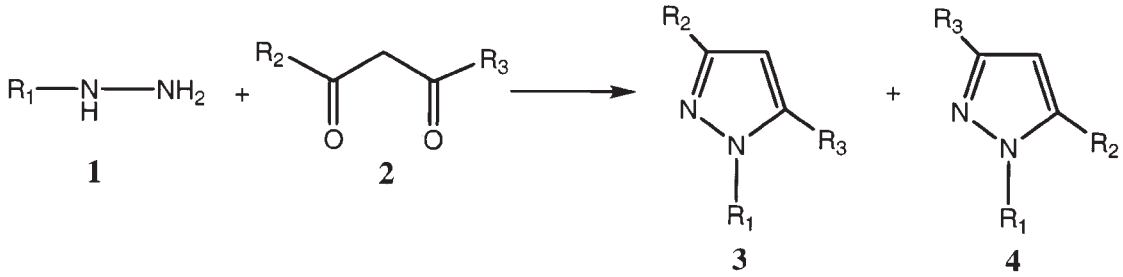
Key words: hydrazines, 1,3-diketones, pyrazolines, pyrazoles, PM3 calculations.

Résumé : La réaction entre des aryl ou hétéroarylhydrazines et des β-dicétones fluorées (CF_3COCH_2COR) donne lieu a une série des 3-, 5- et 3,5-trifluorométhylpyrazoles et 5-trifluorométhyl-5-hydroxy-Δ^2-pyrazolines. Vingt-et-un de ces composés ont été isolés et caractérisés par RMN du ^{13}C et ^{19}F. Avec l'addition des résultats de la littérature, ils donnent une image cohérente de la réaction. Des calculs semi-empiriques PM3 ont été utilisés pour expliquer ces résultats. L'image qui apparaît est celle d'une réaction cinétiquement contrôlée qui correspond à la déshydratation d'une paire de 3,5-dihydroxy-pyrazolidines en équilibre.

Mots clés : hydrazines, 1,3-dicétones, pyrazolines, pyrazoles, calculs PM3.

Introduction

The reaction between a monosubstituted hydrazine (**1**) and a nonsymmetrical β-diketone (**2**) always leads to the formation of a mixture of pyrazole isomers (**3** and **4**) even when one of them is present in a very small amount and the process can be considered regioselective.



This apparently simple reaction, which constitutes the main synthetic approach to pyrazoles (1–5), conceals a complex mechanistic problem. We have summarized in Scheme 1 the different routes that can lead to the two actually isolated compounds making clear where the difficulty of the problem lies. Considering that hydrazine can react initially by the NH (D) or the NH_2 (E) and that a β-diketone has three tautomeric forms (**A**, **B**, and **C**) with two reactive centers, each isomer can be formed by six different routes.

In some cases, it has been possible to isolate the 5-hydroxy-Δ^2-pyrazoline intermediates (**7**) (Scheme 2), but this does not help to solve the mechanistic riddle: which are the route or routes operative in Scheme 1? From low-temperature NMR experiments and from qualitative results, the mechanism represented in Scheme 2 is generally accepted for the synthesis of pyrazoles. The key intermediate is the 3,5-dihydroxypyrazolidine **5** and the formation of both N—C bonds (N2—C3 and N1—C5) of the carbinolamine groups are considered reversible, i.e., when R_2 and R_3 are different, both dihydroxypyrazolidines **5′** and **5″** should be in equilibrium.

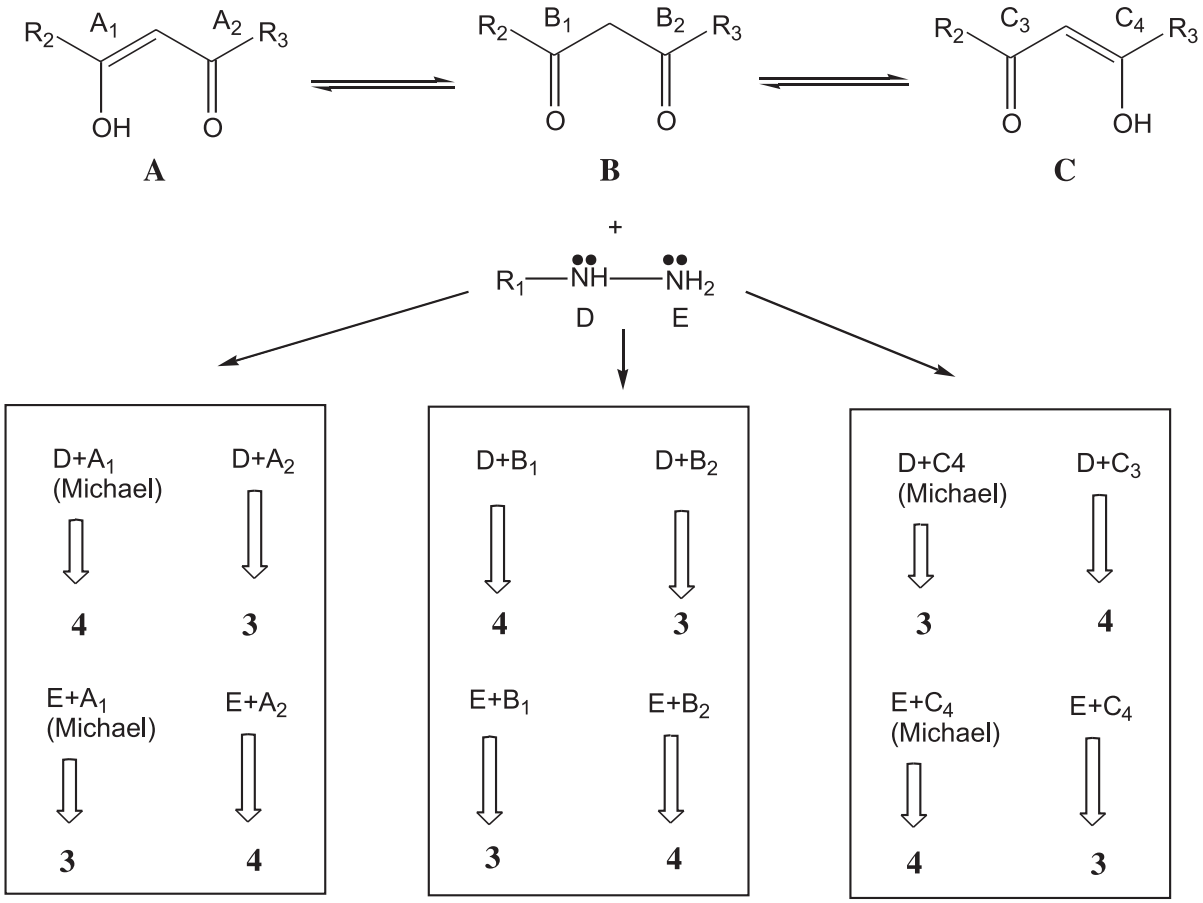
Received May 23, 2000. Published on the NRC Research Press website on August 4, 2000.

S.P. Singh, D. Kumar, H. Batra, and R. Naithani. Department of Chemistry, Kurukshetra University, Kurukshetra-136 119, India. **I. Rozas and J. Elguero.**[1] Instituto de Química Médica, CSIC, Juan de la Cierva 3, E-28006 Madrid, Spain.

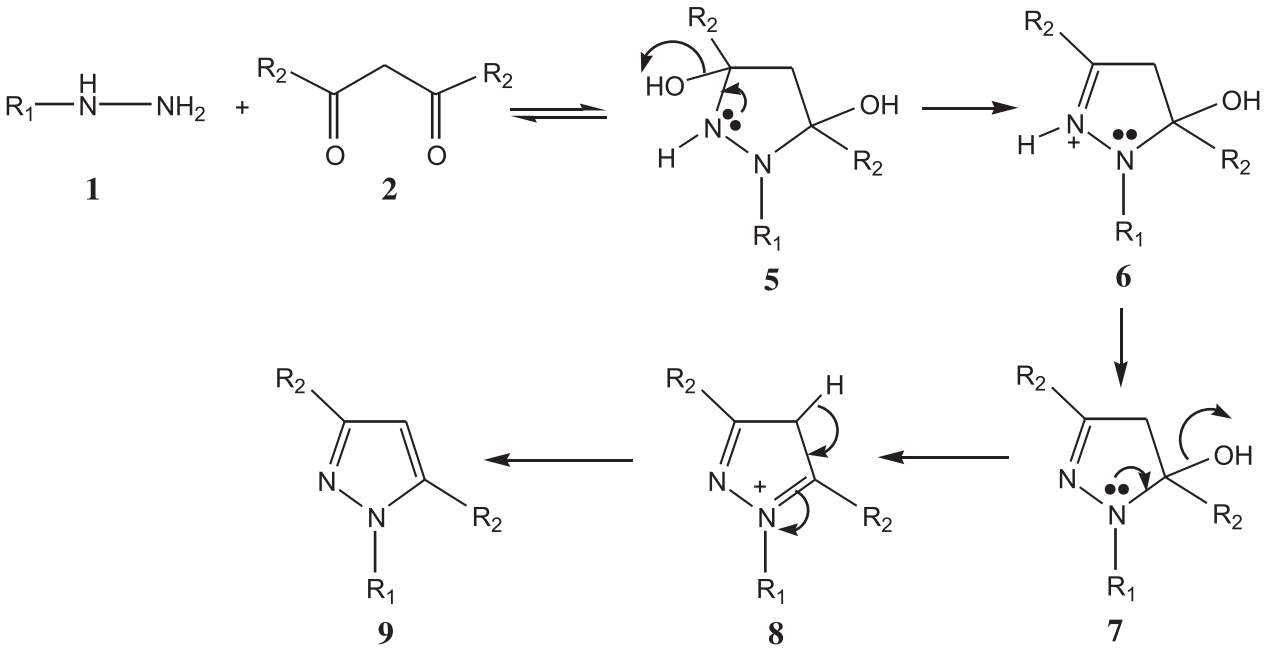
[1]Author to whom correspondence may be addressed. Fax: (34) 91 564 48 53. e-mail: iqmbe17@iqm.csic.es

 © 2000 NRC Canada

Scheme 1.



Scheme 2.



© 2000 NRC Canada

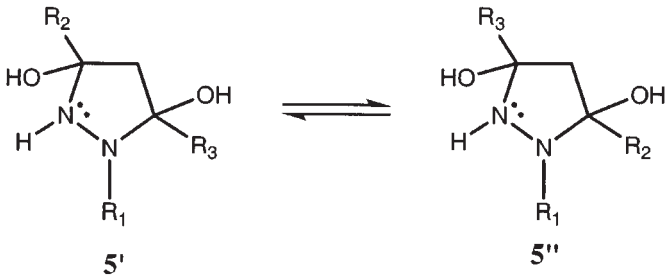
Table 1. Summary of the most relevant results related to the mechanism of the reaction between hydrazines and β-dicarbonyl compounds.

	R_1	R_2	R_3	Isolation of 5-hydroxy-pyrazoline **7**	Dehydration to pyrazole 3-CF_3 **4** and (or) 5-CF_3 **3**	Ratio **4**:**3** or **4**:**7**	Ref.
a	Saccharin[a]	CH_3	CH_3	Yes	Yes (3,5-diCH_3)	—	(6)
b	C_6H_5	CH_3	CF_3	Yes[b]	Yes (5-CF_3).	5:1	(7)
b	C_6H_5	CH_3	CF_3	Yes	No (fails, SO_4H_2)	—	(8)
c	*p*-Fluorophenyl	CH_3	CF_3	No	(5-CF_3 + 3-CF_3)	4:1	This work
d	*p*-Chlorophenyl	CH_3	CF_3	Yes[a]	Yes (5-CF_3)	4:1	(7)
e	*p*-Nitrophenyl	CH_3	CF_3	Yes **7e**	(5-CF_3) **3e**	—	This work
f	2-Benzothiazole	CH_3	CF_3	Yes	Yes (5-CF_3)	—	(9)
g	2-Quinolyl	CH_3	CF_3	Yes	Yes (5-CF_3)	—	(10)
h	Saccharin[a]	CH_3	CF_3	Yes **7h**	Yes (with loss of R_1)	—	This work
i	$CSNH_2$	Cycle[c]	CF_3	Yes	Yes (with loss of R_1)	—	(11)
j	C_6H_5	C_6H_5	CF_3	No	(3-CF_3) **4j**	—	This work
k	*p*-Fluorophenyl	C_6H_5	CF_3	No	(3-CF_3) **4k**	—	This work
l	*p*-Nitrophenyl	C_6H_5	CF_3	No	(3-CF_3) **4l**	—	This work
m	2,4-Dinitrophenyl	C_6H_5	CF_3	Yes **7m**	Yes (5-CF_3) **3m**	—	This work
n	2-Quinolyl	C_6H_5	CF_3	Yes	Yes (5-CF_3)	—	(10)
o	Saccharin[a]	C_6H_5	CF_3	Yes **7o**	Not attempted	—	This work
p	C_6H_5	2-Thienyl	CF_3	No	(3-CF_3) **4p**	—	This work
q	*p*-Fluorophenyl	2-Thienyl	CF_3	No	(3-CF_3) **4q**	—	This work
r	*p*-Nitrophenyl	2-Thienyl	CF_3	No	(3-CF_3) **4r**	—	This work
s	2,4-Dinitrophenyl	2-Thienyl	CF_3	Yes **7s**	Yes (5-CF_3) **3s**	—	This work
t	Saccharine	2-Thienyl	CF_3	Yes **7t**	Yes (with loss of R_1)	—	This work
u	*p*-Fluorophenyl	2-Pyridyl	CF_3	No	(3-CF_3) **4u**	—	This work
v	Saccharin[a]	2-Pyridyl	CF_3	Yes **7v**	Yes (with loss of R_1)	—	This work
x	$CONH_2$	CH_3	CCl_3	Yes		—	(12)
y	$CSNH_2$	CH_3	CCl_3	Yes		—	(12)
z	C_6F_5	CF_3	CF_3	Yes	Yes	—	(13,14)
aa	*p*-Fluorophenyl	CF_3	CF_3	No	(3,5-diCF_3) **9aa**	—	This work
bb	*p*-Nitrophenyl	CF_3	CF_3	Yes	Yes (3,5-diCF_3)	—	(13,14)
cc	2,4-Dinitrophenyl	CF_3	CF_3	Yes	Yes	—	(13)
dd	C_6H_5CO	CF_3	CF_3	Yes	Not reported	—	(13)
ee	2-Quinolyl	CF_3	CF_3	Yes	Yes (3,5-diCF_3)	—	(13)
ff	Saccharin[a]	CF_3	CF_3	Yes **7ff**	Yes (with loss of R_1)	—	This work

[a]Saccharin stands for 1-(1′,2′-benzisothiazol-3′-yl)-1′,1′-dioxide substituent.

[b]From the pyrrolidino adduct on the $COCF_3$.

[c]Cycle stands for a medium size carbocycle (tri, tetra, and pentamethylene pyrazoles).



The dehydration steps (**5** → **6** → **7** and **7** → **8** → **9** in Scheme 2) are irreversible, therefore, the kinetic controlling step is the first dehydration (**5** → **7**). All previous publications dealt with the influence of R_2 and R_3, i.e., the structure of the β-dicarbonyl compound, on the relative ratio of the final pyrazoles **3** and **4**, for a given hydrazine. For instance, the consequences over the **3**:**4** ratio of the fact that aldehydes (R_3 = H) are more reactive than ketones ($R_2 \neq$ H), or that trifluoromethylketones ($R_3 = CF_3$) are more reactive than ordinary ketones ($R_2 = CH_3$ or C_6H_5) have been widely studied.

We will discuss, in the present paper, the effect of R_1 on the **3**:**4** ratio in the case of trifluoromethyl β-diketones and, particularly, when $R_2 = CH_3$ and $R_3 = CF_3$. When R_1 = H, **3** ≡ **4** due to the prototropic tautomerism of pyrazoles.

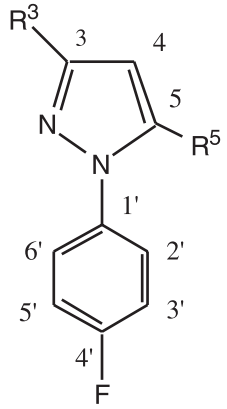
Results and discussion

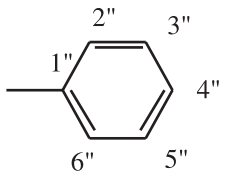
We have gathered in Table 1 the most relevant experimental results for the present work, that is, the isolation of different 5-hydroxypyrazolines (**7**), the dehydration to the corresponding pyrazoles (**9**) (**3**, $R_2 = CH_3$, Ar or Het, $R_3 = CF_3$; **4**, $R_2 = CF_3$, $R_3 = CH_3$, Ar or Het) and the orientation of the reaction (**3**:**4** ratio).

In the present work, we report complementary experiments (marked "this work" in Table 1). This leads us to describe a series of new Δ^2-pyrazolines and pyrazoles, which have been fully characterized by ^{1}H NMR and mass spectrometry (see experimental part). Particularly important for this purpose have been ^{13}C (Table 2) and ^{19}F NMR (Table 3)

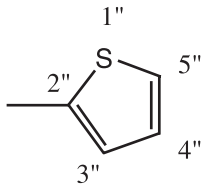
© 2000 NRC Canada

Table 2. ^{13}C chemical shifts (ppm) and ^{13}C – ^{19}F coupling constants (Hz) of *p*-fluorophenylpyrazoles **3c**, **4c**, **9bb**, **4l**, **4r**, **4v**.

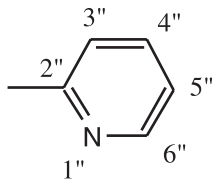




4l



4r



4v

Comp	R^3	R^5	C_3	C_4	C_5	$C_{1'}$	$C_{2'(6')}$	$C_{3'(5')}$	$C_{4'}$	R^3	R^5	$C_{1''}$	$C_{2''}$	$C_{3''}$	$C_{4''}$	$C_{5''}$	$C_{6''}$
3c	CH_3	CF_3	143.32	108.56	149.07	134.93	127.23	116.30	163.83	13.19	121.05	—	—	—	—	—	—
					J = 38		*J* = 10	*J* = 21	*J* = 251		*J* = 269						
4c	CF_3	CH_3	142.75	104.49	140.80	134.91	127.22	116.20	162.38	121.31	12.11	—	—	—	—	—	—
			J = 39				*J* = 9	*J* = 22	*J* = 250	*J* = 268							
9aa	CF_3	CF_3	142.74	107.15	134.81	134.20	127.89	116.41	163.35	119.60	118.71	—	—	—	—	—	—
			J = 43		*J* = 42		*J* = 10	*J* = 23	*J* = 251	*J* = 269	*J* = 270						
4k	CF_3	Phenyl	143.55	105.85	145.08	135.65	127.59	116.36	162.44	121.52	—	129.21	129.43	129.06	129.06	129.06	129.43
			J = 39				*J* = 9	*J* = 24	*J* = 250	*J* = 270							
4q	CF_3	2-Thienyl	143.19	105.00	138.92	134.91	128.27	116.23	162.73	121.59		S	129.36	127.64	128.17	127.57	—
			J = 39				*J* = 9	*J* = 22	*J* = 250	*J* = 268							
4u	CF_3	2-Pyridyl	143.96	106.69	150.00	135.78	127.47	116.09	162.34	121.14		N	148.05	123.60	136.70	122.93	150.00
			J = 43				*J* = 9	*J* = 23	*J* = 250	*J* = 270							

© 2000 NRC Canada

Scheme 3.

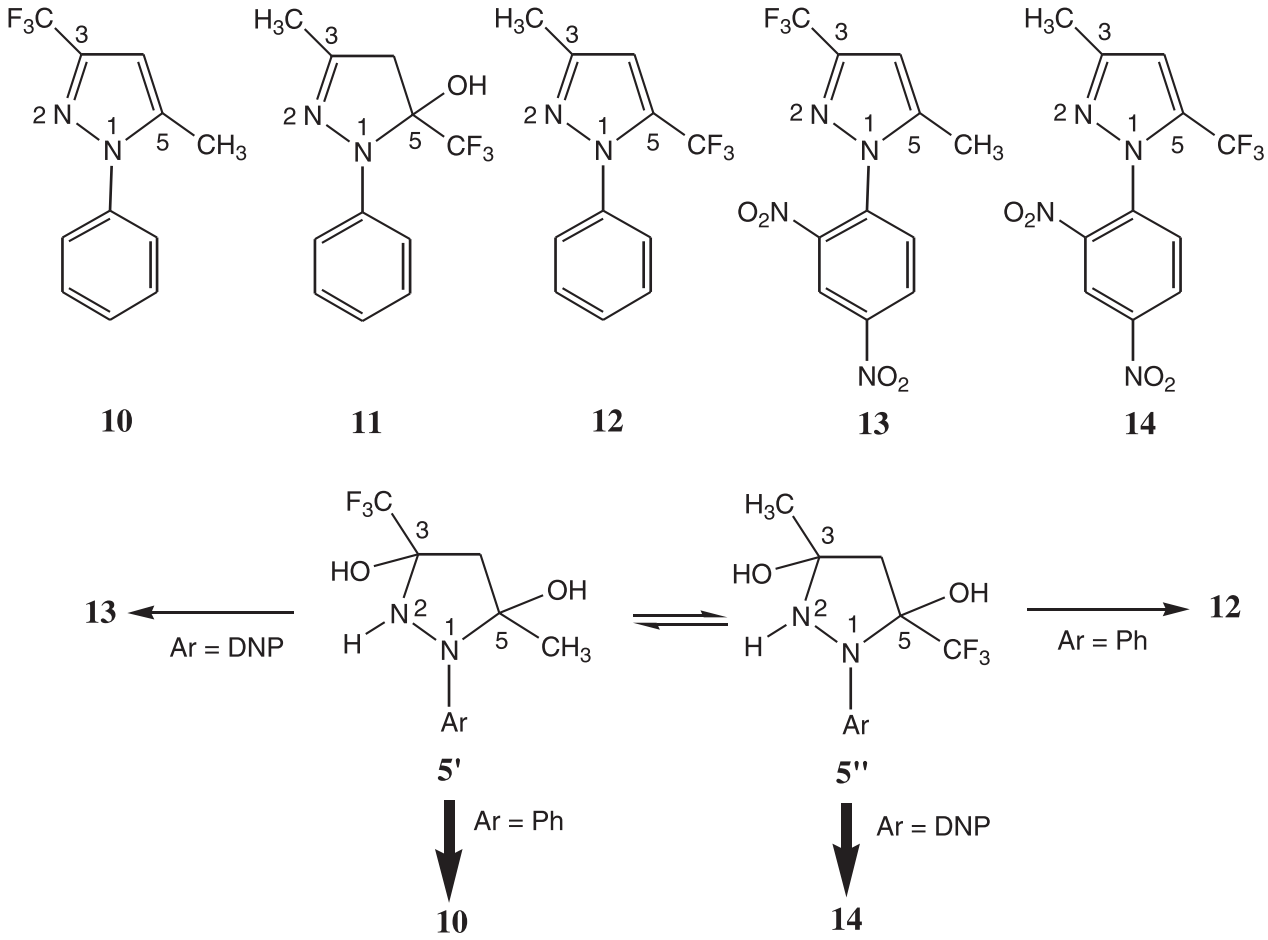


Table 3. ^{19}F chemical shifts (ppm) of some pyrazoles and 5-hydroxypyrazolines.

Comp	CF_3 position	CF_3	*p*-Fluorophenyl
3c	5	–58.2	–112.2
4c	3	–62.8	–112.6
4k	3	–62.8	–112.8
4l	3	–62.9	—
4q	3	–62.8	–111.4
4u	3	–62.7	–110.1
7e	5	–71.2	—
7h	5	–79.3	—
7s	5	–72.1	—
7ff	3	–71.2	—
	5	–78.2	—
9aa	3	–63.0	–110.0
	5	–58.7	—

data since they are characteristic of the different structures (5, 7–10, 12–14).

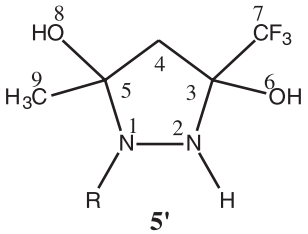
The mechanism of the reaction of β-dicarbonyl compounds and hydrazines has been studied in several occasions, particularly by Selivanov and Ershov and co-workers (15–19), who first used stop-flow NMR techniques to characterize the 3,5-dihydroxypyrazolidines **5** and the 5-hydroxypyrazolines **7** as intermediates and by Elguero and Yranzo (20) who first isolated a 3,5-dihydroxypyrazolidine (**5**, R_1 = H, R_2 = R_2 = CF_3). Russian authors (21, 22) have reported further studies and the reaction has been reviewed (23–25). We have proposed that the dehydration **7** → **9** involves the intermediate **8** to explain why when R_1 is an electron-withdrawing group, the dehydration does not occur or occurs with difficulty (3, 20). Besides, 4-hydroxy-Δ^2-pyrazolines are much more stable than the 5-hydroxy ones and more difficult to aromatize (26).

The results gathered in Table 1 are fully consistent with the role of CF_3 or, more generally, perfluoroalkyl substituents at position 5 and with electron-withdrawing substituents at position 1 to stabilize the 5-hydroxypyrazolines **7**. The role of a 5-trifluoromethyl group is apparent in experiments **b**, **d**, and **z**; that of R_1 in experiment **a** (for brevity's sake, we will use saccharin instead of 1-(1′,2′-benzisothiazol-3′-yl)-1′,1′-dioxide) and that of both in many cases (**e**–**i**, **m**–**o**, s, **t**, **v**, **bb**–**ff**). Note that the CCl_3 group behaves similarly to the CF_3 group (experiments **x** and **y**).

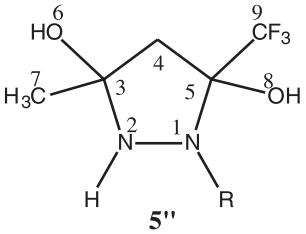
The most difficult point is to rationalize the orientation or **4**:**3** ratio. To advance in this direction, we have carried out a series of semi-empirical calculations, using the PM3 Hamiltonian. We have selected two cases (Scheme 3): the reaction of 1,1,1-trifluoropentane-2,4-dione with phenylhydrazine and 2′,4′-dinitrophenylhydrazine (DNPh). The first yields a mixture of 1-phenyl-3-trifluoro-methyl-5-methyl-

© 2000 NRC Canada

Table 4. PM3 calculations of 1-phenyl-3,5-dihydroxypyrazolidines.



5'



5''

	ΔH_f	Dipole (μ)	q-N1	q-N2	q-O6	q-O8
5′ *ddu*	**–207.7**	4.25	–0.0702	–0.0803	–0.2957	–0.3169
5′ *uuu*	–207.4	3.93	–0.0629	–0.0751	–0.2881	–0.3132
5′ *udu*	–207.2	3.31	–0.0726	–0.0503	–0.2938	–0.3061
5′ *duu*	–206.2	3.44	–0.0632	–0.0708	–0.2882	–0.3022
5′ *dud*	–204.6	3.43	–0.0325	–0.0692	–0.2875	–0.3142
5′ *ddd*	–204.6	3.76	–0.0477	–0.0352	–0.3048	–0.3138
5′ *udd*	–201.5	5.21	0.0078	–0.0365	–0.3096	–0.2716
5′ *uud*	–201.4	4.09	0.0005	–0.0657	–0.2947	–0.2801
5′′ *ddd*	**–205.2**	1.45	–0.0324	–0.0999	–0.3011	–0.2748
5′′ *uuu*	–204.6	3.17	–0.0399	–0.0422	–0.3338	–0.2864
5′′ *duu*	–203.6	4.50	–0.0461	–0.0759	–0.3121	–0.2729
5′′ *ddu*	–199.6	1.88	0.0231	–0.0862	–0.3007	–0.2566
5′′ *udu*	–197.8	1.11	0.0129	–0.0804	–0.3170	–0.2534
5′′ *udd*	–204.9	2.10	–0.0399	–0.0995	–0.3098	–0.2722
5′′ *uud*	–203.7	2.47	–0.0483	–0.0937	–0.3072	–0.2819
5′′ *dud*	–204.0	2.31	–0.0539	–0.0949	–0.2986	–0.2795

Note: ***u*** = up, ***d*** = down.

pyrazole **10** and 1-phenyl-3-methyl-5-trifluoromethyl-5-hydroxypyrazoline **11** in a ratio 5:1 (see Table 1, example **b**) (7) (*p*-fluorophenylhydrazine, example **c** behaves similarly). The pyrazoline can be dehydrated with $HCl–CH_2Cl_2$ into pyrazole **12** (7) although other authors failed using H_2SO_4 (8). From DNPh only 1-(2′,4′-dinitrophenyl)-3-methyl-5-trifluoro-methylpyrazole **14** should be formed considering the **3m** or **3s** examples of Table 1.

The first hypothesis we tested was a thermodynamical control related to the equilibrium **5′**–**5′′** between the 3,5-dihydroxypyrazolidines (Scheme 3). The problem is rather complicated because these compounds present three stereogenic centers N1, C3, and C5 (the inversion at the nitrogen atoms has very low barriers and only that bearing the phenyl ring was considered). The equilibrium between **5′** and **5′′** through the β-diketone implies the epimerization of C3 and C5. In addition, in the case of the dinitrophenyl derivatives, two conformations of this substituent, depending on which side the *o*-nitro group lies, have to be considered. Therefore, 16 and 32 conformations were calculated in the cases of Ar = C_6H_5 and Ar = 2′,4′-$(NO_2)_2$-C_6H_4, respectively. The results are given in Tables 4 and 5, which contain heats of formation (in kcal mol^{-1}), dipole moments μ (in D), and charges (q) of N1, N2, O6, and O8 atoms.

In the case of the phenyl derivative, the most stable structure is **5′** (Ar close to the CH_3) with the conformation represented in Fig. 1 (i.e., Ph *up*, 3-OH *down* and 5-OH *down* (**5′*udd***), –207.7 kcal mol^{-1}). The most stable amongst **5′′** structures is **5′′*ddd***, but it lies 2.5 kcal mol^{-1} higher.

The sixteen values of PM3 heats of formation can be expressed using an additive model with contributions of the different structural features of the compounds. In the **5′** series, a phenyl down is 0 and up is 1 while in the **5** series there is, respectively, 0 and –1. The OH substituents at the 5 position (that close to the phenyl group) is 0 when down and 1 or –1 when up for **5′** and **5′′**. When the Ph and CF_3 substituents are on the same side of the molecule, *cis*, or on opposite sides, *trans*, 1 or 0. The resulting eq. [1] for 16 compounds has an $R^2 = 0.935$

$$[1] \quad \Delta H_f = -(205.2 \pm 0.3) + (3.6 \pm 0.3)\ \text{Ph} - (1.6 \pm 0.3)\ 5\text{OH} + (2.5 \pm 0.4)\ CF_3/\text{Ph}$$

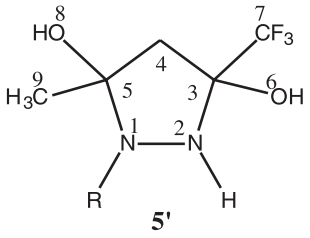
That is, the intercept is close to the average heat of formation for the sixteen compounds. The *N*-phenyl substituent prefers to be down in the **5′** series and up in the **5′′** ones, otherwise it destabilizes the compound by 3.6 kcal mol^{-1}. The contrary happens with the 5-hydroxy substituent, but the effect is lower. Finally, the presence of CF_3 and Ph groups on the same side, *cis*, destabilizes the molecule by an amount of 2.5 kcal mol^{-1}.

Since **5′*udd*** is more stable that **5′′*ddd***, then, if the reaction is thermodynamically controlled, the resulting *N*-phenylpyrazole should have been **10**, which is consistent with the experiment.

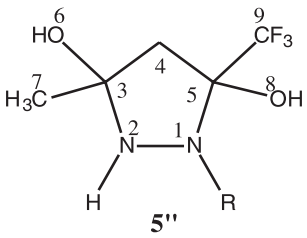
A similar analysis of the thirty-two dinitrophenyl derivatives (DNP), show that, here, the additive model is much less satisfactory (eq. [2], $n = 32$, $R^2 = 0.56$), but the effects are

© 2000 NRC Canada

Table 5. PM3 calculations of 1-(2′,4′-dinitrophenyl)-3,5-dihydroxypyrazolidines.



5'



5''

	ΔH_f	Dipole μ	q-N1	q-N2	q-O6	q-O8
5′*ddda*	–211.4	6.49	–0.0700	–0.0571	–0.2730	–0.3404
5′*udda*	**–220.4**	4.28	–0.1068	–0.0793	–0.2900	–0.3149
5′*ddua*	–211.6	5.55	–0.0587	–0.0939	–0.2857	–0.3448
5′*udua*	–218.5	4.04	–0.1001	–0.0668	–0.2868	–0.2996
5′*duda*	–208.1	4.39	–0.0871	–0.0187	–0.3002	–0.2862
5′*uuda*	–215.7	8.82	–0.0716	–0.0640	–0.2962	–0.2918
5′*duua*	–204.1	5.38	–0.0574	–0.0447	–0.2887	–0.2920
5′*uuua*	–217.2	4.20	–0.1115	–0.0733	–0.2792	–0.3088
5′*dddb*	–216.0	5.35	–0.0826	–0.0247	–0.3089	–0.3128
5′*uddb*	–215.6	7.17	–0.0917	–0.0925	–0.2945	–0.3066
5′*ddub*	–213.8	3.47	–0.0858	–0.0519	–0.2798	–0.3120
5′*udub*	–215.7	5.03	–0.0610	–0.0939	–0.2790	–0.2887
5′*dudb*	–214.5	6.29	–0.0837	–0.0134	–0.3173	–0.2893
5′*uudb*	–219.3	5.99	–0.1119	–0.0470	–0.2916	–0.3045
5′*duub*	–213.8	4.16	–0.0929	–0.0431	–0.2815	–0.2993
5′*uuub*	–216.9	6.67	–0.0774	–0.0929	–0.2825	–0.2930
5″*ddda*	–215.1	6.72	–0.0664	–0.1000	–0.2919	–0.2935
5″*udda*	–214.6	6.43	–0.0590	–0.0983	–0.2953	–0.3030
5″*ddua*	–212.3	3.71	–0.0984	–0.0908	–0.2894	–0.2723
5″*udua*	–209.6	1.72	–0.1038	–0.0481	–0.3054	–0.2832
5″*duda*	–215.1	7.32	–0.0731	–0.0978	–0.3011	–0.2878
5″*uuda*	–204.2	4.99	–0.0212	–0.0627	–0.3260	–0.2752
5″*duua*	–212.5	5.90	–0.0926	–0.0910	–0.3007	–0.2755
5″*uuua*	–205.3	3.93	–0.0829	–0.0339	–0.2978	–0.2798
5″*dddb*	–213.7	4.56	–0.0735	–0.0840	–0.3157	–0.3050
5″*uddb*	–208.0	6.40	–0.0165	–0.0701	–0.2902	–0.2513
5″*ddub*	–212.4	5.79	–0.0629	–0.1090	–0.2913	–0.2771
5″*udub*	–213.9	5.19	–0.0715	–0.0768	–0.3045	–0.2793
5″*dudb*	**–217.5**	3.78	–0.0931	–0.1197	–0.3041	–0.2934
5″*uudb*	–206.1	6.48	–0.0263	–0.0613	–0.3108	–0.2470
5″*duub*	–212.7	5.79	–0.0612	–0.0789	–0.3174	–0.2771
5″*uuub*	–213.2	7.30	–0.0772	–0.0345	–0.3381	–0.2819

Note: ***u*** = up, ***d*** = down, ***a*** = NO_2 towards N2.

the same including a term defining the position of the nitro group (***a*** towards N2, ***b*** towards the OH).

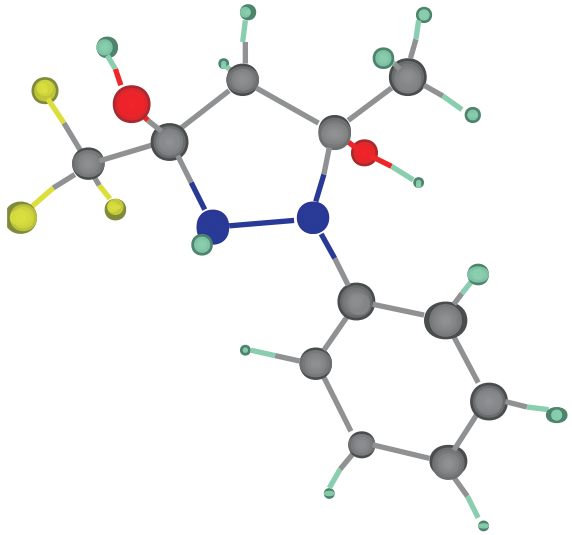
$$[2]\quad \Delta H_f = -(212.6 \pm 0.8) + (4.3 \pm 0.9)\ \text{DNP} - (1.3 \pm 0.9)\ 5\text{OH} + (1.7 \pm 1.4)\ CF_3/\text{DNP} - (1.7 \pm 1.1)\ NO_2$$

The effects are similar to those in eq. [1]: the structures are more stable when the nitro group is ***b*** in dihydroxypyrazolidines **5**″ and ***a*** in the other isomer **5**′. The two most stable compounds (see Fig. 1) are **5′*udda*** (–220.4 kcal mol^{-1}) and **5″*dudb*** (–217.5 kcal mol^{-1}). Here again, the most stable situation (2.9 kcal mol^{-1}) corresponds to the **5′** series. Consequently, isomer **13** should be formed which is contrary to experiment (formation of **14**, see Scheme 3).

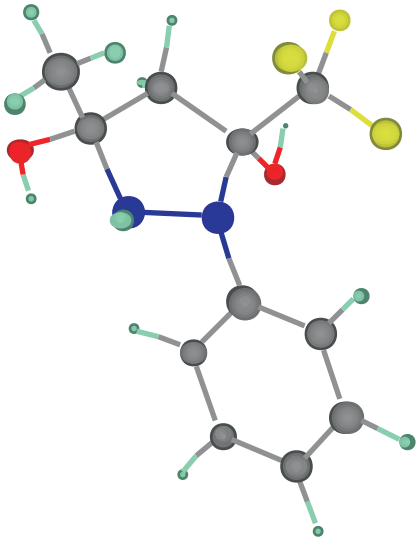
Therefore, this first approach failed. Although the dipole moments are different (Tables 4 and 5), they cannot be used to explain why **14** is preferred over **12**. Since it does not seem to be a thermodynamical control we decided to explore the hypothesis of a kinetic control: the orientation of the pyrazole formation depends on the rate of dehydration of the dihydroxypyrazolidines **5**′ and **5**″. When Ar = Ph, dehydration

© 2000 NRC Canada

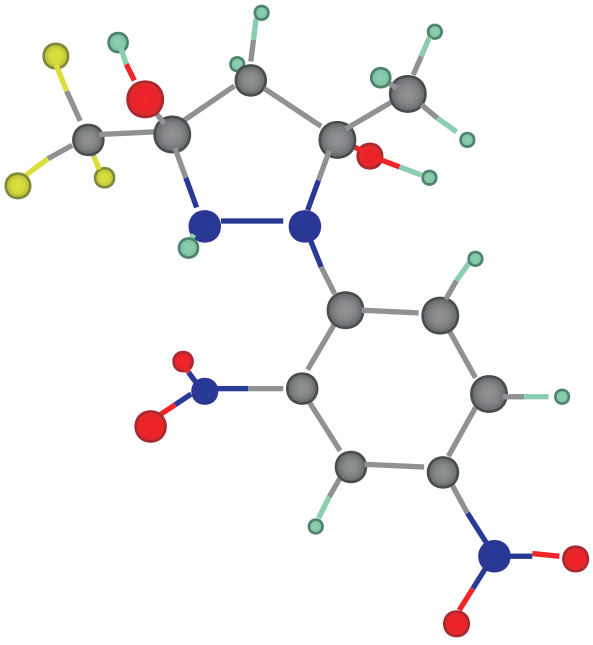
Fig. 1. Optimized PM3 structures of the isomers of minimum energy of derivatives **5′** and **5″** (**5′*udd***, **5″*ddd***, **5′*udda***, and **5″*dudb***).



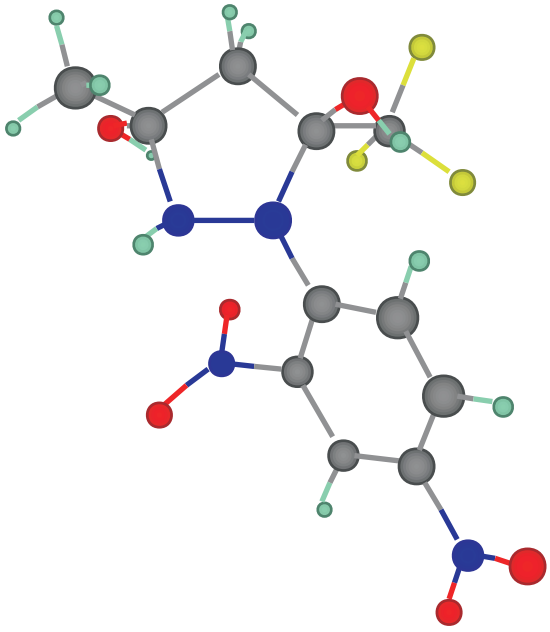
5' *udd*



5'' *ddd*



5' *udda*



5'' *dudb*

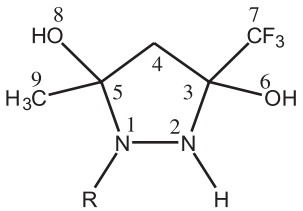
is faster in **5′** than in **5″**; the contrary should happen when Ar = DNP.

In the second case, the dehydration should involve the N2 lone pair and the OH group at position 3. Although less stable, **5″*dudb*** has more negative charge on N2 (+0.0404) and on O6 (+0.0141) than **5′*udda*** (Table 6). Consequently either neutral or assisted by protonation on O6, the easier loss of water should be that from **5″*dudb***, the less stable dihydroxypyrazolidine, yielding **14** in agreement with experimental results (see Scheme 3).

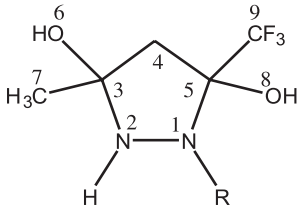
For Ar = Ph, the results are the same, i.e., the less stable dihydroxypyrazolidine **5″*ddd***, would yield **11**, which is the minor isomer, instead of **10**. Note, however, that the differences of q-N2 and q-O6 although positive are smaller

© 2000 NRC Canada

Table 6. PM3 calculations of 3,5-dihydroxypyrazolidines.



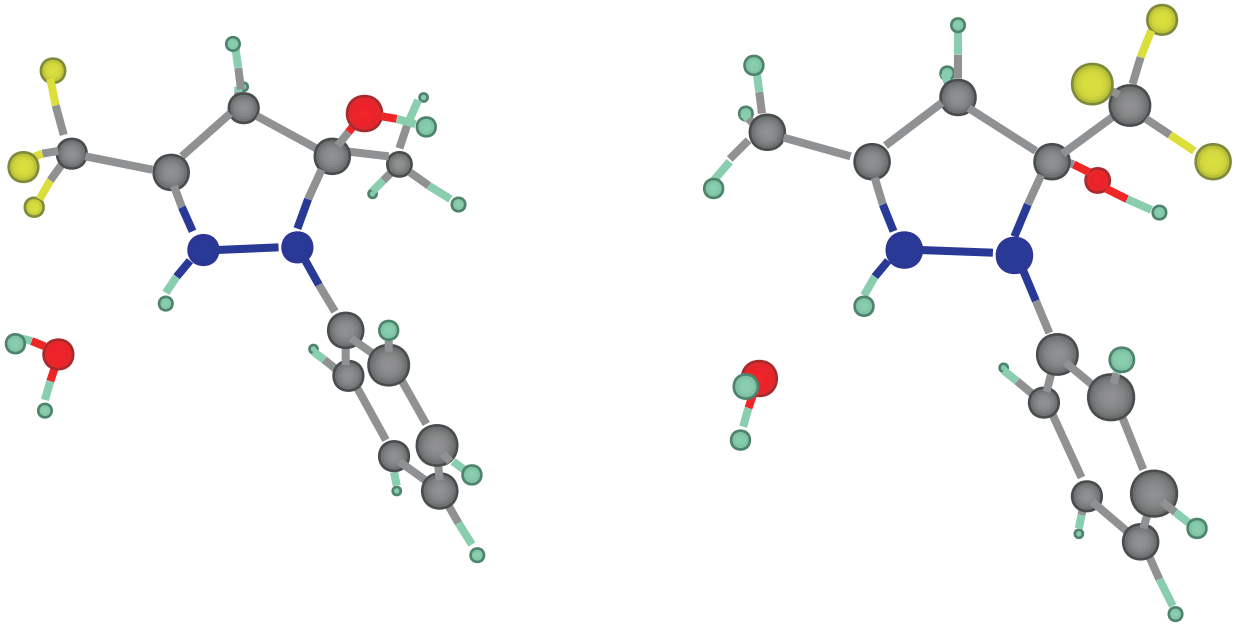
5'



5''

Comp	ΔH_f	q-N1	q-N2	q-O6	q-O8	Experimental result
5′*udd*	–207.7	–0.0702	–0.0803	–0.2957	–0.3169	**10**
5′′*ddd*	–205.2	–0.0324	–0.0999	–0.3011	–0.2748	**11**
Difference	–2.5	–0.0378	+0.0196	+0.0054	–0.0421	ratio **10**:**11** = 5:1
5′*udda*	–220.4	–0.1068	–0.0793	–0.2900	–0.3149	**13**
5′′*dudb*	–217.5	–0.0931	–0.1197	–0.3041	–0.2934	**14**
Difference	–2.9	–0.0137	+0.0404	+0.0141	–0.0215	ratio **13**:**14** = 0

Fig. 2. Optimized PM3 structures corresponding to the protonation on O6 of **5′*udd*** and **5′′*ddd*** to yield **6′*udd***·H_2O and **6′′*ddd***·H_2O.



6' *ddd* · H_2O 6" *ddd* · H_2O

(+0.0196 and +0.0054) than in the preceding case, pointing out that the preference of **11** over **10** should be smaller than that of **13** over **14**, which is what is found experimentally. It is possible that in this case, the experimental rate of formation of **10** and **11** would include the equilibrium constants between **5′*udd*** and **5′′*ddd***.

We tried to calculate the energies of the four dihydroxypyrazolidines protonated on O6 but the resulting cations are not stable and during the process of optimization, they isomerize to cations **6** (see Scheme 2) solvated by a water molecule, something like **5**$H^+ \rightarrow$ **6**·H_2O. We have represented two of such complexes, those formed from **5′*udd*** and **5″*ddd*** in Fig. 2.

Conclusions

Literature results plus those reported in this work prove that the orientation in the reaction of hydrazines with β-diketones depends on the substituent in the hydrazine. Although the differences in orientation between alkyl and arylhydrazines have been assigned to differences in reactivity of both nitrogen atoms (R_1NH, D, in alkyl- and NH_2, E, in aryl-hydrazines, see Scheme 1), this is certainly not the case of the reactions reported in Table 1, because all of them should start reacting by the NH_2. We propose that the orientation is the result of the difference in the rates of dehydration of the two 3,5-dihydroxy-pyrazolidines in equilibrium.

© 2000 NRC Canada

Experimental

Melting points were determined in open capillaries and are uncorrected. The ^{1}H NMR spectra were obtained at 270, 300, and 400 MHz, ^{13}C NMR spectra at 67.5 and 100 MHz, and ^{19}F NMR spectra at 75 and 376 MHz using Jeol-GX270, Jeol-EX400, Bruker-300, and Bruker-400 instruments. The internal standard for ^{1}H and ^{13}C was TMS and for ^{19}F NMR it was $CFCl_3$ ($\delta = 0.00$). The coupling constants reported for the ^{13}C NMR data correspond to couplings with ^{19}F. Mass spectra were recorded on a Kratos-MS-50 instrument and microanalyses were performed on a Perkin–Elmer 2400 instrument.

Synthesis of 1-(*p*-fluorophenyl)-3(5)-trifluoromethylpyrazoles

*1-p-Fluorophenyl-3-methyl-5-trifluoromethylpyrazole (**3c**) and 1-p-fluorophenyl-3-trifluoro-methyl-5-methylpyrazole (**4c**)*

An ethanolic solution (30 mL) of *p*-fluorophenylhydrazine (1 g, 6 mmol) and sodium acetate (0.5 g, 6 mmol) was refluxed for 15 min. 1,1,1-Trifluoropentane-2,4-dione (0.9 g, 6 mmol) was subsequently added and the solution was refluxed for 2 h. The solvent was evaporated and the residue obtained was extracted with chloroform. The organic phase was dried over anhydrous sodium sulfate and the chloroform was distilled off. The TLC and ^{1}H NMR of the gummy mass showed formation of both isomers in a 4:1 (**4c**:**3c**) ratio. Column chromatographic separation using silica gel (60–120 mesh) and light petroleum (60–80°) as eluent afforded **4c**.

4c: Oil, yield 0.8 g (53%). ^{1}H NMR ($CDCl_3$) δ: 2.32 (s, 3H, C_5-CH_3), 6.45 (s, 1H, C_4-H), 7.17 (unresolved dd, 2H, $C_{3'}$- and $C_{5'}$-H, J = 8.1 and 8.8 Hz), 7.42 (m, 2H, $C_{2'}$- and $C_{6'}$-H). Anal. calcd. for $C_{11}H_8F_4N_2$: C 54.11, H 3.30, N 11.47; found C 53.92, H 3.28, N 11.21.

Further elution of the column with light petroleum afforded the other isomer **3c**.

3c: Oil, yield 0.2 g (13%). ^{1}H NMR ($CDCl_3$) δ: 2.35 (s, 3H, C_3-CH_3), 6.59 (s, 1H, C_4-H), 7.25 (unresolved dd, 2H, $C_{3'}$- and $C_{5'}$-H, J = 8.2 and 8.7 Hz), 7.42 (m, 2H, $C_{2'}$- and $C_{6'}$-H). Anal. calcd. for $C_{11}H_8F_4N_2$: C 54.11, H 3.30, N 11.47; found C 54.05, H 3.13, N 11.34.

Three other pyrazoles **4k**, **4q**, **4u** were prepared and purified similarly.

*1-p-Fluorophenyl-3-trifluoromethyl-5-phenylpyrazole (**4k**)*

Mp 102–103°C, yield 72%. ^{1}H NMR ($CDCl_3$) δ: 6.74 (s, 1H, C_4-H), 7.18–7.22 (m, 2H, $C_{2''}$- and $C_{6''}$-H), 7.30 (m, 5H, Ar-H, $C_{3''}$- $C_{4''}$- $C_{5''}$-, $C_{2'}$-, and $C_{6'}$-H), 7.03 (unresolved dd, 2H, $C_{3'}$- and $C_{5'}$-H, J = 8.1 and 8.8 Hz). Anal. calcd. for $C_{16}H_{10}F_4N_2$: C 62.75, H 3.27, N 9.15; found C 62.67, H 3.41, N 8.84.

*1-p-Fluorophenyl-3-trifluoromethyl-5-(2′-thienyl)pyrazole (**4q**)*

Mp 81–82°C, yield 74%. ^{1}H NMR ($CDCl_3$) δ: 6.70 (s, 1H, C_4-H), 6.78 (dd, 1H, $C_{3''}$-H, J = 1.0 and 3.7 Hz), 6.88 (dd, 1H, $C_{4''}$-H, J = 3.7 and 5.0 Hz), 7.03 (unresolved dd, 2H, $C_{3'}$- and $C_{5'}$-H, J = 8.1 and 8.8 Hz), 7.23 (dd, 1H, $C_{5''}$-H, J = 1.0 and 5.0 Hz), 7.28 (m, 2H, $C_{2'}$- and $C_{6'}$-H). Anal. calcd. for $C_{14}H_8F_4N_2S$: C 53.85, H 2.58, N 8.97; found C 54.02, H 2.46, N 8.63.

*1-p-Fluorophenyl-3-trifluoromethyl-5-(2′-pyridyl) pyrazole (**4u**)*

Mp 72–74°C, yield 73%. ^{1}H NMR ($CDCl_3$) δ: 7.01 (s, 1H, C_4-H), 7.08 (m, 2H, $C_{3'}$- and $C_{5'}$-H, J = 8.1 and 8.8 Hz), 7.22–7.35 (m, 4H, $C_{3''}$-, $C_{5''}$-, $C_{2'}$- and $C_{6'}$-H), 7.64 (unresolved dd, 1H, $C_{4''}$-H, J = 1.8 and 7.8 Hz), 8.58 (dd, 1H, $C_{6''}$-H, J = 3.9 and 7.8 Hz). Anal. calcd. for $C_{15}H_9F_4N_3$: C 58.64, H 2.95, N 13.68; found C 58.39, H 3.00, N 13.54.

Synthesis of 1-phenyl-3-trifluoromethylpyrazoles

*1,5-Diphenyl-3-trifluoromethylpyrazole (**4j**)*

An ethanolic solution (30 mL) of phenylhydrazine (0.64 g, 6 mmol) and sodium acetate (0.5 g, 6 mmol) was refluxed for 15 min. An equimolar amount of benzoyltrifluoroacetone (0.9 g, 6 mmol) was subsequently added and the solution was refluxed for 3 h. On cooling, a solid appeared which was recrystallized from ethanol, mp 80°C (lit. (27) mp 95°C), yield 50%. ^{1}H NMR ($CDCl_3$) δ: 6.80 (s, 1H, C_4-H), 6.85 (d, 2H, $C_{3''}$- and $C_{5''}$-H), 6.36 (dd, 1H, $C_{4''}$-H), 7.31 (dd, 2H, $C_{2''}$- and $C_{6''}$-H), 7.42–7.47 (m, 5H, Ar-H). M^+ 288. Anal. calcd. for $C_{16}H_{11}F_3N_2$: C 66.66, H 3.85, N 9.72; found C 66.47, H 3.81; N 9.70.

*1-Phenyl-3-trifluoromethyl-5-thienylpyrazole (**4p**)*

This compound was prepared similarly from thienoyltrifluoroacetone, mp 92°C, yield 51%. ^{1}H NMR ($CDCl_3$) δ: 6.75 (s, 1H, C_4-H), 7.20–7.37 (m, 8H, Ar-H). M^+ 294. Anal. calcd. for $C_{14}H_9F_3N_2S$: C 57.14, H 3.08, N 9.52; found C 57.33, H 3.17, N 9.36.

Synthesis of 1-*p*-nitrophenyl-3-trifluoromethylpyrazoles

*1-p-Nitrophenyl-3-trifluoromethyl-5-phenylpyrazole (**4l**)*

An ethanolic solution (30 mL) of *p*-nitrophenylhydrazine (0.95 g, 6 mmol) and sodium acetate (0.5 g, 6 mmol) was refluxed for 15 min. An equimolar amount of benzoyltrifluoroacetone was subsequently added and the solution was refluxed for 4 h. After solvent evaporation, the residue obtained was crystallized from ethanol, mp 91°C, yield 62%. ^{1}H NMR ($CDCl_3$) δ: 6.79 (s, 1H, C_4-H), 7.23–7.52 (m, 5H, Ar-H), 7.50 (d, 2H, $C_{2'}$- and $C_{6'}$-H), 8.22 (d, 2H, $C_{3'}$- and $C_{5'}$-H). M^+ 333. Anal. calcd. for $C_{16}H_{10}F_3N_3O_2$: C 57.66, H 3.02, N 12.61; found C 57.81, H 2.88; N 12.71.

*1-p-Nitrophenyl-3-trifluoromethyl-5-(2-thienyl)pyrazole (**4r**)*

This compound was prepared similarly from thienoyltrifluoroacetone, mp 97°C, yield 60%. ^{1}H NMR (CDCl3) δ: 6.84 (s, 1H, C_4-H), 6.93 (dd, 1H, $C_{3''}$-H), 7.04 (dd, 1H, $C_{4''}$-H), 7.44 (dd, 1H, $C_{5''}$-H), 7.69 (dd, 1H, $C_{2'}$- and $C_{6'}$-H), 8.28 (dd, 1H, $C_{3'}$- and $C_{5'}$-H). M^+ 339. Anal. calcd. for $C_{14}H_8F_3N_3O_2S$: C 49.56, H 2.38, N 12.38; found C 49.51, H 2.18, N 12.67.

*1-p-Nitrophenyl-3-methyl-5-trifluoromethyl-5-hydroxypyrazoline (**7e**)*

An ethanolic solution (30 mL) of *p*-nitrophenylhydrazine (0.95 g, 6 mmol) and sodium acetate (0.5 g, 6 mmol) was refluxed for 15 min. An equimolar amount of 1,1,1-trifluoropentane-2,4-dione (0.9 g, 6 mmol) was subsequently added and the solution was refluxed for 2 h. After solvent evaporation, the residue obtained was crystallized from ethanol, mp 102°C, yield 54%. ^{1}H NMR ($CDCl_3$) δ : 2.09 (s, 3H,

© 2000 NRC Canada

CH_3), 3.21 and 3.46 (AB system, 2H, CH_2, J = 18 Hz), 7.42 (d, 2H, $C_{2'}$- and $C_{6'}$-H), 8.04 (d, 2H, $C_{3'}$- and $C_{5'}$-H). M^+ 289. Anal. calcd. for $C_{11}H_{10}F_3N_3O_3$: C 45.68, H 3.48, N 14.53; found C 45.81, H 3.60, N 14.68.

*1-p-Nitrophenyl-3-methyl-5-trifluoromethylpyrazole (**3e**)*

An ethanolic solution of (**7e**) and 2 mL of conc. HCl was refluxed for 10 h. The solvent was evaporated and the residue crystallized from ethanol, mp 80–81°C, yield 56%. ^{1}H NMR ($CDCl_3$) δ: 2.36 (CH_3), 6.54 (s, 1H, C_4-H), 7.72 (d, 2H, $C_{2'}$- and $C_{6'}$-H), 8.33 (d, 2H, $C_{3'}$- and $C_{5'}$-H). M^+ 271. Anal. calcd. for $C_{11}H_8F_3N_3O_2$: C 48.72, H 2.97, N 15.49; found C 49.01, H 3.11, N 15.39.

*1-(1′,2′-Benzisothiazol-3′-yl)-3-methyl-5-trifluoromethyl-5-hydroxypyrazoline 1′,1′-dioxide (**7h**)*

An ethanolic solution (50 mL) of 3-hydrazino-2-benzisothiazole-1′,1′-dioxide (1.2 g, 6 mmol) and sodium acetate (0.5 g, 6 mmol) was refluxed for 15 min. An equimolar amount of 1,1,1-trifluoropentane-2,4-dione (0.9 g, 6 mmol) was subsequently added and the solution was refluxed for 2 h. The solvent was evaporated and the residue extracted with chloroform. The organic phase was dried over anhyd sodium sulfate and the chloroform distilled off, mp 180°C (ethanol), yield 54%. ^{1}H NMR ($CDCl_3$ + DMSO-d_6) δ: 2.14 (CH_3), 3.38 (m, 2H, CH_2), 7.72–7.83 (m, 3H, $C_{5'}$-, $C_{6'}$-, and $C_{7'}$-H), 8.67 (m, 1H, $C_{4'}$-H). M^+ 333. Anal. calcd. for $C_{12}H_{10}F_3N_3O_3S$: C 43.25, H 3.02, N 12.61; found C 43.38, H 2.87, N 12.45.

*1-(2′,4′-Dinitrophenyl)-3-phenyl-5-trifluoromethyl-5-hydroxypyrazoline (**7m**)*

An ethanolic solution (50 mL) of 2,4-dinitrophenylhydrazine (0.95 g, 6 mmol) and sodium acetate (0.5 g, 6 mmol) was refluxed for 15 min. An equimolar amount of benzoyltrifluoroacetone (0.9 g, 6 mmol) was subsequently added and the solution was refluxed for 4 h. The solvent was evaporated and the residue crystallized from ethanol, mp 142°C, yield 54%. ^{1}H NMR ($CDCl_3$) δ: 4.51 (m, 2H, CH_2), 7.38–7.99 (m, 5H, ArH), 8.06 (d, 1H, $C_{6'}$-H), 8.45 (dd, 1H, $C_{5'}$-H), 9.05 (d, 1H, $C_{3'}$-H). M^+ 396. Anal. calcd. for $C_{16}H_{11}F_3N_4O_5$: C 48.49, H 2.80. N 14.14; found C 48.22, H 2.66, N 13.81.

*1-(2′,4′-Dinitrophenyl)-3-phenyl-5-trifluoromethylpyrazole (**3m**)*

To a solution of **7m** (0.2 g, 0.5 mmol) in acetic acid was added 2 mL of pure sulfuric acid. The mixture was refluxed for 24 h. The solvent was evaporated and the residue was extracted with chloroform. The organic phase was dried over anhyd sodium sulfate and the chloroform distilled off, mp 56°C (ethanol), yield 53%. ^{1}H NMR ($CDCl_3$) δ: 6.84 (s, 1H, C_4-H), 7.30 (m, 1H, $C_{6'}$-H), 7.92 (d, 1H, $C_{5'}$-H), 8.06–9.05 (m, 6 H, Ar-H). M^+ 378. Anal. calcd. for $C_{16}H_9F_3N_4O_4$: C 50.80, H 2.40, N 15.07; found C 50.66, H 2.37, N 14.86.

*1-(1′,2′-Benzisothiazole-1′,1′-dioxide)-3-phenyl-5-trifluoromethyl-5-hydroxypyrazoline (**7o**)*

With the same method used in the case of **7i**, compound **7o** was obtained, mp 160°C (ethanol), yield 48%. ^{1}H NMR ($CDCl_3$) δ: 3.35 and 3.69 (AB system, 2H, CH_2, J = 18 Hz), 7.26–7.42 (m, 5H, Ar-H), 7.75–7.82 (m, 3H, $C_{5'}$-, $C_{6'}$-, and $C_{7'}$-H), 8.53 (s, 1H, $C_{4'}$-H). M^+ 395. Anal. calcd. for $C_{17}H_{12}F_3N_3O_3S$: C 51.65, H 3.06, N 10.63; found C 51.42, H 321, N 10.65.

*1-(2′,4′-Dinitrophenyl)-3-(2-thienyl)-5-trifluoromethyl-5-hydroxypyrazoline (**7s**)*

This compound was prepared using the procedure described for **7m**, mp 152°C, yield 58%. ^{1}H NMR ($CDCl_3$) δ: 4.42 (m, 2H, CH_2), 7.28 (m, 1H, $C_{3''}$-H), 7.92 (d, 1H, $C_{4''}$-H), 8.02 (d, 1H, $C_{5''}$-H), 8.04 (d, 1H, $C_{6'}$-H), 8.44 (dd, 1H, $C_{5'}$-H), 9.07 (d, 1H, $C_{3'}$-H). Anal. calcd. for $C_{14}H_9F_3N_4O_5S$: C 41.80, H 2.25, N 13.93; found C 42.03, H 2.41, N 13.71.

*1-(2′,4′-Dinitrophenyl)-3-(2-thienyl)-5-trifluoromethylpyrazole (**3s**)*

Following the same procedure as described for **3m**, compound **3s** was prepared, mp 61°C, yield 53%. ^{1}H NMR ($CDCl_3$) δ: 6.88 (s, 1H, C_4-H), 6.92–7.80 (m, 5H, ArH), 7.90 (d, 1H, $C_{6'}$-H), 8.66 (m, 1H, $C_{5'}$-H), 8.88 (d, 1H, $C_{3'}$-H). M^+ 384. Anal. calcd. for $C_{14}H_7F_3N_4O_4S$: C 43.76, H 1.84, N 14.58; found 43.71, H 1.56, N 14.61.

*1-(1′,2′-Benzisothiazol-3′-yl) 3-(2-thienyl)-5-trifluoromethyl-5-hydroxypyrazoline-1′,1′-dioxide (**7t**)*

With the same method used in the case of **7h**, compound **7t** was obtained, mp 190°C, yield 56%. ^{1}H NMR ($CDCl_3$ + DMSO-d_6) δ: 3.75 (m, 2H, CH_2), 7.5–7.7 (m, 3H, thienyl), 8.0–8.3 (m, 3H, $C_{5'}$-, $C_{6'}$-, and $C_{7'}$-H), 8.71 (m, 1H, $C_{4'}$-H). M^+ 401. Anal. calcd. for $C_{15}H_{10}F_3N_3O_3S_2$: C 44.89, H 2.51, N 10.47; found C 45.00, H 2.69, N 10.30.

*1-(1′,2′-Benzisothiazol-3′-yl)-3-(2-pyridyl)-5-trifluoromethyl-5-hydroxypyrazoline 1′,1′-dioxide (**7v**)*

With the same method used in the case of **7h**, compound **7v** was obtained, mp 224°C, yield 67%. ^{1}H NMR ($CDCl_3$ + DMSO-d_6) δ: 3.70 (AB system, 2H, CH_2, J = 19 Hz), 7.70–7.90 (m, 3H, $C_{5'}$-, $C_{6'}$-, and $C_{7'}$-H), 8.70–8.80 (m, 5H, pyridine and C_4-H of the benzisothiazolyl). M^+ 396. Anal. calcd. for $C_{16}H_{11}F_3N_4O_3S$: C 48.49, H 2.80, N 14.14; found C 48.36, H 2.71, N 13.85.

*1-(1′,2′-Benzisothiazol-3′-yl)-3,5-bis-trifluoromethyl-5-hydroxypyrazoline 1′,1′-dioxide (**7ff**)*

Using the same method as in the case of **7h**, compound **7ff** was obtained, mp 208°C (ethanol), yield 54%. ^{1}H NMR ($CDCl_3$ + DMSO-d_6) δ: 3.27 (m, 2H, CH_2), 7.8–7.9 (m, 3H, $C_{5'}$-, $C_{6'}$-, and $C_{7'}$-H), 8.46 (m, 1H, $C_{4'}$-H). M^+ 387. Anal. calcd. for $C_{12}H_7F_6N_3O_3S$: C 37.22, H 1.82, N 10.85; found C 36.98, H 2.07, N 10.70.

*1-(p-Fluorophenyl)-3,5-bis-trifluoromethylpyrazole (**9aa**)*

This compound was prepared like **3c** and **4c** but using 1,1,1,5,5,5-hexafluoropentane-2,4-dione. Mp 54°C (ethanol), yield 65%. ^{1}H NMR ($CDCl_3$) δ: 6.97 (s, 1H, C_4-H), 7.12 (unresolved dd, 2H, $C_{3'}$- and $C_{5'}$-H, J = 8.0 and 8.9 Hz), 7.38 (m, 2H, $C_{2'}$- and $C_{6'}$-H). Anal. calcd. for $C_{11}H_5F_7N_2$: C 44.31, H 1.69, N 9.40; found C 44.28, H 1.41, N 9.12.

© 2000 NRC Canada

Computational details

All the possible isomers considered for compounds **5′** and **5″** (for both R = C_6H_5 (Ph) and R = 2′,4′-$(NO_2)_2$-C_6H_4 (DNP)), see Fig. 1 for four representative examples, have been studied at semi-empirical level, optimizing all the geometrical parameters. The different configuration of the C3 and C5 atoms of the pyrazolidine ring was considered (relative orientation of both OH groups, and of the CH_3 and CF_3 groups). Besides, considering the rotation between the rings, two different orientations for the NO_2 group in *ortho* in the dinitrophenyl derivatives were taken into account. The protonated species of the most stable of each one of the compounds (**5′** and **5″**, R = Ph and DNP) were also computed. At semi-empirical level, the PM3 Hamiltonian (28), as implemented in the MOPAC 6.0 package (29), was used increasing the precision in a factor of 100 and optimizing until a gradient of 0.01 was reached. This Hamiltonian was chosen since good results had been previously obtained predicting the "stereoselectivity" of certain Michael type reactions (for example ref. (30)). In all the cases, the corresponding heats of formation, dipole moments, and charges of the atoms involved in the possible dehydration (N1, N2, O6, and O8) were calculated and gathered in Tables 4 and 5.

Acknowledgements

We are grateful to Ranbaxy Research Laboratories, Council of Scientific and Industrial Research, and to the University Grants Commission, New Delhi for financial assistance. Thanks are due to RSIC, Chandigarh, for NMR spectra and elemental analysis. We are also thankful to Mass Spectrometry Facility, California University, San Francisco, U.S.A., for mass spectra. Two of us (IR and JE) thank the Spanish DGICYT (Project no. SAF 97-0044-C02).

References

1. R. Fusco. *In* Pyrazoles, pyrazolines, pyrazolidines, indazoles, and condensed rings. *Edited by* R.H. Wiley. John Wiley and Sons, New York. 1967.
2. K. Schofield, M.R. Grimmett, and B.T.R. Keene. The Azoles. Cambridge University Press, Cambridge. 1976.
3. (*a*) J. Elguero. *In* Comprehensive heterocyclic chemistry. Vol. 5. *Edited by* A.R. Katritzky and C.W. Rees. Pergamon Press, New York. 1984. pp. 167–303; (*b*) J. Elguero. *In* Comprehensive heterocyclic chemistry II. Vol. 3. *Edited by* A.R. Katritzky, C.W. Rees, and E.F.V. Scriven. Pergamon Press, New York. 1996. pp. 1–75.
4. K. Kirschke. *In* Methoden der Organische Chemie (Houben-Weyl). Vol. 3, Part 2. *Edited by* E. Schaumann. Georg Thieme Verlag, Stuttgart. 1994. pp. 399–763.
5. J. Elguero, A. Fruchier, N. Jagerovic, and A. Werner. Org. Prep. Proced. Int. **27**, 33 (1995).
6. J.J. Traverso, C.W. Whitehead, J.F. Bell, H.E. Boaz, and P.W. Willard. J. Med. Chem. **10**, 840 (1967).
7. J.W. Lyga and R.M. Patera. J. Heterocycl. Chem. **27**, 919 (1990).
8. M.E.F. Braibante, G. Clar, and M.A.P. Martins. J. Heterocycl. Chem. **30**, 1159 (1993).
9. S.P. Singh, D. Kumar, and J.K. Kapoor. J. Chem. Res. Synop. 163 (1993).
10. S.P. Singh, J.K. Kapoor, D. Kumar, and M.D. Threadgill. J. Fluorine Chem. **83**, 73 (1997).
11. H.V. Secor and J.F. DeBardeleben. J. Med. Chem. **14**, 997 (1971).
12. H.G. Bonacorso, M.R. Oliveira, A.P. Wentz, A.D. Wastowski, A.B. de Oliveira, M. Höerner, N. Zanatta, and M.A.P. Martins. Tetrahedron, **55**, 345 (1999).
13. M.D. Threadgill, A.K. Heer, and B.G. Jones. J. Fluorine Chem. **65**, 21 (1993).
14. S.P. Singh, D. Kumar, B.G. Jones, and M.D. Threadgill. J. Fluorine Chem. **94**, 199 (1999).
15. S.I. Selivanov, R.A. Bogatkin, and B.A. Ershov. Zh. Org. Khim. **17**, 886 (1981).
16. S.I. Selivanov, R.A. Bogatkin, and B.A. Ershov. Zh. Org. Khim. **18**, 909 (1982).
17. S.I. Selivanov, K.G. Goldova, Ya.A. Abbasov, and B.A. Ershov. Zh. Org. Khim. **20**, 1494 (1984).
18. S.I. Selivanov, K.G. Golodova, and B.A. Ershov. Zh. Org. Khim. **22**, 2073 (1986).
19. N.S. Zefirov, S.I. Kozhushkov, T.S. Kuznetsova, B.A. Ershov, and S.I. Selivanov. Tetrahedron, **42**, 709 (1986).
20. J. Elguero and G.I. Yranzo. J. Chem. Res. Synop. 120 (1990).
21. P.P. Kondrat'ev, Z.E. Scryabina, V.I. Soloutin, and L.M. Khalilov. Zh. Org. Khim. **28**, 1380 (1992).
22. K.N. Zelenin, V.V. Alekseyev, and A.R. Tygysheva. Tetrahedron, **51**, 11251 (1995).
23. A.R. Katritzky, D.L. Ostercamp, and T.I. Yousaf. Tetrahedron, **43**, 5171 (1987).
24. K.N. Zelenin. Org. Prep. Proced. Int. **27**, 519 (1995).
25. K.N. Zelenin and S.I. Yakimovitch. Targets Heterocycl. Syst. **2**, 207 (1998).
26. C. Dittli, J. Elguero, and R. Jacquier. Bull. Soc. Chim. Fr. 1038 (1971).
27. T.D. Penning, J.J. Talley, S.R. Bertenshaw, J.S. Carter, P.W. Collins, S. Docter, M.J. Graneto, L.F. Lee, J.W. Malecha, J.M. Miyashiro, R.S. Rogers, D.J. Rogier, S.S. Yu, G.D. Anderson, E.G. Burton, J.N. Cogburn, S.A. Gregory, C.M. Koboldt, W.E. Perkins. K. Seibert, A.M. Veenhuizen, Y.Y. Zhang, and P.C. Isakson. J. Med. Chem. **40**, 1347 (1997).
28. J.J.P. Stewart. J. Comput. Chem. **12**, 320 (1991).
29. MOPAC (Version 6.0), QCPE no. 455, Department of Chemistry, Indiana University, Bloomington, Indiana, 1991.
30. M. Ayerbe, I. Morao, A. Arrieta, A. Linden, and F.P. Cossío. Tetrahedron Lett. **37**, 3055 (1996).

© 2000 NRC Canada

Densities, refractive indices and excess properties of mixing of the *n*-octanol + 1,4-dioxane + 2-butanol ternary system at 298.15 K[1]

Alberto G. Camacho, Miguel A. Postigo, Graciela C. Pedrosa, Inés L. Acevedo, and Miguel Katz[2]

Abstract: Excess molar volumes and excess refractive indices of the *n*-octanol + 1,4-dioxane + 2-butanol system and the three corresponding binary mixtures have been determined at 298.15 K by measuring densities and refractive indices. Different expressions exist in the literature to predict these excess properties from binary data. An estimation of excess molar volumes is also evaluated using a modified Heller equation which depends on the refractive indices of the mixtures. A comparison of the predictions of different methods with the experimental values of the physical properties has been made.

Key words: excess molar volumes, densities, refractive indices, *n*-octanol, 1,4-dioxane, 2-butanol, ternary system.

Résumé : Opérant à 298,15 K et faisant appel à des mesures de densités et d'indices de réfraction, on a déterminé les volumes molaires en excès ainsi que les indices de réfraction en excès du système octanol + 1,4-dioxane + butan-2-ol et des trois mélanges binaires correspondants. Il existe différentes expressions dans la littérature pour faire des prédictions relatives aux propriétés en excès de systèmes binaires. Une évaluation des volumes molaires en excès peut aussi être faite en utilisant l'équation de Heller modifiée qui dépend des indices de réfraction des mélanges. On a effectué une comparaison des diverses prédictions obtenues à l'aide de ces différentes méthodes avec les valeurs expérimentales des propriétés physiques.

Mots clés : volumes molaires en excès, indices de réfraction, octanol, 1,4-dioxane, butan-2-ol, système ternaire.

[Traduit par la Rédaction]

Introduction

This paper is a continuation of our studies about excess thermodynamic properties (1, 2). Densities, refractive indices, and excess properties on mixing of the *n*-octanol (1-OC) + 1.4-dioxane (D) + 2-butanol (2-BU) system are reported at 298.15 K. Data on physical properties, like refractive indices and densities, for liquid mixtures are important from a theoretical and practical point of view. The thermodynamics of ternary mixtures of non-electrolytes has not received as much attention as the thermodynamics of binary mixtures. It is therefore interesting to estimate excess molar volumes and excess refractive indices with more than two components. If significant changes of refractivity and volumes during mixing are present as a result of physical and or chemical interactions, some mixing rules will be suitable for predictive calculations. A search of the literature for ternary systems suggests that some empirical correlations can be used to calculate the molar excess volumes and excess refractive indices from binary mixtures, and by knowing refractive indices molar volumes can be calculated.

In this paper we report corresponding densities and refractive indices of the ternary system and the respective three binary mixtures. Some of the components studied here are mentioned in the literature (4–8). Molar excess volumes and excess refractive indices were calculated from those experimental data. As computer design of chemical processes requires mathematical models to predict or describe excess properties of mixtures over the entire range of composition, such information is very useful in chemical engineering. The excess properties are analyzed (in this case two alcohols and a cyclic substance) because of their importance for inferring which type of interaction predominates in liquid mixtures.

Received March 18, 1999. Published on the NRC Research Press website on August 11, 2000.

A.G. Camacho and M.A. Postigo. Cátedra de Fisicoquímica, Depto. de Química. Facultad de Ingeniería U.N. del Comahue, Buenos Aires 1400, Neuquén (8300), Argentina. **G.C. Pedrosa, I.L. Acevedo, and M. Katz.[2]** Cátedra de Fisicoquímica, Instituto de Ingeniería Química, Facultad de Ciencias Exactas y Tecnología, U. N. de Tucumán, Avda. Indpendencia 1800, S. M. de Tucumán (4000), Argentina.

[1]Presented at the 12th Congreso Brasileiro de Engenharia Quimica, Porto Alegre, Brasil, 1998.

[2]Author to whom correspondence may be addressed. Fax: (54) (0381) 436–3004. e-mail: mkatz@herrera.unt.edu.ar

Experimental

Densities were determined with a digital densimeter DA 310, Mettler, and a thermostatically controlled bath constant to 0.01 K was used (with a Digitec digital thermometer with an error of ±0.01 K). Calibration was carried out with air and doubly distilled water with an uncertainty of ±0.01 kg m^{-3} in the densimeter and ±0.02 kg m^{-3} in densities. Refractive

© 2000 NRC Canada

Table 1. Properties characterizing the pure components at 298.15 K.

	$\rho \times 10^{-3}$ (kg m^{-3})		n_D	
	Exp.	Lit.	Exp.	Lit.
1-Octanol	0.82166	0.82157[a]	1.42750	1.4276[a]
1,4-Dioxane	1.02826	1.02797[a]	1.41992	1.42025[a]
2-Butanol	0.80241	0.80241[a]	1.39478	1.39530[a]

[a]Ref. 3.

Table 2. Densities and refractive indices for the 1-OC(1) + D(2) system at 298.15 K.

x_1	$\rho \times 10^{-3}$ (kg m^{-3})	x_1	$\rho \times 10^{-3}$ (kg m^{-3})	x_1	n_D
0.0583	1.00530	0.5521	0.88006	0.0931	1.41973
0.1044	0.98864	0.5975	0.87255	0.2131	1.42008
0.1465	0.97466	0.6538	0.86381	0.3005	1.42053
0.1977	0.95918	0.7022	0.85661	0.3929	1.42118
0.2514	0.94421	0.7484	0.85061	0.4778	1.41188
0.3051	0.93056	0.8037	0.84345	0.6031	1.42297
0.3866	0.91187	0.8458	0.83841	0.7039	1.42409
0.4487	0.89907	0.9045	0.83170	0.7920	1.42500
0.4972	0.88977			0.8996	1.42626

indices were measured at the sodium D line with a Jena dipping refractometer with an accuracy of $\pm 2 \times 10^{-5}$. In this case a thermostatic controlled bath constant was also used with an error of ±0.01 K.

All the substances used were Merck (puriss.). The alcohols were distilled over calcium oxide and the middle fraction collected. 1,4-Dioxane was distilled over sodium at reduced pressure and the middle fraction was also collected.

Mixtures were prepared by mixing weighed amounts of the pure liquids. Caution was taken to prevent evaporation.

Results and discussion

The experimental results for the pure liquids together with literature values for comparison are reported in Table 1.

The excess function of a binary mixture can be represented by a Redlich–Kister equation of the form

$$[1] \qquad X^E = X_j X_j \sum_{k=0}^{n} a_k (x_i - x_j)^k$$

where X^E represents V^E or n_D^E, x_i and x_j are the mole fractions of the component i and j, and a_k are the polynomial coefficients. The method of least squares has been used to determine the values of the coefficients. In each case, the optimum number of coefficients was ascertained from an examination of the standard deviation of the estimate with n

$$[2] \qquad \sigma = [(X^E_{obs} - X^E_{cal})^2 \,/\, ((n_{obs} - (n+1))]^{1/2}$$

Tables 2, 3, and 4 show the values of densities and refractive indices of the binary systems at different mole fractions.

The values adopted for the coefficients and the standard deviation of estimates associated with the use of eq. [1] are summarized in Table 5.

Table 3. Densities and refractive indices for the 1-OC (1) + 2-BU(3) system at 298.15 K.

x_1	$\rho \times 10^{-3}$ (kg m^{-3})	x_1	$\rho \times 10^{-3}$ (kg m^{-3})	x_1	n_D
0.0511	0.80418	0.4974	0.81451	0.1066	1.39987
0.1000	0.80567	0.5565	0.81549	0.2032	1.40432
0.1501	0.80708	0.5979	0.81614	0.3025	1.40832
0.2158	0.80876	0.6970	0.81760	0.3952	1.41179
0.2631	0.80988	0.7425	0.81825	0.4976	1.41518
0.2953	0.81060	0.8119	0.81924	0.5895	1.41787
0.3474	0.81170	0.8524	0.81979	0.6902	1.42076
0.4063	0.81286	0.9428	0.82096	0.7901	1.42314
0.4407	0.81351			0.8930	1.42542

Table 4. Densities and refractive indices for the D (2) + 2-BU(3) system at 298.15 K.

x_2	$\rho \times 10^{-3}$ (kg m^{-3})	x_2	$\rho \times 10^{-3}$ (kg m^{-3})	x_2	n_D
0.0571	0.81340	0.5488	0.91695	0.0999	1.39621
0.0957	0.82094	0.6028	0.92942	0.1608	1.39732
0.1474	0.83127	0.6514	0.94084	0.2067	1.39812
0.2053	0.84290	0.6936	0.95091	0.2924	1.39971
0.2437	0.85079	0.7464	0.96370	0.4139	1.40241
0.2952	0.86146	0.8025	0.97757	0.4951	1.40439
0.3542	0.87397	0.8463	0.98853	0.6020	1.40721
0.3971	0.88318	0.8953	1.00105	0.6790	1.40937
0.4573	0.89550	0.9511	1.01542	0.7723	1.41215
0.5015	0.90625			0.8897	1.41591

Figures 1 and 2 show the experimental values of V^E_{ij} and n^E_{Dij} for the three binary systems.

The experimental values of densities and refractive indices of the ternary system were obtained by adding the third component to a constant ratio of the other two.

Tables 6 and 7 show the experimental values for the densities and refractive indices for the ternary 1-OC (1) + D (2) + 2-BU (3) system at 298.15 K at different mole fractions.

Molar excess volumes and changes in refractive indices on mixing were calculated using the following equations

$$[3] \qquad V^E_{123} = \sum x_i M_i (\rho^{-1} - \rho_i^{-1})$$

$$[4] \qquad n^E_{D123} = n_D - \sum x_i n_{Di}$$

where M_i is the molecular weight of component i, ρ_i is the density of the pure component i, ρ is the density of the mixture, n_{Di} the refractive index of the pure component i, and n_D the refractive index of the solution at the sodium D line. These values are shown in Tables 6 and 7.

Figures 3 and 4 show lines of constant V^E_{123} and n^E_{D123}. These lines were obtained by plotting excess molar volumes and excess refractive indices of the binary systems as a function of x_3 and considering mole fractions with the same excess functions.

In Fig. 1 two binary systems with D show positive excess molar volumes. Alcohols are composed of associated molecules and the addition of the other component produces a rupture of the hydrogen bonding and an expansion of volume. The other system with the two alcohols shows a sigmoid curve with small values for excess molar volume. This

© 2000 NRC Canada

Table 5. Coefficients a_k for eq. [1] and standard deviations for the binary systems at 298.15 K.

Parameters	a_0	a_1	a_2	a_3	a_4	a_5	σ
1-OC (1) + D (2) system							
$V^E_{12} \times 10^6$ (m^3 mol^{-1})	2.6732	–0.1284	0.1863	–1.0271	–0.3181	0.9822	7.7×10^{-3}
n^E_{D12}	-6.64×10^{-3}	2.29×10^{-3}	-9.20×10^{-4}	2.05×10^{-3}	-1.69×10^{-3}	-9.67×10^{-4}	4×10^{-3}
1-OC (1) + 2-BU (3) system							
$V^E_{13} \times 10^6$ (m^3 mol^{-1})	0.0118	0.2891	0.1103	–0.1311	–0.3347	0.1120	$1.5x10^{-3}$
n^E_{D13}	1.64×10^{-2}	-2.50×10^{-3}	1.85×10^{-3}	6.62×10^{-4}	-4.35×10^{-3}	2×10^{-3}	8×10^{-5}
D (2) + 2-BU (3) system							
$V^E_{23} \times 10^6$ (m^3 mol^{-1})	2.0419	–0.1719	–0.1989	0.0627	0.0957	–0.1644	2.3×10^{-3}
n^E_{D23}	-1.14×10^{-2}	1.07×10^{-3}	-1.44×10^{-4}	-6.59×10^{-3}	-1.71×10^{-3}	6.34×10^{-3}	4×10^{-5}

Fig. 1. Excess molar volumes for the three binary systems at 298.15 K. Continuous curves were calculated from eq. [1]. System D(2) + 2-BU(3) in the *x*-axis D, and the other two systems 1-OC(1).

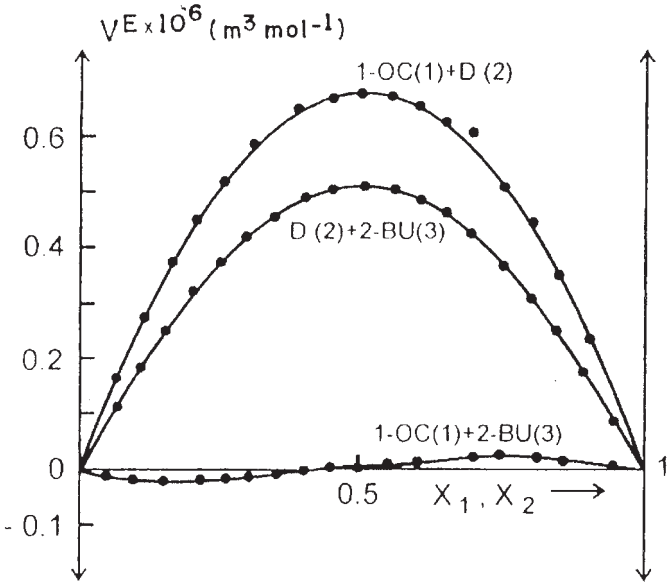
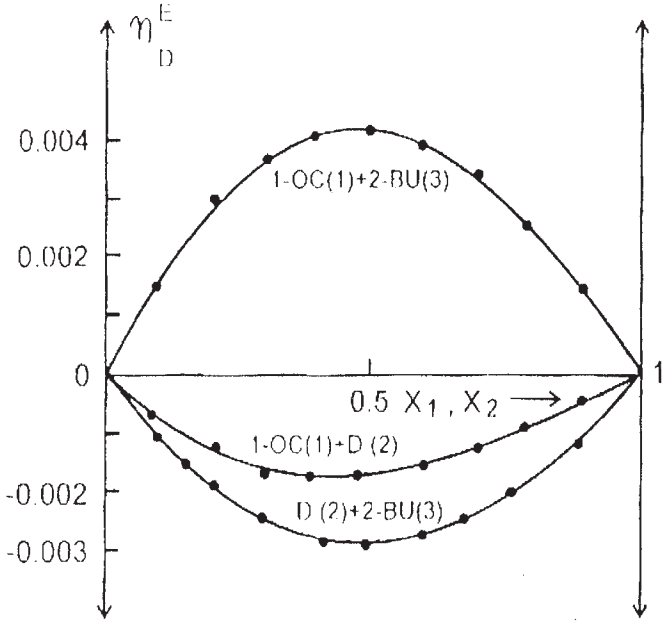


Fig. 2. Excess refractive indices for the three binary systems at 298.15 K. Continuous curves were calculated from eq. [1]. System D(2) + 2-BU(3) in the *x*-axis D, and the other two systems 1-OC(1).



can be explained by the fact that strong interactions between the alcohols is compensated by the broken or formed interactions. Likewise, the differences in molecular sizes between the mixture components must lead to interstitial accommodation of molecules in the mixture and hence to a negative contribution to V^E. A further effect to consider is the difference in free volume between 1,4-dioxane and alcohols. Figure 2 shows positive excess refractive indices for the mixtures of alcohols and negative for the other two systems

Estimation of excess properties

From the different expressions existing in the literature, we applied the equation of Radojkovic et al. (9), which considered an expression proposed by Redlich and Kister. For excess molar volumes for a ternary system,

$$[5] \qquad V^E_{123} = V^E_{12} + V^E_{13} + V^E_{23}$$

where V^E_{12}, V^E_{13}, and V^E_{23} represent the excess molar volumes at x_1, x_2, and x_3 (mole fractions in the ternary system) calculated with eq. [1] using the coefficients of Table 5.

Jacob and Fitzner (10) suggested an equation for estimating the excess properties based on the binary data at the composition nearest the ternary composition, using the following form for the excess molar volume:

$$[6] \qquad V^E_{123} = \frac{x_1 x_2 V^E_{12}}{\left(x_1 + \frac{x_3}{2}\right)\left(x_2 + \frac{x_3}{2}\right)} + \frac{x_1 x_3 V^E_{13}}{\left(x_1 + \frac{x_2}{2}\right)\left(x_3 + \frac{x_2}{2}\right)} + \frac{x_2 x_3 V^E_{23}}{\left(x_2 + \frac{x_1}{2}\right)\left(x_3 + \frac{x_1}{2}\right)}$$

and that, for binary composition x^o_i, x^o_j, is $x_i - x_j = x^o_i - x^o_j$.

© 2000 NRC Canada

Table 6. Densities and excess molar volumes for 1-OC (1) + D (2) + 2-BU (3) system at 298.15 K.

x_1	x_2	$\rho \times 10^{-3}$(kg m^{-3})	$V^E_{123} \times 10^{-6}$(m^3 mol^{-1})
x^o_1/x^o_3 = 0.0457		ρ = 0.80395	V^E_{13} = – 0.017
0.0416	0.0492	0.81286	0.109
0.0390	0.1067	0.82397	0.185
0.0347	0.2062	0.84313	0.353
0.0304	0.3054	0.86305	0.467
0.0264	0.3948	0.88180	0.519
0.0221	0.4954	0.90380	0.527
0.0177	0.5947	0.92651	0.483
0.0129	0.7044	0.95233	0.421
0.0085	0.8046	0.97689	0.327
0.0045	0.8964	1.00058	0.184
0.0020	0.9537	1.01574	0.087
x^o_1/x^o_3 = 0.1111		ρ = 0.80564	V^E_{13} = – 0.018
0.0951	0.0487	0.81398	0.116
0.0896	0.1038	0.82418	0.191
0.0805	0.1954	0.84099	0.367
0.0708	0.2944	0.86028	0.478
0.0595	0.4054	0.88320	0.527
0.0505	0.4951	0.90252	0.537
0.0396	0.6043	0.92727	0.495
0.0297	0.7029	0.95058	0.433
0.0205	0.7948	0.97339	0.335
0.0096	0.9036	1.00163	0.190
0.0056	0.9437	1.01283	0.091
x^o_1/x^o_3 = 0.2508		ρ = 0.80840	V^E_{13} = –0.026
0.1910	0.0472	0.81575	0.123
0.1803	0.1006	0.82489	0.204
0.1681	0.1615	0.83538	0.314
0.1593	0.2056	0.84314	0.390
0.1494	0.2551	0.85217	0.456
0.1250	0.3764	0.87562	0.550
0.1083	0.4601	0.89298	0.558
0.0899	0.5518	0.91283	0.552
0.0685	0.6582	0.93746	0.484
0.0499	0.7511	0.96008	0.412
0.0315	0.8430	0.98382	0.303
x^o_1/x^o_3 = 0.4190		ρ = 0.81059	V^E_{13} = –0.018
0.2801	0.0514	0.81814	0.135
0.2663	0.0982	0.82559	0.217
0.2354	0.2029	0.84279	0.405
0.2076	0.2969	0.85492	0.516
0.1760	0.4038	0.87993	0.565
0.1484	0.4975	0.89916	0.574
0.0873	0.7042	0.94625	0.480
0.0575	0.8051	0.97195	0.373
0.0308	0.8958	0.99706	0.220
0.0161	0.9456	1.01182	0.105
x^o_1/x^o_3 = 0.6895		ρ = 0.81291	V^E_{13} = –0.010
0.3915	0.0406	0.81828	0.131
0.3801	0.0687	0.82225	0.204
0.3424	0.1609	0.83624	0.363
0.3077	0.2460	0.85009	0.474
0.2820	0.3089	0.86096	0.533
0.2595	0.3541	0.87095	0.571
0.2228	0.4540	0.88828	0.596
0.1809	0.5568	0.90961	0.596
0.1397	0.6577	0.93267	0.526
0.1024	0.7492	0.95497	0.471
0.0609	0.8508	0.98242	0.327
x^o_1/x^o_3 = 1.0105		ρ = 0.81456	V^E_{13} = 0.009
0.4762	0.0546	0.82169	0.154
0.4535	0.0998	0.82787	0.259
0.4285	0.1494	0.83511	0.339
0.3995	0.2070	0.84389	0.420
0.3354	0.3342	0.86473	0.568
0.2887	0.4268	0.88152	0.624
0.2557	0.4924	0.89431	0.638
0.2494	0.5048	0.89694	0.624
0.2293	0.5447	0.90523	0.619
0.2064	0.5902	0.91508	0.603
0.1470	0.7082	0.94278	0.520
0.1001	0.8013	0.96699	0.418
0.0487	0.9034	0.99656	0.247
x^o_1/x^o_3 = 1.5426		ρ = 0.81628	V^E_{13} = 0.017
0.5426	0.1056	0.82965	0.272
0.4706	0.2244	0.84664	0.453
0.4213	0.3056	0.85927	0.558
0.3540	0.4165	0.87838	0.633
0.2932	0.5168	0.89766	0.643
0.2532	0.5826	0.91149	0.624
0.2443	0.5974	0.91478	0.613
0.2059	0.6606	0.92927	0.567
0.1838	0.6970	0.93800	0.542
0.1182	0.8051	0.96626	0.421
0.0609	0.8997	0.99431	0.254
x^o_1/x^o_3 = 2.3000		ρ = 0.81759	V^E_{13} = 0.030
0.6602	0.0528	0.82394	0.139
0.6622	0.1073	0.83082	0.244
0.5594	0.1974	0.84280	0.422
0.4895	0.2977	0.85763	0.556
0.4708	0.3962	0.87383	0.636
0.3454	0.5044	0.89387	0.656
0.2731	0.6082	0.91538	0.642
0.2122	0.6956	0.93584	0.568
0.1445	0.7927	0.96131	0.445
0.0684	0.9018	0.99383	0.268
0.0326	0.9532	1.01127	0.132
x^o_1/x^o_3 = 4.0125		ρ = 0.81906	V^E_{13} = 0.028
0.6982	0.1278	0.83400	0.304
0.6656	0.1685	0.83919	0.378
0.5624	0.2975	0.85728	0.553
0.4819	0.3980	0.87325	0.641
0.4209	0.4742	0.88678	0.662
0.3842	0.5201	0.89551	0.666
0.3148	0.6068	0.91340	0.647
0.2316	0.7107	0.93768	0.572

© 2000 NRC Canada

Table 6. (*Concluded*).

x_1	x_2	$\rho \times 10^{-3}$(kg m^{-3})	$V^E_{123} \times 10^{-6}$(m^3 mol^{-1})
0.2106	0.7369	0.94436	0.544
0.1540	0.8076	0.96361	0.453
0.0781	0.9024	0.99289	0.274
x_1^o/x_3^o = 4.3107		ρ = 0.81921	V^E_{13} = 0.028
0.7171	0.1165	0.83281	0.260
0.6139	0.2437	0.84931	0.505
0.5376	0.3377	0.86345	0.584
0.4592	0.4343	0.87948	0.648
0.3754	0.5375	0.89879	0.666
0.3058	0.6232	0.91679	0.645
0.2183	0.7311	0.94267	0.551
0.1392	0.8285	0.96971	0.403
0.0741	0.9087	0.99498	0.251
x_1^o/x_3^o = 9.0100		ρ = 0.82043	V^E_{13} = 0.011
0.8557	0.0493	0.82567	0.131
0.8078	0.1025	0.83175	0.229
0.7230	0.1968	0.84323	0.411
0.6316	0.2983	0.85711	0.550
0.5370	0.4034	0.87344	0.633
0.4513	0.4986	0.89010	0.675
0.3563	0.6041	0.91123	0.660
0.2675	0.7028	0.93398	0.593
0.1824	0.7974	0.95921	0.468
0.0938	0.8958	0.98975	0.280
0.0489	0.9457	1.00745	0.143
x_1^o/x_3^o = 18.3424		ρ = 0.82104	V^E_{13} = 0.005
0.8887	0.0629	0.82758	0.163
0.8483	0.1055	0.83237	0.244
0.7847	0.1725	0.84026	0.376
0.7290	0.2313	0.84777	0.465
0.6034	0.3637	0.86666	0.619
0.5191	0.4526	0.88132	0.663
0.4652	0.4989	0.88962	0.674
0.4261	0.5507	0.89957	0.669
0.3359	0.6458	0.91971	0.640
0.2378	0.7492	0.94503	0.552
0.1343	0.8584	0.97667	0.386

Kohler (11) proposed an equation for a ternary system of the following form:

$$[7] \quad V^E_{123} = (x_1 + x_2)^2 V^E_{12} + (x_1 + x_3)^2 V^E_{13} + (x_2 + x_3)^2 V^E_{23}$$

Kohler's equation is symmetrical in that all three binary systems are treated identically. In this equation V^E_{ij} refers to the excess volumes of x_i^o, x_j^o in the binary system using $x_i^o = 1 - x_j^o = x_i/(x_i + x_j)$.

Tsao and Smith (12) proposed an equation for excess enthalpies, which for excess molar volumes is

$$[8] \quad V^E_{123} = \frac{x_2}{1-x_1} V^E_{12} + \frac{x_3}{1-x_1} V^E_{13} + (1-x_1) V^E_{23}$$

Table 7. Refractive indices and excess refractive indices for 1-OC (1) + D (2) + 2-BU (3) system at 298.15 K.

x_1	x_2	n_D	n^E_{D123}
x_1^o/x_2^o = 0.1098		n_D = 1.41967	n^E_{D12} = – 0.00100
0.0933	0.8499	1.41796	–0.00124
0.0888	0.8094	1.41663	–0.00140
0.0779	0.7103	1.41347	–0.00172
0.0692	0.6301	1.41101	–0.00187
0.0590	0.6376	1.40830	–0.00192
0.0493	0.4497	1.40585	–0.00185
0.0384	0.3496	1.40320	–0.00163
0.0282	0.2568	1.40085	–0.00131
0.0197	0.1799	1.39897	–0.00097
0.0096	0.0873	1.39679	–0.00050
x_1^o/x_2^o = 0.2519		n_D = 1.42001	n^E_{D12} = – 0.00144
0.1910	0.7585	1.41859	–0.00151
0.1810	0.7185	1.41721	–0.00156
0.1690	0.6709	1.41558	–0.00159
0.1548	0.6146	1.41370	–0.00159
0.1354	0.5375	1.41119	–0.00153
0.1129	0.4483	1.40835	–0.00139
0.0958	0.3804	1.40624	–0.00124
0.0737	0.2928	1.40354	–0.00101
0.0573	0.2277	1.40156	–0.00082
0.0402	0.1594	1.39950	–0.00061
0.0195	0.0774	1.39704	–0.00032
x_1^o/x_2^o = 0.6664		n_D = 1.42124	n^E_{D12} = – 0.00172
0.3760	0.5642	1.41982	–0.00145
0.3494	0.5243	1.41823	–0.00116
0.3000	0.4502	1.41527	–0.00064
0.2581	0.3873	1.41273	–0.00023
0.2203	0.3307	1.41038	0.00008
0.1769	0.2655	1.40758	0.00034
0.1399	0.2099	1.40509	0.00045
0.1026	0.1540	1.40247	0.00046
0.0706	0.1059	1.40013	0.00038
0.0337	0.0506	1.39736	0.00021
x_1^o/x_2^o = 1.5176		n_D = 1.42299	n^E_{D12} = – 0.00150
0.5696	0.3754	1.42182	–0.00103
0.5085	0.3337	1.41961	–0.00013
0.4516	0.2976	1.41764	0.00060
0.3695	0.2435	1.41445	0.00146
0.2984	0.1966	1.41138	0.00190
0.2459	0.1621	1.40890	0.00200
0.1807	0.1190	1.40553	0.00185
0.1464	0.0965	1.40365	0.00165
0.1169	0.0771	1.40196	0.00142
0.0493	0.0325	1.39789	0.00068
x_1^o/x_2^o = 3.8757		n_D = 1.42504	n^E_{D12} = – 0.00091
0.7273	0.1877	1.42343	0.00013
0.6602	0.1704	1.42165	0.00099
0.5641	0.1455	1.41884	0.00195
0.4686	0.1209	1.41576	0.00261
0.3967	0.1023	1.41323	0.00290
0.3057	0.0789	1.40976	0.00300
0.2345	0.0605	1.40679	0.00282

© 2000 NRC Canada

Table 7 (*Concluded*).

x_1	x_2	n_D	n^E_{D123}
0.1744	0.0450	1.40408	0.00246
0.1184	0.0305	1.40134	0.00192
0.0632	0.0163	1.39843	0.00117
x_1^o/x_2^o = 9.6680		n_D = 1.42633	n^E_{D12} = – 0.00046
0.8305	0.0860	1.42478	0.00067
0.7553	0.0782	1.42306	0.00160
0.6378	0.0660	1.41989	0.00258
0.5229	0.0541	1.41626	0.00301
0.4285	0.0443	1.41308	0.00316
0.3470	0.0359	1.41026	0.00322
0.2619	0.0271	1.40708	0.00305
0.1642	0.0170	1.40277	0.00219
0.0906	–0.0094	1.39901	0.00103

Table 8. Standard deviations of excess molar volumes (eq. [9]) for 1-OC (1) + D (2) + 2-BU (3) system at 298.15 K.

Equation	$V^E_{123} \times 10^{-6}$ (m^3 mol^{-1})	n^E_{D123}
[5]	0.027	0.0004
[6]	0.027	0.0004
[7]	option (a) = 0.043	option (a) = 0.0007
	option (b) = 0.027	option (b) = 0.0004
	option (c) = 0.059	option (c) = 0.0007
[9]	0.018	0.001
[10]	0.0202	0.00005

Binary contributions were evaluated at $x_i^o = x_1$ and $x_j^o = 1 - x_i^o$ for 1–2 and 1–3 binaries, and $x_2^o = x_2/(x_2 + x_3)$ and $x_3^o = x_3/(x_2 + x_3)$ for 2–3 binary (option a in Table 8). As this model is asymmetric, we evaluate binary contributions alternatively at $x_i^o = x_2$ and $x_j^o = 1 - x_i^o$ for 2–1 and 2–3 binaries, and $x_3^o = x_3/(x_1 + x_3)$ and $x_1^o = x_1/(x_1 + x_3)$ for the 3–1 binary (option b in Table 8). The third alternative (option c in Table 8), was using $x_i^o = x_3$ and $x_j^o = 1 - x_i^o$ for 3–1 and 3–2 binaries and $x_2^o = x_2/(x_2 + x_1)$ and $x_1^o = x_1/(x_2 + x_1)$ for the 1–3 binary system.

These equations were used to calculate V^E_{123} and n^E_{D123} from binary mixture data and were compared with experimental data. Table 8 shows the deviation defined by

$$[9] \qquad SD = \left[\frac{\sum (X^E_{obs} - X^E_{cal})^2}{n}\right]^{1/2}$$

for excess molar volume and excess refraction index using the different expressions in this system.

There exist other equations which introduce fitting parameters like that of Cibulka (13) which propose

$$[10] \qquad V^E_{123} = V^E_{12} + V^E_{13} + V^E_{23} + x_1x_2x_3(A + Bx_1 + Cx_2)$$

where A, B, and C are parameters calculated from experimental data. The parameters obtained for the excess molar volume are A = 1.7391, B = –1.6380, and C = –0.1504. For refraction index, the parameters obtained are A = 0.0786, B = – 0.8660, and C = – 0.1278.

Fig. 3. Lines of constant excess molar volumes for the *n*-octanol (1) + 1,4-dioxane (2) + 2-butanol (3) system at 298.15 K.

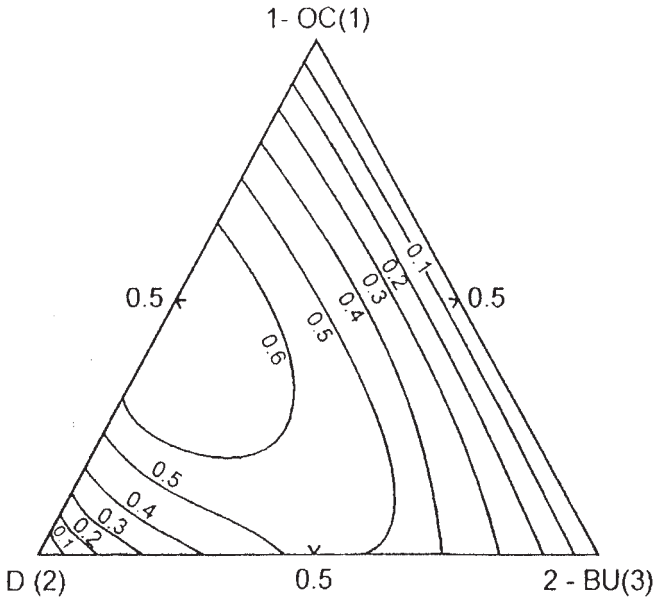
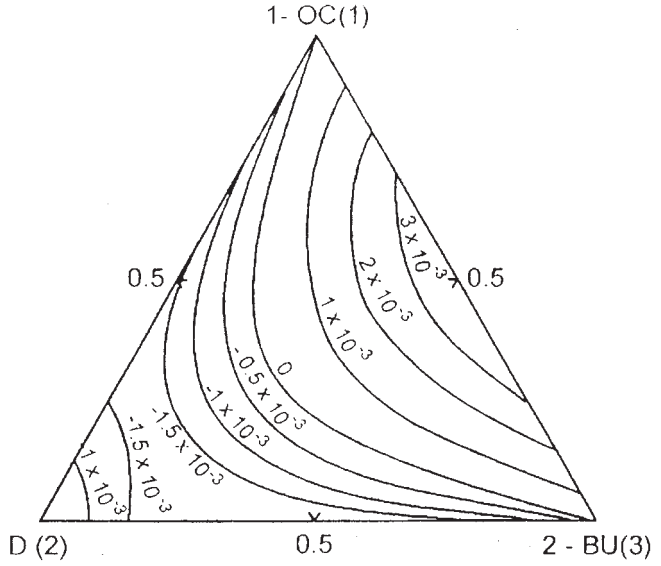


Fig. 4. Lines of constant excess refractive indices for the *n*-octanol (1) + 1,4-dioxane (2) + 2-butanol (3) system at 298.15 K.



Singh et al. (14) proposed an equation of the following form:

$$[11] \qquad V^E_{123} = V^E_{12} + V^E_{13} + V^E_{23} + x_1x_2x_3[A + Bx_1(x_2 - x_3) + Cx_1^2(x_2 - x_3)^2]$$

The parameters obtained for the excess molar volume are A = 1.0378, B = –1.5086, and C = 21.4848. For refraction index, the parameters obtained are A = 0.01517, B = – 0.1889, and C = – 0.9922.

These parameters are also evaluated by the least squares method. These last two equations are modifications of the Radojkovic's equation and the standard deviations are summarized in Table 8.

© 2000 NRC Canada

The models using ternary parameters are superior to the predictive ones (not containing ternary parameters). The fact that so many equations have been developed suggests that no simple equation can describe all types of available systems.

Cibulka's equation shows the best agreement with experimental data for the excess molar volumes and the equation of Singh at al. for the refractive indices of this system.

The prediction of excess molar volumes from refractive index mixing rules has been suggested by some authors (15–17). Following Heller (18)

$$[12] \quad \frac{f(n_D)}{\rho} = \sum_{i=1}^{n} \frac{w_i f(n_{Di})}{\rho_i}$$

where ρ is the density of the mixture, ρ_i is the density of component i in the mixture, w_i is the weight fraction, and f is a mathematical function of the refractive index of the mixture. By substituting $1/\rho$ from eq. [12] and w_i by the mole fraction x_i, we obtain

$$[13] \quad V^E = \frac{\sum_{i=1}^{n} x_i V_i f(n_{Di})}{f(n_D)} - \sum_{i=1}^{n} x_i V_i$$

Expressed in another way, the relation of the excess volumes to the function of the refractive indices would be:

$$[14] \quad V^E = \sum_{i=1}^{n} \left[f(n_{Di}) - f(n_D) \frac{x_i V_i}{f(n_D)} \right]$$

Typical equations for $f(n_D)$ are Lorentz–Lorenz, Dale–Gladstone, Eykman, and Oster. (eq. [15], [16], [17], and [18] respectively). The refractive index mixing rules are:

$$[15] \quad f(n_D) = \frac{(n_D^2 - 1)}{(n_D^2 + 2)}$$

$$[16] \quad f(n_D) = n_D - 1$$

$$[17] \quad f(n_D) = \frac{n_D^2 - 1}{n_D + 0.4}$$

$$[18] \quad f(n_D) = \frac{(n_D^2 + 1)(2n_D^2 + 1)}{n_D^2}$$

Table 9 gives the standard deviation defined by eq. [9] where it could be observed that the Eykman and Oster equations provide the minor deviation for this system to calculate excess molar volumes from refractive indices.

Table 9. Standard deviations of excess molar volumes (eq. [14]) for 1-OC (1) + D (2) + 2-BU (3) system at 298.15 K.

Equation	$V^E_{123} \times 10^{-6}$ (m^3 mol^{-1})
[15]	0.07
[16]	0.06
[17]	0.06
[18]	0.08

Acknowledgment

The present work was financed by a CIUNT research grant.

References

1. S.M. Bardavid, G.C. Pedrosa, M.A. Postigo, and P. García. J. Solution. Chem. **25**, 1125 (1996).
2. S.M. Bardavid, G.C. Pedrosa, and M. Katz. An. Asoc. Quim. Argent. **83**, 141 (1995).
3. J.A. Riddick, W.B. Bunger, and T.K. Sakano. Organic Solvents. 4th. ed. *Edited by* Wiley & Sons, New York. 1988.
4. G.E. Papanastasiou, A.D. Papoutsis, and G.J. Kokkindis. J. Chem. Eng. Data, **32**, 377 (1987).
5. G.C. Pedrosa, J.A. Salas, and M. Katz. Phys. Chem. Liq. **21**, 207 (1990).
6. P.H. García and M.A. Postigo. Inf. Tecnol. **8(4)**, 341 (1997).
7. P. García and M.A. Postigo. An. Asoc. Quim. Argent. **85**, 209 (1997).
8. E. Calvo, P. Brocos, A. Pineiro, M. Pintos, A. Amigo, R. Bravo, A.-.H. Roux, and G.D. Roux. J. Chem. Eng. Data, **44**, 948 (1999).
9. N. Radojkovic, A. Tasic, D. Grozdanic, D. Djordjevic, and D. Malic. J. Chem. Thermodyn. **9**, 349 (1977).
10. K.T. Jacob and K. Fitzner. Thermochim. Acta, **18**, 197 (1977).
11. F. Kohler. Monatsh. Chem. **91**, 738 (1960).
12. C.C. Tsao and J.M. Smith. Chem. Eng. Prog. Symp. Ser. **49**, 107 (1953).
13. I Cibulka. Coll. Czech. Chem. Commun. **47**, 1414 (1982).
14. P.P. Singh, R.K. Nigam, S.P. Sharma, and S. Aggarwal. Fluid Phase Equilib. **8**, 333 (1984).
15. M. Nagata and J. Sakura. J. Chem. Soc. Faraday Trans. 1, **83**, 2449 (1987).
16. E.L. Arancibia and M. Katz. Phys. Chem. Liq. **26**, 107 (1993).
17. M. Iglesias, B. Orge, and J. Tojo. Fluid Phase Equilib. **126**, 203 (1996).
18. W. Heller. J. Phys. Chem. **69**, 1123 (1965).

© 2000 NRC Canada

Coefficient d'activité de l'acide sulfurique déterminé par titrage infrarouge

Christophe Ménichelli, Jean-Joseph Max et Camille Chapados

Résumé : Le titrage fait par spectroscopie infrarouge (IR) en utilisant la technique de la réflexion totale atténuée (Attenuated total reflexion, ATR) des solutions aqueuses de l'acide sulfurique H_2SO_4 est effectué pour des pH variant entre 0 et 14 dans la gamme de concentrations 1,89 à 0,01 M. La soustraction du spectre de l'eau dans les spectres des solutions est faite en tenant compte de l'eau acide, neutre et basique qui ont des spectres différents. Les spectres résultants sont les spectres de mélanges des espèces ioniques HSO_4^- et SO_4^{2-}. Pour chaque concentration, l'analyse par facteurs (AF), donne le spectre des espèces ioniques pures et les facteurs multiplicatifs (FM) dont on tire la distribution des espèces en fonction du pH. Cette distribution est semblable à celle qui est obtenue à partir des équations d'équilibre. La mesure IR permet d'obtenir directement le rapport des coefficients d'activité des ions HSO_4^- et SO_4^{2-}. Ce rapport varie essentiellement avec la concentration des ions sans dépendre de leur concentration relative. L'ajustement des courbes de titrage volumétrique expérimental et théorique dans les régions à haut et à bas pH a permis de déterminer les coefficients moyens d'activité des autres espèces présentes en solution. Les valeurs obtenues sont similaires à celles obtenues par mesures électrochimiques. Ceci montre que la spectroscopie IR peut-être utilisée pour étudier des solutions aqueuses d'acides inorganiques allant de concentrations faibles aux concentrations élevées.

Mots clés : spectroscopie IR, ATR, acide sulfurique, solutions aqueuses, analyse par facteurs, spectres principaux, solvatation, coefficients d'activité, titrage IR.

Abstract: The titration of sulphuric acid by infrared spectroscopy using the attenuated total reflection (ATR) technique was made in the 0 to 14 pH range for solutions ranging from 1.89 to 0.01 M. The subtraction of the water spectrum was made using acidic, neutral, and basic waters which exhibit different spectra. The results gave the spectra of mixtures of the HSO_4^- and SO_4^{2-} ionic species in solutions. For each concentration, factor analysis (FA) sorted the spectra of the pure ionic species and gave through the multiplying factors (MF) the distribution of the species as a function of pH. This distribution is the same as that obtained from the equilibrium equations. The IR measurements gave directly the ratios of the activity coefficients of HSO_4^- and SO_4^{2-} ions. This ratio varies with the total concentration of both ions but is independent of the relative concentration. The fitting of the experimental and theoretical volumetric titration curves in the high and low pH regions gave the mean activity coefficients of the other species present in the solutions. The values obtained are comparable to those obtained by electrochemical measurements. These results show that it is possible to use IR spectroscopy to study aqueous solutions of inorganic acids from low to high concentrations.

Key words : IR spectroscopy, sulfuric acid, aqueous solutions, factor analysis, ATR, principal spectra, solvation, activity coefficients, IR titration.

Introduction

L'acide sulfurique (H_2SO_4) pur et en solution aqueuse est impliqué à tous les niveaux de la chimie, qu'elle soit industrielle ou environnementale. Les propriétés thermodynamiques de ce système ont fait l'objet de nombreuses études au cours des 80 dernières années (1–8). Une de ces propriétés est le coefficient d'activité qui indique l'activité de l'acide différente de sa concentration. Staples (8) a donné une revue complète de la littérature sur le sujet. Les travaux décrits dans cette revue ont été réalisés à l'aide de mesures électrochimiques et thermodynamiques et ils indiquent que ces solutions ont un comportement fortement non idéal. Le désavantage de ces mesures est que les résultats obtenus le sont de façon indirecte et qu'ils donnent peu d'informations sur l'organisation des molécules en solution.

La spectroscopie vibrationnelle est un complément essentiel à ces mesures physico-chimiques car elle permet des mesures directes des espèces en présence tout en fournissant une information de nature structurale sur le système. L'analyse des spectres Raman des solutions aqueuses du H_2SO_4 a fait l'objet de plusieurs études (9–14). Irish et ses collaborateurs ont identifié et quantifié les espèces présentes en solutions (12–14). En spectroscopie

Reçu le 1 février 2000. Publié sur le site Web des Presses scientifiques du CNRC le August 11, 2000.

C. Ménichelli, J.-J. Max[1] et C. Chapados.[2] Département de chimie–biologie, Université du Québec à Trois-Rivières, C.P. 500, Trois-Rivières, QC G9A 5H7, Canada.

[1]Adresse actuelle : Scientech R&D, 2200 Sidbec–S, Trois-Rivières–O, QC G8Z 4H1, Canada.
[2]Auteur à qui adresser toute correspondance. Mél. : Camille_Chapados@uqtr.uquebec.ca

 © 2000 CNRC Canada

infrarouge (IR), peu de travaux ont été effectués sur ces solutions à cause de la forte absorptivité de l'eau qui rend difficile l'analyse quantitative des espèces en solution (15–17).

Récemment, Chapados et ses collaborateurs ont étudié la modification du spectre IR de l'eau par ATR lors de l'ajout d'un sel binaire (NaCl), d'un acide fort (HCl) ou d'une base forte (NaOH) et ont développé une méthode simple pour soustraire quantitativement le spectre d'eau de ces systèmes afin d'obtenir le spectre des autres espèces dissoutes (18–20). Ces études indiquent que la présence d'ions H_3O^+ (ou $H_5O_2^+$), OH^- (ou $H_3O_2^-$), Cl^- ou Na^+ en solution modifie l'organisation naturelle des molécules d'eau et en modifie le spectre.

Dans l'article précurseur à celui-ci (21) (ci-après **I**), nous avons effectué le titrage par spectroscopie IR (titrage IR) d'une solution aqueuse d'acide sulfurique à 0,50 M par des solutions de titrants HCl et NaOH sur la gamme de pH 0 à 14. Des spectres d'eau acide, neutre et basique ont été soustraits quantitativement des spectres des solutions d'acide sulfurique afin d'obtenir les spectres des mélanges HSO_4^- et SO_4^{2-}. L'analyse par facteurs (AF), qui est un traitement mathématique permettant de séparer les spectres des composantes principales (spectres principaux) et d'en déterminer l'abondance, a été effectuée suivant la méthode décrite dans la référence 20. Les facteurs multiplicatifs (FM) déterminés lors de l'AF sont directement proportionnels à la concentration et permettent de calculer les courbes de distribution des espèces en fonction du pH (20–24). Pour l'acide sulfurique 0,50 M, cette méthode a permis de déduire le rapport des coefficients d'activité de l'ion sulfate et de l'ion bisulfate (21). La comparaison des courbes de titrage volumétrique expérimental avec les courbes théoriques obtenues à partir des équations d'équilibre, a conduit à la détermination du coefficient moyen d'activité des autres espèces présentes dans ces solutions.

Le but de ce travail consiste à étudier, suivant la même méthode, le comportement des espèces ioniques de l'acide sulfurique sur une gamme de concentrations de 1,89 à 0,01 M afin d'obtenir les coefficients moyens d'activité dans une gamme étendue de concentrations pour les comparer aux valeurs de la littérature. L'influence du NaCl, un sel binaire, sur les coefficients d'activité sera étudiée afin de tester par IR l'influence d'ions étrangers sur le système sulfate.

Considérations théoriques[3]

Calcul des courbes de la distribution théorique du titrage volumétrique

Introduction

Le développement des équations est le même que dans (**I**). Seul un résumé des étapes essentielles est présenté ici. Lors du titrage, le produit à titrer est en équilibre thermodynamique avec ses différentes espèces ioniques :

$$[1] \qquad H_2SO_4 \overset{pK_1}{\underset{H^+}{\rightleftharpoons}} HSO_4^- \overset{pK_1}{\underset{H^+}{\rightleftharpoons}} SO_4^{2-}$$

L'entité moléculaire de l'acide sulfurique ne coexiste pas en solution aqueuse avec ses deux espèces ioniques (15, 21). L'équation d'équilibre entre les espèces mises en jeu lors de l'ajout de titrant HCl ou NaOH à la solution aqueuse d'acide sulfurique peut s'écrire comme suit :

$$[2] \qquad \begin{array}{c} H_2SO_4 + H_2O + NaOH + HCl \\ A \qquad D \qquad C_1 \qquad C_{-1} \end{array}$$
$$\rightarrow \begin{array}{c} HSO_4^- + SO_4^{2-} + H^+ + OH^- + Na^+ + Cl^- + H_2O \\ y_1 \qquad y_2 \qquad x \qquad x' \qquad c \qquad c' \qquad d \end{array}$$

Pour simplifier, l'équation est écrite comme si HCl et NaOH étaient ajoutés en même temps mais séparés à la fin du traitement. Le côté gauche de l'équation [2] représente l'état de départ et la partie droite l'état d'équilibre du mélange. La seconde ligne représente les quantités (en mol) impliquées dans le titrage. À gauche, A, C_1, C_{-1} et D sont les quantités originales et connues tandis que les quantités à droite (y_1 à d) doivent être déterminées.

Équations d'équilibre de dissociation

L'équilibre de dissociation entre HSO_4^- et SO_4^{2-} dans l'eau est donné par l'équation [3] en utilisant pour simplifier $[H^+]$ au lieu de $[H_3O^+]$ (ou $[H_5O_2^+]$).

$$[3] \qquad \frac{[SO_4^{2-}][H^+]}{[HSO_4^-]} \frac{\gamma_{SO_4^{2-}}\gamma_{H^+}}{\gamma_{HSO_4^-}} = K_2$$

avec

$$[4] \qquad \frac{\gamma_{HSO_4^-}}{\gamma_{SO_4^{2-}}} = \Gamma_2$$

De même pour l'eau :

$$[5] \qquad \frac{[H^+][OH^-]}{[H_2O]} \frac{\gamma_{H^+}\gamma_{OH^-}}{\gamma_{H_2O}} = K_0$$

avec

$$[6] \qquad \frac{\gamma_{H_2O}}{\gamma_{OH^-}} = \Gamma_0$$

Les coefficients d'activité des espèces en solution (γ_i) diffèrent de l'unité dans la gamme de concentrations étudiées et sont exprimés en terme de coefficient moyen d'activité $\gamma_\pm$. (1, 8) :

$$[7] \qquad \gamma_\pm = \frac{\gamma_{H^+}}{\Gamma_2}$$

Distribution des espèces

La mesure obtenue par le pH-mètre conduit à la relation suivante :

$$[8] \qquad X = \frac{V}{\gamma_{H^+}x} = \frac{1}{\gamma_{H^+}[H^+]} = 10^{pH}$$

La quantité (en mol) des espèces est déterminée suivant les équations d'électroneutralité, de conservation des espèces et des constantes d'équilibre (**I**) :

[3] Pour la signification des symboles, voir la liste en annexe.

© 2000 CNRC Canada

$$[9] \qquad y_1 = \frac{A}{1 + K_2 \Gamma_2 X}$$

$$[10] \qquad y_2 = \frac{A}{\frac{1}{K_2 \Gamma_2 X} + 1}$$

L'abondance relative des espèces ioniques HSO_4^- et SO_4^{2-} en fonction du pH est obtenue en divisant les équations [9] et [10] par A et en remplaçant X par 10^{pH}. Les courbes de distribution des espèces en fonction de l'équivalent titrant (P) sont obtenues en transformant la masse de titrant (m_δ) en P par l'équation :

$$[11] \qquad P = \delta \frac{\frac{m_\delta \varepsilon_\delta}{M_\delta}}{\frac{(m - m_\delta)\varepsilon_2}{M_2}}$$

où $\delta = 1$ pour l'ajout de titrant NaOH et $\delta = -1$ pour l'ajout de titrant HCl.

Variation théorique du pH en fonction de la masse de titrant

Le développement des équations (**I**) pour obtenir la variation théorique de la masse de titrant m_δ en fonction du pH conduit à :

$$[12] \qquad m_\delta = \frac{\rho_0 V \left[\frac{\varepsilon_2}{M_2} \frac{1 + 2K_2\Gamma_2 10^{pH}}{1 + 2K_2\Gamma_2 10^{pH}} + \frac{1 - \varepsilon_2}{M_{H_2O}} \frac{K_2\Gamma_2 10^{pH}}{1 + K_2\Gamma_2 10^{pH}} \right] - \frac{V 10^{-pH}}{\gamma_{H^+}}}{\frac{\varepsilon_\delta}{M_\delta} \frac{\delta + \frac{\delta - 1}{2} K_2\Gamma_2 10^{pH}}{1 + K_2\Gamma_2 10^{pH}} + (1 - \rho_\delta) \frac{\varepsilon_\delta}{M_\delta} \frac{1 + 2K_2\Gamma_2 10^{pH}}{1 + K_2\Gamma_2 10^{pH}} - \frac{(1 - \varepsilon_\delta) - (1 - \rho_\delta)(1 - \varepsilon_2)}{M_{H_2O}} \frac{K_2\Gamma_2 10^{pH}}{1 + K_2\Gamma_2 10^{pH}}}$$

où ρ_0 est la densité de la solution aqueuse d'acide sulfurique sans titrant et ρ_δ le coefficient sans dimension de la variation de la densité ρ défini par $\rho_\delta = (\rho - \rho_0)/(m_\delta/V)$. La distribution des espèces et la courbe de titrage volumétrique sont données par les équations [9, 10 et 12]. Les paramètres à déterminer dans ces équations sont les coefficients d'activité Γ_0, Γ_2 et γ_{H^+}. L'étude du comportement aux limites de ces équations permet de déterminer la zone d'influence de chacun de ces paramètres sur les courbes de distribution. Au pH d'équipartition ($[HSO_4^-] = [SO_4^{2-}]$), l'équation [3] est réécrite :

$$[13] \qquad \Gamma_2 = 10^{(pK_2 - pH_{\text{équipartition}})}$$

Cette équation montre que le titrage IR avec une simple mesure de pH permet de déterminer directement le coefficient moyen d'activité (Γ_2) des ions sulfate et bisulfate en équilibre.

À pH élevé, avec ajout de titrant NaOH, ($16 > pH > 13$), où $K_0\Gamma_0 10^{pH} << 1 << K_2\Gamma_2 10^{pH}$, l'équation [12] peut être évaluée par la relation suivante :

$$[14] \qquad m_1 \approx \rho_0 V \frac{2\frac{\varepsilon_2}{M_2} + \frac{1 - \varepsilon_2}{M_{H_2O}} K_0\Gamma_0 10^{pH}}{\frac{\varepsilon_1}{M_1} + 2(1 - \rho_1)\frac{\varepsilon_2}{M_2}} \approx G + \rho_0 V \frac{\frac{1 - \varepsilon_2}{M_{H_2O}} K_0\Gamma_0 10^{pH}}{\frac{\varepsilon_1}{M_1} + 2(1 - \rho_1)\frac{\varepsilon_2}{M_2}}$$

Où G est une constante correspondant à deux équivalents titrants pour la neutralisation totale de l'acide sulfurique. L'équation [14] indique que seul Γ_0 influence la courbe à haut pH. À bas pH, avec ajout de titrant HCl, ($pH < 0{,}5$), où $K_0\Gamma_0 10^{pH} << 1$ et $K_2\Gamma_2 10^{pH} << 1$, l'équation [12] peut être évaluée par la relation suivante :

$$[15] \qquad m_{-1} \approx \frac{\rho_0 V \frac{\varepsilon_2}{M_2} - \frac{V}{\gamma_{H^+}} 10^{-pH}}{\frac{\varepsilon_{-1}}{M_{-1}} + (1 - \rho_{-1})\frac{\varepsilon_2}{M_2}} \approx -H \frac{\frac{V}{\gamma_{H^+}} 10^{-pH}}{\frac{\varepsilon_{-1}}{M_{-1}} + (1 - \rho_{-1})\frac{\varepsilon_2}{M_2}}$$

Où H est une constante correspondant à la première dissociation complète de l'acide en milieu aqueux. L'équation [15] indique que seul γ_{H^+} influence la courbe de titrage à bas pH, tant que la première dissociation de l'acide sulfurique peut-être considérée comme complète.

© 2000 CNRC Canada

La spectroscopie IR par réflexion totale atténuée (ATR)

Les spectres IR de solutions aqueuses obtenus par transmission nécessite l'utilisation de films minces afin d'éviter que l'intensité de la bande d'élongation OH de l'eau ne sature. L'ATR permet de surmonter ces difficultés car le spectre obtenu ne dépend que des propriétés optiques (intensives) du film mesuré. Bien que les effets de dispersion anormale (DA) produisent des variations dans le spectre ATR par rapport à une mesure idéale, les travaux antérieurs sur les effets de la DA dans les spectres ATR de solutions salines montrent que les spectres ATR varient directement avec la concentration de la solution. Il en est de même des spectres de *k*. Ces derniers et les spectres ATR de l'eau varient de façon quasi proportionnelle (25). Il n'est donc pas nécessaire de séparer les effets optiques du spectre ATR pour établir une corrélation entre les modifications des spectres et les modifications chimiques des solutions.

Partie expérimentale

Produits chimiques et solutions

L'acide sulfurique (H_2SO_4) (Aldrich Chemical Co., pureté 98 %) est utilisé sans traitement supplémentaire. De l'eau déionisée est utilisée pour obtenir les solutions aqueuses d'acide sulfurique. Des solutions de NaOH à 49,5 % (±0,7 %) (p/p) et de HCl à 37 % (±0,5 %) (p/p) sont utilisées pour le titrage de l'acide sulfurique afin de travailler sur toute la gamme de pH.

Préparation des échantillons

Les solutions de H_2SO_4 aux concentrations de 1,886; 1,02, 0,500; 0,204; 0,102; 0,0509 et 0,0103 M (±1 %) sont préparées selon la méthode décrite dans **I.** La solution acide salée est préparée en ajoutant du NaCl à du H_2SO_4 0,558 M afin que la solution contienne NaCl 1,00 M.

Mesure de pH

Pour chaque échantillon, les mesures de pH sont effectuées à température ambiante (26,5 ± 0,3°C) avec un pH-mètre Omega, modèle PHH-253, couplé à une électrode combinée (Analytical Sensors, Inc., modèle PH10107B-03-B). Une calibration appropriée (pH = 2,00; 7,00 et 10,00) est effectuée avant chaque série de mesures. Un temps de stabilisation de 20 min est alloué pour chaque prise de mesure. La validité des mesures obtenues avec l'appareil a été vérifiée dans la gamme de pH de –0,25 à 13,89 (20).

Mesures infrarouges

Les mesures IR entre 4800 et 650 cm^{-1} sont effectuées sur un spectromètre FTIR Nicolet, modèle 510P, équipé d'un détecteur TGS. Deux fenêtres de KBr isolent la chambre de mesure de l'extérieur. L'échantillon à analyser est placé dans une cellule ATR cylindrique (SpectraTech, Inc.) équipée d'un cristal de ZnSe cylindrique (11 réflexions internes). Les spectres sont pris sous flux continu d'azote. Pour chaque prise de spectre, une accumulation de 200 balayages est faite avec une résolution de 4 cm^{-1}. Toutes les mesures sont effectuées à 26,5°C ± 0,3°C. Un spectre de référence de la cellule vide est pris avant chaque spectre d'échantillon.

Traitement des données

Les données spectrales pour chaque échantillon (2152 points {I ($\tilde{\nu}$) vs. $\tilde{\nu}$ (en cm^{-1})} sont transférées sur micro-ordinateur et traitées avec le chiffrier Microsoft Excel97. Les intensités I sont transformées en absorbance (log(1/I)). Une légère correction (plus petite que 0,03 UA) de la ligne de base est effectuée par ajustement de la région 4600–4450 cm^{-1} au zéro d'absorbance. Pour chaque série de spectres, la soustraction des différents types d'eau est effectuée sans aucune correction des lignes de base; les spectres principaux des espèces ioniques de l'acide sulfurique sont déterminés et l'AF est appliquée sur l'ensemble des spectres en utilisant la minimisation de la différence quadratique (hors des zones de bruit) comme critère de qualité.

Résultats et discussion

Les spectres et les courbes de distribution relatifs au titrage IR seront présentés suivant l'exemple du titrage de la solution à 1,02 M. Le développement des résultats s'intéressera à l'ensemble des concentrations.

Spectres de mélanges de H_2SO_4 aqueux avec HCl ou NaOH

La figure 1 donne les spectres expérimentaux des solutions aqueuses de H_2SO_4 1,02 M sur la gamme de pH de 0 à 14. La bande large et intense dans la région 3700–2800 cm^{-1} résulte de la vibration d'élongation OH de l'eau (ν_{OH}) et la bande à 1640 cm^{-1} résulte de la vibration de déformation OH de l'eau (δ_{OH}). L'augmentation de l'intensité du spectre dans la région en dessous de 950 cm^{-1} provient de la bande de libration de l'eau. Les bandes relatives aux groupements sulfates sont observées dans la région 1300–800 cm^{-1}. Dans cette région, la variation de l'intensité des bandes en fonction du pH est directement reliée à la variation de la composition ionique des solutions. La modification du spectre d'eau en fonction du pH est due à la présence de l'eau acide, de l'eau neutre et de l'eau basique. La forte absorptivité des spectres des différents types d'eau rend difficile l'analyse quantitative des bandes des espèces ioniques de l'acide sulfurique.

Pour les autres concentrations, les spectres expérimentaux des solutions aqueuses de l'acide sulfurique sur la gamme de pH 0–14 sont obtenus de la même façon. Les intensités des bandes d'eau sont du même ordre de grandeur pour chacune des concentrations alors que les intensités des bandes des espèces ioniques de l'acide sulfurique diminuent avec la concentration. Elles deviennent imperceptibles en dessous de 0,01 M.

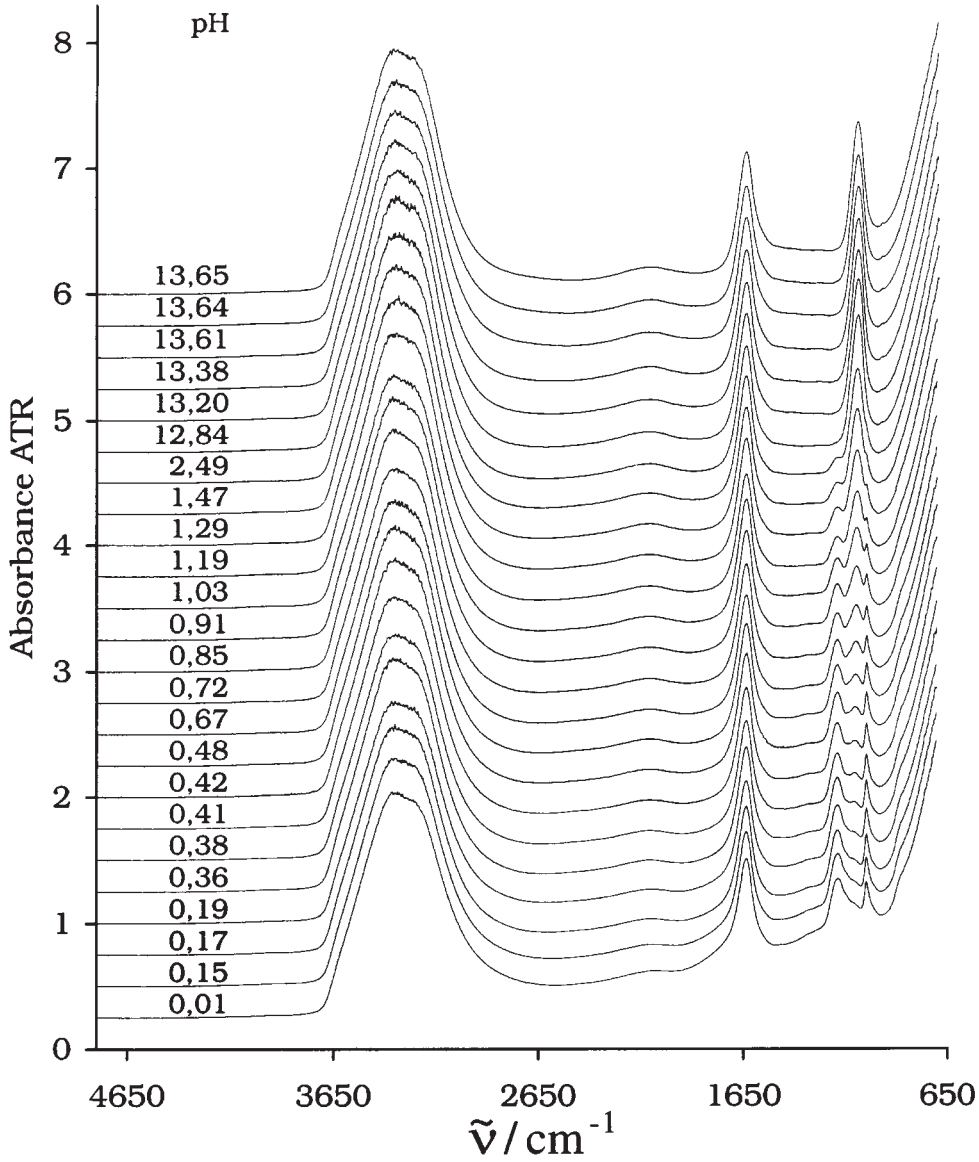
La figure 1 pourrait paraître semblable à celle publiée des spectres de solutions aqueuses d'acide sulfurique à 0,50 M (21). C'est une illusion puisque la différence entre les deux séries de spectres est autre qu'un facteur de concentration puisque l'intensité de la bande à 1098 cm^{-1} est supérieure à celle de la bande à 1637 cm^{-1}, tandis que c'est l'inverse dans la référence 21.

Soustraction des différents types d'eau

La figure 2A présente les spectres d'eau qui sont utilisés comme spectres principaux pour la soustraction des spectres d'eau dans les échantillons titrés : eau acide (HCl 1,54 M);

© 2000 CNRC Canada

Fig. 1. Spectres IR ATR des 24 mélanges de H_2SO_4 1,02 M avec HCl ou NaOH 0 < pH < 14. Chaque spectre est décalé successivement de 0,25 UA.



eau neutre (H_2O); eau basique (NaOH 2,23 M) et eau saline (NaCl 5,00 M). Les spectres de la figure 2A sont superposés afin de mieux souligner leurs différences. La figure 2B donne les spectres des solutions aqueuses de l'acide sulfurique 1,02 M sur la gamme de pH 0–14 après la soustraction des spectres de l'eau acide, de l'eau neutre et de l'eau basique. Pour chaque spectre, la ligne de base est régulière et se situe au 0,00 UA. La figure 2C présente ces spectres d'une façon superposée dans la région des bandes sulfates (1300–800 cm^{-1}). Les points quasi–isobestiques situés à 1147 et 1051 cm^{-1} et la variation de l'intensité des bandes à 1192, 1098, 1050 et 883 cm^{-1} indiquent une transformation unitaire en fonction du pH de HSO_4^- en SO_4^{2-} dans ces solutions. La large bande de faible intensité située dans la région 3700–3050 cm^{-1} et la bande située vers 1640 cm^{-1} (fig. 2B) indiquent que toute l'eau n'a pu être soustraite. Ces bandes résiduelles sont attribuées à l'eau complexée avec les espèces ioniques de l'acide sulfurique et feront l'objet d'un travail subséquent.

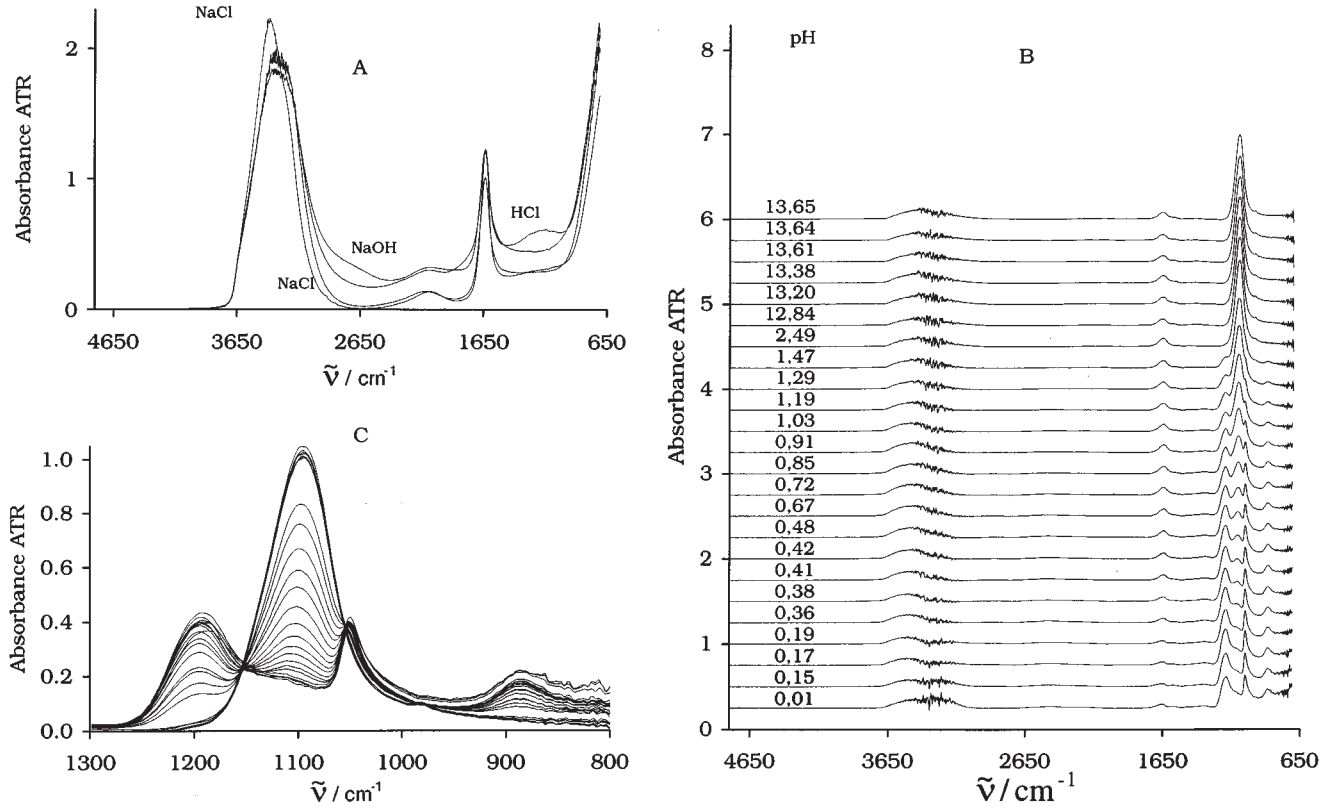
Détermination des spectres des espèces ioniques pures

Les spectres des figures 2B et C représentent les spectres de mélanges des espèces ioniques solvatées HSO_4^- et SO_4^{2-} sur la gamme de pH 0–14 après la soustraction des différents types d'eau. Après la seconde équivalence, tous les groupes HSO_4^- ont été neutralisés. Le spectre le plus basique correspond donc au spectre de l'espèce ionique pure SO_4^{2-}. En fait, il représente le spectre de SO_4^{2-} avec ses contre-ions (ici 2 Na^+) et avec l'eau complexée à cette paire d'ions.

Dans la solution aqueuse d'acide sulfurique sans ajout de titrant, les espèces ioniques présentes en solution sont HSO_4^-, SO_4^{2-}, les deux ayant H_3O^+ comme contre-ion (**I**). Comme l'espèce HSO_4^- n'est jamais pure en solution, le spectre de

© 2000 CNRC Canada

Fig. 2. A, Spectres principaux des espèces d'eau : eau acide (HCl 1,54 M); eau neutre (H_2O); eau basique (NaOH 2,23 M) et eau saline (NaCl 5,00 M). B, Spectres IR ATR des 24 mélanges de H_2SO_4 1,020 M après soustraction des spectres d'eau. Chaque spectre est décalé successivement de 0,25 UA. C Superposition des spectres de 2B dans la région des bandes sulfates.



l'espèce ionique pure HSO_4^- est obtenu en retranchant la contribution du spectre de l'espèce ionique pure SO_4^{2-} du spectre des solutions à bas pH. Ceci est effectué par la minimisation de l'intensité de la bande ν_4 du SO_4^{2-} qui est située à 1098 cm^{-1}.

Comme première approximation, on considère que les bandes propres à chacun des ions HSO_4^- et SO_4^{2-} sont indépendantes du contre-ion H_3O^+ ou Na^+. Ceci est confirmé par la position des bandes à 1192, 1098, 1050 et 883 cm^{-1} en fonction du pH (figs. 2B et C). Cependant, la solvatation de ces espèces est influencée par le contre-ion (**I**). Ainsi, le spectre déterminé de l'espèce pure HSO_4^- est celui de la paire d'ions solvatée (H_3O^+ et HSO_4^-). Le spectre de la paire d'ions solvatée (Na^+ et HSO_4^-) est obtenu quand tous les H_3O^+ sont remplacés par des Na^+ dans la paire d'ions, par l'ajout de titrant NaOH à la solution aqueuse d'acide sulfurique. De même, le spectre de l'espèce pure SO_4^{2-}, qui fut déterminé précédemment, est celui du groupe d'ions ($2Na^+$ et SO_4^{2-}). Les spectres des groupes d'ions (H_3O^+, SO_4^{2-} et Na^+) et ($2H_3O^+$ et SO_4^{2-}) sont obtenus par ajout de NaOH à la solution aqueuse d'acide avant la seconde équivalence. Pour l'AF des espèces ioniques de l'acide sulfurique, on s'est intéressé à la détermination de la concentration des deux espèces HSO_4^- et SO_4^{2-}. Ainsi, pour obtenir la distribution de ces deux espèces, il n'est pas nécessaire de différencier le spectre des groupes ou paires d'ions.

Pour chaque concentration, les spectres des espèces ioniques HSO_4^- et SO_4^{2-} sont déterminés de la même manière que pour la solution à 1,02 M et sont donnés respectivement sur la figure 3 après leur normalisation à 1,00 M. La normalisation des spectres aux plus faibles concentrations a pour effet d'augmenter l'intensité du bruit, notamment au niveau des bandes d'eau de solvatation dans la région 3700–3050 cm^{-1}. Les bandes de chacune des espèces ont une intensité et une position semblables pour chaque concentration. Ceci indique la validité des critères de sélection des spectres des espèces ioniques pures. Les résultats ainsi obtenus sont concordants sur toute la gamme de concentrations étudiées, même aux très faibles concentrations.

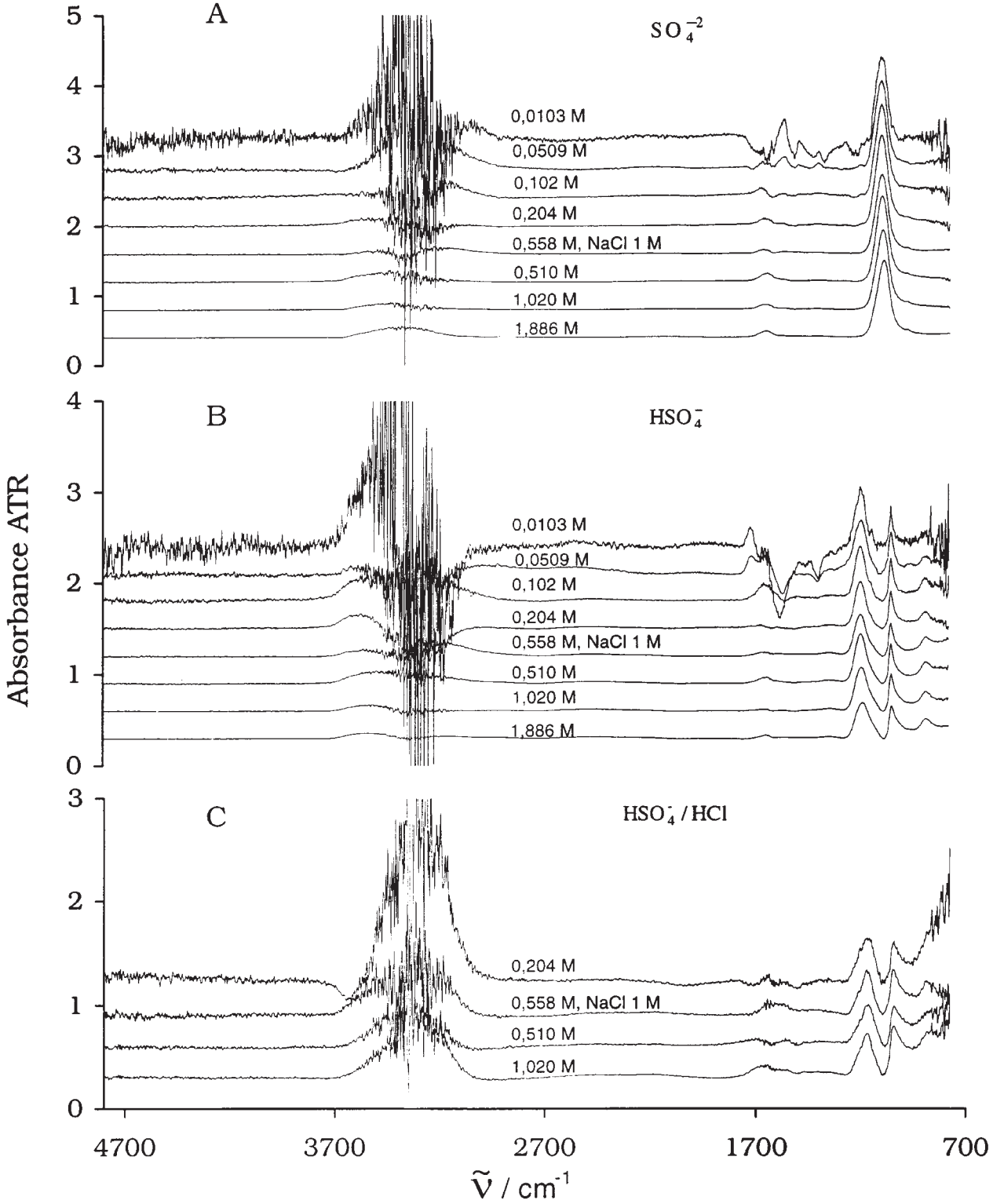
Résultats de l'AF des espèces ioniques de l'acide sulfurique

Pour chaque concentration, les spectres des espèces ioniques pures déterminés précédemment sont soustraits dans tous les spectres auxquels les spectres d'eau ont été retranchés. Les FM impliqués dans la soustraction donnent la proportion de chacune des espèces ioniques.

Dans (**I**), une seconde forme solvatée de l'espèce HSO_4^- a été mise en évidence lors de l'ajout de titrant HCl à la solution aqueuse de l'acide. Ce spectre est observé aux concentrations supérieures à 0,20 M, excepté pour les solutions à 1,89 M dans lesquelles aucun titrant HCl n'a été ajouté. Ce spectre est obtenu en soustrayant les contributions des spectres des espèces ioniques pures HSO_4^- et SO_4^{2-} du spectre sans eau de la solution la plus acide. Ce nouveau spectre de l'espèce que nous appellerons (H_3O^+ et HSO_4^-)$_{\text{-HCl}}$ est ensuite soustrait des spectres des solutions auxquelles du

© 2000 CNRC Canada

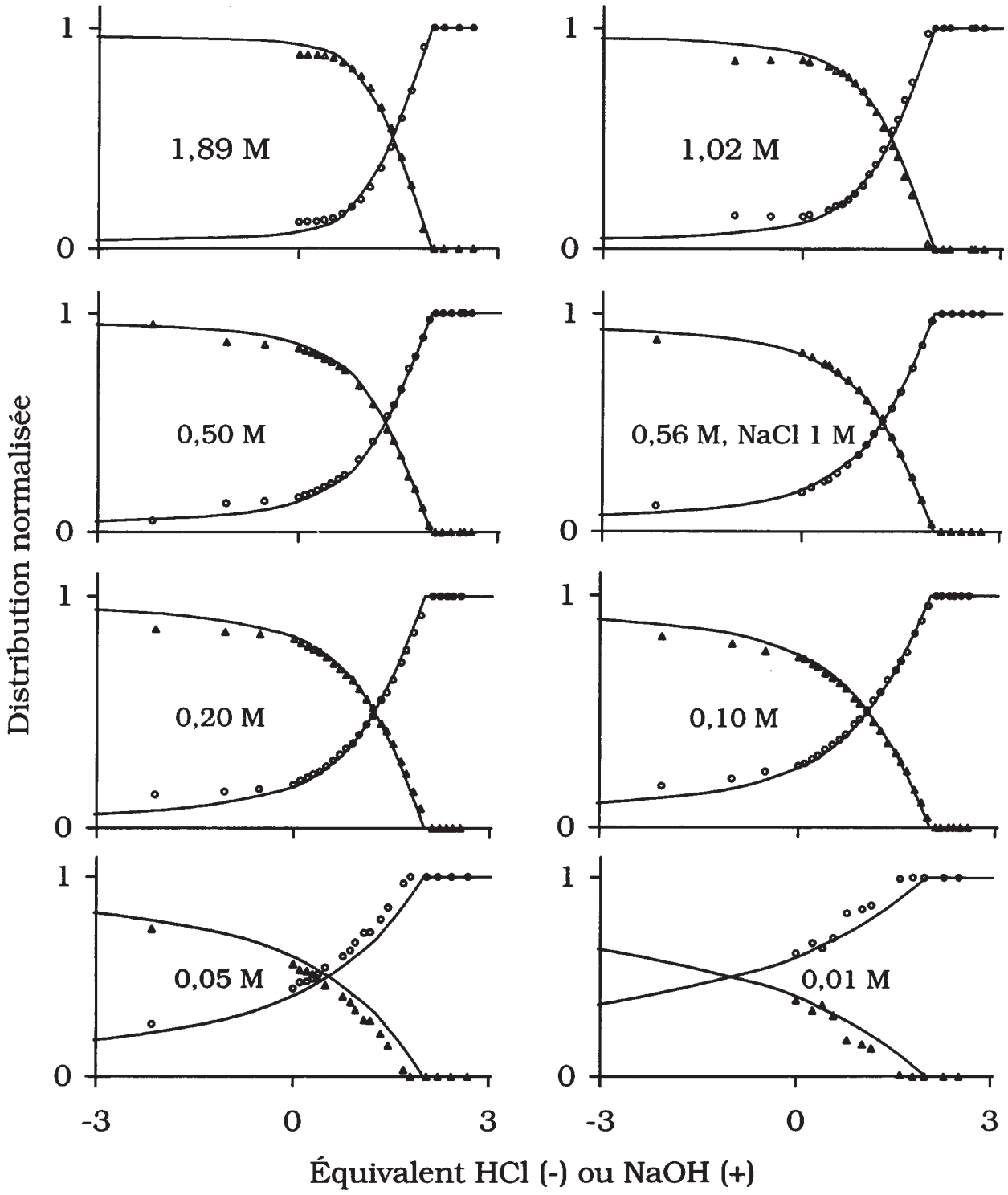
Fig. 3. Spectres IR ATR des espèces ioniques du H_2SO_4 aqueux sur la gamme de concentrations 1,89–0,01 M. Les spectres sont normalisés à 1,00 M de chacune des espèces et sont décalés. À cause de la normalisation, des bandes artifactuelles apparaissent entre 1500 et 1200 cm^{-1} aux concentrations les plus basses (0,0103 et 0,0509 M).



titrant HCl a été ajouté. L'observation de cette espèce à plusieurs concentrations révèle sa présence réelle en solution. Elle résulte de l'influence d'une paire d'ions (H^+ et Cl^-) sur une paire d'ions (H_3O^+ et HSO_4^-). Un élément de preuve supplémentaire est fourni par l'analyse du titrage IR de l'acide sulfurique en présence de NaCl 1,00 M (voir plus loin). Dans les solutions les plus acides, la concentration de cette espèce représente au maximum 20 % de celle de

© 2000 CNRC Canada

Fig. 4. Distribution relative des espèces ioniques de H_2SO_4 aqueux en fonction de l'équivalent titrant sur la gamme de concentration 1,89–0,01 M. Lignes pleines (——), distribution théorique (obtenues avec les équations 9 et 10); points en triangles vides (△△△), HSO_4^- par IR; points en ronds vides (○○○), SO_4^{2-} par IR.

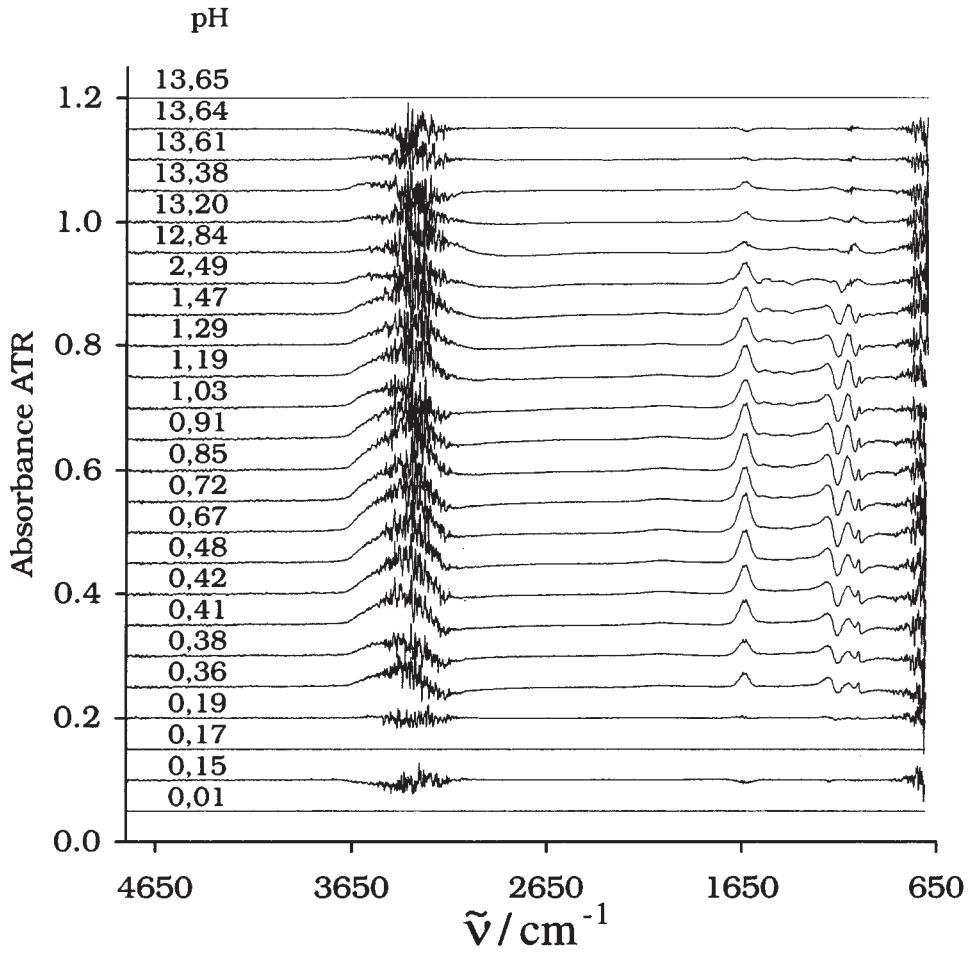


l'espèce (H_3O^+ et HSO_4^-). L'incertitude sur les FM lors de l'AF rend moins précise la normalisation du spectre de cette espèce pure. Ainsi, la figure 3C donne les spectres principaux de l'espèce (H_3O^+ et HSO_4^-)$_{-HCl}$ pour les concentrations précédemment citées.

La figure 4 donne, pour chaque concentration, les résultats de la décomposition par facteurs à partir des spectres principaux en terme de distribution des espèces ioniques HSO_4^- (Δ) et SO_4^{2-} (O) en fonction de l'équivalent titrant. Comme dans **I**, les 2 espèces (H_3O^+ et HSO_4^-) et (H_3O^+ et

© 2000 CNRC Canada

Fig. 5. Résidus résultant de l'AF à partir des spectres principaux pour H_2SO_4 1,02 M pour les pH entre 0 et 14. Les spectres sont décalés successivement de 0,05 UA. Par rapport à la Fig. 2B, l'échelle d'intensité est étalée par un facteur de 5.



$HSO_4^-)_{\text{-HCl}}$ ont été comptabilisées ensemble. Les FM ont été normalisés à 1. Dans la figure 4, les courbes formées de symboles représentent les valeurs réelles de distribution des espèces car elles proviennent de la mesure directe de la concentration des espèces. Les courbes en trait plein représentent les courbes théoriques (équations [9] et [10]) en considérant la contribution des coefficients d'activité du proton, de l'eau et des espèces ioniques de l'acide. Le choix des valeurs des coefficients d'activité dans les courbes de distribution théoriques est expliqué plus loin. Les courbes théoriques et expérimentales montrent une bonne concordance. Aux plus faibles concentrations (0,01 et 0,05 M), l'augmentation du bruit dans les spectres influence l'incertitude des résultats de l'AF. Ces courbes de distribution nous indiquent clairement que l'équilibre se déplace avec la concentration.

Les résidus

La figure 5 donne les résidus de la décomposition par facteurs des solutions aqueuses de l'acide 1,02 M en utilisant trois spectres principaux (Fig. 3). L'AF a été effectuée suivant la minimisation des carrés de la différence entre le spectre expérimental et le spectre calculé. Pour cette raison, les spectres obtenus ont des intensités négatives par endroits. On remarque la présence de bandes résiduelles à 1215, 1116 et 1055 (±3) cm^{-1}. Ces bandes n'ont pas pu être soustraites par l'AF. En effet, la faible intensité des bandes dans la région 1300–800 cm^{-1} ne nous a pas permis de trouver le nombre d'espèces secondaires et leurs spectres. Avec ces résultats, il est évident que plusieurs de ces espèces secondaires existent et qu'elles peuvent s'expliquer par la formation de complexes entre les espèces HSO_4^- et SO_4^{2-}. En **I**, pour l'acide sulfurique 0,50 M, ces bandes résiduelles étaient à peine perceptibles. Dans ce travail, elles ne sont pas visibles aux concentrations inférieures à 0,50 M. Comme ces bandes sont peu intenses, elles peuvent être négligées pour le reste de cette analyse qui porte sur la détermination du coefficient d'activité.

Résultats de la décomposition par facteurs

Les spectres principaux de SO_4^{2-}, de HSO_4^- et de (H_3O^+ et $HSO_4^-)_{\text{-HCl}}$ pour les différentes concentrations sont présentés sur la figure 3. Les spectres sont normalisés à 1,00 M de chacune des espèces. À cause de cette normalisation, les bandes qui apparaissent entre 1500 et 1200 cm^{-1} aux concentrations les plus basses (0,0103 et 0,0509 M) sont artifactuelles. Ces bandes qui sont en dehors de la zone d'absorption des groupes sulfates ne nuisent pas à l'analyse

© 2000 CNRC Canada

Tableau 1. Position et intensité des bandes sulfates des ions SO_4^{2-}, HSO_4^- et du complexe HSO_4^-–HCl en fonction de la concentration.

Concentration (M) ±0,001	SO_4^{2-}		HSO_4^-				HSO_4^-–HCl		
	ν_3 : élong. asy.[a]		SO_3 élong. dégé.[b]		SO_3 élong. sym.[c]	S–OH élong.[d]	SO_3 élong. dégé.[b]	SO_3 élong. sym.[c]	S–OH élong.[d]
	Position (cm^{-1})	Intensité (1200–920 cm^{-1}) (Abs. cm^{-1})	Position (cm^{-1})	Intensité (1300–1086 cm^{-1}) (Abs. cm^{-1})	Position (cm^{-1})	Position (cm^{-1})	Position (cm^{-1})	Position (cm^{-1})	Position (cm^{-1})
1,886	1092±1	100±1	1188±2	35,2±0,4	1047±1	884±3	—	—	—
1,020	1096±1	102±1	1194±2	40,2±0,4	1049±1	887±3	1170±2	1044±2	~886
0,558 (NaCl 1,00 M)	1098±1	99±3	1196±2	40±1	1051±1	891±3	1172±2	1046±2	~888
0,500	1098±1	105±2	1196±2	43,6±0,8	1051±1	889±3	1172±2	1042±2	~886
0,204	1102±1	111±3	1196±2	40±1	1051±1	891±3	1170±2	1045±2	~888
0,102	1102±2	117±7	1198±3	47±3	1051±2	891±4	—	—	—
0,0509	1102±2	107±15	1194±3	52±5	1051±2	~884±5	—	—	—
0,0103	1102±3	—	1196±4	43±10	1051±3	—	—	—	—

[a]Élongation asymétrique.
[b]Élongation dégénérée.
[c]Élongation symétrique.
[d]Élongation S—O.

de ces groupes. L'attribution des bandes qui est donnée dans le tableau 1 est basée sur **I**. La distribution des espèces en fonction des équivalents titrants est donnée sur la figure 4.

Les spectres IR des espèces ioniques de l'acide sulfurique

SO_4^{2-}: Les spectres principaux normalisés (à 1,00 M) de l'espèce ionique SO_4^{2-} sont donnés sur la figure 3A pour chaque concentration. La bande située vers 1098 cm^{-1} est attribuée à la vibration d'élongation SO asymétrique (ν_3). À la concentration de 1,886 M, la bande est située à 1092 cm^{-1} (Tableau 1). Cette position augmente progressivement jusqu'à 1102 cm^{-1} à la concentration de 0,204 M et demeure constante jusqu'à 0,0103 M. L'intensité de la bande tout en ne variant que très peu suit la même tendance : elle est de 100 Abs cm^{-1} à 1,886 M et se stabilise vers 111 Abs cm^{-1} à 0,204 M. Le NaCl 1,00 M ajouté à la solution de 0,558 M n'influence pas la position de la bande et a très peu d'effet sur l'intensité. Ces variations de position et d'intensité sont différentes de la variation du coefficient d'activité avec la concentration (voir ci-après et la figure 7) et ne peuvent par conséquent provenir de la même origine.

Nous apercevons du côté des basses fréquences de la bande ν_3 un épaulement qui devient plus précis au fur et à mesure que la concentration augmente. Cette bande située à 978 cm^{-1} est attribuée à ν_1 de SO_4^{2-}. Avec une symétrie T_d, ce mode, qui n'est pas actif normalement, l'est devenu faiblement à cause des perturbations que subit cet ion en présence de l'eau de solvatation et des contre-ions.

HSO_4^-: Les spectres principaux de l'espèce ionique HSO_4^- sont donnés sur la figure 3B pour chaque concentration. Les spectres de cette espèce obtenus après normalisation à 1,00 M sont semblables mais les positions et les intensités sont un peu modifiées. La bande située vers 1192 cm^{-1} est attribuée à la vibration d'élongation SO_3 dégénérée. À la concentration de 1,886 M, cette bande est située à 1188 cm^{-1}, cette position augmente jusqu'à 1196 cm^{-1} à la concentration de 0,50 M et demeure constante aux plus faibles concentrations. La variation de l'intensité de cette bande est à la limite quand la précision expérimentale mais semble augmenter légèrement si la concentration diminue. Le comportement de cette bande est similaire à celui de ν_3 du SO_4^{2-}. La bande de faible intensité située vers 1150 cm^{-1} est attribuée à une bande harmonique d'une bande fondamentale qui est située en bas de 700 cm^{-1}. Cette bande s'affine lorsque la concentration d'acide diminue.

La bande située vers 1050 cm^{-1} est attribuée à la vibration symétrique du SO_3. La position de cette bande fine ne varie pas avec la concentration de l'acide. Bien que nous ne puissions pas mesurer avec précision l'intensité de cette bande à cause de la ligne de base changeante, elle change peu ou pas.

La faible bande située vers 889 cm^{-1} est attribuée à la vibration d'élongation S—O du groupe SOH. La position et l'intensité de cette bande sont entichées d'une erreur plus grande que les autres bandes parce qu'elle est située à la limite inférieure de nos mesures et que son intensité est faible. Malgré cette limite, la position et l'intensité de cette bande semblent peu varier. L'ajout de sel dans la solution de 0,558 M n'influence ni la position ni l'intensité de la bande.

$(H_3O^+$ et $HSO_4^-)_{\text{-HCl}}$: En interaction avec HCl (Fig. 3C), la bande d'élongation dégénérée du SO_3 passe d'environ 1196 à 1172 cm^{-1}, la bande d'élongation symétrique du SO_3 passe de 1051 à 1044 cm^{-1} pour des déplacement respectifs d'environ 24 et 7 cm^{-1}. La bande d'élongation S—O(H) ne semble pas affectée par l'ajout de sel bien que cette observation soit limitée par la précision de la mesure de cette bande. La bande d'eau située vers 3400 cm^{-1} est plus intense dans les spectres de ces solutions que dans les situations sans HCl.

Le déplacement de la bande principale nous indique que l'ajout de HCl dans une solution aqueuse de H_2SO_4 a pour effet de former un complexe entre les ions H_3O^+, HSO_4^-, Cl^- et les molécules d'eau. Parce que la détermination de ce

© 2000 CNRC Canada

Tableau 2. Coefficients d'activité des solutions aqueuses de H_2SO_4 obtenus par IR.

$[H_2SO_4]$ (M)	pH solution mère	Degré de dissociation solution mère	pH equipartition	$\Gamma_2 = \gamma_{HSO_4^-}/\gamma_{SO_4^{2-}}$	$\gamma_\pm = \gamma_{H^+}/\Gamma_2$
±0,001	±0,02		±0,02	±10 %	±25 %
1,886	0,05	0,13	0,95	10,2	0,067
1,020	0,17	0,15	0,95	9,5	0,072
0,558 (NaCl, 1,00 M)	0,47	0,18	1,00	9,1	0,077
0,500	0,48	0,16	1,25	5,5	0,124
0,204	0,86	0,19	1,35	3,4	0,206
0,102	1,08	0,27	1,44	3,06	0,245
0,0509	1,30	0,44	1,46	3,15	0,270
0,0103	1,90	0,62	1,65	2,04	0,441

complexe dépasse le cadre de ce travail nous réservons cet aspect pour un travail futur.

Titrage volumétrique et coefficients d'activité

Analyse des courbes de distribution

Les tracés de la figure 4 montrent que la position du point d'équipartition en fonction de l'équivalent titrant varie fortement au fur et à mesure que la concentration en acide sulfurique diminue (de haut en bas sur la figure). La seconde dissociation de l'acide sulfurique varie donc avec la concentration ce qui signifie que les coefficients d'activité varient. Les valeurs du pH des solutions sans titrant et celles du point d'équipartition sont données dans le tableau 2. L'évolution de ces valeurs est approximativement logarithmique, ce qui est attendu pour les valeurs de pH qui varient logarithmiquement avec la concentration. Le pH d'équipartition et l'équation [13] permettent d'obtenir directement la valeur de Γ_2, le rapport des coefficients d'activité des ions bisulfate et sulfate (Tableau 2). Dans les équations [9], [10] et [12] (Fig. 4) on a fait l'approximation que Γ_2 est indépendant du pH pour calculer les courbes théoriques de distribution des espèces (lignes pleines de la figure 4). Les valeurs expérimentales obtenues par l'AF des spectres IR (symboles sur la figure 4) qui se situent sur les courbes théoriques confirment que Γ_2 est indépendant du pH. Le phénomène relié au coefficient d'activité serait donc davantage lié à la concentration totale en ions sulfate et bisulfate qu'à la concentration de l'une ou l'autre de ces deux espèces. Plus encore, les valeurs du tableau 2 indiquent qu'en fonction de la concentration, Γ_2 augmente. Ceci indique que l'activité de l'ion sulfate diminue beaucoup plus rapidement que celle de l'ion bisulfate lorsque la concentration augmente.

La figure 6A présente les résultats du titrage volumétrique pour les solutions aqueuses de l'acide à une concentration de 1,02 M. Les valeurs expérimentales de pH en fonction de la masse de titrant (●) sont comparées aux valeurs théoriques dans une situation idéale (équation [12] avec des coefficients d'activité égaux à 1). De même, les courbes de distribution expérimentales des espèces ioniques HSO_4^- (△) et SO_4^{2-} (○) sont comparées aux courbes théoriques idéales de distribution (équations [9] et [10]) en figure 6C. Les différences observées entre les valeurs expérimentales et théoriques proviennent de la déviation des coefficients d'activité des espèces en solution par rapport au comportement idéal. Dans les figures 6A et 6C, ces coefficients sont négligés dans les équations théoriques. En accord avec l'étude aux conditions limites des équations de distribution (équations [13] à [15]) et avec **I**, les coefficients d'activité Γ_2, γ_{H^+} et Γ_0 sont déterminés, le premier par IR et les derniers en ajustant leur contribution dans les équations théoriques pour que la courbe de titrage volumétrique corresponde aux valeurs expérimentales. Les figures 6B et 6D donnent les courbes théoriques pour les valeurs suivantes des coefficients d'activité : $\Gamma_0 = 1{,}5$; $\gamma_{H^+} = 0{,}67$; $\Gamma_2 = 9{,}5$. Ces courbes sont en accord avec les résultats expérimentaux. Sauf aux deux plus basses concentrations étudiees, les coefficients moyens d'activité du proton (γ_{H^+}) et de l'eau (Γ_0) ne sont que faiblement influencés par la concentration d'acide sulfurique : $\gamma_{H^+} = 0{,}70 \pm 0{,}05$ et $\Gamma_0 = 1{,}4 \pm 0{,}2$.

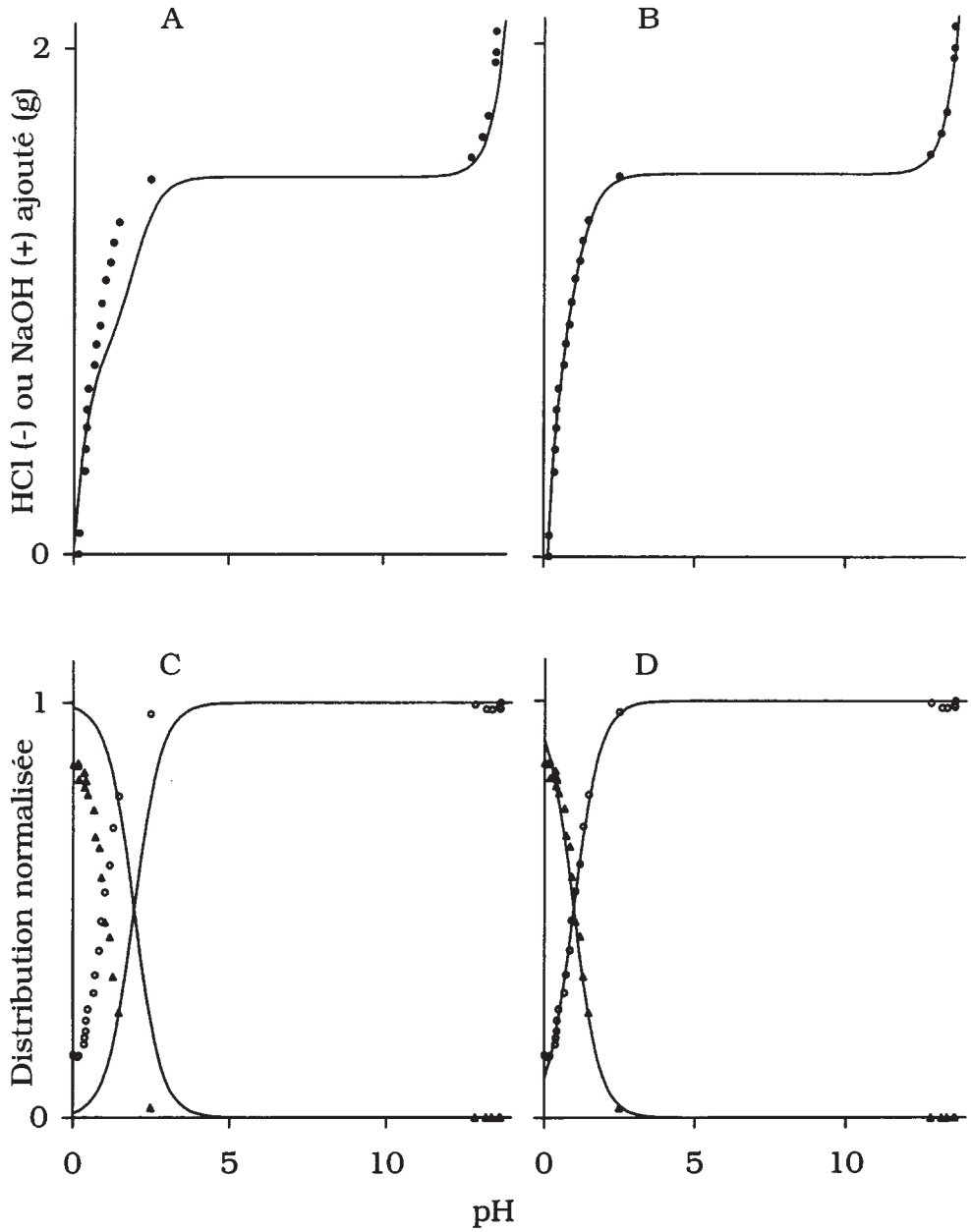
Le coefficient moyen d'activité

La figure 7A présente, sous forme graphique, les valeurs des pH sans titrant et celles d'équipartition en fonction de la concentration en acide sulfurique. Les deux courbes sont monotones et le pH d'équipartition varie peu en fonction de la concentration lorsque celle-ci est supérieure à 1 M. La figure 7B donne la distribution en termes de concentrations relatives des ions bisulfate et sulfate dans les solutions sans titrant. Les lignes pleines correspondent aux valeurs Raman de Chen et Irish (13) et ont été obtenues aux concentrations supérieures à 0,25 mol/kg tandis que les lignes pointillées présentent nos résultats obtenus en IR aux concentrations supérieures à 0,01 M. À la concentration de 0,25 mol/kg, les deux méthodes donnent des résultats identiques ce qui indique que les deux systèmes étudiés étaient semblables. Malgré la concordance observée à cette concentration, les résultats obtenus en spectroscopie Raman montrent une inversion de tendance pour les concentrations supérieures, inversion qui n'est pas confirmée par IR. Les résultats obtenus par Chen et Irish l'ont été par l'analyse du contour des bandes tandis que nos résultats le furent par l'analyse de la totalité du spectre IR dans une gamme plus étendue de concentrations. Ceci nous permet de penser que nos résultats ont une fiabilité plus grande que ceux qui ont été obtenus en Raman.

La figure 7C donne les valeurs du coefficient moyen d'activité de l'acide sulfurique γ_{H^+}/Γ_2 en fonction de la concentration. La courbe en trait plein représente les valeurs de la littérature (26, 27). Les résultats du présent travail sont présentés avec le symbole (○). Il y a une bonne concordance

© 2000 CNRC Canada

Fig. 6. Courbes de titrage volumétrique (A et B) et de distribution (C et D) pour les solutions aqueuses du H_2SO_4 1,02 M. Tracé A : ligne pleine (——), titrage volumétrique théorique (éq. 12) avec $\Gamma_0 = \Gamma_2 = \gamma_{H^+} = 1$; points pleins (●●●), résultats expérimentaux. Tracé B : même que A mais $\Gamma_0 = 1{,}5$; $\Gamma_2 = 9{,}5$ et $\gamma_{H^+} = 0{,}68$. Tracé C ligne pleine (——), distribution théorique (éq. 9 et 10) avec $\Gamma_0 = \Gamma_2 = \gamma_{H^+} = 1$; triangles vides (△△△) et ronds vides (○○○), valeurs obtenues par IR respectivement pour HSO_4^- et SO_4^{2-}. Tracé D, même que C avec $\Gamma_0 = 1{,}5$; $\Gamma_2 = 9{,}5$ et $\gamma_{H^+} = 0{,}68$.



entre les deux séries de valeurs, bien que celles-ci aient été obtenues par des méthodes différentes : électrochimie et IR. Comme sur la figure 7B, une légère divergence que nous ne pouvons pas expliquer apparaît pour les concentrations supérieures à 0,5 mol kg^{-1}. Cependant, comme nos résultats en IR viennent de mesures directes de l'abondance des espèces, ils seraient plus fiables que les mesures électrochimiques qui donnent indirectement ces valeurs.

Le spectre des espèces ioniques pures de l'acide sulfurique est indépendant de la concentration et, par conséquent, la variation des coefficients d'activité des espèces impliquées en solution n'a pas de répercussion sur les spectres de ces espèces. Ce résultat concorde avec les résultats obtenus pour les mélanges NaOH–HCl (20).

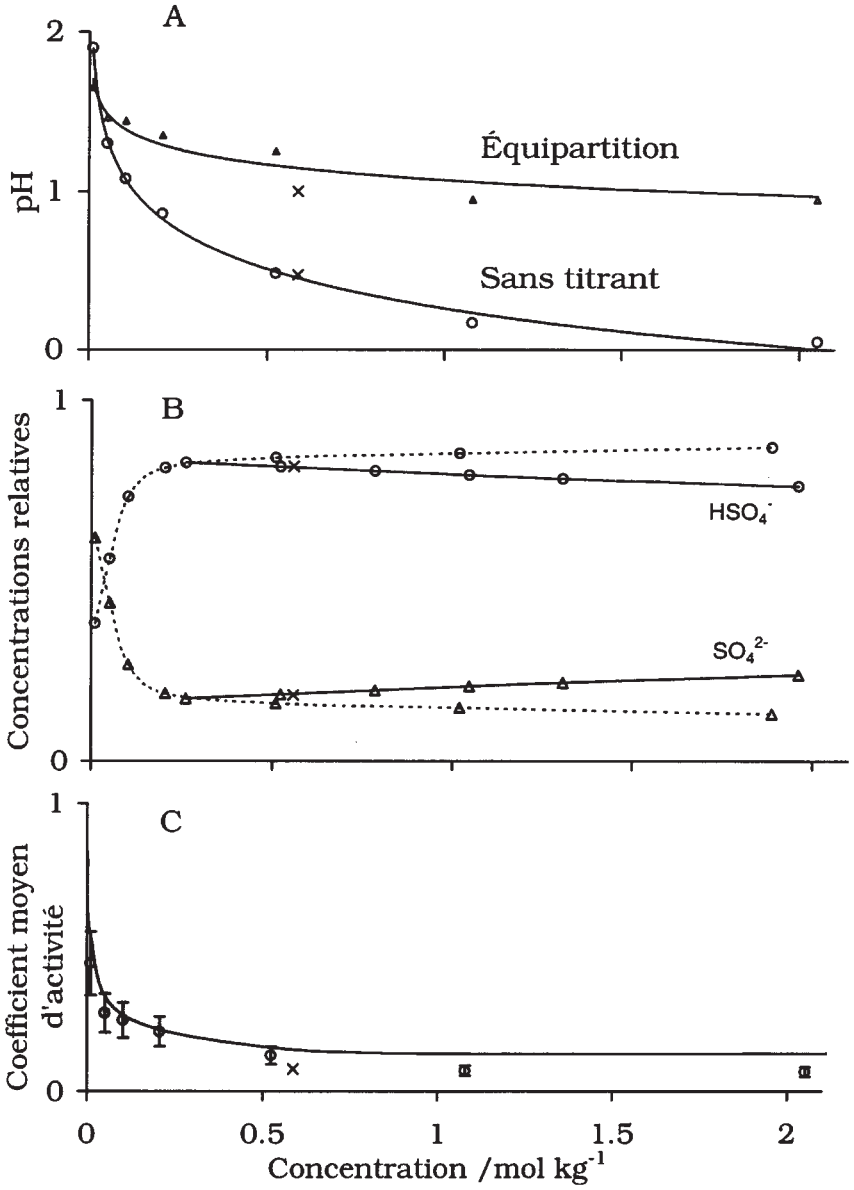
Titrage IR des solutions aqueuses du H_2SO_4 0,56 M dans NaCl 1,00 M

Analyse des spectres des solutions

Pour évaluer l'influence de sels sur les coefficients d'activité et confirmer que le spectre IR des espèces ioniques en solution n'est pas influencé par la variation du coefficient d'activité,[20] le titrage IR d'une solution aqueuse de H_2SO_4, à une concentration de 0,56 M et NaCl 1,00 M, est effectué de

© 2000 CNRC Canada

Fig. 7. Tracé A, pH des solutions sans titrant, ronds vides (○○○) et pH d'équipartition triangles vides (△△△). Tracé B, distribution de HSO_4^-, ronds vides (○○○) et SO_4^{2-}, triangles vides (△△△) sur la gamme de concentration 1,89 à 0,01 M en H_2SO_4. Lignes pointillées (---) mesures IR, lignes pleines (——) mesures par Raman [13]. Tracé C coefficient d'activité moyen dans les solutions aqueuses du H_2SO_4 sur la gamme de concentration 1,89 à 0,01 M. Valeurs obtenues par IR (○○○), valeurs de la littérature obtenues par des mesures électrochimiques [26–27] : ligne pleine (——). Les points indiqués par un × dans les tracés sont pour la solution de H_2SO_4 0,558 M et NaCl 1,00 M.



la même manière que précédemment. Le spectre d'eau salée a aussi été soustrait. Les FM obtenus dans la soustraction de cette eau indiquent que la solvatation des paires d'ions Na^+ et Cl^- reste inchangée en solution en présence d'acide sulfurique comme cela fut rapporté pour le système (HCl, NaCl) (20). Ceci est en accord avec les travaux sur l'eau salée qui indiquent que NaCl en solution reste en forme complexée avec 5 molécules d'eau (28). Les spectres principaux des espèces ioniques montrent que les bandes de vibration sulfate ne sont pas affectées par la présence de sel (Fig. 3). La seconde forme solvatée de HSO_4^- est aussi observée dans les solutions contenant du HCl. Contrairement à l'action de H_3O^+ et Cl^-, la présence des ions Na^+ et Cl^- dans la solution d'acide sulfurique ne modifie pas le spectre des espèces $H_3O^+ - HSO_4^-$ et $Na^+ - HSO_4^-$. Donc, ce ne sont pas les interactions des ions chlorure (Cl^-) seuls avec l'ion HSO_4^- qui produisent le complexe observé lorsque du HCl est ajouté à la solution d'acide sulfurique. Il s'agit là d'une preuve supplémentaire que c'est l'interaction d'une paire H_3O^+–Cl^- solvatée avec une paire $H_3O^+ - HSO_4^-$ solvatée qui produit le complexe $(H_3O^+ - HSO_4^-)_{\text{-HCl}}$. Ceci confirme le fait que la solvatation des ions par l'eau se fait en conservant le cation et l'anion proches l'un de l'autre (20, 28).

Effet du sel sur le coefficient moyen d'activité de l'acide sulfurique

La présente étude n'est pas une étude exhaustive de l'effet de sels neutres sur l'équilibre de l'acide sulfurique en

© 2000 CNRC Canada

solution aqueuse. Une seule concentration d'un seul sel (NaCl 1,00 M) a été appliquée à une seule concentration d'acide sulfurique : 0,56 M). La figure 7A montre que le pH sans titrant n'a pas été affecté par l'ajout de NaCl (symboles ×). Le pH d'équipartition, lui, a été sensiblement abaissé par la présence de NaCl. La figure 7B montre que la dissociation de l'acide sulfurique a été modifiée par l'ajout du NaCl (symboles ×). Le degré de dissociation de HSO_4^-, de 0,16 en l'absence de sel (SO_4^{2-} = 0,16 et HSO_4^- = 0,84) augmente à 0,18 en présence de NaCl 1,00 M (SO_4^{2-} = 0,18 et HSO_4^- = 0,82). Cette variation est dans le sens opposé de celle observée par Chen et Irish dans une solution aqueuse de NH_4HSO_4 (13). Les deux systèmes étudiés et les méthodes d'analyse étant très différents, il n'est pas possible d'établir la raison de cette différence.

Les valeurs des coefficients d'activité $\Gamma_2 = \gamma_{HSO_4^-}/\gamma_{SO_4^{2-}}$ déterminées par le titrage IR sont données dans le tableau 2. L'ajout de NaCl abaisse le coefficient d'activité de l'ion sulfate relativement à celui de l'ion bisulfate. Cette modification est obtenue avec une bonne précision puisqu'elle provient de la mesure par IR de la répartition des deux espèces ioniques. De plus, cette modification des coefficients d'activité des ions n'est aucunement reliée à des modifications spectrales.

Le coefficient moyen d'activité $\gamma_\pm$ (= γ_{H^+}/Γ_2) de l'acide sulfurique est abaissé en présence de NaCl (symbole ×, fig. 7) contrairement à ce qui a été observé pour HCl (20, 29). Les valeurs du coefficient moyen d'activité de l'acide sulfurique sont obtenues dans la présente étude avec une précision de ±25 %. La majeure partie de cette marge d'erreur provient de l'imprécision sur la valeur du coefficient moyen d'activité γ_{H^+} qui est obtenu par mesures de pH. La figure 7C n'a été présentée que pour permettre une comparaison des résultats obtenus par titrage IR avec les valeurs de la littérature.

Conclusion

Le titrage IR des solutions aqueuses d'acide sulfurique est possible sur une gamme étendue de concentrations et de pH en utilisant la technique ATR. La méthode de soustraction des spectres d'eau permet d'obtenir l'information sur les espèces ioniques présentes en solution même à de très faibles concentrations. L'AF appliquée aux spectres de mélanges des espèces ioniques permet de déterminer la concentration réelle des espèces d'une façon directe, ce que ne peuvent faire les méthodes électrochimiques, et d'une manière plus précise que l'analyse du contour de bandes qui a été faite en Raman. La comparaison des courbes expérimentales de distribution obtenues par IR avec les courbes théoriques donne des valeurs du coefficient moyen d'activité qui sont comparables aux valeurs obtenues par mesures électrochimiques. Le rapport des coefficients d'activité des ions sulfate et bisulfate est constant sur toute la gamme de pH et dépend de la concentration totale des ions mais pas de leur concentration relative.

La spectroscopie IR se révèle être un outil performant dans l'étude des solutions aqueuses qui n'est limité que par la qualité des spectres et des traitements numériques. Nous travaillons sur ces aspects qui nous permettront de saisir des informations précises sur la formation des complexes dont nous avons révélé la présence dans ce travail et le précédent (**I**).

Références

1. S.L. Clegg, J.A. Rard et K.S. Pitzer. J. Chem. Soc. Faraday Trans. **90**, 1875 (1994).
2. R. Zhang, P.J. Wooldridge, J.P.D. Abbatt et M.J. Molina. J. Phys. Chem. **97**, 7351 (1993).
3. K.S. Pitzer, R.N. Roy et L.F. Silvester. J. Am. Chem. Soc. **9**9 4930 (1977).
4. A.G. Dickson, D.J. Wesolowski, D.A. Palmer et R.E. Mesmer. J. Phys. Chem. **94**, 7978 (1990).
5. B.A. Bilal et E. Muller. Z. Naturforsch. A: Phys. Sci. **48a**, 1073 (1993).
6. B.A. Bilal et E. Muller. Z. Naturforsch. A: Phys. Sci. **49a**, 939 (1994).
7. J.K. Hovey et L.G. Hepler. J. Chem. Soc. Faraday Trans, **86**, 2831 (1990).
8. B.R. Staples. J. Phys. Chem. Ref. Data, **10**, 779 (1981).
9. J. Balej, F. Hanousek, M. Pisarcik et K. Sarka. J. Chem. Soc. Faraday. Trans. 1, **80**, 521 (1984).
10. R.A. Cox, U.L. Haldna, K.L. Idler et K. Yates. Can. J. Chem. **59**, 2591 (1981).
11. D.E. Irish et M.H. Brooker. Raman and infrared spectral studies of electrolytes. *Dans* Advances in infrared and Raman spectroscopy. Vol. 2. R.J.H. Clark and R.E. Hester, *Editeurs*. Heyden, London, 1976.
12. D.E. Irish et H. Chen. J. Phys. Chem. **74**, 3796 (1970).
13. H. Chen et D.E. Irish. J. Phys. Chem. **75**, 2672 et 2681 (1971).
14. B.S.W. Dawson, D.E. Irish et G.E. Toogood. J. Phys. Chem. **90**, 334 (1986).
15. P.A. Giguère et R. Savoie. Can. J. Chem. **38**, 2467 (1960).
16. M.R. Querry, R.C. Waring, W.E. Holland, L.M. Earls, M.D. Herrman, W.P. Nijm et G.M. Hale. J. Opt. Soc. Am. **64**, 39 (1974).
17. G. Herzberg. Infrared and Raman spectra of polyatomic molecules. D. van Nostrand, Princeton, N.J. 1945.
18. J.-J. Max, M. Trudel et C. Chapados. Appl. Spectrosc. **52**, 234 (1998).
19. J.-J. Max et C. Chapados. Appl. Spectrosc. **52**, 963 (1998).
20. J.-J. Max et C. Chapados. Can. J. Chem. **78**, 64 (2000).
21. J.-J. Max, C. Ménichelli et C. Chapados. J. Phys. Chem. **104**, 2845 (2000).
22. J.-J. Max, M. Trudel et C. Chapados. Appl. Spectrosc. **52**, 226 (1998).
23. J.-J. Max, G. Bérubé, M. Trudel, S. Groleau et C. Chapados. Langmuir, **14**, 5051 (1998).
24. J. Baril, J.-J. Max et C. Chapados. Can. J. Chem. **78**, 490 (2000).
25. J.-J. Max et C. Chapados. Appl. Spectrosc. **53**, 1045 (1999).
26. S. Glasstone. An introduction to electrochemistry. D. van Nostrand Co., Inc., Princeton, N.J. 1942. p. 139.
27. H.S. Harned et W.J. Hamer. J. Am. Chem. Soc. **57**, 27 (1935).
28. J.-J. Max et C. Chapados. Appl. Spectrosc. **53**, 1601 (1999).
29. K. Schwabe. Electrochim. Acta, **12**, 67 (1967).

Liste des symboles

Symboles	Signification
V	volume final de l'échantillon (L)
A	quantité totale (mol) de H_2SO_4 dans l'échantillon
D	quantité initiale totale (mol) d'eau dans l'échantillon
C_1	quantité (mol) de NaOH ajoutée à l'échantillon

© 2000 CNRC Canada

C_{-1} quantité (mol) de HCl ajoutée à l'échantillon
y_1 quantité (mol) de HSO_4^- présent dans l'échantillon à l'équilibre
y_2 quantité (mol) de SO_4^{2-} présent dans l'échantillon à l'équilibre
x quantité (mol) de H^+ présent dans l'échantillon à l'équilibre
x' quantité (mol) de OH^- présent dans l'échantillon à l'équilibre
c quantité (mol) de Na^+ présent dans l'échantillon à l'équilibre
c' quantité (mol) de Cl^- présent dans l'échantillon à l'équilibre
d quantité (mol) d'eau présent dans l'échantillon à l'équilibre
K_2 seconde constante de dissociation de H_2SO_4 dans l'eau
K_0 constante de dissociation de l'eau
$\gamma_{SO_4^{2-}}$ coefficient d'activité du SO_4^{2-} aqueux
$\gamma_{HSO_4^-}$ coefficient d'activité du HSO_4^- aqueux
γ_{H^+} coefficient d'activité du H^+ aqueux (H_3O^+)
γ_{OH^-} coefficient d'activité du OH^- aqueux
γ_{H_2O} coefficient d'activité de l'eau
Γ_2 $\gamma_{HSO_4^-}/\gamma_{SO_4^{2-}}$: rapport des coefficients d'activité de HSO_4^- et SO_4^{2-}
Γ_0 $\gamma_{H_2O}/\gamma_{OH^-}$: rapport des coefficients d'activité de H_2O et OH^-
$\gamma_\pm$ coefficient moyen d'activité : γ_{H^+}/Γ_2
X variable linéaire pour pH : $X = 10^{pH}$
M_{H_2O} masse molaire de l'eau : $18{,}015_2$ g/mol
M_δ masse molaire du titrant : 40,00 g/mol pour NaOH et 36,46 g/mol pour HCl
M_2 masse molaire du H_2SO_4 : 98,06 g/mol
δ δ identifie le titrant utilisé : base, $\delta = +1$; acide, $\delta = -1$
ε_d concentration relative (p/p) de la solution de titrant
ε_2 concentration (p/p) relative de la solution initiale de H_2SO_4
m masse (g) totale de l'échantillon
m_δ masse (g) de titrant ajoutée à l'échantillon
m_2 masse (g) de la solution mère de H_2SO_4 mise dans l'échantillon
m_0 masse (g) de la solution de H_2SO_4 dans l'échantillon sans titrant
ρ_0 densité (g/L) de la solution initiale de H_2SO_4
ρ densité (g/L) de l'échantillon
ρ_δ coefficient sans dimension de la variation de la densité de l'échantillon avec la quantité de titrant : $\rho_d = (\rho - \rho_0)\, V/m_\delta$
P équivalent titrant

© 2000 CNRC Canada

Synthesis of nanocrystalline $Cu_{2-x}Se$ at room temperature by γ-irradiation

Zhengping Qiao, Yi Xie, Jianguang Xu, Xianming Liu, Yingjie Zhu, and Yitai Qian

Abstract: Ten nm nonstoichiometric compound $Cu_{2-x}Se$ was firstly synthesized at room temperature by γ-irradiation, using sodium selenosulfate as the selenium source. The influence of the coordination of copper ions and the pH value of the solutions on the formation of $Cu_{2-x}Se$ has been studied. The $Cu_{2-x}Se$ was prepared here for $x = 0.13$.

Key words: copper selenide, nanocrystalline, γ-irradiation.

Résumé : Opérant à la température ambiante, faisant appel à une irradiation γ et utilisant du sélénosulfate de sodium comme source de sélénium, on a réalisé la première synthèse d'un composé non stoechiométrique de $Cu_{2-x}Se$ de 10 nm. On a étudié l'influence de la coordination des ions cuivre et de la valeur du pH des solutions sur la formation de $Cu_{2-x}Se$. Pour le $Cu_{2-x}Se$ préparé, $x = 0{,}13$.

Mots clés : séléniure de cuivre, nanocristallin, irradiation γ.

[Traduit par la Rédaction]

Introduction

Extensive attention has been paid to the preparation and characterization of selenides owing to their interesting properties and potential applications. Among these materials, copper selenide has recently aroused much interest and attention since it has been widely used in solar cells (1, 2), as an optical filter (3), and as a superionic material (4). For example, $Cu_{2-x}Se$ is a p-type extrinsic semiconductor with an energy gap of 1.1–1.29 eV (5), which is near the optimum value for solar cell applications (6).

Considerable progress has been made in the synthesis of copper selenides in the last few years, such as elemental reactions (7–9) and metathesis reactions (3). However, most of these methods need high temperature (470°C), or dangerous liquid ammonia, or toxic H_2Se, or complex metal precursors. Recently, Wang et al. (10) successfully obtained nanocrystalline $Cu_{2-x}Se$ by heating CuI and Se in an autoclave at 90°C for 4 h. To obtain nanoscale $Cu_{2-x}Se$ under mild conditions, organic ethylenediamine must be used. Thus, it is desirable to find a good selenium source in aqueous solution and appropriate methods to prepare nanocrystalline $Cu_{2-x}Se$ under mild conditions.

In the past twenty years, sodium selenosulfate has been used to prepare bulk selenide materials (5, 11). Padam (12) reported the preparation of chemically deposited polycrystalline $Cu_{2-x}Se$ thin films in a hot water bath maintained at a temperature of 90–95°C, which was proved to be homogeneous with an average grain size of the order of 0.7 μm. Under such conditions it is difficult to grow nanocrystalline materials. To obtain nanocrystalline $Cu_{2-x}Se$, a synthesis method, which can be more easily controlled, is important. Recently, γ-irradiation technique has become an important room temperature, ambient pressure method to prepare nanoscale materials since it can provide high-energy and an evenly distributed irradiation field. We have successfully expanded this method to prepare nanoscale metal sulfide (13). However, it is much easier to get a suitable sulfur source in aqueous solution under γ-irradiation and meanwhile, it is much more difficult but meaningful to find an appropriate selenium source for preparation of nanoscale metal selenides. Here, we firstly report the synthesis of nanocrystalline $Cu_{2-x}Se$ in aqueous solution using sodium selenosulfate as selenium source under γ-irradiation at room temperature and ambient pressure.

Received November 28, 1999. Published on the NRC Research Press website on August 15, 2000.

Z. Qiao, Y. Xie[1], J. Xu, X. Liu, Y. Zhu, and Y. Qian. Structure Research Lab and Department of Chemistry, University of Science and Technology of China, Hefei, Anhui 230026, P.R. China.

[1]Author to whom correspondence may be addressed. Telephone: 86-551-3603987 (O), 86-551-3603085 (H). Fax: 86-551-3631760. e-mail: yxie@ustc.edu.cn

Experimental

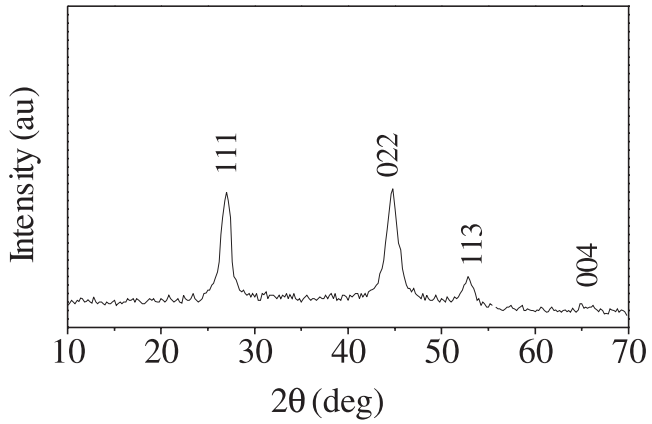
The solutions were prepared by dissolving analytically pure copper acetate (0.001 mol) and freshly prepared sodium selenosulfate (0.5 mol dm^{-3}, 10 dm^{-3}) in 100 dm^{-3} distilled water. Appropriate electrolytes (analytically pure sulfuric acid and sodium hydroxide) were used to adjust the pH value of the solution. Isopropyl alcohol was added as a scavenger for hydroxyl radicals at concentration of 3 mol dm^{-3}. To study the influence of coordination of copper ions on the formation of $Cu_{2-x}Se$, 0.05 mol dm^{-3} sodium chloride and 0.02 mol dm^{-3} $NH_3 \cdot H_2O$–NH_4Cl buffer was used to provide Cl^- and NH_3, respectively, in some solutions (experimental conditions given in Table 1). After the solutions were irradiated in the field of a 2.59×10^{15} Bq ^{60}Co γ-ray source with absorbed dose rate of 1×10^2 Gy min^{-1} for several hours, the black precipitates were collected and washed with dilute acetic acid, distilled water, and absolute alcohol in sequence

© 2000 NRC Canada

Table 1. The influence of ligand and pH value on the products.

Sample	Ligand	pH	$Cu_{2-x}Se$
1	none	1–2	pure
2	none	3	none
3	none	4–14	minor
4	0.05 mol dm^{-3} Cl^-	3–5	minor
5	0.05 mol dm^{-3} Cl^-	6–11	major
6	0.05 mol dm^{-3} Cl^-	12–14	minor
7	(appropriate) $NH_3 \cdot H_2O$	8–11	pure
8	0.02 mol dm^{-3} $NH_3 \cdot H_2O$–NH_4Cl	9	pure

Fig. 1. XRD patterns of sample 8.



to remove the by-products. The final products were dried in vacuum at room temperature for 4 h.

The samples were characterized by powder X-ray diffraction (PXRD) patterns employing a scanning rate of 0.05° s^{-1} in 2θ range from 10° to 70° using a Japan Rigaku Dmax γ_A X-ray diffractometer equipped with a graphite monochromatized CuK_α radiation (λ = 1.54178 Å). The morphology and particle size were determined by transmission electron microscopy (TEM). The TEM images were taken with a Hitachi Model H-800 transmission electron microscope with an accelerating voltage of 200 kV. The purity and composition of the products were examined by X-ray photoelectron spectra (XPS) on an ESCALab MKII instrument with MgKα radiation as the exciting source. The ratio of Cu to Se was determined using an atomic absorption spectrometer (Model WYX-40).

Results and discussion

All the products were examined by XRD. Figure 1 shows the XRD pattern of the as-prepared $Cu_{2-x}Se$ (sample 8 in Table 1) from a solution, which consists of 0.01 mol dm^{-3} copper acetate, 0.05 mol dm^{-3} sodium selenosulfate, 0.02 mol dm^{-3} $NH_3 \cdot H_2O$–NH_4Cl, and 3 mol dm^{-3} isopropyl alcohol. All of the peaks could be indexed as the cubic $Cu_{2-x}Se$ (JCPDS Card File no. 6–680) with cell constant a = 5.741 Å. The broadening of the peaks indicates the product is nanocrystalline. The crystalline size of the product, as calculated from the half-width of diffraction peaks using the Scherrer formula[2] is 9 nm.

The purity and composition of sample 8 were examined by XPS. The survey, the Cu_{2P} region and Se_{3d} region, are shown in Fig. 2. The results indicate that the product was relatively pure. Since $Cu_{2-x}Se$ is stable over a wide range of departures from stoichiometry (the composition parameter x varying from 0 to 0.15) (14, 15), quantification of peaks was done roughly and gave a ratio of Cu to Se as 1.85:1. In addition, the ratio of Cu to Se measured accurately by Atomic Absorption Spectrometer is 1.87:1. So the $Cu_{2-x}Se$ was here prepared for x = 0.13.

Figure 3 is the TEM image of sample 8. From the image, one can see that the product consists of nearly spherical grains with the average size of about 10 nm, which is consistent with the XRD result. This also proved that the broadening of the peaks is caused by the small particle and not the lattice distortion in the crystallite, which is a common phenomenon in nonstoichiometric compounds.

In these γ-irradiation processes, the mechanism of the formation of nanocrystalline selenide is presently not very clear up to now. Few reports have been given on the transformation of the sodium selenosulfate under γ-irradiation. However, it is clear that S^{2-} can be homogeneously released from the decomposition of sodium thiosulfate upon γ-irradiation (16, 17). It is reasonable that Se^{2-} can be released from sodium selenosulfate upon γ-irradiation due to the similarity in the structures of $S_2O_3^{2-}$ and $SeSO_3^{2-}$, shown in Fig. 4.

Meanwhile, hydrated electrons, which are reducers with strong reducibility, were produced from H_2O under γ-irradiation. Isopropyl alcohol was added to scavenge the oxidative free radical OH.

$$H_2O \xrightarrow{\text{radiation}} e^-_{aq},\ H_3O^+,\ H,\ H_2,\ OH,\ H_2O_2$$

$$(CH_3)CHOH + OH \rightarrow (CH_3)COH + H_2O$$

The existence of ligand NH_3 led to the slow release of copper ions and controlled the following nucleation and growth of $Cu_{2-x}Se$ nanocrystalline. Under this condition, the total reaction of the formation of nanocrystalline $Cu_{2-x}Se$ can be formulated as follows

$$(2-x)[Cu(NH_3)_4]^{2+} + Se^{2-} + (2-2x)e^-_{aq} + H_2O \rightarrow Cu_{2-x}Se + (8-4x)NH_3 \cdot H_2O$$

In our experiments, the pH value of the solutions and some coordination of copper ions (Cl^- and NH_3) were studied in detail. The results, as listed in Table 1, showed: (*i*) the existence of ligands (Cl^- and NH_3) takes advantage of the formation of $Cu_{2-x}Se$ in aqueous solution; and (*ii*) without the presence of ligands, the pH value of the solutions is the most important factor for the formation of product. Specifically, when the pH value is 1–2, the products are also pure $Cu_{2-x}Se$ (sample 1). However, the particle size of

[2] Supplementary material has been deposited and may be purchased from the Depository of Unpublished Data, Document Delivery, CISTI, National Research Council of Canada, Ottawa, ON K1A 0S2 (http://www.nrc.ca/cisti/docdel/order_electronic_e.shtml for information on ordering electronically).

© 2000 NRC Canada

Fig. 2. XPS spectra of the sample 8. (*a*) Survey (• ___ Cu, * ___ Se, # ___ O,◦ ___ C); (*b*) Cu_{2p} region; (*c*) Se_{3d} region.

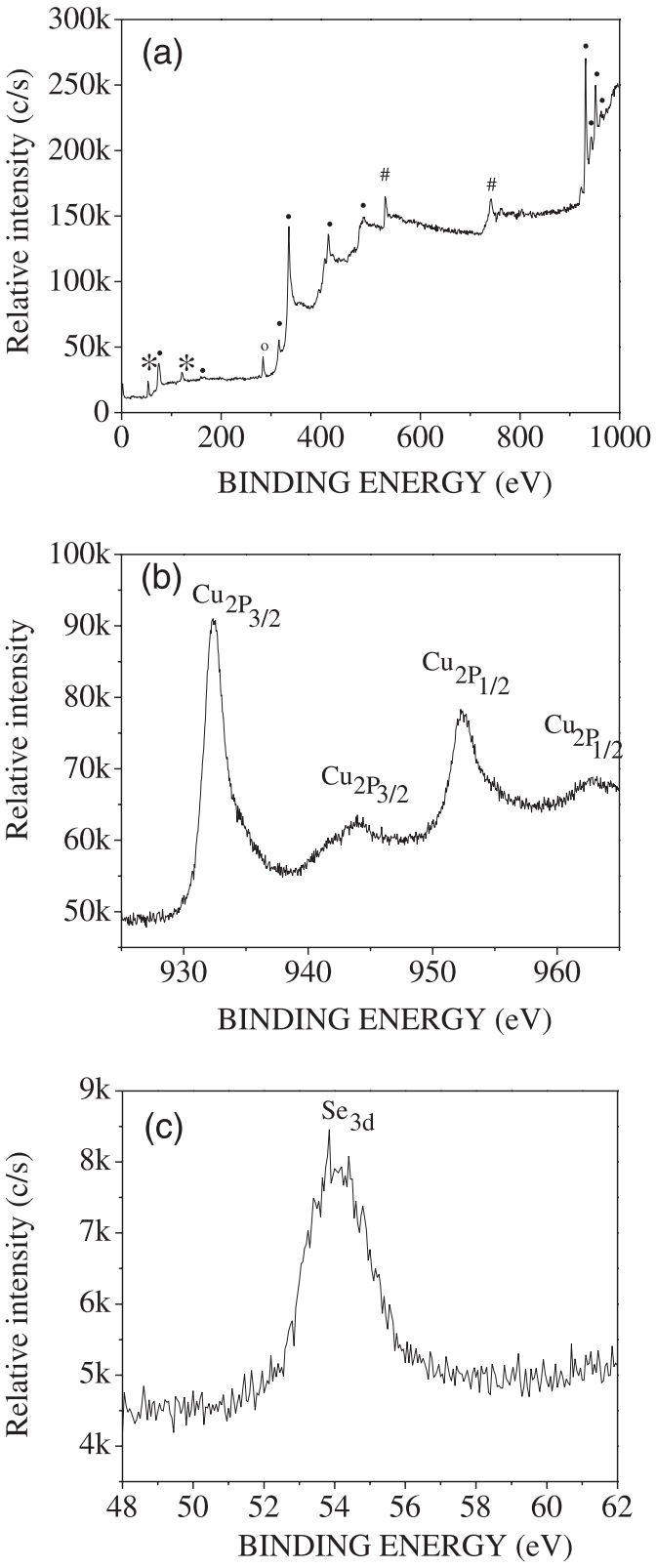


Fig. 3. TEM image of the sample 8.

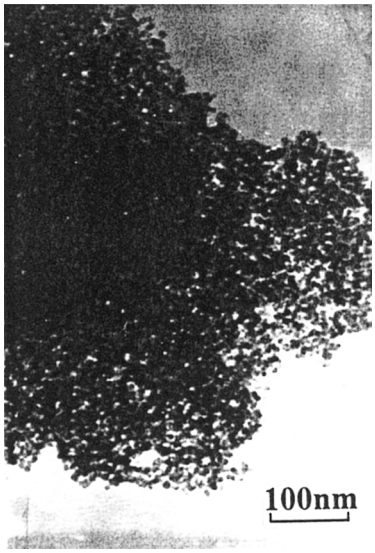
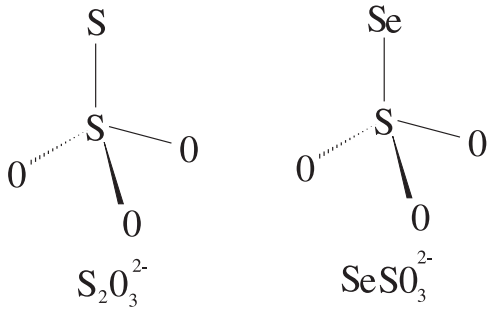


Fig. 4. Schematic structure of $S_2O_3^{2-}$ and $SeSO_3^{2-}$.



$Cu_{2-x}Se$ prepared from acidic solutions (pH = 1, 2, sample 1) — 27 nm, as calculated from the half-width of diffraction peaks using the Scherrer formula[2], is much larger than that of the product from solution with the existence of ligand NH_3 — 9 nm.

As well known, many kinds of metal ions can be slowly reduced by hydrated electrons or solvented electrons produced in water or other organic solvent under γ-irradiation and produced metastable ions by controlling appropriate conditions (18). It is reasonable to expect that the γ-irradiation method can be widely used to prepare other nanocrystalline nonstoichiometric compounds.

Conclusions

In summary, the γ-irradiation method was firstly used to prepare 10 nm $Cu_{2-x}Se$ at room temperature in aqueous solution, using sodium selenosulfate as the selenium source. The influence of the coordination of copper ions and the pH value of solutions were studied in detail. Without the presence of ligand the suitable pH range for the formation of $Cu_{2-x}Se$ is 1–2. Ligand (NH_3) is helpful in the formation and the size control of $Cu_{2-x}Se$. XPS and atomic absorption spectrometer examined the purity of products. The γ-irradiation method is likely to be useful in the preparation of other

© 2000 NRC Canada

nonstoichiometric nanocrystalline selenides at room temperature and ambient pressure.

Acknowledgement

Financial support from the Chinese National Foundation of Natural Research and Outstanding Youth Fund is gratefully acknowledged.

References

1. U. Hiroto. Jpn. Kokai Tokkyo Koho. JP 01 298 010.
2. S.T. Lakshmikvmar. Sol. Energy Mater. Sol. Cells, **32**, 7 (1994).
3. H. Toyoji and Y. Hiroshi. Jpn. Kokai Tokkyo Koho. JP 02 173 622.
4. A.A. Korzhuev. Fiz. Khim. Obrab. Mater. **3**, 131 (1991).
5. P. Pramanik and R.N. Bhattacharya. J. Solid State Chem. **44**, 425 (1982).
6. J.J. Loferski. J. Appl. Phys. **27**, 777 (1956).
7. T. Ohtani and M. Motoki. Mater. Res. Bull. **30**, 1495 (1995).
8. G. Henshaw, I.P. Parkin, and G. Shaw. J. Chem. Soc. Dalton Trans. 231 (1997).
9. G. Henshaw, I.P. Parkin, and G. Shaw. Chem. Commun. 1095 (1996).
10. W. Wang, P. Yan, F. Liu, Y. Xie, Y. Geng, and Y. Qian. J. Mater. Chem. **8**(11), 2321 (1998).
11. A. Mondal and P. Pramanik. J. Solid State Chem. **55**, 116 (1984).
12. G.K. Padam. Thin Solid Films, **150**, L89 (1987).
13. Z. Qiao, Y. Xie, X. Li, C. Wang, Y. Zhu, and Y. Qian. J. Mater. Chem. **9**, 735 (1999).
14. T. Takahashi, O. Yamamoto, F. Matsugawa, and Y. Noda. J. Solid State Chem. **16**, 35(1976).
15. Z. Vucic, O. Milat, V. Horvatic, and Z. Ogorelec. Phys. Rev. B Condens. Matter Mater. Phys. **24**, 5398 (1981).
16. A.J. Elliot, D.R. McCracken, G.V. Buxton, and N.D. Wood. J. Chem. Soc. Faraday Trans. **86**, 1539 (1990).
17. G.V. Buxton and D.C. Walker. Radiat. Phys. Chem. **23**, 207 (1984).
18. A. Henglein. Chem. Rev. **89**, 1861 (1989).

© 2000 NRC Canada

An experimental and theoretical approach to the study of the properties of parabanic acid and related compounds: synthesis and crystal structure of diethylimidazolidine-2-selone-4,5-dione

Massimiliano Arca, Francesco Demartin, Francesco A. Devillanova, Francesco Isaia, Francesco Lelj, Vito Lippolis, and Gaetano Verani

Abstract: The syntheses of the first examples of selenoparabanic acid derivatives (dialkylimidazolidine-2-selone-4,5-dione, $\mathbf{3e^R}$, R = Me, Et, Bu) are presented along with the X-ray crystal structure determination of $\mathbf{3e^{Et}}$. To gain an insight in the properties of parabanic acid derivatives on the basis of their electronic structures, we report the results of comparative hybrid-DFT calculations performed on parabanic, thioparabanic, and selenoparabanic acids ($\mathbf{3a^H}$, $\mathbf{3b^H}$, and $\mathbf{3e^H}$) and on their *N*,*N*′-dimethyl derivatives ($\mathbf{3a^{Me}}$, $\mathbf{3b^{Me}}$, and $\mathbf{3e^{Me}}$). Calculations show that the different nature of the frontier orbitals of $\mathbf{3a^R}$ compared to those of $\mathbf{3b^R}$ and $\mathbf{3e^R}$, might account for the different reactivities of these compounds. Moreover, the weak donor character of $\mathbf{3b^R}$ and $\mathbf{3e^R}$ towards molecular di-iodine, estimated by FT-Raman measurements is in agreement with the calculated NBO-charge distribution.

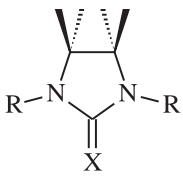
Key words: selenation, selenoparabanic derivatives, crystal structure, DFT calculations.

Résumé : Les synthèses des premiers exemples des dérivés de l'acide sélénoparabanique sont présentés avec la structure des rayons X du composé $\mathbf{3e^{Et}}$. Pour mieux comprendre les propriètés des dérivés de l'acide parabanique sur la base de leurs structures électroniques, nous reportons les résultats des calculs comparatifs hybride-DFT effectués sur les acides parabanique, thioparabanique et sélénoparabanique ($\mathbf{3a^H}$, $\mathbf{3b^H}$ et $\mathbf{3e^H}$) et sur les leurs dérivés *N*,*N*′-dimethyliques ($\mathbf{3a^{Me}}$, $\mathbf{3b^{Me}}$ et $\mathbf{3^{Me}}$). Les calculs montrent que la différente nature des orbitals de frontière de $\mathbf{3a^R}$ comparés avec ceux de $\mathbf{3b^R}$ et $\mathbf{3e^R}$ pourrait expliquer les différentes réactivités de ces composés. De plus, le faible caractère de donneur de $\mathbf{3b^R}$ et $\mathbf{3e^R}$ vers le iode moléculaire, évalué au moyen des mesures FT-Raman, est en accord avec la distribution des charges NBO.

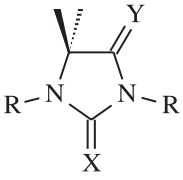
Mots clés : Sélénation, dérivés de l'acide sélénoparabanique, structure cristalline, calculs DFT.

Introduction

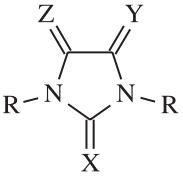
For more than twenty years, our research group has dealt with the synthesis, characterization, and study of the coordination properties of imidazolidine derivatives containing one or two *exo*-chalcogen atoms (**1** and **2** respectively) (1, 2).



1



2



3

As a natural evolution of this research, we have turned our attention to trichalcogen-substituted imidazolidine derivatives **3**, with the aim of synthesizing dischotic metal complexes having a highly delocalized π-system for the preparation of unidimensional conducting materials. Among all the possible compounds (X, Y, Z = O, S, Se; R = H, alkyl, or aryl groups), only the syntheses of $\mathbf{3a^R}$ (X = Y = Z = O, R = H (parabanic acid), alkyl, or aryl groups), (3, 4) $\mathbf{3b^R}$ (X = S, Y = Z = O, R = H (thioparabanic acid), alkyl or aryl groups) (3) and $\mathbf{3c^R}$ (Z = O, X = Y = S, R = Me, dithioparabanic acid derivatives) (5, 6) were reported in the literature. No other member of the possible compounds in this class has

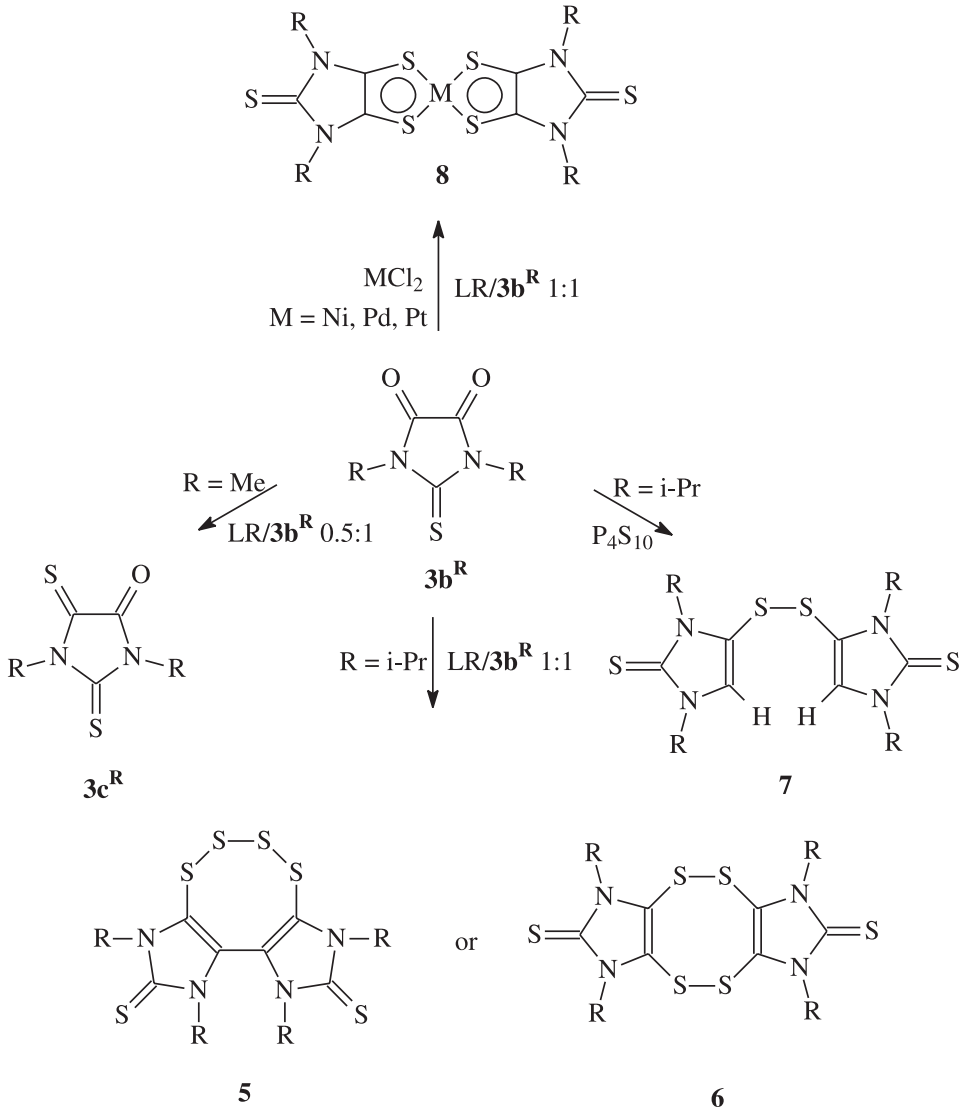
Received March 30, 2000. Published on the NRC Research Press website on August 15, 2000.

M. Arca,[1] F.A. Devillanova, F. Isaia, V. Lippolis,[1] and G. Verani. Dipartimento di Chimica Inorganica e Analitica, SS 554 bivio Sestu, 09042 Monserrato-Cagliari, Italy.
F. Demartin. Dipartimento di Chimica Strutturale e Stereochimica Inorganica, Via G. Venezian 21, 20133 Milano, Italy.
F. Lelj. Dipartimento di Chimica, Via N. Sauro 85, 85100 Potenza, Italy.

[1]Authors to whom correspondence may be addressed. MA: Telephone: +39-070-675-4467/83. Fax: +39-070-675-4456. e-mail: marca@vaxca1.unica.it. VL: e:mail: lippolis@unica.it.

© 2000 NRC Canada

Scheme 1. Reactivity of **3b^R** towards Lawesson's reagent (LR) and P_4S_{10} in refluxing toluene.



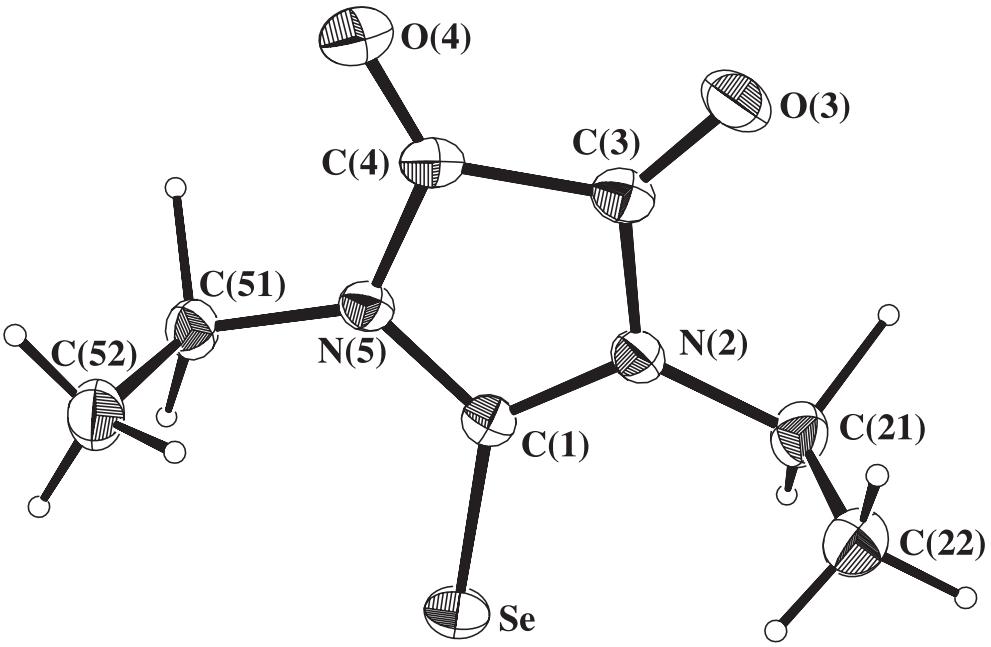
been synthesized and isolated so far. This seems to be in agreement with the alleged instability reported in the literature for five-membered cyclic dithioxamides, (7) which is probably also valid for diselenooxamides. However, the coordination chemistry of these compounds is completely unexplored, with the only exception of **3a^R** (R = $C_6H_5NHCH_2$), for which at any rate just the NH groups seem to be responsible for the coordination to Co(II), Ni(II), and Cu(II) (8). This poverty of data seems to be due to the poor coordination abilities of the chalcogen donor atoms in **3**, rather than to a lack of interest for these compounds by the scientific community.

Many studies (5, 9, 10, 11) have been carried out on the sulphuration reaction of **3a^R** and **3b^R** with P_4S_{10} and Lawesson's reagent (LR) (12) because this reaction represents a possible direct method for synthesizing trithione derivatives **3d^R** (X = Y = Z = S). In particular, while the reaction of **3b^R** with LR in a 1:0.5 ratio leads to **3c^R** (Scheme 1, R = Me) (5) and in a 1:1 ratio to both 4,5,6,7- and 4,5,9,10-tetrathiocino compounds (**5** and **6**, respectively), (9, 10) the reaction with P_4S_{10} leads to bis(1,3-dialkyl-2-thioxoimidazolin-4-yl)disulfide (**7**, alkyl = *i*-Pr, see Scheme 1) (10). When the sulphuration of **3b^R** with LR is carried out in presence of metal powder or salts, (13) the corresponding [M(R_2timdt)$_2$] neutral complexes (**8**) can be obtained (M = Ni, Pd, Pt), where R_2timdt is the monoreduced anion of **3d^R** (11, 14). Complexes **8** represent a brand new class of metal dithiolenes characterized by a very large π-delocalization.

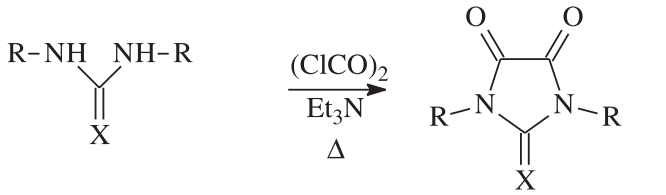
So far, no type **3** compounds containing a Se atom have been reported. In the present paper the synthesis and characterization of imidazolidine-2-selone-4,5-diones having methyl (**3e^{Me}**), ethyl (**3e^{Et}**), and butyl (**3e^{Bu}**) substituents is reported along with the single crystal X-ray structure of **3e^{Et}**. Analogously to **3b^R**, the sulphuration reaction of **3e^R** (synthesized by us according to the method reported here and donated to the authors to study the reactivity of these compounds towards LR) leads again to tetrathiocino analogues (15). By carrying out the sulphuration reaction for longer times, the exocyclic selenium atoms can be replaced by sulphur atoms and move into the octa-membered ring (15).

© 2000 NRC Canada

Fig. 1. View of the molecular structure of compound $\mathbf{3e^{Et}}$ with the numbering scheme adopted. Displacement ellipsoids are drawn at the 30% probability.



Scheme 2. Synthesis of parabanic, thioparabanic, and selenoparabanic acid derivatives from the corresponding ureas, thioureas, and selenoureas.



X = O $\mathbf{4a^R}$ X = O $\mathbf{3a^R}$
X = S $\mathbf{4b^R}$ X = S $\mathbf{3b^R}$
X = Se $\mathbf{4e^R}$ X = Se $\mathbf{3e^R}$

To rationalize the different chemical behavior of $\mathbf{3a,b,e^R}$, especially as far as regarding sulphuration and coordinating ability, we performed hybrid-DFT (16, 17) calculations on $\mathbf{3a^H}$, $\mathbf{3b^H}$, and $\mathbf{3e^H}$ and their methylated derivatives ($\mathbf{3a^{Me}}$, $\mathbf{3b^{Me}}$, and $\mathbf{3e^{Me}}$).

Moreover, the donor properties of imidazolidine-2-selone-4,5-diones towards molecular di-iodine have been explored by electronic and FT-Raman spectroscopy, and the weakness of the interaction has been explained on the basis of the NBO-charge distribution.

Results and discussion

Synthetic aspects

The syntheses of $\mathbf{3a^R}$ and $\mathbf{3b^R}$ have long since been reported, (3, 4) and consist of a cyclization reaction between the corresponding ureas $\mathbf{4a^R}$ or thioureas $\mathbf{4b^R}$ and dicyanogen (the resulting 4,5-diiminoimidazolidine-2-one is hydrolyzed with diluted HCl) or oxalyl chloride (Scheme 2) (3). To prepare selenoparabanic acid derivatives ($\mathbf{3e^R}$), the substitution of the exocyclic sulphur atom of $\mathbf{3b^R}$ with selenium was first attempted without encouraging results by the standard method for replacing S with Se in the > C=S bond, i.e., addition of MeI to > C=S to form the corresponding substituted *S,N,N′*-isothiouronium iodide and subsequent attack to the cation with HSe^- (18). More satisfactory results were achieved by reacting oxalyl chloride and disubstituted selenoureas $\mathbf{4e^R}$ (Scheme 2, R = Me, Et, Bu), which can easily be prepared in good yields by the above method.

X-ray crystallography

A view of the crystal structure of $\mathbf{3e^{Et}}$ is shown in Fig. 1. Table 1 shows a comparison of the interatomic distances with those of $\mathbf{3a^H}$, which is the only other type **3** compound structurally characterized so far (19, 20, 21). The imidazolidine ring displays similar features in both cases, with a slight lengthening of the N(2)—C(3) and N(5)—C(4) bonds and a slight shortening of N(2),N(5)—C(1) bonds, due to an increase in the conjugation of the lone pairs of the two nitrogen atoms towards C(1) in the presence of the Se atom. The five-membered ring is rigorously planar and the atoms Se, O(3), O(4), C(21), and C(51) lie essentially in the plane of the ring (maximum deviation observed 0.05 Å for Se).

Theoretical calculations

With the aim of understanding the effect of the nature of the chalcogen atom bound to the C(1) on the electronic and structural features, and possibly on the reactivity of the molecules of type **3**, DFT (16, 17) calculations have been performed on the molecules reported in Scheme 3. According to the good results recently found on $[M(R_2timdt)_2]$ dithiolenes **8**, (11) hybrid BECKE3LYP functional (22, 23) and Schafer, Horn, and Ahlrichs' (24) pVDZ basis set have been used throughout in the calculations. The Khon–Sham frontier orbital energies are reported in Fig. 2 and a perspective

© 2000 NRC Canada

Table 1. Selected interatomic distances (Å) and angles (°) for compounds **3e**^{Et} and **3a**^{H}.[a]

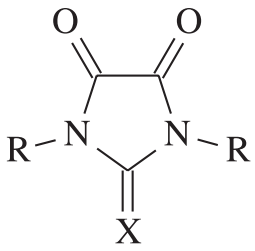
Interatomic distances (Å)	**3e**^{Et}	**3a**^{H}
C(1)—X[b]	1.785(3)	1.203
C(3)—O(3)	1.205(3)	1.213
C(4)—O(4)	1.192(3)	1.205
C(1)—N(2)	1.364(3)	1.399
C(1)—N(5)	1.387(3)	1.396
C(3)—N(2)	1.383(4)	1.362
C(4)—N(5)	1.381(3)	1.360
C(3)—C(4)	1.530(4)	1.551
Angles (°)		
C(1)-N(2)-C(3)	111.5(2)	111.6
C(1)-N(5)-C(4)	110.7(2)	111.3
Se-C(1)-N(2)	126.0(2)	126.6
Se-C(1)-N(5)	125.6(2)	126.1
N(2)-C(1)-N(5)	108.4(2)	107.3
O(3)-C(3)-N(2)	127.6(3)	128.8
O(3)-C(3)-C(4)	127.8(3)	129.1
N(2)-C(3)-C(4)	104.5(2)	104.8
N(5)-C(4)-C(3)	104.8(2)	105.0
O(4)-C(4)-N(5)	127.1(3)	126.1
O(4)-C(4)-C(3)	128.1(3)	126.2

[a]Values taken from ref. (20) accounting for rigid-body libration corrections.

[b]Atom numbering as in Fig. 1. X = O for **3a**^{H}, Se for **3e**^{Et}.

drawing of HOMOs and LUMOs for compounds **3a**, **b**, **e**^{Me} is shown in Fig. 3. The energies of the two highest occupied orbitals (HOMO and HOMO-1) in **3a**^{R} are swapped with respect to those calculated for **3b**^{R} and **3e**^{R} (R = H, Me). As a consequence, while the HOMO in thio- and seleno-

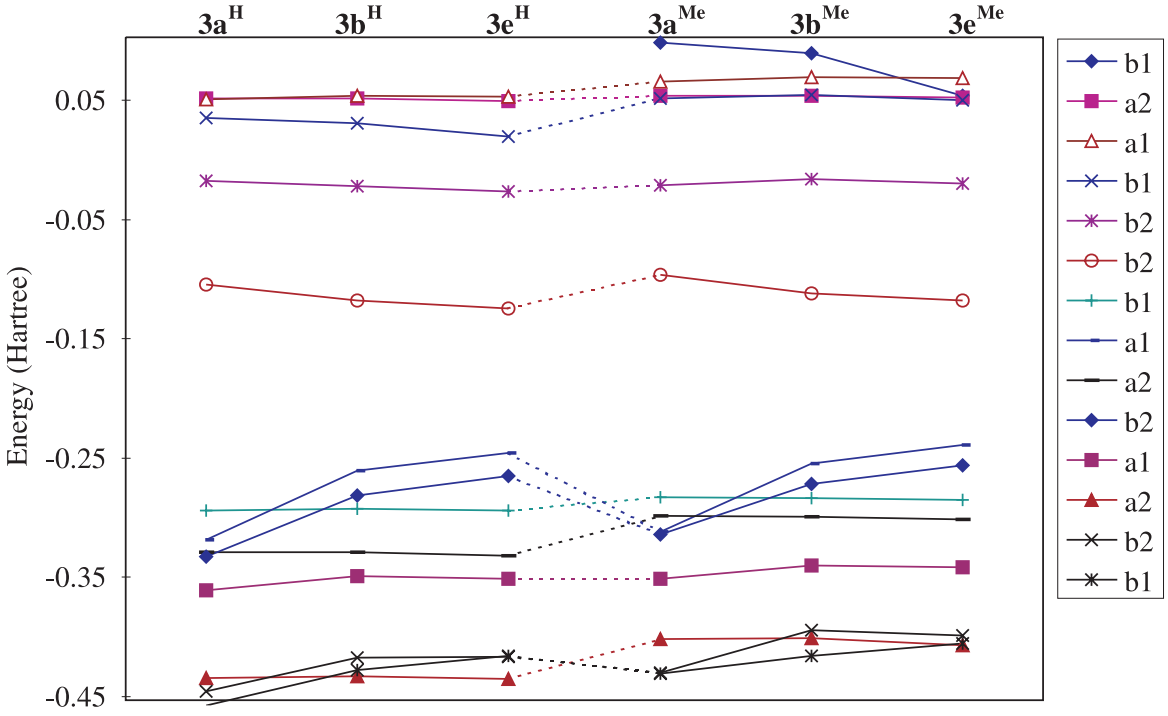
Scheme 3. Naming of the model compounds for DFT-calculations.



		X		
		O	S	Se
R	H	**3a**^{H}	**3b**^{H}	**3e**^{H}
	CH_3	**3a**^{Me}	**3b**^{Me}	**3e**^{Me}

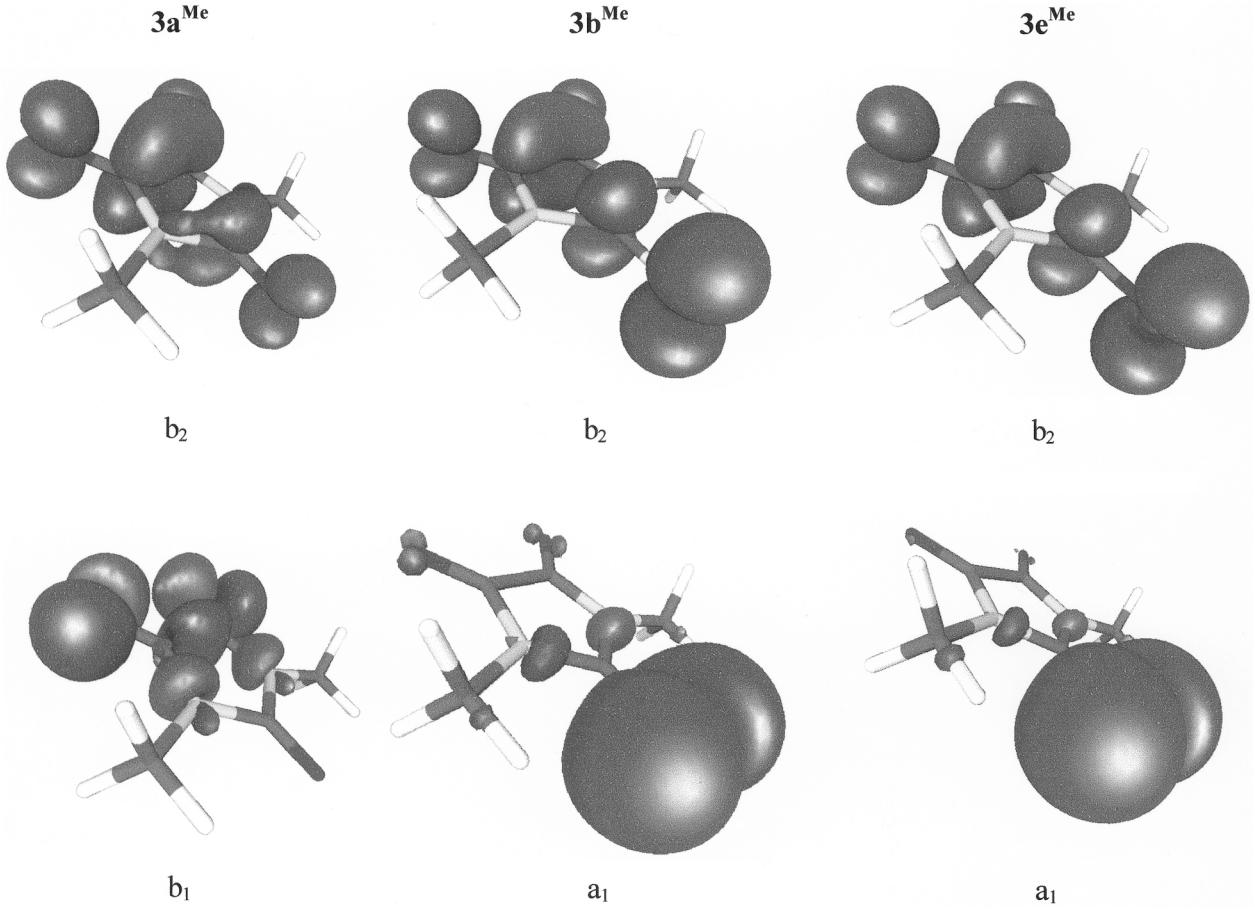
derivatives is an a_1 lone pair centred on the respective chalcogen atom, the HOMO in parabanic acid derivatives is made up of the 2*p* atomic orbitals of O(3) and O(4) lying on the molecular plane, and of the 2*s* and 2*p* atomic orbitals of nitrogen and carbon atoms combining to form a *p*σ bonding molecular orbital extending over the N(2)-C(3)-C(4)-N(5) framework and belonging to the b_1 representation. The different nature of the HOMOs of **3a**^{R} compared to those of **3b**^{R} and **3e**^{R} might be responsible for the different reactivities

Fig. 2. Calculated Kohn–Sham orbital energies (Hartree) of the frontier orbitals for compounds reported in Scheme 3. The box shows the representations of molecular orbitals in the C_{2v} point group.



© 2000 NRC Canada

Fig. 3. HOMOs (bottom row) and LUMOs (upper row) drawings for compounds **3a**^{Me}, **3b**^{Me}, and **3e**^{Me}.



of these substrates, in particular as far as the sulphuration is concerned.

To ascertain whether the change in the nature of the HOMO only depends upon the nature of the X atom, and is common to all systems containing the -NH-C(X)-NH- moiety, the same type of calculations (BECKE3LYP/Ahlrichs basis set) have been performed on **4a**^{H}, **4b**^{H}, and **4e**^{H} (optimized bond lengths and angles: C—N, 1.375, 1.365, 1.351 Å; C=X: 1.228, 1.669, 1.837 Å; N-C-N: 115.29, 115.01, 116.54°) and on **4a**^{Me}, **4b**^{Me}, and **4e**^{Me} (with the substituents arranged in a *cis-cis* configuration, to preserve the C_{2v} symmetry. Optimized bond lengths and angles: C—N, 1.378, 1.366, 1.358 Å; C=X: 1.232, 1.680, 1.846 Å; N-C-N: 114.64, 113.40, 113.81°). The calculated geometries for **4b**^{Me} can be compared with the experimental bond lengths and angles determined by X-ray diffraction for **4b**^{Et}, **4b**$^{i\text{-}Pr}$, and **4b**^{Ph} (C—N, 1.316(4), 1.332(2), 1.384(5) Å; C=X: 1.707(3), 1.711(2), 1.681(5) Å; N-C-N: 117.3(3), 118.3(1), 113.9(4)°, respectively (25)). The best agreement is found with **4b**^{Ph}, possibly because **4b**^{Et} and **4b**$^{i\text{-}Pr}$ adopt a *cis-trans* configuration in the solid state, which leads to the formation of two-dimensional layers of thiourea derivatives. At any rate, as far as regards the N-C and the > C=S moieties, it should be remarked that bond lengths calculated in **4b**^{Me} correspond well to the unweighted mean values determined in thioureas from diffraction techniques (1.346 and 1.681 Å, respectively) (26). Interestingly, while all compounds with R = H, have the same kind of HOMOs, consisting in the lone pair of the chalcogen atom lying on the molecular plane, as found in **3b**^{R} and **3e**^{R}, those with R = Me show the same level inversion between HOMO and HOMO-1 calculated for **3a**^{R}. The NBO-charges (N: –0.87, –0.80, –0.80, –.69, –0.63, –0.63; C: +0.84, +0.29, +0.25, +0.86, +0.32, +0.27; X: –0.68, –0.25, –0.26, –0.70, –0.28, –0.26 e for **4a**^{H}, **4b**^{H}, **4e**^{H}, **4a**^{Me}, **4b**^{Me}, **4e**^{Me}, respectively) and the analysis of the bond order demonstrate that the nitrogen lone pairs are conjugated with the > C=X system in an order that increases on passing from **4a**^{R} to **4e**^{R} (N lone pair occupancies: 1.80, 1.76, 1.73, 1.77, 1.72, 1.70 e for **4a**^{H}, **4b**^{H}, **4e**^{H}, **4a**^{Me}, **4b**^{Me}, and **4e**^{Me}, respectively). At any rate, the charge distributions in **4b**^{H,Me} and **4e**^{H,Me} are very similar, and sensibly differ from those calculated for **4a**^{H,Me}.

Returning to compounds of type **3**, the b_2 LUMOs are π^* molecular orbitals formed by the 2*p* and 3*p* orbitals of all the endocyclic carbon atoms and of the exocyclic chalcogen atom. Some selected optimized bond lengths and angles are reported in Table 2. The agreement between the calculated parameters and experimental data available for **3a**^{H} (20) and for **3e**^{Et} (Table 1) is quite good, with differences within 2%, probably due to solid state effects. We have recently pointed out (11, 14) that although Koopmans'(27) theorem is not valid in DFT, a linear correlation can be found between the Kohn–Sham orbital energies and electronic properties such as molecular electronic transitions and redox potentials. Analogously, in this case a correlation between experimental photoelectron spectra (reported for **3a**^{H} and **3a**^{Me}) (28) and

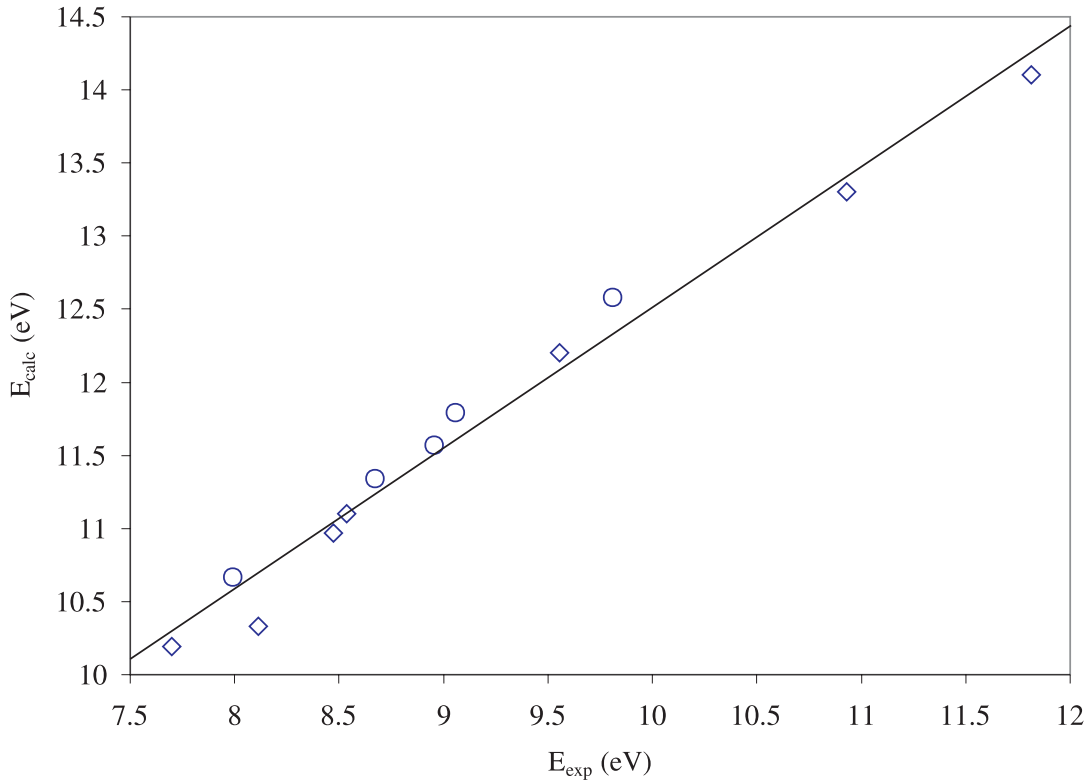
© 2000 NRC Canada

Table 2. Calculated bond lengths (Å) and angles (°) for model compounds reported in Scheme 3.

	3a^{H}	**3b^{H}**	**3e^{H}**	**3a^{Me}**	**3b^{Me}**	**3e^{Me}**
Bond lengths (Å)						
C(1)—X[a]	1.208	1.634	1.791	1.213	1.642	1.801
C(1)—N(2)	1.399	1.387	1.379	1.401	1.394	1.387
N(2)—C(3)	1.386	1.389	1.391	1.384	1.388	1.391
C(3)—O(3)	1.207	1.209	1.208	1.210	1.211	1.212
C(3)—C(4)	1.556	1.549	1.547	1.547	1.535	1.532
Angles (°)						
X-C(1)-N(2)	127.15	127.21	126.94	126.38	126.57	126.36
N(2)-C(1)-N(5)	105.70	105.58	106.11	107.24	106.86	107.28
N(2)-C(3)-C(4)	104.07	103.74	103.64	104.85	104.70	104.63
C(3)-C(4)-O(4)	127.61	128.17	128.39	127.94	128.52	128.70

[a]Atom numbering as in Fig. 1. X = O for **3a^{H,Me}**, S for **3b^{H,Me}**, Se for **3e^{H,Me}**.

Fig. 4. Experimental ionization energies (eV, ref. (28)) vs. calculated Kohn–Sham orbital energies (eV) for **3a^{H}** (circles) and **3a^{Me}** (squares).



calculated Kohn–Sham eigenvalues can be found (Fig. 4 and Table 3). The shifts in the positions of the PES peaks found on passing from **3a^{H}** to **3a^{Me}** due to methylation show the same trend for both experimental and calculated energies (Fig. 5a). Moreover, a new evaluation of the energy values reported for **3a^{Me}**, previously estimated with the help of the results of CNDO/s-CI calculations, (28) leads to a better agreement (Fig. 5*b*). The very good correlation between the shifts in the ionization energies and in the calculated Kohn–Sham orbital energies between methylated and unmethylated parabanic acid indicates that the attribution of π-orbitals perpendicular to the molecular plane (such as HOMO-1 (a_1), HOMO-3 (b_2), and HOMO-5 (a_2) for **3a^{Me}**), in which methyl groups are able to participate sensibly, is correct. As far as

Table 3. Calculated Kohn–Sham orbital energies (eV) and experimental ionization energies[a] (eV) for **3a^{H}** and **3a^{Me}**.

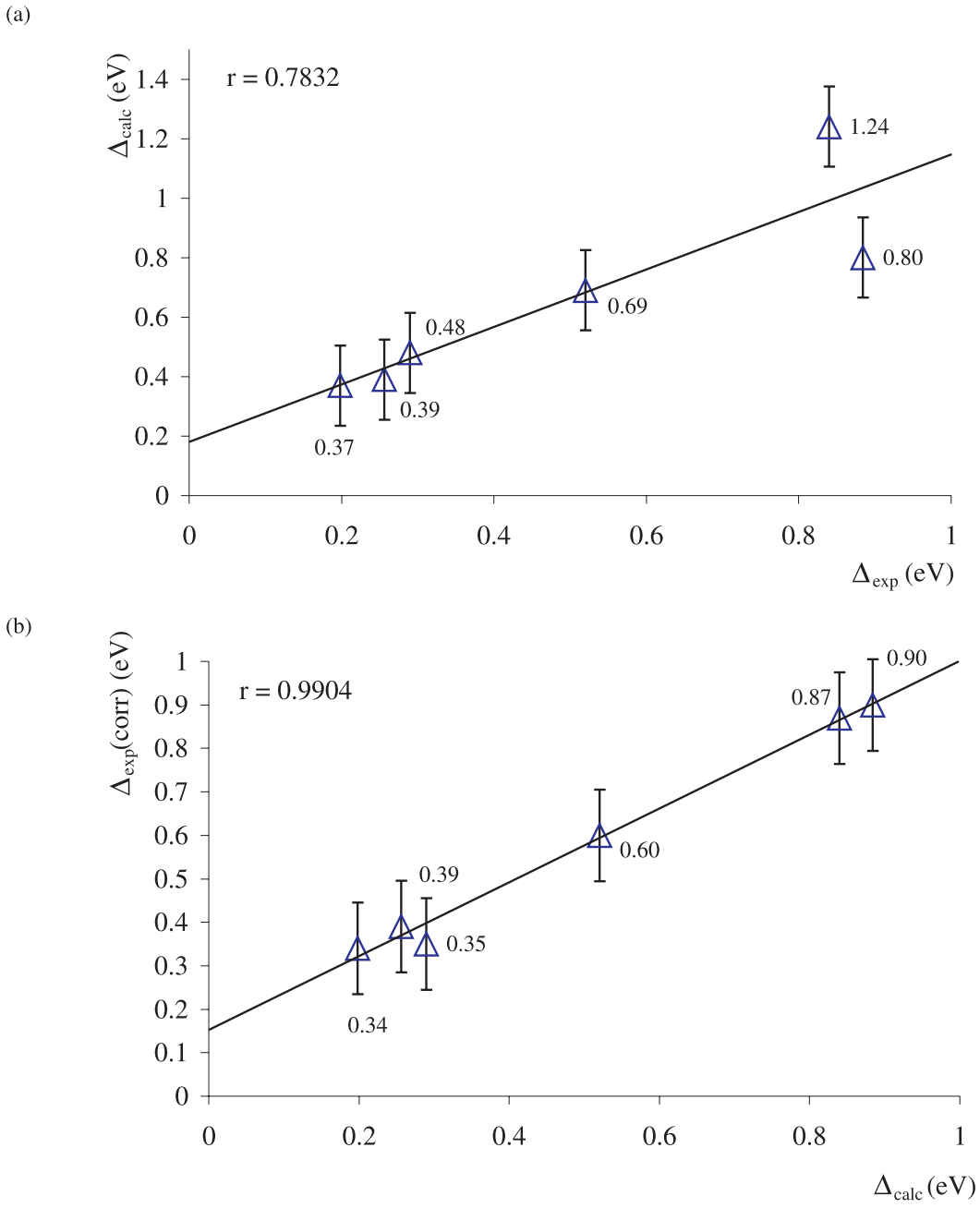
	Calculated eigenvalues (eV)		Exp. ionization energies (eV)[b]		
	3a^{H}	**3a^{Me}**	**3a^{H}**	**3a^{Me}**	
b_1	7.99	7.70	10.67	10.19	(10.32)
a_1	8.67	8.47	11.34	10.97	(10.70)
a_2	8.95	8.11	11.57	10.33	(11.00)
b_2	9.06	8.54	11.79	11.10	(11.19)
a_1	9.81	9.55	12.58	12.19	(12.28)
a_2	11.82	10.93	14.10	13.30	(13.20)

[a]Literature values obtained from PES data (ref. (28)).

[b]In parentheses new energy values extrapolated from data reported in ref. (28) are reported for **3a^{Me}**.

© 2000 NRC Canada

Fig. 5. Correlation and SDs between calculated and experimental shifts Δ (eV) found in the PES of **3a**^{H} and **3a**^{Me}. As experimental data both literature (a, ref. (28)) and newly extrapolated data (b) have been used.



the charge distribution is concerned, NBO (29) charges (which are more reliable (30) than Mulliken charges[2]) are summarized in Table 4. For **3a**^{H,Me} net negative charges are found on all exocyclic O atoms with similar values. In the case of **3b**^{H,Me} and **3e**^{H,Me}, while O(3) and O(4) show very similar NBO-charges, almost identical to those calculated for **3a**^{H,Me}, the S and Se atoms bound to C(1) are almost neutral. Correspondingly, the C(1) atoms in **3a**^{H} and **3a**^{Me} bear a more positive charge than those in **3b**^{H,Me} and **3e**^{H,Me}. While the charge distribution on C(1) and X (X = O, S, and Se for **3a**, **3b**, and **3e**, respectively) strongly depends on the nature of the X atom, in agreement with the trend of the softness of X, the remaining atoms in the molecule show very similar charge distributions. Actually, the almost neutral charges on the sulphur and selenium atoms in **3b**^{H,Me} and **3e**^{H,Me}, respectively suggest a very weak donor character for these compounds towards Lewis acids, such as halogen or interhalogen compounds, compared to that of compounds **1** (31, 32, 33) and **2** (34, 35). This is in accordance with the fact that we have been unable to measure reliable formation

[2] Mulliken charges for X, C(1), N(2,5), C(3,4), O follow: **3a**^{H}: –0.383, +0.240, –0.209, –0.004, –0.027; **3b**^{H}: –0.166, +0.093, –0.200, –0.011, –0.011, –0.042; **3e**^{H}: +0.174, –0.286, –0.175, –0.013, –0.047; **3a**^{Me}: –0.068, +0.112, –0.157, +0.009, –0.033; **3b**^{Me}: –0.136, +0.106, –0.110, +0.006, –0.034; **3e**^{Me}: +0.155, –0.244, –0.087, +0.007, –0.032 e.

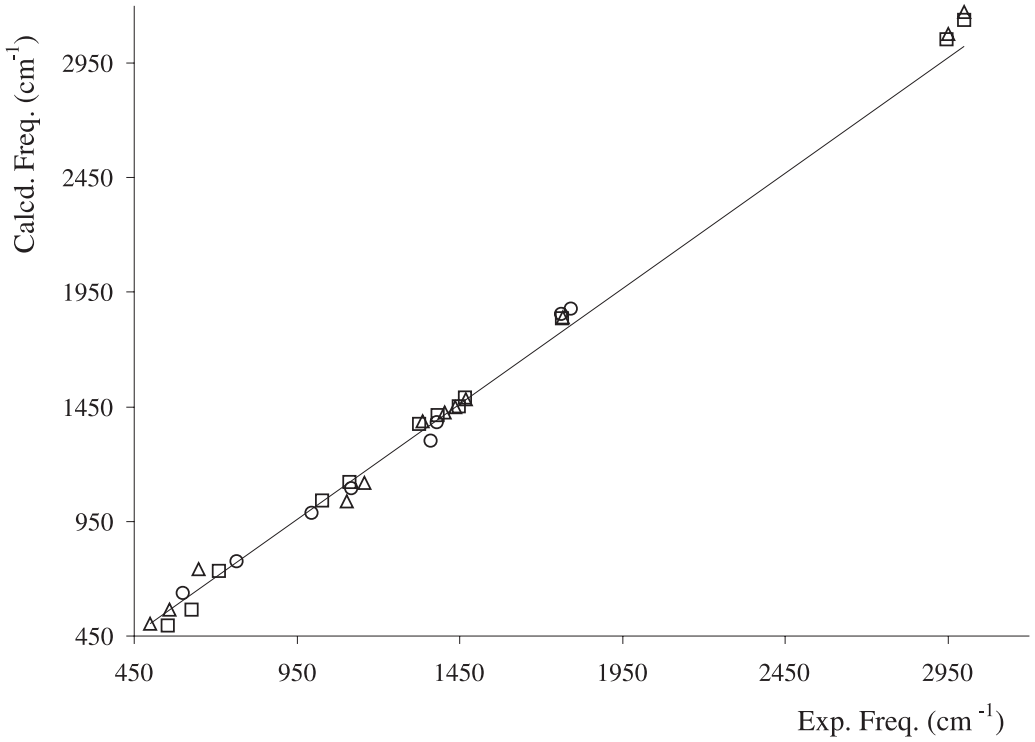
© 2000 NRC Canada

Table 4. NBO-charges (e) for compounds reported in Scheme 3.[a]

Atom	$\mathbf{3a^H}$	$\mathbf{3b^H}$	$\mathbf{3e^H}$	$\mathbf{3a^{Me}}$	$\mathbf{3b^{Me}}$	$\mathbf{3e^{Me}}$
X	–0.573	–0.044	+0.005	–0.592	–0.070	–0.018
C(1)	0.875	+0.249	+0.186	+0.892	+0.277	+0.211
N(2),N(5)	–0.710	–0.660	–0.655	–0.550	–0.505	–0.504
C(3),C(4)	0.636	+0.631	+0.627	+0.647	+0.643	+0.641
O(3),O(4)	–0.519	–0.518	–0.515	–0.532	–0.529	–0.526

[a]Atom numbering as in Fig. 1. X = O for $\mathbf{3a^{H,Me}}$, S for $\mathbf{3b^{H,Me}}$, Se for $\mathbf{3e^{H,Me}}$.

Fig. 6. Experimental vs. calculated mid-IR frequencies (450–3 200 cm^{-1}) for $\mathbf{3a^H}$ (circles), $\mathbf{3b^{Me}}$ (triangles), and $\mathbf{3e^{Me}}$ (squares).



constants of the adduct formed between $\mathbf{3b^R}$ and $\mathbf{3e^R}$ with molecular di-iodine. In fact, when the donor–acceptor interaction is very weak, a spectrophotometric approach (36) is not well-suited, since it is not possible to prepare solutions having a sufficiently high value of the saturation fraction (37, 38). In addition, in this particular class of compounds, an absorption band (λ_{max} = 520 nm, ε = 215 M^{-1} cm^{-1} for $\mathbf{3e^{Me}}$) near to the visible band of molecular di-iodine and a stronger band (λ_{max} = 350 nm, ε = 16 900 M^{-1} cm^{-1} for $\mathbf{3e^{Me}}$) which falls just where the adduct CT-band should appear, make further unreliable simultaneous determinations of the *K* and ε values of the adduct. Nevertheless, it is possible to have a rough estimation of the enthalpy value for the reaction of the 1:1 adduct formation from the lowering of the FT-Raman frequency for the I—I stretching (in methylene chloride solution $\nu_{I\text{-}I}$ falls at 209 cm^{-1} for free I_2 and at 182, 185, and 185 cm^{-1} in the adducts with $\mathbf{3e^{Me}}$, $\mathbf{3e^{Et}}$, and $\mathbf{3e^{Bu}}$, respectively). From the lowering of the $\nu_{I\text{-}I}$ value, a ΔH value of about –15 KJ mol^{-1} can be estimated. This value corresponds to a very weak interaction, and well agrees with the low charges calculated on the S and Se atoms in $\mathbf{3b^R}$ and $\mathbf{3e^R}$. As far as compounds of type **3b** are concerned, an adduct having an elemental analysis indicating a stoichiometry $\mathbf{3b^R}$•I_2 (R = Et) has been isolated in the solid state from $CHCl_3$ solutions. The very low interaction is confirmed by the position of the Raman band (180 cm^{-1}). In fact, their quick decomposition, with ejection of diiodine under the X-ray beam, prevented the crystal structure characterization of this adduct. A low-temperature determination has not been performed because of the scarce diffraction of the crystals.

Vibrational spectroscopy

Finally, DFT calculations can be employed to understand the vibrational spectra of the examined compounds. Calculated harmonic frequencies and experimental values appear to be in fairly good agreement as far as regards the trend in the values of the frequencies and in their intensities. Figure 6 shows a graph reporting the correlation between the experimental FT mid-IR frequencies and the harmonic calculated frequencies for $\mathbf{3b^{Me}}$ and $\mathbf{3e^{Me}}$. For the sake of comparison, the data regarding $\mathbf{3a^H}$ (39) are also reported. A comparison of the data available for all compounds allows to estimate an overall linear average scaling factor of 0.968. Furthermore, the results of our calculations allow to confirm or correct previous attributions based on an exclusively experimental basis. Thus, in Table 5 a comparison between

© 2000 NRC Canada

Table 5. Experimental IR-active frequencies (cm^{-1}) and calculated unscaled and scaled[a] mid-IR frequencies (cm^{-1}), intensities (KM mol^{-1}), old attribution,[b] and description of the vibrations for **3a^{H}**.

Attrib.	Exp. (cm^{-1})[a]	Unscaled (cm^{-1})	Scaled (cm^{-1}) (sc. factor)[b]	Int. (KM mol^{-1})	Old attrib.	Description
1 b_2	595s	640	624 (0.975)	236	b_1	NH out of plane
2 b_2	755s	761	757 (0.995)	28	—	C-N str. + O-C(1)-N bend.
3 b_1	982s	989	984 (0.995)	27	b_1	C-N symm. + N-C-C bend
4 a_1	1125m	1095	1089 (0.995)	10	a_1	C-N str. + O-C(4,5)-N bend.
5 b_1	1360s	1304	1297 (0.995)	134	b_1	C-N str. + O-C(4,5)-N bend.
6 a_1	1380s	1385	1378 (0.995)	247	a_1	C-N symm. + O-C(1)-N bend.
7 b_1	1760vs	1855	1658 (0.942)	1056	a_1	C=O str. + Ring def.
8 a_1	1790s	1878	1769 (0.942)	108	b_1	C=O str. + C-C str.
9 a_1	3160s	3622	3213 (0.887)	182	a_1	NH unsymm. str.
10 b_1	3220s	3624	3214 (0.887)	34	b_1	NH symm. str.

[a]Ref. (39).

[b]Scaling factors taken from ref. (40) according to the nature of the vibration.

the experimental (39) and the harmonic calculated mid-IR frequencies for **3a^{H}** is reported. To obtain a better agreement, the calculated spectra can be scaled by the transferable factors recently reported for a series of organic compounds, according to the nature of the vibrational mode (40). The new attributions generally confirm those previously reported (except for modes 1 and 2 in Table 5 and for the order of modes 7 and 8).

Conclusions

Among compounds of type **3**, only **3a^{R}**, **3b^{R}**, and **3c^{R}** were known, (3–6) and only **3a^{H}** was structurally characterized (19). Now, the synthesis of the first examples of selenoparabanic acid derivatives **3e^{R}** (R = Me, Et, Bu) and the single crystal X-ray structure of **3e^{Et}** are reported. The comparison with the structural features (20) of **3a^{H}** supports a higher degree of electron delocalization on the N(2)-C(1)(Se)-N(5) fragment. Hybrid-DFT (16, 17) calculations performed on the molecules **3a**, **b**, **e^{R}** (R = H, Me) confirm an increase in the electron delocalization on this fragment on passing from O to S and Se derivatives, and indicate a different composition of the HOMOs of **3a^{R}** compared to those of **3b**, **e^{R}**. This might explain the similar reactivities of the latter compounds compared to the former, in particular as far as regards sulphuration with Lawesson's reagent (9–11). Because of experimental difficulties, the donor character of the new compounds towards molecular di-iodine cannot be quantitatively explored by UV–vis spectroscopy (36), but FT-Raman spectroscopy allows to estimate a ΔH value of about –15 kJ mol^{-1}. Such a low value corresponds to a very weak donor character of compounds **3b**, **e^{R}** compared to the donor ability of compounds of type **1** and **2**. This is also in good agreement with the NBO-charge distributions.

Experimental section

All solvents and reagents were Aldrich products used as purchased. All reactions were carried out under dry nitrogen atmosphere. Elemental analyses were performed on a FISONS EA-1108 CHNS-O instrument. FT IR spectra were recorded on a Bruker IFS55 spectrometer at room temperature, purging the sample cell with a flow of dried air. Polythene pellets with a mylar beam-splitter and polythene windows (500–100 cm^{-1}, resolution 2 cm^{-1}) and KBr pellets with a KBr beam-splitter and KBr windows (4 000–400 cm^{-1}, resolution 4 cm^{-1}) were used. FT-Raman spectra were recorded with a resolution of 4 cm^{-1} on a Bruker RFS100 FT-Raman spectrometer, fitted with an In-Ga-As detector (room temperature) operating with a Nd-YAG laser (excitation wavelength 1 064 nm), with a 180° scattering geometry. Electronic spectra were recorded with a quartz cell of an optical path of 1 cm or with cells of an optical path of 0.1 cm in the attempt to determine formation constants, on a Varian Cary 5 spectrophotometer in CH_2Cl_2 solution at 20°C in a thermostated compartment. The ^{1}H NMR and ^{13}C NMR spectra were recorded on a Varian Unity Inova 400 operating at 400 and 100.5 MHz, respectively. Chemical shifts of compounds dissolved in $CDCl_3$ were referred to TMS used as an internal reference.

Procedures

Among the examined compounds (Scheme 3), **3a^{H}** is commercially available, while **3b^{H}**, **3a^{Me}**, and **3b^{Me}** have been prepared according to literature methods (3).

Synthesis of 3e^{Me}, $C_5H_6N_2O_2Se$

Iodomethane (2.4 mL, 38.4 mmol) is added dropwise to a methyl alcohol solution (20 mL) of *N*,*N*′-dimethylthiourea (2 g, 19.2 mmol) and the resulting mixture is refluxed for 1 h and then cooled to 0°C. The *S*,*N*,*N*′-trimethylisothiouronium iodide, separated as a white solid (4.3 g, yield 90%), is dissolved in anhydrous methyl alcohol and reacted at room temperature for 15 h with an absolute ethyl alcohol solution of NaHSe freshly prepared from selenium powder (0.834 g, 10.57 mmol) and sodium borohydride (0.492 g, 13.01 mmol). The mixture is neutralized with diluted acetic acid, 25 mL of distilled water are added, and alcohols are removed under reduced pressure. The *N*,*N*′-dimethylselenourea **4e^{Me}** is extracted with methylene chloride and the solution dried over anhydrous sodium sulfate. Trimethylamine (2.26 mL, 16.3 mmol) and oxalyl chloride (0.78 mL, 8.9 mmol) are added dropwise at 0°C to a methylene chloride solution of **4e^{Me}** containing 8.9 mmol and the reaction mixture is stirred at room temperature for 1 h, washed with water, and the organic phase dried under reduced pressure. The product is purified by crystallization from an ethyl

© 2000 NRC Canada

alcohol–hexane solution. Yield 0.917 g, 55%, mp 119°C. UV–vis (CH_2Cl_2 solution) λ (nm) (ε, M^{-1} cm^{-1}): 347 (6800), 518 (200). IR ν (cm^{-1}): 2948vw, 1760vs, 1664w, 1467m, 1446s, 1379vs, 1323vs, 1229m, 1109s, 1027w, 964w, 785m, 711m, 625m, 554m, 484s, 381m, 325m, 249m. ^{1}H NMR (400.0 MHz, $CDCl_3$, TMS) δ: 3.52 (s). ^{13}C NMR (100.5 MHz, $CDCl_3$, TMS) δ: 186.24, 154.91, 30.07. Anal. calcd.(%): C 29.28, H 2.95, N 13.66; found: C 30.08, H 2.81, N 13.94.

Synthesis of $3e^{Et}$, $C_7H_{10}N_2O_2Se$

3e^{Et} was synthesized following the route outlined for **3e^{Me}**. Yield 1.658 g, 65%, mp 111°C. UV–vis (CH_2Cl_2 solution) λ (nm) (ε, M^{-1} cm^{-1}): 350 (6200), 524 (200). IR ν (cm^{-1}): 2971w, 1766vs, 1454m, 1430m, 1396vs, 1242vs, 1117s, 1074m, 1049w, 1010vw, 901w, 875w, 641m, 367m, 488s, 441w, 395w, 325m, 247vw, 225w, 198w, 187w. ^{1}H NMR (400.0 MHz, $CDCl_3$, TMS) δ: 4.12 (q, 2H), 1.30 (t, 3H). ^{13}C NMR (100.5 MHz, $CDCl_3$, TMS) δ: 184.48, 154.81, 38.89, 13.14. Anal. calcd. (%): C 36.06, H 4.32, N 12.28; found: C 36.84, H 4.72, N 12.28.

Synthesis of $3e^{Bu}$, $C_{11}H_{18}N_2O_2Se$

3e^{Et} was synthesized following the route outlined for **3e^{Me}**. Yield 1.227 g, 70%. m p 35°C. UV–vis (CH_2Cl_2 solution) λ (nm) (ε, M^{-1} cm^{-1}): 352 (5600), 525 (200). IR ν (cm^{-1}): 2960m, 2933w, 2874w, 1767vs, 1434m, 1395vs, 1291m, 1209s, 1164w, 1130m, 1089w, 1061w, 957vw, 703vw, 573w, 495m, 397 w, 300w, 249vw. ^{1}H NMR (400.0 MHz, $CDCl_3$, TMS) δ: 4.05 (t, 2H), 1.70 (m, 2H), 1.37 (m, 2H), 0.96 (t, 3H). ^{13}C NMR (100.5 MHz, $CDCl_3$, TMS) δ: 185.20, 154.99 (s), 43.60, 29.81, 19.85 (s), 13.53. Anal. calcd. (%): C 45.68, H 6.27, N 9.69; found: C 46.80, H 7.01, N 9.86.

X-ray crystallography

Crystal data for **3e^{Et}**: $C_7H_{10}N_2O_2Se$, fw 233.13, orthorhombic, space group $P2_12_12_1$ (no. 19), a = 5.249(1), b = 10.406(3), c = 16.647(1) Å, U = 909,3(3) Å^3, Z = 4, μ(Mo-Kα) = 40.48 cm^{-1}, ρ_{calc} = 1.703 g cm^{-3}; 1721 reflections measured, 1580 unique (R_{int} = 0.018). Intensity data were collected at room temperature with an Enraf–Nonius CAD4 diffractometer using graphite-monochromatised Mo-Kα radiation. Lorentz, polarization, and a semiempirical absorption correction (41) were applied to all the data. The structure was solved by direct methods (MULTAN) (42) and refined by full-matrix least-squares with anisotropic displacement parameters for all the non-hydrogen atoms. The final R and R_w indices were 0.030 and 0.044 for 1339 reflections with $I > 3\sigma(I)$. All H atoms were seen in difference Fourier maps, but not refined. Sources of neutral atomic scattering factors for all atoms are given in ref. (43). Anomalous dispersion effects were included in F_c; and the values for δf′ and δf″ were those of ref. (44). All the calculations were performed using Personal SDP software (45, 46). Atomic coordinates, displacement parameters, bond lengths and angles have been deposited as supplementary material and may be purchased from the Depository of Unpublished Data, Document Delivery, CISTI, National Research Council Canada, Ottawa, ON K1A 0S2 (http://www.nrc.ca/cisti/docdel/order_electronic_e.shtml for information on ordering electronically). This material has also been deposited with the Cambridge Crystallographic Data Centre. Copies of the data can be obtained, free of charge, on application to the Director, CCDC, 12 Union Road, Cambridge CB2 1EZ, U.K. (Fax: 44-1223-336033 or e-mail: deposit@ccdc.cam.ac.uk).

Computations

Quantum chemical calculations were carried out using the commercially available suite of programs Gaussian 94 (47). Density functional calculations (16, 17) (DFT) were performed using the hybrid BECKE3LYP functional (which uses a mixture (22) of Hartree–Fock and DFT exchange along with DFT correlation: the Lee-Yang-Parr correlation functional together with the Becke's gradient correction) (23), Schafer, Horn, and Ahlrichs' (24) pVDZ basis set for C, H, N, O, S, and Se were used for all calculations. Numerical integration was performed using the FineGrid option, which indicates that a total of 7 500 points are used for each atom. After a geometry optimization performed starting from structural data (where available) regularized to satisfy the C_{2v} symmetry, harmonic frequencies were obtained using the second derivatives of the DFT energy, computed by numerical differentiation of the DFT energy gradients. Finally NBO (29) calculations have been performed for each molecule using the converged density matrix corresponding to the equilibrium geometries. All point group representations refer to the model molecules disposed on the *xy* plane with the C(1)=X bond lying on the *y* axis. Calculations have been performed on an IBM Risc 6000 550H, DECServer 4000, and on a VAIER Intel Pentium III 450 MHz Personal Computer running Linux.

Acknowledgments

The project was carried out as a part of the "Progetto Finalizzato Materiali Speciali per Tecnologie Avanzate II" of the "Consiglio Nazionale delle Ricerche." We wish to acknowledge the Advanced Materials Laboratory (LaMI) under the auspices of the European Union and Regione Basilicata for financial support. We also wish to thank Dr. Francesco Usai for help in the synthesis.

Supporting information

Table S1. giving details of the data collection and refinement, atomic coordinates, displacement parameters, bond lengths and angles for **3e^{Et}**. Optimized geometries in Cartesian coordinate form and frontier Kohn–Sham orbital energies at the BECKE3LYP level for all compounds reported in Scheme 3.

References

1. F.A. Devillanova and G. Verani. Aust. J. Chem. **33**, 279 (1980).
2. F.A. Devillanova and G. Verani. Tetrahedron, **37**, 1803 (1981).
3. H. Biltz and E. Topp. Chem. Ber. **46**, 1401 (1913).
4. M. Ponomareff. Bull. Soc. Chim. Fr. **18**, 97 (1872).
5. P. Brix and J. Voss. J. Chem. Res. Miniprint, **8**, 2218 (1993).
6. H. Bredereck. Chem. Ber. **101**, 1863 (1968).

© 2000 NRC Canada

7. H.W. Roesky, H. Hofman, W. Clegg, M. Noltemeyer, and G.M. Sheldrick. Inorg. Chem. **21**, 3798 (1982).
8. A.C. Fabretti, G.C. Franchini, C. Preti, and G. Tosi. Can. J. Chem. **55**, 344 (1977).
9. D. Atzei, F. Bigoli, P. Deplano, M.A. Pellinghelli, and E.F. Trogu. Phosphorus Sulfur Relat. Elem. **37**, 189 (1988).
10. F. Bigoli, P. Deplano, F.A. Devillanova, J.R. Ferraro, V. Lippolis, P.J. Lukes, M.L. Mercuri, M.A. Pellinghelli, and E.F. Trogu. Inorg. Chem. **36**, 1218 (1997).
11. M.C. Aragoni, M. Arca, F. Demartin, F.A. Devillanova, A. Garau, F. Isaia, F. Lelj, V. Lippolis, and G. Verani. J. Am. Chem. Soc. **121**, 7098 (1999), and refs. therein.
12. S. Sheibe, B.J. Pedersen, and S.-O. Lawesson. Bull. Soc. Chim. Belg. **87**, 229 (1978).
13. F. Bigoli, P. Deplano, F.A. Devillanova, V. Lippolis, P.J. Lukes, M.L. Mercuri, M.A. Pellinghelli, and E.F. Trogu. J. Chem. Soc. Chem. Commun. 371 (1995).
14. M. Arca, F. Demartin, F.A. Devillanova, A. Garau, F. Isaia, F. Lelj, V. Lippolis, S. Pedraglio, and G. Verani. J. Chem. Soc. Dalton Trans. 3731 (1998).
15. F. Bigoli, P. Deplano, S. Marcis, M.L. Mercuri, R. Onnis, G. Orrù, M.A. Pellinghelli, and E. F. Trogu. Phosphorus Sulfur Silicon Relat. Elem. **659**, 136 (1998).
16. J. Labanowsky and J. Andzelm. Density functional methods in chemistry. Springer–Verlag, New York. 1991.
17. E.S. Kryachko and E.V. Ludeña. Energy density function theory of many electron systems. Kluver Academic Publisher, NL. 1990.
18. D.L. Klayman and R.J. Shine. J. Org. Chem. **34**, 3549 (1969).
19. D.R. Daviesand and J.J. Blum. Acta Crystallorg. **8**, 129 (1955).
20. X.M. He, S. Swaminathan, B.M. Craven, and R.K. McMullan. Acta Crystallogr. Sect. B: Struct. Sci. **B44**, 271 (1988).
21. B.M. Craven and R.K. McMullan. Acta Crystallogr. Sect. B: Struct. Crystallogr. Cryst. Chem. **B35**, 934 (1979).
22. A.D. Becke. J. Chem. Phys. **98**, 1372 (1993).
23. C. Lee, W. Yang, and R.G. Parr. Phys. Rev. B Condens. Matter Mater. Phys. **37**, 785 (1988).
24. A. Schafer, H. Horn, and R. Ahlrichs. J. Chem. Phys. **97**, 2571 (1992).
25. H.–K. Fun, N. Janarthanan, K. Ramadas, A. Ramnathan, K. Sivakumar, and K. Subramanian. Acta Crystallogr. Sect. C: Cryst. Struct. Commun. **C51**, 2446 (1995).
26. F.H. Allen, O. Kennard, D.G. Watson, L. Brammer, G. Orpen, and R. Taylor. J. Chem. Soc. Perkin Trans 2, **1987**, S1.
27. T.A. Koopmans. Physica, **1**, 104 (1933).
28. J.L. Meeks and S.P. McGlynn. J. Am. Chem. Soc. **97**, 5079 (1975).
29. A.E. Reed, L.A. Curtiss, and F. Weinholt. Chem. Rev. **88**, 899 (1988).
30. F. Jensen. Introduction to computational chemistry. John Wiley, Chichester, U.K. 1999. pp. 229–233.
31. F.A. Devillanova and G. Verani. J. Heterocycl. Chem. **16**, 945 (1979).
32. F.A. Devillanova and G. Verani. Tetrahedron, **35**, 511 (1979).
33. F.A. Devillanova and G. Verani. Tetrahedron, **37**, 1803 (1981).
34. I. Cau, F. Cristiani, F.A. Devillanova, and G. Verani. J. Chem. Soc. Perkin Trans. 2, 759 (1985).
35. F. Cristiani, F.A. Devillanova, A. Garau, F. Isaia, V. Lippolis, and G. Verani. Heteroat. Chem. **5**, 65 (1994).
36. M.C. Aragoni, M. Arca, F.A. Devillanova, A. Garau, F. Isaia, V. Lippolis, and G. Verani. Coord. Chem. Rev. **184**, 271 (1999).
37. G. Carta and G. Crisponi. Tetrahedron, **37**, 2115 (1981).
38. G. Carta and G. Crisponi. J. Chem. Soc. Perkin Trans. 2, 53 (1982).
39. L. Coclers, A. Vanclef, and R. Bouché. Spectrosc. Lett. **11**, 799 (1978).
40. G. Rauhut and P. Pulay. J. Phys. Chem. **99**, 3093 (1995).
41. A.C.T. North, D.C. Phillips, and F.S. Mathews. Acta Crystallogr. Sect. A: Cryst. Phys. Diffr. Theor. Gen. Crystallogr. **A24**, 351 (1968).
42. P. Main, S.J. Fiske, S.E. Hull, L. Lessinger, G. Germain, J.P. Declercq, and M.N. Wolfson. MULTAN 80, Universities of York, England and Louvain, Belgium. 1980.
43. D.T. Cromer and J.T. Waber. International tables for X-ray crystallography. Vol. IV. The Kynoch Press, Birmingham, U.K. 1974. Table 2.2B. p. 1990.
44. D.T. Cromer. International tables for X-ray crystallography. Vol. IV. The Kynoch Press, Birmingham, U.K. Table 2.3.1. 1974.
45. B. Frenz. Comput. Phys. **2**, 42 (1988).
46. B. Frenz. Crystallographic computing 5. Ch. 11. Oxford University Press, Oxford, U.K. 1991. pp. 126–135.
47. Gaussian 94 (Revision D.1 & E.1), M.J. Frisch, G.W. Trucks, H.B. Schlegel, P.M.W. Gill, B.G. Johnson, M.A. Robb, J.R. Cheeseman, T.A. Keith, G.A. Petersson, J.A. Montgomery, K. Raghavachari, M.A. Al-Laham, V.G. Zakrzewski, J.V. Ortiz, J.B. Foresman, C.Y. Peng, P.Y. Ayala, M.W. Wong, J.L. Andres, E.S. Replogle, R. Gomperts, R.L. Martin, D.J. Fox, J.S. Binkley, D.J. Defrees, J. Baker, J.P. Stewart, M. Head-Gordon, C. Gonzalez, and J.A. Pople. Gaussian, Inc., Pittsburgh, Pa. 1995.

© 2000 NRC Canada

The synthesis of pyrido(2,3,4-*kl*)acridine unit of some marine alkaloids

Turan Ozturk and Alexander McKillop

Abstract: A simple and convenient synthesis of pyrido(2,3,4-*kl*)acridine (**1**), the main skeleton of some marine alkaloids, via cyclization and intramolecular nitrene insertion, is described. The importance of the planarity of the molecule during the nitrene insertion is explained.

Key words: pyridoacridine, marine alkaloids, nitrene insertion, quinoline, quinolinone.

Résumé : On décrit une synthèse simple et pratique de la pyrido(2,3,4-*kl*)acridine (**1**), le squelette fondamental de quelques alcaloïdes marins; elle implique une cyclisation et une insertion intramoléculaire de nitrène. On explique l'importance de la planéité de la molécule au cours de l'insertion du nitrène.

Mots clés : pyridoacridine, alcaloïdes marins, insertion de nitrène, quinoléine, quinoléinone.

[Traduit par la Rédaction]

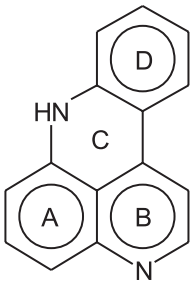
Introduction

Recently, many polycyclic fused-ring alkaloids containing pyrido(2,3,4-*kl*)acridine (**1**) skeleton have been isolated from a variety of marine sources such as sponges, molluscs, and tunicates, most of which have been reported to have cytotoxic, antitumor, and antiviral activities (1). Calliactine (2), 2-bromoleptoclinidinone (3), ascididemin (4), cystodytins A, B, and C (5), petrosamine (6), diplamine (7), varamines (8), dercitin (9), cyclodercitin (10), segolines A (11, 12) and B (12), isosegoline A (11, 12), norsegoline (11, 12), shermilamines A (12), B (13, 14), C (5*b*), D and E (15), styelsamine A, B, C, and D (16), arnoamine A and B (17), kuanoniamine A, B, C, and D (13, 5*b*), eilatin (12), amphimedine (18), neoamphimedine (19), pantherinine (20), lissoclin A and B (21), are among this type of alkaloid. Although elegant synthetic methodologies for most of these alkaloids have been developed and total synthesis of many of these natural products have been achieved, such alkaloids are still continuing to be the focus of many synthetic groups (1, 22). This is due to their interesting biological activities and challenging structures. It seems that any contribution toward the synthesis of pyridoacridine units is worthwhile since most of the strategies involve the synthesis of such units. The route we present here involves two important key steps, cyclization to form the quinolinone moiety and intramolecular nitrene insertion to build a tetracyclic system.

Received March 22, 2000. Published on the NRC Research Press website on August 18, 2000.

T. Ozturk.[1] TUBITAK Marmara Research Center, Chemistry Department, Gebze-Kocaeli, Turkey.
e-mail: turan@mom.gov.tr
A. McKillop. The University of East Anglia, School of Chemical Sciences, Norwich, U.K.

[1]Author to whom correspondence may be addressed. University of Waterloo, Chemistry Department, Waterloo, ON N2L 3G1 Canada. e-mail: turan@muskie.uwaterloo.ca



1

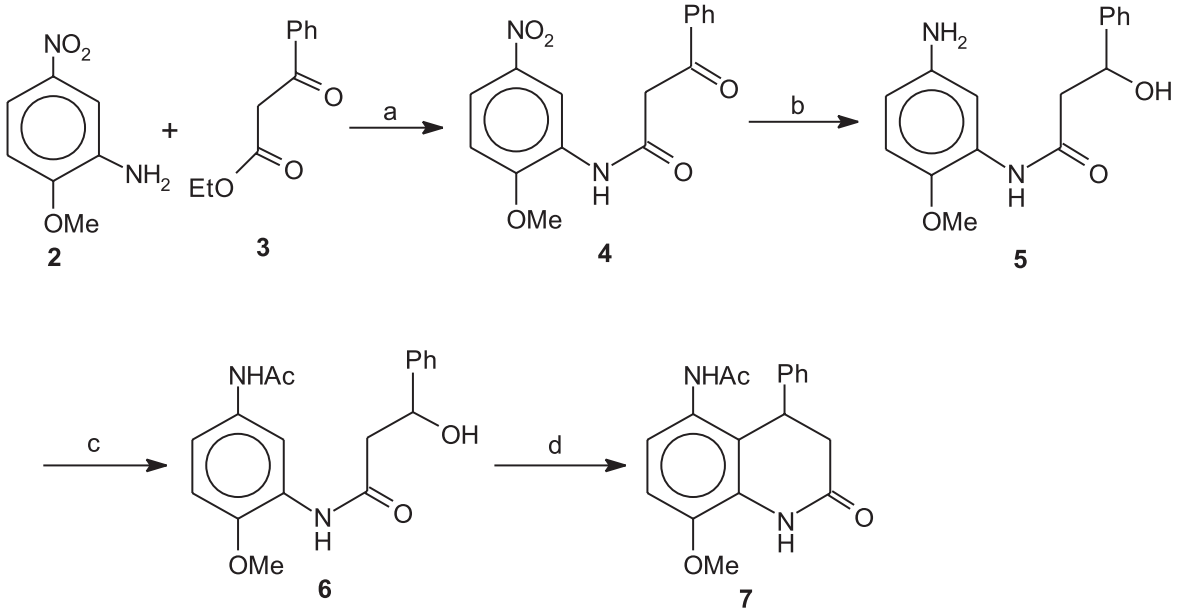
This approach may also be utilized as an easy access for the synthesis of ring B-modified analogues of this type of alkaloid.

Results and discussion

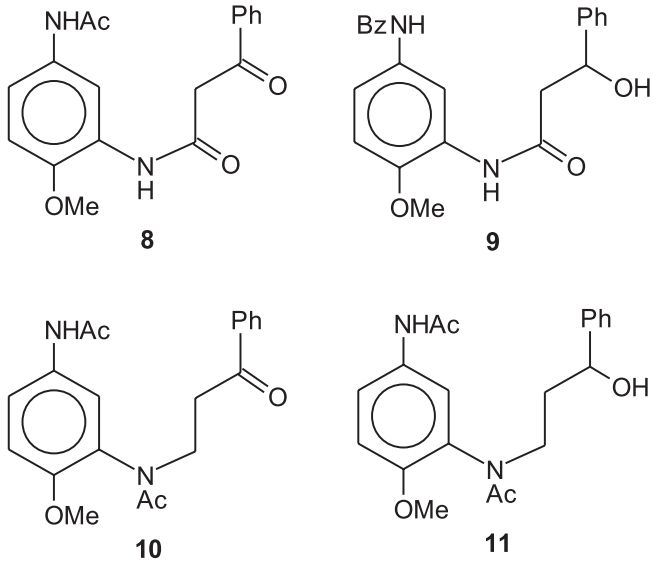
The synthesis of this important pyridoacridine intermediate **21** has been achieved in 10 steps with overall 13.5% yield. Our synthesis started with the condensation of the commercially available reagents 2-methoxy-5-nitroaniline (**2**) and ethyl benzoylacetate (**3**) in toluene, which led to the formation of the amide **4** in 75% yield (Scheme 1) (22*c*). Hydrogenation of the nitro and keto groups of **4**, over palladium on charcoal at room temperature in ethanol, took place at the same time with a 90% yield. Acetylation of the amino group of **5** with acetyl chloride was followed by the cyclization of the corresponding product **6** with 80% H_2SO_4, which smoothly yielded the quinolinone **7** in 92% yield. Unfortunately, our other cyclization attempts with various amides such as **8**, **9**, **10**, and **11** to obtain such an important intermediate were not successful. Although these attempts were carried out in various reagents, conc. H_2SO_4, H_3PO_4, poly.H_3PO_4, $POCl_3$, HCl, and 80% H_2SO_4, in almost all reactions, intractable products or starting materials were obtained, except **8** and **9** which gave hydrolysis of the amide

© 2000 NRC Canada

Scheme 1. (a) Toluene, reflux, 75%; (b) Pd/C, H_2, ethanol, rt, 90%; (c) AcCl, pyridine, 75%; (d) H_2SO_4 (80%), 92%.



when treated with HCl or 80% H_2SO_4, and dehydration with 80% H_2SO_4, respectively.



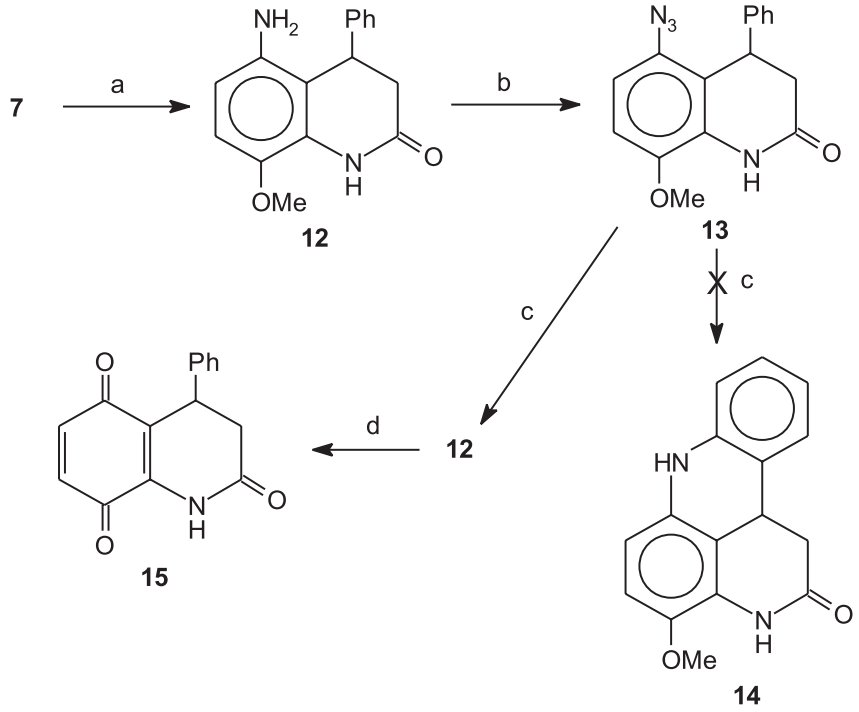
After constructing the quinolinone ring successfully, we concentrated on building the last ring, utilizing the intramolecular nitrene insertion methodology. Initially, deacetylation of **7** was performed, and after some exploratory work, it was found that deacetylation of **7** to **12** best took place in hot 45% sulphuric acid, and **12** was obtained in a very satisfactory, 88% yield (Scheme 2). Conversion of **12** to the corresponding azide **13** was then carried out by the classical nitrous acid followed by sodium azide combination of reactions. With the azide **13** available, conversion to the tetracyclic system **14** was attempted. Thus, **13** was heated in refluxing xylene until no starting material remained in the reaction mixture, as shown by TLC. Examination of the NMR spectrum of the product, however, showed that it was the amine **12**. Further confirmation that **12** had been obtained, was provided by oxidative demethylation with manganese dioxide, which gave the trione **15** in 78% yield, and the analytical and spectroscopic data for **15** were fully consistent with the assigned structure.

In this attempted cyclization of **13** to **14** via the nitrene insertion, which was carried out in xylene, both in the presence and absence of a nitrogen atmosphere, it was assumed that conversion of the nitrene **13** to the aniline **12** was the result of hydrogen abstraction from the solvent. In an attempt to circumvent this, the azide **13** was carefully melted and the liquid azide was stirred under nitrogen in the absence of solvent. After 30 min, NMR and TLC examination of the crude product showed the same result as previously, that is, formation of the amine **12**. Hydrogen abstraction in this case could involve the benzylic hydrogen atom at the 4-position of the dihydroquinolinone ring. Moreover, the stereochemical situation in **13** is probably less than ideal as far as the intended intramolecular cyclisation is concerned. The phenyl group is not on the same plane with the azide, and this is obviously one of the driving forces in such cyclizations (22*g*, *j*, *k*, 23).

To circumvent the problem encountered during intramolecular nitrene insertion, it was decided to introduce a double bond to the system to bring the phenyl group to the same plane with the azide. Then, employment of the one of the most common dehydrogenation reagents DDQ (2,3-dichloro-5,6-dicyanobenzoquinone), unfortunately, did not give any result, only starting material was recovered. This is perhaps not too surprising in view of the large steric bulk of the reagent and the relative steric shielding of the hydrogen atoms at the 3- and 4-positions of the dihydroquinolinone by the 4-phenyl substituent. Then, the conventional method, palladium on charcoal in diphenyl ether, yielded the quinolinone **16** in 65% yield together with 20% of the starting material (Scheme 3). Hydrolysis of the amide group using 45% sulphuric acid proceeded smoothly to give the aminoquinolinone **17** in 96% yield, and conversion of the

© 2000 NRC Canada

Scheme 2. (a) H_2SO_4 (45%), reflux, 2 h, 88%; (b) (*i*) $NaNO_2$, 0–5°C; (*ii*) NaN_3, 0–5°C, 86%; (c) xylene, reflux; (d) MnO_2, H_2SO_4 (35%), 78%.



amino to the azide group, as usual, presented no difficulties. The crude azide **18**, which showed only one spot on TLC, was obtained in 93% yield. It proved to be sensitive to both heat and light and hence no attempt to obtain an analytical sample was made.

The next step in the synthesis was the key intramolecular nitrene insertion reaction. Azide **18** was heated under reflux in xylene for 1.5 h. In contrast to the complete failure to achieve cyclization with the dihydro derivative **13**, the azide **18** reacted quite smoothly to give the required tetracyclic material **19** in 78% yield. Use of the azidoquinolinone rather than the dihydroquinolinone had proved successful, therefore, and would seem to imply that the controlling feature in the reaction as far as nitrene insertion is concerned is sterochemistry.

The synthesis of the tetracyclic compound **19** constitutes achievement of one of the major objectives, namely the synthesis of an advanced tetracyclic intermediate in which the B ring is functionalized. Analogues of natural products containing pyridoacridine units could be available from it by manipulation of the quinolinone ring.

The key compound **21** was then easily prepared from **19** by conversion to the chloroquinoline **20** in 83% yield by reaction with hot phosphorus oxychloride, followed by reductive removal of the chlorine on charcoal in triethylamine in 79% yield.

Experimental

Melting points were determined on a Kofler hotstage microscope melting point apparatus and are uncorrected. Microanalysis were performed with a Carlo Erba 1106 elemental analyzer. Infrared spectra were recorded on Perkin–Elmer 257, 297 grating infrared spectrophotometers using the standard Nujol mull or liquid film techniques between sodium chloride plates. Proton NMR spectra were recorded on JEOL PMX 60 MHz and JEOL GX-400 MHz spectrometers. The ^{13}C NMR spectra were recorded on a JEOL EX-90Q 24 MHz spectrometer. Tetramethylsilane (TMS) was used as the internal standard in all NMR spectra run in $CDCl_3$, DMSO-d_6. Mass spectra were recorded on a Kratos MS-25 mass spectrometer with an ionization potential of 70 eV at 200°C. All column chromatography was performed on silica gel (Merck, Kieselgel 60H, Art 7736) and Merck aluminum oxide 60 PF_{24k}.

N-(2-Methoxy-5-nitrophenyl)-3-oxo-3-phenylpropanamide (4)

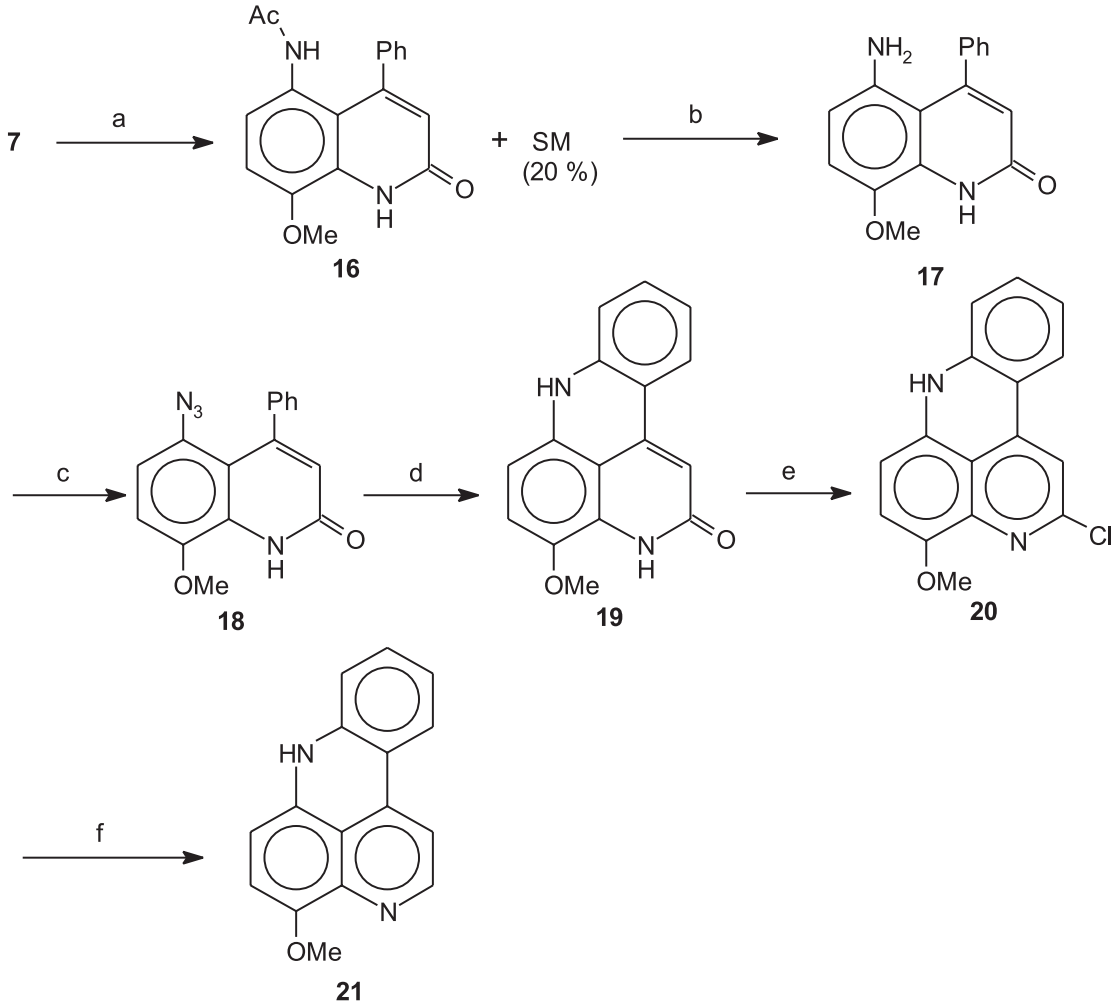
2-Methoxy-5-nitroaniline (**2**) (15 g, 90 mmol) and ethyl benzoylacetate (**3**) (17.29 g, 90 mmol) were condensed in toluene (400 mL) using a Dean and Stark's apparatus for 6 h, and the mixture was then left overnight at room temperature. The solid, which separated, was collected by filtration and recrystallized from ethanol. Yield: 21.9 g, 75%. Light yellow crystals, mp 183–185°C. MS: *m*/*z* 314 (M^+). ^1H NMR ($CDCl_3$) δ: 4.02 (s, 3H), 4.08 (s, 2H), 6.86 (d, J = 8.4 Hz, 1H), 7.60 (s, 5H), 8.0 (m, 2H). Anal. calcd. for $C_{16}H_{14}N_2O_5$: C 61.14, H 4.46, N 8.91; found: C 61.12, H 4.15, N 8.91.

N-(5-Amino-2-methoxyphenyl)-3-hydroxy-3-phenylpropanamide (5)

Compound **4** (6 g, 19 mmol) and C/Pd (0.21 g, 5%) were hydrogenated in ethanol (100 mL) at room temperature until the disappearance of the starting material (TLC). The

© 2000 NRC Canada

Scheme 3. (a) Pd/C, diphenyl ether, reflux, 65%, 20% (starting material); (b) H_2SO_4 (45%), reflux, 96%; (c) (*i*) $NaNO_2$; (*ii*) NaN_3, 93%; (d) xylene, reflux, 78%; (e) $POCl_3$, reflux, 83%; (f) Pd/C, H_2, Et_3N, 79%.



catalyst was filtered off through kieselguhr under suction and the kieselguhr was washed with acetone. After evaporation of the solvent, the crude solid was recrystallized from toluene. Yield: 4.89 g, 90%. Light yellow needles, mp 155–158°C. MS: *m*/*z* 286 (M^+). IR (Nujol) (cm^{-1}): 3420, 3360, 3100–3480, 1654. ^1H NMR ($CDCl_3$) δ: 2.68 (d, *J* = 2.9 Hz, 2H), 3.28 (s, 2H), 3.68 (s, 3H), 5.08 (t, *J* = 2.9 Hz, 1H), 6.26 (dd, *J* = 10.1, 1.2 Hz, 1H), 6.64 (d, *J* = 9.7 Hz, 1H), 7.26 (s, 5H), 7.82 (d, *J* = 1.2 Hz, 1H), 8.06 (s, 1H). Anal. calcd. for $C_{16}H_{18}N_2O_3$: C 67.43, H 6.29, N 9.79; found: C 67.43, H 6.40, N 9.58.

N-(5-Acetamido-2-methoxyphenyl)-3-hydroxy-3-phenylpropanamide (6)

To compound **5** (3 g, 10 mmol), dissolved in pyridine (25 mL) and cooled in an ice bath, was added dropwise freshly distilled acetyl chloride (0.80 mL, 110 mmol). The mixture was stirred for 2 h at room temperature and then poured into water (50 mL). The resulting mixture was extracted with CH_2Cl_2 (3 × 40 mL), dried over Mg_2SO_4. The solvent was evaporated under reduced pressure. Yield: 2.46 g, 75%. Colorless crystalline solid, mp 79–82°C. MS: *m*/*z* 328 (M^+). IR (Nujol) (cm^{-1}): 3110–3400, 1630–1680. ^1H NMR ($CDCl_3$) δ: 2.04 (s, 3H), 2.68 (d, *J* = 3.0 Hz, 2H), 3.00 (s, 3H), 4.04 (s, 1H), 5.08 (t, *J* = 3.0 Hz, 1H), 6.66 (d, *J* = 10.0 Hz, 1H), 7.24 (s, 5H), 7.44 (dd, *J* = 10.0, 1.1 Hz, 1H), 8.20 (d, *J* = 1.0 Hz, 1H), 8.25 (s, 1H). Anal. calcd. for $C_{18}H_{20}N_2O_4$: C 65.85, H 6.09, N 8.53; found: C 65.24, H 6.18, N 8.21.

5-Acetamido-3,4-dihydro-8-methoxy-4-phenylquinolin-2(1*H*)-one (7)

Compound **6** (0.50 g) was stirred in H_2SO_4 (80%, 100 mL) at 80°C for 1 h. The reaction mixture was cooled to room temperature and poured into ice water. The resulting solution was then neutralized with Na_2CO_3 and the Na_2SO_4 which separated was removed by filtration and washed with CH_2Cl_2 (3 × 40 mL) and the combined extracts were dried (Mg_2SO_4) and the solvent was evaporated under reduced pressure. The crude product was recrystallized from toluene. Yield: 0.42 g, 92%. Colorless crystalline solid, mp 218–220°C. MS: *m*/*z* 310 (M^+), 311. IR (Nujol) (cm^{-1}): 3200–3440, 1656, 1650. ^1H NMR ($CDCl_3$) δ: 1.91 (s, 3H), 2.63 (d, *J* = 15.7 Hz, 1H), 2.89 (dd, *J* = 16.1, 6.9 Hz, 1H), 3.80

© 2000 NRC Canada

(s, 3H), 4.53 (d, J = 5.9 Hz, 1H), 6.93 (d, J = 8.8 Hz, 1H), 6.98 (d, J = 8.8 Hz, 1H), 7.02–7.29 (m, 5H), 9.21 (s, 1H), 9.25 (s,1H). Anal. calcd. for $C_{18}H_{18}N_2O_3$: C 69.67, H 5.80, N 9.03; found: C 69.73, H 5.92, N 8.93.

5-Amino-3,4-dihydro-8-methoxy-4-phenylquinolin-2(1*H*)-one (12)

Compound **7** (0.5 g, 1.6 mmol) was refluxed in H_2SO_4 (25 mL, 45%) for 2 h. The mixture was cooled down to room temperature and poured into water (50 mL). The resulting solution was then neutralized with Na_2CO_3, and the aqueous mixture was extracted with CH_2Cl_2 (3 × 40 mL). The organic extracts were dried over Mg_2SO_4, filtered, and the solvent was evaporated under reduced pressure. The crude solid was recrystallized from ethanol. Yield: 0.41 g, 88%. Colorless crystalline solid, mp 225–228°C. MS: m/z 268 (M^+). IR (Nujol) (cm^{-1}): 3460, 3380, 1700. ^{1}H NMR (DMSO-d_6) δ: 2.49 (d, J = 15.7 Hz, 1H), 2.87 (dd, J = 16.1, 6.9 Hz, 1H), 3.71 (s, 3H), 4.40 (d, J = 6.2 Hz, 1H), 4.57 (s, 2H), 6.21 (d, J = 8.4 Hz, 1H), 6.70 (d, J = 8.4 Hz, 1H), 7.09–7.25 (m, 5H), 9.85 (s, 1H). ^{13}C NMR (DMSO-d_6) δ: 35.7, 38.4, 55.7, 102.8, 109.7, 109.8, 126.4, 127.0, 128.3, 132.1, 134.7, 142.1, 142.4, 168.0. Anal. calcd. for $C_{16}H_{16}N_2O_2$: C 71.64, H 5.97, N 10.44; found: C 71.45, H 6.05, N 10.15.

5-Azido-3,4-dihydro-8-methoxy-4-phenylquinolin-2(1*H*)-one (13)

To concentrated H_2SO_4 (1.72 mL) dissolved in water (5.7 mL) was added **12** (1.90 g, 7 mmol). The mixture was stirred for 10 min at room temperature, then more water (3 mL) was added and the mixture was cooled to 0–5°C in an ice water bath. A solution of sodium nitrite (0.63 g, 10 mmol) in water (5 mL) was carefully added dropwise and the mixture was stirred for 45 min. With strong stirring, a solution of sodium azide (0.7 g, 10 mmol) in water (5 mL) was then added dropwise and stirring was continued for a further 40 min. The light yellow solid, which separated, was collected by filtration and washed with plenty of water. The crystalline solid was dried under vacuum, mp 134–137°C. Yield: 1.80 g, 86%. MS: m/z 294 (M^+). IR (Nujol) (cm^{-1}): 2120, 1656. ^{1}H NMR (DMSO-d_6) δ: 2.60 (d, J = 16.2 Hz, 1H), 2.96 (dd, J = 16.2, 7.3 Hz, 1H), 3.82 (s, 3H), 4.43 (d, J = 6.4 Hz, 1H), 6.91 (d, J = 8.8 Hz, 1H), 7.05 (d, J = 8.5 Hz, 1H), 7.08–7.26 (m, 5H), 9.44 (s, 1H). ^{13}C NMR (DMSO-d_6) δ: 36.2, 36.8, 56.0, 111.4, 112.3, 117.7, 126.7, 128.4, 128.6, 129.5, 141.6, 143.0, 143.8, 168.1. Anal. calcd. for $C_{16}H_{14}N_4O_2$: C 65.30, H 4.76, N 19.04; found: C 65.07, H 4.72, N 18.76.

Compound **13** was dissolved in xylene (750 mL) and refluxed for 4 h until the disappearance of the starting material (TLC). Then the reaction mixture was left in the refrigerator for overnight and the formed deep brown solid was filtered and washed with petroleum ether (bp 49–60°C). The crude material was chromatographed using ethyl acetate as an eluent and a brown crystalline solid was then obtained. Its TLC, NMR, and mass analysis showed that the product was indeed 5-amino-3,4-dihydro-8-methoxy-4-phenylquinolin-2(1*H*)-one (**12**).

Compound **13** (1 g) was melted and kept stirring at 150°C under nitrogen atmosphere for 30 min. Examination of the NMR and TLC of the crude product showed that the product is **12**.

3,4-Dihydro-4-phenylquinolin-2(1*H*),5,8-trione (15)

To a stirred solution of the product obtained from attempted insertion reaction of **13** (0.38 g, 1.4 mmol) dissolved in H_2SO_4 (59 mL, 35%) was added activated MnO_2 (0.46 g) portionwise at 0°C. Stirring was carried out 1 h longer, then the mixture was diluted with CH_2Cl_2 (30 mL), neutralized with Na_2CO_3, and filtered. The filtrate was washed with water and the CH_2Cl_2 phase was separated, dried over Mg_2SO_4, filtered, and the solvent was evaporated under reduced pressure. The crude product was crystallized from toluene. Yield: 0.27 g, 78%. Red needles, mp 154–156°C. MS: m/z 253 (M^+). IR (Nujol) (cm^{-1}): 3340, 1740, 1654, 1640. ^{1}H NMR ($CDCl_3$) δ: 2.88 (m, 2H), 4.44 (m, 1H), 6.66 (s, 2H), 7.22 (s, 5H), 8.22 (s, 1H). Anal. calcd. for $C_{15}H_{11}NO_3$: C 71.14, H 4.34, N 5.53; found: C 70.90, H 4.04, N 5.30.

5-Acetamido-8-methoxy-4-phenylquinolin-2(1*H*)-one (16)

A mixture of compound **7** (0.30 g, 1 mmol) and Pd/C (10%, 53 mg) in diphenyl ether (30 mL) was refluxed for 48 h. The reaction mixture was cooled to room temperature, filtered through kiselguhr under suction, and the kiselguhr washed with CH_2Cl_2 (50 mL). The dichloromethane solution was evaporated under reduced pressure and the resulting diphenyl ether solution was poured into petroleum ether (bp 40–60°C, 100 mL). The solid, which separated, was collected by filtration and washed with petroleum ether (25 mL). The crude solid was chromatographed on silica, using ethyl acetate as the first eluent to remove starting material (20%) and then ethanol–ethyl acetate (1:6) to obtain the product. Yield: 0.2 g, 65%. Colorless crystalline solid, mp 193–196°C. MS: m/z 308 (M^+). IR (Nujol) (cm^{-1}): 1615–1654. ^{1}H NMR (DMSO-d_6) δ: 1.12 (s, 3H), 3.93 (s, 3H), 6.22 (s, 1H), 6.84 (d, 1H, J = 8.2 Hz, 1H), 7.18 (d, J = 8.2 Hz, 1H), 7.21–7.41 (m, 5H), 8.81 (s, 1H), 10.88 (s, 1H). ^{13}C NMR (DMSO-d_6) δ: 21.8, 56.4, 110.9, 115.1, 121.6, 124.3, 127.1, 127.3, 127.5, 127.7, 129.9, 139.4, 144.2, 151.1, 159.9, 168.1. Anal. calcd. for $C_{18}H_{16}N_2O_3$: C 70.12, H 5.19, N 9.09; found: C 70.50, H 5.41, N 8.96.

5-Amino-8-methoxy-4-phenylquinolin-2(1*H*)-one (17)

The same reaction conditions and work-up were applied as in the preparation of **12** for the deacetylation of **16** to obtain **17**. The crude product was recrystallized from toluene. Yield: 96%. Yellow needles, mp 216–218°C. MS: m/z 266 (M^+). IR (nujol) (cm^{-1}): 3480, 3440,1650. ^{1}H NMR (DMSO-d_6) δ: 3.80 (s, 3H), 4.12 (s, 2H), 6.05 (s, 1H), 6.30 (d, J = 8.4 Hz, 1H), 7.03 (d, J = 8.8 Hz, 1H), 7.38–7.51 (m, 5H), 10.39 (s, 1H). ^{13}C NMR DMSO-d_6 δ: 56.9, 105.4, 107.1, 114.7, 121.0, 127.5, 128.4, 128.6, 130.1, 137.0,139.4, 139.7, 151.2, 159.9. Anal. calcd. for $C_{16}H_{14}N_2O_2$: C 72.14, H 5.26, N 10.52; found: C 72.14, H 5.19, N 10.29.

5-Azido-8-methoxy-4-phenylquinolin-2(1*H*)-one (18)

Using the same reaction conditions as in the preparation of **13**, compound **17** was converted to the azide **18**. Instead of filtering the precipitate, which formed after the addition of NaN_3, the reaction mixture was poured into water (30 mL), and the resulting solution neutralized with Na_2CO_3

© 2000 NRC Canada

and extracted with CH_2Cl_2 (3 × 40 mL). The organic extracts were dried (Mg_2SO_4), filtered, and the solvent was evaporated under reduced pressure. The yellow crystalline solid, which was obtained in 93% yield, was used directly for the next insertion step. IR (Nujol) (cm^{-1}): 2120, 1640. ^1H NMR ($CDCl_3$) δ: 4.0 (s, 3H), 6.44 (s, 1H), 6.84 (s, 1H), 6.86 (s, 1H), 7.12–7.24 (m, 5H), 9.16 (s, 1H).

3,7-Dihydro-4-methoxy-2-oxo-pyrido(2,3,4-*kl*)acridine (19)

Compound **18** (0.60 g, 2 mmol) was refluxed in xylene (750 mL) for 1.5 h. The reaction mixture was cooled to room temperature and left overnight. The solid, which separated, was collected by filtration and washed with petroleum ether (bp 40–60°C, 25 mL). This crude product was chromatographed on silica using ethyl acetate–ethanol (4:2) as eluent. Yield: 0.41 g, 78%. Brown crystalline solid, mp 270°C (decomp.). MS: *m*/*z* 264 (M^+). IR (Nujol) (cm^{-1}): 1610–1650. ^1H NMR (DMSO-d_6) δ: 3.83 (s, 3H), 6.44 (s, 1H), 6.56 (d, *J* = 8.7 Hz, 1H), 6.97 (t, *J* = 7.1 Hz, 1H), 7.07 (d, *J* = 8.2 Hz, 1H), 7.18 (d, *J* = 8.7 Hz, 1H), 7.41 (t, *J* = 7.3 Hz, 1H), 7.93 (d, *J* = 7.8 Hz, 1H), 10.01 (s, 1H), 10.42 (s, 1H). ^{13}C NMR (DMSO-d_6) δ: 56.7, 101.8, 102.6, 108.2, 114.1, 115.8, 115.9, 120.1, 124.4, 129.6, 131.6, 131.7, 137.5, 139.2, 142.3, 162.4. Anal. calcd. for $C_{16}H_{12}N_2O_2$: C 72.72, H 4.54, N 10.60; found: C 72.39, H 4.56, N 10.34.

2-Chloro-4-methoxy-7*H*-pyrido(2,3,4-*kl*)acridine (20)

Compound **19** (0.20 g, 0.75 mmol) was refluxed in $POCl_3$ (30 mL) for 1 h. The reaction mixture was cooled to room temperature and poured into water (50 mL). The resulting solution was neutralized with Na_2CO_3 and the solid, which separated, was collected by filtration. This gave 0.17 g (83%) of crude red crystalline solid which showed one spot on the TLC and was used directly for the next step. A sample was crystallized from toluene for the analysis, mp 202°C (decomp.). MS: *m*/*z* 282 (M^+). ^1H NMR (DMSO-d_6) δ: 3.85 (s, 3H), 6.69 (d, *J* = 8.4 Hz, 1H), 6.92–7.41 (m, 5H), 7.99 (d, *J* = 8.0 Hz, 1H), 10.57 (s, 1H). ^{13}C NMR (DMSO-d_6) δ: 56.1, 113.6, 114.3, 115.6, 117.9, 120.2, 124.6, 128.1, 128.8, 131.9, 132.4, 139.8, 140.1, 143.7, 144.8, 151.8, 1H. Anal. calcd. for $C_{16}H_{11}ClN_2O$: C 67.97, H 3.92, N 9.91, Cl 12.54; found: C 67.84, H 4.05, N 9.66, Cl 12.20.

4-Methoxy-7*H*-pyrido(2,3,4-*kl*)acridine (21)

Compound **20** (0.50 g, 2 mmol) was catalytically hydrogenated with 10% Pd/C (50 mg) in ethyl alcohol (40 mL) in the presence of triethylamine (0.25 g, 2.7 mmol) for 6 h at room temperature. The catalyst was filtered off through kieselguhr under suction, and then the solvent was evaporated under reduced pressure. This gave 0.34 g (79%) of red crystalline product, which showed one spot on TLC, mp 224°C (decomp.). MS: *m*/*z* 248 (M^+). ^1H NMR (DMSO-d_6) δ: 3.84 (s, 3H), 6.58 (d, *J* = 8.9 Hz, 1H), 6.90 (t, *J* = 8.3 Hz, 1H), 6.95 (d, *J* = 8.3 Hz, 1H), 7.1 (d, *J* = 8.3 Hz, 1H), 7.33 (t, *J* = 7.6 Hz, 1H), 7.41 (d, *J* = 4.9 Hz, 1H), 7.93 (d, *J* = 7.3 Hz, 1H), 8.48 (d, *J* = 4.9 Hz, 1H), 10.30 (s, 1H). ^{13}C NMR (DMSO-d_6) δ: 56.2, 101.5, 107.1, 112.3, 115.1, 119.2, 119.8, 124.0, 130.8, 131.7, 132.1, 139.6, 140.2, 141.1, 145.7, 150.7. Anal. calcd. for $C_{16}H_{12}N_2O$: C 77.42, H 4.48, N 11.29; found: C 77.21, H 4.84, N 11.24.

References

1. (*a*) M.H.G. Munro, R.T. Luibrand, and J.W. Blunt. *In* Bioorganic marine chemistry. Vol. 1. *Edited by* P.J. Scheuer. Springer, New York. 1987; (*b*) T. Ozturk. *In* The alkaloids. Vol. 49. *Edited by* G.A. Cordell. Academic Press, New York. 1997; (*c*) C.J. Moody and R. Thomas. Adv. Heterocycl. Nat. Prod. Synth. **2**, 377 (1992); (*d*) T.F. Molinski. Chem. Rev. **93**, 1825 (1993).
2. E. Lederer, G. Tessier, and C. Huttrer. Bull. Soc. Chim. Fr. **7**, 608 (1940).
3. (*a*) S.J. Bloor and F.J. Schmitz. J. Am. Chem. Soc. **109**, 6134 (1987); (*b*) F.S. de Guzman and F.J. Schmitz. Tetrahedron Lett. **30**, 1069 (1989).
4. J. Kobayashi, J. Cheng, H. Nakamura, Y. Ohizumi, Y. Hirata, T. Sasaki, T. Ohta, and S. Nozoe. Tetrahedron Lett. **29**, 1177 (1988).
5. (*a*) J. Kobayashi, J. Cheng, M.R. Walchli, H. Nakamura, Y. Hirata, T. Sasaki, and Y. Ohizumi. J. Org. Chem. **53**, 1800, (1988); (*b*) L.A. McDonald, G.S. Eldredge, L.R Barrows, and C.M. Ireland. J. Med. Chem. **37**, 3819 (1994).
6. T.F. Molinski, E. Fahy, D.J. Faulkner, G.D. Van Duyne, and J. Clardy. J. Org. Chem. **53**, 1340 (1988).
7. G.A. Charyulu, T.C. McKee, and C.M. Ireland. Tetrahedron Lett. **30**, 4201 (1989).
8. T.F. Molinski and C.M. Ireland. J. Org. Chem. **54**, 4256 (1989).
9. G.P. Gunawardana, S. Kohmoto, S.P. Gunasekara, O.J. McConnell, and F.E. Koehn. J. Am. Chem. Soc. **110**, 4856 (1988).
10. G.P. Gunawardana, S. Kohmoto, and N.S. Barres. Tetrahedron Lett. **30**, 4359 (1989).
11. A. Rudi, Y. Benayahu, I. Goldberg, and Y. Kashman. Tetrahedron Lett. **29**, 3861 (1988).
12. A. Rudi and Y. Kashman. J. Org. Chem. **54**, 5331 (1989).
13 (*a*) A.R. Carroll and P.J. Scheuer. J. Org. Chem. **55**, 4426 (1990); (*b*) C. Eder, P. Schupp, P. Proksch, V. Wray, K. Steube, C.E. Müller, W. Frobenius, M. Herderich, and R.W.M. van Soest. J. Nat. Prod. **61**, 301 (1998).
14. A.R. Carroll, N.M. Cooray, A. Pointer, and P.J. Scheuer. J. Org. Chem. **54**, 4231 (1989).
15. G.K.-Goldhldshlager, M. Aknin, E.M. Gaydou, and Y. Kashman. J. Org. Chem. **63**, 4601 (1998).
16. B.R. Copp, J. Jompa, A. Tahir, and C.M. Ireland. J. Org. Chem. **63**, 8024 (1998).
17. A. Plubrukarn and B.S. Davidson. J. Org. Chem. **63**, 1657 (1998).
18. F.J. Schmitz, S.K. Agarwal, S.P. Gunasekera, P.G. Schmidt, and J.N. Shoolery. J. Am. Chem. Soc. **105**, 4835 (1983).
19. F.S. de Guzman, B. Carte, N. Troupe, D.J. Faulkner, M.K. Harper, G.P. Concepcion, G.C. Mangalindan, S.S. Matsumoto, L.R. Barrows, and C.M. Ireland. J. Org. Chem. **64**, 1400 (1999).
20. J. Kim. E.O. Pordesimo, S.I. Toth, F.J. Schmitz, and I. Van Altena. J. Nat. Prod. **56**, 1813 (1993).
21. P.A. Searle and T.F. Molinski. J. Org. Chem. **59**, 6600 (1994).
22. (*a*) A. Echavarren and J.K. Stille. J. Am. Chem. Soc. **110**, 4051 (1988); (*b*) R.H. Prager and C. Tsopelas. Heterocycles, **29**, 847 (1989); (*c*) A. Kubo and S. Nakahara. Heterocycles, **27**, 2095 (1988); (*d*) F. Bracher. Liebigs Ann. Chem. 205 (1990); (*e*) C.J. Moody, C.W. Rees, and R. Thomas. Tetrahedron Lett. **31**, 4375 (1990); (*f*) F. Bracher. Heterocycles, **29**, 2093 (1989); (*g*) C.V. Labarca, A.R. McKenzie, C.J. Moody, C.W. Rees, and J. Vaquero. J. Chem. Soc. Perkin Trans. 1, 927

© 2000 NRC Canada

(1987); (*h*) C. Subramanyam, M. Noguchi, and S.M. Weinreb. J. Org. Chem. **54**, 5580 (1989); (*i*) M.A. Ciufolini and N.E. Byrne. Tetrahedron Lett. **30**, 5559 (1989); (*j*) N.M. Ali, S.K. Chattopadhyay, A. McKillop, R.M.P.-Gentil, T. Ozturk, and R.A. Rebelo. J. Chem. Soc. Chem. Commun. 1453 (1992); (*k*) S.H. Dunn and A. McKillop. J. Chem. Soc. Perkin Trans. 1, 879 (1993); (*l*) M. Alvarez and J.A. Joule. Heterocycles, **34**, 2385 (1992); (*m*) G. Gellerman, A. Rudi, and Y. Kashman. Tetrahedron, **50**, 12959 (1994); (*n*) B.S. Lindsay, A.N. Pearce, and B.R. Copp. Synth. Commun. **27**, 2587 (1997); (*o*) N. Bontemps, E. Delfourne, J. Bastide, C. Francisco, and F. Bracher. Tetrahedron, **53**, 1743 (1997); (*p*) S. Nakahara, J. Matsui, and A. Kubo. Tetrahedron Lett. **39**, 5521 (1998); (*s*) Y. Kitahara, F. Tamura, M. Nishimura, and A. Kubo. Tetrahedron, **54**, 8421 (1998); (*t*) D. Zhang, I. Llorente, and L.S. Liebeskind. J. Org. Chem. **62**, 4330 (1997); (*v*) M. Alvarez, L. Feliu, W. Ajana, J.A. Joule, and J.L.F.-Puentes. Eur. J. Org. Chem. 849 (2000).

23. (*a*) M.A. Ciufolini and M.J. Bishop. J. Chem. Soc. Chem. Commun. 1463 (1993); (*b*) M.A. Ciufolini and N.E. Byrne. J. Am. Chem. Soc. **113**, 8016 (1991).

© 2000 NRC Canada

A tosyliminium ion-based total synthesis of (±)-schefferine

Darío A. Bianchi and Teodoro S. Kaufman

Abstract: The synthesis of the phenolic tetrahydroprotoberberine alkaloid (±)-schefferine is reported, featuring as key steps a tosyliminium ion-mediated Friedel–Crafts alkylation of eugenol dimethyl ether and an intramolecular Mitsunobu-type amination.

Key words: total synthesis, (±)-schefferine, natural product, tosyliminium ion, Mitsunobu amination.

Résumé : On a réalisé la synthèse de la (±)-schefférine, un alcaloïde phénolique dérivé de la tétrahyroprotoberbérine. Les étapes clés de cette synthèse sont une alkylation de Friedel–Crafts l'éther diméthylique de l'eugénol assistée par l'ion tosyliminium et un amination intramoléculaire du type Mitsunobu.

Mots clés : synthèse totale, (±)-schefférine, produit naturel, ion tosyliminium, amination de Mitsunobu.

[Traduit par la Rédaction]

In 1972, Gellert and Rudzats (1) reported the isolation of schefferine from the bark of *Schefferomitra subaequalis* Diels (Anonaceae), a New Guinea liana found as a climber on rain forest trees. The structure of this phenolic tetrahydroprotoberberine alkaloid, also known as tetrahydropalmatrubine (2), was formulated as **1** on the basis of its ^{1}H NMR and mass spectral data.

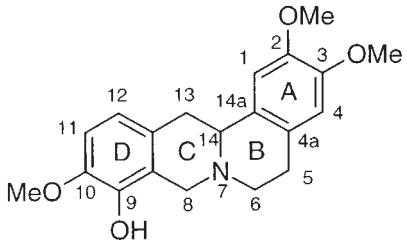
Several syntheses of (±)-schefferine have been previously reported, including reduction of protoberberines as well as Mannich cyclization and photolysis of 1-substituted tetrahydroisoquinolines. Späth and Burger (3) prepared (±)-**1** long before its isolation from a natural source by reduction of palmatrubine, a monodemethylation product of the widely known alkaloid palmatine. A similar approach, involving the synthesis and reduction of a palmatrubine derivative, was followed by Dutta and Bradsher (2*b*).

More recently, Kametani and co-workers informed that the Mannich cyclization of a conveniently substituted 1-benzyltetrahydroisoquinoline under careful pH control, furnished moderate yields of (±)-schefferine (4*a*). The same group also reported the synthesis of this natural product employing the Mannich reaction of a brominated 1-benzyl tetrahydroisoquinoline, produced by a Bischler–Napieralski reaction (4*b*). Noteworthy, they were unable to obtain (±)**–1** by phenolic cyclization of a related substrate (4*c*).

Received May 1, 2000. Published on the NRC Research Press website on August 18, 2000.

D.A. Bianchi and T.S. Kaufman.[1] Instituto de Química Orgánica de Síntesis (CONICET-UNR) and Facultad de Ciencias Bioquímicas y Farmacéuticas, Universidad Nacional de Rosario, Suipacha 531, (2000) Rosario, Argentina.

[1]Author to whom correspondence should be addressed. Telephone: 54-341-4804600. Fax: 54-341-4370477. e-mail: tkaufman@agatha.unr.edu.ar



(±)-Schefferine, (±)-1

In addition, (±)-schefferine was isolated as a minor product resulting from the Mannich reaction of a 1-benzyltetrahydroisoquinoline with formaldehyde generated in situ during the photolysis of the starting heterocycle (5). Interestingly, better yields of (±)**–1** were realized when photolysis of bromoenamides was employed as synthetic strategy (6).

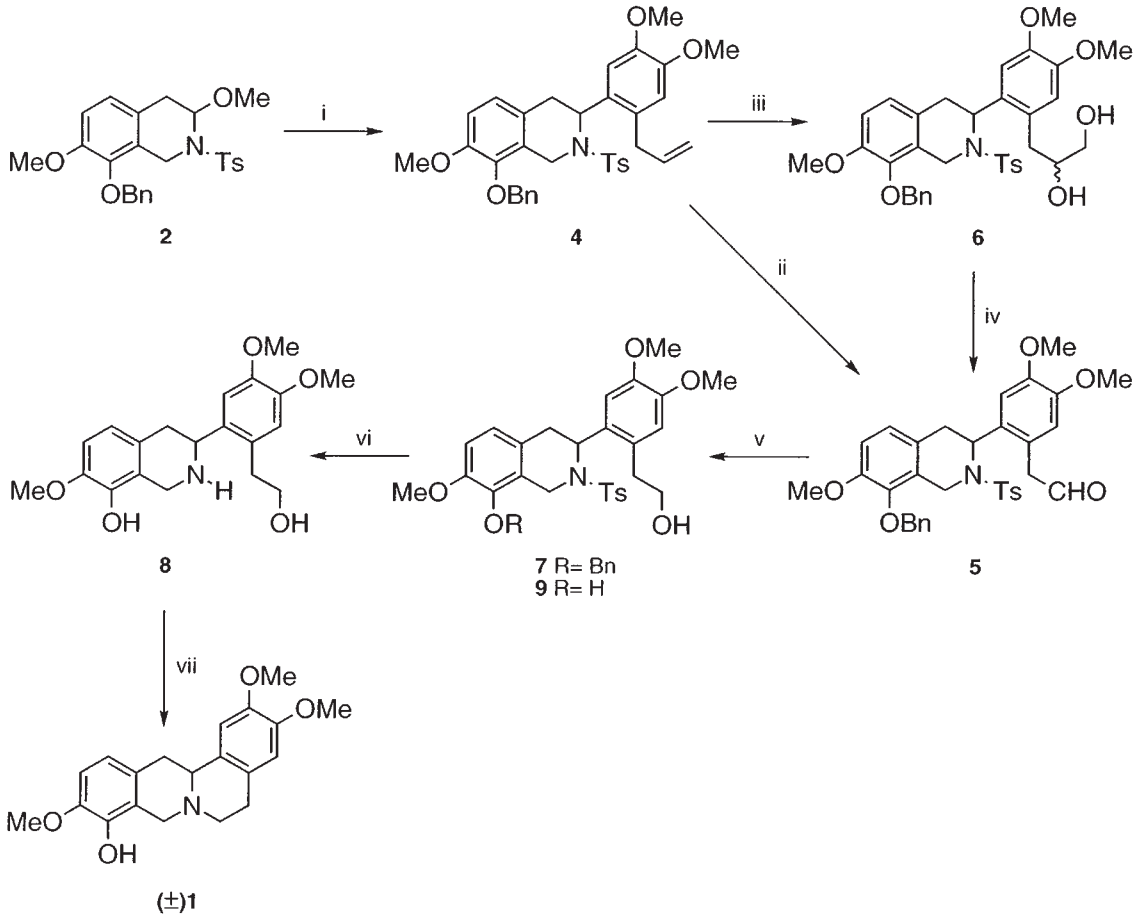
Tracer experiments on *Stephania glabra* Miers (Menispermaceae) evidenced high incorporation of (±)-[aryl-^{3}H]-schefferine into corydalmine but not into stepholidine, indicating that **1** might be a possible intermediate of the biosynthesis of corydalmine from reticuline (7*a*). Likewise, schefferine has been postulated as an intermediate in the biosynthesis of sinactine from reticuline (2*a*) and as a precursor of tetrahydropalmatine (7*b*).

We have reported a convenient entry to 3-substituted tetrahydroisoquinolines featuring the reaction of silicon-based nucleophiles with tosyliminium ions, generated upon addition of Lewis acids to tosylamidals (8). By capturing the tosyliminium ions with electron rich aromatics, such as phenols and their ethers, we recently extended the scope of this transformation to the elaboration of the very useful 3-aryl tetrahydroisoquinolines (9).

Herein, we disclose the details of a new and efficient total synthesis of (±)-schefferine via a new approach, consisting in the tosyliminium ion mediated preparation of a 3-aryl

© 2000 NRC Canada

Scheme 1. Reagents and conditions: (*i*) 4-allyl-1,2-dimethoxybenzene (**3**), $BF_3{\cdot}Et_2O$, CH_2Cl_2, –78°C, 15 min, –30°C, 30 min; (*ii*) OsO_4 (cat.), $NaIO_4$, THF–H_2O (3:1); (*iii*) OsO_4 (cat.), NMO, Me_2CO–H_2O–$_t$BuOH (4:2:1); (*iv*) $NaIO_4$, THF–H_2O (3:1); (*v*) $NaBH_4$, MeOH–Et_2O (4:1); (*vi*) (1) Na, NH_3, –33°C; (2) NH_4Cl, –33°C→ rt; and (*vii*) PPh_3, DEAD, HBF_4, THF, reflux.



tetrahydroisoquinoline intermediate and a Mitsunobu-type intramolecular amination (10).

Although syntheses of alkaloids have made extensive use of acyliminium ion chemistry (11), the reactivity of the related tosyliminium ions has been comparatively less explored.

The known amidal **2** (8) was treated at –78°C with the commercially available 4-allyl-1,2-dimethoxybenzene (3) and $BF_3{\cdot}Et_2O$ to give the 3-aryl tetrahydroisoquinoline derivative **4** in 88% yield. β-Phenethyl alcohol **7** was then synthesized from **4** in two steps. First, sodium periodate-assisted oxidative olefin cleavage with osmium tetraoxide as catalyst in THF–water (12) gave aldehyde **5** in 77% yield; then, reduction of aldehyde **5** with sodium borohydride in dry methanol furnished alcohol **7** in 92% yield.

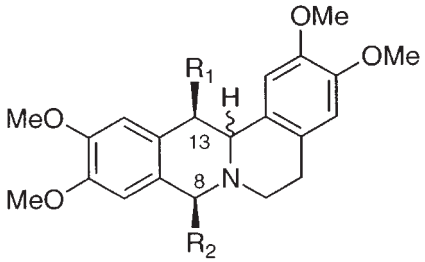
Because phenylacetaldehyde **5** tended to overoxidize, probably through its enol form, the dihydroxylation and oxidative fission steps were carried out separately, employing NMO as cooxidant during the dihydroxylation step, which resulted in an increased overall yield of 89%.

Debenzylation, desulfonylation, and formation of ring B were required to complete the synthesis. Our previous work suggested converting **7** into **8** by a stepwise process, consisting of catalytic debenzylation to yield phenol **9**, followed by sodium-mediated cleavage of the sulfonamide moiety. Although this approach allowed a better control of the delivery of the alkaline metal to the reaction medium to avoid formation of undesirable over-reduced side-products and furnish optimum yields of tetrahydroisoquinolines (13), reaction of **7** with sodium in liquid ammonia was found to cleanly effect simultaneous cleavage of both protective groups (14), providing amino alcohol **8** in 83% yield.

Finally, intramolecular Mitsunobu amination of **8** with the DEAD–PPh_3 couple in dry THF containing 1 equiv of HBF_4 gave 82% of (±)-schefferine [(±)–**1**], exhibiting a melting point and ^{1}H NMR spectrum identical with reported data (4*b*, 5*b*). The use of HBF_4 as additive was key for the success of this transformation to cyclized product in good yields. Protonation of the DEAD-derived hydrazide anion intermediate, is presumed to avoid its involvement as a competing nucleophile in the amination process (10*b*).

Dean and Rapoport (15) reported the syntheses of 8- and 13-methylberbines **10** and **11** by intramolecular cyclizations involving iminium ions formed by α-aminoacid decarbonylation. More recently, Padwa and Waterson (16) described a protoberberine synthesis which furnished **12**, employing a thionium–*N*-acyliminium ion cyclization of amido sulfoxides for the assembly of rings B and C. Unlike the above presented sequence leading to (±)-schefferine, these iminium ion-based synthetic strategies involved construction of ring B by formation of the C_6—N bond prior to the elaboration of the C_{14}—C_{14a} bond between rings A and C. The scope and limitations of this alternative protocol are currently

© 2000 NRC Canada



10 R_1= H, R_2= Me
11 R_1= Me, R_2= H

being evaluated for the synthesis of protoberberine-type natural products.

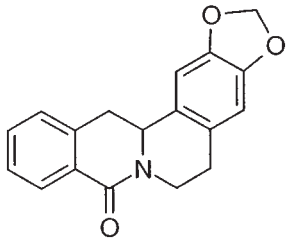
Experimental section

Melting points were measured on an Ernst Leitz hot-stage microscope apparatus and are uncorrected. IR spectra were taken on a Beckman Acculab 8 spectrophotometer with solid samples as KBr pellets and liquid samples as films. ^{1}H and ^{13}C NMR spectra were recorded in $CDCl_3$, on a Bruker AC-200E instrument at 200.13 and 50.33 MHz respectively, with TMS as the internal standard. ^{13}C NMR resonances corresponding to two carbon atoms are designated with an asterisk while those assigned to three carbons are marked with "#." High resolution mass spectra were obtained from UMYMFOR (FCEN, Buenos Aires).

4-Allyl-1,2-dimethoxybenzene was purchased from Aldrich Chemical Co. and used without further purification. All reactions were carried out in a dry oxygen-free nitrogen atmosphere, monitored by thin layer chromatography on Merck's precoated silica gel 60 F_{254} TLC plates developed in hexane–EtOAc (7:3) or $CHCl_3$–EtOH (8:2) and detected by examination under UV light followed by spraying with 2% *p*-anisaldehyde–sulfuric acid reagent in EtOH or 0.2% ninhydrin in EtOH. Careful heating improved the sensitivity of the detection. All new compounds gave a single spot by TLC. Flash chromatography was carried out on Merck Kieselgel 60 (0.04–0.063 mm), packed in hexane; elution was with mixtures of hexane–EtOAc, using gradient techniques. Compounds were preadsorbed from Et_2O or CH_2Cl_2 solutions onto the adsorbent before column chromatography.

3-(2-Allyl-4,5-dimethoxyphenyl)-8-benzyloxy-7-methoxy-2-(toluene-4-sulfonyl)-1,2,3,4-tetrahydroisoquinoline (4)

A CH_2Cl_2 solution of 4-allyl-1,2-dimethoxybenzene (0.88 mL, 0.49 mmol) was added to amidal **2** (110 mg, 0.243 mmol) in anhydrous CH_2Cl_2 (3 mL) and the resulting solution was cooled to –78°C. Then, a solution of $BF_3{\cdot}Et_2O$ in CH_2Cl_2 (0.51 mL, 0.29 mmol) was added dropwise. Stirring continued for 15 min at –78°C and 30 min at –30°C. Then the reaction mixture was rapidly poured over brine (10 mL) and the products were extracted with EtOAc (4 × 25 mL). Drying (Na_2SO_4), concentration, and chromatography of the combined ethereal extracts afforded the 3-aryltetrahydroisoquinoline derivative **4** (128 mg, 88%) as a colourless oil which crystallized on standing, mp 120–121.5°C (hexane–EtOAc). IR (neat) (cm^{-1}): 2920, 2850, 1600, 1500, 1440, 1350, 1280, 1160, 1070, 910, 820, 730, and 660. ^{1}H NMR δ: 2.41 (s, 3H), 2.79 (dd, *J* = 9.0, 11.8 Hz, 1H), 3.36 (brd, 2H), 3.60 (s, 3H), 3.68 (dd, *J* = 5.4, 11.8 Hz, 1H), 3.85 (s, 3H), 3.87 (s, 3H), 3.89 (d, *J* = 15.9 Hz, 1H), 4.38 (dd, *J* = 5.4, 9.0 Hz, 1H), 4.55 (d, *J* = 15.9 Hz, 1H), 4.93–5.10 (m, 2H), 5.03 (d, *J* = 11.1 Hz, 1H), 5.12 (d, *J* = 11.1 Hz, 1H), 5.85–6.06 (m, 1H), 6.23 (s, 1H), 6.48 (d, *J* = 8.7 Hz, 1H), 6.68 (s, 1H), 6.71 (d, *J* = 8.7 Hz, 1H), 7.25 (d, *J* = 8.2 Hz, 2H), 7.30–7.50 (m, 5H) and 7.57 (d, *J* = 8.2 Hz, 2H). ^{13}C NMR δ: 21.37, 36.91, 39.77, 44.31, 49.89, 55.69,* 55.81, 74.22, 111.20, 112.42, 112.71, 115.79, 124.39, 126.77, 127.49,* 127.97,# 128.25,* 129.47,* 130.11, 130.22, 132.34, 133.57, 137.32, 137.42, 143.28,* 147.24, 147.62, and 150.25. HREIMS calcd. for $C_{35}H_{37}NO_6S$: 599.2342; found: 599.2347.



12

2-{2-[8-Benzyloxy-7-methoxy-2-(toluene-4-sulfonyl)-1,2,3,4-tetrahydroisoquinolin-3-yl]-4,5-dimethoxyphenyl}-ethanol (7)

A 2% w/v solution of OsO_4 in *tert*-butanol (0.051 mL) was added to a mixture of allyl tetrahydroisoquinoline **4** (125 mg, 0.21 mmol) and potassium periodate (144 mg, 0.63 mmol) in 3:1 THF–water (4 mL). The mixture was stirred overnight at room temperature and quenched with 10% sodium hydrogensulfite (5 mL); Celite (1 g) was added and stirring continued for an additional 1 h, then the suspension was filtered under reduced pressure through Celite contained in a Büchner funnel and the crude reaction product was exhaustively extracted with EtOAc (5 × 20 mL). The organic portion was dried (Na_2SO_4), concentrated, and chromatographed to furnish aldehyde **5** (96 mg, 77%) as an oil. IR (neat) (cm^{-1}): 2960, 2870, 1750, 1630, 1510, 1480, 1380, 1300, 1190, 1090, 970, 840, 760, and 680. ^{1}H NMR δ: 2.42 (s, 3H), 2.83 (dd, *J* = 8.5, 11.9 Hz, 1H), 3.55–375 (m, 3H), 3.60 (s, 3H), 3.85 (s, 3H), 3.86 (s, 3H), 3.93 (d, *J* = 16.5 Hz, 1H), 4.22 (dd, *J* = 5.0, 8.5 Hz, 1H), 4.47 (d, *J* = 16.5 Hz, 1H), 5.03 (d, *J* = 11.2 Hz, 1H), 5.13 (d, *J* = 11.2 Hz, 1H), 6.34 (s, 1H), 6.52 (d, *J* = 8.6 Hz, 1H), 6.63 (s, 1H), 6.72 (d, *J* = 8.6 Hz, 1H), 7.25 (d, *J* = 8.3 Hz, 2H), 7.35–7.52 (m, 5H), 7.58 (d, *J* = 8.3 Hz, 2H) and 9,70 (s, 1H). ^{13}C NMR δ: 21.32, 40.46, 44.22, 47.64, 49.72, 55.62, 55.72,* 74.16, 111.28, 112.80, 113.41, 122.17, 124.36, 126.61, 127.38,* 127.96, 128.24 (4 carbons), 129.33, 129.49,* 133.41, 133.56, 137.28, 143.18, 143.39, 147.86, 148.19, 150.39, and 198.74. HREIMS calcd. for $C_{34}H_{35}NO_7S$: 601.2134; found: 601.2132.

Without further purification, aldehyde **5** (66 mg, 0.11 mmol) was dissolved in a 4:1 MeOH–Et_2O mixture (10 mL) kept at 0°C in an ice water bath. Sodium

© 2000 NRC Canada

borohydride (10 mg, 0.26 mmol) was added, stirring continued during 15 min and the reaction was quenched with 10% w/v citric acid solution (10 mL). The organic solvent was evaporated under reduced pressure and the reaction product was extracted with EtOAc (4 × 15 mL). The organic extract was dried (Na_2SO_4), concentrated under reduced pressure, and the glassy residue was chromatographed, yielding alcohol **7** (61 mg, 92%), as a solid, mp 148–149.5°C. IR (KBr) (cm^{-1}): 3520, 2960, 2860, 1620, 1530, 1480, 1370, 1310, 1190, 1090, 980, 830, 760, and 680. ^{1}H NMR δ: 1.90 (brs, $w_{1/2}$ = 13 Hz,1H), 2.40 (s, 3H), 2.84 (dd, *J* = 7.4, 10.2 Hz, 1H), 2.88–3.02 (m, 2H), 3.59 (s, 3H), 3.69 (dd, *J* = 4.5, 10.2 Hz, 1H), 3.76–3.90 (m, 2H), 3.84 (s, 3H), 3.87 (s, 3H), 3.91 (d, *J* = 15.9 Hz, 1H), 4.43 (dd, *J* = 4.5, 7.4 Hz, 1H), 4.55 (d, *J* = 15.9 Hz, 1H), 5.03 (d, *J* = 11.2 Hz, 1H), 5.12 (d, *J* = 11.2 Hz, 1H), 6.22 (s, 1H), 6.48 (d, *J* = 8.6 Hz, 1H), 6.70 (d, *J* = 8.6 Hz, 1H), 6.74 (s, 1H), 7.25 (d, *J* = 8.2 Hz, 2H), 7.30–7.51 (m, 5H) and 7.58 (d, *J* = 8.2 Hz, 2H). ^{13}C NMR δ: 21.34, 35.69, 39.60, 44.32, 50.14, 55.64,* 55.77, 63.60, 74.18, 111.16, 112.23, 112.76, 124.35, 126.73, 127.39,* 127.95, 128.20,* 128.25,* 129.04, 129.48,* 130.11, 132.61, 133.54, 137.37, 143.24, 143.33, 147.38, 147.59, and 150.25. HREIMS calcd. for $C_{34}H_{37}NO_7S$: 603.2291; found: 603.2287.

2-{2-[8-Benzyloxy-7-methoxy-2-(toluene-4-sulfonyl)-1,2,3,4-tetrahydroisoquinolin-3-yl]-4,5-dimethoxyphenyl}-acetaldehyde (5)

A 2% w/v solution of OsO_4 in *tert*-butanol (0.100 mL) was added to a mixture of allyl tetrahydroisoquinoline **4** (250 mg, 0.42 mmol) and NMO (103 mg, 0.88 mmol) in 4:2:1 acetone–water–*tert*-butanol (8 mL). The mixture was stirred overnight at room temperature and then quenched with 10% sodium hydrogensulfite (5 mL). Celite (1 g) was added and stirring continued for an additional 1 h, when the suspension was filtered under reduced pressure through Celite contained in a Büchner funnel and the crude reaction product was exhaustively extracted with EtOAc (5 × 20 mL). The organic portion was dried (Na_2SO_4) and concentrated to yield **6**, as an oily 1:1 epimeric mixture (251 mg, 95%). IR (film) (cm^{-1}): 3450, 2950, 2860, 1600, 1500, 1290, 1190, 1070, 920, and 740. Without further purification, the mixture of diols (125 mg) was dissolved in 3:1 THF–water (4 mL) and treated with sodium periodate (101 mg, 0.44 mmol). The reaction was stirred 2 h at room temperature, then it was diluted with brine (5 mL) and extracted with EtOAc (5 × 20 mL). The combined organic extracts were dried (Na_2SO_4), concentrated in vacuum, and chromatographed, providing aldehyde **5** (111 mg, 94%) as an oil.

3-[2-(2-Hydroxyethyl)-4,5-dimethoxyphenyl]-8-hydroxy-7-methoxy-1,2,3,4-tetrahydroisoquinoline (8)

Anhydrous ammonia (10 mL) was condensed in a three-necked flask, fitted with a dry ice – acetone condenser protected with a calcium chloride tube and an ammonia inlet, and containing sulfonamide **7** (50 mg, 0.083 mmol) dissolved in dry THF (3 mL). With rapid stirring, sodium metal contained in a graduated glass tube was added portionwise to the reaction mixture until the characteristic blue colour persisted for 10 min. The reaction was quenched with ammonium chloride (50 mg) and MeOH (2 mL). The ammonia was slowly evaporated and the reaction products were mixed with silica gel. The solvent was removed under reduced pressure and the adsorbed reaction products were chromatographed (CH_2Cl_2–EtOH), furnishing **8** (25 mg, 83%) as an oil. IR (neat) (cm^{-1}): 3550–2500, 2960, 2880, 1630, 1500, 1470, 1280, 1060, 920, and 740. ^{1}H NMR δ: 2.91 (dd, *J* = 8.8, 12.3 Hz, 1H), 2.94 (brd, 2H), 3.31 (dd, *J* = 5.2, 12.3 Hz, 1H), 3.64 (s, 3H), 3.75–3.92 (m, 1H), 3.80 (s, 3H), 3.86 (s, 3H), 4.00–4.30 (m, 6H), 4.35 (dd, *J* = 5.2, 8.8 Hz, 1H), 6.25 (d, *J* = 8.5 Hz, 1H), 6.34 (s, 1H), 6.59 (d, *J* = 8.5 Hz, 1H) and 6.72 (s, 1H). ^{13}C NMR δ: 35.99, 39.31, 43.09, 50.76, 55.72, 55.77, 55.85, 63.62, 106.92, 112.18, 112.84, 119.97, 121.75, 129.17, 131.31, 134.07, 141.37, 144.17, 147.31, and 147.42. HREIMS calcd. for $C_{20}H_{25}NO_5$: 359.1733; found: 359.1736.

(±)-2,3,10-Trimethoxy-9-hydroxy-5,6,13,13a-tetrahydro-8*H*-dibenzo[*a*,*g*]quinolizine ((±)-schefferine, (±)-1)

Diethyl azodicarboxylate (0.022 mL, 0.122 mmol) was added all at once to a stirred solution of **8** (22 mg, 0.061 mmol), triphenylphosphine (32 mg, 0.122 mmol), and ethereal HBF_4 (0.008 mL, 0.067 mmol) in THF (2 mL). The reaction was stirred under reflux until complete conversion of the aminoalcohol was assessed by TLC; then, the volatiles were removed under reduced pressure and the remaining oil was chromatographed, yielding (±)-**1** (17 mg, 82%) as a solid, mp 146.5–148°C (lit. (5*b*) 144–145°C and (4*b*) 147–148°C). IR (KBr) (cm^{-1}): 3430, 2930, 2850, 2800–2720, 1630, 1590, 1500, 1450, 1340, 1290, 1200, 1140, 1070, 990, and 740. ^{1}H NMR δ: 2.18 (dd, *J* = 3.8, 13.3 Hz, 1H), 3.03 (dd, *J* = 2.3, 13.3 Hz, 1H), 3.18–3.56 (m, 5H), 3.68 (brs, 1H), 3.80 (s, 3H), 3.84 (s, 3H), 3.93 (s, 3H), 4.16 (d, *J* = 17.8 Hz, 1H), 4.33 (d, *J* = 17.8 Hz, 1H), 6.49 (s, 1H), 6.54 (d, *J* = 8.4 Hz, 1H), 6.67 (d, *J* = 8.4 Hz, 1H) and 6.82 (s, 1H). ^{13}C NMR δ: 34.15, 43.39, 48.42, 52.19, 55.76, 55.90, 56.06, 56.13, 108.89, 112.96, 114.36, 120.69, 121.95, 129.25, 133.09, 137.89, 140.49, 143.93, 146.45, and 146.51. HREIMS calcd. for $C_{20}H_{23}NO_4$: 341.1627; found: 341.1622.

Acknowledgements

The authors gratefully acknowledge CONICET, SECyT-UNR, and Fundación Antorchas for financial support and a fellowship (D.A.B).

References

1. E. Gellert and R. Rudzats. Aust. J. Chem. **25**, 2477 (1972).
2. (*a*) D.S. Bhakuni, S. Jain, and S. Gupta. Tetrahedron, **39**, 455 (1983); (*b*) N.L. Dutta and C.K. Bradsher. J. Org. Chem. **27**, 2213 (1962).
3. E. Späth and G. Burger. Ber. Dtsch. Chem. Ges. **59**, 1486 (1926).
4. (*a*) S.F. Dyke. The isoquinoline alkaloids. *In* Rodd's chemistry of carbon compounds. Vol. IV H. 2nd ed. *Edited by* S. Coffey. Elsevier, New York, 1978. p. 132; (*b*) T. Kametani, M. Ihara, and T. Honda. J. Chem. Soc. C 1060 (1970); (*c*) T. Kametani, K. Fukumoto, H. Agui, H. Yagi, K. Kigasawa, H. Sugahara, M. Hiiragi, T. Hayasaka, and H. Ishimaru. J. Chem. Soc. C 112 (1968).
5. (*a*) T.R. Govindachari, K. Nagarajan, S. Rajeswari, H. Suguna, and B.R. Pai. Indian J. Chem. Sect. B: Org. Chem. Incl. Med.

© 2000 NRC Canada

Chem. **15B**, 873 (1977); (*b*) T. Kametani, K. Fukumoto, M. Ihara, M. Takemura, H. Matsumoto, B.R. Pai, K. Nagarajan, M.S. Premila, and H. Suguna. Heterocycles, **3**, 811 (1975).
6. T. Kametani, T. Sugai, Y. Shoji, T. Honda, F. Sato, and K. Fukumoto. J. Chem. Soc. Perkin Trans. 1, 1151 (1977).
7. (*a*) D.S. Bhakuni, S. Gupta, and S. Jain. Tetrahedron, **39**, 4003 (1983); (*b*) D.S. Bhakuni, S. Jain, and S. Gupta. Tetrahedron, **36**, 2491 (1980).
8. V.L. Ponzo and T.S. Kaufman. Synlett. 1149 (1995).
9. D.A. Bianchi and T.S. Kaufman. Synlett. 801 (2000).
10. (*a*) R.C. Bernotas and R.V. Cube. Tetrahedron Lett. **32**, 161 (1991); (*b*) P.G. Sammes and S. Smith. J. Chem. Soc. Perkin Trans. 1, 2415 (1984).
11. H. Hiemstra and W.N. Speckamp. Additions to *N*-acyliminium ions. *In* Comprehensive organic synthesis. Vol. 2. *Edited by* B.M. Tost and I. Fleming. Pergamon Press, New York. 1991. pp. 1047–1082.
12. E.J. Corey, R.L. Danheiser, S. Chandrasekaran, P. Siret, G.E. Keck, and J.L. Gras. J. Am. Chem. Soc. **100**, 8031 (1978).
13. T.S. Kaufman. J. Chem. Soc. Perkin Trans. 1, 403 (1993).
14. K. Ito and H. Tanaka. Chem. Pharm. Bull. **25**, 1732 (1977).
15. R.T. Dean and H. Rapoport. J. Org. Chem. **43**, 4183 (1978).
16. A. Padwa and A. G. Waterson. Tetrahedron Lett. **39**, 8585 (1998).

© 2000 NRC Canada

Electrochemical studies of Schiff base compounds derived from antipyrine nucleus in ethanolic buffer solutions

Ibrahim S. El-Hallag, Gad B. El-Hefnawy, Youssef. I. Moharram, and Enass. M. Ghoneim

Abstract: The electrochemical behaviour of Schiff base compounds derived from an antipyrine nucleus was investigated in 30% (v/v) ethanolic buffer solutions (pH 3–11) using various electrochemical techniques at mercury electrode. The results showed that, the total limiting current of each of the studied compounds corresponds to 2-electron transfer process. The mechanistic pathway of the electrode reaction of the investigated compounds at mercury electrode, the effect of the medium, and the evaluation of the electrode reaction parameters were illustrated and discussed.

Key words: Schiff base, antipyrine nucleus, electrode reaction, electrochemical parameters, cyclic voltammetry.

Résumé : Opérant dans des solutions tampons (pH allant de 3 à 11) contenant 30% (v/v) d'éthanol et faisant appel à diverses techniques électrochimiques avec électrode de mercure, on a étudié le comportement électrochimique de diverses bases de Schiff dérivées du noyau antipyrine. Les résultats montrent que, le courant limite total de chacun de composés étudiés correspond à un processus de transfert d'électrons 2-. On illustre et on discute des voies mécanistiques de la réaction à l'électrode, de l'effet du milieu et de l'évaluation des paramètres de la réaction à l'électrode.

Mots clés : base de Schiff, noyau antipyrine, réaction à l'électrode, paramètres électrochimiques, voltampérométrie cyclique.

[Traduit par la Rédaction]

Introduction

The electroreduction of Schiff base compounds was the subject of several interesting investigations (1–6). Generally, the electroreduction of such compounds at mercury electrode in acidic and alkaline solutions consume two electrons per reactant molecule for saturation of a carbon–nitrogen double bond or four electrons for its reductive splitting.

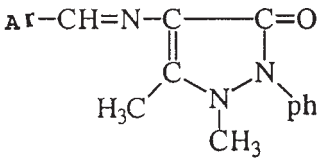
In this paper we report the electrochemical behaviour of some Schiff base compounds derived from an antipyrine nucleus in ethanolic buffer B.R. solutions. The electrochemical parameters of the electrode process were evaluated using dc–polarography, cyclic voltammetry and controlled potential coulometry. Verification of the electrochemical parameters determined experimentally via digital simulation method was also considered. The mechanistic pathway of the electrode reaction was discussed.

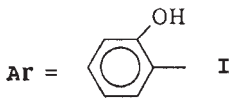
Experimental

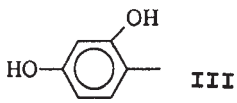
Chemicals and solutions

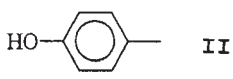
The compounds under consideration were prepared by adding a solution of 4-aminoantipyrine (0.01 mol) dissolved in ethanol to an ethanolic solution of 0.01 mol of salicyladehyde, *p*-hydroxybenzaldehyde, 2,4-dihydroxybenzaldehyde, and 2-hydroxy-1-naphthaldehyde. Then, the mixture was heated and refluxed for about 2 h. On cooling the mixture, the solid compounds were separated and filtered off. The crude products were recrystallized several times from hot ethanol, washed with diethyl ether, and finally dried in a vacuum desiccator. The purity of the compounds was ascertained by crystallization until a constancy of the mp was reached. The structure of the prepared compounds were confirmed by elemental and spectral analysis. The prepared compounds have the general structure formula

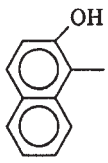
Scheme 1.











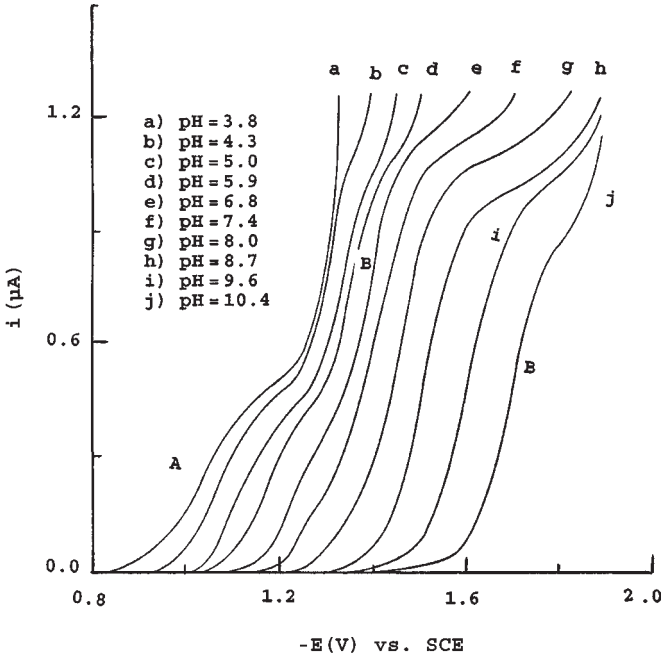
Received January 12, 2000. Published on the NRC Research Press website on September 1, 2000.

I.S. El-Hallag[1], G.B. El-Hefnawy, Y.I. Moharram, and E.M. Ghoneim. Chemistry Department, Faculty of Science, Tanta University, 31527, Tanta, Egypt.

[1]Author to whom correspondence may be addressed.

© 2000 NRC Canada

Fig. 1. Dc–polarograms of **III** in buffer solutions of different pH values, containing 30% (v/v) ethanol.



Stock solutions (2.5×10^{-3} M) of the prepared compounds were obtained by dissolving the accurate mass of the solid compound in appropriate volume of ethanol. Britton–Robinson buffer series (pH 2–12) containing 30% (v/v) ethanol were prepared from analytical grade chemicals and used as supporting electrolyte.

Instrumentation

The dc–polarograms were recorded using a Sargent Welch polarograph model 4001. The capillary characteristics were m = 1.03 mg s^{-1}, t = 3.3 s $drop^{-1}$ at mercury height (h) = 60 cm. The cyclic voltammograms were recorded using a polarographic Analyzer model 264A-PAR (from EG & G) and electrode assembly 303 A with a hanging mercury drop electrode (HMDE) of area = 2.6×10^{-2} cm^2 as a working electrode, Ag–AgCl as a reference electrode, and a Pt-wire as a counter electrode. The number of electrons consumed in the overall electrode reaction was determined using coulometry system model 380-PAR with a mercury pool cathode, saturated calomel electrode as a reference, and a Pt-wire as counter electrode. The electronic spectra were measured using Shimadzu UV–vis spectrophotometer model 160 A. Digital simulation of the extracted parameters for the cyclic voltammetric experiments were run on an PC computer using Condesim software packages (from EG & G) which allows accurate digital simulation for a wide range of mechanisms.

Results and discussion

Dc–polarography

The dc–polarographic behaviour of 2.5×10^{-4} M of Schiff base compounds (**I–IV**) was investigated in Britton–Robinson buffer solutions of pH 3–11 containing 30% (v/v) ethanol. It was found that in strong acidic solutions (pH < 3.0), the polarograms of all compounds under investigation do not show any reduction wave except the hydrogen wave which appears at a potential not more than –1.1 V. However, in solution of 3 ≤ pH ≤ 4.0 the polarograms of the studied compounds show a single reduction wave (A) Fig. 1. At pH > 4.0 a second ill-defined wave (B) appeared. This wave becomes well-defined on increasing the pH up to 7.0, its height increase at the expense of first wave (A) until the two waves merge together and become one wave. This behaviour is characteristic for compounds (**I–III**) while the polarograms of compound (**IV**) exhibit two waves of almost equal height in slightly acidic solutions and the height of the first wave decreases slightly with increasing pH. It is important to note that the total limiting current of the studied compounds corresponds to a two-electron transfer process as evidenced from coulometry studies. Figure 1 gives an example of the recorded dc–polarograms of compound (**III**).

Table 1. Dc–polarographic data obtained for compounds under investigation at 25°C.

Comp.	pH	$-E_{1/2}$ (V)		$(\alpha, n_a = 1)$	
		(*i*)[a]	(*ii*)[b]	(*i*)[a]	(*ii*)[b]
I	4.0	0.85	—	0.42	—
	6.0	0.98	1.25	0.31	0.40
	9.3	—	1.35	—	0.52
II	4.0	1.05	—	0.29	—
	6.0	1.18	1.34	0.35	0.20
	8.6	—	1.48	—	0.49
III	3.8	1.02	—	0.26	—
	5.9	1.16	1.35	0.37	0.40
	9.6	—	1.60	—	0.51
IV	3.9	0.89	—	0.25	—
	6.6	1.02	1.23	0.39	0.29
	9.1	1.25	1.38	0.35	0.31

[a](*i*) First wave.
[b](*ii*) Second wave.

The plots of i_l for compounds (**I–III**) as a function of pH of the medium recall a dissociation curve of two steps denoting the presence of an acid–base equilibrium. The height of the reduction waves is proportional to the square root of mercury height (h). The straight lines obtained on plotting log i_l vs. log h have slope values amounting to 0.45–0.53 revealing that the reduction process of the electrode reaction is mainly diffusion controlled (7). Also, the reduction waves of the Schiff base compounds under consideration were analyzed using the fundamental equation of irreversible polarographic waves (8)

$$[1] \qquad E = E_{1/2} - \frac{0.0591}{\alpha n_a} \log \frac{i}{(i_d - i)}$$

The low values (<0.5) of the cathodic symmetry coefficient (α) obtained from the slope S_1 ($S_1 = 0.0591/\alpha n_a$) of the E vs. log ($i/i_d - i$) plots indicate the irreversible nature of the electrode process. The most probable α-values are obtained for n_a = 1.0 (Table 1), where n_a is the number of electrons participating in the rate-determining step.

On increasing the pH of the electrolysis solution, the half-wave potentials ($E_{1/2}$) of the polarographic wave get shifted to more negative values (Table 1), denoting that the

© 2000 NRC Canada

Table 2. Data of cyclic voltammetry for compounds under investigation at 25°C, v = 0.5 V/s.

Comp.	pH	Mol wt.	$E_p - E_{p/2}$ (mV)		α (n_a = 1)	
			(*i*)[a]	(*ii*)[b]	(*i*)[a]	(*ii*)[b]
I	5.2	307.34	112	—	0.42	—
	10.5		120	135	0.40	0.35
II	6.3	323.34	115	—	0.41	—
	7.5		128	—	0.37	—
III	6.6	307.34	110	115	0.43	0.41
	9.6		125	130	0.38	0.36
IV	6.6	357.39	120	126	0.40	0.38
	10.5		132	138	0.36	0.34

[a](*i*) First wave.
[b](*ii*) Second wave.

hydrogen ions are consumed in the reduction process (9). The $E_{1/2}$–pH plots of the first reduction wave of the studied compounds give a break at pH 4.5–5.5, whereas the $E_{1/2}$–pH plots of the second one exhibit a break at pH 8–9, indicating *the protonation of -CH=N- center and the ionization of OH group of the reactants* at those pH values. From the slope values of logarithmic analysis (S_1) and that of $E_{1/2}$–pH plots (S_2) ($S_2 = (0.0591/\alpha n_a)Z_H^+$), the number of hydrogen ions participating in the rate-determining step is found to equal unity ($Z_H^+ = S_2/S_1$).

Controlled potential coulometry (CPC)

A coulometry measurement is performed by adding 10 mL of Britton–Robinson buffer (slightly acidic or alkaline) to the coulometric cell. The specified potential for each compound was applied to the cell and the electrolysis was continued until the background current attained a constant value. An amount of the reactant solution was then added (1 mL of 10^{-3} M) and the electrolysis was allowed to proceed until completion. The accumulated charge (Q) was read directly from the digital coulometer and the number of electrons (n) consumed for complete reduction of the reactants was calculated using the relation Q = nM/Fw), in which w is the mass (in grams) of the reactant, M is the reactant molecular weight and F is the Faraday's constant. The results obtained denoted that (n) equals two electrons per reactant molecule in both acidic and alkaline media.

Cyclic voltammetry

The voltammograms of the studied compounds in B.R. buffer solution at different scan rates ranging (10–500 mV/s) exhibit one or two well-defined cathodic peaks depending on the pH of the medium and nature of the substituent. In the reverse scan (anodic direction) no oxidation peaks were observed which confirms the irreversible nature of the reduction wave. The extent of the cathodic shift of the peak potential (E_p) as a function of the sweep rate, the difference between the potentials at half-peak ($E_{p/2}$) and at the peak (E_p), confirm the irreversible nature of the electrode process (10). So, the cathodic peak potential (E_p) varies with the logarithm of the potential sweep rate according to the eq. [2] (11)

$$[2]\qquad E_p = -1.14\left(\frac{RT}{\alpha n_a F}\right) + \left(\frac{RT}{\alpha n_a F}\right)\ln\left(\frac{(k_{f,h})}{D^{1/2}}\right) - \left(\frac{RT}{2\alpha n_a F}\right)\ln(\alpha n_a v)$$

On plotting E_p or $E_{p/2}$ for the investigated compounds vs. log v, linear correlations are obtained and the cathodic symmetry coefficient (α) values at selected pH values were calculated from the slopes of these plots. Values of the symmetry coefficient (α) were also determined from the difference of peak and half-peak cathodic potentials by means of the eq. (10)

$$[3]\qquad E_p - E_{p/2} = 1.857(RT/\alpha n_a F)$$

and were found to be less than 0.5 when n_a = 1 (Table 2), confirming the irreversible nature of the reduction process. Good agreement is found between α and n_a values calculated from the cyclic voltammetry data and their values obtained from dc–polarographic measurements.

For the irreversible charge transfer processes (12), the peak current (i_{pirr}) can be expressed by the following equation:

$$[4]\qquad i_{pirr} = 2.99 \times 10^5 n(\alpha n_a)^{1/2} A D^{1/2} C v^{1/2}$$

in which i_{pirr} is the peak current in amp, *and C is the concentration of the reactant species which equals 1.25 × 10^{-4} M in the present study*, and the other terms have their usual meaning.

On plotting the i_{pirr} vs. $v^{1/2}$ at different pH values straight lines with some slight deviation from the origin are obtained revealing the diffusion character of the current (13). Table 2 revealed that the peak width ($E_p - E_{p/2}$) grows larger for the higher molecular weight compounds as well as with increasing pH of the medium, indicating increased irreversibility nature of the electrode process as the molecular weight and (or) the pH are increased (14). The E_p vs. pH plots of the first peak of the investigated compounds give two segments with slope of 60–95 mV/pH which is not much different from the values obtained from dc–polarography experiments and indicates that the species in solution undergoes a fast protonation at the interface, prior to the reduction process (14).

Diffusion coefficient (D) of Schiff base compounds was determined from the following equation (15, 16)

$$[5]\qquad I_{lim} = \frac{i_{pirr}}{3.099(\alpha n_a v)^{1/2}}$$

Also, in the same manner, the ratio $[(dI_1/dt)_f]_{irr}/i_{pirr}$ for irreversible charge transfer can be used for determining the diffusion coefficient of the electroactive species via the following relation (16, 17)

$$[6]\qquad \frac{[dI_l/dt)_f]_{irr}}{i_{pirr}} = 3.73(\alpha/n_a)^{1/2} n v^{1/2}$$

where $[(dI_1/dt)_f]_{irr} = \alpha n^2 F^2 SCD^{1/2} v/3.367RT$ is the height of the forward sweep of the deconvoluted current, and the other terms have their usual meaning. Hence from relation [6], the ratio $[(dI_1/dt)_f]_{irr}$ can be determined which gives another accurate route for determination of the diffusion coefficient.

© 2000 NRC Canada

Table 3. Values of the diffusion coefficient (D) of the compounds under consideration determined via different methods at 25°C.

Comp.	pH	D x10^{10} (m^2/s)		
		(*i*)[a]	(*ii*)[b]	(*iii*)[c]
I	5.2	2.9	2.8	2.7
	10.5	2.5	2.2	2.3
II	6.3	3.1	2.7	2.9
	7.5	2.3	2.2	2.5
III	6.6	3.3	3.2	3.4
	9.6	3.1	2.9	3.3
IV	6.6	2.9	2.7	3.1
	10.5	2.3	2.2	2.4

[a](*i*) Value of D determined from *CV* via eq. [4].
[b](*ii*) Value of D determined from I_{lim} via eq. [5].
[c](*iii*) Value of D determined from $[(dI_1/dt)_f]_{irr}$ via eq. [6].

Table 4. Values of k_{fh} determined via ref. (11) and simulation method and its corresponding ψ of the investigated compounds at 25°C.

Comp.	pH	k_{fh} (m/s)		ψ
		Ref. (11)	Simulation method	
I	5.2	8.2×10^{-6}	9.5×10^{-6}	4.04×10^{-3}
	10.5	5.6×10^{-6}	6.2×10^{-6}	1.28×10^{-3}
II	6.3	7.1×10^{-6}	6.8×10^{-6}	1.81×10^{-3}
	7.5	7.9×10^{-7}	8.5×10^{-7}	4.04×10^{-4}
III	6.6	8.5×10^{-6}	9.3×10^{-6}	4.00×10^{-4}
	9.6	9.1×10^{-7}	9.4×10^{-7}	9.00×10^{-4}
IV	6.6	6.1×10^{-5}	6.3×10^{-5}	1.28×10^{-3}
	10.5	6.3×10^{-7}	6.1×10^{-7}	2.86×10^{-4}

Table 5. Values of peak characteristics, k_c, k_s, D, α, and $E°$ determined via theoretical work at sweep rate 0.5 V/s.

Comp.	pH	i_p (uA)	$E_p - E_{p/2}$ (mV)	k_c (s^{-1})	$k_s \times 10^6$ (m/s)	$D \times 10^{10}$ (m^2/s)	α	$-E°$ (V)
I	5.2	3.33	111	7	8.7	3.1	0.40	0.92
	10.5	5.52	121	8	6.5	1.9	0.35	1.30
II	6.3	5.31	117	5	6.1	2.9	0.42	1.13
	7.5	4.62	130	7	8.0	2.3	0.34	1.18
III	6.6	1.70	109	6	9.7	3.1	0.41	1.08
	9.6	5.35	126	8	0.9	2.6	0.33	1.24
IV	6.6	4.75	121	9	6.7	2.8	0.36	1.14
	10.5	2.91	133	10	0.62	1.9	0.32	1.26

Values of diffusion coefficient (D) determined via different methods (Table 3), indicate a good agreement between the values of D estimated via these methods. As a result of the disappearing of the anodic peak coupled with the cathodic one of the investigated compounds the heterogeneous rate constant (k_{fh}) of the irreversible electrode reaction can be calculated from cyclic voltammetric data using eq. [2] (11). The plot of E_p vs. log v gives the value of the heterogeneous rate constant (k_{fh}). Also, from the values of $E_p - E_{p/2}$ vs. the dimensionless parameter ψ, the heterogeneous rate constant is estimated. The values of k_{fh} is calculated by performing several simulated cyclic voltammograms with various values of k_{fh}. The true value of k_{fh} is established when the values of i_p, E_p, and $E_p - E_{p/2}$ of the simulated cyclic voltammograms agree well with those values of the experimental one. Values of k_{fh} determined from these methods were reported in Table 4 confirming the agreement and the accuracy of the heterogeneous rate constant estimated via different methods.

Verification of the calculated electrochemical parameters via digital simulation

Digital simulation was used for testing the determined accurate values of the cyclic voltammetry parameters as well as obtaining the true information of the type of electrochemical process of the electrode mechanism. In general the testing of parameters is made by matching the simulated voltammogram on the experimental data, using the average experimentally determined parameters. Also, the accuracy of the electrochemical parameters can be tested via the comparison between the peak characteristics (i_p, E_p, $E_p - E_{p/2}$), of the experimental and theoretical cyclic voltammograms (18, 19). The generated cyclic voltammograms have been carried out using CONDESIM software package (from EG & G).

In this work, the nature of the electrode reaction was determined by running digital simulation for the following types of electrochemical reactions: (*i*) $E_{irr}C_{irr}$; (*ii*) $E_{rev}C_{irr}$; (*iii*) $E_{rev}C_{rev}$; (*iv*) E_qC_{irr}; and (*v*) E_{irr}. The electrochemical parameters used are: (*i*) diffusion coefficient of the electroactive species (D); (*ii*) reduction potential ($E°$); (*iii*) concentration of the electroactive species (C); (*iv*) heterogeneous rate constant (k_{fh}); (*v*) scan rate (v); (*vi*) temperature (T); (*vii*) forward homogeneous chemical rate constant (k_f), (*viii*) backward homogenous chemical rate constant (k_b) ($k_c = k_f + k_b$); and (*ix*) symmetry coefficient (α).

Figure 2 shows the comparison between the experimental and generated cyclic voltammograms of $E_{irr}C_{irr}$ model with its convolution and deconvolution voltammetry of the first peak of compound **I** at pH 6.2 and scan rate 0.2 V/s. The value of reduction potential ($E°$) and the values of k_c for chemical steps which following the slow charge transfer were determined using theoretical treatment and their values at the selected pH values are given in Table 5. The values of the measured peak characteristics and the electrochemical parameters used for generating the voltammograms are listed in Table 5 and confirm the accuracy of calculated parameters from experimental cyclic voltammograms. *The slight deviation between the shape of experimental and simulated cyclic*

© 2000 NRC Canada

Fig. 2. Matching between experimental (….) and generating (—) voltammograms of I (A), its convolution (B) and deconvolution voltammetry of experimental voltammogram (C) at T = 298 K, sweep rate 0.2 V/s, pH 6.2.

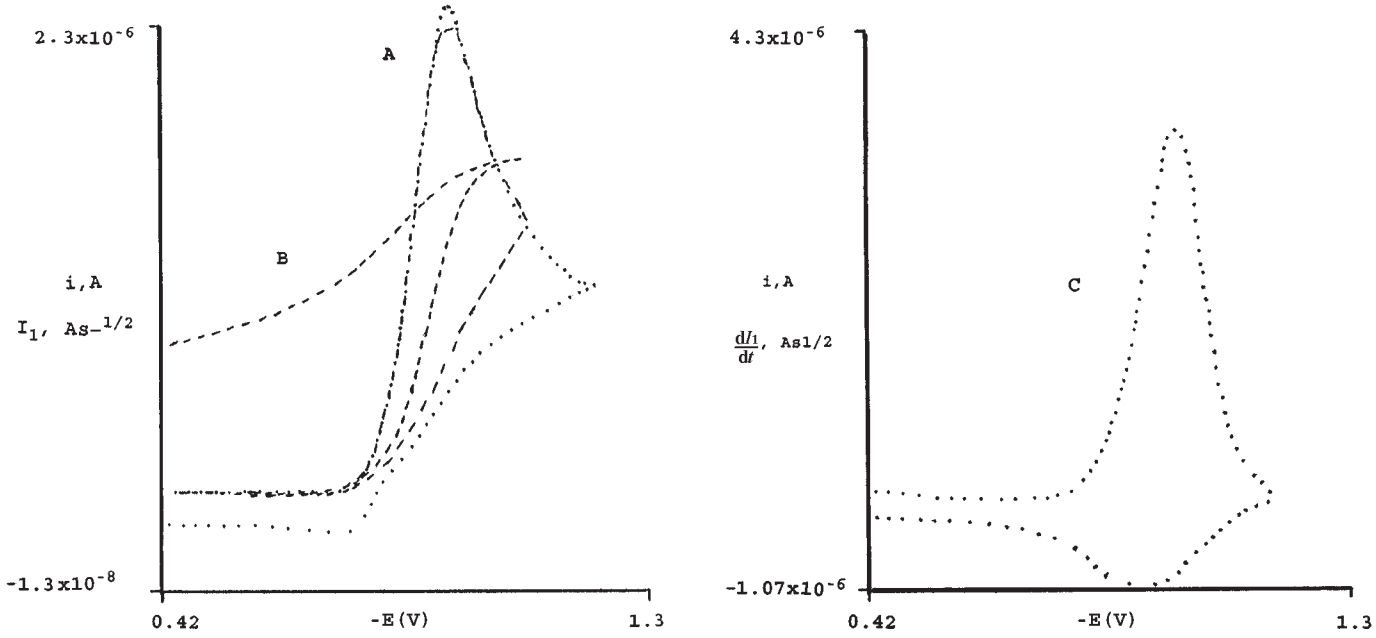
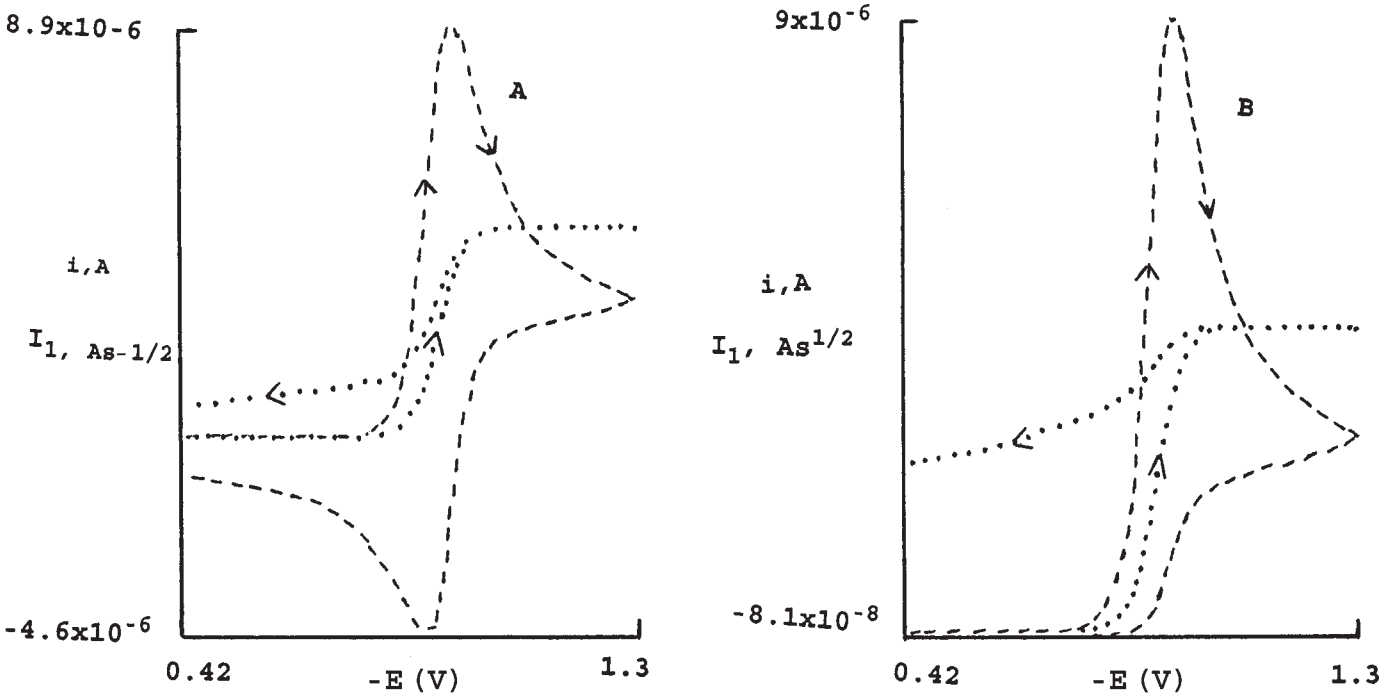


Fig. 3. Generating voltammograms of the models $E_{rev}C_{rev}$ (A) and $E_{rev}C_{irr}$ (B) with their convolution voltammetry at sweep rate 0.5 V/s, T = 298 K.



voltammograms (Fig. 2) is attributed to the weak adsorption of the reactant at electrode surface (20, 21). Figure 3 gives an example response of the simulated cyclic voltammogram along with its convolution voltammetry for the systems $E_{rev}C_{rev}$ and $E_{rev}C_{irr}$ at v = 0.5 V/s which indicate a discrepancy between captured *CV* with these models confirming the validity of the $E_{irr}C_{irr}$ mechanism.

Spectrophotometric determination of the dissociation constants

The spectra of compounds (**I**, **III**, and **IV**) in universal buffer solutions of varying pH values containing 30% (v/v) ethanol are studied within the wavelength range 250–600 nm.

The changes in the absorption spectra on varying the pH of the buffer solution have been used successfully for the de-

© 2000 NRC Canada

termination of the dissociation constant of azomethine group and OH group for the compounds under investigation applying the following methods:

(*i*) The half-height method (22) for which the p*K* is equal to the pH at half height of the absorbance–pH curve, and can be calculated from the following equation

$$[7] \quad pK = pH \text{ at } A_{1/2} = (A_{max} - A_{min})/2;$$

(*ii*) limiting absorbency method (23) using the relation

$$[8] \quad pH = pK + \log\left(\frac{A}{A_{max} - A}\right)$$

Accordingly, a plot of the log $(A/A_{max} - A)$ vs. pH produces a straight line with intercept at log $(A/A_{max} - A) = 0$ equal to p*K*;

(*iii*) The modified limiting absorbency method (24, 25) in which the pK_a is calculated via the following relation

$$[9] \quad pH = pK_a + \log \gamma + \log\left(\frac{A - A_{min}}{A_{max} - A}\right)$$

where the limiting absorbency A_{min} and A_{max} corresponding to the absorbency of the neutral and ionized species liable to exist in the solution of the measuring wavelength and γ is the activity coefficient of the ions which are present in equilibrium. *Since in very dilute solution, log* γ *= 0.0, then eq. [9] takes the following form*

$$[10] \quad pH = pK_a + \log\left(\frac{A - A_{min}}{A_{max} - A}\right)$$

The p*K* value can be evaluated by plotting log $[(A - A_{min})/(A_{max} - A)]$ against pH. Thus, the p*K* value is that corresponding to the value at log $[(A - A_{min})/(A_{max} - A)]$ equals to zero. The values of p*K* obtained from the above three methods are collected in Table 6.

Table 6. pK_a values of the compounds (**I**, **III**, and **IV**) determined from electronic absorption spectra methods.

Comp.	pK_1	pK_2
I	5.2	8.70
III	5.5	9.00
IV	4.5	8.00

Electrode reaction pathway

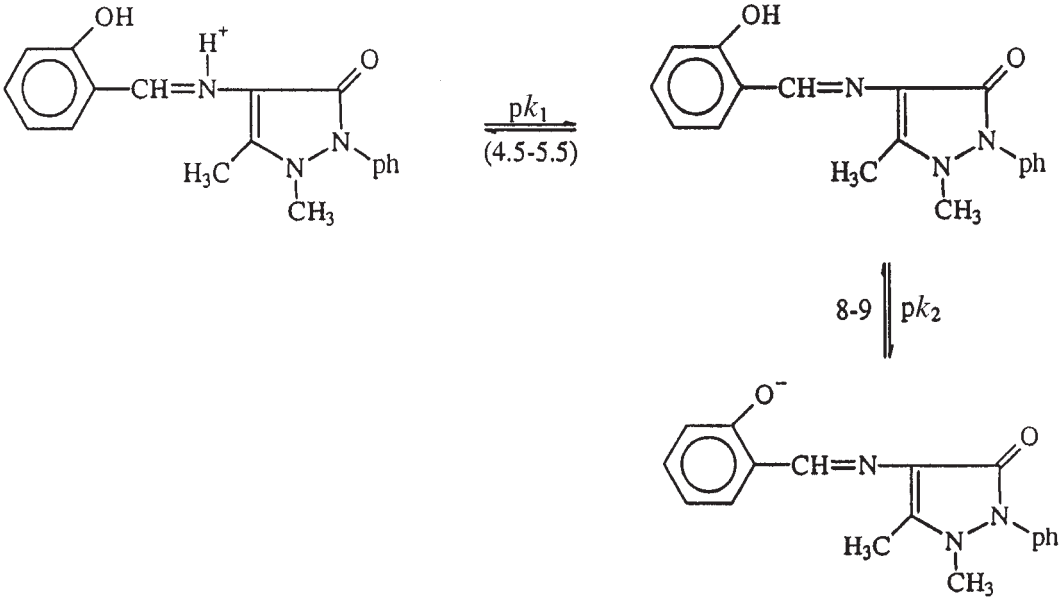
The compounds under consideration are characterized by the presence of azomethine group C=N$^+$H. The number of electrons involved in the reduction is found to be two in acidic as well as in alkaline media as confirmed from a controlled potential coulometry experiments in acidic and alkaline media.

IR (KBr optics) studies of the electrolyzed products gave a broad band at ~3310 cm^{-1} (stretching) which represent the presence of a secondary amine group in the products. Also, it was found that the mp of all the electrolyzed products in the range 338–341°C. All this experimental evidence indicates that the electrode process is irreversible and consumed two-electron reduction transferring the initial electroactive species to an inactive secondary amine (CH_2-NH-).

The $E_{1/2}$–pH plots of the first reduction wave of these compounds give a break at pH 4.5–5.5, whereas the $E_{1/2}$–pH plots of the second one exhibit a break at pH 8–9, indicating the protonation of the azomethine group and dissociation of the OH group of the reactants at these pH values.

On the other hand, calculation of the p*K* values of these compounds using spectrophotometric studies indicated the presence of two p*K* values (Table 6). The equilibria in solution can be represented as follows.

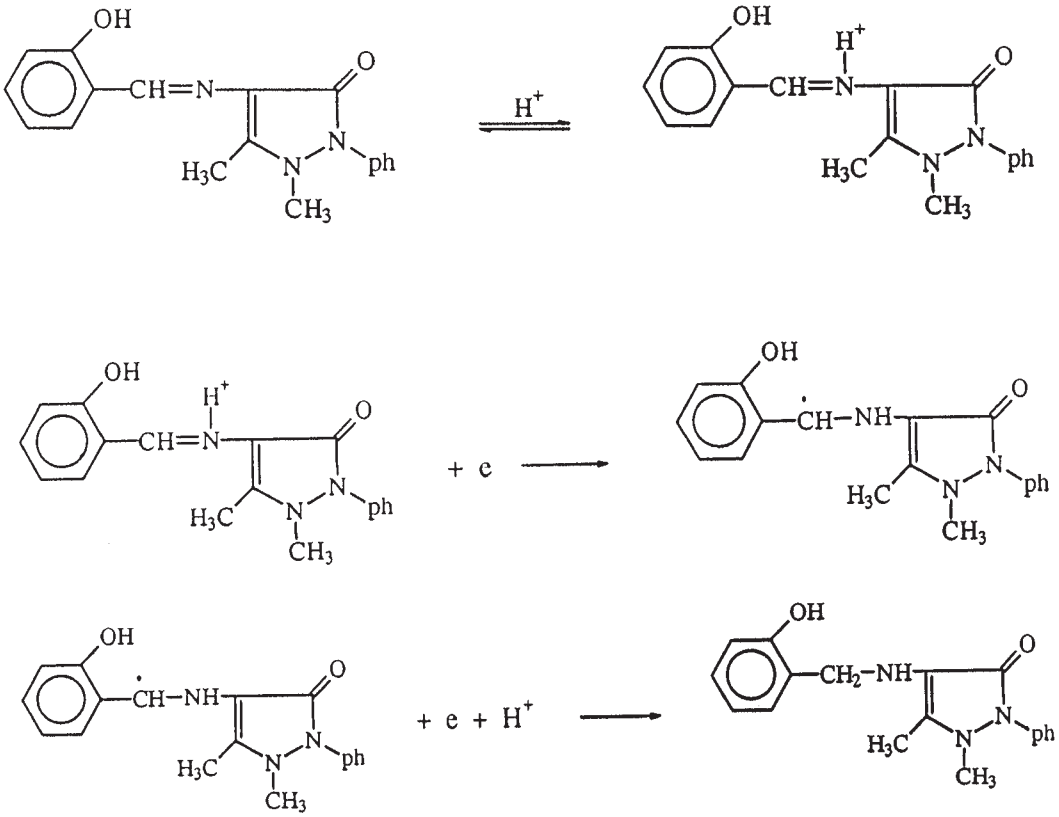
Scheme 2.



© 2000 NRC Canada

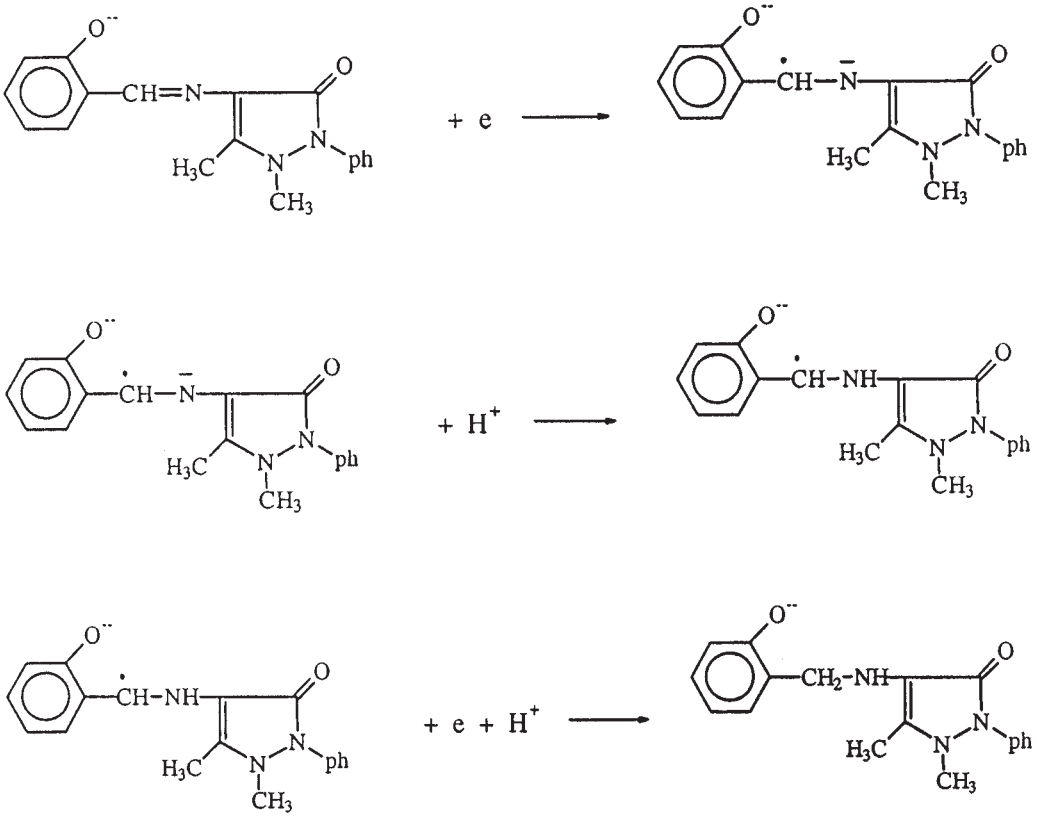
Based on the above results the mechanism of the electrode reaction of the investigated Schiff base compounds can be represented as follows: (*a*) In acidic and slightly alkaline solutions (pH < 8).

Scheme 3.



The electrode reaction mechanism follows the sequence H^+, e, e, H^+. (*b*) In strong alkaline solutions (pH > 8).

Scheme 4.



© 2000 NRC Canada

The electrode reaction mechanism follows the sequence e, H^+, e, H^+.

Acknowledgement

The authors are grateful to Prof. M. Gaber for preparing the investigated compounds.

References

1. J.W. Scottand and W.H. Jura. Can. J. Chem. **45**, 2375 (1967).
2. K. Hadzio. Glas Hem. Tehnol. Bosne Herzegovine, **18**, 47 (1970).
3. S.N. Poddar and N. Saha. J. Indian Chem. Soc. **52**, 57 (1975).
4. M.E. Moustafa, H.E. Megahed, and E.H. El-Mossalamy. B. Electrochem. **9**(**1**), 25 (1993).
5. C.J. Patil, A.S. Madhaua, G. Ramachandraiah, and D.N. Vyas. B. Electrochem. **11**(**3**), 159 (1995).
6. G. Maduavi, P.K. Reddy, and S.J. Reddy. Bull. Electrochem. **11**(**10**), 490 (1995).
7. J. Heyrovsky and J. Kuta. *In* Principle of polarography. *Edited by* R. Brdicka. Academic Press, New York. 1965. p. 61.
8. L. Meites. *In* Polarographic techniques. 4th ed. Interscience Publishers Inc., New York. 1965. pp. 240–248.
9. P. Zuman. *In* The elucidation of organic electrode processes. Academic Press. 1969. p. 21.
10. R.S. Nicholson and I. Shain. Anal. Chem. **36**, 706 (1964).
11. Z. Galus. Fundamentals of electrochemical analysis. *Edited by* G.F. Reynolds. John Wiley, New York. 1976. p. 238.
12. P. Delahay. J. Am. Chem. Soc. **75**, 1190 (1953).
13. A.J. Bard and L.R. Faulkner. *In* Electrochemical methods fundamentals and applications. John Wiley, New York. 1982. p. 218.
14. I.S. El-Hallag, A.M. Hassnien, and M. Gaber. Egypt. J. Chem. **40**, 39 (1997).
15. A. Blagg, S.W. Carr, G.R. Cooper, I.D. Dobson, J.B. Gill, D.C. Goodal, B.L. Shaw, N. Taylor, and T. Boddington. J. Chem. Soc. Dalton Trans. 1213 (1985).
16. I.S. El-Hallag, M.M. Ghoneim, and E. Hammam. Anal. Chim. Acta. **414**, 173 (2000).
17. P.D. Alford, M. Goto, and K.B. Oldham. J. Electroanal. Chem. **49**, 1390 (1977).
18. I.S. El-Hallag, A.M. Hassanien, M. Gaber, and R.M. Issa. B. Electrochem. **10**(**6–7**), 291 (1994).
19. A.M. Hassanein and I.S. El-Hallag. B. Electrochem. **15(12)**, 431 (1999).
20. J.A. Plambeck. *In* Electroanalytical chemistry: basic principles and applications. John Wiley, New York. 1982. p. 321.
21. E.R. Brown and J.R. Sandifer. *In* Physical methods of chemistry. Vol II. *Edited by* B.W. Rossiter and J.F. Hamilton. John Wiley & Sons. 1986. p. 340.
22. R.M. Issa and A.H. Zewail. Egypt. J. Chem. **19**, 53 (1976).
23. R.M. Issa, I.M. Issa, M.S. El-Ezabey, and Y.Z. Ahmed. Z. Phys. Chem. (Leipzig), **242**, 169 (1969).
24. R.M. Issa and A.H. Zewail. Egypt. J. Chem. **14**, 46 (1971).
25. R.M. Issa, N.A. Ibrahim, S.E. Zayan, and G.B. El-Hefnawey. J. Prakt. Chem. (Leipzig), **66**, 169 (1975).

© 2000 NRC Canada

Acidity constants and reactivities of the benzidine and *N,N*-dimethylbenzidine dications, the two electron oxidation intermediates of benzidine carcinogens

Robert A. McClelland, Daniel Ren, Raechelle D'Sa, and Abid R. Ahmed

Abstract: This paper describes the behavior in aqueous solutions of the two electron oxidation products of the carcinogens benzidine and *N,N*-dimethylbenzidine. In biological systems there is evidence that these diamines are oxidized by peroxidases, and that a product of this oxidation may be partly responsible for carcinogenicity. Entry into the oxidation products in the present study was provided through the bis-perchlorate salts of dications obtained upon chemical oxidation and through the irradiation of 4′-amino and 4′-*N,N*-dimethylamino-4-azidobiphenyls. The benzidine oxidation product exists in three conjugate acid–base forms, a dication, a monocation and neutral bisimine, with pK_a(1) = 5.0 and pK_a(2) = 9.0. These values stand in marked contrast to ones previously obtained for the two electron oxidation product of *p*-phenylenediamine, pK_a(1) < 1.5 and pK_a(2) = 5.75. The dimethylamino derivative, blocked from forming the neutral form, exists as a dication and monocation, with pK_a = 5.0. Both systems are quite long-lived in aqueous solution, but they do decay on the minutes-to-hours time scale. The kinetics can be explained by reactions of both the dication and the monocation with water, with a reaction of hydroxide and the monocation becoming important around pH 10. One surprising result is that the monocations are two orders of magnitude more reactive than the dications. Thus, at neutral pH the form that exists in both systems is the monocation, and this is the species that is the most reactive towards the solvent. One of the resonance contributors in the monocation is a 4-biphenylylnitrenium ion. Comparison with other 4′-substituted-4-biphenylylnitrenium ions studied by laser flash photolysis shows that the 4′-amino- and 4′-dimethylamino substituents are highly kinetically stabilizing. These cations, for example, are a billion-fold longer-lived in aqueous solution than the parent 4-biphenylylnitrenium ion.

Key words: quinone bisimine, nitrenium, aryl azide.

Résumé : On décrit le comportement de solutions aqueuses de produits provenant de l'oxydation par deux électrons de la benzidine et de la *N,N*-diméthylbenzidine, deux cancérigènes. Il existe des données qui suggèrent que, dans les systèmes biologiques, ces diamines sont oxydées par les peroxydases et qu'un produit de cette oxydation pourrait être partiellement responsable de leur caractère cancérigène. Dans le présent travail, les produits d'oxydation ont été obtenus par le biais des bis(perchlorates) des dications obtenus par une oxydation chimique, suivie d'une irradiation des 4′-amino- et 4′-*N,N*-diméthylamino-4-azidobiphényles. Le produit d'oxydation de la benzidine existe sous trois formes acide-base, un dication, un monocation et une bisamine neutre avec des pK_a(1) = 5,0 et pK_a(2) = 9,0. Ces valeurs diffèrent fortement de celles obtenues antérieurement pour le produit d'oxydation par deux électrons de la *p*-phénylènediamine, pK_a(1) < 5,0 et pK_a(2) = 5,75. Le dérivé diméthylamino qui ne peut conduire à la forme neutre existe comme dication et monocation avec un pK_a = 5,0. En solution aqueuse, les deux systèmes ont une longue durée de vie, mais leur concentration décroît à l'échelle de temps des minutes et des heures. On peut expliquer la cinétique par des réactions du cation ainsi que du monocation avec l'eau, pour lesquelles une réaction de l'hydroxyde et du monocation devient importante à un pH de près de 10. Il est surprenant que les réactions des monocations soient deux ordres de grandeur plus rapides que celles des dications. Ainsi, à un pH neutre, la forme qui existe dans les deux systèmes est le monocation et c'est l'espèce qui est la plus réactive par rapport au solvant. On retrouve l'ion 4-biphénylylnitrénium parmi les formes de résonance du monocation. Une comparaison avec d'autres ions 4-biphénylylnitrénium substitués en 4′ étudiés par photolyse éclair au laser permet de montrer que les substituants 4′-amino et 4′-diméthylamino ont un effet cinétique fortement stabilisant. Par exemple, en solution ces cations ont des temps de vie un million de fois plus élevées que celle de l'ion 4-biphénylylnitrénium parent.

Received December 10, 1999. Published on the NRC Research Press website on August 25, 2000.

R.A. McClelland,[1] D. Ren, R. D'Sa, and A.R. Ahmed. Department of Chemistry, University of Toronto, Toronto, ON M5A 3H6, Canada.

[1]Author to whom correspondence may be addressed. Telephone: (416) 978-3592. Fax: (416) 978-3592. e-mail: rmcclell@alchemy.chem.utoronto.ca

 © 2000 NRC Canada

Mots clés : bisimine de quinone, nitrénium, azoture d'aryle.

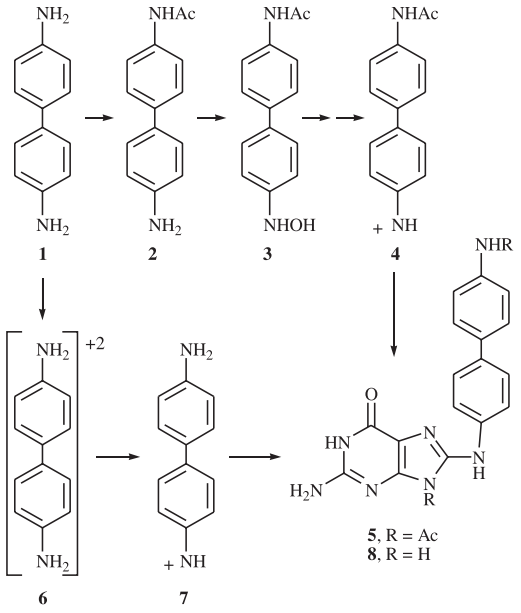
[Traduit par la Rédaction]

Benzidine (**1**) has been recognized as an occupational carcinogen for some time (1) and is now classified as a "proven human" carcinogen (2). Like the majority of carcinogens, the compound is metabolically activated to intermediates that bind covalently to cellular macromolecules, especially DNA. Recent studies have identified the *N*-acetylated guanine adduct **5** (Scheme 1)[2] in peripheral white blood cells (3) and exfoliated urothelial cells (4) obtained from workers exposed to benzidine. This adduct likely arises via an initial acetylation to *N*-acetylbenzidine **2**, a major metabolite (5). Further metabolic activation would lead to an arylnitrenium ion **4**. Such electrophiles are well established as being responsible for the guanine C8 adducts observed with arylamine carcinogens (6–10). Also in parallel with other arylamine carcinogens, *N*-acetylbenzidine is *N*-hydroxylated by cytochrome P-450s (11–13), suggesting that the hydroxylamine **3** is an intermediate between **2** and **4**.

There is also the strong likelihood that non-acetylated intermediates play a role. This appears to be required to explain the formation of urinary bladder tumors in dogs which are deficient in *N*-acetylating enzymes. The parent compound is not a substrate for the P-450s and other enzymes that *N*-hydroxylate other arylamines (11–13). However, it is oxidized by peroxidases (14–21). Although both a cation radical (one electron oxidation) and a dication **6** (two electron oxidation) have been implicated, recent experiments led to the conclusion that it is the two electron product that is responsible for DNA binding (21). The major DNA adducts that are observed are a C8 guanine adduct **8** and a novel cyclic intermediate obtained by further two electron oxidation of this adduct (21). Compound **8** had previously been characterized in nonenzymatic experiments in which DNA was incubated with the bis-perchlorate salt of the dication (22).

It has been suggested that the actual electrophile that reacts with the guanine residue is the monocation **7** (21, 24), an "arylnitrenium ion" when written in the resonance form shown in Scheme 1. We have been interested in substituted biphenylylnitrenium ions of this type (9, 23, 24), and have recently published results pertaining to the *N*-acetyl derivative **4** (25), a cation that can exist as both a more stable tautomer as well as a bisimine conjugate base. In this paper we report a spectroscopic and kinetic investigation of the parent system as well as an *N*,*N*-dimethyl analog. Despite the fact that **6** can be prepared as a stable salt (26), there appears to have been no study of its kinetic behavior in aqueous solutions. Our experiences are that this is not as simple as it seems. Indeed even the acid–base chemistry has not been elucidated, beyond an estimate of a pK_a of ~2 for the dication (20), a number that we show is out by three orders of magnitude. Our results are of additional interest in respect to recent theoretical calculations that suggest that increasing the number of rings separating the ends of benzoquinone bisimines can lead to remarkable enhancements of basicity (27, 28). We indeed find that there is considerable difference between the one ring system (i.e., benzoquinone bisimine) and the two ring benzidine system.

Scheme 1.



Results

Precursors

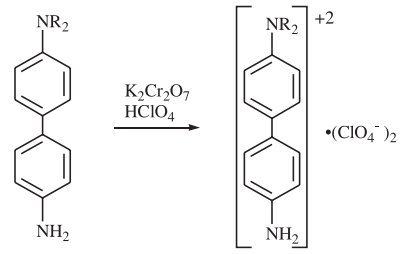
Experiments were conducted with the two electron oxidation products of both benzidine **1** and *N*,*N*-dimethylbenzidine **9**. The respective dications **6** and **10** obtained in the two electron oxidation could be isolated as bis-perchlorate salts, as shown in eq. [1] (26). These salts proved difficult to use in performing quantitative measurements, since the only solvent in which they were stable was a quite concentrated aq acid (i.e., >2 M $HClO_4$). Accordingly the majority of the spectroscopic and kinetic experiments employed a photochemical entry, as shown in eq. [2]. The is a method that we have used extensively for the generation and study of arylnitrenium ions (23–25, 29–35). The precursors in these experiments are aryl azides, whose irradiation results initially in singlet nitrenes (36). In a number of cases now we have found that the nitrene reacts rapidly as a base with solvent water molecules serving as the proton source. This generates the conjugate acid of the nitrene, a singlet arylnitrenium ion. The azides **11** and **12** are the precursors required in the present study, with the monocations **7** and **15** the conjugate acids of the singlet nitrenes **13** and **14**, respectively. It can be seen that **7** and **15** are also conjugate bases of **6** and **10**. With salts of these dications available, it was possible to establish conclusively that the photochemical route does operate as shown in eq. [2]. This was done by comparing the visible

[2] *R* in Scheme 1 is 2-deoxyribose, or a phosphorylated derivative. It can be noted that in experiments involving DNA, the guanine adduct is usually observed and characterized after enzymatic hydrolysis of the DNA.

© 2000 NRC Canada

absorption spectrum following irradiation of an aqueous solution of the azide with one obtained by adding a small amount of the appropriate dication salt to the same solution. Whatever the pH, the spectra were identical.

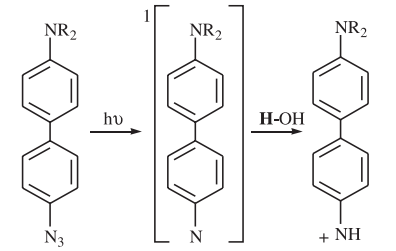
[1]



1, R = H
9, R = Me

6, R=H
10, R=Me

[2]



11, R = H
12, R = Me

13, R = H
14, R = Me

7, R = H
15, R = Me

Spectroscopic acidity constants

Solutions of the azides of 10 μM concentration were placed in a UV cuvette and irradiated at 300 nm for 6 s, a time established by HPLC to result in >95% depletion of the azide. The cuvette was then rapidly loaded into a diode array spectrometer, and spectra obtained every 2 s for about 20 s. The data were transported to a spread sheet, and the absorbance at each wavelength extrapolated to zero time, taken as two seconds after the start of the irradiation. In the oxidized benzidine system one expects three forms — a dication, a monocation, and a neutral bisimine. Figure 1 shows the spectra of each of these, obtained at a pH where that particular form dominates. Representative curves plotting absorbance vs. pH are shown in Fig. 2. These take the form of a titration of a diacid with consecutive loss of two protons (eq. [3], where BH_2^{+2}, BH^+, and B are the dication, monocation, and bisimine, respectively). Data at 30 different wavelengths from 380 to 500 nm were fit to eq. [3]. These gave $pK_a(1) = 5.05 \pm 0.08$ and $pK_a(2) = 8.94 \pm 0.07$. As noted above the same spectra were obtained by adding the solid bis-cation salt to the appropriate solutions. It is also worth noting that the dication has been reported to have a λ_{max} of 429 nm, with an extinction coefficient of 6.0×10^4 (37). Our dication spectrum is in good agreement.

[3] $$\text{Abs} = \left(\frac{\text{Abs}(BH_2^{+2})[H^+]^2 + \text{Abs}(BH^+)K_a(1)[H^+] + \text{Abs}(B)K_a(1)K_a(2)}{[H^+]^2 + K_a(1)[H^+] + K_a(1)K_a(2)} \right)$$

Fig. 1. Absorption spectra extrapolated to zero time following irradiation of 4′-amino-4-biphenylyl azide **11** (10 μM) in aq solution at pH 2 (dication spectrum), pH 7 (cation spectrum), and pH 12 (bisimine spectrum).

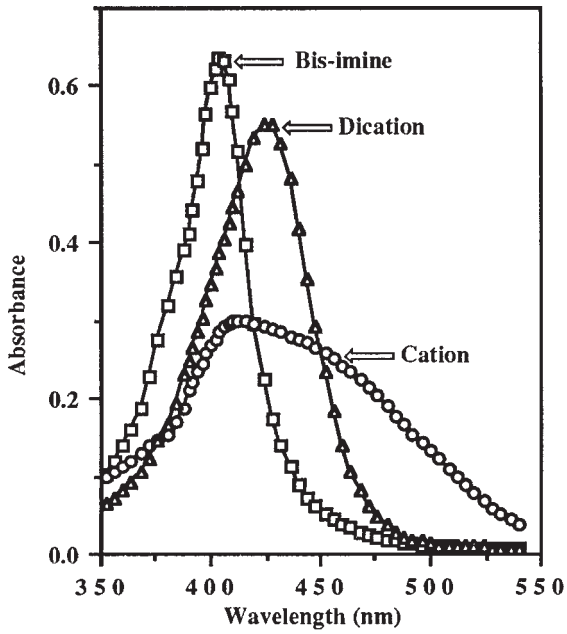
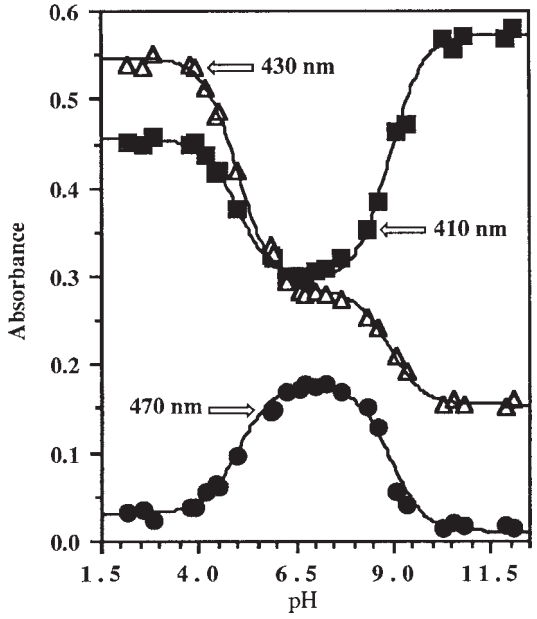


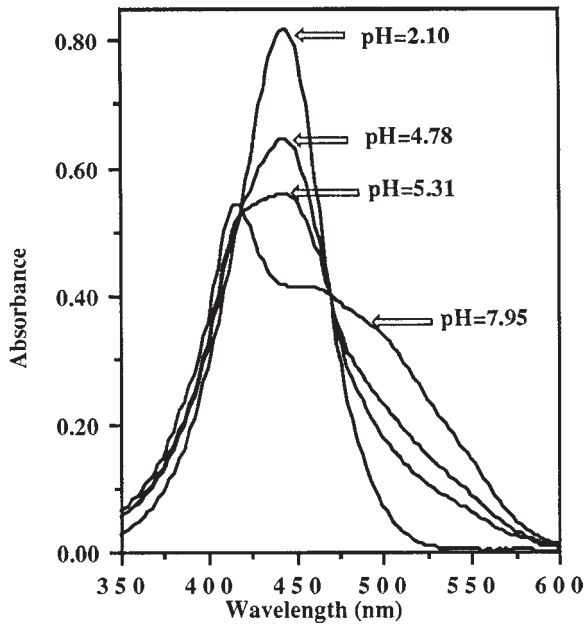
Fig. 2. Absorbance (extrapolate to zero time) vs. pH following irradiation of 4′-amino-4-biphenylyl azide **11** (10 μM) in aq solution. The titration curves drawn through the experimental points are based on a fit of the data to eq. [3] with $pK_a(1)$ and $pK_a(2)$ fixed at 5.05 and 8.94.



Selected spectrum obtained with the dimethylamino derivative are shown in Fig. 3. As expected there is only one spectral change here, from a dication (the spectrum at pH 2.1 in Fig. 3) to a monocation (pH 7.95). The single pK_a obtained in this case is 4.95 ± 0.3. It should be noted that

© 2000 NRC Canada

Fig. 3. Absorption spectra extrapolated to zero time following irradiation of 4′-dimethylamino-4-biphenylyl azide **12** (10 μM) in 75:25 water:acetonitrile.



because of solubility limitations, this refers to an aq solution containing 25% acetonitrile.

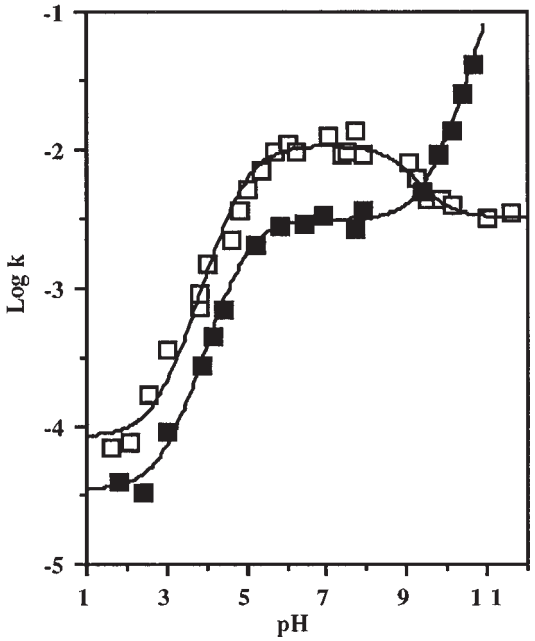
Kinetics of decay

As is apparent from the previous discussion, both systems are sufficiently stable that it is possible to record spectra of the various forms on a regular UV instrument. There is however a reaction, and ultimately the absorbance in the visible region decays to essentially zero. In our initial kinetic experiments, we found that the rate constants were not reproducible, and more importantly the decay did not follow a good single exponential. In fact the rate increased with time, suggesting that a product of the reaction was reacting with the substrate. We finally realized that we could obtain reasonably reproducible rate constants (±5–10%) with adherence to a single exponential by working at the extremely low concentrations of 0.1–0.2 μM. This is possible because of the very strong absorbance of these highly conjugated systems. Even so, optical density changes were only of the order of 0.01–0.02 OD units.

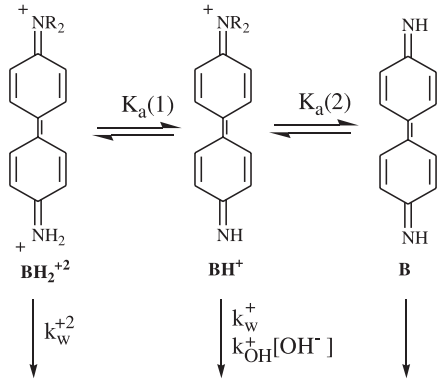
Rate–pH profiles for the two systems are shown in Fig. 4. The data were obtained in aq perchloric acid and sodium hydroxide solutions, and acetate, phosphate, and carbonate buffers. Low concentrations of the buffers (total concentration ~1 mM) were used; at higher concentrations the buffers were found to accelerate the decay. It can be noted that because of the very low concentration of the precursor azide, it was possible to study the dimethylamino system in 100% aq solutions.

We were unable to identify the nature of the products. The problem, we suspect, is that the products are not stable, and indeed the kinetics suggest that the products react with the precursor. This is particular true at the concentrations (i.e., 100 μM) that are required for HPLC product analysis. We did observe a number of small peaks in the HPLC

Fig. 4. Rate–pH profiles for the decay of the two electron oxidation products of benzidine (□) and *N*,*N*-dimethylbenzidine (■). Rate constants have units of s^{-1} and were obtained at 20°C. The curves are drawn on the basis of eqs. [4] and [5] using the parameters given in Table 1.



Scheme 2.



chromatograms, and this was the case whether the dication salt or the azide was employed. These however could not be identified. In particular any attempt at scaling-up to obtain enough material for NMR resulted in a mess.

Discussion

Kinetic analysis

A mechanistic scheme that accounts for the rate–pH profiles is given in Scheme 2. The dimethyl system is the simpler of the two, since there are just the two forms, $\mathbf{BH}_2^{+2}$ and $\mathbf{BH}^+$. The kinetics are explained by reactions of both with the solvent, with a region above pH 9 due to the monocation reacting with hydroxide. Equation [4] applies to this kinetic system, and parameters obtained by fitting the

© 2000 NRC Canada

Table 1. Rate constants and acidity constants for benzidine dications in water at 20°C.

Constant	*N*,*N*-Dimethyl-benzidine dication	Benzidine dication
k^{+2}_{W} (s^{-1})	3×10^{-5}	8×10^{-5}
k^{+}_{W} (s^{-1})	3.1×10^{-3}	1.04×10^{-2}
k^{+}_{OH} (M^{-1} s^{-1})	8.6×10^{1}	3.1×10^{2}
k^{+}_{OH}:k^{+}_{W}	2.8×10^{4}	3.0×10^{4}
pK_a(1) — kinetic	5.04	5.07
pK_a(2) — kinetic	—	9.01
pK_a(1) — spectr.	4.95[a]	5.05
pK_a(2) — spectr.	—	8.95

[a]25% Acetonitrile.

experimental data are given in Table 1. There is good agreement with the value of pK_a(1) obtained spectroscopically, although this is perhaps accidental since the solvents were slightly different.

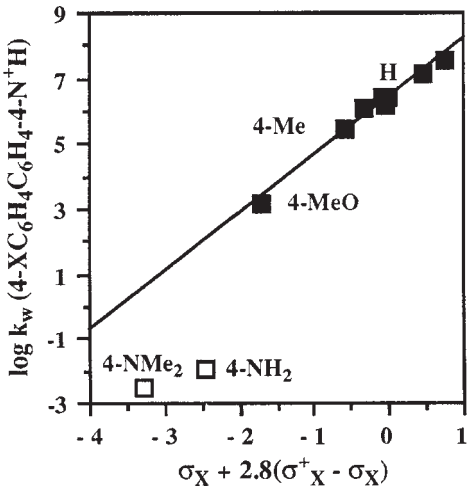
$$[4] \qquad k_{obs} = \left(\frac{k^{+2}_{w}[H^+] + k^{+}_{w}K_a(1) + \frac{k^{+}_{OH}K_a(1)K_w}{[H^+]}}{[H^+] + K_a(1)} \right)$$

There is a third species **B** in the parent system, and therefore a second ionization equilibrium. There is also a kinetic ambiguity in base, where the pH independent region can be explained by either **B** reacting with water, or by $\mathbf{BH}^+$ reacting with hydroxide ion. The analogy with the dimethyl system suggests that it is the latter reaction that is occurring. It is also noteworthy that there is no upswing in rate constant even in 0.01 M NaOH, as would occur if the bisimine were to react with hydroxide ion. The failure to observe such a reaction suggests that the bisimine also does not react with water (or at least does so very slowly). Ignoring the water–bisimine reaction, eq. [5] applies. The five adjustable parameters in this equation obtained by fitting the experimental data are provided in Table 1. There is clearly excellent agreement with the spectroscopic pK_a values. It can also be noted that the ratios k^{+}_{OH}:k^{+}_{w} are essentially the same in the two systems, as is consistent with the parent system reacting in base via the hydroxide–monocation pathway.

$$[5] \qquad k_{obs} = \left(\frac{k^{+2}_{w}[H^+]^2 + k^{+}_{w}K_a(1)[H^+] + k^{+}_{OH}K_a(1)K_w}{[H^+]^2 + K_a(1)[H^+] + K_a(1)K_a(2)} \right)$$

One surprise that emerges from this study is that the dications are less reactive towards water than the monocations. This is counter-intuitive, since one would expect that electrophilicity should increase with protonation. Indeed, in previous studies with the parent 4-biphenylylnitrenium ion (23), the 2-fluorenylnitrenium ion (23) and a series of 4-alkoxyphenylnitrenium ions (32), the dications were the more reactive. All these systems however are inherently many orders of magnitude more reactive than the benzidine derivatives of this study. One possible explanation to explain the differences with the latter is that their dications can localize the two positive charges on the two nitrogens at the end. This is something that cannot be done in, for example, the dication derived from 4-aminobiphenyl, where there is only one amino group. The benzidine monocations on the other hand may have the single positive charge more delocalized throughout the biphenylyl ring system. This would mean that they react more like an arylnitrenium ion, while the dication reacts like an iminium ion.

Fig. 5. Hammett correlation of the water reactivities of 4′-substituted-4-biphenylylnitrenium ions. The substituent constant employed in this plot is calculated as $\sigma + r^{+}(\sigma^{+} - \sigma)$, using $r^{+} = 2.8$ as obtained in a previous study (24) from application of the two parameter Yukawa–Tsuno equation (38). The line drawn in this figure (slope = 1.8) is the least-squares line from that study. Values of σ and σ^{+} are taken from ref. (39).

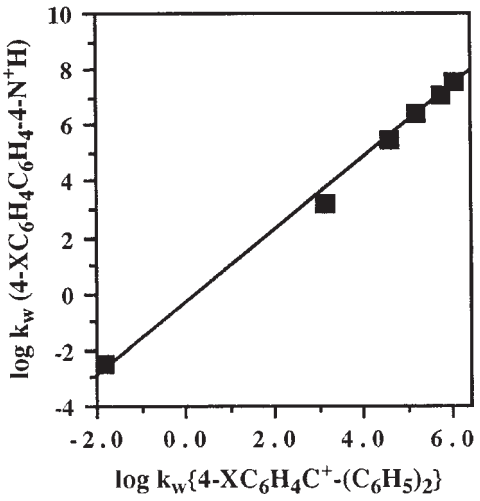


Whatever the reason it is interesting from a biological point of view that it is the monocation or arylnitrenium ion that is the species that is present at neutral pH when benzidine undergoes two electron oxidation. This ion, in water alone, is remarkably long-lived, with a half-life of the order of a minute or so. On the other hand, this ion is the most reactive of the three acid–base forms, being more reactive than both the conjugate acid dication and the conjugate base bisimine. In fact from pH 3 to pH 12, the species that is reacting is the monocation, whether it be the predominant form that is present or not.

Viewing the monocation as a 4-biphenylylnitrenium ion, the amino groups clearly have a very significant stabilization effect. This can be seen in the correlation shown in Fig. 5. This plot was constructed based on a previous study involving 4′-substituted-4-biphenylylnitrenium ions (24) with substituents ranging from CF_3 to MeO. What was observed was that log k_w values plotted against σ^{+} exhibited a poor correlation. In particular, the points for the *para* π-electron donors deviated from the correlation line based on the other substituents, in a direction requiring a more negative substituent parameter for these substituents. The data were satisfactorily fit to the two parameter Yukawa–Tsuno equation (38), giving a parameter r^{+} of 2.8. This means that for the data of the previous series, the substituent constant that provided the best fit in a Hammett plot was $\sigma + 2.8(\sigma^{+} - \sigma)$. Thus the 4-methoxy substituent constant is –1.7, rather than the –0.8 value of σ^{+} alone. Even with the enhanced effects of the *para* π-donors, the data obtained in this study for

© 2000 NRC Canada

Fig. 6. Linear free energy correlation of rate constants for 4′-substituted-4-biphenylylnitrenium ions with rate constants for 4′-monosubstituted trityl cations. Data for the latter are taken from ref. (40) and ref. therein. The slope of the line is 1.3.

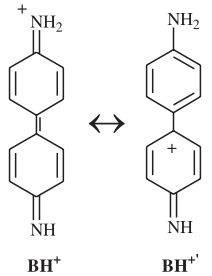


4′-amino- and 4′-dimethylamino- deviate significantly. Again, this deviation is in the direction that says that these substituents are more stabilizing. Thus, for example, the 4-NH_2 system is almost four orders of magnitude less reactive than would be predicted on the basis of the previous correlation line.

Figure 6 shows that this stabilizing effect is not unique to biphenylylnitrenium ions, but it is also seen in arylcarbenium ions. This plot correlates the data for 4-biphenylylnitrenium ions with those of analogously substituted trityl cations. A good correlation with a slope slightly greater than unity is observed, and this includes the point for 4-dimethylamino. Thus, in both the trityl series and the nitrenium series a 4-dimethylamino group makes the cation much less reactive than other substituents, even than 4-methoxy.

A further interesting comparison relates to the pK_a values obtained in the present study for the benzidine dication with values for the dication of *p*-phenylenediamine (or doubly protonated benzoquinone bisimine). The latter pK_as have been obtained in a kinetic study of the hydrolysis of the bisimine and are pK_a(1) < 1.5 and pK_a(2) = 5.75 (41). Thus, the bisimine derived from benzidine is slightly over three orders more basic than benzoquinone bisimine, and there is at least that great a difference in protonating the monocations. The latter is not unexpected, since the positive charges can be more delocalized in the two ring system. Moreover, as noted above, the two positive charges can be placed at the far ends of the two rings, where they would be much further separated than is possible in the one ring dication.

The difference in basicities of the bisimines, on the other hand, seems more surprising, since in both cases protonation is occurring on C=NH. It has been shown theoretically that the greater the number of rings separating the ends of benzoquinonediimines, the greater the proton affinity (27, 28). It was argued that this is associated with increased aromatic character upon protonation of the bisimines with the greater number of rings. Thus, in the present case, one could imagine that the two ring monocation could have a significant contribution from the resonance contributor **$BH^{+'}$**, where the ring bearing the amino group has aromatic character.



Experimental section

4′-Amino-4-azidobiphenyl

N-Acetylbenzidine was obtained by acetylation of hydrazobenzene followed by rearrangement in 80% H_2SO_4 (42). The compound was converted into 4′-(*N*-acetylamino)-4-azidobiphenyl by diazotization and treatment with sodium azide following the procedure given for azidostilbenes in ref. (34). A mixture of *N*-acetylbiphenyl-4-azide in a 1:2 volume ratio of 25% sodium hydroxide solution and ethanol was refluxed for 1 h. The resultant solution was diluted with cold water to give light brown precipitates. These were washed with water and recrystallized with a mixture of ethanol and dichloromethane (5:1). *4′-(N-Acetylamino)-4-azidobiphenyl* (65% yield after column chromatography) had ^{1}H NMR (200 MHz, DMSO-*d*6): 10.10 (s, 1H), 7.67 (m, 6H), 7.20 (d, *J* = 8.4 Hz, 2H), 2.08 (s, 3H). *4′-Amino-4-azidobiphenyl* (90% yield) was obtained as a buff-colored solid that decomposed on heating above 100°C. The solid had ^{1}H NMR (200 MHz, $CDCl_3$): 7.52 (d, *J* = 8.6 Hz, 2H), 7.38 (d, *J* = 8.5 Hz, 2H), 7.05 (d, *J* = 7.6 Hz, 2H), 6.75 (d, *J* = 7.5 Hz, 2H), 5.17 (s, 2H, disappeared upon treatment with D_2O). HRMS (EI, 70 ev): *m*/*z* 210.0911. $C_{12}H_{10}N_4$ requires 210.0905.

N,N-Dimethylbenzidine and 4′-N,N-dimethylamino-4-azidobiphenyl were obtained following procedures previously provided for the preparation of other 4′-substituted-4-amino- and azidobiphenyls (24). *4-(N,N-Dimethylamino)phenylboronic acid,* obtained through the reaction of 4-(*N,N*-dimethylamino)phenyl magnesium bromide and methyl borate, was coupled with 4-bromoaniline to give *N,N*-dimethylbenzidine (24). This was followed by diazotization and treatment with sodium azide to give the azide. *4-(N,N-Dimethylamino)phenylboronic acid* had ^{1}H NMR (DMSO-d_6, 200 MHz): 7.62 (2H, OH), 7.64 (d, *J* = 8.0 Hz, 2H), 6.66 (d, *J* = 8.0 Hz, 2Hz), 2.94 (s, 6H). *N,N-Dimethylbenzidine* had ^{1}H NMR ($CDCl_3$, 200 MHz): 7.42 (d, *J* = 8.6 Hz, 2H), 7.36 (d, *J* = 8.6 Hz, 2H), 6.79 (d, *J* = 8.6 Hz, 2H), 6.73 (d, *J* = 8.6 Hz, 2H), 3.66 (s, 2H), 2.97 (s, 6H). *4′-N,N-Dimethylamino-4-azidobiphenyl* was obtained in 55% after column chromatography. It decomposed on heating above 100°C, and had ^{1}H NMR ($CDCl_3$, 500 MHz): 7.58 (d, *J* = 8.8 Hz, 2H), 7.51 (d, *J* = 8.8 Hz, 2H), 7.10 (d, *J* = 8.8 Hz, 2H), 6.84 (d, *J* = 8.8 Hz, 2H), 3.04 (6H, s). HRMS (EI, 70 ev): *m*/*z* 238.1222. $C_{14}H_{14}N_4$ requires 238.1218.

Benzidine dication bis-perchlorate and *N,N-dimethylbenzidine dication bis-perchlorate* were obtained by

© 2000 NRC Canada

dichromate oxidation in a mixture of acetic acid and aq perchloric acid, as described in the literature (26).

Kinetic experiments were performed by preparing stock solutions of 4′-*N*,*N*-dimethylamino-4-azidobiphenyl and 4′-amino-4-azidobiphenyl in acetonitrile, with a concentration of 0.5 mM. 1–2 μL of this solution were then injected into a UV cuvette containing an aq buffer, and the cuvette irradiated at 300 nm in Rayonet reactor for 6 s. The cuvette was then placed in a Cary 2200 spectrophotometer and the absorbance change followed at 400–440 nm. The exact wavelength was chosen based on the spectrum of the species present at the pH of the experiment (see Figs. 1 and 3). The absorbance–time data were digitized and stored in a computer. Rate constants were obtained by fitting the data to the exponential equation. Kinetic experiments were also performed by adding a very small amount of the solid bisperchlorate salt to an aqueous solution, and transferring this solution to the cuvette. Provided the concentrations were below 0.4 μM there was reasonable agreement (±10%) between experiments in the same solution using the irradiated azide and salt as substrates.

Spectral pK_a determinations were performed in a similar way, except that the stock acetonitrile solutions had concentrations of 10 mM, and the aq solutions concentrations of 10 μM. For a given set of experiments, care was taken to ensure that the final concentration was constant throughout. These experiments were performed by irradiating the cuvette for 6 s in the Rayonet, followed by rapid transfer (2 s) to a Hewlett–Packard 8452A Diode-Array spectrometer. Scans were recorded from 350–600 nm after 2 s for a period of 15–20 s. The diode array apparatus gives an absorbance reading every 2 nm. The data were transferred to an Excel spread sheet, and a linear extrapolation performed at each wavelength to the time 2 s after commencement of the irradiation. The "zero-time" data could be then manipulated into plots of absorbance vs. wavelength (see Figs. 1 and 3) or into plots of absorbance vs. pH (see Fig. 2). The pK_a values were determined from the latter plots by fitting the experimental data to the appropriate titration equation. For each system this was done at a number of wavelengths (where there were significant differences between conjugate acid–base forms), and the average taken.

Acknowledgement

Financial support from the Natural Sciences and Engineering Research Council of Canada (NSERC) is gratefully acknowledged.

References

1. T.J. Haley. Clin. Toxicol. **8**, 13 (1975).
2. H.C. Crabtree, D. Hart, M.C. Thomas, B.H. Witham, I.G. McKenzie, and C.P. Smith. Mutat. Res. **264**, 155 (1991).
3. Q. Zhou, G. Talaska, M. Jaeger, V.K. Bhatnagar, R.B. Hayes, T.V. Zenser, S.K. Kashyap, V.M. Lakshmi, R. Kashyap, M. Dosemeci, F.F. Hsu, D.J. Parikh, B. Davis, and N. Rothman. Mutat. Res. **393**, 199 (1997).
4. N. Rothman, V.K. Bhatnagar, R.B. Hayes, T.V. Zenser, S.K. Kashyap, M.A. Butler, D.A. Bell, V. Lakshmi, M. Jaeger, R. Kashyap, A. Hirvonen, P.A. Schulte, M. Dosemeci, F. Hsu, D.J. Parikh, B.B. Davis, and G. Talaska. Proc. Natl. Acad. Sci. U.S.A. **93**, 5084 (1996).
5. F. Hsu, V. Lakshmi, N. Rothman, V.K. Bhatnager, R.B. Hayes, R. Kashyap, D.J. Parikh, S.K. Kashyap, J. Turk, T. Zenser, and B. Davis. Anal. Biochem. **234**, 183 (1996).
6. A. Dipple. Carcinogenesis, **16**, 437 (1995).
7. M. Novak and S.A. Kennedy. J. Am. Chem. Soc. **117**, 574 (1995).
8. S.A. Kennedy, M. Novak, and B.A. Kolb. J. Am. Chem. Soc. **119**, 7654 (1997).
9. R.A. McClelland, T.A. Gadosy, and D. Ren. Can. J. Chem. **76**, 1327 (1998).
10. R.A. McClelland, A.R. Ahmad, A.P. Dicks, and V.E. Licence. J. Am. Chem. Soc. **121**, 3303 (1999).
11. C.B. Frederick, J.B. Mays, D.M. Ziegler, F.P. Guengerich, and F.F. Kadlubar. Cancer Res. **42**, 2671 (1982).
12. T. Kamataki, K. Maeda, Y. Yamazoe, N. Matsuda, K. Ishii, and R. Kato. Mol. Pharmacol. **24**, 146 (1983).
13. G.J. Hammons, F.P. Guengerich, C.C. Weis, F.A. Beland, and F.F. Kadlubar. Cancer. Res. **45**, 3578 (1985).
14. T.V. Zenser, M.B. Mattamal, H.J. Armbrecht, and B.B. Davis. Cancer Res. **40**, 2839 (1980).
15. F.F. Kadlubar, C.B. Frederick, C.C. Weis, and T.V. Zenser. Biochem. Biophys. Res. Commun. **108**, 253 (1982).
16. P.D. Josephy, T.E. Eling, and R.P. Mason. Mol. Pharmacol. **23**, 766 (1983).
17. P.D. Josephy, T.E. Eling, and R.P. Mason. J. Biol. Chem. **258**, 5561 (1983).
18. J.R. Rice and P.T. Kissinger. Biochem. Biophys. Res. Commun. **104**, 1312 (1982).
19. A. Claiborne and I. Fridovich. Biochemistry, **18**, 2329 (1979).
20. R.W. Wise, T.V. Zenser, and B.B. Davis. Carcinogenesis, **5**, 1499 (1984).
21. Y. Yamozoe, T.V. Zenser, D.W. Miller, and F.F. Kadlubar. Carcinogenesis, **9**, 1635 (1988).
22. Y. Yamozoe, R.W. Roth, and F.F. Kadlubar. Carcinogenesis, **7**, 179 (1986).
23. R.A. McClelland, M.J. Kahley, P.A. Davidse, and G. Hadzialic. J. Am. Chem. Soc. **118**, 4794 (1996).
24. D. Ren and R.S. McClelland. Can. J. Chem. **76**, 78 (1998).
25. A.P. Dicks, A. Ahmad, and R.A. McClelland. J. Chem. Soc. Perkin Trans. 2, 1, (1999).
26. S. Hunig and P. Richters. Chem. Ber. **91**, 442 (1958).
27. B. Kovacevic and Z.B. Maksic. Chem. Phys. Lett. **288**, 289 (1998).
28. Z.B. Maksic and B. Kovacevic. J. Phys. Chem. A. **102**, 7324 (1988).
29. R.A. McClelland, P.A. Davidse, and G. Hadzialic. J. Am. Chem. Soc. **117**, 4173 (1995).
30. P. Sukhai and R.A. McClelland. J. Chem. Soc. Perkin Trans. 2, 1529 (1996).
31. R.A. McClelland, T.A. Gadosy, and D. Ren. Can. J. Chem. **76**, 1327 (1998).
32. P. Ramlall and R.A. McClelland. J. Chem. Soc. Perkin Trans. 2, 225 (1999).
33. T.A. Gadosy and R.A. McClelland. J. Am. Chem. Soc. **121**, 1459 (1999).
34. R. Bose, A.R. Ahmad, A.P. Dicks, M. Novak, K.J. Kayser, and R.A. McClelland. J. Chem. Soc. Perkin Trans. 2, 1591 (1999).
35. P. Ramlall, Y. Li, and R.A. McClelland. J. Chem. Soc. Perkin Trans. 2, 1601 (1999).
36. G.B. Schuster and M.S. Platz. Adv. Photochem. **17**, 143 (1992).
37. T.J. Kemp, P. Moore, and G.R. Quick. J. Chem. Res. **2**, 301 (1981).

© 2000 NRC Canada

38. Y. Yukawa, Y. Tsuno, and M. Sawada. Bull. Chem. Soc. Jpn. **39**, 2274 (1966).
39. H.C. Brown, D.P. Kelley, and M. Periasamy. Proc. Natl. Acad. Sci. U.S.A. **77**, 6956 (1980).
40. R.A. McClelland, V.M. Kanagasabapathy, N. Banait, and S. Steenken. J. Am. Chem. Soc. **111**, 3966 (1989).
41. J.F. Corbett. J. Chem. Soc. B, 213 (1969).
42. D.D. Mysyk. J. Org. Chem. USSR **12**, 2144 (1976).

© 2000 NRC Canada

The tamoxifen cation reacts to give indene products

Cristina Sanchez and Robert A. McClelland

Abstract: The tamoxifen carbocation (Ph(Ar)C=CPh-CH^+-CH_3, Ar = 4-$Me_2NCH_2CH_2OC_6H_4$) is generated from acetate and sulfate precursors by S_N1 ionization in water. The cation exists in (*E*) and (*Z*) forms which equilibrate before reaction. The major products are the α-hydroxytamoxifens Ph(Ar)C=CPh-CHOH-CH_3, both (*E*) 64% and (*Z*) 29%, with the ratio independent of the configuration of the starting ester. Two minor products with a total yield of 7% account for the rest of the products. These have been characterized as indenes derived from intramolecular cyclization, a 4.5% yield of the indene derived from cyclization into the Ar ring with 2.5% due to cyclization into the phenyl ring. Experiments in acid solutions (0.01–0.1 M HCl) starting with pure (*E*)- or (*Z*)-α-hydroxytamoxifen reveal that the two alcohols equilibrate. This occurs by H^+-catalyzed formation of the carbocation followed by water capture. Occurring about 10-fold slower than this isomerization is an irreversible process resulting in the two indenes. This cyclization will result in the destruction of the α-hydroxytamoxifens upon exposure to acidic conditions and also makes the direct observation of the tamoxifen carbocation under super-acid conditions difficult, if not impossible. The indenes do form in low yield whenever the tamoxifen carbocation is generated from an S_N1 precursor. Thus these products could serve as markers for the formation of the tamoxifen carbocation in cellular systems or in in vivo experiments.

Key words: carbocation, indene, allylic cation, isomerization.

Résumé : On a généré le carbocation tamoxifène, [Ph(Ar)C=CPHC$H^+$$CH_3$, Ar = 4-$Me_2NCH_2CH_2OC_6H_4$] à partir de précurseurs acétate et sulfate, par le biais de réactions S_N1, dans l'eau. Le cation existe dans les formes (*E*) et (*Z*) qui se mettent en équilibre avant de réagir. Les produits principaux sont les α-hydroxytamoxifènes Ph(Ar)C=CPH-CHOH-CH_3, *E*, 64 % et *Z*, 29 %, dont le rapport est indépendant de la configuration de l'ester de départ. Deux produits mineurs, qui correspondent à un rendement total de 7 %, forment le reste des produits. Il s'agit d'indènes qui découlent d'une cyclisation intramoléculaire, dont 4,5 % de l'indène dérivé d'une cyclisation dans le noyau aromatique et 2,5 % dû à une cyclisation dans le noyau phényle. Des expériences faites en milieu acide (0,01 à 0,1 M, HCl) faites à partir des (*E*)- ou (*Z*)-α-hydroxytamoxifènes purs révèlent que les deux alcools se mettent en équilibre. Ceci résulte d'une formation acidocatalysée du carbocation, suivie par une fixation d'eau. La vitesse de réaction du processus irréversible conduisant aux deux indènes est dix fois plus faible. Cette cyclisation conduit à la destruction des α-hydroxytamoxifènes lorsqu'ils sont exposés à des conditions acides et elle rend pratiquement impossible toute observation directe du carbocation tamoxifène dans des conditions superacides. Les indènes se forment avec de faibles rendements chaque fois que le carbocation tamoxifène est généré par le biais d'une réaction S_N1. Ces produits pourraient donc servir de marqueurs pour la formation du carbocation tamoxifène dans des systèmes cellulaires ou dans des expériences in vitro.

Mots clés : carbocation, indène, cation allylique, isomérisation.

We have recently reported the direct observation of the tamoxifen carbocation in aqueous solution through the use of the technique of laser flash photolysis (LFP) (1). This cation appears to be responsible for the formation of DNA adducts observed in both animal models (2, 3) and in women treated with the drug tamoxifen (4–7). Such adducts could explain the hepatocarcinogenicity observed in rats (8–10), and the small number of endometrial cancers in women (11–13). The metabolic pathway of Scheme 1 (14–20) accounts for the formation of the cation. The initial metabolic event involves allylic hydroxylation of the parent drug (**Tam**) to form *E*-α-hydroxytamoxifen **E-TOH**, a known metabolite. This is followed by sulfotransferase-mediated conversion to the sulfate **E-TOSO$_3^-$** (21–24). This ester is quite labile in water, undergoing relatively rapid S_N1 ionization, for example, with a half-life around 10 s in water at 20°C (1).

In comparison with other carbocations (25), the tamoxifen intermediate is relatively long-lived. Limiting lifetimes (1/k(decay)) are 160 μs (side-chain amine as free base) and 40 μs (amine protonated).[2] An interesting feature is that the

Received November 30, 1999. Published on the NRC Research Press website on August 30, 2000.

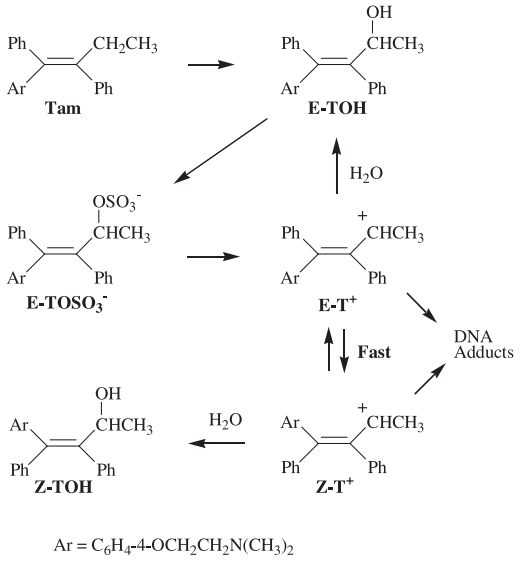
C. Sanchez and R.A. McClelland.[1] Department of Chemistry, University of Toronto, 80 St. George St., Toronto, ON M5S 3H6, Canada.

[1]Author to whom correspondence may be addressed. Telephone: (416) 978-3592. Fax: (416) 978-3592. e-mail: rmcclell@alchemy.chem.utoronto.ca

[2]These numbers are based on measurements in wholly aqueous solutions (E. Sauer, C. Sanchez, and R.A. McClelland, unpublished data). Our previously reported lifetimes (1) of 125 μs and 22 μs refer to a 60:40 water:acetonitrile mixture.

 © 2000 NRC Canada

Scheme 1.



intermediate appears to be a rapidly equilibrating mixture of the two isomers **E-T**$^+$ and **Z-T**$^+$. Thus starting from **E-TOSO$_3^-$**, a mixture of the **E-TOH** and **Z-TOH** is observed (1, 18). The same ratio of these two alcohols is obtained with the (*Z*)-sulfate as the starting material (1). Mixtures of (*E*):(*Z*) products are also observed when the cation reacts with azide ion (1) and with the NH_2 group of guanine (18, 19, 26).

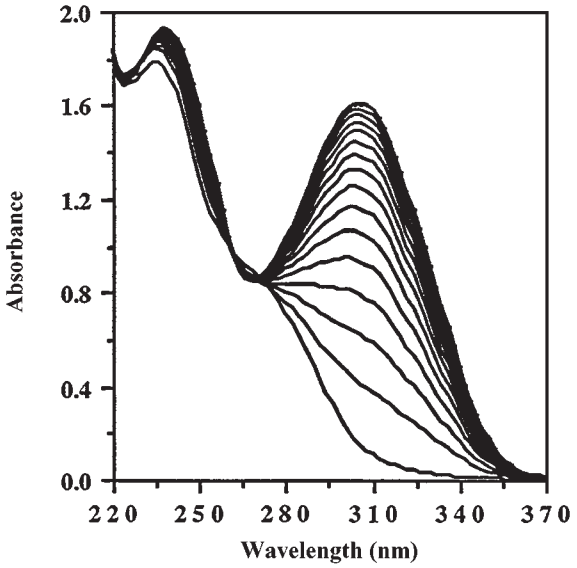
The rapid interconversion can be explained by noting that the cation is better viewed as an α-vinyl substituted diarylmethyl cation such as **E-T**$^{+\prime}$, i.e., where there is little double bond character in the central C—C bond. In fact AM1 calculations show that steric congestion forces the vinyl group to rotate 60–70 degrees out of the plane of the C$^+$-center shown in structure (1). Despite this rotation however we have been unable to detect any products derived from addition of nucleophiles to the C$^+$-center α to the the two aryl groups. In searching for these, we did note two minor peaks in the HPLC chromatogram eluting at considerably longer retention time than the alcohols **E-TOH** and **Z-TOH**. Experiments under acidic conditions where the two alcohols interconvert then revealed that with time an irreversible reaction occurs to produce these same peaks, ultimately as the only peaks in the chromatogram. This provided conditions for isolation of the products responsible. In this paper we provide the details of these experiments, including the characterization of the new products. They turn out to be derived from intramolecular cyclization in the tamoxifen cation. A kinetic analysis shows that the cyclization competes with water addition. Thus, the cyclic products can be taken as an indicator of the formation of the tamoxifen cation.

Results and discussion

Reaction of α-hydroxytamoxifens in acid

The reactions of **E-TOH** and **Z-TOH** in acidic aqueous solutions were first seen in absorption spectra recorded as a function of time in such solutions. As illustrated by the example in Fig. 1, these show the slow growth of a new peak

Fig. 1. Spectra obtained with 2×10^{-4} M (*E*)-α-hydroxytamoxifen (**E-TOH**) in 0.1 M HCl (20°C). Spectra were recorded every 20 min. The absorbance increase at 310 nm fits to a single exponential with a rate constant of 1.1×10^{-4} s^{-1}.



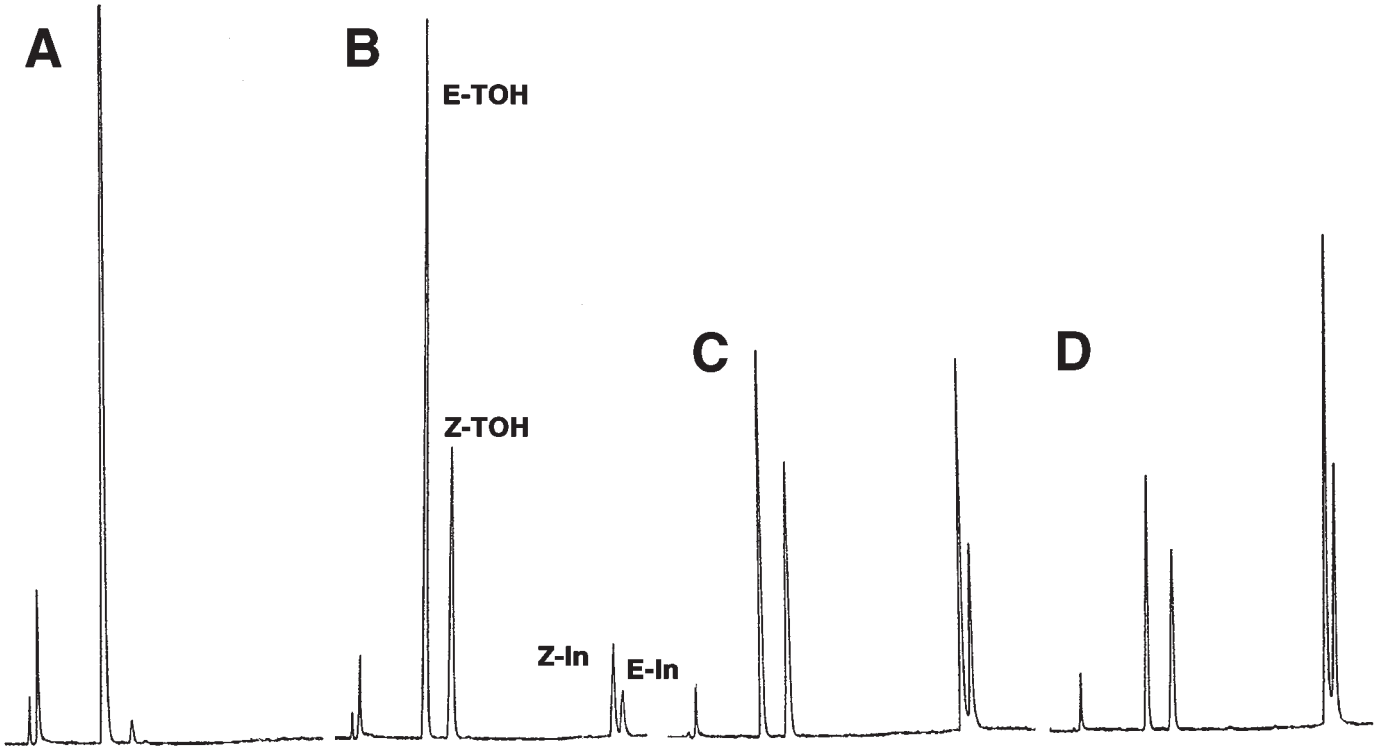
with λ_{max} at 310 nm. The increase at 310 nm follows good single exponential kinetics and there are reasonable isosbestic points at 260 and 270 nm. This suggests a first-order conversion of the starting alcohol to product (or products). However, HPLC chromatograms recorded on the same solution show that the behavior is more complicated. Starting with **E-TOH** as in Fig. 2, this is found to convert to an approximately 1:1 ratio with its (*Z*)-isomer **Z-TOH**, whose HPLC peak appears at a slightly longer retention time (see labels in Fig. 2B). The same interconversion to an ~1:1 **E**:**Z** ratio is obtained with **Z-TOH** as the starting alcohol. At the same time as the isomerization, two new peaks at longer retention time are appearing. This process is considerably slower, and, as will be apparent later, it accounts for the spectral changes in the UV spectra. Ultimately, the two alcohols completely disappear, and the chromatogram contains only the two peaks for the new products.

Identification of Indenes

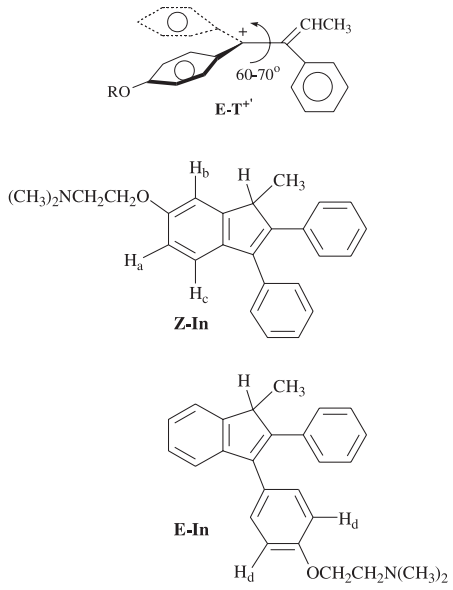
The new products were identified by working on a larger scale in 1 M HCl, and waiting a sufficient time so that there were none of the α-hydroxytamoxifens remaining. An HPLC chromatogram of this mixture was very similar to that obtained at long times on the smaller scales, with the peak at shorter retention time having twice the area of that at the longer retention time. The products were then isolated after neutralization and extraction. Column chromatography unfortunately failed to provide any separation whatsoever, so that identification had to be carried out on the mixture. The mass spectrum showed a molecular ion at *m*/*z* 369 MS, with high resolution MS providing a molecular formula of $C_{26}H_{27}NO$. This indicates that the products are derived from loss of water from the starting material. Considering the chemistry, i.e., that these products arise under acidic conditions where the tamoxifen cations **Z-T**$^+$ and **E-T**$^+$ are being formed, the conclusion is that they are isomeric indenes **Z-In** and **E-In** arising from intramolecular cyclization in the

© 2000 NRC Canada

Fig. 2. HPLC chromatograms (detector at 260 nm) obtained with 2×10^{-4} M (*E*)-α-hydroxytamoxifen (**2**) in 0.1 M HCl (20 ± 1°C). Solutions were injected at 0.8 (**A**), 23.8 (**B**), 95.3 (**C**), and 164.3 (**D**) min after preparation of the solution.



cations. This of course is well established chemistry of phenyl-substituted allylic cations (28–34). The surprising aspect of the present study is that the intramolecular reaction competes with the nucleophilic addition of water. Previous studies of the cyclization have been carried out under strongly acidic conditions where the competing reagents were weakly nucleophilic.



The ^{1}H NMR spectrum of the mixture is consistent with this interpretation. This also shows that the major product at shorter retention time is obtained upon cyclization into the alkoxy-substituted aromatic ring; i.e., the major product is **Z-In**. The indicator here is the aromatic protons next to the alkoxy group, which can be distinguished from the complex multiplet associated with the other aromatic protons. In the indene **Z-In** these protons are nonequivalent. The proton labelled H_a in the representation above appears as a doublet of doublets at 6.87 ppm, with coupling constants of 2.2 and 8.2 Hz representing coupling with H_b and H_c, respectively. The proton H_b is a doublet at 7.18 ppm, with a coupling constant of 2.2 Hz. In **Z-In**, these protons (H_d) are equivalent, and appear as a doublet at 6.95 ppm with a coupling constant of 8.6 ppm. The integration of the doublet of doublets at 6.87 (H_a) vs. the doublet at 6.95 is ~1:1. Since two protons provide the latter doublet, the ratio of **Z**-In**E-In** is ~2:1, so that **Z-In** is the major product eluting at the earlier retention time in the HPLC chromatograms.

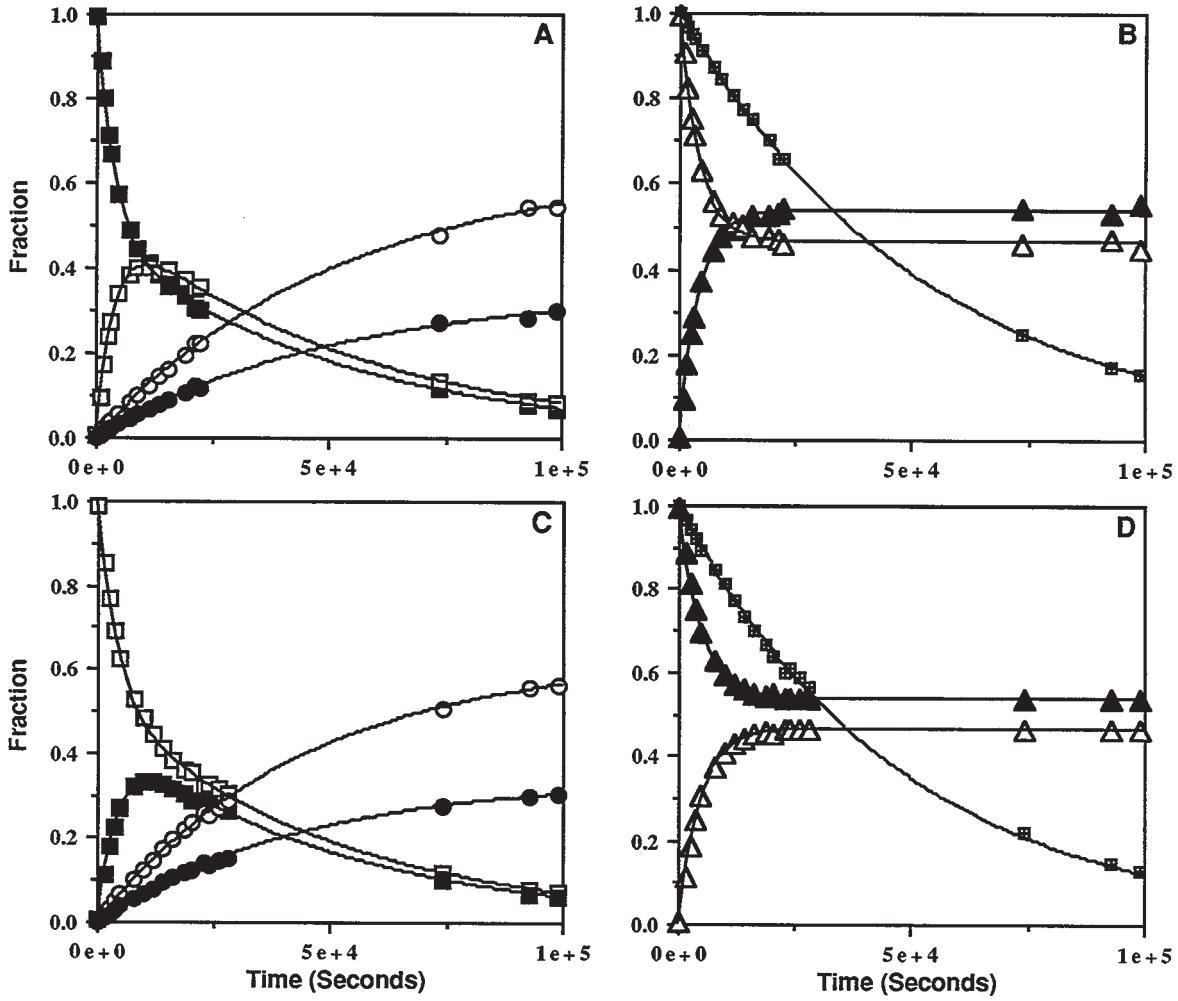
Quantitative analysis

The HPLC chromatograms of Fig. 2 show that there are four species present during the reaction that is occurring in acids. The isosbestic point at 260 nm must therefore mean that these four have essentially identical extinction coefficients at this wavelength. This in turn suggests that by operating at 260 nm in the HPLC, the sensitivities of the four peaks are the same, or, in other works, relative peak areas can be converted directly to relative molar amounts. This was verified for **E-TOH** and **Z-TOH** by injecting known amounts of authentic alcohols. It was further observed that the sum of the areas of the four peaks was constant throughout the reaction, within an experimental error of ±3%. This of course means that the products **E-In** and **Z-In** must have the same sensitivity as the alcohols.

Working on the basis of the HPLC sensitivities being the same at 260 nm, Figs. 3A and 3C were constructed. These

© 2000 NRC Canada

Fig. 3. HPLC analysis of solutions of (*Z*)-α-hydroxytamoxifen (**Z-TOH**) (Figs. 3A, 3B) and (*E*)-α-hydroxytamoxifen (**E-TOH**) (Figs. 3C, 3D) in 0.02 M HCl, 0.08 M NaCl (20°C). Legend for Figs. 3A, 3C: (■) — [**Z-TOH**]:[**Total**], (□) — [**E-TOH**]:[**Total**], (○) — [**Z-In**]:[**Total**], (●) — [**E-In**]:[**Total**], where [**Total**] = [**E-TOH**] + [**Z-TOH**] + [**E-In**] + [**Z-In**]. Legend for Figs. 3B, 3D: (△) — [**Z-TOH**]/([**E-TOH**] + [**Z-TOH**]), (▲) — [**E-TOH**]/([**E-TOH**] + [**Z-TOH**]), (⊠) — ([**E-TOH**] + [**Z-TOH**]):[**Total**]. The points are experimental. The lines are based upon fitting the data to a double exponential or single exponential equation (see Table 1).



plot the fractions of each of the four species as a function of time for experiments starting with **Z-TOH** (Fig. 3A) and **E-TOH** (Fig. 3C) in the same acid solution. It can be seen that the two alcohols interconvert, reaching what appears to be equilibrium position with the ratio [**E-TOH**]:[**Z-TOH**] slightly greater than unity regardless of the starting alcohol. Superimposed on this is the slower process in which the alcohols convert to the indenes. The ratio [**Z-In**]:[**E-In**] is constant throughout each of the runs, and, moreover is the same whether **E-TOH** or **Z-TOH** is the starting material.

The results of kinetic analyses of the data in Figs. 3A and 3C are provided in Table 1. The data for the two alcohols clearly require fitting to an equation that contains two exponential terms, and indeed satisfactory fits are so obtained. The two rate constants determined in such fits differ by a factor of 10–12. The data for the increases in the two indenes, on the other hand, are satisfied by a single exponential. The rate constants so determined are the same as those associated with the slower process of the double exponential fits. Within experimental uncertainty, the same rate constants are obtained whether **Z-TOH** or **E-TOH** is the starting material. Experiments were also performed in solutions with different HCl concentrations with the ionic strength maintained constant at 0.1 M with NaCl. These show that both the fast process and the slow process are first-order in H^+. A final observation is that the slower rate constant obtained from the HPLC data is, within experimental error, the same as the single rate constant obtained from the exponential rise in the UV spectra (obviously for experiments at the same acid concentration). The explanation for this behavior is that the spectra of the two alcohols **E-TOH** and **Z-TOH** are so similar that their interconversion is invisible in the UV. Thus, the spectral change that is observed represents the irreversible process forming the indene products.

Kinetic analysis

Our proposed kinetic model is shown in Scheme 2. This contains the two intermediate carbocations **E-T**$^+$ and **Z-T**$^+$. Each reacts with water to form the corresponding alcohol, and, in competition, cyclizes to an indene. Associated with these reactions are four first-order rate constants k_w(E), k_{cyc}(E), k_w(Z), and k_{cyc}(Z). The carbocations can also form

© 2000 NRC Canada

Table 1. Kinetic analyses of HPLC chromatograms of Fig. 3 obtained with **Z-OH** and **E-TOH** in 0.02 M HCl, 0.08 M NaCl at 20°C.

Constant	Start with **Z-OH**	Start with **E-TOH**
Double exponential decay	k_1 2.57 × 10^4 s^{-1}	2.33 × 10^4 s^{-1}
of starting alcohol[a]	k_2 1.89 × 10^5 s^{-1}	2.01 × 10^5 s^{-1}
Double exponential rise	k_1 2.61 × 10^4 s^{-1}	2.40 × 10^4 s^{-1}
and fall of isomer[b]	k_2 1.87 × 10^5 s^{-1}	2.01 × 10^5 s^{-1}
Single exponential rise of major indene product[c]	1.88 × 10^5 s^{-1}	2.11 × 10^{-5} s^{-1}
Single exponential rise of minor indene product[c]	1.87 × 10^5 s^{-1}	2.07 × 10^{-5} s^{-1}
Ratio of major indene to minor indene[d]	1.86 ± 0.05	1.83 ± 0.04
Single exponential approach to equilibrium — k(isom)[e] [**E-TOH**]/([**Z-TOH**] + [**E-TOH**])	2.37 × 10^{-4} s^{-1}	2.13 × 10^{-4} s^{-1}
[**E-TOH**]([**Z-TOH**]+[**E-TOH**] at equilibrium[f]	0.535 ± 0.02	0.537 ± 0.004
Single exponential decay of ([**E-TOH**] + [**Z-TOH**]):[**total**] – k(cyc)[g]	2.12 × 10^{-5} s^{-1}	1.89 × 10^{-5} s^{-1}

[a]Fit to $A_1 \cdot \mathrm{Exp}(-k_1 t) + A_2 \cdot \mathrm{Exp}(-k_2 t)$ with $A_1 + A_2 = 1$. (Forced to begin at one and end at zero).

[b]Fit to $A_1 \cdot \{\mathrm{Exp}(-k_1 t) - \mathrm{Exp}(-k_2 t)\}$. (Forced to begin and end at zero).

[c]Fit to $(-A_1) \cdot \mathrm{Exp}(-kt) + A_1$. (Forced to begin at zero).

[d]Averaged over all the points.

[e]Fit to eq. [12]. (Forced to begin at zero when **Z-TOH** was starting material and to begin at one when **E-TOH** was starting material).

[f](k_2:(k_1 + k_2)) of eq. [12].

[g]Fit to eq. [13]. (Forced to begin at one and end at zero).

from the appropriate alcohols in H^+-catalyzed processes. The second order rate-constants for these pathways are defined as $k_H(E)$ and $k_H(Z)$; in a solution of a particular acid concentration, the cations will form in pseudo-first-order reactions with rate constants $k_H(E)[H^+]$ and $k_Z(E)[H^+]$.

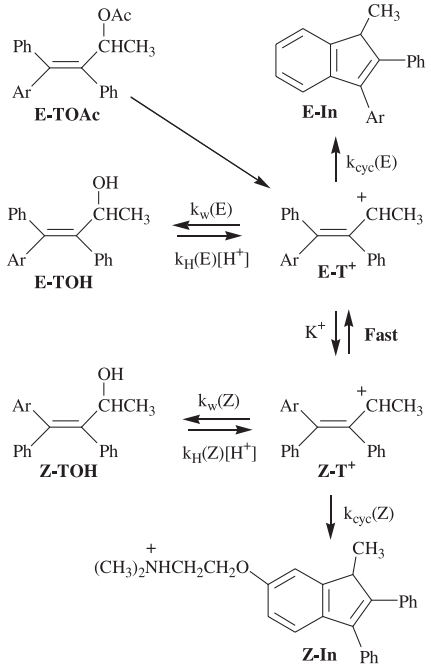
The same carbocations are also the intermediates of the solvolysis of sulfate and acetate precursors. These reactions can be carried out under conditions of kinetic control, i.e., in solutions of very low H^+-concentration such that the alcohol products are stable on the time scale required for complete solvolysis of the ester. An important observation from such experiments is that regardless of whether the ester is (*E*) or (*Z*), **E-TOH** and **Z-TOH** are produced in the same ratio (1), a value of slightly greater than 2:1 in favor of **E-TOH**. The implication is that **E-T**$^+$ and **Z-T**$^+$ achieve equilibrium within their lifetime. These lifetimes (of the equilibrating cations) are known from the LFP experiments, i.e., 40 μs in aq acid. Thus, the (*E*)-(*Z*) interconversion in the cations must be very rapid.[3]

We define the equilibrium constant [**Z-T**$^+$]:[**E-T**$^+$] as K^+. For the solvolysis reactions under conditions of kinetic control, eqs. [1]–[4] can be written for the fraction of each product that is obtained.

[1] $$\mathrm{Fr}(\textbf{E-TOH}) = \left(\frac{k_w(E)}{k_w(E) + k_w(Z)K^+ + k_{cyc}(Z)K^+ + k_{cyc}(E)}\right) = 0.640 \pm 0.005$$

[2] $$\mathrm{Fr}(\textbf{Z-TOH}) = \left(\frac{k_w(Z)K^+}{k_w(E) + k_w(Z)K^+ + k_{cyc}(Z)K^+ + k_{cyc}(E)}\right) = 0.290 \pm 0.003$$

Scheme 2.



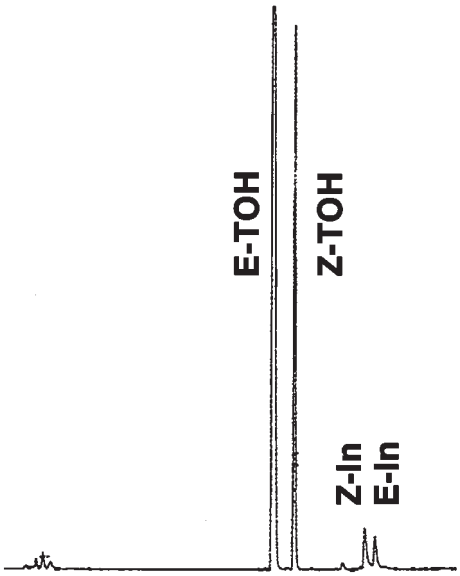
Ar = C_6H_4-4-$OCH_2CH_2N^+H(CH_3)_2$

[3] $$\mathrm{Fr}(\textbf{E-In}) = \left(\frac{k_{cyc}(E)}{k_w(E) + k_w(Z)K^+ + k_{cyc}(Z)K^+ + k_{cyc}(E)}\right) = 0.025 \pm 0.002$$

[3] We have recent evidence that the cations can be trapped before rotation at high concentrations of azide ion, a nucleophile which is a very effective quencher (1).

© 2000 NRC Canada

Fig. 4. HPLC chromatogram obtained after solvolysis of 1×10^{-4} M (*E*)-α-acetoxytamoxifen (**E-TOAc**) in 0.0005 M HCl. Note that the gradient employed to obtain this chromatogram is different from that used in Fig. 2 (see Experimental section). The small peak between the peaks for **Z-TOH** and **Z-In** is due to a small amount of unreacted **E-TOAc**.



[4] $$\mathrm{Fr}(\mathbf{Z\text{-}In}) = \left(\frac{k_{cyc}(Z)K^+}{k_w(E) + k_w(Z)K^+ + k_{cyc}(Z)K^+ + k_{cyc}(E)}\right) = 0.045 \pm 0.002$$

Figure 4 shows a chromatogram obtained in such an experiment, the almost complete solvolysis of (*E*)-α-acetoxytamoxifen (**E-TOAc**) in a very dilute acid solution. The acid was added here to ensure that the products reflect reactions of carbocations where the side-chain amine is protonated. The major products are **E-TOH** and **Z-TOH**, but the peaks for the indenes **Z-In** and **E-In** are present in small amounts. These experiments provide numerical values of the fractions in eqs. [1]–[4]; the ones given above are averages of several experiments. It can be noted that the ratio [**Z-In**]:[**E-In**] is 1.75 ± 0.2, within experimental error the same as the value obtained when these two indenes are formed from alcohol starting materials in more acidic solutions.

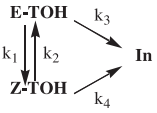
To analyze the experiments with one of the alcohols as starting material, we calculate the steady state concentration of the two carbocations with the assumption that they are in equilibrium. For further simplification we treat the two indene isomers as one, by setting [**In**] = [**E-In**] + [**Z-In**] and Fr(**In**) = (Fr(**E-In**) + Fr(**Z-In**)). This results in the three differential equations of eqs. [5]–[7].

[5] $$\frac{d[\mathbf{E\text{-}TOH}]}{dt} = k_2[\mathbf{Z\text{-}TOH}] - (k_1 + k_3)[\mathbf{E\text{-}TOH}]$$

[6] $$\frac{d[\mathbf{Z\text{-}TOH}]}{dt} = k_1[\mathbf{E\text{-}TOH}] - (k_2 + k_4)[\mathbf{Z\text{-}TOH}]$$

[7] $$\frac{d[\mathbf{In}]}{dt} = k_3[\mathbf{E\text{-}TOH}] + k_4[\mathbf{Z\text{-}TOH}]$$

Scheme 3.



where

[8] $$k_1 = \mathrm{Fr}(\mathbf{Z\text{-}ROH})\cdot k_H(E)[H^+]$$

[9] $$k_2 = \mathrm{Fr}(\mathbf{E\text{-}ROH})\cdot k_H(Z)[H^+]$$

[10] $$k_3 = \mathrm{Fr}(\mathbf{In})k_H(E)[H^+]$$

[11] $$k_4 = \mathrm{Fr}(\mathbf{In})k_H(Z)[H^+]$$

These equations are identical to ones that pertain to the kinetic system of Scheme 3, a model where **E-TOH** and **Z-TOH** interconvert with rate constants k_1 and k_2, and react irreversibly to form the indenes with rate constants k_3 and k_4. The HPLC data of Fig. 3 show that the alcohols equilibrate about 10 times faster than they cyclize to form the indenes. Thus, we make the approximation that $k_1,k_2 > k_3,k_4$. This is equivalent to treating the kinetics in two distinct phases — a rapid phase where the alcohols achieve equilibrium and a slow phase where they react irreversibly to form the indenes. This approximation results in eq. [12] for the equilibration and eq. [13] for the cyclization.

[12] $$\left(\frac{[\mathbf{E\text{-}TOH}]}{[\mathbf{E\text{-}TOH}] + [\mathbf{Z\text{-}TOH}]}\right) = Ae^{-k(\mathrm{isom})t} + \left(\frac{k_2}{k_1 + k_2}\right)$$

where k(isom) = ($k_1 + k_2$), and $A = k_1$:($k_1 + k_2$) or $-k_2$:($k_1 + k_2$) for the cases where **E-TOH** and **Z-TOH**, respectively are the starting alcohols.

[13] $$\left(\frac{[\mathbf{E\text{-}TOH}] + [\mathbf{Z\text{-}TOH}]}{[\mathbf{E\text{-}TOH}] + [\mathbf{Z\text{-}TOH}] + [\mathbf{In}]}\right) = e^{-k(\mathrm{cyc})t}$$

where k(cyc) = ($k_2k_3 + k_1k_4$)/($k_1 + k_2$).

As shown in Figs. 3B and 3D, [**E-TOH**]/([**E-TOH**] + [**Z-TOH**]) and ([**E-TOH**] + [**Z-TOH**])/([**E-TOH**] + [**Z-TOH**] + [**In**]) satisfy a single exponential, as required by eq. [12] and eq. [13] respectively. As seen in Table 1, the rate constant k(isom) from the fit to eq. [12] is essentially the same as the larger of the rate constants obtained by fitting the data for the individual alcohols to equations with two exponentials. The rate constant k(cyc) is the same as the smaller of the rate constants and is also identical to the value obtained from the appearance of the indene products.

From experiments at different acid concentrations, both k(isom) and k(cyc) were found to be proportional to [H^+]. Average values of the second-order rate constants obtained by dividing by H^+ are given in eqs. [14] and [18] below. In the case of the isomerization process, the following relations apply:

[14] $$\left(\frac{k(\mathrm{isom})}{[H^+]}\right) = \left(\frac{k_1 + k_2}{[H^+]}\right) = (1.16 \pm 0.06) \times 10^{-2}\ M^{-1}\ s^{-1} = \mathrm{Fr}(\mathbf{Z\text{-}TOH})\cdot k_H(E) + \mathrm{Fr}(\mathbf{E\text{-}TOH})\cdot k_H(Z)$$

© 2000 NRC Canada

The fit to eq. [12] also provides the fraction of **E-TOH** that is present when the **E-TOH**: **Z-TOH** equilibrium is established:

$$[15]\quad \left(\frac{k_2}{k_1 + k_2}\right) = 0.535 = \left(\frac{[\mathbf{E\text{-}TOH}]_{eq}}{[\mathbf{E\text{-}TOH}]_{eq} + [\mathbf{Z\text{-}TOH}]_{eq}}\right) = \left(\frac{[\mathbf{E\text{-}TOH}]_{eq}}{\mathrm{Fr}[\mathbf{Z\text{-}TOH}] \cdot k_H(E) + \mathrm{Fr}[\mathbf{E\text{-}TOH}] \cdot k_H(Z)}\right)$$

With some algebraic manipulation, inputting the values of Fr(**Z-TOH**) and Fr(**E-TOH**) from eqs. [1] and [2] gives the second-order rate constants:

$$[16]\quad k_H(E) = 2.14 \times 10^{-2}\ M^{-1}\ s^{-1}$$

$$[17]\quad k_H(Z) = 8.42 \times 10^{-3}\ M^{-1}\ s^{-1}$$

It is interesting to note that **E-TOH** forms from the equilibrating cations with a slightly greater than 2:1 preference over **Z-TOH**, but it also undergoes H^+-catalyzed ionization over two-fold faster. The consequence is that the ratio of the two alcohols at equilibrium is close to unity.

For the cyclization process,

$$[18]\quad \left(\frac{k(cyc)}{[H^+]}\right) = (1.01 \pm 0.04) \times 10^{-3}\ M^{-1}\ s^{-1} = \mathrm{Fr}(\mathbf{In})\left(k_H(E)\left(\frac{k_2}{k_1 + k_2}\right) + k_H(Z)\left(\frac{k_1}{k_1 + k_2}\right)\right)$$

where the last term is obtained by substituting the various relations for k(cyc) from eq. [13], and k_3 and k_4 from eqs. [10] and [11]. Numerical values for all the quantities except Fr(**In**) are known from the isomerization kinetics (see eqs. [15]–[17]). Substitution gives FR(**In**) = 0.066. The overall consistency in the analysis is seen in the excellent agreement with the value of 0.070 obtained as the sum of Fr(**E-In**) and Fr(**Z-In**) obtained from the product analysis in the acetate solvolysis.

Summary

These experiments show that the equilibrating tamoxifen carbocations undergo intramolecular cyclization in competition with their reaction with aqueous solvent. The cyclizations represent 7% of the fate of the cations under conditions of kinetic control. Thus they occur with a rate constant of $1.8 \times 10^3\ s^{-1}$, i.e., 7% of the rate constant of $2.5 \times 10^4\ s^{-1}$ obtained by LFP for cation decay (where these rate constants refer to acidic conditions where the side chain amino group is protonated).

We also show that acid conditions must be avoided when performing quantitative analysis of α-hydroxytamoxifens. The H^+-catalyzed formation of the tamoxifen carbocations will occur under these conditions, and the cyclizations represent irreversible processes that result in removal of the alcohols. We had also hoped that we would be able to generate the tamoxifen carbocations under weakly nucleophilic superacid conditions. The occurrence of the rapid intramolecular cyclization however has made this impossible to date, even working at lower temperatures.

Small amounts of the indenes also form at neutral pH when the carbocations are generated in S_N1 solvolysis reactions of acetate and sulfate precursors. Observation of these indenes could be used as an indicator of the formation of the tamoxifen carbocations in cellular systems and even in vivo. To date such experiments have relied upon the formation of the DNA adducts to indicate the formation of the cation (26). The indenes with their λ_{max} at 310 nm and their relatively long retention time should be easily detected by reversed-phase HPLC. Their formation would be unambiguous proof of the formation of the tamoxifen carbocation (and the S_N1 precursor to this cation).

Experimental section

(*E*)-α-Hydroxytamoxifen and (*Z*)-α-hydroxytamoxifen ((*E*)- and (*Z*)-1-[4-[2-(dimethylamino)ethoxy]phenyl]-1,2-diphenyl-1-buten-3-ol) were prepared as a mixture and separated by column chromatography following a literature procedure (27). (*E*)-Acetoxytamoxifen was prepared from the (*E*)-alcohol by treatment with acetic anhydride in pyridine, followed by chromatography as described previously (26, 35).

Z-In (6-(2-dimethylaminoethoxy)-1-methyl-2,3-diphenyl-*1H*-indene) and **E-In** (3-[4-(2-dimethylaminoethoxy)phenyl]-1-methyl-2-phenyl-*1H*-indene) were obtained as a mixture by adding 50 mg of (*E*)-α-hydroxytamoxifen to 100 mL of 1 M HCl. After stirring at ambient temperature for 14 h, the pH was adjusted to 10–11 by the addition of sodium hydroxide, and the indenes extracted with dichloromethane. After drying ($MgSO_4$) and filtration, the solvent was removed to yield a viscous oil. This was purified by chromatography using 8:11:1 ether:hexanes:triethylamine. This failed to provide any separation of the two isomers, as was also the case of TLC experiments using various other solvent combinations. MS (EI): *m*/*z* 369 (100%), 324 (5%), 298 (50%), 265 (75%), 233 (45%), 202 (30%). HRMS *m*/*z* 369.2097; $C_{26}H_{27}NO$ requires 369.2093. The ^1H NMR (400 MHz, $CDCl_3$) of the mixture exhibited peaks that could be assigned to the major isomer (**Z-In**) and minor isomer (**E-In**): 1.315 (major) and 1.320 (minor) (3H, d, J = 7.5 Hz) (CH_3), 2.384 (major and minor) (6H, s) ($N(CH_3)_2$), 2.790 (major) and 2.780 (minor) (2H, t, J = 5.6 Hz) (NCH_2), 4.025 (major) and 4.044 (minor) (1H, q, J = 7.6 Hz) (CH), 4.152 (major) and 4.118 (minor) (2H, t, J = 5.6 Hz), 6.87 (major) (1H, dd, J = 2.2 Hz and 8.2 Hz) (5-H of indene ring of **Z-In**), 6.95 (minor) (2H, d, J = 8.2 Hz) (protons *ortho* to $OCH_2CH_2N(CH_3)_2$ group in **E-In**), 7.16–7.14 (multiplet) (all the other phenyl protons, H7 of the indene ring of **Z-In** could be seen as a doublet at 7.18 Hz with J = 2.2 Hz).

HPLC experiments were conducted with a Waters 600E system, a Waters 486 Tunable Absorbance Detector set at 260 nm, and Waters 746 Data Module. The column was a Water Symmetry C_{18} μm column of dimensions 4.6 mm × 150 mm. The experiments with the α-hydroxytamoxifens as starting material were performed with a flow of 1 mL/min using a programmed eluting system of 0–2 min — isocratic 60% buffer:40% acetonitrile; 2–8 min — linear gradient ending at 15% buffer:85% acetonitrile; and 8–18 min — isocratic 15% buffer:85% acetonitrile, where buffer = 0.025 M sodium acetate:0.025 M acetic acid. Retention times were 4.6 min (**E-TOH**), 5.9 min (**Z-TOH**), 14.2 min

© 2000 NRC Canada

(**Z-In**), and 15.4 min (**E-In**). Experiments starting with α-acetoxytamoxifen used a program of 0–1 min — isocratic 70% buffer:30% acetonitrile; 1–11 min — linear gradient ending at 15% buffer:85% acetonitrile; and 8–18 min — isocratic 15% buffer:85% acetonitrile, where buffer = as above. Retention times were 11.3 min (**E-TOH**), 12.1 min (**Z-TOH**), 13.7 min (**E-TOAc**), 14.8 min (**Z-In**), and 15.3 min (**E-In**). Solutions contained 1×10^{-4} M of the substrate with 60 μL being directly injected into the HPLC.

Acknowledgement

Financial support from the Natural Sciences and Engineering Research Council of Canada (NSERC) is gratefully acknowledged.

References

1. C. Sanchez, S. Shibutani, L. Dasaradhi, J.L. Bolton, P.W. Fan, and R.A. McClelland. J. Am. Chem. Soc. **120**, 13513 (1999).
2. X. Han and J.G. Liehr. Cancer Res. **52**, 1360 (1992).
3. I.N.H. White, F. de Matteis, A. Davies, L.L. Smith, C. Crofton-Sleigh, S. Venitt, A. Hewer, and D.H. Phillips. Carcinogenesis, **13**, 2197 (1992).
4. K. Hemminki, H. Rajaniemi, B. Lindahl, and B. Moberger. Cancer Res. **56**, 4374 (1996).
5. K. Hemminki, H. Rajaniemi, M. Koskinen, and J. Hansson. Carcinogenesis, **18**, 9 (1997).
6. S. Shibutani, L. Dasaradhi, S. Sugarman, A.P. Grollman, and M. Pearl. Proc. Am. Assoc. Cancer Res. **39**, 636 (1998).
7. S. Shibutani. Environ. Mutagen Res. **20**, 201 (1998).
8. G.M. Williams, M.J. Iatropoulos, M.V. Djordjevic, and O.P. Kaltenberg. Carcinogenesis, **14**, 315 (1993).
9. P. Greaves, R. Groonetilleke, G. Nunn, J. Topham, and T. Orton. Cancer Res. **53**, 3919 (1993).
10. G.C. Hard, M.J. Iatropoulos, K. Jordan, L. Radi, O.P. Kaltenberg, A.R. Imondi, and T. Orton. Cancer Res. **53**, 4534 (1993).
11. M.A.-F. Seoud, J. Johnson, and J.C. Weed. Obstet. Gynecol. **82**, 165 (1993).
12. B. Fischer, J.P. Costantino, C.K. Redmond, E.R. Fisher, D.L. Wickerham, and W.M. Cronin. J. Natl. Cancer Inst. **86**, 527 (1994).
13. F.E. van Leeuwen, J. Benraadt, J.W.W. Coebergh, L.A.L. Kiemeney, F.W. Diepenhorst, A.W. van den Belt-Dusebout, and H. van Tinteren. Lancet, **343**, 448 (1994).
14. G.A. Potter, R. McCague, and M. Jarman. Carcinogenesis, **15**, 439 (1994).
15. D.H. Phillips, G.A. Potter, M.N. Horton, A. Hewer, C. Crofton-Sleigh, M. Jarman, and S. Venitt. Carcinogenesis, **15**, 1487 (1994).
16. D.H. Phillips, P.L. Carmichael, A. Hewer, K.J. Cole, and G.K. Poon. Cancer Res. **54**, 5518 (1994).
17. D.H. Phillips, P.L. Carmichael, A. Hewer, K.J. Cole, I.R. Hardcastle, G.K. Poon, A. Keogh and A.J. Strain. Carcinogenesis, **17**, 89 (1994).
18. M.R. Osborne, A. Hewer, I.R. Hardcastle, P.L. Carmichael, and D.H. Phillips. Cancer. Res. **56**, 66 (1996).
19. M.R. Osborne, I.R. Hardcastle, and D.H. Phillips. Carcinogenesis, **18**, 539 (1997).
20. G.K. Poon, B. Walter, P.E. Lonning, M.N. Horton, and R. McCague. Drug. Metabol. Dispos. **23**, 377 (1995).
21. S. Shibutani, L. Dasaradhi, I. Terashima, E. Banoglu, and M.W. Duffel. Cancer Res. **58**, 647 (1998).
22. S. Shibutani, P.M. Shaw, N. Suzuki, L. Dasaradhi, M.W. Duffel, and I. Terashima. Carcinogenesis, **19**, 2007 (1998).
23. W. Davis, S. Venitt, and D.H. Phillips. Carcinogenesis, **19**, 861 (1998).
24. K. Randerath, B. Moorthy, N. Mabon, and P. Sriram. Carcinogenesis, **15**, 2087 (1994).
25. R.A. McClelland. Tetrahedron, **52**, 6823 (1996).
26. L. Dasaradhi and S. Shibutani. Chem. Res. Toxicol. **10**, 189 (1997).
27. A.B. Foster, M. Jarman, O.-T. Leung, R. McCague, G. Leclerq, and N. Devleeschouwer. J. Med. Chem. **28**, 1491 (1985).
28. Chemistry of Carbon Compounds. Vol. III, *Edited by* E.H. Rodd. Elsevier, Amsterdam, 1954.
29. D.Y. Curtin, H.W. Johnston, and E.G. Steiner. **77**, 4566 (1955).
30. D.H.R. Barton and D.W. Jones. J. Chem. Soc. xx, 3563 (1965).
31. M.G. Miller and C.V. Pittman. J. Org. Chem. **39**, 1955 (1974).
32. R. Knorr, E. Lattke, F. Ruf, and H.-U. Reissig. Chem. Ber. **114**, 1592 (1981).
33. R.R. Kostikov, G.S. Varakin, and K.A. Ogloblin. J. Org. Chem. USSR (Engl. Transl.) **19**, 1438 (1983).
34. N.J. Head, G.A. Olah, and G.K.S. Prakash. J. Am. Chem. Soc. **117**, 11205 (1995).
35. M.R. Osborne, A. Hewer, I.R. Hardcastle, P.L. Carmichael, and D.H. Phillips. Cancer Res. **56**, 66 (1996).

© 2000 NRC Canada

Reaction of dimethoxycarbene with strained cyclic carbonyl compounds

Paul C. Venneri and John Warkentin

Abstract: A cyclopropanone, a cyclopropenone, cyclobutanones, a cyclobutane-1,3-dione, and a cyclobutene-1,2-dione reacted with dimethoxycarbene to afford acetals of the next larger ring by formal insertion of the carbene into a C—C bond α to the carbonyl group. When either of two saturated α-ring carbons could be involved in the process, the ring expansion was selective, affording primarily the product of apparent insertion into the more substituted ring bond. With 2,3-dimethoxycyclobutene-1,2-dione, insertion occurred between the carbonyl groups and with β-propiolactone it occurred at the lactone bond. β-Propiolactam, however, reacted by insertion of the carbene into the N—H bond.

Key words: β-propiolactone, cyclobutanone, cyclobutananedione, cyclopropanone, dialkoxycarbene.

Résumé : On a fait réagir du diméthoxycarbène avec unr cyclopropanones, une cyclopropénone, des cyclobutanones, une cyclobuta-1,3-dione et une cyclobutène-1,2-dione pour obtenir les acétals des cycles agrandis par une insertion formelle du carbène dans la liaison C—C en α du groupe carbonyle. Lorsque les deux liaisons C—C en α sont saturées, mais différentes, l'extension de cycle se fait de façon sélective et elle conduit principalement au produit résultant de l'insertion apparente dans la liaison du cycle la plus substituée. Avec la 2,3-diméthoxycyclobutène-1,2-dione, l'insertion se produit entre les groupes carbonyles et avec la β-propiolactone elle se produit au niveau de la liaison lactonique. Toutefois, avec le β-propiolactame, l'insertion du carbène se fait dans la liaison N—H.

Mots clés : β-propiolactone, cyclobutanone, cyclobutanedione, cyclopropanone, dialkoxycarbène.

[Traduit par la Rédaction]

Introduction

Carbenes with one or more donor groups attached to the carbene carbon atom are well known to have singlet ground states and to be relatively long-lived compared to alkylidenes. For example, the singlet state of dimethoxycarbene lies some 76 kcal mol^{-1} below the triplet (1) and several diaminocarbenes are kinetically stable enough to be isolated (2–8). Reduced reactivity is observed with methoxy(methyl)carbene, which undergoes 1,2-migration of H much more slowly than dimethylcarbene (9). The large singlet–triplet gap and the lowered reactivity of such singlets are attributed to conjugative delocalization of electron density from heteroatom substituents (OR, NR_2) into the virtual *p*-orbital of the carbene (10–13). Such delocalization, and analogous delocalization in transition states for reactions of such carbenes with electrophiles, makes them nucleophilic and potentially useful for Michael additions and additions to carbonyl groups. Dialkoxycarbenes do attack isocyanates (14–16), vinyl isocyanates (17–19), isothiocyanates (14, 15), ketenes (20, 21), perchloroketones (22), and anhydrides (23), for example, but they do not attack simple ketones efficiently. Dimethoxycarbene reacts with fluorenone in low yield (24). We now report that strained cycloalkanones and cycloalkanediones react quite cleanly with dimethoxycarbene to afford products of ring expansion (Scheme 1). The only analogous insertions are those of carbenoids into diphenylcyclopropenone (25) and into 1,2-cyclobutenediones (26) reported by Herndon's group.

Received April 10, 2000. Published on the NRC Research Press website on August 30, 2000.

P.C. Venneri and J. Warkentin.[1] Department of Chemistry, McMaster University, Hamilton, ON L8S 4M1, Canada.

[1]Author to whom correspondence may be addressed. Telephone: (905) 525-9140 ext. 23478. Fax: (905) 522-2509. e-mail: warkent@mcmaster.ca

Methods, results, and discussion

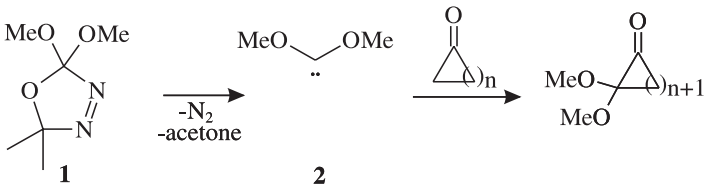
A benzene solution of oxadiazoline **1** and the substrate ketone was degassed and sealed into a Pyrex tube which was then heated for 24 h at 110°C with an oil bath. Thermolysis of oxadiazoline **1**, via loss of nitrogen and acetone (27), generates dimethoxycarbene (**2**), which attacks the ketone and (or) dimerises. A sample of the solution was analyzed by GC and GC–MS prior to work-up to estimate the ratios of products. Major products were isolated by means of chromatographic techniques and they were identified by means of spectroscopy.

Reaction of 2 with cyclobutanone (3)

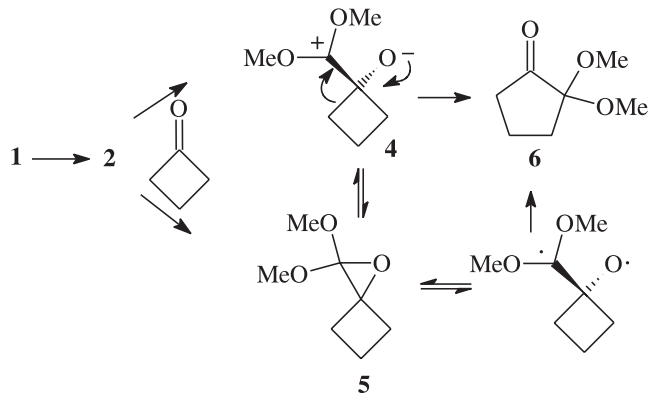
Heating of 2,2-dimethoxy-5,5-dimethyl-Δ^3-1,3,4-oxadiazoline (**1**) with cyclobutanone (**3**) in benzene at 110°C afforded 2,2-dimethoxycyclopentanone (**6**) (Scheme 2) in 75% yield (isolated). The ring expansion is presumably the result of either concerted insertion of dimethoxycarbene (**2**) between the carbonyl group and the α-carbon atom or the result of stepwise reaction in which **2** attacks the electropositive carbon atom of the carbonyl group as a nucleophile, to generate a zwitterionic intermediate (**4**) that is most likely equilibrated with oxirane **5**. Cyclopentanone

 © 2000 NRC Canada

Scheme 1.



Scheme 2.



(**6**) then arises by α-carbon migration (Scheme 2). These mechanisms differ in that **4** is a transition state in the one case and an intermediate, presumably equilibrated with **5**, in the other. Another mechanism that is not ruled out would involve the diradical analogue of **4**, possibly arising from homolytic ring opening of **5**. The latter could arise from **4** or it could be formed by concerted cycloaddition of **2** to cyclobutanone, Scheme 2.

The reaction can be compared to homologations of alkanones with diazomethane (**7**) (28). The first step is thought to be addition to the carbonyl group to generate intermediate **8** (Scheme 3) that, by alkyl migration with loss of nitrogen, gives the homologous ketone (**9**).

The insertion preference was not clearly predictable on the basis of precedents from ring expansions with diazomethane, in which migration of an α-carbon bearing an electron-withdrawing group, such as methoxy or halogen, is disfavoured (28) and one bearing a donor group is generally favoured. For example, 2-methyl-3-benzyloxycyclobutanone affords 3-methyl-4-benzyloxycyclopentanone with a 3:1 preference over 2-methyl-3-benzyloxycyclopentanone (29). On the other hand, steric effects can dominate as indicated by reports that 2-cyclohexylcyclohexanone gave only ca. 5% of ring expansion products (30) and that 3,3,5-trimethylcyclohexanone afforded more 3,3,5-trimethylcycloheptanone (21%), by migration of the less-hindered primary carbon, than 3,5,5-trimethylcycloheptanone (12%), by migration of the more-hindered primary carbon (31, 32). In 2-phenylcyclohexanone, one might expect electronic and steric effects to operate in the same sense, because phenyl is inductively electron withdrawing, to thwart migration of the CHPh group entirely. The fact that one fourth of the product of ring expansion was 3-phenylcycloheptanone, from migration of CHPh (28, 33), and three fourths was 2-phenylcycloheptanone, probably means that phenyl is partially compensating for its steric and inductive effects with weak conjugative stabilization. An early transition state with some cation character in the migrating group could be appropriate.

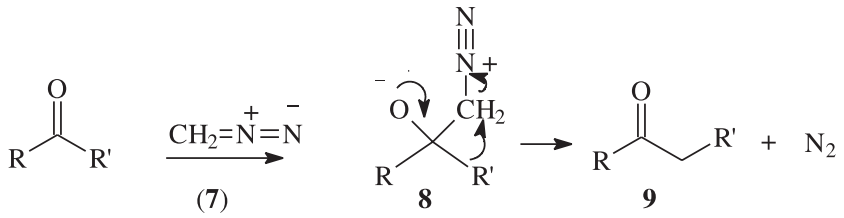
To assess the electronic and steric effects on the insertions of dimethoxycarbene into the cyclobutanone ring, we tested 2-*tert*-butylcyclobutanone (**10**) and 2-methylcyclobutanone (**13**).

Reaction of 2 with 2-*tert*-butylcyclobutanone (10)

Thermolysis of dimethoxy oxadiazoline (**1**) in the presence of 2-*tert*-butylcyclobutanone (**10**) afforded *tert*-butyl-2,2-dimethoxycyclopentanones (**11** and **12**) in 1.5:1.0 ratio, as determined by NMR spectroscopy (Scheme 4). The major product is that from formal carbene insertion between the carbonyl group and the more substituted α-carbon while insertion into the other α-site led to the minor product.

The isomeric structures were established in two ways. First, irradiation of the *tert*-butyl signal of the major isomer (NOE experiment) enhanced both methoxy group signals in the ^{1}H NMR spectrum, while irradiation of the *tert*-butyl signal in the minor component enhanced only one methoxy signal.[2] Second, the fragmentation patterns in the mass spectra of the major and minor isomers were quite different. That of the major isomer had the base peak at m/z = 129 (144 – $CH_3^{\cdot}$), signifying the connectivity $(CH_3O)_2CCHC(CH_3)_2$ of **11**. On the other hand, the base peak in the mass spectrum

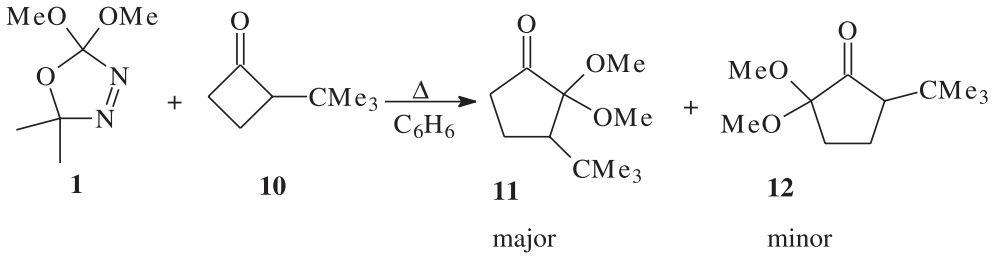
Scheme 3.



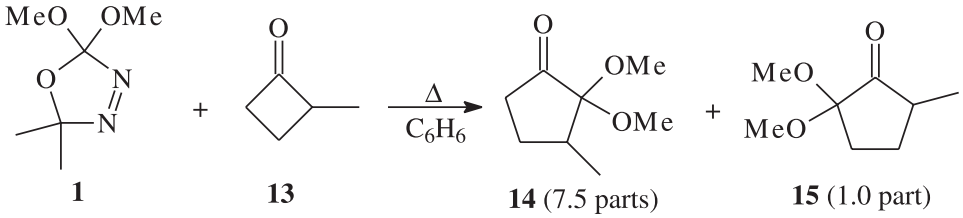
[2] AM-1 geometry optimizations show that rotation brings both methoxy groups of **10** into contact with the *tert*-butyl group. In **11** only one methoxy group is close to the *tert*-butyl group.

© 2000 NRC Canada

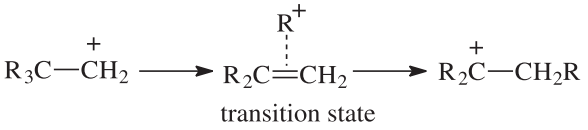
Scheme 4.



Scheme 5.



Scheme 6.



of the minor isomer was at m/z = 88, indicating the connectivity $(CH_3O)_2CCH_2$ of **12**. These results establish the position of the *tert*-butyl group in each isomer.

Preferential migration of the $CHC(CH_3)_3$ group during reaction of **2** with 2-*tert*-butylcyclobutanone indicates that electronic effects must outweigh steric effects. The importance of the latter could be assessed qualitatively with cyclobutanone **13**, which afforded **14** and **15** in 7.5:1.0 ratio (Scheme 5).

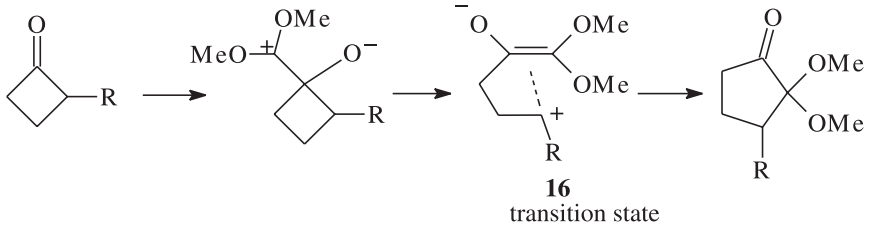
An alkyl substituent exerts an electronic effect that clearly favours migration while its steric effect operates to moderate the electronic influence. The sense of the migration preference is that observed in carbocation rearrangements, which are often described as resembling a π-complex of an alkene and a cation (Scheme 6) (34–36). To retain this model for the rearrangement of a dipolar intermediate from **10** and **13**, one would draw the transition state (**16**) with enolate character; in other words, the carbonyl group of the product would be only weakly expressed at the transition state and the migrating group would move with cation character, rather than anion character (Scheme 7). This mechanism, if correct, means that migration toward a cationic site involves accumulation of some positive charge on the migrating group, even if the cation is delocalized and an anionic group is "pushing".

Treatment of *trans*-di-*tert*-butylcyclopropanone (17), *cis*-2,4-di-*tert*-butylcyclobutanone (19), 2,2,4,4-tetramethylcyclobutanone (22), 1,2-diphenylcyclopropenone (23), and 3,4-dimethoxycyclobutene-1,2-dione (24) with 2

Generation of **2** in the presence of *trans*-di-*tert*-butylcyclopropanone (**17**) gave cyclobutanone **18** in good yield (Scheme 8). The large relief of strain from quaternization of the CO group of a cyclopropanone is presumably responsible. On the other hand, the corresponding reaction of **2** with *cis*-2,4-di-*tert*-butylcyclobutanone (**19**) was not successful.

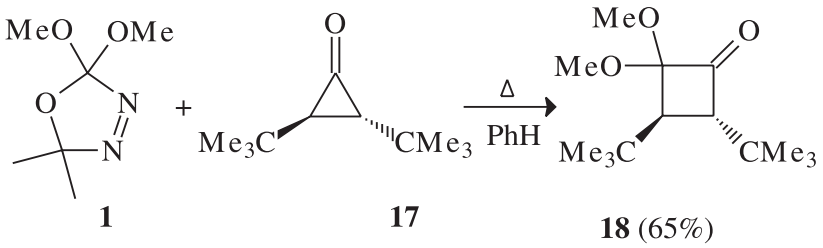
The expected **20** was not detected; only unreacted **19** and carbene dimer **21** could be isolated from the thermolysis mixture (Scheme 9). This result was surprising, because one face of the *cis* disubstituted cyclobutanone would appear to be approachable. Thermal isomerization of **19** to the *trans* isomer was not responsible; the ketone left at the end of the experiment was still *cis* by ^{1}H NMR spectroscopy (37). We propose that attack of **2** at the more accessible face of **19** forces the *tert*-butyl groups, which are probably well separated because the ketone is not planar, closer together and introduces steric interactions with the developing alkoxide

Scheme 7.

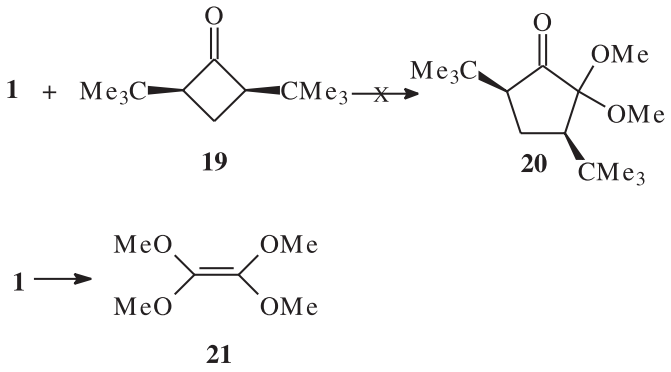


© 2000 NRC Canada

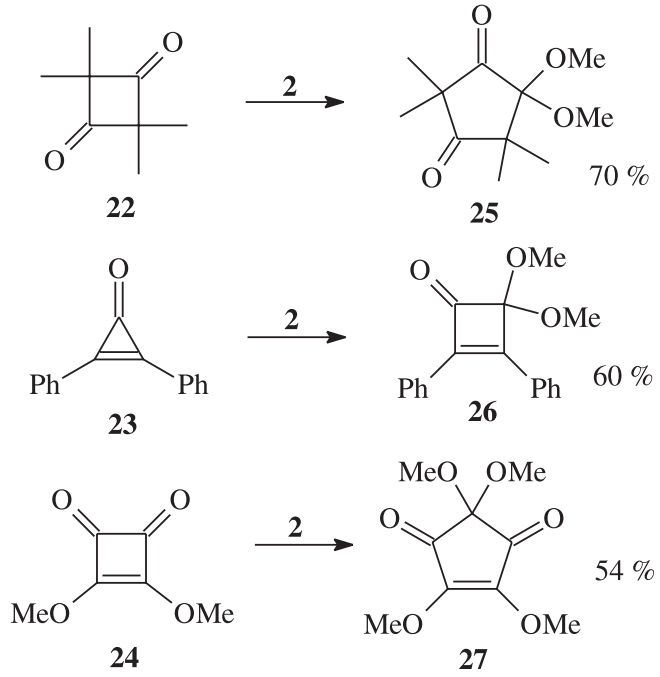
Scheme 8.



Scheme 9.



Scheme 10.



function. That hindrance slows attack by dimethoxycarbene enough to make carbene coupling the predominant reaction. *trans*-Di-*tert*-butylcyclopropanone does react with **2**, in spite of steric hindrance, because of its greater ring strain (Scheme 8).

To test for the importance of ring strain, **2** was generated in the presence of cyclopentanone. A small amount of 2,2-dimethoxycyclohexanone (12% yield) was obtained but the major product was the carbene dimer, which is also the major product from the thermolysis of oxadiazoline **1** in the absence of a carbene trap (27). Thus, as expected, the yield of carbene insertion product is dependent on the ring strain of the cyclic ketone.

Other cycloalkanones that react with **2** to afford products of ring expansion in acceptable yields are **22**, **23**, and **24** (Scheme 10). It is clear that a tricoordinate carbon atom can migrate, as in diphenylcyclopropenone (**23**) and dimethoxycyclobutendione (**24**), whether the attacking group is a carbenoid (25, 26) or **2**. Products of attack in the Michael sense were not found in either case and, in the case of **24**, the product of insertion between the C—C double bond and the carbonyl group was not found.

Compound **27**, although it is an acetal as well as an enol ether, was easily isolated by chromatography. Its resistance to hydrolysis was demonstrated when it was found to be unaffected when stirred with 10% sulphuric acid at room temperature for 2 h. Some reaction to form a complex mixture did occur during stirring for 24 h with a 50:50 solution of 10% sulphuric acid in methanol, although much of the starting material was left unchanged. The resistance of **27** to acid reflects the destabilization of cations that would need to develop during acetal hydrolysis (**28**) or enol ether hydrolysis (**29**), by one or two neighbouring carbonyl groups (Scheme 11).

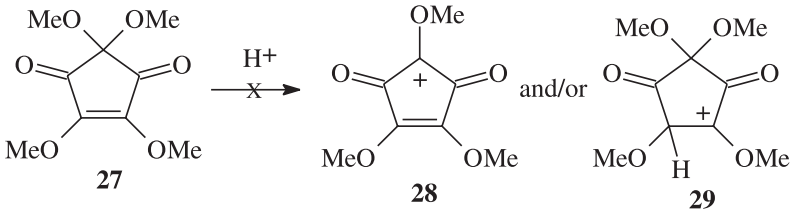
Reaction of 2 with 2-azetidinone (30) and β-propiolactone (34)

The ring-expansion reactions of **2** with small-ring cycloalkanones led us to examine 2-azetidinone (**30**) and β-propiolactone (**34**) also (Scheme 12). With **1** and 2 equiv of 2-azetidinone (**30**), insertion of **2** into the N—H bond (38) was the dominant pathway. Insertion leading to ring expansion products **32** and **33** did not take place. Use of 2 equiv of **1** led to insertion into the N—H bond (76% by GC) but not to subsequent ring expansion of the β-lactam (**31**) via a second carbene insertion. Instead the excess carbene dimerized to **21**. Amide resonance is presumably important enough to reduce the electrophilicity of the carbonyl carbon atom so as to slow ring expansion of **30** and **31**. Whether insertion into the N—H bond is concerted or stepwise is not known.

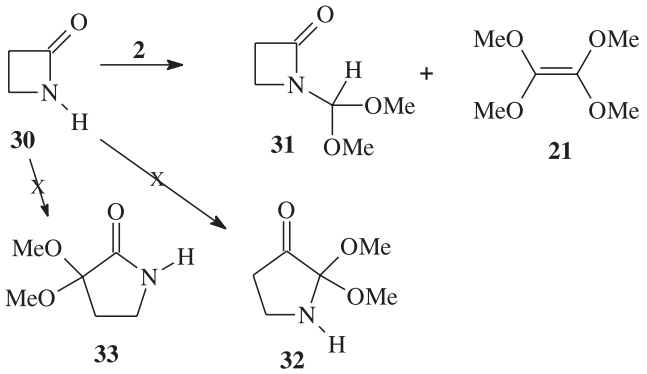
Reaction of **2** with **34** afforded one major ring expansion product (**36**) in 65% yield (Scheme 13). Insertion between the carbonyl carbon atom and the α-oxygen cannot be accommodated within the mechanism invoked to explain the results from 2-*tert*-butylcyclobutanone (**10**) and 2-methylcyclobutanone (**13**). An enolate-like transition state would

© 2000 NRC Canada

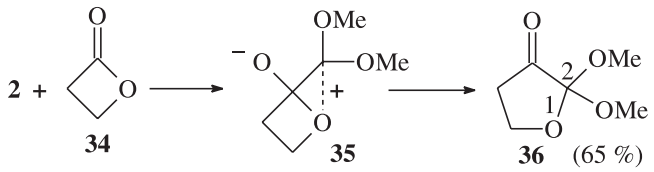
Scheme 11.



Scheme 12.



Scheme 13.



necessarily deplete the migrating ring atom of electron density and lead to migration of the CH_2 group instead of O. We postulate that the ring oxygen interacts with the developing positive site as the carbene begins to bond to the carbonyl carbon. Instead of a zwitterionic intermediate analogous to **4** (Scheme 2) a bicyclic intermediate (or transition state) **35** is reached, with the new bond between O_1 and C_2 partly developed. This picture differs subtly from the previous one in that the migrating atom initially bonds to the migration terminus with an unshared pair rather than with σ-electrons. A similar mechanism fits the insertions of **2** into cyclic anhydrides (23).

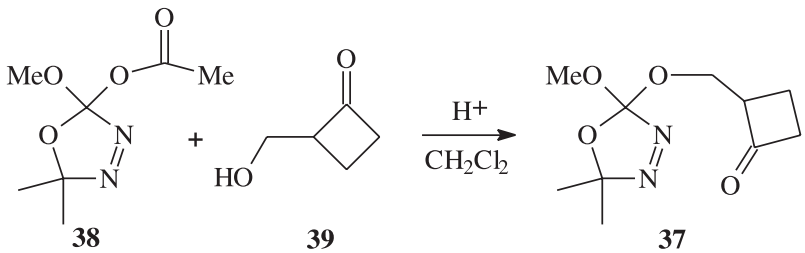
Thermolysis of 2-(2-cyclobutanonemethoxy)-2-methoxy-5,5-dimethyl-Δ^3-1,3,4-oxadiazoline (37)

To investigate the potential of ring expansion reactions for the preparation of bicyclic ketones, an intramolecular variant was examined. The cyclobutanone system illustrated in Scheme 14 was chosen because of the high yield of the product of ring expansion in the intermolecular chemistry of dimethoxycarbene and cyclobutanone. A one carbon link between the oxygen of the oxadiazoline and cyclobutanone would lead to a five-membered transition state from attack of the carbene at the carbonyl group of the cyclobutanone ring.

2-(2-Cyclobutanonemethoxy)-2-methoxy-5,5-dimethyl-Δ^3-1,3,4-oxadiazoline (**37**) was prepared by the acetoxy exchange method (27) (Scheme 14). Acetoxymethoxy oxadiazoline (**38**) and 2-hydroxymethylcyclobutanone (**39**), made by literature procedures (27, 39), reacted in dichloromethane containing a catalytic amount of trifluoroacetic acid to yield the desired oxadiazoline (**37**), which was identified by means of ^1H and ^{13}C NMR spectroscopy and mass spectrometry.

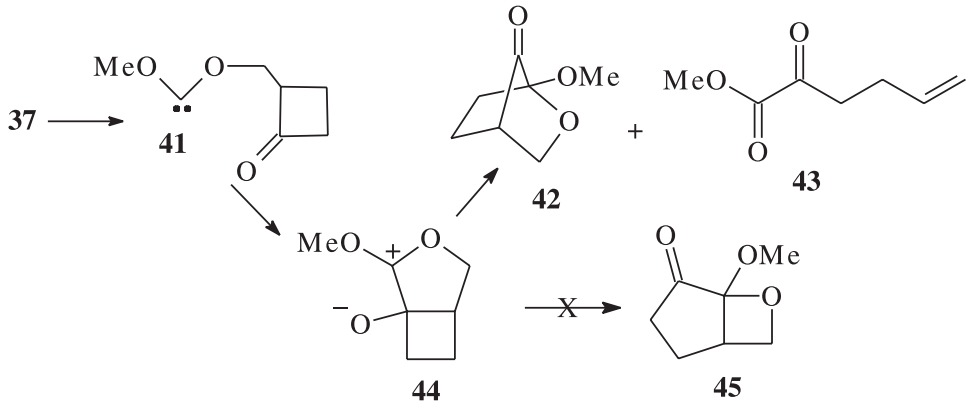
Thermolysis of **37** led to the new bicyclic ketone **42** and to compound **43**, (Scheme 15), which are accounted for as follows. Loss of nitrogen and acetone from **37** gives carbene **41**, and intramolecular carbene addition to the tethered carbonyl group affords intermediate **44**. Substituent migration in **44** could proceed in two ways. Ring enlargement by migration of the least substituted α-carbon atom would give rise to **42** and expansion through migration of the most substituted α-carbon would afford **45**. However, instead of **45**, the product of double ring cleavage (**43**) was obtained. The ratio **42**:**43** was 1.2:1.0 and the combined yield was 60% (isolated). These results can be fitted into the proposed mechanism involving an enolate-like transition state (Scheme 7). Geometric constraints in the cyclic transition state (A, Fig. 1) leading to **42**, with five-membered rings only, should be less severe than those in transition state B leading to **45**, which has a new four-membered ring. Moreover, the electron pair required for rearrangement to **45** is roughly orthogonal to the virtual cation orbital to which it

Scheme 14.



© 2000 NRC Canada

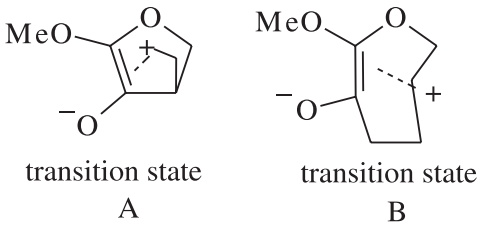
Scheme 15.



would need to migrate. Bond cleavages, to relieve strain and to generate a new carbonyl group, occur instead.

The mono acetals of monocyclic β-dicarbonyl compounds (**6**, **11**, **12**, **14**, **15**, **18**, **25**–**27**) are new compounds and the bicyclic system **42** was unknown. The former are readily accessible by reaction of dimethoxycarbene with small-ring carbonyl compounds and the latter was obtained by an intramolecular variant of the other reactions. The fact that dialkoxycarbenes are now available in a wide variety, and that other nucleophilic carbenes (e.g., $RO(R_2N)C$:) may undergo similar reactions, suggests that the type of reactions introduced above could become useful.

Fig. 1.



Experimental

NMR spectra were acquired with a Bruker DRX-500, AC 300, or AC 200 spectrometer. ^{1}H NMR chemical shifts were referenced to internal TMS or $CHCl_3$ (δ = 7.24) in $CDCl_3$, or C_6HD_5 (δ = 7.15) in C_6D_6, while ^{13}C NMR spectra were referenced to the C_6D_6 triplet (δ = 128.0) or the $CDCl_3$ triplet (δ = 77.0). Mass spectra were recorded with a VGH ZAB-E double focusing mass spectrometer or with a Hewlett–Packard MSD GC–MS. IR spectra are from a Bio-Rad FTS-40 instrument. Semipreparative gas chromatography was performed with a Varian Star 3400 CX gas chromatograph with a thermal conductivity detector and a glass column (6′ × 0.25″) packed with 10% OV-17. Analytical GC work involved a Varian Vista 600 gas chromatograph equipped with a flame ionization detector and a DB-1 megabore capillary column (0.53 mm × 30 m). Unless otherwise stated, benzene was dried with activated molecular sieves and other chromatography solvents were distilled before use. Silica gel from Silicycle (230–400 mesh), in a 30 cm × 2.5 cm glass column, was used for flash chromatography.

General procedure

A Pyrex glass tube (25 mL volume) fitted with a Teflon valve was washed, first with acetone (50 mL), then aq sodium bicarbonate (10%, 50 mL), and finally with distilled water (100 mL). The tube (without the valve) was heated in an oven at 100°C for 2 h. Subsequently, the glass tube (with the valve) was flame dried with the exit port attached to a vacuum line (0.1–0.5 mmHg) to remove most of the residual moisture.

*2,2-Dimethoxy-5,5-dimethyl-Δ^3-1,3,4-oxadiazoline **1***

2,2-Dimethoxy-5,5-dimethyl-Δ^3-1,3,4-oxadiazoline (**1**) was prepared by means of reaction between the corresponding 2-acetoxy-2-methoxy oxadiazoline and methanol catalyzed by trifluoroacetic acid. The crude oxadiazoline was purified by flash column chromatography (silica gel – 10% ethyl acetate in hexanes). MS (EI) *m*/*z*: 132, 129, 105, 91, 90,75, 74, 73, 59, 43 (molecular ion not observed). MS (CI–NH_3) *m*/*z*: 178 ($M^{+\cdot}$ + 18). ^{1}H NMR (200 MHz, $CDCl_3$) δ: 1.53 (s, 6H), 3.45 (s, 6H). ^{13}C NMR (50 MHz, $CDCl_3$) δ: 23.7, 51.5, 118.8, 137.0.

*Thermolysis of **1** in the presence of cyclobutanone **3***

A pyrex glass tube (25 mL) was charged with **1** (0.200 g, 1.25 mmol), cyclobutanone (**3**, Aldrich) (0.175 g, 2.50 mmol), and benzene (5 g). After three freeze–pump–thaw sequences (0.1–0.5 mmHg) with liquid nitrogen as coolant, the glass tube was sealed and immersed for 24 h in an oil bath at 110°C. After the contents had cooled to ambient temperature, the reaction mixture was transferred to a 25 mL round-bottomed flask. The solvent and volatiles were removed with a rotary evaporator and a vacuum pump, yielding 2,2-dimethoxycyclopentanone (**6**) (75% yield). Spectroscopic data were in agreement with those in the literature (40, 41). MS (CI–NH_3) *m*/*z*: 162 ($M^{+\cdot}$ + 18). ^{1}H NMR (500 MHz, C_6D_6) δ: 1.36 (tt, ^3J = 7.0 Hz, ^3J = 7.6 Hz, 2H), 1.61 (t, ^3J = 7.0 Hz, 2H), 1.82 (t, ^3J = 7.6 Hz, 2H), 3.14 (s, 6H). ^{13}C NMR (50 MHz, C_6D_6) δ: 16.9, 33.3, 35.2, 49.9, 100.7, 207.8 (C=O).

© 2000 NRC Canada

*Thermolysis of **1** in the presence of 2-tert-butylcyclobutanone **10***

A 5 mL reaction vessel for thermolysis was charged with **1** (0.078 g, 0.49 mmol), 2-*tert*-butylcyclobutanone (**10**) (38) (0.060 g, 0.48 mmol), and benzene (2.0 g). After three freeze–pump–thaw cycles the tube was sealed and heated at 110°C for 24 h in an oil bath. The contents of the vessel were transferred to a 5 mL round-bottomed flask and the volatiles were removed with a rotary evaporator and then.. a vacuum pump (0.1–0.5 mmHg) leaving a yellow oil. Semipreparatory gas chromatography of the mixture gave two major components in 60% combined yield. 2,2-Dimethoxy-3-*tert*-butylcyclopentanone (**11**) and 2,2-dimethoxy-5-*tert*-butylcyclopentanone (**12**) were obtained in 1.5:1.0 ratio as determined by uncorrected GC analysis and NMR spectroscopy.

11: GC–IR (cm^{-1}): 1762 (C=O). MS (EI) *m*/*z* (rel. intensity): 172 ($M^{+\cdot}$ –28, 5), 153 (3), 144 (13), 129 (100), 113 (10). ^{1}H NMR (500 MHz, C_6D_6) δ: 1.07 (s, 9H), 1.38–1.42 (m, 1H), 1.51–1.65 (m, 3H), 1.95–2.01 (m, 1H), 3.01 (s, 3H, OCH_3), 3.30 (s, 3H, OCH_3). ^{13}C NMR (125 MHz, C_6D_6) δ: 18.9, 29.2, 32.4, 34.7, 48.4, 50.3, 51.5, 103.8, 210.0 (C=O). Irradiation at the frequency of the *tert*-butyl signal (NOE) caused enhancement of both methoxy group signals. In the mass spectrum, the base peak was at *m*/*z* = 129, consistent with loss of a methyl radical from 1,1-dimethoxy-3,3-dimethyl-1-butenyl radical cation (*m*/*z* = 144).

12: IR (CCl_4) (cm^{-1}): 1749 (C=O). MS (EI) *m*/*z* (rel. intensity): 172 ($M^{+\cdot}$ –28, 6), 169 (7), 157 (4), 113 (110), 88 (100). ^{1}H NMR (500 MHz, C_6D_6) δ: 0.95 (s, 9H), 1.30–1.51 (m, 3H), 1.63 (dd, ^3J = 11 Hz, ^3J = 8.8 Hz, 1H), 1.88 (ddd, *J* = 12.7 Hz, *J* = 6.3 Hz, *J*= 1.5 Hz, 1H), 3.13 (s, 3H), 3.16 (s, 3H). ^{13}C NMR (125 MHz, C_6D_6) δ: 20.6, 27.7, 31.5, 33.0, 49.6, 49.9, 56.0, 101.0, 213.3 (C=O). Irradiation at the frequency of the *tert*-butyl signal (NOE) caused enhancement of only one methoxy signal (δ = 3.16). In the mass spectrum the base peak was at *m*/*z* = 88, consistent with 1,1-dimethoxyethene radical cation.

*Thermolysis of **1** in the presence of 2-methylcyclobutanone **13***

A solution of **1** (0.19 g, 1.2 mmol), 2-methylcyclobutanone (**13**, prepared according to the procedure by van Leusen and co-workers ((42, 43), 0.10 g, 1.2 mmol) and benzene (5.0 g) was treated as described above. The residue, a light yellow oil (59%), was a two-component mixture of 2,2-dimethoxy-3-methylcyclopentanone (**14**) and 2,2-dimethoxy-5-methylcyclopentanone (**15**) in 7.5:1.0 ratio, by NMR spectroscopy. The major and minor isomers were distinguished by means of their characteristic mass spectral fragmentation patterns, similar to those observed for **11** and **12**.

14: IR (CCl_4) (cm^{-1}): 1758 (C=O). MS (EI–GC–MS) *m*/*z* (rel. intensity): 158 ($M^{+\cdot}$, 1), 130 ($M^{+\cdot}$–28, 7), 102 ($(CH_3O)_2CCCH_3^{+\cdot}$, 100), 85 (30), 72 (14), 57 (61). MS (CI–NH_3) *m*/*z*: 159 ($M^{+\cdot}$+1), 176 ($M^{+\cdot}$+18). MS (HR) *m*/*z*: calcd. for $(CH_3O)_2CCHCH_3$ (base peak, isomer identification): 102.0703; found: 102.0681. ^{1}H NMR (200 MHz, C_6D_6) δ: 0.79 (d, ^3J = 7.0 Hz, 3H), 1.06–1.24 (m, 1H), 1.60–2.03 (m, 4H), 3.07 (s, 3H), 3.15 (s, 3H). ^{13}C NMR (50 MHz, C_6D_6) δ: 13.9, 25.0, 32.8, 37.3, 49.9 (OCH_3), 50.2 (OCH_3), 102.4 (C_2), 208.3 (C=O).

15: IR (CCl_4) (cm^{-1}): 1758. MS (EI) (GC–MS) *m*/*z* (rel. intensity): 158 ($M^{+\cdot}$, 1), 130 ($M^{+\cdot}$–28, 13), 99 (9), 88 (100), 71(16), 58 (19), 43 (78). ^{1}H NMR (200 MHz, C_6D_6) δ: 0.95 (d, ^3J = 7.0 Hz, 3H), 1.05–1.23 (m, 1H), 1.59–2.02 (m, 4H), 3.13 (s, 3H), 3.16 (s, 3H). ^{13}C NMR (50 MHz, C_6D_6) δ: 15.5, 25.9, 32.0, 41.9, 49.7, 50.2, 101.0, 207.6.

*Thermolysis of **1** in the presence of cyclopentanone*

Thermolysis if **1** (0.100 g, 0.63 mmol) in benzene (5 mL) containing cyclopentanone (0.105 g, 1.25 mmol) as described above for cyclobutanone, gave the known (41) 2,2-dimethoxycyclohexanone in 12% yield.

*Thermolysis of **1** in the presence of cis-2, 4-di-tert-butylcyclobutanone (**19**)*

Thermolysis of **1** (46.1 mg, 0.288 mmol), in benzene (2 g) containing **19** (40.0 mg, 0.219 mmol) did not lead to detectable products of attack by **2** on the ketone. The only species detected were the carbene dimer **21** and unreacted **19**. The latter was still *cis*, as was readily ascertained from the NMR spectrum. ^{1}H NMR (200 MHz, $CDCl_3$) δ: 0.92 (s, 18H), 1.67 (dd, ^3J = 9.4 Hz, ^2J = 19.0 Hz, 1H), 1.96 (dd, ^3J = 10.4 Hz, 1H), 2.86 (dd, ^3J = 9.4 Hz, ^3J = 10.4 Hz, 2H).

*Thermolysis of **1** in the presence of trans-2, 3-di-tert-butylcyclopropanone (**17**)*

A medium-walled NMR tube containing **1** (0.023 g, 0.14 mmol), *trans*-di-*tert*-butylcyclopropanone (**17**) (44–46) (0.020 g, 0.12 mmol) and C_6D_6 (1.0 g) was sealed under vacuum after three cycles of freeze–pump–thaw degassing. The tube was heated for 24 h at 110 °C in an oil bath before it was cut and the contents were transferred to a 3 mL glass vial. Concentration of the sample and semipreparatory gas chromatography gave *trans*-3,4-di-*tert*-butyl-2,2-dimethoxycyclobutanone (**18**) in 65% yield. IR (CCl_4) (cm^{-1}): 1783. MS (EI) *m*/*z* (rel. intensity): 185 ($M^{+\cdot}$ –57, 5), 157 (100), 129 (15), 74 (51), 57 (55). MS (CI–NH_3) *m*/*z*: 260 ($M^{+\cdot}$ + 18), 243 ($M^{+\cdot}$ +1). ^{1}H NMR (300 MHz, C_6D_6) δ: 0.96 (s, 9H), 0.99 (s, 9H), 2.03 (d, ^3J = 7.1 Hz, 1H), 2.62 (d, ^3J = 7.1 Hz, 1H), 2.98 (s, 3H), 3.41 (s, 3H). ^{13}C NMR (75 MHz, C_6D_6) δ: 28.9, 29.0, 30.7, 48.6, 51.0, 51.9, 66.1, 99.6, 111.2, 207.8 (C=O).

*Reaction of **2** with 2,2,4,4-tetramethylcyclobutane-1,3-dione (**22**)*

A 5 mL thermolysis tube was charged with **1** (0.200 g, 1.25 mmol), 2,2,4,4-tetramethylcyclobutane-1,3-dione (**22**, Aldrich, 0.168 g, 1.20 mmol) and benzene (5.0 g). After three freeze–pump–thaw cycles the tube was sealed and heated for 24 h in an oil bath at 110°C. Removal of the volatiles, as described above, left a yellow oil from which the major product (**25**) (70%, estimated by gas chromatography) was isolated, either by semipreparative gas chromatography or by flash column chromatography (silica gel – 10% ethyl acetate in hexanes, R_f = 0.75). IR (CCl_4) (cm^{-1}): 1735. MS (EI) *m*/*z* (rel. intensity): 186 ($M^{+\cdot}$ –28, 12) 149 (8), 116 (32), 101 (16), 84 (28), 43 (100). MS (CI–NH_3) *m*/*z*: 232 ($M^{+\cdot}$ +18). ^{1}H NMR (200 MHz, C_6D_6) δ: 1.06 (s, 6H), 1.09

© 2000 NRC Canada

(s, 6H), 2.91 (s, 6H). ^{13}C NMR (50 MHz, C_6D_6) δ: 18.8, 22.8, 48.6, 50.3, 54.4, 103.9, 208.3 (C=O), 215.5 (C=O).

*Thermolysis of **1** in the presence of 1,2-diphenylcyclopropenone (**23**)*

A solution of **1** (0.200 g, 1.25 mmol) and 1,2-diphenylcyclopropenone (**23**) (Aldrich, 0.450 g, 2.20 mmol) in benzene (5.0 g), in a 25 mL thermolysis tube, was treated as described above. Flash column chromatography (silica gel, 5% ethyl acetate in hexanes, R_f = 0.23) of the residue left after pumping off the volatile components, afforded 4, 4-dimethoxy-2, 3-diphenyl-2-cyclobuten-1-one (**26**) in 60% yield. IR (CCl_4) (cm^{-1}): 1758. MS (EI) *m*/*z* (rel. intensity): 280 ($M^{+\cdot}$, 16), 265 ($M^{+\cdot}$ –15, 6), 249 ($M^{+\cdot}$ –31, 18), 220 (38), 205 (16), 192 (55), 178 (100), 152 (29), 121 (38), 115 (77), 91 (38). MS (HR) *m*/*z*: calcd. for $C_{18}H_{16}O_3$: 280.1090; found: 280.1099. ^{1}H NMR (200 MHz, C_6D_6) δ: 3.47 (s, 6H), 6.98–7.03 (m, 6H), 7.76–7.81 (m, 2H), 7.87–7.92 (m, 2H). ^{13}C NMR (50 MHz, C_6D_6) δ: 53.6, 118.1, 128.3, 128.7, 128.9, 129.0, 129.2, 130.0, 130.9, 131.6, 149.0, 170.7, 193.2.

*Thermolysis of **1** in the presence of 3,4-dimethoxy-3-cyclobutene-1,2-dione (**24**)*

A solution of **1** (0.200 g, 1.25 mmol) and 3,4-dimethoxy-3-cyclobutene-1,2-dione (**24**) (Aldrich, 0.170 g, 1.20 mmol) in benzene (5.0 g) was heated as described above. Flash column chromatography of the residue left after removal of the volatiles (10–30% ethyl acetate in hexanes) gave, from the first yellow band, 2,2,4,5-tetramethoxy-4-cyclopentene-1,3-dione (**27**) in 54% yield as a yellow solid, mp 37.0–38.0°C. IR (CCl_4) (cm^{-1}): 1702. MS (EI) *m*/*z* (rel. intensity): 216 ($M^{+\cdot}$, 100), 185 ($M^{+\cdot}$ –31, 57), 173 (85), 157 (28), 129 (29), 86 (14), 75 (51), 59 (81). MS (CI–NH_3) *m*/*z* : 234($M^{+\cdot}$ +18). MS (HR) *m*/*z*: calcd. for $C_9H_{12}O_6$: 216.0641; found: 216.0634. ^{1}H NMR (200 MHz, C_6D_6) δ: 3.47 (s, 6H), 3.60 (s, 6H). ^{13}C NMR (50 MHz, C_6D_6) δ: 51.8, 59.2, 91.0, 150.8, 188.6 (C=O).

*Thermolysis of **1** in the presence of 2-azetidinone (**30**)*

The procedure described above gave, from **1** (0.200 g, 1.25 mmol) and 2-azetidinone (**30**) (Aldrich, 0.178 g, 2.5 mmol) in benzene (5.0 g), a residue that was worked up by semipreparative gas chromatography. 1-(Dimethoxymethyl)-2-azetidinone (**31**) (76% by GC) was isolated as an oil. IR (CCl_4) (cm^{-1}): 1770. MS (EI) *m*/*z* (rel. intensity): 145 ($M^{+\cdot}$, 1), 130 ($M^{+\cdot}$ –15, 1), 114 (18), 87 (33), 75 ($(MeO)_2CH$, (100), 72 (30), 42 (35). ^{1}H NMR (200 MHz, C_6D_6) δ: 2.24 (t, ^3J = 4.5 Hz, 2H), 2.79 (t, ^3J = 4.5 Hz, 2H), 2.99 (s, 6H), 5.38 (s, 1H). ^{13}C NMR (50 MHz, C_6D_6) δ: 35.5, 36.1, 53.2, 99.5, 166.5.

*Thermolysis of **1** in the presence of β-propiolactone (**34**)*

Heating of a solution of **1** (0.200 g, 1.25 mmol) and β-propiolactone (**34**) (Aldrich, 0.090 g, 1.20 mmol) in benzene (5.0 g), and workup as described above, left a yellow oil. Flash column chromatography (silica gel – 30% ethyl acetate in hexanes, R_f = 0.50) afforded 2,2-dimethoxy-3-oxacyclopentanone (**36**) as an oil in 65% yield. IR (CCl_4) (cm^{-1}): 1741. MS (EI–GC–MS) *m*/*z* (rel. intensity): 118 ($M^{+\cdot}$–28, loss of CO, 29), 115 (40), 91 (90), 59 (100). ^{1}H NMR (500 MHz, C_6D_6) δ: 1.75 (t, ^3J = 7.0 Hz, 2H), 3.25 (s, 6H), 3.50 (t, ^3J = 7.0 Hz, 2H). ^{13}C NMR (125 MHz, C_6D_6) δ: 33.5, 50.2, 60.4, 110.0, 202.8 (C=O).

Synthesis of 1,1-diethoxyethene

1,1-Diethoxyethene was prepared according to the procedure by Thweatt and co-workers (39). A fractional distillation apparatus consisting of a two-necked, round-bottomed flask (50 mL), magnetic stirring bar, addition funnel (20 mL), fractionating column (20 cm), three-way Claisen head with thermometer, condenser (20 cm), and a receiving flask (50 mL) with a vacuum attachment was flame-dried under vacuum. The addition funnel was removed and solid potassium *tert*-butoxide (11.4 g, 102 mmol) was added to the flask. The addition funnel was reattached and 2-bromo-1,1-diethoxyethane (15.3 mL, 20.0 g, 101.5 mmol) was added with a glass syringe to the addition funnel through a rubber septum. The reaction flask was cooled with an ice water mixture (5 min) and 2-bromo-1,1-diethoxyethane was dispensed into the round bottom flask (1 min). A white dense smoke formed immediately. After the reaction appeared to be complete (5 min), the mixture was heated with an oil bath (120–130°C), and *tert*-butyl alcohol (82–83°C/760 mmHg) generated from the reaction was removed by distillation. The system was then attached to a water aspirator and 1,1-diethoxyethene was distilled from the crude reaction mixture (46°C/28 mmHg) (6.70 g, 57%). ^{1}H NMR (200 MHz, C_6D_6) δ: 1.02 (t, ^3J = 7.0 Hz, 6H), 3.17 (s, 2H), 3.55 (q, ^3J = 7.0 Hz, 4H). ^{13}C NMR (25 MHz, C_6D_6) δ: 14.5, 56.6, 63.4, 165.7. The product was used on the same day in the next step.

Synthesis of methyl (2,2-diethoxycyclobutane)carboxylate

A solution of 1,1-diethoxyethene (6.70 g, 58.0 mmol) and methyl acrylate (4.97 g, 58 mmol) was refluxed in dry acetonitrile (40 mL) for eight days. Acetonitrile was distilled out through a Vigreux column, followed by methyl (2,2-diethoxycyclobutane)carboxylate (48°C/0.8 mmHg) (2.0 g, 17%), (lit. (38, 40) 60–63%). ^{1}H NMR (200 MHz, C_6D_6) δ: 0.97–1.24 (m, 1H), 1.01 (t, 3H, 7.0 Hz), 1.11 (t, 3H, 7.0 Hz), 1.58–2.37 (m, 4H), 3.17–3.65 (m, 4H), 3.42 (s, 3H). ^{13}C NMR (125 MHz, C_6D_6) δ: 14.8, 15.3, 15.4, 31.0, 49.6, 51.1, 56.6, 57.1, 102.6, 170.8.

*Synthesis of (2,2-diethoxycyclobutyl)methanol (**47**)*

To a suspension of $LiAlH_4$ (0.25 g, 6.70 mmol) in ether (15 mL) was added, dropwise with stirring, methyl (2,2-diethoxycyclobutane)carboxylate (1.35 g, 6.70 mmol). After the addition the mixture was heated to boiling for 1.5 h before it was cooled with an ice water bath and the excess $LiAlH_4$ was quenched with ethyl acetate (15 mL), followed by water (15 mL, slow addition). The heterogeneous solution left after the fine-grained $Al(OH)_3$ was filtered off with a sintered glass funnel was extracted with diethyl ether (3 × 25 mL) and the combined organic fractions were dried with magnesium sulphate. Filtration through a sintered glass funnel and removal of the volatiles afforded (2,2-diethoxycyclobutyl)methanol in 95% yield. The crude product was used without purification. Purification by distillation (61°C/0.8 mmHg) has been reported (47). ^{1}H NMR (200 MHz, C_6D_6) δ: 0.92 (t, ^3J = 7.1 Hz, 3H), 1.08 (t, ^3J = 7.1 Hz, 3H), 1.35–2.60 (m,

© 2000 NRC Canada

6H), 3.10–3.90 (m, 6H). ^{13}C NMR (25 MHz, C_6D_6) δ: 14.2, 15.3, 15.5, 30.6, 45.9, 56.1, 56.5, 63.1, 103.9.

*Hydrolysis of (2,2-diethoxycyclobutyl)methanol (**48**)*

2,2-(Diethoxycyclobutyl)methanol (0.51 g, 2.93 mmol) was stirred with 3% H_2SO_4 (30 mL) for 20 min in a 50 mL round-bottomed flask. The mixture was extracted with ether (3 × 15 mL) and the combined ether extracts were washed with 5% $NaHCO_3$ (3 × 20 mL). The yellow aq layers were combined in a separatory funnel and CH_2Cl_2 (60 mL) and H_2SO_4 (3%, 30 mL) were added. The yellow aq layer was extracted with CH_2Cl_2 until the yellow colour of the aq layer was completely dissipated. The organic layers were combined and dried with anhyd magnesium sulphate. Filtration through a sintered glass funnel and removal of the solvents yielded the desired 2-hydroxymethylcyclobutanone (**36**) (75%) as an oil. ^{1}H NMR (200 MHz, C_6D_6) δ: 1.45–1.75 (m, 2H), 2.38–2.68 (m, 2H), 2.90–3.10 (m, 2H), 3.37–3.70 (m, 2H). ^{13}C NMR (25 MHz, C_6D_6) δ: 13.5, 45.4, 60.1, 62.8, 210.2.

*Reaction of **38** with 2-hydroxymethylcyclobutanone (**39**)*

Trifluoroacetic acid (4 drops) was added to 2-acetoxy-2-methoxy-Δ^3-1,3,4-oxadiazoline (**38**) (49) (0.700 g, 3.72 mmol), 2-hydroxymethylcyclobutanone (0.220 g, 2.20 mmol), and dichloromethane (35 mL) in a 100 mL round-bottomed flask and the solution was stirred under nitrogen for 48 h at room temperature. Sodium bicarbonate (10%, 20 mL) was added and the contents were stirred for 10 min before the aq layer was separated and discarded. The extraction was repeated before the organic layer was dried with anhyd magnesium sulphate. Filtration and removal of the volatiles afforded a yellow oil. 2-(2-Cyclobutanonemethoxy)-2-methoxy-5,5-dimethyl-Δ^3-1,3,4-oxadiazoline (**37**) was obtained as a 50:50 mixture of diastereomers, in 54% yield, by flash column chromatography on silica gel (20% ethyl acetate in hexanes). IR (CCl_4) (cm^{-1}): 1790 (C=O). MS (EI) *m*/*z* (rel. intensity): (molecular ion not observed) 129 ($M^{+\cdot}$ –99, 14), 117 (7), 83 (35), 73 (31), 55 (100). MS (CI–NH_3): 229 ($M^{+\cdot}$ +1), 246 ($M^{+\cdot}$ +18). ^{1}H NMR (200 MHz, C_6D_6) δ: 1.21 (s, 6H), 1.23 (s, 3H), 1.28 (s, 3H), 1.32–1.71 (m, 4H), 2.34–2.52 (m, 4H), 2.87–2.99 (m, 2H), 3.17 (s, 3H), 3.21 (s, 3H), 3.60–4.00 (m, 4H). ^{13}C NMR (125 MHz, C_6D_6) δ: 14.1, 14.2, 23.7, 23.7, 24.0, 24.1, 45.0, 45.0, 51.6, 51.6, 60.0, 60.0, 62.1, 62.3, 119.3, 119.3, 137.5, 137.5, 206.3, 206.5. The diasteromers could be separated by TLC (20% ethyl acetate in hexanes, R_f = 0.3 and 0.4).

*Thermolysis of 2-(2-cyclobutanonemethoxy)-2-methoxy-5,5-dimethyl-Δ^3-1,3,4-oxadiazoline (**37**)*

2-(2-Cyclobutanonemethoxy)-2-methoxy-5,5-dimethyl-Δ^3-1,3,4-oxadiazoline (**37**, 0.140 g, 0.614 mmol) in benzene (16.5 g) was heated in a 25 mL thermolysis tube as described above. Removal of the volatiles and GC analysis indicated the presence of two major products (**42** and **43**), in 1.2:1.0 ratio. These were isolated by semipreparative gas chromatography in a combined yield of 60%.

42: IR (CCl_4) (cm^{-1}): 1790. MS (EI) *m*/*z* (rel. intensity): 142($M^{+\cdot}$, 20), 124 (21), 97 (25), 81 (53), 55 (100). MS (CI–NH_3) *m*/*z*: 143 ($M^{+\cdot}$ +1), 160 ($M^{+\cdot}$ +18). MS (HR) *m*/*z*: calcd. for $C_7H_{10}O_3$: 142.0629; found 142.0629. ^{1}H NMR (500 MHz, C_6D_6) δ: 1.17 (dt, ^3J = 5.2 Hz, ^2J = 12.0 Hz, ^3J = 12.0 Hz, 1H), 1.28 (m, ^3J = 3.1 Hz, ^4J = 3.0 Hz, ^3J = 12.0 Hz, ^2J = 12.0 Hz, ^3J = 5.0 Hz, 1H), 1.37 (dd, ^3J = 3.0 Hz, ^3J = 3.1 Hz, 1H), 1.63 (ddd, ^3J = 5.2 Hz, ^2J = 13.2 Hz, ^3J = 12.0 Hz, 1H), 1.84 (ddd, ^2J = 13.2 Hz, ^3J = 12.0 Hz, ^3J = 5.0 Hz, 1H), 3.45 (d, ^2J = 7.2 Hz, 1H), 3.48 (s, 3H, OCH_3), 3.76 (dt, ^2J = 7.2 Hz, ^3J = 3.0 Hz, ^4J = 3.0 Hz, 1H). ^{13}C NMR (125 MHz, C_6D_6) δ: 22.4, 28.7, (–)37.8, (–)52.3, 69.6, 99.5, 208.1 (C=O).

43: IR (CCl_4) (cm^{-1}): 1750. MS (EI) *m*/*z* (rel. intensity): 142 ($M^{+\cdot}$, 1), 124 (10), 83 (55), 55 (100). MS (CI–NH_3) *m*/*z*: 160 ($M^{+\cdot}$ +18), 143 ($M^{+\cdot}$ +1). ^{1}H NMR (500 MHz, C_6D_6) δ: 2.08–2.13 (m, 2H), 2.45 (t, ^3J = 7.2 Hz, 2H), 3.20 (s, 3H), 4.84–4.90 (m, 2H), 5.52 (m, 1H). ^{13}C NMR (125 MHz, C_6D_6) δ: 27.1, 38.5, (–) 51.9, 115.6, (–)136.5, 161.8, 192.7.

Acknowledgements

This research was supported with a grant-in-aid from the Natural Sciences and Engineering Research Council of Canada (NSERC). We are indebted to Professor T. S. Sorensen and Dr. F. Sun for samples of *trans*-2, 3-di-*tert*-butylcyclopropanone and *cis*-2,4-di-*tert*-butylcyclobutanone.

References

1. R.A. Moss, M. Włostowski, S. Shen, K. Krogh-Jespersen, and A. Matro. J. Am. Chem. Soc. **110**, 4443 (1988).
2. A.J. Arduengo, III, R.L. Harlow, and M. Kline. J. Am. Chem. Soc. **113**, 361 (1991).
3. A.J. Arduengo, III, H.V. Rasika Dias, R.L. Harlow, and M.J. Kline. J. Am. Chem. Soc. **114**, 5530 (1992).
4. A.J. Arduengo, III, M. Kline, J.C. Calabrese, and F.J. Davidson. J. Am. Chem. Soc. **113**, 9701 (1991).
5. M.K. Denk, A. Thadani, K. Hatano, and A.J. Lough. Angew. Chem. Int. Ed. Engl. **36**, 2607 (1997).
6. A.J. Arduengo, III, J.R. Goerlich, and W.J. Marshall. J. Am. Chem. Soc. **117**, 11027 (1995).
7. A.J. Arduengo, III, F. Davidson, H.V.R. Dias, J.R. Goerlich, D. Khasnis, W.J. Marshall, and T.K. Prakasha. J. Am. Chem. Soc. **119**, 12742 (1997).
8. A.J. Arduengo. Chem. Unserer Zeit, **32**, 6 (1998).
9. R.A. Moss, W. Liu, and C.-S. Ge. J. Phys. Org. Chem. **6**, 376 (1993).
10. P.H. Mueller, N.G. Rondan, K.N. Houk, J.F. Harrison, D. Hooper, B.H. Willen, and J.F. Liebman. J. Am. Chem. Soc. **103**, 5049 (1981).
11. N.C. Baird and K.F. Taylor. J. Am. Chem. Soc. **100**, 1333 (1978).
12. D. Feller, W.T. Borden, and E.R. Davidson. Chem. Phys. Lett. **71**, 22 (1980).
13. C.W. Bauschlicher, Jr., H.F. Schaefer, III, and P.S. Bagus. J. Am. Chem. Soc. **99**, 7106 (1977).
14. R.W. Hoffmann, K. Steinbach, and B. Dittrich. Chem. Ber. **106**, 2174 (1973).
15. R.W. Hoffmann. Angew. Chem. Int. Ed. Engl. **10**, 529 (1971).
16. R.W. Hoffmann and M. Reiffen. Chem. Ber. **109**, 2565 (1976).
17. (*a*) J.H. Rigby, A. Cavezza, and G. Ahmed. J. Am. Chem. Soc. **118**, 12848 (1996); (*b*) J.H. Rigby, S. Laurent, A Cavessa, and M.J. Heeg. J. Org. Chem. **63**, 5587 (1998); (*c*) J.H. Rigby, A. Cavessa, and M.J. Heeg. **120**, 1664 (1998).

© 2000 NRC Canada

18. J.H. Rigby, A. Cavezza, and M.J. Heeg. Tetrahedron Lett. **40**, 2473 (1999).
19. J.H. Rigby and M.D. Danca. Tetrahedron Lett. **40**, 6891 (1999).
20. R.W. Hoffmann, K. Steinbach, and W. Lilienblum. Chem. Ber. **107**, 3395 (1974).
21. J.D. Colomvakos, I. Egle, J. Ma, D.L. Pole, T. Tidwell, and J. Warkentin. J. Org. Chem. **61**, 9522 (1996).
22. J.A. Dunn, J.P. Pezacki, M.J. McGlinchey, and J. Warkentin. J. Org. Chem. **64**, 4344 (1999).
23. D.L. Pole and J. Warkentin. Liebigs Ann. 1907 (1995).
24. D.L. Pole and J. Warkentin. J. Org. Chem. **62**, 4065 (1994).
25. M. Zora and J.W. Herndon. Organometallics, **13**, 3370 (1994).
26. M. Zora, Y. Li, and J.W. Herndon. Organometallics, **18**, 4429 (1999).
27. M. El-Saidi, K. Kassam, D.L. Pole, T. Tadey, and J. Warkentin. J. Am. Chem. Soc. **114**, 8751 (1992).
28. H.N.C. Wong. Houben–Weyl methods of organic chemistry. Vol. E17e. *Edited by* A. de Meijere. Georg Thieme Verlag, Stuttgart. 1997. pp. 513–514.
29. L.M. Reeder and L.S. Hegedus. J. Org. Chem. **64**, 3306 (1999).
30. M. Mousseron and G. Manon. Bull. Soc. Chim. Fr. 392 (1949).
31. M. Stoll and W. Scherrer. Helv. Chim. Acta, **23**, 941 (1940).
32. C.D. Gutsche. J. Am. Chem. Soc. **71**, 3513 (1949).
33. B. Tchoubar. Bull. Soc. Chim. Fr. 164 (1949).
34. S. Winstein, B.K. Morse, E. Grunwald, K.C. Schreiber, and J. Corse. J. Am. Chem. Soc. **74,** 1113 (1952).
35. C. Walling. Acc. Chem. Res. **16**, 448 (1983).
36. T.H. Lowry and K.S. Richardson. Mechanism and theory in organic chemistry. 3rd ed. Harper and Row, New York. 1987. pp. 429–434.
37. J.-M. Conia and J. Salaün. Bull. Soc. Chim. Fr. 2747 (1965).
38. R. Bonneau, I. Reuter, and M.T.H. Liu. J. Am. Chem. Soc. **116**, 3145 (1994).
39. K.C. Brannock, R.D. Burpitt, and J.G. Thweatt. J. Org. Chem. **29**, 940 (1964).
40. C. Kowalski, X. Creary, A.J. Rollin, and M.C. Burke. J. Org. Chem. **43**, 2601 (1978).
41. F. Huet, M. Pellet, A. Lechevallier, and J.M. Conia. J. Chem. Res. Miniprint, 2528 (1982).
42. D. van Leusen, P.H.F.M. Rouwette, and A.M. van Leusen. J. Org. Chem. **46**, 5159 (1981).
43. D. van Leusen and A.M. van Leusen. Synthesis, 325 (1980).
44. J.F. Pazos and F.D. Greene. J. Am Chem. Soc. **89**, 1030 (1967).
45. D.B. Sclove, J.F. Pazos, R.L. Camp, and F.D. Greene. J. Am. Chem. Soc. **92**, 7488 (1970).
46. J.F. Pazos, J.G. Pacifici, F.O. Pierson, D.B. Sclove, and F.D. Greene. J. Org. Chem. **39**, 1990 (1974).
47. W. Kirmse and S. Schneider. Chem. Ber. **102**, 2440 (1969).
48. Ph. Amice and J.-M. Conia. Bull. Soc. Chim. Fr. 1015 (1974).
49. K. Kassam, D.L. Pole, M. El-Saidi, and J. Warkentin. J. Am. Chem. Soc. **116**, 1161 (1994).

© 2000 NRC Canada

Aqueous nonelectrolyte solutions. Part XVII. Formula of hydrogen sulfide hydrate and its dissociation thermodynamic functions

David N. Glew

Abstract: Literature data for the saturation vapor pressure $P(hl_1g)$ of hydrogen sulfide hydrate with water, at 43 temperatures between quadruple points $Q(hs_1l_1g)$ at –0.4°C and $Q(hl_1l_2g)$ at 29.484°C, are properly represented by a six-parameter equation to give a standard error (SE) of 0.13% on a hydrate pressure measurement of unit weight. Equilibrium hydrogen sulfide and water fugacities and the gas and aqueous phase compositions are derived using the Redlich–Kwong equation of state. Literature data for the saturation vapor pressure $P(hs_1g)$ of hydrogen sulfide hydrate with ice, at 15 temperatures between –1.249 and –21.083°C, are properly represented by a two-parameter equation to give a SE of 0.26% on a single hydrate pressure measurement. Quadruple point $Q(hs_1l_1g)$ is evaluated at temperature –0.413° with SE 0.042°C and at pressure 94.7 with SE 0.26 kPa. Using the thermodynamic method, described for deuterium sulfide D-hydrate, the equilibrium fugacities of hydrogen sulfide are used to define 43 equilibrium constants $Kp(h \rightarrow l_1g)$ for hydrate dissociation into water and hydrogen sulfide gas. The temperature dependence of ln $Kp(h \rightarrow l_1g)$ is represented by a three-parameter thermodynamic equation which gives both values and standard errors (*i*) for $Kp(h \rightarrow l_1g)$, and for $\Delta H^{ot}(h \rightarrow l_1g)$ and $\Delta Cp^{ot}(h \rightarrow l_1g)$, the standard enthalpy and heat capacity changes for hydrate dissociation and (*ii*) for $n = r$ the approximate formula number of the hydrate $H_2S \cdot nH_2O$ at each experimental temperature. The formula $H_2S \cdot 6.119H_2O$ with standard error $0.029H_2O$ is found for hydrogen sulfide hydrate with water at lower quadruple point $Q(hs_1l_1g)$ –0.413°C: an approximate formula $H_2S \cdot 5.869H_2O$ with SE $0.026H_2O$ is found at upper quadruple point $Q(hl_1l_2g)$ 29.484°C. These estimates for the formula of hydrogen sulfide hydrate at its quadruple points are not significantly different from those found for the deuterium sulfide D-hydrate.

Key words: clathrate hydrate of hydrogen sulfide, hydrogen sulfide hydrate, formula of hydrogen sulfide hydrate, thermodynamics of clathrate hydrate dissociation, dissociation equilibrium constant of hydrogen sulfide hydrate, standard enthalpy and heat capacity changes for dissociation of hydrogen sulfide hydrate.

Résumé : Les données tirées de la littérature pour la tension de vapeur de saturation (Phl_1g) de l'hydrate du sulfure d'hydrogène avec l'eau, à quarante-trois températures entre les points quadruple $Q(hs_1l_1g)$, à –0,4°C, et $Q(hl_1l_2g)$, à 29,484°C, peuvent être adéquatement représentées par une équation à six paramètres pour laquelle l'erreur standard (ES) est de 0,13 % sur une mesure de tension d'une unité de poids. Les fugacités du sulfure d'hydrogène et de l'eau en équilibre ainsi que les compositions des phases aqueuse et gazeuse sont obtenues à l'aide de l'équation d'état de Redlich-Kwong. Les données de la littérature pour la tension de vapeur de saturation $P(hs_1g)$ de l'hydrate d sulfure d'hydrogène avec la glace, à quinze températures entre –1,249 et –21,083°C peuvent être adéquatement représentées par une équation à deux paramètres pour laquelle l'ES est de 0,26 % pour une seule mesure de la tension de l'hydrate. On a évalué que le point quadruple $Q(hs_1l_1g)$ se situe à –0,413°C avec une ES de 0,042°C et à une pression de 94,7 avec une ES de 0,26 kPa. Faisant appel à la méthode thermodynamique décrite pour l'hydrate deutéré du sulfure de deutérium ainsi que les fugacités à l'équilibre du sulfure d'hydrogène, on a pu définir quarante-trois constantes $Kp(h \rightarrow l_1g)$ pour la dissociation de l'hydrate en eau et en sulfure d'hydrogène gazeux. La relation de ln $Kp(h \rightarrow l_1g)$ avec la température est représentée par une équation thermodynamique à trois paramètres qui conduisent aux valeurs et aux erreurs standards (*i*) pour $Kp(h \rightarrow l_1g)$ ainsi que pour $\Delta H^{ot}(h \rightarrow l_1g)$ et $\Delta Cp^{ot}(h \rightarrow l_1g)$, les changements d'enthalpie et de capacité calorifique standards pour la dissociation de l'hydrate et (*ii*) pour $n = r$, le nombre approximatif de la formule de l'hydrate $H_2S \cdot nH_2O$ à chacune des températures expérimentales. On arrive à une formule de $H_2S \cdot 6{,}119H_2O$ avec une erreur de 0,029 H_2O pour l'hydrate du sulfure d'hydrogène avec l'eau au point quadruple le plus bas, $Q(hs_1l_1g)$, à –0,413°C; pour le point quadruple le plus élevée $Q(hl_1l_1g)$, à 29,484°C, on arrive à une formule approximative de $H_2S \cdot 5{,}869H_2O$ avec une erreur de 0,026 H_2O pour l'hydrate du sulfure d'hydrogène. Ces évaluations de la formule de l'hydrate du sulfure d'hydrogène à ses points quadruples ne diffèrent pas beaucoup de celles trouvées à partir de l'hydrate deutéré du sulfure de deutérium.

Received March 1, 2000. Published on the NRC Research Press website on September1, 2000.

D.N. Glew.[1] 536 Highbury Park, Sarnia, ON N7V 2J9, Canada.

[1]Telephone: (519) 337–3136.

 © 2000 NRC Canada

Mots clés : hydrate clathrate du sulfure d'hydrogène, formule de l'hydrate du sulfure d'hydrogène, thermodynamique de la dissociation, constante de dissociation, changement d'enthalpie standard, changement de capacité calorifique standard.

Introduction

This report is part of a continuing study (1–7) of the thermodynamic properties of aqueous nonelectrolyte solutions and of their clathrate hydrate solid solutions. In this work we evaluate the formula of hydrogen sulfide hydrate with water from literature data (8–20) using the thermodynamic method (7) described in detail for deuterium sulfide D-hydrate. Here a quantitative evaluation is made with standard errors (*i*) of the standard thermodynamic function changes for the ($h \rightarrow l_1 g$) dissociation of hydrogen sulfide hydrate (h) into water (l_1) plus hydrogen sulfide gas (g), and (*ii*) of the formulae for hydrogen sulfide hydrate. These functions and formulae are similar to those reported (7) for the dissociation of deuterium sulfide D-hydrate between its quadruple points $Q(hs_1l_1g)$ and $Q(hl_1l_2g)$.

The literature containing measurements of the saturation pressure $P(hl_1g)$ of hydrogen sulfide hydrate with water goes back to 1882, with the earliest studies (8, 9) having low accuracy, and with the precise measurements of de Forcrand and Villard (10) having an uncertian bias. We fortunately have additional hydrogen sulfide hydrate measurements and careful thermodynamic analyses by Scheffer and his coworkers (11–15) who remeasured and extended the earlier work.

A valuable modern review of the hydrogen sulfide-water system, including both the older (8–15) and more recent hydrate studies (16–19) has been given by Carroll (19). Our assessment of the less reliable hydrate data sets (8, 9, 16–19) generally agrees with the analysis of Carroll et al. (19, 20).

The present study of hydrogen sulfide hydrate with water necessarily uses the same data sets (8–19), but we make an additional quantitative assessment of the reliability of the best data sets (10, 11, 14), and of the resulting formula for hydrogen sulfide hydrate. We find that the measurements of Scheffer et al. (11–15) are the most reliable, but that all of these measurements are not equally reliable. The precise hydrate pressures reported by de Forcrand et al. (10) are unfortunately uniformly biased about 1% lower than the best measurements of Scheffer and Meyer (14), and indicate a temperature significantly higher than –0.4°C for the quadruple point $Q(hs_1l_1g)$ (14, 15). We describe how we weight and combine these three best data sets (10, 11, 14), which to highest accuracy are mutually inconsistent, to provide (*i*) a best equation for $P(hl_1g)$ the saturation pressure of hydrogen sulfide hydrate with water and (*ii*) a best equation for $Kp(h \rightarrow l_1 g)$ the hydrate dissociation equilibrium constant and the values derived for the hydrate formula.

Experimental temperatures are converted to ITS-90, as described in (7), and three digits are retained after the decimal point to enable accurate reconversion, and not to indicate the accuracy of the measurements. The thermodynamic regression equations (21) are evaluated using the method of weighted least-squares (22) and a predicted estimate is qualified with its standard error, written SE. The weights are chosen to indicate the relative importance of measurements within their own data set, and the relative accuracy of the different data sets.

Results and discussion

H_2S hydrate–liquid H_2O-gas (hl_1g) equilibrium

Table 1 presents 43 equilibrium determinations of $P(hl_1g)$, the saturation vapor pressure of hydrogen sulfide hydrate (h) in contact with water-rich liquid (l_1) between 29.484 and –0.413°C.

The second column denotes the data source and datum number. Data S-11 to S-1 are from Scheffer (11, 12): datum S-5 is an outlier and is not included in the regression. Data SM4–16, SM6–8 to SM5–1 are from Tables 4, 6, and 5, respectively, of Scheffer and Meyer (14): datum SM4–10 is an outlier and is not included in the regression. Data dFV-16 to dFV-1 are from de Forcrand and Villard (10). The data listed as Qsol at –0.369°C and QP at –0.413°C are two estimates of the temperature and pressure at the quadruple point temperature $Q(hs_1l_1g)$, evaluated using the equilibrium pressure $P(hs_1g)$ of hydrogen sulfide hydrate with ice (14).

The third column gives the square root of the weights used to combine these data from the various sources into a properly weighted least-squares regression of the logarithm of $P(hl_1g)$ as a function of temperature. The weights are determined by the fit of the best six-parameter equation, using realistic relative weights for the three major data sets (10, 11, 14). Single measurements, which exhibit acceptable large residuals, are given reduced weight; measurements which show unreasonable large residuals (greater than three SE's from their data set) are considered outliers and are excluded from the regression.

The fourth column lists the observed $P(hl_1g)$ MPa and the fifth gives $P(hl_1g)$ calculated from the best (21) equation of the form

$$[1a] \quad \ln P(hl_1g) = b0 + b1{\cdot}u1 + b2{\cdot}u2 + b3{\cdot}u3 + b4{\cdot}u4 + b5{\cdot}u5$$

which is mathematically equivalent to

$$[1b] \quad \ln P(hl_1g) = A + B/T + C \ln T + DT + ET^2 + FT^3$$

and which requires six parameters for a proper representation of the 43 data. The percentage differences between the observed and calculated pressures, shown in the sixth column, yield an overall SE of 0.13% for a single determination of unit weight with 37 degrees of freedom. The seventh column shows the percentage standard error on the pressure estimated from the weighted regression model.

The nine data of unit weight from Scheffer (11, 12) give residuals which indicate a SE of 0.16%: datum S-4 requires the reduced weight $w^{1/2} = 0.05$ to give the same weighted SE. The four data with unit weight from Table 6 of Scheffer and Meyer (14) were measured using a Beckmann thermometer graduated in 1/50°C and their residuals indicate a SE of 0.095%. Data from Tables 4 and 5 of ref. 14 were measured using thermometers graduated in 1/5°C and the six data with $w^{1/2} = 0.4$ correctly reflect their reduced accuracy. The ten residuals with the highest weights from Tables 6, 5, and 4 of ref. 14 indicate a SE of 0.13%. The remaining five measurements from Table 4 of ref. 14 exhibit residuals with large

© 2000 NRC Canada

Table 1. Vapor pressure of hydrogen sulfide hydrate with water.

Temperature (°C)	Datum	$w^{1/2}$	$P(hl_1g)$ Obsd (MPa)	$P(hl_1g)$ Calc (MPa)	Difference (%)	Error on calc pressure (%)
Q 29.484	S-11	1	2.239	2.240	–0.04	0.09
29.184	S-10	1	2.158	2.156	0.12	0.07
28.484	S-9	1	1.976	1.976	0.01	0.06
27.385	S-8	1	1.733	1.735	–0.13	0.07
25.586	S-7	1	1.419	1.421	–0.16	0.07
24.786	S-6	1	1.307	1.305	0.19	0.08
20.988	S-4	0.05	0.871	0.880	–0.97	0.08
19.688	S-3	1	0.770	0.769	0.10	0.08
17.889	S-2	1	0.638	0.638	0.13	0.07
16.290	S-1	1	0.537	0.539	–0.27	0.08
8.844	SM4–16	0.4	0.2452	0.2447	0.19	0.12
7.045	SM6–15	1	0.2036	0.2034	0.07	0.09
6.895	SM5–14	0.4	0.2008	0.2004	0.21	0.09
6.846	SM4–13	0.01	0.2017	0.1993	1.16	0.09
5.027	SM6–12	1	0.1660	0.1659	0.03	0.07
4.897	SM5–11	0.4	0.1641	0.1638	0.20	0.07
3.897	SM4–9	0.01	0.1513	0.1482	2.12	0.08
2.998	SM6–8	1	0.1352	0.1354	–0.14	0.08
2.898	SM5–7	0.4	0.1344	0.1340	0.28	0.08
2.898	SM4–6	0.01	0.1365	0.1340	1.87	0.08
1.899	SM4–5	0.01	0.1241	0.1211	2.54	0.08
0.969	SM6–4	1	0.1100	0.1099	0.09	0.09
0.949	SM5–3	0.4	0.1100	0.1097	0.30	0.09
0.849	SM4–2	0.01	0.1113	0.1085	2.59	0.10
–0.050	SM5–1	0.4	0.0987	0.0985	0.18	0.18
–0.369	Qsol	0.1	0.0949	0.0951	–0.21	0.22
Q –0.413	QP	0.1	0.0947	0.0946	0.10	0.23
5.197	dFV-16	0.1	0.1667	0.1688	–1.27	0.07
4.897	dFV-15	0.1	0.1631	0.1638	–0.45	0.07
4.497	dFV-14	0.1	0.1551	0.1574	–1.47	0.08
3.897	dFV-13	0.1	0.1463	0.1482	–1.30	0.08
3.797	dFV-12	0.1	0.1444	0.1467	–1.58	0.08
3.398	dFV-11	0.1	0.1397	0.1409	–0.86	0.08
2.798	dFV-10	0.1	0.1309	0.1327	–1.31	0.08
2.099	dFV-9	0.1	0.1209	0.1236	–2.13	0.08
1.749	dFV-8	0.1	0.1169	0.1192	–1.91	0.08
1.199	dFV-7	0.1	0.1107	0.1126	–1.71	0.09
0.999	dFV-6	0.1	0.1093	0.1102	–0.83	0.09
0.849	dFV-5	0.1	0.1077	0.1085	–0.73	0.10
0.799	dFV-4	0.1	0.1073	0.1079	–0.57	0.10
0.600	dFV-3	0.1	0.1040	0.1057	–1.58	0.11
0.100	dFV-2	0.1	0.0991	0.1001	–1.05	0.16
0.000	dFV-1	0.1	0.0975	0.0990	–1.58	0.17

positive biases and these data are assigned the very small weight, $w^{1/2} = 0.01$, to reduce their possible bias of the regression equation.

The sixteen data from de Forcrand and Villard (10) require the weight, $w^{1/2} = 0.1$, to make the regression model consistent with a quadruple point temperature $t(hs_1l_1g)$ near to –0.4°C: these residuals indicate an elevated SE of 0.51%, resulting mainly from their bias relative to the more reliable measurements of Scheffer and Meyer (14).

The five temperature variables $u1$–$u5$ in eq. [1*a*] are defined in (21) with $x = (T - 298.15)/298.15$ and the parameters $b0$–$b5$ with their (SEs) are: $b0 = 0.288\,621$ (0.000 75), $b1 = 31.6576$ (0.065), $b2 = 266.610$ (7.0), $b3 = 13915.9$ (680), $b4 = 293\,694$ (19 000), and $b5 = 1\,890\,730$ (150 000). It is seen that the hydrogen sulfide hydrate pressures properly define five temperature parameters, $b1$–$b5$ at 25°C, that all parameters are positive with no alternation of sign, and that the value of the least significant parameter $b5$ could arise by pure chance at a probability level of less than one in 10^{15} times.

Comparison of the fit of the 43 $P(hl_1g)$ data by the four-parameter equation of Carroll (19) and by the six-parameter eq. [1*a*] shows that the residuals are seventeen times smaller and the standard deviations are ten times smaller using eq. [1*a*].

At 25°C the saturation pressure $P(hl_1g)$ of hydrogen sulfide hydrate is 1.3346 with SE 0.0011 MPa and for

© 2000 NRC Canada

Table 2. Properties of gas and aqueous phases in the (hl_1g) equilibrium.

Temperature (°C)	Datum	f_2 (MPa)	f_1 (kPa)	y_1 (× 10^3)	x_2^{l1} (× 10^3)	x_3^{l1} (× 10^6)
Q 29.484	S-11	1.851	4.06	3.95	29.63	7.6
29.184	S-10	1.796	3.99	3.90	28.98	7.5
28.484	S-9	1.669	3.83	3.82	27.42	7.2
27.385	S-8	1.493	3.60	3.73	25.22	6.8
25.586	S-7	1.253	3.24	3.67	22.17	6.2
24.786	S-6	1.165	3.09	3.66	21.04	5.9
20.988	S-4	0.804	2.46	3.78	16.03	4.9
19.688	S-3	0.717	2.27	3.82	14.78	4.6
17.889	S-2	0.600	2.03	3.95	13.00	4.2
16.290	S-1	0.509	1.84	4.11	11.53	3.8
8.844	SM4–16	0.2382	1.130	5.03	6.69	2.5
7.045	SM6–15	0.1985	1.000	5.29	5.90	2.3
6.895	SM5–14	0.1958	0.990	5.30	5.84	2.3
6.846	SM4–13	0.1966	0.987	5.26	5.88	2.3
5.027	SM6–12	0.1623	0.870	5.57	5.14	2.1
4.897	SM5–11	0.1605	0.863	5.58	5.11	2.0
3.897	SM4–9	0.1482	0.804	5.62	4.87	2.0
2.998	SM6–8	0.1325	0.755	5.87	4.48	1.8
2.898	SM5–7	0.1318	0.750	5.87	4.47	1.8
2.898	SM4–6	0.1338	0.750	5.78	4.54	1.8
1.899	SM4–5	0.1218	0.698	5.90	4.28	1.8
0.969	SM6–4	0.1080	0.653	6.19	3.91	1.6
0.949	SM5–3	0.1081	0.653	6.19	3.92	1.6
0.849	SM4–2	0.1094	0.648	6.07	3.98	1.7
–0.050	SM5–1	0.0970	0.607	6.39	3.64	1.6
–0.369	Qsol	0.0933	0.593	6.49	3.54	1.5
Q –0.413	QP	0.0931	0.591	6.48	3.54	1.5
5.197	dFV-16	0.1629	0.881	5.62	5.13	2.1
4.897	dFV-15	0.1595	0.863	5.62	5.07	2.0
4.497	dFV-14	0.1518	0.839	5.73	4.89	2.0
3.897	dFV-13	0.1432	0.804	5.81	4.71	1.9
3.797	dFV-12	0.1414	0.799	5.84	4.66	1.9
3.398	dFV-11	0.1369	0.777	5.86	4.57	1.9
2.798	dFV-10	0.1284	0.745	5.97	4.37	1.8
2.099	dFV-9	0.1187	0.708	6.13	4.14	1.7
1.749	dFV-8	0.1148	0.691	6.18	4.05	1.7
1.199	dFV-7	0.1087	0.664	6.26	3.91	1.7
0.999	dFV-6	0.1074	0.655	6.24	3.89	1.6
0.849	dFV-5	0.1058	0.648	6.27	3.85	1.6
0.799	dFV-4	0.1055	0.646	6.26	3.84	1.6
0.600	dFV-3	0.1022	0.636	6.37	3.75	1.6
0.100	dFV-2	0.0974	0.614	6.43	3.63	1.6
0.000	dFV-1	0.0958	0.609	6.49	3.59	1.5

deuterium sulfide D-hydrate (6) is 1.1701 with SE 0.00011 MPa, a difference of 14%.

Following the work on deuterium sulfide D-hydrate (6), gas phase imperfections of the hydrogen sulfide–water mixtures have been represented by the Redlich–Kwong equation of state. The a_{22} and b_{22} parameters used for hydrogen sulfide vapor are those derived from the high temperature (h.t.) measurements from –30° to +30°C (4): the a_{11} and b_{11} for water vapor are those derived for the solubility measurements (5). The intensive properties of the gas and aqueous phases in equilibrium with hydrogen sulfide hydrate have been evaluated by the same iterative process described in (6) for the D-hydrate. The required modern values (*i*) for p_1°, the saturation vapor pressure of water, are from Haar et al. (23), (*ii*) for V_1^{l1}, the molar volume of water, are from Kell (24), and (*iii*) for V_2^{l1}, the partial molar volume of aqueous hydrogen sulfide, are from Barbero et al. (25), evaluated with proper allowance for the differences of the temperature scales (ITS-27, IPTS-48, IPTS-68, and ITS-90) (26). All temperatures are quoted with Celsius t°C + 273.15 = T K thermodynamic scale ITS-90.

Table 2 presents derived values for the intensive properties of the gas phase (g) and the water-rich phase (l_1) in equilibrium with hydrogen sulfide hydrate (h) under conditions of Table 1. Values shown in columns three to seven are, respectively, for the fugacities f_2 of hydrogen sulfide and f_1 of

© 2000 NRC Canada

Table 3. Equilibrium properties of hydrogen sulfide hydrate with ice.

		$P(hs_1g)$				
Temperature (°C)	Datum	Obsd (MPa)	Calc (MPa)	f_2 (MPa)	f_1 (kPa)	y_1 (× 10^3)
–0.369	Qsol	—	0.0949	0.0933	0.59	6.48
–0.413	QP	—	0.0947	0.0931	0.59	6.47
–1.249	SM2–1	0.0915	0.0914	0.0901	0.55	6.24
–1.998	SM3–2	0.0887	0.0886	0.0873	0.52	6.04
–2.398	SM1–3	0.0873	0.0871	0.0860	0.50	5.93
–2.998	SM2–4	0.0848	0.0850	0.0835	0.48	5.80
–4.946	SM1–5	0.0781	0.0782	0.0770	0.40	5.33
–5.745	SM2–6	0.0753	0.0755	0.0743	0.38	5.16
–6.944	SM3–7	0.0719	0.0717	0.0709	0.34	4.87
–7.944	SM1–8	0.0687	0.0686	0.0678	0.31	4.67
–11.841	SM2–9	0.0574	0.0577	0.0568	0.22	3.94
–11.841	SM1–10	0.0577	0.0577	0.0571	0.22	3.92
–12.840	SM3–11	0.0553	0.0551	0.0548	0.20	3.73
–15.787	SM1–12	0.0483	0.0481	0.0478	0.15	3.25
–16.787	SM2–13	0.0458	0.0459	0.0454	0.14	3.12
–18.735	SM3–14	0.0420	0.0419	0.0416	0.12	2.83
–21.083	SM2–16	0.0373	0.0374	0.0371	0.09	2.54

water, for the gas-phase mole fraction y_1 of water, and for the mole fractions x_2^{l1} of undissociated hydrogen sulfide and x_3^{l1} of hydrogen sulfide anion in the water-rich phase l_1.

H_2S hydrate–ice-gas (hs_1g) equilibrium

Table 3 presents 15 equilibrium measurements by Scheffer and Meyer (14) of $P(hs_1g)$, the saturation total pressure of hydrogen sulfide hydrate (h) in contact with ice (s_1), between –1.249 and –21.083°C.

The second column denotes the data source and datum number, data SM2–1, SM3–7, and SM1–12 are from Tables 2, 3, and 1, respectively, of ref. 14. Three outliers, at the low temperatures –19.734, –24.580, and –25.829°C, exhibit biased and systematically high pressures and are excluded from the regression, to reduce possible bias of the regression model.

The third column shows the observed $P(hs_1g)$ MPa and the fourth column the $P(hs_1g)$ calculated from the best equation

$$[2] \qquad \ln P(hs_1g) = 8.9718 - 3090/T$$

with thermodynamic temperature T K, which gives a SE of 0.26% for a single determination of $P(hs_1g)$ and a SE of 7.4 K on the parameter –3090.

In Table 1 the data listed as Qsol and QP are two estimates of temperature and pressure at the quadruple point $Q(hs_1l_1g)$, based on the (hs_1g) equilibrium eq. [2]. The datum Qsol is evaluated using eq. [2] together with its equilibrium aqueous solution of hydrogen sulfide (5) at its ice-freezing temperature. Our depression for $t(hs_1l_1g)$ is –0.369°C with SE 0.030°C and is in good agreement with the –0.365°C given by Korvezee and Scheffer (15): both values are insignificantly higher than the accepted –0.4°C of $t(hs_1l_1g)$ (14, 15). The datum QP is evaluated from the cut of eq. [2] for $P(hs_1g)$ with the $P(hl_1g)$ data from ref. 14 only: this estimate of $t(hs_1l_1g)$ is –0.413°C with SE 0.042°C, in agreement with the –0.4°C by Scheffer et al. (14, 15).

The fifth to seventh columns in Table 3 present the equilibrium intensive properties f_2, f_1, and y_1 for the binary gas phase, evaluated using the Redlich–Kwong equation of state with the observed total pressures $P(hs_1g)$, as described in ref. 6. The required vapor pressure of ice between –0.369° and –21.083°C is from Dorsey (27).

Lower quadruple point $Q(hs_1l_1g)$

The lower quadruple point $Q(hs_1l_1g)$, determined from the intersection of eq. [1*a*] for $P(hl_1g)$ with eq. [2] for $P(hs_1g)$, is found at temperature –0.398° with SE 0.035°C and at 94.75 kPa pressure with SE 0.25 kPa. If the 16 data of de Forcrand and Villard (10) are excluded and only the 25 data from Scheffer et al. (11, 14) are used for $P(hl_1g)$, $Q(hs_1l_1g)$ is found at –0.413° with SE 0.042°C. These two estimates of $t(hs_1l_1g)$ are not significantly different. We prefer the value –0.413°C for $t(hs_1l_1g)$ because this value does not depend on the data of de Forcrand et al. (10) which contain an uncertain temperature bias.

The temperature difference between the triple and quadruple points (0.010 – (–0.413)) = 0.423°C for water and hydrogen sulfide hydrate is near that (3.8125 – 3.3917) = 0.4208°C found for deuterium oxide and deuterium sulfide D-hydrate (6).

Standard enthalpy change for dissociation of hydrogen sulfide hydrate into ice and hydrogen sulfide gas

Thermodynamic equations from ref. 7 are used here without derivation since all have been discussed for determination of the formula of deuterium sulfide D-hydrate.

Consider the standard dissociation of one gram mole (gram-molar mass) of hydrogen sulfide hydrate of formula $H_2S{\cdot}nH_2O$ into n mole of ice plus one mole of hydrogen sulfide gas. The equilibrium constant $Kp(h{\rightarrow}s_1g)$ for this process is defined by the equation

$$[3] \qquad \ln Kp(h{\rightarrow}s_1g) = \ln f_2 + n[P(hs_1g) - 0.10][V_1^{s1} - (V^h/46)]/RT$$

in which f_2 is the fugacity of hydrogen sulfide, n the hydrate formula number, V_1^{s1} the molar volume of ice, and V^h the unit cell molar volume of hydrate, at thermodynamic

© 2000 NRC Canada

temperature T K and equilibrium pressure $P(hs_1g)$. Equilibrium values for f_2 are given in Table 3 and the gaseous standard state is one MPa fugacity. Formula number $n = 6.10$ is assumed, but this value is not critical because of the low (hs_1g) equilibrium pressures. The molar volume of ice is from Dorsey (27) and the hydrate molar volume is from von Stackelberg and Jahns (28): the standard state of the condensed phases is 0.1 MPa pressure.

Values of $\ln Kp(h \rightarrow s_1g)$ MPa are best (21) represented by

$$[4] \quad \ln Kp(h \rightarrow s_1g) = 8.8351 - 3057/T$$

with the same standard errors as those given for eq. [2].

The standard dissociation enthalpy change $\Delta H^{ot}(h \rightarrow s_1g)$ is found to be 25416 with SE 52 J/mole of hydrogen sulfide and is temperature invariant, with $\Delta Cp^{ot}(h \rightarrow s_1g)$ insignificantly different from zero. This value for the standard enthalpy change is less than the 25500 J/mole found by Scheffer and Meyer (14) using partial pressures.

Standard enthalpy change for dissociation of hydrogen sulfide hydrate into water and hydrogen sulfide gas.

Consider the standard dissociation of one gram mole of hydrogen sulfide hydrate of formula $H_2S{\cdot}nH_2O$ into one mole of gaseous hydrogen sulfide plus n mole of water. The equilibrium constant $Kp(h \rightarrow l_1g)$ for this process is defined by the equation

$$[5] \quad \ln Kp(h \rightarrow l_1g) = \ln f_2 + n \ln x_1^{l1} + n[P(hl_1g) - 0.10][V_1^{l1} - (V^h/46)]/RT$$

in which V_1^{l1} is the molar volume of water at thermodynamic temperature T K and equilibrium pressure $P(hl_1g)$. Equilibrium values of f_2 and for $x_1^{l1} = (1 - x_2^{l1} - 2x_3^{l1})$ are given in Table 2. Formula number $n = 6.10$ is assumed initially, but this value will vary with temperature along the (hl_1g) equilibrium line. The molar volume of water is from Kell (24). Other parameters have the sources given for eq. [3].

Values of $\ln Kp(h \rightarrow l_1g)$ MPa are best (21) represented by

$$[6a] \quad \ln Kp(h \rightarrow l_1g) = d0 + d1{\cdot}u1 + d2{\cdot}u2$$

which is mathematically equivalent to

$$[6b] \quad \ln Kp(h \rightarrow l_1g) = A' + B'/T + C' \ln T$$

and which, differing from (7), uses only three parameters to represent the 43 equilibrium constants between –0.413° and 29.484°C.

Formula of hydrogen sulfide hydrate at lower quadruple point $Q(hs_1l_1g)$

The formula of hydrogen sulfide hydrate is evaluated by the method of Scheffer and Meyer (14) who first derived the thermochemical identity eq. [7] for n

$$[7] \quad \Delta H^{oq}(h \rightarrow l_1g) - \Delta H^{oq}(h \rightarrow s_1g) = n\ \Delta H^{oq}(s_1 \rightarrow l_1)$$

which is exact at the quadruple point $Q(hs_1l_1g)$, with the equilibrium standard enthalpy changes denoted by superscript q. Substitution into eq. [7], of 62088 with SE 165 J/mole H_2S for $\Delta H^{oq}(h \rightarrow l_1g)$, of 25416 with SE 52 J/mole H_2S for $\Delta H^{oq}(h \rightarrow s_1g)$, and of 5993 with SE 4 J/mole H_2O for $\Delta H^{oq}(s_1 \rightarrow l_1)$, evaluated from Osborne (30) and from Giauque and Stout (31), yields $n = 6.119$ with SE 0.029 for the hydrogen sulfide hydrate formula at –0.413°C.

Using this method, which they had developed for the purpose, Scheffer and Meyer (14) determined $n = 6.06$ for the formula of hydrogen sulfide hydrate at the quadruple point –0.4°C: later reevaluation (15) of the same data (14), using only the four most accurate (hl_1g) measurements, confirmed $n = 6.06$ with error 0.13.

Making a t-test of the formula difference (6.119 – 6.06)/0.029 gives $t = 2.03$ with 40 degrees of freedom which indicates that this difference could arise by pure chance with probability 2.5%, that is, there is a 97.5% probability that the difference is significant. Using the 0.13 error given by Korvezee and Scheffer (15) our value of n is well within their error range from $n = 5.93$ to $n = 6.19$.

At 0°C we estimate $n = r = 6.114$ with SE 0.028, this value is in good agreement with the $n = 6.119$ derived from direct hydrate synthesis at 0°C and listed in the Table II by Cady (32).

Formula of hydrogen sulfide hydrate at temperatures above the lower quadruple point

We now extend eq. [7], valid at $Q(hs_1l_1g)$, for more general use at temperature t °C to evaluate an approximate formula number, defined as r, using the thermochemical identity [8]

$$[8] \quad \Delta H^{ot}(h \rightarrow l_1g) - \Delta H^{ot}(h \rightarrow s_1g) = r\ \Delta H^{ot}(s_1 \rightarrow l_1)$$

in which superscript q in [7] is replaced by t in [8]. Values of $\Delta H^{ot}(h \rightarrow s_1g)$ and $\Delta H^{ot}(s_1 \rightarrow l_1)$ at temperature t are equal to their values at the quadruple point plus the integral of their heat capacities from the quadruple point.

The first term in eq. [8] is from the (hl_1g) data (10, 11, 14) of this work. The second term $\Delta H^{ot}(h \rightarrow s_1g)$ is temperature invariant and is 25416 with SE 52 J/mole H_2S, the same as $\Delta H^{oq}(h \rightarrow s_1g)$ in eq. [7]. The final term in eq. [8] is the standard molar enthalpy change for fusion of metastable ice H_2O (s_1) into liquid H_2O (l_1) at t°C. This is evaluated using the Taylor's series expansion

$$[9] \quad \Delta H^{ot}(s_1 \rightarrow l_1) = \Delta H^{oo}(s_1 \rightarrow l_1) + \Delta Cp^{oo}(s_1 \rightarrow l_1)t + d\Delta Cp^{oo}(s_1 \rightarrow l_1)/dt(1/2)t^2 + d^2\Delta Cp^{oo}(s_1 \rightarrow l_1)/dt^2(1/6)t^3$$

about the normal freezing point 0°C, with $\Delta H^{oo}(s_1 \rightarrow l_1) = 6009$ with SE 4 J/mole (30). The standard molar heat capacity change and its temperature derivatives for fusion are evaluated at 0°C using (*i*) the heat capacities of ice between –74° and –2.6°C by Giauque and Stout (31) and (*ii*) the tabulated heat capacities of liquid water between 0° and 100°C (23).

Method for evaluation of dissociation equilibrium constant of hydrogen sulfide hydrate and its formula number *r*

The phase rule requires that the equilibrium water-hydrogen sulfide, two-component, three-phase, (hl_1g) system is univariant and that the intensive properties of the three equilibrium phases are continuous functions of temperature. In particular, the equilibrium hydrate composition and its

© 2000 NRC Canada

component H_2O/H_2S mole ratio $n = r$ are continuous functions of temperature only.

A method is now presented to evaluate the approximate formula number r for the hydrate $H_2S{\cdot}rH_2O$ and its dissociation equilibrium constant $Kp(h{\rightarrow}l_1g)$ at each experimental temperature on the univariant (hl_1g) equilibrium line, from –0.413°C the lower quadruple point $Q(hs_1l_1g)$ up to 29.484°C the upper quadruple point $Q(hl_1l_2g)$.

The method of convergence to a stable solution depends on the temperature continuity of r the approximate hydrate formula number. Initially we assume that $n = r = 6.1$ in eq. [5] for all measurements, giving a first approximation for the logarithm of the equilibrium constant, abbreviated to ln Kp(1st). The ln Kp(1st) values are fitted as a proper function of temperature (21) by the method of least squares (22) to yield the best thermodynamic equation of the form of eq. [6*a*]. These measurements use two temperature variables ($u1$ $u2$) with $x = (T - 298.16)/298.15$, and define (21) three thermodynamic function parameters ($d0$ $d1$ $d2$) and their standard errors at 298.15 K.

Derived from ($d1$ $d2$) of eq. [6*a*], the first approximation standard enthalpy changes $\Delta H^{ot}(h{\rightarrow}l_1g)$, abbreviated to ΔH(1st), for each measurement at its temperature t are substituted into eq. [8], to give a first approximation formula number r(1st).

Values of r(1st) are substituted for n in eq. [5] for each measurement to provide a second approximation for the logarithm of the equilibrium constant ln Kp(2nd); the ln Kp(2nd) values are refitted by eq. [6*a*], thence to obtain second approximation ΔH(2nd) values; these are substituted for $\Delta H^{ot}(h{\rightarrow}l_1g)$ in eq. [8] to give r(2nd) values which are recycled for n in eq. [5], and so on. Iterations for 124 cycles give the converged values of $Kp(h{\rightarrow}l_1g)$ and of r which are presented in Tables 4 and 5.

Equilibrium constant for dissociation of hydrogen sulfide hydrate into water and hydrogen sulfide gas

Table 4 lists 43 determinations between 29.484° and –0.413°C of the equilibrium constant, $Kp(h{\rightarrow}l_1g)$, for dissociation of hydrogen sulfide hydrate to liquid water and hydrogen sulfide gas with $n = r$. Standard thermodynamic function changes refer to dissociation of one mole of $H_2S{\cdot}rH_2O$ (h) at 0.10 MPa pressure to form one mole of H_2S (g) at 1.0 MPa fugacity together with r mole of pure H_2O (l_1) at 0.10 MPa pressure.

The third column of Table 4 gives the square root of the weights used to combine the measurements from the three sources (10, 11, 14) into a properly weighted least-squares regression of the logarithm of $Kp(h{\rightarrow}l_1g)$ as a function of temperature.

The fourth column lists $Kp(h{\rightarrow}l_1g)$ MPa observed, the fifth gives $Kp(h{\rightarrow}l_1g)$ calculated from the best converged eq. [6*a*]. The percentage differences between observed and calculated equilibrium constants, shown in the sixth column, yield an overall SE of 0.11% for a single $Kp(h{\rightarrow}l_1g)$ determination of unit weight with 40 degrees of freedom. The seventh column shows the percentage error on the estimated equilibrium constant defined by the regression eq. [6*a*].

In defining the best values for ($d1$ $d2$) in eq. [6*a*] for the hydrogen sulfide hydrate it is considered that these enthalpy change parameters at 25°C should be of the same sign and numerically smaller than those found in ref. 7 for the deuterium sulfide D-hydrate. Preliminary investigation shows that the hydrogen sulfide hydrate measurements (10, 11, 14) are sufficiently accurate to evaluate only ($d0$ $d1$ $d2$) in eq. [6*a*], but are insufficiently accurate to define any value for $d3$.

The three parameters of the best converged eq. [6*a*] with their (SEs) are: $d0 = 0.019\,008$ (0.000 73), $d1 = 26.6871$ (0.040), $d2 = 19.2499$ (1.2). We note that the equilibrium constants of hydrogen sulfide hydrate properly define only the two enthalpy parameters ($d1$ $d2$) at 25°C, that these two parameters are both positive, and that the value of the least significant parameter $d2$ could arise by pure chance at a probability level of less than one in 10^{15} times.

The SE estimate of 0.11% for a single $Kp(h{\rightarrow}l_1g)$ datum of unit weight given by the three-parameter eq. [6*a*] is seen to be near in value to the SE estimate of 0.13% for a single $P(hl_1g)$ measurement of unit weight given by the six-parameter eq. [1*a*].

The 10 weighted residuals of data by Scheffer (11) show a SE of 0.062%, the 15 weighted residuals of data by Scheffer and Meyer (14) show a SE of 0.083%, and the 16 weighted residuals of data by de Forcrand and Villard (10) show a SE of 0.047%. These low SE estimates, (0.062%, 0.083%, and 0.047%) from the three sets of weighted residuals are all smaller than the overall SE estimate 0.11% and reflect the conservative low weights assigned to the less reliable measurements to reduce possible bias.

The four data at highest pressure by Scheffer (11) give unweighted residuals with SE 0.060%, clearly the most precise of all the measurements. The six data at lower pressure from ref. 11 are given weights equal to the inverse square of their deviations from eq. [6*a*]: these weights are converged to better than one part in 10^4. The six weighted residuals give SE 0.021%, mean bias 0.10% above and root mean squared (RMS) deviation 0.11% above eq. [6*a*]: the six unweighted residuals give SE 0.97%, mean bias 2.2% above and RMS deviation 2.5% above eq. [6*a*].

The four data of unit weight, using the Beckmann thermometer, from Table 6 of Scheffer and Meyer (14) show unweighted residuals with SE 0.095%. The six data with $w^{1/2} = 0.4$ from Tables 5 and 4 of ref. 14 show weighted residuals with SE 0.099% and unweighted residuals with SE 0.25%. The five data with $w^{1/2} = 0.01$ from Table 4 of ref. 14 give weighted residuals with SE 0.0063%, mean bias 0.020% above, and RMS deviation 0.022% above eq. [6*a*]: the five unweighted residuals give SE 0.63%, mean bias 2.0% above, and RMS deviation 2.2% above eq. [6*a*].

The sixteen data with $w^{1/2} = 0.1$ by de Forcrand and Villard (10) give weighted residuals with SE 0.047%, mean bias –0.12% below, and RMS deviation 0.14% below eq. [6*a*]: the sixteen unweighted residuals give SE 0.47%, mean bias –1.2% below, and RMS deviation 1.4% below eq. [6*a*].

Approximate formula number *r* for hydrogen sulfide hydrate

Table 5 presents estimates and SEs for the standard enthalpy change $\Delta H^{ot}(h{\rightarrow}l_1g)$, for the standard heat capacity change $\Delta Cp^{ot}(h{\rightarrow}l_1g)$, and for the approximate formula number $n = r$ for the standard dissociation of hydrogen sulfide hydrate into water and hydrogen sulfide gas. We note that the results listed in Tables 4 and 5 are biased estimates,

© 2000 NRC Canada

Table 4. Equilibrium constant for dissociation of hydrogen sulfide hydrate into water and hydrogen sulfide gas.

Temperature (°C)	Datum	$w^{1/2}$	$Kp(h \rightarrow l_1g)$ Obsd (MPa)	$Kp(h \rightarrow l_1g)$ Calc (MPa)	Difference (%)	Error on *Kp* calc (%)
Q 29.484	S-11	1	1.516	1.517	–0.06	0.06
29.184	S-10	0.96	1.478	1.477	0.03	0.06
28.484	S-9	0.88	1.389	1.389	–0.03	0.06
27.385	S-8	0.77	1.261	1.260	0.09	0.06
25.586	S-7	0.091	1.082	1.074	0.75	0.07
24.786	S-6	0.053	1.014	1.000	1.39	0.07
20.988	S-4	0.049	0.724	0.709	2.07	0.10
19.688	S-3	0.034	0.651	0.630	3.21	0.11
17.889	S-2	0.036	0.552	0.534	3.26	0.12
16.290	S-1	0.046	0.473	0.460	2.63	0.12
8.844	SM4–16	0.4	0.2283	0.2278	0.26	0.09
7.045	SM6–15	1	0.1913	0.1914	–0.10	0.07
6.895	SM5–14	0.4	0.1887	0.1887	0.03	0.07
6.846	SM4–13	0.01	0.1895	0.1878	0.91	0.07
5.027	SM6–12	1	0.1572	0.1573	–0.05	0.05
4.897	SM5–11	0.4	0.1555	0.1553	0.13	0.05
3.897	SM4–9	0.01	0.1437	0.1408	2.06	0.05
2.998	SM6–8	1	0.1289	0.1288	0.05	0.05
2.898	SM5–7	0.4	0.1282	0.1276	0.46	0.05
2.898	SM4–6	0.01	0.1301	0.1276	1.96	0.05
1.899	SM4–5	0.01	0.1186	0.1155	2.60	0.06
0.969	SM6–4	1	0.1055	0.1053	0.14	0.08
0.949	SM5–3	0.4	0.1055	0.1051	0.33	0.08
0.849	SM4–2	0.01	0.1067	0.1041	2.46	0.08
–0.050	SM5–1	0.4	0.0949	0.0951	–0.28	0.10
–0.369	Qsol	0.1	0.0913	0.0921	–0.92	0.10
Q –0.413	QP	0.1	0.0911	0.0917	–0.65	0.11
5.197	dFV-16	0.1	0.1578	0.1599	–1.32	0.06
4.897	dFV-15	0.1	0.1545	0.1553	–0.49	0.05
4.497	dFV-14	0.1	0.1472	0.1493	–1.43	0.05
3.897	dFV-13	0.1	0.1391	0.1408	–1.19	0.05
3.797	dFV-12	0.1	0.1374	0.1394	–1.45	0.05
3.398	dFV-11	0.1	0.1331	0.1340	–0.69	0.05
2.798	dFV-10	0.1	0.1250	0.1263	–1.08	0.05
2.099	dFV-9	0.1	0.1157	0.1179	–1.88	0.06
1.749	dFV-8	0.1	0.1120	0.1138	–1.67	0.06
1.199	dFV-7	0.1	0.1061	0.1078	–1.57	0.07
0.999	dFV-6	0.1	0.1049	0.1057	–0.75	0.08
0.849	dFV-5	0.1	0.1034	0.1041	–0.69	0.08
0.799	dFV-4	0.1	0.1030	0.1036	–0.56	0.08
0.600	dFV-3	0.1	0.0999	0.1015	–1.65	0.08
0.100	dFV-2	0.1	0.0952	0.0966	–1.39	0.09
0.000	dFV-1	0.1	0.0937	0.0956	–1.99	0.10

except for those given at the lower quadruple point $Q(hs_1l_1g)$ –0.413°C, where eq. [8] is exact and the estimates of $Kp(h \rightarrow l_1g)$, $\Delta H^{oq}(h \rightarrow l_1g)$, $\Delta Cp^{oq}(h \rightarrow l_1g)$, and of $n = r$ are true and unbiased.

One bias arises because it is assumed in eq. [8] that $\Delta H^{ot}(h \rightarrow s_1g)$ is temperature-invariant over the extrapolated temperature range –0.413° to 29.484°C, where it is possible that the standard heat capacity change may have a small negative value. This bias is assessed using the datum $\Delta Cp^{ot}(h \rightarrow s_1g) = –8.0$ with SE 24 J/mole deg, found but not significant for the hydrogen sulfide hydrate equilibrium with ice, eq. [3]. Evaluation of *r* at 29.484°C, using eq. [8] with $\Delta H^{ot}(h \rightarrow s1g) = (25\ 413 – 8t)$ J/mole at *t*°C, gives a converged $r = 5.896$ with SE 0.047: a result in agreement with, and not significantly different from, the 5.869 with SE 0.026 given in Table 5.

A second bias arises because it is assumed in eq. [8] that $\Delta H^{ot}(s_1 \rightarrow l_1)$ is given by the Taylor's series eq. [9] over the extrapolated temperature range –0.413° to 29.484°C. Classical error theory (22) shows that the SE on *r* at 29.484°C, due to errors on the Taylor's series parameters of eq. [9], is less than 0.0004 and is not significant. The SE's on the standard enthalpy changes for *r* at 29.484°C are, 145 J/mole on $\Delta H^{ot}(h \rightarrow l_1g)$, 52 J/mole on $\Delta H^{ot}(h \rightarrow s_1g)$, and 9 J/mole on

© 2000 NRC Canada

Table 5. Standard enthalpy and heat capacity changes for dissociation and the formula of hydrogen sulfide hydrate.

Temperature	ΔH^{ot} (J/mole)		ΔCp^{ot} (J/mole deg)			
(°C)	(h→l_1g)	SE	(h→l_1g)	SE	r	SE
Q 29.484	66873	145	160	10	5.869	0.026
29.184	66825	142	160	10	5.871	0.025
28.484	66713	135	160	10	5.874	0.024
27.385	66537	124	160	10	5.880	0.022
25.586	66249	105	160	10	5.891	0.020
24.786	66121	97	160	10	5.896	0.018
20.988	65513	60	160	10	5.920	0.013
19.688	65305	48	160	10	5.929	0.012
17.889	65017	32	160	10	5.942	0.010
16.290	64761	23	160	10	5.954	0.009
8.844	63569	72	160	10	6.018	0.015
7.045	63282	90	160	10	6.035	0.017
6.895	63258	91	160	10	6.037	0.017
6.846	63250	92	160	10	6.037	0.018
5.027	62958	110	160	10	6.056	0.020
4.897	62938	112	160	10	6.057	0.020
3.897	62778	122	160	10	6.068	0.022
2.998	62634	131	160	10	6.078	0.023
2.898	62618	132	160	10	6.079	0.024
2.898	62618	132	160	10	6.079	0.024
1.899	62458	142	160	10	6.091	0.025
0.969	62309	151	160	10	6.102	0.027
0.949	62306	152	160	10	6.102	0.027
0.849	62290	153	160	10	6.103	0.027
–0.050	62146	162	160	10	6.114	0.028
–0.369	62095	165	160	10	6.118	0.029
Q –0.413	62088	165	160	10	6.119	0.029
5.197	62986	109	160	10	6.054	0.020
4.897	62938	112	160	10	6.057	0.020
4.497	62874	116	160	10	6.062	0.021
3.897	62778	122	160	10	6.068	0.022
3.797	62762	123	160	10	6.069	0.022
3.398	62698	127	160	10	6.074	0.023
2.798	62602	133	160	10	6.081	0.024
2.099	62490	140	160	10	6.089	0.025
1.749	62434	143	160	10	6.093	0.025
1.199	62346	149	160	10	6.099	0.026
0.999	62314	151	160	10	6.102	0.027
0.849	62290	153	160	10	6.103	0.027
0.799	62282	153	160	10	6.104	0.027
0.600	62250	155	160	10	6.106	0.027
0.100	62170	160	160	10	6.113	0.028
0.000	62154	161	160	10	6.114	0.028

$\Delta H^{ot}(s_1 \rightarrow l_1)$, showing that the major contribution to the SE on r is the SE on the estimate of $\Delta H^{ot}(h \rightarrow l_1g)$.

It is shown in Table 5 that the value of r decreases monotonously with increasing temperature and asymptotically approaches its theoretical lower limit of 5.75, for a Structure I hydrate (28, 29), at some temperature above the quadruple point $Q(hl_1l_2g)$ at 29.484°C.

This shows a continuous increase with temperature in the number of H_2S hydrate-former molecules per unit cell of $46H_2O$, from 7.518 with SE 0.035 at –0.413°C to about 7.838 with SE 0.034 at 29.484°C, asymptotically trending towards an upper limit of 8.0 (28, 29) above 29.484°C. This requires that an increased fraction of cavities must be occupied by H_2S molecules to stabilize the solid hydrate lattice against collapse at higher temperatures. Although these numbers may be slightly biased, the overall effect of increasing temperature remains unchanged.

The equilibrium hydrogen sulfide hydrate composition at the quadruple point $Q(hl_1l_2g)$ 29.484°C occurs with 2.03% of empty and 97.97% of occupied cavities with SE 0.43% at the saturation activity of liquid H_2S (l_2). This occupancy level is not significantly different from the deuterium sulfide D-hydrate (7) which shows 1.65% of empty and 98.35% of occupied cavities with SE 0.31% at 29.375°C, and 1.54% of empty and 98.46% of occupied cavities with SE 0.32% at the quadruple point $Q(hl_1l_2g)$ 30.770°C.

This agrees well with the work of Scheffer (11), which shows that hydrostatic pressure increases the temperature for hydrogen sulfide hydrate stability above $Q(hl_1l_2g)$ along the three-phase (hl_1l_2) line, where presumably the empty cavities within the hydrate lattice are progressively being filled with additional hydrogen sulfide guest molecules at the higher pressures and temperatures.

The equilibrium hydrogen sulfide hydrate composition at the lower quadruple point $Q(hs_1l_1g)$ –0.413°C occurs with 6.03% of empty and 93.97% of occupied cavities with SE 0.44% at the equilibrium activity of ice H_2O (s_1). Since we considered that this hydrate composition might be a sensitive function of the relative weights assigned to the six data from Tables 5 & 4 by Scheffer and Meyer (14) this effect is tested.

Sensitivity tests are made using the weights $w^{1/2}$ = 0.3, 0.35, 0.4, and 0.5 for the six data: this implies that each of the four data of unit weight from Table 6 by Scheffer and Meyer (14) are, respectively, 11.1, 8.16, 6.25, and 4 times more accurate than each of the six data from Tables 5 and 4. Results indicate 5.97%, 6.00%, 6.03%, and 6.08% of empty cavities, with SE's 0.44%, 0.44%, 0.44%, and 0.43%, respectively, using weights $w^{1/2}$ = 0.3, 0.35, 0.4, and 0.5 for the six data. The hydrate composition at $Q(hs_1l_1g)$ –0.413°C is found not to be a sensitive function of the preferred weight $w^{1/2}$ = 0.4, chosen for the six measurements from Tables 5 and 4 by Scheffer and Meyer (14).

Deuterium sulfide D-hydrate (7) at $Q(hs_1l_1g)$ 3.392°C indicates 5.97% of empty cavities with SE 0.27%, which is not significantly different from the hydrogen sulfide hydrate at $Q(hs_1l_1g)$ –0.413°C.

Formula of hydrogen sulfide hydrate near –0.413°C

Since our (hl_1g) data analysis depends critically on the ten measurements by Scheffer and Meyer (14) taken together with the measurements of Scheffer (11), it is important to discover why our formula $H_2S{\cdot}6.119H_2O$ at –0.413°C does not agree with the earlier formula $H_2S{\cdot}6.06H_2O$ derived (14) and reconfirmed (15) by Scheffer et al. using the same measurements (14).

In the first place our value 25 416 J/mole for $\Delta H^{oq}(h \rightarrow s_1g)$ is 84 J/mole smaller than the 25 500 J/mole used by Scheffer et al. (14, 15): this leads to an increase of 0.014 with SE 0.0087 for n at –0.413°C and the earlier formula is modified to $H_2S{\cdot}6.074H_2O$. In attempts to obtain agreement with the earlier formula $H_2S{\cdot}6.074H_2O$ (14, 15), we have made

© 2000 NRC Canada

numerous least-squares analyses using the three data sets (10, 11, 14) with various relative weights to reduce the effect of all measurements other than the four most important measurements at low temperature (SM6-4, SM6-8, SM6-12, and SM6-15) and the four most important measurements at high temperature (S-11, S-10, S-9, and S-8).

For example, in a regression with the eight measurements (SM6-15, SM6-12, SM6-8, SM6-4, S-8, S-9, S-10, and S-11) with the weights shown in Table 4, with the twenty nine other measurements with their values of $w^{1/2}$ reduced by a factor of 10, and with the six measurements (S-1, S-2, S-3, S-4, S-6, and S-7) with their respective best values of $w^{1/2}$ (0.013, 0.010, 0.010, 0.014, 0.014, and 0.023), we find the SE 0.027% for a datum of unit weight and the parameters with (SE) $d1$ = 26.7292 (0.012) and $d2$ = 21.0337 (0.38) at 25°C. These parameters give estimates with (SE) for n of 6.073 (0.012) at –0.413°C and 5.893 (0.011) at 29.484°C.

The SE 0.027% for a measurement of unit weight is realistic for this extreme weighting scheme and is consistent with the SE 0.021% found for the four measurements (14) using the Beckmann thermometer (SM6–4, SM6–8, SM6–12, and SM6–15). The four measurements at high temperature (S-11, S-10, S-9, and S-8) systematically cut across the regression line and show a larger SE 0.083%.

The value of 21.0337 for the heat-capacity parameter $d2$ is improbably large, because it is significantly larger than the 20.0170 at 25°C found for deuterium sulfide D-hydrate (7), and because the heat capacities of water (23) and of ice (31) are significantly smaller than the heat capacities of liquid deuterium oxide and of D-ice (33).

The 6.073 value for n at –0.413°C is 0.042 smaller than, and the 5.893 value for n at 29.484°C is 0.053 larger than the corresponding values of n found at the quadruple points of deuterium sulfide D-hydrate (7): this cross-over of the values of n for hydrogen sulfide hydrate relative to those found for deuterium sulfide D-hydrate is improbable. The cross-over of the hydrate formulae is even more improbable recognizing that the vapor pressure of hydrogen sulfide hydrate between 2.798° and 29.484°C is an almost constant 14% higher than the vapor pressure of deuterium sulfide D-hydrate (6) at the same temperature.

Only by using the extreme weighting scheme described above, are we able to obtain agreement with the earlier formula (14, 15) $H_2S{\cdot}6.06H_2O$ at –0.4°C, and this extreme weighting scheme is both unreasonable and unrealistic for the three data sets (10, 11, and 14). Use of realistic relative weights always gives estimates for n which are significantly greater than $H_2S{\cdot}6.074H_2O$ at –0.413°C.

In conclusion we suggest that the preferred relative weights listed in Table 4 provide a good, self-consistent and non-unique solution to combine the three data sets (10, 11, and 14) to evaluate the hydrogen sulfide hydrate dissociation equilibrium constants and to derive valid formula for the hydrogen sulfide hydrate with water.

References

1. D.N. Glew and E.A. Moelwyn-Hughes. Discuss. Faraday Soc. **50**, 150 (1953).
2. D.N. Glew. Can. J. Chem. **38**, 208 (1960).
3. D.N. Glew. J. Phys. Chem. **66**, 605 (1962).
4. E.C.W. Clarke and D.N. Glew. Can. J. Chem. **48**, 764 (1970).
5. E.C.W. Clarke and D.N. Glew. Can. J. Chem. **49**, 691 (1971).
6. C.W. Clarke and D.N. Glew. Can. J. Chem. **76**, 1119 (1998).
7. C.W. Clarke and D.N. Glew. Can. J. Chem. **78**, 1 (2000).
8. R. de Forcrand. C. R. Hebd. Seances Acad. Sci. **94**, 967 (1882).
9. L. Cailletet and R. Bordet. C. R. Hebd. Seances Acad. Sci. **95**, 58 (1882).
10. R. de Forcrand and P. Villard. C. R. Hebd. Seances Acad. Sci. **106**, 849 (1888).
11. F.E.C. Scheffer. Proc. K. Ned. Akad. Wet. **13**, 829 (1911).
12. F.E.C. Scheffer. Z. Phys. Chem.: Stoechiom. Verwandtschaftsl. **84**, 734 (1913).
13. F.E.C. Scheffer and G. Meyer. Proc. K. Ned. Akad. Wet., **21**, 1204 (1919).
14. F.E.C. Scheffer and G. Meyer. Proc. K. Ned. Akad. Wet., **21**, 1338 (1919).
15. A.E. Korvezee and F.E.C. Scheffer. Recl. Trav. Chim. Pays-Bas, **50**, 256, (1931).
16. R.H. Wright and O. Maass. Can. J. Res. **6B**, 94 (1932).
17. D.C. Bond and N.B. Russell. Trans. Am. Inst. Min. Metall. Pet. Eng. **179**, 192 (1949).
18. F.T. Selleck, L.T. Carmichael, and B.H. Sage. Ind. Eng. Chem. **44**, 2219 (1952).
19. J.J. Carroll. Ph.D. thesis, University of Alberta, 1990.
20. J.J. Carroll and A.E. Mather. Can. J. Chem. Eng. **69**, 1206 (1991).
21. E.C.W. Clarke and D.N. Glew. Trans. Faraday Soc. **62**, 539 (1966).
22. N.R. Draper and H. Smith. Applied regression analysis. 2nd ed. John Wiley and Sons, New York. 1981.
23. L. Haar, J.S. Gallagher, and G.S.Kell. NBS/NRC steam tables. Hemisphere Publishing Corp., New York. 1984.
24. G.S. Kell. J. Phys. Chem. Ref. Data, **6**, 1109 (1977).
25. J.A. Barbero, K.G. McCurdy, and P.R. Tremaine. Can. J. Chem. **60**, 1872 (1982).
26. R.N. Goldberg and R.D. Weir. Pure Appl. Chem. **10**, 1545 (1992).
27. N.E. Dorsey. Properties of ordinary water-substance. Reinhold Publishing Corp., New York. 1940. pp. 600, 462.
28. M. von Stackelberg and W. Jahns. Z. Elektrochem. **58**, 162 (1954).
29. D.W. Davidson. *In* Water: a comprehensive treatise. Vol. 2. *Edited by* F. Franks. Plenum Press, New York. 1973.
30. N.S. Osborne. J. Res. Natl. Bur. Stand. **23**, 643 (1939).
31. W.F. Giauque and J.W. Stout. J. Am. Chem. Soc. **58**, 1144 (1936).
32. G.H. Cady. J. Phys. Chem. **87**, 4437 (1983).
33. E.A. Long and J.D. Kemp. J. Am. Chem. Soc. **58**, 1829 (1936).

© 2000 NRC Canada

Synthesis, spectroscopic characterization and structural studies of organotin monothiocarbonates. Crystal structures of $Ph_3Sn[SCO_2Me]$ and $Ph_3Sn[SCO_2(i\text{-}Pr)]$

John E. Drake and Jincai Yang

Abstract: *O*-alkyl monothiocarbonate (monoxanthate) derivatives of tin were obtained by the reaction of a sodium salt of the monothiocarbonic acid with an organotin chloride to give $Ph_3Sn[SCO_2R]$, $Ph_2Sn[SCO_2R]_2$, and $Me_3Sn[SCO_2R]$, where R = Me and i-Pr. The compounds have been characterized by infrared, Raman, ^1H NMR, and ^{13}C NMR spectroscopy, as well as mass spectrometry, and in two cases by X-ray crystallography. $Ph_3Sn[SCO_2Me]$ (**1**) and $Ph_3Sn[SCO_2(i\text{-}Pr)]$ (**2**), crystallize in the triclinic space group $P\bar{1}$ (no. 2) with cell parameters a = 10.218(4), b = 10.568(6), c = 9.366(7) Å, α = 106.73(5), β = 96.99(5), γ = 85.55(4)°, V = 960(1) Å^3, and Z = 2 for **1**; and a = 14.793(2), b = 17.856(3), c = 9.813(3) Å, α = 103.86(5), β = 98.36(5), γ = 106.85(4)°, V = 2343(1) Å^3, and Z = 2 for **2**. The latter has two molecules in the asymmetric unit. The immediate environment about tin in both **1** and **2** is that of the expected distorted tetrahedron. However, the orientation of the monothiocarbonate group is such that there is an Sn-O intramolecular interaction of 3.040(8) for **1** and 3.05(2) Å on average for **2**. Thus, the considerable distortion is consistent with a tendency to form a five-coordinate, trigonal bipyramidal species with one of the O-Sn-C angles approaching 180° (153.4(4) for **1** and an average of 157.1(6) for **2**). Estimations of the Pauling partial bond orders suggest this weak Sn-O interaction is slightly stronger than the corresponding Ge-O interaction in the analogous germanium derivative, $Ph_3Ge[SCO_2Me]$.

Key words: structure, tin, methyl, phenyl, isopropyl, monothiocarbonates.

Résumé : On a préparé des dérivés de l'étain avec du monothicarbonate (monoxanthate) de *O*-alkyle ($Ph_3Sn[SCO_2R]$, $Ph_2Sn[SCO_2R]$ et $Me_3Sn[SCO_2R]$ dans lesquels R = Me ou i-Pr) en faisant réagit du sel de sodium de l'acide monothiocarbonique avec un chlorure d'organoétain. On a caractérisé ces composés par spectroscopies infrarouge, Raman et RMN du ^1H et du ^{13}C ainsi que par spectroscopie de masse et, dans deux cas, par diffraction des rayons X. Le $Ph_3Sn[SCO_2Me]$, **1**, et $Ph_3Sn[SCO_2i\text{-}Pr]$, **2**, cristallisent dans le groupe d'espace $P\bar{1}$ (no. 2) avec a = 10,218(4), b = 10,568(6) et c = 9,366(7) Å, α = 106,73(5), β = 96,99(5) et γ = 85,55(4)°, V = 960(1) Å^3 et Z = 2 pour le composé **1** et a = 14,793(2), b = 17,856(3) et c = 9,813(3) Å, α = 103,86(5), β = 98,36(5) et γ = 106,85(4)°, V = 2343(1) Å^3 et Z = 2 pour le composé **2**. Ce dernier composé comporte deux molécules dans la maille asymétrique. L'environnement immédiat autour de l'étain de ces deux composés correspond à celui attendu pour un tétraèdre déformé. Toutefois, l'orientation du groupe monothiocarbonate est tel que l'on observe une interaction Sn-O intramoléculaire de 3,040(8) Å pour **1** et de 3,05(2) Å pour **2**. La déformation importante est donc en accord avec une tendance à former une espèce pentacoordinée trigonale bipyramidale dans laquelle les angles O-Sn-C se rapprochent de 180° (153,4(4) pour **1** et une moyenne de 157,1(6) pour **2**). Des évaluations à partir des ordres partiels de liaison de Paulin suggèrent que cette interaction Sn-O faible est un peu plus forte que l'interaction correspondante Ge-O du composé germaniun analogue, $Ph_3Ge[SCO_2Me]$.

Mots clés : structure, étain, méthyle, phényle, isopropyle, monothiocarbonates.

[Traduit par la Rédaction]

Introduction

O-alkyl dithiocarbonate (xanthate) derivatives have been extensively studied but the chemistry of monothiocarbonates (monoxanthates) has received considerably less attention and most of the relatively few reports have involved transition metal complexes (1). In addition to reports on alkali salts (2), two reports by us have appeared on main group element monothiocarbonates describing some organotellurium (3) and organogermanium (4) derivatives. Considerably more

Received January 20, 2000. Published on the NRC Research Press website on September 1, 2000.

J.E. Drake.[1] Chemistry and Biochemistry, University of Windsor, Windsor, ON N9B 3P4, Canada.
J. Yang. Research and Development, Petro-Canada Lubricants, Mississauga, ON L5K 1A8, Canada.

[1]Author to whom correspondence may be addressed. Telephone: (519) 253-4232. Fax: (519) 973-7098. e-mail: ak4@uwindsor.ca

 © 2000 NRC Canada

work has appeared on dithio derivatives of tin than of germanium, but we were unable to find any reports on monothiocarbonate organotin derivatives. Surprisingly, we found these even more difficult to isolate pure than their germanium analogues but we were able to confirm the formation of five *O*-alkyl monothiocarbonate derivatives $Ph_3Sn[SCO_2R]$ (R = Me and i-Pr), $Ph_2Sn[SCO_2(i\text{-}Pr)]_2$, $Ph_2SnCl[SCO_2(i\text{-}Pr)]$, and $MeSn[SCO_2Me]$ by NMR, infrared, and Raman spectroscopy, as well as mass spectrometry. We also have obtained the X-ray crystal structures of $Ph_3Sn[SCO_2Me]$(**1**) and $Ph_3Sn[SCO_2(i\text{-}Pr)]$(**2**).

Among the many reports on dithio derivatives of tin, those of relevance to this work include discussions of ligand coordination modes and coordination number in a variety of dithiocarbamates (5), a series of publications on dithiocarbonates (6), and a structural study of $Ph_3Sn[S_2CO(i\text{-}Pr)]$ (7). An examination of tin(IV) 1-pyrrolecarbothioates (8), including $Ph_3Sn[SOCNC_4H_4]$, and a comparison of the structures of the monothiocarbamate, $Ph_3Sn[SCON(CH_2)_4O]$, with the analogous dithiocarbamate are also of interest (9). Bidentate linkages appear to be favored in organotin derivatives with dithio-ligands as exemplified in dithiophosphates such as $Ph_2Sn[S_2P(Oi\text{-}Pr)_2]_2$ (10) and dithiocarbamates such as $BuSn[S_2CN(Et)_2]_3$ (11) in both of which tin atoms are in octahedral sites. However, monodentate linkages appear to be often found with triphenyltin derivatives such as in $Ph_3Sn[S_2P(OEt)_2]$ (12). The range of mono-, aniso-, and bidentate ligands will be discussed in some detail.

Experimental

Materials

The starting materials (Ph_3SnCl, Ph_2SnCl_2, and Me_3SnCl) were obtained from Aldrich; all starting materials being used as supplied. All solvents were dried and distilled prior to use and all reactions were carried out under anhydrous conditions. The salts, $NaSCO_2R$, where R = Me and i-Pr, were prepared as described in the literature (4) and their purity checked by ^1H and ^{13}C NMR spectroscopy. No further purification was necessary.

Preparation of $Ph_3Sn[SCO_2Me]$ (1) and $Ph_3Sn[SCO_2(i\text{-}Pr)]$ (2)

Typically, Ph_3SnCl (0.25 g, 0.65 mmol) and an excess of dried $NaSCO_2Me$ (0.10 g, 0.88 mmol) were placed in a previously evacuated flask and solvent (CH_2Cl_2, ca. 15 mL) was added under N_2. The mixture was stirred for 2 h at room temperature, followed by filtration to remove NaCl and excess of starting salt, and then evaporation under vacuum gave $Ph_3Sn[SCO_2Me]$ (**1**) as a colorless solid. Recrystallization from a CH_2Cl_2 – *n*-hexane mixture gave colorless crystals (0.20 g, 0.45 mmol), yield 70%, mp 86°C. Peaks in the mass spectrum corresponding to ^{120}Sn in a typical tin cluster were seen at *m*/*z* (relative intensity): 442 ($(Ph_3SnSCO_2Me)^+$, 3%), 365 ($(Ph_2SnSCO_2Me)^+$, 10%), 351 ($(Ph_3Sn)^+$, 100%), 305 ($(Ph_2SnOMe)^+$, 45%), 274 ($(Ph_2Sn)^+$, 30%), 197 ($(PhSn)^+$, 9%). IR (Raman) (cm^{-1}) main features: ν(O=CSOC) 1669 vs, ν(OSC-OMe) 1148 vs br, ν(OSO-CH_3) 1090 sh, *p*-phenyl [1002 (100)], π(SCO_2) 817 ms, *f*-phenyl 731 vs, *v*-phenyl 698 *vs*, ν(SnS-C) 658 m [658 (55)], *y*-phenyl 447 s, δ(SCO_2) 426 m, ν(Sn-S) [333 (10)]. ^1H NMR: ($CDCl_3$) δ 3.63 [3H, OCH_3, s]; 7.41–7.44 [9H, Sn-C_6H_5 – *meta* + *para*]; 7.63–7.68 [6H Sn-C_6H_5 – *ortho*]. ^{13}C NMR: ($CDCl_3$) δ 54.82 [OCH_3]; 129.03, 130.04, 136.57, 136.74 [Sn-C_6H_5]. In the same fashion $Ph_3Sn[SCO_2(i\text{-}Pr)]$ (**2**) was prepared as a colorless solid. Recrystallization from a CH_2Cl_2 – *n*-hexane mixture gave colorless crystals (0.30 g, 0.71 mmol, yield 86%), mp 92–93°C. Peaks in the mass spectrum corresponding to ^{120}Sn were seen at *m*/*z* (relative intensity): 469 ($(Ph_3SnSCO_2(i\text{-}Pr) - H)^+$, 2%), 393 ($(Ph_2SnSCO_2(i\text{-}Pr))^+$, 8%), 351 ($(Ph_3Sn)^+$, 100%), 333 ($(Ph_3SnO(i\text{-}Pr))^+$, 8%), 291 ($(Ph_2SnOH)^+$, 50%), 274 ($(Ph_2Sn)^+$, 30%), 197 ($(PhSn)^+$, 50%). IR (Raman) ($cm^{-1}$) main features: ν(O=CSOC) 1663 vs, ν((OSC-O(i-Pr)) 1169 vs, ν(OSO-CH(CH_3)$_2$) 1093 vs, *p*-phenyl [1001 (100)], π(SCO_2) 848 m, *f*-phenyl 731 s, *v*-phenyl 698 s, ν(SnS-C) 655 w [657 (45)], *y*-phenyl 446 ms, δ(SCO_2) 433 sh, ν(Sn-S) [335 (15)]. ^1H NMR: ($CDCl_3$) δ 1.04 [6H, OCH(CH_3)$_2$, d, *J*(HH) 6.2 Hz]; 4.88 [1H, OC*H*, sept, *J*(HH) 6.2 Hz]; 7.40–7.42 [9H, Sn-C_6H_5 – *meta* + *para*]; 7.64–7.67 [6H Sn-C_6H_5 – *ortho*]. ^{13}C NMR: ($CDCl_3$) δ 21.61 [OCCH_3]; 72.65 [O*C*H]; 129.98, 129.96, 136.47, 136.71 [Sn-C_6H_5].

Preparation of $Ph_2Sn[SCO_2(i\text{-}Pr)]_2$ (3)

Typically, Ph_2SnCl_2 (0.25 g, 0.72 mmol) and $NaSCO_2(i\text{-}Pr)$ (0.25 g, 1.76 mmol) were placed in a flask and solvent (CH_2Cl_2, ca. 15 mL) was added under N_2. The mixture was stirred for 2 h at room temperature, followed by filtration and evaporation under vacuum to give $Ph_2Sn[SCO_2(i\text{-}Pr)]_2$, **3**, (0.3 g, 0.59 mmol) as a colorless solid, (0.30 g, 0.59 mmol), yield 81.5%, mp 83–84°C. Peaks in the mass spectrum corresponding to ^{120}Sn in a typical tin cluster were seen at *m*/*z* (relative intensity): 512 ($(Ph_2Sn[SCO_2(i\text{-}Pr)]_2)^+$, 1%), 393 ($(Ph_2SnSCO_2(i\text{-}Pr))^+$, 30%), 333 ($(Ph_3SnO(i\text{-}Pr))^+$, 45%), 291 ($(Ph_2SnOH)^+$, 100%), 274 ($(Ph_2Sn)^+$, 65%), 197 ($(PhSn)^+$, 35%). Attempts at recrystallization failed to yield any X-ray quality crystals. IR (Raman) (cm^{-1}) main features: ν(O=CSOC) 1642 vs, ν((OSC-O(i-Pr)) 1176 vs, ν(OSO-CH(CH_3)$_2$) 1091 vs, *p*-phenyl [999 (100)], π(SCO_2) 847 ms, *f*-phenyl 732 ms, *v*-phenyl 695 ms, ν(SnS-C) 655 vw [658 (45)], *y*-phenyl 445 m, δ(SCO_2) 428 m, ν(Sn-S) [344 (15)]. ^1H NMR: ($CDCl_3$) δ 1.06 [12H, OCH(CH_3)$_2$, d, *J*(HH) 6.2 Hz]; 4.86 [2H, OC*H*, sept, *J*(HH) 6.2 Hz]; 7.43–7.45 [6H, Sn-C_6H_5 – *meta* + *para*]; 7.82–7.85 [4H Sn-C_6H_5 – *ortho*]. ^{13}C NMR: ($CDCl_3$) δ 21.58 [OCCH_3]; 73.48 [OCH_3]; 129.07, 130.46, 135.35, 135.73 [Sn-C_6H_5].

Formation and identification of $Ph_2SnCl[SCO_2(i\text{-}Pr)]$ (4) and $Me_3Sn[SCO_2Me]$ (5)

Typically, Ph_2SnCl_2 (0.30 g, 0.87 mmol) and dried $NaSCO_2(i\text{-}Pr)$ (0.12 g, 0.87 mmol) were introduced into a round-bottomed flask, followed by the addition of dried CH_2Cl_2 (ca. 15 mL). The mixture was stirred for ca. 2 h at which time the NaCl that had formed was filtered off and the solvent allowed to evaporate under vacuum to produce $Ph_2SnCl[SCO_2(i\text{-}Pr)]$ (**4**) as a white solid (0.31 g, 0.73 mmol, yield 83%). IR (Raman) (cm^{-1}) main features: ν(O=CSOC) 1629 ms, br, ν((OSC-O(i-Pr)) 1261 s, ν(OSO-CH(CH_3)$_2$) 1095 vs, *p*-phenyl [1000 (100)], π(SCO_2) 803 ms br, *f*-phenyl 728 vs, *v*-phenyl 692 vs, ν(SnS-C) 656 mw [658 (45)], *y*-phenyl 448 m br, δ(SCO_2) 430 sh, ν(Sn-S) [340 (5)], ν(Sn-Cl) [276 (9)]. ^1H NMR: ($CDCl_3$) δ 1.26 [6H,

© 2000 NRC Canada

Table 1. Summary of crystal data, intensity collection, and structural refinement for $Ph_3[SnSCO_2Me]$ (**1**) and $2Ph_3Sn[SCO_2(i\text{-}Pr)]$ (**2**).

Parameter	**1**	**2**
a (Å)	10.218(4)	14.793(2)
b (Å)	10.568(6)	17.856(3)
c (Å)	9.366(7)	9.813(3)
α (°)	106.73(5)	103.86(2)
β (°)	96.99(5)	98.36(2)
γ (°)	85.55(4)	106.85(1)
V (Å^3)	960(1)	2343(1)
Crystal system	Triclinic	Triclinic
Space group	$P\bar{1}$ (no. 2)	$P\bar{1}$(no. 2)
Mol. wt. (g mol^{-1})	444.11	983.33
Z	2	2
Crystal dimensions (mm)	0.41 × 0.36 × 0.21	0.45 × 0.40 × 0.21
ρ (calcd.) (g cm^{-3})	1.52	1.33
μ, cm^{-1}	14.46	11.9
Transmission factors	0.58–1.00	0.73–1.00
Temperature (°C)	23	23
Radiation (Å)	Mo Kα 0.71096	Mo Kα 0.71096
Monochromator	Highly oriented graphite	Highly oriented graphite
Scan method	ω – 2θ	ω – 2θ
Scan speed (°/min)	32	16
Max. (2θ)	50	45
Total reflections measured	3591	5218
No. of unique data	3382	4929
No. of obsd. data ($I \geq 3\sigma(I)$)]	1619	1511
No. of parameters (NP)	127	169
$R = \sum\|\|F_o\| - \|F_c\|\|/\sum\|F_o\|$	0.0543	0.0544
$R_w = [\sum w(\|F_o\| - \|F_c\|)^2/\sum wF_o^2)]^{1/2}$	0.0452	0.0583
Goodness of fit	1.72	1.85
Largest shift/e.s.d, final cycle	0.001	0.001
Largest residual electron density (e Å^{-3})	0.09	0.76

OCH(CH_3)$_2$, d, *J*(HH) 6.2 Hz]; 5.00 [1H, OC*H*, sept, *J*(HH) 6.2 Hz]; 7.47–7.50 [6H, Sn-C_6H_5 – *meta* + *para*]; 7.84–7.87 [4H Sn-C_6H_5 – *ortho*]. ^{13}C NMR: ($CDCl_3$) δ 21.74 [OCCH_3]; 75.38 [OCH_3]; 129.26, 130.98, 135.19, 136.61 [Sn-C_6H_5]. Attempts at recrystallization did not yield any crystals, but rather resulted in decomposition. In a similar manner as described for the preparation of **1** and **2**, $Me_3Sn[SCO_2Me]$ (**5**), was formed as a colorless viscous liquid by starting with Me_3SnCl and an excess of $NaSCO_2Me$. IR (Raman) (cm^{-1}) main features: ν(O=CSOC) 1630 m, ν(OSC-OMe) 1260 vs, ν(OSO-CH_3) 1034 vs br, π(SCO_2) 865 s, ρ($SnCH_3$) 799 vs, ν(SnS-C) 662 m, ν(Sn-C_{asymm}) 532 m, ν(Sn-C_{symm}) 506 mw. ^{1}H NMR: ($CDCl_3$) δ 0.53 [9H, Sn(CH_3)$_3$, *J*(SnH) 64.2 Hz], 3.68 [3H, OCH_3]. ^{13}C NMR: ($CDCl_3$) δ –2.50 [SnCH_3], 53.51 [OCH_3]. For both **4** and **5**, the ^{1}H and ^{13}C NMR spectra taken immediately after separation indicated the presence of only one product.

Attempted formation and identification of $Ph_2Sn[SCO_2Me]_2$ and $Ph_2SnCl[SCO_2Me]$

In a manner similar to the successful preparation of **3** and **4**, substituting $NaSCO_2Me$ for $NaSCO_2(i\text{-}Pr)$ did not result in the formation of pure $Ph_2Sn[SCO_2Me]_2$ or $Ph_2SnCl[SCO_2Me]$ but rather in mixtures. The NMR spectra in each case were consistent with the presence of differing amounts of both of the desired compounds.

Physical measurements

Infrared spectra were recorded on a Nicolet 5DX FT spectrometer as KBr pellets or oils smeared between KBr windows in the region 4000–400 cm^{-1}, and far infrared spectra on a Bomem DA3 infrared spectrometer between polyethylene films as oils or Nujol mulls. The Raman spectra were recorded on samples in sealed glass capillaries on a JEOL-XY Raman spectrometer using the 5145 Å exciting line of an argon ion laser. The ^{1}H and ^{13}C {H} NMR spectra were recorded on a Bruker 300 FT/NMR spectrometer at 300.133 and 75.471 MHz, respectively, in $CDCl_3$ using Me_4Si as internal standard. All NMR spectra were run at ambient temperature and under standard operating conditions. The melting points were determined on a Fisher–Johns apparatus. The mass spectra were recorded on a Kratos Profile GC-MS Spectrometer.

X-ray crystallographic analysis

Colorless block crystals of $Ph_3Sn[SCO_2Me]$ (**1**) and $Ph_3Sn[SCO_2(i\text{-}Pr)]$ (**2**) were sealed in thin-walled glass capillaries and mounted on a Rigaku AFC6S diffractometer, with graphite-monochromated MoKα radiation. Operating at 50 kV and 35 mA.

Cell constants corresponded to triclinic cells whose dimensions are given in Table 1, along with other experimental details. Based on statistical analysis of intensity distribution

© 2000 NRC Canada

Table 2. Selected interatomic distances (Å) and angles (°) for $Ph_3Sn[SCO_2Me]$ (**1**)

Bond	Distance (Å)	Bond	Angle (°)
Sn(1)—S(1)	2.444(4)	S(1)-Sn(1)-C(3)	97.5(3)
Sn(1)—C(3)	2.10(1)	S(1)-Sn(1)-C(9)	112.3(3)
Sn(1)—C(9)	2.12(1)	S(1)-Sn(1)-C(15)	112.2(3)
Sn(1)—C(15)	2.12(1)	C(3)-Sn(1)-C(9)	112.6(4)
S(1)—C(1)	1.76(1)	C(3)-Sn(1)-C(15)	111.4(4)
C(1)—O(1)	1.20(1)	C(9)-Sn(1)-C(15)	109.9(4)
C(1)—O(2)	1.34(1)	Sn(1)-S(1)-C(1)	95.4(5)
O(2)—C(2)	1.43(1)	S(1)-C(1)-O(1)	125(1)
Sn(1)--O(1)	3.040(8)	S(1)-C(1)-O(2)	109.2(9)
S(1)--O(1)	2.636(9)	O(1)-C(1)-O(2)	126(1)
		C(1)-O(2)-C(2)	115(1)
		S(1)-Sn(1)--O(1)	56.2(2)
		O(1)--Sn(1)-C(15)	153.4(4)

Table 3. Selected interatomic distances (Å) and angles (°) for $2Ph_3Sn[SCO_2(i\text{-}Pr)]$ (**2**)

Bond	Distance (Å)	Bond	Angle (°)
Sn(1)—S(1)	2.42(1)	S(1)-Sn(1)-C(5)	113.1(7)
Sn(1)—C(5)	2.12(2)	S(1)-Sn(1)-C(11)	100.7(8)
Sn(1)—C(1)	2.11(2)	S(1)-Sn(1)-C(17)	110.3(8)
Sn(1)—C(1)	2.16(3)	C(5)-Sn(1)-C(11)	106.7(9)
S(1)—C(1)	1.80(4)	C(5)-Sn(1)-C(17)	114.2(8)
C(1)—O(1)	1.16(5)	C(11)-Sn(1)-C(15)	111(1)
C(1)—O(2)	1.35(6)	Sn(1)-S(1)-C(1)	94(2)
O(2)—C(2)	1.52(5)	S(1)-C(1)-O(1)	127(4)
Sn(1)--O(1)	3.04(3)	S(1)-C(1)-O(2)	106(3)
S(1)--O(1)	2.66(3)	O(1)-C(1)-O(2)	127(4)
		C(1)-O(2)-C(2)	118(2)
		S(1)-Sn(1)--O(1)	56.8(6)
		O(1)--Sn(1)-C(11)	157.5(9)
Sn(2)—S(2)	2.46(1)	S(2)-Sn(2)-C(27)	111.2(7)
Sn(2)—C(27)	2.16(2)	S(2)-Sn(2)-C(33)	100.3(8)
Sn(2)—C(33)	2.13(2)	S(2)-Sn(2)-C(39)	100.6(7)
Sn(2)—C(39)	2.08(2)	C(27)-Sn(2)-C(33)	109.5(8)
S(2)—C(23)	1.78(5)	C(27)-Sn(2)-C(39)	114.3(7)
C(23)—O(31)	1.25(5)	C(33)-Sn(2)-C(39)	112(1)
C(23)—O(4)	1.31(6)	Sn(2)-S(2)-C(23)	97(2)
O(4)—C(24a)	1.6(1)	S(2)-C(23)-O(3)	122(4)
O(4)—C(24b)	1.4(1)	S(2)-C(23)-O(4)	113(3)
Sn(2)--O(3)	3.06(3)	O(3)-C(23)-O(4)	125(4)
S(2)--O(3)	2.66(3)	C(23)-O(4)-C(24a)	111(4)
		C(23)-O(4)-C(24b)	108(4)
		S(2)-Sn(2)--O(3)	56.4(6)
		O(3)--Sn(2)-C(33)	156.7(9)

and the successful solution and refinement of the structures, the space group was determined to be $P\bar{1}$ (no. 2) for both **1** and **2**. The data were corrected for Lorentz and polarization effects and an empirical absorption correction was applied. In the case of **2**, data collection stopped automatically at 45.0° because the crystal had decayed, therefore a decay correction was applied.

The structure was solved by direct methods (13) and all calculations were performed using the TEXSAN (14) crystallographic software package of Molecular Structure Corp.[2] All of the non-hydrogen atoms were refined anisotropically for **1**, but for **2** only the thio carbon atom was treated anisotropically along with the other non-hydrogen atoms. The phenyl groups were treated as fixed rings with C—C distances set at 1.39 Å in **2** and an attempt was made to model the i-Pr group of one of the molecules in the asymmetric unit which was badly disordered. Hydrogen atoms, other than those of the disordered group, were included in their idealized position with C—H set at 0.95 Å and isotropic thermal parameters set at 1.2 times that of the carbon to which they were attached.

The unweighted and weighted agreement factors and standard deviation of an observation of unit weight[3] are given in Table 1. Plots of $\sum w(|F_o| - |F_c|)^2$ versus $|F_o|$, reflection order in data collection, $\sin\theta/\lambda$, and various classes of indices showed no unusual trends. Important distances and bond angles are given in Tables 2 and 3 and the molecular structures of the two compounds are displayed as ORTEP diagrams in Figs. 1–3. The final atomic coordinates and equivalent isotropic thermal parameters for the non-hydrogen atoms, anisotropic thermal parameters for non-hydrogen atoms, final fractional coordinates and thermal parameters for hydrogen atoms, and all bond distances and angles have been deposited.[4]

Calculation of Pauling partial bond orders

The formula proposed by Pauling (15) for calculating the bond orders of partial bonds is given by $d_n - d = -0.60 \log n$, where d_n is the bond length for bond number, n, and d is the length of the single bond of the same type. Based on the C—C single bond of 1.54 Å, Pauling's formula gives a bond length of 1.36 Å for $n = 2$; 1.72 Å for $n = 0.5$; and 1.90 Å for $n = 0.25$. These give percentage increases in bond length for the partial bonds of approximately 12 and 23% respectively for $n = 0.5$ and 0.25. It is reasonable to assume that similar relationships relating bond order to interatomic distances for the much longer secondary interactions or partial bonds involving Sn and S should utilize percentage differences "normalized" to 1.54 as follows rather than absolute differences. Pauling's relationship, which can be written as $n = 10^X$, where $X = (d - d_n)/0.6$, can be modified to allow

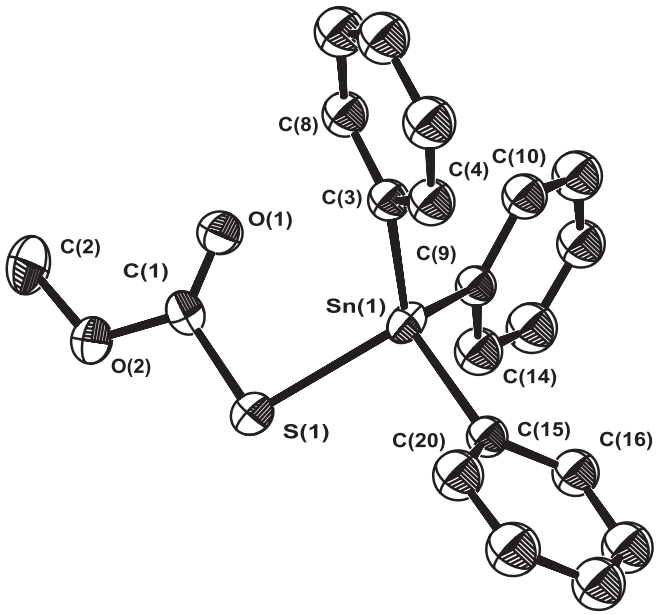
[2] Least-squares function minimized: $\sum w(|F_o| - |F_c|)^2$, where $w = 4F_o^2(F_o^2)$, $\sigma^2(F_o^2) = [S^2C + R^2B) + (pF_o^2)^2]/(Lp)^2$, S = scan rate, C = total integrated peak count, R = ratio of scan time to background counting time, Lp = Lorentz-polarization factor, and $p = p$ factor.

[3] Standard deviation of an observation of unit weight: $[\sum w(|F_o| - |F_c|)^2/N_o - N_v)^{1/2}$, where N_o = number of observations and N_v = number of variables.

[4] Supplementary material may be purchased from the Depository of Unpublished Data, Document Delivery, CISTI, National Research Council Canada, Ottawa, ON, Canada K1A 0S2 (http://www.nrc.ca/cisti/irm/unpub_e.shtml). Tables of atomic coordinates for the structure(s) reported in this paper have been deposited with the Cambridge Crystallographic Data Centre. Copies of the data can be obtained, free of charge, on application to the Director, CCDC, 12 Union Road, Cambridge CB2 1EZ, U.K. (Fax: 44-1223-336033 or e-mail: deposit@ccdc.cam.ac.uk). Structure factor amplitudes are no longer being deposited and may be obtained directly from the author.

© 2000 NRC Canada

Fig. 1. ORTEP plot of the molecule $Ph_3Sn[SCO_2Me]$ (**1**). The atoms are drawn with 30% probability ellipsoids. Hydrogen atoms omitted for clarity.



for percentage differences "normalized" to 1.54 to give $X = [1.54(d - d_n)/d]/0.6$ or $X = 2.57(d - d_n)/d$. Assuming the Sn—S single bond length approximates to the sum of the respective covalent radii (16), the corresponding values for Sn—S single and partial bonds for various values of n are 2.40 Å (n = 1.0), 2.50 (0.75), 2.68 (0.50), 2.95 (0.25), and 3.33 Å (n = 0.10). Similarly, relative to a Sn—O single bond length of 2.14 Å, the corresponding values for Sn—O partial bonds are 2.24 (0.75), 2.40 (0.50) 2.65 (0.25), and 2.97 Å (n = 0.10); relative to a Ge—O single bond length of 1.96 Å, the Ge—O partial bonds are 2.05 (0.75), 2.19 (0.50), 2.43 (0.25), and 2.72 Å (n = 0.10); and relative to a Ge—S single bond length of 2.26 Å, the corresponding values for Ge—S partial bonds are 2.37 (0.75), 2.53 (0.50), 2.79 (0.25), and 3.13 Å (n = 0.10). These calculated values appear to be compatible with the sum of the van der Waals radii of Sn, Ge, S, and O (17) and by way of comparison, the "valencies" for partial Sn—O bonds have been calculated as 2.43 (0.30) and 2.66 (0.20) (18).

Results and discussion

The preparation of *O*-alkyl monothiocarbonate derivatives of triphenyl-, diphenyl-, and trimethyl-tin(IV) compounds was attempted by the reaction of the sodium salt of the monothiocarbonic acid in dried CH_2Cl_2 as solvent with the appropriate organotin chloride using a standard Schlenk line in accord with the reactions

[1] $R_3SnCl + NaSCO_2R' \Rightarrow R_3Sn[SCO_2R'] + NaCl$

[2] $R_2SnCl_2 + 2NaSCO_2R' \Rightarrow R_2Sn[SCO_2R']_2 + 2NaCl$

[3] $R_2SnCl_2 + NaSCO_2R' \Rightarrow R_2SnCl[SCO_2R'] + NaCl$

where R = Me, Ph, R′ = Me, i-Pr.

Fig. 2. ORTEP plot of the two molecules of $Ph_3Sn[SCO_2(i\text{-}Pr)]$ (**2**) in the asymmetric unit. The atoms are drawn with 30% probability ellipsoids. Hydrogen atoms are omitted and only one set of the carbon atoms in partially occupied positions are shown for the disordered i-Pr group for clarity.

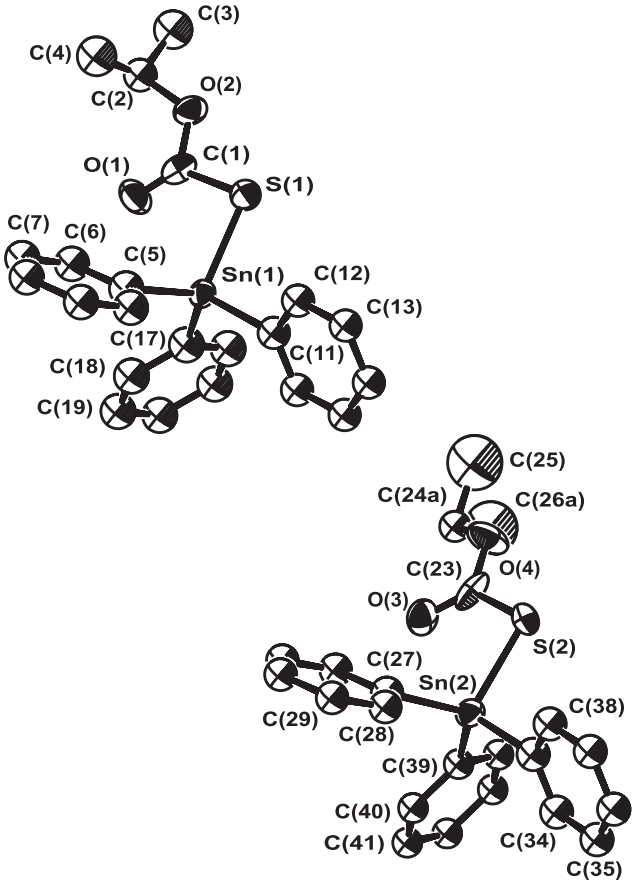
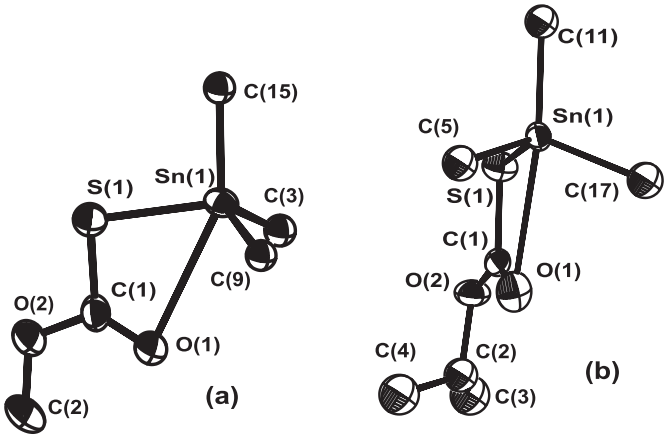


Fig. 3. ORTEP plots illustrating the core around tin including the Sn-O interaction for (*a*) the molecule $Ph_3Sn[SCO_2Me]$ (**1**) and (*b*) the molecule of $Ph_3Sn[SCO_2(i\text{-}Pr)]$ (**2**) that does not contain a disordered i-Pr group. The atoms are drawn with 30% probability ellipsoids. Hydrogen atoms and the carbon atoms of the phenyl rings other than those attached to tin omitted for clarity.



© 2000 NRC Canada

The compounds $Ph_3Sn[SCO_2Me]$ (**1**), $Ph_3Sn[SCO_2(i\text{-}Pr)]$ (**2**), $Ph_2Sn[SCO_2(i\text{-}Pr)]_2$ (**3**), $Ph_2SnCl[SCO_2(i\text{-}Pr)]$ (**4**), and $Me_3Sn[SCO_2Me]$ (**5**) were isolated but only **1** and **2** gave X-ray quality crystals. In reactions [1] and [2], the salts were used in considerable excess relative to the stoichiometric requirements to ensure complete reaction. By contrast, exact stoichiometric amounts were used in reaction [3] to favor the formation of the mixed chloro derivatives. When reactions [2] and [3] were attempted using $NaSCO_2Me$, only mixtures containing $Ph_2Sn[SCO_2Me]_2$ and $Ph_2SnCl[SCO_2Me]$ resulted in both cases. In general, all of the compounds are susceptible to moisture and air on exposure to the atmosphere, and all were readily dissolved in chloroform — which was therefore used as the preferred solvent for recording NMR spectra.

The ^1H NMR spectra of compounds **1**–**5** confirm that the products are over 98% pure relative to any hydrogen-containing impurities and integration ratios are as expected. The signals due to the phenyl groups in compounds **1** and **2** (two sets of peaks between 7.40 and 7.68 ppm) are very similar in appearance and position to those of the analogous germanium derivatives (two sets of peaks between 7.36 and 7.64 ppm) (4). The monothiocarbonate ligands give the expected first order spectra with chemical shifts comparable to those of the corresponding salts. As observed for the corresponding OCH_n-groups in the germanium analogues, the chemical shifts of hydrogen atoms on the carbon atom attached to oxygen are similar for a given monothiocarbonate regardless of the number of phenyl groups attached to tin (4.88 ppm for $Ph_3Sn[SCO_2CH(CH_3)_2]$ (**2**) and 4.86 ppm for $Ph_2Sn[SCO_2CH(CH_3)_2]_2$ (**3**). In $Ph_2SnCl[SCO_2CH(CH_3)_2]$ (**4**), the chemical shifts for the protons in both phenyl and ligand groups are slightly downfield compared to the bis compound, **3**, which is consistent with the electronegativity of Cl being slightly larger than that of the monothiocarbonate group. In $Me_3Sn[SCO_2Me]$ (**5**) the CH_3 chemical shift of the methyl group attached to tin is also very close to the value in $Me_3Ge[SCO_2Me]$ (0.57 ppm). The similarity of all of the spectra is indicative that the environments of the monothiocarbonate groups in solution are identical in all compounds. In the ^{13}C NMR spectra, the chemical shifts of monothiocarbonate groups are similar regardless of whether methyl or phenyl groups are attached to tin or the number of such groups, again as was observed in the analogous germanium derivatives. For the carbon atom in the SCO_2 groups, the chemical shifts range from 170.28 to 172.67 ppm for all compounds except for **4**; again reflecting the presence of the more electronegative Cl atom. The similar values of the ^{13}C NMR chemical shifts in the monothiocarbonate ligands is again consistent with the presence of similar monothiocarbonate linkages in solution.

The crystal structures of $Ph_3Sn[SCO_2Me]$ (1) and $Ph_3Sn[SCO_2(i\text{-}Pr)]$ (2)

Both $Ph_3Sn[SCO_2Me]$ (**1**) and $Ph_3Sn[SCO_2(i\text{-}Pr)]$ (**2**) crystallize in the space group $P\bar{1}$ (No. 2), but with two independent molecules in the asymmetric unit for **2**. The ORTEP diagrams in Figs. 1 and 2 illustrate that the immediate environments about tin in both $Ph_3Sn[SCO_2Me]$ (**1**) and $Ph_3Sn[SCO_2(i\text{-}Pr)]$ (**2**) are that of a distorted tetrahedron. As was found for the analogous germanium derivatives, $Ph_3Ge[SCO_2Me]$ and $Ph_3Ge[SCO_2(i\text{-}Pr)]$ (4), the three C-Sn-C angles range from 109.9(4) to 112.6(4)° in **1** and 106.7(9) to 114.3(7)° in **2** with averages of 111.3(14) and 111.3(29)°, respectively; while those of the S-Sn-C angles range from 97.5(3) to 112.3(3)° in **1** and 100.7(8) to 113.1(7)° in **2** with averages of 107(8) and 107(6)°, respectively. Alternatively, it is notable that one of the S-Sn-C angles is considerably smaller (97.5(3) in **1** and 100.5(3)° average in **2**) than the rest of the five angles around Sn (average 111.7(11) in **1** and 111.1(24)° in **2**); all five being close to or slightly larger than the all-tetrahedral angle. A similar phenomenon was noted for $Ph_3Sn[SCO_2N(CH_2)_4O]$, $Ph_3Sn[SOCNC_4H_4]$, $Ph_3Sn[S_2CO(i\text{-}Pr)]$, and $Ph_3Sn[S_2P(OEt)_2]$ where the smaller S-Sn-C angles were 95.7(1), 98.2(1), 100.0(1), and 100.09(1)°, respectively, (9, 8, 7, 12). The three Sn—C distances, ranging from 2.10(1) to 2.12(1) in **1** and 2.13(3) Å (average) in **2**, are among the shorter reported for the four triphenyltin derivatives mentioned above which range from 2.123(3) to 2.149(5) Å, and similar to that in the cyclic dithiophosphate derivative, $Ph_3Sn[S_2POCMe_2CMe_2O]$ (19) (2.106(8) to 2.134(9) Å).

The Sn—S bond lengths of 2.444(4) in **1** and 2.44(3) Å (average) in **2** are similar to those in $Ph_3Sn[SCO_2N(CH_2)_4O]$ (2.446(2) Å), $Ph_3Sn[S_2CO(i\text{-}Pr)]$ (2.445(1) Å), $Ph_3Sn[SOCNC_4H_4]$ (2.453(1) Å), $Ph_3Sn[S_2P(OEt)_2]$ (2.4582(9) Å), and $Ph_3Sn[S_2POCMe_2CMe_2O]$ (2.436(3) Å); all of which have been described as containing monodentate ligands. Bidentate ligands with essentially identical Sn—S bonds, for example $Ph_2Sn[S_2P(O(i\text{-}Pr)_2]_2$ (10) (2.689 (1) and 2.678 (1) Å), are appreciably longer than the 2.444 (4) Å found in **1**. These bidentate ligands have a partial Pauling bond order of ca. 0.50 compared to the Sn—S bonds in **1** and **2** with bond orders of ca. 0.91. However, examples of bidentate ligands with more variance in Sn—S bond lengths, also referred to as unsymmetrical or anisobidentate, are exemplified by $BuSn[S_2CN(Et)_2]_3$ (11), where Sn—S bonds range from 2.619(7) to 2.860(6) Å, and $Ph_2SnCl[S_2CO(i\text{-}Pr)]_2$ (20), where a range of 2.5 to 2.8 Å is quoted. These have bond orders ranging from ca. 0.78 to 0.32. In $Sn[S_2COEt]_4$ (21), two types of Sn—S distances are reported: those in bidentate ligands ranging from 2.562(2) to 2.627(2) Å) and those in monodentate ligands being 2.494 (2) Å. However, the second sulfur atoms in the latter cases are 2.916(10) Å from tin, giving an Sn—S distance that is only marginally longer than in species where the ligands are described as unsymmetrical bidentate ligands. Given that wave functions are continuous, it is reasonable to assume ever weakening partial bonds as the Sn—S distances increase. Our simplistic calculations based on Pauling's method (15) gave partial bond orders of 0.80 to 0.28 for Sn—S distances of 2.49–2.92 Å.

In the absence of a second sulfur atom, the terminal O atom in both **1** and **2** is oriented towards tin; the Sn—O distances of 3.040(8) and 3.05(1) Å (average) in **1** and **2**, respectively being significantly less than the sum of the van der Waals radii of 3.57 Å. In Fig. 3 and Table 4, the core about tin is shown with the inclusion of the Sn—O bond in the coordination sphere. Similarly, in $Ph_3Sn[S_2CO(i\text{-}Pr)]$ the O atom of the propoxy group, rather than the terminal S atom as is normally the case, is oriented toward tin, and it was proposed that the Sn—O distance of 2.950(3) Å was sufficiently shorter than the sum of the Van der Waals radii

© 2000 NRC Canada

Table 4. Interatomic distances (Å) and angles (°) around M involving the M–O interaction in $Ph_3Sn[SCO_2Me]$ (**1**)[a] $2Ph_3Sn[SCO_2(i\text{-}Pr)]$ (**2**)[b] $Ph_3Sn[SCON(CH_2)_4O]$,[c] and $Ph_3Ge[SCO_2Me]$[b,d].

	$Ph_3Sn[SCO_2Me]$ (**1**)	$2Ph_3Sn[SCO_2(i\text{-}Pr)]$ (**2**)	$Ph_3Sn[SCON(CH_2)_4O]$	$Ph_3Ge[SCO_2Me]$
Sn(1)—S(1)	2.444(4)	2.44(3)	2.446(2)	2.253(3)
Sn(1)—O(1)	3.040(8)	3.05(2)	2.809(2)	3.112(7)
Sn(1)—C(3)	2.10(1)	2.12(1)	2.127(5)	1.931(9)
Sn(1)—C(9)	2.12(1)	2.14(3)	2.127(5)	1.946(9)
Sn(1)—C(15)	2.12(1)	2.12(6)	2.149(5)	1.950(9)
O(1)-Sn(1)-C(15)	153.4(4)	157.1(6)	153.8(1)	155.5(3)
O(1)-Sn(1)-C(9)	86.0(3)	83.7(8)	86.6(1)	89.0(3)
O(1)-Sn(1)-C(3)	79.6(3)	79.5(21)	80.7(1)	75.4(3)
O(1)-Sn(1)-S(1)	56.2(2)	56.2(3)	59.8(9)	56.4(1)

[a]The atom numbering is that used for $Ph_3Sn[SCO_2Me]$.

[b]The average of the corresponding bonds and angles for the two molecules in the asymmetric unit.

[c]Ref. (9).

[d]Ref. (4).

to indicate a significant degree of interaction between the Sn and O atoms (7). Hence the environment around tin can be described as a distorted trigonal bipyramid. By contrast, in a study of organotin(IV)1-pyrrolecarbothioates (8) Sn—O distances ranging from 2.424(3) to 2.523(2) Å were considered bonding, while those from 2.65 to 3.242 Å were described as non-bonding (8), as was the distance of 2.809(4) Å in $Ph_3Sn[SCOCN(CH_2)_4O]$ (9). As discussed above for Sn—S partial bonds, it is reasonable to simply assume that the partial bonds get weaker as the Sn—O distance gets longer. Thus, Sn—O distances of 2.424(3) to 2.523(2) can be assigned partial bond orders of 0.46 to 0.35 and those from 2.65 to 3.242 bond orders from 0.24 to 0.05. This is essentially a spherical model therefore the bond orders are probably underestimated. The Sn—O distance in $Ph_3Sn[SCO_2Me]$ (**1**) of 3.040(8) Å corresponds to a bond order of 0.08 to complement the Sn—S bond length of 2.444(4) Å with a bond order of 0.91. The corresponding Ge—O distance in $Ph_3Ge[SCO_2Me]$ (3.112(7) Å) can be assigned a bond order of only 0.03, compared with a bond order for the Ge—S bond (2.253(3) Å) of 1.02, so on a relative scale the interaction with the terminal C=O bond is less significant for germanium. The comparative features presented in Table 4 for $Ph_3Sn[SCO_2Me]$ (**1**), $Ph_3Sn[SCO_2(i\text{-}Pr)]$ (**2**), $Ph_3Sn[SCON(CH_2)_4O]$, and $Ph_3Ge[SCO_2Me]$ show striking similarities. Quite clearly, each molecule has one O-Sn-C angle much closer to 180° (153.4(4) to 157.1(6)°) and the other two much closer to 90° (75.4 to 89.0°) as expected for distortion based on the trigonal bipyramid.

The terminal C=O bond length of 1.20(1) Å in **1** is similar to that in $Ph_2Te[SCO_2(i\text{-}Pr)]_2$ (1.203(9) Å), where the ligand was considered to be anisobidentate (4). The SC—O bond of 1.34(1) is significantly shorter than the SCO—C bond of 1.43(1) Å. The shortening of the SC—O bond relative to the SCO—C bond is also clear in **2**, despite the poorer refinement, and is consistent with the π-bond character being only of significance within the planar SCO_2 core. The angles in the planar core (e.g., O=C-O (126(1)°), O=C-O (125(1)° and O-C-S 109.2° for **1**) indicate that the C=O bond is clearly most strongly involved in the delocalized π-bonding, as was found for the organogermanium- and organotellurium-monothiocarbonates (3,4). The SnS—C distance of 1.76(1) Å for **1**, which is marginally shorter than the sum of the covalent radii of S and C is also essentially the same as in the Ge and Te analogues, close to the value found in $Ph_3Sn[S_2CO(i\text{-}Pr)]$ (1.748(5) Å), and longer than the typical value (ca. 1.70 Å) for a symmetrical bidentate dithiocarbonate.

Infrared and Raman spectra

In general, monothiocarbonates appear to be relatively poor scatterers and the quality of the Raman spectra is such that no attempt is made at extensive assignments. However, the assignment of distinctive characteristic features is possible by using the same factors described for the analogous germanium (4) and tellurium (3) derivatives, along with comparisons with other related dithioacid tin species (6, 21), and these are provided in linear form for each compound in the experimental section. There is a marked similarity between the spectra of $Ph_2Sn[SCO_2(i\text{-}Pr)]_2$ (**3**) and $Ph_2Te[SCO_2(i\text{-}Pr)]_2$ (3) which is consistent with the similar atomic masses of tin and tellurium and with the similar orientations of the monothiocarbonate groups despite the differences in overall structure. While it is reasonable to assume that there will be significant coupling between the four stretching vibrations of the SCO_2C unit, the positions of the three peaks that dominate the infrared spectra in the 1700–1000 cm^{-1} region suggest these arise primarily from the stretching of the three C—O bonds. Thus, for example, in $Ph_2Sn[SCO_2(i\text{-}Pr)]_2$ (**3**) the three very strong broad peaks are seen at 1642 (mainly C=O stretching), 1176 (mainly C—O stretching), and 1091 cm^{-1} (mainly O—$CH(CH_3)_2$ stretching); compared with 1653, 1149, and 1088 cm^{-1} in $Ph_2Te[SCO_2(i\text{-}Pr)]_2$ and 1698, 1159, and 1087 cm^{-1} in $Ph_2Ge[SCO_2(i\text{-}Pr)]_2$. The strong band corresponding to that at 1640 cm^{-1} is observed at lower wave-number, between 1550 and 1614 cm^{-1}, in $NaSCO_2R$ salts (4), which is consistent with the presence of a strong terminal C=O bond in the monothiocarbonate derivatives. Any association with the metal is apparently similar for tin and titanium and least significant for germanium, as shown by the bond orders calculated for the structures of $Ph_3Sn[SCO_2Me]$ (**1**) in which the band is seen at 1669 cm^{-1} and that of $Ph_3Ge[SCO_2Me]$ in which it is at 1695 cm^{-1}. The fourth stretching vibration associated with the SCO_2C core, which is presumably primarily ν(SnS-C), is seen between 655 and 662 cm^{-1} as a weaker feature in the infrared and

© 2000 NRC Canada

fairly strong feature in the Raman effect. This is within the expected region for a C—S single bond stretch and is at lower wave number than in the salts where the C—S bond would have more partial π-bond character. Two distinctive peaks seen in **1**–**4** within the ranges 813–848 and 412–418 cm^{-1} can be assigned to the out-of-plane mode, $\pi(SCO_2)$, and to one of the in-plane bends, $\delta(SCO_2)$, which were similarly assigned in the tellurium derivatives to ca. 848 and 416 cm^{-1}. The assignment of $\pi(CO_3)$ in a variety of carbonate salts is in the region of 830–873 cm^{-1} suggesting that the π-electron delocalization is similar in all of these planar groups. In **5**, the feature attributable to $\pi(SCO_2)$ is obscured by the very intense and typical peaks assignable to the CH_3 rocking modes of the methyl groups attached to tin.

In the phenyltin derivatives (**1**–**4**) the characteristic and very distinctive *f*-phenyl and *v*-phenyl modes, which are both of similar intensity, are observed at ca. 736 and 695 cm^{-1}, along with *y*-phenyl at ca. 447 cm^{-1}; all three features being essentially the same in the tellurium and germanium analogues (3, 4). In $Me_3Sn[SCO_2Me]$ (**5**) two peaks are seen at 532 and 506 cm^{-1}, which are not seen in the spectra of the phenyltin derivatives. These clearly correspond to the asymmetric and symmetric Sn—C stretching vibrations at almost identical positions to those in Me_3SnSMe (531 and 509 cm^{-1}) (22) suggesting very similar environments about Sn in **5** and the simple sulfide. In the latter, ν(Sn-S) is seen at 341 cm^{-1} but generally for dithioacid derivatives it is assigned at higher wave-number as exemplified by the range 356–394 cm^{-1} for a variety of tin dithiocarbamate derivatives (23). In organotin chlorides, the Sn—Cl stretching vibrations have been typically assigned to the 344–360 cm^{-1} region as they were in a detailed examination of low frequency vibrational spectra of group 14 phenyl compounds including Ph_3SnCl and Ph_2SnCl_2 (24). By contrast, in mixed halide ligand derivatives such as $Me_2SnCl[S_2CNMe_2]$, ν(SnCl) is assigned at a much lower wave-number, 268 cm^{-1}. This was the basis of our assignment of the low frequency modes in **4**.

Concluding comments

The isolation of organotin monothiocarbonates proved to be more difficult than for the corresponding organogermanium derivatives. The X-ray structures of $Ph_3Sn[SCO_2Me]$ (**1**) and $Ph_3Sn[SCO_2(i\text{-}Pr)]$ (**2**) demonstrate a preference for the orientation of the terminal C=O oxygen atom towards tin, at least in the solid state. The resulting weak intermolecular interaction indicates an anisobidentate link that is relatively more significant than in the corresponding germanium derivative. Thus the distortions from "all-tetrahedral" angles around tin are consistent with the formation of a weak Sn—O link that gives a distorted trigonal bipyramidal arrangement around tin. In dithio derivatives, there is often a tendency for Ph_3SnL species with symmetrical bidentate ligands to disproportionate to the bis species, Ph_2SnL_2 on recrystallization giving rise to a trans octahedral structure. This clearly is not the case for $Ph_3Sn[SCO_2Me]$ and $Ph_3Sn[SCO_2(i\text{-}Pr)]$ and indeed we were not able to isolate X-ray quality crystals for $Ph_2Sn[SCO_2Me]_2$ or $Ph_2Sn[SCO_2(i\text{-}Pr)]_2$; consistent with the ligands being essentially monodentate in solution as is indicated by the NMR spectra.

Acknowledgement

We wish to thank the Natural Sciences and Engineering Research Council of Canada for financial support.

References

1. K.K. Pandey and H.L. Wingan. Rev. Inorg. Chem. **6**, 71 (1984); S. Datta and H.L. Agarwala. Indian J. Chem. Sect. A: Inorg. Bio-inorg. Phys. Theor. Anal. **20A**, 1190 (1981); T.V. Ashworth, M. Nolte, and E. Singleton. J. Organomet. Chem. **121**, C57 (1976); T.R. Gaffney and J.A. Ibers. Inorg. Chem. **21**, 2860 (1982); N. Sonoda and T. Tanaja. Inorg. Chim. Acta, **12**, 261 (1975).
2. E.E. Reid. Organic chemistry of bivalent sulfur. Vol. IV. Chemical Publishing, N.Y. 1962, and references therein.
3. J.E. Drake, R.J. Drake, A.G. Mislankar, R. Ratnani, and J. Yang. Can. J. Chem. **74**, 1968 (1996).
4. J.E. Drake and J. Yang. Can. J. Chem. **76**, 319 (1998).
5. E.M. Holt, F.A.K. Nasser, A.Wilson, Jr., and J.J. Zuckerman. Organometallics, 4 2073 (1985).
6. S.W. Cowan, R.W. Gable, B.F. Hoskins, and G. Winter. Inorg. Chim. Acta, **77**, L225 (1983); R.W. Gable, C.L. Raston, G.L. Rowbottom, A.H. White, and G. Winter. J. Chem. Soc. Dalton Trans. 203, (1981); D. Dakterniks, B.F. Hoskins, E.R.T. Tiekink, and G. Winter. Inorg. Chim. Acta, **85**, 215 (1984).
7. E.R.T. Tiekink and G. Winter. J. Organomet. Chem. **314**, 85 (1986).
8. D.K. Srivastave, V.D. Gupta, H. Noth, and W. Rattay. J. Chem. Soc. Dalton Trans. 1533, (1988).
9. S. Chandra, B.D. James, R.J. Magee, W.C. Patalinghug, B.W. Skelton, and A.H. White. J. Organomet. Chem. **346**, 7 (1988).
10. K.C. Molloy, M.B. Hossain, D. Van der Helm, J.J. Zuckerman, and I. Haiduc. Inorg. Chem. **9**, 2041 (1980).
11. J.S. Morris and E.O. Schlemper. J. Cryst. Mol. Struct. **9**, 1 (1979).
12. K.C. Molloy, M.B. Hossain, D. Van der Helm, J.J. Zuckerman, and I. Haiduc. Inorg. Chem. **9**, 3507 (1979).
13. G.M. Sheldrick. Acta Crystallogr. Sect. A: Cryst. Phys. Diffr. Theor. Gen. Crystallogr. **A46**, 467 (1990).
14. TEXSAN-TEXRAY structure analysis package. Molecular Structure Corp., Woodlands, Tex. 1985 and 1992.
15. L. Pauling. J. Am. Chem. Soc. **69**, 542 (1947); The nature of the chemical bond. 3rd ed. Cornell University Press, Ithaca, New York. 1960.
16. A.F. Wells. Structural inorganic chemistry. 4th ed. Clarendon Press, Oxford. 1975.
17. A. Bondi. J. Phys. Chem. **68**, 441 (1964); L. Pauling. The nature of the chemical bond. 3rd ed. Cornell University Press, Ithaca, New York. 1960.
18. I.D. Brown. J. Solid State Chem. **11**, 214 (1974).
19. H. Preut, V.D. Ngo, and F. Huber. Acta Crystallogr. Sect. C: Cryst. Struct. Commun. **C43**, 164 (1987).
20. D. Dakterniks, B.F. Hoskins, P.A. Jackson, E.R.T. Tiekink, and G. Winter. Inorg. Chim. Acta, **101**, 203 (1985).
21. C.L. Raston, P.R. Tennant, A.H. White, and G. Winter. Aust. J. Chem. **31**, 1493 (1978).
22. D.F. van de Vondel, E.V. van den Berghe, and G.P. van de Kelen. J. Organomet. Chem. **23**, 105 (1970).
23. M. Honda, M. Komura, Y. Kawasaki, T. Tanaka, and R. Okawara. J. Inorg. Nucl. Chem. **30**, 3231 (1968).
24. A. Smith. Spectrochim. Acta Part A, **24A**, 695 (1968).

© 2000 NRC Canada

A study of micellization and the thermodynamic properties of a series of aqueous sodium cyclohexyl alkanoate surfactants

Judith A. MacInnis, D. Gerrard Marangoni, and R. Palepu

Abstract: The micellization and the thermodynamic properties of a series of sodium cyclohexyl alkanoates of the general formula $C_6H_{11}(CH_2)_nCOONa$ (where n = 1, 2, 3, 4) were investigated employing conductivity, density, surface tension, viscosity, speed of sound, luminescence probing experiments, and Fourier transform infrared (FT-IR) spectroscopy. The critical micelle concentrations (cmcs) and the aggregation numbers indicate that these surfactants have high cmc values and low aggregation numbers when compared to other single-headed surfactants (most notably the sodium alkanoates). Thermodynamic properties, obtained from the mass action model, indicate that micellization is spontaneous and entropically driven. The saturation area per molecule, the free energies of adsorption, and the efficiency and effectiveness of adsorption were determined through surface tension measurements. The presence of the cylcohexyl ring appears to influence the surface properties of micellization. Both the effectiveness and the efficiency of these surfactants, in lowering the surface tension of water, are lower than that of the straight chain alkanoates.

Key words: thermodynamics, micellization, aggregation numbers, speed of sound, and spectroscopy.

Résumé : Faisant appel à la conductivité, la densité, la tension superficielle, la viscosité, la vitesse du son, des expériences de luminescence ainsi que la spectroscopie infrarouge par transformation de Fourier (« FT-IR »), on a étudié la micellisation et les propriétés thermodynamiques d'une série de cyclohexylalcanoates de sodium de formule générale $C_6H_{11}(CH_2)_nCOONa$ (où n = 1, 2, 3, 4). Par comparaison avec les valeurs correspondantes pour d'autres agents de surface à une seule tête (plus particulièrement les alcanoates de sodium), les concentrations micellaires critiques (cmc) sont élevées alors que les nombres d'agrégation sont faibles. Les propriétés thermodynamiques, obtenues à partir du modèle d'action de masse, indiquent que la micellisation est spontanée et sous l'influence de l'entropie. On a déterminé la superficie de saturation, les énergies libres d'adsorption et l'efficacité de l'adsorption à l'aide de mesures de la tension superficielle. La présence de noyaux cyclohexyles semble influencer les propriétés de surface de micellisation. L'efficacité de ces agents de surface à diminuer la tension superficielle dans l'eau est inférieure à celle des alcanoates en chaîne droite.

Mots clés : thermodynamique, micellisation, nombres d'agrégation, vitesse du son, spectroscopie.

1. Introduction

The study of micellization of aqueous solutions of surfactants in the literature is well established (1–18). The dependence of interfacial activity and micellization on the structure of the hydrophobic part of the surfactant is an area of research that has been receiving increased attention in recent years. The bulk properties of *n*-alkanoate surfactants with linear alkyl chains have been extensively reported in the literature (19–24), however, very little attention has been given to the alkanoate surfactants that contain a cyclohexyl ring. The sodium cyclohexyl alkanoate surfactants have structures similar to those of the petroleum acids. The latter contain mainly short alkyl chains that are attached to various saturated, partially saturated, and aromatic structures. These compounds play an important role in the reduction of interfacial tension during alkaline water flooding of oil reservoirs (10).

Employing techniques such as density, viscosity, conductivity, surface tension, speed of sound, FT-IR spectroscopy, and fluorescence spectroscopy, this paper investigates the bulk thermodynamic and micellar properties of a family of alkanoate surfactants, which contain a cyclohexyl ring in place of a long hydrocarbon chain to address the effects of the cyclohexyl ring and of increasing alkyl chain length on these properties.

Received April 4, 2000. Published on the NRC Research Press website on September 1, 2000.

J.A. MacInnis, D.G. Marangoni, and R. Palepu.[1]
Department of Chemistry, St. Francis Xavier University, P.O. Box 5000, Antigonish, NS B2G 2W5, Canada.

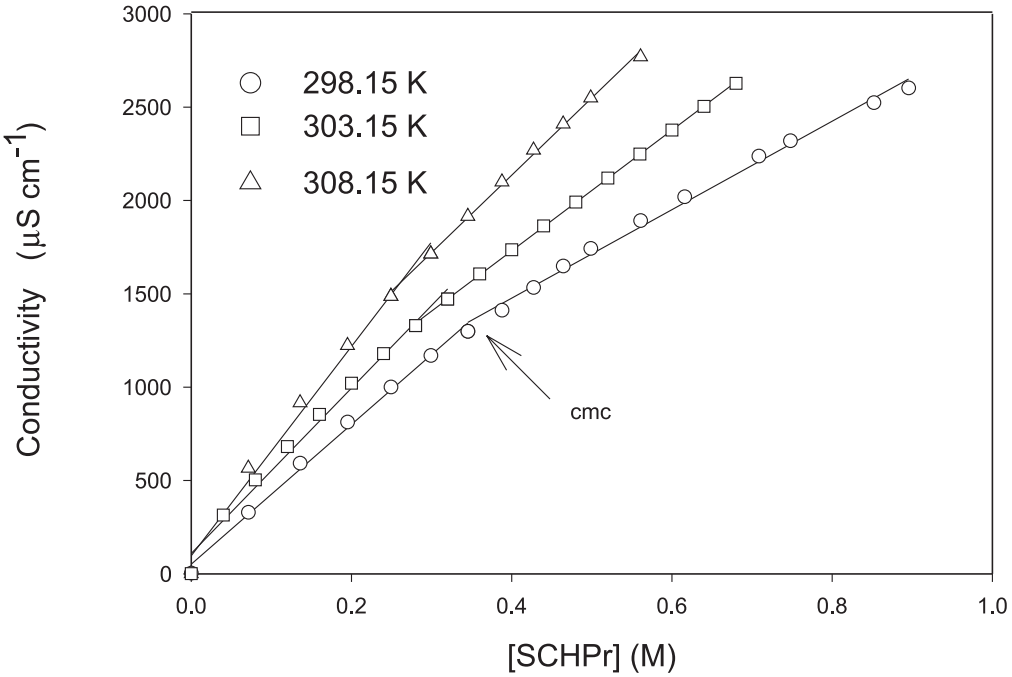
[1]Author to whom correspondence may be addressed. Telephone: (902) 867-3886. Fax: (902) 867-2414. e-mail: rpalepu@stfx.ca

2. Experimental

The cyclohexyl acids were purchased from Aldrich (99% pure). They were dissolved in deionized water, equivalent to triply glass-distilled, and were then converted to the corresponding sodium salts. All of the dried salts were soxhlet extracted with diethyl ether for 2–5 days, dried and stored

 © 2000 NRC Canada

Fig. 1. Conductivity of sodium cyclohexyl propanoate at 298.15, 303.15, and 308.15 K.



under vacuum. Pyrene was also purchased from Aldrich (99%) was purified, by sublimation and recrystallization (twice) from ethanol.

Surface tension measurements were performed on a Fisher surface tensiometer Model 21, equipped with a 13 mm-diameter DuNuoy ring. The solutions were carefully transferred into a double-walled vessel, which was maintained at the appropriate temperature (±0.02°C) with a Haake 4000 temperature bath. The surface tension measurements were carried out at 298.15, 308.15, and 318.15 K. Adsorption processes at the air–water interface were generally completed in 10 min. The repetition rate of individual readings was about 15 min.

The absolute surface tension values (γ) were obtained from the apparent values following the procedure as described in the manual supplied with the instrument. The surface tension of pure water was measured periodically as a calibration. The surface tension measurements of sodium cyclohexyl pentanoate aqueous solutions were performed in a slightly basic solution (pH = 10) to minimize hydrolysis.

The conductivity measurements were made in a thermostated–jacketed beaker with a dip cell having a cell constant of 1.11 cm^{-1}, and an automatic CDM83 conductivity bridge (Radiometer) operating at 1000 Hz. Specific conductivity values, of each set, containing 20–25 different concentrations of surfactant, were measured at different temperatures.

The density measurements at various temperatures were obtained using an Anton–Parr digital densimeter DMA 45 operating in the static mode.

Viscosities of the sodium cyclohexyl salts in water at various concentrations were determined using modified Ostwald viscometers and a viscosity bath (Koehler Instrument), to control temperature.

Speed of sound was measured using a Nusonics (model 6080) concentration analyzer employing the sing around technique. Rapid and accurate measurements of sound velocity as a function of surfactant concentration were made by successive additions of known weights of the surfactant to the water contained in the thermostatted beaker. Speeds of sound measurements are accurate to ±0.10 m s^{-1}.

The FT-IR spectra were obtained using a Biorad FT-IR spectrophotometer (1000 scans at 4 cm^{-1} resolution, triangular apodization) using an ATR cell manufactured by Spectra-Tech Inc. (Stamford, CT: Circle® cell). The reference element of the cell is 45° angle-of-incidence zinc selenide. The reference spectra of pure water and the background spectra of air were obtained at the start of each run. Five hundred to 1000 scans were carried out on each set of solutions. The spectra were obtained by subtracting the water spectra that was run under the same experimental conditions.

For the fluorescence measurements the pyrene probe was held at a constant concentration of 2.5×10^{-5} M. The monolayer method was used to prepare the solutions for fluorescence measurements. Steady state pyrene fluorescence spectra were recorded on a Perkin–Elmer MPF-66 spectrophotometer, using an excitation wavelength of 338 nm and the emission spectra was recorded from 350 to 500 nm. The intensities of the first and third vibronic peaks were recorded and employed to calculate the I_1/I_3 ratio. This ratio gives an indication of the micropolarity sensed by the probe in the micellar solutions. Fluorescence measurements were also used to determine the critical micelle concentration (CMC). The pyrene concentration was again kept constant at 2.0×10^{-5} M. At least 12 solutions were prepared, up to a final concentration of twice the CMC.

3. Results

3.1 Conductivity

Plots of specific conductance (κ) against the concentration of surfactant indicate a break at the CMC, which is temperature dependent for each of the surfactants under study (Fig. 1).

© 2000 NRC Canada

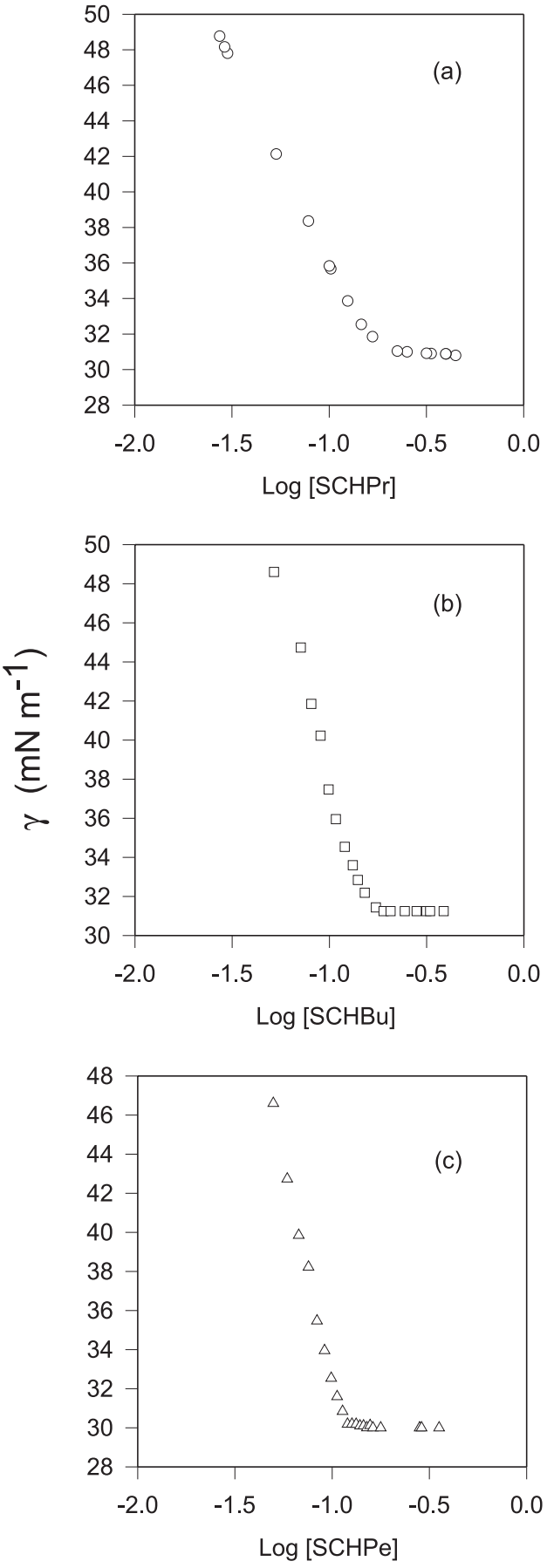


Fig. 2. Surface tension of the sodium cyclohexyl alkanoates at 298.15 K. (*a*) SCHPr. (*b*) SCHBu. c) SCHPe.

Table 1. Comparison of CMC (M) values and degree of ionization for sodium cyclohexyl alkanoates at 298.15 K.

Method	SCHAc	SCHPr	SCHBu	SCHPe
Conductivity	—	0.38	0.16	0.09
Viscosity	0.90	0.45	0.22	0.09
Surface tension	0.93	0.29	0.17	0.12
Ultrasonic velocity	0.87	0.39	0.22	0.12
Fluorescence	—	0.40	0.17	0.10
FT-IR	0.98	0.39	N/A	N/A
α values	0.55[a]	0.59[b]	0.76[b]	0.73[b]

[a]From NMR data ref. (25).

[b]From conductivity data.

The apparent degree of micelle ionization (α) was taken as the ratio of the slopes of the lines above and below the CMC in the plots of conductance (κ) vs. concentration and are presented in Table 1.

3.2 Surface tension

Representative surface tension plots of the cyclohexyl salts, at various temperatures, (298.15, 308.15, and 318.15 K) are given in Figs. 2(*a*), 2(*b*), and 2(*c*). The maximum surface excess concentration, Γ_{max}, the minimum area per surfactant molecule, A_{min} (m^2) at the surfactant–solvent interface, and the values of surface pressure at the CMC, Π_{CMC}, were obtained employing the surface tension data and the following equations (3, 9, 14):

$$[1] \qquad \Gamma_{max} = -\frac{1}{vRT}\left[\frac{\delta\gamma}{\delta \ln C_{T,P}}\right]$$

$$[2] \qquad A_{min} = 1/N_a\Gamma_{max}$$

and

$$[3] \qquad \Pi_{CMC} = \gamma_o - \gamma_{CMC}$$

where v is the number of ions per surfactant molecule, R is the universal gas constant, T is the temperature in K, N_a is Avagadro's number, γ is the surface tension of the solution, and γ_o is the surface tension of the pure solvent. The values of A_{min} are shown in Table 2. The equilibrium surface tension concentration isotherms of the carboxylate salts were analyzed employing the simplified form of the Temkin (14) isotherm (eq. [4]):

$$[4] \qquad \ln X = -\ln B + \Pi^{1/2}\frac{g}{RT}$$

where X is the mol fraction of the compound in the bulk solution, Π is the surface pressure (mN m^{-1}), which is defined as $\Pi = \gamma_{water} - \gamma_{solution}$, B denotes the equilibrium constant of the adsorption process, g is a constant characteristic of each surfactant system. The constant B is related to the extrapolated standard free energy of adsorption:

$$[5] \qquad B = \exp(-\Delta G^{\circ}_{\Pi\rightarrow 0}/RT)$$

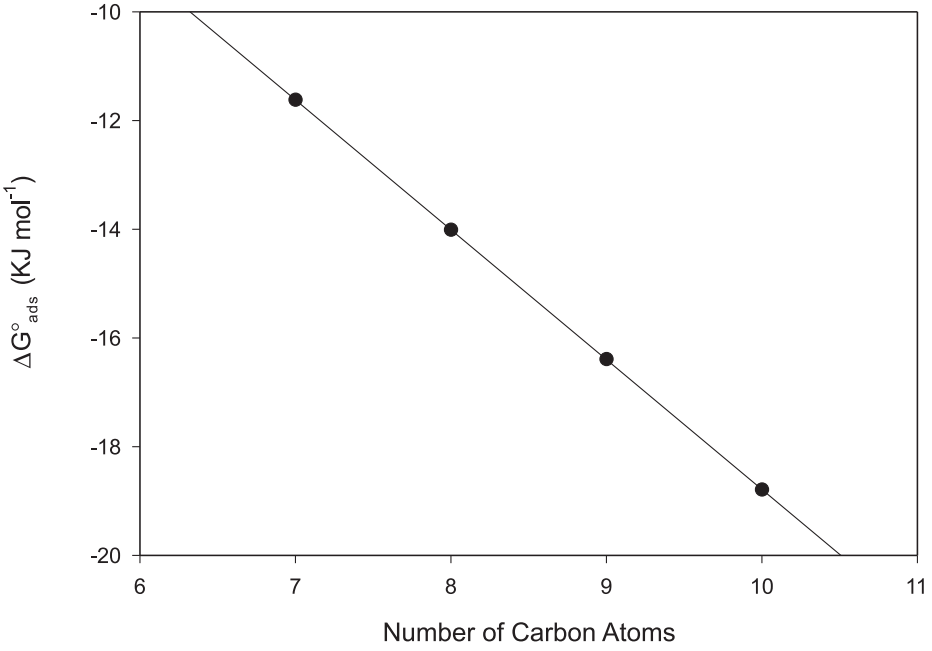
© 2000 NRC Canada

Table 2. Surface properties of the sodium cyclohexyl alkanoates.

	Temp (K)	g × 10^5 ($N^{1/2}$ $m^{3/2}$ mol^{-1})	Ln B	$\Delta G^\circ_{(ad)}$ (KJ mol^{-1})[a]	A_{min} (×10^{-19} m^2)	pC_{20}
SCHPr	298	28.4	13.2	–14.0	2.06	1.50
	308	25.8	12.3	–14.5	1.75	—
	318	11.8	9.6	–14.1	0.58	—
SCHBu	298	26.0	12.9	–16.4	3.50	1.80
	308	5.9	11.1	–16.0	1.42	—
	318	6.3	10.2	–16.3	1.25	—
SCHPe	298	2.42	8.0	–18.8	0.23	1.25
	308	9.96	8.7	–15.8	0.36	—
	318	1.22	9.1	–16.1	0.05	—

[a] $\Delta G^\circ_{(ad)}$ ± 0.8 kJ mol^{-1}.

Fig. 3. Standard free energies of adsorption at 298.15 K as a function of chain length.



From the plots of $\Pi^{1/2}$ vs. ln X, the values of constants B and g were calculated employing the least-squares regression analysis. The values of g and B are also presented in Table 2.

For the sodium carboxylates, v = 2, which accounts for the complete ionization of these salts. At these relatively high concentrations, it is reasonable to assume that the pH is relatively constant and the hydrolysis of the carboxylate ion can be neglected. The values of the standard free energies of adsorption, ΔG°_{ads}, obtained from eq. [5] are presented in Fig. 3, as a function of the number of carbon atoms (excluding the headgroup carbon).

The efficiency of the surface tension reduction, at 298.15 K, was calculated by:

$$[6] \qquad pC_{20} = -\log C_{20}$$

where C_{20} is the surfactant concentration when the surface tension of water is reduced (10) by 20 mN m^{-1} and the values are presented in Table 2.

3.3 Viscosity

The values of the aggregation numbers for the cyclohexyl salts were estimated through the shear solution viscosity assuming the micelles to be spherical and the electroviscous effect to be negligible. The volume fraction of spherical particles (ϕ) was calculated employing the Guth–Simha equation (17):

$$[7] \qquad \eta = \eta_o(1 + 5\phi/2 + 109\phi^2/14)$$

where η and η_o are the shear viscosity of the solution and at the critical micelle concentration, respectively. The volume fraction (ϕ) is related to the aggregation number (N_{agg}) by:

$$[8] \qquad \phi = \frac{4\pi \ell^3 N_a(C_{surf} - CMC)}{3N_{agg}}$$

where ℓ is the length of the hydrated micelle, N_a is Avagadro's number, and C_{surf} is the total surfactant concentration. In this study the value of ℓ was approximated using the dry length of the surfactant from the computer-modeling program "HyperChem" (version 5 AM1 approximation). From this estimate of ℓ, the values of the aggregation

© 2000 NRC Canada

Table 3. Micellar parameters for the sodium cyclohexyl alkanoates.

Surfactant	η_o (cP)	N_{agg} [a]	n_h [b]	n_h [c]	I_1/I_3 [d] (±0.05)	$\phi_{V,1}$ ($cm^3\ mol^{-1}$)	$\phi_{V,2}$ ($cm^3\ mol^{-1}$)	ΔV_{mic} ($cm^3\ mol^{-1}$)	$k_{S,1}$ (10^{-5} bar^{-1})	$k_{S,2}$ (10^{-5} bar^{-1})	Δk_s (10^{-5} bar^{-1})
SCHAc	1.45	5 ± 3 (4 ± 2)[e]	9	12	0.99	130.2	125.0	–5.2	3.54	4.18	0.64
SCHPr	1.26	7 ± 3 (7 ± 2)[e]	12	14	0.96	145.1	130.2	–14.9	–1.39	5.54	6.93
SCHBu	1.06	12 ± 3 (10 ± 2)[e]	14	16	0.95	153.4	133.2	–20.2	–2.38	6.64	9.02
SCHPe	1.01	13 ± 3 (14 ± 2)[e]	16	20	0.94	174.1	145.3	–29.8	–2.67	8.31	10.98

[a]Viscosity.
[b]At cmc.
[c]At infinite dilution.
[d]Water I_1/I_3 = 1.81.
[e]NMR ref. (25).

number were obtained from the slope of the linear plots of ϕ vs. C_{surf} – CMC. The values of N_{agg} and η_o are given in Table 3.

3.4 Apparent molar volumes

Apparent molar volumes, ϕ_v, were calculated from the experimental density data employing the following equation:

$$[9] \qquad \phi_v = \frac{M}{d} - \frac{10^3(\rho - \rho_0)}{m\rho\rho_0}$$

where M is the molecular weight of the surfactant, ρ and ρ_o are the densities of the solution and the solvent, and m is the molality. When ϕ_v is plotted against $C^{1/2,}$ the gradient approaches zero at higher surfactant concentration and this limiting value is subjectively chosen as the apparent molar volume of the micelle (ϕ_v^{mic}) (3, 21).

An alternate method (22) is to fit the data, in the concentration region $m \leq$ CMC, to the following function:

$$[10] \qquad \frac{\phi_v}{\phi_v^{mic}} = \frac{m}{(a + m)}$$

where a is an empirical constant. Rearrangement of eq. [10] in the following form:

$$[11] \qquad \phi_v = -a\left(\frac{\phi_v}{m}\right) + \phi_v^{mic}$$

allows ϕ_v^{mic} to be extrapolated from the plots of ϕ_v, vs. ϕ_v/m.

The values of the apparent molar volumes at infinite dilution, ϕ_v^o, were determined numerically using the following equation:

$$[12] \qquad \phi_v = \phi_v^o + A_v C^{1/2} + B_v C$$

where A_v is the Debye–Huckel limiting law coefficient (1.865 $cm^3\ kg^{1/2}\ mol^{-3/2}$ for a 1:1 electrolyte at 298.15 K), B_v is an adjustable parameter, which measures the deviations from the limiting law, and ϕ_v^o is the apparent molar volume at infinite dilution.

The values of volume change, $\Delta V_m = \phi_v^{mic} - \phi_v^o$, associated with the formation of micelles in the sodium cyclohexyl surfactant solutions are shown in Table 3.

3.5 Speed of sound

The plots of speed of sound against concentration show two linear segments with the intersection occurring at the CMC (Fig. 4(*a*)). Density and speed of sound measurements were combined to calculate the adiabatic compressibility for the sodium cyclohexyl alkanoates using the Laplace equation (Fig. 4(*b*)):

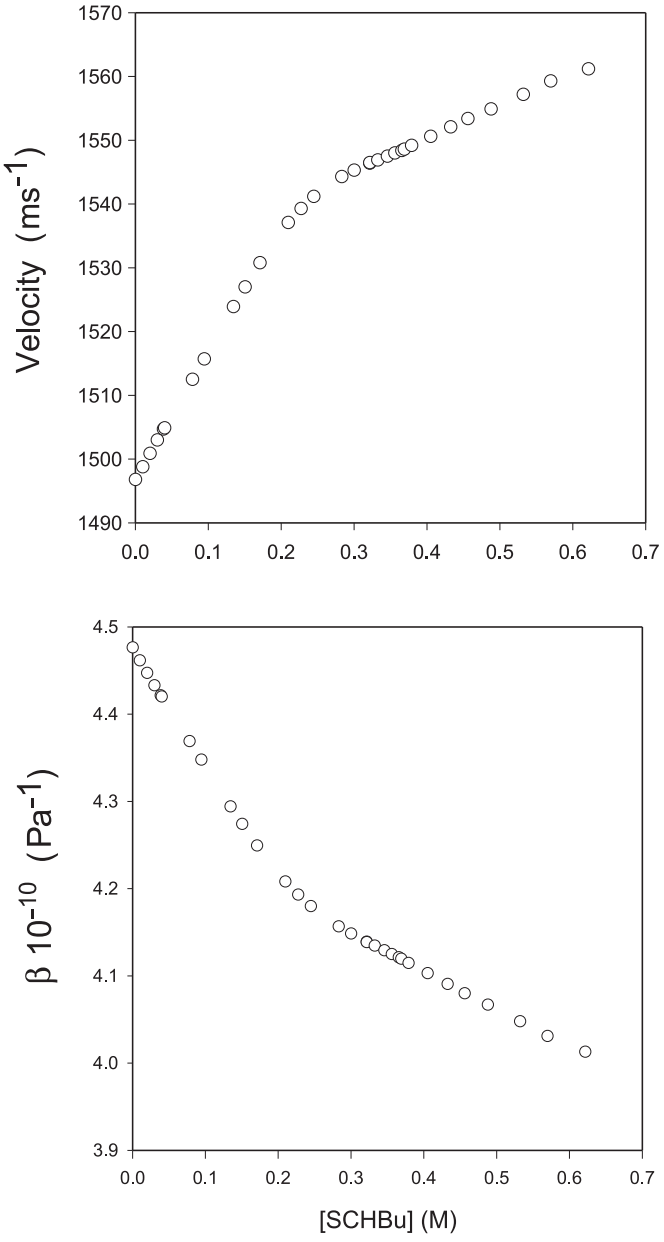
$$[13] \qquad k_s = \frac{1}{\rho u^2}$$

The linear regions may be assigned to the monomeric and micellar forms of the surfactant. The values for the apparent adiabatic compressibilities of the monomeric and micellar forms (11–12) may be calculated from the gradients of the relevant portions of the plots of k_s vs. surfactant concentration using the following equation:

$$[14] \qquad k_s = k_{s,0} + (\tilde{k}_{s,1} - k_{s,0})\tilde{v}_1 c_1 + (\tilde{k}_{s,2} - k_{s,0})\tilde{v}_2 c_2$$

© 2000 NRC Canada

Fig. 4. (*a*) Ultrasonic velocity of sodium cyclohexylbutanoate 298.15 K. (*b*) Adiabatic compressibility of sodium cyclohexylacetate 298.15 K.



where $k_{s,0}$ is the adiabatic compressibility of the solvent, $\tilde{v}_1$ and $\tilde{v}_2$ are the apparent specific volumes of the monomer and the micelle, c_1 and c_2 are the monomer and the micelle concentrations (in g cm^{-3}). The apparent adiabatic compressibilities of the monomer ($\tilde{k}_{s,1}$) and micellar species ($\tilde{k}_{s,2}$) are defined as:

$$[15] \quad \tilde{k}_{s,1} = -\frac{1}{\tilde{v}_1}\left(\frac{\partial \tilde{v}_1}{\partial p}\right)_s$$

and

$$[16] \quad \tilde{k}_{s,2} = -\frac{1}{\tilde{v}_2}\left(\frac{\partial \tilde{v}_2}{\partial p}\right)_s$$

The values of the apparent specific volumes of the monomer, $\tilde{v}_1$ and micelles, $\tilde{v}_2$ required for the calculation of the adiabatic compressibilities were determined from the gradients of linear portions of plots of density against concentration below and above the CMC using eq. [17]:

$$[17] \quad \rho = \rho_0 + (1 - \tilde{v}_1 \rho_0)c_1 + (1 - \tilde{v}_2 \rho_0)c_2$$

The values of $\tilde{k}_{s,1}$, $\tilde{k}_{s,2}$, and $\Delta\kappa_s = \tilde{k}_{s,2} - \tilde{k}_{s,1}$, the change upon micelle formation, are presented in Table 3.

3.6 Fluorescence

The CMC of the sodium cyclohexyl alkanoates was determined using the pyrene I_1/I_3 micropolarity method (24). This procedure relies on the sensitivity of the pyrene vibrational structure to respond to the changes in the surrounding microenvironment. Below the CMC the pyrene fluorescence spectrum corresponds to a polar environment and in the presence of micelles, the probe is assumed to be solubilized in the palisade region and the polarity is drastically decreased, resulting in a lowering of the I_1/I_3 value. The pyrene I_1/I_3 ratios were monitored as a function of surfactant concentration in water and are presented in Table 3.

The CMC values were obtained from the break point as indicated in Fig. 5, and are listed in Table 1. These CMC values are in good agreement with those obtained from other methods.

3.7 FT-IR

The infrared spectra of the sodium cyclohexyl alkanoate surfactants contain various vibrational modes associated with the acyl chain and the carboxylate group. The strongest bands that were used in this study were the antisymmetric CH_2 stretching mode and the antisymmetric and symmetric carboxylate stretching modes. These values are assigned in Table 4. Plots of frequency vs. concentration of the antisymmetrical CH_2, the antisymmetrical COO^- and the symmetrical stretching mode of COO^- for sodium cyclohexyl acetate are shown in Fig. 6. By examining these plots one can see the inflection points at ~1.0 M surfactant concentration. This indicates that the critical micelle concentration occurs at ~1.0 M. Plots of bandwidths at half-height (Fig. 7) also indicate a break point at the CMC.

3.8 Thermodynamics of micellization

The thermodynamic properties of micellization were derived by application of the mass action model as follows. The equilibrium constant, K_m, for the formation of micelles may be written (11–12):

$$[18] \quad \frac{1}{K_m} = \left[n\frac{(2n-z)(4n-2z-1)}{(2n-z-2)}\right] \times \left[\frac{(2n-z)(4n-2z-1)}{(2n-z-1)(4n-2z+2)}X_{cmc}\right]^{2n-z-1}$$

where z is the net charge of the micelle ($z = n\alpha$; n is the aggregation number and α is the fraction of free counterions), and X_{CMC} is the CMC expressed on the mol fraction scale. In the calculation of K_m the values of α and n were determined

© 2000 NRC Canada

Fig. 5. Determination of CMC by fluorescence method for sodium cyclohexyl butanoate.

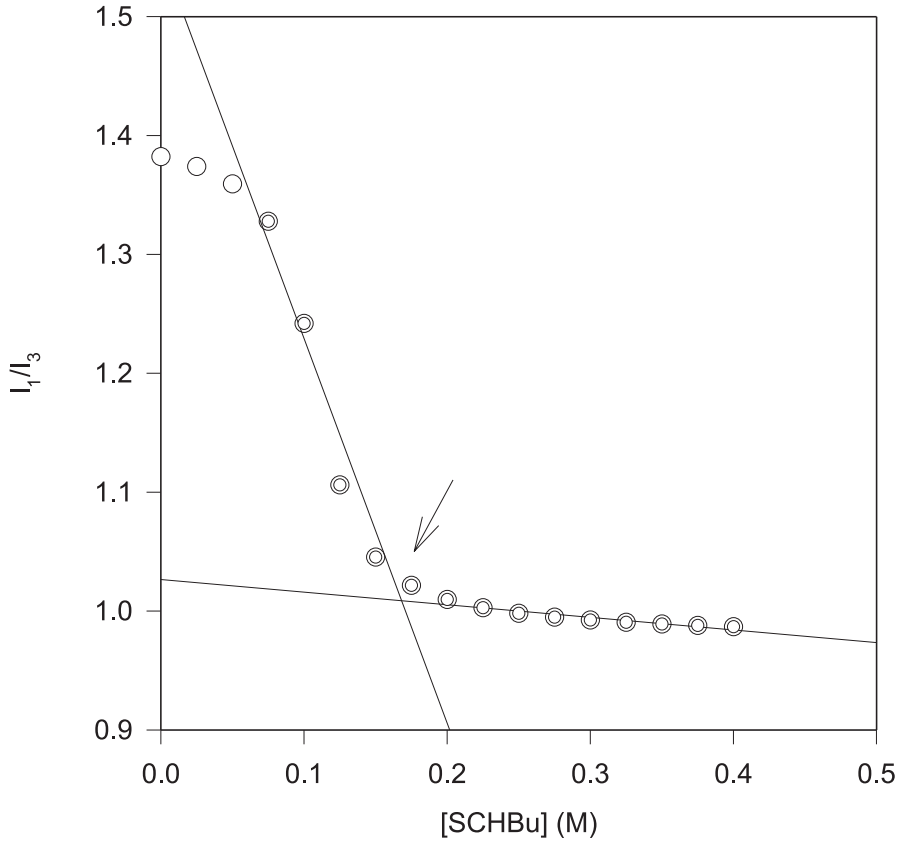


Table 4. Characteristic infrared absorption bands.

Surfactant	0.1 M[a]	2.0 M[a]	Assignment
SCHAc	2932.5	2930.4	ν_{as} CH_2
	1543.5	1548.5	ν_{as} COO-
	1408.6	1406.0	ν_s COO-
SCHPr	0.2 M	0.5 M	
	2928.6	2928.4	ν_{as} CH_2
	1540.9	1542.3	ν_{as} COO-
	1401.9	1407.1	ν_s COO-

[a] Observed frequency.

through conductivity and viscosity measurements, respectively.

The standard Gibbs energy change ΔG_m°, the standard enthalpy change, ΔH_m°, and the standard entropy change, ΔS_m°, on micellization were determined employing the following equations:

[19] $$\Delta G_m^\circ = -(RT/n)\ \ln\ K_m$$

[20] $$\Delta H_m^\circ = -(2-a)RT^2\left(\frac{\partial \ln X_{cmc}}{\partial T}\right)$$

[21] $$\Delta S_m^\circ = \frac{-1}{T}(\Delta G_m^\circ - \Delta H_m^\circ)$$

These values are presented in Table 5.

4. Discussion

The critical micelle concentration has been determined in this study using a variety of experimental techniques including conductivity, density, viscosity, surface tension, speed of sound, FT-IR, and fluorescence (Table 1). All of the CMC values determined using these techniques are in good agreement with each other. Figure 8 shows a plot of log (CMC) against the number of carbon atoms in the surfactant (excluding the headgroup carbon) using the data from the above techniques.

The CMC values determined by the surface tension technique are slightly lower than expected. It is well known in the literature that the CMC values depend on the technique employed in the determination of the CMC (9). The CMC values decrease by approximately half upon the addition of one CH_2 group to the alkyl chain. Similar behavior was also observed for long-chain sodium alkanoate surfactants.

Based on the critical micelle concentration values, the cyclohexyl ring behaves in a similar manner to a five-member alkyl chain (1-CH_3 group and 4-CH_2 groups). The critical micelle concentrations decrease, in the same fashion for the cyclohexyl alkanoates, as for the homologous family of surfactants, sodium hexanoate to sodium decanoate.

An increase of α, as the length of the hydrocarbon chain is increased, is due to a decrease in the surface charge density or an increase in surface area per head group.

The differences between $\phi_{v,1}$ and $\phi_{v,2}$ increase with chain length (Table 3), the free monomer molar volumes being larger that those in the micellar state indicating that the

© 2000 NRC Canada

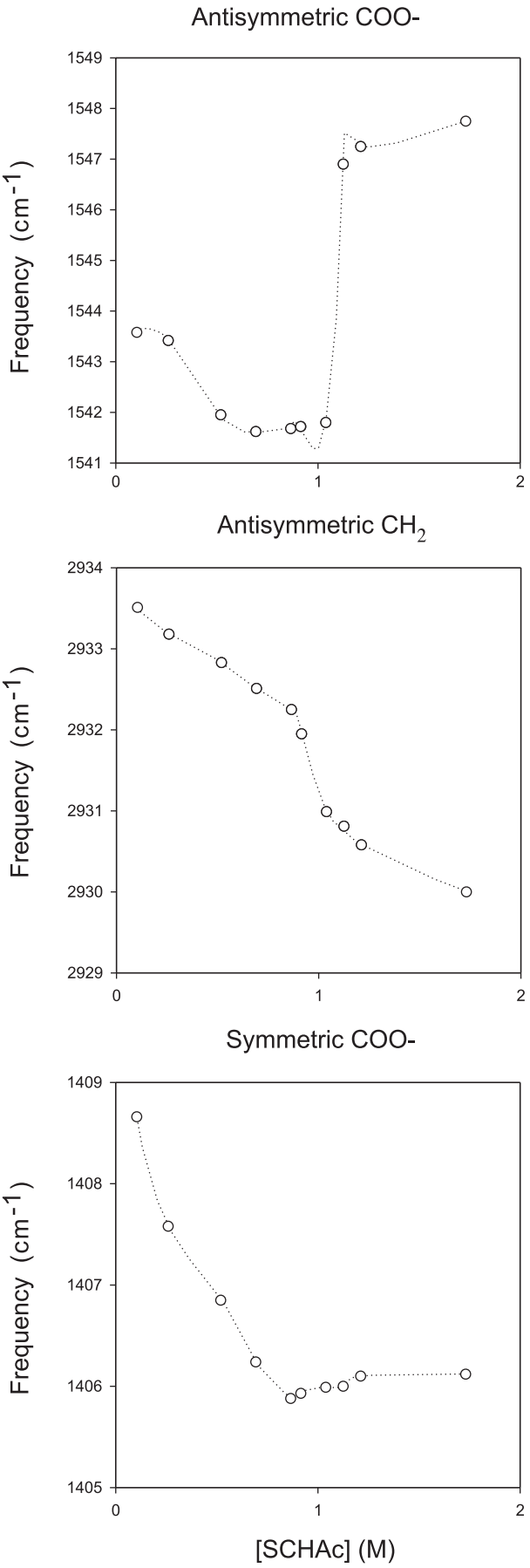
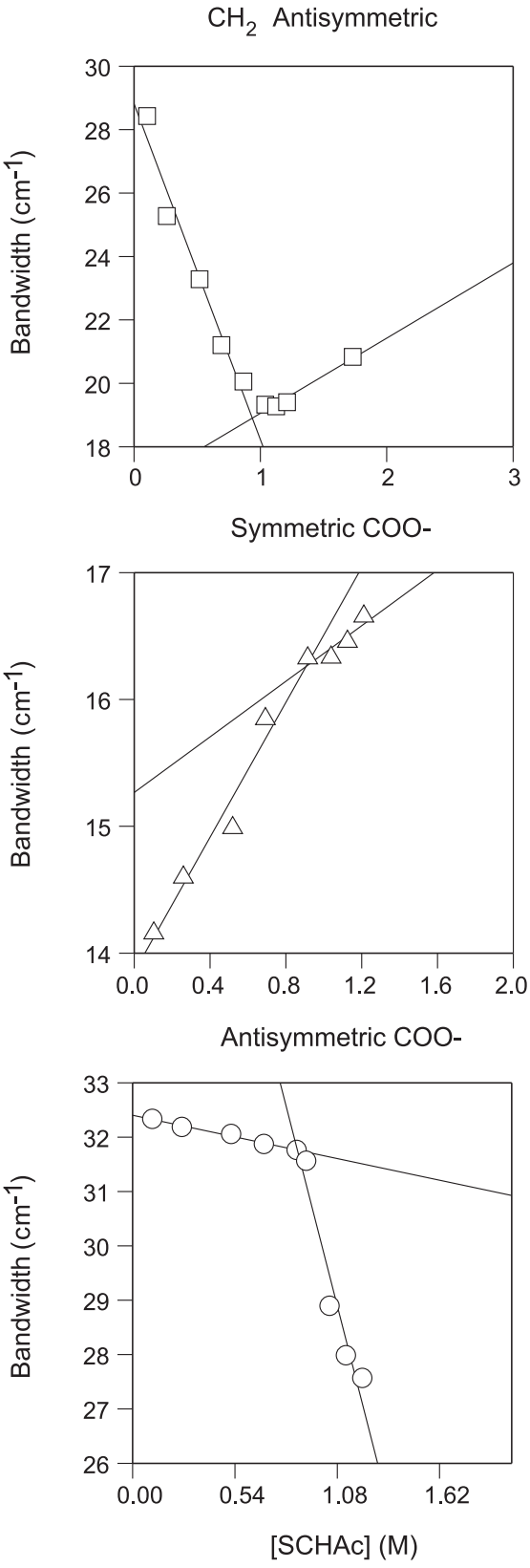


Fig. 6. Concentration dependencies of the infrared frequencies of sodium cyclohexyl acetate.

Fig. 7. Half-height bandwidths for sodium cyclohexyl acetate.



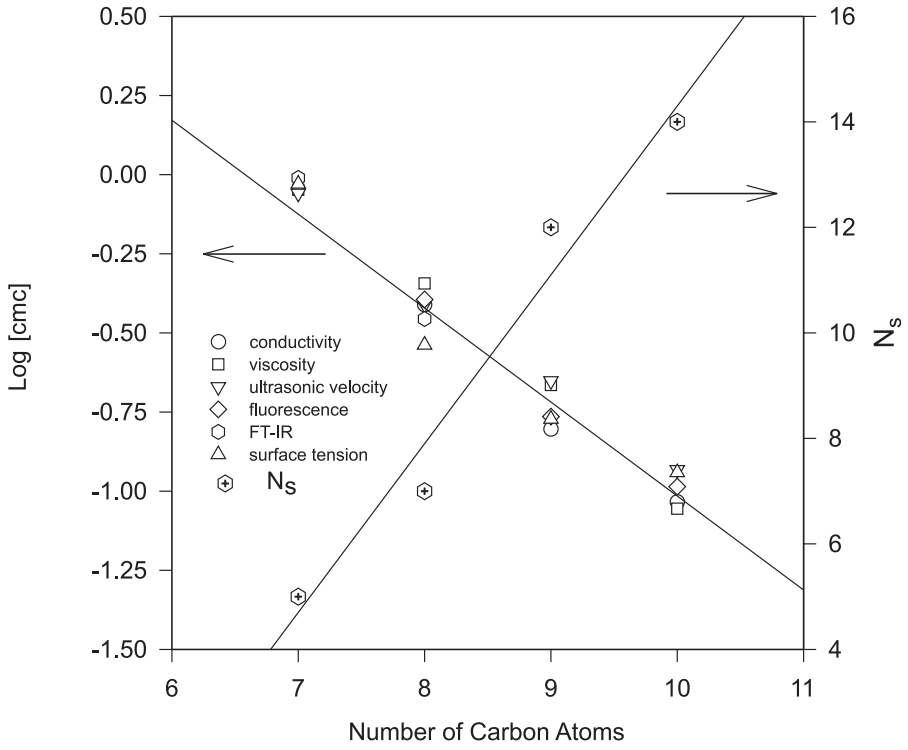
© 2000 NRC Canada

Table 5. Thermodynamics of micellization for the sodium cyclohexyl alkanoates.

Salt	Temperature (K)	ΔG°_{mic} (KJ mol^{-1})[a]	ΔH°_{mic} (KJ mol^{-1})[b]	ΔS°_{mic} (J K^{-1} mol^{-1})[c]
SCHAc	298.15	–12.3	3.9	56.4
	308.15	–12.4	4.2	55.8
	318.15	–12.7	4.4	59.3
SCHPr	298.15	–13.7	13.6	91.6
	308.15	–14.2	14.6	93.5
	318.15	–13.4	15.6	91.2
SCHBu	298.15	–15.4	26.9	141.9
	308.15	–15.7	28.8	144.5
	318.15	–16.7	30.7	149.1
SCHPe	298.15	–17.5	6.1	79.1
	308.15	–17.3	6.6	77.5
	318.15	–17.7	7.1	77.9

[a] ΔG°_{mic} ± 0.5 KJ mol^{-1}.
[b] ΔH°_{mic} ± 0.6 KJ mol^{-1}.
[c] ΔS°_{mic} ± 5 J K^{-1} mol^{-1}.

Fig. 8. Log CMC and aggregation numbers as a function of chain length.



monomer in the micelle is in a more packed structure than the monomer in the free state. The difference between $\phi_{v,1}$ and $\phi_{v,2}$ becomes progressively smaller with the decrease of chain length (Fig. 9(*a*)) suggesting increasing constraints on molecular mobility as the micelle size decreases.

The speed of sound measurements of micellar solutions have been shown to be sensitive to the shape of the aggregate. In the present study, a definite break occurs at the CMC. The plots of adiabatic compressibility coefficients vs. concentration also show a small but definite change in the slopes at the CMC. The values of the apparent adiabatic compressibilities of the monomer $\tilde{k}_{s,1}$, and the micelle $\tilde{k}_{s,2}$, are listed in Table 3 and the values of $\tilde{k}_{s,1}$ decrease while the values for $\tilde{k}_{s,2}$ increase with an increase in chain length.

Adiabatic compressibility is a function of the composition of the system under study and is strongly dependent on the nature and intensity of the molecular interactions. It refers to a volume unit of solution and does not take into account the number of interacting molecules. Changes in adiabatic compressibility may be explained by considering two types of hydration. The monomer in the micellar state has only hydrophilic (or ionic) hydration, whereas the monomer in the free state has both hydrophilic and hydrophobic hydration. In the present study, the hydrophilic hydration would refer to the hydrogen bond interactions between the water molecules and the carboxylate group. The hydrophobic hydration is caused by the strong association of water molecules around the hydrophobe. The increase of hydrophobic interaction with

© 2000 NRC Canada

alkyl chain length leads to the increasing negative values of $\tilde{k}_{s,1}$, as the number of carbon atoms is increased in the alkyl chain. The relatively small difference between $\tilde{k}_{s,1}$ and $\tilde{k}_{s,2}$ for sodium cyclohexyl acetate suggests a higher degree of hydration of the monomer within the micelle. This may be due to the low hydrophobicity of the small alkyl chain in sodium cyclohexyl acetate and the small size makes the aggregates more penetrable to water.

Figure 9(*b*) shows the change of apparent adiabatic compressibility as a result of micelle formation; $\Delta\tilde{k}_2$ is plotted as a function of the number of carbon atoms. The increase of compressibility as the alkyl chain length is increased indicates a transition from an organized micellar structure at low aggregation number to a more fluid structure as the alkyl chain length increases and the monomers have increased mobility.

The standard thermodynamic quantities for this family of surfactants are shown in Table 5. The ΔG_m° values conform to the empirical relationship:

$$[22] \quad \Delta G_m^\circ = s_1 + s_0 n_c$$

where s_1 is a constant which depends on the nature of the ionic headgroup and s_0 is interpreted as the CH_2 (–1.72 kJ per CH_2 group) group contribution to the Gibbs energy of micellization. This is in excellent agreement with the value determined through surface tension measurements. The ΔG_m° is negative and becomes increasingly more negative as the length of the hydrocarbon chain is increased. This suggests that the micelles are readily formed. The increasingly positive value of ΔS_m° indicates an increasing randomness upon transfer of the monomers from the bulk to the micellar interior. For this micellization process $T\Delta S_m$ is much greater than ΔH_m indicating that micellization is primarily governed by entropy.

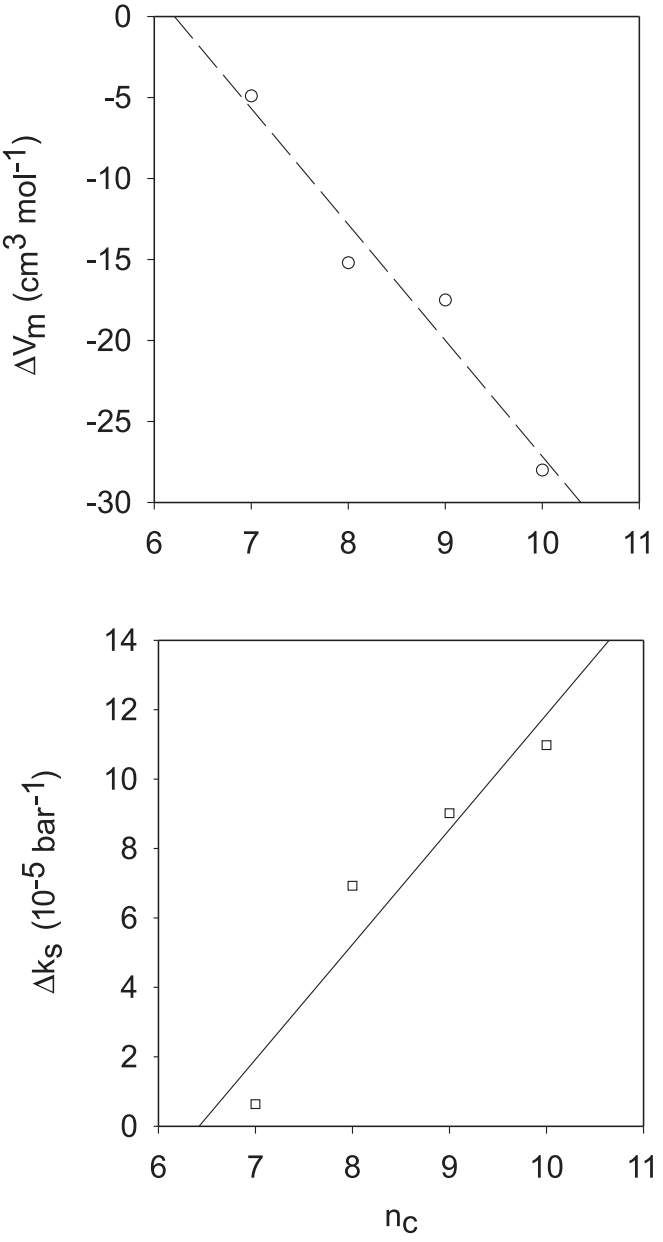
The efficiency and effectiveness of adsorption of the cyclohexyl salts increases with increasing chain length at a constant temperature. The areas decrease as the length of the hydrocarbon chain is increased. This indicates an increasing attraction between the cyclohexyl rings as they are expelled from the aqueous environment by adding CH_2 groups to the alkyl chain.

The free energies of adsorption are plotted in Fig. 3 where the slope is $d(\Delta G_{ad}^\circ)/dN$ is –2.43 KJ per CH_2 group and this is in reasonably good agreement with the "rule of two" ($-RT$ ln 2). From this information it can be concluded that the saturation areas are dependent on the chain length of the alkyl chain. One can conclude, therefore, that the decreasing curvature of the micellar surface, as CH_2 groups are added to the interior of a micelle, does not play a significant role in the micellization process.

The pyrene I_1/I_3 ratio reflects the polarity of the microenvironment around the pyrene probe. For the family of sodium cyclohexyl alkanoates the I_1/I_3 ratios all fall within the same range. Therefore this ratio is essentially constant for the members of this surfactant family.

The aggregation numbers were determined through viscosity measurements and range from four (sodium cyclohexyl acetate) to 14 (sodium cyclohexyl pentanoate). The lower than expected value for sodium cyclohexyl pentanoate is most likely due to the fact that the electroviscous effect

Fig. 9. (*a*) Change in apparent molar volume upon micellization as a function of chain length at 298.15 K. (*b*) Change of adiabatic compressibilities upon micellization as a function of chain length at 298.15 K.



cannot be neglected in solutions of low ionic strength such as these dilute micellar solutions. The aggregation numbers do show an increase as the length of the hydrocarbon chain is increased. These values are in very good agreement with values that were obtained employing NMR (Table 3) methods (25).

From the FT-IR data, the highest CH_2 antisymmetrical stretching mode frequencies occur at low concentrations of surfactant (0.1–0.8 M). It is possible to conclude that the nature of the solvent effect is minimal and that the surfactant is mainly present as monomers. The shift of these values to lower frequencies demonstrates a reduction in the

© 2000 NRC Canada

cyclohexanoate–water interactions. The bandwidths at lower concentration have greater uncertainty and remain relatively constant. The narrowing of bandwidths above the CMC are related to the rates of rotational relaxation of the acyl chain. This is due to the increased solute–solute interactions above the CMC (15). From the FT-IR studies it is clearly evident that micelle formation occurs at ~1.0 M for cyclohexyl acetic acid sodium salt and at ~0.39 M for cyclohexyl propionic acid sodium salt. This is seen as an inflection point in all frequency plots.

The absorption bands of the aggregates (micelles) occur at slightly lower frequency than the monomers. The interactions of the surfactants in solution can be further examined by looking at the density and (or) speed of sound of the cyclohexyl alkanoates at 298.15 K. From the adiabatic compressibility values, the hydration numbers can be calculated using the following equation:

$$[23] \qquad n_h = \frac{x_1}{x_2}\left(1 - \frac{\beta}{\beta_o}\right)$$

n_h is the hydration number, x_1 is the mol fraction of solute, x_2 is the mol fraction of solvent, β is the adiabatic compressibility of the solution, and β_o is the adiabatic compressibility of the solvent. The number of water molecules per surfactant molecule decreases for these surfactants (Table 3) upon micelle formation. Increasing the number of acyl chain carbons, in the hydrocarbon chain that is attached to the cyclohexyl ring, also increases the degree of hydration for the free monomer and surfactant micelles.

5. Conclusion

The presence of the cyclohexyl ring, in the family of sodium cyclohexyl alkanoate surfactants, appears to influence the surface properties of micellization, by lowering both the efficiency and effectiveness of adsorption when compared to that of the straight chain alkanoates. Increasing the chain length of the alkyl chain, which is attached to the cyclohexyl ring, also influences the micellar properties (CMC, degree of counter ion binding, hydration numbers, and aggregation numbers). This family of surfactants tends to be characterized by small degrees of binding, small aggregation numbers, and larger CMC values. These observed micellar properties may find applications in alkaline water flooding of oil reservoirs.

Acknowledgements

RP and DGM greatly appreciate the financial support of the Natural Sciences and Engineering Research Council of Canada (NSERC).

References

1. T. Drakenberg and B. Lindman. J. Colloid Interface Sci. **44**, 184 (1973).
2. Z. Gao, R.E. Wasylishen, and J.C. Kwak. J. Colloid Interface Sci. **137**, 137 (1990).
3. K.D. Gracie, D. Turner, and R. Palepu. Can. J. Chem. **74**, 1616 (1996).
4. H. Gustavsson, B. Lindman, and T.J. Bull. J. Am. Chem. Soc. **100**, 4655 (1978).
5. H. Gustavsson and B.J. Lindman. J. Am. Chem. Soc. **100**, 4647 (1978).
6. J. Lang. J. Phys. Chem. **86**, 992 (1982).
7. B. Perrson, T. Drakenberg, and B.J. Lindman. J. Phys. Chem. **80**, 2124 (1976).
8. B. Perrson, T. Drakenberg, and B.J. Lindman. J. Phys. Chem. **83**, 3011 (1979).
9. M.J. Rosen and S. Aronson. Colloids Surf. **3**, 201 (1981).
10. A. Skauge and J.J Spitzer. J. Phys. Chem. **87**, 2398 (1983).
11. V. Mosquera, J.M. del Rio, D. Attwood, M. Garcia, M.N. Jones, G. Prieto, M.J. Suarez, and F. Sarmiento. J. Colloid Interface Sci. **206**, 66 (1998).
12. R. Zielinski, S. Ikeda, H. Nomura, and S. Kato. J. Colloid Interface Sci. **119**, 398 (1987).
13. Ö. Soderman and P. Guering. Colloid Polym. Sci. **265**, 76 (1987).
14. A. Sokolowski and A. Chebicki. Colloids Surf. **56**, 251 (1991).
15. J. Umemura, D.G. Cameron, and H.H. Mantsch. J. Phys. Chem. **84**, 2271 (1980).
16. C. Tanford. The hydrophobic effect. Wiley, New York. 1980. pp. 42–59.
17. D.J. Jobe and V.C. Reinsborough. Aust. J. Chem. **37**, 303 (1984).
18. N.J. Turro and A.J.Yekta. J. Am. Chem. Soc. **100**, 5951 (1978).
19. J.M. Denton, D.C. Duecker, and E.D. Sprague. J. Phys. Chem. **97**, 756 (1993).
20. T.S. Brun, H. Hoiland, and E. Vikingstad. J. Colloid Interface Sci. **63**, 89 (1978).
21. D. Attwood, R. Blundell, V. Masquera, M. Garcia, and J. Roderigez. Colloid Polym. Sci. **272**, 108 (1994).
22. C.C. Ruiz. Colloid Polym. Sci. **273**, 1033 (1995).
23. B. Lindman and W. Wennerstroem. Top. Curr. Chem. **87**, 1 (1980).
24. D.G. Hall and G.J.T. Tiddy. *In* Anionic surfactants – physical chemistry of surfactant action. Vol. 11. *Edited by* E.H. Lucassen-Reynders. Marcel Dekker, New York. 1981. Chap. 2, p. 55.
25. J.A. MacInnis, R. Palepu, and D.G. Marangoni. Can. J. Chem. **77**, 1994 (1999).

Abbreviations

SCHAc	Sodium cyclohexyl acetate
SCHPr	Sodium cyclohexyl propanoate
SCHBu	Sodium cyclohexyl butanoate
SCHPe	Sodium cyclohexyl pentanoate

© 2000 NRC Canada

Solvation thermodynamics of cyclohexane

Giuseppe Graziano

Abstract: The solvation thermodynamics of cyclohexane in pure liquid phase and in water is analyzed by means of the theoretical approach developed by Lee. The sum of the work of cavity creation and the dispersive solute–solvent interaction energy reproduces well the experimental Gibbs energy values over the whole temperature range 5–100°C. This implies that the purely structural solvent reorganization is an exactly compensating process in both liquids. The dispersive solute–solvent interaction energy is larger in magnitude in cyclohexane than in water, whereas the work of cavity creation is larger in water than in cyclohexane. Therefore, both terms contrast the transfer of cyclohexane from pure liquid phase to water, determining its hydrophobicity. This mechanism qualitatively corresponds to that operative in the case of benzene.

Key words: hydrophobicity, cavity creation, excluded volume, dispersive interactions, enthalpy–entropy compensation.

Résumé : On a fait appel à l'approche théorique développée par Lee pour analyser les données thermodynamiques de solvatation du cyclohexane en phase pure et dans l'eau. La somme de travail pour la création d'une cavité et l'énergie d'interaction de dispersion soluté–solvant permet de bien reproduire les valeurs expérimentales de l'énergie de Gibbs sur l'ensemble des températures entre 5 et 100°C. Ceci implique que la réorganisation purement structurelle du solvant est un processus de compensation exacte dans les deux liquides. L'amplitude de l''énergie d'interaction de dispersion soluté–solvant est plus importante dans le cyclohexane que dans l'eau alors que le travail de création de cavité est plus important dans l'eau que dans le cyclohexane. On peut en déduire que les deux termes sont un reflet du transfert du cyclohexane de la phase liquide pure vers l'eau, ce qui détermine son caractère hydrophobe. Ce mécanisme correspond qualitativement à celui qui influence dans le cas du benzène.

Mots clés : caractère hydrophobe, création de cavité, volume exclu, interactions de dispersion, compensation enthalpie–entropie.

[Traduit par la Rédaction]

Introduction

Recently, we (1) reported on the molecular origin of benzene hydrophobicity, the poor solubility of benzene in water. Such poor solubility is usually called hydrophobicity (2), and according to Ben-Naim (3), is measured by the Gibbs energy change associated with the transfer of a solute molecule from a fixed position in pure liquid phase to a fixed position in water. In performing that study we surprisingly recognized that several physical properties of benzene and cyclohexane are very similar on a quantitative basis. A comprehensive comparison is shown in Table 1. For instance, the normal fusion and boiling points are nearly identical, the vaporization enthalpy changes at 25°C, the critical constants, and the values of surface tension and dielectric constant prove to be close.

The solubility of aromatic and aliphatic rings in water is of great importance: the side-chains of several amino acids consist of aromatic rings, and the cyclohexane ring is the backbone of many sugars. Radzicka and Wolfenden (4), to construct a hydrophobicity scale based on a truly nonpolar reference liquid, determined the distribution coefficients of amino acid side-chains between water and cyclohexane. The latter proved to be closely related to the inside-outside side-chain distribution observed in globular proteins (4), and numerically similar to changes in denaturation Gibbs energy that result from mutating nonpolar side-chains in protein interiors (5). Recently, Wolfenden and co-workers (6) determined also the distribution coefficients of the nucleic acid bases between water and cyclohexane. Thus, a careful analysis of the solvation thermodynamics of cyclohexane and a comparison with that of benzene should be important and useful. This task has recently been attempted by means of sophisticated computer simulations and new intermolecular potential functions; the results were encouraging, and provided satisfactory physical insights (7). We tried to perform the same task by means of the theoretical approach developed by Lee (8), which seemed able to interpret and explain most features of the hydrophobicity puzzle (1, 8–11).

The paper is organized as follows. First, a general theory of solvation is described. Then, the procedures used to perform calculations and to obtain the solvation thermodynamic quantities from experimental data are explained. Next, the solvation processes of cyclohexane in pure liquid phase and in water, in the temperature range 5–100°C, are analyzed.

Received February 10, 2000. Published on the NRC Research Press website on September 1, 2000.

G. Graziano.[1] Department of Chemistry, University of Naples "Federico II," Via Mezzocannone, 4 - 80134 Naples, Italy; and Faculty of Science, University of Sannio, Via Port'Arsa, 11 - 82100 Benevento, Italy.

[1]Telephone: +39 081 2536608. Fax: +39 081 5527771. e-mail: graziano@unisannio.it

© 2000 NRC Canada

Table 1. Some physical properties of cyclohexane and benzene. They come from ref. (53), except the values of the hard-sphere diameter, σ, and molar liquid volume, v_1, which are from ref. (20), those of N_{H2O} that are from ref. (29), and those of $\Delta_{vap}H$ coming from ref. (30).

	Cyclohexane	Benzene
M_w	84.16	78.12
σ (Å)	5.63	5.26
N_{H_2O}	31.0	26.7
v_1 (25°C, cm^3 mol^{-1})	108.75	89.40
T_c (°C)	280.4	288.9
P_c (atm)	40.0	48.6
mp (°C)	6.6	5.5
bp (°C)	80.7	80.1
$\Delta_{fus}H$ (25°C, kJ mol^{-1})	2.6	10.0
$\Delta_{vap}H$ (25°C, kJ mol^{-1})	33.0	33.8
$C_{p,l}$ at (25°C, J K^{-1} mol^{-1})	152	136
γ (20°C, dynes cm^{-1})	25.5	28.9
n_D (25°C)	1.424	1.498
ε (25°C)	2.015	2.274

Finally, the transfer of cyclohexane from pure liquid phase to water is studied and the results are contrasted with those previously obtained for benzene.

Theory of solvation

The process of inserting a solute molecule at a fixed position in a solvent is dissected in two subprocesses that have a clear physical meaning (8): (*i*) creation of a cavity to suitably accommodate the solute molecule; (*ii*) insertion of the solute molecule into the cavity and turning on the solute–solvent interactions. The solvation Gibbs energy change, $\Delta G^{\cdot}$, is:

$$[1] \qquad \Delta G^{\cdot} = \Delta G_c + E_a$$

where ΔG_c, the work of cavity creation, is a positive quantity, and E_a, the average dispersive solute–solvent interaction energy, is a negative quantity. A straightforward application of equilibrium statistical mechanics allows one to demonstrate that the work of cavity creation is purely entropic (12). ΔG_c is a measure of the excluded volume effect due to the reduction in spatial configurations accessible to solvent molecules. Moreover, Madan and Lee (13*a*), and Shimizu and co-workers (13*b*), by means of Monte Carlo computer simulations, showed that the ΔG_c values, at a given density, are similar in both water models and Lennard–Jones fluids constituted by particles having the same size of water molecules. This means that, once the solvent density is fixed, ΔG_c proves to be independent of the intermolecular potential energy existing among the solvent molecules. As a consequence, we set (1, 11)

$$[2] \qquad \Delta G_c = -T\Delta S_x$$

where ΔS_x is the excluded volume entropy contribution. The two terms, ΔG_c and E_a, have to be considered the direct perturbation of the solvent caused by solute insertion; E_a being the enthalpic part, and ΔG_c the entropic one (see the Appendix section). In response to such direct perturbation, the solvent molecules undergo a further reorganization with an associated enthalpy ΔH_r and entropy ΔS_{nx} contributions. Therefore, the total solvation enthalpy and entropy changes are:

$$[3] \qquad \Delta H^{\cdot} = E_a + \Delta H_r$$

$$[4] \qquad \Delta S^{\cdot} = \Delta S_x + \Delta S_{nx}$$

We prefer to use the notation ΔS_{nx} to emphasize that this is the nonexcluded volume entropy contribution, by recognizing that ΔS_x also originates from a reorganization of solvent molecules (see the Appendix section). Lee (14) demonstrated that the solvent response (i.e., which is called the purely structural solvent reorganization) is a compensating process at any temperature when the perturbing potential is weak

$$[5] \qquad T\Delta S_{nx} = \Delta H_r$$

Actually, several authors, using different theoretical approaches, have shown that the purely structural solvent reorganization is a compensating process (15). This physically means that, when the interaction of the inserted solute molecule with the surrounding solvent molecules is given solely by dispersive interactions, the compensation relation is operative (see the Appendix section). Clearly, for nonpolar molecules, such as hydrocarbons, this condition is fulfilled in both pure liquid phase and water (1, 8–11).

Therefore, the purely structural solvent reorganization does not affect the solvation Gibbs energy change and $\Delta G^{\cdot}$, as emphasized by eq. [1], takes into account solely the direct perturbation of the solvent: (*i*) the excluded volume effect due to cavity creation, opposing solvation; (*ii*) the dispersive solute–solvent interactions, favouring solvation. As a consequence, hydrophobicity is mainly determined by the very small size of water molecules, which exaggerates the excluded volume effect with respect to the other solvents (8).

The solvation of cyclohexane in pure liquid phase and in water is analyzed by means of the above equations. For the analysis of the transfer from pure liquid phase to water, we consider that, for all the thermodynamic functions, the following equation holds:

$$[6] \qquad \Delta X^{\cdot}(l\rightarrow w) = \Delta X^{\cdot}(g\rightarrow w) - \Delta X^{\cdot}(g\rightarrow l)$$

where X stands for C_p, H, S, and G. Actually, eq. [6] is only valid when the mutual solubility of the two solvents is very low, as for the pair water and cyclohexane (16). It is not valid for important cases such as the pair water and *n*-octanol, because the water solubility in *n*-octanol is quite large (16).

Calculation procedure

The work of cavity creation is calculated by means of the following equation from Scaled Particle Theory, SPT (17, 18):

$$[7] \qquad \Delta G_c = RT\cdot[K_0 + K_1(\sigma_2/\sigma_1) + K_2(\sigma_2/\sigma_1)^2 + K_3(\sigma_2/\sigma_1)^3]$$

where: $K_0 = -\ln(1-\xi)$, $K_1 = u = 3\xi/(1-\xi)$, $K_2 = u(u+2)/2$, $K_3 = \xi P v_1/RT$.

In these relations R is the gas constant, ξ is the volume packing density of pure solvent, which is defined as the ratio

© 2000 NRC Canada

of the physical volume of a mol of solvent molecules over the molar volume of the solvent, v_1 (i.e., $\xi = \pi\sigma_1^3 N_{Av}/6v_1$), P is the hydrostatic pressure over the liquid, σ_1 and σ_2 are the hard-sphere diameters of the solvent and solute molecules, respectively. For water we use σ = 2.75 Å (8, 9), close to the location of the first peak of the oxygen–oxygen radial distribution function of water (19). For cyclohexane we use σ = 5.63 Å, as determined by Wilhelm and Battino (20). Clearly, water and cyclohexane are not spherical molecules, as can be seen by the large deviations from the law of corresponding states. However, it is customary to consider spherical the water molecules in a series of applications, such as ASA and SPT calculations (21, 22). On the other hand, the local orientation order in liquid cyclohexane should be isotropic, as it is in liquid benzene (23), and thus the assumption of spherical molecules should be physically reliable.

Reiss (17) pointed out that, on increasing temperature, the molecules acquire sufficient kinetic energy to explore different regions of the potential energy surface, implying that the hard-sphere diameter should decrease. However, Wilhelm (24) determined that such a decrease is small for both cyclohexane and water (i.e., in a range of 100°C, the decrease of σ would amount to about 0.08 Å for cyclohexane, and 0.03 Å for water). Therefore, we consider the hard-sphere diameters of water and cyclohexane as temperature independent.

According to eq. [7], ΔG_c is given by the product of two factors: (*i*) the *RT* term, reflecting the kinetic energy contribution of solvent molecules bombarding the cavity surface (17), increases linearly with temperature; (*ii*) the term in square brackets, depending on ξ, a quantity proportional to the liquid density, decreases with temperature (i.e., in general, the liquid density decreases on raising temperature). The first term is equal for all liquids, whereas the density decrease on raising temperature is a specific property of each liquid. In performing calculations, we used the values of liquid density experimentally determined over a large temperature range for both cyclohexane (25), and water (26). In this manner, ξ passes from 0.530 at 5°C to 0.468 at 100°C for liquid cyclohexane; while it passes from 0.364 at 5°C to 0.349 at 100°C for liquid water.

The dispersive interaction energy E_a of cyclohexane in its pure liquid phase is calculated by means of Pierotti's formula (18):

$$[8] \qquad E_a = -(64/3)R\xi\varepsilon$$

where ε is the depth of the well in the Lennard–Jones potential, measuring the magnitude of the maximum attractive potential energy; we use ε/k = 540 K for cyclohexane. This value is reliable considering that the estimates existing in the literature range from 313 K to 573 K (20). The temperature dependence of E_a originates from that of the solvent packing density, which, in turn, reflects the temperature dependence of the liquid density. This is physically reasonable because the magnitude of the dispersive energy is strongly affected by the average distance between the interacting molecules (27).

Pierotti's formula, however, does not work well for hydrocarbons in water, as already pointed out and discussed (10). To calculate E_a for cyclohexane in water at 25°C we use the following relationship:

Table 2. Thermodynamic properties of pure liquid cyclohexane in the temperature range 5–100°C.

T (°C)	p_{eq} (atm)	v_1 (cm^3 mol^{-1})	$\alpha_1 \cdot 10^{-3}$ (K^{-1})	$\Delta_{vap}H$ (kJ mol^{-1})	B (cm^3 mol^{-1})
5	0.048	106.14	1.18	34.0	–2128
25	0.129	108.75	1.24	33.0	–1736
50	0.359	112.25	1.29	31.8	–1391
75	0.841	116.10	1.42	30.6	–1152
100	1.725	120.37	1.54	29.4	–976

Note: Thermodynamic properties are obtained by linear interpolation of the data compiled by Smith and Srivastava (25), and Wilhelm and Battino (30).

$$[9] \qquad E_a = (20.8 \pm 1.6) - (1.9 \pm 0.1)\cdot N_{H_2O} \quad (r = -0.9977)$$

obtained by performing a linear regression over the E_a values for the seven alkanes, computed by Jorgensen et al. (28), versus the hydration number, N_{H_2O}. The analysis of the size dependence of hydrophobic hydration suggested that eq. [9] should give reliable values (10). Accordingly, E_a = –38.1 kJ mol^{-1} for cyclohexane at 25°C, because N_{H_2O} = 31.0 (29). The temperature dependence of E_a for cyclohexane in water is estimated on the basis of the temperature dependence of liquid water density.

The excluded volume entropy contribution, ΔS_x, is calculated by means of eq. [2], and the nonexcluded volume entropy contribution, ΔS_{nx}, is obtained, at any temperature, by the difference $\Delta S^{\cdot} - \Delta S_x$. On the other hand, the contribution of solvent response to the enthalpy change, ΔH_r, is obtained, at any temperature, by the difference $\Delta H^{\cdot} - E_a$.

Experimental data

Thermodynamic solvation functions at a constant pressure for the g→l process of cyclohexane cannot be obtained because the experimental condensation data refer to different pressures. However, Ben-Naim (3) pointed out that a variation in pressure between zero and a few atmospheres causes a negligible effect on $\Delta G^{\cdot}$. Therefore, by assuming that the fugacity of cyclohexane can be represented by the following equation:

$$[10] \qquad f = p\cdot\exp(pB/RT)$$

where B is the second virial coefficient, $\Delta G^{\cdot}$ for the g→l process is given by (1, 8):

$$[11] \qquad \Delta G^{\cdot} = RT \ln (p_{eq}v_1/RT) + Bp_{eq}$$

where v_1 is the molar volume of the liquid and p_{eq} is the equilibrium vapour pressure. Then, by applying the Gibbs–Helmholtz equation, $\Delta H^{\cdot}$ is given by:

$$[12] \qquad \Delta H^{\cdot} = -\Delta_{vap}H + RT(1 - \alpha_1 T) + p_{eq}(B - B'T)$$

where $\Delta_{vap}H$ is the vaporization enthalpy change of the pure liquid, α_1 is its thermal expansion coefficient, and B' denotes the temperature derivative of B. Thermodynamic properties of liquid cyclohexane at different temperatures, obtained from tabulated data (25, 30), are listed in Table 2.

For the g→w process, we use the values of $\Delta H^{\cdot}$, $\Delta S^{\cdot}$, and $\Delta G^{\cdot}$ at 25°C reported by Abraham (31), after correction for

© 2000 NRC Canada

Table 3. Ben-Naim standard thermodynamic quantities for the transfer of cyclohexane from ideal gas phase to pure liquid phase at equilibrium vapour pressure (*a*), and to water at 1 atm (*b*), in the temperature range 5–100°C.

	T (°C)	$\Delta C_p^\cdot$ (J K^{-1} mol^{-1})	$\Delta H^\cdot$ (kJ mol^{-1})	$\Delta S^\cdot$ (J K^{-1} mol^{-1})	$\Delta G^\cdot$ (kJ mol^{-1})
(*a*)	5	40	–32.5	–46.7	–19.5
	25	40	–31.6	–43.9	–18.5
	50	40	–30.4	–39.9	–17.5
	75	40	–29.5	–37.3	–16.5
	100	40	–28.6	–34.6	–15.7
(*b*)	5	420	–39.0	–149.2	2.5
	25	400	–30.8	–120.7	5.2
	50	370	–21.2	–89.7	7.8
	75	335	–12.4	–63.4	9.7
	100	295	–4.5	–41.6	11.0

the Ben-Naim standard (3). For the hydration heat capacity change at 25°C, we add to the value measured for the l→w process by Wadso and co-workers (32), 360 J K^{-1} mol^{-1}, the value calculated by us for the g→l process, 40 J K^{-1} mol^{-1}, obtaining $\Delta C_p^\cdot$ = 400 J K^{-1} mol^{-1}. The temperature dependence of $\Delta C_p^\cdot$ over the range 5–100°C is estimated on the basis of the general relations given by Gill et al. (33) and Makhatadze and Privalov (34). These estimates of $\Delta C_p^\cdot$ are used to calculate $\Delta H^\cdot$, $\Delta S^\cdot$, and $\Delta G^\cdot$ in the whole temperature range 5–100°C, starting from their values at 25°C.

Analysis of the g→l and g→w processes

The experimental values of $\Delta C_p^\cdot$, $\Delta H^\cdot$, $\Delta S^\cdot$, and $\Delta G^\cdot$ for the solvation of cyclohexane in pure liquid phase and in water in the range 5–100°C are collected in Table 3. For the g→l process, it results that: (*i*) the $\Delta G^\cdot$ values are large and negative, and slowly decrease, in absolute value, as a function of temperature, i.e., $\Delta G^\cdot$ = –19.5 kJ mol^{-1} at 5°C and –15.7 kJ mol^{-1} at 100°C; (*ii*) the $\Delta H^\cdot$ and $\Delta S^\cdot$ values are negative and large, showing a temperature dependence similar to that of $\Delta G^\cdot$; (*iii*) $\Delta C_p^\cdot$ is positive and constant, equal to 40 J K^{-1} mol^{-1}. For the g→w process, it results that: (*i*) the $\Delta G^\cdot$ values are positive and increase with temperature, i.e., $\Delta G^\cdot$ = 2.5 kJ mol^{-1} at 5°C and 11.0 kJ mol^{-1} at 100°C; (*ii*) the $\Delta H^\cdot$ and $\Delta S^\cdot$ values are large and negative at 5°C, and increase strongly with temperature; (*iii*) the $\Delta C_p^\cdot$ values are large and positive and decrease with temperature, i.e., $\Delta C_p^\cdot$ = 420 J K^{-1} mol^{-1} at 5°C and 295 J K^{-1} mol^{-1} at 100°C. Under Ben-Naim standard state conditions, for cyclohexane, the g→l process is spontaneous, whereas the g→w process is nonspontaneous, over the whole temperature range 5–100°C.

The calculated values of ΔG_c and E_a, for both the processes, are listed in the second and third columns of Table 4. At any temperature, the ΔG_c estimates in cyclohexane are significantly smaller than those in water. This finding is expected because ΔG_c, being a measure of the excluded volume effect due to the creation of a region of space devoid of solvent molecules, is very large in liquid water owing to the small size of its molecules (8–14, 35). On the other hand, at any temperature, the estimates of E_a in cyclohexane are significantly larger, in absolute value, than those in water. This difference should be simply related to the larger polarizability of cyclohexane with respect to water, because E_a accounts solely for the dispersive solute–solvent interaction energy; such a conclusion agrees with the results of theoretical calculations by Floris and Tomasi (36).

Table 4. Calculated estimates of the Gibbs energy cost of cavity creation (ΔG_c) and of the dispersive interaction energy (E_a), for cyclohexane into pure liquid phase at equilibrium vapour pressure (*a*), and to water at 1 atm (*b*), in the temperature range 5–100°C.

	T (°C)	ΔG_c (kJ mol^{-1})	E_a (kJ mol^{-1})	$\Delta G_c + E_a$ (kJ mol^{-1})	$\Delta G^\cdot$ (kJ mol^{-1})
(*a*)	5	30.6	–50.7	–20.1	–19.5
	25	30.5	–49.5	–19.0	–18.5
	50	30.2	–48.0	–17.8	–17.5
	75	29.8	–46.4	–16.6	–16.5
	100	29.1	–44.8	–15.7	–15.7
(*b*)	5	40.1	–38.2	1.9	2.5
	25	42.7	–38.1	4.6	5.2
	50	45.5	–37.7	7.8	7.8
	75	47.6	–37.1	10.5	9.7
	100	49.3	–36.5	12.8	11.0

Note: The sum $\Delta G_c + E_a$ is also compared to the experimental $\Delta G^\cdot$ values in the same temperature range.

The calculated (i.e., $\Delta G_c + E_a$) and experimental values of $\Delta G^\cdot$ are listed in the fourth and fifth columns of Table 4. There is a very close agreement for both the g→l and g→w processes at any temperature; this has to be considered a demonstration of the general correctness of eq. [1]. Moreover, such good agreement implies that the purely structural solvent reorganization upon solute insertion is a compensating process, as required by eq. [5], in both cyclohexane and water. In particular, this proves that the H-bond reorganization in water upon solute insertion does not contribute to $\Delta G^\cdot$. It is worth mentioning that an essential ingredient of the successful integral equation theory by Pratt and Chandler (37) is the assumption that the contribution of H-bond reorganization can be neglected to calculate hydration Gibbs energies.

In the case of the g→l process, the ΔG_c values are large and positive and decrease very slightly with temperature, whereas the E_a values are large and negative and decrease, in absolute value, with temperature. It proves that $|E_a| > \Delta G_c$ at any temperature, so that $\Delta G^\cdot$ is always large and negative, and its temperature dependence parallels that of $|E_a|$. In the

© 2000 NRC Canada

Table 5. Calculated estimates of the reorganization enthalpy change (ΔH_r) and of the entropy contributions due to the excluded volume effect (ΔS_x) and the nonexcluded volume effect (ΔS_{nx}) associated with the solvation of cyclohexane into pure liquid phase at equilibrium vapour pressure (*a*), and into water at 1 atm (*b*), in the temperature range 5–100°C.

	T (°C)	$\Delta H^{\cdot}$ (kJ mol^{-1})	ΔH_r (kJ mol^{-1})	$\Delta S^{\cdot}$ (J K^{-1} mol^{-1})	ΔS_x (J K^{-1} mol^{-1})	ΔS_{nx} (J K^{-1} mol^{-1})
(*a*)	5	–32.5	18.2	–46.7	–110.0	63.3
	25	–31.6	17.9	–43.9	–102.3	58.4
	50	–30.4	17.6	–39.9	–93.5	53.6
	75	–29.5	16.9	–37.3	–85.6	48.3
	100	–28.6	16.2	–34.6	–78.0	43.4
(*b*)	5	–39.0	–0.8	–149.2	–144.2	–5.0
	25	–30.8	7.3	–120.7	–143.2	22.5
	50	–21.2	16.5	–89.7	–140.8	51.1
	75	–12.4	24.7	–63.4	–136.7	73.3
	100	–4.5	32.0	–41.6	–132.1	90.5

Note: The experimental solvation enthalpy and entropy changes are also reported. Specifically, $\Delta H_r = \Delta H^{\cdot} - E_a$, $\Delta S_x = -\Delta G_c/T$, and $\Delta S_{nx} = \Delta S^{\cdot} - \Delta S_x$.

case of the g→w process, the ΔG_c values are large and positive and increase with temperature, whereas the E_a estimates are large and negative and decrease very slightly, in absolute value, with temperature. It proves that $\Delta G_c > |E_a|$ at any temperature, so that $\Delta G^{\cdot}$ is always positive and its temperature dependence parallels that of ΔG_c. The physical origin of these findings relies in the temperature dependence of the density for the two liquids (1, 11, 38).

In the range 5–100°C the density of liquid cyclohexane decreases by 11.8% (25), causing a significant decrease of $|E_a|$ and a very small decrease of ΔG_c. In contrast, in the same temperature range, the density of liquid water decreases by 4.2% (26), causing a small decrease of $|E_a|$ and an increase of ΔG_c. Therefore, at any temperature, the g→l process is spontaneous because the dispersive interactions between cyclohexane molecules overwhelm the work of cavity creation, whereas the g→w process is non-spontaneous because the work of cavity creation overwhelms the dispersive interactions between cyclohexane and water molecules.

We now analyze the solvation enthalpy changes. The E_a estimates for both the g→l and g→w processes are larger, in absolute sense, than the $\Delta H^{\cdot}$ values, except at 5°C in the g→w case. In cyclohexane at 25°C, E_a = –49.5 kJ mol^{-1} whereas $\Delta H^{\cdot}$ = –31.6 kJ mol^{-1}; in water at 25°C, E_a = –38.1 kJ mol^{-1} whereas $\Delta H^{\cdot}$ = –30.8 kJ mol^{-1}. Therefore, the dispersive interactions of cyclohexane in pure liquid phase and in water are so large that the purely structural solvent reorganization proves to be an endothermic process in both solvents. The ΔH_r values, determined by means of eq. [3], using the experimental $\Delta H^{\cdot}$ values and the E_a estimates, are listed in the third column of Table 5. It proves that, over the range 5–100°C, ΔH_r slightly decreases for the g→l process, whereas it strongly increases for the g→w process (i.e., ΔH_r passes from 18.2 to 16.2 kJ mol^{-1} for the g→l process, whereas it passes from –0.8 to 32.0 kJ mol^{-1} for the g→w process). In this regard, it has to be noted that the purely structural solvent reorganization involves different intermolecular interactions in the two solvents: dispersive interactions in cyclohexane and H-bonds in water. For the g→w process, ΔH_r is slightly negative at 5°C and small positive around room temperature. This means that there is no significant rupture nor gain of H-bonds. Water molecules in the hydration shell, in view of their tetrahedral functionality, are able to avoid the loss of H-bonds by straddling the surface of nonpolar groups (2). This geometrical arrangement has definitely been established by means of direct neutron scattering and X-ray absorption spectroscopy measurements from Finney's group (39, 40). The data emphasized that the hydration shell around nonpolar moieties resembles a disordered clathrate cage, and is not characterized by an increased orientation order with respect to bulk water. In particular, the various radial distribution functions determined indicate that the orientation structure of water in the hydration shell is similar to that existing in the bulk (39, 40). Similar results have emerged from detailed computer simulations (41), confirming the plasticity of the H-bonded network of water. The thermodynamics of H-bond reorganization can be described by means of the modified Muller's model (42), considering that water H-bonds populate two distinct energy states, both in the bulk and in the hydration shell, whose energy gap is not large. Accordingly, the large positive temperature dependence of ΔH_r is simply due to the increase in the population of the higher energy state on raising temperature (11, 42). Recently, Dill and coworkers (43) have confirmed the reliability of the modified Muller's model, in view of its ability to reproduce specific results of Monte Carlo simulations on the Mercedes–Benz model of water.

The two contributions to the solvation entropy change are calculated by means of eqs. [2] and [4]; the values obtained are listed in the fifth and sixth columns of Table 5. The ΔS_x contribution is large and negative for both the g→l and g→w processes and increases with temperature. However, the increase is more pronounced in cyclohexane than in water, as a consequence of the different temperature dependence of ΔG_c in the two liquids, reflecting the different temperature dependence of their density (i.e., in the range 5–100°C, ΔS_x passes from –110.0 to –78.0 J K^{-1} mol^{-1} in cyclohexane, and from –144.2 to –132.1 J K^{-1} mol^{-1} in water). These values indicate unequivocally that the excluded volume effect is the physical cause of the negative solvation entropies of cyclohexane in both pure liquid phase and water (1, 8). The ΔS_{nx} contribution is always positive, except at 5°C for the g→w process; the purely structural solvent reorganization leads to an entropy increase. This term decreases with temperature in

© 2000 NRC Canada

Table 6. Ben-Naim standard thermodynamic quantities for the transfer of cyclohexane from pure liquid phase at equilibrium vapour pressure to water at 1 atm, in the temperature range 5–100°C.

T (°C)	$\Delta C_p^{\cdot}$ (J K^{-1} mol^{-1})	$\Delta H^{\cdot}$ (kJ mol^{-1})	$\Delta S^{\cdot}$ (J K^{-1} mol^{-1})	$\Delta G^{\cdot}$ (kJ mol^{-1})
5	380	–6.5	–102.5	22.0
25	360	0.8	–76.8	23.7
50	330	9.2	–49.8	25.3
75	295	17.1	–26.1	26.2
100	255	24.1	–7.0	26.7

cyclohexane, whereas it strongly increases in water (i.e., in the range 5–100°C, ΔS_{nx} passes from 63.3 to 43.4 J K^{-1} mol^{-1} in cyclohexane, and from –5.0 to 90.5 J K^{-1} mol^{-1} in water); the different temperature dependence corresponds to that of ΔH_r because eq. [5] holds. Overall our work shows that the excluded volume entropy dominates over the entropy of the purely structural solvent reorganization. This analysis of the solvation entropy contrasts with the claims advanced by Frank and co-workers (44), but accords well with the previous analyses of aliphatic hydrocarbons, noble gases, aliphatic alcohols, and benzene, reported in the literature (1, 8–11). Actually, it is strongly supported by direct structural measurements (39, 40), which failed to detect an increased order in the hydration shell of nonpolar groups. In addition, the fundamental role played by the work of cavity creation, and so by the excluded volume effect, in the solvation thermodynamics has been recognized by several scientists, such as Chandler and co-workers (45), Pratt and co-workers (46), Guillot and co-workers (47). Also Paulaitis and co-workers (48), using the multiparticle correlation function expansion for the solvation entropy, truncated at the level of pair correlations, found that the contribution of translational solute–solvent correlation functions, strictly related to the excluded volume effect, is dominant, and larger in water than in nonpolar solvents. Finally, several authors have concluded that the excluded volume effect dominates the energetics of hydrophobic interactions (49, 50), usually considered the partial reversal of hydrophobic hydration.

Analysis of the l→w process

The experimental values of thermodynamic functions associated with the l→w process, in the temperature range 5–100°C, obtained using eq. [6], are listed in Table 6. The process is characterized by a large and positive heat capacity change that leads to a marked temperature dependence of $\Delta H^{\cdot}$ and $\Delta S^{\cdot}$. However, due to an enthalpy–entropy compensation phenomenon, the $\Delta G^{\cdot}$ values increase weakly with temperature and are always large and positive (i.e., $\Delta G^{\cdot}$ passes from 22.0 to 26.7 kJ mol^{-1} in the range 5–100°C).

The values of $\Delta\Delta G_c = \Delta G_c$(water) – ΔG_c(cyclohexane) and $\Delta E_a = E_a$(water) – E_a(cyclohexane) are reported in the second and third columns of Table 7, part (*a*), respectively. Both such quantities are positive and substantial, in the temperature range 5–100°C, because: (*i*) the work of cavity creation is larger in water than in cyclohexane; (*ii*) the dispersive energetic interactions are stronger in cyclohexane than in water. Therefore, both the excluded volume effect and dispersive interactions contrast the transfer of cyclohexane from pure liquid phase to water. The values of $\Delta\Delta G_c + \Delta E_a$, listed in the fourth column of Table 7, part (*a*), prove to be very close to the experimental values of $\Delta G^{\cdot}$ over the whole temperature range considered. Around room temperature, the excluded volume effect and the dispersive interactions contribute roughly to the same extent in determining the positive $\Delta G^{\cdot}$ values, whereas, above 75°C, the excluded volume effect plays the dominant role (i.e., $\Delta\Delta G_c$ = 12.2 kJ mol^{-1} at 25°C and 20.2 kJ mol^{-1} at 100°C, while ΔE_a = 11.4 kJ mol^{-1} at 25°C and 8.3 kJ mol^{-1} at 100°C). It is worth noting that Lee (8), analyzing the l→w process of alkanes (i.e., propane, isobutane, and neopentane), found that the contribution from dispersive interactions was negligible, while the contribution from excluded volume effect was largely dominant in the whole temperature range 0–100°C.

Table 7. Calculated estimates of $\Delta\Delta G_c = \Delta G_c$(water) – ΔG_c(liquid phase) and $\Delta E_a = E_a$(water) – E_a(liquid phase) for the transfer process of cyclohexane (*a*) and benzene (*b*) from pure liquid phase at equilibrium vapour pressure to water at 1 atm, in the temperature range 5–100°C.

	T (°C)	$\Delta\Delta G_c$ (kJ mol^{-1})	ΔE_a (kJ mol^{-1})	$\Delta\Delta G_c + \Delta E_a$ (kJ mol^{-1})	$\Delta G^{\cdot}$ (kJ mol^{-1})
(*a*)	5	9.5	12.5	22.0	22.0
	25	12.2	11.4	23.6	23.7
	50	15.3	10.3	25.6	25.3
	75	17.8	9.3	27.1	26.2
	100	20.2	8.3	28.5	26.7
(*b*)	5	5.7	7.1	12.8	14.4
	25	8.2	6.0	14.2	15.5
	50	10.8	4.9	15.7	16.3
	75	13.1	3.9	17.0	16.7
	100	15.1	3.1	18.2	16.7

Note: The sum $\Delta\Delta G_c + \Delta E_a$ is also compared to the experimental $\Delta G^{\cdot}$ values in the same temperature range. The values for benzene are from ref. (1).

To perform a correct and meaningful comparison, the $\Delta\Delta G_c$ and ΔE_a values already determined for the l→w process of benzene (1) are listed in the second and third columns of Table 7, part (*b*). A look at such values leads to the conclusion that the physical mechanism determining the hydrophobicity of cyclohexane and benzene is identical; the excluded volume effect associated with cavity creation and the dispersive interactions are the solely determinant. Clearly, there are quantitative differences between cyclohexane and benzene, which are important because, at 25°C, $\Delta G^{\cdot}$ = 23.7 kJ mol^{-1} for cyclohexane, but 15.5 kJ mol^{-1} for benzene. In fact, both $\Delta\Delta G_c$ and ΔE_a, at any temperature, are larger for cyclohexane than benzene by about 5 kJ mol^{-1}. The values of both ΔG_c and E_a for benzene and cyclohexane in their own pure liquid phase prove to be closely similar (compare Table 4 with Table 3 of ref. (1)). Instead, the work for creating a cavity suitable to accommodate cyclohexane in water is larger, by about 5 kJ mol^{-1}, than the corresponding work for accommodating benzene (i.e., in water, at 25°C, ΔG_c = 42.7 kJ mol^{-1} for cyclohexane and 38.0 kJ mol^{-1} for benzene). The difference is simply caused by the larger

© 2000 NRC Canada

molecular size of cyclohexane with respect to benzene: σ = 5.63 Å vs. 5.26 Å. On the other hand, the E_a value for cyclohexane in water is smaller, in absolute value, by about 4 kJ mol^{-1} than the corresponding quantity for benzene (i.e., in water, at 25°C, E_a = –38.1 kJ mol^{-1} for cyclohexane and –42.3 kJ mol^{-1} for benzene). The estimate of E_a for benzene in water at 25°C is reliable because it is practically identical to the value, –42.6 kJ mol^{-1}, calculated by Linse (51). He used a modified benzene–water potential with the partial charges characteristic of the aromatic ring switched off (51), yielding an E_a for benzene based solely on dispersive contributions. As a result, the difference in E_a for cyclohexane and benzene should be related to the large polarizability of benzene's π electrons, which strengthen the aromatic ring–water dispersive interactions (i.e., according to the famous London theoretical treatment (27), the dispersive energy is proportional to the polarizabilities of interacting molecules).

In conclusion, the above analysis implies that the hydrophobicity of cyclohexane can be accounted for by only two factors: (*i*) the decrease in the entropy of water due to the excluded volume effect associated with the creation of a cavity suitable to host a cyclohexane molecule; (*ii*) the loss of favourable dispersive interactions among cyclohexane molecules in the pure liquid phase.

Acknowledgements

Work supported by a P.R.I.N. grant from the Italian Ministry for University and Scientific and Technological Research (M.U.R.S.T., Rome).

References

1. G. Graziano. Biophys. Chem. **82**, 69 (1999).
2. W. Blokzijl and J.B.F.N. Engberts. Angew. Chem. Int. Ed. Engl. **32**, 1545 (1993).
3. A. Ben-Naim. Solvation thermodynamics. Plenum Press, New York. 1987.
4. A. Radzicka and R. Wolfenden. Biochemistry, **27**, 1664 (1988).
5. G.D. Rose and R. Wolfenden. Annu. Rev. Biophys. Biomol. Struct. **22**, 381 (1993).
6. P. Shih, L.G. Pedersen, P.R. Gibbs, and R. Wolfenden. J. Mol. Biol. **280**, 421 (1998).
7. J.R. Errington and A.Z. Panagiotopoulos. J. Chem. Phys. **111**, 9731 (1999).
8. B. Lee. Biopolymers, **24**, 813 (1985); Biopolymers, **31**, 993 (1991); Methods Enzymol. **259**, 555 (1995).
9. G. Graziano. Can. J. Chem. **76**, 437 (1998).
10. G. Graziano. J. Chem. Soc. Faraday Trans. **94**, 3345 (1998).
11. G. Graziano. Phys. Chem. Chem. Phys. **1**, 1877 (1999); **1**, 3567 (1999).
12. B. Lee. J. Chem. Phys. **83**, 2421 (1985).
13. (*a*) B. Madan and B. Lee. Biophys. Chem. **51**, 279 (1994); (*b*) M. Ikeguchi, S. Shimizu, S. Nakamura, and K. Shimizu. J. Phys. Chem. B **102**, 5891 (1998).
14. B. Lee. Biophys. Chem. **51**, 271 (1994).
15. A. Ben-Naim. Biopolymers, **14**, 1337 (1975); R. Lumry, E. Battistel, and C. Jolicoeur. Faraday Symp. Chem. Soc. **17**, 93 (1982); E. Grunwald. J. Am. Chem. Soc. **108**, 5726 (1986); H.A. Yu and M.J. Karplus. J. Chem. Phys. **89**, 2366 (1988); H.S. Ashbaugh and M.E. Paulaitis. J. Phys. Chem. **100**, 1900 (1996); H. Qian and J.J. Hopfield. J. Chem. Phys. **105**, 9292 (1996).
16. R. Wolfenden and A. Radzicka. Science (Washington, D.C.), **265**, 936 (1994).
17. H. Reiss. Adv. Chem. Phys. **9**, 1 (1966).
18. R.A. Pierotti. Chem. Rev. **76**, 717 (1976).
19. A.H. Narten and H.A. Levy. Science (Washington, D.C.), **165**, 447 (1969).
20. E. Wilhelm and R. Battino. J. Chem. Phys. **55**, 4012 (1971).
21. B. Lee and F.M. Richards. J. Mol. Biol. **55**, 379 (1971).
22. R.M. Jackson and M.J.E. Sternberg. Protein Eng. **7**, 371 (1994).
23. M.I. Cabaco, Y. Danten, M. Besnard, Y. Guissani, and B. Guillot. J. Phys. Chem. B **101**, 6977 (1997).
24. E. Wilhelm. J. Chem. Phys. **58**, 3558 (1973).
25. B.D. Smith and R. Srivastava. Thermodynamic data for pure compounds, part A, hydrocarbons and ketones. Elsevier, Amsterdam. 1986.
26. G.S. Kell. J. Chem. Eng. Data, **20**, 97 (1975).
27. J.O. Hirschfelder, C.F. Curtiss, and R.B. Bird. Molecular theory of gases and liquids. Wiley, New York. 1964.
28. W.L. Jorgensen, J. Gao, and C. Ravimohan. J. Phys. Chem. **89**, 3470 (1985).
29. P.L. Privalov and S.J Gill. Adv. Protein Chem. **39**, 191 (1988).
30. E. Wilhelm and R. Battino. J. Chem. Phys. **58**, 3561 (1973).
31. M.H. Abraham. J. Am. Chem. Soc. **104**, 2085 (1982).
32. S.J. Gill, N.F. Nichols, and I. Wadso. J. Chem. Thermodyn. **8**, 445 (1976).
33. S.J. Gill, S.F. Dec, G. Olofsson, and I. Wadso. J. Phys. Chem. **89**, 3758 (1985).
34. G.I. Makhatadze and P.L. Privalov. Biophys. Chem. **50**, 285 (1994).
35. M. Lucas. J. Phys. Chem. **80**, 359 (1976); L.S.E. de Souza and D. Ben-Amotz. J. Chem. Phys. **101**, 9858 (1994); A. Wallqvist and D.G. Covell. Biophys. J. **71**, 600 (1996).
36. F. Floris and J. Tomasi. J. Comput. Chem. **10**, 616 (1989).
37. L.R. Pratt and D. Chandler. J. Chem. Phys. **67**, 3683 (1977); J. Chem. Phys. **73**, 3434 (1980).
38. S. Garde, A.E. Garcia, L.R. Pratt, and G. Hummer. Biophys. Chem. **78**, 21 (1999).
39. A.K. Soper and J.L. Finney. Phys. Rev. Lett. **71**, 4346 (1993); J.L. Finney and A.K. Soper. Chem. Soc. Rev. **23**, 1 (1994); J.Z. Turner, A.K. Soper, and J.L. Finney. J. Chem. Phys. **102**, 5438 (1995).
40. A. Filipponi, D.T. Bowron, C. Lobban, and J.L. Finney. Phys. Rev. Lett. **79**, 1293 (1997); D.T. Bowron, A. Filipponi, M.A. Roberts, and J.L. Finney. Phys. Rev. Lett. **81**, 4164 (1998); D.T. Bowron, A. Filipponi, C. Lobban, and J.L. Finney. Chem. Phys. Lett. **293**, 33 (1998).
41. N.T. Skipper, C.H. Bridgeman, A.D. Buckingham, and R.L. Mancera. Faraday Discuss. **103**, 141 (1996); R.L. Mancera. J. Chem. Soc. Faraday Trans. **94**, 3549 (1998); R.D. Mountain and D. Thirumalai. Proc. Natl. Acad. Sci. U.S.A. **95**, 8436 (1998).
42. B. Lee and G. Graziano. J. Am. Chem. Soc. **118**, 5163 (1996).
43. A.D.J. Haymet, K.A.T. Silverstein, and K.A. Dill. Faraday Discuss. **103**, 117 (1996); K.A.T. Silverstein, A.D.J. Haymet, and K.A. Dill. J. Am. Chem. Soc. **120**, 3166 (1998); K.A.T. Silverstein, A.D.J. Haymet, and K.A. Dill. J. Chem. Phys. **111**, 8000 (1999).
44. H.S. Frank and M.W. Evans. J. Chem. Phys. **13**, 507 (1945); H.S. Frank and W.Y. Wen. Discuss. Faraday Soc. **24**, 133 (1957); H.S. Frank and A.S. Quist. J. Chem. Phys. **34**, 604 (1961).

© 2000 NRC Canada

45. D. Chandler. Phys. Rev. E: Stat. Phys. Plasmas Fluids Relat. Interdiscip. Top. **48**, 2898 (1993); G.E. Crooks and D. Chandler. Phys. Rev. E: Stat. Phys. Plasmas Fluids Relat. Interdiscip. Top. **56**, 4217 (1997); K. Lum, D. Chandler, and J.D. Weeks. J. Phys. Chem. B **103**, 4570 (1999).
46. A. Pohorille and L.R. Pratt. J. Am. Chem. Soc. **112**, 5066 (1990); L.R. Pratt and A. Pohorille. Proc. Natl. Acad. Sci. U.S.A. **89**, 2995 (1992); G. Hummer, S. Garde, A.E. Garcia, A. Pohorille, and L.R. Pratt. Proc. Natl. Acad. Sci. U.S.A. **93**, 8951 (1996).
47. B. Guillot, Y. Guissani, and S. Bratos. J. Chem. Phys. **95**, 3643 (1991); B. Guillot and Y. Guissani. J. Chem. Phys. **99**, 8075 (1993).
48. T. Lazaridis and M.E. Paulaitis. J. Phys. Chem. **96**, 3847 (1992); T. Lazaridis and M.E. Paulaitis. J. Phys. Chem. **98**, 635 (1994); S. Garde, G. Hummer, and M.E. Paulaitis. Faraday Discuss. **103**, 125 (1996).
49. A. Ben-Naim. Hydrophobic interactions. Plenum Press, New York. 1980.
50. B.J. Berne. Proc. Natl. Acad. Sci. U.S.A. **93**, 8800 (1996); G. Hummer. J. Am. Chem. Soc. **121**, 6299 (1999); H.S. Ashbaugh, E.W. Kaler, and M.E. Paulaitis. J. Am. Chem. Soc. **121**, 9243 (1999).
51. P. Linse. J. Am. Chem. Soc. **112**, 1744 (1990).
52. B. Widom. J. Chem. Phys. **39**, 2808 (1963); J. Phys. Chem. **86**, 869 (1982).
53. R.C. Weast (*Editor*). Handbook of chemistry and physics. Chemical Rubber Co., Cleveland, OH. 1972.

Appendix: Lee's theory of solvation

Inserting a solute molecule at a fixed point in a solvent corresponds to introducing a perturbing potential $\Psi(\boldsymbol{X})$, where $\boldsymbol{X}$ is a vector describing the position of each of the N molecules of the liquid solvent. According to Widom's (52) potential distribution theory, the standard Gibbs energy change is:

$$[A1] \quad \Delta G^{\cdot} = -RT\ln < \exp[-\Psi(\boldsymbol{X})/RT] >_p$$

where the subscript p means that the canonical average is carried out over the pure solvent configurations, assuming an NPT ensemble. Lee (8) devised the following expression for the perturbing potential:

$$[A2] \quad \exp[-\Psi(\boldsymbol{X})/RT] = \zeta(\boldsymbol{X})\ \exp[-\psi_a(\boldsymbol{X})/RT]$$

where $\zeta(\boldsymbol{X})$ of a configuration is equal to zero or one depending on whether or not the hard core of any solvent molecule in this configuration overlaps with that of the solute molecule, and $\psi_a(\boldsymbol{X})$ represents the attractive potential between the solute molecule and all the solvent molecules in the given configuration. Using eq. [A2], eq. [A1] becomes:

$$[A3] \quad \Delta G^{\cdot} = -RT\ln < \zeta(\boldsymbol{X}) >_p - RT\ln < \exp[-\psi_a(\boldsymbol{X})/RT] >_c$$

where the subscript c means that the canonical average is carried out over the solvent configurations which happen to have a cavity of the desired dimension. Thus, $\Delta G^{\cdot}$ is the sum of two terms: the first one corresponds to the work of creating the cavity, and the second one to the work of turning on the attractive potential around the cavity. Now, let us analyze in detail the two subprocesses.

Creation of the cavity. The work of cavity creation is:

$$[A4] \quad \Delta G_c = -RT\ln < \zeta(\boldsymbol{X}) >_p$$

and corresponds to the work of selecting the configurations containing the cavity from the ensemble of pure solvent configurations; this is an exact result of statistical mechanics (12). Application of equilibrium thermodynamics allows the derivation of the cavity enthalpy and entropy changes (12):

$$[A5] \quad \Delta H_c = < H(\boldsymbol{X}) >_c - < H(\boldsymbol{X}) >_p$$

$$[A6] \quad \Delta S_c = R\ln < \zeta(\boldsymbol{X}) >_p + (\Delta H_c/T) = \Delta S_x + (\Delta H_c/T)$$

The enthalpy change upon cavity creation is entirely due to solvent reorganization. Also the entropy change upon cavity creation is entirely due to solvent reorganization; however, it is made up of two parts: the first one on the right-hand side of eq. [A6] due to the selection of the solvent configurations containing the cavity, and the other due to the reorganization of solvent molecules around the cavity. The latter contribution perfectly cancels the change in enthalpy, so that the work of cavity creation is entirely entropic and due to the excluded volume effect associated with the reduction in the size of the configuration space accessible to the solvent molecules, $\Delta G_c = -T\Delta S_x$. The excluded volume effect has to be considered the entropic part of the perturbing potential.

Turning on the attractive potential. The work of turning on the attractive potential is:

$$[A7] \quad \Delta G_a = -RT\ln < \exp[-\psi_a(\boldsymbol{X})/RT] >_c$$

By applying the Gibbs–Helmholtz equation, the enthalpy change is:

$$[A8] \quad \Delta H_a = < \psi_a(\boldsymbol{X}) >_s + [< H(\boldsymbol{X}) >_s - < H(\boldsymbol{X}) >_c] = < \psi_a(\boldsymbol{X}) >_s + \Delta H_{ar}$$

where the subscript s means that the canonical average is carried out over the solvent configurations that happen to have a cavity occupied by a solute molecule interacting with all the solvent molecules. The enthalpy change is made up of two parts: the first is the average solute-solvent interaction energy, and the other is the enthalpic contribution arising from the solvent reorganization upon turning on the attractive potential. The entropy change is:

$$[A9] \quad \Delta S_a = R\ln < \exp[-\psi_a(\boldsymbol{X})/RT] >_c + [< \psi_a(\boldsymbol{X}) >_s/T] + (\Delta H_{ar}/T)$$

Using an inverse relationship demonstrated by Widom (52), eq. [A9] becomes:

$$[A10] \quad \Delta S_a = -R\ln < \exp[\psi_a(\boldsymbol{X})/RT] >_s + [< \psi_a(\boldsymbol{X}) >_s/T] + (\Delta H_{ar}/T)$$

By setting $\kappa = \psi_a(\boldsymbol{X}) - < \psi_a(\boldsymbol{X}) >_s$, expanding in power series the exponential function, and keeping in mind that $< \kappa >_s \equiv 0$, one obtains:

© 2000 NRC Canada

[A11] $-R\ln < \exp[\psi_a(\boldsymbol{X})/RT] >_s \approx -[< \psi_a(\boldsymbol{X}) >_s/T] - [< \kappa^2 >_s/2RT^2]$

When the attractive potential $\psi_a(\boldsymbol{X})$ is weak (14), the fluctuations in the value of $< \psi_a(\boldsymbol{X}) >_s$ are small, and the second term on the right-hand side of eq. [A11] can be neglected. Thus:

[A12] $\Delta S_a \approx (\Delta H_{ar}/T)$

and the solvent reorganization associated with the process of turning on the attractive potential is a compensating process, because the change in entropy cancels that in enthalpy. The condition of small fluctuations in the value of $< \psi_a(\boldsymbol{X}) >_s$ is verified for nonpolar compounds (8, 28, 36, 51), and the Gibbs energy change is simply given by the average solute–solvent interaction energy:

[A13] $\Delta G_a = < \psi_a(\boldsymbol{X}) >_s \equiv E_a$

Recapitulation. The total solvation Gibbs energy change is:

[A14] $\Delta G^{\cdot} = \Delta G_c + \Delta G_a = -T\Delta S_x + E_a$

The total enthalpy change upon solvation is:

[A15] $\Delta H^{\cdot} = E_a + \Delta H_r$

where E_a, the average solute–solvent interaction energy, has to be considered the enthalpic part of the perturbing potential. The term $\Delta H_r \equiv \Delta H_c + \Delta H_{ar}$ is the enthalpy change due to the purely structural solvent reorganization that happens as a response to full perturbation. The total solvation entropy change is:

[A16] $\Delta S^{\cdot} = \Delta S_r = \Delta S_x + \Delta S_{nx}$

it is entirely due to solvent reorganization because the solute molecule is fixed in space adopting the standard state of Ben-Naim (3, 8). However, the excluded volume effect for cavity creation has to be considered the entropic part of the perturbing potential, not a solvent response; the ΔS_x term is the corresponding entropy contribution. A further reorganization of solvent molecules around the solute happens as a response to full perturbation, both volume exclusion and turning on solute–solvent interaction; the ΔS_{nx} term represents this nonexcluded volume contribution to the total entropy change upon solvation. Finally, it proves that the compensation relation, $T\Delta S_{nx} = \Delta H_r$, is operative for the solvent response.

© 2000 NRC Canada

A study of hydrogenation of benzhydrols in the presence of catalytic amount of triflic acid

Christophe Waterlot, Daniel Couturier, Marc De Backer, and Benoît Rigo

Abstract: The ionic hydrogenation of diarylcarbinols by triethylsilane, in the presence of catalytic amount of triflic acid proceeds via dibenzhydryl ethers. These ethers do not disproportionate to benzophenones and diphenylmethanes but are reduced by triethylsilane to diarylmethanes.

Key words: catalytic reduction, benzhydrols, dibenzhydryl ethers, triethylsilane.

Résumé : L'hydrogénation ionique des benzhydrols par le triéthylsilane en présence d'une quantité catalytique d'acide triflique, passe par la formation d'éthers de dibenzhydryles. Ces éthers ne se dismutent pas en benzophénones et diphénylméthanes correspondants mais sont directement réduit en diarylméthanes par le triéthylsilane.

Mots clés : réduction catalytique, benzhydrols, éthers de dibenzhydryles, triéthylsilane.

1. Introduction

During the course of a program requiring the use of diarylcarbinols (1), we were puzzled by some differences between the reported chemistry (2–6) of these compounds and some of our results (7).

Ionic hydrogenation of ketones (2) and alcohols (3) by triethylsilane can be realized by using four molar equiv. of triflic acid, and is assumed to proceed through carbocations (3, 4) (Scheme 1).

In similar reactions, no symmetrical ethers were observed during the reductions of diaryl ketones by triethylsilane – trifluoroacetic acid (5). In the case of aliphatic or aryl aliphatic ketones only, the reduction performed with triethylsilane – trimethylsilyl triflate yielded symmetrical ethers (6).

It is also reported that in acidic media diarylcarbinols **1** easily yielded dibenzhydryl ethers **2** (8) which rapidly disproportionated into diphenylmethanes **3** and benzophenones **4** (9). These triflic acid-catalyzed disproportionations proceeded via hydride transfer (10). In a previous work (7), it was found that a quantity as low as 0.06 molar equiv. of triflic acid in a chloroform solution of dibenzhydryl ethers **2** promoted this disproportionation. (Scheme 2).

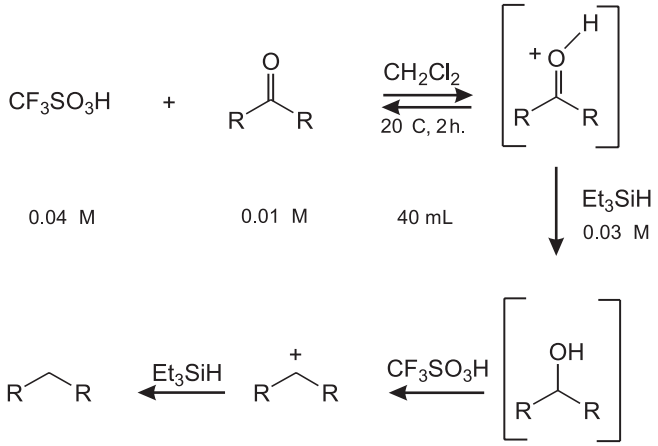
The work reported here is an attempt to elucidate which reaction route is the most probable with the very small amount of triflic acid utilized in the previous works (7). Experimental conditions were selected to answer the following questions

(1) Are the benzhydrols **1**, after protonation, directly reduced to diphenylmethanes **3** (Scheme 3, path A)?

(2) Or do dibenzhydryl ethers **2**, formed in a first step, disproportionate into diphenylmethanes **3** and benzophenones **4**, whose further reduction recycles the starting benzhydrols **1** (Scheme 3, path B)?

(3) Alternatively, are the dibenzhydryl ethers **2** reduced to diphenylmethanes **3** and triethylsilyl benzhydryl ethers which again disproportionate to dibenzhydryl ether **2** (7) (Scheme 3, path C)?

Scheme 1.



Received June 19, 1999. Published on the NRC Research Press website on September 1, 2000.

B. Rigo.[1] Laboratoire d'Ingéniérie Moléculaire, Ecole des Hautes Etudes Industrielles, 13 rue de Toul, 59046 Lille, France.
M. De Backer. LASIR-HEI, UMR 8516, 13 rue de Toul, 59046 Lille, France.
C. Waterlot and D. Couturier. Laboratoire d'Ingéniérie Moléculaire, Université des Sciences et Technologies de Lille, 59655 Villeneuve d'Ascq, France.

[1]Author to whom correspondence may be addressed. Telephone: 03 28 38 48 58. e-mail: rigo@hei.fr

2. Results and discussions

2.1 Reduction of substituted benzhydrols to diarylmethane

To lower the reaction rates and to observe the intermediate products, the reduction of substituted benzhydrols **1** to diarylmethanes **3** was realized with a small amount of triflic acid (benzhydrol – triethylsilane – triflic acid, 1:3:0.3) that is thirteen times lower than that used by others (3) for the

© 2000 NRC Canada

Scheme 2.

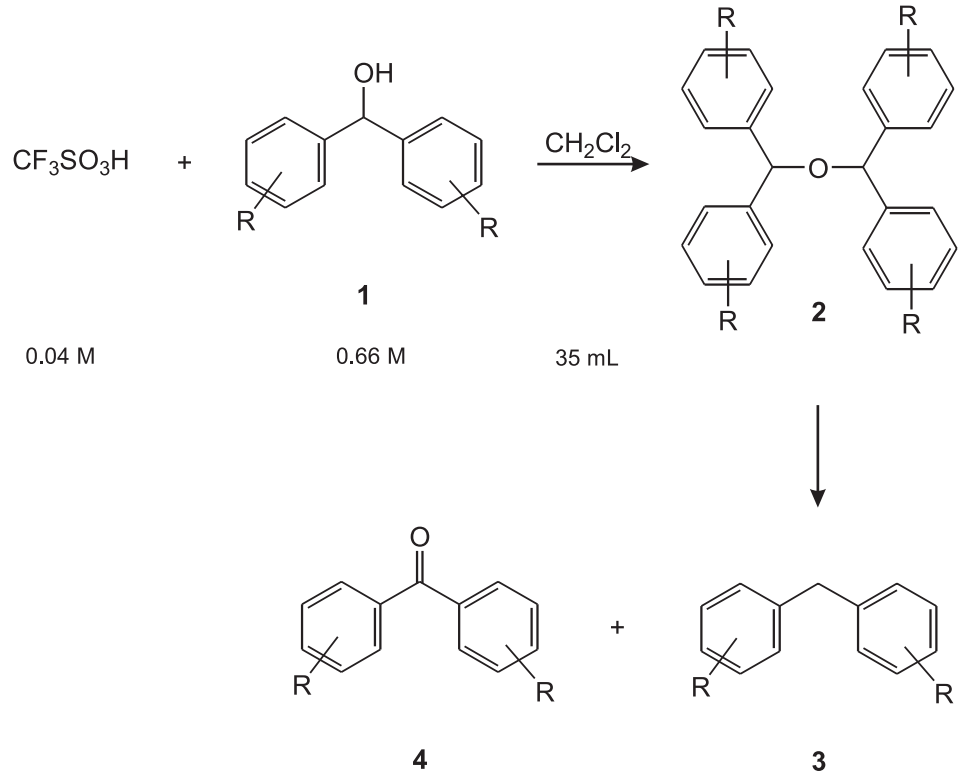


Table 1. Reduction of benzhydrols **1** by Et_3SiH and triflic acid.[a]

Entry	R1	R2	Temp (°C)	Time (min)	Benzhydrol **1** (%)[b]	Ether **2** (%)[b]	$ArCH_2Ar$ **3** (%)[b]
1	H	H	20	240	0	30	70
2	H	4′-Cl	20	240	67	4	29
3	H	4′-Br	20	240	18	11	71
4	4-OMe	4′-OMe	20	90	10	73	17
5	4-OMe	4′-OMe	20	360	0	22	78
6	4-OMe	4′-OMe	60	15	0	22	78
7	4-OMe	4′-OMe	60	30	0	5	95
8	4-OMe	4′-OMe	60	45	0	0	100/(96)[d]
9[e]	$2,5\text{-}(OMe)_2$[e,f]	4′-Cl[c]	5	15	0[f]	29	0
10	$2,5\text{-}(OMe)_2$[f]	4′-Cl[c]	20	45	0	0	(84)[d]
11	$2,5\text{-}(OMe)_2$[f]	4′-Br[c]	20	45	0	0	(90)[d]
12	$2,5\text{-}(OMe)_2$[f]	4′-I[c]	20	45	0	0	(92)[d]

[a]Reaction conditions: benzhydrol **1** 10 mmol, triethylsilane 30 mmol, triflic acid 3 mmol, $CHCl_3$ 40 mL.

[b]Yields were determined by ^1H NMR, ^{13}C NMR, or HPLC.

[c]Triflic acid 3 mmol, triethylsilane 25 mmol.

[d]Isolated yield.

[e]The corresponding benzophenone **4** was used; 71% of the starting ketone was also observed in the reaction mixture.

[f]Synthesis of the starting ketones will be described in a future publication.

reduction of benzophenones (1:3:4) as it was described in Scheme 1. It is shown in Table 1 that dibenzhydryl ethers **2** are important intermediates in the reaction. This is well evidenced by comparing the results in rows 4 and 5; 6–8 where the same reaction has been performed at two different temperatures and for various lengths of time. The same conclusion may be drawn from rows 9 and 10. Thus the already known path A is not the only route for this reaction.

2.2 Reduction of benzhydryl ethers

The reduction of dibenzhydryl ethers[2] **2** to diarylmethanes **3** with 0.01 molar equiv. of triflic acid, in the absence or

[2]The dibenzhydryl ethers **2** were obtained by adding a catalytic amount of triflic acid to a solution of benzhydrol in chloroform (1): R1, R2 = H, 86% (20°C, 2 h); R1 = H, R2 = Cl, 93% (60°C, 2 h); R1 = H, R2 = Br, 95% (60°C, 2 h); R1, R2 = OMe, 85% (20°C, 1.25 h).

© 2000 NRC Canada

Scheme 3.

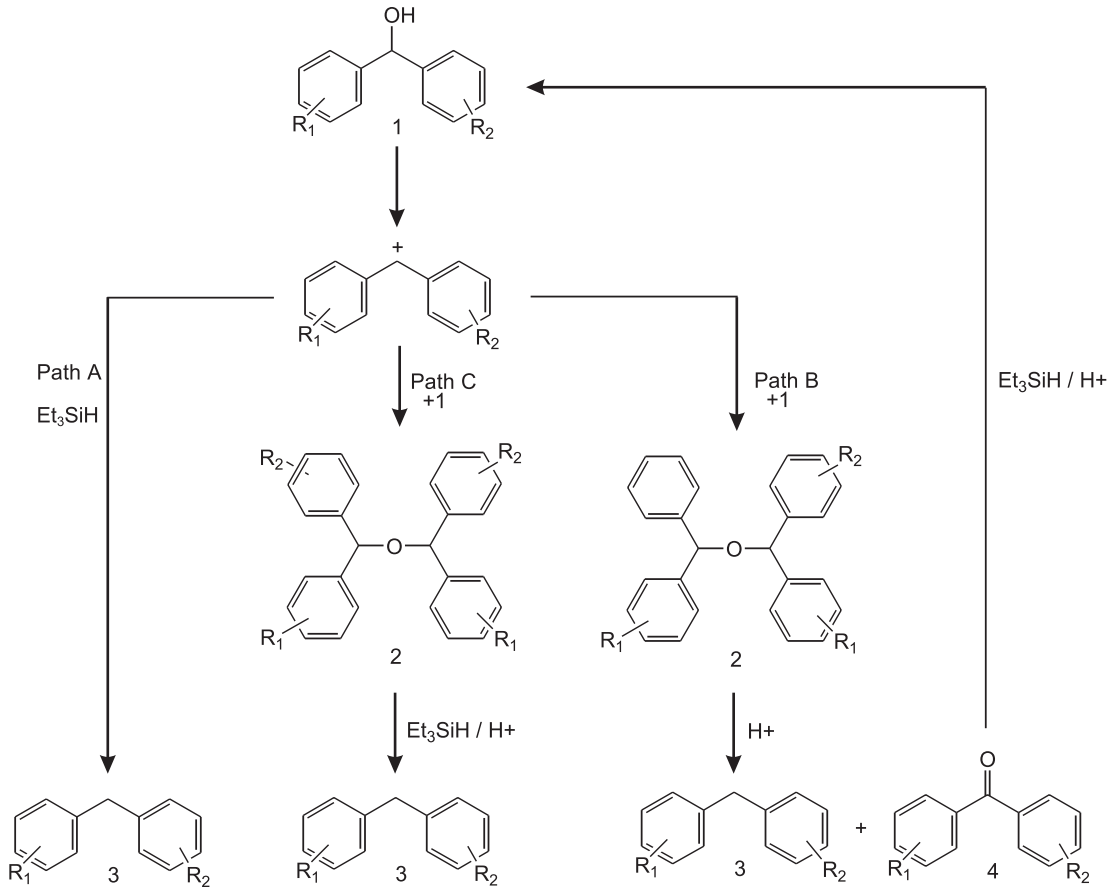


Table 2. Reaction of dibenzhydryl ethers **2** with triflic acid in the presence or absence of triethylsilane.[a]

Entry	R1	R2	Et_3SiH	Temp (°C)	Time (h)	Ether **2** (%)[b]	Ketone **4** (%)[b]	$ArCH_2Ar$ **3** (%)[b]
1	H	H	no	60	0.25	0	50	50
2	H	H	yes[c]	60	0.25	0	0	100
3	H	H	no	20	4	100	0	0
4	H	H	yes[c]	20	4	23	0	77
5	H	4′-Cl	no	60	5	0	50/(38)[d]	50/(34)[d]
6	H	4′-Cl	no	20	48	100	0	0
7	H	4′-Cl	yes[c]	20	4	71	0	29
8	H	4′-Br	no	60	5	0	50/(40)[d]	50/(39)[d]
9	H	4′-Br	no	20	48	100	0	0
10	H	4′-Br	yes[c]	20	4	28	0	72
11	4-OMe	4′-OMe	no	60	0.25	0	50/(42)[d]	50/(44)[d]
12	4-OMe	4′-OMe	no	20	4	48	26	26
13	4-OMe	4′-OMe	yes[c]	60	0.5	0	0	100/(96)[d]
14	4-OMe	4′-OMe	yes[c]	20	4	45	0	55

[a]Reaction conditions: dibenzhydryl ether **2** 10 mmol, triflic acid 0.1 mmol.
[b]Yields were determined by ^1H NMR, ^{13}C NMR, or HPLC.
[c]Triethylsilane 22 mmol.
[d]Isolated yield.

presence of triethylsilane, was studied. Four dibenzhydryl ethers bearing various groups were chosen in such a way that it was possible to identify the reaction intermediates. The reaction was studied at two different temperatures and for various lengths of time. In the absence of triethylsilane, the disproportionation reaction leading to **3** and **4** is the most important while reduction to **3** is preponderant in its presence.

Path B implies that substituted 4,4′-dimethoxybenzophenone **4** should be an important intermediate in this reaction.

© 2000 NRC Canada

However under experimental conditions similar to ours, it has been shown that the reduction of **4** (R = OMe) did not take place[3] due to the extreme stability of the intermediate carbocation formed by the protonation of the carbonyl group (3). If path B was important, there should be in this case an accumulation of **4** (R = OMe) in the course of the reaction. As it can be seen in Table 2 during the reduction of tetramethoxy-dibenzhydryl ether **2** (R1 = R2 = OMe) (rows 13 and 14) benzophenone **4** was never observed when triethylsilane was present; this result allows us to exclude path B.

This point can be further strengthened by observing that in the presence of triethylsilane the production of other substituted benzophenone **4** was never observed. Also, the rate of reduction of dibenzhydryl ethers **2** was greater than the rate of the disproportionation reaction (compare entries 4, 7, 10 with entries 3, 6, 9).

3. Conclusion

Although no formal kinetic studies were reported here, the results presented in Tables 1 and 2 indicate that path C is a favored process when only a small amount of triflic acid is used. In a first step of the ionic reduction of benzhydrols by $Et_3SiH–CF_3SO_3H$, dibenzhydryl ethers are formed and reduction of these ethers is faster than their disproportionation reaction (path C). However, the formation of dibenzhydryl ether is not always considerably faster than the reduction (Table 1, entries 2 and 3). It is then possible that path A contributes in part, to the reduction process. It also must be stressed that the experimental conditions used here are different from previous reported works (3, 11) where super acidic conditions promoted other reaction paths.

4. Experimental

Materials

All benzhydrols were commercially available, except for compounds **1** (R1 = H, R2 = Cl; R1 = H, R2 = I; R1 = H, R2 = Br). Melting points were determined with a Mettler FP1 and are uncorrected. ^{1}H NMR and ^{13}C NMR spectra were recorded on a Brücker AC300 spectrometer operating at, respectively, 300.133 and 75.47 MHz using trimethylsilane as an internal reference. Coupling constants are given in Hz. IR spectra were recorded on a Brücker IFS 48 spectrometer. The reaction mixtures were analyzed by ^{1}H NMR and ^{13}C NMR and by liquid chromatography (C_{18} column and a 60:40 acetonitrile–water as mobile phase). Elemental analyses were performed by the "Service Central de Microanalyses" of CNRS, in Vernaison, France.

Procedure

*4′-Chloro-2,5-dimethoxybenzhydrol (**1**:R1 = H, R2 = Cl)*

To a stirred solution of 2,5-dimethoxy-1-(4′-chlorobenzoyl)benzene (17 g, 0.615 mol) in methanol (160 mL), sodium borohydride (2.8 g, 0.738 mol) was added at 5°C over a period of 15 min. The reaction mixture was then stirred for 60 min at 5°C and brought to room temperature. After removing the methanol, the crude product was quenched with a solution of 1N HCl. The mixture was extracted with diethyl ether (3 × 20 mL), dried over $CaCl_2$, and solvents were evaporated in vacuo; mp 65°C (petroleum ether – diethyl ether), yield 93%. IR (KBr) ν (cm^{-1}): 3419, 3003, 2836, 1591, 1500, 1447, 1276, 1217, 1046, 711. ^{1}H NMR ($CDCl_3$) δ (ppm): 3.24 (s, 1H), 3.73 (s, 6H), 5.95 (s, 1H), 6.80 (m, 3H), 7,27 (m, 4H). ^{13}C NMR ($CDCl_3$) δ (ppm): 55.7, 55.9, 71.6, 111.9, 112.9, 114.0, 127.9, 128.3, 132.6, 132.9, 141.7, 150.7, 153.8 Anal. calcd. for $C_{15}H_{15}ClO_3$: C 64.64, H 5.42, O 17.22; found: C 64.60, H 5.40, O 17.23.

*4′-Iodo-2,5-dimethoxybenzhydrol (**1**:R1 = H, R2 = I)*

This compound was obtained following the same procedure as 4′-chloro-2,5-dimethoxy-benzhydrol; mp 86°C (petroleum ether – diethyl ether), yield 88%. IR (KBr) ν (cm^{-1}): 3345, 3000, 2831, 1590, 1502, 1451, 1278, 1223, 1048, 505. ^{1}H NMR ($CDCl_3$) δ (ppm): 3.35 (s, 1H), 3.64 (s, 6H), 5.83 (s, 1H), 6.68 (m, 2H), 6.77 (d, *J* = 2.7 Hz, 1H), 7.02 (d, *J* = 8.3 Hz, 2H), 7.53 (d, *J* = 8,3 Hz, 2H). ^{13}C NMR ($CDCl_3$) δ (ppm): 55.7, 55.9, 71.6, 92.7, 111.8, 112.9, 113.9, 128.6, 132.5, 137.2, 143.0, 150.7, 153.7.; Anal. calcd. for $C_{15}H_{15}IO_3$: C 48.67, H 4.08, O 12.97; found: C 48.69, H 4.10, O 12.95.

*4′-Bromo-2,5-dimethoxybenzhydrol (**1**:R1 = H, R2 = Br)*

Sodium borohydride (0.85 g, 0.225 mol) was added at 25°C, over a period of 15 min, to a solution of 2,5-dimethoxy-1-(4′-bromobenzoyl)benzene (6 g, 0.187 mol) in methanol (80 mL). The reaction mixture was then stirred for another 90 min at room temperature. After removing the methanol, the crude product was washed with a solution of 1N HCl and the product was extracted with diethyl ether (3 × 10 mL). After drying the organic phase over $CaCl_2$ and evaporating the solvents, the benzhydrol was obtained as an oil which crystallized in a petroleum ether and diethyl ether mixture; mp 70°C (petroleum ether – diethyl ether), yield 92%. IR (KBr) ν (cm^{-1}): 3300, 3000, 2831, 1583, 1499, 1456, 1271, 1223, 1042, 701. ^{1}H NMR ($CDCl_3$) δ (ppm): 3.12 (s, 1H), 3.71 (s, 3H), 3.72 (s, 3H), 5.93 (s, 1H), 6.78 (m, 2H), 6.85 (d, *J* = 2.4 Hz, 1H), 7.24 (d, *J* = 8.4 Hz, 2H), 7.41 (d, *J* = 8.4 Hz, 2H). ^{13}C NMR ($CDCl_3$) δ (ppm): 55.7, 55.9, 71.6, 111.9, 112.9, 113.9, 121.0, 128.3, 131.2, 132.6, 142.3, 150.7, 153.7. Anal. calcd. for $C_{15}H_{15}BrO_3$: C 55.75, H 4.68, O 14.85; found: C 55.72, H 4.69, O 14.87.

Disproportionation of bis-4,4′-dimethoxybenzhydryl ether (2:R1 = R2 = OMe)

A solution of bis-4,4′-dimethoxybenzhydryl ether (4.7 g, 10 mmol) and triflic acid (0.09 mL, 0.1 mmol) in chloroform (5 mL) was heated at 60°C for 15 min. Methylene dichloride (40 mL) and water (40 mL) were added. After washing, the organic phase was dried then evaporated. The solid obtained was filtered, then washed with heptane giving a 42% yield in 4,4′-dimethoxybenzophenone identical to the commercial compound. The heptane solution was evaporated,

[3] We have repeated the reduction of 4,4′-dimethoxybenzophenone in the described conditions (3). After 30 h of reflux, the yield of 4,4′-dimethoxydiphenylmethane was less than 10%.

© 2000 NRC Canada

giving a 44% yield in dianisylmethane, identical to the known compound (9*b*).

Typical procedure: reduction of bis-4,4′-dimethoxybenzhydryl ether (2:R1 = R2 = OMe)

Triflic acid (0.09 mL, 0.1 mmol) was slowly added to a solution of bis-4,4′-dimethoxybenzhydril ether (4.7 g, 10 mmol) and triethylsilane (3.5 mL, 22 mmol) in chloroform (5 mL). The mixture was stirred at room temperature for 45 min. The organic phase was washed with a sodium carbonate solution (30 mL) and dried. After evaporation, the solid was filtered to give a 96% yield in 4,4′-dianisylmethane, identical to the known compound (9*b*).

Typical procedure: reduction of 4,4′-dimethoxybenzhydrol (1:R1 = R2 = OMe)

Triflic acid (0.25 mL, 0.3 mmol) was slowly added (2 min) via syringe, to a stirred solution of 4,4′-dimethoxybenzhydrol (2.5 g, 1 mmol) and triethylsilane (4.8 mL, 3 mmol) in chloroform (40 mL), and the mixture was stirred at 20°C for 90 min. The composition of the solution was obtained by HPLC analysis (C_{18} column, 60:40 acetonitrile–water as the mobile phase, flow 1.3 $mLmin^{-1}$): (*i*) 4.2 min (4,4′-dimethoxybenzhydrol, 10%); (*ii*) 10.8 min (4,4′-dimethoxydiphenylmethane, 73%); and (*iii*) 38.3 min (4,4′-dimethoxydibenzhydryl ether, 17%).

*2,5-Dimethoxy-1-(4′-chlorobenzyl)benzene (**3**:R1 = H, R2 = Cl)*

Triflic acid (0.26 mL, 3 mmol) was added (syringe) at room temperature, to a stirred solution of 2,5-dimethoxy-4′-chlorobenzhydrol (2.8 g, 10 mmol) in dichloromethane (30 mL). The color of the solution turned yellow-red. Subsequently, a solution of triethylsilane (4.02 mL, 25 mmol) in dry dichloromethane (10 mL) was added dropwise. An exothermic reaction took place while the temperature was maintained at 20°C. After 45 min, the mixture was poured into cold saturated sodium hydrogen carbonate solution (20 mL) and extracted with dichloromethane (3 × 10 mL). The organic layer was dried with magnesium sulfate, and evaporated; mp 42°C (petroleum ether – diethyl ether), yield 84%. IR (KBr) ν (cm^{-1}): 2998, 2947, 2831, 1590, 1495, 1459, 1437, 1219, 1045, 711. ^{1}H NMR ($CDCl_3$) δ (ppm): 3.74 (s, 3H), 3.76 (s, 3H), 3.91 (s, 1H),), 6.66 (d, *J* = 3.0 Hz, 1H), 6.73 (dd, *J* = 8.8 Hz, *J* = 3.0 Hz, 1H), 6.80 (d, *J* = 8.8 Hz, 1H), 7.14 (d, *J* = 8.5 Hz, 2H), 7.20 (d, *J* = 8.5 Hz, 2H). ^{13}C NMR ($CDCl_3$) δ (ppm): 35.5, 55.6, 56.0, 111.4, 116.8, 128.3, 130.2, 130.3, 131.6, 139.1, 151.6, 153.5. Anal. calcd. for $C_{15}H_{15}ClO_2$: C 68.57, H 5.75, O 12.18; found: C 68.60, H 5.71, O 12.20.

References

1. (*a*) B. Rigo, P. Gautret, A. Legrand, J.-P. Hénichart, and D. Couturier. Synlett. 998 (1997); (*b*) B. Rigo, P. Gautret, A. Legrand, J.-P. Hénichart, and D. Couturier. J. Heterocycl. Chem. **35**, 567 (1998).
2. (*a*) D.N. Kursanov, Z.N. Parnes, G.I. Bassova, N.M. Loim, and V.I. Zzanovich. Tetrahedron, **23**, 2235 (1967); (*b*) D.N. Kursanov, Z.N. Parnes, and N.M. Loim. Synthesis, 633 (1974).
3. G.A. Olah, M. Arvanaghi, and L. Ohannesian. Synthesis, 770 (1986).
4. F.A. Carey and H.S. Tremper. J. Am. Chem. Soc. **90**, 2578 (1968).
5. (*a*) C.T. West, S.J. Donnelly, D.A. Kooistra, and M.P. Doyle. J. Org. Chem. **38**, 2675 (1973); (*b*) H. Mayr and B. Dogan. Tetrahedron Lett. **38**, 1013 (1997).
6. M.B. Sassaman, G.K.S. Prakash, and G.A. Olah. Tetrahedron Lett. **44**, 3771 (1988).
7. P. Gautret, S. El Ghammarti, A. Legrand, D. Couturier, and B. Rigo. Synth. Commun. **26**, 707 (1996).
8. R. Parades, F. Agudelo, and G. Taborda. Tetrahedron Lett. **37**, 1965 (1996).
9. (*a*) F.G. Kny-Jones and A.M. Ward. J. Chem. Soc. 535 (1930); (*b*) M.P. Balfe, J. Kenyon, and E.M. Thain. J. Chem. Soc. 790 (1952); (*c*) H. Burton and G.W.H. Cheeseman. J. Chem. Soc. 986 (1953).
10. P.D. Bartlett and J.D. McCollum. J. Am. Chem. Soc. **78**, 1441 (1956).
11. G.A. Olah. Angew. Chem. Int. Ed. Engl. **32**, 767 (1993).

© 2000 NRC Canada

COMMUNICATION

Catalysis of the methanolysis of acetylimidazole by lanthanum triflate

Alexei A. Neverov and R.S. Brown

Abstract: Methanolysis of acetylimidazole (**1**) and *N*-acetylimidazolepentamine-Co(III) (**2**) was found to be markedly accelerated in the presence of $La(OTf)_3$. Potentiometric titration of a solution of $La^{3+}(OTf^-)_3$ gave a pK_a for the metal bound CH_3OH of 7.22. The kinetics of methanolysis of **1** and **2** were measured at 25°C at various pH under buffered conditions as a function of increasing La^{3+}. Analysis of both the kinetic and potentiometric data indicates that the catalytically active species is a La^{3+}-dimer, bridged by two methoxides, $(CH_3OH)_nLa^{3+}(CH_3O^-)_2La^{3+}(CH_3OH)_n$. The maximum second-order rate constants for attack of the dimer on **1** and **2** are 1.50×10^3 M^{-1} s^{-1} and 1.42×10^2 M^{-1} s^{-1} respectively and both processes adhere to titration of a $La^{3+}(CH_3OH)$ to generate the active form. The results are explained in terms of a mechanism where the methoxy-bridged La^{3+} dimer transiently breaks a La^{3+}-OCH_3 bond to expose both a CH_3O^- nucleophile and a La^{3+} which can act as a Lewis acid. Unlike the situation in water, the methanol results indicate that the medium greatly stabilizes and solubilizes the active dimer without the necessity of creating specially designed ligands to stabilize the dinuclear core.

Key words: lanthanum ion, catalysis, methanolysis, activated amide.

Résumé : On a observé que la méthanolyse de l'acétylimidazole (**1**) et du *N*-acétylimidazopepentamine-Co(III) (**2**) est fortement accéléré par la présence de $La(OTf)_3$. Un titrage potentiométrique d'une solution de $La^{3+}(OTf^-)_3$ permet d'établir que le pK_a du métal lié au CH_3OH est de 7,22. Opérant à divers pH, dans des conditions tamponnées, on a mesuré les cinétiques de méthanolyse des composés **1** et **2** en fonction d'une concentration croissante de La^{3+}. L'analyse des données tant cinétiques que potentiométriques indique que l'espèce catalytiquement active est un dimère de La^{3+} comportant un pont par deux molécules de méthylates, $(CH_3O)_nLa^{3+}(CH_3O^-)_2La^{3+}(CH_3OH)_n$. Les constantes de vitesse maximales pour les attaques des composés **1** et **2** sont respectivement de $1{,}50 \times 10^3$ M^{-1} s^{-1} et $1{,}42 \times 10^2$ M^{-1} s^{-1} et les deux processus adhèrent au titrage d'un $La^{3+}(CH_3OH)$ pour générer la forme active. On explique les résultats en fonction d'un mécanisme dans lequel il se produit une dissociation transitoire d'une liaison La^{3+}-OCH_3 du dimère de La^{3+} relié par un pont méthoxy qui permet d'exposer un nucléophile CH_3O^- et d'un La^{3+} qui peut agir comme acide de Lewis. Par opposition à la situation dans l'eau, les résultats obtenus avec le méthanol indiquent que le milieu stabilise grandement et solubilise le dimère actif sans avoir à créer des ligands appropriés pour stabiliser le coeur dinucléaire.

Mots clés : ion lanthane, catalyse, méthanolyse, amide activé.

Much recent attention was focussed on the remarkable acceleration provided by lanthanide cations (Ln^{X+}) for the hydrolysis of phosphate esters (1) and, to a lesser degree, amides and peptides (2). However mechanistic study of these Ln^{X+}-promoted hydrolyses is hindered by the fact that in water, formation of insoluble hydroxides and gels of poor definition is a problem, particularly under basic conditions. A few attempts have been made to stabilize the active forms of $Ln^{X+}(OH^-)_n$ by encapsulation into cyclodextrins (1*h*, 2*a*), macrocycles (1*g*), or micelles (1*d*) but most research has been done at neutral or acidic conditions which limits the catalytic ability of those ions. Only a few examples of Ln^{X+}-catalysis of amide bond hydrolysis are known (2), probably due to the poorer M^{X+}-coordinating ability of the neutral > N-C=O moiety compared to that of negatively charged di- and monophosphate esters. Indeed, the reported cases of strong M^{X+}-promoted hydrolysis of amide (peptide) substrates are limited to those having additional binding centers that promote preassociation of the metal (3).

Herein we focus on the La^{3+}-catalyzed methanolysis of the simple activated amide, acetylimidazole, (**1**), and its ligand exchange inert Co^{3+}-complex, *N*-acetylimidazolepentamine-Co(III), ($AcImCo(NH_3)_5^{3+}$, (**2**)) (4). These were chosen because their aqueous hydrolyses are well understood, and because it has yet to be shown that the parent compound

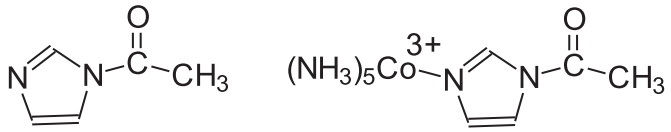
Received June 21, 2000. Published on the NRC Research Press website on August 22, 2000.

A.A. Neverov and R.S. Brown.[1] Department of Chemistry, Queen's University, Kingston, ON K7L 3N6, Canada.

[1]Author to whom correspondence may be addressed. Telephone and Fax: (613) 533-2624. e-mail: rsbrown@chem.queensu.ca

© 2000 NRC Canada

(**1**) is subject to metal ion catalysis in water. This combination allows us to investigate the role of electrostatic effects and the possibility of catalysis arising from the binding of the metal ion to the distal nitrogen of **1**. We report here that in methanol, homogeneous solutions can be obtained throughout the entire pH range surrounding ionization of $La^{3+}(CH_3OH)$. Moreover, through the use of buffered media to control the pH, which can be easily measured using a recently reported glass electrode technique (5), we can study the reaction kinetics in methanol as simply as in water without the annoying problems of metal–alkoxide precipitation. To the best of our knowledge, this is the first time such an approach has been used for kinetic investigations in methanol solutions.[2]

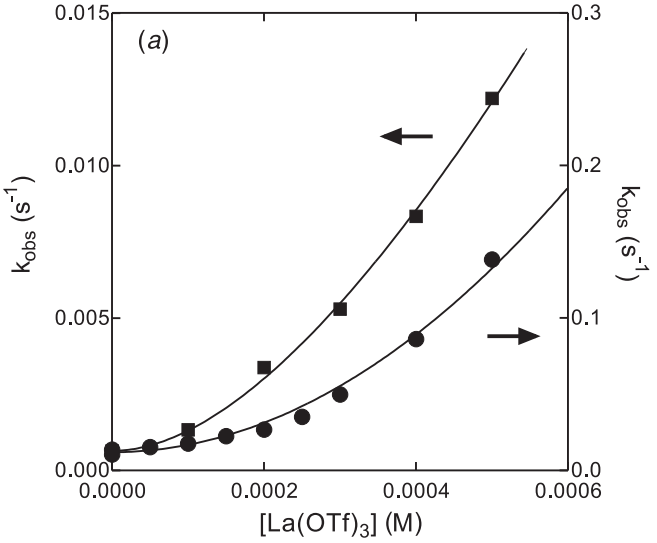


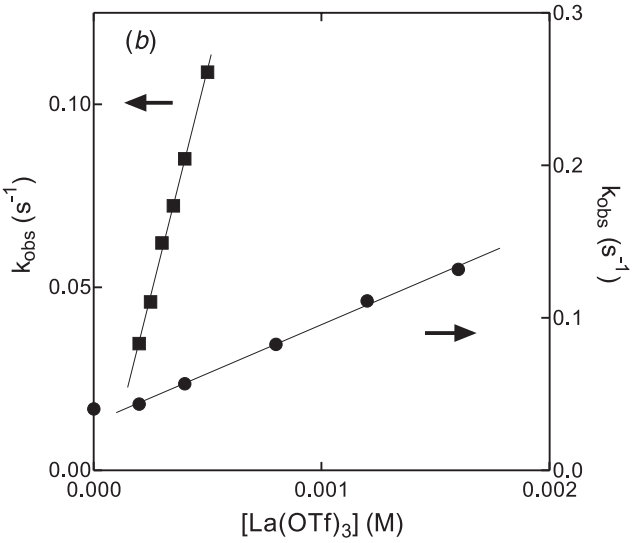
1 **2**

Our preliminary results show that the methanolysis rates[3] of **1** and **2** markedly increase in the presence of lanthanum trifluoromethanesulphonate ($La(OTf)_3$), and this process is very sensitive to pH_{MeOH}. Pseudo-first-order rate constants, k_{obs}, obtained for the methanolysis of **1** and **2** (Fig. 1*a*, *b*) show strong catalysis by $La(OTf)_3$, with the effect being linearly proportional to $[La(OTf)_3]$ at higher concentrations of metal salt but with significant curvature at concentrations lower than $\sim 2 \times 10^{-4}$ M. This indicates the involvement of second- or possibly higher order terms in $[La(OTf)_3]$. Unfortunately, direct analysis of all the experimental k_{obs} vs. $[La^{3+}]_t$ data does not provide us with reliable kinetic parameters, particularly in the case of **2** due to the high rate of the background reaction. However the fact that the k_{obs} vs. $[La(OTf)_3]_t$ dependencies look very similar for both substrates eliminates the possibility that the higher reaction order in $[La^{3+}]$ is due to complexation of a La^{3+} ion by the distal nitrogen of **1**, and rather indicates the catalysis is due to a concentration dependent change in speciation of La^{3+} in methanol such as formation of active dimers. Dimeric structures were previously observed in methanol solutions of $LaCl_3$ using La^{139} and Cl^{35} NMR (6).

Analysis of the linear parts of the plots ($[La^3]_t > 2 \times 10^{-4}$ M, Fig. 1*b*) gives the second-order rate constants (k_2) which are then plotted vs. pH_{MeOH} (as in Fig. 2) to reveal similar profiles for both substrates with apparent kinetic pK_as of 7–7.5. In a separate experiment (not shown), potentiometric titration of $La(OTf)_3$ (1.33 mmol) between pH_{MeOH} 6 and 9 shows ionization of one proton per metal ion with $pK_a^{MeOH} = 7.22$. In combination with the pH-rate profiles (Fig. 2) and k_{obs} vs. $[La(OTf)_3]$ dependencies (Fig. 1*a*, *b*),

Fig. 1. (*a*) Plots of pseudo-first-order rate constants for the methanolysis of AcIm (pH_{MeOH} = 6.7, ■, left axis)) and $AcImCo(NH_3)_5^{3+}$ (pH_{MeOH} = 7.6, μ = 0.2 ($NaClO_4$) ●, right axis) as a function of concentration of $[La(OTf)_3]$ at 25°C. (*b*) Plots of the pseudo-first-order rate constants for methanolysis of AcIm (pH_{MeOH} = 7.33 ■g, left axis) and $AcImCo(NH_3)_5^{3+}$ (pH_{MeOH} = 7.6 ●, right axis) vs. $[La(OTf)_3]$, at 25°C.





this indicates that the kinetically active species is a dimeric complex consisting of two solvated La^{3+} ions and two methoxide anions as shown in Scheme 1.

The equations for the equilibrium constants and the conservation of mass pertaining to the process in Scheme 1 provide the expression given in eq. [1] where k_o is the

[2] *N*-methylimidazole (pK_a^{MeOH} = 7.60) and *N*-ethylmorpholine (pK_a^{MeOH} = 8.28) were used to buffer methanol solutions. Total buffer concentrations were varied between 10^{-3} M and 10^{-2} M, and no buffer catalysis was observed. The $[CH_3OH_2^+]$ was determined using a combination (glass/calomel) electrode, calibrated with Fisher Certified standard aqueous buffers. Values of pH_{MeOH} were calculated by adding a correction constant (2.24) to the experimental meter reading. (R.G. Bates. *In* Determination of pH. Theory and practice. Wiley, New York. (1973); E. Bosch, private communication.)

[3] UV kinetics were monitored by observing the rate of loss of starting material at 240 nm, under pseudo-first-order conditions of excess metal ([amide] = 0.5 – 1.0 × 10^{-4} M) at 25°C. Pseudo-first-order rate constants (k_{obs}) were evaluated by fitting the Abs. vs. time traces to a standard exponential model.

© 2000 NRC Canada

Scheme 1.

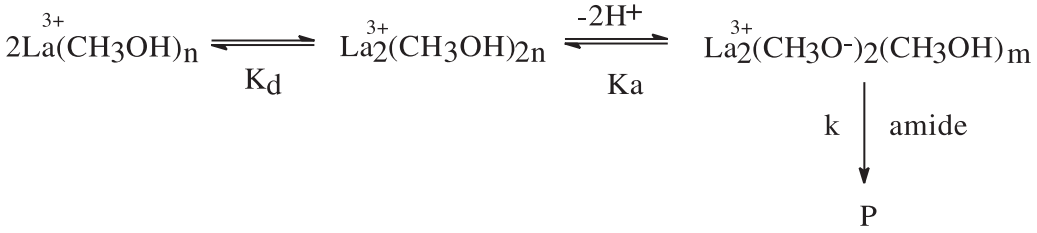
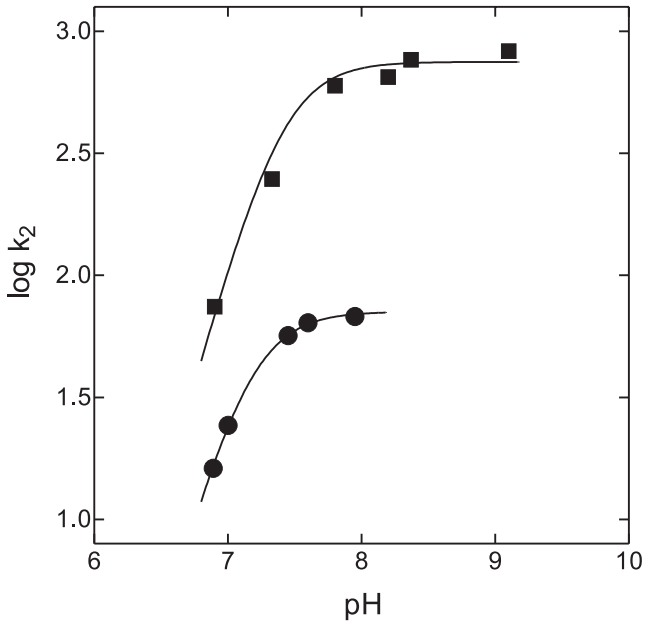


Fig. 2. pH–Second-order rate constant profiles for $La(OTf)_3$-catalyzed methanolysis of AcIm (■) and $AcImCo(NH_3)_5^{3+}$ (●). Curves are the result of NLLSQ fitting of experimental data to eq. [3].



spontaneous rate constant for methanolysis in the absence of metal ion.

$$[1] \quad k_{obs} = k_0 + (kK_a[H^+]^2/K_d)((1 + 8(K_a + [H^+]^2)K_d[La^{3+}]_t/[H^+]^2)^{0.5} - 1)^2/(4(K_a + [H^+]^2))^2$$

The linear part of the plots of k_{obs} vs. $[La^{3+}]_t$, (Fig. 1*b*), used to calculate the second-order rate constant k_2, describe the conditions where $\delta k_{obs}/\delta[La^{3+}]_t$ is constant (eq. [2]),

$$[2] \quad k_2 = \delta k_{obs}/\delta[La]_t = k\alpha\beta(1 - 1/(1 - \beta[La^{3+}]_t)^{0.5})$$

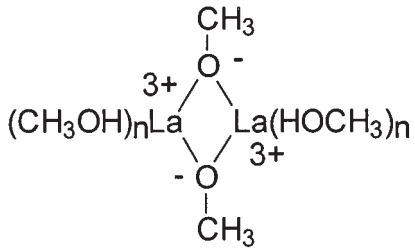
where $\alpha = K_a[H^+]^2/(16K_d(K_d + [H^+]^2)^2)$, and $\beta = 8K_d(K_a + [H^+]^2)/[H^+]^2$.

To satisfy the condition that $\delta k_{obs}/\delta[La^{3+}]_t$ is constant, the range of $[La^{3+}]_t$ for analysis must be chosen such that $(1 - \beta[La^{3+}]_t)^{0.5}$ must be much bigger than 1, thereby providing an expression relating k_2 to K_a, the ionization constant of $La^{3+}(HOCH_3)$, eq. [3].

$$[3] \quad k_2 = kK_a/(2(K_a + [H^+]^2))$$

NLLSQ fitting of pH–k_2 data to eq. [3] gives the following parameters: $k = (1.50 \pm 0.1) \times 10^3\ M^{-1}\ s^{-1}$, $K_a = 10^{(-14.8 \pm 0.1)}\ M^2$ (kinetic $pK_a = 7.40$) for **1**, and $k = (1.42 \pm 0.02) \times 10^2\ M^{-1}\ s^{-1}$, $K_a = 10^{(-14.30 \pm 0.02)}\ M^2$ (kinetic $pK_a = 7.15$) for **2**. The lines through the data in Fig. 2 are those generated by the fits to eq. [3]. That the computed kinetic pK_as are in good agreement with the pK_a^{MeOH} obtained from the potentiometric titration lends strong credence to the idea that both processes relate to the ionization of metal-coordinated methanol. Further, the fact that only one inflection point is present in the potentiometric titration curve indicates strong cooperation between dissociation of both protons from a dimeric species. While the exact structure of this dimer is uncertain, most reasonable is one having two La^{3+} ions bridged by two methoxide anions as in **3**.

Similar double-bridge structures were suggested for $La_2Cl_6(CH_3OH)_{10}$ (6) (with bridging chloride ions) and a



3

La^{3+}-peroxide complex (with bridging peroxide dianions) (7). Hurst et al. (8), from a study of the hydrolysis of an RNA model dimer promoted by La^{3+} in water, proposed a similar catalytically active metal dimer structure having two lanthanide ions bridged by five HO^-.

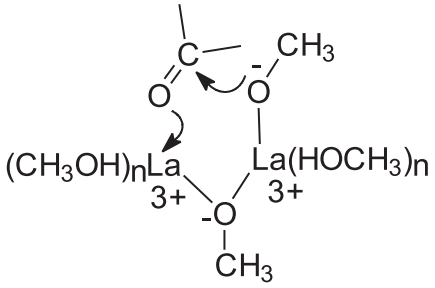
Comparison of the second-order rate constants for La^{3+}-promoted methanolysis of **1** and **2** ($(1.50 \pm 0.1) \times 10^3\ M^{-1}\ s^{-1}$ and $(1.42 \pm 0.02) \times 10^2\ M^{-1}\ s^{-1}$) clearly indicates that coordination of the $(NH_3)_5Co^{3+}$ to the distal nitrogen does not provide any enhancement of the catalytic effect of La^{3+}. Even though **2** has a much better leaving group than does **1** ($pK_a = 10.0$ for $^-ImCo(NH_3)_5^{3+}$ (4) vs. 14 for Im^- (9)), the rate of its La^{3+}-promoted reaction is 10-fold slower. This is in contrast to our results for CH_3O^--catalyzed methanolysis of **2** where the second-order rate constant ($k_{CH3O} = 4.69 \times 10^7\ M^{-1}\ s^{-1}$) is four orders of magnitude higher than that for CH_3O^- attack on **1** ($k_{CH3O} = 7.9 \times 10^3\ M^{-1}\ s^{-1}$).[4] Strong acceleration of methoxide attack on **2** relative to **1** can be explained by a combination of leaving group effects and electrostatic interaction between the positively charged substrate (**2**) and a negatively charged nucleophile. The latter

[4] A.A. Neverov, P. Montoya-Paelez, and R.S. Brown. Submitted for publication.

© 2000 NRC Canada

result thus shows that the La^{3+}-promoted methanolysis mechanism cannot involve attack of free methoxide ion since that should result in much higher rate constants for **2** than for **1**, contrary to what is observed. The slower reaction of the lanthanide reaction with **2** can be accommodated by a process involving the dimeric complex $(La^{3+}{}_2(CH_3O^-)_2(CH_3OH)_m)$ (**3**), having a total positive charge of +4, wherein electrostatic repulsion causes a decrease in the rate for the positively charged substrate **2** relative to neutral **1**.

It has been shown in the case of a structurally similar Co^{3+}-hydroxide dimeric complex, that bridging hydroxides do not possess nucleophilic activity, being at least 10^{10} times less active than the deprotonated oxo-bridged forms (10). For the present methoxy-bridged dimer (**3**) deprotonation is impossible so the only way to generate an active nucleophile within the dimeric complex requires temporary breakage of a lanthanum—methoxy bond. This creates a scissors-like structure where the La^{3+}-bound CH_3O^- is delivered to the C=O carbon with the second La^{3+} functioning as a Lewis acid to stabilize the developing negative charge on the carbonyl oxygen as in **4**.



4

The above study indicates several beneficial features stemming from studying La^{3+}-promoted methanolysis relative to La^{3+} in water. Methanolyses have not been studied as extensively as hydrolyses, undoubtedly due to the problems of controlling and measuring the pH which now have been overcome (5). By a combination of potentiometric titration and kinetic data, we have shown that catalytically active La^{3+} dimers (**3**) are formed above the pK_a of the metal bound CH_3OH. The fact that these dimers are far more soluble in methanol than the corresponding La^{3+}-hydroxides are in aqueous solution simplifies kinetic studies and obviates the necessity of creating complex ligands to stabilize the dinuclear catalytically active core, as is the case in aqueous studies (1, 8, 10). The success observed here with the simple amides and the fact that the La^{3+}-dimer acts on the C=O unit suggests that La^{3+}-catalyzed methanolyses of more biologically relevant amides, peptides, and oligonucleotides would be interesting, and we will report on these studies in due course.

Acknowledgment

The authors gratefully acknowledge financial support of this research by the Natural Sciences and Engineering Research Council of Canada (NSERC). We thank Dr. Elisabeth Bosch for personal communications on determining the pH of buffered methanol solutions.

References

1. (*a*) A. Blasko and T.C. Bruice. Acc. Chem. Res. **32**, 475 (1999) and refs. therein; (*b*) N.H. Williams, B. Tasaki, M. Wall, and J. Chin. Acc. Chem. Res. **32**, 485 (1999) and refs. therein; (*c*) R.A. Moss, B.D. Park, P. Scrimin, and G. Ghirlanda. J. Chem. Soc. Chem. Comm. 1627 (1995); (*d*) R.A. Moss, J. Zhang, and K. Bracken. J. Chem. Soc. Chem. Comm. 1639 (1997); (*e*) J. Sumaoka, S. Miyama, and M. Komiyama. J. Chem. Soc. Chem. Comm. 1755 (1994); (*f*) J.R. Morrow, L.A. Buttrey, and K.A. Berback. Inorg. Chem. **31**, 16 (1992); (*g*) J.R. Morrow, L.A. Buttrey, V.M. Shelton, and K.A. Berback. J. Am. Chem. Soc. **114**,1903 (1992); (*h*) R. Breslow and B. Zhang. J. Am. Chem. Soc. **116**, 7893 (1994); (*i*) N. Takeda, M. Irisawa, and M. Komiyama. J. Chem. Soc. Chem. Comm. 2773 (1994); (*j*) P. Gómez-Tagle and A.K. Yatsimirsky. J. Chem. Soc. Dalton Trans. 2957 (1998).
2. (*a*) T. Takarada, R. Takahashi, M. Yashiro, and M. Komiyama. J. Phys. Org. Chem. **11**, 41 (1998); (*b*) M. Yashiro, T. Takarada, S. Miyama, and M. Komiyama. J. Chem. Soc. Chem. Commun. 1757 (1994).
3. (*a*) T.J. Przystas and T.H. Fife. J. Chem. Soc. Perkin Trans. 2, 393 (1990) and refs. therein; (*b*) J. Suh. Acc. Chem. Res. **25**, 273 (1992) and refs. therein; (*c*) P. Tecilla, U. Tonellato, F. Veronese, F. Fellugg, and P. Scrimin. J. Org. Chem. **62**, 7621 (1997); (*d*) J. Chin, V. Jubian, and K. Mrejen. J. Chem. Soc. Chem. Commun. 1326 (1990); (*e*) L. Meriwether and F. Westheimer. J. Am. Chem. Soc. **78**, 5119 (1956); (*f*) T.J. Grant and R.W. Hay. Aust. J. Chem. **18**, 1189 (1965); (*g*) J.T. Groves and R.M. Dias. J. Am. Chem. Soc. **101**, 1033 (1979); (*h*) J.T. Groves and R.R. Chambers. J. Am. Chem. Soc. **106**, 630 (1984); (*i*) J.T. Groves and J.R. Olson. Inorg. Chem. **24**, 2715 (1985); (*j*) L. Sayre, K.V. Reddy, A.R. Jacobson, and W. Tang. Inorg. Chem. **31**, 935 (1992); (*k*) T.H. Fife. Acc. Chem. Res. **26**, 325 (1993); (*l*) T.H. Fife and R. Bembi. J. Am. Chem. Soc. **115**, 11358 (1993); (*m*) T.N. Parac and N.M. Kostic′. J. Am. Chem. Soc. **118**, 51 (1996); (*n*) L. Singh and R.N. Ram. J. Org. Chem. **59**, 710 (1994); (*o*) P.A. Sutton and D.A. Buckingham. Acc. Chem. Res. **20**, 357 (1987); (*p*) E. Kimura, I. Nakamura, T. Koike, M. Shionoya, Y. Kodama, T. Ikeda, and M. Shiro. J. Am. Chem. Soc. **116**, 4764 (1994); (*q*) T.N. Parac, G.M. Ullman, and N.M. Kostic′. J. Am. Chem. Soc. **121**, 3127 (1999), and refs. therein; (*r*) A.M. Ridder and R.M. Kellogg. *In* Comprehensive supramolecular chemistry. *Edited by* Y. Murakami. Vol. 4. Supramolecular reactivity and transport: bioorganic systems. Chap. 11. Elsevier Science Ltd., Oxford. 1996; (*s*) J. Chin. Acc. Chem. Res. **24**, 145 (1991), and refs. therein.
4. J. MacB. Harrowfield, V. Norris, and A.M. Sargeson. J. Am. Chem. Soc. 7282 (1976).
5. (*a*) E. Bosch, F. Rived, M. Rosés, and J. Sales. J. Chem. Soc. Perkin Trans. 2, 1953 (1999); (*b*) E. Bosch, P. Bou, H. Allemann, and M. Rosés. Anal. Chem. 3651 (1996); (*c*) F. Rived, M. Rosés, and E. Bosch. Anal. Chim. Acta, **374**, 309 (1998).
6. L.S. Smith, D.C. McCain, and D.L. Wertz. J. Am. Chem. Soc. **98**, 5125 (1976).
7. B.K. Takasaki and J. Chin. J. Am. Chem. Soc. **117**, 8582 (1995).
8. P. Hurst, B.K. Takasaki, and J. Chin. J. Am. Chem. Soc. **118**, 9982 (1996).
9. R.J. Sundberg and R.B. Martin. Chem. Rev. **74**, 471 (1974).
10. (*a*) D. Wahnon, A.-M. Lebuis, and J. Chin. Angew. Chem. Int. Engl. **34**, 2412 (1995); (*b*) N.H. Williams, A.-M. Lebuis, and J. Chin. J. Am. Chem. Soc. **121**, 3341 (1999).

© 2000 NRC Canada

1999 R.U. Lemieux Award Lecture Adventures with azo-, azoxy-, and hydrazoarenes: from the Wallach to the benzidine rearrangement. Molecular electronics[1]

Erwin Buncel

Abstract: The author's studies with aromatic azo-, azoxy-, and hydrazo-dye molecules, comprising kinetic and equilibrium investigations, as well as synthesis of novel molecules having photogenic properties, are described under the following highlights: **A.** *Wallach rearrangement and cognate studies with azoxyarenes* — (1) Elucidation of the mechanism of the Wallach rearrangement of azoxybenzene through the kinetic observation of a two-proton process which, together with a pK_a study, was interpreted on the basis of formation of a deoxygenated, dicationic, symmetrical species as a key, short-lived reaction intermediate. (2) The proposal of a general acid-catalyzed pathway in concentrated sulfuric acid (catalysis by H_2SO_4 and $H_3SO_4^+$). (3) Elucidation of the consecutive sulfonations of reaction products of azoxybenzene in the 100% H_2SO_4 region, and the diprotonation equilibria for *p*-hydroxyazobenzene, thus shedding light on past reaction pathway and product studies. (4) The observation of a novel reaction pathway for 2,4,6,2′,4′,6′-hexamethylazoxybenzene. (5) The observation of a dichotomy of reaction pathways for α- and β-2-phenylazoxynaphthalenes: reaction via the dicationic intermediate and via quinoid intermediate species; comprising two isomeric compounds reacting by different pathways to give the same product. (6) Identification and structure proof of α- and β-isomers observed for the first time in the peracid oxidation of phenylazopyridine. (7) Observation of a rate constant ratio of 22 000 in the rearrangement of these α- and β-isomers, and the proposal of differential barriers for transition states leading to a tricationic intermediate. **B.** *Benzidine rearrangement and cognate studies* — (8) Observation of the acid-catalyzed hydroxylation of phenylazopyridine to *p*-hydroxyphenylazopyridine and the proposal of an S_NAr mechanism with formation of an intermediate hydrazo species in the reaction. (9) First study of benzidine type rearrangement–disproportionation of phenylhydrazopyridine in acid media. (10) Proposal of a A → B → C → D type reaction profile for the consecutive hydroxylation→disproportionation processes of phenylazopyridine in aq H_2SO_4. (11) Proposal of 10-π and 14π-electron electrocyclic processes in the benzidine type rearrangement–disproportionation of phenylhydrazopyridine. (12) Identification and structural elucidation of a dimer formed from phenylazopyridine as a minor product and proposal of a reaction mechanism. **C.** *Facile acid-catalyzed demethylation via S_NAr/A-S_E2 mechanisms and studies of tautomerism* — (13) Observation of an abnormally facile acid-catalyzed cleavage (demethylation) of 4-methoxyphenylazopyridine via an S_NAr mechanism. (14) Observation of two reaction pathways, S_NAr and A-S_E2, for the consecutive demethylations of 3,4-dimethoxyphenylazopyridine, with rate constant ratio of 7 000:1 favoring the S_NAr process. (15) Quantitation of the tautomeric and protonation equilibria of 4-hydroxyphenylazopyridine, produced in (13). **D.** *A new solvent polarity scale, molecular switches, and molecular electronics* — (16) Establishment of a π^*_{azo} solvent polarity scale based on solvatochromism of a series of azomerocyanine molecules ("Buncel's dye"). (17) Some glimpses are presented of current forays into molecular electronics, as emanating from the above studies: (*a*) spiropyran (SP) ⇔ merocyanine (MC) thermo- and photochromic "molecular switch" systems; (*b*) synthesis and characterization of azo-functionalized star-burst dendrimers with photoswitchable properties and potential applications in optical data storage systems, holographic gratings, and drug delivery systems as host molecules.

Key words: Wallach rearrangement, benzidine disproportionation, azoarenes, azoxyarenes, dendrimers, hydrazoarenes, dendrimers, solvatochromism, photochromism, thermochromism, spiropyran–merocyanine molecular switch.

Résumé : Dans ce travail, on décrit les travaux de l'auteur avec des molécules de colorants aromatiques de la famille des azo, azoxy et hydrazo, comprenant des études cinétiques et d'équilibres ainsi que les synthèses de nouvelles molécules possédant des propriétés photogéniques; en particulier: **A.** *Réarrangement de Wallach et études apparentées avec des azoxyarènes* — (1) Élucidation du mécanisme du réarrangement de Wallach de l'azoxybenzène par le biais de

Received May 10, 2000. Published on the NRC Research Press website on September 26, 2000.

This paper is dedicated to Professor Joseph F. Bunnett.

E. Buncel.[2] Department of Chemistry, Queen's University, Kingston, ON K7L 3N6, Canada.

[1]Based on R.U. Lemieux Award Lecture, presented at 82nd Canadian Society of Chemistry Conference, Toronto, May 1999.
[2]Fax: (613) 533-6669. e-mail: buncele@chem.queensu.ca

 © 2000 NRC Canada

l'observation cinétique d'un processus à deux protons qui, combinée à une étude de pK_a, a été interprétée sur la base de la formation d'une espèce symétrique, dicationique, désoxygénée comme intermédiaire réactionnel clé, de courte durée de vie. (2) La proposition, pour les réactions en milieu acide sulfurique concentré, d'une voie de réaction impliquant une catalyse acide générale (catalyse par H_2SO_4 et $H_3SO_4^+$). (3) L'élucidation des sulfonations consécutives des produits de réaction du *p*-azoxybenzène qui a permis de voir sous un nouveau jour les voies réactionnelles et les études de produits antérieures. (4) L'observation d'une nouvelle voie réactionnelle pour le 2,4,6,2′,4′,6′-hexaméthylazoxybenzène. (5) L'observation d'une dichotomie dans les voies réactionnelles des α- et β-2-phénylazoxynaphtalènes : une réaction par le biais de l'intermédiaire dicationique et une autre via des espèces intermédiaires quinonoïdes comportant deux composés isomères qui réagissent par des voies différentes pour donner le même produit. (6) L'identification et la preuve de structure des isomères α et β observés pour la première fois lors de l'oxydation de la phénylazopyridine par un peracide. (7) L'observation d'un rapport de constantes de vitesses de 22 000 lors du réarrangement des ces isomères α et β et la proposition de barrières différentielles pour les états de transition conduisant à un intermédiaire tricationique. **B.** *Le réarrangement de la benzidine et les études apparentées* — (8) L'observation d'une hydroxylation catalysée par les acides de la phénylazopyridine en *p*-hydroxyphénylazopyridine et la proposition d'un mécanisme S_NAr avec formation d'une espèce hydrazo intermédiaire au cours de la réaction. (9) La première étude d'un réarrangement/disproportionation de phénylazopyridine de type benzidine en milieu acide. (10) La proposition d'un profile de réaction de type A → B → C → D pour les processus d'hydroxylation–disproportionation consécutives de la phénylazoxypyridine en milieu H_2SO_4 aqueux. (11) La proposition de processus électrocycliques 10-π et 14-π lors de réarrangement–disproportionation de type benzidine de la phénylhydrazopyridine. (12) L'identification et l'élucidation de la structure d'un dimère qui se forme comme produit mineur à partir de la phénylazopyridine et la proposition d'un mécanisme réactionnel. **C.** *La déméthylation acidocatalysée facile par le biais de mécanismes S_NAr/A-S_E2 et les études de tautomérie* — (13) L'observation d'un clivage (déméthylation) acidocatalysée anormalement facile de la 4-méthoxyphénylazopyridine par le biais d'un mécanisme S_NAr. (14) L'observation de deux voies réactionnelles, S_NAr et A-S_E2, pour les déméthylations consécutives de la 3,4-diméthoxyphénylazopyridine pour lesquelles le rapport des constantes de vitesses de 7 000/1 favorise le processus S_NAr. (15) La quantification de l'équilibre tautomère et de protonation de la 4-hydroxyphénylazopyridine obtenue dans la section 13. **D.** *Une nouvelle échelle de polarité des solvants, les commutateurs moléculaires et l'électronique moléculaire* — (16) La mise au point d'une échelle de polarité des solvants π^*_{azo} basée sur la solvatochromie d'une série de molécules azomérocyanines (« colorant de Buncel »). (17) On présente aussi des aperçus des domaines actuels de recherches en électronique moléculaire, telles qu'elles émanent des études mentionnées plus haut: (*a*) systèmes de "commutateurs moléculaires" thermo- et photochromiques spinopyrane (SP) ⇔ mérocyanine (MC); (*b*) synthèse et caractérisation de dendrimères azo fonctionnalisés ayant des propriétés comme commutateurs moléculaires et évaluation des applications potentielles dans le stockage de données optiques, holographiques et dans les systèmes de mises en disponibilité de médicaments comme molécules hôtes.

Mots clés : réarrangement de Wallach, disproportionation de la benzidine, azoarènes, azoxyarènes, hydrazoarènes, dendrimers, solvatochromie, photochromie, thermochromie, commutateur moléculaire spirane–mérocyanine.

1. Introduction

(*a*) Historical

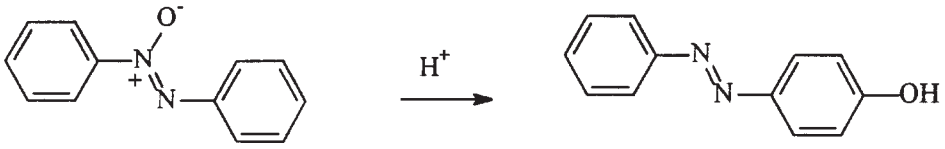
Over the 100 years since the discovery by Peter Griess (1) in 1858 of the versatile diazotization-coupling procedure for the synthesis of aromatic azo compounds, these molecules have earned the distinction of reaching the first rank among industrial dyes and pigments (2). The rich mechanistic chemistry surrounding azoarenes is well documented in texts by Zollinger (3) and the works edited by Patai (4).

The discovery of the transformation of azoxybenzene into *p*-hydroxyazobenzene (eq. [1]) by Wallach and Belli (5) in 1880 has become known as the Wallach rearrangement (WR henceforth). The reaction was found to occur simply by heating in concentrated sulfuric acid.

It was suggested that an initial disproportionation to phenol and diazosulfonic acid would be followed by their recombination to products. Azoxybenzene was formulated as a symmetrical structure which had been proposed by Kekule and Hidegh (6) in 1870; the currently accepted unsymmetrical structure of azoxybenzene (eq. [1]) was established later, 1910–1933 (7). It took roughly 100 years following Wallach's initial discovery for meaningful mechanisms to be proposed (8).

Since the observation by Hoffmann (9) in 1863 of the conversion of hydrazobenzene by dilute acid to 4,4′-diaminobiphenyl, commonly known as benzidine, the mechanism of the rearrangement (BR henceforth) has fascinated chemists for over 100 years. Part of the fascination has been the finding of a variety of products (Scheme 1),

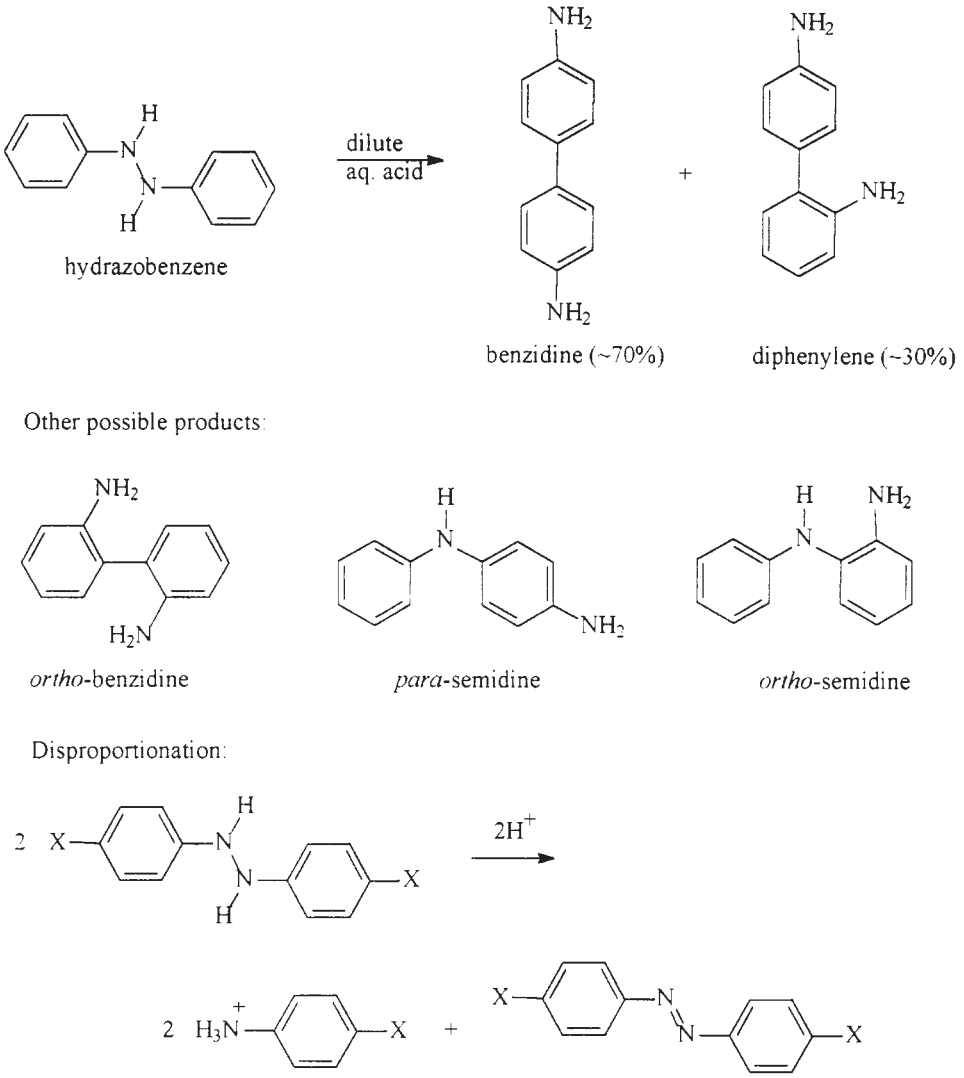
[1]



1

© 2000 NRC Canada

Scheme 1.



complex kinetics, and the intramolecular nature of the processes. The BR thus became regarded as the "holy grail" of molecular rearrangements (10). In that light, Ingold (11) after several decades of study of the BR produced a reaction profile which depicted the transition state as lost in the clouds. Fortunately, recent work has allowed light to filter through the clouds and the holy grail has become within reach.

(*b*) Overview

The author was initiated into the field of azo dyes through a study of the abnormally facile hydrolysis of azoaryl ethers (vide infra), under the guidance of Professor Joseph Bunnett, forming part of the basis of mechanistic criteria for acid-catalyzed processes (12, 13). Azoarenes are found throughout this account, being the precursors of azoxyarenes and the products of their rearrangements, as well as of the rearrangements of hydrazoarenes.

The first project of my independent research at Queen's was directed at a mechanistic study of the WR. Surprisingly, a review of the literature revealed that no kinetic study had as yet been reported of this reaction. This was surprising because proposals of mechanism including postulation of various reaction intermediates were put forward by workers in Australia, Japan, and Russia, without invoking any role of acid!

In the course of our work on the WR during the following years, various structure–reactivity relationships were realized from rate–pK_a studies, including correlations with MO calculations (vide infra). Serendipitous discoveries led us eventually to the benzidine rearrangement (in the heteroaromatic series, which turned out to be even more complex), after we had extended a study of the WR to the two isomers (α and β) of phenylazopyridine (**2a**, **b**). It was envisaged that the WR product, as the deprotonated *N*-alkyl derivative, would exhibit solvatochromic properties due to varying contributions of the zwitterionic merocyanine (**3b**), and quinoid (**3a**), resonance structures (Scheme 2).

The UV–vis spectrum of compound **3** (R = CH_3) exhibited, providentially, one of the largest variations in λ_{max} with solvent polarity (14). This prompted us to synthesize a series of azomerocyanines and to use the solvatochromic method (15) to establish a new solvent polarity scale, π^*_{azo} (16).

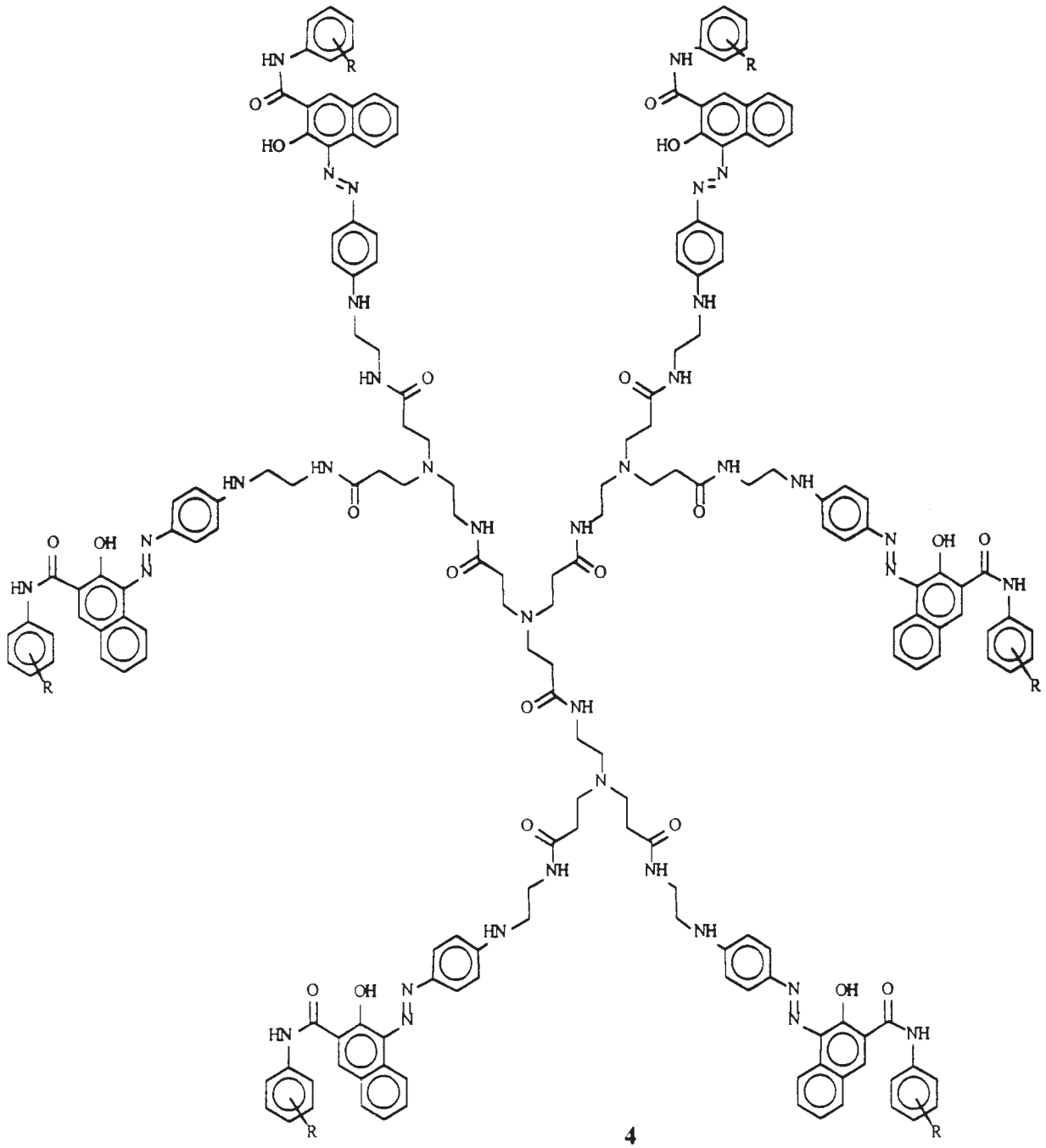
The potential of merocyanines (MCs) in the area of molecular electronics (17) now beckoned us, especially in their usage as the basis of a molecular switch. This would be possible through the interconversion of the colored MC and a

© 2000 NRC Canada

colorless species, as in the case of the spiropyran (SP) structure. The SP ⇔ MC system (18) offers possibilities of thermo- and photochromic interconversion (Scheme 3) and various methods have been explored to stabilize the two forms, including, in our laboratory, chelation of the ring-opened MC form with divalent metal ions.

Azobenzene-functionalized molecules have also been exploited as photoswitches by taking advantage of the azo-functionality as a photoresponsive moiety. Thus, modification of the periphery of dendrimers with azo-functionalities offers applications in materials science — optical data storage, holography, and drug delivery (19). An example from our work is the azobenzene-functionalized polyamide (PAMAM) dendrimer **4**.[3]

With this overview, from the beginning of our work to the present, and having come full circle in these meanderings with the current study of structure properties of azo-functionalities in dendrimers, we can now proceed to flesh



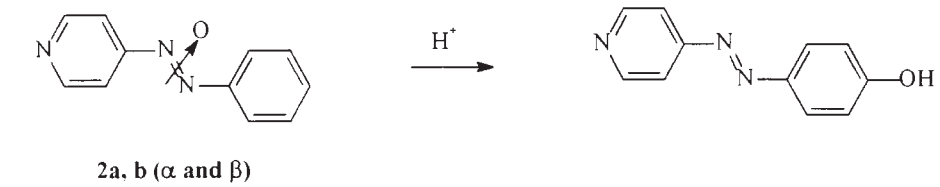
4

R = H, 4'-methoxy, 2', 5'-dimethoxy, 3'-nitro

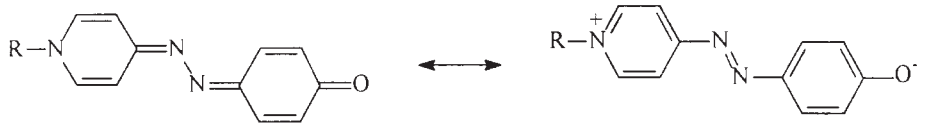
[3] K.S. Cheon, P.M. Kazmaier, S.-R. Keum, and E. Buncel. Unpublished work.

© 2000 NRC Canada

Scheme 2.



2a, b (α and β)



3a **3b**

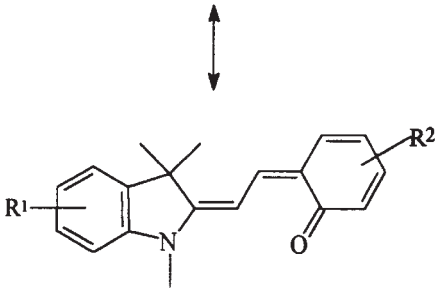
Scheme 3.



R^2 = NO_2, N=N–Ph

State I
Colorless spiro form
SP

IIa



IIb
State II
Colored merocyanine form
MC

out this account. It will be seen that most of our studies did not follow a logical plan but, rather, developed from unexpected observations which then took on a life of their own. Of course, most of the credit goes to the enthusiasm of my co-workers over the years, who will be thanked formally at the end of this account.

2. Wallach rearrangement of azoxyarenes

The Wallach rearrangement (WR) of azoxybenzene in aq H_2SO_4 gives rise, apparently exclusively, to *p*-hydroxyazobenzene (eq. [1]). A small amount of *o*-hydroxyazobenzene has been reported by some workers but this is believed to be formed in a photochemical process. Sulfonated hydroxyazobenzene, also reported previously (20), is, however, a secondary product (21) as a result of the rather harsh conditions typically used in preparative experiments (concd H_2SO_4, elevated temperature, extended reaction time). Contrastingly, kinetic studies performed spectrophotometrically showed that the half-life of the primary reaction in 99.9% H_2SO_4 at 25°C was of the order of 1 min (22). Studies with a number of substituted azoxybenzenes have been reported (23)[4]; these have been reviewed previously (8*a*) and will be referred to only in passing in this account.

Questions that are also pertinent to other molecular rearrangements must be addressed. Is the WR an intramolecular or intermolecular process? Is there evidence for any reaction intermediates? What is the role of acid in the reaction mechanism?

Isotopic tracer studies (24) provide a powerful tool in determination of intra- or inter-molecularity of rearrangement processes. Oxygen-18 tracer studies (25), using labelled substrate and isotopically normal reaction medium, or the reverse, have shown that the *p*-hydroxyazobenzene product

[4] B.T. Newbold. Private communication.

© 2000 NRC Canada

Scheme 4.

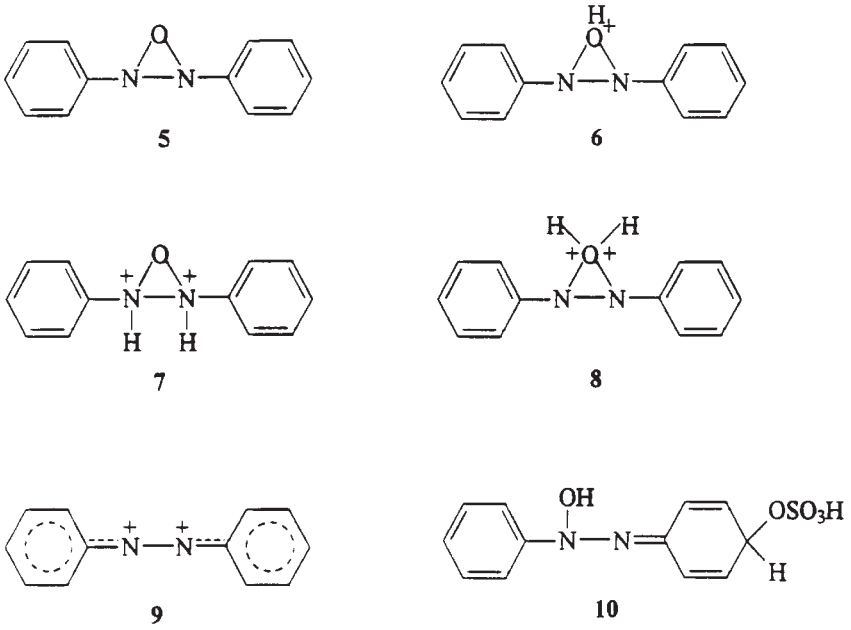


Table 1. Kinetic data for rearrangement of azoxybenzene to 4-hydroxyazobenzene in aq H_2SO_4 at 25°C.

H_2SO_4 (wt%)	X^a	$-H_o{}^b$	$C_{SH^+}{}^c / C_s + C_{SH}$	$10^5 k_\Psi{}^d$ (sec^{-1})
75.30	5.30	6.65	0.967	0.016
80.15	6.17	7.42	0.994	0.208
85.61	7.20	8.35	0.999	2.17
90.37	8.05	9.05	1.000	7.23
95.19	9.04	9.82	1.000	20.90
97.78	10.01	10.35	1.000	43.80
99.00	10.75	10.82	1.000	76.80
99.59	11.21	11.18	1.000	227
99.90	11.48	11.64	1.000	860
99.97	11.54	11.84	1.000	2310
99.99	11.56	11.90	1.000	4160

[a]Data from ref. (33).

[b]Ref. (34).

[c]Calculated using a pK_a for azoxybenzene of –5.15 (ref. (32*a*)).

[d]Pseudo-first-order rate constants as determined spectrophotometrically.

derives its oxygen from the medium, i.e., an intramolecular process. ^{15}N tracer studies (26) with azoxybenzene specifically labelled on one nitrogen produced *p*-hydroxyazobenzene in which the label was equalized on both Ns, pointing to a symmetrical intermediate on the reaction pathway, for which the *N*,*N*-oxide structure **5** was proposed (26). Similar equalization results were obtained on using ^{13}C specifically labelled azoxybenzene (27). Gore (28) was the first to propose the dicationic structure **9** as being in accord with the ^{15}N equalization result and product studies; this structure was later endorsed by Buncel and Lawton (29) on the basis of kinetic studies. However, unsymmetrical intermediates such as **10** continued to be advanced (30). An attempt at assigning the role of acid was made through the proposal of the protonated *N*,*N*-oxide species, i.e., **6, 7**, and **8** (31). Scheme 4 shows the structures of the different intermediates.

It appeared to us that more definitive information concerning the role of acid would be garnered from a kinetic study of the reaction, for which the spectrophotometric method should be ideal. Azoxybenzene in ethanol or in dilute H_2SO_4 (or in basic medium) has an absorption at 323 nm but in strongly acid media protonation occurs on the azoxy function and λ_{max} shifts to 390 nm. A separate pK_a study showed there is 50% O-protonation in 65% H_2SO_4, corresponding to a pK_a of –5.1 (32). The *p*-hydroxyazobenzene product is N-protonated in the acid media with λ_{max} at 460 nm, so the reaction can readily be followed directly (or by quenching in base, with λ_{max} for the azophenolate ion at 430 nm).

In Table 1 are recorded the rate data at various acid concentrations and values of the classical Hammett acidity function H_o (33) as well as the more recent Cox–Yates Excess Acidity X (34) which provide alternate measures of

© 2000 NRC Canada

Scheme 5.

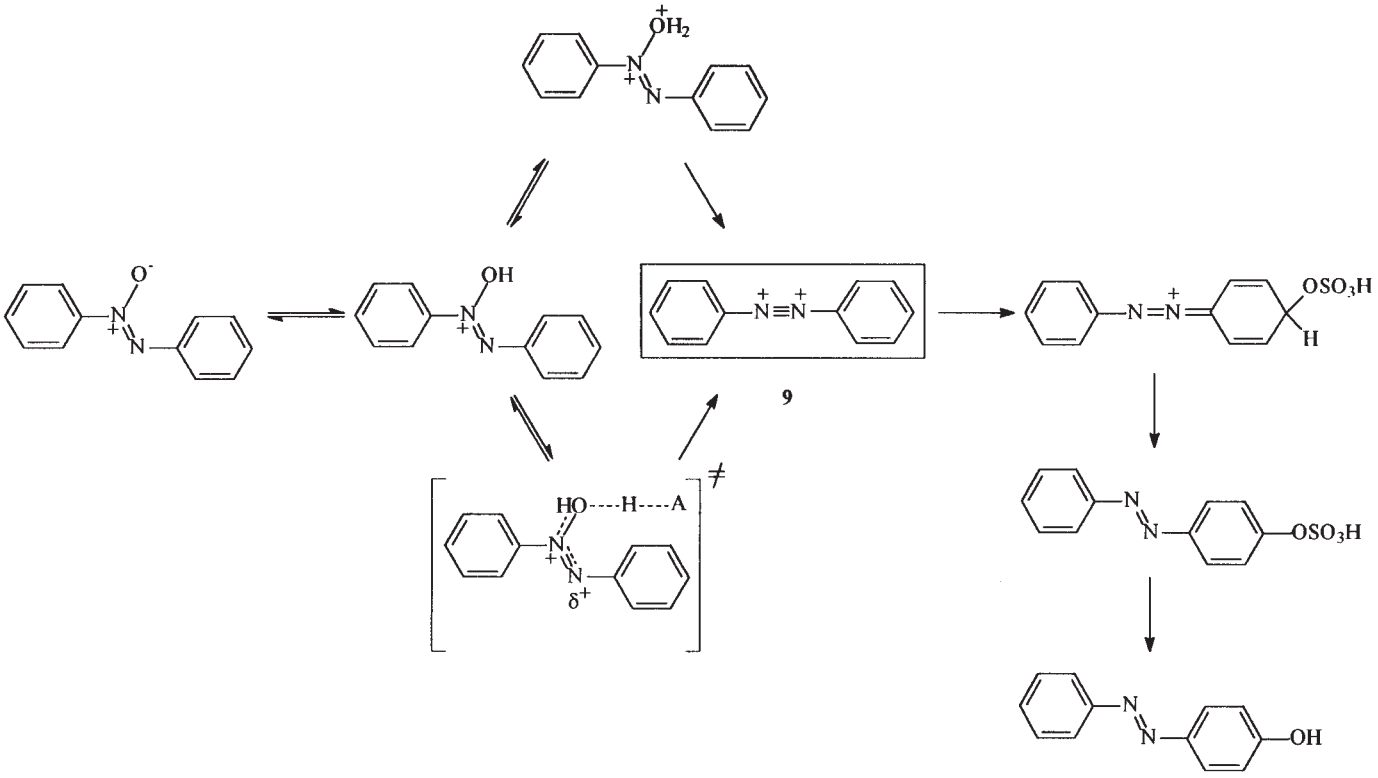
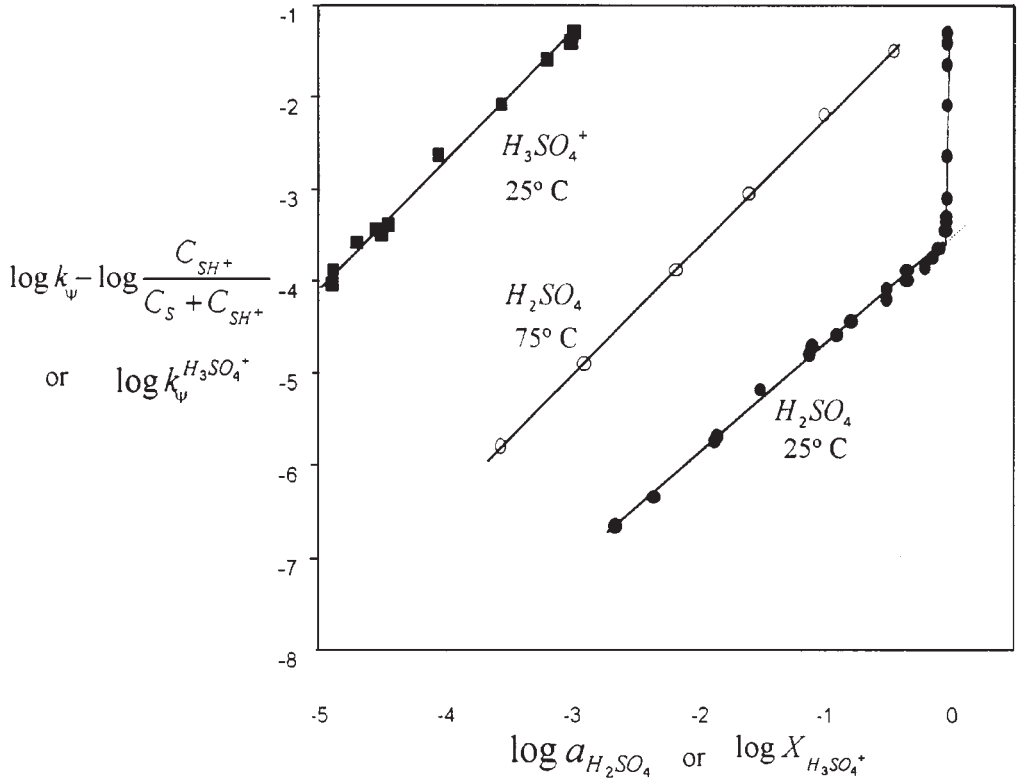
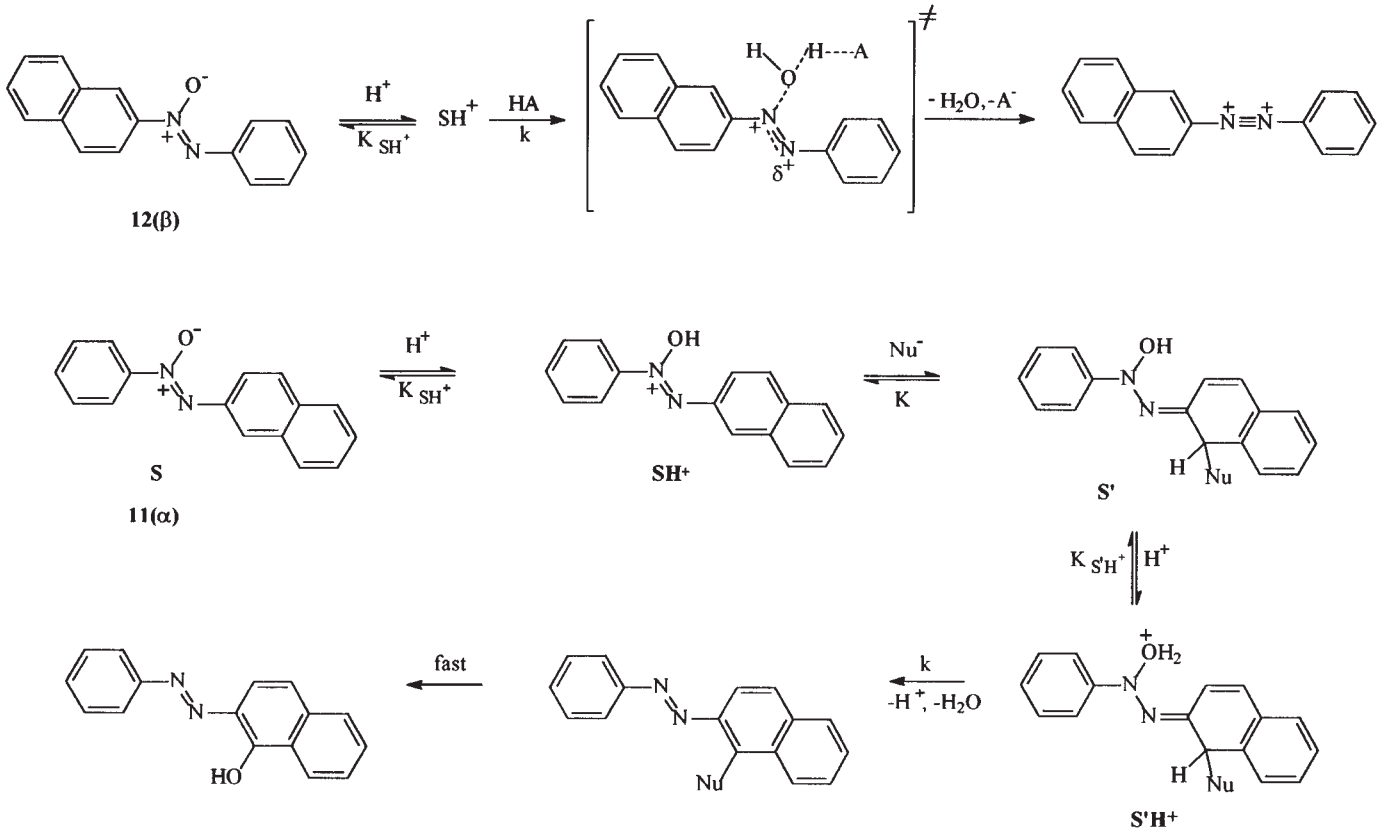


Fig. 1. Graphs of log k_Ψ – log (C_{SH^+}/(C_S + C_{SH^+})) at 25°C (●) and 75°C (○) vs. log $a_{H_2SO_4}$, and of $\log_\psi^{H_3SO_4^+}$ at 25°C (■) vs. log $X_{H_3SO_4^+}$, for the rearrangement of azoxybenzene in H_2SO_4. (Reproduced with permission of the American Chemical Society from ref. (32*b*)).



© 2000 NRC Canada

Scheme 6.



the acidity of the medium. Also shown is the extent of protonation as the quotient $[SH^+]/([S + SH^+])$. The striking result emerges that the rate increases by over 100 000-fold over the acid range studied but the percent protonation increases only very slightly, by 3%. From 85% H_2SO_4 up, there is virtually no increase in protonation but the rate keeps on increasing. Hence a second proton transfer, in addition to the equilibrium protonation must be involved in the overall process.

The mechanism which we proposed as a result of the kinetic study coupled with equilibrium protonation data is shown in Scheme 5 (32). An initial equilibrium protonation on oxygen is followed by a second proton transfer, either as another equilibrium protonation (similar to the protonation of an alcohol) and followed by loss of H_2O, or as a slow process involving concerted general acid-catalyzed removal of H_2O. In either case one obtains the dicationic species **9** as a transient intermediate which is rapidly attacked by solvent on the ring *para* carbon position, followed by rearomatization and hydrolysis to give the final *p*-hydroxyazobenzene product.

The idea of general acid catalysis in concentrated sulfuric acid media, i.e., that undissociated and protonated H_2SO_4 molecules are taking part in rate-determining proton transfer, though unusual, receives support from Fig. 1 (32*b*). This shows that there is good linear correlation of rate with log a_{H2SO4} until 96% of H_2SO_4, when $H_3SO_4^+$ takes over.

The proposal of the dicationic intermediate in the WR appeared to be consistent with other extant studies including the aforementioned isotopic tracer studies, and has also been the subject of a molecular orbital treatment (35). Nevertheless, certain structural features in the substrate could favour a pathway proceeding via an unsymmetrical intermediate.

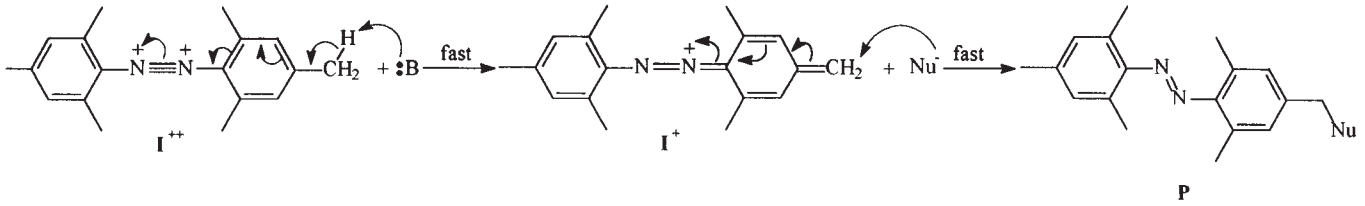
Thus, interestingly, the two isomeric α- and β-2-phenylazoxynaphthalenes, **11** and **12**, were found to react by different mechanisms (36). According to the Cox–Yates excess acidity treatment, **12** reacts by the dicationic mechanism at all acidities but **11** does so at high acidities while the quinoid mechanism shown in Scheme 6 is followed in the low acid regime. Thus for **11** the quinoid intermediate provides a lower energy pathway. Note that **12** cannot react via the quinoid intermediate since the protonated NO function in SH^+ is not correctly oriented with respect to the naphthyl ring for nucleophilic attack, while the phenyl moiety is insufficiently activated to form quinoid intermediates. Hence **12** will react by another mode, namely the dicationic intermediate mechanism as followed by azoxybenzene itself. Thus the two isomeric compounds **11** and **12** react by different mechanisms to give the same product.

In an attempt to stabilize the dicationic intermediate, and possibly have it as a spectroscopically observable species, reaction was performed with 2,4,6,2′,4′,6′-hexamethylazoxybenzene on the basis that, with the *ortho* and *para* positions blocked, attack by solvent should be precluded. The actual result, shown in Scheme 7, was proton loss from a *para* methyl group followed by solvent attack to yield the product corresponding to Nu = OH, thus thwarting observation of the dicationic intermediate (37).

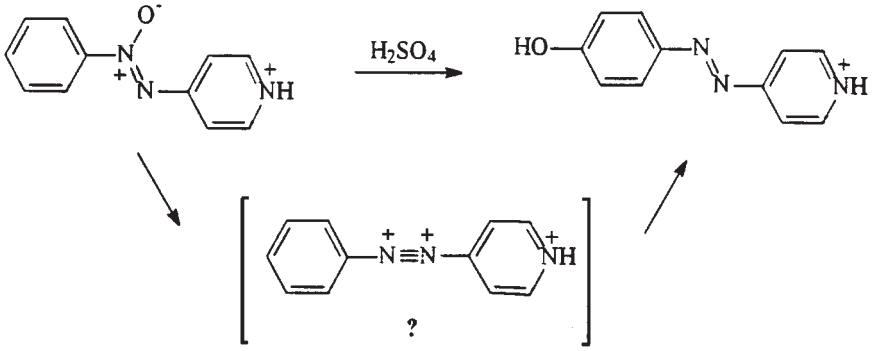
The classical approach by Olah et al. (38) solved the search: when the reaction with azoxybenzene was carried

© 2000 NRC Canada

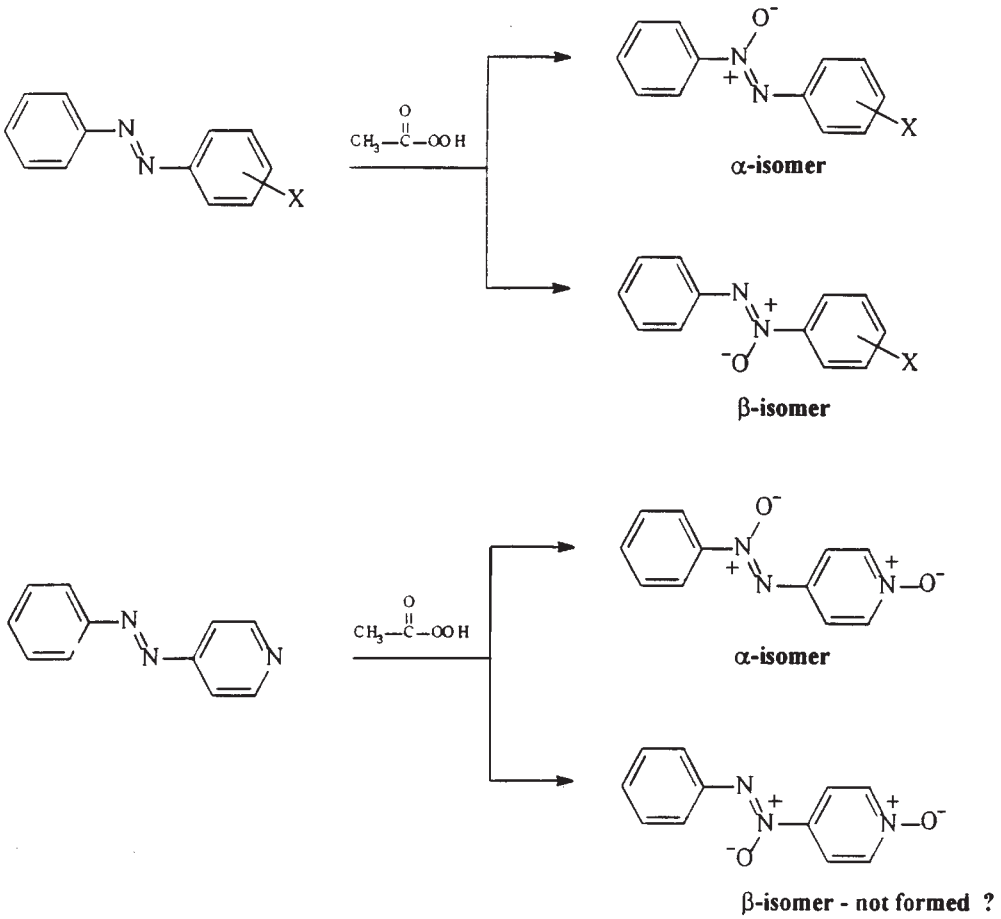
Scheme 7.



Scheme 8.

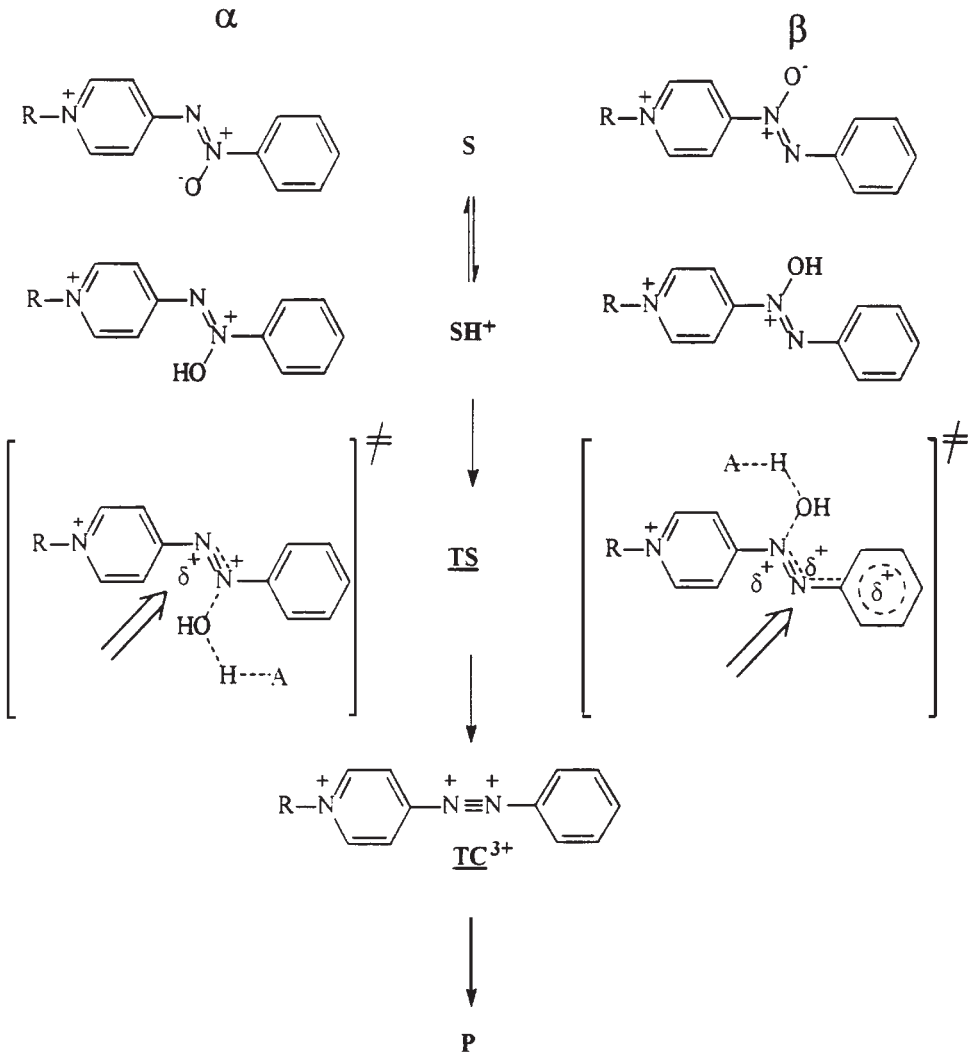


Scheme 9.



© 2000 NRC Canada

Scheme 10.



out in "magic acid," a non-nucleophilic medium, the dicationic intermediate could be observed by its ^{1}H NMR spectrum. Thus ended one chapter on the WR mechanism.

3. Rearrangement of phenylazoxypyridine

We anticipated that a major structural change in substrate could be harnessed toward new questions about products, kinetics, and mechanistic consequences, through extension of the work to the phenylazoxypyridine series. As shown in Scheme 8, an analogous pathway to that of azoxybenzene would now entail formation of a tricationic intermediate. As well, one could envisage the possibility of solvatochromism in the hydroxyazo product in its O-deprotonated, zwitterionic form.

Azoxybenzenes are generally obtained by the peracid oxidation of azobenzenes, and in the case of unsymmetrically substituted azo compounds the reaction usually gives rise to a mixture of isomeric α- and β-azoxybenzenes (Scheme 9). In contrast, oxidation of phenylazopyridine was reported to give rise only to the α-isomer (as the *N*-oxide) and none of the isomeric β-product (39). In our hands, reaction of the oxidation product, under WR conditions and using the usual spectrophotometric method, proceeded to half completion only, approximately half the starting material remaining unreactive. Intuitively, on the assumption that oxidation gave rise in fact to *both* isomeric azoxy compounds only one of which was reactive, the material was chromatographed, yielding two portions whose structures were confirmed by X-ray analysis as the isomeric α- and β-phenylazoxypyridine-*N*-oxides (40).

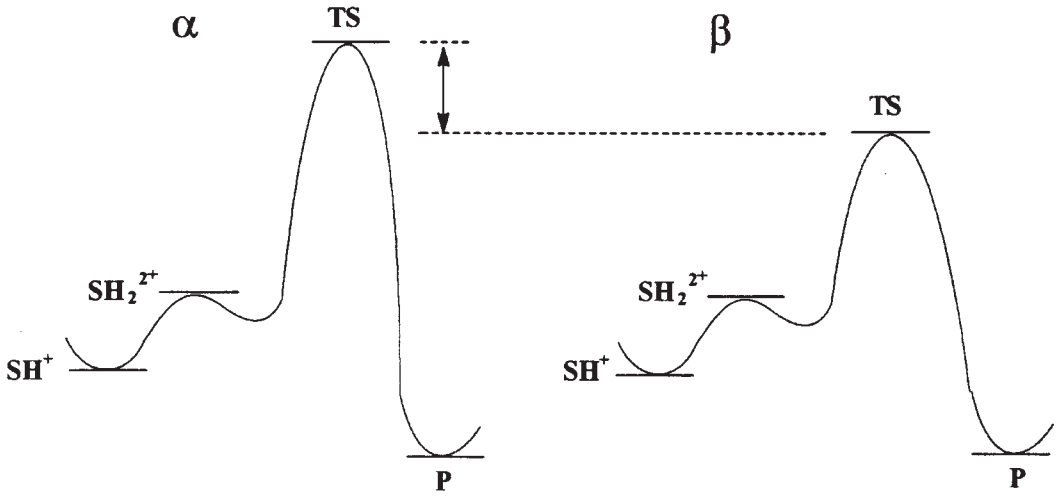
Kinetic study of the authentic α- and β-azoxy isomers then revealed the anticipated remarkable difference in reactivity of these isomeric compounds. In 99.6% of H_2SO_4, at 25°C, the rate constant ratio was found to be 22 000 in favour of the β-isomer (41)[5].

The observed reactivity difference of the α- and β-isomers can be accounted for in terms of the mechanisms illustrated in Scheme 10 in which formation of the tricationic intermediate follows the general acid-catalyzed pathway. Note that

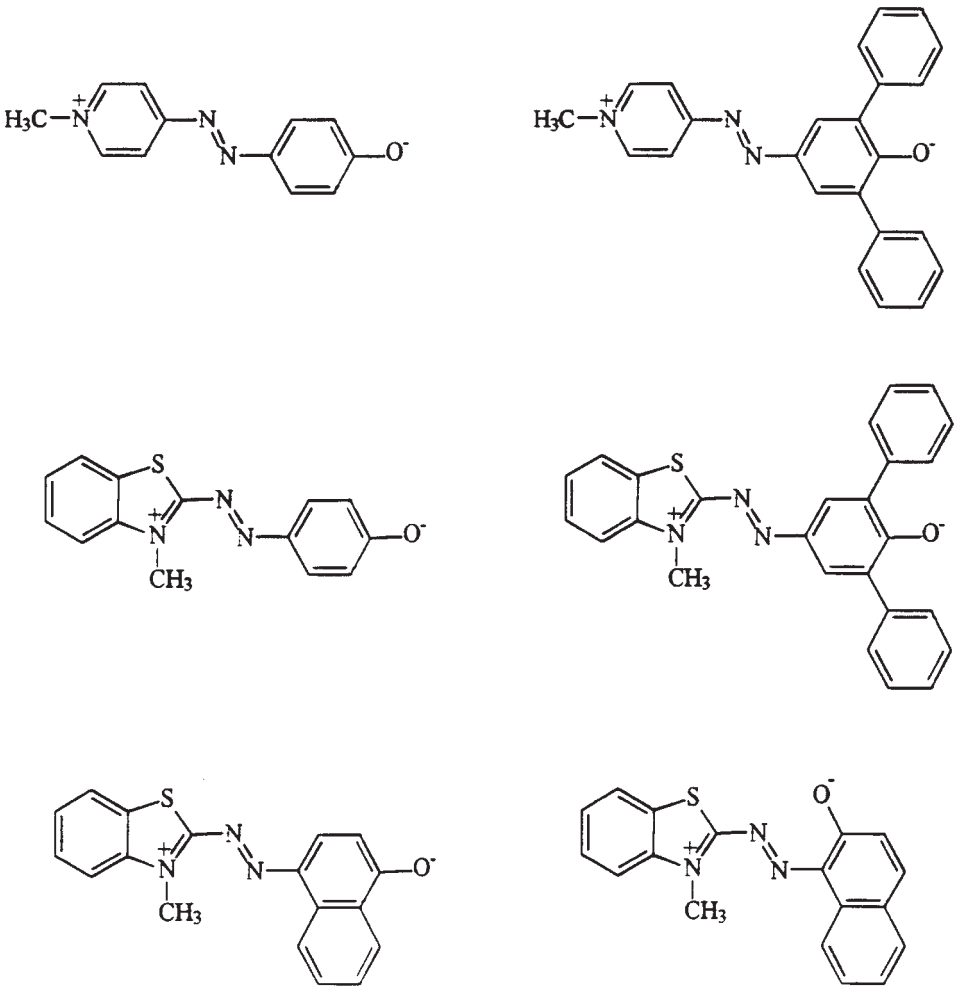
[5] E. Buncel and S. Rajagopal. Unpublished work.

© 2000 NRC Canada

Fig. 2. Energy profiles for rearrangement of α-phenylazoxypyridine (left) and β-phenylazoxypyridine (right).



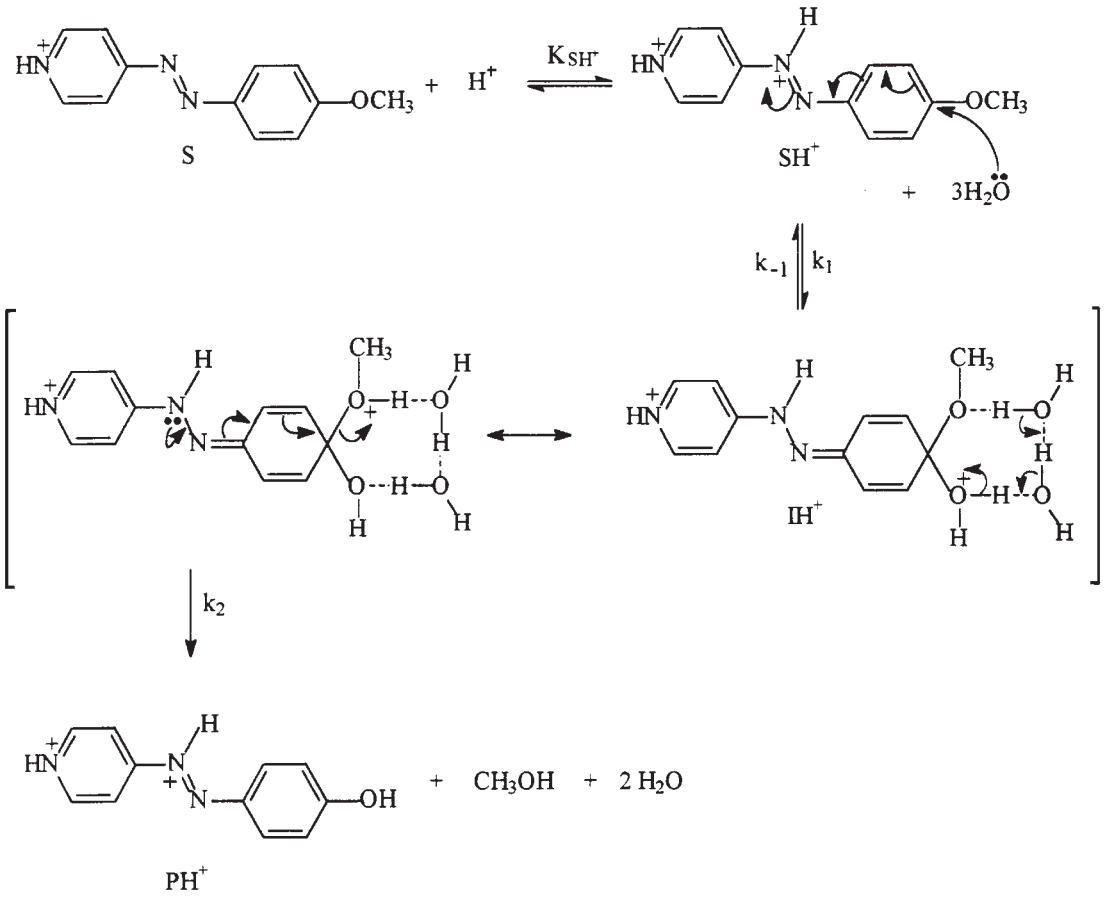
Scheme 11.



in the TS for formation of the trication the nitrogen removed from the azoxy function develops positive charge. In the case of the β-isomer this positive charge can be delocalized on the adjacent phenyl group so this process is facilitated. However, in the case of the α-isomer the positive charge is being developed on the N adjacent to the pyridine nucleus

© 2000 NRC Canada

Scheme 12.



which itself carries a positive charge, so this process will be highly unfavorable, exhibiting a higher energy TS than for the β-isomer, as illustrated in the reaction coordinate diagram in Fig. 2.

4. Meanderings

With the unravelling of the mechanism of rearrangement, first of azoxybenzene and its analogues in the naphthylazoxy series, then of the phenylazoxypyridine compounds, our original aims were essentially completed. However, before closing this chapter altogether it seemed desirable to follow up several avenues which had come to light in the meanwhile. These took on a life of their own, as often happens, and in this section are recorded some of these meanderings. As well, it will be seen that, serependitiously, these meanderings led us eventually to the discovery of novel aspects of the benzidine rearrangement, one of the "holy grails" in organic chemistry.

(*a*) Solvatochromism of azomerocyanines: π^*_{azo} scale

The possible solvatochromic properties of WR products of phenylazoxypyridines in their zwitterionic form was envisaged earlier. Thus, the *N*-methyl betaine **3** was found to exhibit a very large spectral shift with solvent polarity, comparable to Reichardt's well known pyridinium betaine (42). A quantum mechanical study of the solvatochromism in **3** (named "Buncel's dye" by Timothy Clark) yielded satisfactory agreement between calculated and observed solvent-induced spectral shifts (43). The changes in position of the UV–vis absorption band in different polarity solvents result from varying electron distributions in the molecule in response to solvent polarity changes, i.e., varying contributions of the zwitterionic and quinoidal forms **3a** and **3b**, as shown in Scheme 2.

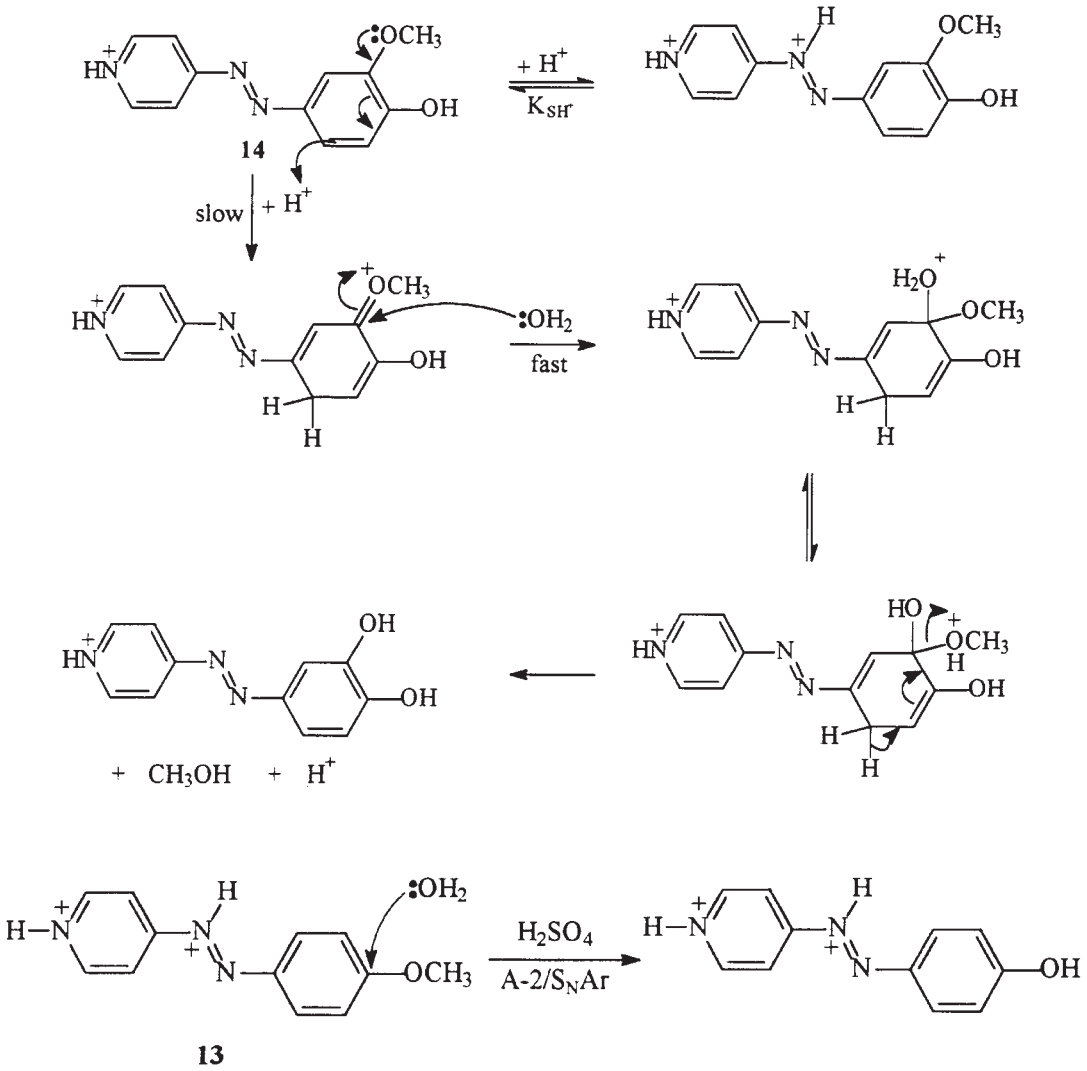
It appeared of interest to utilize a family of azomerocyanines toward establishing a new solvent polarity scale. This was done with the series shown in Scheme 11 and the resulting scale was called π^*_{azo}, following Taft's π^* scale which was established using the solvatochromic method with six compounds of diverse structures (44). The π^*_{azo} scale correlates reasonably well with other solvent polarity scales (15).

(*b*) Sensitivity of azo ethers to acid-catalyzed hydrolysis

The account in the previous section concerning the hydroxyphenylazopyridine system was incomplete in one sense, i.e., that, for completeness, it was desirable to quantitate the various tautomeric and protonation equilibria illustrated in Fig. 3. The spectrophotometrically measured pK_as refer to the macroscopic equilibria on the right hand side, while the microscopic equilibria are shown on the left side; these can be related by standard methods (45). However, to characterize spectrally all species in this system it was required to determine the spectra of a number of model compounds. Unexpectedly, this supposedly routine work led to novel discoveries, ending ultimately with our foray into benzidine rearrangement studies.

© 2000 NRC Canada

Scheme 13.



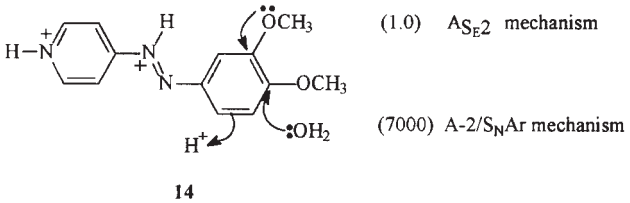
[2]

The first observation was that *p*-methoxyphenylazopyridine **13** undergoes facile hydrolysis in acid media (46) (eq. [2]).

The rate profile exhibited a maximum as a function of percent H_2SO_4, reminiscent of A-2 reactions. One can also view this as an S_NAr process where nucleophilic attack is activated by the protonated azo- and pyridyl-functionality, as illustrated in Scheme 12 (47).

It was of interest to examine the reactivity of a second methoxy group, in the *meta* position, which is not positioned properly with respect to the protonated azopyridyl moiety for the S_NAr mechanism. In fact, the *meta* methoxy group in **14** reacts very much more slowly, with a ratio of 1:7 000 compared with the *para* methoxy group. However, even more interestingly, the Cox–Yates method of analysis showed that the slower reaction followed an A-S_E2 mechanism, i.e., rate-determining proton transfer on the aromatic ring as shown in Scheme 13 (47). The methoxy group activates the aromatic ring towards protonation, which is followed by fast reaction with H_2O and expulsion of methanol concurrent with rearomatization.

The next model compound examined, phenylazopyridine, gave some totally unexpected results which led us to a new facet of the benzidine rearrangement.



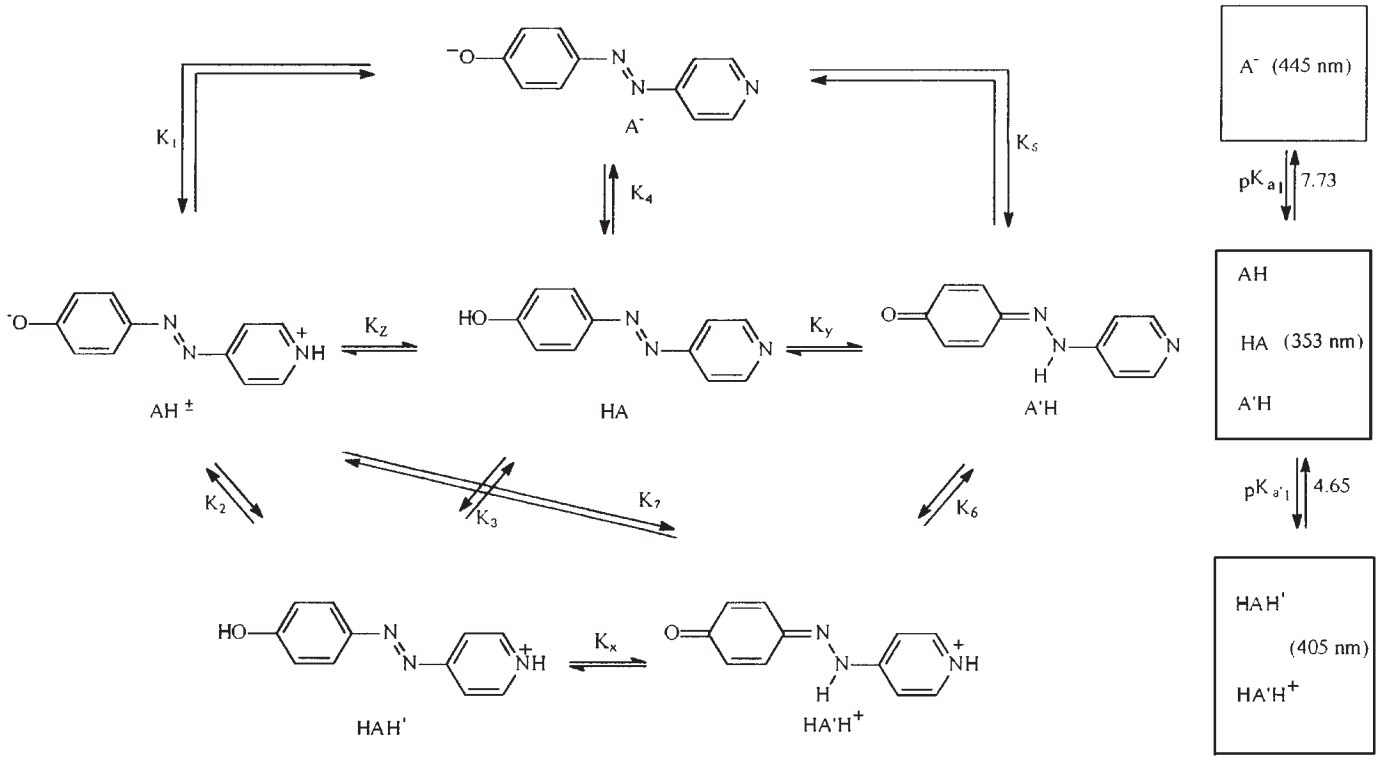
14

5. The benzidine rearrangement and disproportionation of phenylhydrazopyridine

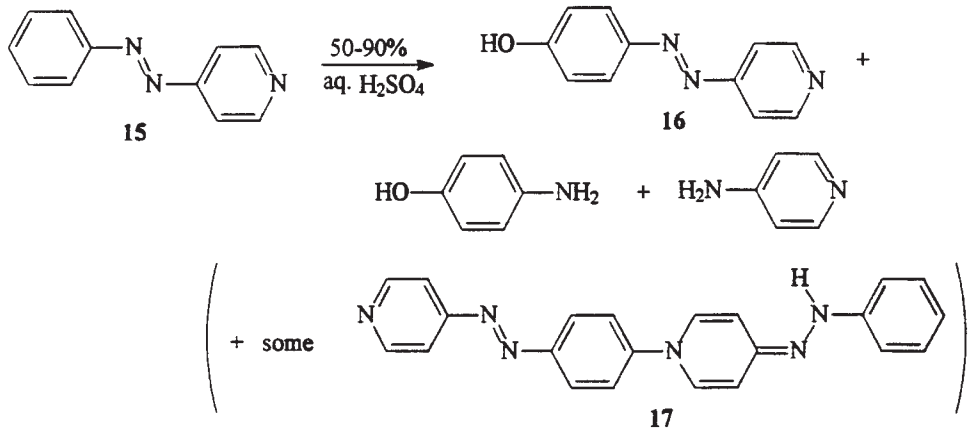
Phenylazopyridine (**15**), when examined spectrophotometrically in acid media was found to be unstable, undergoing hydroxylation to *p*-hydroxyphenylazopyridine (**16**). Chromatographic product analysis showed that the *p*-hydroxyphenylazopyridine is not the sole product, being formed only

© 2000 NRC Canada

Fig. 3. Protonation and tautomeric equilibria of 4-(*p′*-hydroxyphenylazo)pyridine. (Reproduced with permission of Elsevier Science Publishers from ref. (45)).



Scheme 14.

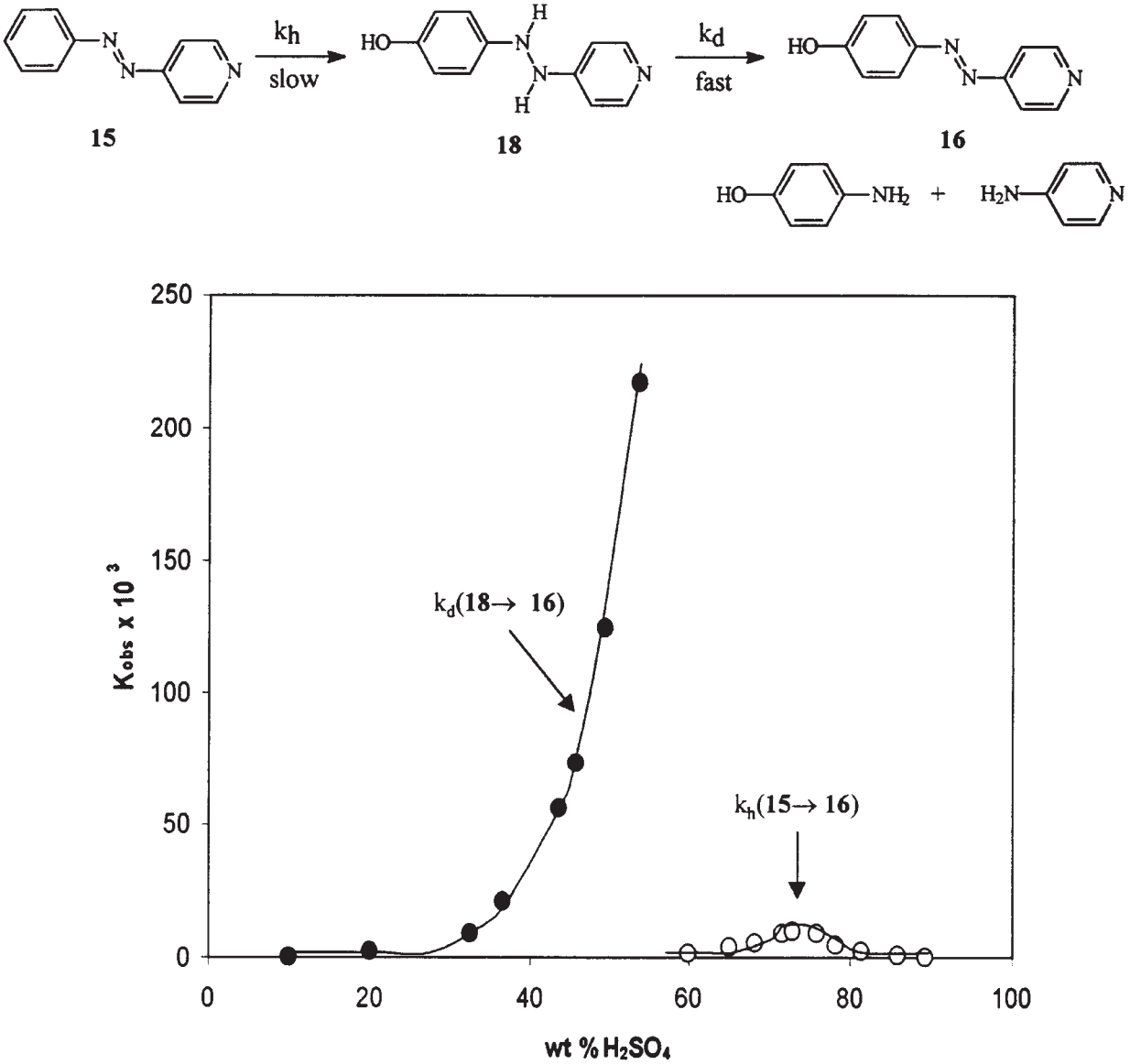


in ca. 45% yield, with *p*-aminophenol and *p*-aminopyridine in 45% yield, while a small amount (5–10%) of a dimeric product, **17**, whose structure was eventually established by NMR and MS, was also obtained (Scheme 14). Disregarding for the moment the latter, it was apparent that a *disproportionation* was occurring, one molecule of reactant being oxidized and another reduced. It is recalled that a similar disproportionation occurs in parallel with the benzidine rearrangement in which hydrazobenzene reacts in acid media to give a variety of products including those from disproportionation (Scheme 1). The classic work of Ingold (11, 48), Banthorpe (49), Shine (10), Olah et al. (38), Bunton and Rubin (51), Dewar (52), Hammond and Claris (53), Vecera (54), Lupes (55), and others (56) revealed different facets of this fascinating intramolecular process, proceeding via 1- and 2-proton pathways.

One could then propose the hypothesis illustrated in Scheme 15, that the overall hydroxylation in our system occurs in two steps: the hydrazo species **18** is formed as an intermediate in a slow step, to be followed by fast disproportionation to products. Accordingly, when the authentic hydrazo compound was subjected to a kinetic and product

© 2000 NRC Canada

Fig. 4. Kinetic behaviour as function of acid concentration of phenylazopyridine and *p*-hydroxyphenylhydrazinopyridine.



analysis study, it was found, indeed, to give the same products of disproportionation as when starting with phenylazopyridine, confirming the validity of Scheme 15 (57).

A plausible mechanism for formation of the hydrazo compound can be proposed, as shown in Scheme 16, i.e., nucleophilic attack of solvent on the activated protonated substrate followed by tautomerization.

The kinetic behaviour for the two processes, hydroxylation and disproportionation, as a function of acid concentration is shown in Fig. 4. The disproportionation of the hydrazo compound **18** occurs readily in the 10–50% H_2SO_4 region and is very fast relative to the hydroxylation of phenylazopyridine **15** for which much higher acidities are required.

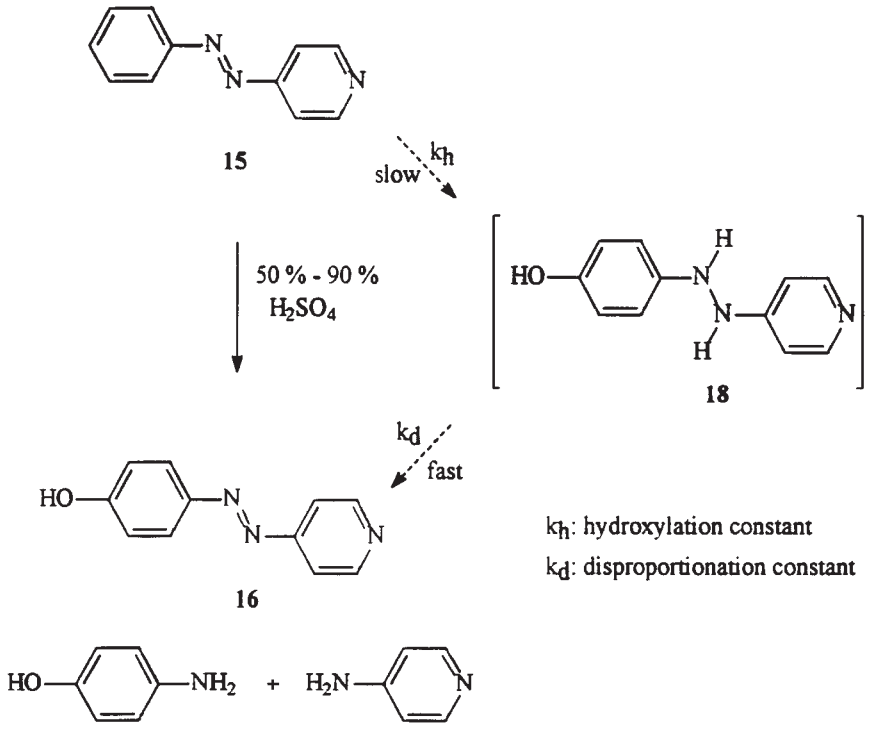
One can now construct a potential energy diagram for these processes (58). As illustrated in Fig. 5, the disproportionation **18** → **16** which occurs in the dilute acid regime is energetically much less demanding than the hydroxylation process **15** → **18** which requires concentrated acid. Thus the hydrazo species **18** becomes a transient intermediate in the **15** → **16** process at the higher acidities.

It then occurred to us to go one step back; that if the hydroxyphenylhydrazopyridine **18** undergoes this disproportionation, then so should also the parent unsubstituted phenylhydrazopyridine **19**, for which one anticipates the reaction sequence **19** → **15** → **18** → **16.** Accordingly, phenylhydrazopyridine was prepared and subjected to kinetic study. In the dilute acid region, the disproportionation **19** → **15** followed similar kinetic behaviour as **18** → **16**, though somewhat slower. As before, **19** undergoes slow hydroxylation to 4-hydroxyphenylazopyridine **16**, for which a higher acid concentration is required. Also in the high acid concentration regime, the **19** → **16** rate is indistinguishable from the **15** → **16** rate. The various kinetic processes are included in Fig. 6.

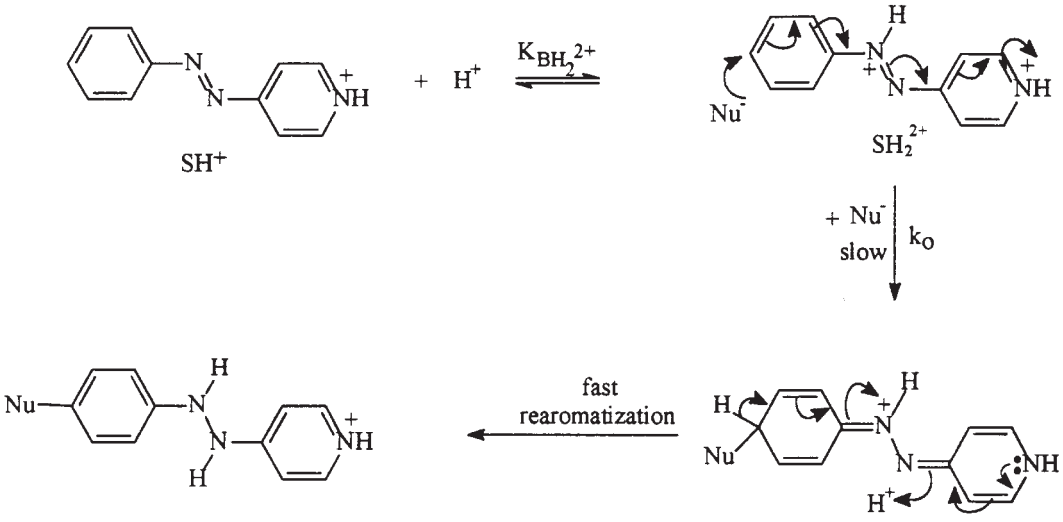
A complete energy profile could then be constructed (Fig. 7) to include the family of azo and hydrazo dyes, starting from **19** going to **15** by disproportionation, then to **18** through

© 2000 NRC Canada

Scheme 15.



Scheme 16.



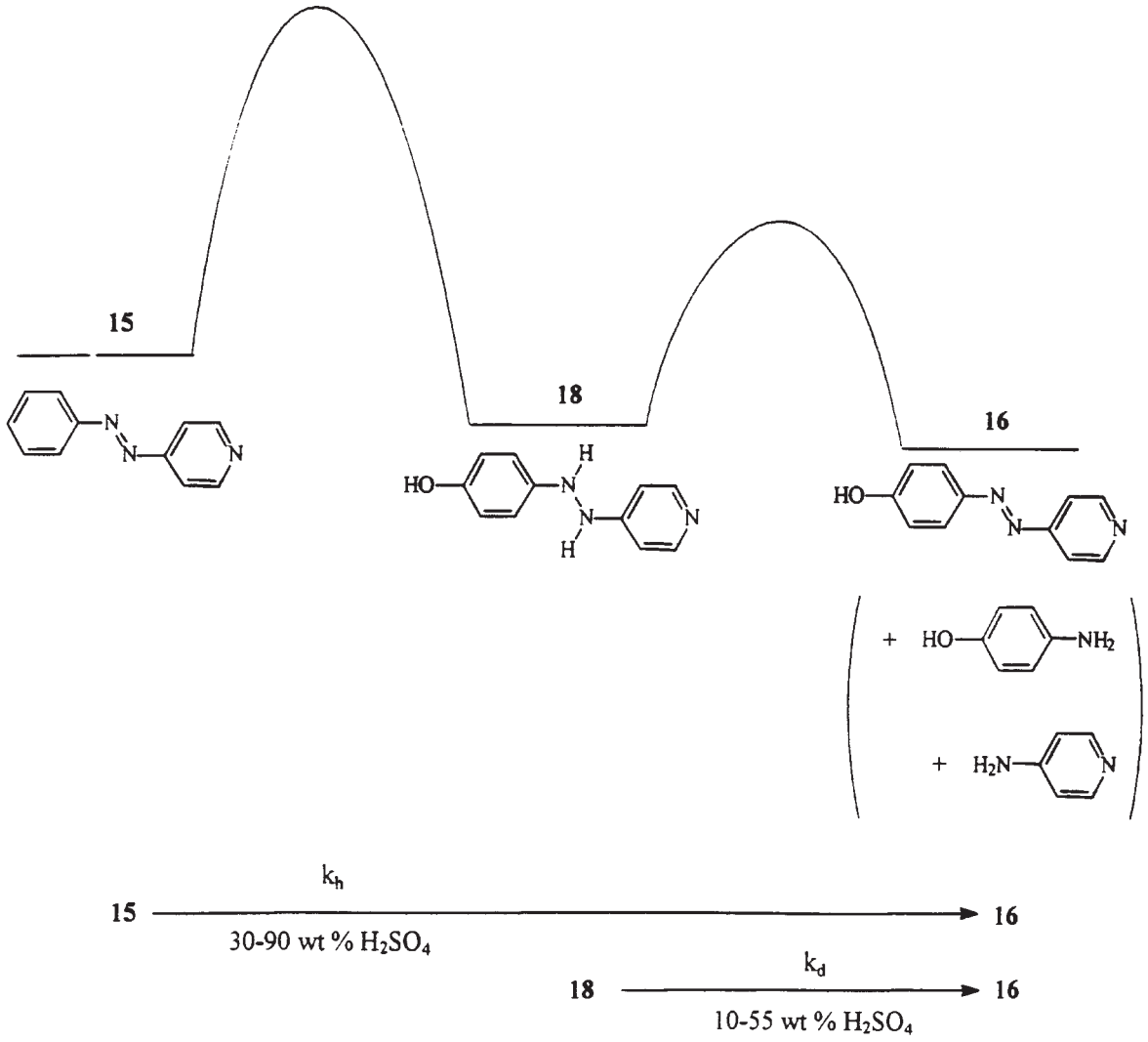
hydroxylation, and finally its disproportionation to **16** (i.e., an A → B → C → D process).

Clearly, Fig. 7 represents a finely balanced series of processes — a cascade — in which some intermediates may be transient under given conditions. For example, **18** is an unobservable, transient intermediate in the reaction **15** → **16** or **19** → **16** in the high acid regime. On the other hand, with **19** as the reactant in the high acid concentration regime, there is an immediate formation of **15** followed by its slow transformation to **16**.

The benzidine rearrangement has been a prolific area of study for over 100 years, and a number of different mechanisms have been proposed (10, 48–59) to account for the variety of products and the unusual kinetic features. The currently most widely accepted mechanism is that due to Henry Shine and his co-workers (50) and this can be nicely adapted to the present system, as shown in Scheme 17. Essentially, there is depicted a rate-determining step involving a thermally allowed 10-electron electrocyclic reaction of the diprotonated substrate giving rise to intermediate **20** which reacts with another molecule of protonated substrate in a thermally allowed 14-electron electrocyclic process to give the observed products of disproportionation. In the case of hydrazobenzene itself, this intermediate would simply rearomatize to

© 2000 NRC Canada

Fig. 5. Energy profiles for the hydroxylation and disproportionation reactions of phenylazopyridine and *p*-hydroxyphenylhydrazinopyridine.



the biphenyl product but this is not possible with the pyridine system (or with 4,4′-disubstituted hydrazobenzenes) so disproportionation results.

The rate equation applicable to the mechanism in Scheme 17 is given by eq. [3]:

$$[3] \quad \log k_\psi - \log (C_{BH_2^{++}}/(C_{BH^+} + C_{BH_2^{++}})) = \log k_o + (m^{\#} - 1)m^* X$$

which correlates the rate constant k_ψ with the excess acidity X. The plot corresponding to eq. [5] is shown in Fig. 8 where PCT is the correction factor for partial protonation. The figure includes results for the *p*-chlorosubstituted substrate, also shown in Scheme 17; clearly a satisfactory correlation is obtained. Other possible mechanisms have been considered as well but could not satisfy the observations (59).

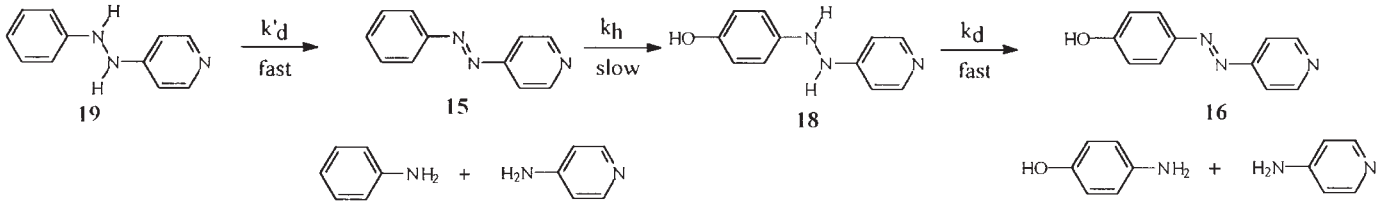
At the outset of this section it was stated that a dimeric product, **17**, was formed in the disproportionation reaction, to a maximum of 10% depending on conditions — acidity and substrate concentration. The mechanism favored for formation of the dimer is shown in Scheme 18 for the *p*-chloro system and involves nucleophilic attack of the pyridino-nitrogen on the *para* carbon of a second molecule of substrate followed by loss of Cl^-. On this basis, dimerization would become less important as the acidity increases since the probability of having an unprotonated pyridine nitrogen present descreases with increasing acidity and, being bimolecular, the reaction would only occur to a detectable extent at the higher substrate concentrations used for the product analysis but not under the kinetic conditions. This is in accord with experimental observations (59).

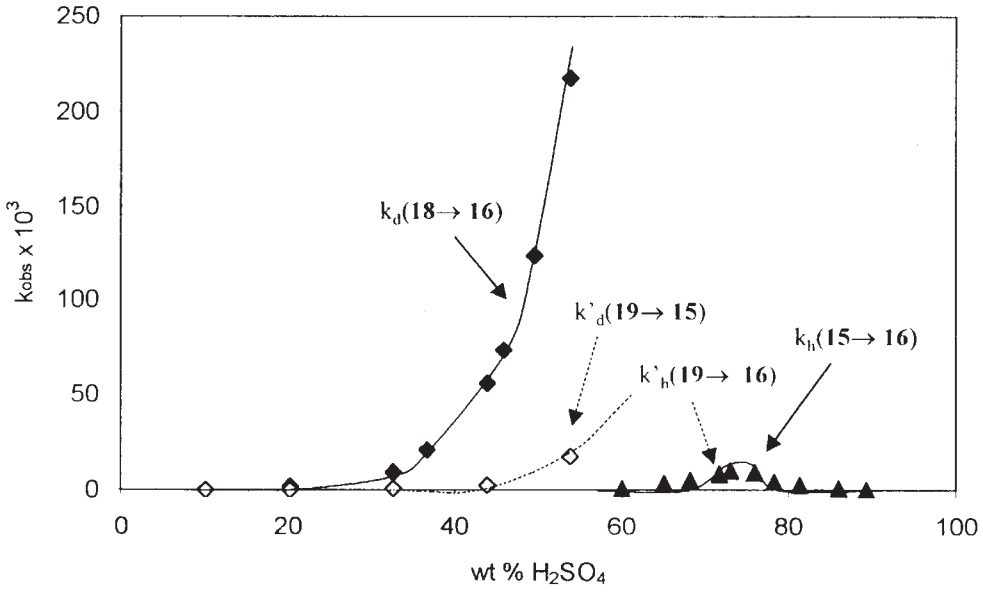
Ackowledgements

I am deeply indebted to a number of co-workers who over the years have worked with me on the related projects described here and without whom none of this would have been possible. The individuals concerned are: B.T. Lawton, W.M.J. Strachan, A. Dolenko, K. Mahendran, S. Rajagopal, S.-R. Keum, K.-S. Cheon, K.-T. Park, J. Wojtyk, M.A.A. Ghani, A. Wasey, I. Onyido, and R.A. Cox. Grateful

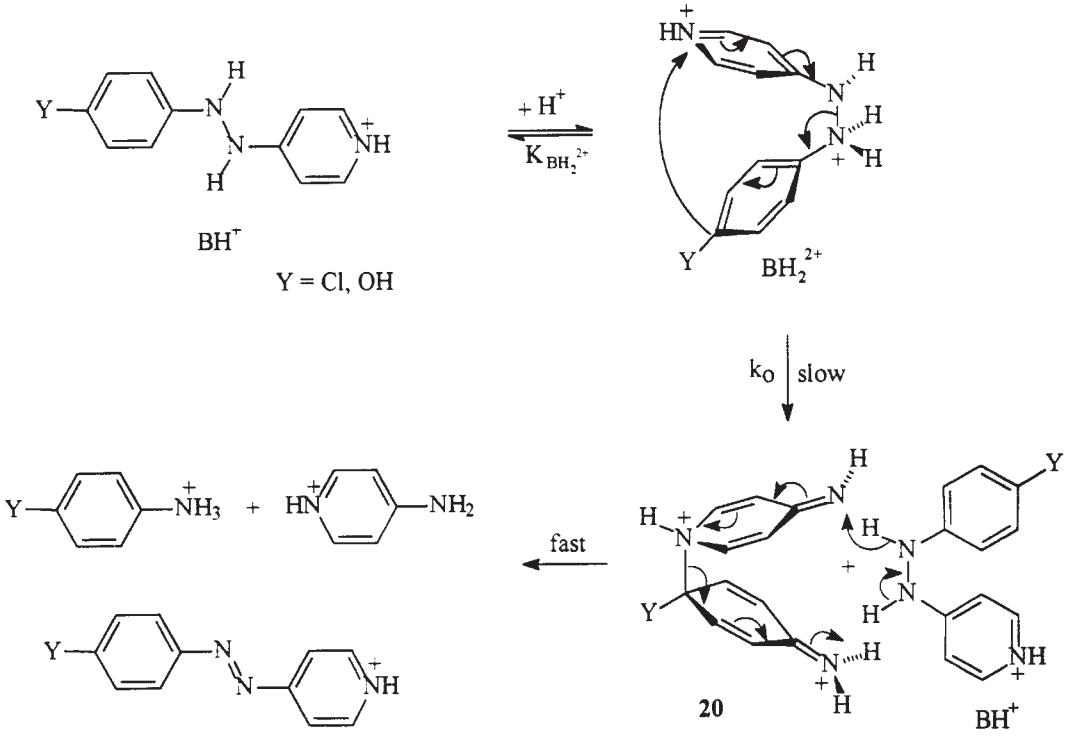
© 2000 NRC Canada

Fig. 6. Kinetic behaviour as function of acid concentration of phenylhydrazinopyridine, phenylazopyridine, and *p*-hydroxyphenylhydrazinopyridine.



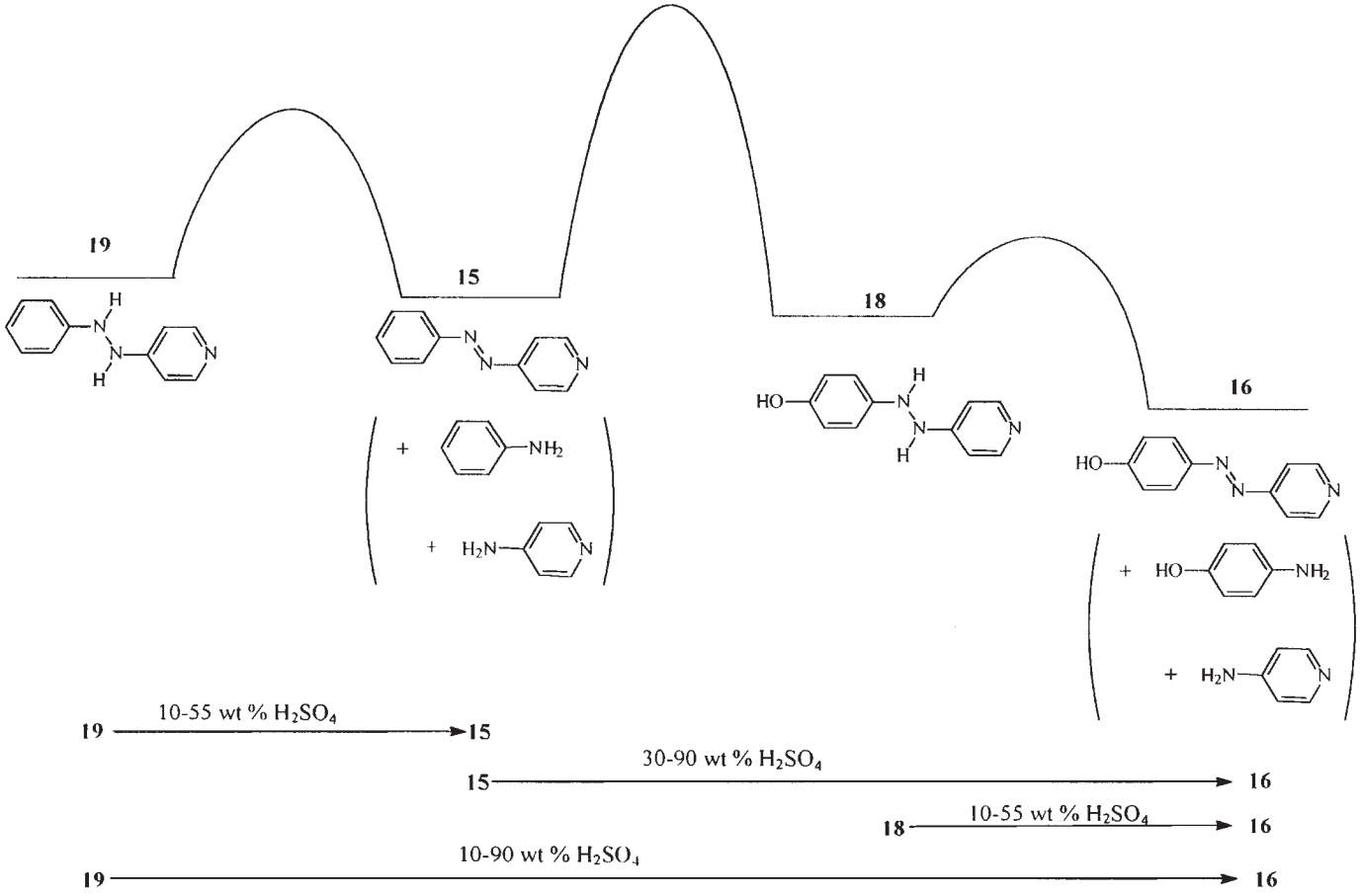


Scheme 17.

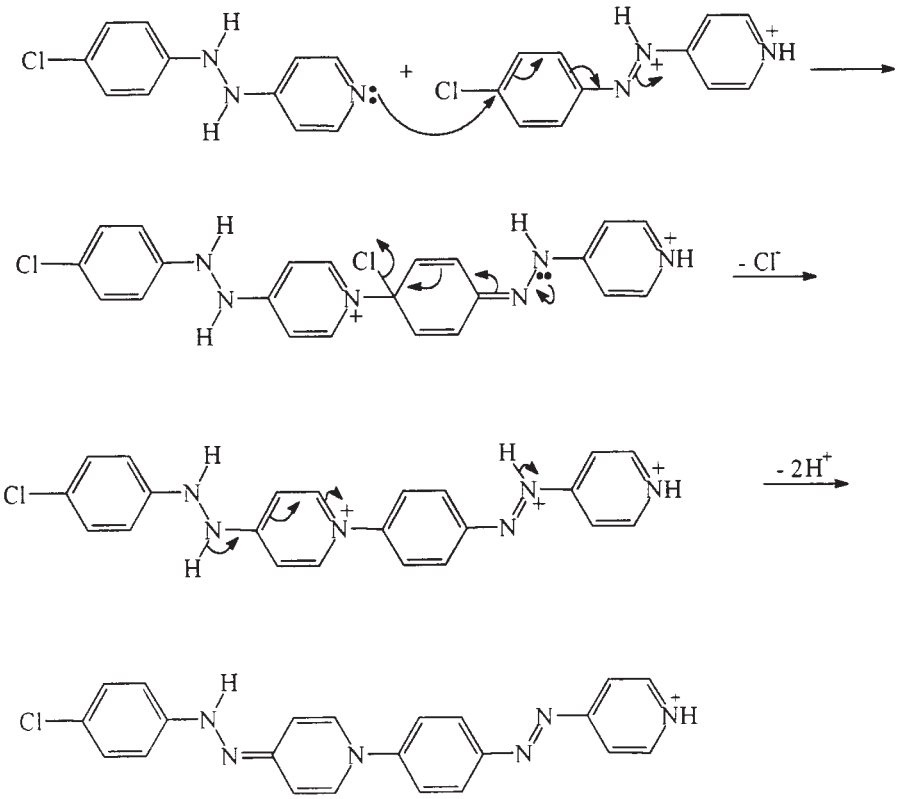


© 2000 NRC Canada

Fig. 7. Energy profiles for the consecutive disproportionation and hydroxylation processes of phenylhydrazinopyridine.

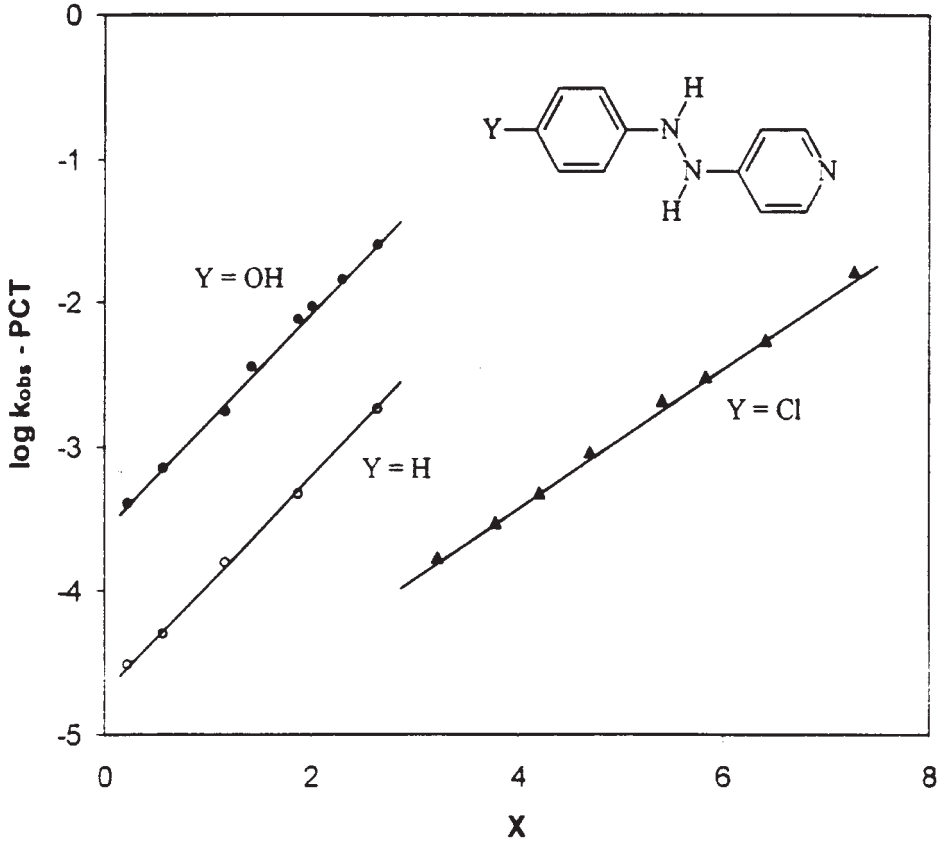


Scheme 18.



© 2000 NRC Canada

Fig. 8. Excess acidity plots of log k_Ψ – log ($C_{BH_2^{++}}/(C_{BH^+} + C_{BH_2^{++}})$) (PCT) vs. X for phenylhydroazinopyridines in aqueous sulfuric acid.



acknowledgement is also made to the Natural Sciences and Engineering Research Council of Canada for generous funding of our research under the heading Dynamics of Organic Reactions.

References

1. P. Griess. Liebigs Ann. Chem. **106**, 123 (1858).
2. Kirk–Othmer encyclopedia of chemical technology. Vol. 3. 4th ed. Wiley, New York. 1992. p. 821.
3. (*a*) H. Zollinger. Diazo chemistry. I. Aromatic and heteroaromatic compounds. VCH, Weinheim. 1994; (*b*) H. Zollinger. Color chemistry. Syntheses, properties, and applications of organic dyes and pigments. VCH, Weinheim. 1991; (*c*) H. Zollinger. Color: a multidisciplinary approach. Wiley, Weinheim. 1999.
4. (*a*) S. Patai (*Editor*). The chemistry of diazonium and diazo groups. Parts 1 and 2. Wiley, London. 1978; (*b*) S. Patai (*Editor*). The chemistry of hydrazo, azo, and azoxy groups. Parts 1 and 2. Wiley, London. 1975; (*c*) S. Patai (*Editor*). The chemistry of hydrazo, azo, and azoxy groups, Vol. 2. Wiley, Interscience, New York. 1997.
5. O. Wallach and L. Belli. Chem. Ber. **13**, 525 (1880).
6. A. Kekule and C. Hidegh. Chem. Ber. **3**, 233 (1870).
7. (*a*) A. Angeli. Atti. Accad. Lincei. **19**, **I**, 793 (1910); Chem. Abstr. **4**, 2634 (1910); (*b*) T.T. Chu and C.S. Marvel. J. Am. Chem. Soc. **55**, 2841 (1933).
8. (*a*) E. Buncel. *In* Mechanisms of molecular migrations. Vol. 1. *Edited by* B.S. Thyagarajan. Wiley, New York. 1968. pp. 61–119; (*b*) R.A. Cox and E. Buncel. *In* The chemistry of the hydrazo, azo, and azoxy groups. *Edited by* S. Patai. Wiley, London. 1975. pp. 775–859.
9. A.W. Hoffmann. Proc. Roy. Soc. (London), **12**, 576 (1863).
10. (*a*) H.J. Shine. Aromatic rearrangements. Elsevier, New York. 1967; (*b*) H.J. Shine. *In* Mechanisms of molecular migrations. *Edited by* B.S. Thyagarajan. Vol. 2. Interscience, New York. 1969. p. 191; (*c*) H.J. Shine. J. Phys. Org. Chem. **2**, 491 (1989); (*d*) H.J. Shine. *In* Isotopes in organic chemistry. Vol. 8. *Edited by* E. Buncel and W.H. Saunders. Elsevier, Amsterdam. 1992. pp. 1–40.
11. C.K. Ingold. *In* The transition state. Chem. Soc. London, Spec. Pub. No. 16, 132 (1962).
12. (*a*) J.F. Bunnett and E. Buncel. J. Am. Chem. Soc. **83**, 1117 (1961); (*b*) J.F. Bunnett, E. Buncel, and K.V. Nahabedian. J. Am. Chem. Soc. **84**, 4136 (1962).
13. (*a*) J.F. Bunnett. J. Am. Chem. Soc. **83**, 4956, 4968, 4973, 4978 (1961); (*b*) J.F. Bunnett and F.P. Olsen. Can. J. Chem. **44**, 1899, 1917 (1966).
14. S. Rajagopal and E. Buncel. Dyes Pigm. **17**, 303 (1991).
15. E. Buncel and S. Rajagopal. Acc. Chem. Res. **23**, 226 (1990).
16. E. Buncel and S. Rajagopal. J. Org. Chem. **54**, 798 (1989).
17. G.J. Ashwell (*Editor*). Molecular electronics. Wiley, New York. 1992.
18. (*a*) S.-R. Keum, S.-S. Hur, P.M. Kazmaier, and E. Buncel. Can. J. Chem. **69**, 1940 (1991); (*b*) S.-R. Keum, K.-B. Lee, P.M. Kazmaier, R.A. Manderville, and E. Buncel. Mag. Res. Chem, **30**, 1128 (1992); (*c*) S.-R. Keum, K.-B. Lee, P.M. Kazmaier, and E. Buncel. Tetrahedron Lett. **35**, 1015 (1994); (*d*) S.-R. Keum, S.S. Lim, B.H. Min, P.M. Kazmaier, and E. Buncel. Dyes Pigm. **30**, 225 (1996); (*e*) J.T.C. Wojtyk, P.M. Kazmaier, and E. Buncel. J. Chem. Soc. Chem. Commun. 1703 (1998); (*f*) S.-R. Keum, M.-J. Lee, S. Swansburg, E. Buncel, and R.P. Lemieux. Dyes Pigm. **39**, 383 (1998); (*g*) S.

© 2000 NRC Canada

Swansburg, E. Buncel, and R.P. Lemieux. J. Am. Chem. Soc. **122**, 6594 (6000); (*h*) J.T.C. Wojtyk, P.M. Kazmaier, and E. Buncel. J. Phys. Chem. in press.
19. A. Archut and G.C. Azzellini. Chem. Soc. Rev. **27**, 233 (1998).
20. (*a*) P.H. Gore and G.K. Hughes. Aust. J. Sci. Res. **3A**, 136 (1950); (*b*) P.H. Gore and G.K. Hughes. Aust. J. Sci. Res. **4A**, 185 (1951).
21. (*a*) E. Buncel and W.M.J. Strachan. Can. J. Chem. **48**, 377 (1970); (*b*) W.M.J. Strachan and E. Buncel. Can. J. Chem. **47**, 4011(1969); (*c*) E. Buncel, W.M.J. Strachan, R.J. Gillespie, and R. Kapoor. J. Chem. Soc. Chem. Commun. 765 (1969); (*d*) W.M.J. Strachan, A. Dolenko, and E. Buncel. Can. J. Chem. **47**, 4011 (1969); (*e*) E. Buncel, W.M.J. Strachan, and H. Cerfontain. Can. J. Chem. **49**, 152 (1971).
22. E. Buncel and W.M.J. Strachan. Can. J. Chem. **48**, 377 (1970).
23. (*a*) C.S. Hahn, K.W. Lee, and H.H. Jaffe. J. Am. Chem. Soc. **89**, 4975 (1967); (*b*) C.S. Hahn and H.H. Jaffe. J. Am. Chem. Soc. **84**, 946 (1962); (*c*) M.H. Akhtar. M.Sc. Thesis. University of Moncton, 1967; (*d*) V.O. Lukashevich and T.N. Kurdyumova. Zh. Obshch. Khim. **18**, 1963 (1948); (*e*) J. Singh, P. Singh, J.L. Boivin, and P.E. Gagnon. Can. J. Chem. **41**, 499 (1963); (*f*) D. Duffey and E.C. Hendley. J. Org. Chem. **33,** 1918 (1968).
24. A.J. Dolenko and E. Buncel. *In* The chemistry of the hydrazo, azo, and azoxy groups. *Edited by* S. Patai. Wiley, London. 1975. pp. 725–773.
25. (*a*) S. Oae, T. Fukumoto, and M. Yamagami. Bull. Chem. Soc. Jpn. **34**, 1873 (1961); (*b*) S. Oae, T. Fukumoto, and M. Yamagami. Bull. Chem. Soc. Jpn. **36**, 601 (1963); (*c*) M.M. Shemyakin, T.E. Agadzhanyan, V.I. Maimind, R.V. Kudryavtsev, and D.N. Kursanov. Dokl. Adak. Nauk SSSR. **135**, 346 (1960); Chem. Abstr. **55**, 11337 (1961).
26. (*a*) M.M. Shemyakin, V.I. Maimind, and B.K. Vaichunaite. Zh. Obshch. Khim. **28**, 1708 (1958); Chem. Abstr. **53**, 1201 (1959); (*b*) M.M. Shemyakin, V.I. Maimind, and B.K. Vaichunaite. Chem. Ind. (London), 755 (1958).
27. L.C. Behr and E.C. Hendley. J. Org. Chem. **31**, 2715 (1966).
28. P.H. Gore. Chem. Ind. (London), 191 (1959).
29. E. Buncel and B.T. Lawton. Chem. Ind. (London), 1835 (1963).
30. E.C. Hendley and D. Duffey. J. Org. Chem. **35**, 3579 (1970).
31. C.S. Hahn and H.H. Jaffe. J. Am. Chem. Soc. **84**, 949 (1962).
32. (*a*) E. Buncel and B.T. Lawton. Can. J. Chem. **43**, 862 (1965); (*b*) E. Buncel. Acc. Chem. Res. **8**, 132 (1975).
33. M.A. Paul and F.A. Long. Chem. Rev. **57**, 1 (1957); M.J. Jorgenson and D.R. Hartter. J. Am. Chem. Soc. **85**, 878 (1963).
34. R.A. Cox. Acc. Chem. Res. **20**, 27 (1987); R.A. Cox and K. Yates. Can. J. Chem. **57**, 2944 (1979).
35. E. Buncel, A. Dolenko, I.G. Csizmadia, J. Pincock, and K. Yates. Tetrahedron, **24**, 6671 (1968).
36. (*a*) E. Buncel and A. Dolenko. Tetrahedron Lett. 113 (1971); (*b*) A. Dolenko and E. Buncel. Can. J. Chem. **52,** 623 (1974); (*c*) E. Buncel, R.A. Cox, and A. Dolenko. Tetrahedron Lett. no. 3, 215 (1975); (*d*) R.A. Cox, A.J. Dolenko, and E. Buncel. J. Chem. Soc. Perkin Trans. 2, 471 (1975).
37. (*a*) E. Buncel and R.A. Cox. J. Chem. Soc. Chem. Commun. 1259 (1972); (*b*) R.A. Cox and E. Buncel. Can. J. Chem. **51**, 3143 (1973); (*c*) R.A. Cox and E. Buncel. J. Am. Chem. Soc. **97**, 1871 (1975).
38. G.A. Olah, K. Dunne, D.P. Kelly, and Y.K. Mo. J. Am. Chem. Soc. **94**, 7438 (1972).
39. E. Buncel and S.R. Keum. Heterocycles, **20**, 1751 (1983).
40. E. Buncel, S.-R. Keum, M. Cygler, K.I. Varughese, and G.I. Birnbaum. Can. J. Chem. **62**, 1628 (1984).
41. E. Buncel and S.-R. Keum. J. Chem. Soc. Chem. Commun. 578 (1983).
42. C. Reichardt. Solvents and solvent effects in organic chemistry. 2nd ed. VCH, Weinheim. 1990.
43. G. Rauhut, T.Clark, and T. Steinke. J. Am. Chem. Soc. **115**, 9174 (1993).
44. M.J. Kamlet, J.-L. M.Abboud, M.H. Abraham, and R.W. Taft. J. Org. Chem. **48**, 2877 (1983).
45. E. Buncel and S.R. Keum. Tetrahedron, **39**, 1091 (1983).
46. E. Buncel and I. Onyido. Can. J. Chem. **64**, 2115 (1986).
47. R.A. Cox, I. Onyido, and E. Buncel. J. Am. Chem. Soc. **114**, 1358 (1992).
48. (*a*) C.K. Ingold and H.V. Kidd. J. Chem. Soc. 984 (1933); (*b*) C.A. Bunton, C.K. Ingold, and M. Mhala. J. Chem. Soc. 1906 (1957); (*c*) D.V. Banthorpe, E.D. Hughes, and C.K. Ingold. J. Chem. Soc. 2418 (1962).
49. (*a*) D.V. Banthorpe and J.G. Winter. J. Chem. Soc. Perkin Trans. 2, 874 (1972); (*b*) D.V. Banthorpe. Chem. Rev. **70**, 295 (1970); (*c*) D.V. Banthorpe. Top. Carbocyclic Chem. **1**, 1 (1969).
50. (*a*) H.J. Shine, L. Kupczyk-Subotkowska, and W. Subotkowski. J. Am. Chem. Soc. **107**, 6674 (1985); **109**, 1286 (1987); (*b*) E.S. Rhee and H.J. Shine. J. Am. Chem. Soc. **108**, 1000 (1986); **109**, 5052 (1987).
51. C.A. Bunton and R.J. Rubin. J. Am. Chem. Soc. **98**, 4236 (1976).
52. M.J.S. Dewar. *In* Molecular rearrangements. Vol. 1. *Edited by* P. De Mayo. Interscience, New York. 1963. p. 323.
53. J.S. Clovis and G.S. Hammond. J. Org. Chem. **28**, 3290 (1963).
54. M. Vecera. Chem. Listy, **52**, 1373 (1958).
55. M.E. Lupes. Rev. Roum. Chim. **17**, 1253 (1972).
56. (*a*) D.L.H. Williams and E. Buncel. *In* Isotopes in organic chemistry. Vol. 5. *Edited by* E. Buncel and C.C. Lee. Elsevier, Amsterdam. 1980. pp. 184–197; (*b*) R.A. Cox and E. Buncel. *In* The chemistry of the hydrazo, azo, and azoxy groups. Vol. 1. *Edited by* S. Patai. Wiley, London. 1975. pp. 775–859.
57. K.-S. Cheon, R.A. Cox, S.-R. Keum, and E. Buncel. J. Chem. Soc. Perkin Trans. 2, 1231 (1998).
58. E. Buncel and K.-S. Cheon. J. Chem. Soc. Perkin Trans. 2, 1241 (1998).
59. R.A. Cox, K-S. Cheon, and E. Buncel. Can. J. Chem. **76**, 896 (1998).

© 2000 NRC Canada

Thermodynamics of mixtures with strongly negative deviations from Raoult's law. Part 3. Application of the DISQUAC model to mixtures of triethylamine with alkanols. Comparison with Dortmund UNIFAC and ERAS results

Juan Antonio González, Isaias Garcia de la Fuente, and Jose Carlos Cobos

Abstract: Binary mixtures of triethylamine (TEA) and alkanols have been investigated in the framework of DISQUAC. The systems are built by three contacts: aliphatic–hydroxyl, aliphatic–nitrogen, and hydroxyl–nitrogen. The corresponding interaction parameters are reported and discussed. The former are avalilable in the literature but were modified (particularly the third dispersive (DIS) and quasichemical (QUAC) interchange coefficients) for *sec*- and *tert*-alkanols + *n*-alkanes using recent data on excess heat capacities at constant pressure (C_p^E) for systems of these alkanols with *n*-heptane. The interaction parameters for aliphatic–nitrogen contacts are purely dispersive. The structure dependence of the DIS and QUAC interchange coefficients of the hydroxyl–nitrogen contacts in 1-alkanols + TEA systems is similar to that found in other solutions previously investigated. The QUAC interchange coefficients remain constant from ethanol and are also valid for 2-alkanols and *tert*-butanol. Methanol behaves differently. A short discussion in terms of effective dipole moments is also included. DISQUAC represents well the thermodynamic properties examined: vapor-liquid equilibria (VLE), molar excess Gibbs energies (G^E) and molar excess enthalpies (H^E). DISQUAC provides better results than the Dortmund version of UNIFAC using the published geometrical and interaction parameters. ERAS parameters for 1-alkanols + TEA systems are also reported. Interactions between unlike molecules are stronger for solutions with methanol or ethanol. DISQUAC improves ERAS results on H^E, while both models give similar results for G^E. However, ERAS needs an specific parameter, with unknown temperature-dependence, to describe properly G^E. The main advantage of ERAS is its ability to provide information on V^E. Its main limitation is that can be only applied to those systems where association is expected. DISQUAC, a purely physical model, can be applied to any type of binary mixture, as it is followed from this and previous studies.

Key words: theory, liquids, associated, thermodynamics, group contributions.

Résumé : On a étudié des mélanges binaires de triéthylamine (TEA) et d'alkanols dans le cadre du DISQUAC. On a construit les systèmes par trois contacts : aliphatique–hydroxyle, aliphatique–azote et hydroxyle–azote. On rapporte et on discute des paramètres d'interaction correspondants. Les premiers sont disponibles dans la littérature, mais on les a modifiés [en particulier, les troisièmes coefficients d'échange dispersifs (« DIS ») et quasichimiques (« QUAC »)] pour les alcanols (secondaires et tertaires) + alcanes en utilisant des données récentes sur les capacités calorifiques en excès à pression constante (C_p^E) pour les systèmes de ces alcanols dans l'heptane. Les paramètres d'interaction pour les contacts aliphatique–azote sont strictement dispersifs. La relation entre la structure et les d'échange « DIS » et « QUAC » pour les systèmes alcan-1-ols + TEA sont semblables à ceux observés avec d'autres systèmes étudiés antérieurement. Les coefficients d'échange « QUAC » demeurent constants à partir de l'éthanol et ils sont aussi valides pour la alcan-2-ols et pour le *tert*-butanol. Le méthanol se comporte différemment. On inclut aussi une courte discussion en termes des moments dipolaires effectifs. Le modèle « DISQUAC » permet de bien représenter les propriétés thermodynamiques examinées : équilibre vapeur-liquide (EVL), énergies molaires de Gibbs en excès (G^E) et les enthalpies molaires en excès (H^E). Il donne de meilleurs résultats que la version de Dortmund de l'« UNIFAC » en utilisant les paramètres géométriques et d'interaction publiés. On rapporte aussi les paramètres « ERAS » pour les systèmes alcan-1-ols + TEA. Les interactions entre les molécules dissemblables sont plus fortes pour des solutions avec du méthanol ou de l'éthanol. La méthode « DISQUAC » améliore les résultats « ERAS » pour H^E alors que les deux modèles conduisent à des résultats semblables pour G^E. Toutefois, « ERAS » nécessite un paramètre spécifique, pour lequel on ne connaît pas la relation avec la température qui permettrait de décrire correctement G^E. Le principal

Received November 28, 1999. Published on the NRC Research Press website on September 26, 2000.

J.A. González[1], I. Garcia de la Fuente, and J.C. Cobos. G.E.T.E.F. Dpto. de Termodinámica y Física Aplicada, Facultad de Ciencias, Universidad de Valladolid, 47071 Valladolid, Spain.

[1]Author to whom correspondence may be addressed. e-mail: jagl@termo.uva.es

 © 2000 NRC Canada

avantage de « ERAS » réside dans sa facilité de fournir des informations sur V^E. Sa principale limitation a trait au fait qu'on ne peut l'appliquer qu'aux systèmes où on prévoit des associations. Comme il en découle de la présente étude et des autres faites antérieurement, « DISQUAC » est un modèle purement physique qui peut être appliqué à tous les types de systèmes binaires.

Mots clés : théorie, liquides, associés, thermodynamique, contributions de groupes.

[Traduit par la Rédaction]

Table 1. Critical temperatures (T_c), pressures (P_c), molar volumes (V), dipole moments in vapor phase (μ), effective dipole moments ($\bar{\mu}$, eq. [1]), and reduced dipole moments ($(\mu^*)'$, eq. [3]) in liquid phase for some of the compounds considered in this work.

Compound	T_c (K)	P_c (bar)	V^a (cm^3 mol^{-1})	μ (D)	$\bar{\mu}$	$(\mu^*)'$
Methanol	512.6[b]	80.9[b]	40.51[b]	1.7[b]	1.023	0.216
Ethanol	513.9[b]	61.4[b]	58.39[b]	1.7[b]	0.852	0.188
1-Propanol	536.8[b]	51.7[b]	74.75[b]	1.7[b]	0.752	0.165
2-Propanol	508.3[b]	47.6[b]	76.46[b]	1.7[b]	0.744	0.167
1-Butanol	563.1[b]	44.2[b]	91.51[b]	1.66[c]	0.664	0.142
2-Butanol	536.1[b]	41.8[b]	91.85[b]	1.7[b]	0.679	0.148
tert-Butanol	506.2[b]	39.7[b]	94.18[b]	1.7[b]	0.670	0.153
1-Pentanol	588.2[b]	39.1[b]	108.16[b]	1.7[b]	0.626	0.131
1-Hexanol	610.7[c]	34.7[c]	125.48[b]	1.7[d]	0.580	0.119
TEA	535.0[b]	30.3[b]	139.00[b]	0.9[b]	0.292	0.067
TPA	626.7[e]	26.7[e]	189.52[c]	0.76[d]	0.211	0.045
TBA	643.0[b]	18.2[b]	237.94[b]	0.8[b]	0.198	0.038

[a]Data at 293. K.
[b]Ref. 78.
[c]Ref. 79.
[d]Ref. 80.
[e]Calculated using the Joback's method (78).

1 Introduction

Alkanols and TEA are polar compounds which differ substantially in their permanent dipole moment (μ) and consequently also in their effective dipole moment ($\bar{\mu}$ (Table 1)) a useful magnitude to investigate the impact of polarity in bulk properties (1–6). It is defined as (5)

$$[1] \qquad \bar{\mu} = [\mu^2 N_A / 4\pi\varepsilon_0 V k_B T]^{1/2}$$

where N_A is the Avogadro's constant; ε_0, the permittivity of the vacuum; k_B, the Boltzmann's constant; V, the molar liquid volume; and T, the temperature.

In exchange, for the purpose of characterizing the effective polarity of a a single, isolated molecule with a given μ, it is defined a reduced dipole moment according to (3–5)

$$[2] \qquad \hat{\mu} = [\mu^2 / 4\pi\varepsilon_0 \sigma^3 \varepsilon]^{1/2}$$

where σ is an appropiate molecular size parameter, and ε the corresponding interaction energy parameter. This expression may advantageously be transformed by virtue of the corresponding states principle to

$$[3] \qquad \mu^* = [\mu^2 N_A / 4\pi\varepsilon_0 V_c k_B T_c]^{1/2}$$

$$[4] \qquad (\hat{\mu})' = [\mu^2 P_c / 4\pi\varepsilon_0 k_B^2 T_c^2]^{1/2}$$

Here V_c, T_c, and P_c are the critical values of molar volume, temperature, and pressure, respectively.

In the case of 1-alkanols + TEA mixtures, thermal and volumetric data (7–11) are indicative of strong intermolecular interactions between unlike molecules (negative deviations from Raoult's law) through the formation of hydrogen-bonded complexes. This may be related to amines (primary, secondary, tertiary, and aromatic) are good proton acceptors because the electrons around the N atoms have less *s* and more *p* character than in other groups (e.g., nitrile or carbonile groups) (12, 13).

DISQUAC (14, 15) a purely physical model based on the rigid lattice theory developed by Guggenheim (16) has been successfully applied to the characterization of other binary liquid mixtures which also show strong negative deviations from Raoult's law (1, 17) (parts I and II of this series). Particularly, the systems investigated so far are: methanol or ethanol with propanal (17), *n*-alkanones with $CHCl_3$ (17); or oxaalkanes (linear or cyclic) with $CHCl_3$ or CH_2Cl_2 (1). It is remarkable that DISQUAC and different continuous association models yield similar results for such systems (17). As a continuation, we now present the DISQUAC treatment of TEA + alkanols mixtures.

A systematic comparison between DISQUAC calculations and predictions from the Dortmund version of UNIFAC model (18) (hereafter, merely UNIFAC) is shown. At this end, the corresponding published geometrical and interaction parameters were used without modification (18).

Mixtures containing 1-alkanols and TEA have been studied (19, 20) in terms of the ERAS (21) model, which combines the real association solution model (22–25) with a physical term, namely the Flory's equation of state (26). In (19), the equation which represents the chemical contribution to V^E was incorrectly written (27), and solutions of

© 2000 NRC Canada

Table 2. Relative group increments for molecular volumes, $r_G = V_G/V_{CH4}$, and areas, $q_G = A_G/A_{CH4}$, calculated using Bondi's method (30) ($V_{CH4} = 17.12 \times 10^{-6}$ m^3 mol^{-1}; $A_{CH4} = 2.90 \times 10^{-5}$ m^2 mol^{-1}).

Group	r_G	q_G	Ref.
CH_3	0.79848	0.73103	(31)
CH_2	0.59755	0.46552	(31)
CH	0.39603	0.19655	(81)
C	0.19451	0.	(81)
N	0.25290	0.07930	(48)
OH	0.46963	0.50345	(32)

methanol and TEA were not considered. So, here new ERAS parameters for 1-alkanols + TEA mixtures are reported.

Finally, it should be mentioned that the UNIQUAC associated solution model (28), which uses the UNIQUAC equation (29) to describe the physical contribution to the excess functions has been also applied to the 1-propanol + TEA system (28).

2. Theory

2.1 Disquac

In the framework of DISQUAC, mixtures of alkanols with TEA are regarded as possessing three types of surfaces: (*i*) type a, (aliphatic: CH_3, CH_2, CH, or C in alkanols or TEA); (*ii*) type n (nitrogen, N, in TEA); (*iii*) type h (hydroxyl, OH, in alkanols)

2.1.1 Assessment of geometrical parameters

When DISQUAC is applied, the total relative molecular volumes (r_i) surfaces (q_i) and the molecular surface fractions (α_{si}) of the compounds present in the mixture are usually calculated additively on the basis of the group volumes V_G and surfaces A_G, recommended by Bondi (1968) (30). As volume and surface units, the volume V_{CH_4} and surface A_{CH_4} of methane are taken arbitrarily (31). The geometrical parameters of the groups referred to in this work are listed in Table 2.

2.1.2 Equations

The equations used to calculate G^E and H^E are the same as in other applications (32). The interactional terms in the excess thermodynamic properties G^E and H^E contain a DIS and a QUAC contribution which are calculated independently by the classical formulas and then simply added. The degree of non-randomness is thus expressed by the relative amounts of dispersive and quasichemical terms

$$[5] \qquad G^E = G^{E,COMB} + G^{E,DIS} + G^{E,QUAC}$$

$$[6] \qquad H^E = H^{E,DIS} + H^{E,QUAC}$$

where $G^{E,COMB}$ is the Flory–Huggins combinatorial term (31, 33).

For the QUAC part, as coordination number the reference value was chosen, that is $z = 4$.

The temperature dependence of the interaction parameters g_{st}, h_{st}, and c_{pst} has been expressed in terms of the DIS and (or) QUAC interchange coefficients (32) $C_{st,1}^{DIS}$ and $C_{st,1}^{QUAC}$, where s, $t = a$; h, n, and $l = 1$ (Gibbs energy; $C_{st,1}^{DIS/QUAC} = g_{st}^{DIS/QUAC}(T_0)/RT_0$); $l = 2$ (enthalpy; $C_{st,2}^{DIS/QUAC} = h_{st}^{DIS/QUAC}(T_0)/RT_0$) and $l = 3$ (heat capacity; $C_{st,3}^{DIS/QUAC} = c_{pst}^{DIS/QUAC}(T_0)/R$).

$T_0 = 298.15$ K is the scaling temperature.

2.2 Modified UNIFAC (Dortmund version)

Modified UNIFAC (18) differs from the original UNIFAC (34) by the combinatorial term and the temperature dependence of the group interaction parameters (a_{nm}, b_{nm}, c_{nm}). This dependence is as follows

$$[7] \qquad \psi_{nm} = \exp[-(a_{nm} + b_{nm}T + c_{nm}T^2)/T]$$

The equations used to calculate G^E and H^E are obtained from the fundamental equation for the activity coefficient γ_i of component i

$$[8] \qquad \ln\gamma_i = \ln\gamma_i^{COMB} + \gamma_i^{RES}$$

where $\ln\gamma_i^{COMB}$ is the combinatorial term and $\ln\gamma_i^{RES}$ is the residual term.

2.2.1 Assessment of geometrical and interaction parameters

In modified UNIFAC, alkanols are characterized by two main groups, OH and CH_3OH. The former is subdivided in three subgroups: OH(p), OH(s), and OH(t), which represent the hydroxyl group in primary, secondary, and tertiary alcohols. CH_3OH is a group itself which characterizes methanol. Tertiary amines are characterized by the main group (C)3N, subdivided in two subgroups: CH_3N and CH_2N. The subgroups have different geometrical parameters, but the subgroups within the same main group are assumed to have identical group energy-interaction parameters. The geometrical parameters, the relative van der Waals volumes, and the relative van der Waals surfaces of the different subgroups are not calculated from molecular parameters like in the original UNIFAC but fit together with (a_{nm}, b_{nm}, c_{nm}) to the experimental values of the thermodynamic properties considered. The geometrical and interaction parameters are taken from literature (18) and used without modification.

2.3 The ERAS model

This model combines the real association solution model (22–25) with Flory's equation of state (26). The excess functions are written as

$$[9] \qquad X^E = X_{phys}^E + X_{chem}^E$$

where $X = G$ (Gibbs energy), H (enthalpy), V (volume). In eq. [9], X_{chem}^E is the chemical contribution, mainly due to association reactions, and X_{phys}^E represents the physical contribution, a consequence of the physical interactions between molecules. Correct expressions for these terms when cross-association between compounds exist are given elsewhere (27, 35, 36) for $X = H$ and V, and will not repeated here. The chemical contribution to the excess properties arises from chemical interactions between the molecules, in particular hydrogen bonding. It is assumed that TEA (B) molecules are not associated, while alcohol molecules (A) build linear chains of associated multimers

$$[10] \qquad A_n + A \xleftrightarrow{K_A} A_{n+1}$$

© 2000 NRC Canada

Table 3. Interchange coefficients, dispersive $C_{ah,1}^{DIS}$ and quasichemical $C_{ah,1}^{QUAC}$ (l = 1, Gibbs energy; l = 2, enthalpy; l = 3, heat capacity) for contacts (a,h) (Type a, CH_3, CH_2, CH, or C in secondary or tertiary alkanols and n-alkanes; Type h, OH in secondary or tertiary alkanols). The coordination number used for the QUAC part is z = 4.

Alkanol	$C_{ah,1}^{DIS}$	$C_{ah,2}^{DIS}$	$C_{ah,3}^{DIS}$	$C_{ah,1}^{QUAC}$	$C_{ah,2}^{QUAC}$	$C_{ah,3}^{QUAC}$
***sec*-Alkanols + *n*-alkanes**						
2-Propanol	3.00	2.50	10.00	10.00	9.75	38.00
2-Butanol	4.15	5.70	21.00	10.00	9.75	38.00
2-Pentanol	4.20	6.80[a]	21.00	10.00	9.75	38.00
3-Pentanol	3.00	4.40[a]	21.00	10.00	12.75	38.00
2-Hexanol	4.80[a]	7.90	21.00	10.00	9.75	38.00
3-Hexanol	3.70[a]	5.35	21.00	10.00	12.75	38.00
2-Heptanol	5.40[a]	6.80[a]	21.00	10.00	9.75	38.00
3-Heptanol	4.40[a]	3.60[a]	21.00	10.00	12.75	38.00
2-Octanol	6.10	5.65	21.00	10.00	9.75	38.00
3-Octanol	5.10	1.20	21.00	10.00	12.75	38.00
4-Octanol	5.10	1.20	21.00	10.00	12.75	38.00
***tert*-Alkanols + *n*-alkanes**						
2M-2-Propanol[b]	1.90	6.10	–12.00	10.00	7.50	85.00
2M-2-Butanol[b]	1.35	0.30	–21.50	10.00	13.00	80.00
2M-2-Pentanol[b]	0.85[a]	1.20	–21.50	10.00	13.00	80.00
3M-3-Pentanol[b]	0.50[a]	0.80	–21.50	10.00	17.00	80.00

[a]Estimated value.

[b]The abbreviations used are: 2M-2-propanol, 2-methyl-2-propanol; 2M-2-butanol, 2-methyl-2-butanol; 2M-2-pentanol, 2-methyl-2-pentanol; 3M-3-pentanol, 3-methyl-3-pentanol;

where n is the degree of self association, ranging from 1 to ∞. The cross-association between A and B molecules is represented by

$$[11] \quad A_n + B \xleftrightarrow{K_{AB}} A_nB$$

The association constants K_i are assumed to be independent from the chain length. Their temperature dependence is given by

$$[12] \quad K_i = K_o \exp[-(\Delta h_i^*/R)(1/T - 1/T_o))$$

where K_o is the equilibrium constant at the standard temperature T_o and h_i^* is the enthalpy variation for reactions 10–11, which corresponds to the hydrogen bonds energy. Reactions 10–11 are also characterized by the volume change (Δv_i^*) which is related to the formation of the linear chains.

X_{phys}^E is derived from Flory's equation of state (26), which is assumed to be valid not only for pure components but also for the mixture

$$[13] \quad \overline{P}_i \overline{V}_i / \overline{T}_i = \overline{V}_i^{1/3}/(\overline{V}_i^{4/3} - 1) - 1/\overline{V}_i \overline{T}_i$$

where i = A, B, M(mixture). In eq. [13], $\overline{V}_i = V_i/V_i^*$; $\overline{P}_i = P/P_i^*$ and $\overline{T}_i = T/T_i^*$ are the reduced parameters, volume, pressure, and temperature, respectively. The reduction parameters for pure components V_i^*, P_i^*, and T_i^* are calculated previous determination of density, thermal expansion coefficient, and compressibility which can be obtained from experimental P-V-T data. They also depend on K_i, Δh_i^*, and Δv_i^*. The method is clearly explained elsewhere (35, 36). The reduction parameters for the mixture P_M^* and T_M^* are calculated via certain mixing rules (36–37), where X_{AB}, the energetic interaction parameter characterizing the difference of dispersive intermolecular interactions between molecules A and B in the solution and in the pure components is introduced. It is the only adjustable parameter of the physical part of H^E and V^E.

3. Estimation of models parameters

3.1 Disquac

The three types of surface generate three pairs of contacts: (a,n), (a,h) and (h,n).

3.1.1 Alkanols + n-alkane mixtures: the (a,h) contacts

In the framework of DISQUAC, primary, secondary, and tertiary alkanols differ by their interaction parameters obtained from data for alkanol + *n*-alkane systems (32, 38, 39). The respective $C_{ah,1}^{DIS/QUAC}$ coefficients change regularly with the alkanol structure (32, 38, 39). This approach has been shown to be successful in treating more complex mixtures: 1-alkanols + C_6H_6 or C_7H_8 (40), + CCl_4 (41), + linear monocarboxylic acids (42), + 1-alkanols (43), + ketones (44), or *sec*-alkanols + C_6H_6, + C_7H_8 or + ketones (45).

In this work, new values of $C_{ah,3}^{DIS/QUAC}$ for *sec*- or *tert*-alkanols were obtained on the basis of recent C_p^E data for the following systems: 2-propanol, 2-butanol, 2-pentanol, 3-pentanol, or *tert*-butanol + heptane (46). The $C_{ah,1}^{DIS/QUAC}$ coefficients for *sec*- and *tert*-alkanols are collected in Table 3. These new $C_{ah,3}^{DIS/QUAC}$ coefficients may modify interaction parameters of more complex mixtures where the (a,h) contacts are also involved. This occurs for *sec*-alkanols + cyclohexane, + C_6H_6, or + C_7H_8, or for *tert*-alkanols + cyclohexane (Tables 1 and 2 of Appendix 1). For *sec*-alkanols + ketones, the corresponding parameters remain unchanged (45).

3.1.2 N,N,N-trialkylamines + n-alkanes mixtures: the (a,n) contacts

Mixtures of tertiary amines with alkanes, particularly with homomorphic alkanes, are nearly ideal. It has been attributed

© 2000 NRC Canada

Table 4. Interchange energy coefficients, dispersive $C^{DIS}_{sn,1}$ and quasichemical $C^{QUAC}_{sn,1}$ (l = 1, Gibbs energy; l = 2, enthalpy, l = 3, heat capacity) for contacts (s,n) (s = a,h; type a, CH_3, CH_2, CH, or C in 1-alkanols or *N*,*N*,*N*-Trialkylamines; type h, OH in 1-alkanols); type n, N in *N*,*N*,*N*-Trialkylamines).

System	$C^{DIS}_{sn,1}$	$C^{DIS}_{sn,2}$	$C^{DIS}_{sn,3}$	$C^{QUAC}_{sn,1}$	$C^{QUAC}_{sn,2}$	$C^{QUAC}_{sn,3}$
***N*,*N*,*N*-Trialkylamines + *n*-alkanes (s = a)**						
TEA + *n*-C_6	34.0	83.7	0.0	0.0	0.0	0.0
TPA + *n*-C_6	100.0[a]	15.0	0.0	0.0	0.0	0.0
TBA + *n*-C_6	240.0[a]	–13.8	0.0	0.0	0.0	0.0
TEA + 1-alkanols (s = h)						
TEA + methanol	–47.0	–142.0	0.0	–8.50	–3.0	0.0
TEA + ethanol	–44.0	–133.0	0.0	–7.50	–1.5	0.0
TEA + 1-propanol	–64.0	–141.0	0.0	–7.50	–1.5	0.0
TEA + 1-butanol	–67.5	–159.0[a]	0.0	–7.50	–1.5	0.0
TEA + 1-pentanol	–67.5[a]	–159.0[a]	0.0	–7.50	–1.5	0.0
TEA + 1-hexanol	–67.5[a]	–159.0[a]	0.0	–7.50	–1.5	0.0
TEA + 2-alkanols (s = h)						
TEA + 2-propanol	–24.5	–115.0[a]	0.0	–7.50	–1.5	0.0
TEA + 2-butanol	–42.5	–131.0[a]	0.0	–7.50	–1.5	0.0
TEA + 2-pentanol	–42.5[a]	–131.0[a]	0.0	–7.50	–1.5	0.0
TEA + *tert*-alkanols (s = h)						
TEA + *tert*-butanol	4.0	–118.0[a]	0.0	–7.50	–1.5	0.0
TPA + 1-alkanols (s = h)						
TPA + 1-propanol	–55.0[a]	–114.6	0.0	–7.50	–1.5	0.0

[a]Estimated values.

to physical properties of tertiary amines are close to those of the mentioned alkanes (47, 48). The very low polarity of amines, represented by small $\bar{\mu}$ values (Table 1), should be also remarked.

H^E measurements for *N*,*N*,*N*-trialkylamines + *n*-alkanes show that this magnitude depends rather strongly on the relative size of the components (49, 50). For shorter amines, TEA, tripropylamine (TPA), or tributylamine (TBA), which are globular molecules, H^E increases with the length of the *n*-alkane (49, 50). In exchange, an opposite behaviour is encountered for tridodecylamine + *n*-alkane systems (50).

These systems have been treated in the framework of the Flory theory (51). The main conclusion is that the shorter amines are order breakers of the long *n*-alkanes (Patterson effect, (52)) and that tridodecylamine is an ordered molecule and the shorter *n*-alkanes act as breakers of such order (51). This has been confirmed by H^E measurements of systems containing two *N*,*N*,*N*-trialkylamines (53).

In DISQUAC, the aliphatic–nitrogen (a,n) interactions in *N*,*N*,*N*-trialkylamines + *n*-alkane mixtures are represented by dispersive parameters which can be calculated using data on these type of solutions. The same procedure has been applied to *N*,*N*-dialkylmethylamines + *n*-alkanes (48); where the Patterson effect is of minor importance, probably due to the small degree of branching in the amines (48). Unfortunately, the available interaction parameters are not valid for *N*,*N*,*N*-trialkylamines (48).

Previous calculations show that, as a consequence of the Patterson's effect, each *N*,*N*,*N*-trialkylamine + *n*-alkane system should be characterized by its own set of interaction parameters. The same occurs in, for example, mixtures of cyclohexane (34), benzene, toluene, or CCl_4 (54) + *n*-alkanes, also studied in the zeroth approximation. For the present work, only the $C^{DIS}_{an,1}$ coefficients for TEA; TPA or TBA + *n*-C_6 are needed (see below). They were calculated using data from refs. (48–50) and are listed in Table 4.

3.1.3 Alcohols + triethylamine mixtures: the (h,n) contacts

These systems are characterized by three contacts: (a,h), (a,n) and (h,n). Because the (a,s) (s = h,n) parameters are known, only those for the (h,n) contacts must now be obtained. The general procedure applied has been explained in detail elsewhere (32, 33). Along with the fitting of the $C^{DIS/QUAC}_{hn,1}$ coefficients, the interaction parameters corresponding to TEA + *n*-hexane were used in spite of the rather different size of the other molecules involved (e.g., methanol and 1-butanol). Calculations show that the $C^{QUAC}_{hn,1}$ (l = 1, 2, 3) coefficients are not essentially affected by the $C^{DIS}_{an,1}$ values. As well the relative variation of the interaction parameters of the (h,n) contacts remains unchanged.

On the other hand, the estimation of the $C^{DIS/QUAC}_{hn,2}$ coefficients is somewhat difficult due to the lack of accurate experimental data (see the H^E values at equimolar composition from different sources in Table 9 for example). In solutions of 1-alkanols and secondary amines (e.g., dibutylamine) for example, the transition of H^E from methanol to ethanol is much steeper compared to the transition from ethanol to butanol (55, 56) (see below). The $C^{DIS/QUAC}_{hn,2}$ coefficients for 1-alkanols + TEA systems were estimated assuming that such fact is still valid, as it is suggested from measurements reported by Findlay (1961) (57).

To reduce the number of interaction parameters, it was assumed that the QUAC coefficients are common for all the alkanols. In absence of H^E data for *sec*- or *tert*-alkanols + TEA mixtures, the DIS enthalpic parameters were determined

© 2000 NRC Canada

Table 5. ERAS parameters of pure compounds at temperature T (K).

Compound	T (K)	K	P^* (J mol^{-1})	V^{mol} (cm^3 mol^{-1})	V^* (cm^3 mol^{-1})	Δh^*_A (J mol^{-1})	Δv^*_A (cm^3 mol^{-1})
Methanol	298.15	986[a]	443.6[a]	40.73[a]	32.13[a]	–25 100[a]	–5.6[a]
	313.15[b]	607[b]	412.1[b]	41.47[b]	32.40[b]	–25 100[a]	–5.6[a]
Ethanol	293.15	377[c]	422.7[c]	58.37[c]	46.83[c]	–25 100[a]	–5.6[a]
	298.15	317[a]	426.4[a]	58.67[a]	47.11[a]	–25 100[a]	–5.6[a]
	303.15	267[c]	403.9[c]	58.99[c]	47.10[c]	–25 100[a]	–5.6[a]
	307.95	230[c]	393.6[c]	59.30[c]	47.20[c]	–25 100[a]	–5.6[a]
1-Propanol	293.15	234[c]	428.4[c]	74.74[c]	60.93[c]	–25 100[a]	–5.6[a]
	298.15	197[a]	414.0	75.16[a]	61.22[a]	–25 100[a]	–5.6[a]
	313.15	121[c]	390.2[c]	76.72[c]	62.00[c]	–25 100[a]	–5.6[a]
1-Butanol	298.15	175[a]	422.7[a]	91.97[a]	75.70[a]	–25 100[a]	–5.6[a]
	313.15[c]	108[c]	392.9[c]	92.77[c]	75.70[c]	–25 100[a]	–5.6[a]
TEA	293.15	0[c]	471.3[c]	139.11[c]	107.20[c]	0[c]	0[c]
	298.15	0[c]	467.6[c]	140.01[c]	107.40[c]	0[c]	0[c]
	307.95	0[c]	451.2[c]	141.78[c]	108.00[c]	0[c]	0[c]
	313.15	0[c]	447.0[c]	142.72[c]	108.10[c]	0[c]	0[c]
TPA	293.15	0[d]	488.0[d]	190.30[d]	146.50[d]	0[d]	0[d]

[a]Ref. 35.
[b]Ref. 37.
[c]Ref. 19.
[d]Ref. 77.

Table 6. ERAS parameters (this work) for mixtures at temperature T (K).

Mixture	T (K)	K_{AB}	Δh^*_{AB} (J cm^{-3})	Δv^*_{AB} (cm^3 mol^{-1})	Q_{AB} (J cm^{-3} K^{-1})	X_{AB} (J cm^{-3})
Methanol +TEA	298.15	725	–35 500	–13.8	—	10.0
Ethanol + TEA	298.15	140	–34 300	–13.8	—	10.0
	307.95	90	–34 300	–13.8	0.0045	10.0
1-Propanol + TEA	293.15	126	–33 200	–13.8	0.016	10.0
	298.15	100	–33 200	–13.8	—	10.0
	313.15	53	–33 200	–13.8	0.022	10.0
1-Butanol + TEA	298.15	84	–33 200	–13.8	—	10.0
	313.15	44	–33 200	–13.8	0.031	10.0
1-Propanol + TPA	298.15	140[a]	–26 600[a]	–9.5[a]	—	15.0[a]

[a]Ref. 77.

in such way that the temperature dependence of VLE is well represented.

The calculated $C_{hn,1}^{DIS/QUAC}$ coefficients are listed in Table 4.

3.2 Estimation of the adjustable ERAS parameters

The parameters adjustable to excess properties are K_A, K_{AB}, Δh^*_A, Δh^*_{AB}, Δv^*_A, Δv^*_{AB}, X_{AB}, and Q_{AB} (needed to represent G^E (37, 58–63)). K_A, Δh^*_A, Δv^*_A are known for all alcohols and are fitted to H^E and V^E data of alcohol + alkane mixtures. The values used in this work are listed in Table 5. It is remarkable that Δh^*_A = –25.1 kJ mol^{-1} and Δv^*_A = –5.6 cm^3 mol^{-1} are values widely used (see 37, 58–63). On the contrary, in (20), Δv^*_A = –7.6 cm^3 mol^{-1} was applied.

The remaining parameters K_{AB}, Δh^*_{AB}, Δv^*_{AB}, X_{AB}, and Q_{AB} are adjusted to H^E, V^E, and VLE data of 1-alkanols + TEA systems. More details are given in literature (35, 37, 58–61). Final parameters are listed in Table 6. It is remarkable that the relative variation of Δh^*_{AB} with the size of the alcohol is similar to that found in 1-alkanols + primary amines systems (35).

4. Results

4.1 Comparison of DISQUAC with experiment

The new DIS and QUAC coefficients for hydroxyl–aliphatic contacts in *sec*- or *tert*-alkanols + *n*-alkanes mixtures improve results for the thermodynamic properties usually considered, G^E, H^E, C_p^E. So, the shape of C_p^E for 2-propanol or *tert*-butanol + *n*-C_7 systems is well represented (Fig. 1). The model also predicts a small region, at very high dilution of the alkanol, where $C_p^E < 0$ for mixtures of 2-butanol, 2-pentanol, or 3-pentanol with *n*-C_7. However, these systems show a point of inflection in the mole fraction range of alcohol >0.1 (46), which are not reproduced by the model.

Regarding alkanols + TEA mixtures, experimental data are compared to results obtained using DISQUAC along Tables 7–9, and shown graphically, for selected systems, in Figs. 2–7.

For the sake of clarity, Table 7 includes standard relative deviations in pressure (P) defined as

$$[14] \quad \sigma_r(P) = \{1/N \sum[P_{exp} - P_{calc}) / P_{exp}]^2\}^{1/2}$$

© 2000 NRC Canada

Fig. 1. C_p^E of alkanols + *n*-heptane mixtures at 298.15 K. Solid lines, DISQUAC results. Points, experimental data (46): (●), 2-propanol; and (▲), *tert*-butanol.

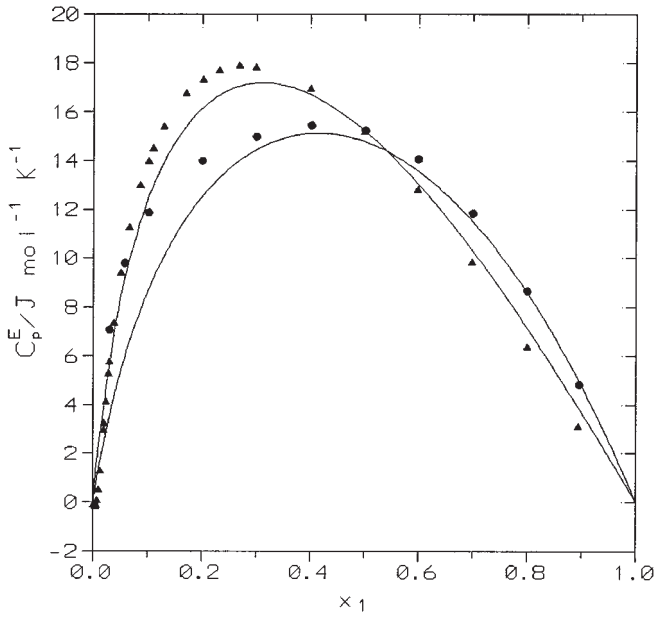


Fig. 2. VLE phase diagrams for methanol(1) or ethanol(1) + TEA(2) mixtures at several temperatures. Solid lines, DISQUAC results. Points, experimental results: (●), methanol (T = 313.15 K) (82); (■), ethanol (307.95 K) (82); and (▲), ethanol (322.75 K) (83).

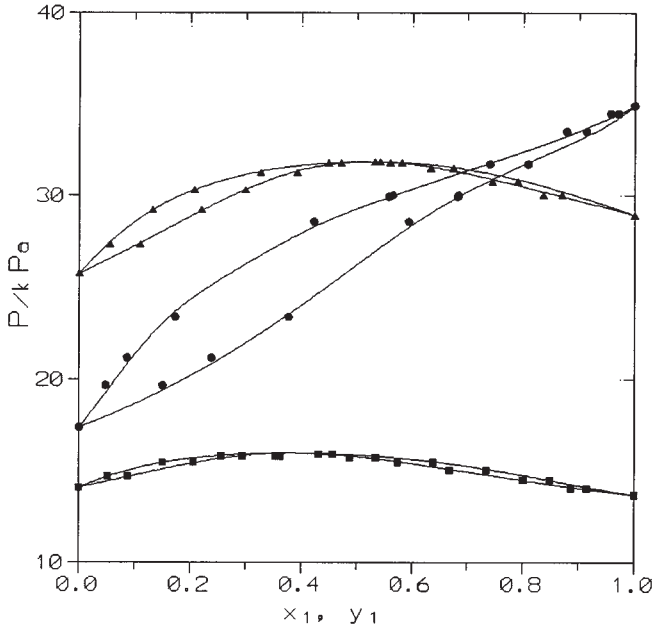


Table 9 lists the standard deviation for H^E:

$$[15] \quad \sigma(H^E) = [1/N \sum H^E_{exp} - H^E_{calc})^2]^{1/2}$$

In eqs. [14] and [15], N is the number of data points of each system. In view of the results, one can conclude that DISQUAC represents well the thermodynamic properties of the systems investigated over a rather wide range of temperature.

Fig. 3. VLE phase diagrams at 313.15 K for TEA(1) + butanols(2) mixtures. Solid lines, DISQUAC results. Points, experimental results (85): (■), 1-butanol; (●), 2-butanol; and (▲), *tert*-butanol

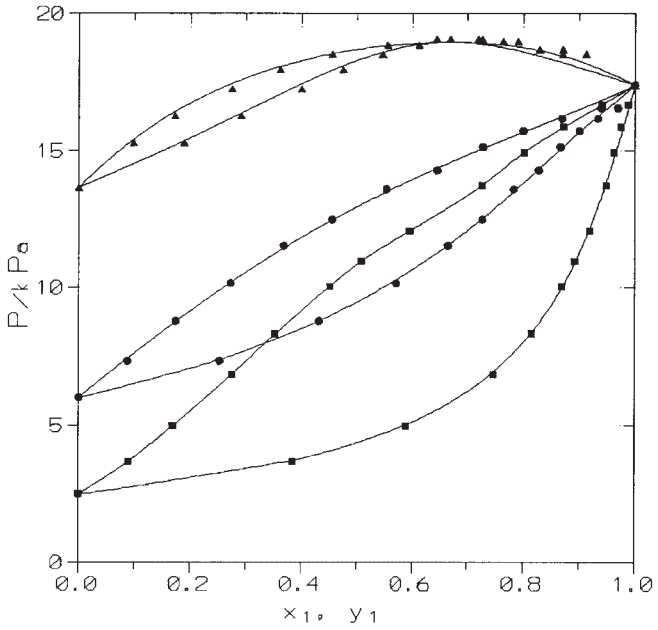
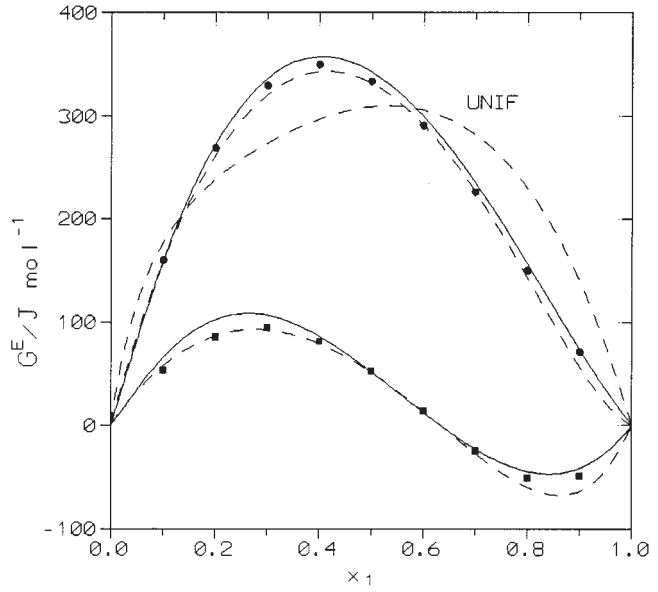


Fig. 4. G^E at several temperatures for 1-alkanols(1) + TEA(2) mixtures. Points, experimental data: (●), ethanol (307.95 K) (82) and (■), 1-propanol (293.15 K) (84). Solid lines, DISQUAC results; dashed lines, ERAS calculations or UNIFAC results with parameters from literature (18) for the system with ethanol.



4.2 Comparison between the DISQUAC and the UNIFAC models

This comparison is presented in detail in Tables 7–9 (see also Figs. 4–6). DISQUAC provides better results. The temperature dependence of the thermodynamic properties considered here is not well reproduced by UNIFAC, which predicts a decreasing of H^E when T increases. An opposite behaviour is expected, as it occurs in other similar systems.

© 2000 NRC Canada

Table 7. Molar excess Gibbs energies (G^E) at equimolar composition and at various temperatures (T/K) for alkanols(1) + TEA(2) mixtures. Comparison of experimental results (exp) with DISQUAC values (DQ) calculated using the coefficients from Tables 3–4; or with UNIFAC results (UNIF) obtained with geometrical and interaction parameters from literature (18); or with ERAS calculations using parameters from Tables 5–6.

Solvent	T (K)	N^a	G^E (J mol^{-1})				$\sigma_r(P)^b$			
			exp.	DQ	UNIF	ERAS	exp.	DQ	UNIF	Ref.
Methanol	283.15	11	145	140	–63		0.0054	0.010	0.065	(82)
	293.20	11	217	212	0		0.0053	0.010	0.068	(82)
	303.20	11[c]	284	281	64		0.0056	0.009	0.067	(82)
	313.15	9	349	348	128		0.0068	0.011	0.065	(82)
		13	345	—	—		0.0037	0.011	0.079	(10)
	333.05	15	479	471	256		0.0016	0.013	0.078	(10)
Ethanol	283.15	10	192	191	182		0.0065	0.007	0.032	(82)
	293.20	10	262	254	232		0.0048	0.008	0.025	(82)
	303.20	10[c]	312	314	284		0.0052	0.009	0.026	(82)
	307.95	10	334	343	309	331 354[d]	0.0021	0.003	0.020	(82)
		10	338	—	—		0.0014	0.003	0.019	(83)
	322.75	10	421	421	385		0.0015	0.003	0.017	(83)
1-Propanol	283.15	11	–5	–1.0	75		0.012	0.018	0.057	(84)
	293.20	11	53	52	121	51 140[d]	0.0054	0.008	0.044	(84)
	303.20	11[c]	117	103	169		0.0035	0.008	0.032	(84)
	313.15	11	160	150	218	160 293[d]	0.0021	0.004	0.031	(84)
	343.20	22	324	262	364		0.0024	0.021	0.018	(10)
	353.25	19	366	285	410		0.0013	0.025	0.019	(10)
	363.40	13	394	300	454		0.0014	0.026	0.022	(10)
1-Butanol	283.15	11	–94	–74	1		0.016	0.030	0.096	(85)
	293.20	11	–15	–22	43		0.0070	0.024	0.068	(85)
	303.20	11	26	27	88		0.0040	0.016	0.055	(85)
	313.15	11	74	72	133	80 293[d]	0.0068	0.016	0.045	(85)
	337.65	13	177	165	247		0.0032	0.014	0.037	(10)
	352.95	13	229	205	316		0.0050	0.019	0.036	(10)
2-Propanol	283.15	12	331	288	–28		0.0066	0.017	0.12	(84)
	293.20	11	383	339	14		0.0055	0.018	0.12	(84)
	303.20	12[c]	374	385	57		0.0028	0.008	0.095	(84)
	313.15	12	431	427	102		0.0019	0.012	0.096	(84)
2-Butanol	283.15	11	125	130	–87		0.02	0.025	0.087	(85)
	293.20	11	174	171	–48		0.008	0.011	0.081	(85)
	303.20	11[c]	207	208	–8		0.0054	0.008	0.071	(85)
	313.15	11	256	241	34		0.011	0.008	0.064	(85)
t-Butanol	283.15	11	502	416	–157		0.0033	0.050	0.19	(85)
	303.20	11[c]	445	437	–139		0.0013	0.008	0.16	(85)
	313.15	11	466	477	–102		0.0017	0.010	0.15	(85)

[a]Number of data points.

[b]Eq. [14].

[c]System used in the estimation of the interaction parameters.

[d]Calculated with $Q_{AB} = 0$.

It is interesting to compare results for mixtures containing methanol, considered in UNIFAC as a main group with interaction parameters which differ from those of other alcohols (18). So, both models are applied in a similar way. In the case of methanol, we note that UNIFAC does not represent simultaneously G^E and H^E (Tables 7–9). The use of the UNIFAC parameters lead, at low temperatures to erroneous results (Table 7, (18)). This may be due to the applied database in the determination of the UNIFAC parameters does not cover a wide enough range of temperature as to obtain six interaction parameters.

4.3 Comparison between DISQUAC and ERAS models

This comparison is shown in Tables 7 and 9 and Figs. 4–6. ERAS properly describes G^E while the results of H^E are improved by DISQUAC. ERAS can provide information on V^E

© 2000 NRC Canada

Table 8. Comparison of some experimental (exp.) coordinates of azeotropes: pressure (P_{az}), temperature (T_{az}), and mole fraction (x_{1az}) for alkanols(1) + TEA(2) mixtures with values calculated (calc.) using the coefficients from Tables 3–4 or with UNIFAC results (UNIF) obtained with geometrical and interaction parameters from literature (18).

		P_{az} (KPa)			x_{1az}			
Alkanol	T_{az} (K)	exp.	DQ	UNIF	exp.	DQ	UNIF	Ref.
Ethanol	283.15	4.25	4.27	4.27	0.163	0.161	0.081	(82)
	307.95	15.923	15.980	15.625	0.380	0.383	0.501	(82)
	—	15.814	—	—	0.397	—	—	(83)
	322.75	31.861	31.861	31.722	0.513	0.513	0.635	(83)
2-Propanol	303.20	11.725	11.641	11.398	0.199	0.207	0.047	(84)
	313.15	18.987	18.684	17.742	0.285	0.317	0.085	(84)
t-Butanol	303.20	11.859	11.717	11.288	0.217	0.222	0.006	(85)
	313.15	19.070	18.926	17.445	0.292	0.331	0.031	(85)

Table 9. Molar excess enthalpies (H^E) at equimolar composition and at various temperatures (T/K) for alkanols(1)+ TEA(2) mixtures. Comparison of experimental results (exp) with DISQUAC values (DQ) calculated using the coefficients from Tables 3–4, with UNIFAC results (UNIF) obtained with geometrical and interaction parameters from literature (18), or with ERAS calculations using the parameters from Tables 5 and 6.

			H^E (J mol^{-1})				$\sigma(H^E)^b$ (J mol^{-1})				
Solvent	T (K)	N^a	exp.	DQ	UNIF	ERAS	exp.	DQ	UNIF	ERAS	Ref.
Methanol	298.15	9[c]	–1871	–1821	–1871	–1878	23	45	25	180	(8)
		10	–1887	—	—	—	78	93	86	203	(7)
	313.15	9	–2143	–1700	–1895	–1866	110	250	152	231	(57)
	318.15	7	–1737	–1647	–1899	—	88	110	145	—	(7)
Ethanol	293.15	9	–1522	–1545	–1266	—	63	76	323	137	(86)
	298.15	9	–1333	–1502	–1284	–1513	12	130	307	181	(8)
		15[c]	–1520	—	—	—	69	75	361	127	(57)
	313.15	10	–1316	–1337	–1297	—	50	66	306	—	(57)
1-Propanol	298.15	10	–1500	–1432	–1285	–1424	44	68	381	98	(57)
		13[c]	–1413	—	—	—	7	53	335	128	(20)
	313.15	9	–1411	–1266	–1328	–1443	59	150	293	97	(57)
1-Butanol	298.15	10	–1550	–1458	–1259	–1421	44	100	386	112	(57)
	313.15	9	–1538	–1300	–1316	–1441	56	180	306	94	(57)
1-Pentanol	298.15	—	—	–1352	–1223	—	—	—	—	—	—
1-Hexanol	298.15	—	—	–1268	–1184	—	—	—	—	—	—
2-Propanol	298.15	—	—	–1013	–1270	—	—	—	—	—	—
2-Butanol	298.15	—	—	–910	–1242	—	—	—	—	—	—
2-Methyl-2-propanol	298.15	—	—	–885	–1222	—	—	—	—	—	—

[a]Number of data points.

[b]Eq. [15].

[c]System used in the fitting of the interaction parameters.

(Fig. 7), which is its main advantage. The more important limitations are:

(*i*) The temperature dependence of properties of pure compounds is needed to determine the temperature dependence of thermodynamic properties.

(*ii*) The problems to simultaneously represent VLE and LLE for 1-alkanols + alkanes mixtures have been already underlined (37); and although $Q_{AB} = 0$ has been used to predict VLE for such systems (59), here Q_{AB} is needed to obtain an accurate representation of G^E (Table 7).

(*iii*) ERAS is only applicable to those systems where association is expected.

It should be mentioned that the ERAS parameters obtained in this work for 1-alkanols + TEA systems (Table 6) are valid only for such type of mixtures. While the Δh^*_{AB} and Δv^*_{AB} parameters are probably common to solutions with 2-alkanols, as it occurs for $\Delta h^*_A = -25\,100$ J mol^{-1} and $\Delta v^*_A = -5.6$ cm mol^{-1} in the case of alkanols + *n*-alkanes (58, 61), experimental data are needed to calculate K_{AB} and X_{AB}.

5. Discussion

5.1 The effect of increasing the chain length of the alcohol for a given amine

The $\bar{\mu}$ of alcohols decreases (Table 1) and consequently also the alcohol–alcohol interactions in the condensed phase in the sequence methanol > ethanol > … > decanol.

It seems that the H^E transition from methanol to ethanol is much steeper compared to the transition from ethanol to

© 2000 NRC Canada

Fig. 5. H^E at 298.15 K for 1-alkanols(1) + TEA(2) mixtures. Points, experimental data: (●), methanol (8) and (■), ethanol (57). Solid lines, DISQUAC calculations; dashed lines, ERAS results or UNIFAC calculations with parameters from literature (18).

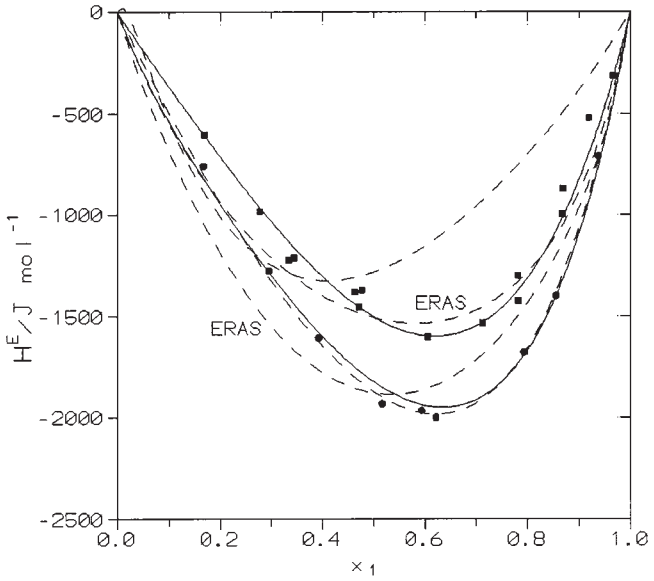
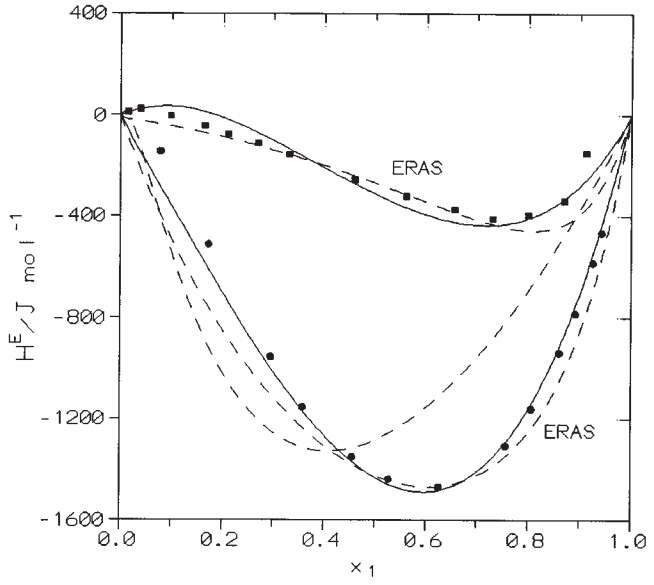
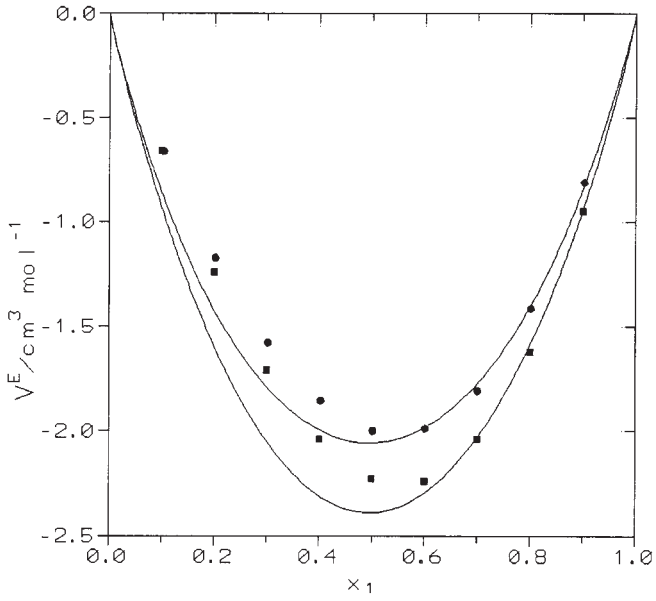


Fig. 6. H^E at 298.15 K for 1-propanol(1) + *N*,*N*,*N*-trialkylamines(2) mixtures. Points, experimental data: (●), TEA (20) and (■), TPA (71). Solid lines, DISQUAC calculations; dashed lines, ERAS results, or UNIFAC calculations for the system with TEA using parameters from literature (18).



1-butanol (Table 9). Therefore it occurs, for example, in mixtures of methanol, ethanol, propanol, or butanol with propyl or butylamine (35). Systems of 1-alkanols and secondary amines (55, 56), pyridines (64, 65), or polyethers (66) behave similarly. Excess volumes confirm this point (11, 67–69). Therefore interactions between methanol and TEA (or primary or secondary amines) are much stronger than with other alcohols.

Fig. 7. V^E at 298.15 K for 1-alkanols(1) + TEA(2) mixtures. Points, experimental data: (■), methanol (10) and (●), 1-propanol (20). Solid lines, ERAS results.



5.2 The effect of passing from a primary alkanol to an isomeric secondary or tertiary alkanol

When passing from 1-alkanols to 2-alkanols, it is observed that not only the μ values of isomeric alkanols are constant, but also that their $\bar{\mu}$s have similar values (Table 1). Therefore, H^E (2-alkanols) > H^E (1-alkanols), as it occurs for solvents such as ketones, C_6H_6, or C_7H_8 (45), may be due to steric hindrance to H-bond formation (45, 70), in such a way that at a given alcohol concentration fewer hydrogen bonds would be formed in 2-butanol (or *tert*-butanol) (for example) than in 1-butanol. This implies that more bonds are also broken in 2-alkanols than in 1-alkanols (46), leading to a higher value of H^E. A similar behaviour is expected for TEA as solvent (Table 9).

5.3 The effect of increasing the size of the amine for a given alcohol

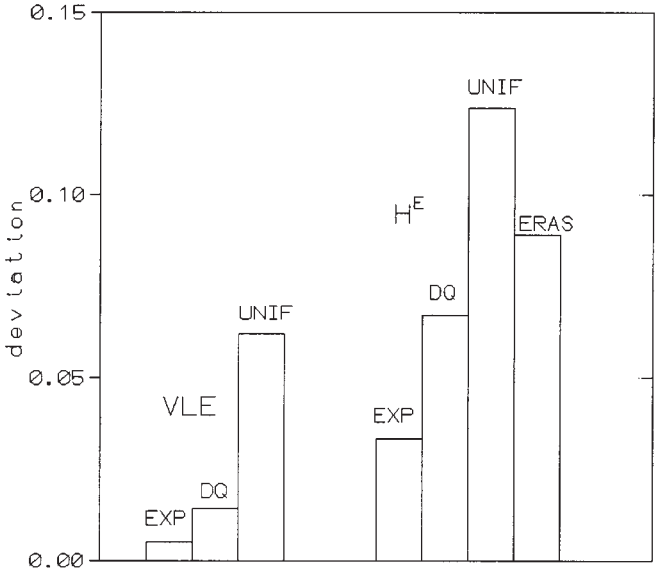
In this case, $\bar{\mu}$ of the amine decreases (Table 1) indicating that amine–amine interactions in the condensed phase decrease in the sequence TEA > TPA > TBA. Hence, H^E should increase in the inverse order. However, this increase in much stronger than the expected. At 298.15 K, atmospheric pressure, and equimolar composition H^E (J mol^{-1}) = –283 for 1-propanol + TPA (71), while for 1-propanol + TEA, this value is –1413 (20). This large difference underlines the fact that steric factors play a major role in mixtures containing tertiary amines (72).

5.4 Structure dependence of the DISQUAC interaction parameters

Strictly speaking, a comparison between interchange coefficients corresponding to different OH–X contacts (X being a given group) is not possible because they depend: (*i*) on the values of the interaction parameters of the remainder contacts which build the mixture; and (*ii*) on the geometrical

© 2000 NRC Canada

Fig. 8. Comparison between mean deviations (obtained as Σ deviations/number of systems) between experimental data and calculated values from different models. For VLE, mean standard relative deviations in pressure (eq. [14]) are given. For H^E, deviations for each system are calculated as $\sigma(H^E)$ (eq. [15]) / H^E_{exp} (x = 0.5)



parameters of the molecule where the X group is placed. Nevertheless, regarding the structure dependence of our interaction parameters, some results can be highlighted:

(*a*) the $C^{QUAC}_{hn,2}$ coefficients are negative. So it occurs in other solutions which show strong negative deviations from Raoult's law (1, 17). In contrast, mixtures with positive deviations from Raoult's law are characterized by positive enthalpic QUAC parameters. This is the case, for example, of OH–CO interactions in 1-alkanols + *n*-alkanones (44) or of OH–O interactions in 1-alkanols + monooxaalkanes (73).

(*b*) In 1-alkanols + TEA mixtures, the QUAC coefficients remain constant from ethanol. Similarly it occurs in other many alcoholic solutions previously investigated (seefor example (17, 39, 44)). The different values of the interchange coefficients for methanol merely underline the different character of this alcohol (stronger self-association and higher dielectric constants (74, Table 5) when compared to the longer ones. Similar effects appear when 1-alkanols + CCl_4 systems are treated using DISQUAC (41) or the Barker's theory (75), or from the analysis of 1-alkanols + aromatic mixtures in terms of DISQUAC (40), or in the framework of the quasilattice theory (76). From the point of view of ERAS, Δh^*_{AB} is lower for methanol or ethanol than for the remainder alcohols (Table 6), indicating that interactions between unlike molecules are stronger for mixtures with these two alkanols.

(*c*) The $C^{QUAC}_{hn,1}$ coefficients in alkanols + *N*,*N*,*N*-trialkylamines are independent of both components of the mixture. So, 1-propanol + TEA, or + TPA can be represented by the same coefficients (Table 4). That is, the increase of steric factors in the system, as occurs when 2-alkanols, *tert*-butanol or TPA are present, lead to an increase of the corresponding DIS coefficients (Table 4). However, this behaviour is not general, depending on the type of mixture considered. In the framework of ERAS, note that Δh^*_{AB} (1-propanol + TEA) = –33 200 J mol^{-1} (this work, Table 6) < Δh^*_{AB} (1-propanol + TPA) = –26 600 J mol^{-1} (77). That is, interactions between the hydroxyl and nitrogen groups are weaker for the latter system.

6. Conclusions

Figure 8 summarizes results obtained using the different models considered. It is concluded that DISQUAC is an useful tool to represent alkanol + TEA mixtures. DISQUAC improves ERAS results on H^E, while both models give similar results for G^E. However, ERAS needs a specific parameter, with an unknown temperature-dependence, to properly describe G^E. The main advantage of ERAS is its ability to provide information about V^E. Its main limitation is that can be only applied to those systems where association is expected. DISQUAC, a purely physical model, can be applied to any type of binary mixture because it is followed from this and previous studies (see for example 1, 2, 17).

Acknowledgements

This work was supported by the Programa Sectorial de Promoción General del Conocimiento de la S.E.U.I. y D. del M.E.C. (Spain), Project no. PB97–0488 and by the Consejería de Educación y Cultura de la Junta de Castilla y León (Spain), under the Project VA54/98.

References

1. J.A. González, I. García de la Fuente, and J.C. Cobos. Phys. Chem. Chem. Phys. **1**, 275 (1999).
2. J.A. González, I. García de la Fuente, and J.C. Cobos. Fluid Phase Equilib. **154**, 11 (1999).
3. J.S. Rowlinson and F.L. Swinton. Liquid and liquid mixtures. 3rd ed. Butterworths, GB. 1982.
4. E. Wilhelm, A. Laínez, and J.-P.E. Grolier. Fluid Phase Equilib. **49**, 233 (1989).
5. E. Wilhelm. Thermochim. Acta, **162**, 179 (1990).
6. E. Wilhelm, W. Egger, M. Vencour, A.H. Roux, M. Polednicek, and J.-P.E. Grolier. J. Chem. Thermodyn. **30**, 1509 (1998).
7. N. Nakanishi, H. Touhara, and N. Watanabe. Bull. Chem. Soc. Jpn. **43**, 2671 (1970).
8. A. Chand and D.V. Fenby. J. Chem. Eng. Data, **22**, 289 (1977).
9. M.H. Abraham and A. Nasehzadeh. J. Chem. Thermodyn. **13**, 549 (1981).
10. J.L. Copp and T.J.V. Findlay. Trans. Faraday Soc. **56**, 13 (1960).
11. A. Kumar, O. Prakash, and S. Prakash. J. Chem. Eng. Data, **26**, 64 (1981).
12. J.S. Rowlinson. Liquids and liquid mixtures. 1st ed. Butterworths, London. 1959.
13. R. Thacker and J.S. Rowlinson. Trans. Faraday Soc. **50**, 1036 (1954).
14. H.V. Kehiaian. Fluid Phase Equilib. **13**, 243 (1983).
15. H.V. Kehiaian. Pure Appl. Chem. **57**, 15 (1985).
16. E.A. Guggenheim. Mixtures. Oxford University Press, London. 1952.
17. J.A. González, I. García de la Fuente, and J.C. Cobos. J. Chem. Soc. Faraday Trans. **93**, 3773 (1997).
18. J. Gmehling, J. Li, and M. Schiller. Ind. Eng. Chem. Res. **32**, 178 (1993).

© 2000 NRC Canada

19. H. Funke, M. Wetzel, and A. Heintz. Pure Appl. Chem. **61**, 1429 (1989).
20. M. Bender, J. Hauser, and A. Heintz. Ber. Bunsen-Ges.**95**, 801 (1991).
21. A. Heintz. Ber. Bunsen-Ges. **89**, 172 (1985).
22. C.B. Kretschmer and R. Wiebe. J. Chem. Phys. **22**, 1697 (1954).
23. H. Renon and J.M. Prausnitz. Chem. Eng. Sci. **22**, 299 (1967).
24. H.V. Kehiaian. Bull. Acad. Pol. Sci. **16**, 165 (1968).
25. H.V. Kehiaian and A.J. Treszczanowicz. Bull. Acad. Pol. Sci, **16**, 171 (1968).
26. P.J. Flory. J. Am. Chem. Soc. **87**, 1833 (1965).
27. T.M. Letcher and A. Goldon. Fluid Phase Equilib. **114**, 147 (1996).
28. I. Nagata, M. Rogalski, and K. Miyamoto. Thermochim. Acta, **224**, 43 (1993).
29. D.S Abrams and J.M. Prausnitz. AIChE J. **21**, 116 (1974).
30. A. Bondi. Physical properties of molecular crystals, liquids and glasses. John Wiley and Sons, N.Y. 1968.
31. H.V. Kehiaian, J.-P.E. Grolier, and G.C. Benson. J. Chim. Phys. Phys-Chim. Biol. **75**, 1031 (1978).
32. J.A. González, I. García de la Fuente, J.C. Cobos, and C. Casanova. Ber. Bunsen-Ges. **95**, 1658 (1991).
33. J.A. González, I. García de la Fuente, J.C. Cobos, C. Casanova, and A. Ait-Kaci. Fluid Phase Equilib. **112**, 63 (1995).
34. A. Fredenslund, R.L. Jones, and J.M. Prausnitz. AIChE J. **21**, 1086 (1975).
35. A. Heintz and D. Papaioannou. Thermochim. Acta, **310**, 69 (1998).
36. A. Heintz, P.K. Naicker, S.P. Verevkin, and R. Pfestorf. Ber. Bunsen-Ges. **102**, 953 (1998).
37. M. Bender and A. Heintz. Fluid Phase Equilib. **89**, 197 (1993).
38. J.A. González, I. García de la Fuente, and J.C. Cobos. Fluid Phase Equilib. **123**, 39 (1996).
39. J.A. González, I. García de la Fuente, J.C. Cobos, and U. Domanska. Fluid Phase Equilib. **119**, 81 (1996).
40. J.A. González, I. García de la Fuente, J.C. Cobos, and C. Casanova. Fluid Phase Equilib. **93**, 1 (1994).
41. J.A. González, I. García de la Fuente, J.C. Cobos, and C. Casanova. Thermochim. Acta, **237**, 261 (1994).
42. J.A. González, I. García de la Fuente, and J.C. Cobos. Fluid Phase Equilib. **135**, 1 (1997).
43. J.A. González, I. García de la Fuente, J.C. Cobos, and C. Casanova. Fluid Phase Equilib. **78**, 61 (1992).
44. J.A. González. Can. J. Chem. **75**, 1412 (1997).
45. J.A. González, I. García de la Fuente, and J.C. Cobos. Can. J. Chem. **76**, 1418 (1998).
46. R. Tanaka and S. Toyama. J. Chem. Thermodyn. **28**, 1403 (1996).
47. K. Sosnkowska-Kehiaian, R. Hryniewicz, and H.V. Kehiaian. Bull. Acad. Pol. Sci. Ser. Sci. Chim. XVII, 185 (1969).
48. I. Ferino, B. Marongiu, V. Solinas, S. Torraza, and H.V. Kehiaian. Fluid Phase Equilib. **9**, 49 (1982).
49. R. Philippe and G. Delmas. Int. Data Ser. Selec. Data Mixtures Ser. A, 1983, 2, 154 (1982).
50. R. Philippe and G. Delmas. Int. Data Ser. Selec. Data Mixtures Ser. A, 1, 51 (1982).
51. R. Philippe, G. Delmas, and P.N. Hong. Can. J. Chem. **57**, 517 (1979).
52. D. Patterson. Pure Appl. Chem. **47**, 305 (1976).
53. R. Philippe, G. Delmas, and P.N. Hong. Can. J. Chem. **56**, 2856 (1978).
54. A. Ait-Kaci. PhD. thesis. Lyon, France. 1982.
55. F. Ratkovics, Zs. Guti, Acta Chim. Acad. Sci. Hung., 83, 63 (1974).
56. J. Fernández, M.I. Paz Andrade, M. Pintos, F. Sarmiento, and R. Bravo. J. Chem. Thermodyn. **15**, 581 (1983).
57. T.J.V. Findlay. Aust. J. Chem. **14**, 520 (1961).
58. A. Heintz, E. Dolch, and R.N. Lichtenthaler. Fluid Phase Equilib. **27**, 61 (1986).
59. A. Cabañas, B. Coto, C. Pando, and J.A.R. Renuncio. Ber. Bunsen-Ges. **98**, 777 (1994).
60. M. Keller, S. Schnabel, and A. Heintz. Fluid Phase Equilib. **110**, 231 (1995).
61. R. Garriga, F. Sánchez, P. Pérez, and M. Gracia. Ber. Bunsen-Ges. **102**, 1 (1998).
62. T.M. Letcher, J. Mercer-Chalmers, S. Schnabel, and A. Heintz. Fluid Phase Equilib. **112**, 131 (1995).
63. T.M. Letcher and P.U. Govender. Fluid Phase Equilib. **140**, 207 (1997).
64. T. Kasprzycka-Guttman, K. Izycka, and M. Kurzela. J. Therm. Anal. **14**, 127 (1978).
65. P.P. Singh, D.V. Verma, and P.S. Arora. Thermochim. Acta, **15**, 267 (1976).
66. F.J. Carmona, F.J. Arroyo, I. García de la Fuente, J.A. González, and J.C. Cobos. Can. J. Chem. **77**, 1608 (1999)
67. D. Papaioannou, M. Bridakis, and C.G. Panayiotou. J. Chem. Eng. Data, **38**, 370 (1993).
68. D. Papaioannou and C.G. Panayiotou. J. Chem. Eng. Data, **40**, 202 (1995).
69. I.M.S. Lampreia and E.F.G. Barbosa. Fluid Phase. Equilib. **71**, 125 (1992).
70. M. Cáceres-Alonso, M. Costas, L. Andreoli-Ball, and D. Patterson. Can. J. Chem. **66**, 989 (1988).
71. T.M. Letcher and B.C. Bricknell. J. Chem. Eng. Data, **41**, 166 (1996).
72. J. Hine and M. Hine. J. Am. Chem. Soc. **74**, 5266 (1952).
73. S. Delcros, J.R. Quint, J.-P. Grolier, and H.V. Kehiaian. Fluid Phase Equilib. **113**, 1 (1995).
74. J.A. González, J.C. Cobos, I. García, and C. Casanova. Thermochim. Acta, **171**, 153 (1990).
75. B. Dacre and G.C. Benson. Can. J. Chem. **41**, 278 (1963).
76. J.R. Goates, R.L. Snow, and J.B. Ott. J. Phys. Chem. **66**, 1301 (1962).
77. T.M. Letcher and B.C. Bricknell. J. Chem. Eng. Data, **41**, 639 (1996).
78. R.C. Reid, J.M. Prausnitz, and B.E. Poling. The properties of gases and liquids. 4th ed. McGraw-Hill, U.S.A. 1987.
79. CRC Handbook of Chemistry and Physics. D.R. Lide (*Editor in Chief*). 75th ed. CRC Press, U.S.A. 1995.
80. A.L. McClellan. Tables of experimental dipole moments. Vols. 1, 2, 3. Rahara Enterprises, U.S. 1974.
81. H.V. Kehiaian, M.R. Tiné, L. Lepori, E. Matteoli, and B. Marongiu. Fluid Phase Equilib. **46**, 131 (1989).
82. K.W. Chun and R.R. Davison. J. Chem. Eng. Data, **17**, 307 (1972).
83. J.L. Copp and D.H. Everett. Discuss. Faraday Soc. **15**, 174 (1953).
84. K.W. Chun, J.C. Drummond, and R.R. Davison. J. Chem. Eng. Data, **19**, 142 (1974).
85. K.W. Chun, J.C. Drummond, and R.R. Davison. J. Chem. Eng. Data, **20**, 58 (1975).
86. F. Ratkovics, J. Liszi, M. László, B. Szeiler,and J. Dévay. Acta. Chim. Acad. Sci. Hung. **77**, 249 (1973).

© 2000 NRC Canada

Appendix 1.

Table A1. Interchange coefficients, dispersive $C_{ch,1}^{DIS}$ and quasichemical $C_{ch,1}^{QUAC}$ (l = 1, Gibbs energy; l = 2, enthalpy; l = 3, heat capacity) for contacts (c,h) (Type c, c-CH_2 in cyclohexane; Type h, OH in secondary or tertiary alkanols). The coordination number used for the QUAC part is z = 4.

Alkanol	$C_{ch,1}^{DIS}$	$C_{ch,2}^{DIS}$	$C_{ch,3}^{DIS}$	$C_{ch,1}^{QUAC}$	$C_{ch,2}^{QUAC}$	$C_{ch,3}^{QUAC}$
***sec*-Alkanols + cyclohexane**						
2-Propanol	3.10	2.60	12.00	10.00	9.75	38.00
2-Butanol	4.05	5.80	12.00	10.00	9.75	38.00
***tert*-Alkanols + cyclohexane**						
2M-2-Propanol[a]	2.00	6.10	–12.00	10.00	7.50	85.00
2M-2-Nutanol[a]	1.55	0.30[b]	–21.50	10.00	13.00	80.00
2M-2-Pentanol[a]	1.10[b]	0.90[b]	–21.50	10.00	13.00	80.00
3M-3-Pentanol[a]	0.75[b]	0.40[b]	–21.50	10.00	17.00	80.00

[a]For abbreviations see Table 3 in text.

[b]Estimated value.

Table A2. Interchange coefficients, dispersive $C_{sh,1}^{DIS}$ and quasichemical $C_{sh,1}^{QUAC}$ (l = 1, Gibbs energy; l = 2, enthalpy; l = 3, heat capacity) for contacts (s, h) (Type s = b, C_6H_6; Type s = p, C_6H_5 in toluene; Type h, OH in *sec*-alkanols).

Alkanol	$C_{sh,1}^{DIS}$	$C_{sh,2}^{DIS}$	$C_{sh,3}^{DIS}$	$C_{sh,1}^{QUAC}$	$C_{sh,2}^{QUAC}$	$C_{sh,3}^{QUAC}$
***sec*-Alkanols + benzene (s = b)**						
2-Propanol	2.90	1.30	10.00	8.50	12.75	32.50
2-Butanol	3.95	5.10	13.00	8.50	12.75	32.50
2-Pentanol	4.50[a]	6.50[a]	13.00	8.50	12.75	32.50
≥2-Hexanol	4.50[a]	7.50[a]	13.00	8.50	12.75	32.50
3-Pentanol	3.00[a]	7.50[a]	13.00	8.50	12.75	32.50
≥3-Hexanol	3.00[a]	8.50[a]	13.00	8.50	12.75	32.50
***sec*-Alkanols + toluene (s = p)**						
2-Propanol	2.80	1.70	10.00	8.50	12.75	32.50
2-Butanol	3.65	5.70[a]	13.00	8.50	12.75	32.50
2-Pentanol	4.30[a]	5.20[a]	13.00	8.50	12.75	32.50
≥2-Hexanol	4.30[a]	5.90[a]	13.00	8.50	12.75	32.50
3-Pentanol	2.70[a]	6.20[a]	13.00	8.50	12.75	32.50
≥3-Hexanol	2.70[a]	7.00[a]	13.00	8.50	12.75	32.50

[a]Estimated value.

© 2000 NRC Canada

Synthesis of 5-alkyl- and 5-aryl-1,5-dihydro-2*H*-pyrrol-2-ones via coupling of *5*-chloro-1,5-dihydro-2*H*-pyrrol-2-ones with organometallic compounds

Kirill V. Nikitin and Nonna P. Andryukhova

Abstract: 5-Chloro-1,5-dihydro-2*H*-pyrrol-2-ones are easily alkylated at the 5-position by organomagnesium or organozinc compounds and diethyl sodiomalonate leading to corresponding 5-alkyl-1,5-dihydro-2*H*-pyrrol-2-ones in high yields.

Key words: organometallic compounds, alkylation, 1,5-dihydro-2*H*-pyrrol-2-one.

Résumé : Les réactions du sodiomalonate de diéthyle ou de composés organomagnésiens ou organozinciques avec les 5-chloro-1,5-dihydro-2*H*-pyrrol-2-ones provoquent des réactions faciles d'alkylation en position 5 qui conduisent à la formation des 5-alkyl-1,5-dihydro-2*H*-pyrrol-2-ones avec des rendements élevés.

Mots clés : composés organométalliques, alkylation, 1,5-dihydro-2*H*-pyrrol-2-one.

Substituted 5-alkyl-1,5-dihydro-2*H*-pyrrol-2-ones (**2**) are well known as herbicides and can be prepared (1) by consecutive alkylation of an amine by an α-halogenated ketone followed by acylation of the product and final intramolecular condensation. Transformation of *exo* methylene isoindolin-1-one leading to **2** (R_2 + R_2 = fused benzene ring) was documented (2). Recently, an unusual [4+1] cyclization (3) was applied in the synthesis of **2**. To produce a wider variety of **2** a general method to introduce various R_3 groups is sought. Several known examples (4) of organometallic coupling at the 5-position of tetrahydropyrrol-2-ones (pyrrolidin-2-ones) show great synthetic potential of that method but no report has been documented for the alkylation of partially unsaturated 1,5-dihydro-2*H*-pyrrol-2-ones. Since α-halogenated amides (5) and imides (6) are versatile reactants under nucleophilic conditions and in organometallic coupling (7) the substitution of chlorine for an alkyl or an aryl moiety is expected to be useful pathway leading to **2**. The addition of RMgX to substituted phthalic (8) and succinic (9) imides has been studied and may lead to methylenation as an alternative to Tebbe reaction (10).

The starting material (**1)** can be easily prepared from the corresponding 5-hydroxy (11) as well as 5-methoxy derivative. Compounds **1** are readily hydrolyzed and should be handled in dry atmosphere.

In the present study compounds **1a** (R_1 = *t*-Bu, R_2 = Me), **1b** (R_1 = $PhCH_2$, R_2 + R_2 = fused benzene ring) and **1c** (R_1 = $PhCH_2$, R_2 = Me) were subjected to coupling with R_3MX organomagnesium (R_3 = Me, R_3 = Ph), organozinc (R_3 = Me, R_3 = Ph) reagents, and diethyl sodiomalonate (R_3 = $CH(COOEt)_2$). We also carried reactions of the same organometallics with *N*-chloromethylphthalimide (6, 7) (**3**) and compared the results.

We found that compounds **1** undergo cross-coupling with organometallic reagents leading to **2** in high yields (Table 1). The difference in product yields between organomagnesium and organozinc reagents may be accounted for by the considerable CH acidity at the 5-position of **1** and formation of 5–5 coupled dipyrrolines. Indeed a blue-colored byproduct was formed in the reaction of **1b** with Grignard reagents. The coupling with R_3ZnBr may be preferable in complex cases or for sensitive substituents. Reactions with diethyl sodiomalonate proceed unexpectedly fast and lead to products **2** in high yields (Table 1).

In contrast to the coupling of pyrrolinones **1**, reactions of *N*-chloromethylphthalimide (**3**) are diverse. Substrate **3** does not react with organozinc R_3ZnBr (R_3 = Me, Ph) under ambient conditions for 10 h and can be quantitatively recovered. We found that with MeMgCl, **3** undergoes consecutive chlorine substitution and carbonyl addition to furnish **4**, and elimination of water under mild acidic treatment leads to product **5**. Reaction of **3** with phenylmagnesium chloride leads to expected product **6** (substitution and addition) and unusual by-product **7** as a result of intermolecular coupling of **6** with **3**. These processes are illustrated by Scheme 2.

In conclusion the coupling of 5-chloropyrrolinones **1** with organometallic reagents is an effective method for the preparation of 5-alkyl-, 5-ethoxycarbonylmethyl-, and 5-aryl-pyrrolin-2-ones **2**.

Experimental

Commercially available reagents and solvents were used without further purification. Melting points were measured

Received December 9, 1999. Published on the NRC Research Press website on September 26, 2000.

K.V. Nikitin[1] and N.P. Andryukhova. Department of Chemistry, Moscow State University, Moscow 119899, Russia.

[1]Author to whom correspondence may be addressed. e-mail: newscientist@mtu-net.ru

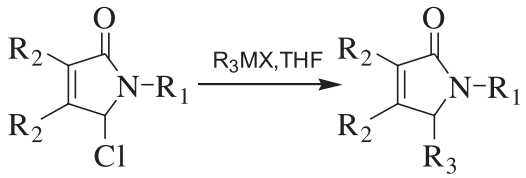
© 2000 NRC Canada

Table 1. Synthesis of **2** by coupling of **1** with organometallics R_3MX.

Product	Substrate	R_1	R_2	R_3	MX	Time (h)	Yield (%)
2a	1a	*t*-Bu	Me	Me	MgCl	0.5	66
2a	1a	*t*-Bu	Me	Me	ZnBr	1	70
2b	1a	*t*-Bu	Me	Ph	MgCl	0.5	62
2b	1a	*t*-Bu	Me	Ph	ZnBr	0.5	65
2c	1b	Bn	benz[a]	Me	MgCl	2	55
2c	1b	Bn	benz	Me	ZnBr	2	84
2d	1b	Bn	benz	Ph	MgCl	1	74
2d	1b	Bn	benz	Ph	ZnBr	1	74
2e	1a	*t*-Bu	Me	$CH(COOEt)_2$	Na	0.5	80
2f	1b	Bn	benz	$CH(COOEt)_2$	Na	0.5	82
2g	1c	Bn	benz	$CH(COOEt)_2$	Na	0.5	78

[a] – R_2 + R_2 = fused benzene ring.

Scheme 1. Coupling of 5-chloro-1,5-dihydro-2*H*-pyrrolones with organometallic compounds.



1 **2**

with a Thomas–Hoover capillary melting point apparatus and are not corrected. ^{1}H NMR specrta were recorded on a Varian GEMINI-200 with deuterochlorofom as solvent. All chemical shifts are in ppm (δ) downfield from tetramethylsilane and coupling constants are given in Hz. Mass spectra were recorded on a Shimadzu GCMS-OP 1000 mass spectrometer. FTIR spectra were recorded on a Mattson Genesis II spectrophotometer. Chromatographic separations were carried out on a silica gel column (Merck, 60 μm). Substituted 5-hydroxy and 5-methoxy-1,5-dihydro-2*H*-pyrrol-2-ones were prepared by known procedures (4, 5).

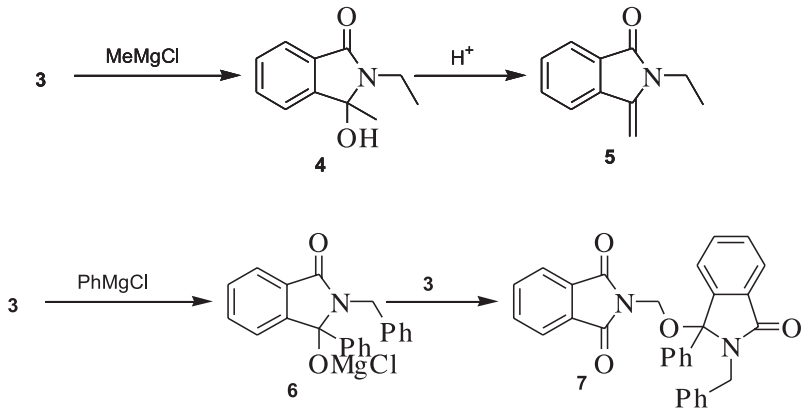
1-tert-*Butyl-5-chloro-3,4-dimethyl-1,5-dihydro-2*H-*pyrrol-2-one (**1a**)*: To a suspension of 1-*tert*-butyl-5-methoxy-3,4-dimethyl-1,5-dihydro-2*H*-pyrrol-2-one (3.94 g, 20 mmol) in hexane (40 mL), phosphorus pentachloride (4.4 g, 21 mmol) was added, and the mixture was heated under reflux for 2 h during which time PCl_5 dissolved completely. The mixture was evaporated at reduced pressure (1 torr, 1 torr = 133.322 Pa) to remove $POCl_3$ to afford **1a** (3.95 g, 98%) as a glassy solid. IR (KBr): 1681 (C=O) cm^{-1}. ^{1}H NMR ($CDCl_3$–TMS) δ: 1.55 (s, 9H), 1.78 (s, 3H), 1.99 (s, 3H), 5.94 (s, 1H). MS *m*/*z*: 201 (M^+).

*2-Benzyl-3-chloroisoindolin-1-one (**1b**)*: This compound was obtained in the same manner as described for **1a** as a glassy solid. IR (KBr): 1678 (C=O), 1439, 1065 cm^{-1}. ^{1}H NMR ($CDCl_3$–TMS) δ: 4.27 (d, 1H, *J* = 14.7 Hz), 5.40 (d, 1H, *J* = 14.7 Hz), 6.16 (s, 1H), 7.3–7.4 (m, 5H), 7.5–7.6 (m, 3H), 7.9 (d, 1H, *J* = 5.5 Hz). MS *m*/*z*: 257 (M^+).

*1-Benzyl-5-chloro-3,4-dimethyl-1,5-dihydro-2*H-*pyrrol-2-one (**1c**)*: This compound was obtained in the same manner as described for **1a** as a glassy solid. IR (KBr): 1685 (C=O) cm^{-1}. ^{1}H NMR ($CDCl_3$–TMS) δ: 1.88 (s, 3H), 1.99 (s, 3H), 4.15 (d, 1H, *J* = 14.8 Hz), 5.18 (d, 1H, *J* = 14.8 Hz), 5.45 (s, 1H), 7.3–7.4 (m, 5H). MS *m*/*z*: 235 (M^+).

1-tert-*Butyl-3,4,5-trimethyl-1,5-dihydro-2*H-*pyrrol-2-one (**2a**)*: Method A: to a solution of **1a** (0.20 g, 1 mmol) in dry THF (3 mL) at 0°C under nitrogen atmosphere a 3 M solution of methylmagnesium chloride in dry THF (0.4 mL, 1.2 mmol) was added. The reaction mixture was stirred at room temperature for 0.5 h, water (0.2 mL) was added, THF was evaporated, residue mixed with water (5 mL), extracted with ethyl acetate, and dried ($MgSO_4$). The solvent was evaporated and

Scheme 2.



© 2000 NRC Canada

crude product was purified by column chromatography to give **2a** as a liquid, yield 0.12 g (66%). Method B: to a solution of freshly sublimed zinc bromide (0.34 g, 1.5 mmol) in dry THF (2 mL), a 3 M solution of methylmagnesium chloride (0.4 mL, 1.2 mmol) was added under a nitrogen atmosphere. The mixture was stirred 20 min at room temperature, cooled to 0°C, and a solution of **1a** (0.20 g, 1 mmol) in dry THF (1 mL) was added. The mixture was stirred 1 h at room temperature, water (0.2 mL) was added, THF was evaporated, and the residue was mixed with water (5 mL), extracted with ethyl acetate, and dried ($MgSO_4$). The solvent was evaporated and crude product was purified by column chromatography to give **2a** as a liquid, yield 0.126 g (70%). IR (KBr): 1675 (C=O), 1395, 1370, 1227 cm^{-1}. ^1H NMR ($CDCl_3$–TMS) δ: 1.32 (d, 3H, *J* = 6.5 Hz), 1.49 (s, 9H), 1.72 (s, 3H), 1.85 (s, 3H, CH_3), 3.9 (q, 1H, CH, *J* = 6.5 Hz). MS *m*/*z*: 182 (M^+ + 1). Anal. calcd. for $C_{11}H_{19}NO$: C 72.88, H 10.56, N 7.73; found: C 73.06, H 10.40, N 8.11.

*1-*tert*-Butyl-1,5-dihydro-3,4-dimethyl-5-phenyl-2*H*-pyrrol-2-one (**2b**)*: Method A: from **1a** (0.201 g, 1 mmol) and 2 M phenylmagnesium chloride (0.6 mL, 1.2 mmol) **2b** was obtained as a solid, yield 0.15 g (62%), mp 133°C. Method B: from **1a** (0.201 g, 1 mmol), zinc bromide (0.34 g, 1.5 mmol) and 2 M phenylmagnesium chloride (0.6 mL, 1.2 mmol) **2b** was obtained as a solid, yield 0.16 g (65%), mp 133°C. IR (KBr): 1656 (C=O), 1366, 1225 cm^{-1}. ^1H NMR ($CDCl_3$–TMS) δ: 1.34 (s, 9H), 1.57 (s, 3H), 1.79 (s, 3H), 4.85 (s, 1H), 7.05–7.33 (m, 5H). MS *m*/*z*: 243 (M^+). Anal. calcd. for $C_{16}H_{21}NO$: C 78.97, H 8.70, N 5.76; found: C 79.10, H 8.89, N 5.70.

*2-Benzyl-3-methylisoindolin-1-one (**2c**) (**2**)*: Method A: from **1b** (0.257 g, 1 mmol) and 3 M methylmagnesium chloride (0.4 mL, 1.2 mmol) **2c** was obtained as a liquid, yield 0.13 g (55%). Method B: from **1b** (0.257 g, 1 mmol), zinc bromide (0.34 g, 1.5 mmol) and 3 M methylmagnesium chloride (0.4 mL, 1.2 mmol) **2c** was obtained as a liquid, yield 0.20 g (84%). IR (KBr): 1690 (C=O), 1408, 761 cm^{-1}. ^1H NMR ($CDCl_3$–TMS) δ: 1.43 (d, 3H, *J* = 7 Hz), 4.26 (d, 1H, *J* = 15 Hz), 4.38 (quartet, 1H, *J* = 7 Hz), 5.34 (d, 1H, *J* = 15 Hz), 7.3–7.6 (m, 8H, Ar), 7.88 (d, 1H, *J* = 5 Hz). MS *m*/*z*: 237 (M^+).

*2-Benzyl-3-phenylisoindolin-1-one (**2d**)*: Method A: from **1b** (0.257 g, 1 mmol) and 2 M phenylmagnesium chloride (0.6 mL, 1.2 mmol) **2d** was obtained as a solid, yield 0.22 g (74%); mp 124°C. Method B: from **1b** (0,257 g, 1 mmol), zinc bromide (0.34 g, 1.5 mmol) and 2 M phenylmagnesium chloride (0.6 mL, 1.2 mmol) **2d** was obtained as a solid, yield 0.22 g (74%). IR (KBr): 1690 (C=O), 1401, 702 cm^{-1}. ^1H NMR ($CDCl_3$–TMS) δ: 3.72 (d, 1H, *J* = 15 Hz), 5.23 (s, 1H), 5.39 (d, 1H, *J* = 15 Hz), 7.0–7.5 (m, 13H), 7.93 (d, 1H, *J* = 5 Hz). MS *m*/*z*: 299 (M^+). Anal. calcd. for $C_{21}H_{17}NO$: C 84.25, H 5.72, N 4.68; found: C 84.55, H 5.76, N 4.43.

*1-Benzyl-5-bis(ethoxycarbonyl)methyl-1,5-dihydro-3,4-dimethyl-2*H*-pyrrol-2-one (**2g**)*: To a suspension of sodium hydride (0.044 g 60% dispersion, 1.1 mmol) in dry THF (2 mL) a solution of diethyl malonate (0.176 g, 1.1 mmol) in 1 mL THF was added dropwise with stirring under nitrogen at 0°C. After 5 min a solution of **1c** (0.235 g, 1 mmol) in dry THF (1 mL) was added dropwise. The reaction mixture was stirred at room temperature 30 min and was quenched with water (1 mL). The solvents were evaporated, water (15 mL) was added, the mixture was extracted with ethyl acetate (3 × 3 mL), the combined organic layers were dried ($MgSO_4$), the solvent was evaporated, and crude product was purified by column chromatography to give **2g** as a solid, yield 0.28g (78%), mp 72°C. IR (KBr): 1741, 1672 (C=O), 1293, 1179 cm^{-1}. ^1H NMR ($CDCl_3$–TMS) δ: 1.15–1.26 (m, 6H), 1.84 (s, 3H), 1.93 (s, 3H), 3.87 (d, 1H, CH(COOEt), *J* = 3 Hz), 4.03–4.23 (m, 5H, CH_2 + CH-Ph), 4.43 (broad s, 1H), 5.18 (d, 1H, *J* = 15.7 Hz), 7.22–7.31 (m, 5H, Ph). MS *m*/*z*: 359 (M^+). Anal. calcd. for $C_{20}H_{25}NO_5$: C 66.83, H 7.01, N 3.90; found: C 67.05, H 7.22, N 3.68.

*1-(*tert*-Butyl)-3,4-dimethyl-5-bis(ethoxycarbonyl)methyl-1,5-dihydro-2*H*-pyrrol-2-one (**2e**)*: was obtained from **1a** (0.201 g, 1 mmol) as a liquid, yield 0.20 g (80%). IR (KBr): 1738, 1686 (C=O), 1363, 1112 cm^{-1}. ^1H NMR ($CDCl_3$–TMS) δ: 1.16 (t, 3H, *J* = 6 Hz), 1.31 (t, 3H, *J* = 6 Hz), 1.50 (s, 9H) 1.70 (s, 3H), 1.90 (s, 3H), 4.05 (q, 2H, *J* = 6 Hz), 4.26 (q, 2H, *J* = 6 Hz), 4.16 (d, 1H, *J* = 2.6 Hz), 4.72 (d, 1H, *J* = 2.6 Hz). MS: *m*/*z* = 326 (M^+ + 1). Anal. calcd. for $C_{17}H_{27}NO_5$: C 62.75, H 8.36, N 4.30; found: C 62.75, H 8.20, N 4.11.

*2-Benzyl-3-bis(ethoxycarbonyl)methylisoindolin-1-one (**2f**)*: was obtained from **1b** (0.257 g, 1 mmol) as a liquid, yield 0.25 g (82%). IR (KBr): 1741, 1672 (C=O), 1293, 1179 cm^{-1}. ^1H NMR ($CDCl_3$–TMS) δ: 0.94 (t, 3H, *J* = 7 Hz), 1.23 (t, 3H, *J* = 7 Hz), 3.8–3.95 (m, 2H), 4.08 (d, 1H, *J* = 3.5 Hz), 4.28 (d, 1H, *J* = 16 Hz), 4.1–4.25 (m, 2H), 5.05 (d, 1H, *J* = 3.5 Hz), 5.4 (d, 1H, *J* = 16 Hz), 7.2–7.35 (m, 5H), 7.45–7.55 (m, 3H), 7.9 (m, 1H, Ar). MS *m*/*z*: 381 (M^+). Anal. calcd. for $C_{22}H_{23}NO_5$: C 69.28, H 6.08, N 3.67; found: C 69.49, H 6.20, N 3.51.

*2-Ethyl-3-methyleneisoindolin-1-one (**5**)*: Method A: to a solution of **3** (0.195 g, 1 mmol) in dry THF (3 mL) at 0°C under nitrogen atmosphere a 3 M solution of methylylmagnesium chloride (0.5 mL, 1.5 mmol) was added. The reaction mixture was stirred at room temperature for 0.5 h, water (0.2 mL) was added, THF was evaporated, and the residue was mixed with aqueous ammonium chloride (5 mL), extracted with ethyl acetate, and dried ($MgSO_4$). The solvent was evaporated and crude **4** was heated in benzene (10 mL) using a Dean-Stark trap and the product was purified by column chromatography to give **5** as a liquid, yield 0.125 g (75%). IR (KBr): 1773, 1710 (C=O), 1645, 1398 cm^{-1}. ^1H NMR ($CDCl_3$–TMS) δ: 1.24 (t, 3H, *J* = 5 Hz), 3.82 (q, 1H, *J* = 5 Hz), 4.80 (d, 1H, *J* = 2 Hz), 5.17 (d, 1H, *J* = 2Hz), 7.4–7.5 (m, 2H), 7.65 (d, 1H, *J* = 4Hz), 7.80 (d, 1H, *J* = 4 Hz). MS *m*/*z*: 173 (M^+).

Method B: to a solution of freshly sublimed zinc bromide (0.34 g, 1.5 mmol) in dry THF (2 mL), a 3 M solution of methylmagnesium chloride (0.4 mL, 1.2 mmol) was added under a nitrogen atmosphere. The mixture was stirred 20 min at room temperature, cooled to 0°C, and a solution of **3** (0.20 g, 1 mmol) in dry THF (1 mL) was added. The mixture was stirred 1 h at room temperature, water (0.2 mL) was added, THF was evaporated, and the residue was mixed with water (5 mL), extracted with ethyl acetate, and dried ($MgSO_4$). The solvent was evaporated and the residue was

© 2000 NRC Canada

purified by column chromatography to give starting **3** (0.18 g, 92%).

Reaction of 3 with phenylmagnesium chloride

To a solution of **3** (0.195 g, 1 mmol) in dry THF (3 mL) at 0°C under nitrogen atmosphere, a 2 M solution of phenylmagnesium chloride (0.7 mL, 1.4 mmol) was added. The reaction mixture was stirred at room temperature for 0.5 h, water (0.2 mL) was added, THF was evaporated, and the residue was mixed with water (5 mL), extracted with ethyl acetate, and dried ($MgSO_4$). The solvent was evaporated and crude product was purified by column chromatography to give **6** (12) as a solid, yield 0.19 g (60%). mp 143°C. IR (KBr): 3271, 1669 (C=O) cm^{-1}. ^1H NMR ($CDCl_3$–TMS) δ: 3.40 (s, 1H, OH), 4.05 (d, 1H, *J* = 15 Hz), 4.70 (d, 1H, *J* = 15 Hz), 7.1–7.35 (m, 10H), 7.4–7.5 (m, 2H), 7.7–7.8 (m, 2H). MS: *m*/*z* = 316 (M^+ + 1).

Additionally **7** was isolated as a solid, yield 0.050 g (21%). mp 203°C. IR (KBr): 1777, 1720 (C=O), 1355, 1049 cm^{-1}. ^1H NMR ($CDCl_3$–TMS) δ: 4.28 (d, 1H, *J* = 14.6 Hz), 4.50 (d, 1H, *J* = 10.2 Hz), 4.60 (d, 1H, *J* = 10.2 Hz), 4.73 (d, 1H, *J* = 14.6 Hz), 7.0–7.3 (m, 13H), 7.7–7.85 (m, 4H), 7.92 (d, 1H, *J* = 7.5 Hz). MS *m*/*z*: 474 (M^+). Anal. calcd. for $C_{30}H_{22}N_2O_4$: C 75.94, H 4.67, N 5.90; found: C 75.66, H 4.90, N 6.01.

References

1. N. Ohba, A. Ikeda, K. Matsunari, Y. Yamada, M. Hirata, Y. Nakamura, A. Takeuchi, and H. Karino. U.S. Patent 5 006 157, 1991; (Chem. Abstr. **114**, 247 145 (1991)).
2. J.-M. Ferland, C.A. Demerson, and L.G. Humber. Can. J. Chem. **63**, 361 (1985).
3. T. Morimoto, N. Chatani, and S. Murai. J. Am. Chem. Soc. **121**(8), 1758 (1999).
4. (*a*) Z.Y. Wei and E.E. Knaus. Org. Prep. Proced. Int. **25(2)**, 255 (1993); (*b*) Y. Arai, M. Matsui, A. Fujii, T. Kontani, T. Ohno, T. Koizumi, and M. Shiro. J. Chem. Soc. Perkin Trans. 1, 25 (1994).
5. F. Weygand, W. Steglich, I. Lengyel, F. Fraunberger, A. Maierhofer, and W. Oettmeier. Chem. Ber. **99**, 1944 (1966).
6. (*a*) A. Korenova, P. Netchitailo, and B. Decroix. J. Heterocycl. Chem. **35**(1), 9 (1988); (*b*) Y.-D. Gong and N. Iwasawa. Chem. Lett. 2139 (1994).
7. C. Germon, A. Alexakis, and J.F. Normant. Synthesis, 40 (1984).
8. P. Pigeon and B. Decroix. Bull. Soc. Chim. Fr. **134**(2), 153 (1997).
9. (*a*) A.I. Meyers, B.A. Lefker, T.J. Sowin, and L.J. Westrum. J. Org. Chem. **54**, 4243 (1989); (*b*) H.-D. Stachel and J. Schachtner. Z. Naturforsch. B: Chem. Sci. **51**(9), 1334 (1996).
10. S.H. Pine, R.J. Pettit, G.D. Geib, S.G. Cruz, C.G. Gallego, T. Tijerina, and R.D. Pine. J. Org. Chem. **50**, 1212 (1985).
11. M.S. Kitching, W. Clegg, M.R.J. Elsegood, R.J. Griffin, and B.T. Golding. Synlett. 997 (1999).
12. T. Nishino, N. Okuda, Y. Mori, and C. Kashima. Synthesis, 396 (1989).

© 2000 NRC Canada

Co(II) and Mn(II) complexes of 2,2′-thiodiethanol: $[Co^{II}(2,2'\text{-thiodiethanol})_2Cl_2]$ and $[Mn(2,2'\text{-thiodiethanol})Cl_2]_n$

Yousheng Zhang, Suning Wang, Craig Bridges, and John E. Greedan

Abstract: $[Co(2,2'\text{-thiodiethanol})_2Cl_2]$ (**1**) and $[Mn(2,2'\text{-thiodiethanol})Cl_2]_n$ (**2**), have been synthesized and characterized structurally. Compound **1** is a six-coordinate, mononuclear Co(II) complex. The mononuclear units in the crystal lattice of **1** are linked together through intermolecular hydrogen bonds between hydroxy and chloride groups to form a three-dimensional array. Compound **2** consists of six-coordinate Mn(II) units that are linked by covalently bound 2,2′-thiodiethanol and chloride ligands to form an alternating one-dimensional chain, which is further linked together by inter-chain hydrogen bonds to form a two-dimensional sheet. Antiferromagnetic exchange is present in compound **2**.

Key words: cobalt, manganese, 2,2′-thiodiethanol, structure, magnetism.

Résumé : On a synthétisé les complexes $[Co(2,2'\text{-thiodiéthanol})_2Cl_2]$ (**1**) et $[Mn(2,2'\text{-thiodiéthanol})Cl_2]_n$ (**2**) et on en a caractérisé la structure. Le composé **1** est un complexe mononucléaire de Co(II) hexacoordiné. Les unités mononucléaires du réseau cristallin du composé **1** sont reliées par de liaisons hydrogènes intermoléculaires entre les groupes hydroxy et chlorure qui conduisent à la formation d'un arrangement tridimensionnel. Le composé **2** consiste d'unités Mn(II) hexacoordinées reliées par le 2,2′-thiodiéthanol attaché de façon covalente et par des ligands chlorures qui conduisent à la formation de chaînes unidimensionnelles alternantes qui sont liées entre elles par des liaisons hydrogènes interchaînes pour former un feuillet bidimensionnel. Le composé **2** donne lieu à un échange antiferromagnétique.

Mots clés : cobalt, manganèse, 2,2′-thioéthanol, structure, magnétisme.

Introduction

The construction of polynuclear metal complexes that display interesting structures and magnetic properties has been one of the research interests of our group. Previously we reported the results of our investigation on polynuclear copper(II) and cobalt(II) complexes where aminoalcohols or tetraacetylethane dianions are used as the bridging ligands (1). Recently we have been studying the syntheses and structures of polynuclear metal complexes that contain 2,2′-thiodiethanol ligands. 2,2′-Thiodiethanol has three potential binding sites, the sulfur atom and two hydroxy groups. Therefore, it can function as either a bidentate chelate ligand, a tridentate chelate ligand, or a bridging ligand. The removal of the proton from the hydroxy group can lead to additional bonding modes such as μ_2- or μ_3-bridging by the oxygen atom. Indeed our earlier study on lanthanide and copper polynuclear complexes containing 2,2′-thiodiethanol ligands confirmed the versatile bonding modes of 2,2′-thiodiethanol and its usefulness in the formation of polynuclear compounds (2). We report herein the structures and properties of a cobalt(II) complex and a Mn(II) complex of 2,2′-thiodiethanol.

Received May 10, 2000. Published on the NRC Research Press website on September 26, 2000.

Y. Zhang and S. Wang.[1] Department of Chemistry, Queen's University, Kingston, ON K7L 3N6, Canada.
C. Bridges and J.E. Greedan. Department of Chemistry, McMaster University, Hamilton, ON L8S 4M1, Canada.

[1]Author to whom correspondence may be addressed. Telephone: (613) 533-2616. Fax: (613) 533-6669. e-mail: wangs@chem.queensu.ca

Experimental

All syntheses were carried out under a dry nitrogen atmosphere by using the standard Schelenk line techniques. All chemicals and solvents used for syntheses were reagent grade. Elemental analyses were performed at Canadian Microanalytical Service Ltd. Delta, BC. Magnetic susceptibility measurements were carried out in the 4–300 K temperature range at 100 G on a SQUID magnetometer from Quantum Design.

Synthesis of $CoCl_2[S(CH_2CH_2OH)_2]_2$ (1)

200 mg of $CoCl_2 \cdot 6H_2O$ (0.73 mmol) was dissolved in 5 mL of methanol. With stirring, 10 mL of a methanol solution of 300 mg of 2,2′-thiodiethanol (excess) was added into the flask. The mixture was left stirring for one day, then concentrated to 5 mL in vacuo. Crystals of **1** were obtained under the slow diffusion of diethylether vapor into the solution with 87% yield. Anal. calcd. for $C_8H_{20}O_4S_2Cl_2Co$: C 25.68, H 5.39; found: C 25.41, H 5.19.

© 2000 NRC Canada

Table 1. Crystallographic data.

Compound	**1**	**2**
Formula	$C_8H_{20}O_4Cl_2S_2Co$	$C_8H_{20}O_4S_2Cl_4\ Mn_2$
fw	374.19	496.04
Space group	P 2_1/c	P 2_1/c
a (Å)	6.7824(8)	6.511(1)
b (Å)	11.228(2)	16.226(4)
c (Å)	10.319(2)	8.715(2)
ζ (°)	109.167(7)	107.18(2)
V (Å^3)	742.3(2)	879.6(3)
Z	2	2
D_c (g cm^{-3})	1.674	1.873
T (°C)	23	23
μ (cm^{-1})	18.0	22.8
Max and min transmission	1.000, 0.850	0.862, 0.654
$2\theta_{max}$ (°)	50	50
Reflns measured	729	1 678
Reflns used (R_{int})	729 (0.0005)	1 540 (0.0106)
No. of variables	81	93
Final *R* [$I > 2s(I)$]	R_1 = 0.0313	$R_1{}^a$ = 0.0271
	wR_2 = 0.0790	$wR_2{}^b$= 0.0783
R (all data)	R_1 = 0.0350	R_1 = 0.0281
	wR_2 = 0.0815	wR_2 = 0.0795
Goodness-of-fit on F^2	1.120	1.279

$^a R_1 = \Sigma||F_o| - |F_c|| / \Sigma|F_o|$.

$^b wR_2 = [\Sigma w[(F_o^2 - F_c^2)^2] / \Sigma[w(F_o^2)^2]]^{1/2}$.

$w = 1/[\sigma^2(F_o^2) + (0.075P)^2]$, where $P = [\text{Max}(F_o^2, 0) + 2F_c^2]/3$.

Synthesis of $\{MnCl_2[S(CH_2CH_2OH)_2]\}_n$ (2)

200 mg of $MnCl_2 \cdot 4H_2O$ (1.01 mmol) was ground first, then added into 2 mL of 2,2′-thiodiethanol (excess) with stirring. The color of the mixture changed to dark purple after being stirred for one day. The mixture was evacuated to dryness by vacuum overnight with stirring. 5 mL of methanol was added to dissolve the residue and a purple solution was obtained. The solution was left under diethylether vapor for one week. Pink crystals of **2** were obtained with 83% yield. Anal. calcd. for $C_4H_{10}O_2S_1Cl_2Mn$: C 19.37, H 4.06; found: C 19.66, H 4.08.

X-ray diffraction analyses

Crystals were obtained from the slow diffusion of diethylether into the methanol or methanol–water solution. The crystals were mounted on glass fibers with epoxy glue. All data was collected on a Siemens P4 single-crystal diffractometer with graphite-monochromated Mo-Kα radiation, operated at 50 kV and 35 mA at 23°C. The data for **1** and **2** were collected over 2θ 3–50°. Three standard reflections were measured every 197 reflections. No significant decay was observed for all samples during the data collection. Data were processed on a Pentium PC using Siemens SHELXTL software package (version 5.0) (3). The semiempirical from ψ-scans absorption corrections were applied for both compounds. Neutral atom scattering factors were taken from Cromer and Waber (4). The crystals of **1** and **2** belong to the monoclinic space group $P2_1/c$. The structures were solved by direct methods. The positions for all hydrogen atoms except those attached to the oxygen atoms were calculated and their contributions in structural factor calculation were included. The hydrogen atoms attached to the oxygen were located directly from difference Fourier maps and refined successfully. All non-hydrogen atoms in **1** and **2** were refined anisotropically. The crystal data for both compounds are given in Table 1.

Results and discussion

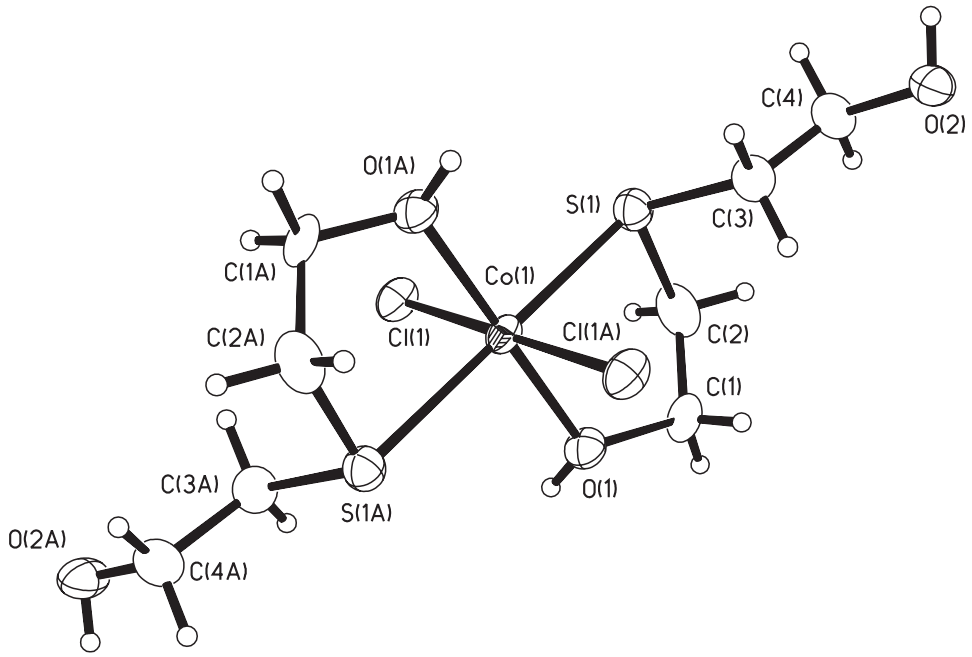
Structures

The title compounds were initially reported by Sen and Johnson (5). Based on analytical, IR, room temperature magnetic moments in solution, and conductivity data, Sen and Johnson (5) suggested that compound **1** is mononuclear and has an octahedral structure with two of the hydroxy groups of the two 2,2′-thiodiethanol lignads coordinating to the cobalt(II) center while compound **2** is also mononuclear with a five-coordinate structure. Our earlier work (2) on 2,2′-thiodiethanol copper(II) complexes indicates that 2,2′-thiodiethanol has a tendency to act as a bridiging ligand and form polynuclear compounds which contradicts the conclusions made by Sen and Johnson. We therefore decided to re-examine these two compounds.

Compounds **1** and **2** were obtained by a modified Sen and Johnson's (5) procedure. In Sen and Johnson's (5) report, only the 1:1 (metal:2,2′-thiodiethanol) compound **2** was described for manganese(II) while both 1:1 and 1:2 compounds were described for cobalt(II). As observed by Sen and Johnson (5), compound **2** is the only product that can be isolated from the reaction regardless of the ratio of Mn(II) to 2,2′-thiodiethanol used in the reaction, the cause of which has not been understood yet. The 1:1 cobalt(II) analog of **2** is

© 2000 NRC Canada

Fig. 1. A diagram showing the molecular structure of **1** with 50% thermal ellipsoids and labeling schemes.



believed to have the same structure as that of **2**. Therefore, the structural study focused on compounds **1** and **2**.

The crystal structure of **1** is shown in Fig. 1. Selected bond lengths and angles are given in Table 2. The crystal structure of compound **1** is composed of discrete mononuclear molecules. The Co(II) atom is six-coordinate, in agreement with Sen and Johnson's (5) suggestions. The cobalt atom is located on the inversion center. Two 2,2′-thiodiethanol ligands are chelated to the Co(II) ion via one sulfur and one oxygen atom. Two chlorine ions are bound to the Co(II) ion in a *trans* fashion. The Co(1)—S, Co(1)—O, and Co(1)—Cl bond lengths are typical (1*b*, 1*c*, 6). The O(1)-Co(1)-Cl(1) angle is nearly 90° (90.66(7)°), but the O(1)-Co(1)-S(1) angle is slightly less than 90° (85.50(3)°). Thus, the geometry of the Co(II) ion is best described as a distorted octahedron.

In the crystal lattice of **1** the hydrogen atoms in the hydroxyl groups of the 2,2′-thiodiethanol ligand link the monomeric molecules through O—H···O hydrogen bonds (7) and O—H···Cl hydrogen bonds as evidenced by the distances of O(2)···O(1′) (2.626 Å) and O(2)···Cl(1′) (3.13 Å). As a result, compound **1** has a three-dimensional hydrogen bonded structure in the solid-state (Fig. 2). The Co—Co separation distances in the crystal lattice are 6.782(1) and 7.625(2) Å, respectively.

The structure of compound **2** is shown in Fig. 3. Selected bond lengths and angles are given in Table 2. As shown in Fig. 3, compound **2** has a polymeric structure. The unique portion of the structure is Mn(1) which is coordinated by three chlorine atoms, two oxygen atoms, and one sulfur atom from two 2,2′-thiodiethanol ligands. The Mn—Cl bond lengths vary considerably, (Mn(1)—Cl(1) = 2.4214(8) Å, Mn(1)—Cl(2) = 2.5125(10) Å, Mn(1)—Cl(2A) = 2.5603(8) Å) while the Mn—O bond lengths are quite similar (Mn(1)—O(1) = 2.234(2) Å and Mn(1)—O(2A) = 2.191(2) Å). The Mn(1)—S(1) bond is much longer than the Co—S bond in **1** but similar to previously reported values (8). The O(1)-Mn(1)-O(2A), Cl(2)-Mn(1)-S(1), and Cl(1)-Mn(1)-Cl(2A) bond angles are 167.98(8), 165.59(3), and 175.86(3)°, respectively, a substantial deviation from an ideal octahedral geometry. The geometry of the Mn(II) ion in compound **2** can be therefore also best described as a distorted octahedron. There are two possible geometric isomers for compound **2**, *fac* and *mer*. The observed structure of **2** is the *mer* isomer where two of the chlorine atoms are *trans* to each other.

The thiodiethanol ligand has three forms: (*i*) the neutral ligand ($S(CH_2CH_2OH)_2$ (H_2tde)); (*ii*) the anion ($S(CH_2CH_2OH)(CH_2CH_2O)^-$ ($Htde^-$)); and (*iii*) the dianion ($S(CH_2CH_2O)_2^{2-}$ (tde^{2-})). In addition being a chelate ligand, the $Htde^-$ and tde^{2-} ligands can function as a bridging ligand where the negatively charged oxygen atom binds two metal ions as established by our previous studies (2). $Htde^-$ and tde^{2-} are therefore excellent ligands for the formation of polynuclear metal complexes (2). In contrast, the oxygen atoms of the neutral H_2tde ligand in both compounds **1** and **2** function as terminal donors only, which could be attributed to the fact that the negatively charged oxygen of $Htde^-$ and tde^{2-} is a much better donor than the neutral OH group of H_2tde, hence capable of binding to two metal ions.

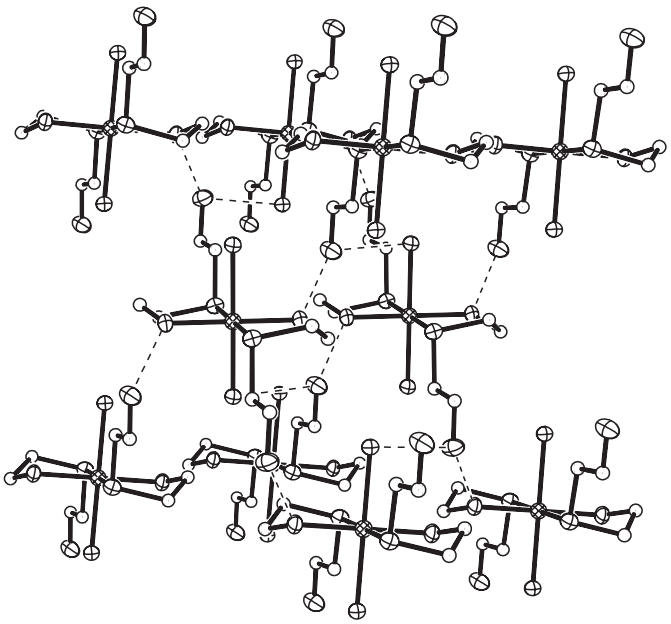
2,2′-Thiodiethanol in **2** functions as a chelating and bridging ligand. The second OH group of H_2tde in compound **2** is coordinated to a second Mn(II) ion of a neighboring Mn(II) unit, resulting in a cyclic dinuclear $Mn_2(H_2tde)_2Cl_4$ unit. The Mn(1)—Mn(1B) separation distance in the cyclic unit is 6.504(1) Å. The dimension of this 12-membered ring is approximately 6.50 × 3.90 Å. The cyclic dinuclear $Mn_2(H_2tde)_2Cl_4$ units are further linked together through two chloride bridges Cl(2) and Cl(2A). The chloride bridges are almost symmetric with the Mn(1)—Cl(2) bond length (2.5125(10) Å) being slightly longer than that of Mn(1)—Cl(2A) (2.5603(8) Å). The two metal ions, Mn(1)

© 2000 NRC Canada

Table 2. Selected bond lengths (Å) and angles (°).

Bond lengths	(Å)	Angles	(°)
(A) Compound **1**			
Co(1)—O(1)	2.060(4)	O(1)-Co(1)-O(1A)	180.0(2)
Co(1)—Cl(1)	2.4145(9)	O(1)-Co(1)-Cl(1)	90.62(7)
Co(1)—S(1)	2.5054(9)	O(1A)-Co(1)-Cl(1)	89.38(7)
S(1)—C(3)	1.803(3)	O(1)-Co(1)-S(1)	84.09(7)
S(1)—C(2)	1.812(5)	O(1A)-Co(1)-S(1)	95.91(7)
		Cl(1)-Co(1)-S(1)	85.49(3)
		Cl(1A)-Co(1)-S(1)	94.51(3)
		S(1)-Co(1)-S(1A)	180.00(3)
(B) Compound **2**			
Mn(1)—O(2A)	2.191(2)	O(2A)-Mn(1)-O(1)	167.98(8)
Mn(1)—O(1)	2.234(2)	O(1)-Mn(1)-Cl(1)	92.59(6)
Mn(1)—Cl(1)	2.4214(8)	O(2A)-Mn(1)-Cl(2)	96.01(6)
Mn(1)—Cl(2)	2.5125(10)	O(1)-Mn(1)-Cl(2)	95.83(6)
Mn(1)—Cl(2A)	2.5603(8)	Cl(1)-Mn(1)-Cl(2)	97.21(3)
Mn(1)—S(1)	2.7224(10)	O(2A)-Mn(1)-Cl(2A)	88.49(6)
S(1)—C(2)	1.805(3)	O(1)-Mn(1)-Cl(2A)	90.42(6)
S(1)—C(3)	1.814(3)	Cl(1)-Mn(1)-Cl(2A)	175.86(3)
		Cl(2)-Mn(1)-Cl(2A)	85.30(3)
		O(2A)-Mn(1)-S(1)	91.53(6)
		O(1)-Mn(1)-S(1)	76.45(6)
		Cl(1)-Mn(1)-S(1)	95.31(3)
		Cl(2)-Mn(1)-S(1)	165.59(3)
		Cl(2A)-Mn(1)-S(1)	82.63(3)
		Mn(1)-Cl(2)-Mn(1A)	94.70(3)

Fig. 2. A diagram showing hydrogen bonds in the crystal lattice of **1**.



and Mn(1A) are separated by the two chloride bridges by 3.731(1) Å. As a result of the chloride bridges, compound **1** has a one-dimensional polymeric structure in the solid state.

There are extensive hydrogen bonds between the polymeric chains as shown in Fig. 4. The first type of hydrogen bond in **2** is between the bridging chlorine atoms Cl(2) and Cl(2A) and the terminal OH groups O(2) and O(2A) from two neighboring polymer chains, as evidenced by the distance of Cl(2)···O(2′) (3.223 Å). The second type of hydrogen bond in **2** is between the terminal chloride ligands Cl(1) and Cl(1A) and the chelate OH groups O(1) and O(1A) from neighboring chains (Cl(1)···O(1′) = 3.144 Å). The hydrogen bonds extend the polymeric structure of **2** into a two-dimensional infinite sheet. The shortest Mn···Mn separation distance between the hydrogen bonded polymer chains is 5.577(1) Å.

Sen and Johnson (5) suggested a five-coordinate trigonal bipyramidyl geometry for compound **2** based on electronic spectral data in solution and the solid state which contradicts the results of our investigation. Because the physical properties (IR, mp, and elemental analysis) of our compound **2** are identical to that reported by Sen and Johnson (5) they must have the same structure. Therefore, we believe that Sen and Johnson made an error in their assignment of the structure of compound **2**.

Magnetic properties

As established by Sen and Johnson (5), the cobalt(II) ion in compound **1** has a high spin configuration. Due to the lack of covalent bonds and the large separation distance between the mononuclear units, compound **1** is essentially paramagnetic with negligible intermolecular magnetic interactions as supported by Sen and Johnson's (5) data. Therefore, we did not study its magnetic properties in detail. On the other hand, the Mn(II) ions in compound **2** are covalently linked together by chloride and H_2tde ligands with

© 2000 NRC Canada

Fig. 3. A diagram showing a portion of the extended structure of **2** with 50% thermal ellipsoids and labeling schemes.

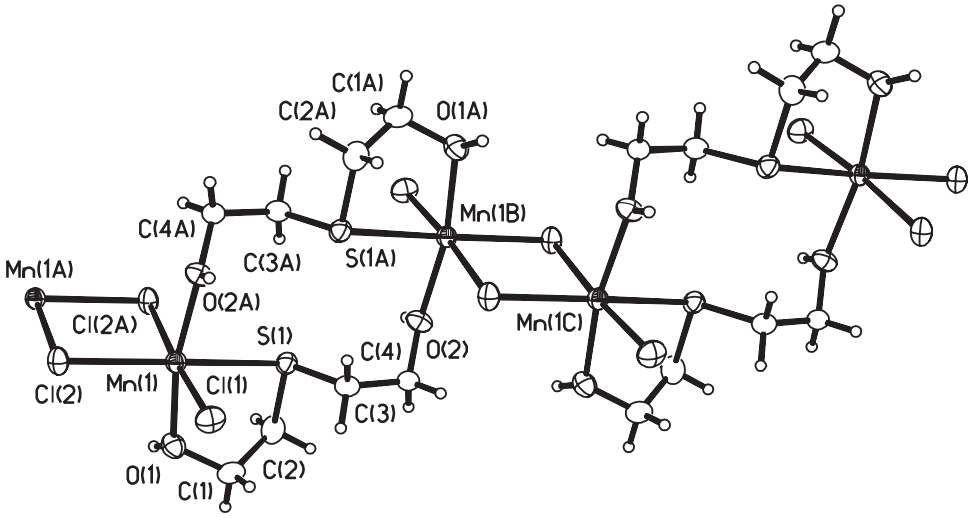
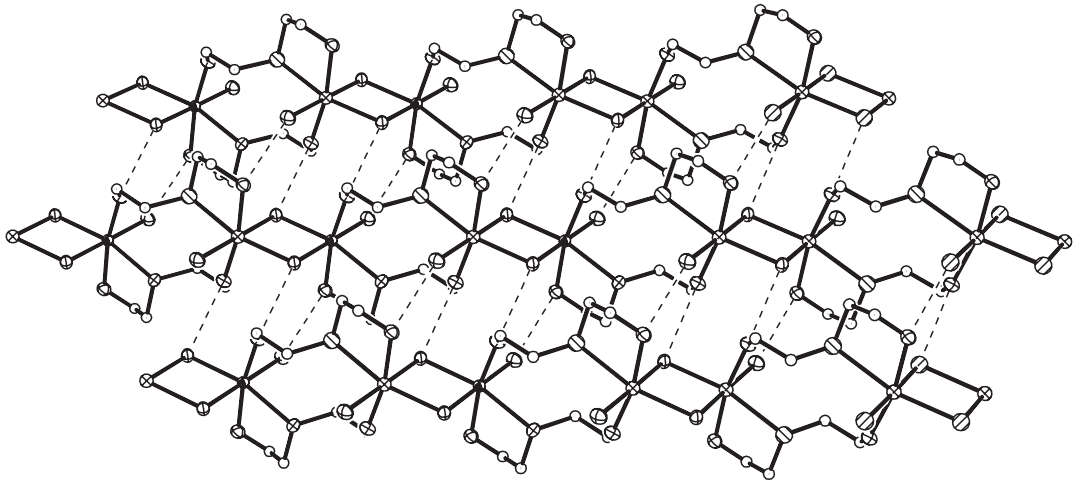


Fig. 4. A diagram showing interchain hydrogen bonds in the crystal lattice of **2**.

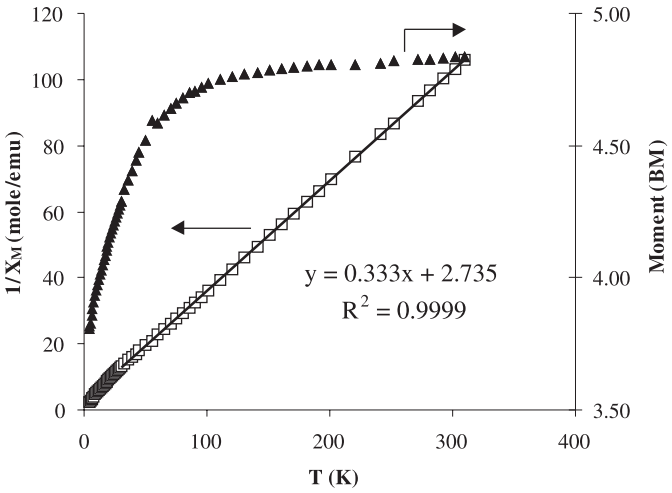


considerably shorter metal–metal separation distances (3.731 Å and 6.504 Å) within the one-dimensional chain than those of compound **1**. Some magnetic interactions between Mn(II) ions are therefore anticipated. Therefore, we examined the magnetic properties of compound **2** by measuring its magnetic susceptibility in the solid-state over the temperature range of 4–310 K. There is not a max in the χ_M vs. *T* plot. As a result, the data cannot be fitted into a $S = 5/2$ dimer model. The magnetic data (χ_M^{-1} and μ vs. *T*) corrected for diamagnetism by using Pascal constants of **2** is shown in Fig. 5. The magnetic moment at 310 K is 4.83 BM, much less than the expected value (5.90 BM) for a high spin and noninteracting Mn(II) ion. The magnetic moment of **2** decreases gradually from 310 to ~50 K, then decreases rapidly at temperatures below 50 K, indicative of the presence of antiferromagnetic exchange. The plot of the reciprocal molar susceptibility χ_M^{-1} vs. *T* is essentially a straight line from 30 to 310 K. There is a slight deviation from the straight line at temperatures below 30 K. The χ_M^{-1} vs. *T* plot in the 30–310 K range is fitted into a linear equation which produces a perfect fit ($R^2 = 0.9999$). From the fitting parameters, we obtained the θ value of Curie–Weiss law ($\chi_M = C/(T - \theta)$), $\theta = -8.213$ K), which further supports the presence of antiferromagnetic exchange in compound **2** (9). The antiferromagnetic exchange in **2** occurs most likely between the Mn(1) and Mn(1A) pair because they have the shortest Mn—Mn separation distance and are directly linked by two chloride ligands with a Mn-Cl-Mn bond angle of 94.70(3)° (9). Similar antiferromagnetic exchange has been observed in a number of chloride bridged, high spin Mn(II) compounds (10). The deviation of χ_M^{-1} vs. *T* plot from a straight line at temperatures below 30 K could be caused by additional magnetic interactions, perhaps magnetic interactions between the hydrogen bonded polymeric chains of **2**.

In summary, our studies have established unambiguously that the 1:2 compound **1** is a mononuclear, six-coordinate, and hydrogen bonded system while the 1:1 compound **2** is a six-coordinate covalent polymer. The neutral ligand 2,2′-thioethanol is capable of forming polynuclear complexes as the corresponding anion ($Htde^-$) and dianion (tde^{2-}) ligands are. Further investigation on 2,2′-thiodiethanol polynuclear complexes is in progress.

© 2000 NRC Canada

Fig. 5. Plots of χ_M^{-1} and μ vs. T for compound **2**. The solid line is the linear fit for χ_M^{-1} vs. *T* plot in the 30–310 K region.



Acknowledgment

We thank the Natural Sciences and Engineering Research Council of Canada for financial support.

References

1. (*a*) S. Wang. J. Cluster Sci. **6**, 463 (1995); (*b*) Y. Zhang, S.R. Breeze, S. Wang, J.E. Greedan, N.P. Raju, and L.J. Li. Can. J. Chem. **77**, 1424 (1999); (*c*) Y. Zhang, S. Wang, G.D. Enright, and S.R. Breeze. J. Am. Chem. Soc. **120**, 9398 (1998); (*d*) S. Kawata, S.R. Breeze, S. Wang, J.E. Greedan, and N.P. Raju. J. Chem. Soc. Chem. Commun. 717 (1997); (*e*) S.R. Breeze, S. Wang, J.E. Greedan, and N.P. Raju. Inorg. Chem. **35**, 6944 (1996); (*f*) L. Chen, S.R. Breeze, R. Rousseau, S. Wang, and L.K. Thompson. Inorg. Chem. **34**, 454 (1995).
2. S.R. Breeze, S. Wang, J.E. Greedan, and N.P. Raju. J. Chem. Soc. Dalton Trans. 2327 (1998).
3. SHELXTL Version 5. Crystal structure analysis package. Bruker Axs, Analytical X-ray System, Madison, WI. U.S.A. 1995.
4. D.T. Cromer and J.T. Waber. International Tables for X-ray crystallography. Vol. 4. Kynoch Press, Birmingham, AL. 1974. Table 2.2A.
5. B. Sen and D.A. Johnson. J. Inorg. Nucl. Chem. **34**, 609 (1972).
6. (*a*) S.O.H. Gutschke, M. Molinier, A.K. Powell, and P.T. Wood. Angew. Chem. Int. Ed. Engl. **36**, 991 (1997); (*b*) A.J. Kinneging, W.J. Vermin, and S. Gorter. Acta Crystallogr. Sect B: Struct. Crystallogr. Cryst. Chem. **B38**, 1824 (1982); (*c*) G.R. Newkome, D.K. Kohli, and F. Fronczek. J. Chem. Soc. Chem. Commun. 9 (1980); (*d*) D.A. Buckinghum and C.R. Clark. *In* Comprehensive coordination chemistry. Vol. 4. *Edited by* G. Wilkinson, R.D. Gillard, and J.A. McCleverty. Pergamon Press, Oxford. 1987. Chap. 4.
7. (*a*) W.C. Hamilton and J.A Ibers. Hydrogen bonding in solids. W.A. Benjamin, New York. 1968; (*b*) A. Novak. Struct. Bonding (Berlin), **18**, 177 (1974); (*c*) J. Emsley. Chem. Soc. Rev. **9**, 91 (1980); (*d*) S.N. Vinogradov and R.H. Linnell. Hydrogen bonding. Van Nostrand–Reinhold, New York. 1971.
8. (*a*) R.D. Willett. Acta Crystallogr. Sect B: Struct. Crystallogr. Cryst. Chem. **B35**, 178 (1979); (*b*) A.L. Gillon, A.G. Orpen, J. Starbuck, X.M. Wang, Y. Rodríguez-Martin, and C. Ruiz-Pérez. J. Chem. Soc. Chem. Commun. 2287 (1999); (*c*) A.H. Othman, K.L. Lee, H.K. Fun, and B.C. Yip. Acta Crystallogr. Sect. C: Cryst. Struct. Commun. **C52**, 602 (1996); (*d*) H.O. Stephan and G. Henkel. Polyhedron, **15**, 501 (1996); (*e*) H.O. Stephan, M.G. Kanatzidis, and G. Henkel. Angew. Chem. Int. Ed. Engl. **35**, 2135 (1996).
9. (*a*) W.E. Hatfield. *In* Magneto-structural correlations in exchange coupled systems. *Edited by* R.D. Willett, D. Gatteschi, and O. Kahn. NATO ASI. Reidel, Dordrecht. 1985. p. 555; (*b*) R.L. Carlin. Magnetochemistry. Springer–Verlag, Berlin. 1986.
10. (*a*) W. Zhang, J.R. Jeitler, M.M. Turnbull, C.P. Landee, M. Wei, and R.D. Willett. Inorg. Chim. Acta, **256**, 183 (1997); (*b*) J.S. Sun, H. Zhao, X. Ouyang, R. Clérac, J.A. Smith, J.M. Clemente-Juan, C. Gómez-Garcia, E. Coronado, and K.R. Dunbar. Inorg. Chem. **38**, 5841 (1999).

© 2000 NRC Canada

Thermodynamics of methanesulfonic acid revisited

J. Peter Guthrie and Roger T. Gallant

Abstract: Recently we reported a study of the thermodynamics of methanesulfonic acid and some of its derivatives. The foundation of these results was a measurement of the heat of reaction of *S*-methyl thioacetate with aq sodium hypochlorite, leading to methanesulfonic acid. We have reinvestigated this reaction and discovered that contrary to the initial stoichiometry experiments, the stoichiometry under the reaction conditions is not as was believed and that the heat of reaction observed was spuriously high. We have found a new reaction, that of sulfite ion with methyl methanesulfonate, which does allow a clean determination of the heat of formation of methanesulfonic acid. Revised thermodynamic quantities for methanesulfonic acid, methanesulfonyl chloride, and methyl methanesulfonate are reported here.

Key words: sulfonic acid, heat of reaction, free energy of formation, S_N2 reaction.

Résumé : On a récemment rapporté une étude sur les propriétés thermodynamiques de l'acide méthanesulfonique et de ses dérivés. La base de ces résultats était une mesure de la chaleur de réaction du thioacétate de *S*-méthyle avec de l'hypochlorite de sodium aqueux conduisant à la formation d'acide méthanesulfonique. On a repris l'étude de cette réaction et on a trouvé que, contrairement aux expériences initiales de stoechiométrie, cette dernière n'est pas toujours celle que l'on croyait et que la chaleur de réaction observée était faussement élevée. On a trouvé une nouvelle réaction, celle de l'ion sulfite avec le méthanesulfonate de méthyle qui permet de faire une détermination propre de la chaleur de formation de l'acide méthanesulfonique. On rapporte les valeurs révisées des quantités thermodynamiques pour l'acide méthanesulfonique, le chlorure de méthanesulfonyle et le méthanesulfonate de méthyle.

Mots clés : acide sulfonique, chaleur de réaction, énergie libre de formation, réaction S_N2.

Introduction

Recently we reported a study of the thermochemistry and thermodynamics of methaneulfonic acid and some of its derivatives (1). Two colleagues knowledgeable in this area pointed out that the heat of formation we reported was inconsistent with heats of formation of related compounds or other indirect sources of heat of formation data. To settle the point we have determined the heat of formation of methanesulfonic acid independently, by a reaction of sulfite ion with methyl methanesulfonate (methyl mesylate). With some embarrassment we now report that the initial value we reported was in error and herewith revise the thermochemistry of methanesulfonic acid.

Results

Heats of reaction were measured using a Tronac isoperibol calorimeter. The results are given in Table 1. The apparent heat of hydrolysis of methyl trifluoromethanesulfonate in pH 10 aq borate buffer was –7.85 ± 0.35 kcal mol^{-1}.

[1] $CH_3\text{-}O\text{-}SO_2\text{-}CF_3(1) + (HO)_4B^-(soln) \rightarrow CH_3\text{-}OH(soln) + {}^-O_3S\text{-}CF_3(soln) + (HO)_3B(soln)$

The heat of reaction of methyl trifluoromethanesulfonate with aq sodium sulfite was –11.76 ± 0.12 kcal mol^{-1}.

[2] $CH_3\text{-}O\text{-}SO_2\text{-}CF_3(1) + SO_3^{2-}(soln) \rightarrow CH_3\text{-}SO_3^-(soln) + {}^-O_3S\text{-}CF_3(soln) + (HO)_3B(soln)$

The heat of reaction of hydroxide with boric acid can be calculated from the known heats of ionization of boric acid and water (2) to be –9.97 ± 0.01 kcal mol^{-1}.

[3] $(HO)_3B(soln) + HO^-(soln) \rightarrow (HO)_4B^-(soln)$

Combining these values allows calculation of the heat of reaction for the convenient hypothetical process, [4], for which $\Delta H_{reaction}$ = +6.06 ± 0.37 kcal mol^{-1}. From the heats of formation of the other species involved (see Table 2), we can now calculate the heat of formation of methanesulfonate ion in aqueous solution as –149.64 ± 0.70 kcal mol^{-1}.

[4] $CH_3\text{-}OH(soln) + SO_3^{2-}(soln) \rightarrow CH_3 + SO_3^-(soln) + HO^-(soln)$

The heat of solution of methanesulfonic acid in water was –11.40 ± 0.41 kcal mol^{-1}.

Received September 2, 1999. Published on the NRC Research Press website on September 26, 2000.

J.P. Guthrie[1] and R.T. Gallant. Department of Chemistry, University of Western Ontario. London, ON N6A 5B7, Canada.

[1]Author to whom correspondence may be addressed. Telephone: (519) 661-2111 ext. 86352. Fax: (519) 661-3022. e-mail: peter.guthrie@uwo.ca

© 2000 NRC Canada

Table 1. Heats of reaction and solution.[a]

Compound	ΔH	Av
$CH_3OSO_2CF_3$ + borate buffer	–7.92[b], –8.25[b], –7.39[b]	–7.85 ± 0.35[b]
$CH_3OSO_2CF_3$ + sulfite	–11.58[c], –11.93[c], –11.75[c], –11.75[c], –11.78[c]	–11.76 ± 0.12[c]
CH_3SO_3H	–11.70[d] –10.69[d], –11.51[d], –11.68[d]	–11.40 ± 0.41[d]
$CH_3OSO_2CH_3$ + sulfite	–37.89[e], –37.11[e], –36.80[e], –36.38[e]	–37.05 ± 0.55

[a]All at 25°C, units are kcal mol^{-1}; heat of reaction unless noted.
[b]In pH 10 aq borate buffer l.
[c]In 0.1 M aq Na_2SO_3.
[d]Heat of solution in water.
[e]In 0.5 M aq Na_2SO_3.

[5] $CH_3\text{-}SO_3H(1) \rightarrow CH_3\text{-}SO_3^-(soln) + H^+(soln)$

This permits calculation of the heat of formation of liquid methanesulfonic acid as –138.24 ± 0.81.

This value was closer to the previous literature estimates, but still differed by 10 kcal mol^{-1} from these estimates. Nagging concerns about this discrepancy, prompted by similar concerns expressed by a referee reviewing an early version of this paper, led us to do further analysis of the results, and then to do further experiments. From the previous results (1) we can calculate the heat of hydrolysis for methyl methanesulfonate. This heat of reaction does not depend on the absolute value of the heat of formation of methanesulfonic acid from our original paper, but only on the heats of reaction of methanesulfonyl chloride with water or methanol, and this heat of hydrolysis is consistent with the literature estimates. The heat of hydrolysis for the process

[6] $CH_3SO_2OCH_3(1) + HO^-(soln) \rightarrow CH_3SO_3^-(soln) + CH_3OH(soln)$

is –27.31 kcal mol^{-1}, while for the analogous reaction of methyl trifluoromethanesulfonate

[7] $CF_3SO_2OCH_3(1) + HO^-(soln) \rightarrow CF_3SO_3^-(soln) + CH_3OH(soln)$

we calculate from the results given above that the heat of hydrolysis is –17.82 kcal mol^{-1}. That the heat of hydrolysis of the ester of the stronger acid should be less than that of the ester of the weaker acid seems wildly unlikely.

We turned next to measurement of the heat of reaction of sulfite ion with methyl methanesulfonate. With 0.1 M sodium sulfite in water the reaction was not quite fast enough for convenient calorimetry, but at 0.5 M sodium sulfite the reaction was fast enough to give a well-defined post reaction trace and thus allow good determination of the heat of reaction. For the process:

[8] $CH_3\text{-}O\text{-}SO_2\text{-}CH_3(1) + SO_3^{2-}(soln) \rightarrow 2CH_3\text{-}SO_3^-(soln)$

the heat of reaction was –37.05 ± 0.55. This is much more exothermic than the corresponding value from experiments with methyl trifluoromethanesulfonate (–11.76 ± 0.12 kcal mol^{-1}). Again it seems wildly unlikely that the more reactive ester would have the smaller heat of reaction. These experiments with methyl methanesulfonate, also reported in Table 1, permitted calculation of the heat of reaction for the hypothetical process [4], based on the heat of reaction of methyl methanesulfonate, as –7.89 ± 0.85 kcal mol^{-1}, which is quite different from the value based on the heats of reaction of methyl trifluoromethanesulfonate, namely +6.06 ± 0.37 kcal mol^{-1}. In this calculation process [8] minus process [6] yields process [4].

Table 2. Heats of formation.[a]

Compound	Phase	$\Delta H_f°$
H_2O	l	–68.32 ± 0.01[b]
NaOH	soln	–112.36 ± 0.01[b]
NaCl	soln	–97.25 ± 0.02[b]
Na_2SO_3	l	–266.70 ± 0.59[b]

[a]All at 25°C, heats of formation in kcal mol^{-1}.
[b]Reference (10).

From the new value for the heat of reaction of process [4], we derive a heat of formation of methanesulfonate ion in aqueous solution as –163.79 ± 1.04 kcal mol^{-1}, and hence a value of –152.39 ± 1.12 kcal mol^{-1} for liquid methanesulfonic acid. This requires revision of all the thermodynamic quantities dependent upon the heat of formation of methane sulfonic acid, in Table 4 of ref. (1). The revised values are given in Table 3 below.

The stoichiometry of the reaction of methyl thioacetate with hypochlorite was reexamined. In the original work it had been demonstrated by NMR analysis that the only products were acetate and methanesulfonate, in equimolar amounts. This experiment involved reaction with full strength, 5%, hypochlorite solution, to allow concentrations of products high enough for analysis by 200 MHz ^{1}H NMR spectroscopy. However there was a difference in concentration between the stoichiometry determinations and the calorimetry, since full strength 5% sodium hypochlorite was used for stoichiometry determinations (ca. 0.67 M OCl^-, 0.11 M thioester), and 15:35 sodium hypochlorite:water was used for calorimetry (ca. 0.28 M OCl^-, 0.0054 M thioester). The distilled water could significantly lower the hydroxide concentration of this very weakly buffered solution, and thus have affect the relative rates of hydroxide dependent and hypochlorite dependent reactions.

When the analyses were repeated at lower concentrations of hypochlorite, and consequently lower concentrations of products, using 500 MHz ^{1}H NMR spectroscopy, we found that the amount of methane sulfonate was less than the amount of acetate. This result requires that there be a process consuming methanethiol equivalents which does not lead

© 2000 NRC Canada

Table 3. Thermodynamic quantities for compound discussed in this paper.[a]

Compound	$\Delta Hf(l)$	ΔH_{vap}[b]	$\Delta Hf(g)$	$S°(g)$[b]	$\Delta Gf(g)$	ΔGt[b]	$\Delta Gf(aq)$
CH_3SO_3H	–152.39 ± 1.12	17.97 ± 2.0	–134.42 ± 2.29	74.03 ± 2.0	–113.29 ± 2.37	–12.73 ± 0.79	–126.02 ± 2.50
CH_3SO_2Cl	–101.20 ± 1.20	11.50 ± 0.28	–89.70 ± 1.21	74.76 ± 2.0	–72.80 ± 1.35	–2.97 ± 0.27	–75.58 ± 1.36
$CH_3SO_3CH_3$	–138.63 ± 1.24	13.96 ± 0.70	–124.67 ± 1.43	82.33 ± 2.0	–96.30 ± 1.55	–5.27 ± 0.18	–101.57 ± 1.84

[a]All at 25°C, enthalpies and free energies are in kcal mol^{-1}, entropies are in cal deg^{-1} mol^{-2}, standard states are the ideal gas at 1 atm and 1 M aqueous solution with an infinitely dilute reference state. Standard entropies in the gas-phase and free energies of transfer (from the gas at 1 atm to 1 M aqueuos solution) were calculated as described in the text. Free energies of formation in the gas-phase are calculated from the corresponding enthalpies of formation and the standard entropies, and free energies of formation in aqueous solution are calculated from the corresponding free energies of formation in the gas and free energies of transfer.

[b]Reference (1).

to methanesulfonate, and thus implies that the measured heat of reaction will be spuriously high.

In other experiments we measured the concentration of hypochlorite by UV before and after adding *S*-methyl thioacetate, and found that the amount of hypochlorite used was greater than required for the simple stoichiometry previously assumed.

Thus it seems clear that the basis for the initial calorimetry was incorrect, despite apparently clear evidence from a stoichiometry experiment carried out before these measurements were performed.

Discussion

It seems clear that we were mistaken in thinking that we knew the stoichiometry of the reaction used to determine the heat of formation of methanesulfonic acid. The distressing thing is that the stoichiometry had been determined by direct analysis for methanesulfonate and acetate, admittedly under slightly different conditions than were used for the actual calorimetry. The difference, amounting to a factor of 3.3 in hypochlorite concentration, had not seemed important but obviously was. In addition, the logical consistency of the results had been checked by a γ plot (3) (admittedly a novel extrapolation of the idea of a γ plot, but one which seemed reasonable). Clearly, this too was misleading. Work in progress suggests that γ is indeed relevant to these equilibria, but is not the whole story.

We do not know what reactions could have led to consumption of methanethiolate equivalents so that they did not become methanesulfonate, but it is tempting to speculate that under the alkaline reaction conditions elimination of HCl from an initial S^+Cl species could lead to a $CH_2{=}S^+$ species which would quickly release formaldehyde, and leave a sulfide equivalent. Oxidation of sulfide to sulfate is strongly exothermic.

The new calorimetric results reported here are for an inherently simpler reaction. When methyl trifluoromethanesulfonate was added to a 1 M solution of Na_2SO_3 in D_2O, to give a final concentration of organic material of 0.2 M, the ^1H NMR spectrum showed essentially only one peak, at the chemical shift expected for methanesulfonate ion. The only nucleophiles in the solution are water, hydroxide, and sulfite ion. Hydroxide is at quite low concentration and therefore should be of negligible significance. The Swain–Scott *n* value for sulfite ion is 5.1, (4), while that for water is 0.0. Thus it seems highly reasonable that the only reaction would be that of sulfite attacking methyl trifluoromethanesulfonate as was observed. Sulfite is potentially an oxygen nucleophile instead of a sulfur nucleophile, but as an oxygen nucleophile it would be expected to have a Swain–Scott n value, 3.8, similar to that of HPO_4^{2-} which has a very similar pK_a. This implies a reaction rate only one twentieth that of the sulfur. In any case NMR analysis of the product solution (for an experiment done in D_2O) showed only traces of additional products. There was about 2% of a peak which might be methanol, and an even tinier trace of a peak to lower field. An amount of competing hydrolysis or reaction at oxygen of sulfite amounting to no more than this would have an effect on the heat of reaction less than the observed experimental error.

NMR analysis of the product solution from the reaction of sulfite with methyl methanesulfonate shows only the peak expected for methanesulfonate ion, with no other products amounting to more than 0.5% of the total.

Why then are the results of reactions with methyl trifluoromethanesulfonate so out of line with expectations? The only explanation we have been able to devise is that the reactions are fast and exothermic, and so may have caused significant amounts of volatilization of ester before reaction, leading to anomalously low measured heats of reaction. Trifluoromethanesulfonic acid is 4 pK_a units stronger than methanesulfonic acid (5), so an initial guess using a Brønsted exponent of 0.5 suggests that the reactions of methyl trifluoromethanesulfonate would be 100 times faster than those of methyl methanesulfonate. Reactions of methanesulfonyl chloride with aqueous hydroxide could not be studied because of spattering from the exothermic reaction, leading to obvious scatter and unreacted droplets (1). This reaction could only be studied in solutions buffered at pH 10, and this experience guided our use of buffer for the hydrolysis reaction of methyl trifluoromethanesulfonate. Methyl trifluoromethanesulfonate boils at 95°C (6), and thus would volatilize before water, unlike methanesulfonyl chloride, bp 159 (7); this may explain the difference in behavior.

The present approach to the heat of formation of methanesulfonic acid, though free of the problems which affected the hypochlorite oxidation procedure, is less general, since it requires that there be a rapid nucleophilic displacement. Examination of the literature showed that the S_N2 reactions of CH_3X were not likely to be fast enough for calorimetry without an extremely good leaving group, such as trifluoromethanesulfonate or methanesulfonate. For alkyl groups other than methyl, the reaction becomes slower, and side reactions become increasingly likely as the group gets larger.

© 2000 NRC Canada

The values reported in the present paper for the heats of formation of liquid methanesulfonic acid, methyl methanesulfonate, and methanesulfonyl chloride are much closer to the values in the earlier literature than those in our original paper. The values we now report are respectively –152, –139, and –101 as opposed to –178, –164, and –127 (1) kcal mol^{-1}; Liebman(8) gave –147, –135, and –101 kcal mol^{-1}.

Experimental

Materials

S-Methyl thioacetate was a fresh bottle from Lancaster Chemicals, and was used without further purification. NMR spectroscopy showed no impurities. Sodium hypochlorite as a 5% solution in water was Malinckrodt analytical reagent grade. Methyl trifluoromethanesulfonate was a fresh bottle from Aldrich, used without further purification. ^{1}H and ^{19}F NMR spectra each showed only one peak with the expected chemical shift. Methyl methanesulfonate was taken from a fresh bottle (Aldrich 99%). The ^{1}H NMR spectrum showed only the two peaks expected for methyl methanesulfonate. Boric acid, potassium chloride, sodium hydroxide, and sodium sulfite were analytical reagent grade. pH 10 borate buffer was made up following ref. (9).

Methods

Reaction calorimetry was carried out as previously described (1). ^{1}H NMR spectra were recorded on Varian Gemini 200 or Unity 500 MHz spectrometers, the latter through the cooperation of Dr. G. Shaw, of the Departments of Biochemistry and Chemistry at this university.

Acknowledgments

We thank the Natural Sciences and Engineering Research Council of Canada for financial support of this work. We thank Dr. G. Shaw, Departments of Biochemistry and Chemistry, for recording the 500 MHz NMR spectra. We thank Professors John Bartmess and Joel Liebman for helpful discussions which provoked the work reported here.

References

1. J.P. Guthrie, A.R. Stein, and A.P. Huntington. Can. J. Chem. **76**, 929 (1998).
2. J.W. Larson and L.G. Hepler. *In* Solvent solute interactions. Vol. 1. *Edited by* J.F. Coetzee and C.D. Ritchie. Marcel Dekker, New York. 1969.
3. E.G. Sander and W.P. Jencks. J. Am. Chem. Soc. **90**, 6154 (1968).
4. C.G. Swain and C.B. Scott. J. Am. Chem. Soc. **75**, 141 (1953).
5. J.P. Guthrie. Can. J. Chem. **56**, 2342 (1978).
6. Beilstein. Handbuch der Organischen Chemie. **3**(4) 34.
7. Beilstein. Handbuch der Organischen Chemie. **4**(2) 525.
8. J. Liebman. *In* The chemistry of sulphonic acids, esters, and their derivatives. *Edited by* S. Patai and Z. Rappoport. John Wiley and Sons Ltd., Chichester. 1991. pp. 283.
9. S.P. Datta and A.K. Grzybowski. *In* Biochemist's handbook. *Edited by* C. Long. E. & F.N. Spon Ltd., London. 1961. pp. 40.
10. D.D. Wagman, W.H. Evans, V.B. Parker, R.H. Schumm, I. Halow, S.M. Bailey, K.L. Churney, and R.L. Nuttall. J. Phys. Chem. Ref. Data. Suppl. **2**, **11**, (1982).

© 2000 NRC Canada

Oxidative coupling-type mechanism of *N*,*N*-dialkylanilines in solvent-free conditions forming crystal violet derivatives. A clay-mediated and microwave-promoted approach

J.G. López-Cortés, G. Penieres-Carrillo, M.C. Ortega-Alfaro, R. Gutiérrez-Pérez, R.A. Toscano, and C. Alvarez-Toledano

Abstract: In the clay-mediated reaction of *N*,*N*-disubstituted anilines using microwave radiation as an energy source in the absence of solvent, crystal violet and derivatives, diphenylmethanes, and biphenyls were isolated along with intermediates supporting an oxidative coupling-type mechanism.

Key words: clay, dyes, microwave radiation, solvent-free reactions.

Résumé : Les réactions d'anilines *N*,*N*-disubstituées effectuées en présence d'argile, sans solvant et en utilisant un rayonnement de micro-ondes comme source d'énergie, on a isolé du cristal violet et de ses dérivés, des diphénylméthanes et des biphényles, en plus d'intermédiaires qui sont en accord avec un mécanisme de type couplage oxydant.

Mots clés : argile, colorants, rayonnement, réactions sans solvant.

Introduction

Much attention has been recently focused on bis(4-*N*,*N*-dialkylaminophenyl)methanes because these kinds of compounds are employed as precursors of dyes and (or) indicators (1), as well as in materials science and other fields (2). 4-Bis(*N*,*N*-dialkylamino)biphenyls also have many uses, such as nonaqueous electrolytes in lithium batteries (3), and in photosensitive reduction on de-chloration of chloroaromatic pesticides (4). On the other hand, crystal violet and analogues have also attracted considerable interest in recent years owing to their newer applications on surface phenomena in materials science (5), in biochemical genetics (6), etc. Some transformations of *N*,*N*-dialkylanilines to obtain the aforementioned compounds are, inter alia, oxidation reactions (7) and several oxidizing catalysts containing different metals (8). Some other methods involve e.g., the condensation of formaldehyde and aniline with concentrated HCl (9), the reduction of 4,4′-(*N*,*N*-dialkylamino)benzophenones (10), using heterocyclic compounds (11) or by alkylation of methylenebisanilines (12).

In the last years, our laboratory has been involved in the development of new synthetic strategies employing a bentonitic earth as catalyst and (or) reaction medium in solvent-free systems (13) and with the use of microwave (for leading reviews see ref. 14) or infrared energy sources. The simplicity of experimental conditions, ease of isolation of the end products, as well as avoidance of byproducts and likewise the availability of the clay, have been important and valuable features for the growing increase of studies with the bentonite-mediated approach as a performing and attracting synthetic tool for a wide-ranging assortment of organic reactions, such as oxidative couplings of naphthols, etc. (15, 16*a*, 16*b*; for reviews concerning oxidative couplings see ref. 16*c*). The vast majority of clay catalysts used in organic synthetic chemistry are based on the naturally occurring smectite clay, montmorillonite, also known as bentonite. Clay catalysts have been shown to contain both Brønsted and Lewis acid sites, with the Brønsted mainly associated

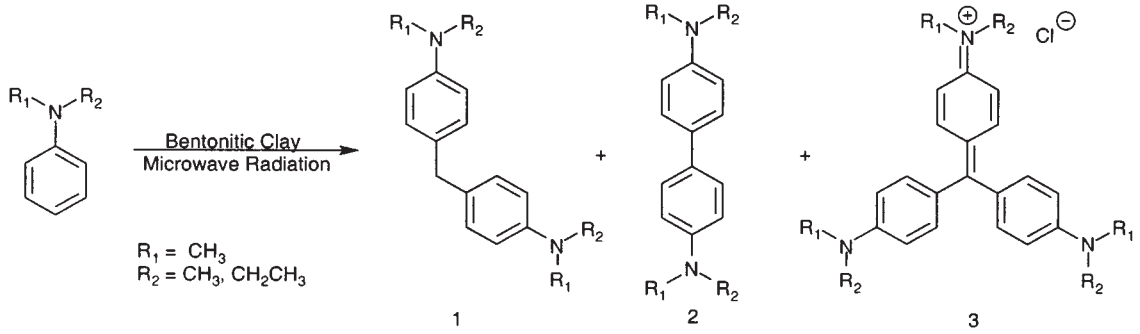
Received February 1, 2000. Published on the NRC Research Press website on September 26, 2000.

J.G. López-Cortés, M.C. Ortega-Alfaro, R.A. Toscano, and C. Alvarez-Toledano.[1] Instituto de Química, U.N.A.M., Cd. Universitaria, Circuito Exterior, Coyoacán, C.P.04510, México, D.F.
G. Penieres-Carrillo. Facultad de Estudios Superiores Cuautitlán, U.N.A.M., Av. 1 de Mayo s/n, Campo 1, Colonia Santa María Las Torres, Cuautitlán-Izcalli, Edo. de México, C.P. 54740.
R. Gutiérrez-Pérez. Centro de Investigación. Facultad de Ciencias Químicas. Universidad Autónoma de Puebla. Apdo. Postal 1067, C.P. 72001, Puebla, Pue., México.

[1]Author to whom correspondence may be addressed. Telephone: (525) 622 45 13. Fax: (525) 616 22 17.
e-mail: cecilio@servidor.unam.mx

 © 2000 NRC Canada

Scheme 1.



Compound	R_1	R_2	Reaction Time (min)	Yields[a] (%) 1	2	3
a	CH_3	CH_3	25	34	19	36
			60	Traces	21	70
b	CH_3	CH_2CH_3	40	37	Traces	50
			60	15	Traces	65

[a]Yields were determined by the weight of purified products according to the moles required for their formation.

with the interlamellar region and the Lewis sites mainly associated with edge sites (17)[2].

Results and discussion

Thus, we wish to report our results concerning the reaction of several *N*,*N*-disubstituted anilines with a bentonitic clay in solvent-free conditions, using microwave radiation as an energy source affording diphenylmethanes (**1**), biphenyls (**2**), and crystal violet and analogues (**3**) (Scheme 1). Reactions were carried out by mixing *N*,*N*-dialkylaniline with bentonitic clay in the aforementioned conditions and irradiating in a conventional microwave oven at the higher power. It must be pointed out that the reactions were also performed employing infrared irradiation, but lower yields and longer reaction times than those observed by using microwave radiation were registered. On the other hand, unresolvable mixtures reactions were obtained by using conventional heating (oil bath) along with other serious inconveniences, as decomposition of the starting materials due to the severe and drastic conditions involved in slowly reaching the gradient temperature needed for such chemical transformations, and that can be easily accomplished by means of rapid microwave heating. The use of solvents such as xylene, hexane, DMSO, and methanol, etc. combined with bentonite was also tested but there was no reaction at all in any case, evidencing the important role of the substrate's adsorption over the clay. Finally, allowing the reaction to proceed with montmorillonite K-10,[3] the yields and reaction time were almost identical to those observed with our protocol, but the difference in prices address the bentonite as the best choice.

The structure of the products was established by spectroscopic techniques (IR, ^1H and ^{13}C NMR, and mass spectrometry). Compounds **1a**, **2a**, **3a**, and **1b** were found to be identical with authentic samples obtained from commercial suppliers (Aldrich and Fluka). With regard to compound **2b**, a spot was observed in TLC which could correspond to such a compound, but since it is formed in traces we were not able to isolate it from the reaction mixture. The novel compound **3b** displayed in its mass spectrum a molecular ion at 414 *m*/*z*, which corresponds to the expected molecular weight for the cationic structure. However, in the ^1H NMR spectrum each signal appeared as sets of four lines, suggesting that compound **3b** actually occurs as a mixture of rotamers in dynamic equilibrium (18). It must be pointed out that some authors have discussed the existence of isomers in solution of such compounds (19).

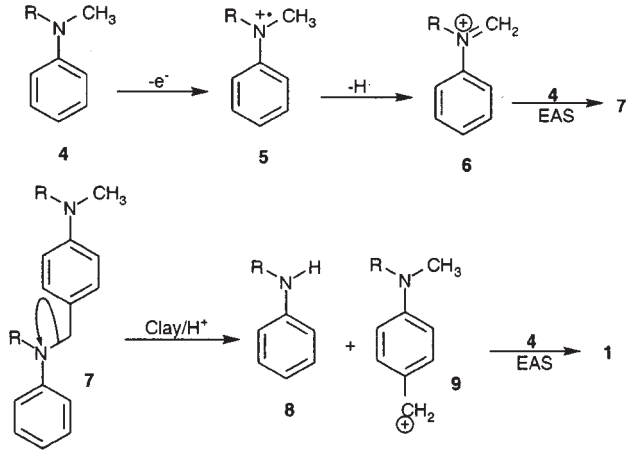
To observe the methyl group role, the *N*,*N*-diethylaniline was employed as substrate and there was no reaction at all, as stated by several authors (8*b*, 20, 21), indicating that the C atom between two or three aromatic rings stems from the methyl group of the aniline molecule and accordingly, if this

[2]Clay used is Tonsil Actisil FF (commercial name). Chemical composition: on examination by X-ray fluorescence, the clay employed in this study was found to have the following composition (in %): SiO_2 63.5, Al_2O_3 12.7, MgO 3.1, Fe_2O_3 4.9, CaO 1.5, K_2O 3.1, TiO_2 0.6, MnO 0.03, Na_2O 0.8, P_2O_5 0.1, H_2O (110°) 9.5. The commercial acid-activated material was obtained from Tonsil Mexicana and analyzed with a Phillips spectrometer using Cr primary radiation. The measured specific surface area was 161.074 $m^2\ g^{-1}$ (B.E.T. N_2), and the pore volume was 0.3235 $cm^3\ g^{-1}$. The acidity by NH_3 thermodesorption was 12.107 mmol mg^{-1}. The particle size was 325 mesh. Commercial price to date: $ 0.35 US/Kg.

[3]Available from Aldrich.

© 2000 NRC Canada

Scheme 2. Proposed formation of Michler's base derivative **1**.



methyl group is absent, the reaction does not proceed. A mechanism which would account for the formation of compounds **1** is proposed in Scheme 2.

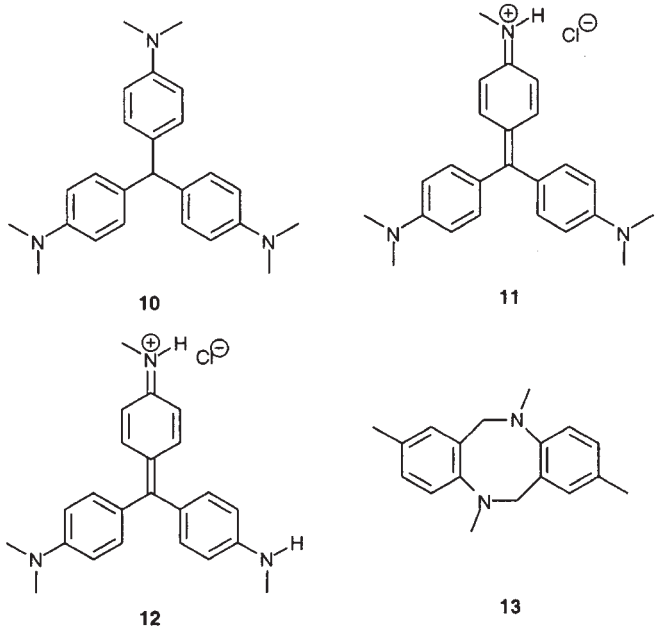
The reaction proceeds by an oxidation of *N*-methyl-*N*-alkylaniline (**4**) forming the radical cation **5**, which we consider as the key intermediate in the reaction. This intermediate has recently been proposed in the N-dealkylation of methylanilines (22, 23) and gives rise to the cation **6** reacting by an electrophilic aromatic substitution (EAS) to generate the compound **7**. Further reaction on the clay acidic sites produces both the monoalkylaniline **8** and the benzylic cation **9**, which subsequently reacts with another aniline molecule **4** to yield **1**.

When *N*,*N*-dimethylaniline is employed as starting material, after 4 min the formation of diphenylmethane (**1a**) is observed. This compound is the prevailing product even after 10 min, and then the formation of another product corresponding to crystal violet (**3a**) is detected by TLC, as well as the formation of the crystal violet leucobase (**10**) (Fig. 1). If the reaction is stopped at this moment, the three aforementioned products can be isolated but, allowing the reaction to proceed, after 25 min the diphenylmethane spot begins to vanish and the formation of at least five byproducts is observed by TLC. After 1 h, diphenylmethane had completely disappeared and only two TLC spots became neatly visible besides the crystal violet spot. HPLC allows a 70% yield of crystal violet to be isolated along with the two byproducts **11** and **12**, formed by the incorporation of methylaniline (**8**) in the reaction. It must be pointed out that with the other substrate the yields are quite similar.

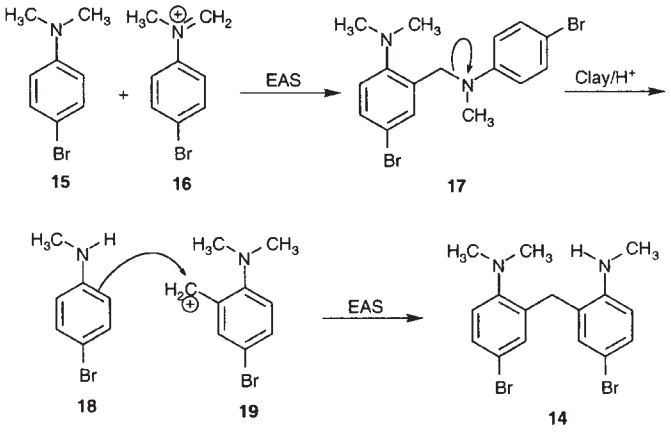
Furthermore, reaction with *p*-substituted anilines was also carried out to observe if the reaction proceeds when the key position is blocked. Thus, when *p*-methyl-*N*,*N*′-dimethylaniline was employed, compound **13** was obtained, whose structure was elucidated by spectroscopic methods and confirmed by single-crystal X-ray diffraction studies, finding the crystal data quite similar to those reported (24).

As can be seen, this compound presents the same structural sequence found in the intermediate **7** (consisting of an aromatic ring, a nitrogen atom, a methylene group, and an aromatic ring and so on). Isolation of this compound is significant given that it brings to light the existence of intermediate **7** and also by the fact that the carbon atom connecting

Fig. 1.



Scheme 3. Proposed formation of compound **14**.

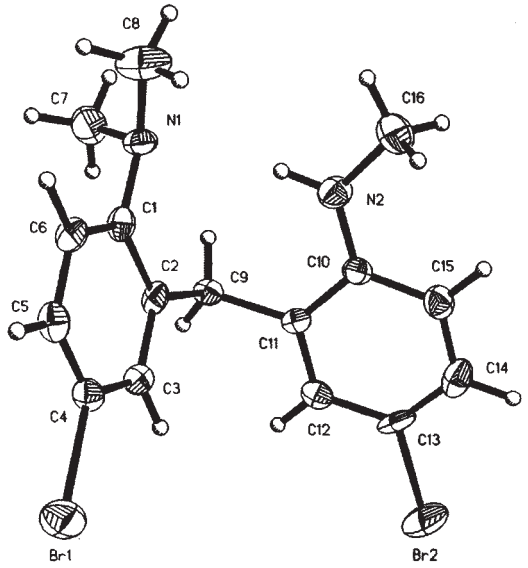


the aromatic rings in compounds **1** and **3** stems from the methyl group of aniline. It is worth notingthat this class of compounds have been obtained by other methods involving, inter alia, metallic salts (25), etc. and, in our case, there are just the bentonitic clay and microwave radiation, without any other reagents, and the role of such essential physical and chemical catalysts appear to be clearly established as fundamental. Also worth mentioning is that bentonite's oxidizing performance can be attributed to redox systems such as Fe^{2+}/Fe^{3+}, present in the clay, as reported by Chang and co-workers (26).

Other strong evidence supporting the proposed mechanism in the formation of **1** was the isolation of (2-*N*,*N*-dimethylamino-5-bromophenyl)-(2′-*N*-methylamino-5′-bromophenyl) methane (**14**) when the reaction was carried out with *N*,*N*-dimethylamino-4-bromobenzene (**15**), a molecule chosen because of the hindrance on the key position (Scheme 3).

© 2000 NRC Canada

Fig. 2. ORTEP-type drawing of compoooound **14**. Thermal ellipsoids at 30% probability level.



Formation of **14** can be explained from intermediate **16**, an analogue of cation **6**, which reacts with another molecule of *N*,*N*-dimethylamino-4-bromobenzene (**15**) giving rise to **17**, which undergoes an heterolytic rupture on the C—N bond between the rings affording the secondary amine **18** and the benzylic cation **19**. Further EAS of this species on the *ortho* position of **18** leads finally to **14**.

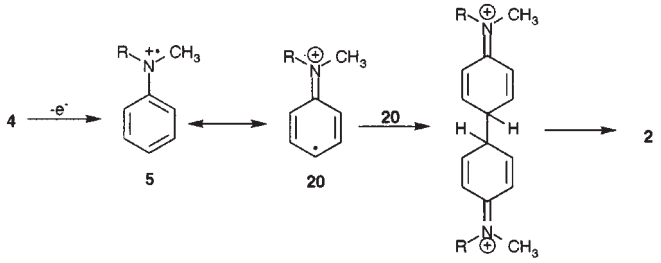
On the other hand, **14** can also be considered as an *ortho* analogue of **1**, with one of the aniline moieties possessing two methyl groups and the other aniline molecule only one. The aniline moiety containing one methyl group must certainly be issued from the rupture of intermediate **17**, demonstrating that the methyl group of the aniline is lost giving rise to **18** and **19**.

Compound **14** was characterized by spectroscopic methods and its structure confirmed by an X-ray crystal analysis. Figure 2 shows compound **14** as possessing a *syn*-parallel orientation of the mono- and di-*N*-methylated *p*-bromoanilines, joined to the methylene group. This orientation seems to be locked by an intramolecular H—bond between the secondary and tertiary amine groups (H2···N1 2.23(11) Å, N2···N1 3.118(14) Å, N2-H2···N1 168(10)°). The angle between the phenyl rings (100.8°) deviates significantly from the tetrahedral value observed for the methylene C-atom (C2-C9-C11 111.9°). The sum of bond angles around the N-atoms clearly shows a different hybridization for N1 (sp^3, sum = 339.8°) and N2 (sp^2, sum = 359.6°) with an important interaction with the aromatic system for the latter, as judging by the shortening in the N—C_{phenyl} bond length (N1—C1 1.423(13) Å, N2—C10 1.369(14) Å).

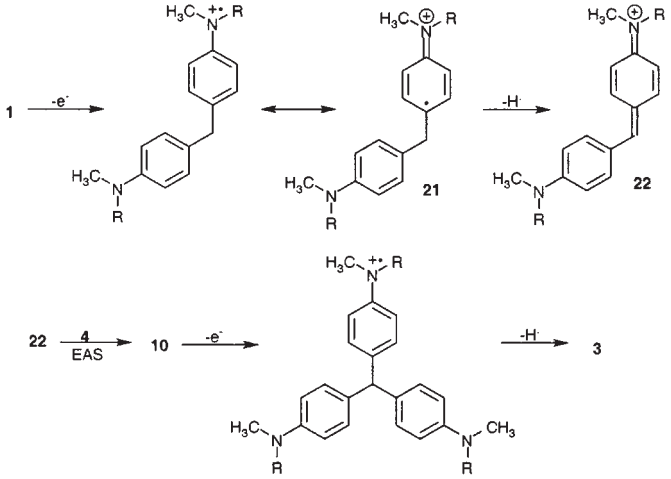
With regard to compounds **2***a* and **2***b*, their formation can be explained by a coupling of radical ions such as **20** (Scheme 4), generated from radical cation **5,** involved as a key intermediate in our proposed mechanisms.

Concerning the crystal violet derivatives (Scheme 5), the formation of radical ion **21** from the Michler's base **1** leads to **22**, which reacts with a molecule of the starting material **4** via an EAS to give the leuco-base intermediate **10**.

Scheme 4. Proposed formation for compound **2**.



Scheme 5. Proposed formation of crystal violet derivatives **3**.



Further loss of an electron and a hydrogen atom affords, finally, the **3** derivatives. Intermediate **10** has been detected by TLC by comparison with a sample of commercial leucocrystal violet, i.e., when R is a methyl group. An interesting point is that crystal violet leuco-base **10** in the aforementioned conditions oxidizes to crystal violet almost quantitatively in 3 min.

In summary, crystal violet derivatives, diphenylmethanes, and biphenyls were isolated along with some important intermediates supporting a clay-mediated oxidative coupling of *N*,*N*-disubstituted anilines using microwave radiation as an energy source in solvent-free conditions.

Experimental section

Melting points, which are uncorrected, were determined using a MEL-TEMP II apparatus. Infrared spectra were obtained on a Perkin–Elmer 283-B instrument as KBr discs or liquid films. NMR spectra were recorded in $CDCl_3$ or CD_3CN solution on a JEOL GX300 or Varian ST spectrometer (500 MHz). Chemical shifts are reported in ppm while the coupling constant (*J* values) are in Hz. Mass spectra were measured on a JEOL JMS-AX505, using the technique of electronic impact. High-resolution mass spectrometry and FAB spectra were obtained at an accelerating voltage of 10 KV, samples were desorbed from a nitrobenzyl alcohol matrix using 6 KeV xenon atoms. Mass measurements in FAB were performed at 10 000 resolution using electric field scans and the polyethylene glycol ions as the reference material.

© 2000 NRC Canada

Reactions were carried out by mixing 1 g of *N*,*N*-dialkylaniline with 5 g of bentonitic clay in dry medium and irradiating with a conventional microwave oven (2450 MHz, Goldstar model NOMA-1465M, single phase) at the higher power. After extraction of the products in a Soxhlet apparatus for 30 min using ethyl acetate:hexane (20:80) and methanol as eluents, reaction products were separated by silica gel chromatography using as eluent either ethyl acetate–hexane or isopropanol–formic acid in different ratios.

HPLC (27) was carried out in a Waters Delta Prep 4000 apparatus, with a Waters 486 tunable absorbance detector. The detector was set at 560 nm of wavelength. Chromatographic separation was on a 19 × 300 mm Waters μBondapack C_{18} preparative column. Mobile phase was 80:20 acetonitrile–buffer, with a concentration of 0.1 M of ammonium acetate and pH was then adjusted to 3.6 with glacial acetic acid. Flow rate was 10 mL/min.

Compound 1a

Yellow plates, (228 mg, 34% at 25 min), mp 85°C (from hexane). MS–EI (*m*/*z*): 254 (M^+). IR ν_{max} (cm^{-1}) (KBr): 3074, 2889, 2811, 1615, 1520, 1440. ^{1}H NMR (300 MHz, $CDCl_3$) δ_H (ppm): 6.9, 6.6 (AB system, 8H, Ph), 3.8 (s, 2H, C*H*$_2$Ph), 2.8 (s, 12H, Me). ^{13}C NMR (75 MHz, $CDCl_3$) δ_C (ppm): 40 (MeN), 55 (*C*H$_2$Ph), 113 (*C*H$_{ar}$), 130 (*C*H$_{ar}$,), 135 (*C*CH$_2$Ph), 150 (C_{ar}NMe$_2$).

Compound 2a

White solid, (200 mg, 21% at 60 min), mp 192°C. MS–EI (*m*/*z*): 240 (M^+). IR ν_{max} (cm^{-1}) (KBr): 3005, 2926, 1611, 1517. ^{1}H NMR (300 MHz, $CDCl_3$) δ_H (ppm): 7.0, 6.7 (AB system, 8H, Ph), 2.9 (s, 12H, Me). ^{13}C NMR (75 MHz, $CDCl_3$) δ_C (ppm): 43(MeN), 113 (*C*H$_{ar}$), 128 (*C*H$_{ar}$), 126 (*C*Ph), 144 (C_{ar}NMe$_2$).

Compound 3a

Green solid, (563 mg, 70% at 60 min), mp 213°C. MS–EI (*m*/*z*): 372 (M^+). IR ν_{max} (cm^{-1}) (film): 3384, 2920, 2582, 1357, 1171. ^{1}H NMR (300 MHz, CD_3CN) δ_H (ppm): 7.3, 6.9 (AB system, 8H, Ph), 3.3 (s, 18H, Me). ^{13}C NMR (75 MHz, CD_3CN) δ_C (ppm): 40 (MeN), 112 (*C*H$_{ar}$), 126 (C_{ar}CPh), 139 (*C*H$_{ar}$), 155 (C_{ar}NMe$_2$) 176 (*C*Ph$_3$).

Compound 1b

Yellow solid, (243 mg, 37% at 40 min), mp 80°C. MS–EI (*m*/*z*): 282 (M^+). IR ν_{max} (cm^{-1}) (KBr): 2969, 2957, 1614, 1517. ^{1}H NMR (300 MHz, $CDCl_3$) δ_H (ppm): 7.1, 6.7 (AB system, 8H, Ar), 3.88 (s, 2H, C*H*$_2$Ph), 3.43 (q, 4H, NC*H*$_2$CH$_3$), 2.97 (s, 6H, NC*H*$_3$), 1.17 (t, 6H, NCH$_2$C*H*$_3$). ^{13}C NMR (75 MHz, $CDCl_3$) δ_C (ppm): 11 (NCH$_2$*C*H$_3$), 38 (Me), 40 (N*C*H$_2$CH$_3$), 47 (*C*H$_2$Ph), 113 (*C*H$_{ar}$), 128 (C_{ar}CH$_2$Ph), 130 (*C*H$_{ar}$), 148 (C_{ar}N(Me)(Et).

Compound 3b

Purple solid, (512 mg, 65% at 60 min), mp 278°C. MS–EI (*m*/*z*): 414 (M^+). IR ν_{max} (cm^{-1}) (film): 2924, 1581, 1368, 1186. ^{1}H NMR (500 MHz, CD_3CN) δ_H (ppm): 6.917, 7.312 (AB system, 12H, Ph), 6.741, 7.643 (AB system, 12H, Ph), 6.643, 6.917 (AB system, 12H, Ph), 6.66, 6.717 (AB system, 12H, Ph), 3.62 (q, 6H, NC*H*$_2$CH$_3$), 3.492 (q, 6H, NC*H*$_2$CH$_3$), 3.354 (q, 6H, NC*H*$_2$CH$_3$), 3.263 (q, 6H, NC*H*$_2$CH$_3$), 3.166 (s, 9H, NMe), 2.996 (s, 9H, NMe), 2.837 (s, 9H, NMe), 2.761 (s, 9H, NMe), 1.234 (t, 9H, NCH$_2$C*H*$_3$), 1.141 (t, 9H, NCH$_2$C*H*$_3$), 1.048 (t, 9H, NCH$_2$C*H*$_3$), 1.023 (t, 9H, NCH$_2$C*H*$_3$). ^{13}C NMR (125 MHz, CD_3CN) δ_C (ppm): 11.141 (NCH$_2$*C*H$_3$), 11.339 (NCH$_2$*C*H$_3$), 12.155 (NCH$_2$*C*H$_3$), 37.827 (NMe), 38.556 (NMe), 47.152 (N*C*H$_2$CH$_3$), 47.443 (N*C*H$_2$CH$_3$), 47.997 (N*C*H$_2$CH$_3$), 111.493 (*C*H$_{ar}$), 113.212 (*C*H$_{ar}$), 113.314 (*C*H$_{ar}$), 116.360 (*C*H$_{ar}$), 116.753(*C*H$_{ar}$), 127.331 (C_{ar}CPh), 130.667(*C*H$_{ar}$), 132.911(*C*H$_{ar}$), 140.721(*C*H$_{ar}$), 152.756 (*C*Ph$_3$), 155.903 (C_{ar}NMe). HR-MS $C_{28}H_{36}N_3$ (M^+) calcd.: 414.2909; found: 414.2900.

Compound 13

Colorless prism, (525 mg, 57%), mp 136°C. MS–EI (*m*/*z*): 266 (M^+). IR ν_{max} (cm^{-1}) (film): 2877, 1510, 1480. ^{1}H NMR (300 MHz, $CDCl_3$) δ_H (ppm): 7.0, 6.7 (m, 6H, Ph), 4.1 (s, 4H, C*H*$_2$), 2.8 (s, 6H, NMe), 2.3 (s, 6H, Me). ^{13}C NMR (75 MHz, $CDCl_3$) δ_C (ppm): 20 (*Me*Ph), 39 (*Me*N), 58 (PhCH$_2$N), 115 (*C*H$_{Ar}$), 127 (C_{Ar}), 128 (C_{Ar}), 129 (*C*H$_{Ar}$), 132 (*C*H$_{Ar}$), 145 (C_{Ar}N).

Compound 14

Yellow crystals, (605 mg, 63%). MS–EI (*m*/*z*): 398 (M^+). IR ν_{max} (cm^{-1}) (KBr): 3425, 2924, 1597, 1502, 1317, 812. ^{1}H NMR (300 MHz, $CDCl_3$) δ_H (ppm): 7.35 (dt, 1H, Ph), 7.21, (dt, 1H, Ph), 6.99 (d, 1H, Ph), 6.77 (dt, 1H, Ph), 6.52 (dt, 1H, Ph), 6.34 (d, 1H, Ph), 4.17 (s, 1H, N*H*), 3.73 (s, 2H, C*H*$_2$Ph), 2.80 (s, 3H, MeN), 2.75 (s, 6H, MeN). ^{13}C NMR (300 MHz, $CDCl_3$) δ_C (ppm): 37 (MeN), 30 (*C*H$_2$Ph), 45 (MeN), 110 (C_{ar}Br), 111 (C_{ar}Br), 116, (*C*H$_{ar}$), 117 (*C*H$_{ar}$) 130 (C_{ar}CH$_2$), 131 (C_{ar}CH$_2$), 132.0 (*C*H$_{ar}$), 132.1 (*C*H$_{ar}$), 132.8 (*C*H$_{ar}$), 133 (*C*H$_{ar}$), 146 (C_{ar}N), 147 (C_{ar}N).

X-ray crystallographic data for 14

14: $C_{16}H_{18}N_2Br_2$, MW = 398.14; light-yellow prism (0.44 × 0.28 × 0.28 mm); monoclinic, *P*2/*n*, *a* = 11.095 (2) Å, *b* = 9.008 (1) Å, *c* = 17.058 (2) Å, β = 105.93 (1), *V*= 1639.4 (4) Å^3; *Z*= 4, *D*c = 1.613 g cm^{-3}. Data were collected on a SIEMENS P4 diffractometer at room temperature, with graphite-monochromated Mo-Kα radiation (λ = 0.71073 Å). The cell parameters were obtained from 39 reflections in the range 9.62 < 2θ < 20.48. The data collection (2θ max= 50.0°, scans θ/2θ, range 0 < h < 13, 0 < k < 10, –20 < l < 19) give 2884 unique reflections (R_{int} = 5.25%) with 682 (F > 4.0 s(F)) observed reflections. All these reflections were used for structure refinement after the intensity data was corrected for background and Lorentz-polarization effects. Absorption correction based on ψ-scans (min/max transmission 0.346/0.254) and the crystal decay negligible. The structure was solved by Direct Methods and refined by full-matrix least-squares using the SHELXL-97 (28) program, which gave final discrepancy indices R = 7.45%, wR_2 = 12.54% for "observed" ($I > 2\sigma(I)$) data. Non-hydrogen atoms refinement anisotropically; the hydrogen atoms included in idealized positions with a fixed temperature factor U = 1.2 times the U_{eq} or the parent C-atom. Final difference Fourier map was 0.452 and –0.454 e Å^{-3}. Atomic coordinates, bond lengths and angles, and thermal parameters have been deposited at the Cambridge Crystallographic Data Centre (CCDC 146746). Copies of the data can be obtained, free of charge,

© 2000 NRC Canada

on application to the Director, CCDC, 12 Union Road, Cambridge CB2 1EZ, U.K. (Fax: 44-1223-336033 or e-mail: deposit@ccdc.cam.ac.uk).

Acknowledgment

Thanks are due to CONACyT 27500E for financial support and Carmen Márquez, Rocío Patiño, Isabel Chávez, as well as, Luis Velasco, for their technical assistance.

References

1. (*a*) K. Venkataraman. The chemistry of synthetic dyes. Vol. IV. Academic Press, New York. 1971. pp. 103–160; (*b*) H. Zollinger. Color chemistry. Synthesis, properties and applications of organic dyes and pigments. VCH, New York. 1987. pp. 59–65.
2. (*a*) Sanyo Chem. Industries Ltd. Jpn. Pat. Doc. JP 59 208 546 (1984); Chem. Abst. 102, P212 749 1985; (*b*) Nippon Mining Co., Ltd. Jpn. Pat. Doc. JP 59 230 094 (1984); Chem. Abst. Jpn. 103, P73 675 1985; (*c*) W. Kleeberg, H. Hacker, and K.R. Hauschildt. Dtsch. Pat. Doc. 3 327 712 (1985); Chem. Abst. 102, P 221 664 1985; (*d*) W. Kleeberg, H. Hacker, and K.R. Hauschildt. Dtsch. Pat. Doc. 3 327 711 (1985); Chem. Abst. 102, P221 663 1985; (*e*) H. Otani. Jpn. Pat. JP 06 216 420 (1994); Chem. Abst. Jpn. 122, P253 985f 1995; (*f*) D. Daly. U.S. Pat US 5 376 154 (1994); Chem. Abst. 122, P269 865c 1995.
3. M. Yamasaki. Jpn Pat. JP 06 333 595 (1994); Chem. Abst. 122, P244 109w 1995.
4. A. Galadi. Chemosphere, **30**, 1655 (1995); Chem. Abst. 122, 308 731c 1995.
5. (*a*) N. Batina, M. Kunitake, and K. Itaya. J. Electroanal. Chem. **405**, 245 (1996); (*b*) D. Fischer, W.R. Caseri, and G. Hahner. J. Colloid Interface Sci. **198**, 337 (1998); (*c*) W. Haiss, R.J. Nichols, and J.K. Sass. Surf. Sci. **388**, 141 (1997).
6. A.E. Ehrenhofer-Murray, M.K. Seitz, and C. Sengstag. Yeast, **14**, 49 (1998).
7. (*a*) L. Horner, H. Brüggemann, and K. Knapp. Ann. **626**, 1 (1959); (*b*) L. Horner and E. Schwenk. Angew. Chem. **61**, 411 (1949); (*c*) J. Cadogan, D. Hey, and W. Sanderson. J. Chem. Soc. 3203 (1960); (*d*) G. Sosnovsky and N. Yang. J. Org. Chem. **25**, 899 (1960); (*e*) D. Krüger and F. Oberlies. Chem. Ber. **77**, 663 (1941).
8. (*a*) H. Sato. Bull. Chem. Soc. Jpn. **38**, 1719 (1965); (*b*) S. Murata, M. Miura, and M. Nomura. J. Chem. Soc. Chem. Commun. 116 (1989); (*c*) J. Barluenga, P.J. Campos, M.A. Roy, and G. Asencio. J. Chem. Soc. Chem. Commun. 339 (1979); (*d*) J. Barluenga, P.J. Campos, M.A. Roy, and G. Asencio. J. Chem. Soc. Perkin Trans. **1**, 1420 (1980); (*e*) R.C. Cambie, P.S. Rutledge, T. Smith-Palmer, and P.D. Woodgate. J. Chem. Soc. Perkin Trans. **1**, 1161 (1976); (*f*) C.C. Yin and A.J. Deeming. J. Organomet. Chem. **144**, 351 (1978).
9. (*a*) N. Cohn. Chem. Ztg. **24**, 564 (1900); (*b*) J.T. Scanlan. J. Am. Chem. Soc. **57**, 887 (1935); (*c*) E.C. Wagner. J. Am. Chem. Soc. **56**, 1944 (1934); (*d*) E.C. Wagner. J. Org. Chem. **19**, 1862 (1954).
10. S.R. Wann, P.T. Thorsen, and M.M. Kreevoy. J. Org. Chem. **46**, 2579 (1981).
11. (*a*) A. Katritzky, X. Lan, and J. Lam. Synthesis, 341 (1990); (*b*) A. Katritzky, B. Galuszka, S. Stanislaw, and M. Black. J. Heterocycl. Chem. **31**, 917 (1994).
12. T.D. Greenwood, R.A. Kahley, and J.F. Wolfe. J. Polym. Sci. Part A, **18**, 1047 (1980).
13. (*a*) G. Penieres, V. Soto, C. Alvarez, O. García, and J.G. García. Heterocyclic Commun. **4**, 31 (1998); (*b*) G. Penieres, J.M. Aceves, A. Flores, G. Mendoza, O. García, and C. Alvarez. Heterocyclic Commun. **3**, 507 (1997); (*c*) M. Jiménez, A. Navarro, J.L. Eusebio, C. Alvarez, O. García, G. Penieres, and R. Gutiérrez. Steroids, **62**, 500 (1997); (*d*) G. Penieres, C. Alvarez, K. Franco, O. García, and O. Espinoza. Heterocyclic Commun. **2**, 359 (1996).
14. (*a*) S. Deshayes, M. Liagre, A. Loupy, J. Luche, and A. Petit. Tetrahedron, **55**, 10851 (1999); (*b*) S.L. Cresswell and S.J. Haswell. Chem. Ind. (London), 621 (1999); (*c*) A. Loupy, A. Petit, J. Hamelin, F. Texier-Boullet, P. Jaquault, and D. Mathe. Synthesis, 1213 (1998); (*d*) S. Caddick. Tetrahedron, **51**, 10403 (1995).
15. D. Villemin and F. Sauvaget. Synlett. 435 (1994).
16. (*a*) M. Smrcina, J. Poláková, S. Vyskocil, and P. Kocovsky. J. Org. Chem. **58**, 4534 (1993); (*b*) M. Smrcina, M. Lorenc, V. Hanus, P. Sedmera, and P. Kokovsky. J. Org. Chem. **57**, 1917 (1992); (*c*) B.M. Trost. Comprenhensive organic synthesis. Vol. 3. Pergamon Press, New York. 1991. pp. 659–703.
17. K. Smith. Solid supports and catalysts in organic synthesis. Prentice Hall, West Sussex. 1992. pp. 3–39.
18. O. Michinori. Applications of dynamic NMR spectroscopy to organic chemistry. VCH, Deerfield Beach. 1985. pp 17–18, 352–354.
19. (*a*) Y. Murayama, M. Ishikawa, and H. Satozono. J. Am. Chem. Soc. **118**, 6257 (1996); (*b*) H. Lueck, J. McHale, and W. Edwards. J. Am. Chem. Soc. **114**, 2342 (1992); (*c*) G. Lewis, T. Magel, and D. Lipkin. J. Am. Chem. Soc. **64**, 1774 (1942).
20. J.R. Lindsay, R.O.C. Norman, and W.M. Walker. J. Chem. Soc. 269 (1968).
21. M. Grodowski and T. Latowski. Tetrahedron, **30**, 767 (1974).
22. R.N. Loeppky, S.P. Sing, S. Elomari, R. Hastings, and T. Theiss. J. Am. Chem. Soc. **120**, 5193 (1998).
23. E. Baciochi, O. Lanzalunga, A. Lapi, and L. Manduchi. J. Am. Chem. Soc. **120**, 5783 (1998).
24. S.M. Prasad, S.P. Narayan, D.K. Mandal, and S.C. Gupta. Acta Crystallogr. Sect. C: Cryst. Struct. Commun. **C49**, 531 (1993).
25. (*a*) Y. Cheng, O. Meth-Cohn, and D. Taylor. J. Chem. Soc. Perkin Trans. **1**, 1257 (1998); (*b*) T. Sakakibara and H. Matsuyama. Chem. Lett. 131 (1980).
26. Y. Teng, I. Chang, and C.M. Wang. J. Phys. Chem. B, **101**, 10386 (1997).
27. (*a*) S. Turnipseed, J. Roybal, H. Rupp, J. Hurlbut, and A. Long. J. Chromatogr. B. **670**, 55 (1995); (*b*) L. Rushing and E. Hansen. J. Chromatogr. B. **700**, 223 (1995).
28. G.M. Sheldrick. SHELXL-97 Program for refinement of crystal structures. University of Göettingen, Germany. 1997.

© 2000 NRC Canada

Molecular and electronic structure of $An^{IV}Fe^{II}(CN)_6 \cdot xH_2O$ (An = Th, U, Np) compounds: an X-ray absorption spectroscopy investigation

Isabelle Bonhoure, Christophe Den Auwer, Christophe Cartier dit Moulin, Philippe Moisy, Jean-Claude Berthet, and Charles Madic

Abstract: $An^{IV}Fe^{II}(CN)_6 \cdot xH_2O$ (An = Th, U, Np) molecular compounds have been prepared by precipitation from acidic media. These microcrystalline compounds have been characterized by infrared spectroscopy, X-ray diffraction, and X-ray absorption spectroscopy. They have been found to be isostructural with the $Ln^{III}KFe^{II}(CN)_6 \cdot 4H_2O$ compounds. The molecular structures of these compounds are presented and their chemical formulas are given: in all compounds, the $Fe(CN)_6$ octahedra is conserved and the An ion is linked to the N atoms of the CN ligands. The formal oxidation states are also discussed.

Key words: hexacyanoferrate, actinide, EXAFS, XANES, X-ray absorption spectroscopy.

Résumé : Les composés moléculaires $An^{IV}Fe^{II}(CN)_6 \cdot xH_2O$ (An = Th, U, Np) ont été synthétisés par précipitation en milieu acide. Ces composés microcristallins ont été caractérisés par spectroscopie infrarouge, diffraction des rayons X et par spectroscopie d'absorption des rayons X. Nous montrons que ces composés sont isostructuraux avec les composés $Ln^{III}KFe^{II}(CN)_6 \cdot 4H_2O$ correspondants. Leurs structures moléculaires et électroniques sont présentées et les formules chimiques sont proposées: dans tous les composés l'octaèdre $Fe(CN)_6$ est conservé et l'ion actinide est lié à l'azote du ligand cyano. Les degrés d'oxydation sont également discutés.

Mots clés : hexacyanoferrate, actinide, EXAFS, XANES, spectroscopie d'absorption des rayons X.

Introduction

It is well-known that new three-dimensional molecular structures can be obtained by using well-characterized building blocks (1, 2). Such methods have been widely used to obtain preorganized three-dimensional entities (3–8). Among the possible building blocks, the hexacyanometallate ions $[M(CN)_6]^{n-}$ are often used to form polymeric inorganic networks such as Prussian Blue ($Fe_4[Fe(CN)_6]_3 \cdot 15H_2O$). The structure of this compound is a cubic lattice in which alternating Fe^{II} and Fe^{III} ions are linked by cyanide bridges (9–11). A great number of isomorphic compounds called "Prussian Blue analogs" have also been intensively studied (12–17) and a wide number of structures containing $Fe(CN)_6$ units are known.

Among others, numerous studies report on mixed hexacyanoferrate ($M_x[Fe(CN)_6]_y \cdot zH_2O$ where M = transition metal or lanthanide). In particular, mixed transition metal hexacyanoferrates are studied for their magnetic properties. For instance, Sato et al. (18) recently reported the synthesis of a cobalt–iron cyanide compound that exhibits photoinduced long-range magnetic ordering. The interactions between the two metal atoms via the CN ligands have been also theoretically studied so as to predict the magnetic behavior of this kind of complexes (19). Mixed transition metal hexacyanoferrates are also known for their alkali metal cation storage capabilities (20) and it has been demonstrated that Cs could efficiently be sorbed on $Cu^{II}{}_2Fe^{II}(CN)_6 \cdot xH_2O$ complexes (21). In most cases, transition metal hexacyanoferrates exhibit a cubic structure (9–11, 22) but they can also present trigonal or rhomboedral structures (22, 23).

Lanthanide hexacyanoferrates are known for their possible semipermeable membrane (24) and ion-exchange properties (25). These properties are considered to be related to the nature of the zeolitic water molecules. As a consequence, great attention has been paid to the structure determination of these compounds so as to investigate the zeolitic water molecule environment. $Ln^{III}Fe^{III}(CN)_6 \cdot 5H_2O$ and $Ln^{III}KFe^{II}(CN)_6 \cdot 4H_2O$ (Ln = La, Ce, Pr, Nd) crystallize in the $P6_3/m$ group for the early lanthanide ions (26–30).

Received March 14, 2000. Published on the NRC Research Press website on September 26, 2000.

I. Bonhoure,[1,2] C. Den Auwer,[2] and P. Moisy. CEA Marcoule, DCC/DRRV/SEMP, 30207 Bagnols s/ Ceze, France.
C. Cartier dit Moulin.[2] Laboratoire de Chimie Inorganique et Matériaux Moléculaires, ESA CNRS 7071, Université Pierre et Marie Curie, 4, Place Jussieu, 75252 Paris CEDEX 05, France.
J.-C. Berthet. CEA Saclay, DSM/DRECAM/SCM, 91190 Gif s/ Yvette, France.
C. Madic. CEA Saclay, DCC, 91190 Gif s/ Yvette, France.

[1]Author to whom correspondence may be addressed. Telephone: 33-1-64-46-80-99. Fax: 33-1-64-46-41-48.
e-mail: bonhoure@lure.u-psud.fr
[2]LURE, Centre Universitaire Paris-Sud, Bat 209 D, BP 34, 91898 Orsay CEDEX, France.

© 2000 NRC Canada

Hexacyanoferrate $Fe(CN)_6$ entities complexed with actinide ions (An = Pu) were first mentioned during the 1950s (31). Some various $M_x(UO_2)_y[Fe(CN)_6]_z{\cdot}wH_2O$ compounds have also been synthesized and used as sorbants (32, 33) but none of these $[An/Fe(CN)_6]$ complexes has been structurally characterized. Only the X-ray powder diffraction of the complex $Th^{IV}Fe^{II}(CN)_6{\cdot}5H_2O$ has been reported (34) showing that it crystallizes in the hexagonal $P6_3/m$ space group as $Ln^{III}KFe^{II}(CN)_6{\cdot}4H_2O$ (Ln = La...Nd) complexes do. However neither the nature of the Ln—NC bond nor the one of An—NC bond have been extensively investigated.

The structural study of these $[An/Fe(CN)_6]$ complexes is of great interest; all the more they have possible applications in nuclear fuel reprocessing. Indeed, in our group, fundamental studies in actinide inorganic chemistry are linked to further applications in the frame of nuclear fuel cycle. For instance, the selective complexation of the actinide vs. the lanthanide ions is one of the main challenges, the final purpose being the separation of the so-called minor actinides, americium (Am) and curium (Cm), from the abundant lanthanides fission products both present in the acidic highly radioactive effluents issuing the reprocessing of nuclear spent fuels. Recently, Kulyako et al. (35–37) used the $[Fe(CN)_6]^{3-}$ molecular entity to complex trivalent actinide ions (An = Am, Cm). They observed the different behavior of the Ln^{III} ions which do not form precipitates in the conditions used to perform the An^{III} precipitation. The potential different affinity of $[Fe(CN)_6]^{3-}$ for these two *f* elements series is at the starting point of this work.

The aim of this paper is to describe the molecular and electronic structure of the edifices formed by the $[Fe(CN)_6]^{n-}$ building blocks and the actinide ions (An = Th, U, Np) and to compare these new materials to the analogs obtained with lanthanide. We decided here to synthesize the $An^{IV}Fe^{II}(CN)_6{\cdot}xH_2O$ entities with An = Th^{IV}, U^{IV}, Np^{IV} so as to investigate the early actinide complexes of these series. For comparison, Np^{III} and Fe^{III} have also been used as starting materials to determine if the not so stable Np^{III} is maintained or oxidized into Np^{IV} in these compounds. The $La^{III}KFe^{II}(CN)_6{\cdot}4H_2O$ structurally well characterized compound has also been synthesized and investigated by the same spectroscopic techniques for further comparisons.

As microcrystalline materials were obtained, X-ray powder diffraction (XPD), infrared (IR), and X-ray absorption (XAS) spectroscopies were of particular help to probe the An and Fe environments. We investigated the long-range order by XRPD. The IR vibration bands of the cyano groups probe the chemical bonds of the carbon and nitrogen atoms in these new materials. XAS provides both information about the electronic structure via X-ray absorption near edge spectroscopy (XANES) and about the local structure around the metals via extended X-ray absorption fine structures spectroscopy (EXAFS).

Experimental section

Synthesis

The reference and starting compounds, $K_4Fe^{II}(CN)_6{\cdot}3H_2O$, $K_3Fe^{III}(CN)_6$, $UO_2(NO_3)_2{\cdot}6H_2O$ were commercially purchased (Aldrich) and used as received. $UO_{2.0}$ and NpO_2 (obtained from CEA inventory) were kindly supplied by the University of Rennes I (Pr. H. Noel, Matériaux intermétalliques d'éléments de transition *d* et (ou) *f*) and by the LCAA laboratory (DCC/DRRV/SEMP) of CEA Marcoule. $Np^{IV}(C_2O_4)_2{\cdot}6H_2O$ and UCl_4 were synthesized as described in the literature (38, 39).

Synthesis of the $[An/Fe(CN)_6]$ compounds were performed by precipitation upon the addition of hexacyanoferrate ions and actinide ions solutions. The actinide aqueous acid media allows the stabilization of the chosen actinide oxidation state. All Np solutions were handled in radiological glove boxes.

Hexacyanoferrate stock solutions were obtained by dissolving the corresponding solids in acidic or neutral distilled water (solution acidity specified below). Actinide stock solutions were obtained in the following way: the Th^{IV} initial solution ([Th] = 0.71 mmol g^{-1} in 4 M HCl obtained by attack of metallic Th by HCl) was diluted to obtain the final solution ([Th] = 0.079 mmol g^{-1} in 0.44 M HCl); U^{IV} solution was obtained by dissolving 1 g of UCl_4 in 30 mL 0.5 M HCl ([U] = 0.09 M) in a glove box filled with Ar; Np^{IV} solution was obtained by dissolving 73 mg of NpO_2 (obtained from CEA inventory) in $HClO_4$/HF (2.4 mL 9.37 M $HClO_4$ and 0.5 mL 2.3 M HF) under reflux. After evaporation of HF and dilution in 0.1 M $HClO_4$, the final solution was obtained: [Np] = 0.027 M in 10 mL 2.34 M $HClO_4$. Np^{III} solution was obtained by galvanostatic reduction of the former Np^{IV} solution under argon with a current fixed to –1 mA with platinum electrodes for working and separated auxiliary electrodes and a calomel electrode as reference. The exclusive presence of Np^{IV} or Np^{III} ions in the stock solutions was checked by UV–vis spectrometry (UV–vis–NIR SCHIMADZU 3101 PC spectrometer, characteristic absorption bands (nm): Np^{III}: 550, 601, 658, 783; Np^{IV}: 724, 939, 964; Np^{V}: 981)).

The $[An/Fe(CN)_6]$ precipitates were obtained at room temperature by the slow simultaneous addition of the two reagents (An solution and $Fe(CN)_6$ solution) in a vortex. After mixing (about 20 min), the solution was stirred for 30 min. After 12 h, a fine precipitate was separated from the solution by centrifugation, washed with ethanol and acetone, and dried at room temperature overnight. The synthesis of $Th^{IV}Fe^{II}(CN)_6{\cdot}5H_2O$ was carried out as described in the literature (34).

In the following, the compounds will be formally written as $An^I/Fe^J(CN)_6$, meaning that An ions at the +I oxidation state and Fe ions at the iron +J oxidation state were used as starting materials.

Compound 1: $Th^{IV}/Fe^{II}(CN)_6$

5.493 g of a colorless Th^{IV} solution was heated to 45°C and 5 mL of a pale yellow $K_4Fe^{II}(CN)_6$ neutral solution ([Fe] = 0.09 M) was slowly added. An abundant precipitate was immediately obtained. After washing (H_2O, EtOH) a blue solid was recovered. The X-ray diffraction pattern registered on this powder corresponds to the $P6_3/m$ space group and the found lattice parameters are close to those published by Xu and Hullinger (34) (present work: a = 7.38 ± 0.01 Å, c = 13.95 ± 0.02 Å; Xu. and Hullinger: a = 7.408 Å, c = 13.943 Å).

As elemental analysis was not available for thorium compounds, we evaluated the stoichiometry of the iron and

© 2000 NRC Canada

thorium elements in the material by measurement of the X-ray absorption atomic coefficients on both the Fe K edge and the Th L_3 edge. The McMaster atomic absorption parameters (40) have been used to extract the molar ratio corresponding to the edge jump. We found a molar ratio Th:Fe equal to 1.1 for compound **1**, which confirms the stoichiometry found by Xu and Hullinger (34).

Compound 2: $U^{IV}/Fe^{II}(CN)_6$

Synthesis was carried out in a glove box filled with Ar (less than 2 ppm O_2) because of the air sensitivity of U^{IV}. 15 mL of a pale yellow $K_4Fe^{II}(CN)_6$ solution (0.11 M in 0.5 M HCl) was mixed with 15 mL of the green U^{IV} solution and a green precipitate was instantaneously obtained. If exposed to air, the precipitate turned brown due to a massive oxidation of U^{IV} into U^{VI}. All the analyses were therefore carried out under argon or vacuum. Elemental analysis was performed at Analytische Laboratorien GMBH (Germany). Anal. calcd. for $UFeC_6N_6H_6O_3$: U 47.22, Fe 11.11, C 14.28, N 16.67; found: U 47.70, Fe 12.75, C 15.12, N 17.83. The U:Fe ratio was found equal to 0.9.

Compound 3: $Np^{IV}/Fe^{II}(CN)_6$

3 mL of the green Np^{IV} stock solution was mixed with 2 mL of a pale yellow $K_4Fe^{II}(CN)_6$ neutral solution (0.041 M) and a deep pink precipitate was instantaneously obtained.

Compound 4: $Np^{III}/Fe^{III}(CN)_6$

3 mL of the violet Np^{III} stock solution was mixed with 2 mL of a yellow $K_3Fe^{III}(CN)_6$ neutral solution (0.041 M) and a deep pink precipitate was instantaneously obtained.

The iron and Np stoichiometries for **3** and **4** were determined as for **1**. However, since McMaster coefficients are not available for Np, we used in first approximation the parameters tabulated for U element. We found a molar ratio Np:Fe equal to 1.1 for compound **3** and 1.0 for compound **4**.

It should be noted here that the reaction between Np^{III} and $Fe^{II}(CN)_6$ ions was not undertaken due to the lack of Np^{III}.

Compound 5: $La^{III}KFe^{II}(CN)_6.4H_2O$

Single crystals were obtained by very slow diffusion of dilute $LaCl_3$ and $K_4Fe^{II}(CN)_6$ water solutions into an U-tube filled with H_2O as described elsewhere (26). X-ray diffraction measurements on the single crystals allowed us to obtain the same crystallographic parameters as those previously published by Beall et al. (26).

IR spectroscopy

IR spectra were recorded between 400 and 4000 cm^{-1} on a Nicolet Magna 560 spectrometer equipped with a ZnSe horizontal attenuated transmitted reflectance crystal. The solid samples were crushed with Nujol (2 mg of solid sample into 100 μL of Nujol) and the mixture obtained positioned on the ZnSe crystal.

X-ray absorption spectroscopy

Data acquisition

EXAFS and XANES measurements were carried out at the LURE (Laboratoire pour l'Utilisation du Rayonnement Electromagnétique, France) facility on the DCI ring (1.8 GeV, λc = 3.7 keV) on D44 experimental hutch. Because all samples are radiologically hazardous, they were placed in a house-made shroud (41). Uranium air-sensitive samples were kept under primary vacuum during the experiment. A double crystal monochromator was used and X-ray absorption was measured in transmission mode with ionization chambers. For XANES measurements, a reference metallic foil was positioned after the second ionization chamber and its spectra was recorded simultaneously with a diode detector.

Actinide L_3 edge: A Si 311 monochromator for both EXAFS and XANES spectra and argon-filled ionization chambers were used. Calibration was done at the Zr K edge of a Zr metallic foil at 18014.0 eV (42) at the absorption maximum. The energy resolution was 8.4 eV at 17000 eV.

Iron K edge: A Si 111 monochromator for EXAFS spectra and a Si 311 monochromator for XANES spectra were used. The ionization chambers were filled with air. Harmonic rejection was achieved by detuning the two crystals of the monochromator (30% loss of flux). Energy calibration was done at the Eu L_3 edge of an $EuPd_2$ alloy foil at 6982.0 eV at the absorption maximum. Energy resolution at 7000 eV was 2.7 eV for Si 111 and 1.3 eV for Si 311 crystal.

EXAFS data treatment

EXAFS data treatments were carried out using the set of programs "EXAFS pour le Mac" (43). A linear function was used for pre-edge extrapolation, atomic absorption was modeled by a polynomial function of the 6th order for Fe and by spline smoothing for An (polynom of the 6th order, smoothing coefficient equal to 0.94 for **1**, 0.96 for **2**, 0.91 for **3**, 0.94 for **4**). The nonreduction of the neighbor contribution by the spline smoothing has been checked. Normalization was done using the Heitler–Heisenberger method. The pseudo-radial distribution functions (PRDF) were obtained by Fourier transformation (FT) of the EXAFS oscillations in k^3 space between 1.8 and 14.6 $Å^{-1}$ for Fe K edge and between 2.2 and 14.7 $Å^{-1}$ for An L_3 edge using a Kaiser window with $\tau = 3$ for the Fe K edge, $\tau = 5$[3] for the An L_3 edge.

XANES data treatment

After pre-edge linear extraction and energy calibration with respect to the in situ reference foil using the Bragg formula, the XANES spectra were normalized to 1.0 at the middle of the first EXAFS oscillation.

EXAFS data fitting procedure

It is well known that EXAFS data analysis highly depends on the choice of reliable electronic parameters (backscattering phase $\varphi(\theta, k)$, backscattering amplitude $f(\theta, k)$, electron mean free path $\lambda(k)$, and inelastic losses S_0^2) (44). Best sets of such parameters are often extracted from model compounds that account for the electronic and crystallographic structures of the unknown compound. This is the case here where hexacyanoferrate starting material is the best candidate as a model compound at the Fe K edge. This is, however, not the case at the An L_3 edge since the synthesis of

[3] The high τ value for the actinide L_3 edge is made to decrease the effect of the side PRDF peaks.

© 2000 NRC Canada

reference compounds with only An—N bonds (such as ThN, UN, and NpN materials) required drastic conditions not available at the present time in our laboratory. To analyze the An L_3 EXAFS oscillations, calculated electronic parameters have to be used. In all cases, the EXAFS oscillations were back-Fourier transformed before adjustment. Fits of the $k\chi(k)$ EXAFS oscillations were carried out with the Round Midnight code[4] (43).

Fe K edge analysis: Fe-C and Fe-N electronic functions were extracted from the EXAFS spectrum of $K_3Fe^{III}(CN)_6$ complex ([1.23 Å, 2.00 Å] back-Fourier transformation for Fe-C, [2.00 Å, 3.10 Å] back-Fourier transformation for Fe-N). The electronic functions Fe-N contain several single and multiple scattering contributions which are known to be present for this kind of geometry (45, 46). A mean contribution is hence taken into account.

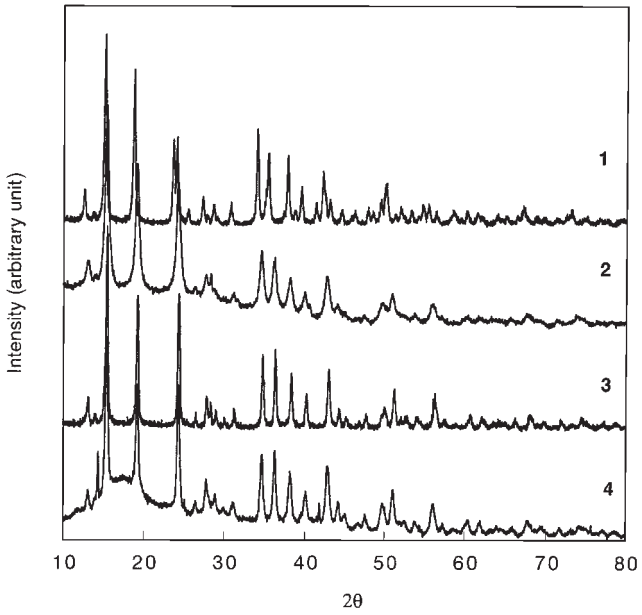
The fitted EXAFS oscillations of the first (C) and second (N) peaks of the PRDF of compounds **1** to **4** were obtained by inverse FT between 1.23 and 3.10 Å. Floating parameters in the 2-shell fit were: the two Debye–Waller factors $\sigma_{Fe\text{-}C}$ and $\sigma_{Fe\text{-}N}$, the global energy threshold ΔE_o, and the backscatterer distances R_C and R_N. N, the number of neighbors, was fixed to 6, S_0^2 and $\lambda(k)$ are included in the experimental amplitude.

An L_3 edge analysis: Calculated electronic parameters were obtained with Feff7.02 code (47). Many studies have already proved the efficiency of this code for actinide compounds (48–50). The amplitude and phase shift functions were obtained with one pair An/N with an An—N distance fixed reasonably to 2.50 Å, which is a typical An—N or An—O distance in compounds whose structures have been determined (38, 51–56). The Hedin–Lundqvist potential was used with Nleg = 2 (cf. appendix). The fitted EXAFS oscillations of the first peak of the PRDF were obtained by back-Fourier transformation of the FT between 1.38 and 2.37 Å. S_0^2 and Γ (= k/λ) functions calculated by Feff7.02 were fixed in the fit. Floating parameters in the 1-shell fit were: the Debye–Waller factor $\sigma_{An\text{-}N}$, the global energy threshold E, and the backscatterer distance R_N. The number of first neighbors around the actinide was fixed to nine by analogy to the corresponding lanthanide complexes. In a first approximation all the neighbors were considered equivalent. Then, to take into account the probable coordination of water molecules at different distances, two distances were fitted.

X-ray powder diffraction

The X-ray powder diffraction of **1**, **3**, and **4** were collected at COGEMA Marcoule with a Jobin-Yvon CGR apparatus in a glove box using a Cu Kα ray. The X-ray powder diffraction of **2** was collected on an INEL CPS120-equipped powder diffractometer set up in a horizontal Debye–Scherrer geometry (using the Cu $K\alpha_1$ radiation as incident beam, a sealed capillary of 0.1 mm internal diameter as sample holder, and a curved gaseous detector –6.5 × 10^5 Pa of 15% ethane and 85% argon).

Fig. 1. X-ray powder diffraction patterns for **1**, **2**, **3**, **4** (10° < 2θ < 70°). The refined lattice parameters are listed in Table 1. The spectra are shifted in ordinates for clarity.



Results

X-ray powder diffraction

The X-ray powder diffraction patterns of compounds **1**, **2**, **3**, and **4** are presented on Fig. 1. Compound **1** ($Th^{IV}Fe^{II}(CN)_6{\cdot}5H_2O$) is known to crystallize in the $P6_3/m$ space group (34) and contains most probably nine-coordinated $MN_6(H_2O)_3$ groups linked to octahedral FeC_6 groups by cyanide bridges like in the case of $KLa^{III}Fe^{II}(CN)_6{\cdot}4H_2O$ (26).

The structure of the X-ray patterns of **2**, **3**, and **4** are similar to those of **1**. This observation means that these complexes are isostructural with $La^{III}KFe^{II}(CN)_6{\cdot}4H_2O$. The lattice parameters have been determined with the ERACEL program (57). Moreover, all the peaks of the compound **3** spectrum are present in the spectrum of **4**, at the same 2θ values suggesting that, starting from different oxidation states for the metal ions, the precipitation reactions lead to the same compound.

The 2θ peaks are nevertheless shifted to higher θ values going from Th (**1**) to U (**2**) complexes and from U (**2**) to Np (**3** and **4**) complexes. This shift is due to a shortening of the lattice parameters from Th to Np complexes. The parameters range indeed from 7.38 to 7.30 Å for **a** and from 13.95 to 13.47 Å for **c** (Table 1) for U and Np, respectively.

Infrared spectroscopy

The absorption bands between 2000 and 2200 cm^{-1} for compounds **1**–**5** are listed in Table 2. There is only one peak in this energy range for each compound. This peak can be assigned to the cyano stretching vibration by analogy with the IR spectra of similar compounds found in the literature

[4] EXAFS fits were carried out in $(k^{q+1}/A)\text{chi}(k)$ weighting mode (where A is the mean of the standard deviation pondered by q which is equal to 1.5 for Fe K edge, 1 for An L_3 edge).

© 2000 NRC Canada

Table 1. Refined lattice parameters for compounds **1**–**4**.

Complexes	$a = b$ (Å)	c (Å)	R
1	7.38 ± 0.01	13.95 ± 0.02	0.56
2	7.332 ± 0.008	13.55 ± 0.01	0.46
3	7.302 ± 0.005	13.497 ± 0.008	0.36
4	7.310 ± 0.008	13.47 ± 0.01	0.36

Note: Space group = $P6_3/m$ (no. 176) $\alpha = b = 90°$ $\gamma = 120°$.
$R = \frac{\Sigma(\theta_{obs} - \theta_{calc})^2}{N_{reflexion} - N_{paramter}}$.

Table 2. Position of the CN infrared stretching mode in reference compounds and in complexes **1**–**5**.

Complexes	ν(CN) (cm^{-1})	References and notes
$K_3Fe^{III}(CN)_6$	2 118	(62)
$K_4Fe^{II}(CN)_6{\cdot}3H_2O$	2 044	(63)
$Pr^{III}KFe^{II}(CN)_6{\cdot}4H_2O$	2 061	(26)
$La^{III}KFe^{II}(CN)_6{\cdot}4H_2O$ (**5**)	2 064	this work
$Th^{IV}/Fe^{II}(CN)_6{\cdot}xH_2O$ (**1**)	2 059	this work
$U^{IV}/Fe^{II}(CN)_6{\cdot}xH_2O$ (**2**)	2 061	this work
$Np^{IV}/Fe^{II}(CN)_6{\cdot}xH_2O$ (**3**)	2 060	this work
$Np^{III}/Fe^{III}(CN)_6{\cdot}xH_2O$ (**4**)	2 060	this work

Note: The formal oxidation states of An and Fe in $An/Fe(CN)_6$ compounds in this table correspond to those of the starting ions.

(15, 18, 28, 58) and is located in the $Fe^{II}(CN)_6$ energy range since the peak position is known to be mostly sensitive to the oxidation state of the metal ion linked to the C atom (58, 59). These positions indicate then the presence of Fe^{II}-CN entities for **1**–**4**. While the band of non-bridging CN ligands (2044 cm^{-1} for Fe^{II}-CN) is not observed (58) in the spectra of compounds **1**–**5** higher energy shifted vibration bands of about 20 cm^{-1} (as observed here with respect to free CN ligands linked to Fe^{II} ion) indicates that all CN are bridging. This CN-bridging IR signature indicates that the actinide is linked to the nitrogen atom of the CN ligands. Moreover, this position is very close to the one of the CN stretching vibrations for $Ln^{III}KFe^{II}(CN)_6{\cdot}4H_2O$ (Ln = La, Pr) containing the Fe^{II}-CN-Ln^{III} motif.

XANES

It is well known that the X-ray absorption edge (position and structure) is sensitive to both local and electronic structure of the absorbing atom (symmetry, formal oxidation state of the metal, nature of the ligands, and distances (metal–ligands)). However, this sensitivity highly depends on the orbital probed. Here, we chose to probe: (*i*) the actinide L_3 edge ($2p^6 6d^n \rightarrow 2p^5 6d^{n+1}$ transition), since many studies have reported the influence of the actinide formal oxidation state on the L_3 edge position (50, 60–62); (*ii*) the iron K edge ($1s^2 4p^0 \rightarrow 1s^1 4p^1$ transitions), which is sensitive to both iron oxidation state (63, 64), point symmetry, and electronic structure (64–66) via the edge and pre-edge feature analysis.

A high-energy shift is generally to be expected with the increase of the oxidation state and (or) decrease of the metal–ligand distances (50, 60–64, 67).

Fig. 2. Iron K edge XANES spectra of compounds **1**, **2**, **3**, and **4**, and reference compounds $K_3Fe^{III}(CN)_6$ and $K_4Fe^{II}(CN)_6{\cdot}3H_2O$. The spectra are shifted in ordinates for clarity.

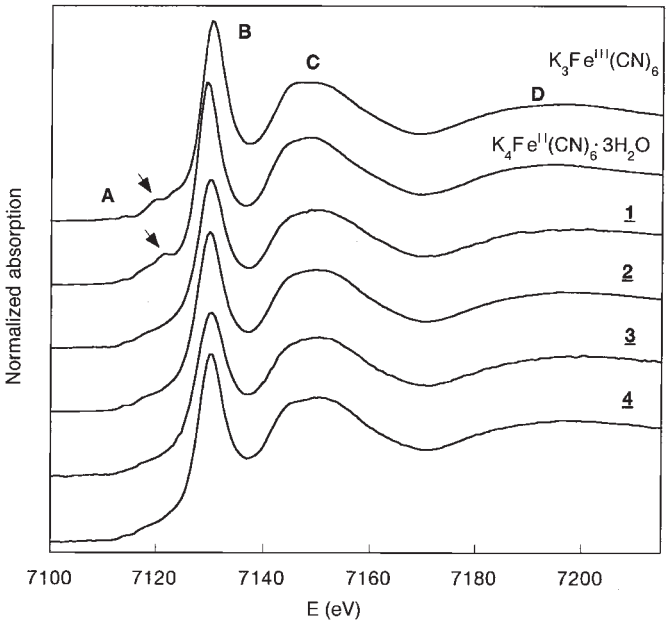


Table 3. Absorption edge maximum energy of the Fe K edge XANES spectra (E_{max}).

Compounds	E_{max} (eV) (±0.25 eV)
$K_3Fe^{III}(CN)_6$	7 130.5
$K_4Fe^{II}(CN)_6{\cdot}3H_2O$	7 129.5
1	7 130.2
2	7 130.0
3	7 130.2
4	7 130.0

Iron XANES

The iron K edge XANES spectra of compounds **1**–**4** are reported in Fig. 2 and compared to the reference compounds spectra of $K_3Fe^{III}(CN)_6$ and $K_4Fe^{II}(CN)_6{\cdot}3H_2O$. All the spectra resemble each other (presence of the principal structures B, C, and D) and are characteristic of the $Fe(CN)_6$ entity. Nevertheless, a weak structure A in the pre-edge is modified with respect to the two references. This prepeak A disappears in the spectra of compounds **1**–**4**.

The energies of the edge maxima are listed in Table 3. A high-energy shift of 1 eV is observed going from $Fe^{II}(CN)_6$ to $Fe^{III}(CN)_6$ references (67). The position of the edge maximum in the complexes **1**–**4** is intermediate between those of these two references.

Actinide XANES

The XANES of the three actinide ions (i.e., Th, U, and Np) are reported on Fig. 3 and compared to the spectra of reference compounds. First, note the similarity of all spectra. They present only two major features: the first one called white line is intense and relatively sharp; the second one corresponds to the first EXAFS oscillation. The Np L_3 edges of **3** and **4** (Fig. 3*c*) are identical which means that the two

© 2000 NRC Canada

Fig. 3. (*a*) An L_3 edge XANES spectra of compounds **1**. (*b*) **2**, $U^{IV}O_{2.0}$, and $U^{VI}O_2(NO_3)_2{\cdot}6H_2O$. **(*c*) 3**, **4**, and $Np^{IV}(C_2O_4)_2{\cdot}6H_2O$.

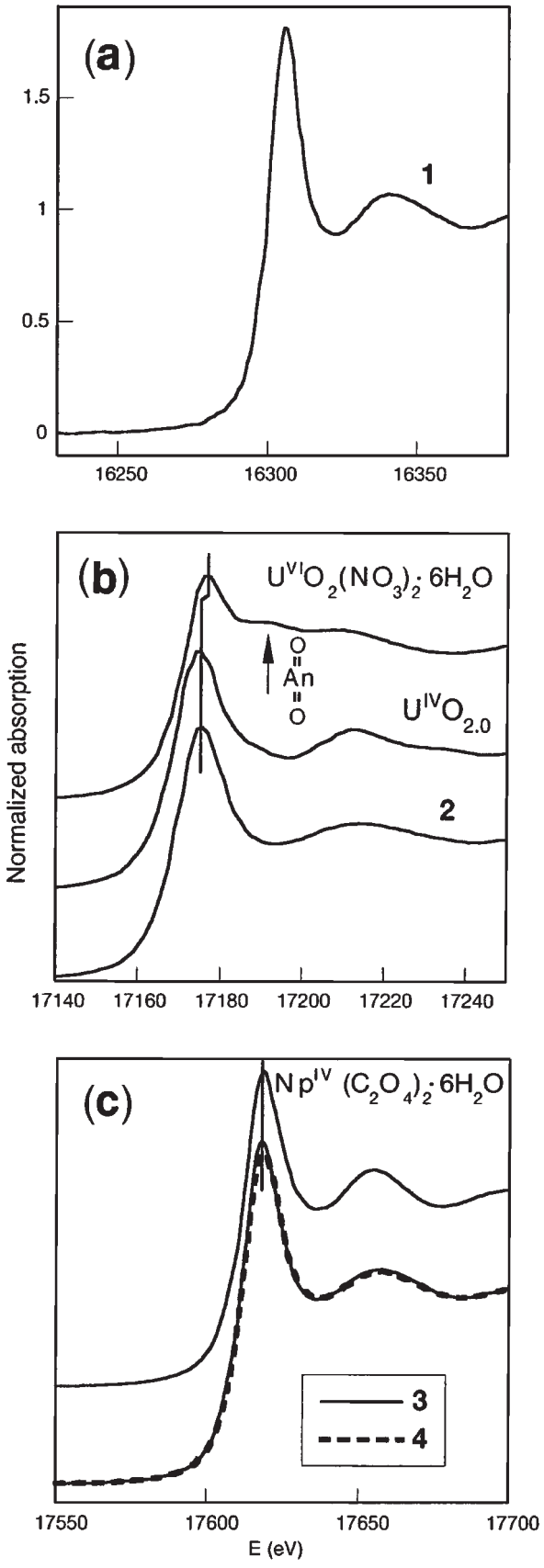


Table 4. Absorption edge maximum energy of the An L_3 edge XANES spectra (E_{max}).

Compounds	E_{max} (eV) (±0.5 eV)
1	16 305.8
$U^{VI}O_2(NO_3)_2{\cdot}6H_2O$	17 176.5
$U^{IV}O_{2.0}$	17 175.1
2	17 175.5
$Np^{IV}(C_2O_4)_2{\cdot}6H_2O$	17 618.5
3	17 618.1
4	17 618.5

starting systems $Np^{III}/Fe^{III}(CN)_6$ or $Np^{IV}/Fe^{II}(CN)_6$ yield compounds with the same Np formal oxidation state and the same actinide environment. According to Table 4, the position of the Np absorption maximum of **3**, **4**, and Np^{IV} reference compounds are similar. Further proof is brought by the following: the XANES of the actinyl ion $[AnO_2]^{n+}$ (n = 1, 2) presents a typical signature (50, 62, 68). The multiple scattering along the linear O=An=O chain creates a shoulder at ~15 eV after the absorption maximum. This shoulder that is present in the spectrum of the reference compound $U^{VI}O_2(NO_3)_2{\cdot}6H_2O$ (Fig. 3*b*) is absent in the spectra of compounds **1**–**4**. The absence of such a feature in the XANES spectra precludes then the occurrence of +V or +VI oxidation states in compounds **1**–**4**.

Similarly, the XANES maximum position of compound **2** corresponds to U^{IV} with respect to the reference ($U^{IV}O_{2.0}$). The XANES spectrum of **1** (Fig. 3*a*) is not compared to the one of a reference compound since the formal oxidation state +IV is the only one possible for Th.

EXAFS

Fe K edge and An (Th, U, Np) L_3 edges were recorded for compounds **1**–**4** to investigate the local structure around these atoms. The pseudo-radial distribution function around Fe and An allows us, moreover, to study the geometry of the An-N-C-Fe motif.

Iron EXAFS

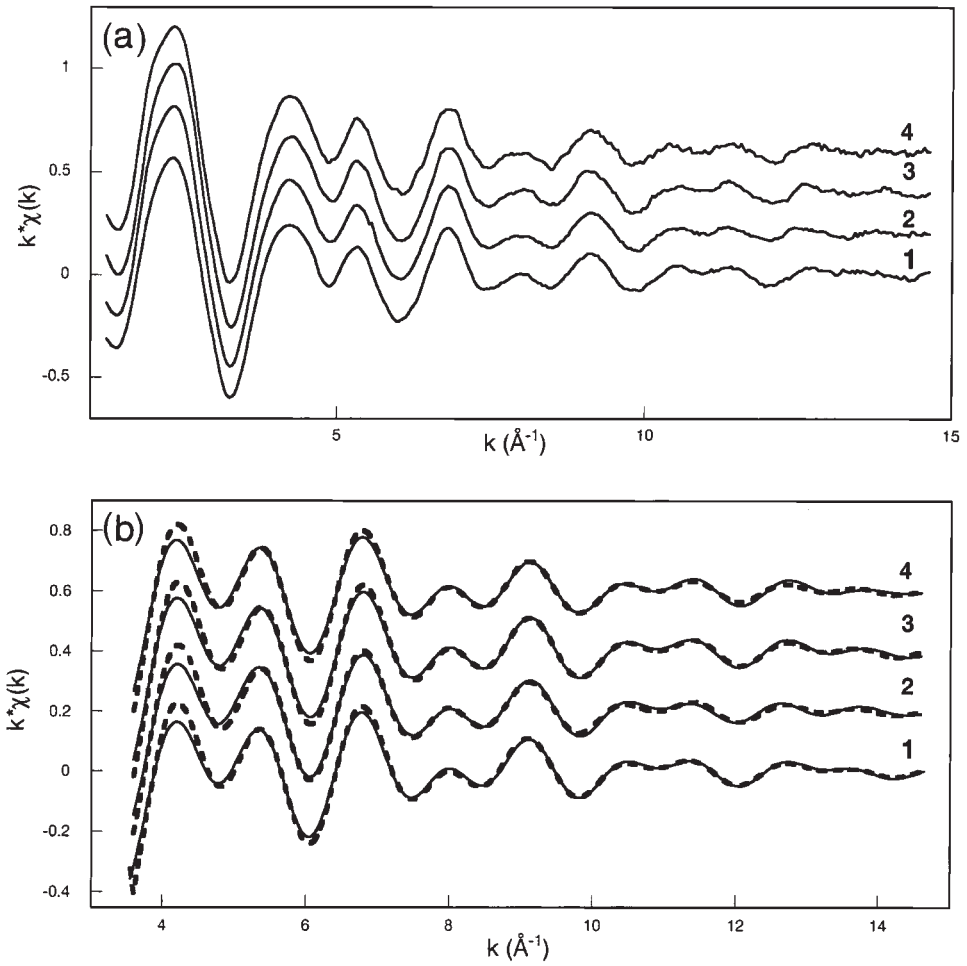
The EXAFS oscillations of **1**–**4** at the Fe K edge are presented in Fig. 4*a*. The EXAFS signals are quite similar. As the three PRDF are similar, only the PRDF of uranium compound **2** is presented on Fig. 5 for clarity.

Two major contributions A and B are present in the PRDF. Contribution A is assigned to the carbon first neighbors linked to the iron ion while contribution B is attributed to the nitrogen second neighbors. The second neighbor contribution is unusually high. The contribution of a second shell constituted of light atoms usually provides a less intense peak than the first shell due to the increase of the dumping factor $(1/kRj^2)\ e^{-2Rj/\lambda}$ of the EXAFS oscillations with R. Here, contribution B is as intense as A due to focusing effect along the Fe-C-N motif. It has been demonstrated that the linearity of this chain increases the number and the amplitudes of multiple scattering paths that occurs at the same frequency as the single scattering ones, thus increasing the contribution of the second shell atoms (45, 46).

Given the XANES results, the number of neighbors have been fixed to 6C and 6N in the two shell fitting procedure. With these values satisfactory fits have been obtained

© 2000 NRC Canada

Fig. 4. (*a*) EXAFS oscillations at the Fe K Edge for complexes **1**–**4**. (*b*) Filtered (—) (first and second neighbors shells) and calculated (--) oscillations at the Fe K edge for complexes **1**, **2**, **3**, and **4** using a two-shell fit (cf. Table 5) (bottom). Oscillations are shifted in ordinate for clarity.

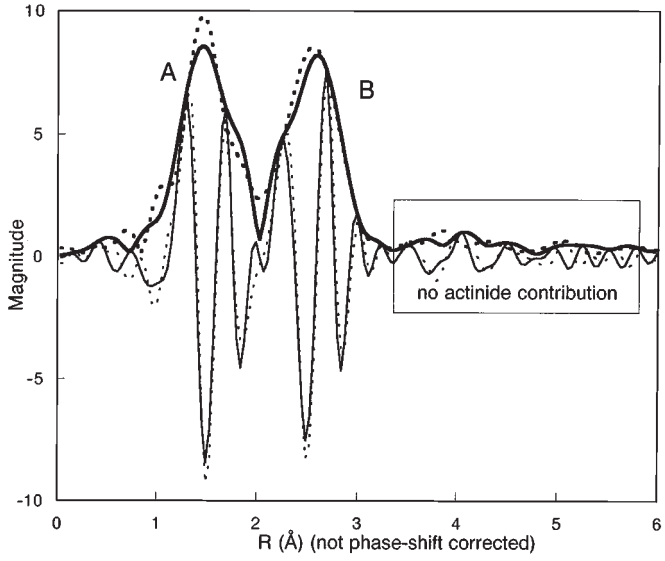


(Fig. 4*b* and Table 5). The Fe—C distances found by EXAFS (1.90 Å) in **1**–**4** are smaller to those of $K_3Fe^{III}(CN)_6$ (69) and $K_4Fe^{II}(CN)_6{\cdot}3H_2O$ (70) (1.94 and 1.93 Å, respectively). The Fe—N distances range from 3.05 to 3.06 Å. The deduced C—N distances range then from 1.15 to 1.16 Å supposing the linearity of the Fe-C-N chain. These fitted distances are in good agreement with those found by X-ray single crystal diffraction of $KLa^{III}Fe^{II}(CN)_6{\cdot}4H_2O$ which contains Fe-C-N-La chains ($R_{Fe\text{-}C}$ = 1.90 Å, $R_{C\text{-}N}$ = 1.15 Å, $R_{Fe\text{-}N}$ = 3.05 Å) (26).

Actinide EXAFS

The EXAFS oscillations at the An L_3 edge for complexes **1**–**4** are presented in Fig. 6*a*. The EXAFS oscillations of **1** are shifted to lower *k* in comparison with compounds **2**–**4** indicating a longer Th–ligand distance than U and Np–ligand distances. Given the similarity of the PRDF general shape for compounds **1**–**4**, only the PRDF of **2** is presented in Fig. 7. Three contributions D, E, and F are present in all PRDF. Contribution D is assigned to the nitrogen first neighbors and should probably contain oxygen neighbors of water molecules. Contribution E is due to the second carbon neighbors. The distances between the first two peaks of the nonphase shift corrected PRDF (i.e. 1.17 Å for **1**, 1.14 Å for

Fig. 5. Modulus (bold) and imaginary part (fine) of the PRDF of the Fe EXAFS oscillations for compound **2** (—) and model $La^{III}KFe^{II}(CN)_6{\cdot}4H_2O$ compound (--).



© 2000 NRC Canada

Table 5. Best-fit parameters of the filtered EXAFS oscillations (peaks A and B of the PRDF) at the Fe K edge.

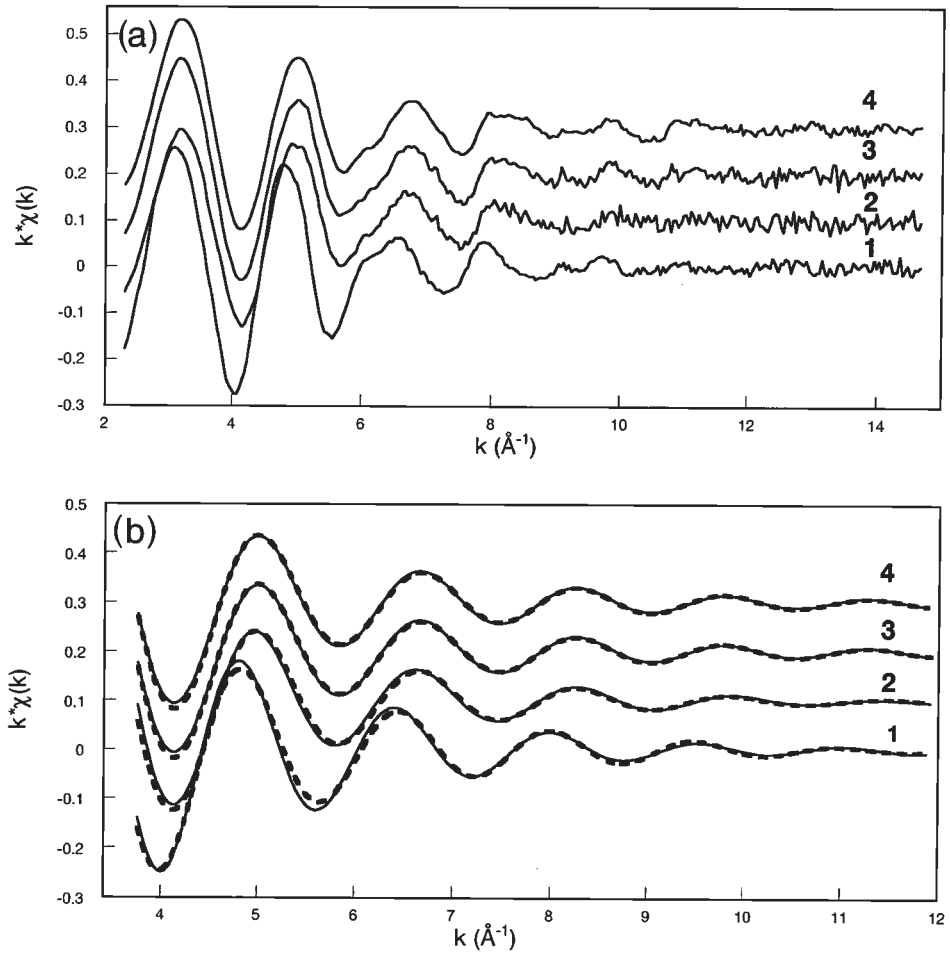
Compound	A^a	First shell (Fe—C)	Second shell (Fe—N)	ΔE_0 (eV)	rf^b (%)
1		N = 6	N = 6		
	0.014	$\boldsymbol{R_1}$ **= 1.90 ± 0.01**	$\boldsymbol{R_2}$ **= 3.06 ± 0.01**	–0.3 ± 0.7	3.0
		σ^2_1 = 0.0004	σ^2_2 = 0.0009		
		±0.0004	±0.0001		
2		N = 6	N = 6		
	0.008	$\boldsymbol{R_1}$ **= 1.90 ± 0.01**	$\boldsymbol{R_2}$ **= 3.06 ± 0.01**	–0.1 ± 0.4	3.8
		σ^2_1 = 0.0016	σ^2_2 = 0.0009		
		±0.0001	±0.0001		
3		N = 6	N = 6		
	0.018	$\boldsymbol{R_1}$ **= 1.90 ± 0.01**	$\boldsymbol{R_2}$ **= 3.05 ± 0.01**	–0.3 ± 0.8	2.5
		σ^2_1 = 0.0004	σ^2_2 = 0.0004		
		±0.0004	±0.0004		
4		N = 6	N = 6		
	0.023	$\boldsymbol{R_1}$ **= 1.90 ± 0.01**	$\boldsymbol{R_2}$ **= 3.06 ± 0.01**	–0.5 ± 1	4.0
		σ^2_1 = 0.0016	σ^2_2 = 0.0009		
		±0.0004	±0.0004		

Note: N is the number of neighbors, R_1 and R_2 are the Fe—C and Fe—N distances (Å), σ is the Debye–Waller factor (Å).

[a] A is the mean standard deviation of the EXAFS oscillations.

[b] The residual factor ($rf = \frac{\sum_{i=1}^{n}[k\chi_{exp} - k\chi_{theo}]^2}{\sum_{i=1}^{n}[k\chi_{exp}]^2}$) represents the quality of the fit.

Fig. 6. (*a*) EXAFS oscillations ($k^*\chi(k)$) at the An L_3 Edge for complexes **1**–**4**. (*b*) First shell filtered (—) and calculated (--) oscillations at the An L_3 edge for complexes **1**–**4** (cf. Table 6). Oscillations are shifted in ordinate for clarity.

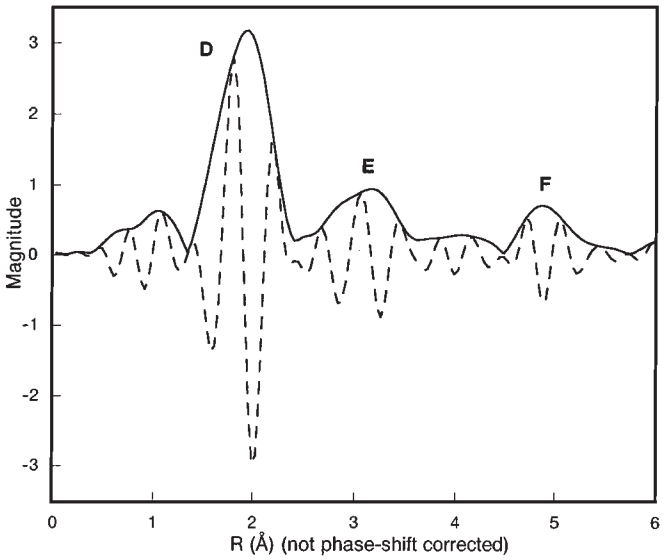


© 2000 NRC Canada

Table 6. Best-fit parameters of the filtered EXAFS oscillations (peak D of the PRDF) at the An L_3 edge. *N* is the number of neighbors, *R*, R_1, and R_2 are the An—N distances (Å), σ is the Debye–Waller factor (Å). The definitions of the other parameters are given in Table 5.

	A	One shell analysis	rf (%)	Two shell analysis	rf (%)	
		$N = 9$		$N = 6$	$N = 3$	
1		$\boldsymbol{R = 2.52 \pm 0.01}$		$\boldsymbol{R_1 = 2.48 \pm 0.01}$	$\boldsymbol{R_2 = 2.61 \pm 0.03}$	
	0.016	$\sigma^2 = 0.0064 \pm 0.0001$	2.5	$\sigma^2 = 0.0025 \pm 0.004$	$\sigma^2 = 0.0004 \pm 0.0016$	1.8
		$\Delta E_0 = 0.6 \pm 1$		$\Delta E_0 = 0.7 \pm 1$	$\Delta E_0 = 0.7 \pm 1$	
2		$\boldsymbol{R = 2.44 \pm 0.01}$		$\boldsymbol{R_1 = 2.41 \pm 0.01}$	$\boldsymbol{R_2 = 2.54 \pm 0.03}$	
	0.013	$\sigma^2 = 0.0081 \pm 0.0001$	1.8	$\sigma^2 = 0.0049 \pm 0.0001$	$\sigma^2 = 0.0036 \pm 0.0009$	1.2
		$\Delta E_0 = 0.2 \pm 1$		$\Delta E_0 = 0.4 \pm 1$	$\Delta E_0 = 0.4 \pm 1$	
3		$\boldsymbol{R = 2.43 \pm 0.01}$		$\boldsymbol{R_1 = 2.40 \pm 0.01}$	$\boldsymbol{R_2 = 2.52 \pm 0.03}$	
	0.012	$\sigma^2 = 0.0081 \pm 0.0001$	0.6	$\sigma^2 = 0.0049 \pm 0.0001$	$\sigma^2 = 0.0049 \pm 0.0009$	0.7
		$\Delta E_0 = 0.5 \pm 1$		$\Delta E_0 = 0.8 \pm 1$	$\Delta E_0 = 0.8 \pm 1$	
4		$\boldsymbol{R = 2.43 \pm 0.01}$		$\boldsymbol{R_1 = 2.40 \pm 0.01}$	$\boldsymbol{R_2 = 2.52 \pm 0.03}$	
	0.014	$\sigma^2 = 0.0081 \pm 0.0001$	0.6	$\sigma^2 = 0.0049 \pm 0.0001$	$\sigma^2 = 0.0049 \pm 0.0009$	0.7
		$\Delta E_0 = 0.5 \pm 1$		$\Delta E_0 = 0.8 \pm 1$	$\Delta E_0 = 0.8 \pm 1$	

Fig. 7. Modulus (—) and imaginary part (--) of the PRDF of the U L_3 EXAFS oscillations for complex **2**.



2, 1.17 Å for **3** and **4**) which is close to the C—N distance in $Fe(CN)_6$ (1.14 Å) confirms this assignment. The third peak F has two possible origins: multiple scattering paths along the An-N-C chain or multiple scattering paths including the Fe atom along the An-N-C-Fe chain. These two assumptions can hardly be verified due to the great number of possible multiple scattering paths in this peak. In all cases, peak E intensity is weak, indicating the nonlinearity of the An-N-C chain which does not create an important focusing effect like at the Fe K edge where the Fe-C-N chain is quite linear. The best fit results of the first peak D filtered oscillations are presented in Table 6 and Fig. 6*b*. The number of neighbors has been fixed to nine in a first approximation (usual value between eight and nine) by structural analogy with corresponding $Ln^{III}KFe^{II}(CN)_6 \cdot 4H_2O$ complexes evidenced by our XPD measurements. This approximation is well beyond the EXAFS sensitivity to coordination numbers that is known to be at least 10%. Two types of fits have been performed: (*i*) using only one shell with nine atoms at the same *R* distance; and (*ii*) using two shells with six atoms at the R_1 distance and three atoms at R_2 (Fig. 6*b*). We suppose that the first nearest-neighbor shell contains both the An-N(NC) and An-O(OH_2) contributions. These two neighbors are not distinguishable by XAS due to their close *Z* numbers ($Z = 7$ and $Z = 8$). This first shell was hence analyzed using only the An-N parameters obtained with the Feff7.02 code. If all surrounding atoms are supposed to be equivalent, the average An—N distance is equal to 2.52 Å for Th (**1**), 2.44 Å for U (**2**), and 2.43 Å for Np (**3** and **4**). The high value of the Debye–Waller factor for this fit ($\sigma^2 = 0.0081$ Å^2) suggests, nevertheless, a large distribution of neighbor distances. In the two shell fit procedure: $R_{Th\text{-}O} = 2.61$ Å and $R_{Th\text{-}N} = 2.48$ Å are found in the thorium complex **1**; $R_{U\text{-}O} = 2.54$ Å and $R_{U\text{-}N} = 2.41$ Å are found in the uranium complex **2**; and $R_{Np\text{-}O} = 2.52$ Å and $R_{Np\text{-}N} = 2.40$ Å are obtained for the neptunium complexes **3** and **4**. The mean An—N,O distances decrease from Th to Np.

Discussion

The above spectroscopic results lead us to draw a structural and to a lesser extent electronic picture of these complexes that is discussed below.

First of all, the two neptunium complexes **3** and **4** exhibit equivalent spectroscopic results (IR, XANES, EXAFS, XRPD). Starting with two different couples of metal ions (Np^{III}/Fe^{III} and Np^{IV}/Fe^{II}) results in the formation of the same compound.

The An (Th, U, Np) XANES spectra (Fig. 3) suggest that the compounds contain Th^{IV} (**1**), U^{IV} (**2**), and Np^{IV} (**3**, **4**) ions. This tetravalent state is quite common in the complexes of U and Np and is the only one possible for Th (71). The chemical analysis for **2** and the molar ratio An/LFe for **1**, **2**, **3**, and **4** attest that there is one Fe for one An in **1**–**4**. To take into account the electroneutrality of the compounds, two possible formula can arise from this stoichiometry: $An^{IV}Fe^{II}(CN)_6 \cdot xH_2O$ or $An^{IV}XFe^{III}(CN)_6 \cdot xH_2O$ (X = Cl^-, ClO_4^-). As the possible X anions were not detected (absence of ClO_4^- characteristic vibration mode (72, 73) at 1099 cm^{-1} on the infrared spectra of **3** and **4**, absence of Cl in **2** elemental analysis) the second formula can be rejected. Thus,

© 2000 NRC Canada

the Fe oxidation state is II in all the complexes. Nevertheless the Fe XANES maximum absorption of compounds **1**–**4** is shifted at higher energy (0.5 eV) compared to the Fe^{II} reference spectrum. This small but significant shift can be attributed to the decrease of the Fe—C distance, as emphasized by EXAFS analysis (67). The Fe^{II} oxidation state attribution is also in agreement with the infrared spectra. The position of the stretching mode ν_{CN} (2060 cm^{-1}) for **2**, **3**, and **4** is the same as the one observed for model compounds **1** and **5** for which the Fe oxidation state is II.

The formation of identical species (**3** and **4**) starting from Np^{III} or Np^{IV} is in agreement with the oxido-reduction potentials of the couples, i.e., 0.36 V/ENH for $Fe^{III}(CN)_6/Fe^{II}(CN)_6$ and 0.18V/ENH for Np^{IV}/Np^{III}. The oxido-redox process ($Fe^{III}(CN)_6 + Np^{III} \rightarrow Fe^{II}(CN)_6 + Np^{IV}$) might be thus invoked as a reaction driving force even if it can be considered as a schematic view of the reaction mechanism. Further experiments are in progress to clarify the features that govern the species formation. It should be noticed here that the unstable Np^{III} ions can be oxidized to Np^{IV} by air but that the $Fe^{III}(CN)_6$ ion is stable in solution. Thus this redox reaction can not be attributed to an air oxidation process.

As suggested by EXAFS and XANES Fe K edge analysis, the structural entity $Fe(CN)_6$ is conserved in compounds **1**–**4**. The IR spectroscopy shows besides that the six cyano ligands surrounding the iron are bridging as only one peak accounting for the ν_{CN} stretching vibration observed. The effect of this bridging is confirmed by the Fe pre-edge analysis: pre-peak A (Fig. 2) disappears in the Fe K edge XANES of complexes **1**, **2**, **3**, and **4** with respect to the two references in which the CN ligands are monodentates. This feature between 7118 and 7122 eV is principally attributed to the Fe 1*s*-4t_{1u} transition, the 4t_{1u} orbital being mainly built from the antibonding π^* orbitals of the CN ligands (64). According to the same author it may also contains dipole-forbidden transitions of the Fe 1*s* electron into nonbonding 2t_{1g} and 2t_{2u} and antibonding 3t_{2g}. The later are also mainly built from π^* orbitals of the CN ligands. Variations of A (position and occurrence) indicates a change in the molecular orbitals localized on the CN ligands due to the creation of an An—N bond. The formation of this bond changes the symmetry of the molecular orbitals and (or) due to actinide back-bonding into CN ligands, fills the empty orbitals. Moreover, the CN molecular orbitals are delocalized both on the actinide and the iron ion, which can explain the decrease of the intensity of the transition.

Given the CN ligands are linked by the carbon and the nitrogen atoms, the absence of the actinide contribution in the Fe PRDF which should appear near 5 Å could seem surprising (Fig. 5). In fact, the same kind of behavior has already been analyzed in a recent paper in the case of an Fe-C-N-Cu chain (74) where the decrease of the Cu-N-C angle from 174 to 147° creates the disappearance of the Cu contribution on the Fe PRDF. It has also been shown that the Cu-N-C bending could prevent copper signature to be observable in the iron PRDF. The interpretation of this phenomena has been checked on the $La^{III}KFe^{II}(CN)_6 \cdot 4H_2O$ (**5**) EXAFS spectrum: the contribution of La is absent on the Fe PRDF (Fig. 5). The absence of a visible La contribution is not surprising taking into account the Feff7.02 simulation results. Starting from the crystallographic Fe environment of **5** (6C at 1.90 Å, 6N at 3.05 Å, 6La at 5.52 Å), the Fe EXAFS oscillations were simulated using the Feff7.02 parameters described in Appendix. The simulated EXAFS oscillations (Fig. 8*a*) and PRDF (Fig. 8*b*) are in very good agreement with the experimental ones. However, when the Feff7.02 calculation is performed with a linear Fe-C-N-La geometry (180°), the PRDF reported in Fig. 8 shows a strong contribution from the La backscatter (very intense third peak). This is a nice illustration of the intensity decrease of the multiple scattering contributions when the geometry deviates from the linearity. The absence of the An signature in the iron PRDF of compounds **1**, **2**, **3**, and **4** therefore indicates that the An-N-C angle is most certainly smaller than 180°, as in the case of **5**.

The An L_3 edge EXAFS treatment allows to investigate the local environment of the An ions. The decrease of the average An-Ligands fitted distances (Table 6) from Th to Np (2.52 Å, 2.44 Å, and 2.43 Å, respectively) is significant from Th to U and of the uncertainty order from U to Np. This constant decrease is in agreement with the ionic radii actinide contraction from Th^{IV} to Np^{IV} (ionic radii of eight coordinate An^{IV} ions for Th, U, and Np are respectively, equal to 1.19, 1.14, and 1.12 Å) (75). This trend is the same when the two-shell model is used (3O + 6N) for **1**–**4** ($R_{Th\text{-}N}$ = 2.48 Å > $R_{U\text{-}N}$ = 2.41 Å > $R_{Np\text{-}N}$ = 2.40 Å and $R_{Th\text{-}O}$ = 2.61 Å > $R_{U\text{-}O}$ = 2.54 Å > $R_{Np\text{-}O}$ = 2.52 Å).

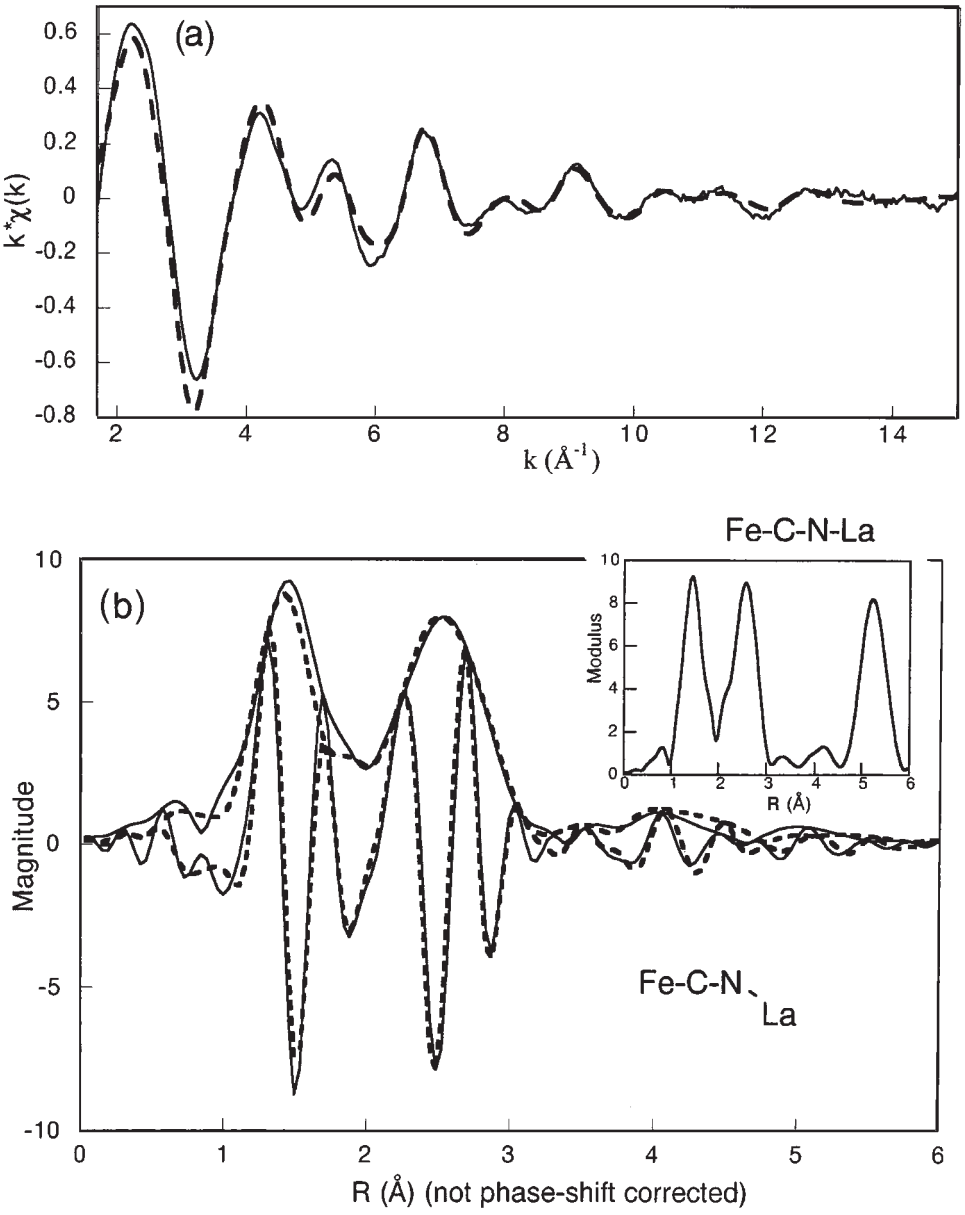
In Table 6, the two-shell fit procedure of the first peak (six nitrogen neighbors and three oxygen neighbors) is devoted to mimic the lanthanide coordination sphere. The distances obtained for **1**–**4** are smaller than in the case of $La^{III}KFe^{II}(CN)_6 \cdot 4H_2O$ (24) ($R_{La\text{-}N}$ = 2.60 Å, $R_{La\text{-}O}$ = 2.73 Å) which is consistent with the decrease of ionic radii from Ln to An. For instance, $R_{U\text{-}N}$ in **2** is found 0.19 Å shorter than $R_{La\text{-}N}$. This difference is very close to the difference in ionic radii between eight-coordinated La^{III} and U^{IV}: 0.16 Å (75). The distance difference between $O(H_2O)$ and N(NC) neighbors is found to be the same for all our complexes **1**–**4** (~0.13 Å) and is similar to the one obtained in lanthanide series (26–29). Our results show that the environment of An in **1**–**4** is probably constituted of six nitrogen atoms coming from the cyano ligands and of three water molecules to complete the coordination sphere number to 9. These distances are consistent with the An—N and An—O distances determined by X-ray diffraction analysis on other compounds (38, 51–56). Thermogravimetric measurements (that are not available at this moment for nuclear species in our laboratory) should confirm this water content.

X-ray powder diffraction also demonstrates that complexes **2**, **3**, and **4** are isostructural with the $Ln^{III}KFe^{II}(CN)_6 \cdot 4H_2O$ (Ln = La to Nd) family of complexes and with complex **1** whose structure was previously described (34). The lattice parameters of **2**, **3**, and **4** are found to be shorter than for $La^{III}KFe^{II}(CN)_6 \cdot 4H_2O$ (a = 7.412 Å, c = 13.943 Å). This result is consistent with the smaller An-ligands distances with respect to Ln-ligands distances.

The combination of the diffraction and the EXAFS results allows us to estimate a value for the (AnNC) angle. Knowing the space group ($P6_3/m$) and the An (1/3,2/3,1/4) and Fe (0,0,0) positions, the lattice parameters values lead to determine the An—Fe distance (5.51 Å for **1**, 5.42 Å for **2**, 5.40 Å for **3** and **4**). The (AnNC) angle is then deduced,

© 2000 NRC Canada

Fig. 8. (*a*) Experimental EXAFS oscillations (—) for complex **5** at the Fe K edge compared with calculated Feff7.02 oscillations (--) (cf. Appendix) (*b*) corresponding experimental (—) and calculated (--) PRDF. The insert corresponds to the PRDF obtained with Feff7.02 supposing that the entity Fe-C-N-La is linear.



thanks to the An—N and Fe—N EXAFS-fitted distances. We found angles equal to 168 ± 3° for **1**, 164 ± 3° for **2**, 163 ± 3° for **3** and **4**. All these angles are comparable and are however slightly higher than the (LnNC) angle in $LaKFe(CN)_6 \cdot 4H_2O$ (155°). These angles differ sufficiently from 180° to explain the absence of An contribution in Fe K edge PRDF.

Conclusion

Only a few three-dimensional structures have been reported with 5*f* elements. Neptunyl cation–cation complex with mellitic acid, $Na_4(NpO_2)_2C_{12}O_{12} \cdot 8H_2O$ (51), zeolitic actinide material (76, 77), and $Rb_4U_4P_4Se_{26}$ which contains pentavalent uranium (78) or neptunium perovskite structures (79) can be cited as examples. In this work, two new three-dimensional solid state complexes $An^{IV}Fe^{II}(CN)_6 \cdot xH_2O$ (An = U, Np) have been synthesized and characterized. Spectroscopic investigations (XAS, IR) of these complexes show that for the two complexes the $Fe(CN)_6$ entity is present in the network. The first shell An analysis is consistent with the presence of three water molecules linked to the actinide, to complete the coordination sphere to 9 which is the classical geometry for these ions. These complexes can be viewed as a three-dimensional framework where the building blocks ($Fe(CN)_6$ entities) are connected through the actinide ions via the cyano bridging ligands. Thus, all the cyano ligands are bridging and the powder X-ray diffractograms show that the 3D network is isostructural with the $Ln^{III}KFe^{II}(CN)_6 \cdot 4H_2O$ analogs network. The space group is $P6_3/m$ and the cell parameters have been determined and used to propose a (AnNC) angle value which is: 164° for **2**,

© 2000 NRC Canada

163° for **3** and **4**. This angle value also explains the absence of the An contribution in the iron PRDF as modeled by multiple scattering Feff7.02 simulations.

Clearly, the early actinide and lanthanide hexacyanoferrates exhibit structural similarities despite some electronic discrepancies between the Ln and early An ions that can be pointed out. For instance the redox process invoked to explain the formation of the $Np^{IV}[Fe^{II}(CN)_6]\cdot xH_2O$ species ($Fe^{III}(CN)_6 + Np^{III} \rightarrow Fe^{II}(CN)_6 + Np^{IV}$) is not acceptable with the lanthanide ions. Indeed, only oxidation state +III is available for the early lanthanide series except for the case of Ce^{IV}. The Fe^{II}/Ce^{IV} couple has been already investigated by Xu and Hullinger (34), however the solid compound $Ce^{IV}Fe^{II}(CN)_6\cdot xH_2O$ was not obtained.

The greater covalence within the An—N bond vs. the Ln—N bond (80) is not evidenced by our EXAFS analysis which reflects only the decrease of the ionic radii going from Ln^{III} to Th^{IV}, U^{IV}, and Np^{IV}. Such results may be surprising knowing that the early actinide ions are considered to have the possibility to form more covalent-like character bonds. This propensity is not shared by the later actinides (Am, Cm, Cf) (81, 82). Thus, comparison between Ln^{III} and Am^{III} or Cm^{III} hexacyanoferrate compounds needs to be investigated to see if the tuning of the An ion leads to structural discrepancies between Ln and An species. This would be however surprising, given the similarities between the later actinide ions and lanthanide ions, as evidenced by previous work on Nd/Am coordination complexes where no structural differences have been observed (83).

Acknowledgments

The authors are very grateful to J. Vaissermann (LCIMM, Jussieu) F. Boucher (IMN, Nantes), J.-M. Blanchard (COGEMA, Marcoule), and E. Elkaïm (LURE, Orsay) for their contribution in diffraction measurements and interpretation. They thank also N. Dacheux (IPN, Orsay), F. Villain (LCIMM, Jussieu), and C. Neskovic (Laboratoire Pierre Süe, Saclay) for very fruitful discussions.

References

1. B.B. Kaul, W.S. Durfee, and T.Y. Gordon. J. Am. Chem. Soc. **121**, 6862 (1999).
2. A. Mayr and J. Guo. Inorg. Chem. **38**, 921 (1999).
3. M. Wachhold and M.G. Kanatzidis. Inorg. Chem. **38**, 4178 (1999).
4. N. Fukita, M. Ohba, H. Okawa, K. Matsuda, and H. Iwamura. Inorg. Chem. **37**, 842 (1998).
5. S. Triki, J. Sala Pala, M. Decoster, P. Molinié, and L. Toupet. Angew. Chem. Int. Ed. **38**, 113 (1999).
6. M.P. Shores, L.G. Beauvais, and J.R. Long. J. Am. Chem. Soc. **121**, 775 (1999).
7. M.S. El Fallah, E. Rentschler, A. Caneshi, R. Sessoli, and D. Gatteshi. Angew. Chem. Int. Ed. Engl. **35,** 1947 (1996).
8. T. Niu and A.J. Jacobson. Inorg. Chem. **38**, 5346 (1999).
9. H.J. Buser and A.J. Ludi. J. Chem. Soc. Chem. Commun. 1299 (1972).
10. H.J. Buser, D. Schwarzenbach, W. Petter, and A.J. Ludi. J. Inorg. Chem. **16**, 2704 (1977).
11. F. Herren, P. Fischer, and A. Ludi. Inorg. Chem. **19**, 956 **(**1980).
12. T. Mallah, S. Thiébault, M. Verdaguer, and P. Veillet. Science (Washington, D.C.), **262**, 1554 (1993).
13. W.R. Entley, G.S Girolami, and A. Ludi. Science (Washington, D.C.), **268**, 397 (1995).
14. S. Ferlay, T. Mallah, R. Ouahès, P. Veillet, and M. Verdaguer. Nature (London), **378**, 701 (1995).
15. O. Sato, T. Iyoda, A. Fujishima, and K. Hashimoyo. Science (Washington, D.C.), **271**, 49 (1996).
16. L.C. Brousseau, D. Williams, J. Kouvetakis, and M. O'Keefe. J. Am. Chem. Soc. **119**, 6292 (1997).
17. S. Ohkoshi, A. Fujishima, and K. Hashimoto. J. Am. Chem. Soc. **120**, 5349 (1998).
18. O. Sato, Y. Einaga, A. Fujishima, and K. Hashimoto. Inorg. Chem. **38**, 4405 (1999).
19. M. Nishino, Y. Yoshioka, and K. Yamaguchi. Chem. Phys. Lett. **297**, 51 (1998).
20. C. Loos-Neskovic and M. Fedoroff. Solv. Extr. Ion Exch. **7**, 131 (1989).
21. S. Ayrault, B. Jimenez, E. Garnier, M. Fedoroff, D.J. Jones, and C. Loos-Neskovic. J. Solid State Chem. **141**, 475 (1998).
22. C. Loos-Neskovic, M. Fedoroff, and E. Garnier. Talanta, 749 (1989).
23. E. Garnier, P. Gravereau, and A. Hardy. Acta Crystallogr. Sect B: Struct. Crystallogr. Cryst. Chem. **B38**, 1401 (1982).
24. W.O. Milligan, M. Uda, M.L. Beasley, D.R. Dillin, W.E. Bailey, and J.J. MacCoy. Office of Saline Water Research and Development progress report no. 594. 1970.
25. A.K. Jain, R.P. Singh, and C. Bala. Analyst (Cambridge, U.K.), **107**, 770 (1982).
26. G.W. Beall, D.F. Mullica, and W.O. Milligan. Acta Crystallogr. Sect. B: Struct. Crystallogr. Cryst. Chem. **B34**, 1446 (1978).
27. D.F. Mullica, W.O. Milligan, and J.D. Oliver. Inorg. Nucl. Chem. Lett. **15**, 1 (1979).
28. D.F. Mullica, E.L. Sappenfield, and H.O. Perkins. J. Solid State Chem. **73**, 65 (1988).
29. W.O. Milligan, D.F. Mullica, and H.O. Perkins. Inorg. Chim. Acta, **60**, 35 (1982).
30. W.E. Bailey, R.J. Williams, and W.O. Milligan. Acta Crystallogr. Sect. B: Struct. Crystallogr. Cryst. Chem. **B29**, 1365 (1973).
31. G.T. Seaborg and J.J. Katz. The actinide elements. Vol. 14B. Mc Graw–Hill Book Co., Inc., New York, Toronto, London. 1954. p. 427.
32. V.M. Vdovenko. The chemistry of uranium and transuranium elements. Academy of Sciences, USSR. Moscow, Leningrad. 1960. p. 182.
33. J. Krtill. Radiochim. Acta, **7**, 30 (1967).
34. X.L. Xu and F. Hulliger. J. Solid State Chem. **80**, 120 (1989).
35. Y.M. Kulyako, T.I. Trofimov, D.A. Malikov, I.A. Lebedev, and B.F. Myasoedov. Radiochemistry, **35(4)**, 399 (1993).
36. Y.M. Kulyako, T.I. Trofimov, D.A. Malikov, I.A. Lebedev, and B.F. Myasoedov. Radiochemistry, **35(5)**, 549 (1993).
37. Y.M. Kulyako, D.A. Malikov, T.I. Trofimov, and B.F. Myasoedov. Mendeleev Commun. 173 (1996).
38. M.S. Grigor'ev, I.A. Charushnikova, N.N. Krot, A.I. Yanovskii, and Y.T. Struchkov. Radiochemistry, **39(5)**, 420 (1997).
39. J.A. Hermann and J. F. Suttle. Inorg. Synth. **5**, 143 (1957).
40. W.H. McMaster, N. Kerr Del Grande, J. Mallet, and H. Hubbel. Compilation of X-ray cross sections. U.S. NTIS. Springfield.
41. A. Chabane. Ph.D. Thesis. Univ. Paris XI Orsay, France. 1997.
42. Reference X-ray spectra of metal foils, EXAFS MATERIALS, 871, El Cerro Blvd, Danville, CA 94526, U.S.A.

© 2000 NRC Canada

43. A. Michalowicz. J. Phys. IV, **7**, C2-235 (1997).
44. B.K. Teo. EXAFS: basic principles and data analysis. Inorganic chemistry concepts. Vol. 9. Springer–Verlag (*Editors*). Berlin, Heidelberg, New York. 1986.
45. T.E. Westre, A. Di Cicco, A. Filipponi, C.R. Natoli, B. Hedman, E.I. Solomon, and K.O. Hodgson. J. Am. Chem. Soc. **117**, 1566 (1995).
46. M. Giorgetti, M. Berrettoni, A. Filipponi, P.J. Kulesza, and R. Marassi. Chem. Phys. Lett. **275**, 108 (1997).
47. A.L. Ankudinov and J.J. Rehr. Phys. Rev. B: Condens. Matter, **56**, 1712 (1997).
48. H. Moll, M.A. Denecke, F. Jalilehvand, M. Sandström, and I. Grenthe. Inorg. Chem. **38**, 1795 (1999).
49. W.W. Lukens, P.G. Allen, J.J. Bucher, N.M. Edelstein, E.A. Hudson, D.K Shuh, T. Reich, and R.A. Andersen. Organometallics, **18**, 1253 (1999).
50. E.A. Hudson, J.J. Rehr, and J.J. Bucher. Phys. Rev. B: Condens. Matter, **52**, 13815 (1995).
51. A. Cousson, S. Dabos, H. Abazli, F. Nectoux, M. Pagés, G. Choppin. J. Less-Common Met. **99**, 233 (1984).
52. P.A. Tanner and T.C.W. Mak. Inorg. Chem. **38**, 6024 (1999).
53. R.O. Willey, R.B. von Dreele, and T.M. Brown. Inorg. Chem. **19**, 3351 (1980).
54. R. Countryman and W.S. McDonald. J. Inorg. Nucl. Chem. **31**, 2213 (1971).
55. N.W. Alcock, S. Esperas, K.W. Bagnall, and W. Hsian-Yun. J. Chem. Soc. Dalton Trans. 638 (1978).
56. N.W. Alcock and M.M. Roberts. Acta Crystallogr. Sect. B: Struct. Crystallogr. Cryst. Chem. **B38**, 2870 (1982).
57. A. Le Bail. ERACEL, modified version of CELREF (J. Laughier and A. Filhol, 1978). Université de Le Mans. 1996.
58. K. Nakamoto. Infrared and Raman spectra of inorganic and coordination compounds. 4th ed. Wiley, New York. 1986.
59. B.W. Pfennig, J.C. Cohen, I. Sosnowski, N.M. Novotny, and D.M. Ho. Inorg. Chem. **38**, 606 (1999).
60. S.D. Conradson, I.A. Mahamid, D.L. Clark, N.J. Hess, E.A. Hudson, M.P. Neu, P.D. Palmer, W.H. Runde, and C.D. Tait. Polyhedron, **17**, 599 (1998).
61. C. Den Auwer, R. Revel, M.C. Charbonnel, M.T. Presson, S.D. Conradson, E. Simoni, J.F. Le Du, and C. Madic. J. Synchrotron Radiat. **6**, 101 (1999).
62. C. Den Auwer, C. Lecouteux, M.C. Charbonnel, C. Madic, and R. Guillaumont. Polyhedron, **16**, 2233 (1997).
63. P.J. Kulesza, M.A. Malik, M. Berrettoni, M. Giorgetti, S. Zamponi, R. Schmidt, and R. Marassi. J. Phys. Chem. B **102**, 1870 (1998).
64. M. Obashi. Jpn. J. Appl. Phys. **17**, 563 (1978).
65. T.E. Westre, P. Kennepohl, J.G. DeWitt, B. Hedman, K.O. Hodgson, and E.I. Solomon. J. Am. Chem. Soc. **119**, 6297 (1997).
66. S. Bajt, S.R. Sutton, and J.S. Delaney. Physica B: (Amsterdam), **208** & **209**, 243 (1995).
67. A. Bianconi, M. Dell'Ariccia, P.J. Durham, and J.B. Pendry. Phys. Rev. B: Condens. Matter, **26**, 6502 (1982).
68. A.L. Ankudinov, S.D. Conradson, J. Mustre de Leon, and J.J. Rehr. Phys. Rev. B: Condens. Matter, **57**, 7518 (1998).
69. Y. Morioka, K. Toriumi, T. Ito, A. Saito, and I. Nakagawa. J. Phys. Soc. Jpn. **54**, 2184 (1985).
70. J.C. Taylor, M.H. Mueller, and R.L. Hitterman. Acta Crystallogr. Sect. A: Cryst. Phys. Diffr. Theor. Gen. Crystallog. **26**, 559 (1970).
71. G. Wilkinson. Comprehensive coordination chemistry. Vol. 7. Pergamon Press, Oxford. 1986.
72. N.H. Pilkington and R. Robson. Aust. J. Chem. **23**, 2225 (1970).
73. B.H. Hataway and A.E. Underhill. J. Chem. Soc. 3091 (1961).
74. H.H. Zhang, A. Filipponi, A. Di Cicco, M.J. Scott, R.H. Holm, B. Hedman, and K.O. Hodgson. J. Am. Chem. Soc. **119**, 2470 (1997).
75. Anonymous. Webelements. <http://www.webelements.com> (accessed 30 January 2000).
76. P.S. Halasyamani, S.M Walker, and D. O'Hare. J. Am. Chem. Soc. **121**, 7415 (1999).
77. S.M. Walker, P.S. Halasyamani, S. Allen, and D. O'Hare. J. Am. Chem. Soc. **121**, 10513 (1999).
78. K. Chondroudis and M.G. Kanatzidis. J. Am. Chem. Soc. **119**, 2574 (1997).
79. E. Simoni, H. Abezeli, A. Cousson, and M. Pages. Radiochem. Radioanal. Lett. **49**, 37 (1981).
80. J.C. Bailar, H.J. Emeleus, R. Nyholm, and A.F. Trotman-Dickenson. Comprehensive inorganic chemistry. Vol. 5. Pergamon Press, Oxford. 1973.
81. G.T. Seaborg. Radiochemistry, **61**, 115 (1993).
82. S.A. Bartenev, G.S. Markov, V.N. Romanovskii, and N.N. Khramov. Radiochemistry (Moscow), **40**, 3 (1998).
83. C. Den Auwer, M.C. Charbonnel, M.G.B. Drew, M. Grigoriev, M.J. Hudson, P.B. Iveson, C. Madic, M. Nierlich, M.T. Presson, R. Revel, M.L. Russel, and P. Thuery. Inorg. Chem. **39**, 1487 (2000).

Appendix

Feff7 parameters

The following parameters are used for the Feff7.02 calculation at the Fe K edge for complex **5**: (*i*) RMAX = 8 (Å) which represents the maximum effective distance of a given path; (*ii*) SIG2 = 0.003 (Å) which is the square the global Debye–Waller factor to be used for all paths; (*iii*) CRITERIA 7 2 = represents the filter devoted to eliminate the paths beyond 2% of largest path (in a first plane wave approximation) and then to eliminate the scattering paths beyond 7% (in a full curved wave calculation);(*iv*) NLEG = 8 stands for the maximum number of scattering paths; (*v*) CORRECTION = –13 1.0: increase the E_0 value taken by Feff by 13.0 eV and add 1 eV of broadening.

© 2000 NRC Canada

The one-electron oxidation of hydroxy(tetramesitylporphyrinato)iron(III)

David H. Jones and A. Scott Hinman

Abstract: The oxidation of hydroxy(tetramesitylporphyrinato)Fe(III) ([Fe(tmp)]OH) has been investigated by voltammetric and spectroelectrochemical techniques in CH_2Cl_2 containing tetra(*n*-butyl)ammonium hexafluorophosphate as supporting electrolyte. In this medium, the first one-electron oxidation is reversible on the time scale of cyclic voltammetry. The UV–vis spectrum, as obtained by double potential step chronoabsorptometry, indicates that the oxidation is centered at the porphyrin ring to form the corresponding π-cation radical. At longer times, or higher potentials, oxidation of [Fe(tmp)]OH leads to loss of hydroxide and formation of [Fe(tmp$^+$)]PF_6 π-cation radical. The time-dependent process is consistent with an ECE type mechanism, with the chemical step being slow conversion to neutral [Fe(tmp)]PF_6. At higher potentials, the initial oxidation product loses a second electron. The overpotential dependent oxidation suggests an EEC type mechanism with the second electrochemical step being a slow heterogeneous electron transfer from the Fe-OH moiety.

Key words: hydroxy(tetramesitylporphyrinato)iron(III), oxidation, electrochemistry, spectroelectrochemistry, π-cation radical.

Résumé : Faisant appel à des techniques voltampérométriques et spectroélectrochimiques, on a étudié l'oxydation de l'hydroxy(tétramésitylporphyrinato)Fe(III) ([Fe(tmp]OH) dans du CH_2Cl_2 contenant de l'hexafluorophosphate de tétra(*n*-butyl)ammonium comme électrolyte de support. Dans ce milieu, à l'échelle de temps de la voltampérométrie cyclique, la première oxydation à un électron est réversible. Le spectre UV–vis, tel qu'obtenu par la chronoabsorptométrie, indique que l'oxydation est centrée sur le noyau porphyrine et qu'elle conduit au radical cation-π correspondant. À des temps plus grands ou à des potentiels plus élevés, l'oxydation du [Fe(tmp]OH conduit à une perte de l'hydroxyde et à la formation du radical cation-π [Fe(tmp$^+$)]PF_6. Le processus qui varie avec le temps est en accord avec un mécanisme de type ECE dans lequel la première étape est une transformation lente en [Fe(tmp)]PF_6 neutre. À des potentiels plus élevés, le produit de l'oxydation initiale perd un deuxième électron. L'oxydation qui varie avec le surpotentiel suggère que le mécanisme impliqué est de type EEC dans lequel la deuxième étape électrochimique est un transfert hétérogène lent à partir de la portion Fe-OH.

Mots clés : hydroxy(tétramésitylporphyrinato)fer(III), oxydation, électrochimie, spectroélectrochimie, radical cation-π.

Introduction

The anodic oxidation of the sterically bulky five-coordinate iron(III) tetramesitylporphyrin with hydroxide as the axial ligand ([Fe(tmp)]OH), was first reported by Bruice and co-workers (1) in 1985. The cyclic voltammetry in dichloromethane containing 0.1 M tetra(*n*-butyl)ammonium perchlorate (TBAP) showed two oxidations separated by ca. 140 mV in a potential region where the chloro derivative, [Fe(tmp)]Cl, showed a single oxidation. It was proposed that the two oxidation waves were associated with step-wise formation of an iron(IV) porphyrin and an iron(IV) porphyrin π-cation radical and low-temperature thin-layer UV–vis spectroelectrochemistry was subsequently used to spectrally characterize two electrogenerated intermediates (2).

Received November 9, 1999. Published on the NRC Research Press website on October 4, 2000.

D.H. Jones and A.S. Hinman.[1] Department of Chemistry, The University of Calgary, Calgary, AB T2N 1N4, Canada.

[1]Author to whom correspondence may be addressed. Fax: (403) 289-9488. e-mail: ashinman@ucalgary.ca

Different cyclic voltammetry was reported by Groves and Gilbert (3) for [Fe(tmp)]OH in dichloromethane containing 0.1 M TBAP and saturated with Na_2CO_3. In this case only one oxidation process at 1.0 V vs. SCE was observed. Low-temperature bulk electrolysis of the hydroxy iron(III) porphyrin complex in the presence of excess tetra(*n*-butyl)ammonium hydroxide produced a species with a UV–vis spectrum reminiscent of an oxoferryl porphyrin and not a porphyrin π-cation radical.

The difference between Groves and Gilbert's (3) voltammetry and that of Bruice and co-workers (1) was ascribed by Groves to the presence of chloride in Bruice's experiments. In response to Groves and Gilbert's (3) report, Calderwood and Bruice (4) published evidence that no chloride was present in their system and that Groves and Gilbert's voltammetry could be reproduced if wet dichloromethane was used as solvent.

Following these communications Kadish and co-workers (5) described a thorough investigation of both the oxidative and reductive electrochemistry and spectroelectrochemistry of [Fe(tmp)]OH using dc and steady-state voltammetries as well as thin-layer UV–vis spectroelectrochemistry. Their work suggested that the one-electron oxidized hydroxy iron

 © 2000 NRC Canada

porphyrin was unstable at room temperature and underwent one or more reactions producing either the chloro- or the perchlorato derivative as the final product(s).

Groves et al. (6) more recently observed that the potentials for oxidation of a series of hydroxy iron(III) porphyrins with different ring substituents correlated linearly with the potentials of the same series of chloroiron(III) porphyrins. Since chloroiron(III) porphyrins are widely accepted to undergo one-electron oxidation at the porphyrin ring, this correlation of potentials was taken as evidence that hydroxy iron(III) porphyrins also underwent initial ring oxidation.

In the studies described above, spectral characterization of the electrogenerated intermediates was not possible on the voltammetric timescale at ambient temperature. In view of the reported instability of the initial electrode product (5, 6) it was felt that further study of the electrochemical oxidation of [Fe(tmp)]OH was in order. In addition to more conventional voltammetric and thin-layer spectroelectrochemical techniques, we have applied double potential step chronoabsorptometry (7) under conditions of semiinfinite linear diffusion to determine the UV–vis spectrum of the initial one-electron oxidation product.

Experimental

Materials

Tetramesitylporphyrin ($tmpH_2$)was prepared according to literature methods (8–10). Chloro(tetramesitylporphyrinato)iron(III) ([Fe(tmp)]Cl) was obtained from $tmpH_2$ and $FeCl_2 \cdot 4H_2O$ according to Adler et al.'s (11) DMF method. This material was converted to the hydroxide form by stirring a 1 mM toluene solution of the iron porphyrin against an equal volume of 1 M NaOH according to a published procedure (12). The UV–vis spectrum (toluene) was identical to that previously reported.

Dichloromethane was shaken with alumina, distilled from P_2O_5 onto CaH_2, and stored over CaH_2 prior to use. Tetra(*n*-butyl)ammonium perchlorate (TBAP) from Fluka was recrystallized from isopropanol–water and dried at 80°C in vacuo for several days. Tetra(*n*-butyl)ammonium hexafluorophosphate ($TBAPF_6$) was prepared as previously described (13).

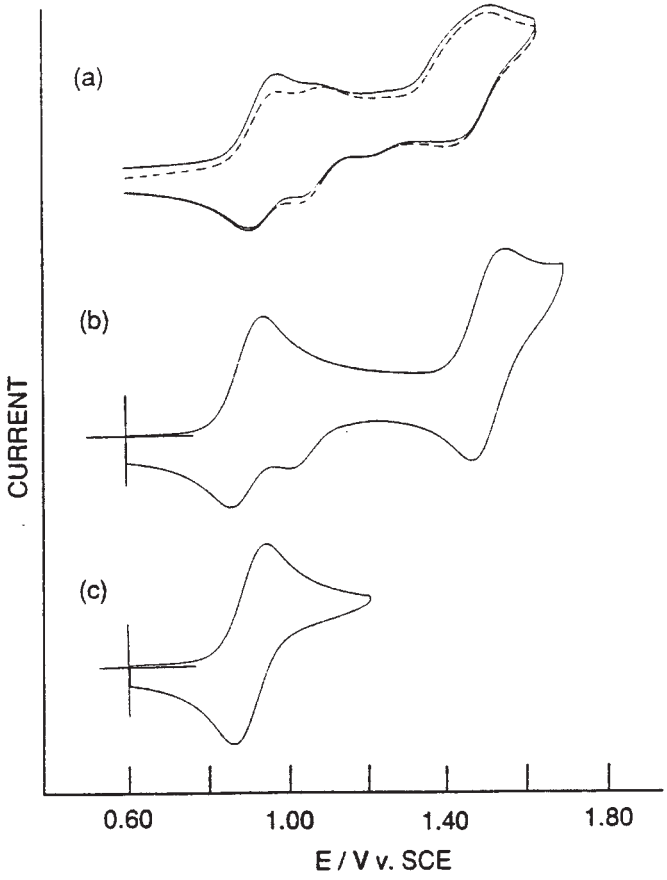
Electrochemistry

The cells and instrumentation used for conventional cyclic voltammetry and potential pulse measurements (14), and for thin-layer voltammetric measurements (15) have been described previously. Either a homemade aqueous SCE (16) or a Ag–$AgPF_6$ quasi reference electrode was employed. The latter was prepared by immersing a Ag wire in CH_2Cl_2 containing $TBAPF_6$ and a crystal of $AgPF_6$ for 24 h prior to use.

Spectroelectrochemistry

Thin-layer UV–vis and in situ FTIR reflectance spectroelectrochemistry employed the same cell as used for thin-layer voltammetry (15). The instrumentation and methodology for the in situ FTIR measurements are as in ref. (15). For thin-layer UV–vis measurements, a reflectance optical arrangement was employed along with a spinning, grating monochromator to facilitate rapid spectral measurement. The instrumentation and methodology have been fully described elsewhere (17). The cell, instrumentation, and methodology for double potential step chronoabsorptometry are fully described in ref. (18).

Fig. 1. Cyclic voltammetry of 1 mM [Fe(tmp)]OH in dichloromethane containing (*a*) 0.1 M TBAP and (*b*), (*c*) 0.1 M $TBAPF_6$. The sweep rate for all experiments was 100 mV s^{-1}.



Results

Cyclic voltammetry

The room temperature dc cyclic voltammetry of [Fe(tmp)]OH in dichloromethane containing 0.1 M TBAP is shown in Fig. 1. The voltammetry is essentially identical to that previously reported by Kadish and co-workers (5) and shows two oxidation processes with half-wave potentials of 0.97 and 1.08 V vs. At higher potentials further oxidation is evident. Close inspection suggests the presence of a very weak anodic peak near 1.28 V apparently coupled to a cathodic peak at 1.22 V on the reverse scan. Another anodic peak at 1.55 V is coupled to a cathodic peak at 1.44 V. An apparent shoulder on the 1.55 V peak suggests there may be two closely spaced oxidations occuring in this potential region.

During a subsequent scan (Fig. 1*a*, dashed line) initiated immediately following completion of the first cycle, it is seen that the relative magnitude of the anodic peak currents corresponding to the oxidations at 0.97 and 1.08 V is altered. Thus, in the initial experiment the oxidation process at 0.97 V has the larger peak current (solid line). During the

© 2000 NRC Canada

repeat cycle (dashed line) it is the oxidation at 1.08 V which gives rise to the larger peak current.

The voltammetry of the hydroxide complex in CH_2Cl_2 containing $TBAPF_6$ is shown in Fig. 1*b*. The use of hexafluorophosphate over perchlorate as the supporting electrolyte anion produces significant changes in the voltammetry. Two oxidation processes are observed at 0.90 V and 1.51 V vs. SCE. In addition a cathodic wave is observed at 1.01 V. Thus, a comparison of Figs. 1*a* and 1*b* shows that the forward oxidation wave for the oxidation process at 1.08 V in CH_2Cl_2 containing 0.1 M TBAP is not clearly evident when $TBAPF_6$ is the supporting electrolyte. Steady-state cycling between 0.4 V and 1.7 V causes a new anodic peak at 1.08 V to grow in, resulting in voltammetry very similar to that observed in CH_2Cl_2 – 0.1 M TBAP. The half-wave potential of this oxidation in CH_2Cl_2 containing 0.1 M $TBAPF_6$ is estimated to be 1.04 V vs. SCE.

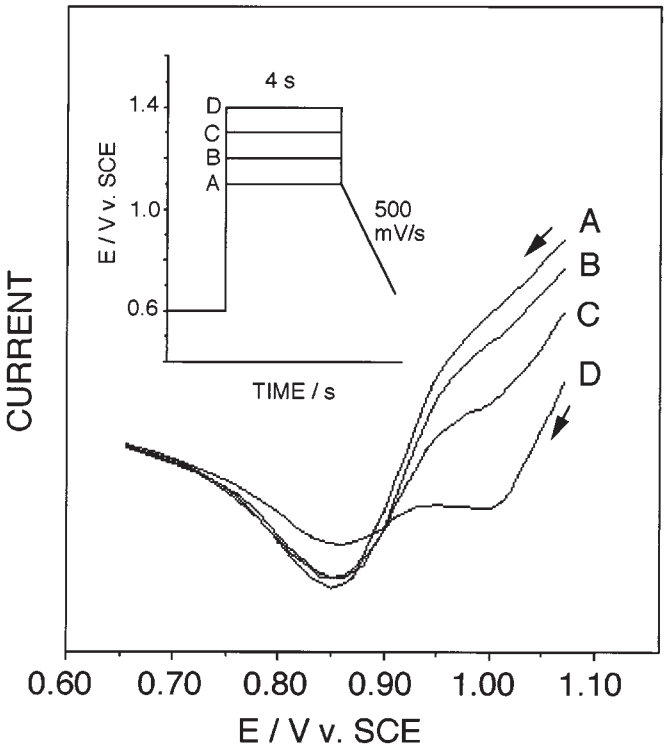
If the potential is switched at 1.20 V instead of 1.75 V then the initial oxidation process becomes completely reversible with a half-wave potential of 0.90 V vs. SCE (Fig. 1*c*). No evidence of the oxidation process at 1.04 V is seen. The reverse to forward peak current ratios for the process at 0.90 V are unity in the range 50–150 mV s^{-1}. The peak current is also proportional to the square root of the sweep rate for sweep rates in the range 50–150 mV s^{-1}. At a sweep rate of 25 mV s^{-1} the reverse to forward peak current ratio was 0.9. All subsequent electrochemical and spectroelectrochemical experiments utilized 0.1 M $TBAPF_6$ as supporting electrolyte.

In comparing the voltammetries of Figs. 1*b* and 1*c*, it is not clear whether the apparent irreversibility of the first oxidation and the appearance of the new cathodic peak at 1.01 V in 1*b* is due to the higher potentials reached on the anodic sweep, or to the longer time which the initial oxidation product exists in the diffusion layer prior to initiating its reduction. A combination of potential steps and a potential sweep was used to further probe the voltammetry of [Fe(tmp)]OH. In a first experiment (A), the potential was stepped from 0.6 V to 1.1 V for a 4 s period. The potential was then immediately swept back to 0.6 V at 500 mV s^{-1}. After a 30 s delay to allow the analyte solution to relax, experiment B was initiated whereby the potential was stepped from 0.6 V to 1.2 V for a 4 s period, and then immediately stepped back to 1.1 V and swept back to 0.6 V. Experiments C and D are similar to experiment B except that the potential steps were to 1.3 and 1.4 V, respectively. Thus, the overall time of the four experiments (A–D) is the same but the 4 s electrolysis occurs at increasingly positive potentials.

The potential sweeps from 1.1 V to 0.6 V resulting from experiments A–D are shown in Fig. 2. It is seen that the cathodic peak at 1.01 V increases as higher potentials are accessed, and this occurs concomitant with a decrease in the reduction wave for the initial oxidation process. This dependence on overpotential indicates that at least one step in the formation of the species giving rise to the reduction peak at 1.01 V involves a slow, irreversible heterogeneous electron transfer process

It was observed that over extended periods of time, [Fe(tmp)]OH in CH_2Cl_2 spontaneously converted to [Fe(tmp)]Cl. This is consistent with other workers' observations (6). In our case, the use of the aqueous SCE reference

Fig. 2. Current vs. potential during the potential sweep portion of the potential programs illustrated in the inset. The solution was 0.25 mM [Fe(tmp)]OH in CH_2Cl_2 – 0.1 M $TBAPF_6$.



electrode appeared to accelerate this problem, likely through slow leakage of either chloride or water into the CH_2Cl_2 solutions. Use of a Ag–$AgPF_6$ quasi reference electrode in subsequent electrochemical experiments prevented any observable formation of [Fe(tmp)]Cl.

Double potential step chronoabsorptometry

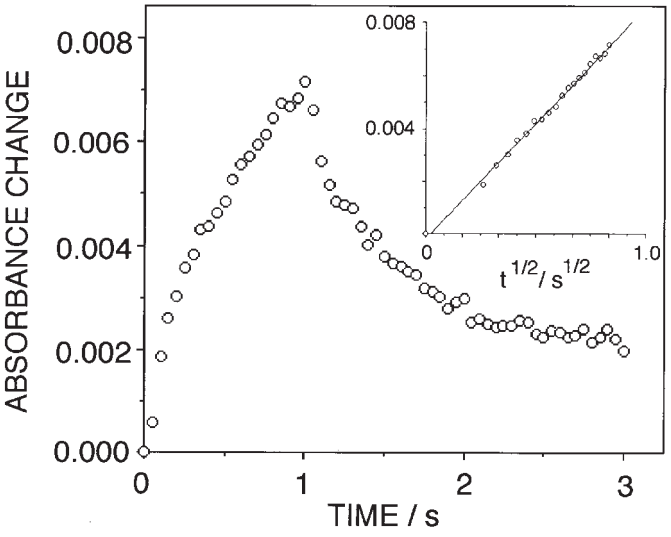
Since the initial oxidation wave with half-wave potential at 0.90 V is reversible at moderate sweep rates provided that the switching potential is not too positive, it was possible to generate the UV–vis spectrum of the one-electron oxidized species using short timescale chronoabsorptometric experiments carried out under conditions of semiinfinite linear diffusion. In this technique, a potential step is applied, and the change in absorbance (ΔA) of monochromatic light reflected from the electrode surface is monitored as function of time. For a reversible electron transfer process, the change in absorbance is given (7) by:

$$[1] \qquad \Delta A = \frac{4\Delta\varepsilon C D^{1/2} t^{1/2}}{\pi^{1/2}\cos\theta}$$

Here, $\Delta\varepsilon$ is the difference between the molar absorptivities of the product and starting material in the electrode reaction, D is the diffusion coefficient of the electroactive species, θ is the angle of incidence of the reflected light beam, and other terms have their usual significance. If the diffusion coefficient of the electroactive species is known, it is possible to determine the difference between molar absorptivities of the product and starting material for the electrode reaction from the slope of a plot of ΔA vs. $t^{1/2}$.

© 2000 NRC Canada

Fig. 3. Absorbance–time transient recorded at 350 nm for 0.05 mM [Fe(tmp)]OH during double potential step chronoabsorptometry of the first one-electron oxidation in CH_2Cl_2 containing 0.1 M $TBAPF_6$. The transient is the average of 64 experiments. Data reduction and smoothing was done with a 10 point box car averaging routine. The inset is a plot of the absorbance change against the square root of time for the forward step.



If the molar absorptivity of the starting material is known, then the molar absorptivity of the product is readily determined. Linearity of the ΔA vs. $t^{1/2}$ plot is an indication of reversibility of the electron transfer reaction. In double potential step chronoabsorptometry, the potential is stepped back to its intial value after a period τ. For a reversible reaction, the ratio ΔA ($t = 2\tau$)/ΔA ($t = \tau$) will be equal to 0.414, providing further indication of the reversibility.

Absorbance–time transients were recorded at single wavelengths in the range 350–690 nm at intervals of 20 nm. A total of 64 transients were collected at each wavelength and averaged. Data reduction and smoothing was done with a 10-point boxcar average. Analyte concentrations were adjusted to produce an absorbance in the range 1.0–1.5 in the chronoabsorptometric cell at the analytical wavelength and were in the range 10^{-4}–10^{-5} M. The potential was stepped to a point 120 mV beyond the forward voltammetric peak potential of the initial oxidation for 1 s and then stepped back to the base potential for 12 s prior to initiating a subsequent potential step. The spectra of the analyte solutions recorded prior to and after the experiments indicated that the iron(III) porphyrin remained in the hydroxide form. Cyclic voltammetry recorded before and after each spectroelectrochemical experiment indicated that reversibility was maintained and that there were no local fluctuations of the analyte concentration in the vicinity of the working electrode.

The absorbance–time transient for the experiment performed at 350 nm is shown in Fig. 3. The ratio of the absorbance at time 2τ relative to that at time τ is 0.414 ± 0.017 in excellent agreement with theory (0.414). Absorbance–time responses at other wavelengths also indicated that the absorbance changes were due to a reversible one-electron oxidation process without any complications during the timescale of the experiment.

A plot of the absorbance change for the forward step against the square root of the elapsed time is shown in the inset of Fig. 3. The plot is linear for data collected at 100 ms and beyond and yields a zero intercept as predicted by theory. Since the bulk analyte concentration is known, and the diffusion coefficient was determined by chronoamperometry to be 5.33×10^{-6} cm^2 s^{-1}, the change in molar absorptivity, $\Delta\varepsilon$ may be calculated from the slope according to eq. [1].

Figure 4 shows the UV–vis spectrum of the species produced from the reversible one-electron oxidation of [Fe(tmp)]OH (circles). The spectrum has been calculated from the molar absorptivity changes determined from chronoabsorptometric experiments carried out at different wavelengths. The spectrum of the parent hydroxy iron(III) porphyrin is shown for comparison (solid line). The spectral changes associated with the one-electron oxidation of [Fe(tmp)]Cl in dichloromethane containing TBAP as measured by time-resolved thin-layer UV–vis spectroelectrochemistry are also shown in the inset of Fig. 4. Chloroiron porphyrins are generally accepted to give π-cation radicals on one-electron oxidation. To confirm that [Fe(tmp)]Cl is not an exception, the in situ FTIR difference spectrum associated with its one-electron oxidation in CH_2Br_2 containing 0.1 M $TBAPF_6$ was carried out. The oxidized product had a strong new infrared band at 1280 cm^{-1} which is a marker for ring-oxidation in tetraphenylporphyrins (13).

The UV–vis spectral changes accompanying the 1 e^- oxidation of [Fe(tmp)]OH and [Fe(tmp)]Cl both involve a broadening and blue-shifting of the Soret band and the appearance of a broad absorbance in the visible region, as evident in Fig. 4. Such changes are characteristic of porphyrin π-cation radical formation. These results strongly suggest that the site of one-electron oxidation is the same for both complexes and is centred at the porphyrin ring forming iron(III) porphyrin π-cation radicals.

In situ FTIR spectroelectrochemistry of 2 mM [Fe(tmp)]OH in CH_2Br_2 containing 0.1 M $TBAPF_6$ was carried out. A band at 1278 cm^{-1} appeared during electrolysis at 1.1 V indicating formation of a porphyrin π-cation radical. However, this infrared band cannot be unambiguously ascribed to the $1e^-$ oxidized [Fe(tmp)]OH since there is evidence (vide infra) that hydroxide would not remain coordinated to the iron porphyrin during the thin-layer experiment.

Thin-layer voltammetry and simultaneous linear potential sweep UV–vis spectroelectrochemistry

Figure 5 shows the thin-layer voltammetry of 0.5 mM [Fe(tmp)]OH in dichloromethane containing 0.1 M $TBAPF_6$ carried out in an external reflectance thin-layer spectroelectrochemical cell. On the positive sweep it is seen that there are three major oxidation processes with anodic peak potentials at 0.26, ca. 0.35 (shoulder), and 0.53 V vs. the Ag–$AgPF_6$ quasi reference electrode. On the reverse sweep only one major reduction with a reverse peak potential at 0.26 V vs. the Ag–$AgPF_6$ quasi reference electrode is observed. It is notable that the main reduction peak is actually 10 mV *anodic* of the main oxidation peak. The theoretical response for a chemically reversible process is expected to

© 2000 NRC Canada

Fig. 4. UV–vis spectra of Fe(tmp)OH (solid line) and its one-electron oxidation product (circles) in dichloromethane solvent. The inset shows time-resolved thin-layer UV–visible spectra for the oxidation of Fe(tmp)Cl in dichloromethane containing 0.1 M TBAP. Thin-layer spectra were recorded at 2.7 s intervals.

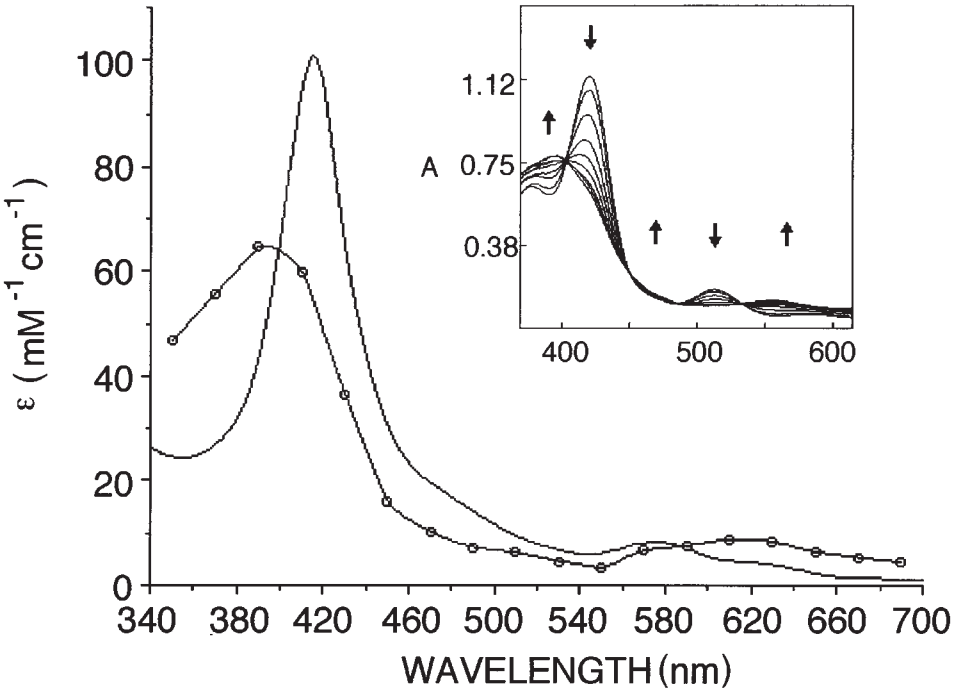
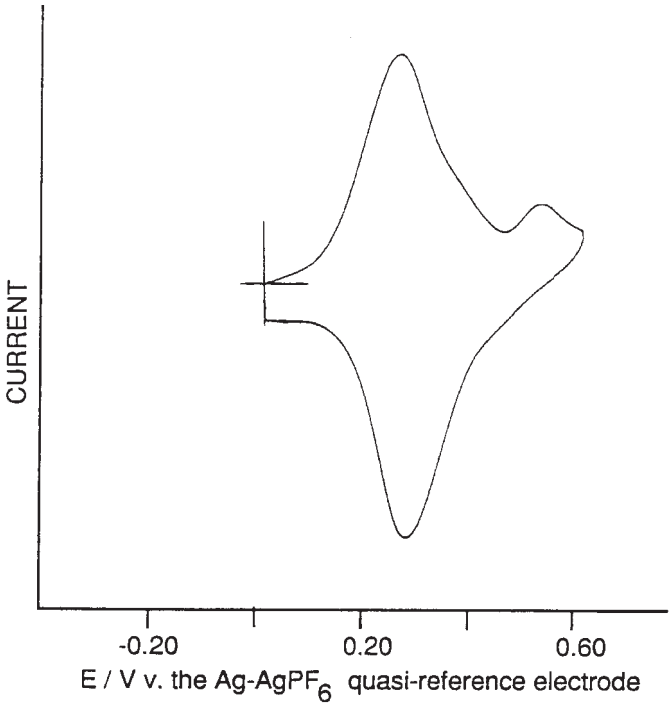


Fig. 5. Thin-layer cyclic voltammetry of 0.5 mM [Fe(tmp)]OH in CH_2Cl_2 containing 0.1 M Bu_4NPF_6. Sweep rate is 5 mV s^{-1}. Potentials are vs. the Ag–$AgPF_6$ quasi reference electrode.



have coincident forward and reverse peak potentials. However, in a real thin-layer cell iR drops arising from solution resistance will tend to make the reduction peak potential more cathodic than the corresponding oxidation peak potential. For this thin-layer cell and solvent system, the cathodic peak typically lies 100 mV negative of the anodic peak for a reversible redox couple under similar conditions. The clear inference here is that the reduction peak does not correspond to reduction of the initial oxidation product.

The thin layer UV–vis spectral changes recorded during the thin-layer cyclic voltammetry experiment shown in Fig. 5 at potentials between 0.00 V to 0.42 V vs. the Ag–$AgPF_6$ quasi reference electrode on the forward sweep are shown in Fig. 6*a*. The spectra show the average absorbance change in sequential 14 s time periods. This translates into a potential separation between spectra of ca. 70 mV. Comparison of the spectral changes with the calculated spectrum of one-electron oxidized [Fe(tmp)]OH (Fig. 4) show that this species is formed initially. However, loss of isosbestic points associated with the oxidation at ca. 0.35 V indicates that at least one additional porphyrin species is formed.

The thin-layer UV–vis spectral changes recorded during the thin-layer cyclic voltammetry experiment at potentials between 0.42 V on the forward sweep and 0.51 V on the reverse sweep show formation of another porphyrin species with peaks at 520 and 589 nm (Fig. 6*b*). This species is associated with the irreversible oxidation at 0.53 V. The thin-layer UV–vis spectral changes recorded during the thin-layer cyclic voltammetry experiment at potentials between 0.5 V and 0.00 V on the reverse scan are shown in Fig. 6*c*. This process shows loss of the species with bands at 520 and 589 nm and reduction of one or more oxidized porphyrin species to form a final spectrum of an unoxidized iron(III) porphyrin which is not due to either [Fe(tmp)]OH or

© 2000 NRC Canada

[Fe(tmp)]Cl. Since the only other counter-ion available is PF_6^-, the spectrum is indicated to be due to [Fe(tmp)]PF_6. This species has not, to our knowledge, been isolated, and its spectrum has not been previously reported.

Discussion

Cyclic voltammetry of [Fe(tmp)]OH shows that the first one-electron oxidation at 0.90 V vs. SCE is chemically reversible in dichloromethane at room temperature at moderate sweep rates provided $TBAPF_6$ is used as the supporting electrolyte and that potentials do not become too positive. The UV–vis spectrum of one-electron oxidized [Fe(tmp)]OH as evidenced by chronoabsorptometry is qualitatively similar to that of one-electron oxidized [Fe(tmp)]Cl and is typical of iron(III) porphyrin π-cation radicals (19). That one-electron oxidation of the chloro complex produces a porphyrin π-cation radical is further evidenced by the strong appearance band at 1280 cm^{-1} in the in situ FTIR difference spectrum associated with the electrode reaction. This clearly indicates that the changes occurring to the porphyrin infrared bands are consistent with a porphyrin ring-centred process (13).

On the basis of this evidence it is proposed that both [Fe(tmp)]Cl and [Fe(tmp)]OH undergo one-electron oxidation centred at the porphyrin ring to produce iron(III) porphyrin π-cation radicals. Thus, one hydroxide axial ligand does not appear capable of stabilizing an iron(IV) porphyrin under the experimental conditions.

At the lower sweep rates associated with thin-layer voltammetry, the first one-electron oxidation is no longer reversible. The initial oxidation product reacts to form a new species which undergoes a further oxidation, as indicated by the shoulder at 0.35 V vs. Ag–$AgPF_6$ quasi reference electrode (Fig. 5). Reduction of the product of this second oxidation produces an Fe(III) porphyrin which is neither the hydroxide nor the chloride, as evidenced by the spectral changes in Fig. 6*c*. In CH_2Cl_2 containing TBAP, the oxidation of [Fe(tmp)]OH has been suggested (5, 6) to follow an ECE mechanism in which hydroxide is lost to produce [Fe(tmp)]ClO_4, which is then subject to a further reversible one-electron oxidation. A similar mechanism in CH_2Cl_2–$TBAPF_6$ to produce [Fe(tmp)]PF_6, as indicated in rxns. [2]–[4], would account for our observations.

[2] [Fe(tmp)]OH – $1e^-$ ⇌ Fe(tmp^+)OH

[3] [Fe(tmp^+)]OH + PF_6^- → [Fe(tmp)]PF_6 + OH

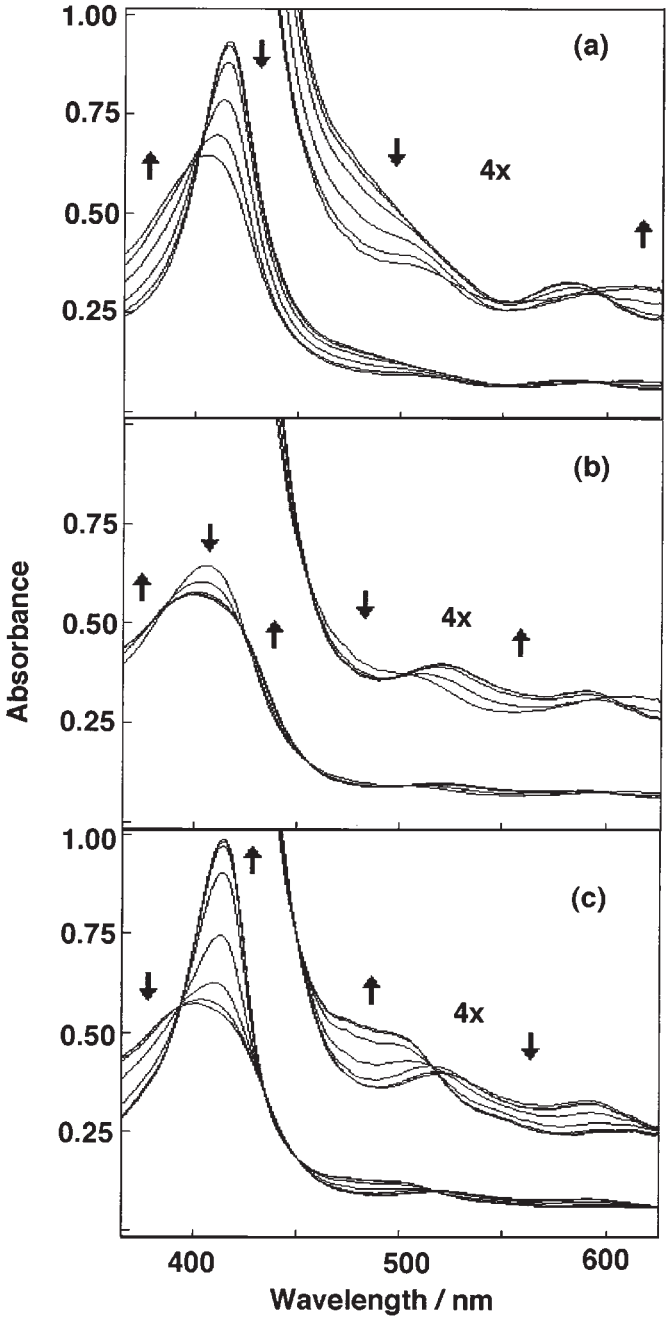
[4] [Fe(tmp)]PF_6 $-1e^-$ ⇌ [Fe(tmp^+)]PF_6

Since PF_6^- is less strongly coordinating than ClO_4^-, rxn. [3] would be less favoured with PF_6^- as the supporting electrolyte anion than ClO_4^-. This would account for the greater stability of the [Fe(tmp^+)]OH π-cation radical observed in CH_2Cl_2–$TBAPF_6$.

We have not investigated supporting electrolyte anions other than perchlorate and hexafluorophosphate with this system.

The appearance of an additional anodic peak at 0.53 V vs. the Ag–$AgPF_6$ quasi reference electrode in the thin-layer voltammetry of Fig. 5 indicates that the initial one-electron oxidation product may also react by a different pathway than rxn. [4], to produce a species which oxidizes at higher potential than does [Fe(tmp)]PF_6. This oxidation is accompanied by the appearance of bands at 520 and 589 nm in the UV–vis. spectra of Fig. 6*b*. The identity of this porphyrin species cannot be unambiguously assigned on the basis of the results. The bands at 520 and 589 nm are not characteristic of either iron(III) porphyrin π-cation radicals (19) or oxoferryl porphyrins (20). On the other hand, the UV–vis spectrum of iron(III) tetramesitylporphyrin *N*-oxide — which

Fig. 6. Thin-layer UV–visible spectral changes recorded during the thin-layer cyclic voltammetry experiment shown in Fig. 5 at potentials between (*a*) 0.00–0.42 V vs. the Ag–$AgPF_6$ quasi reference electrode on the forward sweep; (*b*) 0.42 V on the forward sweep and 0.51 V on the reverse sweep; (*c*) 0.51 and 0.00 V on the reverse sweep.



© 2000 NRC Canada

has oxo-bridging iron and a pyrrole nitrogen — and that of the *N*-hydroxy cation formed by protonation of the *N*-oxide, do exhibit similar spectral features (21). These species are formed on oxidation of [Fe(tmp)]OH by *meta*-chloroperoxybenzoic acid. It seems possible that such species might also be formed on heterogeneous oxidation. Thus, rxns. [5] and [6], provide a plausible account for our observations.

[5] $[Fe(tmp^+)]OH + PF_6^- \rightarrow [Fe(tmpOH)]PF_6$

[6] $[Fe(tmpOH)]PF_6 - 1e^- \rightarrow [Fe(tmp^+OH)]PF_6$

In [5], hydroxide migrates from Fe to one of the pyrrole nitrogens of the porphyrin π-cation radical to give an *N*-hydroxy porphyrin. This could undergo electron loss to produce the *N*-hydroxy porphyrin cation, as in [6]. It is possible for the *N*-hydroxy cation to lose a proton to form the bridged *N*-oxide species.

The combined potential step – potential sweep experiments of Fig. 2 indicate that the initial one-electron oxidation product is susceptible to further oxidation. This process is over-potential dependent, indicating a slow heterogeneous electron transfer process, and results in loss of hydroxide to form $[Fe(tmp+)]PF_6$, as evident from its reduction potential. The process is represented in rxn. [7].

[7] $[Fe(tmp^+)]OH - 1e^- + PF_6^- \rightarrow [Fe(tmp^+)]PF_6 + OH$

The over-potential dependence of this process is not consistent with porphyrin ring oxidation, clearly suggesting the oxidation is associated with the Fe-OH moeity of the porphyrin complex to give, at least formally, a hydroxy iron(IV) species. This species then eliminates OH to give the Fe(III) cation-radical. The overall conversion of [Fe(tmp)]OH to the $[Fe(tmp^+)]PF_6$ π-cation radical in this case follows an EEC type mechanism.

Acknowledgements

The authors are grateful to the Natural Sciences and Engineering Research Council of Canada for financial support.

References

1. W.A. Lee, T.S. Calderwood, and T.C. Bruice. Proc. Natl. Acad. Sci. U.S.A. **82**, 4301 (1985).
2. T.S. Calderwood, W.A. Lee, and T.C. Bruice. J. Am. Chem. Soc. **107**, 8272 (1985).
3. J.T. Groves and J.A. Gilbert. Inorg. Chem. **25**,125 (1986).
4. T.S. Calderwood and T.C. Bruice. Inorg. Chem. **25**, 3722 (1986).
5. C. Swistak, X.H. Mu, and K.M. Kadish. Inorg. Chem. **26**, 4360 (1987).
6. J.T. Groves, Z. Gross, and M.K. Stern. Inorg. Chem. **33**, 5065 (1994).
7. D.H. Jones and A.S. Hinman. Can. J. Chem. **74**, 1403 (1996).
8. M. Kihn-Botulinski and B. Meunier. Inorg. Chem. **26**, 210 (1988).
9. J.S. Lindsey, I.C. Shreiman, H.C. Hsu, P.C. Kearney, and A.M. Marguerettaz. J. Org. Chem. **52**, 827 (1987).
10. R.W. Wagner, D.S. Lawrence, and J.S. Lindsey. Tetrahedron Lett. **28**, 3069 (1987).
11. A.D. Adler, F.R. Longo, F. Kampas, and J. Kim. J. Inorg. Nucl. Chem. **32**, 2443 (1970).
12. R.J. Cheng, L. Latos-Grazynski, and A.L. Balch. Inorg. Chem. **21**, 2412 (1982).
13. D.H. Jones and A.S. Hinman. J. Chem. Soc. Dalton Trans. 1503 (1992).
14. A.S. Hinman, B.J. Pavelich, A.E. Kondo, and S. Pons. J. Electroanal. Chem. **234**, 145 (1987).
15. A.S. Hinman and B.J. Pavelich. Can. J. Chem. **65**, 919 (1987).
16. R.N. Adams. Electrochemistry at solid electrodes. Marcel Dekker, New York. 1969.
17. D.H. Jones and A.S. Hinman. Can. J. Chem. **68**, 2234 (1990).
18. D.H. Jones and A.S. Hinman. Can. J. Chem. **74**, 1403 (1996).
19. P. Gans, G. Buisson, E. Duee, J.-C. Marchon, W.F. Scholz, and C.A. Reed. J. Am. Chem. Soc. **108**, 1223 (1986).
20. A. Gold, K. Jayaraj, P. Doppelt, R. Weiss, G. Chottard, E. Gill, X. Ding, and A.X. Trautwein. J. Am. Chem. Soc. **110**, 5756 (1988).
21. H. Tsurumaki, Y. Watanabe, and I. Morishima. J. Am. Chem. Soc. **115**, 11784 (1993).

© 2000 NRC Canada

Nitrones and oximes of bifunctional carbonyl compounds and their reaction products with diarylborinic acids. Crystal and molecular structure of examples of five-, six-, and seven-membered boron chelates[1]

Wolfgang Kliegel, Gottfried Lubkowitz, Jens O. Pokriefke, Steven J. Rettig, and James Trotter

Abstract: Synthesis has been carried out of diarylboron chelates of 2- and 3-hydroxynitrones, of 2- and 3-hydroxyoximes, and of 2-carboxynitrones and a 2-carboxyoxime. The structures have been determined from spectroscopic data and from X-ray analyses of **5*d***, **9*a***, **11*b***, and **19**. Crystals (at 180 K) of **5*d*** are monoclinic, a = 10.543(2), b = 19.085(4), c = 10.2667(3) Å, β = 90.4978(7)°, Z = 4, space group $P2_1/c$; those of **9*a*** are orthorhombic, a = 10.9913(5), b = 14.9329(7), c = 10.2460(13) Å, Z = 4, space group $P2_12_12_1$; those of **11*b*** are monoclinic, a = 11.227(2), b = 9.967(2), c = 17.0537(4) Å, β = 105.4179(5)°, Z = 4, space group $P2_1/n$; those of **19** are monoclinic, a = 11.1847(15), b = 13.715(3), c = 11.5559(5) Å, β = 104.8730(10)°, Z = 4, space group $P2_1/n$. The structures were solved by direct methods and refined by full-matrix least-squares procedures to $R(F, I \geq 3\sigma(I))$ = 0.049, 0.047, 0.042, and 0.047, respectively, for CCD data for **5*d***, **9*a***, **11*b***, and **19**. The four molecules contain five-, seven-, six-, and five-membered rings, respectively, with O-B-N groups in the **5*d***, **11*b***, and **19**, and O-B-O in **9*a***; the rings exhibit various deviations from planarity, particularly the seven-membered ring.

Key words: diarylboron chelates, hydroxyoximes, hydroxynitrones, carboxyoximes, carboxynitrones, organoboron compounds, crystal structure.

Resumé : On a réalisé la synthèse de chélates du diarylbore avec de 2- et 3-hydroxynitrones, de 2- et 3-hydroxyoximes, de 2-carboxynitrones et d'une 2-carboxyoxime. On a déterminé les structures à partir de données spectroscopiques et d'analyses par diffraction des rayons X des composés **5*d***, **9*a***, **11*b*** et **19**. Les cristaux du composé **5d** sont monocliniques (à 180 K), groupe d'espace $P2_1$/c avec a = 10,543(2), b = 19,085(4) et c = 10,2667(3) Å, β = 90,4978(7)° et Z = 4; ceux du composé **9*a*** sont orthorhombiques, groupe d'espace $P2_12_12_1$, avec a = 10,9913(5), b = 14,9329(7) et c = 10,2460(13) Å et Z = 4; ceux du composé **11*b*** sont monocliniques, groupe d'espace $P2_1/n$ avec a = 11,227(2), b = 9,967(2) et c = 17,0537(4) Å, β = 105,4179(5)° et Z = 4 et ceux du composé **19** sont monocliniques, groupe d'espace $P2_1/n$ avec a = 11,1847(15), b = 13,715(3) et c = 11,5559(5) Å, β = 104,8730(10)° et Z = 4. On a résolu les structures par des méthodes directes et on les a affinées par la méthode des moindres carrés (matrices entières) jusqu'à des valeurs de $R(F, I \geq 3\sigma(I))$ = 0,049, 0,047, 0,042 et 0,047 respectivement pour les données pour les molécules **5*d*, 9*a*, 11*b*** et **19**. Les quatre molécules comportent respectivement des cycles à cinq, sept, six et cinq chaînons et des groupes O-B-N dans les molécules **5*d*, 11*b*** et **19** et O-B-O pour la molécule **9*a***; les cycles présentent des déviations diverses par rapport à la planéité, en particulier pour le cycle à sept chaînons.

Mots Clés : chélates de dialkylbores, hydroxyoximes, hydroxynitrones, carboxyoximes, carboxynitrones, composés organiques du bore, structure cristalline.

Received May 26, 2000. Published on the NRC Research Press website on October 11, 2000.

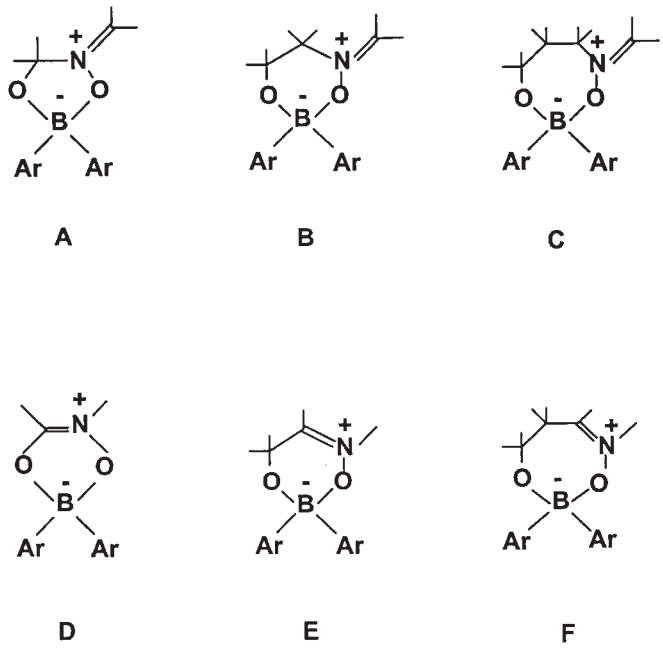
W. Kliegel, G. Lubkowitz, and J.O. Pokriefke. Institut für Pharmazeutische Chemie der Technischen Universität Braunschweig, Beethovenstrasse 55, 38106 Braunschweig, Germany.
S.J. Rettig and J. Trotter.[2] Department of Chemistry, University of British Columbia, 2036 Main Mall, Vancouver, BC V6T 1Z1, Canada.

[1]Structural studies of organoboron compounds LXXII. Previous paper in this series: ref. 38.
[2]Author to whom correspondence may be addressed. Telephone: (604) 822-4865. Fax: (604) 822-2847.
e-mail: jtrt@xray4.chem.ubc.ca

 © 2000 NRC Canada

Introduction

In the course of our investigations on cyclic boron nitrogen betaines (1) we synthesized a series of five-, six-, and seven-membered boron chelates containing bidentate nitrone ligands with an *N*-(1-hydroxyalkyl) group (2) (ring system **A**), an *N*-(2-hydroxylalkyl) group (3) or *N*-(1-carboxyalkyl) group (4) (ring system **B**), and an *N*-(3-hydroxylalkyl) group (5) (ring system **C**), all having the nitrone C=N bond located outside of the chelate ring ("exocyclic" or "semicyclic" (6, see footnote for exocyclic double bonds, p. 954)). As an extension of our work in this area we investigated comparable chelate ring structures with an "endocyclic" C=N double bond, as depicted in the ring systems **D**, **E**, and **F**. Five-membered boron chelates of type **D** had been obtained previously from various hydroxamic acid derivatives (7). We now report, continuing and completing this series, the synthesis and structural characteristics of six- and seven-membered boron chelates, type **E** and **F**, derived from the corresponding bidentate nitrones. In connection with these compounds we describe also the synthesis and structural features of several boron chelates of analogous bifunctional oximes. Unambiguous proof of coordination sites and ring geometries is furnished by X-ray crystallographic analyses in selected cases.



Experimental

General procedures

Oxybis(diphenylborane) was prepared according to literature methods (8). All reactions were carried out under normal conditions, without protective gas atmosphere. Melting points (uncorrected): Linström apparatus and Büchi SMP 20. IR: PYE-Unicam SP 3-200, Philips PU 9800 FT-IR-Spectrometer, V 3.00, and ATI Mattson Genesis Series FT-IR™ Rev. I. ^{1}H NMR: Varian EM 390 and Bruker AM 400. ^{11}B NMR: Bruker AC 200. Elemental analyses: Carlo Erba CHNO elemental analyzer 1106; boron and chlorine titrimetrically after Schöniger-oxidation with Metrohm Potentiograph E 536/Dosimat 655.

2-(Methylimino)ethanol *N*-oxide (2*a*)

Hydroxyacetaldehyde (1.20 g, 20 mmol) and *N*-methylhydroxylamine hydrochloride (1.67 g, 20 mmol) are dissolved in 20 mL of ethanol (96%) and mixed with a solution of K_2CO_3 (1.38 g, 10 mmol) in 5 mL of water under stirring. After 48 h, KCl is filtered off, the solvent removed in vacuo, and the residue taken up in 50 mL of absolute ethanol. After filtration the solvent is distilled off in vacuo. The remaining oil is not purified further, and is characterized only with NMR data. ^{1}H NMR (90 MHz, $CDCl_3$–TMS) δ (ppm): 3.65 (s, N-CH_3), 4.15 (s, broad, exchangeable, OH), 4.35 (d, J = 4 Hz, O-CH_2), 6.92 (t, J = 4 Hz, N=CH).

N-(Benzylimino)ethanol *N*-oxide (2*b*)

Hydroxyacetaldehyde (1.20 g, 20 mmol), *N*-benzylhydroxylamine hydrochloride (3.19 g, 20 mmol), and K_2CO_3 (1.38 g, 10 mmol) are reacted as described above for **2*a***. The remaining solid is recrystallized from ethanol–ether. Yield: 2.30 g (70%) of colorless plates, mp 82–84°C. IR (KBr, cm^{-1}): 3 300 and 3 170 (broad, O-H), 1610 (C=N). ^{1}H NMR (90 MHz, $CDCl_3$–TMS) δ (ppm): 4–5 (s, very broad, exchangeable, OH), 4.35 (d, J = 4 Hz, O-CH_2), 4.83 (s, N-CH_2), 6.88 (t, J = 4 Hz, N=CH), 7.37 (s, C_6H_5). Anal. calcd. for $C_9H_{11}NO$: C 65.44, H 6.71, N 8.48; found: C 65.41, H 6.71, N 8.57.

1-(Methylimino)-2-propanol *N*-oxide (2*c*)[3]

This compound was prepared as described previously (9).

1-(*tert*-Butylimino)-2-propanol *N*-oxide (2*d*)

2-Hydroxypropanal (1.48 g, 20 mmol) and *N*-*tert*-butylhydroxylamine (1.80 g, 20 mmol) are dissolved in 20 mL of absolute ethanol and stirred for 48 h at room temperature. The solvent is distilled off in vacuo. The remaining oily residue is not purified further, and is characterized only with NMR data. ^{1}H NMR (90 MHz, $CDCl_3$–TMS) δ (ppm): 1.37 (d, J = 7 Hz, OC-CH_3), 1.51 (s, $C(CH_3)_3$), 4.68 (m, 1 H exchangeable, OH and O-CH), 6.93 (d, J = 5 Hz, N=CH).

1-(Cyclohexylimino)-2-propanol *N*-oxide (2*e*)

2-Hydroxypropanal (2.22 g, 30 mmol) and *N*-cyclohexylhydroxylamine (3.45 g, 30 mmol) are reacted as described above for **2*d***. The remaining solid is recrystallized from absolute ethanol. Yield: 4.42 g (86%) of colorless needles, mp 129°C. IR (KBr, cm^{-1}): 3 210 (broad, O-H), 1 600 (C=N). ^{1}H NMR (90 MHz, $CDCl_3$–TMS) δ (ppm): 1.04–2.20 (m, $(CH_2)_5$), 1.39 (d, J = 7 Hz, CH_3), 3.64 (m, N-CH), 4.71 (m, O-CH), 5.61 (s, exchangeable, OH), 6.85 (d, J = 5 Hz, N=CH). Anal. calcd. for $C_9H_{17}NO_2$: C 63.13, H 10.01, N 8.18; found: C 63.09, H 10.15, N 7.97.

1-(Benzylimino)-2-propanol *N*-oxide (2*f*)

This compound was prepared as described previously (9).

[3] Alternative nomenclature for the compounds of type **2** (generally): *N*-(2-hydroxyalkylidene) alkanamine *N*-oxide, as used in ref. 9.

© 2000 NRC Canada

1-(Benzhydrylimino)-2-propanol *N*-oxide (2*g*)

2-Hydroxypropanal (1.48 g, 20 mmol) and *N*-benzhydrylhydroxylamine (3.98 g, 20 mmol) are reacted as described above for **2*d***. The remaining solid is recrystallized from ethanol–ether. Yield: 4.21 g (82%) of colorless crystals, mp 110–111°C. IR (KBr, cm^{-1}): 3 290 (broad, O-H), 1 590 (C=N). ^{1}H NMR (90 MHz, $CDCl_3$–TMS) δ (ppm): 1.34 (d, J = 7 Hz, CH_3), 4.71 (m, O-CH), 5.47 (s, broad, exchangeable, OH), 6.15 (s, N-CH), 6.82 (d, J = 5 Hz, N=CH), 7.32 (s, $C(C_6H_5)_2$). Anal. calcd. for $C_{16}H_{17}NO_2$: C 75.27, H 6.71, N 5.49; found: C 75.47, H 6.71, N 5.64.

3-(Cyclohexylimino)-2-butanol *N*-oxide (2*h*)

3-Hydroxy-2-butanone (0.88 g, 10 mmol) and *N*-cyclohexylhydroxylamine (1.15 g, 10 mmol) are dissolved in 30 mL of benzene and refluxed for 5 h using a Dean–Stark trap for continuous removal of water. The solution is evaporated down to one-quarter of the initial volume. After addition of 10 mL of hexane and cooling down to –18°C crystallization starts after 48 h. The air-sensitive compound can be recrystallized carefully from chloroform–ether. Yield: 0.90 g (49%) of colorless crystals, mp 118°C. IR (KBr, cm^{-1}): 3 221 (broad, O-H), 1 587 (C=N). ^{1}H NMR (90 MHz, $CDCl_3$–TMS) δ (ppm): 0.67–2.67 (m, $(CH_2)_5$), 1.37 (d, J = 6 Hz, OC-CH_3), 2.13 (s, NC-CH_3), 3.93 (m, N-CH), 4.67 (q, J = 6 Hz, O-CH), 6.53 (s, broad, exchangeable, OH). Anal. calcd. for $C_{10}H_{19}NO_2$: C 64.83, H 10.34, N 7.56; found: C 64.92, H 10.41, N 7.46.

4-Methyl-2,2-diphenyl-1,3-dioxa-4-azonia-2-borata-4-cyclohexene (3*a*)

2*a* (0.2 g of the crude product) in 1 mL of ethanol and oxybis(diphenylborane) (0.35 g, 1 mmol) in 1 mL ethanol are mixed under stirring. After 5 h at room temperature, the analytically pure crystals are filtered off and washed with ether.[4] Yield: 0.31 g (61%) of colorless crystals[6], mp 104–105°C (decomp.). IR (KBr, cm^{-1}): 1 665 (C=N). ^{1}H NMR (90 MHz, $CDCl_3$–TMS) δ (ppm): 3.14 (s, CH_3), 4.23 (m, O-CH_2), 6.25 (s, N=CH), 6.87–7.40 (m, $B(C_6H_5)_2$). Anal. calcd. for $C_{15}H_{16}BNO_2$: C 71.18, H 6.37, N 5.53; found: C 71.17, H 6.37, N 5.49. (Boron elemental analyses and NMR data were obtained only for some of the examples of compounds of type **3**.)

4-Cyclohexyl-2,2-diphenyl-1,3-dioxa-4-azonia-2-borata-4-cyclohexene (3*b*)

Hydroxyacetaldehyde (0.12 g, 2 mmol) and *N*-cyclohexylhydroxylamine (0.23 g, 2 mmol) are dissolved in 5 mL of ethanol. After addition of oxybis(diphenylborane) (0.35 g, 1 mmol) in 1 mL of ethanol the crystallization commences at room temperature or after several hours of cooling. The analytically pure crystals are filtered off and washed with ether.[4] Yield: 0.43 g (77%) of colorless crystals[6], mp 131°C (decomp.). IR (KBr, cm^{-1}): 1 653 (C=N). ^{1}H NMR (90 MHz, $CDCl_3$–TMS) δ (ppm): 0.80–2.47 (m, $(CH_2)_5$), 3.53 (m, N-CH), 4.47 (s, O-CH_2), 6.90 (s, N=CH), 6.97–7.67 (m, $B(C_6H_5)_2$). ^{11}B NMR (64 MHz, $CDCl_3$–Et_2OBF_3) δ (ppm): 7.1 ($w_{1/2}$ = 300 Hz). Anal. calcd. for $C_{20}H_{24}BNO_2$: C 74.78, H 7.53, B 3.37, N 4.36; found: C 74.84, H 7.84, B 3.35, N 4.15.

4-Benzyl-2,2-diphenyl-1,3-dioxa-4-azonia-2-borata-4-cyclohexene (3*c*)

2*b* (0.33 g, 2 mmol) and oxybis(diphenylborane) (0.35 g, 1 mmol) are reacted as described above for **3*a***. Yield: 0.53 g (80%) of colorless needles[6], mp 125°C (decomp.). IR (KBr, cm^{-1}): 1 655 (C=N). ^{1}H NMR (90 MHz, $CDCl_3$–TMS) δ (ppm): 4.49 (m, O-CH_2), 4.84 (s, N-CH_2), 6.92 (s, N=CH), 7.02–7.45 (m, 15 aromatic H). Anal. calcd. for $C_{21}H_{20}BNO_2$: C 76.62, H 6.12, N 4.26; found: C 76.60, H 6.15, N 4.19.

4-Benzhydryl-2,2-diphenyl-1,3-dioxa-4-azonia-2-borata-4-cyclohexene (3*d*)

Hydroxyacetaldehyde (0.30 g, 5 mmol), *N*-benzhydrylhydroxylamine (1.00 g, 5 mmol), and oxybis (diphenylborane) (0.87 g, 2.5 mmol) are reacted as described for **3*b***. Yield: 1.05 g (52%) of colorless crystals[6], mp 126°C. IR (KBr, cm^{-1}): 1 638 (C=N). ^{1}H NMR (90 MHz, $CDCl_3$–TMS) δ (ppm): 4.60 (s, CH_2), 6.30 (s, N-CH), 7.00–7.67 (m, 20 aromatic H and N=CH). ^{11}B NMR (64 MHz, $CDCl_3$–Et_2OBF_3) δ (ppm): 6.4 ($w_{1/2}$ = 257 Hz), 26.0, ratio of peak areas 20:1.[7] Anal. calcd. for $C_{27}H_{24}BNO_2$: C 80.00, H 5.97, B 2.67, N 3.46; found: C 80.08, H 6.04, B 2.68, N 3.34.

4-Cyclohexyl-2,2-di(4-chlorophenyl)-1,3-dioxa-4-azonia-2-borata-4-cyclohexene (3*e*)

Hydroxyacetaldehyde (0.12 g, 2 mmol), *N*-cyclohexylhydroxylamine (0.23 g, 2 mmol), and di(4-chlorophenyl)borinic acid (11) (0.50 g, 2 mmol) are reacted as described for **3*b***. Yield: 0.55 g (71%) of colorless crystals[6], mp 141°C (decomp.). IR (KBr, cm^{-1}): 1 650 (C=N). ^{1}H NMR (90 MHz, $CDCl_3$–TMS) δ (ppm): 0.93–2.43 (m, $(CH_2)_5$), 3.73 (m, N-CH), 4.60 (s, CH_2), 7.00–7.53 (m, aromatic H and N=CH). ^{11}B NMR (64 MHz, $CDCl_3$–Et_2OBF_3) δ (ppm): 6.7 ($w_{1/2}$ = 300 Hz). Anal. calcd. for $C_{20}H_{22}BCl_2NO_2$: C 61.58, H 5.68, B 2.77, N 3.59; found: C 61.58, H 5.71, B 2.80, N 3.37.

4-Cyclohexyl-2,2-di(1′-naphthyl)-1,3-dioxa-4-azonia-2-borata-4-cyclohexene (3*f*)

Hydroxyacetaldehyde (0.12 g, 2 mmol), *N*-cyclohexylhydroxylamine (0.23 g, 2 mmol), and di(1′-naphthyl)borinic acid (12) (0.56 g, 2 mmol) are reacted as described for **3*b***. Yield: 0.66 g (78%) of colorless crystals[6], mp 153°C (decomp.). IR (KBr, cm^{-1}): 1 640 (C=N). ^{1}H NMR

[4] Recrystallization should be avoided because of a thermally induced rearrangement reaction with an aryl 1,4-shift leading to heterocyclic arylboronates.[5] Very careful recrystallization without thermal stress or reprecipitation from chloroform with petroleum ether at mild temperature is possible in some cases.

[5] W. Kliegel, G. Lubkowitz, J.O. Pokriefke, S.J. Rettig, and J. Trotter. To be published.

[6] The product gives a blue-colored solution upon the addition of diphenylcarbazone in ethanol, indicating the presence of the chelated diarylborenium (Ar_2B^+) ion (10).

[7] The signals with very small peak areas originate from impurities caused by thermally induced rearrangement of the type **3** compounds, resulting in heterocyclic arylboronates **3**′ (see discussion below).

© 2000 NRC Canada

(90 MHz, $CDCl_3$–TMS) δ (ppm): 0.87–2.27 (m, $(CH_2)_5$), 3.33 (m, N-CH), 4.17 (s, O-CH_2), 6.63 (s, N=CH), 7.00–8.13 (m, 12 aromatic H), 8.33–8.70 (m, 2 aromatic H). ^{11}B NMR (64 MHz, $CDCl_3$–Et_2OBF_3) δ (ppm): 9.1 ($w_{1/2}$ = 514 Hz). Anal. calcd. for $C_{28}H_{28}BNO_2$: C 79.82, H 6.70, B 2.57, N 3.32; found: C 79.64, H 6.51, B 2.63, N 3.02.

4-Cyclohexyl-2,2-di[(2′, 2″-ethylene)phenyl]-1,3-dioxa-4-azonia-2-borata-4-cyclohexene (3*g*)

Hydroxyacetaldehyde (0.24 g, 4 mmol), *N*-cyclohexylhydroxylamine (0.46 g, 4 mmol), and 5,5′-oxybis(10,11-dihydro-5*H*-dibenzo[b,f]borepin) (12) (0.18 g, 2 mmol) are reacted as described for **3*b***. Yield: 1.10 g (79%) of colorless crystals[6], mp 132°C. IR (KBr, cm^{-1}): 1 643 (C=N). ^1H NMR (90 MHz, $CDCl_3$–TMS) δ (ppm): 0.90–2.33 (m, $(CH_2)_5$), 3.23 (s, ar-CH_2CH_2-ar), 3.67 (m, N-CH), 4.43 (s, O-CH_2), 6.67–7.67 (m, 8 aromatic H and N=CH). ^{11}B NMR (64 MHz, $CDCl_3$–Et_2OBF_3) δ (ppm): 3.6 ($w_{1/2}$ = 342 Hz). Anal. calcd. for $C_{22}H_{26}BNO_2$: C 76.09, H 7.55, B 3.11, N 4.03; found: C 76.27, H 7.58, B 3.22, N 3.77.

4,6-Dimethyl-2,2-diphenyl-1,3-dioxa-4-azonia-2-borata-4-cyclohexene (3*h*)

2*c* (0.41 g of the crude product, about 4 mmol) and oxybi(diphenylborane) (0.69 g, 2 mmol) are reacted as described for **3*a***. Yield: 0.80 g (75%) of colorless crystals[6], mp 113–114°C (decomp.). IR (KBr, cm^{-1}): 1 660 (C=N). ^1H NMR (90 MHz, $CDCl_3$–TMS) δ (ppm): 1.36 (d, J = 7 Hz, C-CH_3), 3.27 (s, N-CH_3), 4.40 (m, O-CH), 6.51 (s, N=CH), 6.88–7.40 (m, $B(C_6H_5)_2$). Anal. calcd. for $C_{16}H_{18}BNO_2$: C 71.94, H 6.79, B 4.05, N 5.24; found: C 71.99, H 6.82, B 4.05, N 5.21.

4-*tert*-Butyl-6-methyl-2,2-diphenyl-1,3-dioxa-4-azonia-2-borata-4-cyclohexene (3*i*)

2*d* (0.58 g of the crude product, about 4 mmol) and oxybis(diphenylborane) (0.69 g, 2 mmol) are reacted as described for **3*a***. Yield: 1.10 g (89%) of colorless crystals[6], mp 106–107°C (decomp.). IR (KBr, cm^{-1}): 1 620 (C=N). ^1H NMR (90 MHz, $CDCl_3$–TMS) δ (ppm): 1.38 (d, J = 7 Hz, OC-CH_3), 1.56 (s, $C(CH_3)_3$), 4.72 (m, O-CH), 7.00–7.50 (m, $B(C_6H_5)_2$ and N=CH). Anal. calcd. for $C_{19}H_{24}BNO_2$: C 73.80, H 7.82, B 3.50, N 4.53; found: C 73.97, H 7.92, B 3.52, N 4.50.

4-Cyclohexyl-6-methyl-2,2-diphenyl-1,3-dioxa-4-azonia-2-borata-4-cyclohexene (3*j*)

2*e* (0.34 g, 2 mmol) and oxybis(diphenylborane) (0.35 g, 1 mmol) are reacted as described for **3*a***. Yield: 0.51 g (76%) of colorless crystals[6], mp 117–118°C (decomp.). IR (KBr, cm^{-1}): 1 625 (C=N). ^1H NMR (90 MHz, $CDCl_3$–TMS) δ (ppm): 1.00–2.17 (m, $(CH_2)_5$), 1.44 (d, J = 7 Hz, CH_3), 3.57 (m, N-CH), 4.60 (q, J = 7 Hz, O-CH), 6.95 (s, N=CH), 7.00–7.53 (m, $B(C_6H_5)_2$). Anal. calcd. for $C_{21}H_{26}BNO_2$: C 75.24, H 7.82, N 4.18; found: C 75.03, H 7.87, N 4.32.

4-Benzyl-6-methyl-2,2-diphenyl-1,3-dioxa-4-azonia-2-borata-4-cyclohexene (3*k*)

2*f* (0.36 g, 2 mmol) and oxybis(diphenylborane) (0.35 g, 1 mmol) are reacted as described for **3*a***. Yield: 0.59 g (86%) of slightly yellow crystals[6], mp 107–108°C (decomp.). IR (KBr, cm^{-1}): 1 635 (C=N). ^1H NMR (90 MHz, $CDCl_3$–TMS) δ (ppm): 1.38 (d, J = 7 Hz, CH_3), 4.53 (q, J = 7 Hz, O-CH), 4.74 (s, N-CH_2), 6.82 (s, N=CH), 6.97–7.44 (m, 15 aromatic H). ^1H NMR (400 MHz, $CDCl_3$–TMS) δ (ppm): 1.39 (d, J = 7 Hz, CH_3), 4.59 (q, J = 7 Hz, O-CH), 4.81 (q, AB system, N-CH_2), 6.88 (d, J = 1 Hz, N=CH), 7.07–7.49 (m, 15 aromatic H). Anal. calcd. for $C_{22}H_{22}BNO_2$: C 76.99, H 6.46, N 4.08; found: C 77.09, H 6.45, N 4.19.

4-Benzhydryl-6-methyl-2,2-diphenyl-1,3-dioxa-4-azonia-2-borata-4-cyclohexene (3*l*) (·EtOH)

2*g* (0.51 g, 2 mmol) and oxybis(diphenylborane) (0.35 g, 1 mmol) are reacted as described for **3*a***. Yield: 0.85 g (91%) of slightly yellow plates[6], mp 86–90°C (decomp.). IR (KBr, cm^{-1}): 3 390 (broad, O-H), 1 650 (C=N). ^1H NMR (90 MHz, $CDCl_3$–TMS) δ (ppm): 1.22 (t, J = 7 Hz, CH_3 of ethanol), 1.48 (d, J = 7 Hz, CH_3), 3.66 (q, J = 7 Hz, O-CH_2 of ethanol), 4.73 (m, O-CH), 6.31 (s, N-CH), 7.06–7.50 (m, 20 aromatic H, N=CH, and OH of ethanol). Anal. calcd. for $C_{28}H_{26}BNO_2$ + C_2H_5OH: C 77.42, H 6.93, N 3.01; found: C 77.30, H 6.94, N 3.22.

4-Cyclohexyl-5-methyl-2,2-diphenyl-1,3-dioxa-4-azonia-2-borata-4-cyclohexene (3*m*)

Hydroxyacetone (0.37 g, 5 mmol) and oxybis(diphenylborane) (0.87 g, 2.5 mmol) are dissolved in 5 mL of absolute ethanol, if necessary under slight warming. A solution of *N*-cyclohexylhydroxylamine (0.58 g, 5 mmol) in 5 mL of ethanol is added without stirring, after precooling of both solutions. At –18°C, crystallization starts spontaneously or after rubbing with a glass stick. The crystals are filtered off and are washed rapidly with a small amount of ethanol and small portions of ether.[4] Yield: 0.52 g (32%) of colorless crystals[6], mp 156°C (decomp.). IR (KBr, cm^{-1}): 1 647 (C=N). ^1H NMR (90 MHz, $CDCl_3$–TMS) δ (ppm): 0.90–2.67 (m, $(CH_2)_5$), 1.83 (s, CH_3), 3.90 (m, N-CH), 4.50 (s, O-CH_2), 6.9 7.73 (m, $B(C_6H_5)_2$). ^{11}B NMR (64 MHz, $CDCl_3$–Et_2OBF_3) δ (ppm): 6.4 ($w_{1/2}$ = 257 Hz). Anal. calcd. for $C_{21}H_{26}BNO_2$: C 75.24, H 7.82, B 3.22, N 4.18; found: C 75.24, H 7.96, B 3.22, N 3.98.

4-Benzyl-5-methyl-2,2-diphenyl-1,3-dioxa-4-azonia-2-borata-4-cyclohexene (3*n*)

Hydroxyacetone (0.37 g, 5 mmol) and oxybis(diphenylborane) (0.87 g, 2.5 mmol) are dissolved in 5 mL of absolute ethanol, if necessary under slight warming. To a solution of *N*-benzylhydroxylamine hydrochloride (0.80 g, 5 mmol), triethylamine (0.51 g, 5 mmol) is added. Both solutions are cooled and mixed without stirring. Crystallization starts during storage at –18°C spontaneously or upon rubbing with a glass stick. The crystals are filtered off and washed rapidly with a small amount of ethanol and small portions of ether.[4] Yield: 1.3 g (66%) of colorless crystals[6], mp 118°C. IR (KBr, cm^{-1}): 1 654 (C=N). ^1H NMR (90 MHz, $CDCl_3$–TMS) δ (ppm): 1.93 (s, CH_3), 4.53 (s, O-CH_2), 5.07 (s, N-CH_2), 6.90–7.90 (m, 15 aromatic H). ^{11}B NMR (64 MHz, $CDCl_3$–Et_2OBF_3) δ (ppm): 6.9 ($w_{1/2}$ = 257 Hz), 27.0, ratio of peak areas 10:1.[7] Anal. calcd. for $C_{22}H_{22}BNO_2$: C 76.99, H 6.46, B 3.15, N 4.08; found: C 76.48, H 6.31, B 3.07, N 3.88.

© 2000 NRC Canada

5-Methyl-4-(4′-methylphenyl)-2,2-diphenyl-1,3-dioxa-4-azonia-2-borata-4-cyclohexene (3*o*)

Hydroxyacetone (0.37 g, 5 mmol), oxybis(diphenylborane) (0.87 g, 2.5 mmol), and *N*-(4-methylphenyl)hydroxylamine (0.62 g, 5 mmol) are reacted as described for **3*m***. Yield: 0.85 g (50%) of colorless crystals[6], mp 113°C. IR (KBr, cm^{-1}): 1 636 (C=N). ^{1}H NMR (90 MHz, $CDCl_3$–TMS) δ (ppm): 1.70 (s, N=C-CH_3), 2.43 (s, aryl-CH_3), 4.73 (s, O-CH_2), 6.77–8.03 (m, 14 aromatic H)[8]. ^{11}B NMR (64 MHz, $CDCl_3$–Et_2OBF_3) δ (ppm): 7.6 ($w_{1/2}$ = 257 Hz), 29.2, ratio of peak areas 20:1.[7] Anal. calcd. for $C_{22}H_{22}BNO_2$: C 76.99, H 6.46, B 3.15, N 4.08; found: C 77.12, H 6.63, B 3.28, N 3.93.

4-Benzhydryl-5-ethyl-2,2-diphenyl-1,3-dioxa-4-azonia-2-borata-4-cyclohexene (3*p*)

1-Hydroxy-2-butanone (0.44 g, 5 mmol), oxybis(diphenylborane) (0.87 g, 2.5 mmol), and *N*-benzhydrylhydroxylamine (1.00 g, 5 mmol) are reacted as described for **3*m***. Yield: 1.23 g (57%) of colorless crystals[6], mp 120°C. IR (KBr, cm^{-1}): 1 626 (C=N). ^{1}H NMR (90 MHz, $CDCl_3$–TMS) δ (ppm): 0.97 (t, J = 7 Hz, CH_3), 2.33 (q, J = 7 Hz, N=C-CH_2), 4.67 (s, O-CH_2), 6.50 (d, N-CH), 6.83–7.90 (m, 20 aromatic H). ^{11}B NMR (64 MHz, $CDCl_3$–Et_2OBF_3) δ (ppm): 7.4 ($w_{1/2}$ = 257 Hz). Anal. calcd. for $C_{29}H_{28}BNO_2$: C 80.38, H 6.51, B 2.49, N 3.23; found: C 80.58, H 6.57, B 2.55, N 2.96.

4,5,6-Trimethyl-2,2-diphenyl-1,3-dioxa-4-azonia-2-borata-4-cyclohexene (3*q*)

3-Hydroxy-2-butanone (0.44 g, 5 mmol), oxybis(diphenylborane) (0.87 g, 2.5 mmol), *N*-methylhydroxylamine hydrochloride (0.42 g, 5 mmol), and triethylamine (0.51 g, 5 mmol) are reacted as described for **3*n***. Yield: 0.79 g (56%) of colorless crystals[6], mp 120°C. IR (KBr, cm^{-1}): 1 655 (C=N). ^{1}H NMR (90 MHz, $CDCl_3$–TMS) δ (ppm): 1.57 (t, J = 7 Hz, O-C-CH_3), 1.67 (s, N=C-CH_3), 3.47 (s, N-CH_3), 4.53 (q, J = 7 Hz, O-CH), 6.90–8.03 (m, B(C_6H_5)$_2$)[9]. ^{11}B NMR (64 MHz, $CDCl_3$–Et_2OBF_3) δ (ppm): 6.6 ($w_{1/2}$ = 214 Hz), 27.0, ratio of peak areas 20:1.[7] Anal. calcd. for $C_{17}H_{20}BNO_2$: C 72.62, H 7.17, B 3.85, N 4.98; found: C 72.65, H 7.28, B 3.86, N 4.84.

5,6-Dimethyl-2,2-diphenyl-4-propyl-1,3-dioxa-4-azonia-2-borata-4-cyclohexene (3*r*)

3-Hydroxy-2-butanone (0.44 g, 5 mmol), oxybis(diphenylborane) (0.87 g, 2.5 mmol), *N*-propylhydroxylamine hydrochloride (0.56 g, 5 mmol), and triethylamine (0.51 g, 5 mmol) are reacted as described for **3*n***. Yield: 0.79 g (51%) of colorless crystals[6], mp 115°C. IR (KBr, cm^{-1}): 1 637 (C=N). ^{1}H NMR (90 MHz, $CDCl_3$–TMS) δ (ppm): 0.97 (t, J = 7 Hz, N-C-C-CH_3), 1.57 (d, J = 7 Hz, O-C-CH_3), 1.63–2.30 (m, N-C-CH_2-C), 1.83 (s, N=C-CH_3), 3.73 (t, J = 7 Hz, N-CH_2), 4.33–4.60 (m, O-CH), 6.80–8.03 (m, B(C_6H_5)$_2$)[10]. ^{11}B NMR (64 MHz, $CDCl_3$–Et_2OBF_3) δ (ppm): 7.0 ($w_{1/2}$ = 214 Hz), 27.0, ratio of peak areas 20:1.[7] Anal. calcd. for $C_{19}H_{24}BNO_2$: C 73.80, H 7.82, B 3.50, N 4.53; found: C 73.84, H 7.99, B 3.53, N 4.40.

4-Isopropyl-5,6-dimethyl-2,2-diphenyl-1,3-dioxa-4-azonia-2-borata-4-cyclohexene (3*s*)

3-Hydroxy-2-butanone (0.44 g, 5 mmol), oxybis(diphenylborane) (0.87 g, 2.5 mmol), *N*-isopropylhydroxylamine hydrochloride (0.56 g, 5 mmol), and triethylamine (0.51 g, 5 mmol) are reacted as described for **3*n***. Yield: 0.99 g (64%) of colorless crystals[6], mp 133°C. IR (KBr, cm^{-1}): 1 625 (C=N). ^{1}H NMR (90 MHz, $CDCl_3$–TMS) δ (ppm): 1.30–1.67 (m, N-C(CH_3)$_2$ and O-C-CH_3), 1.83 (s, N=C-CH_3), 4.20 (sept, J = 7 Hz, N-CH), 4.36 (q, J = 7 Hz, O-CH), 6.80–7.70 (m, B(C_6H_5)$_2$)[10]. ^{11}B NMR (64 MHz, $CDCl_3$–Et_2OBF_3) δ (ppm): 6.2 ($w_{1/2}$ = 171 Hz). Anal. calcd. for $C_{19}H_{24}BNO_2$: C 73.80, H 7.82, B 3.50, N 4.53; found: C 73.86, H 7.98, B 3.49, N 4.80.

4-Cyclohexyl-5,6-dimethyl-2,2-diphenyl-1,3-dioxa-4-azonia-2-borata-4-cyclohexene (3*t*)

Method A

2*h* (0.19 g, 1 mmol) and oxybis(diphenylborane) (0.17 g, 0.5 mmol) are reacted as described for **3*a***. Yield: 0.14 g (40%).

Method B

3-Hydroxy-2-butanone (0.44 g, 5 mmol), oxybis(diphenylborane) (0.87 g, 2.5 mmol), and *N*-cyclohexylhydroxylamine (0.55 g, 5 mmol) are reacted as described for **3*m***. Yield: 1.10 g (63%) of colorless crystals[6], mp 132°C. IR (KBr, cm^{-1}): 1 614 (C=N). ^{1}H NMR 90 MHz, $CDCl_3$–TMS) δ (ppm): 0.93–2.57 (m, $(CH_2)_5$), 1.53 (d, J = 7 Hz, O-C-CH_3), 1.93 (s, N=C-CH_3), 3.87 (m, N-CH), 4.63 (q, J = 7 Hz, O-CH), 6.90–7.70 (m, B(C_6H_5)$_2$). ^{11}B NMR (64 MHz, $CDCl_3$–Et_2OBF_3) δ (ppm): 6.4 ($w_{1/2}$ = 257 Hz). Anal. calcd. for $C_{22}H_{28}BNO_2$: C 75.65, H 8.08, B 3.10, N 4.01; found: C 75.64, H 8.16, B 3.05, N 3.84.

4-Benzyl-5,6-dimethyl-2,2-diphenyl-1,3-dioxa-4-azonia-2-borata-4-cyclohexene (3*u*)

3-Hydroxy-2-butanone (0.44 g, 5 mmol), oxybis(diphenylborane) (0.87 g, 2.5 mmol), *N*-benzylhydroxylamine hydrochloride (0.80 g, 5 mmol), and triethylamine (0.51 g, 5 mmol) are reacted as described for **3*n***. Yield: 1.21 g (68%) of colorless crystals[6], mp 120°C. IR (KBr, cm^{-1}): 1 630 (C=N). ^{1}H NMR (90 MHz, $CDCl_3$–TMS) δ (ppm): 1.50 (d, J = 7 Hz, O-C-CH_3), 1.83 (s, N=C-CH_3), 4.40–4.70 (m, O-CH), 4.87/5.07 (d/d, AB system, J = 15 Hz, N-CH $_2$), 7.00–7.90 (m, 15 aromatic H)[11]. ^{1}H NMR (400 MHz, CD_3Cl_2–TMS, –17°C) δ (ppm): 1.53 (d, J = 7 Hz, O-C-CH_3), 1.93 (s, N=C-CH_3), 4.65 (q, J = 7 Hz, O-CH), 5.02/5.12 (d/d, AB system, J = 15 Hz, N-CH_2), 7.03–7.96 (m, 15 aromatic H). ^{11}B NMR (64 MHz, $CDCl_3$–Et_2OBF_3) δ (ppm): 7.1 ($w_{1/2}$ = 214 Hz), 27.8, ratio of peak areas 5:1. Anal. calcd. for $C_{23}H_{24}BNO_2$: C 77.33, H 6.77, B 3.03, N 3.92; found: C 77.48, H 6.91, B 2.99, N 3.72.

[8] Additional small peaks at: 1.47 (s, N-C-CH_3), 2.77 (s, aryl-CH_3).[7]
[9] Additional small peaks at: 1.03 (d, J = 7 Hz, O-C-CH_3), 1.43 (s, N-C-CH_3), 2.50 (s, N-CH_3).[7]
[10] Additional small peaks at: 0.83 (t?, J = 7 Hz, N-C-C-CH_3), 1.40 (s, N-C-CH_3).[7]
[11] Additional small peaks at: 1.00 (d, J = 7 Hz, O-C-CH_3), 1.53 (s, N-C-CH_3), 3.63 (s, N- CH_2).[7]

© 2000 NRC Canada

4-Benzhydryl-5,6-dimethyl-2,2-diphenyl-1,3-dioxa-4-azonia-2-borata-4-cyclohexene (3*v*)

3-Hydroxy-2-butanone (0.44 g, 5 mmol), oxybis(diphenylborane) (0.87 g, 2.5 mmol), and *N*-benzhydrylhydroxylamine (1.00 g, 5 mmol) are reacted as described for **3*m***. Yield: 1.05 g (49%) of colorless crystals[6], mp 105°C (rearr.). MS (CI, NH_3, pos. mode, 90°C) *m/z*: 433 (26%, M^+), 434 (100%, $M^+ + H$). IR (KBr, cm^{-1}): 1 607 (C=N/C=C). ^1H NMR (90 MHz, $CDCl_3$–TMS) δ (ppm): 1.57 (d, *J* = 7 Hz, O-C-CH_3), 1.97 (s, N=C-CH_3), 4.37 (q, *J* = 7 Hz, O-CH), 6.40 (s, N-CH), 6.67–7.97 (m, $B(C_6H_5)_2$)[12]. ^{11}B NMR (64 MHz, $CDCl_3$–Et_2OBF_3) δ (ppm): 6.4 ($w_{1/2}$ = 257 Hz), 27.0, ratio of peak areas 10:1. Anal. calcd. for $C_{29}H_{28}BNO_2$: C 80.38, H 6.51, B 2.49, N 3.23; found: C 80.07, H 6.74, B 2.47, N 3.02.

2,2-Di(4′-chlorophenyl)-4-cyclohexyl-5,6-dimethyl-1,3-dioxa-4-azonia-2-borata-4-cyclohexene (3*w*)

3-Hydroxy-2-butanone (0.18 g, 2 mmol), di(4-chlorophenyl)borinic acid (11) (0.5 g, 2 mmol), and *N*-cyclohexylhydroxylamine (0.23 g, 2 mmol) are reacted as described for **3*m***. Yield: 0.39 g (47%) of colorless crystals[6], mp 150°C. IR (KBr, cm^{-1}): 1 579 (C=N/C=C). ^1H NMR (90 MHz, $CDCl_3$–TMS) δ (ppm): 0.90–2.50 (m, $(CH_2)_5$), 1.50 (d, *J* = 7 Hz, O-C-CH_3), 1.97 (s, N=C-CH_3), 3.90 (m, N-CH), 4.57 (q, *J* = 7 Hz, O-C-CH_3), 7.00–7.50 (m, 8 aromatic H). ^{11}B NMR (64 MHz, $CDCl_3$–Et_2OBF_3) δ (ppm): 5.7 ($w_{1/2}$ = 258 Hz). Anal. calcd. for $C_{22}H_{26}BCl_2NO_2$: C 63.19, H 6.27, B 2.59, N 3.35; found: C 63.21, H 7.03, B 2.64, N 3.14.

4-Benzhydryl-2,2-di(4-chlorophenyl)-5,6-dimethyl-1,3-dioxa-4-azonia-2-borata-4-cyclohexene (3*x*)

3-Hydroxy-2-butanone (0.88 g, 10 mmol), di(4-chlorophenyl)borinic acid (11) (2.50 g, 10 mmol), and *N*-benzhydrylhydroxylamine (1.99 g, 10 mmol) are reacted as described for **3*m***. Yield: 2.42 g (48%) of colorless crystals[6], mp 130°C (rearr.). MS (CI, NH_3, pos. mode, 100°C) *m/z*: 502 (2%, M^+). IR (KBr, cm^{-1}): 1 578 (C=N/C=C). ^1H NMR (90 MHz, $CDCl_3$–TMS) δ (ppm): 1.57 (d, *J* = 7 Hz, O-C-CH_3), 2.10 (s, N=C-CH_3), 4.67 (q, *J* = 7 Hz, O-C-CH), 6.43 (s, N-CH), 6.63–7.90 (m, 18 aromatic H). ^{11}B NMR (64 MHz, $CDCl_3$–Et_2OBF_3) δ (ppm): 6.9 ($w_{1/2}$ = 342 Hz). Anal. calcd. for $C_{29}H_{26}BCl_2NO_2$: C 69.35, H 5.22, B 2.15, Cl 14.12, N 2.79; found: C 69.29, H 5.20, B 2.28, Cl 14.22, N 2.71.

4-Cyclohexyl-5,6-dimethyl-2,2-di(1′-naphthyl)-1,3-dioxa-4-azonia-2-borata-4-cyclohexene (3*y*)

3-Hydroxy-2-butanone (0.18 g, 2 mmol), di(1-naphthyl)borinic acid (11) (0.56 g, 2 mmol), and *N*-cyclohexylhydroxylamine (0.23 g, 2 mmol) are reacted as described for **3*m***. Yield: 0.51 g (57%) of colorless crystals[6], mp 157°C. IR (KBr, cm^{-1}): 1 625 (C=N). ^1H NMR (90 MHz, $CDCl_3$–TMS) δ (ppm): 0.87–2.42 (m, $(CH_2)_5$), 1.47 (d, *J* = 7 Hz, O-C-CH_3), 1.87 (s, N=C-CH_3), 3.93 (m, N-CH), 4.37 (q, *J* = 7 Hz, O-CH), 7.00–8.00 (m, 12 aromatic H), 8.43–8.87 (m, 2 aromatic H). ^{11}B NMR (64 MHz, $CDCl_3$–Et_2OBF_3) δ (ppm): 9.2 ($w_{1/2}$ = 342 Hz). Anal. calcd. for $C_{30}H_{32}BNO_2$: C 80.18, H 7.18, B 2.41, N 3.12; found: C 80.21, H 7.25, B 2.45, N 3.00.

4-Cyclohexyl-5,6-tetramethylene-2,2-diphenyl-1,3-dioxa-4-azonia-2-borata-4-cyclohexene (3*z*)

2-Hydroxycyclohexanone (0.57 g, 5 mmol) and oxybis(diphenylborane) (0.87 g, 2.5 mmol) are dissolved in 10 mL of absolute ethanol under slight heating and stirring for a further 10 min. After cooling down to room temperature, a solution of *N*-cyclohexylhydroxylamine (0.58 g, 5 mmol) in 5 mL of absolute ethanol is added, and the mixture stored at room temperature. Crystallization starts spontaneously or upon cooling. The usually analytically pure crystals are filtered off after 1 h and can be recrystallized from ethanol. Yield: 1.20 g (64%) of colorless crystals[6], mp 151°C. IR (KBr, cm^{-1}): 1 619 (C=N). ^1H NMR (90 MHz, $CDCl_3$–TMS) δ (ppm): 1.00–2.90 (m, $(CH_2)_4$ and $(CH_2)_5$), 4.10 (m, N-CH), 4.47 (dd, *J* = 12 Hz, *J* = 7 Hz, O-CH), 6.83–7.67 (m, $B(C_6H_5)_2$). ^{11}B NMR (64 MHz, $CDCl_3$–Et_2OBF_3) δ (ppm): 6.1 ($w_{1/2}$ = 214 Hz). Anal. calcd. for $C_{24}H_{30}BNO_2$: C 76.81, H 8.06, B 2.88, N 3.73; found: C 76.87, H 8.24, B 2.87, N 3.56.

4-Benzyl-5,6-tetramethylene-2,2-diphenyl-1,3-dioxa-4-azonia-2-borata-4-cyclohexene (3*aa*)

2-Hydroxycyclohexanone (0.57 g, 5 mmol) and oxybis(diphenylborane) (0.87 g, 2.5 mmol) in 10 mL of ethanol are reacted with *N*-benzylhydroxylamine hydrochloride (0.80 g, 5 mmol) and triethylamine (0.51 g, 5 mmol) in 5 mL of ethanol as described for **3*z***. Yield: 1.50 g (78%) of colorless crystals[6], mp 138°C. IR (KBr, cm^{-1}): 1 632 (C=N). ^1H NMR (90 MHz, $CDCl_3$–TMS) δ (ppm): 0.87–2.83 (m, $(CH_2)_4$), 4.40 (dd, *J* = 12 Hz, *J* = 6 Hz, O-CH), 5.03/5.17 (d/d, AB system, *J* = 15 Hz, N-CH_2), 6.87–7.87 (m, 15 aromatic H). ^{11}B NMR (64 MHz, $CDCl_3$–Et_2OBF_3) δ (ppm): 6.1 ($w_{1/2}$ = 257 Hz). Anal. calcd. for $C_{25}H_{26}BNO_2$: C 78.34, H 6.84, B 2.82, N 3.65; found: C 78.31, H 6.88, B 2.88, N 3.48.

4-Benzhydryl-5,6-tetramethylene-2,2-diphenyl-1,3-dioxa-4-azonia-2-borata-4-cyclohexene (3*bb*)

2-Hydroxycyclohexanone (0.57 g, 5 mmol), oxybis(diphenylborane) (0.87 g, 2.5 mmol), and *N*-benzhydrylhydroxylamine (1.00 g, 5 mmol) are reacted as described for **3*z***. Yield: 1.50 g (65%) of colorless crystals[6], mp 144°C. IR (KBr, cm^{-1}): 1 610 (C=N/C=C). ^1H NMR (400 MHz, $CDCl_3$–TMS) δ (ppm): 0.94–2.91 (m, $(CH_2)_4$), 4.57 (dd, *J* = 12 Hz, *J* = 6 Hz, O-CH), 6.66 (s, N-CH), 6.90–7.82 (m, 20 aromatic H). ^{11}B NMR (64 MHz, $CDCl_3$–Et_2OBF_3) δ (ppm): 6.9 ($w_{1/2}$ = 257 Hz). Anal. calcd. for $C_{31}H_{30}BNO_2$: C 81.05, H 6.58, B 2.35, N 3.05; found: C 81.08, H 6.63, B 2.39, N 2.79.

5,5-Tetramethylene-4-(4′-methylphenyl)-2,2-diphenyl-1,3-dioxa-4-azonia-2-borata-4-cyclohexene (3*cc*)

2-Hydroxycyclohexanone (0.57 g, 5 mmol), oxybis(diphenylborane) (0.87 g, 2.5 mmol), and *N*-(4-methylphenyl)hydroxylamine (0.62 g, 5 mmol) are reacted as described for **3*z***. Yield: 1.28 g (67%) of colorless crystals[6], mp 140°C. IR (KBr, cm^{-1}): 1 657 (C=N), 1625 (C=C). ^1H NMR (90 MHz, $CDCl_3$–TMS) δ (ppm): 1.00–2.90 (m, $(CH_2)_4$), 2.40 (s, CH_3), 4.63 (dd, *J* = 12 Hz, *J* = 6 Hz, O-CH), 6.90–7.80 (m, 14 aromatic

[12]Additional small peaks at: 0.90 (d, *J* = 7 Hz, O-C-CH_3), 0.97 (s, N-C-CH_3), 4.97 (s, N-CH)[7].

© 2000 NRC Canada

H). ^{11}B NMR (64 MHz, $CDCl_3$–Et_2OBF_3) δ (ppm): 6.3 ($w_{1/2}$ = 299 Hz). Anal. calcd. for $C_{25}H_{26}BNO_2$: C 78.34, H 6.84, B 2.82, N 3.65; found: C 78.87, H 7.01, B 2.89, N 3.48.

4,5-Dimethyl-2,2-diphenyl-1-oxa-3-azonia-2-borata-3-cyclopenten-3-ol (5*a*)

3-Hydroxy-2-butanonoxime (13) (0.52 g, 5 mmol) and oxybis(diphenylborane) (0.87 g, 2.5 mmol) are dissolved separately in 5 mL of absolute ethanol each. The solutions are mixed at room temperature under continuous stirring. Crystallization commences after a few minutes, if necessary after slight cooling or addition of petroleum ether. The usually analytically pure substance can be recrystallized from ethanol. Yield: 1.02 g (76%) of colorless crystals[6], mp 170°C. IR (KBr, cm^{-1}): 2 598 (broad, O-H), 1 664 (C=N). ^{1}H NMR (90 MHz, DMSO-d_6–TMS) δ (ppm): 1.40 (d, J = 7 Hz, O-C-CH_3), 2.10 (s, N=C-CH_3), 4.83 (q, J = 7 Hz, O-CH), 6.80–7.80 (m, $B(C_6H_5)_2$), 11.93 (s, exchangeable, OH). ^{11}B NMR (64 MHz, DMSO-d_6–Et_2OBF_3) δ (ppm): 9.7 ($w_{1/2}$ = 385 Hz). Anal. calcd. for $C_{16}H_{18}BNO_2$: C 71.94, H 6.79, B 4.05, N 5.24; found: C 71.92, H 6.80, B 4.02, N 5.22.

4-Ethyl-2,2-diphenyl-1-oxa-3-azonia-2-borata-3-cyclopenten-3-ol (5*b*)

1-Hydroxy-2-butanonoxime (14) (0.52 g, 5 mmol) and oxybis(diphenylborane) (0.87 g, 2.5 mmol) are reacted as described for **5*a***. Yield: 0.35 g (26%) of colorless crystals[6], mp 145°C. IR (KBr, cm^{-1}): 2 775 (broad, O-H), 1 668 (C=N). ^{1}H NMR (90 MHz, DMSO-d_6–TMS) δ (ppm): 1.10 (t, J = 7 Hz, CH_3), 2.57 (q, J = 7 Hz, N=C-CH_2), 4.73 (s, O-CH_2), 7.00–8.00 (m, $B(C_6H_5)_2$), 11.9 (s, exchangeable, OH). ^{11}B NMR (64 MHz, DMSO-d_6–Et_2OBF_3) δ (ppm): 10.1 ($w_{1/2}$ = 470 Hz). Anal. calcd. for $C_{16}H_{18}BNO_2$: C 71.94, H 6.79, B 4.05, N 5.24; found: C 71.98, H 6.90, B 3.99, N 5.20.

4,5-Tetramethylene-2,2-diphenyl-1-oxa-3-azonia-2-borata-3-cyclopenten-3-ol (5*c*)

2-Hydroxycyclohexanonoxime (15) (0.39 g, 3 mmol) and oxybis(diphenylborane) (0.52 g, 1.5 mmol) are reacted as described for **5*a***. Yield: 0.71 g (81%) of colorless crystals[6], mp 180°C. IR (KBr, cm^{-1}): 2 472 (broad, O-H), 1 674 (C=N). ^{1}H NMR (90 MHz, DMSO-d_6–TMS) δ (ppm): 1.00–3.23 (m, $(CH_2)_4$), 4.60 (m, O-CH), 7.00–7.83 (m, $B(C_6H_5)_2$), 11.83 (s, exchangeable, OH). ^{11}B NMR (64 MHz, DMSO-d_6–Et_2OBF_3) δ (ppm): 10.2 ($w_{1/2}$ = 470 Hz). Anal. calcd. for $C_{18}H_{20}BNO_2$: C 73.75, H 6.88, B 3.69, N 4.78; found: C 73.67, H 6.99, B 3.69, N 4.74.

2,2,4,5-Tetraphenyl-1-oxa-3-azonia-2-borata-3-cyclopenten-3-ol (5*d*)

α-Benzoinoxime (commercial product "Cupron") (0.23 g, 1 mmol) and oxybis(diphenylborane) (0.17 g, 0.5 mmol) are reacted as described for **5*a***. Yield: 0.32 g (82%) of colorless crystals[6], mp 170°C. IR (KBr, cm^{-1}): 2 734 (broad, O-H), 1 637 (C=N), 1596 (C=C). ^{1}H NMR (90 MHz, DMSO-d_6–TMS) δ (ppm): 6.53 (s, O-CH), 6.93–7.90 (m, 20 aromatic H), 12.77 (s, exchangeable, OH). ^{11}B NMR (64 MHz, DMSO-d_6–Et_2OBF_3) δ (ppm): 8.0. Anal. calcd. for $C_{26}H_{22}BNO_2$: C 79.81, H 5.67, B 2.76, N 3.58; found: C 97.91, H 5.70, B 2.89, N 3.42. Single crystals suitable for X-ray crystallographic analysis were obtained by very slow crystallization from absolute ethanol.

3-(Methylimino)-2,2-dimethylpropanol *N*-oxide (8*a*)

3-Hydroxy-2,2-dimethylpropanal (16) (1.02 g, 10 mmol), *N*-methylhydroxylamine hydrochloride (0.84 g, 10 mmol), and K_2CO_3 (0.7 g) are suspended in 10 mol of water and stirred for 10 min. After addition of 20 mL of benzene the mixture is refluxed using a Dean–Stark trap for continuous removal of water. After 5 h, the precipitated KCl is filtered off and the solvents removed in vacuo. The oily residue is purified by destillation in vacuo. Yield: 0.61 g (47%) of slightly orange oil, bp 135°C/5 torr (1 torr = 133 Pa). MS (CI, NH_3, pos. mode) *m*/*z*: 132 (100%, M^+ + H). IR (NaCl, film, cm^{-1}): 3 323 (broad, O-H), 1 606 (C=N). ^{11}H NMR ($CDCl_3$–TMS) δ (ppm): 1.23 (s, $C(CH_3)_2$), 3.63 (s, O-CH_2), 3.70 (s, N-CH_3), 4.57 (s, broad, exchangeable, OH), 6.53 (s, N=CH). Anal. calcd. for $C_6H_{13}NO_2$: C 54.94, H 9.99, N 10.86; found: C 54.92, H 9.84, N 10.10.

3-(Propylimino)-2,2-dimethylpropanol *N*-oxide (8*b*)

3-Hydroxy-2,2-dimethylpropanol (1.02 g, 10 mmol), *N*-propylhydroxylamine hydrochloride (0.12 g, 10 mmol), and K_2CO_3 (0.7 g) are reacted as described for **8*a***. Yield: 0.75 g (47%) of a slightly yellow oil, bp 142°C/10 torr (1 torr = 133 Pa). MS (CI, NH_3, pos. mode) *m*/*z*: 160 (100%, M^+ + H). IR (NaCl, film, cm^{-1}): 3 338 (broad, O-H), 1 595 (C=N). ^{11}H NMR ($CDCl_3$–TMS) δ (ppm): 0.97 (t, J = 6 Hz, N-C-C-CH_3), 1.27 (s, $C(CH_3)_2$), 1.67–2.20 (m, N-C-CH_2), 3.57 (s, O-CH_2), 3.73 (t, J = 6 Hz, N-CH_2), 6.00 (s, broad, exchangeable, OH), 6.60 (s, N=CH). Anal. calcd. for $C_8H_{17}NO_2$: C 60.35, H 10.76, N 8.80; found: C 60.42, H 10.26, N 8.49.

3-(Cyclohexylimino)-2,2-dimethylpropanol *N*-oxide (8*c*)

3-Hydroxy-2,2-dimethylpropanal (1.02 g, 10 mmol) and *N*-cyclohexylhydroxylamine are refluxed in 20 mL of benzene using a Dean–Stark trap for continuous removal of water. After 5 h, the solvent is distilled off and the remaining orange-colored oil is dissolved in a small amount of ethanol. Crystallization is achieved upon cooling and addition of *n*-hexane. Yield: 1.30 g (66%) of colorless crystals, mp 72°C (from EtOH–hexane). IR (KBr, cm^{-1}): 3 284 (broad, O-H), 1 595 (C=N). ^{1}H NMR (90 MHz, $CDCl_3$–TMS) δ (ppm): 0.57–2.33 (m, $(CH_2)_5$), 1.23 (s, $C(CH_3)_2$), 3.40–3.87 (m, N-CH), 3.60 (d, J = 6 Hz, O-CH_2), 6.07 (t, J = 6 Hz, broad, exchangeable, OH), 6.53 (s, N=CH). Anal. calcd. for $C_{11}H_{21}NO_2$: C 66.30, H 10.62, N 7.03; found: C 66.29, H 10.61, N 6.82.

3-(Benzylimino)-2,2-dimethylpropanol *N*-oxide (8*d*)

3-Hydroxy-2,2-dimethylpropanal (2.04 g, 20 mmol), *N*-benzylhydroxylamine hydrochloride (3.19 g, 20 mmol), and K_2CO_3 (1.40 g) are reacted as described for **8*a***. After the refluxing, about two-thirds of the benzene is distilled off and crystallization is achieved by addition of ether. Yield: 1.77 g (43%) of colorless crystals, mp 98°C (from benzene–ether). IR (KBr, cm^{-1}): 3 243 (broad, O-H), 1 600 (C=N/C=C). ^{1}H NMR (90 MHz, $CDCl_3$–TMS) δ (ppm): 1.23

© 2000 NRC Canada

(s, $C(CH_3)_2$), 3.63 (d, J = 6 Hz, O-CH_2), 4.87 (s, N-CH_2), 5.70 (t, J = 6 Hz, exchangeable, OH), 6.53 (s, N=CH), 7.43 (s, C_6H_5). Anal. calcd. for $C_{12}H_{17}NO_2$: C 69.54, H 8.27, N 6.76; found: C 69.52, H 8.27, N 6.67.

3-(Benzhydrylimino)-2,2-dimethylpropanol *N*-oxide (8*e*)

3-Hydroxy-2,2-dimethylpropanal (1.02 g, 10 mmol) and *N*-benzhydrylhydroxylamine (1.99 g, 10 mmol) are reacted as described for **8*c***. After the refluxing about two-thirds of the benzene is distilled off and crystallization is achieved upon cooling and addition of petroleum ether. Yield: 1.84 g (65%) of colorless crystals, mp 123°C (from abs ethanol–petroleum ether). IR (KBr, cm^{-1}): 3 400 (broad, O-H), 1 587 (C=N/C=C). ^{1}H NMR (90 MHz, $CDCl_3$-TMS), δ (ppm): 1.20 (s, $C(CH_3)_2$), 3.63 (d, J = 6 Hz, O-CH_2), 5.67 (t, J = 6 Hz, exchangeable, OH), 6.20 (s, N-CH), 6.57 (s, N=CH), 7.37 (s, $C(C_6H_5)_2$). Anal. calcd. for $C_{18}H_{21}NO_2$: C 76.30, H 7.47, N 4.94; found: C 76.31, H 7.46, N 4.71.

4,6,6-Trimethyl-2,2-diphenyl-1,3-dioxa-4-azonia-2-borata-4-cycloheptene (9*a*)

Solutions of **8*a*** (0.13 g, 1 mmol) in 1 mL of ethanol and of oxybis(diphenylborane) (0.17 g, 0.5 mmol) in 1 mL of ethanol are mixed under stirring at room temperature. Crystallization commences usually after a few minutes or upon cooling and rubbing with a glass stick. If necessary the substance can be recrystallized from absolute ethanol. Yield: 0.21 g (71%) of colorless crystals[6], mp 176°C. IR (KBr, cm^{-1}): 1 664 (C=N). ^{1}H NMR (90 MHz, $CDCl_3$–TMS) δ (ppm): 1.27 (s, $C(CH_3)_2$), 3.03 (s, N-CH_3), 3.70 (s, O-CH_2), 6.80 (s, N=CH), 7.00–7.97 (m, $B(C_6H_5)_2$). ^{11}B NMR (64 MHz, $CDCl_3$–Et_2OBF_3) δ (ppm): 10.6 ($w_{1/2}$ = 257 Hz). Anal. calcd. for $C_{18}H_{22}BNO_2$: C 73.24, H 7.51, B 3.66, N 4.57; found: C 73.37, H 7.53, B 3.77, N 4.67. Single crystals suitable for X-ray crystallographic analysis were obtained by very slow crystallization from ethanol.

6,6-Dimethyl-2,2-diphenyl-4-propyl-1,3-dioxa-4-azonia-2-borata-4-cycloheptene (9*b*)

8*b* (0.16 g, 1 mmol) and oxybis(diphenylborane) (0.17 g, 0.5 mmol) are reacted as described for **9*a***. Yield: 0.22 g (68%) of colorless crystals[6], mp 170°C. IR (KBr, cm^{-1}): 1 655 (C=N). ^{1}H NMR (90 MHz, $CDCl_3$–TMS) δ (ppm): 0.77 (t, J = 6 Hz, N-C-C_3), 1.27 (s, $C(CH_3)_2$), 1.47–1.97 (m, N-C-CH_2), 3.10 (t, J = 6 Hz, N-CH_2), 3.73 (s, O-CH), 6.90 (s, N=CH), 7.00–7.90 (m, $B(C_6H_5)_2$). ^{11}B NMR (64 MHz, $CDCl_3$–Et_2OBF_3) δ (ppm): 10.3 ($w_{1/2}$ = 257 Hz), 44.6, ratio of peak areas 10:1.[13] Anal. calcd. for $C_{20}H_{26}BNO_2$: C 74.32, H 8.11, B 3.34, N 4.33; found: C 74.20, H 8.10, B 3.40, N 4.17.

4-Cyclohexyl-6,6-dimethyl-2,2-diphenyl-1,3-dioxa-4-azonia-2-borata-4-cycloheptene (9*c*)

8*c* (0.20 g, 2 mmol) and oxybis(diphenylborane) (0.35 g, 1 mmol) are reacted as described for **9*a***. Yield: 0.64 g (88%) of colorless crystals[6], mp 178°C. IR (KBr, cm^{-1}): 1 636 (C=N). ^{1}H NMR (90 MHz, $CDCl_3$–TMS) δ (ppm): 0.67–2.27 (m, $(CH_2)_5$), 1.30 (s, $C(CH_3)_2$), 2.97 (m, N-CH), 3.77 (s, O-CH_2), 6.93 (s, N=CH), 7.07–8.00 (m, $B(C_6H_5)_2$). ^{11}B NMR (64 MHz, $CDCl_3$–Et_2OBF_3) δ (ppm): 10.6 ($w_{1/2}$ = 342 Hz), 46.7, ratio of peak areas 10:1.[13] Anal. calcd. for $C_{23}H_{30}BNO_2$: C 76.06, H 8.32, B 2.98, N 3.86; found: C 76.22, H 8.36, B 3.05, N 3.66.

4-Benzyl-6,6-dimethyl-2,2-diphenyl-1,3-dioxa-4-azonia-2-borata-4-cycloheptene (9*d*)

8*d* (0.42 g, 2 mmol) and oxybis(diphenylborane) (0.35 g, 1 mmol) are reacted as described for **9*a***. Yield: 0.73 g (98%) of colorless crystals[6], mp 174°C. IR (KBr, cm^{-1}): 1 652 (C=N), 1 605 (C=C). ^{1}H NMR (90 MHz, $CDCl_3$–TMS) δ (ppm): 1.23 (s, $C(CH_3)_2$), 3.77 (s, O-CH_2), 4.27 (s, N-CH_2), 6.73 (s, N=CH), 6.93–8.00 (m, 15 aromatic H). ^{11}B NMR (64 MHz, $CDCl_3$–Et_2OBF_3) δ (ppm): 10.7 ($w_{1/2}$ = 258 Hz), 47.3, ratio of peak areas 10:1.[13] Anal. calcd. for $C_{24}H_{26}BNO_2$: C 77.64, H 7.06, B 2.91, N 3.77; found: C 77.75, H 7.21, B 3.01, N 3.69.

4-Benzhydryl-6,6-dimethyl-2,2-diphenyl-1,3-dioxa-4-azonia-2-borata-4-cycloheptene (9*e*)

8*e* (0.57 g, 2 mmol) and oxybis(diphenylborane) (0.35 g, 1 mmol) are reacted as described for **9*a***. Yield: 0.76 g (85%) of colorless crystals[6], mp 168°C. IR (KBr, cm^{-1}): 1 664 (C=N), 1 586 (C=C). ^{1}H NMR (90 MHz, $CDCl_3$–TMS) δ (ppm): 1.30 (s, $C(CH_3)_2$), 3.83 (s, O-CH_2), 5.60 (s, N-CH), 6.67–8.00 (m, 20 aromatic H and N=CH). ^{11}B NMR (64 MHz, $CDCl_3$–Et_2OBF_3) δ (ppm): 10.5 ($w_{1/2}$ = 342 Hz), 46.0, ratio of peak areas 10:1.[13] Anal. calcd. for $C_{30}H_{30}BNO_2$: C 80.54, H 6.76, B 2.42, N 3.13; found: C 80.37, H 6.80, B 2.49, N 2.91.

5,5-Dimethyl-2,2-diphenyl-1-oxa-3-azonia-2-borata-3-cyclohexen-3-ol (11*a*)

3-Hydroxy-2,2-dimethylpropionaldoxime (16) (0.12 g, 1 mmol) and oxybis(diphenylborane) (0.17 g, 0.5 mmol) are reacted as described for **5*a***. Yield: 0.25 g (89%) of colorless crystals[6], mp 165°C (from ethanol). IR (KBr, cm^{-1}): 2 566 (broad, O-H), 1 638 (C=N). ^{1}H NMR (90 MHz, $CDCl_3$–TMS) δ (ppm): 1.30 (s, $C(CH_3)_2$), 3.57 (s, O-CH_2), 7.13–7.67 (m, 1 H exchangeable, OH and $B(C_6H_5)_2$, and N=CH). ^{1}H NMR (400 MHz, $CDCl_3$–TMS) δ (ppm): 1.30 (s, $C(CH_3)_2$), 3.53 (s, O-CH_2), 7.13 (m, exchangeable, OH), 7.23–7.57 (m, $B(C_6H_5)_2$), 7.60 (s, N=CH). ^{11}B NMR (64 MHz, $CDCl_3$–Et_2OBF_3) δ (ppm): 4.00 ($w_{1/2}$ = 257 Hz). Anal. calcd. for $C_{17}H_{20}BNO_2$: C 72.62, H 7.17, B 3.84, N 4.98; found: C 72.67, H 7.22, B 3.98, N 4.84.

2,2-Di(4′-methoxyphenyl)-5,5-dimethyl-1-oxa-3-azonia-2-borata-3-cyclohexen-3-ol (11*b*)

3-Hydroxy-2,2-dimethylpropionaldoxime (16) (0.23 g, 2 mmol) and di(4-methoxyphenyl)-borinic acid (obtained from the 2-aminoethyl ester (19) by hydrolysis (11)) (0.48 g, 2 mmol) are reacted as described for **5*a***. Yield: 0.33 g (49%)

[13]Side signals with a small peak area at about 46 ppm have also been observed in the ^{11}B NMR spectra of diphenylboron chelates from other nitrone ligands (17) indicating a trivalent (sp^2) boron atom of a Ph_2B-O-R species (18). It is not yet clear whether the signal originates from an open-chain diphenylborinate (scission of the nitrone O-B coordination in **9**), or from free diphenylborinic acid caused by partial solvolysis.

© 2000 NRC Canada

of colorless crystals[6], mp 128°C (from ethanol). IR (KBr, cm^{-1}): 2 517 (broad, O-H), 1 640 (C=N), 1 599 (C=C). ^1H NMR (90 MHz, $CDCl_3$–TMS) δ (ppm): 1.27 (s, $C(CH_3)_2$), 3.60 (s, O-CH_2-C), 6.67–8.00 (m, 1 H exchangeable, OH and N=CH, and 8 aromatic H). ^{11}B NMR (64 MHz, $CDCl_3$–Et_2OBF_3) δ (ppm): 9.9 ($w_{1/2}$ = 342 Hz). Anal. calcd. for $C_{19}H_{24}BNO_4$: C 66.88, H 7.09, B 3.17, N 4.11; found: C 66.81, H 7.15, B 3.28, N 3.95. Single crystals suitable for X-ray crystallography were obtained by very slow crystallization from absolute ethanol.

4,5-Dimethyl-2,2-diphenyl-1-oxa-3-azonia-2-borata-3-cyclohexen-3-ol (11*c*)

4-Hydroxy-3-methyl-2-butanonoxime (15) (0.59 g, 5 mmol) and oxybis(diphenylborane) (0.87 g, 2.5 mmol) are reacted as described for **5*a***. Instead of petroleum ether, diethyl ether is added to initiate the crystallization. Yield: 0.85 g (58%) of colorless crystals[6], mp 151°C (from ethanol–ether). IR (KBr, cm^{-1}): 2 691 (broad, O-H), 1 638 (C=N). ^1H NMR (90 MHz, $CDCl_3$–TMS) δ (ppm): 1.40 (d, J = 7 Hz, N=C-C-CH_3), 2.23 (s, N=C-CH_3), 2.40–3.00 (m, X of ABX system, N=C-CH), 3.47/3.90 (m/m, AB of ABX system, O-CH_2), 7.07 (s, broad, exchangeable, OH), 7.20–7.67 (m, $B(C_6H_5)_2$). ^{11}B NMR (64 MHz, $CDCl_3$–Et_2OBF_3) δ (ppm): 6.6 ($w_{1/2}$ = 235 Hz). Anal. calcd. for $C_{17}H_{20}BNO_2$: C 72.62, H 7.17, B 3.84, N 4.98; found: C 72.66, H 7.16, B 3.87, N 4.85.

4,6,6-Trimethyl-2,2-diphenyl-1-oxa-3-azonia-2-borata-3-cyclohexen-3-ol (11*d*)

4-Hydroxy-4-methyl-2-pentanonoxime (20) (0.66 g, 5 mmol) and oxybis(diphenylborane) (0.87 g, 2.5 mmol) are reacted as described for **5*a***. Yield: 0.60 g (41%) of colorless crystals[6], mp 124°C (from ethanol). IR (KBr, cm^{-1}): 2 702 (broad, O-H), 1 650 (C=N). ^1H NMR (90 MHz, $CDCl_3$–TMS) δ (ppm): 1.37 (s, $C(CH_3)_2$), 2.30 (s, N=C-CH_3), 2.50 (s, N=C-CH_2-C), 7.10–7.90 (m, 1 H exchangeable, OH and $B(C_6H_5)_2$). ^{11}B NMR (64 MHz, $CDCl_3$–Et_2OBF_3) δ (ppm): 6.2 ($w_{1/2}$ = 128 Hz). Anal. calcd. for $C_{18}H_{22}BNO_2$: C 73.24, H 7.51, B 3.66, N 4.75; found: C 73.27, H 7.65, B 3.71, N 4.58.

(Methylimino)acetic acid *N*-oxide (16*a*)

Method A

Glyoxylic acid monohydrate (0.46 g, 5 mmol), dried $MgSO_4$ (0.60 g), *N*-methylhydroxylamine hydrochloride (0.42 g, 5 mmol), and triethylamine (0.51 g, 5 mmol) are refluxed in 50 mL of ether for 5 min. The solid residue is filtered off and extracted several times with boiling ether. The combined ether solutions are partially evaporated and, if necessary, cooled for crystallization. Yield: 0.12 g (24%) of colorless crystals, mp 78°C (from ether). IR (KBr, cm^{-1}): 2 600–2 000 ("curtain," O-H assoc.), 1 711 (C=O), 1 580 (C=N). ^1H NMR (90 MHz, $CDCl_3$–TMS) δ (ppm): 3.93 (s, CH_3), 7.43 (s, N=CH), 14.67 (s, very broad, exchangeable, OH). Anal. calcd. for $C_3H_5NO_3$: C 34.96, H 4.89, N 13.59; found: C 34.72, H 4.87, N 13.32.

Method B

Large quantities (up to 40 mmol) can be prepared advantageously also by the procedure described in the literature (21) for **16*d*** (see below), which gives better yields, but requires more time.

(*tert*-Butylimino)acetic acid *N*-oxide (16*b*)

Method A, as described above for **16*a***, is applied for *N*-*tert*-butylhydroxylamine (0.45 g, 5 mmol), without triethylamine in *n*-hexane as the solvent. Yield: 0.58 g (68%) of colorless crystals, mp 62°C (from hexane). IR (KBr, cm^{-1}): 2 600–2 170 (curtain, O-H assoc.), 1 703 (C=O), C=N band not identified. ^1H NMR (90 MHz, $CDCl_3$–TMS) δ (ppm): 1.60 (s, $C(CH_3)_3$), 7.47 (s, N=CH), 14.63 (s, broad, exchangeable, OH). Anal. calcd. for $C_6H_{11}NO_3$: C 49.65, H 7.64, N 9.65; found: C 49.42, H 7.73, N 9.42.

(Cyclohexylimino)acetic acid *N*-oxide (16*c*)

Method A, as described above for **16*b***, is applied for *N*-cyclohexylhydroxylamine (0.58 g, 5 mmol). Yield: 0.46 g (54%) of colorless crystals, mp 87°C (from hexane). IR (KBr, cm^{-1}): 2 500–2 340 (curtain, OH assoc.), 1 727/1 699 (C=O), 1 609 (C=N). ^1H NMR (90 MHz, $CDCl_3$–TMS) δ (ppm): 1.00–2.37 (m, $(CH_2)_5$), 3.90 (m, N=CH), 7.43 (s, N=CH), 14.77 (s, broad, exchangeable, OH). Anal. calcd. for $C_8H_{13}NO_3$: C 56.13, H 7.65, N 8.18; found: C 56.02, H 7.80, N 8.05.

(Benzylimino)acetic acid *N*-oxide (16*d*)

The compound was prepared as described in the literature (21), using *N*-benzylhydroxylamine hydrochloride and triethylamine in equimolar amounts.

4-Methyl-2,2-diphenyl-1,3-dioxa-4-azonia-2-borata-4-cyclohexen-6-one (17*a*)

Method A

16*a* (0.21 g, 2 mmol) in 5 mL of absolute ethanol and oxybis(diphenylborane) (0.35 g, 1 mmol) in 5 mL of absolute ethanol are mixed. Under stirring at room temperature crystallization commences. After complete precipitation, the crystals are washed with 3 × 5 mL of warm ether. Yield: 0.40 g (75%) of colorless crystals[6], mp 114°C.[14] IR (KBr, cm^{-1}): 1 719/1 705 (C=O), 1 602 (C=N/C=C). ^1H NMR (90 MHz, DMSO-d_6–TMS) δ (ppm): 3.97 (s, CH_3), 7.00–8.00 (m, $B(C_6H_5)_2$), 8.53 (s, N=CH). A ^{11}B NMR spectrum could not be obtained because of poor solubility. Anal. calcd. for $C_{15}H_{14}BNO_3$: C 67.45, H 5.28, B 4.05, N 5.24; found: C 67.26, H 5.26, B 4.06, N 5.03.

Method B

Glyoxylic acid monohydrate (0.46 g, 5 mmol) and oxybis(diphenylborane) (0.87 g, 2.5 mmol) are dissolved in 5 mL of absolute ethanol under stirring at room temperature for 5 min. A solution of *N*-methylhydroxylamine hydrochloride (0.42 g, 5 mmol) and triethylamine (0.51 g, 5 mmol) in 5–10 mL of ethanol is added and stirred briefly for homogenization. Yield: 1.00 g (75%) of colorless crystals as described for method A.

[14]The usually analytical pure compound rearranges under thermal stress in solution[5]; therefore, recrystallization was not possible.

© 2000 NRC Canada

4-*tert*-Butyl-2,2-diphenyl-1,3-dioxa-4-azonia-2-borata-4-cyclohexen-6-one (17*b*)

16*b* (0.58 g, 4 mmol) and oxybis(diphenylborane) (0.70 g, 2 mmol) are reacted as described for **17*a*** (method A). Yield: 0.95 g, (77%) of colorless crystals[6], mp 132°C[14]. IR (KBr, cm^{-1}): 1 703 (C=O), 1 605 (C=N/C=C). ^1H NMR (90 MHz, $CDCl_3$–TMS) δ (ppm): 1.47 (s, $C(CH_3)_3$), 7.00 – 7.60 (m, $B(C_6H_5)_2$), 7.70 (s, N=CH). ^{11}B NMR (64 MHz, $CDCl_3$–Et_2OBF_3) δ (ppm): 10.5 ($w_{1/2}$ = 300 Hz), 30.0, ratio of peak areas 40:1.[15] Anal. calcd. for $C_{18}H_{20}BNO_3$: C 69.93, H 6.52, B 3.50, N 4.53; found: C 69.93, H 6.50, B 3.60, N 4.36. The compound is also available by a three component reaction of equimolar amounts of glyoxylic acid, *N*-*tert*-butylhydroxylamine, and diphenylborinic acid (method B as described for **17*a***, omitting triethylamine).

4-Cyclohexyl-2,2-diphenyl-1,3-dioxa-4-azonia-2-borata-4-cyclohexen-6-one (17*c*)

16*c* (0.34 g, 2 mmol) and oxybis(diphenylborane) (0.35 g, 1 mmol) are reacted as described for **17*a*** (method A). Yield: 0.21 g, (32%) of colorless crystals[6], mp 121°C[14]. IR (KBr, cm^{-1}): 1 706 (C=O), 1 603 (C=N/C=C). ^1H NMR (90 MHz, $CDCl_3$–TMS) δ (ppm): 0.80–2.33 (m, $(CH_2)_5$), 3.73 (m, N-CH), 7.00–7.67 (m, $B(C_6H_5)_2$ and N=CH). ^{11}B NMR (64 MHz, $CDCl_3$–Et_2OBF_3) δ (ppm): 10.3 ($w_{1/2}$ = 385 Hz), 30.1, ratio of peak areas 40:1[15]. Anal. calcd. for $C_{20}H_{22}BNO_3$: C 71.66, H 6.62, B 3.23, N 4.18; found: C 71.69, H 6.64, B 3.35, N 4.00. The compound is also available by a three component reaction of equimolar amounts of glyoxylic acid, *N*-cyclohexylhydroxylamine, and diphenylborinic acid (method B as described for **17*a***, omitting triethylamine).

4-Benzyl-2,2-diphenyl-1,3-dioxa-4-azonia-2-borata-4-cyclohexen-6-one (17*d*)

16*d* (0.18 g, 1 mmol) and oxybis(diphenylborane) (0.17 g, 0.5 mmol) are reacted analogous as described for **17*a*** (method A). Yield: 0.16 g, (47%) of colorless crystals[6], mp 199°C[13]. IR (KBr, cm^{-1}): 1 719 (C=O), 1 615 (C=N/C=C). ^1H NMR (90 MHz, $CDCl_3$–TMS) δ (ppm): 4.87 (s, N-CH_2), 6.67–7.73 (m, aromatic H and N=CH). ^{11}B NMR (64 MHz, $CDCl_3$–Et_2OBF_3) δ: C 73.50, H 5.29, B 3.15, N 4.08; found: C 73.20, H 5.39, B 3.16, N 4.12. The compound is also available by a three component reaction of equimolar amounts of glyoxylic acid, *N*-benzylhydroxylamine (hydrochloride + triethylamine), and diphenylborinic acid (method B as described for **17*a***).

4-Benzyl-2,2-di(4′-chlorophenyl)-1,3-dioxa-4-azonia-2-borata-4-cyclohexen-6-one (17*e*)

16*d* (0.36 g, 2 mmol) and di(4-chlorophenyl)borinic acid (11) (0.50 g, 2 mmol) are reacted as described for **17*a*** (method A). Yield: 0.45 g, (55%) of colorless crystals[6], mp 113°C[14]. IR (KBr, cm^{-1}): 1 709 (C=O), 1 616 (C=N). ^1H NMR (90 MHz, $CDCl_3$–TMS) δ (ppm): 4.93/5.13 (d/d, J = 15 Hz, AB system, N-CH_2), 6.67–8.00 (m, 13 aromatic H and N-CH). ^{11}B NMR (64 MHz, $CDCl_3$–Et_2OBF_3) δ (ppm): 11.6 ($w_{1/2}$ = 684 Hz), 31.3, ratio of peak areas 50:1.[15] Anal. calcd. for $C_{21}H_{16}BCl_2NO_3$: C 61.21, H 3.91, B 2.62, N 3.40; found: C 61.13, H 3.85, B 2.90, N 3.30. The compound is also available by a three component reaction of glyoxylic acid, *N*-benzylhydroxylamine (hydrochloride + triethylamine), and di(4-chlorophenyl)borinic acid (method B as described for **17*a***).

4-Methyl-2,2,5-triphenyl-1,3-dioxa-4-azonia-2-borata-4-cyclohexen-6-one (17*f*)

Phenylglyoxylic acid (0.75 g, 5 mmol) and oxybis(diphenylborane) (0.87 g, 2.5 mmol) are dissolved in 5 mL of absolute ethanol under stirring. After addition of a solution of *N*-methylhydroxylamine hydrochloride (0.42 g, 5 mmol) and triethylamine (0.51 g, 5 mmol) in 5 mL of ethanol and short heating, crystallization of the analytically pure product starts, at room temperature, eventually after cooling. Yield: 1.52 g, (89%) of colorless crystals[6], mp 132°C (from ethanol). IR (KBr, cm^{-1}): 1 711 (C=O), 1 594 (C=N/C=C). ^1H NMR (90 MHz, $CDCl_3$–TMS) δ (ppm): 3.60 (s, CH_3), 6.80–7.83 (m, 15 aromatic H). ^{11}B NMR (64 MHz, $CDCl_3$–Et_2OBF_3) δ (ppm): 10.2 ($w_{1/2}$ = 214 Hz). Anal. calcd. for $C_{21}H_{18}BNO_3$: C 73.50, H 5.29, B 3.15, N 4.08; found: C 73.45, H 5.36, B 3.33, N 3.90.

2,2,5-Triphenyl-4-propyl-1,3-dioxa-4-azonia-2-borata-4-cyclohexen-6-one (17*g*)

Phenylglyoxylic acid (0.75 g, 5 mmol), oxybis(diphenylborane) (0.87 g, 2.5 mmol), *N*-propylhydroxylamine hydrochloride (0.56 g, 5 mmol), and triethylamine (0.51 g, 5 mmol) are reacted as described for **17*f***. Yield: 0.66 g, (36%) of colorless crystals[6], mp 117°C (from ethanol). IR (KBr, cm^{-1}): 1 717 (C=O), 1 594 (C=N/C=C). ^1H NMR (90 MHz, $CDCl_3$–TMS) δ (ppm): 0.80 (t, J = 7 Hz, CH_3), 1.67–2.17 (m, N-C-CH_2), 3.70 (t, J = 7 Hz, N-CH_2), 6.80–7.73 (m, 15 aromatic H). ^{11}B NMR (64 MHz, $CDCl_3$–Et_2OBF_3) δ (ppm): 11.1 ($w_{1/2}$ = 257 Hz). Anal. calcd. for $C_{23}H_{22}BNO_3$: C 74.41, H 5.97, B 2.91, N 3.77; found: C 74.33, H 5.97, B 2.96, N 3.80.

4-Cyclohexyl-2,2,5-triphenyl-1,3-dioxa-4-azonia-2-borata-4-cyclohexen-6-one (17*h*)

Phenylglyoxylic acid (0.75 g, 5 mmol), oxybis(diphenylborane) (0.87 g, 2.5 mmol), and *N*-cyclohexylhydroxylamine (0.58 g, 5 mmol) are reacted as described for **17*f***, omitting triethylamine. Yield: 1.34 g, (65%) of colorless crystals[6], mp 139°C (from ethanol). IR (KBr, cm^{-1}): 1 719 (C=O), 1 586 (C=N/C=C). ^1H NMR (90 MHz, $CDCl_3$–TMS) δ (ppm): 0.83–2.67 (m, $(CH_2)_5$), 3.73 (m, N-CH), 6.70–7.87 (m, 15 aromatic H). ^{11}B NMR (64 MHz, $CDCl_3$–Et_2OBF_3) δ (ppm): 9.2 ($w_{1/2}$ = 342 Hz). Anal. calcd. for $C_{26}H_{26}BNO_3$: C 75.93, H 6.37, B 2.63, N 3.41; found: C 75.82, H 6.36, B 2.57, N 3.27.

4-Benzyl-2,2,5-triphenyl-1,3-dioxa-4-azonia-2-borata-4-cyclohexen-6-one (17*i*)

Phenylglyoxylic acid (0.75 g, 5 mmol), oxybis(diphenylborane) (0.87 g, 2.5 mmol), *N*-benzyhlhydroxylamine hydrochloride (0.80 g, 5 mmol), and triethylamine (0.51 g, 5 mmol) are reacted as described for **17*f***. Yield: 1.31 g, (63%) of colorless crystals[6], mp 112°C (from ethanol). IR (KBr, cm^{-1}): 1 713 (C=O), 1 596 (C=N/C=C). ^1H NMR

[15]The signal with very small peak area originates from impurities caused by a thermally induced rearrangement reaction.[5]

© 2000 NRC Canada

Table 1. Crystallographic data.[a]

Compound	**5*d***	**9*a***	11***b***	19
Formula	$C_{26}H_{22}BNO_2$	$C_{18}H_{22}BNO_2$	$C_{19}H_{24}BNO_4$	$C_{20}H_{16}BNO_3$
fw	391.28	295.19	341.21	329.16
Crystal system	Monoclinic	Orthorhombic	Monoclinic	Monoclinic
Space group	$P2_1/c$	$P2_12_12_1$	$P2_1/n$	$P2_1/n$
a (Å)	10.543(2)	10.9913(5)	11.227(2)	11.1847(15)
b (Å)	19.085(4)	14.9329(7)	9.967(2)	13.715(3)
c (Å)	10.2667(3)	10.2460(13)	17.0537(4)	11.5559(5)
β (°)	90.4978(7)	90	105.4179(5)	104.8730(10)
V (Å^3)	2065.6(4)	1681.7(2)	1839.7(3)	1713.2(3)
Z	4	4	4	4
ρ_{calc} (g/cm^3)	1.258	1.166	1.232	1.276
F(000)	824	632	728	688
Radiation	Mo	Mo	Mo	Mo
μ (cm^{-1})	0.78	0.74	0.85	0.85
Size (mm)	0.25 0.3 0.4	0.25 0.35 0.4	0.3 0.35 0.4	0.35 0.4 0.5
Corr. factors[b]	0.83–1.00	0.79–1.00	0.86–1.00	0.84–1.00
φ range (χ = –90°)	0–190	0–190	0–190	0–190
ω range (χ = –90°)	–23–18	–23–18	–22–18	–22–18
Osc. width (deg)	0.5	0.5	0.5	0.5
Images, time	462, 80 s	462, 80 s	460, 60 s	460, 90 s
$2\theta_{max}$ (deg)	60.1	60.1	60.0	60.4
Total reflections	19617	15953	17151	15767
Unique reflections	5150	4438 [c]	4331	3996
R_{merge}	0.069	0.069	0.040	0.025
No. with $I \geq 3\sigma(I)$	3392	3338	2807	2739
No. of variables	359	287	322	287
R (F) ($I \geq 3\sigma(I)$)	0.049	0.047	0.042	0.047
R_w (F^2) (all data)	0.128	0.111	0.085	0.095
gof	1.27	1.16	2.07	2.72
Max Δ/σ (final cycle)	0.0003	0.006	0.0003	0.0004
Residual density (e/Å^3)	–0.50–0.46	–0.49–0.46	–0.34–0.36	–0.29–0.32

[a]Temperature 180 K, Rigaku/ADSC CCD diffractometer, Mo K_a (l = 0.71069 Å), graphite monochromator, takeoff angle 6.0°, aperture 94.0 × 94.0 mm at a distance of 39.2 mm from the crystal, $\sigma^2(F^2) = (C + B)/Lp^2$ (C = scan count, B = background count), function minimized $\sum w(|F_o^2| - |F_c^2|)^2$ where $w = 1/\sigma^2(F_o^2)$, $R(F) = \sum||F_o| - |F_c||/\sum|F_o|$, $R_w(F^2) = (\sum w(|F_o^2| - |F_c^2|)^2/\sum w|F_o^2|^2)^{1/2}$, and gof = $[\sum w(|F_o^2| - |F_c^2|)^2/(m - n)]^{1/2}$.

[b]Includes crystal decay (if any), absorption, and scaling corrections performed in a single step.

[c]Includes Friedel pairs, 3 144 are unique.

(90 MHz, $CDCl_3$–TMS) δ (ppm): 4.90 (s, N-CH_2), 6.80–7.70 (m, 15 aromatic H). ^{11}B NMR (64 MHz, $CDCl_3$–Et_2OBF_3) δ (ppm): 11.5 ($w_{1/2}$ = 385 Hz). Anal. calcd. for $C_{27}H_{22}BNO_3$: C 77.35, H 5.29, B 2.58, N 3.34; found: C 77.36, H 5.33, B 2.63, N 3.17.

3-Hydroxy-2,2,4-triphenyl-1-oxa-3-azonia-2-borata-3-cyclopenten-5-one (19)

2-(Hydroxyimino)phenylacetic acid (22) (0.83 g, 5 mmol) is dissolved in 50 mL of refluxing $CHCl_3$. After the addition of oxybis(diphenylborane) (0.87 g, 2.5 mmol), dissolved in 2 mL of $CHCl_3$, the mixture is refluxed briefly. The solvent is distilled off until the volume is reduced to 10 mL. Crystallization is achieved after addition of small amount of petroleum ether and cooling to –18°C for 1 h. Yield: 1.16 g (70%) of colorless crystals[6], mp 181°C (from $CHCl_3$–petroleum ether). IR (KBr, cm^{-1}): 3 156–2 737 (curtain, O-H assoc.), 1 725 (C=O), 1 657 (C=N), 1597 (C=C). ^{1}H NMR (90 MHz, $CDCl_3$–TMS) δ (ppm): 7.23–7.73 (m, 13 aromatic H), 8.90 (d, J = 7 Hz, 2 aromatic H), signal for OH not detectable. ^{11}B NMR (64 MHz, $CDCl_3$–Et_2OBF_3) δ (ppm): 9.3 ($w_{1/2}$ = 300 Hz). Anal. calcd. for $C_{20}H_{16}BNO_3$: C 72.98, H 4.90, B 3.28, N 4.26; found: C 73.03, H 4.89, B 3.21, N 4.25. Single crystals suitable for X-ray crystallography were obtained by very slow crystallization from chloroform–petroleum ether (bp 30–70°C) using the liquid diffusion method (23).

X-ray crystallographic analyses of 5*d*, 9*a*, 11*b*, 19

Crystallographic data appear in Table 1. The final unit-cell parameters were obtained by least-squares based on 12 693, 12 078, 8 118, and 9 840 reflections with 2θ = 4–64° for **5*d***, **9*a***, **11*b***, and **19**, respectively. The data were processed,[16] corrected for Lorentz and polarization effects, and absorption (based on analysis of symmetry-equivalent data).

The structures were solved by direct methods, the coordinates of the atoms being determined from *E*-maps or from

[16]teXsan: Crystal structure analysis package. Unix version 1.7. Molecular Structure Corp. The Woodlands, TX, U.S.A. 1995; and d*TREK: Area Detector Software. Molecular Structure Corp. The Woodlands, TX, U.S.A. 1997.

© 2000 NRC Canada

Table 2. Selected bond lengths (Å, σ = 0.002 Å) and angles (deg, σ = 0.1°).

Structure	**5*d***	**9*a***	**11*b***	**19**
Ring size	5	7	6	5
(A) Bond lengths (Å)				
B—N	1.613	—	1.626	1.608
B—O	1.503	1.464, 1.593	1.491	1.517
B—C	1.604, 1.612	1.616, 1.621	1.605, 1.612	1.601, 1.608
N=C	1.289	1.284	1.275	1.294
N—O	1.380	1.357 (ring)	1.394	1.360
O—C	1.427	1.417	1.430	1.311
C—C (ring)	1.518	1.498, 1.536	1.498, 1.528	1.512
(B) Angles (deg)				
O-B-N	94.9	107.0 (OBO)	102.8	95.3
C-B-C	115.7	117.0	117.6	118.5
B-N=C	114.1	112.4 (BON)	126.1	115.3
B-O-C	112.0	113.6	113.8	113.3

subsequent difference Fourier syntheses. The non-hydrogen atoms were refined with anisotropic thermal parameters, and the hydrogen atoms were refined with isotropic thermal parameters. No corrections for secondary extinction were necessary. Neutral atom scattering factors for all atoms and anomalous dispersion corrections for the non-hydrogen atoms were taken from the *International Tables for X-Ray Crystallography*. For **9a**, the absolute configuration for the crystal used could not be determined from the small anomalous scattering effect. Selected bond lengths and angles are listed in Table 2. Complete tables of atomic coordinates and equivalent isotropic thermal parameters, bond lengths and angles, hydrogen atom parameters, anisotropic thermal parameters, torsion angles, intermolecular contacts, and least squares planes are included as supplementary material.[17]

Results and discussion

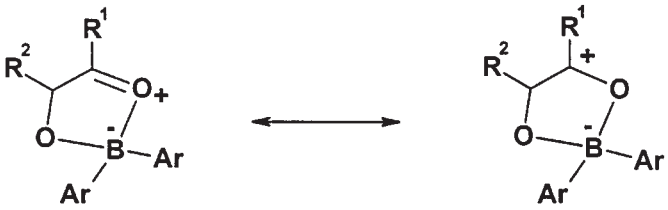
Nitrones 2

The *N*-alkylnitrones **2** which were required as intermediates for the synthesis of the six-membered boron chelates **3** could be prepared in the case of the aldonitrone species by condensation of *N*-alkylhydroxylamines with 2-hydroxycarbaldehydes **1** (R^1 = H) (9). The preparation of ketonitrones from 2-hydroxyketones (R^1 = alkyl) by condensation with *N*-alkylhydroxylamines appeared ineffective and led to some nitrone only in the case of **2*h***.

Since it has been recognized that the (*Z*)-configuration of aldonitrones is generally favored (24), it can be assumed that the aldonitrones **2** exist entirely in the (*Z*)-form which should be stabilized additionally by the intramolecular O-H···O bond in this case. The ready formation of **3**, described below, might corroborate this supposition.

Typical for the nitrones **2** are infrared spectra showing a C=N absorption band between 1 587 and 1 600 cm^{-1} and a broadened band of the associated O-H group at about 3 250 cm^{-1}. The ^1H NMR spectra of the aldonitrones **2** are characterized by the signals for the N=CH methine proton between 6.76 and 6.93 ppm and signals for an exchangeable OH proton which is present also in the spectrum of the ketonitrone **2*h***.

Scheme 1.



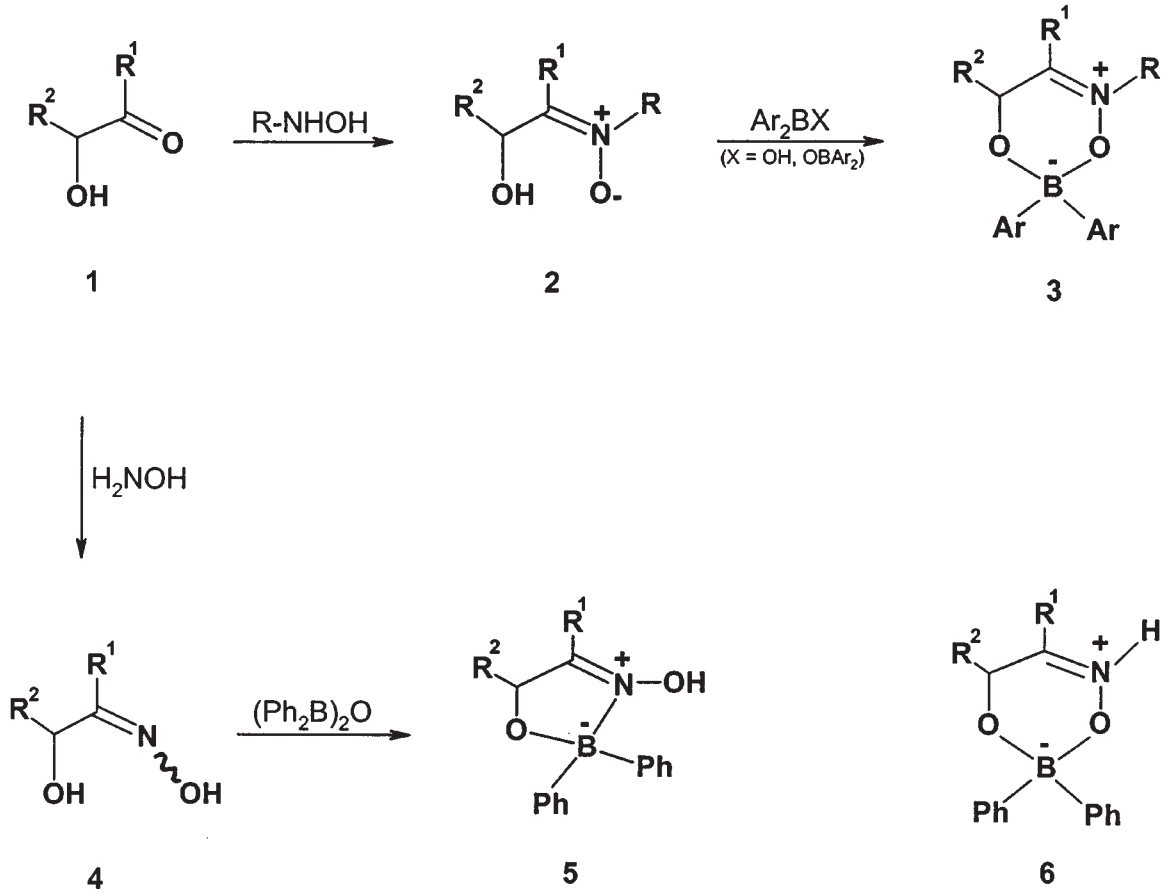
Nitrone complexes 3

Reaction of **2** with a diarylborinic acid or anhydride gave the diarylboron chelates **3** readily and in good yields. However, the preformation of the nitrone **2**, which is quite difficult with ketones, could be avoided by a three-component one-pot reaction of **1**, a diarylborinic acid, and an *N*-alkylhydroxylamine, which proved an advantage for the synthesis of ketonitrone derivatives applying the 2-hydroxyketones **1** (R^1 = alkyl). In the latter case, a preceding complex formation between the 2-hydroxyketone and the Lewis-acid boron compound (see Scheme 1)[18] might facilitate the nucleophilic attack of the hydroxylamine at the carbonyl carbon atom. Thus, only one of the ketonitrones (**2*h***) could be isolated in a satisfying yield and applied as an educt for the diphenylboron complex (**3*t***). All the other ketonitrone chelates **3** were prepared by the one-pot method without isolation of an intermediate **2**.

The infrared spectra of **3** are characterized by the disappearance of the stretching vibration of the O-H group of the free ligand **2**, and display an N=C band between 1 578 and 1 665 cm^{-1}, generally shifted to higher wave numbers

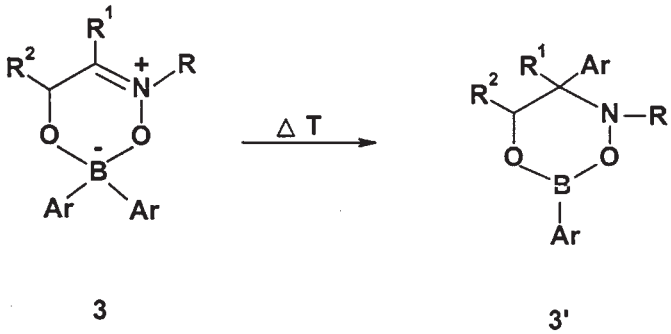
[17]Copies of material on deposit may be purchased from the Depository of Unpublished Data, Document Delivery, CISTI, National Research Council Canada, Ottawa, Canada K1A 0S2 (http://www.nrc.ca/cisti/irm/unpub_e.shtml for information on ordering electronically).
[18]Diarylboron complexes of this type could not be isolated as crystalline products or intermediates in the reactions of the various 2-hydroxycarbonyl compounds used in this investigation.

© 2000 NRC Canada



		R	R^1	R^2
2	*a*	CH_3	H	H
	b	$PhCH_2$	H	H
	c	CH_3	H	CH_3
	d	$(CH_3)_3C$	H	CH_3
	e	C_6H_{11}	H	CH_3
	f	$PhCH_2$	H	CH_3
	g	Ph_2CH	H	CH_3
	h	C_6H_{11}	CH_3	CH_3

Scheme 2.

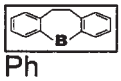


compared to the N=C bands of the corresponding educts **2**. In the ^{1}H NMR spectra of the aldonitrone derivatives (**3*a*–*l***), the N=CH methine proton shows a signal between 6 and 7 ppm. The ^{11}B NMR spectra of **3** indicate the tetracoordinate boron nucleus with signals between 3.6 and 9.2 ppm. In some of the spectra a second signal with very small peak area appears between 26.0 and 29.2 ppm, pointing to a trivalent boron atom in the trigonal arrangement of an arylboronate derivative (18). Small additional peaks were also observed in some of the ^{1}H NMR spectra and originate from impurities caused by a thermally induced rearrangement reaction (Scheme 2), leading to the isomeric arylboronates **3′**.[5] The isomerization can be retarded mostly by avoiding thermal stress during the preparation, recrystallization, and spectroscopy of **3**. The thermal stability of **3** depends on the substitution pattern. Thus the compounds **3*f*, *g*, *y*** can be recrystallized from the boiling solvent, and especially **3*z*–*cc*** show a high stability at all temperatures in various solvents.

Oxime complexes 5

Several 2-hydroxyketoximes **4** were reacted with diphenylborinic acid anhydride and gave readily crystalline compounds which show an elemental analysis consistent with both of the isomeric structures, **5** and **6**. An intact diphenylboron moiety is proved by the color reaction with

© 2000 NRC Canada

		R	R^1	R^2	Ar
3	***a***	CH_3	H	H	Ph
	b	C_6H_{11}	H	H	Ph
	c	$PhCH_2$	H	H	Ph
	d	Ph_2CH	H	H	Ph
	e	C_6H_{11}	H	J	4-ClC_6H_4
	f	C_6H_{11}	H	H	1-naphthyl
	g	C_6H_{11}	H	H	Ar_2B= 
	h	CH_3	H	CH_3	Ph
	i	$(CH_3)_3C$	H	CH_3	Ph
	j	C_6H_{11}	H	CH_3	Ph
	k	$PhCH_2$	H	CH_3	Ph
	l	Ph_2CH	H	CH_3	Ph
	m	C_6H_{11}	CH_3	H	Ph
	n	$PhCH_2$	CH_3	H	Ph
	o	4-$CH_3C_6H_4$	CH_3	H	Ph
	p	Ph_2CH	C_2H_5	H	Ph
	q	CH_3	CH_3	CH_3	Ph
	r	n-C_3H_7	CH_3	CH_3	Ph
	s	i-C_3H_7	CH_3	CH_3	Ph
	t	C_6H_{11}	CH_3	CH_3	Ph
	u	$PhCH_2$	CH_3	CH_3	Ph
	v	Ph_2CH	CH_3	CH_3	Ph
	w	C_6H_{11}	CH_3	CH_3	4-ClC_6H_4
	x	Ph_2CH	CH_3	CH_3	4-ClC_6H_4
	y	C_6H_{11}	CH_3	CH_3	1-naphthyl
	z	C_6H_{11}	—$(CH_2)_4$—		Ph
	aa	$PhCH_2$	—$(CH_2)_4$—		Ph
	bb	Ph_2CH	—$(CH_2)_4$—		Ph
	cc	4-$CH_3C_6H_4$	—$(CH_2)_4$—		Ph

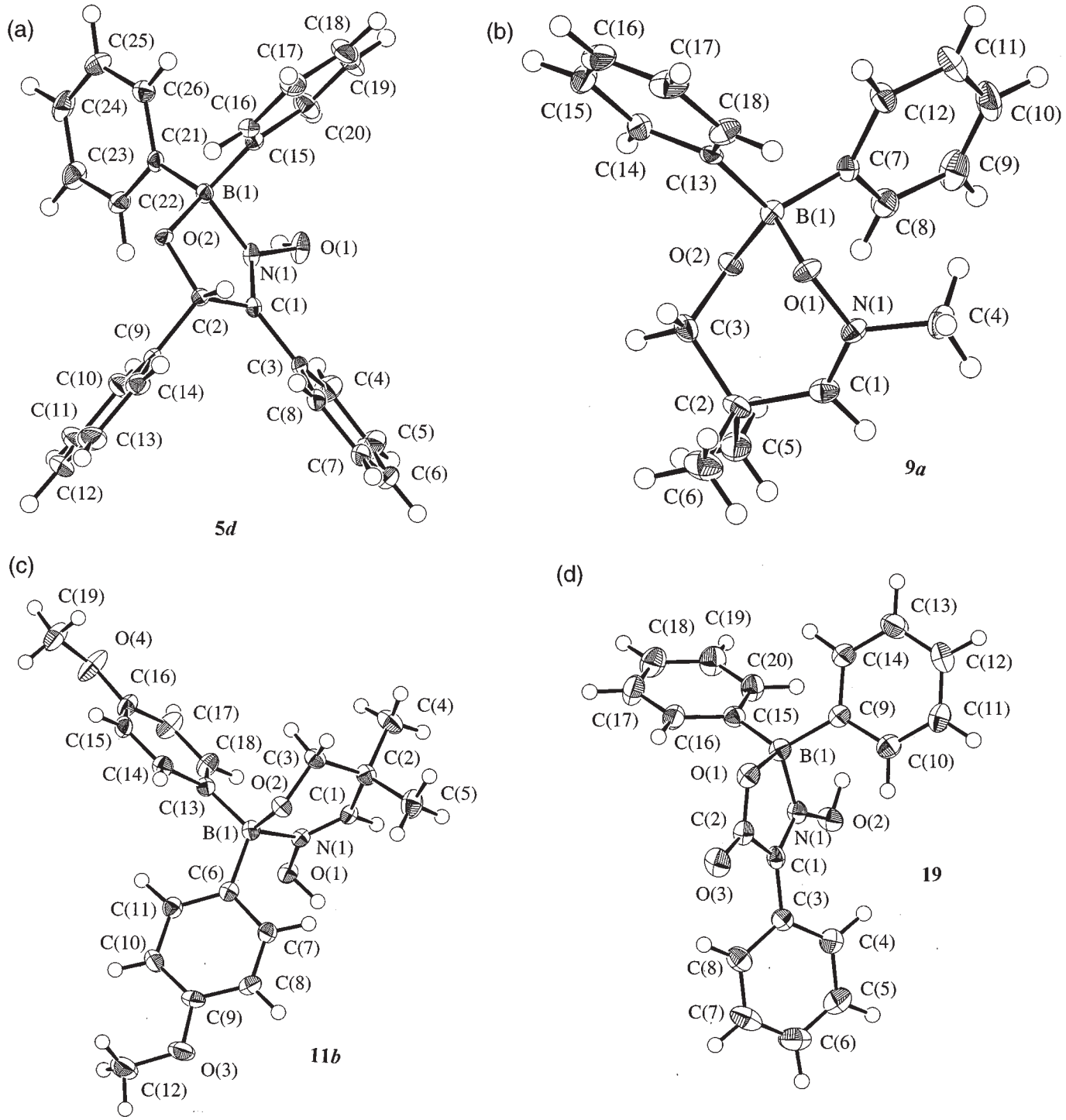
diphenylcarbazone (10). The infrared spectra, displaying a C=N absorption between 1 637 and 1 674 cm^{-1} and a broad band in the region of stretching vibrations of associated N-H/O-H groups (2 400–2 800 cm^{-1}), do not allow an unambiguous assignment to the five-membered ring system **5** with N-B coordination, or to the six-membered O-B-O chelate **6**, which is an *N*-unsubstituted derivative of **3**. From the ^1H NMR spectra, as well as from ^{11}B NMR spectra, no positive proof for one of the ring systems can be obtained. One exchangeable proton giving a ^1H signal about 12 ppm for acidic N-H or O-H, and a ^{11}B signal between 8.0 and 10.2 ppm, indicating the tetracoordinate boron nucleus (18), might characterize either of the structures **5** and **6**. For most of the metal complexes of 2-hydroxyoximes a five-membered O-*M*-N chelate structure is assumed (25), but evidence is presented also for six-membered O-*M*-O ring systems (26), even from the stereochemically defined (*E*)-benzoinoxime (α-benzoinoxime) as an educt (26*b*). The geometrical isomerism of the educt seems to be of minor significance, anyway, because *E*/*Z*-isomerization of oximes (inversion and (or) rotation) can take place easily, especially in the presence of an acid (27) or Lewis acid like a boron compound (28). Of the ketoximes **4** used in this work only α-benzoinoxime ((*E*)-**4**) (R^1 = R^2 = Ph), was stereochemically defined. An X-ray crystallographic analysis of **5*d*** proves the five-membered chelate ring structure presenting the oxime ligand in the (*E*)-conformation. Since the spectroscopic data of the other derivatives, **5*a*–*c***, are very similar, this structure should be applicable to all of the compounds **5**. To the best of our knowledge, **5*d*** is the first X-ray structurally characterized boron (or any other element) chelate of α-benzoinoxime.

The crystal structure of **5*d*** consists of discrete molecules (Fig. 1), linked by NO-H···O hydrogen bonds, the acceptor oxygen atom being the O(2) ring member:

O (1)···O (2) = 2.583(1), O(1)-H = 0.90(2),
H···O(2) = 1.71(2) Å, O(1)-H···O(2) = 162(2)°

© 2000 NRC Canada

Fig. 1. Views of the molecules of (*a*) ***5d***, (*b*) ***9a***, (*c*) ***11b***, and (*d*) **19**; 50% probability thermal ellipsoids are shown for the non-hydrogen atoms.



The C-C=N-B system in the five-membered ring in ***5d*** shows some deviation from exact planarity, torsion angle 9.6(2)°, and the ring conformation is best described as a half-chair, with B and O displaced on opposite sides of the C-C=N plane. A relatively narrow "bite" of the oxime ligand leads to a compressed O-B-N angle of 94.9(1)° (Table 2), thus distorting the tetrahedral grouping around the boron atom slightly. This angle is even smaller than the O-B-N angle between 98.2 and 99.9° in other five-membered COBNC rings derived from 2-aminoethanols and diarylborinic acids (29). The O-B, B-N, and N=C bond lengths are of the same order as those found in the diphenylboron chelate of

© 2000 NRC Canada

salicylaldoxime (cf. formula **13** below), which represents a six-membered analogue (30):

5*d*: 1.503, 1.613, and 1.289(2) Å, respectively.

13: 1.516, 1.609, and 1.284(2) Å, respectively.

The B—C (phenyl) bond lengths (1.604 and 1.612 Å) are about normal.

Nitrones 8

The 3-hydroxyaldehyde nitrones **8** were prepared by condensation of 3-hydroxy-2,2-dimethylpropanal with various *N*-alkylhydroxylamines to obtain bidentate ligands for the synthesis of the seven-membered boron chelate type **9**. Depending on the *N*-alkyl residue the nitrones **8** are high boil-

		R^1	R^2	Ar
5	*a*	CH_3	CH_3	Ph
	b	C_2H_5	H	Ph
	c	— $(CH_2)_4$ —		Ph
	d	Ph	Ph	Ph

ing liquids or crystalline substances under normal conditions. In the IR spectra the most characteristic absorptions are found in the 3 400–3 200 cm^{-1} region where stretching modes of hydrogen bonded O-H groups appear, and between 1 587 and 1 606 cm^{-1} where the C=N group of the nitrone function absorbs. The ^1H NMR spectra of **8** display some typical signals, common to all of the samples, such as the resonance of the N=CH methine proton between 6.53 and 6.60 ppm and a signal for the hydroxyl proton between 4.57 and 6.07 (in $CDCl_3$), as well as from the singlet of the 2,2-dimethyl grouping at about 1.23 ppm. As mentioned above for the aldonitrones **2**, it can be assumed that **8** exists in the (*Z*)-form and thus presents a suitable ligand for the diphenylborenium (Ph_2B^+) ion to form the chelate **9**.

Nitrone complexes 9

From the reaction of **8** with diphenylborinic acid anhydride the diphenylboron chelates **9** resulted as crystalline compounds in high yields, favored by larger *N*-alkyl substituents. The IR spectra of **9** show C=N absorptions be-

		R
8, 9	*a*	CH_3
	b	n-C_3H_7
	c	C_6H_{11}
	d	$PhCH_2$
	e	Ph_2CH

tween 1 636 and 1 664 cm^{-1}, a shift of 30–60 cm^{-1} to higher frequencies compared to the free ligand **8**. Similar observations have been made from the IR spectra of **2** and **3** and of other boron chelates and their nitrone ligands (31). In the ^1H NMR spectra of **9** the most significant signal is that of the N=CH methine proton between 6.73 and 6.93 ppm, shifted to lower field by 0.2–0.4 ppm compared to the ligand nitrone **8**. The ^{11}B NMR spectra of **9** show the expected signals of a tetravalent boron nucleus at about 10.5 ppm. A thermally induced 1,4-phenyl shift (from the diphenylboron group to the N=CH methine carbon), as observed from the spectra of **3**, obviously does not occur in **9**, even in boiling ethanol.

To prove the molecular structure, an X-ray crystallographic analysis of **9*a*** was carried out and confirmed the seven-membered ring structure derived from the (*Z*)-form of the nitrone ligand (Fig. 1). This is a new crystallographic example of a boron chelate with a stable seven-membered ring system. Similar chelate rings (**14**) containing a bidentate ligand with an *N*-oxide and a phenolate donor group have been described by X-ray crystallographic analyses in earlier work (17*c*, 32, 33). Two of these are derivatives of salicylaldehyde nitrones (**14**, X = Y = H, *R* = Me (32); X = NEt_2, Y = H, *R* = CH_2-C_6H_4-2-OH (17*c*)). Unlike the boron chelate rings of the salicylaldehyde nitrones **14**, which possess a somewhat distorted envelope (or sofa) conformation with the boron atom on the flap displaced by 0.8–1 Å from the mean plane formed by the remaining ring atoms, the seven-membered ring of **9*a*** has a distorted half-chair conformation (Fig. 1). The ring contains a planar segment, O(1)-N(1) = C(1)-C(2) of the nitrone moiety (torsion angle 0.1°), with the other three ring atoms considerably displaced from this plane (torsion angles as large as 95.5(2)°). This ring conformation places the B-phenyl groups quite far from the nitrone carbon atom C(1), the distance between the nearest boron-bound phenyl carbon atom C(7) and the nitrone carbon atom C (1) being 3.75 Å (with C(13)···C(1) = 4.40 Å). These distances are probably too long to facilitate the 1,4-migration of the phenyl group as observed in the diphenylboron chelate of *N*-methylsalicylaldonitrone (32). The higher thermal stability of the compounds **9** could be explained at least partially by that structural difference. As in other diphenylboron chelates with an *N*-oxide and an alcoholate or phenolate ligand (ref. 32 and refs. therein), the O—B bond between the nitrone oxygen atom and boron in **9*a*** (O(1)—B(1) = 1.593(2) Å) is longer than the O—B bond from the alcoholate (O(2)—B(1) = 1.464(2) Å). The mean O—B (1.528(2) Å) and C—B (1.619(2) Å) distances are similar to the average O—B and C—B bonds lengths in **14** (*R* = Me, X = Y = H) of 1.528 and 1.610 Å, respectively, (32), and the mean C—B:O—B bond length ratio of 1.059 for **9*a*** is only slightly larger than the value of 1.054 for **14** (*R* = Me, X = Y = H), indicating a minor increase of overall binding strength (34) of the ligand to the Ph_2B^+ nucleus in both of the seven-membered diphenylboron chelates. **9*a*** has no hydrogen-bond donating functional group, and the molecules in the crystal are linked by van der Waals forces, with a possibly significant C-H···O interaction: C···O = 3.235(2), C-H = 0.93(2), H···O = 2.33(2) Å, C-H···O = 153(2)°.

Oxime complexes 11

The stability of the nitrone chelates **9** led us to investigate diarylboron complexes of 3-hydroxyoxime which might have a six-membered ring structure **11** with N-B coordination or the seven-membered isomeric structure **12** corresponding to the nitrone O-B-O chelates **9**. The reaction of 3-hydroxyaldoximes (**10**, R^1 = H) and ketoximes (**10**, R^1 = alkyl)

© 2000 NRC Canada

		R^1	R^2	R^3	R^4	R^5	Ar
11	***a***	H	CH_3	CH_3	H	H	Ph
	b	H	CH_3	CH_3	H	H	4-$CH_3OC_6H_4$
	c	CH_3	CH_3	H	H	H	Ph
	d	CH_3	H	H	CH_3	CH_3	Ph

(which were prepared according to the literature (15, 16, 20) without regard to geometrical isomerism) with a diarylborinic acid or anhydride gave crystalline compounds in quite good yields. The elemental analyses and the spectroscopic data confirm the 1:1 condensation of oxime and diarylborinic acid. In the IR spectra distinct C=N stretching modes at about 1 640 cm^{-1} and broad absorption bands between 2 700 and 2 400 cm^{-1} in the N-H/O-H region are characteristic but do not allow an unambiguous assignment to either **11** or **12**. The same holds for the ^1H NMR spectra, which give no specific indication of one of the two isomeric structures. The ^{11}B NMR spectra show the expected signals in the shift region of tetracoordinate boron nuclei between 4.0 and 9.9 ppm. An intact diphenylboron grouping was proved by the color reaction with diphenylcarbazone (10). Positive evidence of the molecular structure however, was furnished by an X-ray crystallographic analysis of **11*b*** (Fig. 1) which gave the best single crystals. The six-membered O-B-N chelate structure **11** based upon the (*E*)-form of the oxime ligand **10** corresponds to the structure of the salicylaldoximediphenylboron chelate **13** (30). Like **13** and also like **5*d*** (see above), the crystal structure of **11*b*** consists of discrete molecules (Fig. 1) linked by strong O-H···O hydrogen bonds:

O(1)···O(2) = 2.569(1), O (1)-H = 0.98(2),
H···O (2) = 1.59(2) Å; O(1)-H···O = 175(2)°

Compared to **13** and **5*d*** the hydrogen bond in **11*b*** is the shortest with the least bent angle:

	11*b*	**13**	**5*d***
O···O	2.569	2.737	2.583 Å
O-H···O	175	167	162°

A half-chair conformation, with a nearly planar B(1)-N(1) = C(1)-C(2) segment (torsion angle = 0.9(2)°), and O(2) and C(3) displaced on opposite sides of the six-membered ring, characterizes the overall structure, as a result of the presence of the C=N double bond within the otherwise saturated ring skeleton of **11**. The O-B-N angle in **11*b*** (102.8(1)°, Table 2) is less compressed than the O-B-N angle in **5*d*** (94.9°), allowing a less distorted tetrahedral arrangement around the boron atom. Compared to **13** and also to **5*d***, the oxime C=N bond in **11*b*** (1.275(2) Å) is slightly shorter by about 0.01 Å, which is in accordance with a lengthened (by 0.01 Å) N—B bond.

Nitrones 16

As described in the literature (21), the aldonitrones **16** (R^1 = H) can be obtained by condensation of glyoxylic acid with an *N*-alkylhydroxlamine. The IR spectra of **16** show a

		R	R^1
16	***a***	CH_3	H
	b	$(CH_3)_3C$	H
	c	C_6H_{11}	H
	d	$PhCH_2$	H

broadened band of low intensity (curtain) in the region of associated O-H groups between 2 700 and 2 000 cm^{-1}, carboxyl-C=O stretching modes at about 1 700, and C=N vibrations at about 1 600 cm^{-1}, often hidden by aromatic C=C vibrations. In the ^1H NMR spectra, a typical N=CH methine proton signal between 7.43 and 8.13 ppm and a broad low field singlet (13–14 ppm) of the carboxyl-OH identify the nitrone and the carboxylic acid functions of **16**. It can be assumed that the aldonitrones **16** exist in the (*Z*)-form, stabilized additionally by an intramolecular O-H···O hydrogen bridge, as has been discussed above for the nitrones **2**.

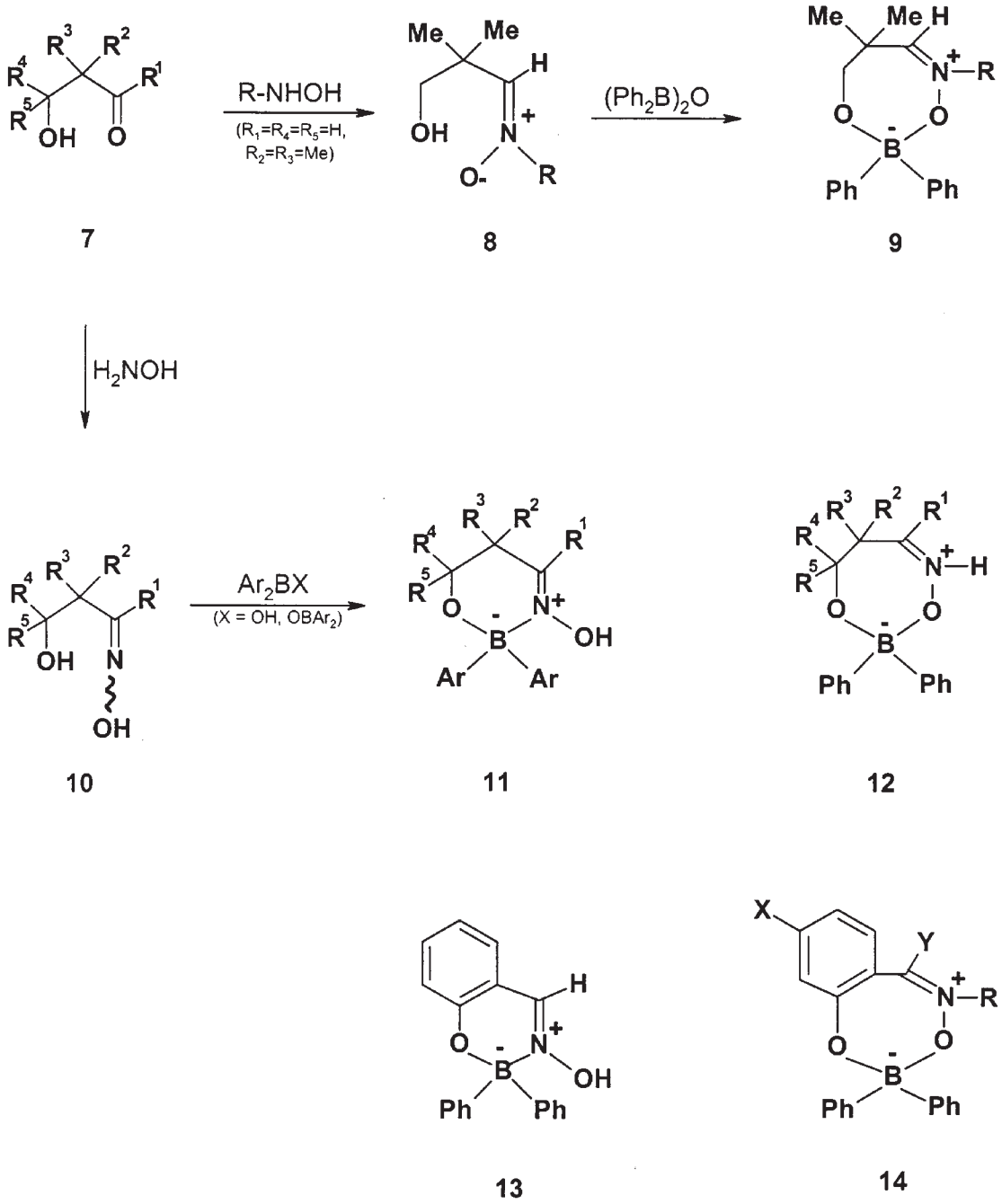
Nitrone complexes 17

Reaction of the aldonitrones **16** (R^1 = H) with a diarylborinic acid (or anhydride) resulted in the crystalline diarylboron chelates **17*a*–*e*** which can be isolated under avoidance of thermal stress leading to isomerization similar to that mentioned above for some type **3** nitrones.[5] For the synthesis of ketonitrone chelates **17**, the difficulties of preparing the nitrone of an α-ketocarbonic acid **16** could be avoided by a three-component one-pot reaction of **15** (R^1 = Ph), diarylborinic acid, and *N*-alkylhydroxylamine, with the advantage of a Lewis acid catalysis of the nitrone formation, as described above for the ketonitrone complexes **3**. The ketonitrone derivatives **17*f*–*i*** turned out to be thermally more stable, which suggests that they are less susceptible to an isomerization by 1,4-phenyl migration. In the IR spectra of the chelates **17** there is not much change as compared with the free ligands **16**, except for the absence of the O-H absorption. The disappearance of the OH signal is also the most significant change in the ^1H NMR spectra of the chelates **17** compared to the nitrone ligand **16**. In the ^{11}B NMR spectra of **17** the typical signals for tetracoordinate boron appear between 9.2 and 11.6 ppm. The compounds **17** are functionally related to the six-membered boron chelates of *N*-carboxymethylnitrones (4), with the difference of an *endo*cyclic nitrone-C=N group.

Oxime complex 19

To obtain at least one reaction product of an oxime of a 2-oxocarbonic acid and diphenylborinic acid, the phenylglyoxylic acid oxime **18** (22) was chosen. Because of the easy isomerization, even at room temperature in aqueous

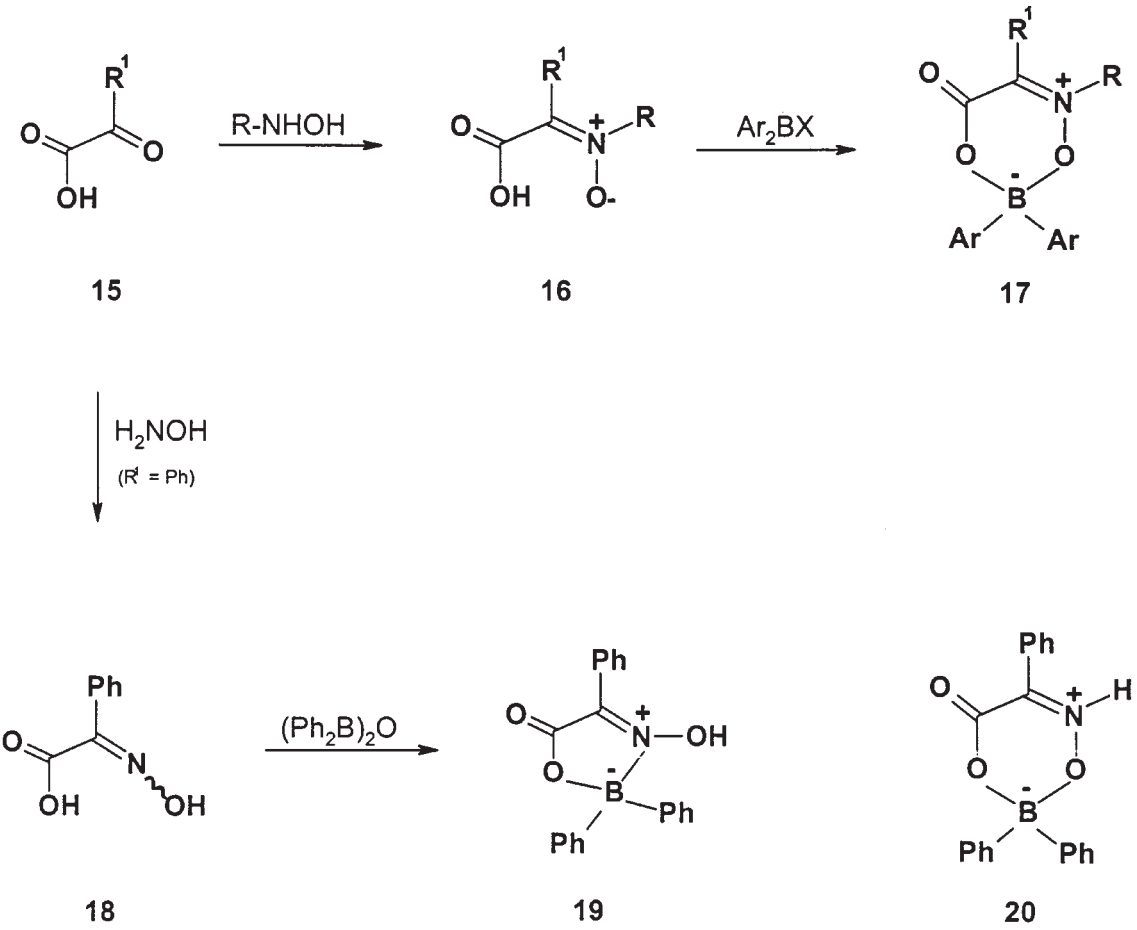
© 2000 NRC Canada



solution (22*a*, *b*), the oxime was applied without separation of the *E*/*Z*-isomers. The high-melting crystalline product is obtained in good yield and has an elemental analysis corresponding to the isomeric molecular structures **19** and **20**. The IR spectrum shows the expected bands in the N-H/O-H region between 2 737 and 3 156 cm^{-1}, as well as the carboxylate C=O and the oxime C=N absorptions at 1 725 and 1 657 cm^{-1}, respectively. An ^{11}B NMR signal for tetracoordinate boron at 9.3 ppm and the blue color reaction with diphenylcarbazone indicate the diphenylboron–chelate character of the compound. The unambiguous discrimination between the five-membered ring **19** with N-B coordination, and the six-membered O-B-O chelate system **20** representing an *N*-unsubstituted derivative of **17**, was made possible by an X-ray crystallographic analysis. The X-ray analysis confirms the five-membered boron chelate structure **19** incorporating the (*E*)-form of the ligand **18**. The ring dimensions are similar to that of **5**, with the ring conformation being more near planar (B-N=C-C torsion angle = 2.7(2)°). As in **5*d***, the O-B-N angle in **19** is distinctly compressed (to 95.3(1)°). The ring C(2)-O(1) distance in **19** (1.311(2) Å, Fig. 1, Table 2), part of the carboxylate function, is shorter than the ring alcoholate-C(2)-O(2) distance in **5*d*** (1.427(2) Å), according to expectation. The crystal structure of **19** consists of discrete molecules linked by N-O-H···O=C hydrogen bonds:

O(2)···O(3) = 2.600(1), O(2)-H = 0.96(2),
H···O (3) = 1.76(2) Å; O-H···O = 144(2)°

© 2000 NRC Canada



		R	R^1	Ar
17	*a*	CH_3	H	Ph
	b	$(CH_3)_3C$	H	Ph
	c	C_6H_{11}	H	Ph
	d	$PhCH_2$	H	Ph
	e	$PhCH_2$	H	4-ClC_6H_4
	f	CH_3	Ph	Ph
	g	n-C_3H_7	Ph	Ph
	h	C_6H_{11}	Ph	Ph
	i	$PhCH_2$	Ph	Ph

To the best of our knowledge **19** is the first boron complex of a 2-(hydroxyimino)carboxylic acid reported on and structurally established. The coordination chemistry of 2-(hydroxyimino)carboxylic acids has not been a subject of extensive investigation until recently (35). Previous reviews (25) do not mention this species of ligand. However, a cobalt complex of phenylglyoxylate oxime is described by NMR data earlier (36). Structural details of 2-(hydroxyimino)propionate complexes of different metals have been determined by X-ray analyses (35). All of these complexes possess five-membered O-*M*-N chelate moieties with a near planar ring conformation like **19**.

The large number of compounds of type **3** with various substituents has been synthesized for a broader investigation of the thermal rearrangement reaction of these materials, and for the interest in new boron compounds with potentially herbicidal, insecticidal, and other biological effects (37).

Acknowledgments

We thank the Natural Sciences and Engineering Research Council of Canada and the Fonds der Chemischen Industrie, Frankfurt am Main, for financial support. We are grateful to the Chemische Institute der Technischen Universität Braunschweig for ^{1}H and ^{11}B NMR and mass spectra.

References

1. W. Kliegel. Organomet. Chem. Rev. Sect. A: **8**, 153 (1972).
2. W. Kliegel, U. Riebe, S.J. Rettig, and J. Trotter. Can. J. Chem. **73**, 835 (1995).
3. (*a*) W. Kliegel. Tetrahedron Lett. 223 (1969); (*b*) W. Kliegel and H. Becker. Chem. Ber. **110**, 2067 (1977); (*c*) Chem. Ber. **110**, 2090 (1977); (*d*) W. Kliegel, B. Enders, and H. Becker. Liebigs Ann. Chem. 1712 (1982); (*e*) Chem. Ber. **116**, 27 (1983).
4. W. Kliegel and J. Graumann. Liebigs Ann. Chem. 1545 (1984).
5. (*a*) W. Kliegel and L. Preu. Liebigs Ann. Chem. 1937 (1983); (*b*) Chem. Ztg. **108**, 283 (1984).
6. (*a*) G. Zinner. Chem. Ztg. **109**, 436 (1985); (*b*) H. Hopf and G. Maas. Angew. Chem. **104**, 953 (1992).

© 2000 NRC Canada

7. (*a*) S.J. Rettig, J. Trotter, W. Kliegel, and D. Nanninga. Can. J. Chem. **55**, 1 (1977); (*b*) Can. J. Chem. **56**, 1676 (1978); (*c*) W. Kliegel and D. Nanninga. Chem. Ber. **116**, 2616 (1983); and refs. therein.
8. (*a*) R. Neu. Chem. Ber. **87**, 802 (1954); (*b*) G.N. Chremos, H. Weidmann, and H.K. Zimmerman. J. Org. Chem. **26**, 1683 (1961).
9. W. Kliegel, G. Lubkowitz, S.J. Rettig, and J. Trotter. Can. J. Chem. **70**, 2809 (1992).
10. (*a*) R. Neu. Z. Anal. Chem. **176**, 334 (1960); (*b*) B. Friese and F. Umland. Anal. Chim. Acta **96**, 303 (1978).
11. G.E. Coates and J.G. Livingstone. J. Chem. Soc. 4909 (1961).
12. R.L. Letsinger and I.H. Skoog. J. Am. Chem. Soc. **77**, 5176 (1955).
13. G. Rindorf. Acta Chem. Scand. **25**, 774 (1971).
14. A. Dornow and A. Müller. Chem. Ber. **93**, 26 (1960).
15. A. Balsamo, D. Gentili, A. Lapucci, M. Macchia, and A. Martinelli. Farmaco (Pavia), **49**, 759 (1994).
16. (*a*) L. Wessely. Monatsh. Chem. **21**, 216 (1900); (*b*) J.M. Kern and P. Ferlin. Bull. Soc. Chim. Fr. 4379 (1972).
17. (*a*) W. Kliegel, J. Metge, S.J. Rettig, and J. Trotter. Can. J. Chem. **75**, 1830 (1997); (*b*) Can. J. Chem. **76**, 389 (1998); (*c*) Can. J. Chem. **76**, 1082 (1998).
18. (*a*) H. Nöth and B. Wrackmeyer. Nuclear magnetic resonance spectroscopy of boron compounds. Springer, Berlin. 1978; (*b*) R. Köster (*Editor*). Houben-Weyl: Organobor-Verbindungen III. Vol. XIII/3c. Georg Thieme, Stuttgart. 1984.
19. T.P. Povlock and W.T. Lippincott. J. Am. Chem. Soc. **80**, 5409 (1958).
20. M. Kohn and G. Lindauer. Monatsh. Chem. **23**, 755 (1902).
21. D. Keirs and K. Overton. Heterocycles, **28**, 841 (1989).
22. (*a*) A. Hantzsch. Ber. Dtsch. Chem. Ges. **24**, 36 (1891); (*b*) A. Ahmad and I.D. Spenser. Can. J. Chem. **39**, 1340 (1961); (*c*) J. Armand and J.-P. Guetté. Bull. Soc. Chim. Fr. 2849 (1969).
23. P.G. Jones. Chem. Ber. **17**, 222 (1981).
24. (*a*) H. Stamm. *In* Methodicum Chimicum. Vol. 6. *Edited by* F. Zymalkowski. Georg Thieme, Stuttgart. 1974. p. 337; (*b*) E. Breuer. *In* The chemistry of amino, nitroso and nitro compounds and their derivatives. Part 1. *Edited by* S. Patai. Wiley, Chichester. 1982. p. 459; (*c*) E. Breuer. *In* Nitrones, nitronates, and nitroxides. *Edited by* S. Patai and Z. Rapoport. Wiley, Chichester. 1989. p. 245; (*d*) D. Döpp and H. Döpp. *In* Houben-Weyl, Organische Stickstoff-Verbindungen mit C,N-Doppelbindungen.. Vol. E 14b. *Edited by* D. Klamann and H. Hagemann. Georg Thieme, Stuttgart. 1990. p. 1372.
25. (*a*) A. Chakravorty. Coord. Chem. Rev. **13**, 1 (1974); (*b*) R.C. Mehrotra, A.K. Rai, A. Singh, and R. Bohra. Inorg. Chim. Acta, **13**, 91 (1975); (*c*) M.E. Keeney, K. Osseo-Asare, and K.A. Woode. Coord. Chem. Rev. **59**, 141 (1984); (*d*) R.C. Mehrotra. *In* Comprehensive coordination Chemistry. Vol. 2. *Edited by* G. Wilkinson. Pergamon, Oxford. 1987. p. 269; (*e*) J. Szymanowski and A. Borowiak-Resterna. Crit. Rev. Anal. Chem. **22**, 65 (1991); (*f*) A. Borowiak-Resterna and J. Szymanowski. J. Radioanal. Nucl. Chem. **150**, 235 (1991).
26. (*a*) J.S. Fritz, D.R. Beuerman, and J.J. Richard. Talanta, **18**, 1095 (1971); (*b*) N.S. Biradar, V.B. Mahale, and V.H. Kulkarni. J. Inorg. Nucl. Chem. **35**, 2565 (1973).
27. (*a*) C.G. McCarthy. *In* The chemistry of the carbon–nitrogen double bond. *Edited by* S. Patai. Interscience, London. 1970. p. 363; (*b*) W.B. Jennings and V.E. Wilson. *In* Acyclic organonitrogen stereodynamics. *Edited by* J.B. Lambert and Y. Takeuchi. VCH, Weinheim. 1992. p. 191.
28. C.E. Hauser and D.S. Hoffenberg. J. Org. Chem. **20**, 1491 (1955).
29. S.J. Rettig and J. Trotter. Can. J. Chem. **51**, 1288 (1973); Acta Crystallogr. Sect. B: Struct. Crystallogr. Cryst. Chem. **B30**, 2139 (1974); Can. J. Chem. **54**, 3130 (1976); Can. J. Chem. **61**, 2334 (1983).
30. W. Kliegel, S.J. Rettig, and J. Trotter. Can. J. Chem. **62**, 1363 (1984).
31. W. Kliegel, J. Metge, S.J. Rettig, and J. Trotter. Can. J. Chem. **75**, 1830 (1997) and refs. therein.
32. W. Kliegel, U. Lauterbach, S.J. Rettig, and J. Trotter. Can. J. Chem. **65**, 1457 (1987).
33. W. Kliegel, M. Tajerbashi, S.J. Rettig, and J. Trotter. Can. J. Chem. **66**, 2621 (1988).
34. W.R. Cullen, S.J. Rettig, J. Trotter, and E.B. Wickenheiser. Can. J. Chem. **66**, 2007 (1988).
35. (*a*) Yu.A. Simonov, T.Yu. Sliva, M.D. Mazus, A.A. Dvorkin, and R.D. Lampeka. Russ. J. Inorg. Chem. **34**, 489 (1989); (*b*) A.A. Dvorkin, Yu.A. Simonov, T.Yu. Sliva, R.D. Lampeka, M.D. Mazus, V.V. Skopenko, and T.I. Malinovskii. Russ. J. Inorg. Chem. **34**, 1475 (1989); (*c*) V.V. Skopenko, T.Yu. Sliva, Yu.A. Simonov, A.A. Dorkin, N.D. Mazus, R.D. Lampeka, and T.I. Malinovskii. Russ. J. Inorg. Chem. **35**, 993 (1990); (*d*) R.D. Lampeka, Z.D. Uzakbergenova, and V.V. Skopenko. Z. Naturforsch. B: Chem. Sci. **48 b**, 409 (1993); (*e*) R.D. Lampeka, R. Bergs, R. Krämer, K. Polborn, and W. Beck. Z. Naturforsch. B: Chem. Sci. **49 b**, 225 (1994) and refs. therein.
36. G. Occupati and L. Pratt. J. Chem. Soc. Dalton Trans. 1699 (1973).
37. (*a*) W. Kliegel. Bor in Biologie, Medizin und Pharmazie. Springer, Berlin. 1980; (*b*) M.F. Hawthorne. Angew. Chem. **105**, 997 (1993); Angew. Chem. Int. Ed. Engl. **105**, 950 (1993); (*c*) C. Morin. Tetrahedron, **50**, 12521 (1994); (*d*) R.F. Schinazi and R.F. Lesnikowski. Nucleosides Nucleotides, **17**, 635 (1998); (*e*) A.H. Solway, W. Tjarks, B.A. Barnum, F.G. Rong, R.F. Barth, I.M. Codogni, and G. Wilson. Chem. Rev. **98**, 1515 (1998); (*f*) M.P. Groziak. Prog. Heterocycl. Chem. **12**, (2000), in press.
38. W. Kliegel, J.O. Pokriefke, S.J. Rettig, and J. Trotter. Can. J. Chem. **78**, 546 (2000).

© 2000 NRC Canada

New syntheses of dillapiol [4,5-dimethoxy-6-(2-propenyl)-1,3-benzodioxole], its 4-methylthio and other analogs

Sherry L. Majerus, Najma Alibhai, Sasmita Tripathy, and Tony Durst

Abstract: Three syntheses of the natural synergist dillapiol from the natural, commercially available sesamol as starting material, are described. A major difference between these is the order of introduction of the additional methoxy and allyl substituents. In one of the syntheses, a formyl group is introduced at C4 via an electrophilic aromatic substitution reaction and then converted into the methoxy group using a Baeyer–Villiger reaction and subsequent methylation; in the other two, a directed ortho-metalation, Baeyer–Villiger, methylation sequence was employed. Various intermediates along the synthetic route were used to generate more than 30 analogs, including the 4-thiomethyldillapiol, to investigate the structure activity relationships of the pesticide synergism of these compounds. Radio-labeled dillapiol, bearing ^{14}C at the C4 methoxy group was also prepared. Initial screening with mosquito larvae showed that most of the derivatives prepared in this study had signifacant synergistic activities in combination with the phototoxic larvicide α-therthiophene.

Key words: dillapiol, insecticide synergists, dillapiol analogs, 4-methylthiodillapiol.

Résumé : On décrit trois synthèses du dillapiol, un produit naturel de synergie, qui ont été réalisées à partir du sésamol, un produit naturel disponible commercialement. Ces trois ces synthèses diffèrent principalement par l'ordre d'introduction des substituants méthoxy et alkyles additionnels. Dans l'une de ces synthèses, le groupe formyle est introduit en C-4 par le biais d'une réaction de substitution aromatique électrophile et elle est ensuite transformée en groupe méthoxy à l'aide d'une réaction de Baeyer–Villiger et une réaction de méthylation subséquente; dans les deux autres, on fait appel à la séquence de réaction impliquant une métalation ortho dirigée, une réaction de Baeyer–Villiger et une méthylation. On a utilisé divers intermédiaires obtenus au cours de ces voies de synthèses pour générer plus de 30 analogues, y compris le 4-thiométhyldillapiol, afin d'en étudier les relations structure-activité de synergie de ces composés comme pesticide. On a aussi préparé du dillapiol radioactivement marqué par du ^{14}C dans le groupe méthoxy en C-4. Des évaluations initiales avec des larves de moustiques montrent que la plupart des dérivés préparés au cours de cette étude présentent des activités importantes de synergie lorsqu'on les utilise en combinaison avec l'α-therthiophéne, un larvicide phototoxique.

Mots clés : dillapiol, effet de synergie pour les insecticides, analogues de dillapiol, 4-méthylthiodillapiol.

Introduction

During the past few years we have been involved in a project aimed at developing natural insecticides (1). Part of this includes the use of the naturally occurring synergist dillapiol (**1**). Dillapiol is a member of a group of both natural and synthetic synergists known as polysubstrate mono-oxygenase inhibitors (PMSO) whose key structural unit is a benzene ring bearing a methylenedioxy unit (2). This unit binds strongly to the heme portion of the cytochrome P-450 thereby inhibiting the oxidation of various other substrate such as insecticides and delaying their rate of elimination from the insects. Examples of natural lignans with known synergistic activity, in addition to the dillapiol, are myristicin (**2**), safrole (**3**), and sessamin (**4**). Piperonyl butoxide (**5**) the commonly used commercial synergist for pyrethroids and carbamates, is also known to inhibit PSMOs.

Dillapiol is a monolignan and a major constituent of the essential oils of a number of plants, including Indian dill (*Antheum graveolus*) (3), and *Piper aduncum*, (4), a species in the Piperaceae family. The latter grows as a small shrub in many tropical areas such as Central America, the West Indies, and Southeast Asia. The development of dillapiol for commercial purposes requires either an inexpensive reliable natural source or a viable synthetic source. Additionally for registration purposes both the toxicity to nontarget species and pharmacokinetics including the nature of the metabolites need to be known. The latter studies can be carried out best with isotopically labeled material.

Three syntheses of dillapiol have previously been reported. 3,4,5-Tri-methoxyacetophenone (**5**), 2-hydroxy-3-methoxybenzaldehyde (*o*-vanillin) (**6**), and 1,2,3-trimethoxybenzene (**7**) were used as starting materials. These syntheses required

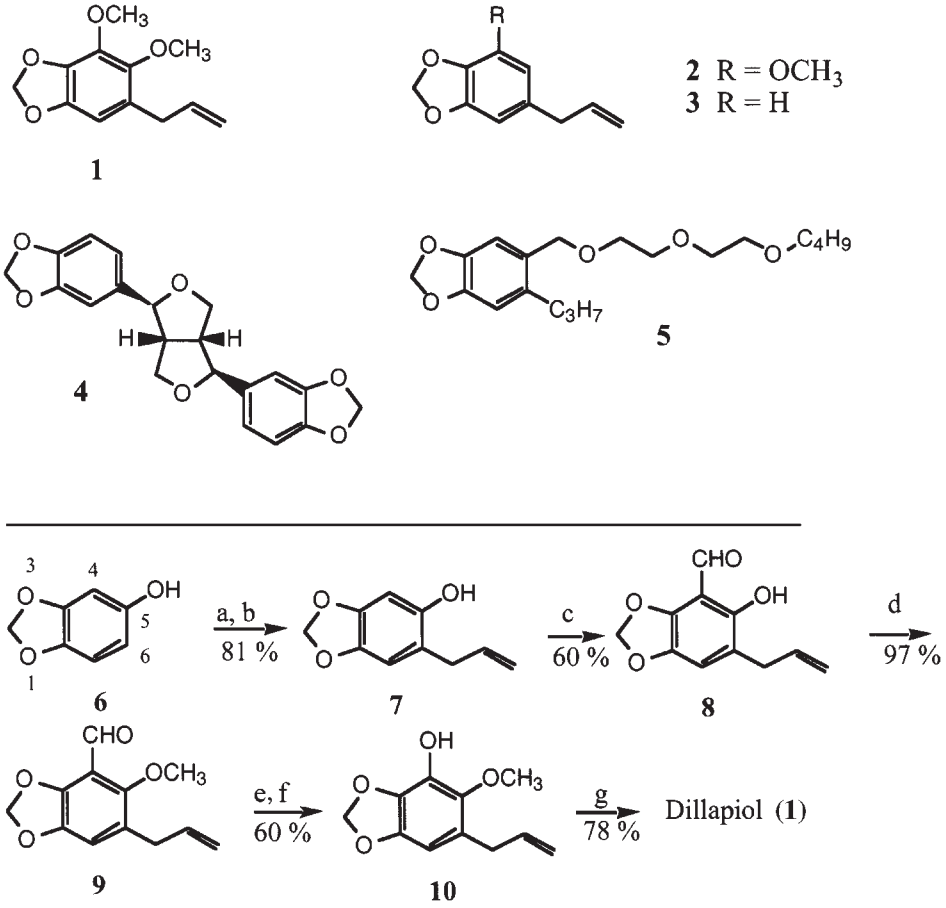
Received October 1, 1999. Published on the NRC Research Press website on October 16, 2000.

S.L. Majerus, N. Alibhai, S. Tripathy, and T. Durst.[1]
Departments of Chemistry and Biology, University of Ottawa, Ottawa, ON KIN 6N5, Canada.

[1]Author to whom correspondence may be addressed.
Telephone: (613) 562-5800 ext. 6072. Fax: (613) 562-5170.
e-mail: tdurst@science.uottawa.ca

© 2000 NRC Canada

Scheme 1. Reagents: (*a*) K_2CO_3–CH_2=$CHCH_2Br$; (*b*) *N*,*N*-dimethylaniline (180°C); (*c*) $(CH_2O)n$–$SnCl_4$–Bu_3N; (*d*) CH_3I–K_2CO_3; (*e*) MCPBA–$CHCl_3$ (18 h, 0°C); (*f*) LiOH–THF–H_2O; (*g*) CH_3I–K_2CO_3–acetone.



5–7 steps and occurred in 2, 10, and 6% yield, respectively. None of the three syntheses is efficient or amenable to the introduction of isotopic carbon in the form of the relative inexpensive methyl iodide. We therefore decided to investigate several new syntheses which would be not only more efficient and enable us to introduce the labeled CH_3I in the last synthetic step, but also enable us to generate a family of derivatives to initiate a structure–activity relationship study. Finally, access to various intermediates is expected to help in the identification of metabolites.

Discussion of results

Three syntheses have been completed starting with sesamol (**6**). These are shown in Schemes 1–3. The structure of the intermediates generated in each sequence were determined mainly by ^{1}H NMR. The assignments were supported by ^{13}C NMR, IR, and HRMS data. These are given in the experimental section.

In the first synthesis, Scheme 1, sesamol (**6**)[2] was converted to the *ortho*-allylated phenol **7** in 81% overall yield via *O*-allylation, followed by a Claisen rearrangement. Introduction of the formyl group into the 4 position in **7** was accomplished by treatment with formaldehyde, $SnCl_4$, and tributylamine (8) to afford **8** in 60% isolated yield. Replacement of tributylamine by other tertiary amines such as triethyl- or trioctylamine either reduces or did not improve the yield of **8**. The variation of other reaction parameters such as temperature and reaction time also did not result in yield improvements.

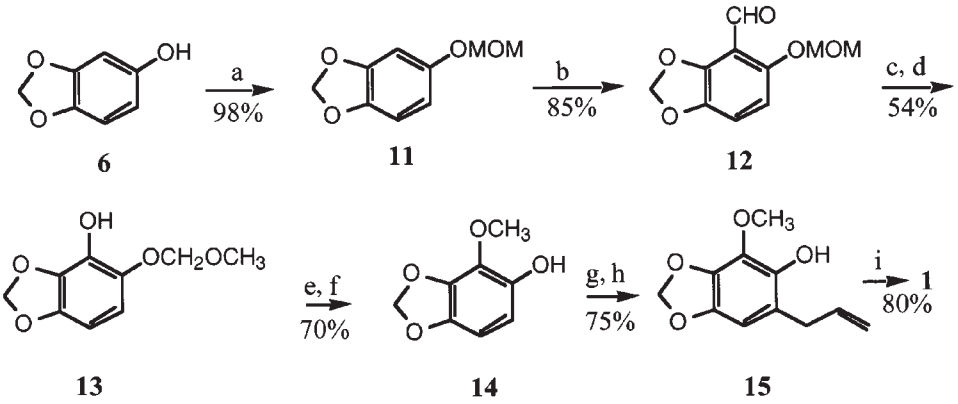
This compound was quantitatively methylated to **9** in preparation for the Baeyer–Villiger and subsequent hydrolysis of the formate ester to form **10**. The conversion of **9** to **10** was carried out using 1 equiv. of MCPBA in $CHCl_3$ at 0°C for 18 h and afforded the formyl intermediate in 71% isolated yield, saponification of which gave **10.** Under these conditions competition by the alkene moiety for the peracid to give an epoxide was minor; at room temperature the rates of desired Baeyer–Villiger and the epoxidation were quite comparable. Finally, methylation of **10** with CH_3I–K_2CO_3 in acetone afforded pure dillapiol. Replacement of cold methyl iodide with carbon-14 labeled material afforded radiolabeled dillapiol, suitable for metabolism studies.

The overall yield of dillapiol from sesamol via Scheme 1, based on the isolated yields of each intermediate, is more than 21%. The major shortcomings of this route are the rather stringent conditions required for the introduction of the formyl group and the problem of the competing

[2] The numbering used throughout this paper is based on the IUPAC numbering of the 1,3-benzodioxole ring system. See structure **6**, Scheme 1.

© 2000 NRC Canada

Scheme 2. Reagents: (*a*) MOM-Cl–*n*BuLi; (*b*) *n*BuLi, THF, (–78°C), then DMF; (*c*) MCPBA; (*d*) 10% KOH; (*e*) K_2CO_3 and CH_3I; (*f*) CH_3CO_2H, NaI; (*g*) K_2CO_3, CH_2=$CHCH_2Br$; (*h*) *N*,*N*-dimethylaniline (180°C); (*i*) K_2CO_3 and CH_3I.



epoxidation of the terminal double bond during the Baeyer–Villiger reaction of **9**. These difficulties became more severe on attempted scale-up.

Considerable effort was expended to avoid the sensitive reactions and shorten the synthesis by going directly from **7** to the resorcinol **20** and hence to dillapiol. Direct *o*-hydroxylation of **7** using H_2O_2–$AlCl_3$ according to Kurz and Johnson (9) or by use of oxygen and copper metal in the presence of $CuCl_2$ as developed by Capdevielle and Maumy (10) was unsuccessful and gave mainly recovered **7**.

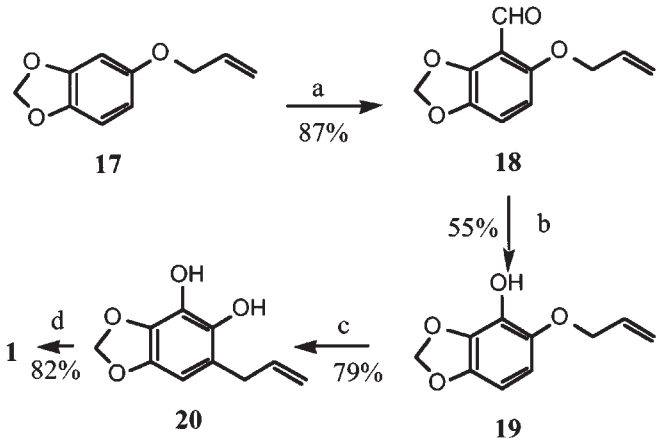
In the second synthesis, Scheme 2, the MOM-protected sesamol **11** was *o*-metallated (11) and treated with DMF to produce the aldehyde **12** in 85% yield. The protection of phenol as a THP derivative, thus avoiding the rather expensive MOM-chloride, was not possible since reaction of **6** with dihydopyran in the presence of acid resulted in the introduction of the THP unit at C6 via an electrophile aromatic substitution to afford **16** rather than the desired phenol protection.

Baeyer–Villiger oxidation followed by basic hydrolysis afforded phenol **13** which was methylated to give **14**. Removal of the MOM group set the stage for alkylation and subsequent Claisen rearrangement to afford phenol **15**, methylation of which gave dillapiol **1**. The overall yield of dillapiol via Scheme 2 was 19%.

After this synthesis was completed we realized that one might be able to avoid the protection–deprotection sequence if *ortho*-directed metallation and subsequent introduction of the formyl group could be carried out on the allyl ether **17** to give **18**. The conversion of **18** to dillapiol would require first a Baeyer–Villiger reaction and hydrolysis to the resorcinol **19** and then double methylation to dillapiol. Such a sequence would save three steps from the synthesis shown in Scheme 2.

We were concerned that **17** would undergo a 1,2-Wittig rearrangement rather than the directed *ortho*-metallation. Fortunately, this fear was unfounded and reaction of **17** with 1 equiv. of *n*Buli followed addition of DMF gave **18** in 87% isolated yield. Conversion to **19** was successful upon stirring with MCPBA at 0°C for 24 h. The reduced nucleophilicity of the double bond in **18** relative to **9** allows the Baeyer–Villiger reaction to proceed without competition from the epoxidation of the allyl ether. The intermediate formate ester was hydrolyzed to **19** without purification. Claisen rearrangement of **19** at 190°C afforded the resorcinol **20** which was methylated to dillapiol. The overall yield of dillaiol from sesamol via Scheme 3 is 31%.

Scheme 3. Reagents: (*a*) *n*BuLi, THF, (–78°C), then DMF; (*b*) MCPBA (25°C), then KOH; (*c*) *N*,*N*-dimethylaniline (180°C); (*d*) CH_3I, K_2CO_3, acetone.

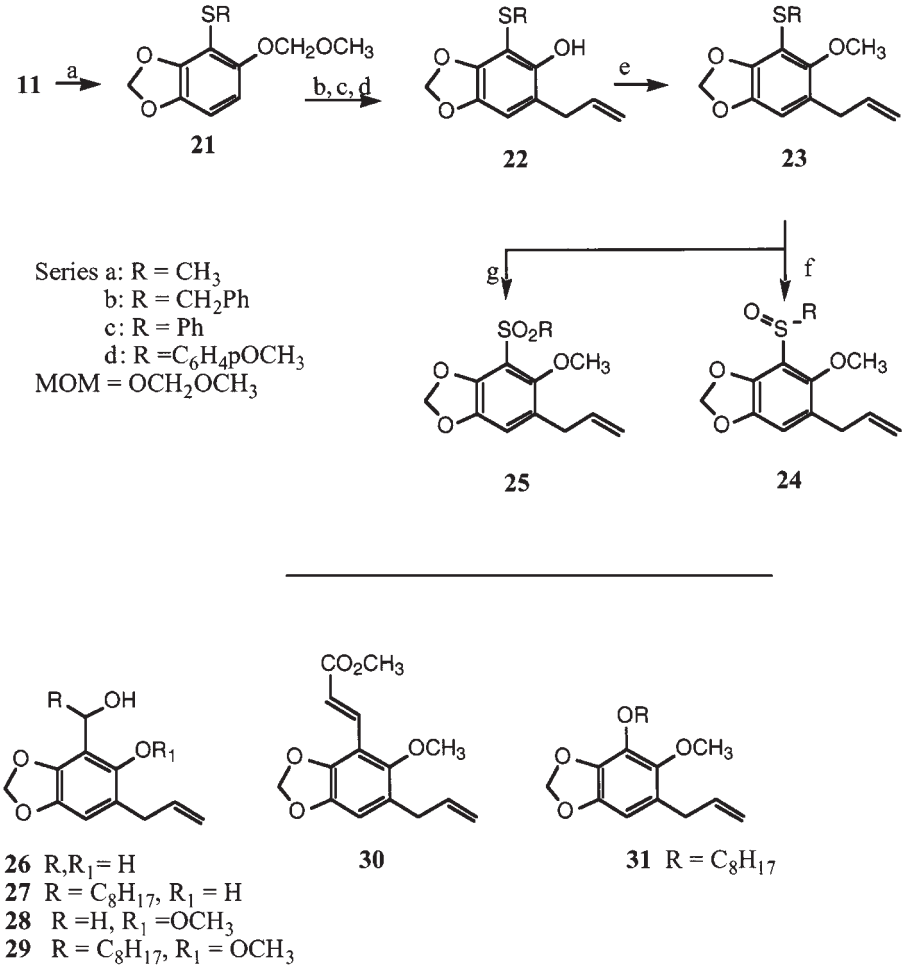


Synthesis of dillapiol analogues

Several of the intermediates in Schemes 1 and 2 were suitable for the preparation of dillapiol analogues. These compounds have been evaluated for their ability to synergize the insecticidal property of α-terthienyl when determined in the presence of light (12). For example, *ortho*-metalation of the MOM-protected sesamol **11**, followed by treatment with dimethyl disulfide afforded the *S*-methyl derivative **21** in 91% yield. This compound was converted via **22a** into the 3-thiomethyl analog of dillapiol **23a** in four steps in 48% overall yield. Oxidation afforded the sulfoxide and sulfone analogs **24a** and **25a**, respectively (Scheme 4). A number of other sulfide, sulfoxide, and sulfone analogs were also prepared in a similar manner simply by replacing dimethyl disulfide with other disulfides (Scheme 4). Surprisingly, reaction of the *ortho*-lithiated allyl ether with dimethyl disulfide was not nearly as efficient as reaction with DMF and afforded only about 55% of the desired product. In addition, a significant amount of a by-product which was difficult to separate from the desired product was obtained. The

© 2000 NRC Canada

Scheme 4. Reagents: (*a*) *n*BuLi, THF, (–78°C), then RSSR; (*b*) Hcl–MeOH–NaI; (*c*) allyl bromide – K_2CO_3 – acetone; (*d*) *N*,*N*-dimethylaniline (180°C); (*e*) CH_3I–K_2CO_3–acetone; (*f*) MCPBA (1.1 equiv.); (*g*) MCPBA (2.2 equiv.).



by-product has not been identified and this route to sulfur analogues of dillapiol was not pursued further.

The aldehydes **8** and **9** served as a source of a number of derivatives. Thus, reduction of **8** with $NaBH_4$, or reaction with *n*-octylmagnesium iodide, gave the derivatives **26** and **27**, respectively.

Similarly, the methoxyaldehyde **9** was reduced to **28**, or converted to **29** upon addition of *n*-octylmagnesium bromide. Reaction of **9** with methyl (triphenylphosphoranylidene) acetate resulted in formation of the unsaturated ester **30**. The ^{1}H NMR of both **27** and **29** show nonequivalence of each of the methylene hydrogens both α and β to the chiral benzylic center. The β methylene hydrogen nonequivalence is somewhat surprising and may be due to a combination of both steric crowding and intramolecular hydrogen bonding resulting in a preferred conformation in which each of these sets of geminal hydrogens continue to show nonequivalence.

The use of the phenol **10** allowed us to generate ethers such as **31** and thereby test how increased lipophilicity relative to dillapiol affects the synergism of these compounds.

Biological results

Detailed SAR studies of the compounds described in this paper and a number of other analogs as synergists for the light α-terthienyl (α-T) is being published elsewhere (12). Qualitatively, only a few derivatives showed activity comparable to or greater than dillapiol. The most active derivative was the cinnamate ester **30** with a synergism factor 30% higher than dillapiol. In the sulfur series the sulfides showed synergism effects of approximately 1.1–1.3, relative to dillapiol equals. In contrast the corresponding sulfoxides and sulfones had effects which were approximately 40–60% of that observed for dillapiol.

Experimental

General comments

Unless stated otherwise, ^{1}H NMR were obtained at 200 or 500 MHz, and ^{13}C NMR spectra at 125 MHz. Solvents used in reactions were distilled prior to use. BuLi was purchased from Aldrich as a hexane solution and titrated [diphenylacetic acid] prior to use. Usual work-up refers to partitioning of the reaction mixture between an organic solvent such as ether, ethyl acetate, or dichloromethane and water or 5% NH_4Cl solution, drying of the organic phase with anhydrous $MgSO_4$, and evaporating the solvents at reduced pressure. Yields, unless indicated otherwise, refer to chromatograpically pure fractions.

© 2000 NRC Canada

5-Hydroxy-6-(2-propenyl)-1,3-benzodioxole (7)

This compound was prepared in 81% overall yield following the procedure of Grubbs et al. (13). Melting point 74–76°C, lit. (13) mp 74–76°C.

4-Formyl-5-hydroxy-6-(2-propenyl)-1,3-benzodioxole (8)

Paraformaldehyde (0.56 g, 18.5 mmol) was added to toluene (5.6 mL) containing 1.5 g (8.4 mmol) of **7**, 0.1 mL (0.84 mmol) of tin tetrachloride, and 0.8 mL (3.37 mmol) of tri-*n*-butylamine. The resulting yellow solution was heated 8 h at 100°C, then cooled, acidified with 2 N HCl to pH 2, and extracted with ether. Purification by silica gel chromatography (1:1, hexane :CH_2Cl_2) afforded 1.05 g (60%) of **8** as a bright yellow solid, mp 68–70°C. IR (cm^{-1}): 1658, 3215. ^1H NMR δ: 3.27–3.29 (m, 2H), 5.03–5.07 (m, 2H), 5.86–5.94 (m, 1H), 6.00 (s, 2H), 6.87 (s, 1H), 10.09 (s, 1H), 10.65 (s, 1H). ^{13}C NMR δ: 32.8, 102.5, 106.7, 116.0, 117.6, 119.0, 136.1, 140.1, 148.5, 152.3, 191.3. HRMS calcd. for $C_{11}H_{10}O_4$: 206.0579; found: 206.0568.

4-Formyl-5-methoxy-6-(2-propenyl)-1,3-benzodioxole (9)

Potassium carbonate (1.31 g, 9.45 mmol) and methyl iodide (3.92 mL, 63.0 mmol) were added sequentially to a solution of aldehyde **8** (1.30 g, 6.30 mmol) in acetone (10 mL). The resulting solution was allowed to stir at rt for 48 h, after which time the solvent was evaporated under reduced pressure. The remaining K_2CO_3 was dissolved in water and the aqueous phase extracted with ether (3 × 15 mL). Chromatography (5:1, hexane:EtOAc) of the crude product gave 1.35 g (97%) of **9** as a pale yellow solid, mp 101–102°C. ^1H NMR δ: 3.32 (dt, 2H, J = 6.4, 1.5 Hz), 3.77 (s, 3H), 5.03–5.08 (m, 2H), 5.86–5.91 (m, 1H), 6.05 (s, 2H), 6.83 (s, 1H), 10.23 (s, 1H). ^{13}C NMR δ: 33.0, 64.1, 102.9, 114.2, 114.7, 116.4, 125.7, 136.5, 144.9, 146.9, 153.6, 188.1. IR (cm^{-1}): 1689. HRMS calcd. for $C_{12}H_{12}O_4$: 220.0736; found: 220.0754.

4-Hydroxy-5-methoxy-6-(2-propenyl)-1,3-benzodioxole (10)

To a cooled (0°C) solution of aldehyde **9** (210 mg, 0.95 mmol) in dry $CHCl_3$ (6 mL) was added in one portion MCPBA (0.30 g, 0.95 mmol, 55%). After 18 h, the reaction mixture was allowed to reach rt and washed with sodium sulfite (sat., 2 × 10 mL), sodium bicarbonate (sat., 1 × 10 mL), and water (1 × 10 mL). The extract was dried over Na_2SO_4, filtered and evaporated to dryness. The resulting oily residue was purified by flash chromatography (3:1, Hex:EtOAc) to give the formyl derivative of **10** as a colorless oil (160 mg, 71%). IR (cm^{-1}): 1759. ^1H NMR δ: 3.32 (d, 2H, J = 6.5 Hz), 3.69 (s, 3H), 5.03–5.06 (m, 2H), 5.86–5.93 (m, 1H), 5.94 (s, 2H), 6.56 (s, 1H), 8.26 (s, 1H). ^{13}C NMR δ: 33.6, 61.8, 102.3, 107.0, 116.1, 126.3, 126.8, 136.8, 144.6, 144.8, 157.9. HRMS calcd. for $C_{12}H_{12}O_5$: 236.0685; found: 236.0690.

To a solution of the above formyl derivative (250 mg, 1.06 mmol) in THF (9 mL) was added 1 mL of a 3 N NaOH solution. The resulting homogeneous solution was stirred at rt for 1 h and diluted with brine. Usual work-up gave **10** (180 mg, 82%) as a pale yellow solid, mp 61–63°C. IR (cm^{-1}): 3523. ^1H NMR δ: 3.31 (dt, 2H, J = 6.5, 1.4 Hz), 3.73 (s, 3H), 5.03–5.07 (m, 2H), 5.50 (s, 1H), 5.87–5.93 (m, 1H), 5.90 (s, 2H), 6.25 (s, 1H). ^{13}C NMR δ: 33.6, 61.8, 101.0, 101.7, 115.9, 125.2, 132.7, 133.5, 137.0, 141.1, 144.9. HRMS calcd. for $C_{11}H_{12}O_4$: 208.0736; found: 208.0740.

4,5-Dimethoxy-6-(2-propenyl)-1,3-benzodioxole)(dillapiol) (1)

A mixture of **10** (100 mg, 0.48 mmol), CH_3I (0.28 mL), and K_2CO_3 (0.1 g) was stirred at rt for 72 h. The solvent was evaporated. Usual work-up afforded, after chromatography (5:1, hexane:EtOAc), 80 mg (78%) of dillapiol. The physical and spectroscopic properties were identical to those of the commercial material.

5-(Methoxymethoxy)-1,3-benzodioxole (11)

To a solution of sesamol (5.0 g, 36.2 mmol) in 20 mL of dry THF at 0°C was added 1 equiv. of BuLi (16.5 mL, 2.2 M). The reaction mixture was stirred for 30 min and then 1.5 equiv. of chloromethyl methyl ether (4.4 g, 4.1 mL) was added. The resulting mixture was stirred at rt for 24 h and then quenched with 10 mL of saturated NH_4Cl. The usual work-up gave 6.5 g (98%) of **11** as a colorless liquid. The product was used as such. EI–MS (m/z, %): 182 ($M^{+\cdot}$, 100), 152 (75), 137 (30). ^1H NMR δ: 3.47 (s, 3H), 5.08 (s, 2H), 5.91 (s, 2H), 6.49 (dd, 1H, J = 8.4 Hz, 2.4 Hz), 6.62 (d, 1H, J = 2.2 Hz), 6.70 (d, 1H, J = 8.4 Hz). ^{13}C NMR δ: 55.9, 95.5, 99.7, 101.2, 108.0, 108.4, 142.5, 148.1, 152.5. HRMS calcd. for $C_9H_{10}O_4$: 182.0579; found: 182.05830.

4-Formyl-5-(methoxymethoxy)-1,3-benzodioxole (12)

BuLi (12.5 mL, 2.2 M) was added to a solution of 5.0 g (27.5 mmol) of **11** in dry THF (20 mL) at 0°C. The reaction mixture was stirred for 30 min and 1.5 equiv. of DMF (3.00 g, 3.18 mL) was added. The resulting mixture was stirred at room temperature for 4 h and quenched with 10 mL of NH_4Cl solution. Work-up gave the crude product as an orange powder. Purification by flash column chromatography (3:1, hexane:ethyl acetate) gave **12** as pale yellow crystals (4.9 g, 85%), mp 85–87°C. EI–MS (m/z, %): 210 ($M^{+\cdot}$, 92), 178 (53), 164 (82). IR (cm^{-1}): 1687. ^1H NMR δ: 3.48 (s, 3H), 5.17 (s, 2H), 6.09 (s, 2H), 6.58 (d, 1H, J = 8.6 Hz), 6.86 (d, 1H, J = 8.6 Hz), 10.35 (s, 1H). ^{13}C NMR δ: 56.4, 95.7, 102.9, 106.4, 111.7, 113.1, 143.4, 148.1, 153.6, 188.0. HRMS calcd. for $C_{10}H_{10}O_5$: 210.0528; found: 210.05317.

4-Hydroxy-5-(methoxymethoxy)-1,3-benzodioxole (13)

MCPBA (5.30 g, 30.7 mmol) was added in one portion to a solution of aldehyde **12** (3.00 g, 14. 3 mmol) in dry $CHCl_3$ (25 mL) at 0°C. The reaction mixture was warmed up to rt and stirred for 24 h, washed with sodium sulfite solution (sat., 2 × 15 mL), sodium bicarbonate (sat., 2 × 20 mL), and water (2 × 20 mL). The extract was dried over anhyd. $MgSO_4$, filtered, and evaporated to dryness. The resulting oily residue was purified by flash column chromatography (5:1, hexane:ethyl acetate) affording the expected formate ester as a pale yellow liquid (2.76 g, 91%). EI–MS (m/z, %): 226 ($M^{+\cdot}$, 6), 45 (100). IR (cm^{-1}): 1752. ^1H NMR δ: 3.45 (s, 3H), 5.06 (s, 2H), 5.96 (s, 2H), 6.64 (d, 1H, J = 8.6 Hz), 6.62 (d, 1H, J = 8.6 Hz), 8.24 (s, 1H). ^{13}C NMR δ: 56.2, 96.2, 102.3, 105.5, 108.5, 124.1, 139.8, 143.9, 144.6, 157.7. HRMS calcd. for $C_{11}H_{10}O_6$: 226.077; found: 226.04806.

© 2000 NRC Canada

To the above compound (20 mg, 0.94 mmol) in 5 mL of THF was added 25% NaOH solution (2 mL). The reaction mixture was stirred for 4 h at rt and extracted with water (4 × 5 mL). The resulting oily residue, obtained after usual work-up was purified using flash chromatography (9:1, hexane:ethyl acetate). Phenol **13** was obtained as a pale yellow liquid, (11 mg, 59%). EI–MS (*m*/*z*, %): 198 ($M^{+\cdot}$, 100), 166 (29), 153 (33). IR (cm^{-1}): 3540. ^1H NMR δ: 3.51 (s, 3H), 5.07 (s, 2H), 5.92 (s, 1H), 6.20 (s, 1H), 6.30 (d, 1H, *J* = 8.4 Hz), 6.54 (d, 1H, *J* = 8.4 Hz, the OH proton was not located). ^{13}C NMR δ: 56.5, 97.6, 99.2, 101.7, 109.4, 132.3, 134.5, 141.5, 144.5. HRMS calcd. for $C_9H_{10}O_5$: 198.0528; found: 198.05296.

5-Hydroxy-4-methoxy-1,3-benzodioxole (14)

Phenol **13** (4.9 g, 24.7 mmol) was *O*-methylated following the procedure for formation of **9**. The yield of 4-methoxy-5-methoxymethyl-1,3-benzodioxole, a pale yellow liquid, was 5.05 g, (96%). EI–MS (*m*/*z*, %): 212 ($M^{+\cdot}$, 100), 182 (89), 167 (69). ^1H NMR δ: 3.49 (s, 3H), 3.99 (s, 3H), 5.08 (s, 2H), 5.88 (s, 2H), 6.41 (d, 1H, *J* = 8.4 Hz), 6.57 (d, 1H, *J* = 8.6 Hz). ^{13}C NMR δ: 56.1, 60.1, 96.6, 101.2, 101.4, 110.1, 135.4, 137.7, 144.1, 144.2. HRMS calcd. for $C_{10}H_{12}O_5$: 212.0685; found: 212.0709.

The above compound (4.86 g, 22.9 mmol) in acetone (15 mL) containing 5.15 g, (34.3 mmol) of NaI was stirred for 30 min. 3 N Methanol HCl (40 mL) was added and the resulting reaction mixture stirred for 4 h. Most of the solvent was evaporated and the crude residue dissolved in water (10 mL). The aqueous phase was extracted with ether (3 × 15 mL) and the combined organic extracts were then washed with 10% NaOH solution (3 × 15 mL). The combined aqueous phase was acidified using conc. HCl and extracted with ether (3 × 20 mL). Further work-up afforded 2.81 g (73%) of **14** as pale orange crystals, mp 53–55°C. EI–MS (*m*/*z*, %): 168 (M^+, 100), 153 (76). IR (cm^{-1}): 3541. ^1H NMR δ: 4.02 (s, 3H), 5.43 (s, 1H), 5.87 (s, 2H), 6.39 (s, 2H). ^{13}C NMR δ: 59.9, 101.1, 101.8, 105.9, 131.4, 136.2, 142.1, 142.7. HRMS calcd. for $C_8H_8O_4$: 168.0422; found: 168.0408.

5-Hydroxy-4-methoxy-6-(2-propenyl)-1,3-benzodioxole (15)

A solution of **14** (2.55 g, 15.2 mmol), allyl bromide (2.0 mL, 23 mmol), and anhyd. K_2CO_3 (3.15 g, 23 mmol) in acetone (15 mL) was refluxed for 30 h. The solvent was removed under reduced pressure and the crude residue was dissolved in 20 mL water and 10 mL of 10% NaOH solution. Further work-up gave 5-*O*-allyl-4-methoxy-1,3-benzodioxole as a yellow liquid (2.72 g, 86%). EI–MS (*m*/*z*, %): 208 ($M^{+\cdot}$, 39), 167 (100). IR (cm^{-1}): 977, 929.; ^1H NMR δ: 3.97 (s, 3H), 4.47 (dt, 2H, *J* = 5.4 Hz, 1.4 Hz), 5.22 (ddt, 1H, *J* = 10.5 Hz, 1.6 Hz, 1.4 Hz), 5.35 (ddt, 1H, *J* = 17.3 Hz, 1.6 Hz, 1.6 Hz), 5.86 (s, 1H), 6.00–6.06 (m, 1H), 6.32 (d, 1H, *J* = 8.5 Hz), 6.38 (d, 1H, *J* = 8.5 Hz). ^{13}C NMR δ: 60.2, 71.2, 101.1, 101.2, 107.2, 117.5, 133.6, 134.9, 138.1, 143.4, 146.2. HRMS calcd. for $C_{11}H_{12}O_4$: 208.0736; found: 208.0755.

A solution of the above allyl ether (460 mg, 2.0 mmol) in 5 mL *N*,*N*-dimethylaniline was heated at 190°C for 2.5 h. The solution was cooled, diluted with 7 mL of ether, and washed several times with 10% NaOH solution. The alkaline extract was acidified with conc. HCl and extracted with ether (3 × 15 mL). The crude residue obtained after work-up was purified by flash column chromatography (9:1, hexane:ethyl acetate) to give **15** as pale yellowish liquid (400 mg, 87%). EI–MS (*m*/*z*,%): 208 ($M^{+\cdot}$, 100). IR (cm^{-1}): 926, 987. ^1H NMR δ: 3.30 (d, 2H, *J* = 6.6 Hz), 4.03 (s, 3H), 5.00–5.11 (m, 2H), 5.43 (s, 1H), 5.84 (s, 2H), 5.85–6.02 (m, 1H), 6.33 (s, 1H). ^{13}C NMR δ: 33.7, 59.9, 100.9, 102.8, 115.4, 117.5, 131.1, 143.2, 136.7, 139.9, 141.6. HRMS calcd. for $C_{11}H_{12}O_4$: 208.0736; found: 208.0731.

4,5-Dimethoxy-6-(2-propenyl)-1,3-benzodioxole (1)

The phenol **15** (140 mg, 0.70 mmol), K_2CO_3 (140 mg, 0.10 mmol), and 0.50 mL (0.8 mmol) of methyl iodide was reacted in 5 mL of acetone as with **9**. Work-up and chromatography gave 130 mg (80%) of **1**.

5-Allyloxy-4-formyl-1,3-benzodioxole (18)

To a solution of compound **17** (0.3 g, 1.68 mmol) in anhyd. THF (5 mL), *n*-BuLi (1.35 mL, 2.01 mmol, 1.5 molar solution in hexane) was added dropwise at 78°C. The resulting yellow solution was allowed to stir for 45 min and then *N*,*N*-dimethylformamide (0.26 mL, 3.37 mmol) was added. After 30 min, the reaction mixture was quenched with sat. NH_4Cl solution and extracted with ether. Flash column chromatography of the crude ether extracts using ethyl acetate:hexane (1:5) furnished the aldehyde **18** (302 mg, 87%) as a yellow solid, mp = 98–100°C. ^1H NMR: δ 4.52 (m, 2H), 5.25 – 5.34 (m, 2 H), 6.04 (s, 2H), 5.81–6.11 (m, 1H), 6.27 (d, 1H, *J* = 8.6 Hz), 6.83 (d, 1H, *J* = 8.5 Hz), 10.37 (s, 1H). ^{13}C NMR δ: 70.6, 103.5, 104.2, 111.7, 113.5, 118.5, 133.1, 143.2, 148.9 155.7, 188.8. HRMS calcd. for $C_{11}H_{10}O_4$: 206.0593; found: 206.0581.

5-Allyloxy-4-hydroxy-1,3-benzodioxole (19)

To a solution of aldehyde **18** (0.3 g, 1.45 mmol) in dry chloroform (5 mL) at 0°C, was added in one portion MCPBA (0.61 g, 1.74 mmol, 50%). The resulting mixture was stirred at 0°C for 24 h. The mixture was diluted with chloroform (20 mL) and was washed with sat. sodium sulfite (1 × 15 mL), sat. sodium bicarbonate solution (1 × 15 mL) and water (1 × 15 mL). The crude formate ester (0.25 g, 78%) was obtained as an oil and used for the next reaction without any further purification. ^1H NMR δ: 4.45 (m, 2H), 5.25 (m, 2 H), 5.96 (s, 2H), 5.95–6.01 (m, 1H), 6.34 (d, 1H, *J* = 8.5 Hz), 6.59 (d, 1H, *J* = 8.5 Hz), 8.24 (s, 1H). To a solution of the ester (0.25 g, 1.13 mmol) in THF (5 mL), was added 1 mL of a 3 N NaOH solution. The resulting homogeneous solution was stirred at rt for 1 h and was extracted with water (4 × 10 mL). The aqueous phase was then acidified with 2 N HCl and was extracted with CH_2Cl_2 (3 × 20 mL). Further work-up afforded an oily residue. Purification by silica gel flash column chromatography using ethyl acetate–hexane (1:5) as eluent gave **19** (0.15 g, 70%) as a yellow liquid. ^1H NMR δ: 4.48 (m, 2H), 5.32 (m, 2H), 5.92 (s, 2 H), 5.90–6.10 (m, 1 H), 6.30 (s, 2 H). ^{13}C NMR δ: 71.6, 99.3, 102.3, 105.3, 119.1, 132.2, 133.5, 137.1, 142.8, 144.0. HRMS calcd. for $C_{10}H_{10}O_4$:194.0593; found: 194.0602.

© 2000 NRC Canada

4,5-Dihydroxy-6-(2-propenyl)-1,3-benzodioxole (20)

A solution of **19** (0.15 g, 0.77 mmol) in *N*,*N*-dimethylaniline (2 mL) was heated at 190°C for 1 h and then was allowed to cool to rt The reaction mixture was extracted into ethyl acetate and was washed with 1 N HCl solution (3 × 10 mL), brine (2 × 10 mL), followed by water (10 mL). The crude rearranged product was purified via silica gel flash chromatography using ethyl acetate–hexane (3:7) as eluent to yield **20** (0.12 g, 79%) as a brown syrup. ^{1}H NMR δ: 3.31 (m, 2 H), 5.44 (m, 2H), 5.87 (s, 2H), 5.85–6.02 (m, 1H), 6.22 (s, 1H). ^{13}C NMR δ: 35.4, 101.82, 102.0, 116.7, 118.4, 129.6, 133.4, 137.1, 138.2, 142.6. HRMS calcd. for $C_{10}H_{10}O_4$: 194.0579; found 194.5965.

4,5-Dimethoxy-6-(2-propenyl)-1,3-benzodioxole (1)

To a solution of **20** (0.02 g, 0.103 mmol) in acetone (3 mL), was added sequentially potassium carbonate (28 mg, 0.21 mmol), and methyl iodide (0.10 mL, 0.206 mmol). The resulting reaction mixture was allowed to stirred at rt for 60 h. Solvent was removed under reduced pressure. The crude product obtained after the usual work-up was purified by silica gel flash column chromatography using ethyl acetate–hexane (1:5) as eluent to furnish the dillapiol (**1**) (18 mg, 82%) as a yellow liquid.

Reaction of 11 with disulfides

General procedure

*n*BuLi (1 equiv.) was added to 1 equiv. of **11** in THF at 0°C. After 30 min, 1.5 equiv. of disulfide was added and the solution was stirred for 1 h. Further work-up followed by silica gel chro-matography afforded the desired 4-thio derivatives.

4-Methylthio-5-methoxymethoxy-1,3-benzodioxole (21a)

This reaction was carried out starting with 5.0 g (27.5 mmol) of **11**. The yield of **21a**, a pale yellow liquid, was 5.70 g (91%). EI–MS (*m*/*z*, %): 228 (M^+, 100), 198 (63), 182 (17). ^{1}H NMR δ: 2.41 (s, 3H), 3.47 (s, 3H), 5.92 (s, 2H), 5.11 (s, 2H), 5.92 (s, 2H), 6.52 (d, 1H, *J* = 8.6 Hz), 6.59 (d, 1H, *J* = 8.6 Hz). ^{13}C NMR δ: 16.9, 56.1, 95.9, 101.2, 106.7, 107.8, 108.8, 142.3, 148.5, 151.7. HRMS calcd. for $C_{10}H_{12}O_4S$: 228.0456; found: 228.04679.

4-Phenylmethanethio-5-methoxymethoxy-1,3-benzodioxole (21b)

From 3.0 g, (16 mmol) of **11** and 5.35 g (22 mmol) of benzyl disulfide was obtained 2.37 g (58%) of **21b** as yellow oil. EI–MS (*m*/*z*, %): 304 (M^+, 29), 259 (18), 182 (26), 91 (100). ^{1}H NMR δ: 3.45 (s, 3H), 4.07 (s, 2H), 5.03 (s, 2H), 5.85 (s, 2H), 6.54 (d, 1H, *J* = 8.5 Hz), 6.63 (d, 1H, *J* = 8.5 Hz), 7.20 (s, 5H). ^{13}C NMR δ: 38.0, 56.1, 96.0, 101.2, 106.5, 107.4, 107.9, 126.9, 128.1, 128.8, 138.0, 142.2, 149.5, 152.5. HRMS calcd. for $C_{16}H_{16}O_4S$: 304.0792; found: 304.0758.

4-Phenylthio-5-methoxymethoxy-1,3-benzodioxole (21c)

Reaction of 1.50 g (8.0 mmol) of **11** (1.5 g, 8.0 mmol) and 1.80 g (8.0 mmol) of diphenyl disulfide gave 0.67 g (30%) of **21c** as white crystals, mp 67–69°C. EI–MS (*m*/*z*, %): 290 (M^+, 51), 260 (25), 91 (50). ^{1}H NMR δ: 3.33 (s, 3H), 5.05 (s, 2H), 5.93 (s, 2H), 6.63 (d, 1H, *J* = 8.5 Hz), 6.77 (d, 1H, *J* = 8.5 Hz), 7.08–7.20 (m, 5H). ^{13}C NMR δ: 56.1, 95.7, 101.6, 104.2, 1007.8 08.8, 125.5, 127.1, 128.7, 136.2, 142.5, 150.4, 152.7. HRMS calcd. for $C_{15}H_{14}O_4S$: 290.0613; found: 290.0600.

4-(4′-Methoxyphenylthio)-5-methoxymethoxy-1,3-benzodioxole (21d)

Reaction of 420 mg of **11** with 530 mg of *p*-methoxyphenyl disulfide gave 250 mg (40%) of **21d** as white crystals, mp 82–84°C. EI–MS (*m*/*z*, %): 320 (M^+, 8.6), 278 (46), 139 (100). ^{1}H NMR δ: 3.34 (s, 3H), 3.69 (s, 3H), 5.03 (s, 2H), 5.88 (s, 2H), 6.56 (d, 1H, *J* = 8.5 Hz), 6.68 (d, 1H, *J* = 8.5 Hz), 6.74 (d, 2H, *J* = 8.9 Hz), 7.22 (d, 2H, *J* = 8.9 Hz). ^{13}C NMR δ: 55.0, 55.9, 95.7, 101.4, 106.3, 107.7, 108.1, 114.2, 126.2, 130.7, 142.3, 149.8, 152.3, 158.3. HRMS calcd. for $C_{16}H_{16}O_5S$: 320.0718; found: 320.0706.

Removal of the MOM group

General procedure

Each MOM derivative **21** was dissolved in a mixture of acetone and 3 N methanolic HCl containing NaI. The mixture was stirred for about 4 h and most of the solvent was removed under reduced pressure. The residue was partitioned between ether and 10% NaOH solution. The basic extracts were acidified and reextracted with ether. The crude products obtained after further work-up were purified by recrystallization or chromatography.

5-Hydroxy-4-methylthio-1,3-benzodioxole

From 4.0 g of **21a** and 3.94 g of NaI in 15 mL of acetone and 40 mL of 3 N methanolic HCl was obtained 2.65 g (80%) of the title compound as a white powder, mp 51–53°C. EI–MS (*m*/*z*, %): 184 (M^+, 100), 169 (30). IR (cm^{-1}): 3428. ^{1}H NMR δ: 2.31 (s, 3H), 5.98 (s, 2H), 6.22 (s, 1H), 6.42 (d, 1H, *J* = 8.4 Hz), 6.69 (d, 1H, *J* = 8.4 Hz). ^{13}C NMR δ: 18.0, 101.6, 103.4, 105.4, 109.4, 140.7, 149.3, 151.2. HRMS calcd. for $C_8H_8O_3S$: 184.0194; found: 184.0163.

5-Hydroxy-4-phenylmethanethio-1,3-benzodioxole

Reaction of 2.51 g of **21b** with 1.86 g of NaI in 50 mL of acetone–methanol–conc. HCl (1:3:1) for 1 h afforded 1.68 g (91%) of the deprotected phenol as a yellowish oil. EI–MS (*m*/*z*, %): 260 (M^+, 36), 169 (8.2), 91 (100). IR (cm^{-1}): 3434. ^{1}H NMR δ: 3.87 (s, 2H), 5.85 (s, 2H), 6.03 (s, 1H), 6.35 (d, 1H, *J* = 8.4 Hz), 6.68 (d, 1H, *J* = 8.4 Hz), 7.10–7.25 (m, 5H). ^{13}C NMR δ: 39.3, 101.0, 101.5, 105.3, 109.8, 127.4, 128.4, 128.7, 137.2, 140.4, 149.8, 151.7. HRMS calcd. for $C_{14}H_{12}O_3S$: 260.0510; found: 260.0512.

5-Hydroxy-4-phenylthio-1,3-benzodioxole

Compound **21c** (670 mg, 2.3 mmol), 5.2 g of NaI in 10 mL of acetone and 8 mL of 3 N methanolic HCl was stirred for 1 h. The yield of the title compound, a white powder, mp 119–122°C, was >99%. EI–MS (*m*/*z*, %): 246 (M^+, 100), 162 (23), 140 (49). IR (cm^{-1}): 3441. ^{1}H NMR δ: 5.96 (s, 2H), 6.18 (s, 1H), 6.52 (d, 1H, *J* = 8.5 Hz), 6.81 (d, 1H, *J* = 8.6 Hz), 7.12–7.26 (m, 5H). ^{13}C NMR δ (ppm): 99.5, 101.9, 105.9, 110.8, 126.5, 127.0, 129.3, 134.2, 141.0,

© 2000 NRC Canada

150.1, 151.9. HRMS calcd. for $C_{13}H_{10}O_3S$: 246.0351; found: 246.0334.

5-Hydroxy-4-(4′-methoxyphenylthio)-1,3-benzodioxole

Compound **21d** (250 mg, 0.78 mmol) in acetone (10 mL) and 8 mL of 3 N methanolic HCl containing 180 mg NaI was stirred for 2 h. The yield of the above phenol (mp 82–83°C) was 180 mg (83%). EI–MS (*m*/*z*, %): 276 (M^+,100), 162 (18), 140 (44). IR (cm^{-1}): 3443. ^1H NMR δ: 3.74 (s, 3H), 5.94 (s, 2H), 6.31 (s, 1H), 6.47 (d, 1H, *J* = 8.5 Hz), 6.75 (d, 1H, *J* = 8.4 Hz), 6.79 (d, 1H, *J* = 6.9 Hz), 7.20 (d, 1H, *J* = 7.6 Hz). ^{13}C NMR δ: 55.3, 101.5, 101.7, 105.8, 110.4, 114.9, 124.5, 130.4, 140.9, 149.8, 151.6, 159.0. HRMS calcd. for $C_{14}H_{12}O_4S$: 276.0456; found: 276.0466.

Allylation of the 4-thio-5-hydroxy derivatives

General procedure

The above phenols were dissolved in acetone containing about 10–20% excess of anhydrous potassium carbonate. The mixture was refluxed for up to 24 h. The solvent was evaporated under reduced pressure and the residue was partitioned between ether and 10% NaOH solution. Further processing of the ether phase gave the desired product.

5-Allyoxy-4-methylthio-1,3-benzodioxole

From 1.89 g of 5-hydroxy derivative, series **a**, 2.13 g of potassium carbonate and 0.90 mL of allyl bromide in 15 mL acetone was obtained after 23 h of reflux, 2.03 g (88%) of the desired product as a clear liquid. EI–MS (*m*/*z*, %): 224.1 ($M^{+\cdot}$, 100), 184 (13), 137 (98). ^1H NMR δ: 2.46 (s, 1H), 4.53 (dt, 2H, *J* = 5.1 Hz, 1.4 Hz), 5.28 (dd, 1H, *J* = 10.5 Hz, 1.5 Hz), 5.44 (dd, 1H, *J* = 17.0 Hz, 1.6 Hz), 5.97 (s, 2H), 6.00–6.09 (m, 1H), 6.31 (d, 1H, *J* = 8.5 Hz), 6.63 (d, 1H, *J* = 8.5 Hz). ^{13}C NMR δ: 16.9, 70.3, 101.2, 104.5, 106.4, 117.4, 133.1, 133.8, 141.5, 148.7, 153.3. HRMS calcd. for $C_{11}H_{12}O_3S$: 224.0507; found: 224.0533.

5-Allyoxy-4-phenylmethanethio,3-benzodioxole

A solution of the 5-phenol, series **b** (1.68 g, 6.5 mmol), anhyd. K_2CO_3 (1.10 g, 8.0 mmol and 0.63 mL of allyl bromide in 15 mL of acetone when refluxed for 23 h, yielded 1.39 g (83%) of the desired allyl ether as a clear oil. EI–MS (*m*/*z*, %): 300 (M^+, 30), 259 (38), 91 (100). IR (cm^{-1}): 953, 995. ^1H NMR δ: 4.09 (s, 2H), 4.46 (d, 2H, *J* = 5.1 Hz), 5.27 (dd, 1H, *J* = 10.5 Hz, 1.5 Hz), 5.43 (dd, 1H, *J* = 15.6 Hz, 1.6 Hz), 5.84 (s, 2H), 5.95–6.11 (m, 1H), 6.30 (d, 1H, *J* = 8.4 Hz), 6.62 (d, 1H, *J* = 9.2 Hz), 7.21 (s, 5H). ^{13}C NMR δ: 37.9, 70.3, 101.1, 104.6, 105.5, 107.1, 117.3, 126.8, 128.1, 128.8, 133.1, 138.0, 141.3, 149.7, 153.9. HRMS calcd. for $C_{17}H_{16}O_3S$: 300.0821; found: 300.0820.

5-Allyoxy-4-phenylthio-1,3-benzodioxole

A mixture of phenol, series **c** (1.62 g, 6.6 mmol), anhyd. K_2CO3 (1.10 g, 8.0 mmol), and 0.63 mL of allyl bromide when refluxed for 23 h in acetone (15 mL) gave 1.25 g (84%) of the expected allyl ether. EI–MS (*m*/*z*, %): 268 ($M^{+\cdot}$, 52), 245 (52), 91 (100). IR (cm^{-1}): 943, 996. ^1H NMR δ: 4.44 (dt, 2H, *J* = 5.0 Hz, 1.6 Hz), 5.15 (ddt, 1H, *J* = 10.5 Hz, 1.6 Hz, 1.5 Hz), 5.25 (ddt, 1H, *J* = 17.0 Hz, 1.7 Hz, 1.6 Hz), 5.76–5.95 (m, 1H), 5.93 (s, 2H), 6.35 (d, 1H, *J* = 8.5 Hz), 6.75 (d, 1H, *J* = 8.5 Hz), 7.07–7.22 (m, 5H). ^{13}C NMR δ: 70.3, 101.6, 103.5, 104.9, 108.4, 117.2, 125.4, 127.3, 128.6, 132.8, 136.2, 141.7, 150.5, 145. HRMS calcd. for $C_{16}H_{14}O_3S$: 286.0664; found: 286.0649.

5-Allyoxy-4-(4′-methoxyphenylthio)-1,3-benzodioxole

Reaction of the phenol, series **d** (1.10 g, 4.0 mmol), anhyd. K_2CO_3 (0.83 g, 6.0 mmol) and 0.41 mL of allyl bromide in acetone (15 mL) at reflux for 23 h gave 0.96 g (76%) of the expected product as a clear oil. EI–MS (*m*/*z*, %): 316 ($M^{+\cdot}$, 32), 275 (30), 149 (100). IR (cm^{-1}): 931, 953. ^1H NMR δ: 3.72 (s, 3H), 4.43 (dt, 2H, *J* = 5.1 Hz, 1.5 Hz), 5.18 (ddt, 1H, *J* = 12 Hz, 1.6 Hz, 1.5 Hz), 5.31 (ddt, 1H, *J* = 18 Hz, 1.7 Hz, 1.6 Hz), 5.90 (s, 2H), 5.83–5.97 (m, 1H), 6.30 (d, 1H, *J* = 8.5 Hz), 6.67 (d, 1H, *J* = 8.5 Hz), 6.75 (d, 2H, *J* = 9.0 Hz), 7.26 (d, 2H, *J* = 9.0 Hz). ^{13}C NMR δ: 55.1, 70.3, 101.4, 104.8, 105.6, 107.8, 114.2, 117.2, 126.3, 131.0, 132.9, 141.6, 149.9, 153.7, 158.4. HRMS calcd. for $C_{17}H_{16}O_4S$: 316.0770; found: 316.0766.

Claisen rearrangement of the 5-allyl ethers

General procedure

The 5-allyl ethers obtained as described above were dissolved in a small quantity of *N*,*N*-dimethylaniline and heated to 190°C for 1–3 h. The cooled reaction mixture was diluted with ether and extracted with 10% NaOH solution. The combined basic extracts were acidified and extracted with ether. Further work-up and purification yielded the desired Claisen rearrangement products.

5-Hydroxy-4-methylthio-6-(2-propenyl)-1,3-benzodioxole (22a)

Allyl ether, series **a** (1.0 g, 4.0 mmol) when heated in 5 mL of *N*,*N*-dimethylaniline (5 mL) at 190°C for 2.5 h, gave 0.87 g (87%)of **22a** as a colourless liquid. EI–MS (*m*/*z*, %): 224 ($M^{+\cdot}$, 100), 197 (9), 176 (18). IR (cm^{-1}): 927, 953, 3425. ^1H NMR δ (ppm): 2.31 (s, 3H), 3.32 (dt, 2H, *J* = 6.8 Hz, 1.4 Hz), 5.01–5.11 (m, 2H), 5.95 (s, 2H), 5.88–6.02 (m, 1H), 6.40 (s, 1H), 6.62 (s, 1H).^{13}C NMR δ: 18.0, 34.4, 101.3, 102.9, 110.4, 115.5, 117.1, 136.6, 140.3, 147.5, 148.2. HRMS calcd. for $C_{11}H_{12}O_3S$: 224.0507; found: 224.0493.

5-Hydroxy-4-phenylmethanethio-6-(2-propenyl)-1,3-benzodioxole (22b)

Allyl ether, series **b** (4.30 g, 14.0 mmol) when treated as above gave 0.42 g (98%) of **22b** as a colourless oil. EI–MS (*m*/*z*, %): 300 (M^+, 48), 224 (91), 209 (28), 176 (48). IR (cm^{-1}): 954, 997, 1638, 3429. ^1H NMR δ: 3.25 (d, 2H, *J* = 6.4 Hz), 3.87 (s, 2H), 4.93–5.04 (m, 2H), 5.82–5.96 (m, 1H), 5.83 (s, 2H), 6.18 (s, 1H), 6.61 (s, 1H), 7.08–7.25 (m, 5H). ^{13}C NMR δ: 34.4, 39.4, 100.6, 101.2, 10.9, 115.3, 116.9, 127.4, 128.5, 128.7, 136.6, 137.2, 140.1, 148.0, 148.8. HRMS calcd. for $C_{17}H_{16}O_3S$: 300.0821; found: 300.08240.

5-Hydroxy-4-phenylthio-6-(2-propenyl)-1,3-benzodioxole (22c)

From 1.5 g of allyl ether, series **c**, was obtained 550 mg (37%) of **22c** as a pale yellow oil. EI–MS (*m*/*z*, %): 286 (M^+, 100), 162 (8). IR (cm^{-1}): 953, 997, 1638, 3443. ^1H NMR δ: 3.35 (dt, 2H, *J* = 6.4 Hz, 1.4 Hz), 5.05–5.09

© 2000 NRC Canada

(m, 2H), 5.92 (s, 2H), 5.93–5.99 (m, 1H), 6.31 (s, 1H), 6.73 (s, 1H), 7.13–7.23 (m, 5H). ^{13}C NMR δ: 34.4, 99.0, 101.5, 111.9, 115.7, 117.6, 126.5, 127.0, 129.3, 134.3, 136.5, 40.6, 148.3, 148.9. HRMS calcd. for $C_{16}H_{14}O_3S$: 286.0664; found: 286.0641.

5-Hydroxy-4-(4′-methoxyphenylthio)-6-(2-propenyl)-1,3-benzodioxole (22d)

The allyl ether from series **d** (310 mg, 0.9 mmol) when heated for 2.5 h in 3 mL of *N*,*N*-dimethylaniline gave 0.29 g (97%) of **22d** as pale yellow oil. EI–MS (*m*/*z*, %): 316 (M^+, 100), 208 (22), 180 (47). IR (cm^{-1}): 949, 995, 1638, 3440. ^{1}H NMR δ: 3.32 (d, 2H, *J* = 6.5 Hz), 3.74 (s, 3H), 5.02 (s, 1H), 5.05 (d, 2H, *J* = 6 Hz), 5.91 (s, 2H), 5.89–5.97 (m, 1H), 6.42 (s, 3H), 6.67 (s, 1H), 6.78 (d, 2H, *J* = 8.7 Hz), 7.19 (d, 2H, *J* = 8.7 Hz). ^{13}C NMR δ: 34.5, 55.4, 101.1, 101.5, 111.5, 114.9, 115.6, 117.5, 124.7, 130.4, 136.6, 140.6, 148.0, 148.7, 159.0. HRMS calcd. for $C_{17}H_{16}O4S$: 316.0770; found: 316.0749.

Methylation of phenols (22)

These reactions were carried out in the same manner as the conversion **8** to **9**.

5-Methoxy-4-methylthio-6-(2-propenyl)-1,3-benzodioxole (23a)

Phenol **22a** (400 mg, 1.8 mmol), was converted in 87% yield (372 mg) to **23a**. EI–MS (*m*/*z*, %): 238 (M^+,100), 223 (13), 176 (41). IR (cm^{-1}): 949, 996. ^{1}H NMR δ: 2.45 (s, 3H), 3.30 (dt, 2H, *J* = 6.5 Hz, 1.4 Hz), 3.75 (s, 3H), 5.01–5.05 (m, 2H), 5.93 (s, 2H), 5.84–5.92 (m, 1H), 6.53 (s, 1H). ^{13}C NMR δ: 16.9, 34.0, 61.4, 101.3, 108.2, 112.3, 115.7, 125.8, 137.1, 143.4, 146.8, 151.8. HRMS calcd. for $C_{12}H_{14}O_3S$: 238.0664; found: 238.0682.

5-Methoxy-4-phenylmethanethio-6-(2-propenyl)-1,3-benzodioxole (23b)

Phenol **22b** (420 mg, 1.4 mmol) was converted into 0.420 mg (96%) of **23b**. EI–MS (*m*/*z*, %): 314 ($M^{+\cdot}$, 72), 223 (11), 91 (100). IR (cm^{-1}): 950, 994, 1638. ^{1}H NMR δ: 3.30 (dt, 2H, *J* = 6.4 Hz, 1.5 Hz), 3.65 (s, 3H), 4.12 (s, 2H), 4.96–5.07 (m, 2H), 5.88 (s, 2H), 5.83–5.95 (m, 1H), 6.55 (s, 1H), 7.17–7.24 (m, 5H). ^{13}C NMR δ: 34.0, 37.9, 61.6, 101.3, 108.9, 109.9, 115.7, 125.7, 127.0, 128.3, 128.9, 137.2, 138.0, 43.2, 147.6, 152.5. HRMS calcd. for $C_{18}H_{18}O_3S$: 314.0977; found: 314.0953.

5-Methoxy-4-phenylthio-6-(2-propenyl)-1,3-benzodioxole (23c)

The title compound **23c** was obtained as a yellowish oil in 87% yield starting with 550 mg of **22c**. EI–MS (*m*/*z*, %): 300 ($M^{+\cdot}$, 100), 176 (48), 162 (15). IR (cm^{-1}): 948, 995, 1639. ^{1}H NMR δ: 3.35 (dt, 2H, *J* = 6.4 Hz, 1.4 Hz), 3.73 (s, 3H), 5.02–5.11 (m, 2H), 5.91 (s, 2H), 5.86–6.05 (m, 1H), 6.71 (s, 1H), 7.10–7.22 (m, 5H). ^{13}C NMR δ: 34.2, 62.2, 101.6, 107.6, 110.4, 116.0, 125.6, 126.2, 127.1, 128.9, 136.2, 137.1, 143.7, 148.6, 153.2. HRMS calcd. for $C_{17}H_{16}O_3S$: 300.0821; found: 300.0802.

5-Methoxy-4-(4′-methoxyphenylthio)-6-(2-propenyl)-1,3-benzodioxole (23d)

Phenol **22d** (170 mg) was converted in 96% yield into **23d** as a pale yellow oil. EI–MS (*m*/*z*, %): 330 ($M^{+\cdot}$, 100), 176 (21), 121 (68). IR (cm^{-1}): 949, 995, 1638. ^{1}H NMR δ: 3.34 (dt, 2H, *J* = 6.5 Hz, 1.5 Hz), 3.73 (s, 3H), 3.75 (s, 3H), 5.03–5.07 (m, 2H), 5.87 (s, 2H), 5.88–5.94 (m, 1H), 6.63 (s, 1H), 6.77 (d, 2H, *J* = 8.9 Hz), 7.24 (d, 2H, *J* = 8.9 Hz). ^{13}C NMR δ: 34.1, 55.2, 62.0, 101.5, 109.7, 109.8, 114.5, 115.9, 126.0, 126.3, 130.7, 137.1, 143.6, 148.1, 152.7, 158.5. HRMS calcd. for $C_{18}H_{18}O_4S$: 330.0926; found: 330.0942.

Oxidation of the sulfides (23) to sulfoxides (24) and sulfones (25)

General procedures

For the oxidation to the sulfoxides, a solution of the sulfide in ethyl acetate was cooled to approx. –40°C and 1.2 equiv. of MCPBA was added. The reaction mixture was allowed to warm to rt and stirred for 24 h. Work-up consisted of washing first with sat. sodium bisulfite solution, then with sat. sodium bicarbonate, and finally with water. The organic soluble product was purified by column chromatography.

The oxidation to sulfones was carried out with 3–4 equiv. of MCPBA in ethyl acetate at rt for 24 h. The work-up of the reaction mixture was similar to that of the sulfoxides.

5-Methoxy-4-methylsulfinyl-6-(2-propenyl)-1,3-benzodioxole (24a)

Sulfide **23a** (100 mg, 0.42 mmol) was reacted with 0.5 mmol of MCPBA in 6 mL of ethyl acetate to afford 67 mg (63%) of **24a** as a pale yellowish liquid. EI–MS (*m*/*z*, %): 254 ($M^{+\cdot}$, 83), 237 (100). IR (cm^{-1}): 942, 994, 1050. ^{1}H NMR δ: 3.01 (s, 3H), 3.16 (dd, 2H, *J* = 6.4 Hz, 1.5 Hz), 3.78 (s, 3H), 5.03–5.09 (m, 2H), 5.84–5.89 (m, 1H), 6.06 (s, 2H), 6.74 (s, 1H). ^{13}C NMR δ: 33.1, 39.7, 63.4, 102.7, 112.3, 116.5, 120.8, 126.1, 136.3, 145.0, 145.5, 149.1. HRMS calcd. for $C_{12}H_{14}O_4S$: 254.0613; found: 254.0607.

5-Methoxy-4-methylsulfonyl-6-(2-propenyl)-1,3-benzodioxole (25a)

Oxidation of 50 mg, (0.21 mmol) of sulfide **23a** afforded 45 mg (80%) of sulfone **25a** as a pale yellow solid. EI–MS (*m*/*z*, %): 270 ($M^{+\cdot}$, 100). IR (cm^{-1}): 950, 993, 1136, 1316. ^{1}H NMR δ: 3.26 (s, 3H), 3.54 (d, 2H, *J* = 6.5 Hz), 3.84 (s, 3H), 5.06–5.13 (m, 2H), 5.84–5.92 (m, 1H), 6.05 (s, 2H), 6.83 (s, 1H). ^{13}C NMR δ: 32.1, 44.8, 63.8, 102.8, 113.9, 117.0, 118.1, 127.0, 135.9, 145.0, 145.2, 149.2. HRMS calcd. for $C_{12}H_{14}O_5S$: 270.0562; found: 270.0541.

5-Methoxy-4-phenylmethanesulfinyl-6-(2-propenyl)-1,3-benzodioxole (24b)

From 110 mg, (0.4 mmol) of **23b** was obtained 70 mg (61%) of sulfoxide **24b** as a yellowish oil. EI–MS (*m*/*z*, %): 330 ($M^{+\cdot}$, 21), 283 (47), 91 (100). IR (cm^{-1}): 951, 992, 1049, 1071. ^{1}H NMR (500 MHz) δ: 3.24 (d, 2H, *J* = 6.3 Hz), 3.56 (s, 3H), 4.34 (d, 1H, *J* = 12.5 Hz), 4.45 (d, 1H, *J* = 12.5 Hz), 5.00–5.06 (m, 2H), 5.82 (d, 1H, *J* = 1.34), 5.90 (d, 1H, *J* = 1.4 Hz), 5.81–5.87 (m, 1H), 6.67 (s, 1H), 7.10–7.24 (m, 5H). ^{13}C NMR δ: 33.0, 59.2, 63.0, 102.6, 112.3, 116.3, 118.6,

© 2000 NRC Canada

125.8, 128.1, 128.4, 130.2, 130.3, 136.4, 145.2, 145.8, 149.4. HRMS calcd. for $C_{18}H_{18}O_4S$: 330.0926; found: 330.0910.

5-Methoxy-4-phenylmethanesulfonyl-6-(2-propenyl)-1,3-benzodioxole (25b)

Oxidation of 80 mg (0.25 mmol) of sulfide **23b** in 6 mL of ethyl acetate gave 40 mg (45%) of sulfone **25b** as a white solid, mp 133–136°C. EI–MS (*m*/*z*, %): 346 ($M^{+\cdot}$, 34), 139 (16), 91 (100). IR (cm^{-1}): 1149, 1320. ^1H NMR δ: 3.35 (d, 2H, *J* = 6.4 Hz), 3.88 (s, 3H), 4.57 (s, 2H), 5.05–5.15 (m, 2H), 5.82 (s, 2H), 5.88–5.93 (m, 1H), 6.77 (s, 1H), 7.20–7.24 (m, 5H). ^{13}C NMR δ: 33.2, 62.2, 63.9, 102.6, 114.1, 116.8, 126.7, 128.1, 128.3, 128.5, 130.9, 133.9, 144.9, 146.3, 1494. HRMS calcd. for $C_{18}H_{18}O_5S$: 346.0875; found: 346.0852.

5-Methoxy-4-lphenylsulfinyl-6-(2-propenyl)-1,3-benzodioxole (24c)

Sulfide **23c** (100 mg, 0.30 mmol) was oxidized to sulfoxide **24c**, mp 83–87°C, in 76% yield. EI–MS (*m*/*z*, %): 316 ($M^{+\cdot}$, 39), 299 (100), 190 (59). IR (cm^{-1}): 948, 994, 1054,1639. ^1H NMR δ: 3.29 (d, 2H, *J* = 6.4 Hz), 3.85 (s, 3H), 5.00–5.07 (m, 2H), 5.82 (s, 1H), 5.82–5.88 (m, 1H), 5.97 (s, 1H), 6.68 (s, 1H), 7.24–7.71 (m, 5H). ^{13}C NMR δ: 33.0, 63.2, 102.6, 112.4, 116.5, 124.3, 125.8, 128.8, 130.3, 136.2, 143.8, 145.4. HRMS calcd. for $C_{17}H_{16}O_4S$: 316.0770; found: 316.0766.

5-Methoxy-4-phenylsulfonyl-6-(2-propenyl)-1,3-benzodioxole (25c)

Oxidation of 90 mg (0.21 mmol) of sulfide **23c** in ethyl acetate (6 mL) with 2 equiv. of MCPBA for 24 h provided the sulfone **25c** as a white solid, mp 86–88°C, in 71% yield. EI–MS (*m*/*z*, %): 332 ($M^{+\cdot}$, 100), 176 (34). IR (cm^{-1}): 992, 953, 1148, 1319. ^1H NMR δ: 3.23 (dt, 2H, *J* = 6.4 Hz, 1.5 Hz), 3.80 (s, 3H), 5.03–5.07 (m, 2H), 5.77–5.82 (m, 1H), 6.08 (s, 2H), 6.78 (s, 1H), 7.41–7.57 (m, 5H). ^{13}C NMR δ: 33.0, 63.6, 102.8, 114.0, 116.9, 118.7, 126.9, 127.5, 128.7, 133.2, 136.0, 142.6, 145.0, 145.4, 149.3. HRMS calcd. for $C_{17}H_{16}O_5S$: 332.0719; found: 332.0699.

5-Methoxy-4-(4′-methoxyphenylsulfinyl)-6-(2-propenyl)-1,3-benzodioxole (24d)

Sulfide **23d** (140 mg) was oxidized to give 100 mg (68%) of sulfoxide **25c** as a pale yellow oil. EI–MS (*m*/*z*, %): 330 ($M^{+\cdot}$, 60), 190 (28), 121 (100). IR (cm^{-1}): 949, 993,1044,1639. ^1H NMR δ: 3.27 (dt, 2H, *J* = 6.4 Hz, 1.4 Hz), 3.77 (s, 3H), 3.82 (s, 3H), 4.99–5.06 (m, 2H), 5.81–5.84 (m, 1H), 5.87 (s, 1H), 5.98 (s, 1H), 6.66 (s, 1H), 6.92 (d, 2H, *J* = 8.9 Hz), 7.64 (d, 2H, *J* = 8.9 Hz). ^{13}C NMR δ: 33.1, 55.4, 63.2, 102.6, 112.1, 114.4, 116.5, 122.1, 125.9, 126.4, 135.4, 136.4, 144.7, 145.5, 149.2, 161.5. HRMS calcd. for $C_{18}H_{18}O_5S$: 346.0875; found: 346.0875.

5-Methoxy-4-(4′-methoxyphenylsulfonyl)-6-(2-propenyl)-1,3-benzodioxole (25d)

Sulfide **23d** (90 mg) was oxidized to sulfone **25d**, mp 82–85°C, in 71% yield. EI–MS (*m*/*z*, %): 362 ($M^{+\cdot}$, 38), 300 (100), 176 (52). IR (cm^{-1}): 953, 992, 1145, 1315. ^1H NMR δ: 3.22 (dt, 2H, *J* = 6.4 Hz, 1.4 Hz), 3.80 (s, 3H), 3.81 (s, 3H), 4.99–5.07 (m, 2H), 5.75–5.83 (m, 1H), 6.05 (s, 2H), 6.92 (s, 1H), 6.84 (d, 2H, *J* = 8.9 Hz), 7.93 (d, 2H, *J* = 8.9 Hz). ^{13}C NMR δ: 33.1, 55.5, 63.6, 102.7, 113.7, 113.9, 116.9, 126.9, 129.8, 134.4, 136.0, 144.9, 145.1, 149.2, 163.4. HRMS calcd. for $C_{18}H_{18}O_6S$: 362.0824; found: 362.0821.

5-Hydroxy-4-hydroxymethyl-6-(2-propenyl)-1,3-benzodioxole (26)

To a solution of the aldehyde **8** (238 mg, 1.15 mmol) in 2.5 mL of ethanol was added 44 mg of sodium borohydride. The solution was stirred for 40 min, diluted with 2 mL of water, and then acidified with 2 N HCl. Work-up afforded 256 mg of crude product which was purified by chromatography to yield 198 mg (83%) of **26** as a white solid, mp 82–84°C. EI–MS (*m*/*z*, %): 208 ($M^{+\cdot}$, 26), 190 (100), 189 (50). IR (cm^{-1}): 3404, 3587. ^1H NMR δ: 2.55 (s, 1H), 3.28 (dt, *J* = 6.5, 1.4 Hz), 4.81 (s, 2H), 5.05–5.10 (m, 2H), 5.83 (s, 2H), 5.91–5.96 (m, 1H), 6.53 (s, 1H), 6.85 (s, 1H). ^{13}C NMR δ: 34.2, 57.8, 101.0, 108.9, 115.7, 118.3, 136.9, 140.4, 143.3, 148.8. HRMS calcd. for $C_{11}H_{12}O_4$: 208.0736; found: 208.0736.

5-Hydroxy-4-(1-hydroxyoctyl)-6-(2-propenyl)-1,3-benzodioxole (27)

A solution of 300 mg (1.45 mmol) of aldehyde **8** in 2 mL of ether was added to a freshly prepared solution (approx. 3 mmol) of *n*-octylmagnesium bromide in 3 mL of ether. The reaction mixture was refluxed for 45 min and quenched with sat. NH_4Cl solution. Work-up afforded 108 mg (25%) of **27**, mp 91–93°C. EI–MS: (*m*/*z*, %): 320 ($M^{+\cdot}$-H_2O, 100), 191 (53). IR (cm^{-1}): 3372, 3586. ^1H NMR δ: 0.86 (t, 3H, *J* = 6.7 Hz), 1.24–1.33 (m, 11H), 1.41–1.46 (m, 1H), 1.75–1.81 (m, 1H), 1.85–1.91 (m, 1H), 2.54 (s, 1H), 3.23–3.33 (m, 2H), 5.02–5.07 (m, 3H), 5.79 (d, 1H, *J*= 1.3 Hz), 5.83 (d, 1H, *J* = 1.4 Hz), 5.91–5.99 (m, 1H), 6.52 (s, 1H), 7.65 (d, 1H, *J* = 4.5 Hz). ^{13}C NMR δ: 14.1, 22.6, 25.5, 29.2, 29.3, 29.5, 31.8, 33.9, 36.6, 70.4, 100.8, 108.4, 111.4, 115.4, 119.0, 137.1, 139.8, 142.6, 147.8. HRMS calcd. for $C_{19}H_{28}O_4$: 320.1998; found: 320.1998.

4-Hydroxymethyl-5-methoxy-6-(2-propenyl)-1,3-benzodioxole (28)

The aldehyde **9** (350 mg) was reduced with $NaBH_4$ following the procedure for **8** to give **28** as an oil in 75% purified yield. IR (cm^{-1}): 3598. ^1H NMR δ: 2.45 (s, 1H), 3.30 (dt, 2H, *J* = 6.5, 1.4 Hz), 3.72 (s, 3H), 4.68 (s, 2H). ^{13}C NMR δ: 33.6, 55.7, 62.5, 101.4, 108.9, 115.9, 116.4, 125.4, 137.2, 143.7, 144.7, 150. EI–MS (*m*/*z*, %): 222 ($M^{+\cdot}$, 100). HRMS calcd. for $C_{12}H_{14}O_4$: 222.0892; found: 222.0906.

4-(1-Hydroxyoctyl)-5-methoxy-6-(2-propenyl)-1,3-benzodioxole (29)

This compound was prepared in 68% yield in a manner similar to the preparation of **27**. The yield of **29**, a clear yellowish oil, was 65%. EI–MS (*m*/*z*, %): 334 ($M^{+\cdot}$, 5), 316 (100), 190 (42), 43 (75). IR (cm^{-1}): 3588. ^1H NMR δ: 0.84–0.87 (m, 3H), 1.24–1.30 (m, 11H), 1.45–1.50 (m, 1H), 1.76–1.78 (m, 1H), 1.90–1.91 (m, 1H), 3.31 (dd, 2H, *J* = 6.4, 1.0 Hz), 3.70 (s, 3H), 4.88 (s, 1H), 5.02–5.06 (m, 2H), 5.87–5.93 (m, 1H), 5.91 (s, 2H), 6.56 (s, 1H). ^{13}C NMR δ: 14.1,

© 2000 NRC Canada

22.6, 26.1, 29.2, 29.5, 29.7, 31.9, 33.7, 37.6, 62.5, 68.3, 101.3, 108.4, 115.9, 120.8, 125.5, 137.2, 143.6, 143.9, 149.7. HRMS calcd. for $C_{20}H_{30}O_4$: 334.2145; found: 334.2157.

Cinnamate ester (30)

Methyl (triphenylphosphoranylidene)acetate (0.16 g, 0.47 mmol) was added to a solution of aldehyde **24** (85.5 mg, 0.39 mmol) in toluene (2 mL) and the mixture was refluxed for 22 h. After this time, the mixture was cooled to rt and the solvent was removed under vacuum. Purification by flash chromatography (5:1, hexane–ethyl acetate) afforded the desired product **30** as a pale yellow solid, mp 76–78°C, (98.4 mg, 91%). EI–MS (*m*/*z*, %): 276 ($M^{+\cdot}$, 100), 245 (41). IR (cm^{-1}): 1713 ^{1}H NMR δ: 3.32 (dt, 2H, *J* = 6,5, 1.4 Hz), 3.69 (s, 3H), 3.79 (s, 3H), 5.03–5.07 (m, 2H), 5.87–5.93 (m, 1H), 6.00 (s, 2H), 6.66 (s, 1H), 6.78 (d, 1H, *J* = 16.3 Hz), 7.81 (d, 1H, *J* = 16.3 Hz). ^{13}C NMR δ: 33.6, 51.6, 62.7, 101.8, 110.7, 112.3, 116.0, 121.8, 125.5, 135.0, 137.0, 143.9, 145.6, 151.2, 167.9. HRMS calcd. for $C_{15}H_{16}O_5$: 276.0998; found: 276.0999.

5-Methoxy-4-octyloxy-6-(2-propenyl)-1,3-benzodioxide (31)

A solution of phenol **10** (88 mg), K_2CO_3 (90 mg), and octyl bromide (0.09 mL) in 6 mL of acetone was refluxed for 64 h. The acetone was evaporated and the residue partitioned between water and ether. The yield of **31**, a yellow oil, was 60%. EI–MS (*m*/*z*, %): 320 ($M^{+\cdot}$, 64), 208 (74), 84 (62), 49 (100). ^{1}H NMR δ: 0.87 (t, 3H, *J* = 6.8 Hz), 1.24–1.32 (m, 8H), 1.42–1.45 (m,2H), 1.72–1.75 (m, 2H), 3.29 (dt, 2H), *J* = 6.6, 1.1 Hz), 3.75 (s, 3H), 4.16 (t, 2H, *J* = 6.7 Hz), 5.00–5.04 (m, 2H), 5.85 (s, 2H), 5.87–5.93 (m, 1H), 6.33 (s, 1H). ^{13}C NMR δ: 14.1, 22.6, 25.8, 29.2, 29.3, 30.1, 31.8, 34.0, 61.2, 72.6, 101.0, 102.7, 115.4, 126.0, 136.3, 136.9, 137.5, 144.4, 144.7. HRMS calcd. for $C_{19}H_{28}O_4$: 320.1988; found: 320.1984.

Acknowledgements

Funding was provided by Natural Sciences and Engineering Research Council of Canada (NSERC) (Strategic Program). S.L. Majerus was the recipient of an NSERC PGS A scholarship.

References

1. R. Assabgui, F. Lorenzetti, L. Terradot, C. Regnault-Roger, N. Malo, P. Wiriyachitra, P.E. Sanchez-Vindas, L. San Roman, M.B. Isaman, T. Durst, and J.T. Arnason. *In* Phytochemicals for pest control. ACS Symposium series 658. *Edited by* P.A. Hedin, R.M. Hollingworth, E.P. Masler, J. Miyamoto, and D.G. Thompson. Chap. 4. 1997.
2. J.E. Casida. J. Agri. Food Chem. **18**, 753 (1970).
3. E.P. Lichtenstein, T.T. Liang, K.R. Schultz, H.K. Schnoes, and G.T. Carter. J. Agri. Food Chem. **22**, 658 (1974).
4. (*a*) B. Burke and M. Nair. Phytochemistry, **25**, 1427 (1986); (*b*) J.F. Ciccio and C.M. Ballestero. Rev. Biol. Trop. **45**, 783 (1997).
5. W. Baker and E.H.T. Subrahmanyam. J. Chem. Soc. 1681 (1934).
6. F. Dallacker. Chem. Ber. **102**, 2663 (1969).
7. J.R. Cannon, E.L. Chisalherti, and V. Lojanapiwatna. J. Sci. Soc. Thailand, 59 (1980).
8. G. Casiraghi, G. Casnati, G. Puglia, G. Sartori, and G. Terenghi. J. Chem. Soc. Perkin Trans. **1**, 1862 (1980).
9. M.E. Kurz and G.J. Johnson. J. Org. Chem. **36**, 3184 (1971).
10. P. Capdeville and M. Maumy. Tetrahedron Lett. **23**, 1573 (1982).
11. V. Snieckus. Chem. Rev. **90**, 880 (1990).
12. A.-S. Belzile, S.L. Majerus, C. Podesfinski, G. Guillet, T. Durst, and J.T. Arnason. Pesticide Biochem. Physiol. **66**, 33 (2000).
13. R.H. Grubbs, O. Fu, and G.C. Fu. J. Org. Chem. **59**, 4029 (1994).

© 2000 NRC Canada

Canadian Journal of Chemistry

Author Index
Volume 78, 2000

Revue canadienne de chimie

Index des auteurs
Volume 78, 2000

Abraham, M.H., 184
Abrams, S.R., 963
Acevedo, I.L., 1121
Acree, Jr., W.E., 184, 449, 459
Ahmed, A.R., 1178
Aicken, F.M., 415
Aknin, M., 986
Aliaga, C., 1052
Alibhai, N., 1345
Alper, H., 920
Alvarez-Toledano, C., 1299
Alvaro, G., 809
An, H., 884
Andraos, J., 508
Andreotti, D., 772
Andryukhova, N.P., 1285
Arakawa, H., 291
Arca, M., 1147
Arslan, T., 884
Arya, P., 920
Atay, E., 84, 520
Aue, W.A., 95
Aumelas, A., 248
Back, M.H., 16
Bailey, M., 739
Baisch, G., 892
Ball, J.M., 464
Balsevich, J.J., 963
Balzarini, J., 1081
Baril, J., 490
Batchelor, R.J., 598
Batra, H., 1109
Beck, E.J., 1060
Belzile, N., 51
Benn, M., 542
Bennet, A.J., 577
Berg, D.J., 255, 454
Bernard, G.M., 614
Bernardinelli, G., 280
Bertani, B., 809
Berthet, J.-C., 1305
Bianchi, D.A., 1165
Biondi, S., 772
Birahda, K., 568
Blagoeva, I.B., 84, 520
Blais, P., 10
Bodo, B., 487
Boeré, R.T., 583
Bonhoure, I., 1305
Bossard, A.R., 16
Botta, M., 925
Bottomley, F., 383
Bourque, S.C., 920
Braekman, J.C., 1030
Bridges, C., 1289
Brossard, L., 307
Brown, M.A., 536
Brown, R.S., 1247
Brown, W., 800
Brun, P., 128
Buchanan, G.W., 316
Buncel, E., 474, 1251
Camacho, A.G., 1121
Camerman, A., 26, 1045
Camerman, N., 26, 1045
Cameron, T.S., 118
Cartier dit Moulin, C., 1305
Castan, P., 280
Castellan, A., 73
Chabot, C., 852
Chan, T.H., 776
Chang, J.-C., 224
Chapados, C., 64, 490, 1128
Chapleur, Y., 708
Charlton, J.L., 553
Chênevert, R., 275
Chiltz, F., 307
Chivers, T., 10
Chrusciel, J.J., 1233
Chubb, F.L., 84, 520
Chuca, I., 184
Clarke, C.W., 1
Classon, B., 829
Clement, O., 474
Cobos, J.C., 1272
Collins, C., 151
Corelli, F., 925
Coumbarides, G.S., 935
Couture, P., 356
Couturier, D., 1242
Cow, C., 553
Crasto, C.F., 884
Crespo-Pinilla, M.S., 521
Cristobal-Telésforo, E., 248
Csizmadia, I.G., 362, 395, 626
Curran, D.P., 791
Cyr, A., 307
Dag, Ö., 516
Daloze, D., 1030
Dapporto, P., 723
Das, S.K., 191, 838
Dass, G., 444
Dasser, M., 275
Dawes, R., 1035
De Backer, M., 1242
De Clercq, E., 1081
De Fina, K.M., 184, 449, 459
de Rossi, R.H., 233
De, A.K., 139
Dean, P.A.W., 590
Decken, A., 270
Demartin, F., 1147
Den Auwer, C., 1305
Denmark, S.E., 673
Devillanova, F.A., 1147
Dhawan, R., 784
Di Fabio, R., 809
Dogra, S.K., 191
Dominique, R., 838
Donati, D., 772
Donnadieu, B., 280
Downard, A., 10
Drake, J.E., 1214
Driega, A.B., 316
Drouin, M., 212
D'Sa, R., 1178
Duceppe, J.-S., 739
Dufresne, C., 784
Duran, M., 328
Durst, T., 1345
Dwyer, J.R., 1035
Eames, J., 935
Edward, J.T., 84, 520
Eichele, K., 118, 614
Einstein, F.W.B., 598
Ekelmans, D., 1030
Elguero, J., 1109
El-Hallag, I.S., 1170
El-Hefnawy, G.B., 1170
El-Saidi, M., 356
Enriz, R.D., 626

© 2000 NRC Canada

Ernst, B., 892
Fabre, P.-L., 280
Fattori, D., 925
Faure, R., 986
Fisher, L., 409
Fletcher, K.A., 449
Foster, J., 1019
Foster, K., 800
Fradera, X., 328
Frank, S.A., 757
Franzén, R., 957
Fryzuk, M.D., 1003
Fu, J.-m., 905
Fujita, K., 1089
Fusar-Bassini, D., 925
Futatsuki, K., 1089
Gable, K.P., 704
Galibert, A.M., 280
Gallant, R.T., 1295
Ganguly, T., 139
Garcia de la Fuente, I., 1272
Gauvin, A., 986
Gay, I.D., 598
Gaydou, E.M., 986
Gee, M., 118
Gendron, R.A.L., 255, 454
Genêt, J.-P., 846
Gentile, G., 925
Ghoneim, E.M., 1170
Giacobbe, S., 809
Gibson, H.W., 347
Giesbrecht, G.R., 1003
Girard, C., 816
Glaser, R., 212
Glew, D.N., 1, 1204
González, J.A., 1272
Gough, K.M., 1035
Grand-Maître, C., 739
Graziano, G., 1233
Greedan, J.E., 1289
Green, C.E., 184
Grenier, L., 739
Grzegozek, M., 950
Gu, J.-H., 598
Guérin, B., 852
Guindon, Y., 852
Guthrie, J.P., 1295
Gutiérrez-Pérez, R., 1299
Hallberg, A., 829
Handerson, S., 527
Hecht, S.M., 884
Heilporn, S., 1030
Hempel, A., 26, 1045
Hennigar, T.L., 568
Hernández-Ortega, S., 248
Hinman, A.S., 1318
Hou, X., 963
Hu, Y.-J., 838
Huang, X., 577
Hughes, G., 868
Hum, G., 642
Hursthouse, M.B., 1073
Hussein, S.M.I., 436
Iftime, G., 409
Igarashi, K., 657
Ikariya, T., 697
In, Y., 31
Infante, A.B., 521
Irvine, N., 963
Isaia, F., 1147
Ishitani, H., 666
Jankowski, C.K., 248
Jeanson, P., 307
Jefferson, G.R., 920
Jeffrey, K.R., 46
Jenkins, H.A., 590
Jiang, Z.-H., 322
Jiménez-Estrada, M., 248
Jobe, D.J., 464
Johnson, M., 133
Joly, H.A., 51
Jones, D.H., 1318
Jordan, R.W., 527
Jurkauskas, V., 800
Kabanyane, S., 270
Kagan, H.B., 816
Kagayama, A., 657
Karginov, V.A., 884
Katopodis, A., 892
Katz, M., 1121
Kaufman, T.S., 1165
Kelly, D.G., 1073
Kim, J.-H., 673
Kirby, C.W., 614
Klassen, V., 583
Kliegel, W., 546, 1325
Knaus, E.E., 1081
Kobayashi, S., 666
Koerner, T., 1067
Kresge, A.J., 508
Krishnamoorthy, G., 191
Kumar, D., 1109
Kumar, H., 427
Kvarnström, I., 829
Laikhter, A.L., 884
Lamarque, L., 128
Lamba, D., 925
Laporte, F., 118
Larsen, G., 206
Lautens, M., 868
Lavallée, P., 739
Leblanc, Y., 784
Leclercq, S., 1030
Lee, J., 642
Lee, S.-H., 347
Lelj, F., 1147
Lessard, J., 307
Leung, C., 553
Lewars, E., 297
Leznoff, C.C., 167
Li, H., 51
Liao, D.-Z., 322
Light, M.E., 1073
Lin, A.C., 362
Lin, Y.-S., 224
Lin, Z.-P., 95
Lipari, F., 577
Lippolis, V., 1147
Lissi, E.A., 1052
Littke, A., 784
Liu, P., 133
Liu, X., 1143
Lociuro, S., 772
Lodder, M., 884
López-Cortés, J.G., 1299
Lubkowitz, G., 1325
Machado, A.A.S.C., 1013
MacInnis, J.A., 1222
Mackintosh, N., 800, 852
Madic, C., 1305
MaGee, D.I., 1060
Majerus, S.L., 1345
Mak, M.L., 626
Malonga, H., 291
Manzer, L.E., 920
Marangoni, D.G., 1222
Martel, A.A., 307
Mastropaolo, D., 26, 1045
Mata-Pérez, F., 521
Mathey, F., 118
Matsunaga, S., 31
Max, J.-J., 64, 490, 1128
McClelland, R.A., 1178, 1186
McKillop, A., 1158
Ménard, H., 307
Ménichelli, C., 1128
Meou, A., 128
Merkley, N., 356, 942
Messanga, B.B., 487
Mestres, J., 328
Mislow, K., 41
Mogren, T., 800
Moharram, Y.I., 1170
Moisy, P., 1305
Mukaiyama, T., 657
Nagashima, T., 791
Naithani, R., 1109
Natansohn, A., 409

© 2000 NRC Canada

Neault, J.F., 291
Neverov, A.A., 1247
Nickel, P., 26
Nikitin, K.V., 1285
Nishino, H., 31
Norstrom, T., 963
Novetta-Delen, A., 291
Noyori, R., 697
Ogilvie, W.W., 739, 852
Öhrlein, R., 892
Ohtsu, H., 31
Okanga, F.I., 338
Ollerenshaw, J., 784
Onyido, I., 474
Ortega-Alfaro, M.C., 1299
Oscarsson, K., 829
Overman, L.E., 732
Ozturk, T., 1158
Padwa, A., 749
Pain, G., 772
Pal, A., 427, 444
Palepu, R., 151, 1222
Paoli, P., 723
Paquette, L.A., 689
Parvez, M., 10
Pedras, M.S.C., 338
Pedrosa, G.C., 1121
Pena, C., 280
Penieres-Carrillo, G., 1299
Penner, G.H., 46
Pennington, L.D., 732
Perczel, A., 395
Pincock, A.L., 1019
Pincock, J.A., 1019
Pinto, B.M., 598
Plehiers, M., 1030
Poirier, R.A., 1067
Pojarlieff, I.G., 84, 520
Pokriefke, J.O., 546, 1325
Popelier, P.L.A., 415
Postigo, M.A., 1121
Poupart, M.-A., 739
Qian, Y., 1143
Qiao, Z., 1143
Rajalingam, U., 590
Ratovelomanana-Vidal, V., 846
Reger, T.S., 749
Ren, D., 1178
Rettig, S.J., 546, 1003, 1325
Rey, F., 1013
Reyes-Chilpa, R., 248
Rifai, S., 1019
Rigo, B., 1242
Rivkin, A., 791
Roberts, E., 800
Rochon, P., 409
Roelens, S., 723
Roscoe, J.M., 16
Roush, W.R., 757
Roy, R., 838
Rozas, I., 1109
Ruffin, B., 73
Salpietro, S.J., 362, 626
Samuelsson, B., 829
Sanchez, C., 1186
Sanchez, V., 383
Sangermano, M., 1030
Sanipelli, G.G., 464
Schmid, R., 265
Sham, S., 975
Shanmugham, M.S., 704
Shao, P., 255
Sharma, S., 427
Sharp, T.L., 184
Shaver, M.P., 568
Shiftan, D., 212
Short, III, G.F., 884
Shvedov, D., 151
Sibi, M.P., 133
Sikorski, M., 963
Simoneau, B., 739
Singh, S.P., 1109
Sinha, H.K., 963
Smadja, J., 986
Smolik, M., 993
Snieckus, V.A., 905
Sondengam, B.L., 487
Sosa, C.P., 395
Soula, B., 280
Spurgin, M.A., 184
St-Denis, Y., 776
Steer, R.P., 963
Stephenson, C.R.J., 800
Strunz, G.M., 270
Sumi, K., 697
Sun, B.-W., 322
Sung, K., 562
Surylo, P., 950
Şüzer, S., 516
Tae, J., 689
Taillefumier, C., 708
Tajmir-Riahi, H.A., 291
Tam, W., 527
Tanaka, K.S.E., 577
Tanaka, R., 31
Taylor, S.D., 642
Tee, O.S., 436, 1100
Thavonekham, B., 739
Thompson, K.A., 1019
Thompson, R.C., 383
Tobin, J., 151
Tokuda, H., 31
Tokuhisa, K., 238
Toner, A.J., 1073
Torres-Collín, L., 248
Toscano, R.A., 1299
Toteva, M.M., 84, 520
Tranmer, G.K., 527
Tremaine, P.R., 151
Trimble, L.A., 784
Tripathy, S., 1345
Trotter, J., 546, 1325
Tsou, N.N., 784
Tsuzuki, H., 238, 1089
Tuck, D.G., 536
Turner, I.E., 436
Van Calsteren, M.R., 248
Van, T., 449, 459
Vank, J.C., 395
Veglia, A.V., 233
Venneri, P.C., 1194
Verani, G., 1147
Vogels, C.M., 568
Wachner, A.M., 46
Wagner, B., 892
Wallbank, A.I., 568
Wang, B.-C., 224
Wang, G.-L., 322
Wang, H.-G., 322
Wang, P.-Y., 224
Wang, S., 975, 1289
Wang, Y., 1067
Wang, Z.-X., 1081
Warkentin, J., 356, 942, 1194
Wasylishen, R.E., 118, 614
Waterlot, C., 1242
Weerassooriya, N., 935
Westaway, K.C., 1067
Westcott, S.A., 568
White, J.D., 704
Wiebe, L.I., 1081
Wienberg, N., 41
Williams, P., 542
Winkler, T., 892
Wolmershäuser, G., 583
Womiloju, O.O., 383
Wong, A., 975
Wooler, K., 642
Works, A.B., 757
Wozniak, M., 950
Wren, J.C., 464
Wu, G., 118, 614, 975
Xie, Y., 1143
Xu, J., 1143
Xu, Z., 383
Yadav, V.K., 542
Yamashita, Y., 666
Yamato, T., 238, 1089

© 2000 NRC Canada

Yan, S.-P., 322
Yang, H., 800
Yang, J., 1214
Yao, X.-K., 322
Yap, G.P.A., 316
Yazbeck, O.J., 436, 1100
Yip, C., 527
Yu, C.-M., 270
Zaworotko, M.J., 568
Zhang, Y., 1289
Zhao, Q.-H., 322
Zhou, X.-M., 598
Zhu, J., 577
Zhu, Y., 1143
Ziegler, T., 265
Zunic, V., 868

© 2000 NRC Canada

IUPAC Recommendations

Macromolecular Division
Commission on Macromolecular Nomenclature

Generic source-based nomenclature for polymers

Synopsis

The commission has already published two documents on the source-based names of linear copolymers and nonlinear polymers; however, in some cases this nomenclature leads to ambiguous names. The present document proposes a generic source-based nomenclature that solves these problems and yields clearer source-based names. A generic source-based name comprises two parts: (1) a polymer class (generic) name followed by a colon; and (2) the actual or hypothetical monomer name(s), parenthesized in the case of a copolymer.

The formula, the structure-based name, the source-based name, and the generic source-based name are given for each example in the document. In some cases, only generic source-based nomenclature gives unambiguous names — for example, when a polymer has more than one name or when it is obtained through a series of intermediate structures. The rules concern mostly polymers with one or more types of functional group or heterocyclic system in the main chain, but to some extent they are also applicable to polymers with side-groups, carbon-chain polymers such as vinyl or diene polymers, spiro and cyclic polymers, and networks.

Comments on these recommendations are welcome and should be submitted by February 28, 2001 to Prof. Ernest Maréchal, Laboratoire de Synthèse Macromoléculaire, Université Pierre et Marie Curie (Paris VI), Boîte 184 - Tour 54, 4e étage, 4 place Jussieu, F-75252 Paris CEDEX 05, France. Telephone: +33-1-44-27-38-04. Fax: +33-1-44-27-70-54. e-mail: marechal@ccr.jussieu.fr

A copy of the full recommendation is available from Dr. J.W. ApSimon, Vice-President (Research and External), Carleton University, 1125 Colonel By Drive, Ottawa, Ontario, Canada, K1S 5B6. Telephone: (613) 520-3570. Fax: (613) 520-2689.

Analytical Chemistry Division
Commission on Separation Methods in Analytical Chemistry

The hold-up volume concept in column chromatography

Synopsis

Revised recommendations are presented for the nomenclature of the *hold-up volume* in chromatography, updating those originally presented in the IUPAC document *Nomenclature for Chromatography (IUPAC Recommendations 1993)* (Pure Appl. Chem. **65**, 819 (1993)). A number of related and derived definitions for retention parameters are described, including a definition of the term "chromatographic system". The paper also compares methods used in the literature to determine the hold-up volume.

Comments on these recommendations are welcome and should be submitted by February 28, 2001 to Prof. José Antonio García Domínguez, Institute of Physical Chemistry "Rocasolano", Calle Serrano 119, E-28006 Madrid, Spain. Telephone: +34-91-651-9400. Fax: +34-91-564-2431. e-mail: jagd@iqfr.csic.es

A copy of the full recommendation is available from Dr. J.W. ApSimon, Vice-President (Research and External), Carleton University, 1125 Colonel By Drive, Ottawa, Ontario, Canada, K1S 5B6. Telephone: (613) 520-3570. Fax: (613) 520-2689.

© 2000 NRC Canada

Analytical Chemistry Division
Commission on Separation Methods in Analytical Chemistry

Retention parameters in gas chromatography

Synopsis

This paper presents a revision of terms in Chapter 3.6 The Mobile Phase and Chapter 3.7 Retention Parameters in Column Chromatography in *Nomenclature for Chromatography (IUPAC) Recommendations 1993)* (Pure Appl. Chem. **65**, 819 (1993)), with the aims of: (*i*) emphasizing the physical meaning of the terms; and (*ii*) specifying the temperatures and pressures for the terms for gas volumes and flow rates. A number of the original terms were found to be misleading or superfluous, including such terms as *corrected retention time*, *net retention time*, *total retention volume (time)*, *specific retention volume at 0°C*, *relative pressure*; and their usage is strongly discouraged. Chapter 1.1 Basic Definitions was supplemented with the terms *chromatographic system* and *chromatographic process*.

Comments on these recommendations are welcome and should be submitted by February 28, 2001 to Prof. Vadim A. Davankov, Institute of Organo-Element Compounds, Russian Academy of Sciences, Vavilov Street 28, RU-117813 Moscow, Russia. Telephone: +7-095-135-6471. Fax: +7-095-135-6471. e-mail: davank@ineos.ac.ru

A copy of the full recommendation is available from Dr. J.W. ApSimon, Vice-President (Research and External), Carleton University, 1125 Colonel By Drive, Ottawa, Ontario, Canada, K1S 5B6. Telephone: (613) 520-3570. Fax: (613) 520-2689.

© 2000 NRC Canada

PREVIEW / APERÇU

Forthcoming special issues / Numéros spécials à paraître

November 2000	In honour of Professor A. Brook
June 2001	In honour of Professor B. James
November 2001	In honour of Professor V. Snieckus

Forthcoming articles / Articles à paraître

Synthesis and reactivity of the stable silylene *N,N′*-di-*tert*-butyl-1,3-diaza-2-sila-2-ylidene	M. Haaf, T.A. Schmedake, B.J. Paradise, and R. West
Reactions of the stable bis(amino)silylene Si[{N((CH$_2$*t*Bu)}$_2$C$_6$H$_4$-1,2] with group 3 or lanthanide metal organic compounds. Crystal structures of [Ln(η^5-C$_5$H$_5$)$_3$Si{[N(CH$_2$*t*Bu)]$_2$C$_6$H$_4$-1,2}]·C$_7$H$_8$ (Ln = Y or Yb)	X. Cai, B. Gehrhus, P.B. Hitchcock, and M.F. Lappert
A novel route to chlorodimethylsilane	J.J. Chruściel
Reduction of conjugate double bonds with trichlorosilane	M. Chauhan and P. Boudjouk
The one- and two-photon photochemistry of benzylsilacyclobutanes, acyclic benzylsilanes, and 1,1,2-triphenylsilacyclobutane	W.J. Leigh and T.R. Owens
Alkoxides of *o*-silyl benzyl alcohols in cleavage reactions: approaches to benzyl and silyl anion equivalents	P.F. Hudrlik, J.O. Arango, Y.M. Hijji, C.O. Okoro, and A.M. Hudrlik
Dehydrocoupling reactions of hydrosilanes with group 4 metallocenes Cp$_2$MY$_2$ (M = Ti, Zr, Hf; Y = F, OPh, NMe$_2$)	Q. Wang and J.Y. Corey
Trichlorovinylsilane, lithium-*tert*-butyl, and 1,3-enynes: a versatile combination for the competitive formation of silacyclobutanes and silacyclobutenes	N. Auner, M. Grasmann, B. Herrschaft, and M. Hummer
Neutral hyperconjugation and one-bond couplings between heavy atoms	J.B. Lambert, C.E. Shawl, and E. Basso
Improved simple synthesis of cyclic sulfates from trimethylsilyl chlorosulfonate	A.R. Bassindale, I. Katampe, and P.G. Taylor
Formation of organosilicon compounds 117: *C*-brominated 1,3,5-trisilacyclohexanes and their reactions with BuLi	G. Fritz, M. Keuthen, F. Kirschner, E. Matern, H. Goesmann, K. Peters, E.-M. Peters, and H.G. von Schnering
The photolysis of Si,Si-di-*tert*-butyltetramesitylsiladigermirane in the presence of methylmagnesium iodide	M.S. Samuel, K.M. Baines, and D.W. Hughes
Di[(hydroxyalkyl)dimethylammonium] tris[benzene-1,2-diolato(2–)]silicates and their germanium analogs: syntheses, crystal structure analyses, and NMR studies	R. Tacke, A. Stewart, J. Becht, C. Burschka, and I. Righter
Metal-supported catalysts obtained by sol-gel in the hydrosilylation of phenylacetylene with R$_3$SiH organosilanes (R$_3$ = Ph$_3$, Ph$_2$Me, and PhMe$_2$)	R. Jiménez, J.M. López, and J. Cervantes
Photolysis of tris(trimethylsilyl)silane: trapping of sisyl radicals	M. Mohamed and M.A. Brook
Addition reactions of a dialkyl- and a diarylsilylene to cyanides RCN: different pathways?	M. Weidenbruch, F. Meiners, and W. Saak
Preparation and characterization of organic–inorganic hybrid materials incorporating diphosphino moieties. Study of the accessibility of the phosphorus atoms included into the material	J.-P. Bezombes, C. Chuit, R.J.P. Corriu, and C. Reyé
Adducts of sila-, germa-, and stannaethenes (Me$_2$E=C(SiMe$_3$)$_2$) (E = Si, Ge, Sn) with anthracene: syntheses, structures, thermolyses	N. Wiberg, S. Wagner, S.-K. Vasisht, and K. Polborn
Bis(trimethylsilyl)methylamine (BSMA): tool or toy?	J.-P. Picard

© 2000 NRC Canada

The insertion of germylene into the H—H bond; rate constant limits and thermochemistry. Ab initio and DFT calculations on the reactions of GeH_2 and SiH_2 with H_2 — R. Becerra, S.E. Boganov, M.P. Egorov, V.I. Faustov, O.M. Nefedov, and R. Walsh

On the possible formation of Si=O, Si=S, and Si=Se double bonds via the reaction of silylenes with oxirane, thiirane, and selenirane, respectively. An ab initio theoretical study — Y. Apeloig and S. Sklenak

Geminal bis(hypersilyl) compounds — the synthesis and structure of bis[tris(trimethylsilyl)silyl]silanes — T. Gross, H. Reinke, and H. Oehme

A low-temperature reversible phase transition for 1,1′-bis-(ferrocenyldimethylsilyl)ferrocenylene ($(\eta^5\text{-}FcSiMe_2C_5H_4)_2Fe$). An oligomeric model for silyleneferrocenylene polymers — M. Yu. Antipin, I.I. Vorontsov, I.I. Dubovik, V. Papkov, F. Cervantes-Lee, and K.H. Pannell

Photolysis of tris(trimethylsilyl)silane: trapping of sisyl radicals

Mustafa Mohamed and Michael A. Brook

Abstract: The photolysis of tris(trimethylsilyl)silane (TTMSS) was studied in the absence and in the presence of added trapping agents such as alkenes and alcohols. It was found that, unlike the case with pyrolysis, silyl radicals rather than silylenes are produced. They may be efficiently trapped with alkenes, to give the hydrosilylation products, but not with alcohols. The major product from the photolysis of TTMSS in the absence of added trapping agent (or with alcohols as trapping agents) was tetrakis(trimethylsilyl)silane. Possible mechanisms to account for the photoproducts are presented.

Key words: hydrosilane, photolysis, silylenes, silyl radical, sisyl hydride.

Résumé : On a étudié la photolyse du tris(triméthylsilyl)silane (TTMSS) en l'absence et en présence d'agents de piégeage tels les alcènes et les alcools. On a trouvé qu'il se forme des radicaux silyles plutôt que des silylènes contrairement à ce qui se passe lors de la pyrolyse. Ces produits peuvent être piégés efficacement avec des alcènes, mais pas avec les alcools, pour donner des produits d'hydrosilylation. Le produit majoritaire de la photolyse du TTMSS en l'absence d'agents de piégeage (ou avec des alcools comme agents de piégeage) est le tétrakis(triméthylsilyl)silane. On présente un mécanisme possible qui justifie la formation des produits observés.

Mots clés : hydrosilane, photolyse, silylènes, radical silyle, hydrure de silyle.

[Traduit par la Rédaction]

Introduction

Unlike their carbon analogues, and in spite of the absence of π bonds, catenated oligosilanes are UV-active molecules. The long wavelengths of maximum UV absorption, which increase dramatically with chain length before levelling off at about 320 nm (for poly(dimethylsilylene), (1), have been attributed to extended σ conjugation (2). Even longer UV absorptions accompany polysilanes with appropriate (π-conjugating) substituents.

The chemistry of oligosilanes that can be initiated photochemically is indeed rich (3). The photoinduced silyl group rearrangement of oligosilanes led to the isolation of the first stable silicon–carbon double bond (4); many related sigmatropic photorearrangements of oligosilanes are known (for some selected examples, see ref. 5). In the absence of receptor functional groups to which they can rearrange, oligosilanes undergo photodecomposition via both silyl radical and silylene intermediates (6–9). These reactive species may be trapped by a variety of reagents, the most useful of which include hydrosilanes (R_3SiH), alcohols, and dienes for the silylenes, and alkenes for the silyl radicals (8).

Synthetically, one of the most useful oligosilanes is tris(trimethylsilyl)silane (sisyl hydride, TTMSS). Due in part to the relative weakness of the hydrogen–silicon bond in this molecule (ca. 85 kcal mol^{-1}, (10) the molecule can be used under radical conditions to reduce a wide variety of organic functional groups including alkyl halides, carbonyl groups, xanthates, etc. The compound also undergoes facile hydrosilylation with isolated alkenes and hydrosilylative coupling of α,ω-dialkenes (Scheme 1).

We have recently reported the use of the tris(trimethylsilyl)silyl group (sisyl) as a photoremovable protecting group for alcohols (11). The sisyl ethers undergo photodecomposition primarily via silylenes (12) as shown by trapping experiments; the regiochemistry of decomposition is affected by the steric bulk on the alcohol (Scheme 2, (13)). We were interested in establishing if sisyl hydride ($(Me_3Si)_3SiH$) could similarly be induced to undergo photodecomposition by silylene routes, as this would be complementary to the radical chemistry noted above. In this paper we describe studies of the photochemical decomposition of sisyl hydride on its own and in the presence of various trapping agents.

Results

Tris(trimethylsilyl)silane (**1**), tris(trimethylsilyl)methylsilane (**2**), and tetrakis(trimethylsilyl)silane (**3**) were prepared by the method of Gilman and Harrel, Jr. (14). Photolyses were undertaken in a Rayonet reactor with irradiation at 254 nm using low pressure mercury lamps. Major

Received August 20, 1999. Published on the NRC Research Press website on October 18, 2000.

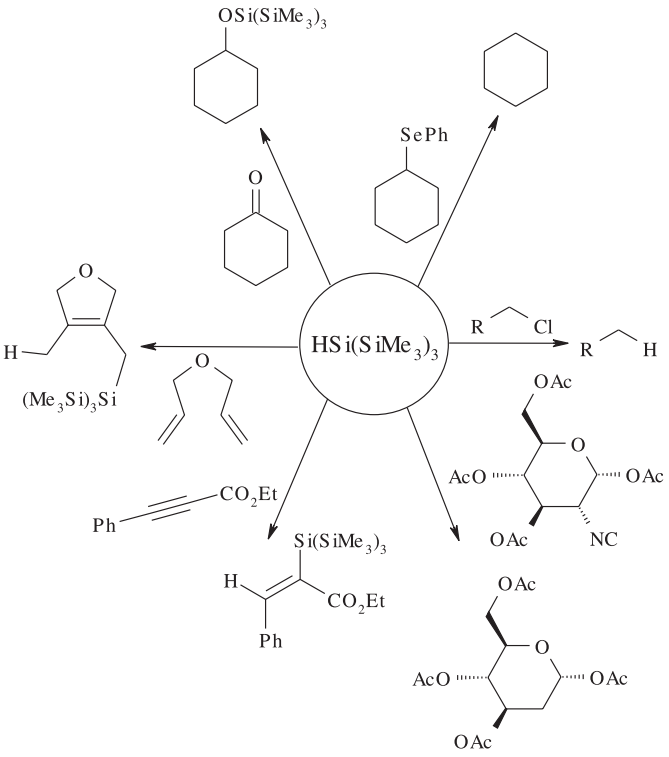
Dedicated to Professor Adrian Brook for his seminal contributions to organosilicon chemistry.

M. Mohamed and M.A. Brook.[1] Department of Chemistry, McMaster University, 1280 Main St. W., Hamilton, ON L8S 4M1, Canada.

[1]Author to whom correspondence may be addressed. Telephone: (905) 525-9140 ext. 23483. Fax: (905) 522-2509. e-mail: mabrook@mcmaster.ca

© 2000 NRC Canada

Scheme 1.



products and (some) minor products were identified by comparison of retention time and GC–mass spectra with those of authentic samples.

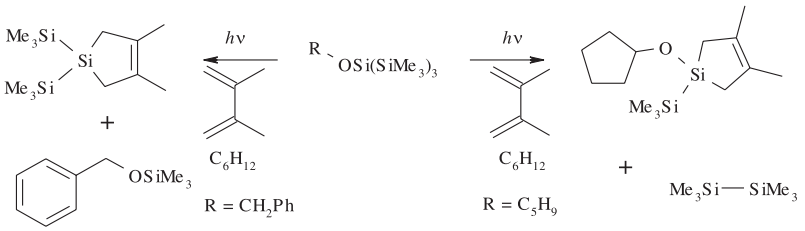
Photolyses of TTMSS

When a hexane solution of TTMSS was photolyzed over 8 h in the absence of added traps, GC–MS analysis of the volatile products showed formation of three different products and the presence of a great deal of residual starting material (78%). The major products are **2** and **3**; their identities were confirmed by comparison with authentic samples (Scheme 3). The formation of such products could be consistent with the intermediacy of either silylenes or silyl radicals. To throw light on this, TTMSS was photolyzed in the presence of alkenes and alcohols, which are known to be excellent traps for silyl radicals and silylenes, respectively.

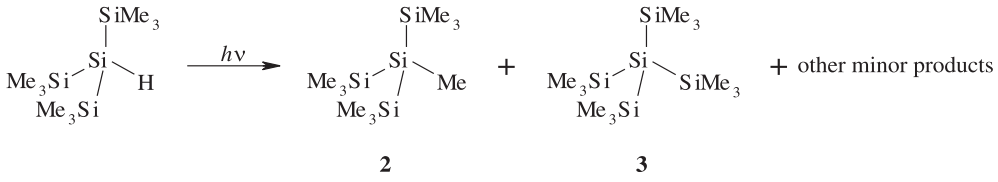
Reaction with alkenes

The radically induced hydrosilylation of alkenes using TTMSS has been reported previously (15). To establish whether these reactions could similarly be photoinduced, the reaction of TTMSS with a series of alkenes was examined in hexane at room temperature in the absence of any radical initiators such as AIBN. The hydrosilylation products were obtained in good yield in less than 3 h of photolysis time, in all cases (Scheme 4).

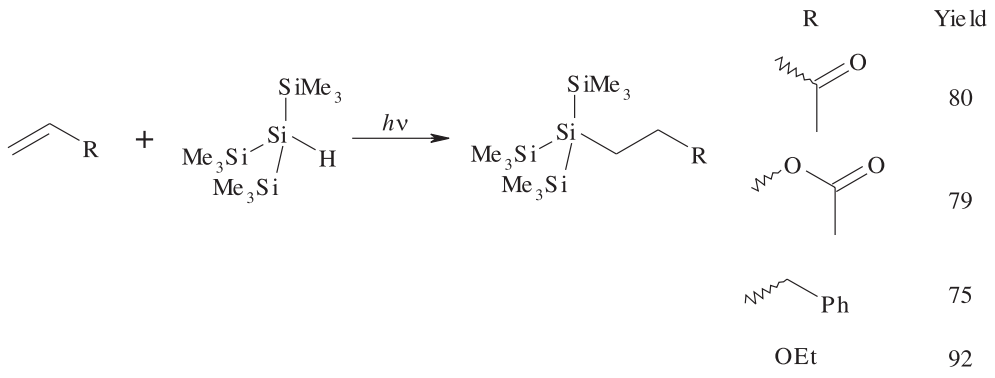
Scheme 2.



Scheme 3.

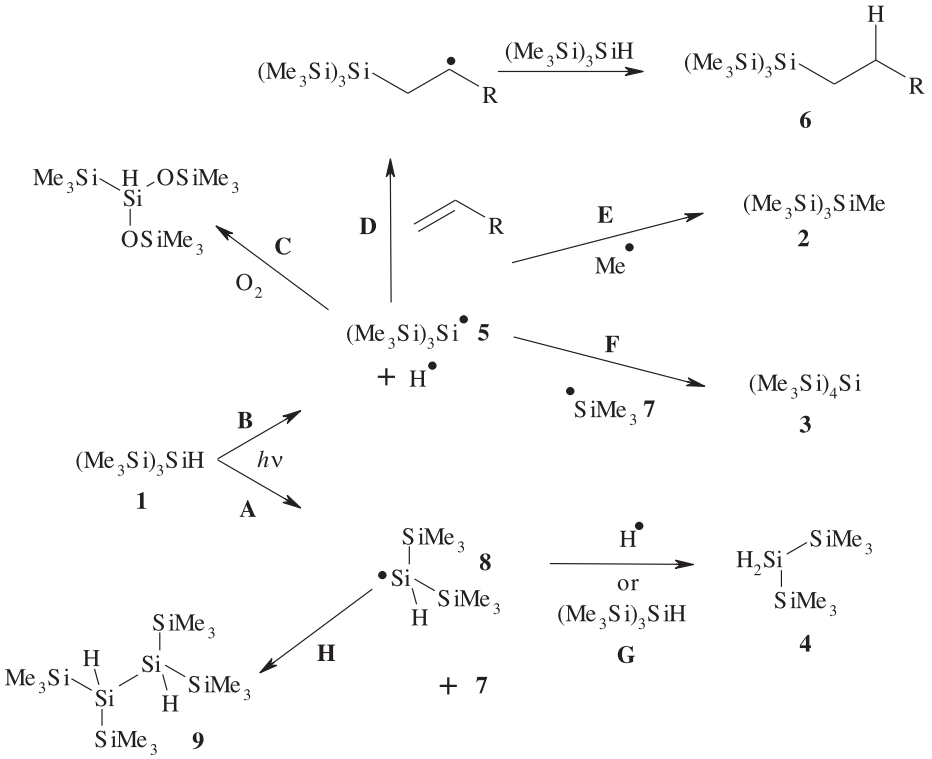


Scheme 4.



© 2000 NRC Canada

Scheme 5.



Reaction with alcohols

The photolysis of TTMSS in the presence of cyclopentanol was not very efficient; after 24 h mostly starting material (80%) remained. The major products included $(Me_3Si)_4Si$ (**3**), $(Me_3Si)_2SiH_2$ (**4**), $(C_5H_9O)SiMe_3$, and two others that have not yet been conclusively identified. In addition, the product of autoxidation of TTMSS, $(Me_3SiO)_2SiH(SiMe_3)$, previously described by Chatgilialoglu et al. (16), was also observed (Scheme 5, Path C). The latter product was also detected when methanol was used as a trap, but in none of the other experiments performed.

Photoreactions in the presence of methanol were similarly inefficient. After 2.5 h more than seven different volatile products with a total yield of less than 10% were present; the remaining 90% was unreacted starting material. Analysis of the products was complicated by the fact that few of the products showed a molecular ion in the mass spectrum. Three of the detected products were similar to those observed from the photolysis of TTMSS in the absence of added trapping agent: **2**, **3**, and **4** (Scheme 5). With prolonged photolysis of 24 h, over 80% of TTMSS remained. The character of the remainder of the GC–MS trace was, however, profoundly different than that from the shorter reaction time. Most of the volatile photoproducts had disappeared, and there was a concomitant increase in the relative concentration of $Si(SiMe_3)_4$.

Discussion

The behaviour of TTMSS in the presence of alkenes, activated by photolysis, exactly mirrors the chemistry that takes place in the presence of radical initiators. Silyl radical hydrosilylation to form the terminal sisylalkane in good yield is observed. The process is efficient, going to completion within 3 h. There is no evidence of chemistry occurring via the intermediacy of silylenes.

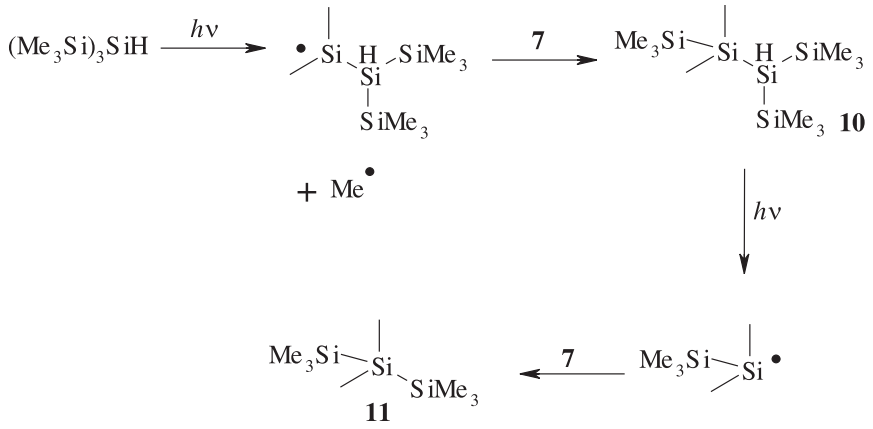
When a radical trap, such as an alkene, is not present, TTMSS is presented with fewer accessible reaction pathways, and instead reacts inefficiently via silyl radicals to generate a myriad of photoproducts. The most stable of these, as evidenced by its increasing significance during the photolyses over time, is **3**.

Gaspar et al. (12) observed degradation via silylene intermediates during the pyrolysis of TTMSS; a major product was $(Me_3Si)_3Si\text{-}Si(SiMe_3)_2H$ which, as noted by them, could have its origins either in the silylene:$Si(SiMe_3)_2$ or the disilene $(SiMe_3)_2Si{=}Si(SiMe_3)_2$ derived from the silylene. No evidence for compounds of this type was obtained in the photolysis of TTMSS in the absence of trapping agents. Similarly, no evidence of trapping of silylenes by alcohols to form hydroalkoxysilanes (8) was observed. All this evidence, in addition to the radical hydrosilylation noted above, is consistent with radical formation as the predominant reaction for TTMSS under photolysis (9).

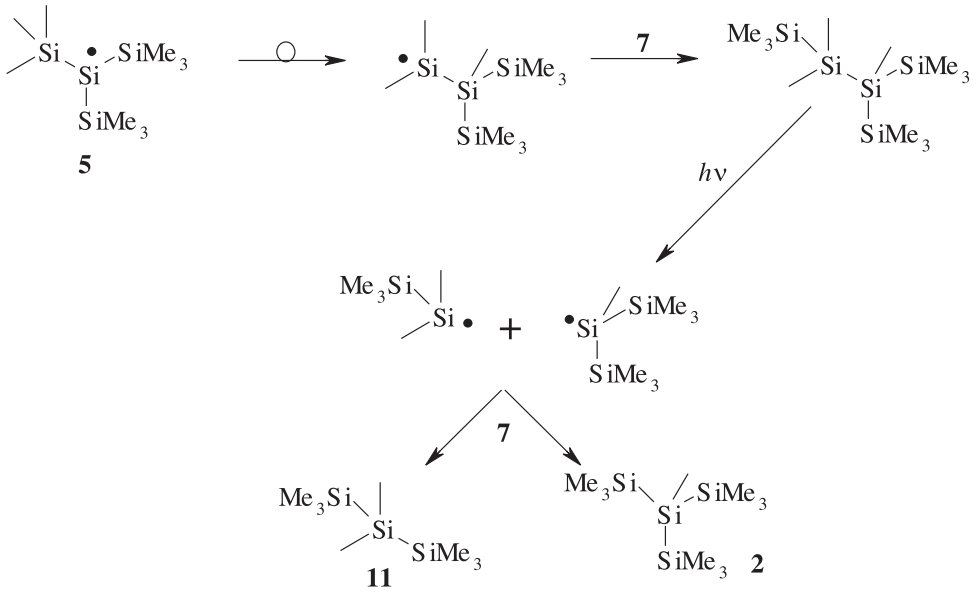
The presence of $Si(SiMe_3)_4$ as a major product in the absence of efficient radical traps such as alkenes can be explained by the following mechanism. Primary photocleavage of the relatively weak Si—H bond (85 kcal mol^{-1}, (7)), provides the sisyl radical **5** (Scheme 5, Path B). In the presence of alkenes, radical chain hydrosilylation is initiated, to give the products **6** shown in Path D, Scheme 5. In the absence of such traps, the sisyl radical can, among other reactions,

© 2000 NRC Canada

Scheme 6.



Scheme 7.



recombine with (adventitious) methyl (Path E → **2**) or trimethylsilyl radicals **7** (Path F → **3**), also likely generated from TTMSS (Path A), which is present throughout the photolyses in relatively high concentration. Hydrogen abstraction by the sisyl radical from TTMSS is, of course, a transparent reaction. The generation of **8** in Path A (Scheme 5) can also account for the formation of **4** via $H^{\cdot}$ recombination or abstraction from TTMSS (Path G). **8** can also lead to $(Me_3Si)_2Si(H)Si(H)(SiMe_3)_2$ (**9**) by dimerization (Scheme 5, Path H).

The most difficult molecules to account for mechanistically are the mono- and dimethylated compounds **2**, **10**, and **11**, respectively. The photocleavage of a Si-Me group is not very favourable. However, as noted this mechanism could account for the formation of **2** (Scheme 5, Path E) and compounds **10** and **11** (Scheme 6). A more reasonable proposal involves 1,2-methyl migration from **5** to give new oligosilanes that can then fragment to react with (readily available) $Me_3Si^{\cdot}$ to produce **2** and **11** (Scheme 7). It should be reiterated that these are mechanistic speculations; other mechanisms involving recombination and rearrangements are also possible. However, compounds derived from silylenes, which would have been particularly easy to identify in the photolyses in the presence of alcohols (11, 13), were not detected.

$(Me_3Si)_4Si$ was observed to be a major photoproduct and, over more extensive photolysis, the dominant photoproduct of TTMSS in the absence of trapping agents. This suggests that $(Me_3Si)_4Si$ does not easily undergo photoinduced degradation, particularly when compared with the other photoproducts. That is, the other photoproducts undergo further preferential photolysis or reaction with the dominant radicals $(Me_3Si)_3Si^{\cdot}$, $H^{\cdot}$, and $Me_3Si^{\cdot}$, eventually to give nonvolatile oligo- or polysilanes (2). The lack of photoreactivity of $(Me_3Si)_4Si$ has previously been shown, at least in the absence of photosensitizers (17).

These experiments indicate that TTMSS readily participates in radical reactions that are synthetically useful, particularly

© 2000 NRC Canada

when radical traps such as alkenes are present. However, the photochemical formation of silylenes from TTMSS could not be observed in the presence of standard silylene traps.

Experimental section

^1H and ^{13}C NMR spectra were recorded on a Bruker AC-200 spectrometer with $CDCl_3$ or C_6D_6 as an internal standard. IR spectra were recorded on a Biorad spectrometer. Electron impact (EI) and chemical ionization (CI, NH_3) mass spectra were recorded at 70 eV with a source temperature of 200°C on a VG Instruments analytical ZAB-R mass spectrometer equipped with a VG 11–250 data system.

Gas chromatographic (GC) analyses were carried out using a Hewlett–Packard 5890A gas chromatography equipped with a conventional heated injector, a flame ionization detector, a Hewlett–Packard 3393A integrator, and a DB-1 megabore capillary column (30 m × 0.54 mm, Chromatographic Specialties, Inc.). Mass spectra and GC–MS analyses were recorded on a Hewlett–Packard 5890II gas chromatograph equipped with a HP-5971A mass selective detector and a DB-5 fused silica capillary column (30 m × 0.25 mm, Chromatograph Specialties, Inc.). All syntheses were performed with dry glassware under an atmosphere of anhydrous nitrogen. Prior to photolysis, all the solutions were degassed with dry argon.

With the exception noted below, all reagents were purchased from Aldrich: vinyl acetate, ethyl vinyl ether, methyl vinyl ketone, allylbenzene, diethyl ether, chlorotrimethylsilane, MeMgBr, MeLi-Br hexane (Omni solvent), and THF. THF was distilled from benzophenone ketyl just before to use. Silicon tetrachloride was purchased from Gelest. $(Me_3Si)_4Si$, $(Me_3Si)_3SiH$, and $(Me_3Si)_3Me$ (14) were prepared by standard literature routes or are commercially available (Gelest).

Photolyses

With alkenes: hydrosilylation

A mixture of alkene and 1.2 equiv. of silane in a quartz tube was irradiated for 3 h in a Rayonet photochemical reactor equipped with low pressure mercury lamps emitting 254 nm radiation.

1-[Tris(trimethylsilyl)silyl]ethyl acetate: Vinyl acetate (0.53 g, 62 mmol), TTMSS (1.8 g, 7.4 mmol), hexane (10 mL); product was purified on silica gel (petroleum ether, 1.64 g, 79%). MS (EI, *m*/*z* (%)): 319 (M^+-15 (1.0)), 291 (3.2), 275 (4.2), 233 (39), 191 (33), 174 (20), 73 (100), 43 (50). IR (cm^{-1}) ν: 2954, 2897, 1742, 1247, 1046. ^1H NMR (300 MHz, C_6D_6) δ: 4.27–4.22 (t, 2H, *J*= 8), 1.70 (s, 3H), 1.32–1.26 (t, 2H), 0.17 (s, 27 H). ^{13}C NMR (MHz, C_6D_6) δ: 170.05, 64.60, 20.78, 8.9, 0.98.

2-(Ethoxy)-1-[tris(trimethylsilyl)silyl]ethane: Ethyl vinyl ether (0.35 g, 5 mmol), TTMSS (1.5 g, 6 mmol), hexane (10 mL); product was purified on silica gel (petroleum ether, 1.47 g, 92%). MS (EI, *m*/*z* (%)): 305 (M^+-15 (1.6)), 275 (0.5), 247 (2.1), 219 (12), 191 (12), 131 (11), 117 (15), 73 (100), 45 (27). IR (neat) ν: 2951, 2895, 2861, 1245, 1122, 1097. ^1H NMR (200 MHz, C_6D_6) δ: 3.53–3.47 (t, 2 H, *J*= 6), 3.35–3.28 (q, 2 H, *J* = 4), 1.28–1.22 (t, 2 H *J*= 6), 1.15–1.10 (t, 3H, *J*= 6), 0.20 (s, 27 H). ^{13}C NMR (50.3 MHz, C_6D_6) δ: 70.52, 65.83, 15.52, 9.81, 1.31.

3-Oxo-1-[tris(trimethylsilyl)silyl]butane: Methyl vinyl ketone (0.46 g, 6.6 mmol), TTMSS (1.9 g, 7.9 mmol), hexane (10 mL); product was purified on silica gel (petroleum ether, 1.58 g, 80%). IR (neat) ν: 2951, 2895, 1720, 1409, 1356, 1245, 840, 623. ^1H NMR (200 MHz, C6D6) δ: 2.38–2.32 (m, 2 H), 2.05 (s, 3 H), 0.96–0.91 (m, 2 H), 0.08 (s, 27H). ^{13}C NMR (50.3 MHz, C_6D_6) δ: 209.0, 42.65, 28.99, 1.45, 1.24. MS (EI, *m*/*z* (%)): 303 (M^+-15, 2.6), 245 (18), 191 (8), 175 (8), 131 (12), 117 (19), 73 (100), 45 (24).

3-Phenyl-1-tris(trimethylsilyl)silylpropane: Allylbenzene (0.96 g, 8.1 mmol), TTMSS (2.4 g, 9.7mmol), and 20 mL of hexane was placed in a quartz cell. After 8 h of photolysis, the reaction mixture was concentrated in vacuo, and the product purified on silica gel (5% ethyl acetate–hexane) to give (0.72 g, 75%). MS (EI, *m*/*z*): 366 (5.0), 351 (3.0), 293 (40), 219 (8.0), 204 (6.0), 175 (71), 117 (20), 73 (100). IR ν (cm^{-1}): 3086, 3064, 3028, 2950, 2894, 2856, 1604, 1496, 1453, 1397, 1245, 1069, 835, 746, 695, 623. ^1H NMR (200 MHz, $CDCl_3$) δ: 7.18 (m, 5 H, Ph), 2.61 (t, 2 H, *J* = 7), 1.68 (dd, 2 H, *J* = 7 and 4), 0.12 (s, 27 H $(CH_3)_3Si)_3$). ^{13}C NMR (50.3 MHz, $CDCl_3$) δ: 142.3, 128.4, 128.2, 125.6, 40.49, 30.91, 7.42, 1.15.

Without traps

A solution of TTMSS (0.30 g, 1.2 mmol) in hexane 10 mL was irradiated for 2 h to 20% conversion in the absence of added trapping agent. GC–MS analysis of the crude mixture led to many products in which the major product is $(Me_3Si)_4Si$, (4%, refers to GC area%, Table 1).

With alcohols as traps

Photolysis of TTMSS in the presence of methanol for 2.5 h: $(Me_3Si)_3SiH$ (90%), $(Me_3Si)_2SiH_2$ (0.8%) MS: 176 (M^+), 162, 161, 131,117, 101, 88, 73; $(Me_3SiO)_2Si(H)SiMe_3$ (1.5%) MS: 280 (6.4), 265 (6.4), 207 (47), 191 (100), 177 (18), 147 (14), 133 (18), 117 (18), 103 (4.3), 73 (21); $(Me_3Si)_3SiMe$ (**2**) (0.3%), $(Me_3Si)_4Si$ (**3**) (0.6%).

Prolonged photolysis of TTMSS in the presence of MeOH over 24 h led to the formation of two products: **3** (92%), unidentified product (5%), GS–MS: 353 (13), 264 (91), 235 (26), 219 (38), 205 (73), 189 (18), 175 (43), 159 (9), 131 (38), 117 (27), 89 (18), 73 (100), 59 (34), and TTMSS (3%).

A solution of TTMSS (0.248 g, 1.0 mmol) in hexane (10 mL) was photolyzed in the presence of cyclopentanol (0.086 g, 1 mmol) for 2.35 h. Six major products were produced: **3** (2.5%,), **4** (3%, for mass spectral data, see Table 1), $(C_5H_9O)SiMe_3$ (1.7%), GC–MS: 158, 143, 129, 115, 101, 75, 73; $(Me_3SiO)_2Si(H)SiMe_3$ (3.2%), GC–MS: 280, 265, 207, 191, 177, 147, 133, 117, 103, 87, 73, 59. The other two products could not be identified. Residual starting material (80%) accounted for the remainder of the products.

Acknowledgements

We gratefully acknowledge the financial support of the Natural Sciences and Engineering Research Council of Canada (NSERC). The authors would also like to thank

© 2000 NRC Canada

Table 1. Product distribution of the photolysis of TTMSS in the absence of trapping agent.

Time (min)	% Composition	Probable structure	Mass spectral fragment
3.1	2.7	$(Me_3Si)_2SiH_2$ (**4**)	176 (17), 161 (20), 131 (2.1), 117 (4), 115 (4), 101 (11), 88 (54), 73 (100), 57 (4.8)
4.9	0.7	$(Me_3Si)_2SiMe_2$ (**11**)	204 (30), 189 (22), 145 (4.3), 131 (100), 116 (62), 101 (10), 73 (62)
6.2	0.8		281 (24), 265 (3), 207 (100), 193 (35), 133 (10), 119 (2), 73 (60)
7.0	4.0		297 (36), 281 (100), 265 (12), 249 (9), 193 (27), 133 (10), 119 (3), 73 (56)
8.6	78	$(Me_3Si)_3SiH$ (**1**)	248 (23), 233 (15), 174 (60), 160 (65), 159 (58), 131 (14), 129 (16) 73 (100)
9.5	0.2	$(Me_3Si)_3SiMe$ (**2**)	262 (26), 247 (10), 207 (12), 189 (33), 174 (100), 159 (35), 131 (34), 115 (19), 73 (90)
12.6	0.4	$(Me_3Si)Me_2SiSi(Me_3Si)_2H$ (**10**)	306 (6.9), 232 (100), 217 (26), 173 (26), 158 (44), 144(31), 129 (16), 99 (18), 85 (6.4), 73 (60)
13.4	4.0	$(Me_3Si)_4Si$ (**3**)	320 (15), 305 (10), 247 (2.1), 232 (79), 173 (34), 158 (31), 131 (19), 115 (12), 99 (13), 73 (100)
15.5	1.7		276 (33), 261 (5.8), 215 (4), 202 (100), 187 (11), 171 (10), 157 (23), 143 (12), 125 (10), 99 (9), 73(42)
19.6	0.4	$(Me_3Si)_2Si(H)Si(H)(SiMe_3)_2$ (**9**)	348 (31), 275 (22), 259 (12), 201 (46), 199 (33), 171 (15), 157 (29), 131 (20), 115 (14), 99 (13), 73 (100)

W.J. Leigh (McMaster University) for the use of the Rayonet reactor.

References

1. R.D. Miller. Angew. Chem. Int. Ed. Engl. Adv. Mater. **28**, 1733 (1989).
2. M.G. Steinmetz. Chem. Rev. **61**, 9455 (1996); N. Ishikawa and M. Kumada. Adv. Organomet. Chem. **19**, 51 (1981); G. Raabe and J. Michl. Chem. Rev. **85**, 419 (1985).
3. A.G. Brook. The photochemistry of organosilicon compounds. *In* The chemistry of organic silicon compounds. Vol..2. *Edited by* Z. Rappoport and Y. Apeloig. Wiley, Chichester, U.K. 1998. Chap. 21, p. 1233; A.G. Brook. The photochemistry of organosilicon compounds. *In* The chemistry of organic silicon compounds. Vol. 1. *Edited by* S. Patai and Z. Rappoport. Wiley, Chichester, U.K. 1989. Chap. 15, p. 965.
4. A.G. Brook and M.A. Brook. Adv. Organomet. Chem. **39**, 71 (1996).
5. H. Sakurai, Y. Kamiyama, and Y. Nakadaira. J. Am. Chem. Soc. **98**, 7424 (1976); M. Ishikawa, Y. Nishimura, and H. Sakamoto. Organometallics, **10**, 2701 (1991); M. Ishikawa, K.-I. Nakagawa, R. Enokida, and M. Kumada. J. Organomet. Chem. **201**, 151 (1980); K.M. Baines, A.G. Brook, R.R. Ford, P. Lickiss, A.K. Saxena, W.J. Chatterton, J.F. Sawyer, and B.A. Behnam. Organometallics, **8**, 693 (1989); A.G. Brook, A. Baumegger, and A.J. Lough. Organometallics, **11**, 3088 (1992).
6. C. Chatgilialoglu, D. Griller, and M. Lesage. J. Org. Chem. **53**, 3641 (1988); C. Chatgilialoglu, B. Kopping, M. Zehnder, and B. Giese. J. Org. Chem. **57**, 3994 (1992).
7. C. Chatgilialoglu. Acc. Chem. Res. **25**, 188 (1992).
8. M. Ishikawa. Pure Appl. Chem. **50**, 11 (1978); M. Kira, K. Sakamoto, and H. Sakurai. J. Am. Chem. Soc. **105**, 7469 (1983).
9. G.W. Sluggett and W.J. Leigh. Organometallics, **11**, 3731 (1992); G.W. Sluggett and W.J. Leigh. J. Am. Chem. Soc. **114**, 1195 (1992).
10. C. Chatgilialoglu, C. Ferreri, and T. Gimisis. Tris(trimethylsilyl)silane in organic synthesis. *In* The chemistry of organic silicon compounds. Vol. 2. *Edited by* Z. Rappoport and Y. Apeloig. Wiley, Chichester. 1998. Chap. 25, p. 1539.
11. M.A. Brook, C. Gottardo, S. Balduzzi, and M. Mohamed. Tetrahedron Lett. **38**, 6997 (1997).
12. Y.-S. Chen and P.P. Gaspar. Organometallics, **1**, 1410 (1982).
13. M.A. Brook, C. Gottardo, S. Balduzzi, and M. Mohamed. Tetrahedron, **55**, 10027 (1999).
14. H. Gilman and R.L. Harrel, Jr. J. Organomet. Chem. **9**, 67 (1967).
15. M. Ballestri, C. Chatgilialoglu, K.B. Clark, D. Griller, B. Giese, and B. Kopping. J. Org. Chem. **56**, 678 (1991).
16. C. Chatgilialoglu, A. Guarini, A. Guerrini, and G. Seconi. J. Org. Chem. **57**, 2201 (1992).
17. K. Mizuno, K. Nakanishi, J.-I. Chosa, and Y. Otsuji. J. Organomet. Chem. **473**, 35 (1994).

© 2000 NRC Canada

Bis(trimethylsilyl)methylamine (BSMA): tool or toy?[1]

Jean-Paul Picard

Abstract: Bis(trimethylsilyl)methylamine, BSMA, an original primary amine, was proven to be the source of a large variety of *N*-bis(trimethylsilyl)methylamino derivatives that otherwise have to be prepared indirectly. Because of the bulkiness of the bissilylmethyl group, regio- and stereoselectivities resulted in appropriated examples. Apart from the potential biological properties associated with the Si-C-N framework, these derivatives were powerful synthetic intermediates. Special emphasis was given to the chemistry of corresponding imines. Cleavage of Si—C bonds or abstraction of the methine proton afforded α-nitrogen carbanions in very mild conditions. Application of these results to the β-lactam chemistry allowed the introduction of new synthetic methodologies in this field. It results the $(Me_3Si)_2CH$- group could now be regarded as a Me_3SiCH_2- or a CH_3- group or a proton equivalent.

Key words: bis(silyl)methylamine, preparations, reactivity, nitrogen heterocycles, α-nitrogen carbanions.

Résumé : Il a été montré que la bis(triméthylsilyl)méthylamine, BSMA, une amine primaire originale, peut être à la base d'une large variété de composés *N*-bis(triméthylsilyl)méthylaminés, qui ne pouvaient être obtenus qu'indirectement. La présence du groupe $(Me_3Si)_2CH$-, volumineux, sur l'azote induit une régio- et stéréosélectivité dans les cas appropriés. Mis à part la possibilité qu'ils puissent présenter une activité biologique (lie à l'enchaînement Si-C-N), ces composés sont des intermédiaires de synthèse puissants. Une attention spéciale a été portée aux imines correspondantes. La coupure des liaisons Si—C ou l'arrachement du proton méthine donne accès à des carbanions α-azotés dans des conditions douces. La chimie des β-lactames a largement tiré bénéfice de ces résultats. Finalement, le groupe $(Me_3Si)_2CH$- peut être considéré comme un équivalent synthétique des groupes Me_3SiCH_2- et CH_3-, et du proton.

Mots clés : bis(silyl)méthylamine, préparations, réactivité, hétérocycles azotés, carbanions α-azotés.

I. Introduction

Since the first α-C-silylated amino derivatives were reported independently by Speier and co-workers (1) and Sommer and Rocket (2), in 1951, compounds having a Si-C(sp^3)-N framework have been the subject of nearly 700 publications and 100 patents (Fig. 1).

Two important features characterize this type of compound:

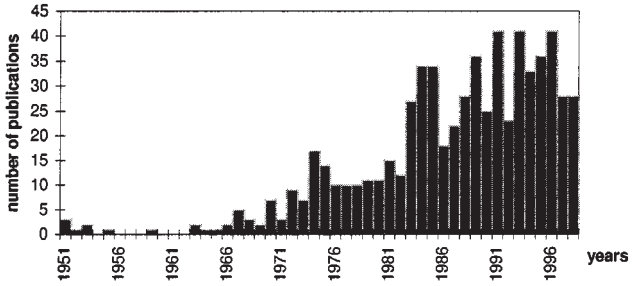
Cleavage of the carbon—silicon bond

This can be achieved under mild and neutral conditions, leading to the corresponding α-nitrogen carbanions as exemplified by Katritzky and Sengupta (3) and Patel and Joule (4) (Scheme 1).

Biological activity

A number of α-C-silylated amino derivatives show significant biological activities (5–10) (Scheme 2). For example, flusilazole is an active fungicide, produced in tons. Aminomethyl(trimethyl)silane inhibits monoamine oxidase (MAO-B) whereas its carbon analogue, neopentylamine, is a substrate for the same enzyme.

Fig. 1. The publication history of compounds having a Si-C(sp^3)-N framework.



General comments

The above two features triggered our interest in the chemistry of α-C-silylated amines (or "silylmethylamines," SMA) which we divided into four classes according to their substitution patterns: monosilylmethylamine (MSMA), arylsilylmethylamine (ASMA), alkylsilylmethylamine (RSMA), and bissilylmethylamine (BSMA), respectively, (Scheme 3).

The purpose of this paper is to review the syntheses and the reactivity of BSMA and its derivatives, showing BSMA

Received July 7, 1999. Published on the NRC Research Press website on October 31, 2000.

Dedicated to Professor Adrian Gibbs Brook for his outstanding contribution to the development of organosilicon chemistry.

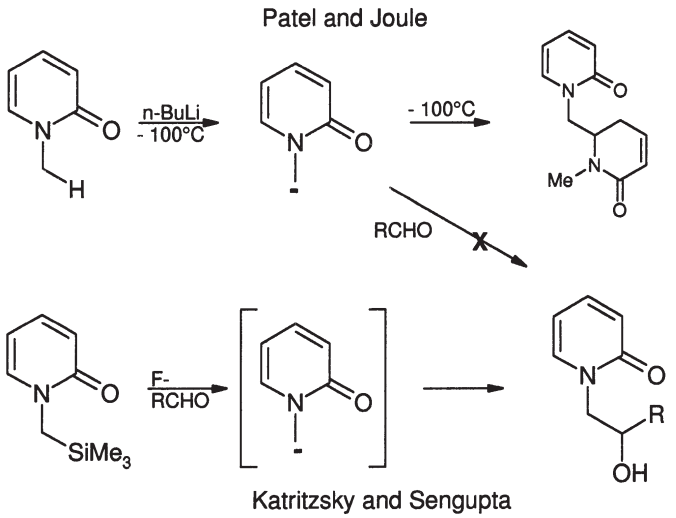
J.-P. Picard.[2] Laboratoire de Chimie Organique et Organométallique, UMR 5208 CNRS, Université Bordeaux 1, F-33405 Talence, France.

[1]Part of this material has been presented at the 12th International Symposium on Organosilicon Chemistry, Sendai, Japan (May 1999).

[2]Telephone: ++ 33 556 846 285. Fax: ++ 33 556 846 646. e-mail: j-p.picard@lcoo.u-bordeaux.fr

© 2000 NRC Canada

Scheme 1.



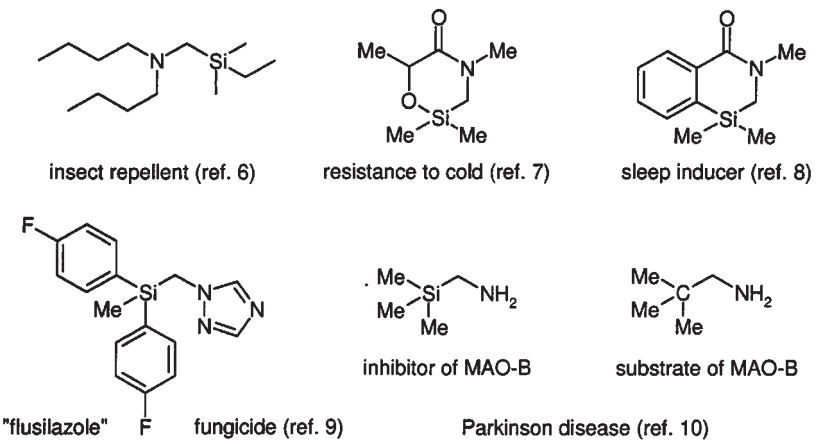
is a very useful and easily handled synthon at the disposal of organic synthetic chemists, as exemplified by the new developments these compounds have permitted in the chemistry of β-lactams.

The BSMA derivatives (BSMa) were obtained through successive replacement of two methyl hydrogens of *N*-methyl amino derivatives (11–15) (Scheme 4), and the strategy was successfully used in the preparation of BSMA benzamide (Scheme 5), BSMA isonitrile (Scheme 6), and BSMA benzotriazole (Scheme 7).

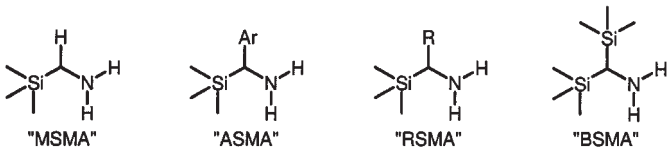
II. Syntheses of BSMA

We, on the other hand, thought bis(trimethylsilyl)methylamine derivatives (BSMa) could be obtained directly from parent amine (BSMA) using classical amine chemistry, which would provide an organometallic-free approach towards these derivatives.

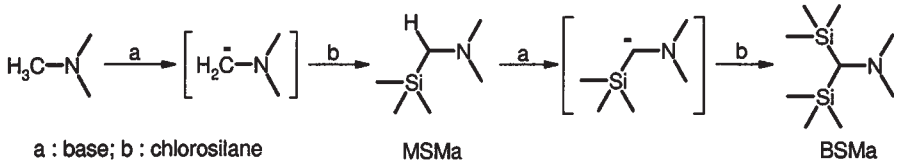
Scheme 2.



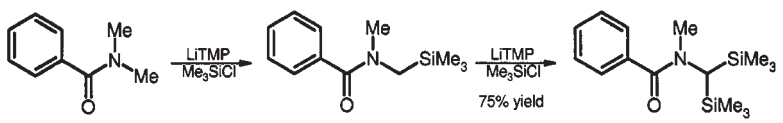
Scheme 3.



Scheme 4.

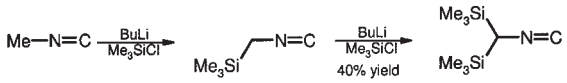


Scheme 5.

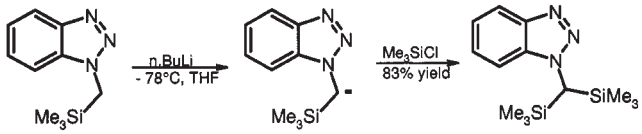


© 2000 NRC Canada

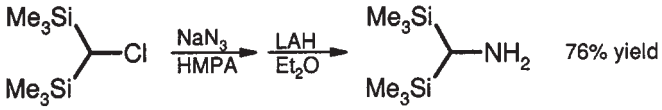
Scheme 6.



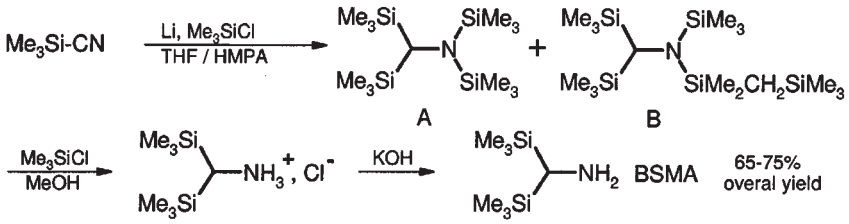
Scheme 7.



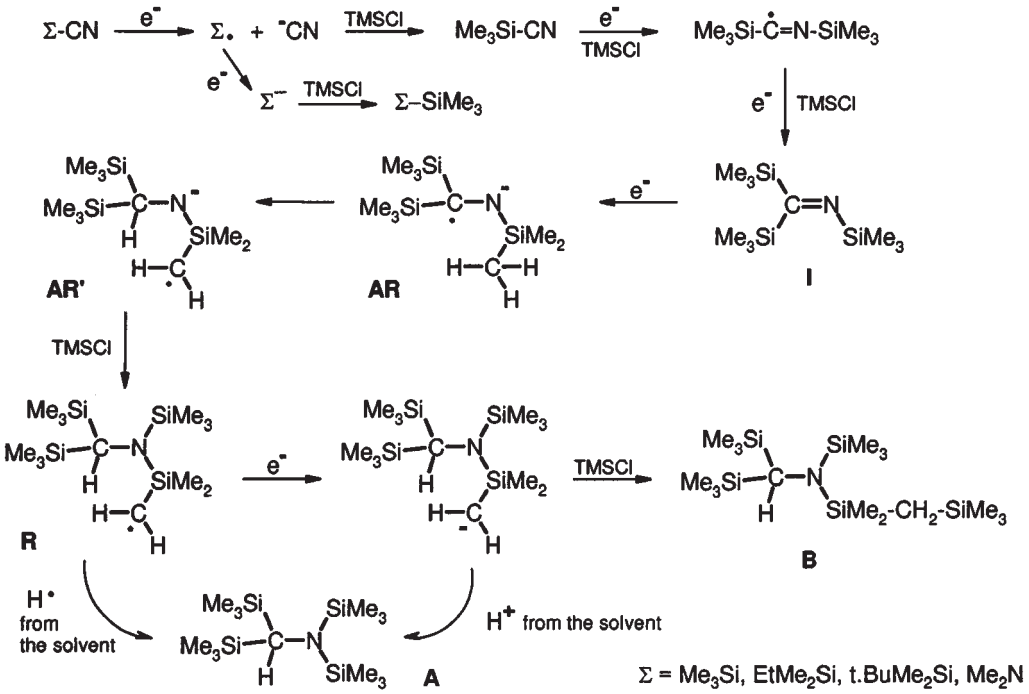
Scheme 8.



Scheme 9.



Scheme 10.



Amination

Bis(trimethylsilyl)methyl amine was first prepared by amination of the corresponding chloride (16) (Scheme 8), following a procedure parallel to that described by Letellier for MSMA (17), but the difficulty in obtaining the starting chloride made this synthesis undesirable for large scale preparations.

Reductive silylation

Reductive silylation of trimethylsilylcyanide (TMS-CN) provided an attractive solution. Thus, TMS-CN, when reacted with trimethylsilylchloride (TMSCl) and lithium sand in a THF–HMPA mixture,[3] afforded a mixture of the silazanes A and B, with the latter predominating (18). Hydrolysis of the N—Si bonds with TMSCl in MeOH[4] quantitatively produced the hydrochloride of BSMA, which was neutralized by solid KOH to give BSMA in good yields on a multigram scale (Scheme 9).

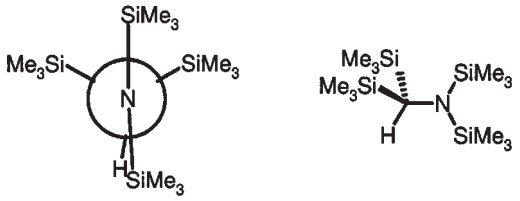
Other cyanides ($EtMe_2Si$-CN, *t*-$BuMe_2Si$-CN, Me_2N-CN) and *t*-butyl isonitrile were also tested as starting materials,

[3] This molecule that has been referred to as a "potential carcinogenic compound," is now referred to as a "useful aprotic solvent": cf. for instance, Sigma–Aldrich 1999–2000 catalogue, p. 919.

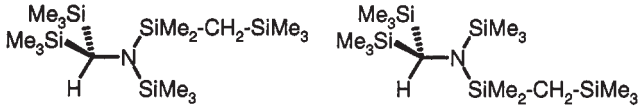
[4] Under these conditions, even tris(trimethylsilyl)amine was hydrolysed quantitatively within a minute into methoxytrimethylsilane and ammonium chloride (18*b*).

© 2000 NRC Canada

Scheme 11.



Scheme 12.



which gave rise to mixtures of the same silazanes A and B in different ratios.

A mechanism leading to the formation of the silazanes A + B has been proposed. Thus, successive electron transfer to the substrate to form anion-radicals and capture by TMSCl leads to the intermediate imine I (18) (Scheme 10). Imine I has never been isolated, probably because it is fast reduced to the intermediate AR. A facile [1,5]-H shift in AR gives rise to the new intermediate AR′, which, via successive electron transfer and reaction with TMSCl, leads to the silazanes A and B.

An equally efficient electrochemical version of this preparation, using a sacrificial anode technique (see for example ref. 19), has also been published (20).

Particular Properties of Silazanes A and B

The silazane A, previously obtained by another route (21), showed unusual ^{1}H, ^{13}C, and ^{29}Si NMR spectra (three lines for the trimethylsilyl groups), which were explained by a restricted rotation around the C—N bond, resulting in a favoured conformation with one N—Si bond eclipsing the C—H bond. A similar phenomenon has been observed with *N*,*N*-dimethylisopropylamine in the gaseous state (22).

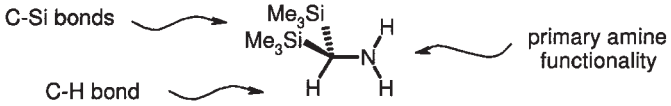
A careful NMR study using 2D ^{13}C-^{1}H and ^{29}Si-^{1}H correlation methods confirmed this hypothesis and allowed complete assignment of signals. It also showed that two Me_3Si groups were linked to the central carbon atom and two other magnetically non-equivalent groups were attached to the nitrogen atom. The respective coupling constants $^{n}J(^{1}H$-$^{29}Si)$ were also determined.

Theoretical calculations estimated the energy of free rotation at ~35 Kcal/mol.[5] However, no change in the NMR spectra of silazane A were observed up to 180°C. This was quite surprising as rotation has been observed above 80°C with the symmetrical tetrakis(trimethylsilyl)ethane (23).

The silazane B was obtained as a 50:50 mixture of two rotamers, which were fully assigned by their NMR spectra (18) (Scheme 12).

III. Chemistry of BSMA and its derivatives

A priori, one may consider three sites of reactivity for BSMA: the amine function, the Si—C bonds, and the C—H bond. Reactions involving the latter two, however, require prior transformation of the amine group into another nitrogen functionality.



Reactivity of the amine function

General

Like other organic primary amines, BSMA reacted easily with a large variety of reactants to directly and quantitatively yield BSMa derivatives: phthalimide with phthalic anhydride, formamidine with dimethylformamide dimethylacetal, sulphonamides with sulfonyl chlorides, carbamates with carbamoyl chlorides, isocyanate with phosgene and triethylamine, β-aminoesters with acrylates, pyrrole with 2,5-dimethoxy tetrahydrofurane, and β-aminoenones with β-diketones (24) (Scheme 13). It is important to note that the bis(silyl)methyl group was not affected during these transformations.

The above strategy allowed the direct preparation of BSMA amides and isonitrile (24) (Schemes 14 and 15), in a more practical way than those reported previously (Schemes 5 and 6). This isonitrile has been used by Battaglia to prepare the corresponding isothiocyanate (25).

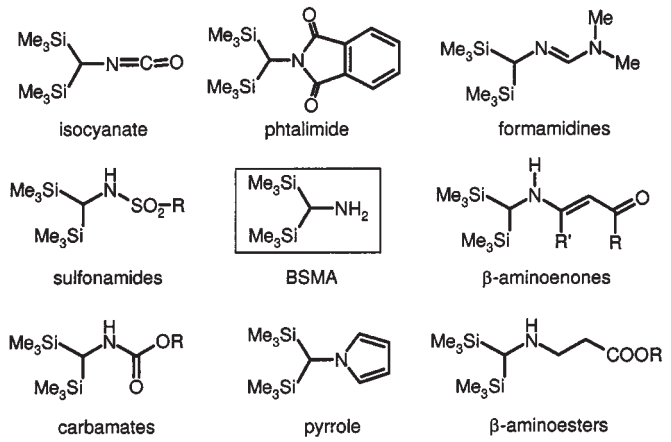
A series of BSMA-cumulenes were also synthesized from BSMA iminophosphorane (25) (Scheme 16).

Aminolysis of epoxides

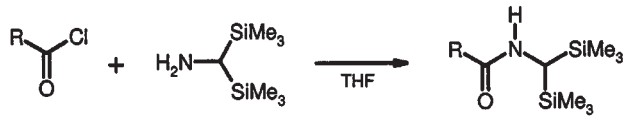
The opening of oxiranes by a primary amine is a useful way to get β-amino alcohols, an important class of organic compounds, especially in biochemical studies.

Using BSMA as the primary amine, ring opening of unsymmetrical epoxides yielded β-amino alcohols with high regiochemistry (26) (Scheme 17).

Scheme 13.



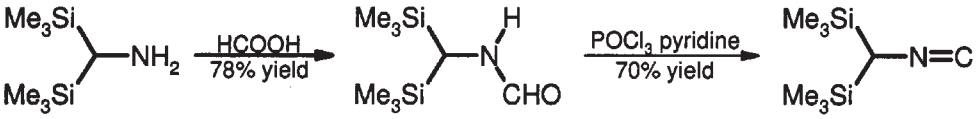
Scheme 14.



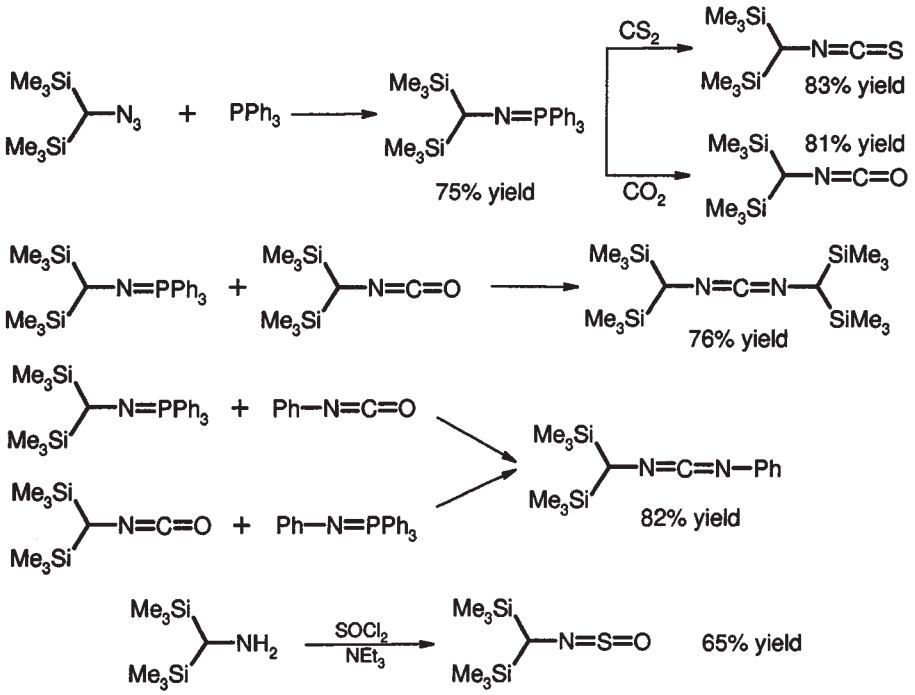
[5] M.T. Rayez, J.C. Rayez, and J.P. Picard. Unpublished result.

© 2000 NRC Canada

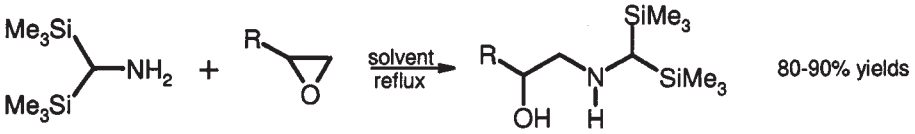
Scheme 15.



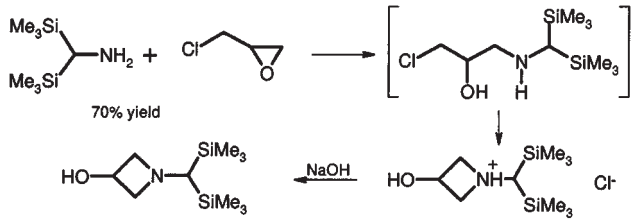
Scheme 16.



Scheme 17.



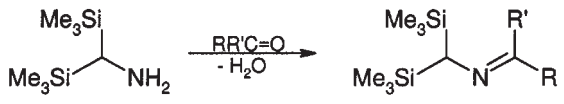
Scheme 18.



With epichlorohydrin, subsequent cyclization of the ring-opened intermediate led to the azetidinol as the sole product (26) (Scheme 18). This was particularly interesting as the silyl groups could be potentially removed (vide infra) to yield the *N*-methyl derivative, a compound that is not easily accessible via reaction of methylamine with epichlorohydrin (27).

Formation of imines

Condensation of BSMA with carbonyl compounds proceeds rapidly to produce the corresponding aldimines and ketimines almost quantitatively at room temperature in the presence of molecular sieves.



It was worth noting that the synthesis of *N*-[bis(trimethylsilyl)methyl]methylen imine occurred even in water medium (entry 1 in Table 1) in excellent yield. Moreover, this imine was quite stable and distillable (28), a feature that is not found for other methylene imines, except for those where the nitrogen atom is linked to a tertiary carbon atom (29).

Ultraviolet photoelectron, electron transmission, and ab initio studies of the factors which determine the stability of the BSMA aldimines has been made, which showed that the bissilylmethyl group altered the energy ordering and localisation properties of the valence molecular orbital where the lone pair orbital was no longer the HOMO (30).

© 2000 NRC Canada

Table 1. Aldimines (R′ = H, selected examples).

Entry	R-	Conditions[a]	Yield%	References
1	H- [from formaline]	Water	77	31
2	H- [from $(CH_2O)_n$]	MS[b] 4Å, Et_2O, RT°[c]	80	28
3	CH_3-	MS 4Å, Et_2O, RT°	90	28, 32, 33
4	Ph-	MS 4Å, Et_2O, RT°	97	34
5	$(CH_3)_3C$-	MS 4Å, PhH, RT°	78	35
6	PhCH=C(Me)-	MS 4Å, Et_2O, RT°		34, 36
7	EtCH=CH-	MS 4Å, PhH, RT°		16, 37
8	MeOOC-	MS 4Å, Et_2O, RT°		34

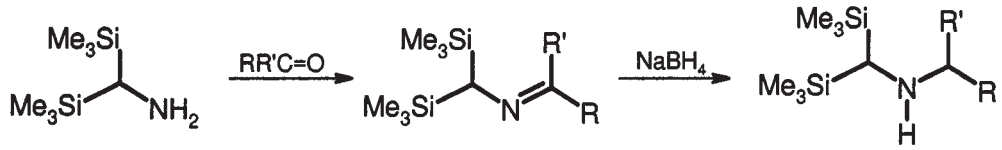
[a]In CH_2Cl_2 at RT°.
[b]MS: molecular sieves.
[c]RT°: room temperature.

Table 2. Ketimines (selected examples).

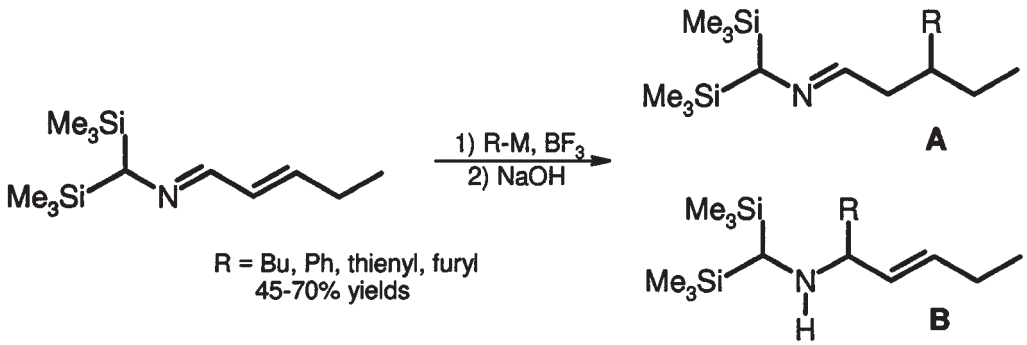
Entry	R-	R′-	Conditions[a]	Yield (%)	Reference
1	Me-	Me-	MS[b] 4Å, RT°[c]	91	32
2	Me	Et	Excess of ketone, RT°	90	32, 39
5	Me-	-COOMe	MS 4Å, CH_2Cl_2,RT°	97	32

[a]Excess of ketone was used as the solvent.
[b]MS: molecular sieves.
[c]RT°: room temperature.

Scheme 19.



Scheme 20.



Some representative exemples are listed in Table 1 (16, 28, 31–37) and Table 2 (32, 38).

BSMA imines have also been prepared from aldehydo- and ketosugars (39).

Alkylation

Imine formation with BSMA, followed by reduction of the double bond with sodium borohydride, provided an easy access to the corresponding secondary amines in good yields (16) (Scheme 19).

Addition of cuprates to 1-aza-1,3-butadienes obtained from BSMA and α,β-ethylenic aldehydes, occurred under mild conditions in the presence of BF_3,Et_2O with high regioselectivity (37). The latter was somewhat dependent on the nature of the ligand to be transferred from the organometallic reagent, alkyl and aryl ligands leading to imine A, and thienyl and furyl ligands to allylamine B (Scheme 20).

Deamination

Nitrous acid deamination of BSMA produced bis(trimethylsilyl)methanol in a moderate yield (Scheme 21).[6]

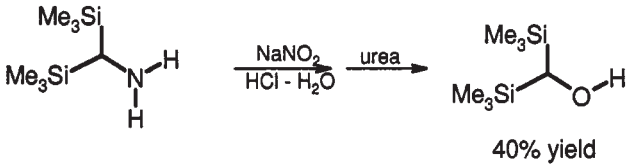
Cleavage of the Si—C bond

The importance of this cleavage reaction for SMA derivatives has long been appreciated. For BSMa, additional interest

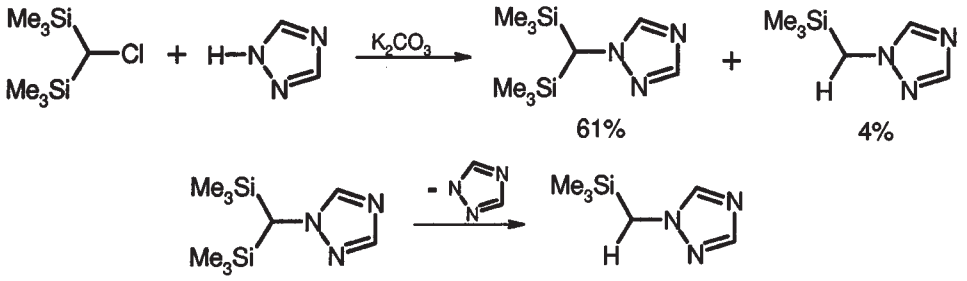
[6]J.P. Picard and R. Ernst. Unpublished result.

© 2000 NRC Canada

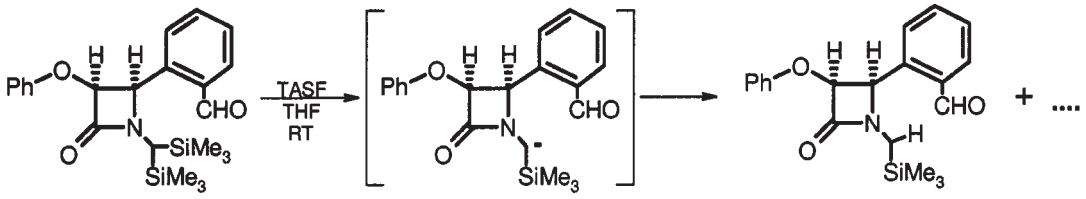
Scheme 21.



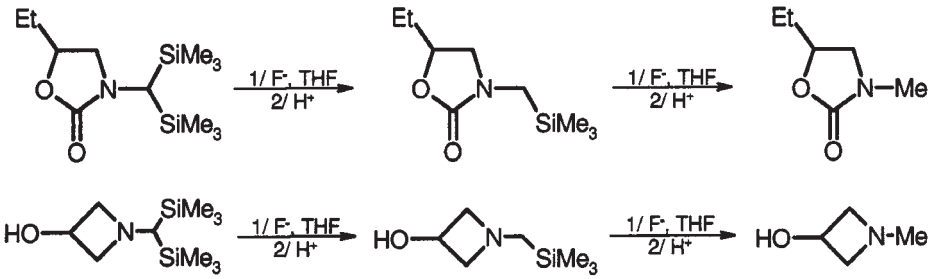
Scheme 22.



Scheme 23.



Scheme 24.



came from the presence of a second Si—C bond which allowed developing new chemistry.

Protonation (C-Si →C-H)

Protolytic cleavage of one Si—C bond of BSMa led to the parent MSMa. Some examples of this kind already existed, but as a side reaction. For instance, during preparation of *N*-[bis(trimethylsilyl)methyl]triazole, some monosilylated derivative was formed, probably under the action of the triazolyl anion onto the desired product (40) (Scheme 22).

Similar protodesilylation during cyclization reaction to form the B ring of a carbacephem (vide infra) has been observed (41) (Scheme 23).

Protodesilylation can also be achieved by treating BSMa with one equivalent of fluoride anion and quenching with diluted acid in THF medium. Complete desilylation can also occur in a stepwise fashion with a second equivalent of fluoride anion (Scheme 24).[7]

These protodesilylation reactions show the importance of the bis(trimethylsilyl)methyl group as a methyl group equivalent.

Oxidation (C-Si → C-O)

Ceric ammonium nitrate (CAN) was found to easily oxidize the C—Si bonds of BSMa to a formyl group. The formamide thus quantitatively formed could be hydrolyzed to the corresponding N-H derivative in excellent yields (31, 32). Thus, bis(trimethylsilyl)methyl group appeared to be an effective N-protecting group (Scheme 25). This was particularly useful in β-lactam synthesis.

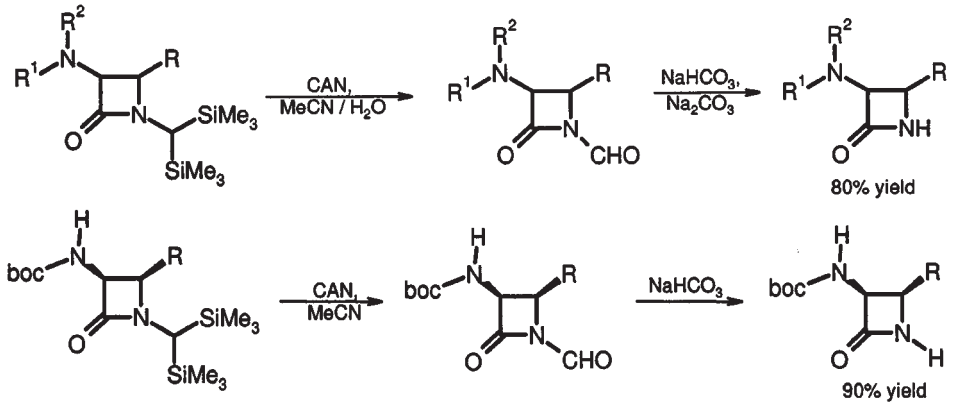
Alkenation (C-Si → C=C)

Fluoride ion induced cleavage of the C—Si bond in presence of a carbonyl compound opens a direct and easy access to enamine derivatives. In these reactions, initial desilylative formation of a α-nitrogen carbanion followed by reaction with the carbonyl compounds yielded the corresponding

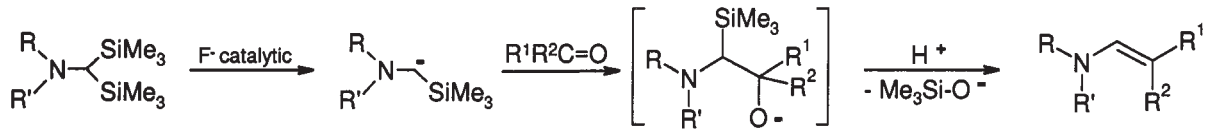
[7] J.P. Picard, S. Grelier, and T. Constantieux. Unpublished results.

© 2000 NRC Canada

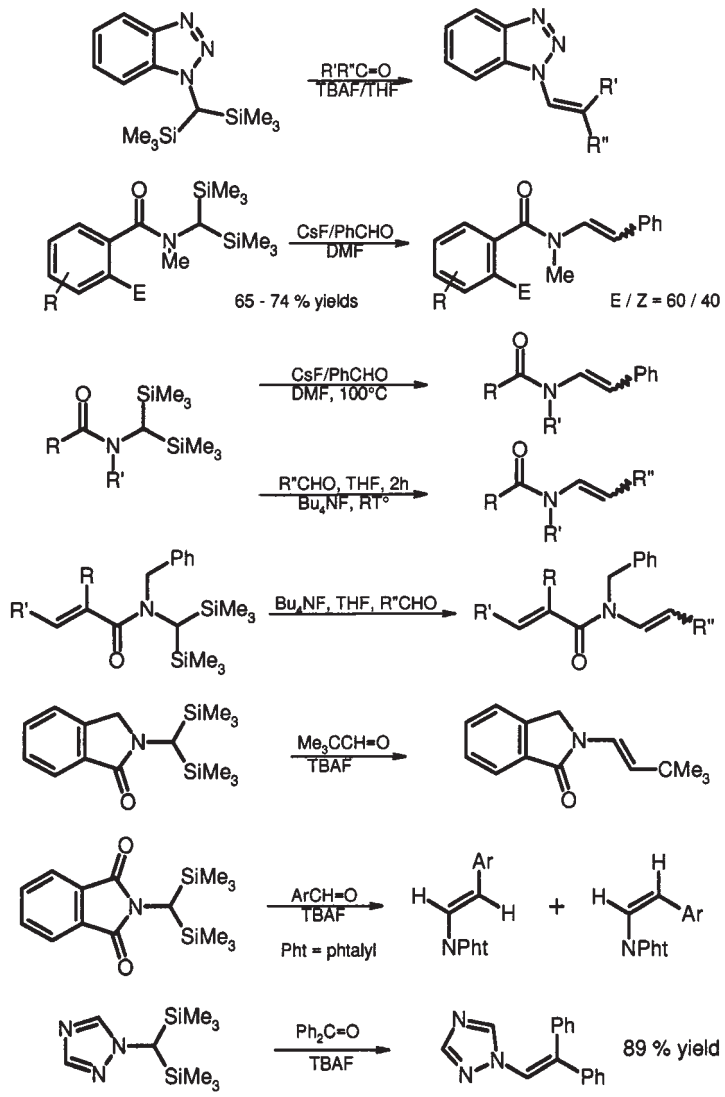
Scheme 25.



Scheme 26.

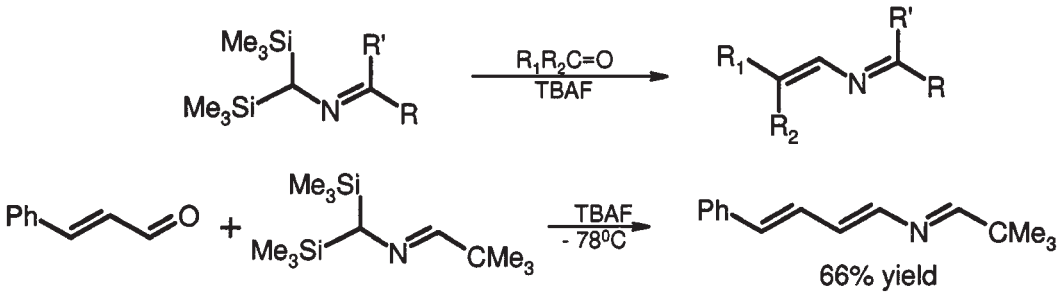


Scheme 27.

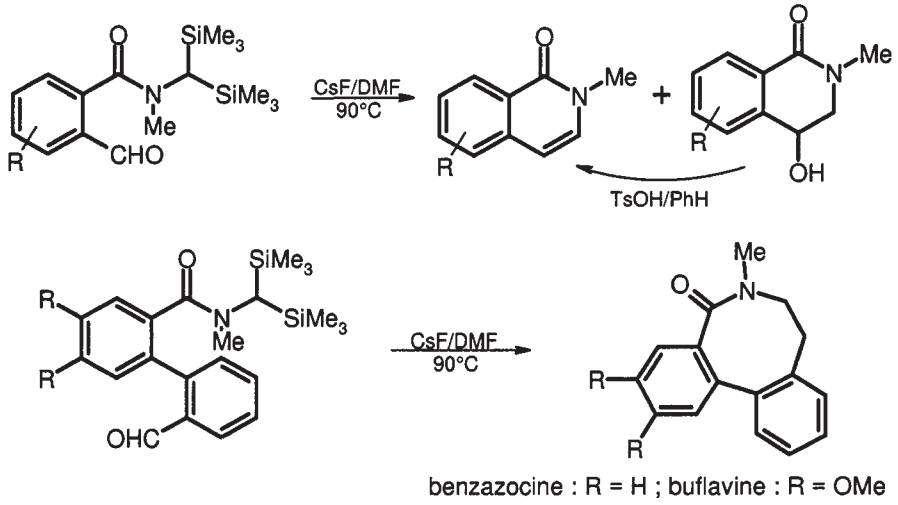


© 2000 NRC Canada

Scheme 28.



Scheme 29.



aminoalcohols which underwent a Peterson elimination through loss of silanol to give the enamines (Scheme 26).

This has been exploited to prepare *N*-vinyl benzotriazoles (42), *N*-vinyl amides (13, 16, 43), *N*-vinyl phtalimidine (24), *N*-vinyl phtalimide (34), and *N*-vinyl triazole (40) (Scheme 27).

Using BSMA imines as the starting materials, 2-aza-1,3-dienes were obtained under very mild conditions with good yields, avoiding the formation of any polymer, even when the reacting carbonyl was an α,β-ethylenic aldehyde (34) (Scheme 28).

An intramolecular version of this reaction has led to a rapid access to isoquinolones, benzazocine (43), buflavine (44) (Scheme 29), and β-lactams (vide infra).

This methodology has been also applied to a facile synthesis of dihydroisoquinoline derivatives (16). Incidentally, it was discovered that mono BSMA imine of *ortho*-phtalaldehyde was not stable, as attack of the lone pair electrons of nitrogen on the remaining aldehyde functionality took place, followed by an internal Cannizzaro reaction, to give rise to the corresponding phtalimidine with good yields (24) (Scheme 30). The condensation reaction of *o*-phtalic aldehyde with primary aromatic and aliphatic amines has some precedents (see for instance ref. 45).

Sometimes, results depended upon the geometry of the intermediate alcoxyde, as shown, for instance, by the addition to benzaldehyde of the carbanion generated from BSMA isothiocyanate. The expected oxazolidine-2-thione was formed in low yield whereas styryl isothiocyanate was obtained in much higher yield (46, 47) (Scheme 31).

Precursors to 1,3-dipoles

SMA derivatives (imines, amides, etc…) haven proven to be excellent sources of unstabilized nitrogen ylids (or 1,3-dipoles) suitable for heterocyclic ring construction after reaction with dipolarophiles (48–53) (Scheme 32).

Benzamide and thiobenzamide have been converted to 1,3-dipoles via treatment with methyltriflate and caesium fluoride and reacted with methyl acrylate followed by DDQ oxidation, affording a mixture of 2-H and 2-silylpyrroles (13) (Scheme 33).

BSMA imines, upon reaction (quaternarization of the nitrogen atom) with an acyl chloride led to an ylid that was intercepted by dimethyl acetylenedicarboxylate to yield the corresponding *N*-acyl pyrrole. Reactions of aliphatic BSMA imines needed to be catalyzed with fluoride anion (TASF) (24) (Scheme 34).

However, BSMA imine derived from acetone did not give rise to cycloaddition reaction, instead leading to amide formation (24)[8] (Scheme 35).

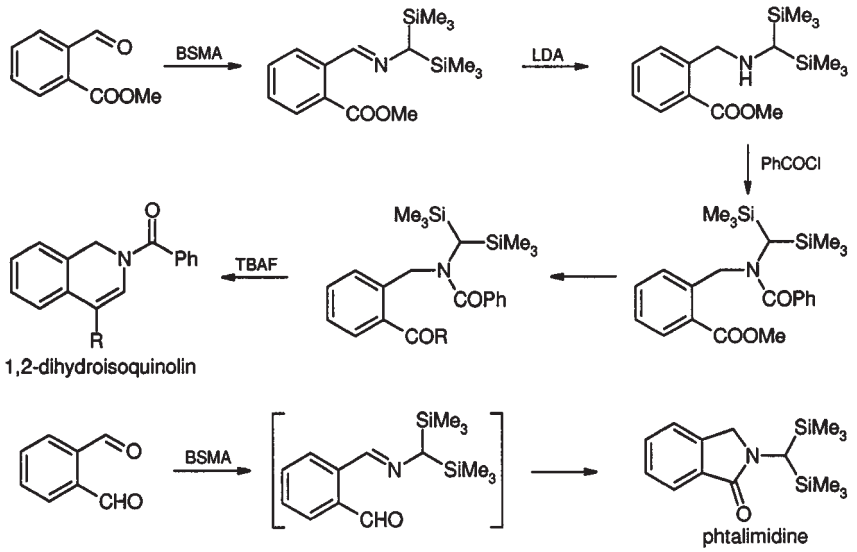
Radical induced cleavage

In a study done by Walton et al. (54) dealing with the behaviour of different silylmethylamines in the presence of *t*-butyl peroxide, the radical induced cleavage of the C—Si bond has been reported. First formed at low temperature was

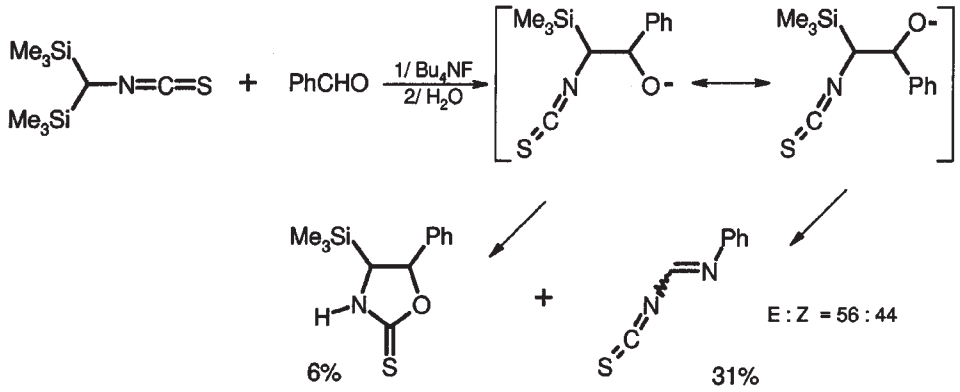
[8] Also formed in the reaction performed in THF was the adduct of THF to DMAD (40% yield).

© 2000 NRC Canada

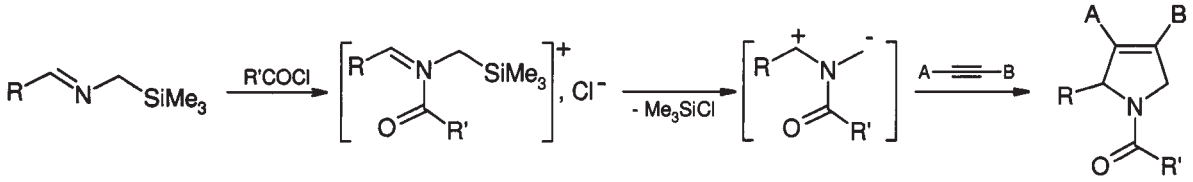
Scheme 30.



Scheme 31.



Scheme 32.



a mixture of the aminoalkyl and the aminyl radicals through abstraction of one hydrogen respectively from the methine and the amine. Aminyl radical was not directly detectable as it rearranged at upper temperature into a new carbon-centred radical in which the silyl group was located on nitrogen. Based on mechanistic evidences, intramolecular migration of the silyl group has been favoured, implying valence shell expansion of the silicon to five (Scheme 36).

Thermally induced rearrangement

When *N*-[bis(trimethylsilyl)methyl]-1-aza-1,3-dienes were heated (neat) in a Kügelrohr oven at 200–240°C, ring closure occurred with migration of one trimethylsilyl group from carbon to nitrogen, to yield Δ^2-pyrroline derivatives in high yields and high stereo selectivity (*trans* only). From these Δ^2-pyrrolines, corresponding 1-trimethylsilyl-2,3-disubstituted pyrrolidines were easily prepared (55) (Scheme 37). The total stereocontrol of the three substituents was established by NOE experiments. Independently in the same year, Komatsu and co-workers (56) published a similar stereocontrolled cyclization from *N*-(α-trimethylsilyl) benzyl-1-aza-2, 3-dienes.

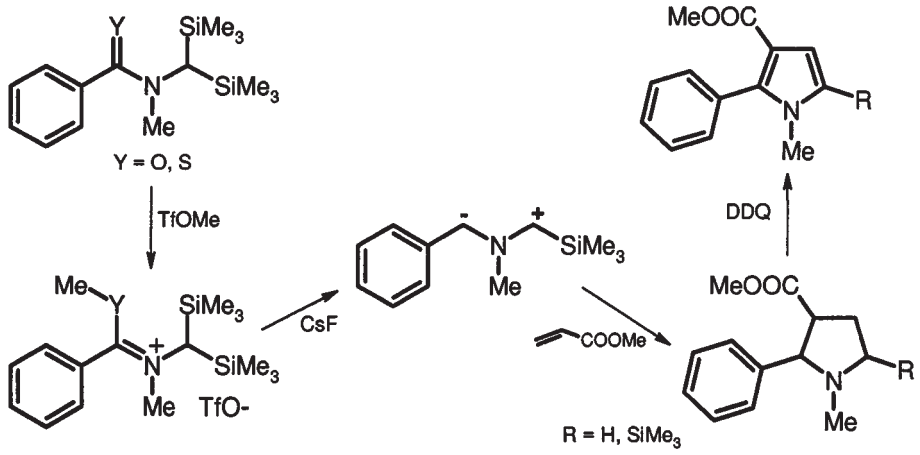
N-Trimethylsilyl-5-trimethylsilyl-3, 4-disubstituted Δ^2-pyrrolines, after treatment with an acyl chloride, were converted almost quantitatively into corresponding *N*-acyl pyrroles upon oxidation with DDQ, providing a novel route to 3,4-disubstituted pyrroles (57) (Scheme 37).

Cleavage of the C—H bond

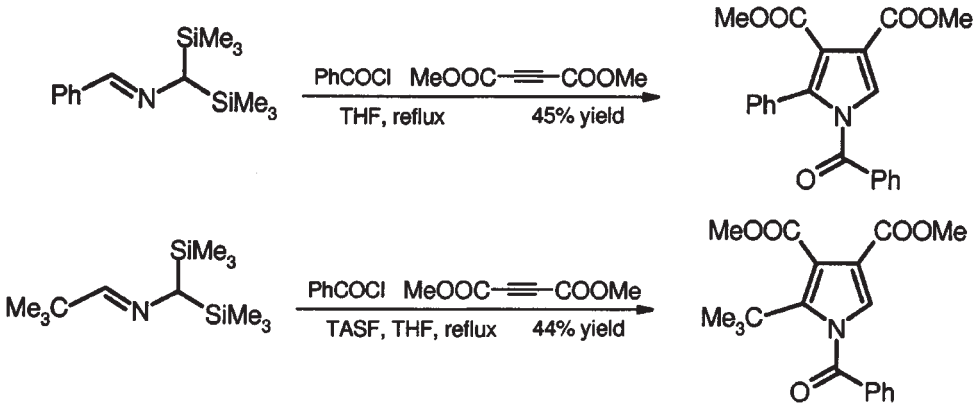
Owing to the electron withdrawing effect of the α-nitrogen atom on the one side and the ability of trimethylsilyl

© 2000 NRC Canada

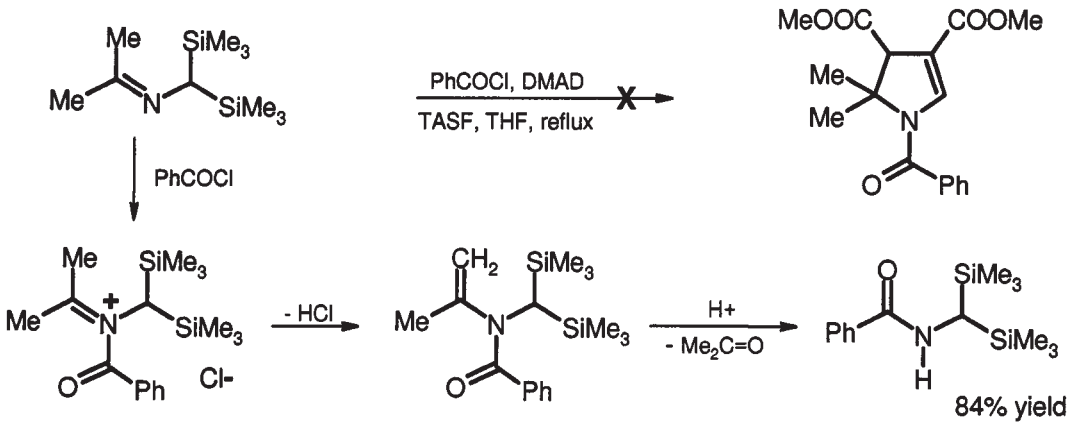
Scheme 33.



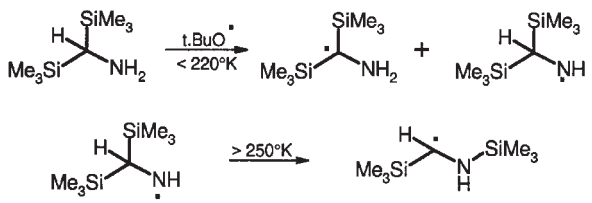
Scheme 34.



Scheme 35.



Scheme 36.



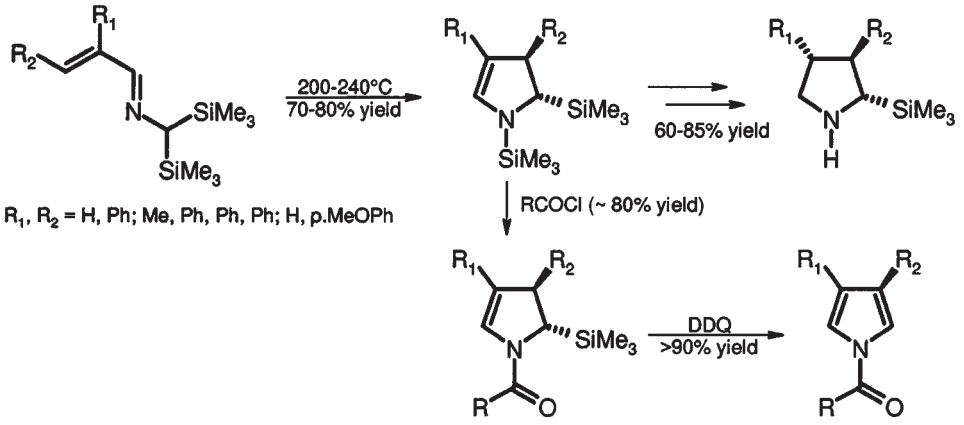
groups to stabilize a carbanion in α-position on the other side, abstraction of the central hydrogen atom in BSMA was expected to be quite facile. This has been shown starting from a benzotriazole derivative (42) (Scheme 38).

BSMA imines

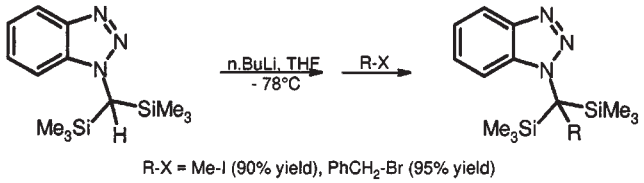
Abstraction of this hydrogen should be even easier in BSMA imines, as it is present in an "allylic" position. However, several bases (*n*-BuLi at –78°C, LDA, etc…) were tested unsuccessfully. It was subsequently found that "Lidakor" ("Schlosser base" (58)) and methyl lithium at

© 2000 NRC Canada

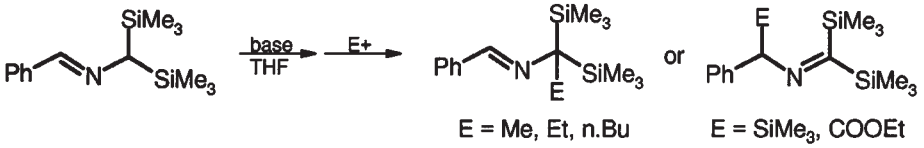
Scheme 37.



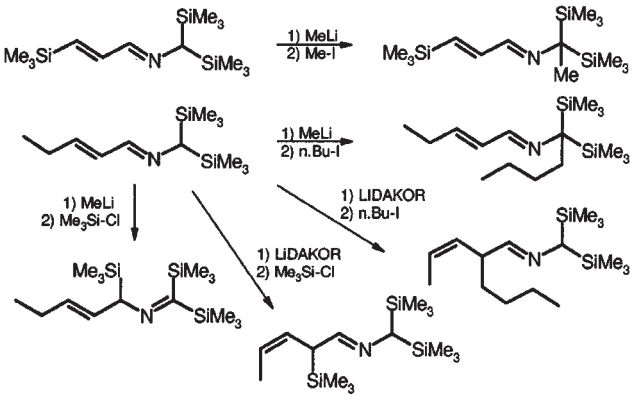
Scheme 38.



Scheme 39.



Scheme 40.

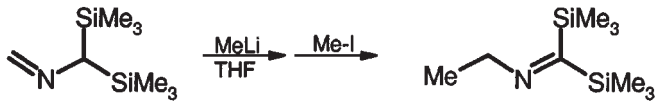


room temperature were able to deprotonate BSMA imines (35). Quenching with various electrophiles then afforded either the direct substitution product or the rearranged product, depending on the nature and the size of the electophile (Scheme 39).

BSMA imines from α,β*-ethylenic carbonyl compounds*

The same sequence on 1-aza-1,3-dienes led to the formation of products whose structure depended not only on the nature and the size of the electophile, but also on the nature of the base (35) (Scheme 40).

Scheme 41.



BSMA formaldimine

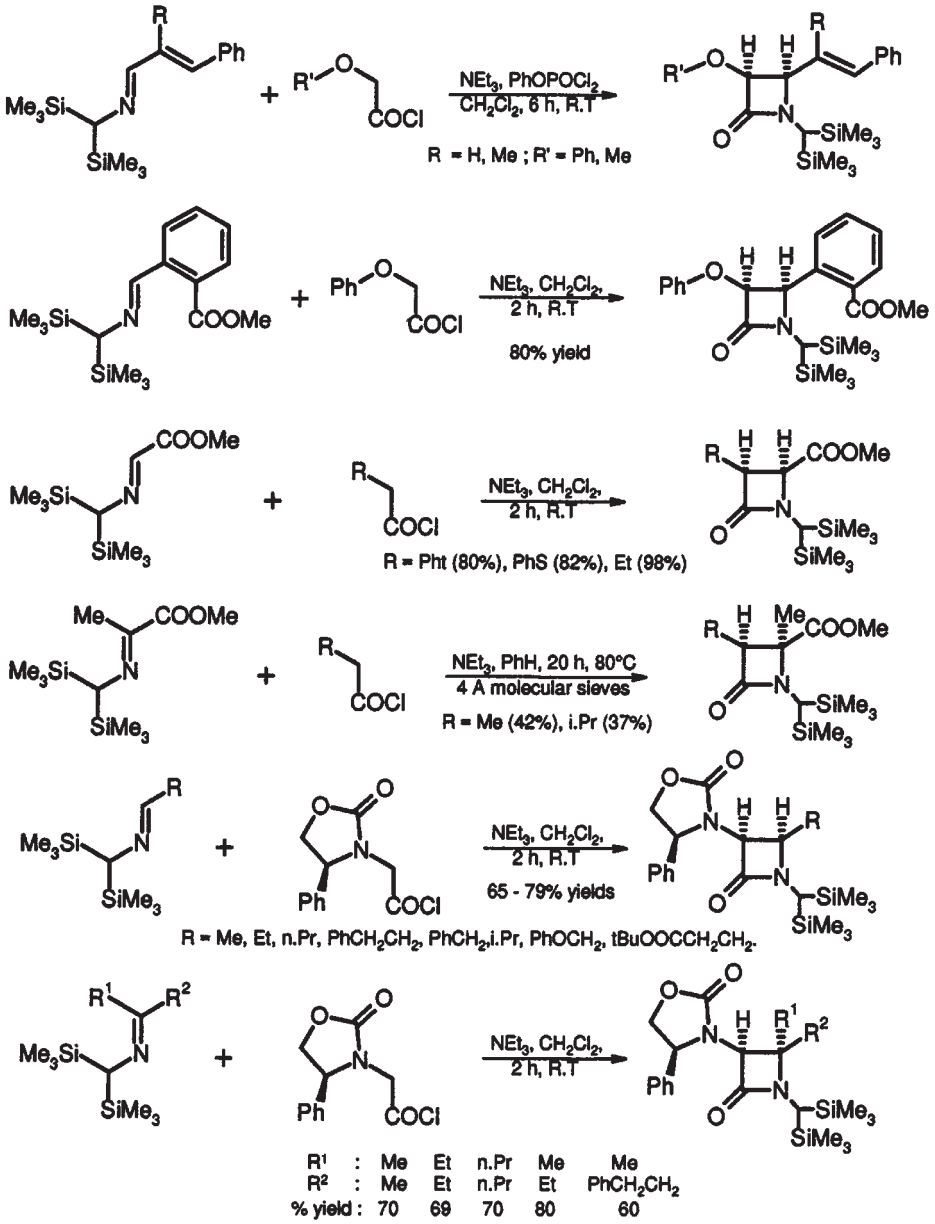
In the case of BSMA methylene imine, this reaction always occurred with transposition of the double bond, even when methyl iodide was used as the electrophile[9] (Scheme 41).

This sequence consisting of imine formation from formaldehyde followed by imine alkylation and hydrolysis, represents a one-carbon homologation of an organic halide into a primary amine. Another interesting feature is the formation of the new imine which can be considered to be derived from the quite sensible carbonyl compound, $(Me_3Si)_2C{=}O$. Such a type of imine was previously obtained by Y. Ito and co-workers (59, 60) (vide infra).

[9] J.P. Picard and L. Puysegu. To be published.

© 2000 NRC Canada

Scheme 42.

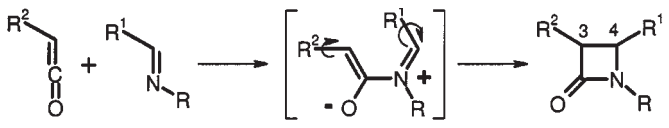


Application to β-lactam chemistry

Stereocontrolled formation of the azetidin-2-one ring

Staudinger reaction (62) of BSMA imines with ketenes in the presence of triethyl amine led to the corresponding β-lactams in excellent yields. Moreover, an unexpectedly high *cis* stereoselectivity was observed in these reactions (33, 34, 36, 38, 41, 62) (Scheme 42). In contrast, using *N*-(trimethylsilyl)methyl imines (MSMA imines) lead to a mixture of *cis* and *trans* β-lactams (63).

In the first step of this formal (2 + 2) cycloaddition reaction, nitrogen to carbonyl carbon bond is formed. Ring closure then occurs by a conrotatorial movement of the substituents on C_3 and C_4. Opposed to MSMA imines, conformation of BSMA imines is fixed, which leads to the strict stereochemical control in the formation of the C_3—C_4 bond of the ring:



Propagation of the chirality

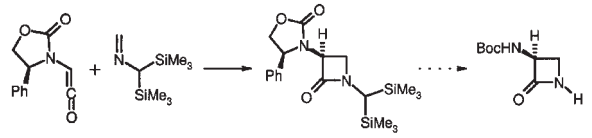
Advantage of the stereocontrolled ring closure was the propagation of the chirality from a chiral auxiliary at C_3 to C_3 and C_4 of the ring. Examples are given in Scheme 42 in which chiral azetidin-2-ones were obtained with excellent diastereoisomeric excesses (31, 38).

C_4 – Unsubstituted azetidin-2-ones

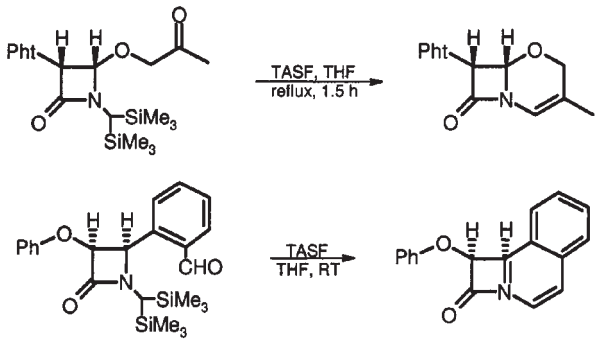
The readily availability of BSMA formaldimine allowed the synthesis of a class of synthetically interesting azetidin-2-ones, as they are valuable synthons in β-lactam antibiotics chemistry (see for instance ref. 64). As an example,

© 2000 NRC Canada

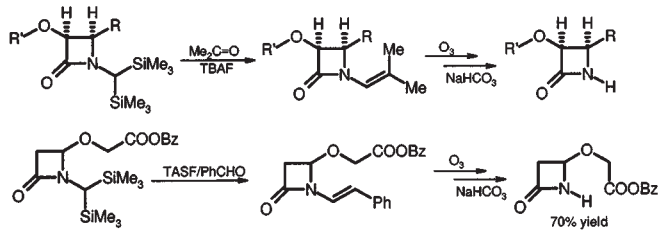
Scheme 43.



Scheme 44.



Scheme 45.



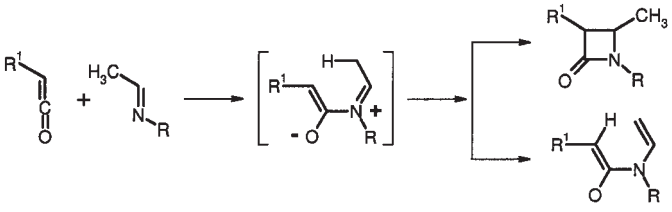
precursor of 3-amino-4-unsubstituted azetidin-2-one was easily obtained through the condensation of this imine with the ketene derived from Evans–Sjögren acetic acid (65) (Scheme 43).

This is a remarkable feature, as MSMA formaldimine, which exits only under the form of a trimer, did not lead to any azetidin-2-one.

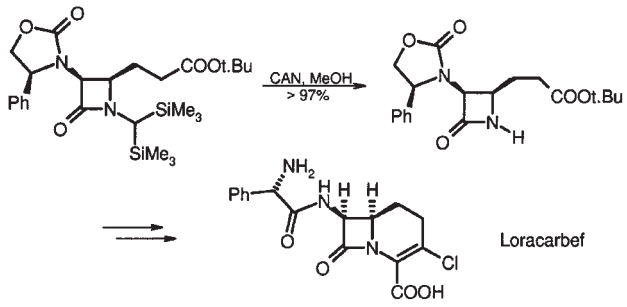
Azetidin-2-ones from enolizable carbonyl derivatives

Generally, condensation of ketenes with imines from enolizable carbonyl derivatives led to *N*-vinyl enamides. Interestingly, the use of the bis(trimethylsilyl)methyl group allowed the synthesis of azetidin-2-ones for the first time (33) (Scheme 42).

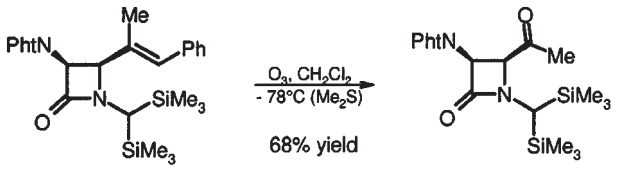
Probably, the inductive effect of the trimethylsilyl groups lowered the electron deficiency on nitrogen in the zwitterion, making the allylic proton less acidic and less available for undergoing a 1,5-migration through a concerted electronic transfer to give the enamide.



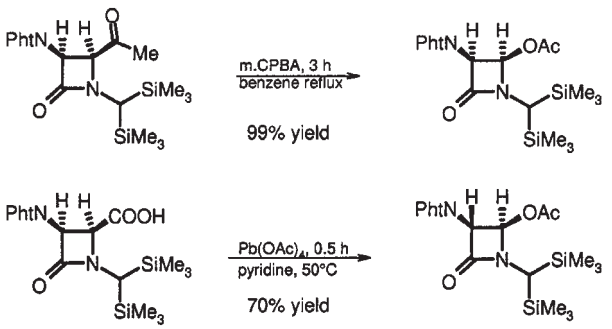
Scheme 46.



Scheme 47.



Scheme 48.



Formation of the B-ring of β-lactams

Many β-lactamic antibiotics are bicyclic compounds. Thus, Peterson olefination methodology has been applied to the construction of the B-ring of oxa- and carbacephem skeletons, starting from BSMA azetidin-2-ones bearing a substituent on C_4 with a carbonyl moiety at the suitable position (36, 41) (Scheme 44).

Deprotection of the N-atom (N-CHSi$_2$ – >> N-H)

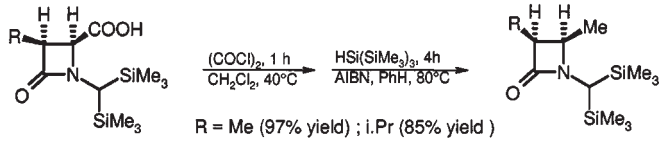
The benefit of using BSMA imines to built azetidin-2-one derivatives has now been well established. However, key compounds for further chemistry in the β-lactam area are N-H azetidin-2-ones. It results that the bis(silyl)methyl group has to be cleaved off selectively. Two methodologies were proposed.

The first method is based on Peterson olefination reaction combined with ozonolysis of the double bond of the resulting vinyl amine, followed by decomposition of the formamide thus formed (34, 36) (Scheme 45).

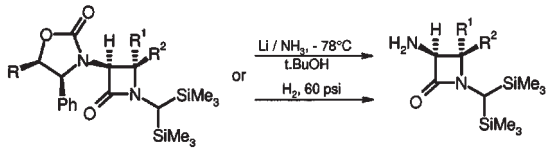
The second method using ceric ammonium nitrate (CAN) has already been described (cf. Scheme 25, § B-b) and has been used several times (31, 62, 65), particularly as a key step in the synthesis of β-lactam Loracarbef (33) (Scheme 46).

© 2000 NRC Canada

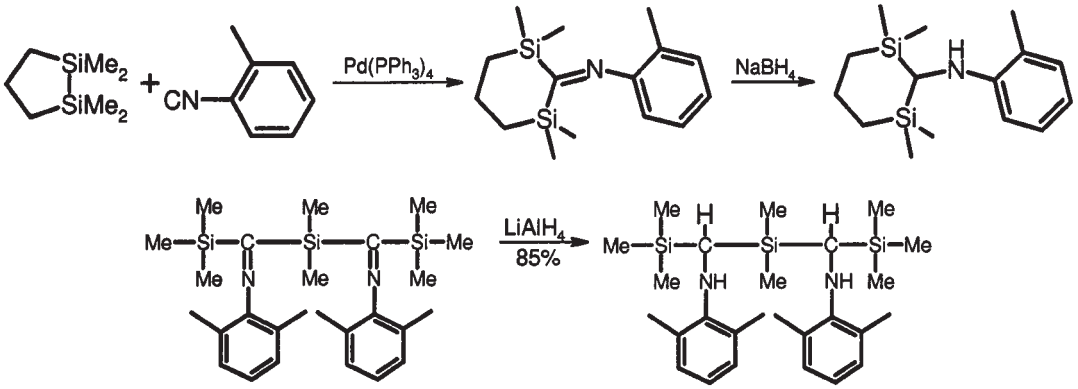
Scheme 49.



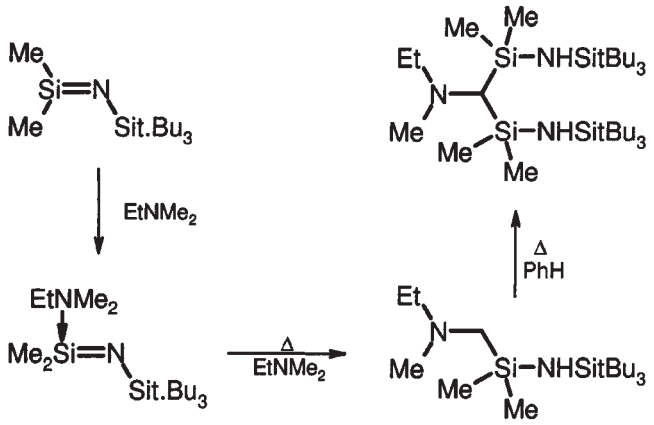
Scheme 50.



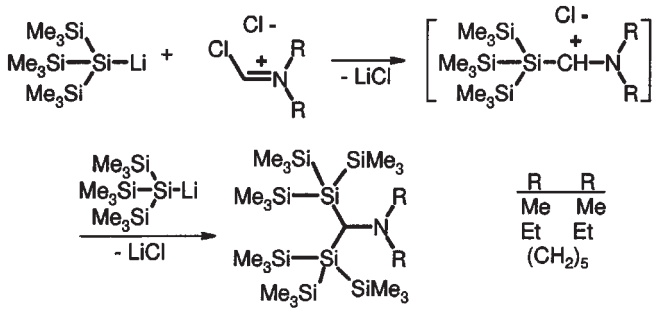
Scheme 51.



Scheme 52.



Scheme 53.



Reactions not involving the bis(trimethylsilyl)methyl group

Many chemical transformations have been performed on BSMA azetidin-2-ones that kept the bis(silyl)methyl group intact. For instance, 4-acyl azetidinones were obtained through ozonolysis of the corresponding 4-vinyl derivatives (36) (Scheme 47).

Similarly, neither Baeyer–Villiger oxidation with m.chloroperbenzoic acid (36), nor oxidation with lead tetra acetate (36) did not affect this group (Scheme 48).

Katritzky and Lam (12) observed the cleavage of the C—Si bond of *N*-(trimethylsilyl)methyl benzotriazoles with acid chlorides. Such a cleavage has not been observed with BSMA azetidinones in a sequence where a carboxylic functionality was reduced into a methyl group (62) (Scheme 49).

Deprotection of an amine on C_3 can be also performed using Li in liquid ammonia (31, 33, 62, 65) or hydrogen (60 psi) in the presence of $Pd(OH)_2$ catalyst (31) (Scheme 50).

IV. Miscellaneous

Obtention of some BSMa

It should be mentioned that some particular BSMa have been obtained by specific routes.

Thus, sodium borohydride reduction of bis(trimethylsilyl) carbonyl imines formed by insertion of isonitriles into the Si—Si bond, led to the obtention of secondary BSMA amines (59, 60) (Scheme 51).

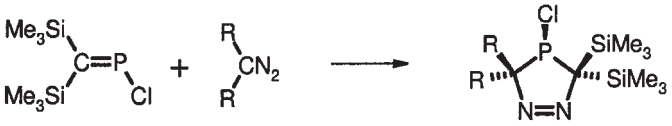
Under heating, trialkylamine stabilized silanimine gave rise to the formation of bis(aminosilyl)methylamine (66, 67) (Scheme 52).

Very recently, Oehme and co-workers (68, 69) published the synthesis of the very congested BSMA $[(Me_3Si)_3Si]_2C\text{-}NR_2$, (Scheme 53).

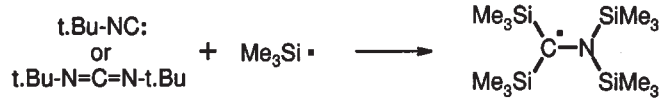
Cycloaddition of dialkyl, diaryl, and arylalky diazomethanes with C-bis(silyl)-P-chlorophosphaalkene yielded quantitatively not very stable BSMA cycloadducts (70) (Scheme 54).

© 2000 NRC Canada

Scheme 54.



Scheme 55.



Bis(trimethylsilyl) [bis(trimethylsilyl)amino]carbinyl radical

Reacting trimethylsilyl radical with *t*-butyl isocyanide or carbodiimide led to this C-centred radical after a series of addition and elimination reactions (71–73) (Scheme 55).

V. Conclusions

Bis(trimethylsilyl)methylamine, BSMA, a very easily accessible original amine was proven to be an efficient synthon at disposal to organic synthetic chemists. It is the source of a large variety of derivatives (BSMa) that can be expected to have biological activity. The presence of the bis(trimethylsilyl)methyl group gives BSMa an enhanced solubility in less polar solvents and induces a selective (or specific) regio- and stereochemistry because of its bulkiness. Thus, a quite different chemistry can be performed, in comparison with current chemistry of methylamine and *N*-methyl nitrogen derivatives. Moreover, this group can be readily transformed into a trimethylsilylmethyl or a methyl group (Scheme 56).

More interesting is the easy cleavage of bis(trimethylsilyl)methyl group and its replacement by a proton that has given benefit, in particular, in β-lactam chemistry.

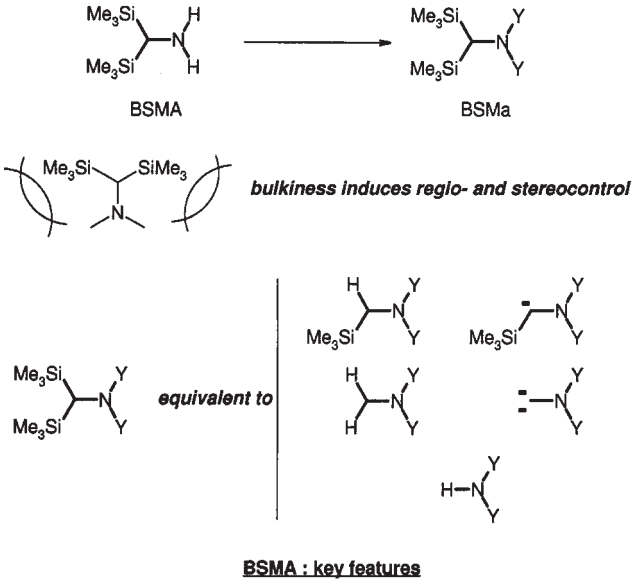
An important feature is that the catalytic cleavage of a silyl group by a fluoride anion delivers the corresponding α-nitrogen carbanion in very mild conditions. However, the remaining silyl group allows performing chemistry different from that performed using monosilylmethylamino derivatives.

In other words, BSMA is not simply another molecule in the extremely large collection of organic molecules. It is a real tool with which one can play efficiently. We are convinced that there is even more that can be done with BSMA, and new investigations are already underway in this domain.

VI. Acknowledgements

The author is very pleased to acknowledge all the persons who have contributed to this work. He would like to particularly thank his former students S. Grelier and T. Constantieux and Prof. J.M. Aizpurua, a former post-doc in his group, who initiated the research and established the basis of the chemistry of BSMA. Also acknowledged are the colleagues and their co-workers whose names appear along the references. Assistance by B. Barbe and M. Petraud (Cesamo, Université Bordeaux I) in solving difficult problems encountered in NMR analysis is well appreciated. Acknowledgements are due also to CNRS, Bordeaux I University, Aquitaine Regional Council and European Economic Community (Project SCI CT91/0648) whose financial support made this research possible.

Scheme 56.



VII. References

1. J.E. Noll, J.L. Speier, and B.F. Daubert. J. Am. Chem. Soc. **73**, 3867 (1951).
2. L.H. Sommer and J. Rocket. J. Am. Chem. Soc. **73**, 5130 (1951).
3. A.R. Katritzky and S. Sengupta. Tetrahedron Lett. **28**, 5419 (1987).
4. P. Patel and J. Joule. J. Chem. Soc. Chem. Commun. 1021 (1985).
5. R. Tacke and U. Wannagat. Topics Curr. Chem. **84**, 1 (1979).
6. E. Chang and V.K. Jain. Med. Chem. **9**, 433 (1966).
7. Ye.A. Mamayeva, O.V. Agafonova, V.N. Negrebetsky, A.G. Shipov, Yu.I. Baukov, and A.S. Losev. Khim. Farm. Zh. **28**, 26 (1994).
8. S. Barcza. U.S. Patent, 4 132 725 (1979); Chem. Abstr. **90**, 121 795 (1979).
9. K.W. Moberg. U.S. Patent, 4 510 136 (1983); R. Tacke, B. Becker, and D. Schomburg. Appl. Organometal. Chem. **3**, 133 (1989).
10. G.M. Banik and R.B. Silverman. J. Amer. Chem. Soc. **112**, 4499 (1990).
11. R. West and G.A. Gornowicz. J. Organometal. Chem. **25**, 385 (1970).
12. A.R. Katritzky and J.N. Lam. Heteroatom Chem. **1**, 21 (1990).
13. J.C. Cuevas, P. Patil, and V. Snieckus. Tetrahedron Lett. **30**, 5841 (1989).
14. C.J. Moody, C.W. Rees, and R.G. Young. J. Chem. Soc. Perkin Trans. 1, 323 (1991).
15. L. Brandsma, N.A. Nedolya, H.D. Verkruijsse, and B.A. Trofimov. Synthesis, 423 (1997).
16. C. Palomo, J.M. Aizpurua, M. Legido, J.P. Picard, J. Dunoguès, and T. Constantieux. Tetrahedron Lett. **33**, 3903 (1992).

© 2000 NRC Canada

17. M. Letellier, D.J. MacPhee, and D. Griller. Synth. Commun. **18**, 1975 (1988).
18. (*a*) J.P. Picard, S. Grelier, J. Dunoguès, J.M. Aizpurua, and C. Palomo. J. Organometal. Chem. **419**, C1 (1991); (*b*) J.P. Picard, S. Grelier, T. Constantieux, J. Dunoguès, J.M. Aizpurua, C. Palomo, M. Petraud, B. Barbe, L. Lunazzi, and J.M. Leger. Organometallics, **12**, 1378 (1993).
19. M. Heintz, O. Sock, C. Saboureau, J. Perichon, and M. Troupel. Tetrahedron, **44**, 1631 (1988).
20. S. Grelier, T. Constantieux, D. Deffieux, M. Bordeau, J. Dunoguès, J.P. Picard, C. Palomo, and J.M. Aizpurua. Organometallics, **13**, 3711 (1994).
21. A. Ekouya, R. Calas, J. Dunoguès, C. Biran, and N. Duffaut. J. Organometal. Chem. **177**, 137 (1979).
22. D.G. Anderson and D.W.H. Rankin. J. Chem. Soc. Dalton Trans. 779 (1989).
23. S. Brownstein, J. Dunoguès, D. Lindsay, and K. Ingold. J. Amer. Chem. Soc. **99**, 2073 (1977).
24. S. Grelier. Thesis, Bordeaux, France. 1991.
25. G. Barbaro, A. Battaglia, P. Giorgianni, A. Guerrini, and G. Seconi. J. Org. Chem. **60**, 6032 (1995).
26. T. Constantieux, S. Grelier, and J.P. Picard. Synlett, 510 (1998).
27. R.H. Higgins, Q.L. Eaton, L. Worth, and M.V. Peterson. J. Heterocyclic Chem. **24**, 255 (1987).
28. A. Capperucci, A. Ricci, G. Seconi, J. Dunoguès, S. Grelier, J.P. Picard, C. Palomo, and J.M. Aizpurua. J. Organometal. Chem. **458**, C1 (1993).
29. M.D. Hurwitz. U.S. Patent, 2 582 128; Chem. Abstr. **46**, 8146 (1954)]. See also: K.N. Campbell, A.H. Sommers, and B.K. Campbell. J. Amer. Chem. Soc. **66**, 82 (1944); M. Fischer and C. Djerassi. Chem. Ber. **99**, 1541 (1966).
30. M. Dal Colle, G. Distefano, D. Jones, A. Guerrini, G. Seconi, and A. Modelli. J. Chem. Soc. Perkin Trans. 2, 789 (1994).
31. C. Palomo, J.M. Aizpurua, M. Legido, A. Mielgo, and R. Galarza. Chem. Eur. J. 1432 (1997).
32. R. Galarza. Thesis, San Sebastian, Spain. 1997.
33. C. Palomo, J.M. Aizpurua, M. Legido, R. Galarza, P.M. Deya, J. Dunoguès, J.P. Picard, A. Ricci, and G. Seconi. Angew. Chem. Int. Ed. Engl. **35**, 1239 (1996).
34. J. Lasarte, C. Palomo, J.P. Picard, J. Dunoguès, and J.M. Aizpurua. J. Chem. Soc. Chem. Commun. 72 (1989).
35. A. Ricci, A. Guerrini, G. Seconi, A. Mordini, T. Constantieux, J.P. Picard, J.M. Aizpurua, and C. Palomo. Synlett, 955 (1994).
36. C. Palomo, J.M. Aizpurua, J.M. Garcia, J.P. Picard, and J. Dunoguès. Tetrahedron Lett. **31**, 1921 (1990).
37. B.F. Bonini, M. Fochi, M.C. Franchini, G. Mazzanti, A. Ricci, J.P. Picard, J. Dunoguès, J.M. Aizpurua, and C. Palomo. Synlett, 1321 (1997).
38. C. Palomo, J.M. Aizpurua, J.M. Garcia, R. Galarza, M. Legido, R. Urchegui, P. Roman, A. Luque, J. Server-Carrio, and A. Linden. J. Org. Chem. **62**, 2070 (1997).
39. Z. Gonzalez Glaria. Thesis, Pamplona, Spain. 1997.
40. S. Shimizu and M. Ogata. J. Org. Chem. **52**, 2314 (1987).
41. C. Palomo, J.M. Aizpurua, J.M. Garcia, I. Ganboa, F.P. Cossio, B. Lecea, and C. Lopez. J. Org. Chem. **55**, 2498 (1990).
42. A.R. Katritzky, R.J. Offerman, P. Cabildo, and M. Soleiman. Rec. Trav. P.-B. **107**, 641 (1988).
43. V. Snieckus. Pure Appl. Chem. **62**, 671 (1990).
44. P.A. Patil and V. Snieckus. Tetrahedron Lett. **39**, 1325 (1998).
45. J. Thiele and J. Schneider. Liebigs Ann. Chim. **347**, 117 (1906), and 369, 287 (1909). I. Takahashi, T. Kawakami, E. Hirano, H. Yokota, and H. Kitajima. Synlett, 353 (1996). S.M. Allin and C.C. Hodkinson. Synlett, 781 (1996).
46. T. Hirao, A. Yamada, Y. Ohshiro, and T. Agawa. Angew. Chem. Int. Ed. Engl. **20**, 126 (1980).
47. T. Hirao, A. Yamada, K. Hayashi, Y. Ohshiro, and T. Agawa. Bull. Soc. Chim. Jpn. **55**, 1163 (1981).
48. N. Imai, Y. Terao, and K. Achiwa. J. Syn. Org. Chem. Jpn. **43**, 862 (1985).
49. E. Vedejs and F.G. West. Chem. Rev. **86**, 941 (1986).
50. Y. Terao, M. Aono, and K. Achiwa. Heterocycles, **27**, 981 (1988).
51. K. Achiwa, T. Motoyama, and M. Sekiya. Chem. Pharm. Bull. **31**, 3939 (1983).
52. O. Tsuge, S. Kanemasa, A. Hatada, and K. Matsuda. Bull. Chem. Soc. Jpn. **59**, 2537 (1986).
53. A. Padwa, J.R. Gasdaska, G. Haffsmanns, and H. Rebello. J. Org. Chem. **52**, 1027 (1987). See also references 1–8 cited therein.
54. J.M. Harris, J.C. Walton, B. Maillard, S. Grelier, and J.P. Picard. J. Chem. Soc. Perkin Trans. 2, 2119 (1993).
55. C. Palomo, J.M. Aizpurua, J.M. Garcia, and M. Legido. J. Chem. Chem. Commun. 524 (1991).
56. M. Ohno, H. Miyata, M. Komatsu, and Y. Ohshiro. Tetrahedron Lett. **32**, 5093 (1991).
57. T. Constantieux. Thesis, Bordeaux, France. 1994.
58. M. Schlosser. Pure Appl. Chem. **60**, 1627 (1988).
59. Y. Ito, S. Nishimura, and M. Ishikawa. Tetrahedron Lett. **28**, 1293 (1987).
60. Y. Ito, T. Matsuura, and M. Murakami. J. Amer. Chem. Soc. **110**, 3692 (1988).
61. H. Staudinger. Liebigs Ann. Chem. **351**, 51 (1907).
62. C. Palomo, J.M. Aizpurua, R. Galarza, M. Iturburu, and M. Legido. Bioorg. Med. Chem. Lett. **3**, 2461 (1993).
63. A. Arrieta, F.P. Cossio, J.M. Garcia, B. Lecea, and C. Palomo. Tetrahedron Lett. **29**, 3129 (1988).
64. W. Dürkheimer, J. Blumbach, R.Latrell, and K.H. Sheunemann. Angew. Chem. Int. Ed. Engl. **24**, 180, 1985; O. Nakaguchi, T. Oku, H. Takeno, M. Hashimoto, and T. Kamiya. Chem. Pharm. Bull. **35**, 3885 (1987).
65. C. Palomo, J.M. Aizpurua, M. Legido, and R. Galarza. Chem. Commun. 233 (1997).
66. N. Wiberg, G. Preiner, P. Karampatses, C-K. Kim, and K. Schurz. Chem. Ber. **120**, 1357 (1987).
67. N. Wiberg and K. Schurz. J. Organomet. Chem. **341**, 145 (1988).
68. T. Gross, R. Kempe, and H. Oehme. Inorg. Chem. Commun. **1**, 128 (1998).
69. T. Gross, R. Kempe, and H. Oehme. Eur. J. Inorg. Chem. 21 (1999).
70. J.Y. Thoraval, W. Nagaï, Y.Y.C. Yeung Lam Ko, and R. Carrié. Tetrahedron Lett. **46**, 3859 (1990).
71. R.A. Kaba, D. Griller, and K.U. Ingold. J. Am. Chem. Soc. **96**, 6202 (1974).
72. G. Brunton, J.F. Taylor, and K.U. Ingold. J. Am. Chem. Soc. **98**, 4879 (1976).
73. G. Brunton, D. Forrest, D. Griller, K.U. Ingold, and A.H. Reddoch. J. Am. Chem. Soc. **100**, 3721 (1978).

© 2000 NRC Canada

Di[(hydroxyalkyl)dimethylammonium] tris[benzene-1,2-diolato(2–)]silicates and their germanium analogs: syntheses, crystal structure analyses, and NMR studies

Reinhold Tacke, Alistair Stewart, Joachim Becht, Christian Burschka, and Ingo Richter

Abstract: Treatment of $Si(OMe)_4$ with three molar equivalents of 1,2-$C_6H_4(OH)_2$ (= 1,2-dihydroxybenzene) and two molar equivalents of $HO(CH_2)_nNMe_2$ (n = 2, 3) in acetonitrile at room temperature yields the λ^6Si-silicates $(HO(CH_2)_nNMe_2H)_2(SiL_3)$ (**5**: n = 2; **6**: n = 3; L^{2-} = 1,2-$C_6H_4(O)_2^{2-}$ (= benzene-1,2-diolato(2–))). The analogous λ^6Ge-germanates $(HO(CH_2)_nNMe_2H)_2(GeL_3)$ (**7**: n = 2; **8**: n = 3) were synthesized analogously starting from $Ge(OMe)_4$. Compounds **5**·2CH_3CN and **6**–**8** were structurally characterized by single-crystal X-ray diffraction. In addition, aqueous solutions of the Si/Ge analogs **5**/**7** and **6**/**8** were studied by NMR spectroscopy. The title compounds may be regarded as model systems for the transport and storage of silicon in biological systems and as tools to investigate biosilification.

Key words: hexacoordinate silicon, hexacoordinate germanium, silicon biochemistry

Résumé : Le traitement de $Si(OMe)_4$ avec trois équivalents molaires de 1,2-dihydroxybenzène (= 1,2-$C_6H_4(OH)_2$) et deux équivalents molaires de $HO(CH_2)_nNMe_2$ (n = 2, 3), dans l'acétonitrile, à la température ambiante, conduit aux λ^6Si-silicates $(HO(CH_2)_nNMe_2H)_2(SiL_3)$ (**5**: n = 2; **6** n = 3; L^{2-} = 1,2-$C_6H_4(O)_2^{2-}$ (= benzène-1,2-diolato(2–))). Utilisant le $Ge(OMe)_4$ comme produit de départ, on a synthétisé les λ^6Ge-germanates analogues $(HO(CH_2)_nNMe_2H)_2(GeL_3)$ (**7**: n = 2; **8** n = 3). Faisant appel à la diffraction des rayons X, on a caractérisé la structure des composés **5**·CH_3CN et **6**–**8**. De plus faisant appel à la spectroscopie RMN, on a étudié les analogues Si/Ge **5**/**7** et **6**/**8** en solution. On peut considérer que les composés mentionnés dans le titre sont des systèmes modèles pour le transport et l'emmagasinage du silicium dans les systèmes biologiques et comme des instruments pour étudier la biosilification.

Mots clés : silicium hexacoordiné, germanium hexacoordiné, biochimie du silicium.

[Traduit par la Rédaction]

Introduction

As reported recently (1), tetramethoxysilane reacts with α-hydroxycarboxylic acids and aminoalkanols (molar ratio 1:2:1) in acetonitrile to yield zwitterionic λ^5Si-silicates with an SiO_5 skeleton, such as compounds **1** and **2** (for a comprehensive review dealing with zwitterionic λ^5Si-silicates see ref. 2). Surprisingly, all attempts to synthesize the related zwitterionic pentacoordinate silicon compounds **3** and **4** by using 1,2-dihydroxybenzene instead of 2-methyllactic acid failed. Even when using the required stoichiometric ratio 1:2:1 ($Si(OMe)_4$:1,2-$C_6H_4(OH)_2$:$HO(CH_2)_nNMe_2$), we rather isolated the ionic λ^6Si-silicates **5**·2CH_3CN and **6**. The corresponding germanium analogs, the ionic λ^6Ge-germanates **7** and **8**, can be prepared analogously starting from tetramethoxygermane. We report here on the optimized synthesis of compounds **5**·2CH_3CN and **6**–**8** and their structural characterization in the solid state (crystal structure analyses, ^{29}Si CP/MAS NMR studies) and in solution (^{1}H, ^{13}C, and ^{29}Si NMR investigations) (for a comprehensive review dealing with hexacoordinate silicon and germanium compounds see ref. 3). As will be discussed in the "Biological aspects" section, the title compounds may be regarded as model systems for the transport and storage of silicon in biological systems and as tools to investigate biosilification.

Experimental

Materials

All syntheses were carried out under dry nitrogen. The organic solvents and reagents were dried and purified according to standard procedures and stored under nitrogen.

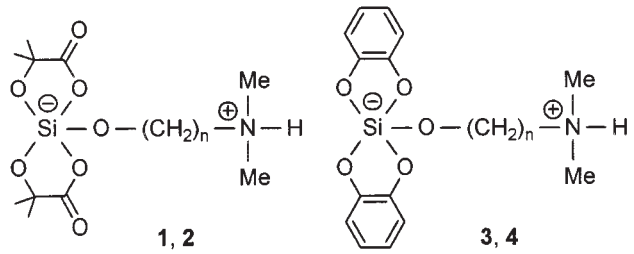
Received July 15, 1999. Published on the NRC Research Press website on October 20, 2000.

This paper is dedicated to Professor Adrian Brook in recognition of his outstanding contributions to organosilicon chemistry.

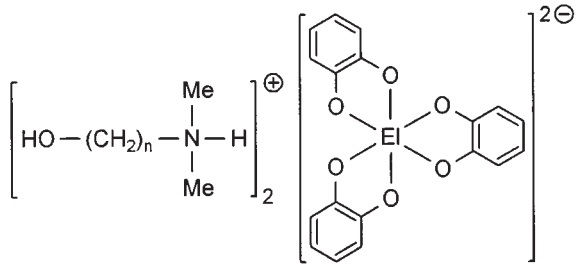
R. Tacke,[1] A. Stewart, J. Becht, C. Burschka, and I. Richter. Institut für Anorganische Chemie, Universität Würzburg, Am Hubland, D-97074 Würzburg, Germany.

[1]Author to whom correspondence may be addressed. Telephone: (931)888-5250. Fax: (931)888-4609. e-mail: r.tacke@mail.uni-wuerzburg.de

 © 2000 NRC Canada



1, 2 3, 4



5–8

	n
1, 3	2
2, 4	3

	5	6	7	8
El	Si	Si	Ge	Ge
n	2	3	2	3

Tetramethoxysilane, tetramethoxygermane, 1,2-dihydroxybenzene, 2-(dimethylamino)ethanol, and 3-(dimethylamino)propanol were purchased from Aldrich Chemical Co.

Physical measurements

Melting points were determined with a Büchi Melting Point B-540 apparatus using samples in sealed capillaries. The ^{1}H, ^{13}C, and ^{29}Si solution NMR spectra were recorded at room temperature on a Bruker DRX-300 NMR spectrometer (^{1}H, 300.1 MHz; ^{13}C, 75.5 MHz; ^{29}Si, 59.6 MHz). D_2O was used as solvent. Chemical shifts (ppm) were determined relative to internal DHO (^{1}H, δ = 4.70) and external TMS (^{13}C, δ = 0; ^{29}Si, δ = 0). The ^{1}H NMR spectra of **5** and **6** were additionally recorded on a Bruker DRX-600 NMR spectrometer (^{1}H, 600.1 MHz) to resolve the ^{1}H spin systems of the benzene-1,2-diolato(2–) ligands. The ^{1}H spin systems were analyzed by using the Bruker program WINDAISY (4). Assignment of the ^{13}C NMR data was supported by DEPT 135 experiments. ^{29}Si CP/MAS NMR spectra were recorded at room temperature on a Bruker DSX-400 NMR spectrometer with bottom layer rotors of ZrO_2 (diameter 7 mm) containing ca. 300 mg of sample (79.5 MHz; TMS as external standard (δ = 0); spinning rate 5000 Hz; contact time 5 ms; 90° ^{1}H transmitter pulse length 3.6 μs; repetition time 4 s).

Syntheses

*Synthesis of di[(2-hydroxyethyl)dimethylammonium] tris[benzene-1,2-diolato(2–)]silicate–diacetonitrile (**5**·2CH$_3$CN)*

2-(Dimethylamino)ethanol (891 mg, 10.0 mmol) and then tetramethoxysilane (761 mg, 5.00 mmol) were added to a stirred solution of 1,2-dihydroxybenzene (1.65 g, 15.0 mmol) in acetonitrile (25 mL) at room temperature (formation of a precipitate after a few seconds). After the reaction mixture was kept for 24 h at room temperature, the precipitate was isolated by filtration, recrystallized from acetonitrile (slow cooling of a saturated boiling solution to room temperature and then to –20°C), washed with diethyl ether and dried in vacuo (0.01 torr (1 torr = 133.322 Pa), 20°C, 1 h) to give 2.46 g (92% yield) of a colorless crystalline product (loss of CH_3CN at ca. 80°C, mp 230°C, dec.). ^{1}H NMR (600.1 MHz, D_2O) δ: 1.99 (CH_3CN), 2.73 (s, 12 H, NCH_3), 3.07 (m, centered, 4 H, CCH_2N), 3.76 (m, centered, 4 H, CCH_2O), 6.56 (δ_A) and 6.58 (δ_B) (AA′BB′ system, $^{3}J_{AB} = {}^{3}J_{A'B'} = 7.6$ Hz, $^{3}J_{BB'} = 7.6$ Hz, $^{4}J_{AB'} = {}^{4}J_{A'B} = 1.5$ Hz, $^{5}J_{AA'} = 0.3$ Hz, 12 H, silicate anion); 6.75–6.87 (m, free 1,2-dihydroxybenzene). ^{13}C NMR (D_2O) δ: 1.19 CH_3CN), 43.2 (NCH_3), 55.9 (CCH_2N), 59.1 (CCH_2O), 111.3 (aromatic C-4/C-5), 118.3 (aromatic C-3/C-6), 119.6 (CH_3CN), 149.7 (aromatic C-1/C-2); 116.6, 121.0, 145.2 (free 1,2-dihydroxybenzene). ^{29}Si NMR (D_2O) δ: –144.0. ^{29}Si CP/MAS NMR (45 transients) δ: –141.2. Anal. calcd. for $C_{30}H_{42}N_4O_8Si$: C 58.61, H 6.89, N 9.11; found: C 58.57, H 6.74, N 9.02.

*Synthesis of di[(3-hydroxypropyl)dimethylammonium] tris[benzene-1,2-diolato(2–)]silicate (**6**)*

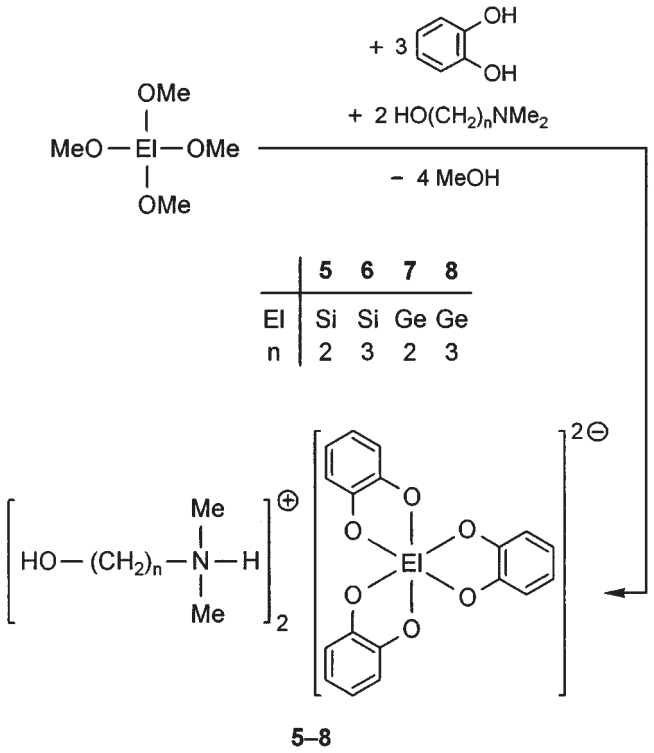
The same procedure was followed as described for the synthesis of **5**·2CH$_3$CN (tetramethoxysilane (761 mg, 5.00 mmol), 3-(dimethylamino)propanol (1.03 g, 10.0 mmol), 1,2-dihydroxybenzene (1.65 g, 15.0 mmol), acetonitrile (25 mL)). Compound **6** was isolated in 75% yield (2.09 g) as a crystalline solid (mp 238°C, dec.). ^{1}H NMR (600.1 MHz, D_2O) δ: 1.84 (m, centered, 4 H, CCH_2C), 2.74 (s, 12 H, NCH_3), 3.06 (m, centered, 4 H, CCH_2N), 3.59 (m, centered, 4 H, CCH_2O), 6.56 (δ_A) and 6.58 (δ_B) (AA′BB′ system, $^{3}J_{AB} = {}^{3}J_{A'B'} = 7.6$ Hz, $^{3}J_{BB'} = 7.7$ Hz, $^{4}J_{AB'} = {}^{4}J_{A'B} = 1.5$ Hz, $^{5}J_{AA'} = 0.4$ Hz, 12 H, silicate anion); 6.75–6.87 (m, free 1,2-dihyroxybenzene). ^{13}C NMR (D_2O) δ: 26.9 (CCH_2C), 43.1 (NCH_3), 55.9 (CCH_2N), 59.1 (CCH_2O), 111.3 (aromatic C-4/C-5), 118.3 (aromatic C-3/C-6), 149.7 (aromatic C-1/C-2); 116.5, 121.0, 145.2 (free 1,2-dihydroxybenzene). ^{29}Si NMR (D_2O) δ: –144.0. ^{29}Si CP/MAS NMR (830 transients) δ: –141.5. Anal. calcd. for $C_{28}H_{40}N_2O_8Si$: C 59.98, H 7.19, N 5.00; found: C 59.89, H 7.13, N 5.24.

*Synthesis of di[(2-hydroxyethyl)dimethylammonium] tris[benzene-1,2-diolato(2–)]germanate (**7**)*

The same procedure was followed as described for the synthesis of **5**·2CH$_3$CN, however, the product was crystallized by slow cooling to room temperature without further cooling to –20°C (tetramethoxygermane (492 mg, 2.50 mmol), 2-(dimethylamino)ethanol (445 mg, 4.99 mmol), 1,2-dihydroxybenzene (825 mg, 7.49 mmol), acetonitrile (15 mL)). Compound **7** was isolated in 81% yield (1.17 g) as a colorless crystalline solid (mp 266°C, dec.). ^{1}H NMR (D_2O) δ: 2.70 (s, 12 H, NCH_3), 3.04 (m, centered, 4 H, CCH_2N), 3.69 (m, centered, 4 H, CCH_2O), 6.54 (δ_A) and 6.59 (δ_B) (AA′BB′ system, $^{3}J_{AB} = {}^{3}J_{A'B'} = 7.7$ Hz, $^{3}J_{BB'} = 7.7$ Hz, $^{4}J_{AB'} = {}^{4}J_{A'B} = 1.5$ Hz, $^{5}J_{AA'} = 0.3$ Hz, 12 H, germanate anion). ^{13}C NMR (D_2O) δ: 43.0 (NCH_3), 55.4 (CCH_2N), 59.0 (CCH_2O), 112.3 (aromatic C-4/C-5), 118.3 (aromatic C-3/C-6), 149.2 (aromatic C-1/C-2). Anal. calcd. for $C_{30}H_{42}N_2O_8Ge$: C 54.12, H 6.29, N 4.86; found: C 54.00, H 6.02, N 4.85.

© 2000 NRC Canada

Scheme 1.



5–8

*Synthesis of di[(3-hydroxypropyl)dimethylammonium] tris[benzene-1,2-diolato(2–)]germanate (**8**)*

The same procedure was followed as described for the synthesis of **5**·2CH_3CN, however, the product was crystallized by slow cooling to room temperature without further cooling to –20°C (tetramethoxygermane (492 mg, 2.50 mmol), 3-(dimethylamino)propanol (515 mg, 4.99 mmol), 1,2-dihydroxybenzene (825 mg, 7.49 mmol), acetonitrile (15 mL)). Compound **8** was isolated in 84% yield (1.27 g) as a crystalline solid (mp 266°C, dec.). ^{1}H NMR (D_2O) δ: 1.80 (m, centered, 4 H, CCH_2C), 2.72 (s, 12 H, NCH_3), 3.04 (m, 4 H, CCH_2N), 3.54 (m, 4 H, CCH_2O), 6.55 (δ_A) and 6.60 (δ_B) (AA′BB′ system, $^3J_{AB} = {}^3J_{A'B'} = 7.7$ Hz, $^3J_{BB'} = 7.7$ Hz, $^4J_{AB'} = {}^4J_{A'B} = 1.5$ Hz, $^5J_{AA'} = 0.3$ Hz, 12 H, germanate anion). ^{13}C NMR (D_2O) δ: 26.7 (CCH_2C), 43.1 (NCH_3), 55.9 (CCH_2N), 59.0 (CCH_2O), 112.3 (aromatic C-4/C-5), 118.3 (aromatic C-3/C-6), 149.2 (aromatic C-1/C-2). Anal. calcd. for $C_{28}H_{40}N_2O_8Ge$: C 55.57, H 6.66, N 4.63; found: C 55.67, H 6.57, N 4.65.

Crystal structure analyses[2]

Suitable single crystals of **5**·2CH_3CN and **6**–**8** were obtained by crystallization from solutions in acetonitrile. The crystals were mounted in inert oil on a glass fiber and then transferred to the cold nitrogen stream of the diffractometer (Stoe IPDS, monochromated Mo Kα radiation (λ = 0.71073 Å)). No absorption correction was applied. The structures were solved by direct methods (5). All non-hydrogen atoms were refined anisotropically (6). A riding model was employed in the refinement of the C*H* hydrogen atoms. Except for **7**, the positions of the N*H* and O*H* hydrogen atoms were localized in difference fourier syntheses and refined freely. In the structure of **7**, the cation was found to be disordered at 263 K and hence none of its hydrogen atoms could be localized. As **7** undergoes a phase transition on cooling, a crystal structure analysis at 173 K failed.

Results and discussion

Syntheses

The ionic λ^{6}Si-silicates **5** and **6** were synthesized according to Scheme 1 by treatment of tetramethoxysilane with 1,2-dihydroxybenzene and the respective aminoalkanol (molar ratio 1:3:2). The corresponding λ^{6}Ge-germanates **7** and **8** were prepared analogously starting from tetramethoxygermane (Scheme 1). All syntheses were performed in acetonitrile at room temperature and the products **5**·2CH_3CN and **6**–**8** were isolated in high yields as crystalline solids (yields after recrystallization from acetonitrile: **5**·2CH_3CN, 92%; **6**, 75%; **7**, 81%; **8**, 84%). The identity of these compounds was established by elemental analyses (C, H, N), crystal structure analyses, as well as solid-state (^{29}Si) and solution (^{1}H, ^{13}C, ^{29}Si) NMR studies.

Physical and chemical properties

Compounds **5**·2CH_3CN and **6**–**8** are high-melting solids that are almost insoluble in non-polar and even in most polar organic solvents at room temperature. However, they were found to be soluble in DMSO and sparingly soluble in water.

Studies with freshly prepared aqueous solutions of **5**–**8** at room temperature (c = ca. 4×10^{-2} mol L^{-1}) revealed pH values of ca. 8.3 (λ^{6}Si-silicates) and ca. 7.4 (λ^{6}Ge-germanates), respectively (in this context, see also section "NMR studies"). Preliminary studies with **5** and **6** demonstrated breakdown of these λ^{6}Si-silicates upon a lowering of the pH value by addition of hydrochloric acid: At pH 6 (initial value) and after standing for three days at room temperature, a gel (silica gel; composition not yet studied in detail) was formed from aqueous solutions of **5** and **6**. Further experiments are necessary to study the kinetics of this process and to characterize the nature of the silica gel formed.

Crystal structure analyses

The crystal structures of compounds **5**·2CH_3CN and **6**–**8** were determined by single-crystal X-ray diffraction. The crystal data and experimental parameters used for these studies are given in Table 1 (for further details, see "Experimental section").

Compounds **5**·2CH_3CN and **7** crystallize in the space groups *C*2/*c* and *Fdd*2, respectively. The central silicon and germanium atom of the respective anions is located on a 2–fold axis (special positions: 0, *y*, 1/4 (**5**·2CH_3CN); 0, 0, *z* (**7**)). Thus, the asymmetric unit contains half of the anion and one cation (and one additional acetonitrile molecule in

[2] Crystallographic data (excluding structure factors) for the structures reported in this paper have been deposited with the Cambridge Crystallographic Data Centre (CCDC 129242 (**5**·2CH_3CN), CCDC 129243 (**6**), CCDC 129244 (**7**), and CCDC 129245 (**8**)). Copies of the data can be obtained, free of charge, on application to the Director, CCDC, 12 Union Road, Cambridge CB2 1EZ, U.K. (Fax: 44-1223-336033 or e-mail: deposit@ccdc.cam.ac.uk).

© 2000 NRC Canada

Table 1. Crystal data and experimental parameters for the crystal structure analyses of **5**·2CH_3CN and **6**–**8**.

Compound	**5**·2CH_3CN	**6**	**7**	**8**
Empirical formula	$C_{30}H_{42}N_4O_8Si$	$C_{28}H_{40}N_2O_8Si$	$C_{26}H_{36}GeN_2O_8$	$C_{28}H_{40}GeN_2O_8$
Formula mass (g mol^{-1})	614.77	560.71	577.16	605.21
Collection *T* (K)	173(2)	173(2)	263(2)	173(2)
λ(Mo Kα) (Å)	0.71073	0.71073	0.71073	0.71073
Crystal system	monoclinic	monoclinic	orthorhombic	monoclinic
Space group (no.)	*C*2/*c* (15)	$P2_1/c$ (14)	*Fdd*2 (43)	$P2_1/c$ (14)
a (Å)	14.4222(13)	12.9455(16)	14.752(3)	13.081(3)
b (Å)	10.8328(13)	10.1656(9)	35.790(7)	10.165(2)
c (Å)	20.5638(16)	21.326(3)	9.992(2)	21.412(4)
β (deg)	90.670(10)	91.985(14)	–	92.62(3)
V ($Å^3$)	3212.5(5)	2804.9(5)	5275.8(18)	2844.0(10)
Z	4	4	8	4
D(calcd) (g cm^{-3})	1.271	1.328	1.453	1.413
μ (mm^{-1})	0.127	0.136	1.213	1.129
F(000)	1312	1200	2416	1272
Crystal dimensions (mm)	0.6 × 0.5 × 0.4	0.5 × 0.4 × 0.4	0.5 × 0.5 × 0.4	0.5 × 0.5 × 0.4
2θ range (deg)	4.70–56.16	5.10–56.14	4.56–54.10	5.08–54.12
Index ranges	$-19 \le h \le 19$, $-14 \le k \le 14$, $-25 \le l \le 25$	$-17 \le h \le 17$, $-13 \le k \le 13$, $-28 \le l \le 28$	$-18 \le h \le 14$, $-45 \le k \le 45$, $-12 \le l \le 11$	$-16 \le h \le 15$, $-13 \le k \le 12$, $-27 \le l \le 27$
No. of collected reflections	17619	21528	8127	20938
No. of independent reflections	3595	6650	2636	6041
R_{int}	0.0478	0.0455	0.0283	0.0351
No. of reflections used	3595	6650	2636	6041
No. of parameters	204	368	214	368
No. of restraints	0	0	71	0
S^a	1.055	0.999	1.026	1.014
Weight parameters $(a/b)^b$	0.0697/0.7947	0.0684/0.0000	0.0664/0.0000	0.0472/0.0688
$R1^c$ ($I > 2\sigma(I)$)	0.0394	0.0381	0.0332	0.0268
$wR2^d$ (all data)	0.1131	0.1063	0.0879	0.0723
Max/min residual electron density (e $Å^{-3}$)	+0.471/–0.310	+0.379/–0.349	+0.491/–0.432	+0.290/–0.350

[a] $S = \{\Sigma[w(F_o^2 - F_c^2)^2]/(n-p)\}^{0.5}$; *n* = no. of reflections; *p* = no. of parameters.
[b] $w^{-1} = \sigma^2(F_o^2) + (aP)^2 + bP$, with $P = (\text{Max } F_o^2, 0 + 2F_c^2)/3$.
[c] $R1 = \Sigma||F_o| - |F_c||/\Sigma|F_o|$.
[d] $wR2 = \{\Sigma[w(F_o^2 - F_c^2)^2]/\Sigma[w(F_o^2)^2]\}^{0.5}$.

the case of **5**·2CH_3CN). The Si/Ge analogs **6** and **8** crystallize in the space group $P2_1/c$ with two cations and one anion in the asymmetric unit, the crystal structures being isotypic.

The crystal structure analyses of **5**·2CH_3CN and **6**–**8** reveal the silicon and germanium atoms of the respective λ^{6}Si-silicate and λ^{6}Ge-germanate anions to be octahedrally coordinated (Figs. 1–3, Tables 2 and 3). There are only small distortions from the ideal octahedral geometry with O–Si–O (O–Ge–O) angles in the ranges 87.53(4)–95.00(5)° (86.01(17)–96.10(5)°) and 174.42(6)–176.80(5)° (172.93(18)–174.76(4)°). The Si–O (Ge–O) distances are in the range 1.7742(10)–1.7984(10) Å (1.8758(11)–1.9002(10) Å). The structural features observed for the SiO_6 and GeO_6 skeletons of **5**·2CH_3CN and **6**–**8** are similar to those already reported for other compounds containing the tris[benzene-1,2-diolato(2–)]silicate (7–9) and tris[benzene-1,2-diolato(2–)]germanate anion (10).

As expected from the presence of the potential N–H and O–H donor functions of the cations and the six potential oxygen acceptor atoms of the anions, both N–H···O and (except for **7**) O–H···O hydrogen bonds are observed in the crystals of **5**·2CH_3CN and **6**–**8**. Considering the relevant geometric parameters (11), the existence of intermolecular bifurcate N1–H1···O2/O3A and intermolecular nonfurcate O4–H4···O3A hydrogen bonds in the crystal of **5**·2CH_3CN can be assumed (Fig. 1, Table 4). In the case of compounds **6** and **8**, intermolecular bifurcate N1–H1···O3/O5 and N2–H2···O2/O6 hydrogen bonds as well as intermolecular nonfurcate O7A–H7A···O4 and O8A–H8A···O1 hydrogen bonds were observed (Fig. 2, Table 4). For compound **7**, the existence of an intermolecular bifurcate N1–H1···O2/O3A hydrogen bond can be assumed (Fig. 3).

A closer inspection of the hydrogen bonding systems observed for **5**·2CH_3CN, **6**, and **8** reveals that the protonated aminoalkanols are particularly useful cations for stabilizing the crystal structures of salts that contain anions of the tris[benzene-1,2-diolato(2–)]silicate and tris[benzene-1,2-diolato(2–)]germanate type. In addition to N–H···O interactions, cations of this particular type can also form O–H···O hydrogen bonds between cation and anion.

NMR studies

The silicon compounds **5**·2CH_3CN and **6** were investigated by ^{29}Si CP/MAS NMR experiments. The isotropic ^{29}Si

© 2000 NRC Canada

Fig. 1. Structure of the cation and anion in the crystal of **5**·2CH_3CN (probability level of thermal displacement ellipsoids 50%). The dashed lines indicate hydrogen bonds between the cation and anion.

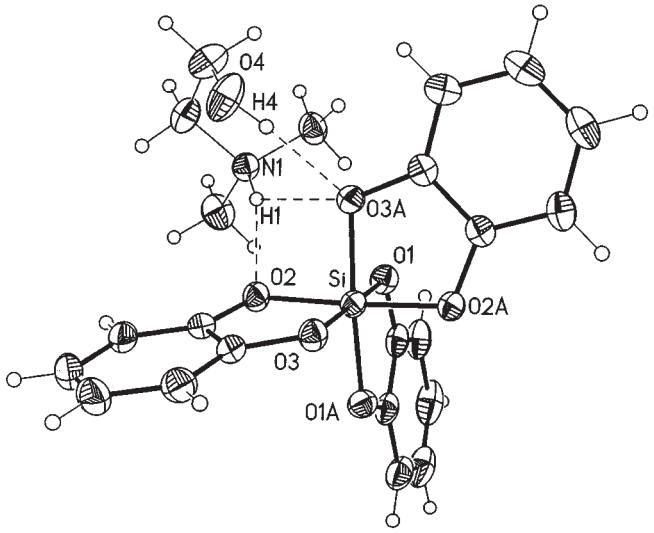
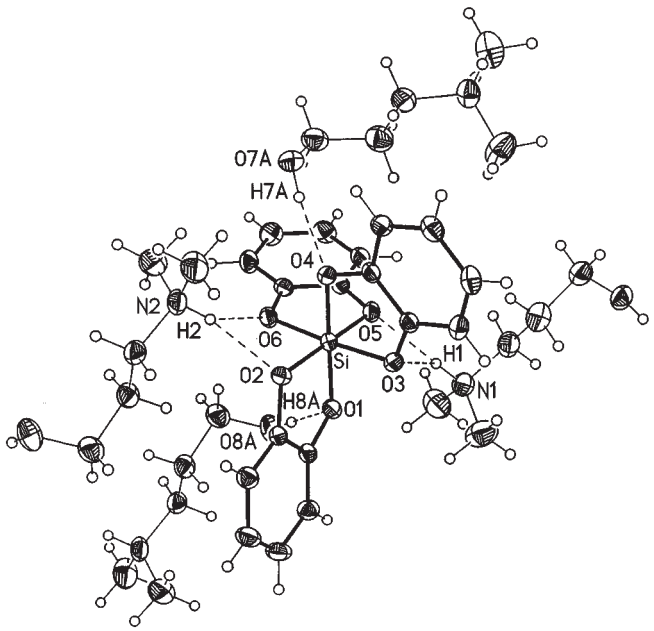


Fig. 2. Structure of the two crystallographically independent cations and the anion in the crystal of **6** (probability level of thermal displacement ellipsoids 50%). The dashed lines indicate hydrogen bonds between the cations and the anion. The crystal structure of the germanium analog **8** is isotypic.



chemical shifts obtained in these studies (**5**·2CH_3CN, δ = –141.2; **6,** δ = –141.5) clearly characterize the ^{29}Si resonances as arising from hexacoordinate silicon atoms. As these ^{29}Si chemical shifts are very similar to those obtained for **5** (δ = –144.0) and **6** (δ = –144.0) in D_2O, it is concluded that hexacoordinate silicon is also present in aqueous solution. Furthermore, both the ^1H and ^{13}C solution NMR data of **5**–**8** (solvent D_2O; $c = 4 \times 10^{-2}$ mol L^{-1}, room temperature) were found to be compatible with the presence of the λ^6Si-silicate and λ^6Ge-germanate anion of these compounds, the spectra of the respective Si/Ge analogs **5**/**7** and **6**/**8** being very similar. Thus, the results of the solid-state and solution NMR experiments unequivocally demonstrate that the tris[benzene-1,2-diolato(2–)]silicate and tris[benzene-1,2-diolato(2–)]germanate anion also exists in aqueous solution (for NMR studies of related λ^6Si-silicates with three bidentate ligands of the benzene-1,2-diolato(2–) type in aqueous solution, see ref. 13).

Interestingly, the ionic λ^6Si-silicates **5** and **6** are not sufficiently stable in D_2O to obtain ^1H and ^{13}C NMR spectra without resonance signals of the respective breakdown products: Even with fast measurement of freshly prepared solutions resonance signals corresponding to free 1,2-dihydroxybenzene were observed (Fig. 4). Formation of 1,2-dihydroxybenzene was found to occur immediately upon addition of **5**·2CH_3CN and **6** to D_2O; however, ^1H NMR studies showed this to be a

Fig. 3. Structure of the cation and anion in the crystal of **7** (probability level of thermal displacement ellipsoids 50%). The dashed lines indicate hydrogen bonds between the cation and anion.

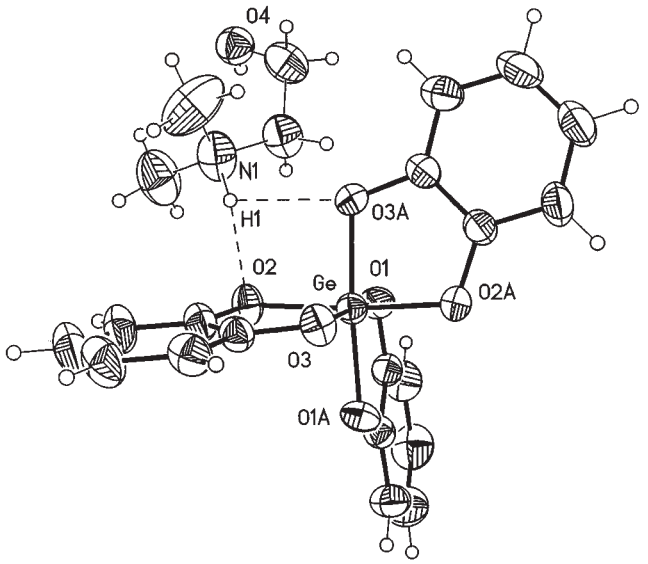


Table 2. Selected interatomic distances (Å) and angles (°) for **5**·2CH_3CN and **7**.[a, b]

	5·2CH_3CN	**7**
El—O1 (El—O1A)	1.7736(9)	1.893(3)
El—O2 (El—O2A)	1.7907(8)	1.893(2)
El—O3 (El—O3A)	1.7979(9)	1.886(3)
O1–El–O1A	89.59(6)	86.01(17)
O1–El–O2 (O1A–El–O2A)	89.41(4)	90.19(11)
O1–El–O2A (O1A–El–O2)	94.55(4)	94.99(12)
O1–El–O3 (O1A–El–O3A)	176.09(4)	174.01(15)
O1–El–O3A (O1A–El–O3)	88.30(4)	89.18(10)
O2–El–O2A	174.42(6)	172.93(18)
O2–El–O3 (O2A–El–O3A)	87.48(4)	86.66(11)
O2–El–O3A (O2A–El–O3)	88.72(4)	88.60(11)
O3–El–O3A	93.98(6)	95.82(19)

[a] **5**·2CH_3CN: El = Si; **7**: El = Ge.

[b] Atoms suffixed with "A" are generated by a crystallographic 2-fold axis, which bisects the ligand with the atoms O1 and O1A.

Interestingly, the ionic λ^6Si-silicates **5** and **6** are not sufficiently stable in D_2O to obtain ^1H and ^{13}C NMR spectra without resonance signals of the respective breakdown products: Even with fast measurement of freshly prepared solutions resonance signals corresponding to free 1,2-dihydroxybenzene were observed (Fig. 4). Formation of 1,2-dihydroxybenzene was found to occur immediately upon addition of **5**·2CH_3CN and **6** to D_2O; however, ^1H NMR studies showed this to be a

© 2000 NRC Canada

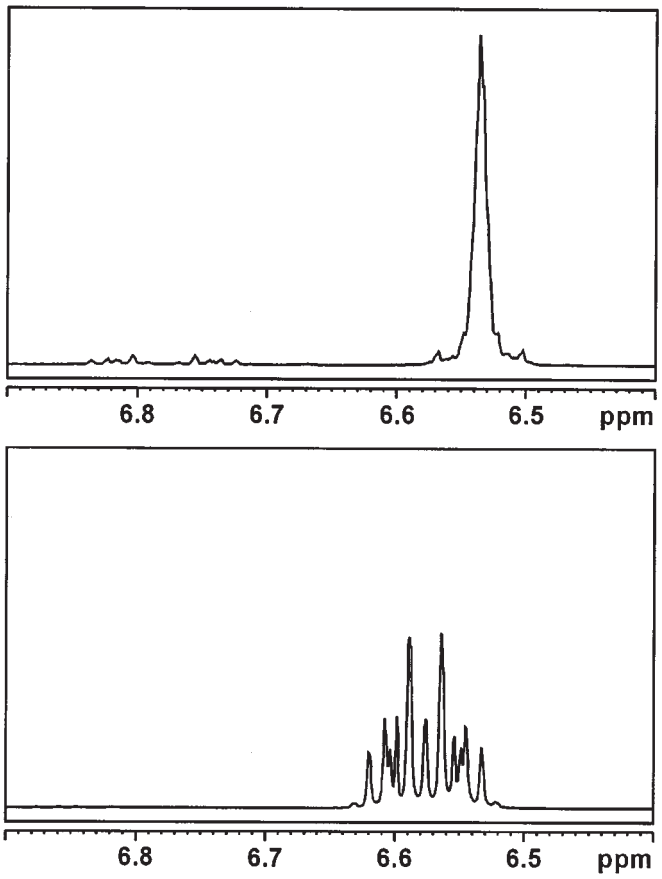
Table 3. Selected interatomic distances (Å) and angles (°) for **6** and **8**.[a]

	6	**8**
El—O1	1.7928(9)	1.8945(10)
El—O2	1.7879(10)	1.8868(11)
El—O3	1.7812(10)	1.8844(10)
El—O4	1.7964(10)	1.9002(10)
El—O5	1.7832(10)	1.8831(11)
El—O6	1.7767(10)	1.8758(11)
O1–El–O2	88.65(4)	86.95(5)
O1–El–O3	88.20(4)	88.90(5)
O1–El–O4	175.88(4)	174.18(4)
O1–El–O5	89.06(4)	89.37(5)
O1–El–O6	95.00(5)	96.10(5)
O2–El–O3	93.93(5)	95.09(5)
O2–El–O4	88.83(4)	89.52(5)
O2–El–O5	176.80(5)	174.76(4)
O2–El–O6	88.86(4)	89.37(5)
O3–El–O4	88.72(4)	86.80(4)
O3–El–O5	88.23(5)	88.58(5)
O3–El–O6	175.81(5)	173.48(4)
O4–El–O5	93.58(5)	94.44(5)
O4–El–O6	88.21(4)	88.48(5)
O5–El–O6	89.11(4)	87.30(5)

[a]**6**: El = Si; **8**: El = Ge.

slow process. As demonstrated in Fig. 5, the molar ratio (λ^6Si-silicate anion):(1,2-dihydroxybenzene) was 86:14 after 30 min and after ca. 12 h the system achieved an apparent steady state at 65:35 and remained virtually unchanged for at least 7 days. An analogous behaviour was not observed for either **7** or **8**, both ionic λ^6Ge-germanates proving to be stable in aqueous solution (D_2O) with no formation of 1,2-dihydroxybenzene after two weeks.

Fig. 4. ^{1}H NMR partial spectra (300.1 MHz, room temperature) of 4×10^{-2} M aqueous solutions (D_2O) of the λ^6Si-silicate **6** (above) and the analogous λ^6Ge-germanate **8** (below). The spectrum of **6** shows already traces of free 1,2-dihydroxybenzene (concentration increasing with time; see Fig. 5), whereas the spectrum of **8** shows no free 1,2-dihydroxybenzene.



Biological aspects

A variety of marine organisms (e.g., diatoms, radiolarians, and sponges) and many higher plants (e.g., *Equisetum* species) are known to accumulate silicon and to deposit it as amorphous silica (14). Although significant progress in silicon biochemistry of marine organisms has been made in recent years (for a short review see ref. 15), still little is known about the chemical mechanisms that control the transport of silicon, its concentration (as soluble silicon pool), and its deposition (as silica). It has been speculated that organic chelate complexes of silicon, including hexacoordinate species, may be involved in these processes (16–18). Bidentate ligands of the benzene-1,2-diolato(2–) type are particularly promising candidates to form such complexes: Diols of the 1,2-dihydroxybenzene type are well known natural products that are found in many biological systems (see for example the derivatives identified in *Equisetum* species, such as caffeic acid esters (19, 20)) and that form hexacoordinate silicon complexes in aqueous solution.

The ionic λ^6Si-silicates **5**·2CH_3CN and **6** may be useful model compounds and tools to investigate the potential role of anionic species of the tris[benzene-1,2-diolato(2–)]silicate type in the above-mentioned biological processes. Both compounds can be easily synthesized and are soluble in aqueous solution. These solutions provide a source of orthosilicic acid ($Si(OH)_4$) which can be liberated in a controlled manner by regulating the pH value. The kinetics of this process can be monitored by ^{1}H NMR experiments (integration of the characteristic resonance signals of the aminoalkanol, tris[benzene-1,2-diolato(2–)]silicate anion, and free 1,2-dihydroxybenzene). Studies on silica formation from aqueous solutions of related tris[benzene-1,2-diolato(2–)]silicates under approximately neutral pH conditions have already been reported (21, 22) and the results obtained have been discussed with reference to biologically produced silica (21).

Related studies with the λ^6Ge-germanates **7** and **8** might also be of interest. Due to the lack of a convenient and practicable radioisotope of silicon (the half-life of ^{31}Si is 156 min), the radioisotope ^{68}Ge (half-life: 282 days) has been used as a probe for silicon in many biological studies (23, 24). However, the application of this particular tracer technique presupposes very similar chemical properties of the respective silicon and germanium species under investigation. Thus, comparative studies of the coordination chemistry of silicon and germanium in aqueous solution are desirable. The importance of such investigations is emphasized by the different chemical behaviour observed for the Si/Ge analogs **5**/**7** and **6**/**8** in aqueous solution.

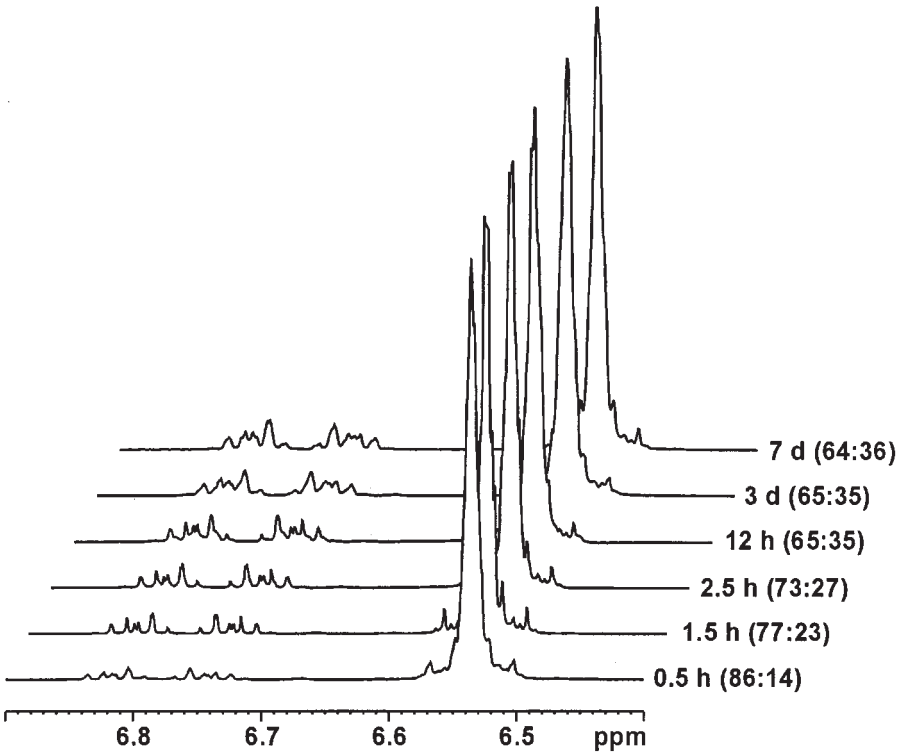
© 2000 NRC Canada

Table 4. Hydrogen-bonding geometries for **5**·2CH_3CN and **6**–**8**.[a]

Compound	D–H···A[b]	D–H (Å)	H···A (Å)	D···A (Å)	D–H···A (°)
5·2CH_3CN[c]	N1–H1···O2	0.901(16)	1.926(16)	2.7770(13)	156.8(15)
	N1–H1···O3A	0.901(16)	2.477(16)	3.1744(13)	134.5(13)
	O4–H4···O3A	0.84(2)	1.88(2)	2.7239(14)	175(2)
6[d]	N1–H1···O3	0.944(19)	2.314(19)	3.0743(17)	137.2(15)
	N1–H1···O5	0.944(19)	1.972(19)	2.8387(16)	151.6(17)
	N2–H2···O2	0.918(19)	2.078(19)	2.8880(17)	146.5(17)
	N2–H2···O6	0.918(19)	2.27(2)	3.0528(16)	143.2(16)
	O7A–H7A···O4	0.85(2)	1.95(2)	2.7879(14)	167(2)
	O8A–H8A···O1	0.87(2)	2.03(2)	2.8958(16)	172(2)
7[e]	N1–H1···O2	0.9095	2.0805	2.983(12)	171.22
	N1–H1···O3A	0.9095	2.5069	3.055(13)	119.15
8[f]	N1–H1···O3	0.85(2)	2.43(2)	3.120(2)	138.0(18)
	N1–H1···O5	0.85(2)	2.07(2)	2.846(2)	151(2)
	N2–H2···O2	0.87(2)	2.11(2)	2.892(2)	149(2)
	N2–H2···O6	0.87(2)	2.39(2)	3.103(2)	139.4(18)
	O7A–H7A···O4	0.89(2)	1.90(2)	2.7812(17)	167(2)
	O8A–H8A···O1	0.76(3)	2.14(3)	2.8893(18)	166(3)

[a]Data calculated by using the program PLATON (12); in this context, see also ref. 11.
[b]D: donor atom; A: acceptor atom.
[c]O2···H1···O3A = 68.2(5)°.
[d]O3···H1···O5 = 70.2(6)°, O2···H2···O6 = 69.9(6)°.
[e]O2···H1···O3A = 69.54°.
[f]O3···H1···O5 = 71.0(7)°, O2···H2···O6 = 71.7(7)°.

Fig. 5. ^1H NMR partial spectra (300.1 MHz, room temperature) of a 4×10^{-2} M aqueous solution (D_2O) of the λ^6Si-silicate **6** as a function of time. The molar ratios (λ^6Si-silicate anion):(free 1,2-dihydroxybenzene) obtained by integration of the respective resonance signals are given in brackets.



© 2000 NRC Canada

Acknowledgments

This work was supported by the *Deutsche Forschungsgemeinschaft* and the *Fonds der Chemischen Industrie*.

References

1. R. Tacke, B. Pfrommer, M. Pülm, and R. Bertermann. Eur. J. Inorg. Chem. 807 (1999).
2. R. Tacke, M. Pülm, and B. Wagner. Adv. Organomet. Chem. **44**, 221 (1999).
3. C.Y. Wong and J.D. Woollins. Coord. Chem. Rev. **130**, 175 (1994).
4. WIN-DAISY 4.0, Bruker-Franzen GmbH, Bremen, Germany (1998); U. Weber, A. Germanus, H. Thiele. Fresenius J. Anal. Chem. **359**, 46 (1997).
5. G.M. Sheldrick. SHELXS-97, University of Göttingen, Germany (1997); G.M. Sheldrick. Acta Crystallogr. Sect. A: Fundam. Crystallogr. **46**, 467 (1990).
6. G.M. Sheldrick. SHELXL-97, University of Göttingen, Germany (1997).
7. J.J. Flynn and F.P. Boer. J. Am. Chem. Soc. **91**, 5756 (1969).
8. F.E. Hahn, M. Keck, and K.N. Raymond. Inorg. Chem. **34**, 1402 (1995).
9. D. Sackerer and G. Nagorsen. Z. Anorg. Allg. Chem. **437**, 188 (1977).
10. J. Parr, A.M.Z. Slawin, J.D. Woollins, and D.J. Williams. Polyhedron, **13**, 3261 (1994).
11. G.A. Jeffrey and W. Saenger. Hydrogen bonding in biological structures. Springer-Verlag, Berlin. 1991. pp. 15–24.
12. A.L. Spek. PLATON, University of Utrecht, The Netherlands (1998).
13. D.F. Evans, J. Parr, and E.N. Coker. Polyhedron, **9**, 813 (1990).
14. T.L. Simpson and B.E. Volcani (*Editors*). Silicon and siliceous structures in biological systems. Springer-Verlag, New York. 1981.
15. R. Tacke. Angew. Chem. **111**, 3197 (1999); Angew. Chem. Int. Ed. Engl. **38**, 3015 (1999).
16. R.K. Iler. The chemistry of silica: solubility, polymerization, colloid and surface properties, and biochemistry. John Wiley & Sons, New York. 1978. pp. 783–784.
17. T.L. Simpson and B.E. Volcani (*Editors*). Silicon and siliceous structures in biological systems. Springer-Verlag, New York. 1981. pp. 442–446.
18. D. Evered and M. O'Connor (*Editors*). Silicon biochemistry. *Edited by* John Wiley & Sons, Chichester. 1986. pp. 70–73.
19. M. Veit, K. Bauer, C. Beckert, B. Kast, H. Geiger, and F.-C. Czygan. Biochem. Syst. Ecol. **23**, 79 (1995).
20. M. Veit, C. Beckert, C. Höhne, K. Bauer, and H. Geiger. Phytochemistry, **38**, 881 (1995).
21. C.C. Perry and Y. Lu. J. Chem. Soc. Faraday Trans. **88**, 2915 (1992).
22. C.C. Harrison and N. Loton. J. Chem. Soc. Faraday Trans. **91**, 4287 (1995).
23. T.L. Simpson and B.E. Volcani (*Editors*). Silicon and siliceous structures in biological systems. Springer-Verlag, New York. 1981. pp. 43–67.
24. M. Hildebrand, B.E. Volcani, W. Gassmann, and J.I. Schroeder. Nature (London), **385**, 688 (1997).

© 2000 NRC Canada

Formation of organosilicon compounds 117:[1] C-brominated 1,3,5-trisilacyclohexanes and their reactions with BuLi

G. Fritz, M. Keuthen, F. Kirschner, E. Matern, H. Goesmann, K. Peters, E.-M. Peters, and H.G. von Schnering

Abstract: The photobromination of 1,1,3,3,5,5-hexamethyl-1,3,5-trisilacyclohexane (**1**) almost exclusively attacks CH_2 groups and results in 2,2-dibromo-trisilacyclohexane (**2**) as well as 2,2,4,4-tetrabromo-trisilacyclohexane (**3**) in high yields. Starting from a mixture of C-brominated trisilacyclohexanes the isomeric 2,2,9-tribromo-1,3,3,5,5,8,8,10,10,13,13-undecamethyl-1,3,5,8,10,13-hexasilabicyclo[7.2.2]tridec-6-yne (**6**) had been obtained in very low yield in an attempt to establish a preparative route to adamantanes with a C_4Si_6 skeleton, i.e., with C bridgeheads and SiR_2 bridges. By ICl-cleavage of a Si—methyl bond in **2** and subsequent substitution with Br_3CLi, the trisilacyclohexane **4** with functional groups in opposite positions of the ring can be obtained. Linking the step-by-step synthesized Cl-Me_2Si-C≡C-SiMe_2-CH_2-SiMe_2-Ph to the CBr_3 group of **4** results after HBr-cleavage of the Si—Ph bond in (ω-bromo-octynyl)-trisilacyclohexane (**12**). A ring closure of **12** would result in an isomeric hexasila-bicyclo[7.2.2]tridec-6-yne. The compounds were characterized by ^{1}H, ^{13}C, and ^{29}Si NMR spectra. Additionally, the molecular structures of **4** and **6** were confirmed by X-ray single crystal investigations.

Key words: 1,1,3,3,5,5-hexamethyl-1,3,5-trisilacyclohexane, bromination, 2,2,9-tribromo-1,3,3,5,5,8,8,10,10,13,13-undecamethyl-1,3,5,8,10,13-hexasilabicyclo[7.2.2]tridec-6-yne, carbosilane synthesis, NMR data, crystal structure investigation.

Résumé : La photobromation du 1,1,3,3,5,5-hexaméthyl-1,3,5-trisilacyclohexane (**1**) se fait presque exclusivement par une attaque des groupes CH_2 et elle conduit à la formation de 2,2-dibromotrisilacyclohexane (**2**) ainsi que de 2,2,4,4-tétrabromo-trisilacyclohexane (**3**) avec des rendements élevés. Dans un essai de démontrer la possibilité de préparer des adamantanes comportant un squelette C_4Si_6, c'est-à-dire les atomes de ponts C et les ponts SiR_2, on a déterminé que, en partant d'un mélange de trisilacyclohexanes C-bromé, on obtient le 2,2,9-tribromo-1,3,3,5,5,8,8,10,10,13,13-undécaméthyl-1,3,5,8,10,13-hexasilabicyclo[7.2.2]tridéc-6-yne (**6**) avec un faible rendement. Un clivage d'une liaison C—méthyle du composé **2** à l'aide de ICl, suivie d'une substitution subséquente avec du Br_3CLi permet d'obtenir le trisilacyclohexane **4** portant des groupes fonctionnels dans des positions opposées du cycle. La liaison du groupe CBr_3 du produit **4** au Cl-Me_2Si-C≡C-SiMe_2-CH_2-Ph synthétisé étape par étape conduit au (ω-bromo-octynyl)-trisilacyclo-hexane (**12**) après clivage de la liaison Si—Ph avec du HBr. Une fermeture du cycle du produit **12** devrait conduire à l'hexasilabicyclo[7.2.2]tridéc-6-yne. Les composés ont été caractérisés par spectroscopie RMN du ^{1}H, du ^{13}C et du ^{29}Si. De plus, on a confirmé les structures des composés **4** et **6** par diffraction des rayons X par des cristaux uniques.

Mots clés : 1,1,3,3,5,5-hexaméthyl-1,3,5-trisilacyclohexane, bromation, 2,2,9-tribromo-1,3,3,5,5,8,8,10,10,13,13-undécaméthyl-1,3,5,8,10,13-hexasilabicyclo[7.2.2]tridéc-6-ène, synthèse de carbosilanes, données de RMN, étude de structures cristallines.

[Traduit par la Rédaction]

1. Introduction

The gas phase pyrolysis of methylsilanes, among many other carbosilanes, yields 1,3,5,7-tetrasilaadamantanes, but only those with a Si_4C_6 skeleton were observed, i.e., Si occupies the bridgehead positions and CH_2 groups form the bridges in these adamantanes (1). Nevertheless, C bridgeheads exist in the barrelane $Si_4C_{11}H_{28}$ (2), in the asterane

Received July 2, 1999. Published on the NRC Research Press website on October 20, 2000.

Dedicated to Professor Adrian G. Brook on the occasion of his 75th birthday.

G. Fritz,[2] M. Keuthen, F. Kirschner, E. Matern, and H. Goesmann. Institut für Anorganische Chemie der Universität (TH), Karlsruhe, Germany.
K. Peters, E.-M. Peters, and H.G. von Schnering. Max-Planck-Institut für Festkörperforschung, Stuttgart, Germany.

[1]Part 116: H. Wendt, I. Odenwald, P. Scheer, E. Matern, G. Fritz, Z. Anorg. Allg. Chem. **623**, 853 (1997).

[2]Author to whom correspondence may be addressed. Prof. Dr. Dr.h.c. G. Fritz, Institut für Anorganische Chemie der Universität (TH), Engesserstr. Geb. Nr. 30.45, D-76128 Karlsruhe, Germany. E-mail: gerhard.fritz@chemie.uni-karlsruhe.de

© 2000 NRC Canada

Scheme 1. Photobromination products of $(Me_2Si\text{-}CH_2)_3$ (**1**).

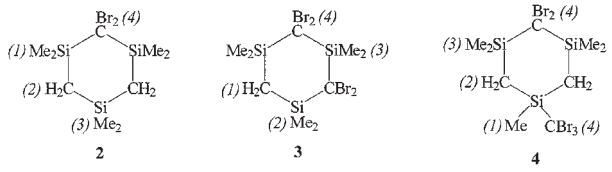
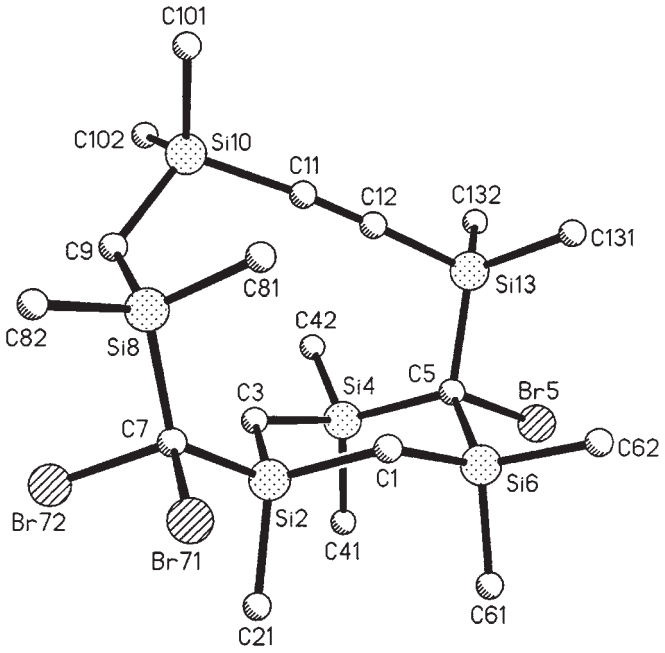


Fig. 1. Structure of 2,2,9-tribromo-1,3,3,5,5,8,8,10,10,13,13-undecamethyl-1,3,5,8,10,13-hexasilabicyclo[7.2.2]tridec-6-yne $Si_6C_{18}H_{39}Br_3$ (**6**) with the atomic labelling (hydrogen atoms omitted). For bond lengths and angles see Tables 4 and 5, respectively.

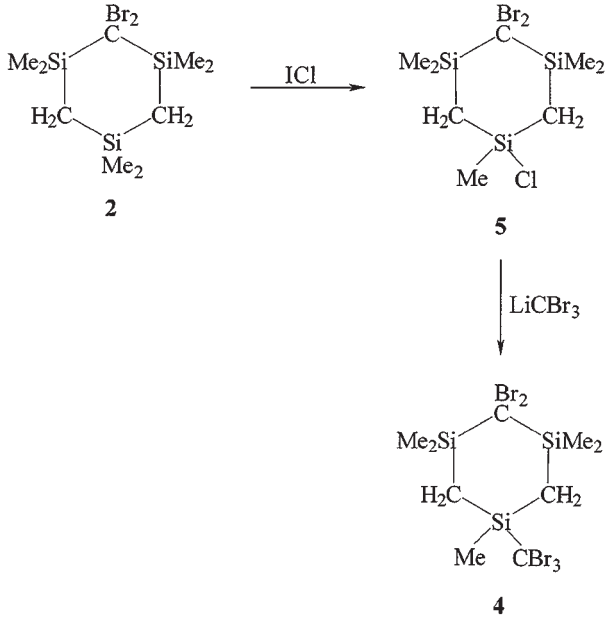


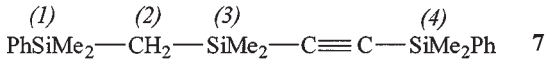
$Si_6Cl_8C_6H_8$ (3), in the di-adamantane $Si_7C_{16}H_{36}$ (4) and in the octamethyl-octasilaheptacyclooctadecane $Si_8C_{18}H_{40}$ (5), e.g., obtained either by pyrolysis or by organometallic synthesis. The synthetic approach to adamantanes with the "inverse" skeleton C_4Si_6 has to start from C-functional carbosilanes which at the same time carry less or non-reactive groups at Si. Unfortunately, these cannot simply be obtained by alkylating the readily available perchlorinated carbosilanes, because MeMgCl, for example, does not substitute the Si atoms in $(Cl_2Si\text{-}CCl_2)_3$. Instead, the reaction starts at a ring C atom and proceeds via ring contraction and ring cleavage to eventually lead to the linear $Me_3Si\text{-}CH_2\text{-}SiMe_2\text{-}C{\equiv}C\text{-}SiMe_3$ (6).

In addition, the photochlorination of Si-methylated carbosilanes does not provide a suitable pathway to the desired starting material, because photochlorination attacks both CH_3 and CH_2 groups at the same time. In contrast, the photobromination of hexamethyl-1,3,5-trisilacyclohexane **1** can be guided in a way that nearly exclusively attacks CH_2 groups (7) (Scheme 1).

In a first attempt to link the CBr_2 groups in a mixture of such C-functional trisilacyclohexanes by adding ^{n}BuLi, the compound $Si_6C_{18}H_{39}Br_3$ was isolated in a very low yield.

Scheme 2. Organometallic preparation of **4**.





According to the sum formula it might consist of two triply C-C linked trisilacyclohexanes in a wurtzite-like structure. The single crystal structure investigation of this product confirmed the heavy-atom formula $Si_6C_{18}Br_3$, while revealing a completely different and unexpected molecular structure (molecule **6** in Fig. 1). In this paper we first present a convenient preparative access to C-brominated derivatives of $(Me_2Si\text{-}CH_2)_3$ **1**, then we deal with the reactions of such derivatives with metal alkyls, and eventually we describe a reaction path for the synthesis of **6** as far as these steps have already been realized.

The structures of all mentioned compounds are to be found in Schemes 1–4 and NMR data are given in Table 1.

2. Results and discussion

2.1 Photobromination of $(Me_2Si\text{-}CH_2)_3$ (1)

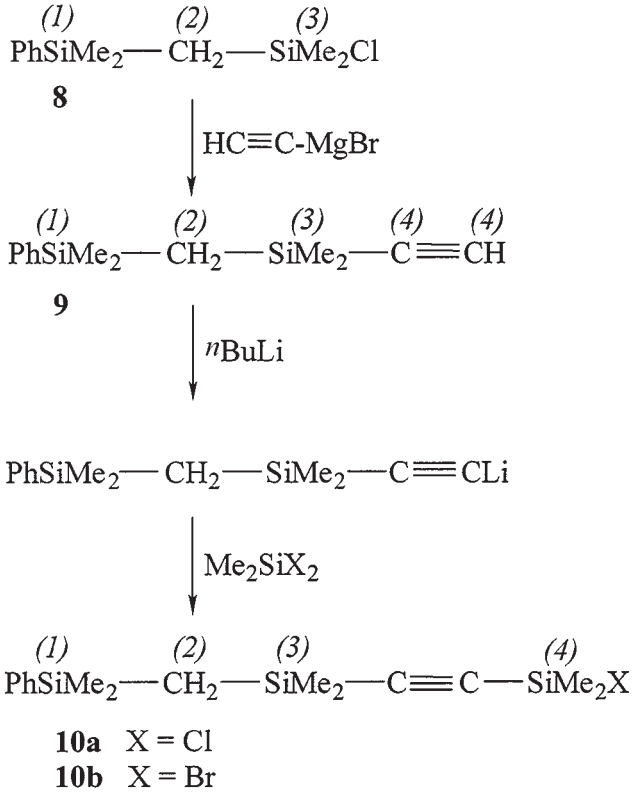
A solution of $(Me_2Si\text{-}CH_2)_3$ (**1**) and *N*-bromosuccinimide in CCl_4 was irradiated (UV) until **2** and **3** reached a ratio of 1:1 and about 10% of **1** remained. If **2** and **3** are isolated at this point the compounds can be obtained in pure form. In the same manner **2** was further brominated to give **3** in an overall yield of about 90%. Only when trying to gain higher yields of the ring **3** with two CBr_2 groups or when trying to introduce a third CBr_2 group, some of the remaining ring **2** suffers bromination of a CH_3 to a CBr_3 group in opposite position to the CBr_2 group. This side product **4** is formed in a yield of 5–10% at most.

2.2 The reactions of 3 and 4 with metal alkyls

Whereas **3** is lithiated and subsequently alkylated by ^{n}BuLi, the reactions with ^{t}BuLi or MeMgBr proceed under ring

© 2000 NRC Canada

Scheme 3. Preparation of the functional trisilaoct-3-ynes **10a** and **10b**.



contraction and ring opening to $BrMe_2Si\text{-}CH_2\text{-}SiMe_2\text{-}C{\equiv}C\text{-}SiMe_2Br$ or $Me_3Si\text{-}CH_2\text{-}SiMe_2\text{-}C{\equiv}C\text{-}SiMe_3$, respectively, quite analogously to the reactions of $(Cl_2Si\text{-}CCl_2)_3$ (6) or of 1,3-disila-4-trimethylsilylcyclopentene (8) with MeMgCl.

In **4,** ^{t}BuLi first attacks the CBr_3 group as was proven by trapping the lithiated intermediate with MeI.

With the formation of **4** in the photobromination of **2**, and with $BrMe_2Si\text{-}CH_2\text{-}SiMe_2\text{-}C{\equiv}C\text{-}SiMe_2Br$ resulting from the rearrangement of the lithiated derivative of **3**, two molecules were independently isolated which may have been combined to give **6** in our orientating experiment. However, **6** could not be detected in repeated experiments when treating a mixture of **3** and **4** with ^{t}BuLi.

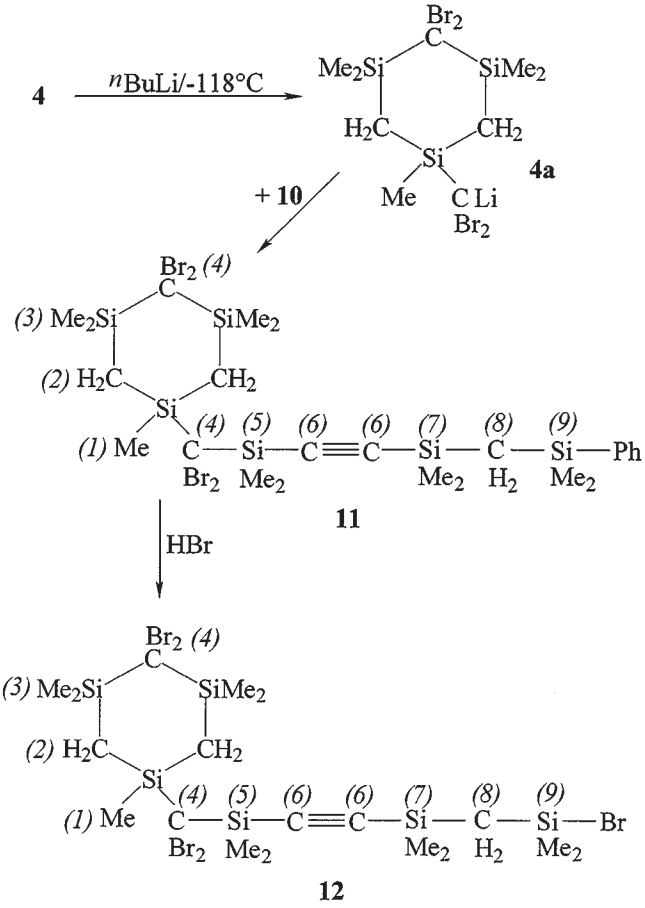
2.3 Organometallic synthesis of 6

On the way to **6**, the organometallic synthesis of **4** is quite a decisive step because **4** was not obtained in sufficient amounts by photobromination. Starting from **2**, a Si—Me bond has to be cleaved using ICl (9), then the intermediate -SiCl- unit can be substituted by Br_3CLi. In this manner, **4** could be prepared in a yield of 70% as shown in Scheme 2.

As a second building block, initially compound **7** was synthesized (Scheme 2). However it wasdecomposed by HBr to $BrMe_2Si\text{-}CH_2\text{-}SiMe_2Br$ and further products while cleaving the Ph—Si bonds. Therefore, the Si-functional 2,5,7-trisilaoct-3-yne **10** had to be synthesized according to a slightly changed reaction path (Scheme 3).

The linking of **4** with **10** was achieved via the Br_2CLi intermediate **4a** (10) as shown in Scheme 4. Then the remaining

Scheme 4. Linking of **10** and **4**, and reaction with HBr to give (ω-bromo-octynyl)-trisilacyclohexane **12**.



terminal Si atom of **11** could be functionalized using HBr. As CBr_2 groups are readily lithiated by ^{n}BuLi, a cyclization of **12** via elimination of LiBr was attempted. However, only oxygen-containing products, probably resulting from ether cleavage, were obtained. Therefore, a ring closure using metallic Li was tried. In mass spectra of two out of fifteen HPLC fractions (11) of this product mixture, a compound with the molecular mass of $Si_6C_{18}H_{41}Br$ could be detected which can be tentatively assigned to a partially hydrogenated isomer of **6**.

2.4 Conclusion

As only few crystals of **6** were initially obtained, it is not reasonable to derive a synthetic procedure from this single experiment. However, the investigations demonstrate a reproducible synthetic path from $(Me_2Si\text{-}CH_2)_3$ to 2,2,9-tribromo-1,3,3,5,5,8,8,10,10,13,13-undecamethyl-1,3,5,8,10,13-hexasilabicyclo[7.2.2]tridec-6-yne **6** even if the last step, i.e., the final ring closure has not yet been done.

2.5 Molecular structure determinations

The crystal structures of **6** and **4** were determined by X-ray single crystal methods. The crystallographic data are

© 2000 NRC Canada

Table 1. ^{1}H, ^{13}C, and ^{29}Si NMR data (δ in ppm) of the compounds **2**–**12**. Bruker AMX 300, standard TMS (ext.); solvent $CDCl_3$, where indicated for ^{1}H also C_6D_6; high field shifts with negative sign. Where the same number is used to mark different positions in this table and in the reaction schemes, the signals could not unambigously be assigned.

Compound		
2	$\delta^{1}H$	*(1)* 0.35; *(2)* 0.03; *(3)* 0.09
	$\delta^{13}C$	*(1)* –0.3; *(2)* 1.7; *(3)* 3.0; *(4)* 56.7
	$\delta^{29}Si$	*(1)* 10.95; *(3)* –0.3
3	$\delta^{1}H$	*(3)* 0.74; *(2)* 0.39; *(1)* 0.24
	$\delta^{13}C$	*(1)* –1.4; *(2)* 0.5; *(3)* –2.8; *(4)* 47.5
	$\delta^{29}Si$	*(3)* 10.9; *(2)* 11.4
4	$\delta^{1}H$	*(3)* 0.5 0.33; *(2)* 0.23 0.83; *(1)* 0.45; $^{2}J_{AB}$ 13.95 Hz
	$\delta^{13}C$	*(1)* –1.7; *(2)* –1.4; *(3)* –0.3; *(4)* 48.6 53.9
	$\delta^{29}Si$	*(3)* 10.6; *(1)* 20.5
5	$\delta^{1}H$, C_6D_6	*(3)* 0.5 0.42; *(2)* 0.16 0.23; *(1)* 0.37; $^{2}J_{AB}$ 13.6 Hz
	$\delta^{13}C$	*(1)* 6.5; *(2)* 5.2; *(3)* –0.8; *(4)* 54.9
	$\delta^{29}Si$	*(3)* 10.5; *(1)* 27.6
6	$\delta^{1}H$, C_6D_6	0.21 (6H); 0.26 (6H); 0.48(6H); 0.59 (3H); 0.86 (AA′); 0.35 (XX′ + 12H + 2H)
7	$\delta^{1}H$, C_6D_6	*(1)* 0.39; *(2)* 0.08; *(3)* 0.12; *(4)* 0.37; *(Ph)* 7.6 7.2
8	$\delta^{1}H$, C_6D_6	*(1)* 0.25; *(2)* 0.32; *(4)* 0.32; *(Ph)* 7.25
	$\delta^{13}C$	*(1)* –0.4; *(2)* 7.0; (3) 4.5; *(Ph)* 139.6 139.4 133.2 127.8
	$\delta^{29}Si$	*(1)* –4.5; *(3)* 30.5
9	$\delta^{1}H$, C_6D_6	*(1)* 0.33; *(2)* 0.0; *(3)* 0.08; *(4)* 2.12; *(Ph)* 7.32
	$\delta^{13}C$	*(1)* 1.0; *(2)* 2.6; *(3)* –0.3; *()* 90.4 93.9; *(Ph)* 141.1 140.3 133.2 127.7
	$\delta^{29}Si$	*(1)* –3.7; *(3)* –17.1
10a X = Cl	$\delta^{1}H$, C_6D_6	*(1)* 0.36; *(2)* 0.0; *(3)* 0.06; *(4)* 0.44; *(Ph)* 7.34
	$\delta^{29}Si$	*(1)* –3.9; *(3)* –18.0; *(4)* –1.5
11	$\delta^{1}H$, C_6D_6	*(2)* 0.09; *(1)* 0.57; *(2)* 0.29 1.10; *(3,3,5,7,9)* 0.18 0.26 0.43 0.56 0.6; *(Ph)* 7.39; $^{2}J_{AB}$ 14.1 Hz
	$\delta^{13}C$	*(1)* 0.4; *(2)* 0.2; *(4)* 54.9 56.7; *(6)* 110.6 118.3; *(8)* 2.5; *(3,3,5,7,9)* 0.9 –0.2 –0.3 –0.5 –0.6; *(Ph)* 140.7 133.3 128.8 127.7
	$\delta^{29}Si$	*(3)* 10.6; *(1)* 10.3; *(5)* –14.4; *(7)* –18.7; *(9)* –4.3
12	$\delta^{1}H$, C_6D_6	*(8)* 0.26; *(1)* 0.51; *(2)* 0.25 1.01; *(3,3,5,7,9)* 0.21 0.25 0.52 0.54 0.58
	$\delta^{13}C$	*(1)* –0.6; *(2)* 0.2; *(4)* 54.8 56.4; *(8)* 7.7; *(9)* 5.4; *(6)* 111.7 116.7; *(3,3,5,7)* –0.7 –0.5 –0.2 0.7
	$\delta^{29}Si$	*(3)* 10.6; *(1)* 10.3; *(5)* –14.6; *(7)* –20.0; *(9)* 25.6

listed in Table 2, and structural information is summarized in Tables 3–8.[3]

2,2,9-Tribromo-1,3,3,5,5,8,8,10,10,13,13-undecamethyl-1,3,5,8,10,13-hexasilabicyclo[7.2.2]tridec-6-yne $Si_6C_{18}H_{39}Br_3$ (**6**) crystallizes in the monoclinic space group $P2_1/a$ with 4 molecules in the unit cell (12). The molecule of **6** with the atomic labelling is shown in Fig. 1. Bond lengths and angles are listed in Table 4 and 5, respectively.

The standard deviations of about 1 pm do not allow for a sophisticated analysis. Nevertheless, some tendencies are obvious because the standard deviation of the averaged bond length *d*(Si—C) = 188(3) is three times as large as those for the single values. This results from two significantly different groups of bonds to be considered, namely the elongated ones to the atoms C5 and C7, which are bonded to bromine (*d*(Si—C5,7) = 192(1) pm); and the other ones (*d*(Si—C) = 186(1) pm). Moreover, the latter show a small differentiation of *d*(Si—C)*endo* = 187(1) > *d*(Si—C)*exo* = 186(1) > *d*(Si—CC) = 184(2) pm. At first glance the Si—CC bond shortening may indicate an influence of the C≡C triple bond. On the other hand, the internal tension of the seven-membered section (C7 → Si13) is reflected by the small bond angle C5-Si13-C12 (105.8°) and the large bond angles Si6-C5-Si13 (118.2°), Si8-C9-Si10 (122.0°), and Si2-C7-Si8 (125.5°) as well as by the deviation of the Si10-C11-C12-Si13 fragment from linearity (7–8°). This tension seems to be responsible for the shortening and bending of this fragment (Fig. 1). The axial ligands C21, C41, C61, and Si13 are shifted away from the central axis of the trisilacyclohexane ring. This demonstrates the six-membered ring to be arched, which is indicated, too, by the enlarged endocyclic angles at C1 and C3 (117–120°) and the smaller endocyclic angles at Si2 and Si4 (108–109°) as described by Fritz et al. (13).

Neglecting the C≡C group, the framework of **6** almost perfectly displays a diamond fragment with all six-membered rings being in the chair conformation (Fig. 2). It is noticeable,

[3] Additional material has been deposited as supplementary material and may be purchased from the Depository of Unpublished Data, Document Delivery, CISTI, National Research Council Canada, Ottawa, ON, Canada K1A 0S2 (http://www.nrc.ca/cisti/irm/unpub_e.shtml). Crystallographic data for the structure(s) reported in this paper have been deposited with the Cambridge Crystallographic Data Centre (CCDC 132465). Copies of the data can be obtained, free of charge, on application to the Director, CCDC, 12 Union Road, Cambridge CB2 1EZ, U.K. (Fax: 44-1223-336033 or e-mail: deposit@ccdc.cam.ac.uk).

© 2000 NRC Canada

Table 2. Crystallographic data for **6** and **4**.

	Compound; formula	
	6; $C_{18}H_{39}Br_3Si_6$	**4**; $C_9H_{19}Br_5Si_3$
Molar mass	663.7 amu	610.5 amu
Crystal system	monoclinic	orthorhombic
Space group	$P2_1/a$ (no. 14)	*Pbca* (no. 61)
a	1425.2(4) pm	1262.3(12) pm
b	1856.2(5) pm	2355.5(18) pm
c	1152.7(3) pm	1285.2(26) pm
β	101.81(2)°	
V	2986×10^6 pm^3	3821×10^6 pm^3
ρ calc	1.477 g cm^{-3}	2.124 g cm^{-3}
Z	4	8
Diffractometer	Syntex P3	Siemens AED 2
Radiation	Mo *K*α graphite monochromator	Mo *K*α graphite monochromator
Scan type	ω	ω – 2θ
2θ range	3.5–55°	3–56°
Temperature	293 K	293 K
Total observed reflections	7077	3937
Total independent reflections	4636	2728
Reflections	4279 with $I > 3\sigma(I)$	1452 with $I > 2\sigma(I)$
Absorption correction	Ψ-scan	Ψ-scan
Absorption coefficient	45.33 cm^{-1}	105.9 cm^{-1}
R; R_w	0.067; 0.054	0.078; 0.065

Table 3. Atomic positional parameters and U_{eq} (10^4 pm^2) of **6**. Estimated standard deviations are given in parentheses.

Atom	*x/a*	*y/b*	*z/c*	U_{eq}[a]
Br(5)	0.3283(1)	0.9461(1)	1.0745(1)	0.052(1)
Br(71)	0.0188(1)	0.6908(1)	0.5455(1)	0.051(1)
Br(72)	0.2245(1)	0.6818(1)	0.4771(1)	0.049(1)
Si(2)	0.1940(2)	0.7667(1)	0.7008(2)	0.031(1)
Si(4)	0.3666(2)	0.8657(1)	0.8465(2)	0.037(1)
Si(6)	0.1637(2)	0.8591(1)	0.9198(2)	0.035(1)
Si(8)	0.0958(2)	0.8175(1)	0.4165(2)	0.037(1)
Si(10)	0.2260(2)	0.9634(1)	0.4158(2)	0.040(1)
Si(13)	0.2445(2)	1.0112(1)	0.8341(2)	0.037(1)
C(1)	0.1134(5)	0.8236(4)	0.7696(7)	0.033(3)
C(3)	0.3083(5)	0.8180(4)	0.7068(7)	0.033(3)
C(5)	0.2702(3)	0.9191(4)	0.9066(7)	0.031(3)
C(7)	0.1349(5)	0.7464(4)	0.5394(7)	0.035(3)
C(9)	0.2058(6)	0.8646(4)	0.3882(8)	0.049(4)
C(11)	0.2166(6)	0.9844(4)	0.5711(7)	0.037(3)
C(12)	0.2213(6)	0.9950(4)	0.6748(8)	0.037(3)
C(21)	0.2160(6)	0.6787(5)	0.7767(8)	0.051(4)
C(41)	0.4295(6)	0.7977(5)	0.9543(8)	0.061(4)
C(42)	0.4603(6)	0.9245(5)	0.8090(9)	0.066(4)
C(61)	0.2010(7)	0.7844(5)	1.0306(8)	0.054(4)
C(62)	0.0681(6)	0.9061(5)	0.9795(9)	0.061(4)
C(81)	0.0073(6)	0.8790(5)	0.4630(9)	0.058(4)
C(82)	0.0362(7)	0.7701(5)	0.2768(8)	0.058(4)
C(101)	0.1355(7)	1.0171(5)	0.3137(8)	0.058(4)
C(102)	0.3489(7)	0.9861(5)	0.4047(8)	0.058(4)
C(131)	0.1416(7)	1.0598(5)	0.8711(9)	0.063(4)
C(132)	0.3457(7)	1.0770(5)	0.8682(9)	0.065(4)

[a]Equivalent isotropic *U* defined as one third of the trace of the orthogonalized tensor.

that only minor modifications are necessary to insert the C≡C group into this diamond fragment, namely rotations around the C9—Si10 and Si8—C9 bonds by angles of about 60° and 30°, respectively. These modifications result in the skew boat conformation of the six-membered ring fragment C81-Si8-C9-Si10-C11 (one atom is missing between C81 and C11).

A colourless single crystal of 2,2-dibromo-5-tribromomethyl-1,1,3,3,5-pentamethyl-1,3,5-trisilacyclohexane $Si_3C_9H_{19}Br_5$ **4** was selected for the X-ray structure determination and the results are summarized in Table 2. The molecule of (**4**) with the atomic labelling is shown in Fig. 3; fractional coordinates are given in Table 6; bond lengths and angles are listed in Table 7 and 8, respectively.

The trisilacyclohexane ring adopts the chair conformation with an equatorial CBr_3 group, which is the necessary conformation for a successful further synthesis. Also in this molecule the bond distances from the brominated carbon atoms to Si as well as to Br are significantly larger than standard average values (Table 7). The endocyclic angles Si-C-Si with an average value of 118.2° are larger than the tetrahedral angle whereas the angles C-Si-C don't show a common tendency. Due to the sterically requiring CBr_3 group, the angle C4-Si2-C7 of 111.1° is remarkably larger than those at Si1 and Si3 (Table 8). The mean value of 113.0° for all endocyclic angles indicates a slightly flattened conformation of the trisilacyclohexane chair.

3. Experimental

3.1 General procedures

All solvents were thoroughly dried, and the reactions run in a N_2 atmosphere. Gaseous Cl_2 was passed through a P_2O_5

© 2000 NRC Canada

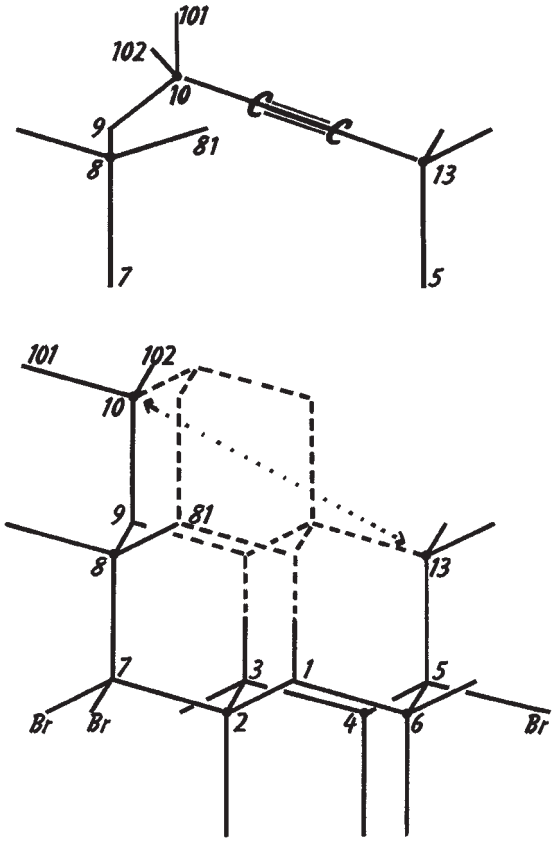
Table 4. Bond lengths (in pm) for **6**.

Bond	Length	Bond	Length	Bond	Length
Br(5)-C(5)	200.6 (7)	Br(71)-C(7)	196.3 (8)	Br(72)-C(7)	199.2 (8)
Si(2)-C(1)	185.5 (9)	Si(2)-C(3)	187.6 (8)	Si(2)-C(7)	191.6 (8)
Si(2)-C(21)	184.8 (9)	Si(4)-C(3)	187.7 (8)	Si(4)-C(5)	193.4 (8)
Si(4)-C(41)	186.6 (9)	Si(4)-C(42)	184.4 (9)	Si(6)-C(1)	185.4 (8)
Si(6)-C(5)	191.4 (8)	Si(6)-C(61)	188.6 (9)	Si(6)-C(62)	186.4 (9)
Si(8)-C(7)	193.3 (8)	Si(8)-C(9)	188.1 (9)	Si(8)-C(81)	185.9 (9)
Si(8)-C(82)	187.9 (9)	Si(10)-C(9)	187.4 (9)	Si(10)-C(11)	186.3 (9)
Si(10)-C(101)	185.0 (9)	Si(10)-C(102)	183.1 (9)	Si(13)-C(5)	190.6 (8)
Si(13)-C(12)	182.3 (9)	Si(13)-C(131)	184.4 (9)	Si(13)-C(132)	186.8 (9)
C(11)-C(12)	120.0 (9)				

Table 5. Bond angles (in deg) for **6**.

Bond	Angle	Bond	Angle
C(1)-Si(2)-C(3)	107.7(4)	C(1)-Si(2)-C(7)	109.8(3)
C(1)-Si(2)-C(21)	111.2(4)	C(3)-Si(2)-C(7)	110.0(4)
C(3)-Si(2)-C(21)	111.7(4)	C(7)-Si(2)-C(21)	106.5(4)
C(3)-Si(4)-C(5)	109.1(3)	C(3)-Si(4)-C(41)	108.7(4)
C(3)-Si(4)-C(42)	107.0(4)	C(5)-Si(4)-C(41)	112.8(4)
C(5)-Si(4)-C(42)	112.4(4)	C(41)-Si(4)-C(42)	106.6(4)
C(1)-Si(6)-C(5)	107.1(4)	C(1)-Si(6)-C(61)	111.9(4)
C(1)-Si(6)-C(62)	109.8(4)	C(5)-Si(6)-C(61)	111.3(4)
C(5)-Si(6)-C(62)	114.1(4)	C(61)-Si(6)-C(62)	102.7(4)
C(7)-Si(8)-C(9)	108.6(4)	C(7)-Si(8)-C(81)	108.6(4)
C(7)-Si(8)-C(82)	108.7(4)	C(9)-Si(8)-C(81)	113.4(4)
C(9)-Si(8)-C(82)	108.4(4)	C(81)-Si(8)-C(82)	108.7(4)
C(9)-Si(10)-C(11)	109.3(4)	C(9)-Si(10)-C(101)	110.8(4)
C(9)-Si(10)-C(102)	109.2(4)	C(11)-Si(10)-C(101)	108.7(4)
C(11)-Si(10)-C(102)	106.1(4)	C(101)-Si(10)-C(102)	112.6(4)
C(5)-Si(13)-C(12)	105.8(4)	C(5)-Si(13)-C(131)	115.3(4)
C(5)-Si(13)-C(132)	115.0(4)	C(12)-Si(13)-C(131)	108.9(4)
C(12)-Si(13)-C(132)	107.0(4)	C(131)-Si(13)-C(132)	104.4(4)
Si(2)-C(1)-Si(6)	116.5(4)	Si(2)-C(3)-Si(4)	120.0(5)
Br(5)-C(5)-Si(4)	106.9(3)	Br(5)-C(5)-Si(6)	104.3(4)
Br(5)-C(5)-Si(13)	101.7(3)	Si(4)-C(5)-Si(6)	111.3(4)
Si(4)-C(5)-Si(13)	112.9(4)	Si(6)-C(5)-Si(13)	118.2(4)
Br(71)-C(7)-Br(72)	107.7(4)	Br(71)-C(7)-Si(2)	106.0(4)
Br(71)-C(7)-Si(8)	105.5(3)	Br(72)-C(7)-Si(2)	106.3(3)
Br(72)-C(7)-Si(8)	104.9(4)	Si(2)-C(7)-Si(8)	125.5(4)
Si(8)-C(9)-Si(10)	122.0(5)	Si(10)-C(11)-C(12)	172.3(7)
C(11)-C(12)-Si(13)	172.9(8)		

Fig. 2. Below: the diamond fragment of the molecule **6** after abstracting the C≡C group (arrows). Real bonds are shown by full lines, dotted lines help to complete the six-membered rings (all in chair conformation) of the diamond fragment. Above: very small modifications allow for the insertion of the C≡C group (see text) by formation of only one skew boat fragment (atoms 81, 8, 9, 10, 11, and one atom missing between atoms 81 and 11).



tube (2 m × 8 cm). The photoreactions were run in quartz flasks using a water cooled Original Hanau mercury high pressure immersion lamp. HPLC analyses were performed according to ref. 11.

3.2 Photobromination of $(Me_2Si\text{-}CH_2)_3$ 1 to give 2,2-dibromo-1,1,3,3,5,5-hexamethyl-1,3,5-trisilacyclohexane (2)

Method 1: 21.6 g (100 mmol) of **1** + 3 drops of Br_2 without any solvent were irradiated. Only after the colour of Br_2 disappeared was a new portion of Br_2 added. Evolving HBr was collected in a cooling trap (slightly reduced pressure, liquid N_2). Whenever the mixture turned black from suspended carbon it had to be filtered. These steps were repeated until **3** became detectable in the ^1H NMR spectrum after a total irradiation time of about 150 h. The mixture was diluted in pentane and prepurified using a silicagel column (Merck 40–63 μm). Pentane and remaining **1** (10.6 g; 49 mmol) were removed, then 11.3 g (30.6 mmol, 60%) of **2** could be obtained as colourless crystals (mp 52°C).

Method 2: 21.6 g (100 mmol) of **1** + 19.6 g (110 mmol) of *N*-bromosuccinimide in CCl_4 were irradiated for 7 d. The insoluble succinimide was removed by filtration, Br_2 and CCl_4 stripped, the oily brown residue eluted with 1 L of pentane from an Al_2O_3 column (10 × 2 cm; Riedel de Haen Al_2O_3 S neutral active), and the solvent removed. With

© 2000 NRC Canada

Table 6. Fractional atomic coordinates and U_{eq} of **4** with standard deviations in parentheses.

Atom	*x*/*a*	*y*/*b*	*z*/*c*	U_{eq}
Br(1)	0.3701(1)	0.08540(7)	0.3884(1)	0.0511(5)
Br(2)	0.2553(1)	–0.01401(6)	0.5127(1)	0.0513(6)
Br(3)	0.3554(4)	0.28645(8)	0.4277(1)	0.0625(7)
Br(4)	0.3303(2)	0.32302(7)	0.6618(1)	0.0684(7)
Br(5)	0.1377(2)	0.33136(7)	0.5098(2)	0.0742(8)
Si(1)	0.1381(3)	0.1009(2)	0.4620(3)	0.030(1)
Si(2)	0.2202(3)	0.2103(2)	0.5814(3)	0.027(1)
Si(3)	0.3365(3)	0.0939(2)	0.6259(3)	0.031(1)
C(1)	0.2706(9)	0.0683(5)	0.5025(9)	0.025(4)
C(2)	0.038(1)	0.0785(7)	0.559(1)	0.047(6)
C(3)	0.101(1)	0.0765(7)	0.330(1)	0.053(6)
C(4)	0.157(1)	0.1790(6)	0.466(1)	0.032(5)
C(5)	0.128(1)	0.2174(7)	0.693(1)	0.044(5)
C(6)	0.259(1)	0.2864(6)	0.546(1)	0.042(5)
C(7)	0.343(1)	0.1725(6)	0.615(1)	0.033(5)
C(8)	0.255(1)	0.0734(7)	0.740(1)	0.050(6)
C(9)	0.469(1)	0.0605(8)	0.638(1)	0.057(7)

Fig. 3. Structure of 2,2-dibromo-5-tribromomethyl-1,1,3,3,5-pentamethyl-1,3,5-trisilacyclohexane $Si_3C_9H_{19}Br_5$ (**4**) with the atomic labelling (hydrogen atoms omitted). For bond lengths and angles see Table 7 and 8, respectively.

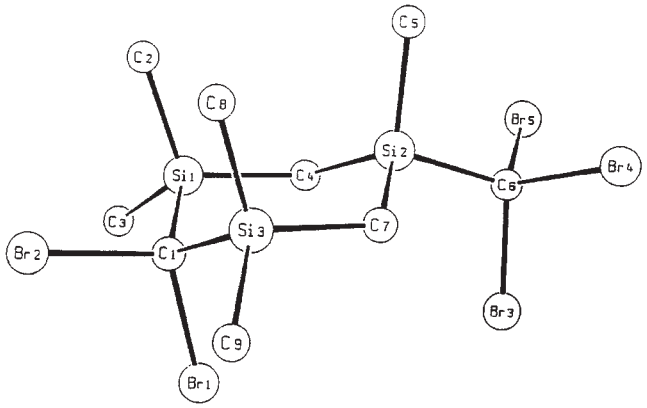


Table 7. Bond lengths (in pm) for **4**.

Bond	Length	Bond	Length	Bond	Length
Br(1)—C(1)	197(1)	Br(5)—C(6)	192(1)	Si(1)—C(4)	186(1)
Si(2)—C(6)	191(1)	Si(3)—C(9)	186(2)	Br(3)—C(6)	194(1)
Si(1)—C(2)	185(2)	Si(2)—C(7)	184(1)	Si(3)—C(7)	186(1)
Br(2)—C(1)	195(1)	Si(1)—C(1)	191(1)	Si(2)—C(4)	184(1)
Si(3)—C(1)	189(1)	Br(4)—C(6)	195(1)	Si(1)—C(3)	185(2)
Si(2)—C(5)	185(1)	Si(3)—C(8)	185(2)		

another 19.6 g (110 mmol) of NBS, the full procedure was repeated. In a short path distillation apparatus (oil pump vacuum) first 2.3 g (11 mmol) of **1**, then 26.6 g (55 mmol) of **2** were collected. A third fraction of 8.3 g consisted of about 50 mol% of **2** and 50 mol% of **3**. 20.6 g of **2** (55%) remained after recrystallization from pentane. As the recovered starting material was re-used for further photobrominations, **2** could be obtained in an overall yield of 90%.

3.3 Photobromination of $(Me_2Si\text{-}CH_2)_3$ 1 to give 2,2,4,4-tetrabromo-1,1,3,3,5,5-hexamethyl-1,3,5-trisilacyclohexane 3 and 2,2-dibromo-5-tribromomethyl-1,1,3,3,5-pentamethyl-1,3,5-trisilacyclohexane (4)

According to method 2, 36.4 g of a mixture of about 10 mol% of **1**, 80 mol% of **2** and 10 mol% of **3** (^{1}H NMR analysis) + 19.6 g (110 mmol) of NBS in CCl_4 were irradiated for 10 d, and the procedure repeated for a second time. At 30–50°C, the collected residues were distilled in the mentioned apparatus yielding a main fraction which after recrystallization gave 12.4 g (33 mmol; 33%) of **2**, 16.5 g (31 mmol; 31%) of **3** as well as 1.8 g (3 mmol; 3%) of **4**. From the distillation residue another small amount of **4** and **3** was obtained by crystallization.

3.4 Cleavage of a Si—Me bond in 2 to give 2,2-dibromo-5-chloro-1,1,3,3,5-pentamethyl-1,3,5-trisilacyclohexane (5)

To 10 g (26.8 mmol) of **2** in 60 mL of CCl_4, a solution of 1.4 g of I_2 (20 mol%) was added; in the dark a slow stream of dry Cl_2 was applied for 2 min, and the mixture stirred for 15 min. This was repeated until the signals of **2** disappeared from the ^{1}H NMR spectrum of the solution. After all volatile components had been removed, 9.9 g (25.2 mmol; 94%) of **5** crystallized (mp 87.5°C).

3.5 Preparation of 4 from 5

At –110°C, 9 mL (13.5 mmol) of ^{n}BuLi were added dropwise to a solution of 5.0 g (15.2 mmol) of CBr_4 in 200 mL THF:pentane:Et_2O (4:1:1). After stirring for 1 h at this temperature the solution was frozen (liquid N_2). A solution of 5.4 g (13.7 mmol) of **5** in 50 mL THF–pentane–Et_2O was added, the reaction flask allowed to warm to –80°C and the mixture stirred for another 3 h at this temperature. After gradually warming to room temperature the solvents were removed, hexane added and the solution filtered. 5.9 g of **4** (9.7 mmol; 72%) were recrystallized from hexane (mp 137°C, decomp.).

3.6 Preparation of 5-phenyl-3,3,5-trimethyl-3,5-disilahex-1-yne (9)

75 g (0.31 mol) of **8** in 100 mL THF were added at 0°C to a solution of HC≡CMgBr (14) (8.5 g (0.35 mol) Mg turnings; 21.6 mL (0.35 mol) EtBr; 400 mL THF). After refluxing for 2 h, the ether was removed, the residue suspended in pentane and filtered, and the solvent stripped. A vacuum distillation yielded 51.7 g (0.22 mol; 71%) of **9** (bp 60°C; 2×10^{-3} mm Hg).

© 2000 NRC Canada

Table 8. Bond angles (in deg) for **4**.

Bond	Angle	Bond	Angle
C(1)-Si(1)-C(2)	107.6(6)	C(2)-Si(1)-C(3)	110.9(8)
C(4)-Si(2)-C(7)	111.1(6)	C(7)-Si(2)-C(5)	112.9(6)
C(1)-Si(3)-C(7)	105.9(6)	C(7)-Si(3)-C(8)	110.3(7)
Br(1)-C(1)-Br(2)	108.4(6)	Br(2)-C(1)-Si(1)	109.2(6)
Si(1)-C(4)-Si(2)	118.3(7)	Si(2)-C(6)-Br(5)	111.9(7)
Br(4)-C(6)-Br(5)	108.0(7)	C(1)-Si(1)-C(3)	110.2(7)
C(2)-Si(1)-C(4)	110.7(7)	C(4)-Si(2)-C(5)	113.1(7)
C(7)-Si(2)-C(6)	107.1(6)	C(1)-Si(3)-C(8)	109.7(6)
C(7)-Si(3)-C(9)	112.7(7)	Br(1)-C(1)-Si(1)	105.8(6)
Br(2)-C(1)-Si(3)	107.7(6)	Si(2)-C(6)-Br(3)	110.4(7)
Br(3)-C(6)-Br(4)	107.8(7)	Si(2)-C(7)-Si(3)	117.3(7)
C(1)-Si(1)-C(4)	106.1(6)	C(3)-Si(1)-C(4)	111.3(7)
C(4)-Si(2)-C(6)	106.9(6)	C(5)-Si(2)-C(6)	105.2(7)
C(1)-Si(3)-C(9)	109.2(6)	C(8)-Si(3)-C(9)	108.9(7)
Br(1)-C(1)-Si(3)	106.2(6)	Si(1)-C(1)-Si(3)	119.0(6)
Si(2)-C(6)-Br(4)	110.4(7)	Br(3)-C(6)-Br(5)	108.3(7)

3.7 Preparation of Me_2SiBr_2

To 4.2 g (70 mmol) of Me_2SiH_2 (no solvent) at –35°C (cooling bath) very cautiously and as slowly as possible 22.1 g (140 mmol) of Br_2 were dropwise added. The reflux condenser of the apparatus was connected to a cryostate (–35°C). When the mixture turned brown, the remaining Br_2 was added at room temperature. Eventually the mixture was heated to 55°C until the ^{1}H NMR peak of Me_2SiHBr was no longer detectable. Distillation at normal pressure yielded 12.3 g (40 mmol) of Me_2SiBr_2.

3.8 Preparation of 2-chloro-7-phenyl-2,5,5,7-tetramethyl-2,5,7-trisilaoct-3-yne 10a and of 2-bromo-7-phenyl-2,5,5,7-tetramethyl-2,5,7-trisilaoct-3-yne (10b)

At 0°C, 15.7 mL (23.8 mmol) of ^{n}BuLi were added over 45 min to 5.8 g (25 mmol) of **9** dissolved in 50 mL hexane. After another 45 min stirring at room temperature, the mixture is transferred with 250 mL hexane into a dropping funnel and added over 7 h to 3.25 g (25 mmol) of Me_2SiCl_2 in 100ml hexane. Dry work-up with filtration and distillation yielded 3.3 g (10.2 mmol; 43%) of **10a** (bp 78°C; 5×10^{-3} mm Hg).

Similarly, from 13.5 g (58.2 mmol) of **9**, 35.5 mL (57.5mmol) of ^{n}BuLi and 12.6 g (58.3 mmol) of Me_2SiBr_2 a yield of 10.1 g (27.4 mmol; 48%) of **10b** (bp 91°C; 5×10^{-3} mm Hg) resulted.

3.9 Linking of 10 and 4 to give (ω-phenyl-octynyl)-trisilacyclohexane (11)

At –105°C, 4.0 mL (6.3 mmol) of ^{n}BuLi were added to 3.87 g (6.4 mmol) of **4** in 90 mL THF:pentane:Et_2O (4:1:1). After stirring for 30 min, 2.1g (6.5 mmol) of **10a** in 50 mL pentane were added at this temperature. The mixture was stirred at –105 to –85°C for another 2 h, then filtered and distilled in vacuo. 4.93 g of **11** were obtained as a slightly yellow, highly viscous oil.

Similarly, 8.2 g of **11** resulted from 6.8 g (11.2 mmol) of **4**, 6.9 mL ^{n}BuLi (11.2 mmol) and 4.2 g (11.4 mmol) of **10b**.

3.10 Reaction of 11 with HBr to give (ω-bromo-octynyl)-trisilacyclohexane (12)

4.3 g (5.25 mmol) of **11** were placed in an ampoule and frozen (liquid N_2). 6 mmol of HBr were added, the ampoule sealed and stored at –78°C. After 1 d, the ampoule was warmed to room temperature, vigorously shaken and stored again at –78°C. This was repeated for 7 d. A raw yield of 3.9 g of **12** remained when all volatile components had been removed.

3.11 Reaction of 12 with Li granules

Over 11 h, 1.95 g (2.4 mmol) of **12** in 500 mL THF were added to a vigorously stirred suspension of 44.3 mg (6.4 mmol) of Li (metal granules) in 50 mL THF. Dry work-up gave 1.28 g of raw product of which 533 mg were separated by HPLC.

Acknowledgements

We gratefully acknowledge the financial support of this work by “Deutsche Forschungsgemeinschaft” and “Fonds der Chemischen Industrie.”

References

1. G. Fritz and E. Matern. Carbosilanes. Springer–Verlag, Berlin, Heidelberg, New York, Tokyo. 1986.
2. G. Fritz and M. Hähnke. Z. Anorg. Allg. Chem. **390**, 191 (1972); A. Lipka, H.G. v. Schnering, Z. Anorg. Allg. Chem. **419**, 20 (1976).
3. A. Lipka and H.G. v. Schnering. Z. Anorg. Allg. Chem. **399**, 257 (1973); G. Fritz, H.J. Dannappel, and E. Matern. Z. Anorg. Allg. Chem. **399**, 263 (1973).
4. G. Fritz, H. Köhler, and D. Kummer. Z. Anorg. Allg. Chem. **374**, 54 (1970); G. Fritz and G. Marquardt. Z. Anorg. Allg. Chem. **404**, 1 (1974); G. Sawitzki and H.G. v. Schnering. Z. Anorg. Allg. Chem. **425**, 1 (1976).
5. G. Fritz, K.-P. Wörns, K. Peters, E.-M. Peters, and H.G. v. Schnering. Z. Anorg. Allg. Chem. **512**, 126 (1984).
6. G. Fritz and N. Szczepansky. Z. Anorg. Allg. Chem. **367**, 44 (1969).
7. G. Fritz, U. Finke, and W. Speck. Z. Anorg. Allg. Chem. **481**, 51 (1981); G. Fritz and W. Speck. Z. Anorg. Allg. Chem. **481**, 60 (1981).
8. G. Fritz and P. Böttinger. Z. Anorg. Allg. Chem. **395**, 159 (1973).
9. G. Fritz and J. Honold. Z. Anorg. Allg. Chem. **556**, 23 (1988); M. Bordeau, S.M. Djamei, J. Dunogues, and R. Calas. Bull. Soc. Chim. Fr. **1982**, II-159.
10. R.H. Fischer and G. Köbrich. Chem. Ber. **101**, 3230 (1968).
11. G. Fritz and K.-P. Wörns. Z. Anorg. Allg. Chem. **512**, 103 (1984); G.Fritz, H. Reuss, K.-P. Wörns, and A. Wörsching. Z. Anorg. Allg. Chem. **512**, 93 (1984).
12. G.M. Sheldrick. SHELXTL-Plus, Siemens Industrial Automation, Inc. 1994.
13. G. Fritz, H. Volk, M. Straub, H.G. v. Schnering, K. Peters, and E.-M. Peters. J. Organomet. Chem. **341**, 109 (1988).
14. L. Skattebol, E.R.H. Jones, and M.C. Withing. Org. Synthesis. **4**, 792 (1963).

© 2000 NRC Canada

Reduction of conjugate double bonds with trichlorosilane

Moni Chauhan and Philip Boudjouk

Abstract: A variety of α,β-unsaturated esters and cyclic ketones underwent smooth reduction of the carbon–carbon double bond with a combination of inexpensive and readily available trichlorosilane and $CoCl_2$. The reactions are performed under very mild conditions and products are obtained in high yields.

Key words: reduction, carbonyl compounds, trichlorosilane, ketones, chemoselectivity.

Résumé : Une grande variété d'esters et de cétones cycliques α,β-insaturés subissent une réduction facile de la double liaison carbone–carbone sous l'influence combinée du $CoCl_2$ et du trichlorométhane facilement accessible et peu dispendieux. Les réactions se produisent dans des conditions très douces et les produits sont obtenus avec des rendements élevés.

Mots clés : réduction, composés carbonyles, trichlorosilane, cétones, chimiosélectivité.

[Traduit par la Rédaction]

Introduction

Among the various reducible substrates of great relevance are those containing both a carbonyl group and a C=C bond such as α,β-unsaturated esters and ketones. Indeed, the capability of reducing only one group, leaving the other one unaffected, is a challenging task in organic synthesis, particularly for the preparation of pharmaceutical and agrochemical products. Chemoselective hydrogenation of double bonds in α,β-unsaturated carbonyl compounds has attracted much interest for more than two decades. A very convenient and fundamentally important route to these reactions is by metal-catalyzed hydrogenation (1). Practical motivations arise from the fact that such reactions are convenient in large scale synthesis since there is no need to employ a high hydrogen pressure or to use hazardous reducing agents. Transfer of organic groups of organosilanes to metallic species, transmetalation, and subsequent homocoupling reactions under mild conditions are well known (2). Recently, there have been reports of generating copper hydride species via transmetalation of a hydrogen atom on silicon to copper (3). Although this combination of a Cu(I) salt and dimethylphenylsilane is a useful reagent for conjugate reduction of α,β-unsaturated compounds, the hydrosilane is a fairly expensive starting material. Consequently this report introduces the use of the cheapest and most readily available silane, trichlorosilane, as a hydride source catalyzed by $CoCl_2$ in the presence of small amounts of DMI (1,3-dimethyl-2-imidazolidinone) or DMPU (1,3-dimethyl-3,4,5,6-tetrahydro-2(1 *H*)-pyrimidinone).

In our effort to find a new catalyst for hydrosilylation of acrylonitriles (4) and acrylates, we found that $CoCl_2$ and TMEDA (*N*,*N*,*N′*,*N′*-tetramethylethylenediamine) catalyzed the reduction of the double bond in acrylates and hydrosilylation (eq. [1]).

[1] $$CH_2{=}CHCO_2Me + HSiCl_3 \xrightarrow[CD_3CN,\,70°C,\,8\,h]{CoCl_2,\,TMEDA} Cl_3SiCH_2CH_2CO_2Me + CH_3CH_2CO_2Me$$

In contrast, in the presence of DMI or DMPU reduction of the carbon–carbon double bond was the exclusive reaction path resulting in efficient, high yield syntheses of saturated ketones and esters under mild conditions.

Experimental

General procedure

All reactions and manipulations were routinely performed under an argon atmosphere by using standard Schlenk techniques. Commercially available hexahydrated $CoCl_2$ was oven dried. All acrylates and ketones are commercial products and were distilled in an inert atmosphere prior to use. Trichlorosilane was purified by distillation over magnesium metal. TMEDA, DMI, or DMPU were used as received without further purification. Deuterated acetonitrile for the reaction was dried over molecular sieves. ^1H and ^{13}C NMR spectra were recorded on a JEOL GSX270 and JEOL GSX400 (operating at 100.53 MHz for ^{13}C) spectrometers respectively. All chemical shifts are reported in ppm and were measured relative to residual ^1H or ^{13}C resonances in a deuterated solvent (CD_3CN, δ 1.94).

Received April 23, 1999. Published on the NRC Research Press website on October 20, 2000.

M. Chauhan and P. Boudjouk.[1] Center for Main Group Chemistry, Department of Chemistry, North Dakota State University, Fargo ND 58105–5516, U.S.A.

[1]Author to whom correspondence may be addressed. Telephone: (701) 231-8601. Fax: (701) 231-7947. e-mail: boudjouk@plains.nodak.edu

© 2000 NRC Canada

Table 1.

Entry	Alkenes (mmol) / Silane (mmol)	$CoCl_2$ (mmol)	DMI or DMPU (mmol)	Rxn. Conditions	Product, Yield
1	CH_2=$CHCO_2Me$(8) / $HSiCl_3$(16)	1.4	4.0	CD_3CN (2 mL) 70°C, 5 h	$CH_3CH_2CO_2Me$, 90%
2	CH_2=$CHCO_2Et$(8) / $HSiCl_3$(16)	1.4	4.0	CD_3CN (2 mL) 70°C, 5 h	$CH_3CH_2CO_2Et$, 70%
3	PhCH=$CHCO_2Et$(8) / $HSiCl_3$(16)	1.4	4.0	CD_3CN (2 mL) 70°C, 5 h	$PhCH_2CH_2CO_2Et$, 50%
4	2-Cyclohexen-1-one(8) / $HSiCl_3$(16)	1.4 or 0.4	4.0 or 2.0	Neat or CD_3CN (2 mL), R.T., 5 h	1-cyclohexanone, 88%
5	2-Cyclopenten-1-one(8) / $HSiCl_3$(16)	1.4	4.0	Neat or CD_3CN (2 mL), R.T., 4 h	1-cyclopentanone, 92%
6	1-Acetyl-1-cyclohexene(8) / $HSiCl_3$(16)	1.4	4.0	CD_3CN (2 mL) 70°C, 2 h	1-acetyl cyclohexane, 75%
7	3,5-Dimethyl-2-cyclohexen-1-one(8) / $HSiCl_3$(16)	1.4	4.0	CD_3CN (2 mL) 70°C, 12 h	3,5-dimethyl-1-cyclohexanone, 50%
8	CH_2=$CHCO_2Et$(8) / Me_2PhSiH(16)	1.4	4.0	CD_3CN (2 mL) 80°C, 10 h	$CH_3CH_2CO_2Et$, 85%, $Me_2PhSiOSiMe_2Ph$.
9	2-Cyclopenten-1-one(8) / $HSiMe_2Ph$(16)	1.4	4.0	Neat, 80°C, 10 h	1-cyclopentanone 65%, $Me_2PhSiOSiMe_2Ph$.

Catalysis experiments

A typical procedure is given as follows: to a mixture of $CoCl_2$ (0.180 g, 1.4 mmol) and DMI (0.5 mL, 4 mmol) in CD_3CN (2 mL), methylacrylate (0.72 mL, 8 mmol) and then trichlorosilane (1.76 mL, 16 mmol) was added at room temperature. The resulting mixture was refluxed at 70°C and was monitored by ^1H and ^{13}C NMR. After 5 h the color of the reaction solution changed from blue to green, which indicated the complete consumption of methylacrylate. The solid formed in the reaction was filtered through a short-column chromatography (Florisil, CD_3CN:pentane = 1:2) to furnish pure reduction product.

Results and discussion

The catalysis was found to be quite general for the selective reduction of C=C bonds of α,β-unsaturated esters and ketones. Our results are summarized in Table 1 and show that all reactions exhibit excellent chemoselectivity, good catalytic activity, and essentially only one product: the corresponding saturated ester or ketone. The optimum reaction conditions from entry 1 were applied to ethylacrylate (entry 2) and ethylcinnamate (entry 3). This last reaction proceeds much slower and gives a lower yield of the desired product (50%) in comparison to the reactions in entry 1 (90%) and 2 (70%). We attribute this to a combination of steric and electronic effects arising from the phenyl ring.

We applied our reduction system to the α,β-unsaturated cyclic ketones. As is evident from Table 1, 2-cyclohexen-1-one (entry 4) and 2-cyclopenten-1-one (entry 5) underwent reduction reactions at room temperature which resulted in excellent yields (88–92%). It was observed that a reduction in the amounts of catalyst did not affect the rate or the yields of the reaction. In fact, the amount of $CoCl_2$ in this reaction can be reduced to 5 mmol% and DMI or DMPU can be used as low as 25 mmol%. On the other hand, 1-acetyl-1-cyclohexene and 3,5-dimethyl-2-cyclohexen-1-one were not reactive at room temperature. 1-acetyl cyclohexane was obtained in 75% yield after heating at 70°C for 2 h (entry 6) and 3,5-dimethyl-2-cyclohexane was obtained only in 50% yield after 12 h. Steric influence from methyl groups at the *meta*-position might be responsible for its low reactivity. Unfortunately, the silicon species formed in the present catalysis were difficult to identify.

To get an insight into the mechanism of these reactions, we treated dimethylphenylsilane with ethylacrylate and with 2-cyclopenten-1-one (entry 8 and 9). Notably, both reactions were homogeneous to give the corresponding saturated products. The silicon compounds formed in these reactions were isolated by dissolving the crude product in pentane and were identified by NMR as dimethylphenyldisiloxane. It is relevant to note that Mori et al. (3*b* and 3*c*) have recently reported the formation of this disiloxane from the reaction of CuCl and $PhMe_2SiH$ in DMF at room temperature for 1 h. The authors suggested that CuH and chlorodimethylphenylsilane first formed are converted to disiloxane via hydrolytic condensation. By analogy, we assume a similar pathway for the reactions in entry 8 and 9.

Conclusions

Trichlorosilane effects conjugate reduction with the aid of $CoCl_2$. This reduction method constitutes a simple and cheap alternative to literature procedures for the selective conjugate reduction of α,β-unsaturated carbonyl compounds. Further characterization of the reactive intermediates and elucidation of the mechanism is under active investigation.

Acknowledgements

The financial Support of the National Science Foundation through Grant no. 9452892 is gratefully acknowledged. Fruitful discussions with Bhanu P. S. Chauhan are also gratefully acknowledged.

References

1. (*a*) H.O. House (*Editor*). Modern synthetic reactions. 2nd ed. W.A. Benjamin. Menlo Park, Calif. 1972 and refs therein; (*b*) P.N. Rylander (*Editor*). Catalytic hydrogenation in organic synthesis. Acedemic Press, New York. 1979; (*c*) H.C. Brown and S. Krishnamurthy. Tetrahedron, **35**, 567 (1979); (*d*) D.C.

© 2000 NRC Canada

Wigfield. Tetrahedron, **35**, 449 (1979); (*e*) J.P. Collman, R.G. Finke, P.L. Matlok, R. Wahren, R.G. Komoto, and J.I. Brauman. J. Am. Chem. Soc. **100**, 1119 (1978); (*f*) H. Chikashita, M. Miyazaki, and K. Itoh. Synthesis, 308 (1984), and refs therein; (*g*) F. Yoneda, K. Kurodo, and K. Tanaka. J. Chem. Soc. Chem. Commun. 1199 (1984); (*h*) A. Alba, M.A. Aramendia, V. Borau, A. Garcia-Raso, C. Jimenez, J.M. Marinas. Can. J. Chem. **62**, 917 (1984).

2. (*a*) K. Ikegashira, Y. Nishihara, K. Hirabayashi, A. Mori, and T. Hiyama. J. Chem. Soc. Chem. Commun. 1039 (1997); (*b*) H. Ito, K. Aromoto, H. Sensui, and A. Hosomi. Tetrahedron Lett. **38**, 3977 (1997); (*c*) H. Ito, H. Sensui, K. Aromoto, K. Miura, and A. Hosomi. Chem. Lett. 639 (1997); (*d*) Y. Nishihara, K. Ikegashira, A. Mori, and T. Hiyama. Chem. Lett. 1233 (1997); (*f*) Y. Nishihara, K. Ikegashira, A. Mori, and T. Hiyama. Tetrahedron Lett. **39**, 4075 (1998).
3. (*a*) H. Ito, T. Ishizuka, K. Aromoto, K. Miura, and A. Hosomi. Tetrahedron Lett. **38**, 8887 (1997); (*b*) A. Mori, A. Fujita, Y. Nishihara, and T. Hiyama. J. Chem. Soc. Chem. Commun. 2159 (1997); (*c*) A. Mori, A. Fujita, H. Kajiro; Y. Nishihara, and T. Hiyama. Tetrahedron, **55**, 4573 (1999).
4. M. Chauhan, B.P.S. Chauhan, and P. Boudjouk. Tetrahedron Lett. **40**, 4127 (1999).

© 2000 NRC Canada

Geminal bis(hypersilyl) compounds — the synthesis and structure of bis[tris(trimethylsilyl)silyl]silanes

Thoralf Gross, Helmut Reinke, and Hartmut Oehme

Abstract: Protodesilylation of diphenylsilane with trifluoromethanesulfonic acid and subsequent reaction of the obtained bis(trifluoromethanesulfonyloxy)silane with tris(trimethylsilyl)silyllithium (**1**) (molar ratio 1:2) afforded bis[tris(trimethylsilyl)silyl]silane (**8**). Methyl-bis[tris(trimethylsilyl)silyl]silane (**3**) and phenyl-bis[tris(trimethylsilyl)silyl]silane (**10**) were obtained by coupling reactions of **1** with $MeHSiCl_2$ or $PhHSiCl_2$, respectively, (2:1). By treatment with $HCBr_3$, the H-silanes **3**, **8**, and **10** were converted into the bromosilanes $[(Me_3Si)_3Si]_2SiR^1R^2$ (**9**: $R^1 = R^2 = Br$; **11**: $R^1 = Me$, $R^2 = Br$; **12**: $R^1 = Ph$, $R^2 = Br$). X-ray crystal structure analyses, performed for **3**, **10** and **12**, confirmed the expected distortions of the molecular skeletons of the compounds. Thus, e.g., in **10**, the spatial demand of the two extended hemispherical hypersilyl groups forces a widening of the Si-Si-Si angle at the central Si atom to a value of 128.3°.

Key words: silanes, sterically congested, bis(hypersilyl)silanes, hypersilylsilanes, bis(hypersilyl)germanes, tris(trimethylsilyl)silylsilanes.

Résumé : La protodésilylation du diphénylsilane par l'acide trifluorométhanesulfonique et la réaction du bis(trifluorométhanesulfonyloxy)silane qui en résulte avec du tris(triméthylsilyl)silyllithium (**1**) (rapport molaire 1:2) conduit à la formation de bis[tris(triméthylsilyl)silyl]silane (**8**). Les réactions de couplage de **1** avec le $MeHSiCl_2$ et le $PhHSiCl_2$ conduisent à la formation respectivement de méthyl-bis[tris(triméthylsilyl)silyl]silane (**3**) et de phényl-bis[tris(triméthylsilyl)silyl]silane (**10**). Par traitement avec du $HCBr_3$, les silanes **3**, **8** et **10** sont transformés en bromosilanes $[(Me_3Si)_3Si]_2SiR^1R^2$ (**9**: $R^1 = R^2 = Br$; **11**: $R^1 = Me$, $R^2 = Br$; **12**: $R^1 = Ph$, $R^2 = Br$). L'examen des composés **3**, **10** et **11** par diffraction des rayons X a permis de confirmer les déformations attendues pour les squelettes moléculaires de ces composés. Ainsi, par exemple, dans le composé **10**, la demande spatiale des deux groupes hypersilyles hémisphériques étendus provoque un agrandissement, jusqu'à une valeur de 128,3°, de l'angle Si-Si-Si au niveau de l'atome de Si central.

Mots clés : silanes, congestion stérique, bis(hypersilyl)silanes, hypersilylsilanes, bis(hypersilyl)germanes, tris(triméthylsilyl)silylsilanes.

[Traduit par la Rédaction]

Introduction

The tris(trimethylsilyl)silyl group, the hypersilyl group, proved to be a function with unusual steric and electronic properties, gaining increasing interest as a substituent suitable for protecting and stabilizing uncommon bonding states of main group as well as transition elements (1, 2). The spherical extension of the $(Me_3Si)_3Si$ group was found to cause considerable distortions of the molecular skeletons of respective hypersilyl derivatives (3) and, of course, particularly serious deviations from regular molecular structures were expected for compounds, in which two of these bulky groups are bound to the same central atom. Geanangel and co-workers (4) calculated the cone angles for $(Me_3Si)_3Si$-E fragments of, e.g., group 14 elements to be 168° for E = Sn, 175° for E = Ge, 182° for E = Si, and 199° for E = C, respectively, indicating that the access to geminal bis(hypersilyl) derivatives, especially to those with a nonlinear arrangement of the two groups, might be difficult. Nevertheless, in recent years a number of geminal bis(hypersilyl) compounds, preferably of the heavier main group elements, was synthesized and, in part, structurally characterized. Thus, bis(hypersilyl)galliumchloride (5*a*), the chlorobis(hypersilyl)gallium and indium complexes $[(Me_3Si)_3Si]_2MCl{\cdot}LiCl$ (M = Ga, In) (5*b*) as well as tetrakis-[tris(trimethylsilyl)silyl]digallium (5*c*), and tetrakis[tris(trimethylsilyl)silyl]dithallium (5*d*) were described. Biffar and Nöth (5*e*) succeeded in synthesizing methoxy-bis[tris(trimethylsilyl)silyl]boron and dimethylamino-bis[tris(trimethylsilyl)silyl]boron. Bis(hypersilyl) selenane (6*a*) and

Received June 28, 1999. Published on the NRC Research Press website on October 20, 2000.

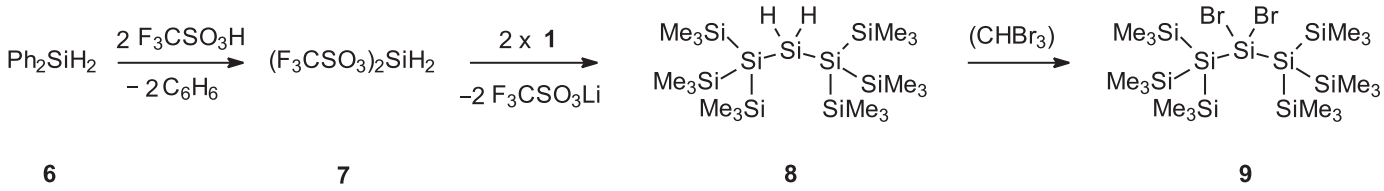
This paper is dedicated to Professor Adrian G. Brook.

T. Gross, H. Reinke, and H. Oehme.[1] Fachbereich Chemie der Universität Rostock, D-18051 Rostock, Germany.

[1]Author to whom correspondence may be addressed. Telephone: 49(0) 381-498-1765. Fax: 49(0) 381-498-1763. e-mail: hartmut.oehme@chemie.uni-rostock.de

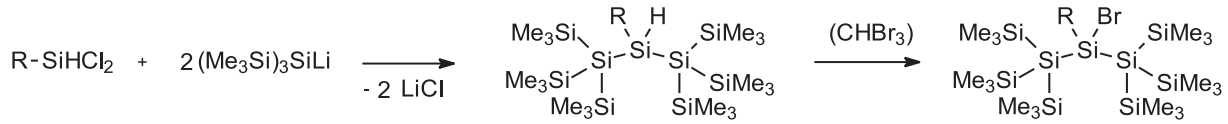
© 2000 NRC Canada

Scheme 1.



6 **7** **8** **9**

Scheme 2.



1

R = Me, Ph

3: R = Me
10: R = Ph

11: R = Me
12: R = Ph

bis(hypersilyl) tellurane (6*a*, 6*b*) were described, also bis(hypersilyl) derivatives of iron, chromium, manganese (7*a*), and of zinc and mercury (7*b*) are known.

Concerning group 14 elements, which are of special interest in the context of this paper, the carbene analogues $[(Me_3Si)_3Si]_2Sn$ (8*a*) and $[(Me_3Si)_3Si]_2Pb$ (8*b*) and their dimers were synthesized and structurally characterized. Bis(hypersilyl)tin dichloride was obtained by the reaction of tris(trimethylsilyl)silyllithium with tin tetrachloride (8*c*), and Klinkhammer (2) succeeded in synthesizing $NaSn[Si(SiMe_3)_3]_3$, the first compound bearing three hypersilyl groups at one central atom. There are reports in the literature about unsuccessful attempts of the synthesis of bis(hypersilyl) derivatives of germanium (8*c*, 8*d*) and silicon (8*d*, 8*e*), but recently Apeloig et al. (8*f*) described the synthesis of $[(Me_3Si)_3Si]_2SiHCl$ (**2**) by a coupling reaction of tris(trimethylsilyl)silyllithium (**1**) with trichlorosilane and its conversion into $[(Me_3Si)_3Si]_2SiHMe$ (**3**), $[(Me_3Si)_3Si]_2Si(Cl)Me$ (**4**), and $[(Me_3Si)_3Si]_2SiMe_2$ (**5**). Very recently Marschner (8*g*) obtained the nonasilane **5** by the reaction of $(Me_3Si)_3SiSiMe_2Br$ with tris(trimethylsilyl)silylpotassium.

Of particular interest from a structural point of view are geminal bis(hypersilyl) compounds with a central carbon atom, and rather unexpectedly we found that the placement of two bulky $(Me_3)Si)_3Si$ groups at one comparatively small sp^3 carbon atom can easily be achieved. Thus, we succeeded in synthesizing methoxybis[tris(trimethylsilyl)silyl]methane by the reaction of **1** with dichloromethyl-methylether (9*a*). Bis(hypersilyl)methanol was obtained from **1** and *tert*-butyl formate (9*b*) and, furthermore, **1** reacts with dialkyl(chloromethylene)ammonium chlorides to give dialkylaminobis[tris(trimethylsilyl)silyl]methanes (9*c*). Recently, we were also able to describe the parent compound of the series, bis[tris(trimethylsilyl)silyl]methane (9*d*). The structures of all these compounds are characterized by tremendous distortions of the molecular skeletons. In particular, the Si-C-Si bond angles at the central sp^3 carbon atoms are extremely widened to values up to 136.2°, the individual values being dependent on the space demand of the further *C*-substituents. In the present paper we describe the extension of these studies to geminal bis(hypersilyl) compounds with a central silicon atom with the aim of comparing the structural parameters of the silicon centered bis(hypersilyl) compounds with their carbon analogues.

Results and discussion

The syntheses of geminal bis(hypersilyl)silanes 8–12

Bis[tris(trimethylsilyl)silyl]silane (**8**) was obtained by treatment of bis(triflouromethanesulfonyloxy)silane (**7**) with tris(trimethylsilyl)silyllithium (**1**) (molar ratio 1:2) in toluene (Scheme 1). The silyltriflate **7** was prepared by protodesilylation of diphenylsilane (**6**) with trifluoromethanesulfonic acid (10) and was used without isolation and purification. The method gave **8** in a total yield of 19% (based on **6**).

In a very straightforward reaction dichloromethylsilane with two equiv. of **1** afforded methylbis(hypersilyl)silane (**3**). Similarly, dichlorophenylsilane with **1** gave phenylbis(hypersilyl)silane (**10**) (Scheme 2).

Despite the steric congestion of the molecules, the Si—H bonds in **3**, **8**, and **10** proved to be reactive and were converted into Si—Br functions. Thus, refluxing of **8** in tribromomethane for 10 h gave 40% of dibromobis[tris(trimethylsilyl)silyl]silane (**9**). For the comparable replacement of hydrogen by bromine in **3** and **10** the solutions of the H-silanes in $HCBr_3$ had to be heated for several days. Nevertheless the conversions of **3** and **10** were incomplete and in case of the synthesis of **11**, we did not succeed in a clean separation of the starting compound **3** from the formed bromosilane. The bromosilane **12** was obtained in a yield of 70%.

The direct coupling of **1** with dichlorodimethylsilane (2:1) appears not to be a practicable method for the synthesis of dimethylbis(hypersilyl)silane (**5**). Independent of the molar ratio of the components, we always obtained chlorodimethyl[tris(trimethylsilyl)silyl]silane $((Me_3Si)_3SiSi(Cl)Me_2)$ (**13**) (8*e*, 11). Obviously, the steric situation in **13** prevents the replacement of the chlorine atom by a second hypersilyl group.

© 2000 NRC Canada

Fig. 1. Molecular structure of **3** in the crystal (ORTEP, 30% probability, H atoms omitted except for Si1 H). Selected bond lengths (Å): Si1—C1 1.784(9), Si1—Si2 2.374(9), Si1—Si3 2.360(10), Si2—Si4 2.343(8), Si2—Si5 2.350(8), Si2—Si6 2.362(9), Si3—Si7 2.375(11), Si3—Si8 2.370(8), Si3—Si9 2.381(6); and selected bond angles (deg): Si2-Si1-Si3 128.34(7), C1-Si1-Si2 113.0(5), C1-Si1-Si3 107.7(4), Si1-Si2-Si4 117.8(3), Si1-Si2-Si5 103.4(3), Si1-Si2-Si6 110.8(4), Si1-Si3-Si7 115.5(4), Si1-Si3-Si8 113.0(4), Si1-Si3-Si9 104.1(3); dihedral angles: Si2-Si1-Si3-Si7 48.9(7), Si2-Si1-Si3-Si8 78.1(6), Si2-Si1-Si3-Si9 166.1(5), Si3-Si1-Si2-Si4 49.6(7), Si3-Si1-Si2-Si5 164.7(5), Si3-Si1-Si2-Si6 80.2(6).

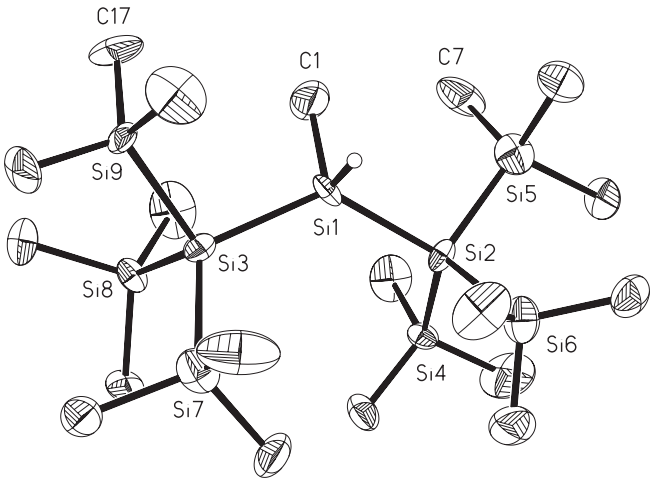
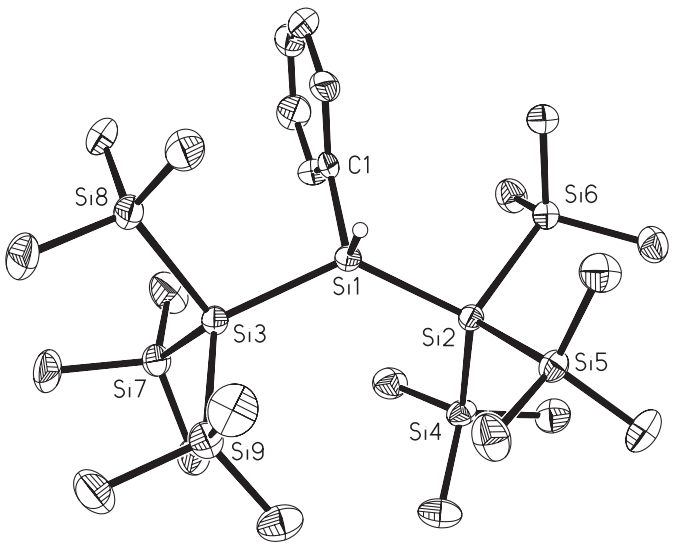


Fig. 2. Molecular structure of **10** in the crystal (ORTEP, 30% probability, H atoms omitted except for Si1 H). Selected bond lengths (Å): Si1—C1 1.891(9), Si1—Si2 2.380(3), Si1—Si3 2.390(3), Si2—Si4 2.359(3), Si2—Si5 2.369(3), Si2—Si6 2.368(3), Si3—Si7 2.371(3), Si3—Si8 2.373(3), Si3—Si9 2.354(4); and selected bond angles (deg): Si2-Si1-Si3 128.66(12), Si1-Si2-Si4 118.69(12), Si1-Si2-Si5 108.18(12), Si1-Si2-Si6 106.93(11), Si1-Si3-Si7 119.89(13), Si1-Si3-Si8 102.32(11), Si1-Si3-Si9 112.81(12); Si2-Si1-Si3-Si7 66.9(2), Si2-Si1-Si3-Si8 173.15(15), Si2-Si1-Si3-Si9 59.7(2), Si3-Si1-Si2-Si4 33.2(2), Si3-Si1-Si2-Si6 153.96(14), Si3-Si1-Si2-Si5 94.37(17).



The structures of geminal bis(hypersilyl)silanes

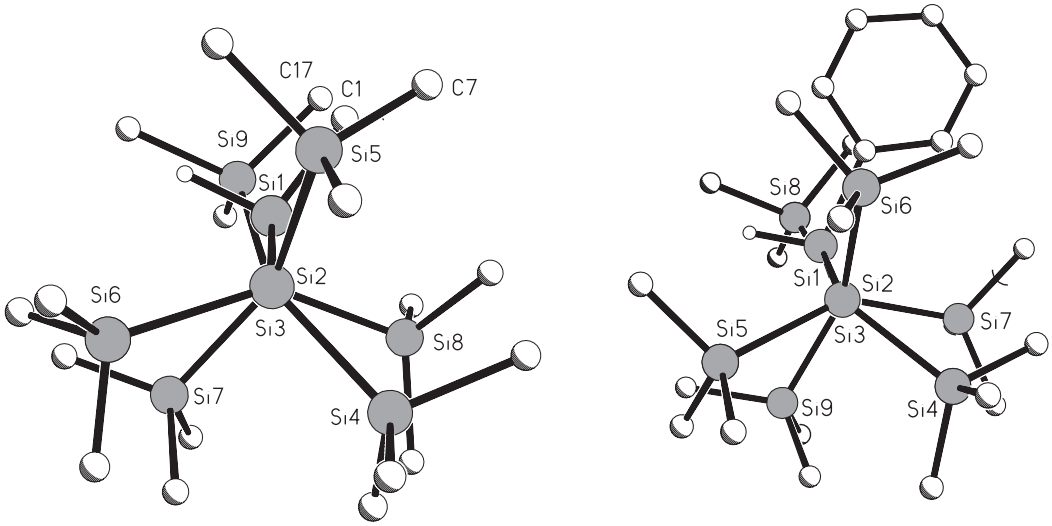
The structures of the products obtained were elucidated by IR, NMR, and MS studies (see Experimental section). As found already for geminal bis(hypersilyl) carbon derivatives (9), in the ^{1}H, ^{13}C, and ^{29}Si NMR spectra of the synthesized bis(hypersilyl) silicon compounds (**8**–**12**) only one signal appeared for all trimethylsilyl substituents, indicating a considerable mobility of these groups in the congested molecules.

X-ray crystal structure analyses were performed for **3**, **10**, and **12**. Unfortunately, the crystal quality of **8** was insufficient for a structure determination. Thus, a direct comparison of the structural parameters of **8** with those of the carbon homologue $[(Me_3Si)_3Si]_2CH_2$ (9*d*) could not be realized. Crystals of **12** contained disordered acetone in special positions (origin of the unit cell), which impedes accurate results. In addition to this, experimental problems with the low-temperature device led to an unfinished ψ scan. So absorption correction calculations on the basis of experimental results could not be performed. Anyhow, the crystal structure of **12** was refined down to $R1 = 0.0661$ for the observed reflections when the structure of the solvent molecule was calculated with both distance and distant restraints as well as a restraint to force the acetone atoms in one plane. Thus, the constitution of **12** was confirmed and, e.g., the central Si-Si-Si angle could be determined to be 130.7°.

For a detailed discussion of molecular structures we have chosen compounds **3** and **10**. As expected, the results of the X-ray analyses of the two compounds, which are illustrated in Figs. 1 and 2, reveal considerable distortions of the molecular skeletons of these polysilanes. The structures are mainly determined by the two extended hemispherical hypersilyl groups, which are separated by a MeSiH or PhSiH unit, respectively, as spacers, causing the angles in the molecular axes of **3** and **10**. As expected, the spatial demand of the $(Me_3Si)_3Si$ substituents forces a widening of the Si-Si-Si angles at the central silicon atoms. In **10**, the small Si1-hydrogen atom and the phenyl ring, whose plain is arranged orthogonal to the line connecting the two central hypersilyl silicon atoms, allow the angle to open to a value of 128.66(12)°. The Si1—Si2 and Si1—Si3 bond distances in **10** (2.380(3) and 2.390(3) Å, respectively) are slightly elongated. The structural parameters obtained for **3** (Si2-Si1-Si3 angle 128.34(7)°, bond distances Si1—Si2 2.374(9) and Si1—Si3 2.360(10) Å, respectively) are comparable with those obtained for **10**, indicating that in these particular compounds the space demand of the methyl and the phenyl group is almost the same. As reported by Marschner (8*g*) for dimethylbis[tris(trimethylsilyl)silyl]silane (**5**), replacement of the hydrogen atom at the central silicon atom of **3** by a further methyl group leads to a decrease of the Si-Si-Si angle to a value of 125.7°, which is in agreement with the picture that increasing space demand of the further substituents at Si1 should reduce the $(Me_3Si)_3Si$-Si-Si-$Si(SiMe_3)_3$ angle. Actually, all the central Si-Si-Si angles of the bis(hypersilyl)silanes mentioned are extraordinarily wide, but increasing bulk of the substituents may lead to even wider angles. Thus, e.g., Lambert et al. (12) and Suzuki et al. (12) found the Si(1)-Si(2)-Si(3) angles in the dendritic polysilane $[(Me_3Si)_3Si(3)\text{-}Si(2)Me_2]_3Si(1)Me$ to amount to a value of 130.4°.

© 2000 NRC Canada

Fig. 3. Projection of the molecular structures of **3** and **10**, looking along the Si2—Si3 axes. Dihedral angles (deg): **3**: Si4-Si2-Si3-Si8 26.11(36), Si5-Si2-Si3-Si8 91.81(40), Si5-Si2-Si3-Si9 36.42(15), Si6-Si2-Si3-Si9 90.49(42), Si6-Si2-Si3-Si7 28.75(42), Si4-Si2-Si3-Si7 86.42(10); **10**: Si4-Si2-Si3-Si7 27.91(13), Si6-Si2-Si3-Si7 90.23(15), Si6-Si2-Si3-Si8 41.42(20), Si5-Si2-Si3-Si8 85.78(16), Si5-Si2-Si3-Si9 32.16(13), Si4-Si2-Si3-Si9 82.50(12).



3 **10**

A direct comparison of the Si-Si-Si angles of **3**, **5**, and **10** with the Si-C-Si angles of carbon centered bis(hypersilyl) compounds is not possible, since derivatives with an identical substitution pattern are not available. But the trend is obvious. Due to shorter Si—C bond distances, the angles at the central carbon atoms are even wider and correlate with the space demand of the further substituents at the carbon atom (e.g., Si-C-Si angles found for $[(Me_3Si)_3Si]_2CHR$: R = H 136.2(2)° (9*d*), R = OH 135.5(2)° (9*b*), R = OMe 132.7(4)° (9*a*), R = NMe_2 132.6(3)° (9*c*), R = OC(O)Me 131.3(2)° (9*e*), R = $N(CH_2)_5$ 128.7(2)° (9*c*)).

The steric strain in the molecules of **3** and **10** leads to considerable deformations of the usually tetrahedral configuration at the central Si atoms of the hypersilyl substituents. Thus, the average MeHSi-Si-$SiMe_3$ angles in **3** are 110.7° or 110.9°, respectively, but the individual angles differ markedly. At positions, where the two hypersilyl hemispheres contact each other, the angles are wider (Si1-Si2-Si4 117.8°, Si1-Si3-Si7 115.5°) and at the opposite positions the Me_3Si groups evade the steric strain making the angle much smaller (Si1-Si2-Si5 103.4°, Si1-Si3-Si9 104.1°). In **10** the situation is quite comparable, the average Si1-Si-Si angles are 111.3° and 111.7°, respectively, the angles Si1-Si2-Si4 (118.7°) and Si1-Si3-Si7 (119.9°) are considerably widened, consequently the angles Si1-Si2-Si6 (106.9°) and Si1-Si3-Si8 (102.3°) are compressed.

Very instructive is a view along the Si2—Si3 axes of **3** and **10**, which again reveals that the structure of the compounds is predominantly determined by the space filling trimethylsilyl groups of the two hypersilyl moieties, the bridging MeSiH and PhSiH groups playing a minor role. No trimethylsilyl group is in gauche conformation with Si1, since this, of course, would lead to an extreme approach of the Me_3Si groups in the anti positions (Fig. 3). At the positions, where the two hypersilyl hemispheres contact each other, the trimethylsilyl groups evade the steric strain by rotating the hypersilyl shells, opening the dihedral angle Si4-Si2-Si3-Si7 in **3** to a value of 86.4°. The dihedral angle Si4-Si2-Si3-Si9 in **10** was found to be 82.5°. Consequently the dihedral angles in the opposite positions, which frame the bridging Si1 atom and its substituents, become very small (**3**: Si5-Si2-Si3-Si9 36.4°; **10**: Si6-Si2-Si3-Si8 41.4°). As a result of that, in **3** the methyl group at Si1 and the neighboring groups of Me_3Si substituents approach to exceptionally short distances (C1—C7 3.31(3), C1—C17 3.51(3) Å). Due to the steric stress in the molecule, the methyl groups at the opposite positions of the hypersilyl hemispheres are also pressed together (C4—C13 3.80(1), C8—C13 3.89(3) Å), resulting in distances significantly shorter than the sum of the van der Waals radii of two methyl groups, which amounts to about 4.00 Å (13). Also in compound **10**, there are short distances between the *ortho* carbon atoms of the phenyl ring and some methyl carbon atoms in the wing groups, ranging from 3.46 Å for C2—C16 to 3.79 Å for C6—C21. Further dihedral angles characterizing the molecular structures of the polysilanes **3** and **10** are given in the captions of Figs. 1 and 2.

Experimental section

All reactions involving organometallic reagents were carried out under purified argon. NMR: Bruker AC 250 or Bruker ARX 300, tetramethylsilane as internal standard. IR: Nicolet 205 FT-IR. MS: Intectra AMD 402 (EI, 70 eV). $(Me_3Si)_3SiLi \cdot 3$ THF was prepared as reported in the literature (14). All yields given refer to amounts obtained after chromatographic separation and purification. Due to

© 2000 NRC Canada

incomplete combustion the results of the elemental analyses were unsatisfactory; therefore HRMS data are given.

Methylbis[tris(trimethylsilyl)silyl]silane (3)

At –78°C, 0.23 g (2.0 mmol) of dichloromethylsilane, dissolved in 20 mL of toluene, were added to a vigorously stirred solution of 1.85 g (4.0 mmol) of $(Me_3Si)_3SiLi \cdot 3$ THF in 20 mL of toluene. After warming up to room temperature, stirring was continued for 2 h and the solution was evaporated in vacuo. Recrystallization of the residue from ethyl acetate gave 0.75 g (71%) of pure **3**. Single crystals were obtained by recrystallization from toluene at –50°C, mp 188–191°C (under partial sublimation). IR (Nujol) $\tilde{\nu}$ (cm^{-1}): 2068 (SiH). MS (*m*/*z*) (%): 538 (1) [M^+], 523 (1) [M^+-CH_3], 464 (88) [M^+-$HSiMe_3$], 217 (100) [M^+-$HSi(SiMe_3)_3$]. ^{1}H NMR (benzene-d_6) δ: 0.35 (s, $Si(CH_3)_3$, 54 H), 0.59 (d, ^3J = 5.2 Hz, $SiCH_3$, 3 H), 4.24 (q, ^3J = 5.2 Hz, SiH, 1 H). ^{13}C NMR (benzene-d_6) δ: –0.4 (SiMe), 3.5 ($SiMe_3$). ^{29}Si NMR (benzene-d_6) δ: –124.7 (*Si*$SiMe_3$), –65.45 (d,^1J = 167.8 Hz, SiH), –9.1 ($SiMe_3$). HRMS calcd. ($C_{19}H_{58}Si_9$): 538.212; found: 538.246.

Bis[tris(trimethylsilyl)silyl]silane (8)

At 0°C, 0.78 g (5.2 mmol) of trifluormethanesulfonic acid were gradually added to a solution of 0.48 g of diphenylsilane in 20 mL of toluene. After warming up to room temperature, the solution was stirred for 3 h and subsequently given at –78°C within 30 min to 2.43 g (5.2 mmol) of $(Me_3Si)_3SiLi \cdot 3$ THF, dissolved in 20 mL of toluene. The mixture was allowed to warm again to room temperature and after stirring for a further 2 h and filtration over silica gel the solvent was removed in vacuo. Chromatography of the residue (silica gel, heptane) gave 0.26 g (19%) of **8**, mp 172–176°C (under partial sublimation). IR (KBr) $\tilde{\nu}$ (cm^{-1}): 2074 (SiH). MS (CI, isobutane as the reactant gas) (*m*/z) (%): 525 (1) [M^+-H], 509 (0.5) [M^+-CH_3], 450 (17) [M^+-$HSiMe_3$], 376 (100) [M^+-2 ($HSiMe_3$)], 303 (52) [M^+- 2($HSiMe_3$)-$SiMe_3$]. ^{1}H NMR (benzene-d_6) δ: 0.35 (s, $SiCH_3$, 54 H), 3.60 (s, SiH_2, 2 H). ^{13}C NMR (benzene-d_6) δ: 2.59 ($SiCH_3$). ^{29}Si NMR (benzene-d_6) δ: = –131.5 (*Si*$SiMe_3$), –107.3 (t, ^1J = 169.5 Hz, SiH_2), – 9.1 ($SiMe_3$). HRMS studies could not be performed. HRMS measurements with chemical ionization were not possible, and under EI conditions no molecular peak was found.

Dibromobis[tris(trimethylsilyl)silyl]silane (9)

A solution of 0.17 g (0.3 mmol) of **8** in 2 mL of bromoform was refluxed for two days. Evaporation and chromatographic purification of the residue (silica gel, heptane) gave 0.08 g (40%) of **9**, sublimation beginning at 160°C. MS (*m*/z) (%): 665 (14) [M^+-CH_3], 608 (9) [M^+-$SiMe_3$], 528 (43) [M^+-$BrSiMe_3$], 354 (46) [M^+-$BrSi(SiMe_3)_3$], 73 (100) [$SiMe_3^+$]. ^{1}H NMR (benzene-d_6) δ: 0.43 (s, $SiCH_3$). ^{13}C NMR (benzene-d_6) δ: 3.68 ($SiCH_3$). ^{29}Si NMR (benzene-d_6) δ: –88.2 (*Si*$SiMe_3$), –7.9 ($SiMe_3$), 32.9 ($SiBr_2$). HRMS calcd. ($C_{17}H_{51}Br_2Si_9$): 665.045; found: 665.028.

Phenylbis[tris(trimethylsilyl)silyl]silane (10)

As described for the preparation of **3**, 1.80 g (3.8 mmol) of $(Me_3Si)_3SiLi \cdot 3$ THF and 0.34 g (1.9 mmol) of dichlorophenylsilane gave, after recrystallization from acetone, 0.82 g (71%) of **10**, mp 223–225°C (under partial sublimation). IR (Nujol) $\tilde{\nu}$ (cm^{-1}): 2065 (SiH). MS (*m*/z) (%): 600 (5) [M^+], 526 (21) [M^+-$HSiMe_3$], 353 (94) [M^+-$Si(SiMe_3)_3$], 279 (100) [M^+-$Si(SiMe_3)_3$-$SiMe_3$], 247 (10) [$Si(SiMe_3)_3^+$]. ^{1}H NMR (benzene-d_6) δ: 0.29 (s, $SiCH_3$, 54 H), 4.83 (s, SiH, 1 H), 7.06–7.08, and 7.67–7.70 (m, arom. H, 5 H). ^{13}C NMR (benzene-d_6) δ: 3.42 ($SiCH_3$), 128.12, 128.71, 137.21, and 138.45 (arom. C). ^{29}Si NMR (benzene-d_6) δ: –123.5 (*Si*$SiMe_3$), –54.7 (d, ^1J = 169.5 Hz, SiH), –9.0 ($SiMe_3$). HRMS calcd. ($C_{24}H_{60}Si_9$): 600.246; found: 600.261.

Bromophenylbis[tris(trimethylsilyl)silyl]silane (12)

0.50 g of **10** were dissolved in 5 mL of bromoform and heated under reflux. The progress of the reaction was monitored by means of ^{1}H NMR spectroscopy. After 3–5 days the conversion was complete. The solution was evaporated and the residue recrystallized from acetone to give 0.4 g (68%) of **12**, mp > 230°C (under partial sublimation). MS (*m*/z) (%): 663 (21) [M^+-CH_3], 605 (8) [M^+-$SiMe_3$], 526 (6) [M^+-$BrSiMe_3$], 433 (100) [M^+-$Si(SiMe_3)_3$]. ^{1}H NMR (benzene-d_6) δ: 0.32 (s, $SiCH_3$, 54 H), 7.00–7.13 and 7.84–7.88 (m, arom. H, 5 H). ^{13}C NMR (benzene-d_6) δ: 3.92 ($SiCH_3$), 128.29, 129.18, 135.05 and 138.40 (arom. C). ^{29}Si NMR (benzene-d_6) δ: –105.2 (*Si*$SiMe_3$), –8.3 ($SiMe_3$), 10.6 (SiBrPh). HRMS calcd. (for M^+-CH_3, $C_{23}H_{56}BrSi_9$): 663.148; found: 663.142.

Crystal structure determination of 3, 10, and 12

The X-ray diffraction results were obtained on a Siemens P4 four circle diffractometer with monochromated Mo-K_α radiation. After taking rotational photos and determining reasonable reduced cells, a data collection was started in routine ω-scan. The structures were solved with direct methods (SHELXTL, Siemens Analytical X-ray Instruments Inc., 1990) and refined with the full-matrix least-squares method of SHELXL-97 (Bruker, SHELXL, 1997, Bruker Analytical X-ray Systems). All non-hydrogen atoms were refined anisotropically whereas the hydrogen atoms were put into theoretical positions and refined according to the riding model. For the presentation of ORTEP plots the Bruker SHELXTL graphical software was used.

Crystallographic data (Table 1) (excluding structure factors) for the structures reported in this paper can be purchased from the Depository of Unpublished Data, Document Delivery, CISTI, National Research Council Canada, Ottawa, Canada K1A OS2 (http://www.nrc.ca/cisti/irm/unpub_e.shtml for information on ordering electronically). This material has also been deposited with the Cambridge Crystallographic Data Centre as supplementary publication no. CCDC-121792 for **3**, CCDC-121793 for **10**, and CCDC-121793 for **12**. Copies of the data can be obtained free of charge on application to The Director, CCDC, 12 Union Road, Cambridge CB2 1EZ, U.K. (Fax: 44-1223-336033 or e-mail: deposit@ccdc.cam.ac.uk).

Acknowledgement

We gratefully acknowledge the support of our research by the Deutsche Forschungsgemeinschaft and the Fonds der Chemischen Industrie. We thank Dr. M. Michalik,

© 2000 NRC Canada

Dr. W. Baumann, and Prof. N. Stoll for recording the NMR and MS spectra, respectively.

References

1. R.J. Sipe and R. West. J. Organomet. Chem. **70**, 353 (1974); H. Bock, J. Meuret, and H. Schnödel. Chem. Ber. **126**, 2227 (1993); H. Bock, J. Meuret, R. Baur, and K. Ruppert. J. Organomet. Chem. **446**, 113 (1993); M. Haase and U. Klingebiel. Angew. Chem. **97**, 335 (1985); Angew. Chem. Int. Ed. Engl. **24**, 324 (1985); F.H. Elsner and T.D. Tilley. J. Am. Chem. Soc. **110**, 313 (1988).
2. K.W. Klinkhammer. Chem. Eur. J. **3**, 1418 (1997), and refs. therein.
3. H. Bock, J. Meuret, and K. Ruppert. Angew. Chem. **105**, 413 (1993); Angew. Chem. Int. Ed. Engl. **32**, 414 (1993); A. Heine, R. Herbst-Irmer, G.M. Sheldrick, and D. Stalke. Inorg. Chem. **32**, 2694 (1993).
4. M. Aggarwal, M.A. Ghuman, and R.A. Geanangel. Main Group Met. Chem. **14**, 263 (1991).
5. (*a*) G. Linti, W. Koestler, and A. Rodig. Eur. J. Inorg. Chem. 745 (1998); (*b*) A.M. Arif, A.H. Cowley, T.M. Elkins, and R.A. Jones. J. Chem. Soc. Chem. Commun. 1776 (1986); (*c*) W. Koestler and G. Linti. Organosilicon chemistry III: from molecules to materials. *Edited by* N. Auner and J. Weis. WILEY–VCH, Weinheim. 1996. p. 182; G. Linti and W. Koestler. Angew. Chem. **10**8 593 (1996); Angew. Chem. Int. Ed. Engl. **35**, 550 (1996); (*d*) S. Henkel, K.W. Klinkhammer, and W. Schwarz. Angew. Chem. **106**, 721 (1994); Angew. Chem. Int. Ed. Engl. **33**, 681 (1994); (*e*) W. Biffar and H. Nöth. Z. Naturforsch. Anorg. Chem. Org. Chem. **36b**, 1509 (1981).
6. (*a*) D.R. Cary and J. Arnold. Inorg. Chem. **33**, 1791 (1994); (*b*) V. Christou and J. Arnold. J. Am. Chem. Soc. **114**, 6240 (1992); D.R. Cary and J. Arnold. J. Am. Chem. Soc. **115**, 2520 (1993); A. Seligson and J. Arnold. J. Am. Chem. Soc. **115**, 8214 (1993).
7. (*a*) D.M. Roddick, T.D. Tilley, A.L. Rheingold, and S.J. Geib. J. Am. Chem. Soc. **109**, 945 (1987); (*b*) J. Arnold, T.D. Tilley, A.L. Rheingold, and S.J. Geib. Inorg. Chem. **26**, 2106 (1987).
8. (*a*) K.W. Klinkhammer and W. Schwarz. Angew. Chem. **107**, 1448 (1995); Angew. Chem. Int. Ed. Engl. **34**, 1334 (1995); K.W. Klinkhammer, T.F. Fassler, and H. Gruetzmacher. Angew. Chem. **110**, 114 (1998); Angew. Chem. Int. Ed. Engl. **37**, 124 (1998); (*b*) M. Stuermann, M. Weidenbruch, K.W. Klinkhammer, F. Lissner, and H. Marsmann. Organometallics, **17**, 4425 (1998); (*c*) S.P. Mallela and R.A. Geanangel. Inorg. Chem. **29**, 3525 (1990); (*d*) S.P. Mallela and R.A. Geanangel. Inorg. Chem. **30**, 1480 (1991), and **33**, 1115 (1994); (*e*) Y. Derouiche and P.D. Lickiss. J. Organomet. Chem. **407**, 41 (1991); (*f*) Y. Apeloig, M. Yuzefovich, M. Bendikov, D. Bravo-Zhivotovskii, and K. Klinkhammer. Organometallics, **16**, 1265 (1997); (*g*) C. Marschner. Eur. J. Inorg. Chem. 221 (1998).
9. (*a*) E. Jeschke, T. Gross, H. Reinke, and H. Oehme. Chem. Ber. **129**, 841 (1996); (*b*) T. Gross, R. Kempe, and H. Oehme. J. Organomet. Chem. **534**, 229 (1997). T. Gross, R. Kempe, and H. Oehme. Chem. Ber./Recueil **130**, 1709 (1997); (*c*) T. Gross, R. Kempe, and H. Oehme. Inorg. Chem. Commun. **1**, 128 (1998); T. Gross, R. Kempe, and H. Oehme. Eur. J. Inorg. Chem. 21 (1999); (*d*) T. Gross, R. Kempe, and H. Oehme. Organometallics, **18**, 1815 (1999); (*e*) T. Gross, H. Oehme, R. Kempe. Organosilicon chemistry IV — from molecules to materials. *Edited by* N. Auner and J. Weiss. VCH, Weinheim. 2000. p. 356.
10. W. Uhlig. Chem. Ber. **129**, 733 (1996).
11. S.M. Whittaker, M.C. Brun, F.C. Lee, and K.H. Pannell. J. Organomet. Chem. **499**, 247 (1995).
12. J.B. Lambert, J.L. Pflug, and C.L. Stern. Angew. Chem. **107**, 106 (1995); Angew. Chem. Int. Ed. Engl. **34**, 98 (1995); H. Suzuki, Y. Kimata, S. Satoh, and A. Kuriyama. Chem. Lett. 292 (1995).
13. H. Bock, K. Ruppert, C. Näther, Z. Havlas, H.-F. Herrmann, C. Arad, I. Göbel, A. John, J. Meuret, S. Nick, A. Rauschenbach, W. Seitz, T. Vaupel, and B. Solouki. Angew. Chem. **104**, 564 (1992); Angew. Chem. Int. Ed. Engl. **31**, 550 (1992).
14. G. Gutekunst and A.G. Brook. J. Organomet. Chem. **225**, 1 (1982).

© 2000 NRC Canada

A novel route to chlorodimethylsilane

Jerzy J. Chruściel

Abstract: A new efficient laboratory method of preparation of chlorodimethylsilane ($Cl(CH_3)_2SiH$) has been elaborated, which is a modification of the Eaborn et al. method (34) and is based on a *transsilylation reaction of substituted (amino)dimethylhydrosilanes, R_2NSiMe_2H* (R_2 = Me_2, Et_2, $(CH_2)_n$, etc.) with *dimethyldichlorosilane (Me_2SiCl_2)*. The reaction proceeds at reflux, at 70°C, preferably with an excess of Me_2SiCl_2. The most important feature of this novel method is a recovery of intermediate (amino)chlorodimethylsilanes (R_2NSiMe_2Cl), which can be again reduced to R_2NSiMe_2H. *The transsilylation mechanism* has been proven by reaction of (diethylamino)methylphenylsilane with Me_2SiCl_2. The products of this latter reaction are HMePhSiCl and R_2NSiMe_2Cl, thus a disproportionation mechanism has been excluded. New substituted bis(amino)dimethylsilanes ($(R_2N)_2SiMe_2$), (amino)dimethylchlorosilanes (R_2NSiMe_2Cl), and (amino)dimethylhydrosilanes (R_2NSiMe_2H) have been synthesized and characterized by NMR and IR.

Key words: chlorodimethylsilane, $(CH_3)_2SiHCl$, synthesis, new laboratory method, transsilylation mechanism.

Résumé : On a développé une nouvelle méthode de préparation du chlorodiméthylsilane, $Cl(CH_3)_2SiH$, efficace au niveau du laboratoire. Il s'agit d'une modification de la méthode de Eaborn et al. (34) et elle est basée sur une réaction de transsilylation de (amino)diméthylhydrosilanes substitués, R_2NSiMe_2H (R_2 = Me_2, Et_2, $(CH_2)_n$, etc.). Avec le diméthyldichlorosilane, Me_2SiCl_2. La réaction se produit à reflux, à 70°C, de préférence dans un excès de Me_2SiCl_2. La caractéristique la plus importante de cette nouvelle méthode est la récupération des intermédiaires (amino)chlorodiméthylsilanes, $R_2NSiMe_2Cl_2$, qui peuvent être soumis à une nouvelle réduction pour donner du R_2NSiMe_2H. On a démontré le mécanisme de transsilylation par la réaction du (diéthylamino)méthylphénylsilane avec le Me_2SiCl_2. Les produits de cette dernière réaction sont le HMePhSiCl et le R_2NSiMe_2Cl qui permettent d'exclure la possibilité d'une réaction de dismutation. On a synthétisé de nouveaux bis(amino)diméthylsilanes, $(R_2N)_2SiMe_2$, (amino)diméthylchlorosilanes, R_2NSiMe_2Cl, et (amino)diméthylhydrosilanes, R_2NSiMe_2H, que l'on a caractérisés par RMN et IR.

Mots clés : chlorodiméthylsilane, $(CH_3)_2SiHCl$, synthèse, nouvelle méthode de synthèse, mécanisme de transsilylation.

[Traduit par la Rédaction]

Introduction

Chlorodimethylsilane ($(H)Me_2SiCl$) (CDMS) is a very useful and valuable organosilicon monomer and reagent, bearing two different functional groups: ≡Si-Cl and ≡Si-H. The ≡Si-Cl bond can react with Grignard and organolithium reagents, or undergo alcoholysis and hydrolysis reactions. The ≡Si-H group enables preparation of complex derivatives, mainly through hydrosilylation reaction. HMe_2SiCl finds many synthetic applications in organosilicon synthesis and silicone technology (2–6), as well as in general polymer chemistry (7–12). Most often HMe_2SiCl is used in a preparation of 1,1,3,3-tetramethyldisiloxane ($HMe_2SiOSiMe_2H$), other Si-H terminated polysiloxanes (13–20), and multifunctional hydrosiloxanes (e.g., $Si(OSiMe_2H)_4$ (11), octa(hyridodimethylsiloxy)octasilsesquioxane $(HMe_2SiOSiO_{3/2})_8$ (21–23)), or hydropolysilanes (e.g., $Si(SiMe_2SiH)_4$ (24–27) and *o*-(bisdimethylsilyl)benzene (28)).

Yields of HMe_2SiCl in an industrial "direct process" (from elemental silicon and methyl chloride) are poor, usually 0.1–1% (29–31), although, when H_2 was added to the methyl chloride gas phase, yields can be significantly improved up to 8% (32), or 2.2–33% (33), depending on reaction conditions.

Many synthetic methods lead to chlorodimethylsilane, but some are unattractive due to expense and unavailability of intermediates. In the present paper a new laboratory procedure for preparation of HMe_2SiCl is described, which is a modification of the Eaborn et al. (34) method. The key of our method is a transsilylation of substituted (amino)dimethylhydrosilanes R_2NSiMe_2H with dimethyldichlorosilane Me_2SiCl_2.

Received September 21, 1999. Published on the NRC Research Press website on October 20, 2000.

This paper is dedicated to Professor Adrian G. Brook, very distinguished organosilicon and organic chemist, and my briliant teacher, on the occasion of his 75th birthday. In 1982–83 Professor A.G. Brook gave me a chance to join his research group, at the Department of Chemistry of the University of Toronto. In the Lash Miller Chemical Laboratories I had the pleasure to continue studies on a very well known Brook rearrangement, work out some details of its mechanism, and discover a new silyl anion rearrangement (1). I have learned a lot from Professor Adrian G. Brook, who opened for me a world of international science, and I will be always grateful to him.

J.J. Chruściel. Institute of Polymers, Faculty of Chemistry, Technical University, 90-924 Łódź 40, Poland (e-mail: jchrusci@ck-sg.p.lodz.pl).

© 2000 NRC Canada

Experimental

General procedures

All reactions were carried out under an atmosphere of dry nitrogen. Most of the substrates and reaction products were distilled through a Vigreux column (120 cm).

NMR spectra were determined with Tesla BS-487C (80 MHz) and Bruker MSL-300 (300 MHz); ~10% solutions of studied silanes in CCl_4, $CDCl_3$, or CD_2Cl_2 were used. Infrared spectra were recorded for neat samples on a Carl Zeiss Jena 75R spectrometer.

Reagents

Dimethyldichlorosilane (70.5–71.0°C) and methyltrichlorosilane (66°C) were purified by fractional distillation. Diethylamine (POCh, Gliwice, Poland), triethylamine (POCh), pyrrolidine (Aldrich), piperidine (Loba Chem.) were dried with KOH (POCh) and purified by distillation over small amounts of P_2O_5 (POCh). Dimethylamine (Fluka), magnesium (POCh), and lithium aluminium hydride (Aldrich) were used as received. Bromobenzene (POCh) was distilled over CaH_2 (Aldrich). Diethyl ether and tetrahydrofuran were dried with KOH and distilled over fresh sodium wire. Methylphenyldichlorosilane was prepared by a Grignard method (35), from $MeSiCl_3$ and PhMgBr, in ether, and fractionally distilled (bp 103–104°C/20 mmHg).

Bis(diethylamino)dimethylsilane

Bis(diethylamino)dimethylsilane (142.2 g, yield 85%) was prepared from 2.9 mol of diethylamine and 0.7 mol of Me_2SiCl_2, in dry ether (36, 37). Solution of Me_2SiCl_2 was added dropwise to a stirred solution of Et_2NH in 1300 mL of Et_2O, followed by reflux for 7 h. The reaction mixture was left overnight. A precipitate of diethylamine hydrochloride was filtered off and washed with dry ether. The product was fractionally distilled (bp 86°C/20 mmHg).

Preparation of (diethylamino)dimethylchlorosilane

Into a 500 mL four-neck flask, fitted with a condenser and a mechanical stirrer, was placed 116.3 g (0.575 mol) of bis(diethylamino)dimethylsilane. Stirring was turned on and the substrate was cooled down to –5°C. 70 mL (0.578 mol) of Me_2SiCl_2 was added dropwise from an addition funnel, at –5°C, within 2 h. The cooling bath was removed and stirring was continued at room temperature for 6 h. The products were fractionally distilled to give 152.4 g (80% yield) of Et_2NSiMe_2Cl (bp 152°C) (36, 37).

Preparation of (diethylamino)dimethylsilane

(*a*) Into a 500 mL four-neck flask, fitted with a condenser and a mechanical stirrer, was placed 10.63 g (0.28 mol) of $LiAlH_4$ and 250 mL of dry ether. 148.5 g (0.90 mol) of (diethylamino)dimethylchlorosilane in 80 mL of dry ether was added dropwise from an addition funnel, within 1.5 h. The reaction mixture was refluxed for 2.5 h, and cooled to room temperature. Solids were filtered off and washed with dry ether. Fractional distillation of the filtrate gave 94.0 g (80% yield) of Et_2NSiMe_2H (bp 110–111°C).

(*b*) Similarly, from 5.43 g (0.14 mol) of $LiAlH_4$ and 75.7 g (0.46 mol) of (diethylamino)dimethylchlorosilane, with 170 mL of dry ether, after 4 h of reflux and an identical work-up 37.9 g (63% yield) of Et_2NSiMe_2H was obtained.

Reaction of (diethylamino)dimethylsilane with dimethyldichlorosilane

(*a*) Into a 250 mL two-neck flask was placed 74.4 g (0.567 mol) of (diethylamino)dimethylsilane and 74.0 g (0.573 mol) of dimethyldichlorosilane. The reaction flask was connected to a Vigreux column and heated to reflux. A fraction of HMe_2SiCl (containing traces of Me_2SiCl_2) was continously distilled and collected to give 40.8 g (76% yield) of HMe_2SiCl (bp 36°C). Distillation of the reaction flask residue gave 74.8 g (80% yield) of Et_2NSiMe_2Cl (bp 152°C).

(*b*) A similar reaction of 33.0 g (0.252 mol) of (diethylamino)dimethylsilane was carried out with double excess of dimethyldichlorosilane (61 mL, 0.573 mol). 20 mL of Me_2SiCl_2 was added to a flask containing Et_2NSiMe_2H, the reagents were heated to reflux under Vigreux column, and the remaining amount of Me_2SiCl_2 was added dropwise at reflux. Products were recovered by distillation: (*i*) 20.7 g (87% yield) of HMe_2SiCl (bp 36°C); and (*ii*) 37.7 g (90% yield) of Et_2NSiMe_2Cl (bp 152°C) were obtained.

Preparation of bis(pyrrolidino)dimethylsilane

Into a four-neck 2.5 L sulphonation reactor, fitted with a condenser and a mechanical stirrer, was added 126 mL (1.04 mol) of Me_2SiCl_2, 309 mL (2.22 mol) of Et_3N, and 1800 mL of dry ether. 175 mL (2.10 mol) of dry pyrrolidine was added dropwise, within 2 h. A precipitate of triethylamine hydrochloride was filtered off and washed with dry ether (3 × 100 mL). The ether was distilled off and the residue was distilled to give $[(CH_2)_4N]_2SiMe_2$ (73% yield, bp 107–110°C/15 mmHg).

Preparation of (pyrrolidino)dimethylchlorosilane

(*a*) Into a 500 mL four-neck flask, fitted with a condenser and a mechanical stirrer, was placed 90.9 g (0.458 mol) of bis(pyrrolidino)dimethylsilane. The substrate was cooled to –10°C and 56 mL (2.10 mol) of Me_2SiCl_2 was added dropwise, within 2 h. Stirring was continued at –5°C for 4 h and reaction mixture was left overnight. Products were fractionally distilled to give 123.1 g (82% yield) of $(CH_2)_4NSiMe_2Cl$ (bp 80–81°C/40 mmHg).

(*b*) Into a four-neck 1.5 L sulphonation reactor, fitted with a condenser and mechanical stirrer, was added 124 mL (1.02 mol) of Me_2SiCl_2, 139 mL (1.00 mol) of Et_3N, and 900 mL of dry ether. 83.5 mL (1.00 mol) of dry pyrrolidine was added dropwise, within 2 h. Reaction mixture was stirred and refluxed for 2 h, and cooled to room temperature. Triethylamine hydrochloride was filtered off and washed with dry ether (2 × 150 mL). Ether was distilled off and a residue was distilled to give 72.8 g (44% yield) of $(CH_2)_4NSiMe_2Cl$ (bp 60–62°C/15 mmHg).

Preparation of (pyrrolidino)dimethylsilane

Into a 500 mL four-neck flask, fitted with a condenser and a mechanical stirrer, was placed 7.50 g (0.197 mol) of $LiAlH_4$ and 200 mL of dry ether. 64.3 g (0.393 mol) of $(CH_2)_4NSiMe_2Cl$ in 70 mL of dry ether was added dropwise, within 40 min. The reaction mixture was refluxed for 4 h,

© 2000 NRC Canada

cooled to room temperature, and left overnight. Solids were filtered off, washed with dry ether. The filtrate was fractionally distilled to give an ether fraction and 21.8 g (43% yield) of $(CH_2)_4NSiMe_2H$ (bp 47–48°C/40 mmHg).

Reaction of (pyrrolidino)dimethylsilane with dimethyldichlorosilane

Into a 250 mL two-neck flask was placed 18.1 g (0.14 mol) of (pyrrolidino)dimethylsilane and 34 mL (0.28 mol) of dimethyldichlorosilane. The reaction flask was heated to reflux, and HMe_2SiCl (with traces of Me_2SiCl_2) was continously distilled off through a Vigreux columnto give 9.0 g (68% yield) of HMe_2SiCl (bp 36°C). Distillation of the residue gave $(CH_2)_4NSiMe_2Cl$ (17.1 g, 74% yield; bp 80–81°C/40 mmHg).

Preparation of (diethylamino)methylphenylchlorosilane

Into a 1.5 L four-neck reactor, fitted with a condenser and a mechanical stirrer, was placed 116.3 mL (0.72 mol) of methylphenyldichlorosilane and 900 mL of dry ether. 151 mL (1.46 mol) of Et_2NH was added dropwise, within 5 h, followed by reflux for 2 h. On the next day a precipitate of $Et_2NH{\cdot}HCl$ was filtered off (under nitrogen) and washed three times with ether. After removal of ether, the liquid residue was distilled to give 130.2 g (79% yield) of $Et_2NSiMePhCl$ (bp 108–110°C/5 mmHg).

Preparation of (diethylamino)methylphenylsilane

Into a 0.5 L three-neck flask, fitted with a condenser and a mechanical stirrer, was placed 5.50 g (0.145 mol) of $LiAlH_4$ and 90 mL of dry THF. 65.8 g (0.289 mol) of (diethylamino)methylphenylchlorosilane in 70 mL of dry THF was added dropwise, within 30 min. The reaction mixture was refluxed for 4 h, and cooled to room temperature. Solids were filtered off and washed with dry pentane (3 × 30 mL). Solvents were removed and the residue fractionally distilled to give 7.5 g of $MePhSiH_2$ (bp 25–26°C/5 mmHg; n_D^{20} = 1.5051 (Lit. (38) value: 1.5058) and 52.2 g (58% yield) of $Et_2NSiMePhH$ (bp 87–90°C/5 mmHg).

Reaction of (diethylamino)methylphenylsilane with dimethyldichlorosilane

Into a 250 mL two-neck flask was added 13.75 g (0.071 mol) of (diethylamino)methylphenylsilane. 17 mL (0.140 mol) of Me_2SiCl_2 was added dropwise at ~30°C. Reaction mixture was heated to reflux and then fractionally distilled through a Vigreux column. Four fractions were collected and analyzed by means of ^1H NMR (and IR): (1) bp 69–72°C (11.5 g, Me_2SiCl_2); (2) bp 82–86°C/63 mmHg (4.9 g, ~95% of Et_2NSiMe_2Cl and ~5% of HMePhSiCl); (3) bp 97–115°C/65 mmHg (7.2 g, 35% of Et_2NSiMe_2Cl and 65% of HMePhSiCl); (4) bp 130–140°C/64 mmHg (7.0 g, 70% of $Et_2NSiMePhH$ (conversion 64.4%)); and 30% of HMePhSiCl). Contents of the above fractions are based on integrations of their ^1H NMR spectra (80 MHz, in CCl_4).

Analytical data for the products

HMe_2SiCl

Boiling point 36.0°C. IR (neat (cm^{-1})): 2170 (Si-H). ^1H NMR (80 MHz, δ (ppm)), in $CDCl_3$): 0.50 (d, 6H, $(CH_3)_2Si$), 4.88 (sept., 1H, Si-H); in CCl_4: 0.45 (d, J = 3.0 Hz, 6H, $(CH_3)_2Si$), 4.80 (sept., J = 3.0 Hz, 1H, Si-H).

Et_2NSiMe_2Cl

Boiling point 152–154°C. ^1H NMR: 0.38 (s, 6H, $(CH_3)_2Si$), 0.98 (t, J = 7 Hz, 6H, CH_3-C), 2.85 (q, J = 7 Hz, 4H, CH_2-N).

$Et_2NSiMe_2(H)$

Boiling point 111–112°C. IR (neat (cm^{-1})): 2120 (Si-H). ^1H NMR (300 MHz, $CDCl_3$, δ (ppm)): 0.185 (d, 6H, J = 2.79 Hz, $(CH_3)_2Si$), 1.11 (t, 6H, J = 7.14 Hz, CH_3-C), 2.65 (q, 4H, J = 7.15 Hz, CH_2-N), 4.68 (sept., 1H, J = 2.78 Hz, Si-H). ^{13}C NMR: –1.49 (s, CH_3-Si), 15.63 (s, CH_3), 41.00 (s, CH_2-N). ^{29}Si NMR: –7.77 (s).

$Et_2NSiMePhCl$

Boiling point 136–140°C/25 mmHg, 108–110°C/5 mmHg. n_D^{20} 1.5073. IR (neat (cm^{-1})): 3068, 1800–2000, 1588 (Ph), 1426 (Si-Ph), 1253 (Si- CH_3), 2966, 2927, 2866 (C-H aliphat.), 1202, 1166, 1055 (C-N), 1028, 931 (Si-N), 640, 460, 413 (Si-Cl). ^1H NMR (80 MHz, CCl_4, δ (ppm)): 0.79 (s, 3H, CH_3-Si), 1.21 (t, J = 6.4 Hz, 6H, CH_3-C), 3.08 (q, J = 6.4 Hz, 4H, CH_2-N), 7.47–7.65 (m, 3H (Ph, *m*-, *p*-)), 7.8–8.0 (m, C-H (Ph, *o*-)). ^{13}C NMR (300 MHz, $CDCl_3$, δ (ppm)): 1.63 CH_3-Si, 15.12 CH_3-C, 39.37 CH_2-N, 128.06, 130.06, 134.32, 135.14 (Ph). Anal. calcd. (%): C 57.99, H 7.96, N 6.14, Cl 15.56; found (%): C 57.59, 57.59, H 8.02, 8.14, N 5.83, 5.63, Cl 15.16, 15.38.

$Et_2NSiMePh(H)$

Boiling point 115–117°C/21 mmHg, 86–89°C/5 Tr. n_D^{20} 1.4969. IR (neat (cm^{-1})): 3067, 1800–2000, 1591 (Ph), 1428 (Si-Ph), 1252 (Si- CH_3), 2965, 2927, 2864 (C-H aliphat.), 2126, 2085 (Si-H), 1211, 1180, 1065 (C-N), 1028, 931 (Si-N), 1030, 930 (Si-N). ^1H NMR (80 MHz, CCl_4, δ (ppm)): 0.33 (d, J = 3.2 Hz, 3H, CH_3-Si), 0.94 (t, J = 7 Hz, 6H, CH_3-C), 2.82 (q, J = 7 Hz, 4H, CH_2-N), 4.80 (q, J = 3.2 Hz, 1H, Si-H), 7.25 (m, 3H (Ph, *m*-, *p*-)), 7.50 (m, C-H (Ph, *o*-)). Anal. calcd. (%): C 68.33, H 9.90, N 7.24; found (%): C 67.63, 67.56, H 9.86, 9.89, N 6.67, 6.83.

HMePhSiCl

Boiling point 174–176°C, bp 92–95°C/65 mmHg. n_D^{20} 1.5073. IR (neat (cm^{-1})): 2170 (Si-H). ^1H NMR (80 MHz, $CDCl_3$, δ (ppm)): 0.65 (d, J = 3.4 Hz, 3H, CH_3-Si), 5.25 (q, J = 3.4 Hz, 1H, Si-H), 7.35 (m (t), 3H, Ph (*m*-, *p*-), 7.55 (m (d), 2H, Ph (*o*-)).

$[(CH_2)_4N]_2SiMe_2$

Boiling point 107–110°C/15 mmHg. n_D^{20} 1.4682. ^1H NMR (80 MHz, CCl_4, δ (ppm)): 0.24 (s, 6H, $(CH_3)_2Si$), 1.46 (m, 4H, $(CH_2)_2$), 2.73 (m, 4H, $(CH_2)_2N$). ^{13}C NMR (300 MHz, $CDCl_3$, δ (ppm)): –3.33 CH_3-Si, 26.61 $(CH_2)_2$, 46.73 $(CH_2)_2N$. Anal. calcd. (%): C 60.54, H 11.18, N 14.12, Si 14.16; found (%): C 60.63, 60.71, H11.31, 11.31, N 13.54, 13.54, Si 14.10.

$(CH_2)_4NSiMe_2Cl$

Boiling point 80–81°C/40 mmHg, 60–62°C/15 mmHg. $n^{20}{}_D$ 1.4533. ^1H NMR (80 MHz, δ (ppm)) in CCl_4: 0.44 (s,

© 2000 NRC Canada

6H, $(CH_3)_2Si$), 1.75 (quintette, J = 3.6 Hz, 4H, $(CH_2)_2$), 3.01(m, J = 6.4 Hz, 4H, $(CH_2)_2N$); in $CDCl_2$: 0.44 (s, 6H, $(CH_3)_2Si$), 1.36 (quintette, J = 4.3 Hz, 4H, $(CH_2)_2$), 2.28 (m, J = 6.4 Hz, 4H, $(CH_2)_2N$).

$(CH_2)_4NSiMe_2(H)$

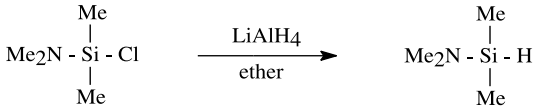
Boiling point 47–48°C/40 mmHg, 59–63°C/15 mmHg. IR (neat (cm^{-1})): 2960, 2869, 2820, 1591 (C-H), 2120, 2074 (Si-H), 1457, 1420, 1352 (C-H, CH_3), 1252 (Si- CH_3), 1125, 1200, 1080 (C-N), 896, 835 (Si-N), 764, 628 (Si-C). ^{1}H-NMR (80 MHz, $CDCl_2$, δ (ppm)): 0.07 (d, J = 4.6 Hz, 6H, $(CH_3)_2Si$), 1.22 (quintette, J = 4.6 Hz, 4H, $(CH_2)_2$), 2.11 (m, 4H, $(CH_2)_2N$), 3.14 (sept., J = 4.3 Hz, 1H, Si-H). Anal. calcd. (%): C 55.74, H 11.70, N 10.83; found (%): C 54.35, 54.21, H 11.33, 11.21, N 10.07, 9.95.

Results and discussion

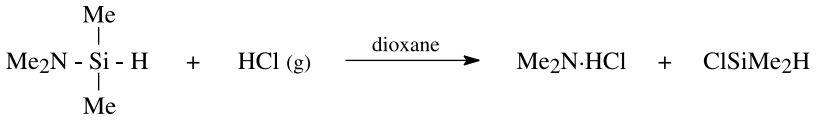
Since yields of chlorodimethylsilane obtained in a direct Rochow and Müller process are very low, many attempts have been made to find new efficient synthetic methods, especially useful on a laboratory scale. HMe_2SiCl has been prepared by the following methods: (*i*) the direct synthesis from elemental silicon and methyl chloride (29–33, 39–44); (*ii*) Grignard reaction between $MeHSiCl_2$ and MeMgBr (45); (*iii*) selective reduction of dimethyldichlorosilane Me_2SiCl_2 (DDS) with Na_3AlH_6, NaH, $NaBH_4$, $LiAlH_4$ (46–49), Et_3Al (50), or $Me_2SiCl(OMe)$ with i-Bu_2AlH (51), and Me_2NSiMe_2Cl with $LiAlH_4$ (followed by cleavage of the intermediate silane with HCl) (34); (*iv*) disproportionation of hydrochlorosilanes (52) or organohydrosilanes and -siloxanes with chlorosilanes (53–59); (*v*) cleavage of $HMe_2SiOSiMe_2H$ with HCl (60, 61), HCl and $AlCl_3$ (62), BCl_3 (63), and polymethylhydrolsiloxanes with Me_2SiCl_2, catalyzed by BF_3, n-Bu_4NCl, BCl_3 and HMPT (64); and with $MeSiCl_3$, Me_2SiCl_2, $PhSiCl_3$, catalyzed by HMPT and HCl (65); (*vi*) photolytic cleavage of polydimethylsilanes (66) and Me_3SiMe_2SiCl (67) with HCl; cleavage of disilanes with HCl towards phosphine–nickel complexes (68) and hydrogenation of chlorodisilanes obtained from the direct process, with copper catalysts (69) and phosphine–nickelocene (and nickel) complexes (70, 71); (*vi*) selective (and quantitative) chlorination of Me_2SiH_2 with $SnCl_4$ (72).

All of these procedures have limitations. Mainly due to safety precautions, the application of metal hydrides is limited to a relatively small scale. According to Eaborn (2) partial reduction of organohalogenosilanes with $LiAlH_4$ is not possible. Reductions of Me_2SiCl_2 with NaH afforded low yields of HMe_2SiCl: 11–17% (46) or 38% (at 150°C) (47). Reduction of Me_2SiCl_2 with Et_3Al, in c-C_6H_{12}, at 500°C, requires very short reaction time (1 s) and gives 17.7% of CDMS (50). Although reduction of DDS with i-Bu_2AlH, carried out at high temperature (at 330°C), gave 76% of CDMS (73). Also reaction of $Me_2Si(OMe)Cl$ with i-Bu_2AlH, at –23°C, gave good, 83% yield of CDMS. Similar reduction of DDS with $NaBH_4$ in HMPT, at 50°C, within 2 h, gave 71% yield of HMe_2SiCl (50). The symmetrical 1,1,3,3-tetramethyldisiloxane cannot be recommended as a substrate for the preparation of chlorodimethylsilane, and $HMe_2SiOSiMe_2H$ is synthesized from HMe_2SiCl. Synthesis of polydimethylsilanes is difficult, and the photolysis is limited to a small scale, requiring a special apparatus. The gaseous dimethylsilane and $SnCl_4$ are expensive substrates as well. The above reasons encouraged us to search for a new laboratory method of synthesis of HMe_2SiCl.

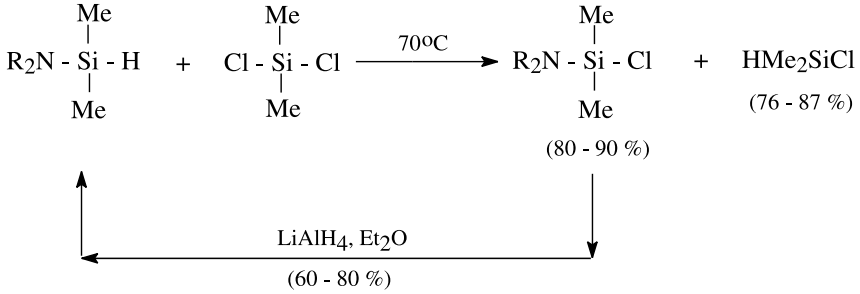
Our new method of preparation of Me_2SiHCl (74, 75) is a modification of the Eaborn et al. method (34), which involves the reduction of the Si—Cl bond to the Si—H bond, in the presence of the Si—N bond:

[1] 

and a subsequent cleavage of of the Si-N bond with gasous hydrogen chloride

[2] 

Our method is based on reaction of (dialkylamino)dimethylhydrosilanes (R_2NSiMe_2H) with dimethyldichlorosilane

[3] 

© 2000 NRC Canada

[4] $$2\,R_2NH + Me_2SiCl_2 + Et_3N \xrightarrow[25\text{ - }35^oC]{Et_2O} Me_2Si(NR_2)_2 + 2\,Et_3N{\cdot}HCl$$

As a single step, the yield of chlorodimethylsilane was in the range 76–87%, with respect to Et_2NSiMe_2H. The overall yield of four-step (or three-step) reaction, including synthesis of Et_2NSiMe_2Cl (see rxns. [4]–[6]), its reduction to (diethylamino)dimethylsilane, followed by reaction (3) with Me_2SiCl_2, ranged from 45 to 58%. However, intermediate Et_2NSiMe_2Cl and other (dialkylamino)dimethylchlorosilanes R_2NSiMe_2Cl were recovered, in a high yield (80–90%), and may be used again for synthesis of $HSiMe_2Cl$, after reduction with $LiAlH_4$. When we are considering the recovery of R_2NSiMe_2Cl, the overall yields of HMe_2SiCl are much higher (within the range of 150–240% (!!!)), than yields calculated for the single step reaction (3).

The starting (amino)chlorosilanes can be prepared either in two steps (36, 37)

[5] $$Me_2Si(NR_2)_2 + Me_2SiCl_2 \xrightarrow[-5\text{ - }0^oC]{Et_2O} \underset{\sim 85\ \%}{2\,R_2N\text{-}Me_2Si\text{-}Cl}$$

or in one step (36, 37)

[6] $$R_2NH + Me_2SiCl_2 + Et_3N \xrightarrow[-5\text{ - }0\ ^oC]{Et_2O} R_2N\text{-}Me_2Si\text{-}Cl$$

Alternatively a secondary amine can be used as an HCl acceptor.

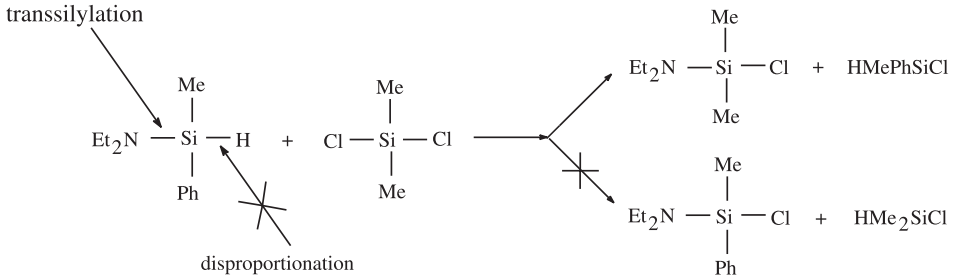
(Dialkylamino)chlorodimethylsilanes were reduced with excess $LiAlH_4$ in dry ether (or THF) at reflux. Yields of R_2NSiMe_2H depend on reaction time, and amount of reducing agent. Longer reaction times lead to lower yields, presumably due to reduction of Si—N bond; for Et_2NSiMe_2H: 80% after 2.5 h and 63% after 4 h (crude yields). Yields of reduction of $(CH_2)_4NSiMe_2Cl$ with $LiAlH_4$ were lower than in reduction of Et_2NSiMe_2Cl. Presumably a steric hinderance in this case diminishes the cleavage of the Si—N bond as a side reaction. In the case of reduction of $Et_2NSiMePh(Cl)$, small amounts of $MePhSiH_2$ were isolated. It has been reported (76), that (dimethylamino)trichlorosilane and bis(dimethylamino)dichlorosilane are reduced to monosilane SiH_4, as a result of the cleavage of Si—N bonds.

The final step of the synthesis of HMe_2SiCl, reaction of substituted (amino)dimethylchlorosilanes with Me_2SiCl_2, was carried out at reflux (~70°C), using a fractionation Vigreux column. During dropwise addition of Me_2SiCl_2 to Et_2NSiMe_2H, crude HMe_2SiCl was distilled off. When stoichiometric amounts of both substrates were used the reaction began at reflux and it was quite vigorous (a bleeding of the column appeared); thus 76% of CDMS was obtained. With excess Me_2SiCl_2, the yield of HMe_2SiCl reached 87%. Other substituted (amino)dimethylsilanes (R_2 = Me_2, n-Bu_2, $(CH_2)_5$), can be used for the synthesis of HMe_2SiCl, in the same manner.

Reaction mechanism

The Si—N bond (bond energy: 335 kJ/mol (77)) is slightly weaker than that of the Si—H bond (377 kJ/mole (78)). Thus it seems that reaction of (amino)dimethylsilanes ($R_2NSiMe_2(H)$) with Me_2SiCl_2 proceeds through a transsilylation mechanism, with a cleavage of the Si—N bond, rather than through a *disproportionation mechanism*, which would require breaking of the Si—H bond, in the aminosilane substrate. To prove this mechanism, $Et_2NSiMePhH$ was reacted with Me_2SiCl_2 to yield methylphenylchlorosilane (HMePhSiCl) and Et_2NSiMe_2Cl

[7]



The formation of HMePhSiCl confirms that the reaction of $Et_2NSiMePh(H)$ with Me_2SiCl_2 proceeds through the transsilylation mechanism, with the cleavage of the Si—N bond. The alternative disproportionation process, which would require breaking of the Si—H bond, would give $Et_2NSiMePhCl$ and $HSiMe_2Cl$, as reaction products. $HSiMe_2Cl$ was not detected in products of the above reaction. Moreover in disproportionation reactions of chlorosilanes with hydrosilanes the presence of various catalysts (e.g., $AlCl_3$ or H_2PtCl_6) is necessary. So far we have not conducted comprehensive mechanistic studies of reaction of (amino)hydrosilanes with chlorosilanes. It seems quite obvious, that this interesting and useful reaction is a next example of the nucleophilic displacement at silicon and may be catalyzed by traces of amine hydrochlorides or (amino)silanes hydrochlorides, which could be formed in the presence of traces of moisture, during the course of synthesis.

© 2000 NRC Canada

Conclusions

(1.) The new efficient laboratory method of the synthesis of HMe_2SiCl has been described, based on reaction of (dialkylamino)chlorodimethylsilanes (R_2NSiMe_2H) with dimethyldichlorosilane.

(2.) The main features of this novel method are as follows: (*a*) the intermediate products (dialkylamino)dimethylchlorosilanes (R_2NSiMe_2Cl) are recovered in high yields and are reused, in the synthesis cycle by reduction with $LiAlH_4$ to give R_2NSiMe_2H; (*b*) a very simple procedure and good yields of HMe_2SiCl are obtained (usually above 80%).

(3.) The reaction of substituted (amino)dimethylchlorosilanes with Me_2SiCl_2 proceeds through a nucleophilic substitution (transsilylation mechanism), and was confirmed by reaction of $Et_2NSiMePhH$ with Me_2SiCl_2. Products of this reaction are: HMePhSiCl and Et_2NSiMe_2Cl.

(4.) New compounds, not described in a literature, have been prepared: (*i*) bis(pyrrolidino)dimethylsilane $[(CH_2)_4N]_2SiMe_2$, from pyrrolidine and Me_2SiCl_2, in ether, in the presence of Et_3N; (*ii*) (pyrrolidino)dimethylchlorosilane $(CH_2)_4NSiMe_2Cl$, from reactions of bis(pyrrolidino)dimethylsilane or pyrrolidine with Me_2SiCl_2, in ether (in the presence of Et_3N, in the latter case); (*iii*) (diethylamino)methylphenylchlorosilane, from diethylamine and $MePhSiCl_2$, in ether; (*iv*) (diethylamino)methylphenylsilane, by reduction of $Et_2NSiMePh(Cl)$ with $LiAlH_4$, in THF.

(5.) (Pyrrolidino)dimethylsilane was synthesized by reduction of (pyrrolidino)dimethylchlorosilane $(CH_2)_4NSiMe_2Cl$ with $LiAlH_4$, in ether.

Acknowledgement

This work was supported by the Polish State Committee for Scientific Research under the Research Project 1359/T09/95/08.

References

1. A.G. Brook and J. Chruściel. Organometallics, **3**, 1317 (1984).
2. C. Eaborn. Organosilicon compounds. Butterworth Sci. Publ., London. 1960, and refs. therein.
3. W. Noll. Chemistry and technology of silicones. Academic Press, New York and London. 1968, and refs. therein.
4. B. Hardman and A. Torkelson. Silicones chapter. *In* Encyclopedia of Polymer Science and Engineering. Second ed. Vol. 15. J. Wiley & Sons, New York. 1989. pp. 271–289.
5. B. Marciniec, J. Guliński, W. Urbaniak, and Z.W. Kornetka. Comprehensive handbook on hydrosilylation. *Edited by* B. Marciniec. Pergammon Press, Oxford, New York, Seoul, Tokyo. 1992, and refs. therein.
6. H.R. Kricheldorf (*Editor*). Silicon in polymer synthesis. Springer–Verlag, Berlin, Heidelberg, New York. 1996, and refs. therein.
7. Y. Nakagawa and K. Matyjaszewski. Polym. Prepr. (Am. Chem. Soc. Div. Polym. Chem.), **37**(2), 270 (1996).
8. J.F. Miravet and J.M.J. Fréchet. Proceedings of the Am. Chem. Soc. Div. of PMSE, Fall Meeting, Sept. 8–11, 1997, Las Vegas, NV. Polym. Mater. Sci. Eng. **77**, 141 (1997).
9. J. Hu and D.Y. Son. Polym. Prepr. (Am. Chem. Soc. Div. Polym. Chem), **39**(1), 410 (1998).
10. D.Y. Son and K. Yoon. Proceeding of the Am. Chem. Soc. Div. of PMSE, Fall Meeting, March 21–25, 1999, Anaheim, CA. Polym. Mater. Sci. Eng. **80**, 200 (1999).
11. L. Wilczek and J.P. Kennedy. Int. Symp. Organosilicon Chem. 8th. June 7–12, 1987, St. Louis, MO. Abstracts of Papers, P.-2.10 (1987).
12. (*a*) A. Hirao, T. Hatayama, and S. Nakahama. Macromolecules, **20**, 1505 (1987); (*b*) S. Lu and E.M. Pearce. Macromolecules, **26**, 3514 (1993).
13. J. Chruściel and Z. Lasocki. Pol. J. Chem. **57**, 1383 (1979).
14. J. Chruściel and Z. Lasocki. Pol. J. Chem. **57**, 113 (1983); Pol. J. Chem. **57**, 121 (1983).
15. J. Chruściel. Polimery (Warsaw), **44**, 462 (1999), and refs. therein.
16. J.V. Crivello, J.L. Lee, and D.A. Conlon. *In* Advances in elastomers and rubber elasticity. *Edited by* J. Lal and J.E. Mark. Plenum Press, New York & London. 1986. pp. 157–173.
17. L.N. Lewis, D.S. Johnson, and J.D. Rich. J. Organomet. Chem. **448**, 15 (1993).
18. M. Pintela, V. Harabagiu, C. Cotzur, and B.C. Simionescu. Eur. Polym. J. **30**, 309 (1994).
19. M.A. Sherman and J.P. Kennedy. Proceeding of the Am. Chem. Soc. Div. of PMSE, Fall Meeting, Sept. 8–11, 1997, Las Vegas, NV. Polym. Mater. Sci. Eng. **77**, 321 (1997).
20. P.J. Madec and E. Maréchal. Polym. Prepr. (Am. Chem. Soc. Div. Polym. Chem.), **34**(1), 814 (1993).
21. A. Sellinger and R.M. Laine. Chem. Mater. **8**, 1592 (1996).
22. A.R. Bassindale and T.R. Gentle. J. Mater. Sci. **3**, 1319 (1993).
23. I. Majoros, T.M. Marsalko, and J.P. Kennedy. Polym. Bull. **38**, 15 (1997).
24. H. Gilman and C.L. Smith. J. Organomet. Chem. **8**, 245 (1967).
25. J. Maxka, J. Chruściel, M. Sasaki, and K. Matyjaszewski. Makromol. Chem. Macromol. Symp. **77**, 79 (1994).
26. K. Matyjaszewski, J. Chruściel, J. Maxka, and M. Sasaki. J. Inorg. Organomet. Polym. **5**(3), 261 (1995).
27. J. Chruściel. 26th Silicon Symposium. Indianapolis, Ind. (U.S.A.), March 26–27, 1993, Abstracts, C-11 (1993).
28. W. Fink. Helv. Chim. Acta, **57**, 1010 (1974).
29. E.G. Rochow and W.F. Gilliam. J. Am. Chem. Soc. **67**, 963 (1945).
30. R. Müller. Ger. Pat. Anm. C 7411 (1942).
31. L.N. Lewis. Polym. Prepr. (Am. Chem. Soc. Div. Polym. Chem.), **39**(1), 443 (1998).
32. N.G. Morozov, S.A. Golubtsov, L.P. Morozova-Sukreeva, and I.V. Trofimova-Volkova. Fr. Patent 1 523 912 (1968); Chem. Abstr. **72**, 90 613 (1970).
33. M.G.R.T. De Cooker, J.H.N. De bruyn, and P.J. van den Berg. J. Organomet. Chem. **99**, 371 (1975).
34. C. Eaborn, B.N. Ghose, and D.R.M. Walton. J. Organomet. Chem. **18**, 371 (1969).
35. J. Hetflejs, F. Mares, and V. Chvalovský. Collect. Czech. Chem. Commun. **30**, 1643 (1965).
36. K. Rühlmann and M. Mansfeld. J. Prakt. Chem. (Leipzig), **24**, 226 (1964).
37. E.W. Abel, D.A. Armitage, and R.P. Bush. J. Chem. Soc. 7098 (1965); Chem. Abstr. **64**, 5129 (1966).
38. V. Bazant, V. Chvalovský, and J. Rathouský. Organosilicon compounds. Vol. 1. *In* Chemistry of organosilicon compounds. *Edited by* V. Bazant and V. Chvalovský. Publ. House of the Czechoslovak Academy of Sciences, Prague. (1965), and refs. therein.
39. G.S. Popeleva, K.A. Andrianov, A.A. Larionov, and S.A. Golubtsov. Zh. Obshch. Khim. **34**, 1111 (1964).

© 2000 NRC Canada

40. N.P. Lobusevich, S.A. Golubtsov, Yu. P. Endovin, L.I. Kleimeneva, L.P. Sporikhina, G.S. Volkov, and B.V. Moshalev. Patent SU 392 694 (1973); Chem. Abstr. **80**, 37 275 (1974).
41. N.P. Lobusevich, S.A. Golubtsov, V.N. Penskii, B.A. Golovnya, M.A. Ezerets, E.S. Starodubtsev, A.I. Masliukov, Yu. V. Martinovskii, M.G. Ufimtsev, and V.I. Panasenko. Patent SU 186 480 (1960); Chem Abstr. **66**, 105 048 (1967).
42. R. Schrader, H. Henneck, K. Dreier, R. Bugge, J. Frohnert, and W. Eichler. Patent DD 63 744 (1968); Chem. Abstr. **71**, 91 634 (1969).
43. D. Snobl, M. Dvorak, and J. Cermak. Patent CS 118 723 (1966); Chem Abstr. **66**, 95 178 (1967).
44. S.A. Golubtsov, V.V. Ponomariev, A.S. Shapatin, B.A. Golovnya, M.A. Ezerets, E.S. Starodubtsev, G.N. Kondrasheva, and G.I. Krasnova. Fr. Patent 1 590 075 (1970); Chem. Abstr. **78**, 43 690 (1973).
45. H. Kriegsman and G. Engelhardt. Z. Anorg. Allg. Chem. **310**, 100 (1961).
46. L.M. Antipin, L.M. Blekh, and V.F. Mironov. Zh. Obshch. Khim. **40**, 812 (1970).
47. M. Matsumoto. Jpn. Patent 77 151 130 (1977); Chem. Abstr. **88**, 105 557 (1978).
48. K.W. Michael. Ger. Patent 2 053 195 (1971); Chem. Abstr. **75**, 36 322 (1971).
49. (*a*) N.G. Morozov, S.A. Golubtsov, and L.P. Morozova. Br. Patent 1 089 726 (1968); Chem. Abstr. **68**, 13 166 (1968); (*b*) V.N. Penskii, S.A. Golubtsov, and V.V. Ponomariev. Patent SU 278 694 (1968); Chem. Abstr. **74**, 88 121 (1971).
50. T. Hiiro, H. Sakurai, and F. Kondo. Jpn. Patent 7 895 222 (1978); Chem Abstr. **90**, 6529 (1979).
51. K.W. Michael. Ger. Patent 2 007 001 (1970); Chem. Abstr. **73**, 109 897 (1970).
52. (*a*) H. Schuman and C. Dathe. Ger. Patent 2 851 984 (1979); Chem. Abstr. **91**, 175 511 (1979); (*b*) Br. Patent 2 012 787 (1979); Chem. Abstr. **92**, 181 351 (1980).
53. A. Berger. U.S. Patent 3 362 977 (1968); Chem Abstr. **68**, 95 944 (1968).
54. (*a*) A.G. Viego and H.R. McEntee. U.S. Patent 3 769 310 (1973); Chem. Abstr. **80**, 3624 (1974); (*b*) Ger. Patent 2 163 213 (1962); Chem. Abstr. **77**, 126 838 (1972).
55. M. Lefort and G. Simon. Fr. Patent 2 467 855 (1981); Chem. Abstr. **96**, 6861 (1982).
56. M.G. Voronkov and L.A. Abramas. Izv. Akad. Nauk SSSR, Ser. Khim., 699 (1974).
57. S.A. Golubtsov, V.N. Penskii, and V.V. Ponomariev. Patent SU 415 269 (1974); Chem. Abstr. **80**, 133 619 (1974).
58. J. James. Ger. Patent 1 111 183 (1960); Chem. Abstr. **56**, 8746 (1962); (*b*) Br. Patent 881 179 (1959); Chem. Abstr. **56**, 8745 (1962).
59. U. Scheim and K. Rühlmann. Ger. (East) Patent 259 867 (1988); Chem. Abstr. **111**, 23 714 (1974).
60. R. Müller, R. Köhne, and S. Sliwinski. J. Prakt. Chem. (Leipzig), **9**, 63 (1959).
61. G. Maass and K. Brändle. Ger. Patent 3 133 885 (1983); Chem. Abstr. **99**, 5812 (1983).
62. H.J. Emeleus and M. Onyszchuk. J. Chem. Soc. 604 (1958).
63. N.S. Nametkin, V.M. Vdovin, V.N. Karelskii, B.V. Katcharmin, and E.D. Babich. Izv. Akad. Nauk SSSR, Ser. Khim., 2149 (1973).
64. M. Takamisawa, T. Hayashi, and M. Umamura. Jpn. Patent 7 731 854 (1977); Chem. Abstr. **88**, 121372y (1978).
65. N. Shinohara, M. Arai, and S. Ichinohe. Jpn. Patent 7 765 226; Chem. Abstr. **87**, 135 905r (1977).
66. (*a*) M. Kumada and M. Ishikawa. J. Chem. Soc. 10 (1971); Chem. Abstr. **75**, 36 219 (1971); (*b*) M. Kumada and M. Ishikawa. Jpn. Patent 7 238 930 (1972); Chem. Abstr. **78**, 58 615 (1973).
67. M. Kumada. J. Chem. Soc. Jpn. Ind. Chem. Sect. **60**, 1395 (1957).
68. H. Matsumoto, T. Motegi, M. Hasagawa, and Y. Nagai. J. Organomet. Chem. **142**, 149 (1977).
69. R. Calas and G.D.J. Dunogues. J. Organomet. Chem. **148**, 119 (1978).
70. G. Deleris, M. Lefort, and E. Simonnet. Ger. Patent 2 709 137 (1977); Chem Abstr. **88**, 7047 (1978).
71. R.S. Nale. U.S. Patent 4 079 071 (1978) Chem. Abstr. **89**, 43 758h (1978).
72. S. Cradock and E.K.V. Ebsworth. Inorg. Chim. Acta, **72**, 181 (1983).
73. K.W. Michael. Br. Patent 1 258 852 (1971); Chem. Abstr. **76**, 59 733 (1971).
74. J. Chruściel and Z. Lasocki. Pol. Patent 150 116 (1990); Chem. Abstr. **114**, 82111w (1991).
75. J. Chruściel. Int. Symp.Organosilicon Chem. 11th. Université Montpellier II, France. Abstracts, PC22 (1996).
76. R. Cass and G. Coates. J. Chem. Soc. 2347 (1952).
77. F.A. Cotton and G. Wilkinson. Advanced inorganic chemistry. Interscience Publ. 1972.
78. R. Walsh. Acc. Chem. Res. **14**, 246 (1981).

© 2000 NRC Canada

Adducts of sila-, germa-, and stannaethenes $Me_2E=C(SiMe_3)_2$ (E = Si, Ge, Sn) with anthracene: syntheses, structures, thermolyses[1]

Nils Wiberg, Susanne Wagner, Sham-Kumar Vasisht, and Kurt Polborn

Abstract: The [4 + 2] cycloadducts of $Me_2E=C(SiMe_3)_2$ (E = Si, Ge, Sn) and anthracene are prepared by reaction of an excess of anthracene in benzene with the [2 + 2] cycloadduct of $Me_2Si=C(SiMe_3)_2$ and $Ph_2C=NSiMe_3$ at 130°C, with $Me_2Ge(OPh)$-$CLi(SiMe_3)_2$ at 100°C, and with Me_2SnBr-$CNa(SiMe_3)_2$ at 80°C, respectively. The mentioned adducts act as sources for the ethenes $Me_2E=C(SiMe_3)_2$ above 100°C, the intermediate formation of which has been demonstrated by trapping experiments with 2,3-dimethylbutadiene (formation of a [4 + 2] and an ene reaction product). The half life time of the anthracene adducts with E = Si, Ge, and Sn in the presence of DMB (= 2,3-dimethylbutadiene) in benzene on thermolysis at 130°C (first order reactions) is found to be 141, 12, and 0.3 h, respectively. In the absence of DMB, thermolysis of the cycloadducts leads in benzene as reaction medium exclusively to the dimers of the $Me_2E=C(SiMe_3)_2$ intermediates. In toluene as reaction medium ene products of $Me_2E=C(SiMe_3)_2$ are observed in addition to the dimers. The ene products are not isolable as such, but only after migration of the $Me_2E–CH(SiMe_3)_2$ substituents. The formed derivatives $C_6H_5CH_2EMe_2CH(SiMe_3)_2$ of toluene in part give a second ene reaction with another $Me_2E=C(SiMe_3)_2$ molecule. X-ray structure analyses of the mentioned sources in fact prove the latter to be normal [4 + 2] cycloadducts of $Me_2E=C(SiMe_3)_2$ and anthracene.

Key words: silaethene, germaethene, stannaethene, [4 + 2] anthracene adducts, [4 + 2] cycloadditions and reversions, ene reactions, X-ray structure analyses.

Résumé : On a préparé les cycloadduits [4 + 2] du $Me_2E=C(SiMe_3)_2$ (E = Si, Ge, Sn) avec l'anthracène en faisant réagir un excès d'anthracène, en solution dans le benzène, avec respectivement le cycloadduit [2 + 2] du $Me_2Si=C(SiMe_3)_2$ et le $Ph_2C=NSiMe_3$ à 130°C, avec le $Me_2Ge(OPh)$-$CLi(SiMe_3)_2$ à 100°C et avec le Me_2SnBr-$CNa(SiMe_3)_2$ à 80°C. À des températures supérieures à 100°C, les produits mentionnés agissent comme sources d'éthènes $Me_2E=C(SiMe_3)_2$ dont on a démontré la formation par des expériences de piégeage à l'aide de 2,3-diméthylbutadiène qui donne lieu à la formation d'un produit d'addition [4 + 2] ainsi que d'un produit de réaction ène. On a trouvé que les temps de demi-vie des adduits de l'anthracène avec E = Si, Ge et Sn en présence de DMB (= 2,3-diméthylbutadiène), en solution dans le benzène, lors d'une thermolyse à 130°C (réactions du premier ordre) sont respectivement de 141, 12 et 0,3 h. En absence de DMB, la thermolyse des cycloadduits dans le benzène comme milieu réactionnel conduit exclusivement aux dimères des intermédiaires $Me_2E=C(SiMe_3)_2$. Lorsque le milieu réactionnel est le toluène, on observe aussi des produits de réaction ène, en plus de la formation des dimères. Il n'est pas possible d'isoler les produits ène comme tels, uniquement après la migration des substituants Me_2E-$CH(SiMe_3)_2$. Une partie des dérivés qui se forment dans le toluène, $C_6H_5CH_2EMe_2CH(SiMe_3)_2$, donne lieu à une deuxième réaction ène, avec une autre molécule $Me_2E=C(SiMe_3)_2$. Une analyse des structures déterminées par diffraction des rayons X pour les sources mentionnées prouve en fait que ces derniers sont des cycloadduits [4 + 2] normaux des $Me_2E=C(SiMe_3)_2$ avec l'anthracène.

Mots clés : silaéthène, germaéthène, stannaéthène, adduits [4 + 2] de l'anthracène, cycloadditions et cycloréversions [4 + 2], réactions ène, détermination de structures par diffraction des rayons X.

Received July 8, 1999. Published on the NRC Research Press website on October 20, 2000.

This paper is dedicated to Professor A.G. Brook on the occasion of his 75th birthday.

N. Wiberg,[2] S. Wagner, S.-K. Vasisht, and K. Polborn.[3] Department Chemie der Universität München, Butenandtstr. 5–13 (Haus D), D-81377 München, Germany.

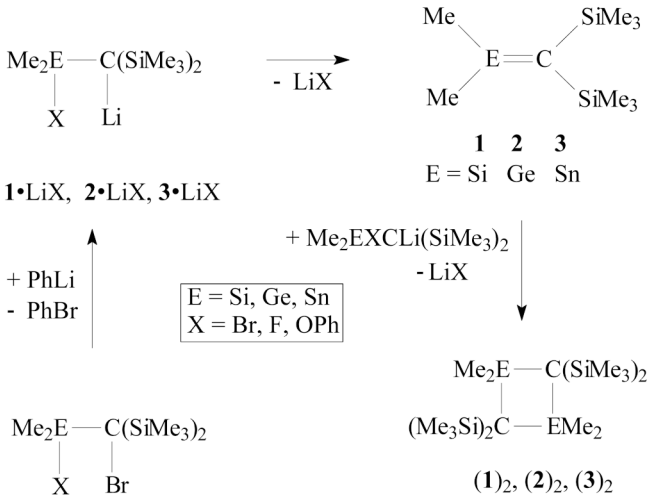
[1]Compounds of silicon and homologues, part 130, and unsaturated compounds of silicon and homologues, part 55. Part 129: N. Wiberg, T. Blank, A. Purath, G. Stößer, H. Schnöckel. Angew. Chem. Int. Ed. Engl. **38**, 2563 (1999); Part 54: N. Wiberg, H.-W. Lerner, S.-K. Vasisht, S. Wagner, K. Karaghiosoff, H. Nöth, W. Ponikwar. Eur. J. Inorg. Chem. 1211 (1999).

[2]Author to whom correspondence should be addressed: Telephone: +49(0)89-2180-7456. Fax: +49(0)89-2180-7865. e-mail: Niw@cup.uni-muenchen.de

[3]X-ray structure analyses.

 © 2000 NRC Canada

Scheme 1. Generation of **1**, **2**, **3** by thermal salt elimination.



Introduction

In the past years we attempted to generate silaethene $Me_2Si=C(SiMe_3)_2$ (**1**), germaethene $Me_2Ge=C(SiMe_3)_2$ (**2**) and stannaethene $Me_2Sn=C(SiMe_3)_2$ (**3**) as short-lived reaction intermediates, which immediately dimerize to $(\mathbf{1})_2$, $(\mathbf{2})_2$, and $(\mathbf{3})_2$. If a solution of PhLi in ether is added to a cold solution of $Me_2EX\text{-}CBr(SiMe_3)_2$ (E = Si, Ge, Sn; X = Br, F, OPh) in ether, **1**, **2**, and **3** will be formed (1–3). According to Scheme 1, the compounds $Me_2EX\text{-}CBr(SiMe_3)_2$ react by exchange of bromine bonded to carbon for lithium; thus the sila-, germa-, and stannaethene sources $Me_2EX\text{-}CLi(SiMe_3)_2$ (**1**·LiX, **2**·LiX, **3**·LiX)[4] are formed. The latter decompose via thermal salt elimination to ethenes **1**, **2**, and **3.** The reaction rate is found to increase in the order **1**·LiX < **2**·LiX < **3**·LiX and depending on X in the order X = OPh < F < Br (1, 2, 3).

Thus, salt elimination takes place for **1**·LiBr at –78°C during hours (1), for **2**·LiBr at –78°C during minutes (2), for **1**·LiF at +8°C during hours (1), and for **2**·LiOPh at –40°C during one hour (2). The reactive intermediates **1**, **2**, and **3** react with their precursors $Me_2EX\text{-}CLi(SiMe_3)_2$ via the insertion products $Me_2EX\text{-}C(SiMe_3)_2\text{-}EMe_2\text{-}CLi(SiMe_3)_2$ to $(\mathbf{1})_2$, $(\mathbf{2})_2$, and $(\mathbf{3})_2$ (Scheme 1, (4)).

The intermediate formation of **1**, **2**, and **3** could be proved by trapping experiments among others, with organic dienes and enes (formation of Diels–Alder and ene reaction products (5–7)). Due to the high dimerization tendency (even growing in the direction **1**, **2**, **3**, see above) and the reduced reactivity of dienes and enes at lower temperatures, the cycloadditions and ene reactions have to be carried out with an excess of the trapping reagent and not at too low reaction temperatures (see Experimental).

The less reactive dienes and enes are by no means effective trapping reagents for **1**, **2**, and **3** even when the relevant ethenes are released from more stable sources **1**·LiX, **2**·LiX, and **3**·LiX. In the latter case it is advantageous to use "stores" of **1**, **2**, and **3**, which are formed by reaction of the ethenes from **1**·LiX, **2**·LiX, and **3**·LiX with appropriate reactants, able to fix the unsaturated compounds at low temperatures and able to set them free at slightly higher temperatures.

An example are the adducts **1**·$Ph_2C=NSiMe_3$, which can be generated from **1** (from **1**·LiF) and benzophenonimine $Ph_2C=NSiMe_3$ at room temperature via [2 + 2] and [4 + 2] cycloadditions (Scheme 2, first equation). Above 60°C the cycloadducts decompose reversibly into **1** and comparatively unreactive[5] $Ph_2C=NSiMe_3$ (8). Unfortunately it is impossible to "store" **2** and **3** with $Ph_2C=NSiMe_3$. Meanwhile we succeeded in synthesizing the [4 + 2] cycloadducts **1a**, **2a**, and **3a** from **1**, **2**, **3** and anthracene (**a**). They act as "stores" for silaethene as well as germaethene and stannaethene, and are able to decompose above 100°C via thermal cycloreversion into the unsaturated compounds **1**, **2**, and **3** which dimerize in a fast reaction (Scheme 2, second equation).

Syntheses of the anthracene adducts 1, 2, and 3

The adducts **1a**, **2a**, and **3a** must be synthesized at higher temperatures because of the low reactivity of the ethenes **1**, **2**, **3** towards anthracene. Due to the decreasing reactivity in the order **3**, **2**, **1**, the applied reaction temperature is higher for **1** than for **2**, and for **2** higher than for **3**. The adduct **3a** is prepared from $Me_2SnBr\text{–}CBr(SiMe_3)_2$ and sodium (formation of **3** via **3**·NaBr, see Schemes 1 and 2) in the presence of excess anthracene at 80°C using toluene as solvent (molar ratio $Me_2SnBr\text{–}CBr(SiMe_3)_2$:sodium:anthracene = 1:2:20; benzophenone is added to the reaction mixture for activation of sodium; nearly quantitative formation of **3a**). Compound **2a** can be prepared by adding a –50°C cold solution of **2**·LiOPh in *tert*-butylbenzene to a 100°C hot solution of anthracene (added in excess) in *tert*-butylbenzene (molar ratio **2**·LiOPh to anthracene = 1:2; ca. 50% yield of **2a** besides $(\mathbf{2})_2$, see Schemes 1 and 2). The adduct **1a** is synthesized by heating a solution of **1**·$Ph_2C=NSiMe_3$ and an excess of anthracene in benzene at 130°C for 14 h (molar ratio **1**·$Ph_2C=NSiMe_3$ to anthracene = 1:2, nearly quantitative formation of **1a**, see Scheme 2).

In this context it should be mentioned that the rate constants for the formation of the anthracene adducts increase in the order **1a** < **2a** < **3a** (see above), as do the rate constants for the thermal cycloreversions of the adducts, leading to **1**, **2**, **3** and anthracene (ratio of the rate constants about 1:10:100; see below). Thus, going from **1** over **2** to **3**, both activation energies for the formation of the source and for the decomposition of the source are decreasing. Therefore, the absolute reaction enthalpies (equivalent to the difference in both activation energies) for the presumably exothermic formation of the "sources" are obviously very similar. In contrast to **2a** and **3a**, the adduct **1a** shows a low tendency towards cycloreversion even at 130°C. Therefore, it is favorable to use the adducts **1**·$Ph_2C=NSiMe_3$, **2a**, and **3a** as "sources" for **1**, **2**, and **3** (5–7) to perform reaction studies for sila-, germa-, and stannaethenes at temperatures between 100 and 130°C.

[4] The also possible (but unwanted) exchange of X bonded to silicon, germanium, or tin for phenyl under formation of $Me_2EPh\text{–}CBr(SiMe_3)_2$ is only important for $Me_2EX\text{–}CBr(SiMe_3)_2$ with X = Br at reaction temperatures above –78°C (E = Si, Ge) and at –78°C (E = Sn).
[5] $Ph_2C=NSiMe_3$ slowly and irreversibly traps **1** by formation of the insertion product $Ph_2C=N\text{–}SiMe_2\text{-}C(SiMe_3)_3$ (8).

© 2000 NRC Canada

Scheme 2. Generation of **1**, **2**, **3** by thermal cycloreversion.

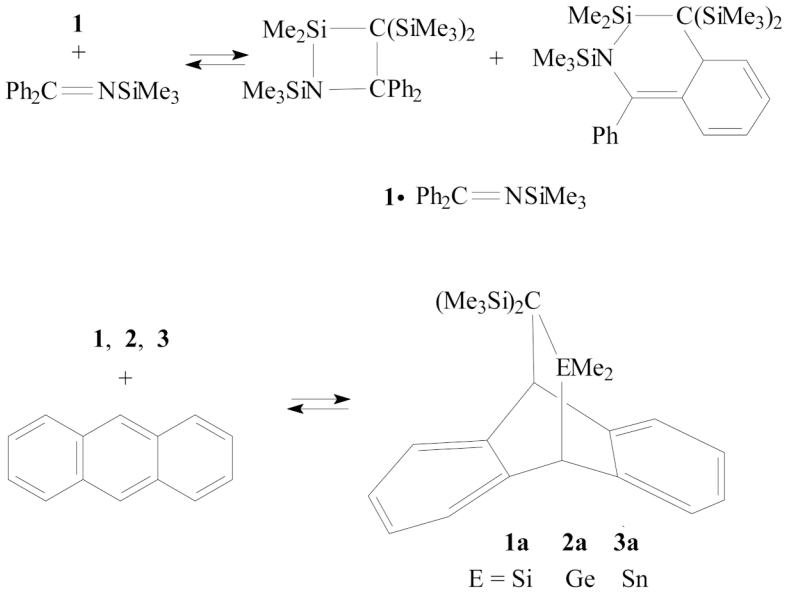


Fig. 1. Kinetic (first order presentation) of the thermolyses of **3a** in the absence or presence of DMB (mol ratio **3a**:DMB = 1:10) in C_6D_6 at 130°C.

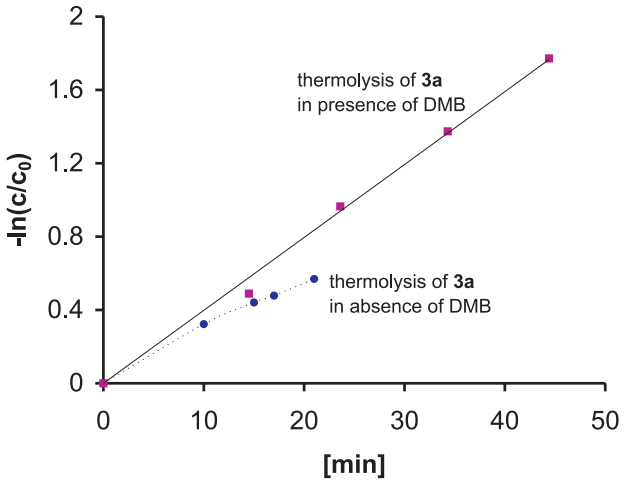
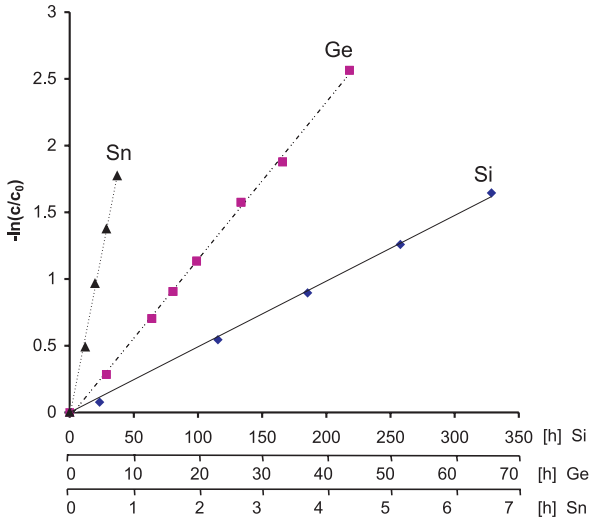


Fig. 2. Kinetic (first order presentation) of the thermolyses of **1a, 2a,** and **3a** in the presence of DMB (mol ratio adduct: DMB = 1:10) in C_6D_6 at 130°C.



Thermolyses of 1a, 2a, and 3a

It is difficult to determine the reaction order and the rate constants for the thermolysis of **1a**, **2a**, and **3a** in benzene, leading to dimers $(\mathbf{1})_2$, $(\mathbf{2})_2$, $(\mathbf{3})_2$, and anthracene. The reason for this fact is the increasing rate of the reverse reaction (that is to say, the rate for the adduct formation from **1**, **2**, **3**, and anthracene) due to the increase of free anthracene in the reaction mixture in the course of the reaction (Scheme 2, second equation). If ln (c/c_0) (c = adduct concentration at time t, c_0 = sum of concentration of adduct and dimer) is plotted against time t in the sense of a first order reaction, a graph with a significant decrease in the ascent will be obtained instead of a straight line (Fig. 1). If the decomposition of **1a**, **2a**, and **3a** is carried out in the presence of a suitable trapping reagent like DMB (= 2,3-dimethylbutadiene), which removes the sila-, germa-, and stannaethene **1**, **2**, and **3** from the adduct equilibrium (Scheme 2, second equation), the thermolysis of the adducts takes place according to a first order reaction as expected (Fig. 2). At the starting point the ascents of first order plots of adduct thermolysis in the presence and the absence of DMB are similar (Fig. 1).

In the presence of DMB, the thermal cycloreversion reactions of the adducts **1a**, **2a**, and **3a** in benzene at 100–130°C lead to [4 + 2] cycloadducts **4** and ene reaction products **5** (Scheme 3). Rate constants and half life times for these thermolyses are shown in Table 1.

Using toluene as solvent instead of benzene for the 130°C thermolyses of **1**·$Ph_2C{=}NSiMe_3$, **2a**, and **3a**; the ene products of **1**, **2**, and **3** with toluene are formed to our surprise, together with the dimers $(\mathbf{1})_2$, $(\mathbf{2})_2$, and $(\mathbf{3})_2$. The highly reactive compounds **1**, **2**, and **3** force the chemically quite

© 2000 NRC Canada

Scheme 3. Thermolyses of **1a**, **2a**, **3a** in the presence of DMB.

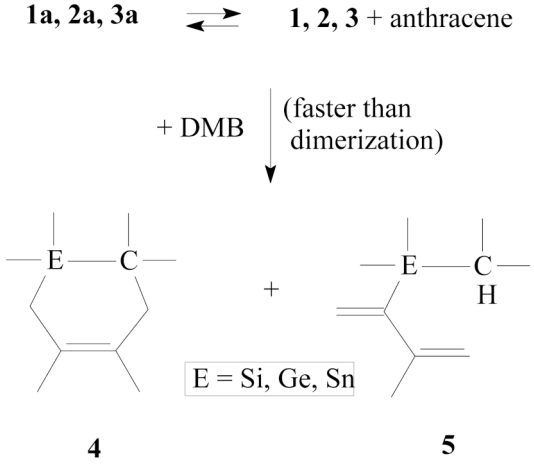


Table 1. Rate constants k and half life times $\tau_{1/2}$ of the thermolyses of **1a, 2a**, and **3a** in C_6D_6 at variable temperatures in the presence of DMB (mol ratio adducts: DMB = 1:10).

		k (s^{-1})	$\tau_{1/2}$ (h)
1a	(130°C)	1.37×10^{-6}	141
2a	(130°C)	1.60×10^{-5}	12
3a	(130°C)	6.60×10^{-4}	0.3
	(100°C)	2.44×10^{-5}	7.9

unreactive toluene to act as an ene reagent. Certainly **1**, **2**, and **3** (generated from **1**·Ph_2C=$NSiMe_3$, **2a**, **3a**) first form the ene products **6** (Scheme 4). These are only intermediates, which finally react to the toluene derivatives **8** and **10**. The products **8** are obtained from **6** via rearrangement of Me_2E–$CH(SiMe_3)_2$ groups, whereas there are three possible ways that may lead to **10** as the product (Scheme 4): (*i*) Products **6** rearrange to the non-isolable products **7** (according to experimental studies a rearrangement of **8** to **7** does not occur), whereby the latter reacts with **1**, **2**, or **3** via ene products **9** to isolable compounds **10** (as no traces of products **7** were found, reaction path (*i*) is less probable). (*ii*) Products **10** are formed by reaction of **8** with **1**, **2**, or **3** via the ene products **11** (according to preliminary studies these reactions do not occur, therefore reaction path (*ii*) is less probable). (*iii*) Products **6**, which certainly are very reactive intermediates, form directly with **1**, **2**, or **3** the ene products **10**.

Table 2 shows the yields of the products after complete thermolysis of **1**·Ph_2C=$NSiMe_3$, **2a**, and **3a** at 130°C in toluene. It reveals that if complete educt thermolysis needs a long time, a decrease in the yields of dimers $(\mathbf{1})_2$, $(\mathbf{2})_2$, and $(\mathbf{3})_2$ will be observed. This fact can be explained as follows: the stationary concentration of intermediates **1**, **2**, and **3** decreases with decreasing rate for the decomposition of the sources **1a**, **2a**, **3a**. As a consequence, the ene reactions of **1**, **2**, and **3** with toluene (which take place according to a first order reaction) are more dominant than the dimerization reactions (which represents a second order reaction). This important result indicates that the formation of $(\mathbf{1})_2$, $(\mathbf{2})_2$, and $(\mathbf{3})_2$ — via the thermal cycloreversion of **1**·Ph_2C=$NSiMe_3$, **1a**, and **2a**, respectively — takes place through a direct dimerization of **1**, **2**, and **3** (compare however the formation of dimers in the course of salt elimination of **1**·LiX, Scheme 1).

Scheme 4. Thermolyses of **1a**, **2a**, **3a** in toluene (in addition to **8** and **10**, the dimers $(\mathbf{1})_2$, $(\mathbf{2})_2$, $(\mathbf{3})_2$ are formed).

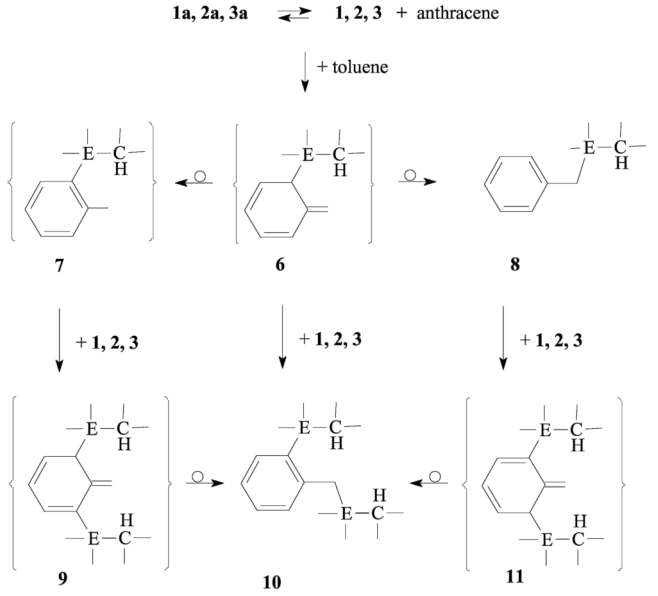


Table 2. Relative yields of dimers $(\mathbf{1})_2$, $(\mathbf{2})_2$, $(\mathbf{3})_2$, and products **8**, **10** [mole %] after complete thermolysis of 0.08 molar solutions of **1**·Ph_2C=$NSiMe_3$, **2a** and **3a** in toluene at 130°C.

Sources	T (°C)	t (d)	dimers	**8**	10
1·Ph_2C=$NSiMe_3$	130	9	37%	57%	6%
2a	130	44	12%	49%	39%
3a	130	1	83%	13%	4%

Of course, both the ratio of yields of dimers to ene reaction products and the ratio of yields of **8** to **10**, in addition depend on the relative reactivity of ethenes **1**, **2**, or **3** towards themselves, toluene and toluene derivatives **6**, **7**, and **8**, respectively. Obviously, on going from toluene to **6**, **7**, or **8**, the ene reactivity has significant effect in the case of the germaethene **2,** a smaller effect in the case of the stannaethene **3** and the smallest effect in the case of the silaethene **1**, regarding the ratio of yields of **8** to **10** (Table 2). Nevertheless, for direct formation of **10** from **6** – being the most favoured reaction course – the stationary concentrations of **1**, **2**, or **3** are important, as the transformations of **6** into **8** and **10**, respectively, are zero order in the first and first order in the second case concerning the mentioned ethenes.

Structures of 1a, 2a and 3a

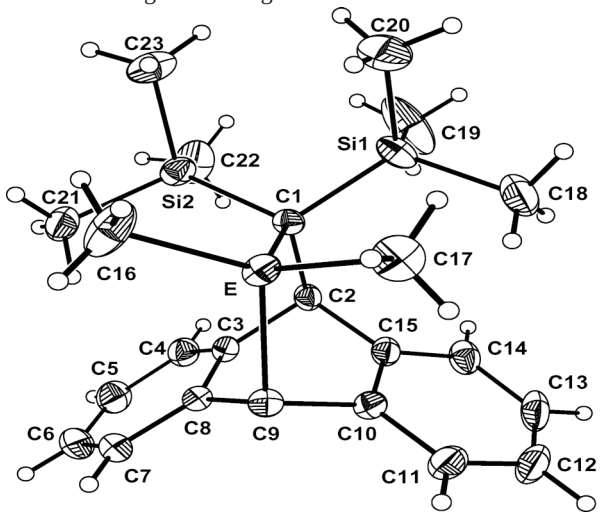
The anthracene adducts **1a**, **2a**, and **3a** precipitate from benzene as colourless, moisture- and air-insensitive crystals, which melt at 144, 136, and 140°C, respectively, and are thermolabile above 100°C. Figure 3 shows their molecular structure in the crystal determined by X-ray structure analysis.

© 2000 NRC Canada

Table 3. Selected bond distances (Å) and angles (°) for **1a**, **2a**, and **3a** (for atom numbering see Fig. 3). The unit cells of the adducts contain one, three, or two independent molecules in the case of **1a**, **2a**, or **3a**.

1a, **2a**, **3a**	E = Si	E = Ge	E = Sn
E—C9	1.907(2)	1.999(5), 1.982(5), 1.993(5)	2.194(4), 2.199(4)
E—C1	1.905(2)	2.001(4), 2.001(5), 1.998(5)	2.201(3), 2.206(3)
C1—C2	1.612(2)	1.603(6), 1.619(7), 1.619(6)	1.604(5), 1.621(4)
E—C17	1.875(3)	1.956(6), 1.961(6), 1.947(6)	2.147(5), 2.141(5)
E—C16	1.873(3)	1.940(6), 1.954(6), 1.962(7)	2.133(4), 2.149(5)
Si1—C1	1.923(2)	1.911(5), 1.921(6), 1.933(5)	1.897(3), 1.911(3)
Si2—C1	1.923(2)	1.930(5), 1.914(5), 1.915(5)	1.914(4), 1.900(4)
C9—C8	1.498(3)	1.506(7), 1.501(7), 1.492(7)	1.498(5), 1.491(5)
C8—C3	1.386(3)	1.389(7), 1.385(7), 1.402(7)	1.409(5), 1.399(5)
C3—C2	1.515(3)	1.517(7), 1.514(7), 1.509(7)	1.523(5), 1.512(5)
C2—C15	1.515(3)	1.524(6), 1.522(7), 1.516(6)	1.521(5), 1.521(5)
C15—C10	1.392(4)	1.391(7), 1.386(7), 1.391(7)	1.401(5), 1.397(5)
C10—C9	1.496(4)	1.502(7), 1.509(7), 1.501(7)	1.501(5), 1.497(5)
C17-E-C16	104.4(2)	104.6(3), 104.5(3), 104.4(4)	107.1(2), 104.8(3)
C16-E-C1	117.8(1)	117.8(2), 117.1(3), 118.0(3)	117.9(2), 118.8(2)
C17-E-C1	117.6(1)	118.2(2), 119.0(3), 117.8(3)	117.3(2), 120.5(2)
C16-E-C9	111.1(2)	113.3(3), 111.4(3), 107.6(3)	115.6(2), 109.9(2)
C17-E-C9	105.9(1)	104.8(3), 107.0(3), 114.4(3)	106.2(2), 109.9(2)
C1-E-C9	99.4(1)	97.5(2), 97.3(2), 97.3(2)	91.7(1), 91.7(1)
E-C1-Si1	109.1(1)	108.4(2), 111.7(2), 111.9(2)	108.8(2), 110.3(2)
E-C1-Si2	114.1(1)	112.8(2), 109.2(3), 110.3(2)	108.6(1), 108.7(2)
E-C1-C2	105.6(1)	104.0(3), 105.1(3), 104.8(3)	105.4(2), 105.0(2)
C8-C9-C10	107.3(2)	107.8(4), 108.0(4), 108.7(4)	107.7(3), 109.7(3)
C3-C8-C9	115.2(2)	115.6(4), 115.7(5), 115.5(4)	117.4(3), 116.6(3)
C2-C3-C8	115.5(2)	115.6(4), 116.2(5), 115.7(4)	116.4(3), 117.4(3)
C15-C2-C3	103.8(2)	105.0(4), 104.9(4), 105.2(4)	103.7(3), 104.7(3)
C10-C15-C2	114.7(2)	115.4(4), 115.7(5), 116.6(4)	117.0(3), 117.0(3)
C9-C10-C15	115.8(2)	115.9(4), 115.8(5), 115.0(4)	117.2(3), 116.7(3)

Fig. 3. View of the molecular structures of **1a**, **2a**, and **3a** (E = Si, Ge, Sn) in the crystal (ORTEP plot; 25% thermal probability ellipsoids; local symmetry of the molecules $\approx c_n$) (for clarity hydrogen atoms are not shown) and atom numbering scheme. For selected bond lengths and angles see Table 3.



In Table 3, selected bond length and angles are given. It is evident from Fig. 3 that the anthracene part is bent roof-shaped at the central C-atoms in **1a**, **2a**, and **3a**. Both parts of the roof are planar (each angular sum at C3, C8, C10, and C15 is about 360°). The ridge is bridged with a Me_2E–$C(SiMe_3)_2$ group (Fig. 4). The exchange of silicon for germanium and of germanium for tin practically doesn't change most of the bond lengths and angles in **1a**, **2a**, and **3a,** except the E—C bond length and C-E-C bond angles (Fig. 5).

Experimental

All experiments were carried out in the absence of air and moisture. According to literature procedures were prepared: **1**·$Ph_2C{=}NSiMe_5$ (8), $Me_2Ge(OPh)$-$CBr(SiMe_3)_2$ (2), Me_2SnBr-$CBr(SiMe_3)_2$ (3). The NMR-spectra were recorded on multinuclear instruments Jeol GSX 270 and Jeol EX 400. The product seperation was done by preparative HPLC on Waters 600 (column 21.2 mm × 250 mm; Zorbax C18; flow 21 mL/min.; detection: UV at 230 nm and refractometer). Mass spectrometry (EI): Varian CH7; found and calculated isotopic patterns were in perfect agreement.

Thermolyses of 1·LiBr, 2·LiBr, 3·LiBr in the presence of DMB at low temperatures

To a solution of *x* mmol Me_2EBr-$CBr(SiMe_3)_2$ and *y* mmol DMB in ether, *x* mmol PhLi in ether are added dropwise at temperature T (Table 4). After warming up to ambient temperature the types and yields of products formed were identified by ^{1}H NMR (Table 4) and by comparison of

© 2000 NRC Canada

Table 4. Reactions of Br/Br ($Me_2EBr–CBr(SiMe_3)_2$, E = Si, Ge, Sn) with PhLi in the presence of DMB at low temperatures *T*; (dimers = $(\mathbf{1})_2$, $(\mathbf{2})_2$, $(\mathbf{3})_2$, Ph/Br = $Me_2EPh–CBr(SiMe_3)_2$, for **4** and **5** see Scheme 3; % = reaction yields).

	$Me_2EBr-CBr(SiMe_3)_2$, E =					
	Si		Ge		Sn	
Br/Br (mmol)	0.45	0.27	0.27	0.76	3.2	3.2
DMB (mmol)	13.5	0.27	0.27	8.8	32	64
Et_2O (mL)	9	10	10	25	10	10
T (°C)	–78	–78	–40	–40	–78	–40
Dimers (%)	14	80	7	6	60	19
4 (%)	75	16	54	56	10	18
5 (%)	11	4	11	5	—	—
Ph/Br (%)	—	—	28	33[a]	30	63

[a] *n*BuLi was used instead of PhLi, therefore $Me_2GeBu–CBr(SiMe_3)_2$ (2) was formed.

Fig. 4. Projection of **1a**, **2a**, and **3a** in the direction of the middle C atoms of the anthracene parts of the molecules. Dihedral and folding angles in (°) (first data for E = Si, second for E = Ge and third for E = Sn, see the legend of Table 3).

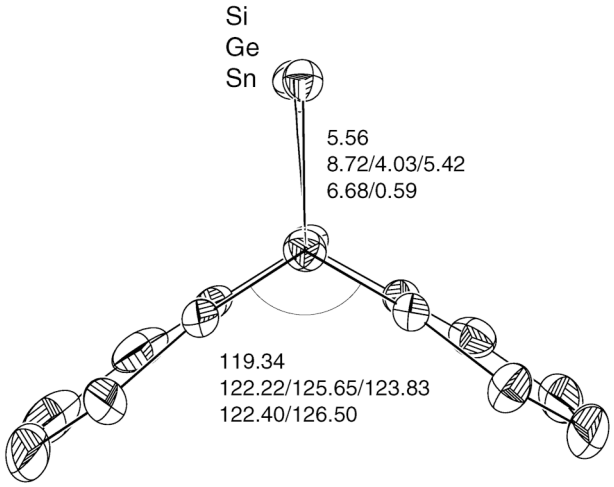
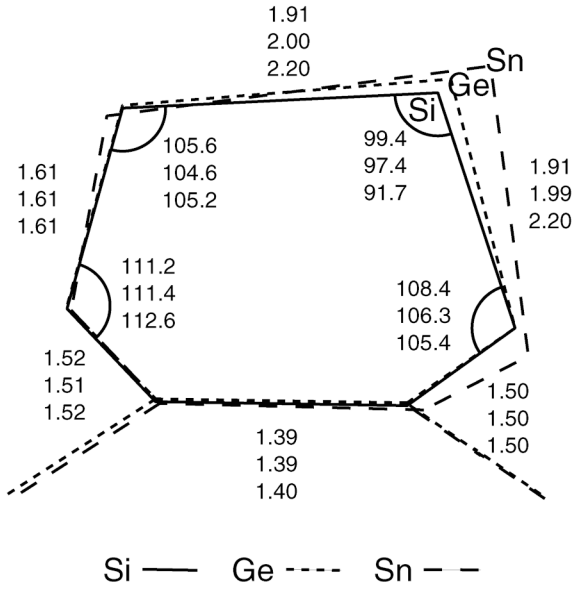


Fig. 5. Projection of **1a**, **2a**, and **3a** in the direction of the normals of the two benzene rings. Bond distances in (Å) and bond angles in (°) (first data for E = Si, second for E = Ge and third for E = Sn, mean values in case of **2a** and **3a**, see Table 3).



the NMR data with those of authentic compounds (dimers of **1**, **2**, **3**, Diels-Alder adducts **4**, ene reaction products **5**, and $Me_2EPh-CBr(SiMe_3)_2$ (1–3)).

Synthesis of 1a

A solution of 0.132 g (0.28 mmol) **1**•$Ph_2C=NSiMe_3$ and 0.100 g (0.56 mmol) anthracene in 2.4 mL benzene was heated for 14 h at 130°C. According to ^{1}H NMR, 94% **1a**, 2% $(\mathbf{1})_2$ and 4% $Ph_2C=N-SiMe_2-C(SiMe_3)_3$ were formed. The reaction mixture was treated with 0.5 mL MeOH – 1.0 mL *t*BuOMe, and separation was done by HPLC using MeOH and *t*BuOMe as mobile phase (0–8 min: 100% MeOH, 8–20 min with gradient to 80% MeOH – 20% *t*BuOMe, 20–25 min with gradient to 100% MeOH). Retention time: 5.1 min (anthracene), 9.2 min (**1a**), 14.7 min ($Ph_2C=N–SiMe_2–C(SiMe_3)_3$).

*9,10-Dihydro-9,10-[11,11-dimethyl-12,12-bis(trimethylsilyl)-11-silaethano]-anthracen (**1a**):* colourless solid, mp 144°C. ^{1}H NMR (C_6D_6, iTMS) δ: –0.083 (s; 2 $SiMe_3$), 0.085 (s; $SiMe_2$), 3.51 (s, SiCH), 4.56 (s; CCH), 6.90–7.10 (m; =CH). $^{13}C\{^1H\}$ NMR (C_6D_6, iTMS) δ: 1.91 ($SiMe_2$), 4.52 (2 $SiMe_3$), 12.51 (Si_3C), 43.27 (SiCH), 50.68 (CCH), 124.5/125.4/126.0/126.4 (8 =CH-), 143.4/143.5 (4 =C<). ^{29}Si NMR (C_6D_6, eTMS) δ: 1.68 ($SiMe_2$), 3.16 (2 $SiMe_3$). MS: *m*/*z* 394 (M^+). Anal. calcd. for $C_{23}H_{34}Si_3$: C 69.98, H 8.68; found: C 69.54 H 8.46.

Synthesis of 2a

A solution of 1.17 mmol $Me_2Ge(OPh)–CLi(SiMe_3)_2$ in $tBuC_6H_5$ (synthesized by reaction of 1.17 mmol $Me_2Ge(OPh)-CBr(SiMe_3)_2$ with 1.17 mmol *n*BuLi in Et_2O at –78°C, ether replaced by $tBuC_6H_5$ at –78°C) at –50°C, was added dropwise (over a period of one hour) to a solution of 0.456 g (2.56 mmol) anthracene in 20 mL $tBuC_6H_5$, which was heated to 100°C. According to ^{1}H NMR, **2a** and $(\mathbf{2})_2$ were formed in the molar ratio 1.2:1, besides $Me_2GeR–CH(SiMe_3)_2$ (*R* = OPh, *n*Bu) (2). The reaction mixture was allowed to cool to room temperature, 0.3 mL Me_3SiCl (to form Me_3SiOPh of LiOPh) were added, and all volatile

© 2000 NRC Canada

fractions (tBuC$_6$H$_5$, Me$_3$SiCl, Me$_3$SiOPh) were condensed in oil pump vacuum at 30°C. The residue was dissolved in 8 mL benzene and insoluble LiBr was removed. The solution was concentrated to 4 mL, and 1.5 mL MeOH – 2.5 mL tBuOMe were added. Some hours later anthracene and (**2**)$_2$ had crystallized partially and were removed by decantation. The further separation of the reaction mixture was done by HPLC using MeOH as mobile phase. Retention times: 6.0 min (anthracene), 11.4 min (**2a**), 41.6 min ((**2**)$_2$).

*9,10-Dihydro-9,10-[11,11-dimethyl-12,12-bis(trimethylsilyl)-11-germaethano]-anthracene (**2a**)*: colourless solid, mp 136°C. ^{1}H NMR (C$_6$D$_6$, iTMS) δ: –0.102 (s; 2 SiMe$_3$), 0.232 (s; GeMe$_2$); 3.66 (s; GeCH), 4.69 (s; CCH), 6.90–7.10 (m; =CH–). ^{13}C{^{1}H} NMR (CDCl$_3$, iTMS) δ: 2.19 (GeMe$_2$), 3.96 (2 SiMe$_3$), 13.57 (Si$_2$C), 42.38 (GeCH), 50.19 (CCH), 124.0/124.5/125.6/126.5 (8 =CH–), 142.1/143.2 (4 =C<). ^{29}Si NMR (CDCl$_3$, eTMS) δ: 3.49 (2 SiMe$_3$). MS: *m*/*z* 440 (M$^+$).

Synthesis of 3a

A mixture of 0.23 g (10.0 mmol) sodium metal, 9.10 g (50.0 mmol) benzophenone and 17.80 g (100 mmol) anthracene in 200 mL toluene was stirred and heated to 100°C for 1/2 hour to obtain a deep blue coloured solution. The reaction mixture was cooled to 80°C and a solution of 2.33 g (5.00 mmol) of Me$_2$SnBr-CBr(SiMe$_3$)$_2$ in 50 mL toluene was added over a period of two hours. According to ^{1}H NMR 88% **3a**, 10% (**3**)$_2$ and 2% **8** were formed. The reaction mixture was cooled down to 0°C, unsoluble compounds (NaBr, anthracene) were separated, solvent was removed and benzophenone was sublimed out at 60°C and 10^{-3} mbar over 2 days. The residue was treated with 5 mL MeOH – 10 mL tBuOMe and separation of the reaction mixture was done by HPLC using MeOH and tBuOMe as mobile phase (0–8 min: 100% MeOH, 8–14 min with gradient to 80% MeOH – 20% tBuOMe, 20–25 min with gradient to 100% MeOH). Retention times: 5.0 min (anthracene), 8.4 min (**3a**), and 18.5 min ((**3**)$_2$).

*9,10-Dihydro-9,10-[11,11-dimethyl-12,12-bis(trimethylsilyl)-11-stannaethano]-anthracene (**3a**)*: colourless solid, mp 140°C. ^{1}H NMR (C$_6$D$_6$, iTMS) δ: –0.098 (s; 2 SiMe$_3$), 0.166 (s; SnMe$_2$), 3.92 (s, SnCH), 4.90 (s; CCH), 6.83–7.15 (m; =CH). ^{13}C{^{1}H} NMR (C$_6$D$_6$, iTMS) δ: – 4.18 (SnMe$_2$), 3.87 (2 SiMe$_3$), 16.93 (SnSi$_2$C), 39.33 (SnCH), 50.60 (CCH), 123.6/123.8/125.7/127.3 (8 =CH-), 141.0/143.5 (4 =C<). ^{29}Si NMR (C$_6$D$_6$, eTMS) δ: = 3.01 (2 SiMe$_3$). ^{119}Sn NMR (C$_6$D$_6$, eTMS) δ: = –3.14 (SnMe$_2$). MS: *m*/*z* 486 (M$^+$). Anal. calcd. for C$_{23}$H$_{34}$Si$_2$Sn: C 57.06, H 7.03; found: C 56.73 H 6.82.

Thermolysis of 3a in benzene at 130°C

A sealed NMR tube, containing 0.029 g (0.06 mmol) of **3a** in 0.6 mL C$_6$D$_6$, was heated at 130°C. The progress of the reaction was monitored by ^{1}H NMR after 10, 15, 17, 21 min. The intensities of the ^{1}H NMR signals as resulting from the evaluation of the integrals were determined for **3a** and the dimer of **3** as follows: 10 min: 72% **3a**, 28% (**3**)$_2$; 15 min: 64% **3a**, 36% (**3**)$_2$; 17 min: 62% **3a**, 38% (**3**)$_2$; 21 min: 57% **3a**, 43% (**3**)$_2$. In the further course of the reaction (**3**)$_2$ precipitates.

Thermolysis of anthracene adducts 1a, 2a, 3a in presence of DMB at 100°C and 130°C

Sealed NMR tubes containing 0.016 g (0.04 mmol) of **1a** and 0.045 mL (0.40 mmol) DMB in 0.5 mL C$_6$D$_6$ (**A**); 0.018 g (0.04 mmol) of **2a** and 0.045 mL (0.40 mmol) DMB in 0.6 mL C$_6$D$_6$ (**B**); 0.029 g (0.06 mmol) of **3a** and 0.068 mL (0.60 mmol) DMB in 0.6 mL C$_6$D$_6$ (**C**); 0.029 g (0.06 mmol) of **3a** and 0.081 mL (0.72 mmol) DMB in 0.6 mL C$_6$D$_6$ (**D**); were heated at 130°C (**A**, **B**, **C**) and 100°C (**D**). The progress of the reaction was monitored by ^{1}H NMR. The intensities of the ^{1}H NMR signals as resulting from the evaluation of the integrals were determined for **1a**, **2a**, **3a**, **4**, and **5**. To determine the reaction order, –ln (c/c_0) was plotted against time t, with c being the ^{1}H NMR signal area of anthracene adducts and c_0 being the sum of ^{1}H NMR signal areas of anthracene adducts + **4** + **5**. For the plots, rate constants, and half life times see Table 1 and Fig. 2.

Thermolysis of 1·Ph$_2$C=NSiMe$_3$ in toluene

A solution of 0.075 g (0.16 mmol) **1**·Ph$_2$C=NSiMe$_3$ in 2.0 mL toluene was heated at 130°C for 9 d in a sealed, evacuated NMR tube. The ^{1}H NMR spectrum indicated complete conversion to Ph$_2$C=N–SiMe$_2$–C(SiMe$_3$)$_3$ (59%), (**1**)$_2$ (15%), **8** (23%), and **10** (3%). After removal of volatile constituents, the residue was treated with 1.0 mL tBuOMe – 0.5 mL MeOH and separation was done by HPLC using MeOH as mobile phase. Retention times: 10.2 min (**8**), 18.1 min (Ph$_2$C=N–SiMe$_2$–C(SiMe$_3$)$_3$), 34.4 min (**10**), and 44 min ((**1**)$_2$).

*Benzyldimethylsilyl-bis(trimethylsilyl)methane (**8**, E = Si)*: colourless liquid. ^{1}H NMR (C$_6$D$_6$, iTMS) δ: –0.750 (s, Si$_3$CH), 0.078 (s; 2 SiMe$_2$), 0.148 (s; 2 SiMe$_3$), 2.17 (s; SiCH$_2$), 6.99–7.15 (m; *o*-/*p*-/*m*-CH of Ph). ^{13}C{^{1}H} NMR (C$_6$D$_6$, iTMS) δ: 0.645 (SiMe$_2$), 2.28 (Si$_3$C), 3.35 (2 SiMe$_3$), 28.76 (SiCH$_2$), 124.3/128.2/128.5/140.4 (*p*-/*o*-/*m*-/i-C of Ph). ^{29}Si NMR (C$_6$D$_6$, eTMS) δ: –0.15 (2 SiMe$_3$), 0.68 (SiMe$_2$). MS: *m*/*z* 308 (M$^+$).

*1-[1,1-Dimethyl-2,2-bis(trimethylsilyl)-1-silaethyl]-2-[2,2-dimethyl-3,3-bis(trimethylsilyl)-2-silapropyl]-benzene (**10**, E = Si)*: colourless solid, mp 96°C. ^{1}H NMR (C$_6$D$_6$, iTMS) δ: = –0.458 (s, Si$_3$CH), –0.041 (s, Si$_3$CH), 0.148 (s; 2 SiMe$_3$), 0.199 (s; 2 SiMe$_3$), 0.199 (s; SiMe$_2$), 0.521 (s; SiMe$_2$), 2.56 (s; SiCH$_2$), 7.06 (t; J = 7 Hz; 1 CH of Ph), 7.12 (d; J = 7 Hz; 1 CH of Ph), ? (1 CH of Ph; hidden by solvent), 7.50 (d; J = 7 Hz; 1 CH of Ph). ^{1}H NMR (d_6-acetone, iTMS) δ: –0.410 (s, Si$_3$CH), –0.105 (s, Si$_3$CH), 0.064 (s; 2 SiMe$_3$), 0.179 (s; 2 SiMe$_3$), 0.105 (s; SiMe$_2$), 0.450 (s; SiMe$_2$), 2.44 (s; SiCH$_2$), 7.04 (t; J = 7 Hz; 1 CH of Ph), 7.09 (d; J = 7 Hz; 1 CH of Ph), 7.21 (t; J = 7 Hz; 1 CH of Ph), 7.42 (d; J = 7 Hz; 1 CH of Ph). ^{13}C{^{1}H} NMR (CDCl$_3$, iTMS) δ: 1.71 (SiMe$_2$), 3.25 (SiMe$_2$), 3.44 (2 SiMe$_3$), 3.61 (2 SiMe$_3$), 3.18 (Si$_3$C), 4.58 (Si$_3$C), 29.53 (SiCH$_2$), 123.4/128.5/128.5/135.2 (=CH of Ph), 139.3/146.4 (=C< of Ph). ^{29}Si NMR (C$_6$D$_6$, eTMS) δ: –4.79 (SiMe$_2$), 0.15 (2 SiMe$_3$), 0.69 (2 SiMe$_3$), 1.84 (SiMe$_2$). MS: *m*/*z* 509 (M$^+$ – CH$_3$).

© 2000 NRC Canada

Table 5. Summary of crystal data collections for **1a, 2a**, and **3a**.

	1a	**2a**	**3a**
Empirical formula	$C_{23}H_{34}Si_3$	$C_{23}H_{34}GeSi_2$	$C_{23}H_{34}SnSi_2$
Formula weight (g mol^{-1})	394.77	439.27	483.36
Temperature (K)	293(2)	293(2)	293(2)
Wavelength (Å), (MoKα)	0.71073	0.71073	0.71069
Crystal system	monoclinic	triclinic	monoclinic
Space group	*Cc*	*P*-1	*P*21/*n*
a (Å)	11.752(2)	9.5615(8)	16.621(2)
b (Å)	14.575(2)	15.430(2)	9.6809(14)
c (Å)	13.6361(13)	25.350(4)	30.447(6)
α (°)	90.000(10)	89.063(14)	90.000(14)
β (°)	93.585(11)	81.005(14)	101.979(13)
γ (°)	90.000(14)	73.980(11)	90.000(12)
Volume (Å^3)	2331.0(6)	3549.2(9)	4792.3(13)
Z	4	6	8
Density (calculated) (Mg/m^3)	1.125	1.233	1.340
Absorption coefficient (mm^{-1})	0.209	1.401	1.171
F (000)	856	1392	1984
Crystal size (mm)	0.53 × 0.43 × 0.13	0.53 × 0.47 × 0.20	0.53 × 0.37 × 0.27
Theta range for data collection (°)	2.23 to 25.01	2.16 to 23.97	2.45 to 24.97
Index ranges	$-13 \le h \le 13$, $-17 \le k \le 0$, $-16 \le l \le 16$	$-10 \le h \le 10$, $-17 \le k \le 0$, $-28 \le l \le 28$	$-19 \le h \le 0$, $-11 \le k \le 0$, $-35 \le l \le 36$
Reflections collected	6225	11551	8717
Independent reflections	4092	11078	8402
Max. and min. transmission	0.9993 and 0.9474	0.9945 and 0.7262	0.9987 and 0.9525
Data / restraints / parameters	4092 / 2 / 243	11078 / 0 / 727	8402 / 6 / 485
Goodness-of-fit on F^2	1.064	1.103	1.113
$R1$ ($I > 2\sigma(I)$)	0.0353	0.0535	0.0345
$wR2$	0.0882	0.1148	0.0818
Largest diff. peak and hole (e/Å^3)	0.193 and –0.180	0.862 and –0.665	0.718 and –0.636

Thermolysis of 2a in toluene

A solution of 0.026 g (0.06 mmol) **2a** in 0.75 mL toluene was heated at 130°C for 44 d in a sealed, evacuated NMR tube. The ^{1}H NMR spectrum indicated complete conversion to (**2**)$_2$ (12%), **8** (49%), and **10** (39%). After removal of volatile constituents, the residue was treated with 1.0 mL *t*BuOMe – 0.5 mL MeOH and separation was done by HPLC using MeOH as mobile phase. Retention times: 10.1 min (**8**), 34.2 min (**10**), and 41.0 min ((**2**)$_2$).

*Benzyldimethylgermyl-bis(trimethylsilyl)methane (**8**, E = Ge)*: colourless liquid. ^{1}H NMR (C_6D_6, iTMS) δ: –0.659 (s, Si_2CH), 0.137 (s; 2 $SiMe_3$), 0.185 (s; $GeMe_2$), 2.30 (s; $GeCH_2$), 6.99–7.15 (m; *o*-/*p*-/*m*-CH of Ph). – ^{13}C{^{1}H} NMR ($CDCl_3$, iTMS) δ: 0.244 ($GeMe_2$), 2.80 ($GeSi_2C$), 3.15 (2 $SiMe_3$), 28.52 ($GeCH_2$), 123.9/127.9/128.1/141.0 (*p*-/*o*-/*m*-/i-C of Ph). ^{29}Si NMR (C_6D_6, eTMS) δ: 0.53 (2 $SiMe_3$). MS: *m*/*z* 339 ($M^+ - CH_3$).

*1-[1,1-Dimethyl-2,2-bis(trimethylsilyl)-1-germaethyl]-2-[2,2-dimethyl-3,3-bis(trimethylsilyl)-2-germapropyl]-benzene (**10**, E =Ge)*: colourless solid. ^{1}H NMR (C_6D_6, iTMS) δ: –0.374 (s, Si_2CH), –0.037 (s, Si_2CH), 0.142 (s; 2 $SiMe_3$), 0.182 (s; 2 $SiMe_3$), 0.287 (s; $GeMe_2$), 0.620 (s; $GeMe_2$), 2.64 (s; $GeCH_2$), 7.04 (t; *J* = 7 Hz; 1 CH of Ph), 7.07 (d; *J* = 7 Hz; 1 CH of Ph), ? (1 CH of Ph; hidden by solvent), 7.44 (d; *J* = 7 Hz; 1 CH of Ph). ^{1}H NMR (d_6-acetone, iTMS) δ: –0.326 (s, Si_2CH), –0.090 (s, Si_2CH), 0.055 (s; 2 $SiMe_3$), 0.152 (s; 2 $SiMe_3$), 0.211 (s; $GeMe_2$), 0.560 (s; $GeMe_2$), 2.53 (s; $GeCH_2$), 7.04 (t; *J* = 7 Hz; 1 CH of Ph), 7.06 (d; *J* = 7 Hz; 1 CH of Ph), 7.20 (t; *J* = 7 Hz; 1 CH of Ph), 7.37 (d; *J* = 7 Hz; 1 CH of Ph). ^{13}C{^{1}H} NMR (C_6D_6, iTMS) δ: 1.23 ($GeMe_2$), 2.89 ($GeMe_2$), 3.15 (2 $SiMe_3$), 3.19 (2 $SiMe_3$), 3.50 ($GeSi_2C$), 4.41 ($GeSi_2C$), 30.30 ($GeCH_2$), 124.1/128.4/128.5/134.3 (=CH of Ph), 141.1/146.0 (=C< of Ph). ^{29}Si NMR (C_6D_6, eTMS) δ: 0.76 (2 $SiMe_3$), 1.28 (2 $SiMe_3$). MS: *m*/*z* 509 ($M^+ - SiMe_3 - 2CH_4 - H_2$).

Thermolysis of 3a in toluene

A solution of 0.097 g (0.200 mmol) **3a** in 2.5 mL toluene was heated at 130°C for 26 h in a sealed, evacuated NMR tube. The ^{1}H NMR spectrum indicated complete conversion to (**3**)$_2$ (83%), **8** (13%), and **10** (4%). After removal of volatile constituents, the residue was treated with 1.0 mL *t*BuOMe/0.5 mL MeOH, and separation was done by HPLC using MeOH as mobile phase. Retention times: 10.7 min (**8**), 36.6 min ((**3**)$_2$), and 40.4 min (**10**).

*Benzyldimethylstannyl-bis(trimethylsilyl)methane (**8**, E = Sn)*: colourless liquid. ^{1}H NMR (C_6D_6, iTMS) δ: –0.672 (s, Si_2CH), 0.108 (s; 2 $SiMe_3$), 0.289 (s; $SnMe_2$), 2.35 (s; $SnCH_2$), 6.99–7.29 (m; *o*-/*p*-/*m*-CH of Ph). ^{13}C{^{1}H} NMR ($CDCl_3$, iTMS) δ: –6.85 ($SnMe_2$), 0.13 ($SnSi_2C$), 3.27 (2 $SiMe_3$), 23.19

© 2000 NRC Canada

($SnCH_2$), 123.4/127.0/128.4/142.7 (*p*-/*o*-/*m*-/i-C of Ph). ^{29}Si NMR (C_6D_6, eTMS) δ: 0.33 (2 $SiMe_3$). ^{119}Sn NMR (C_6D_6, eTMS) δ: 8.00 ($SnMe_2$). MS: *m*/*z* 385 ($M^+ - CH_3$).

*1-[1,1-Dimethyl-2,2-bis(trimethylsilyl)-1-stannaethyl]-2-[2,2-dimethyl-3,3-bis(trimethylsilyl)-2-stannapropyl]-benzene (**10**, E = Sn)*: colourless solid. ^{1}H NMR (C_6D_6, iTMS) δ: –0.408 (s, Si_2CH), –0.197 (s, Si_2CH), 0.150 (s; 2 $SiMe_3$), 0.158 (s; 2 $SiMe_3$), 0.181 (s; $SnMe_2$), 0.507 (s; $SnMe_2$), 2.64 (s; $SnCH_2$), 7.02 (t; *J* = 7 Hz; 1 CH of Ph), 7.06 (d; *J* = 7 Hz; 1 CH of Ph), ? (1 CH of Ph; hidden by solvent), 7.46 (d; *J* = 7 Hz; 1 CH of Ph). ^{13}C{^{1}H} NMR ($CDCl_3$, iTMS) δ: –6.18 ($SnMe_2$), –4.47 ($SnMe_2$), 1.11 ($SnSi_2C$), 1.32 ($SnSi_2C$), 3.32 (4 $SiMe_3$), 22.76 ($SnCH_2$), 122.9/127.9/128.2/134.9 (=CH of Ph), 142.5/146.6 (=C< of Ph). ^{29}Si NMR (C_6D_6, eTMS) δ: 1.48 (2 $SiMe_3$), 1.88 (2 $SiMe_3$). ^{119}Sn NMR ($CDCl_3$, eTMS) δ: –28.58 ($SnMe_2$), 9.88 ($SnMe_2$). MS: *m*/*z* 603 ($M^+ - SiMe_3 - C_2H_6$).

Thermolysis of 8 in benzene

A solution of 0.022 g (0.07 mmol) **8** (E = Si) in 0.6 mL benzene was heated at 160°C for 5 d and at 170°C for 11 d. According to ^{1}H NMR spectrum no reaction (formation of **7**) occurred.

Thermolysis of 8 and 1·Ph_2C=$NSiMe_3$ in benzene

A solution of 0.008 g (0.026 mmol) **8** and 0.016 g (0.034 mmol) **1**·Ph_2C=$NSiMe_3$ in 0.6 mL C_6D_6 was heated at 130°C for 9 d. According to ^{1}H NMR spectrum no formation of **10** occurred.

Crystal structures of 1, 2 and 3

Single crystals were crystallized from benzene as colourless plates. For structure determinations a Nonius CAD4 diffractometer was used. All structures were solved by SHELXS86 and refined with SHELXL93. The non-hydrogen atoms were refined anisotropically. The H atoms were considered as a riding model. Crystallographic parameters and details of the data collection are summarized in Table 5.[6]

Acknowledgements

We are grateful to the Deutsche Forschungsgemeinschaft, Bonn, for the generous financial support.

References

1. N. Wiberg, G. Preiner, and O. Schieda. Chem. Ber. **114**, 2087, 3518 (1981); N. Wiberg, G. Preiner, O. Schieda, and G. Fischer. Chem. Ber. **114**, 3505 (1981).
2. N. Wiberg and Ch.-K. Kim. Chem. Ber. **119**, 2966, 2980 (1986).
3. N. Wiberg and S.-K. Vasisht. Angew. Chem. Int. Ed. Engl. **30**, 93 (1991).
4. N. Wiberg, T. Passler, S. Wagner, and K. Polborn. Unpublished.
5. N. Wiberg, K. Schurz, and G. Fischer. Chem. Ber. **119**, 3498 (1986) and **120**, 1605 (1987); N. Wiberg, G. Fischer, and S. Wagner. Chem. Ber. **124**, 769, 1981 (1991); N. Wiberg and S. Wagner. Z. Naturforsch. **51b**, 629, (1996).
6. N. Wiberg and S. Wagner. Z. Naturforsch. **51b**, 838 (1996).
7. N. Wiberg, S. Wagner, and S.-K. Vasisht. Chem. Eur. J. 2571 (1998).
8. N. Wiberg, G. Preiner, G. Wagner, H. Köpf, and G. Fischer. Z. Naturforsch. **42b**, 1055 (1987); N. Wiberg, G. Preiner, G. Wagner, and H. Köpf. Z. Naturforsch. **42b**, 1062 (1987).

[6] Crystallographic data for the structures reported in this paper have been deposited with the Cambridge Crystallographic Data Centre (CCDC 127654 for **1a**, 127655 for **2a**, and 127656 for **3a**). Copies of the data can be obtained, free of charge, on application to the Director, CCDC, 12 Union Road, Cambridge CB2 1EZ, U.K. (Fax: 44-1223-336033 or e-mail: deposit@ccdc.cam.ac.uk).

© 2000 NRC Canada

Alkoxides of *o*-silyl benzyl alcohols in cleavage reactions: approaches to benzyl and silyl anion equivalents

Paul F. Hudrlik, Jose O. Arango, Yousef M. Hijji, Cosmas O. Okoro, and Anne M. Hudrlik

Abstract: The alkoxides of *o*-silyl benzyl alcohols **4** undergo cleavage reactions under mild conditions allowing transfer of a benzyl or silyl group to an electrophile. Reactions **3a** → **8**, and **3c** or **4c** → **11** illustrate their potential as benzyl and silyl anion equivalents.

Key words: silyl migration, benzyl anion equivalent, silyl anion equivalent, β-silyl ketone, γ-hydroxysilane.

Résumé : Les alcoolates d'alcools benzyliques *o*-silylés (**4**) subissent des réactions de clivage dans des conditions douces qui permettent d'effectuer le transfert d'un groupe benzyle ou silyle vers un électrophile. Les réactions **3a** → **8** et **3c** ou **4c** → **11** illustrent leur potentiel comme équivalents des anions respectivement benzyle et silyle.

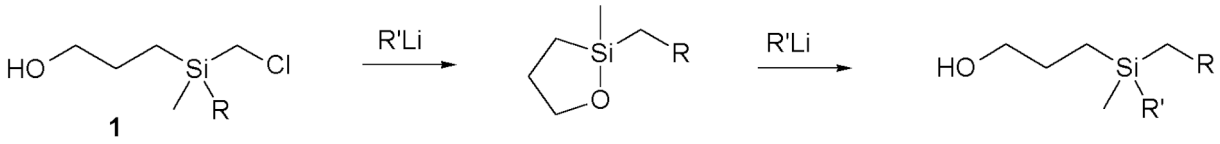
Mots clés : migration d'un silyle, équivalent de l'anion benzyle, équivalent de l'anion silyle, β-silylcétone, γ-hydroxysilane.

Introduction

Reactions involving nucleophilic attack at silicon have been used in organic synthesis for the removal of protecting groups (1), for the formation of multiple bonds (elimination reactions) (2), and for the generation of anionic intermediates (3). We have been interested in the use of intramolecular nucleophilic attack for some of these reactions. Organosilicon compounds with a protected internal nucleophile could, in principle, be carried through a synthetic sequence, and later activated (deprotected) to form a more readily cleaved silicon group.

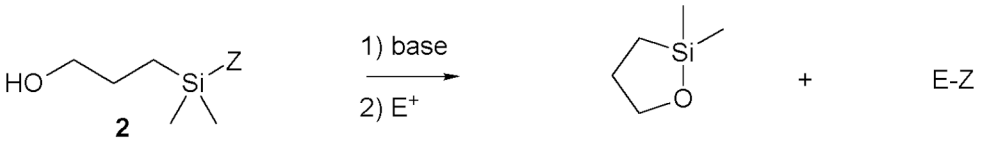
We have previously found that the γ-oxidopropyl group on silicon is effective as an internal nucleophile. We have reported the use of γ-hydroxysilanes **1** in rearrangement reactions (eq. [1]) (4*a*), and of γ-hydroxysilanes **2a**,**b** in cleavage reactions (for generation of benzyl and allyl anion equivalents) (eq. [2]) (4*b*).

[1]



1: R = Ph, Me, 2-furyl, allyl

[2]



2a: Z = CH_2Ph; **2b**: Z = $CH_2CH{=}CH_2$; **2c**: Z = $SiMe_3$

Received July 5, 1999. Published on the NRC Research Press website on October 25, 2000.

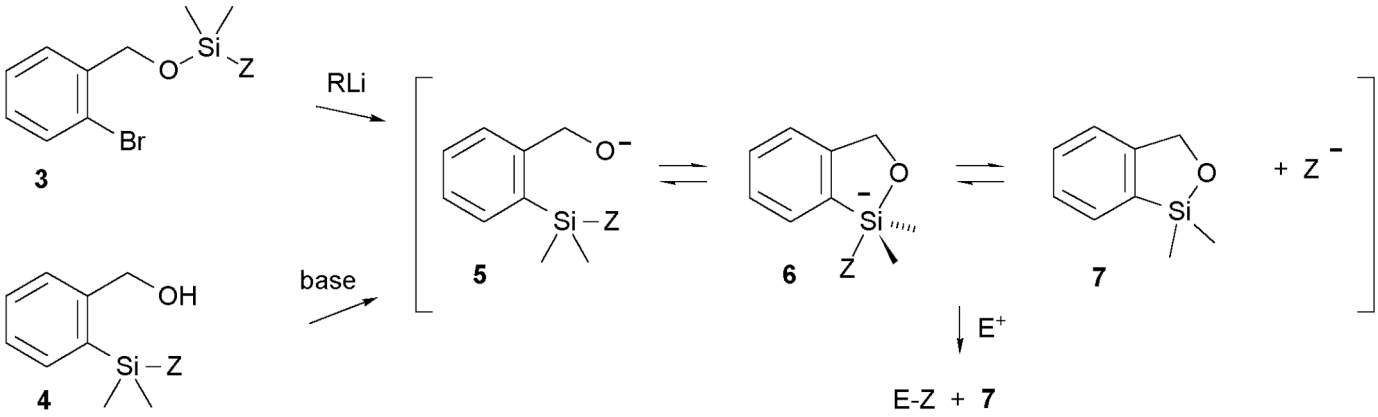
Dedicated to Professor Adrian Brook in recognition of his outstanding contributions to organosilicon chemistry.

P.F. Hudrlik,[1] **J.O. Arango, C.O. Okoro, and A.M. Hudrlik.** Department of Chemistry, Howard University, Washington, DC 20059, U.S.A.
Y.M. Hijji. Department of Chemistry, Morgan State University, Baltimore, MD 21251, U.S.A.

[1]Author to whom correspondence may be addressed. Telephone: (202) 806-4245. Fax: (202) 806-5442.
e-mail: phudrlik@fac.howard.edu

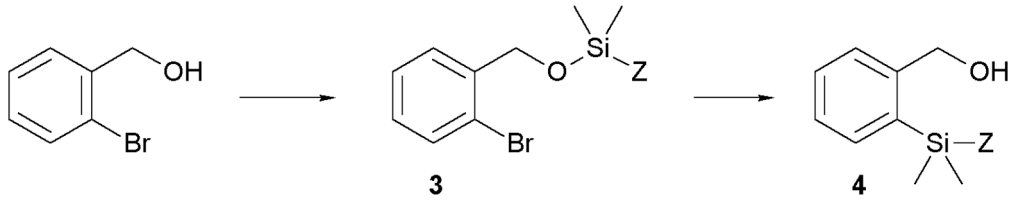
© 2000 NRC Canada

Scheme 1.



a: Z = CH_2Ph; **b**: Z = CH_2-CH=CH_2; **c**: Z = $SiMe_3$

[3]



a: Z = CH_2Ph; **b**: Z = $CH_2CH=CH_2$; **c**: Z = $SiMe_3$; **d**: Z = Me

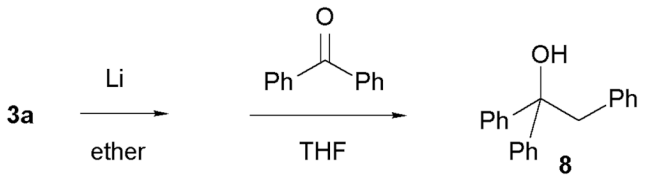
We felt that the use of a more rigid *ortho*-substituted aromatic ring in a γ-hydroxysilane such as **4** should facilitate the cleavage reactions. We report that this appears to be the case, and that these reactions can be used for the generation of benzyl and silyl anion equivalents.

Results and discussion

o-Silyl benzyl alcohol **4a** was prepared from *o*-bromobenzyl alcohol by treatment with $PhCH_2SiMe_2Cl$ and triethylamine (to give silyl ether **3a** in 87% yield) followed by treatment of **3a** with lithium wire in ether to give **4a** (92%) (5). Lithium alkoxide **5a** (Scheme 1), a presumed intermediate in the rearrangement of **3a** to **4a**, appears to be relatively stable in ether, but undergoes a facile cleavage reaction in the presence of THF. Treatment of benzyl silyl ether **3a** with *n*-BuLi in ether at room temperature resulted in disappearance of **3a** after 1.5 h, with appearance of alcohol **4a** (analysis of aliquots (with aqueous workup) by GC). Addition of THF to the reaction mixture resulted in almost complete disappearance of **4a** within 1 h with the appearance (after aqueous workup) of toluene and a product assigned as oxasilacyclopentane **7** by the mass spectrum [*m*/*z* 164 (18%, M^+), 149 (100%, M^+ – Me)]. By contrast, treatment of the acyclic analog **2a** with *n*-BuLi–THF resulted in no reaction in 1 day (although cleavage of the benzyl group was observed under more polar conditions, e.g., KH–ether or NaH–THF) (4*b*).

A mechanistic rationale appears in Scheme 1. Treatment of **3** with RLi or of **4** with base should lead to alkoxide **5**. Lithium alkoxide **5a** appears to be stable in ether, although in the presence of THF it yields oxasilacyclopentane **7**, most likely via pentacoordinate intermediate **6**. In the case of **3a**, presumably an anionic intermediate such as **6** or Z^- was trapped with water to form toluene, and could in principle be trapped with a number of electrophiles, allowing **3** and **4** to be used to generate anion equivalents.

We were able to demonstrate that the **3a**–**4a** system can serve as a benzyl anion equivalent by treating silyl ether **3a** with Li in ether (2 h) followed by benzophenone in THF (12 h, room temperature). Benzyldiphenylcarbinol (**8**) was isolated in 57% yield after chromatography (not optimized). In contrast, the analogous reaction with the acyclic γ-hydroxysilane **2a** required the use of a more polar solvent (HMPA) (4*b*).



Evidence for the intermediacy of oxasilacyclopentane **7** in the cleavage reactions was obtained by trapping with MeLi. Treatment of γ-hydroxysilane **4c** (5) with KH–THF–0°C fol-

© 2000 NRC Canada

lowed by excess MeLi–ether (15 h, room temperature) gave γ-hydroxysilane **4d** (5, 7) in 82% yield. Initial attempts to isolate and more fully characterize oxasilacyclopentane **7** led to samples which appeared pure by GC and GC/MS, but had sizeable OH signals in the IR, suggesting the oxasilacyclopentane might be forming a dihydroxy compound during workup or partially forming oligomers.

To isolate oxasilacyclopentane **7**, we decided to use γ-hydroxy(allyl)silane **4b** (5) as a substrate because the expected by-product, propene, would be volatile. Compound **4b** was prepared by treatment of silyl ether **3b** with Li–Et_2O (5). Treatment of **4b** with KH in ether (1 h, room temperature), followed by removal of solvent under vacuum (no aqueous workup) and bulb-to-bulb distillation (room temperature, oil pump vacuum) gave a product with an ^{1}H NMR spectrum expected for **7** (singlets at δ 0.40 and 5.15, and a multiplet at 7.2–7.6 in a ratio of 6:2:4), but with an IR spectrum having a rather large OH (3438 cm^{-1}). Because we felt the allylmetallic species generated in this reaction might be causing oligomerization of oxasilacyclopentane **7**, we added 1,2-dibromoethane as a trapping agent. Treatment of **4b** with *t*-BuLi (1.1 equiv) in THF (0°C, 1.5 h) followed by 1,2-dibromoethane (removal of cold bath, 30 min) followed by removal of solvent (no aqueous workup) and distillation gave a sample of **7** having an IR spectrum which did not have the OH peak. The ^{1}H NMR spectrum was essentially identical to that above, except for considerable amounts of dibromoethane (as well as small amounts of ether and THF); the GC showed two major peaks corresponding to dibromoethane (26%) and oxasilacyclopentane **7** (70%).

We were especially interested to study the possibility of using these reactions to generate silyl anion equivalents. Silylmetallic reagents (8) such as trimethylsilyllithium and phenyldimethylsilyllithium have found considerable use in synthesis, but existing methods for the preparation of silylmetallic reagents have disadvantages. Trimethylsilyllithium is most often prepared from the reaction of hexamethyldisilane with MeLi in HMPA (9), which is highly polar, nonvolatile, and a suspected carcinogen. Trimethylsilyllithium can also be made from silylmercury compounds which are undoubtedly highly toxic. Phenyldimethylsilyllithium is easily prepared by the reaction of the disilane (or the silyl chloride) with lithium, but this type of reaction cannot be used for tri*alkyl*silylmetallic reagents (8), and has been found to fail with a number of substituted aryldimethylsilyl groups (10). We are interested in developing general methods to generate trimethylsilyl- and other silylmetallic reagents in solvents which are not highly polar, nonvolatile, or toxic.

Compounds **2c**, **3c**, and **4c** were prepared as potential substrates for generation of silyl anion equivalents. Alcohol **2c** was prepared from $Me_3SiSi(Me_2)F$ by treatment with allylmagnesium bromide (54% yield) followed by hydroboration-oxidation of the product (64% yield). Silyl ether **3c** was prepared from *o*-bromobenzyl alcohol by treatment with $Me_3SiSi(Me)_2Cl$ and triethylamine in 92% yield.

Alcohol **4c** was prepared via rearrangement of **3c** (eq. [3]) with lithium or magnesium followed by aqueous workup. This transformation was studied with several different conditions, and the yields have been improved over those reported (5). Use of magnesium turnings in ether–THF gave good (72%) yields of **4c**, but the Grignard reaction was hard to initiate and keep going. Use of activated (Rieke) magnesium (11) in THF (room temperature) resulted in a facile reaction to give 89% crude yield of a product which appeared to be pure **4c**. Use of lithium wire (containing 1% sodium) in ether (0°C → room temperature) resulted in 78–92% yields of **4c**. In preliminary experiments, lithium powder (~0.5% Na) was also found to give **4c** in a similar manner.

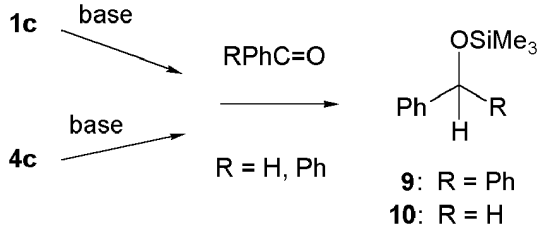
The lithium wire procedure was convenient, and was the procedure we used to prepare alcohol **4c**. In all cases, the progress of the reaction was followed by GC or GC/MS of aliquots before aqueous workup of the entire reaction. The pentamethyldisilyl ether of benzyl alcohol (hydrolysis product of the intermediate from the metal-exchange reaction) could be seen in small amounts in some of the early aliquots from the reactions with lithium wire, and in larger amounts in early aliquots from the reactions with magnesium and activated magnesium.

Relative reactivities of the γ-hydroxysilanes were studied in reactions which were followed by GC and GC/MS of aliquots using an internal hydrocarbon standard (with aqueous workup). γ-Hydroxysilane **4c** was considerably more reactive to cleavage than the acyclic analog **2c** (and **2c** was less reactive than the corresponding benzyl compound **2a**). For example, with NaH in THF at room temperature, reaction of **4c** was complete by 30 min, while reaction of **2c** was complete by 4 h (and reaction of **2a** by 30 min (4*b*)). With KH in Et_2O at room temperature, cleavage reactions of **2a** and **4c** were complete within 3–5 min, and that of **2c** was mostly complete by 90 min.

As mentioned above, the lithium alkoxide of **4a** (generated from **3a**) appeared to be stable in ether, but disappeared within an hour upon the addition of THF. The lithium alkoxide of **4c** was more stable; 70% of alcohol **4c** remained one hour after treatment of **4c** with MeLi in THF. Treatment of alcohol **2c** with MeLi–THF for 22 h resulted in no reaction (after workup).

To study the possible utility of these substrates as silyl anion equivalents, alcohols **2c** and **4c** were treated with base and bromo silyl ether **3c** was treated with lithium wire to generate the corresponding alkoxides (**5** in the case of **3c** and **4c**), and then they were treated with electrophiles, sometimes in a more polar solvent.

Compounds **2c** and **4c** were each treated with base followed by Ph_2C=O or PhCHO. The products were the Me_3Si ethers of benzhydrol (**9**) and of benzyl alcohol (**10**), respectively, presumably from trapping of the Me_3Si group followed by Brook (12) rearrangement. Benzhydrol and benzyl alcohol were also present in the product mixtures, presumably from hydrolysis of the silyl ethers.

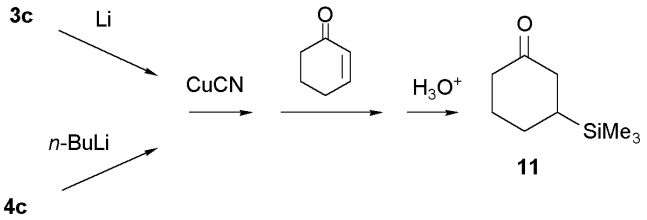


© 2000 NRC Canada

For example, treatment of alcohol **4c** with KH–THF and benzaldehyde (mixed at 0°C, then room temperature, 1 h) gave a mixture of silyl ether **10**, benzyl alcohol, and oxasilacyclopentane **7** in GC area ratios of 13%, 33%, and 47%, respectively. Silyl ether **10** (13) was isolated by chromatography in 39% yield. Treatment of **4c** with KH–THF followed by benzophenone similarly gave a mixture containing silyl ether **9**. Use of MeLi–THF followed by benzophenone in THF–HMPA (mixed at 0°C, then room temperature, 15 h) gave a similar mixture from which silyl ether **9** (13) was isolated in 35% yield.

When silyl ether **3c** was treated with lithium wire in ether followed by benzyl bromide in THF, and when alcohol **4c** was treated with *n*-BuLi followed by benzyl bromide or chloride in THF, little or no benzyltrimethylsilane was formed. However, when **4c** in THF was treated with MeLi followed by benzyl bromide in THF–HMPA (0°C, 1 h; room temperature, 14 h), benzyltrimethylsilane was formed, along with comparable amounts of oxasilacyclopentane **7** and benzyl bromide, and small amounts of bibenzyl.

The generation of anionic intermediates for a conjugate addition reaction was studied using both silyl ether **3c** and alcohol **4c**. As mentioned above, silyl ether **3c** could be converted to alcohol **4c** (or alkoxide **5c**) with either lithium or magnesium. Since both copper and zinc reagents are known to promote conjugate addition reactions (14), we have studied several combinations of these reagents with **3c** and 2-cyclohexenone to try to effect conjugate addition to form 3-trimethylsilylcyclohexanone (**11**). β-Silyl ketones such as **11** are of interest (for a recent method for preparing β-silyl ketones via silylcopper reagents see ref. 15) because of the directing effect of the silyl group on reactions such as the Baeyer–Villiger reaction (16), the Beckman fragmentation reaction (9*b*, 17), and alkylation reactions (18).



Reactions of silyl ether **3c** with lithium, CuCN, and cyclohexenone gave moderate yields of silyl ketone **11**. The corresponding reactions with activated magnesium instead of lithium gave no evidence for the formation of **11**. The reactions of **3c** with lithium, Et_2Zn, and cyclohexenone gave small amounts of silyl ketone **11** in two reactions. In most cases (Mg–CuCN and Li–Et_2Zn reactions) alcohol **4c** and oxasilacyclopentane **7** were major products.

The best procedure of those we tried used lithium wire and CuCN. An ice-cooled solution of **3c** in ether was treated with lithium wire until conversion to alkoxide **5c** was complete (from GC or GC/MS analysis of aliquots); the resulting solution was cannulated away from the unreacted lithium into a flask containing about 0.5 equiv of CuCN and ether or THF. Cyclohexenone in THF was added at low temperature (–90 to –75°C), and the solution was allowed to gradually warm to room temperature. The progress of the reaction was followed by analysis of aliquots. Two major products were seen in the GC and GC/MS, oxasilacyclopentane **7** and silyl ketone **11**. Silyl ketone **11** was generally not observed at low temperatures, but began to appear above 0°C. Two reactions were run in the presence of tridecane as an internal standard, and in two other reactions tridecane was added to a portion of the crude product. The yields of silyl ketone **11** at completion were determined by GC to be 61–65%.

Following the progress of the reaction by aliquots appeared to be important. In one case the reaction time (3–4 days) was longer than the others (~1 day), and a reaction in which 1.2 equiv of CuCN was used was faster (~7 h), but the GC yields at completion were all about the same.

The use of alcohol **4c** as a precursor to silyl ketone **11** was also investigated. Reactions of **4c** with *n*-BuLi followed by cyclohexenone were carried out using CuCN and Et_2Zn. The use of CuCN gave good yields of silyl ketone **11**. (An attempt to improve the reaction using Me_3SiCl as an additive (19) led to the trimethylsilyl ether of alcohol **4c**.) The use of Et_2Zn instead of CuCN resulted in mostly recovered **4c**; in one reaction silyl ketone **11** was formed in 14% yield by GC.

The role of copper in these reactions was demonstrated by the reaction of **4c** with *n*-BuLi in ether followed by cyclohexenone in THF. The major product was oxasilacyclopentane **7**; there was no evidence for silyl ketone **11**, the 1,2-addition product (1-trimethylsilyl-2-cyclohexenol (20)), or its Brook rearrangement product, the trimethylsilyl ether (21) of 2-cyclohexenol.

In the best procedure, the reactions were run in a very similar manner to those with silyl ether **3c** and lithium wire followed by CuCN: An ice-cooled ether solution of alcohol **4c** was treated with *n*-BuLi, 0.5–0.6 equiv of CuCN, cooled to about –78°C, then cyclohexenone in THF was added. The mixture was gradually warmed to room temperature following the reaction by GC and (or) GC/MS of aliquots. GC and GC/MS showed only oxasilacyclopentane **7** and silyl ketone **11** as major products. In one reaction, the crude product was purified by chromatography, yielding silyl ketone **11** in 50% yield. In another reaction, tridecane was added as an internal standard, and GC yields were determined. As in the case with the reactions of silyl ether **3c** with lithium wire and CuCN, silyl ketone **11** did not begin to appear in the aliquots until the reaction temperature rose above 0°C (e.g., 11% yield of **11** at 14°C, 8.75 h after addition of cyclohexenone). At reaction completion, the GC yield of silyl ketone **11** was 73%.

In summary, we have found that easily available *o*-silyl benzyl alcohols **4** and their precursor silyl ethers **3** can be used to generate alkoxides **5** which undergo facile cleavage reactions. Alcohols **4** and silyl ethers **3** are therefore of potential use for the generation of anionic intermediates.

Experimental section

General procedures

All reactions were carried out under a nitrogen or argon atmosphere, and liquids were transferred with nitrogen- or argon-flushed syringes. The verb "concentrated" refers to removal of the solvent by a rotary evaporator. Column chromatography was carried out as flash chromatography (22)

© 2000 NRC Canada

using 200–425 mesh silica gel. Nuclear magnetic resonance (NMR) spectra were obtained in $CDCl_3$ (^1H at 300 MHz and ^{13}C at 75 MHz) and chemical shifts are reported in δ using $CHCl_3$ (δ 7.26) for ^1H NMR, and $CDCl_3$ (δ 77.00) for ^{13}C NMR as internal standard. Methylene chloride (δ 5.32) was used as an internal standard for ^1H NMR for compounds containing aromatic hydrogens. Gas chromatography (GC) analyses were carried out with a flame ionization detector and using helium as the carrier gas using a Shimadzu GC-14A instrument with a 15 m × 0.32 mm × 25 μm cross-linked methyl silicone gum capillary column, and the following temperature program: 50°C (5 min), 10°C/min to 230°C (15 min) unless otherwise noted. Most reactions were followed by GC or GC/MS of aliquots (using the aqueous workup of the reaction). GC yields were determined using tridecane calibrated with an authentic sample (9) of 3-trimethylsilylcyclohexanone (**11**). In a few cases where noted, GC analyses were carried out with a Hewlett-Packard HP 5880 instrument with 12.5 and 25 m cross-linked polymethyldisiloxane capillary columns and the following temperature program: 50°C (1 min), 10°C/min to 250° (5 min).

Materials

Chloropentamethyldisilane was prepared by a procedure of Ishikawa et al. (23) and was purchased from Gelest. Anhydrous ether and tetrahydrofuran (THF) were distilled from sodium and benzophenone. Lithium wire contained 1% sodium. 2-Cyclohexenone was dried over magnesium sulfate and fractionally distilled under reduced pressure. Triethylamine was distilled from calcium hydride.

*3-Hydroxypropylpentamethyldisilane (**2c**)*

Allylpentamethyldisilane (24) was prepared from fluoropentamethyldisilane (25) and allylmagnesium bromide, and had IR, ^1H NMR, and mass spectra corresponding to those reported (24).

To an ice-cooled solution of 2.43 g (14 mmol) of allylpentamethyldisilane in 10 mL of THF was added 42 mL (42 mmol) of BH_3·THF (1.0 M in THF) dropwise. The ice bath was replaced with a water bath, and the mixture was stirred for 24 h. The mixture was recooled in ice, and the following additions were made: (1) 10 mL of H_2O, (2) 10 mL of 3 M NaOH, (3) 10 mL of 30% H_2O_2 (dropwise). The resulting mixture was heated at 50°C for 3 h, cooled to room temperature, and then 9.0 g of K_2CO_3 was added. The mixture was stirred an additional 5 min, then the layers were allowed to separate, and the aqueous layer was extracted with ether (2 × 10 mL), and the combined organic layers were washed with saturated $NaHCO_3$, dried ($MgSO_4$), concentrated, chromatographed (50 g of Florisil, ether:petroleum ether (3:7)), and Kugelrohr distilled (oven temperature 70°C, oil pump vacuum) to give 1.72 g (64%) of 3-hydroxypropylpentamethyldisilane (**2c**) (26): IR (film) 3340 (b), 2956, 1461, 1246 (m), 1069, 834 cm^{-1}; mass spectrum *m*/*z* (relative intensity, tentative assignment) 190 (M^+, not visible), 147 (5, $(Me_3SiOSiMe_2)^+$), 133 (20), 131 (20, $Me_3SiMe_2Si^+$), 117 (60, $Me_2Si^+CH_2CH_2CH_2OH$), 75 (100, $(Me_2SiOH)^+$). GC analysis (HP 5880, dodecane = 6.42 min) showed one peak at 6.13 min (100%). The ^1H NMR spectrum is the same as that reported (26).

*Reaction of silyl ether 3a with lithium and benzophenone: Formation of benzyldiphenylcarbinol (**8**)*

To a solution of 0.20 g (0.60 mmol) of silyl ether **3a** (5) in 5 mL of anhydrous ether was added 0.1 g (14 mmol) of lithium wire (flattened and washed with petroleum ether). The reaction was stirred at room temperature for 2 h (following the progress by GC analysis of an aliquot). Then 0.12 g (0.66 mmol) of benzophenone was added, and the reaction mixture was stirred at room temperature for 30 min (aliquots showed little or no reaction). Then 5 mL of THF was added, and the progress of the reaction was followed by aliquots taken after 5 min, 30 min, and 12 h. The reaction mixture was then added to saturated $NaHCO_3$ and extracted twice with ether. The organic layer was dried ($MgSO_4$), concentrated, and chromatographed on 20 g of silica gel using 8:2 pet ether:ether giving 0.094 g (57%) of benzyldiphenylcarbinol (**8**) as a white solid: mp 88–89°C (lit. (27) mp 89–90°C).

*o-Bromobenzyloxypentamethyldisilane (**3c**)*

A solution of 6.30 g (33.7 mmol) of *o*-bromobenzyl alcohol, 14 mL of triethylamine, and 110 mL of anhydrous ether was cooled in an ice bath, and 5.80 g (34.8 mmol) of pentamethylchlorodisilane in 15 mL of anhydrous ether was added dropwise. The mixture was stirred at room temperature for about 2 h, and then added to 170 mL of aqueous $NaHCO_3$ overlaid with 50 mL of ether. The organic layer was washed with water (4 × 30 mL), dried ($MgSO_4$), concentrated, and placed under oil pump vacuum (3 mm, 4 h). Chromatography on silica gel (26.7 × 4.4 cm) using petroleum ether gave 10.2 g (92%) of silyl ether **3c** (5): IR (neat) 3066, 2950, 2891, 1443, 1375, 1247, 1090, 1026, 837, 806, 749 cm^{-1}; ^1H NMR δ 0.17 (s, 9 H), 0.34 (s, 6 H), 4.76 (s, 2 H), 7.15 (crude t, *J* = 7 Hz, 1 H), 7.37 (crude t, *J* = 7 Hz, 1 H), 7.5–7.6 (m, 2 H); ^{13}C NMR (assignments by DEPT) δ –2.01 (CH_3), –0.75 (CH_3), 64.99 (CH_2), 121.08 (C), 127.23 (CH), 127.62 (CH), 128.15 (CH), 131.98 (CH), 140.12 (C). GC analysis showed one major peak at 15.3 min (100%). The mass spectrum was equivalent to that reported (5).

*o-Pentamethyldisilylbenzyl alcohol (**4c**)*

A solution of 10.77 g (33.9 mmol) of *o*-bromobenzyloxypentamethyldisilane (**3c**) in 130 mL of anhydrous ether was cooled in an ice bath. Lithium wire was wiped with paper towels to remove oil, weighed, placed between weighing papers, flattened with a hammer, and cut into small pieces. To the above solution 2.18 g (314 mmol) of the lithium was added. Typically, the reaction was stirred at ice temperature until the slurry turned from slightly turbid to light brown-yellow or until GC or GC/MS indicated the reaction had begun. Then the ice bath was removed, and the reaction was stirred at room temperature until GC and (or) GC/MS indicated the reaction was complete (and the reaction mixture had turned cloudy gray). In this case, the reaction was stirred at ice temperature 1.5 h after the addition of lithium, and 1 h after removal of the ice bath. The reaction mixture was transferred to a beaker, and the remaining lithium pieces were quickly removed. The mixture was then immediately poured into 120 mL of aqueous $NaHCO_3$ overlaid with 50 mL of ether. The organic layer was dried ($MgSO_4$), concentrated, placed under oil pump vacuum (0.75 mm,

© 2000 NRC Canada

2.5 h), and chromatographed on silica gel (35 × 4.4 cm) using petroleum ether:ether (1:0, 7:3, and then 1:1) giving 6.82 g (84%) of alcohol **4c**. The IR, ^{1}H NMR, ^{13}C NMR, and mass spectra were equivalent to those reported (5).

*Reaction of silyl ether **3c** with lithium, CuCN, and 2-cyclohexenone*: *Formation of 3-trimethylsilylcyclohexanone (**11**)*

A solution of 1.10 g (3.47 mmol) of silyl ether **3c** and 40 mL of anhydrous ether was cooled in an ice bath, and 0.22 g (31.7 mmol) of lithium wire (for handling, see the synthesis of **4c**) was added. The progress of the reaction was followed visually and by GC/MS as described for the synthesis of **4c**. In this case, the reaction was stirred in an ice bath for 35 min, and then the ice bath was removed and stirring was continued (total 2 h). The reaction mixture was transferred via cannula into an ice-cooled mixture of 0.20 g (2.23 mmol) of CuCN in 40 mL of THF. The resulting dark brown slurry was stirred for 35 min at ice temperature, and then cooled to –75°C. After 15 min, 0.6 mL (6.2 mmol) of cyclohexenone in 20 mL of THF was added dropwise. The slurry was kept at –80°C for 1 h, then allowed to warm up gradually to room temperature, and the progress of the reaction was monitored by GC/MS and GC analysis of aliquots. After 21 h, the mixture was added to 160 mL of aqueous NH_4Cl overlaid with 50 mL of ether. The organic layer was dried ($MgSO_4$) and concentrated. The GC analysis showed peaks at 7.91 min (59%, oxasilacyclopentane **7**), 9.35 min (29%, silyl ketone **11**), and 16.32 min (12%), and the GC/MS showed two peaks in the GC chromatogram having mass spectra corresponding to **7** (major) and **11**. The product was placed under oil pump vacuum (2.5 mm, 0.5 h) giving 1.65 g of a light brown crude product. The IR, ^{1}H NMR, and ^{13}C NMR were consistent with the presence of predominantly **7** and **11**. A portion of the product was mixed with tridecane in ether, and the GC yield of **11** was calculated to be 65%.

An analogous reaction was done in which the reaction mixture was cannulated into CuCN in ether rather than in THF. GC analysis of the crude product showed two major peaks at 7.99 min (57%, **7**) and 9.45 min (43%, **11**). The spectra were all consistent with predominantly **7** and **11**. A portion of the crude product was mixed with tridecane in ether, and the GC yield of silyl ketone **11** was calculated to be 62%.

A similar reaction was done in which the standard was present when the aliquots were taken (and 1.2 equiv of CuCN were used), and GC yields were calculated at various reaction times: 0.76 g (2.39 mmol) of silyl ether **3c** in 45 mL of anhydrous ether, 0.25 g (36 mmol) of lithium wire, 0°C for 2.5 h; mixture transferred via cannula into an ice-cooled mixture of 0.25 g (2.79 mmol) of CuCN, 0.074 g of tridecane, and 15 mL of anhydrous ether (0°C for 35 min), then cooled to –90°C for 20 min; cyclohexenone (0.55 mL, 5.68 mmol) in 35 mL of THF added, –80 to –85°C for about an hour, and then mixture warmed gradually to room temperature, monitoring progress of the reaction by GC and GC/MS of aliquots. GC yields are given in Table 1.

After 10.3 h, the reaction was quenched by adding it to aqueous NH_4Cl overlaid with ether, the organic layer was dried ($MgSO_4$), and the GC yield of **11** was determined to be 62%. After removal of solvent, the spectra (IR, ^{1}H NMR, ^{13}C NMR, GC/MS) were all consistent with the presence of oxasilacyclopentane **7**, silyl ketone **11**, and tridecane, and the GC analysis showed peaks at 7.93 min (31%, **7**), 9.38 min (16%, **11**), and 11.22 min (10%, tridecane).

Table 1. GC yields of aliquots.

Time (h)	Temp (°C)	% GC yield of **11**
1.1	–83	0
4.1	5	33.0
7.3	16	61.0
9.8	15	60.6

Table 2. GC yields of aliquots.

Time (h)	Temp (°C)	% GC yield of **11**
0.5	–80	0
3.5	–7	0
6.75	9	3.2
8.75	14	11.3
11.25	16	39.8
21.75	22	73.1

*Reaction of alcohol **4c** with n-BuLi, CuCN, and 2-cyclohexenone: Formation of 3-trimethylsilylcyclohexanone (**11**)*

A solution of 1.05 g (4.40 mmol) of alcohol **4c** in 100 mL of anhydrous ether was cooled in an ice bath and 3.9 mL (6.24 mmol) of *n*-butyllithium (1.6 M in hexane) was added. The reaction mixture was stirred and cooled in an ice bath for about 0.5 h at which time the slurry turned light yellow. Then 0.23 g (2.6 mmol) of CuCN was added, within 5 min 40 mL of THF was added, and the mixture was stirred at 0°C for 20 min. Then the slurry was cooled to –80°C, and after 35 min, a solution of 0.74 mL (7.64 mmol) of cyclohexenone in 80 mL of THF was added. The reaction mixture was allowed to warm up gradually, and the progress of the reaction was monitored by GC analysis and GC/MS of aliquots. The reaction mixture was quenched after 13 h by adding it to a mixture of 200 mL of aqueous NH_4Cl overlaid with 85 mL of ether, and the organic layer was dried ($MgSO_4$) and concentrated. GC analysis showed two major peaks at 6.17 min (55%, oxasilacyclopentane **7**) and 7.82 min (19%, silyl ketone **11**), and a number of small peaks from 10–25 min. The product was placed under oil pump vacuum (6–7 mm, 2 h). The spectra were consistent with the presence of **7** and **11**. The crude product was chromatographed on silica gel (24 × 2.9 cm). Elution with petroleum ether:ether (4:1) gave 0.372 g (50% yield) of silyl ketone **11** as a colorless liquid: ^{13}C NMR (assignments by APT) δ –3.90 (CH_3), 25.85 (CH_2), 27.82 (CH), 29.75 (CH_2), 41.77 (CH_2), 42.19 (CH_2), 212.41 (C=O); GC/MS *m*/*z* (relative intensity, tentative assignment) 170 (16, M^+), 169 (15), 155 (24, M^+ – Me), 127 (20), 75 (65), 73 (100, Me_3Si^+). The spectra were essentially identical to those of an authentic sample of silyl ketone **11** (9), and the IR and ^{1}H NMR were identical to those reported (15).

An analogous reaction was done in which the standard was present when the aliquots were taken, and GC yields

© 2000 NRC Canada

were calculated at various reaction times: 0.63 g (2.64 mmol) of alcohol **4c** in 45 mL of anhydrous ether and 0.135 g of tridecane, 1.7 mL (3.4 mmol) of *n*-butyllithium (2.0 M in cyclohexane) (0.5 h at 0°C), 0.135 g (1.5 mmol) of CuCN (30 min), cooled to –75°C for 15 min, dropwise addition of 0.45 mL (4.65 mmol) of cyclohexenone in 40 mL of THF, gradual warming to room temperature, monitoring the reaction by GC analysis of aliquots. GC yields are given in Table 2.

After 22.75 h the reaction was quenched by adding it to aqueous NH_4Cl overlaid with ether, the organic layer was dried ($MgSO_4$), and the GC yield of **11** was determined to be 73%. After removal of solvent, the spectra (IR, ^{1}H NMR, ^{13}C NMR, GC/MS) were all consistent with the presence of oxasilacyclopentane **7**, silyl ketone **11**, and tridecane.

Acknowledgements

Financial support from the National Science Foundation (CHE-9505465 and CHE-9007879) and NIGMS (SO6GM08016) is gratefully acknowledged.

References

1. Review: T.D. Nelson and R.D. Crouch. Synthesis, 1031 (1996).
2. Review: D.J. Ager. Org. React. (N.Y.) **38**, 1 (1990).
3. For example, see A.S. Pilcher and P. DeShong. J. Org. Chem. **61**, 6901 (1996).
4. (*a*) P.F. Hudrlik, Y.M. Abdallah, and A.M. Hudrlik. Tetrahedron Lett. **33**, 6743 (1992); see also ref. 6; (*b*) P.F. Hudrlik, Y.M. Abdallah, and A.M. Hudrlik. Tetrahedron Lett. **33**, 6747 (1992).
5. Y.M. Hijji, P.F. Hudrlik, C.O. Okoro, and A.M. Hudrlik. Synth. Commun. **27**, 4297 (1997).
6. Y.M. Hijji, P.F. Hudrlik, and A.M. Hudrlik. Chem. Commun. (Cambridge), 1213 (1998).
7. N. Meyer and D. Seebach. Chem. Ber. **113**, 1304 (1980).
8. For a review, see J. Belzner and U. Dehnert. *In* The chemistry of organic silicon compounds. Vol. 2. Part 1. *Edited by* Z. Rappoport and Y. Apeloig. Wiley, New York, N.Y. 1998. pp. 779–825.
9. (*a*) W.C. Still. J. Org. Chem. **41**, 3063 (1976); (*b*) P.F. Hudrlik, M.A. Waugh, and A.M. Hudrlik. J. Organomet. Chem. **271**, 69 (1984).
10. N. Abd. Rahman, I. Fleming, and A.B. Zwicky. J. Chem. Res. Synop. 292 (1992).
11. R.D. Rieke, S.E. Bales, P.M. Hudnall, T.P. Burns, and G.S. Poindexter. Org. Syn. Coll. Vol. VI, 845 (1988).
12. (*a*) A.G. Brook. Acc. Chem. Res. **7**, 77 (1974); (*b*) A.G. Brook and A.R. Bassindale. *In* Rearrangements in ground and excited states. Vol. 2. *Edited by* P. de Mayo. Academic Press, New York, 1980. pp. 149–227.
13. W. Gerrard and K.D. Kilburn. J. Chem. Soc. 1536 (1956).
14. (*a*) W. Tückmantel, K. Oshima, and H. Nozaki. Chem. Ber. **119**, 1581 (1986); (*b*) R.A.N.C. Crump, I. Fleming, and C. J. Urch. J. Chem. Soc. Perkin Trans. **1**, 701 (1994).
15. H. Ito, T. Ishizuka, J. Tateiwa, M. Sonoda, and A. Hosomi. J. Am. Chem. Soc. **120**, 11 196 (1998).
16. (*a*) P.F. Hudrlik, A.M. Hudrlik, G. Nagendrappa, T. Yimenu, E.T. Zellers, and E. Chin. J. Am. Chem. Soc. **102**, 6894 (1980). Correction: J. Am. Chem. Soc. **104**, 1157 (1982); (*b*) P.F. Hudrlik, A.M. Hudrlik, T. Yimenu, M.A. Waugh, and G. Nagendrappa. Tetrahedron, **44**, 3791 (1988); (*c*) T. Aida, M. Asaoka, S. Sonoda, and H. Takei. Heterocycles, **36**, 427 (1993).
17. H. Nishiyama, K. Sakuta, N. Osaka, H. Arai, M. Matsumoto, and K. Itoh. Tetrahedron, **44**, 2413 (1988).
18. R.A.N.C. Crump, I. Fleming, J.H.M. Hill, D. Parker, N.L. Reddy, and D. Waterson. J. Chem. Soc. Perkin Trans. **1**, 3277 (1992).
19. (*a*) B.H. Lipshutz, S.H. Dimock, and B. James. J. Am. Chem. Soc. **115**, 9283 (1993), and refs. therein; (*b*) S.H. Bertz, G. Miao, B.E. Rossiter, and J.P. Snyder. J. Am. Chem. Soc. **117**, 11 023 (1995).
20. (*a*) G. Altnau, L. Rösch, and G. Jas. Tetrahedron Lett. **24**, 45 (1983); (*b*) P.F. Hudrlik, L. Tafesse, and A.M. Hudrlik. J. Am. Chem. Soc. **119**, 11 689 (1997).
21. P.F. Hudrlik, C.-N. Wan, and G.P. Withers. Tetrahedron Lett. 1449 (1976).
22. W.C. Still, M. Kahn, and A. Mitra. J. Org. Chem. **43**, 2923 (1978).
23. M. Ishikawa, M. Kumada, and H. Sakurai. J. Organomet. Chem. **23**, 63 (1970).
24. (*a*) Yu.P. Egorov, G.G. Kirei, S.A. Samoilenko, E.A. Chernyshev, and N.G. Tolstikova. Bull. Acad. Sci. USSR Div. Chem. Sci. (Eng. Trans.) 515 (1963); (*b*) T.A. Dixon, K.P. Steele, and W.P. Weber. J. Organomet. Chem. **231,** 299 (1982).
25. M. Kumada, M. Yamaguchi, Y. Yamamoto, J. Nakajima, and K. Shiina. J. Org. Chem. **21**, 1264 (1956).
26. Y. Nakadaira, A. Sekiguchi, Y. Funada, and H. Sakurai. Chem. Lett. 327 (1991).
27. R.O.C. Norman and R.A. Watson. J. Chem. Soc. B, 692 (1968). See also ref. 4*b*.

© 2000 NRC Canada

The insertion of germylene into the H—H bond; rate constant limits and thermochemistry. Ab initio and DFT calculations on the reactions of GeH_2 and SiH_2 with H_2

Rosa Becerra, Sergey E. Boganov, Mikhail P. Egorov, Valery I. Faustov, Oleg M. Nefedov, and Robin Walsh

Abstract: The technique of laser flash photolysis in the gas-phase has been used to set limits on the rate constants for the bimolecular reaction of germylene (GeH_2) with deuterium (D_2) at both ambient and elevated temperatures (585 K). These limits show that the activation energy for the insertion of GeH_2 into the H—H bond is at least 19 (±6) kJ mol^{-1}. Thermochemical arguments place the activation energy approximately in the range 63–84 kJ mol^{-1}. DFT B3LYP/6–311++G(3df,2pd) and ab initio QCISD(T)/6–311G++(3df,2pd)//QCISD/6–311G(d,p) calculations have been carried out on the potential energy surfaces of reactions $ZH_2 + H_2 \rightarrow ZH_4$ (Z= Ge, Si). Both methods predict the same mechanisms for germylene and silylene insertion which include formation of loose prereaction complexes and transition states of similar structure. The prereaction complex is only about half as strong in the case of germylene (ΔH (298 K) = –9 (–11) kJ mol^{-1}) as in the case of silylene (ΔH (298 K) = –16 (–21) kJ mol^{-1}) (QCISD values cited with B3LYP values in parentheses). The differences in activation energies are even more significant. Germylene insertion has a very high barrier of 58 (56) kJ mol^{-1} compared to that of silylene 13 (6) kJ mol^{-1}. Calculated activation parameters for both reactions are in reasonable consistency with experimental results. Reasons for the enhanced H-H insertion barrier for germylene compared with silylene are discussed.

Key words: laser flash photolysis, germylene, silylene, deuterium, activation energy, thermochemistry, ab initio calculation, DFT B3LYP calculation.

Résumé : On a fait appel à la technique de la photolyse éclair au laser pour déterminer les limites des constantes de vitesse de la réaction bimoléculaire du germylène (GeH_2) avec le deutérium (D_2) à des températures tant ambiantes qu'élevées (585 K). Ces limites montrent que l'énergie d'activation pour l'insertion du GeH_2 dans la liaison H—H est d'au moins 19 ± 6 kJ mol^{-1}. Des arguments thermodynamiques suggèrent que la valeur de l'énergie d'activation est de l'ordre de 63 à 84 kJ mol^{-1}. On a effectué des calculs DFT B3LYP/6–311++G(3df,2pd) et des calculs ab initio QCISD(T)/6–311G ++(3df,2pd)//QCISD/6–311G(d,p) sur les surfaces d'énergie potentielle des réactions $ZH_2 + H_2 \rightarrow ZH_4$ (Z = Ge, Si). Les deux méthodes prédisent les mêmes mécanismes pour la réaction d'insertion du germylène et du silylène; ils comportent la formation de complexes préréactionnels lâches et des états de transition de structure similaire. La force du complexe préréactionnel du germylène est approximativement la moitié (ΔH (298 K) = –9 (–11) kJ mol^{-1}) que dans le cas du silylène (ΔH (298 K) = –16 (–21) kJ mol^{-1}) (dans lesquelles la valeur citée correspond à QCISD et la valeur entre parenthèses aux calculs B3LYP). Les différences dans les énergies d'activation sont plus significatives. La valeur de la barrière pour l'insertion du germylène est très élevée 58 (56) kJ mol^{-1} par comparaison avec celle du silylène 13 (6) kJ mol^{-1}. Les paramètres d'activation calculés pour les deux réactions sont en accord raisonnable avec les résultats expérimentaux. On discute des raisons de la barrière d'insertion H—H plus élevée pour le germylène par comparaison avec le silylène.

Mots clés : photolyse éclair au laser, germylène, silylène, deutérium, énergie d'activation, thermochimie, calculs ab initio, calculs DFT B3LYP.

[Traduit par la Rédaction]

Received July 5, 1999. Published on the NRC Research Press website on October 25, 2000.

This paper is dedicated to Adrian Brook in recognition of his special contribution to organosilicon chemistry

R. Becerra. Instituto de Quimica-Fisica "Rocasolano," C.S.I.C., C/Serrano 119, 28006 Madrid, Spain.
S.E. Boganov, M.P. Egorov, V.I. Faustov, and O.M. Nefedov. N.D. Zelinsky Institute of Organic Chemistry, Russian Academy of Sciences, Leninsky Prospekt 47, 117913 Moscow, Russian Federation.
R. Walsh.[1] Department of Chemistry, University of Reading, Whiteknights, P.O. Box 224, Reading RG6 6AD, U.K.

[1]Author to whom correspondence may be addressed. Telephone: +44 (0)118 931 6347. Fax: +44 (0)118 931 6331. e-mail: r.walsh@reading.ac.uk

 © 2000 NRC Canada

Introduction

Germylene(GeH_2) is thought to be an important intermediate in the chemical vapour deposition (CVD) of semiconductor germanium from GeH_4 (1, 2). It is certainly the key intermediate in the thermal decomposition of GeH_4 (3). Interest in this species has grown, not only because of its involvement in the materials formation process, but also because in recent years it has become accessible to direct monitoring by laser resonant absorption (4–7). Studies in our laboratories have shown that GeH_2 inserts into Ge—H bonds with a negative activation energy which is greater (i.e., more negative) for the Ge—H bond in Et_3GeH (5) than that in GeH_4 (6). In this respect the kinetic and mechanistic behaviour of GeH_2 parallels that of SiH_2 (8–10) which undergoes the equivalent Si—H bond insertion processes. However GeH_2 is less reactive than SiH_2 in its counterpart reactions and shows greater selectivity (alkyl substituents enhance the reactivity of Ge—H bonds to GeH_2 more than of Si—H bonds to SiH_2). This can be explained in terms of the involvement, and binding strengths, of the H bridged complexes formed as intermediates, whose relative stabilities have been calculated by ab initio methods (6).

The question naturally arises of the ability of GeH_2 to insert into the H—H bond, viz.

[1] $GeH_2 + H_2 \rightarrow GeH_4$

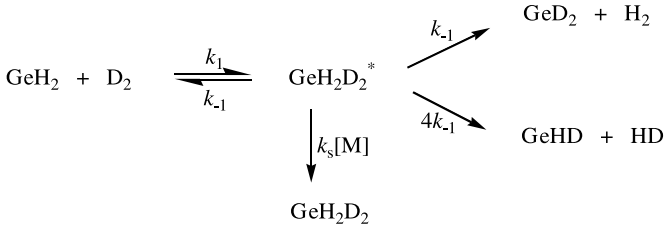
This is arguably the simplest insertion reaction of all and is potentially of great significance in CVD systems where H_2 is present. The kinetics of the silylene analogue of [1] were first investigated by Jasinski (11), viz.

[2] $SiH_2 + H_2 \rightarrow SiH_4$

This study made a dramatic impact. Not only was it amongst the earliest of absolute rate measurements for SiH_2, but the rate constant obtained (2.6×10^{-12} cm^3 $molecule^{-1}$ s^{-1} for $SiH_2 + D_2$) was more than 10^4 times greater than expected from earlier indirect experimental measurements (12) or available theoretical calculations (13–16). Thus, this paper caused a significant re-evaluation of the reactivity and thermochemistry of SiH_2.

At the present time there has been no reported (or attempted) measurement of the rate constant of rxn. [1] nor any published calculation of the energy barrier of reaction [1]. Thus unlike for rxn. [2] there is no prior history. The reaction is however ripe for investigation. It is an important point to note that we have chosen to study the deuterium variant of [1], following the logic of Jasinski (11) who studied the deuterium version of [2] (viz. $SiH_2 + D_2$). The reason for this is straightforward; it is to avoid the potential complications arising from studying a third-body assisted association process at pressures below the high-pressure (true bimolecular) limit. The reaction of GeH_2 with D_2 can be described by the mechanism shown in Scheme 1. In this reaction the initial insertion product is vibrationally excited $GeH_2D_2^*$. This species can then either be collisionally stabilized by the third body, or decompose unimolecularly by one of the three pathways shown. Of these three pathways, assuming there are no unexpectedly large isotope effects, reversion to $GeH_2 + D_2$ is only one, and indeed on probability grounds represents only one in six of the possible decomposition channels for $GeH_2D_2^*$. Thus the monitoring of the disappearance of GeH_2 (with its unique isotopic absorption signature) should correspond, to a good approximation, to the rate constant k_1 for the true bimolecular process.

Scheme 1.



We have also carried out ab initio QCISD and DFT B3LYP calculations on the potential energy surfaces of both rxns. [1] and [2]. Silylene insertion [2] was naturally chosen as a reference reaction, not only because of the intrinsic interest in comparing Ge with Si, but also because there is a wealth of experimental (8, 9) and theoretical data (13–17) for [2]. Both reactions may be considered as test systems for comparison of the accuracy of various levels of quantum chemical calculations against kinetic and thermochemical data.

Experimental

Rate measurements

Germylene kinetic studies have been carried out by the laser flash photolysis technique, details of which have been published previously (4–6). Only essential details are therefore included here. GeH_2 was produced by photodecomposition of 3,4-dimethylgerma-cyclopentene-3 (DMGCP) using the 193 nm line of a pulsed excimer laser (Coherent Compex 100). GeH_2 was detected and monitored in real time by use of a single mode dye laser (Coherent 699–21) pumped by an argon ion laser (Coherent Innova 90–5), tuned to a known strong vibration–rotation transition at 17 111.31 cm^{-1} in the visible A ← X absorption band. Experiments were carried out in a variable temperature spectrosil quartz vessel with demountable windows which were regularly cleaned. Signal decays from 3–10 photolysis laser shots (at 60 mJ/pulse) were averaged and found to give good first order linear fits (ln (abs) vs. t plots up to 90% signal decay). These experiments yielded values for the first order rate coefficient, k_{obs}, for removal of GeH_2 in the presence of known partial pressures of D_2. Gas mixtures for study consisted of a few mtorr (1 torr = 133.322 Pa) of DMGCP and various amounts of substrate D_2 (limited by pressures which caused signal quenching). DMGCP was synthesised by us previously (4). Deuterium (British Oxygen Co) was 99.8% pure (0.2% of HD). It contained no GC detectable impurities and was handled carefully to avoid contamination by non-condensibles (air).

Ab initio and DFT calculations

In the ab initio calculations geometry optimisations, vibrational analyses and reaction paths were performed at the frozen core, QCISD/6–311G(d,p) level (18). All the structures obtained here were verified, by examination of the frequency matrix, as minima (all frequencies real) or transition

© 2000 NRC Canada

Table 1. First order rate constants[a] for GeH_2 decay in the presence of D_2.

Temp (K)[b]	D_2 (torr) (1 torr = 133.322 Pa)	k_{obs} (10^4 s^{-1})	Temp (K)[c]	D_2 (torr) (1 torr = 133.322 Pa)	k_{obs} (10^4 s^{-1})
293	0[d]	4.2 ± 0.4	585	0[d]	2.3 ± 0.4
	9.4	5.5 ± 0.3		9.5	2.1 ± 0.4
	29.4	6.2 ± 0.1		51.0	3.4 ± 0.3
	79.4	6.6 ± 0.2		—	—

[a]Average of three or four measurements.
[b]Precursor (DMGCP): 3.0 mtorr.
[c]Precursor (DMGCP): 5.0 mtorr.
[d]Pressurized to 10 torr with SF_6.

states (TSs) (one imaginary frequency). Final energies were refined by single point QCISD(T)/6–311G++(3df,2pd) calculations, which are denoted subsequently in this paper as QCISD(T)/6–311G++(3df,2pd)//QCISD/6–311G(d,p). The DFT calculations, including the finding and verification of stationary points, were done with the B3LYP functional (19) using the 6–311++G(3df,2pd) basis. Energies from both levels of theory were corrected to include zero point vibrational energy contributions. For all stationary points we also calculated enthalpies and Gibbs free energies at 298 K. For these other thermodynamic functions, harmonic oscillator and rigid rotor models were used throughout, employing geometries and frequencies (unscaled) from the appropriate set of calculations.

Transition states were confirmed by calculations along the minimum energy paths (intrinsic reaction coordinate, IRC) connecting them with local minima. Most of the calculations carried out here were performed using GAUSSIAN 94 (20) on the SGI POWER CHALLENGE L supercomputer at the computer center of IOC RAS, Moscow.

Results and discussion

Kinetics and thermochemistry

The reaction was studied at 293 K and 585 K at several partial pressures of D_2. The results are shown in Table 1. It is clear from the extremely small variation in values of k_{obs} under the operational conditions that there is very little if any reaction. Even at the maximum pressures of D_2 at each temperature the values of k_{obs} are barely beyond the uncertainties of the measurements without D_2. At intermediate pressures of D_2 the values are consistent. It is certainly possible that the small increases observed could have been caused by as little as 0.01% of an impurity reacting at the collision rate. To obtain an upper limit to the true second-order rate constants, the maximum values of k_{obs} at the highest D_2 pressures were combined with the zero D_2 values and the difference attributed to reaction. This yielded for k_1, maximum values of 1.0×10^{-14} cm^3 $molecule^{-1}$ s^{-1} at 293 K and 1.7×10^{-14} cm^3 $molecule^{-1}$ s^{-1} at 585 K. The difference between these values, which for the reasons given only represent upper limiting values, is not significant, and we therefore saw no point in investigating intermediate temperatures (or further D_2 pressures).

Because these measurements have only given limiting values, the magnitudes of the true rate constants remain to be obtained. Nevertheless each value can be used independently to obtain a lower limiting value for the activation energy $E_a[1]$ through the use of an estimated A factor, $A_1 = 10^{-12.07}$ cm^3 $molecule^{-1}$ s^{-1}. This is obtained by analogy with the measured A factor (8,9) for $SiH_2 + D_2$ (deuterium analogue of rxn. [2]). Use of this value leads to the activation energy values shown in Table 2. Clearly the advantage of the higher temperature study is to have provided a better (higher) limit. While the value of A_1 has been assumed by analogy with A_2, it is worth noting that the values of the A factors for the reverse reactions, A_{-1} and A_{-2}, obtained by study of the thermal decompositions of GeH_4 (3) and SiH_4 (21) respectively, are both $10^{15.5}$ s^{-1}. Since the entropy changes for these isostructural reactions are likely to be close to one another, this adds weight to the assumption of similar forward reaction A factors. The activation energies quoted in Table 2 nevertheless allow for an uncertainty of $10^{\pm 0.5}$ in the estimate of A_1.

Table 2. Limiting values for rate constants and derived activation energies[a] for $GeH_2 + D_2$

Temp (K)	k_1 (cm^3 $molecule^{-1}$ s^{-1})	$E_a[1]$ (kJ mol^{-1})
293	$< 1.0 \times 10^{-14}$	> 10.8 (±3)
585	$< 1.7 \times 10^{-14}$	> 19.2 (±6)

[a]Based on assumed A factor (see text).

There are no previous measurements of this activation barrier by direct means. However this result can be illuminated by consideration of the expected value based on thermochemistry. For the reverse reaction, viz.

[–1] $GeH_4 \rightarrow GeH_2 + H_2$

$\Delta H°$ may be estimated from $\Delta H_f°(GeH_4) = 90.4 \pm 2.1$ kJ mol^{-1} (22) together with $\Delta H_f°(GeH_2) = 237.2 \pm 12$ kJ mol^{-1} by experiment (6), or 250–258 kJ mol^{-1} (6, 23, 24) by theoretical calculation. This puts $\Delta H°[-1]$ in the range 147–168 kJ mol^{-1}; at the lower end from experimental data alone, at the higher end using theoretical information. The thermal decomposition of GeH_4 in static systems is highly perturbed by surface reactions (for previous studies of the kinetics of GeH_4 decomposition see ref. 3). Only one study by Newman et al. (3) in a shock tube in the temperature range 950–1060 K yields reliable kinetic measurements of rate constants of the purely homogeneous rxn. [–1]. Under these conditions the reaction is in its unimolecular fall-off region and RRKM modelling was required to obtain the true infinite pressure value of $E_a[-1]$ for which a figure of 227 kJ mol^{-1} was obtained (error limits are not quoted). If this value is assumed reasonably independent of temperature, then $E_a[1]$ can be

© 2000 NRC Canada

Fig. 1. Stationary points of reactions [1] (Z = Ge) and [2] (Z = Si) calculated at the QCISD/6–311G(d,p) and B3LYP/6–311++G(3df,2pd) levels. The symmetry group is given below each structure.

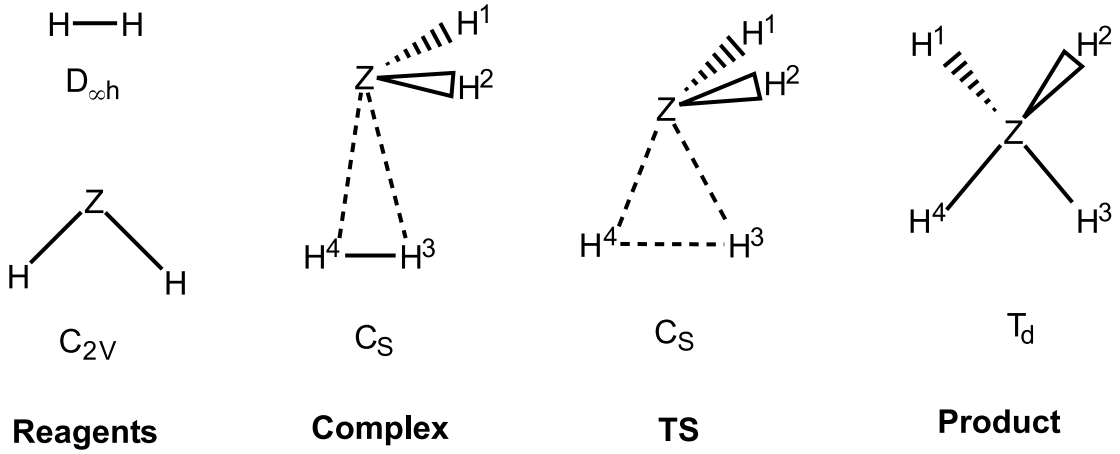


Table 3. QCISD/6–311G(d,p) and B3LYP/6–311++G(3df,2pd) calculated geometric parameters (*R, A*) and the lowest harmonic wavenumber (ν (cm^{-1})) of stationary points of reactions $ZH_2 + H_2 \rightarrow ZH_4$ (Z = Si, Ge). Distances *R* are in Angstroms, angles *A* in degrees. For atom numbering see Fig. 1.[a]

Structure	Method	ν (cm^{-1})	$R(Z\text{-}H^1)$	$R(Z\text{-}H^3)$	$R(Z\text{-}H^4)$	$R(H^3\text{-}H^4)$	$A(H^1\text{-}Z\text{-}H^2)$	Reference
Z = Si								
Complex	QCISD	437	1.509	1.936	1.859	0.783	95	This work
	B3LYP	493	1.513	1.870	1.778	0.805	95	This work
	MP2	609	1.505	1.858	1.787	0.792	94	17
TS	QCISD	–1272	1.479	1.661	1.522	1.117	110	This work
	B3LYP	–1172	1.484	1.647	1.522	1.140	110	This work
	MP2	–1205	1.477	1.636	1.515	1.135	110	17
	MRD-CI	—	1.494	2.001	1.548	1.974	118	16
	HF	—	1.484	1.691	1.547	1.103	113	15
Z = Ge								
Complex	QCISD	261	1.589	2.276	2.225	0.758	92	This work
	B3LYP	330	1.590	2.108	2.033	0.773	92	This work
TS	QCISD	–1347	1.539	1.742	1.573	1.215	111	This work
	B3LYP	–1252	1.539	1.721	1.568	1.250	111	This work

[a]For reagents and products calculated QCISD (B3LYP) parameters are: H_2, *R*(H—H) = 0.744 (0.743); GeH_2, *R*(Ge—H) = 1.592 (1.596), *A*(H-Ge-H) = 91.8 (90.9); GeH_4, *R*(Ge—H) = 1.535 (1.534); SiH_2, *R*(Si—H) = 1.516 (1.523), *A*(H-Si-H) = 92.6 (91.6); SiH_4, *R*(Si—H) = 1.476 (1.480).

obtained via $E_a[1] = E_a[-1] - (\Delta H° - RT)$. From the figures cited this puts $E_a[1]$ in the range 63–84 kJ mol^{-1} (estimated at a temperature of 500 K). Because of the assumptions concerning $E_a[-1]$ the uncertainty must be considered slightly larger than this. Nevertheless this thermochemical estimate is well above the limit set by experiment and therefore shows that unless the thermochemical data are seriously in error, a fast reaction between GeH_2 and H_2 is not to be expected.

Quantum chemical calculations

Apart from the reactants, $GeH_2 + H_2$, and the product, GeH_4, we find two stationary points on the potential energy surface (PES) corresponding to a local minimum and a transition state, both of C_s symmetry. These are shown in Fig. 1. The same set of stationary points was found for the silylene rxn. [2]. For the latter reaction this agrees with earlier studies at the MP4(SDQ)/6–31G*//HF/3–21G level (15), MRD-CI/TZ+P level (16) and MP4/6–311G++(3df,3pd)//MP2/6–311G(2d,2p) level (17). The geometrical parameters of these structures are shown in Table 3, including comparisons with earlier work in the silylene case. The geometries from the B3LYP and QCISD calculations are in good agreement with each other not only for the stable species (reagents and products) but also for the TSs and complexes. The bigger differences found between silylene and germylene complexes reflect the rather loose nature of these structures. The calculated energies are shown in Table 4.

The prereaction complex in the germylene reaction is only about half as strong (ΔH (298 K) = –9 (–11) kJ mol^{-1}) as that in silylene case (ΔH (298 K) = –16 (–21) kJ mol^{-1}). Both here and subsequently the QCISD values are given first, with the B3LYP values following in parentheses. Despite the weakness of these species the interactions of the two fragments are significant enough to stretch the H—H bond (H^4—H^3) by 0.015 (0.030) Å in the germylene complex and by 0.039 (0.062) Å in the silylene complex. The

© 2000 NRC Canada

Table 4. QCISD(T)/6–311G++(3df,2pd)//QCISD/6–311G(d,p) and B3LYP/6–311++G(3df,2pd) calculated energies (E /hartree, ΔE, ΔH, ΔG in kJ/mol) of stationary points on the PES of reactions [1] and [2].[a]

	Z = Si			Z = Ge		
	Complex	TS	SiH_4	Complex	TS	GeH_4
QCISD(T)						
E	–291.35054	–291.34032	–291.43606	–2077.74926	–2077.72484	–2077.81231
ΔE	–28	–1	–252	–17	47	–183
ΔE + ZPE	–9	13	–226	–4	58	–160
ΔE 298 K	–13	7	–232	–6	53	–165
ΔH 298 K	–16	5	–234	–9	50	–168
ΔG 298 K	15	38	–194	19	84	–128
B3LYP						
E	–291.83611	–291.82650	–291.91909	–2079.34896	–2079.32428	–2079.40668
ΔE	–32	–7	–250	–20	44	–172
ΔE + ZPE	–14	6	–225	–5	56	–150
ΔE 298 K	–19	0	–231	–9	50	–155
ΔH 298 K	–21	–2	–234	–11	48	–157
ΔG 298 K	12	33	–198	20	83	–122

[a]Calculated QCISD (B3LYP) total energies of reagents (hartree): H_2, –1.17235 (–1.180013); GeH_2, –2076.57037 (–2078.16115); SiH_2, –290.16762 (–290.643748).

characteristics of the silylene complex are in close similarity to those of the previous highest level of calculation by Gordon et al. (17) although our complex is slightly looser especially in the QCISD calculations.

According to our calculations rxns. [1] and [2] have similar TSs. The distinction between them is only of the degree to be expected from the characteristic differences in Ge—H and Si—H bond lengths. The breaking H^4—H^3 bond of the germylene TS is stretched by 0.472 (0.508) Å compared to 0.373 (0.398) Å for the silylene TS. This implies that the PES maximum in the germylene insertion [1] is shifted towards the product compared to the silylene case [2] in agreement with expectations from Hammond's postulate (25) for a less exothermic process. The TS structure for the silylene insertion [2] found here is very similar to those calculated earlier by Sosa and Schlegel (15) and Gordon et al. (17) but differs somewhat from that of Sax and Olbrich (16) (Table 3). The latter has a much more extended H^4—H^3 bond, which looks (with hindsight) out of keeping with the early nature of the transition state (based on energy). This was probably a deficiency of the calculation.

The values for $\Delta H°$[1] calculated by the QCISD and B3LYP methods are –168 and –157 kJ mol^{-1}, respectively, (Table 4). Both fall within the range –147 to –168 kJ mol^{-1} estimated from thermochemistry and indicated above, and are consistent with our ab initio calculations on the reaction of GeH_2 with GeH_4 (6). The ab initio barrier ($E_a = \Delta E$ + ZPE) of 53 (50) kJ mol^{-1} at 298 K is slightly lower than the thermochemically estimated range of 63–84 kJ mol^{-1} at 500 K. However for the reasons given in the previous section this must be considered quite good agreement. The calculations may be judged by the results for the silylene case for which both methods give the same value of $\Delta H°$[2] of –234 kJ mol^{-1} (Table 4). This compares well with the current best value of –239 ± 3 kJ mol^{-1} (derived from $\Delta H_f°(SiH_4)$ = 34.3 ± 1.2 kJ mol^{-1} (26) and $\Delta H_f°(SiH_2)$ = 273.2 ± 2 kJ mol^{-1} (8, 10)). The QCISD barrier, ΔE[2] of 7 kJ mol^{-1} is slightly higher than the measured E_a of – 2 kJ mol^{-1} (8, 9) but as reasonably close as the previous best calculation of Gordon et al. (17) who also obtained 7 kJ mol^{-1} (the other earlier calculations (13–16) gave significantly higher barriers). Even better agreement for the barrier ΔE[2] was obtained in B3LYP calculations (0 kJ mol^{-1}). It appears that DFT methods, with their markedly lower computational demands, can produce good results for these quite large systems. Thus B3LYP may be considered as the best choice for studying this type of reaction.

The calculations carried out here show that, despite the mechanistic similarity, rxn. [1] has a significant barrier compared with rxn. [2] and so a fast reaction between GeH_2 and H_2, like that between SiH_2 and H_2, is not to be expected. It prompts the question as to why there is a significant increase of activation barrier from [2] to [1]. Sax and Olbrich (16) actually predicted this qualitatively on the basis of a valence-bond configuration mixing (VBCM) model (27, 28) which was employed to explain the differences between the silylene and methylene ($^1A_1$ states) reactions with H_2. The VBCM model involves energy surface mixing with surfaces derived from triplet state species. Despite the slight deficiencies of structure and energy in the calculations mentioned above (16), Sax and Olbrich make their prediction for GeH_2 + H_2 on the basis that the singlet-to-triplet excitation of GeH_2 is ca 17 kJ mol^{-1} higher than that of SiH_2. Whatever the merits of this argument we would point out that our calculations show unequivocally the extra extension of the H—H bond in the TS for rxn. [1] compared to [2] and this is consistent with the need to satisfy the less favourable H···Ge overlap compared to that of H···Si, due to the more diffuse nature of the germanium atomic orbitals. This reasoning also qualitatively supports a more demanding energy requirement for germylene than silylene in reaching the transition state.

The existence of pre-TS complexes of GeH_2 and SiH_2 with H_2 as predicted here, presents a challenge to experiment. The possibility exists of direct spectral observation at low temperatures. In this respect, the germylene complex may be more amenable to isolation than its silylene counterpart,

© 2000 NRC Canada

despite its weaker binding. This is because of the existence of the substantial barrier to formation of GeH_4, in contrast to the low barrier separating the silylene complex from SiH_4. The positive ΔG of complexation at 298 K makes equilibrium detection of either species totally unlikely.

We finish by noting the contrasts between GeH_2 and SiH_2 insertion reactions. Both species insert readily and rapidly into Ge—H bonds (5, 6) and also Si—H bonds (29).[2] Activation energies for these processes are all negative but are more negative for GeH_2 than for SiH_2 insertions although potential energy surfaces show many similarities. For H—H bond insertion, despite some similarity of the potential energy surfaces, GeH_2 requires significant activation whereas SiH_2 does not. For C—H bond insertion, reactions of both GeH_2 and SiH_2 with CH_4 require significant activation. For GeH_2 a recent DFT calculation gives a barrier of 138 kJ mol^{-1} (30), whereas for $SiH_2 + CH_4$ the best estimate of the barrier is 59 kJ mol^{-1} (31).

Acknowledgements

We wish to thank the following: (*i*) the Royal Society of Great Britain for support under its joint project scheme with States of the Former Soviet Union (Grant P851); (*ii*) INTAS-RFBR (Grant N IR-97-1658); (*iii*) the Russian Foundation for Basic Research (Grants N 00-03-33001 and N 00-15-97387); (*iv*) the Russian Academy of Sciences for a young scientists grant 1998, for support to S.E.B.; (*v*) the CACR Computer Center at the Zelinsky Institute for computer time on the SGI Power Challenge L; and (*vi*) the Direccion General de Investigacion Cientifica y Technica (DGICYT), Spain, for support to R.B. under project PB97-1214.

References

1. C. Isobe, H. Cho, and J.E. Sewell. Surf. Sci. **295**, 117 (1993).
2. W. Du, L.A. Keeling, and C.M. Greenlief. J.Vac. Sci. Technol. A, **12**, 2281 (1994).
3. C.G. Newman, J. Dzarnoski, M.A. Ring, and H.E. O'Neal. Int. J. Chem. Kinet. **12**, 661 (1980).
4. R. Becerra, S.E. Boganov, M.P. Egorov, O.M. Nefedov, and R. Walsh. Chem. Phys. Lett. **260**, 433 (1996).
5. R. Becerra, S.E. Boganov, M.P. Egorov, O.M. Nefedov, and R. Walsh. Mendeleev Commun. 87 (1997).
6. R. Becerra, S.E. Boganov, M.P. Egorov, V.I. Faustov, O.M. Nefedov, and R. Walsh. J. Am. Chem. Soc. **120**, 12657 (1998).
7. U.N. Alexandra, N.A. Trout, K.D. King, and W.D. Lawrance. Chem. Phys. Lett. **299**, 291 (1999).
8. J.M. Jasinski, R. Becerra, and R. Walsh. Chem. Rev. **95**, 1203 (1995).
9. R. Becerra and R. Walsh. *In* Research in chemical kinetics. Vol. 3. *Edited by* R.G. Compton and G. Hancock. Elsevier, Amsterdam. 1995. p. 263.
10. R. Becerra, H.M. Frey, B.P. Mason, R. Walsh, and M.S. Gordon. J. Chem. Soc. Faraday Trans. **91**, 2723 (1995).
11. J.M. Jasinski. J. Phys. Chem. **90**, 555 (1986).
12. P. John and J.H. Purnell. J. Chem. Soc. Faraday Trans. 1, **69**, 1455 (1973).
13. M.S. Gordon. J. Chem. Soc. Chem. Commun. 890 (1981).
14. R.S. Grev and H.F. Schaefer, III. J. Chem. Soc. Chem. Commun. 785 (1983).
15. C. Sosa and H.B. Schlegel. J. Am. Chem. Soc. **106**, 5847 (1984).
16. A. Sax and G. Olbrich. J. Am. Chem. Soc. **107**, 4868 (1985).
17. M.S. Gordon, D.R. Gano, J.S. Binkley, and M.J. Frisch. J. Am. Chem. Soc. **108**, 2191 (1986).
18. J.B. Foresman and A. Frisch. Exploring chemistry with electronic structure methods. 2nd ed. Gaussian Inc., Pittsburgh, Pa. 1995, and refs. therein.
19. A.D. Becke. J. Chem. Phys. **98**, 5648 (1993).
20. M.J. Frisch, G.W. Trucks, H.B. Schlegel, P.M.W. Gill, B.G. Johnson, M.A. Robb, J.R. Cheeseman, T. Keith, G.A. Petersson, J.A. Montgomery, K. Raghavachari, M.A. Al-Laham, V.G. Zakrzewski, J.V. Ortiz, J.B. Foresman, J. Cioslowski, B.B. Stefanov, A. Nanayakkara, M. Challacombe, C.Y. Peng, P.Y. Ayala, W. Chen, M.W. Wong, J.L. Andres, E.S. Replogle, R. Gomperts, R.L. Martin, D.J. Fox, J.S. Binkley, D.J. Defrees, J. Baker, J.P. Stewart, M. Head-Gordon, C. Gonzales, and J.A. Pople. Gaussian 94. Revision D.1. Gaussian Inc., Pittsburgh, Pa. 1995.
21. C.G. Newman, H.E. O'Neal, M.A. Ring, F. Leska, and N. Shipley. Int. J. Chem. Kinet. **11**, 1167 (1979).
22. S.R. Gunn and L.G. Green. J. Phys. Chem. **65**, 779 (1961).
23. B. Ruscic, M. Schwartz, and J. Berkowitz. J. Phys. Chem. **92**, 1865 (1990).
24. J. Karolczak, W.W. Harper, R.S. Grev, and D.J. Clouthier. J. Chem. Phys. **103**, 2839 (1995).
25. G.S. Hammond. J. Am. Chem. Soc. **77**, 334 (1955).
26. R. Becerra and R. Walsh. Thermochemistry. *In* The chemistry of organic silicon compounds. Vol. 2. *Edited by* Z. Rappoport and Y. Apeloig. Wiley, Chichester. 1998. Chap. 4. p. 153.
27. S.S. Shaik. J. Am. Chem. Soc. **103**, 3692 (1981).
28. A. Pross and S.S. Shaik. Acc. Chem. Res. **16**, 363 (1983).
29. R. Becerra and R. Walsh. Phys. Chem. Chem. Phys. **1**, 5301 (1999).
30. M-D. Su and S-Y. Chu. J. Am. Chem. Soc. **121**, 4229 (1999).
31. R. Becerra and R. Walsh. Int. J. Chem. Kinet. **31**, 393 (1999).

[2] R. Becerra, S.E. Boganov, M.P. Egorov, V.I. Faustov, O.M. Nefedov, and R. Walsh. Submitted to Phys. Chem. Chem. Phys.

© 2000 NRC Canada

Dehydrocoupling reactions of hydrosilanes with group 4 metallocenes Cp_2MY_2 (M = Ti, Zr, Hf; Y = F, OPh, NMe_2)

Qingzheng Wang and Joyce Y. Corey

Abstract: Dehydrocoupling polymerization of phenylsilane with group 4 metallocene precatalysts Cp_2MY_2 (M = Ti, Zr, Hf; Y = F, OPh, NMe_2) under comparable conditions has been examined. All nine title metallocenes produced polysilane products which ranged in molecular weight from 1100 to 4400 and exhibited ratios of linear to cyclic products from ~2 to 30. The highest molecular weight polysilanes observed for each metal were obtained from $Cp_2M(NMe_2)_2$ and the highest percentage of linear polysilane was found with $Cp_2Hf(NMe_2)_2$. The near stoichiometric reactions of Cp_2MY_2 with $PhSiH_3$, $PhMeSiH_2$, and Ph_2MeSiH were monitored by ^1H, ^{19}F and ^{29}Si NMR spectroscopy and in all cases exchange products containing Si-Y were identified. Metal hydride species could be observed only with Cp_2TiY_2.

Key words: metallocene, dehydrocoupling, polymerization, hydrosilanes, polysilane.

Résumé : On a étudié la polymérisation par déshydrocouplage du phénylsilane avec des précatalyseurs métallocènes du groupe 4, Cp_2MY_2 (M = Ti, Zr, Hf; Y = F, OPh, NMe_2) dans des conditions comparables. Les neuf métallocènes mentionnés dans le titre ont tous conduit à la formation de polysilanes dont les poids moléculaires varient de 1100 à 4400 et pour lesquels les rapports de produits linéaires à cycliques vont d'environ 2 à 30. Pour chacun des métaux, les poids moléculaires les plus élevés de polysilanes ont été obtenus avec le $Cp_2M(NMe_2)_2$; le pourcentage de polysilane le plus élevé a été obtenu avec le $Cp_2Hf(NMe_2)_2$. La spectroscopie RMN du ^1H, ^{19}F et ^{29}Si a permis de suivre les réactions pratiquement stoechiométriques des Cp_2MY_2 avec $PhSiH_3$, $PhMeSiH_2$ et Ph_2MeSiH; dans chacun des cas, on a pu identifier des produits d'échange comportant la liaison Si-Y. On n'a pu observer des espèces hydrures métalliques qu'avec le Cp_2TiY_2.

Mots clés : métallocène, déshydrocouplage, polymérisation, hydrosilanes, polysilane.

Introduction

Polysilanes exhibit unusual electronic, optical, and chemical properties that have potential technological applications (1). The polymers are traditionally prepared through Wurtz-type coupling of a dichlorosilane by an alkali metal (1). However, the vigorous nature of Wurtz coupling conditions limits the incorporation of some functional groups on the substituents at silicon. Alternative approaches, such as dehydrocoupling (2), ring-opening polymerization of cyclosilanes (3), and anion induced polymerization of masked disilenes (4), have been developed as alternate methods for the synthesis of polysilanes.

Group 4 transition metal catalyzed dehydrocoupling reactions of primary silanes ($RSiH_3$) by metallocenes, Cp_2MR_2 (Cp = η^5-C_5H_5; M = Ti, Zr; R = Me, Ph) were reported in the 1980's by Harrod and co-workers (5). Since then other Group 4 metallocene precursors have been found to be effective including CpCp*M[$Si(SiMe_3)_3$]R (Cp* = η^5-C_5Me_5; M = Zr, Hf; *R* = H, Cl, Me) developed by Tilley and co-workers (2*a*, *e*), Cp_2MCl_2/*n*-BuLi developed by Corey and co-workers (6), and $Cp_2M(OAr)_2$ [M = Ti, Zr; Ar = *p*-XC_6H_4 (X = MeO, Me, Cl, CN)] reported by Corriu and co-workers (7). Recently, we (8*a*) and Marschner's group (8*b*) concurrently discovered that Cp_2MF_2 (M = Ti, Zr) could function as a catalyst precursor for the dehydrocoupling of hydrosilanes. In this report we describe our continued work on the dehydrocoupling of hydrosilanes utilizing Cp_2MY_2 (X = F, OPh, NMe_2) as single component catalysts.

Received June 29, 1999. Published on the NRC Research Press website on October 30, 2000.

Dedicated to Professor Adrian Brook in appreciation of his fundamental contributions to silicon chemistry.

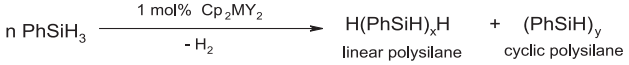
Q. Wang and J.Y. Corey.[1] Department of Chemistry, University of Missouri-St. Louis, St. Louis, MO 63121, U.S.A.

[1]Author to whom correspondence may be addressed. Telephone: (314) 516-5360. Fax: (314) 516-5342. e-mail: corey@umsl.edu

Results

Dehydropolymerization of $PhSiH_3$

After varying induction periods, which occurred when Cp_2MY_2 was added to $PhSiH_3$, gas evolution and color changes were observed followed by dehydropolymerization of the silane (eq. [1]).



© 2000 NRC Canada

Table 1. Dehydropolymerization of $PhSiH_3$ by group 4 metallocenes, Cp_2MY_2.

		Induction period[a]			Polysilane GPC data[b]		
Y in Cp_2MY_2	M	Temp. (°C)	Time (min)	Color Change	MW	*M*n	*L*/*C*
F	Ti	rt	~20–30	Brt. yellow→dk. blue	1667(1620[c])	1410(1040[c])	1.9
	Zr	rt	<5	Cream→yellow	2695(2200[d])	1875(1400[d])	6.3
	Hf	50	~45–60	Cream→yellow	2433	1802	11.5
OPh	Ti	50	~15–20	Yellow→dk. blue	2030(2400[e])	1460(1900[e])	1.9
	Zr	50	~10–15	White→yellow	2810(3200[f])	1950(2200[f])	6.1
	Hf	85	~120–150	White→yellow	1071	1009	>30[g]
NMe_2	Ti	rt	Immediate	Dk. brown→dk. blue	1909	1285	3.1
	Zr	rt	Immediate	Brt. yellow→yellow	3135	2024	6.1[h]
	Hf	rt	~3	Yellow→yellow	4366	2608	27
Cl (with *n*BuLi) (9)	Ti	rt	Immediate	Red→dk. blue	1480	900	2.2
	Zr	rt	Immediate	Cream→brown	1740	1140	2.5
	Hf	rt	Immediate	Cream→tan	3340	—	>20[i]

[a]The end of the induction period is signaled by gas evolution and the indicated color change (dk = dark, brt. = bright). Reactions were run neat with 1 mol% catalyst precursor and conducted at room temperature after the induction period.

[b]Unless otherwise indicated, polymerization reactions were terminated after 2 days. The molecular weights were determined relative to polystyrene standards; UV detector.

[c]From ref. 8b; condensations performed neat with 1 mol% catalyst precursor, for 1 week. Sample contains about 30% cyclics.

[d]From ref. 8b; 1 mol% catalyst precursor for 3 days. Sample contains <10% cyclics.

[e]From ref. 7; reaction performed neat with 0.1 mol% catalyst precursor for 1 day. Sample contains 25% cyclic.

[f]From ref. 7; reaction performed neat with 0.1 mol% catalyst precursor for 3 days. Sample contains 10% cyclics.

[g]Data obtained after 5 days.

[h]Data obtained after 3 days.

[i]4 mol% Cp_2HfCl_2 (ref. 9*b*).

The reactions of $Cp_2M(OPh)_2$ (M = Ti, Zr, Hf) and Cp_2HfF_2 required heat to initiate catalyst formation but the polymerizations were conducted at room temperature. Reactions of Cp_2MY_2 (1 mol%) with $PhSiH_3$ are summarized in Table 1 as well as the molecular weights of the polysilane products obtained after 48 h.[2] Molecular weight data collected after 24 h and 72 h were similar. When mixtures were examined before the color change and gas evolution occurred, no polysilane oligomers or polymers were observed. Regardless of the nature of Y in Cp_2MY_2 (Y = F, OPh, NMe_2), titanium systems became dark blue and zirconium and hafnium systems became yellow when an active catalyst was generated. In general, conversion of Cp_2HfY_2 to a catalytically active hafnium complex required longer induction periods compared to the corresponding titanium and zirconium complexes. A phenoxide substituent on the metal required a longer induction period relative to the fluoride and the amide.

Of the three classes of complexes (Y = F, OPh, NMe_2) polysilane with the highest MW values were obtained when Y = NMe_2 for all three metals. The amides also exhibited the shortest induction period. The highest linear to cyclic ratio was usually produced with the hafnium complexes and the percent cyclic material followed the sequence Ti > Zr > Hf. These observations are consistent with those reported by Tilley (2*a*, *e*; 10) and demonstrated by Harrod in the reaction of $PhSiH_3$ with Cp_2MCl_2/*x*MeLi (M = Ti, Zr, Hf) (11). The linear/cyclic ratio for the polysilanes produced from the zirconium complexes (Y = F, OPh, NMe_2) exhibited approximately the same value independent of the substituent Y. The ^1H and ^{29}Si spectra of the polysilanes formed from Cp_2MY_2 systems also revealed similar features to those obtained from the previously studied combination, Cp_2MCl_2/2 *n*-BuLi (M = Ti, Zr) (6, 12).

When *p*-$TolSiH_3$ was used as the starting monomer, a longer induction period and (or) a higher temperature was required to initiate the polymerization reaction. A mixture of *p*-tolylsilane and Cp_2TiF_2 (0.5 mol%) required 40 min at 40°C before the onset of the polymerization reaction. The mixture was still fluid after 2 days in contrast to the phenylsilane case (0.5 mol% Cp_2TiF_2) which became very viscous after 1 day. The polymerization of *p*-tolylsilane in the presence of $Cp_2Zr(NMe_2)_2$ (1 mol%) at room temperature provided a product where the linear:cyclic ratio was 2.2, a higher ratio of cyclic products than was observed for phenylsilane under the same conditions.

The reaction of secondary silanes with Cp_2MY_2 occurred relatively slowly. As an example, at 60–85°C only 12% disilane was obtained from Ph_2SiH_2 after 50 hs (2 mol% Cp_2TiF_2). The reaction of $Cp_2Ti(OPh)_2$ and Ph_2SiH_2 provided only 10% disilane after 5 h at 100°C (7).

Exchange reactions of hydrosilanes with Cp_2MY_2

The original motivation in the current study was to utilize excess reacting silane to transfer hydride to the metal center, thus producing a potentially active catalyst for dehydrocoupling of the remaining silane as generally depicted in Scheme 1. To probe the suspected exchange reaction Cp_2MY_2 was mixed with primary, secondary, and tertiary silanes in a Si:M molar ratio of about 4:1 in C_6D_6. Once a color change occurred (either at room temperature or with heating to temperatures indicated in Table 1) the products

[2]MW values are influenced by the mol% catalyst and tend to decrease with increasing concentration of the metal (9*c*).

© 2000 NRC Canada

Scheme 1.

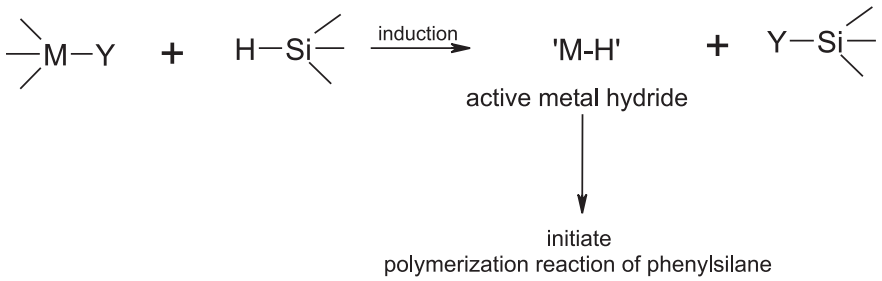


Table 2. Silicon products identified by ^{1}H NMR spectroscopy in the reaction of Cp_2MY_2 with hydrosilanes.[a]

Cp_2My_2		Starting silane		
Y	M	Ph_2MeSiH	$PhMeSiH_2$	$PhSiH_3$
F	Ti	Ph_2MeSiF[b]	PhMeSiHF,[c] $PhMeSiF_2$,[c] disilane[c]	$PhSiF_3$,[b] polysilane[d]
	Zr	Ph_2MeSiF[b]	disilane[c]	polysilane[d]
	Hf	Ph_2MeSiF[b]	PhMeSiHF,[b] disilane[c]	polysilane[d]
OPh	Ti	$Ph_2MeSi(OPh)$[c]	PhMeSiH(Oph),[c] $PhMeSi(OPh)_2$,[c] disilane[c]	$PhSiH(OPh)_2$,[c] polysilane[d]
	Zr	$Ph_2MeSi(OPh)$[c]	PhMeSiH(Oph),[c] $PhMeSi(OPh)_2$,[c] disilane[c]	polysilane[d]
NMe_2	Ti	$Ph_2MeSi(NMe_2)$[e]	$PhMeSiH(NMe_2)$,[f] disilane[c]	$PhSiH_2(NMe_2)$, polysilane[c]
	Zr	—	$PhMeSiH(NMe_2)$,[f] disilane[c]	$PhSiH_2(NMe_2)$,[g] $PhSiH(NMe_2)_2$,[g] polysilane[d]

[a]Pertinent NMR data for the current study as well as literature values may be found in the supplemental material.
[b]By comparison to literature values (13).
[c]By comparison to authentic sample.
[d]By comparison to previously published data (6*b*, 9*a*).
[e]By comparison to typical values observed for dimethylaminosilanes (14).
[f]By comparison to literature values found in supplemental data to ref. 15.
[g]By comparison to literature values found in supplemental data to ref. 16.

were analyzed through ^{1}H, ^{19}F, ^{29}Si NMR, and GCMS. Silicon products were identified by comparison to literature data or to authentic samples prepared by literature methods and are summarized in Table 2. In all three types of silanes the substituent originally on the metal complex was found in one or more silicon products and suggested that the exchange between M-Y and Si-H did indeed occur.

The initial product of exchange with the silane might be expected to be Cp_2MHY although such species may react further. If reduction to a paramagnetic M(III) species occurs identification of the metal complex by NMR spectroscopy could be difficult. The formation of a Ti(III) species from Cp_2TiF_2 and $PhSiH_3$ in toluene has been verified by EPR spectroscopy (8*b*). A doublet of triplets (g = 1.9924) was observed which had been assigned previously to $(Cp_2TiH)_2(\mu\text{-}H)$ by Harrod in an earlier study (17). A second radical species was also present in the Cp_2TiF_2–$PhSiH_3$ solution but was not identified (8*b*). We examined the variable temperature ^{1}H NMR spectrum of solutions of Cp_2TiF_2–$PhSiH_3$ in tol-d_8 and observed the same data in the bridging hydride region (upfield of TMS; see Fig. 1) as reported by Harrod for the isolated dimers, $(Cp_2TiSiH_2Ph)_2$ and $[Cp_2Ti(\mu\text{-}H)(\mu\text{-}HSiPh)TiCp_2]$ (Fig. 2) (17*b*).

In an effort to trap one or more of the metal products, PMe_3 was added to the dark-blue mixture from Cp_2TiF_2 and $PhSiH_3$. A deep purple solution formed that exhibited three new resonances in the ^{31}P NMR spectrum between 20 and 28 ppm. The most intense of the new signals appeared at 23.8 ppm and is essentially identical to that reported for $Cp_2Ti(\eta^2\text{-}HSiH_2Ph)PMe_3$ (literature value in tol-d_8, 23.9) (18). The only other system that exhibited resonances in the bridging hydride region occurred in the mixture of $Cp_2Ti(NMe_2)_2$ and $PhSiH_3$.

In another attempt to identify hydride resonances, acetone was added to mixtures of Cp_2MY_2 and $PhSiH_3$. A heptet for O-C*H*Me_2 which would result from the addition of M-H to >C=O (or from the metal activated addition of Si-H to >C=O) could be identified at 4.17 ppm (literature value, 4.11 ppm) (19). Unfortunately, it was not possible to assign any resonances in the original spectrum of Cp_2MY_2–$PhSiH_3$ to M-H. Addition of acetone to the yellow solution produced from $Cp_2Zr(OPh)_2$–$PhSiH_3$ system resulted in the formation of $Cp_2Zr(OCHMe_2)_2$ by comparison to data reported for reaction of Cp_2ZrH_2 with acetone (19).

Discussion

Other substituents that may be removed from the metal center prior to initiation of the dehydrocoupling reaction include the alkyl groups of Cp_2MR_2 [R = Me and CH_2Ph; M = Ti, Zr (the original catalyst precursors studied by Harrod (20))] and $Si(SiMe_3)_3$ in $CpCp^*M[Si(SiMe_3)_3]R$ (R = Me, Cl; Cp* = C_5H_5, (21), C_5Me_5 (2*a*, *e*, 21)). The rate of removal of M-$Si(SiMe_3)_3$ by $PhSiH_3$ is considerably faster than that of M-CH_3 by $PhSiH_3$. This results in varying induction periods for the dehydrocoupling reaction in the case of Cp_2MMe_2. After addition of $PhSiH_3$ to $CpCp^*Hf[Si(SiMe_3)_3]R$ (R = Cl, Me), $HSi(SiMe_3)_3$ and $CpCp^*Hf[SiH_2Ph]R$ are formed initially followed by

© 2000 NRC Canada

Fig. 1. Bridging hydride region generated from Cp_2TiF_2–$PhSiH_3$ in tol-d_8 at –63°C. Signal labeled A (–8.8 ppm) is assigned to the dimer $[Cp_2Ti(H_cSiHPh)]_2$ and those labeled B are assigned to $[Cp_2Ti(\mu\text{-}H)(\mu\text{-}HSiPh)TiCp_2]$ according to ref. 13*b*.

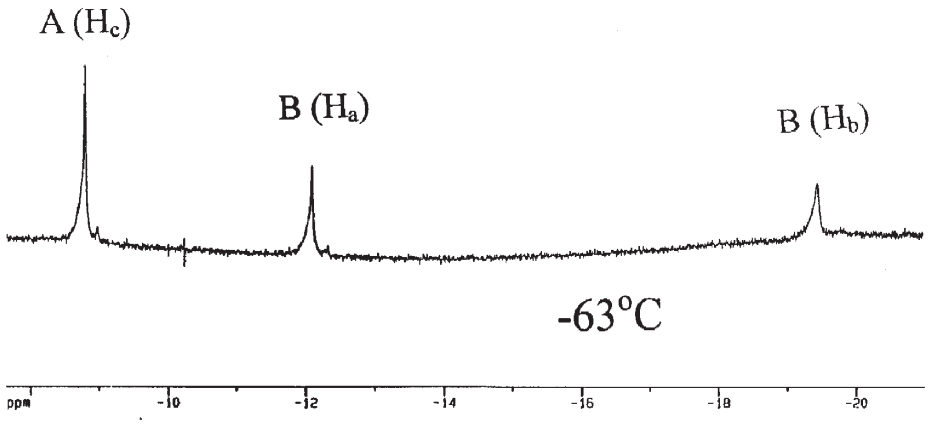
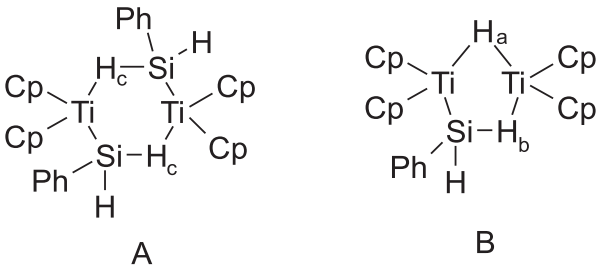


Fig. 2. Titanium hydride dimers.



decomposition or reaction of the later with excess $PhSiH_3$ to give $[CpCp^*HfHR]_2$ (22). Observations with the slow coupling system involving hafnium complexes led Tilley to conclude that metal hydrides are the actual catalysts in dehydropolymerization.

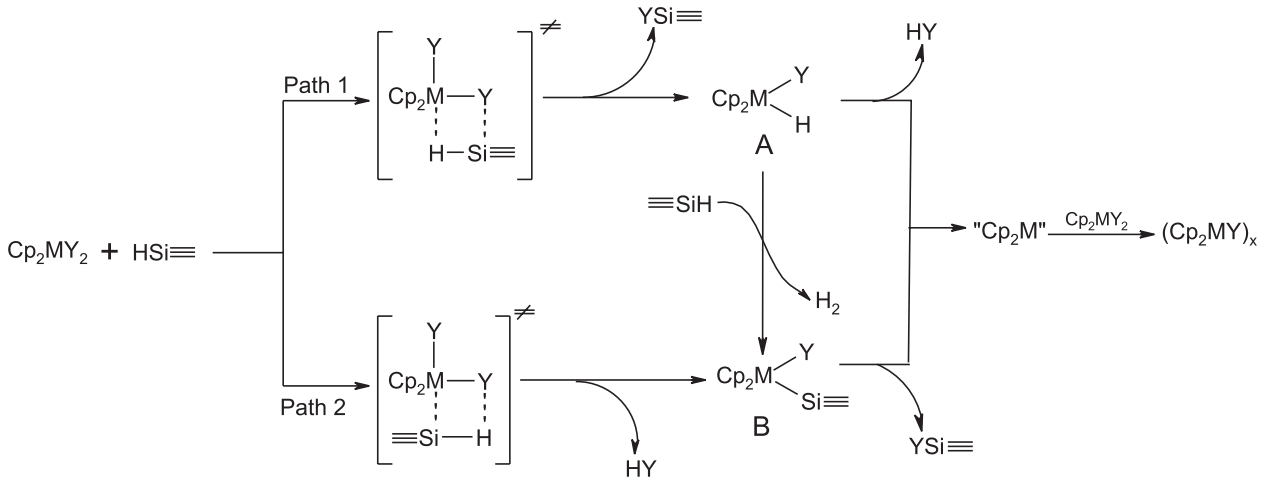
With the less sterically hindered Cp substituents in Cp_2TiMe_2, reaction with $PhSiH_3$ produced three hydride bridged dimers of Ti(III) after the induction period. The concentrations of the Ti(III) species could be monitored by NMR spectroscopy. Quantitative yields of $Cp_2(\mu\text{-}HSiHPh)(\mu\text{-}H)TiCp_2$ were initially produced along with CH_4, $PhMeSiH_2$ and polysilane. The original metal dimer then partially converts to the two dimers, $[Cp_2Ti(\mu\text{-}HSiHPh)]_2$ and $[Cp_2Ti(H)]_2(\mu\text{-}H)$ until an equilibrium was reached in which $[Cp_2Ti(\mu\text{-}HSiHPh)]_2$ dominated (23). In the presence of PEt_3 as a trapping agent, high yields of the paramagnetic monomer, $Cp_2Ti(PEt_3)(SiH_2Ph)$, were isolated (23*e*). From kinetic studies of Cp_2TiMe_2-catalyzed reactions, it was concluded that the probable catalytic species was $Cp_2Ti(SiH_2Ph)H$ possibly formed from reaction of the originally formed dimer with $PhSiH_3$. Such a Ti(IV) species has not yet been isolated although the η^2-SiH complex, $Cp_2Ti(\eta^2\text{-}HSiH_2Ph)PMe_3$, has been isolated by Buchwald and co-workers (24). In contrast, the Zr(IV) dimer, $Cp_2Zr(SiMePhH)(\mu\text{-}H)_2(PhH_2Si)ZrCp_2$, (23*a*) precipitated from the reaction of Cp_2ZrMe_2 and $PhSiH_3$. For both Cp_2TiMe_2 and Cp_2ZrMe_2 the Me group originally on the metal is transferred to the silicon center although several different processes are possible by which this occurs (23). Hydride bridged Zr(IV) dimers as well as phosphine adducts of Zr(IV) have been isolated and crystallographically characterized from addition of Ph_2SiH_2 and PMe_3 to the combination of Cp_2ZrCl_2/2*n*-BuLi (25).

In the present study it has been demonstrated that F, OPh, and NMe_2 bound to the metal site in group IV metallocenes can be transferred to primary, secondary, and tertiary hydrosilanes. By implication, hydride is transferred to the metal although it was not possible to identify unequivocally the resonances in the ^1H NMR spectrum that could be attributed to either bridging or terminal hydrides except in the case of Cp_2TiF_2. However, since all nine metallocenes (Cp_2MY_2) were able to dehydrocouple $PhSiH_3$, it is probable that a metal hydride was generated. All three titanium systems appeared to generate Ti(III) species as indicated by the dark blue colored solutions that formed although this is not necessarily the only oxidation state in the solution. It is less likely, but not impossible, that M(III) species are produced in the zirconium and hafnium cases as well. No observable radicals detectable by EPR spectroscopy were reported in the reaction of Cp_2ZrF_2 and $PhSiH_3$ (8*b*).

It is possible that exchange of substituents between Cp_2MY_2 and the hydrosilane occurs initially through a σ-bond metathesis step. There are two possibilities as illustrated in the two transition states depicted in Scheme 2. In Path 1 the hydride from the silicon is transferred to the metal and the substituent on the metal forms a bond to silicon. In Path 2, silicon forms a bond to the metal and HY is eliminated. We originally selected the Y substituents on the basis of those that would form strong bonds to silicon (such as F). This suggests that Path 1 would be favored over Path 2 (Scheme 2). Since CH_4 is eliminated when $PhSiH_3$ is added to $Cp_2M(CH_3)_2$, Path 2 must be followed (in part) when Y = CH_3 (13*a*). Similarly, in Tilley's system, if the reacting Y represents a small silyl group (the nonreacting Y was Me or Cl), Path 1 would provide the observed $CpCp^*MYH$ (Y = Me, Cl) (18*c*). A second metathesis from A to B replaces MH with MSi. Reductive elimination from A or B would produce M(II) and could lead further to M(III) species although reductive elimination of HF, HOPh, or $HNMe_2$ has little precedence. It is interesting to note that the reaction of

© 2000 NRC Canada

Scheme 2.



$R'_3SiZr(NR_2)_3$ (R′ = Me, $SiMe_3$) gives $R'_3SiZrH(NR_2)_2$ which in turn reacts with an aminosilane to return to $R'_3SiZr(NR_2)_3$ (15).

In this study a major difference in the type of substituent on the reacting metallocene compared to the earlier systems examined by Harrod and by Tilley is that the Y substituents (F, OPh, NMe_2) all form stronger bonds to silicon than do either carbon or another silicon. In addition, all these substituents contain lone pairs. The presence of such lone pairs could promote the formation of dimers (or oligomers) through M-Y-M bridges. This was elegantly demonstrated recently by Xue in the the reaction of $Zr(NMe_2)_4$ with Ph_2SiH_2 where a novel trinuclear complex of "$HZr(NMe_2)_3$" was isolated (15). In the metallocene systems, such bridges could also connect metals in different oxidation states. Elimination of HY (Path 2) could lead to adducts such as $Cp_2MY{\cdot}HY$ (particularly with HOPh or $HNMe_2$).[3] If a number of monomeric or oligomeric metal complexes form, it would be fortuitous to isolate crystalline metal products from the near stoichiometric reactions.

Although Cp_2MHCl (A in Scheme 2) is known for Zr, and Hf (and possibly for Ti (22*c*)), Cp_2MHF, $Cp_2MH(OPh)$, and $Cp_2MH(NMe_2)$ do not appear to have been reported. A few examples of monomeric Cp^*_2MHY (M = Hf, Y = Cl, NMe_2; M = Zr, Y = F) do exist (26). This suggests that a study of $Cp^*_2MY_2$ or of other substituted metallocenes complexes with hydrosilanes may provide a less complex system in which to identify intermediate products which could not be identified with Cp_2MY_2 reactants. In general, however, metallocenes with overly substituted rings are not good dehydrocoupling catalysts (2*c*, 9*b*).

Conclusion

Metallocenes, Cp_2MY_2, with electronegative Y substituents such as F, OPh, and NMe_2 function as single component catalysts for the dehydrocoupling of $PhSiH_3$. The molecular weights of the polysilane products are comparable to those produced from the previously studied combination catalyst system, Cp_2MCl_2–2*n*-BuLi, and in most cases exceed those produced from this system. An induction period was observed for Cp_2MF_2 and $Cp_2M(OPh)_2$ but essentially none was found with $Cp_2M(NMe_2)_2$. The amide system also produced the highest molecular weights for all three metals.

Reactions of Cp_2MY_2 with primary, secondary, and tertiary silanes on a near stoichiometric scale shows that one or more Y groups could be transferred from the metal to the silicon center. The formation of Y-SiRR′R′′ suggests that hydride was transferred to the metal center during the induction period to form a metallocene hydride species that functioned as the actual catalyst for the dehydrocoupling reaction. However, efforts to observe these MH systems by NMR spectroscopy or by trapping reactions (with PMe_3) were not successful even in reactions of tertiary silanes where dehydrocoupling has not been observed. During the induction period, reduction of Ti(IV) to Ti(III) also occurred and Ti(III) hydride dimers analogous to those reported in the literature were identified spectroscopically (^{1}H NMR). It is possible that reactions of metallocenes with bulkier cyclopentadiene substituents would lead to MH-containing products that could be trapped as monomers and crystallographically characterized.

The single reagent precatalysts exhibit certain disadvantages over the two component precatalyst system, Cp_2MCl_2–2*n*-BuLi, the components of which are commercially available. Since none of the Cp_2MY_2 (M = F, OPh, NMe_2) are commercially available additional synthetic steps from Cp_2MCl_2 are required. The metallocene (Cp_2TiF_2) has the attractive advantage of being air and water stable in contrast to all the other catalyst systems that have been discussed. The facile reaction of an NMe_2 group in $Cp_2M(NMe_2)_2$ and the higher molecular weight polysilane products that are produced suggest that such substituents could be usefully developed in new catalyst systems. On the other hand, the results described in this report also suggest that the development of precatalysts for dehydrocoupling that do not contain Cp-substituents must take into consideration the possible removal of coordinated O-based or N-based ligands by reacting hydrosilanes. Developing such catalysts will be a challenge in the future.

[3] Formation of $Cp_2TiH{\cdot}NH_3$ has been proposed in the catalytic loop for the reaction of $PhSiH_3$ and NH_3 (23*f*).

© 2000 NRC Canada

Experimental

General methods

All reactions were carried out under an atmosphere of nitrogen in sealed Schlenk flasks that were flame-dried before use. Solvents were freshly distilled under nitrogen from sodium/benzophenone prior to use. ^{1}H, ^{29}Si, and ^{19}F NMR spectra were recorded using a Varian Unity 300 (^{1}H and ^{29}Si referenced to TMS) and an XL-300 (^{19}F, referenced to $CFCl_3$). Unless otherwise stated, the solvent for NMR data collection was benzene-d_6. GPC data were collected using an SSI 222D HPLC pump to elute the samples through a bank of 10^4, 10^2, and 500 Å Waters 78 × 300 mm Ultrastyragel columns in HPLC grade THF solvent. A Linear UV-vis detector set to 254 nm was used for the detection of the polymers. Molecular weights are reported with respect to polystyrene standards.

The following compounds were prepared according to literature procedures: Cp_2MF_2 (M = Ti (27), Zr (28), Hf (28)), $Cp_2M(OPh)_2$ (M = Ti, (29) Zr, (30) Hf (31)), $Cp_2M(NMe_2)_2$ (M = Ti (32), Zr (32), Hf (32)), $PhSiH_3$ (33), (p-$CH_3C_6H_4$)SiH_3 (34), $PhMeSiH_2$ (35), Ph_2SiH_2 (36), $PhSiF_3$ (13), PhMeSiHF (13), $PhMeSiF_2$ (13), PhMeSiH(OPh) (37), $PhMeSi(OPh)_2$ (37), $Ph_2MeSi(OPh)$ (37), and HPhMeSiSiMePhH (38). Ph_2MeSiH was a commercial sample.

General procedures for the dehydropolymerization of $PhSiH_3$

A mixture of Cp_2MY_2 (0.08 mmol, 1 mol%) and $PhSiH_3$ (~1 mL, 8 mmol) in a 25 mL Schlenk tube was magnetically stirred at the indicated temperatures for a period of time until the color of the mixture changed and gas evolution was observed (Table 1). The reaction mixture was cooled immediately to room temperature and was continually stirred for two or more days. To obtain an NMR sample, an aliquot from the reaction mixture was added to a dried, N_2-filled NMR tube containing C_6D_6. For the GPC sample an aliquot was removed, added to THF and air passed through the solution. Solutions were filtered before injection onto the GPC columns. Molecular weight data are also summarized in Table 1.

General procedure for NMR studies

Under a nitrogen atmosphere a mixture of Cp_2MY_2 (0.06 mmol) and hydrosilanes (0.25 mmol; approximate ratio of Si:M = 4:1) in a NMR tube was placed in an oil bath of desired temperature and periodically shaken until the color change described in Table 1 was observed. The solvent C_6D_6 was added to the tube by syringe and the spectrum was obtained. Trapping reagents (acetone or PMe_3; stoichiometry relative to the metal) were added to selected samples and the NMR spectrum again was obtained. In selected cases, excess acetone or PMe_3 were added but no new information was obtained.[4]

Acknowledgements

We are grateful for partial support of this work from a Research Award from the University of Missouri-St. Louis. We also wish to thank Ziling "Ben" Xue for providing a sample of $Cp_2Ti(NMe_2)_2$ in the initial stages of the investigation.

References

1. (*a*) R.D. Miller and J. Michl. Chem. Rev. **89**, 1359 (1989); (*b*) R. West. J. Organomet. Chem. **300**, 327 (1986).
2. (*a*) T.D. Tilley. Comments Inorg. Chem. **10**, 49 (1990); (*b*) R.M. Laine. *In* Aspects of homogeneous catalysis. *Edited by* R. Ugo. Kluwer Academic Publishers, Amsterdam. 1990. pp. 37; (*c*) J.Y. Corey. *In* Advances in silicon chemistry. Vol. 1. *Edited by* G. Larson. JAI Press Inc., Greenwich, Conn. 1991. p. 327; (*d*) J.F. Harrod, Y. Mu, and E. Samuel. Polyhedron, **10**, 1239 (1991); (*e*) T.D. Tilley. Acc. Chem. Res. **26**, 22 (1993); (*f*) J.F. Harrod. Adv. Organomet. Chem. **42**, 363 (1998).
3. M. Cypryk, Y. Gupta, and K. Matyjaszewski. J. Am. Chem. Soc. **113**, 1046 (1991).
4. K. Sakamoto, K. Obata, H. Hirata, M. Nakajima, and H. Sakurai. J. Am. Chem. Soc. **111**, 641 (1989).
5. (*a*) C. Aitken, J.F. Harrod, and E. Samuel. J. Organomet. Chem. **279**, C11 (1985); (*b*) J.P. Barry, F. Gauvin, J.F. Harrod, A. Malek, and D. Rosseau. Organometallics, **8**, 1732 (1989).
6. (*a*) J.Y. Corey and X.H. Zhu. J. Organomet. Chem. **439**, 1 (1992); (*b*) R.M. Shaltout and J.Y. Corey. Tetrahedron, **51**, 4309 (1995).
7. S. Bourg, R.J.P. Corriu, M. Enders, and J.J.E. Moreau. Organometallics, **14**, 564 (1995).
8. (*a*) Q. Wang and J.Y. Corey. Abstracts of papers, 31st organosilicon symposium. New Orleans, LA. May 1998, P-5; (*b*) F. Lunzer, C. Marschner, and S. Landgraf. J. Organomet. Chem. **568**, 253 (1998).
9. (*a*) J.L. Huhmann, J.Y. Corey, and N.P. Rath. J. Organomet. Chem. **533**, 61 (1997); (*b*) R.M. Shaltout and J.Y. Corey. Main Group Chem. **1**, 115 (1995); (*c*) J.L. Huhmann. Ph.D. Thesis. University of Missouri-St. Louis, St. Louis, MO. 1996.
10. (*a*) J.F. Walzer, H.-G. Woo, and T.D. Tilley. Polym. Prepr. (Am. Chem. Soc. Div. Polym. Chem.) **32**, 441 (1991); (*b*) T.D. Tilley and H.-G. Woo. Inorganic and organometallic oligomers and polymers. *Edited by* J.F. Harrod and R.M. Laine. Kluwer Academic Publishers. Netherlands. 1991. pp. 3–11.
11. H. Li, F. Gauvin, and J.F. Harrod. Organometallics, **12**, 575 (1993).
12. B.J. Grimmond and J.Y. Corey. Organometallics, **18**, 2223 (1999).
13. A. Kunai, T. Sakurai, E. Toyoda, and M. Ishikawa. Organometallics, **15**, 2478 (1996).
14. (*a*) R.J.P. Corriu, H. Leclercq, P.H. Mutin, J.M. Planeix, and A. Vioux. J. Organomet. Chem. **406**, C1 (1991); (*b*) R.H. Cragg and R. D. Lane. J. Organomet. Chem. **277**, 199 (1984); (*c*) R.H. Cragg and R.D. Lane. J. Organomet. Chem. **294**, 7 (1985); (*d*) L.W. Breed, R.L. Elliott, and J.C. Wiley, Jr. J. Organomet. Chem. **31**, 179 (1970); (*e*) S.S. Washburne and W.R. Peterson, Jr. J. Organomet. Chem. **21**, 59 (1970).
15. X. Liu, Z. Wu, Z. Peng, Y-D. Wu, and Z. Xue. J. Am. Chem. Soc. **121**, 5350 (1999). We thank Professor Xue for providing a preprint prior to publication.
16. D.S. Hays and G.C. Fu. J. Org. Chem. **62**, 7070 (1997) and its supporting information.
17. (*a*) E. Samuel and J.F. Harrod. J. Am. Chem. Soc. **106**, 1859 (1984); (*b*) C.T. Aitken, J.F. Harrod, and E. Samuel. J. Am. Chem. Soc. **108**, 4059 (1986).

[4] Supplementary material may be purchased from the Depository of Unpublished Data, Document Delivery, CISTI, National Research Council Canada, Ottawa, ON, Canada K1A OS2 (http://www.nrc.ca/cisti/irm/unpub_e.shtml for information on ordering electronically).

© 2000 NRC Canada

18. R. Shu, L. Hao, J.F. Harrod, H.-G. Woo, and E. Samuel. J. Am. Chem. Soc. **120**, 12988 (1998).
19. P.C. Wailes and H. Weigold. J. Organomet. Chem. **24**, 413 (1970).
20. C.A. Aitken, J.F. Harrod, and E. Samuel. J. Organomet. Chem. **279**, C11 (1985).
21. T. Imori and T.D. Tilley. Polyhedron, **13**, 2231 (1994).
22. (*a*) H-G. Woo and T.D. Tilley. J. Am. Chem. Soc. **111**, 3757 (1989); (*b*) H-G. Woo and T.D. Tilley. J. Am. Chem. Soc. **111**, 8043 (1989); (*c*) H.-G. Woo, J.F. Walzer, and T.D. Tilley. J. Am. Chem. Soc. **114**, 7047 (1992).
23. (*a*) C. Aitken, J.F. Harrod, and E. Samuel. Can. J. Chem. **64**, 1677 (1986); (*b*) C. Aitken, J.F. Harrod, and U.S. Gill. Can. J. Chem. **65**, 1804 (1987); (*c*) Y. Mu, C. Aitken, B. Cote, J.F. Harrod, and E. Samuel. Can. J. Chem. **69**, 264 (1991); (*d*) J.F. Harrod, Y. Mu, and E. Samuel. Can. J. Chem. **70**, 2980 (1992); (*e*) E. Samuel, Y. Mu, J.F. Harrod, Y. Dromzee, and Y. Jeannin. J. Am. Chem. Soc. **112**, 3435 (1990); (*f*) H.Q. Liu and J.F. Harrod. Organometallics, **11**, 822 (1992).
24. E. Spaltenstein, P. Palmer, K.A. Kreutzer, C.A. Willoughby, W.M. Davis, and S.L. Buchwald. J. Am. Chem. Soc. **116**, 10308 (1994).
25. T. Takahashi, M. Hasegawa, N. Suzuki, M. Saburi, C.J. Rousset, P.E. Fanwick, and E-i. Negishi. J. Am. Chem. Soc. **113**, 8564 (1991).
26. D.J. Cardin, M.F. Lappert, and C.L. Raston. Chemistry of organo-zirconium and -hafnium compounds. Ellis Horwood Limited, Chichester. 1986. Chap. 12.
27. P.M. Druce, B.M. Kingston, M.F. Lappert, T.R. Spalding, and R.C. Srivastava. J. Chem. Soc. A, 2106 (1969).
28. E.F. Murphy, P. Yu, S. Dietrich, and H.W. Roesky. J. Chem. Soc. Dalton Trans. 1983 (1996).
29. K. Andra. J. Organomet. Chem. **11**, 567 (1968).
30. K. Andra and E. Hille. Z. Naturforsch. B: Anorg. Chem. Org. Chem. Biochem. Biophys. Biol. **24B**, 169 (1969).
31. E.M. Brainina, L.A. Fedorov, and M.Kh. Minacheva. Dokl. Akad. Nauk. SSSR, **96**, 1085 (1971).
32. G. Chandra and M.F. Lappert. J. Chem. Soc. A, 1940 (1968).
33. A.E. Finholt, A.C. Bond, Jr., K.E. Wilzback, and H.I. Schlesinger. J. Am. Chem. Soc. **69**, 2692 (1947).
34. Y. Nagai, H. Matsumoto, M. Hayashi, E. Tajima, M. Ohtsuki, and N. Sekikawa. J. Organomet. Chem. **29**, 209 (1971).
35. L.I. Zakharkin. Izv. Akad. Nauk. SSSR, Otdel. Khim. Nauk. 2244 (1960).
36. R.A. Benkesser, H. Landesman, and D. Foster. J. Am. Chem. Soc. **74**, 648 (1952).
37. Z-Y. Zhang and Z-B. Xia. Youji Huaxue, 63 (1993).
38. J.Y. Corey, X-H. Zhu, T.C. Bedard, and L.D. Lange. Organometallics, **10**, 924, 1991.

© 2000 NRC Canada

Neutral hyperconjugation and one-bond couplings between heavy atoms

Joseph B. Lambert, Catherine E. Shawl, and Ernani Basso

Abstract: The relationship has been examined between bond order and one-bond couplings involving heavy atoms, as modulated by neutral hyperconjugation. Two systems have been studied in which either an aromatic ring or a double bond can influence, through hyperconjugation, the α and β bonds (respectively, C—C and C—M in =C-C-M). Hyperconjugation may be modulated by substituents on the aromatic ring or double bond or by placement of different atoms (M = C, Si, Ge, or Sn) at the β position. The α bond exhibits no relationship between coupling constant and neutral hyperconjugation, but the β bond shows a strong relationship.

Key words: hyperconjugation, germanium, σ-π conjugation, silicon, tin.

Résumé : On a examiné la relation entre l'ordre de liaison et les couplages à travers une liaison impliquant des atomes lourds, tels que modulée par l'hyperconjugaison neutre. On a étudié deux systèmes dans lesquels l'hyperconjugaison permet d'influencer un noyau aromatique ou une double liaison, soit les liaisons α et β (respectivement C—C et C—M dans =C-C-M). On peut moduler l'hyperconjugaison en fixant divers substituants sur le noyau aromatique ou en plaçant divers atomes (M = C, Si, Ge ou Sn) en position de la double liaison. Pour la liaison α, il n'existe aucune relation entre la constante de couplage et l'hyperconjugaison neutre; toutefois, pour la liaison β, il existe une grande relation.

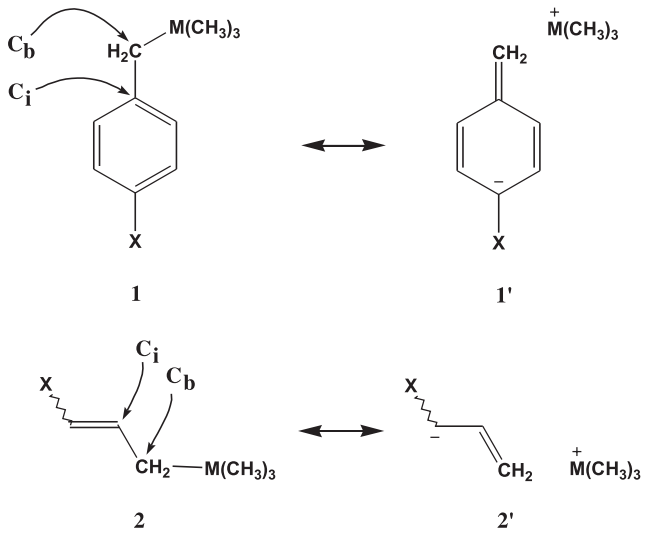
Mots clés : hyperconjugaison, germanium, conjugaison σ-π, silicium, étain.

Introduction

The donation of σ electrons to π orbitals has been termed hyperconjugation or double-bond, no-bond resonance (1, 2). Valence structures **1** and **1′** illustrate hyperconjugation within neutral aromatics and structures **2** and **2′** illustrate the phenomenon within neutral alkenes. As the structures suggest, hyperconjugation is associated with important changes in bond order. These changes have been well documented in positively charged systems. Thus hyperconjugation is not doubted as the underlying cause for the stabilization of carbocations by alkyl groups and, to an even greater extent, stabilization of carbocations by electropositive elements such as silicon at the β position (3, 4). Electron demand in charged systems thus brings about large kinetic and thermodynamic effects.

Because the effects are much smaller or even negligible in neutral systems, neutral hyperconjugation has been a more controversial subject than charged hyperconjugation (2). There have been no systematic crystallographic studies that would provide unambiguous evidence for neutral hyperconjugation. A theoretical study has concluded that neutral hyperconjugation can alter bond lengths in hydrocarbons by about 0.015 Å (5). The systems studied had been selected because of structural anomalies suggested by crystallography. Even in these systems, however, the bond length changes were rather small.

We suggested that one-bond coupling constants between heavy atoms might provide a novel approach to assessing neutral hyperconjugation (6). The hypothesis is that these one-bond couplings reflect the bond order changes induced by neutral hyperconjugation in structures **1** and **2**. Thus in



Received May 19, 1999. Published on the NRC Research Press website on October 30, 2000.

This paper is dedicated to Professor Adrian G. Brook on the occasion of his 75th birthday.

J.B. Lambert[1] and C.E. Shawl. Department of Chemistry, Northwestern University, Evanston IL 60208-3113, U.S.A.
E. Basso. Departamento de Química, Universidade Estadual de Maringá, Av. Colombo 5790, 87020–900 Maringá – PR Brazil.

[1]Author to whom correspondence should be addressed. Fax: 847-491-7713.

© 2000 NRC Canada

the aromatic case, neutral hyperconjugation should enhance the coupling between the ipso and the benzylic carbons ($^1J(C_i\text{-}C_b)$ in **1**) and diminish the coupling between the benzylic carbon and the β atom M ($^1J(C_b\text{-}M)$). In the alkenic case **2**, the allylic carbon replaces the benzylic carbon in these couplings.

As the ionic resonance structures (**1′** and **2′**) indicate, neutral hyperconjugation should be enhanced by electron-withdrawing groups X (which stabilize the negative charge) or by electron-donating atoms M (which stabilize the positive charge). We previously explored the phenomenon in the aromatic series (6) and concluded that neutral hyperconjugation is unimportant when M is carbon but increases in significance down the 14th column, from silicon to germanium to tin. This study involved measurement of one-bond $^{13}C\text{-}^{13}C$ couplings by the INADEQUATE method and direct measurement of one-bond $^{13}C\text{-}^{29}Si$ and $^{13}C\text{-}^{119}Sn$ couplings.

In the course of this study, we measured 71 $^{13}C\text{-}^{13}C$ coupling constants and all the corresponding chemical shifts (6). We found that the chemical shifts and the couplings between aromatic carbons provided little or no information on hyperconjugation. The one-bond couplings to the benzylic carbon, however, did reflect neutral hyperconjugation, but only for the atoms (M) below carbon. Subsequently, Kamieńska-Trela (7) found that two of these couplings were mismeasured. We concurred with this observation (8), and suggested that two others also had been mismeasured because of peak overlap in the INADEQUATE spectra in each case. These were the $^1J(C_i\text{-}C_b)$ for the four carbon compounds, that is, **1** with M = C and X = MeO, Me, H, and NO_2. We now have remeasured all the $C_i\text{-}C_b$ and $C_b\text{-}M$ couplings for molecules **1**. In addition, we have prepared several examples from the alkene series **2** and measured the analogous couplings. We report these measurements herein and assess the results in terms of the relationship between one-bond couplings and neutral hyperconjugation.

Results and discussion

We have prepared the aromatic series **1** anew with M = C and X = MeO, Me, H, and NO_2; with M = Si and Sn and X = MeO, Me, H, and CN; and with M = Ge and X = MeO, Me, and H. We have prepared the alkene series **2** with M = C and X = MeO (*cis* and *trans*), Me (*trans*), H, and CN (*cis* and *trans*); with M = Si and X = Me; and with M = Ge and X = H (in this case the group on M is butyl rather than methyl). The newly measured couplings are given in Tables 1–3. All $^{13}C\text{-}^{13}C$ couplings were obtained by the INADEQUATE method, and all $^{29}Si\text{-}^{13}C$ and $^{119}Sn\text{-}^{13}C$ couplings were measured directly. In each case the $^{13}C\text{-}^{13}C$ couplings were measured twice, as they appear in the INADEQUATE spectra for each coupled carbon. Except for the four cases already mentioned (7, 8), all $^{13}C\text{-}^{13}C$ couplings were very close to those previously measured in the aromatic series, but the results must be reinterpreted in light of the four corrected measurements.

According to the double-bond, no-bond resonance structure for the aromatic series (**1′**), the bond order between the ipso and benzylic carbons should increase with increased electron-withdrawing nature of X and electron-donating nature of M. The $^1J(C_i\text{-}C_b)$ coupling, however, does not reflect this trend. In any given M series (C, Si, Ge, Sn for constant X), the trend begins with the highest value for C, continues with the lowest value for Si, and then rises slightly for Ge and Sn, for example, 45.1, 41.7, 43.7, 43.9 Hz for X = MeO. If this coupling constant reflected increased neutral hyperconjugation from C to Sn, the value should have increased monotonically. The variation in fact follows a simple dependence on the electronegativity of M. The Pauling–Allred electronegativities (9) for C, Si, Ge, and Sn respectively, are 2.55, 1.90, 2.01, and 1.96. Thus a prime factor controlling this coupling constant is the electron density provided through the σ framework rather than neutral hyperconjugation.

Table 1. One-bond couplings (Hz) in the aromatic series **1**.

X	M	$^1J(C_i\text{-}C_b)^a$	$^1J(C_b\text{-}M)$
MeO	C	45.1 (45.1, 45.1)	33.9
	Si	41.7 (41.5, 41.9)	47.3
	Ge	43.7 (43.9, 43.4)	
	Sn	43.9 (43.9, 43.8)	309
Me	C	44.3 (44.5, 44.1)	33.9
	Si	41.0 (40.8, 41.2)	46.7
	Ge	42.7 (42.7, 42.6)	
	Sn	43.2 (42.9, 43.4)	301
H	C	43.9 (43.9, 43.9)	32.9
	Si	40.9 (40.8, 41.0)	46.3
	Ge	42.8 (42.7, 42.9)	
	Sn	42.7 (42.4, 42.9)	288
CN	Si	40.3 (40.3, 40.3)	43.3
	Sn	42.6 (42.4, 42.7)	252
NO_2	C	42.8 (42.9, 42.7)	33.1

[a]Respectively, the mean, the coupling measured from the CH_2 (C_b) signal and the coupling measured from the C_{ipso} (C_i) signal.

For the X series with constant M, this same coupling constant, $^1J(C_i\text{-}C_b)$, decreases with increased electron withdrawal, for example, 45.1, 44.3. 43.9, 42.8 Hz for M = C and X = MeO, Me, H, NO_2. The values decrease for other M to a lesser extent, contrary to the expectation for neutral hyperconjugation, which should increase with larger M. This effect again is along the lines expected for electron withdrawal through the σ framework. Thus variation of the C-C coupling between the ipso and benzylic carbons appears to depend primarily on σ (inductive) rather than π (neutral hyperconjugative) effects. This conclusion is contrary to our earlier study, which was misled by the incorrect values of 36.0 Hz measured for the four C systems, thereby generating a monotonic increase from C to Sn for a given X series.

According to resonance structure **1′**, the bond order between the benzylic carbon and M should decrease with increased electron-withdrawing nature of X and electron-donating nature of M. This prediction cannot be tested for the M series with constant X, as the identity of the coupling partners changes, from C-C to C-Si to C-Sn. The only test therefore is for the X series with constant M. For M = C $^1J(^{13}C\text{-}^{13}C)$ is 33.9, 33.9, 32.9, and 33.1 Hz for X = MeO, Me, H, and NO_2. This invariance suggests no dependence on either neutral hyperconjugation or inductive effects of X. For the carbon series, neutral hyperconjugation must be negligible according to this coupling constant probe, and the X

© 2000 NRC Canada

Table 2. One-bond couplings (Hz) in the alkene series **2**.

X	M	^1J(C=C)[a]	^1J(=C-C_b)[b]	^1J(C_b-M)
cis-MeO	C	81.5 (81.5, 81.5)	45.0 (44.0, 45.9)	36.6
trans-MeO	C	81.9 (81.6, 82.1)	45.9 (46.0, 45.8)	36.6
trans-Me	C	74.5 (73.8, 75.2)	49.7 (45.5, 43.9)	33.8
trans-Me	Si	71.6 (71.8, 71.4)	39.1 (39.0, 39.2)	67.1
H	C	69.2 (69.4, 69.0)	42.3 (42.0, 42.6)	33.8
H	Ge[c]	69.4 (69.3, 69.5)	40.6 (40.7, 40.5)	
cis-CN	C	72.6	41.7 (41.7, 41.7)	33.6
trans-CN	C	73.6	41.7	33.2

[a]Respectively, the mean, the coupling measured from the X-**C**H=C signal, and the coupling measured from the C=**C**H-CH_2 signal.
[b]Respectively, the mean, the coupling measured from the =**C**H-CH_2 signal, and the coupling measured from the CH-**C**H_2M signal.
[c]The alkyl group on germanium is butyl rather than methyl.

group is too far away to manifest an effect through the σ framework. For M = Si, ^1J(^{13}C-^{29}Si) is 47.3, 46.7, 46.3, and 43.3 Hz for X = MeO, Me, H, and CN. This monotonic decrease with increasing electron withdrawal is the expectation for both neutral hyperconjugation and induction. Since induction had no effect in the C series, it is doubtful that it should suddenly bring about a significant effect in coupling constants that are only some 30% larger for the Si series. Consequently, there is a strong likelihood that neutral hyperconjugation is causing this coupling variation.

There is no germanium nuclide for which couplings to carbon can be measured. For M = Sn, ^1J(^{13}C-^{119}Sn) is 309, 301, 288, and 252 Hz for X = MeO, Me, H, and CN. As with Si, this trend is in agreement with either inductive or neutral hyperconjugative effects. As inductive effects should be constant for the series C, Si, Sn, this large increase in the modulation of the coupling is explicable only by neutral hyperconjugation. This coupling therefore appears to be strongly sensitive to hyperconjugation and demonstrates that the effect increases remarkably from C to Si to Sn. The large sensitivity of ^1J(C_b-M) to neutral hyperconjugation compared with ^1J(C_i-C_b) can be attributed to the closeness of M to the C_b-M bond and the greater distance of X to the C_i-C_b bond.

We have more limited data in the alkene series, with a full set only for M = C. Of particular interest is the coupling between the doubly bonded carbons, ^1J(C=C). The analogous couplings in the aromatic series (6) are those between adjacent aromatic carbons. We found little dependence of these couplings on M. Thus for X = H in the aromatic series **1**, the values of ^1J(C_m-C_p) were 55.9 Hz for the entire series of M = C, Si, Ge, and Sn. The values of ^1J(C_o-C_m) for this series were 56.6, 57.2, 57.2, and 57.2 Hz for X = Me, and the values of ^1J(C_i-C_o) were 57.0, 57.3, 57.3, and 57.3 Hz for X = MeO. The only variation of any size was for ^1J(C_m-C_p), which is most affected by direct connection to X, for example, for M = C, 67.6, 56.9, and 55.9 Hz for X = MeO, Me, H. The coupling ^1J(C=C) between the two sp^2 atoms in the alkene series is structurally analogous to ^1J(C_m-C_p), in the sense that the X group is attached to one of the coupled carbons. The variation with X is somewhat similar: for M = C, 81.9, 74.5, and 69.2 Hz for the same substituents, X = MeO, Me, H, indicating greater double bond character for C_m-C_p with electron donation.

Effects of neutral hyperconjugation must then be sought from other couplings. The values of ^1J(=C-CH_2), analogous to ^1J(C_i-C_b) in the aromatic series, for M = C are 45.9, 44.7, 42.3, and 41.7 Hz for X = MeO, Me, H, and CN. This is the identical trend observed in the aromatic series, contrary to neutral hyperconjugation (the coupling should increase with electron withdrawal according to resonance structure **2′**) but in agreement with induction, whereby σ electron withdrawal decreases the coupling. As we have only single values for Si and Ge, we cannot examine this coupling as a function of M.

Table 3. Further one-bond couplings (Hz) in the alkene series **2**, X-CH=CH-CH_2-M(CH_3)$_3$.

X	M	^1J(X-CH=)[a]	^1J(M-CH_3)[a]
trans-Me	C	43.6 (43.5, 43.7)	
trans-Me	Si	43.2 (43.0, 43.4)	65.2
H	C		36.1
cis-CN	C	79.8	36.1
trans-CN	C	78.3	36.1

[a]Respectively, the mean, the coupling measured from the X signal (CH_3 or CN), and the coupling measured from the X-**C**H signal.

In the aromatic series, we found ^1J(C_b-M) to be sensitive to neutral hyperconjugation. The analogous coupling in the alkene series is ^1J(CH_2-M). The only data we have for this series is for M = C for which the values are 36.6, 33.8, 33.8, and 33.2 Hz for X = MeO, Me, H, and CN. There is a possibility that neutral hyperconjugation is having some effect here, as the coupling decreases monotonically with increased electron withdrawal, as expected for resonance structure **2′**. The absolute change, however, is relatively small. Confirmation would have to await preparation of an entire Si or Sn series, which, however, we found synthetically impractical.

The alkene series can exist as either cis or trans isomers, and our syntheses sometimes resulted in stereoisomeric mixtures. The data in Tables 2 and 3 indicate that none of the measured coupling constants exhibits any important dependence on the stereochemistry of the double bond.

Conclusions

The one-bond ^{13}C-^{13}C coupling across the partial double bonds in the aromatic ring and the alkene exhibit significant changes with the nature of the X substituent, but these variations appear to depend primarily on the inductive effect of X. The C-C coupling between the methylene-substituted aromatic or alkenic carbon and the methylene (benzylic, allylic) carbon exhibits small variations with X that also parallel the

© 2000 NRC Canada

inductive effect of X. In the aromatic series, this coupling exhibits small variations with M that parallel the electronegativity of M. The only C-C coupling that exhibits the variation expected for neutral hyperconjugation is that between the allylic methylene carbon and the *tert*-butyl carbon (M = C in the alkene series), and this variation is only 3 Hz. In contrast, the Si-C and particularly the Sn-C couplings in the aromatic series exhibit large variations with change in X that are consistent with neutral hyperconjugation. These couplings are larger to begin with than the corresponding C-C couplings, but the critical consideration probably is the larger magnitude of neutral hyperconjugation in the silicon and tin systems because of the higher polarizability and electropositivity of these elements than carbon.

Experimental section

Aromatic systems **1** were prepared by the methods described earlier (6). 4,4-Dimethyl-1-pentene (**2**, M = C, X = H) and allyltributylgermane (M = Ge, X = H, but with butyl replacing methyl on M) are commercially available. *trans*-5,5-Dimethyl-2-hexene (M = C, X = CH_3) was prepared by the reaction of *tert*-butyllithium with 1,3-butadiene, followed by slow distillation through a Vigreux column (10). 1-Cyano-4,4-dimethyl-1-pentene (M = C, X = CN) was obtained as a *cis*/*trans* mixture by the Wittig reaction of triphenyl(cyanomethyl)phosphonium chloride (from triphenylphosphine and chlorocyanomethane) and 3,3-dimethylbutanal (11). 1-Methoxy-4,4-dimethyl-1-pentene (M = C, X = OMe) was obtained in an analogous fashion with methoxychloromethane as the starting material (11). *trans*-2-Butenyltrimethylsilane was prepared by the reaction of 1-bromo-1-propene with the Grignard reagent (trimethylsilyl)methylmagnesium chloride ($(CH_3)_3SiCH_2MgCl$) in the presence of ($Ni(II)(dppp)Cl_2$) catalyst (12).

Spectra were obtained on a Bruker AMX600 NMR spectrometer with ^{13}C at 150.91 MHz. The standard 1D INADEQUATE pulse was performed, 90°(*x′*)-τ-*180°(y′)*-τ-90°(*x′*) with phase cycling. The GARP decoupling sequence was used, with a 90° pulse of 150 μs. Because the substrates were all liquids, samples were run as 90% solutions with the remaining 10% either $CDCl_3$ or acetone-d_6. The relaxation reagent chromium(acetylacetonate) was added to shorten the delay time between acquisitions, which typically dropped from 10 to 0.5 s. Acquisitions normally required overnight runs with about 50 000 transients. The constant delay time τ in the pulse sequence, $1/4J(^{13}C\text{-}^{13}C)$, was optimized for the coupling constant of interest. For example, for J = 70 Hz τ was 3.57 ms and for J = 35 Hz τ was 7.14 ms. Couplings to ^{29}Si and ^{119}Sn were read directly from the spectra.

Acknowledgements

This work was supported by the National Science Foundation (Grant no. CHE-9725652).

References

1. N. Muller and R.S. Mulliken. J. Am. Chem. Soc. **80**, 3489 (1958).
2. M.J.S. Dewar. Hyperconjugation. Ronald Press, N.Y. 1962.
3. T.G. Traylor, W. Hanstein, H.J. Berwin, N.A. Clinton, and R.S. Brown. J. Am. Chem. Soc. **93**, 5715 (1971).
4. J.B. Lambert. Tetrahedron, **46**, 2677 (1990); J.B. Lambert, Y. Zhao, R.W. Emblidge, L.A. Salvador, X. Liu, J.-H. So, and E.C. Chelius. Acc. Chem. Res. **32**, 183 (1999).
5. N.L. Allinger, K. Chen, J.A. Katzenellenbogen, S.R. Wilson, and G.M. Anstead. J. Comput. Chem. **17**, 747 (1996).
6. J.B. Lambert and R.A. Singer. J. Am. Chem. Soc. **114**, 10246 (1992).
7. K. Kamieńska-Trela. Magn. Reson. Chem. **33**, 406 (1995).
8. J.B. Lambert and R.A. Singer. J. Am. Chem. Soc. **117**, 2122 (1995).
9. A.L. Allred. J. Inorg. Nucl. Chem. **17**, 215 (1961); D.F. Shriver, P. Atkins, and C.H. Langford. Inorganic chemistry. 2nd ed. W.H. Freeman Co., N.Y. 1994.
10. W.H. Glaze, J.E. Hanicak, M.L. Moore, and J. Chaudhuri. J. Organomet. Chem. **44**, 39 (1972).
11. A.I. Meyers and R.C. Strickland. J. Org. Chem. **37**, 2579 (1972).
12. M. Kumada, K. Tamao, and K. Sumitani. Org. Syn. **58**, 127 (1978).

© 2000 NRC Canada

Silaheterocycles 36 (1). Trichlorovinylsilane, lithium-*tert*-butyl, and 1,3-enynes: A versatile combination for the competitive formation of silacyclobutanes and silacyclobutenes

N. Auner, M. Grasmann, B. Herrschaft, and M. Hummer

Abstract: Equimolar amounts of trichlorovinylsilane **(9)**, lithium-*tert*-butyl, and 1,3-enynes were reacted to yield the corresponding isomeric silacyclobutanes and silacyclobutenes competitively. As reaction pathway the mixture **9**/^{t}BuLi is discussed to give a silene equivalent, $Cl_2Si{=}CHCH_2{}^tBu$ **(10)**, yielding the four-membered ring silacycles by formal [2 + 2] cycloaddition reactions of **10** with the C=C double or the C≡C triple bond of the 1,3-enyne. The relative ratio of the products formed depends on the polarity of the multiple bonds in the enyne, which is mainly determined by the substituent pattern. Thus, from the organosubstituted 1,3-enynes $R^1C{\equiv}C\text{-}C(R^2){=}CR^3R^4$ (R^1 = Me, Et, $SiMe_3$, Ph; R^2 = H, Me, Ph; R^3=Me, OMe, Ph; R^4=H; and $R^1C{\equiv}C\text{-}R'$ (R′ = 1-cyclohexenyl, cyclohexanevinylidyne)) and **9**/^{t}BuLi the silacyclobutanes **12**, **13**, and **15** and the silacyclobutenes **14**, **16**–**24,** and **27** (from **10** and 3-hexyne) are prepared in a one-step synthesis and isolated from the reaction mixtures. The silacyclobutanes and -butenes are thermally stable and can be distilled under vacuo up to temperatures of about 150°C without decomposition. The experimental results are confirmed qualitatively by semiempiric calculations at the AM-1 level and their analysis using FMO theory. The solid state structure of the silacyclobutene **19** ($C_{17}H_{30}Cl_2Si_2$) has been determined by single crystal X-ray diffractometry. **19** is orthorhombic, space group $P2_12_12_1$, a = 1030.94(2) pm, b = 1244.6(2) pm, c = 1605.5(3) pm, Z = 4.

Key words: neopentylsilene, dichloroneopentylsilene, silacyclobutenes, silacyclobutanes, 1,3-enynes.

Résumé : La réaction de quantités équimoléculaires de trichlorovinylsilane (**9**), de *tert*-butyllithium et de 1,3-énynes conduit à la formation compétitive des silacyclobutanes et silacyclobutènes isomères correspondants. On suggère que la voie réactionnelle du mélange de **9**/^{t}BuLi conduit à un silène équivalent, $Cl_2Si{=}CHCH_2{}^tBu$ (**10**), qui, par une réaction de cycloaddition [2 + 2] avec les liaisons double, C=C, ou triple, C≡C, du 1,3-ényne conduit à la formation de cycles silylés à quatre chaînons. Les rapports relatifs des produits qui se forment dépendent de la polarité des liaisons multiples de l'ényne qui est déterminée principalement par les motifs de substitution. Ainsi, les 1,3-énynes substitués par des groupes organiques ($R^1\text{-}C{\equiv}C\text{-}C(R^2){=}CR^3R^4$ (R^1 = Me, Et, $SiMe_3$, Ph; R^2 = H, Me, Ph; R^3 = Me, OMe, Ph; R^4 = H) et $R^1\text{-}C{\equiv}C\text{-}R'$ (R′ = 1-cyclohexényle; cyclohexavinylidyne)) qui réagissent avec **9**/^{t}BuLi permettent de préparer, en une seule étape, les composés **12**, **13** et **15** ainsi que les silacyclobutènes **14** et **16**–**24** et **27** (qui dérive de **10** et de l'hex-3-yne) et de les extraire des milieux réactionnels. Les silacyclobutanes/butènes sont thermiquement stables et on peut les distiller sous vide jusqu'à des températures d'environ 150°C sans décomposition. Les résultats expérimentaux sont confirmés de façon qualitative par des calculs semiempiriques au niveau AM-1 et par leur analyse à l'aide de la théorie « FMO ». La structure de silacyclobutène (**19**) à l'état solide a été déterminée par diffraction des rayons-X. Le composés **19** est orthorhombique, groupe d'espace $P2_12_12_1$ avec a = 1030,94(2), b = 1244,6(2) et c = 1605,5(3) pm et Z = 4.

Mots clés : néopentylsilène, dichloronéopentylsilène, silacyclobutènes, silacyclobutanes, 1,3-énynes.

Received July 28, 1999. Published on the NRC Research Press website on November 2, 2000.

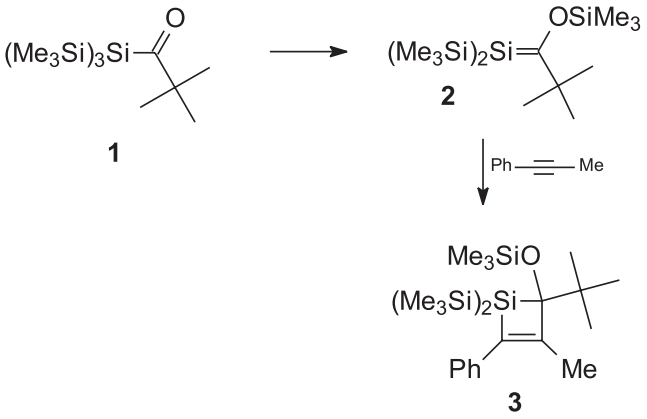
Dedicated to Prof. Dr. A. Brook for his outstanding contributions to organosilicon chemistry.

N. Auner[1] and B. Herrschaft. Johann Wolfgang Goethe University, Institute of Inorganic Chemistry, Marie-Curie-Str. 11, 60439 Frankfurt am Main, Germany.
M. Grasmann and M. Hummer. Humboldt-University, Institute of Inorganic and Analytical Chemistry, Hessische Str. 1–2, 10115 Berlin, Germany.

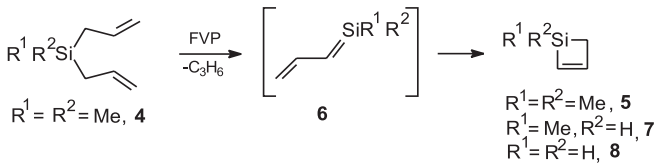
[1]Author to whom correspondence should be addressed. Telephone: + 49-(0)69-798-29591. Fax: + 49-(0)69-798-29188. e-mail: Auner@chemie.uni-frankfurt.de

 © 2000 NRC Canada

Scheme 1.



Scheme 2.



Introduction

While synthetic methods for the preparation of silacyclobutanes are well established since more than fourty years (2, 3), much less is known about the chemistry of silacyclobutenes. Although the first multi step syntheses for such compounds were already published starting in 1964 (4), only in 1979 Brook et al. (5) reported the first general route for the formation of a silacyclobutene by silene [2 + 2] cycloaddition reactions: thermolysis or photolysis of pivaloyltris(trimethylsilyl)silane **1** in the presence of 1-phenyl propine as trapping reagent for the intermediate silene **2** yields the sterically crowded silacyclobutene **3** (Scheme 1).

Nearly at the same time Block and Revelle (6) published the flash vacuum pyrolysis (FVP) of dimethyldiallylsilane **4** giving dimethylsilacyclobutene **5** via the intermediate formation and intramolecular rearrangement of 1-silabutadiene **6**. Grobe et al. extended this synthetic method including the formation of the methyl hydrogen substituted derivative **7** and even of the parent silacyclobutene **8** (Scheme 2) (7)[2] starting from the corresponding diallylsilanes.

All synthetic routes to silacyclobutenes reported until 1981 exhibit some common features: they require a multi step synthesis including low yields of products; especially the gas phase reactions described in Scheme 2 lead to complex product mixtures and the isolation of the silacyclobutenes often includes gaschromatographic separation of the thermally not very stable compounds. For the series investigated the thermal stability decreases with increasing hydrogen substitution at the silicon center, $Me_2SiCH{=}CHCH$ > $Me(H)SiCH{=}CHCH$ > $H_2SiCH{=}CHCH$.[2] Moreover, the variation of the organo substituents at the ring carbon atoms is difficult and no silicon chlorinated compound was reported, consequently excluding following reactions using the silicon functionality. Similar arguments hold for the syntheses of silacyclobutanes: Although the ring closure of γ-halopropylhalogenosilanes proved to be a facile entry to silacyclobutanes, the preparation of differently substituted starting γ-halopropylsilanes very often includes multi-step syntheses and suffers from low product yields especially in that case when different functional groups in α- and β-positions are required.

In 1981 we reported a preparatively facile one step synthesis of silicon dichloro substituted silacyclobutenes using vinyltrichlorosilane (**9**), lithium-*tert*-butyl and differently organo- and silyl substituted acetylenes as trapping agents for the intermediate formed dichloroneopentylsilene, $Cl_2Si{=}CHCH_2{}^tBu$ (**10**) (8). Using this synthetic method, the variation of the substitution pattern at the silicon and carbon four-membered ring moiety can easily been performed (9) and the yields of silacyclobutenes are sufficiently high; especially silacyclobutene **11** ($Cl_2SiCH(Ph){=}CH(Ph)CHCH_2Bu^t$) can be isolated nearly quantitatively from mixtures of vinyltrichlorosilane **9**, ^{t}BuLi and tolane. Notably, these silacyclobutenes exhibit an outstanding thermal[3] and chemical stability (10): using the chlorine functionality at silicon, **11** can be easily incorporated into silicones (10), polycarbosilanes,[4] polyorganosiloxanes (11), and polysilanes[5] containing the "closed" four-membered ring subunit as building block and thus transferring extraordinary physical and chemical properties into the polymeric backbones (12). For the formation of high molecular weight polymers the intermolecular linkage of the four-membered ring moieties is required requesting carbon carbon functionalities such as alkenyl- and alkinyl groups at the silacyclobutenes and -butanes carbon atoms; preliminary results reported for silacyclobutanes show that the four-membered rings can be linked together by hydrosilylation reactions (10).

In this paper we report on the preparatively facile competitive synthesis of silacyclobutanes and -butenes containing carbon and silicon functionalities using mixtures of vinyltrichlorosilane, lithium-*tert*-butyl and 1,3-enynes as reaction partners (Scheme 3).

Results and discussion

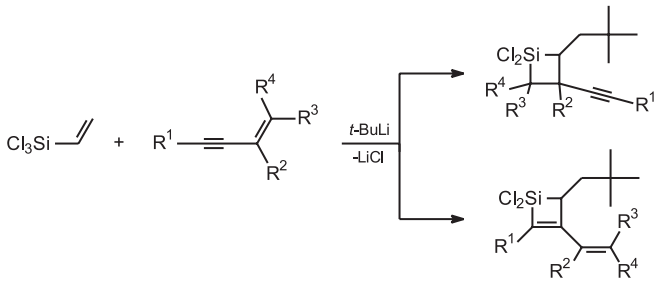
Preparation of 1,3-enynes and their reactions with mixtures of $H_2C{=}CHSiCl_3/{}^t$BuLi

The synthesis of most of the 1,3-enynes $HC{\equiv}C(R^2)C{=}CR^3R^4$ used in this experimental study is basically described in the literature (13). We focused on a series of compounds which (*i*) could easily been obtained in good yields from readily available starting materials and (*ii*) could easily been transferred into their organo substituted derivatives

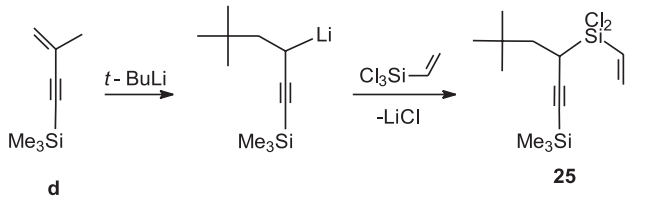
[2] N. Auner. J. Prakt. Chem. **337**, 79 (1995): work done under ref. 7 cited therein. Because of an overlap of signals, the NMR signals and (or) the coupling constants could not be assigned.
[3] According to DTA analyses of silacyclobutenes obtained from silene **10** and organo substituted acetylenes, these compounds are thermally stable up to about 300°C: D. Filsinger and N. Auner. In preparation.
[4] B. Goetze, B. Herrschaft, and N. Auner. Chem. Eur. J. 948 (1997). Because of an overlap of signals, the NMR signals and (or) the coupling constants could not be assigned.
[5] N. Auner and B. Biebl. Ph.D. Thesis, München. 1997. Paper in preparation.

© 2000 NRC Canada

Scheme 3.



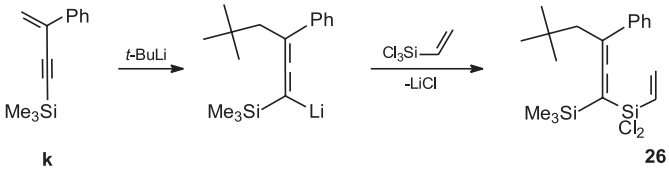
Scheme 4.



$R^1C{\equiv}C(R^2){=}CR^3R^4$. The C,H acidity of the hydrogen substituted precursors does not allow the use of Li-*tert*-butyl as reaction partner for the vinyl group of the starting trichlorovinylsilane **9**. In a general experimental procedure equimolar amounts of Li-*tert*-butyl were slowly added to equimolar mixtures of vinyltrichlorsilane **9** and the corresponding 1,3-enynes listed in Table 1. *n*-Pentane was used as solvent and the reactions were performed at room temperature. Mixing the reactions partners, in most cases LiCl elimination started immediately. The reaction is completed after stirring the solutions for some hours at room temperature. After filtration the silicon carbon four-membered ring compounds can be isolated by vacuum distillation as colourless, highly viscous liquids or as white crystalline solids. The reactions performed from vinylchlorosilane **9**, ^{t}BuLi and the 1,3-enynes **a** to **k** are summarized in Table 1 and clearly prove the extraordinary cycloaddition potential of the dichloroneopentylsilene **10**.

From Table 1 (and Table 4, Exp. section) it becomes obvious that: (*i*) the formation of silacyclobutanes and -butenes occurs regio- but not stereo-specific; (*ii*) the reaction of the C1 phenyl substituted enyne **a** with the **9**/^{t}BuLi mixture exclusively leads to the formation of silacyclobutane **12**; (*iii*) the reactions of the C1 trimethylsilyl substituted enyne **b** and the C1 ethyl substituted derivative **c** with the **9**/^{t}BuLi mixture result in the competitive formation of 1,1-dichloro substituted silacyclobutanes (**13**, **15**) and -butenes (**14**, **16**); (*iv*) the reactions with the C1 trimethylsilyl- and methyl substituted 1,3-enynes **e** to **j** yield the 1,1-dichlorosilacyclobutenes **18**–**23** exclusively; (*v*) the reaction of the **9**/^{t}BuLi mixture with (but-1-ene-3-yne)trimethylsilane **d** is exceptional: besides dichlorosilacyclobutene **17**, the 1,2 addition product **25** (Scheme 4) is formed in yields ranging from 7 up to 22% in different runs. Only small amounts of silacyclobutene **24** are obtained from the reaction with the C3 phenyl substituted enyne **k**. The formation of the main product **26** obviously results from a coupling reaction of an allenylic α-silyllithio species and trichlorovinylsilane **9** as discussed in Scheme 5; and (*vi*) all compounds are formed in good yields: except **25** and **26** no other side products can be detected by gaschromatographic investigations on the product mixtures. The overall yields listed in Table 4 are generally diminished by the high temperatures required for the vacuum distillation to purify the viscous and oily silacycles.

Scheme 5.



Summarizing the experimental work, the results clearly prove that the 1,2-addition of the lithium organyl to the vinyl group of the chlorosilane **9** dominates the usually favored 1,4 addition to conjugated carbon–carbon multiple bonds of 1,3-enynes in non polar solvents and at room temperature. In order to understand the directive influence of the substituents at the 1,3-enynes on the LiR addition and to predict the product formation "silacyclobutane vs. silacyclobutene" qualitatively, semiempiric calculations at the AM-1 level (14)[6] were performed and analyzed using FMO theory.

For simplification of the product forming pathway it is assumed that due to the chlorine substitution at silicon highly polar dichloroneopentylsilene **10** is formed by addition of ^{t}BuLi to vinyltrichlorosilane **9** followed by subsequent 1,2-LiCl elimination. The participation of lithiated species for the product formation is neglected.

For a rough estimation of the cycloaddition behaviour of **10** the FMO model is used.[6] Silene reactions are usually highly exothermic and should react via early transition states. Consequently the reactivity can be derived by discussion of the electron distribution in the starting material. The reactivity of the 1,3-enynes **a**–**k** is qualitatively estimated by inspecting the frontier orbitals based on the data listed in Table 2. Silene **10** is not included into the calculations because no reliable results might be expected[7] from semiempiric calculations with standard parameters. The question, whether silene **10** reacts with the double and (or) the triple bond of the 1,3-enyne is answered by the polarization of the multiple bonds. The order of polarization is given by the ratio of the HOMO orbital coefficients c_1/c_2 and c_4/c_3 at the carbon atoms C1, C2, C3, and C4 (Table 2): the polarization is getting larger the stronger it deviates from one.

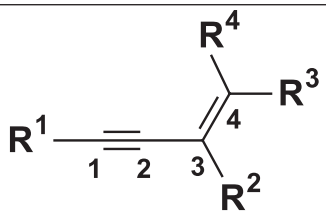
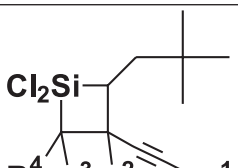
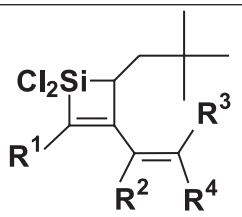
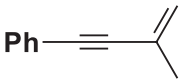
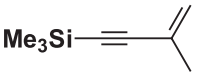
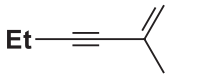
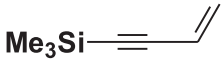
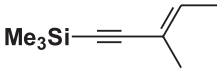
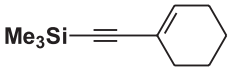
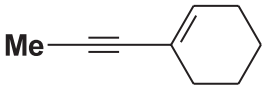
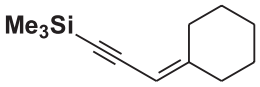
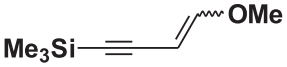
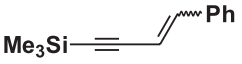
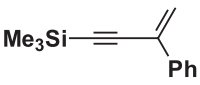
Usually the reactions of dienes and alkynes with neopentylsilenes are regiospecific, but not stereospecific (22). Refering to the eigenvektor coefficients of the LUMO this

[6] All calculations were done with: Hyperchem® 3.0, 1996. Hypercube, Inc. 419 Phillip Street, Waterloo, ON N2L 3X2, Canada.

[7] The geometry of **10** calculated at the AM1 level strongly deviates from that calculated for similar substituted silenes by ab initio methods (21). Thus, the Si=C bond distance is by more than 10 pm smaller than the experimentally measured and with ab initio methods calculated value of about 170 to 175 pm. Consequently, the HOMO–LUMO interaction between enophile and enyne cannot be determined precisely. Nevertheless, knowing the order of magnitude of the eigenvektor coefficients of the HOMO–LUMO interaction, the most favorable conformation of the reactants in the transition state is predictable; preferably the orientation occurs in such a way that bonding results from those atoms with the biggest (smallest) coefficients.

© 2000 NRC Canada

Table 1. Silacyclobutanes and silacyclobutenes prepared from $H_2C{=}CHSiCl_3$/Li-*tert*-butyl/1,3-enyne mixtures.

		
 **a**	**12**[a] R^1=Ph, R^2=Me R^3=R^4=H	
 **b**	**13**[a] R^1=$SiMe_3$, R^2=Me R^3=R^4=H	**14** R^1=$SiMe_3$, R^2=Me R^3=R^4=H
 **c**	**15**[a] R^1=Et, R^2=Me R^3=R^4=H	**16** R^1=Et, R^2=Me R^3=R^4=H
 **d**		**17** R^1=$SiMe_3$ R^2=R^3=R^4=H
 **e**		**18** R^1=$SiMe_3$ R^2=R^3=Me, R^4=H
 **f**		**19** R^1=$SiMe_3$ R^2=R^3=$(CH_2)_2$, R^4=H
 **g**		**20** R^1=Me R^2=R^3=$(CH_2)_2$, R^4=H
 **h**		**21** R^1=$SiMe_3$, R^2=H $R^{3,4}$ =cyclo-C_6H_{11}
 **i**		**22**[b] R^1=$SiMe_3$, R^2=H R^3=OMe, R^4=H
 **j**		**23**[b] R^1=$SiMe_3$, R^2=H R^3=Ph, R^4=H
 **k**		**24** R^1=$SiMe_3$, R^2=Ph R^3=R^4=H

[a]For silacyclobutanes **12**, **13**, and **15** the *E*/*Z*-isomeric ratio refers to the relative positions of the neopentyl- and the alkinyl groups.
[b]For the silacyclobutenes **22** and **23** *E*/*Z*-isomers relative to the exocyclic C=C double bond are formed.

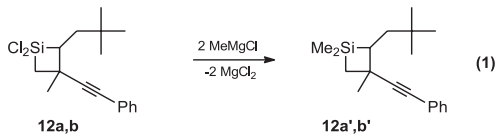


10

© 2000 NRC Canada

Table 2. Calculated coefficients and energies of the frontier orbitals of 1,3-enynes.

1,3-enynes	HOMO coefficients						LUMO coefficients						orbital energies (eV)		
	*C*1	*C*2	*C*3	*C*4	*C*1/*C*2	*C*4/*C*3	*C*1	*C*2	*C*3	*C*4	*C*1/*C*2	*C*4/*C*3	π	π*	π–π*
a	0.35	0.38	–0.29	–0.42	0.92	1.45	–0.31	0.36	0.23	–0.37	0.86	1.61	–8.8	–0.2	8.6
b	0.45	0.31	–0.47	–0.60	1.45	1.28	0.44	–0.34	–0.48	0.62	1.29	1.29	–9.5	0.3	9.8
c	–0.45	–0.35	0.46	0.60	1.29	1.30	0.45	–0.31	–0.51	0.63	1.45	1.24	–9.3	0.6	9.9
d	0.47	0.35	–0.43	–0.52	1.34	1.21	–0.43	0.33	0.45	–0.58	1.30	1.29	–9.7	0.3	10.0
e	–0.42	–0.25	0.51	0.57	1.68	1.11	–0.43	0.33	0.48	–0.61	1.30	1.27	–9.2	0.4	9.6
f	–0.46	–0.28	0.52	0.52	1.64	1.00	–0.43	0.33	0.48	–0.61	1.30	1.27	–9.2	0.3	9.5
g	0.39	0.27	–0.47	–0.53	1.44	1.13	0.41	–0.28	–0.47	0.58	1.46	1.23	–8.9	0.6	9.4
h	0.33	0.18	–0.43	–0.36	1.83	0.84	0.29	–0.17	–0.42	0.39	1.70	0.93	–8.8	0.5	9.3
i	–0.43	–0.25	0.52	0.49	1.72	0.94	0.41	–0.32	–0.43	0.60	1.28	1.39	–9.0	0.4	9.4
j	0.43	0.26	–0.51	–0.57	1.72	1.11	0.42	–0.32	–0.49	0.62	1.31	1.27	–9.2	0.3	9.5
k	0.24	0.13	–0.35	–0.51	1.84	1.45	0.25	–0.16	–0.36	0.55	1.56	1.53	–9.0	0.3	9.3



becomes understandable: the biggest coefficient is found at the silicon and compared to the parent silene, $H_2Si{=}CH_2$, the two silicon chlorine substituents of silene **10** even result in an additional increase of the orbital coefficent c_{Si}. Consequently, the resulting regiochemistry of the silacyclobutanes and silacyclobutenes might be explained by an electrophilic attack of silicon at the C1 ($c_1 > c_2$: formation of silacyclobutenes) and C4 ($c_4 > c_3$: formation of silacyclobutanes) of the 1,3-enyne, respectively. According to that the product formation from equimolar mixtures of $Cl_3SiCH{=}CH_2$ (**9**), ^{t}BuLi and 1,3-enynes (Tables 1 and 2) becomes predictable: (*i*) A strong polarization of the C3=C4 double bond and a weak polarization of the C1≡C2 triple bond (e.g., enyne **a**) results in a selective formation of silacyclobutanes; (*ii*) if both multiply bonded centers are polarized, a competitive formation of silacyclobutanes and silacyclobutenes (e.g., enyne **b** and **c**) is expected and experimentally found; and (*iii*) A strong polarization of the C1≡C2 triple bond and an only weak one of the C4=C3 double bond as exhibited by the enynes **d**, **e**, **f**, **g**, **h**, **i**, **j**, and **k**, yield in a selective formation of silacyclobutenes.

The experimental results listed in Table 1 and the calculations (Table 2) fit very well together: from an estimation of the polarization of the carbon carbon multiple bonds in 1,3-enynes the silacyclobutane/butene formation and their regiochemistry is clearly predictable using **9**/^{t}BuLi mixtures as synthetic equivalent for silene **10**.

Spectroscopic characterization of the reaction products

Although the *E*/*Z* isomeric silacyclobutanes and the regioisomeric silacyclobutenes/butanes can not be separated by distillation, the mixtures are fully characterized by the usual analytical and spectroscopical methods. The relative ratio of the formal [2 + 2] cycloadducts is determined gaschromatographically or by comparison of the intensities of the resonance signals of the *tert*-butyl groups in the ^{1}H NMR spectrum of the sample. Although the NMR data for the silacyclobutanes and silacyclobutenes obtained are completely listed in the Experimental Part, some characteristic ^{29}Si and ^{13}C NMR spectroscopic shifts are given in Table 3 and the data sets for the 2-neopentyl-1-silacyclobutane/butene moieties are examplarily discussed in detail.

As expected each isomer *E* and *Z* of the silacyclobutanes **12a**, **b**; **13a**, **b**; and **15a**, **b** shows two isolated spin systems in the ^{1}H NMR spectrum.[8] In agreement to the corresponding correlations in the ^{1}H^{1}H COSY NMR experiments, the diastereotopic protons H4 are split into two dublets each by geminal couplings (^2J = 12.81–15.82 Hz), while H2 shows a dublet of dublets by two vicinal couplings (^3J = 11.68–12.43, ^3J = 1.89–3.40 Hz) to both of the diastereotopic protons H7 of the neopentyl group. Each of the methylene protons H7 couples to a dublet of dublets due to vicinal coupling to H2 and the geminal coupling. These couplings are characteristic for the silacyclobutane moieties and prove the regiospecific [2 + 2] addition of dichloroneopentylsilene **10** to the 1,3-enynes **a**–**c**. The spin correlations of the exocyclic ethyl group of **15a**, **b** are identified by the ^{1}H^{1}H COSY NMR spectrum. The quaternic acetylenic carbon atoms are assigned according to the literature (17).

For proof of the NMR assignment, a diastereoisomeric mixture of the *E*/*Z*-isomeric dimethyl substituted silacyclobutane **12a′**, **b′** was exemplarily separated by column

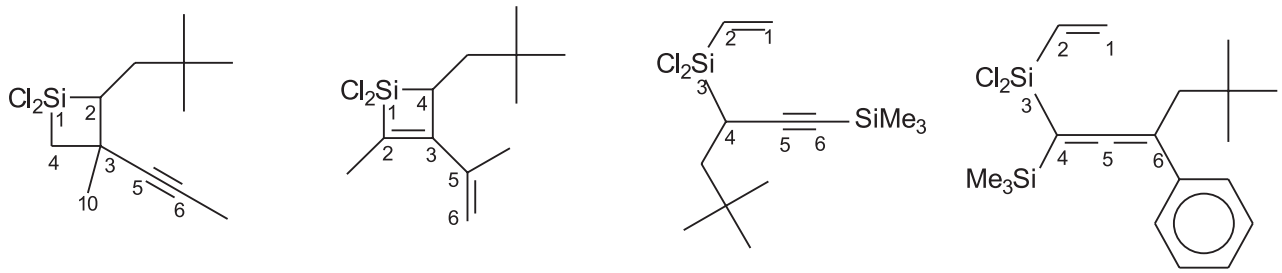
[8] By GC/MS the two *E*/*Z*-stereo isomeric silacylobutanes can be detected as a low boiling isomer **a** and a higher boiling isomer **b** (**a** having a shorter retention time compared to **b**). For compound **12a′**, **b′** the two isomers could be separated but not been assigned to *E* and *Z* configurated silacyclobutane **12**. However, separation was successfully performed with the silacyclobutane **33a**, **b**. In this case the low boiling compound is the *Z*-isomer, **b** is the higher boiling *E*-isomer. As there is no distinctive *E*/*Z*-assignment for the two isomers of the silacyclobutanes **12**, **13**, and **15**, they are differentiated as isomers **a** and **b**.

© 2000 NRC Canada

Table 3. Characteristic ^{29}Si and ^{13}C NMR spectroscopic parameters for the silacyclobutanes **12a**, **b**, **13a**, **b**, and **15a**, **b** and the silacyclobutenes **14** and **16**–**24** and the by-products **25** and **26**.

Comp.	$SiCl_2$	C2	C3	C4	C5	C6
12a, b	15.9/19.9	50.80/50.90	34.35/32.21	40.71/40.73	92.97/96.96	84.17/79.89
13a, b	19.8/15.8	51.01/50.41	32.29/34.45	40.60/40.66	83.19/88.33	113.95/109.91
14	0.6	142.64	175.69	45.38	148.14	116.84
15a, b	20.1/16.1	50.43/50.99	33.84/34.45	40.80/40.66	85.75/87.12	81.17/82.77
16	–2.2	138.97	158.44	40.42	148.22	117.77
17	–1.0	152.34	168.90	43.48	132.67	122.16
18	–1.5	149.69	175.10	40.28	134.50	122.53
19	–0.5	145.69	176.32	44.81	136.10	129.65
20	–2.4	138.74	160.39	40.10	132.64	130.58
21	–1.0	150.34	171.74	48.21	119.30	147.31
22-*E*/*Z*	3.5	144.84	167.85	43.78/48.08	102.26/102.79	156.16/151.00
23-*E*/*Z*	–0.4	153.73/152.08	171.05/168.64	46.54/43.74	133.58/135.80	126.25/123.88
24	–1.7	152.18	173.92	46.80	146.89	115.98
25	–1.6	139.25	129.61		105.16	88.41
26	–0.8	137.38	132.92	89.12	217.29	94.99

Numbering of the atoms:



chromatography (eluent: *n*-hexane, ratio **a′**:**b′** = 61:39). The methylation of the chlorinated precursor **12a**, **b** was performed using Grignard Reagent (eq. [1]).

Although the NMR data set was determined for both isomers **a** and **b** separately and is in excellent agreement with the data obtained for the isomeric mixtures, a distinctive assignment to the *E* or *Z* configuration of **12** failed.

As expected, the ^1H NMR spectra of the silacyclobutenes **14**, **16**–**21**, ***E***/***Z*-22**, and ***E***/***Z*-23** show two separate spin systems. Both diastereotopic protons H7 exhibit a dublet of dublets each, resulting from geminal (^3J = 13.56–13.94 Hz) and vicinal couplings (^3J = 10.27–12.06, ^3J = 1.13–3.37 Hz). Similarily, for the ring protons H4 a dublet of dublets is detected, caused by vicinal couplings to the protons H7. Compared to the corresponding δ H2 of the silacyclobutanes (δ = 1.90–2.62 ppm), δ H4 of the silacyclobutenes is characteristically shifted to lower fields (δ = 2.51–2.96 ppm). The spin system of the exocyclic ethyl group of **16** is identified by the $^1H^1H$ COSY NMR spectrum. The second spin sequence corresponds to the olefinic protons H6: for the silacyclobutenes **14** and **16** they appear at the lowest field. Only the protons H6 of **14** are splitted into a dublet by geminal coupling, the allylic coupling to the protons of the methyl group R^2 is detected for only one of the diastereoisomers. The protons H6 of **16** exhibit a multiplet and show no coupling to R^2.

According to the rule $J_{trans} > J_{cis}$ for vicinal couplings of alkenes (17), the *E*- or *Z*- configurations of the exocyclic double bonds in ***E***/***Z*-22** and ***E***/***Z*-23** are assigned by the value of the vicinal coupling constants of H5 and H6: thus, the relative isomeric ratio for ***E***/***Z*-22** = 84:16 and for ***E***/***Z*-23** = 24:76.[9]

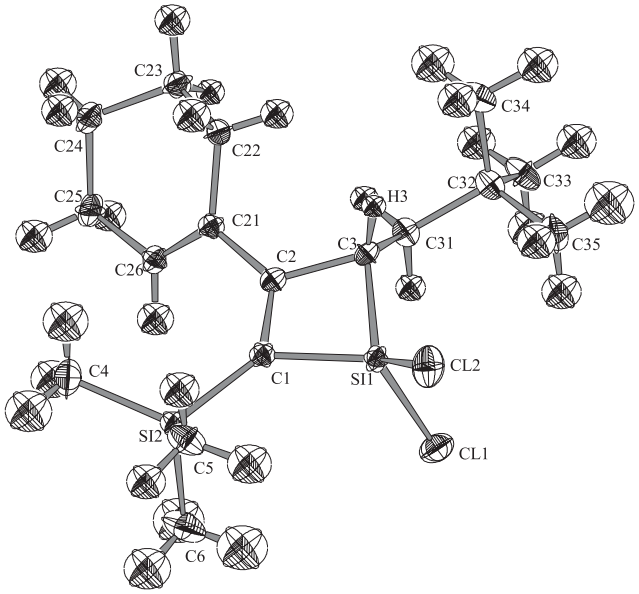
The silacyclobutenes **19**, **20**, and **21** show the characteristic couplings for the strongly low field shifted protons H4 and the diastereotopic methylene protons; the data are given in the Experimental Part. The protons of the cyclohexenyl substituents in **19** and **20** exhibit two multiplets attributed to the protons at C8/C9 and C7/C10 by $^1H^{13}C$ correlation. An assignment of the methylene protons of the cyclohexylidene ring of **21** is difficult even using the $^1H^{13}C$ correlation method: the two multiplets of H7/H11 and H8/H9/H10 detected in the proton NMR spectra are assigned to the carbon atoms C7/C11 and C8/C9/C10.

The ^{29}Si NMR spectroscopy proved to be an excellent tool for a fast decision between silacyclobutanes and silacyclobutenes formed in the reaction mixtures: both classes of compounds exhibit characteristic and relatively narrow ranges of the chemical shift. Thus, ^{29}Si resonance signals for

[9] Obviously the *E*/*Z* isomeric ratios in both silacyclobutenes are very different compared to those of the 1,3-enynes used [*E*/*Z*-(4-phenylbut-3-ene-1-inyl)-trimethylsilane, **i**: *E*/*Z* = 55:45; and *E*/*Z*-(4-methoxy-but-3-ene-1-inyl)trimethyl-silane, **j**: *E*/*Z* = 92/8]; related to the exocyclic double bonds the formation of the *Z*-isomeric silacyclobutenes is favoured. Assuming that there is no inversion of configurations performing the distillation (bp ***E***/***Z*-22**: 74°C/10^{-3} mbar; ***E***/***Z*-23:** 81–84°C/7 × 10^{-5} mbar) it becomes evident that the *Z*-isomeric enynes preferably react with the mixtures of $Cl_3SiCH{=}CH_2$/^{t}BuLi.

© 2000 NRC Canada

Fig. 1. Molecular structure of 1,1-dichloro-2-trimethylsilyl-3-cyclohex-1-enyl-4-neopentyl-1-sila-cyclobut-2-ene (50% envelopes). Bonding distances (Å) and angles (°):
Cl1—Si1 2.0629(6), Cl2—Si1 2.0656(6), Si1—C1 1.835(1), Si1—C2 2.237(1), Si1—C3 1.871(1), Si2—C1 1.867(1), Si2—C4 1.867(2), Si2—C5 1.880(2), Si2—C6 1.881(2), C1—C2 1.372(2), Si1-C1-C2 87.18(8),C1-C2-C3 110.54(10), C2-C3- Si1 80.90(7), C3-Si1-C1 81.13(1).



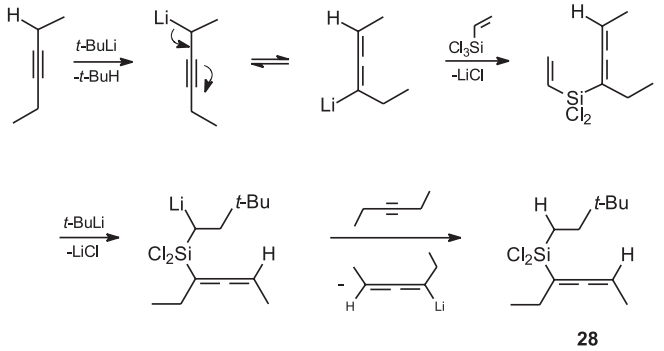
the silacyclobutanes are found between 14 and 21 ppm (18), while the shielding effect of the endocyclic double bond in 1,1-dichlorosilacyclobutenes causes a shift to higher field (δ^{29}Si ≈ –5 to 0 ppm) (8, 9). The δ^{29} silicon shifts determined for the silacyclics described in this paper fit very well into these ranges and are listed in Table 3.

X-ray structure analysis of the silacyclobutene 19

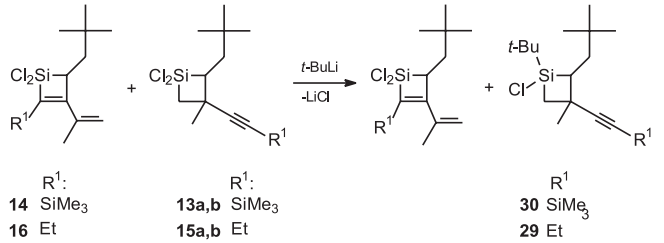
From the crude reaction mixture crystalline **19** was isolated. After recrystallization from *n*-pentane a suitable single crystal was investigated by X-ray structure analysis (Fig. 1).

The silacyclobutene **19** crystallizes in the non-centrosymmetric chiral space group $P2_12_12_1$ (no. 19) with a complete dissymmetric molecule as asymmetric unit. For refinement a racemic twin with a *R*:*S* ratio of 0.25 was assumed. With respect to the over-optimistic standard deviations the central, markedly distorted SiC four-membered ring is almost planar (interplanar angle of the planes Si2-C1-C2-C3 and Si2-C1-C2-C21: 5.25 (3)°). The bond lengths and angles are largely determined by the influence of the two chlorine substituents at the Si atom and the shortness of the endocyclic C=C double bond. Due to the chlorine substituents the Si1—C1 and Si1—C3 bond length — in comparison to the structural parameters of other silacyclobutanes (19) — are clearly shortened to 1.835(1) and 1.871(1) Å respectively, and consequently the endocyclic angle at Si1 is widened to 81.13(1)°, whereas the C=C bond distorts the angle Si1-C1-C2 to 87.18(8)°. As a result there are two external angles of 134.8(2)° and 137.9(2)° at C1. The silacyclobutene C1=C2-bond is with 1.372(2) Å slightly longer than the C=C-double bond of the cyclohexenyl substituent (1.340(1) Å). The Si—Cl bonds also differ slightly with 2.0628(6) and 2.0655(5) Å. Within the unit cell no exceptionally short intermolecular contacts are detected. As expected the molecular structure of **19** shows great similarities to that of 1,1-dichloro-2-trimethylsilyl-3-phenyl-4-neopentyl-1-silacyclobut-2-ene published recently (8).

Scheme 6.



Scheme 7.



Formation of side products from mixtures of trichlorovinylsilan, Li-*tert*-Bu, and 1,3-enynes

From the reaction of vinylchlorosilane **9**, Li^{t}Bu, and the 1,3-enyne **d**, the "open" isomer **25** of silacyclobutene **17** was isolated in 7–22% yield from several runs. This can easily been understood following the reaction sequence shown in Scheme 4.

In competition to the silacyclobutene formation (**17**), the lithium organyl is added to the enyne double bond in an 1,2 fashion followed by a chlorosilane coupling reaction giving **25**.

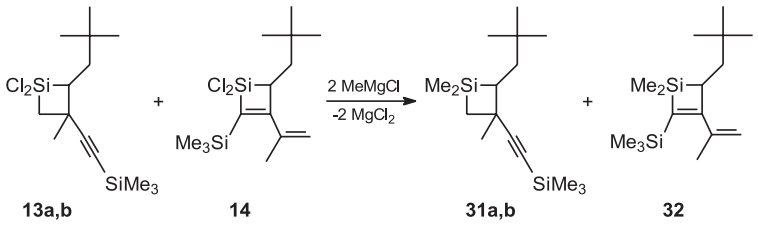
In the reaction of vinylchlorosilane **9**, ^{t}BuLi and (3-phenyl-but-3-ene-1-enyne)-trimethylsilane **k**, compound **26** is formed competitively to silacyclobutene **24** (**26**:36%, **24**:9%) and results from an 1,4-addition of ^{t}BuLi to the 1,3-enyne to give a lithiated allenyl derivative. Coupling reaction with chlorosilane **9** yields **26** (Scheme 5).

In this case the side reaction clearly dominates over the silacyclobutene formation. The reaction pathway discussed in Scheme 5 is confirmed by the reaction of the mixture **9**/^{t}BuLi with a *di*alkyl substituted alkyne such as 3-hexyne. From that a 1,2-dichloro-2,3-diethyl substituted silacyclobutene (**27**) and the allenylsilane **28** are isolated. The reaction sequence giving **28** is shown in Scheme 6: deprotonation of 3-hexyne gives a lithiated allenylsilane; chlorovinylsilane coupling yields a dichloroallenylsilane which can not be isolated and serves as starting material to give **28** (19%) after ^{t}BuLi-addition, followed by subsequent deprotonation of 3-hexyne.

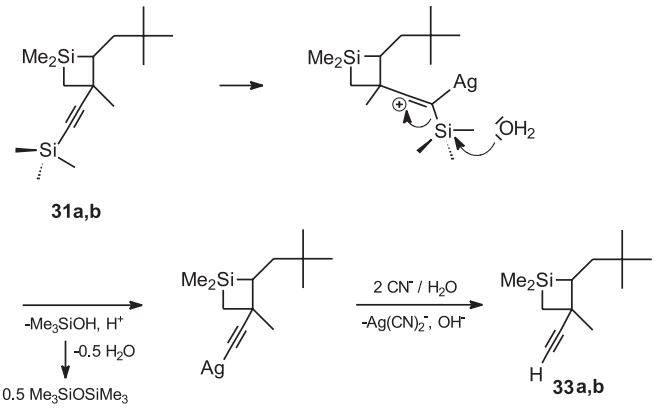
Silacyclobutene **27** can be separated as a pure liquid (yield: 30%) by reacting the mixture **27, 28** with bromine:

© 2000 NRC Canada

Scheme 8.



Scheme 9.



while the allenylsilane **28** adds bromine to the carbon double bonds immediately, the silacyclobutene does *not* react; it is isolated from the reaction mixture by distillation, the brominated silane remains as a residue (see Exp. section).

Silacyclobutene/butane separation from isomeric product mixtures

With respect to their comparable boiling points a silacyclobutene/butane separation of the isomeric mixtures **13a**, **b**/**14** and **15a**, **b**/**16** by distillation is impossible; due to the dichlorosilyl functionality even a gaschromatogaphic separation failed. However, for a successful "chemical" separation the two mixtures are reacted with silacyclobutane equivalent molar amounts of ^{t}BuLi each giving the mono-*tert*-butylated silacyclobutanes **29** and **30** nearly quantitatively; notably, the silacyclobutenes **14** and **16** do not react under comparable conditions (Scheme 7). The silacyclobutenes are then easily separated by distillation, the silacyclobutanes **29** and **30** remain as high boiling residues.[10] Electronic and steric reasons might be responsible for the selective substitution of only *one* silacyclobutane Si-Cl function: although the ethyl substituent at C2 of **16** is sterically less demanding than the trimethylsilyl group in **14**, even in that case only the mono substitution to give **29** took place. Nevertheless, methylation of the mixture **13a**, **b**/**14** by methyl Grignard Reagent gives the dimethyl substituted product mixture **31a**, **b**, and **32** (Scheme 8).

Loosing the dichlorosilyl functionality this clean reaction opens possibilities for derivatization and separation: reacting a mixture of **31a**, **b**, and **32** under the conditions of the Arens–Schmidt reaction (desilylation by use of $AgNO_3$/KCN (20)) yields the stereoisomeric silacyclobutane **33a**, **b**, while the silacyclobutene **32** is not affected. The metallated trimethylsilyl—alkyne bond in **31a**, **b** is quantitatively and selectively cleaved by use of a double molar amount of an aqueous solution of cyanide as shown in Scheme 9 and described in the Experimental part.

The high stereospecificity of the Schmidt–Arens reaction is surprising: by addition of an ethereal ethanolic solution of silver nitrate equimolar to the higher boiling isomer **31b**, this isomer is selectively desilylated (95% de). Notably, only after completion the trimethyl—silyl bond of the low boiling isomer **31a** is cleaved. The configuration of **31a** was assigned to be the *Z* isomer by NOE difference NMR spectroscopy; consequently **31b** represents the *E*-isomer. From the experimental results it is obvious that the attack of the silver atoms on the alkinyle triple bond of the *E*-isomer **31b** is kinetically preferred over that at the *Z*-isomer **31a**.

Experimental part

General remarks

All manipulations were performed under purified argon using standard Schlenk techniques. Solvents were dried by refluxing under nitrogen with the appropriate drying agent and were distilled prior before use. $CDCl_3$ was dried with molecular sieves, while [D6]benzene was dried with potassium/sodium and distilled prior to NMR sample preparation. NMR spectra: Bruker AM 300 (^{29}Si), DPX 300 (^{1}H, ^{13}C) and AMX 600 (^{1}H, ^{13}C), ^{1}H and ^{13}C NMR chemical shifts (δ) were internally referenced (δ (C*H*Cl$_3$) = 7.24, δ (*C*DCl$_3$) = 77.00, δ (C_6D_5H) = 7.15, δ (C_6D_6) = 128.00); ^{29}Si NMR spectra were measured using either the INEPT pulse sequence or the inversed gated decoupling technique, the ^{29}Si NMR shifts were externally referenced to TMS. GC: Varian Chromstar 3400 (15 m × 0.32 mm, 1µ film, Fison J & W scientific DB 1 column). GC/MS: Chrompack CP 9000 (capillary column CP-SIL/5CB-MS, diameter 0.25 mm, 12.5 m length) coupled with a Finnigan MAT Ion Trap Detector 800 (electron impact, space current 3000 µA, ionisation energy 70 eV, ion-source temperature 250°C), for chemical ionization methanol was used. Elemental analyses: Microanalytical Laboratory of the Department of Chemistry, Humboldt-University, Berlin. Leco CHNS-932. Trichlorovinylsilane was distilled from sodium carbonate prior before use. *tert*-Butyllithium was used as 1.7 M solution in pentane. All other chemicals were used as purchased by Aldrich and Fluka.

Preparation of 1,3-enynes

2-Methyl-4-phenyl-but-1-ene-3-yne (**a**) was prepared according to ref. 21 (yield 59%) and following the general

[10]Due to very complex isomeric mixtures (from eight expected stereoisomers, four can be detected by GC/MS) a listing of the NMR and mass spectroscopic data for **29** and **30** is avoided.

© 2000 NRC Canada

procedures described in ref. 17. For the syntheses of the 1,3-enynes **b**, **d**, **e**, **f**, **g**, **h**, **i**, **j** see ref. (17), **k** was synthesized according to ref. 21 and **c** is commercially available.

General procedure for the preparation of silacyclobutanes and silacyclobutenes

Trichlorovinylsilane (**9**, 50 mmol, 8.1 g) and the corresponding 1,3-enyne (50 mmol) are dissolved in 150 mL of *n*-pentane. Then 29.4 mL of 1.7 M ^{t}BuLi/*n*-pentane (50 mmol) are added dropwise over a period of 15 min. Generally, the solution warms slightly, and after 4 h stirring at room temperature the solution is separated from the precipitated LiCl by filtration. The solvent and an access of the 1,3-enyne is removed by destillation. Finally, the oily residue is distilled at 10^{-2} mbar for purification.

The syntheses carried out following this procedure are listed in Table 4.

Spectroscopic and analytical characterization of the silacyclobutanes and silacyclobutenes

E/Z-*1,1-dichloro-3-methyl-(2′-phenylethinyl)-2-neopentyl-1-silacyclobutane (**12a**)*: ^{1}H NMR ($CDCl_3$) δ: 0.95 (s, 9H, C(CH_3)$_3$), 1.58 (s, 3H, CH_3), 1.90 (d, ^2J = 15.07 Hz, 1H, H4), 1.92 (dd, ^2J = 12.44 Hz, ^3J = 12.43 Hz, 1H, CH_2), 1.94 (dd, ^2J = 12.44 Hz, ^3J = 1.89 Hz, 1H, CH_2), 2.00 (dd, ^3J = 12.43 Hz, ^3J = 1.89 Hz, 1H, H2), 2.37 (d, ^2J = 15.07 Hz, 1H, H4), 7.27–7.43 (m, 5H, C_6H_5); ^{13}C NMR ($CDCl_3$) δ: 29.61 (C(*C*H$_3$)$_3$), 30.08 (*C*(CH$_3$)$_3$), 31.51 (*C*H$_3$), 34.35 (C3), 40.71 (C4), 41.24 (*C*H$_2$), 50.80 (C2), 84.17 (C≡*C*-Ph), 92.97 (*C*≡C-Ph), 128.19 (2*C*H aromat), 128.58 (*C*H aromat), 123.49 (C*q* aromat), 131.54 (2*C*H aromat); ^{29}Si NMR ($CDCl_3$) δ: 15.9. **12b**: ^{1}H NMR ($CDCl_3$) δ: 0.97 (s, 9H, C(CH_3)$_3$), 1.49 (s, 3H, CH_3), 1.96 (d, ^2J = 15.45 Hz, 1H, H4), 2.44 (d, ^2J = 15.45 Hz, 1H, H4), 2.62 (dd, ^3J = 12.05 Hz, ^3J = 3.39 Hz, 1H, H2), 7.28–7.44 (m, 5H, C_6H_5);[2] ^{13}C NMR ($CDCl_3$) δ: 25.03 (*C*H$_3$), 29.51 (C(*C*H$_3$)$_3$), 30.41 (*C*(CH$_3$)$_3$), 32.21 (C3), 40.73 (C4), 40.55 (*C*H$_2$), 50.90 (C2), 79.89 (C≡*C*-Ph), 96.96 (*C*≡C-Ph), 127.84 (2*C*H aromat), 128.31 (*C*H aromat), 123.52 (C*q* aromat), 131.50 (2*C*H aromat); ^{29}Si NMR ($CDCl_3$) δ: 19.9. Anal. calcd. (found) for $C_{17}H_{22}Cl_2Si$ (325.35): C 62.76 (62.32), H 7.29 (7.61), Cl 21.79 (21.23).

E/Z-*1,1-dichloro-3-methyl-(2′-trimethylsilylethinyl)-2-neopentyl-1-silacyclobutane (**13a (Z)**)*: ^{1}H NMR ($CDCl_3$) δ: 0.14 (s, 9H, Si(CH_3)$_3$), 0.92 (s, 9H, C(CH_3)$_3$), 1.34 (s, 3H, CH_3), 1.40 (dd, ^2J = 13.56 Hz, ^3J = 3.39 Hz, 1H, CH$_2$), 1.56 (dd, ^2J = 13.56 Hz, ^3J = 11.69 Hz, 1H, CH$_2$), 1.83 (d, ^2J = 12.81 Hz, 1H, H4), 2.23 (d, ^2J = 12.81 Hz, 1H, H4), 2.46 (dd, ^3J = 11.68 Hz, ^3J = 3.39 Hz, 1H, H2); ^{13}C NMR ($CDCl_3$) δ: 0.19 (Si(*C*H$_3$)$_3$), 24.84 (*C*H$_3$), 29.43 (C(*C*H$_3$)$_3$), 29.97 (*C*(CH$_3$)$_3$), 32.29 (C3), 39.21 (*C*H$_2$), 40.60 (C4), 51.01 (C2), 83.19 (*C*≡C-SiMe$_3$), 113.95 (C≡*C*-SiMe$_3$); ^{29}Si NMR ($CDCl_3$) δ: 19.8 ($SiCl_2$), –18.3 (Si(CH$_3$)$_3$). **13b** (***E***): ^{1}H NMR ($CDCl_3$) δ: 0.12 (s, 9H, Si(CH_3)$_3$), 0.92 (s, 9H, C(CH_3)$_3$),1.45 (s, 3H, CH_3), 1.90 (m, 1H, H2), 1.96 (d, ^2J = 13.20 Hz, 1H, H4), 2.27 (d, ^2J = 13.19 Hz, 1H, H4);[4] ^{13}C NMR ($CDCl_3$) δ: 0.06 (Si(*C*H$_3$)$_3$), 29.59 (C(*C*H$_3$)$_3$), 30.00 (*C*(CH$_3$)$_3$), 31.34 (*C*H$_3$), 34.45 (C3), 40.66 (C4), 41.37 (*C*H$_2$), 50.41 (C2), 88.33 (*C*≡C-SiMe$_3$), 109.91 (C≡*C*-SiMe$_3$); ^{29}Si NMR ($CDCl_3$) δ: 15.8 ($SiCl_2$), –18.5 (Si(CH$_3$)$_3$); MS (70 eV), *m*/*z* (%): 305 (4.4) (M^+ – CH_3), 250 (24.5) (M^+ – 2Cl), 247 (11.8) (M^+ – Si(CH$_3$)$_3$); analysis together with **14**.

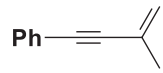
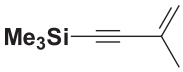
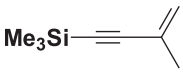
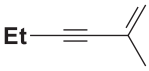
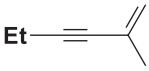
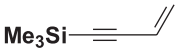
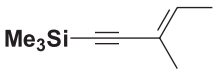
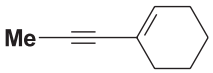
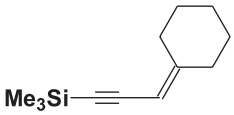
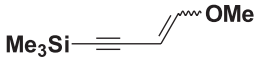
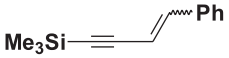
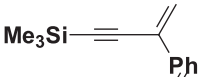
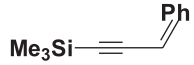
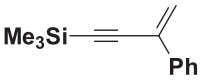
*1,1-dichloro-2-trimethylsilyl-3-(1′-methylethenyl)-4-neopentyl-1-silacyclobut-2-ene (**14**)*: ^{1}H NMR ($CDCl_3$) δ: 0.13 (s, 9H, Si(CH_3)$_3$), 0.92 (s, 9H, C(CH_3)$_3$), 1.82 (m, ^4J = 1.51 Hz, 3H, CH_3), 1.42 (dd, ^2J = 13.56 Hz, ^3J = 3.01 Hz, 1H, CH_2), 1.51 (dd, ^2J = 13.56 Hz, ^3J = 11.68 Hz, 1H, CH_2), 2.81 (dd, ^3J = 11.67 Hz, ^3J = 3.02 Hz, 1H, H4), 4.96 (m, ^2J = 1.89 Hz, 1H, =CH_2), 5.07 (dq, ^2J = 1.89 Hz, ^4J = 1.51 Hz, 1H, =CH_2); ^{13}C NMR ($CDCl_3$) δ: 0.10 (Si(*C*H$_3$)$_3$), 20.52 (*C*H$_3$), 29.37 (C(*C*H$_3$)$_3$), 30.38 (*C*(CH$_3$)$_3$), 40.93 (*C*H$_2$), 45.38 (C4), 116.84 (=*C*H$_2$), 142.64 (^1J(^{13}C^{29}Si) = 25.60 Hz, ^1J(^{13}C^{29}Si) = 90.57 Hz, C2), 148.14 (^3J(^{13}C^{29}Si) = 55.58 Hz, =C), 175.69 (^2J(^{13}C^{29}Si) = 59.07 Hz, C3); ^{29}Si NMR ($CDCl_3$) δ: –0.6 ($SiCl_2$), –12.3 (Si(CH$_3$)$_3$); MS (70 eV), *m*/*z* (%): 305 (4.4) (M^+ – CH_3), 250 (24.5) (M^+ – 2Cl), 247 (11.8) (M^+ – Si(CH$_3$)$_3$). Anal. calcd. (found) for $C_{14}H_{26}Cl_2Si_2$ (321.43): C 52.31 (52.08), H 8.15 (8.32), Cl 22.06 (22.21).

E/Z-*1,1-dichloro-3-methyl-3-(1′-butinyl)-2-neopentyl-1-silacyclobutane (**15a**)*: ^{1}H NMR ($CDCl_3$) δ: 0.81 (s, 9H, C(CH_3)$_3$), 0.96 (tr, ^3J = 7.54 Hz, 3H, CH$_2$CH_3), 1.25 (d, ^2J = 12.05 Hz, 2H, CH_2), 1.32 (s, 3H, CH_3), 1.71 (dd, ^2J = 12.05 Hz, ^3J = 3.01 Hz, 1H, CH_2), 1.72 (d, ^2J = 15.07 Hz, 1H, H4), 2.01 (d, ^3J = 3.01 Hz, 1H, H2), 2.04 (q, ^3J = 7.54 Hz, 2H, CH_2CH$_3$), 2.09 (d, ^2J = 15.07 Hz, 1H, H4).[2] ^{13}C NMR ($CDCl_3$) δ: = 12.46 (*C*H$_2$CH$_3$), 14.22 (CH$_2$*C*H$_3$), 29.24 (C(*C*H$_3$)$_3$), 30.40 (*C*(CH$_3$)$_3$), 31.89 (*C*H$_3$), 33.84 (C3), 39.26 (*C*H$_2$), 40.80 (C4), 50.43 (C2), 81.17 (C≡*C*-CH$_2$), 85.75 (*C*≡C-CH$_2$); ^{29}Si NMR ($CDCl_3$) δ: 20.1. **15b**: ^{1}H NMR ($CDCl_3$) δ: 0.80 (s, 9H, C(CH_3)$_3$), 1.00 (tr, ^3J = 7.54 Hz, 3H, CH$_2$CH_3), 1.21 (s, 3H, CH_3), 1.30 (dd, ^2J = 13.19 Hz, ^3J = 3.40 Hz, 1H, CH_2), 1.44 (dd, ^2J = 13.19 Hz, ^3J = 12.05 Hz, 1H, CH_2), 1.85 (d, ^2J = 15.82 Hz, 1H, H4), 2.04 (q, ^3J = 7.54 Hz, 2H, CH_2CH$_3$), 2.14 (d, ^2J = 15.82 Hz, 1H, H4), 2.31 (dd, ^3J = 12.05 Hz, ^3J = 3.40 Hz, 1H, H2); ^{13}C NMR ($CDCl_3$) δ: 12.41 (*C*H$_2$CH$_3$), 14.31 (CH$_2$*C*H$_3$), 25.40 (*C*H$_3$), 29.42 (C(*C*H$_3$)$_3$), 29.48 (*C*(CH$_3$)$_3$), 34.45 (C3), 40.66 (C4), 39.26 (*C*H$_2$), 50.99 (C2), 82.77 (C≡*C*-CH$_2$), 87.12 (*C*≡C-CH$_2$); ^{29}Si NMR ($CDCl_3$) δ: 16.1; MS (CI, MeOH), *m*/*z* (%): 277 (4.1) (M^+ + 1), 276 (3.8) (M^+), 247 (6.4) (M^+ – C_2H_5), 241 (22.1) (M^+ – Cl), 219 (25.8) (M^+ – C(CH$_3$)$_3$). Anal. calcd. (found) for $C_{13}H_{22}Cl_2Si$ (277.30): C 52.31 (52.08), H 8.15 (8.32), Cl 22.06 (22.21).

*1,1-dichloro-2-ethyl-3-(1′-methylethenyl)-4-neopentyl-1-silacyclobut-2-ene (**16**)*: ^{1}H NMR ($CDCl_3$) δ: 0.80 (s, 9H, C(CH_3)$_3$), 0.98 (tr, ^3J = 7.54 Hz, 3H, CH$_2$CH_3), 1.36 (m, 2H, CH_2), 1.73 (s, 3H, CH_3), 2.17 (q, ^3J = 7.54 Hz, 2H, CH_2CH$_3$), 2.51 (dd, ^3J = 10.17 Hz, ^3J = 3.77 Hz, 1H, H4), 4.83 (m, 1H, =CH_2), 5.06 (m, =CH_2); ^{13}C NMR ($CDCl_3$) δ: 14.11 (CH$_2$*C*H$_3$), 20.88 (*C*H$_3$), 21.35 (*C*H$_2$CH$_3$), 29.60 (C(*C*H$_3$)$_3$), 30.01 (C(CH$_3$)$_3$), 40.92 (*C*H$_2$), 40.42 (C4), 117.77 (=*C*H$_2$), 138.97 (C2), 148.22 (=*C*CH$_3$), 158.44 (C3); ^{29}Si NMR ($CDCl_3$) δ: –2.2; MS (CI, MeOH), *m*/*z* (%): 277 (4.1) (M^+ + 1), 276 (3.8) (M^+), 247 (6.4) (M^+ – C_2H_5), 241 (22.1) (M^+ – Cl), 219 (25.8) (M^+ – C(CH$_3$)$_3$). Anal. calcd. (found) for $C_{13}H_{22}Cl_2Si$ (277.30): C 52.31 (52.08), H 8.15 (8.32), Cl 22.06 (22.21).

© 2000 NRC Canada

Table 4. Preparation of silacyclobutanes and silacyclobutenes.[a]

	1,3-enyne	products	bp/mp [°C / 10^{-3} mbar]	yield [g / mmol / %]
a		**12a,b** (61/39)[b]	108-120	6.83/21.0/42
b		**13a,b** (41/59)[b]	55-59	6.68/29.8/42
b		**14**	55-59	4.66/14.5/29
c		**15a,b** (47/53)[b]	82-96	4.46/16.1/32
c		**16**	82-96	2.60/9.4/19
d		**17**	85[d]	4.46/14.5/29
e		**18**	60-63	13.05/36.8/74
f		**19**	88-89[e]	12.11/33.5/67
g		**20**	110	6.82/22.5/45
h		**21**	83-84[e]	12.58/33.5/67
i		**22a,b** (84/16)[c]	78	9.51/28.2/56
j		**23a,b** (24/76)[c]	81-84[e]	13.99/36.5/73
k		24	93	1.73/4.5/9
d		25	85[d]	1.08-3.38/3.5-11.0/7-22
k		26	93[e]	6.90/18.00/36

[a]The silacyclobutanes and silacyclobutenes as well as the by-products are colourless, viscous liquids; only **19** was isolated as a crystalline solid.

[b]The *cis*/*trans* isomeric ratios **a**/**b** are given in parentheses.

[c]The *E*/*Z* isomeric ratios **a**/**b** corresponding to the exocyclic double bond of the silacyclobutenes are given in parentheses. The mixtures of isomers were subjected to elemental analysis (see Experimental section).

[d]Product formation according to Scheme 5.

[e]Product formation according to Scheme 6.

© 2000 NRC Canada

1,1-dichloro-2-trimethylsilyl-3-ethenyl-4-neopentyl-1-silacyclobut-2-ene ***(17)***: ^{1}H NMR ($CDCl_3$) δ: 0.16 (s, 9H, Si(CH_3)$_3$), 0.94 (s, 9H, C(CH_3)$_3$), 1.56 (dd, ^2J = 13.94 Hz, ^3J = 12.05 Hz, 1H, CH_2), 1.78 (dd, ^2J = 13.94 Hz, ^3J = 1.13 Hz, 1H, CH_2), 2.96 (dd, ^3J = 12.06 Hz, ^3J = 1.13 Hz, 1H, H4), 5.45 (dd, ^2J = 1.13 Hz, ^3J = 17.71 Hz, 1H, =CH_2); 5.49 (dd, ^2J = 1.13 Hz, ^3J = 10.55 Hz, 1H, =CH_2); 6.49 (dd, ^3J = 10.55 Hz, ^3J = 17.71 Hz, 1H, =C*H*); ^{13}C NMR ($CDCl_3$) δ: –0.29 (Si(CH_3)$_3$), 29.18 (C(CH_3)$_3$), 30.76 (*C*(CH_3)$_3$), 40.65 (*C*H_2), 43.48 (^2J($^{13}C^{29}Si$) = 35.61 Hz, C4), 122.16 (=*C*H_2), 132.67 (=*C*H), 152.34 (C2), 168.90 (C3). ^{29}Si NMR ($CDCl_3$) δ: –1.0 ($SiCl_2$), –12.3 (Si(CH_3)$_3$); Anal. calcd. (found) for $C_{13}H_{24}Cl_2Si_2$ (307.40): C 52.31 (52.08), H 8.15 (8.32), Cl 22.06 (22.21).

1,1-dichloro-2-trimethylsilyl-3-(1′-methylprop-1′-enyl)-4-neopentyl-1-silacyclobut-2-ene ***(18)***: ^{1}H NMR ($CDCl_3$) δ: 0.08 (s, 9H, Si(CH_3)$_3$), 0.89 (s, 9H, (CH_3)$_3$), 1.33 (dd, ^2J = 13.57 Hz, ^3J = 2.26 Hz, 1H, CH_2), 1.46 (dd, ^2J = 13.57 Hz, ^3J = 12.06 Hz, 1H, CH_2), 1.52 (q, ^4J = 6.78 Hz, 3H, =CCH_3), 1.72 (s, 3H, =CHCH_3), 2.80 (dd, ^3J = 12.06 Hz, ^3J = 2.26 Hz, 1H, H4), 5.37 (q, ^4J = 6.78 Hz, 1H, =C*H*); ^{13}C NMR ($CDCl_3$) δ = –1.17 (Si(*C*H_3)$_3$), 15.28 (2CH_3), 29.28 (C4), 29.35 (C(*C*H_3)$_3$), 30.17 (*C*(CH_3)$_3$), 40.28 (*C*H_2), 122.53 (=*C*H), 134.50 (^3J($^{13}C^{29}Si$) = 25.33 Hz, =C), 149.69 (^1J($^{13}C^{29}Si$) = 48.69 Hz, ^1J($^{13}C^{29}Si$) = 61.76 Hz, C2), 175.10 (^2J($^{13}C^{29}Si$) = 33.42 Hz, C3); ^{29}Si NMR ($CDCl_3$) δ: –1.5 ($SiCl_2$), –12.0 (Si(CH_3)$_3$); MS (CI, MeOH), *m*/*z* (%): 335 (4.8) (M^+ + 1), 319 (85.5) (M^+ – CH_3), 299 (43.0) (M^+ – Cl), 277 (30.1) (M^+ – C(CH_3)$_3$). Anal. calcd. (found) for $C_{15}H_{28}Cl_2Si_2$ (335.46): C 53.71 (53.11), H 8.41 (8.17), Cl 21.13 (21.67).

1,1-dichloro-2-trimethylsilyl-3-cyclohex-1-enyl-4-neopentyl-1-silacyclobut-2-ene ***(19)***: ^{1}H NMR ($CDCl_3$) δ: –0.10 (s, 9H, Si(CH_3)$_3$), 0.89 (s, 9H, (CH_3)$_3$), 1.40 (dd, ^2J = 13.94 Hz, ^3J = 3.01 Hz, 1H, C4CH_2), 1.48 (dd, ^2J = 13.94 Hz, ^3J = 11.30 Hz, 1H, C4CH_2), 2.09–2.14 (m, 4H, =CHCH_2, =CCH_2), 1.58–1.62 (m, 4H, 2CH_2), 2.80 (dd, ^3J = 11.30 Hz, ^3J = 3.01 Hz, 1H, H4), 5.73 (m, 1H, =C*H*); ^{13}C NMR ($CDCl_3$) δ: 0.04 (Si(*C*H_3)$_3$), 21.85, 22.29 (2*C*H_2), 25.32, 26.25 (=CH*C*H_2, =*C*CH_2), 29.27 (C(*C*H_3)$_3$), 30.37 (C(CH_3)$_3$), 41.04 (C4*C*H_2), 44.81 (C4), 129.65 (=*C*H), 136.10 (^3J($^{13}C^{29}Si$) = 26.81 Hz, *C*=CH), 145.69 (^1J($^{13}C^{29}Si$) = 48.09 Hz, ^1J($^{13}C^{29}Si$) = 62.89 Hz, C2), 176.32 (^2J($^{13}C^{29}Si$) = 23.12 Hz, C3). ^{29}Si NMR ($CDCl_3$) δ: –0.5 ($SiCl_2$), –12.7 (Si(CH_3)$_3$); MS (CI, MeOH), *m*/*z* (%): 325 (2.8) (M^+ – Cl), 303 (21.2) (M^+ – C(CH_3)$_3$), 287 (17.6) (M^+ – SiC(CH_3)$_3$). Anal. calcd. (found) for $C_{17}H_{30}Cl_2Si_2$ (361.40): C 52.31 (52.08), H 8.15 (8.32), Cl 22.06 (22.21).

X-ray structure determination of 1,1-dichloro-2-trimethylsilyl-3-cyclohex-1-enyl-4-neopentyl-1-silacyclobut-2-ene

A crystal of the approximate dimensions 0.5 × 0.6 × 0.6 mm was mounted on a glass fibre tip glued with silicon grease and transfered to the goniometer. The crystal was cooled to 100 K (Oxford CryoStream, U.K.) for all subsequent manipulations. The intensity data collection was performed by means of a one-circle diffraktometer (Stoe IPDS, Darmstadt, FRG) equipped with a image plate (IP: ⌀ = 180 mm, BaFBr(Eu^{2+}), scanning head: He–Ne laser (632 nm), photomultiplier (400 nm), resolution (max.) 150 μm), a sealed fine focus X-ray tube (MoKα radiation, λ = 0.71073 Å) and a graphite monochromator. The indexing procedure for estimating the initial lattice constants used 158 reflections ($I > 12\sigma_I$) out of a total of 260 recorded reflections (5 frames, φ-increment: 72°, 50 kV, 40 mA). The raw intensities (data collection: 21 h, 200 frames, 0° < φ < 240°, φ-increment: 1.2°, 50 kV, 30 mA, 5.1° < 2θ < 63.4°, 23613 reflns: 3 overlapped, 43 overloaded, 23 565 reflns merged (R_{int} = 0.0903), 7690 unique, 6963 observed ($I > 2\sigma_I$)) were corrected for Lorentz and polarization effects. To refine the lattice constants 5000 reflections (φ = 174°, 6.8° < 2θ < 63.3°, 12.0 < I/σ_I < 1020.8) were chosen from the data set. Atom form factors (22) for neutral atoms were implemented in the used program system. Direct Methods (SHELXS86 (23)) were applied to the data set to gain an initial model of the molecular structure. After four cycles of Difference Fourier Syntheses (24) and subsequent Least Squares Refinement the structure model was completed. All second row elements were allowed to refine anisotropically, the next 30 strongest electron densities taken from the Fourier map occured in most plausible positions for hydrogen atoms and were refined isotropically. After the final refinement cycle no meaningful electron densities remained. Details of the crystal structure analysis are given in Table 5. Crystallographic data (excluding structure factor listings) for the

Table 5. Crystal data for 1,1-dichloro-2-trimethylsilyl-3-cyclohexenyl-4-neopen-tyl-1-silacyclobut-2-ene.

Empirical formula	$C_{17}H_{30}Cl_2Si_2$
Formula weight	361.49
Crystal system	orthorhombic
Space group	$P2_12_12_1$ (no. 19)
Unit cell dimensions (Å):	
a	10.309(2)
b	12.446(2)
c	16.055(3)
V (Å^3)	2060.0(6)
Z	4
σ_{calc} (g/cm^3)	1.166
F_{000}	776
$\mu_{MoK\alpha}$ (mm^{-1})	0.4
Crystal size (mm)	0.5 × 0.6 × 0.6
Temperature (K)	100
Radiation (Å)	MoKα (0.71073)
Scan range	3.3 < θ < 29.1
	h:–14/14, *k*:–17/17; *l*:–21/21
Data	
Total	25806
Unique data (R_{int})	5500 (0.052)
Observed ($I > 2.0\ \sigma_I$)	5213
N_{par}	311
R	0.0303
WR	0.0781
	$w = 1/[\sigma^2F_o^2) + (0.0608P)^2 + 0.0000P]$
	$P = (F_O^2 + 2F_C^2)/3$
Goodness-of-fit	1.03
Shift/error (max./aver.)	0.00, 0.00
Resd. dens. (e/Å^3)	–0.35, 0.24

© 2000 NRC Canada

structure reported in this paper have been deposited with the Cambridge Crystallographic Data Centre (CCDC 132182). Copies of the data can be obtained, free of charge, on application to the Director, CCDC, 12 Union Road, Cambridge CB2 1EZ, U.K. (Fax: 44-1223-336033 or e-mail: deposit@ccdc.cam.ac.uk).

*1,1-dichloro-2-methyl-3-cyclohex-1-enyl-4-neopentyl-1-silacyclobut-2-ene (**20**)*: ^{1}H NMR ($CDCl_3$) δ: 0.91 (s, 9H, (CH_3)$_3$), 1.45 (dd, ^2J = 13.57 Hz, ^3J = 3.02 Hz, 1H, C4CH_2), 1.47 (dd, ^2J = 13.57 Hz, ^3J = 10.55 Hz, 1H, C4CH_2), 1.60–1.64 (m, 4H, 2CH_2), 1.80 (s, 3H, CH_3), 2.13–2.17 (m, 4H, =CHCH_2, =CCH_2), 2.61 (dd, ^3J = 10.55 Hz, ^3J = 3.02 Hz, 1H, H4), 5.75 (m, 1H, =C*H*); ^{13}C NMR ($CDCl_3$) δ: 13.04 (*C*H_3), 21.96, 22.47 (2*C*H_2), 25.47, 26.74 (=CH*C*H_2, =C*C*H_2), 29.27 (C(*C*H_3)$_3$), 30.45 (*C*(CH_3)$_3$), 40.10 (C4), 40.91 (C4*C*H_2), 130.58 (C=*C*H), 132.64 (*C*=CH), 138.74 (C2), 160.39 (C3). ^{29}Si NMR ($CDCl_3$) δ: –2.4. MS (CI, MeOH), *m*/*z* (%): 303 (31.7) (M^+ + 1), 302 (31.6) (M^+), 287 (14.7) (M^+ – CH_3), 267 (35.3) (M^+ – Cl), 245 (69.7) (M^+ – C(CH_3)$_3$). Anal. calcd. (found) for $C_{15}H_{24}Cl_2Si$ (303.34): C 59.39 (59.10), H 7.98 (7.81), Cl 23.37 (23.62).

*1,1-dichloro-2-trimethylsilyl-3-methylidencyclohexyl-4-neopentyl-1-silacyclobut-2-ene (**21**)*: ^{1}H NMR ($CDCl_3$) δ: 0.10 (s, 9H, Si(CH_3)$_3$), 0.90 (s, 9H, (CH_3)$_3$), 1.50 (dd, ^2J = 13.56 Hz, ^3J = 11.67 Hz, 1H, C4CH_2), 1.57 (dd, ^2J = 13.56 Hz, ^3J = 3.01 Hz, 1H, C4CH_2), 1.56–1.61 (m, 3 CH_2), 2.14–2.18 (m, 4H, 2=CCH_2), 2.87 (dd, ^3J = 11.67 Hz, ^3J = 3.01 Hz, 1H, H4), 5.71 (m, 1H, =C*H*); ^{13}C NMR ($CDCl_3$) δ: –0.64 (Si(*C*H_3)$_3$), 26.34, 27.88, 28.58, 30.60, 37.54 (*C*H_2), 29.45 (C(*C*H_3)$_3$), 30.49 (*C*(CH_3)$_3$), 40.84 (C4*C*H_2), 48.21 (C4), 119.30 (C=*C*H), 147.31 (*C*=CH), 150.34 (C2), 171.74 (C3). ^{29}Si NMR ($CDCl_3$) δ: –1.0 ($SiCl_2$), –12.4 (Si(CH_3)$_3$); MS (CI, MeOH), *m*/*z* (%): 339 (34.8) (M^+ – Cl), 317 (78.1) (M^+ – C(CH_3)$_3$), 301 (8.3) (M^+ – SiC(CH_3)$_3$). Anal. calcd. (found) for $C_{18}H_{32}Cl_2Si_2$ (375.52): C 57.57 (57.23), H 8.59 (8.25), Cl 18.88 (18.69).

E/Z-*1,1-dichloro-2-trimethylsilyl-3-(2-methoxyvinyl)-4-neopentyl-1-silacyclobut-2-ene (**22-E**)*: ^{1}H NMR ($CDCl_3$) δ: 0.14 (s, 9H, Si(CH_3)$_3$), 0.94 (s, 9H, (CH_3)$_3$), 1.61 (dd, ^2J = 13.94 Hz, ^3J = 12.05 Hz, 1H, CH_2), 1.74 (dd, ^2J = 13.94 Hz, ^3J = 1.89 Hz, 1H, CH_2), 2.83 (dd, ^3J = 12.05 Hz, ^3J = 1.89 Hz, 1H, H4), 3.64 (s, 3H, OCH_3), 5.52 (d, ^3J = 12.81 Hz, 1H, =C*H*OCH_3), 6.82 (d, ^3J = 12.81 Hz, 1H, C*H*=CHOCH_3); ^{13}C NMR ($CDCl_3$) δ: –0.31 (Si(*C*H_3)$_3$), 29.21 (C(*C*H_3)$_3$), 30.81 (*C*(CH_3)$_3$), 41.08 (*C*H_2), 43.78 (C4), 56.82 (*C*H_3O), 102.26 (*C*H=CHOCH_3), 144.84 (C2), 156.16 (=*C*HOCH_3), 167.85 (C3); ^{29}Si NMR ($CDCl_3$) δ: 3.5 ($SiCl_2$), –12.9 (Si(CH_3)$_3$). **22-Z**: ^{1}H NMR ($CDCl_3$) δ: 0.18 (s, 9H, Si(CH_3)$_3$), 0.91 (s, 9H, (CH_3)$_3$), 3.69 (s, 3H, CH_3O), 5.07 (d, ^3J = 6.78 Hz, 1H, =C*H*OCH_3), 6.06 (d, ^3J = 6.78 Hz, 1H, C*H*=CHOCH_3);[4] ^{13}C NMR ($CDCl_3$) δ: –0.43 (Si(*C*H_3)$_3$), 29.51 (C(*C*H_3)$_3$), 30.96 (*C*(CH_3)$_3$), 41.49 (*C*H_2), 48.08 (C4), 56.85 (O*C*H_3), 102.79 (*C*H=CHOCH_3),151.00 (=*C*HOCH_3) (13); ^{29}Si NMR ($CDCl_3$): (13) MS (CI, MeOH), *m*/*z* (%): 295 (17.6) (M^+ + 1), 294 (28.9) (M^+), 279 (100) (M^+ – CH_3), 237 (48.6) (M^+ – C(CH_3)$_3$). Anal. calcd. (found) for $C_{14}H_{26}Cl_2OSi_2$ (337.43): C 57.57 (57.23), H 8.59 (8.25), Cl 18.88 (18.89).

E/Z-*1,1-dichloro-2-trimethylsilyl-3-(2′-phenylethenyl)-4-neopentyl-1-silacyclobut-2-ene (**23-Z**)*: ^{1}H NMR ($CDCl_3$) δ: 0.01 (s, 9H, Si(CH_3)$_3$), 0.48 (s, 9H, (CH_3)$_3$), 1.17 (dd, ^2J = 13.56 Hz, ^3J = 2.64 Hz, 1H, CH_2), 1.30 (dd, ^2J = 13.56 Hz, ^3J = 13.57 Hz, 1H, CH_2), 2.80 (dd, ^3J = 13.57 Hz, ^3J = 2.64 Hz, ^4J = 1.13 Hz, 1H, H4), 6.08 (d, ^3J = 12.05 Hz, ^4J = 1.13 Hz, 1H, C*H*=CHPh), 6.56 (d, ^3J = 12.05 Hz, 1H, =C*H*Ph), 7.13–7.33 (m, 5H, C_6H_5 aromat); ^{13}C NMR ($CDCl_3$) δ: –0.88 (Si(*C*H_3)$_3$), 29.27 (C(*C*H_3)$_3$), 30.08 (*C*(CH_3)$_3$), 40.80 (*C*H_2), 46.54 (C4), 126.24 (=*C*HPh), 127.18 (*C*H aromat), 128.20 (2*C*H aromat), 129.10 (2*C*H aromat), 136.51 (C*q* aromat), 133.58 (*C*H=CHPh), 153.73 (C2), 171.05 (C3); ^{29}Si NMR ($CDCl_3$) δ: –0.4 ($SiCl_2$), –12.0, –12.3 (Si(CH_3)$_3$). **23-E**: ^{1}H NMR ($CDCl_3$) δ: 0.12 (s, 9H, Si(CH_3)$_3$), 0.90 (s, 9H, (CH_3)$_3$), 1.55 (dd, ^2J = 13.94 Hz, ^3J = 12.06 Hz, 1H, CH_2), 1.76 (dd, ^2J = 13.94 Hz, ^3J = 1.51 Hz, 1H, CH_2), 2.96 (dd, ^3J = 12.06 Hz, ^3J = 1.51 Hz, 1H, H4), 6.64 (d, ^3J = 16.21 Hz, 1H, C*H*=CHPh), 6.74 (d, ^3J = 16.21 Hz, 1H, =C*H*Ph), 7.13–7.33 (m, 5H, C_6H_5 aromat); ^{13}C NMR ($CDCl_3$) δ: –0.08 (Si(*C*H_3)$_3$), 29.22 (C(*C*H_3)$_3$), 30.87 (C(CH_3)$_3$), 40.96 (*C*H_2), 43.74 (C4), 123.88 (=*C*HPh), 128.14 (*C*H aromat), 128.88 (2*C*H aromat), 129.06 (2*C*H aromat), 135.86 (C*q* aromat), 136.80 (*C*H=CHPh), 152.08 (C2), 168.64 (C3); ^{29}Si NMR ($CDCl_3$) δ: –0.4 ($SiCl_2$), –12.0, –12.3 (Si(CH_3)$_3$); MS (CI, MeOH), *m*/*z* (%): 383 (8.4) (M^+ + 1), 382 (8.5) (M^+), 347 (29.2) (M^+ – Cl), 325 (22.8) (M^+ – C(CH_3)$_3$), 309 (29.2) (M^+ – SiC(CH_3)$_3$), 305 (19.7) (M^+ – C_6H_5). Anal. calcd. (found) for $C_{19}H_{28}Cl_2Si_2$ (383.50): C 59.51 (59.02), H 7.35 (7.67), Cl 18.49 (18.91).

*1,1-dichloro-2-trimethylsilyl-3-(1′-phenylethenyl)-4-neopentyl-1-silacyclobut-2-ene (**24**)*: ^{1}H NMR ($CDCl_3$) δ: 0.28 (s, 9H, Si(CH_3)$_3$), 0.75 (s, 9H, (CH_3)$_3$), 1.35 (dd, ^2J = 13.56 Hz, ^3J = 2.27 Hz, 1H, CH_2), 1.98 (dd, ^2J = 13.56 Hz, ^3J = 12.06 Hz, 1H, CH_2), 2.84 (dd, ^3J = 12.06 Hz, ^3J = 2.27 Hz, 1H, H4), 5.23 (d, ^2J = 1.51 Hz, 1H, =CH_2), 5.58 (d, ^2J = 1.51 Hz, 1H, =CH_2), 7.13–7.33 (m, 5H, C_6H_5 aromat); ^{13}C NMR ($CDCl_3$) δ: –0.47 (Si(*C*H_3)$_3$), 29.05 (C(*C*H_3)$_3$), 31.50 (*C*(CH_3)$_3$), 40.73 (*C*H_2), 46.80 (C4), 115.98 (=*C*H_2), 125.95 (2*C*H aromat), 126.82 (*C*H aromat), 128.29 (2*C*H aromat), 137.49 (C*q* aromat), 146.89 (*C*Ph=), 152.18 (C2), 173.92 (C3); ^{29}Si NMR ($CDCl_3$) δ: –1.7 ($SiCl_2$), –16.5 (Si(CH_3)$_3$); MS (CI, MeOH), *m*/*z* (%): 384 (100) (M^+ + 2), 382 (73.20) (M^+), 347 (64.1) (M^+ – Cl), 325 (3.92) (M^+ – C(CH_3)$_3$), 309 (17.7) (M^+ – SiC(CH_3)$_3$). Anal. calcd. (found) for $C_{19}H_{28}Cl_2Si_2$ (383.50): C 59.51 (59.13), H 7.35 (7.01), Cl 18.49 (18.32).

*4,4-dichloro-3-neopentyl-1-trimethylsilyl-4-silahexa-5-ene-1-yne (**25**)*: ^{1}H NMR ($CDCl_3$) δ: 0.11 (s, 9H, Si(CH_3)$_3$), 0.97 (s, 9H, (CH_3)$_3$), 1.58 (dd, ^2J = 14.31 Hz, ^3J = 10.17 Hz, 1H, CH_2), 1.78 (dd, ^2J = 14.31 Hz, ^3J = 2.64 Hz, 1H, CH_2), 2.25 (dd, ^3J = 10.17 Hz, ^3J = 2.64 Hz, 1H, C*H*), 6.26 (dd, ^2J = 1.89 Hz, ^3J = 19.60 Hz, 1H, =CH_2), 6.26 (dd, ^3J = 9.80 Hz, ^3J = 19.60 Hz, 1H, =C*H*), 6.29 (dd, ^2J = 1.89 Hz, ^3J = 9.80 Hz, 1H, =CH_2); ^{13}C NMR ($CDCl_3$) δ: –0.09 (Si(*C*H_3)$_3$), 21.43 (*C*H), 29.63 (C(*C*H_3)$_3$), 32.27 (*C*(CH_3)$_3$), 41.66 (*C*H_2), 88.41 (C≡*C*Si(CH_3)$_3$), 105.16 (*C*≡CSi(CH_3)$_3$), 139.25 (=*C*H_2), 129.61 (=*C*H); ^{29}Si NMR ($CDCl_3$) δ: –1.6 ($SiCl_2$), –18.3 (Si(CH_3)$_3$); MS (70 eV), *m*/*z* (%): 307 (8.6) (M^+ + 1), 291 (47.6) (M^+ – CH_3), 271 (28.6) (M^+ – Cl),

© 2000 NRC Canada

249 (12.4) (M^+ – $C(CH_3)_3$). Anal. calcd. (found) for $C_{13}H_{24}Cl_2Si_2$ (307.40): C 52.31 (52.08), H 8.15 (8.32), Cl 22.06 (22.21).

*3,3-dichloro-8,8-dimethyl-6-phenyl-4-trimethylsilyl-3-silanona-1,4,5-triene (**26**)*: ^{1}H NMR ($CDCl_3$) δ: 0.26 (s, 9H, $Si(CH_3)_3$), 0.95 (s, 9H, $(CH_3)_3$), 2.35 (d, ^2J = 14.32 Hz, 1H, CH_2), 2.45 (d, ^2J = 14.32 Hz, 1H, CH_2), 6.14 (dd, ^2J = 5.65 Hz, ^3J = 16.95 Hz, 1H, =CH_2), 6.20 (dd, ^2J = 5.65 Hz, ^3J = 12.44 Hz, 1H, =CH_2), 6.28 (dd, ^3J = 12.44 Hz, ^3J = 16.95 Hz, 1H, =CH), 7.14–7.41 (C_6H_5 aromat); ^{13}C NMR ($CDCl_3$) δ: 0.14 ($Si(CH_3)_3$), 30.23 ($C(CH_3)_3$), 32.66 ($C(CH_3)_3$), 42.73 (CH_2), 89.12 ($^1J(^{13}C^{29}Si)$ = 77.02 Hz, $^1J(^{13}C^{29}Si)$ = 49.40 Hz, Cl_2SiC=), 94.99 ($^3J(^{13}C^{29}Si)$ = 55.67 Hz, =CPh), 125.85 (2CH aromat), 126.96 (CH aromat), 128.37 (2CH aromat), 132.92 ($^1J(^{13}C^{29}Si)$ = 94.46 Hz, =CH), 137.21 (C*q* aromat), 137.38 (=CH_2), 217.29 ($^2J(^{13}C^{29}Si)$ = 75.57 Hz, C=C=C); ^{29}Si NMR ($CDCl_3$) δ: –0.8 ($SiCl_2$), –12.9 ($Si(CH_3)_3$); MS (CI, MeOH), *m/z* (%): 383 (81.6) (M^+ + 1), 382 (42.1) (M^+), 347 (100) (M^+ – Cl), 309 (4.37) (M^+ – $SiC(CH_3)_3$), 305 (17.9) (M^+ – C_6H_5). Anal. calcd. (found) for $C_{19}H_{28}Cl_2Si_2$ (383.50): C 59.51 (59.13), H 7.35 (7.01), Cl 18.49 (18.32).

*Preparation of silacyclobutene **27** and separation from **28***: The preparation of **27** followed the general procedure given in the Experimental section. From the equimolar mixture of H_2C=$CHSiCl_3$/^{t}BuLi/3-hexyne (50 mmol each), **27** (3.98 g, 15 mmol, 30%) and **28** (1.75 g, 9.5 mmol, 19%) were obtained as a mixture of colorless liquids, bp 64–68°C, 10^{-2} mbar. The analysis was performed from the mixture; Anal. calcd. (found) for $C_{12}H_{22}Cl_2Si$ (265.29): C 52.31 (52.08), H 8.15 (8.32), Cl 22.06 (22.21).

*Separation of **27** from **28***: To a mixture of 6.63 g (25 mmol) of **27**/**28**, solved in 30 mL CCl_4, 1.82 g (11.42 mmol) Br_2, solved in 20 mL of CCl_4, were slowly added at –10°C. The reaction was controlled by its color lost and by IR spectroscopy (**28**: $\nu_{C=C=C}$: 1938 cm^{-1}). After the bromine color remains and the band at 1938 cm^{-1} has disappeared, the solvent is removed and the residue is distilled under vacuo. While brominated **28** remains as high boiling residue, the silacyclobutene **27** was isolated as a pure liquid.

*1,1-dichloro-2,3-diethyl-4-neopentyl-1-silacyclobut-2-ene (**27**)*: ^{1}H NMR ($CDCl_3$) δ: 0.93 (s, 9H, H7), 1.00, 1.04 (tr, ^3J = 7.53 Hz, 3H, H8, H10), 1.43 (dd, ^2J = 13.57 Hz, ^3J = 11.68 Hz, 1H, H5), 1.53 (dd, ^2J = 13.57 Hz, ^3J = 2.64 Hz, 1H, H5), 2.13, 2.14 (q, ^3J = 7.53 Hz, ^5J = 0.76 Hz, 2H, H8, H10), 2.49 (dd, ^3J = 11.68 Hz, ^3J = 2.64 Hz, 1H, H4). ^{13}C NMR ($CDCl_3$) δ: 11.17, 13.93 (C9, C11), 20.04, 21.51 (C8, C10), 29.41 (C7), 30.44 (C6), 40.05 (C4), 40.42 (C5), 146.89, 162.17 (C2, C3). ^{29}Si NMR ($CDCl_3$) δ: –2.9. MS (70 eV), *m/z* (%): 305 (4.4) (M^+ –15), 291 (22.3) (M^+ -Et), 263 (34.9) (M^+ – ^{t}Bu), 250 (24.5) (M^+ – 2Cl).

*6,6-dichloro-5,9,9-trimethyl-6-siladecadi-3,4-ene (**28**)*: IR: 1938 cm^{-1} ($\nu_{C=C=C}$); ^{1}H NMR ($CDCl_3$) δ: 0.87 (s, 9H, H9), 1.00 (dd, ^3J = 7.54 Hz, ^3J = 7.54 Hz, 3H, H11), 1.13 (m, 2H, H6), 1.37 (m, 2H, H7), 1.68 (d, ^3J = 7.16 Hz, 3H, H1), 2.08 (dq, ^2J = 13.94 Hz, ^3J = 7.54 Hz, 1H, H10), 2.36 (dq, ^2J = 13.94 Hz, ^3J = 7.54 Hz, 1H, H10), 5.15 (pn, ^3J = 7.16 Hz, ^5J = 3.01 Hz, ^5J = 4.15 Hz, 1H, H2). ^{13}C NMR ($CDCl_3$) δ: 13.14 (C11), 14.61 (C6), 21.67 (C10), 27.04 (C1), 28.69 (C9), 30.88 (C8), 36.07 (C7), 85.35 (C2), 95.86 (C4), 208.55 (C3). ^{29}Si NMR ($CDCl_3$) δ: 18.1.

*Methylation of **13a**, **b**/**14** and performance of the Arens–Schmidt reaction*: The mixture **13a**, **b**/**14** was reacted with a double molar amount of methyl Grignard reagent. Silacyclobutane **31a**, **b** and silacyclobutene **32** were obtained nearly quantitatively (93%) as a mixture of colorless liquids, bp 48–49°C/10^{-2} mbar. Both compounds were characterized by GC/MS methods. The isomeric mixture was then reacted under the conditions of the Arens–Schmidt reaction (29). To a solution of 19.78 g (70.5 mmol) of **31a**, **b**/**32** (28.9 mmol of **32**; 24.7 mmol of **31a** and 16.9 mmol of **31b**: the molar ratio was determined from the intensities of the resonance signals of the *tert*-butyl groups in the ^{1}H NMR spectrum of the sample), solved in 100 mL of ether and 50 mL of ethanol, 2.87 g (16.9 mmol) of $AgNO_3$, solved in a mixture of 20 mL of water and 40 mL of ethanol, were added. Immediately a brown solid precipitated. After 10 min of stirring at room temperature 4.16 g NaCN (85 mmol), solved in 40 mL of water, were added. The reaction solution was extracted three times with ether, the organic layer was separated, washed with aequous NaCl solution, and dried over $MgSO_4$. After removal of the solvent the residue was distilled at 1 mbar. The compound isolated contained 98% of ***E*-33** and 2% of the *Z*-isomer. Treating the residue then with a solution of 4.21 g (24.8 mmol) $AgNO_3$, the *Z*-isomer of **31** is obtained in 98%, while the amount of ***E*-31** is 2% (bp 58°C/1 mbar). Repeating the distillation of the residue gave pure **32** (bp 48–49°C/10^{-2} mbar).

*1,1-dimethyl-2-trimethylsilyl-3-(1′-methyl-ethenyl)-4-neopentyl-1-silacyclobut-2-en (**32**)*: ^{1}H NMR ($CDCl_3$) δ: 0.03 (s, 9H, $Si(CH_3)_3$), 0.21 (s, 6H, $Si(CH_3)_2$), 0.86 (s, 9H, H9), 1.22 (dd, ^2J = 13.56 Hz, ^3J = 12.43 Hz, 1H, H7), 1.43 (dd, ^2J = 13.56 Hz, ^3J = 2.26 Hz, 1H, H7), 1.77 (d, ^4J = 1.5 Hz, 3H, H10), 1.95 (dd, ^3J = 12.43 Hz, ^3J = 2.26 Hz, 1H, H4), 4.81 (d, ^2J = 2.64 Hz, 1H, H6), 4.88 (dq, ^2J = 2.64 Hz, ^4J = 1.51 Hz, 1H, H6). ^{13}C NMR ($CDCl_3$) δ: –0.06, –1.68 ($SiCH_3$), 0.44 ($Si(CH_3)_3$), 20.76 (C10), 29.57 (C9), 30.52 (C8), 31.68 (C4), 41.94 (C7), 113.77 (C6), 145.15, 146.58 (C2, C5), 174.96 (C3). MS (70 eV), *m/z* (%): 280 (9.3) (M^+), 265 (11.7) (M^+ – Me), 223 (100) (M^+ – ^{t}Bu), 207 (34.2) (M^+ – $SiMe_3$). Anal. calcd. (found) for $C_{16}H_{32}Si_2$ (280.60 : C 68.48 (68.11), H 11.49 (11.17).

E/Z-*1,1-dimethyl-3-methyl-(2′-ethinyl)-2-neopentyl-1-silacyclobutane (**33a**, **b**)*: **33a**(***Z***)**: ^{1}H NMR ($CDCl_3$) δ: 0.36, 0.25 (s, 3H, $SiCH_3$), 0.83 (s, 9H, H9), 0.99 (d, ^2J = 13.94 Hz, 1H, H4a), 1.07 (dd, ^3J = 12.43 Hz, ^3J = 3.01 Hz, 1H, H2), 1.32 (dd, ^2J = 13.56 Hz, ^3J = 3.02 Hz, 1H, H7a), 1.36 (s, 3H, H10), 1.42 (d, ^2J = 13.94 Hz, 1H, H4b), 1.60 (dd, ^2J = 13.57 Hz, ^3J = 12.43 Hz, 1H, H7b), 2.17 (s, 1H, H6). ^{13}C NMR ($CDCl_3$) δ: = 1.69, –2.36 ($SiCH_3$), 29.25 (C4), 29.81 (C9), 30.18 (C8), 32.72 (C10), 36.10 (C3), 37.88 (C2), 42.08 (C7), 69.87 (C6), 91.64 (C5). ^{29}Si NMR ($CDCl_3$) δ: = 11.6.

33b(***E***)**: ^{1}H NMR ($CDCl_3$) δ: 0.28, 0.30 (s, 3H, $SiCH_3$), 0.84 (s, 9H, H9), 1.16 (d, ^2J = 14.69 Hz, 1H, H4), 1.24 (s, 3H, H10), 1.34 (dd, ^2J = 13.18 Hz, ^3J = 6.41 Hz, 1H, H7), 1.37 (dd, ^2J = 13.18 Hz, ^3J = 9.79 Hz, 1H, H7), 1.48 (d, ^2J = 14.69 Hz,

© 2000 NRC Canada

1H, H4), 1.60 (dd, ^3J = 9.79 Hz, ^3J = 6.41 Hz, 1H, H2), 2.18 (s, 1H, H6). ^{13}C NMR ($CDCl_3$) δ: –1.27, 2.01 (Si*C*H$_3$), 25.50 (C10), 29.42 (C4), 29.72 (C9), 30.14 (C8), 33.54 (C3), 38.50 (C2), 40.42 (C7), 65.79 (C6), 95.21 (C5). ^{29}Si NMR ($CDCl_3$) δ: 15.6. MS (for *E*/*Z* mixture): MS (70 eV), *m*/*z* (%): 193 (4.8) (M^+ – Me), 151 (100) (M^+ – ^{t}Bu). Anal. calcd. (found) for $C_{13}H_{24}Si$ (208.23): C 74.92 (74.41), H 11.60 (11.03).

Acknowledgements

We thank Dow Corning for financial support, Wacker–Chemie and Chemetal for gifts of chlorosilanes and lithium alkyls.

References

1. N. Auner, H.-U. Steinberger, and B. Herrschaft. Eur. J. Inorg. Chem. 1095 (1999).
2. R. Damrauer. Chem. Rev. A, 67 (1972).
3. N. Auner and J. Grobe. J. Organomet. Chem. **188**, 25 (1980).
4. H. Gilman and W.H. Atwell. J. Am. Chem. Soc. **86**, 2687 (1964); H. Gilman and W.H. Atwell. J. Am. Chem. Soc. **86**, 5589 (1964); H. Gilman and W.H. Atwell. J. Am. Chem. Soc. **87**, 2678 (1965).
5. A.G. Brook, J.W. Harris, J. Lennon, and M. El Sheikh. J. Am. Chem. Soc. **101**, 83 (1979).
6. E. Block and L.K. Revelle. J. Am. Chem. Soc. **100**, 1630 (1978).
7. A. Ellmann. Ph.D. Thesis, Münster. 1986.
8. N. Auner, C. Seidenschwarz, and E. Herdtweck. Angew. Chem. **103**, 1172 (1991); Angew. Chem. Int. Ed. Engl. **30**, 1151 (1991).
9. N. Auner, C.-R. Heikenwälder, and C. Wagner. Organometallics, **12**, 4135 (1993).
10. C.R. Heikenwälder. Ph.D. Thesis, Humboldt Universität, Berlin. 1997; N. Auner, C. Wagner, E. Herdtweck, M. Heckel, and W. Hiller. Bull. Soc. Chim. Fr. **132**, 599 (1995).
11. N. Auner, O. Nuyken, and B. Biebl. J.M.S.-Pure Appl. Chem. **A 34**, 225 (1997).
12. N. Auner, M. Backer, U. Pernisz, and H. Roskos. Photoluminescence of organosilicon based materials. *In* Abstracts of The 12th Internat. Symp. on Organosiliccon Chemistry. Sendali, May 1999, p. 124; U. Pernisz, N. Auner, and M. Backer. Polym. Preprints, **39**(1) 450 (1998); U. Pernisz, N. Auner, and M. Backer. *In* Silicones and silicon-modified materials. *Edited by* S.J. Clarson, J.J. Fitzgerald, M.J. Owen, and S.D. Smith. ACS Symp. Ser. No. 729, Dallas, TX. 1998. Chap. 7.
13. L. Brandsma. *In* Preparative acetylenic chemistry. Elsevier, Amsterdam. 1992.
14. M.J.S. Dewar. J. Am. Chem. Soc. **107**, 3902 (1985).
15. Y. Apeloig and M. Karni. J. Am. Chem. Soc. **106**, 6676 (1984).
16. N. Sewald, W. Ziche, A. Wolff, and N. Auner. Organometallics, **12**, 4123 (1993).
17. E. Pretsch, T. Clerk, J. Seibl, and W. Simon. Tabellen zur Strukturaufklärung organischer Verbindungen mit spektroskopischen Methoden, 3. Aufl., Springer-Verlag, Berlin Heidelberg. 1986.
18. W. Ziche, N. Auner, and J. Behm. Organometallics, **11**, 2494 (1992).
19. M. Ishikawa, S. Matruzawa, K. Hirotsu, S. Kamitori, and T. Higuchi. Organometallics, **3**, 1930 (1984); M. Ishikawa, H. Sugisawa, H. Akimoto, and K. Matsusaki. **5**, 2447 (1986); M. Weidenbruch, B. Brand-Roth, S. Pohl, and W. Saak. J. Organomet. Chem. **379**, 271 (1989); D.B. Puranik, M.P. Johnson, and M.J. Fink. J. Chem. Soc. Chem. Commun. 706 (1989); M.J. Fink, D.B. Puranik, and M.P. Johnson. J. Am. Chem. Soc. **110**, 1315 (1988).
20. H.M. Schmidt and J.F. Arens. Recl. Trav. Chim. Pays-Bas, **86**, 1138 (1967).
21. C. Hurd. J. Am. Chem. Soc. **53**, 1074 (1931); R.M. Fantazier and M.L. Poutsma. J. Am. Chem. Soc. **90**, 5490 (1968).
22. G.M. Sheldrick. *In* Crystallographic computing 3. *Edited by* G.M. Sheldrick, C. Krüger, and R. Goddard. Oxford University Press, Oxford, U.K. 1985.
23. G.M. Sheldrick. SHELXL93. A Program for the refinement of crystal structures. Universität Göttingen, Germany. 1993.
24. International Tables for Crystallography, Vol. C Table 4.2.6.8, Table 6.1.1.4. Kluwer Academic Publishers, Dordrecht, Boston, London. 1993.

© 2000 NRC Canada

The one- and two-photon photochemistry of benzylsilacyclobutanes, acyclic benzylsilanes, and 1,1,2-triphenylsilacyclobutane

William J. Leigh and Thomas R. Owens

Abstract: The photochemistry of several α-silylbenzyl compounds has been investigated in hexane and in methanol solution. Direct photolysis of 1-benzyl-1-methylsilacyclobutane (**1**) in methanolic hexane solution produces 1-propyl-1-methyl-2,3-benzosilacyclobutene (**6**) in quantitative yield, by a sequential two-photon process involving the photoactive isotoluene derivative 1-methylene-6-(1-methylsilacyclobutyl)-2,4-cyclohexadiene (**13a**), which has been identified on the basis of its ^{1}H NMR and UV absorption spectra. In contrast, direct irradiation of 1-benzyl-1-phenylsilacyclobutane (**2**) under similar conditions results in the formation of a complex mixture of products consistent with the competing formation of 1-benzyl-1-phenylsilene and benzyl- and 1-phenylsilacyclobutyl radicals. The silene is a transient which has been detected directly by laser flash photolysis of **2** (λ_{max} = 315 nm, $\tau \sim 4.5$ μs). Free radical formation is shown to be due to secondary photolysis of a second primary product, 1-methylene-6-(1-phenylsilacyclobutyl)-2,4-cyclohexadiene (**13b**), which has also been detected and identified by static UV absorption (λ_{max} = 335 nm) and ^{1}H NMR spectroscopy. In a reaction with some analogy to the acid-catalyzed desilylation of allylsilanes, both **13a** and **13b** can be intercepted in neutral or acidic methanol solution to yield toluene and 1-methyl- or 1-phenyl-1-methoxysilacyclobutane, respectively. Direct photolysis of benzyldimethylphenylsilane (**4**) also leads to the formation of the corresponding isotoluene derivative, while benzyltrimethylsilane (**3**) exhibits negligible photoreactivity. The endocyclic benzylsilane 1,1,2-triphenylsilacyclobutane (**5**) is shown to undergo competing [2 + 2]-cycloreversion and [1,3]-silyl migration to yield a bicyclic isotoluene analogue, which reacts rapidly with methanol to yield the acyclic methoxysilane reported previously to be the main product of photolysis of this silacyclobutane in methanol solution. Relative quantum yields for isotoluene formation from photolysis of **1**–**4** and absolute rate constants for methanolysis of several of these compounds under neutral and acidic conditions have also been determined.

Key words: photochemistry, organosilicon, benzylsilane, silacyclobutane, silene, kinetics, isotoluene.

Résumé : On a étudié la photochimie de plusieurs composés α-silylbenzyles en solutions dans l'hexane ou dans le méthanol. La photolyse directe du 1-benzyl-1-méthylsilacyclobutane (**1**), en solution méthanolique d'hexane, conduit à la formation de 1-propyl-1-méthyl-2,3-benzosilacyclobutène (**6**) avec un rendement quantitatif; la réaction se produit par un processus séquentiel à deux photons impliquant le dérivé photoréactif isotoluène, 1-méthylène-6-(1-méthylsilacyclobutyl)cyclohexa-2,4-diène (**13a**) que l'on a identifié sur la base de son spectre RMN du ^{1}H et de son spectre d'absorption UV. Par ailleurs, l'irradiation directe du 1-benzyl-1-phénylsilacyclobutane (**2**) dans des conditions semblables conduit à un mélange complexe de produits qui pourraient résulter d'une compétition entre la formation des radicaux 1-benzyl-1-phénylsilène, et benzyl- et 1-phénylsilacyclobutyles. Le silène est une espèce transitoire que l'on a détectée directement par photolyse éclair à l'aide d'un laser du produit **2** (λ_{max} = 315 nm, $\tau \sim 4{,}5$ μs). On a démontré que la formation du radical libre est due à une photolyse secondaire d'un deuxième produit primaire, la 1-méthylène-6-(1-phénylsilacyclobutyl)cyclohexa-2,4-diène (**13b**) que l'on a aussi détecté et identifié par absorption UV statique (λ_{max} = 335 nm) et spectroscopie RMN du ^{1}H. Dans une réaction qui présente une certaine analogie avec la désilylation acidocatalysée des allylsilanes, on peut intercepter les composés **13a** ainsi que **13b**, en solutions méthanoliques tant neutre qu'acide, pour obtenir du toluène et respectivement du 1-méthyl- et du 1-phényl-1-méthoxysilacyclobutane. La photolyse directe du benzyldiméthylphénylsilane (**4**) conduit aussi à la formation du dérivé isotoluène correspondant alors que la photoréactivité du benzyltriméthylsilane (**3**) est négligeable. On a démontré que le benzylsilane endocyclique, 1,1,2-triphénylsilacyclobutane (**5**), est soumis à des réactions en compétition de cycloréversion [2 + 2] et de migration de silyle [1,3] qui conduisent à un analogue isotoluène bicyclique qui réagit rapidement avec le méthanol pour fournir le méthoxysilane acyclique reconnu antérieurement comme le produit principal de la photolyse de ce silacyclobutane en solution dans le méthanol. On a aussi déterminé les rendements quantiques

Received July 30, 1999. Published on the NRC Research Press website on November 2, 2000.

This paper is dedicated to Professor Adrian Brook in honour of his many contributions to organosilicon chemistry.

W.J. Leigh[1] and T.R. Owens. Department of Chemistry, McMaster University, 1280 Main Street West, Hamilton, ON L8S 4M1, Canada.

[1]Author to whom correspondence may be addressed. Telephone (905) 525-9140 ext. 23715. e-mail: leigh@mcmaster.ca

 © 2000 NRC Canada

pour la formation de l'isotoluène par photolyse des composés **1**–**4** ainsi que les constantes de vitesse absolues de méthanolyse de plusieurs de ces composés dans des conditions neutres et acides.

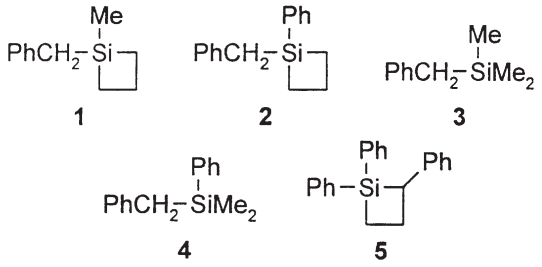
Mots clés : photochimie, organosilicium, benzylsilane, silacyclobutane, silène, cinétique, isotoluène.

Introduction

Silacyclobutanes are well-known photochemical and thermal precursors to transient Si=C containing compounds ("silenes") (1–8), and are tremendously useful in experiments aimed at detecting these reactive intermediates directly and studying the kinetics and mechanisms of their various characteristic reactions (9–17). Photochemical silene formation proceeds with useful efficiencies from silacyclobutanes bearing a wide range of substituents at silicon, ranging from compounds in which the silacyclobutane ring is the primary chromophore (e.g., 1,1-dialkylsilacyclobutanes) to those in which the lowest excited state is localized more in the substituent (e.g., 1-arylsilacyclobutanes). The only known exception to this generalization is alkoxy-substituted derivatives; substituents of this type, either directly at silicon or on the aromatic rings of phenylated derivatives, renders the silacyclobutane moiety inert to photocycloreversion (13, 17).

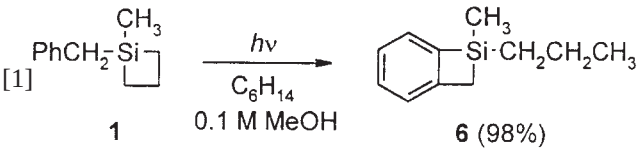
Recent work in our laboratory has been directed at exploring the versatility of arylsilacyclobutanes as photochemical silene precursors, through systematic variation of the structure and photophysical properties of the aryl chromophore (18). These studies have also afforded new detail on the mechanism of silene photoextrusion from arylsilacyclobutanes. For example, the reaction proceeds from the lowest excited singlet state, probably via a 1,4-biradical intermediate that partitions between silene and the ground state of the silacyclobutane. If this mechanism is correct, then the overall quantum yield for reaction will be a function of two factors. The first is the partitioning of the silacyclobutane excited singlet state between Si—C bond cleavage and nonproductive decay via internal conversion, intersystem crossing, and fluorescence; this tends to not vary dramatically as a function of aryl substituent, at least within the series of compounds that we have studied to date. The second is the partitioning of the biradical intermediate between silene and starting material. This does appear to vary as a function of substituent at silicon, most likely due to substituent-induced variations in the conformational properties of the biradical.

In this paper, we describe the results of a study of the photochemistry in solution of two 1-benzylsilacyclobutanes (**1** and **2**). These two compounds exemplify two different photophysical situations – one in which the benzyl group is the primary chromophore in the molecule (**1**) and one in which the role of primary chromophore is shared between it and the silacyclobutane ring via a second phenyl group attached to silicon (**2**). Previous work suggests that benzylsilanes generally exhibit very low photoreactivity upon direct excitation in condensed phases (19). We thus wondered whether benzylsilacyclobutanes might show similar reactivity toward silene photoextrusion as is possessed by other simple silacyclobutane derivatives, with minimal complications from competing reactions due to the benzylic substituent. It quickly became clear that this is not the case, prompting us to expand our studies to include three additional benzylsilane derivatives, two of which have been studied previously: benzyltrimethylsilane (**3**) (19), benzyldimethylphenylsilane (**4**), and 1,1,2-triphenylsilacyclobutane (**5**) (4, 9, 20).

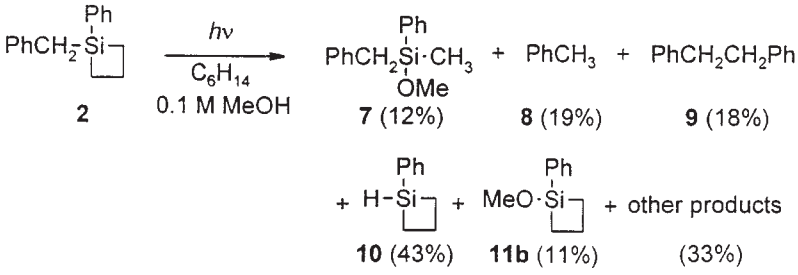


Results and discussion

Direct photolysis of 1-benzyl-1-methylsilacyclobutane (**1**; 0.05 M) in deoxygenated hexane solution containing methanol (0.1 M) with the light from a low pressure mercury lamp (254 nm) affords the single product **6** in quantitative (>98%) yield (eq. [1]). The same product was formed, again quantitatively, when the photolysis was conducted in the absence of methanol.

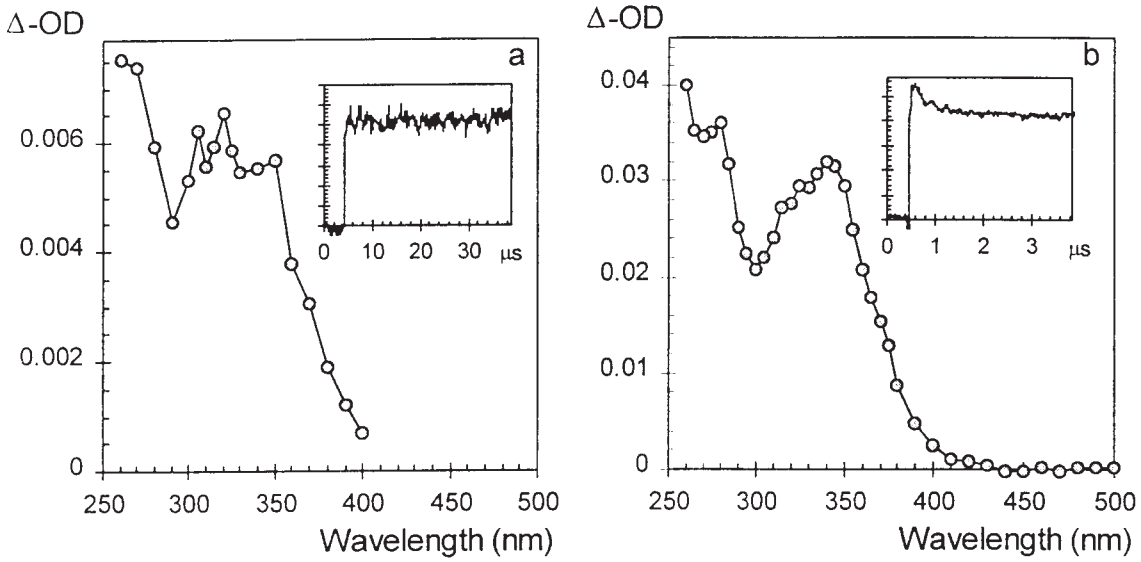


In contrast, photolysis of **2** as a deoxygenated 0.05 M solution in hexane containing 0.1 M methanol led to the more complex mixture of products shown in eq. [2]. Alkoxysilane **7** is the product expected from trapping of 1-benzyl-1-phenylsilene (**12**) by methanol, while **8**–**10** are most likely the products of hydrogen abstraction or coupling of benzyl



© 2000 NRC Canada

Fig. 1. UV absorption spectra, recorded by laser flash photolysis of deoxygenated hexane solutions of (*a*) 1-benzyl-1-methylsilacyclobutane (**1**; 0.002 M), 10–15 μs after the pulse and (*b*) 1-benzyl-1-phenylsilacyclobutane (**2**; 0.001 M), 3–3.5 μs after the pulse. The inserts show typical traces, recorded at 335 nm.



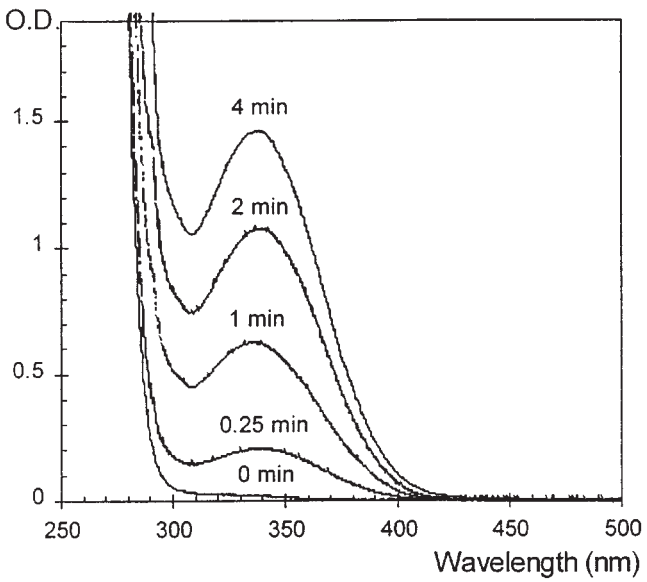
and phenylsilacyclobutyl radicals. Several other products were also formed, in yields which were too low to enable identification. The mass balance was ~93% at 20% conversion of **2**.

Flash photolysis of a deoxygenated hexane solution of **1** (0.007 M) with a KrF excimer laser (248 nm) led to the formation of a weakly absorbing species which was stable over 10 ms, the longest timescale able to be monitored with our system. The UV spectrum recorded 10–15 μs after laser excitation is shown in Fig. 1*a*, along with a ΔOD vs. time profile. No short-lived transient species could be detected at any monitoring wavelength between 260–600 nm from this compound. Similar experiments with **2** (0.008 M) led to the results shown in Fig. 1*b*: the formation of a long-lived species which exhibits a similar spectrum to that observed from **1**, on which is superimposed a weak transient absorption which decayed with pseudo-first order kinetics ($\tau \sim 4.5$ μs). Subtraction of the spectrum of the long-lived species from the spectrum recorded immediately after the laser pulse revealed an absorption centered at 310–315 nm, which can be associated with the short-lived transient species. The lifetime of this transient was shortened upon addition of methanol to the solution; a plot of k_{decay} vs. [MeOH] according to eq. [3] was linear, with slope $k_{MeOH} = (9 \pm 2) \times 10^7$ M^{-1} s^{-1}. The spectrum and sensitivity of the lifetime of this transient to the presence of methanol are consistent with its assignment to 1-benzyl-1-phenylsilene (**12**). Neither of the long-lived species formed from **1** and **2** were affected detectably by the addition of up to 0.1 M methanol, over the 10 ms timescale.

$$[3] \qquad k_{decay} = k_o + k_{MeOH}[MeOH]$$

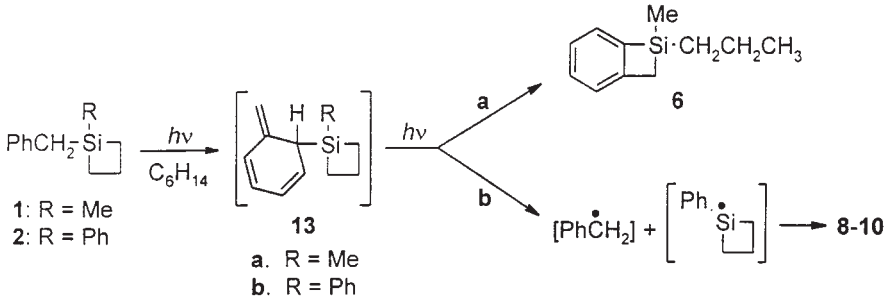
The stable species produced in the flash photolysis experiments with **1** and **2** could also be detected by static UV absorption spectroscopy, and by ^{1}H NMR spectroscopy when the reactions were carried out in cyclohexane-d_{12}. For example, the static UV spectrum of a 0.017 M solution of **1** as a function of photolysis time is shown in Fig. 2. The ^{1}H NMR spectra of a cyclohexane-d_{12} solution of this compound after

Fig. 2. Static UV absorption spectra of a 0.017 M solution of **1** in hexane solution after various time intervals of photolysis with 254-nm light, illustrating the formation of isotoluene **13a** (λ_{max} = 335 nm).



photolysis for similar periods of time showed the growth of a broad singlet at δ 3.18 ppm and a number of resonances in the vinylic region which integrate to a total of six protons relative to the signal at δ 3.18. These signals grow in during the early stages of the photolysis and then remain roughly constant in relative intensity upon continued irradiation, and can thus be identified as arising from the same initially-formed product that is responsible for the 335 nm UV absorption. On the basis of these data, we assign the structure of this product to 1-methylene-6-(1-methylsilacyclobutyl)-2,4-cyclohexadiene (**13a**; eq. [4]). The spectral data observed agree very well with those reported for other

© 2000 NRC Canada

[4] 

isotoluene derivatives (21–24). Compounds of this type are surprisingly quite stable in non-nucleophilic solvents.

In the case of **1**, these experiments indicated **13a** to be the sole primary photolysis product, building up steadily in concentration over a conversion range of 0–15% to a level roughly 6% of that of the starting material, after which it decreased in parallel with **1** upon continued photolysis. Compound **6** could only be detected in significant yields after the formation of **13a** had nearly reached its initial plateau, suggesting that it is a secondary product resulting from photolysis of the latter species. This was verified by photolyzing a solution of **1** with 248 nm light to ca. 10% conversion, and then continuing the photolysis with 337 nm light; this caused **13a** to disappear, with concomitant formation of **6** and no further consumption of **1**, consistent with the fact that the latter is nonabsorbing above ~280 nm.

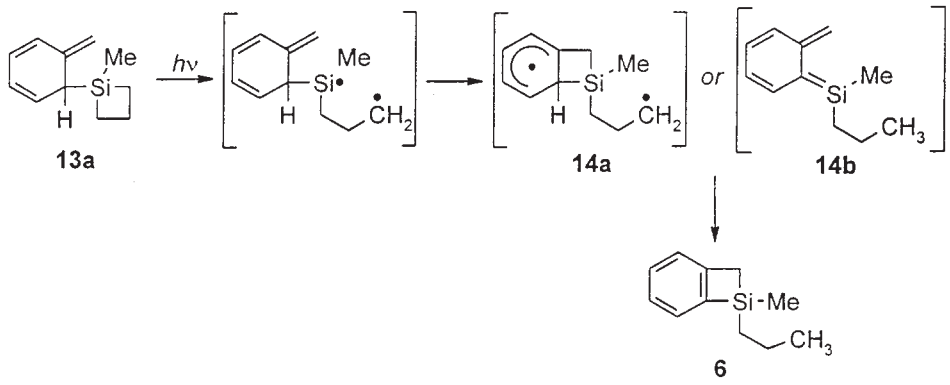
Similar experiments with **2** indicated that only alkoxysilane (**7**), ethylene, and a product identifiable as isotoluene **13b** are formed upon photolysis in hexane or cyclohexane-d_{12} solution to low (<ca. 10%) conversions. Again, the isotoluene derivative could be detected by both static UV and ^{1}H NMR spectroscopy, and products **8**–**10** were found to be produced only after the concentration of **13b** rose to ~5% of that of **2**. Alternating 248 and 337 nm irradiation experiments verified that **8**–**10** are formed as a result of secondary photolysis of **13b**.

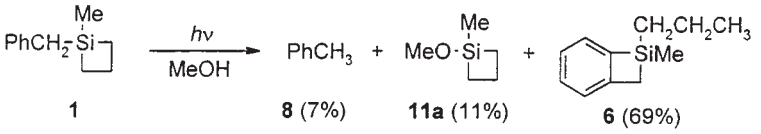
The formation of **13a**, **b** as the major primary products of photolysis of **1** and **2** indicates that the photochemistry of these compounds is in both cases dominated by reactivity specific to the benzyl chromophore rather than the silacyclobutane moiety, unlike the case with other silacyclobutanes that have been studied. Silene formation competes significantly only in **2**, where the silacyclobutane ring bears a second phenyl chromophore which competes effectively with the benzyl group for direct light absorption. The reactive excited states in both **1** and **2** are most likely the lowest singlet states, since our flash photolysis experiments indicate that **13a**, **b** are both formed within the duration of the laser pulse (~25 ns), consistent with either a concerted sigmatropic rearrangement or a singlet radical-pair recombination mechanism for their formation. No evidence for the competing formation of benzyl radicals in the primary photochemical event could be obtained by flash photolysis in either case, which provides strong evidence against a mechanism for the formation of **13** which involves the triplet excited states of **1** and **2**. For that matter, no evidence for benzyl radical formation could be obtained either in two-laser flash photolysis experiments with **2**, where the second (337 nm) laser pulse was delivered 5–10 μs after **13b** was formed by the primary (248 nm) pulse. Since product studies clearly indicate that free benzyl radicals *must* be formed upon secondary photolysis of **13b**, this result merely suggests that the quantum yield for photolysis of the intermediate is exceedingly low. This is also indicated by the fact that only slight irreversible bleaching of the 335 nm absorption due to **13b** could be detected in these experiments. Flash photolysis experiments carried out with optically matched (at 248 nm) solutions of **1** and **2** indicated that the quantum yield for formation of **13b** from **2** is only slightly higher than that for formation of **13a** from **1** (Φ_{13b}/Φ_{13a} ~ 1.3). This suggests that the main effect of replacing the methyl substituent in **1** with phenyl (in **2**) is to promote silene formation in minor amounts, via [2 + 2]-cycloreversion of the silacyclobutane ring. The spectra shown in Fig. 1 were recorded with solutions which were not optically-matched, and with different excitation laser intensities.

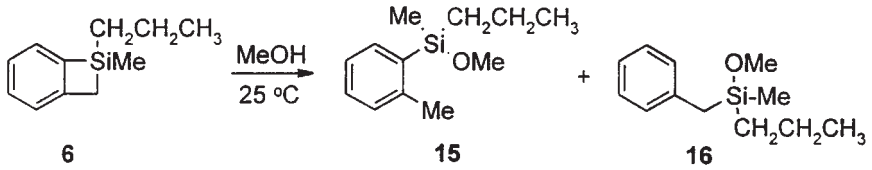
Interestingly, the identity of the second silyl substituent has a far more substantial effect on the photochemistry of the corresponding isotoluene derivatives **13a**, **b**. The formation of **6** from **13a** can be formulated in terms of a nonconcerted mechanism involving rearrangement of the 1,4-biradical intermediate formed by cleavage of the one of the endocyclic silacyclobutyl Si—C bonds (eq. [5]). If this mechanism is correct, then the photochemistry of **13a** initially follows a course typical of 1-substituted methylsilacyclobutanes (18). Unlike other methylsilacyclobutane-derived 1,4-biradicals however, that derived from **13a** has available two possible reaction pathways that are both likely to be less energetically demanding than cleavage to the corresponding silene and ethylene: rearrangement to yield the more stable cyclohexadienyl biradical **14a** which can then aromatize to **6** via intramolecular disproportionation, or intramolecular abstraction of the cyclohexadienyl proton to form an *ortho*-silaxylylene intermediate (**14b**) followed by electrocyclic ring closure. We favour the former mechanism, on the basis of the fact that none of the expected trapping product of **14b** was observed in the photolysis of **1** in 0.3 M MeOH solution; however, its possible intermediacy in the formation of **6** from **13a** cannot be rigorously ruled out.

The photochemistry of **13b**, on the other hand, is evidently initiated by preferential cleavage of the weaker of the *exocyclic* silacyclobutyl Si—C bonds, yielding benzyl- and phenylsilacyclobutyl radicals. To our knowledge, no other examples of exocyclic Si—C bond cleavage are known in silacyclobutane photochemistry. One possible explanation for the difference in the photochemistry of **13a** and **13b** is that the latter has available to it a conformer in which a reasonable degree of π-overlap is possible between the methylenecyclohexadienyl and phenyl rings; this could lead to preferential weakening of the exocyclic Si—C bond due to charge-transfer interactions between the two moieties in the lowest excited singlet state. While no evidence for such interactions could be obtained from the UV absorption spectra

© 2000 NRC Canada

[5] 

[6] 

[7] 

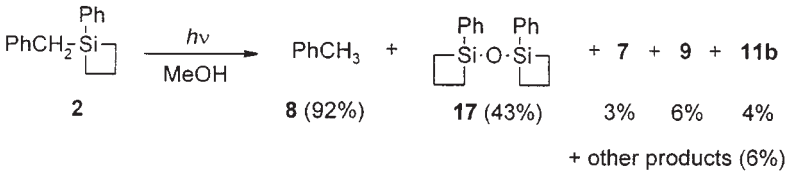
of the two compounds, the vinylic resonances in the ^{1}H NMR spectrum of **13b** appear at consistently lower fields than those in the spectrum of **13a**, indicative of significant deshielding of the vinyl protons by the phenyl ring. Neither compound appears to undergo the 4π electrocyclic ring closure that is typical of other isotoluene derivatives that have been studied (24), to any detectable extent.

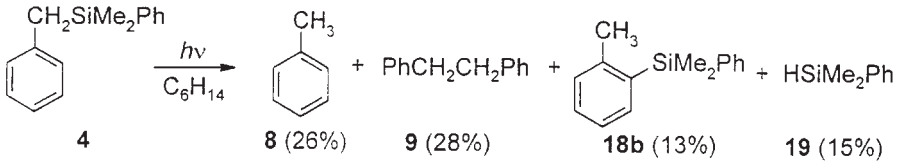
To gain additional evidence for the primary involvement of **13a**, **b** in the photochemistry of **1** and **2**, we examined the photolyses of the latter two compounds in neat methanol solution. One of the common properties of isotoluene derivatives is their sensitivity towards acid-catalyzed aromatization, the exact course of which (isomerization vs. solvolysis) depends on the nature of the substituents at the *bis*-allylic position of the methylenecyclohexadienyl ring (21, 24). Judging from the well-known reactivity of allylsilanes toward acid-catalyzed desilylation (25, 26), the present compounds should be expected to react readily with aliphatic alcohols to yield toluene and the corresponding methoxysilacyclobutane. Thus, it seemed very likely that the formation of the secondary products of photolysis of **1** and **2** might be suppressed in methanol solution due to interception of the primary products (**13**) by reaction with the solvent. This might also explain the formation of methoxyphenylsilacyclobutane (**11b**) in trace amounts in the photolysis of **2** in hexane containing 0.1 M methanol (eq. [2]).

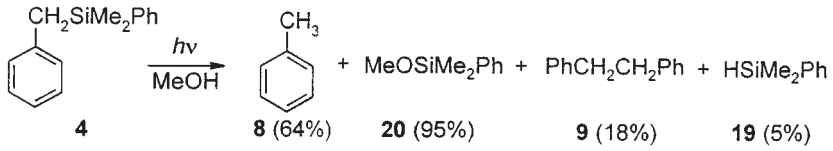
As expected, photolysis of **1** in neat methanol produced **6** (69%), toluene (**8**; 7%), and 1-methoxy-1-methylsilacyclobutane (**11a**; 11%), as shown in eq. [6]. The reaction mixture was actually somewhat more complicated than this, because like other benzosilacyclobutenes (27), **6** reacts rapidly in methanol solution, in this case to yield two methoxysilanes in a 8:1 ratio. These were tentatively identified as **15** and **16**, respectively, on the basis of ^{1}H NMR and GC/MS evidence (eq. [7]). The actual amount of **6** detected in the photolysis mixture therefore varied depending on the time taken between photolysis and GC analysis. The yields of **8** and **11a** increased to a combined yield of ~73% upon photolysis of a methanol solution of **1** containing 0.1 M HCl, and as expected (27), the relative yields of **15** and **16** changed to 1.4:1. Evaporation of the solvent after photolysis of a hexane solution of **1** to ca. 10% conversion and redissolution of the mixture in methanol confirmed that the formation of toluene (**8**) and 1-methoxy-1-methylsilacyclobutane (**11a**) are due to reaction of **13a** with the alcohol. Monitoring of this reaction by UV spectroscopy revealed that the isotoluene disappears with pseudo-first order kinetics and a rate constant of $k_{\mathbf{-13a}} = (1.10 \pm 0.05) \times 10^{-3}$ s^{-1} in neutral methanol solution at 25°C. In methanol containing 0.1 M HCl, disappearance of **13a** was too rapid for a rate constant to be measured by conventional UV absorption spectroscopy.

Steady state photolysis of **2** in deoxygenated methanol solution led to the formation of two main products, toluene (**8**) and disiloxane **17**, and only traces of bibenzyl (**9**) and the silene-derived methoxysilane **7** (eq. [8]). The mass balance in this experiment was ~92% after ca. 40% conversion of **2**. Disiloxane **17** most likely arises from condensation of **11b** due to the presence of small amounts of water in the solvent, a process which can be expected to proceed more readily in **11b** than in **11a** under neutral (as well as acidic) conditions (28). As before, evaporation of the solvent after photolysis of a hexane solution of **2** to ca. 10% conversion and redissolution of the mixture in methanol resulted in the disappearance of the 335 nm UV absorption due to **13b** and the formation of **8** and **17**. The reaction is complete within ~5 s under these conditions, but was found to be too slow for a rate constant to be obtained by flash photolysis. Thus, while an absolute rate constant for the reaction of **13b** with methanol could not be easily determined, it is clearly at least

© 2000 NRC Canada

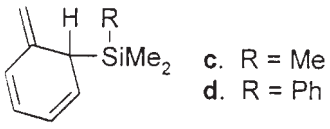
[8] 

[9] 

[10] 

two orders of magnitude greater than that for reaction of **13a** under similar conditions. The much higher reactivity of **13b** toward dark reaction with methanol more effectively lowers its steady-state concentration during the photolysis of **2** in this solvent, resulting in much lower yields of secondary photolysis products relative to what is observed in hydrocarbon solvents, compared to **13a**.

While the photoisomerization of **1** and **2** to the corresponding isotoluene derivatives has precedent in the photochemistry of other benzyl compounds (24), it has not been reported previously for benzylsilanes. Benzyltrimethylsilane (**3**) was first reported to be inert to photolysis in solution (20), but Kira et al. (19) later found that extended photolysis of the compound in hydrocarbon solution leads to the inefficient formation of *ortho*-tolyltrimethylsilane (**18a**), which they suggested to arise from a minor reaction of benzyl and trimethylsilyl radicals produced by homolysis of the benzyl carbon-silicon bond in the benzylsilane. More recently, spectroscopic evidence for the formation of free benzyl radicals upon photolysis of **3** in an ethanol matrix at 77 K has been reported by Hiratsuka et al. (29).



c. R = Me
d. R = Ph

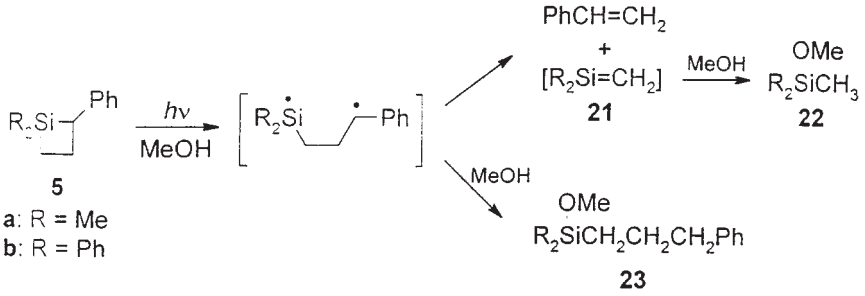
13

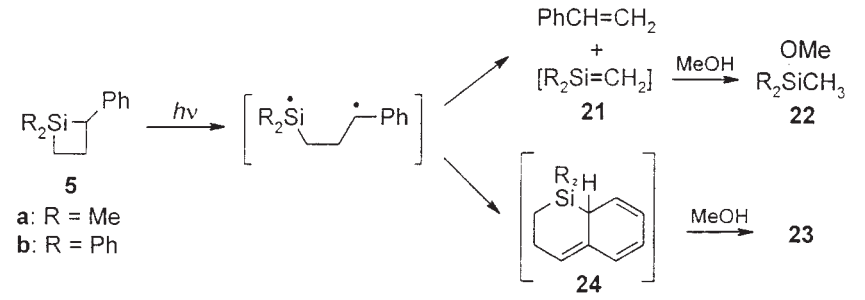
We also find that the parent benzylsilane exhibits very low photoreactivity in solution at room temperature. Extended photolysis of **3** in hexane with 254 nm light produces very weak UV absorptions on the long-wavelength edge of the absorption band due to **3**, but the ^{1}H NMR spectrum of the mixture shows no evidence of vinylic resonances consistent with the formation of isotoluene **13c** in detectable amounts. The quantum yield for formation of this product from **3** is thus no greater than ~5% of that for the formation of **13a** from **1** under similar conditions.

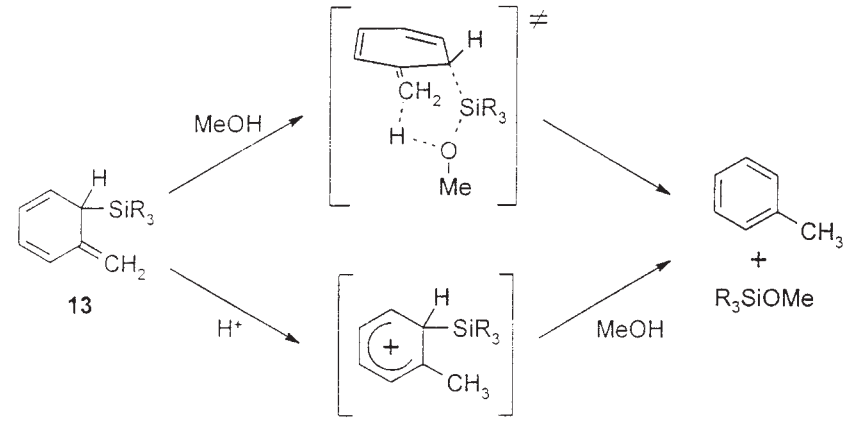
On the other hand, photolysis of benzyldimethylphenylsilane (**4**) in hexane results in the fairly efficient formation of a long-wavelength absorbing species which can be identified as the isotoluene derivative **13d** on the basis of its UV and ^{1}H NMR spectra. This compound, the only detectable product at low (<5%) conversion of **4**, is formed with a similar quantum yield to that for formation of **13b** from **2**. It also behaves similarly to **13b** with respect to secondary photolysis and reaction with methanol. For example, eqs. [9] and [10] show the product mixtures obtained from photolysis of **4** in deoxygenated hexane and methanol solutions, respectively, to 40–50% conversion of the starting material. Interestingly, a product tentatively identified as *ortho*-tolyldimethylphenylsilane (**18b**) could be detected in significant yield by GC/MS analysis of the hexane photolyzate. It is barely resolved from **4** under our GC/MS conditions, and coelutes with **4** under those employed for our GC/FID analyses. A closer inspection of the product mixture from photolysis of **2** in hexane revealed that an analogous isomeric product is formed in this case as well, but in yields of less than 10%. These products are most likely formed by a free radical pathway initiated by hydrogen abstraction from **13b/d** by benzyl radicals, since they are not formed in detectable yields in methanol solution, where the steady state concentration of **13** is substantially lower due to reaction with the solvent. As was found with **13b**, dissolution of **13d** in neutral methanol results in its immediate disappearance and the concomitant formation of **8** and **20**. It is possible that the higher photoreactivity of **4** compared to **3** with respect to isotoluene formation is due to similar factors as those suggested above to explain the different photoreactivities of **13a**, **b**. However, we are at a loss to explain why the methylsilacyclobutyl derivative **1** is also more reactive than **3** toward this photorearrangement.

The results reported above provide a reasonable explanation for one or two unusual aspects of the photochemistry of 2-phenylsilacyclobutanes (**5**) which have been reported previously (4, 9, 20). Both 1,1-dimethyl-2-phenyl- and 1,1,2-triphenylsilacyclobutane (**5a** and **5b**, respectively), yield styrene and the corresponding silene **21a**, **b** upon photolysis in methanol solution, as evidenced by the formation of the methoxysilane (**22**) expected from trapping of the silene by the solvent (eq. [11]) (4, 20). Also formed are the methoxysilanes **23a**, **b**, which were originally ascribed to nucleophilic trapping of the 1,4-biradical/zwitterion formed

© 2000 NRC Canada

[11] 

[12] 

[13] 

by cleavage of a single carbon—silicon bond in the excited state of the silacyclobutane (eq. [11]. The formation of these products was offered as the first evidence for a stepwise reaction mechanism for the formal [2 + 2]-photocycloreversion of silacyclobutanes (4, 20).

Our results for **1**–**4** suggest that a more likely explanation for the formation of **23** is that it arises from reaction of methanol with the isotoluene derivative (**24**) formed by [1,3]-silyl migration into the *ortho*-position of the 2-phenyl ring in **5** (eq. [12]). The isotoluenes **24a**, **b** would be expected to be stable enough that they should build up to significant concentrations, at least in non-nucleophilic solvents. However, their secondary photolysis should result mainly in reversion to the biradical precursor, so no additional products that might have signalled their presence would be expected.

In fact, we have already published evidence consistent with this interpretation, although we failed to recognize it at the time (9). Laser flash photolysis of **5b** in isooctane leads to the formation of a transient species identified as 1,1-diphenylsilene (**21b**), whose absorptions (λ_{max} = 325 nm) are superimposed on those due to a species which is stable over the timescale of our experiment and exhibits λ_{max} ~ 335 nm. We originally reported that this species did not persist over a timescale of several minutes, but this conclusion was based on examination of photolyzed solutions containing small amounts of methanol. In fact, inspection of photolyzed hexane or cyclohexane-d_{12} solutions of **5b** in the absence of added methanol reveals that the species is quite stable, and exhibits a ^{1}H NMR spectrum consistent with isotoluene **24b**. The compound reacts within ~5 s upon dissolution in neutral methanol to yield the previously reported methoxysilane **23**.

The three phenylsilyl-substituted isotoluenes (**13b**, **13d**, and **24b**) all react with methanol under neutral conditions at least two orders of magnitude faster than the trialkylsilyl derivative **13a**. This difference in reactivity, which has been documented previously in other systems (25, 30), suggests that desilylation proceeds by an S_N2 mechanism under these conditions, probably with simultaneous protonation at the exocyclic double bond of the leaving group (eq. [13]).

On the other hand, little difference in reactivity as a function of substitution at silicon is observed in acidic methanol solution. For example, **13a**, **13b**, **13d**, and **24b** were all found (by laser flash photolysis) to have lifetimes in the 12–17 ms range in methanol containing 0.3 M HCl. This suggests that under acidic conditions, the rate-determining step for reaction is protonation of the exocyclic double bond,

© 2000 NRC Canada

Table 1. Pseudo-first order rate constants for decay of isotoluenes in methanol and methanol containing 0.3 M HCl at 23°C.

	k_{decay} (s^{-1})			
	13a	**13b**	**13d**	**24b**
MeOH	0.0011±0.0001	>0.2	>0.2	>0.2
0.3 M HCl–MeOH	85 ± 1	61 ± 2	77 ± 1	58 ± 4

the rate of which is not expected to depend on substitution at silicon. The resulting β-silyl-substituted cyclohexadienyl carbenium ion then undergoes rapid methanol-assisted desilylation (30) to yield toluene and the corresponding methoxysilane. The pseudo-first-order rate constants for decay of the four isotoluenes in methanol and methanol containing 0.3 M HCl are summarized in Table 1.

Summary and conclusions

The direct photolysis of benzylsilanes in solution results mainly in the formation of the corresponding 6-silylisotoluene derivatives, which are sufficiently stable in hydrocarbon solvents that they build up in concentration and start to compete with the precursor for light absorption after conversions of only 5–6%. Secondary photolysis of the isotoluene derivatives is responsible for the formation of most of the products of benzylsilane photolysis that are detected chromatographically. Isotoluene formation results formally from a photochemically allowed [1,3]-sigmatropic rearrangement, although a singlet radical pair recombination mechanism cannot be ruled out, and is generally more efficient in benzyldialkylphenylsilanes than in benzyltrialkylsilanes. Phenyl substitution at silicon also affects the photochemistry of the corresponding 6-silylisotoluene derivative, promoting Si—C bond homolysis to yield benzyl and silyl free radicals. The isotoluene derivatives undergo rapid desilylation in neutral or acidic methanol solution, which allows the formation of secondary photolysis products to be suppressed. The rate of solvolysis under neutral conditions is at least two orders of magnitude greater for the phenylsilyl derivatives, suggesting that it proceeds by an S_N2 mechanism in neutral methanol. The rates are accelerated by up to five orders of magnitude in methanol containing 0.3 M HCl and show no dependence on silyl substituent, consistent with protonation being the rate determining step for isotoluene desilylation under acidic conditions. The photochemical [1,3]-rearrangement also occurs in "masked" benzylsilanes such as 1,1,2-triphenylsilacyclobutane and accounts for the formation of silacyclobutane-ring-opening products in the photolyses of 2-phenylsilacyclobutanes in methanol solution.

Experimental

^1H, ^{13}C, and ^{29}Si NMR spectra were recorded using Bruker AC200, Bruker AC300, or DRX500 NMR spectrometers. Infrared spectra were recorded on a BioRad FTS-40 FT/IR spectrometer and are reported in wavenumbers (cm^{-1}). Ultraviolet absorption spectra were recorded on Cary–Varian Model 50 or Model 400 spectrometers. Gas chromatographic separations employed a Hewlett–Packard 5890 gas chromatograph equipped with a 3396A integrator, flame ionization detector, a conventional splitless injector (heated), and a DB-1 fused silica capillary column (15 m × 0.2-mm; Chromatographic Specialties, Inc.). Low resolution mass spectra were recorded using a Hewlett–Packard 5890 gas chromatograph equipped with a HP-5971A mass selective detector and a DB-5 fused silica capillary column (30 m × 0.25 mm; Chromatographic Specialties, Inc.). High-resolution electron impact mass spectra and exact masses were determined using a VGH ZABE mass spectrometer.

Radial chromatographic separations were carried out using a Chromatotron® (Harrison Research, Inc.), with 2 or 4 mm silica gel 60 thick layer plates using hexane as the eluant.

Hexanes and methanol (BDH Omnisolv), cyclohexane-d_{12} (Cambridge Isotope Laboratories), benzyl bromide (Aldrich), benzyltrimethylsilane (**3**, Aldrich), dimethylphenylsilane (**19**, Aldrich), and chlorodimethylphenylsilane (Aldrich) were used as received from the suppliers. Tetrahydrofuran (BDH) was distilled from sodium. 1-Chloro-1-methylsilacyclobutane (31), 1-chloro-1-phenylsilacyclobutane (32), and benzyldimethylphenylsilane (**4**) (33) were prepared as previously described. 1,1,2-Triphenylsilacyclobutane (**5**) (9), 1-methoxy-1-methylsilacyclobutane (**11a**) (17), 1-phenylsilacyclobutane (**10**) (18), and dimethylmethoxyphenylsilane (**20**) (18) were available from previous studies. Benzylmethoxymethylphenylsilane (**7**) was prepared by reaction of benzylmethylphenylsilane with methanol in the presence of $PdCl_2$ (17).

1-Benzyl-1-methylsilacyclobutane (**1**) (34) was synthesized as follows. Magnesium filings (2.55 g, 0.105 g-atom) were placed in a 500 mL 2-neck round bottom flask fitted with an addition funnel, reflux condenser with nitrogen inlet, and magnetic stirrer. The entire apparatus was flame-dried under nitrogen and after cooling, anhydrous diethyl ether (100 mL) and 1-chloro-1-methylsilacyclobutane (4.0 mL, 2.75 g, 0.0299 mol) were added. Benzyl bromide (3.3 mL, 2.29 g, 0.0136 mol) was dissolved in anhydrous ether (50 mL) and added dropwise over a 30 min period with stirring. The mixture was stirred for 48 h at room temperature, during which time it turned a light gray color. Ice water (30 mL) was added slowly, and the resulting mixture was then filtered. The filtrate was placed in a 500 mL separatory funnel, the aqueous layer was removed, and the ether solution was washed with cold water (3 × 50 mL). After drying with anhydrous magnesium sulfate and filtering, the solvent was removed on a rotary evaporator to afford a slightly yellow oil (2.01 g). Compound **1** (1.04 g, 0.006 mol, 29%) was isolated as a colourless oil in >99% purity by radial chromatography on silica gel using hexane as eluant, and identified on the basis of the following spectroscopic data: ^1H NMR, δ = 0.289 (s, 3H), 1.03 (m, 2H), 1.09 (m, 2H), 2.08 (m, 2H), 2.36 (s, 2H), 7.13 (m, 3H), 7.26 (d, 1H), 7.28 (d, 1H); ^{13}C NMR, δ = –1.79, 13.8, 17.85, 22.68, 26.56, 31.61, 124.16, 128.02, 128.29, 128.60, 139.40; ^{29}Si NMR, δ = 18.85; 3082(s), 3062(s), 3027(s), 2964(m), 2926(w), 2798(m), 1934(m), 1868(m), 1801(m), 1600(s), 1494(s), 1452(s), 1410(m), 1250 (s), 1206(s), 1152(s), 1121(m), 1055(s), 1031(s), 903(s), 873(s), 755(s), 698(m), 653(s); UV (λ_{max}) = 220, 260 nm; MS (EI), *m/z* (I) = 176 (27), 148 (100), 133 (68), 119 (18), 107 (17), 105 (28), 91 (40), 85 (95), 65 (38), 43 (47); HRMS calcd. for $C_{11}H_{16}Si$: 176.1022; found: 176.1025.

© 2000 NRC Canada

1-Benzyl-1-phenylsilacyclobutane (**2**) was synthesized and purified by a similar procedure to the one given above for **1**. It was isolated as a colourless oil and identified on the basis of the following spectroscopic data: ^{1}H NMR, δ = 0.90 (s), 0.98 (t), 1.33 (m, 2H), 1.96 (m, 2H), 2.64 (t, 2H), 7.17 (m, 3H), 7.29 (m, 3H), 7.46 (m, 2H), 7.63 (m, 2H); ^{13}C NMR, δ = 12.88, 18.05, 22.68, 25.32, 31.59, 124.40, 127.88, 128.30, 128.36, 129.51, 133.67, 137.20,138.74; ^{29}Si NMR, δ = 12.00; 3067(w), 3025(m), 2969(m), 2924(w), 1954(m), 1881(m), 1816(m), 1600(s), 1493(s), 1428(s), 1395(m), 1207(s), 1184(s), 1152(m), 1117(m), 1056(s), 1030(s), 999(s), 924(s), 902(s), 858(m), 820(s), 801(s), 766(m), 735(s), 697(w); UV (λ_{max}) = 262, 222; MS (EI), *m*/*z* (I) = 238 (33), 210 (25), 161 (25), 147 (48), 132 (60), 105 (100), 93 (60), 91 (67), 65 (25), 53 (55); HRMS calcd. for $C_{16}H_{18}Si$: 238.1179; found: 238.1177.

Compound **6** was isolated from a semi-preparative scale photolysis of a hexane solution of 1-benzyl-1-methylsilacyclobutane (**1**, 0.22 g, 1.25 mmol) in hexane (20 mL). The solution was placed in a quartz photolysis tube, sealed with a rubber septum, deoxygenated with dry argon, and then irradiated in a Rayonet reactor fitted with seven RPR-2537 lamps The photolysis was monitored periodically by GC, and terminated after ca. 95% conversion of **1** (59 hs). After evaporation of the solvent, the single product was isolated by radial chromatography, further purified by silica gel column chromatography (hexane as eluent), and identified as 1-methyl-1-propyl-3,4-benzosilacyclobutene (**6**; 0.023 g, 0.125 mmol, 10%) on the basis of the following spectroscopic data: ^{1}H NMR, δ = 0.43 (s, 3H), 0.93 (t, 2H), 0.97 (t, 3H), 1.48 (m, 2H), 2.11 (d, 1H), 2.14 (d, 1H), 7.13 (d, 1H), 7.16 (d, 1H), 7.24 (d, 1H), 7.30 (d, 1H); ^{13}C NMR, δ = –2.173, 17.39, 17.66, 18.35, 19.08, 126.12, 126.82, 130.30, 130.57, 145.71, 150.95; ^{29}Si NMR, δ = 10.82; IR (neat), 3078(m), 2969(m), 2938(w), 2875(m), 2360(m), 2313(m), 1718(s), 1703(s), 1671(s), 1625(s), 1546(s), 1531(s), 1500(s), 1422(s), 1407(m), 1375(s), 1281(s), 1250(m), 1125(m), 1063(m), 1047(m), 812(s), 750(w); MS (EI), *m*/*z* (I) = 176(8), 161(3), 134(14), 119(15), 105(4), 85(43), 56(76), 57(74), 43(91), 41(100); HRMS calcd. for $C_{11}H_{16}Si$: 176.1022; found: 176.0995.

Steady state photolysis experiments were carried out in a Rayonet reactor fitted with 6–10 RPR-2537 lamps, on argon-saturated solutions contained in quartz tubes. In some cases, KrF excimer (248 nm) or nitrogen (337 nm) lasers, operated at 0.5 Hz with the intensity reduced using neutral density filters, were employed as excitation sources. Product yields were estimated in small scale runs, from the GC peak areas relative to that of an internal standard (usually decane). These were not corrected for differences in FID response factors.

The products of photolysis of **1** in deoxygenated methanol solution containing 0.1 M HCl were identified by GC/MS and GC coinjection with authentic samples. The major product of dark reaction of **6** with methanol was tentatively identified as methylmethoxy(*o*-tolyl)(1-propyl)silane (**15**; 76%) by ^{1}H NMR and GC/MS, on the crude mixture obtained from stirring a sample of **6** (0.1 g) in methanol (5 mL) for fourteen hours at 25°C, followed by evaporation of the solvent and redissolution in $CDCl_3$. The ^{1}H NMR spectrum of the compound exhibited singlets at δ 0.41 ($SiCH_3$), 2.46 (*o*-tolyl CH_3), and 3.41 (OCH_3) and resonances assignable to the *n*-propyl group (δ 0.90 (t, 2H), 0.95 (t, 3H), 1.38 (m, 2H)), and the following mass spectrum: *m*/*z* (I) = 208 (4), 193 (2), 165 (100), 151 (12), 135 (33), 119 (12), 105 (18), 91 (11), 59 (20). Both the photolysis and dark reaction mixtures also contained a second minor isomer in the same yield relative to **15** (1:8) which was tentatively identified as benzylmethylmethoxy(1-propyl)silane (**16**, 21%) on the basis of its mass spectrum: *m*/*z* (I) = 208 (17), 165 (15), 151 (10), 133 (12), 117 (90), 91 (30), 75 (100), 59 (30)). The latter clearly shows the fragmentation pattern expected for a benzylsilane.

The products of steady state photolysis of **2**–**4** in hexane, hexane containing 0.1 M methanol, or neat methanol were identified by GC coinjection with authentic samples. In the few cases where these were not available, tentative identification was made on the basis of GC/MS. For example photolysis of **2** in hexane yielded an isomer in ~10% yield, which was barely resolved from **2** under our GC/MS conditions. It exhibited the following mass spectral data: MS, *m*/*z* (I) = 226 (7), 211 (100), 195 (7), 181 (10), 165 (15), 148 (67), 133 (15), 105 (22), 91 (10). An analogous product was formed in ~35% yield from photolysis of **4** in hexane solution, and tentatively identified as dimethylphenyl(*o*-tolyl)silane (**18b**) *m*/*z*: (I) = 226 (7), 211 (100), 195 (7), 181 (10), 165 (15), 148 (67), 133 (15), 105 (22), 91 (10). Disiloxane **17** from photolysis of **2** in methanol solution was identified on the basis of its ^{1}H NMR (δ 1.45 (m, 8H), 1.67 (m, 2H), 2.06 (m, 2H), 7.41 (m, 6H), 7.61 (m, 4H)) and mass spectrum: *m*/*z* (I) = 310 (3), 282 (25), 269 (100), 254 (50), 241 (78), 227 (27), 197 (36), 195 (28), 181 (39), 119 (27), 105 (59), 93 (16), 78 (19) (35).

The isotoluene derivatives **13a**, **b**, **d**, and **24b** were detected by UV absorption and ^{1}H NMR spectroscopy on the crude mixtures from 254-nm photolysis of **1**–**5** (0.01–0.02 M) to 5–10% conversion in hexane or cyclohexane-d_{12}. The four compounds exhibited identical UV spectra (λ_{max} = 335 nm; see Fig. 1 for **13a**) and the following ^{1}H NMR spectra: **13a** (from **1**; silacyclobutyl Hs excluded), δ = 0.49 (s, 3H), 3.18 (m, 1H), 4.12 (s, 1H), 4.46 (s, 1H), 5.74 (m, 3H), 5.97 (d, 1H, *J* = 8.7 Hz); **13b** (from **2**; phenyl and silacyclobutyl Hs excluded), δ = 3.34 (m, 1H), 4.42 (s, 1H), 4.58 (s, 1H), 5.60 (m, 1H), 5.72 (m, 2H), 5.94 (d, 1H, *J* = 6.3 Hz); **13d** (from **4**; phenyl Hs excluded), δ = 3.33 (m, 1H), 4.41 (s, 1H), 4.76 (s, 1H), 5.82 (m, 1H), 5.86 (m, 2H), 6.14 (d, 1H, *J* = 7.4 Hz); **24b** (from **5**; phenyl Hs excluded), δ = 3.20 (m, 1H), 4.55 (m, 1H), 5.75 (m, 1H), 5.94 (m, 2H), 6.08 (d, 1H, *J* = 7.5 Hz). Photolysis of a 0.01 M solution of **3** under the same conditions resulted in the appearance of weak edge absorptions in the 300–340 nm range, even after photolysis for roughly 5 times longer than the other compounds. The ^{1}H NMR spectrum of the photolysate (after evaporation of the solvent and redissolution in cyclohexane-d_{12}) showed no evidence of absorptions in the 3–6 ppm range.

Nanosecond laser flash photolysis experiments employed the pulses (248 nm; ca. 25 ns; 70–140 mJ) from a Lambda Physik Compex 120 excimer laser filled with F_2–Kr mixtures in neon, and a microcomputer-controlled detection system (36). The laser beam was unfocussed, and its intensity was reduced to 10–15 mJ at the cell using a series

© 2000 NRC Canada

of stainless steel wire meshes as neutral density filters. Solutions were prepared at concentrations such that the absorbance at the excitation wavelength was ca. 0.7 (~8×10^{-4} M), and were flowed continuously through a 3 × 7 mm Suprasil flow cell connected to a calibrated 100 mL reservoir. Nitrogen was bubbled continuously through the reservoir throughout the experiments.

Acknowledgements

We wish to thank D. Hughes for his assistance with high-resolution NMR spectra, the McMaster Regional Centre for Mass Spectrometry for high-resolution mass spectra and exact mass determinations, and Dr. R. Boukherroub and E.C. Lathioor for technical assistance. The financial support of the Natural Sciences and Engineering Research Council (NSERC) of Canada is also gratefully acknowledged.

References

1. L.E. Gusel'nikov and M.C. Flowers. J. Chem. Soc. Chem. Commun. 864 (1967).
2. P. Boudjouk and L.H. Sommer. J. Chem. Soc. Chem. Commun. 54 (1973).
3. N. Auner and J. Grobe. J. Organomet. Chem. **197**, 147 (1980).
4. P. Jutzi and P. Langer. J. Organomet. Chem. **202**, 401 (1980).
5. L.E. Gusel'nikov, N.S. Nametkin, and V.M. Vdovin. Acc. Chem. Res. **8**, 18 (1975).
6. G. Raabe and J. Michl. Chem. Rev. **85**, 419 (1985).
7. A.G. Brook. *In* The chemistry of organic silicon compounds. *Edited by* S. Patai and Z. Rappoport. John Wiley and Sons, New York. 1989. pp. 965–1005.
8. A.G. Brook and M.A. Brook. Adv. Organomet. Chem. **39**, 71 (1996).
9. W.J. Leigh, C.J. Bradaric, and G.W. Sluggett. J. Am. Chem. Soc. **115**, 5332 (1993).
10. C.J. Bradaric and W.J. Leigh. J. Am. Chem. Soc. **118**, 8971 (1996).
11. W.J. Leigh, C.J. Bradaric, C. Kerst, and J.H. Banisch. Organometallics, **15**, 2246 (1996).
12. R.K. Vatsa, A. Kumar, P.D. Naik, H.P. Upadhyaya, U.B. Pavanaja, R.D. Saini, J.P. Mittal, and J. Pola. Chem. Phys. Lett. **255**, 129 (1996).
13. C.J. Bradaric and W.J. Leigh. Can. J. Chem. **75**, 1393 (1997).
14. C. Kerst, R. Boukherroub, and W.J. Leigh. J. Photochem. Photobiol. A, **110**, 243 (1997).
15. C.J. Bradaric and W.J. Leigh. Organometallics, **17**, 645 (1998).
16. W.J. Leigh, C. Kerst, R. Boukherroub, T.L. Morkin, S. Jenkins, K. Sung, and T.T. Tidwell. J. Am. Chem. Soc. **121**, 4744 (1999).
17. W.J. Leigh, R. Boukherroub, and C. Kerst. J. Am. Chem. Soc. **120**, 9504 (1998).
18. W.J. Leigh, R. Boukherroub, C.J. Bradaric, C. Cserti, and J.M. Schmeisser. Can. J. Chem. **77**, 1136 (1999).
19. M. Kira, H. Yoshida, and H. Sakurai. J. Am. Chem. Soc. **107**, 7767 (1985).
20. P.B. Valkovich, T.I. Ito, and W.P. Weber. J. Org. Chem. **39**, 3543 (1974).
21. W.J. Bailey and R.A. Baylouny. J. Org. Chem. **27**, 3476 (1962).
22. D. Hasselmann and K. Loosen. Angew. Chem. Int. Ed. Engl. **17**, 606 (1978).
23. K.R. Kopecky and M.-P. Lau. J. Org. Chem. **43**, 525 (1978).
24. F.L. Cozens, A.L. Pincock, J.A. Pincock, and R. Smith. J. Org. Chem. **63**, 434 (1998).
25. E.W. Colvin. Silicon in organic synthesis. London, Butterworths. 1981. pp. 97–124.
26. T. Morita, Y. Okamoto, and H. Sakurai. Tetrehedron Lett. 835 (1980).
27. C. Eaborn, D.R.M. Walton, and M. Chan. J. Organomet. Chem. **9**, 251 (1967).
28. L.H. Sommer. Stereochemistry, mechanism, and silicon. McGraw–Hill, New York. 1965. p. 132.
29. H. Hiratsuka, Y. Kadokura, H. Chida, M. Tanaka, S. Kobayashi, T. Okutsu, M. Oba, and K. Nishiyama. J. Chem. Soc. Faraday Trans. **92**, 3035 (1996).
30. C.S.Q. Lew and R.A. McClelland. J. Am. Chem. Soc. **115**, 11516 (1993).
31. R. Damrauer, R.A. Davis, D.R. Burley, M. Karni, and J.L. Goodman. J. Organomet. Chem. **43**, 121 (1972).
32. G. Bertrand, J. Dubac, P. Mazerolles, and J. Ancelle. Nouv. J. Chim. **6**, 381 (1982).
33. A. Hosomi and H. Sakurai. Bull. Chem. Soc. Jpn. **45**, 248 (1972).
34. V.M. Vdovin, N.S. Nametkin, and P.L. Grinberg. Dokl. Akad. Nauk. SSSR, **150**, 799 (1963).
35. A.I. Mikaya, N.V. Ushakov, V.G. Zaikin, and V.M. Vdovin. Zh. Obshch. Khim. **54**, 1008 (1984).
36. W.J. Leigh, M.S. Workentin, and D. Andrew. J. Photochem. Photobiol. A, **57**, 97 (1991).

© 2000 NRC Canada

Addition reactions of a dialkyl- and a diarylsilylene to cyanides RCN: Different pathways? (1)

Manfred Weidenbruch, Frank Meiners, and Wolfgang Saak

Abstract: Di-*tert*-butylsilylene, generated by photolysis of hexa-*tert*-butylcyclotrisilane, reacts with the triple bond of adamantane-1-carbonitrile to furnish the 1,3-diaza-2,5-disilacyclohexa-3,6-diene **5**. However, treatment of 2,2-dimethylpropanenitrile with dimesitylsilylene affords the azadisilacyclobutene ring system **6**. The structures of **5** and **6** were determined by X-ray crystallography.

Key words: silicon, silylene, silaheterocycles, X-ray crystallography.

Résumé : Le di-*tert*-butylsilylène, obtenu par photolyse de l'hexa-*tert*-butylcyclotrisilane, réagit avec la triple liaison de l'adamantane-1-carbonitrile pour conduire à la formation du 1,3-diaza-2,5-disilacyclohexa-3,6-diène, **5**. Toutefois, si on soumet le 2,2-diméthylpropanenitrile au même traitement, il y a formation du système cyclique **6** de l'azadisilacyclobutène. Les structures des composés **5** et **6** ont été déterminées par diffraction des rayons X.

Mots clés : silicium, silylène, hétérocycles silylés, diffraction des rayons X.

Introduction

Dialkyl- and diarylsilylenes, R_2Si:, are versatile and reactive intermediates that undergo numerous addition and insertion reactions. When the substituent R is relatively small the primary products are usually unstable, with rearrangement and other subsequent reactions occurring spontaneously (2). In contrast, the reactions of sterically encumbered silylenes follow a more simple course. For example, treatment of some cyanides with di-*tert*-butylsilylene furnished the diazadisilacyclohexadiene derivatives **1** and **2** (Scheme 1); the structure of the latter has been confirmed by X-ray crystallography (3).

The reaction pathway proposed for the formation of the six-membered ring compounds **1** and **2** involves an initial [2 + 1] cycloaddition of the silylene to the C≡N triple bond followed by a σ-dimerization of the highly strained, three-membered ring intermediate. Indirect support for this proposal was provided by the reactions of di-*tert*-butylsilylene with phosphaalkynes from which the phosphasilirenes **3** were isolated. In these compounds the C=P double bonds are markedly longer than the corresponding C=N bonds so that the three-membered ring system is probably less strained and thus shows no tendency to undergo σ-dimerization (4). It was, therefore, most surprising to find that the analogous reactions of dimesitylsilylene with the phosphaalkynes furnished the phosphadisilacyclobutene derivatives **4**. The appealing hypothesis that two silylene molecules initially dimerize to give $Mes_2Si{=}SiMes_2$ (5) which would then undergo a subsequent [2 + 2] cycloaddition cannot be verified experimentally, since mixtures of the disilene with the phosphaalkyne showed no signs of a reaction. (6)

Received May 27, 1999. Published on the NRC Research Press website on November 2, 2000.

Dedicated to Professor Adrian G. Brook in appreciation of his outstanding contributions to organosilicon chemistry.

M. Weidenbruch,[1] F. Meiners, and W. Saak. Fachbereich Chemie, Universität Oldenburg, D-26111 Oldenburg, Germany.

[1]Author to whom correspondence may be addressed. Telephone: +(441)7983655. Fax: +(441)7983352.

Results and discussion

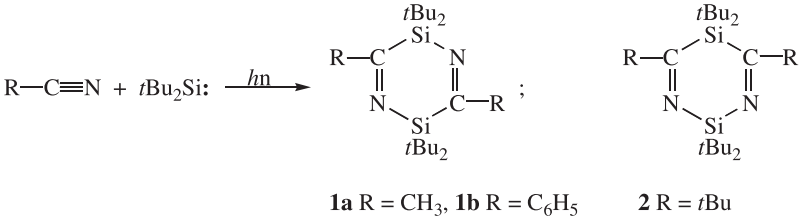
To test whether the formation of the different products in the reactions of a dialkyl- and a diarlysilylene with phosphaalkynes (4, 6) may have possibly been the result of different reaction pathways, we have reinvestigated the reactions of silylenes with cyanides R-C≡N and now report the results which lend support to this hypothesis (Scheme 2).

For the cyanide partner we selected 1-adamantanecarbonitrile because its alkyl group has even higher steric requirements than the *tert*-butyl group of 2,2,-dimethylpropanenitrile (7). After photolysis of the former nitrile in the presence of hexa-*tert*-butylcyclotrisilane (8), that smoothly furnishes di-*tert*-butylsilylene under these conditions, yellow crystals were isolated in 54% yield. The analytical and spectral data of this product are indicative for the formation of the 1,3-diaza-2,5-disilacyclohexadiene derivative **5**. For example, the ^{29}Si NMR spectrum of this product contains two signals at –20.82 and –35.69 ppm, demonstrating the presence of two silicon atoms in differing environments.

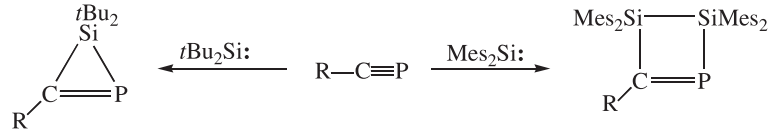
The structure of the obtained product was confirmed by X-ray crystallography (Fig. 1) albeit with some noteworthy aspects. Compound **5** crystallizes as two independent molecules with four of each occupying the unit cell. The six-membered ring is completely planar and possesses a C_2-axis passing through the two silicon atoms. The most surprising features of the molecular structure are the unusually long endocyclic Si—C bonds which, with 2.012(2) (molecule 1) and 2.032(2) Å (molecule 2) are among the largest yet known and, for example, are appreciably longer than the stretched Si—C bonds in the sterically crowded 1,3-disilacyclobutanes (9) and even the corresponding bonds in **2** (2.005(3) Å). The

© 2000 NRC Canada

Scheme 1.



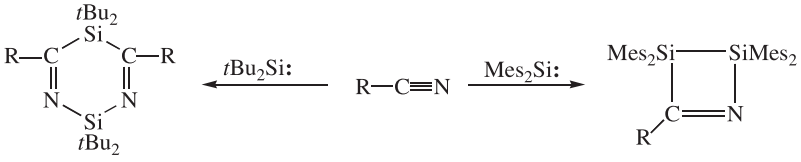
1a R = CH_3, **1b** R = C_6H_5 **2** R = *t*Bu



3a R = 1-adamantyl
3b R = *t*Bu

4a R = 1-adamantyl
4b R = 2-Me-cC_6H_{10}

Scheme 2.



5 R = 1-adamantyl

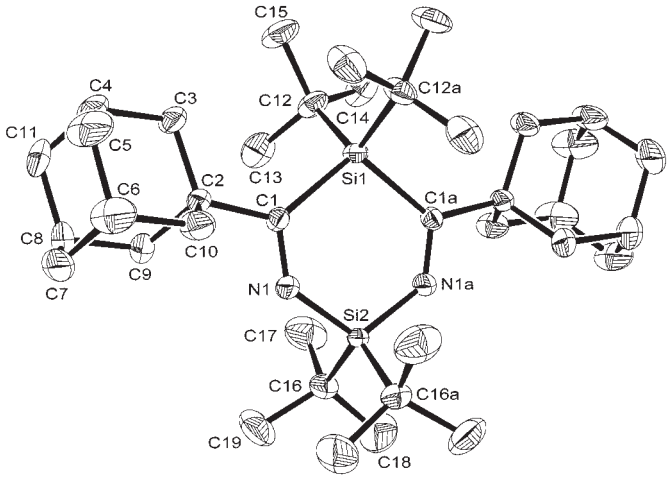
6 R = *t*Bu

reason for this is the direct adjacency of the *tert*-butyl and the adamantyl groups, the mutual repulsions of which forcibly stretch these bonds. We cannot as yet explain why just the cyanides with spatially demanding substituents should react to give the ring systems **2** or **5**, respectively, instead of **1** in which only three organic groups would be directly adjacent.

Attempts to confirm the differing reaction behavior of dialkyl- and diarylsilylenes by means of the reaction of dimesitylsilylene with adamantanecarbonitrile have not yet resulted in any uniform products. The mass spectrum of the reaction mixture, however, does suggest the probable existence of a four-membered ring product of the type **6** in the mixture. On the other hand, photolysis of 2,2-dimethylpropanenitrile with dimesitylhexamethyltrisilane (10), which decomposes on irradiation to afford hexamethyldisilane and dimesitylsilylene, resulted in the formation of colorless crystals in 43% yield. The analytical and spectral data of this product are indicative for the four-membered ring structure **6**.

Again the structure of the isolated product was confirmed by X-ray crystallography (Fig. 2). The only conspicuous feature of this structure is that the Si—Si bond length of 2.365(1) Å is only slightly larger than the normal bond length of 2.34 Å in spite of the adjacency of the four mesityl groups. The 2,3-disila-1-azetidine ring skeleton of compound **6** has been obtained previously by the addition of tetra-*tert*-butyldisilene to the extremely sterically crowded tri-*tert*-butylsilyl cyanide. (11) We have thus examined the question as to whether dimesitylsilylene may have first dimerized to the disilene $Mes_2Si{=}SiMes_2$ before undergoing

Fig. 1. Molecular structure of **5** in the crystal (hydrogen atoms omitted). Ellipsoids are drawn at 50% probability. Selected bond lengths (Å) and angles (°): Si1—C1 2.012(2), C1—N1 1.279(2), N1—Si2 1.716(2), C1-Si1-C1a 104.3(1), Si1-C1-N1 119.8(1), C1-N1-Si2 110.7(2), N1-Si2-N1a 110.5(1), C12-Si1-C12a 115.3(1), C16-Si2-C16a 116.6(1).



the [2 + 2] cycloaddition to furnish product **6**. However, no signs of any reaction between this disilene and 2,2-dimethylpropanenitrile were observed either under photochemical or thermal conditions. Thus, the formation of **6** must be attributed to a two-fold reaction of dimesitylsilylene with 2,2-dimethylpropanenitrile.

© 2000 NRC Canada

Scheme 3.

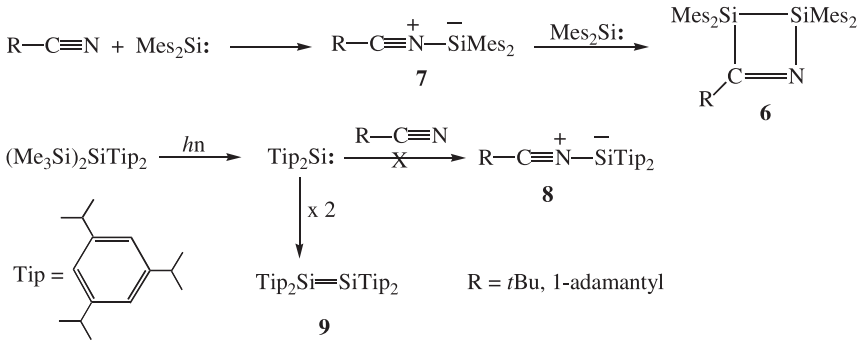
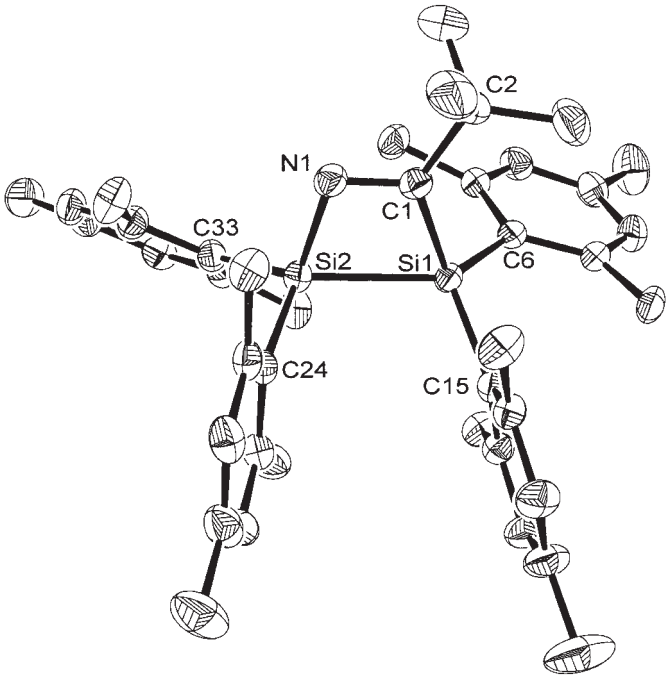


Fig. 2. Molecular structure of **6** in the crystal (hydrogen atoms omitted). Ellipsoids are drawn at 50% probability. Selected bond lengths (Å) and angles (°): Si1—Si2 2.365(1), Si1—C1 1.948(3), Si2—N 1.807(2), C1—N 1.295(4), Si1-Si2-N 77.62(8), Si2-N-C1 104.6(2), N-C1-Si1 107.9(2), C1-Si1-Si2 69.24(8).



Together with the results of previous investigations, (3, 4, 6) the observations described here clearly support the hypothesis that the additions of dialkyl- and diarylsilylenes to cyanides and phosphaalkynes probably proceed by different mechanisms. Thus, the reactions of the weakly nucleophilic di-*tert*-butylsilylene seem to be initiated by [2 + 1] cycloadditions which, in the case of the phosphaalkynes, furnish the stable, three-membered ring products **3** while, in the case of the cyanides, a subsequent σ-dimerization occurs to afford the six-membered ring products **2** or **5**. The more electrophilic dimesitylsilylene, on the other hand, appears to react initially to form an ylide **7** by addition to the free electron pair of the nitrogen atom, followed by addition of a second silylene molecule and ring closure to afford **6** (Scheme 3). However, the formation of a three-membered ring of type **3** (with N instead of P), followed by the addition of a second silylene molecule across the double bond to form a bicyclo[1.1.0]butane derivative as an intermediate cannot be completely excluded. Movement of two bonds from this intermediate then could give **6**. Attempts to trap the postulated ylide **8** by use of the sterically highly overcrowded bis(2,4,6-triisopropylphenyl)silylene were unsuccessful; the disilene **9** (12) and the respective cyanide were isolated from these reactions. In this case the dimerization of the silylene to **9** seems to proceed more rapidly than the possible addition to the nitrogen atom of the cyanide.

Experimental section

General procedures

All reactions were carried out in oven-dried glassware under an atmosphere of dry argon. Photolyses were carried out by using a high-pressure mercury immersion lamp (Heraeus TQ 150). The ^{1}H and ^{13}C NMR spectra were obtained on a Bruker AMX 500 spectrometer using C_6D_6 as solvent. The ^{29}Si NMR spectra were recorded on a Bruker AMX 300 spectrometer. Mass spectra were taken on a Finnigan MAT 95 instrument. Elemental analyses were performed by Analytische Laboratorien, D-51779 Lindlar, Germany.

*4,6-Diadamantyl-2,2,5,5-tetra-tert-butyl-1,3-diaza-2,5-disilacyclohexa-1,3-diene (**5**)*: A solution of hexa-*tert*-butylcyclotrisilane (0.75 g, 1.8 mmol) and adamantanecarbonitrile (0.31 g, 1.9 mmol) in *n*-hexane (80 mL) was irradiated for 6 h at room temperature. After this time the reaction was shown to be complete by the disappearance of the cyclotrisilane (TLC monitoring). The resulting yellow solution was concentrated, cooled at –20°C, and filtered. The isolated yellow needles were recrystallized from a minimum amount of *n*-pentane to provide 0.29 g (54% yield) of yellow, cuboid crystals of **5**: mp 260–268°C (dec). ^{1}H NMR: 1.27 (s, 18 H), 1.28 (s, 18 H), 1.68 (q, 12 H), 2.02 (s, 6 H), 2.15 (d, 12 H). ^{13}C NMR: 19.47, 21.00, 29.33, 29.76, 33.31, 37.36, 42.14, 52.82, 214.84 (*C*N). ^{29}Si NMR: –20.8, –35.7. Mass spectra (CI, isobutane) *m/z*: 606 (MH^+, 10%). Anal. calcd. for $C_{38}H_{66}N_2Si_2$: C 75.18, H 10.96, N 4.62; found: C 74.92, H 11.05, N 4.56.

*4-tert-Butyl-2,2,3,3-tetrakis(2,4,6-trimethylphenyl)-2,3-disila-1-azetine (**6**)*: A solution of 2,2-dimesitylhexamethyltrisilane (1.0 g, 2.4 mmol) and 2,2-dimethylpropanenitrile (0.40 g, 4.8 mmol) in *n*-hexane (80 mL) was irradiated for 5 h at room temperature. After this time the reaction was shown to be complete by the disappearance of the trisilane

© 2000 NRC Canada

Table 1. Crystallographic data for **5** and **6**.

	5	6
Empirical formula	$C_{38}H_{66}N_2Si_2$	$C_{41}H_{53}NSi_2$
Formula weight	607.11	616.02
a (Å)	16.6601(7)	10.1018(7)
b (Å)	16.4799(9)	11.3976(11)
c (Å)	26.5881(18)	17.7146(16)
α (°)	90	77.300(11)
β (°)	90	73.485(9)
γ (°)	90	70.585(10)
V (Å^3)	7299.9(7)	1826.4(3)
Z	8	2
D_x (g cm^{-3})	1.105	1.120
Crystal size (mm)	0.57 × 0.41 × 0.19	0.48 × 0.18 × 0.13
Temperature (K)	193(2)	213(2)
Crystal system	Orthorhombic	Triclinic
Space group	*Pnna*	*P*-1
2θ range (°)	52	52
No. of reflns measd.	60302	22136
No. of unique reflns	6884	6675
Lin. abs. coeff. (mm^{-1})	0.125	0.125
Parameters	381	397
R ($I > 2\sigma(I)$)	0.0477	0.0547
w*R*2 (all data)	0.1218	0.1673
GOF (F^2)	0.977	1.018

(TLC monitoring). The resulting yellow solution was concentrated to a volume of 10 mL and cooled at –20°C. The yellow precipitate was filtered off and recrystallized from *n*-pentane to furnish 0.32 g (43% yield) of colorless, rhombohedral crystals of **6**, mp 192–194°C. ^{1}H NMR: 1.30 (s, 9 H), 2.04 (s, 6 H), 2.06 (s, 6 H), 2.23 (s, 12 H), 2.63 (s, 12 H), 6.62 (s, 4 H), 6.66 (s, 4 H). ^{13}C NMR: 19.60, 23.29, 24.22, 27.82, 131.90, 132.29, 137.56, 141.91, 143.36, 222.11 (*C*N). ^{29}Si NMR: 3.91, 10.21. Mass spectrum (CI, isobutane) *m*/*z*: 616 (MH^+, 100%). Anal. calcd. for $C_{41}H_{53}NSi_2$: C 79.94, H 8.67, N 2.27; found: C 79.67, H 8.51, N 2.26.

Crystallographic analyses of 5 and 6

Crystal data and numerical data of the structure determinations are given in Table 1. In each case, the crystal was mounted in an inert oil. Data collection was performed with an STOE-IPDS area-detector using graphite-monochromated Mo Kα (λ = 0.71073 Å) radiation. The structures were solved by direct phase determination and refined by full-matrix least-squares against F^2 with the SHELXL-97 program system (13). Hydrogen atoms were placed in calculated positions, and all other atoms were refined anisotropically.[2]

Acknowledgements

Financial support of our work by the Deutsche Forschungsgemeinschaft and the Fonds der Chemischen Industrie is gratefully acknowledged.

References

1. A. Grybat, S. Boomgarden, W. Saak, H. Marsmann, and M. Weidenbruch. Angew. Chem. **111**, 2161 (1999); Angew. Chem. Int. Ed. **38**, 2010 (1999).
2. Reviews: (*a*) M. Weidenbruch. Coord. Chem. Rev. **130**, 275 (1994); (*b*) P.P. Gaspar and R. West. *In* The chemistry of organic silicon compounds II. *Edited by* Z. Rappoport and Y. Apeloig. John Wiley and Sons, Chichester. 1998. Chap. 43, p. 2463.
3. M. Weidenbruch, A. Schäfer, K. Peters, and H.G. von Schnering. J. Organomet. Chem. **314**, 25 (1986).
4. A. Schäfer, M. Weidenbruch, W. Saak, and S. Pohl. Angew. Chem. **99**, 806 (1987); Angew. Chem. Int. Ed. Engl. **26**, 776 (1987).
5. R. West, M.J. Fink, and J. Michl. Science (Washington, D.C.), **214**, 1343 (1981).
6. M. Weidenbruch, S. Olthoff, K. Peters, and H.G. von Schnering. Chem. Commun. 1433 (1997).
7. J.E. Anderson, H. Pearson, and D.I. Rawson. J. Am. Chem. Soc. **107**, 1446 (1985).
8. A. Schäfer, M. Weidenbruch, K. Peters, and H.G. von Schnering. Angew. Chem. **96**, 311 (1984); Angew. Chem. Int. Ed. Engl. **23**, 302 (1984).
9. K.M. Baines, A.G. Brook, P.D. Lickiss, and J.F. Sawyer. Organometallics, **8**, 709 (1989).
10. M.J. Fink, M.J. Michalczyk, R. West, and J. Michl. Organometallics, **3**, 793 (1984).
11. M. Weidenbruch, B. Flintjer, S. Pohl, and W. Saak. Angew. Chem. **89**, 101 (1989); Angew. Chem. Int. Ed. Engl. **28**, 95 (1989).

[2] Crystallographic data (excluding structure factors) for the structures reported in this paper have been deposited with the Cambridge Crystallographic Data Centre (CCDC 121796 (**5**) and 121795 (**6**)). Copies of the data can be obtained, free of charge, on application to the Director, CCDC, 12 Union Road, Cambridge CB2 1EZ, U.K. (Fax: 44-1223-336033 or e-mail: deposit@ccdc.cam.ac.uk).

© 2000 NRC Canada

12. (*a*) H. Watanabe, K. Takeuchi, N. Fukawa, M. Kato, M. Goto, and Y. Nagai. Chem. Lett. 1341 (1987); (*b*) A.J. Millevolte, D.R. Powell, S.G. Johnson, and R. West. Organometallics, **11**, 1091 (1992).

13. G.M. Sheldrick. SHELXL-97. Program for crystal structure refinement. University of Göttingen, Germany. 1997.

© 2000 NRC Canada

The photolysis of Si,Si-di-*tert*-butyltetramesitylsiladigermirane in the presence of methylmagnesium iodide

Mini S. Samuel, Kim M. Baines, and Donald W. Hughes

Abstract: The photolysis of Si,Si-di-*tert*-butyltetramesitylsiladigermirane in the presence of methylmagnesium iodide at 15°C has been investigated. Five products were isolated and identified from the complex product mixture: mesityldimethylgermane, dimesitylmethylgermane, (di-*tert*-butylmethylsilyl)mesitylmethylgermane, *meta*-(di-*tert*-butylmethylsilyl)toluene, and *para*-(di-*tert*-butylmethylsilyl)toluene. The characterization of these compounds and proposed mechanisms for their formation will be discussed.

Key words: germasilene, Grignard reagents, germylmagnesium compounds.

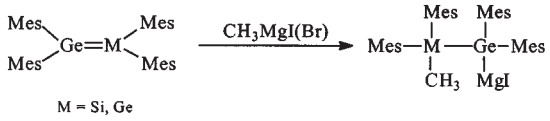
Résumé : Opérant à 15°C, on a étudié la photolyse du Si,Si-di-*tert*-butyltétramésitylsiladigerminane en présence d'iodure de méthylmagnésium. À partir du mélange complexe de produits, on a isolé et identifié cinq produits: mésityldiméthylgermane, dimésitylméthylgermane, (di-*tert*-butylméthylsilyl)mésitylméthylgermane, *méta*-(di-*tert*-butylméthylsilyl)toluène et *para*-(di-*tert*-butylméthylsilyl)toluène. On discute de la caractérisation de ces produits et des mécanismes proposés pour leur formation.

Mots clés : germasilène, réactifs de Grignard, composés germylmagnésium.

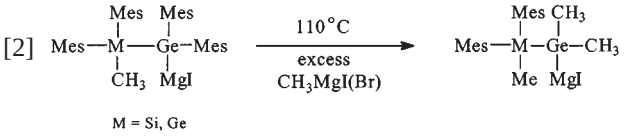
[Traduit par la Rédaction]

Introduction

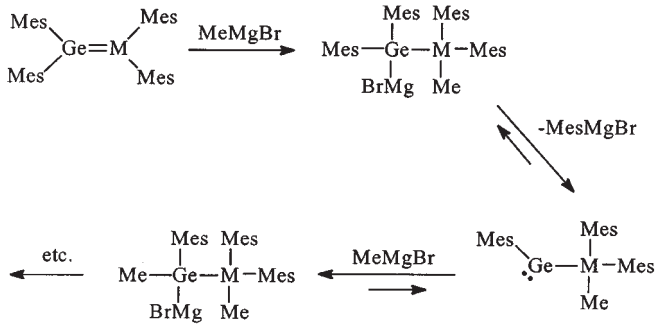
In a recent publication, we reported on a novel route to germyl Grignard reagents by the addition of methylmagnesium halide to $Mes_2Ge{=}GeMes_2$ and $Mes_2Si{=}GeMes_2$ at low temperature (Mes = 2,4,6-trimethylphenyl) (1). The addition to the germasilene is completely regioselective with the alkyl group adding to the silicon atom (eq. [1]).

[1] 

Furthermore, we discovered that thermolysis of the germyl Grignard reagents in the presence of excess MeMgX lead to a facile ligand exchange reaction in which the mesityl groups on the germanium bonded to the magnesium were exchanged for methyl groups (eq. [2]). A mechanism involving the α-elimination of MesMgX followed by the addition of MeMgX to the intermediate germylene has been proposed to explain the observed ligand exchange (Scheme 1). Evidence for the formation of the germylene was provided by trapping the intermediate with 2,3-dimethylbutadiene.

[2] 

Scheme 1.



To our knowledge, this novel ligand exchange in germyl Grignard reagents has no precedent in the literature. Considering the recent interest in the generation and chemistry of both germyl (2) and silyl (3) Grignard reagents and the importance of germylenes as intermediates in organogermanium chemistry, it was desirable to investigate not only

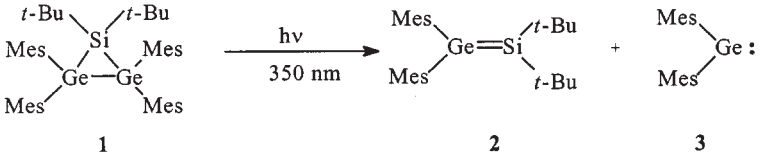
Received July 1, 1999. Published on the NRC Research Press website on November 2, 2000.

Dedicated to Professor Adrian G. Brook in recognition of his seminal contributions to the field of organosilicon chemistry.

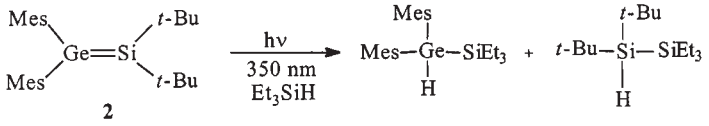
M.S. Samuel and K.M. Baines.[1] Department of Chemistry, University of Western Ontario, London, ON N6A 5B7, Canada.
D.W. Hughes. Department of Chemistry, McMaster University, Hamilton, ON L8S 4M1, Canada.

[1]Author to whom correspondence should be addressed. Telephone: (519) 661-2111 ext. 86302. Fax: (519) 661-3022. e-mail: kbaines2@julian.uwo.ca

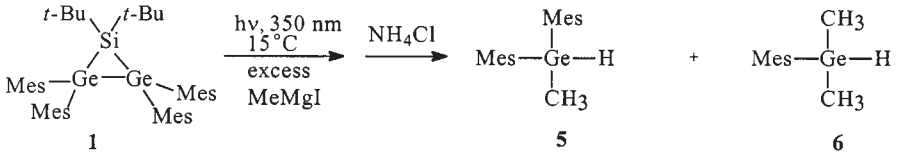
© 2000 NRC Canada

[3] 

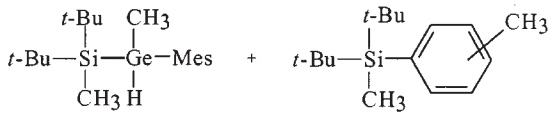
1 2 3

[4] 

2

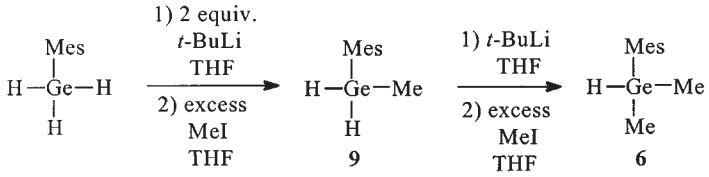


1 5 6

[5] 

7 8

(3:1 mixture of *m*-isomer and *p*-isomer)

[6] 

the generality of the Grignard addition to germasilenes as a novel approach for the synthesis of germyl Grignard reagents but also the generality of the ligand exchange reaction. For this reason, the addition of methylmagnesium iodide to $(t\text{-Bu})_2Si{=}GeMes_2$, generated photochemically from Si,Si-di-*tert*-butyltetramesitylsiladigermirane, was investigated.

Results

The photolysis of Si,Si-di-*tert*-butyltetramesitylsiladigermirane **1** has been shown to give di-*tert*-butyldimesitylgermasilene and dimesitylgermylene, regioselectively (eq. [3]) (4). Although stable solutions of tetramesityldigermene and tetramesitylgermasilene can be prepared by photolysis of hexamesitylcyclotrigermane and hexamesitylsiladigermirane, respectively, at –78°C in the presence of triethylsilane, this methodology cannot be used to generate a solution of Si,Si-di-*tert*-butyldimesitylgermasilene; germasilene **2** undergoes photodissociation to yield dimesitylgermylene **3** and di-*tert*-butylsilylene **4**, both of which can be trapped by triethylsilane (eq. [4]) (4). As a result, the study of the reactivity of Si,Si-di-*tert*-butyldimesitylgermasilene must be carried out in the presence of the trapping reagent.

Si,Si-di-*tert*-butyltetramesitylsiladigermirane is unreactive toward methylmagnesium iodide in the dark. Photolysis of Si,Si-di-*tert*-butyltetramesitylsiladigermirane **1** dissolved in toluene, in the presence of excess methylmagnesium iodide at 15°C, yielded a complex product mixture. Through preparative thin layer and centripetal chromatography, five products, **5**, **6**, **7**, and **8** were isolated and identified in a ratio of approximately 5:1:2:3, respectively, and were estimated to account for 75% of the crude product mixture. Although the major products from the reaction mixture were identified, there were several minor unidentified products (eq. [5]).

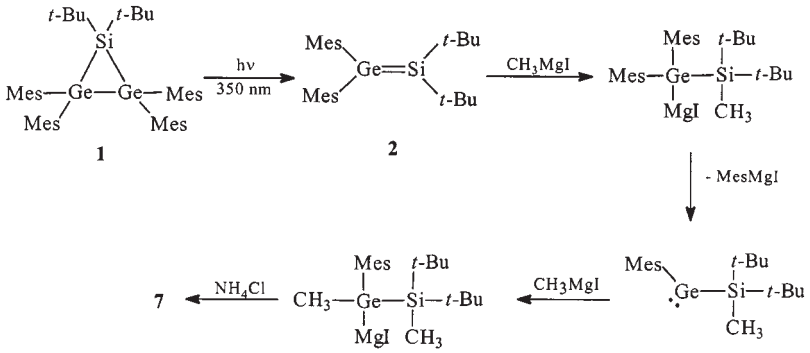
Compounds **5**, **7**, and **8** were isolated in quantities of 19, 3.5, and 4.5%, respectively, (as determined by assuming that formation of each of these compounds occurred independently of the others), and were characterized by ^1H, ^{13}C, and ^{29}Si NMR, IR, and mass spectrometry. Compound **6** could not be isolated free of compound **7**, and thus, compound **6** was independently synthesized and fully characterized.

Compound **5** was isolated in yields ranging from 14 to 23%. The identification was based on comparison of the ^1H NMR spectral data to literature values (5).

The volatility of **6** largely contributes to the fact that it could not be obtained in pure form; it was difficult to isolate it during the work-up and purification stages. Since **6** could not be isolated, the structural assignment is based upon data obtained from a ^1H NMR spectrum of a mixture of **6** and **7**. To confirm the structure of **6**, it was independently synthesized from $MesGeH_3$ by stepwise deprotonation using *tert*-butyllithium followed by methylation using methyl iodide. We were unable to synthesize **6** in one step from $MesGeH_3$ as has been reported in the literature (eq. [6]) (6).

© 2000 NRC Canada

Scheme 2.



The ^{1}H NMR spectrum of compound **7** revealed the presence of two nonequivalent *tert*-butyl groups, one mesityl group, a doublet at 0.63 ppm (^3J = 4.4 Hz, 3H), a quartet at 4.70 ppm (^3J = 4.4 Hz, 1H) and a methyl singlet at 0.23 ppm. The ^{29}Si/^{1}H heteronuclear multiple bond correlation (HMBC) spectrum showed correlations between the signal at 10.9 ppm in the ^{29}Si dimension to the singlets at 1.08, 0.93, and 0.23 ppm in the ^{1}H dimension. These data together with the molecular ion at 366 amu, support our assignment of the structure of compound **7**.

From the ^{1}H, ^{13}C NMR, and mass spectra, compound **8** was determined to be an isomeric mixture of (di-*tert*-butylmethylsilyl)toluenes in a ratio of 3:1. The multiplet at 7.54 ppm in the ^{1}H NMR spectrum of **8** appears to be one half of a typical AA′XX′ pattern associated with 1,4-disubstituted benzenes, and thus, the minor component of the mixture was assigned as the para isomer. Examination of the multiplicity of the remaining four signals in the aromatic region of the ^{1}H NMR spectrum and the correlations observed in the 2-D COSY spectrum indicated that the major component of the mixture was the *meta*-substituted isomer. This was based on the observation that all the signals in the aromatic region, with the exception of the signal at 7.51 ppm, were split by a coupling of 7.5–8.0 Hz. Confirmation of the assignment of the *meta*- and *para* isomers of **8** was made using COSY, ^{13}C-^{1}H, and ^{29}Si-^{1}H HSQC and HMBC experiments, TOCSY and standard spin decoupling experiments. Full details can be found in the supplementary material.[2]

Discussion

Despite the low isolated yields of the compounds reported herein and the complexity of the reaction mixture, we believe we can add to our understanding of the addition of Grignard reagents to germasilenes and the subsequent behaviour of the newly formed germyl Grignard reagents.

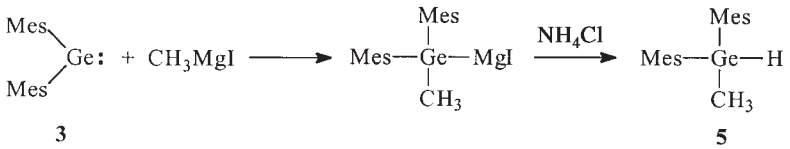
Following what we have previously proposed (see Scheme 1) (1), compound **7** is believed to arise from attack of the Grignard reagent on the silicon atom of the germasilene followed by an α-elimination of mesitylmagnesium iodide. Methylmagnesium iodide could then add to the resulting silylgermylene, giving **7** after hydrolysis (Scheme 2). The regioselectivity of the addition is the same as that of tetramesitylgermasilene: the alkyl portion of the Grignard reagent adds only to the silicon atom of the germasilene. The other regioisomer was not detected.

The mechanism for the formation of compound **8** is indeed intriguing. There is ample precedence for the addition of silyl radicals to aromatic compounds (7, 8). Thus, the most reasonable explanation for the formation of **8** is from the addition of the di-*tert*-butylmethylsilyl radical to toluene followed by loss of a hydrogen atom. The source of the silyl radical is unknown. It is possible that the germyl Grignard reagent, *t*-Bu$_2$MeSiGeR$_2$MgI, undergoes homolysis of the Si-Ge bond. Alternatively, the silyl radical may be derived from *t*-Bu$_2$MeSiMgBr. The germasilene **2** is known to photodissociate to give *t*-Bu$_2$Si: and Mes$_2$Ge: (4). Addition of MeMgI to the silylene may give *t*-Bu$_2$MeSiMgBr which may decompose to give the silyl radical. Further work is required to learn more about the nature of this reaction.

Compound **5** has previously been observed in the photolysis of both hexamesitylcyclotrigermane and -siladigermirane in the presence of excess methylmagnesium iodide followed by hydrolysis. The formation of compound **5** is most likely the result of addition of methylmagnesium iodide to dimesitylgermylene followed by hydrolysis to the germane (eq. [7]).

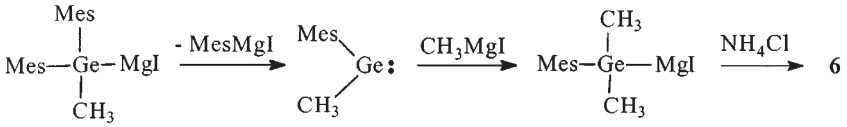
Compound **6**, on the other hand, is believed to arise from dimesitylmethylgermylmagnesium iodide by elimination of mesitylmagnesium iodide to yield mesitylmethylgermylene

[7]



[2] Copies of material on deposit may be purchased from the Depository of Unpublished Data, Document Delivery, CISTI, National Research Council Canada, Ottawa, ON, Canada K1A 0S2 (http://www.nrc.ca/cisti/irm/unpub_e.shtml).

© 2000 NRC Canada

[8] 

and subsequent addition of methylmagnesium iodide to give $MesMe_2GeMgI$, which upon hydrolysis gives **6** (eq. [8]).

Thermolysis of hexamesitylcyclotrigermane in the presence of excess methylmagnesium bromide leads to the formation not only of $Mes_2MeGeGeMe_2H$, but also mesitylene and trimethylgermane (1). Trimethylgermane is believed to be derived from *two* successive α-eliminations of mesitylmagnesium halide from $Mes_2MeGeMgX$ followed, each time, by addition of methylmagnesium iodide. Mesitylmethylgermylene, the first formed intermediate germylene, was trapped with 2,3-dimethylbutadiene to give the germacyclopentene, providing convincing evidence for the proposed mechanism (1). The isolation of compound **6** provides further evidence for the formation of this intermediate germylene.

Compounds **6** and **7**, which are believed to originate from the α-elimination of MesMgI from germyl Grignard reagents, have been observed in the photolysis of Si,Si-di-*tert*-butyltetramesitylsiladigermirane with excess methylmagnesium iodide at 15°C. This is in contrast to the previously studied systems (1), where ligand exchange products were observed well above room temperature (~105°C). The difference in the ease of the proposed α-elimination of the Grignard reagents may be the result of the need to relieve steric congestion in the case of the bulkier di-*tert*-butylmethylsilyl-substituted germylmagnesium halide. However, at 15°C the elimination of a second equivalent of MesMgI does not appear to take place, allowing for the formation of **6** and **7** rather than the products of complete ligand exchange.

In summary, the addition of Grignard reagents to germasilenes to give germyl Grignard reagents and the α-elimination of mesitylmagnesium halide from mesitylgermylmagnesium halides to give the germylenes do appear to be general reactions.

Experimental

All experiments were carried out in flame-dried glassware under an inert argon atmosphere. Toluene, diethyl ether and THF were freshly distilled from sodium–benzophenone. Methylmagnesium iodide was prepared from commercially available methyl iodide (BDH) and magnesium (Lancaster Chemical Co.), stored under argon and the concentration was determined by titration, prior to use. Mesitylgermane was prepared following the published procedure (9). Chromatography was carried out using a Chromatotron (Harrison Research) or on conventional silica gel preparative plates. Photolyses were carried out at 350 nm using a Rayonet Photochemical Reactor.

An acidic work-up entails the separation of the aqueous and organic phases following quenching of the reaction mixture. The aqueous phase was extracted with four portions of an organic solvent (hexanes for the photolyses and diethyl ether for the synthesis of $Me_2MesGeH$) and the extracts were combined with the organic phase. The organic phase was dried over anhydrous magnesium sulfate and then filtered to remove the solid.

NMR spectra were recorded on a Varian Gemini 200, an XL-300, a Varian Gemini 300 or a Bruker Avance DRX-500 using benzene-d_6 as a solvent. The 2-D spectra were acquired using standard techniques. IR spectra were recorded (cm^{-1}) as thin films on a Perkin-Elmer 2000 FT IR spectrometer. A Finnegan MAT model 8230 mass spectrometer, with an ionizing voltage of 70 eV, was used to obtain electron impact mass spectra (recorded in mass-to-charge units, *m*/*z*, with ion identity and peak intensities relative to the base peak in parentheses).

Photolysis of Si,Si-di-*tert*-butyltetramesitylsiladigermirane in the presence of excess methylmagnesium iodide

A solution of $(t\text{-}Bu)_2SiGe_2Mes_4$ (100 mg, 0.131 mmol) and freshly prepared methylmagnesium iodide (3 mL, 84 mmol in Et_2O) in toluene (15 mL) was photolyzed for 16 h at 15°C. Following the photolysis, the reaction mixture was quenched with aqueous ammonium chloride, followed by an acidic work-up. Removal of the solvent in vacuo yielded an oily residue (106.5 mg), which contained several compounds including dimesitylmethylgermane **5** (5), mesityldimethylgermane **6**, (di-*tert*-butylmethylsilyl)mesitylmethylgermane **7** and a mixture of the *meta*- and *para*-isomers of (di-*tert*-butylmethylsilyl)toluene **8**. Separation of the components was accomplished using preparative thin layer chromatography (Chromatotron) with hexanes:CH_2Cl_2 (8:2) as the eluent. Compounds **5**, **7**, and **8** were isolated in 19% (16.25 mg), 3.5% (1.65 mg), and 4.5% (1.5 mg) yields, respectively. Compound **6** could not be separated from **7**.

*(Di-*tert*-butylmethylsilyl)mesitylmethylgermane (**7**)*: Colourless, waxy solid. IR (thin film, cm^{-1}): 2022 (m) (Ge-H); ^{1}H NMR (ppm): 6.78 (s, 2H, Mes **H**), 4.70 (q, 1 H, J = 4.4 Hz, Ge-**H**), 2.45 (s, 6 H, Mes *o*C**H**$_3$), 2.11 (s, 3 H, Mes *p*C**H**$_3$), 1.08 (s, 9 H, *tert*-butyl C**H**$_3$), 0.93 (s, 9 H, *tert*-butyl C**H**$_3$), 0.63 (d, 3 H, J = 4.4 Hz, Ge-C**H**$_3$), 0.23 (s, 3 H, Si-C**H**$_3$); ^{13}C NMR (ppm): 143.05, 137.58, 136.21 (Mes **C**), 128.93 (Mes **C**H), 29.18, 29.00 (C(**C**H$_3$)$_3$), 25.45 (Mes *o*C**H**$_3$), 21.35, 21.18 (**C**(CH$_3$)$_3$), 21.03 (Mes *p*C**H**$_3$), –3.01 (Ge-C**H**$_3$), –7.23 (Si-C**H**$_3$); ^{29}Si NMR (ppm): 10.9; MS (*m*/*z*): 366 (M^+, 3), 208 (MesGeMe, 34), 193 (MesGe, 39), 119 (Mes, 19), 84 (42), 73 ($SiMe_3$, 100), 49 (69); High resolution MS: calc. for $C_{19}H_{36}SiGe$: 366.1798, found: 366. 1801.[3]

*(Di-*tert*-butylmethylsilyl)toluene (mixture of meta-isomer and para-isomer) (**8**)*: Colourless, waxy solid. IR (thin film, cm^{-1}): 3020 (w), 2962 (s), 2930 (s), 2892 (m), 2857 (s), 1471 (m), 1388 (m), 1364 (m), 1252 (m), 1119 (m), 1098 (w), 1012 (w), 935 (w), 853 (w), 821 (m); ^{1}H NMR

[3] Due to the small quantities of samples, it was very difficult to separate the compounds from grease and, therefore, the compounds were unsuitable for elemental analysis.

© 2000 NRC Canada

(ppm)[4]: 7.54 (half of an AA′XX′ pattern, Ar **H-3/5** of *p*-isomer), 7.51 (bs, ^5J = 0.6 Hz, ^4J = 1.3, 1.9 Hz, Ar **H-2** of *m*-isomer), 7.46 (pseudo d, ^3J = 7.5 Hz, ^4J = 1.3, 1.3 Hz, Ar **H-4** of *m*-isomer), 7.17 (pseudo t, ^3J = 7.5, 7.6 Hz, ^5J = 0.6 Hz, Ar **H-5** of *m*-isomer), 7.06 (m, Ar **H-2/6** of *p*-isomer), 7.05 (m, ^3J = 7.6 Hz, ^4J = 1.3, 1.9 Hz, Ar **H-6** of *m*-isomer), 2.17 (s, Ar C**H**$_3$ of *m*-isomer), 2.14 (s, Ar C**H**$_3$ of *p*-isomer), 1.050 (s, *tert*-butyl C**H**$_3$ of *m*-isomer), 1.047 (s, *tert*-butyl C**H**$_3$ of *p*-isomer), 0.29 (s, Si-C**H**$_3$ of *m*-isomer), 0.27 (s, Si-C**H**$_3$ of *p*-isomer); ^{13}C NMR (ppm): 136.8, 136.76 (Ar **C-1/C-3** of *m*-isomer), 136.10 (Ar **C-2** of *m*-isomer), 132.73 (Ar **C-4** of *m*-isomer) 129.77 (Ar **C-6** of *m*-isomer), 127.8 (Ar **C-5** of *m*-isomer), 138.5 (Ar **C-1/C-4** of *p*-isomer), 135.59 (Ar **C-3** and **C-5** of *p*-isomer), 128.61 (Ar **C-2** and **C-6** of *p*-isomer), 29.10 (C(**C**H$_3$)$_3$ of both isomers), 21.66 (Ar **C**H$_3$ of *m*-isomer), 21.34 (Ar **C**H$_3$ of *p*-isomer), 19.51 (**C**(CH$_3$)$_3$ of both isomers), –8.59 (Si-**C**H$_3$ of both isomers); ^{29}Si NMR (ppm): 4.5 (*m*-isomer), –10.9 (*p*-isomer); MS (*m*/*z*): 248 (M$^+$, 2), 233 (M$^+$-CH$_3$, 3), 191 (M$^+$-*tert*-butyl, 100), 149 (63), 73 (SiMe$_3$, 93); High resolution MS: calcd. for $C_{16}H_{28}Si$: 248.1960; found: 248.1959.

Preparation of mesitylmethylgermane

Tert-butyllithium (1.7 M in hexanes, 5 mmol) was added to a solution of crude mesitylgermane (0.480 g, 2.5 mmol) in THF (10 mL) at –50°C. The orange-yellow mixture was allowed to stir at –50°C for 10 min before the addition of methyl iodide (1.77 g, 13 mmol). After 20 min at –50°C, the reaction mixture was warmed to room temperature and allowed to stir for 1 hour. The reaction mixture was then quenched with 1 M HCl, followed by an acidic work-up. Removal of the solvent in vacuo yielded a yellow oil. Isolation and purification of **9** was accomplished by Kugelrohr distillation (60°C, 2 mm Hg) which yielded 131.85 mg (24% yield) of **9** as a clear, colourless oil.

*Mesitylmethylgermane (**9**)*: IR (thin film, cm^{-1}): 2064 (s, Ge-H); ^{1}H NMR (ppm): 6.74 (s, 2 H, Mes **H**), 4.53 (q, 2 H, *J* = 3.9 Hz, Ge-**H**), 2.32 (s, 6 H, Mes *o*C**H**$_3$), 2.11 (s, 3 H, Mes *p*C**H**$_3$), 0.34 (t, 3 H, *J* = 3.9 Hz, Ge-C**H**$_3$); ^{13}C NMR (ppm): 143.30, 138.44, 131.6 (Mes **C**), 128.5 (Mes **C**H), 24.00 (Mes *o*C**H**$_3$), 21.10 (Mes *p*C**H**$_3$), –6.78 (Ge-**C**H$_3$); MS (*m*/*z*): 210 (M$^+$, 21), 193 (MesGe, 64), 121 (MesH$_2$, 100), 105 (MeGeH, 43), 91 (M$^+$ – Mes, 26); High resolution MS: calcd. for $C_{10}H_{16}Ge$: 210.0464; found: 210.0451.

Preparation of mesityldimethylgermane

Tert-butyllithium (1.7 M in hexanes, 0.85 mmol) was added to a solution of mesitylmethylgermane (0.131 g, 0.63 mmol) in THF (5 mL) at –50°C. The orange-yellow mixture was allowed to stir at –50°C for 10 min before the addition of methyl iodide (0.45 g, 3.2 mmol). After 20 min at –50°C the reaction mixture was warmed to room temperature and allowed to stir for 1 h. The reaction mixture was then quenched with 1 M HCl, followed by an acidic work-up. Removal of the solvent in vacuo yielded a yellow oil. Isolation and purification of **6** was accomplished by Kugelrohr distillation (85°C, 2 mm Hg) which yielded 42.4 mg (30% yield) of **6** as a clear, colourless oil.

*Mesityldimethylgermane (**6**)*: IR (thin film, cm^{-1}): 2050 (s, Ge-H); ^{1}H NMR (ppm): 6.75 (s, 2 H, Mes **H**), 4.85 (septet, 1 H, *J* = 3.7 Hz, Ge-**H**), 2.34 (s, 6 H, Mes *o*C**H**$_3$), 2.13 (s, 3 H, Mes *p*C**H**$_3$), 0.42 (d, 6 H, *J* = 3.7 Hz); ^{13}C NMR (ppm): 143.27, 138.19, 134.01 (Mes **C**), 128.79 (Mes **C**H), 24.11 (Mes *o*C**H**$_3$), 21.04 (Mes *p*C**H**$_3$), –2.18 (Ge-**C**H$_3$); MS (*m*/*z*): 224 (M$^+$, 26), 209 (M$^+$ -CH$_3$, 100), 191 (MesGe, 12), 119 (Mes, 32), 105 (M$^+$ – Mes, 19), 89 (GeCH$_3$, 29); High resolution MS: calcd. for $C_{11}H_{18}Ge$: 224.0620; found: 224.0608.

Acknowledgements

The financial support of the Natural Sciences and Engineering Council of Canada is gratefully acknowledged.

References

1. C.E. Dixon, M.R. Netherton, and K.M. Baines. J. Am. Chem. Soc. **120**, 10365 (1998).
2. (*a*) A. Castel, P. Rivière, J. Satgé, and Y.-H. Ko. J. Organomet. Chem. **342**, C1 (1988); (*b*) A. Castel, P. Rivière, J. Satgé, M. Ahbala, C. Abdennadher, and D. Desor. Main Group Met. Chem. **16**, 291 (1993); (*c*) K. Mochida and H. Chiba. J. Organomet. Chem. **473**, 45 (1994); (*d*) K.S. Nosov, A.V. Lalov, M.P. Egorov, and O.M. Nefedov. Russ. Chem. Bull. **45**, 2673 (1996).
3. (*a*) H.J. Reich, R.C. Holtan, and C. Bolm. J. Am. Chem. Soc. **112**, 5609 (1990); (*b*) D.L. Comins and M.O. Killpack. J. Am. Chem. Soc. **114**, 10972 (1992); (*c*) C. Krempner and H. Oehme. J. Organomet. Chem. **464**, C7 (1994); (*d*) C. Krempner, H. Reinke, and H. Oehme. Angew. Chem. Int. Ed. Engl. **33**, 1615 (1994); (*e*) R. Goddard, C. Krüger, N.A. Ramadan, and A. Ritter. Angew. Chem. Int. Ed. Engl. **34**, 1030 (1995).
4. G.M. Kollegger, W.G. Stibbs, J.J. Vittal, and K.M. Baines. Main Group Met. Chem. **19**, 317 (1996).
5. A. Castel, P. Rivière, and J. Satgé. Organometallics, **9**, 205 (1990).
6. A. Castel, P. Rivière, J. Satgé, and D. Desor. J. Organomet. Chem. **433**, 49 (1992).
7. R.A. Jackson. *In* Adv. Free Radical Chem. Vol. III. *Edited by* G.H. Williams. Academic Press, New York. 1969. pp. 231–288.
8. H. Sakurai. *In* Free radicals. *Edited by* J.K. Kochi. Wiley, New York. Vol. II. 1973. pp. 741–808.
9. P. Rivière, M. Rivière-Baudet, and J. Satgé. *In* Organometallic Syntheses. Vol. IV. *Edited by* R.B. King and J.J. Eisch. Elsevier, Amsterdam. 1988. pp. 545–548.

[4] Coupling constants were measured from the homonuclear decoupled ^{1}H NMR spectrum (irradiated at 2.17 ppm; see Supplementary Material).

© 2000 NRC Canada

Improved simple synthesis of cyclic sulfates from trimethylsilyl chlorosulfonate

Alan R. Bassindale, Ibrahim Katampe, and Peter G. Taylor

Abstract: Reaction of iodosobenzene and trimethylsilyl chlorosulfonate followed by removal of the solvent and trimethylchlorosilane gives phenyliodosulfate. This can be used without further purification to prepare cyclic sulfates from alkenes, including vinylsilanes. Previous results have shown that if the trimethylchlorosilane is not removed, sultones are formed and a possible explanation of this behaviour is given.

Key words: silicon, vinylsilanes, cyclic sulfate, phenyliodosulfate.

Résumé : La réaction de l'iodosobenzène et du chlorosulfonate de triméthylsilyle, suivie de l'élimination du solvant et du triméthylchlorosilane, conduit à la formation du phényliodosulfate. On peut l'utiliser sans purification subséquente pour préparer des sulfates cycliques à partir d'alcènes, y compris les vinylsilanes. Des résultats antérieurs ont montré qu'il y a formation de sultones si l'on n'enlève pas le triméthylchlorosilane; on propose une explication pour ce comportement.

Mots clés : silicium, vinylsilanes, sulfate, phényliodosulfate.

Introduction

Cyclic sulfates are vicinally substituted electrophiles (for reviews see ref. 1). Like epoxides, they have a unique role in organic synthesis: they simultaneously activate and protect adjacent functionalized carbon atoms for nucleophilic attack. They are usually superior to their acyclic counterparts because their cyclic nature renders competing elimination processes stereoelectronically unfavourable (2). Cyclic sulfates have been shown by Sharpless and his group to react readily with a wide variety of nucleophiles with apparent complete selectivity (3) to give aziridines and amino alcohols as shown in Scheme 1.

We are interested in the preparation of silylaziridines from simple precursors such as vinyl silanes. Thus, the synthesis of aziridines from the corresponding cyclic sulfates seemed very attractive. However, the preparation of silyl substituted cyclic sulfates is not straightforward. Unfortunately in our hands traditional methods of preparation of silyl substituted cyclic sulfates, such as from the corresponding diol, usually resulted in desilylated products. Xu and co-workers (4), however, was successful in preparing one silylated cyclic sulfate by this method and subsequently converting it to the corresponding 2-trialkylsilyl aziridine. In this paper we report an alternative synthesis of cyclic sulfates based on the reaction of iodosobenzene with trimethylsilyl chlorosulfonate to give phenyliodosulfate. This reagent reacted with vinyl silanes to give the corresponding silyl substituted cyclic sulfate which could subsequently be converted to aziridines.

Received July 22, 1999. Published on the NRC Research Press website on November 1, 2000.

Dedicated to A.G. Brook — a great chemist, teacher, and friend.

A.R. Bassindale, I. Katampe, and P.G. Taylor.[1] The Open University, Milton Keynes, MK6 7AA, England, U.K.

[1]Author to whom correspondence may be addressed. Telephone: (+44) 1908 652512. Fax: (+44) 1908 858327. e-mail: P.G.Taylor@open.ac.uk

Results and discussion

Ethylene cyclic sulfate and the 4-butyl derivative have previously been prepared in 70–85% yield by the reaction of the corresponding olefin with the hypervalent organoiodine complex, phenyliodosulfate **1**, as shown in Scheme 2 (5).

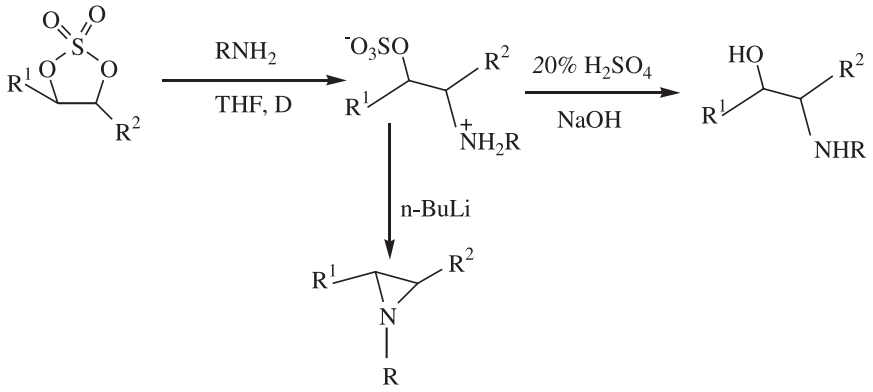
The authors prepared the phenyliodosulfate by the reaction of sulfur trioxide with iodosobenzene. However, the preparation and handling of dry sulfur trioxide is not always straightforward and thus we looked for alternative ways of preparing phenyliodosulfate. We found that the reaction of iodosobenzene with trimethylsilyl chlorosulfonate at –78°C followed by warming to room temperature and removal of the solvent and trimethylsilyl chloride, gave the reagent **1** in good yield (procedure A). This could then be stored for further reaction; however, we found it more convenient to proceed with a "one pot" synthesis and to immediately react the iodosulfate, without further purification, with vinyltrimethylsilane. This gave the corresponding cyclic sulfate in a reasonable yield as listed in Table 1.

Alternatively, trimethylsulfonyl chloride could be added to 1,4-dioxane at low temperature and the solvent removed to give a sulfur trioxide – 1,4-dioxane adduct (6). Further reaction of this with iodosobenzene gave phenyliodosulfate which could be used as before to give the cyclic sulfate. This second procedure (procedure B) gave slightly improved yields, as shown in Table 1.

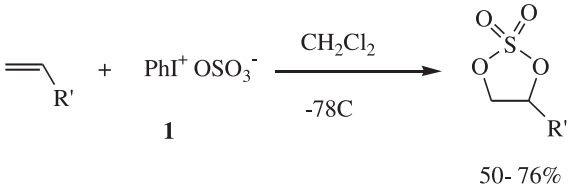
The addition of 1,4-dioxane to trimethylsulfonyl chloride lead to the equilibrium found in Scheme 4.

© 2000 NRC Canada

Scheme 1.



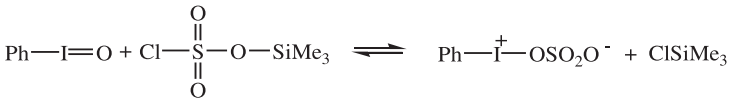
Scheme 2.



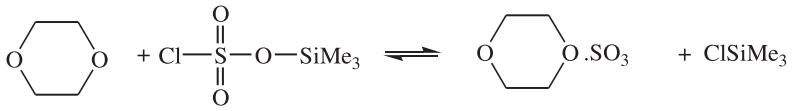
Presumably removal of the trimethylchlorosilane shifts the equilibrium in favour of the sulfur trioxide – 1,4-dioxane complex. We have previously found that direct reaction of iodosobenzene with trimethylsilyl chlorosulfonate at –78°C followed by addition of the alkene, without removal of the trimethylsilyl chloride generates the corresponding sultone (7) as shown in Scheme 5.

We suggest that the iodosobenzene – trimethylsilyl chlorosulfonate system exists as a series of equilibria as shown in Scheme 6.

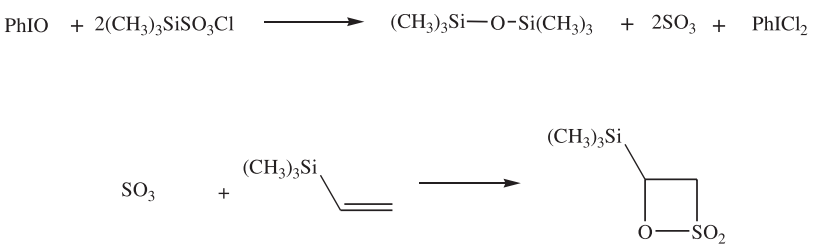
Scheme 3.



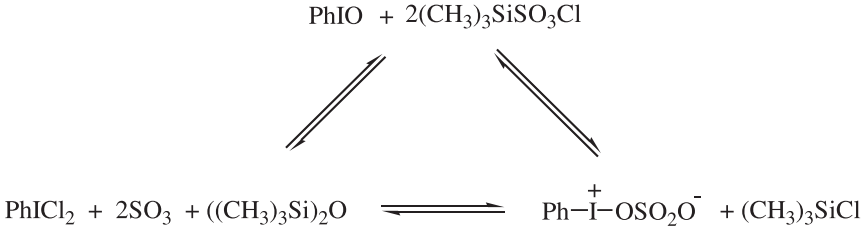
Scheme 4.



Scheme 5.

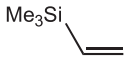
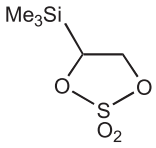
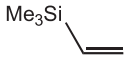
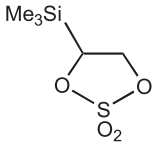
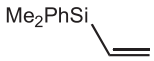
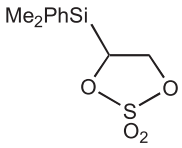
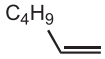
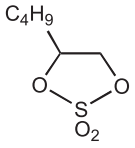
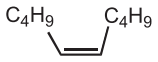
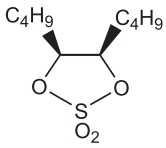


Scheme 6.



© 2000 NRC Canada

Table 1. Yields of cyclic sulfates obtained from reaction of an alkene with phenyliodosulfate.

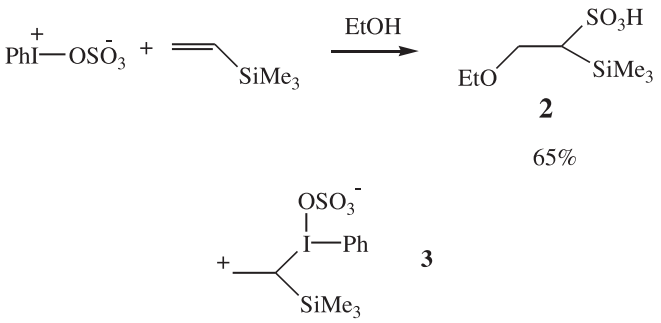
Alkene	Cyclic Sulfate	Procedure	Yield
		A	64%
		B	76%
		B	65%
		B	66%
		B	50%

At –78°C generation of sulfur trioxide, rather than the phenyliodosulfate, is favoured, such that addition of the alkene results in sultone formation. Alternatively, both species may be available for reaction; however, sulfur trioxide is more reactive than phenyliodosulfate, leading to the preferential formation of the sultone. In the absence of the alkene, warming to room temperature and removal of the trimethylsilyl chloride leads to formation of the phenyliodosulfate. The boiling points of trimethylsilylchloride and hexamethyldisiloxane are 58 and 101°C respectively, suggesting that the equilibria may be driven by preferential loss of the trimethylsilyl chloride. However, we may also expect loss of sulfur trioxide to favour generation of the hexamethyldisiloxane and the iodosobenzene dichloride. We would suggest that at room temperature the equilibria favour the formation of the phenyliodosulfate.

Reaction of phenyliodosulfate with vinyltrimethylsilane leads to the corresponding cyclic sulfate. However, if the reaction is carried out in the presence of ethanol, an ethoxy group ends up β to the trimethylsilyl group, giving the sulfonic acid **2**, as shown in Scheme 7.

In this case addition of the phenyliodosulfate occurs in two steps via the formation of the more stable β-silyl carbocation **3**. Formation of the cyclic sulfate followed by ring opening with ethanol is unlikely because it should yield the corresponding α-ethoxy trimethylsilyl compound. In this case the geometry of the ring prevents hyperconjugative stabilisation of the incipient carbocation. Nucleophilic attack α to the silicon is likely as observed with α-silylepoxides and aziridines (8).

Scheme 7.



In conclusion, the formation of phenyliodosulfate from iodosobenzene and trimethylsilyl chlorosulfonate provides a route to cyclic sulfates that avoids the use of sulfur trioxide. The preparation of the cyclic sulfate can be carried out in one pot and provides a route into trimethylsilyl substituted aziridines which we are at present exploring (9).

© 2000 NRC Canada

Experimental

Melting points were determined on a Buchi 510 melting point apparatus and are uncorrected. Infrared spectra were obtained as Nujol mulls or thin films using sodium chloride plates or as KBr discs on a Nicolet 205 FT-IR spectrometer. NMR spectra were recorded as solutions in deuteriochloroform with tetramethylsilane as internal standard on a JEOL EX 400 NMR spectrometer. Mass spectra were obtained using a VG20–250 quadrupole instrument equipped with an Ion Tech fast atom bombardment (FAB) gun.

*Iodosobenzene sulfate (**1**)*: To a slurry of iodosobenzene (10) (5.50 g, 25 mmol) in dry dichloromethane (100 mL), at –78°C under a nitrogen atmosphere, was added trimethylsilyl chlorosulfonate (3.0 mL, 20 mmol) with continuous stirring to produce a clear yellow solution. The reaction mixture was allowed to slowly warm up to room temperature and allowed to stir at this temperature for another 30 min before removal of the solvent under vacuum, to give a very moisture-sensitive yellow solid: mp 110°C (dec.). Physical properties were in agreement with published data (5).

Trimethylsilylethene-1,2-sulfate: *Procedure A*: To a slurry of iodosobenzene (2.20 g, 10 mmol) in dry dichloromethane (50 mL), at –78°C under a nitrogen atmosphere was added trimethylsilyl chlorosulfonate (1.5 mL, 10 mmol) with continuous stirring to produce a clear yellow solution. The solution was allowed to slowly warm up to about –10°C and then subjected to vacuum distillation until all the solvent had been removed to leave a yellow powder. Dry CH_2Cl_2 (50 mL) was immediately added and the mixture re-cooled to –78°C. To this was added vinyltrimethylsilane (1.5 g, 15 mmol). The reaction mixture, which turned colourless, was allowed to warm up to room temperature and stirring continued at this temperature for another 1 h. Removal of the solvent from the reaction mixture using a rotary evaporator gave a black residue. Purification of the crude product over silica gel using hexane–dichloromethane as the eluent gave 1-trimethylsilylethylene-1, 2- sulfate (1.9 g, 64%) as a white solid: IR (Nujol): 2960, 2930, 2857, 1376, 1254, 1202, 943, 843 cm^{-1}; ^1H NMR (400 MHz, $CDCl_3$) δ: 0.00 (s, 9H, $SiMe_3$), 4.38 (m, 1H, CHSi), 4.50 (m, 2H, CH_2); ^{13}C (100 MHz, $CDCl_3$) δ: 4.52 ($SiMe_3$), 72.19 (CH_2), 76.68 (CH); (EI) *m*/*z* 181 (M^+-O_2, 1%), 165 (1%), 153 (1%), 147 (12%), 101 (61%), 80 (10%), 75 (33%), 73 (100%), 64 (12%), 59 (37%), 48 (9%), 45 (33%), 43 (19%), 28 (10%). Anal. calcd. for $C_5H_{12}SiSO_4$: C 30.6, H 6.2, S 16.3; found: C 30.7, H 5.7, S 16.2.

Procedure B: To 1,4-dioxane (1.32 g, 15 mmol,) in dry dichloromethane (25 mL), under a nitrogen atmosphere at –5°C was added dropwise trimethylsulfonyl chloride (1.5 mL, 10 mmol). The reaction mixture was allowed to warm up to room temperature and the solvent removed under vacuum to leave a white crystalline moisture-sensitive solid. To this was added dry dichloromethane (50 mL) and the mixture re-cooled to –78°C before addition of iodosobenzene. The mixture was allowed to warm up to 0°C and vinyltrimethylsilane (1.5 g, 15 mmol) was added dropwise. The reaction mixture was allowed to warm up to room temperature and stirring continued at this temperature for another 1 h. Removal of the solvent from the reaction mixture using a rotary evaporator gave a black residue. Purification of the crude product over silica gel using hexane–dichloromethane as the eluent gave 1-trimethylsilylethylene-1,2- sulfate **(**2.2 g, 76%) as a white solid.

1-Dimethylphenylsilylethene-1,2-sulfate: Reaction of iodosobenzene sulfate, generated in situ as described in Procedure B, with (1.62 g, 10 mmol) of vinyldimethylphenylsilane gave 1-dimethylphenylsilyl-ethylene-1, 2-sulfate (0.7 g, 65%) as a white solid; IR (Nujol): 2960, 1375, 1254, 1200, 1119, 935, 852, 832 cm^{-1}; ^1H NMR (400 MHz, $CDCl_3$) δ: 0.52 (s, 3H, SiMe), 0.53 (s, 3H, SiMe), 4.52 (dd, 1H, *J* = 8.8, 12.0 Hz, CH_2), 4.56 (dd, 1H, *J* = 6.4, 8.8 Hz, CH_2), 4.86 (dd, 1H, *J* = 6.4, 12 Hz, CH), 7.54 (m, 5H, Ph); ^{13}C NMR (100 MHz, $CDCl_3$) δ: –6.5 ($SiMe_2$), –5.5 ($SiMe_2$), 72.37 (CH_2), 77.48 (CHSi), 128.7, 130.99, 131.75, 134.00 (Ph); (EI) *m*/*z* 258 (M^+, 51%), 257 (30%), 123 (51%), 96 (94%), 80 (100%), 64 (22%). This product was very unstable and hence could not be characterized further.

1-n-*butylethene-1,2-sulfate*: Addition of 1-hexene (1.3 g, 15 mmol), to iodosobenzene sulfate, generated as described above (Procedure B), gave after purification 1-*n*-butylethene-1,2-sulfate (1.8 g, 66%); IR (Nujol): 2962, 2936, 1469, 1387, 1212, 1191, 997, 832 cm^{-1}; ^1H NMR (400 MHz, $CDCl_3$) δ: 0.95 (t, 3H, *J* = 6.8 Hz, CH_3), 1.26–2.1 (m, 6H, $(CH_2)_3$), 4.33 (dd, 1H, *J* = 5.3, 12.2 Hz, CH_2O), 4.75 (dd, 1H, *J* = 7.5, 12.2 Hz, CH_2O), 5.12 (m, 1H, CHO); ^{13}C NMR (400 MHz, $CDCl_3$) δ: 13.83 (CH_3), 22.15, 26.56, 32.12 $(CH_2)_3$, 72.86 (CH_2O), 83.30 (CHO); (EI) *m*/*z* 181 (MH^+, 2%), 164 (7.8%), 149 (3%), 139 (3.4%), 129 (6%), 123 (10%), 100 (13%), 87 (16%), 83 (100%), 82 (69%), 81 (19%), 71 (20%). Anal. calc. for $C_6H_{12}SO_4$: C 40.0, H 6.7; found: C 40.6, H 6.8.

Cis-*1,2- dibutylethene cyclic sulfate*: Addition of *cis*-5-decene (0.70 g, 5 mmol) to iodosobenzene sulfate, generated as described above (Procedure B), gave after purification 1,2-*n*-dibutylethylene cyclic sulfate (0.6 g, 50%). The physical properties were in agreement with published data (3).

*1-Trimethylsilyl-2-ethoxyethane sulfonic acid (**2**)*: To a slurry of iodosobenzene (2.20 g, 10 mmol) in dry dichloromethane,(50 mL) at –78°C under a nitrogen atmosphere was added trimethylsilyl chlorosulfonate (1.5 mL, 10 mmol) with continuous stirring to produce a clear yellow solution. The solution was allowed to slowly warm up to about –10°C and then subjected to vacuum distillation. When all the solvent had been removed, a yellow powder remained. A further 50ml of dry CH_2Cl_2 "spiked" with ethanol was added and the mixture re-cooled to –78 °C. To this was added vinyltrimethylsilane (1.5 g, 15 mmol) and the reaction mixture, which turned colourless, was allowed to warm up to room temperature and stirring continued at this temperature for another 1 h. Removal of the solvent from the reaction mixture using a rotary evaporator gave a black residue. Purification of the crude product over silica gel using hexane–dichloromethane as the eluent gave an oil (2.2 g, 65%). IR (neat): 2986, 1388, 1254, 1192, 923, 848 cm^{-1}; ^1H NMR (400 MHz, $CDCl_3$) δ: 0.00 (s, 9H, $SiMe_3$), 1.42 (t, 3H, *J* = 6.8 Hz, CH_3), 3.64 (m, 2H, OCH2CH3), 3.87 and 4.02 (dd, 1H, *J* = 6.4, 12.8 Hz and dd, 1H, *J* = 3.6, 12.8 Hz, CH_2-),

© 2000 NRC Canada

4.67 (dd, 1H, J = 3.6, 6.4 Hz, CHO); ^{13}C NMR (400 MHz, $CDCl_3$) δ: –2.83 ($SiMe_3$), 14.51 (CH_3), 44.85 (CH_2O-), 69.95 (OCH_2CH_3), 80.89 (CHO); MS (EI+) *m*/*e* 225 (1, (M–H)), 197 (4), 181(1), 167 (4), 155 (17), 152 (7), 147 (3), 139 (4), 124 (17), 117 (6), 103 (10), 93 (23), 75 (56), 73 (100), 59 (12), 45 (22), 44 (20), 43 (17), 29 (28), 27 (11).

References

1. (*a*) D.S. Breslow and H. Skolnik. Multi-sulphur and sulphur and oxygen five- and six-membered heterocycles. Part 1. Wiley–Interscience, New York. 1966, p. 17; (*b*) G.W. Fisher and T. Zimmermann. *In* Comprehensive heterocyclic chemistry. Vol 6. *Edited by* A.R. Katritzky and C.W. Rees. Pergamon, Oxford. 1984. p. 851.
2. D. Seebach, J.D. Aebi, M. Gander-Coquoz, and R. Naef. Helv. Chim. Acta, **70**, 1194 (1987), and refs. therein.
3. Y. Gao and K.B. Sharpless. J. Am. Chem. Soc. **110**, 7538 (1988).
4. A.R. Bassindale, P.G. Taylor, and Y. Xu. J. Chem Soc. Perkins Trans. 1, 1061 (1994).
5. (*a*) N.S. Zefirov, V.V. Zhadankin, Yu.V. Dan'kov, V.D. Sorokin, V. Semerikov, A.S. Kozmin, R. Caple, and B.A. Berglund. Tetrahedron Lett. **27**, 3971 (1986); (*b*) N.S. Zefirov, V.V. Zhadankin, V.D. Sorokin, and A.S. Kozmin. Zh. Org. Khim. **22**, 450 (1986).
6. K. Hofmann and G. Simchen. Synthesis, 699 (1979).
7. A.R. Bassindale, I. Katampe, M.G. Maesano, P. Patel, and P.G. Taylor. Tetrahedron Lett. **40**, 7417 (1999).
8. A.R. Bassindale, S.J. Glynn, and P.G. Taylor. *In* The chemistry of organic silicon compounds. Vol. 1. *Edited by* Z. Rappoport and Y. Apeloig. John Wiley and Sons, New York. 1998. p. 355.
9. B.B. Lohray, Y. Gao, and K.B. Sharpless. Tetrahedron Lett. **30**, 2623 (1989).
10. (*a*) H.J. Lucas, E.R. Kennedy, and M.W. Formo. Organic Synthesis. Vol. 3. John Wiley and Sons, New York. 1955. p. 483; (*b*) H. Saltzman and J.G. Sharefkin. Organic Synthesis. Vol. 5. John Wiley and Sons, New York. 1973, p. 683.

© 2000 NRC Canada

Reactions of the stable bis(amino)silylene Si[{N(CH$_2$*t*Bu)}$_2$C$_6$H$_4$-1,2] with group 3 or lanthanide metal organic compounds. Crystal structures of [Ln(η^5-C$_5$H$_5$)$_3$Si{[N(CH$_2$*t*Bu)]$_2$C$_6$H$_4$-1,2}]·C$_7$H$_8$ (Ln = Y or Yb)

Xiaoping Cai, Barbara Gehrhus, Peter B. Hitchcock, and Michael F. Lappert

Abstract: Treatment of the thermally stable aminosilylene Si[{N(CH$_2$*t*Bu)}$_2$C$_6$H$_4$-1,2] [≡ Si(NN)] with a tris(cyclopentadienyl)- group 3 or -lanthanide metal compound LnCp$_3$ (Cp = η^5-C$_5$H$_5$ and Ln = Y or Yb) in toluene at ambient temperature afforded the first earliest transition or f-block metal–silylene complexes [LnCp$_3${Si(NN)}]·C$_7$H$_8$ (Ln = Y (**1**) or Yb (**2**)), characterized by NMR spectroscopy and X-ray crystallography: complex **1** (monoclinic, space group $P2_1/c$ (no. 14), a = 15.641(5), b = 15.895(7), c = 14.876(5) Å, β = 112.93(3), Z = 4, $R1$ = 0.067 for 6194 observed data), and **2** (monoclinic, space group $P2_1/c$ (no. 14), a = 15.635(3), b = 15.795(2), c = 14.842(2) Å, β = 112.87(2), Z = 4, $R1$ = 0.044 for 9829 observed data). The Ln atom in each of the isoleptic complexes **1** and **2** has distorted trigonal monopyramidal geometry, with the approximately trigonal silicon atom in the apical position. The Ln—Si bond length is 3.038(2) (**1**) or 2.984(2) Å (**2**). Variable temperature ^{29}Si{^{1}H} NMR spectra in toluene-d_8 show that each complex readily dissociates (Y > Yb) into its factors; at 188 K, the ^{29}Si{^{1}H} signal for (**1**) was a doublet centred at δ 119.5, $^1J(^{29}\text{Si}\text{-}^{89}\text{Y})$ = 59 Hz.

Key words: crystallography, NMR, silylene, yttrium, ytterbium, organometallic complexes.

Résumé : La réaction de l'aminosilylène thermiquement stable Si[{N(CH$_2$*t*Bu)}$_2$C$_6$H$_4$-1,2] [≡ Si(NN)] avec un composé comportant un groupe tris(cyclopentadiényl) attaché à un métal du groupe 3 ou à un lanthanide, LnCp$_3$ (Cp = η^5-C$_5$H$_5$ et Ln = Y ou Yb), dans du toluène à la température ambiante, a permis d'obtenir les premiers complexes de silylène attaché à un métal prémier de transition ou du bloc f, [LnCp$_3${Si(NN)}]·C$_7$H$_8$ (Ln = Y (**1**), ou Yb (**2**)), qui ont été caractérisés par spectroscopie RMN et par diffraction des rayons X. Le complexe **1**, monoclinique, groupe d'espace $P2_1/c$ (no. 14), avec a = 15,641(5), b = 15,895(7) et c = 14,876(5) Å, β = 112,93(3)°, Z = 4 et $R1$ = 0,067 pour 6194 données observées. Le complexe **2**, monoclinique, groupe d'espace $P2_1/c$ (no. 14), avec a = 15,635(3), b = 15,795(2) et c = 14,842(2) Å, β = 112,87(2)°, Z = 4 et $R1$ = 0,044 pour 9829 données observées. Dans chacun des complexes isoleptiques **1** et **2**, l'atome Ln présente une géométrie monopyramidale trigonale déformée dans laquelle l'atome de silicium trigonal est approximativement en position apicale; la longueur de la liaison Ln—Si est de 3,038(2) (**1**) et de 2,984(2) (**2**) Å. Les spectres RMN du ^{29}Si{^{1}H} à température variable, dans le toluène-d$_8$, montrent que chacun des complexes peut facilement se dissocier (Y > Yb) en ses composants; à 188 K, le signal ^{29}Si{^{1}H} du composé **1** est un doublet centré à un δ de 119,5 avec un $^1J(^{29}\text{Si}\text{-}^{89}\text{Y})$ = 59 Hz.

Mots clés : cristallographie, RMN, silylène, yttrium, ytterbium, complexes organométalliques.

[Traduit par la Rédaction]

Introduction

Compounds containing a group 3 or lanthanide metal atom (Ln) bound to silicon are exceedingly rare and invariably have involved a tetravalent organosilyl ligand [SiXX′X″]$^-$ bound to a Ln(II) or Ln(III) metal, as in [Yb(η^5-C$_5$H$_5$){Si(SiMe$_3$)$_3$}(THF)$_2$] (1*a*), [Sm(η^5-C$_5$H$_5$)$_2${SiH(SiMe$_3$)$_2$}]$_2$ (1*b*), or [Yb(SiPh$_3$)$_2$(THF)$_4$] (1*c*).

Another class of silicon-containing ligands which has recently attracted attention, in the context of lower oxidation state d^6, d^8, or d^{10} metal complexes, is a neutral silylene SiX$_2$ (with or without a stabilizing neutral base bound to

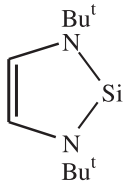
Received August 6, 1999. Published on the NRC Research Press website on November 2, 2000.

This paper is dedicated to Professor Adrian Brook, in recognition of his many important contributions to organosilicon chemistry, as a mark of esteem and (by MFL) friendship.

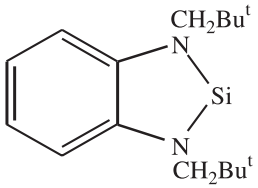
X. Cai, B. Gehrhus, P.B. Hitchcock, and M.F. Lappert.[1] The Chemistry Laboratory, University of Sussex, Brighton, BN1 9QJ, U.K.

[1]Author to whom correspondence may be addressed. e-mail: m.f.lappert@sussex.ac.uk

 © 2000 NRC Canada



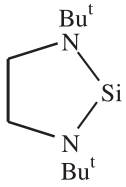
A



B [abbreviated as Si(NN)]



C



D

silicon). Among these are those derived from the thermally stable silylenes **A** (2), **B** (3), and **C** (4); the silylene **D** is somewhat less robust than its unsaturated analog **A** (5). The transition metal complexes which had previously been reported were derivatives of Cr(0), Mo(II), Fe(0), Ru(II), Ni(0), Ni(II), Pt(0), Pt(II), and Au(I): [Cr(CO)$_2$(C$_6$H$_3$Me$_3$-1,3,5)(**A**)] (6), [Mo(Cp)$_2$ (**A**)] (7), [Fe(CO)$_4$(**A**)] (6), [Ru(η^5-C$_5$H$_5$)(PMe$_3$)$_2$(SiX$_2$)]$^+$ [X = SEt (8*a*), SC$_6$H$_4$Me-4 (8*b*) or Ph], [Ni(CO)$_2$(**A**)$_2$] (9), [Ni(PPh$_3$)(**B**)$_3$] (10), *trans*-[Pt{Si(NN)Cl}$_2${Si(NN)}$_2$] (10), *trans*-[PtH{P(C$_6$H$_{11}$-c)$_3$}$_2${Si(SEt)$_2$}]$^+$ (11*a*), [PtH{P(Pr^i)$_2$CH$_2$}$_2${Si(C$_6$H$_2$Me$_3$-2,4,6)$_2$}]$^+$ (11b), [Pt{P(C$_6$H$_{11}$-c)$_3$}$_2${ Si(C$_6$H$_2$Me$_3$-2,4,6)$_2$}] (12), and [AuCl(**C**)] (13).

Of the above silylene–transition metal complexes, only those derived from one of the silylenes **A**–**C** were directly accessible from the parent silylene SiX$_2$. Two methods of synthesis have been employed: (*i*) a nucleophilic displacement of carbon monoxide (**A** or **C**), or (**B**) cycloocta-1,4-diene (COD), or a tertiary phosphine (**A** or **B**) from an appropriate transition metal precursor; and (*ii*) for **B**, displacement of PPh$_3$ and concomitant reductive Cl atom elimination, eq. [1]. The methods for the silylene Si[{N(CH$_2$Bu^t)}$_2$C$_6$H$_4$-1,2] [≡ Si(NN)] (**B**) are illustrated in eqs. [1]–[4] (10).

[1] $$[Ni(COD)_2] + 4\ Si(NN) \rightarrow [Ni\{Si(NN)\}_4] + 2\ COD$$

[2] $$[NiCl_2(PPh_3)_2] + 4\ Si(NN) \rightarrow [Ni(PPh_3)\{Si(NN)\}_3] + Si(NN)Cl_2 + PPh_3$$

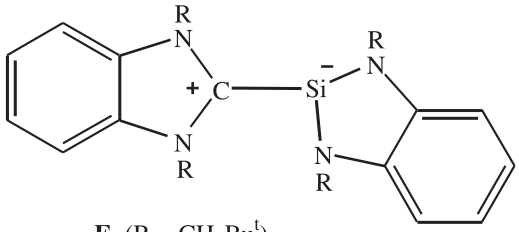
[3] $$[NiCl_2(PPh_3)_2] + 5\ Si(NN) \rightarrow [Ni\{Si(NN)\}_4] + Si(NN)Cl_2 + 2\ PPh_3$$

[4] $$[PtCl_2(PPh_3)_2] + 4\ Si(NN) \rightarrow \textit{trans}\text{-}[Pt\{Si(NN)Cl_2\{Si(NN)\}_2] + 2\ PPh_3$$

The isolation and mode of formation of the above silylene–transition metal complexes is consistent with the notion that silylenes probably are rather "soft" ligands and hence bind strongly to low oxidation state (M(0), M(I), or M(II)) soft Lewis acid metal (M) centers.

The present work represents an extension of a previous study (10) of the coordination chemistry of the silylene Si(NN) **B** to the earliest transition and the lanthanide metals, collectively abbreviated as Ln. As for the former, yttrium was chosen as a representative group 3 metal, in part because of its possession of an NMR-friendly nucleus, ^{89}Y, I = 1/2, 100% natural abundance; for the latter, ytterbium was selected, in part because it more than any other Ln metal shows a facile Ln(III) → Ln(II) reduction. The Ln metal complexes are ubiquitously found in the +3 oxidation state and are regarded as having rather "hard" metal centers, showing a preference for binding to hard Lewis acids. For example, LnCp$_3$ complexes form 1:1 adducts with tetrahydrofuran or ammonia, but more rarely with carbon monoxide, an alkene, or a tertiary phosphine.

The data here presented are also complementary to our studies of the role of the silylene **B** as a ligand in main group element chemistry. However, the present indications are that **B** behaves more akin to a Lewis acid than base in the complex 1,2-C$_6$H$_4$[N(CH$_2$*t*Bu)]$_2$C$^+$-$^-$Si[N(CH$_2$*t*Bu)]$_2$C$_6$H$_4$-1,2 **E** (14).



E (R = CH$_2$Bu^t)

Experimental section

General techniques

All operations and manipulations were carried out under purified argon, by conventional Schlenk techniques. Solvents were dried and degassed before use. The silylene Si(NN) (3) and the tris(cyclopentadienyl)metal complexes LnCp$_3$ (15) were obtained by published procedures. Other chemicals were purchased and purified by standard techniques. Microanalyses were carried out by Medac Ltd. (Brunel University). The NMR spectra were recorded in benzene-d_6 or toluene-d_8 using Bruker Instruments: Bruker DPX 300 (^{1}H and ^{13}C) and AMX 500 (^{29}Si), and referenced internally to residual solvent resonances (data in δ). Electron impact mass spectra were taken from solid samples using a Kratos MS 80 RF instrument. Melting points were taken in sealed capillaries and are uncorrected.

Synthesis of the crystalline complex 1

A solution of Si(NN) (0.48 g, 1.76 mmol) in toluene (10 mL) was slowly added to a suspension of YCp$_3$ (0.25 g, 0.88 mmol) in toluene (30 mL) at 0°C. The cloudy solution was stirred for one day at room temperature. After filtration, the filtrate was concentrated and cooled (–25°C) yielding colorless crystals of complex **1** (0.35 g, 61.4%), mp 75–80°C. MS: 284 [YCp$_3$]$^+$, 219 [YCp$_2$]$^+$, 274 [Si(NN)]$^+$, 217 [Si(NN) – CMe$_3$]$^+$, 147 [Si(NN) – CH$_2$*t*Bu-CMe$_3$]$^+$, 93 [C$_7$H$_8$H]$^+$, 66 [CpH]$^+$, 57 [CMe$_3$]$^+$. ^{1}H NMR (C$_6$D$_6$, 300.13 MHz, 298 K, δ): 7.12, 7.10, 7.06 (phenyl, 5H), 7.02

© 2000 NRC Canada

(phenyl, 4H, s), 5.92 (Cp, 15H, s), 3.56 (CH_2, 4H, s), 2.10 (Me, 3H, s), 0.89 (CMe_3, 18H, s). ^{13}C NMR (C_6D_6, 75.46 MHz, 298 K, δ): 111.19 (Cp), 21.38 (Me), 137.82, 129.27, 128.00, 125.64 (phenyl), 28.74 (CMe_3), 33.28 (CMe_3), 54.50 (CH_2), 141.24, 111.02, 118.75 (phenyl). $^{29}Si\{^1H\}$ NMR (C_7D_8, 99.33 MHz, 188 K, δ): 119.5 (d, $^1J(^{29}Si\text{-}^{89}Y)$ = 59 Hz), 93.5. For some variable temperature $^{29}Si\{^1H\}$ NMR spectral data, see the discussion. Anal. calcd. for $C_{38}H_{49}N_2SiY$ (%): C 70.1, H 7.59, N 4.30; found (%): C 69.5, H 7.55, N 4.68.

Synthesis of of the crystalline complex 2

A solution of Si(NN) (0.22 g, 0.82 mmol) in toluene (10 mL) was added slowly to a suspension of the dark green $YbCp_3$ (0.15 g, 0.41 mmol) in toluene (20 mL) at 0°C. The cloudy solution was stirred overnight at room temperature. After filtration, the filtrate was concentrated and cooled (–25°C) affording deeper green crystals of complex **2** (0.24 g, 80%), mp 61–65°C. MS: 643 $(M)^+$, 369 $[YbCp_3]^+$, 304 $[YbCp_2]^+$, 239 $[YbCp]^+$, 276 $[Si(NN)H_2]^+$, 91 $[C_7H_8]^+$, 66 $[CpH]^+$. ^1H NMR (C_6D_6, 300.13 MHz, 298 K, δ): 10.18 (CH_2, 2H, s), 8.92 (CH_2, 2H, s), 8.68 (phenyl, 4H, s), 7.08, 6.99, 6.90 (phenyl, 5H), 3.22 (CMe_3, 18H, s), 2.01 (Me, 3H, s), –61.56 (Cp, 15H, s). ^{13}C NMR (C_6D_6, 75.46 MHz, 298 K, δ): –124.81 (Cp), 20.48 (Me), 137.35, 128.91, 128.00, 125.38 (phenyl), 31.04 (CMe_3), 36.91(CMe_3), 62.05 (CH_2), 149.13, 114.55, 121.07 (phenyl). Anal. calcd. for $C_{38}H_{49}N_2SiYb$ (%): C 62.1, H 6.72, N 3.81; found (%): C 60.2, H 6.74, N 3.97.

Lack of reaction between $LaCp_3$ and Si(NN)

A solution of Si(NN) (0.41 g, 1.50 mmol) in toluene (10 mL) was added slowly to a suspension of $LaCp_3$ (0.25 g, 0.75 mmol) in toluene (30 mL) at 0°C. Unlike in the preparation of **1** or **2**, for which the sparingly soluble $LnCp_3$ largely dissolved upon addition of Si(NN), the almost insoluble $LaCp_3$ appeared not to dissolve. The mixture was heated to 80–90°C for 24 h, then filtered. The precipitate was dried under vacuum to yield a white powder (0.2 g), which was shown by its ^1H NMR spectrum and X-ray crystal data to be the $LaCp_3$ starting material.

X-ray crystallographic analysis of $[YCp_3\{Si(NN)\}]\cdot C_7H_8$ (1) and $[YbCp_3\{Si(NN)\}]\cdot C_7H_8$ (2)

Crystallographic data for complexes **1** and **2** are displayed in Table 1. Crystallographic data collection was carried out on an Enraf–Nonius CAD4 diffractometer using Mo-K_α radiation, λ = 0.71073 Å. The crystal was coated with a layer of hydrocarbon oil, attached to a glass fiber, and cooled to 173(2) K. The structures were solved by direct methods (SHELXS-97) (16) and refined on all F^2 by the full-matrix, least-squares procedure (SHELXL-97) (17).

Results and discussion

Treatment of a tris(cyclopentadienyl)metal complex $LnCp_3$ (Ln = Y or Yb) with an excess of the thermally stable bis(amino)silylene Si[{N(CH_2*t*Bu)}$_2$$C_6H_4$-1,2] [≡Si(NN)] at ambient temperature afforded (eq. [5], forward reaction) the first of the earliest (group 3–5) transition (Y) or lanthanide (Yb) metal–silylene complexes, the crystalline $[LnCp_3\{Si(NN)\}]\cdot C_7H_8$ (Ln = Y (**1**) or Yb (**2**)).

Table 1. Summary of crystallographic data for complexes **1** and **2**.

	1	**2**
Empirical formula	$C_{38}H_{49}N_2SiY$	$C_{38}H_{49}N_2SiYb$
Formula weight *M*	650.79	734.9
Crystal system	monoclinic	monoclinic
Space group	$P2_1/c$ (no. 14)	$P2_1/c$ (no. 14)
a (Å)	15.641(5)	15.635(3)
b (Å)	15.895(7)	15.795(2)
c (Å)	14.876(5)	14.842(2)
β (deg)	112.93(3)	112.87(3)
V (Å^3)	3406(2)	3377.2(9)
Z	4	4
D_{calc} (mg m^{-3})	1.27	1.45
Absorption coefficient (mm^{-1})	1.77	2.83
Reflections collected (unique)	6194	10161
Independent (*n*) (R_{int})	5972 (0.072)	9829 (0.035)
Observed (*n*) ($I > 2\sigma(I)$)	3388	6791
No. of parameters (*p*)	379	379
θ range for data collcn (deg)	2 – 25	2 – 30
R1 [$I > 2\sigma(I)$]	0.067	0.044
wR2 (all data)	0.160	0.086
Max, min peaks in final difference map (e Å^{-3})	+0.46, –0.59	+0.75, –0.72

$$[5] \quad LnCp_3 + Si(NN) \overset{PhMe}{\rightleftarrows} [LnCp_3\{Si(NN)\}]\cdot PhMe$$

The colorless (Y) or green (Yb) crystals of each of the complexes **1** or **2** were thermally stable in the solid state, mp 75–80°C (Y) or 61–65°C (Yb) without obvious decomposition. The EI mass spectrum showed the parent molecular ion only for the Yb complex **2**, indicating that the latter is thermally more robust than **1**.

In toluene-d_8 solution, however, it was evident from variable temperature $^{29}Si\{^1H\}$ NMR spectroscopic measurements that there was Ln(III)—Si(II) bond dissociation (eq. [5], back reaction). This occurred more readily for Ln = Y than Ln = Yb and, as appropriate for an equilibrium process, was temperature-dependent. Thus, at 298 K, the proportion of the diamagnetic complex **1** to its factors was 1:14; at 188 K, it was 6:10; while at 338 K essentially the sole silicon-containing species in solution was the free silylene, δ 97.4. For the case of the paramagnetic Yb(III) complex **2**, no free silylene was detected at 298 K (nor at temperatures down to 238 K), while at 343 K a significant silylene signal at δ 94.6 was present. Despite the evident kinetic lability of the Ln(III)—Si(II) bond in a solution of each of **1** or **2**, the magnitude of the coupling constant $^1J(^{29}Si\text{-}^{89}Y)$ = 59 Hz, suggests that there is strong YSi bond orbital overlap. This *J* value may be compared with the $^1J(^{13}C_{sp3}\text{-}^{89}Y)$ = 33 Hz found in $[Y\{\eta\text{-}C_8H_6(SiMe_3)_2\text{-}1,4\}\{CH(SiMe_3)_2\}(THF)]$.[2] The ^{29}Si NMR spectral signal at 188 K was at the higher frequency of δ 119.5 in **1** than the free silylene (δ 93.5); cf. δ 136.5 in $[Ni(PPh_3)\{Si(NN)\}_3]$ (10).

[2] F.G.N. Cloke. University of Sussex. Personal communication, 2000.

© 2000 NRC Canada

Table 2. Bond lengths (Å) and angles (deg) for complexes **1** and **2**.[a]

Bond lengths (Å)	**1**	**2**
Ln—Si	3.038(2)	2.984(2)
Ln—M(1)	2.432(7)	2.407(5)
Ln—M(3)	2.437(7)	2.403(3)
Si—N(2)	1.725(5)	1.729(4)
N(1)—C(22)	1.463(8)	1.4639(6)
N(2)—C(27)	1.477(8)	1.463(6)
C(16)—C(21)	1.387(9)	1.403(7)
C(17)—C(18)	1.408(9)	1.392(7)
C(19)—C(20)	1.376(11)	1.373(8)
Ln—M(2)	2.427(7)	2.398(5)
Si—N(1)	1.729(6)	1.734(4)
N(1)—C(16)	1.409(8)	1.398(6)
N(2)—C(17)	1.399(8)	1.401(6)
C(1)—C(5)	1.411(10)	1.403(7)
C(16)—C(17)	1.402(9)	1.408(7)
C(18)—C(19)	1.370(9)	1.387(7)
C(20)—C(21)	1.379(10)	1.393(7)
Angles (deg)		
M(2)-Ln-M(3)	116.0(2)	116.0(2)
M(3)-Ln-M(1)	118.2(2)	118.4(2)
M(2)-Ln-Si	95.9(2)	96.3(1)
N(2)-Si-N(1)	90.1(3)	90.4(2)
N(1)-Si-Ln	130.8(2)	130.9(1)
C(16)-N(1)-Si	112.6(5)	112.0(3)
C(17)-N(2)-C(27)	123.1(5)	122.2(4)
C(27)-N(2)-Si	124.1(4)	125.1(3)
N(1)-C(16)-C(21)	128.4(7)	127.5(5)
N(2)-C(17)-C(16)	112.3(6)	111.5(4)
M(2)-Ln-M(1)	119.9(2)	119.8(2)
M(1)-Ln-Si	98.1(2)	97.9(1)
M(3)-Ln-Si	100.5(2)	100.2(1)
N(2)-Si-Ln	136.2(3)	136.2(1)
C(16)-N(1)-C(22)	122.8(6)	123.4(4)
C(22)-N(1)-Si	124.5(5)	124.4(3)
C(17)-N(2)-Si	112.8(4)	112.7(3)
N(1)-C(16)-C(17)	111.3(6)	112.5(4)
N(1)-C(22)-C(23)	116.0(5)	116.1(4)

[a]M (1), M(2), and M(3) are the centroids of the C(1)–C(5), C(6)–C(10), and C(11)– C(15) rings, respectively.

The ^{1}H NMR spectrum in benzene-d_6 of the complex **1** showed signals of each of the individual components of the equilibrium mixture of eq. [5] (Ln = Yb): (*i*) the sparingly soluble YCp_3 ($\delta[^1H]$: 5.93 and $\delta^{13}C\{^1H\}$]: 113.9); (*ii*) Si(NN) ($\delta[^1H]$: 7.01, 3.58, and 0.89; $\delta[^{13}C\{^1H\}]$: 141.5, 118.5, 110.7, 54.9, 33.2, and 28.7 (3)); and (*iii*) toluene. We conclude that the rate of exchange at 298 K between **1** and its factors is fast on the NMR time scale. As for the paramagnetic complex **2**, we consider that the rate of exchange at 298 K between **2** and its factors in benzene-d^6 is slow on the NMR time scale. Thus, no signals close to those of Si(NN) were observed and others differed significantly from those found for the sparingly soluble (in C_6D_6) $YbCp_3$: $\delta[^1H]$: –65.7, $\delta[^{13}C\{^1H\}]$: –127.2.

Molecular structures of the crystalline complexes 1 and 2

The molecular structures of the isomorphous, crystalline complexes $[LnCp_3\{Si(NN)\}]\cdot C_7H_8$ (Ln = Y (**1**) or Yb (**2**)) are illustrated in Fig. 1, the unit cell being shown in Fig. 2. Non-hydrogen bond lengths and angles are listed in Table 2. In Table 3 are shown some comparative geometric data for the mononuclear complexes $[YbCp_3]$ (18), $[YbCp_3(THF)]$ (19), $[LuCp_3(THF)]$ (20), **1**, and **2**. Comparison is not so readily made with YCp_3, since this crystalline complex is polymeric $[\{Y(\eta^5\text{-}C_5H_5)_2(\mu\text{-}\eta^2\text{-}C_5H_5)\}_\infty]$ (21), having average Y—C distances for the two $[\eta^5\text{-}C_5H_5]^-$ ligands of 2.67 Å for one ring and 2.75 Å for the other, while the two Y—C distances to the $[\eta^2\text{-}C_5H_5]^-$ ligands are 3.35 ± 0.25 Å. The molecule $[LuCp_3(THF)]$, an f^{14} complex, is taken as a model for the f^{13} Yb(III) analog for which data are not available. Table 4 shows some structural comparison relating to the silicon environment in the crystalline free ligand Si(NN) **B** (3) and its Y (**1**) and Yb (**2**) tris(cyclopentadienyl) complexes.

The Ln atom in each of the crystalline complexes **1** and **2** is in a distorted trigonal monopyramidal environment, being almost coplanar with each of the centroids of the three Cp^- ligands; the distorted trigonal silicon atom occupies the apical site. This arrangement is close to that found in the related THF complexes (Table 3), in which the ligating oxygen atoms of the neutral donor is similarily situated. The Ln—Si bond in the yttrium complex **1** of 3.038(2) Å is longer than in the ytterbium analog **2**, 2.984(2) Å (and may be compared with the Yb—Si bond length of 3.158(2) Å in $[Yb(SiPh_3)_2(THF)_4]$ (1*c*)). The ca. 2% longer Y—Si than Yb—Si bond is matched by the comparable trend in the Ln—C or Ln—M bond lengths (Y > Yb).

Conclusions

It has been shown that the bis(amino)silylene Si[{N(CH$_2$*t*Bu)}$_2$C$_6$H$_4$-1,2] [Si(NN)] (**B**) forms well characterized crystalline 1:1-complexes with tris(cyclopentadienyl)metal complexes $LnCp_3$ of formula $[Ln(\eta^5\text{-}C_5H_5)_3\{Si(NN)\}]\cdot C_7H_8$ (Ln = Y (**1**) or Yb (**2**)), by treating $LnCp_3$ with Si(NN) in toluene at ambient temperature. By

Table 3. Some comparative structural data for $[YCp_3(THF)]$, $[YbCp_3(THF)]$, $[LuCp_3(THF)]$, **1**, and **2**.

Complex	Av Ln-C (Å)	Av Ln-M (Å)[a]	Av M-Ln-M′ (deg)[a]	ΣLn (deg)[b]	Av M-Ln-O (or Si) (deg)	Ref.
$[YbCp_3]$	2.64	2.35	120	359.8		18
$[YbCp_3(THF)]$	2.71	2.45	117.4	352.1	99.3	19
$[LuCp_3(THF)]$	2.69	2.42	117.6	352.6	99.0	20
1	2.71	2.43	118.0	354.1	98.2	This work
2	2.68	2.40	118.1	354.2	98.5	This work

[a]M represents the centroid of a Cp ring.

[b]Σ Ln represents the sum of the three M-Ln-M′ angles.

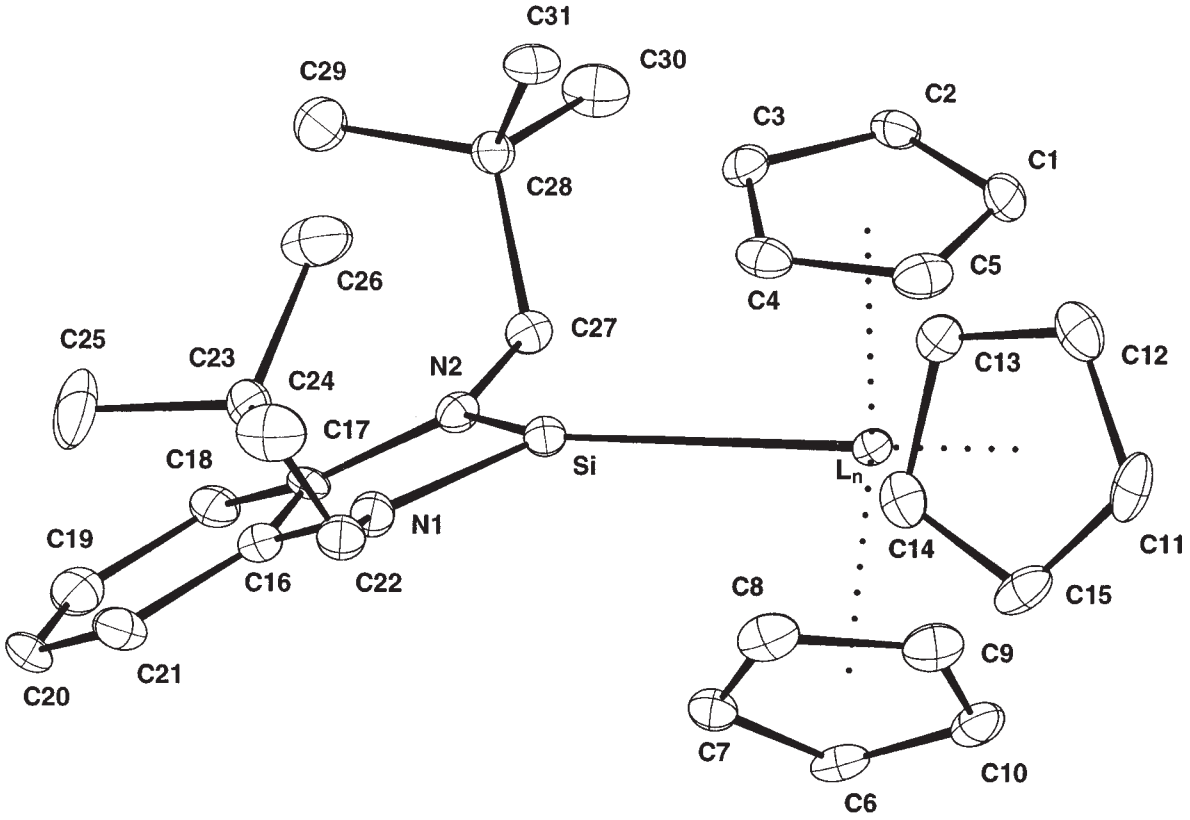
© 2000 NRC Canada

Table 4. Some comparative structural data for Si(NN) and **1** and **2**.

Complex	Av Si-N (Å)	Av N-C_{sp2} (Å)	Av N-Si-N′ (deg)	ΣSi[a] (deg)	Ref.
Si(NN)	1.750	1.382	88.2	88.2	3
1	1.727	1.404	90.1	357.1	This work
2	1.732	1.400	90.4	357.5	This work

[a] ΣSi represents the sum of the angles at silicon.

Fig. 1. Cameron representation of the molecular structure of the isomorphous, crystalline complexes $[LnCp_3\{Si(NN)\}]\cdot C_7H_8$ (Ln = Y (**1**) or Yb (**2**)), with the atom numbering system. Thermal ellipsoids correspond to 50% probability.



contrast, under similar conditions, $LaCp_3$ proved to be unreactive. Each of the complexes **1** and **2** in toluene was found to be in equilibrium with its factors, the yttrium complex **1** being the more readily dissociated. We interpret these findings on the three $LnCp_3$ complexes in the following manner. Only the ytterbium complex is a monomer in the crystal, the other two being polymeric, of structure $[\{Ln(\eta^5\text{-}C_5H_5)_2(\mu\text{-}\eta^2\text{-}C_5H_5)\}_\infty]$, and of these the bridge-binding is more effective for lanthanum than yttrium. The thermodynamics of the formation of a silylene-tris(cyclopentadienyl)metal complex $[LnCp_3\{Si(NN)\}]$ requires an additional term for Ln = La or Y than for Ln = Yb, namely ΔG for $[\{LnCp_3\}_\infty]$ depolymerization. This is greater for Ln = La than Ln = Y. Evidently, the ΔG (depolym.) term for Ln = La is sufficiently large to prevent formation of the La(III)-Si(NN) complex, while for Ln = Y it is responsible for making complex **1** more readily prone to Ln—Si bond dissociation than its isoleptic ytterbium analog **2**. On steric grounds, a silylene–Ln complex might have been expected to be favored by a large Ln(III) radius (La > Y > Yb), an effect which is evidently less important.[3]

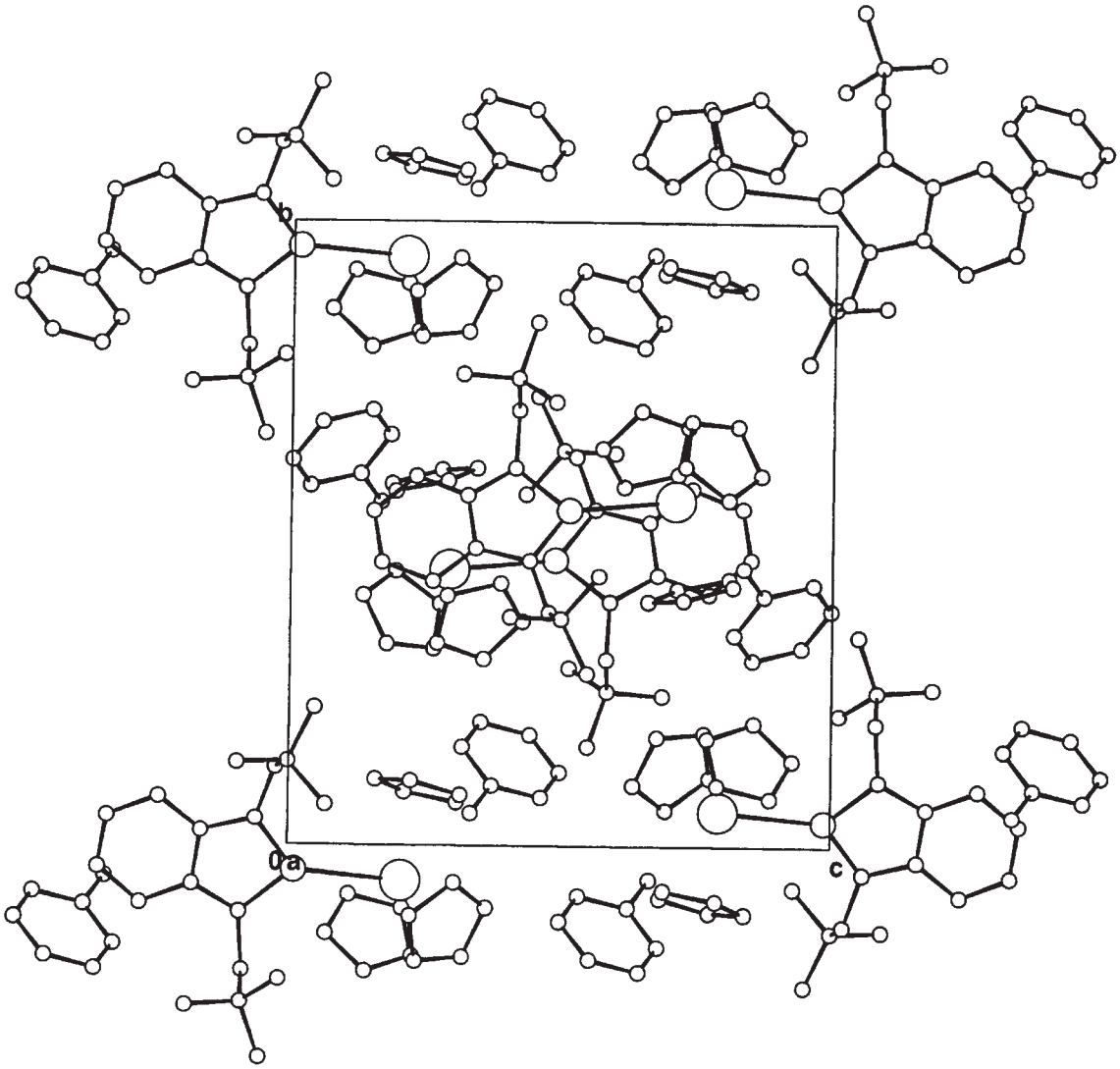
Acknowledgement

We are grateful to the Royal Society for the award of a K.S. Wong fellowship to X.C. and the E.P.S.R.C. for the award of a fellowship to B.G. and for other support.

[3] Crystal data and structure refinement, atomic coordinates, anisotropic and isotropic displacement parameters, bond lengths and angles, hydrogen coordinates, and crystal packing diagrams have been deposited as supplementary material and may be purchased from the Depository of Unpublished Data, Document Delivery, CISTI, National Research Council of Canada, Ottawa, ON K1A 0S2 (http://www/nrc.ca/cisti/docdel/order_electronic_e.shtml for information on ordering electronically). Crystallographic data for the structure(s) reported in this paper have been deposited with the Cambridge Crystallographic Data Centre (CCDC). Copies of the data can be obtained, free of charge, on application to the Director, CCDC, 12 Union Road, Cambridge CB2 1EZ, U.K. (Fax: 44-1223-336033 or e-mail: deposit@ccdc.cam.ac.uk).

© 2000 NRC Canada

Fig. 2. Cameron representation of the unit cell of the isomorphous, crystalline complexes $[LnCp_3\{Si(NN)\}]\cdot C_7H_8$ (Ln = Y (**1**) or Yb (**2**)).



References

1. (*a*) M.M. Corradi, A.D. Frankland, P.B. Hitchcock, M.F. Lappert, and G.A. Lawless. Chem. Commun. 2323 (1996); (*b*) N.S. Radu, T.D. Tilley, and A.L. Rheingold. J. Am. Chem. Soc. **114**, 8293 (1992); (c) L.M. Bochkarev, V.M. Makarov, Y.N. Hrzhanovskaya, L.N. Zakharov, G.F. Fukin, A.I. Yanovsky, and Yu. T. Struchkov. J. Organomet. Chem. **467**, C3 (1994).
2. M. Denk, R. Lennon, R. Hyashi, R. West, A.V. Belyakov, H.P. Verne, A. Haaland, M. Wagner, and N. Metzler. J. Am. Chem. Soc. **116**, 2691 (1994).
3. B. Gehrhus, M.F. Lappert, J. Heinicke, R. Boese, and D. Bläser. J. Chem. Soc. Chem. Commun. 1931 (1995); J. Organomet. Chem. **521**, 211 (1996).
4. P. Jutzi, H. Holtmann, D. Kanne, C. Krüger, R. Blom, R. Gleiter, and I. Hyla-Kryspin. Chem. Ber. **122**, 1629 (1989).
5. A.J. Arduengo, H. Bock, H. Chen, M. Denk, D.A. Dixon, J.C. Green, W.A. Herrmann, N.L. Jones, M. Wagner, and R. West. J. Am. Chem. Soc. **116**, 6641 (1994).
6. R. West and M. Denk. Pure Appl. Chem. **68**, 785 (1996).
7. S.H. Petri, D. Eikenberg, B. Neumann, H.-G. Stammler, and P. Jutzi. Organometallics, **18**, 2615 (1999).
8. (*a*) D.A. Straus, S.D. Grumbine, and T.D. Tilley. J. Am. Chem. Soc. **112**, 7801 (1990); (*b*) S.K. Grumbine, T.D. Tilley, F.P. Arnold, and A.L. Rheingold. J. Am. Chem. Soc. **116**, 5495 (1994), and refs. therein.
9. M. Denk, R.K. Hayashi, and R. West. J. Chem. Soc. Chem. Commun. 33 (1994).
10. B. Gehrhus, P.B. Hitchcock, M.F. Lappert, and H. Maciejewski. Organometallics, **17**, 5599 (1998).
11. (*a*) S.D. Grumbine, T.D. Tilley, F.P. Arnold, and A.L. Rheingold. J. Am. Chem. Soc. **115**, 7884 (1993); (*b*) G.P. Mitchell and T.D. Tilley. Angew. Chem. Int. Ed. Engl. **37**, 2524 (1998).
12. J.D. Feldman, G.P. Mitchell, J.-O. Nolte, and T.D. Tilley. J. Am. Chem. Soc. **120**, 11184 (1998).
13. P. Jutzi and A. Möhrke. Angew. Chem. Int. Ed. Engl. **29**, 893 (1990).
14. W.M. Boesveld, B. Gehrhus, P.B. Hitchcock, M.F. Lappert, and P. von R. Schleyer. Chem. Commun. 755 (1999).
15. J.M. Birmingham and G. Wilkinson. J. Am. Chem. Soc. **78**, 42 (1956).
16. G.M. Sheldrick. SHELXS-86, a package for solution of crystal structures. University of Göttingen. 1985.

© 2000 NRC Canada

17. G.M. Sheldrick. SHELXS-93, a package for crystal structure refinement. University of Göttingen. 1993.
18. S.H. Eggers, J.Kopf, and R.D. Fischer. Acta Crystallogr. Sect. C: Cryst. Struct. Commun. **43C**, 2288 (1987).
19. R.D. Rogers, J.L.Atwood, A. Emad, D.J. Sikora, and M.D. Rausch. J. Organomet. Chem. **216**, 383 (1981).
20. C. Ni, D. Deng, and C. Qian. Inorg. Chim. Acta, **110**, L7 (1985).
21. M. Adam, U. Behrens, and R.D. Fischer. Acta Crystallogr. Sect. C: Cryst. Struct. Commun. **47C**, 968 (1991).

© 2000 NRC Canada

Metal supported catalysts obtained by sol-gel in the hydrosilylation of phenylacetylene with R_3SiH organosilanes (R_3 = Ph_3, Ph_2Me, and $PhMe_2$)

Rafael Jiménez, Juan Manuel López, and Jorge Cervantes

Abstract: The hydrosilylation reaction of phenylacetylene, generated on the surface of solid catalysts (such as Pt and Ru) supported on inorganic matrices such as MgO obtained by the sol-gel process, yields vinylsilanes as the main products. The products' distribution, specific activity, and turnover reactions were determined for the case of the hydrosilylation reaction of PhC≡CH with R_3SiH (R = Ph_3, Ph_2Me, and $PhMe_2$). For Ph_3SiH and Ph_2MeSiH, the presence of β-*trans* and α isomers is observed. Addition of $PhMe_2SiH$ to phenylacetylene leads to the formation of β (*cis* and *trans*) and α isomers. These catalytic systems provide a new synthetic route to Si—C bond formation.

Key words: Vinylsilanes, sol-gel catalysts, hydrosilylation and phenylacetylene.

Résumé : La réaction d'hydrosilylation du phénylacétylène, effectuée à la surface d'un catalyseur solide tel le Pt ou le Ru fixé sur des matrices inorganiques tel le MgO obtenu selon le procédé de sol-gel, donne des vinylsilanes comme produits majoritaires. On a déterminé, la distribution des produits, l'activité spécifique et les réactions d'échange dans le cas de la réaction d'hydrosilylation du PhC≡CH avec R_3SiH (R = Ph_3, PH_2Me, et $PhMe_2$). On a observé la présence d'isomères β-*trans* et α dans le cas du Ph_3SiH, PH_2MeSiH. L'addition du PH_2MeSiH sur le phénylacétylène conduit à la formation d'isomères β(*cis* et *trans*) et α. Ces systèmes catalytiques fournissent une nouvelle voie de synthèse pour la formation de la liaison Si—C.

Mots clés : vinylsilanes, catalyseur sol-gel, hydrosilylation et phénylacétylène.

[Traduit par la Rédaction]

Introduction

Catalysts prepared by the sol-gel method show good catalytic activity for a broad range of chemical reactions. Ni–SiO_2 aerogel catalysts have been used for the hydrogenation of toluene to methylcyclohexene (1). Willey et al. (2) studied the selective catalytic reduction of nitric oxide by ammonia over iron oxide-chromia-alumina aerogels. On the other hand, Armor et al. (3) found that Pd–Al_2O_3 aerogel catalysts were highly active toward hydrogenation for the quantitative and selective production of aniline from nitrobenzene. In it has also been found that aerogel catalysts can be used for the nitration of toluene into nitrobenzene (4); the synthesis of methanol from CO_2–H_2 mixtures (5); and the transformation of isobutylene by NO into methacrylonitrile, acrylonitrile, and acetonitrile (6). They also show a good hydrogenation-dehydrogenation activity (7). The sol-gel method provides an useful method of preparing supported metal systems because several reaction parameters can be adjusted to modify the structure of the samples. Ru–MgO has been used in the benzene hydrogenation reaction (8) and in the hydrogenolysis of cyclopentene (9). A high turnover value and considerably smaller deactivation rate have been observed for Ru–MgO, Ru–SiO_2, Ru–Al_2O_3, or Ru–TiO_2. Alumina-supported platinum, prepared by the sol-gel process by Balakrishan and Gonzalez (10), was active in *n*-hexane hydrogenation.

Received July 12, 1999. Published on the NRC Research Press website on November 2, 2000.

This paper is dedicated to Professor Adrian Brook, an outstanding person and chemist for his contributions to modern organosilicon chemistry.

R. Jiménez, J.M. López, and J. Cervantes.[1] Facultad de Química, University of Guanajuato, Guanajuato, Gto. 36050. Mexico.

[1]Author to whom correspondence may be addressed. Telephone: 52-473-26885. Fax: 52-473-24250. e-mail: address: jauregi@quijote.ugto.mx

Sol-gel catalysts used in the hydrosilylation reaction

The hydrosilylation reaction represents one of the most important routes to obtain organosilicon compounds. The addition of Si—H bonds to unsaturated compounds can be carried out by free radical chain reactions, or more conveniently by the use of catalysts such as platinum or other transition metals (11, 12). One of the most important features in the development of this reaction is the use of heterogeneous catalysts (13–16). For example, Polizzi et al. (14) reported studies of specific activity, selectivity, and turnover reactions of heterogeneous catalytic systems, prepared by treatment of solids supports such as graphite, γ-Al_2O_3, and carbon with mesitylene solvated platinum atoms. They found that Pt–C, Pt–graphite, and Pt–γ-Al_2O_3 systems are able to promote the hydrosilylation of 1- and 2-hexyne. The hydrosilylation of 1-hexyne with $HSiMeCl_2$ took place at room temperature when the Pt–C was used. However, other systems also show good catalytic activity at 70°C.

© 2000 NRC Canada

Fig. 1. Hydrosilylation reaction of phenylacetylene promoted by Pt–MgO, 0.5% Pt wt% with Ph_3SiH, Ph_2MeSiH, and $PhMe_2SiH$.

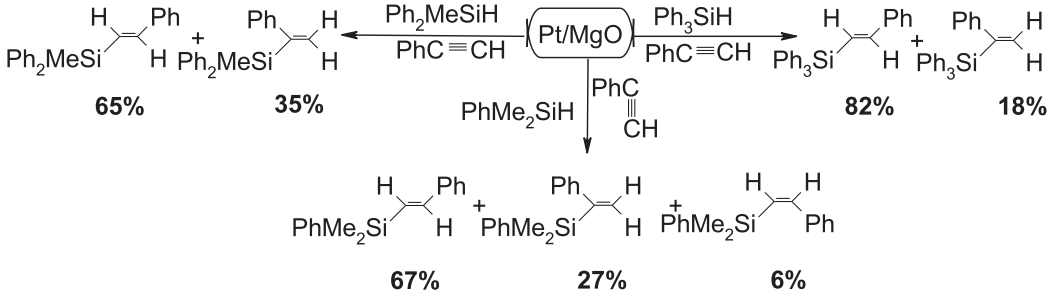
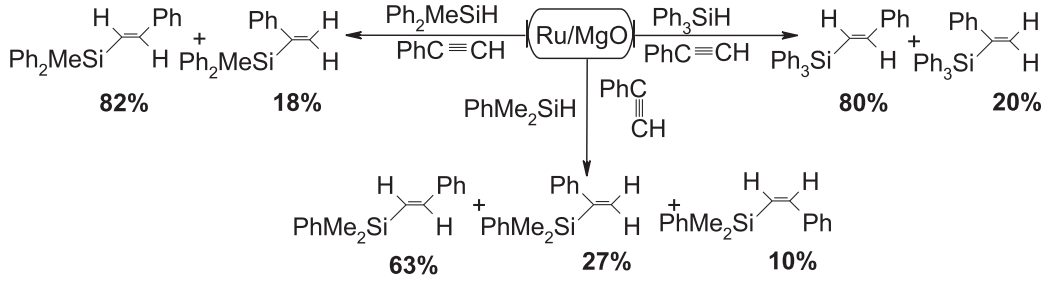


Fig. 2. Hydrosilylation reaction of phenylacetylene promoted by Ru–MgO, 0.5% Ru wt% with Ph_3SiH, Ph_2MeSiH, and $PhMe_2SiH$.



Schubert et al. (17) reported the activity of $Rh(CO)Cl(PR_3)_2$ heterogenised by the sol-gel process in the hydrosilylation of 1-hexene with triphenylsilane.

Considering that there are only a few examples of hydrosilylation reactions catalyzed by heterogeneous systems obtained by sol-gel we have studied this reaction catalyzed by Ru–MgO and Pt–MgO generated by this route. We found that Ru–MgO and Pt–MgO systems are able to promote the selective hydrosilylation of phenylacetylene with Ph_3SiH, Ph_2MSiH, and $PhMe_2SiH$. The reactions and general results are illustrated in Fig. 1 and Fig. 2.

Experimental

The catalysts used (Pt–MgO, 0.5% Pt and Ru–MgO, 0.5% Ru) were prepared by the sol-gel method in the Department of Chemistry at the Universidad Autonoma Metropilitana-Iztapalapa, Mexico. Synthetic methods of these catalytic systems have been described already in the literature (18–22). The BET areas were determined by air adsorption at the temperature of liquid nitrogen. The values reported are 46.3 m^2/g for Pt–MgO and 23.2 m^2/g for Ru–MgO. Catalysts were activated in air at 400, 450, and 540°C during 4 h and then reduced in hydrogen atmosphere for 1 h. The chemicals used were all reagent-grade and available from suppliers such as Aldrich. All the glassware used was treated with a 1 M of KOH in EtOH solution, washed carefully with deionized water and acetone, and dried in an oven at 110°C for several hours. Any contact with other organic materials such as silicon grease was avoided. All reactions were carried out under nitrogen atmosphere.

Liquid hydrosilanes were purified by distillation under nitrogen atmosphere. NMR measurements were performed in $CDCl_3$ solutions using a Varian Gemini 200 MHz spectrometer and a Varian Unity-Plus 300 MHz spectrometer.

General procedure for the preparation of vinylsilanes

In a typical experiment, the previously activated catalyst (25 mg Pt–MgO, 0.5% Pt), were mixed at room temperature with 4.066 mmol of Ph_2MeSiH and 4.473 mmol of phenylacetylene in a 50 mL two-necked flask equipped with a reflux condenser and a thermometer. After the addition was completed, the mixture was stirred and heated at 80–90°C for 2 h. Progress of the reaction was monitored by ^1H NMR spectroscopy and aliquots from the mixture reaction were taken every half and hour. The isomeric ratio of the hydrosilylation products was derived from the areas of olefinic protons. Decrease of the ≡**C-H** bond was comparable with the increase of the vinylic protons signals. The specific activity was calculated as moles of phenylacetylene transformed per g-atom of metal per hour. Products were conveniently purified by distillation or crystallization. For Ph_3SiH with PhC≡CH, the product mixture was washed with CH_2Cl_2–methanol (2:1) solution and crystallized at –5°C to separate the β-*trans* and α-isomer from the solution.

We also studied the turnover reaction for these catalytic systems. The product mixture was separated from the catalyst by decantation and then equal amounts of fresh silane and phenylacetylene were added to the catalyst to start the next hydrosilylation reaction. The decrease in integrals of the ≡**C-H** bond were comparable with the increase of the vinylic protons signals, and then the specific activity was again measured as moles of phenylacetylene transformed per g-atom of metal per hour.

Results and discussion

It is important to discuss the effect of the activation temperature in the observed catalytic activity. In the MgO synthesis by the sol-gel process, hydrolysis is improved by the presence of acid and basic catalysts, leading to $Mg(OH)_2$

© 2000 NRC Canada

Table 1. Reaction conditions and product distribution on the hydrosilylation of phenylacetylene by R_3SiH promoted by Pt–MgO.

R_3SiH	Time (h)	*T* (°C)	Product (%)		
			Trans	*Gem*	*Cis*
Ph_3SiH	2	80–90	82	18	——
Ph_2MeSiH	2	80–90	65	35	——
$PhMe_2SiH$	2	80–90	67	27	6

Table 2. Reaction conditions and product distribution in the hydrosilylation of phenylacetylene by R_3SiH promoted by Ru–MgO.

R_3SiH	Time (h)	*T* (°C)	Product (%)		
			Trans	*Gem*	*Cis*
Ph_3SiH	2	80–90	80	20	——
Ph_2MeSiH	2	80–90	82	18	——
$PhMe_2SiH$	2	80–90	63	27	10

formation that persists after gelation (23–24). López et al. (18) reported, in MgO synthesis by sol-gel process, hydrolysis is improved by the presence of acid an basic catalysts leading to $Mg(OH)_2$ large formation. We found that if the catalysts were activated at 400°C, reaction time was about 25 h, which is caused by $Mg(OH)_2$ brucite phase, affecting specifically the catalytic activity. When the catalysts were activated at 450 or 540°C, the support crystallized completely as MgO periclase phase, and the reaction time was reduced to only 2 h. This particular behavior has not been completely understood. However, some explanation has been suggested: temperature very easily modifies morphology and crystalline structure, and the hydroxyl groups found in the surface of the support are directly related to the catalytic activity.

The reactivity and products distribution ratio of the hydrosilylation reactions of phenylacetylene using the Pt–MgO and Ru–MgO as catalysts are shown in Fig. 1 and 2. Model reactions used were hydrosilylation of phenylacetylene by Ph_3SiH, Ph_2MeSiH, and $PhMe_2SiH$ under nitrogen atmosphere at constant organosilane:catalyst ratio (4.066 mmol/25 mg). In terms of product distribution, we observe that the hydrosilylation reaction with Ph_3SiH and Ph_2MeSiH using Pt–MgO or Ru–MgO as catalysts generates a mixture of *trans* (63–82%) and *gem* (17–34%) vinylsilanes. In the hydrosilylation reaction of Ph_3SiH with PhC≡CH, the mixture formed by catalyst and Ph_3SiH was heated to 50°C to melt the triphenylsilane before the addition of phenylacetylene. After 2 h, the reagents have been consumed and the reaction products mixture was washed with CH_2Cl_2:methanol (2:1) solution and crystallized at –5°C to separate the β-*trans* (mp 149–152°C) and α-isomer (mp 115–119°C) from the solution. The use of $PhMe_2SiH$ in the hydrosilylation of phenylacetylene with both catalysts resulted in a different ratio of isomers, containing: *trans* (63–67%), *gem* (27%), and *cis* (6–10%) isomers. Results obtained in the two catalytic systems are listed in Tables 1 and 2.

To compare results, Table 3 illustrates the product distribution for the same model reactions using the well known catalytic systems of Karsted, Speier, and Wilkinson (25–28).

Reaction products were characterized by ^1H, ^{29}Si, and ^{13}C NMR spectroscopy, and the properties for the entire set of compounds prepared according to Figs. 1 and 2 are the same as those reported previously (14, 29). The isolated *trans* and *gem* isomers obtained in the hydrosilylation of phenylacetylene with Ph_3SiH and Ph_2MeSiH were identified. In the ^1H NMR spectrum two doublets are seen in 5.6–6.1 ppm region, which are typical signals of an AB spin system (J = 2.8 Hz) and correspond to protons in geminal position.

Table 3. Product distribution for hydrosilylation of phenylacetylene with different catalysts and several hydrosilanes.

Catalysts	R_3SiH	*Trans*	*Gem*	*Cis*	Ref.
Karsted's	Ph_3	78	7	15	25–26
H_2PtCl_6	Ph_3	90	10	0	27
	Ph_2Me	78	22	0	27
	$PhMe_2$	69	31	0	27
$(PPh_3)_3RhCl$	Ph_3	67	6	26	28
	Ph_2Me	83	17	0	28
	$PhMe_2$	19	5	76	28

The signals in the downfield region of 6.6–7.0 ppm are assigned to the AX spin system (J = 19.1 Hz) and indicate vicinal protons of the HC=CH fragment in the *trans* position. According to the ^{29}Si NMR spectrum, negative peaks are observed for all silicon atoms linked to a double bond as is shown in Table 4. All these signals agree with information reported in the literature (14, 29–32). On the other hand, the hydrosilylation reaction of the phenylacetylene with $PhMe_2SiH$ using the two catalytic systems produces a mixture of β-*trans*, *cis*, and α-vinylsilanes. The β-*trans* and α-vinylsilanes were easily identified by ^1H, ^{13}C, and ^{29}Si NMR spectroscopy and compared to those reported elsewhere in the literature (14, 29–33). The *cis* isomer was identified by ^{29}Si NMR; we observed a negative chemical shift value for the silicon atom linked to a double bound at –8.2 ppm.

Specific activity is illustrated in the hydrosilylation of phenylacetylene with Ph_2MeSiH. The Ru–MgO catalysts showed a specific activity of 17989 with 45% of conversion in the first half and hour to 18943 with 96% of conversion in the first hour. 98% of conversion was reached after 2 h of reaction. The Pt–MgO specific activity was 47555 with 75% of conversion in the first half and hour but higher conversion (93%) was achieved after 1 h of reaction. The results are shown in Tables 5 and 6. The same study also revealed that hydrosilylation of phenylacetylene catalyzed by Pt–MgO and Ru–MgO is often accompanied by olefin isomerization. During the first half and hour, *trans–gem* isomerization was observed and measured from ^1H NMR areas of olefinic protons calculated for both catalytic systems. The results summarized in Table 7 shows that isomeric ratio depends on the total reaction time. Turnover reactions are illustrated in the hydrosilylation of phenylacetylene with Ph_2MeSiH using Pt–MgO as catalyst. As it can be seen, after three cycles the specific activity remained unchanged. The catalysts do not lose any activity even after several months.

© 2000 NRC Canada

Table 4. ^{1}H, ^{29}Si, and ^{13}C NMR chemical shifts for *trans* and *gem* isomers.

R_3SiH	Compound	$\delta(^{29}Si)$	$\delta(^{1}Ha)$	$\delta(^{1}Hb)$	J(Ha-Hb)	$\delta(^{13}C)$					
						Cα	Cβ	C_6H_5			
								C_1	C_o	C_m	C_p
Ph_3SiH	β-*Trans*	–16.6	7.0	7.0	19.0						
Ph_2MeSiH	β-*Trans*	–13.5	6.8	7.0	19.0						
$PhMe_2SiH$	β-*Trans*	–10.3	6.6	7.0	19.1	134.1	145.5	138.7	127.6	129.2	128.7
Ph_3SiH	*Gem*	–14.3	5.8	6.0	2.7						
Ph_2MeSiH	*Gem*	–10.7	5.6	6.1	2.7						
$PhMe_2SiH$	*Gem*	–8.2	5.7	6.3	2.8	136.0	148.8	136.4	127.9	129.6	128.5

Table 5. Specific activity and isomeric ratio as a function of reaction time of Ru–MgO system in the hydrosilylation of phenylacetylene with Ph_2MeSiH.[a]

Time (h)	Conv. (%)	Specific Activity	Products (%)	
			Trans	*Gem*
1/2	45	17989	47	53
1	96	18943	85	15
1 1/2	97	12824	81	19
2	98	9743	82	18

[a]Specific activity is calculated as moles of phenylacetylene transformed/g-atom of Ru per hour. The isomeric ratio was derived from the ^{1}H NMR integrals of the olefinic protons.

Table 6. Specific activity and isomeric ratio as a function of reaction time of Pt–MgO system in the hydrosilylation of phenylacetylene with Ph_2MeSiH.[a]

Time (h)	Conv. (%)	Specific Activity	Products (%)	
			Trans	*Gem*
1/2	75	47555	65	35
1	93	29542	65	35

[a]Specific activity is calculated as moles of phenylacetylene transformed/g-atom of Pt per hour. The isomeric ratio was derived from the ^{1}H NMR integrals of the olefinic protons.

Table 7. Turnover reactions and specific activity of Pt–MgO from the hydrosilylation of phenylacetylene with Ph_2MeSiH.

Specific Activity[a]	Cycles	Time (h)	Products (%)	
			Trans	*Gem*
29542	1	2	65	35
29542	2	2	65	35
29542	3	2	64	36

[a]Specific activity is calculated as moles of phenylacetylene transformed/g-atom of Pt per hour.

Conclusions

The supported catalysts Pt–MgO and Ru–MgO, synthesized by the sol-gel process, catalyze selective hydrosilylation of phenylacetylene. A good selectivity and specific activity are observed. Reactions can be run without solvent, products can be easily separated, and the catalyst can be recycled.

The use of heterogeneous catalysts prepared by the sol-gel method appears to offer new options that can be widely used for the synthesis of organosilicon compounds.

We are currently performing studies on the reaction mechanism and the isomerization reaction observed during the hydrosilylation. These results will be help us to understand the applications of these catalytic systems in the hydrosilylation reaction. An investigation of the use of other catalytic systems prepared by sol-gel process are underway.

Acknowledgements

We would like to acknowledge CONCyTEG (Consejo Estatal de Ciencia y Tecnología del Estado de Guanajuato) for lending support to this project.

We want to thank Dr. Tessy Lopez and Dr. Ricardo Gómez (UAM-Izpatalapa-Mexico City) for providing the catalysts used in this work.

References

1. D. Klavana, J. Chaoki, D. Kusohorsky, and C. Chavarie. Appl. Catal. **42**, 121 (1988).
2. R.J. Willey, H. Kai, and J.B. Peri. J. Catal. **130**, 319 (1991).
3. J.N. Armor, E.J. Carlson, and P.M. Zambri. Appl. Catal. **19**, 339 (1985).
4. S. Abouarnadasse, G.M. Pajonk, and S.J. Teichner. *In* Proceedings 9th international congress on catalysis. Vol. 4. *Edited by* M.J. Phillips and Ternan. Calgary, Canada. 1988. p. 1936.
5. B. Pommier and S. J. *In* Proceedings 9th international congress on catalysis. Vol. 2. *Edited by* M.J. Phillips and Ternan. Calgary, Canada. 1988. p. 610.
6. H. Zarrouk, A. Ghorbel, G.M. Pajonk, and S.J. Teichner. Proceedings 9th iberoamerican symposium on catalysts. Vol. 1. Lisbon. 1984. p. 338.
7. M. Astier, A. Bertrand, D. Bianch, A. Chenard, G.E. Gardcs, G. Pajonk, M.B. Taghavi, S.J. Teichner, and B.L. Villenin. *In* Preparation of catalysts I. *Edited by* B. Delmon, P.A. Jacobs, and G. Poncelet. Elsevier, Amsterdam. 1976. p. 315.
8. M. Viniega, R. Gómez, and R.D. González. J. Catal. **111**, 429 (1988).
9. P. Villamil, J. Reyes. N. Rosas, and R. Gómez. J. Mol. Catal. **54**, 205 (1989).
10. K. Balakrishnan and R.D. Gonzalez. J. Catal. **144**, 395 (1993).
11. I. Ogima. *In* The chemistry of organic silicon compounds. *Edited by* S. Patai and Z. Rappoport. Wiley, New York. 1989. Part 2, Chap. 25.
12. B. Marciniec, J. Gulinski, W. Urbaniak, and Z. Kornetka. *In* Comprehensive handbook on hydrosilylation. *Edited by* B.

© 2000 NRC Canada

Marciniec. Pergamon Press Inc., Tarrytown, New York. 1992. Chap. 2, p. 84.
13. M.G. Pomerantseva and Z.V. Belyakova. Zh. Obshch. Khim. **54**, 2, 354 (1984).
14. C. Polizzi, A.M. Caporusso, G. Vitulli, P. Salvatori, and M. Pasero. J. Mol. Catal. **91**, 83 (1994).
15. T. Baba, A. Kato, H. Yuasa, and F. Toriyama. Catal. Today, **44**, 271 (1998).
16. G. Schmid, H. West, H. Mehles, and A. Lehnert. Inorg. Chem. **36**, 891 (1997).
17. U. Schubert, C. Egger, and K. Rose. J. Mol. Catal. **55**, 330 (1989).
18. T. López, I. García, and R. Gómez. J. Catal. **127**, 75 (1991).
19. T. López, M. Asomoza, P. Boch, E. García-Figueroa, and R. Gómez. J. Catal. **138**, 463 (1992).
20. K. Balakrishnan and R.D. Gonzalez. J. Catal. **144**, 395 (1993).
21. T. López, R. Gómez, O. Novaro, A. Ramírez-Solis, E. Sánchez-Mora, S. Castillo, E. Poulain, and J.M. Martínez-Magadán. J. Catal. **141**, 114 (1993).
22. P. Moggi, G. Predieri, F. Di Silvestri, and A. Ferreti. Appl. Catal. A, **182**, 257 (1999).
23. J. Livage. Catalysis, **41**, 3 (1998).
24. G. Pacchioni and A. Ferrari. Catal. Today, **50**, 533 (1999).
25. L.N. Lewis, K.G. Sy, G.L. Bryant, Jr., and P.E. Donahue. Organometallics, **10**, 350 (1991).
26. L.N. Lewis. J. Am. Chem. Soc. **112**, 5998 (1990).
27. E. Lukevics, R.Ya. Sturkovich, and O.A. Pudova. J. Organomet. Chem. **292**, 151 (1985).
28. H. Watanabe, T. Kitahara, T. Motegi, and Y. Nagai. J. Organomet. Chem. **139**, 215 (1977).
29. E. Liepens, Y. Golberg, I. Lovel, and E. Lukevicks. J. Organomet. Chem. **335**, 301 (1987).
30. S.P. Chou, H. Kuo, Ch. Wang, Ch. Tsai, and Ch. Sun. J. Org. Chem. **54**, 868 (1989).
31. M.G. Voronkov and V.B. Pukhnarevich. Inorg. Chim. Acta, **68**, 103 (1983).
32. E.A. Williams. *In* The chemistry of organic silicon compounds. *Edited by* S. Patai and Z. Rappoport. Wiley, New York. 1989. Part 1, Chap. 8.
33. M. Grignon-Dubois and M. Laguerre. Organometallics, **7**, 1443 (1988).

© 2000 NRC Canada

On the possible formation of Si=O, Si=S, and Si=Se double bonds via the reaction of silylenes with oxirane, thiirane, and selenirane, respectively. An ab initio theoretical study

Yitzhak Apeloig and Stepan Sklenak

Abstract: The reactions between silylene, H_2Si, and the three-membered ring compounds, oxirane (**9**), thiirane (**10**), and selenirane (**11**), which provide possible routes to Si=X (X = O, S, Se) double bonds were studied by ab initio calculations at the MP2 and QCISD correlated levels of theory employing the polarized 6-31G** basis set. The calculations show that the three reactions are all *highly exothermic*, (–61.8, –45.2, –52.9 kcal/mol at MP2/6-31G**//MP2/6-31G** for X = O, S, Se, respectively). In the gas phase, at 0 K, these reactions are predicted to be also spontaneous (i.e., the calculated transition states are lower in energy than the reactants). At 298 K, entropy contributions result in small barriers on the ΔG surface for X = O, S (7.4 kcal/mol for both reactions at QCISD (full)/6-31G**), but for X = Se the reaction remains spontaneous. Thus, the calculations suggest that these reactions are viable routes for the preparation of compounds with Si=X (X = O, S, Se) double bonds. The first step in all the reactions is the barrier-less formation of an encounter-complex between the silylene and the X atom of the precursor. For X = O, S, these complexes are predicted to be sufficiently stable to be observed in a matrix. The reaction steps which follow depend on X; for X = O fragmentation of the silylene–XC_2H_4 complex proceeds in two steps via a *biradical* intermediate, while for X = S and X = Se the fragmentation occurs in *a single step*. The first ab initio calculations for H_2Si=Se are reported.

Key words: silylene, silanone, silanethione, silaneselone.

Résumé : Faisant appel à des calculs ab initio aux niveaux MP2 et QCISD apparentés de la théorie et utilisant l'ensemble polarisé 6-31G**, on a étudié les réactions entre le silylène, H_2Si, et les composés cycliques à trois chaînons oxirane (**9**), thiirane (**10**) et sélénirane (**11**) qui pourraient servir de voies à la formation de doubles liaisons Si=X (X = O, S, Se). Les calculs montrent que les trois réactions sont toutes *très exothermiques* (–61,8, –45,2 et –52,9 kcal/mol au niveau MP2/6-31G**//MP2/6-31G** pour X = O, S et Se respectivement). En phase gazeuse, à 0 K, il est aussi prédit que ces réactions seront spontanées (c'est-à-dire que l'énergie des états de transitions est plus faible que l'énergie des réactifs). À 298 K, les contributions de l'entropie conduisent à de faibles barrières sur la surface du ΔG pour X = O et S (7,4 kcal/mol pour chacune des réactions au niveau QCISD(plein)/6-31G**)); toutefois, pour X = Se, la réaction reste spontanée. Ainsi les calculs suggèrent que ces réactions sont viables pour la préparation de composés comportant une double liaison Si=X (X = O, S, Se). La première étape de toutes ces réactions est une formation sans barrière d'énergie d'un complexe de rencontre entre le silylène et l'atome X du précurseur. Pour X = O et S, il est prédit que ces complexes sont suffisamment stables pour être observés dans une matrice. Les étapes réactionnelles qui suivent dépendent de la nature de X; pour X = O, la fragmentation du complexe silylène–XC_2H_4 se produit en deux étapes par le biais d'un intermédiaire *biradical* alors que pour X = S et X = Se, la fragmentation se produit en *une seule étape*. On rapporte aussi les premiers calculs ab initio pour le H_2Si=Se.

Mots clés: silylène, silanone, silathione, silanesélone.

[Traduit par la Rédaction]

Introduction

The synthesis of compounds with multiple bonds to silicon is one of the important contemporary challenges in silicon chemistry (1). For many years such compounds were known only as transients and stable compounds with multiple bonds to silicon were isolated only in the last two decades (1). Of the R_2Si=X (X = O, S, Se) family, a stable

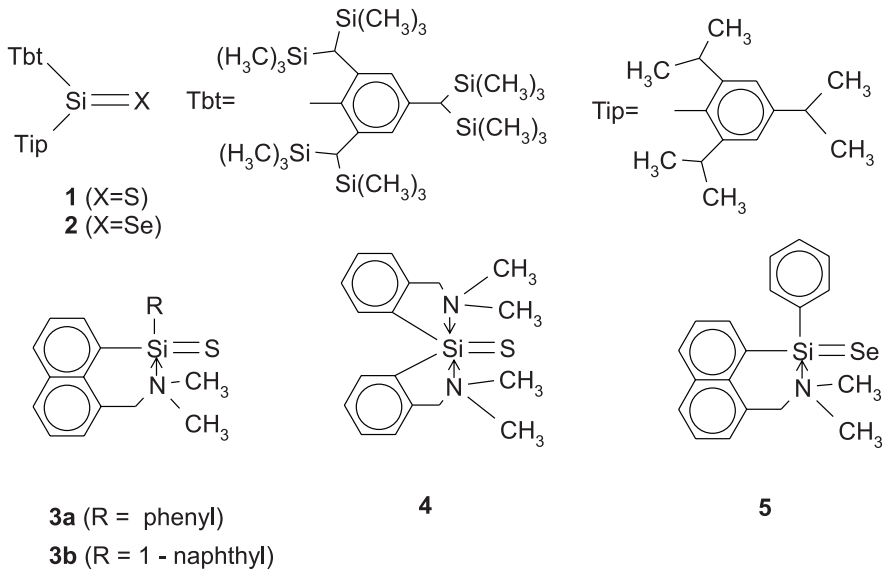
Received April 8, 1999. Published on the NRC Research Press website on November 2, 2000.

Dedicated to Professor Adrian G. Brook, one of the great pioneers of modern organosilicon chemistry.

Y. Apeloig[1] and S. Sklenak. Department of Chemistry and the Lise Meitner - Minerva Center for Computational Quantum Chemistry, Technion-Israel Institute of Technology, Haifa 32000, Israel.

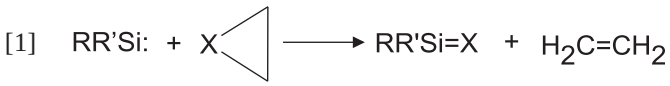
[1]Author to whom correspondence may be addressed. Telephone: + 972-4-829-3721. Fax: + 972-4-823-3735. e-mail: chrapel@techunix.technion.ac.il

 © 2000 NRC Canada



silanethione $R_2Si{=}S$ (**1**) (2) and a stable silaneselone $R_2Si{=}Se$ (**2**), (3) which are kinetically stabilized by the very bulky substituents Dip (2,6-$^i Pr_2C_6H_3$), Tip (2,4,6-$^i Pr_3C_6H_2$), and Tbt (2,4,6–$[(Me_3Si)_2CH]C_6H_2$) were recently isolated by Okazaki and co-workers (2, 3) in two spectacular achievements. All other known silanethiones or silaneselones with a tricoordinated silicon atom are transient species (1, 4, 5). Si=X double bonds can also be stabilized by substituents which can coordinate intramolecularly to the low-coordinated silicon atom. Three such "internally coordinated silanethiones," **3a**, **3b**, and **4**, were recently isolated (6); **3** and **4** have tetracoordinate (6*a*) and pentacoordinate (6*b*) silicon atoms, respectively. An internally coordinated silaneselone (**5**), with a tetracoordinated silicon atom, was also isolated (6*a*). Stable silanones, $R_2Si{=}O$, are not yet known (not even as internally coordinated species as in **3**–**5**), but several transient silanones, including the parent $H_2Si{=}O$ (**6**), (7*a*, *b*) were detected spectroscopically in matrix (7) and in the gas phase (8). The parent silanone $H_2Si{=}O$ (**6**) (1*b*, (for a related theoretical study see ref. 8*c* and 8*e*), 9) and silanethione $H_2Si{=}S$ (**7**) (9*c*, 10) were studied theoretically. In contrast, nothing is currently known, either theoretically or experimentally, on silaneselone $H_2Si{=}Se$ (**8**).

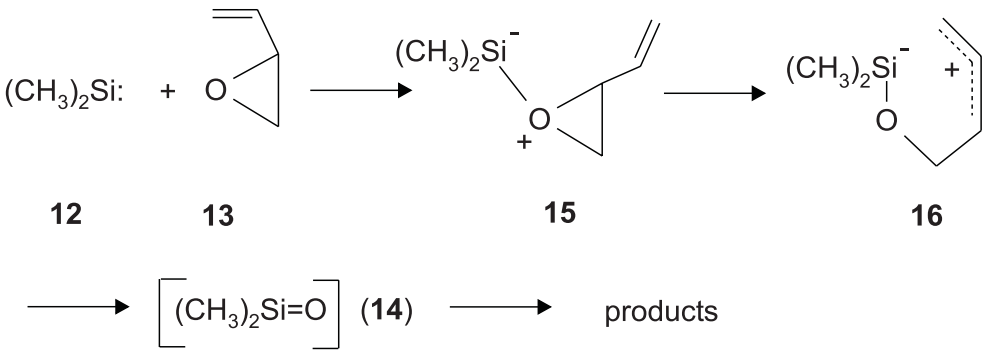
A possible route leading to compounds with a Si=X (X = O, S, Se) double bond is the reaction between a silylene, R_2Si:, and a strained chalcagenide three-membered ring compound, c-C_2H_4X, such as oxirane (X = O, **9**), thiirane (X = S, **10**), or selenirane (X = Se, **11**), as shown in eq. [1].



Several experimental studies of the reaction of silylenes with oxiranes have been reported (11). Tzeng and Weber (11*a*) studied the reaction between dimethylsilylene (**12**) and 2-vinyl oxirane (**13**) and based on the observed products they suggested that dimethylsilanone (**14**) is formed as an intermediate (Scheme 1). The proposed mechanism (Scheme 1) involves the initial formation of a silylene–oxirane ylide intermediate **15**, which opens to an allylic ion-pair (**16**), which dissociates to give $(CH_3)_2Si{=}O$. Although the observed products are consistent with the intermediacy of $(CH_3)_2Si{=}O$, the desired dimethylsilanone (**14**) was not directly observed.

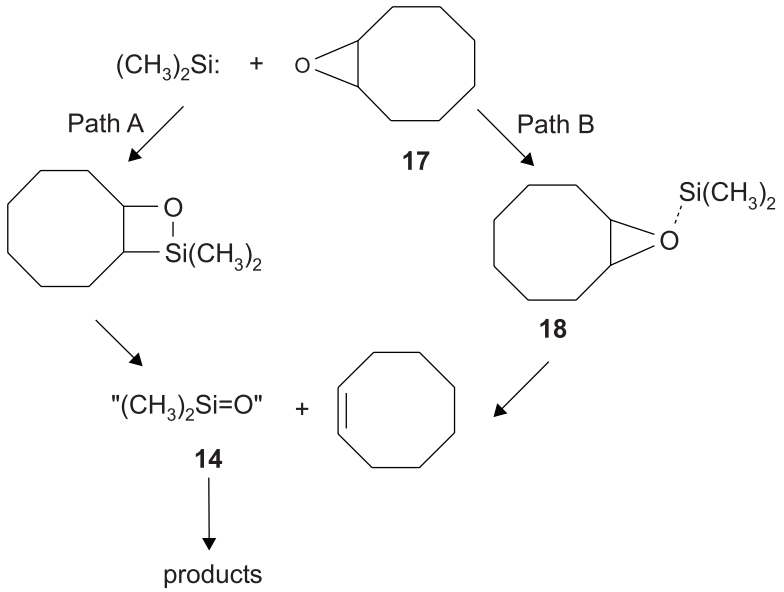
Barton (11*b*) and Goure and Barton (11*c*) studied the reaction of $(CH_3)_2Si$ with cyclooctene oxide (**17**). They concluded (Scheme 2) that the ylide **18** is formed, but they could not establish unequivocally if **18** extrudes $(CH_3)_2Si{=}O$, or whether it acts as a "silanone transfer agent" yielding products which are consistent with the presence of **14**. They also could not differentiate between paths A and B in Scheme 2.

Scheme 1.

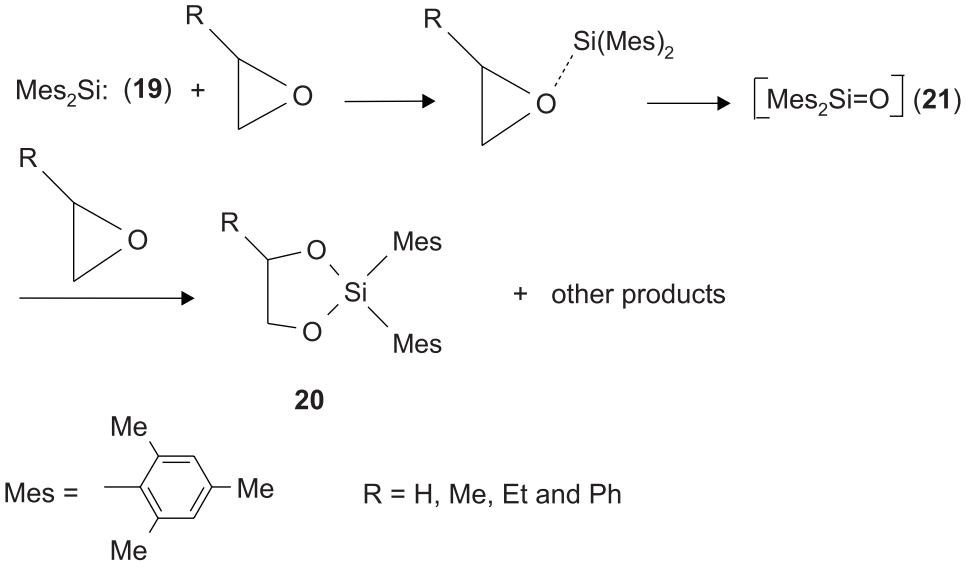


© 2000 NRC Canada

Scheme 2.



Scheme 3.



Ando et al. (11*d*), suggested the intermediacy of dimesitylsilanone ($Mes_2Si=O$, Mes = 2,4,6-$Me_3C_6H_2$) (**21**) in the reaction of Mes_2Si (**19**) with oxiranes and with several 2-substituted oxiranes (Scheme 3).

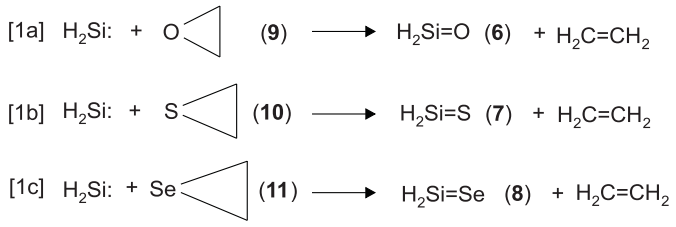
In a recent study, Walsh and co-workers (11*e*) studied the gas phase reactions of $(CH_3)_2Si$ with oxirane and interpreted their results in terms of the transient formation of $(CH_3)_2Si=O$.

Although a variety of thiiranes, are known (12*a*), only one example of rxn. [1], X = S, between a disilyloxy silylene, $(Me_3SiO)_2Si$ (generated in situ on a reactive silica surface) and a thiirane, was reported, and the intermediacy of a silanethione was suggested (12*b*). There are no reports on the reaction of silylenes with seleniranes; which is not surprising, as the number of available seleniranes is limited. Only one stable tetra-substituted selenirane (13*a*, 13*b*) and two relatively unstable tri-substituted seleniranes (13*c*) are known.

To shed further light on the mechanism of the reactions of silylenes with chalcogenide-3-membered ring compounds and to test whether these reactions are potentially useful for generating Si=X double bonds we have studied rxn. [1] by high-level ab initio molecular orbital calculations. We have attempted to answer questions such as: "Is rxn. [1] exothermic, despite the formation of the high energy $H_2Si=X$? Do large energy barriers separate the reactants from the desired products? Are there lower energy channels leading to other products?." Three major model reactions were studied: i.e., the reactions between H_2Si and oxirane (**9**), thiirane (**10**), and selenirane (**11**), potentially leading to $H_2Si=X$, X = O,

© 2000 NRC Canada

S, Se, respectively, (eqs. [1*a*]–[1*c*]), as well as the reactions of the larger Me_2Si and Mes_2Si (Mes = 2,4,6-$Me_3C_6H_2$-) with oxirane. The computational results and our conclusions about the mechanisms of these reactions are reported in this paper.



Computational methods

Ab initio molecular orbital calculations (14) at the correlated Møller–Plesset MP2 (15) and QCISD (16) levels of theory were performed, using the Gaussian 94 series of programs (17). The fully polarized 6-31G** basis set (18) was used throughout and all electrons were included in the calculations (including for Se). Equilibrium geometries and transition structures were fully optimized at both the MP2(full)/6-31G** and the QCISD(full)/6-31G** (except for H_2Si=Se) levels of theory. Vibrational frequencies at the MP2/6-31G** level were computed for all species, to characterize them as minima, transition structures, or higher order saddle points on the potential energy surface (PES) and for evaluating their zero-point vibrational energies (ZPE). IRC calculations (19) were applied to all the MP2/6-31G** calculated transition structures to secure that they indeed connect the reactants with the desired products.

Enthalpies at 0 K (H°_0) were calculated as the sum of the total energies (either at MP2 or at QCISD) and the corresponding ZPEs calculated at MP2/6-31G**. Entropies (S°_{298}), Gibbs free energies (G°_{298}), and ZPEs at 298 K, were calculated using the ideal gas approximation, as implemented in Gaussian 94 (17). S°_{298} and thus G°_{298} could be calculated directly at the MP2 level. At the QCISD level (where the vibration energies were not calculated) G°_{298} was estimated using the S°_{298} values calculated at MP2/6-31G**.

To simplify the presentation the following designations are used throughout the paper: (*i*) S° and G° (without a subscript) denote these values at 298 K (i.e., $S^\circ = S^\circ_{298}$ and $G^\circ = G^\circ_{298}$, respectively), while ΔH° denotes this value at 0 K; (*ii*) MP2 and QCISD denote such calculations with the 6-31G** basis set using the optimized geometries at the same levels, i.e., MP2 and QCISD denote MP2/6-31G**/ /MP2/6-31G** and QCISD/6-31G**//QCISD/6-31G** calculations, respectively.

Results

The calculated total energies, ZPEs, entropies, and Gibbs free energies of all species involved in eqs. [1*a*]–[1*c*] are listed in Table 1. Selected geometrical parameters of the optimized structures of the reactants and products are shown in Fig. 1, those of the intermediates and the transition states are given in Table 2 and the atom numbering used is shown in Scheme 4. The calculated enthalpies and Gibbs free energies of eqs. [2*a*]–[2*c*] are given in Table 3. The supplementary material includes the calculated vibration frequencies of the $H_2S\cdots XC_2H_4$ complexes.

The effect of the level of theory which was used on the calculated reaction energies is small for X = S, but somewhat more significant for X = O, where the MP2/6-31G** calculations overestimate ΔH° of rxn. [1*a*] by 5 kcal/mol (the difference is even higher for the individual reaction steps) relative to QCISD/6-31G**. In general the QCISD/6-31G** values are believed to be the more reliable and therefore QCISD values are generally used in the discussion (unless stated otherwise). The very small difference between the MP2 and QCISD results for eq. [1*b*] (X = S) suggest that this is the case also for eq. [1*c*] (X = Se), where QCISD calculations are beyond our current capabilities.

Discussion

The calculations reported in this paper apply directly to the isolated molecules in the gas-phase and we wish first to point out some of the consequences of this fact. In connection to the bimolecular reactions discussed in this paper, two types of potential energy surfaces (PES), shown in Fig. 2, should be considered: (*i*) an exothermic multistep reaction in which the energy of the reactants is higher than the energy of all the transition states involved (Fig. 2*a*). Such a reaction is spontaneous at 0 K and is expected to occur extremely rapidly. The encounter-complex is produced in a vibrationally excited state having sufficient internal energy to overcome the activation barrier, $\Delta E(1)$, and to proceed to yield the products; (*ii*) an exothermic multistep reaction in which one of the transition states is higher in energy than the energy of the reactants (Fig. 2*b*). In this case the reaction is not spontaneous and the encounter-complex (or other intermediates) will have a significant life time (depending on the height of the $\Delta E(3)$ barrier), because on average the vibrationnally excited molecules do not have the required energy to cross the $\Delta E(3)$ barrier. An additional energy of at least $\Delta E(3)$ has to be supplied to allow the reaction to proceed to the products.

The situation is different in solution (or in high-pressure gas-phase reactions) because the energy gained in the formation of the first encounter-complex (or intermediate) can be rapidly distributed to the environment and the complex can reach its vibrational ground state. So even in case (*i*) (Fig. 2*a*) the encounter-complex will have a significant lifetime and an additional energy of $\Delta E(1)$ has to be supplied to the system to overcome the barrier separating the first encounter-complex from the products. In case (*ii*) (Fig. 2*b*), the energy required in solution to overcome the activation barrier of $\Delta E(2)$ is higher than for the isolated molecules in the gas-phase ($\Delta E(3)$).

The discussion below applies generally to the gas-phase reactions to which the calculations are directly applicable, but in some cases the conclusions are extended to the liquid phase based on the guidelines discussed above.

1. Energetics and mechanism of the reactions of silylene with chalcogenide three-membered rings

Reactions [2*a*]–[2*c*] are calculated to be highly exothermic, both on the enthalpy and on the free energy surfaces (Table 3) i.e., by (ΔG°_{298} values at MP2, kcal/mol): –61.8 for

© 2000 NRC Canada

Table 1. Calculated absolute energies (Hartrees), zero point energies (ZPE, kcal/mol), entropies (cal mol^{-1} K^{-1}), and Gibbs free energies (Hartrees).

Molecule (level)	MP2/6–31G**[a]	QCISD/6–31G**[b]	ZPE[c]	S°_{298}[c]	G°_{298}[c]
Silanone (**6**)	–365.213082	–365.226555	12.06	56.09	–365.216484
Silanethione (**7**)	–687.821243	–687.848974	11.18	58.94	–687.827266
Silaneselone (**8**)	–2687.911768		10.82	61.85	–2687.919636
Oxirane (**9**)	–153.348235[d]	–153.373619	37.16[e]	57.86	–153.312440
Thiirane (**10**)	–475.982236	–476.015201	35.90	60.63	–475.949604
Selenirane (**11**)	–2476.059698		35.06	63.82	–2476.029732
Dimethylsilylene (**12**)	–368.499000		46.32		
Dimethylsilanone (**14**)	–443.626979		49.63		
O-zwitterion (**22**)	–443.479700	–443.524871	48.48	72.37	–443.430556
S-zwitterion (**23**)	–766.113835	–766.165433	46.65	76.84	–766.069175
Se-zwitterion (**24**)	–2766.207981		45.79	79.66	–2766.165775
O-biradial complex (**25**)	–443.480586	–443.510428	47.29	75.10	–443.434037
O-transition state (**26**)	–443.445958	–443.498331	46.62	71.91	–443.399624
O-transition state (**27**)	–443.474872	–443.505329	45.98	74.07	–443.430206
S-transition state (**28**)	–766.086683	–766.138443	45.10	78.72	–766.045223
Se-transition state (**29**)	–2766.194380		44.71	79.32	–2766.153826
Silaoxetane (**30a**)	–443.597940		49.63		
Silathietane (**30b**)	–766.202552		48.15		
Silaselenetane (**30c**)	–2766.292564		47.47		
Silaoxetane TS (**31a**)	–443.528756		47.57		
Silathietane TS (**31b**)	–766.134320		46.57		
Silaselenetane TS (**31c**)	–2766.229162		46.11		
Dimethylsilanethione (**32**)	–766.233346		48.82		
Dimethylsilaneselone (**33**)	–2766.328298		48.65		
Diphenylsilylene (**34**)	–749.137953[f]		121.75[f]		
Diphenylsilanone (**35**)	–824.064648[f]		124.96[f]		
H_2Si	–290.093976	–290.118691	7.76	49.48	–290.101309
$H_2C{=}CH_2$	–78.327231[g]	–78.355922	32.89[h]	52.29	–78.295689

[a]Using MP2/6–31G** optimized geometries.
[b]Using QCISD/6–31G** optimized geometries.
[c]At MP2/6–31G**.
[d]–152.874064 at HF/6–31G**.
[e]38.86 kcal/mol at HF/6–31G**.
[f]At HF/6–31G**.
[g]–78.038841 at HF/6–31G**.
[h] 34.20 kcal/mol at HF/6–31G**.

oxirane (eq. [1*a*]), –45.2 for thiirane (eq. [1*b*]) and –52.9 for selenorane (eq. [1*c*]). The calculated reaction enthalpies, $\Delta H°$, are very similar to the $\Delta G°$ values (Table 3). The energies of eqs. [1*a*]–[1*c*] are significantly lower than those calculated for the analogous reactions of singlet methylene, CH_2, ($\Delta H°$ values at MP2, kcal/mol) with oxirane (–110.0), thiirane (–85.8), and selenorane (–80.0). However, although these reactions are highly exothermic, rxns. [1*a*] and [1*b*] are calculated not to occur spontaneously at 298 K even in the gas-phase because significant barriers (ΔG surface) of 7.4 and 7.3 kcal/mol, respectively, separate the reactants from the products. This result has, of course, important experimental consequences which will be discussed below. Only rxn. [1*c*], for X =Se is predicted to occur spontaneously in the gas-phase.

The first step in all three reactions is the attack of H_2Si on the heteroatom X of the three-membered ring to give the corresponding encounter-complex intermediates: (*i*) **22** (X = O, eq. [2*a*]); (*ii*) **23** (X = S, eq. [2*b*]); and (*iii*) **24** ((X = Se, eq. [2*c*]). This step is exothermic and does not involve an energy barrier and it occurs spontaneously both on the enthapy and on the free energy surfaces. However, due to the contribution of entropy this step is much less exothermic (by ca. 9–10 kcal/mol at 298 K) on the ΔG_{298} surface than on the ΔH_{298} surface. The geometries (Table 2) and the electronic nature of the intermediate silylene–XC_2H_4 complexes **22**–**24** are discussed below.

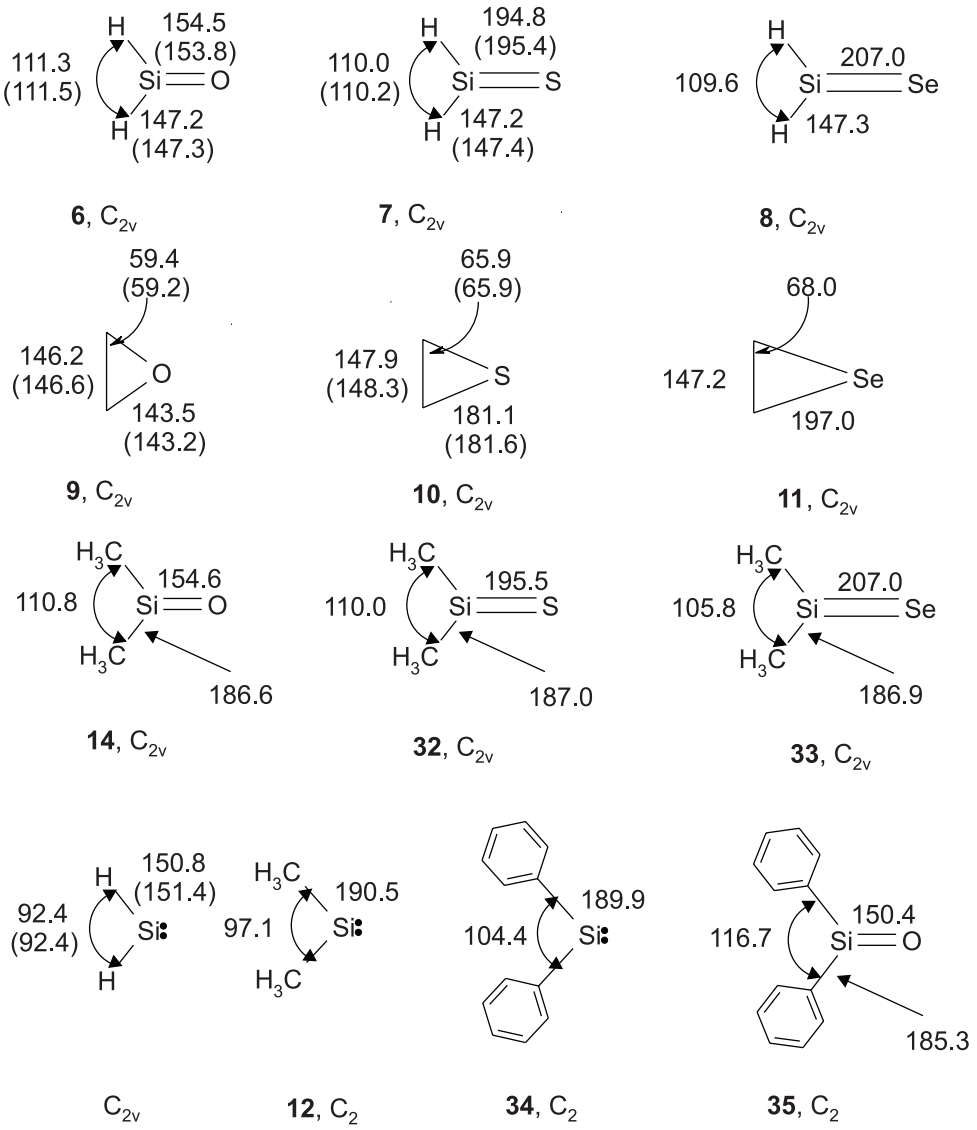
The subsequent reaction steps, leading from the encounter-complex intermediates to the final $H_2Si{=}X + CH_2{=}CH_2$ products, are different for the silylene reaction with oxirane (eq. [2*a*]) and for the reactions with thiirane and selenirane (eq. [2*b*] and eq. [2*c*], respectively), and these reactions are therefore discussed separately.

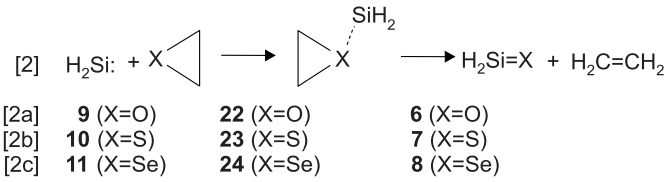
1. (a) The reaction of silylene with oxirane

The calculated enthalpies and Gibbs free energies (at 298 K) for the reaction between H_2Si and oxirane (rxn. [2*a*]) are shown in Figs. 3*a* and 3*b*, respectively. These figures and the

© 2000 NRC Canada

Fig. 1. Selected optimized geometrical parameters at MP2/6–31G** and QCISD/6–31G** (values in parenthesis) of species of interest. Species **34** and **35** are at HF/6-31G**. Bond lengths are given in pm, bond angles in degrees.





discussion below are based on the QCISD/6-31G** values, which are believed to be the more reliable (the MP2/6-31G** values are given in parenthesis). As pointed out above, rxn. [2*a*], although it is very exothermic, $\Delta G°$ = –56.6 kcal/mol (at QCISD/6-31G**) is predicted not to occur spontaneously at 298 K even in the gas-phase, as it involves a significant barrier (i.e., the PES is of type (*b*) in Fig. 2) on the ΔG surface (Fig. 3*b*). On the other hand at 0 K, where the contribution of entropy is zero (Fig. 3*a*), the reaction is spontaneous (i.e., the PES is of type (*a*) in Fig. 2).

In the first step of the reaction, a donor–acceptor complex between H_2Si and oxirane (**22**), which is kinetically stable, is formed. This step is spontaneous and quite exothermic ($\Delta H°$ = –17 – –20, $\Delta G°$ = –7 – –11 kcal/mol), pointing to a stable complex, which should be detectable spectroscopically at low temperatures. Similar complexes between silylenes and ethers or alcohols have been reported and also characterized spectroscopically (20). The calculated vibrational frequencies of the complexes **22**–**24** are reported in the supplementary material to assist in their future spectroscopic identification. The cleavage of the complex **22** to give the $H_2Si{=}O$ and $H_2C{=}CH_2$ products is also exothermic ($\Delta G°$ = –49.3 kcal/mol), however a significant energy barrier of 14.8 kcal/mol ($\Delta H°$) and 14.9 kcal/mol ($\Delta G°$) (at QCISD/6-31G**, 19.3 and 19.4 kcal/mol, respectively, at MP2/6-31G**) separates **22** from the products. The cleavage of **22** occurs in two steps: in the first step, one of the C—O bonds cleaves via transition state (TS) **26** to give the biradical intermediate **25**, which then fragments (via TS **27**) to produce

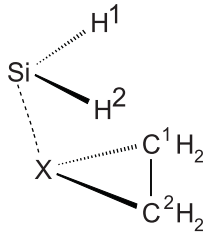
© 2000 NRC Canada

Table 2. Selected optimized geometry parameters at MP2/6–31G** and QCISD/6–31G** (in parenthesis) for intermediates and transition states in rxns. [2*a*]–[2*c*].[a]

Molecule	r(Si-X)	r(X-C_1)	r(X-C_2)	r(C_1-C_2)	<(Si-X-C_1)	<(Si-X-C_2)	<(C_1-Si-C_2)	<(H_1-Si-X-C_1)	<(H_1-Si-X-C_2)	<(H_2-Si-X-C_1)	<(H_2-Si-X-C_2)	<(Si-X-C_2-C_1)
O-zwitterion (**22**) C_1	203.6	146.0	146.1	146.3	116.7	120.3	–105.3	–41.6	27.8	–135.2	–65.8	111.2
	(205.7)	(145.5)	(145.6)	(146.6)	(117.5)	(120.6)	(–106.4)	(–41.2)	(29.1)	(–134.7)	(–64.4)	(111.4)
S-zwitterion (**23**) C_s	236	182.1	182.1	147.2	101.2	101.2	–95.0	108.1	156.8	–156.8	–108.1	95.0
	(239)	(182.8)	(182.8)	(147.6)	(101.9)	(101.9)	(–95.3)	(108.2)	(156.9)	(–156.9)	(–108.2)	(95.3)
Se-zwitterion (**24**) C_s	243.3	198.1	198.1	146.7	98.3	98.3	–93.3	110.9	154.9	–154.9	–110.9	93.3
O-transition state (**26**) C_1	177.3	146.3	188.9	144.5	121.3	130.5	–99.4	–31.3	29.4	–135.9	–75.2	118.6
	(181)	(143.8)	(185.5)	(145.8)	(119.1)	(128.7)	(–98.6)	(–39.1)	(22.0)	(–140.4)	(–79.3)	(117.9)
O-biradical intermediate (**25**) C_1	165.8	146.1	234.3	147.5	126.1	135.5	–93.1	–12.2	36.3	–134.9	–86.4	119.9
	(169.9)	(141.9)	(236.0)	(147.4)	(110.2)	(108.6)	(–99.0)	(–47.3)	(–9.0)	(–162.5)	(–124.2)	(94.1)
O-transition state (**27**) C_1	163.9	167.8	240.4	140.5	126.8	127.3	–103.0	27.5	71.5	–100.7	–56.6	104.4
	(162.8)	(169.6)	(244.4)	(140.3)	(124.1)	(121.7)	(–105.2)	(36.2)	(76.7)	(–92.0)	(–51.4)	(97.5)
S-transition state (**28**) C_s	212	212.9	212.9	139.7	120.8	120.8	–102.0	32.9	77.9	–77.9	–32.9	102.0
	(214.4)	(216.8)	(216.8)	(139.3)	(118.7)	(118.7)	(–100.7)	(33.2)	(76.2)	(–76.1)	(–33.2)	(100.7)
Se-transition state (**29**) C_s	224.5	222.4	222.4	140.3	119.6	119.6	–100.9	32.9	75.4	–75.4	–32.9	100.9

[a]For atom numbering see Scheme 4. Bond lengths are given in pm, angles in degrees.

Scheme 4. Definition of geometrical paramters for species **22**–**29**.



22-29

Table 3. Calculated enthalpies and Gibbs free energies (in parentheses) for various reactions (kcal/mol).

	ΔH°_0 (ΔG°_{298})	
Equation	MP2/6–31G**	QCISD/6–31G**
2*a*	–61.5 (–61.8)	–56.5 (–56.8)
2*b*	–44.9 (–45.2)	–44.2 (–44.4)
2*c*	–52.6 (–52.9)	
3*a*	–68.1	
3*b*	–50.3	
3*c*	–60.6	
4[a]	–58.9	

[a]At HF/6-31G**.

the desired silanone **6** (and ethylene). The biradical intermediate (**25**) lies higher in energy than **22** on both the ΔH and the ΔG surfaces (at QCISD)[2] and as the barrier for its cleavage is only ca. 2 kcal/mol, it is expected to have a very short lifetime.

These computational results are consistent with the only experimental kinetic study of the reaction of dimethylsilylene with oxirane (11*e*). Yet, the high value of the measured rate constant together with the observation of C_2H_4 formation, suggest that the calculated barrier of 14.9 kcal/mol (QCISD) separating **22** from **25** (i.e., TS **26**) is probably too high. This small theoretical–experimental discrepancy may result from real differences in the reactions of H_2Si (used in the calculations) and of $(CH_3)_2Si$ (used experimentally), or from errors in the calculations. B3LYP/6-31G**//B3LYP/6-31G** calculations indeed give a lower barrier of 10.4 kcal/mol for the conversion of **22** to **25** ($\Delta H°$ for the formation of **22** is –16.6 kcal/mol at this level). A more detailed theoretical study of the reaction of $(CH_3)_2Si$ with oxirane, as well as additional experiments are however required to reach a fully consistent theoretical–experimental picture of this reaction.

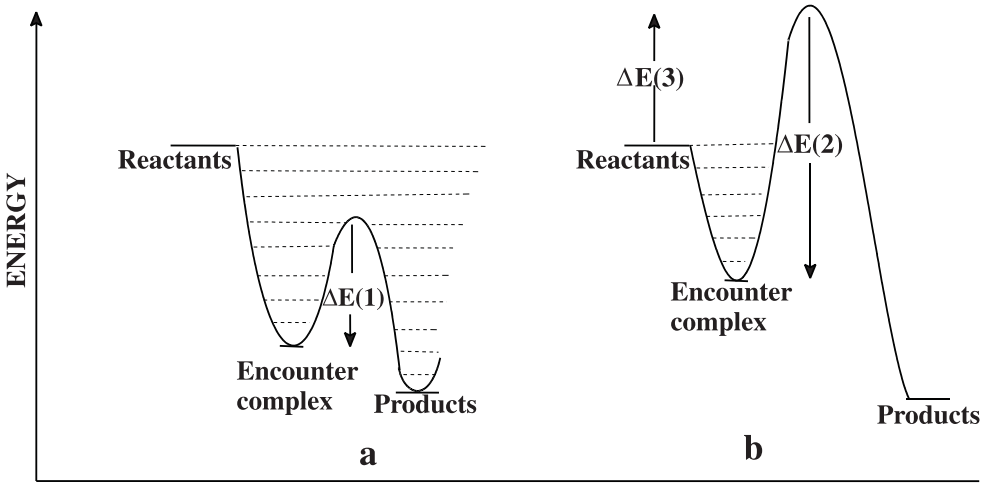
1. (b) The reaction of H_2Si with thiirane and selenirane

In contrast to the multistep fragmentation of the oxirane–silylene complex **22**, the fragmentation of the analagous S- and Se-complexes (**23** and **24**) to produce the desired products (silanethione **7** or silaneselone **8** (and ethylene), respectively) occurs in a single step via transition states **28** and

[2]At MP2/6–31G** **25** is slightly lower in energy than **22** (Table 1), but based on previous experience with biradicals (e.g., ref. 23) we prefer the QCISD/6–3IG** results.

© 2000 NRC Canada

Fig. 2. Schematic potential energy surfaces for an exothermic multi-step bimolecular gas-phase reaction: (*a*) the energy of the reactants is higher than that of the transition state for the conversion of the encounter-complex to products; (*b*) the energy of the reactants is lower than the energy of the transition state for the conversion of the encounter-complex to products.



29, respectively, in which the two C—X bonds are equally elongated.[3]

Reaction [2*b*] and each of its two steps are highly exothermic on both the ΔH and the ΔG surfaces (Fig. 4). Thus, $\Delta H°$ at 0 K for the overall reaction and for the first and second steps are: (QCISD, kcal/mol): –44.2, –16.8, and –27.4, respectively, and $\Delta G°$ = –44.4, –7.6, and –36.8, respectively. However, rxn. [2*b*], similarly to rxn. [2*a*], is spontaneous at 0 K but not at 298 K. The rate-determining step, as in rxn. [2*a*], is the cleavage of the intermediate silylene–thiirane complex **23**. The Gibbs free energy of activation for this step is calculated to be relatively high, ca. 15.0 kcal/mol at both QCISD and MP2 ($\Delta H°$ is very similar, 15.4 kcal/mol).[3] As the complexation energy released in the formation of **23** from the reactants of 7.6 kcal/mol is smaller than the energy required for its fragmentation (14.9 kcal/mol), **23** is predicted to be a long-lived entity even in the gas-phase. This conclusion applies even more strongly to the solution phase, where the energy gained by complexation can be speedily distributed to the environment and therefore it might be possible to observe **23** spectroscopically in matrices (the calculated vibrational frequencies of **23** are given in the supplementary material).

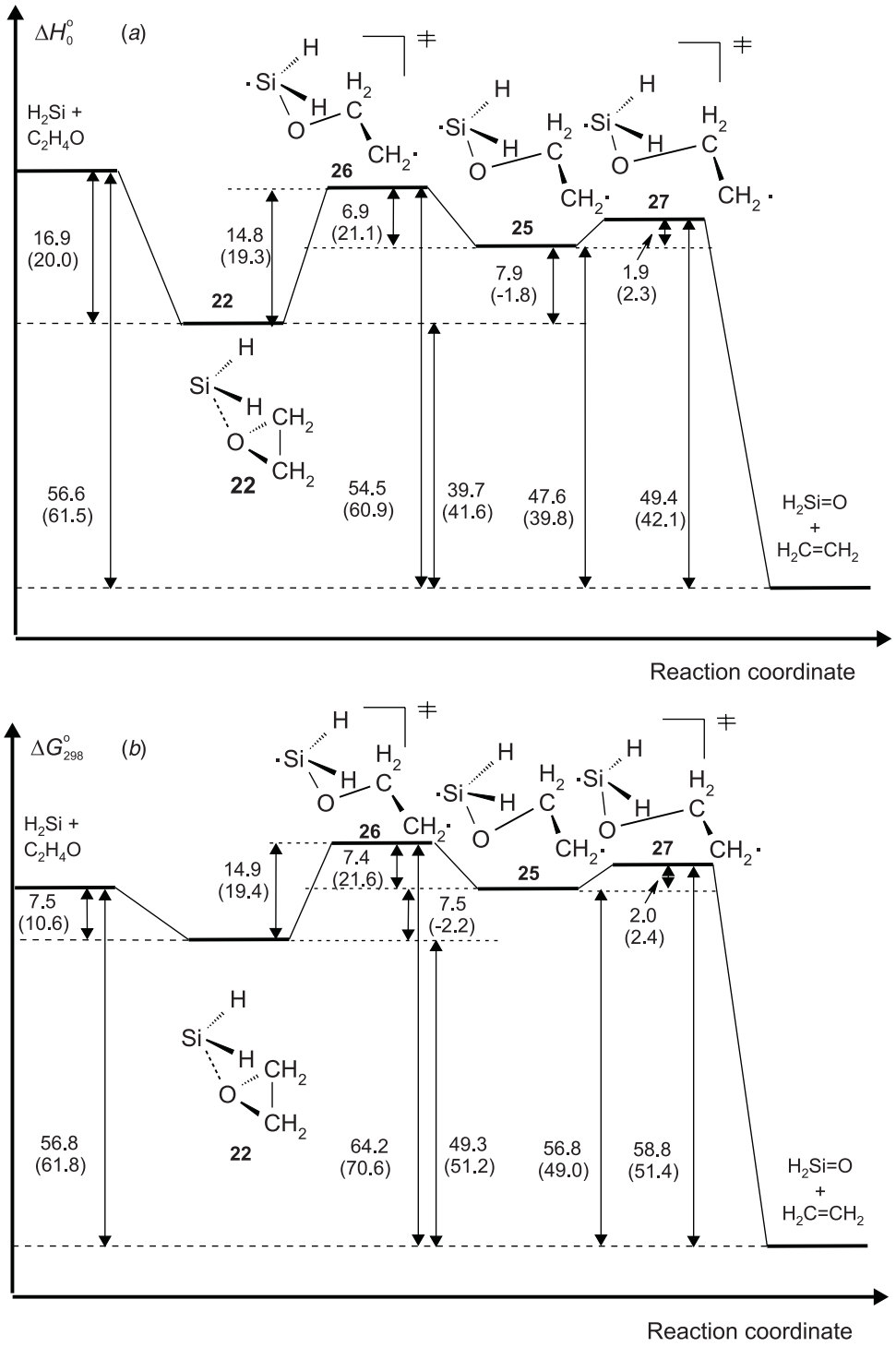
Reaction [2*c*] (Fig. 5) is the only reaction of the three reactions studied here in which no energy barrier exists between reactants and products either on the ΔH or on the ΔG surfaces (i.e., the reaction is of type (*a*) in Fig. 2). Reaction [2*c*] in contrast to rxns. [2*a*] and [2*b*], is therefore predicted to occur spontaneously in the gas-phase, as the barrier for the fragmentation of the silylene–selenirane intermediate **24** ($\Delta G°$ = 7.5 kcal/mol) is significantly lower than the energy released ($\Delta G°$ = –21.8 kcal/mol) upon its formation (Fig. 5). Reaction [2*c*] is predicted to be very facile also in solution as the barrier for the fragmentation of complex **24** is small, only 7.5 kcal/mol.

In summary, the calculations show that rxns. [2*a*]–[2*c*] are highly exothermic, both on the ΔH and ΔG energy surfaces, in the range of –44 – –56 kcal/mol (QCISD/6-31G**) depending on the heteroatom X of the reactant three-membered ring. All reactions proceed via intermediate $H_2Si\cdots XC_2H_4$ donor–acceptor complexes which are formed spontaneously. These complexes are quite stable kinetically (less so for

[3] It is noteworthy that the synchronous single-step fragmentation of the $H_2Si\cdots XC_2H_4$ encounter-complexes, **22–24**, to the corresponding $H_2Si{=}X$ and ethylene is formally a "symmetry-allowed" reaction in a "linear-type" process (see ref. 24). Thus, assuming a linear-type process with C_s-symmetry the relevant occupied orbitals of the reactant (**22**) are: (*i*) the two σ(C—X) bonds — one symmetric (S) and one *anti*-symmetric (A); (*ii*) the Si···X bond (S); (*iii*) and the silylene lone-pair (S). These orbitals correlate with those of the ground state orbitals of the products, $H_2C{=}CH_2 + CH_2{=}X$, i.e., σ(C—X) (S), π(C=X) (S), π(C=C) (S), and the lone-pair on O (A). A close analogy to rxns. [2*a*]–[2*c*] is the abstraction of NR from *N*-alkylaziridines by dichlorocarbenes producing olefins in which the relative configuration of the substituents is retained, indicating a synchronous symmetry-allowed process (see for example ref. 25). However, a closer examination of the reaction reveals that the fragmentation step has, to some extent a "symmetry-forbidden" contribution due to the very high polarity of the $H_2Si{=}X$ molecules which are better described as $H_2Si^+—X^-$ (the calculated charges on X are: –0.96, –0.55, –0.46 for X = O, S, Se, respectively). To better understand this point it is more convenient to analyze the fragmentation reaction in the reverse direction, i.e., as an addition reaction of $H_2Si^+—X^-$ to $CH_2{=}CH_2$. Such a reaction is a symmetry-forbidden $\pi 2s + \omega 2s$ reaction. In agreement with this analysis, the fragmentation reactions of **22**–**24**, although highly exothermic, have significant activation barriers and for X = O, the preferred reaction path is indeed nonconcerted, i.e., it proceeds via a two-step mechanism, as expected for a symmetry–forbidden reaction (a C_s species having two imaginary frequencies and closely corresponding to TS **28** for X = S and to TS **29** for X = Se, is 5.9 kcal/mol higher in energy than the biradicaloid TS **26**) The contribution of the polarity to the degree of symmetry-forbiddeness of the fragmentation reactions is smaller for X = S and Se than for X = O, due to the lower polarity of $H_2Si{=}S$ and $H_2Si{=}Se$ relative to $H_2Si{=}O$, and with these chalcogonites fragmentation occurs in a single step. Another factor contributing to the significant barriers of the fragmentation step is the high degree of electron reorganization required along the fragmentation process (see for example ref. 26).

© 2000 NRC Canada

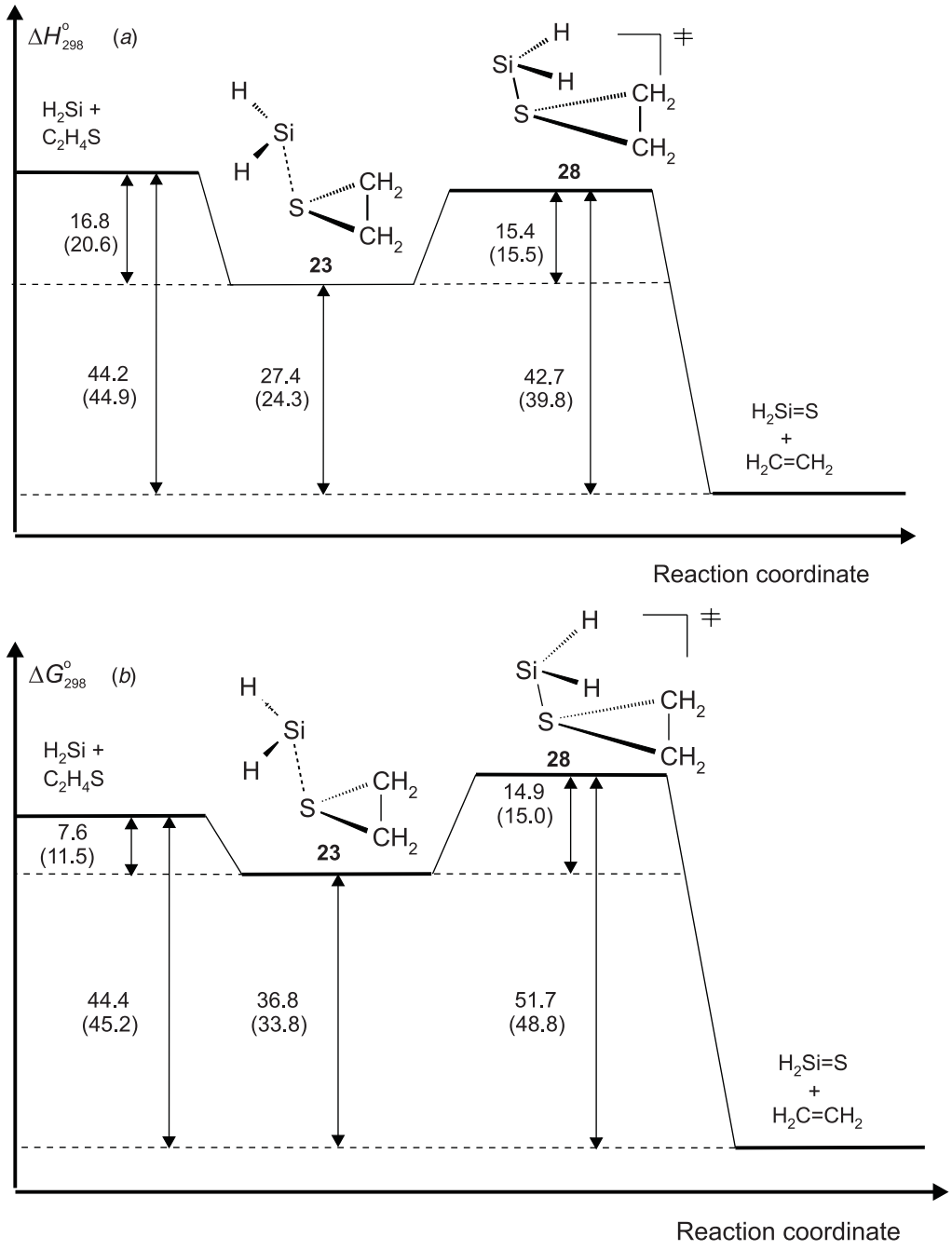
Fig. 3. Calculated reaction scheme for eq. [2*a*] at QCISD/6–31G** and at MP2/6–31G** (values in parenthesis). The figure is drawn according to the QCISD/6–31G** values and the relative energies are given in kcal/mol. (*a*) Reaction enthalpies. (*b*) Gibbs free energies at 298 K.



X = Se) and according to the calculations should be detectable in low-temperature matrices. The cleavage of these complexes is also highly exothermic and in the gas-phase at 0 K it is also spontaneous (i.e., represented by a PES of type (*a*) in Fig. 2). However, at 298 K, even in the gas-phase, the cleavage of the donor–acceptor complex is spontaneous only for X = Se. For X = O and X = S, a significant barrier (ΔG = 7.4 kcal/mol for both reactions) exists and the energy gained in the complexation step is not sufficient to overcome the barrier separating the complex from the products. In solution, where the silylene–XC_2H_4 complexes may have the possibility to relax, the barriers which have to be overcome are larger and become quite significant, i.e., 14.9 kcal/mol for both reactions (at QCISD).

© 2000 NRC Canada

Fig. 4. Calculated reaction scheme for eq. [2*b*] at QCISD /6–31G** and at MP2/6–31G** (values in parenthesis). The figure is drawn according to the QCISD/6–31G** values and the relative energies are given in kcal/mol. (*a*) Reaction enthalpies. (*b*) Gibbs free energies at 298 K.

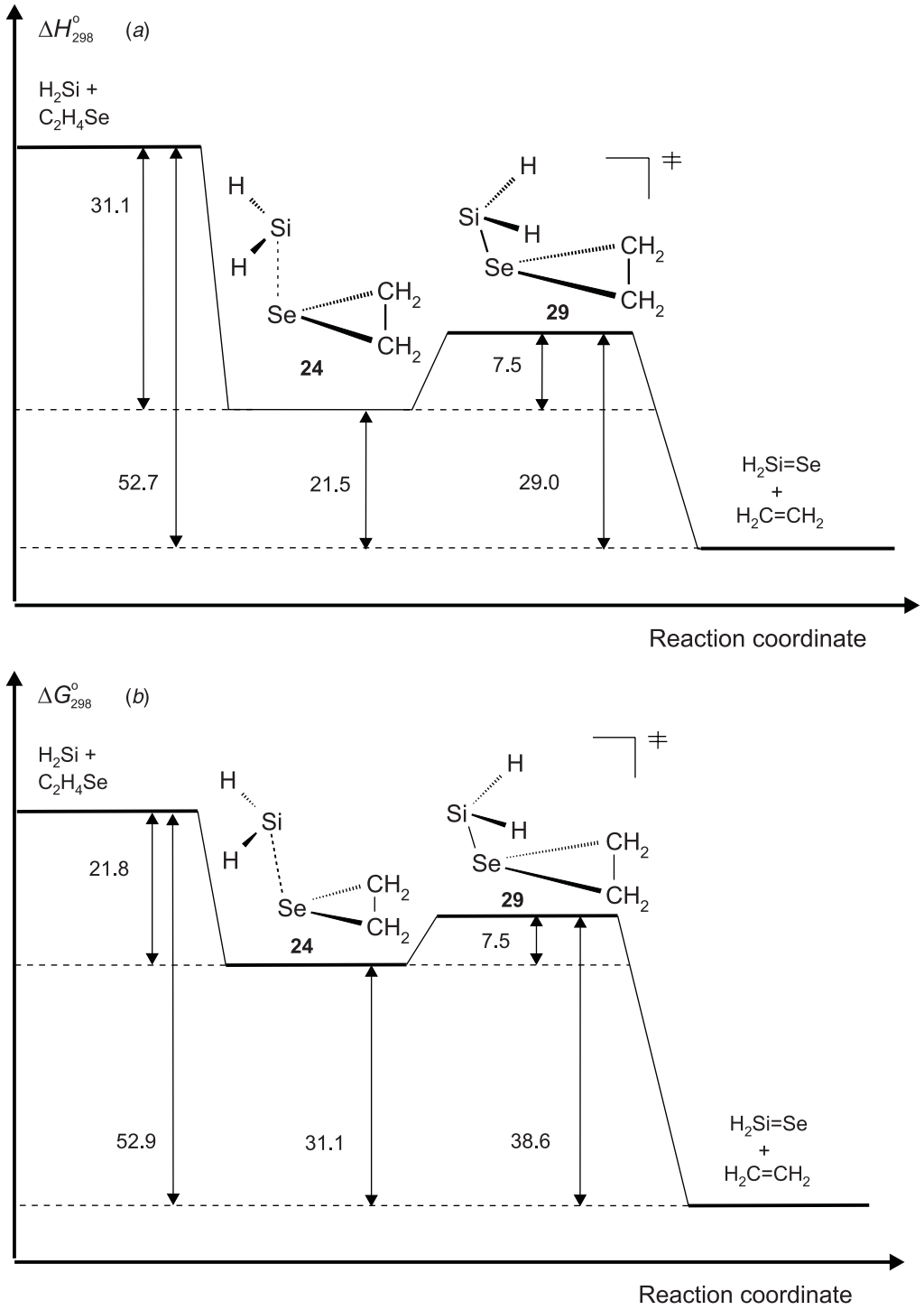


1. (c) The silatane route

Barton (11*b*) and Barton and Goure (11*c*), who studied experimentally the reaction of dimethylsilylene with cyclohexane oxide, pointed out that an alternative mechanism to that shown in Fig. 3, i.e., via the corresponding silaoxetanes (see path A in Scheme 2), could not be excluded. To evaluate the viability of this mechanistic possibility, we have calculated the "silatane route" for the reaction of H_2Si with **9**–**11**, shown in Scheme 5. Our results reveal that the rearrangement of **22** to **30***a* is very sluggish since the calculated barrier $E_a(1)$ is 32.0 kcal/mol. Unfortunately, we could not locate the corresponding transition states connecting the silylene complexes **23**–**24** with the corresponding silatanes **30b**–**30c**, and thus could not compare directly these barriers ($E_a(1)$) with the corresonding barriers for fragmentation of the complexes **23**–**24** to the corresponding $H_2Si{=}X + C_2H_4$, $E_a(4)$ in Scheme 5 ($E_a(4)$ are the barriers to the fragmentation of **22**–**24** given in Figs. 3*a*–3*c*, respectively). However, even without this direct comparison the calculations (at the MP2/6-31G**//MP2/6-31G** level), show clearly (Table 4)

© 2000 NRC Canada

Fig. 5. Calculated reaction scheme (kcal/mol) for eq. [2*c*] at MP2/6–31G**. The relative energies are given in kcal/mol. (*a*) Reaction enthalpies. (*b*) Gibbs free energies at 298 K.



that in solution the silatane route is not a likely mechanism for the production of $H_2Si{=}X$. Thus, the silatanes **30a**–**30c,** even if formed in the reaction, are significantly more stable than the final products of rxn. [2] (i.e., by 31.5, 29.8, 29.9 kcal/mol for X = O, S, and Se, respectively (see $\Delta H(2)$ values in Table 4). Furthermore, the cleavage of the silatanes involves additional activation barriers ($E_a(-2)$ values in Table 4) of 9.9, 11.4, and 8.6 kcal/mol for X = O, S, Se, respectively, so that the overall activation barriers, $E_a(2)$, for the cleavage of the silatanes **30a**–**30c** to the corresponding $H_2Si{=}X$ are 41.4, 41.2, and 38.4 kcal/mol, respectively, (Table 4). Thus, if the silatanes were indeed formed as intermediates in the reactions of silylenes with chalcogenide three-membered rings, they would not be expected to extrude $H_2Si{=}X$ under the reaction conditions used in the literature experiments and therefore they should have been

© 2000 NRC Canada

detected experimentally. At the moment experiments are available only for X = O and in agreement with the above theoretical analysis, silaoxetanes were not detected in solution experiments (11*a*–11*c*, 21)[4]. Also, in gas-phase reactions the silatanes are not expected according to the calculations to be observed experimentally, as the energy released in their production $\Delta H(1)$, far exceeds the energy, $E_a(2)$, required for their fragmentation. This is in agreement with the available gas-phase experiments (11*e*, 21)[4].

Attempts to locate a reaction path connecting directly the reactants with the corresponding silatanes, i.e., a direct insertion of the silylene into the strained C—X bond of the XC_2H_4 molecule (a reaction which is exothermic ($\Delta H(3)$ in Scheme 5) by –97.7, –79.3, and –87.1 kcal/mol (MP2/6–31G**) for X = O, S, and Se, respectively) have failed, but we believe that these pathways are higher in energy than via the silylene–XC_2H_4 complexes.

Our computational results combined with the fact that silaoxetanes were not observed experimentally in these reactions (11) strongly support the conclusion that silaoxetanes are not involved as intermediates in the reactions of silylenes with chalcogenide three-membered rings. The calculations also show that silatanes are not good precursors for the production of Si=X multiple bonds (e.g., via pyrolysis), because the activation barriers for their fragmentation, $E_a(2)$, are high, ca. 38–41 kcal/mol, requiring relatively high reaction temperatures.

2. Reactions of dimethylsilylene and diphenylsilylene with chalcogenide three-membered rings

Do the calculations for the parent H_2Si discussed above apply also to silylenes, which experimentally are used more widely than H_2Si, such as dimethylsilylene and diphenylsilylene? To answer this question we have calculated the reaction enthalpies of rxn. [3] (at MP2/6–31G**//MP2/6–31G**) and of rxn. [4] (at HF/6–31G**//HF/6–31G**). The calculated reaction energies (Table 3) are quite similar to those obtained for the parent rxns. [2*a*]–[2*c*] and although a full scan of the PES was not carried out, this result suggests that alkyl- and aryl-substituted silylenes can also serve as precursors for producing the desired $R_2Si{=}X$ compounds. Of particular interest is the computational prediction that even with the relatively stable Ph_2Si the reaction with oxirane to give $Ph_2Si{=}O$ is still highly exothermic, i.e., by –58.9 kcal/mol. This suggests that it might be possible to use even sterically protected silylenes, such as Mes_2Si and even Tbt_2Si, to produce sterically stabilized silanones, e.g., $Mes_2Si{=}O$ and $Tbt_2Si{=}O$. We encourage experimentalists to test this suggestion.

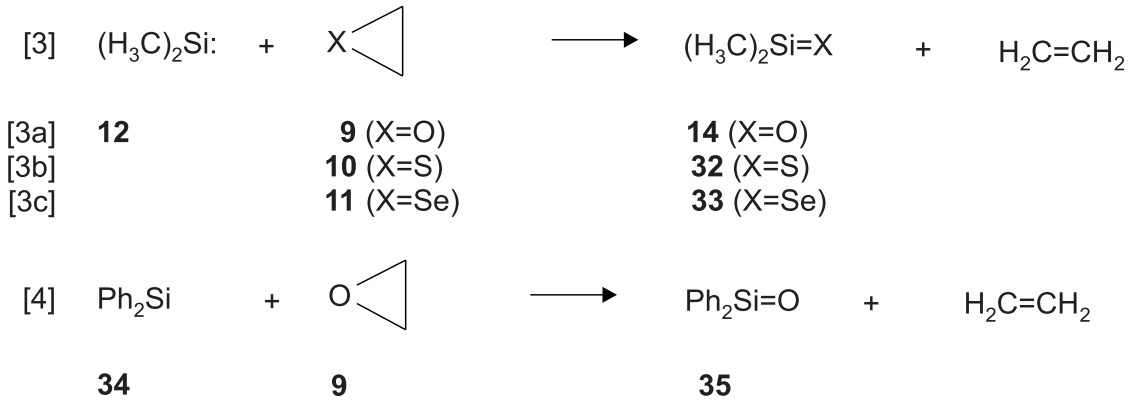
Table 4. Calculated enthalpies and activation energies (kcal/mol) at MP2/6–31G**//MP2/6–31G** for the silatane route (Scheme 5).

X	$\Delta H(1)$	$\Delta H(2)$	$E_a(2)$	$E_a(-2)$
O	–73.1	31.5	41.4	9.9
S	–54.2	29.8	41.2	11.4
Se	–51.4	29.9	38.5	8.6

Equilibrium geometries

The differences between the QCISD and the MP2 calculated geometries are relatively small (see Fig. 1 and Table 2), and the discussion below is based on the QCISD geometries (except for X = Se, where only MP2 values are available) which are believed to be more reliable.

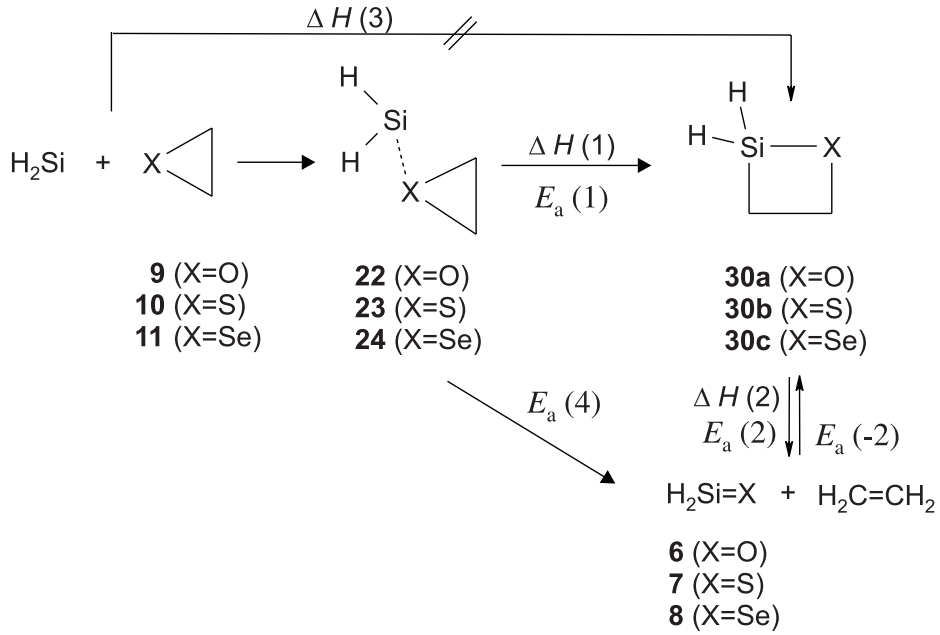
The doubly bonded compounds: silanone (**6**), silanethione (**7**), and silaneselone (**8**) are all planar, i.e., have C_{2v} symmetry. The calculated Si=X bond lengths (pm) of: 153.8 (X = O), 195.4 (X = S), and 207.0 (X = Se) are all significantly shorter (by ca. 8–9%) than the corresponding Si—X single



[4] For X = O, the silaoxetane **30a** can be formed from the silylene–oxirane complex **22** via ring-closure of the biradical **25**. This ring-closure requires rotation around the Si—O and C—C bonds in **25**. The fact that a silaoxetane was not observed experimentally (11*a*–11*c*, 11*e* indicates that the fragmentation of **25** to $H_2Si{=}O$ and $H_2C{=}CH_2$ is faster than its ring closure to **30a**. This is reasonable, as the activation barrier for the fragmentation of **25** is only ca. 2 kcal/mol and it essentially involves only elongation of the C—O bond, while ring-closure to **30a** requires rotation around two bonds, reducing the dynamic probability of this process (for a discussion of the rates of rotation around C—C bonds in biradicals, see for example ref. 21). The actual substituents used in the experiments, which are significantly larger than H used in the calculations, may further slow down the ring-closure relative to fragmentation. The fact that silaoxetanes were not observed experimentally implies that the free energy of activation for the ring-closure of **25** is by at least 3 kcal/mol higher in energy than that for its fragmentation. For X = S and Se we could not locate the transition state which separates the S–silylene and Se–silylene complexes (**23** and **24**, respectively) from the corresponding silatanes, **30b** and **30c**. We assume that also in these cases these barriers are higher than the corresponding fragmentation barriers to the products (15.4 and 7.5 kcal/mol, respectively), but this point will have to be rechecked when such experiments will become available.

© 2000 NRC Canada

Scheme 5. The silatane route.



bond distances, (166.7, 214.3, 226.6 pm, respectively in H_3SiXH), indicating the multiple bonding nature of the Si=X bond in these molecules. The calculated (H-Si-H) bond angles are: 111.5° (X = O), 110.2° (X = S), and 109.6° (X = Se) and the Si—H bond lengths in all species are 147.3 pm. The calculated QCISD geometry of silanone **6** agrees well with the recently measured experimental values (8*b*) (r(Si=O) = 151.5 pm, r(Si—H) = 147.2 pm, < (H-Si-H) = 112.0°) as well as with the best available calculated geometry at CCSD/TZ2P(f,d)//CCSD/TZ2P(f,d) (8*c*). Substitution of the hydrogens in $H_2Si=X$ by two methyl groups has a minor effect on the geometry of the Si=X.

The calculated charges and geometries of the silylene–XC_2H_4 complexes (Table 2) are consistent with the description of these species as involving a modest donor–acceptor interaction between one of the lone pairs of X (donor) and the vacant 3*p*(Si) orbital (acceptor).[5] Thus, in the encounter complexes **22**–**24**, the calculated total charge transferred from C_2H_4X to the SiH_2 unit (using the Natural Population Analysis at MP2(full)/6–31G**) is: 0.15 el. in **22**, 0.31 el. in **23**, and 0.34 el. in **24**. Consistent with the modest charge transfer is the fact that the Si···X distances in the complexes **22**–**24** are quite long, r(Si—X) = 205.7 (X = O), 239.0 (X = S), and 243.3 (X = Se) pm, in comparison with the corresponding Si—X single bonds in H_3SiXH: 166.7 (X = O), 214.3 (X = S), and 226.6 (X = Se) pm. Similarly, the C—X bond lengths in the complexes are only slightly elongated (by 1–2 ppm) compared to those calculated for the corresponding three-membered ring precursors. The silylene is tilted above the three-membered ring; the Si-X-Y bond angle (where Y is the center of the C—C bond) is 124° for **22,** and ca. 102° for **23** and **24**. Rotation of the silylene around the Si···X axis is facile (barriers of 0.6–2 kcal/mol), with **22** preferring the "inside" conformation (i.e., where the ∠HSiXC dihedral angle is ca. 0°), while **23** and **24** are more stable in the "outside" conformation (e.g., ∠HSiXC is ca. 180°). Although, the geometrical parameters of **22**–**24** indicates a relatively weak complexation, the calculated complexation energies show that these complexes are bound quite strongly; i.e., by 20.0, 20.6, and 31.1 kcal/mol for X = O, S, Se, respectively, (at MP2). This apparent dichotomy between the geometries and the complexation energies reflects the high energies of the Si—X bonds (22).

The transition states for the concerted fragmentation of the silylene–XC_2H_4, X = S, Se intermediates (**28** and **29**, respectively) are structurally similar to those of the corresponding silylene–XC_2H_4 complexes (**23** and **24**, respectively), but they have much shorter Si···X distances (r(Si—X) = 214.4 and 224.5 pm), much longer C—X bonds (r(C—X) = 216.8 and 222.4 pm), significantly shorter C—C bonds (ca. 140 pm) and significantly wider Si-X-C bond angles (ca. 120°), compared to those parameters in the corresponding complexes. Actually, the r(Si—X) distances in **28** and **29** are very close to those of the corresponding Si—X single bonds (214.3 and 226.6 pm for X = S and Se, respectively) and these transition states can be described as occurring relatively "late" along the fragmentation reaction coordinate.

In the silylene–oxirane reaction the intermediate complex **22** undergoes cleavage in two steps: (*i*) first only one of the C—O bonds breaks (via TS **26**) to give the biradical complex **25**; (*ii*) followed by cleavage of the second C—O bond (TS **27**) to give $H_2Si=O$ and ethylene. Along the progression: **22** → **26** → **25** → **27** → **6**, the Si—O bond length is gradually shortened (205.7, 181.0, 169.9, 162.8, and 153.8 pm respectively) and the C—O bond length is gradually elongated (143.2 (**9**), 145.6 (**22**), 185.5 (**26**), 236.0 (**25**), and 244.4 (**27**), pm). The largest differences between the QCISD and MP2 geometries are found for the *biradical* **25** (Table 2).

[5] Silylene–XR_2 complexes are often referred to in the literature as "zwiterionic." According to the calculations this description is not justified and we prefer to refer to them as donor–acceptor complexes.

© 2000 NRC Canada

Conclusions

High level ab initio calculations for the reactions between silylene and oxirane (**9**), thiirane (**10**), and selenirane (**11**) which are possible routes to Si=X double bonds (X = O, S, Se, eqs. [2*a*]–[2*c*]), show that these reactions are highly exothermic ($\Delta H°$ = –61.5, –44.9, and –52.7 kcal/mol for X = O, S, Se, respectively at MP2/6–31G**) and in the gas-phase at 0 K they are also spontaneous. The first step of these reactions involves the barrierless formation of a donor–acceptor complex between the silylene and the X atom of the precursor, C_2H_4X. The reaction steps which follow depend on X. For X = O, fragmentation of the silylene–C_2H_4X complex **22** proceeds in two steps via a biradical intermediate. In contrast, fragmentation of the S (**23**) and the Se (**24**) complexes occurs in a single step. At 298 K in the gas-phase, the contributions of entropy lead for X = O and S, to a small energy barrier (ΔG) of 7.4 kcal/mol on the path between the silylene–XC_2H_4 complex and the products, but for X = Se the reaction is spontaneous also at 298 K. In solution, a barrier of 7.5 kcal/mol separates the silylene complexes from the products also for X = Se and this barrier is somewhat higher (14.9 kcal/mol) for X = O, and S. However, these barriers can be easily surmounted, making these reactions synthetically attractive.

In conclusion, the computational results suggest that the reaction of silylenes with chalcogenide three-membered ring compounds (eq. [1]) is indeed a viable route for the preparation of compounds with a Si=X double-bond (X = O, S, Se), both in the gas-phase and in solution. We call for an experimental testing of this prediction.

Acknowledgements

This work was supported by the U.S. – Israel Binational Science Foundation (BSF), the German Federal Ministry for Science, Research, Technology, and Education (BMBF) and the Minerva Foundation in Munich, and the Technion Fund for the Promotion of Research. S.S. is grateful to the Israel Ministry for Higher Education for a postdoctoral scholarship. We are also grateful to the supercomputer centers in Israel (Machba) and in the Czech Republic (in Prague and Brno) for a generous donation of computer time.

Supplementary material

Tables of calculated vibrational frequencies for the silylene–XC_2H_4 complexes **22**, **23**, and **24**. A copy of the supplementary material may be purchased from the Depository of Unpublished Data, Document Delivery, CISTI, National Research Council Canada, Ottawa, ON K1A 0S2 (http://www.nrc.ca/cisti/irm/unpub_e.shtml for information on ordering electronically).

References

1. (*a*) G. Raabe and J. Michl. *In* The chemistry of organic silicon compounds. *Edited by* S. Patai and Z. Rappoport. Wiley, Chichester, U.K. 1989. Chap. 17; (*b*) Y. Apeloig. *In* The chemistry of organic silicon compounds. *Edited by* S. Patai and Z. Rappoport. Wiley, Chichester, U.K. 1989. Chap. 2; (*c*) N. Tokitoh and R. Okazaki. *In* The chemistry of organic silicon compounds. Vol. 2. *Edited by* Z. Rappoport and Y. Apeloig. Wiley, Chichester, U.K. 1998. Chap. 17.
2. (*a*) H. Suzuki, N. Tokitoh, S. Nagase, and R. Okazaki. J. Am. Chem. Soc. **116**, 11578 (1994); (*b*) H. Suzuki, N. Tokitoh, R. Okazaki, S. Nagase, and M. Goto. J. Am. Chem. Soc. **120**, 11096 (1998).
3. N. Tokitoh, T. Sadahiro, N. Takeda, and R. Okazaki. The 12th international symposium on organosilicon chemistry. Sendai, Japan, May 23–28, 1999. Abstract 4A-23.
4. (*a*) R. Koppe and H.Z. Schnockel. Z. Anorg. Allg. Chem. **607**, 41 (1992); (*b*) V. Lefevre and J.L. Ripoll. Phosp. Sulfur Silicon, **120**, 37 (1997).
5. (*a*) D.P. Thompson and P. Boudjouk. J. Chem. Soc. Chem. Commun. 1466 (1987); (*b*) P. Boudjouk, S.R. Bahr, and D.P. Thompson. Organometallics, **10**, 778 (1991).
6. (*a*) P. Arya, J. Boyer, F. Carre, R. Corriu, G. Lanneau, J. Lapasset, M. Perrot, and C. Priou. Angew. Chem. Int. Ed. Engl. **28**, 1016 (1989); (*b*) J. Belzner, I. Heiko, B.O. Kneisel, and R. Herbst-Irmer. Chem. Ber. **129**, 125 (1996).
7. (*a*) R. Withnall and L. Andrews. J. Phys. Chem. **89**, 3261 (1985); (*b*) R.J. Glinski, J.L. Gole, and D.A. Dixon. J. Am. Chem. Soc. **107**, 5891 (1985); (*c*) R. Withnall and L. Andrews. J. Phys. Chem. **92**, 594 (1989), and refs. therein.
8. (*a*) R. Srinivas, D.K. Boehme, D. Suelzle, and H. Schwarz. J. Phys. Chem. **95**, 9836 (1991); (*b*) S. Bailleaux, M. Bogey, C. Demuynck, J. Destombes, and A. Walters. Chem. Phys. **101**, 2729 (1994); (*c*) B. Ma and H.F. Schaefer, III. J. Chem. Phys. **101**, 2734 (1994); (*d*) M. Bogey, B. Delcroix, A. Walters, and J.C. Guillemin. J. Mol. Spectrosc. **175**, 421 (1996); (*e*) B. Ma, N.L. Allinger, and H.F. Schaefer, III. J. Chem. Phys. **105**, 5731 (1996).
9. (*a*) T. Kudo and S. Nagase. J. Phys. Chem. **88**, 2833 (1984); (*b*) T. Kudo and S. Nagase. Chem. Phys. Lett. **128**, 507 (1986); (*c*) T. Kudo and S. Nagase. J. Am. Chem. Soc. **107**, 2589 (1985); (*d*) M.S. Gordon and L.A. Pederson. J. Phys. Chem. **94**, 5527 (1990); (*e*) J. Kapp, M. Remko, P. von R. Schleyer. J. Am. Chem. Soc. **118**, 5745 (1996); (*f*) T. Kudo, F. Hashimoto, and M.S. Gordon. J. Comput. Chem. **17**, 1163 (1996); (*g*) J.M.L. Martin. J. Phys. Chem. **102**, 1294 (1998); (*h*) J. Koput, S. Carter, and N.C. Handy. Chem. Phys. Lett. **301**, 1 (1999).
10. (*a*) T. Kudo and S. Nagase. Organometallics, **5**, 1207 (1986); (*b*) P.J. Bruna and F. Grein. Chem. Phys. **165**, 265 (1992); (*c*) M.W. Schmidt, P.N. Truong, and M.S. Gordon. J. Am. Chem. Soc. **109**, 5217 (1987); (*d*) L. Nyulaszi, A. Belghazi, S.K. Szetsi, T. Veszpremi, J. Heinicke. THEOCHEM. **119**, 73 (1994).
11. (*a*) D. Tzeng and W.P. Weber. J. Am. Chem. Soc. **102**, 1451 (1980); (*b*) T.J. Barton. Pure Appl. Chem. **52**, 615 (1980); (*c*) W.F. Goure and T.J. Barton. J. Organomet. Chem. **199**, 33 (1980); (*d*) W. Ando, M. Ikeno, Y. Hamada. J. Chem. Soc. Chem. Commun. 621 (1981); (*e*) J.E. Baggott, M.A. Blitz, H.M. Frey, P.D. Lightfoot, and R. Walsh. Int. J. Chem. Kinet. **24**, 127 (1992).
12. (*a*) D.C. Dittmer. *In* Comprehensive heterocyclic chemistry. Vol. 7, Part 5. *Edited by* A.R. Katritzky and C.W. Rees. Pergamon Press, Oxford. 1984. Chap. 5; (*b*) Yu V. Razskazovskii, M.V. Roginskaya, and M.Ya. Mel'nikov. J.Organomet. Chem. **486**, 249 (1995).
13. (*a*) W. Ando, Y. Kumamoto, and N. Tokitoh. Tetrahedron Lett. **28**, 2867 (1987); (*b*) W. Ando, Y. Kumamoto, and N. Tokitoh. J. Phys. Org. Chem. **1**, 317 (1988); (*c*) S. Watanabe, T. Kawashima, and R. Okazaki. Chem. Lett. 1289 (1994).
14. W.J. Hehre, L. Radom, P.v.R. Schleyer, and J.A. Pople. Ab initio molecular orbital theory. Wiley, New York. 1986.

© 2000 NRC Canada

15. (*a*) M. Head-Gordon, J.A. Pople, and M.J. Frisch. Chem. Phys. Lett. **153**, 503 (1988); (*b*) M.J. Frisch, M. Head-Gordon, and J.A. Pople. Chem. Phys. Lett. **166**, 275 (1990); (*c*) M.J. Frisch, M. Head-Gordon, and J.A. Pople. Chem. Phys. Lett. **166**, 281 (1990).
16. J.A. Pople, M. Head-Gordon, and K. Raghavachari. J. Chem. Phys. **87**. 5968 (1987).
17. M.J. Frisch, G.W. Trucks, H.B. Schlegel, P.M.W. Gill, B.G. Johnson, M.A. Robb, J.R. Cheeseman, T.A. Keith, G.A. Petersson, J.A. Montgomery, K. Raghavachari, M.A. Al-Laham, V.G. Zakrzewski, J.V. Ortiz, J.B. Foresman, J. Cioslowski, B.B. Stefanov, A. Nanayakkara, M. Challacombe, C.Y. Peng, P.Y. Ayala, W. Chen, M.W. Wong, J.L. Andres, E.S. Replogle, R. Gomperts, R.L. Martin, D.J. Fox, J.S. Binkley, D.J. Defrees, J. Baker, J.J.P. Stewart, M. Head-Gordon, C. Gonzalez, and J.A. Pople. Gaussian 94. Gaussian, Inc., Pittsburgh, Pa. 1995.
18. (*a*) W.J. Hehre, R. Ditchfield, and J.A. Pople. J. Chem. Phys. **56**, 2257 (1972); (*b*) P.C. Hariharan and J.A. Pople. Theor. Chim. Acta, **28**, 213 (1973); (*c*) M.S. Gordon, J.S. Binkley, J.A. Pople, W.J. Pietro, and W.J. Hehre. J. Am. Chem. Soc. **104**, 2797 (1982); (*d*) M.M. Francl, W.J. Pietro, W.J. Hehre, J.S. Binkley, M.S. Gordon, D.J. DeFrees, and J.A. Pople. J. Chem. Phys. **77**, 3654 (1982).
19. (*a*) C. Gonzalez and H.B. Schlegel. J. Chem. Phys. **90**, 2154 (1989); (*b*) C. Gonzalez and H.B. Schlegel. J. Phys. Chem. **94**, 5523 (1990).
20. P.P. Gaspar and R. West. *In* The chemistry of organic silicon compounds. Vol. 2. *Edited by* Z. Rappoport, and Y. Apeloig. Wiley, Chichester, U.K. 1998. Chap. 43.
21. C. Doubleday, M. Nedel, K.N. Houk, D. Thweatt, and M. Page. J. Am. Chem. Soc. **121**, 4720 (1999), and refs. therein.
22. R. Walsh. *In* The chemistry of organic silicon compounds. Vol. 2. *Edited by* Z. Rappoport and Y. Apeloig. Wiley, Chichester, U.K. 1998. Chap. 4.
23. K. Raghavachari, J.A. Pople, and M. Head-Gordon. J. Phys. Chem. **94**, 5579 (1990).
24. R.B. Woodward and R. Hoffmann. The conservation of orbital symmetry. Verlag Chemie, Weinheim, Germany. 1971.
25. Y. Hata and M. Watanabe. J. Am. Chem. Soc. **95**, 8450 (1973); Tetrahedron Lett. **46**, 4659 (1972).
26. S. Shaik and A. Shurki. Angew Chem. Int. Ed. Engl. **39**, 586 (1999).

© 2000 NRC Canada

A low temperature reversible phase transition for 1,1′-bis-(ferrocenyldimethylsilyl)ferrocenylene, $(\eta^5\text{-FcSiMe}_2\text{C}_5\text{H}_4)_2\text{Fe}$, an oligomeric model for silyleneferrocenylene polymers

Mikhail Yu Antipin, Ivan I. Vorontsov, Irene I. Dubovik, Vladimir Papkov, Francisco Cervantes-Lee, and Keith H. Pannell

Abstract: We have reinvestigated the solid state structure of 1,1′-*bis*-(ferrocenyldimethylsilyl)ferrocenylene, $(\eta^5\text{-FcSiMe}_2\text{C}_5\text{H}_4)_2\text{Fe}$, Fc = $(\eta^5\text{-C}_5\text{H}_5)\text{Fe}(\eta^5\text{-C}_5\text{H}_4)$. Using a DSC technique we observed a reversible phase transition for this compound at 169(3)K with ΔH = 1.1 kJ/mol, and ΔS = 6.54 J/mol K. A single crystal X-ray diffraction study has demonstrated that this phase change involves a transformation from a high temperature phase, space group $P2_1/c$, Z = 2, to a triclinic low temperature phase, space group $P\bar{1}$, Z = 4. The phase transition involves the loss of the molecular crystallographic center of symmetry and rotations about the terminal and central cyclopentadienyl ring pairs. The results are compared to those reported for ferrocene.

Key words: solid state, phase transition, silyleneferrocenylene.

Résumé : On a réexaminé la structure à l'état solide du 1,1′-*bis*-(ferrocényldiméthylsilyl)ferrocénylène, $[\eta^5\text{-FcSiMe}_2\text{C}_5\text{H}_4)_2\text{Fe}$, Fc = $\eta^5\text{-C}_5\text{H}_5)\text{Fe}(\eta^5\text{-C}_5\text{H}_4)]$. Faisant appel à la technique de l'analyse calorimétrique différentielle (ACD), il a été possible d'observer une transition de phase réversible pour ce composé à 169(3)K, avec un ΔH de 1,1 kJ/mol et un ΔS de 6,54 J/mol K. La diffraction des rayons X par un seul cristal a permis de démontrer que ce changement de phase implique une transformation d'une phase de température élevée, groupe d'espace $P2_1/c$ avec Z = 2, vers une phase triclinique de température plus faible, groupe d'espace $P\bar{1}$ avec Z = 4. La transition de phase implique la perte du centre de symétrie cristallographique moléculaire et des rotations autour les paires de cycles cyclopentadiényles centraux et terminaux. On compare ces résultats avec ceux rapportés pour le ferrocène.

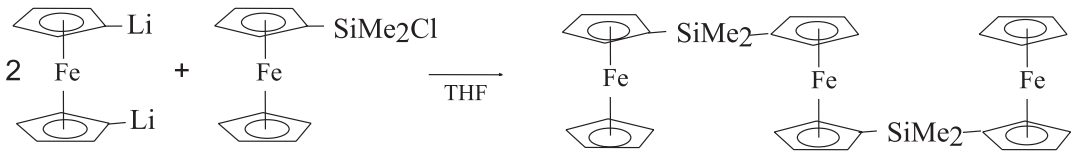
Mots clés : état solide, transition de phase, silylèneferrocénylène.

[Traduit par la Rédaction]

Introduction

The potential of inorganic-based polymers to produce materials with novel electrical, electrooptic and physical properties has been understood for some time (1). Ferrocene is a compound of particular interest since it forms easily handled, thermally stable materials, but has a readily accessible and useful redox system (2). Early attempts to make group 14 [1]-ferrocenophanes often resulted in the formation of oligomeric materials (3); however, more recently the thermal, anionic, and transition metal-catalyzed ring opening of such ferrocenophanes has been shown to produce a range of well-behaved high molecular weight polymers (4–6). Such polymers can be semi-crystalline or amorphous depending upon the various substituents on the group 14 element and the thermal history of the sample.

Models of the structures of such polymers have been published and the structures of oligomeric complexes have been determined by single crystal X-ray diffraction (4, 5). We have published the synthesis and the structure of 1,1′-*bis*-(ferrocenyldimethylsilyl)ferrocenylene, $(\eta^5\text{-FcSiMe}_2\text{C}_5\text{H}_4)_2\text{Fe}$ (**1**), eq. [1] (5*e*):

[1] 

Received June 30, 1999. Published on the NRC Research Press website on November 2, 2000.

Adrian, I am very happy to dedicate this article to you and to B[3].

M.Y. Antipin, I.I. Vorontsov, I.I. Dubovik, and V. Papkov. Institute of Organoelement Compounds (INEOS), Russian Academy of Sciences, 28 Vavilov St. B-334, Moscow, 117813, Russia.
F. Cervantes-Lee and K.H. Pannell.[1] Department of Chemistry, The University of Texas at El Paso, El Paso, TX 79968, U.S.A.

[1]Author to whom correspondence may be addressed. Telephone: (915) 747-5796. Fax: (915) 747-5748. e-mail kpannell@utep.edu

 © 2000 NRC Canada

Table 1. Crystal data and refinement results for the structure of (1).

	HT-phase	LT-phase
Temperature (K)	185(2)	135(2)
Symmetry (*Z*)	monoclinic, *Z* = 2	triclinic, *Z* = 4
Space group	*P*21/*c*	$P\bar{1}$
a (Å)	10.053(3)	11.375(3)
b (Å)	14.801(4)	17.746(6)
c (Å)	11.084(4)	17.805(9)
α (deg)	90	117.83(3)
β (deg)	114.81(2)	105.50(3)
γ (deg)	90	95.61(2)
V (Å^3)	1496.9(8)	2956(2)
d (calc) (Mg/m^3)	1.487	1.506
Formula mass	670.37	670.37
F(000)	696	1392
Reflections collected	2800	9150
Independent reflections	2645	8448
Observed reflections, $I > 2.0\sigma$	1803	7063
Number of params. refined	179	703
Refined method	L.S. on *F*	L.S. on F^2
R (obs. refl.) on *F*	0.047	0.114[a]
R (all data) on *F*	0.095	0.135
Goodness-of-Fit	1.93	1.101

[a]For observed reflections *wR*2 = 0.211 (calculated on F^2).

We also synthesized **1** by the addition of ferrocenyllithium with 1,1′-*bis*-(chlorodimethylsilyl)ferrocene (5*e*) and the Manners group isolated **1** (4*g*), along with other oligomers, from the anion-catalyzed ring opening of [1]-(dimethylsilylene)ferrocenophane. The crystal structure of **1** derived from data obtained at room temperature showed the terminal ferrocenyl groups to be orthogonal to the central group and although the structure was satisfactory, we observed that certain portions of the molecule exhibited very large thermal motions. We have revisited the structure of **1** and now report a low-temperature study which demonstrates that it undergoes a reversible phase change at approximately 160 K. This phase change can also be observed and quantified by differential scanning calorimetry.

Experimental section

Differential scanning calorimetric measurements were performed with a DSM-3 calorimeter (Pushino Biopribar, Russia) using a sample of 18 mg and a heating/cooling rate of 8 K/min.

X-ray diffraction analysis was carried out for single crystal samples with the approximate dimensions 0.20 × 0.20 × 0.35 mm at two temperatures 185 ± 2 (HT) and 135 ± 2 K (LT). Fast cooling in the temperature interval near the phase transition severely reduced the diffraction quality of the crystal (the width of the diffraction maxima increased significantly). Thus, before data collection for the LT-phase at 135 K the sample crystal was cooled slowly (≈ 30 K/h) from 180 to 135 K and this preserved the diffraction quality of the single crystal.

Unit cell parameters and intensities of reflections for both HT and LT phases were measured with two different samples of **1** using 4-circle diffractometer (Siemens P3/PC, MoKα-radiation, λ = 0.71073 Å, graphite monochromator, θ/2θ-scan, 2θ ≤ 50°, scan range in ω = 1.80 deg) equipped with a low-temperature device. To establish precisely the temperature dependence of the unit cell dimensions and the relationship between the two phases during the phase transition, special measurements of the unit cell parameters and unit cell volume were performed at eight temperature points in the temperature interval 200–130 K. During this process the crystal sample was cooled at a rate about 8 K/h.

Both structures were solved with the direct methods and refined by least-squares in the anisotropic approximation for non-hydrogen atoms. Hydrogen atoms were placed at the calculated positions and refined with a riding-model. All calculations were made with a personal computer using SHELXTL PLUS program package. Selected crystal data and results of the refinement for both HT and LT phases are summarized in Table 1. No absorption correction was applied because it was small (μ = 1.54 mm^{-1}) and extinction corrections were found to be negligible.

Atomic coordinates and their displacement parameters for the non-hydrogen atoms in both structures are given in Supplementary Materials, selected bond lengths and bond angles are presented in Table 2. Figure 1 shows a general view of the molecule **1** at 185 K (HT phase) and one of the two independent molecules of **1** in the LT phase in projection on the planes of the central five-membered rings.

Results and discussion

By DSC analysis we established that a phase transition in **1** takes place at the temperature 169 ± 3 K. Upon heating a sample of **1** at a rate of 8 K/min it displayed a small but very sharp endothermic peak centered at 169 K. The cooling runs of the same sample (also at 8 K/min) revealed the expected exothermic event; the DSC traces are presented in Fig. 2.

© 2000 NRC Canada

Table 2. Selected bond lengths (Å) and bond angles (deg) in the structure of (1).[a]

Parameter	185 K	135 K	Room temp.
Bond lengths			
Fe(1)—C(1)	2.054(4)	2.061	2.065(4)
Fe(2)—C(6)	2.052(5)	2.053	2.062(6)
< Fe—C(Cp) > $_{centr}$	2.041	2.045	—
< Fe—C(Cp) > $_{term}$	2.031	2.033	—
Si—C(1)	1.842(5)	1.842	1.861(6)
Si—C(6)	1.866(4)	1.870	1.870(5)
< Si—C(Me) >	1.843(9)	1.863	1.860
Bond angles[b]			
X-Fe(1)-X′	180.0	177.4 / 177.1	—
X-Fe(2)-X′	179.0	172.9–178.6	—
C(1)-Si-C(6)	107.6(2)	108.1	—
Me-Si-Me	108.7(4)	111.1	—

[a]For chemically equivalent bond lengths and angles averaged values are given, for data at 135 K the results are averaged for both independent molecules as well. The mean standard deviation in the Fe—C bond lengths at 135 K is 0.01 Å. Atomic numbering scheme corresponds the data at 185 K. For comparison, available data for the same structure at room temperature from ref. (1) are given.

[b]X and X′ are Cp-ring centroids.

The areas of the *exo*- and the endothermic peaks are essentially identical and analysis provides the enthalpy and entropy of the phase change as 1.1 KJ/mol and 6.54 J/mol K respectively. Such values are typical for phase transitions in molecular crystals (7). In particular it should be noted that a similar phase transition has been reported for solid ferrocene itself at 163.4 K with the enthalpy and entropy parameters of 0.87 KJ/mol and 5.32 J/mol K, respectively, (8).

Two low temperature X-ray diffraction experiments were performed on either side of the transition temperature noted by DSC, i.e., at 185(2) (HT) and 135(2) K (LT). From the unit cell parameters it is clear that the phase transition is accomplished by a doubling of the unit cell volume and the changing of the crystal symmetry. The latter changes from the monoclinic HT phase (space group $P2_1/c$, $Z = 2$, molecules in the inversion centers) to a triclinic LT phase (space group $P\bar{1}$, $Z = 4$, two independent molecules in the unit cell).

The molecular geometry parameters (bond lengths and bond angles) in each of the two crystal phases of **1** have values that are essentially the same as those previously published for the monoclinic modification of **1** measured at room temperature (*4g*, 5*e*). These data are compared in Table 2. For both phases the mean Fe—C distances in the central ferrocenylene fragments are systematically larger than in the terminal ferrocenyl groups. This can be explained by the steric demands of the two bulky Me_2SiFc-substituents. In addition, the corresponding Fe—C_{ipso} bond lengths are also systematically larger than all other Fe—C bonds.

The Si atoms have a distorted tetrahedral coordination, the bong angles C(1)-Si-C(6) being slightly smaller than the corresponding Me-Si-Me angles; however, the scatter of the individual values is rather large. All Si atoms deviate from the mean ring planes by 0.02–0.03 Å in the directions opposite to the Fe atoms. In all the molecules, for both phases of **1,** the endocyclic C-C(Si)-C angles in the rings are smaller (by ~4.0°) in comparison with other similar angles (i.e., 104.6° vs. 108.5°). The terminal ferrocenyl fragments are slightly bent with dihedral ring angles in the range 0.7–4.3° and the angles X-Fe-X′ (X and X′ are centroids of the rings) in the range 172.9–178.6°. The Cp rings of the central ferrocenylene fragment in the monoclinic phase are strictly parallel due to a crystal symmetry. The pseudo-torsion angles Fe-Si-Si-Fe characterizing the relative orientation of the Fc-fragments are equal to 180.0° for monoclinic phase (atoms Fe(1), Si(1), Fe(2), Fe(1a), Si(1a), and Fe(2a) are strictly coplanar), and 175.7°, 172.3° for triclinic phase (angles Fe(1)-Si(1)-Si(2)-Fe(3) and Fe(4)-Si(3)-Si(4)-Fe(6), respectively). The angles Si(1)-Fe(2)-Si(2) and Si(3)-Fe(5)-Si(4) are close to linear (166.9 and 167.5°), so all Fe and Si atoms in the molecule are almost coplanar.

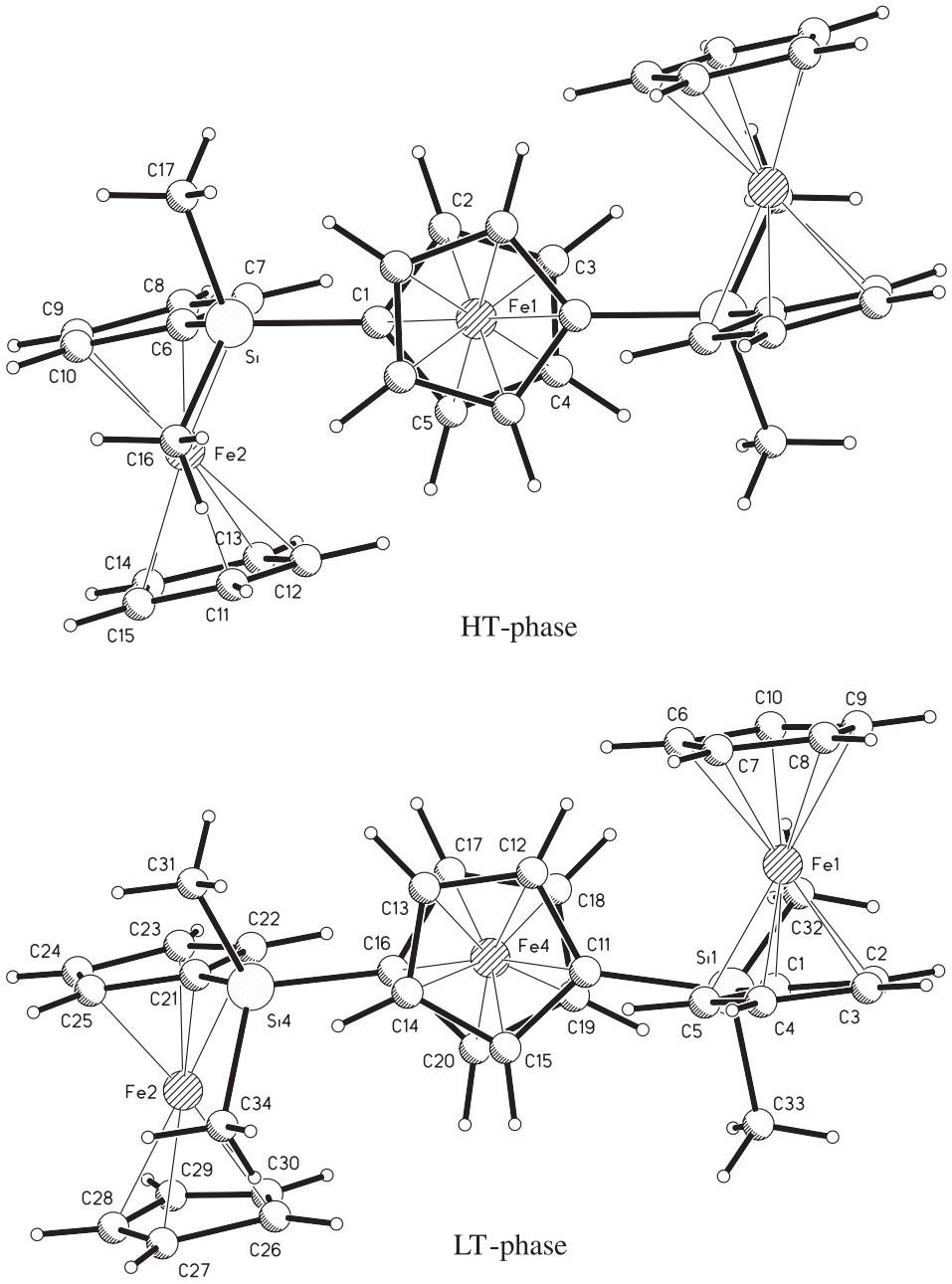
Table 3. Mutual orientation of the 5-member rings (degrees) in monoclinic (HT) and triclinic (LT) phases of (1). Values X and X′ are centroids of the rings and Cp/Cp are interplanar angles.

	HT phase	LT phase
Central rings		
Fe(1) : C(1)-X-X′-C(3a)	36.0	—
Cp / Cp and X-Fe(1)-X′	180.0 and 180.0	—
Fe(2) : C(11)-X-X′-C(19)	—	15.3
C(11)-X-X′-C(16)	—	160.4
Cp / Cp and X-Fe(2)-X′	—	0.7 and 177.4
Fe(5) : C(51)-X-X′-C(58)	—	–17.8
C(51)-X-X′-C(56)	—	–163.4
Cp / Cp and X-Fe(5)-X′	—	1.1 and 177.1
Terminal rings		
Fe(2) : C(6)-X-X′-C(11)	6.1	—
Cp / Cp and X-Fe(2)-X′	1.3 and 179.0	—
Fe(1) : C(1)-X-X′-C(10)	—	–13.3
Cp / Cp and X-Fe(1)-X′	—	2.2 and 178.0
Fe(3) : C(21)-X-X′-C(26)	—	–28.3
Cp / Cp and X-Fe(3)-X′	—	4.3 and 172.9
Fe(4) : C(41)-X-X′-C(47)	—	–22.4
Cp / Cp and X-Fe(4)-X′	—	3.8 and 176.0
Fe(6) : C(61)-X-X′-C(70)	—	10.3
Cp / Cp and X-Fe(6)-X′	—	2.8 and 178.6

The most interesting feature of the molecular structure of both phases of **1** is the mutual orientation (staggered,

© 2000 NRC Canada

Fig. 1. General view of the molecule **1** in the HT- and LT-phase(one of the two independent molecules) and atomic numbering scheme. Molecules are shown in projection on the central ring planes.



eclipsed, or intermediate) of the cyclopentadienyl groups in the central and terminal ferrocenylene and ferrocenyl fragments. The parameters describing various orientations of rings for both phases are presented in Table 3.

At room temperature and 185 K, in accord with the crystal symmetry, the central ferrocenylene fragment has an ideal staggered conformation of rings, Fig. 1. In the terminal ferrocenyl fragments the orientation of the rings is close to the eclipsed one (torsion angle C(6)-X-X′-C(11) = 6.1°) with a very small ring bending (angle X-Fe(2)-X′ = 179.0°, dihedral angle = 1.3°).

The phase transition is accomplished by a loosening of the molecular and crystallographic center of symmetry, and in the LT phase the central rings have an intermediate orientation between the eclipsed and staggered ones (torsion angles C-X-X′-C = 15.3 and –17.8°, see Table 3), Fig 1. Some small bending of the central Fc-fragment is also observed. In the terminal ferrocenyl fragments the ring orientation is also intermediate (ring rotation angles from 10.3 to –28.3°), and for some of them, in particular for the Fe(3) atom, it is even closer to staggered. Thus, during the phase transition both the central and terminal Fc-fragments have changed a mutual ring orientation.

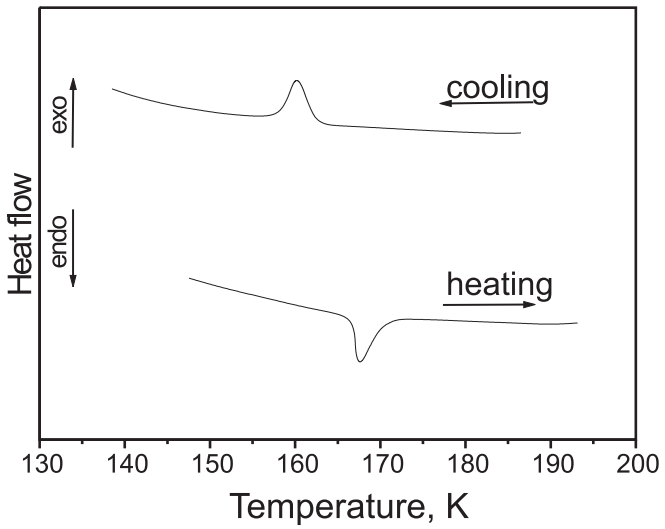
The present result is close to that exhibited for the parent compound ferrocene, $Fe(C_5H_5)_2$, which has a well-established phase transition at 164 K. This transition occurs from a disordered monoclinic high-temperature phase (space group $P2_1/a$, $Z = 2$) to the low-temperature triclinic one with

© 2000 NRC Canada

Table 4. The temperature dependence of the unit cell parameters in the crystal of (**1**).

Temp (K)	200	184	176	169	161	153	143	131
a' (Å)	10.036(3)	10.028(3)	10.024(3)	10.021(3)	10.020(3)	20.071(3)	20.112(7)	20.113(5)
b' (Å)	14.821(4)	14.803(3)	14.791(4)	14.784(4)	14.765(4)	29.487(5)	29.467(9)	29.421(7)
c' (Å)	11.407(4)	11.401(3)	11.400(3)	11.399(3)	11.393(4)	11.387(4)	11.366(4)	11.358(3)
α' (deg)	89.94(3)	89.94(2)	89.94(2)	89.93(2)	89.89(3)	89.81(3)	89.67(3)	89.65(2)
β' (deg)	118.10(2)	118.12(2)	118.13(2)	118.15(2)	118.19(2)	118.36(2)	118.60(2)	118.66(2)
γ' (deg)	90.07(2)	90.07(2)	90.07(2)	90.09(2)	90.11(20)	90.14(3)	90.23(3)	90.25(2)
V (Å^3)	1497(10)	1493(1)	1491(1)	1489(10)	1486(1)	5931(3)	5910(3)	5897(3)

Fig. 2. DSC thermogram of a sample of **1** on cooling (*left*) and heating (*right*). Sample weight = 18.1 mg; heating rate = cooling rate = 8 K/min; Δ = 1.7 J g^{-1}.



two independent molecules in the unit cell. For the high-temperature phase, due to the crystal symmetry, the molecules must possess D_{5d} symmetry. However, this is not the case since an analysis of the atomic anisotropic displacement parameters clearly indicated that the structure is characterized by the static disorder related to a superposition of a few ring orientations in the crystal. It has been shown (9) that two independent molecules in the ordered triclinic low-temperature phase of ferrocene have approximate D_5 symmetry, but are neither eclipsed nor staggered. A very similar situation is observed for **1**. However, our analysis of the high-temperature data for **1** did not reveal clearly the central ring disorder although for both sets of HT data (room temperature and 185 K) there is some extra elongation of the central ring atom thermal ellipsoids.

The data on the temperature dependence of the unit cell parameters of **1** are presented in Table 4. For better comparison of the two unit cells their initial parameters (Table 1) were transformed to their similar crystal settings. Thus, the monoclinic HT phase was transformed into a new monoclinic phase ($P2_1/n$) with the a', b', c' axes and the monoclinic angle β' = 118.63(2)°, and the triclinic LT phase was transformed into a *C*-centered triclinic phase with new parameters a' and b' doubled in comparison with those in the HT phase. The corresponding transformation matrices are given below

HT-phase, from β to β' monoclinic setting LT-phase, from triclinic P to triclinic C-centered setting

$$\begin{pmatrix} a' \\ b' \\ c' \end{pmatrix} = \begin{pmatrix} 1 & 0 & 0 \\ 0 & -1 & 0 \\ -1 & 0 & -1 \end{pmatrix} \begin{pmatrix} a \\ b \\ c \end{pmatrix} \qquad \begin{pmatrix} a' \\ b' \\ c' \end{pmatrix} = \begin{pmatrix} 1 & 1 & 0 \\ -1 & -1 & -2 \\ -1 & 0 & 0 \end{pmatrix} \begin{pmatrix} a \\ b \\ c \end{pmatrix}$$

The temperature dependence of these parameters is presented in Figs. 3 and 4 where the a' and b' values for HT phase were doubled, and the unit cell volume was multiplied by the factor of 4 for a more clear comparison of the data.

It is seen from these data that on cooling the crystal, the $b'$and c' parameters smoothly decrease, while a' attains a minimum at nearly 160 K, and then increases. This behaviour correlates with the estimated temperature of the phase transition at about 159 K. The α' and γ' angles which are very close to ideal value of 90° above the transition point ($\Delta\alpha'$ and $\Delta\gamma'$ are less than 3σ), deviate significantly from this value below the transition point, and at 131 K the corresponding deviations $\Delta\alpha'$ and $\Delta\gamma'$ are equal to 0.35(2) and 0.25(2)°. The β' angle is increased on cooling by 0.56(2)°. In principle, the LT phase could be considered as strongly distorted pseudo-monoclinic *C*-centered, and some non-direct indications were found for it, namely the presence of small number of weak additional reflections at 143 K corresponding to this setting. Nevertheless, our attempts to solve and (or) refine the structure of this phase in the *C*-centered monoclinic space group failed. We believe therefore that the true symmetry of the LT phase is triclinic, and only for easy comparison with the HT-phase it might be transformed to monoclinic *C*-centered one.

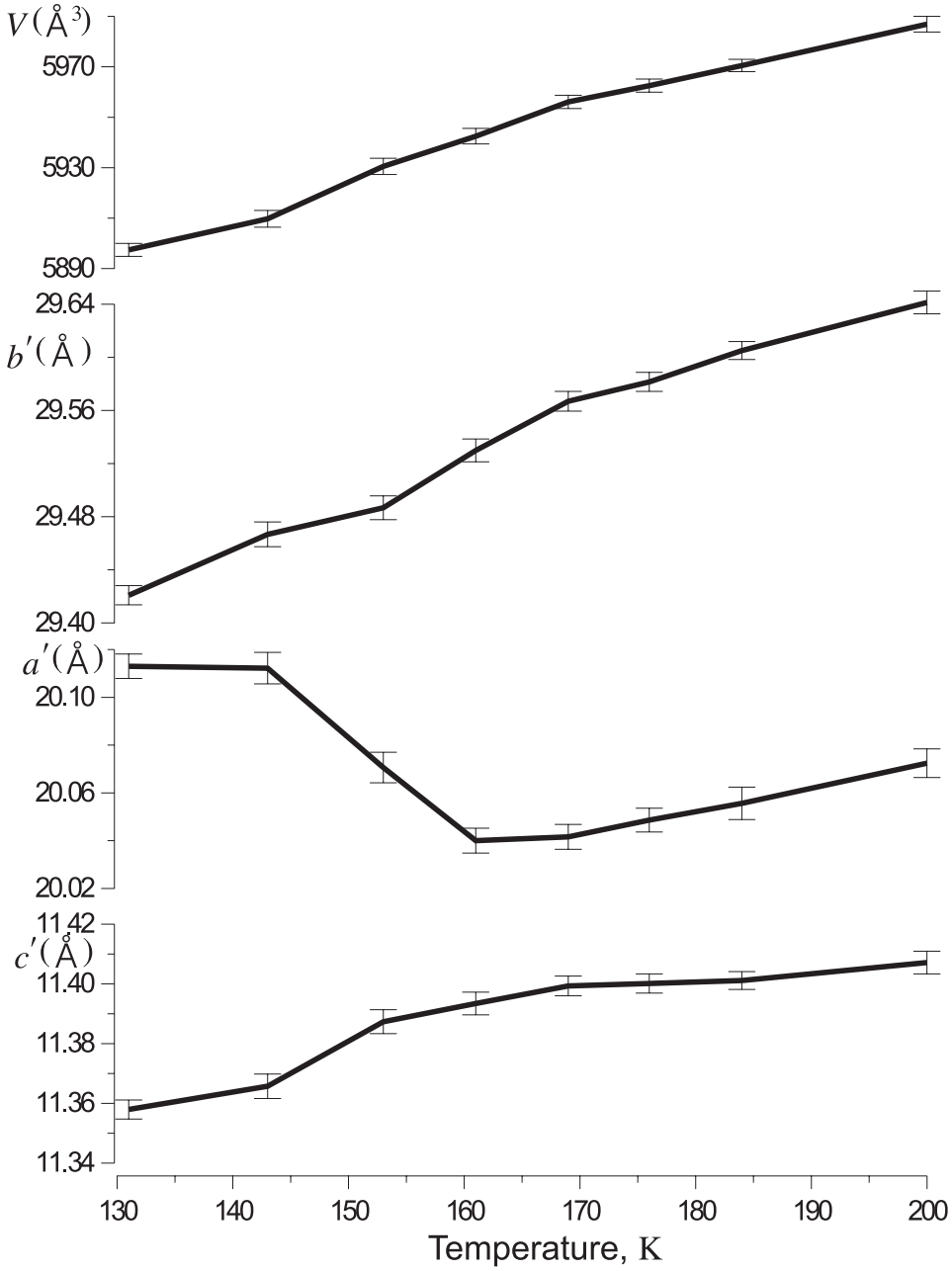
Concluding remarks

The phase transition we have observed in **1** is related to the change of C_i-symmetry of the central ferrocenyl fragment at the transition point. In this respect the transition might be similar to those found in 3d and 4d metallocenes, namely ferrocene (9) or decamethylosmocene (10). In the HT phase of decamethylosmocene the Cp* rings are strictly eclipsed (space group $P2_1/m$, Z = 2), and below the transition (in the LT phase crystal space group is $P2_1/c$, Z = 4) there is some small but significant mutual ring rotation that increases gradually on further cooling the sample.

This is probably not the case for **1** where the transition is much closer to that in ferrocene. The fact that during this transition the ring orientation changes, and both central and terminal ferrocenyl fragments are involved in this process, allows one to suggest that transition might result from an

© 2000 NRC Canada

Fig. 3. Temperature dependence of the unit call dimensions in **1**. The values shown for *a*, *b*, *c* and *V* are given as 2*a′*, 2*b′*, *c′* and 4*V* (HT-phase in the β-monoclinic setting, see explanations in the text) at $T > 160$ K (transition temperature), and *a′*, *b′*, *c′* and *V* (LT-phase, C-centered triclinic cell) at $T < 160$ K.



interplay between intermolecular and intramolecular interactions among the ferrocene moieties. The occurrence of a similar transition in higher molecular weight dimethylsilylferrocenylene oligomers and polymer is therefore an interesting issue in further investigation.

The temperature dependence of the unit cell volume in crystal of **1** is also of special interest. As shown in Fig. 3, there is no sharp change in the volume of the doubled cell near the transition point. In this respect the transition appears to proceed nearly continuously although it is accompanied by the well-defined but small sharp change in the enthalpy of the crystal (1.1 kJ/mol).

Acknowledgements

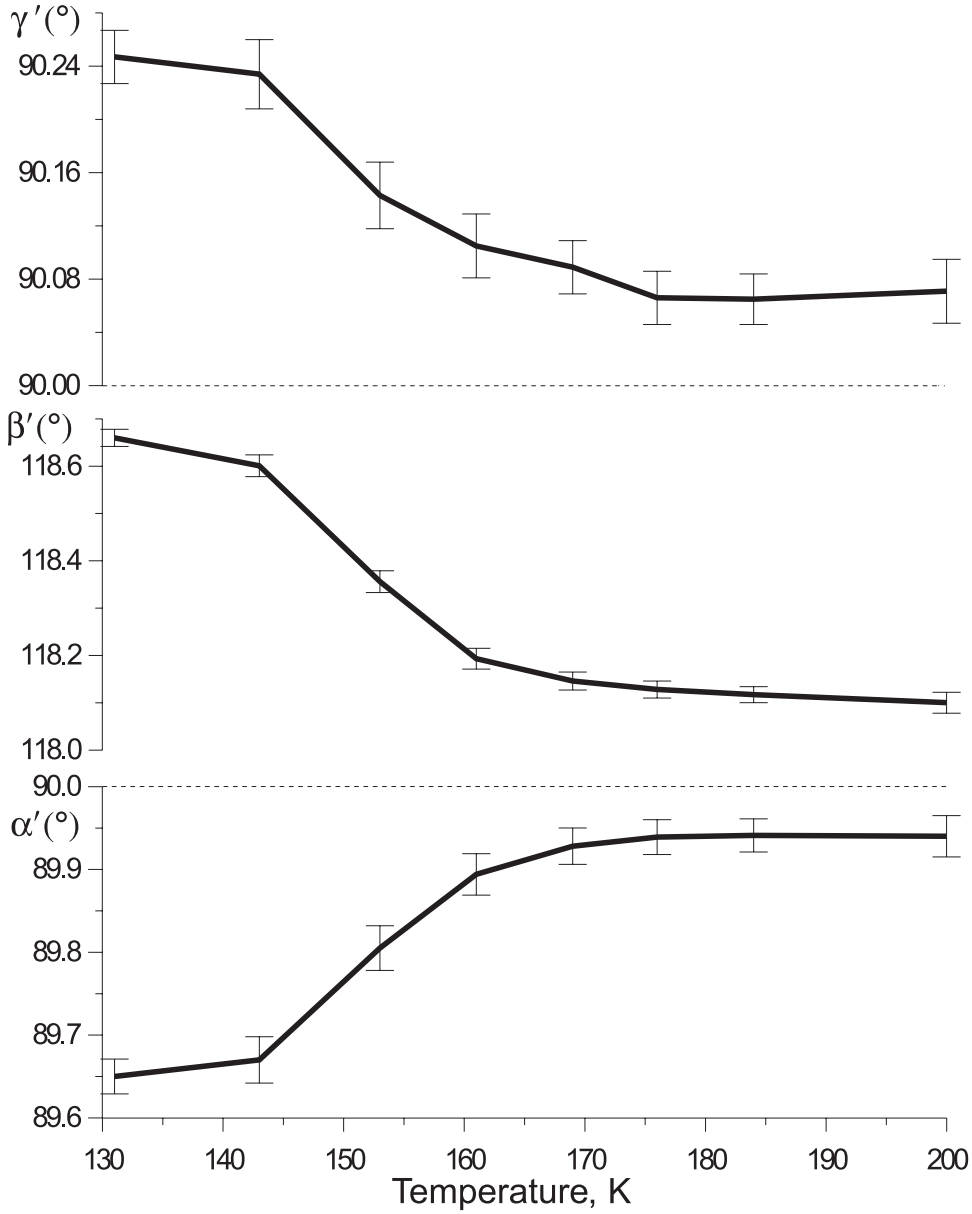
This research was supported by the NSF and the Civilian Research Development Fund (CRDF) for collaborative research between the U.S.A. and former Soviet Union countries, (Grant # RC1–276). We thank Dr. Chuck Campana for initial data that illustrated the new LT phase of **1**.

Supporting information available

Tables of the X-ray determination summary, tables of the non-hydrogen atom coordinates and their equivalent displacement parameters, bond lengths, anisotropic displacement

© 2000 NRC Canada

Fig. 4. Temperature dependence of the unit cells angular parameters in **1**. HT-Unit cell is in β′ monoclinic setting at $T > 160$ K, and LT-unit cell is in the *C*-centered triclinic setting at $T < 160$K.



parameters for non-hydrogen atoms, hydrogen atom coordinates and their isotropic displacement parameters, and ORTEP views of molecules have all been deposited as supplementary material and may be purchased from the Depository of Unpublished Data, Document Delivery, CISTI, National Research Council Canada, Ottawa, ON, Canada K1A 0S2 (http://www.nrc.ca/cisti/irm/unpub_e.shtml).

References

1. (*a*) M. Zeldin, K.J. Wynne, and H.R. Allcock. Inorganic and organometallic polymers. Advances in Chemistry series **360**. American Chemical Society, Washington, D.C. 1988; (*b*) J.E. Mark, H.R. Allcock, and R. West. Inorganic polymers. Prentice Hall, New Jersey. 1992.
2. A. Togni and T. Hayashi (*Editors*). Ferrocenes, VCH, New York, 1995.
3. (*a*) A.G. Osborne, R.H. Whiteley, and R.E. Meads. J. Organomet. Chem. **193**, 345 (1980); (*b*) A. Clearfield, C.J. Simmons, H.P. Withers, and D. Seyferth. Inorg. Chim. Acta, **75**, 139 (1983).
4. (*a*) D.A. Foucher, B.-Z. Tang, and I. Manners. J. Am. Chem. Soc. **114**, 6246 (1992); (*b*) B.-Z. Tang, D.A. Foucher, A. Lough, N. Coombs, R. Sodhi, and I. Manners. J. Chem. Soc. Chem. Commun. 523 (1993); (*c*) D.A. Foucher, R. Ziembinski, B.-Z. Tang, P.M. Macdonald, J. Massey, C.R. Jaeger, G.J. Vancso, and I. Manners. Macromolecules, **26**, 2878 (1993); (*d*) D.A. Foucher, R. Ziembinski, R. Petersen, J. Pudelski, M. Edwards, Y. Ni, J. Massey, C.R. Jaeger, G.J. Vansco, and I. Manners. Macromolecules, **27**, 3992 (1994); (*e*) D.I. Zechel, K.C. Hultzsch, R. Rulkens, D. Balaishis, Y. Ni, J.K. Pudelski, A.L. Lough, I. Manners, and D.A. Foucher.

© 2000 NRC Canada

Organometallics, **15**, 1972 (1996); (*f*) I. Manners. Adv. Organomet. Chem. **37**, 131(1995); (*g*) Y. Ni, R. Rulkens, and I. Manners. J. Am. Chem. Soc. **118**, 4102 (1996); (*h*) A.J. Lough, I. Manners, and R. Rulkens. Acta Crystallogr. Sect. C: Crystl. Struct. Commun. **50**, 1667 (1994).

5. (*a*) M.T. Nguyen, A.F. Diaz, V.V. Dementiev, H. Sharma, and K.H. Pannell. SPIE Proceedings **1910**, 230 (1993); (*b*) M.T. Nguyen, A.F. Diaz, V.V. Dementiev, and K.H. Pannell. Chem. Mater. **5**, 1389 (1993); (*c*) V.V. Dementiev, F. Cervantes-Lee, L. Párkányi, H.K. Sharma, K.H. Pannell, M.-T. Nguyen, and A.F. Diaz. Organometallics, **12**, 1983 (1993); (*d*) M.T. Nguyen, A.F. Diaz, V.V. Dementiev, and K.H. Pannell. Chem. Mater. **6**, 952 (1994); (*e*) K.H. Pannell, V.V. Dementiev, H. Li, F. Cervantes-Lee, M.T. Nguyen, and A.F. Diaz. Organometallics, **13**, 3644 (1994); (*f*) K.H. Pannell and H.K. Sharma. Organometallics, **16**, 3077 (1997); (*g*) K.H. Pannell, H.K. Sharma, F. Cervantes-Lee, and J.S. Mahmoud. Organometallics, **18**, 399 (1999).
6. (*a*) M. Tanaka and T. Hayashi. Bull. Chem. Soc. Jpn. **66**, 334 (1993); (*b*) N.P. Reddy, H. Yamashita, and M. Tanaka. J. Chem. Soc. Chem. Commun. 2263 (1995); (*c*) M. Hmyene, A. Yasser, M. Escorne, A. Percheron-Guegan, and F. Garnier. Adv. Mater. (Weinheim Ger.), **6**, 564 (1994**)**.
7. N.G. Parsonage and L.A.K. Staveley. Disorder in crystals. Clarendon Press, Oxford. Chap. 10. 1978.
8. (*a*) J.W. Edwards and G.L Kington. Trans. Faraday Soc. **58,** 1334 (1962); (*b*) J.W. Edwards, G.L. Kington, and R. Mason. Trans. Faraday Soc. **56**, 660 (1960).
9. C.P. Brock and Y. Fu. Acta Crystallogr. B: Struct. Crystallogr. Cryst. Chem. **B53**, 928 (1997).
10. I.I. Vorontsov, K.A. Potekhin, M.Yu Antipin, and I.E. Zanin. Kristallografiya. In press.

© 2000 NRC Canada

Preparation and characterization of organic-inorganic hybrid materials incorporating diphosphino moieties. Study of the accessibility of the phosphorus atoms included into the material

Jean-Philippe Bezombes, Claude Chuit, Robert J.P. Corriu, and Catherine Reyé

Abstract: The hydrolysis-polycondensation by the sol-gel process of the aromatic diphosphines $(X_3SiC_6H_4)_2PC_6H_4P(C_6H_4SiX_3)_2$, which are rigid molecules bearing four hydrolysable SiX_3 groups (X = O^iPr, H), leads to new organic-inorganic hybrid materials, characterized by solid state ^{13}C, ^{29}Si, and ^{31}P NMR spectroscopies. The accessibility of the phosphorus centres incorporated into the xerogel obtained from the diphosphine with X = O^iPr has been studied. All the phosphorus atoms reacted quantitatively with H_2O_2, S_8, and CH_3I but only 20% with the more bulky reagent $W(CO)_5$·THF. This result is explained by the rigidity of the inorganic network resulting from the high number of hydrolysable Si-O^iPr groups in the precursor.

Key words : Diphosphines, sol-gel process, xerogels, solid ^{31}P NMR.

Résumé : L'hydrolyse-polycondensation via le procédé sol-gel des diphosphines aromatiques $(X_3SiC_6H_4)_2PC_6H_4P(C_6H_4SiX_3)_2$, molécules rigides portant quatre groupements SiX_3 hydrolysables (X = O^iPr, H), conduit à de nouveaux matériaux hybrides organique-inorganiques qui ont été caractérisés par la RMN à l'état solide du ^{13}C, du ^{29}Si et du ^{31}P. L'étude de l' accessibilité des centres phosphorés incorporés dans le xérogel obtenu à partir de la diphosphine avec X = O^iPr est décrite. Tous les atomes de phosphore réagissent quantitativement avec H_2O_2, S_8, et CH_3I, mais seulement 20% réagissent avec $W(CO)_5$·THF réactif plus volumineux que les précédents. Ce résultat est expliqué par la rigidité du réseau inorganique qui est la conséquence du nombre élevé de groupements hydrolysables Si-O^iPr porté par le précurseur.

Mots clés : diphosphines, procédé sol-gel, xérogels, RMN solide ^{31}P.

Introduction

The sol-gel process allows the preparation of organic–inorganic hybrid materials under smooth conditions (1–4). In a recent publication (5) we described the preparation of phosphines **1**, **2**, and **3** as well as their hydrolysis and polycondensation via the sol-gel process, giving rise to the corresponding xerogels. The accessibility of the phosphorus centres included in these xerogels was investigated by using some classical reactions at phosphorus. We found that the phosphorus centres react quantitatively with H_2O_2, S_8, and MeI, whilst their reactivity towards $W(CO)_5$·THF (6) varied depending on the xerogel studied. We noticed that the phosphorus atoms became more readily accessible when the number of $Si(OR)_3$ groups in the precursor is low. Thus the phosphorus atoms in the xerogel derived from precursor **1** (with two $Si(O^iPr)_3$ groups) reacts more readily with $W(CO)_5$·THF than when included into the xerogels derived from precursors **2** and **3** (with three SiX_3 groups).

As a continuation of this study, we prepared the aromatic diphosphines **4** and **5** (with four SiX_3 groups) and studied their hydrolysis and polycondensation as well as the accessibility of the phosphorus centres included into the xerogel **X4** obtained from the diphosphine **4**. This diphosphine was chosen with rigid substituents around the phosphorus centres as in the case for the phosphines **1** and **2**. This study was undertaken to verify if the high number of $Si(O^iPr)_3$ groups in the precursor **4** gives rise to a low accessibility of the phosphorus centres included into the corresponding xerogel as predicted by our previous study (6).

Results and discussion

1) Preparation of diphosphines 4 and 5 and of phosphine derivatives 7–9.

The diphosphine **4** was prepared in 53% yield by reaction of the previously described functional Grignard reagent **6** (5) with *P,P,P′,P′*-tetrachloro-*p*-phenylenediphosphine (7) in

Received July 5, 1999. Published on the NRC Research Press website on November 2, 2000.

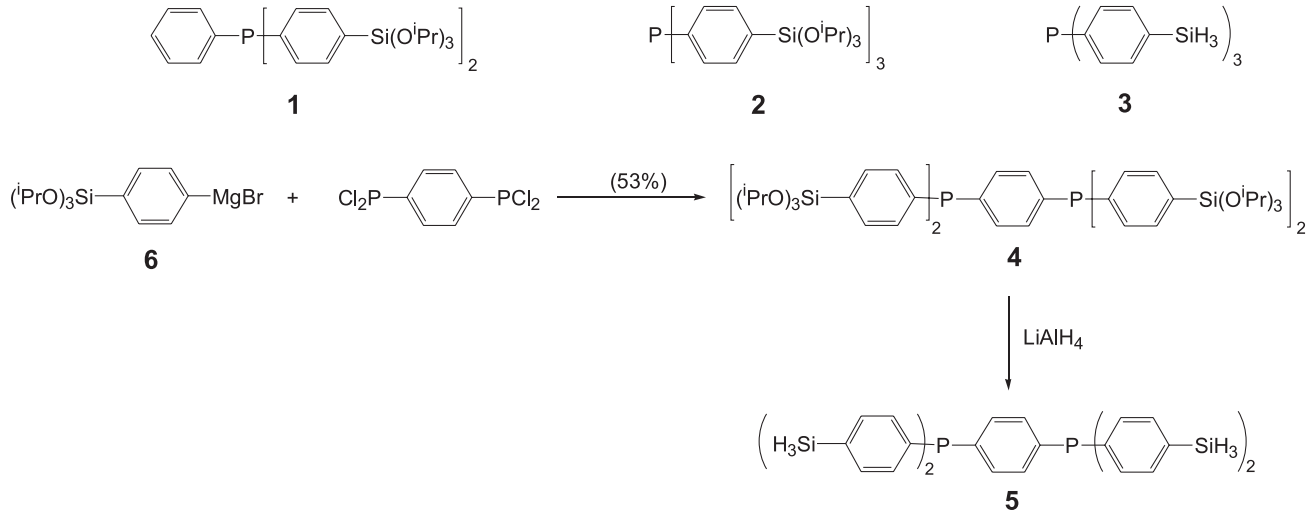
This paper is dedicated to Professor Adrian Brook in recognition to his very important contribution in silicon chemistry.

J.-P. Bezombes, C. Chuit, R.J.P. Corriu,[1] and C. Reyé. Laboratoire de Chimie Moleculaire et Organisation du Solide. UMR 5637, Université Montpellier II, Case 007, F-34095 Montpellier CEDEX 5, France.

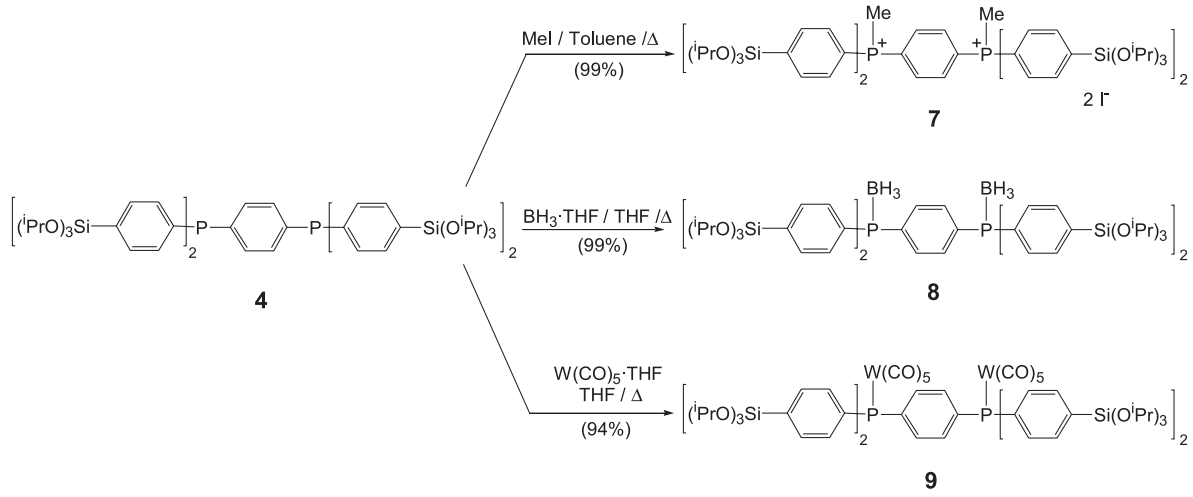
[1]Author to whom correspondence may be addressed. Telephone : 0467143801. Fax : 0467143852.
e-mail: corriu@crit.univ.montp2.fr

 © 2000 NRC Canada

Scheme 1.



Scheme 2.



THF (Scheme 1). $LiAlH_4$ reduction of **4** gave the diphosphine **5** in good yield (Scheme 1). Treatment of **4** by methyl iodide, BH_3·THF, and $W(CO)_5$·THF gives rise respectively and quantitatively to the diphosphonium salt **7**, to the diphosphine borane complex **8**, and to the diphosphine tungsten pentacarbonyl complex **9** (Scheme 2).

2) Sol-gel processing of diphosphines 4 and 5 and of diphosphine derivatives 7–9

We previously showed (5) that phosphines **1** and **2** required an acidic catalyst to be hydrolyzed, therefore diphosphine **4** was hydrolyzed and polycondensed with 6 equivalents of water in the presence of 10% of HCl in THF solution (eq. [1] and Table 1). At 30°C, the gelation occurs within 2 h which is close to the gelation time for phosphine **2** (5). Xerogel **X4** was obtained after ageing at 30°C for five days. It was then powdered and washed twice with ethanol, acetone, and diethyl ether and dried in vacuo at 120°C for two hours. The solid state ^{31}P NMR spectrum of **X4** displays only one signal at –5.0 ppm which indicates that no oxidation of the phosphorus atom occurred during the sol-gel process. The solid state ^{13}C NMR spectrum of **X4** displays one signal at 134.4 ppm attributed to the aromatic carbons and two further signals at 24.8 and 66.7 ppm attributed to remaining O^iPr groups. Thus the hydrolysis is incomplete; however the elemental analysis indicates that only about 10% of the $Si(O^iPr)_3$ groups were not hydrolyzed. The solid state ^{29}Si NMR spectrum of **X4** displays two main resonances at –60.5 ppm [substructure T^1, C-$Si(OR)_2OSi$] and –69.1 ppm [substructure T^2, C-$Si(OR)(OSi)_2$]. A minor resonance assigned to the substructure T^3 [C-$Si(OSi)_3$] was observed while substructure T° was absent. The ratio of the T groups was estimated from deconvoluted T peaks (8, 9) at 42% for T^1, 52% for T^2, and 6% for T^3 corresponding to a degree of condensation τ of 55%.[2] Thus while the hydrolysis is important, the polycondensation is rather weak. The absence of any Q signal corresponding to the SiO_4 substructure (region of –100ppm) is noteworthy indicating that the

[2] The degree of condensation was calculated according to the equation: $\tau = [(0.5)(\text{area } T^1) + (1.0)(\text{area } T^2) + (1.5)(\text{area } T^3)]/1.5$.

© 2000 NRC Canada

Table 1. Textural and solid state NMR data for xerogels **X4**, **X5**, and **X7**–**X9**.

Precursor	Gelification time	S_{BET} (m^2 g^{-1})	^{31}P CP-MAS NMR (δ)	^{13}C CP-MAS NMR (δ)	^{28}Si CP-MAS NMR (δ)
4	2 h	460	–5.0	24.8, 66.7, 134.4	–60.5 (T^1), –69.1 (T^2)
7	1 min	<10	+22.0		–67.7 (T^2)
8	15 min	75	–5.8, +22.0 (50/50)		
9	20 min	380	+20.9		
5	30 h	570	–5.1		–61.6 (T^1), –69.3 (T^2), –77.0 (T^3) –50 to –30 (D)

Table 2. Textural data for the materials prepared by hydrolysis and polycondensation of phosphines **1**, **2**, and **4**.

Precursor	Xerogel	S_{BET} (m^2 g^{-1})	τ[a]	N^b	Micropore vol. (mL g^{-1})	Mean pore dia. (Å)
1 (f^c = 6)	**X1**[d]	< 10	62	3.7	—	—
2 (f^c = 9)	**X2**[d]	400	57	5.1	0.175	15
4 (f^c = 12)	**X4**[d]	460	55	6.6	0.182	15.5

[a] Degree of condensation, determined by ^{29}Si CP-MAS NMR.

[b] Average number of Si—O—Si bonds by precursor ($N = f \times \tau$).

[c] Functionality at silicon.

[d] HCl, 10% as catalyst.

integrity of the organic moiety had been maintained during the sol-gel process. The surface area (N_2 BET measurement) is of 460 m^2/g, value comparable to that found for the hydrolysis of phosphine **2** (Table 2). The adsorption–desorption isotherms for **X4** indicated that the solid is microporous with a microporous volume of 0.182 mL g^{-1} and mean pore diameter of 15.5 Å.

The hydrolysis of diphosphine **5** was performed in THF solution in the presence of a catalytic amount of tetrabutylammonium fluoride (10) with 6 equivalents of water. The reagents were mixed at 0°C and the solution was allowed to warm to 24°C after 8 min. The gel was formed after 30 h. After the usual work-up, xerogel **X5** was obtained. Its N_2 BET surface area was found of 570 m^2 g^{-1}, with a microporous volume of 0.247 mL g^{-1}. There is no oxidation of the phosphorus atoms during the hydrolysis as indicated by the solid state ^{31}P NMR spectrum of **X5** which displays only one signal at –5.1 ppm. The solid state ^{29}Si NMR spectrum of **X5** displays a set of three resonances at –61.6 ppm (substructure T^1), –69.3 ppm (substructure T^2), and –77.0 ppm (substructure T^3); and a broad resonance (–50 to –30 ppm) corresponding to $CSi(H)O_2$ substructures. This is consistent with the FTIR spectrum which shows a Si—H absorption band at 2160 cm^{-1}. No peak corresponding to an SiO_4 substructure was found around –100 ppm indicating that no Si—C cleavage occurred during the sol-gel process.

Phosphorus derivatives **7**–**9** were hydrolyzed and polycondensed under the same conditions as those previously described for phosphine **4** to give xerogels **X7**-**X9** (eqs. [2]–[4] and Table 1). The solid state ^{31}P NMR spectra of xerogels **X7** and **X9** showed that there was neither oxidation nor decomplexation during the polycondensation reactions. In the case of the diphosphine derivative **8** partial decomplexation took place during the hydrolysis. The P—B bond cleavage was estimated by ^{31}P NMR spectroscopy to be about 40% after reaction without drying the xerogel. After heating for one night at 120°C, the cleavage of the P—B bond was increased to 70%. This P—B bond cleavage occurred probably either by hydrolysis or by reaction of the Si-OH present in the xerogel or by both processes. The participation of the Si-OH groups in the cleavage of the P—B bonds is likely as elemental analysis showed that most of the B atoms are incorporated in the xerogel after washing, probably as Si-O-B groups.

Thus the behaviour of diphosphines **4** and **5** and diphosphine derivatives **7**–**9** during the hydrolysis process is very similar to those of phosphines **2** and **3** as well as that of the corresponding derivatives of phosphine **2** (5).

3) Reactivity of the xerogel X4 with H_2O_2, S_8, CH_3I, and $W(CO)_5$·THF

To investigate the accessibility of the phosphorus centers included into **X4**, we treated it with an excess of the following reagents: H_2O_2, S_8, CH_3I, and $W(CO)_5$·THF (Scheme 3).

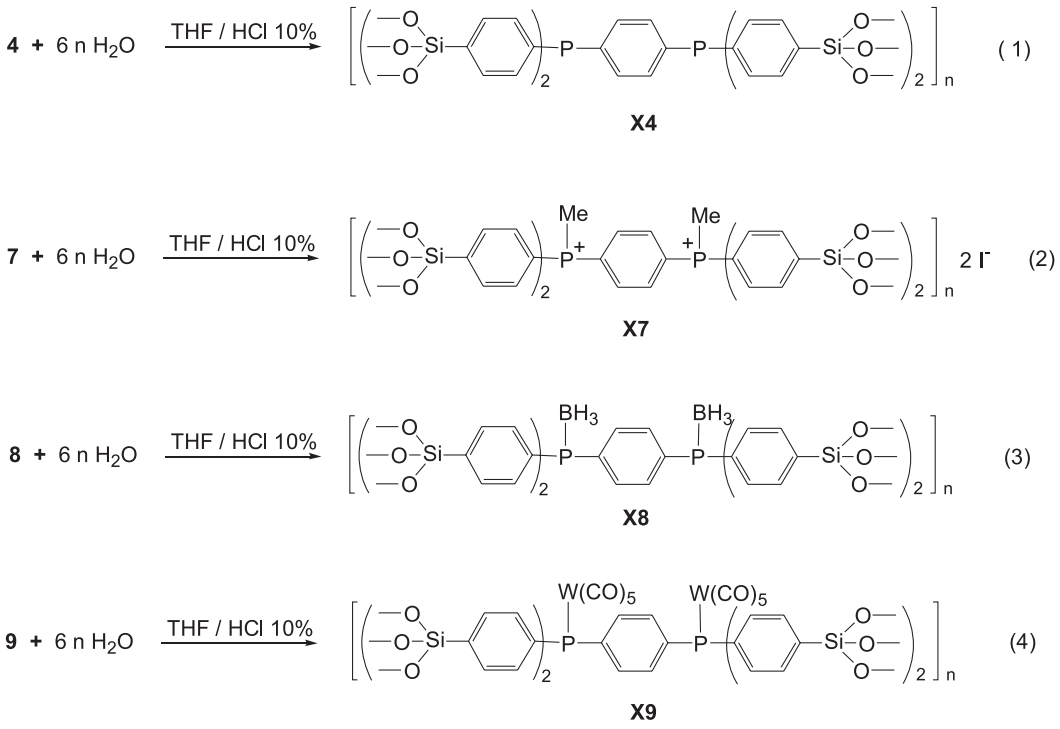
First we studied the oxidation of the phosphorus centres by reacting **X4** with an aqueous solution of H_2O_2 (60 equiv). The solid state ^{31}P NMR spectrum of the resulting xerogel showed the absence of the signal attributed to the phosphino group (–5.0 ppm) and the presence of a signal at 28.1 ppm assigned to the phosphine oxide centers (5).

X4 was treated with sulphur (13 equiv) in *n*-butanol heated under reflux for 48 h. The solid state ^{31}P NMR spectrum of the resulting xerogel exhibited only a signal at 41.3 ppm assigned to the thiophosphoryl centres (5).

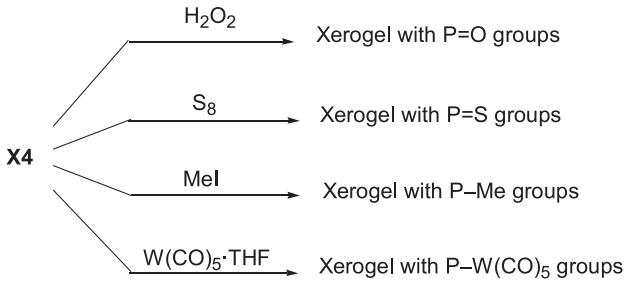
Treatment of **X4** with an excess of methyl iodide for 48 h in toluene heated under reflux gave rise to a xerogel, the solid state ^{31}P NMR spectrum of which displayed a signal at 21.5 ppm, close to that for **X7** (δ = 22 ppm). This signal indicates that all the phosphino groups were transformed into phosphonium salts.

Finally **X4** was treated with an excess of $W(CO)_5$·THF (4 equiv) in THF heated under reflux for 96 h. After the usual work-up, FTIR analysis of the resulting xerogel revealed the presence of the same CO stretching bands as those observed in **X9**, which characterize the expected $LW(CO)_5$. The solid state ^{31}P NMR spectrum of this xerogel displays a weak signal at 22.0 ppm corresponding to about 20% of complexed

© 2000 NRC Canada



Scheme 3.



phosphino centres and a large signal at –7.3 ppm corresponding at about 80% of unchanged phosphino groups (Fig. 1). Thus, most of the phosphino groups in xerogel **X4** are not accessible by $W(CO)_5$·THF under the conditions used for the reaction.

Discussion

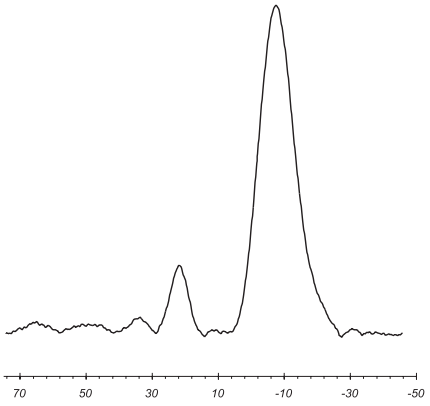
All the phosphorus atoms of the xerogel **X4** are accessible to the small reagents H_2O_2, S_8, and CH_3I as was previously observed for the xerogels **X1** and **X2** obtained from the phosphines **1** and **2** respectively (Table 2) (5). In contrast, the reaction with the rather bulky reagent $W(CO)_5$·THF allowed discrimination between the xerogels **X1**, **X2**, and **X4**. Indeed, only 20% of phosphorus atoms included into **X4** were complexed by $W(CO)_5$ while the complexation was complete for **X1** and was 80% for **X2** (Table 3).

In our previous publication (6) we have observed that the average number (N) of Si-O-Si bonds attached to each organophosphorous moiety in the material was an important parameter controlling the accessibility of the phosphino centres. This number N is a function of both the degree of condensation τ of the xerogel and the number f of hydrolysable SiX_3 groups of the precursor ($N = f \times \tau$) (see Table 2). We observed that the greater the N value, the more difficult was the accessibility of the phosphorus centres by the rather bulky reagent $W(CO)_5$·THF. The present study of the accessibility of the phosphorus centres incorporated into **X4** confirms this observation.

We consider that the number of Si—O—Si bonds should have an influence on the mobility of the network of the xerogel. The more important the mobility of the organic moieties, the easier is the penetration and the diffusion of the reagents into the hybrid organic-inorganic material (11, 12). Thus the diffusion of the reagent through **X1**, material in which the average number of Si—O—Si bonds by organic moiety is $N = 3.7$, is much easier than through **X4** in which the organic moieties are more rigid ($N = 6.6$). This interpretation is supported by ^{31}P NMR data of xerogels **X1**, **X2**, and **X4**. Indeed as shown on Fig. 2, the broadening of the ^{31}P NMR signals for xerogels increases with the average number N of Si—O—Si bonds attached to the organic moieties. The less flexible the organophosphorus moieties, the larger is the ^{31}P NMR signal of the phosphorus atoms (13).

© 2000 NRC Canada

Fig. 1. Solid state ^{31}P NMR spectrum of the xerogel **X4** after reaction with $W(CO)_5$·THF



Thus these NMR data confirm that the mobility of organophosphorous moieties decreases as *N* increases, the phosphorus atoms being less readily accessible to reagents owing to a lower swellability of the matrix.

In conclusion, this study and the preceding one (6) clearly show that the average number *N* of Si—O—Si bonds attached to the organic moiety is an important parameter controlling the accessibility of the phosphorus centers included in an hybrid organic-inorganic material. This shows the importance of the number of the hydrolysable SiX_3 bonds in the organic precursor. This parameter has been well evidenced because the precursors **1**, **2**, as well as **4** all bear rigid groups around the phosphorus centres. It is likely that in the case of phosphines with flexible groups around the phosphorus atoms, the situation is different.

Experimental

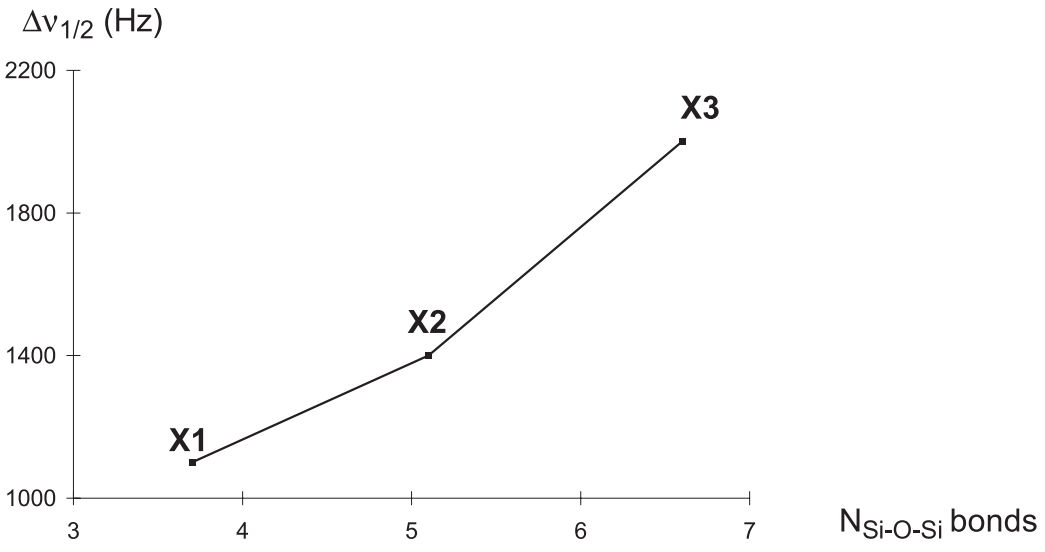
All reactions were carried out under argon by using a vacuum line. Solvents were dried and distilled just before use. Melting points were determined with a Gallenkamp apparatus and are uncorrected. IR data were obtained on a Perkin-Elmer 1600 FTIR spectrophotometer by the DRIFT method. The solution NMR spectra were recorded on a Bruker AC-200 (^{29}Si), Bruker DPX-200 (^{1}H and ^{13}C), and Bruker WP 250 SY (^{31}P, ^{11}B). Chemical shifts (δ in ppm) were referenced to Me_4Si (^{1}H, ^{13}C, ^{29}Si), BF_3·THF (^{11}B), or H_3PO_4 (^{31}P). The CP MAS solid state ^{29}Si NMR spectra were recorded on a Bruker FTAM 300 as well as CP MAS ^{13}C solid state NMR spectra in that case by using the TOSS technique. In both cases the repetition time was 5 and 10 s with contact times of 5 and 2 milliseconds. The HPDEC MAS ^{31}P solid state NMR spectra were recorded on a Bruker FTAM 300, a Brucker ASX 200, or a Brucker ASX 400 with repetition time of 5 s. FAB mass spectra (matrix, *m*-nitrobenzyl alcohol (NBA), thioglycerol (GT)) were registered on Jeol JMS-D3000 spectrometer. Specific surface areas were determined by the Brunauer-Emmett-Teller (BET) method on Micromeritics ASAP 2010 and Micromeritics Gemini III 2375 analysers. Elemental analyses were carried out by the Service Central de Micro- Analyse du CNRS.

Table 3. Solid state ^{31}P NMR chemical shifts (δ in ppm) of phosphorus atoms after treatment of the xerogels **X1**, **X2**, and **X4** with $W(CO)_5$·THF. The percent of each signal is indicated in parentheses.

	^{31}P HPDEC MAS NMR	
Xerogel	Complexed centers	Unchanged centers
X1 (f = 6)	21.1 (100%)	—
X2 (f = 9)	20.8 (80%)	–7.3 (20%)
X4 (f = 12)	22.0 (20%)	–5.9 (80%)

*P,P,P′,P′-tetrakis(4-triisopropyloxysilylphenyl)p-phenylenediphosphine (**4**)*: *P,P,P′,P′*-tetrachloro-*p*-phenylenediphosphine (14) (5.28 g, 18.9 mmol) in THF (50 mL) are added dropwise, at 0°C, to a solution of 4-triisopropyloxysilylphenylmagnesium bromide (77.4 mmol) in THF (200mL). The reaction mixture was stirred for 12 h at room temperature and then was heated under reflux for one hour. The THF was removed under vacuum and pentane (250 mL) was

Fig. 2. Half line width ($\Delta\nu_{1/2}$, 1100 Hz for **X1**, 1400 Hz for **X2**, 2000 Hz for **X4**) of the solid state ^{31}P NMR signals of xerogels **X1**, **X2**, and **X4** as a function of the average number *N* of Si-O-Si bonds (3.7 for **X1**, 5.1 for **X2**, 6.6 for **X4**).



© 2000 NRC Canada

added. After filtration and removal of the solvent under vacuum, 2-propanol (30 mL) was added under stirring to the oily residue (23.6 g). The resulting powder was recrystallised from 2-propanol to give 11.7 g, (10.1 mmol, 53%) of white crystals. Mp (2-propanol) 172–175°C; ^{1}H NMR (δ, 200 MHz, $CDCl_3$) 1.24 (d, $^{3}J_{H\text{-}H}$ = 6.1 Hz, 72H, Me), 4.30 (spt, $^{3}J_{H\text{-}H}$ = 6.1 Hz, 12H, OCH), 7.25–7.36 (m, 12H, aromatic), 7.65–7.70 (m, 8H, aromatic); ^{13}C NMR (δ, 50 MHz, $CDCl_3$) 25.9 (Me), 65.9 (OCH), 133–139 (aromatic); ^{29}Si NMR (δ, 40 MHz, $CDCl_3$) –61.9; ^{31}P NMR (δ, 100 MHz, $CDCl_3$) –4.9; MS (FAB+, GT) 1263 [$(M + H)^+$, 32%], 1295 [$(M + 2 \text{ oxygen} + H)^+$, 45%]. Anal. calc. for $C_{66}H_{104}O_{12}P_2Si_4$: C 62.75, H 8.24%; found: C 62.76, H 8.39.

*P,P,P′,P′-tetrakis(4-trihydrosilylphenyl)p-phenylenediphosphine (**5**)*: Diphosphine **4** (10.4 g, 8.23 mmol) in diethyl ether (80 mL) was added dropwise at 0°C to a suspension of $LiAlH_4$ (1.92 g, 50.5 mmol) in diethyl ether (60 mL). The reaction mixture was stirred for 3 h at room temperature and the solvent was then evaporated under vacuum to give a white solid which was dissolved in pentane (500 mL). After filtration of the salts and evaporation of the solvent under vacuum, 4.24 g (7.49 mmol) of raw diphosphine was obtained. Mp 172 (decomp.); ^{1}H NMR (δ, 200 MHz, $CDCl_3$) 4.23 (s and d (satellite ^{29}Si, $^{1}J_{Si\text{-}H}$ = 202 H), 9H, SiH), 7.23–7.62 (m, 20H, aromatic ; ^{13}C NMR (δ, 50 MHz, $CDCl_3$) 130–139 (aromatic) ; ^{29}Si NMR (δ, 40 MHz, $CDCl_3$) –58.7 ; ^{31}P NMR (δ, 80 MHz, $CDCl_3$) –4.6 ; IR (ν/cm^{-1}, CCl_4) 2160; MS (FAB+, NBA) 567 [$(M + H)^+$, 40%], 583 [$(M + 1 \text{ oxygen} + H)^+$, 56%]. Anal. calc. for $C_{30}H_{32}P_2Si_4$: C 63.60, H 5.65%; found: C 61.86, H 5.96.

*Dimethyl[P,P,P′,P′-tetrakis(4-triisopropyloxysilylphenyl)p-phenylene]diphosphonium diiodide (**7**)*: Diphosphine **4** (2.38 g, 1.88 mmol) and methyl iodide (0.5 mL, 8.03 mmol) were heated under reflux in toluene (20 mL) for 3 h. After evaporation of the solvent, 2.87 g (1.86 mmol, 99%) of crude **7** was obtained. Mp (2-propanol) 284.6 (decomp.) ; ^{1}H NMR (δ, 200 MHz, $CDCl_3$) 1.20 (d, $^{3}J_{H\text{-}H}$ = 6.1 Hz, 72H, Me), 3.23 (d, $^{2}J_{P\text{-}H}$ = 13.3 Hz, 6H, PMe), 4.28 (spt, $^{3}J_{H\text{-}H}$ = 6.1 Hz, 12H, OCH), 7.78–8.03 (m, 20H, aromatic); ^{13}C NMR (δ, 50 MHz, $CDCl_3$) 11.8 (d, $^{1}J_{P\text{-}C}$ = 56.7 Hz, PC), 25.9 (Me), 66.5 (OCH), 112–143 (aromatic) ; ^{29}Si NMR (δ, 40 MHz, $CDCl_3$) –65.8 ; ^{31}P NMR (δ, 100 MHz, $CDCl_3$) 22.7 ; MS (FAB+, GT) 1293 [$(M - 2I)^+$, 100%]. Anal. calc. for $C_{68}H_{110}O_{12}P_2Si_4$: C 52.78, H 7.11%; found: C 52.01, H 7.41.

*P,P,P′,P′-tetrakis(4-triisopropyloxysilylphenyl)p-phenylenediphosphine diborane (**8**)*: A molar solution of BH_3·THF in THF (4.1 mL, 4.1 mmol) was added dropwise, at 0°C, to 2.56 g (2.03 mmol) of **4** in THF (10 mL). After stirring one hour at room temperature the solvent was removed to give 2.61 g (2.02 mmol, 99%) of crude **8**. Mp 163.7 (decomp.); ^{1}H NMR (δ, 200 MHz, $CDCl_3$) 1.25 (d, $^{3}J_{H\text{-}H}$ = 6.1 Hz, 78H, Me+BH), 4.31 (spt, $^{3}J_{H\text{-}H}$ = 6.1 Hz, 12H, OCH), 7.54–7.81 (m, 20H, aromatic); ^{13}C NMR (δ, 50 MHz, $CDCl_3$) 25.9 (Me), 66.1 (OCH), 128–138 (aromatic); ^{11}B NMR (δ, 80 MHz, $CDCl_3$) –38.5 (broad signal); ^{29}Si NMR (δ, 40 MHz, $CDCl_3$) –63.5 (d, $^{5}J_{P\text{-}Si}$ = 1.2 Hz); ^{31}P NMR (δ, 100 MHz, $CDCl_3$) 22.1 (broad signal); MS (FAB+, GT) 1263 [$(M - 2BH_3 + H)^+$, 41%]. Anal. calc. for $C_{66}H_{110}O_{12}B_2P_2Si_4$: C 61.39, H 8.53%; found: C 60.86, H 8.35.

*P,P,P′,P′-tetrakis(4-triisopropyloxysilylphenyl)p-phenylenediphosphine bis tungsten pentacarbonyl (**9**)*: A THF solution of $W(CO)_5$·THF (15) (150 mL, 8.55 mmol) was added to 2.61 g (2.07 mmol) of **4**. After stirring for two hours at room temperature, the solvent was evaporated under vacuum. After elimination of excess of $W(CO)_5$·THF by sublimation at 60°C under vacuum, 3.71 g (1.94 mmol, 94%) of crude **9** was obtained. Mp (2-propanol) 203.6 (decomp.); ^{1}H NMR (δ, 200 MHz, $CDCl_3$) 1.25 (d, $^{3}J_{H\text{-}H}$ = 6.1 Hz, 72H, Me), 4.31 (spt, $^{3}J_{H\text{-}H}$ = 6.1 Hz, 12H, OCH), 7.44–7.80 (m, 20H, aromatic); ^{13}C NMR (δ, 50 MHz, $CDCl_3$) 25.9 (Me), 66.1 (OCH), 132.4–138.9 (aromatic), 197.4 (s and d $^{2}J_{P\text{-}C}$ = 6.8 Hz, CO cis), 199.4 (s and d $^{2}J_{P\text{-}C}$ = 22 Hz, CO trans); ^{29}Si NMR (δ, 40 MHz, $CDCl_3$) –63.3 (d, $^{5}J_{P\text{-}Si}$ = 1.2 Hz); ^{31}P NMR (δ, 100 MHz, $CDCl_3$) 21.7 (s d, $^{5}J_{P\text{-}Si}$ = 1.2 Hz); IR (ν/cm^{-1}, CCl_4) 1942, 1980, 2071; MS (FAB+, NBA) 1911 [$(M + H)^+$, 14%], 1587 [$(M - W(CO)_5 + H)^+$, 18%], 1263 [$(M - 2W(CO)_5 + H)^+$, 16%]. Anal. calc. for $C_{76}H_{104}O_{22}P_2Si_4$ W_2: C 47.75, H 5.44%; found: C 47.89, H 5.84.

Xerogel X4: To a THF (3.2 mL) solution of **4** (2.00 g, 1.58 mmol) in a 12.5 mL flask were added dropwise at room temperature 1.6 mL of a 6 M H_2O (9.6 mmol) and 0.1 M HCl (0.16 mmol) solution in THF. The mixture was stirred for 5 min, then the flask was placed in a water-bath at 30°C without stirring. Gelation occurred after 3h. The wet whitish gel was allowed to age for 5 days at 30°C after which it was powdered and washed with ethanol, acetone and ether. The powdering and washing were repeated once and the gel was powdered again and dried in vacuum for 2 h at 120°C to yield 1.14 g of **X4** as a white powder. Specific surface area, ^{31}P, ^{13}C, and ^{29}Si CP-MAS NMR are indicated in Table 1. Elemental anal. calc. for $C_{30}H_{20}O_6PSi_4$: C 55.38, H 3.07, O 14.77, P 9.54, Si 17.23; found: C 51.80, H 5.13, O 20.87, P 8.05, Si 14.15 which corresponds to $C_{33.24}H_{39.51}O_{10\cdot04}P_{2.00}Si_{3.89}$.

Xerogel X5: To a THF (5.7 mL) solution of **5** (1.76 g, 3.10 mmol) in a 20 mL test tube was added dropwise at 0°C in 5 min, under stirring, 3.1 mL of a 6 M H_2O (16.2 mmol) and 0.01 M nBu_4NF (0.03 mmol) solution in THF. The reaction mixture was then kept at room temperature without stirring. A release of dihydrogen was observed until gel formation (30h). The wet gel was left to age for 5 days at room temperature and the solid was subsequently treated as it was described before to give 1.93 g of white xerogel **X5**. Specific surface area, ^{31}P and ^{29}Si CP-MAS NMR are indicated in Table 1. IR (DRIFT) (ν/cm^{-1}) 2159 (Si-H). Elemental anal. calc. for $C_{30}H_{20}O_6PSi_4$: C 55.38, H 3.07, O 14.77, P 9.54, Si 17.23; found: C 53.82, H 4.36, O 15.87, P 9.25, Si 16.70 which corresponds to $C_{30.06}H_{29.22}O_{6.65}P_{2.00}Si_{3.99}$.

Xerogel X7: To a THF (1.3 mL) solution of 2 g (1.29 mmol) of **7** in a 12.5 mL flask were added dropwise at room temperature 1.3 mL of a 6 M H_2O (7.8 mmol) and 0.1 M HCl (0.13 mmol) solution in THF. The reaction mixture was stirred and gel formation occurred after one min. After drying, 1.32g of yellow **X7** was obtained. Elemental anal. calcd. for

© 2000 NRC Canada

$C_{32}H_{26}I_2O_6P_2Si_4$: C 41.11, H 2.78, I 27.20, O 10.28, P 6.64, Si 11.99; found: C 41.30, H 4.80, I 20.45, O 17.50, P 5.80, Si 10.15 which corresponds to $C_{36.79}H_{41.30}I_{1.72}O_{11.69}P_{2.00}Si_{3.87}$.

Xerogel X8: To a THF (1.55 mL) solution of 2.0 g (1.55 mmol) of **8** in a 12.5 mL flask were added dropwise at room temperature 1.55mL of a 6 M H_2O (9.3 mmol) and 0.1 M HCl (0.15 mmol) solution in THF. The reaction mixture was stirred for 5 min and kept at 30°C without stirring. Gel formation occurred after 15 min. However, after about 10 min a slight release of gas was observed so that the cork of the flask was pierced. After ageing, powdering and washing, 1.31 g of white powder was obtained. Drying 2 h at 120°C of 1.01 g of crude xerogel gave 882 mg of **X8**. ^{31}P CP MAS NMR spectra indicated a cleavage of P—B bonds of 50%. Elemental anal. calcd. for $C_{30}H_{26}B_2O_6P_2Si_4$: C 53.10, H 3.83, B 3.24, O 14.16, P 9.14, Si 16.52; found: C 50.47, H 5.17, B 1.95, O 22.01, P 6.20, Si 14.20 which corresponds to $C_{42.06}H_{51.7}B_{1.77}O_{13.76}P_{2.00}Si_{5.07}$. The cleavage of the P—B bond of the crude xerogel is 40%. It is of 70% if the crude xereogel is heated one night at 120°C.

Xerogel X9: To a THF (1.0 mL) solution of 2.0 g (1.05 mmol) of **9** in a 12.5 mL flask were added dropwise at room temperature 1.1mL of a 6 M H_2O (6.6 mmol) and 0.1 M HCl (0.11 mmol) solution in THF. The reaction mixture was stirred for 5 min and kept at 30°C without stirring. Gel formation occurred after 20min. After drying, 1.38 g of light beige **X9** was obtained. IR (DRIFT ν/cm^{-1}, KCl) 1934, 1986, 2072. Specific surface area and ^{31}P CP-MAS NMR data are indicated in Table 1. Elemental anal. calcd. for $C_{40}H_{20}O_{16}P_2Si_4W_2$: C 36.98, H 1.54, O 19.72, P 4.78, Si 8.63, W 28.30; found : C 30.33, H 2.88, O 28.55, P 3.81, Si 7.58, W 26.85 which corresponds to $C_{41.13}H_{46.86}O_{29.03}P_{2.00}Si_{4.40}W_{2.37}$.

Reactivity of X4 with H_2O_2

To a suspension of 325 mg (0.50 mmol) of **X4** in CH_2Cl_2 (20ml) were added dropwise at room temperature 5 mL of a 35% aqueous H_2O_2 solution (60 mmol). After 13 h stirring at room temperature, the suspension was filtered off and the precipitate was washed with water, ethanol, acetone, and diethyl ether. After drying, 296 mg of a white powder were obtained. ^{31}P NMR (δ, 162 MHz, HPDEC MAS) 28.1. S_{BET} < 370 m^2/g. Elemental anal. calc for $C_{30}H_{20}O_8P_2Si_4$: C 52.78, H 2.93, O 18.77, P 9.09, Si 16.42; found: C 47.39, H 4.34, O 26.07, P 7.35, Si 14.85 which corresponds to $C_{33.31}H_{36.61}O_{13.74}P_{2.00}Si_{4.47}$.

Reactivity of X4 with S_8

333 mg (0.51 mmol) of **X4**, 426 mg (13.3 mmol) of sulphur, and 24 mL of *n*-butanol were heated under reflux for 48 h. The hot suspension was then filtered (to remove the excess of sulphur) and the precipitate was washed twice with hot *n*-butanol (2 × 20 mL) then with acetone and diethyl ether. After drying under vacuum for 2 h at 120°C, 346 mg of a whitish solid was obtained. ^{31}P NMR (δ, 120 MHz, HPDEC MAS) 41.3. S_{BET} = 415 m^2/g. Elemental anal. calc. for $C_{30}H_{20}O_6P_2S_2Si_4$: C 50.42, H 2.80, O 13.45, P 8.68, S 8.96, Si 15.69%; found: C 49.91, H, 4.68, O 18.75, P 6.90, S 6.19, Si 13.75%, which corresponds to $C_{37.37}H_{42.00}O_{10.53}P_{2.00}S_{1.74}Si_{4.41.}$

Reactivity of X4 with MeI

334 mg (0.514 mmol) of **X4** and 0.25 mL (4.0 mmol) of methyl iodide were heated under reflux in toluene (10ml) for 48 h. After filtration, the precipitate was washed with ethanol, acetone and diethyl ether, and dried to give 398 mg of a yellow powder. ^{31}P NMR (δ, 162 MHz, HPDEC MAS) 21.4. S_{BET} < 10 m^2/g. Elemental anal. calc. for $C_{36}H_{26}I_2O_6P_2Si_4$: C 41.11, H 2.78, I 27.20, O 10.28, P 6.64, Si 11.99%; found: C 43.40, H 4.53, I 15.32, O 17.25, P 7.30, Si 12.20 which corresponds to $C_{30.72}H_{38.47}$ $I_{1.02}$ $O_{9.16}P_{2.00}Si_{3.70}$.

Reactivity of X4 with $W(CO)_5$·THF

302 mg (0.46 mmol) of **X4** and 70 mL of a 0.057 M THF solution of $W(CO)_5$·THF (4.0 mmol) were heated under reflux and stirring for 96 h. The greenish suspension was then filtered and the precipitate was washed twice with THF (2 × 30 mL) then with ethanol, acetone, and ethyl ether. After drying under vacuum for 2 h at 120°C, 344 mg of a pale green solid was obtained. ^{31}P NMR (δ, 120 MHz, HPDEC MAS) 20.8 (20%), –5 (80%). IR (DRIFT ν/cm^{-1}, KCl) 1935, 1984, 2072. S_{BET} = 380 m^2/g. Elemental anal. calc for $C_{40}H_{20}O_{16}P_2Si_4W_2$: C 36.98, H 1.54, O 19.72, P 4.78, Si 8.63, W 28.35; found: C 43.67, H 3.58, O 23.25, P 5.90, Si 11.80, W 11.80% which corresponds to $C_{38.24}H_{37.62}O_{15.27}P_{2.00}Si_{4.43}W_{0.67}$.

References

1. U. Schubert, N. Hüsing, and A. Lorenz. Chem. Mater. **7**, 2010 (1995).
2. D.A. Loy and K.J. Shea. Chem. Rev. **95**, 1431 (1995).
3. R.J.P. Corriu and D. Leclercq. Angew. Chem. Int. Ed. Engl. **35**, 1420 (1996); G. Cerveau and R.J.P. Corriu. Coord. Chem. Rev. **178–180**, 1051 (1998).
4. R. Corriu. C. R. Acad. Sci. Ser. II 83 (1998); R. Corriu. Polyhedron, **5–6**, 925 (1998).
5. J.P. Bezombes, C. Chuit, R.J.P. Corriu, and C. Reyé. J. Mater. Chem. **8**, 1749 (1998).
6. J.P. Bezombes, C. Chuit, R.J.P. Corriu, and C. Reyé. J. Mater. Chem. **9**, 1727 (1999).
7. E.M.J. Evleth, L.V.D. Freeman, and R.I. Vagner. J. Org. Chem. **27**, 2192 (1962).
8. K.J. Shea, D.A. Loy, and O. Webster. J. Am. Chem. Soc. **114**, 6700 (1992).
9. G. Cerveau, R.J.P. Corriu, C. Lepeytre, and P.H. Mutin. J. Mater. Chem. **8**, 2707 (1998).
10. R.J.P. Corriu, J.J.E. Moreau, and M. Wong Chi Man. J. Sol-Gel Sci. Technol. **2**, 87 (1994).
11. E. Lindner, M. Kemmler, T. Schneller, and H.A. Mayer. Inorg. Chem. **34**, 5489 (1995).
12. E. Lindner, T. Schneller, H.A. Mayer, H. Bertagnolli, T.S. Ertel, and W. Hörner. Chem. Mater. **9**, 1524 (1997).
13. E. Lindner, R. Schreiber, M. Kemmler, T. Schneller, and H.A. Mayer. Chem. Mater. **7**, 951 (1995).
14. E.M.J. Evleth, L.V.D. Freeman, and R.I. Wagner. J. Org. Chem. **27**, 2192 (1962).
15. R.B. King and N.D. Sadanani. Inorg. Chem. **24**, 3136 (1985).

© 2000 NRC Canada

Synthesis and reactivity of the stable silylene *N,N′*-di-*tert*-butyl-1,3-diaza-2-sila-2-ylidene

Michael Haaf, Thomas A. Schmedake, Bryan J. Paradise, and Robert West

Abstract: The synthesis and several reactions of the stable silylene **1** (*N,N′*-di-*tert*-butyl-1,3-diaza-2-sila-2-ylidene) are reported. Overreduction of **1** with alkali metals results in the formation of a dimeric dianion, which can be trapped with a proton source to give the dihydride derivative **9**. In the solid state or in concentrated solutions, **1** undergoes a reversible conversion into the novel tetrameric disilene, **10**. **1** reacts with ethanol, phenol, and water via insertion into the O—H bond, and with iodomethane by insertion into the C—I bond. A reaction of **1** with the diene 2,3-dimethyl-1,3-butadiene affords the silacyclopentene, **15**. This reaction is markedly different from the one found for the unsaturated analog of the silylene, **2**, which catalyzes the conversion of this diene into a highly cross-linked polymer.

Key words: silylene, carbene analog, disilene, divalent compounds, *N*-heterocycles.

Résumé : On a réalisé la synthèse du *N,N′*-di-*tert*-butyl-1,3-diaza-2-sila-2-ylidène (**1**), un silylène stable, sur lequel on a effectué plusieurs réactions. Une surréduction de **1** avec des métaux alcalins conduit à la formation d'un dianion dimère que l'on peut piéger avec une source de proton pour obtenir le dérivé dihydrure **9**. À l'état solide ou en solutions concentrées, **1** subit une conversion réversible en un nouveau disilène tétramère, **10**. Le produit **1** réagit avec l'éthanol, le phénol et l'eau par le biais d'une insertion dans la liaison O—H et avec l'iodométhane par insertion dans la liaison C—I. Une réaction de **1** avec le 2,3-diméthylbuta-1,3-diène conduit à la formation du silacyclopentène, **15**. Cette réaction est très différente de celle qui est observée avec le composé **2**, l'analogue insaturé du silylène, qui catalyse la conversion de ce diène en un polymère hautement réticulé.

Mots clés : silylène, analogue de carbène, disilène, composés bivalents, hétérocycles azotés.

[Traduit par la Rédaction]

Introduction

Silylenes (R_2Si:), the silicon analogs to carbenes in organic chemistry, are key intermediates in numerous thermal and photochemical reactions of organosilicon compounds and hence are extremely important in the field of silicon chemistry (for recent reviews, see ref. (1)). Until recently, silylenes have been observed only at low temperatures in argon or hydrocarbon matrices, disappearing quickly at temperatures above 77 K.

In 1994, syntheses were reported for two novel silylenes, **1** (2) and **2** (3). The unsaturated silylene **2** has truly remarkable thermal stability; it can be sublimed or distilled at 85°C (1 torr, 1 torr = 133.322 Pa), survives heating in toluene at 150°C indefinitely, and decomposes only at its melting point of 220°C. The properties of **2** reflect the electron donation from the nitrogen to the silicon, stabilizing the vacant *p*-orbital on the silicon atom, as well as aromatic delocalization in the six π-electron ring (4, 5). By comparison, silylene **1**, which does not benefit from aromaticity, is significantly less stable, converting into a red product in concentrated solutions or in the solid state at room temperature. Since the synthesis of **1** and **2**, four additional stable silylenes **3a** (6)**, 3b** (7), **4** (8), and **5** (9), have subsequently been reported.

The reactions of **2** (10) and **3a** (11) have been explored and reactions common to these silylenes are shown in eq. [1]. However, no reactions of the saturated analog, **1**, have been reported. Herein we report an improved variation of a previously reported synthesis for silylene **1** (2), several reactions involving insertion of the silylene into a variety of chemical bonds, and a discussion of the novel disilene formed from the saturated silylene in the solid state or in concentrated solutions (12).

Results and discussion

The synthetic pathway for **1** is outlined in eq. [2]. Diamine **6**, formed from dibromoethane and *tert*-butylamine in refluxing hexane, was treated with silicon tetrachloride in the presence of triethylamine (TEA) to give **7**, the five-membered

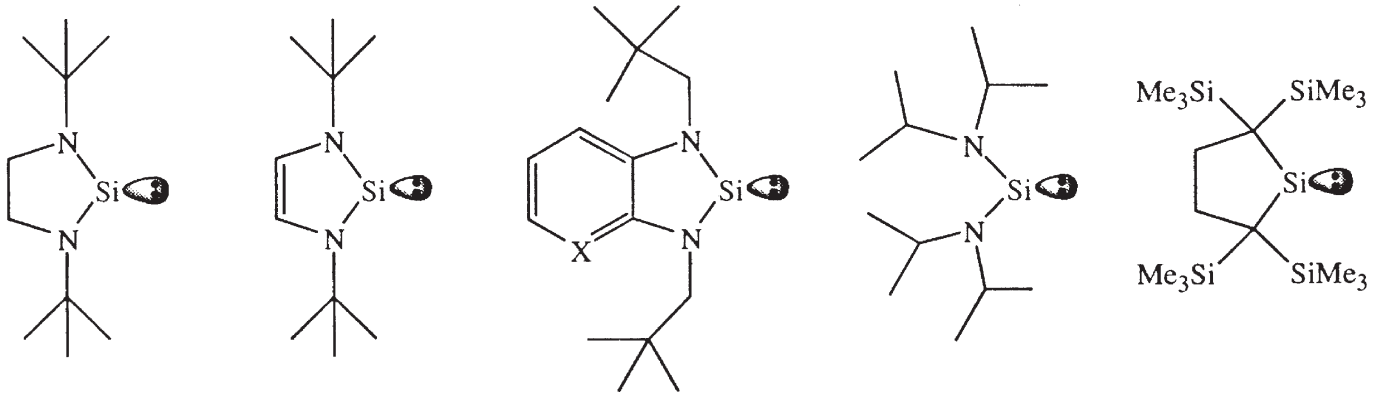
Received August 3, 1999. Published on the NRC Research Press website on November 2, 2000.

Dedicated to Professor Adrian Brook, the father of silenes, a true pioneer of organosilicon chemistry.

M. Haaf, T.A. Schmedake, B.J. Paradise, and R. West.[1] Department of Chemistry, University of Wisconsin-Madison, Madison, WI 53706, U.S.A.

[1]Author to whom correspondence may be addressed. Telephone: (608) 262-1873. Fax: (608) 262-6143. e-mail: west@chem.wisc.edu

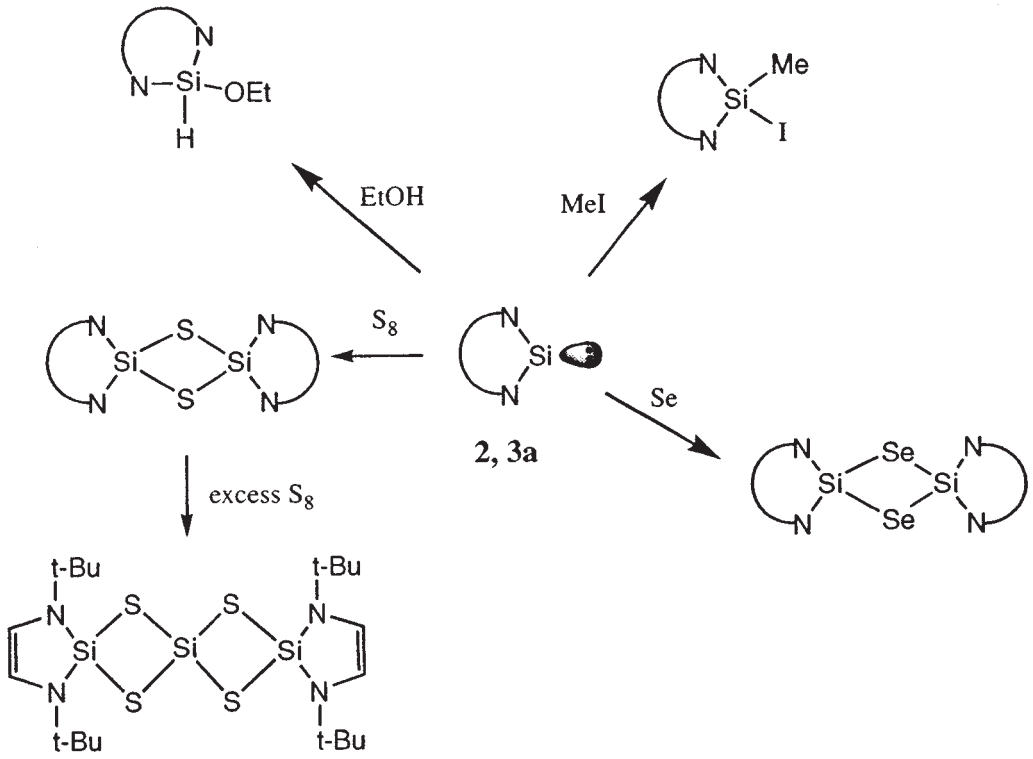
 © 2000 NRC Canada



1 **2** **3** **4** **5**

a X = C
b X = N

[1]



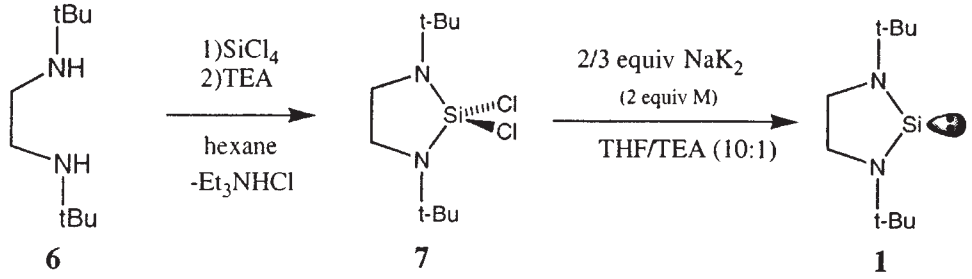
N-heterocyclic precursor to **1**. Sublimation of the dichloride precursor **7** at 53°C and 0.1 torr (1 torr = 133.322 Pa) affords clear, colorless crystals.

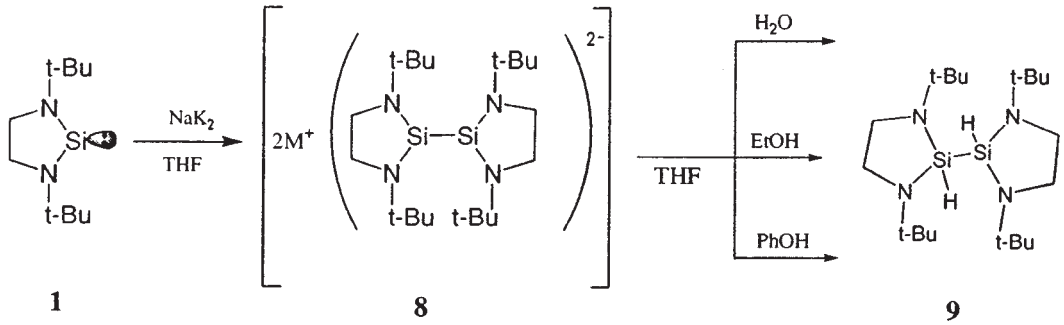
Dechlorination of **7** to produce **1** took place upon treatment with sodium potassium alloy in a 10:1 THF–TEA solution for approximately 3 h.

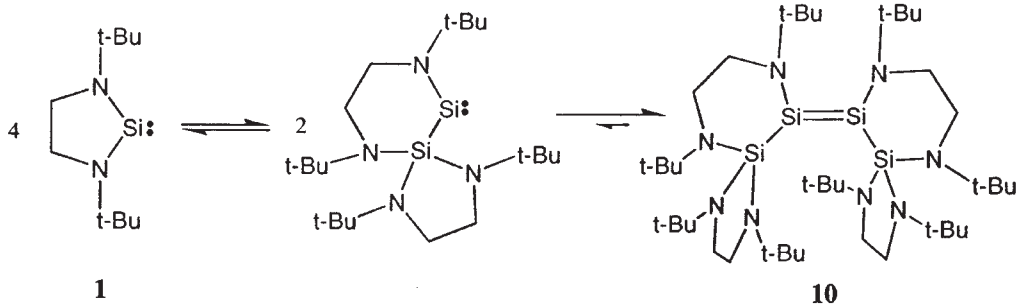
Although the reduction of **7** can be performed at room temperature with Na–K alloy in neat THF, these reaction conditions often result in the formation of overreduced products, such as the dimeric dianion **8** shown in eq. [3]. Evidently, the reduction of the silylene **1** competes with the reduction of the dichloride **7**, resulting in a lower yield of silylene. The anionic species of the silylene has yet to be fully characterized, but it can be trapped in nearly quantitative yields. Formation of the dihydride **9**, by trapping of the dianion with a proton source, provides evidence for the dimeric nature of the overreduced silylene. The crystal structure of **9** is displayed in Fig. 1.

The presence of triethylamine in the reaction mixture appears to decrease the rate of reduction for the silylene, affording silylene **1** in yields in excess of 95% according to NMR. However, overreduction of the silylene can still take place once the dichloride is used up. Consequently, the reaction must be carefully monitored by ^{1}H NMR and the

© 2000 NRC Canada

[2] 

[3] 

[4] 

reducing agent must be filtered away from the reaction mixture as soon as all of the dichloride is consumed.

Evaporation of the solvent leaves a red-black residue, which can be sublimed (60°C, 0.1 torr (1 torr = 133.322 Pa)) as colorless crystals of **1**. Although crystals of the unsaturated silylene, **2**, are stable under inert conditions, the crystals of **1** "decompose" over a period of days to a red powdery material, which has been characterized as the novel tetrameric disilene **10** (12; similar insertions into metal–nitrogen bonds have been observed. See for example ref. (13)). Remarkably, the interconversion between **1** and **10** is reversible (eq. [4]). Dissolving crystals of **10** in an inert solvent produces a concentration dependent equilibrium mixture of silylene and disilene, with dilution favoring silylene formation. A 0.013 M solution of disilene in THF will effectively convert to a solution containing 100% silylene over a period of 2 h. Conversely, attempts to crystallize silylene from solution inevitably lead to crystallization of **10**. Unlike **1**, disilene **10** can be stored indefinitely in a dry box and dissolved prior to use.

Reactions of 1

The reactivity of silylene **1** (eq. [5]) appears to be similar in many ways to that of the unsaturated silylene **2** (10). It does not insert into Si—H bonds, nor does it behave as a Lewis acid, even in the presence of relatively strong bases (THF, triethylamine).

However, like the more reactive transient silylenes, **1** does insert into O—H bonds of hydroxyl compounds. With alcohols such as ethanol and phenol, the product formed is the corresponding ethoxysilane **11** (liquid, bp = 38°C, 0.1 torr (1 torr = 133.322 Pa)) or phenoxysilane **12** (Fig. 2). Water reacts with **1** to give disiloxane **13**, presumably through condensation of an intermediate silanol. **1** will also readily insert into the C—I bond of iodomethane to form the corresponding alkyliodosilane, **14**.

Not all reactions of **1** and **2** are identical. Contrary to the unsaturated silylene **2**, which catalyzes the conversion of 2,3-dimethyl-1,3-butadiene into a highly cross-linked, insoluble polymer, the saturated silylene undergoes a 1 + 4 cycloaddition reaction with the diene to give the 1-sila-3-cyclopentene **15**. Clear, colorless crystals of **15** were obtained in nearly quantitative yields by reacting **1** with 2,3-dimethyl-1,3-butadiene. The crystal structure is shown in Fig. 3. The two five-membered rings in **15** are nearly perpendicular (89.5°).

Experimental

All reactions and manipulations were conducted under an argon atmosphere using standard Schlenk techniques.

© 2000 NRC Canada

[5]

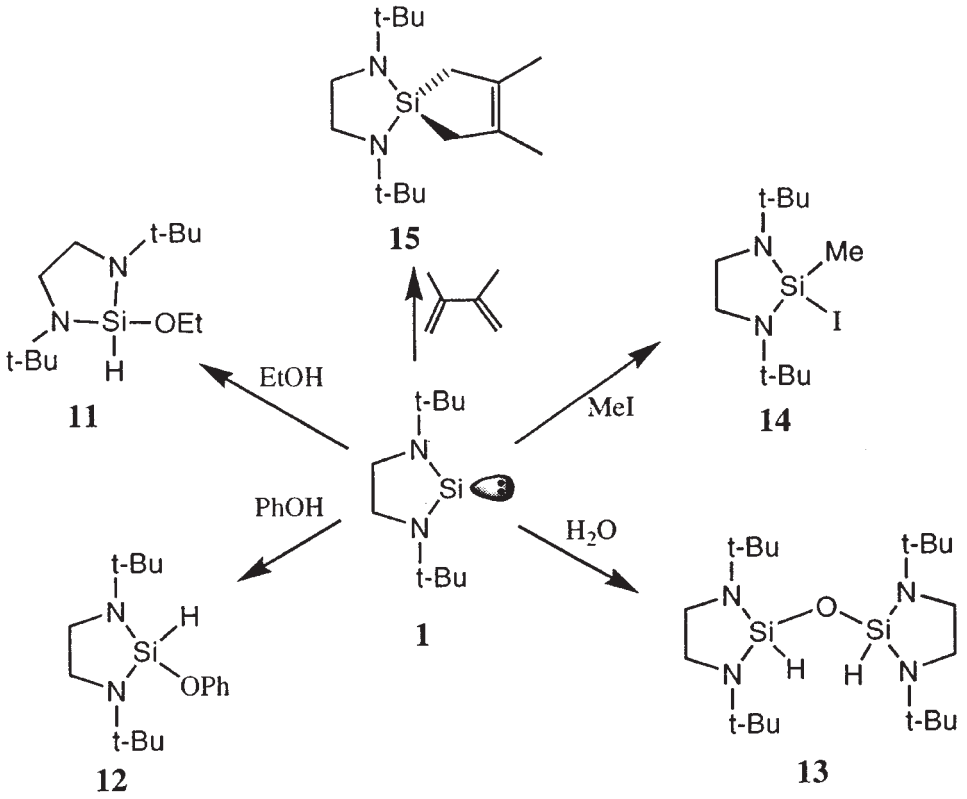
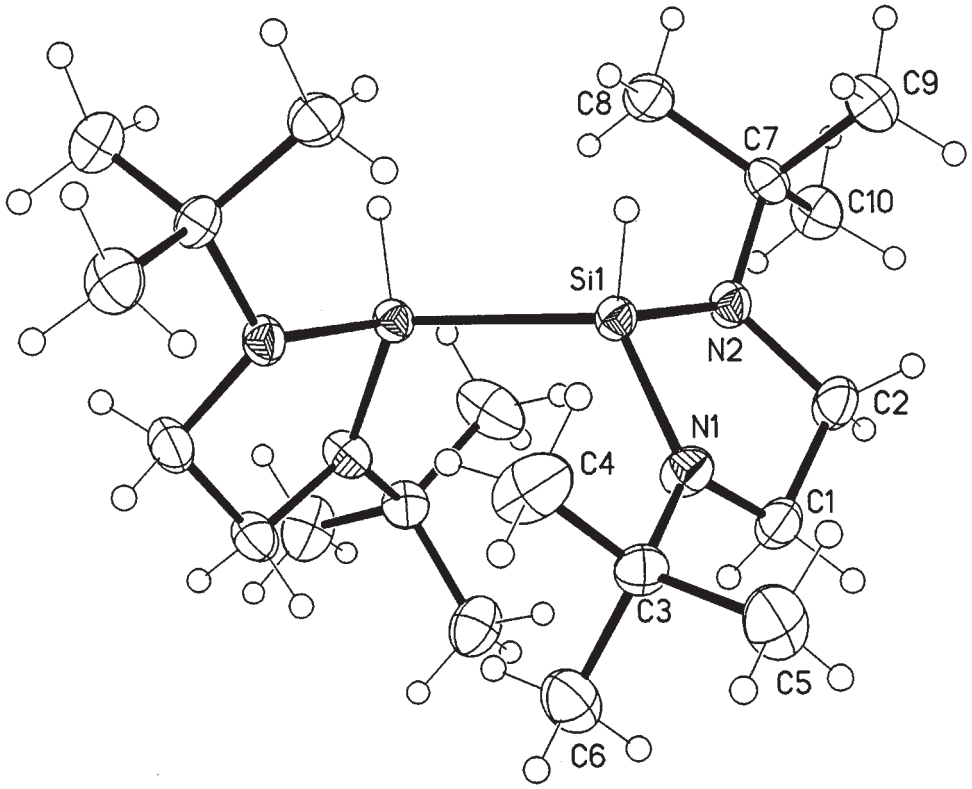
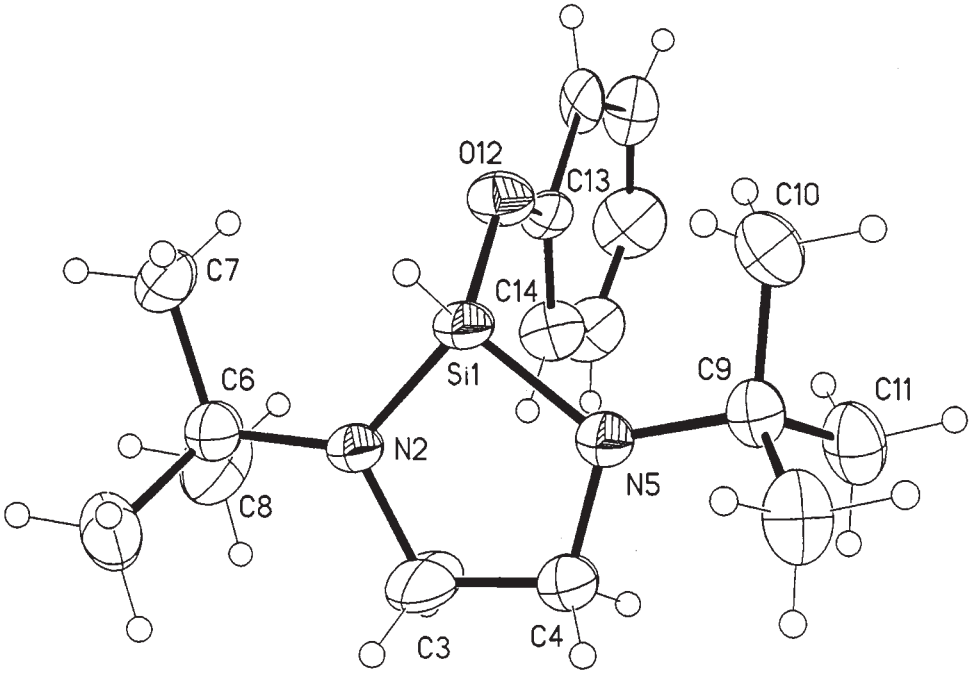


Fig. 1. Crystal structure of **9** (50% probability ellipsoids). Selected bond lengths: Si(1)—N(1) = 1.7373(19) Å, Si(1)—N(2) = 1.7508(18) Å, Si(1)—Si(1)′ = 2.4081(11) Å. Selected bond angles: N(1)-Si(1)-N(2) = 93.94(9)°, N(1)-Si(1)-Si(1)′ = 118.87(7)°, N(2)-Si(1)-Si(1)′ = 112.76(7)°. Selected torsion angles: N(1)-Si(1)-Si(1)′-N(1)′ = –38.5(2)°, N(1)-Si(1)-Si(1)′-N(1)′ = 70.0(2)°



© 2000 NRC Canada

Fig. 2. Molecular structure of phenoxysilane **12** (50% probability ellipsoids). Selected bond lengths: Si(1)—O(12) = 1.789(7) Å, Si(1)—N(5) = 1.690(6) Å, Si(1)—N(2) = 1.696(6) Å. Selected bond angles: N(5)-Si(1)-N(2) = 96.1(3)°, N(5)-Si(1)-O(12) = 110.4(3)°, N(2)-Si(1)-O(12) = 109.9(3)°, Si(1)-O(12)-C(13) = 132.1(5)°. Selected torsion angle: Si(1)-O(12)-C(13)-C(14) = 12.7(15)°.



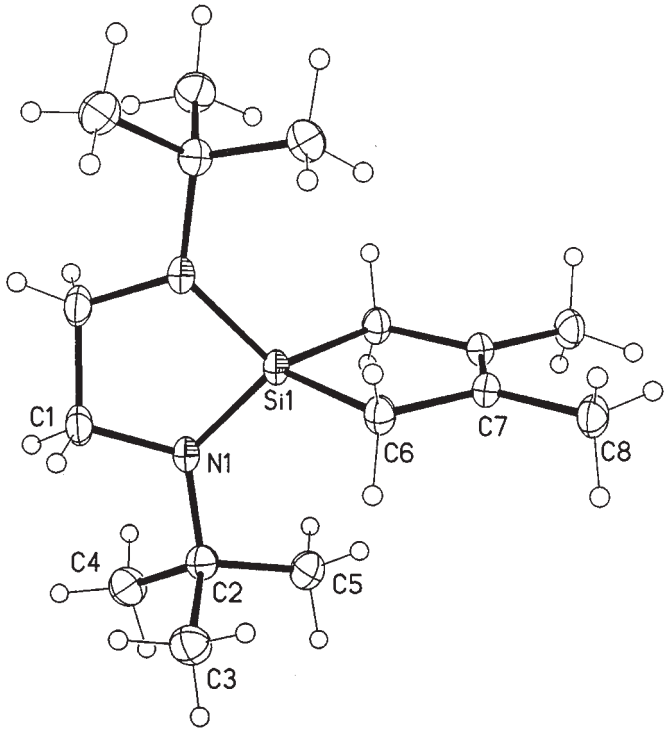
Dibromoethane, *tert*-butylamine, silicon(IV) chloride, 2,3-dimethyl-1,3-butadiene and phenol, were purchased and used without further purification. All of the reaction solvents were dried and distilled in an inert atmosphere. Lithium and potassium were purchased in mineral oil and washed with hexane or pentane before use.

Proton NMR spectra were recorded on either a Bruker AC-250 or a Bruker AC-300 spectrometer. Silicon-29 NMR spectra were collected on a Bruker 500 MHz spectrometer. Carbon-13 NMR spectra were taken on a Bruker AC-300 spectrometer. Solid state ^{29}Si NMR spectra were determined on a Varian 500 MHz spectrometer or a Bruker 360 MHz spectrometer. All NMR spectra were taken in solutions of deuterated benzene.

Synthesis of *N*,*N*′-di-*tert*-butylethylenediamine (6)

Into a 1 L three-necked round bottom flask fitted with a condenser, a gas inlet, a stopper and a septum, dibromoethane (141 g, 65 mL, 0.75 mol), *tert*-butylamine (274 g, 394 mL, 3.75 mol), hexane (100 mL), and water (100 mL) were added. The reaction mixture was brought to a boil and was allowed to reflux for three days. During this time period, a precipitate formed and two layers became apparent. After refluxing, the mixture was cooled in an ice bath and three portions of 27.0 g of NaOH (81.0 g total) were sequentially added to the reaction mixture. The heat generated from this addition caused the reaction to begin refluxing again. After cooling, the reaction mixture was decanted away from the precipitate and into a separatory funnel. The hexane (top) layer was saved and stored over NaOH. This organic layer was then distilled to remove the hexane and any unreacted dibromoethane or *tert*-butylamine. The distillation was then continued under vacuum and 93 g

Fig. 3. Crystal structure of the butadiene trap, **15** (50% probability ellipsoids). Selected bond lengths: Si(1)—N(1) = 1.7377(11) Å, Si(1)—N(1)′ = 1.7378(11) Å, Si(1)—C(6) = 1.9010(12) Å, C(6)—C(7) = 1.5214(17) Å, C(7)—C(7)′ = 1.349(3) Å. Selected bond angles: N(1)-Si(1)-N(1)′ = 94.38(7)°, N(1)-Si(1)-C(6) = 119.51(5)°, N(1)-Si(1)-C(6)′ = 115.74(6)°. Angle of intersection between planes defined by N(1)-Si(1)-N(1)′ and C(6)-Si(1)-C(6)′ = 86.9(15)°.



© 2000 NRC Canada

(72%) of product **6** was collected (49°C, 0.1 torr (1 torr = 133.322 Pa)) The product was stored over NaOH to keep it dry. ^{1}H NMR δ: 1.014 (s,18H), 2.541 (s, 4H). ^{13}C NMR δ: 29.5, 43.6, 49.8.

Synthesis of *N,N′-di-tert*-butyl-1,3-diaza-2,2-dichloro-2-silacyclopentane (7)

Into a three-necked 2 L flask equipped with a condenser, gas inlet, stopper, stir bar, and septum was added *N,N′*-di-*tert*-butylethylenediamine **6** (20.0 g, 116 mmol) and hexane (250 mL). The solution was stirred at 0°C while $SiCl_4$ (20.0 g, 118 mmol) was added via syringe. The solution was then allowed to warm to room temperature, at which time triethylamine (40 mL) was added. The solution was heated to reflux and left stirring overnight, and was then allowed to cool to room temperature. The reaction mixture was filtered under vacuum and the ammonium salt precipitate was washed with two aliquots of hexane (300 mL each). The hexane filtrate was subsequently concentrated to dryness. The remaining white solid was purified by distillation (90°C, 1 torr (1 torr = 133.322 Pa)), affording 21.0 g (67.2%) of a colorless, crystalline solid. This product can be stored indefinitely under an atmosphere of nitrogen. ^{1}H NMR δ: 1.20 (s, 18H), 2.71 (s, 4H). ^{13}C NMR δ: 29.0, 41.7, 51.8.

Synthesis of *N,N′*-di-*tert*-butyl-1,3-diaza-2-sila-2-ylidene (1)

A solution of *N,N′*-di-*tert*-butyl-1,3-diaza-2,2-dichloro-2-silacyclopentane, **7**, (10 g, 37.1 mmol) in THF (100 mL) was made up in a flame-dried, degassed Schlenk flask. A three-necked, 250 mL flask was equipped with a stir bar, frit, septum, and stopper. On the other end of the frit was placed a 250 mL Schlenk flask equipped with a stir bar and attached to the Schlenk line. The apparatus was rigorously flame-dried and charged with argon. Freshly cut potassium (2.0 g) and sodium (0.6 g) were added to the three-necked flask under a heavy flow of argon. The apparatus was then evacuated, and the flask heated with a heat gun to melt the potassium and sodium chunks to generate NaK_2. The apparatus was again charged with argon, and cooled to room temperature at which point 50 mL freshly distilled THF and 20 mL freshly distilled TEA were added to the flask. The apparatus was then cooled in a dry ice – acetone bath. The solution of **7** in THF was added to the flask, and the apparatus was warmed to room temperature. The reaction was monitored by ^{1}H NMR and filtered when complete (approximately 2–3 h). It is important to filter immediately upon completion for maximal yield. The filtrate was concentrated to give 6 g (80%) of crude product and recrystallized from THF to give crystals of disilene **10** (5.0 g, 68%). ^{1}H NMR (for **1**) δ: 1.269 (s, 18H), 3.140 (s, 4H). ^{13}C NMR δ: 31.68, 46.46, 52.46. ^{29}Si NMR δ: 118.9.

Synthesis of dihydride (9)

A solution of *N,N′-di-tert*-butyl-1,3-diaza-2,2-dichloro-2-silacyclopentane, **7**, (1.0 g, 3.7 mmol) in THF (20 mL) was made up in a flame-dried, degassed Schlenk flask. A three-necked, 250 mL flask was equipped with a stir bar, frit, septum, and stopper. On the other end of the frit was placed a 250 mL Schlenk flask equipped with a stir bar and attached to the Schlenk line. The apparatus was rigorously flame-dried and charged with argon. Freshly cut potassium (1.0 g, 25.5 mmol) and sodium (0.33 g, 14.3 mmol) were added to the three-necked flask under a heavy flow of argon. The apparatus was then evacuated, and the flask heated with a heat gun to melt the potassium and sodium chunks to generate NaK_2. The apparatus was again charged with argon, and cooled to room temperature at which point 30 mL freshly distilled THF was added to the flask. The apparatus was then cooled in a dry ice – acetone bath. The solution of **7** in THF was added to the flask via cannula, and the apparatus was warmed to room temperature. Upon warming the solution turned black. Regular monitoring by ^{1}H NMR indicated a gradual formation and then disappearance of silylene over a 3 h period. Eventually no silylene peaks were observed in the NMR. At this point the solution was filtered. The filtrate was cooled in a dry ice – acetone bath and reacted with 1 equiv of a proton source (water, EtOH, phenol) to produce the dihydride in 95% yield (by NMR). Crystals suitable for X-ray analysis were grown from THF. HRMS : *m/z* 398 [M^+]. Exact mass calcd. for $C_{20}H_{46}N_4Si_2$ *m/z*: 398.3261; found: 398.3210. ^{1}H NMR δ: 1.293 (s, 36H), 2.965 (s, 8H), 5.739 (s, 2H). ^{13}C NMR δ: 29.71, 44.78, 50.73. ^{29}Si NMR δ: –23.9.

Synthesis of tetramer (10)

Disilene **10** was produced by recrystallization of **1** from THF or diethyl ether. Alternatively, crystals of **1** will slowly convert in the solid state to disilene **10**. ^{1}H NMR δ: 1.368 (s, 18H), 1.416 (s, 18H), 1.429 (s, 18H), 1.575 (s, 18H), 2.9–3.1 (m, 16H). ^{13}C NMR δ: 30.16, 30.22, 31.0, 31.20, 42.50, 42.56, 45.41, 51.36, 51.55, 51.67, 55.59, 55.67. ^{29}Si NMR δ: 119.0, –25.0.

Reaction of 1 with ethanol

A dried, degassed Schlenk flask was charged with 0.222 mL of ethanol (3.8×10^{-3} mol) and 10 mL THF, then placed in a dry ice – acetone bath. A solution of **1** (0.075 g (3.8×10^{-3} mol)/50 mL THF) was added and the flask was allowed to warm to room temperature. The ethanol insertion product **11** is a liquid, which can be isolated by fractional distillation (38°C, 0.1 torr (1 torr = 133.322 Pa)) (60%). ^{1}H NMR δ: 1.207 (s, 18H), 1.207 (t, 3H, J = 6.9 Hz), 2.88–2.94 (m, 4H), 3.736(q, 2H, J = 6.9 Hz), 5.090 (s, 1H). ^{13}C NMR δ: 18.41, 29.58, 43.05, 50.50, 56.92. ^{29}Si NMR δ: –44.5.

Reaction of 1 with phenol

A dried, degassed Schlenk flask was charged with 0.475 g of phenol (5.0×10^{-3} mol) and 30 mL THF, then placed in a dry ice – acetone bath. A solution of **1** (1.0 g (5.05×10^{-3} mol)/50 mL THF) was added and the flask was allowed to warm to room temperature. The insertion product **12** was formed in 80% yield by NMR. Recrystallization from THF provided crystals of **12** suitable for X-ray analysis. ^{1}H NMR δ: 1.130 (s, 18H), 2.9–3.0 (m, 4H), 5.354 (s, 1H), 6.7–7.2 (m, 5H). ^{13}C NMR δ: 29.38, 42.81, 50.69, 116.5,121.6, 123.3, 129.9. ^{29}Si NMR δ: –46.6.

Reaction of 1 with water

A dried, degassed Schlenk flask was charged with 0.034 mL of water (1.9×10^{-3} mol) and 10 mL THF, then placed in a dry ice – acetone bath. A solution of **1** (0.075 g

© 2000 NRC Canada

Table 1. Crystallographic data for **9**, **12**, and **15**.

	9	12	15
Formula	$C_{20}H_{46}N_4Si_2$	$C_{16}H_{28}N_2OSi$	$C_{16}H_{32}N_2Si$
Fw	398.79	292.49	280.53
Cryst size (mm^3)	0.40 × 0.40 × 0.30	0.30 × 0.20 × 0.17	0.40 × 0.30 × 0.10
a (Å)	15.6331(7)	12.7614(12)	15.087(2)
b (Å)	13.3956(7)	9.3774(12)	10.1328(13)
c (Å)	11.7738(6)	14.3743(14)	11.9175(15)
α (deg)	90	90	90
β (deg)	90.679(2)	90	112.040(3)
γ (deg)	90	90	90
Cryst syst	monoclinic	orthorombic	monoclinic
Space group	C2/c	Pnma	C2/c
Vol ($Å^3$)	2465.4(2)	1720.2(3)	1688.8(4)
D_{calc} (mg m^{-3})	1.074	1.129	1.103
Z	4	4	4
Temp (K)	143(2)	138(2)	133(2)
Abs coeff (mm^{-1})	0.155	0.136	0.131
No. reflns collected	4692	8778	3966
No. indep reflns	2154	1615	2034
θ range (deg)	2.61–25.0	2.13–25.0	2.48–29.04
*R*1 (final *R* indices)	0.0547	0.1017	0.0377
*wR*2 (final *R* indices)	0.1096	0.2388	0.1057

(3.8×10^{-3} mol)/10 mL THF) was added and the flask was allowed to warm to room temperature. The water insertion product **13** was the major product (55% yield by NMR). Excess water produces *N*,*N*′-di-*tert*-butylethylenediamine (**6**) as a significant byproduct. HRMS: *m*/*z* 414 [M^+]. Exact mass calcd. for $C_{20}H_{46}ON_4Si_2$ *m*/*z*: 414.3210; found: 414.3210. ^{1}H NMR δ: 1.292 (s, 36H), 2.95–3.05 (m, 8H), 5.282 (s, 2H). ^{13}C NMR δ: 29.66, 42.86, 50.76. ^{29}Si NMR δ: –54.7.

Reaction of 1 with iodomethane

A dried, degassed Schlenk flask was charged with 0.236 mL of freshly distilled iodomethane (3.8×10^{-3} mol) and 10 mL THF, then placed in a dry ice – acetone bath. A solution of **1** (0.075 g, 3.8×10^{-3} mol) in 50 mL THF was added and the flask was allowed to warm to room temperature. The insertion product, **14**, was produced cleanly (90% yield by NMR). ^{1}H NMR δ: 0.390 (s, 3H), 1.176 (s, 18H), 2.8–2.95 (m, 4H). ^{13}C NMR δ: 29.54, 29.68, 42.91, 60.70.

Reaction of 1 with 2,3-dimethyl-1,3-butadiene

A dried, degassed Schlenk flask was charged with 0.414 g of 2,3-dimethyl-1,3-butadiene (5.05×10^{-3} mol) and 30 mL THF, then placed in a dry ice – acetone bath. A solution of **1** (1.0 g, 5.05×10^{-3} mol) in 50 mL THF was added and the flask was allowed to warm to room temperature. The major product was the silacyclopentene, **15** (85% by NMR). Crystals suitable for X-ray analysis were grown from THF. HRMS: *m*/*z* 280 [M^+]. Exact mass calcd. for $C_{16}H_{32}N_2Si$ *m*/*z*: 280.2334; found: 280.2334. ^{1}H NMR δ: 1.173 (s, 18H), 1.55 (s, 4H), 1.756 (s, 6H), 2.940 (s, 4H). ^{13}C NMR δ: 19.44, 29.29, 29.76, 43.63, 50.98, 130.48. ^{29}Si NMR δ: –10.2.

Crystal structure determination

Intensity data for compounds **9** and **12** were collected using a Bruker SMART ccd area detector mounted on a Bruker Platform goniometer equipped with graphite-monochromated Mo Kα radiation. Intensity data for **15** was collected using a Siemens SMART ccd area detector mounted on a Siemens P4 diffractometer equipped with graphite-monochromated Mo Kα radiation. All structures were determined at temperatures below 150 K. The structures of all compounds were solved by direct methods and refined by full-matrix least-squares on F^2 (SHELXTL, Version 5). Hydrogen atoms were initially determined by geometry and refined by a riding model. Non-hydrogen atoms were refined with anisotropic displacement parameters. Compound **12** sits on a crystallographic mirror that includes the silicon and nitrogens. The mirror symmetry causes the phenyl group and the hydrogen on the silicon to be disordered. Restraints on the positional and displacement parameters of the phenyl group were required to achieve convergence in the refinement. Details of the data collection and refinement are given in Table 1.

Acknowledgment

This research was supported by a grant from the National Science Foundation. We thank Douglas R. Powell and Randy K. Hayashi for crystal structure determinations and the National Science Foundation and the University of Wisconsin for funds to purchase the X-ray instrument and computers.

Supporting information available

Tables of crystallographic data, atomic coordinates, thermal parameters, and bond lengths and angles for **9**, **12**, and **15** have been deposited as supplementary material and may be purchased from the Depository of Unpublished Data, Document Delivery, CISTI, National Research Council Canada, Ottawa, ON K1A 0S2 (http://www.nrc.ca/irm/unpub_e.shtml for information on ordering electronically).

© 2000 NRC Canada

Crystallographic data for the structure(s) reported in this paper have deposited with the Cambridge Crystallographic Data Centre (CCDC). Copies of the data can be obtained, free of charge, on application to the Director, CCDC, 12 Union Road, Cambridge CB2 1EZ, U.K. (Fax: 44-1223-336033 or e-mail: deposit@ccdc.cam.ac.uk).

References

1. (*a*) P.P. Gaspar and R. West. *In* The chemistry of organic silicon compounds. Vol. 2. *Edited by* Z. Rappoport and Y. Apeloig. John Wiley & Sons, Chichester, U.K. 1998. Chap. 43, pp. 2464–2568; and (*b*) O.M. Nefedov, M.P. Egerov, A.I. Ioffe, C.G. Menchikov, P.S. Zuev, V.L. Minikin, B.Y. Simkin, and M.N. Glukhovstev. Pure Appl. Chem. **64**, 265 (1992).
2. R. West and M. Denk. Pure Appl. Chem. **68**, 785 (1996).
3. M. Denk, R. Lennon, R. Hayashi, R. West, A.V. Belyakov, H.P. Verne, A. Haaland, M. Wagner, and N. Metzler. J. Am. Chem. Soc. **116**, 2691 (1994).
4. C. Heinemann, T. Mueller, Y. Apeloig, and H. Schwartz. J. Am. Chem. Soc. **118**, 2023 (1996).
5. R. West, J. Buffy, M. Haaf, T. Mueller, B. Gehrhus, M.F. Lappert, and Y. Apeloig. J. Am. Chem. Soc. **120**, 1639 (1998).
6. B. Gehrhus, P. Hitchcock, M.F. Lappert, J. Heinicke, R. Boese, and D. Bläser. J. Organomet. Chem. **521**, 211 (1996).
7. J. Heinicke and A. Oprea. Abstracts from the 11th Int. Symp. Organosilicon Chem. Montpellier, France. 1996. PA28.
8. S. Tsutsui, K. Sakamoto, and M. Kira. J. Am. Chem. Soc. **120**, 9955 (1998).
9. S. Ishida, T. Iwamoto, C. Kabuto, and M. Kira. Abstract from the 12th Int. Symp. Organosilicon Chem. 1999. Sendai, Japan. p. 191.
10. M. Haaf, A. Schmiedl, T.A. Schmedake, D.R. Powell, A.J. Millevolte, M. Denk, and R. West. J. Am. Chem. Soc. **120**, 12714 (1998).
11. B. Gehrhus, P.B. Hitchcock, and M.F. Lappert. Organometalics, **17**, 1378 (1998); **18**, 4861 (1997).
12. T.A. Schmedake, M. Haaf, Y. Apeloig, T. Müller, S. Bukalov, and R. West. J. Am. Chem. Soc. In press.
13. (*a*) A. Schäfer, W. Saak, and M. Weidenbruch. Z. Anorg. Allg. Chem. **624**, 1405 (1998); (*b*) B. Gehrhus, P.B. Hitchcock, and M.F. Lappert. Angew. Chem. Int. Ed. Engl. **22**, 36 (1997); *(c)* A. Schäfer, W. Saak, M. Weidenbruch. H. Marsmann, and G. Henkel. Chem. Ber./Recl. **130**, 1733 (1997).

© 2000 NRC Canada

Canadian Journal of Chemistry

Author Index
Volume 78, 2000

Revue canadienne de chimie

Index des auteurs
Volume 78, 2000

Abraham, M.H., 184
Abrams, S.R., 963
Acevedo, I.L., 1121
Acree, Jr., W.E., 184, 449, 459
Ahmed, A.R., 1178
Aicken, F.M., 415
Aknin, M., 986
Aliaga, C., 1052
Alibhai, N., 1345
Alper, H., 920
Alvarez-Toledano, C., 1299
Alvaro, G., 809
An, H., 884
Andraos, J., 508
Andreotti, D., 772
Andryukhova, N.P., 1285
Antipin, M.Y., 1511
Apeloig, Y., 1496
Arakawa, H., 291
Arango, J.O., 1421
Arca, M., 1147
Arslan, T., 884
Arya, P., 920
Atay, E., 84, 520
Aue, W.A., 95
Aumelas, A., 248
Auner, N., 1445
Back, M.H., 16
Bailey, M., 739
Baines, K.M., 1474
Baisch, G., 892
Ball, J.M., 464
Balsevich, J.J., 963
Balzarini, J., 1081
Baril, J., 490
Bassindale, A.R., 1479
Basso, E., 1441
Batchelor, R.J., 598
Batra, H., 1109
Becerra, R., 1428
Becht, J., 1380
Beck, E.J., 1060
Belzile, N., 51
Benn, M., 542
Bennet, A.J., 577
Berg, D.J., 255, 454
Bernard, G.M., 614
Bernardinelli, G., 280
Bertani, B., 809
Berthet, J.-C., 1305
Bezombes, J.-P., 1519
Bianchi, D.A., 1165
Biondi, S., 772
Birahda, K., 568
Blagoeva, I.B., 84, 520
Blais, P., 10
Bodo, B., 487
Boeré, R.T., 583
Boganov, S.E., 1428
Bonhoure, I., 1305
Bossard, A.R., 16
Botta, M., 925
Bottomley, F., 383
Boudjouk, P., 1396
Bourque, S.C., 920
Braekman, J.C., 1030
Bridges, C., 1289
Brook, M.A., 1357
Brossard, L., 307
Brown, M.A., 536
Brown, R.S., 1247
Brown, W., 800
Brun, P., 128
Buchanan, G.W., 316
Buncel, E., 474, 1251
Burschka, C., 1380
Cai, X., 1484
Camacho, A.G., 1121
Camerman, A., 26, 1045
Camerman, N., 26, 1045
Cameron, T.S., 118
Cartier dit Moulin, C., 1305
Castan, P., 280
Castellan, A., 73
Cervantes, J., 1491
Cervantes-Lee, F., 1511
Chabot, C., 852
Chan, T.H., 776
Chang, J.-C., 224
Chapados, C., 64, 490, 1128
Chapleur, Y., 708
Charlton, J.L., 553
Chauhan, M., 1396
Chênevert, R., 275
Chiltz, F., 307
Chivers, T., 10
Chruściel, J.J., 1405
Chubb, F.L., 84, 520
Chuca, I., 184
Chuit, C., 1519
Clarke, C.W., 1
Classon, B., 829
Clement, O., 474
Cobos, J.C., 1272
Collins, C., 151
Corelli, F., 925
Corey, J.Y., 1434
Corriu, R.J.P., 1519
Coumbarides, G.S., 935
Couture, P., 356
Couturier, D., 1242
Cow, C., 553
Crasto, C.F., 884
Crespo-Pinilla, M.S., 521
Cristobal-Telésforo, E., 248
Csizmadia, I.G., 362, 395, 626
Curran, D.P., 791
Cyr, A., 307
D'Sa, R., 1178
Dag, Ö., 516
Daloze, D., 1030
Dapporto, P., 723
Das, S.K., 191, 838
Dass, G., 444
Dasser, M., 275
Dawes, R., 1035
De Backer, M., 1242
De Clercq, E., 1081
De Fina, K.M., 184, 449, 459
de Rossi, R.H., 233
De, A.K., 139
Dean, P.A.W., 590
Decken, A., 270
Demartin, F., 1147
Den Auwer, C., 1305
Denmark, S.E., 673
Devillanova, F.A., 1147
Dhawan, R., 784
Di Fabio, R., 809
Dogra, S.K., 191
Dominique, R., 838

Can. J. Chem. Downloaded from www.nrcresearchpress.com by San Diego (UCSD) on 09/06/12
For personal use only.

© 2000 NRC Canada

Can. J. Chem. Downloaded from www.nrcresearchpress.com by San Diego (UCSD) on 09/06/12
For personal use only.

Donati, D., 772
Donnadieu, B., 280
Downard, A., 10
Drake, J.E., 1214
Driega, A.B., 316
Drouin, M., 212
Dubovik, I., 1511
Duceppe, J.-S., 739
Dufresne, C., 784
Duran, M., 328
Durst, T., 1345
Dwyer, J.R., 1035
Eames, J., 935
Edward, J.T., 84, 520
Egorov, M.P., 1428
Eichele, K., 118, 614
Einstein, F.W.B., 598
Ekelmans, D., 1030
Elguero, J., 1109
El-Hallag, I.S., 1170
El-Hefnawy, G.B., 1170
El-Saidi, M., 356
Enriz, R.D., 626
Ernst, B., 892
Fabre, P.-L., 280
Fattori, D., 925
Faure, R., 986
Faustov, V.I., 1428
Fisher, L., 409
Fletcher, K.A., 449
Foster, J., 1019
Foster, K., 800
Fradera, X., 328
Frank, S.A., 757
Franzén, R., 957
Fritz, G., 1388
Fryzuk, M.D., 1003
Fu, J.-m., 905
Fujita, K., 1089
Fusar-Bassini, D., 925
Futatsuki, K., 1089
Gable, K.P., 704
Galibert, A.M., 280
Gallant, R.T., 1295
Ganguly, T., 139
Garcia de la Fuente, I., 1272
Gauvin, A., 986
Gay, I.D., 598
Gaydou, E.M., 986
Gee, M., 118
Gehrhus, B., 1484
Gendron, R.A.L., 255, 454
Genêt, J.-P., 846
Gentile, G., 925
Ghoneim, E.M., 1170
Giacobbe, S., 809
Gibson, H.W., 347
Giesbrecht, G.R., 1003
Girard, C., 816
Glaser, R., 212
Glew, D.N., 1, 1204
Goesmann, H., 1388
González, J.A., 1272
Gough, K.M., 1035
Grand-Maître, C., 739
Grasmann, M., 1445
Graziano, G., 1233
Greedan, J.E., 1289
Green, C.E., 184
Grenier, L., 739
Gross, T., 1399
Grzegozek, M., 950
Gu, J.-H., 598
Guérin, B., 852
Guindon, Y., 852
Guthrie, J.P., 1295
Gutiérrez-Pérez, R., 1299
Haaf, M., 1526
Hallberg, A., 829
Handerson, S., 527
Hecht, S.M., 884
Heilporn, S., 1030
Hempel, A., 26, 1045
Hennigar, T.L., 568
Hernández-Ortega, S., 248
Herrschaft, B., 1445
Hijji, Y.M., 1421
Hinman, A.S., 1318
Hitchcock, P.B., 1484
Hou, X., 963
Hu, Y.-J., 838
Huang, X., 577
Hudrlik, A.M., 1421
Hudrlik, P.F., 1421
Hughes, D.W., 1474
Hughes, G., 868
Hum, G., 642
Hummer, M., 1445
Hursthouse, M.B., 1073
Hussein, S.M.I., 436
Iftime, G., 409
Igarashi, K., 657
Ikariya, T., 697
In, Y., 31
Infante, A.B., 521
Irvine, N., 963
Isaia, F., 1147
Ishitani, H., 666
Jankowski, C.K., 248
Jeanson, P., 307
Jefferson, G.R., 920
Jeffrey, K.R., 46
Jenkins, H.A., 590
Jiang, Z.-H., 322
Jiménez, R., 1491
Jiménez-Estrada, M., 248
Jobe, D.J., 464
Johnson, M., 133
Joly, H.A., 51
Jones, D.H., 1318
Jordan, R.W., 527
Jurkauskas, V., 800
Kabanyane, S., 270
Kagan, H.B., 816
Kagayama, A., 657
Karginov, V.A., 884
Katampe, I., 1479
Katopodis, A., 892
Katz, M., 1121
Kaufman, T.S., 1165
Kelly, D.G., 1073
Keuthen, M., 1388
Kim, J.-H., 673
Kirby, C.W., 614
Kirschner, F., 1388
Klassen, V., 583
Kliegel, W., 546, 1325
Knaus, E.E., 1081
Kobayashi, S., 666
Koerner, T., 1067
Kresge, A.J., 508
Krishnamoorthy, G., 191
Kumar, D., 1109
Kumar, H., 427
Kvarnström, I., 829
Laikhter, A.L., 884
Lamarque, L., 128
Lamba, D., 925
Lambert, J.B., 1441
Laporte, F., 118
Lappert, M., 1484
Larsen, G., 206
Lautens, M., 868
Lavallée, P., 739
Leblanc, Y., 784
Leclercq, S., 1030
Lee, J., 642
Lee, S.-H., 347
Leigh, W.J., 1459
Lelj, F., 1147
Lessard, J., 307
Leung, C., 553
Lewars, E., 297
Leznoff, C.C., 167
Li, H., 51
Liao, D.-Z., 322
Light, M.E., 1073
Lin, A.C., 362

© 2000 NRC Canada

Lin, Y.-S., 224
Lin, Z.-P., 95
Lipari, F., 577
Lippolis, V., 1147
Lissi, E.A., 1052
Littke, A., 784
Liu, P., 133
Liu, X., 1143
Lociuro, S., 772
Lodder, M., 884
López, J.M., 1491
López-Cortés, J.G., 1299
Lubkowitz, G., 1325
Machado, A.A.S.C., 1013
MacInnis, J.A., 1222
Mackintosh, N., 800, 852
Madic, C., 1305
MaGee, D.I., 1060
Majerus, S.L., 1345
Mak, M.L., 626
Malonga, H., 291
Manzer, L.E., 920
Marangoni, D.G., 1222
Martel, A.A., 307
Mastropaolo, D., 26, 1045
Mata-Pérez, F., 521
Matern, E., 1388
Mathey, F., 118
Matsunaga, S., 31
Max, J.-J., 64, 490, 1128
McClelland, R.A., 1178, 1186
McKillop, A., 1158
Meiners, F., 1469
Ménard, H., 307
Ménichelli, C., 1128
Meou, A., 128
Merkley, N., 356, 942
Messanga, B.B., 487
Mestres, J., 328
Mislow, K., 41
Mogren, T., 800
Mohamed, M., 1357
Moharram, Y.I., 1170
Moisy, P., 1305
Mukaiyama, T., 657
Nagashima, T., 791
Naithani, R., 1109
Natansohn, A., 409
Neault, J.F., 291
Nefedov, O.M., 1428
Neverov, A.A., 1247
Nickel, P., 26
Nikitin, K.V., 1285
Nishino, H., 31
Norstrom, T., 963
Novetta-Delen, A., 291
Noyori, R., 697
Oehme, H., 1399
Ogilvie, W.W., 739, 852
Öhrlein, R., 892
Ohtsu, H., 31
Okanga, F.I., 338
Okoro, C.O., 1421
Ollerenshaw, J., 784
Onyido, I., 474
Ortega-Alfaro, M.C., 1299
Oscarsson, K., 829
Overman, L.E., 732
Owens, T.R., 1459
Ozturk, T., 1158
Padwa, A., 749
Pain, G., 772
Pal, A., 427, 444
Palepu, R., 151, 1222
Pannell, K.H., 1511
Paoli, P., 723
Papkov, V., 1511
Paquette, L.A., 689
Paradise, B.J., 1526
Parvez, M., 10
Pedras, M.S.C., 338
Pedrosa, G.C., 1121
Pena, C., 280
Penieres-Carrillo, G., 1299
Penner, G.H., 46
Pennington, L.D., 732
Perczel, A., 395
Peters, E.-M., 1388
Peters, K., 1388
Picard, J.-P., 1363
Pincock, A.L., 1019
Pincock, J.A., 1019
Pinto, B.M., 598
Plehiers, M., 1030
Poirier, R.A., 1067
Pojarlieff, I.G., 84, 520
Pokriefke, J.O., 546, 1325
Polborn, K., 1412
Popelier, P.L.A., 415
Postigo, M.A., 1121
Poupart, M.-A., 739
Qian, Y., 1143
Qiao, Z., 1143
Rajalingam, U., 590
Ratovelomanana-Vidal, V., 846
Reger, T.S., 749
Reinke, H., 1399
Ren, D., 1178
Rettig, S.J., 546, 1003, 1325
Rey, F., 1013
Reyé, C., 1519
Reyes-Chilpa, R., 248
Richter, I., 1380
Rifai, S., 1019
Rigo, B., 1242
Rivkin, A., 791
Roberts, E., 800
Rochon, P., 409
Roelens, S., 723
Roscoe, J.M., 16
Roush, W.R., 757
Roy, R., 838
Rozas, I., 1109
Ruffin, B., 73
Saak, W., 1469
Salpietro, S.J., 362, 626
Samuel, M.S., 1474
Samuelsson, B., 829
Sanchez, C., 1186
Sanchez, V., 383
Sangermano, M., 1030
Sanipelli, G.G., 464
Schmedake, T.A., 1526
Schmid, R., 265
Sham, S., 975
Shanmugham, M.S., 704
Shao, P., 255
Sharma, S., 427
Sharp, T.L., 184
Shaver, M.P., 568
Shawl, C.E., 1441
Shiftan, D., 212
Short, III, G.F., 884
Shvedov, D., 151
Sibi, M.P., 133
Sikorski, M., 963
Simoneau, B., 739
Singh, S.P., 1109
Sinha, H.K., 963
Sklenak, S., 1496
Smadja, J., 986
Smolik, M., 993
Snieckus, V.A., 905
Sondengam, B.L., 487
Sosa, C.P., 395
Soula, B., 280
Spurgin, M.A., 184
St-Denis, Y., 776
Steer, R.P., 963
Stephenson, C.R.J., 800
Stewart, A., 1380
Strunz, G.M., 270
Sumi, K., 697
Sun, B.-W., 322
Sung, K., 562
Surylo, P., 950
Şüzer, S., 516
Tacke, R., 1380

Can. J. Chem. Downloaded from www.nrcresearchpress.com by San Diego (UCSD) on 09/06/12
For personal use only.

© 2000 NRC Canada

Tae, J., 689
Taillefumier, C., 708
Tajmir-Riahi, H.A., 291
Tam, W., 527
Tanaka, K.S.E., 577
Tanaka, R., 31
Taylor, P.G., 1479
Taylor, S.D., 642
Tee, O.S., 436, 1100
Thavonekham, B., 739
Thompson, K.A., 1019
Thompson, R.C., 383
Tobin, J., 151
Tokuda, H., 31
Tokuhisa, K., 238
Toner, A.J., 1073
Torres-Collín, L., 248
Toscano, R.A., 1299
Toteva, M.M., 84, 520
Tranmer, G.K., 527
Tremaine, P.R., 151
Trimble, L.A., 784
Tripathy, S., 1345
Trotter, J., 546, 1325
Tsou, N.N., 784
Tsuzuki, H., 238, 1089
Tuck, D.G., 536
Turner, I.E., 436
Van Calsteren, M.R., 248
Van, T., 449, 459
Vank, J.C., 395
Vasisht, S.-K., 1412
Veglia, A.V., 233
Venneri, P.C., 1194
Verani, G., 1147
Vogels, C.M., 568
von Schnering, H.G., 1388
Vorontsov, I.I., 1511
Wachner, A.M., 46
Wagner, B., 892
Wagner, S., 1412
Wallbank, A.I., 568
Walsh, R., 1428
Wang, B.-C., 224
Wang, G.-L., 322
Wang, H.-G., 322
Wang, P.-Y., 224
Wang, Q., 1434
Wang, S., 975, 1289
Wang, Y., 1067
Wang, Z.-X., 1081
Warkentin, J., 356, 942, 1194
Wasylishen, R.E., 118, 614
Waterlot, C., 1242
Weerassooriya, N., 935
Weidenbruch, M., 1469
West, R., 1526
Westaway, K.C., 1067
Westcott, S.A., 568
White, J.D., 704
Wiberg, N., 1412
Wiebe, L.I., 1081
Wienberg, N., 41
Williams, P., 542
Winkler, T., 892
Wolmershäuser, G., 583
Womiloju, O.O., 383
Wong, A., 975
Wooler, K., 642
Works, A.B., 757
Wozniak, M., 950
Wren, J.C., 464
Wu, G., 118, 614, 975
Xie, Y., 1143
Xu, J., 1143
Xu, Z., 383
Yadav, V.K., 542
Yamashita, Y., 666
Yamato, T., 238, 1089
Yan, S.-P., 322
Yang, H., 800
Yang, J., 1214
Yao, X.-K., 322
Yap, G.P.A., 316
Yazbeck, O.J., 436, 1100
Yip, C., 527
Yu, C.-M., 270
Zaworotko, M.J., 568
Zhang, Y., 1289
Zhao, Q.-H., 322
Zhou, X.-M., 598
Zhu, J., 577
Zhu, Y., 1143
Ziegler, T., 265
Zunic, V., 868

Can. J. Chem. Downloaded from www.nrcresearchpress.com by San Diego (UCSD) on 09/06/12
For personal use only.

© 2000 NRC Canada

Can. J. Chem. Downloaded from www.nrcresearchpress.com by San Diego (UCSD) on 09/06/12
For personal use only.

This issue is dedicated to

Professor Adrian G. Brook

to honour his scientific contributions and to wish him further discoveries in silicon chemistry

Associate Editors: Victor A. Snieckus and Michael A. Brook

Ce tirage est dédié au

Professeur Adrian G. Brook

pour souligner ses contributions scientifiques et pour lui souhaiter beaucoup d'autres découvertes dans le domaine de la chimie du silicium.

Rédacteurs associés : Victor A. Snieckus et Michael A. Brook

© 2000 NRC Canada

Can. J. Chem. Downloaded from www.nrcresearchpress.com by San Diego (UCSD) on 09/06/12
For personal use only.



Professor Adrian Brook

© 2000 NRC Canada

Can. J. Chem. Downloaded from www.nrcresearchpress.com by San Diego (UCSD) on 09/06/12
For personal use only.

PREVIEW / APERÇU

Forthcoming special issues / Numéros spécials à paraître

June 2001	In honour of Professor B. James
November 2001	In honour of Professor V. Snieckus

Forthcoming articles / Articles à paraître

Potentiometric study of cadmium(II) and lead(II) complexation by a cross-linked poly(acrylic acid). Comparison with linear analogue	C. Morlay, Y. Mouginot, M. Cromer, M. Chatelut, and O. Vittori
A thermodynamic study of aqueous acetonitrile: excess chemical potentials, partial molar enthalpies, entropies and volumes, and fluctuations	P.V. Nikolova, S.J.B. Duff, P. Westh, C.A. Haynes, Y. Kasahara, K. Nishikawa, and Y. Koga
Interactions of 6-aminopurine (adenine) in water and aqueous urea solutions	J.D. Pandey, S. Haroon, K.K. Dubey, M. Upadhyaya, R. Dey, and K. Misra
Preparation, X-ray structure, and dynamic solution behaviour of *N*,*N*′,*N*″-tris (2,6-diisopropylphenyl)guanidine and its reaction with molybdenum carbonyl	R.E. Boeré, R.T. Boeré, J. Masuda, and G. Wolmershäuser
An approximate ab initio method based on the DIM model	J. Cullen
Synthesis and characterization of two new "pincer" complexes of zinc(II). The X-ray crystal structures of the five coordinate complexes $[ZnCl_2\{\eta^3\text{-}N,N',N\text{-}2,6\text{-}(R_2NCH_2)_2C_5H_3N\}]$ (R = *n*-Bu or Me)	I. del Río, R.A. Gossage, M.S. Hannu, M. Lutz, A.L. Spek, and G. van Koten
Syntheses and electrochemical characterization of heteroleptic cyclopentadienyl–bisdithiolene complexes of niobium and tantalum	I.V. Jourdain and F. Guyon
AIM study on the transferability of the oxygen atom in linear ethers	A. Vila, E. Carballo, and R.A. Mosquera
Asymmetric synthesis based on chiral (arene)tricarbonylchromium acetal complexes	M.K. McKay and J.R. Green
Synthesis and X-ray structure of 1,2,2,2-tetrakis(3-methoxyphenyl)ethanone	L.H. Klemm and T.J.R. Weakley
Bis(trimethylsilyl)methanesulfonyl and tris(trimethylsilyl)methanesulfonyl chlorides and their reactions by way of sulfenes	J.F. King, K.M. Baines, M.R. Netherton, and V. Dave
Anhydrous perchlorato complexes of palladium(II): $Pd(ClO_4)_2$, $(ClO_2)_2Pd(ClO_4)_4$, and $(NO_2)_2Pd(ClO_4)_4$. Syntheses and structural analyses	F. Cunin, F. Favier, and J.L. Pascal
Dew points of ternary methane + water + methanol. Measurement and correlation	S.T. Blanco, I. Velasco, E. Rauzy, and S. Otín
Determination of the acidity constant of isothiocyanic acid in aqueous solution	Y. Chiang and A.J. Kresge

© 2000 NRC Canada

Can. J. Chem. Downloaded from www.nrcresearchpress.com by San Diego (UCSD) on 09/06/12
For personal use only.

Professor Adrian G. Brook, FCIC,

**University Professor of Chemistry Emeritus,
University of Toronto**

This Special Issue of *The Canadian Journal of Chemistry* honours the scientific contributions of Adrian Brook. We are pleased to present this collection of papers whose contents indicate the richness and diversity of research areas and themes taken by his many students, research associates, colleagues, and friends in their own careers.

Adrian Brook has enriched the discipline of chemistry in Canada and worldwide through manifold contributions in research, teaching, and administration. From the early days of his independent career, he established an international reputation for work on organosilicon chemistry. His research in the synthesis of a wide variety of functionally substituted organometalloid compounds and the study of their properties is of particular significance. From these fundamental studies evolved important synthetic and other applications, including the use of organosilicon compounds as unusual synthons that take advantage of altered functional reactivity. Particularly noteworthy are: the first synthesis of acylsilanes, compounds whose utility is being increasingly exploited; the synthesis of silylcarbinols and his discovery of their base-catalyzed rearrangement to alkoxysilanes which all chemists recognize as the Brook rearrangement; the photoinduced rearrangement of polysilylacylsilanes leading to the first synthesis, isolation, and characterization of silenes, stable compounds containing a silicon–carbon double bond, a testament of Brook's ingenious and methodical pursuit of a long sought goal which had eluded organometallic chemists. Even as we celebrate his contributions, Brook continues to pursue research on the thermal chemistry and photochemistry of silenes and silene precursors.

Adrian Brook received the Frederick Stanley Kipping Award in Organosilicon Chemistry of the American Chemical Society in 1973 for his work in organosilicon chemistry. The neighbours at his favourite residence, a cottage north of Toronto, were somewhat surprised to observe the sailboat, "Miss Silicone", on the lake after the award had been received. He also received the Chemical Institute of Canada Medal in 1985 and the Izaak Walton Killam Memorial Prize in 1994 for his contributions to organic chemistry.

As a teacher, Brook is well-known for the clarity of his lectures and the high standards he inculcates in his students. As an administrator he brought the same high standards to the positions that he has held, which include the chairmanships of the Research Board of the University of Toronto and of the Chemistry Grants Selection Committee of NRC (currently NSERC).

Brook is an enthusiastic do-it-yourselfer. His *magnum opus* was the construction of a cedar plank cottage on a small Ontario lake using as his only assistants a col-

Professeur Adrian G. Brook, MICC,

**Professeur hors rang émérite de chimie
University of Toronto**

Le présent numéro spécial de la *Revue canadienne de chimie* rend hommage aux contributions scientifiques de M. Adrian Brook. Nous sommes ravis de présenter ce recueil d'articles qui témoigne de la richesse et de la diversité des domaines qu'explorent ses nombreux étudiants, agrégés de recherche, collègues et amis.

Adrian Brook a enrichi la discipline de la chimie au Canada et dans le monde entier grâce à ses précieuses interventions en recherche, en enseignement et en administration. Dès le début de sa carrière de chercheur autonome, il a acquis une réputation internationale d'excellence pour ses travaux sur la chimie des organosiliciés, en particulier sur la synthèse d'un grand nombre de composé organométalloïdes ayant subi une substitution fonctionnelle et sur leurs propriétés. Ces études fondamentales ont été la source d'applications de synthèse et d'autres applications, y compris le recours aux composés organosiliciés comme synthons atypiques en vue de tirer avantage de la réactivité fonctionnelle ainsi modifiée. Parmi ses réalisations les plus notables figurent la première synthèse d'acylsilanes, composés dont l'utilité devient de plus en plus apparente; la synthèse de silylcabinols et la découverte de leur réarrangement par catalyse basique en alkoxysilanes, que tous les chimistes appellent aujourd'hui le « réarrangement de Brook »; et le réarrangement photo-induit des polysilylacylsilanes ayant découlé en la première synthèse, isolation et caractérisation des silènes, composés stables révélant une double liaison silicium–carbone. Ces travaux reflètent l'engagement indéfectible de Brook à atteindre un objectif qui constituait une pierre d'achoppement pour les autres chimistes organométalliques. Au moment de publier le présent recueil qui célèbre ses réussites, Brook poursuivait ses recherches sur la chimie thermique et la photochimie des silènes et de leurs précurseurs.

En 1973, la American Chemical Society a remis à Adrian Brook le prix Frederick Stanley Kipping de chimie des organosiliciés pour ses contributions dans ce domaine. Les voisins de sa résidence de prédilection, un chalet au nord de Toronto, ont dû être fort surpris de constater le nom du bateau d'Adrian, « Miss Silicone », après son retour de la cérémonie de remise des prix! Adrian a aussi vu ses efforts applaudis par la Médaille de l'Institut de chimie du Canada, en 1985, et par le Prix commémoratif Izaak-Walton Killam, en 1994, pour ses contributions à la chimie organique.

À titre d'enseignant, Brook était réputé pour la précision de ses exposés et pour les normes élevées qu'il visait avec ses étudiants. Ces normes ne manquaient pas à l'appel lorsqu'il a assumait des fonctions d'administrateur, y compris la présidence du Conseil d'administration de la recherche de la University of Toronto et du Comité de sélection des boursiers en chimie du CNRC (programme qui relève maintenant du CRSNG).

Brook est un bricoleur enjoué. Le projet dont il est le plus fier à ce chapitre est la construction d'un chalet en cèdre sur la rive d'un petit lac de l'Ontario. Ses seuls assistants dans cette

© 2000 NRC Canada

Can. J. Chem. Downloaded from www.nrcresearchpress.com by San Diego (UCSD) on 09/06/12
For personal use only.

league (for beams, joists and floor), graduate students (for walls), and his brother and then 10-year-old son (for the roof). The later advent of hydroelectricity at the lake led to exploits in wiring and plumbing. As well, his stable of homemade watercraft include a fibreglass kayak and a sailing pram.

Adrian Gibbs Brook was born in Toronto in 1924. He received B.A. and Ph.D. degrees from the University of Toronto in 1947 and 1950, respectively, his research for the latter being carried out with Professor George F. Wright on oxymercuration chemistry. He was appointed Lecturer in Chemistry at the University of Saskatchewan (1950-51) and then was awarded first a Nuffield Fellowship at the Imperial College of Science and Technology, University of London (1951–53), with Professor R. P. Linstead, and then a Research Fellowship at Iowa State University with Professor Henry Gilman. In 1953, he returned to the University of Toronto as Lecturer in Chemistry, becoming Assistant Professor in 1956, Associate Professor in 1960, and Professor of Chemistry in 1962. During the 1968–74 period, Brook served as Associate Chairman, Acting Chairman, and Chairman of the Department of Chemistry. In 1967, he held a NRC Senior Research Fellowship at Princeton University. He also held Visiting Professorships at the University of Sussex (1974–75), Cambridge University (1982) and Indiana University (1988). In 1977, Brook was elected Fellow of the Royal Society of Canada.

On behalf of all of the contributors and, we have no doubt, chemists worldwide, we are pleased to offer this Special Issue to Adrian Brook and to wish him further discoveries in silicon chemistry.

Michael A. Brook

entreprise ont été un de ses collègues (pour l'installation des poutres, des poutrelles et du plancher), quelques-uns de ses étudiants diplômés (pour l'érection des murs) ainsi que son frère et le fils de ce dernier, qui n'avait alors que dix ans (pour la construction du toit). L'arrivée de l'électricité dans le secteur a marqué un retour aux outils pour Adrian, qui a alors entrepris des travaux de câblage et de plomberie dans son chalet. Constructeur d'esquifs à ses heures, il a à son actif la construction d'un kayak en fibre de verre et d'une prame à voiles.

Adrian Gibbs Brook est né à Toronto en 1924. Il a reçu son baccalauréat et son doctorat de la University of Toronto en 1947 et 1950, respectivement. Son doctorat, supervisé par le professeur George F. Wright, a porté sur la chimie de l'oxymercuration. Il a été nommé maître de conférences en chimie à la University of Saskatchewan (1950–51). Il a ensuite obtenu une bourse Nuffield au Imperial College of Science and Technology, à la University of London (1951–53), auprès du professeur R. P. Linstead, puis une bourse de recherche de la part de la Iowa State University, auprès du professeur Henry Gilman. En 1953, il a regagné la University of Toronto à titre de maître de conférences en chimie. Il y est ensuite devenu professeur adjoint (1956), professeur agrégé (1960) puis professeur de chimie (1962). De 1968 à 1974, Brook a été tour à tour directeur adjoint, directeur intérimaire et directeur du Département de chimie de l'Université. En 1967, il a été nommé chargé de recherche du NRC à la Princeton University. Il a également été professeur invité à la University of Sussex (1974–75), à la Cambridge University (1982) et à la Indiana University (1988). En 1977, Brook a été élu membre de la Société royale du Canada.

Au nom de tous les collaborateurs du présent ouvrage et, nous osons le dire, de tous les chimistes du monde, nous sommes heureux de dédier ce numéro spécial à Adrian Brook. Nous lui souhaitons de faire encore de nombreuses découvertes dans le domaine de la chimie du silicium.

Michael A. Brook

© 2000 NRC Canada

AIM study on the transferability of the oxygen atom in linear ethers

Antonio Vila, Enrique Carballo, and Ricardo A. Mosquera

Abstract: The integrated values of the electron population, electron energy, nucleus–electron potential energy interaction, dipole moment and volume of the oxygen atoms, and the main properties of the O—C bond critical points, were determined by employing the theory of atoms in molecules and 6–31++G**//6–31G* wave functions for a series of 25 unbranched alkyl monoethers. These results were used to assess the degree of approximate transferability of the oxygen atom along this series in terms of the particular alkyl radicals bonded to it. It has been found that a set of six different oxygen atoms is necessary to classify all the computed values. It can be established that the oxygen atoms bonded to propyl and larger radicals can be treated, in practice, as a transferable fragment, while those bonded to at least one smaller radical are specific. Though the total HF energy and the available experimental heats of formation are well fitted by a traditional additivity scheme that distinguishes only among O, CH_2, and CH_3 units, it has been found that the energy properties are influenced by the size of the molecule.

Key words: transferability, AIM theory, ethers.

Résumé : Utilisant la théorie des atomes dans les molécules et des fonctions d'onde 6–31++G**//6–31G*, on a déterminé les valeurs intégrées de la population électronique, de l'énergie électronique, de l'énergie potentielle d'interaction noyau-électron, du moment dipolaire et du volume des atomes d'oxygène ainsi que les propriétés principales des points critiques de la liaison O—C d'une série de 25 éthers monoalkylés et non ramifiés. On a utilisé ces résultats pour évaluer le degré approximatif de transférabilité de l'atome d'oxygène dans cette série en fonction des radicaux alkyles particuliers qui lui sont liés. On a trouvé qu'un ensemble de six atomes d'oxygène différents est nécessaire pour classifier toutes les valeurs calculées. On a pu établir que, en pratique, les atomes d'oxygène liés à des groupes propyle ou plus importants peuvent être traités comme des fragments transférables alors que ceux liés à des groupes à au moins un radical plus petit sont spécifiques. Même si le schéma d'additivité traditionnelle qui ne distingue que des unités O, CH_2 et CH_3 permet d'établir une bonne corrélation entre l'énergie totale selon HF et les chaleurs de formation expérimentales disponibles, on a trouvé que les propriétés d'énergie sont influencées par la taille de la molécule.

Mots clés : transférabilité, théorie des atomes dans une molécule, éthers.

[Traduit par la Rédaction]

Introduction

The transferability of the physical properties of atoms and groups of atoms (especially those known as functional groups) has been a basic idea for the development of chemistry allowing researchers to systematize the reactivity and the physical properties of a huge amount of chemical compounds. It is also employed as the basic concept sustaining many different theoretical or computational methodologies ranging from the straightforward calculation of thermochemical quantities by using the additivity of functional groups or bonds schemes (1), to the employment of solution molecular models to compute thermodynamic properties of liquid mixtures (2). Even such a widespread and powerful methodology as molecular mechanics (3) can be easily related to the functional group concept. In accordance with this practical importance the concept of functional group has been the subject of several recent theoretical research papers (4–9).

Though it has been demonstrated that the perfect transferability is an unattainable limit (10, 11), the development of the theory of atoms in molecules (AIM) (12, 13) has provided the physical basis, methodology, and computational tools required to carry out quantitative analysis of the degree of approximate transferability of atoms and groups of atoms (9, 14, 15). In fact, this theory was applied a long time ago to the study of the methyl and methylene fragments of *n*-alkanes giving rise to the distinction of the methylene group bonded to a methyl group from the remaining methylenes (16, 17). In spite of the increasingly amount of applications of the AIM theory, there are not many series of compounds for which this theory has been

Received June 1, 2000. Published on the NRC Research Press website on November 21, 2000.

A. Vila and E. Carballo. Departamento de Física Aplicada, Universidade de Vigo, Facultade de Ciencias, Campus de Ourense, 32004 Ourense, Spain.
R.A. Mosquera.[1] Departamento de Química Física, Universidade de Vigo, Facultade de Ciencias, Campus de Vigo, 36200 Vigo, Spain.

[1]Author to whom correspondence may be addressed. Telephone: +34-986-812298. Fax: +34-986-812382. e-mail: mosquera@uvigo.es

© 2000 NRC Canada

Table 1. Total energies, virial coefficient (γ), errors in the integrated energies and populations, and experimental heats of formation for various $CH_3(CH_2)_nO(CH_2)_mCH_3$ molecules as obtained from HF/6–31++G**//6–31G* wave functions.

n	m	E (au)	γ	$E-\sum E(\Omega)$ (kJ mol^{-1})	$N-\sum N(\Omega)$ (au)	$\sum L(\Omega)$ (au)	$\Delta H^\circ_{f\ exp}$ (kJ mol^{-1})
0	0	–154.07863	2.00145	2.86	0.0039	0.0049	–184.01 (27)
0	1	–193.12221	2.00124	0.25	0.0012	0.0013	–216.4 (27)
0	2	–232.16017	2.00111	–1.28	–0.0026	0.0031	–237.7 (27)
0	3	–271.19808	2.00101	–1.53	–0.0025	0.0048	–258.08 (28)
0	4	–310.23614	2.00092	–0.24	–0.0027	–0.0032	
0	5	–349.27416	2.00087	–0.72	–0.0037	–0.0035	
0	7	–427.3509	2.00074	2.08	0.0006	–0.0001	
0	9	–505.42605	2.00111	1.83	–0.0014	–0.0006	–381.09 (28)
1	1	–232.16562	2.00093	–3.91	–0.0068	–0.0087	–252.2 (27)
1	2	–271.20358	2.00087	1.83	0.0018	0.0024	–272.1 (28)
1	3	–310.24148	2.00083	2.33	0.0031	0.0032	
1	4	–349.28065	2.00076	3.11	0.0005	0.0003	
1	5	–388.31749	2.00093	2.61	0.0014	0.0012	
1	7	–466.39352	2.00087	4.70	0.0029	0.0033	
2	2	–310.24141	2.00083	–1.83	–0.0061	–0.0071	–292.8 (29)
2	3	–349.27995	2.00079	1.53	0.0024	0.0036	
2	4	–388.31736	2.00074	1.83	0.0018	0.0023	
2	5	–427.35535	2.00082	1.53	0.0016	0.0021	
2	7	–505.42137	2.00079	1.91	–0.0126	–0.0142	
3	3	–388.31712	2.00076	2.61	–0.0002	0.0001	–334.1 (29)
3	4	–427.35529	2.00071	1.28	0.0008	0.0021	
3	5	–466.39322	2.00076	3.66	0.0047	0.0055	
3	7	–544.46907	2.00074	1.83	–0.0068	0.0082	
4	4	–466.39324	2.00024	6.00	0.0029	0.0056	–390.0 (30)
4	5	–505.43123	2.00072	–0.50	–0.0011	–0.0006	

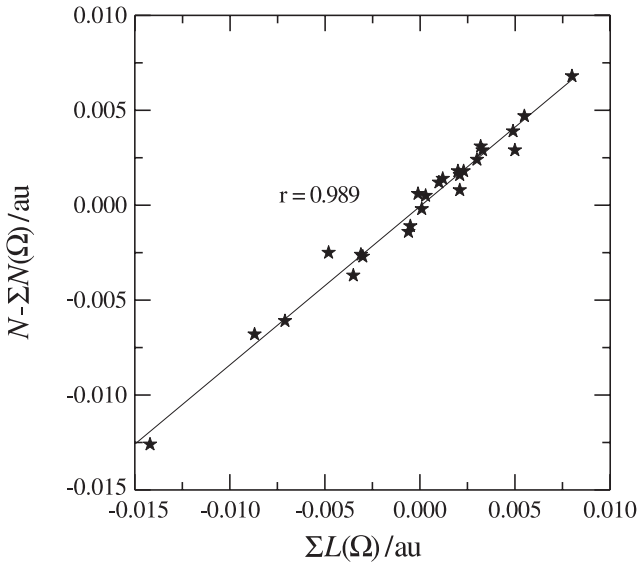
employed to make a detailed study of the variability or approximate transferability of atomic groups containing hetheroatoms. In one recent paper (18) the application of the AIM theory has proportioned a classification of the carbonyl groups presented in these compounds, and has pointed out that the energy of the carbonyl group along a series of aldehydes and ketones exhibited a dependence on the size of the molecule that had not been reported previously. The same trend was also found in another study on protonated ketones (19). In this work we try to confirm if this dependence is also shown for the oxygen atom in other molecular environments. At the same time, the evolution of the atomic and bond properties of the oxygen atom along the series of alkyl monoethers is analyzed aiming to define molecular environments for which an oxygen atom can be considered approximately transferable, along the series of ethers, within the known limits of experimental errors and the accuracy of numerical calculations. The definition of such environments would establish a transferability scheme of general applicability, which would provide rationalization of chemical facts and prediction of physical properties or chemical behaviours. As an example, the definition of transferable fragment in unbranched alkanes and esters done in a previous work and based upon the distances between nuclei and the bond critical points surrounding them were employed to define parameters sets for the Nitta–Chao liquid-state molecular solution theory based on a group contribution model (20). Though this definition was based only on a not very sensitive property, the parameter sets developed according to it improved the prediction of activity coefficients in mixtures alkane + ester by a factor of two and allowed the reproduction of the evolution of these activity coefficients with temperature (21).

Computational details

The calculations of the atomic and bond properties were carried out using the AIMPAC program series (22, 23) with wave functions obtained with the GAUSSIAN 94 program (24) using the 6–31++G** (25) basis set on the geometries optimized with the 6–31G* basis (26). The calculations were carried out on the 25 molecules of unbranched monoethers (CH_3-$(CH_2)_n$-O-$(CH_2)_m$-CH_3) shown in Table 1 and named by their n and m coefficients ($n \leq m$). Table 1 also displays ab initio energies, experimental heats of formation (27–30), virial ratios, and integration errors expressed as differences between total properties and those obtained by summation of properties of the fragments ($\Sigma N(\Omega) - N$ or $\Sigma E(\Omega) - E$) and as the summation of the integrated values of the laplacian of the charge density in all the atomic fragments ($\Sigma L(\Omega)$). The linear relationship between both forms of integration errors previously observed in a series of aldehydes and ketones (18) has also been found here (Fig. 1). For all the compounds concerned, we took into account only the conformer corresponding to the optimization of the antiperiplanar disposition of all the dihedral angles of the main skeleton and the alternate disposition of the terminal methyl groups with regard to the main skeleton. In this work we have studied the following atomic properties for the oxygen atom: (*i*) electron population (N(O)); (*ii*) electronic energy (E(O)); (*iii*) potential

© 2000 NRC Canada

Fig. 1. Linear relationship between $N - \Sigma N(\Omega)$ and $\Sigma L(\Omega)$.



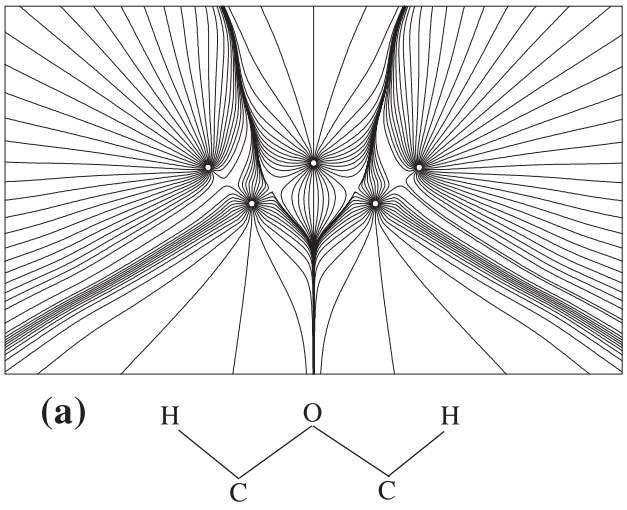
energy of interaction of the nucleus with the electron charge of the fragment (V_{NEO}(O)); (*iv*) dipole moment of the fragment (μ(O)); and (*v*) atomic volume (*v*(O)) of the region delimited by the interatomic surface and the boundary defined by an electron charge density of 0.002 au. We also include the integrated value of the laplacian of the charge density (*L*(O)); this parameter is a measure of the accuracy with which the interatomic surface was determined. Oxygen fragments were also characterized in terms of the properties at the O—C bond critical points, viz. the positive eigenvalue of the Hessian matrix for the electron charge density at this point (λ_3), bond ellipticity (ε) (defined as $\varepsilon = (\lambda_1/\lambda_2) - 1$ where $|\lambda_1| > |\lambda_2|$ are the two negative eigenvalues of the Hessian of the charge density at the bond critical point), charge density at the bond critical point (ρ_c), and distance from the nucleus to the bond critical point (*R*).

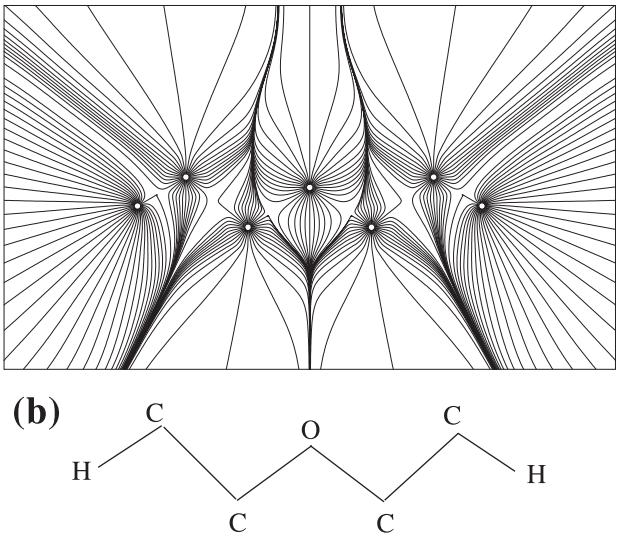
Results and discussion

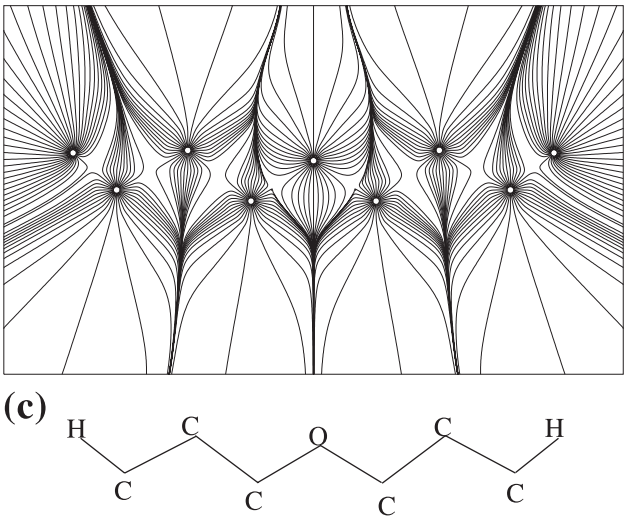
As it could be expected, the geometries obtained for the completely antiperiplanar conformer of the 25 compounds here studied are very similar; it can be mentioned only the well-known difference between O—CH_3 (1.391 Å) and O—CH_2 (1.396 Å) bond length distances as well as the even less significant differences between bond angles (for example the value of the C-O-C bond angle is 113.8° and 114.2° for compounds labelled as **00** and **01**, respectively).

Figure 2 shows the plots of the charge density gradient field in the main plane of the methoxymethane (**00**), ethoxyethane (**11**), and 1-propoxypropane (**22**) molecules. The oxygen atoms are represented by the central lens-shaped fragments. It is clear that the form of the enveloping surface of the gradient lines changes substantially from methoxymethane to ethoxyethane. Thus, the properties of an atom are a function of its boundary surface, its change necessarily results in significant variations of the properties (31). On the other hand, the basins of the oxygen atom display a more similar form in ethoxyethane and 1-propoxypropane molecules, suggesting that the values of the integrated properties in both systems have to be closer.

Fig. 2. Vector field for the charge density gradient in the principal plane of: (*a*) the methoxymethane molecule; (*b*) the ethoxyethane molecule; and (*c*) the 1-propoxypropane molecule.







© 2000 NRC Canada

Table 2. Atomic and bond properties for the oxygen fragment in the $CH_3(CH_2)_nO(CH_2)_mCH_3$ ethers studied in this work. All values are given in au.

n	m	N(O)	$-E$(O)	$-V_{NEO}$(O)	μ(O)	ν(O)	L(O) × 10^3	λ_3^-	λ_3^+	ε^- × 10^3	ε^+ × 10^3	ρ_c^-	ρ_c^+	R^-	R^+
0	0	9.3088	75.4867	185.2320	0.185	88.38	0.9	0.9523	0.9523	14.2	14.2	0.2686	0.2686	1.7984	1.7984
0	1	9.3155	75.4827	185.2773	0.183	88.25	–0.7	0.9531	0.9371	12.0	31.3	0.2684	0.2650	1.7984	1.8026
0	2	9.3165	75.4729	185.2832	0.184	88.24	0.0	0.9530	0.9414	12.2	26.7	0.2682	0.2650	1.7949	1.8022
0	3	9.3156	75.4652	185.2793	0.184	88.22	0.3	0.9523	0.9373	12.2	26.7	0.2683	0.2647	1.7948	1.8027
0	4	9.3152	75.4600	185.2788	0.184	88.07	0.9	0.9525	0.9371	12.2	26.9	0.2683	0.2647	1.7947	1.8028
0	5	9.3152	75.4559	185.2789	0.183	88.01	0.9	0.9527	0.9371	12.2	26.8	0.2683	0.2647	1.7947	1.8028
0	7	9.3162	75.4500	185.2818	0.186	88.17	–0.3	0.9524	0.9371	12.2	26.6	0.2684	0.2646	1.7947	1.8029
0	9	9.3156	75.4454	185.2794	0.184	88.03	0.9	0.9538	0.9386	12.2	26.5	0.2683	0.2645	1.7947	1.8030
1	1	9.3191	75.4840	185.3123	0.171	87.75	2.2	0.9377	0.9377	29.4	29.4	0.2648	0.2648	1.8026	1.8026
1	2	9.3233	75.4767	185.3274	0.181	88.10	–1.3	0.9380	0.9429	29.7	24.9	0.2646	0.2648	1.8027	1.8021
1	3	9.3229	75.4710	185.3253	0.182	88.17	–1.3	0.9378	0.9398	29.4	24.9	0.2647	0.2646	1.8025	1.8025
1	4	9.3218	75.4671	185.3234	0.179	87.89	0.0	0.9377	0.9396	29.3	25.2	0.2648	0.2646	1.8025	1.8026
1	5	9.3217	75.4639	185.3233	0.179	87.79	0.1	0.9379	0.9396	29.3	25.0	0.2648	0.2645	1.8024	1.8026
1	7	9.3220	75.4586	185.3234	0.178	87.77	0.3	0.9392	0.9407	29.3	24.8	0.2647	0.2644	1.8025	1.8027
2	2	9.3221	75.4728	185.3292	0.175	87.62	2.3	0.9441	0.9442	24.8	24.8	0.2647	0.2647	1.8021	1.8021
2	3	9.3237	75.4676	185.3321	0.181	87.87	–0.4	0.9441	0.9406	24.8	25.1	0.2648	0.2645	1.8019	1.8225
2	4	9.3235	75.4642	185.3315	0.179	87.74	0.3	0.9455	0.9413	24.6	25.3	0.2648	0.2644	1.8020	1.8026
2	5	9.3234	75.4616	185.3315	0.179	87.68	0.5	0.9458	0.9413	24.6	25.2	0.2648	0.2644	1.8020	1.8027
2	7	9.3237	75.4575	185.3321	0.180	87.65	0.2	0.9458	0.9414	24.6	25.0	0.2648	0.2643	1.8019	1.8027
3	3	9.3229	75.4646	185.3297	0.179	87.79	0.3	0.9407	0.9407	25.1	25.1	0.2646	0.2646	1.8024	1.8024
3	4	9.3242	75.4609	185.3318	0.182	87.85	–1.0	0.9421	0.9415	24.9	25.3	0.2646	0.2645	1.8024	1.8025
3	5	9.3230	75.4599	185.3306	0.180	87.71	0.3	0.9419	0.9414	24.9	25.2	0.2647	0.2646	1.8022	1.8023
3	7	9.3241	75.4553	185.3317	0.183	87.88	–0.8	0.9425	0.9416	24.9	25.0	0.2646	0.2644	1.8023	1.8026
4	4	9.3218	75.4594	185.3262	0.176	87.48	2.3	0.9418	0.9419	25.2	25.2	0.2645	0.2645	1.8025	1.8025
4	5	9.3241	75.4569	185.3320	0.182	87.79	–0.7	0.9421	0.9417	25.2	25.1	0.2645	0.2645	1.8025	1.8025

Note: $^-$ and $^+$ represent bond properties referring to the bond point between the oxygen atom and the carbon atom bonded to it on the left and right, respectively.

© 2000 NRC Canada

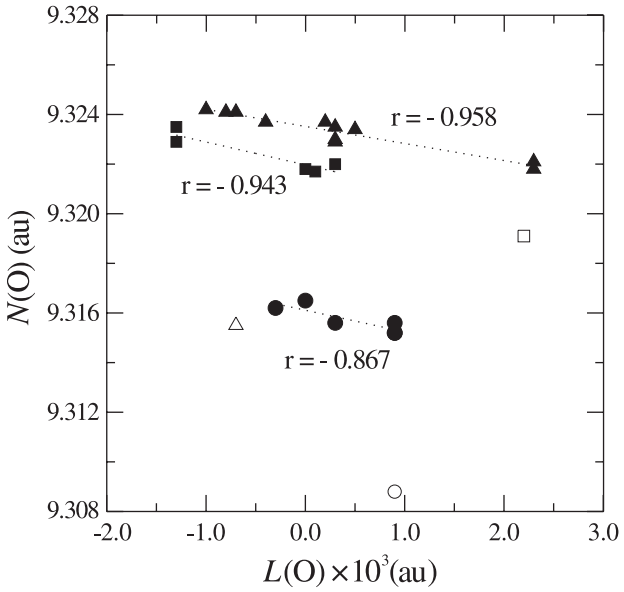
Table 3. Influence of the basis set used on the electron population, electronic energy, dipole moment, combined distances to bond points, and bond point densities for the oxygen fragments in various $CH_3(CH_2)_nO(CH_2)_mCH_3$ molecules.

Basis	N(O)	$-E$(O)	μ(O)	$R^- + R^+$	ρ_c^-	ρ_c^+	L(O) × 10^3
n = 2, m = 2							
6–31G	9.0374	75.1741	0.207	3.4734	0.2283	0.2283	2.0
6–31G*	9.3171	75.4849	0.219	3.6026	0.2648	0.2648	2.0
6–31++G**	9.3221	75.4728	0.175	3.6042	0.2647	0.2647	2.3
n = 2, m = 3							
6–31G	9.0384	75.1688	0.203	3.4730	0.2284	0.2282	0.3
6–31G*	9.3187	75.4807	0.224	3.6024	0.2649	0.2646	–0.2
6–31++G**	9.3237	75.4676	0.181	3.6044	0.2648	0.2645	–0.4
n = 3, m = 3							
6–31G	9.0364	75.1651	0.207	3.4726	0.2283	0.2283	2.4
6–31G*	9.3163	75.4783	0.218	3.6032	0.2647	0.2647	2.4
6–31++G**	9.3229	75.4646	0.179	3.6049	0.2646	0.2646	0.3
n = 3, m = 4							
6–31G	9.0396	75.1616	0.1979	3.4728	0.2282	0.2282	–1.4
6–31G*	9.3189	75.4755	0.2254	3.6034	0.2647	0.2646	–0.8
6–31++G**	9.3242	75.4609	0.1827	3.6049	0.2646	0.2645	–1.0

Note: All values are given in au. $^-$ and $^+$ represent bond properties referring to the bond point between the oxygen atom and the carbon atom bonded to it on the left and right, respectively.

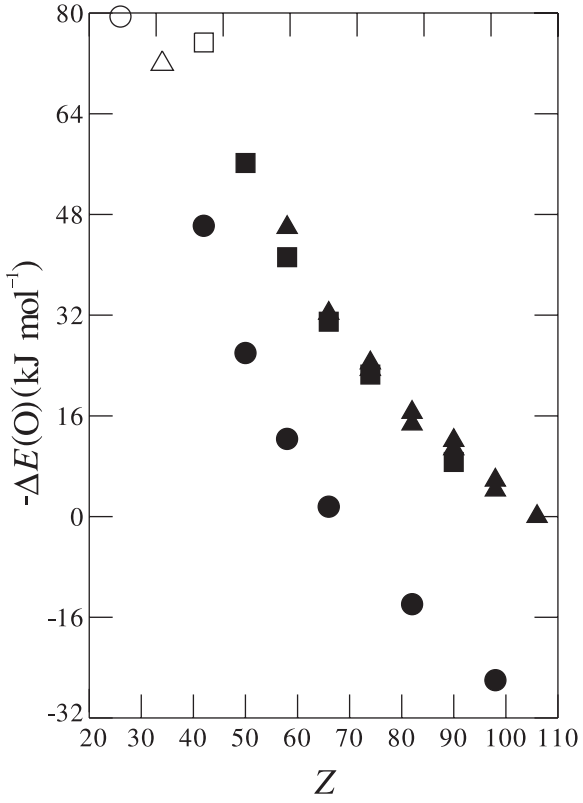
Table 2 presents the main atomic and bond properties computed for the oxygen atom from the HF/6–31++G**//6–31G* wave functions. It can be observed that the values of L(O) never exceed 0.0023 au — what makes them susceptible to be employed to study the transferability of the computed properties — being one order of magnitude larger than those obtained for the carbonyl oxygen in a previous work (18). This fact can be explained bearing in mind that two boundary surfaces have to be determined for oxygen atom in ethers. On the other hand, these larger values of L(O) allow us to employ N(O) vs. L(O) plots to distinguish among different transferable oxygen atoms as it was previously done for carbonyl carbon (18), and carbons of methyl and methilene groups in aldehydes and ketones (32). Though these linear relationships are empirical and they can be only applied along a certain range of $L(\Omega)$ values (typically $L(\Omega)$ values should verify: 10^{-2} au > $|L(\Omega)|$ > 10^{-4} au), the classification of the oxygen atoms provided by them is supported by the remaining properties (as it also happened with the atoms studied in the above mentioned works (18, 32)). In fact, the properties evaluated at bond critical points, which are not affected by integration errors, and which have been proposed to span an abstract space for similarity measures (33), and were used to classify alkyl esters (20), can be successfully classified according to this partition (Table 2). These N(O) vs. L(O) plots, presented in Fig. 3, indicate that the N(O) values can be classified in six groups: three specific values for the smallest molecules (methoxymethane, methoxyethane, and ethoxyethane) and other three values which can be considered transferable within methylethers (n = 0, m > 1), ethyl ethers (n = 1, m > 1), and the remaining dialkyl ethers (n > 1, m > 1). This conclusion can be also obtained at lower computational levels (just as an example of that, Table 3 shows the constancy of the integrated and bond properties of the dialkyl ethers' oxygen computed with smaller basis sets). It can be observed that though the addition of polarization functions over 6–31G basis set yields electron populations of the oxygen that are around 0.28 au larger and the addition of diffuse functions raises them by further 5–6 × 10^{-3} au, the differences among values computed at different levels for every molecule are almost constant. The linear relationship between N(O) and L(O) is maintained for all these computational levels (r coefficients are: 0.98, 0.97 and 0.97 for 6–31G//6–31G, 6–31G*//6–31G* and 6–31++G**//6–31G*, respectively).

Fig. 3. Variation of the electron population (N(O)) for the oxygen fragment with the error integral in the $CH_3(CH_2)_nO(CH_2)_mCH_3$ molecular series, r being the linear correlation coefficient. (○) n = m = 0; (△) n = 0, m = 1; (□) n = m = 1; (●) n = 0, m > 1; (■) n = 1, m > 1; (▲) n, m > 1.



© 2000 NRC Canada

Fig. 4. Plot of the electronic energy (ΔE(O)) for oxygen in $CH_3(CH_2)_nO(CH_2)_mCH_3$ relative to that in $CH_3(CH_2)_3O(CH_2)_7CH_3$ against the total nuclear charge Z of the molecule. (○) n = m = 0; (△) n = 0, m = 1; (□) n = m = 1; (●) n = 0, m > 1; (■) n = 1, m > 1; (▲) n, m > 1.



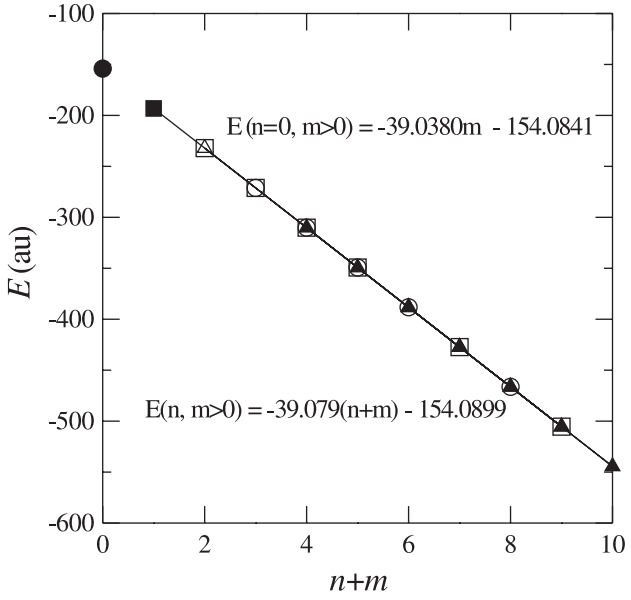
It has to be remarked that, though the employment of N(O) absolute values to establish this classification can lead to wrong conclusions because of the influence of L(O) over N(O), N(O) absolute values are consistent with the strong electronegativity of the O atom (electron populations are always greater than 9.3 au). Both the transferable values extrapolated to L(O) = 0 (9.3161, 9.3219, and 9.3235 au for methyl ethers, ethyl ethers, and dialkyl ethers, respectively) and the specific values mentioned before indicate that the oxygen electron populations increases with the size of the substituents (methyl, ethyl, or a substituent larger than ethyl).

The evolution of the values of the oxygen energies (E(O)) (Fig. 4), obtained after correcting the electron kinetic energy (T(O)) with the (γ – 1) factor, also support the partition for the O atoms proposed above from N(O) values. As it has been found for carbonyl, methyl, and methylene groups in neutral (18, 32) and protonated (19) aldehydes and ketones, oxygen energies in alkyl ethers are also dependent of the molecule size (expressed by Z, sum of the atomic numbers of the molecule). The possibility that the molecular size effect on E(O) could be an artifact due to the incompleteness of the basis set was studied in a work on alkyl alcohols (34).[2] In no case did the changes observed in that work for the E(O) values modify the relative ΔE(O) by more than a 3% (i.e., for 1-penthanol ΔE(O), referred to 1-dodecanol, changed from –61.1 to –60.8 kJ mol^{-1}). Figure 4 shows the variation of the electronic energy ΔE(O) for oxygen atom relative to that in $CH_3(CH_2)_3O(CH_2)_7CH_3$ (the largest value of E(O) found in the molecules here studied) against the total nuclear charge Z of the molecule. So, E(O) increases with increasing m at fixed n. For example, the oxygen atoms in 1-methoxybutane and 1-methoxypentane, which are so similar as regards all other properties (Table 2), exhibit an energy difference of 13.7 kJ mol^{-1}. If we consider the difference between the energy of the smallest and the largest molecule in every series, it reaches 72.1 kJ mol^{-1} in methyl ethers, 66.6 kJ mol^{-1} in ethyl ethers, and 45.9 kJ mol^{-1} in the remaining dialkyl ethers. As a general result, we have found that oxygen atom is more stabilized for the dialkyl ether isomer than for the ethyl ether one and the latter is more stable than the corresponding methyl ether isomer. It can be concluded from Fig. 4 that it is not possible to establish transferable values for E(O) because of the influence of the molecular size Z on this magnitude. Nevertheless, this fact does not mean that the different models of group contribution traditionally applied to the calculation of energy properties in these systems cannot be employed. In fact, both HF total molecular computed energies and ΔH_f° experimental values can be very well fitted to expressions of the form:

$$E_{HF} = E(CH_2)\cdot(n + m) + E_0$$

where (n + m) represents the number of CH_2 groups in the molecule, $E(CH_2)$ is the CH_2 contribution to the total energy, and E_0 is the sum of the remaining groups contributions (the oxygen atom and the two CH_3 groups). We have considered two independent fittings, with no inclusion of methoxymethane molecule: one for methyl ethers and another one for the remaining molecules (Fig. 5) which allow an excellent reproduction of the HF/6–31++G** energies (Table 1) with maximum discrepancies of 2.2 kJ mol^{-1}

Fig. 5. HF/6–31++G** vs. number of CH_2 groups n + m for molecules in Table 1. (●) n = m = 0; (■) n = 0, m = 1; (△) n = m = 1; (□) n = 0, m > 1; (○) n = 1, m > 1; (▲) n, m > 1.



[2] M. Mandado, A.M. Graña, and R.A. Mosquera. To be published.

© 2000 NRC Canada

Fig. 6. Difference between the HF/6–31++G** calculated energy and that obtained from the fitting in Fig. 5. (●) $n = m = 0$; (■) $n = 0$, $m = 1$; (△) n = m = 1; (□) $n = 0$, $m > 1$; (○) $n = 1$, $m > 1$; (▲) n, $m > 1$.

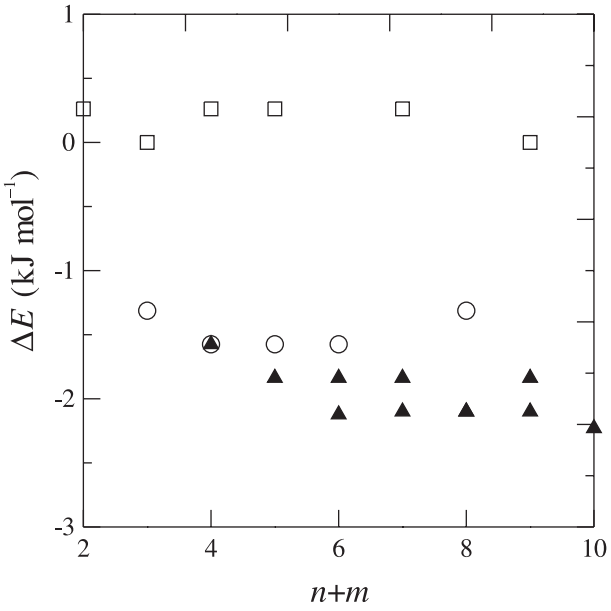


Fig. 7. Experimental $\Delta H^{\circ}_{f\,exp}$ vs. number of CH_2 groups $n + m$ for molecules in Table 1. (▲) n = m = 0; (●) $n = 0$; $m > 0$; (◆) n, $m > 0$.

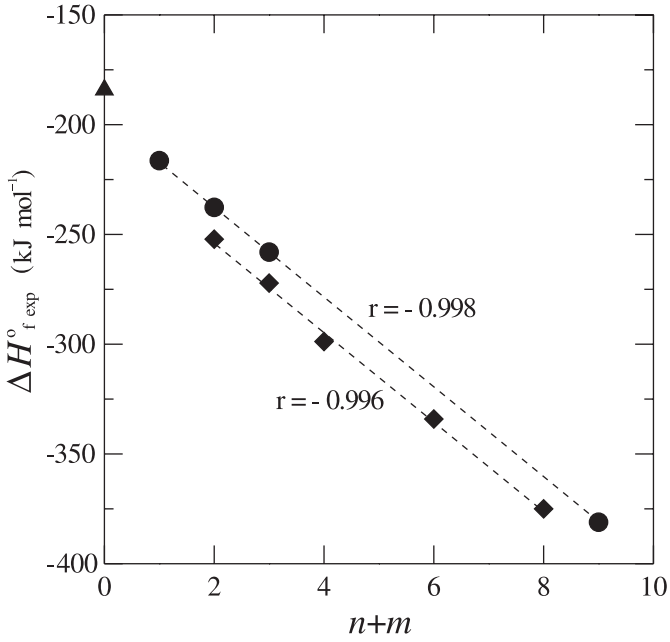


Table 4. Transferable values of electron population extrapolated to $L(O) = 0$, $[N(O)]_{L(O)=0}$, and mean values of the molar volume ($v(O)$) for the partition proposed in this work.

	$[N(O)]_{L(O)=0}$ (au)	$v(O)$ ($cm^3\ mol^{-1}$)	RMS$[v(O)] \times 10^4$
Methoxymethane	—	7.89	—
Methoxyethane	—	7.88	—
Ethoxyethane	—	7.83	—
Methylethers ($n = 0$, $m > 1$)	9.3161	7.86	3.9
Ethylethers ($n = 1$, $m > 1$)	9.3219	7.85	10.5
Dialkylethers (n, $m > 1$)	9.3235	7.83	11.8

(Fig. 6). Though the difference between the energy of the CH_2 groups for methyl ethers and remaining dialkyl ethers does not reach 1 kcal mol^{-1} according to these fittings, the difference in the intercepts justifies the consideration of two independent fittings for each series. We have also applied the same treatment to the experimental $\Delta H^{\circ}_{f\ exp}$ values available for these compounds (Table 1), though the quality of the fitting decreases (Fig. 7) as it could be expected bearing in mind the magnitude of the experimental errors and the diversity of the experimental methods employed. We have also found that there was no meaningful improvement when three independent fittings were considered for methyl ethers, ethyl ethers, and the remaining dialkyl ethers.

Also, the different evolutions of the values of the potential energy for the nucleus–electron charge interaction in the oxygen fragment ($V_{NEO}(O)$) (Table 2), allow one to distinguish methyl ethers, ethyl ethers, and dialkyl ethers with longer chains than those in the previous series.

The volumes ($v(O)$) of the region bound by the interatomic C-O surfaces and the boundary defined by an electron charge density of 0.002 au are significantly smaller than those obtained for the carbonyl oxygen (18). The evolution of the magnitude along the alkyl ethers indicates the volume decreases slightly in the series: $v(n = 0) > v(n = 1) > v(n > 2)$ as shown in Table 2. Mean values and RMS obtained for each of these series are consistent with the partitioning of the alkyl ethers proposed from the properties we have analyzed above. In Table 4 we present the transferable values of the atomic population extrapolated to $L(O) = 0$ and molar volume for the partition proposed in this work.

Though the values of the dipole moment of the electron charge distribution ($\mu(O)$) for the oxygen fragments are very similar (Table 2), it is clear the charge distribution of the oxygen in methyl ether is more polarized and that a symmetric substitution reduces the value of this magnitude.

Bond properties, which are not affected by the errors and uncertainties involved in the numerical determination of the zero-flux surfaces, clearly reflect the specific character of the oxygen fragments observed from the previous analysis. Table 2 contains the main critical bond properties for C—O bonds. Opposite to what was found for the energetic properties, bond properties do not exhibit any dependence on the total nuclear charge Z.

The ellipticity values obtained for both C—O bonds (ε^+ and ε^-) can be classified also considering three specific pairs of values for (methoxymethane, methoxyethane, and

© 2000 NRC Canada

Table 5. Average values, RMS values, and maximum deviations for bond properties of the transferable oxygen fragments proposed for the $CH_3(CH_2)_nO(CH_2)_mCH_3$ molecules studied in this work.

Mean value	λ_3^-	λ_3^+	$\varepsilon^- \times 10^3$	$\varepsilon^+ \times 10^3$	ρ_c^-	ρ_c^+	R^-	R^+
$n = 0$, $m > 1$	0.9528	0.9381	12.2	26.7	0.2683	0.2647	1.7984	1.8027
RMS	0.0005	0.0016	0.0	0.1	0.0001	0.0002	0.0001	0.0003
Max deviation	0.0005	0.0033	0.0	0.2	0.0001	0.0003	0.0002	0.0005
$n = 1$,$m > 1$	0.9381	0.9405	29.4	24.9	0.2647	0.2646	1.8025	1.8025
RMS	0.0005	0.0013	0.1	0.1	0.0001	0.0001	0.0001	0.0002
Max deviation	0.0004	0.0024	0.3	0.2	0.0001	0.0002	0.0002	0.0004
n, $m > 1$	0.9433	0.9416	24.8	25.1	0.2647	0.2645	1.8022	1.8043
RMS	0.0017	0.0009	0.2	0.1	0.0001	0.0001	0.0002	0.0058
Max deviation	0.0025	0.0026	0.2	0.3	0.0002	0.0002	0.0003	0.0012

Note: $^-$ and $^+$ represent bond properties referring to the bond point between the oxygen atom and the carbon atom bonded to it on the left and right, respectively. All values are given in au.

ethoxyethane) and three groups of molecules (the same above defined to classify atomic properties) where the ellipticity values present small oscillations (never larger than 3×10^{-4} au) around certain transferable and clearly different values presented in Table 5. This table also contains the mean values (with RMS and maximum deviations) of the positive eigenvalue of the Hessian matrix of the charge density at the C—O bond critical points (λ_3^+, λ_3^-).The larger value of the O—CH_3 bond can be associated to a smaller dependence on the environment for the properties of this bond (35).

The values obtained for the charge density at the bond critical points display a smaller variation in the series and could be grouped distinguishing only between methyl ethers the remaining alkyl ethers and the specific behaviour of the methoxymethane molecule. In fact the main difference among the values listed in Table 2 correspond to the values of ρ_c for an O—CH_3 bond (0.268 au) and an O—CH_2 bond (0.265 au). The same can be said for the R values (1.798 au and 1.795 au for O-CH_3 and O-CH_2, respectively), which can also be classified according to the partition described for ρ_c. As it has been previously stated by Wiberg and Breneman (36) a large part of the variation in ρ_c is associated with the change in bond length and so O-Et is almost the same as O-R (R > Et). Table 5 includes mean values of R and ρ_c with RMS and maximum deviation for each of the groups considered for previous properties.

Conclusions

To sum up, the different trends followed by the energy properties (which cannot be considered transferable because of a strong dependence with the size of the molecule already reported for aldehydes and ketones), the different linear relationships between N(O) and L(O), and the different values of other integrated properties and the main C—O bond properties, support the consideration of six different oxygen atoms along the series of the unbranched dialkyl ethers. These atoms are the O of: MeOMe, MeOEt, EtOEt, MeOR, EtOR, and ROR′ (R, R′ > Et).

Acknowledgements

This paper is in memory of Prof. Julia Franco. We thank the Autonomous Government of Galicia for funding this research by XUGA 380301B93 and Centro de Supercomputacion de Galicia for access to their computational facilities.

References

1. S.W. Benson and J.H. Buss. J. Chem. Phys. **29**, 546 (1958).
2. I. Prigogine, V. Mathot, and A. Bellemans. The molecular theory of solutions. North Holland, Amsterdam. 1957.
3. U. Burkert and N.L. Allinger. Molecular mechanics. American Chemical Society, Washington, D.C. 1982.
4. R.F.W. Bader. Can. J. Chem. **77**, 13 (1999).
5. R.F.W. Bader, P.L.A. Popelier, and C. Chang. J. Mol. Struct. (THEOCHEM), **225**, 145 (1992).
6. J. Cioslowsky and A. Nanayakkara. J. Am. Chem. Soc. **115**, 11 213 (1993).
7. E. Besalú, R. Carbó, and M. Solà. Top. Curr. Chem. **173**, 31 (1995).
8. P.G. Mezey. Adv. Quant. Chem. **27**, 163 (1996).
9. J. Cioslowski, B.B. Stefanov, and P. Constans. J. Comput. Chem. **17**, 1352 (1996).
10. R.F.W. Bader and P. Becker. Chem. Phys. Lett. **148**, 452 (1988).
11. J. Riess and W. Münch. Theor. Chim. Acta, **58**, 295 (1981).
12. R.F.W. Bader. Atoms in molecules — a quantum theory. *In* International series of monographs on chemistry. No. 22. Oxford University Press, Oxford. 1990.
13. R.F.W. Bader. Chem. Rev. **91**, 893 (1991).
14. R.F.W. Bader and K.E. Laidig. J. Mol. Struct. (THEOCHEM), **234**, 75 (1991).
15. R.F.W. Bader, P.L.A. Popelier, and T.A. Keith. Angew. Chem. Int. Ed. Engl. **33**, 620 (1994).
16. R.F.W. Bader, M.T. Carroll, J.R. Cheeseman, and C. Chang. J. Am. Chem. Soc. **109**, 7968 (1987).
17. K.B. Wiberg, R.F.W. Bader, and C.D.H. Lau. J. Am. Chem. Soc. **109**, 1001 (1987).
18. A. Graña and R.A. Mosquera. J. Chem. Phys. **110**, 6606 (1999).
19. A. Graña and R.A. Mosquera. Chem. Phys. **243**, 17 (1999).
20. E. Carballo, R. Mosquera, J.L. Legido, and L. Romaní. J. Chem. Soc. Faraday Trans. **93**, 3437 (1997).
21. V.J. Comanita, R.A. Grrencorn, and K.C. Chao. J. Chem. Eng. Data, **21**, 491 (1976).
22. F.W. Biegler-König, R.F.W. Bader, and T.H. Tang. J. Comput. Chem. **3**, 17 (1982).
23. R.F.W. Bader. (*Editor*). AIMPAC: a suite of programs for the theory of atoms in molecules. McMaster University, Hamilton, ON L8S 4M1, Canada. Contact bader@mcmail.cis.mcmaster.ca

© 2000 NRC Canada

24. M.J. Frisch, G.W. Trucks, H.B. Schlegel, P.M.W. Gill, B.G. Johnson, M.A. Robb, J.R. Cheeseman, T. Keith, G.A. Petersson, J.A. Montgomery, K. Raghavachari, M.A. Al-Laham, V.G. Zakrzewski, J.V. Ortiz, J.B. Foresman, J. Cioslowski, B.B. Stefanov, A. Nanayakkara, M. Challacombe, C.Y. Peng, P.Y. Ayala, W. Chen, M.W. Wong, J.L. Andres, E.S. Replogle, R. Gomperts, R.L. Martin, D.J. Fox,. S. Binkley, D.J. Defrees, J. Baker, J.P. Stewart, M. Head-Gordon, C. Gonzalez, and J.A. Pople. Gaussian 94, Revision C.3. Gaussian, Inc., Pittsburgh, Pa. 1995.
25. T. Clark, J Chandrasekar, G.W. Spitznagel, and P.V.R. Schleyer. J. Comput. Chem. **4**, 294 (1983).
26. P.C. Hariharan and J.A. Pople. Theor. Chim. Acta, **28**, 213 (1973).
27. G. Pilcher, A.S. Pell, and D.J. Coleman. Trans. Faraday Soc. **60**, 499 (1964).
28. J.O. Fenwick, D. Harrop, and A.J. Head. J. Chem. Thermodyn. **7**, 943 (1975).
29. M. Colomina, A.S. Pell, H.A. Skiner, and D.J. Coleman. Trans. Faraday Soc. **61**, 2641 (1965).
30. J.W. Murrin and S. Goldhagen. NAVORD Report no. 5491. 1 (1957).
31. R.F.W. Bader and F.J. Martín. Can. J. Chem. **76**, 284 (1998).
32. A. Graña and R.A. Mosquera. J. Chem. Phys. **113**, 1492 (2000).
33. P.L.A. Popelier. J. Phys. Chem. **103**, 2883 (1999).
34. M. Mandado. Estudio AIM de la transferabilidad en alcoholes alifáticos primarios. Tesina de Licenciatura, Universidade de Vigo. 2000.
35. T. Slee. J. Am. Chem. Soc. **108**, 606 (1986).
36. K.B. Wiberg and C.M. Breneman. J. Am. Chem. Soc. **112**, 8765 (1990).

© 2000 NRC Canada

Anhydrous perchlorato complexes of palladium(II): $Pd(ClO_4)_2$, $(ClO_2)_2Pd(ClO_4)_4$, and $(NO_2)_2Pd(ClO_4)_4$. Syntheses and structural analyses

Frédérique Cunin, Frédéric Favier, and Jean Louis Pascal

Abstract: Chlorine trioxide (Cl_2O_6) reacts with $PdCl_2$ to yield "$ClO_2Pd(ClO_4)_3$" which is, in fact, an equimolar mixture of $Pd(ClO_4)_2$ and $(ClO_2)_2Pd(ClO_4)_4$. The chloryl salt decomposes under vacuum to give $Pd(ClO_4)_2$. $(NO_2)_2Pd(ClO_4)_4 \cdot 0.5\ NO_2ClO_4$ is prepared using $Pd(NO_3)_2 \cdot 0.5\ (H_2O, HNO_3)$ as the starting salt. Excess NO_2ClO_4 sublimes easily and pure $(NO_2)_2Pd(ClO_4)_4$ is obtained. $Pd(ClO_4)_2$ and $(NO_2)_2Pd(ClO_4)_4$ crystallize poorly; however, a $P2_1/m$ space group is proposed for the latter. A complete assignment of vibrational modes, and DFT calculations, show that $Pd(ClO_4)_2$ is monomeric with chelating bidentate [ClO_4] groups and Pd is in a square planar environment. In nitryl and chloryl salts, individual anions ($Pd(ClO_4)_4^{2-}$), where unidentate [ClO_4] groups interact partially with the cation or the Pd core, were characterized.

Key words: palladium(II), chlorine trioxide, perchlorato complexes, chelating bidentate, vibrational spectroscopy, DFT calculations, powder X-ray diffraction.

Résumé : Le trioxyde de chlore (Cl_2O_6) réagit avec $PdCl_2$ pour donner « $ClO_2Pd(ClO_4)_3$ ». Ce sel est en fait un mélange équimoléculaire de $Pd(ClO_4)_2$ et de $(ClO_2)_2Pd(ClO_4)_4$. Ce dernier se décompose sous vide dynamique en $Pd(ClO_4)_2$ et Cl_2O_6. $(NO_2)_2Pd(ClO_4)_4 \cdot 0{,}5\ NO_2ClO_4$ est obtenu à partir de $Pd(NO_3)_2 \cdot 0{,}5\ (H_2O, HNO_3)$. NO_2ClO_4 additionnel se sublime facilement et $(NO_2)_2Pd(ClO_4)_4$ pur est isolé. La cristallinité de $Pd(ClO_4)_2$ et $(NO_2)_2Pd(ClO_4)_4$ est médiocre cependant il est possible de proposer le groupe d'espace $P2_1/m$ pour le sel de nitryle. Une attribution complète des modes de vibration et un calcul DFT montrent que $Pd(ClO_4)_2$ est un monomère et que les groupements [ClO_4] sont bidentés chélatants. Pd est dans un environnement plan carré. Les sels de nitryle et de chloryle comportent des anions individuels $Pd(ClO_4)_4^{2-}$ ou les groupements [ClO_4] monodentés interagissent fortement avec les cations ou le centre métallique Pd.

Mots clés : palladium(II), trioxyde de chlore, complexes perchlorato, bidenté chélatant, spectroscopie de vibration, calculs DFT, rayons X sur poudre.

Introduction

In spite of advancing knowledge of perchlorato complexes (1) they still remain an attractive subject of interest (2) in view of their versatile structural properties (1), their potential use as catalysts (3) or electrolytes (4), and as a source of materials such as chlorides, oxides, or oxychlorides (5) or oxygen (6). Perchlorates of precious metals are little studied for reasons less linked to the cost of starting materials than to their difficult synthesis. According to Pearson's HSAB concept (7), the hard base ClO_4^- interacts more readily with hard acids than boundary or soft acids. The latter are mainly found in the platinum group family. Since these metals can exist in high oxidation states they should bind more easily to O^{2-} than ClO_4^-, and O^{2-} can be formed from efficient perchlorating reagents such as anhydrous $HClO_4$ or Cl_2O_6 which are also very strong oxidizers. Since the most stable oxidation state of Pd is II, the synthesis of palladium perchlorato complexes should be easier than that of the other perchlorato complexes of the platinum series. In fact, this has been demonstrated previously when it was shown that $Pd(ClO_4)_2$ and $ClO_2Pd(ClO_4)_3$ could be prepared without the formation of oxides (8). However, their IR spectra did not allow a molecular geometry to be proposed. In this paper, synthesis and structural studies of the above complexes are revisited and a previously unknown perchlorate ($(NO_2)_2Pd(ClO_4)_4$) has been synthesized and analyzed. For the first time, a DFT optimization of the geometry of a perchlorato complex involving a chelating bidentate [ClO_4] group was performed and a complete assignment of vibrational modes is proposed.

Received May 21, 2000. Published on the NRC Research Press website on November 21, 2000.

F. Cunin, F. Favier, and J.L. Pascal.[1] Laboratoire des Agrégats Moléculaires et Matériaux Inorganiques (CNRS UMR 5072), Case Courrier 15, Université de Montpellier 2, 34095 Montpellier CEDEX 5, France.

[1]Author to whom correspondence may be addressed. Telephone: 33 4 67 14 33 32. Fax: 33 4 67 14 33 04. e-mail: pasfav@univ-montp2.fr

Results and discussions

Synthesis

Reaction of a perchlorating reagent with various salts has been described in a recent review (1), where the choice of Cl_2O_6 as perchlorating reagent as well as strategies to improve reactions have been explained.

© 2000 NRC Canada

If a hydrated chloride is used as the starting salt, [Cl] is replaced by [ClO_4] and eliminated as Cl_2 and as the acids that are produced when Cl_2O_6 reacts with water (9). Extra Cl_2O_6 adds to the neutral molecule $M(ClO_4)_n$ (n = oxidation state of M) to give well-characterized salts $(ClO_2)_mM(ClO_4)_{n+m}$ or mixtures $M(ClO_4)_n$, mCl_2O_6, ($0.5 < m < 2$) (1).

With $PdCl_2 \cdot \varepsilon H_2O$ ($\varepsilon \approx 0.1$), the reaction proceeds as follows:

[1] $$PdCl_2 \cdot \varepsilon H_2O + (3 + \varepsilon)Cl_2O_6 \rightarrow ClO_2Pd(ClO_4)_3 + \varepsilon HClO_3\uparrow + \varepsilon HClO_4\uparrow + Cl_2\uparrow$$

[2] $$ClO_2Pd(ClO_4)_3 \underset{\Delta / \text{vacuum}}{\rightarrow} Pd(ClO_4)_2 + Cl_2O_6$$

Nitrate salts behave differently since NO_3^- is transformed into the nitryl cation (NO_2^+) in acidic medium (10, 11) and is replaced simultaneously by ClO_4^- according to:

[3] $$M(NO_3)_n + 2nCl_2O_6 \underset{10°C}{\rightarrow} (NO_2)_nM(ClO_4)_{2n} + 2nClO_2\uparrow + n/2O_2\uparrow$$

$(NO_2)_nM(ClO_4)_{2n}$ is generally formed as the mixture: $NO_2M(ClO_4)_{n+1}/n - 1\ NO_2ClO_4$. Nitryl perchlorate sublimes under vacuum at $T > 60°C$ and pure $NO_2M(ClO_4)_{n+1}$ is obtained. When $T > 100°C$, nitryl perchlorato metallate salts decompose to yield $M(ClO_4)_n$ (1). Well-defined $(NO_2)_nM(ClO_4)_{2n}$ salts are rarely prepared in a single step. Until the present study, only Cu (11) and Hg (12) salts of such stoichiometry had been obtained.

With $Pd(NO_3)_2 \cdot 0.5(H_2O, HNO_3)$ as the starting material, the reactions can be summarized as follows:

[4] $$Pd(NO_3)_2 + 4Cl_2O_6 \underset{10°C}{\rightarrow} (NO_2)_2M(ClO_4)_4 + 4ClO_2\uparrow + O_2\uparrow$$

[5] $$H_2O + HNO_3 + 2Cl_2O_6 \underset{10°C}{\rightarrow} NO_2ClO_4 + 2ClO_2\uparrow + 1/2O_2\uparrow + HClO_3\uparrow + 2HClO_4\uparrow \quad (13)$$

therefore:

[6] $$Pd(NO_3)_2 \cdot 0.5(H_2O, HNO_3) + 5Cl_2O_6 \underset{10°C}{\rightarrow} (NO_2)_2Pd(ClO_4)_4 + NO_2ClO_4 + 5ClO_2\uparrow + 1.25O_2\uparrow + 0.5HClO_3\uparrow + 2HClO_4\uparrow$$

Powder X-ray diffraction analysis

The powder diffraction pattern of $Pd(ClO_4)_2$ is of poor quality, only 14 well-defined lines were found in the 2θ range: 10–50° and at higher angles, the line intensities vanish rapidly, therefore an indexing program such as TREOR 90 (TREOR 90: A semiexhaustive TRial and ErrOR powder indexing program. Basic principles: see ref. 14*a*; for all symmetries: see ref. 14*b*) could not give an accurate determination of the crystallographic symmetry. For $(NO_2)_2Pd(ClO_4)_4$, 24 lines could be used and determination of the unit cell was straightforward. This compound crystallizes with monoclinic symmetry (a = 15.063(4), b = 9.666(1), c = 5.436(2) Å, β = 103.29(2)° (M(24) = 23 av. eps. = 0.0000316) (15); F24 = 35 (0.009554, 72) (16))).

Table 1. Powder X-ray diffraction lines for $Pd(ClO_4)_2$.

d_{obs}	I	d_{obs}	I
7.626	28	2.482	sh
5.975	100	2.471	7
5.315	27	2.439	3
4.622	45	2.416	3
4.475	2	2.376	4
4.118	40	2.311	<1
3.980	45	2.286	<1
3.850	3	2.266	<1
3.777	5	2.250	3
3.681	4	2.198	1
3.644	8	2.153	3
3.411	19	2.140	3
3.359	33	2.102	1
3.272	6	2.093	1
3.266	5	2.060	5
3.125	7	2.046	2
3.081	10	1.992	13
2.986	33	1.984	sh
2.924	16	1.946	1
2.871	11	1.915	3
2.744	8	1.872	3
2.692	4	1.859	<1
2.604	16	1.839	<1
2.519	14		

$P2_1/m$ appears as a possible space group. With $Z = 2$, the calculated density is 2.57. It is in the expected range for a such perchlorato complex (17). An X-ray diffraction pattern finger print is given in Table 1 for $Pd(ClO_4)_2$. The indexed X-ray lines for $(NO_2)_2Pd(ClO_4)_4$ are listed in Table 2.

Vibrational analysis

$Pd(ClO_4)_2$

IR and Raman spectra of bis(perchlorato)palladium(II) are shown in Fig. 1. The distribution of lines and their frequencies in the range of the stretching modes (800–1350 cm^{-1}) are consistent with bidentate bonding for the [ClO_4] groups (1). The region containing deformation modes (400–700 cm^{-1}) is very perturbed. Comparison of these data with those found for $Ti(ClO_4)_4$ (18) or $Yb(ClO_4)_3$ (high-temperature form) (2*a*) (Fig. 2) suggests that [ClO_4] is a chelating bidentate group in $Pd(ClO_4)_2$ and that therefore, the complex is a monomeric unit (Fig. 3). This is very surprising because the chloride salt (from which the geometry of perchlorato complexes generally derives (19)) ($PdCl_2$) is a two-dimensional polymer with bridging Cl atoms (20) and because some carboxylate and phosphate complexes, ligands act as bridging entities. $(Pd(OAc)_2$ is a cyclic trimer (21) while $Pd(PO_3)_2$ is built on a three-dimensional network (22)). However, the geometry of $Pd(ClO_4)_2$ is similar to that of $Pd(AlCl_4)_2$ (23). Assignment of bands and lines was improved by a DFT geometry optimization which provided the vibrational frequencies (24). A starting model was built on the basis of the relation $\nu = f$(dCl—O) established elsewhere (1) for a bidentate chelating [ClO_4] group and a square planar geometry around palladium with 4 Pd—O

© 2000 NRC Canada

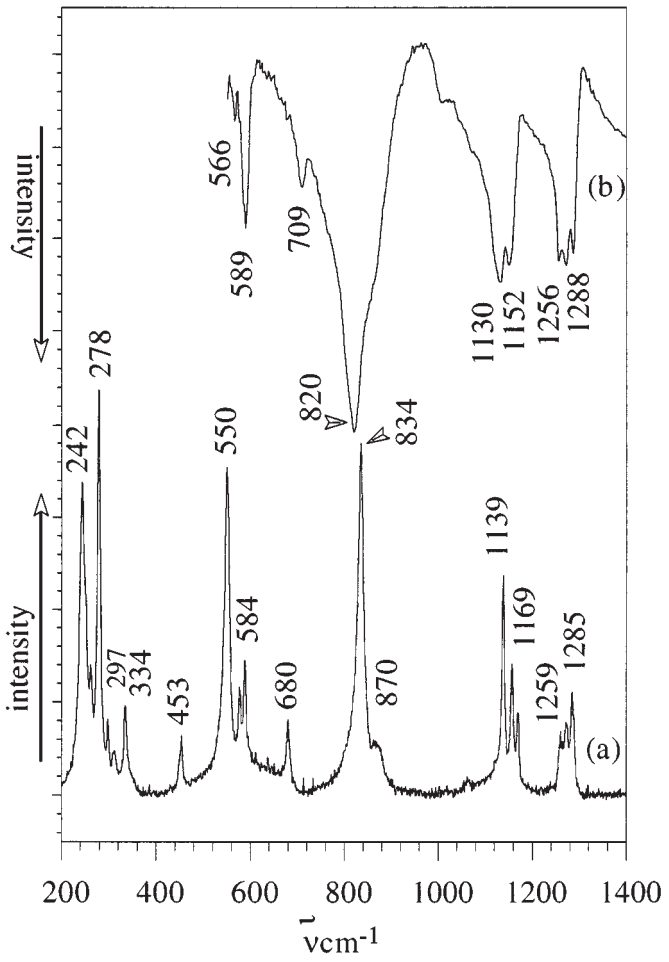
Table 2. Indexed X-ray powder diffraction lines for $(NO_2)_2Pd(ClO_4)_4$.

hkl	d_{obs}	d_{calc}	I_{obs}	*hkl*	d_{obs}	d_{calc}	I_{obs}
	8.87		1	–222		2.353	
011	8.044	8.069	100		2.355		<1
002	7.312	7.330	47	–214		2.353	
012	5.744	5.840	<1	202	2.323	2.323	3
–101	5.407	5.387	<1	042	2.295	2.295	10
100	5.286	5.290	26	133	2.285	2.284	
–102	4.843	4.851	94	212	2.260	2.259	14
–111	4.701	4.706	15	221	2.225	2.224	1
110	4.638	4.641	4	026	2.180	2.180	1
021	4.586	4.590	4	035	2.169	2.168	14
–112	4.335	4.336	19	043	2.167	2.166	14
111	4.187	4.188	4	–142	2.165	2.163	10
022	4.022	4.035	<1	–135	2.139	2.138	sh
102	3.885	3.887	35	222	2.095	2.094	7
–113	3.765	3.765	64	213	2.081	2.080	2
112		3.606		–143	2.078	2.080	6
	3.600		30	–231	2.075	2.076	6
–121		3.597		142		2.052	
120	3.570	3.568	8		2.049		3
–122	3.423	3.423	46	017		2.045	
–104	3.400	3.400	35	044	2.017	2.017	5
–114	3.208	3.209	12	231	1.978	1.977	5
031	3.145	3.147	51	–144	1.971	1.969	3
–123	3.123	3.121	sh	036	1.947	1.947	3
113	3.069	3.070	29	–234	1.938	1.938	1
122	3.029	3.029	5	027	1.921	1.921	1
032	2.949	2.949	14	135	1.896	1.896	2
015	2.806	2.806	17	232		1.884	
–124	2.779	2.781	sh		1.884		4
–131	2.765	2.765	19	126		1.884	
104	2.733	2.733	4	–108		1.869	
123		2.690			1.869		2
	2.691		22	052		1.869	
033		2.690		–145	1.841	1.845	5
131	2.649	2.648	19	008	1.832	1.832	sh
–211	2.615	2.613	2				
–212	2.597	2.595	2				
210	2.559	2.551	<1				
–133	2.531	2.531	18				
025	2.506	2.507	<1				
006	2.444	2.443	6				
–204	2.426	2.426	11				
124	2.379	2.379	6				

distances around 2.00 Å. For this closed shell compound ($S = 0$), we searched for a local minimum on the potential energy surface at three levels (HF, B3LYP, and B3PW91). The calculated geometry converged to a deformed square planar environment for Pd and chelating bidentate $[ClO_4]$ groups (Fig. 3) which was independent of the level of theory and basis sets used. Geometrical data are summarized in Table 3. As expected, the higher the level of calculation and the more complex the basis sets, the closer the result of the calculation to the experimental data. The calculated vibrational frequencies (unscaled) are compared with the experimental frequencies in Table 4. A description of vibrational modes is also given. Regardless of the level of theory and basis sets used, the same classification of vibrational energy levels and coupling were obtained. Best agreement was found with B3PW91 hybrid density functional level and selected basis sets for Pd, Cl, and O (LANL2DZ for Pd, cc-pVQZ for Cl and O). Although a maximum symmetry of D_{2h} was expected, assignments correspond to C_{2v} symmetry. In contrast crystal effects which are associated mainly with stretching modes cannot be accounted for. Shifts between experimental and calculated frequencies are consistent with those observed in several solids for which a similar procedure was carried out (25). The stretching modes are located, as expected, at frequencies higher than 800 cm^{-1}. The three groups of lines or bands are close to those observed in other

© 2000 NRC Canada

Fig. 1. (*a*) Raman and (*b*) IR spectra of $Pd(ClO_4)_2$.

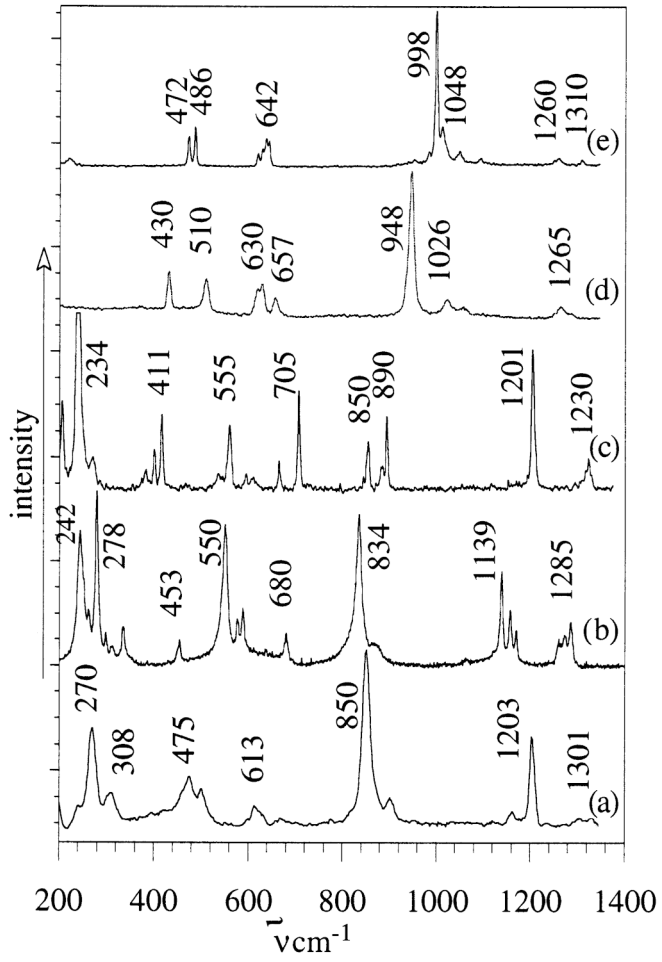


complexes involving bidentate $[ClO_4]$ (1) (Fig. 2). The most striking feature appears for the deformation modes. Previous results using guidelines from Hathaway and Underhill (26) and from a simple force constant calculation (27), but which did not take into account coupling between ClO_4 and MO_n vibrational modes, led to the following scale: $\rho_r > \rho_w > \delta ClO_t > \rho_t > \delta ClO_b$. Present results show that $\delta ClO_b > \rho_w > \rho_t > \delta ClO_t > \rho_r$, and that these modes are coupled with PdO_4 vibrations. The distribution seems consistent with constraints imposed by the chelation of $[ClO_4]$ groups.

Chloryl- and nitryl-perchloratopalladates

The Raman spectra for these salts are shown in Fig. 4. They are compared with those of $Pd(ClO_4)_2$ and $ClO_2Au(ClO_4)_4$ (2*f*). The ClO_2^+ and NO_2^+ cations are clearly identified by their very strong lines resulting from their symmetric stretching vibrations at 1033 cm^{-1} and 1406 cm^{-1} (1), respectively. The strong line around 1050 cm^{-1}, the broad doublet near 1200 cm^{-1}, and lines in the range 750–900 cm^{-1} are characteristic of perturbed unidentate $[ClO_4]$ groups (28). For the chloryl salt, additional lines appear at 555, 835, 1150, and 1280 cm^{-1}, which are interpreted as characteristic of a bidentate $[ClO_4]$. A close comparison of these lines with those found for $Pd(ClO_4)_2$ show that they are identical. Subtraction of the $Pd(ClO_4)_2$ contribution leads to a clean spectrum of $ClO_2Pd(ClO_4)_3$ in which only unidentate $[ClO_4]$ appears

Fig. 2. Comparison of the Raman spectra of: (*a*) $Fe(ClO_4)_3$ (43); (*b*) $Pd(ClO_4)_2$; (*c*) $Ti(ClO_4)_4$; (*d*) $Yb(ClO_4)_3$ (high-temperature form); and (*e*) $Yb(ClO_4)_3$ (low-temperature form). Shifts in the deformation mode range (400–700 cm^{-1}) distinguish bridging and chelating bonding modes for bidentate (a, b, c) and tridentate (d, e) $[ClO_4]$ groups.



as found in $ClO_2Au(ClO_4)_4$ or $(ClO_2)_2Pt(ClO_4)_6$ (2*f*). Since Pd(II) is generally found in a square planar environment, we can conclude that the chloryl salt is $(ClO_2)_2Pd(ClO_4)_4$ and that the product obtained in a first step is an equimolar mixture of $Pd(ClO_4)_2$ and $(ClO_2)_2Pd(ClO_4)_4$.

X-ray diffraction and vibrational spectroscopic analyses of Cl_2O_6 (27, 29), $(ClO_2)_2Sn(ClO_4)_6$ (28), and $ClO_2Au(ClO_4)_4$ (2*f*) indicate strong anion–cation interactions. This is demonstrated in metal salts by a shift and a splitting of the νClO_b modes (750–920 cm^{-1} range) as well as by the appearance of new lines between 1000 and 1250 cm^{-1}. Only some $[ClO_4]$ interacts with ClO_2^+ leading to pseudo-bidentate $[ClO_4]$ groups (Fig. 5), whereas the remaining $[ClO_4]$ groups are classical unidentate groups (1). These two kinds of bonding modes are distinguished. They appear in Table 5 where their vibrational assignments are given and where couplings found from the DFT optimization of $ClO_2Au(ClO_4)_4$ are included.

The nitryl salt, $(NO_2)_2Pd(ClO_4)_4$, behaves like the chloryl salt, however, the lines assigned to the stretching modes of bridged Cl—O (Cl—O_b) are shifted to higher frequencies,

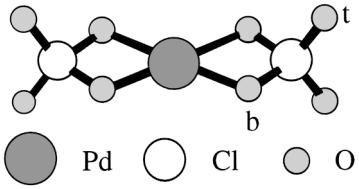
© 2000 NRC Canada

Table 3. Calculated and experimental structural data for $Pd(ClO_4)_2$. (*a*) distances (Å) and angles (°); (*b*) levels of theory and basis sets; (*c*) from dMO = *f*(eir) (ref. 1); (*d*) from ν = *f*(dClO) (ref. 1).

(a) (b)>	HF[a]	B3LYP[a]	B3LYP[b]	B3PW91[a]	B3PW91[b]	B3PW91[c]	B3PW91[d]	Experiment
Pd—O_b	2.080	2.071	2.072	2.056	2.054	2.043	2.043	1.995 (c)
Cl—O_b	1.515	1.590	1.552	1.577	1.539	1.539	1.525	1.526 (d)
Cl—O_t	1.412	1.456	1.431	1.450	1.423	1.423	1.413	1.393 (d)
O_b-Cl-O_b	98.9	97.5	98.5	97.7	98.7	98.4	99.0	
O_t-Cl-O_t	114.8	115.0	114.4	115.0	114.3	114.3	114.2	
O_b-Pd-O_b	112.7	109.4	110.8	109.4	110.7	110.4	110.8	
Pd-O_b-Cl	96.8	95.9	96.1	95.8	96.0	95.9	95.9	
E(au) *–1	753.294365440	757.660714588	1648.58123364	757.53398475	1648.30218484	1648.30770521	1648.40551240	

[a]Pd and Cl: LANL2DZ polarization on Cl, O: 6–31G*.
[b]Pd: LANL2DZ, Cl and O: cc-pVTZ.
[c]Pd: LANL2DZ with polarization, Cl and O: cc-pVTZ.
[d]Pd: LANL2DZ, Cl and O: cc-pVQZ.

Fig. 3. Molecular geometry of $Pd(ClO_4)_2$.



indicating stronger interactions between $[ClO_4]$ and a positive center. Generally NO_2^+ is relatively free (17), but in this nitryl salt ν_s NO_2^+ is located at 1406 cm^{-1} instead of at 1396 cm^{-1} (30) and δNO_2^+ is assigned at 596 cm^{-1} (the same position as the line arising from δ_{as} ClO_{3t}) instead of 570 cm^{-1}. This implies weak bonding of the nitryl cation to $[ClO_4]$ with a shortening of N—O bonds and an angular deformation, but this does not account entirely for the large observed shift. A secondary interaction between $[ClO_4]$ and the Pd center probably occurs leading to a pseudo-bidentate $[ClO_4]$ and a strained octahedron around Pd. Such a geometry was suggested in $Au(NO_3)_4^-$ (31). However in $(NO_2)_2Pd(ClO_4)_4$, $O_3ClO_b\cdots Pd$ distances should be shorter than those observed for $O_2NO_b\cdots Au$ (2.86 Å) in $Au(NO_3)_4^-$ or $O_3ClO_b\cdots Au$ (≈2.90 Å) in $Au(ClO_4)_4^-$ and the Pd-O_b-Cl angle lower to support formation of pseudo-bidentate $[ClO_4]$ and to explain the observed frequency shifts in the νClO_b range. Frequency assignments are compared to those of $ClO_2Au(ClO_4)_4$ (2*f*) and $(ClO_2)_2Pd(ClO_4)_4$ in Table 5.

Experimental

Caution: Chlorine trioxide, perchlorato complexes prepared in this work are very hazardous reagents. They can explode spontaneously when mixed with organic compounds. They must be handled with an efficient protective shield. Reactions have to be continuously checked and monitored. Only small amounts of products should be prepared and used.

Starting products

The perchlorating reagent (Cl_2O_6) was prepared and purified as previously described (9). The starting salts were anhydrous $PdCl_2$ (Alpha 99%) and $Pd(NO_3)_2{\cdot}xH_2O$ (Aldrich, $x \approx 2$). To facilitate the reaction between $PdCl_2$ and Cl_2O_6, $PdCl_2$ was dissolved in distilled water (17) then dried under dynamic vacuum (1.33 Pa) to give a slightly hydrated chloride $PdCl_2{\cdot}\varepsilon H_2O$ ($\varepsilon \approx 0.1$). Behaviour of the nitrate salt toward Cl_2O_6 (2*f*) showed that this commercial compound should be written as $Pd(NO_3)_2{\cdot}0.5(H_2O, HNO_3)$ rather than as $Pd(NO_3)_2{\cdot}2H_2O$.

Syntheses

Reactions were performed as previously described on a vacuum line (1) by reacting an excess of Cl_2O_6 with the starting salts for several hours. Weight and Raman spectroscopic tests were carried out regularly to check the progress of the reactions. Products are very hygroscopic and they were handled in a JACOMEX glove box (model B 5531 NMT) filled with ultra-purified and dried N_2.

In a typical reaction, 0.196 g of $PdCl_2$ gave 0.496 g of a brown-black solid which should be formulated as

© 2000 NRC Canada

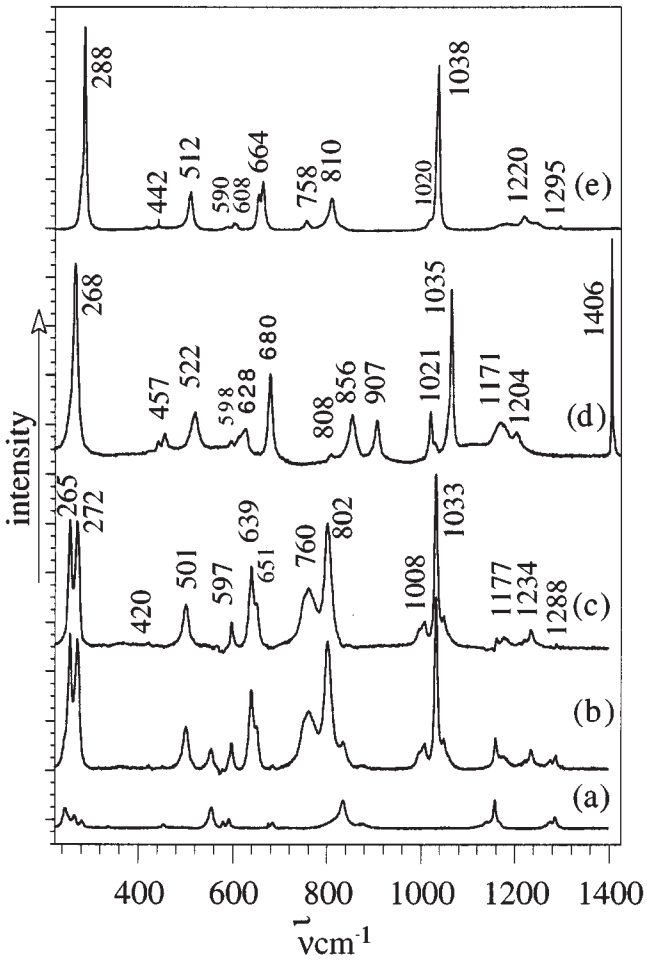
Table 4. Experimental and unscaled calculated frequencies, assignments, and mode descriptions for $Pd(ClO_4)_2$.

Experimental		HF[a]	B3LYP[a]	B3LYP[b]	B3PW91[a]	B3PW91[c]	B3PW91[d]	Assignments
IR	Raman							
1288(m)	1285 (35)	1338 (63)	1208 (48)	1249 (51)	1250 (48)	1292 (51)	1311 (51)	B_1 $\boldsymbol{\nu_{as}ClO_t}$
1272(m)	1260 (18)	1336 (0)	1207 (0)	1247 (0)	1249 (0)	1291 (0)	1310 (0)	A_2
1255(m)	1260 (15)							
1152(m)	1169 (20)	1233 (0)	1093 (0)	1134 (0)	1132 (0)	1176 (0)	1195 (0)	A_1 $\boldsymbol{\nu_sClO_t}$
1130(m)	1156 (32)	1215 (100)	1079 (100)	1118 (100)	1117 (100)	1160 (100)	1177 (100)	B_2
1005(w)	1060 (4)							?
864(sh)	870 (12) (br)	973 (44)	753 (26)	791 (28)	784 (27)	829 (28)	847 (27)	A_1 $\boldsymbol{\nu_{as}ClO_b}$ + ρ_w
		955(0)	739 (0)	783 (0)	772 (0)	824 (0)	843 (0)	B_2
820(s)	834 (87)	899 (0)	716 (0)	765 (0)	754 (0)	805 (0)	827 (0)	A_1 $\boldsymbol{\nu_sClO_b}$ + δOPdO
		894 (20)	714 (16)	759 (25)	750 (19)	799 (25)	820 (27)	B_2
708(w)	680 (19)	745 (0)	628 (0)	653 (0)	641 (0)	668 (0)	678 (0)	A_1 $\boldsymbol{\delta ClO_b}$ + δClO_t + νPdO + δClOPd
	636(vw)	720 (52)	605 (67)	633 (53)	617 (64)	647 (53)	657 (49)	B_2
	595(sh, vw)							
590(m)	587 (33)	649 (3)	520 (0)	561 (0.2)	541 (0)	583 (0.2)	602 (3)	A_1 $\boldsymbol{\nu_{as}PdO}$ + ρ_w
	577 (27)	629 (0)	509 (0)	552 (0)	528 (0)	571 (0)	589 (0)	B_2
566(w)	550 (100)	610 (11)	481 (6)	529 (5)	494 (6)	542 (5)	557 (5)	B_1 $\boldsymbol{\rho_t}$
		604 (0)	479 (0)	526 (0)	491 (0)	539 (0)	554 (0)	A_2
		548 (10)	475 (14)	502 (14)	488 (12)	517 (12)	529 (12)	B_2 $\boldsymbol{\delta ClO_t}$ + δClO_b + ν_sPdO
		548 (0)	468 (0)	502 (0)	479 (0)	516 (0)	528 (0)	A_1
	453(14)							
	448 sh	456 (10)	408 (2)	416 (1.5)	419 (3)	433 (1.5)	441 (10)	A_1 $\boldsymbol{\rho_w}$ + ν_{as}PdO
	431 < 1	423 (0)	327 (0)	363 (0)	336 (0)	371 (0)	383 (0)	A_2 $\boldsymbol{\rho_r}$ + ΠPdO_4
		411 (0)	323 (0)	353 (0)	329 (0)	360 (0)	372 (0)	B_1
	334(22)							
320(m)	312 (11)	331 (18)	317 (0)	323 (10)	324 (0)	332 (9)	335 (9)	B_2 $\boldsymbol{\nu_{as}PdO}$ + δOPdO + δClO_t
290(w)	297 (17)							
	278 (100)	245 (0)	288 (0)	283 (0)	298 (0)	303 (0)	311 (0)	B_2 $\boldsymbol{\nu_sPdO}$ + ρ_w
	261 (32)							
230(w)	242 (77)							
		214 (0)	203 (0)	202 (0)	207 (0)	210 (0)	212 (0.02)	A_1 $\boldsymbol{\delta ClOPd}$

Note: Main contribution is printed in bold. Basis sets are specified in the footnotes of Table 3. Observed (Raman) and calculated (IR) intensities are given between brackets. Experimental IR values from ref. 8: s = strong, m = medium, w = weak, sh = shoulder, br = broad, v = very.

© 2000 NRC Canada

Fig. 4. Raman spectra of (*a*) $Pd(ClO_4)_2$; (*b*) raw $ClO_2Pd(ClO_4)_3$; (*c*) $(ClO_2)_2Pd(ClO_4)_4$; (*d*) $(NO_2)_2Pd(ClO_4)_4$; and (*e*) $ClO_2Au(ClO_4)_4$.



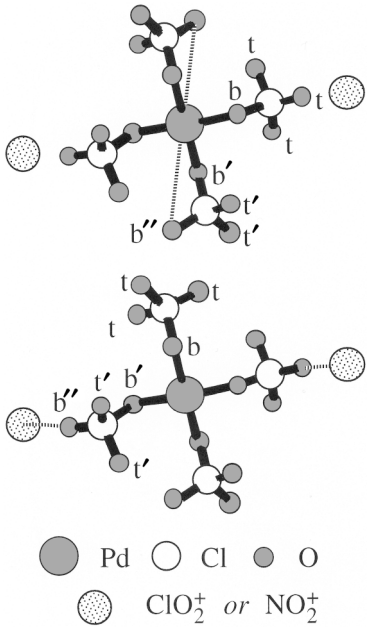
$ClO_2Pd(ClO_4)_3$ (expected: 0.498 g). This compound decomposes over a period of 3 weeks at room temperature under dynamic vacuum (1.33 Pa) to yield a brown solid $Pd(ClO_4)_2$ (anal. calcd.: Pd 34.8, ClO_4 65.2; found: Pd 34.8, ClO_4 66.6). Warming the chloryl salt to 60°C under dynamic vacuum increased the decomposition rate and limited the duration of synthesis of pure $Pd(ClO_4)_2$ to a few hours. In so doing, some of the $Pd(ClO_4)_2$ sublimed, without decomposition, onto the cold part of the reactor as a thin brown metallic film.

When 0.305 g of $Pd(NO_3)_2 \cdot 0.5(H_2O,HNO_3)$ reacted with an excess of Cl_2O_6, 0.752 g of the pale brown solid $(NO_2)_2Pd(ClO_4)_4 \cdot 0.5\ NO_2ClO_4$ (expected: 0.749 g) was obtained after removal of the unreacted Cl_2O_6 under vacuum at room temperature. Extra NO_2ClO_4 was removed above 60°C to yield $(NO_2)_2Pd(ClO_4)_4$. At higher temperature, this nitryl salt sublimed to form thin brown metallic films and microcrystals which were not suitable for X-ray diffraction studies.

Structural studies

Powder X-ray diffraction analysis of $Pd(ClO_4)_2$ and $(NO_2)_2Pd(ClO_4)_4$ were collected at the IMN in Nantes on an INEL PSD PCS 120 diffractometer equipped with a curved

Fig. 5. Molecular geometry of $(A)_2Pd(ClO_4)_4$ (A = ClO_2^+, NO_2^+).



detector. Cu-$K_{\alpha 1}$ radiation (1.54059 Å) was used. $Na_2Ca_3Al_2F_{14}$ was the external standard (a = 10.25012 Å). Finely ground and sieved (0.45 μ) powder was introduced into a thin Lindeman capillary (0.3 mm) that was sealed under dry N_2. TREOR90 (14) was used to determine cell parameters and lattice symmetry. A complete analysis of the observed lines with DTETA (32) and application of extinction rules led to determination of the space groups.

For IR spectroscopy, finely ground solids were pressed between very clean and polished AgCl plates (2*f*). Plates were placed in an airtight holder. Spectra were recorded on a Bomem DA8 FTIR spectrometer. Calibration was performed with a polystyrene film. For Raman analysis, a LABRAM DILOR spectrometer, equipped with a RX40 OLYMPUS microscope, was used. Samples sealed in thin Pyrex capillaries (≈1 mm) were illuminated with an He–Ne laser (6328 Å, 0.12 mW on the sample). Lines of a neon tube were used as standard.

Computational details

All calculations on the complex $Pd(ClO_4)_2$ were carried out with the GAUSSIAN 98 set of programs (24). Palladium was represented using Los Alamos relativistic core potential (ECP) for the 32 innermost electrons and its associated double ζ basis set (33) with or without polarization *f* function (34). Chlorine atoms were also described with the Los Alamos ECPs and their associated double ζ basis set (35) augmented by polarization *d* functions (34). A 6–31G (d,p) was used for the oxygen atoms (36). For calculations at higher levels of theory, chlorine and oxygen atoms were described with the double, triple, or quadruple ζ correlation consistent basis set of Dunning and co-workers (37). Calculations were performed by the Hartree–Fock method or within the framework of density functional theory with two different hybrid functions. The exchange potential was that proposed by Becke (38) and included in part, the exact Hartree–Fock exchange (39). Correlation potentials of Perdew and Wang (40) (B3PW91) and of Lee et al. (41)

© 2000 NRC Canada

Table 5. Assignments of vibrational modes for $(A)_2Pd(ClO_4)_4$ ($A = ClO_2^+$, NO_2^+) compared to $ClO_2Au(ClO_4)_4$ data (ref. 2*f*).

$ClO_2Au(ClO_4)_4$	$(ClO_2)_2Pd(ClO_4)_4$	$(NO_2)_2Pd(ClO_4)_4$	Assignments
		1410(sh)	$\nu_s\ NO_2^+$
		1400 (100)	
1295 (2)	1288 (2)		$\nu_{as}\ ClO_2^+$
1282 (2)			
1243 (4)	1234 (11)		
1220 (7)	1221 (6)	1204 (15)	$\nu_{as}\ ClO_t$ (M)
	1177 (7)	1171 (20)	
1180 (4)	1161 (6)	1113 (11) (br)	$\nu_{as}\ ClO_{t'}$ (B)
1038 (84)	1050 (19)	1065 (80)	$\nu_s\ ClO_t$ (M)
1035(sh)	1033 (100)		$\nu_s\ ClO_2^+$
1020(sh)	1008 (15)	1031(sh)	$\nu_s\ ClO_{t'}$ (B)
	997(sh)	1021 (sh)	
810(16)	801(72) br	907 (19)	$\nu\ ClO_{b''}$ (B)
798(sh)		856 (19)	$\nu\ ClO_{b'}$ (B)
758 (5)	760 (35)	808 (4)	$\nu\ ClO_b$ (M)
664 (24)		680 (41)	$\delta_{as}\ ClO_t + \Pi XO_4$
655(18)	651(sh)		$+\delta\ XOCl$
	639 (47)	628 (16)	
608 (3)			
603 (4)	597 (14)	598 (10)	$\delta_s\ ClO_t + \Pi XO_4 + \delta XOCl$
589(sh)			
		[598 (10)]	$\delta\ NO_2^+$
544 (<1)			$\delta_s\ ClO_t + \rho ClO_4 + \delta XO_4$
512 (19)	501 (25)	522 (19)	
[512 (19)]			δClO_2^+
442 (3)		457(14)	$\delta_s\ ClO_t + \Pi XO_4$
417 (2)	420 (2)	442 (9)	
371 (<1)	360 (<1)	360 (<1)	$\rho ClO_4 + \Pi XO_4$
288 (100)	272 (73)	268 (92)	$\nu_a + \nu_s XO_4$
	256 (73)	253(sh)	

Note: M: unidentate, B: pseudobidentate (see text and Fig. 5). X = Au or Pd.

(B3LYP) were used. The nature of the optimized structure was assigned by analytical calculations of the vibrational frequencies. Vibrational modes were displayed with the MOLDEN program (42).

Conclusion

Whereas $[ClO_4]$ generally acts as an assembling ligand leading to polymeric channeled or layered structures (1), results on Pd perchlorato complexes show that it can behave differently to give monomeric units which are less frequently encountered in the list of known perchlorato complexes. Such behaviour should improve their reactivity.

Acknowledgment

The authors are grateful to Catherine Deudon of the IMN in Nantes for the powder X-ray data recording. They thank Deborah J. Jones and Bernard Mula for helpful discussion and CNRS for financial support.

References

1. J.L. Pascal and F. Favier. Coord. Chem. Rev. **178–180**, 865 (1998).
2. (*a*) F. Favier, J.L. Pascal, F. Cunin, A.N. Fitch, and G. Vaughan. Inorg. Chem. **37**, 1776 (1998); (*b*) J.L. Pascal, F. Favier, F. Cunin, A.N. Fitch, and G. Vaughan. J. Solid State Chem. **139**, 259 (1998); (*c*) M.S. Wickleder. Z. Anorg. Allg. Chem. **625**, 11, 309, 1156 (1999); (*d*) K.S. Gavrichev, G.A. Sharpataya, V.E. Gorbunov, L.N. Golushina, and Z.K. Nikitina. Inorg. Mater. **35**, 1075 (1999); (*e*) T. Cui, J.T. Chen, and J.S. Huang. Inorg. Chim. Acta, **293**, 129 (1999); (*f*) F. Cunin. Ph.D. Thesis, Université Montpellier 2, Montpellier, France. 2000.
3. (*a*) H. Cheradame, G. Rissoan, F. Favier, J.L. Pascal, and F.J. Chen. C. R. Acad. Sci. Paris Serie, II. **18**, 329 (1994); (*b*) I. Hachiya and S. Kobayashi. Tetrahedron Lett. **35**, 3319 (1994); (*c*) S.S. Springer, C. Elam, A. Edwards, C. Bowe, D. Boyles, J. Bartems, M. Chandlers, K. West, J. Williams, J. Green, R.M. Pagni, and G.W. Kabalka. J. Org. Chem. **64**, 2202 (1999); (*d*) N. Jain and K.G. Krisnamurthy. Indian J. Chem. B. **38**, 865 (1999); (*e*) I.A. Motarina and D.S. Grierson. Tetrahedron Lett. **40**, 7215 (1999); (*f*) ALDRICH. Inorg. Chem. **36**(**8**), cover IV (1997).
4. (*a*) A.A. Schilt. *In* Perchloric acid and perchlorates. C. Frederick Smith Co., Columbus, OH. 1979; (*b*) T. Li and P.B. Balbuena. J. Electrochem. Soc. **146**, 3613 (1999); (*c*) D.S. Gill, L. Byrne, and T.I. Quickenden. Z. Naturforsch. A: Phys. Sci. **53**, 1004 (1999).
5. (*a*) F. Solymosi. *In* Structure and stability of salts of halogen oxyacids in the solid phase. John Wiley and Sons, London.

© 2000 NRC Canada

1977; (*b*) F. Favier and J.L. Pascal. Ecole thématique, Chimie de Coordination. Gujan Mestras, France. 1996.
6. (*a*) Z.K. Nikitina, N.I. Nikitina, and V.Ya Rosolovskii. Zh. Neorg. Khim. **43**, 1259 (1998); (*b*) G.P. Dolganova, D.B. Lempert, and G.N. Nechiparenko. Russ. J. Appl. Chem. **71**, 1726 (1998); (*c*) S. Halawy and S.S. Alshihry. J. Therm. Anal. Calorim. **55**, 833 (1999).
7. R.G. Pearson. *In* Chemical hardness. Wiley–VCH, Weinheim. 1997.
8. M. Chaabouni, J.L. Pascal, A.C. Pavia, J. Potier, and A. Potier. C. R. Acad. Sci. Serie C. **291**, 125 (1980).
9. F. Favier and J.L. Pascal. J. Chem. Soc. Dalton Trans. 1997 (1992).
10. R.N. Kust and F.R. Duke. J. Am. Chem. Soc. **85**, 3338 (1963).
11. J.L. Pascal, J. Potier, and C.S. Zhang. J. Chem. Soc. Dalton Trans. 297 (1985).
12. M. Fourati, M. Chaabouni, J.L. Pascal, and J. Potier. Can. J. Chem. **65**, 2783 (1987).
13. J.L. Pascal, A. Hassan, and J. Potier. C. R. Acad. Sci. Serie II, **302**, 817 (1986).
14. (*a*) P.E. Werner. Z. Kristallogr. **120**, 375 (1964); (*b*) P.E. Werner, L. Erikson, and N. Westdahl. J. Appl. Crystallogr. **18**, 367 (1985).
15. P.M. de Wolff. J. Appl. Crystallogr. **1**, 108 (1968).
16. G.S. Smith and R.L. Snyder. J. Appl. Crystallogr. **12**, 60 (1979).
17. C.S. Zhang. Thèse d'Etat. Université Montpellier 2, Montpellier, France. 1984.
18. M. Fourati, M. Chaabouni, C.H. Belin, M. Charbonnel, J.L. Pascal, and J. Potier. Inorg. Chem. **25**, 1386 (1986).
19. J.L. Pascal, J. Potier, J. Roziere, D.J. Jones, and A. Michalowicz. Inorg. Chem. **24**, 238 (1985).
20. A.F. Wells. *In* Structural inorganic chemistry. 5th ed. Clarendon Press, Oxford. 1984.
21. A. Carrondo and A. Skapski. J. Chem. Soc. Chem. Comm. 410 (1976).
22. K.K. Palkina, S.I. Maksimova, A.V. Lavrov, and N.A. Chalisova. Dokl. Akad. Nauk. SSSR. **242**, 829 (1978).
23. (*a*) G.N. Papatheodorou. J. Phys. Chem. **77**, 472 (1973); (*b*) W. Lenhard, H. Shaefer, H.U. Huerter, and B. Krebs. Z. Anorg. Allg. Chem. **482**, 19 (1981).
24. M.J. Frisch, G.W. Trucks, H.B. Schlegel, G.E. Scuseria, M.A. Robb, J.R. Cheeseman, V.G. Zakrzewski, J.A. Montgomery, R.E. Stratmann, J.C. Burant, S. Dapprich, J.M. Milam, A.D. Daniels, K.N. Kudin, M.C. Strain, O. Farkas, J. Tomasi, V. Barone, M. Cossi, R. Cammi, B. Mennucci, C. Pomelli, C. Adamo, S. Clifford, J. Ochterski, G.A. Petersson, P.Y. Ayala, Q. Cui, K. Morokuma, D.K. Malick, A.D. Rabuck, K. Raghavachari, J.B. Foresman, J. Cioslowski, J.V. Ortiz, B.B. Stefanov, G. Liu, A. Liashenko, P. Piskorz, I. Komaromi, R. Gomperts, R.L. Martin, D.J. Fox, T. Keith, M.A. Al-Laham, C.Y. Peng, A. Nanayakkara, C. Gonzalez, M. Challacombe, P.M.W. Gill, B.G. Johnson, W. Chen, M.W. Wong, J.L. Andres, M. Head-Gordon, E.S. Replogle, and J.A. Pople. Gaussian 98, Révision A.1. Gaussian, Inc., Pittsburgh, Pa. 1998.
25. (*a*) K.O. Christe, W.W.W. Wilson, J.A. Sheehy, and J.A. Boatz. Angew. Chem. Int. Ed. **38**, 2004 (1999); (*b*) W.J. Casteel, Jr., D.A. Dixon, N. Leblond, P.E. Lock, H.P.A. Mercier, and G.J. Schrobilgen. Inorg. Chem. **38**, 2340 (1999).
26. B.J. Hathaway and A.E. Underhill. J. Chem. Soc. 3091 (1961).
27. J.L. Pascal. Thèse d'Etat. Université Montpellier 2, Montpellier, France. 1978.
28. M. Fourati, M. Chaabouni, C.H. Belin, J.L. Pascal, and J. Potier. New. J. Chem. **14**, 695 (1990).
29. K.M. Tobias and M. Jansen. Z. Anorg. Allg. Chem. **550,** 16 (1987).
30. K. Nakamoto. *In* Infrared and Raman spectra of inorganic and coordination compounds. 5th ed. Wiley, New York. 1997.
31. C.D. Garner and S.C. Wallwork. J. Chem. Soc. 3092 (1976).
32. A. Norbert. Rev. Chim. Miner. **6**, 687 (1969).
33. P.J. Hay and W.R. Wadt. J. Chem. Phys. **82**, 299 (1985).
34. A. Höllwardt, M Böhme, S. Dapprich, A.W. Ehlers, A. Gobbi, V. Jonas, K. Köhler, R. Stegmann, A. Veldkamp, and G. Frenking. Chem. Phys. Lett. **208,** 237 (1993).
35. W.R. Wadt and P.J. Hay. J. Chem. Phys. **82**, 284 (1985).
36. P.C. Harchman and J. Pople. Theor. Chim. Acta, **28**, 213 (1973).
37. (*a*) D.E. Wuon and T.H. Dunning, Jr. J. Chem. Phys. **98**, 1358 (1993); (*b*) R.A. Kendall and T.H. Dunning, Jr. J. Chem. Phys. **96**, 6796 (1992); (*c*) T.H. Dunning, Jr. J. Chem. Phys. **90**, 1007 (1989).
38. A.D. Becke. Phys. Rev. A: At. Mol. Opt. Phys. **38**, 3098 (1966).
39. A.D. Becke. J. Chem. Phys. **98**, 5648 (1993).
40. P. Perdew and Y. Wang. Phys. Rev. B: Condens. Matter, **45**, 13244 (1992).
41. C. Lee, W. Yang, and R.G. Parr. Phys. Rev. B: Condens. Matter, **37**, 785 (1988).
42. G. Schaftenaar. MOLDEN. CAOS/CAMN, University of Nijmegen. The Netherlands.
43. (*a*) M. Chaabouni, J.L. Pascal, A.C. Pavia, J. Potier, and A. Potier. C. R. Acad. Sci. Paris Ser. C. **297**, 419 (1978); (*b*) F. Favier. Ph.D. Thesis. Université Montpellier 2, Montpellier, France. 1992.

© 2000 NRC Canada

A thermodynamic study of aqueous acetonitrile: excess chemical potentials, partial molar enthalpies, entropies and volumes, and fluctuations

Penka V. Nikolova, Sheldon J. B. Duff, Peter Westh, Charles A. Haynes, Yasutoshi Kasahara, Keiko Nishikawa, and Yoshikata Koga

Abstract: We measured vapour pressures of aqueous acetonitrile (abbreviated as ACN) at 6, 20, and 37°C, from which excess chemical potentials of ACN (μ^{E}_{ACN}) were calculated. We also determined excess partial molar enthalpies of ACN (H^{E}_{ACN}) at 6, 20, 30, 37, and 45°C. From these data, excess partial molar entropies of ACN (S^{E}_{ACN}) were calculated at 6, 20, and 37°C. Using density data by Benson's group, excess partial molar volumes of ACN (V^{E}_{ACN}) were evaluated. The response function data by the same group were also used to evaluate amplitude and wavelength of mean-square fluctuations in terms of volume, entropy, and cross between volume and entropy. All the above quantities and their dependence on the mol fraction of solute, i.e., the effect of additional solute on the above quantities were used to study the effect of acetonitrile on the molecular organization of H_2O. It was found that acetonitrile works as a stronger structure-making solute than methanol. Rather its effect on H_2O is about the same as that of propan-1-ol.

Key words: aqueous acetonitrile, interaction functions, fluctuations.

Résumé : On a mesuré les tensions de vapeur de solutions aqueuses d'acétonitrile (ACN) à 6, 20 et 37°C et, à partir des valeurs obtenues, on en a calculé les potentiels chimiques en excès d'ACN (μ^{E}_{ACN}). On a aussi déterminé les enthalpies molaires partielles en excès d'ACN (H^{E}_{ACN}) à 6, 20, 30, 37 et 45°C. À partir de ces données, on a calculé les entropies molaires partielles en excès d'ACN (S^{E}_{ACN}) à 6, 20 et 37°C. En utilisant des données relatives à la densité obtenues par le groupe de Benson, on a calculé les volumes molaires partiels en excès, d'ACN (V^{E}_{ACN}). On a aussi utilisé les données relatives à la fonction de réponse obtenues par ce même groupe pour évaluer l'amplitude et la longueur d'onde des fluctuations quadratiques moyennes en termes de volume, entropie et mélange de volume et d'entropie. Dans le but d'étudier l'effet de l'acétonitrile sur l'organisation moléculaire de H_2O, on a aussi utilisé toutes les valeurs mentionnées plus haut ainsi que leur dépendance sur la fraction molaire du soluté, c'est-à-dire l'effet de soluté additionnel sur les quantités mentionnées plus haut. On a trouvé que, par rapport au méthanol, l'acétonitrile agit comme un soluté provoquant une mise en place plus grande de la structure. Son effet sur H_2O est à peu près égal à celui du propan-1-ol.

Mots clés : acétonitrile aqueux, fonctions d'interaction, fluctuations.

[Traduit par la Rédaction]

Introduction

As a part of our continuing effort to study binary aqueous solutions by using partial molar quantities and response functions (1–9), we report here the results of our study on aqueous acetonitrile (abbreviated as ACN). Our earlier studies on aqueous alcohols (AL) including methanol (ME) (4, 7) indicated that there are three composition regions in each of which the mixing scheme is qualitatively different from those of other regions. In the most H_2O-rich region, what we

Received March 24, 2000. Published on the NRC Research Press website on November 21, 2000.

P.V. Nikolova, P. Westh, and C.A. Haynes.[1] Biotechnology Laboratory, The University of British Columbia, 6174 University Boulevard, Vancouver, BC V6T 1Z3, Canada.
S.J.B. Duff. Department of Chemical Engineering, The University of British Columbia, 6174 University Boulevard, Vancouver, BC V6T 1Z3, Canada.
P. Westh. Department of Chemistry, Roskilde University, DK-4000 Roskilde, Denmark.
Y. Kasahara and K. Nishikawa. Department of Diversity Science, Graduate School of Science and Technology, Chiba University, Yayoi, Inage-ku, Chiba 263-8522, Japan.
Y. Koga.[2] Department of Chemistry, The University of British Columbia, 2036 Main Mall, Vancouver, BC V6T 1Z1, Canada.

[1]Also at: Department of Chemical Engineering, The University of British Columbia.
[2]Also at: Materials and Structures Laboratory, Tokyo Institute of Technology, Nagatsuta, Midori-ku, Yokohama 226-8503, Japan. Author to whom correspondence may be addressed. Telephone: (604) 822-3491. Fax: (604) 822-2847. e-mail: koga@chem.ubc.ca

 © 2000 NRC Canada

call Mixing Scheme I is operative. Alcohol enhances the hydrogen bond network of H_2O in its immediate vicinity with a concomitant reduction of the hydrogen bond probability of bulk H_2O away from solute. However, the hydrogen bond probability of bulk H_2O is still high enough so that the hydrogen bond network is connected throughout of the entire bulk. Namely, the hydrogen bond network is still bond-percolated.

In the intermediate composition, there is no bond-percolation and the solution consists of two kinds of clusters, each rich in AL or H_2O. We call this Mixing Scheme II. The transition from Mixing Scheme I to II occurs in a certain narrow mol fraction range. We call the starting point of transition X and the end point Y. This is apparent in an anomalous behaviour in the thermodynamic quantities proportional to the third derivatives of Gibbs energy (G) (as demonstrated later on in this paper). The longer the alkyl chain of AL, the stronger the effect of solute. The transition region occurs at a lower mol fraction of AL (x_{AL}) and the interaction between solutes is stronger.

In the AL-rich region, Mixing Scheme III becomes apparent, in which AL molecules cluster. H_2O molecules then interact with AL clusters as a single molecule (1, 2, 4, 7). Thus, the characteristics of liquid H_2O are lost completely in this region.

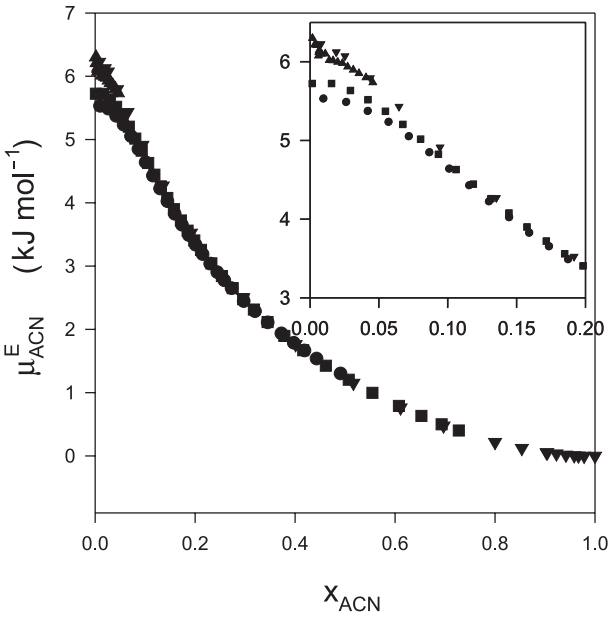
ME–H_2O mixtures follow this general trend, although the effect of ME is not as dramatic as those of higher alcohols. The transitions of mixing scheme are still observable in ME–H_2O. Point X occurs at x_{ME} = 0.07, Y at x_{ME} = 0.25, and at x_{ME} = 0.45 the transition from Mixing Scheme II to III takes place (4, 7).

Our interest in studying aqueous acetonitrile lies on the effect of change from -OH of ME to -CN on the thermodynamic behaviour of aqueous solutions, on one hand. On the other, our preliminary study on a cellulolytic enzyme in a mixed solvent, ACN–H_2O, shows a strong, step-wise dependence of enzyme function on the mol fraction of ACN (x_{ACN}) hinting at the effect of the change in mixing scheme in the solvent system, ACN–H_2O, on enzyme kinetics. To gain insight in the mixing schemes, we measured the excess partial molar enthalpy of ACN (H^E_{ACN}) and the vapour pressures to calculate excess chemical potential of ACN (μ^E_{ACN}). For density and response functions, there are extensive data by Benson and co-workers (10, 11). We use these data for evaluating partial molar volume, and fluctuation functions (5–7, 12, 13).

Experimental

Acetonitrile (ACROS, nonaqueous titration grade, 99+%) was handled in a dry nitrogen atmosphere. H_2O was distilled three times; the last two times in a Pyrex glass still immediately before use. Excess partial molar enthalpy of ACN (H^E_{ACN}) was determined by a microtitration calorimeter, Calorimetry Science Corp. (Provo, UT) Model 4209, at 20, 30, 37, and 45°C. For 6°C, a homemade titration calorimeter (14), similar to an LKB Bromma model, was used. The uncertainty in H^E_{ACN} is about ±0.05 kJ mol^{-1}. Since the absolute sensitivity of the former calorimeter is higher by some 100-fold, the amount of titre is reduced by the same ratio. As a result, the data increments are much smaller. This turned out to be crucial in detecting anomalous behaviour in a very dilute range (x_{ACN} < 0.01). Vapour pressure was measured by a static method (15).

Fig. 1. Excess chemical potential of acetonitrile (μ^E_{ACN}). Circle (6°C), square (20°C), triangle up (37°C), triangle down (35°C) (17).



Results

The total vapour pressure data (p) corrected by the Gibbs–Konovalov relation (15), for a small temperature variation during the measurement, are listed in Table I, deposited in CISTI.[3] The 37°C data are limited to a dilute range (x_{ACN} < 0.05) since the total pressure reached 100 torr (1 torr = 133.322 Pa), the upper limit of the Baratron gauge used. The partial pressure of ACN (p_{ACN}) and that of H_2O (p_W) were calculated by the Boissonnas method (15), and they are listed in Table I.[3] The excess chemical potential of ACN (μ^E_{ACN}) was calculated as,

$$[1] \qquad \mu^E_{ACN} = RT \ln (p_{ACN}/x_{ACN}p^0_{ACN})$$

where p^0_{ACN} is the vapour pressure of pure ACN at the same temperature (16). The correction term due to nonideality of the gas-phase is negligibly small in comparison with the value calculated by the right hand side of eq. [1]. The resulting μ^E_{ACN} data are also listed in Table I,[3] and plotted in Fig. 1. Also plotted in Fig. 1 are the data by French (17) for 35°C. As is evident in Fig. 1, the temperature dependence of μ^E_{ACN} is small. Our 37°C data are almost identical to the 35°C data by French in the range x_{ACN} > 0.03. The first few

[3] Tables I, II, and III have been deposited. Copies of the material on deposit may be purchased from the Depository of Unpublished Data, Document Delivery, CISTI, National Research Council Canada, Ottawa, ON, Canada K1A 0S2 (http://nrc.ca/cisti/irm/unpub_e.shtml for information on ordering electronically).

© 2000 NRC Canada

Fig. 2. Excess partial molar enthalpy of acetonitrile (H^{E}_{ACN}) and entropy times temperature (TS^{E}_{ACN}). (*a*) Diamond (6°C), square (20°C), triangle down (30°C), circle (37°C), triangle up (45°C); (*b*) Filled symbols (H^{E}_{ACN}), hollow symbols (TS^{E}_{ACN}), circle (6°C), square (37°C).

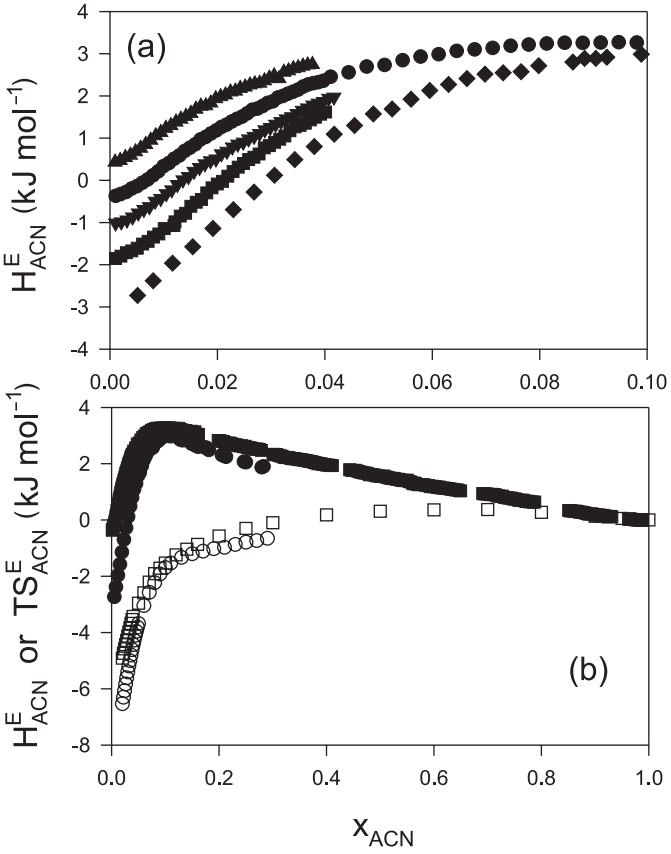
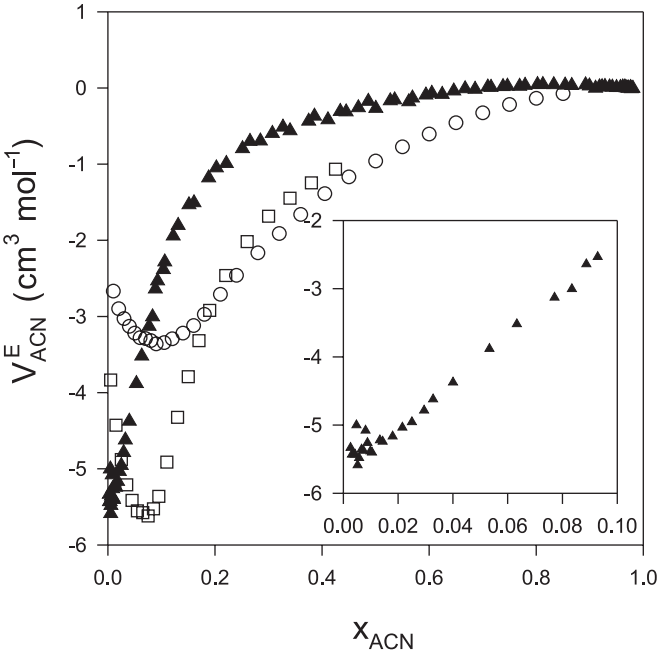


Fig. 3. Excess partial molar volume of acetonitrile (V^{E}_{ACN}) at 25°C. Hollow circle, methanol (V^{E}_{ME}), hollow square, ethanol (V^{E}_{ET}) (7), filled triangle (V^{E}_{ACN}).



points ($x_{ACN} < 0.03$) calculated by the Boissonnas method are not reliable (18).

The excess partial molar enthalpies of ACN (H^{E}_{ACN}) are listed in Table II[3] and plotted in Fig. 2. In Fig. 2*b* are also plotted the values of TS^{E}_{ACN}, the excess partial molar entropy of ACN times temperature for 6 and 37°C calculated as,

[2] $$TS^{E}_{ACN} = H^{E}_{ACN} - \mu^{E}_{ACN}$$

For 37°C, French's data of μ^{E}_{ACN} at 35°C (17) were used. The excess partial molar volume of ACN (V^{E}_{ACN}) was calculated using the density data by Handa and Benson (10) in the same manner as described elsewhere (19). The resulting V^{E}_{ACN} data were plotted in Fig. 3.

The density (10), the heat capacity, and the speed of sound data by Benson et al. (11) were treated in the same way as in a previous paper on fluctuations in aqueous alcohols (7). Briefly, the following quantities related to mean-square fluctuation were calculated using molar volume (V_m), heat capacity (C_p), isothermal compressibility (κ_T), and thermal expansivity (α_p):

[3] $$^{V}\delta = T\kappa_T$$

[4] $$^{S}\delta = C_p/V_m$$

[5] $$^{SV}\delta = T\alpha_p$$

[6] $$^{V}\Delta = RT\kappa_T/V_m$$

[7] $$^{S}\Delta = RTC_p/V_m{}^2$$

[8] $$^{SV}\Delta = RT\alpha_p/V_m$$

As discussed at some length earlier (7), $^{q}\delta$ (q = *V*, *S*, or *SV*) shows the amplitude of fluctuation in q, while $^{q}\Delta$ contains qualitative information about the wavelength as well as the amplitude of fluctuation in q. The functions calculated by eqs. [3]–[8] are listed in Table III[3] and plotted in Figs. 4–6.

Discussion

Second derivatives of *G*

We discuss first what the data of H^{E}_{ACN}, S^{E}_{ACN}, V^{E}_{ACN}, $^{q}\delta$s, and $^{q}\Delta$s indicate in terms of the nature of ACN–H_2O. The latter quantities are all proportional to the second derivatives of G with respect to a combination of independent variables (p, T, n_{ACN}) in the Gibbs ensemble. The fact that μ^{E}_{ACN} is positive and decreases as x_{ACN} increases (Fig. 1), hints at a possibility of liquid–liquid phase separation (1, 2, 20). The H^{E}_{ACN} and TS^{E}_{ACN} data in Fig. 2 indicate that in the H_2O-rich region, $x_{ACN} < 0.1$, the slopes are positive, i.e., $(\partial H^{E}_{ACN}/\partial x_{ACN}) > 0$ and $(\partial S^{E}_{ACN}/\partial x_{ACN}) > 0$. Together with $(\partial \mu^{E}_{ACN}/\partial x_{ACN}) < 0$, this is a necessary but not sufficient requirement for phase separation with a lower critical solution temperature (LCST) (1, 2, 20). Thus, if there were to be a phase separation in the range $x_{ACN} < 0.1$, it must be that with an LCST. In the range $x_{ACN} > 0.1$, on the other hand, the slopes turn negative $(\partial H^{E}_{ACN}/\partial x_{ACN}) < 0$ in Fig. 2, which hints together with $(\partial \mu^{E}_{ACN}/\partial x_{ACN}) < 0$ a possibility of a phase separation with an upper critical solution temperature

© 2000 NRC Canada

Fig. 4. Volume fluctuations at 25°C. (*a*) Amplitude of volume fluctuation ($^{V}\delta$); (*b*) amplitude and wavelength of volume fluctuation ($^{V}\Delta$).

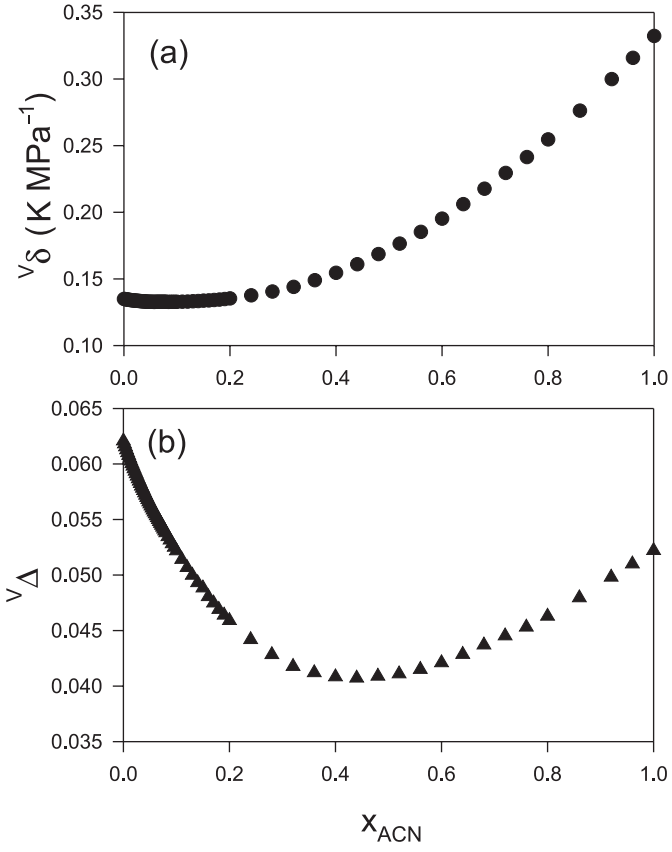
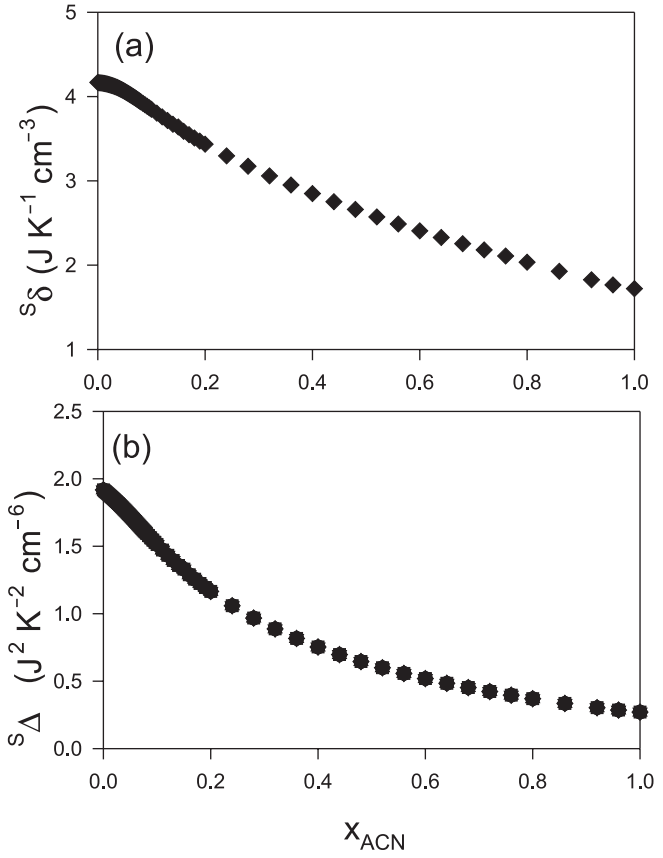


Fig. 5. Entropy fluctuation at 25°C. (*a*) Amplitude of entropy fluctuation ($^{S}\delta$); (*b*) amplitude and wavelength of entropy fluctuation ($^{S}\Delta$).

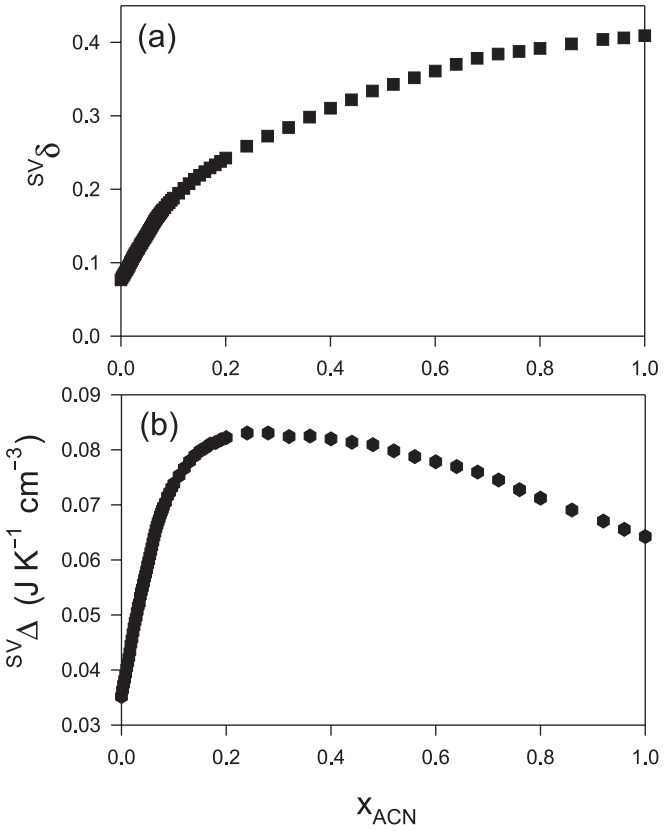


(UCST) (1, 2, 20), although $(\partial S^{E}_{ACN}/\partial x_{ACN})$ is weakly positive. Indeed, there is a UCST at –1°C at x_{ACN} = 0.38 (21). Hence, at temperatures higher than –1°C, the solution in this composition region consists of two kinds of clusters, rich in each component, which would grow to a macroscopic size at –1°C; a typical behaviour of Mixing Scheme II as discussed earlier (1–9). Indeed, our preliminary X-ray scattering measurement shows a sharp increase in the forward scattering intensity near the UCST, suggesting growth of such clusters. In the H_2O-rich region (x_{ACN} < 0.1), on the other hand, a qualitatively different mixing scheme must be operative, since the slopes of H^{E}_{ACN} and TS^{E}_{ACN} do not support a phase separation with UCST. Figure 2 shows that at the infinite dilution H^{E}_{ACN} is negative and TS^{E}_{ACN} is more negative. Also, the slopes $(\partial H^{E}_{ACN}/\partial x_{ACN})$ and $(\partial S^{E}_{ACN}/\partial x_{ACN})$ are both positive which is similar to aqueous alcohols (1, 2, 4). These observations indicate that a typical Mixing Scheme I is operative in ACN–H_2O in this region. Namely, the ACN molecule enhances the hydrogen bond network of H_2O in its immediate vicinity. However, the excess partial molar volume (V^{E}_{ACN}) (Fig. 3), does not show very clearly an initial decrease, although there is a hint at it below x_{ACN} < 0.005. An initial decrease in the partial molar volume would indicate a progressive decrease of the hydrogen bond probability of bulk H_2O away from solutes, typical for Mixing Scheme I of aqueous alcohols (1, 2, 7). The excess partial molar volume of a solute at the infinite dilution is determined basically by the following two effects: (*i*) a negative effect due to size difference between solute and H_2O; and (*ii*) a positive effect due to bulkiness of H_2O depending on the hydrogen bond probability (1, 2, 22). The second effect would be the same for any solute since at the infinite dilution the bulkiness of H_2O, i.e., the hydrogen bond probability, depends only on temperature. Now, the molar volume of pure ACN is 52.9 cm^3 mol^{-1}, while that of ME is 40.8 and that of ethanol (ET) 58.7 cm^3 mol^{-1}. Unless there is some additional direct effect between ACN and H_2O that makes V^{E}_{ACN} a very negative value, it is expected V^{E}_{ACN} at the infinite dilution to be not far away from V^{E}_{ET}. Thus, there could be a sharp initial decrease that has not been detected by the present method used (10), determining density as composition is changed. Dilatometry, by which a change in volume on addition of a solute is directly measured, may be required to detect such a sharp decrease in this very dilute region.

Next, we discuss the behaviours of fluctuation functions (Figs. 4–6) in comparison with those for aqueous alcohols, methanol in particular, dealt with extensively in a previous publication (7). The volume fluctuation density ($^{V}\delta$) (Fig. 4*a*) shows very little decrease on addition of ACN. The amplitude of volume fluctuation in ACN–H_2O depends much less on composition than that for ME–H_2O (7). A decrease in $^{V}\delta$ is consistent with a progressive loss of the hydrogen bond probability of bulk H_2O away from solute. Thus, the effect of reduction of the hydrogen bond probability of bulk H_2O, if any, is apparently little. Alternatively this could be related

© 2000 NRC Canada

Fig. 6. Entropy–volume cross-fluctuation at 25°C. (*a*) Amplitude of cross fluctuation (Sνδ); (*b*) amplitude and wavelength of cross-fluctuation ($^{SV}\Delta$).



to an apparent lack of an initial decrease in V^{E}_{ACN} in Fig. 3. For the normalized volume fluctuation ($^{V}\Delta$) Fig. 4*b* shows an appreciable decrease to almost the same extent as that for ME–H_2O (7), suggesting that ACN works to decrease the wavelength as well as the amplitude of volume fluctuation. The wavelength of fluctuation is related to collectiveness of fluctuation, which is one of the characteristics of liquid H_2O (7, 13). Thus, ACN does reduce H_2O-likeness of solvent H_2O, just as alcohols (5–7).

The entropy fluctuations (Fig. 5) seem to behave in almost the same manner as those in ME–H_2O (7). Entropy fluctuation is equivalent of enthalpy fluctuation ($< (\Delta S)^2 > = < (\Delta H)^2 > /T^2$) showing fluctuation in the hydrogen bond strength, and hence in the degree of hydrogen bond bending. For higher alcohols than ME, there is an initial increase in $^{S}\delta$, presumably due to an enhanced bending near the hydration structures or the so-called "iceberg." The larger the hydrophobic alkyl moiety, the stronger the effect (7). For ME–H_2O, its effect is not apparent. As is evident in Fig. 5*a*, the effect of ACN on $^{S}\delta$ is almost the same as that of ME. The same is true for $^{S}\Delta$ (Fig. 5*b*). Hence, in terms of the effect on the hydrogen bond bending, or on the hydrogen bond strength, ACN works in the same way as ME.

The entropy–volume cross fluctuations (Fig. 6) shows an initial rapid increase as for ME–H_2O. Namely, a negative contribution to $^{SV}\delta$ and $^{SV}\Delta$ that is characteristic to liquid H_2O diminishes rapidly on addition of either ACN or ME. While the amplitude of volume fluctuation ($^{V}\delta$) is not affected by ACN as much as ME, the amplitude plus the wavelength of volume fluctuation ($^{V}\Delta$) is equally affected. As for entropy fluctuations, both ACN and ME have almost the same effect on H_2O. Now the cross fluctuations show almost the same trend in both ACN–H_2O and ME–H_2O. We are thus in favour of the notion that ACN does affect the molecular organization of H_2O equally as well as alcohols, at least as ME, and that Mixing Scheme I is operative in the most H_2O-rich region.

Third derivatives of *G*

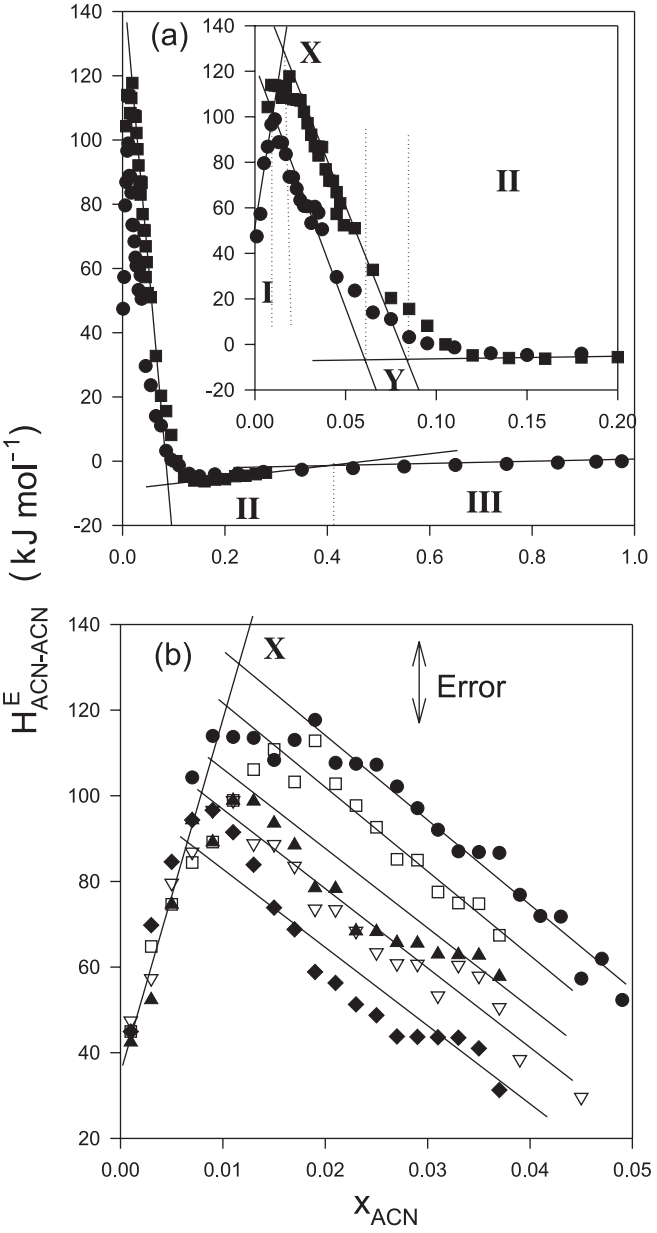
The quantities shown in Figs. 2–6 are all proportional to the second derivatives of *G* with respect to *p*, *T*, or n_{ACN}, or a combination thereof. We now take one more derivative with respect to the amount of ACN (n_{ACN}) to evaluate the effect of additional ACN on the quantity in question (1, 2, 4, 8, 9). Thus, the enthalpic interaction function ($H^{E}_{ACN-ACN}$) is calculated as,

$$[9] \qquad H^{E}_{ACN-ACN} = N(\partial H^{E}_{ACN}/\partial n_{ACN}) = (1 - x_{ACN})(\partial H^{E}_{ACN}/\partial x_{ACN})$$

In evaluating $H^{E}_{ACN-ACN}$, we use a graphical method. As argued to some length earlier (1, 2), a more common practice of numerical method, curve-fitting or some variation thereof, has a tendency of introducing a systematic error in derivatives. Davis et al. (23), recognizing that no single analytic function can fit thermodynamic data of aqueous solutions in the entire composition range, used several analytic functions at separate segments. However, there is arbitrariness in determining a segment boundary. We measured H^{E}_{ACN} accurately and in small increments (Fig. 2), and thus we could take the derivative (eq. [9]) graphically with a reasonable uncertainty, an order of %. Smooth curves are drawn by means of a flexible ruler through all the data points in Fig. 2. The values of H^{E}_{ACN} were read off a smooth curve at the interval of $\delta x_{ACN} = 0.002$ for $x_{ACN} < 0.1$ and at a larger increment for $x_{ACN} > 0.1$, where H^{E}_{ACN} changes slowly. Then, $(\partial H^{E}_{ACN}/\partial x_{ACN})$ is approximated by $(\delta H^{E}_{ACN}/\delta x_{ACN})$. The uncertainty in $H^{E}_{ACN-ACN}$ is estimated as ±10 kJ mol^{-1}, shown in Fig. 7(*b*). This quantity ($H^{E}_{ACN-ACN}$), is the effect of additional ACN on the enthalpic situation of ACN in the system. Thus, as we argued earlier (1, 2), $H^{E}_{ACN-ACN}$ signifies the degree of ACN–ACN interaction in terms of enthalpy. Figure 7 indicates the x_{ACN}-dependence of $H^{E}_{ACN-ACN}$ is similar to the x_{ME}-dependence of H^{E}_{ME-ME} (4). Thus, we assign similarly the regions of Mixing Scheme I, II, and III as shown in Fig. 7. The boundary region between Mixing Scheme I and II, starting at point X and completing at point Y, is also shown in Fig. 7. The loci of points X and Y and the values of $H^{E}_{ACN-ACN}$ are listed in Table 1. In Table 1 are also listed equivalent values for aqueous alcohols (7). We recall that in a series of alcohols, the larger the hydrophobic alkyl moiety, the stronger the effect on H_2O, the smaller the value of mol fraction at point X and the larger the value of enthalpic interaction function. It is striking that ACN appears to work as a stronger hydrophobic solute than ME. In terms of the locus of point X, it is stronger than 2-butoxyethanol, while in terms of the value of $H^{E}_{ACN-ACN}$, it seems to lie between ethanol and propan-1-ol.

© 2000 NRC Canada

Fig. 7. Enthalpic interaction between acetonitrile molecules ($H^{E}_{ACN-ACN}$). (*a*) Circle (37°C), square (6°C); (*b*) filled diamond (45°C), hollow triangle down (37°C), filled triangle up (30°C), hollow square (20°C), filled circle (6°C).



We also calculate the partial molar fluctuation functions (eq. [5]–[7]) as,

[10] $${}^{q}\delta_{ACN} = N(\partial^{q}\delta/\partial n_{ACN}) = (1 - x_{ACN})(\partial^{q}\delta/\partial x_{ACN})$$

[11] $${}^{q}\Delta_{ACN} = N(\partial^{q}\Delta/\partial n_{ACN}) = (1 - x_{ACN})(\partial^{q}\Delta/\partial x_{ACN})$$

where $q = V, S,$ or $SV,$ specifying volume, entropy, and cross (entropy–volume) fluctuations. These quantities show the effect of additional ACN on the respective fluctuations. They are plotted in Figs. 8–10.

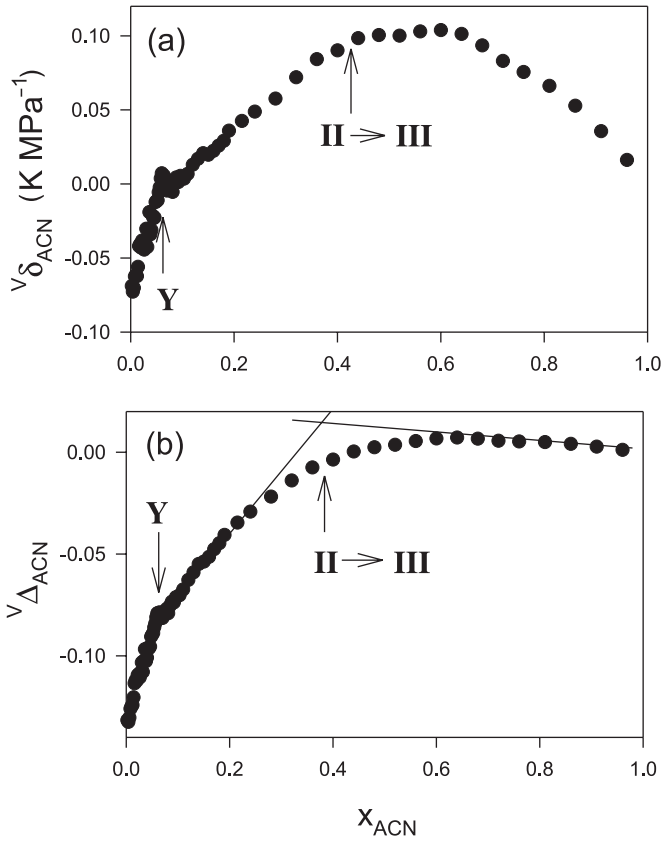
The partial molar volume fluctuations of alcohols in aqueous alcohols start off negative, and progressively increase to about zero at point Y (7). There is no sign of anomaly at point X (7). For ACN–H_2O (Fig. 8) the situation is the same,

Table 1. Loci of mixing scheme boundaries and the value of enthalpic interaction function (H^{E}_{A-A} at point X, A = ACN, ME, ET, or 1P).

	Temp. (°C)	X	H^{E}_{A-A} (kJ mol^{-1})	Y	II → III
Acetonitrile	6	0.0125	133	0.085	
	20	0.0106	122		
	30	0.0088	110		
	37	0.0080	100	0.060	0.45
	45	0.0065	90		
Methanol	25	0.07	32	0.25	0.45
Ethanol	25	0.06	73	0.19	
Propan-1-ol	25	0.05	210	0.09	

Note: See text for detail.

Fig. 8. Partial molar volume fluctuations of acetonitrile at 25°C. (*a*) Amplitude ($^{V}\delta_{ACN}$); (*b*) amplitude and wavelength ($^{V}\Delta_{ACN}$).



although the absolute value of $^{V}\delta_{ACN}$ at the infinite dilution is smaller than the counter part of alcohol, even of ME. However, both $^{V}\delta_{ACN}$ and $^{V}\Delta_{ACN}$ show an anomalous break in slope at point Y (x_{ACN} = 0.07). For alcohols–H_2O, it is propan-1-ol (1P) that shows a bend at point Y, and there is no apparent anomaly at point Y for ME–H_2O, and ET–H_2O (7). For *tert*-butanol (TBA–H_2O) and 2-butoxyethanol (BE–H_2O), $^{V}\Delta_{TBA}$ (6) and $^{V}\Delta_{BE}$ (5) show anomalous behaviours not only at point Y but also at X. This observation hints that the larger the hydrophobic moiety, the more apparent the anomaly at point Y and X, and that the effect of ACN on $^{V}\delta_{ACN}$ and $^{V}\Delta_{ACN}$ in this regard is equivalent to that of propan-1-ol.

© 2000 NRC Canada

Fig. 9. Partial molar entropy fluctuations of acetonitrile at 25°C. (*a*) Amplitude ($^{S}\delta_{ACN}$); (*b*) amplitude and wavelength ($^{S}\Delta_{ACN}$).

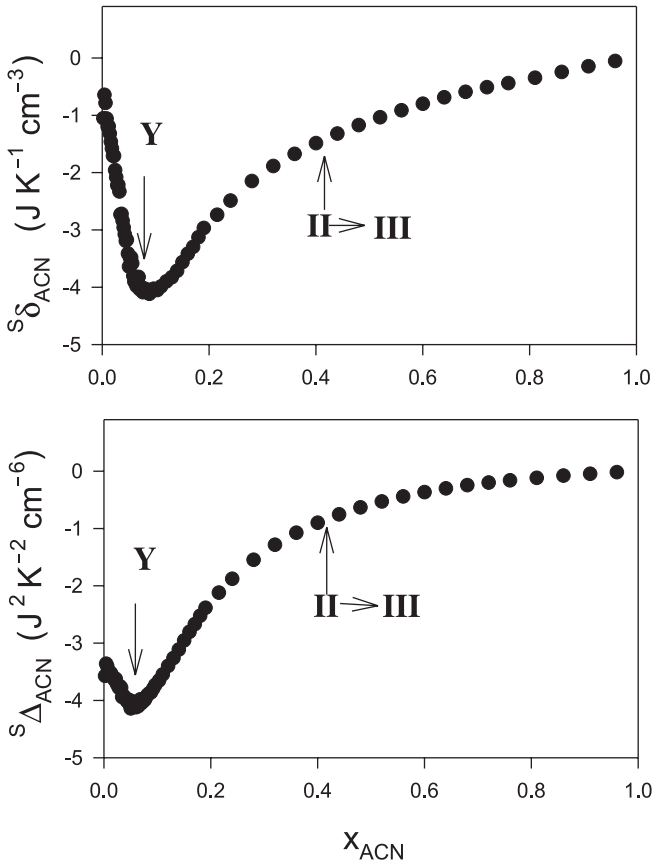


Figure 9*a* shows that $^{S}\delta_{ACN}$ starts at a value very close to zero, similar to ME (7), continues to decrease linearly to point Y and then turns around. There is no indication of anomaly at point X. It is again 1P–H_2O that has a conspicuous anomaly at point X and Y in $^{S}\delta_{1P}$ (7). For ET and ME, both points, X and Y, are obscure (7). For 1P, $^{S}\delta_{1P}$ stays constant to point X, and then drops sharply to point Y (7). For the present case, there is no sign of point X, but $^{S}\delta_{ACN}$ starts to decrease immediately. The situation for the normalized fluctuation is similar and $^{S}\Delta_{ACN}$ (Fig. 9*b*) starts to decrease immediately without a sign of point X. Thus, in terms of entropy fluctuation, ACN seems to start driving the system to point Y without going through point X.

The peculiarity of H_2O and aqueous solutions manifests itself in the cross entropy–volume fluctuations, since there is a characteristic negative contribution in $< (\Delta S)(\Delta V) >$ (5–7, 13). Earlier, it was pointed out that the x_{AL}-dependence of $^{SV}\delta_{AL}$ and $^{SV}\Delta_{AL}$ is the same as that of the enthalpic interaction function (H^{E}_{AL-AL}) (6, 7). In particular, $^{SV}\Delta_{AL}$ and H^{E}_{AL-AL} are identical with a scaling factor on the ordinate (6, 7). Here, subscript AL stands for alcohol, ME, ET, 1P, TBA, and BE. Indeed, the x_{ACN}-dependence of $^{SV}\delta_{ACN}$ and $^{SV}\Delta_{ACN}$ (Fig. 10) looks similar to that in Fig. 7 ($H^{E}_{ACN-ACN}$) except that the existence of point X is not perfectly unequivocal, due to inevitable uncertainty in determining α_p by using density data at two temperatures. Dilatometry, in which the volume change due to temperature rise is directly measured, is required for an attempt to resolve the existence of X in

Fig. 10. Partial molar cross-fluctuations of acetonitrile at 25°C. (*a*) Amplitude ($^{SV}\delta_{ACN}$); (*b*) amplitude and wavelength ($^{SV}\Delta_{ACN}$).

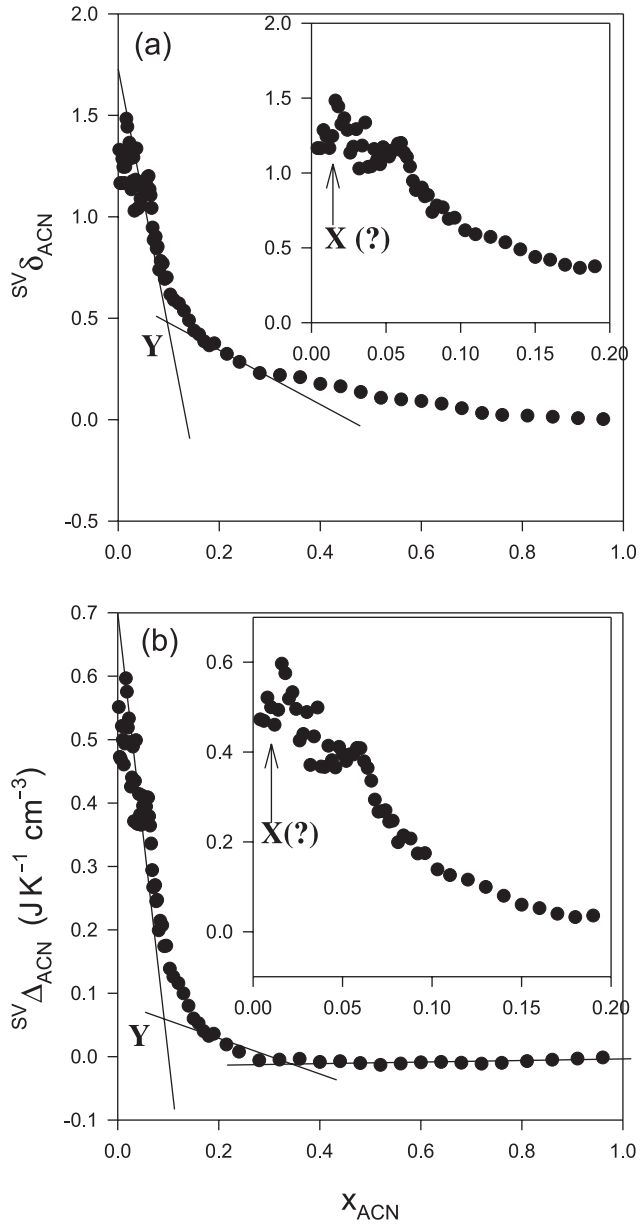
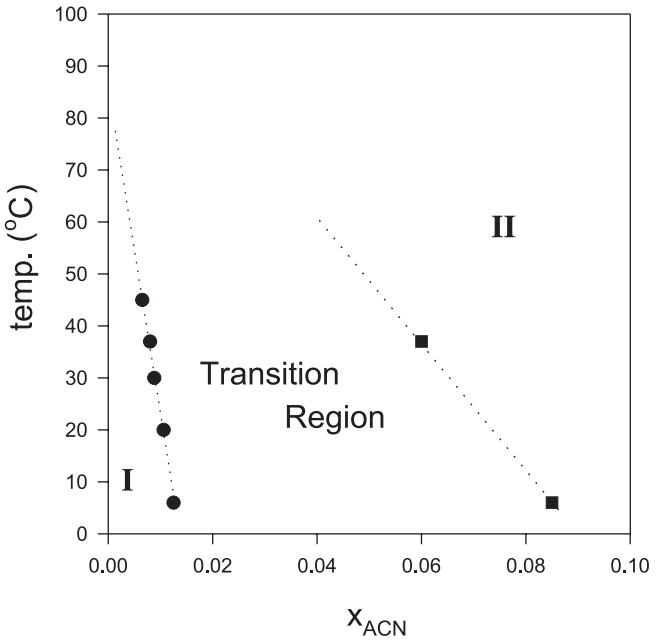


Fig. 10. We point out, however, the values of $^{SV}\delta_{ACN}$ and $^{SV}\Delta_{ACN}$ at a presumed point X in Fig. 10 are the same as those of $^{SV}\delta_{1P}$ and $^{SV}\Delta_{1P}$ for 1P–H_2O.

Turning back to Fig. 7, high sensitivity of the titration calorimeter that we used was the key to obtain many data points in a very dilute region ($x_{ACN} < 0.01$), which made locating points X and Y possible in $H^{E}_{ACN-ACN}$ plots. The loci of X and Y thus obtained are plotted in Fig. 11 as functions of temperature. In the figure, the region between X and Y is the transition region. The transition from Mixing Scheme I to II starts at point X and ends at Y. Beyond point Y is the region where Mixing Scheme II is operative. Extrapolation of the data points in Fig. 11 hints, though not quite conclusively, that the region of Mixing Scheme I disappears above about 80°C, and above this temperature Mixing Scheme II is operative right from $x_{ACN} = 0$. According to Stanley and

© 2000 NRC Canada

Fig. 11. The loci of the transition region from Mixing Scheme I to II.



Teixeira's (24) estimate, at about 80°C the hydrogen bond probability of H_2O decreases to 0.39, which is the bond percolation threshold of ice Ih lattice. Namely, above 80°C the hydrogen bond network of liquid H_2O is no longer bond-percolated. This suggests that in Mixing Scheme I in Fig. 11 the hydrogen bond network of H_2O is percolated and that ACN–H_2O also has Mixing Scheme I as typical as aqueous alcohols. In turn, Fig. 11 provides other evidence, though circumstantial, of the loss of percolation at about 80°C for pure liquid H_2O, together with the similar graphs for TBA–H_2O and BE–H_2O (1, 2).

Conclusion

We conclude that in ACN–H_2O there are three qualitatively different mixing schemes are operative, Mixing Scheme I, II, and III, just as in aqueous alcohols (1, 2, 4, 7). However, the effect of ACN on H_2O is stronger than that of ME. In terms of the locus of the transition from Mixing Scheme I to II, ACN appears to be stronger than BE, while the strength of the enthalpic interaction is equivalent to 1P. The equivalence to 1P is also apparent in the behaviours of volume, entropy, and cross (entropy–volume) fluctuation functions.

The above conclusion is pending, however, on future direct determination by dilatometry of V^{E}_{ACN} and α_p at a very dilute region, $x_{ACN} < 0.01$. Furthermore, there are still many unresolved issues. (1) Why does $^{V}\delta$ show an extremely slow decrease, while $^{V}\Delta$ behaves similar to alcohols? (2) Why is the locus of point X smaller than that for BE, while all other indications are that ACN's effect on H_2O is the same as 1P? (3) Why is ACN much stronger in its effect on H_2O than ME? Clearly, answers to all the above and other questions ought to be sought in the function of the -CN group as opposed to the -OH of alcohols. Further elucidation of these questions may be possible in studies of aqueous solution of cyanide with a higher alkyl group.

Acknowledgement

We thank A. Louise Creagh for her invaluable help throughout of this work. Thanks are also due to Candy Cheung and Jonathan Lau for assistance in the enthalpy measurements. This work was supported by the Natural Sciences and Engineering Research Council of Canada (NSERC). The guest professorship to one of us (YK) at Tokyo Institute of Technology was financed by Monbusho of Japan.

References

1. Y. Koga. J. Crystallogr. Soc. Jpn. **37**, 172 (1995).
2. Y. Koga. J. Phys. Chem. **100**, 5172 (1996).
3. Y. Koga, K. Tamura, and S. Murakami. J. Solution Chem. **24**, 1125 (1995).
4. S.H. Tanaka, H.I. Yoshihara, A.W.-C. Ho, F.W. Lau, P. Westh, and Y. Koga. Can. J. Chem. **74**, 713 (1996).
5. Y. Koga and P. Westh. Bull. Chem. Soc. Jpn. **69**, 1505 (1996).
6. K. Tamura, A. Osaki, and Y. Koga. Phys. Chem. Chem. Phys. **1**, 121 (1999).
7. Y. Koga. Can. J. Chem. **77**, 2039 (1999).
8. E.C.H. To, J.V. Davies, M. Tucker, P. Westh, Ch. Trandum, K.S.H. Suh, and Y. Koga. J. Solution Chem. **28**, 1137 (1999).
9. K. Tamura, J. Hu, Ch. Trandum, P. Westh, C.A. Haynes, and Y. Koga. Phys. Chem. Chem. Phys. **2**, 355 (2000).
10. Y.P. Handa and G.C. Benson. J. Solution Chem. **10**, 291 (1981).
11. G.C. Benson, P.J. D'Arcy, and Y.P. Handa. Thermochim. Acta, **46**, 295 (1981).
12. Y. Koga. Chem. Phys. Lett. **240**, 340 (1995).
13. Y. Koga, P. Westh, S. Sawamura, and Y. Taniguchi. J. Chem. Phys. **105**, 2028 (1996).
14. Y. Koga. Can. J. Chem. **66**, 1187 (1988).
15. Y. Koga, W.W.Y. Siu, and T.Y.H. Wong. J. Phys. Chem. **94**, 7700 (1990).
16. Chem. Soc. Jpn. (*Editor*). Chemistry handbook. 3rd ed. Maruzen, Tokyo. 1984. p. II–111.
17. H.T. French. J. Chem. Thermodyn. **19**, 1155 (1987).
18. Y. Koga. J. Phys. Chem. **99**, 6231 (1995).
19. Y. Koga, J. Kristiansen, and Aa. Hvidt. J. Chem. Thermodyn. **25**, 51 (1993).
20. T.Y.H. Wong, K.C. Wong-Moon, L.J. Beach, Y.-F. Chuang, and Y. Koga. J. Phys. Chem. **96**, 10 025 (1992).
21. D.A. Armitage, M. J. Blandamer, M.J. Foster, N.J. Hidden, K.W. Morcom, M.C.R. Symons, and M.J. Wootten. Trans. Faraday Soc. **64**, 1193 (1968).
22. Y. Koga, J. Phys. Chem. **96**, 10466 (1992).
23. M.I. Davis, M.C. Molina, and G. Douheret. Thermochim. Acta, **131**, 153 (1988).
24. H.E. Stanley and J. Teixeira. J. Chem. Phys. **73**, 3404 (1980).

© 2000 NRC Canada

Interactions of 6-aminopurine (adenine) in water and aqueous urea solutions

J.D. Pandey, S. Haroon, Krishna K. Dubey, Madhulika Upadhyaya, Ranjan Dey, and K. Misra

Abstract: Density (ρ), ultrasonic velocity (*U*), viscosity (η), and absorbance (*A*) of adenine in water, 1 M, 3 M, and 6 M aqueous urea solutions have been measured in the presence (and absence) of different concentrations of salts, i.e., NaCl, KCl, and $CaCl_2$. From these measured values, the apparent molar volume (ϕ_v), experimental slope (S_v), apparent molar compressibility (ϕ_K), viscosity coefficients A and B of Jones–Dole equation, specific acoustic impedance (*Z*), hydration number (S_n), internal pressure (P_i), molar absorptivity (ε), hypochromicity (*h*), and oscillator strength (*f*) have been calculated at 298.15 K. The increasing and (or) decreasing trends of all these parameters indicate a strong interaction of urea in moderate concentration (1 M and 3 M) with adenine especially at the hydrophilic/polar and ionic sites, particularly by hydrogen bonding. However, the interaction at hydrophobic sites are relatively weaker. Higher concentrations of urea (6 M) have more denaturation effect. The π–π interactions (stacking) in adenine are more prominent in concentrated solutions and are also strengthened by the presence of cations up to an optimum concentration of salts (cut-off point). The self-association of urea and adenine is more significant in concentrated aqueous solutions and becomes negligible on dilution.

Key words: interaction, adenine, urea, density, viscosity, and ultrasonic velocity.

Résumé : On a mesuré la densité (ρ), la vélocité ultrasonique (*U*), la viscosité (η) et l'absorbance (*A*) de l'adénine dans l'eau et dans des solutions aqueuses à 1 M, 3 M et 6 M d'urée, en présence et en absence de sels (tels que NaCl, KCl et $CaCl_2$) à diverses concentrations. Sur la base de ces valeurs mesurées, on a calculé le volume molaire apparent (ϕ), la pente expérimentale (S_v), la compressibilité molaire apparente (ϕ_k), les coefficients de viscosité A et B de l'équation de Jones–Dole, l'impédance acoustique spécifique (*Z*), le nombre d'hydratation (S_n), la pression interne (P_i), l'absorptivité molaire (ε), l'hypochromicité (*h*) et la force de l'oscillateur (*f*) à 298,15 K. Les tendances à l'augmentation/diminution de tous ces paramètres indiquent la présence d'une forte interaction de l'urée avec l'adénine aux concentrations modérées (1 M et 3 M), particulièrement au niveau des sites ioniques et hydrophiles/polaires principalement par le biais de liaisons hydrogènes. Toutefois, l'interaction au niveau des sites hydrophobes est relativement faible. Des concentrations plus élevées d'urée (6 M) ont un effet de dénaturation. Les interactions π–π (empilement) de l'adénine sont plus importantes en solutions concentrées et elles sont aussi renforcées par la présence de cations jusqu'à des concentrations optimales de sels (point de rupture). L'autoassociation de l'urée et de l'adénine est aussi plus importante en solutions aqueuses concentrées et elle devient négligeable par dilution.

Mots clés : interaction, adénine, urée, densité, viscosité, vélocité ultrasonique.

[Traduit par la Rédaction]

Introduction

Molecular interactions in general and protein–nucleic acid interactions in particular are of immense importance in understanding the life processes. Despite exhaustive researches being carried out in this field during the last two decades we do not have a clear idea about the geometry of repressor–operator recognition. Simultaneous observations of two associated macromolecules makes this study rather highly complex.

The most plausible solution to this problem is to study model compounds using both theoretical and experimental approaches. Urea with its highly polar >C=O and -NH_2 functional groups can be the best model substitute for peptide bond of proteins. In earlier work (1, 2) thermodynamic studies of urea and its derivatives in water and in water–dioxan solutions at different temperatures have been carried out.

Aqueous urea solutions have been widely reported to be nucleic acid denaturants. The effects of urea on the secondary structure of nucleic acids has been investigated by some workers (3). Hemmes et al. (4) have reported that urea concentration larger than 7 M effectively eliminated stacking in a model of 6-methyl purine. On the basis of partial molar heat capacities and volumes, studies (5), it has been found that urea in high concentrations (3–6 mol kg^{-1}) showed

Received August 6, 1999. Published on the NRC Research Press website on November 21, 2000.

J.D. Pandey, S. Haroon, K.K. Dubey, M. Upadhyaya, R. Dey, and K. Misra.[1] Department of Chemistry, University of Allahabad, Allahabad-211 002, India.

[1]Author to whom correspondence may be addressed. Telephone: +91-532-461236 (Office) / 465462 / 467154 (Residence). Fax: +91-532-623221 / 607367. e-mail: krishnamisra@hotmail.com

© 2000 NRC Canada

strong hydrophilic–hydrophilic ionic group interactions of nucleic acid bases, nucleosides, and nucleotides, thereby supporting its denaturing characteristics. Various types of interactions are encountered in biomolecules, the predominant being π—π bond, hydrogen bond, and ionic interactions.

Base–base interaction through hydrogen bonding has been investigated by thermodynamic methods to derive association constants as well as enthalpies and entropies for this process. Stacking interactions are mainly due to π-electrons resulting in dispersion and dipole induced dipole forces and hydrophobic bonding.

The role of water in these interactions is extremely important. Hydration of proteins and nucleic acids is mainly responsible for stabilization of their secondary and tertiary structure (4–6) and is responsible for the conformational transitions of DNA. The bases are known to self-assemble into ordered structures by active participation of water molecules. High relative humidity favours the B-form of DNA and reduced humidity leads to transitions from B-form to C or A and with specific sequences to D and Z-DNA. Nucleic acid–water interactions have been studied by a number of workers (7–9). We have reported earlier the interaction of nucleic acid components in water–dioxan mixtures (10–12) and also of urea and its derivatives in water (13).

The concentration of ions significantly effects the conformational changes in both, i.e., DNA and (or) RNA and proteins. Besides phosphate oxygen, metal ions also coordinate with ribose hydroxyls, base ring nitrogens, and keto substituents. Since metal ions like Na^+, K^+, and Ca^{++} are present in the body in millimolar concentrations, proteins and nucleic acids occur as complexes coordinated with these metal ions. Therefore, the interaction between these two macromolecules is greatly affected by the presence of these metal ions.

To explicitly study the contribution of purine and (or) pyrimidine bases of DNA towards their interaction with urea, the purine base viz., adenine has been investigated separately in water, aqueous urea solutions of different concentrations, without metal ions, and in the presence of different concentrations of metal ions, e.g., Na^+, K^+, and Ca^{2+}. Ultrasonic, volumetric, and viscometric techniques have been used in addition to spectroscopic (UV) technique. Ultrasonic velocity, density, and viscosity data have been used to deduce a number of interesting and important thermodynamic parameters viz., apparent molar volume, apparent molar compressibility, viscosity coefficients A and B of the Jones–Dole equation, apparent hydration number, internal pressure, acoustic impedance, and molar absorptivity, hypochromicity, and oscillator strength, etc. Interestingly, the use of all these parameters reported in this paper yielded comparable results which is certainly a step forward in the direction of solving the complexities involved in such macromolecular interactions at unimolecular level.

Materials and methods

Ultrasonic velocity, density, and viscosity for all the systems were measured at 298.15 ± 0.01 K over the entire composition range (i.e., three solutions in 0.1–0.5 M range).

Ultrasonic velocity (U) was measured using a variable path ultrasonic interferometer (frequency 2 MHz). Density was measured with the help of a standard double capillary pycknometer technique used by other workers (14, 15). Viscosity was measured by a calibrated Ubbelhode type viscometer, UV absorption was recorded on 220 S Hitachi UV–vis spectrophotometer. Temperature was maintained by a SB-16 shaking thermostatic bath with an accuracy of ±0.01 K. The uncertainties in the measurements of velocity and density were within $\pm 1 \times 10^{-2}$ ms^{-1} and $\pm 1 \times 10^{-4}$ g cm^{-3}, respectively. Uncertainties in the measurements of viscosity and ε values were within $\pm 1 \times 10^{-2}$ g cm^{-1} ms^{-1} and 1×10^{-6} unit, respectively. Time was measured by a calibrated stopwatch. The details of the experimental procedures and method of calibration have been reported earlier (16).

Adenine was purchased from Sigma Chemical Co. U.S.A. and used after drying under vacuum for 12 h. Salts (NaCl, KCl, $CaCl_2$) and urea were obtained from E. Merck, India and were used after drying in an air oven and kept dry over CaO and P_2O_5 in a dessicator. Purity of all the chemicals was checked by TLC. All the solutions were prepared by weight in double-distilled and degassed water.

Solutions of urea and adenine were prepared in concentrations of 2×10^{-2} M, individually. 1 M stock solutions of NaCl, KCl, and $CaCl_2$ were prepared separately and these were diluted to make solutions in the range of 0.1–0.5 M.

Experimental values of density (ρ), ultrasonic velocity (U), and viscosity (η) along with the computed values of apparent molar compressibility (ϕ_k), apparent molar volume (ϕ_v) and Jones–Dole parameters ($\eta_{rel}^{-1}/\sqrt{m}$) and hydration number (S_n) of adenine–water, adenine–1 M, 3 M, and 6 M urea have been recorded in Table 1. The same parameter for equimolar mixtures of adenine (10^{-4} M) – aqueous urea (10^{-4} M) in the presence of varying concentration (0.1–0.5 M) of the salts NaCl, KCl, and $CaCl_2$ have been presented in Table 2. The partial molar volume (ϕ_v^0), experimental slope (S_v), apparent molar compressibility (ϕ_k^0), and viscosity coefficient A and B of the Jones–Dole equation for all the systems under the present investigation have been depicted in Table 3. Computed values of internal pressure (P_i), acoustic impedance (Z) of adenine–water and adenine–1 M, 3 M, and 6 M aqueous urea at different concentrations (0.1–0.5 mol L^{-1}) of salts, i.e., NaCl, KCl, and $CaCl_2$ are presented in Table 4.

Absorbance (A), molar absoptivity (ε), hypochromicity (h), and oscillator strength (f) of all the systems under the present study have been listed in Table 5.

The systems chosen for the present investigation are: (1) adenine in water; and (2) adenine in 1 M, 3 M, and 6 M aqueous urea with and without the presence of different concentrations of salts, i.e., NaCl, KCl, and $CaCl_2$.

Ultrasonic velocity (U), density (ρ), viscosity (η) data of various solutions have been employed to deduce a number of useful parameters viz., apparent molar volume (ϕ_v), partial molar volume (ϕ_v^0), apparent molar compressibility (ϕ_k), partial molar compressibility (ϕ_k^0), viscosity interaction coefficient A and B of the Jones–Dole equation, apparent hydration number (S_n), acoustic impedance (Z), and internal pressure (P_i) using the following equations (17),

$$K_s = (U^2\rho)^{-1}$$

$$\phi_v = \frac{M_{soln}}{\rho} - \frac{\rho - \rho_0}{m\rho\rho_0}v$$

© 2000 NRC Canada

Table 1. Experimental values of density (ρ), ultrasonic velocity (*U*), viscosity (η), apparent molar volume (ϕ_v), apparent molar compressibility (ϕ_K), apparent hydration number (S_n), and Jones–Dole parameter ($\eta_{rel}^{-1}/\sqrt{m}$) of adenine in water and aqueous urea solutions at 298.15 K.

Conc. of adenine (mol L^{-1})	$\rho \times 10^{-3}$ (kg m^{-3})	U (m s^{-1})	η (kg m^{-1} s^{-1})	$\phi_v \times 10^{-3}$ (m^3 mol^{-1})	$\phi_K \times 10^{-14}$ (cm^3 mol^{-1})	S_n	$\eta_{rel}^{-1}/\sqrt{m}$
Adenine–water system							
0.011	0.9983	1498.9	0.1260	14.66	–1.77	22.00	3.9657
0.010	0.9980	1498.8	0.1233	31.74	–1.69	21.00	3.8571
0.009	0.9979	1498.6	0.1207	33.65	–1.70	21.04	3.7603
0.008	0.9977	1498.4	0.1195	36.03	–1.70	21.09	3.8531
0.007	0.9976	1498.4	0.1195	47.70	–1.80	11.32	4.0959
Adenine – 1 M urea system							
0.011	1.0125	1476.4	0.1406	92.07	–0.01	12.01	0.9479
0.010	1.0124	1479.3	0.1388	92.84	–0.19	22.40	0.8535
0.009	1.0124	1479.3	0.1371	93.76	–0.21	25.10	0.7595
0.008	1.0123	1479.1	0.1365	101.02	–0.21	26.03	0.7531
0.007	1.0122	1479.1	0.1359	103.39	–0.25	30.02	0.7490
Adenine – 3 M urea system							
0.011	1.03827	1585.9	0.1357	121.58	–1.44	185.42	0.5450
0.010	1.03825	1585.9	0.1346	122.60	–1.59	204.42	0.4859
0.009	1.03824	1585.6	0.1337	122.81	–1.76	225.75	0.4383
0.008	1.03822	1585.4	0.1332	124.22	–1.97	253.04	0.4213
0.007	1.03820	1585.4	0.1327	126.05	–2.26	289.84	0.4039
Adenine – 6 M urea system							
0.011	1.06925	1598.2	0.1268	123.23	–1.11	141.74	–0.1948
0.010	1.06923	1598.1	0.1256	124.68	–1.22	155.80	–0.2970
0.009	1.06921	1597.8	0.1244	126.44	–1.34	171.76	–0.4108
0.008	1.06920	1597.5	0.1232	127.56	–1.50	191.82	–0.5393
0.007	1.06918	1597.4	0.1228	130.25	–1.72	219.05	–0.6135

$$\phi_v = \phi_v^0 + S_v\sqrt{m}$$

$$\phi_k = \frac{10^3(K_s - K_{s,0})}{m\rho_0} + \phi_v K_s$$

$$\phi_k = \phi_k^0 + S_k\sqrt{m}$$

$$\frac{\eta}{\eta_0} = 1 + A\sqrt{m} + Bm$$

$$S_n = \frac{n_1}{n_2}1 - \left(\frac{K_s}{K_{s,0}}\right)$$

$$Z = \rho U$$

$$P_i = bRT\left(\frac{k\eta^{1/2}}{U}\right)\left(\frac{\rho^{2/3}}{M_{soln}^{7/6}}\right)$$

$$\varepsilon = \frac{A}{c\lambda}$$

$$h = 1 - \frac{[\varepsilon\,(\text{solution})]}{[\varepsilon\,(\text{solvent})]}$$

$$f = 4.32 \times 10^{-9}.\int_0^{\nu} \varepsilon_a(\nu)d\nu$$

Where all the symbols have their usual notations.

Results and discussion

In the present study, the hydration cosphere, i.e., the region occupied by water that is significantly affected by the presence of solute molecule viz. adenine (**1**) and urea is extremely important. When the cospheres of both these molecules, i.e., adenine and urea overlap due to their proximity caused by van der Waals hydrogen bonding or electrostatic interactions, some of the cosphere material is displaced, causing changes in thermodynamic parameters (5, 18–20). The hydrogen bonding capability of water leads to its interactions with adenine acid groups such as O and N atoms that are hydrogen bonding acceptors and protons that are hydrogen bonding donors. It also leads to extensive though imperfect and transitory hydrogen-bonded network in water itself. Formation or disruption of such networks leads to a decrease or increase, respectively, in the entropy (*S*), thus affecting the thermodynamics of processes that affect water hydrogen bonding. Introduction of a hydrophobic residue like adenine base in water leads to the formation of hydrogen-bonded water cluster and leads to negative ΔS. This is partially responsible for low solubility of adenine base in water and consequently for its tendency to self-associate by stacking in aqueous solution (21). A structure breaking species such as urea disrupts water hydrogen bonding and thereby increases the entropy of the system. The large dipole moment of water

© 2000 NRC Canada

Table 2. Experimental values of density (ρ), ultrasonic velocity (*U*), apparent molar volume (ϕ_v), viscosity (η), specific acoustic impedance (*Z*), and apparent molar compressibility (ϕ_K) of adenine (10^{-4} M) – aqueous urea (10^{-4} M) in the presence of varying concentrations (0.1–0.5 M) of NaCl, KCl, and $CaCl_2$ salts at 298.15 K.

Conc. of salt (mol L^{-1})	$\rho \times 10^3$ (kg m^{-3})	*U* (m s^{-1})	$\phi_v \times 10^3$ (m^3 mol^{-1})	η (kg m^{-1} s^{-1})	$Z \times 10^{-3}$	$\phi_K \times 10^{-14}$ (m^3 mol^{-1} Pa^{-1})
1	2	3	4	5	6	7
Adenine - Urea System						
NaCl						
0.10	0.9990	1 604.4	58.5464	0.1316	1 602.79	22.592
0.15	0.9998	1 610.2	58.4983	0.1320	1 609.87	22.375
0.20	1.0005	1 615.5	58.4751	0.1356	1 616.30	22.176
0.25	1.0008	1 617.6	58.4412	0.1367	1 618.89	22.113
0.30	1.0017	1 621.2	58.3877	0.1374	1 623.95	21.994
0.35	1.0025	1 626.7	58.3407	0.1266	1 630.76	21.864
0.40	1.0034	1 630.0	58.2877	0.1207	1 635.54	21.227
0.45	1.0041	1 638.8	58.2471	0.1167	1 640.49	21.596
0.50	1.0052	1 637.9	58.1825	0.1165	1 646.41	21.394
KCl						
0.10	1.0000	1 607.70	74.4779	0.1323	1 607.70	28.563
0.15	1.0006	1 612.06	74.4312	0.1344	1 611.11	28.512
0.20	1.0009	1 616.75	74.4174	0.1355	1 615.30	28.273
0.25	1.0010	1 620.91	74.4071	0.1378	1 619.30	28.213
0.30	1.0017	1 626.25	74.3605	0.1380	1 623.50	27.366
0.35	1.0032	1 633.51	74.2468	0.1338	1 628.30	27.776
0.40	1.0038	1 639.70	74.2031	0.1328	1 635.50	27.533
0.45	1.0044	1 645.10	74.1589	0.1311	1 637.90	27.368
0.50	1.0047	1 647.70	74.1376	0.1311	1 640.00	27.295
$CaCl_2$						
0.10	0.9998	1 609.9	147.0093	0.1342	1 609.57	56.443
0.15	1.0010	1 611.0	146.8339	0.1349	1 621.61	56.427
0.20	1.0019	1 615.3	146.7040	0.1357	1 618.36	55.918
0.25	1.0032	1 616.5	146.5084	0.1390	1 621.67	55.708
0.30	1.0047	1 619.3	146.2870	0.1399	1 626.91	55.329
0.35	1.0065	1 622.3	146.0252	0.1429	1 632.84	55.092
0.40	1.0078	1 624.6	145.8351	0.1367	1 637.27	54.726
0.45	1.0088	1 629.9	145.6857	0.1334	1 644.24	54.224
0.50	1.0094	1 632.6	145.6079	0.1330	1 647.94	53.903

Table 3. Partial molar volume (ϕ_v^0), experimental slope (S_v), partial molar compressibility (ϕ_K^0), viscosity coefficients A and B of the Jones–Dole equation for adenine in water, aqueous urea, and in presence of salts, NaCl, KCl, and $CaCl_2$ at 298.15 K.

	System	$\phi_v^0 \times 10^3$ (m^3 mol^{-1})	S_v	$\phi_K^0 \times 10^{-14}$	A	B
	1	2	3	4	5	6
(*a*) Adenine (conc. range 0.011–0.007 M)						
1	Adenine–water	53	1.00	–0.182	4.10	1.23
2	Adenine – 1 M urea	105	0.58	–0.260	0.74	1.41
3	Adenine – 3 M urea	127	0.27	–2.360	0.39	1.40
4	Adenine – 6 M urea	132	0.26	–1.800	0.09	1.32
(*b*) Adenine (10^{-4} M) – urea (10^{-4} M) (salt conc. 0.1–0.5 M)						
1	NaCl	58.4412	2.006	21.310	0.3810	6.5662
2	KCl	74.4471	2.0155	26.229	0.3855	8.7562
3	$CaCl_2$	146.8339	8.0985	51.364	0.3912	9.1786

makes it a good solvent for ions. Cations interact favourably with the O and anions interact with H atoms. Since, a high dipole moment leads to a high dielectric constant, ε, coulumbic interactions between ions, whose energy is $E = q_1q_2/\varepsilon r$ (where q_1 and q_2 are the ion charges and r is their separation) will be weaker in water ($\varepsilon \approx 80$) than in organic

© 2000 NRC Canada

Table 4. Internal pressure ($P_i \times 10^{-5}$ Pa) and acoustic impedance ($Z \times 10^{-3}$) of adenine in water and aqueous urea at 298.15 K.

Conc. of adenine (mol L^{-1})	$P_i \times 10^{-5}$ (Pa)	$Z \times 10^{-3}$ (kg m^{-2} s^{-1})
1	2	3
Adenine–water system		
0.011	2909	1496.35
0.010	2878	1495.80
0.009	2858	1495.45
0.008	2834	1494.95
0.007	2833	1494.80
Adenine – 1 M urea system		
0.011	2884	1494.85
0.010	2866	1497.64
0.009	2849	1497.64
0.008	2823	1497.29
0.007	2837	1497.14
Adenine – 3 M urea system		
0.011	2640	1646.59
0.010	2629	1646.48
0.009	2621	1646.16
0.008	2616	1645.64
0.007	2611	1645.64
Adenine – 6 M urea system		
0.011	2328	1708.79
0.010	2318	1708.68
0.009	2307	1708.36
0.008	2296	1708.47
0.007	2292	1708.47

Adenine (10^{-4} M) – aq. urea (10^{-4} M)					
Salt conc. (mol L^{-1})	$P_i \times 10^{-5}$ (Pa)	Salt conc. (mol L^{-1})	$P_i \times 10^{-5}$ (Pa)	Salt conc. (mol L^{-1})	$P_i \times 10^{-5}$ (Pa)
NaCl		KCl		$CaCl_2$	
0.10	490.6	0.10	491.7	0.10	494.2
0.15	305.0	0.15	308.6	0.15	309.6
0.20	221.0	0.20	221.3	0.20	221.3
0.25	171.3	0.25	172.3	0.25	173.5
0.30	139.6	0.30	139.6	0.30	140.7
0.35	111.1	0.35	114.0	0.35	118.5
0.40	92.8	0.40	97.2	0.40	99.2
0.45	79.5	0.45	84.1	0.45	85.3
0.50	70.2	0.50	74.4	0.50	75.3

solvents ($\varepsilon \approx 2$). Moreover, in the present case the adenine moiety is interacting with highly polar urea molecule and the properties of water as a solvent for ions becomes crucial. However, this effect may be more important if in place of adenine more ionic adenosine or adenylic acid are used.

The ϕ_v values for adenine in water and 1 M, 3 M, and 6 M urea solutions are positive and increase regularly with dilution, indicating the decrease in stacking interactions. These values are highest for adenine in 6 M urea, indicating maximum denaturation (Table 1).

The effects of salts NaCl, KCl, and $CaCl_2$ on ϕ_v values can be observed from the results reported in Table 2. The calculated values of ϕ_v gradually decrease with increase in concentration of each salt, indicating that these salts do contribute to the strengthening of interactions between adenine and urea. The values of partial molar volumes are highest for the adenine–urea–$CaCl_2$ system as compared to adenine–urea–KCl and adenine–urea–NaCl systems, indicating the interaction strengthening contribution of salts in the order $CaCl_2$ > KCl > NaCl.

Table 2 shows the values of ϕ_v calculated from the intercept of the linear plot of ϕ_v against the square root of the concentration. The plot is in accordance with Masson's equation. The increase in S_v values (Table 3) is indicative of stronger solute–solvent interaction. In case of adenine in aqueous urea (1 M, 3 M, and 6 M) this value decreases with an increase in concentration of urea and is minimum in 6 M urea indicating the disruption of adenine water interaction

© 2000 NRC Canada

Table 5. Absorbance (*A*), molar absorptivity (ε), hypochromicity (*h*), and oscillator strength (*f*) of the adenine (10^{-4} M) – aq. urea

Salt conc. (mol L^{-1})	*A*	ε × 10^{-30} (mol L^{-1} cm^{-1})	*h*	*f*
Adenine – aq. urea system				
NaCl				
0.10	0.951	9.9	0.2500	49.3455
0.15	0.922	9.6	0.2727	47.8502
0.20	0.921	9.6	0.2727	47.8502
0.25	0.910	9.5	0.2803	47.3518
0.30	0.912	9.5	0.2803	47.3578
0.35	0.892	9.3	0.2954	46.3549
0.40	0.906	9.4	0.2878	46.8533
0.45	0.920	9.6	0.2727	46.8592
0.50	0.937	9.7	0.2651	48.3486
KCl				
0.10	1.000	10.4	0.2121	51.8377
0.15	0.962	10.0	0.2424	49.8440
0.20	0.961	10.0	0.2424	49.8440
0.25	0.954	9.9	0.2500	49.3455
0.30	0.944	9.8	0.2575	48.8471
0.35	0.891	9.3	0.2954	46.3549
0.40	0.940	9.8	0.2575	48.8471
0.45	0.941	9.8	0.2575	48.8471
0.50	0.999	10.3	0.2196	51.3393
$CaCl_2$				
0.10	1.080	10.4	0.2121	51.8377
0.15	0.990	10.3	0.2196	51.3393
0.20	0.969	10.0	0.2424	49.8440
0.25	0.966	10.0	0.2424	49.8440
0.30	0.928	9.6	0.2727	47.8502
0.35	0.928	9.6	0.2727	47.8502
0.40	0.926	9.6	0.2727	47.8502
0.45	0.899	9.3	0.2954	46.3549
0.50	0.895	9.3	0.2954	46.3549

with urea. The presence of salts apparently increases S_v values and the contribution of $CaCl_2$ is maximum as compared to KCl and NaCl.

Degree of hydration of DNA and (or) RNA plays an important role in their conformational transitions. The solvation parameter (S_n) is responsible in deciding the "effective" density gradient and therefore, the relative molecular weights. Hydration number also varies with the nature and concentration of salts. High values of apparent hydration number are indicative of strong solute–solvent interactions. This is evident from the results obtained in the present study (Table 1). It is observed that in the case of the adenine–water system, the value of S_n decreases with dilution. Since the stacking interactions in the case of purine bases having flat aromatic rings, i.e., adenine are mainly hydrophobic in nature, it is maximum in concentrated solutions and decreases with dilution. This may also be due to water molecules forming a cage around $-N^+H_3$ of adenine. However, stacking interactions are not important. Similarly, when urea is added the polar interactions increase and there is a broad gamut of intermolecular interactions. However, maximum values of η are observed in adenine – 3 M urea, while these decrease in 6 M urea. It may be due to a higher degree of denaturation in more concentrated urea solutions. The molecules of urea, such that they correspond to those of the cages in the ice-like structure of water, arrange themselves in the aqueous urea environment so that >C=O groups are located in the structures existing in water, whereas the $-NH_2$ groups are enclosed in clathrates and are unable to interact with added solute molecules. Hence, in the systems, urea–water and adenine–urea–water, the concentration dependence of the apparent hydration number (S_n) also depends on the number of cages not occupied by the $-NH_2$ group of urea. Finally, these observations can be interpreted by the cosphere overlap model developed by Gurney (22).

Negative values of apparent molar compressibility (ϕ_K) in all systems studied are indicative of the loss of structural compressibility of the solvent molecules due to increased population of bonded water molecules in the aqueous urea. The ϕ_K values for adenine–water systems decreases with decrease in concentration. In aqueous urea this value increases for adenine in comparison to pure water. However, the highest value of ϕ_K are obtained in adenine – 1 M urea solution. These values increase on increasing concentration of salts, the highest values being obtained with $CaCl_2$. The sequence of increase is in the order $CaCl_2$ > KCl > NaCl.

The B coefficient of the Jones–Dole equation (Table 3) has positive values for all the systems indicating a strong alignment of the solvent molecules with solute. This B coefficient is known to be sensitive to the nature of solute–solvent interaction. Comparatively higher values of B coefficient are observed for the adenine–urea–$CaCl_2$ system as compared to adenine–urea–KCl, while, adenine–urea–NaCl values are still lower. Thus Ca^{2+} causes stronger interactions as compared to K^+ or Na^+.

A coefficient is positive for adenine in 6 M urea solution indicating the structure-breaking (denaturation) behaviour of urea (Table 3). The values of A coefficient for adenine–urea is negligibly small as compared to aqueous adenine. Although the values of A coefficient are positive in the presence of salts, there is no significant variation. This indicates that solute–solute interactions in these systems are unimportant.

The viscosity values (Table 1) show a regular trend in case of all systems, i.e., decrease with dilution whereas it shows a small upward trend with decrease in concentration of urea.

The "cut-off" point for increasing viscosity is 0.3 M concentration of the salts (Table 2). Evidently, the solute–solvent interaction increases beyond this concentration considerably and, therefore, the viscosity decreases due to denaturation. The system which become more viscous at the highest salt concentration contain NaCl or KCl. Systems having $CaCl_2$ always show a decrease in viscosity after a certain point. This can be explained due to the larger ionic size and higher charge on Ca^{2+} as compared to Na^+ and K^+. NaCl and KCl ionize to form two ions each while $CaCl_2$ produces three ions. Moreover, smaller ions have a better chance of electrostatic bonding than a larger ion. The strength of these ionic bonds also differ because of the size and number of orbitals in these atoms. In the present case it appears that the higher concentrations of ions enhance the denaturing capacity of urea, although in some cases it is not

© 2000 NRC Canada

quite apparent. Urea appears to act as denaturant even in very dilute solutions.

Internal pressure (P_i) is an important parameter for study of solute–solvent interaction of biomolecules. The higher values of P_i indicate strong solute–solvent interactions. Table 4 shows that P_i values for the adenine–water system are higher as compared to those in 1 M, 3 M, and 6 M urea solutions at 298.15 K. Values of P_i in 1 M urea solutions are higher as compared to those in 3 M and 6 M urea solutions. P_i values decrease with decrease in solute concentration. Apparently, the solute–solvent interactions are stronger for adenine in water than in urea solutions and among different concentration of urea solutions. Such interactions become stronger in 1 M urea and weak in 6 M urea solution.

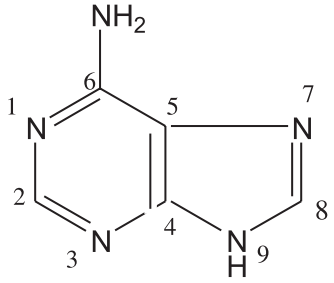
The values of internal pressure change significantly with a slight change in concentration of salts (Table 4). These values were found to decrease with an increase in concentration of NaCl, KCl, $CaCl_2$ in adenine–urea salt. A dissolving electrolyte is known to lower the compressibility of the solvent due to the influence of the electrostatic field of the ions on the surrounding solvent molecules and thus the total P_i of the solution increases. Contrary to this in the present study the internal pressure decreases with increase in concentration of salt. This anomalous behaviour can be accounted for, due to several reasons viz.: (*i*) the denaturing effect of urea on adenine, bringing about abnormal changes in both the molecules. The presence of salts further affects this denaturation; (*ii*) different neutral salts may have striking effects on the stacking interactions of adenine; (*iii*) the hydrogen bonding between urea and adenine are affected by salts; (*iv*) cohesive forces may be loosened; and (*v*) the upsurge in various types of interactions may take place in the system.

Specific acoustic impedance (Table 2) is another parameter used during the present study for revealing the nature of interactions in the medium. The *Z* value has a greater significance as a characteristic property of the medium than either density (ρ), ultrasonic velocity (*U*), individually. Its value has been found to decrease with dilution in the case of adenine–water and adenine–water–urea systems, and with increasing concentration of salts. However, the changes are not very significant.

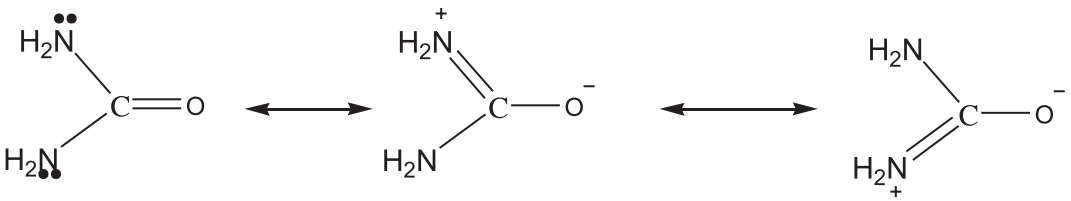
To confirm the findings of the solute–solvent interactions of nucleic acids components viz. adenine in water and urea–water systems by the use of various thermodynamic parameters presented, in this paper, the UV spectral studies were also carried out and measured values of absorbance (*A*) and calculated values of molar extinction coefficient (ε) were used as parameters. UV spectra of nucleic acids are sensitive to base stacking affects and hypochromicity (reduction in UV absorption) is specific for base composition and conformational transitions. UV spectra are effected by any modification in the purine and (or) pyrimidine base, e.g., protonations and (or) deprotonations or hydrogen bonding or any change in electronic state of the π electrons.

As shown in Table 5, the absorbance value (*A*) of adenine shows considerable variation with concentration, the trend being a decrease in *A* values with decrease in concentration of the solution which is in accordance with Lambert–Beer law, ε value being specific for π electron system are fairly constant for a particular set. In 1 M, 3 M, and 6 M urea solution, the ε values for adenine indicate a regular decrease with increase in urea concentration indicating strong interactions of adenine with urea.

Adenine (**1**) is planar, aromatic, and has strong π–π* transitions. The exocyclic amino group can act as a weak acid and therefore as a donor for the hydrogen bond. The N1, N3, and N7 positions of adenine can act as proton acceptors. Urea is a resonance hybrid having the following canonical forms (**2**):



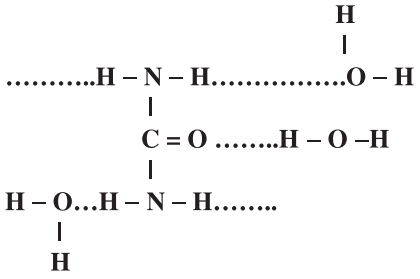
1



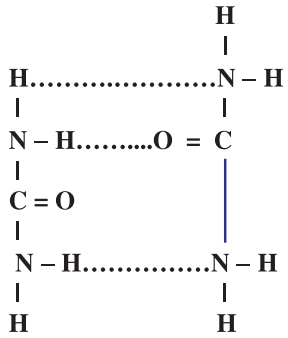
2

© 2000 NRC Canada

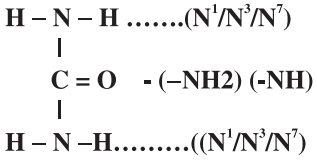
It can therefore act as both a proton acceptor and a proton donor. The possibilities of hydrogen bond formation between urea–water (**2**a), urea–urea (**2**b), and urea–adenine (**2**c) are shown below



2a



2b



2c

The equilibrium constant for self-association of two urea molecules in water is very low, i.e., the association constant (M^{-1}) of the urea dimer is 0.04 and for the benzene dimer (van der Waals interaction) in water the $K_{benzene}$ (M^{-1}) value is 0.442.

In aqueous solution, adenine forms hydrogen bonds with water. When urea is added, complete loss of structure is observed due to hydrogen bonding between urea and water. Due to the very low concentration of adenine used, the interactions between these molecules are not so important. Interaction between urea and polar hydrophilic and (or) ionic sites of adenine through overlap of hydration cosphere lead to increased hydrogen bonding interactions. This increase in hydrogen bonding with increase in urea concentration as solvent is reflected in increased hypochromicity and, therefore, indicating stronger solute–solvent interactions. It can be seen from Table 5 that due to the increase in concentration of urea from 1 to 3 M there is a decrease in molar absorptivity of adenine by a factor of 49.49 mol cm^{-1} and for the increase in urea concentration from 3 to 6 M, there is a decrease in molar absorptivity of 40.63 mol cm^{-1}. It may be due to H-bonding at $-NH_2$ and >NH groups of adenine with urea and also due to the extended π electron cloud present in adenine, responsible for hydrophobic interaction.

Interesting observation has been made in the case of adenine–urea salt systems. The absorbance and molar absorptivity values fall initially with increasing concentration of NaCl and KCl salts in the case of adenine but after a certain limit start rising, while with $CaCl_2$ these values regularly fall and there is no cut-off point. A decrease in *A* and ε values is an indication of stronger interaction. It is evident that interaction increases with an increase in concentration of NaCl, KCl until a saturation point is reached after which it starts decreasing. This optimum concentration of salt is about 0.35–0.4 mol λ^{-1} for equimolar solution of adenine (10^{-4} M) and urea (10^{-4}M). In case of $CaCl_2$, the values regularly decrease indicating a comparatively stronger interaction. The cut-off point can be explained due to the fact that as the salt concentration goes on increasing, higher numbers of Na^+, K^+, and Ca^{2+} ions are released in the system which counteract with the charges already present. In case of Ca^{2+} there are two counter ions for each cation. Another reason may be that the cations help in binding the extended π electron systems in adenine and more availability of cations helps in increasing π–π interaction. However, beyond a certain extent the interaction decreases because of the limited interaction sites.

Hypochromicity values (Table 5) also show a similar trend as *A* and ε, i.e., increase up to a certain concentration of NaCl, KCl and thereafter decrease, while in the case of $CaCl_2$ these values continuously increase with increasing concentration of salt. Since, increase in *h* values indicates a more extended chromophore. This can be explained by stronger interactions between π–π electrons of the adenine base. The cations increase these interactions by getting sandwiched in between the electron clouds.

Oscillator strength (Table 5) depends upon the ε values and decides whether the transitions are allowed or forbidden. The values either decrease or first increase and then decrease with the increase in concentration of salt. This trend indicates that the interaction goes on increasing, or initially increases and then decreases as the concentration of salts is increased.

Conclusion

All the thermodynamic and spectroscopic parameters used under the present study for the interpretation of interactions of adenine in water, aqueous urea, and in the presence of salts i.e., NaCl, KCl, and $CaCl_2$ leads to parallel conclusions. The trend is the same in all cases. The interaction of urea with adenine is dependent on the concentration of urea and presence of salts.

In adenine there are hydrophobic (delocalized π electrons) as well as hydrogen bond donor ($-NH_2$/-NH) and (or) acceptor (N1, N3, N7) sites (**2**c) responsible for base pairing with complementary bases, i.e., thymine in DNA and uracil in RNA. The hydration cospheres around adenine molecules having both hydrophobic and hydrophilic sites in the adenine–water system result in a transitory and rather imperfect

© 2000 NRC Canada

hydrogen-bonded network of water. The hydrophobicity of adenine being responsible for the π–π stacking interactions, which are effected by the presence of metal ions, being strongest in presence of Ca^{2+} ions. However, the hydrophilic sites on adenine result in an increase in entropy of the system by disrupting the hydrogen-bonded network. The highly polar urea molecule can interact with polar and (or) hydrophilic sites on adenine (especially -NH_2 / -NH) and also with the hydrophobic sites, although the former are much more important than the latter. The stacking π–π interactions due to hydrophobicity of the purine base are more evident by the study of absorption spectroscopy. The measured absorbance values of ε, *h*, and *f* indicate a strong π–π stacking interaction which is strong in the presence of cations like, Na^+, K^+, and Ca^{2+} up to a certain optimum concentration of salts after which it falls.

The self-association in urea and adenine resulting in the corresponding dimers is more important in relatively concentrated solutions. In more dilute solutions salts play an important role and the role of water becomes crucial. Urea acts as a denaturant in concentrated solutions since it disrupts intermolecular hydrogen bonds between adenine and water and itself interacts at the hydrophobic and (or) hydrophilic polar and ionic sites of the adenine moiety.

Acknowledgement

Financial assistance from CSIR, New Delhi (KKD) is gratefully acknowledged.

References

1. J.D. Pandey, K. Misra, A. Shukla, V. Mushran, and R.D. Rai. Thermochim. Acta, **17**, 245 (1987).
2. K. Misra, A. Mishra, R.D. Rai, and S. Srivastava. Acoust. Lett. **2**, 173 (1988).
3. H. Edilhoch and J.C. Osporne, Jr. Adv. Protein Chem. **30**, 183 (1976).
4. P. Hemmes, E.I. Dudchenlso, A.P. Sarvazyan, and V.A. Buchin. J. Phys. Chem. **84**, 696 (1980).
5. J.C. Ahluwalia and N. Kishore. J. Chem. Soc. Faraday Trans. **86**, 905 (1990).
6. J.C. Ahluwalia and N. Kishore. J. Solution Chem. **19**, 51 (1990).
7. J. Texter. Proc. Biophys. Mol. Biol. **33**, 83 (1978).
8. J.E. Hanst and J. Vinogod. Proc. Natl. Acad. Sci. U.S.A. **47**, 825 (1961).
9. M. Flak, K.A. Hartman, and R.C. Locop. J. Am. Chem. Soc. **82**, 921 (1963).
10. J.D. Pandey, A.K. Puri, and K. Misra. Thermochim. Acta, **74**, 313 (1984).
11. J.D. Pandey, K. Misra, and V. Mushran. Acustica, **81**, 97 (1994).
12. J.D. Pandey, A.K. Puri, A.K. Shukla, and S. Haroon. Indian J. Chem. Sect. A: Inorg. Bio-inorg. Phys. Theor. Anal. **36A**, 560 (1997).
13. J.D. Pandey, A. Misra, N. Hasan, and K. Misra. Acoust. Lett. **15**, 105 (1991).
14. S. Magazir, P. Magliardo, A.M. Musclino, and M.T. Sciortino. J. Phys. Chem. **101**, 2348 (1997).
15. J.M. Leal, C. Herrera, and B. Garcila. J. Chem. Eng. Data, **36**, 269 (1991).
16. J.D. Pandey, P. Jain, and V. Vyas. Can. J. Chem. **72**, 2486 (1994).
17. J.D. Pandey, K. Misra, A. Shukla, and R.D. Rai. Can. J. Chem. **65**, 303 (1987); J. Chem. Eng. Data, **34**, 29 (1989); X.X. Vishnu, R. Wadhwani, Y. Akhtar, and J.D. Pandey. Proc. Indian Acad. Sci. Chem Sci. **109** (**5**), 353 (1997); J.D. Pandey, K. Misra, A. Shukla, V. Mushran, and D. Rai. Thermochim. Acta, **117**, 245 (1987); V. Dhari and R. Wadhwani. Acustica, **84**, 976, (1998).
18. J.C. Ahluwalia and A.K. Mishra. Intl. J. Pept. Protein Res. **21**, 322 (1983).
19. J.C. Ahluwalia, B.S. Lark, I.S. Ranipal, and P.K. Ranipal. J. Chem. Soc. Faraday Trans. **93**, 81 (1997).
20. J.E. Desnoyers, G. Perron, and C. Visser. J. Chem. Soc. **99**, 5854 (1977).
21. D.M. Crothers and D. Ratner. Biochemistry, **7**, 1823 (1968).
22. R.W. Gurney. Ionic processes in solutions. McGraw Hill, New York. 1950.

© 2000 NRC Canada

Syntheses and electrochemical characterization of heteroleptic cyclopentadienyl–bis(dithiolene) complexes of niobium and tantalum

I.V. Jourdain and F. Guyon

Abstract: Diamagnetic niobium and tantalum complexes of general formula [M(η^5-C_5Me_5)(dithiolene)$_2$] have been prepared (M = Nb, dithiolene = dddt^{2-} (5,6-dihydro-1,4dithiine-2,3-dithiolate) (**1**); M = Ta, dithiolene = dddt^{2-} (**2**); M = Nb, dithiolene = dddt^{2-} and dmit^{2-} (1,3-dithiole-2-thione-4,5-dithiolate) (**3**)). All these complexes exhibit temperature-dependent ^{1}H NMR spectra which result from a fluxional behavior of the dithiolene ligands. Their redox properties have been investigated by cyclic voltammetry and reversible oxidation processes involving the dithiolene ligands have been evidenced for the complexes **1** and **2**.

Key words: niobium, tantalum, dithiolene, voltammetry cyclic, variable-temperature ^{1}H NMR.

Résumé : On a préparé des complexes diamagnétiques du niobium et du tantale de formule générale [M(η^5-C_5Me_5)(dithiolène)$_2$] [M = Nb, dithiolène = dddt^{2-} (5,6-dihydro-1,4-dithiine-2,3-dithiolate) (**1**); M = Ta, dithiolène = dddt^{2-} (**2**); M = Nb, dithiolène = dddt^{2-} et dmit^{2-}(1,3-dithiole-2-thione-4,6-dithiolate) (**3**)]. Les spectres RMN ^{1}H de chacun de ces complexes varient avec la température en raison d'un comportement dynamique des ligands dithiolènes. Les propriétés redox ont été par voltampérométrie cyclique et, pour chacun des complexes **1** et **2**, a été mis mettre en évidence un processus d'oxydation réversibles impliquant les ligands dithiolènes.

Mots clés : niobium, tantale, dithiolène, voltampérométrie cyclique, RMN ^{1}H à température variable.

[Traduit par la Rédaction]

Introduction

Coordination chemistry of sulfur-rich dithiolenes such as dmit^{2-} (1,3-dithiole-2-thione-4,5-dithiolate) or dddt^{2-} (5,6-dihydro-1,4dithiine-2,3-dithiolate) has attracted considerable interest in the past two decades (1) since the discovery of (TTF)[Ni(dmit)$_2$]$_2$ the first molecular superconductor containing a transition metal complex (2). For our part, we have been interested in the synthesis of heteroleptic complexes bearing both such dithiolene and cyclopentadienyl ligands with regards to the elaboration of novel conducting or magnetic materials. Our attention was mainly concentrated on complexes of general formula [M(cp)$_2$(dithiolene)] (cp = η-C_5H_5). We have shown that the radical cations [M(cp)$_2$(dithiolene)]$^{+}$ (M = Mo and W) organize in the solid-state into various supramolecular structures from quasi-regular chains to spin ladder with relatively strong antiferromagnetic interactions (3). However, in those paramagnetic species the spin density on the metal is far from negligible. This restricts the strength of the intermolecular interactions which result from dithiolene–dithiolene interactions via short S···S contacts. Thus we turned our effort to the synthesis of compounds in which the spin density is fully supported by the dithiolene ligand. For example, this property was expected in the oxidative form of the M(cp)$_2$(dithiolene) complexes of group 4 metals (d^0), but any oxidation process in these series ended up with the destruction of the molecules (4). So, the modification of these complexes by substituting cyclopentadienyl for electron-rich dithiolene seems a prerequisite to realize our goal. In that respect, the heteroleptic complexes M(cp)(dithiolene)$_2$ of group 5 metals (d^0) are particularly promising. Compounds of this class are very scarce in the literature, only two studies involving the synthesis of three complexes of vanadium (5) and tantalum (6) have been published. Note that their redox properties have not been investigated. Another consideration which led us to choose this family as precursors of molecular materials is the report by Fourmigué and Coulon (7) on an ordered three-dimensional antiferromagnetic ground state in the Mo(cp*)(dmit)$_2$ (cp* = η^5-C_5Me_5) complex.

Here, we describe the syntheses, characterization, and the electrochemical properties of M(cp*)(dddt)$_2$ (M = Nb and Ta) and Nb(cp*)(dmit)(dddt) complexes. The use of cp* instead of the unsubstituted cp ligands was settled to favor the formation of stable radical cation. Indeed the stabilizing effect of higher oxidation states by using cp* is well established (8).

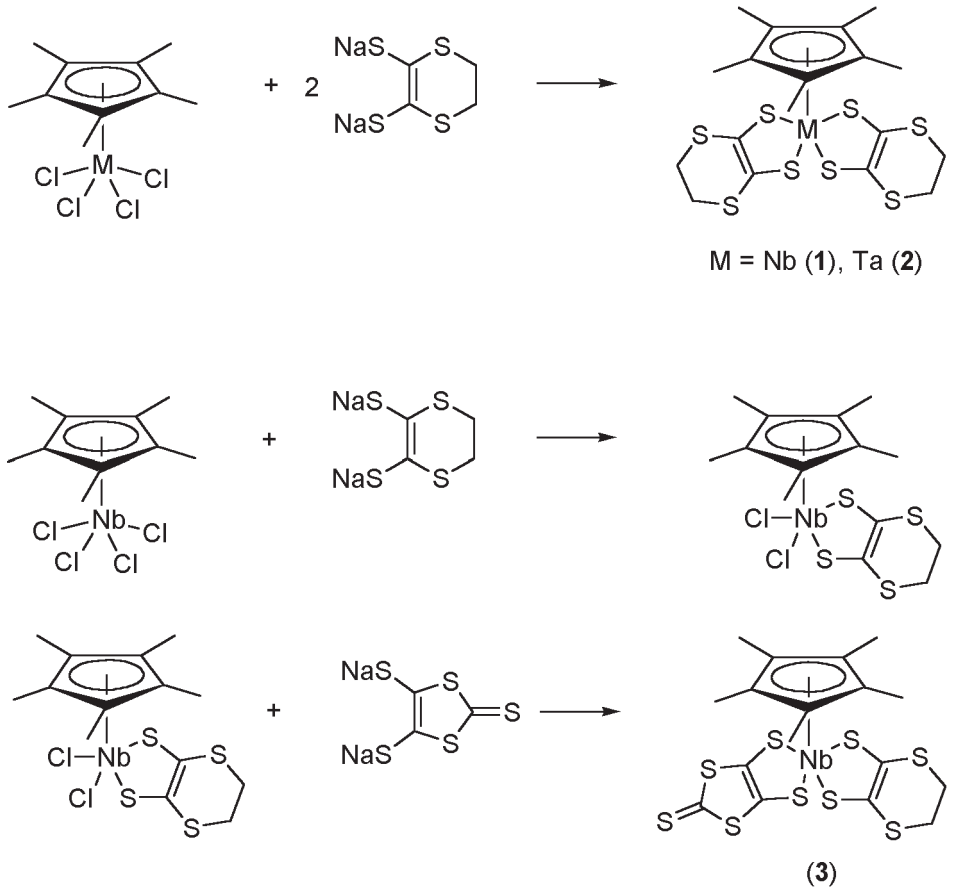
Received May 21, 2000. Published on the NRC Research Press website on November 21, 2000.

I.V. Jourdain and F. Guyon.[1] Laboratoire de Chimie des Matériaux et Interfaces, UFR des Sciences et Techniques, 25030 Besançon CEDEX, France.

[1]Author to whom correspondence may be addressed. Telephone: 03 81 66 62 68. Fax: 03 81 66 64 38. e-mail: fabrice.guyon@univ-fcomte.fr

© 2000 NRC Canada

Scheme 1.



Results and discussion

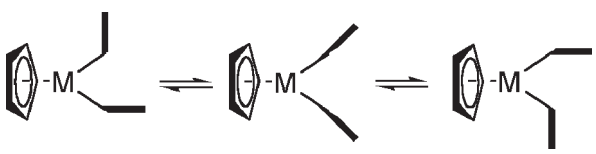
The synthesis of M(cp*)(dddt)$_2$ (M = Nb (**1**) and Ta (**2**)) was achieved by nucleophilic substitution of halides from the highly air sensitive precursors M(cp*)Cl$_4$ (M = Nb and Ta) by two equivalents of the dithiolene Na$_2$dddt. The reactivity of Ta(cp*)Cl$_4$ proved to be inferior to that of Nb(cp*)Cl$_4$ and the complex (**2**) was isolated in low yield (<10%). All our attempts to prepare the analogous M(cp*)(dmit)$_2$ remained unsuccessful. However we were able to isolate Nb(cp*)(dddt)(dmit) (**3**) by treating successively Nb(cp*)Cl$_4$ by one equivalent of Na$_2$dddt and one equivalent of Na$_2$dmit. To the best of our knowledge, this compound represents the first example of a mixed bis(dithiolene) in the class of heteroleptic cyclopentadienyl–dithiolene complexes. The formation of the intermediate Nb(cp*)(dddt)Cl$_2$ was evidenced by the ^{1}H NMR spectrum which shows two signals integrating four and 15 protons, respectively.

All the bis(dithiolene) complexes were identified by elemental analysis and ^{1}H NMR spectroscopy (Table 1). The IR spectra are poor of distinctive bands except the $\upsilon_{C=S}$ vibration in **3** at 1060 cm^{-1}. An interesting feature is the temperature-dependence of the ^{1}H NMR spectra (Fig. 1). At low temperature, two symmetric signals are observed for the protons of the dddt ligands which coalesce at higher temperatures. Such behaviour is consistent with a fluxional process of the ligands which has been already reported in Ta(cp*)(S$_2$C$_2$H$_2$)$_2$ by Nakamura and co-workers (6). These observations are in agreement with the *exo–endo* geometry observed in the isoelectronic [Ti(cp)(dithiolene)$_2$]$^-$ (4, 9). Indeed this geometry involves the presence of two conformers in equilibrium in which the dithiolene ligands are not equivalent. At high temperature, the interconversion between the two conformers is fast and the ^{1}H NMR spectra correspond to an averaged hypothetical C_{2v} conformer.

Table 1. ^{1}H NMR data in CDCl$_3$ (δ in ppm and T = 293 K).

Compound	C$_5$(C**H**$_3$)$_5$	SC**H**$_2$C**H**$_2$S
Nb(cp*)Cl$_4$	2.50 (s)	—
Nb(cp*)(dddt)Cl$_2$	2.39 (s)	3.73 (m)
Nb(cp*)(dddt)$_2$ (**1**)	2.13 (s)	3.30 (m)
Nb(cp*)(dddt)(dmit) (**3**)	2.18 (s)	3.50 (m)
Ta(cp*)Cl$_4$	2.73 (s)	—
Ta(cp*)(dddt)$_2$ (**2**)	2.30 (s)	3.37 (m)

Scheme 2.



This dynamic exchange occurs concomitantly with the fluxional process involving the ethylenic fragment of the

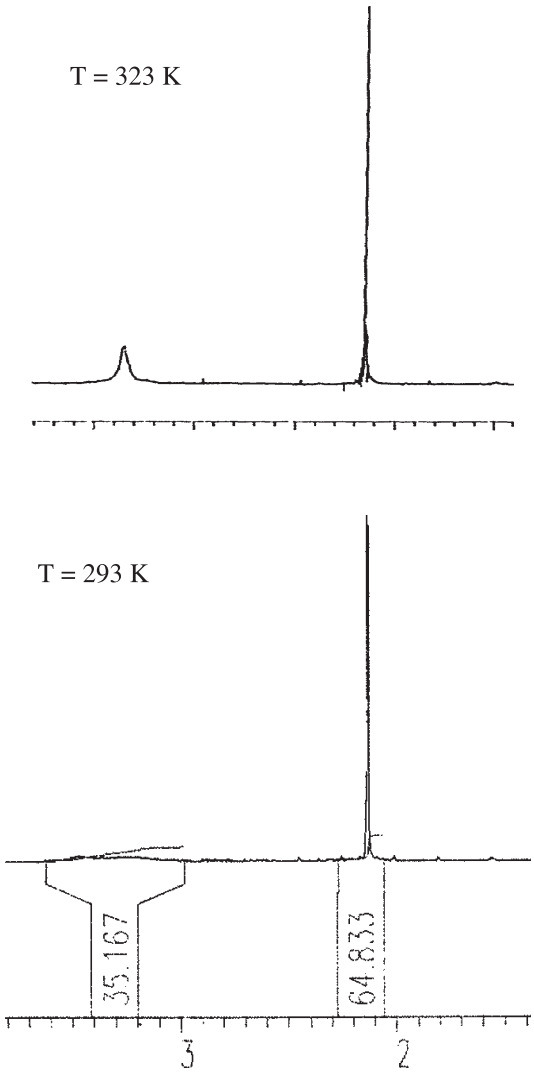
© 2000 NRC Canada

Table 2. Electrochemical data (E in V vs. Ag – 0.1 mol dm^{-3} $AgClO_4$).

Compound	$E_{1/2}$ (M^{IV}–M^{III})	$E_{1/2}$ (M^{V}–M^{IV})	$E_{1/2}$ ($[M]^{\cdot+}$/[M])
Nb(cp*)(dddt)$_2$ (**1**)	–1.92	–0.88	0.12
Ta(cp*)(dddt)$_2$ (**2**)	—	–0.96	0.15
Nb(cp*)(dddt)(dmit) (**3**)	–1.68	–0.70	0.40[a]

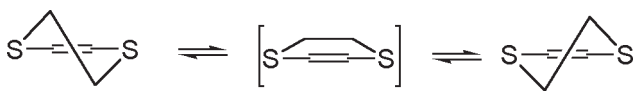
[a] $E_{p,a}$

Fig. 1. ^{1}H NMR spectrum of **1** in $CDCl_3$ at 293 and 323 K.



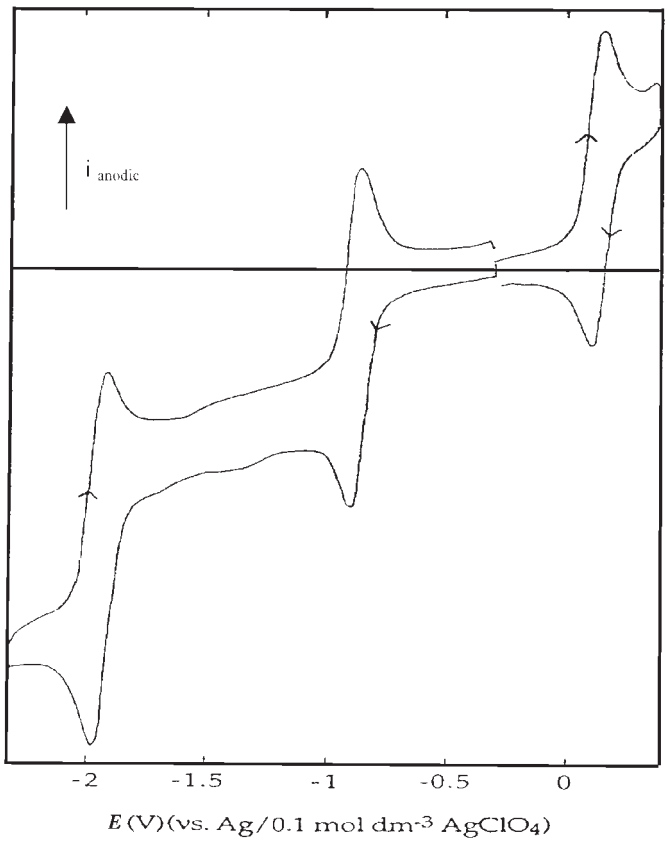
dddt ligand. Indeed the SCH_2CH_2S protons exhibit a AA′BB′ pattern at low temperature whereas they appear as a singlet at higher temperature.

Scheme 3.



Note that the *exo–endo* geometry has been rationalized with the aid of molecular orbital considerations and extended Hückel calculations in the case of Ta(cp*)$(S_2C_2H_2)_2$ and [Ti(cp)(dithiolene)$_2$]$^-$ complexes (4, 6).

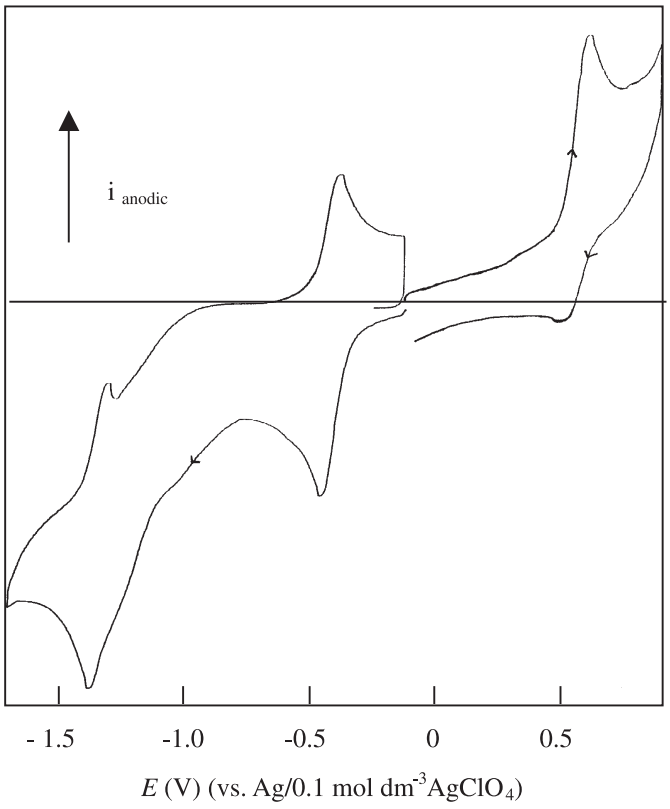
Fig. 2. Cyclic voltammogram of Nb(cp*)(dddt)$_2$ (**1**). Scan rate 100 mV s^{-1}.



Cyclic voltammetry experiments were performed in MeCN for complexes **1**–**3** to study their redox properties (Table 2). The cyclic voltamogramm of **1** and **3** are presented in Figs. 2 and 3. Each complex exhibits one reversible reduction wave corresponding to the formation of the d^1 species. The reduction occurs at lower potential in the case of the tantalum compound and is limited to one electronic process in the range investigated (–2 V/+1 V vs. Ag/Ag^+), whereas another reversible reduction process is observed in the case of niobium complexes. This second monoelectronic wave is attributed to the couple Nb^{IV}/Nb^{III}. The substitution of one dddt ligand by one dmit ligand induces a potential shift of about 0.2 V toward more anodic potentials of each electrochemical process involving the metal. This may be a consequence of the global electron impoverishment of the resulting complex. The electron-rich character of the dddt ligand appears also in the oxidative process which should derived from one electron oxidation of the dithiolene ligands. Indeed, for a scan rate of 100 mV/s, the ratio of peak currents $i_{p,a}/i_{p,c}$ are equal to 1 for the complexes **1** and **2** whereas this value is lower than 0.5 for compound **3**. The

© 2000 NRC Canada

Fig. 3. Cyclic voltammogram of Nb(cp*)(dddt)(dmit) (**3**). Scan rate 100 mV s^{-1}.



formation of a stable radical cation requires also complexes bearing two dddt ligands. Contrary to what is observed in reduction, the nature of the metal has no significant effect which confirms that the oxidation involves the dithiolene ligands.

Further studies will concern the isolation of the species $[Mcp^*(dddt)_2]^{+\cdot}$ (M= Nb or Ta) by using electrocrystallization technique. Interesting magnetic properties may be expected from these radicals in the solid-state since the spin density is assumed to be strongly localized on the dithiolene ligands.

Experimental

General data

All reactions were carried out under an atmosphere of dry argon using standard Schlenk techniques. Solvents were dried and distilled just prior to use under nitrogen. The compounds $M(\eta^5\text{-}C_5Me_5)Cl_4$ were prepared according to the literature method (M = Nb (10) and Ta (11)) and characterized by ^1H NMR spectroscopy. IR spectra were measured with a Bruker IFS45 WHR FTIR spectrophotometer on KBr pellets. NMR spectra were recorded in $CDCl_3$, with TMS as an internal standard, on a Bruker 200 MHz spectrometer. Elemental analysis were performed at the Service Central d'Analyse, CNRS, Vernaison, France.

Synthesis of $Nb(\eta^5\text{-}C_5Me_5)(dddt)_2$ (1)

A solution of $Nb(\eta^5\text{-}C_5Me_5)Cl_4$ (0.5 mmol) in dichloromethane (40 mL) is added to a suspension of Na_2dddt (8*b*) (1 mmol) in dichloromethane (10 mL) at 0°C. After allowing the mixture to warm to room temperature, it was stirred for 15 h, then filtered, and the filtrate was concentrated under vacuum. Chromatography (SiO_2, $CHCl_3$) afforded a purple crystalline solid, yield: 135 mg, 45%. IR (υ (KBr)/cm^{-1}): 2985, 2955 (C-H), 1450 (C=C). Anal. calcd: C 36.7, H 3.9, S 43.6; found: C 36.0, H 3.9, S 43.8%.

Synthesis of $Ta(\eta^5\text{-}C_5Me_5)(dddt)_2$ (2)

A solution of $Ta(\eta^5\text{-}C_5Me_5)Cl_4$ (0.5 mmol) in dichloromethane (40 mL) is added to a suspension of Na_2dddt (1 mmol) in dichloromethane (10 mL) at 0°C. The cooling bath was removed, allowing the mixture to warm to room temperature and stirring was continued for 15 h in refluxing dichloromethane. The green solution was then filtrered and the filtrate was concentrated under vacuum. Chromatography (SiO_2, $CHCl_3$) afforded a green solid, yield; 25 mg, 8%. IR (υ (KBr)/cm^{-1}): 2985, 2950 (C-H), 1450 (C=C). Anal. calcd: C 34.5, H 3.7, S 41.0; found: C 33.8, H 3.6, S 39.8%.

Synthesis of $Nb(\eta^5\text{-}C_5Me_5)(dddt)(dmit)$ (3)

A solution of $Nb(\eta^5\text{-}C_5Me_5)Cl_4$ (0.5 mmol) in dichloromethane (40 mL) is added to a suspension of Na_2dddt (0.5 mmol) in dichloromethane (10 mL) at 0°C. After allowing the mixture to warm to room temperature, it was stirred for 15 h, then filtered, and the filtrate was concentrated under vacuum. After washing with three portions of hexane (10 mL), the green solid obtained (m = 0.132 g) is reacted with Na_2dmit (12) (70 mg, 0.29 mmol) in refluxing dichloromethane (30 cm^3) during 15 h. After filtration, the brown-red solution is concentrated under vacuum. Chromatography (SiO_2, $CHCl_3$) afforded a yellow-brown solid, yield: 130 mg, 42%. IR (υ (KBr)/cm^{-1}): 2985, 2950w (C-H), 1450 (C=C), 1060 (C=S). Anal. calcd: C 34.9, H 3.4, S 46.6; found: C 34.7, H 3.4, S 44.3%.

Electrochemical measurements

Cyclic voltammetry experiments were performed with a radiometer PGP 201 potentiostat. The electrolyte consisted of 0.1 M $N^nBu_4PF_6$ solution in acetonitrile dried on molecular sieves. A three-compartment cell was used with a platinum working electrode (diameter 2 mm), a platinum counter electrode, and an Ag – 0.1 mol dm^{-3} $AgClO_4$ reference electrode. Experiments were performed under argon flow. After each measurement the reference electrode was checked against the ferrocene–ferricinium couple (+0.025 V).

References

1. (*a*) R.-M. Olk, B. Olk, W. Dietzsch, R. Kirmse, and E. Hoyer. Coord. Chem. Rev. **117**, 99 (1992); (*b*) A. E. Pullen and R.-M. Olk. Coord. Chem. Rev. **188**, 211 (1999); (*c*) M. Fourmigué. Coord. Chem. Rev. **178**–**180**, 823 (1998).
2. M. Bousseau, L. Valade, J.P. Legros, P. Cassoux, M. Garbauskas, and L.V. Interrante. J. Am. Chem. Soc. **108**, 1908 (1986).
3. (*a*) I.V. Jourdain, M. Fourmigué, F. Guyon, and J. Amaudrut. J. Chem. Soc. Dalton Trans. 483 (1998); (*b*) M. Fourmigué, B.

© 2000 NRC Canada

Domercq, I.V. Jourdain, P. Molinié, F. Guyon, and J. Amaudrut. Chem. Eur. J. **4**, 1714 (1998).
4. F. Guyon, C. Lenoir, M. Foumigué, J. Larsen, and J. Amaudrut. Bull. Soc. Chim. Fr. **131**, 217 (1994).
5. C.M. Bolinger, T.B. Rauchfuss, and A.L. Rheingold. Organometallics, **1**, 1551 (1982).
6. K. Tatsumi, J. Takeda, Y. Sekiguchi, M. Kohsada, and A. Nakamura. Angew. Chem. Int. Ed. Engl. **24**, 332 (1985).
7. M. Fourmigué and C. Coulon. Adv. Mater. (Weinheim, Ger.) **6**, 948 (1994).
8. (*a*) P. Gassman, D. Macomber, and J. Hershberger. Organometallics, **2**, 1470 (1983); (*b*) F. Guyon, M. Fourmigué, P. Audebert, and J. Amaudrut. Inorg. Chim. Acta, **239**, 117 (1995).
9. H. Köpf, K. Lange, and J. Pickardt. J. Organomet. Chem. **420**, 345 (1991).
10. T. Okamoto, H. Yasuda, A. Nakamura, Y. Kai, N. Kanehisa, and N. Kasai. J. Am. Chem. Soc. **110**, 5008 (1988).
11. T. Okamoto, H. Yasuda, A. Nakamura, Y. Kai, N. Kanehisa, and N. Kasai. Organometallics, **7**, 2266 (1988).
12. K.S. Varma, A. Bury, N.J. Harris, and A.E. Underhill. Synthesis, 837 (1987).

© 2000 NRC Canada

An approximate ab initio method based on the DIM model

John M. Cullen

Abstract: Using a second quantized formulation, an approximate diatomics in molecules (DIM) theory is presented in which all three- and four-centered electronic integrals are neglected. To ameliorate the effects of this approximation, the DIM one electron operator is constructed so that the true ab initio first-order density matrix and total energy are reproduced at the Hartree–Fock level. The resulting model was extensively tested for a variety of basis sets for its capability of capturing both the dynamic and nondynamic components of the electron correlation energy as well as the energies of excited electronic states. A modified method in which the DIM one-electron operator is formed from the initial extended Hückel guess of the Hartree–Fock orbitals was also found to produce excellent results.

Key words: DIM, electron correlation energy, excited states, semiempirical.

Résumé : Faisant appel à une deuxième formulation quantifiée, on propose une approximation de la théorie des molécules diatomiques (« DIM ») dans laquelle on néglige les intégrales électroniques à trois et à quatre centres. Afin d'améliorer les effets de cette approximation, on construit l'opérateur à un électron de la « DIM » de façon à ce que la vraie matrice de densité du premier ordre ainsi que l'énergie totale ab initio soient reproduites au niveau Hartree–Fock. On a vérifié le modèle qui en résulte de façon extensive pour une variété d'ensembles de base pour évaluer sa capacité de capturer les composantes dynamiques et non dynamiques de la corrélation d'énergie de l'électron ainsi que les énergies des états électroniques excités. On a aussi trouvé qu'il est possible d'obtenir d'excellents résultats à l'aide d'une méthode modifiée dans laquelle l'opérateur à un électron de la « DIM » est formé à partir d'évaluations initiales des orbitales de Hartree–Fock, faites sur la base de la théorie étendue de Hückel.

Mots clés : molécules diatomiques (« DIM »), énergie de corrélation des électrons, états excités, semi-empirique.

[Traduit par la Rédaction]

Introduction

Possibly one of the most underrated methods in quantum chemistry is the diatomics in molecules (DIM) approach originated by Ellison (1). This theory begins with the recognition that the two-body nature of the nonrelativistic molecular electronic Hamiltonian allows one to express the operator as a sum of diatomic and atomic terms (for reviews of DIM method see ref. 2). Unlike standard quantum chemical methods no electronic integral evaluations are performed. There is no hierarchy of procedures as found in molecular orbital methods to include electron correlation. Instead a Hamiltonian-like matrix is constructed from overlap integrals and eigenvalues of the isolated atomic and diatomic fragments. Diagonalization gives results which automatically include electron correlation. The calculation of excited electronic states becomes as easy to obtain as the ground state. The multireference nature of the DIM wave function also ensures accurate results for molecular geometries in which chemical bonds are being broken or formed.

Received June 1, 2000. Published on the NRC Research Press website on November 21, 2000.

J.M. Cullen.[1] Department of Chemistry, University of Manitoba, Winnipeg, MB R3T 2N2, Canada.

[1]Telephone: (204) 474-6441. Fax: (204) 474-7608. e-mail: cullen@cc.umanitoba.ca

Though the DIM formulation is exact for a complete set of electronic eigenstates of the constituent atoms and diatomics, for an incomplete set the results are nonvariational. In fact results of DIM calculations can be quite sensitive to the basis set used (see for example ref. 3). Unfortunately the size of the atomic and diatomic eigenstate basis needed for reliable results precludes most molecular applications. A notable exception has been the successful work done on argon gas clusters interacting with one or two open-shell atoms or ions (4). To curtail the large basis set requirement, recent work (5) has focused on incorporating electrostatic terms into the DIM Hamiltonian and using a second-order perturbation expansion to include the effects of less dominant terms in the polyatomic basis set.

In this paper we take a different tack expanding out in second quantized form the molecular electronic Hamiltonian by the method of increments (6) to obtain an approximate DIM model in which all three- and four-centered electronic integrals vanish. Using a modified one-electron operator which reproduces the exact Fock matrix, calculations were performed at the Moller–Plesset second-order perturbation (MP2), generalized valence bond (GVB), and configuration interaction of all single excitations (CIS) levels to test the accuracy of this model for predicting the dynamic electron correlation, nondynamic electron correlation, and electronically excited state energies respectively. A faster computational form of the DIM one-electron operator based on an initial extended Hückel guess of the Hartree–Fock molecular

© 2000 NRC Canada

orbitals was also tested and found to work surprisingly well. Before presenting theory and results we comment on the relationship of our model to the linearized class of quantum chemical methods.

Today groups such as those led by Scuseria (7, 8) and Head-Gordon (9) are recasting standard quantum chemical methods such as density functional theory and Hartree–Fock theory into procedures which computationally scale linearly with system size. For the most part this is being accomplished through the use of fast multipole moment expansions (10, 11) and exploiting the local nature of the first-order density matrix (12). For a double ζ basis set typically these linear algorithms do not become more effective over traditional ones until the problem size has exceeded 300 atomic orbitals (11). This is a result of the large prefactor for the integral generation and subsequent Fock matrix construction step. In comparison standard matrix diagonalization routines which are often used in these linear programs scale with the cube of the system size. Because these latter methods have relatively small prefactors, they do not become computational bottlenecks until the molecular size exceeds 3000 atomic orbitals (7).

To compare our approximate ab initio DIM approach to these theories we first examine the case of small molecules where linearized programs offer no advantage over the traditional methods. Using the ratio of the number of two electron integrals generated by both programs as a rough measure of the relative computational times we find at the 6-31G double ζ level, that for benzene (66 orbitals), the standard ab initio procedure already uses eleven times more two-electron integrals than our DIM method. By the time we have reached buckminsterfullerene (540 orbitals) this ratio has increased to 157:1. Though the number of two-electron integrals grows roughly quadratically with molecular size for both ab initio and our DIM model, the scaling is N^2 where N is the number of atomic orbitals in the ab initio case (7*b*), and m^2, where m is the number of atoms in the molecule in the DIM case. For very large molecules the methods used to linearize standard quantum chemical programs could also be applied to our DIM model.

Theory

The second quantized form of the molecular electronic Hamiltonian consisting of m atoms and n electrons is

$$[1a] \qquad H = \sum_{i,j}^{N} h_{ij}\, a_i^{+} a_j + \frac{1}{2} \sum_{i,j}^{N} \sum_{k,l}^{N} (ij|kl) a_i^{+} a_k^{+} a_l a_j$$

Here sums are over the orthonormal basis set of N atomic spin orbitals which span the entire molecule. The one- and two-electron matrix elements are defined by the usual expressions

$$[1b] \qquad h_{ij} = \langle \phi_i \left| -\frac{1}{2}\nabla^2 - \sum_{K}^{m} \frac{Z_K}{|R_k - r|} \right| \phi_j \rangle$$

$$[1c] \qquad (ij|kl) = \langle \phi_i(r_1)\, \phi_k(r_2) \left| \frac{1}{r_{12}} \right| \phi_j(r_1)\, \phi_l(r_2) \rangle$$

For an isolated atom "A" embedded within the molecule, the Hamiltonian is similarly given by

$$[2a] \qquad H_{\mathrm{A}}^{0} = \sum_{i,j \in \mathrm{A}}^{N} h_{ij}\, a_i^{+} a_j + \frac{1}{2} \sum_{i,j \in \mathrm{A}}^{N} \sum_{k,l \in \mathrm{A}}^{N} (ij|kl) a_i^{+} a_k^{+} a_l a_j$$

where now sums are over the subset of orbitals associated with atom A and these are only orthogonalized within this local subset. As a zero-order approximation the molecule can be considered as being composed of collection of the m isolated atoms. Then the resulting Hamiltonian of this system is then

$$[2b] \qquad H^{0} = \sum_{\mathrm{A}}^{m} H_{\mathrm{A}}^{0}$$

To improve upon this approximation we now consider the interaction of pairs of atoms within the molecule. The Hamiltonian of a diatomic fragment consisting of atoms A and "B" is

$$[3a] \qquad H_{\mathrm{AB}}^{1} = \sum_{i,j \in \mathrm{AB}}^{N} h_{ij}\, a_i^{+} a_j + \frac{1}{2} \sum_{i,j \in \mathrm{AB}}^{N} \sum_{k,l \in \mathrm{AB}}^{N} (ij|kl) a_i^{+} a_k^{+} a_l a_j$$

Again only those orbitals associated with the atoms A and B are included and orthogonalized to each other. To extract the diatomic interactions from the atomic ones we define

$$[3b] \qquad \Delta H_{\mathrm{AB}}^{1} = H_{\mathrm{AB}}^{1} - H_{\mathrm{A}}^{0} - H_{\mathrm{B}}^{0}$$

Included in $\Delta H_{\mathrm{AB}}^{1}$ are one-centered atomic terms which result from the reorthogonalization that occurs when the separate sets of atomic orbitals on atoms A and B are joined to form one orthonormal set. Therefore the approximate molecular Hamiltonian to first-order can be written as

$$[4a] \qquad H_1 = \sum_{\mathrm{A}}^{m} H_{\mathrm{A}}^{0} + \sum_{\mathrm{A>B}}^{m} \Delta H_{\mathrm{AB}}^{1}$$

Substituting eq. [3*b*] for $\Delta H_{\mathrm{AB}}^{1}$ yields

$$[4b] \qquad H_1 = \sum_{\mathrm{A}}^{m} H_{\mathrm{A}} + \sum_{\mathrm{A>B}}^{m} H_{\mathrm{AB}}^{1} - \frac{1}{2} \sum_{\mathrm{A} \neq \mathrm{B}}^{m} (H_{\mathrm{A}}^{0} + H_{\mathrm{B}}^{0}) = \sum_{\mathrm{A>B}}^{m} H_{\mathrm{AB}}^{1} - (m-2) \sum_{\mathrm{A}}^{m} H_{\mathrm{A}}^{0}$$

In comparison to this result the original DIM Hamiltonian (1) is given by

$$[5] \qquad H_{\mathrm{DIM}} = \sum_{\mathrm{A>B}}^{m} H_{\mathrm{AB}} - (m-2) \sum_{\mathrm{A}}^{m} H_{\mathrm{A}}$$

where H_{A} and H_{AB} are the usual Hamiltonians consisting of differential kinetic and classical potential energy terms for the isolated atom A and the isolated diatomic molecule composed of atoms A and B, respectively. Formally eq. [5] is exact and for a finite orthonormal atomic orbital basis the second quantized form will contain all three- and four-centered integrals. For a common set of atomic orbitals spanning the molecule, the calculation of fragment Hamiltonian matrix elements will not only involve basis

© 2000 NRC Canada

functions within the fragment but also basis functions or so-called ghost orbitals external to the fragment. Normally DIM methods ignore these latter orbitals and a variational calculation will not necessarily produce an upper bound to the exact energy. This omission however, can either be minimized by the use of extensive basis sets for the internal spaces of the respective atomic and diatomic fragments, or accounted for by explicit incorporation into the Hamiltonian of three-body empirical potentials (4, 5).

Equation [4*b*] which is developed from a perturbative-like expansion contains only one- and two- centered electronic integrals over an atomic orbital basis which is only approximately orthogonal. For diatomic molecules this model becomes exact. Our test calculations on polyatomics further show a cancellation of errors between those made from the neglect of three- and four-centered electronic integrals and the assumption of othogonality of the atomic orbital basis. These results however systematically overestimate chemical binding energies and produce optimized molecular geometries with chemical bond lengths predicted too short. Since the intended use of our model Hamiltonian is for applications where electron correlation plays a significant role, it can be improved with exact results obtained within the same calculation at the Hartree–Fock level. Therefore we reformulate the DIM one-electron operator to reproduce the exact Hartree–Fock energy as well as the exact Fock density within a symmetrically orthogonalized atomic orbital (OAO) basis set, i.e.,

$$[6a] \quad P^{\mathrm{OAO}}_{\mathrm{exact}} = P^{\mathrm{DIM}}$$

$$[6b] \quad E^{\mathrm{exact}}_{\mathrm{HF}} = E^{\mathrm{DIM}}_{\mathrm{HF}}$$

To satisfy eq. [6a] we set

$$[7a] \quad f^{\mathrm{DIM}} = f^{\mathrm{OAO}}_{\mathrm{exact}} + \sigma I$$

Here I, f^{DIM}, and $f^{\mathrm{OAO}}_{\mathrm{exact}}$ are the identity matrix, corresponding DIM and exact Fock operators, respectively. Expanding out eq. [7*a*] results in

$$[7b] \quad h^{\mathrm{DIM}} = h^{\mathrm{OAO}} + (g^{\mathrm{OAO}} - g^{\mathrm{DIM}}) + \sigma I$$

where matrices h^{OAO}, g^{OAO} and h^{DIM}, g^{DIM} are the two-electron contributions to the respective Fock operators. In the closed shell case over the atomic orbital basis, $\{\chi_m\}$, g takes the form

$$[7c] \quad g_{\mu\nu} = \sum_{\lambda\sigma}^{N} P_{\lambda\sigma}\left[(\mu\nu|\lambda\sigma) - \frac{1}{2}(\mu\sigma|\lambda\nu)\right]$$

In similar fashion expanding out eq. [6*b*] leads to

$$[8a] \quad \frac{1}{2} TrP^{\mathrm{OAO}}_{\mathrm{exact}}(2h^{\mathrm{OAO}} + g^{\mathrm{OAO}}) = \frac{1}{2} TrP^{\mathrm{DIM}}(2h^{\mathrm{DIM}} + g^{\mathrm{DIM}})$$

Substitution of eqs. [6*a*], [7*b*] produces

$$[8b] \quad \sigma = \frac{1}{2n} TrP^{\mathrm{OAO}}_{\mathrm{exact}}(g^{\mathrm{DIM}} - g^{\mathrm{OAO}})$$

where n is the number of electrons in the molecule. Another possibility is to directly use the ab initio Fock operator as our DIM one-electron operator in the molecular orbital basis, however for multireference electron correlation treatments of the ground and excited states we would need to make an intermediate transformation to the MO basis and ensure that our programs use the two-electron integrals in normal product form.

For open shell molecules we shall only consider high-spin cases in this initial paper. One can partition the Fock matrix into its α- and β-spin components. Over a canonical molecular orbital basis this yields

$$[9a] \quad f^{\alpha}_{ii} = h_{ii} + \sum_{j}^{N_\alpha}[(ii|jj) - (ij|ij)] + \sum_{j}^{N_\beta}(ii|jj)$$

$$[9b] \quad f^{\beta}_{ii} = h_{ii} + \sum_{j}^{N_\beta}[(ii|jj) - (ij|ij)] + \sum_{j}^{N_\alpha}(ii|jj)$$

where N_α and N_β are the number of occupied and -spin molecular orbitals with, $N_\alpha > N_\beta$. To have a spin independent one-electron DIM operator we define the Fock operator

$$[10a] \quad f_{ii} = h_{ii} + \sum_{j}^{N_\beta}[2(ii|jj) - (ij|ij)] + \sum_{j=N_\beta+1}^{N_\alpha}\left[(ii|jj) - \frac{1}{2}(ij|ij)\right]$$

Then

$$[10b] \quad f^{\alpha}_{ii} = f_{ii} - \frac{1}{2}\sum_{j=N_\beta+1}^{N_\alpha}(ii|jj)$$

$$[10c] \quad f^{\beta}_{ii} = f_{ii} + \frac{1}{2}\sum_{j=N_\beta+1}^{N_\alpha}(ii|jj)$$

Therefore this is equivalent to choosing an average Fock operator (i.e., $f = 1/2(f^{\alpha} + f^{\beta})$). Equations [8*b*] and [7*b*] then can be used in these high-spin cases with the density matrix generalized to

$$[10d] \quad P_{\mu\nu} = \sum_{j}^{N_\alpha} c^{\alpha}_{\mu j} c^{\alpha}_{\nu j} + \sum_{j}^{N_\beta} c^{\beta}_{\mu j} c^{\beta}_{\nu j}$$

Results and discussion

Moller–Plesset second-order (MP2) perturbation calculations were performed for a range of Pople-type basis sets (see for example ref. 13) over a variety of molecules to test the capability of our ab initio DIM model to capture the dynamic electron correlation energy, responsible for the London or van der Waals forces in a molecule. These results are compared with exact values in Table 1 where energies are reported in millihartrees (mH) and all molecular geometries set to their 6-31G(d) MP2 optimized values. Due to the two-body nature of our model Hamiltonian and the approximate nature of the orthonormal basis used, one might expect that errors should increase in cases where atoms are crowded in as found in cyclic molecules or when atomic orbitals from multiple centers overlap to a significant extent as in the case

© 2000 NRC Canada

Table 1. Comparison of MP2 energies for various basis sets.[a]

Molecule	Basis set	Exact MP2	DIM MP2	Error	Relative % error
Acetate	6-31G	–430.842	–431.932	–1.090	0.253
	6-31G(d)	–617.041	–620.521	–3.480	0.564
	6-31G(2d)	–679.369	–676.892	2.477	–0.365
	6-311G(d,p)	–696.048	–698.271	–2.222	0.319
	6-311G(d,p)++	–708.089	–713.401	–5.313	0.750
Acetic acid	6-31G	–429.222	–428.895	0.327	–0.076
	6-31G(d)	–612.209	–615.953	–3.744	0.612
	6-31G(2d)	–671.873	–669.621	2.252	–0.335
	6-311G(d,p)	–694.513	–696.399	–1.887	0.272
	6-311G(d,p)++	–699.889	–705.410	–5.521	0.789
B_2H_6	6-31G	–135.432	–140.319	–4.887	3.608
	6-31G(d)	–180.641	–185.293	–4.653	2.576
	6-31G(2d)	–189.956	–192.539	–2.583	1.360
	6-311G(d,p)	–230.623	–231.950	–1.326	0.575
	6-311G(d,p)++	–230.976	–233.809	–2.832	1.226
BF_3	6-31G	–417.869	–422.098	–4.228	1.012
	6-31G(d)	–584.838	–587.290	–2.452	0.419
	6-31G(2d)	–688.926	–693.563	–4.637	0.673
	6-311G(d,p)	–711.469	–713.841	–2.371	0.333
	6-311G(d,p)++	–717.968	–720.407	–2.439	0.340
BF_3NH_3	6-31G	–532.206	–534.997	–2.791	0.524
	6-31G(d)	–764.704	–768.769	–4.065	0.532
	6-31G(2d)	–885.549	–888.006	–2.457	0.277
	6-311G(d,p)	–917.683	–922.693	–5.010	0.546
	6-311G(d,p)++	–927.662	–934.505	–6.843	0.738
Borazine	6-31G	–466.044	–465.876	0.168	–0.036
	6-31G(d)	–705.370	–716.338	–10.968	1.555
	6-31G(2d)	–760.544	–763.464	–2.920	0.384
	6-311G(d,p)	–790.161	–801.353	–11.192	1.416
	6-311G(d,p)++	–793.343	–816.243	–22.901	2.887
Acetylene	6-31G	–185.069	–188.130	–3.061	1.654
	6-31G(d)	–251.396	–255.522	–4.126	1.641
	6-31G(2d)	–268.474	–269.091	–0.617	0.230
	6-311G(d,p)	–274.780	–275.930	–1.151	0.419
	6-311G(d,p)++	–275.052	–276.518	–1.466	0.533
Eclipsed ethane	6-31G	–187.543	–185.786	1.757	–0.937
	6-31G(d)	–265.977	–267.443	–1.466	0.551
	6-31G(2d)	–284.472	–283.871	0.601	–0.211
	6-311G(d,p)	–321.727	–322.127	–0.400	0.124
	6-311G(d,p)++	–322.322	–323.973	–1.652	0.512
Staggered ethane	6-31G	–188.037	–186.060	1.977	–1.051
	6-31G(d)	–266.222	–267.716	–1.494	0.561
	6-31G(2d)	–284.203	–284.009	0.194	–0.068
	6-311G(d,p)	–321.920	–322.224	–0.303	0.094
	6-311G(d,p)++	–322.369	–324.034	–1.665	0.517
Pyrrole	6-31G	–474.200	–472.284	1.917	–0.404
	6-31G(d)	–691.045	–697.491	–6.446	0.933
	6-31G(2d)	–738.284	–740.575	–2.290	0.310
	6-311G(d,p)	–762.919	–768.024	–5.105	0.669
	6-311G(d,p)++	–766.938	–768.024	–1.086	0.142
Benzene	6-31G	–516.139	–517.068	–0.929	0.180
	6-31G(d)	–755.910	–764.749	–8.838	1.169
	6-31G(2d)	–806.300	–809.103	–2.804	0.348
	6-311G(d,p)	–834.929	–842.396	–7.466	0.894
	6-311G(d,p)++	–837.558	–857.534	–19.976	2.385
CH_3CN	6-31G	–301.976	–306.451	–4.476	1.482
	6-31G(d)	–416.053	–420.390	–4.338	1.043

© 2000 NRC Canada

Table 1 (*continued*).

Molecule	Basis set	Exact MP2	DIM MP2	Error	Relative % error
	6-31G(2d)	–442.333	–442.066	0.267	–0.060
	6-311G(d,p)	–457.878	–460.848	–2.970	0.649
	6-311G(d,p)++	–459.398	–463.163	–3.766	0.820
CH_3NC	6-31G	–281.918	–283.230	–1.313	0.466
	6-31G(d)	–401.688	–404.398	–2.710	0.675
	6-31G(2d)	–428.012	–427.242	0.770	–0.180
	6-311G(d,p)	–444.130	–446.272	–2.142	0.482
	6-311G(d,p)++	–445.751	–450.418	–4.667	1.047
Methanol	6-31G	–215.950	–214.904	1.046	–0.485
	6-31G(d)	–312.019	–312.710	–0.691	0.221
	6-31G(2d)	–343.972	–341.535	2.437	–0.708
	6-311G(d,p)	–367.187	–366.979	0.208	–0.057
	6-311G(d,p)++	–371.206	–371.896	–0.690	0.186
cis-Butene	6-31G	–361.942	–359.512	2.430	–0.671
	6-31G(d)	–516.686	–520.506	–3.820	0.739
	6-31G(2d)	–551.416	–549.975	1.441	–0.261
	6-311G(d,p)	–598.607	–601.557	–2.950	0.493
	6-311G(d,p)++	–600.432	–609.797	–9.365	1.560
trans-Butene	6-31G	–361.987	–359.469	2.519	–0.696
	6-31G(d)	–516.551	–520.540	–3.989	0.772
	6-31G(2d)	–550.990	–549.754	1.236	–0.224
	6-311G(d,p)	–598.334	–601.057	–2.723	0.455
	6-311G(d,p)++	–599.870	–608.553	–8.683	1.447
Cyclopropane	6-31G	–270.531	–266.870	3.661	–1.353
	6-31G(d)	–390.106	–391.877	–1.771	0.454
	6-31G(2d)	–414.702	–415.075	–0.373	0.090
	6-311G(d,p)	–452.552	–453.063	–0.511	0.113
	6-311G(d,p)++	–453.997	–457.837	–3.840	0.846
Ethylene oxide	6-31G	–304.915	–303.296	1.619	–0.531
	6-31G(d)	–438.367	–440.267	–1.900	0.433
	6-31G(2d)	–474.987	–474.405	0.582	–0.122
	6-311G(d,p)	–499.029	–499.715	–0.686	0.137
	6-311G(d,p)++	–502.908	–506.076	–3.168	0.630
F_2O_2	6-31G	–543.702	–542.802	0.900	–0.166
	6-31G(d)	–749.191	–748.645	0.546	–0.073
	6-31G(2d)	–854.510	–853.630	0.879	–0.103
	6-311G(d,p)	–869.028	–869.157	–0.129	0.015
	6-311G(d,p)++	–877.427	–878.898	–1.471	0.168
Furan	6-31G	–472.832	–474.331	–1.499	0.317
	6-31G(d)	–688.228	–695.553	–7.326	1.064
	6-31G(2d)	–741.571	–743.490	–1.919	0.259
	6-311G(d,p)	–760.666	–764.804	–4.138	0.544
	6-311G(d,p)++	–764.030	–775.614	–11.584	1.516
Hydrogen peroxide	6-31G	–256.969	–255.767	1.203	–0.468
	6-31G(d)	–370.086	–369.819	0.266	–0.072
	6-31G(2d)	–415.539	–413.432	2.107	–0.507
	6-311G(d,p)	–425.424	–424.526	0.898	–0.211
	6-311G(d,p)++	–431.261	–431.027	0.234	–0.054
Hexatriene	6-31G	–527.495	–527.428	0.068	–0.013
	6-31G(d)	–757.076	–764.828	–7.753	1.024
	6-31G(2d)	–808.748	–808.214	0.534	–0.066
	6-311G(d,p)	–848.859	–853.773	–4.914	0.579
	6-311G(d,p)++	–851.634	–866.642	–15.008	1.762
N_2H_2	6-31G	–230.194	–230.151	0.043	–0.019
	6-31G(d)	–325.453	–326.452	–0.999	0.307
	6-31G(2d)	–347.811	–347.329	0.482	–0.139
	6-311G(d,p)	–359.765	–360.171	–0.407	0.113
	6-311G(d,p)++	–362.508	–363.328	–0.820	0.226

© 2000 NRC Canada

Table 1 (*concluded*).

Molecule	Basis set	Exact MP2	DIM MP2	Error	Relative % error
Ammonia	6-31G	–116.268	–115.160	1.108	–0.953
	6-31G(d)	–170.390	–170.229	0.161	–0.094
	6-31G(2d)	–186.243	–185.381	0.861	–0.463
	6-311G(d,p)	–201.124	–200.548	0.576	–0.286
	6-311G(d,p)++	–203.580	–203.214	0.367	–0.180
Propene	6-31G	–270.545	–269.869	0.677	–0.250
	6-31G(d)	–384.951	–388.588	–3.636	0.945
	6-31G(2d)	–411.186	–410.689	0.498	–0.121
	6-311G(d,p)	–445.425	–447.157	–1.732	0.389
	6-311G(d,p)++	–446.519	–451.298	–4.779	1.070
Pyridine	6-31G	–539.260	–540.117	–0.858	0.159
	6-31G(d)	–789.095	–798.849	–9.754	1.236
	6-31G(2d)	–840.218	–842.995	–2.777	0.331
	6-311G(d,p)	–863.866	–871.488	–7.622	0.882
	6-311G(d,p)++	–867.920	–886.664	–18.744	2.160
Trioxane	6-31G	–622.343	–619.467	2.876	–0.462
	6-31G(d)	–913.448	–919.658	–6.211	0.680
	6-31G(2d)	–1003.031	–994.734	8.297	–0.827
	6-311G(d,p)	–1035.312	–1040.745	–5.433	0.525
	6-311G(d,p)++	–1045.451	–1066.413	–20.962	2.005

[a]All energies are in millihartrees relative to the Hartree–Fock value for each given basis set.

of basis sets having diffuse functions. Comparing the linear vs. cyclic types of molecules in Table 1 shows that with the exception of the 6-311G(d,p)++ results in cases such as benzene, borazine, pyrimidine, and trioxane, there really is no significant increase in error. The root mean square (RMS) errors made by the DIM method to the exact results for the 6-31G, 6-31G(d), 6-31G(2d), 6-311G(d,p) basis sets are 2.3, 5.0, 2.5, 4.0 mH, respectively, while the RMS error for the 6-311G(d,p)++ basis is 9.7 mH. The last basis with its diffuse orbitals appears problematic for our model. In comparison, the RMS relative errors are 1.0, 0.96, 0.45, 0.54,and 1.3% for the corresponding basis sets ranging from 6-31G to 6-311G(d,p)++. These results are similar to those found by the resolution of the identity methods for computing MP2 energies when they were first introduced (14, 15). It may be possible to "tune" the basis to minimize these errors, the 6-31G(2d) results when compared to the 6-31G(d) values demonstrate this possibility.

We can also extract from Table 1 electron correlation contributions to conformational energy differences as well as to chemical reaction enthalpies.[2] Focusing on results at the 6-311G(d,p) level and using the notation ΔE^{exact} (ΔE^{DIM}) we find that the MP2 electron correlation energy favors staggered ethane by 0.5 (0.3) kJ mol^{-1} over the eclipsed conformer. Similarly *cis*-2-butene is favored by 0.7 (1.3) kJ mol^{-1} over *trans*-2-butene. For the isomerization of propene into cyclopropane and acetonitrile into methylisocyanide there is, respectively, a 18.7 (15.5) kJ mol^{-1} contribution in favor of cyclopropane and 36.1 (38.3) kJ mol^{-1} for acetonitrile. The formation of the Lewis adduct trifluoroboronamine over the reactants ammonia and trifluoroboron is also favored by an electron correlation contribution of 13.4 (21.8) kJ mol^{-1}. Finally the gas phase energy difference between acetate, H^+, and acetic acid, known as the absolute acidity (see for example ref. 13), has an MP2 contribution of 4.0 (4.9) kJ mol^{-1} at the 6-311G(d,p) level and for the more anion appropriate 6-311G(d,p)++ basis, 21.5 (21.0) kJ mol^{-1}. These cases demonstrate that errors in the DIM computed dynamic electron correlation energy are generally small, much smaller than the basis set incompletion errors occurring at the 6-311G(d,p) level. Similar results were also found at the coupled cluster singles, doubles level of theory.

In contrast to the dynamic electron correlation energy, the nondynamic electron correlation energy arises from constraining spin paired orbitals in the restricted Hartree–Fock (RHF) wave function to have the same spatial function. As a chemical bond is stretched or twisted this constraint causes the Hartree–Fock energy to rise more rapidly than the true energy. The remedy is to replace the single Slater determinant representation of the RHF wave function with a multideterminant spin adapted one. The generalized valence bond (GVB) approach accomplishes this in a computationally simple and quick way (16, 17). In Table 2, GVB as well as RHF results are presented for ethylene in which first the π bond is broken as one CH_2 group is twisted perpendicular to the other and then both carbon–carbon π and σ bonds are simultaneously stretched to twice their equilibrium distance. Agreement between the exact GVB energies and those generated by the DIM Hamiltonian with the one-electron operator constructed at the Hartree–Fock level is within a millihartree.

To complete the examination of our DIM model to post Hartree–Fock treatments, vertical excitation energies computed at the configuration interaction singles (CIS) level of theory are presented in Table 3. The 6-31G and 6-31G+ basis sets are identical to those employed by Foresman et al.

[2]For comparison later to experiment we report ethalpies in kJ mol^{-1} where 1 mH = 2.626 kJ mol^{-1}. Typically quantum calculations strive for an accuracy with experiment of a kcal mol^{-1} which corresponds to 4.184 kJ mol^{-1}.

© 2000 NRC Canada

Table 2. Bond breaking in ethylene at the 6-311G(d,p) level.[a]

	Exact results		DIM results		HDIM results[b]	
	RHF	GVB	RHF	GVB	RHF	GVB
Equilibrium geometry	–78.054043	–78.152048	–78.054043	–78.151990	–78.054583	–78.152267
p bond twisted 30 deg	20.03	18.38	20.03	18.37	20.02	18.36
p bond twisted 60 deg	79.33	70.81	79.33	70.79	79.34	70.79
p bond twisted 90 deg	204.68	123.41	204.68	124.38	204.34	125.14
C—C bond stretched 1.5 × R_0	223.21	153.73	223.21	153.98	223.19	154.33
C—C bond stretched 2.0 × R_0	424.70	257.78	424.70	258.35	424.42	259.09

[a]Energies are in atomic units for the equilibrium geometry and in millihartrees relative to this reference for all other molecular geometries.
[b]The HDIM method uses a density matrix generated from the initial extended Hückel guess to construct the DIM one-electron operator.

(18), however our molecular geometries for formaldehyde and ethylene differ slightly since we use 6-31G(d) MP2 optimized coordinates. In the case of formaldehyde these differences are for the CO bond: 0.0089 Å; CH bond: 0.0003 Å; and CHO angle: 0.24°. Examining the sensitivity of the vertical excitation energies to these molecular geometry variations at the 6-31G+ level shows that the Foresman results are 0.04 eV higher for the valence state $^1A_2$ n-π* transition and 0.08 eV lower for the Rydberg $^1B_2$ n-3s transition. Examining our exact results with the DIM computed values for the same transitions and basis set yields excitation energies which are 0.03 eV higher for the $^1A_2$ n-π* case and 0.09 eV lower in the $^1B_2$ n-3s transition. Therefore these errors are comparable to the errors made from the uncertainties in the molecular geometry. Overall, inspection of Table 3 reveals good agreement between the DIM and exact computed values. However when excited states lie close to one another as for example, in the case of $^1B_1$ π-3s, $^1B_2$ π-3p Rydberg transitions in pyrrole (for the calculated value see ref. 29), reversals in the ordering of the states can occur.

In place of the converged Fock–Dirac density matrix used to generate the one-electron operator in our DIM model Hamiltonian, the initial guess density matrix generated from an extended Hückel calculation was also used. The results with this modified DIM Hamiltonian, which we denote as HDIM are displayed in Table 4. Compared to the exact energies computed with the same basis set the agreement at the Hartree–Fock level is surprisingly good with RMS errors of 2.8, 2.0, and 2.4 mH for the corresponding 6-31G, 6-311G(d,p), and 6-311G(d,p)++ basis sets. This good agreement also holds when bonds are stretched or twisted as seen in the ethylene case of Table 2, where the HDIM RHF energies lie within 0.3 mH of the exact RHF values. The corresponding errors at the GVB level are 1.5 mH or less showing the capability of the HDIM model to capture accurately the nondynamic electron correlation energy. In comparison, the computed MP2 dynamic electron correlation results have, with the exception of the 6-31G basis, errors slightly larger than seen in our original DIM model but still quite acceptable when compared to the basis set incompletion errors that occur at these levels. In Table 4 we find RMS errors for the respective 6-31G, 6-311G(d,p), and 6-311G(d,p)++ basis sets of 4.8, 4.3, and 10.5 mH.

Using the notation ΔE^{exact} (ΔE^{HDIM}) we compare the total 6-311G(d,p) conformational energy differences as well as reaction enthalpies to experiment. Because zero-point energies are not taken into account and 6-31G(d) MP2 optimized molecular geometries are used, one can only hope for semi-quantitative accuracy. In the case of staggered vs. eclipsed ethane, the RHF energy difference is 12.9 (13.1) kJ mol^{-1} while the contribution from MP2 electron correlation is 0.5 (0.3) kJ mol^{-1}. Both exact and HDIM calculations yield an identical 13.4 kJ mol^{-1} energy gap compared to the experimental

Table 3. Comparison of vertical excitation energies computed at the CIS level.[a]

Transition	6-31G Basis set		6-31G+ Basis set		Experiment
	Exact	DIM	Exact	DIM	
Formaldehyde					
$^1A_2$ n-p*	4.229	4.269	4.188	4.219	4.10[b]
$^1B_2$ n-3s	11.816	10.629	9.000	8.912	7.13[c]
$^1B_2$ n-3s	13.000	13.474	9.635	9.648	7.98[c]
$^1A_1$ n-3p	14.489	13.703	10.125	10.089	8.14[b]
Ethylene					
$^1B_{1u}$ π-π*	8.671	8.655	7.893	7.895	7.66[d]
$^1B_{3u}$ π-3s	10.191	10.076	7.770	7.773	7.15[d]
$^1B_{1g}$ π-3p	10.350	10.041	8.204	8.219	7.83[e]
$^1B_{2g}$ π-3p	11.629	11.098	8.316	8.325	8.00[f]
Benzene					
$^1B_{2u}$ π-π*	6.416	6.396	6.230	6.093	4.72[g]
$^1B_{1u}$ π-π*	6.629	6.692	6.404	6.260	6.07[g]
$^1E_{1u}$ π-π*	8.635	8.364	7.210	7.178	6.93[g]
Pyridine					
$^1B_1$ n-π*	5.963	5.864	5.904	5.800	4.59[h]
$^1B_2$ π-π*	6.512	6.481	6.350	6.211	4.99[i]
$^1A_2$ n-π*	7.474	7.398	7.374	7.253	5.43[j]
$^1A_1$ π-π*	6.854	6.901	6.663	7.178	6.93[i]
Pyrrole					
$^1A_2$ π-3 s	6.664	6.346	6.176	6.037	5.22[k]
$^1B_1$ π-3s	7.023	6.915	6.430	6.385	5.70[l]
$^1B_2$ π-3p	8.156	8.009	6.447	6.364	5.86[m]

[a]Energies are in eV.
[b]Ref. 19.
[c]Ref. 20.
[d]Ref. 21.
[e]Ref. 22.
[f]Ref. 23.
[g]Ref. 24.
[h]Ref. 25.
[i]Ref. 26.
[j]Ref. 27.
[k]Ref. 28.
[l]Ref. 29.
[m]Ref. 30.

© 2000 NRC Canada

Table 4. Comparison of exact and HDIM energies at the RHF and MP2 levels.[a]

Molecule	Basis Set	HDIM RHF	Exact RHF	Error	HDIM MP2	Exact MP2	Error
Acetate	6-31G	–227.128451	–227.122127	–6.324	–433.715	–430.842	–2.873
	6-311G(d,p)	–227.288926	–227.286257	–2.669	–699.341	–696.048	–3.292
	6-311G(d,p)++	–227.307736	–227.304839	–2.897	–714.322	–708.089	–6.234
Acetic acid	6-31G	–227.701905	–227.696827	–5.077	–429.552	–429.222	–0.330
	6-311G(d,p)	–227.874849	–227.872571	–2.278	–696.849	–694.513	–2.336
	6-311G(d,p)++	–227.881632	–227.878118	–3.514	–706.030	–699.889	–6.141
B_2H_6	6-31G	–52.780331	–52.774745	–5.586	–139.817	–135.432	–4.385
	6-311G(d,p)	–52.828308	–52.827701	–0.606	–232.430	–230.623	–1.807
	6-311G(d,p)++	–52.828397	–52.827826	–0.570	–234.269	–230.976	–3.293
BF_3	6-31G	–323.092350	–323.085473	–6.877	–422.604	–417.869	–4.735
	6-311G(d,p)	–323.275884	–323.277865	1.981	–714.619	–711.469	–3.149
	6-311G(d,p)++	–323.283185	–323.283957	0.772	–721.274	–717.968	–3.307
BF_3NH_3	6-31G	–379.315345	–379.307600	–7.745	–538.756	–532.206	–6.550
	6-311G(d,p)	–379.518183	–379.518821	0.637	–923.672	–917.683	–5.989
	6-311G(d,p)++	–379.529801	–379.527602	–2.199	–936.140	–927.662	–8.478
Borazine	6-31G	–241.058208	–241.068171	9.963	–469.899	–466.044	–3.855
	6-311G(d,p)	–241.208578	–241.214521	5.944	–803.917	–790.161	–13.756
	6-311G(d,p)++	–241.214355	–241.218728	4.373	–819.290	–793.343	–25.948
Acetylene	6-31G	–76.791115	–76.791296	0.181	–187.983	–185.069	–2.914
	6-311G(d,p)	–76.838753	–76.838727	–0.026	–276.098	–274.780	–1.318
	6-311G(d,p)++	–76.840298	–76.840418	0.121	–276.678	–275.052	–1.626
Eclipsed ethane	6-31G	–79.192698	–79.192871	0.173	–185.659	–187.543	1.884
	6-311G(d,p)	–79.247144	–79.246689	–0.456	–322.077	–321.727	–0.350
	6-311G(d,p)++	–79.247503	–79.246949	–0.554	–324.027	–322.322	–1.706
Staggered ethane	6-31G	–79.197077	–79.197260	0.183	–185.935	–188.037	2.102
	6-311G(d,p)	–79.252127	–79.251594	–0.534	–322.179	–321.920	–0.259
	6-311G(d,p)++	–79.252414	–79.251821	–0.593	–324.086	–322.369	–1.718
Pyrrole	6-31G	–208.532079	–208.517727	–14.352	–473.511	–474.200	0.690
	6-311G(d,p)	–208.681907	–208.677802	–4.106	–767.845	–762.919	–4.926
	6-311G(d,p)++	–208.687510	–208.682527	–4.983	–781.018	–766.938	–14.080
Benzene	6-31G	–230.622691	–230.623165	0.474	–516.826	–516.139	–0.686
	6-311G(d,p)	–230.753588	–230.753003	–0.585	–841.651	–834.929	–6.722
	6-311G(d,p)++	–230.757222	–230.755744	–1.478	–857.220	–837.558	–19.662
CH_3CN	6-31G	–131.863259	–131.862290	–0.969	–306.206	–301.976	–4.230
	6-311G(d,p)	–131.954713	–131.954644	–0.069	–461.065	–457.878	–3.187
	6-311G(d,p)++	–131.957089	–131.956760	–0.329	–463.393	–459.398	–3.995
CH_3NC	6-31G	–131.831533	–131.831622	0.089	–283.512	–281.918	–1.595
	6-311G(d,p)	–131.924459	–131.924448	–0.011	–447.001	–444.130	–2.871
	6-311G(d,p)++	–131.927311	–131.926904	–0.407	–451.083	–445.751	–5.332
Methanol	6-31G	–114.985232	–114.986282	1.050	–214.661	–215.950	1.289
	6-311G(d,p)	–115.074743	–115.074319	–0.424	–366.808	–367.187	0.379
	6-311G(d,p)++	–115.079647	–115.078895	–0.752	–371.774	–371.206	–0.568
cis-Butene	6-31G	–156.047105	–156.047856	0.751	–359.387	–361.942	2.554
	6-311G(d,p)	–156.148068	–156.147706	–0.362	–601.365	–598.607	–2.758
	6-311G(d,p)++	–156.149926	–156.149189	–0.737	–609.894	–600.432	–9.461
trans-Butene	6-31G	–156.049425	–156.050255	0.830	–359.374	–361.987	2.613
	6-311G(d,p)	–156.150922	–156.150253	–0.669	–600.900	–598.334	–2.566
	6-311G(d,p)++	–156.152610	–156.151695	–0.916	–608.642	–599.870	–8.772
Cyclo-propane	6-31G	–117.011261	–117.007407	–3.854	–266.166	–270.531	4.364
	6-311G(d,p)	–117.089825	–117.088298	–1.526	–453.103	–452.552	–0.551
	6-311G(d,p)++	–117.091140	–117.088823	–2.317	–458.070	–453.997	–4.073
Ethylene oxide	6-31G	–152.787727	–152.783332	–4.395	–302.668	–304.915	2.247
	6-311G(d,p)	–152.908032	–152.905794	–2.238	–499.405	–499.029	–0.376
	6-311G(d,p)++	–152.912919	–152.909650	–3.269	–505.941	–502.908	–3.034
F_2O_2	6-31G	–348.107003	–348.105024	–1.979	–543.836	–543.702	–0.134
	6-311G(d,p)	–348.297447	–348.296006	–1.442	–869.353	–869.028	–0.325
	6-311G(d,p)++	–348.307350	–348.305555	–1.795	–879.266	–877.427	–1.839

© 2000 NRC Canada

Table 4 (*Concluded*).

Molecule	Basis Set	HDIM RHF	Exact RHF	Error	HDIM MP2	Exact MP2	Error
Furan	6-31G	–228.527770	–228.522932	–4.838	–473.373	–472.832	–0.541
	6-311G(d,p)	–228.679876	–228.678108	–1.768	–764.522	–760.666	–3.856
	6-311G(d,p)++	–228.684462	–228.681989	–2.473	–775.730	–764.030	–11.700
Hydrogen peroxide	6-31G	–150.706796	–150.707224	0.428	–255.844	–256.969	1.125
	6-311G(d,p)	–150.814478	–150.814260	–0.218	–424.298	–425.424	1.126
	6-311G(d,p)++	–150.819300	–150.819346	0.046	–430.849	–431.261	0.413
Hexatriene	6-31G	–231.721777	–231.723263	1.486	–527.717	–527.495	–0.222
	6-311G(d,p)	–231.864446	–231.863535	–0.911	–853.713	–848.859	–4.854
	6-311G(d,p)++	–231.868069	–231.866566	–1.503	–866.964	–851.634	–15.330
N_2H_2	6-31G	–109.924946	–109.924764	–0.182	–230.423	–230.194	–0.229
	6-311G(d,p)	–110.023040	–110.022439	–0.601	–359.968	–359.765	–0.203
	6-311G(d,p)++	–110.027012	–110.026613	–0.399	–363.164	–362.508	–0.656
Ammonia	6-31G	–56.160167	–56.160462	0.295	–115.086	–116.268	1.182
	6-311G(d,p)	–56.209758	–56.209793	0.034	–200.366	–201.124	0.758
	6-311G(d,p)++	–56.213849	–56.213981	0.132	–203.067	–203.580	0.513
Propene	6-31G	–117.027409	–117.027498	0.089	–269.835	–270.545	0.710
	6-311G(d,p)	–117.103329	–117.102667	–0.663	–447.087	–445.425	–1.662
	6-311G(d,p)++	–117.105007	–117.104174	–0.833	–451.399	–446.519	–4.880
Pyridine	6-31G	–246.593709	–246.591962	–1.747	–540.427	–539.260	–1.168
	6-311G(d,p)	–246.748694	–246.747421	–1.273	–870.713	–863.866	–6.847
	6-311G(d,p)++	–246.753406	–246.751109	–2.297	–886.598	–867.920	–18.679
Trioxane	6-31G	–341.477995	–341.473807	–4.188	–618.260	–622.343	4.082
	6-311G(d,p)	–341.739710	–341.735250	–4.461	–1040.440	–1035.31	–25.128
	6-311G(d,p)++	–341.748947	–341.742358	–6.589	–1066.769	–1045.45	–21.318

[a]RHF energies are in au, MP2 energies are in mH relative to their respective HDIM, exact RH*F* values. Errors are mH for both RHF and MP2 results.

value of 12.1 kJ mol^{-1} (31). Similarly, the *cis*/*trans*-2-butene conformational energy difference is 6.7 (7.5) kJ mol^{-1} at the RHF level and 6.0 (6.3) kJ mol^{-1} at the MP2 level compared to the estimated experimental value of 4.2 kJ mol^{-1} (32). For the isomerization of acetonitrile to methylisocyanide, the experimental enthalpy of reaction is 99 kJ mol^{-1} (33). At the RHF and MP2 levels energy differences of 79.3 (79.4) kJ mol^{-1} and 36.1 (36.9) kJ mol^{-1}, respectively, produce a total of 115.4 (116.4) kJ mol^{-1}. In contrast to this overestimation, the experimental isomerization energy of propene to cyclopropane of 35.1 kJ mol^{-1} (34) is underestimated with computed RHF and MP2 contributions of 37.7 (35.5) kJ mol^{-1} and –18.7 (–15.8) kJ mol^{-1} yielding a net energy of 19.0 (19.7) kJ mol^{-1}. Finally, the formation of trifluoroboron from ammonia and BF3 is predicted to be 81.8 (85.4) kJ mol^{-1} at the RHF level and when MP2 electron correlation contributions are added in, 95.2 (108.2) kJ mol^{-1}. Experimentally the gas-phase reaction enthalpy is unknown. The best theoretical estimate is 80.3 kJ mol^{-1} (35).

Results of the determination of equilibrium geometries by numerically minimizing the energy with respect to the molecular coordinates are presented in Table 5. A comparison between exact and HDIM values shows excellent agreement both at the RHF and MP2 6-311G(d,p) levels of theory with bond distances predicted to within 0.002 Å and bond angles to within 0.3°. Also included in Table 5 are three examples of open shell systems, the lowest lying triplet states of ethylene (CH_2 groups twisted 90° to one another) and cyclopropenylidene as well as the doublet methyl radical (planar D_{3h} conformation). Even though our one-electron DIM operator is constructed from densities of an averaged Fock operator, eqs. [10*a*]–[10*c*], geometries and energies show similar accuracies as found in the closed shell molecules.

The only dihedral angle reported in Table 5 is for hydrogen peroxide where there is 0.2° agreement at the RHF level but a 2.4° difference at the MP2 level. One reason for this is as seen from Table 4 is that the HDIM MP2 errors are larger than the RHF errors for hydrogen peroxide. However, a more significant factor is likely the shallow H_2O_2 torsional potential well causing a deterioration in the accuracy of the numerical optimization used. The error in the BC bond distance in borane carbonyl also is an exception to the 0.002 Å accuracy found in most compounds. There is a substantial 0.015 Å deviation at the Hartree–Fock level which would seem to indicate that the extended Hückel guess used to generate the initial density matrix employed in the construction of our HDIM one-electron operator is not sufficiently accurate. However the computed exact and HDIM RHF energies differ by only 0.6 mH. Therefore, it is likely our numerical minimization is again suspect in this weakly bound intermolecular complex.

Occasionally, one comes across molecules where the HDIM method fails to be sufficiently accurate. Two examples are pyrrole and C_{60} at the 6-31G level. In the case of buckminsterfullerene, the exact RHF calculation which requires just under 3 billion two-electron integrals yields an energy of –2270.9496 Hartrees. In comparison, the HDIM calculation uses 19 million two-electron integrals but the predicted RHF energy of –2271.0205 Hartrees is in error by 70.9 mH. However, the converged density matrix can be used to reconstruct a more accurate DIM one-electron operator from eqs. [7*b*] and [8*b*]. Repeating the Hartree–Fock step

© 2000 NRC Canada

Table 5. Predicted equilibrium geometries at the 6-311G(d,p) level.[a]

Molecule	Variable		HF	HF-HDIM	MP2	MP2-HDIM	Experiment
Hydrogen peroxide	OO	Distance	1.3846	1.3826	1.4446	1.4425	1.452[b]
	OH	Distance	0.9424	0.9414	0.9629	0.9616	0.965[b]
	OOH	Angle	102.75	102.67	99.319	99.446	100.0[b]
	HOOH	Dihedral	116.29	116.11	120.08	117.60	119.1[b]
		Energy	–150.8212	–150.8217	–151.2402	–151.2394	
Formaldehyde	CO	Distance	1.1783	1.1781	1.2103	1.2105	1.208[b]
	CH	Distance	1.0950	1.0954	1.1060	1.1054	1.116[b]
	HCO	Angle	122.95	122.04	122.24	122.01	121.8[b]
		Energy	–113.8993	–113.8997	–114.2408	–114.2412	
Acetylene	CC	Distance	1.1822	1.1822	1.2150	1.2158	1.203[b]
	CH	Distance	1.0557	1.0557	1.0650	1.0661	1.061[b]
		Energy	–76.8416	–76.8416	–77.1135	–77.1146	
Ethane	CC	Distance	1.5273	1.5259	1.5282	1.5280	1.531[b]
	CH	Distance	1.0862	1.0868	1.0931	1.0944	1.096[b]
	CCH	Angle	111.19	111.13	111.15	110.89	111.1[b]
		Energy	–79.2518	–79.2523	–79.5735	–79.5743	
Fluoromethane	CF	Distance	1.3638	1.3632	1.3824	1.3816	1.383[b]
	CH	Distance	1.0827	1.0827	1.0916	1.0921	1.100[b]
	FCH	Angle	108.95	108.94	109.18	109.10	108.3[b]
		Energy	–139.0784	–139.0788	–139.4450	–139.4456	
Benzene	CC	Distance	1.3855	1.3852	1.3982	1.3972	1.397[c]
	CH	Distance	1.0756	1.0757	1.0863	1.0869	1.073[c]
		Energy	–230.7544	–230.7550	–231.5879	–231.5952	
Acetonitrile	CN	Distance	1.1284	1.1291	1.1719	1.1734	1.156[d]
	CC	Distance	1.4656	1.4632	1.4632	1.4623	1.457[d]
	CH	Distance	1.0823	1.0838	1.0912	1.0928	1.10[e]
	CCH	Angle	109.70	109.70	109.94	109.73	109.7[e]
		Energy	–131.9613	–131.9611	–132.4126	–132.4159	
Cyclopropane	CC	Distance	1.4994	1.4986	1.5086	1.5091	1.512[c]
	CH	Distance	1.0758	1.0762	1.0834	1.0841	1.083[c]
	HCH	Angle	114.24	114.43	114.95	115.33	118.2[e]
		Energy	–117.0887	–117.0902	–117.5409	–117.5430	
BH_3CO	BC	Distance	1.6192	1.6343	1.5555	1.5611	1.540[f]
	BH	Distance	1.2035	1.2045	1.2041	1.2062	1.194[f]
	CO	Distance	1.0992	1.0983	1.1363	1.1357	1.131[f]
	CBH	Angle	103.02	102.98	104.00	103.68	104.6[f]
		Energy	–139.1799	–139.1805	–139.6162	–139.6186	
B_2H_6[g]	BB	Distance	1.7826	1.782	1.7672	1.766	1.763[b]
	BH_b	Distance	1.3224	1.3208	1.3154	1.3138	1.320[b]
	BH_a	Distance	1.1850	1.1862	1.1870	1.1893	1.201[b]
	H_aBH_a	Angle	122.08	122.28	122.36	122.78	121.0[b]
		Energy	–52.8280	–52.8286	–53.0584	–53.0608	
Singlet ethylene	CC	Distance	1.3163	1.3161	1.3364	1.3374	1.339[b]
	CH	Distance	1.0767	1.0772	1.0849	1.0862	1.085[b]
	CCH	Angle	121.69	121.68	121.40	121.33	121.1[b]
		Energy	–78.0548	–78.0553	–78.3473	–78.3484	
Triplet ethylene	CC	Distance	1.4654	1.4661	1.4578	1.4571	
	CH	Distance	1.0768	1.0762	1.0862	1.0851	
	CCH	Angle	121.24	121.29	121.38	121.45	
		Energy	–77.9804	–77.9802	–78.2395	–78.2393	
Singlet cyclopropenylidene	CC	Distance	1.4059	1.4059	1.4325	1.4320	1.422[h]
	CCC	Angle	55.59	55.56	55.59	55.54	56[h]
	CH	Distance	1.0693	1.0694	1.0800	1.0799	1.072[h]
	CCH	Angle	147.75	147.81	147.91	148.063	150[h]
		Energy	–114.6489	–114.6484	–115.0299	–115.0283	

© 2000 NRC Canada

Table 5 (*Concluded*).

Molecule	Variable		HF	HF-HDIM	MP2	MP2-HDIM	Experiment
Triplet cyclopropenylidene	CC	Distance	1.3292	1.3284	1.3570	1.3560	
	CCC	Angle	71.48	71.35	73.66	73.51	
	CH	Distance	1.0597	1.0601	1.0706	1.0706	
	CCH	Angle	158.84	158.82	164.62	164.30	
		Energy	–114.5426	–114.5429	–114.9384	–114.9370	
Methane	CC	Distance	1.0843	1.0842	1.0909	1.0898	1.092[i]
		Energy	–40.2092	–40.2090	–40.3801	–40.3805	
Methyl radical	CC	Distance	1.0724	1.0721	1.0797	1.0799	1.079[j]
		Energy	–39.5689	–39.5687	–39.7085	–39.7086	

[a]Bond distances are in Å, bond and dihedral angles are in deg, and energies are in au.
[b]Ref. 13: pp. 147–151.
[c]Ref. 34.
[d]Ref. 33.
[e]Ref. 36.
[f]Ref. 13: p. 218.
[g]H_b is a bridging H.
[h]Ref. 37.
[i]Ref. 13: p. 138.
[j]Ref. 13: p. 196.

produces a new energy of –2270.9790 Hartrees reducing the error to 29.4 mH. A second iteration yields –2270.9565 Hartrees further reducing the error to 6.9 mH.

Conclusions

Molecular applications of the diatomics in molecules (DIM) method often prove impractical due to the large basis set size of atomic and diatomic eigenstates needed to obtain reliable and accurate results. We have presented a semiempirical DIM theory which sidesteps this problem by using a second quantized approach. In this method all three- and four-centered electronic integrals are discarded. This is equivalent to ignoring the overlaps between atomic and diatomic fragments. To compensate for this approximation, the one-electron DIM operator is constructed to reproduce the density matrix and energy in a Hartree–Fock calculation. The resulting method is found to reproduce accurately the energies from both the dynamic and nondynamic electron correlation as well as excited stated states. A modified model in which the DIM one-electron operator is formed from the initial extended Hückel guess density matrix was also examined and found to work surprisingly well.

In this initial work no attempt has been made at the post Hartree–Fock level to take advantage of the reduced number of two-electron integrals which formally scale as m^2, where m is the number of atoms. Even so, our DIM MP2 energies computed over a canonical molecular orbital basis, using the segmented integral transformation algorithms of the GAMESS program (38) are three to four times faster than the exact MP2 results for the same basis computed in the same fashion. More suitable electron correlation treatments for our DIM model would be to use the atomic orbital (AO) based MP2 and coupled cluster approaches of Scuseria and Ayala (8). Alternatively, due to the orthogonal AO basis used in our model, transforming integrals to a strictly localized one- and two-centered molecular orbital basis (39) would scale as m^2 and allow localized electron correlation treatments.

For the future we plan to examine the possibility of reducing computational times of the DIM one- and two-centered orthogonal AO two-electron integrals by constructing interpolation tables to directly reproduce these integrals for a given basis set as a function of internuclear separation. Transformations would still be required to rotate these results from their local frames into the external molecular frame. Also in the case of our HDIM model we would like to improve the extended Hückel starting guess of Hartree–Fock molecular orbitals which is used to form the density matrix that in turn is used to form g^{DIM} and g^{OAO} in eqs. [7] and [8] which in turn is used to construct our DIM one-electron operator. Because these starting guesses are projections of a minimum AO basis set onto our larger target basis, it may be possible to form g^{OAO} by first building the g matrix over the two-electron integrals of the minimum basis set rather than the two-electron integrals of our target AO basis, then projecting these results onto the symmetrically orthogonalized target atomic orbital basis.

References

1. F.O. Ellison. J. Am. Chem. Soc. **85**, 3540 (1963).
2. J.C. Tully. Adv. Chem. Phys. **42**, 63 (1980); J.C. Tully. Modern theoretical chemistry: Semiempirical methods of electronic structure calculations. Part B. Vol. 7. *Edited by* G.A. Segal. Plenum Press, New York. 1977. p. 173; P.J. Kuntz. Ber. Bunsenges. Phys. Chem. **86**, 367 (1982).
3. P.J. Kuntz and A.C. Roach. J. Chem. Phys. **74**, 3420 (1981); A.C. Roach and P.J. Kuntz. J. Chem. Phys. **74**, 3435 (1981); J.L. Schreiber and P.J. Kuntz. J. Chem. Phys. **76**, 1872 (1982); P.J. Kuntz and J.L. Schreiber. J. Chem. Phys. **76**, 4120 (1982).
4. W.R. Wadt. Appl. Phys. Lett. **38**, 1030 (1980); P.J. Kuntz and J. Valldorf. Z. Phys. D: At. Mol. Clusters, **D8**, 195 (1988); F.Y. Naumkin, P.J. Knowles, and J.N. Murrell. Chem. Phys. **193**, 27 (1995); F.Y. Naumkin and D.J. Wales. Mol. Phys. **96**, 1295 (1999); N.L. Doltsinis and P.J. Knowles. Mol. Phys. **94**, 981 (1998).
5. M. Ovchinnikov and V.A. Apkarian. J. Chem. Phys. **110**, 9842 (1999).

© 2000 NRC Canada

6. J. Cullen. J. Comput. Chem. **13**, 901 (1992); P. Fulde. Electron correlation in molecules and solids. Springer, Berlin. 1995. p. 94, p. 200; J. Cullen. J. Comput. Chem. **20**, 999 (1999).
7. G.E. Scuseria. J. Phys. Chem. **A103**, 4782 (1999); (*b*) D.L. Strout and G.E. Scuseria. J. Chem. Phys. **102**, 8448 (1995).
8. G.E. Scuseria and P.Y. Ayala. J. Chem. Phys. **111**, 8330 (1999).
9. C.A. White, B.G. Johnson, P.M.W. Gill, and M. Head-Gordon. Chem. Phys. Lett. **253**, 268 (1996); C. Ochsenfeld, C.A. White, and M. Head-Gordon. J. Chem. Phys. **109**, 1663 (1998).
10. L. Greengard and V. Rokhlin. J. Comput. Chem. **73**, 325 (1987).
11. M.C. Strain, G.E. Scuseria, and M.J. Frisch. Science (Washington, D.C.), **271**, 51 (1996).
12. W. Kohn. Int. J. Quantum Chem. **56**, 229 (1995); S. Goedecker. Rev. Mod. Phys. **71**, 1085 (1999).
13. W.J. Hehre, L. Radom, P.v.R. Schleyer, and J.A. Pople. Ab initio molecular orbital theory. John Wiley & Sons, New York. 1985.
14. M.W. Feyereisen, D. Feller, and D.A. Dixon. J. Chem. Phys. **100**, 2993 (1996).
15. F. Weigand and M. Haser. Theor. Chem. Acc. **97**, 331 (1997).
16. F.W. Bobrowicz and W.A. Goddard, III. Modern theoretical chemistry: methods of electronic structure theory. Vol. 3. *Edited by* H.F. Schaefer, III. Plenum Press, New York. 1977. p. 79.
17. J. Cullen. Chem. Phys. **202**, 217 (1996).
18. J.B. Foresman, M. Head-Gordon, J.A. Pople, and M.J. Frisch. J. Phys. Chem. **90**, 135 (1992).
19. M. Weiss, C.E. Kuyatt, and S. Mielczarek. J. Chem. Phys. **54**, 4147 (1971).
20. A. Chutjian. J. Chem. Phys. **61**, 4279 (1974).
21. A.J. Merer and R.S. Mulliken. Chem. Rev. **69**, 639 (1969); M. Zelikoff and K. Watanabe. J. Opt. Soc. Am. **43**, 756 (1953).
22. E.H. van Veen. Chem Phys. Lett. **41**, 540 (1976).
23. K.E. Johnson, D.B. Johnston, and S. Lipsky. J. Chem. Phys. **70**, 3844 (1979).
24. J.E. Parkin and K.K. Innes. J. Mol. Spectrosc. **15**, 407 (1965).
25. L. Goodman. J. Mol. Spectrosc. **6**, 109 (1961).
26. A. Bolovinos, P. Tsekeris, J. Philis, E. Pantos, and G. Andritsopoulos. J. Mol. Spectrosc. **103**, 240 (1984).
27. I.C. Walker, M.H. Palmer, and A. Hopkirk. Chem. Phys. **141**, 365 (1989).
28. M.B. Robin. Higher excited states of polyatomic molecules. Vol. II. Academic, New York. 1975. p. 184; M.B. Robin. Higher excited states of polyatomic molecules. Vol. III. Academic, New York. 1985. p. 334.
29. H. Nakano, T. Tsuneda, T. Hashimoto, and K. Hirao. J. Chem. Phys. **104**, 2312 (1996).
30. M. Bavia, F. Bertinelli, C. Taliani, and C. Zauli. Mol. Phys. **31**, 479 (1985).
31. P.W. Payne and L.C. Allen. Modern theoretical chemistry. Vol. 4. *Edited by* H.F. Schaefer, III. Plenum Press, New York. 1977. p. 29.
32. V.M. Bedanov, W. Tsang, and M.R. Zachariah. J. Phys. Chem. **99**, 11452 (1995), and refs. therein.
33. S.G. Lias, J.E. Bartmess, J.F. Liebman, J.L. Holmes, R.D. Levin, and W.G. Mallard. J. Phys. Chem. Ref. Data Suppl. **17**, 1 (1988); P.M. Mayer, M.S. Taylor, M.W. Wong, and L. Radom. J. Phys. Chem. A, **A102**, 7074 (1998).
34. D. Feller and D.A. Dixon. J. Phys. Chem. A, **A104**, 3048 (2000).
35. C.W. Bauschlicher and A. Ricca. Chem. Phys. Lett. **237**, 14 (1995).
36. H.J. Bowen, J. Donahue, D.G. Jenkin, O. Kennard, and D.H. Whiffen. Tables of interatomic distances and configuration in molecules and ions. Special Publication no. 11. The Chemical Society, London. 1958.
37. R.A. Seburg, E.V. Patterson, J.F. Stanton, and R.J. McMahon. J. Am. Chem. Soc. **119**, 5847 (1997).
38. M.W. Schmidt, K.K. Baldridge, J.A. Boatz, S.T. Elbert, M.S. Gordon, J.H. Jensen, S. Koseki, N. Matsunaga, K.A. Nguyen, S.J. Su, T.L. Windus, M. Dupuis, and J.A. Montgomery. J. Comput. Chem. **14**, 1347 (1993).
39. H. Stoll, G. Waggenblast, and H. Preuss. Theor. Chim. Acta, **57**, 169 (1980); J. Cullen. Int. J. Quantum Chem. **S25**, 193 (1991); G.F. Smits and C. Altona. Theor. Chem. Acta, **67**, 461 (1985).

© 2000 NRC Canada

Dew points of ternary methane + water + methanol. Measurement and correlation

Sofía T. Blanco, Inmaculada Velasco, Evelyne Rauzy, and Santos Otín

Abstract: A water and methanol dew point generation device has been built up and tested. Experimental measurements of dew point for ternary methane + water + methanol were carried out between 1.01×10^5 Pa to 97.84×10^5 Pa and the temperature range from 248.71 to 282.93 K. A EOS–CR method (equation of state – chemical reticular) reproduces very accurately the experimental curves independently of the pressure and temperature ranges.

Key words: dew point, experimental method, equation of state, excess function.

Résumé : On a mis au point et évalué un appareil permettant de générer le point de rosée de l'eau et du méthanol. On a déterminé expérimentalement le point de rosée du mélange ternaire méthane + eau + méthanol entre $1{,}01 \times 10^5$ et $97{,}84 \times 10^5$ Pa et à des températures entre 248,71 et 282,93 K. Une méthode « EOS–CR » (équation d'état chimique réticulaire) permet de reproduire avec beaucoup de précision les courbes expérimentales quelles que soient les variations de pression et de température.

Mots clés : point de rosée, méthode expérimentale, équation d'état, fonction d'excès.

Introduction

Methanol is one of the main additives added to natural gases. This chemical is used firstly as a hydrate inhibitor and secondly as a secant after hydraulic tests, which constitute one of the first phases in the starting of gas transport pipelines. In both of two submitted applications, methanol is found with water in natural gases. To know the influence of these two components in vapour–liquid equilibrium of natural gases, water and methanol dew points in methane have been generated and the conditions of them determinated. Taking into account that natural gas is composed of more than 90% methane, the study of the methane + water + methanol system constitutes an approximated knowledge of natural gas + water + methanol behaviour.

A water and methanol dew point generation device has been built up and tested to determine the experimental dew points of methane + water + methanol mixtures. The results obtained on these mixtures between 1.01×10^5 and 97.84×10^5 Pa and temperatures from 248.71 to 282.93 K are presented here.

The demand for reliable calculation procedures to estimate these dew points in natural gases is becoming more and more important. Therefore the experimental results obtained on the ternary system were analyzed in terms of an EOS–CR method, which reproduces very well the experimental dew point curves.

Received December 11, 1999. Published on the NRC Research Press website on December 1, 2000.

S.T. Blanco, I. Velasco, and S. Otín.[1] Departamento de Química Orgánica y Química Física, Facultad de Ciencias, Universidad de Zaragoza, 50.009 – Zaragoza, Spain.
E. Rauzy. Laboratoire de Chimie Physique de Marseille, Faculté des Sciences de Luminy, Université de la Méditerranée, 13.288 – Marseille CEDEX 9, France.

[1]Author to whom correspondence may be addressed. Telephone: +34 976 761 199. e-mail: santos@posta.unizar.es

Experimental

Apparatus

The experimental method used for this work is based on the generation of saturated gases with water and methanol by condensation of these compounds in one temperature-controlled condenser with continuous gas flow at specified pressures. The concentrations of water and methanol in the gas are measured at the outlet of the dew point generation system, using a Karl Fischer titration, according to the standard method ISO 10101 (1) at atmospheric pressure, and a gas chromatography analysis, respectively. By doing so, the water and methanol contents reference values of the gaseous phase are obtained. The dew point values are measured by means of a chilled mirror instrument. The chilled mirror instrument input pressure is set using a regulator valve, when the apparatus reaches a stable value of dew temperature, both pressure and temperature are recorded. In this way, the values of the temperature and pressure of the dew point curve of the mixture generated are obtained.

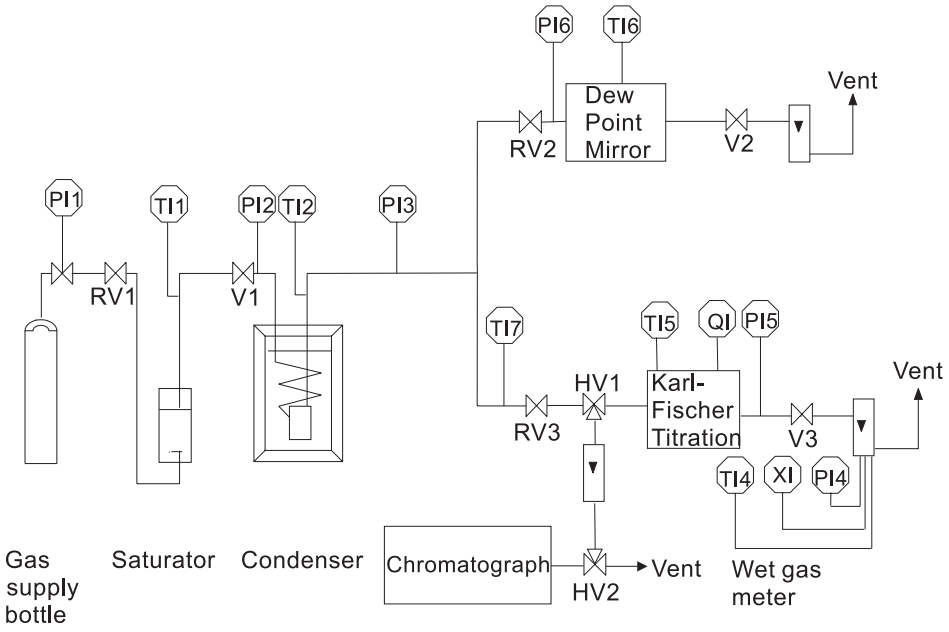
Operating procedure

The dew point pressure values range from 1.01×10^5 Pa to 97.84×10^5 Pa and the temperature values range from 248.71 to 282.93 K. The methane gas was supplied by Air Liquide with the specified purity of 99.95 vol.% and was used without further treatment.

The dew point generation device used for our experimental data collecting is presented in Fig. 1. After controlled expansion (PI1), the gas is saturated with water and methanol vapour by flowing through a liquid mixture of these compounds in an isolated saturator held at laboratory temperature. The condensation temperature of water and methanol is then achieved in a controlled-temperature stainless steel condenser.

© 2000 NRC Canada

Fig. 1. Experimental apparatus used in this work. RV: control valve; V: ball valve; HV: three-way valve; TI: temperature measurement; PI: pressure measurement; QI: coulometric measurement; XI: volume measurement.



To avoid any recondensation, the expansion before the Karl–Fischer titrator inlet is made using a heated valve (RV3). To analyze the contents of water and methanol and to carry out the dew point measurements the following instrumentation is used: (*i*) Mitsubishi CA 06 Karl–Fischer titrator, coupled with an Elster wet gas meter Type Gr. 00, E51, 0.2% accuracy; (*ii*) HP 5890 gas chromatograph with TCD detector adjusted to maximum sensitivity; (*iii*) MBW dew point instrument model DP3-D. The cooling of the mirror is achieved by a Peltier cooling device with automatic mirror check. The uncertainty on the dew temperature is better than ±0.4 K; and (*iv*) pressure transmitter with a maximum error of 0.2% in the calibrated range.

Previously to the study of methane + water + methanol, the performance of both analysis methods and experimental procedures was determined. Repeatability and reproducibility of the Karl–Fischer titration, the gas chromatography analysis, and the dewpoint generation were calculated according to ISO 5725 (2) after repetitive measurements. The results obtained in the performance evaluation are presented in Table 1. Reference conditions for volume are 273.15 K and 1.01325×10^5 Pa. The test was achieved on a water and methanol dew point of 283.15 K and 5×10^5 Pa in pure nitrogen. The reliability tests results are taken as consistency criteria; the maximum acceptable standard deviation of measurements is derived from the repeatability value, and the maximum acceptable discrepancy with measurements from external laboratories is derived from the reproducibility value.

Results

The water and methanol contents in the vapour phase and the dew point curve of the mixtures generated at the dew point generation system were determined and the results of the experiments are collected on Table 2.

Table 1. Performance evaluation of water and methanol content measurements.

	Water content analysis ($\times 10^{-6}$ kg m^{-3})	Methanol content analysis ($\times 10^{-6}$ kg m^{-3})
Mean value(n)	899.64	12301.1
Repeatability (n)	15.96	316.7
Reproducibility (n)	36.32	294.0

Theory

Introduction

Classical models such as UNIQUAC or NRTL yield good results for vapour–liquid equilibrium of binary systems under low pressures containing one self-associating compound such as alcohol, but are not suitable for high-pressure phase equilibrium calculations.

In this work, EOS–CR is used and is derived from the excess function equations of state model (3) and founded on the zeroth approximation on the quasireticular model. The values of dew temperature and composition of the vapour phase for the studied system are calculated by means of this theoretical method using the experimental values of pressure obtained in the present work.

To know the ability of this method to predict the dew point curves of the ternary system in the temperature and pressure studied ranges, the comparison between experimental and calculated values is carried out obtaining very good results.

Description of the model

To represent the vapour–liquid equilibrium of mixtures containing one self-associating component, we use a model founded on the zeroth approximation of Guggenheim's reticular model, which answers two conditions: (*i*) the

© 2000 NRC Canada

Table 2. Experimental dew points temperatures and pressures for ternary mixtures {(1 – y_1 – y_2) methane + $y_1$water + $y_2$methanol}.

T (K)	P (×10^5 Pa)	T (K)	P (×10^5 Pa)
y_1 = 0.00004		y_2 = 0.0009	
251.15	5.30	270.55	54.48
255.36	9.01	271.19	59.87
259.40	16.04	271.91	66.28
261.03	19.56	272.22	70.13
263.23	24.94	273.07	75.74
264.59	29.12	273.07	76.78
266.10	33.38	273.56	85.07
266.66	35.31	273.73	86.63
267.60	38.67	274.42	90.47
268.50	43.17	274.36	93.97
269.53	48.53	274.05	97.84
y_1 = 0.00005		y_2 = 0.0011	
252.07	5.19	274.78	59.60
256.77	9.96	275.51	65.43
260.81	14.95	275.68	67.11
263.81	19.96	275.93	70.06
266.21	24.90	276.40	75.54
268.07	30.00	276.68	79.94
269.48	34.26	277.08	80.67
271.20	40.50	277.34	84.34
272.40	45.24	277.61	90.05
273.62	52.16	277.98	95.59
274.24	56.08		
y_1 = 0.00008		y_2 = 0.0014	
254.54	5.23	277.34	55.98
259.68	9.88	278.13	61.85
263.27	14.07	278.71	66.19
266.92	20.19	279.16	69.94
269.29	25.59	279.57	75.71
271.13	29.93	280.00	80.30
272.78	35.06	280.23	85.78
274.20	40.61	280.43	91.18
275.09	44.21	280.68	94.91
276.49	51.16		
y_1 = 0.00010		y_2 = 0.0014	
253.85	5.53	277.47	44.51
257.92	7.99	278.24	48.06
262.63	12.10	279.00	52.34
265.40	15.59	279.74	56.51
268.40	20.29	280.33	58.81
270.54	23.95	280.86	63.23
272.37	28.27	281.47	69.25
274.11	32.72	281.85	71.37
275.17	35.51	282.12	75.22
276.45	40.44	282.69	81.66
y_1 = 0.00008		y_2 = 0.0007	
248.71	4.80	267.59	32.16
253.48	7.83	268.73	36.12
257.69	12.17	270.02	40.21
260.52	16.01	270.83	43.86
260.16	16.18	271.74	47.90
262.57	20.08	272.56	52.43
264.78	24.16	273.19	56.74
266.03	28.00	274.04	59.21

Table 2 (*continued*).

T (K)	P (×10^5 Pa)	T (K)	P (×10^5 Pa)
y_1 = 0.00012		y_2 = 0.0008	
250.91	4.83	271.74	36.03
256.22	8.31	272.98	40.17
259.96	12.09	274.02	44.01
263.01	16.05	275.00	47.97
265.34	19.95	275.88	51.84
267.47	23.76	276.53	56.13
269.09	28.23	277.40	60.47
270.43	32.12		
y_1 = 0.00016		y_2 = 0.0008	
251.59	4.18	275.22	36.04
259.37	8.41	276.67	40.06
263.21	11.90	277.68	43.89
266.55	16.10	278.72	48.13
269.20	20.40	279.54	51.89
271.00	24.01	280.34	55.81
272.74	28.10	281.35	61.22
274.29	32.33		
y_1 = 0.00022		y_2 = 0.0013	
254.73	3.40	276.60	24.12
260.91	6.21	278.00	27.19
265.06	9.14	279.10	29.99
268.24	12.02	280.14	32.91
270.79	14.85	281.26	36.32
273.32	18.22	282.05	39.01
274.90	20.99	282.91	42.04
y_1 = 0.00020		y_2 = 0.0006	
251.48	4.08	266.56	15.89
253.83	4.99	267.89	17.93
256.11	6.18	269.03	19.88
259.17	8.16	270.16	22.01
261.30	9.88	271.08	23.91
263.53	12.08	271.98	25.93
265.17	14.03	272.93	28.10
y_1 = 0.00023		y_2 = 0.0009	
254.77	3.94	271.36	17.84
256.92	4.89	272.69	20.10
259.18	6.04	273.75	22.07
262.13	7.94	274.75	24.13
264.59	9.90	275.56	25.96
266.69	11.96	276.35	27.89
268.40	13.90	277.03	29.41
270.03	15.88		
y_1 = 0.00036		y_2 = 0.0015	
252.90	2.00	274.89	13.85
259.50	3.57	276.26	15.59
263.18	5.05	277.22	16.97
265.77	6.45	278.24	18.51
268.36	8.04	279.17	19.92
270.08	9.35	279.96	21.35
272.00	11.02	281.05	23.06
273.53	12.04		
y_1 = 0.00057		y_2 = 0.0023	
255.67	1.13	276.46	8.87

© 2000 NRC Canada

Table 2. (*concluded*).

T (K)	P ($\times 10^5$ Pa)	T (K)	P ($\times 10^5$ Pa)
260.84	2.11	277.89	9.97
264.44	3.05	278.99	11.06
267.53	4.05	280.16	12.31
270.04	4.72	280.84	12.94
272.08	6.04	281.55	13.93
274.02	7.12	282.63	14.81
275.45	8.08		
y_1 = 0.00078		y_2 = 0.0022	
253.40	1.23	266.29	3.53
255.75	1.50	266.45	3.62
257.96	1.81	267.43	3.91
259.72	2.10	268.41	4.21
261.43	2.41	269.23	4.51
261.54	2.44	270.05	4.81
261.76	2.47	270.88	5.12
262.77	2.67	271.54	5.42
262.86	2.71	272.13	5.69
264.09	3.00	272.99	6.04
265.42	3.32		
y_1 = 0.00110		y_2 = 0.0023	
255.80	1.13	270.39	3.63
256.58	1.22	271.29	3.90
259.21	1.50	272.31	4.21
261.55	1.81	273.17	4.51
263.42	2.10	273.95	4.79
265.23	2.43	274.79	5.12
265.60	2.50	275.58	5.40
266.53	2.70	276.30	5.69
267.90	3.01	277.08	6.04
269.03	3.30		
y_1 = 0.00175		y_2 = 0.0031	
259.82	1.01	274.10	3.04
260.88	1.11	274.86	3.22
262.09	1.22	275.63	3.38
263.99	1.41	275.98	3.46
265.63	1.60	276.42	3.60
265.72	1.61	277.21	3.81
267.34	1.82	277.79	3.98
268.79	2.03	278.49	4.20
269.90	2.21	279.18	4.41
271.13	2.42	279.78	4.60
272.15	2.63	280.40	4.80
273.03	2.81	281.05	5.02
y_1 = 0.00263		y_2 = 0.0035	
264.44	1.02	278.04	2.83
266.44	1.19	278.82	3.00
268.61	1.40	279.77	3.22
270.45	1.60	280.58	3.40
272.10	1.82	281.36	3.61
273.54	2.03	281.94	3.74
275.07	2.25	282.13	3.81
275.98	2.42	282.93	4.02
276.96	2.62		

Helmholtz energies of pure components are calculated by equations of state; (*ii*) the excess functions are defined at constant packing fraction, the latter described by $v°/v$, $v°$ being the molar close-packed volume and v the molar volume. It is assumed that it is possible to define a "covolume" b proportional to $v°$, which enables evaluation of the packing fraction by the ratio $\eta = b/v$. If the packing fraction for the pure components and for the mixture is assumed to be the same, then:

$$[1] \qquad \eta = \frac{b}{v} = \frac{b_1}{v_1} \qquad (i = 1, \ldots p)$$

The equation of state used in this model is the translated Peng–Robinson cubic equation of state (4, 5) of the form:

$$[2] \qquad P = \frac{RT}{\bar{v} - \bar{b}} - \frac{a(T)}{\bar{v}(\bar{v} + \gamma\bar{b})}$$

where P and T are the system pressure and temperature, R is the gas constant, $\bar{v}$ is a translated molar volume called the pseudo-molar volume and $\bar{b}$ is the pseudo covolume and it is calculated as follows for each component of the mixture:

$$[3] \qquad \bar{b} = 0.045572\frac{RT_c}{P_c}$$

where T_c and P_c are the critical temperature and pressure, respectively, for each component.

The parameter a in eq. [2] is the attractive parameter and is a function of the temperature; the equations used for its calculation are the proposed by Carrier (6) and Carrier et al. (7).

The molar Helmholtz energy of a mixture, A, may be written as follows:

$$[4] \qquad A = A^{id} - RT \ln (1 - \eta) - \sum_{i=1}^{p} \frac{x_i a_i}{b_i} Q(\eta) + A^E_{res}$$

where A^{id} is the ideal mixture molar Helmholtz energy, a_i is the attractive parameter of the translated Peng–Robinson cubic equation of state for the component i (4, 5), b_i is the molar covolume for the component i, A^E_{res} is the residual excess Helmholtz energy which will be explained later, and $Q(\eta)$ is expressed as follows:

$$[5] \qquad Q(\eta) = \int_0^\eta \frac{Q'(\eta)}{\eta}\, d\eta$$

where

$$[6] \qquad Q'(\eta) = \frac{\eta}{1 + \gamma\eta}$$

and

$$\gamma = 2(\sqrt{2} + 1)$$

The value used for the parameter γ is characteristic of the equation of state under consideration, in our case the translated Peng–Robinson cubic equation of state (4, 5).

The residual excess Helmholtz energy (A^E_{res}) is separated into two terms (eq. [7]): (*i*) the physical interactions between different compounds are represented by the physical term (A^E_{fis}) using the eq. [8] (8); (*iii*) the molecular associations

© 2000 NRC Canada

Table 3. Values of the group interaction parameters, ${}_1A^0_{kl}$, ${}_1B^0_{kl}$, ${}_2A^0_{kl}$ and ${}_2B^0_{kl}$, used in this work.

Binary	${}_1A^0_{kl}$ ($\times 10^6$ J m^{-3})	${}_1B^0_{kl}$ ($\times 10^6$ J m^{-3})	${}_2A^0_{kl}$ ($\times 10^6$ J m^{-3})	${}_2B^0_{kl}$ ($\times 10^6$ J m^{-3})
methane + water	1279.540 (8)	–0.7259 (8)	135246.231[a]	1.076[a]
methane + methanol	161.791[a]	2.3900[a]	1761.995[a]	–11.605[a]

[a] This work.

are described by the chemical term ($A^{\mathrm{E}}_{\mathrm{qui}}$). For its calculation, the CREE model (Chimique Réticulaire Equation d'Etat) is used, which is a continuous association model defined by Rauzy and Berro (9, 10).

$$[7] \qquad A^{\mathrm{E}}_{\mathrm{res}} = A^{\mathrm{E}}_{\mathrm{fis}} + A^{\mathrm{E}}_{\mathrm{qui}}$$

where the physical part, $A^{\mathrm{E}}_{\mathrm{fis}}$, is written by means of a formalism which enables to separate the composition and packing fraction variables:

$$[8] \qquad A^{\mathrm{E}}_{\mathrm{fis}} = E(T,x)\,Q(\eta)$$

For the first factor on the right hand side of eq. [8] the following equations are used (8):

$$[9] \qquad E(T,x) = \frac{1}{2q_{\mathrm{m}}}\left[\sum_{i=1}^{p} q_i x_i \left[\sum_{j=1}^{p} q_j x_j K_{ij}\right] + \sum_{i=1}^{p} q_i x_i \left[\sum_{j=1}^{p} q_j^{1/3} x_j L_{ji}^{1/3}\right]\right]$$

with

$$K_{ij} = \frac{E^1_{ij} + E^2_{ij}}{2}$$

$$[10] \qquad L_{ij} = E^2_{ij} - E^1_{ij}$$

$$L_{ij} = -L_{ji}$$

$$[11] \qquad q_{\mathrm{m}} = \sum_{i=1}^{p} q_i x_i$$

and

$$q_i = \delta_i b_i$$

where the subscripts i and j are referred to the components i and j of the mixture with p components, q_i is the molecular surface of the component i and it is supposed that $q_i/q_j = (b_i/b_j)\delta$, being an adjustable parameter. K_{ij} and L_{ij} are two binary interaction parameters between components i and j, which depend on the terms of the binary interchange energy (E^1_{ij} and E^2_{ij}) calculated using a group contribution method as follows (8):

$$[12] \qquad E^1_{ij} = -\frac{1}{2}\sum_{k=1}^{N}\sum_{l=1}^{N}(\alpha_{ik} - \alpha_{jk})(\alpha_{il} - \alpha_{jl})\,A^1_{kl}(T)$$

with

$$A^1_{kl} = {}_1A^0_{kl}\left(\frac{T^\circ}{T}\right)^{{}_1B^0_{kl}}$$

$$[13] \qquad E^2_{ij} = -\frac{1}{2}\sum_{k=1}^{N}\sum_{l=1}^{N}(\alpha_{ik} - \alpha_{jk})(\alpha_{il} - \alpha_{jl})\,A^2_{kl}(T)$$

with

$$A^2_{kl} = {}_2A^0_{kl}\left(\frac{T^\circ}{T}\right)^{{}_2B^0_{kl}}$$

where ${}_1A^0_{kl}$, ${}_1B^0_{kl}$, ${}_2A^0_{kl}$ and ${}_2B^0_{kl}$ are group interaction parameters. In this work, these parameters for the interchange energy between methane and methanol are obtained using the experimental results of vapour–liquid equilibrium for methane + methanol system from the literature (11). New values for ${}_2A^0_{kl}$ and ${}_2B^0_{kl}$ group interaction parameters for the binary interchange energy E^2_{ij} between methane and water are obtained using dew point experimental results available in Enagás, S. A. The values for these parameters used in later calculations of this work are presented in Table 3.

The chemical contribution to the residual molar excess Helmholtz energy of a mixture ($A^{\mathrm{E}}_{\mathrm{qui}}$) is based on the self-association model of Rauzy and Berro (9, 10) where the alcohol (methanol in this work) is assumed to form continuous linear hydrogen-bounded polymers M_1, M_2, …, M_i, … by successive chemical reactions:

$$M_1 + M_1 \xleftrightarrow{k_{\mathrm{M}}} M_2$$

$$M_2 + M_1 \xleftrightarrow{k_{\mathrm{M}}} M_3$$

$$\vdots$$

$$M_i + M_1 \xleftrightarrow{k_{\mathrm{M}}} M_{i+1}$$

described by a single equilibrium constant (k_{M}) of the form:

$$[14] \qquad k_{\mathrm{M}} = \frac{\eta RT}{[b(1-\eta)]}\exp\left(\frac{-\Delta A}{RT}\right)\exp\left(\frac{\beta Q(\eta)}{RT}\right)$$

The self-association Helmholtz energy (A) is obtained as follows:

$$[15] \qquad \Delta A = \Delta U^\circ + C_{\mathrm{T}}(T - T^\circ) - T\left(\Delta S^\circ + C_{\mathrm{T}}\ln\left(\frac{T}{T^\circ}\right)\right)$$

The values of U°, C_{T} are from the literature (8) but a new value for S° of –127.767 J K^{-1} mol^{-1} is obtained in this work using the experimental data of vapour–liquid equilibrium of methane + methanol system from the literature (11).

The chemical contribution to the residual molar excess Helmholtz energy ($A^{\mathrm{E}}_{\mathrm{qui}}$) of a mixture with p components where the component M is self-associated is calculated as:

$$[16] \qquad A^{\mathrm{E}}_{\mathrm{qui}} = A_{\mathrm{qui}} - A^{\mathrm{id}}_{\mathrm{qui}}$$

with

© 2000 NRC Canada

Fig. 2. Comparison between experimental dew point curves (symbol) and calculated with the EOS–CR method (line) for the system {$(1 - y_1 - y_2)$methane + $y_1$water + $y_2$methanol}: ■, y_1 = 0.00004, y_2 = 0.0009; □, y_1 = 0.00005, y_2 = 0.0011; ●, y_1 = 0.00008, y_2 = 0.0014; ○ y_1 = 0.00010, y_2 = 0.0014.

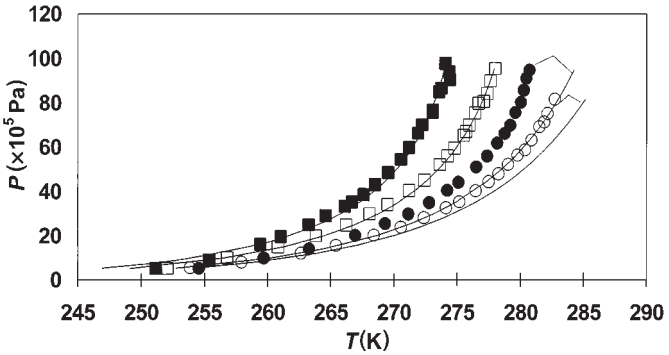


Fig. 3. Comparison between experimental dew point curves (symbol) and calculated with the EOS–CR method (line) for the system {$(1 - y_1 - y_2)$methane + $y_1$water + $y_2$methanol}: ■, y_1 = 0.00008, y_2 = 0.0007; □, y_1 = 0.00012, y_2 = 0.0008; ●, y_1 = 0.00016, y_2 = 0.0008; ○ y_1 = 0.00022, y_2 = 0.0013.

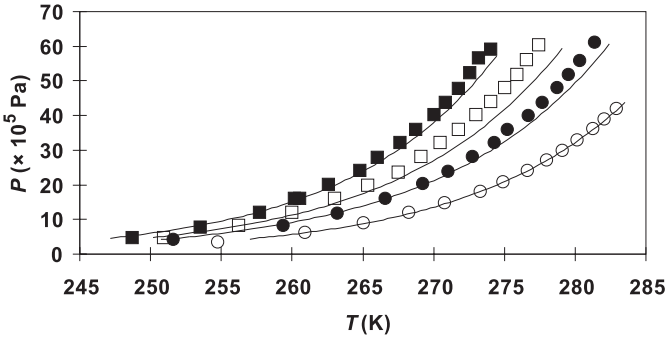


Fig. 4. Comparison between experimental dew point curves (symbol) and calculated with the EOS–CR method (line) for the system {$(1 - y_1 - y_2)$methane + $y_1$water + $y_2$methanol}: ■, y_1 = 0.00020, y_2 = 0.0006; □, y_1 = 0.00023, y_2 = 0.0009; ●, y_1 = 0.00036, y_2 = 0.0015; ○ y_1 = 0.00057, y_2 = 0.0023.

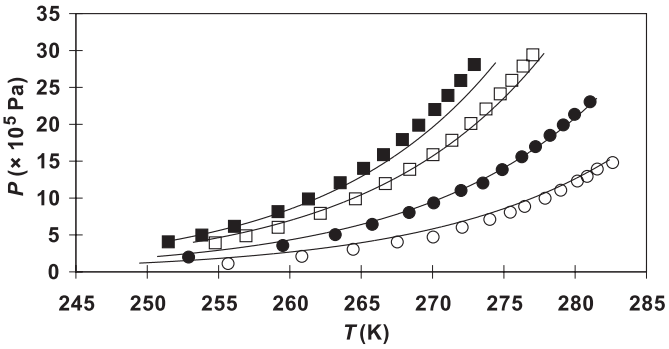
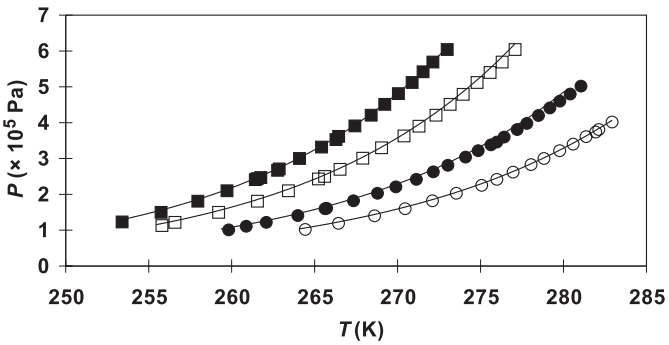


Fig. 5. Comparison between experimental dew point curves (symbol) and calculated with the EOS–CR method (line) for the system {$(1 - y_1 - y_2)$methane + y_1 water + y_2 methanol}: ■, y_1 = 0.00078, y_2 = 0.0022; □, y_1 = 0.00110, y_2 = 0.0023; ●, y_1 = 0.00175, y_2 = 0.0031; ○ y_1 = 0.00263, y_2 = 0.0035.



[17] $$A_{qui} = (x_M - X)\Delta A$$

[18] $$A_{qui}^{id} = x_M(1 - X_p)\Delta A$$

and

[19] $$X = \frac{X_1}{1 - k_M X_1}$$

where X_1 is the monomer molar fraction that is expressed as:

[20] $$X_1 = \frac{(1 + 2k_M x_M) - (1 + 4k_M x_M)^{1/2}}{2k_M^2 x_M}$$

The water self-association is not accounted for and the same for cross-association between water and methanol.

Discussion

The pressure and temperature values ranges studied in this work include *P–T* conditions in which methane gas hydrate is stable and can be obtained from the gas phase. However, the presence of methanol in the studied mixtures avoids the formation of hydrates and, on the other hand, the generation of hydrates in the device produces the quick interruption of gas flow, not observed in this work.

The experimental dew point curves and calculated with the ESO–CR method are represented in Fig. 2–5, as it can be seen in them an increase of contents of water and methanol in the mixtures of the system studied leads to a displacement of the dew point curves to higher values of dew temperatures and pressures.

After comparing the experimental and calculated dew point curves in Figs. 2–5, it can be concluded that the EOS–CR method used in this work reproduces very accurately the dew point curves independently of the pressure and temperature ranges. The mean deviations obtained are between 0.21 and 2.26 K. For each mixture studied in the present work the calculated values for molar fraction of both water and methanol in vapour phase are exactly the same as the experimental values.

Acknowledgements

The authors acknowledge financial and technical support from Enagás, S. A. during the experimental part of this work.

© 2000 NRC Canada

References

1. ISO 10101. Natural gas — Determination of water by the Karl–Fischer method. International Organization of Standardization, Geneva, Switzerland. 1993.
2. ISO 5725. Precision of test methods — Determination of repeatability and reproducibility for a standard test method by interlaboratory tests. International Organization of Standardization, Geneva, Switzerland. 1986.
3. A. Péneloux, W. Abdoul, and E. Rauzy. Fluid Phase Equilib. **47**, 115 (1989).
4. A. Péneloux, E. Rauzy, and R. Fréze. Fluid Phase Equilib. **8**, 7 (1982).
5. E. Rauzy. Les méthodes simples de calcul des équilibres liquide–vapeur sous pression. Thèse d'Etat — Sciences, Université Aix Marseille II, France, 1982.
6. B. Carrier. Modélisation des coupes lourdes des fluides pétroliers. Thèse de Docteur en Sciences, Université Aix Marseille III, France, 1989.
7. B. Carrier, M. Rogalski, and A. Péneloux. Ind. Eng. Chem. Res. **27**, 1714 (1988).
8. H. Hocq. Etude expérimentale et modélisation thermodynamique des mélanges méthanol – eau – hydrocarbures. Thèse en Sciences, Université de Droit, d'Economie et des Sciences d'Aix Marseille III, France, 1994.
9. E. Rauzy and C. Berro. Act. Colloq. Fluides Supercritiques Applications, (INPL 905267), 107 (1987).
10. E. Rauzy and C. Berro. International symposium of supercritical fluids. M. Perrut (*Editor*). 153 (1988).
11. J.H. Hong, P.V. Malone, M.D. Jett, and R. Kobayashi. Fluid Phase Equilib. **38**, 83 (1987).

List of Symbols

a equation of state energy parameter (Pa m^6 mol^{-2})
A molar Helmholtz energy (J mol^{-1})
A_{kl} group interaction parameter between groups k and l (J m^{-3})
b covolume; equation of state size parameter (m^3 mol^{-1})
$\bar{b}$ pseudo-covolume (m^3 mol^{-1})
C_T coefficient of CREE (Chimique Réticulaire Equation d'Etat) model (J K^{-1} mol^{-1})
E^1_{ij}, E^2_{ij} terms of the interchange energy (J m^{-3})
k constant of self-association equilibrium
K_{ij}, L_{ij} binary interaction parameters (J m^{-3})
N number of groups in a solution
p number of components in the mixture
P pressure (Pa)
q molecular surface (m^2)
Q Q'/η integral between 0 and η
Q' a packing fraction function
R gas constant (8.314 J mol^{-1} K^{-1})
T temperature (K)
$T°$ reference temperature (298.15 K)
v molar volume (m^3 mol^{-1})
$\bar{v}$ pseudo-molar volume (m^3 mol^{-1})
$v°$ molar close-packed fraction (m^3 mol^{-1})
x_M nominal molar fraction of component M in the mixture
X sum of molar fractions of polymer in the mixture
X_1 molar fraction of monomer in the mixture
X_p value of X when x_M is the unity
z compressibility factor

Greek letters

α_{ik} surface area fraction of group k in molecule i
γ constant of the translated Peng–Robinson cubic equation of state
δ adjustable parameter, proportionality coefficient between the surface measure (q) and the covolume (v)
ΔA molar Helmholtz energy of self–association (J mol^{-1})
$\Delta S°$ molar entropy of methanol self–association at $T°$ (J K^{-1} mol^{-1})
$\Delta U°$ molar energy of methanol self–association at $T°$ (J mol^{-1})
η packing fraction

Subscripts

c critical property
fis physical contribution
i, j referring to components i, j
k, l referring to groups k, l
M referring to component M, which is considered self–associated
qui chemical contribution
res residual

Superscripts

E excess property
id ideal solution property

© 2000 NRC Canada

Rate and equilibrium constants for formation and hydrolysis of 9-formylfluorene oxime: diffusion-controlled trapping of a protonated aldehyde by hydroxylamine

R.A. More O'Ferrall, D.M. O'Brien, and D.G. Murphy

Abstract: Equilibrium constants K_{add} = 440 and K_{ox} = 3.0 × 10^8 for formation of a carbinolamine adduct and oxime, respectively from 9-formylfluorene and hydroxylamine, and pK_a = –1.62 for protonation of the oxime, have been evaluated at 25°C in aqueous solution, based on measurements in hydroxylamine buffers, acetic acid buffers, and dilute HCl. Rate constants for hydrolysis of the oxime have been measured in the acidity range pH 4–12 M $HClO_4$. At the highest acidities, a reaction pathway via protonated carbinolamine has been identified: evidence is presented that the reverse of this reaction involves rate-determining attack of hydroxylamine upon protonated 9-formylfluorene. By assuming that the attack of hydroxylamine is diffusion-controlled, with rate constant 3 × 10^9 M^{-1} s^{-1}, a pK_a for *O*-protonation of the aldehyde (–4.5) is derived. Taking account of the equilibrium constant for enolization of 9-formylfluorene (K_E = 16.6), a pK_a for for *C*-protonation of the enol tautomer (–5.7) may also be obtained. Comparison of this pK_a with that of the enol of acetophenone shows that the enol of 9-formylfluorene is less basic by a factor of 10^{10}. By combining pK_as for protonation of the aldehyde and oxime with measured or estimated equilibrium constants for addition of water, hydroxide ion, and hydroxylamine to 9-formylfluorene, it is also possible to obtain values of pK_R = –5.3, 4.1, and 12.25 for the protonated 9-formylfluorene, protonated oxime, and 9-formylfluorene, respectively. The usefulness of pK_R in providing a general measure of equilibrium constants for electrophile–nucleophile combination reactions is discussed.

Key words: oxime, formyfluorene, hydrolysis, protonation, diffusion-control.

Résumé : En se basant sur des mesures faites en solutions aqueuses, à 25°C, dans des tampons d'hydroxylamine ou d'acide acétique et dans des solutions diluées de HCl, on a établi les valeurs des constantes d'équilibre pour la formation de l'adduit carbinolamine (K_{add} = 440) et de l'oxime ((K_{ox} = 3,0 × 10^8) entre le 9-formylfluorène et l'hydroxylamine ainsi que le pK_a (= –1,62) de la protonation de l'oxime. On a mesuré les constantes de vitesse d'hydrolyse de l'oxime dans les domaines d'acidité allant de pH 4 à 12 M, $HClO_4$. Aux acidités les plus élevées, on a identifié la présence d'une voie réactionnelle impliquant la carbinolamine protonée: on présente des données suggérant que l'étape déterminante de la réaction inverse implique une attaque de l'hydroxyle sur le 9-formylfluorène protoné. En faisant l'hypothèse que l'attaque de l'hydroxylamine est soumise à un contrôle par la diffusion, on en déduit que sa constante de vitesse est de 3 × 10^9 M^{-1} s^{-1} et que le pK_a de la *O*-protonation de l'aldéhyde est de –4,5. Si l'on tient compte de la constante d'équilibre de l'énolisation du 9-formylfluorène (K_E = 16,6), on a aussi obtenu une valeur de pK_a (–5,7) pour la *C*-protonation de l'éther énolique. Une comparaison de ce pK_a avec celui de l'énol de l'acétophénone montre que l'énol du 9-formylfluorène est moins basique par un facteur de 10^{10}. En combinant les valeurs de pK_a de protonation de l'aldéhyde et de l'oxime avec les constantes de vitesse mesurées ou évaluées pour l'addition de l'eau, de l'ion hydroxyde et de l'hydroxylamine au 9-formylfluorène, on peut aussi obtenir les valeurs de pK_R = –5,3, 4,1 et 12,25 respectivement pour le 9-formylfluorène protoné, l'oxime protoné et le 9-formylfluorène. On discute de l'utilité des pK_R comme mesure générale des constantes d'équilibre pour les réactions de combinaison électrophile–nucléophile.

Mots clés : formylfluorène, hydrolyse, protonation, contrôle par diffusion.

[Traduit par la Rédaction]

Received March 28, 2000. Published on the NRC Research Press website on December 4, 2000.

This paper is dedicated to Jerry Kresge in honour of his many achievements in physical organic chemistry.

R.A. More O'Ferrall,[1] D.M. O'Brien, and D.G. Murphy. Department of Chemistry, University College Dublin, Belfield, Dublin 4, Ireland.

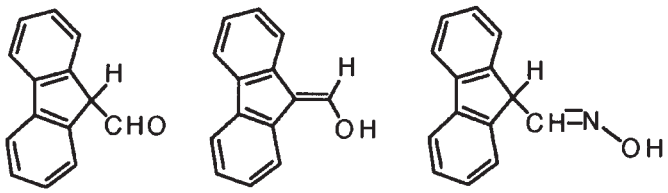
[1]Author to whom correspondence may be addressed. Telephone: 353-1-706-2285. Fax: 353-1-706-2127. e-mail: rmof@macollamh.ucd.ie

 © 2000 NRC Canada

Introduction

The main features of the mechanism of formation and hydrolysis of oximes are now fairly well understood based on studies extending over more than 30 years (1–13). Nucleophilic attack of hydroxylamine upon an aldehyde or ketone yields initially a carbinolamine adduct which undergoes acid- or base-catalysed dehydration to form the oxime; depending on the pH either formation or reaction of the adduct may be rate-determining. Less well understood, however, is the structural dependence of rate and equilibrium constants for these reactions (2). Thus for oximes of aldehydes measurements have focused largely on aromatic aldehydes (1–6), presumably because these are easily prepared and show a strong UV absorbance convenient for monitoring the reactions. Studies of aliphatic aldehydes have either been less comprehensive (7, 8) or have involved reactions of *N*-alkyl or *N*-aryl hydroxylamines leading to nitrones (9).

In this paper we report measurements for formation and hydrolysis of the oxime of the (aryl-substituted) aliphatic aldehyde, 9-formylfluorene (**1**). This aldehyde is unusual in that it exists in aqueous solution predominantly as its enol tautomer **2** (14). The chromophore associated with the enol eases kinetic and equilibrium measurements, while the availability of rate and equilibrium constants for enolization and hydration (14) allows reactions of the enol to be transformed to those of the aldehyde.



1 **2** **3**

The main aim of the study was to obtain rate and equilibrium constants for overall formation of the oxime **3** and for the individual steps of this reaction. Of particular interest were the protonation and hydration of the oxime. Measurement of the equilibrium constant K_R for the hydration reaction, shown in the first steps of eq. [1], identifies the protonated oxime **4** as a carbocation and allows comparisons of its stability with that of other carbocations (15).

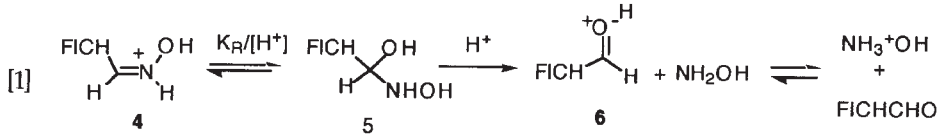
Also of interest are the mechanism and equilibria asssociated with hydrolysis of the oxime in acidic media. It is proposed that in strongly acidic solutions the carbinolamine intermediate **5** is subject to protonation and reacts initially to form hydroxylamine and the *O*-protonated 9-formylfluorene (**6**). If this is correct, and we assume that the reverse reaction, attack of hydroxylamine on the protonated aldehyde, is diffusion-controlled, rate constants for the forward and reverse reactions can be combined to assign an equilibrium constant for conversion of protonated oxime to protonated aldehyde. This in turn leads to values of K_a and K_R for the conjugate acid of 9-formylfluorene.

Results

Hydrolysis of the oxime

Formation and hydrolysis of the oxime of 9-formylfluorene have been studied as forward and reverse reactions. The hydrolysis occurs at a convenient rate for measurement in the pH range 0–4 and in concentrated solutions of HCl and $HClO_4$. The reaction is much slower than keto–enol tautomerization of 9-formylfluorene and except at highest acid concentrations, where the tautomeric equilibrium is displaced in favour of the aldehyde, it could be monitored by the appearance of the chromophore of the enol. A repetitive scan for the conversion of oxime to enol is shown in Fig. 1, and demonstrates that the product has the distinctive chromophore of fluorene. In Fig. 2, a pH profile for the hydrolysis is shown with logs of first-order rate constants (k_{obs}) plotted against pH – X, where X is the usual solvent free energy parameter (16) measuring the effect of a strong acid medium upon the protonation of an aniline base. The X-function was formulated by Cox and Yates (17) for correlating measurements of rate and equilibrium constants in aqueous mixtures of strong acids. Thus plots of log ($k_{obs}/[H^+]$) against $-X$ are normally linear and are characterized by a slope m^*. The value of pH – X also provides a convenient formal extension of pH equivalent to the "acidity function" H_o. In principle, correlations based on X should be independent of the nature of the acid but it is evident from the figure that hydrolysis of the oxime shows significant divergence between $HClO_4$ (open circles) and HCl (closed circles) at high acidities; similar relative effects of HCl and $HClO_4$ have been observed in the hydrolysis of triaryl carbocations (18). Values of k_{obs}, X (18), and pH are listed in Table S1.[2]

It can be seen from Fig. 2 that the hydrolysis reaction is acid-catalyzed above pH 2. Below pH 2 it approaches pH independence, and after passing through a weak max decreases with increasing acidity at high acid concentrations (>5 M $HClO_4$). This rather complex behaviour receives a fairly straightforward interpretation in terms of the expected mechanism of hydrolysis which, as we will see, is confirmed by studies of the reverse reaction forming the oxime. A similar acidity dependence has been described by Gregory and Moodie (10) for hydrolysis of the oxime of acetophenone.



(FlCH_2 denotes fluorene)

[2] Tables of kinetic and equilibrium data (S1–S4) have been deposited and may be purchased from: The Depository of Unpublished Data, Document Delivery, CISTI, National Research Council Canada, Ottawa, ON K1A OS2, Canada.

© 2000 NRC Canada

Fig. 1. Repetitive scan of spectra during hydrolysis of the oxime of 9-formylfluorene (3×10^{-5} M) in 0.1 M $HClO_4$.

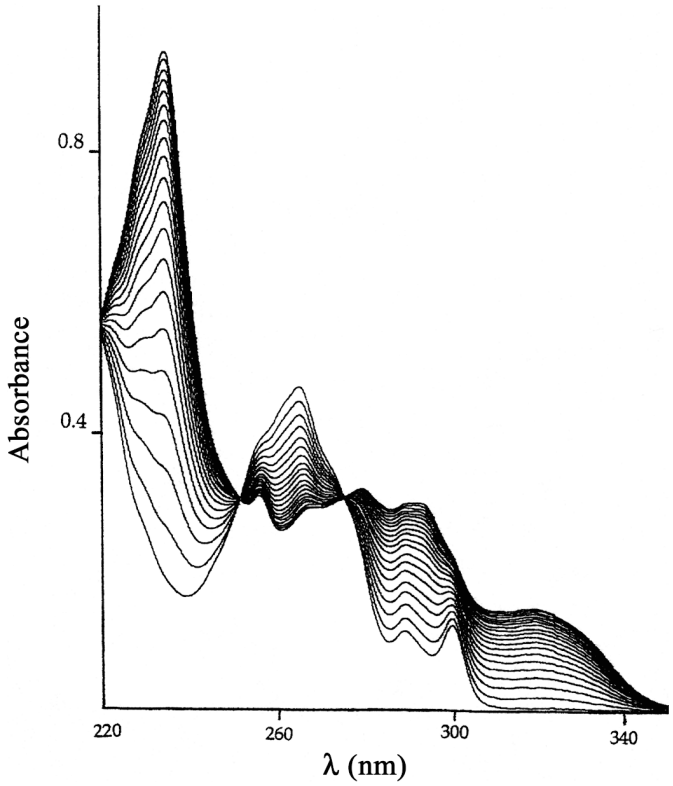
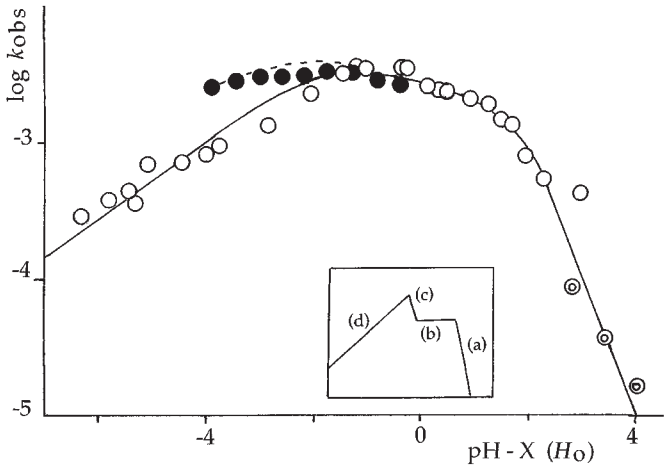


Fig. 2. Dependence of log k_{obs} upon pH – X (pH or H_0) for hydrolysis of the oxime of 9-formylfluorene in $HClO_4$ (○), aqueous chloroacetic acid buffers (◎), and HCl (●) at 25°C. The inset shows schematically limiting acidity dependences inferred.

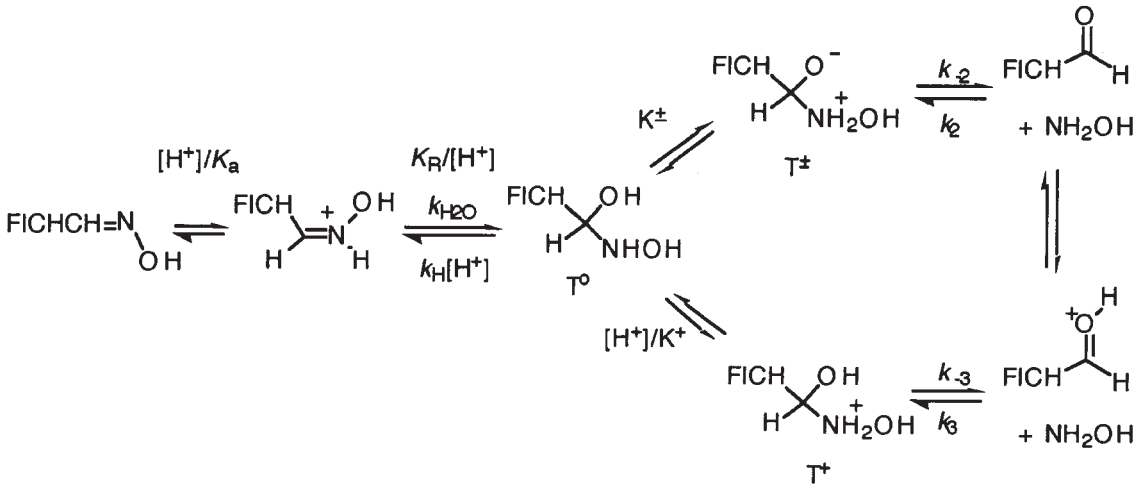


The sequence of steps expected to occur in the hydrolysis reaction is shown in Scheme 1 (10). It comprises: (*i*) rapid protonation of the oxime (with equilibrium constant K_a); (*ii*) attack of H_2O on the protonated species to form a carbinolamine intermediate; and (*iii*) reaction of the carbinolamine to form the product aldehyde via zwitterionic and (or) protonated intermediates $T^{\pm}$ and T^+, respectively.

In Scheme 1, rate constants for attack of water on the protonated oxime and for reaction of the zwitterionic and *N*-protonated forms of the adduct are denoted k_{H_2O}, k_{-2}, and k_{-3}, respectively; k_H is the rate constant for acid-catalyzed reversion of carbinolamine to protonated oxime. Negative subscripts are used for rate constants to retain positive values for oxime formation. By analogy with previous studies (1–6) the acid-dependent reaction at high pH corresponds to the k_{H_2O} step being rate-determining, while the transition to pH independence around pH 2 indicates that the k_{-2} step has become rate-determining. The weak max in the pH profile should correspond to protonation of the oxime and the transition from reaction via $T^{\pm}$ to reaction via T^+ as an intermediate.

It should be noted that, in principle, protonation of the oxime could be associated with the break in the pH dependence at either pH – X = –1.5 or +2. Evidence that it is the former comes from measurements of the UV spectra of the oxime prior to hydrolysis which show a significant change in the acid concentration range (3–6 M $HClO_4$). The spectrum of the oxime is dominated by the chromophore for fluorene but shows an end absorption and a weaker than normal long-wavelength peak at 300 nm ($\varepsilon = 1.1 \times 10^4$). The end absorption disappears between 1.0 and 2.5 M and the peak at 300 nm decreases with a satisfactorily defined isosbestic point (290 nm) between 3.0 and 6.0 M $HClO_4$. The latter

Scheme 1.



© 2000 NRC Canada

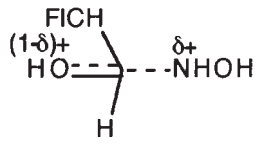
change is attributed to protonation; the former may reflect changes in solvation similar to those occurring prior to protonation of aliphatic carbonyl compounds (19). The protonation is also associated with a small increase and shift to shorter wavelengths of the peak at 260 nm. A plot of log K_a, calculated from the absorbance changes at 300 nm at different acid concentrations, against $-X$ has an intercept giving an aqueous pK_a = –1.5 and a slope m^* = 0.91. As discussed below, it is likely that these values correspond to an equilibrium mixture of *syn*- and *anti*-forms of neutral and protonated oxime. It is difficult to determine whether the protonated species is the oxime or oxime plus carbinolamine (T^+). An estimate of the pK = –2.12 for conversion of T^+ to the oxime, included in an appendix to this paper, suggests that the protonated oxime and T^+ are not very different in stability. Strictly speaking, therefore, the measured pK_a is an apparent value representing an equilibrium mixture of protonated species. Correcting for this, using the estimated pK for T^+, yields pK_a = –1.62 for the protonated oxime, although this value is clearly subject to some uncertainty.

The assumption that the reaction in strong acids is proceeding with the formation of T^+ as an intermediate is consistent with a reverse reaction in which attack of hydroxylamine upon the aldehyde is acid-catalyzed. This reaction has been well-characterized for aromatic aldehydes reacting with hydroxylamine, methoxylamine, and a range of weakly basic amines by Jencks and co-workers (2) and Sayer et al. (3). In principle reaction of the protonated oxime, which will be the reactant species in strongly acidic media (possibly in equilibrium with a fraction of T^+), should be independent of acid concentration. In practice it can be seen in Fig. 2 that there is a significant decrease in rate with increasing acid concentration, which is more pronounced in $HClO_4$ than HCl. We believe that this decrease is a result of a medium effect reflecting a reduced solvation requirement for the transition state compared with the reactant. For the closely analogous hydrolysis of the oxime of *p*-chlorobenzaldehyde, the reverse reaction, in which the oxime is formed from the aldehyde, is independent of acid concentration in strongly acidic media under conditions that the hydroxylamine reactant is fully protonated (3). This implies that hydrolysis of the protonated *oxime* of *p*-chlorobenzaldehyde is also independent of acid concentration.

Strictly speaking the decrease in rate with increasing acid concentration in Fig. 2 does not exclude the possibility of rate-determining loss of NH_2OH from the zwitterionic form of the tetrahedral intermediate $T^{\pm}$, a reaction which would be inversely dependent on stoichiometric acid concentration. However, comparison with the hydrolysis of *p*-chlorobenzaldehyde-*N*-phenyl imine (20), a reaction which almost certainly does proceed via $T^{\pm}$, shows that a plot of log k vs. X implies a much sharper decrease in rate with increasing acid concentration ($m^* \cong 1.3$) than for the oxime of 9-formylfluorene (m^* = 0.3). Moreover, reaction via $T^{\pm}$ would be expected to show a fairly large "normal" solvent isotope effect (k_{H_2O}/k_{D_2O} = 2–3) as a consequence of the preequilibrium deprotonation of the (protonated) oxime reactant in strongly acidic media. The experimentally observed isotope effect, k_{H_2O}/k_{D_2O} = 1.3, is not consistent with this.

An alternative acid-independent reaction (for hydrolysis of the protonated oxime) could involve deprotonation of T^+ to form $T^{\pm}$ (2, 3). However, this mechanism is viable only when expulsion of hydroxylamine from $T^{\pm}$ is faster than reprotonation to form T^+. This is not expected of $T^{\pm}$ intermediates derived from aliphatic aldehydes because such intermediates should be relatively stable; nor is it likely at high acid concentrations. The scope of the T^+ mechanism and different modifications of the $T^{\pm}$ mechanism for hydrolysis and formation of oximes and other imines has been summarised by Sayer and co-workers (3). (Although, as will be discussed below, we differ from these authors in believing that loss of NH_2OH from T^+ is a stepwise process and not a concerted one).

Returning to Fig. 2, the line drawn through the points is based on a best fit of rate constants and m^* values for rate-determining expulsion of NH_2OH from the zwitterionic and protonated carbinolamine intermediates ($T^{\pm}$ and T^+ in Scheme 1) at low pH and hydration of the protonated oxime at high pH. Each m^* corresponds to the slope of a plot of log ($k_{obs}/[H^+]$) vs. X (or, for acid-independent reactions, log k_{obs} vs. X) in concentrated solutions for the appropriate reaction step or mechanism; details are given in the experimental section. The limiting acidity dependences assigned in different acid regions are shown schematically in the inset to the figure and are labelled (*a*)–(*d*) in the direction of increasing acid concentration. For protonation of the oxime m^* and K_a were taken as their equilibrium values (above). The transition from reaction via the zwitterionic ($T^{\pm}$) to protonated (T^+) tetrahedral intermediate is presumed to occur just before the onset of protonation of the oxime. This is not well-defined by the results for $HClO_4$ but is suggested by the near constancy of the rate in hydrochloric acid solutions in the range 3–11 M (filled circles). As noted above, the weak but distinctive decrease in rate constants at high concentrations of $HClO_4$ implies a transition state with greater solvation demands than the protonated oxime (16). This is consistent with the expected structure of the transition state for reaction of T^+ which should lead to relocation of charge to the solvation sensitive hydrogen-bearing oxygen atom, as shown in **7**. Indeed, it will be argued below that for 9-formylfluorene oxime the bond to nitrogen is completely broken and the charge fully transferred to oxygen. The decrease in log k_{obs} at high acid concentrations corresponds to an m^* value (slope of log k_{obs} vs. X) of –0.3.



7

A source of uncertainty in the pH profile is the influence of *syn*- and *anti*-tautomerism of the oxime on the hydrolysis reaction. The NMR spectrum of the oxime indicates that its configuration is *syn* and this form must be the reactant at high pH. However, below pH 2 where nucleophilic attack of water on the protonated oxime becomes reversible, *syn–anti* tautomerization should be faster than hydrolysis. Nucleophilic catalysis of *syn–anti* tautomerization of aldehyde oximes has been studied previously by Cocivera et al. (7). The equilibrium ratio of isomers is expected to be about 1:2

© 2000 NRC Canada

$$[2]\qquad k_{obs} = \frac{k_{H2O}k_{-2}K^{\pm}}{(k_H[H^+] + k_{-2}K^{\pm})(1 + K_a/[H^+])} + \frac{k_{H2O}k_3}{(1 + K_a/[H^+])k_HK^+}$$

$$(a)\quad \frac{k_{H2O}[H^+]}{K_a} = 0.10[H^+] \qquad (b)\quad \frac{k_{H2O}k_{-2}K^{\pm}}{k_HK_a} = 2.5 \times 10^{-3}$$

$$(c)\quad \frac{k_{-3}k_{H2O}[H^+]}{k_HK^+K_a} = 6.0 \times 10^{-4}[H^+] \qquad (d)\quad \frac{k_{H2O}k_3}{k_HK^+} = 1.1 \times 10^{-2}$$

(21) and establishing this equilibrium should slow the reaction. However, it was not possible to separate the effect on the rate of isomerization from that of the subsequent (presumed) change from the $T^{\pm}$ to T^+ reaction pathway, and it is assumed that the rate constant for the pH-independent process below pH 2 represents reaction of the equilibrated isomers. In principle the onset of tautomerization should be detectable as a perturbation of first-order kinetics in the hydrolysis reaction. However, no significant departure from first-order kinetics was detected, and this is probably a consequence of the similarity of spectra, lack of pronounced difference in reactivities of the two isomers, and possibly rapidity of isomerization.

If *syn–anti* tautomerism is neglected the appropriate rate expression to fit the experimental dependence of first-order rate constants for hydrolysis (k_{obs}) on acid concentration in the limit of low acid concentrations is given by eq. [2]. In this equation the notation for rate and equilibrium constants follows that of Scheme 1. The equilibrium constants K^+ and $K^{\pm}$ refer to formation of the tetrahedral intermediates T^+ and $T^{\pm}$, respectively from the carbinolamine adduct (T°). Limiting rate expressions corresponding to the different sections of the pH – *X* profile ((*a*)–(*d*)) are indicated below the equation together with the numerical values used to obtain the best fit. For the reactions in concentrated acid solutions the expressions were modified by inclusion of *m** values. However, as noted above, these modifications are described in the experimental section and here *m** values are summarized only.

Thus the region (*a*) in Fig. 2 is well fitted by $k_{H_2O}/K_a = 0.10$. If the pK_a of the protonated oxime is assigned its independently measured value of –1.62 we then derive $k_{H_2O} = 4.2\ s^{-1}$. The value of *m** for the protonation was assumed to be the same as its equilibrium value (0.9) and the same value was assumed for the acid-catalyzed expulsion of NH_2OH from T° (via T^+). The analysis is rather insensitive to choice of the latter *m** or to dissection of *m** = 1.2 implied for the equilibrium conversion of T° to protonated oxime into kinetic values for the forward and reverse constants k_H (*m** = –0.8) and k_{H_2O} (*m** = 0.4).

The limiting rate constant accommodated by the pH profile in region (*b*) was 2.5×10^{-3}. Correction of this for the contribution of $k_{H_2O}/K_a = 0.10$ and $k_H = 8.5 \times 10^4$, evaluated from the reverse oxime forming reactions in hydroxylamine buffers, yields $k_{-2}K^{\pm} = 2.1 \times 10^3\ s^{-1}$. For the reaction at the highest acidities (*d*), extrapolation to *X* = 0 yields values of $k_{H_2O}k_{-3}/k_HK^+ = 1.1 \times 10^{-2}\ s^{-1}$ for $HClO_4$ and 9.0×10^{-3} for HCl. The difference in the values reflects the divergence of rate constants between the two acids at high acid concentrations, which appears to be due partly to a different dependence of *X* upon stoichiometric acid concentration and possibly to small differences in *m** values between the two acids. Taking 1.0×10^{-2} as an average value for this rate constant yields $k_{-3}/K^+ = 200\ s^{-1}$. In principle, at more moderate acidities (*c*), where the oxime is unprotonated, the rate expression for region (*d*) is modified by dividing by $K_a/[H^+]$; however, as already implied, region (*c*) makes little impact on the pH profile.

As a general comment, although it might appear that the pH and X dependence of Fig. 2 is relatively featureless and should offer considerable flexibility in choice of the several rate constants and *m** values implicated in the fit, in practice the rate constants defined by regions (*a*) and (*b*) and even (*d*) are sharply constrained. Probably the main uncertainty resides in the pK_a for protonation of the oxime, arising partly from the possible formation of T^+ as well as protonated oxime.

In addition to measurements for HCl in H_2O rate constants were measured for DCl in D_2O. There was little variation in the isotope effect with acid concentration, with values of k_{H_2O}/k_{D_2O} in the range 1.25–1.35 between 1 M and 6 M acid concentration (Table 1). These isotope effects should correspond to regions (*d*) and (*b*) of the pH profile, i.e., to reaction of the protonated oxime by the T^+ pathway and of the neutral oxime via the $T^{\pm}$ pathway, as discussed below. The smallness of the variation may reflect a rough coincidence of the pH at which the change between $T^{\pm}$ and T^+ pathways occurs and the pK_a of the protonated oxime. Similar isotope effects have been found for the hydrolysis of acetophenone oxime (10).

Formation of oxime from 9-formylfluorene

Hydrolysis of the oxime of 9-formylfluorene was monitored by the appearance of the chromophore of the enol. The reverse oximation could be monitored by its disappearance. The reaction was studied by introducing a small amount of enol from a stock solution in acetonitrile into aqueous solutions containing hydroxylamine. In acetonitrile the enol is the only isomer detectable by NMR, and it was presumed that at low concetrations of hydroxylamine (in aqueous solution) the enol exists in rapid equilibrium with a few percent

© 2000 NRC Canada

Table 1. First-order rate constants for hydrolysis of 9-formylfluorene oxime in aq. HCl and DCl, measured at 270 nm and 25°C.

Solution	pH	H_o	$k_{obs} \times 10^3$ (s^{-1})
[HCl] (M)			
6.10	–0.79	–2.15	3.19
4.88	–0.69	–1.74	3.25
3.66	–0.56	–1.32	3.31
2.44	–0.39	–0.87	2.86
1.22	–0.086	–0.32	2.62
[DCl] (M)			
6.10	–0.79	–2.15	2.51
3.03	–0.48	–1.09	2.34
2.02	–0.31	–0.697	2.25
1.35	–0.13	–0.386	2.14

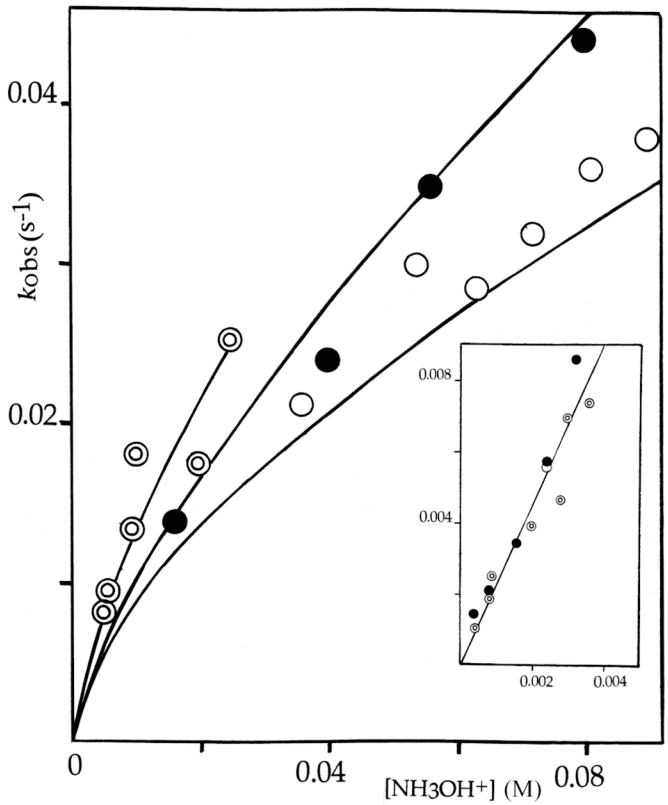
of aldehyde (K_E = [enol]/[aldehyde] = 16.6) (14). At higher concentrations of NH_2OH, where oxime formation is rapid, conversion of the enol to aldehyde becomes rate determining in the oximation reaction. At low pH and low concentrations of NH_2OH competing hydration of the aldehyde may also occur, giving at equilibrium, together with the aldehyde and enol, about 30% of hydrate (K_h = 5.6 for the aldehyde). By use of these equilibrium constants measured rate constants could be adjusted so that rate constants refer specifically to reaction of the aldehyde.

Several measurements of rate and equilibrium constants for reaction of the enol with hydroxylamine were undertaken: (*i*) the equilibrium conversion of enol to carbinolamine adduct in aqueous hydroxylamine buffers; (*ii*) the corresponding equilibrium between enol and oxime in aq. HCl in the presence of hydroxylammonium chloride; (*iii*) rates of formation of the oxime in hydroxylamine and acetic acid buffers (in which dehydration of the carbinolamine intermediate is rate determining); and (*iv*) rates of formation of the oxime in dilute aq. HCl and $HClO_4$ (for which the rate-determining step is attack of hydroxylamine upon the 9-formylfluorene).

Enol–carbinolamine equilibrium

Injection of a small quantity of a 10^{-2} M stock solution of the enol of 9-formylfluorene into hydroxylamine buffers led to a rapid buffer concentration-dependent drop in absorbance consistent with the formation of an aldehyde–hydroxylamine adduct **5** as shown in eq. [3]. This initial drop in absorbance was followed by a slower decrease attributed to the reaction forming the oxime. Initial absorbances were extrapolated to times of mixing and yield an effective equilibrium constant K = 25.0 between **5** and the equilibrated enol and aldehyde species (and hydroxylamine). This may be corrected to K_{add} = 440 for the aldehyde by division by 0.057 (= $1/(1 + K_E)$), the fraction of aldehyde present at equilibrium. Under the conditions of the reaction conversion of the aldehyde to hydrate is expected to be slow, so this species is not included in the equilibration.

Fig. 3. Plot of k_{obs} against [NH_3OH^+] for oxime formation from 9-formylfluorene enol in aqueous hydroxylamine buffers at 25°C with [acid]/[base] buffer ratios 1:1 (◎), 4:1 (●), 9:1 (○). The inset shows measurements at low buffer concentrations with rate constants (k_{obs}) corrected for carbinolamine adduct formation; [acid]/[base] buffer ratios 3:7 (○), 1:4 (●), 1:9 (◎).

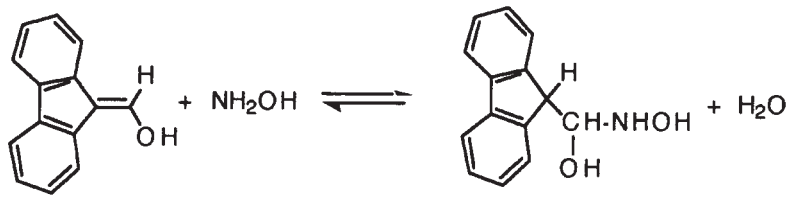


Oxime formation in hydroxylamine buffers

In hydroxylamine buffers, 9-formylfluorene is converted to its oxime with strong buffer catalysis, predominantly by the acidic component of the buffer. This is apparent from the plot of first-order rate constants at different buffer concentrations and buffer ratios against [NH_3^+OH] for the more acidic buffers investigated in Fig. 3. The measured rate constants are listed in Table S2.[2]

From the figure it can be seen that the buffer plots are curved. This curvature occurs at too low a concentration of hydroxylamine to be attributed solely to conversion of the enol reactant to the hydroxylamine adduct of the aldehyde,

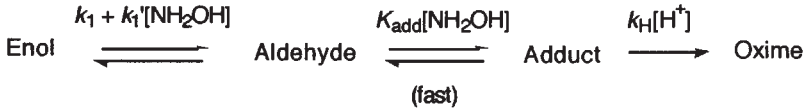
[3]



5

© 2000 NRC Canada

Scheme 2.



and it is apparent that there is a change in rate-determining step from dehydration of the adduct at low hydroxylamine concentrations to conversion of the enol to aldehyde at high concentrations. The curvature is not more pronounced because conversion of the enol to aldehyde is catalyzed by the basic component of the buffer, NH_2OH.

The curves drawn in Fig. 3 represent a best-fit of rate constants to a kinetic expression based on Scheme 2, in which k_H is the rate constant for acid-catalyzed dehydration of the adduct and k_1 and k_1' are rate constants for uncatalyzed and hydroxylamine-catalyzed ketonisation of the enol of 9-formylfluorene. This expression is given in the experimental section of the paper. The dependence of the rate of the overall reaction upon $[NH_3OH^+]$ arises from the combination of $k_H[H^+]$ for dehydration with $K_{add}[NH_2OH]$ from the preceding rapid equilibrium.

The analysis yields the rate constants k_H and k_1'. The value of k_1' was 3.1 which fits satisfactorily a Bronsted plot for general base-catalyzed ketonization of the enol (14). Values of k_1 and K_{add} were those determined previously (k_1 = 0.254/16.6 =.0153) (14) or as described above (K_{add} = 440).

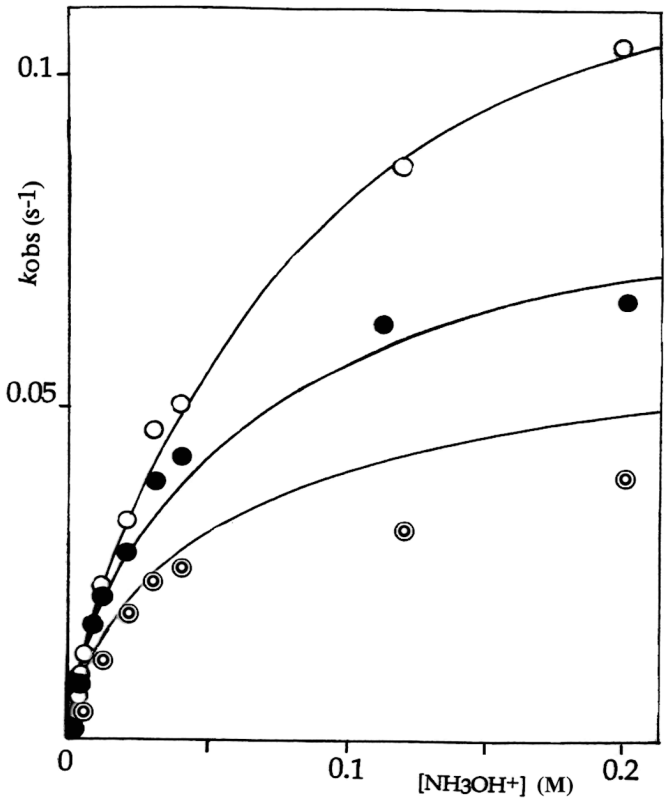
In practice the value of k_H was best determined from the slope of a linear plot of k_{obs} against $[NH_3OH^+]$ at high concentrations of NH_2OH, i.e., for basic hydroxylamine buffers with a high ratio of $[NH_2OH]$:$[NH_3OH^+]$. Under these conditions the k_H step is fully rate-determining and the slope of the plot is given by $k_H K_a K_{add}/K_E$, where K_a is the ionization constant of NH_3OH^+ (pK_a = 6). This plot is shown as an inset in Fig. 3. Values of k_{obs} are corrected for partial conversion to adduct by multiplying by $\{1 + (K_{add}/K_E)[NH_2OH]\}$. The value of k_H obtained was 8.5×10^4 M^{-1} s^{-1}. The lack of dependence of this value upon buffer ratio indicates that there is no appreciable catalysis by NH_3OH^+.

Oxime formation in acetic acid buffers

Similar measurements to those in hydroxylamine buffers were made in 1:1 acetic acid buffers with concentrations of the buffer components 0.025, 0.05, and 0.1 M. First-order rate constants (k_{obs}) for different stoichiometric concentrations of hydroxylamine hydrochloride are listed in Table S3[2] and plotted against $[NH_3OH^+]$ in Fig. 4. The figure shows more pronounced kinetic saturation at high concentrations of NH_3OH^+ than Fig. 3. This reflects the lower concentration of NH_2OH present at lower pH and hence weaker catalysis of ketonization at high concentrations of NH_3OH^+, when this step becomes rate-determining.

The kinetic expression describing the reaction in acetic acid buffers was similar to that in hydroxylamine buffers save that the initial ketonization step is catalyzed by acetate ion ($k_1 + k_1'[NH_2OH] + k_1''[AcO^-]$) and a small allowance is made for catalysis of dehydration by acetic acid. The dependence of the rate of ketonization upon concentration of acetate ion accounts for the strong dependence of the limiting rate constants at high concentrations of NH_3OH^+ seen in Fig. 4 upon buffer concentrations since under these conditions the ketonization step becomes rate-determining.

Fig. 4. Plot of k_{obs} against $[NH_3OH^+]$ for oxime formation from 9-formylfluorene enol in 1:1 aqueous acetic acid buffers at 25°C. [AcOH] = [AcO^-] = 0.1 M (○), 0.05 M (●), and 0.025 M (◎).



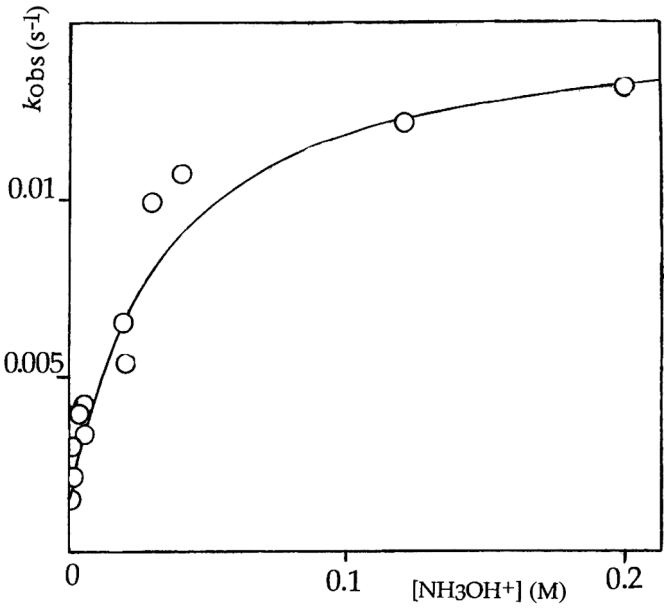
The lines drawn through the points in the figure are based on the same rate and equilibrium constants as for the hydroxylamine buffers but with k_1'' = 1.00 for the acetate-catalyzed ketonization, which compares reasonably well with the previously determined value of 0.88 (14). Account was taken of the change in concentrations of acetic acid and acetate ion at the relatively high concentrations of NH_3OH^+. A contribution of 20% to the rate from general acid-catalyzed dehydration in the 0.1 M acetic acid buffers (and proportionately less at lower concentrations) was assumed, taking Reimann and Jencks (1) study of *p*-chlorobenzaldehyde as a guide for this small correction. The fit to the data is satisfactory, except at the lowest concentration of acetic acid buffers; there it appears that the contribution of the water reaction and catalysis by hydroxylamine to the ketonization of 9-formylfluorene has been slightly overestimated relative to that of the acetate ion.

Oxime formation in aq. HCl

Measurements were also made of oxime formation in solutions of 0.05 M HCl. First-order rate constants are shown

© 2000 NRC Canada

Fig. 5. Plot of k_{obs} against [NH_3OH^+] for oxime formation from 9-formylfluorene enol in 0.05 M HCl at 25°C.



in Table S4[2] and are plotted against [NH_3OH^+] in Fig. 5. Pronounced kinetic saturation at high concentrations of NH_3OH^+ is again observed and as before can be attributed to a change in rate-determining step from oxime formation to ketonization. However, in this case the slowness of the reaction at low concentrations of NH_3OH^+ also signals a change in rate-determining step relative to higher pHs in the oximation reaction. The same change is apparent in the reverse hydrolysis reaction from the break in pH dependence between pH 1 and 3 seen in Fig. 2. In the oxime-forming direction this corresponds to the well-known transition from rate-determining dehydration of the hydroxylamine adduct at high pH to attack of hydroxylamine on the aldehyde at low pH (1–6).

In 0.05 M HCl the low concentration of hydroxylamine in equilibrium with hydroxylamine hydrochloride also renders the overall oxime forming reaction appreciably reversible if the concentration of NH_3OH^+ falls below 0.02 M. Taking account of this a kinetic expression for the reaction may be based on the reaction steps shown in Scheme 3.

In Scheme 3, k_2 is the rate constant for the attack of hydroxylamine upon the aldehyde. The rate constant for the reverse reaction is k_2/K_{ox} where K_{ox} = ([oxime]/[NH_2OH][FlCHCHO]) is the equilibrium constant for oxime formation from the aldehyde. The rate constant for the uncatalyzed enolization is k_1 and, as before, K_E is the keto–enol tautomeric constant. The line drawn through the data points in Fig. 5 corresponds to $k_1 = 0.0135\ s^{-1}$, $k_2 = 4.8 \times 10^5\ L\ mol^{-1}\ s^{-1}$, and intercept $k_2/K_{ox} = 1.6 \times 10^{-3}\ s^{-1}$.

Scheme 3 is oversimplified in that it neglects hydration of the aldehyde. At low pH the hydration reaction is acid-catalyzed and, in contrast to the reaction in hydroxylamine or acetic acid buffers, water now competes effectively with the low concentration of hydroxylamine present in trapping the aldehyde. In Fig. 5 it was assumed that equilibration is complete; therefore the measured value of k_2 (4.8×10^5) has been corrected for the presence of an equilibrium concentration of the hydrate in addition to the enol. Equilibration is probably incomplete at high concentrations of NH_3OH^+ and the value of $k_o = 0.0135\ s^{-1}$ compares with an independently measured value of 0.0170 for the enol alone. The latter value would be reduced to 0.0120 in the presence of an equilibrium concentration of hydrate, and it may be significant that the value measured here falls between these extremes.

Scheme 3.

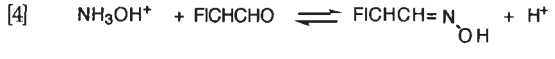


The oxime-enol equililibrium

Evaluation of the intercept in Fig. 5 and its identification with the rate constant for the reverse reaction of hydrolysis of the oxime k_2/K_{ox} allows us to evaluate an equilibrium constant for oxime formation (from the aldehyde) as $K_{ox} = 3.0 \times 10^8\ L\ mol^{-1}$. The value for the intercept (k_2/K_{ox}) is confirmed by measurements for the hydrolysis reaction in Fig. 2. This is the rate constant stemming from the break in the pH profile and change in rate-determing step below pH 2 corresponding to $k_{H_2O}k_{-2}K^{\pm}/k_HK_a$ (= k_2/K_{ox}). Although subject to a rate-enhancing medium effect in strong acid media, the rate constant extrapolated to dilute acid has the value of 2.5×10^{-3}, which is in acceptable agreement with 1.6×10^{-3} from Fig. 5 considering the uncertainties in extracting this rate constant from the experimental measurements in both cases. This agreement also provides confirmation that the break in the pH profile close to pH 2 in Fig. 2 does not correspond to the pK_a of the oxime.

The equilibrium between oxime and enol is also reflected in the incomplete conversion of enol to oxime. This indeed provides a more direct measurement of the equilibrium constant for this reaction. Because measurements are made at low pH, the equilibrium encountered experimentally (after correction for conversion of the enol to aldehyde) is that shown in eq. [4] and is sensitive to concentrations of both H^+ and NH_3OH^+. Analysis of measurements of enol absorbance as a function of concentration of H^+ and NH_3OH^+ gives a value of $K_{ox} = 2.2 \times 10^8\ M^{-1}\ s^{-1}$. In principle this value is preferred to that derived above (3.0×10^8) based on the slope and the intercept of the plot on Fig. 5 which is only approximately corrected for competition between oxime formation and hydration of the 9-formylfluorene.

However, yet another value of K_{ox} can be obtained from



rate constants for the reaction at higher pH where acid-catalyzed dehydration of the aldehyde–hydroxylamine adduct is rate-determining in the oxime forming direction. For the H^+-catalyzed reaction, we can write Scheme 4, in which the forward rate constant is k_HK_{add} and the reverse rate constant is k_{H_2O}/K_a. The value of k_{H_2O}/K_a is again obtainable from the pH profile for hydrolysis of the oxime at the highest pHs measured as $0.10\ M^{-1}\ s^{-1}$. The forward rate constant comes from the measurement of oxime formation in hydroxylamine buffers and yields a value of $k_HK_{add} = 3.7 \times 10^7$. The equilibrium constant is then given by

© 2000 NRC Canada

Scheme 4.

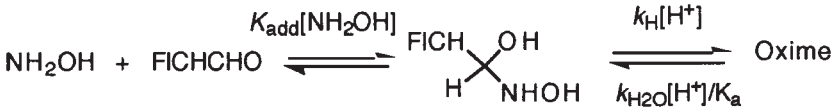


Table 2. Rate and equilibrium constants for oxime formation from 9-formyl-fluorene,[a] *p*-chlorobenzaldehyde[b], acetone[c], and acetophenone[d] in water at 25°C.[e]

	FlCHCHO	*p*-Cl-C_6H_4CHO	CH_3COCH_3	$PhCOCH_3$
K_{ox}	2.0×10^8	6.1×10^7	7.4×10^5	5.1×10^5
K_{add}[f]	440	23.5	1.0	
pK_a^{Ox} [g]	–1.62	–1.25	1.75	0.44
pK_R^{Ox} [h]	4.24	5.16	7.39	
pK_a^{ald} [j]	–4.52	–4.7	–3.07	–3.87
pK_R^{ald} [k]	–5.27	–2.9	0	(0.6)[m]
k_2	6.0×10^5	3.85×10^4	6×10^4	
k_H	7.5×10^4 [n]	5.55×10^4	1.5×10^6	
k_{H_2O}	4.6[n]	0.37	0.036	0.0042
k_H' [p]	5.2×10^4	5800	3300	300
k_3	(3×10^9)[q]	2.9×10^8	3.9×10^6	1.6×10^6

[a]The constants are presumed to refer to equilibrated mixtures of *syn*- and *anti*-oximes.

[b]References (1) and (3).

[c]References (5) and (12).

[d]Reference (10).

[e]The notation for rate and equilibrium constants follows that of Scheme 1.

[f]Further comparisons are provided by K_{add} = 105 for isobutyraldehyde (ref. (8)) and K_{add} = 1480 for trifluoroacetophenone (ref. (11)).

[g]pK_a of protonated oxime.

[h]pK_R of protonated oxime.

[j]pK_a of protonated aldehyde or ketone.

[k]pK_R of protonated aldehyde or ketone.

[m]From the pK_a of the ketone and an estimate of 3×10^{-5} for the equilibrium constant for hydration of acetophenone based on the experimental equilibrium constant for acetal formation (55).

[n]Because of over determination of rate and equilibrium constants, values of k_H and k_{H_2O} are adjusted relative to those determined experimentally.

[p]Rate constant for acid-catalyzed reaction of aldehyde or ketone with NH_2OH.

[q]Diffusion rate constant; the brackets indicate that this is an estimated value (cf. ref. (46)).

$k_H K_{add} K_a / k_{H_2O} = 3.7 \times 10^8$. This is in relatively poor agreement with 2.2×10^8 from direct monitoring of the equilibrium. However, it is possible that the larger value from the pH profile arises because reaction there is believed to involve hydration of the (possibly less reactive) *syn*-oxime whereas in the equilibrium measurements we should be dealing with an equilibrated mixture of *syn*- and *anti*-isomers.

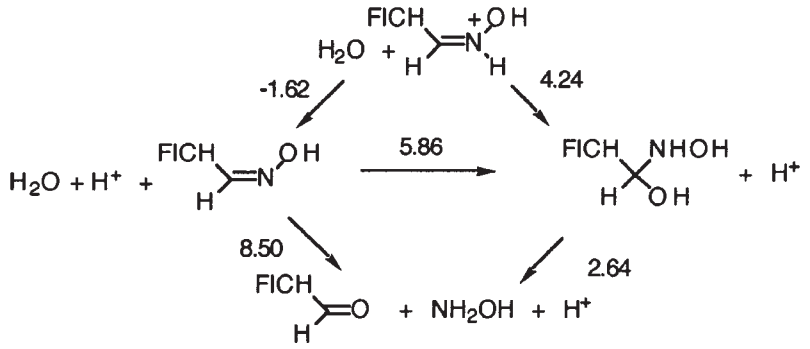
In practice we have taken $K_{ox} = 3.0 \times 10^8$. Since this does not correspond precisely to the ratio of experimentally determined forward and reverse rate constants, $k_{H_2O}/K_a = 0.1$ and $k_H K_{add} = 3.7 \times 10^7$, we have assigned "best" values of k_H and k_{H_2O} consistent with this value of K_{ox} which involve a minimum correction of the experimental values, i.e., $k_{H_2O}/K_a = 0.11$ and $k_H K_{add} = 3.3 \times 10^7$. With $pK_a = -1.62$ and $K_{add} = 440$, these yield $k_{H_2O} = 4.6 s^{-1}$ and $k_H = 7.5 \times 10^4$. These are the rate constants shown in the first column of Table 2. Corresponding values of $k_{-2}K^{\pm}$ and k_{-3}/K^+ are 1.4×10^3 and 160 s^{-1}, respectively. The value of $k_2 = 6.0 \times 10^5$ in Table 2 comes from the average of values of $k_2 K_{ox}$ (2.0×10^{-3}) together with $K_{ox} = 3 \times 10^8$.

Discussion

Equilibrium measurements for the formation and hydrolysis of the oxime of 9-formylfluorene provide access to equilibrium constants for the elementary reactions summarized in Scheme 5. The equilibrium constants are shown as negative logs (p*K*s), and, following Guthrie et al. (22), the p*K*s are expressed to two decimal places to avoid round-off errors. The arrows in the scheme indicate the direction of reactions to which the constants refer. Three of the equilibrium constants, those for formation of the oxime and carbinolamine adduct and for ionization of the protonated oxime, have been measured directly, and because the equilibria can be written as thermodynamic cycles (Scheme 5) two additional equilibrium constants, for addition of water to the oxime (pK = 5.86) and for the reaction of water with the protonated oxime (pK_R = 4.24), can be inferred. The p*K*s for these equilibria are summarized in Table 2. Also shown are values for the few oximes for which a comparable range of equilibrium constants can be evaluated. Apart from 9-formylfluorene, the table includes the oximes of acetone (5, 12), acetophenone (10), and *p*-chlorobenzaldehyde (1, 3).

© 2000 NRC Canada

Scheme 5.



A principal focus of the following discussion will be rate and equilibrium constants for electrophile–nucleophile combination reactions. Examples of these from Scheme 5 include the reactions of the protonated oxime with water and of 9-formylfluorene with hydroxylamine. Reactions of electrophiles with nucleophiles have been extensively discussed in the literature (23–25), but here attention will be confined to: (*i*) the use of the equilibrium constant K_R to measure the relative stability and affinity of electrophiles and nucleophiles; and (*ii*) the possibility of deriving values of pK_a and pK_R for the conjugate acid of 9-formylfluorene.

pK_R and stabilities of nucleophiles and electrophiles

Use of the equilibrium constant K_R as a measure of carbocation stability (15) is based on the reaction of the carbocation with water shown in eq. [5].

$$[5]\qquad R^+ + H_2O \overset{K_R}{\rightleftharpoons} ROH + H^+ \qquad K_R = \frac{[H^+][ROH]}{[R]}$$

Some years ago, Hine (23) suggested use of the equilibrium constant K_c to characterize the general reaction of electrophiles with nucleophiles shown in eq. [6].

$$[6]\qquad E^+ + N^- \overset{K_c}{\rightleftharpoons} EN \qquad K_c = \frac{[EN]}{[E^+][N^-]}$$

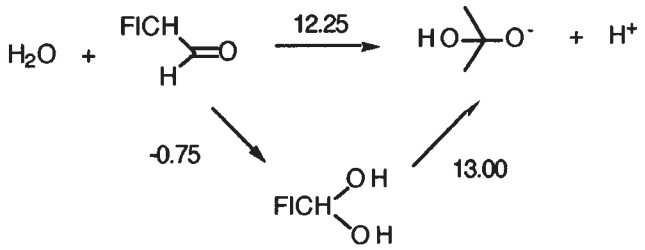
It was pointed out by Bunting (26) that when the nucleophile is a hydroxide ion, K_c and K_R provide equivalent measures of electrophile stability. Thus, Bunting reexpressed equilibrium constants for pseudo-base formation from reaction of hydroxide ion with a range of heterocylic cations as pK_R values, by using the relationship $K_R/K_c = K_w$ (where K_w is the autoprotolysis constant of water).

The same analysis can be applied to addition of hydroxide ion to a carbonyl group. This is illustrated by and provides a value of K_R for 9-formylfluorene. The appropriate equilibrium is shown in eq. [7].

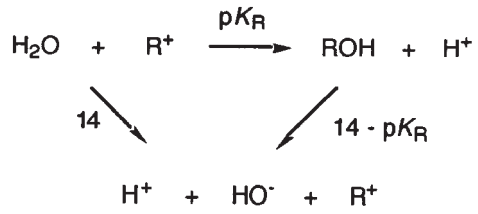
$$[7]\qquad H_2O + \text{>C=O} \overset{K_R}{\rightleftharpoons} HO\text{-C<}\,O^- + H^+$$

For most aldehydes K_R can be obtained from a direct measurement of K_c (27). For 9-formylfluorene, however, reaction in aqueous sodium hydroxide yields not the required hydroxide adduct but an enolate anion. K_R is then best obtained from the thermodynamic cycle of Scheme 6 which relates pK_R to the equilibrium constants for hydration of the aldehyde and ionisation of the hydrate to its monoanion.

Scheme 6.



Scheme 7.



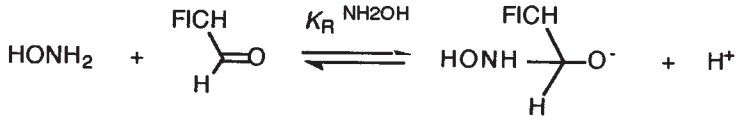
In this cycle the equilibrium constant for hydrate formation is known (K_h = 5.6) and the pK_a of the hydrate may be estimated as 13.0 from a Taft relationship for gem diols by taking σ^* = 0.41 for the fluorenyl group, on the assumption that this is the same as for Ph_2CH (28). Then, from pK_a = 13.57 for the hydrate of acetaldehyde (29) and ρ^* = 1.45 (30), we obtain pK_R = pK_h + pK_a = 12.25.

Again following arguments of Hine (23), we can write a further cycle of p*K*s as in Scheme 7 to show that pK_R measures the relative affinity (Lewis basicity) of a proton (H_3O^+) and an electrophile (R^+) towards hydroxide ion. This is apparent from the lower arms of the cycle which correspond to values of log K_c for reactions of H^+ and R^+ with hydroxide.

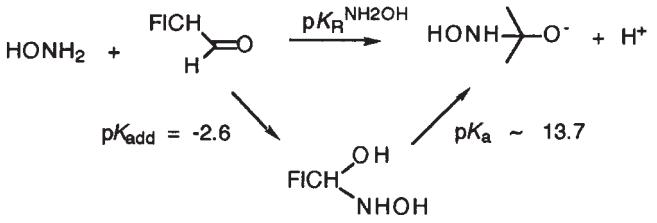
Hine (23) also used K_c to compare affinities (Lewis basicities) of electrophiles for nucleophiles other than hydroxide ion. For any nucleophile, we can again derive a value of "K_R" using the relationship $K_R/K_c = K_a$, where K_a is the ionization constant of the conjugate acid of the nucleophile. Thus in eq. [8] we write the equilibrium for reaction of 9-formylfluorene with hydroxylamine and denote the equilibrium constant $K_R^{NH_2OH}$.

A value for $pK_R^{NH_2OH}$ can be obtained in the same way as pK_R by combining equilibrium constants for formation and

© 2000 NRC Canada

[8] 

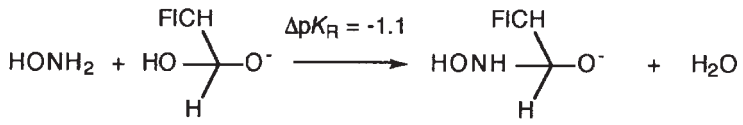
Scheme 8.



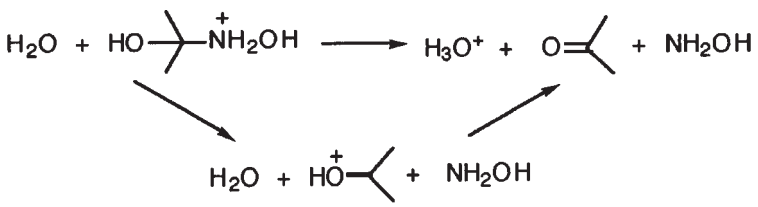
ionization of the carbinolamine adduct as shown in Scheme 8. The equilibrium constant for adduct formation pK_{add} is 2.64 and that for ionization may be estimated from pK_R = 13 for 9-formylfluorene hydrate by adding $\rho^*\Delta\sigma^*$, where ρ^* = 1.45 (30) and $\Delta\sigma^*$ is the difference in values of σ^* for OH and NHOH. Unfortunately the effect of NHOH on the ionization of an alcohol has not been determined directly and there is some doubt as to the value of σ^* to use. We took a value of 1.1 which may be compared with values of 1.2 for PhNH and 0.62 for NH_2 used recently by Guthrie et al. (22) for estimating pK_as of tetrahedral intermediates and with a value of 1.61 for OH based on the ionization constants of ethanol and formaldehyde hydrate. This gives pK_a = 13.7 and $pK_R^{NH_2OH}$ = 11.06. Jencks and co-workers (31) used σ_I = 0.18 for NHOH which implies a value of σ^* ~ 0.9 which is comparable with ours.

The difference between pK_R values of 9-formylfluorene with respect to the two nucleophiles (HO^- and $HONH^-$) indicates a difference in relative "carbon" and hydrogen basicities, $\Delta pK_R = pK_R^{NH_2OH} - pK_R^{H_2O} = -1.15$. The negative value implies that hydroxide ion has a smaller affinity for the carbonyl group relative to a proton (bound to water) than the hydroxylamide ion (eq. [9]). Identification of ΔpK_R as a measure of carbon basicity again follows Hine (23, 32). Although the difference between the nucleophiles in this instance is small, differences for other nucleophiles are much larger (32).

An advantage of using K_R rather than K_c to characterize equilibria for nucleophile–electrophile combination reactions is that K_R can sometimes be determined when K_c cannot, e.g., evaluation of K_c for NH_2OH in eq. [8] would require knowledge of the ionization constant of NH_2OH. On the other hand, K_c is required for investigating rate equilibrium correlations (23) so both equilibrium constants are of interest. In the light of current preoccupation with reactions between electrophiles and nucleophiles (25) it is possible that Hine's analysis has received less attention than it deserves (24).

[9] 

Scheme 9.



The mechanism of hydrolysis in strong acid

We may also derive values of pK_a and pK_R for the conjugate acid of 9-formylfluorene. To do so, however, it is necessary to consider the mechanism of hydrolysis of the oxime in strongly acidic media. As noted above, at high acid concentrations this reaction occurs exclusively via the protonated tetrahedral intermediate T^+ (Scheme 1). Twenty-five years ago, Jencks and co-workers (2), Sayer and co-workers (2, 3), and Sayer and Conlon (33) concluded that the reaction takes place by a concerted mechanism in which breaking of the C—N^+ bond occurs simultaneously with deprotonation of T^+ to form the hydroxylamine and aldehyde products in a single step. After reexamining the experimental data, however, and in the light of new measurements, we conclude that the mechanism is stepwise, with C—N bond-breaking preceding proton transfer and an *O*-protonated aldehyde being formed as a reactive intermediate. The alternative mechanisms are shown in the upper and lower pathways of Scheme 9.

Jencks and Sayer advanced two main arguments in favour of a concerted reaction. Firstly, they suggested that aldehydes were too weakly basic for their conjugate acids to be discrete intermediates in the acid-catalyzed oxime forming and hydrolysis reactions. Secondly, they argued that a stepwise mechanism was unlikely on the grounds that the rate of reaction in the oxime forming direction was insensitive to substituent effects in the aldehyde.

The first of these arguments was based on an estimate of the basicity of aldehydes which has since been revised. Thus, Reiman and Jencks (1) and Sayer regarded –8 as a reasonable value for the pK_a of *p*-chlorobenzaldehyde, which is more than three units more negative than the value accepted today. At the time (1972), the qualitative magnitudes

© 2000 NRC Canada

of pK_as of carbonyl compounds (34) were still under discussion. Indeed, more recently, Toullec (35) has argued in favour of the larger negative values on the grounds that they are consistent with α-hydroxy and α-alkoxy carbocations having similar stabilities. If the ketones were 3–4 orders of magnitude more basic than supposed by Jencks and Sayer (2), a substantially greater stability would be implied for the α-hydroxycarbocations, which Toullec (35) considered unlikely.

However, it is now clear that the large negative pK_as for aldehydes were based on an inadequate extrapolation of equilibrium measurements in strongly acidic media to aqueous solution. Methods for correcting equilibrium constants (and measurements of UV–vis spectra used to monitor the equilibria) for medium effects in concentrated solutions of strong acids are now well understood (16, 36, 37). This means that pK_as, at least of compounds in which conjugation of the carbonyl group and the aromatic ring provides an intense π-π* chromophore for reliably monitoring the extent of protonation (such as pK_a = –3.87 for acetophenone (36, 37) and –4.5 for benzaldehyde (38)), can no longer be considered in doubt. It also seems clear that the large difference in stabilities of carbocations containing α-hydroxy and α-alkoxy substituents derives from the stabilization conferred by aqueous solvation of a hydroxyl group conjugated to the charge centre (39). This stabilization is not available to the alkoxy group.

The basis of Jencks's and Sayer's (2) second argument, that the rates of acid-catalyzed oxime-forming reactions are insensitive to substituents in the carbonyl reactant, is illustrated by rate constants for acid-catalyzed attack of *O*-methyl hydroxylamine upon *p*-methoxy, *p*-chloro, and *p*-nitro benzaldehydes. For these reactions Jencks and Sayer obtained values of 1 500, 2 070, and 1 930 M^{-1} s^{-1}, respectively (2). They concluded that the rate constants for attack of hydroxylamine on the *protonated* benzaldehydes, which are obtained by correction of the experimental rate constants for the extent of protonation of the aldehyde, were too *sensitive* to the structure of the aldehyde to represent reactions which should be close to diffusion control.

However, if we widen the range of structures of ketones and aldehydes to include acetone (5, 12), acetophenone (10), and 9-formylfluorene, this insensitivity to substituents is no longer apparent. We find that rate constants for their acid-catalyzed reactions vary by 250-fold, as is indicated by values of k_H' listed in Table 2. Explicit values of the rate constants for attack of NH_2OH on the protonated conjugate acids of these compounds are considered below, and it is argued that they show a rational dependence on the structure of the substrate.

Further evidence cited by Sayer et al. (3) in support of the concerted mechanism, was the observation of general acid catalysis in oxime-forming reactions. However, because the T^+ pathway is normally observed only at fairly high concentrations of strong acid, most studies demonstrating general acid catalysis pertain to the alternative acid-catalyzed mechanism occurring at higher pH and involving rate-determining formation of T^+ through trapping of the zwitterionic tetrahedral intermediate $T^\pm$ by protonation (40).

At this point, we might conclude that there is little evidence to support the concerted reaction in Scheme 9. However, Brown and Guthrie and co-workers (41) have recently inferred such a mechanism for the H_3O^+-catalyzed hydrolysis of acetanilides. They monitored C—N^+ bond-breaking in the protonated tetrahedral intermediate formed from attack of water on the protonated anilide by measuring the extent of oxygen isotope exchange occurring in the reactant in competition with hydolysis. Their principal evidence that the reaction of T^+ is concerted came from the measurement of a solvent isotope effect (k_{H_2O}/k_{D_2O}) close to 1.0 for ^{18}O exchange. This strongly implicated the contribution of a primary isotope effect k_H/k_D = 2.5 to compensate an expected solvent isotope effect in the opposite direction arising from protonation of the anilide by H_3O^+ in a preequilibrium (42).

The isotope effect for hydrolysis of the oxime of 9-formylfluorene is also close to unity: k_{H_2O}/k_{D_2O} = 1.3. However, a fundamental difference from the hydrolysis of the anilides is that the reactants are not the oxime and H_3O^+, but the *protonated* oxime (Scheme 5). In contrast to the anilides, therefore, there is no preequilibrium protonation so the value of k_{H_2O}/k_{D_2O} points to the *absence* of a primary isotope effect in the reaction. We found that the magnitude of k_{H_2O}/k_{D_2O} does not change appreciably on going to lower acid concentrations, where the oxime is no longer protonated. However, reaction then occurs via the $T^\pm$ pathway of Scheme 1 and is not subject to catalysis by H_3O^+. Again therefore an inverse solvent isotope effect is not to be expected.

It is not clear why the mechanisms for reaction via T^+ in the hydrolysis of anilides and oximes should differ. Possibly that the greater acidity of the protonated carboxylic acid than protonated aldehyde as a reactive intermediate, coupled with a less acidic medium, implies a greater preference for concerted proton transfer in the reaction of anilides than oximes.

pK_R and pK_a for protonated 9-formylfluorene

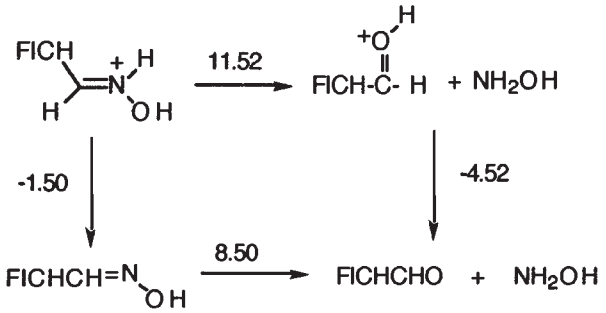
Summarizing the above arguments, we conclude, on the basis of the isotope effect, and the fact that the reaction takes place at acidities at which the extent of protonation of the aldehyde renders its conjugate acid a viable intermediate, that C—N bond-breaking of T^+ derived from the 9-formylfluorene oxime is unlikely to be concerted with proton transfer.

If this conclusion is correct the immediate products of the reaction of T^+ are protonated 9-formylfluorene and hydroxylamine. If formation of these products is rate-determining, then by the principle of microscopic reversibility the rate-determining step of the reverse reaction is attack of hydroxylamine on the protonated 9-formylfluorene. It follows that we can infer a pK_a for the protonated aldehyde if we make the assumption that its reaction with hydroxylamine is diffusion-controlled.

An experimental rate constant for the reaction in the oxime-forming direction can be deduced by combining the rate constant for the acid-catalyzed hydrolysis with the equilibrium constant for the overall reaction. This rate constant corresponds to k_3/K_a where k_3 is the rate constant for attack of hydroxylamine on, and K_a is the acid dissociation constant of, the protonated aldehyde (Scheme 1). If k_3 corresponds to a diffusion-controlled reaction then, since the magnitude of rate constants for diffusion are known, K_a can be determined.

© 2000 NRC Canada

Scheme 10.



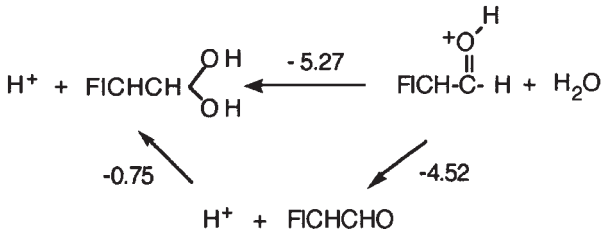
What evidence is there that attack of hydroxylamine on the protonated aldehyde is diffusion-controlled? Diffusion control for reactions of carbocations with nucleophiles has been invoked most commonly for azide (43) or sulphur (44) anions. NH_2OH is a reactive α-nucleophile which is more basic and more reactive towards methyl iodide than azide ion (45). Although its N^+ value is somewhat lower than that of azide (5.1 compared with 7.5 (24)) it is still large. Its rate constant for reaction with 9-formylfluorene itself is 3.4×10^5. It is very likely that the increase in reactivity conferred by protonation of the carbonyl group would increase this by the factor of 10^4 required to achieve the expected diffusion rate constant of 3×10^9 M^{-1} s^{-1} for attack of a neutral molecule upon an ion in aqueous solution (46).

This argument is reinforced below by assessing the activating effect of protonation of 9-formylfluorene on nucleophilic attack in the case of water as a nucleophile. However, further evidence for diffusion control comes from examination of rate constants for acid-catalyzed attack of hydroxylamine on other protonated ketones and aldehydes for which pK_as are known. Again the experimental rate constant corresponds to a ratio of the rate constant for attack by hydroxylamine to the ionization constant of the protonated ketone (k_3/K_a). Now, however, we deduce the magnitude of the rate constant from knowledge of the equlibrium constant rather than vice versa.

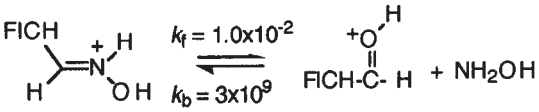
Rate constants (k_3) for attack of hydroxylamine on protonated acetone, acetophenone, and *p*-chlorobenzaldehyde and the pK_as on which they are based are shown in Table 2. The rate constants are rather large. For acetophenone and acetone they are 1.6×10^6 and 3.9×10^6 respectively and for *p*-chlorobenzaldehyde 5.8×10^8. As expected the aldehyde is more reactive than the ketones. The order of reactivities is confirmed if we deduce a value for *p*-methoxybenzaldehyde by assuming that the ratio of acid-catalyzed rate constants for reactions of hydroxylamine and methoxylamine (2) are the same for the *p*-methoxy and *p*-chlorobenzaldehydes. The value obtained, 1.1×10^8, is somewhat less than for *p*-chlorobenzaldehyde and is again consistent with expected relative stabilities of the carbonyl compounds.

It is clear that the rate constant for the *p*-chlorobenzaldehyde is within an order of magnitute of the value of 3×10^9 for diffusion. 9-Formylfluorene should be significantly more reactive than an aromatic aldehyde and we conclude that any error from assuming that the reaction of hydroxylamine with the protonated aldehyde is diffusion-controlled must be small.

Scheme 11.



If we assume that the reaction of hydroxylamine with protonated 9-formylfluorene does indeed occur at the diffusion limit we can combine the rate constant for diffusion (3×10^9) with the experimental rate constant $k = 1.0 \times 10^{-2}$ for the forward, weakly acid-dependent, hydrolysis reaction occurring in concentrated acid solutions, to obtain an equilibrium constant for the hydrolysis reaction. As shown in eq. [10], the reactant in this equilibrium is the protonated oxime, which is the predominant form of the oxime existing at the acid concentrations at which the T^+ reaction path prevails.

[10] 

Thus we derive an equilibrium constant between protonated 9-formylfluorene and protonated oxime of $1.0 \times 10^{-2}/3 \times 10^9 = 3.3 \times 10^{-12}$ (pK = – 11.52). As shown in Scheme 10, this can be combined in a cycle with equilibrium constants for protonation and formation of the oxime to derive pK_a = –4.52 for the protonated 9-formylfluorene. (The apparent pK_a = –1.50 for protonation of the oxime to yield a mixture of protonated oxime and protonated carbinolamine is used in Scheme 10). The pK_a of the 9-formylfluorene may be compared with directly measured values of pK_a = –4.4 and –5.0 for protonated benzaldehyde and *p*-chlorobenzaldehyde, respectively (38).

An alternative way of deriving K_a is by converting the hydrolysis rate constant 1.0×10^{-2} M^{-1} s^{-1} into a rate constant for the reverse acid-catalyzed attack of hydroxylamine upon 9-formylfluorene and identifying this rate constant with k_3/K_a where k_3 is again the rate constant (3×10^9) for diffusion-controlled attack of hydroxylamine on protonated aldehyde. Correcting for the contribution from k_3 then yields the value of K_a.

The pK_a for protonation of 9-formylfluorene so obtained may be further combined with an equilibrium constant for hydration of the aldehyde to yield a value of pK_R = –5.27 for the protonated aldehyde by taking advantage of the cycle of Scheme 11. This value is compared with pK_R values for protonated *p*-chlorobenzaldehyde, acetone and acetophenone in Table 2. It is noteworthy that the pK_R for 9-formylfluorene is considerably more negative than that for *p*-chlorobenzaldehyde (–2.9) even though the pK_as of the two compounds are practically the same. The trend in pK_R values is similar to that of the protonated oximes, for which pK_Rs are also shown in Table 2.

Finally, we derive $pK_R^{NH_2OH} = -7.14$ for the protonated 9-formylfluorene based on the cycle of Scheme 12. The pK_R

© 2000 NRC Canada

Scheme 12.

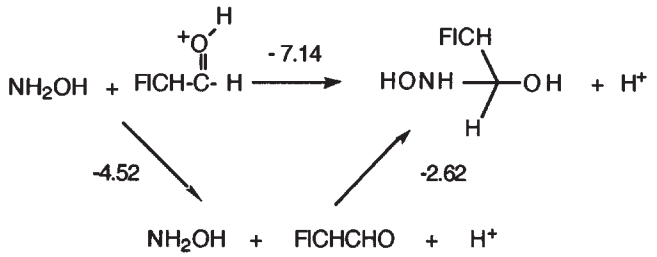


Table 3. Values of pK_R for 9-formylfluorene, its conjugate acid, and protonated oxime in water at 25°C.

	pK_R	p$K_R^{NH_2OH}$
FlCHCH=OH^+	–5.27	–7.14
FlCHCH=NH^+OH	4.10	—
FlCHCH=O	12.25	11.1

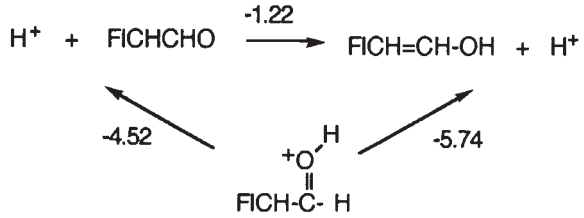
values for 9-formylfluorene, its conjugate acid, and protonated oxime are summarized in Table 3.

We return now to the question of diffusion control of attack by NH_2OH on the protonated 9-formylfluorene and compare the activating effect of protonation upon attack by water and attack by hydroxylamine. In a previous study of the hydration reaction a rate constant for catalysis by H_3O^+ was measured as 12.5 M^{-1} s^{-1}. Combining this with K_R = 3.7×10^5 yields a rate constant $k_{H_2O} = 3.4 \times 10^6$ s^{-1} for attack of water on the protonated 9-formylfluorene. This may be compared with $k = 2.86 \times 10^{-2}$ s^{-1} for hydration of the unprotonated aldehyde. The ratio of these rate constants, 1.2×10^8, measures the activating effect of protonation of the carbonyl oxygen atom upon nucleophilic attack by water. Such a ratio has been called by Stewart and Srinivasan (47) a proton activating factor (paf).

It should be noted that the evaluation of paf implies that attack of water occurs on a fully protonated carbonyl group whereas it has usually been considered that in the acid-catalyzed hydration of aldehydes attack of water is concerted with proton transfer from H_3O^+ (48). Strictly speaking, therefore, 1.2×10^8 should be an upper limit for the activation of water attack. The possibility of concertedness and the difficulty of distinguishing this from direct reaction with water exists for other carbocation reactions. However, Ritchie (24) has shown that relative rates of reactions of electrophiles with H_2O are often correlated with those of nucleophiles not reacting by a concerted pathway, such as hydroxide ion. It seems likely therefore that the qualitative significance of the comparison of rates of reaction of water with those of NH_2OH remains valid.

By assuming that reaction of NH_2OH with the protonated aldehyde is indeed diffusion-controlled ($k = 3 \times 10^9$ M^{-1} s^{-1}) an activation factor for NH_2OH may be calculated from the value of $k_2 = 6.0 \times 10^5$ for attack of NH_2OH on the unprotonated aldehyde (Table 2) to give a value of paf = 5×10^3. This is more than 10^4 times smaller than the value for water. An unexpectedly slow reaction between a nucleophile and a carbocation is commonly used as an argument for diffusion control (44). Put another way, the ratio of rate constants for attack of NH_2OH and H_2O on the unprotonated 9-formylfluorene (2.1×10^7) is much larger than the corresponding ratio (900) for attack on the protonated compound, even though the reaction of hydroxylamine is assumed to be diffusion-controlled. A low selectivity between water and a reactive nucleophile is again an established argument for diffusion control. The measured ratio of 900 may also be compared with a value of $>10^5$ predicted by the N^+ relationship.

Scheme 13.



Finally, we note that in principle the limiting rate constant for NH_2OH might even exceed that for diffusion if, as seems likely, the encounter complex with protonated aldehyde is generated by proton tranfers to and from 9-formylfluorene and NH_3OH^+ already associated within a solvent cage. However, it seems unlikely that this would increase the rate sufficiently to affect the estimated pK_a of the protonated 9-formylfluorene by more than a few tenths of a log unit.

Protonation of the enol of 9-formylfluorene

We may now use the pK_a for protonation of 9-formylfluorene to complete the cycle of equilibria associated with the enolization and ionization of its aldehyde tautomer shown in Scheme 13. This cycle allows us to assign a pK_a = –5.74 to the *C*-protonated enol. This pK_a is of interest for comparison with corresponding values for the enols of acetone and acetophenone. These may be derived in the same way as for 9-formylfluorene by combining keto–enol tautomeric constants measured by Chiang et al. (49) and Kresge and co-workers (49, 50) (7.90 for acetophenone and 8.33 for acetone) with the pK_as of the ketones measured by Bagno (36) (–3.87 for acetophenone and –3.06 for acetone). We then obtain as pK_as for the enols of acetophenone and acetone 4.03 and 5.27, respectively. Thus, these enols are more basic than the enol of formylfluorene by factors of 10^{10} and 10^{11}.

The exceptionally low basicity of the enol of 9-formylfluorene partly reflects the greater stabilizing effect on the protonated species of the α-methyl or α-phenyl substituent of the ketones than hydrogen of the aldehyde. Another factor is the electron-withdrawing effect of the fluorenyl group. However, these also influence the basicities of the keto tautomers, and the most important factor specifically affecting the enol is undoubtedly the influence of the fluorenyl group on the stability of the enolic double bond (51). Thus K_E = 16.6 for 9-formylfluorene is more than 10^9-fold greater than that of K_E for acetone or acetophenone. Accordingly the difference in basicity of the enols is much greater than that of their keto tautomers.

Summary

The pK_as for protonation of 9-formylfluorene and its enol represent the principal results of this study. The pK_a of the aldehyde tautomer is derived from measurements of rate constants for formation and hydrolysis of its oxime and

© 2000 NRC Canada

depends on evidence: (*i*) that the mechanism of acid-catalyszd formation involves attack of hydroxylamine on the protonated aldehyde (rather than concerted attack and protonation); and (*ii*) that this reaction is diffusion-controlled. The value of the pK_a = –4.5 (and pK_R = –5.2) is consistent with p*K*s of other aldehydes based on measurements of protonation equilibria in concentrated solutions of strong acids (38).

The study also yields values of pK_a and pK_R for the protonated oxime and equilibrium constants for the reaction of hydroxylamine with 9-formylfluorene to form the tetrahedral adduct and the oxime itself. Such a set of equlibrium constants has not previously been obtained for an aldehyde group bound to an aliphatic carbon atom.

Experimental

The kinetics of reactions described in this paper were monitored spectrophotometrically using Phillips PU 8600, Perkin–Elmer Hitachi 124, or Spectronic Genesys 2PC UV–vis spectrophotometers. Measurements of pH were made with a Radiometer PHM 26 or Metronohm pH meter 744. Solutions of strong acids or buffers were prepared from commercial reagents usually of AR quality. The acids were standardized with solutions of NaOH prepared from Merck "Titrisol" ampoules. Reactions were carried out in aqueous solutions using doubly distilled water.

9-Formylfluorene was prepared as previously described (14, 52) and purified by Kugelrohr distillation to give a pale yellow oil. To prepare the oxime, 9-formylfluorene (1.57 g, 8.4 mmol) was dissolved in ethanol (20 mL). Sodium (0.195 g, 8.4 mmol) in ethanol (3.5 mL) was added, followed by hydroxylamine hydrochloride (0.59 g, 8.4 mmol) in water (3.5 mL) to give a light brown solution and white precipitate. The mixture was heated at 60°C for 1 h to give a clear solution from which a water soluble white precipitate formed after leaving overnight in a freezer. Addition of water (50 mL) led to precipitation of the oxime which was filtered and dried. Careful recrystallization gave white needles, mp 160–165°. ^{1}H NMR (CD_3CN) δ: 5.66 (d, *J* = 7.0 Hz, 1H), 6.60 (d, *J* = 7.0 Hz, 1H), 7.3 – 7.9 (m, 8H), 9.23 (s, 1H) (in $CDCl_3$, the peak at 9.23 was broadened and shifted upfield to δ 8.2). ^{13}C NMR ($CDCl_3$) δ: 44.4, 120.0, 125.5, 127.5, 127.9, 141, 142.5, 150.5. Anal. calcd. for $C_{14}H_{11}NO$: C 80.36, H 5.36, N 6.61; found: C 80.35, H 5.3, N 6.69.

Based on the work of Karabatsos and Taller (21), it was expected that the oxime that crystallized was the *syn*-isomer. This was confirmed by the magnitude of the chemical shift of the vinyl hydrogen when compared, e.g., with *syn*- and *anti*-oximes from phenylacetaldehyde (21). No conversion to the *anti*-isomer was observed after leaving the NMR solution for several days. However, excessive heating of solutions during recrystallization produced a product with a broad melting range which was presumed to be a mixture of *syn*- and *anti*-oximes.

Equilibrium measurements

Protonation of 9-formylfluorene

A pK_a for the protonated oxime was obtained from measurements of (small) changes in absorbance in the UV spectrum in solutions of perchloric acid in the concentration range 2.5–8.0 M. Below 2.5 M there was interference from a significant end absorption from the oxime. Absorbances were measured following injection of 10 μL of a 10^{-2} M solution of the oxime in acetonitrile into 2 mL of different concentrations of aq $HClO_4$. Measured absorbances at the indicated acid concentrations were: 0.40 (3.01 M), 0.36 (3.76 M), 0.337 (4.14 M), 0.32 (4.35 M), 0.322 (4.51 M), 0.314 (4.70 M), 0.305 (5.08 M), 0.29 (5.64 M). The pK_a was obtained as the intercept of a plot of –log *K* against *X* based on eq. [11], in which 0.27 and 0.45 are absorbances for ionized and unionized oxime, respectively (which were interpolated by assuming that log *K* depends linearly upon the medium acidity function *X*) and *A* is the measured absorbance at the acid concentration [H^+] (16–18).

$$[11] \quad -\log K = -\log\left\{\frac{(A - 0.27)[H^+]}{(0.45 - A)}\right\} = m^*X + pK_a$$

The plot gave m^* = 0.9 and pK_a = –1.50 with an error estimated qualitatively as ±0.2. The pK_a is confirmed by the fact that it yields a satisfactory fit of calculated to experimental rate constants in the pH – *X* profile for hydrolysis of the oxime (Fig. 2). However, it should be noted that protonation of the oxime may be associated with partial hydration to form the protonated carbinolamine (T^+). The pK_a used in the text (–1.62) includes a correction for this described in the appendix.

Formation of carbinolamine

An equilibrium constant for the addition of hydroxylamine to 9-formylfluorene was measured by injecting a small amount of a solution of the substrate in acetonitrile (typically 20 μL) into 2 mL of aq hydroxylamine buffer and measuring the absorbance at 319 nm. The absorbance decreased with time, but an initial value A_I was extrapolated to the time of injection. This and the limiting absorbance (A_{max}), referring to a solution without added hydroxylamine, are related to the ratio of concentrations of carbinolamine and enol (and aldehyde) as shown in eq. [12].

$$[12] \quad \frac{A_{max} - A_I}{A_I} = \frac{[\text{carbinolamine}]}{[\text{enol}] + [\text{aldehyde}]}$$

Combination of eq. [12] with the equilibrium constant for formation of carbinolamine from equilibrated enol and aldehyde, K_{eff} (eq. [13]), gives eq. [14], which shows that $1/A_I$ may be plotted against [NH_2OH] to give $1/A_{max}$ as intercept and K_{eff}/A_{max} as slope.

$$[13] \quad K_{eff} = \frac{[\text{carbinolamine}]}{([\text{enol}] + [\text{aldehyde}])[NH_2OH]}$$

$$[14] \quad \frac{1}{A_I} = \frac{1}{A_{max}} + \frac{K_{eff}\,[NH_2OH]}{A_{max}}$$

Two sets of measurements were carried out. The first with [NH_2OH]/[NH_3OH^+] = 1 gave the following absorbances (A_I) at the indicated concentrations of NH_2OH: 0.34 (0.025 M), 0.45 (0.01 M), 0.49 (0.005 M), 0.52 (0.0025 M), 0.53

© 2000 NRC Canada

(0.00125 M). The second with $[NH_2OH]/[NH_3OH^+]$ = 9 gave: 0.24 (0.04 M), 0.39 (0.009 M), 0.47 (0.0045 M). The average value of K_{eff} derived from the two sets of data was 25, with an estimated error of ±2. The corresponding equilibrium constant for formation of the carbinolamine from the aldehyde was obtained from $K_{add} = K_{eff}(1 + K_E)$ where K_E is the keto–enol equilibrium constant (=16.6). This gave K_{add} = 440.

Formation of oxime

An equilibrium constant was also measured for the complete reaction of enol with hydroxylamine to form oxime. In practice the equilibrium was approached both from the oxime-forming direction and the reverse direction of oxime to enol. Because the equilibrium strongly favours the oxime, measurements were made in solutions of HCl, in which the hydroxylamine is fully protonated. Practically speaking the equilbrium studied corresponds closely to that of eq. [4] and, taking account of the presence of the small fraction of aldehyde, has an equilibrium constant K given by eq. [15]. In this equation the ratio of concentrations of oxime to enol plus aldehyde may be replaced by $(\Delta A_{max} - \Delta A)/\Delta A$ where ΔA is the change in absorbance between the oxime initially present and the equilibrium concentration of oxime and enol (plus aldehyde and hydrate) and ΔA_{max} is the value of ΔA for complete conversion of the oxime to "enol". Making this substitution the value of K could be determined from a plot of $1/\Delta A$ vs. $[NH_3OH^+]/[H^+]$ based on rearrangement of eq. [15] to eq. [16].

$$[15] \qquad K = \frac{[\text{carbinolamine}]}{([\text{enol}] + [\text{aldehyde}] + [\text{hydrate}])[NH_3OH^+]}$$

$$[16] \qquad \frac{1}{\Delta A} = \frac{1}{\Delta A_{max}} + \frac{K}{\Delta A_{max}} \frac{[NH_3OH^+]}{[H^+]}$$

From this plot, a value of K = 9.9 was obtained based on the following sets of measurements of ΔA at different concentrations of acid and $[NH_3OH^+]$. For $[H^+]$ = 0.2 M values of ΔA and $[NH_3OH^+]$ were: 0.559, 0.02 M; 0.591, 0.016 M; 0.630, 0.012 M; 0.683, 0.01 M; 1.145, 0 M. For $[H^+]$ = 0.1 M they were 0.551, 0.01 M; 0.627, 0.008 M; 0.733, 0.005 M; 1.137, 0.0 M. For $[H^+]$ = 0.05 M they were: 0.512, 0.005 M; 0.566, 0.004 M; 0.642, 0.003 M; 0.703, 0.002 M; 1.064, 0.0 M.

Similar measurements were made at 319 nm with the enol and protonated hydroxylamine as reactants. At this wavelength, the oxime does not absorb and the ratio [oxime]/[enol] at equilibrium is given by $(A_I - A_F)/A_F$, where A_I and A_F are absorbances at the beginning and completion of the reaction. Measured values of A_I and A_F (in that order) at different concentrations of NH_3OH^+ in 0.1 M HCl were as follows: 0.428, 0.145, 0.02 M; 0.435, 0.25, 0.008 M; 0.430, 0.390, 0.001 M. These gave an average value of K = 9.4 and the combined results gave K = 9.7. The value of K is related to K_{ox} for oxime formation from the aldehyde tautomer of 9-formylfluorene by $K_{ox} = K/(0.044 \times K_a)$ where $K_a = 10^{-6}$ is the ionization constant of NH_3OH^+ and 0.044 is the ratio of the concentration of the aldehyde tautomer to the combined concentrations of aldehyde, enol, and hydrate (9). The derived value is $K_{ox} = 2.20 \times 10^8$.

Kinetic measurements

Hydrolysis of the oxime

Rate constants for hydrolysis of the oxime in acidic media were monitored from the spectrum of the enol product at 234, 260, and 270 nm (Fig. 1). In solutions of HCl, care had to be taken to avoid oxidation to fluorenone with the formation of a characteristic peak at 260 nm. In concentrated solutions of $HClO_4$, there was a shift in the equilibrium between keto and enol tautomers in favour of the keto isomer. The reaction was then monitored from a decrease in absorption of the peak for the protonated oxime at 270 nm.

In principle microscopic rate constants for the hydrolysis reaction could be obtained from a best fit of eq. [2] based on Scheme 1 to the pH-dependence of log k_{obs} shown in Fig. 2. In practice measurements were made mainly with concentrated solutions of HCl or $HClO_4$. Log k_{obs} is then correlated not by pH but pH – X, where X measures the acidity of the medium based on the protonation of weakly basic anilines (12, 13) and account must be taken of the acidity dependence of limiting rate constants in different acidity ranges. In practice, therefore, the line drawn through the points in Fig. 2 is based on the modified form of eq. [2] shown as eq. [17].

The limiting kinetic expressions for different reaction paths and numerical values of their composite rate coefficients extrapolated to aqueous solution are those shown below eq. [2]. In eq. [17] the dependence of these rate coefficients upon X in strong acids is described by multiplying microscopic rate or equilibrium constants by 10^{m^*X} where m^* is the slope of a plot of the log of the limiting rate constant against $-X$ (16, 17). The constants to which these m^* refer are shown in Scheme 14, which is an abbreviated form of Scheme 1 with the oxime and protonated oxime denoted Ox and OxH^+, respectively, and rate and equilibrium constants k and K replaced by $k \times 10^{-m^*X}$ or $K \times 10^{-m^*X}$.

Assignments of values of m^* include the measured value of 0.9 for the dissociation constant of the protonated oxime and $m^* = m_2^* + m_4^* - m_3^* = 0.3$ for the measured limiting dependence of log k_{obs} upon $-X$ at the highest concentrations of $HClO_4$. If we take m_4^* for the acidity dependence of k_{-3}/K^+ (the reaction of T° via T^+) as –0.9, the same as for the protonation of the oxime, and m^* for the corresponding reaction of T^o via $T^\pm$ as 0, then the implied value of m^* for reaction of the protonated oxime via the $T^\pm$ pathway is 1.2, which is close to the value (1.3) previously observed for the hydrolysis of the *N*-phenylimine of *p*-chlorobenzaldehyde (20). Finally, m_2^* and m_3^* are assigned by noting that $m_2^* - m_3^* = 1.2$ and giving m_2^* and m_3^* the arbitrary but reasonable values of 0.4 and –0.8. These values provide the satis-

$$[17] \qquad k_{obs} = \frac{k_{H2O}k_{-2}K^\pm 10^{m_2^*X}}{(k_H 10^{m_3^*X}[H^+] + k_{-2}K^\pm)(1 + K_a 10^{m_1^*X}/[H^+])} + \frac{k_{H2O}k_{-3}10^{(m_4^* + m_2^* - m_3^*)X}}{k_H K^+(1 + K_a 10^{m_1^*X}/[H^+])}$$

© 2000 NRC Canada

Scheme 14.

$$H^+ + Ox \underset{}{\overset{[H^+]/K_a 10^{m_1^* X}}{\rightleftharpoons}} OxH^+ \underset{k_H 10^{m_3^* X}[H^+]}{\overset{k_{H2O}10^{m_2^* X}}{\rightleftharpoons}} T^{\circ} \xrightarrow{k_{-2}K^{\pm} + (k_{-3}/K^+)10^{m_4^* X}[H^+]}$$

factory fit to the measurements for $HClO_4$ shown in Fig. 2. However, the dominant influences on the acidity dependence are the measured limiting value, which is established at X – pH < –2, and the fact that X approaches zero at pH > 0. The flexibility in assignments of m^* values is: (*i*) more limited than appears therefore; and (*ii*) confined to reactions making little contribution in the strong acid region such as the reaction via $T^{\pm}$.

For HCl, slighly different values of m* were used: $m_1^* = m_4^* = 0.8$, $m_2^* = 0.45$, and $m_3^* = -0.55$. The rate and equilibrium constnats were the same as for $HClO_4$ except for the limiting rate constant extrapolated from high acidities ($k_{H_2O}k_{-3}/k^H K^+$) being 9×10^{-3} instead of 1.1×10^{-2} s^{-1}.

The solvent isotope effect upon hydrolysis of the oxime was based on the measurements of rate constants at the concentrations of DCl shown in Table 1. When combined with interpolated rate constants at the same concentrations of HCl the following isotope effects (k_{H_2O}/k_{D_2O}) at the indicated acid concentrations were obtained.

$$k_{H_2O}/k_{D_2O} = 1.3 \text{ (4.8–6.1 M)}$$
$$= 1.25 \text{ (1.2–2.4 M)}$$

Oxime formation in hydroxylamine buffers

The dependence of k_{obs} upon concentration of NH_3OH^+ in hydroxylamine buffers at different buffer ratios is shown in Fig. 3 and Table S2.[2] The lines drawn through the points in Fig. 3 are based on a kinetic expression derived from Scheme 2 which allows for a change in rate-determining step from H^+-catalyzed dehydration of the carbinolamine adduct of 9-formylfluorene and hydroxylamine at low buffer concentrations to ketonization of the enol at high buffer concentrations. This expression is shown in eq. [18] and con-

$$[18] \qquad k_{obs} = \frac{ax(b + Rcx)}{ax + (b + Rcx)}$$

tains parameters a, b, and c which may be defined in terms of the symbols for rate and equilibrium constants of Schemes 1 and 2, as $a = k_H K_{add} K_a / K_E$, $b = k_1'$, $c = k_1$, $x = [NH_3OH^+]$, and $R = [NH_2OH]/[NH_3OH^+]$ (and where k_1' is the rate constant for ketonization catalysed by NH_2OH). As noted above, at high concentrations of NH_2OH a correction is applied for partial conversion of the enol of 9-formylfluorene to the carbinolamine adduct by replacing a by $a/(1 + K_{eff}[NH_2OH])$ where $K_{eff} = K_{add}/(1 + K_E) = 25$ is the apparent equilibrium constant for adduct formation from the enol (14).

A value of $a = 2.25$ was obtained from the limiting slope of the plot of k_{obs} against $[NH_3OH^+]$ for relatively basic buffers shown in the inset of Fig. 3. In this plot the correction for adduct formation is applied by multiplying k_{obs} by $(1 + K_{eff}[NH_2OH])$ as described. The value of a allowed evaluation of k_H. It was also used, together with independently determined values of k_1 (.0153) and K_{add} (440) and a value of $k_1' = 3.1$ based on a best-fit to the data at high concentrations of NH_3OH^+, in fitting the curved buffer plots shown in Fig. 3.

Oxime formation in acetic acid buffers

The behaviour observed in acetic acid buffers in the presence of hydroxylammonium chloride was similar to that in hydroxylamine buffers. The dependence of k_{obs} upon $[NH_3OH^+]$ and the concentration of acetic acid buffer was also fitted to eq. [18] but with b replaced by $k_1 + k_1''[AcO^-]$ where k_1 and k_1'' are rate constants for uncatalyzed and acetate-catalyzed ketonization of the enol of 9-formylfluorene, respectively. The term a was also modified to allow for a 20% contribution from general acid catalysis of dehydration of the carbinolamine intermediate by acetic acid at 0.1 M concentration. This was based on previous work for *p*-chlorobenzaldehyde (1) but has little influence on the results. Otherwise the parameters used in eq. [18] were the same for acetic as for hydroxylamine buffers. When calculating concentrations of buffer components and hydroxylamine, allowance had to be made for modification of added concentrations of hydroxylamine hydrochloride, acetic acid, and acetate ion through equilibration according to eq. [19].

$$[19] \qquad CH_3COOH + NH_2OH \overset{K}{\rightleftharpoons} CH_3COO^- + NH_3OH^+$$

The concentration of NH_2OH (x) from mixing $NH_3OH^+Cl^-$ and a 1:1 acetic acid buffer to give formal concentrations A and B, respectively is given by eq. [20]. In this equation the equilibrium constant K is given by the ratio of acid dissociation constants of the acetic acid buffer and NH_3OH^+. Values of x and the concentration of acetate ion $(A - x)$ and acetic acid $(B - x)$ were obtained by solution of eq. [20] as a quadratic.

$$[20] \qquad \frac{(A - x)(B - x)}{x \quad (B + x)} = K$$

To correct for ionic strength, K was replaced by $K' = K \times 10^y$ where $y = I^{1/2}/(1 + 1.6I^{1/2})$ and I is the ionic strength.

Oxime formation in aq. HCl

The dependence of first-order rate constants for oxime formation in 0.05 M aq HCl shown in Table S4[2] and Fig. 4 is described by eq. [21], which is based on and uses the symbols of Scheme 3. The equation takes account of the reversibility of the reaction at low concentrations of NH_2OH

$$[21] \qquad k_{obs} = \frac{k_1 k_2 [NH_2OH]}{k_1 K_E + k_2 [NH_2OH]} + k_2/K_{ox}$$

© 2000 NRC Canada

and also of the difference in rate-determining step for the oxime-forming reaction from that for the measurements with acetic acid or hydroxylamine buffers. However, it does not take account of the competing hydration reaction which equilibrates enol and hydrate at low concentrations of hydroxylamine. The concentration of hydroxylamine used in the equation was calculated as $K_a[NH_3OH^+]/[H^+]$ where K_a is the acid dissociation constant of NH_3OH^+.

Acknowledgment

Support for this work by Zeneca Fine Chemicals Manufacturing Organization is gratefully acknowledged.

References

1. J.E. Reimann and W.P. Jencks. J. Am. Chem. Soc. **86**, 3973 (1966).
2. S. Rosenberg, S.M. Silver, J.M. Sayer, and W.P. Jencks. J. Am. Chem. Soc. **96**, 7986 (1974).
3. J.M. Sayer, B. Pinsky, A. Schonbrunn, and W. Washtien. J. Am. Chem. Soc. **96**, 7998 (1974).
4. M. Calzadilla, A. Malpica, and T. Cordova. J. Phys. Org. Chem. **12**, 708 (1999).
5. W.P. Jencks. J. Am. Chem. Soc. **81**, 475 (1959).
6. I.M.C. Brighente, L.R. Vottero, A.J. Terezani, and R.A. Yunes. Bull. Chem. Soc. Jpn. **66**, 2289 (1993); I.M.C. Brighente, R. Budal, and R.A. Yunes. J. Chem. Soc. Perkin. Trans. 2, 1861 (1991).
7. M. Cocivera, C.A. Fyfe, A. Effio, S.P. Vaish, and H.E. Chen. J. Am. Chem. Soc. **98**, 1573 (1976).
8. J. Hine, F.A. Via, J.K. Gotkis, and J.C. Craig. J. Am. Chem. Soc. **92**, 5186 (1970).
9. M. Masui and C. Yijima. J. Chem. Soc. B, 56 (1966).
10. B.J. Gregory and R.B. Moodie. J. Chem. Soc. B. 862 (1970).
11. C.D. Ritchie. J. Am. Chem. Soc. **106**, 7187 (1984).
12. R.B. Martin. J. Phys. Chem. **68**, 1369 (1964).
13. G. Lamaty, J. Roque, A. Naltat, and T. Silou. Tetrahedron, **42**, 2667 (1986).
14. M.P. Harcourt and R.A. More O'Ferrall. J. Chem. Soc. Perkin. Trans. 2, 1415 (1995).
15. T.L. Amyes, J.P. Richard, and M. Novak. J. Am. Chem. Soc. **114**, 8032 (1992); N. Mathivanan, R.A. McClelland, and S. Steenken. J. Am. Chem. Soc. **112**, 8454 (1990).
16. A. Bagno, G. Scorrano, and R.A. More O'Ferrall. Rev. Chem. Intermed. **7**, 313 (1987).
17. R.A. Cox and K. Yates. J. Am. Chem. Soc. **100**, 3861 (1978); A.J. Kresge, H.J. Chen, G.L. Capen, and M.F. Powell. Can. J. Chem. **61**, 249 (1983).
18. C.A. Barton and S.K. Huang. J. Am. Chem. Soc. **94**, 3536 (1972).
19. A. Bagno, V. Lucchini, and G. Scorrano. Bull. Soc. Chim. Fr. 563 (1987).
20. E.H. Cordes and W.P. Jencks. J. Am. Chem. Soc. **84**, 832 (1962).
21. G.J. Karabatsos and R.A. Taller. Tetrahedron, **24**, 3347 (1968).
22. J.P. Guthrie, J. Barker, P.A. Cullimore, J. Lu, and D.C. Pike. Can. J. Chem. **71**, 2109 (1993).
23. J. Hine. J. Am. Chem. Soc. **93**, 3701 (1971).
24. C.D. Ritchie. Can. J. Chem. **64**, 2239 (1986).
25. H. Mayr, O. Kuhn, M.F. Gotta, and M. Patz. J. Phys. Org. Chem. **11**, 642 (1998), and refs. cited; R.A. McClelland, V.M. Kanagasabapathy, N.S. Banait, and S. Steenken. J. Am. Chem. Soc. **114**, 1816 (1992); R. Ta Shma and Z. Rappaport. J. Am. Chem. Soc. **105**, 6082 (1983); C.D. Johnson and P. Denton. J. Chem. Soc. Perkin Trans. 2, 477 (1995); L.A.P. Kane-Maguire, E.D. Honig, and D.A. Sweigart. Chem. Rev. **84**, 525 (1984); J.P. Richard. Tetrahedron, **57**, 1535 (1995); J.P. Guthrie and D.C. Pike. Can. J. Chem. **65**, 1951 (1987); C.F. Bernasconi. Adv. Phys. Org. Chem. **27**, 119 (1992).
26. J.W. Bunting. Adv. Heterocycl. Chem. **25**, 1 (1979).
27. R.A. McClelland and M. Coe. J. Am. Chem. Soc. **105**, 2718 (1983).
28. D.D. Perrin, B. Dempsy, and E.P. Serjeant. pK_a prediction for organic acids and bases. Chapman and Hall, London. 1981.
29. R.P. Bell and D.P. Onwood. Trans. Faraday Soc. **58**, 1557 (1962).
30. J. Fastrez. J. Am. Chem. Soc. **99**, 7004 (1977).
31. H. Fischer, F.X. DeCandis, S.D. Ogden, and W.P. Jencks. J. Am. Chem. Soc. **102**, 1340 (1980); J.P. Fox and W.P. Jencks. J. Am. Chem. Soc. **96**, 1436 (1974).
32. J. Hine and R.D. Weimar, Jr. J. Am. Chem. Soc. **87**, 3387 (1965).
33. J.M. Sayer and P. Conlon. J. Am. Chem. Soc. **102**, 3952 (1980).
34. C.C. Grieg and C.D. Johnson. J. Am. Chem. Soc. **90**, 6453 (1968); E.M. Arnett, R.P. Quirke, and J.W. Larsen. J. Am. Chem. Soc. **92**, 3977 (1970).
35. J. Toullec. Tetrahedron Lett. **29**, 5541 (1988).
36. A. Bagno, V. Lucchini, and G. Scorrano. J. Phys. Chem. **95**, 345 (1991).
37. R.A. Cox, C.R. Smith, and K. Yates. Can. J. Chem. **57**, 2952 (1979).
38. M.R. Sharif and R.I. Zalewski. Bull. Acad. Pol. Sci. Ser. Sci. Chim. **29**, 38 (1981).
39. R.A. McClelland and J.P. Potter. Can. J. Chem. **58**, 2318 (1980); R.A. McClelland. J. Am. Chem. Soc. **100**, 1844 (1978); A.J. Kresge, H.J. Chen, L.E. Hakka, and J.E. Kouba. J. Am. Chem. Soc. **93**, 6174 (1971); T.L. Amyes and W.P. Jencks. J. Am. Chem. Soc. **111**, 7888 (1989).
40. J.M. Sayer and W.P. Jencks. J. Am. Chem. Soc. **95**, 5637 (1973).
41. A.J. Bennett, H. Slebocka-Tilk, R.S. Brown, J.P. Guthrie, and A. Jodhan. J. Am. Chem. Soc. **112**, 8497, (1990); J.P. Guthrie. J. Am. Chem. Soc. **96**, 3608 (1974).
42. A.J. Kresge, R.A. More O'Ferrall, and M.F. Powell. *In* Isotopes in organic chemistry. *Edited by* E. Buncel and C.C. Lee. Elsevier, Amsterdam. 1987.
43. J.P. Richard, M.E. Rothenburg, and W.P. Jencks. J. Am. Chem. Soc. **106**, 1361 (1984).
44. P.R. Young and W.P. Jencks. J. Am. Chem. Soc. **99**, 8238 (1977).
45. R.G. Pearson, H. Sobel, and J. Songstad. J. Am. Chem. Soc. **90**, 319 (1968).
46. M. Eigen. Angew. Chem. Int. Ed. Engl. **3**, 1 (1964).
47. R. Stewart and R. Srinivasan. Acc. Chem. Res. **11**, 271 (1978).
48. P.E. Sorenson and W.P. Jencks. J. Am. Chem. Soc. **109**, 4675 (1987).
49. Y. Chiang, A.J. Kresge, and J. Wirz. J. Am. Chem. Soc. **106**, 6392 (1984).
50. J.R. Keeffe, A.J. Kresge, and N.P. Schepp. J. Am. Chem. Soc. **112**, 4862 (1990).
51. J. Andraos, Y. Chiang, A.J. Kresge, and V.V. Popik. J. Am. Chem. Soc. **119**, 3417 (1997).
52. L.A. Carpino. J. Org. Chem. **45**, 4250 (1980).
53. J. Hine and F.C. Kokesh. J. Am. Chem. Soc. **92**, 4383 (1970).
54. J. Hine, J.C. Craig, J.G. Underwood, and I.A. Via. J. Am. Chem. Soc. **92**, 5194 (1970).
55. J. Toullec and M. El-Alaoui. J. Org. Chem. **51**, 4058 (1986).

© 2000 NRC Canada

APPENDIX

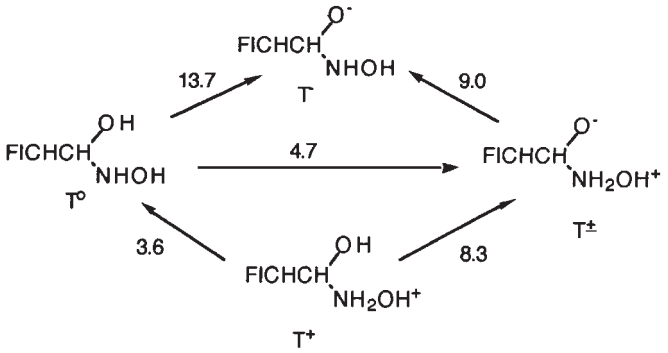
Following Sayer and Jencks (40) and Guthrie (22), the set of rate and equilibrium constants for formation and hydrolysis of the oxime shown in Scheme 1 can be completed by estimating equilibrium constants for formation of cationic and zwitterionic forms of the carbinolamine adduct T^+ and $T^{\pm}$. As these estimates are of lower precision than measurements of rate and equilibrium constants in the body of the paper they are presented in an appendix.

The relationships between the carbinolamine adducts of 9-formylfluorene T°, T^-, T^+, and $T^{\pm}$ are summarized in Scheme 1. The pK_a for ionization of T° to T^- has already been estimated as 13.7. We can estimate a pK_a for conversion of T^+ to T° based on pK_a = 6.1 for $CH_3NH_2OH^+$ by correcting for the substituent effects of the OH group and fluorenyl group present in T^o (for which σ* = 1.31 and 0.41, respectively). Thus, if ρ* for the ionization of substituted methylamines is 1.4 (28), the required pK_a is calculated as 6.1 – (1.31 + 0.41) × 1.4 = 3.6.

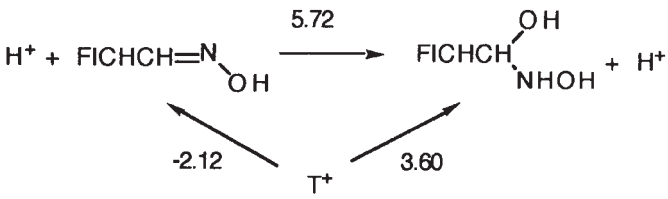
To evaluate a pK_a for conversion of T^+ to $T^{\pm}$ we begin with Hine and Kokesh's (53) estimate of pK_a = 9.98 for the ionization of $MeNH_2^+CH_2OH$ to $MeNH_2^+CH_2O^-$ based on the measured ionization constant for $Me_3N^+CH_2OH$ of 9.33 (54). If we replace the methyl group on $MeNH_2^+CH_2OH$ by OH and presume that ρ* is the same as if NH_2^+ was replaced by CH_2, then from σ*= 0.62 and –0.1 for CH_3 and CH_2OH[28], we obtain pK_a = 9.98 – 1.45(0.62 – 0.1) = 8.85 for $HONH_2^+CH_2OH$. Finally, correcting for the substituent effect of the fluorenyl group, taking σ* = 0.41 for Ph_2CH as usual, we obtain pK_a = 8.85 – 1.45 × 0.41 = 8.25 for T^+. This allows completion of the cycle shown below (Scheme A1).

A noteworthy feature of this cycle is that the proton activating factor (PAF), i.e., effect of protonation of nitrogen upon ionization of the hydroxyl group (47) is given by log PAF = 5.4. This value is roughly consistent with other estimates of pK_as of tetrahedral intermediates for which log PAF values of 3.6 (22), 4.7 (40), 4.8 (31), and 5.3 (2, 22) have been recorded, including in particular the value 5.3 for the adduct of methylhydroxylamine and three substituted benzaldehydes (2). It seems likely that the greatest uncertainty in pKs in the cycle is ±0.5 log units.

Scheme A1.



Scheme A2.



If we combine the pK_a for conversion of T^+ to T° with the equilibrium constant between T° and the oxime, we obtain an effective ionization constant for conversion of T^+ to the oxime, pK_a^{eff} = 2.12, as shown in Scheme A2. This value is used to correct the experimentally measured value of –1.50 for conversion of the oxime to protonated oxime and T^+ to a pK_a = –1.62 for protonation specifically of the oxime.

The equilibrium constants of Scheme A1 can be used to derive rate constants for reaction of T^+ in the hydrolysis of the oxime from the measurements of $k_{-2}K^{\pm} = 1.4 \times 10^3$ and $k_{-3}/K^+ = 160$ based on the pH-profile of Fig. 2 and shown under eq. [2]. Thus the rate constant k_{-2} for expulsion of NH_2OH from T± is calculated as 2.8×10^8 and the corresponding reaction from T^+ is $k_{-3} = 4.0 \times 10^{-2}$ s^{-1}.

© 2000 NRC Canada

Preparation, X-ray structure, and dynamic solution behaviour of *N*,*N*′,*N*″-tris(2,6-diisopropylphenyl)-guanidine, and its reaction with molybdenum carbonyl

Robyn E. Boeré, René T. Boeré, Jason Masuda, and Gotthelf Wolmershäuser

Abstract: The reaction of *N*,*N*′-bis(2,6-diisopropylphenyl)carbodiimide with lithium 2,6-diisopropylanilide, quenching with water and recrystallization from heptane produces the symmetric guanidine $[DipNH]_2C{=}NDip$ which crystallizes in the triclinic system, space group $P\bar{1}$, a = 10.6513(11), b = 10.8997(11), c = 16.2961(17) Å, α = 80.524(12), β = 78.921(13), γ = 70.060(12)°, V = 1735.2(3) Å^3, Z = 2. The molecule crystallizes with three perpendicular 2,6-diisopropylphenyl groups, which surround and shield the central CN_3 unit, and provide (almost) three-fold symmetry around the central atom. Its dynamic solution behaviour has been studied by VT NMR between –90 and +180°C, and is consistent with three distinct barriers to N—C_{Ar} rotation. Preliminary estimates of the Gibbs free energy of activation for the lower two barriers are 56 ± 2 and 73 ± 2 kJ mol^{-1}. Reaction of the title compound with $Mo(CO)_6$ in refluxing *n*-heptane produces $[DipNH]_2C{=}NDip{\cdot}Mo(CO)_3$, a complex in which $Mo(CO)_3$ is η^6-coordinated to one of the diisopropylphenyl rings.

Key words: crystal structure, diisopropylaniline, guanidine, bulky ligands.

Résumé : La réaction du *N*,*N*′-bis(2,6-diisopropylphényl)carbodiimide avec le 2,6-diisopropylanilure, suivie d'un piégeage avec de l'eau et d'une recristallisation à partir de l'heptane permet d'isoler la guanidine symétrique $[DipNH]_2C{=}NDip$ qui cristallise dans le système triclinique, groupe d'espace $P\bar{1}$, avec a = 10,6513(11), b = 10,8997(11) et c = 16,2961(17) Å, α = 80,524(12), β = 78,921(13) et γ = 70,060(12)°, V = 1735,2(3) Å^3 et Z = 2. La molécule cristallise avec trois groupes 2,6-diisopropylphényles perpendiculaires qui entourent et protègent l'unité CN_3 centrale et qui assurent une symétrie pratiquement ternaire autour de l'atome central. On a étudié son comportement dynamique en solution à l'aide de la RMN à température variable entre –90 et 180°C et il est en accord avec trois barrières distinctes pour la rotation autour de la liaison N—C_{Ar}. Sur la base d'évaluations préliminaires, les énergies libres d'activation de Gibbs des deux barrières les plus faibles sont respectivement de 56 ± 2 et 73 ± 2 kJ mol^{-1}. La réaction des composés mentionnés dans le titre avec du $Mn(CO)_6$ dans l'heptane au reflux conduit à la formation de $[DipNH]_2C{=}NDip{\cdot}Mo(CO)_3$, un complexe dans lequel le $Mo(CO)_3$ est η^6-coordiné à l'un des noyaux diisopropylphényles.

Mots clés : structure cristalline, diisopropylaniline, guanidine, ligands encombrants.

[Traduit par la Rédaction]

Introduction

We have recently reported the synthesis of a series of superamidines (**1**) and their molybdenum carbonyl adducts (**2**) (1, 2), which contain the sterically demanding 2,6-diisopropylphenyl (Dip) substituent on nitrogen. The reactions of carbodiimides with nucleophiles is a well-established organic synthetic route for the preparation of amidines, and in particular for amidinate anions used in coordination chemistry (3), and we are interested in exploring this route to amidines and related compounds bearing Dip substituents using the known *N*,*N*′-bis-(2,6-diisopropylphenyl)carbodiimide.

There is currently a strong interest in the use of guanidines (4) and guanidinate anions (5, 6) as ligands in coordination chemistry. Symmetrically trisubstituted guanidines are the nitrogen analogues of carbonic acid. In this work we report on the preparation of a guanidine (**3**) with a Dip substituent on all three nitrogen atoms using the carbodiimide route. Thermal reaction of the guanidine with $Mo(CO)_6$ leads to a single product (**4**) in which $Mo(CO)_3$ is coordinated in an η^6 fashion by one of the Dip groups, which is the dominant reaction previously observed for Dip-substituted amidines (1, 2).

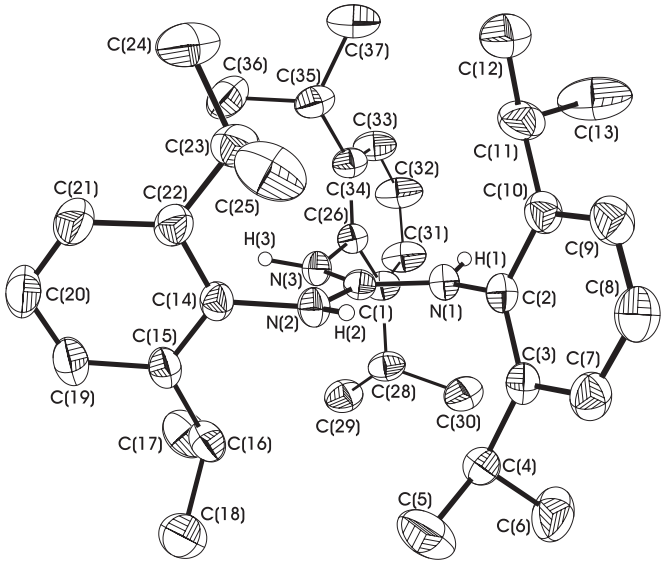
Received September 10, 1999. Published on the NRC Research Press website on November 27, 2000.

R.E. Boeré, R.T. Boeré[1], and J. Masuda. Department of Chemistry and Biochemistry, University of Lethbridge, Lethbridge, AB T1K 3M4, Canada.
G. Wolmershäuser. Fachbereich Chemie der Universität Kaiserslautern, Erwin-Schrödinger-Straβe, D-67663 Kaiserslautern, Germany.

[1]Author to whom correspondence may be addressed. Telephone: (403) 329-2045. Fax: (403) 329-2057. e-mail: boere@uleth.ca

© 2000 NRC Canada

Fig. 1. ORTEP diagram (50% probability) of the structure of **3** as found by X-ray crystallography, with the atom numbering scheme. Hydrogen atoms on carbon are omitted for clarity. The occupancy of H(1) is 30%, and of H(2) 70%.



Results and discussion

Synthesis and structure of 3

Bis-(2,6-diisopropylphenyl)carbodiimide was prepared from *N*,*N*′-2,6-diisopropylphenylisocyanate according to a literature method (7). Attempts to prepare the guanidine by direct addition of the carbodiimide with 2,6-disopropyl aniline in refluxing toluene or xylenes failed, although this is precisely how *N*,*N*′,*N*″-triphenylguanidine is prepared (5). However, when the lithium anilide is prepared in situ in THF (rxn. [1]), it reacts quantitatively with the carbodiimide (rxn. [2]), to provide, after quenching, the desired guanidine (rxn. [3]).

[1] $DipNH_2 + n\text{BuLi} \rightarrow DipNH^-Li^+ + n\text{BuH}$

[2] $DipNH^-Li^+ + DipN{=}C{=}NDip \rightarrow [DipN]_2CNHDip^-Li^+$

[3] $[DipN]_2CNHDip^-Li^+ + H_2O \rightarrow [DipNH]_2C{=}NDip + LiOH$

The guanidine **3** is easily purified by recrystallization from acetonitrile, which removes coloured impurities. Since these crystals tend to retain solvent, we performed a second recrystallization from *n*-heptane to give solvent-free colourless crystals that have been fully characterized by elemental analysis, mass spectrometry, and solution NMR.

The structure of **3** has been determined in the solid state by X-ray diffraction (Figs. 1 and 2, Tables 1 and 2). The side view of the structure shown in Fig. 1 is particularly instructive, showing the three Dip groups arranged almost perpendicular to the planar central CN_3 unit. A similarly rotated aryl group disposition was observed previously in the structure of 2-(2,6-dichlorophenyl)-1-methylguanidine, and seems to be a feature of *ortho*-disubstituted aryl amidine or guanidine derivatives (8). Figure 2 shows the central triazamethane unit in **3** with directly attached atoms. Noteworthy is the similarity of all the C—N distances [from 1.316(2) to 1.357(2) Å]. A representative C=N bond distance has been established as 1.283(3) Å (9), and a value close to this has been obtained for the neutral guanidine (*E*)-*N*,*N*′-dicyclohexyl-4-morpholinecarboxamidine for which the C=N distance was measured as 1.276(3) Å (10). The related C—N single bonds in the latter guanidine were measured as 1.414(2) and 1.381(2) Å. Häfelinger and Kuske (11) have defined the parameter $\Delta_{CN} = d(C{-}N) - d(C{=}N)$ for the central N-C-N linkage found in all amidines (including guanidines). We have previously found that two almost identical Dip-substituted amidine structures, (**1**, R = 4-$CH_3C_6H_4$ and R = 4-$CH_3OC_6H_4$) possessed the very different Δ_{CN} values of 0.027(6) and 0.057(3) (1). In the former case, i.e., where the difference in interatomic distance in the supposed "double" and "single" bonds was very small, we were able to detect the presence of two N—H hydrogen atom positions, and refined a disorder model with 72 and 28% occupancy of the two structures. We propose that a similar positional disorder is operative in the crystal structure of **3**, for which $\Delta_{CN} = 0.032(6)$ Å. Indeed, peaks corresponding

Fig. 2. ORTEP diagram of the central triazamethane fragment in **3** with directly attached atoms. The disordered H atoms were located on a difference Fourier map, and correspond to positional disorder in the crystal packing of the molecule.

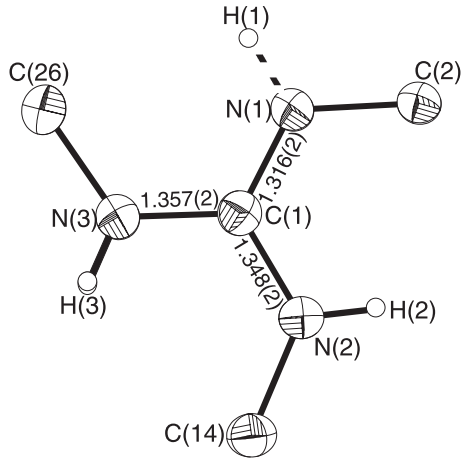


Table 1. Selected interatomic distances and angles for **3**.

Bond lengths	(Å)
N(1)-C(1)	1.3163(19)
N(1)-C(2)	1.4295(18)
N(2)-C(1)	1.3480(19)
N(2)-C(14)	1.421(2)
N(3)-C(1)	1.3567(18)
Bond angles	**(°)**
C(1)-N(1)-C(2)	120.16(12)
C(1)-N(2)-C(14)	124.30(12)
C(1)-N(3)-C(26)	122.81(14)
N(1)-C(1)-N(2)	121.99(13)
N(1)-C(1)-N(3)	119.52(13)
N(2)-C(1)-N(3)	118.47(14)

© 2000 NRC Canada

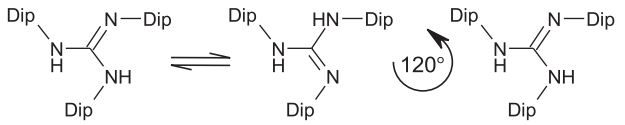
Table 2. Crystal data for **3**.[a]

Formula	$C_{37}H_{53}N_3$
Fw	539.82
Crystal system	triclinic
Space group	$P\bar{1}$ (no. 2)
a (Å)	10.6513(11)
b (Å)	10.8997(11)
c (Å)	16.296(17)
α (deg)	80.542(12)
β (deg)	78.921(13)
γ (deg)	70.060(12)
V (Å^3)	1735.2(4)
Z	2
d_{calc} (g cm^{-3})	1.033
Crystal dim. (mm)	0.52 × 0.32 × 0.21
Radiation, MoK$_\alpha$ (Å)	0.71073
Temperature (K)	293
μ (cm^{-1})	0.60
Absorption correction	none
Total reflections	20 256
Unique reflections	5206
Parameters refined	382
R (all data)	0.0586
R_w (all data)	0.1268
g.o.f. (all data)	1.052
Largest Δ/σ	0.01
Final diff. map [e Å^{-3}]	0.152, –0.104

[a]Weighting scheme used: $w = 1/[\sigma^2(Fo^2) + (0.0135P)^2]$ where $P = (Fo^2 + 2Fc^2)/3$.

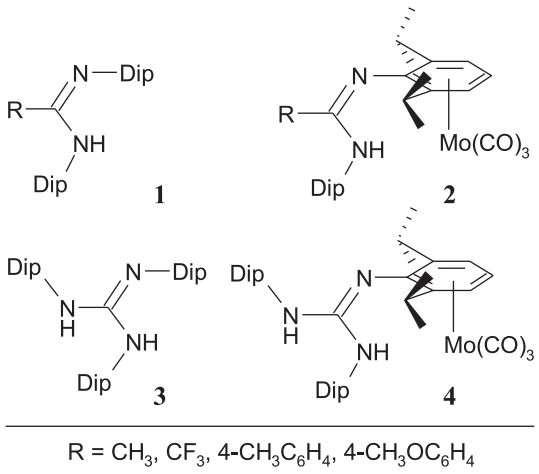
to the three N—H hydrogen atom locations were observed on a difference Fourier map, and their occupancies were allowed to vary. Convergence was achieved with H(3) as 100, H(2) 70, and H(1) 30%. In a structure so large we do not put a great deal of weight in the refinement of these occupancies, and our disorder model is based primarily on the metric parameters. As Fig. 2 clearly shows, the atoms in the triazamethane fragment are well-defined with almost spherical thermal ellipsoids.

Tautomeric disorder was postulated (without location of the H atoms) in the 2-(2,6-dichlorophenyl)-1-methylguanidine mentioned above (8). In this system, the three C···N distances are 1.364(5), 1.339(4), and 1.308(4) Å, only a slightly larger range than that found in the structure of **3**. These authors conclude only that the tautomer that identifies the 1.308(4) Å distance as the C=N bond "is predominant." In **3**, unlike our previously determined amidine structure (**1**, R = 4-$CH_3C_6H_4$) (1), the tautomeric forms are degenerate, and the apparent bond length averaging can be achieved by simple positional disorder in the crystal packing, as shown in the following graphic:



What these results emphasize is that the large Dip groups dominate the crystal packing and small variations in position of the remaining atoms can be tolerated with little cost to the lattice energy.

Scheme 1.



Reaction of 3 with $Mo(CO)_6$

The reaction of **3** with $Mo(CO)_6$ in refluxing *n*-heptane, conditions that were identical to our previous reactions of superamidines with molybdenum carbonyl (1, 2), resulted in a slow reaction that deposited yellow crystalline solid at the reflux temperature. Careful cooling of the solution resulted in the formation of essentially pure **4**, which has been characterized by solution IR, NMR and mass spectroscopies, and combustion analysis. The similarity in the NMR and IR spectroscopic parameters with those observed previously for type **2** complexes strongly suggests that the metal is coordinated in an η^6 fashion to the aromatic ring of one of the Dip groups. A parent ion for the complex is observed in the high-resolution mass spectrum. In the ^{1}H NMR spectrum, the aromatic C—H signals of *one* of the three Dip rings (a pseudo doublet and a pseudo triplet) are shifted ~1.5 ppm upfield as a consequence of π-coordination to the molybdenum atom. One of the two N—H signals is shifted ~2 ppm downfield (as observed for **2**), while the other retains a chemical shift similar to that in free **3**. The ν(C≡O) bands in the solution IR spectra are diagnostic of a "piano stool" coordination geometry for the $Mo(CO)_3$ group. Almost certainly it is the *imino* Dip group that attaches to the metal, as seen in all the superamidine complexes. Moreover, among the three X-ray structures previously determined for type **2** complexes, the ligand environment is extremely similar, and we note that this same arrangement can be obtained in **4** with the ligand in the conformation obtained for **3** in the solid state. This proposed structure is indicated in Scheme 1.

If we compare the solution IR data of **4** with those of **2** (Table 3), a distinct pattern emerges (1, 2). The electron withdrawing CF_3 group in **2** (R = CF_3) despite being three bonds removed from the diisopropylphenyl ring, nevertheless reduces the electron density at the ring. This leads to weaker back-bonding to Mo, and hence to about 5 cm^{-1} higher ν(C≡O) frequencies than in the methyl- and aryl-substituted amidine complexes **2** (R ≠ CF_3). In **4**, where an electron-donating DipNH group is attached to the amidine backbone, the ν(C≡O) frequencies are about 3 cm^{-1} lower in energy than in the methyl- and aryl-substituted amidine complexes **2** (R ≠ CF_3) consistent with stronger back-bonding by a more electron-rich aromatic ring.

© 2000 NRC Canada

Table 3. Solution IR data for **3**, **4**, and related compounds.[a]

Compound	ν(N-H) (cm^{-1})	ν(N-C-N) (cm^{-1})	ν(C≡O) (cm^{-1})	Reference
3	3415, 3392	1650	—	this work
1 (R = CH_3)	3391, 3378, 3366, 3350	1643	—	(1)
1 (R = CF_3)	3453, 3356	1657	—	(2)
1 (R = 4-$CH_3C_6H_4$)	3431, 3366	1620	—	(1)
1 (R = 4-$CH_3OC_6H_4$)	3431, 3366	1620	—	(1)
4	3403, 3272 br[b]	1640	1963, 1893, 1870	this work
2 (R = CH_3)	3193 br[b]	1640	1966, 1896, 1876	(1)
2 (R = CF_3)	—	1665	1971, 1906, 1883	(2)
2 (R = 4-$CH_3C_6H_4$)	3216 br[b]	1615	1966, 1896, 1879	(1)
2 (R = 4-$CH_3OC_6H_4$)	3216 br[b]	1615	1966, 1896, 1879	(1)

[a] *n*-Heptane solution in 0.2 mm NaCl solution cell.
[b] $CHCl_3$ solution in 0.2 mm NaCl solution cell; these weak bands are not observed in *n*-heptane because of limited solubility of the complexes.

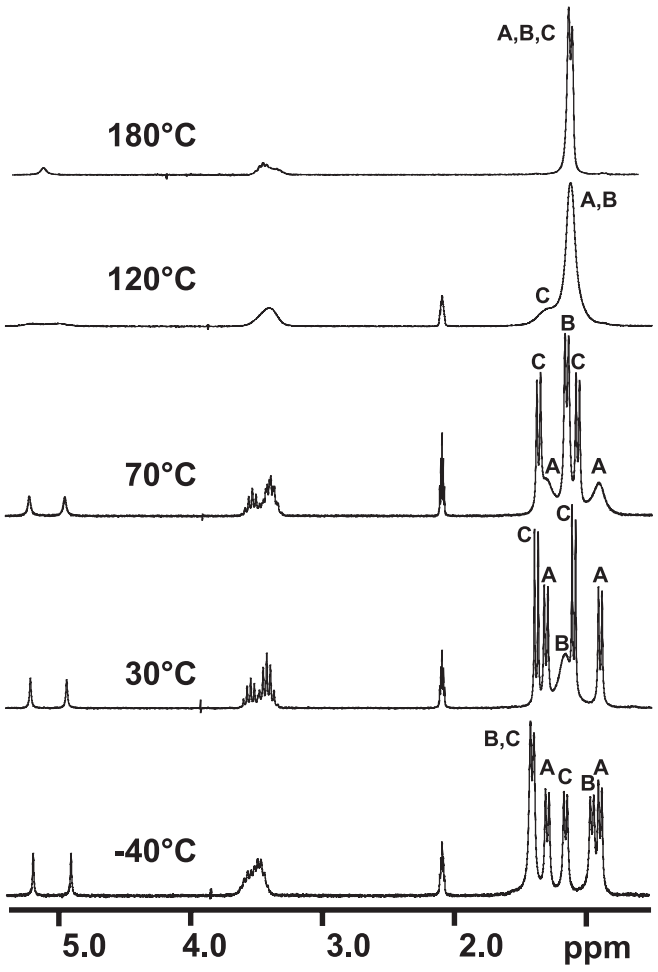
The large difference in NH environments observed for **4** in the NMR spectrum (δ 5.06 and 7.28) is also seen in solution IR spectra. Thus there is a broad band at 3272 cm^{-1} quite similar to the NH bands found in **2**, but there remains a sharp NH stretch at 3403 cm^{-1} for the additional DipNH group. In summary, the spectroscopic evidence for similarity with the previously characterized superamidine adducts strongly supports the proposed structure of **4** shown in Scheme 1.

Dynamic processes in solution

The room temperature ^1H NMR spectra of both the guanidine **3** and its metal complex **4** contain exchange-broadened signals as well as many sharp peaks. The room temperature ^{13}C spectrum of **3** also contains exchange-broadened peaks. Thus, there is some sort of dynamic process operative in both the guanidine and its complex with $Mo(CO)_3$. In this respect, the Dip-substituted guanidine differs from the Dip-substituted amidines **1** and their metal complexes **2**. The predominant isomers of **1** and the sole isomers of **2** have sharp, nonexchanging room temperature NMR signals. We have undertaken a preliminary VT-NMR study of the ^1H NMR spectra of **3** to try and sort out the complexities in the spectra. No attempt has been made to analyze the VT ^{13}C spectra of this compound; the RT spectrum is reported in the experimental section. Metal complex **4** is far too unstable in $CDCl_3$ solution to allow for VT-NMR studies.

The room temperature ^1H NMR spectrum of **3** in $CDCl_3$ solution as reported in the experimental section, or in $CD_3C_6D_5$ as shown in Fig. 3 at 30°C, is quite complex. Two very distinct NH proton signals, each integrating to one, are observed at δ 5.00 and 4.76. The isopropyl CH protons occur as three different septets, two of which have almost coincident chemical shifts, upfield of the remaining set. The most unusual feature is the isopropyl CH_3 protons, which exist as four sharp doublets in a 1:1:1:1 ratio, as well as a large exchange-broadened singlet between the inner two sharp doublets. These data strongly suggest that **3** exists in solution as a single isomer in which some sort of internal exchange is occurring that is slow on the NMR timescale. The NMR parameters of **3** closely resemble the predominant *Z-anti* isomer found for **1** (this conformation is that drawn in Scheme 1). This is the predominant solid-state form when H-bonding is not involved, as well as the lowest energy isomer by gas-phase computation (AM1 method) (1). Moreover, this is the geometry uniquely adopted by the $Mo(CO)_3$ adducts **2** in the solid-state and in solution (1, 2). Indeed, the solid-state structure of **3** can be considered as an amidine in the *Z-anti* geometry, with an additional DipNH group attached as the "R" group on the C atom of the backbone.

Fig. 3. NMR spectra of **3** at various temperatures (–40°C to +120°C in $CD_3C_6D_5$, 180°C in 1,2-$Cl_2C_6H_4$). Spectra were monitored at 10 degree intervals, and in the intervening spectra to those displayed here, smooth transitions between the peaks were observed.



© 2000 NRC Canada

Our VT-NMR spectroscopic study was conducted in a variety of solvents, namely CD_2Cl_2 and $CDCl_3$ for the low-temperature range, $CD_3C_6D_5$ for the intermediate, and 1,2-$Cl_2C_6H_4$ for the high-temperature range. There is indeed some solvent dependence of the chemical shifts of the signals, but the general process seems to be the same, and is clearly of an intramolecular nature. The solvent that covers the widest temperature range is $CD_3C_6D_5$. We independently checked the low-temperature range of this solvent by using the less viscous deuterated halocarbons, and find that essentially the same effects occur in all solvents studied. For simplicity we discuss the dynamic NMR behaviour using the data collected in $CD_3C_6D_5$ (except at the highest temperatures beyond the boiling point of this solvent, where 1,2-$Cl_2C_6H_4$ is used.)

Consider the representative NMR spectra presented in Fig. 3. At –40°C, rotational exchange of the Dip groups is frozen out, and in $CD_3C_6D_5$ solution there are five sharp methyl doublets in 2:1:1:1:1 ratio corresponding to two sets of two symmetry equivalent methyl groups of the imino Dip groups labeled "C" in the figure (δ 1.15 and 1.41), as well as two sets of two for each of the *amino* Dip groups, labeled "A" (δ 0.89 and 1.29) and "B" (δ 0.95 and 1.41). These data are consistent with three different Dip environments and a single plane of symmetry in the molecule, as seen in the solid-state structure. The shift equivalence of the deshielded B and C resonances is accidental (in CD_2Cl_2 their shifts are different). We note also that over the temperature range –90 to +80°C, the NH resonances remain sharp and distinct, with remarkably temperature-independent chemical shifts. This also agrees with the structure of **3** shown in Fig. 1 in which there are two different kinds of NH environments [i.e., H(2) and H(3)], and supports the notion that there is only a single geometrical isomer in solution over the whole temperature range that we have studied. There are of course several possible conformations that **3** may adopt in solution. We have modeled several of these by gas-phase AM1 calculations, and find that the geometry found in our crystal structure is indeed the lowest energy isomer we could find, lying 26.5 kJ mol^{-1} below the next higher form. Since this structure is fully consistent with the dynamic NMR data we will for the sake of argument consider this to be the isomer in solution, though we recognize that the actual solution geometry has not been proven.

Rotation of an amino Dip group exchanges the "inner" and "outer" methyl groups of the ^{i}Pr substituents, which appear to possess quite distinct shielding environments. On warming to 30°C, the two doublets labeled B have coalesced to a broad singlet at δ 1.15, indicating slow rotation of a single amino Dip group. This leaves four sharp doublets labeled A and C now in a 1:1:1:1 ratio for the shielded and deshielded methyl groups of the remaining amino and imino Dip groups, respectively. Spectra were obtained at 10 deg. intervals, and the changes in peak intensities and locations between the selected spectra presented in Fig. 2 underwent smooth transitions in the intermediate stages. At 70°C the coalesced signal B has grown into a sharp doublet at δ 1.14 (effectively the average of the two separate signals at –40°C) due to the four methyl groups on the rapidly rotating Dip substituent, while the second amino Dip CH_3 signals have collapsed into two exchange-broadened singlets labeled A. The two doublets C remain sharp, which we assign to the more rigid imino ring. Thus there are again five different CH_3 environments, integrating in a 1:1:2:1:1 ratio. At 120°C, line broadening of the NH signals to produce two extremely broad lines has (finally) set in, indicating the onset of slow NH tautomerism. This exchange process interconverts the amino and imino Dip sites, breaking down the rigidity of the latter. Now wholesale exchange of all the CH_3 *and* the CH environments sets in, the latter signals having remained sharp at lower temperatures, and all resonances are either coalesced or almost coalesced. Finally, at 180°C, NH tautomerism and rotation of the Dip groups are all fast on the NMR time-scale, and a simple high-symmetry spectrum containing a single Dip environment occurs. These changes are also reflected in the aromatic region, but we have not interpreted the observed patterns in detail; they are partly obscured by the residual toluene signals, and have thus been omitted from Fig. 3 for the sake of clarity.

An important piece of additional evidence for the interpretation of the dynamic phenomena put forth above for **3** is the RT spectrum in $CDCl_3$ of the metal complex **4**. The NMR signals that are sharp are virtually identical to those obtained for the two Dip groups of the type **2** amidine complexes, i.e., a coordinated imino and an uncoordinated amino group (1, 2). The CH_3 resonances of the third DipNH group are exchange-broadened at RT. This suggests that one amino DipNH group is undergoing slow rotation on the NMR time-scale, while the other is not, and that it must be the DipNH group on the amidine backbone that is dynamic. Sample instability has prevented us from performing the same kind of VT studies with **4** that were done with **3**. Ligand fluxionallity in a Pt{COD} complex of the dianion of *N*,*N*′,*N*″-triphenylguanidine has recently been reported, but the mechanism of intramolecular motion in this complex is not directly comparable to that observed in **4** (6).

A preliminary estimate of the activation energies for some of these dynamic processes can be obtained from the half-height line widths of the NMR signals at the coalescence temperature, using the classical expression of Gutowsky and Holm (12). Eyring absolute rate theory (13) leads to a value of $\Delta G^{\ddagger} = 56 \pm 2$ kJ mol^{-1} for the interconversion of the A set of signals, which we have attributed to the rotation of one of the Dip groups about an N—C_{Ar} bond. Similarly, $\Delta G^{\ddagger} = 73 \pm 2$ kJ mol^{-1} for the interconversion of the B set of signals. The final process that interconverts A, B, and C signals at the highest temperature is too complex to analyze by simple coalescence-point measurement. Although a full understanding of the dynamic processes that operate in **3** will require complete line-shape analysis and spectral simulation, we note that similar free energies of activation have been measured for hindered rotation about P—C_{Ar} bonds bearing the related bulky supermesityl substituent. Thus in Mes*P=C=PMes*, $\Delta G^{\ddagger} = 59 \pm 1$ kJ mol^{-1} (14), while in Mes*As=C=PMes*, $\Delta G^{\ddagger} = 57$ kJ mol^{-1} (15).

In conclusion, an *N*,*N*′,*N*″-trisubstituted guanidine bearing super-bulky Dip substituents has been prepared by the carbodiimide route, and shows interesting conformational effects due to hindered rotation in solution as shown by NMR spectroscopy. It forms a piano stool complex with $Mo(CO)_3$, in which the imino aryl ring acts as a six-electron donor to the organometallic fragment.

© 2000 NRC Canada

Experimental section

Starting materials and general procedures

All experimental procedures were performed under a nitrogen atmosphere using modified Schlenk techniques. 2,6-Diisopropylaniline and *n*-butyllithium (Aldrich) were commercial products and used as received. Bis-2,6-diisopropylphenylcarbodiimide was prepared using the published procedure (7). Solvents were reagent grade, or better, and were used as received (acetonitrile) or dried and distilled under a nitrogen atmosphere from $LiAlH_4$ (*n*-heptane) and sodium–benzophenone (tetrahydrofuran). ^1H and ^{13}C NMR spectra were recorded on a Bruker AC250/Tecmag Macspect spectrometer operating at 250.13 and 62.90 MHz, respectively. The ^1H and ^{13}C chemical shifts δ (ppm) for $CDCl_3$ solutions are referenced to TMS, while $CD_3C_6D_5$ solutions were referenced to the residual CHD_2 signal at δ 2.09. VT-NMR spectra were recorded using the Bruker VT accessory, and temperatures are considered accurate to ±2° below RT and ±1° above RT. IR spectra were recorded on a Bomem MB-100 spectrometer as KBr pressed pellets (solids) or in NaCl solution cells. Mass spectra were undertaken in the Department of Chemistry, University of Alberta and elemental analyses by MHW Laboratories, Phoenix, AZ.

Preparation of *N,N′,N″*-tris(2,6-diisopropylphenyl)guanidine (3)

A solution of 0.495 g (2.75 mmol) 2,6-diisopropylaniline in 10 mL of anhyd THF was treated with 3.03 mmol of 2.25 M *n*BuLi in hexanes at 0°C, and stirred for an additional 20 min at the same temperature. After warming to RT, 1.00 g (2.75 mmol) of *N,N′*-bis(2,6-diisopropylphenyl)carbodiimide in 6 mL of THF was added dropwise to the orange solution, whereupon the mixture was refluxed for 2 h. After cooling to RT, 1 mL H_2O was added, the mixture dried with anhyd $MgSO_4$ and evaporated to dryness. Crystallization from CH_3CN afforded 1.05 g (1.94 mmol, 70.5% yield) of **3**, mp 261–262°C. Additional product could be won from the mother liquor, but this tended to be slightly discoloured. Analytical material and data crystals were obtained by recrystallization from *n*-heptane. MS (70 eV): *m/z* 539.42351 (M^+ within 0.8 ppm, 100%), 524 ($M - CH_3^+$, 8%); 496 ($M - {}^iPr^+$, 92%). IR (KBr) cm^{-1}: ν(N-H) 3407, 3398; ν(C=N) 1646. ^1H NMR ($CDCl_3$): δ 0.98 (d, *J*(H-H) = 6.8 Hz, 12H), 1.09 (br s, 12H), 1.31 (d, *J*(H-H) = 6.8 Hz, 6H), 1.36 (d, *J*(H-H) = 6.8 Hz, 6H), 3.26 (sept, *J*(H-H) = 6.8 Hz, 2H), 3.31 (sept, *J*(H-H) = 6.8 Hz, 2H), 3.46 (sept, *J*(H-H) = 6.8 Hz, 2H), 4.77 (s, 1 H), 5.00 (s, 1 H), 6.93–7.30 (m, 9H). ^{13}C NMR δ: 22.55, 23.00, 24.31 (br), 24.88, 26.04, 28.66, 28.80, 28.89, 122.54, 123.07, 124.09, 127.30, 128.76, 132.47, 133.92, 141.15, 144.15, 145.63, 147.09, 147.92. Anal. calcd. for $C_{37}H_{53}N_3$ (539.9): C 82.32, H 9.90, N 7.78%; found: C 82.12, H 9.89, N 7.93%.

Preparation of *N,N′N″*-tris(2,6-diisopropylphenyl)guanidinotricarbonylmolybdenum(0) (4)

A mixture of **3** (0.482 g, 0.895 mmol) and $Mo(CO)_6$ (0.236 g, 0.895 mmol) was heated in *n*-heptane (24 mL) to reflux. After 18 h, a solid precipitate formed. On cooling, the solid was filtered off, and recrystallized from a minimum quantity of boiling heptane, hot filtering, and cooling to –35°C to give small, bright yellow crystals of **4** which were analytically pure. Yield: 0.17 g, (0.24 mmol, 26%), mp 210°C dec. ^1H NMR ($CDCl_3$) δ: 0.91 (d, *J*(H-H) = 6.8 Hz, 6H), 1.1 (br s, 12H), 1.20 (d, *J*(H-H) = 6.8 Hz, 6H), 1.29 (d, *J*(H-H) = 6.8 Hz, 6H), 1.39 (d, *J*(H-H) = 6.8 Hz, 6H), 2.87 (sept, *J*(H-H) = 6.8 Hz, 2H), 3.11 (sept, *J*(H-H) = 6.8 Hz, 2H), 3.49 (sept, *J*(H-H) = 6.8 Hz, 2H), 5.06 (s, 1 H), 5.50 (d, *J*(H-H) = 6 Hz, 2 H), 5.77 (t, *J*(H-H) = 6 Hz), 1 H), 7.06–7.37 (m, 6H), 7.28 (s, 1 H). ^{13}C NMR spectrum not obtained due to sample instability. MS (70 eV) reported on ^{98}Mo isotopomers: *m/z* 721.31377 (M^+ within 1.8 ppm, 2%), 635.31446 ($M - 3CO - 2H^+$ within 0.2 ppm, 17%); 539 (ligand$^+$, 62%), 496 (ligand–$^iPr^+$, 100%). IR (KBr) (cm^{-1}): ν(N-H) 3400, 3252 br; ν(C≡O) 1952, 1882, 1833; ν(C=N) 1635. Anal. calcd. for $C_{40}H_{53}MoN_3O_3$ (719.83): C 66.74, H 7.42, N 5.84%; found: C 67.00, H 7.16, N 5.95%.

X-ray analysis

The crystal structure of **3** was determined using a Stoe IPDS diffractometer. 277 Frames with an angle increment of 1.3° were measured. Therefore the full φ range of 360° was covered and each reflection was thus measured twice. Experimental details are summarized in Table 1. The structure was solved by direct methods using SHELXS-97 (16) and refined by full-matrix least-squares on F^2 using SHELXL-97 (17) using all reflections. The non-hydrogen atoms were refined anisotropically, and although most of the H atoms on C were located on the difference map, they were refined using a riding model (C—H = 0.95 Å). For CH_3 groups, a geometrically fixed trigonal pyramidal unit was fitted to the electron density for H by refining a torsion angle that defined the rotation of the group on the C—C bond (a standard procedure in SHELXL). The H atoms attached to N were refined freely. Isotropic *U* values were bound to 1.2 times the *U* values of the corresponding N atoms. Disorder is encountered with respect to the position of one such H atom. The disorder ratio was freely refined (the sum was fixed to 1). The refinement converged with occupancy of 0.3 for the hydrogen attached to N(1) and 0.7 for N(2). Crystallographic data (excluding structure factors) for the structures in this paper have been deposited.[2]

Electronic structure calculations

All calculations were performed using the AM1 method as implemented in HyperChem 5.1 running on a Pentium III computer under Windows NT 4.0 (18).

[2] A detailed structure report including atom positions and the anisotropic temperature factors has been deposited. Copies of materials on deposit may be purchased from the Depository of Unpublished Data, Document Delivery, CISTI, National Research Council Canada, Ottawa, ON, Canada K1A 0S2 (http://www.nrc.ca/cisti/irm/unpub_e.shtml for information on ordering electronically). Crystal data, atomic coordinates, bond lengths and angles, and hydrogen coordinates of the structure(s) reported in this paper have been deposited with the Cambridge Crystallographic Data Centre. Copies of the data can be obtained, free of charge, on application to the Director, CCDC, 12 Union Road, Cambridge, CB2 1EZ, U.K. (Fax: 44-1223-336033 or e-mail: deposit@ccdc.cam.ac.uk).

© 2000 NRC Canada

Acknowledgments

We thank the Natural Sciences and Engineering Research Council of Canada (NSERC) for financial support (RTB), and the University of Lethbridge for purchase of the NMR spectrometer and the Macspect controller.

References

1. R.T. Boeré, V. Klassen, and G. Wolmershäuser. J. Chem. Soc. Dalton Trans. 4147 (1998).
2. R.T. Boeré, V. Klassen, and G. Wolmershäuser. Can. J. Chem. **78**, 583 (2000).
3. Y. Zhou and D.S. Richeson. Inorg. Chem. **36**, 501 (1997).
4. P.J. Bailey, K.J. Grant, S. Pace, S. Parsons, and L.J. Stewart. J. Chem. Soc. Dalton Trans. 4263 (1997).
5. P.J. Bailey, L.A. Mitchell, and S. Parsons. J. Chem. Soc. Dalton Trans. 2839 (1996).
6. M.B. Dinger, W. Henderson, and B.K. Nicholson. J. Organomet. Chem. **556**, 75 (1998).
7. G. Himbert and W. Schwickerath. Liebigs Ann. Chem. 85 (1984).
8. A. Carpy, J.-M. Leger, C.-G. Wermuth, and G. Leclerc. Acta Crystallogr. Sect. B: Struct. Crystallogr. Cryst. Chem. **B37**, 885 (1981).
9. G. Argay, A. Kalman, A. Karpor, and B. Ribar. Acta Crystallogr. Sect. B: Struct. Crystallogr. Cryst. Chem. **B36**, 363 (1980).
10. F. Bellucci, V. Bertolasi, V. Ferretti, and G. Gilla. Acta Crystallogr. Sect. C: Cryst. Struct. Commun. **C41**, 544 (1985).
11. G. Häfelinger and K. H. Kuske. *In* The chemistry of amidines and imidates. Vol. 2. *Edited by* S. Patai and Z. Rappoport. Wiley, Chichester. 1991. Chap. 1. pp. 1–100.
12. H.S. Gutowsky and C.H. Holm. J. Chem. Phys. **25**, 1228 (1956).
13. J. Sandström. *In* Dynamic NMR spectroscopy. Academic Press, London. 1982.
14. M. Yoshifuji, S. Sasaki, T. Niitsu, and N. Inamoto. Tetrahedron Lett. **30**, 187 (1989).
15. H. Ranaivonjatovo, H. Ramadane, H. Gornitzka, J. Escudié, and J. Satgé. Organometallics, **17**, 1631 (1998).
16. G. Sheldrick. SHELXS-97. University of Göttingen, Göttingen, Germany. 1997.
17. G. Sheldrick. SHELXL-97. University of Göttingen, Göttingen, Germany. 1997.
18. HyperChem Pro Release 5.1, HyperCube. Waterloo, ON.

© 2000 NRC Canada

Synthesis and characterization of two new "pincer" complexes of zinc(II). The X-ray crystal structures of the five coordinate complexes [$ZnCl_2$\{η^3-*NN′N*-2,6-$(R_2NCH_2)_2C_5H_3N$\}] (R = *n*-Bu or Me)

Ignacio del Río, Robert A. Gossage, Milja S. Hannu, Martin Lutz, Anthony L. Spek, and Gerard van Koten

Abstract: The potentially terdentate *NN′N* donor ligand 2,6-bis[di-(*n*-butyl)aminomethyl]pyridine (**1**) does not form a stable, isolable Ru complex using any standard Ru starting materials. This is in contrast to the dimethylamino derivative **2**. In the presence of Zn metal as a reducing agent, the treatment of hydrated ruthenium trichloride with **2** leads instead to the isolation of a diamagnetic Zn(II) complex (**3**) of general formula [$ZnCl_2$(**1**)]. Analysis of **3** (NMR, X-ray) reveals the complex to be a mononuclear Zn halide compound containing ligand **1** in an η^3-*NN′N* bonding motif. The Zn atom is found to be five-coordinate and in a geometry best described as midway between trigonal bipyramidal and square pyramidal in structure. Similar experiments using **2** produce an analogous Zn species (**4**) which has likewise been fully characterized (NMR, X-ray) and found to be similar to **3** although the metal is in a distinctly square pyramidal environment. These compounds are viewed as relatives of the class of Zn "pybox" catalysts.

Key words: pincer complexes, zinc(II) compounds, X-ray crystal structure.

Résumé : Lorsqu'on le met en présence de dérivés du ruthénium appropriés, le ligand donneur, potentiellement terdentate *NN′N*, 2,6-bis[di(butyl)aminométhyl]pyridine (**1**) ne forme aucun complexe stable ou isolable du Ru. Ceci est en opposition avec le comportement du dérivé diméthylamino, **2**. En présence de Zn métallique comme agent de réduction, le traitement du trichlorure de ruthénium hydraté avec du produit **2** conduit plutôt à un complexe diamagnétique de Zn(II), de formule générale [$ZnCl_2$(**1**)] que l'on peut isoler. L'analyse de ce complexe (**3**) par RMN et diffraction des rayons X indique que le complexe est un composé mononucléaire d'halogénure de zinc contenant un ligand **1** dans un motif de liaison η^3-*NN′N*. On a observé que le zinc est pentacoordonné et qu'une structure intermédiaire entre une bipyramide trigonale et une pyramide à base carrée est la meilleure façon de décrire sa géométrie. Des expériences semblables avec le complexe **2** conduisent à la formation d'une espèce analogue contenant du zinc (**4**) que l'on a aussi caractérisée par RMN et diffraction des rayons X; on a trouvé que ce complexe est semblable à **3**, même si le métal se trouve dans un environnement à pyramide à base carrée bien caractérisée. On considère que ces composés sont apparentés aux catalyseurs de la classe « pybox ».

Mots clés : complexes en forme de pince, composés du Zn(II), structure cristalline par diffraction des rayons X.

[Traduit par la Rédaction]

Received May 1, 2000. Published on the NRC Research Press website on November 27, 2000.

I. del Río.[1] Departamento de Quimica Organica e Inorganica, Facultad de Quimica, Universidad de Oviedo, E-33071 Oviedo, Spain.
R.A. Gossage.[1] Department of Chemistry, Acadia University, Wolfville, NS B0P 1X0, Canada.
M.S. Hannu and G. van Koten.[1] Debye Institute, Department of Metal-Mediated Synthesis, Utrecht University, Padualaan 8, 3584 CH Utrecht, The Netherlands.
M. Lutz and A.L. Spek.[2] Bijvoet Centre for Biomolecular Research, Department of Crystal and Structural Chemistry, Utrecht University, Padualaan 8, 3584 CH Utrecht, The Netherlands.

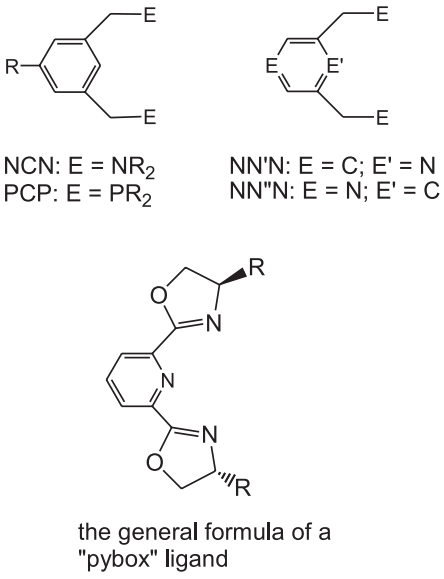
[1]Authors to whom correspondence may be addressed: IdR: Telephone: +34-98-5102985 or +34-98-5103449. Fax: +34-98-5103446. e-mail: irc@sauron.quimica.uniovi.es; RAG: Telephone: (902) 585-1109. Fax: (902) 585-1114. e-mail: rob.gossage@acadiau.ca; GvK: Telephone: +31-30-2533120. Fax: +31-30-2523615. e-mail: g.vankoten@chem.uu.nl.
[2]Author to whom correspondence may be addressed concerning the crystallographic portion of this work. e-mail: a.l.spek@chem.uu.nl.

 © 2000 NRC Canada

Introduction

The use of multidentate ligands in the stabilization of transition metal fragments is an important aspect of modern inorganic and organometallic synthesis. Of the large number of ligands that are currently known, the group of potentially terdentate ligands referred to as the "pincer" class of ligands (Fig. 1) has been yielding a rich body of interesting and novel chemistry (1). In particular, pincer complexes of the platinum group metals have been used in a number of diverse applications which include molecular sensor technology (1, 2) and in the modelling of reaction intermediates (1, 3). Several other properties, many of which have direct industrial relevance, have also been reported for metal complexes containing a pincer ligand. These aspects include a number of catalytic organic transformations involving C—C (4), C—N (5), and C—halogen bond formation (6), in addition to the polymerization of activated olefins via ROMP[3] or ATRP[4]. One of our areas of interest revolves around the inorganic chemistry of Ru containing a neutral, potentially terdentate *NN′N*-donor ligand derived from 2,6-bis(aminomethyl)pyridine (**1**: R = *n*-Bu; **2**: R = Me, Fig. 1). We have previously shown that **2** can be used to produce a number of useful Ru containing starting materials and reagents for the catalytic and stoichiometric activation of a variety of substrates including olefins, amines, and sulphur containing compounds (5, 7–10). We wished to expand our investigations to include Ru pincer complexes containing **1**. However, our attempts to coordinate this particular pincer ligand to a Ru metal centre have instead led to the isolation of a new *NN′N* complex of Zn(II). The incorporation of a Zn metal atom was the result of a failed attempt to produce a reactive source of Ru(II) (i.e., Ru(III) reduced via Zn) in situ in the presence of **1**. From this result, we have expanded this Zn chemistry and have fully characterized (NMR, X-ray) two novel Zn complexes, incorporating ligands **1** or **2**. In contrast to the plenitude of work involving platinum group metal pincer compounds (1–3, 5–9), relatively little is known about the Group XII transition metal chemistry of these ligands (1). This work has obvious relevance to Zn pybox (Fig. 1) complexes and their derivatives (pybox = [2,6-bis{oxazolin-2-yl}pyridine]) (11*a*). Several halide and pseudohalide complexes of Zn(II) in the presence of a pybox ligand are known to be potent enantioselective catalysts (e.g., Diels–Alder, aldol reactions, etc.) (11*b*, 11*c*) and surmised to have the general formula [$ZnX_2(\eta^3$-*NN′N*-pybox)]. In addition, complexes of this general class have recently been used as models for hydrolytic metallo-enzymes (11*d*).

Fig. 1.



Experimental section

General

All synthetic manipulations were carried out under inert atmosphere (Schlenk) techniques. Solvents were dried and degassed by standard methods. Diethyl ether was predried with NaOH and distilled from sodium–benzophenone; halocarbons were distilled from CaH_2 and hydrocarbon solvents and tetrahydrofuran (THF) was distilled from sodium–benzophenone. NMR spectra (^{1}H, ^{13}C, and ^{31}P) were recorded on a Bruker AC-200 or AC-300 spectrometer at RT (RT = room temperature). Chemical shifts (^{1}H and ^{13}C) are reported in ppm referenced to external $SiMe_4$ ($\delta_{H\ or\ C}$ = 0.00) and coupling constants (*J*) are given in Hz. Elemental analyses were performed by Kolbe Microanalytisches Laboratorium, Mülheim, Germany. The compounds $[RuCl_2(PPh_3)_3]$ (12), $[RuCl_2(nbd)]_n$ (nbd = 1,5-norbornadiene) (13), and 2,6-bis(dimethylaminomethyl)pyridine (**2**) (14) were synthesized according to previously published procedures. All other reagents and solvents were used as received from commercial sources.

Synthesis of 2,6-bis(di-*n*-butylaminomethyl)pyridine (1)

A sample of HBr (0.210 L, 48% in water) was added dropwise to a precooled solution (0°C) of 2,6-pyridinedimethanol (15.99 g, 43.0 mmol) in 500 mL of acetic anhydride. After addition was complete, the flask was removed from the ice bath and the mixture stirred overnight at 100°C. The resulting brown solution was cooled again to 0°C and a white precipitate formed. The solid was filtered, washed with ethylacetate (2 × 50 mL), and then dried under reduced pressure to give 29.0 g (73%) of a white solid presumed to be the HBr salt of 2,6-bis(bromomethyl)pyridine. A 150 mL portion of di-*n*-butylamine was added to a 15.0 g (4.44 mmol) portion of the above salt suspended in 150 mL of benzene. The mixture was then heated to reflux temperature for 48 h. Pentane was then added to the resulting light brown suspension to precipitate any salts. The solid was removed by filtration and washed with ether (3 × 20 mL). Volatile components of the combined organic fractions were then removed under reduced pressure to give 10.9 g (69%) of **1** which was deemed to be of sufficient purity (>95%: NMR) for further use. ^{1}H NMR ($CDCl_3$): 7.45 (t, 1H, py-*H*,

[3] ROMP = Ring Opening Metathesis Polymerization (7*a*).
[4] ATRP = Atom Transfer Radical Polymerization (6*b*, 7*b*).

© 2000 NRC Canada

J = 7.6), 7.23 (d, 2H, py-*H*), 3.56 (s, 4H, CH_2), 2.37–2.32 (m, 8H, NCH_2), 1.38–1.29 (m, 8H, CH_2), 1.24–1.14 (m, 8H, CH_2), 0.77–0.72 (m, 12H, CH_3). ^{13}C NMR ($CDCl_3$): 160.1 (*o*-C, py), 136.4 (*m*-C, py), 120.5 (*p*-C, py), 60.9 (NCH_2), 54.3 (CH_2), 29.6 (CH_2), 20.7 (CH_2), 14.1 (CH_3).

Synthesis of [{η^3-*NN′N*-2,6-bis(di-*n*-butylaminomethyl)pyridine} zinc(II) chloride] (3)

Method A

A solution of hydrated ruthenium trichloride (0.35 g, 3.44 mmol) and **1** (1.64 g, 4.54 mmol) was dissolved in EtOH (25 mL) and heated to 40°C in the presence of excess Zn powder for a period of 48 h. The resulting black suspension was centrifuged, the green-brown layer was then removed, and a black solid portion was isolated. This material was dissolved in 30 mL of dichloromethane, filtered, and the solution concentrated to a volume of about 5–10 mL. Pentane (10 mL) was then added and the resulting precipitated solid was collected and dried in vacuo to afford crude **3** in the form of a brown-grey solid (1.51 g, 88%).

Method B

A solution of anhyd zinc dichloride (0.13 g, 0.95 mmol) and **1** in EtOH (25 mL) was stirred at RT for 12 h. The liquid layer was removed from the resulting white suspension and the remaining solid was then dried under reduced pressure. The white solid thus obtained was dissolved in 5 mL of dichloromethane and filtered. The resulting light grey solution was mixed with 10 mL of pentane to precipitate **3** in the form of a white solid (yield: 0.30 g, 57%). ^{1}H NMR ($CDCl_3$): 7.88 (t, 1H, py-*H*, *J* = 7.2), 7.27 (d, 2H, py-*H*), 3.86 (s, 4H, CH_2), 2.80–2.72 (m, 8H, NCH_2), 1.59–1.43 (m, 8H, CH_2), 1.33–1.15 (m, 8H, CH_2), 0.92–0.84 (m, 12H, CH_3). ^{13}C NMR ($CDCl_3$): 158.6 (*o*-C, py), 141.1 (*m*-C, py), 122.4 (*p*-C, py), 57.5 (NCH_2), 52.5 (CH_2), 26.0 (CH_2), 21.0 (CH_2), 14.3 (CH_3). Anal. calcd. for $C_{23}H_{43}N_3Cl_2Zn$ (497.89): C 55.48, H 8.71, N 8.44; found: C 55.39, H 8.65, N 8.39.

Synthesis of [{η^3-*NN′N*-2,6-bis(dimethylaminomethyl)pyridine} zinc(II) chloride] (4)

Method A

A solution of hydrated ruthenium trichloride (0.52 g, 5.12 mmol) and **2** (1.61 g, 8.33 mmol) was dissolved in EtOH (25 mL) and stirred at RT in the presence of excess Zn powder for a period of 12 h. The resulting black suspension was centrifuged, the brown-black layer was then removed and a black solid portion was isolated. This material was dissolved in 30 mL of dichloromethane, filtered, and the solution concentrated to a volume of about 5–10 mL. Pentane (10 mL) was then added and the resulting precipitated solid was collected and dried in vacuo to afford crude **4** in the form of a light yellow solid (0.31 g, 17%).

Method B

A solution of zinc dichloride (0.41 g, 3.0 mmol) and **2** in EtOH (25 mL) was stirred at RT for 12 h. The yellow liquid layer was removed from the resulting suspension and the remaining solid was then dried under reduced pressure. The white solid thus obtained was dissolved in 5 mL of dichloromethane and the yellow solution was filtered thereafter. The mixture was then treated with a 10 mL portion of pentane to precipitate **4** in the form of a white solid (yield: 0.37 g, 37%). ^{1}H NMR ($CDCl_3$): 7.92 (t, 1H, py-*H*, *J* = 7.9), 7.29 (d, 2H, py-*H*), 3.77 (s, 4H, CH_2), 2.49 (s, 12H, CH_3). ^{13}C NMR ($CDCl_3$): 155.5 (*o*-C, py), 141.5 (*m*-C, py), 122.8 (*p*-C, py), 65.2 (NCH_2), 46.5 (CH_3). Anal. calcd. for $C_{11}H_{19}N_3Cl_2Zn$ (329.57): C 40.09, H 5.81, N 12.75; found: C 40.15, H 5.75, N 12.66.

Crystal structure determinations

General

Intensities were measured on a Nonius Kappa CCD diffractometer with rotating anode (Mo-Kα, λ = 0.71073 Å) at a temperature of 150 K. The structures were solved with direct methods (SHELXS-97 (15)) and refined with the program SHELXL-97 (16) against F^2 of all reflections up to a resolution of $(\sin\theta/\lambda)_{max}$ = 0.65 Å^{-1}. Non-hydrogen atoms were refined freely with anisotropic displacement parameters, hydrogen atoms were refined freely with isotropic parameters. The drawings, calculations, and checking for higher symmetry were performed with the PLATON package (17).

Crystal structure determination of 3

Formula: $C_{23}H_{43}Cl_2N_3Zn$; fw = 497.87; colourless-brownish plate, 0.25 × 0.25 × 0.11 mm^3; monoclinic, *C*2/*c* (no. 15), *a* = 13.1705(1) Å, *b* = 9.1163(1) Å, *c* = 21.7754(2) Å, β = 92.0916(6)°, *V* = 2612.75(4) Å^3, *Z* = 4, ρ = 1.266 g cm^{-3}, analytical absorption correction (PLATON (17), μ = 1.158 mm^{-1}, 0.73–0.88 transmission). Measured reflections = 27 704, 3003 unique reflections (R_{int} = 0.0466), *R* ($I > 2\sigma(I)$): *R*1 = 0.0188, *wR*2 = 0.0507. *R* (all data): *R*1 = 0.0195, *wR*2 = 0.0512. *S* = 1.040. –0.218 < Δρ < 0.278 e Å^{-3}.

Crystal structure determination of 4

Formula: $C_{11}H_{19}Cl_2N_3Zn$; fw = 329.56; yellow block, 0.63 × 0.28 × 0.28 mm^3; tetragonal, $P4_12_12$ (no. 92), *a* = *b* = 10.5893(1) Å, *c* = 25.9157(3) Å, *V* = 2906.01(5) Å^3, *Z* = 8, ρ = 1.507 g cm^{-3}, analytical absorption correction (PLATON (17), μ = 2.041 mm^{-1}, 0.30–0.60 transmission). Measured reflections = 19 719, 3323 unique reflections (R_{int} = 0.0316), *R* ($I > 2\sigma(I)$): *R*1 = 0.0183, *wR*2 = 0.0484. *R* (all data): *R*1 = 0.0186, *wR*2 = 0.0486. *S* = 1.071. –0.364 < Δρ < 0.609 e Å^{-3}.

Results and discussion

Our desire to use a Bu derivative of the *NN′N* ligand (i.e., **1**) was a direct consequence of the observation that several of our catalysts containing ligand **2** have low-solubility characteristics in organic solvents. Thus, derivative **1** was synthesized to evaluate its potential as a ligand for metal complexation where the resulting species will ideally present more favourable solubility properties. In addition, the trialkyl *N*-donor atoms of **1** are expected to have a stronger (Lewis) basic character when compared with the analogous *N*-atoms of **2**. Thus, one can evaluate the effect of increased ligand basicity on complexation behaviour, stability, and catalytic performance. Ligand **1** was produced according to a

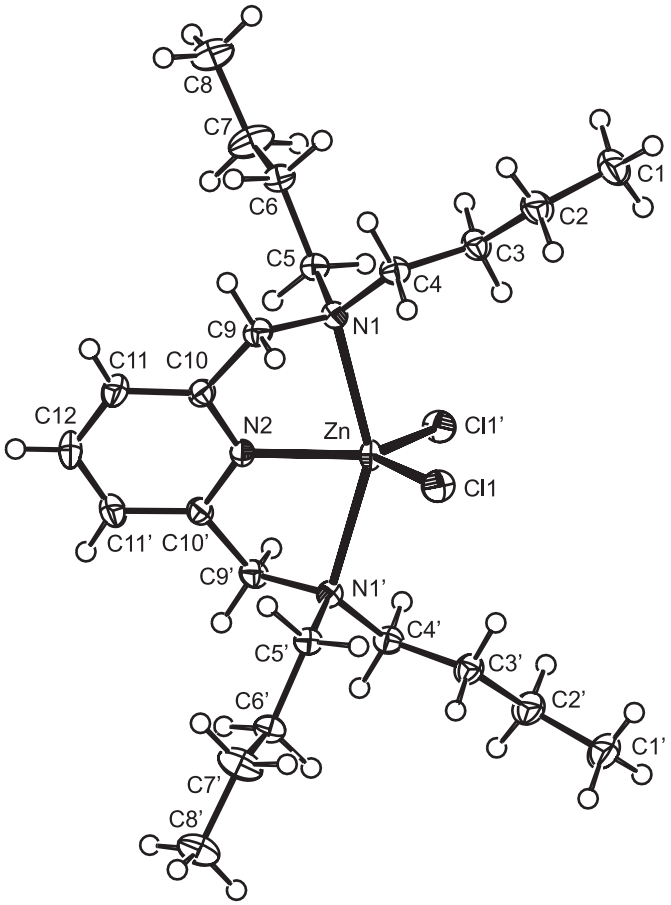
© 2000 NRC Canada

modified version of a simple two-step procedure (18). The treatment of 2,6-pyridinedimethanol with aq HBr, followed by heating in the presence of excess $HNBu_2$, gives **1** in 51% overall yield (see Experimental section).

The typical synthesis of Ru complexes containing **2** involves the reaction of the ligand with 1 equiv of $[RuCl_2(PPh_3)_3]$ in a halocarbon solvent. However, the treatment of **1** with this Ru precursor (CH_2Cl_2 or $C_2H_4Cl_2$ as solvent) gave no reaction at RT (NMR). Heating of these mixtures to reflux temperature gave a complicated mixture of products (NMR) including both starting materials, free PPh_3, and a number of other phosphine containing complexes in an inseparable mixture. The use of a hydrocarbon solvent such as toluene gave only starting materials at both RT and upon addition of heat. We then attempted the use of the polymeric form of $[RuCl_2(nbd)]$ as the Ru starting material. Unfortunately, this also gave a complex mixture upon treatment with **1**, using either toluene or THF as solvent. Following these failures, we attempted the use of hydrated $RuCl_3$ as the source of Ru under reducing conditions (Zn metal in EtOH) in the presence of **1**. To our surprise, a new complex was formed which appeared to contain the reducing agent (i.e., Zn) and not a Ru metal centre. Elemental analysis indicated a formula which corresponds to $[ZnCl_2(\mathbf{1})]$ (i.e., **3**). Although the yield of **3** was low, heating of the mixture to 40°C gave **3** in over 88% isolated yield. Complex **3** can also be produced in moderate yield from anhyd zinc dichloride (EtOH, reflux, 12 h) in the absence of ruthenium halide source. The ^1H and ^{13}C NMR spectra of **3** indicates a high degree of molecular symmetry and the diamagnetic nature of this inorganic Zn complex. The ^1H NMR spectrum reveals a singlet resonance assigned to the benzylic methylene protons of the *NN′N* ligand fragment (δ_H = 3.86 ppm) and a corresponding ^{13}C resonance for the corresponding benzylic carbon (δ_C = 57.5 ppm). These results cannot distinguish between an η^3-*NN′N*, or η^1-N_{py} binding motif of **1** to the metal centre nor the possibility that a multinuclear complex has been formed.

Therefore, a single crystal X-ray structure determination of **3** was carried out to confidently assign the structural properties of this compound. A suitable crystal was obtained by the slow evaporation of a dichloromethane solution of the complex which had been layered by a blanket of pentane and THF. The solid-state molecular structure of **3** is depicted in Fig. 2. The list of relevant bond lengths and angles appears in Table 1. The coordination sphere around the Zn atom is best described as midway between trigonal bipyramidal (TBP) and square pyramidal (SQP) in structure. The τ-value for estimating the distortion from these two extremes was found to be 0.47 (the τ-values range from 1.0 for a true trigonal bipyramidal geometry to 0.0 for an idealized square pyramidal structure. See ref. 19). However, the compound is not on a true Berry pseudo-rotation pathway between these two ideal geometries. Thus, a numerical description such as the τ-value is very approximate (19). Since complex **3** has an exact C_2 symmetry plane in the solid-state, the Zn atom is in the plane formed by the three N atoms. The bond lengths between the metal and the N and halogen ligands are typical for a complex that is formally Zn(II) and can be compared with that of other Zn complexes containing the 3N-2X (X = halogen or pseudo-

Fig. 2. Representation of the solid-state structure of **3**.



halogen) ligand set. These include such complexes as $[ZnCl_2(\eta^3\text{-terpy})]$ (terpy = 2:6,2′,2″-terpyrdine) (20*a*) and others (crystallographically characterized examples of the general formula $[ZnX_2(\eta^3\text{-}NN'N'')]$ can be found in ref. 20*b*–20*j*; for a discussion of the bond length properties of coordination complexes, including Zn(II) compounds, see ref. 21; for a general discussion on the coordination properties of zinc(II) ions see ref. 22). Complex **3** may also be viewed as an analogue of compounds having the general formula $[ZnX_2(\eta^3\text{-pybox})]$. Such complexes have recently found application in a variety of Lewis acid-catalyzed asymmetric organic transformations including Diels–Alder reactions (11*b*), aldol (Mukaiyama) reactions (11*b*), and for the enantioselective addition of enol silanes to ketomalonate (11*c*).

The robust nature of **3** was demonstrated by the following experiments. No reaction was observed (NMR) when a solution of **3** was heated to reflux temperature under a nitrogen atmosphere in a CCl_4 (12 h), acetonitrile (12 h), benzene (48 h), or toluene (48 h) solution. No spectral changes were observed when a RT solution of **3** is treated with a basic trialkyl phosphine (e.g., PMe_3) or a phosphite (e.g., $P[OMe]_3$), even in the presence of excess $AgBF_4$. However, treatment of **3** with an ether solution of HCl resulted in some decomposition of the material (a black precipitate was noted). Compound **3** was also found to be unstable to the presence

© 2000 NRC Canada

Table 1. Important bond lengths (Å) and angles (deg) for complexes **3** and **4**.[a]

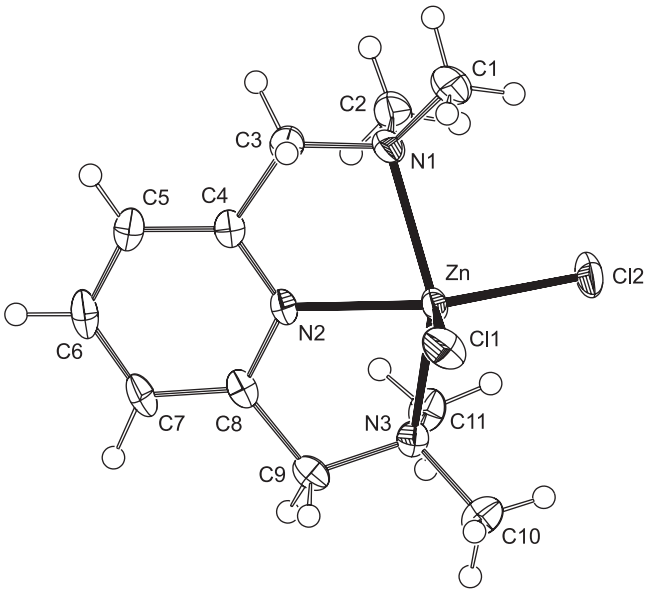
Bond length	Complex **3**	Complex **4**
Zn—Cl(1)	2.2293(3)[b]	2.2636(4)
Zn—Cl(2)	n.a.[c]	2.2882(5)
Zn—N(1)	2.3883(8)‡	2.2554(13)
Zn—N(2)	2.0498(12)	2.0980(12)
Zn—N(3)	n.a.	2.2512(14)
Bond and torsion angles		
Cl(1)-Zn-N(1)	95.35(2)	135.63(4)
Cl(1)-Zn-N(2)	119.10(1)	103.54(4)
Cl(1)-Zn-Cl(1A)	121.81(1)	n.a.
Cl(1)-Zn-Cl(2)	n.a.	108.94(2)
Cl(1)-Zn-N(1A)	99.07(2)	n.a.
Cl(1)-Zn-N(3)	n.a.	109.57(4)
N(1)-Zn-Cl(1A)	150.11(3)	n.a.
Cl(2)-Zn-N(1)	n.a.	95.06(4)
Cl(2)-Zn-N(2)	n.a.	147.50(5)
Cl(2)-Zn-N(3)	n.a.	94.28(4)
N(2)-Zn-Cl(1A)	119.10(1)	n.a.
N(1)-Zn-N(2)	n.a.	74.89(5)
N(1)-Zn-N(3)	n.a.	138.17(5)
N(2)-Zn-N(3)	n.a.	75.52(5)
N(2)-Zn-N(1A)	75.06(2)	n.a.
Cl(1A)-Zn-N(1A)	95.35(2)	n.a.
N(1)-C(9)-C(10)-N(2)	35.68(11)	n.a.
N(1)-C(3)-C(4)-N(2)	n.a.	27.54(19)
N(2)-C(8)-C(9)-N(3)	n.a.	–21.33(18)

[a]Standard deviations are given in parenthesis.
[b]Also the Zn—Cl(1A) or Zn—N(1A) bond length.
[c]n.a. = not applicable.

of sulphur dioxide or phenylacetylene[5] when a silver salt was present ($AgBF_4$ or AgOTf). Under these conditions, the bis HX salt (X = BF_4 or OTf) of ligand **1** can be isolated from the reaction mixture[6].

Despite our failure to produce the desired Ru complexes by the above route, we were intrigued as to the possibility of forming the related Zn(II) complex using the prototypical *NN′*N ligand **2** described earlier. Thus, treatment of a solution of anhyd zinc dichloride with a solution of **2** in EtOH solution gave complex **4** in 37% isolated yield. Interestingly, treatment of a solution of **2** with Zn metal in the presence of hydrated ruthenium trichloride under a nitrogen atmosphere leads to the formation of both **4** (17%) and the known complex $[RuCl_2(NN'N)]_2(\mu\text{-}N_2)$ (15%: NMR) (5b). Thus, it appears that the higher nucleophilicity of the nitrogen atoms in **1**, when compared with ligand **2**, may be detrimental to forming stable Ru(II) species.

Fig. 3. Representation of the solid-state structure of **4**.



As in the case of **3**, an X-ray structural determination of **4** was also carried out. The compound has a somewhat similar molecular structure when compared with **3** (i.e., a mononuclear complex (Fig. 3)). However, the Zn atom in **4** is more accurately described as being in a slightly distorted square pyramidal environment (τ = 0.16 (19)). Also, compound **4** has an approximate, non-crystallographic C_s (mirror) symmetry and hence the Zn atom, unlike in **3**, is not in the plane formed by the three N atoms (a deviation of 0.726(1) Å). The important bond lengths and angles for complex **4** can be found in Table 1. The *NN′N* pincer ligand is in a typical geometry (5*b*–5*c*, 7*b*, 8–10). Compound **4** was also found to be stable to prolonged heating (12 h) under a nitrogen atmosphere in CCl_4 solution.

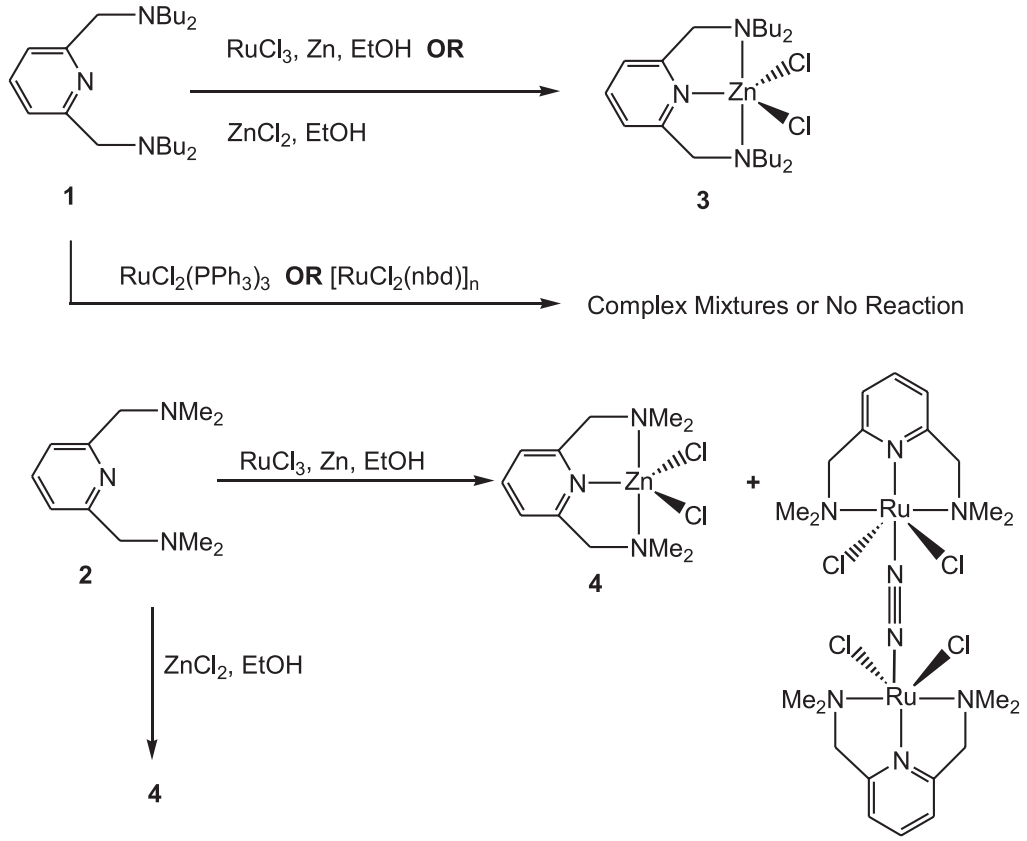
Conclusions

Attempts to synthesise Ru complexes under standard conditions (5*b*, 5*c*) with the basic *NN′N* ligand **1** leads to complex mixtures or a complete absence of any reaction. The former result may be due to the more basic nature of the trialkylamine donor atoms when compared with the complimentary ligand **2**. Treatment of hydrated $RuCl_3$ with **1** in the presence of Zn metal in EtOH solution leads to a thermally stable compound (**3**), which is an *NN′N* complex of Zn(II). Complex **3** and its methyl analogue **4** can also be produced in moderate yields using anhyd zinc chloride as the metal source (Scheme 1). Both **3** and **4** have been characterized by elemental analysis, NMR, and by a single crystal X-ray structure determination.[7] The latter results show that both

[5] Our interest in the activation of SO_2 and PhC≡CH stems from earlier work (2, 8, 10).
[6] Compound **1**·2(HBF_4)·0.5(H_2O): Selected data: ^{1}H NMR ($[CD_3]_2CO$): 11.54 (s, 2H, N*H*), 8.13 (t, 1H, *J* = 7.8, py-*H*), 7.73 (d, 2H, py-*H*), 4.87 (d, 4H, CH_2), 3.49–3.43 (m, 8H, NCH_2), 1.92–1.81 (m, 8H, CH_2), 1.44–1.31 (d, 8H, CH_2), 0.94–0.85 (m, 12H, CH_3). ^{19}F NMR ($[CD_3]_2CO$): 145.3 (s, BF_4). Anal. calcd. for $C_{23}H_{46}N_3B_2F_4O_{0.5}$ (527.24): C 50.57, H 8.49, N 7.69; found: C, 50.51, H 8.32, N 7.09.
[7] Supplementary material may be purchased from the Depository of Unpublished Data, Document Delivery, CISTI, National Research Council Canada, Ottawa, ON K1A 0S2, Canada (http://www.nrc.ca/cisti/irm/unpub_e.shtml for information on ordering electronically). Crystal data and structure refinement, atomic coordinates, bond lengths and angles, and hydrogen coordinates for the structure(s) reported in this paper have been deposited with the Cambridge Crystallographic Centre. Copies of the data can be obtained, free of charge, on application to the Director, CCDC, 12 Union Road, Cambridge CB2 1EZ, U.K. (Fax: 44-1223-336033 or e-mail: deposit@ccdc.cam.ac.uk).

© 2000 NRC Canada

Scheme 1.



compounds are mononuclear, five coordinate Zn species but the geometry about the metal is notably different between the two species. Compound **3** is best described as midway between TBP and SQP geometry while compound **4** has a slightly distorted SQP geometry about the metal centre. These results clearly emphasize that subtle changes in ligand structure can have a large effect on metal geometry, even with the two closely related cases of pincers **1** and **2**. This observation may have a profound impact on catalytic applications, especially as both **3** and **4** may be viewed as simple relatives to the Zn pybox systems which are known to be mediators of regio- and enantio-selective organic reactions (11*a*–11*c*).

Acknowledgements

IdR and MSH would like to thank the European Union for financial support under the auspices of the Training and Mobility of Researchers Program (Grant ERBFMBICT961634) and the Eramus Program, respectively. RAG is indebted to Acadia University for funding and computer support. This work has been further supported (ML, ALS, and GvK) by the Netherlands Organization for Scientific Research (CW-NWO).

References

1. (*a*) G. van Koten. Pure Appl. Chem. **61**, 1681 (1989), and refs. therein; (*b*) M.H.P. Rietveld, D.M. Grove, and G. van Koten. New J. Chem. **21**, 751 (1997), and refs. therein; (*c*) P. Steenwinkel, R.A. Gossage, and G. van Koten. Chem. Eur. J. **4**, 759 (1998), and refs. therein; (*d*) B. Rybtchinski and D. Milstein. Angew. Chem. Int. Ed. **38**, 870 (1999), and refs. therein; (*e*) C.M. Jensen. Chem. Commun. 2443 (1999), and refs. therein.
2. (*a*) M. Albrecht, R.A. Gossage, A.L. Spek, and G. van Koten. Chem. Commun. 1003 (1998); (*b*) M. Albrecht and G. van Koten. Adv. Mater. **11**, 171 (1999).
3. (*a*) J.A.M. van Beek, G. van Koten, W.J.J. Smeets, and A.L. Spek. J. Am. Chem. Soc. **108**, 5010 (1986); (*b*) G. van Koten. Pure Appl. Chem. **62**, 1155 (1990); (*c*) A.J. Canty and G. van Koten. Pure Appl. Chem. **28**, 406 (1995); (*d*) P. Dani, T. Karlen, R.A. Gossage, W.J.J. Smeets, A.L. Spek, and G. van Koten. J. Am. Chem. Soc. **119**, 11317 (1997); (*e*) R.A. Gossage, A.D. Ryabov, A.L. Spek, D.J. Stufkens, J.A.M. van Beek, R. van Eldik, and G. van Koten. J. Am. Chem. Soc. **121**, 2488 (1999); (*f*) M. Albrecht, R.A. Gossage, A.L. Spek, and G. van Koten. J. Am. Chem. Soc. **121**, 11898 (1999); (*g*) A. Vigalok, B. Rybtchinski, L.J.W. Shimon, Y. Ben-David, and D. Milstein. Organometallics, **18**, 895 (1999).
4. J.G. Donkervoort, J.L. Vicario, J.T.B.H. Jastrzebski, R.A. Gossage, G. Cahiez, and G. van Koten. J. Organomet. Chem. **558**, 61 (1998).
5. (*a*) Q. Jiang, D. van Plew, S. Murtuza, and X. Zhang. Tetrahedron Lett. **37**, 797 (1996); (*b*) R.A.T.M. Abbenhuis, I. del Río, M.M. Bergshoef, J. Boersma, N. Veldman, A.L. Spek, and G. van Koten. Inorg. Chem. **37**, 1749 (1998); (*c*) R.A.T.M. Abbenhuis, J. Boersma, and G. van Koten. J. Org. Chem. **63**, 4282 (1998).
6. (*a*) J.W.J. Knapen, A.W. van der Made, J.C. de Wilde, P.W.N.M. van Leeuwen, P. Wijkens, D.M. Grove, and G. van Koten. Nature (London), **372**, 659 (1994); (*b*) R.A. Gossage, L.A. van de Kuil, and G. van Koten. Acc. Chem.

© 2000 NRC Canada

Res. **31**, 423 (1998); (*c*) R.A. Gossage, J.T.B.H. Jastrzebski, J. van Ameijde, S.J.E. Mulders, A.J. Brouwer, R.M.J. Liskamp, and G. van Koten. Tetrahedron Lett. **40**, 1413 (1999); (*d*) G. van Koten and J.T.B.H. Jastrzebski. J. Mol. Catal. A: Chem. **146**, 317 (1999); (*e*) A.W. Kleij, R.A. Gossage, J.T.B.H. Jastrzebski, J. Boersma, and G. van Koten. Angew. Chem. Int. Ed. **39**, 176 (2000).

7. (*a*) I. del Río and G. van Koten. Tetrahedron Lett. **40**, 1401 (1999); (*b*) I. del Río and G. van Koten. Organometallics, **19**, 361 (2000).
8. I. del Río, R.A. Gossage, M. Lutz, A.L. Spek, and G. van Koten. Inorg. Chim. Acta, **287**, 113 (1999).
9. I. del Río, R.A. Gossage, M. Lutz, A.L. Spek, and G. van Koten. J. Organomet. Chem. **583**, 69 (1999).
10. I. del Río, R.A. Gossage, M.S. Hannu, M. Lutz, A.L. Spek, and G. van Koten. Organometallics, **18**, 1097 (1999).
11. (*a*) M. Gómez, G. Muller, and M. Rocamora. Coord. Chem. Rev. **193**–**195**, 769 (1999) and refs. therein; (*b*) D.A. Evans, M.C. Kozlowski, and J.S. Tedrow. Tetrahedron Lett. **37**, 7481 (1996); (*c*) F. Reichel, X. Fang, S. Yao, M. Ricci, and K.A. Jørgensen. Chem. Commun. 1505 (1999); (*d*) P. Molenveld, W.M.G. Stikvoort, H. Kooijman, A.L. Spek, J.F.J. Engbersen, and D.N. Reinhoudt. J. Org. Chem. **64**, 3896 (1999).
12. R. Holm, Jr. Inorg. Synth. **12**, 238 (1970).
13. E.W. Abel, M.A. Bennett, and G. Wilkinson. J. Chem. Soc. 3178 (1959).
14. B.M. Markies, P. Wijkens, H. Kooijman, N. Veldman, A.L. Spek, J. Boersma, and G. van Koten. Organometallics, **13**, 3244 (1994).
15. G.M. Sheldrick. SHELXS-97. Program for crystal structure solution. University of Göttingen, Göttingen, Germany. 1997.
16. G.M. Sheldrick. SHELXL-97. Program for crystal structure refinement. University of Göttingen, Göttingen, Germany. 1997.
17. A.L. Spek. PLATON, a multipurpose crystallographic tool. Utrecht University, The Netherlands. 1999.
18. J.A.M. van Beek, G. van Koten, G.P.C.M. Dekker, E. Wissing, M.C. Zoutberg, and C.H. Stam. J. Organomet. Chem. **394**, 659 (1990).
19. A.W. Addison, T.N. Rao, J. Reedijk, J. van Rijn, and G.C. Verschoor. J. Chem. Soc. Dalton Trans. 1349 (1984).
20. (*a*) M. Vlasse, T. Rojo, and D. Beltran-Porter. Acta Crystallogr. Sect. C: Struct. Commun. **C39**, 560 (1983); (*b*) P.J.M.W.L. Birker, A.J. Schierbeek, G.C. Verschoor, and J. Reedijk. J. Chem. Soc. Chem. Commun. 1124 (1981); (*c*) G.A. Nicholson, J.L. Petersen, and B.J. McCormick. Inorg. Chem. **21**, 3274 (1982); (*d*) H. Plenio and D. Burth. Organometallics, **15**, 4054 (1998); A. Abufarang and H. Vahrenkamp. Inorg. Chem. **34**, 2207 (1995); (*e*) A. Hazell, C.J. McKenzie, and L.P. Nielsen. J. Chem. Soc. Dalton Trans. 1751 (1998); (*f*) M. Graf, B. Greaves, and H. Stoeckli-Evans. Inorg. Chim. Acta, **204**, 239 (1993); (*g*) E. Amadei, M. Carcelli, S. Ianelli, P. Cozzini, P. Pelagatti, and C. Pelizzi. J. Chem. Soc. Dalton Trans. 1025 (1998); (*h*) A.L. Vance, N.W. Alcock, J.A. Heppert, and D.H. Busch. Inorg. Chem. **37**, 6912 (1998); (*i*) H.W. Smith. Acta Crystallogr. Sect. B: Struct. Crystallogr. Cryst. Chem. **B31**, 2701 (1975); (*j*) J. Wirbser and H. Vahrenkamp. Z. Naturforsch. B: Chem. Sci. **47B**, 962 (1992).
21. A.G. Orpen, L. Brammer, F.H. Allen, O. Kennard, D.G. Watson, and R. Taylor. J. Chem. Soc. Dalton Trans. S1 (1989).
22. (*a*) C.W. Bock, A.K. Katz, and J.P. Glusker. J. Am. Chem. Soc. **117**, 3754 (1995); (*b*) Y.-H. Chiu, O. dos Santos, and J.W. Canary. Tetrahedron, **55**, 12069 (1999).

© 2000 NRC Canada

Determination of the acidity constant of isothiocyanic acid in aqueous solution

Y. Chiang and A.J. Kresge

Abstract: Changes in absorbance of the thiocyanate ion (SCN^-) at λ = 220 nm, measured in concentrated aqueous perchloric acid solution, were analyzed using a titration curve expression containing the X_o excess acidity function; this provided the acidity constant K_a = 19.2 ± 1.1 M, pK_a = –1.28 ± 0.03, for isothiocyanic acid (SCNH).

Key words: isothiocyanic acid (acidity of), thiocyanate ion (basicity of), acid–base titration in concentrated aqueous acids, X_o excess acidity function, Cox–Yates method.

Résumé : Utilisant une expression pour la courbe de titrage contenant la fonction d'acidité en excès X_α, on a analysé les changements d'absorbance de l'ion thiocyanate (SCN^-) à λ = 220 nm, mesurés dans une solution concentrée d'acide perchlorique aqueux; cette analyse nous a permis d'évaluer la constante d'acidité, K_a = 19,2 ± 1,1 M (pK_a = –1,28 ± 0,03) de l'acide isothiocyanique (SCNH).

Mots clés : acide isothiocyanique (acidité), ion thiocyanate (basicité), titrage acide–base dans des acides concentrés aqueux, fonction d'acidité en excès X_α, méthode de Cox–Yates.

The thiocyanate ion (SCN^-) is a strong nucleophile, useful for studies of nucleophilic displacement and carbocation–nucleophile combination reactions. Analysis of quantitative data obtained in such studies, carried out in aqueous solution under conditions of acid catalysis, requires accurate knowledge of the acid dissociation constant of the conjugate acid of SCN^-. The literature contains reports of a number of determinations of this constant, but there is little agreement among the results obtained: a recent compilation, for example, lists nine values, but these differ by three orders of magnitude (1).

The thiocyanate ion has a strong UV absorption max at λ = 220 nm, which is replaced by another, somewhat weaker, max at λ = 235 nm as the ion is protonated. We used this spectral change to determine the acidity constant of the conjugate acid of SCN^- in aqueous solution. The thiocyanate ion is only weakly basic, and measurements had to be made in concentrated acid solutions. The data so obtained were then extrapolated to a dilute solution standard-state using the X_o excess acidity function (2). This scale appears to be the best function currently available for this purpose (3), and we believe that its use here eliminated many of the difficulties experienced in previous attempts to determine this acidity constant.

The thiocyanate ion is an ambident species that bonds to hard metals through its nitrogen atom and to soft metals through its sulfur (1). No definitive determination of the site of protonation of SCN^- in aqueous solution appears to have been made, but, since the proton is a hard species, it seems likely that SCN^- bonds with H^+ in aqueous solution on its nitrogen atom, forming isothiocyanic acid, as shown in eq. [1]. This conclusion is supported by the fact that isothiocyanic acid rather than the isomeric thiocyanic acid (HSCN) is the species present in the gas-phase (4).

[1] $SCN^- + H^+ \rightleftarrows SCNH$

Experimental section

Absorbance measurements were made at λ = 220 nm in perchloric acid solutions over the concentration range $[HClO_4]$ = 0.1–8.3 M using NaSCN as the source of thiocyanate ion. A Cary 2200 spectrometer, whose cell compartment was thermostated at 25.1 ± 0.05°C, was employed. Measurements were made in triplicate at some 20 different perchloric acid concentrations. The stoichometric concentration of thiocyanate ([SCN] + [SCNH]) in these solutions was held constant at 5×10^{-4} M.

The data so obtained are summarized in Table S1.[2]

Results and discussion

The conventional way of converting measurements made in concentrated acid solutions into acidity constants refer-

Received August 9, 2000. Published on the NRC Research Press website on November 27, 2000.

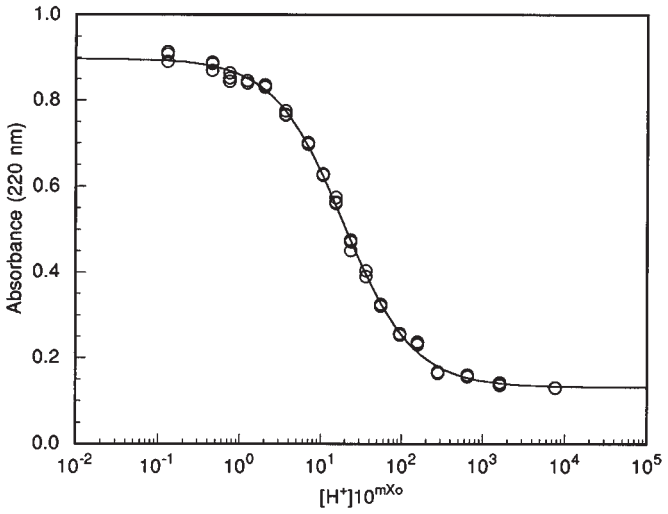
Y. Chiang and A.J. Kresge.[1] Department of Chemistry, University of Toronto, Toronto, ON M5S 3H6, Canada.

[1]Author to whom correspondence may be addressed. Telephone: (416) 978-7259. Fax: (416) 978-7259. e-mail: akresge@chem.utoronto.ca

[2]Table S1 of absorbance and acid concentration data has been deposited and may be purchased from the Depository of Unpublished Data, Document Delivery, CISTI, National Research Council Canada, Ottawa, ON, Canada K1A OS2 (http://www.nrc.ca/cisti/irm/unpub_e.shtml for information on ordering electronically).

© 2000 NRC Canada

Fig. 1. Absorbance data for the protonation of thiocyanate ion in aqueous perchloric acid solution at 25°C plotted according to eq. [4].



enced to the usual infinitely dilute standard-state is to extrapolate values of I, where I is the ratio of concentrations of protonated (SH^+) to unprotonated (S) forms of the substrate, down an appropriate acidity function. Values of I are generally calculated from absorbance measurements made at constant total substrate concentration ($[SH^+] + [S]$) using the relationship shown in eq. [2] where A_{SH} and A_S are the limiting absorbances of solutions

$$[2] \qquad I = \frac{[SH^+]}{[S]} = \frac{A_S - A}{A - A_{SH}}$$

containing only SH^+ or S, respectively, and A is the absorbance of solutions containing both SH^+ and S. When the extrapolation is done using the X_o acidity function, the quantity extrapolated is $\log (I/[H^+])$ (5). Since the limiting value of X_o in dilute solution is zero, the pK_a is then obtained as the y-intercept at $X_o = 0$, as shown in eq. [3]. The quantity m in this equation is a slope parameter that

$$[3] \qquad \log (I/[H^+]) = pK_a + mX_o$$

takes into account the fact that the acidity function appropriate to the system under investigation may not be X_o, but that it will in that case be a simple multiple of X_o.

This method has the advantages inherent in a linear extrapolation, e.g., analysis of the experimental data can be done by simple linear least-squares fitting. It suffers, however, from the fact that the limiting absorbances A_{SH} and A are used to calculate each value of I, and accurate knowledge of these quantities is consequently required. Values of I, moreover, are less reliable the farther they are from unity (6), and measurement should either be confined to a region not too distant from $I = 1$, or $\log (I/[H^+])$ values should be weighted appropriately.

These difficulties may be avoided by using a least-squares fitting function in which A is the sole dependent variable and A_{SH} and A_S are parameters to be determined by the fit. Such an expression, eq. [4] has the form of a titration curve; it can be derived by combining eqs. [2] and

$$[4] \qquad A = \frac{A_{SH}[H^+]10^{mX_o} + A_S K_a}{[H^+]10^{mX_o} + K_a}$$

[3] and then solving for A. The resulting function has two independent variables, $[H^+]$ and X_o, and four parameters to be determined by the fit: K_a, A_{SH}, A_S, and m. Analysis of experimental data using this function requires nonlinear least-squares fitting, but, with the current widespread availability of powerful desktop computers and appropriate software, that is not a problem. This method has the advantages of not requiring prior knowledge of A_{SH} and A_S, not being restricted to a narrow range of experimental data, and, since all values of A are likely to have similar uncertainties (7), not requiring special weighting of the data.

As Fig. 1 demonstrates, the present experimental data conform to the expression of eq. [4] quite well. Least-squares analysis using Grafit software gave $K_a = 19.2 \pm 1.1$ M, $pK_a = -1.28 \pm 0.03$, $A_{SH} = 0.131 \pm 0.004$, $A_S = 0.897 \pm 0.004$, and $m = 0.851 \pm 0.027$.

The acidity constant determined here is consistent with $pK_a = -1.1 \pm 0.3$ obtained by Raman spectroscopy (8). This agreement, however, must be considered to be fortuitous, for the data obtained in the previous work were analyzed, not by extrapolating down an acidity function, but rather by applying activity coefficients estimated using a method of dubious validity.

Acknowledgement

We are grateful to the Natural Sciences and Engineering Research Council of Canada (NSERC) for financial support of this work.

References

1. A. Bahta, G.A. Parker, and D.G. Tuck. Pure Appl. Chem. **69**, 1489 (1997).
2. R.A. Cox and K. Yates. Can. J. Chem. **59**, 2116 (1981).
3. A.J. Kresge, H.J. Chen, G. Capen, and M.F. Powell. Can. J. Chem. **61**, 249 (1983).
4. C.I. Beard and B.P. Dailey. J. Chem. Phys. **15**, 762 (1947).
5. R.A. Cox and K. Yates. J. Am. Chem. Soc. **100**, 3861 (1978); R.A. Cox. Adv. Phys. Org. Chem. **35**, 1 (2000).
6. A.J. Kresge and H.J. Chen. Anal. Chem. **41**, 74 (1969).
7. L. Cahn. J. Opt. Soc. Am. **45**, 953 (1955).
8. A.K. Covington and R.A. Matheson. J. Solution Chem. **5**, 781 (1976).

© 2000 NRC Canada

Asymmetric synthesis based on chiral (arene)tricarbonylchromium acetal complexes. Addition reactions to the *ortho*-formyl complex

M. Kevin McKay and James R. Green

Abstract: The addition reactions of organolithium and Grignard reagents to chiral, enantiomerically pure *ortho*-formyl (arene)tricarbonylchromium acetal complex (**2**) have been studied. The diastereoselectivity of the addition process is fair in the absence of an additional Lewis acid, and good in the presence of $Ti(O^iPr)_4$. The nature of the newly formed chiral centre, and studies on the possible nature of the nucleophilic species suggest that the Lewis acid acts through monodentate coordination to the aldehyde carbonyl, and thereby alters the carbonyl rotamer population more heavily in favour of the *s-trans* conformation. Nucleophilic attack then occurs on the face *anti-* to that bearing the $Cr(CO)_3$ unit.

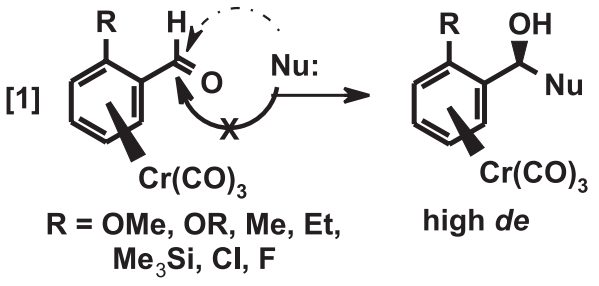
Key words: (arene)tricarbonylchromium complexes, asymmetric synthesis, carbonyl additions, Lewis acids.

Résumé : On a étudié les réactions d'addition de réactifs organolithiens et de Grignard sur le complexe chiral, énantiomériquement pur *ortho*-formyl(arène)tricarbonylchrome acétal (**2**). La diastéréosélectivité du processus d'addition est correcte en l'absence d'un acide de Lewis additionnel et elle est bonne en présence de $Ti(O^iPr)_4$. La nature du centre chiral qui se forme et les études sur la nature possible de l'espèce nucléophile suggèrent que l'acide de Lewis agit par le biais d'une coordination monodentate du groupe carbonyle de l'aldéhyde et que celle-ci modifie la population des rotamères du groupe carbonyle de façon à favoriser la conformation *s-trans*. L'attaque nucléophile se produit alors sur la face *anti-* par rapport à celle qui porte l'unité $Cr(CO)_3$.

Mots clés : complexes (arène)tricarbonylchrome, synthèse asymétrique, additions sur des carbonyles, acides de Lewis.

The chemistry of (arene)tricarbonylchromium complexes has been the subject of considerable attention in organic synthesis, due to the relative ease of preparation of compounds of this class, the change in electronic properties of the arene ring upon complexation, and the presence of a large functional group (the $Cr(CO)_3$ unit) on one face of the ring (1). Recently, much of the focus of work in this area has been concerned with the chemistry of chiral and enantiomerically pure versions of these complexes. In particular, the enantiopure complexes have seen wide application in the chemistry of nucleophilic attack on the arene ring (2), in stereoselective functionalization of prochiral centres adjacent or near the ring (3), and in enantioselective catalysis (4). A former bottleneck to research in this area, namely that of reliable access to enantiomerically enriched complexes, has been eliminated to a large degree by several important recent advances (5, 6, 7). Among these developments is the diastereoselective ortho lithiation of tartrate-derived benzaldehyde acetal tricarbonylchromium complex **1**, which allows highly selective *ortho* functionalization of the pro-(*R*) site (ca. 90% de) (5*a*). As a result, we consider the framework in **1** to be promising in the field of asymmetric synthesis, and therefore the systematic investigation of the reactions of prochiral centres attached to the ring in these systems is warranted. We have shown that homobenzylic ketones derived from **1** a capable of undergoing highly diastereoselective reductions at very low temperatures (8).

In the field of *ortho*-disubstituted arenetricarbonylchromium complexes, study of the additions to the arylaldehyde function has become the most important measure of the system in asymmetric synthesis (3*a*). A substantial number of types of nucleophiles have been shown to participate in the addition process. These include alkyl-, aryl-, and alkynylmetals (9), enolates and their equivalents (10), nitronate anions (11), Reformatsky reagents (10*a*, 12), α-halo carbonyl enolates (13), and active methylene compounds (14). In most cases the diastereoselectivity of addition is good to excellent at the benzylic site, and is consistent with a predominant *s-trans* conformation of the aldehyde function, and nucleophile addition *anti-* to the face bearing the $Cr(CO)_3$ fragment (eq. [1]). In the vast majority of these cases, however, the



Received July 6, 2000. Published on the NRC Research Press website on December 4, 2000.

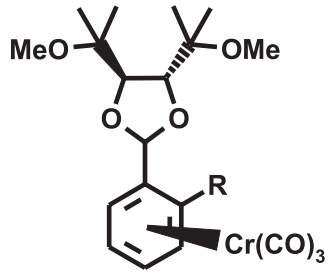
M.K. McKay and J.R. Green.[1] Chemistry and Biochemistry, School of Physical Sciences, University of Windsor, Windsor, ON N9B 3P4, Canada.

[1]Author to whom correspondence may be addressed. Telephone: (519) 253-4232, ext. 3545. Fax: (519) 973-7098. e-mail: jgreen@uwindsor.ca

© 2000 NRC Canada

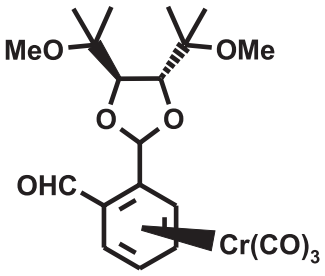
ortho-substituent is simple and, saving the aryl ether complexes, not containing any Lewis basic centres. In contrast, Koide and Uemura's (15) work on complexes containing an *ortho*-benzamide function has shown more complex behaviour, where the degree and disposition of asymmetry in alkylmetal additions varies greatly with the metal counterion and the presence of additional Lewis acids.

Extension of these studies to the compound based on the arylaldehyde system derived from **1**, namely **2**, would give ether-alcohols **3**, with a 1,6-dioxygen relationship. Other classes of enantiomerically pure ether-alcohols which are capable of making seven membered chelates with transition metal fragments have seen recent use in enantioselective catalysis of protonation reactions (16), enol silane isomerizations (17), and aldol type condensations (18, see also ref. 19). Therefore, we have chosen the *ortho*-benzaldehyde complex **2** for study in its addition reactions with a variety of nucleophiles. The results are contained in this report.

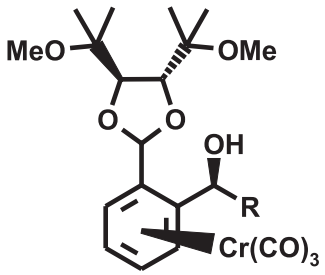


1, R = H

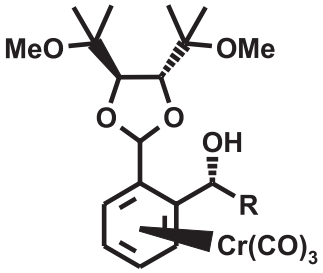
2, R = CHO



2' R = CHO



3



3'

a, R = Me
b, R = Et
c, R = *n*-Pr
d, R = H
e, R = *n*-Bu
f, R = *t*-Bu
g, R = 1-hexynyl
h, R = Ph
i, R = 2-thienyl

The diastereomerically and enantiomerically pure *ortho*-formyl complex **2** was prepared by adaptation of the previously reported procedure (5*a*). Lithiation of the chiral acetal **1** under the literature conditions (–35°C, slow addition of BuLi, 4.5 h total) followed by addition of *N*-methylformanilide afforded **2** in 78% yield after aqueous workup, a slight increase from the yields resulting from the use of DMF as the electrophile (70%). In addition, the ^{1}H NMR spectrum of the crude reaction products employing *N*-methylformanilide showed no evidence for the presence of the minor diastereomer **2′**, and therefore we consider the diastereoselectivity for this transformation to be >94% de.

With ready access to **2**, conditions were investigated for optimization of the addition reactions; methyllithium was chosen as a representative nucleophile for this process. Addition of methyllithium to **2** was investigated in Et_2O and THF, and at several reaction temperatures.[2] Reaction was most straightforwardly evidenced by a change in solution colour from dark orange to yellow, indicative of destruction of the conjugation between the aldehyde carbonyl and the arene ring, and was rapid under most sets of conditions. For example, based on this very approximate parameter, reaction was instantaneous at –35°C and –78°C, and required approximately 1 min at –110°C (in Et_2O). The stereoselectivity of the process was evaluated by the ^{1}H NMR spectra of the crude reaction products; most diagnostic was the acetal proton of addition product **3a**, which resonated at 6.02 in the major diastereomer, and at 6.26 in the minor diastereomer (**3a′**).

Between the two solvent systems, greater diastereoselectivity was observed in Et_2O (4.6:1 at –78°C) relative to THF (2.9:1 at –78°C). Diastereoselectivity also increased with decreasing reaction temperature; in Et_2O, this varied from 2.4:1 at –35°C to 4.6:1 at –78°C, and to 4.9:1 at –110°C.

The possibility of a significant effect of the presence of Lewis acids on the addition reaction was also investigated. BF_3–OEt_2, $Ti(O^iPr)_4$, $Ti(O^nPr)_4$, and $ZnCl_2$ (3 equiv relative to **2**) were investigated for their effect. The presence of BF_3–OEt_2 or $ZnCl_2$ were deleterious to the addition reaction with MeLi; BF_3–OEt_2 caused complete decomplexation of **2**, while $ZnCl_2$ gave partial decomplexation of **1** and partial transformation to **3a**. We have previously observed ready decomplexation of (arene)tricarbonylchromium complexes bearing this acetal unit in the presence of Lewis- or protic acid reagents containing halide ion (5*a*, 20). Conversely, in the presence of both $Ti(O^iPr)_4$ and $Ti(O^nPr)_4$, decomplexation of **2** was negligible, and the diastereoselectivity of the addition process improved substantially at –78°C.[3] In view of the lower viscosity of $Ti(O^iPr)_4$, this Lewis acid was chosen for all addition reactions; the diastereoselectivity of the MeLi/$Ti(O^iPr)_4$ combination in Et_2O at –78°C was 16:1 or 88% de (75% yield of diastereomerically and enantiomerically pure **3a**, Table 1).

With optimized conditions of MeLi addition reactions delineated, the basic transformation was expanded to a wider range of nucleophiles. Representative organolithium and organomagnesium halides were chosen for investigation based on ready availability, and included *n*-BuLi, *t*-BuLi, 1-lithio-1-hexyne, phenyllithium, EtMgBr, *n*-PrMgBr, *i*-PrMgCl, phenylmagnesium bromide, and 1-thienylmagnesium bromide. In each case, aldehyde **2** was subjected to $Ti(O^iPr)_4$ mediated addition of the nucleophile at –78°C in Et_2O. While the nucleophiles derived from smaller organic units reacted noticeably more rapidly than those of the aryl

[2] Methyllithium addition to the analogue of **2** lacking the $Cr(CO)_3$ unit occurred in total stereorandom fashion.
[3] In the presence of $Ti(O^iPr)_4$, the reaction became very sluggish at –110°C.

© 2000 NRC Canada

Table 1. Nucleophilic additions to aldehyde **2**.

Entry	Nucleophile	Product	Yield (%)	de (%)
1	MeLi	**3a**	75	88
2	EtMgBr	**3b**	73	85
3	*n*-PrMgBr	**3c**	76	87
4	*i*-PrMgCl	**3d**	65	—
5	*n*-BuLi	**3e**	72	86
6	*t*-BuLi	**3f**	61	85
7	1-Hexynyllithium	**3g**	42	94
8	PhLi	**3h**	60	88
9	PhMgBr	**3h**	62	82
10	2-BrMgthiophene	**3i**	73	86

nucleophiles and 2° and 3° alkylmetals, consumption of **2** was complete after 3 h in all cases except for the *t*-BuLi case. With *t*-BuLi, very little conversion had occurred after the 3 h time period, and the reaction was allowed to gradually warm to room temperature overnight prior to workup.

The results are summarized in Table 1. In general, addition products **3a–c, e–i** were obtained in good chemical yield and in diastereomerically and enantiomerically homogeneous form following chromatographic purification. Diastereoselectivities of addition were good (82–94% de) and were in general consistent across the nucleophiles examined. In three cases, the results deserve specific comment. In the one case where the organolithium and the organomagnesium reagent derived from the same organic unit (entries 8 and 9), the organolithium reagent was observed to give slightly higher de. This trend is the converse of that observed previously in organometallic addition reactions to *o*-trimethylsilylbenzaldehyde complexes (9*c*), and stands in complete contrast to change in direction of asymmetry observed in the additions to *o*-diethylcarbamoylbenzaldehyde complexes reported recently by Koide and Uemura (15). In the case of hexynyllithium nucleophile, the initial addition products were quite clean; these, however, underwent extensive decomplexation upon attempted chromatographic purification. Repeated precipitation from petroleum ether gave pure material, with a compromise of the isolated yield of **3g** (42%). Finally, *i*-PrMgCl did not give the addition product, but rather the product of aldehyde reduction, namely **3d** (21).

With the presence of several Lewis basic groups in the vicinity of the aldehyde carbonyl, the disposition of the addition process was open to question. Fortunately, the *n*-BuLi/Ti(O^i-Pr)$_4$ addition product, **3e**, gave crystals from petroleum ether suitable for X-ray diffraction (Fig. 1, Table 2). This revealed the major diastereomeric product to possess the (*S*)-configuration at the benzylic carbinol carbon. The analogous stereochemical assignments have therefore been made to the other addition products (**3a–c, e–i**). Additional support for uniformity in the stereochemical assignments may be derived from the ^{1}H NMR spectra of the crude adducts, as the acetal hydrogen atoms of the major diastereomers resonated further upfield than those of the minor diastereomer in all cases. These additions are also consistent with the dominant mode of nucleophilic additions to simpler *ortho*-substituted benzaldehyde–Cr(CO)$_3$ complexes (3*a*).

There are several alternative possibilities for the role played by Ti(O^{i}Pr)$_4$ in the addition process. For example, the Lewis acid could complex to the carbonyl oxygen, could complex to one or several oxygen atoms of the acetal unit, or could react with the nucleophile to give a different nucleophilic species. In the case of Ti(O^{i}Pr)$_4$, the "different" nucleophilic reagent may conceivably be the titanium ate complex, formally [RTi(O^{i}Pr)$_4$]$^-$ (the nature of these ate complexes have not been determined rigourously, see ref. 22), or the organotitanium triisopropoxide, RTi(O^{i}Pr)$_3$. To evaluate the latter set of possibilities, CH$_3$Ti(O^{i}Pr)$_3$ was prepared by the addition of MeLi to ClTi(O^{i}Pr)$_3$ (23). Addition of this reagent to **2** under the standard addition conditions gave no **3a** and predominantly recovered **2** (84% recovery). In a similar fashion, the ate complex [CH$_3$Ti(O*i*-Pr)$_4$]$^-$Li$^+$ was prepared by the addition of Ti(O^i-Pr)$_4$ to MeLi in Et$_2$O at –30°C. Addition of this ate complex to **2** under the standard addition conditions gave no addition products, and starting material **2** was recovered (75% recovery).

Fig. 1. ORTEP drawing of **3e**.

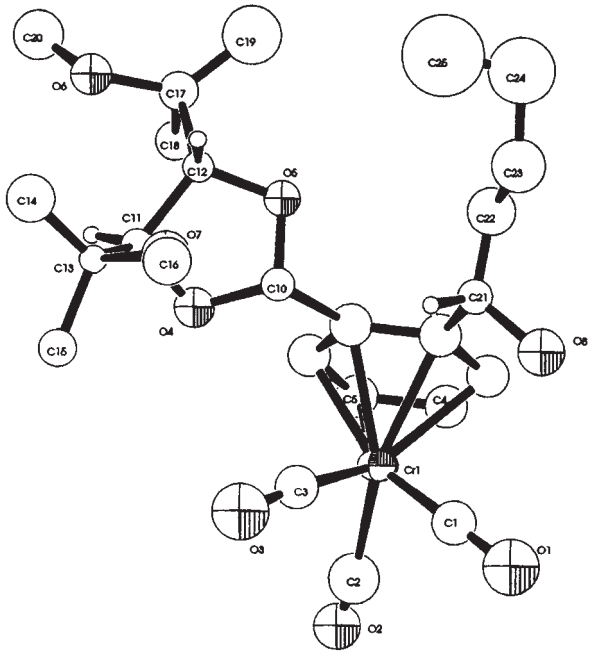


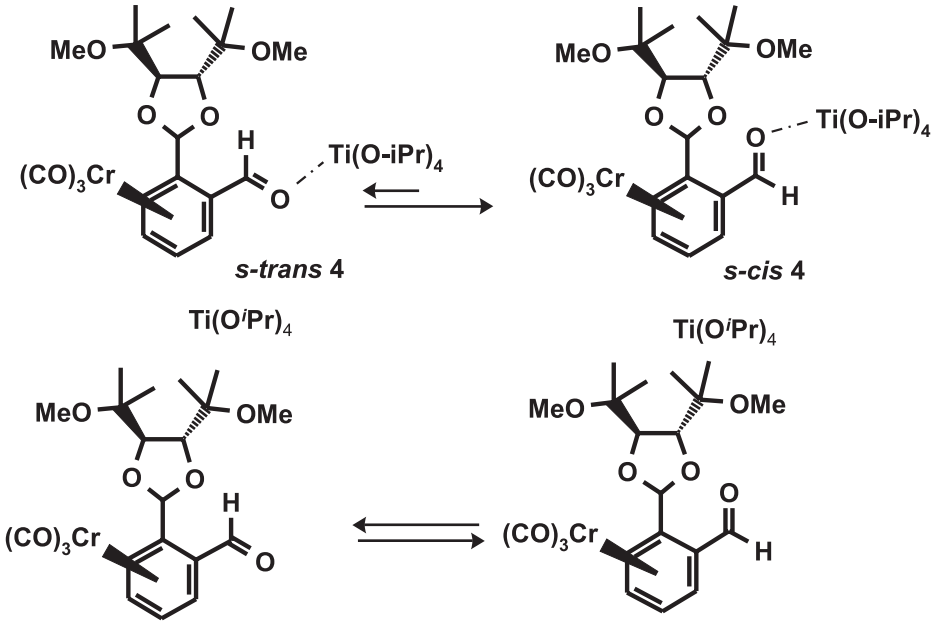
Table 2. Crystallographic data for **3e**.

Formula	$C_{25}H_{36}CrO_8$
Fw	516.55
Space group	$P2_12_12_1$ (no. 19)
a (Å)	11.303(4)
b (Å)	11.295(1)
c (Å)	21.528(2)
V (Å^3)	2748.4(9)
Z	4
λ (Å)	0.71069
ρ (g cm^{-3})	1.25
μ (cm^{-1})	4.59
R^a	0.089
$R_w{}^b$	0.071

$^aR = \Sigma||Fo| - |Fc||/\Sigma|Fo|$.
$^bR_w = [\Sigma\omega(|Fo| - |F_c|)^2/\Sigma\omega Fo^2]^{1/2}$.

© 2000 NRC Canada

Fig. 2. Lewis acid coordination to **2**.



In view of the lack of reactivity of $MeTi(O^iPr)_3$ and $[CH_3Ti(O^iPr)_4]^-Li^+$, the most economical interpretation of the reaction characteristics features monodentate coordination of $Ti(O^iPr)_4$ to the aldehyde oxygen lone-pair (**4**), in the plane of the carbonyl and the arene. Nucleophilic attack then occurs on the face of arylaldehyde *anti-* to the $Cr(CO)_3$ unit (Fig. 2). Bidentate or tridentate coordination of $Ti(O^iPr)_4$ to the carbonyl and acetal oxygen(s) is considered unlikely in that it would then require attack of the nucleophile *syn-* to the $Cr(CO)_3$ unit to obtain the observed major diastereomer of **3**. Similarly, there is no evidence in these systems of out-of-plane Lewis acid coordination and resultant reversal of facial selectivity, as has been observed in conjugate additions to aryl enone chromium complexes (24). The increased stereoselectivity observed in the presence of the Ti Lewis acid in the current case most likely stems from the resultant effective increase in size of the carbonyl oxygen and therefore an increase in the bias for the *s-trans* conformer drawn in Fig. 2 (***s-trans* 4**). This is the more commonly established role of Lewis acids in related additions (9*c*). Coordination of an additional molecule of $Ti(O^iPr)_4$ to the acetal unit of **2** cannot be ruled out with certainty.

This work, in conjunction with our work on reductions of homobenzylic ketones, demonstrates the utility of tartrate-derived benzaldehyde acetal tricarbonylchromium complexes in the induction of chirality in side chain alkyl functions. Further work on materials derived from this study will be reported in due course.

Experimental section

General methods

All solvents were used after distillation from the appropriate drying agent. Diethyl ether and tetrahydrofuran were distilled from benzophenone ketyl immediately prior to use. *n*-BuLi, *s*-BuLi, *t*-BuLi, MeLi, and PhLi were obtained from Aldrich Chemical Co., Ltd. Their titres were determined using 2,5-dimethoxybenzyl alcohol (25) or diphenylacetic acid as standards (26). $ClTi(O^iPr)_3$ and $MeTi(O^iPr)_3$ were prepared according to literature methods (27). Melting points are uncorrected. Flash chromatography followed the protocol described by Still et al. (28).

NMR spectra were run at 300 MHz or 500 MHz for ^1H, and 75 MHz or 125 MHz for ^{13}C, in $CDCl_3$ solution at 25°C; chemical shifts are given in ppm and coupling constants (*J*) are given in Hz. Mass spectra were run at the Chemistry and Biochemistry Mass Spectrometry Facility, University of Windsor.

All reactions were performed under nitrogen or argon unless otherwise noted.

*(1′R,2′*S,*4*R,*5*R*)-[4,5-Bis(1-methoxy-1-methylethyl)-2-(2′-formyl)phenyl)-1,3-dioxolane]tricarbonylchromium(0) (2)*

To a solution of acetal **1** (1.500 g, 3.49 mmol) in diethyl ether (150 mL) at –35°C was added *n*-BuLi (3.78 mL, 2.21M, 8.364 mmol, 2.4 equiv) over 90 min. The solution was kept at –35°C for 3h, at which point *N*-methylformanilide (1.03 mL, 8.36 mmol, 2.4 equiv) was added. The reaction mixture was stirred for a further 1 h. Standard aqueous workup afforded a red viscous oil, which was subjected to column chromatography using petroleum ether:ethyl acetate (5:1) as the eluent to afford **2** (1.246 g, 78%) as a red crystalline solid, mp 104–105°C (hexanes). $[\alpha]_D$ = 296° (c 0.6, Et_2O). IR (KBr) ν_{max} (cm^{-1}): 1984, 1924, 1692. ^1H NMR δ: 9.91 (s, 1H), 6.42 (s, 1H), 6.06 (d, 1H, *J* = 6.5), 5.60–5.68 (m, 2H), 5.26 (t, 1H, *J* = 6.0), 4.22, (d, 1H, *J* = 3.3), 4.05 (d, 1H, *J* = 3.3), 3.22 (s, 3H), 3.13 (s, 3H), 1.31 (s. 3H), 1.14 (s, 3H), 1.12 (s, 3H), 1.03 (s, 3H). ^{13}C NMR δ: 230.2, 187.3, 110.9, 99.7, 94.1, 93.7, 92.3, 88.7, 86.8, 85.1, 83.2, 75.4, 49.4, 49.3, 22.1, 21.2, 20.9, 19.4. MS *m/e*: 458 (M^+). HRMS *m/e* calcd. for $C_{21}H_{26}CrO_8$ (M^+): 458.1032; found: 458.1031.

Standard nucleophilic addition procedure

To a solution of *o*-formyl complex **2** (0.075–0.100 g) in Et_2O (10 mL) at –78°C was added $Ti(O^iPr)_4$ (3 equiv), and the solution allowed to stir for 20 min. The nucleophile

© 2000 NRC Canada

(3 equiv) was added dropwise by syringe and stirring was continued for 3 h at –78°C. The reaction was quenched by the addition of distilled water (ca. 2 mL), and a standard aqueous work-up resulted in a crude product whose ^{1}H NMR spectrum was examined to determine the diastereomeric ratio.

*(1′*R*,2′*S*,4*R*,5*R*)-[4,5-Bis(1-methoxy-1-methylethyl)-2-(2′-(*S*-1-hydroxyethyl)phenyl)-1,3-dioxolane]tricarbonylchromium(0) (**3a**) (methyl derivative)*

o-Formyl complex **2** (0.0983 g, 0.215 mmol) was subjected to the standard procedure with MeLi (0.43 mL, 1.5 M in Et_2O, 0.64 mmol) as the nucleophile. A standard aqueous work-up resulted in a crude product whose ^{1}H NMR spectrum revealed a resonance at δ 5.99 (**3a**) and 6.26 (**3a′**) with a relative integral of 15.6:1 (88% de). Purification by silica gel chromatography using petroleum ether:ethyl acetate (5:1) as eluent gave **3a** (0.076 g, 75%) as a yellow solid, mp 77–78°C (pentane). $[\alpha]_D$ = –36° (c 0.5, Et_2O). IR (KBr pellet) ν_{max} (cm^{-1}): 3436, 1966, 1886. ^{1}H NMR δ: 6.01 (s, 1H), 5.76 (d, 1H, *J* = 6.0), 5.66 (d, 1H, *J* = 6.1), 5.34 (m, 2H), 4.82 (m, 1H), 4.16 (d,1H, *J* = 3.2), 3.98 (d, 1H, *J* = 3.2), 3.22 (s, 3H), 3.16 (s, 3H), 2.02 (s, 1H), 1.48 (d, 3H, *J* = 6.3), 1.26 (s, 3H), 1.17 (s, 3H), 1.13 (s, 3H), 1.03 (s, 3H). ^{13}C NMR δ: 232.8, 117.5, 105.5, 99.6, 92.3, 91.6, 90.0, 88.9, 84.6, 82.6, 75.4, 64.4, 49.4, 49.3, 25.7, 22.3, 21.1, 19.1. MS *m*/*e*: 474 (M^+). HRMS *m*/*e* calcd. for $C_{22}H_{30}CrO_8$ (M^+): 474.1346; found: 474.1357.

*(1′*R*,2′*S*,4*R*,5*R*)-[4,5-Bis(1-methoxy-1-methylethyl)-2-(2″-(*S*-1-hydroxypropyl)phenyl)-1,3-dioxolane]tricarbonylchromium(0) (**3b**) (ethyl derivative)*

o-Formyl complex **2** (0.0890 g, 0.194 mmol) was subjected to the standard procedure with EtMgBr (0.49 mL, ca. 1.2 M in Et_2O, 0.58 mmol) as the nucleophile. A standard aqueous work-up resulted in a crude product whose ^{1}H NMR spectrum revealed a resonance at 6.00 (**3b**) and 6.26 (**3b′**) with a relative integral of 12.4:1 (85% de). Purification by silica gel chromatography using petroleum ether:ethyl acetate (5:1) as eluent gave **3b** (0.069 g, 73%) as a yellow oil, $[\alpha]_D$ = –40.4° (c 0.54, Et_2O). IR (NaCl, neat) ν_{max} (cm^{-1}): 3452, 1966, 1892. ^{1}H NMR δ: 6.00 (s, 1H), 5.77 (d, 1H, *J* = 5.9), 5.61 (d, 1H, *J* = 5.9), 5.33 (m, 2H), 4.61 (br d, 1H, *J* = 8.2), 4.17 (d, 1H, *J* = 3.1), 3.98 (d, 1H, *J* = 3.1), 3.23 (s, 3H), 3.17 (s, 3H), 1.94 (s, 1H), 1.90 (m, 1H), 1.67 (m, 1H), 1.31 (s, 3H), 1.14 (s, 3H), 1.12 (s, 3H), 1.05 (s, 3H), 1.03 (t, 3H, *J* = 7.3). ^{13}C NMR δ: 232.8, 116.7, 105.9, 99.5, 92.2, 91.7, 90.3, 89.2, 84.6, 82.6, 75.4, 69.2, 49.5, 49.3, 32.4, 22.4, 21.2, 19.2, 10.4. MS *m*/*e*: 488 (M^+). HRMS *m*/*e* calcd. for $C_{23}H_{32}CrO_8$ (M^+): 488.1502; found: 488.1517.

*(1′*R*,2′*S*,4*R*,5*R*)-[4,5-Bis(1-methoxy-1-methylethyl)-2-(2″-(*S*-1-hydroxybutyl)phenyl)-1,3-dioxolane]-tricarbonylchromium(0) (**3c**) (*n*-propyl derivative)*

o-Formyl complex **2** (0.1102 g, 0.2406 mmol) was subjected to the standard procedure with *n*-PrMgBr (0.56 mL, ca. 1.14 M in Et_2O, 0.63 mmol) as the nucleophile. A standard aqueous work-up resulted in a crude product whose ^{1}H NMR spectrum revealed a resonance at 6.00 (**3c**) and 6.24 (**3c′**) with a relative integral of 14.4:1 (87% de). Purification by silica gel chromatography using petroleum ether:ethyl acetate (5:1) as eluent gave **3c** (0.092 g, 76%) as a yellow oil. $[\alpha]_D$ = –55° (c 0.50, Et_2O). IR (NaCl, neat) ν_{max} (cm^{-1}): 3457, 1966, 1886. ^{1}H NMR δ: 6.00 (s, 1H), 5.77 (d, 1H, *J* = 6.4), 5.61 (d, 1H, *J* = 6.4), 5.35 (t, 1H, *J* = 6.0), 5.31 (t, 1H, *J* = 6.2), 4.67 (br d, 1H, *J* = 8.6), 4.17 (d, 1H, *J* = 3.3), 3.97 (d, 1H, *J* = 3.3), 3.22 (s, 3H), 3.18 (s, 3H), 1.93 (s, 1H), 1.78 (m, 1H), 1.57 (m, 2H), 1.47 (m, 1H), 1.31 (s, 3H), 1.22 (s, 3H), 1.12 (s, 3H), 1.06 (s, 3H), 0.92 (t, 3H, *J* = 7.2). ^{13}C NMR δ: 232.9, 117.0, 105.7, 99.4, 92.2, 91.5, 90.2, 89.1, 84.6, 82.6, 77.4, 75.4, 68.0, 49.5, 49.3, 39.2, 28.2, 22.40, 22.37, 21.2, 19.2, 13.9. MS *m*/*e*: 502 (M^+). HRMS *m*/*e* calcd. for $C_{24}H_{34}CrO_8$ (M^+): 502.1659; found: 502.1667.

*(1′*R*,2′*S*,4*R*,5*R*)-[4,5-Bis(1-methoxy-1-methylethyl)-2-(2″-(hydroxymethyl)phenyl)-1,3-dioxolane]tricarbonylchromium(0) (**3d**) (reduction product from* i*-PrMgCl)*

o-Formyl complex **2** (0.1102 g, 0.2406 mmol) was subjected to the standard procedure with *i*-PrMgCl (0.32 mL, 2.0 M in Et_2O, 0.64 mmol) as the nucleophile. A standard aqueous work-up followed by purification by silica gel chromatography using petroleum ether:ethyl acetate (5:1) as eluent gave **3d** (0.077 g, 70%) as a yellow solid, mp 65–67°C (petroleum ether. $[\alpha]_D$ = –38.7 (c 0.714, Et_2O). IR (NaCl, neat) ν_{max} (cm^{-1}): 3461, 1967, 1890. ^{1}H NMR δ: 6.12 (s, 1H), 5.76 (m, 1H), 5.39 (m, 1H), 5.32 (m, 2H), 4.67 (br d, 1H, *J* = 12.9), 4.24 (d, 1H, *J* = 3.3), 4.12 (dd, 1H, *J* = 12.9, 10.0), 4.00 (d, 1H, *J* = 3.3), 3.32 (br d, 1H, *J* = 10.0), 3.25 (s, 3H), 3.17 (s, 3H), 1.31 (s, 3H), 1.19 (s, 3H), 1.09 (s, 3H), 1.06 (s, 3H). ^{13}C NMR δ: 232.2, 108.0, 106.5, 100.9, 93.8, 92.2, 90.8, 90.4, 84.9, 82.6, 77.1, 75.5, 62.0, 49.3, 21.7, 21.2, 20.7, 19.5. MS *m*/*e*: 460 (M+). HRMS *m*/*e* calcd. for $C_{21}H_{28}CrO_8$ (M^+): 460.1189; found: 460.1176.

*(1′*R*,2′*S*,4*R*,5*R*)-[4,5-Bis(1-methoxy-1-methylethyl)-2-(2′-(*S*-1-hydroxy-2,2-pentyl)phenyl)-1,3-dioxolane]tricarbonylchromium(0) (**3e**) (*n*-butyl derivative)*

o-Formyl complex **2** (0.0823 g, 0.180 mmol) was subjected to the standard procedure with *n*-BuLi (0.24 mL, 2.21 M in hexanes, 0.54 mmol) as the nucleophile. A standard aqueous work-up resulted in a crude product whose ^{1}H NMR spectrum revealed a resonance at δ 5.99 (**3e**) and δ 6.26 (**3e′**) with a relative integral of 13.2:1 (86% de). Purification by silica gel chromatography using petroleum ether:ethyl acetate (5:1) as eluent gave **3e** (0.067 g, 72%) as a yellow solid, mp 93–94°C (pentane). $[\alpha]_D$ = –50.6 (c 0.480, Et_2O). IR (KBr pellet) ν_{max} (cm^{-1}): 3489, 1968, 1893. ^{1}H NMR δ: 5.99 (s,1H), 5.77 (d, 1H, *J* = 6.5), 5.62 (d, 1H, *J* = 6.5), 5.35 (t, 1H, *J* = 6.0), 5.31 (t, 1H, *J* = 6.3), 4.66 (br d, 1H, *J* = 8.9), 4.16 (d, 1H, *J* = 3.3), 3.98 (d, 1H, *J* = 3.3), 3.22 (s, 3H), 3.17 (s, 3H), 1.98 (s, 1H), 1.85 (m, 1H), 1.30–1.68 (m, 5H), 1.35 (s, 3H), 1.14 (s, 3H), 1.11 (s, 3H), 1.04 (s, 3H), 0.88 (t, 3H, *J* = 7.3). ^{13}C NMR δ: 232.9, 117.0, 105.7, 99.4, 92.2, 91.5, 90.2, 89.1, 84.6, 82.6, 77.4, 75.4, 68.0, 49.5, 49.3, 39.2, 28.2, 22.4, 21.2, 19.2, 13.9. MS *m*/*e*: 516 (M^+). HRMS *m*/*e* calcd. for $C_{25}H_{36}CrO_8$ (M^+): 516.1815; found: 516.1812.

*(1′*R*,2′*S*,4*R*,5*R*)-[4,5-Bis(1-methoxy-1-methylethyl)-2-(2′-(*S*-1-hydroxy-2,2-dimethylpropyl)phenyl)-1,3-dioxolane]tricarbonylchromium(0) (**3f**) (*tert*-butyl derivative)*

o-Formyl complex **2** (0.0753 g, 0.164 mmol) was subjected to the standard procedure with *t*-BuLi (0.33 mL, 1.5 M in pentane, 0.49 mmol) as the nucleophile, with the

© 2000 NRC Canada

exception that the bath temperature was allowed to gradually warm to room temperature over 8 h after the 3 h period at –78°C. A standard aqueous work-up resulted in a crude product whose ^{1}H NMR spectrum revealed a resonance at δ 6.12 (**3f**) and δ 6.48 (**3f′**) with a relative integral of 12.3:1 (85% de). Purification by silica gel chromatography using petroleum ether:ethyl acetate (5:1) as eluent gave **3f** (0.052 g, 61%) as a yellow oil. $[\alpha]_D$ = –14.7° (c 0.300, Et_2O). IR (NaCl, neat) ν_{max} (cm^{-1}): 3480, 1968, 1891. ^{1}H NMR δ: 6.12 (s, 1H), 5.74 (d, 1H, *J* = 5.5), 5.58 (d, 1H, *J* = 6.0), 5.33 (m, 2H), 4.57 (d, 1H, *J* = 2.0), 4.16 (d, 1H, *J* = 3.3), 3.94 (d, 1H, *J* = 3.3), 3.22 (s, 3H), 3.20 (s, 3H), 1.67 (s, 1H), 1.34 (s, 3H), 1.17 (s, 3H), 1.14 (s, 3H), 1.10 (s, 3H), 0.97 (s, 9H). ^{13}C NMR δ: 232.6, 115.8, 109.6, 99.3, 92.4, 91.2, 90.5, 90.4, 84.6, 82.2, 77.7, 75.5, 73.6, 49.3, 49.2, 36.7, 26.4, 22.5, 21.6, 21.0, 19.1. MS *m*/*e*: 516 (M^+). HRMS *m*/*e* calcd. for $C_{25}H_{36}CrO_8$ (M^+): 516.1815; found: 516.1838.

*(1′*R*,2′*S*,4*R*,5*R*)-[4,5-Bis(1-methoxy-1-methylethyl)-2-(2′-(*S*-1-hydroxy-2-heptynyl)phenyl)-1,3-dioxolane]-tricarbonylchromium(0) (**3g**) (hexynyl derivative)*

o-Formyl complex **2** (0.1240 g, 0.271 mmol) was subjected to the standard procedure with hexynyllithium (0.50 mL, ca. 1.64 M in Et_2O, 0.81 mmol) as the nucleophile. A standard aqueous work-up resulted in a crude product whose ^{1}H NMR spectrum revealed a resonance at δ 6.52 (**3g**) and δ 6.71 (**3g′**) with a relative integral of 15.6:1 (88% de). Filtration of an acetone solution of the crude product through Florisil®, followed by concentration under reduced pressure and precipitation from petroleum ether at –10°C afforded **3g** (0.0519 g, 42%) as a yellow oil (at room temperature). $[\alpha]_D$ = –33.7° (c 1.08, Et_2O). IR (KBr, neat) ν_{max} (cm^{-1}): 3410 (br), 1968, 1893. ^{1}H NMR δ: 6.52 (s, 1H), 5.68 (d, 1H, *J* = 6.5), 5.63 (d, 1H, *J* = 6.0), 5.35 (t, 1H, *J* = 6.3), 5.26 (d, 1H, *J* = 7.9), 5.20 (t, 1H, *J* = 6.3), 4.23 (d, 1H, *J* = 3.3), 4.02 (d, 1H, *J* = 3.3), 3.29 (d, 1H, *J* = 7.9), 3.21 (s, 3H), 3.15 (s, 3H) 2.21 (t, 2H, *J* = 7.1), 1.51 (m, 2H), 1.41 (m, 2H), 1.30 (s, 3H), 1.15 (s, 3H), 1.13 (s, 3H), 1.06 (s, 3H), 0.87 (t, 3H, *J* = 7.3). ^{13}C NMR δ: 232.2, 110.9, 107.3, 99.9, 93.5, 92.0, 89.9, 88.6, 87.9, 84.8, 82.6, 78.7, 77.1, 75.5, 62.2, 49.4, 49.3, 30.4, 22.1, 22.0, 21.3, 20.9, 19.4, 18.5, 13.5. MS *m*/*e*: 456 (M^+ – 3CO). HRMS *m*/*e* calcd. for $C_{27}H_{36}CrO_8$ (M^+ – 3CO): 456.1968; found: 456.1964.

*(1′*R*,2′*S*,4*R*,5*R*)-[4,5-Bis(1-methoxy-1-methylethyl)-2-(2′-(*S*-1-hydroxy-1-phenylmethyl)phenyl)-1,3-dioxolane]tricarbonylchromium(0) (**3h**) (phenyl derivative)*

o-Formyl complex **2** (0.0924 g, 0.202 mmol) was subjected to the standard procedure with phenylmagnesium bromide (0.42 mL, ca. 1.44 M in Et_2O, 0.61 mmol) as the nucleophile. A standard aqueous work-up resulted in a crude product whose ^{1}H NMR spectrum revealed a resonance at δ 6.11 (**3h**) and δ 6.32 (**3h′**) with a relative integral of 10.1:1 (82% de). Purification by silica gel chromatography using petroleum ether:ethyl acetate (5:1) as eluent gave **3h** (0.067 g, 62%) as a yellow oil. $[\alpha]_D$ = –49.4° (c 0.56, Et_2O). IR (NaCl, neat) ν_{max} (cm^{-1}): 3421, 1966, 1887. ^{1}H NMR δ: 7.45 (d, 2H, *J* = 7.0), 7.29 (m, 3H), 6.11 (s, 1H), 5.88 (d, 1H, *J* = 2.7), 5.74 (d, 1H, *J* = 6.5), 5.69 (d, 1H, *J* = 6.5), 5.35 (t, 1H, *J* = 6.3), 5.30 (t, 1H, *J* = 6.3), 4.11 (d, 1H, *J* = 3.3), 3.98 (d, 1H, *J* = 3.3), 3.21 (s, 3H), 3.15 (s, 3H), 2.54 (d, 1H, *J* = 2.7), 1.34 (s, 3H), 1.11 (s, 3H), 1.08 (s, 3H), 1.04 (s, 3H). ^{13}C NMR δ: 232.5, 141.8, 128.3, 127.9, 127.0, 115.3, 107.3, 99.5, 91.9, 91.3, 90.5, 89.6, 84.8, 82.4, 77.4, 75.4, 69.4, 49.4, 49.2, 22.3, 21.3, 21.1, 19.0. MS *m*/*e*: 536 (M^+). HRMS *m*/*e* calcd. for $C_{27}H_{32}CrO_8$ (M^+): 536.1502; found: 536.1492.

*(1′*R*,2′*S*,4*R*,5*R*)-[4,5-Bis(1-methoxy-1-methylethyl)-2-(2′-(*S*-1-hydroxy-1-thiophene-1-ylmethyl)phenyl)-1,3-dioxolane]-tricarbonylchromium(0) (**3i**) (thiophene derivative)*

o-Formyl complex **2** (0.0763 g, 0.167 mmol) was subjected to the standard procedure with 2-bromomagnesiothiophene (0.47 mL, ca. 1.14 M in Et_2O, 0.50 mmol) as the nucleophile. A standard aqueous work-up resulted in a crude product whose ^{1}H NMR spectrum revealed a resonance at δ 6.10 (**3i**) and δ 6.40 (**3i′**) with a relative integral of 13.3:1 (86% de). Purification by silica gel chromatography using dichloromethane:petroleum ether (7:1) as eluent gave **3i** (0.066 g, 73%) as a yellow oil. $[\alpha]_D$ = –25.2° (c 0.456, Et_2O). IR (NaCl, neat) ν_{max} (cm^{-1}): 3402, 3090, 1965, 1903, 1879. ^{1}H NMR δ: 7.26 (d, 1H, *J* = 4.9), 7.01 (d, 1H, *J* = 3.8), 6.92 (dd, 1H, *J* = 3.8, 4.9), 6.15 (d, 1H, *J* = 3.1), 6.10 (s, 1H), 5.78 (m, 2H), 5.38 (m, 2H), 4.14 (d, 1H, *J* = 3.6), 4.01 (d, 1H, *J* = 3.6), 3.22 (s, 3H), 3.18 (s, 3H), 2.59 (d, 1H, *J* = 3.1), 1.36 (m, 3H), 1.13 (s, 3H), 1.12 (s, 3H), 1.07 (s, 3H). ^{13}C NMR δ: 232.4, 145.7, 126.5, 126.0, 125.5, 113.9, 106.9, 99.5, 91.6, 91.5, 89.9, 89.7, 84.8, 82.3, 77.4, 75.4, 66.2, 49.4, 49.2, 22.3, 21.4, 21.0, 19.0. MS *m*/*e*: 542 (M^+), 458 (M^+ – 3CO). MS (electrospray) *m*/*e*: 565 (M + Na^+), 581 (M + K^+), 445 (M + K^+-$Cr(CO)_3$), 429 (M + Na^+-$Cr(CO)_3$). HRMS *m*/*e* calcd. for $C_{25}H_{30}CrO_8S$ (M^+): 542.1066; found: 542.1070.

Addition of $CH_3Ti(O^iPr)_3$ to o*-formyl complex **2***

To a solution of the *o*-formyl complex **2** (0.100 g, 0.218 mmol) in diethyl ether (10 mL) at –78°C was added $CH_3Ti(O^iPr)_3$ (1.64 mL, 0.40 M in Et_2O, 0.66 mmol) in a dropwise manner. The reaction was allowed to proceed for 3 h, at which time H_2O (10 mL) was added. A standard aqueous work-up afforded a red residue which was subjected silica gel chromatography (petroleum ether:ethyl acetate, 5:1) to afford starting material **2** (0.084 g).

Addition of the ate complex $[CH_3Ti(O^iPr)_4Li]$ to o*-formyl complex **2***

To a solution of MeLi (0.66 mL, 1.0 M, 0.66 mmol) in Et_2O (10 mL) at –30°C was added $Ti(O^iPr)_4$ (0.19 mL, 0.66 mmol, 3 equiv) in a dropwise fashion. After 30 min, the solution was cooled to –78°C, and *o*-formyl complex **2** (0.100 g, 0.218 mmol) was added as a solution in Et_2O (2.0 mL). The solution allowed to stirred for 3 h, at which point distilled water (10 mL) was added. A standard aqueous work-up afforded a red residue which was subjected silica gel chromatography (petroleum ether:ethyl acetate, 5:1) to afford starting material **2** (0.075 g).

X-ray analysis of 3e

Yellow plates of **3e** were obtained from petroleum ether at –10°C. Accurate cell dimensions and a crystal orientation matrix were obtained on a Rigaku AFC5R diffractometer by a least-squares fit of the scattering angles of 25 reflections in

© 2000 NRC Canada

the range $10.5° < 2\theta < 22.9°$. Intensity data were collected by the ω-2θ method using a scan speed of 16° min^{-1}, scan width 1° above $K\alpha_1$ / 1° below $K\alpha_2$, and monochromatic MoK_α radiation in the range $4.5° < 2\theta < 50.0°$.

The intensities of 2778 unique reflections were measured of which 681 had $F_o^2 > 3\sigma(F_o^2)$. Data were corrected for Lorentz polarization and absorption effects. The structure was solved by direct methods and expanded using Fourier techniques. The non-hydrogen atoms were refined anisotropically. Hydrogen atoms were included but not refined. Scattering factors were those of Cromer and Waber (29) and allowance was made for anomalous dispersion. All calculations were performed using teXsan.

Material on deposit

The ^{13}C NMR spectra of **2** and **3a**–**i** and the details of the X-ray structural characterization of **3e** (details of data collection and refinement, tables of atomic coordinates, anisotropic displacement parameters, bond distances and angles) (29 pages) have been deposited as supplementary material.[4]

Acknowledgements

We are grateful for the research support of the Natural Sciences and Engineering Research Council of Canada (NSERC) and the University of Windsor. We wish to thank the Windsor Molecular Structure Centre (WINMOL) for the crystallographic structural work on **3e**. We wish to thank the Wayne State University Central Instrumentation Facility for mass spectral work on **3i**.

References

1. V.N. Kalinin. Usp. Khim. **56**, 1190 (1987); Russ. Chem. Rev. (Engl. Transl.) **56**, 682 (1987); S.G. Davies, S.J. Coote, and C.L. Goodfellow. *In* Advances in metal-organic chemistry. Vol. 2. *Edited by* L. Liebeskind. JAI, Greenwich. 1991. pp. 1–57; M. Uemura. *In* Advances in metal-organic chemistry. Vol. 2. *Edited by* L. Liebeskind. JAI, Greenwich. 1991. pp. 159–245; M.F. Semmelhack. *In* Comprehensive organic synthesis. Vol. 4. *Edited by* B.M. Trost and I. Fleming. Pergamon, Oxford. 1991. pp. 517–549; M.F. Semmelhack. *In* Comprehensive organometallic chemistry II. Vol. 12. *Edited by* E.W. Abel, F.G.A. Stone, and G. Wilkinson. Pergamon, Oxford. 1995. pp. 979–1015 and 1017–1038; F. Rose-Munch, V. Gagliardini, C. Renaud, and E. Rose. Coord. Chem. Rev. **178**–**180**, 249 (1998).
2. S.G. Davies and T.J. Donohoe. Synlett. 323 (1993).
3. A. Solladie-Cavallo. *In* Advances in metal-organic chemistry. Vol. 1. *Edited by* L. Liebeskind. JAI, Greenwich. 1989. pp. 99–133; S.G. Davies and T.D. McCarthy. *In* Comprehensive organometallic chemistry II. Vol. 12. *Edited by* E.W. Abel, F.G.A. Stone, and G. Wilkinson. Pergamon, Oxford. 1995. pp. 1039–1070.
4. M. Sodeoka and M. Shibasaki. Synthesis, 643 (1993); C. Bolm and K. Muniz. Chem. Soc. Rev. **28**, 51 (1999).
5. Y. Kondo, J.R. Green, and J. Ho. J. Org. Chem. **58**, 6182 (1993) and refs. therein; F. Rose-Munch and E. Rose. Curr. Org. Chem. **3**, 445 (1999) and refs. therein; J. Aubé, J.A. Heppert, M.L. Milligan, M.J. Smith, and P. Zenk. J. Org. Chem. **57**, 3563 (1992); S.G. Davies and W.E. Hume. J. Chem. Soc. Chem. Commun. 251 (1995); S.G. Davies, T. Loveridge, and J.M. Clough. J. Chem. Soc. Chem. Commun. 817 (1995); J.W. Han, S.U. Son, and Y.K. Chung. J. Org. Chem. **62**, 8264 (1997).
6. R.A. Ewin, A.M. MacLeod, D.A. Price, N.S. Simpkins, and A.P. Watt. J. Chem. Soc. Perkin Trans. 1, 401 (1997) and refs. therein; A. Ariffin, A.J. Blake, W.S. Li, and N.S. Simpkins. Synlett. 1453 (1997); A. Quattropani, G. Bernardinelli, and E.P. Kündig. Helv. Chim. Acta, **82**, 90 (1999); M. Uemura, Y. Hayashi, and Y. Hayashi. Tetrahedron: Asymmetry, **5**, 1427 (1994); M. Siwek and J.R. Green. J. Chem. Soc. Chem. Commun. 2359 (1996); H.-G. Schmalz and K. Schellhaas. Tetrahedron Lett. **36**, 5515 (1995); E.M.L. Cowton, S.E. Gibson, M.J. Schnider, and M. H. Smith. Chem. Commun. 839 (1996).
7. A. Fretzen and E.P. Kündig. Helv. Chim. Acta, **80**, 2023 (1997); M. Uemura, H. Nishimura, and T. Hayashi. J. Organomet. Chem. **473**, 129 (1994).
8. R. Thangarasa, J.R. Green, and T.T. Nadasdi. J. Chem. Soc. Chem. Commun. 501 (1994).
9. A. Solladié-Cavallo and J. Suffert. Tetrahedron Lett. **25**, 1897 (1984); A. Solladié-Cavallo, D. Farkhani, S. Fritz, T. Lazrak, and J. Suffert. Tetrahedron Lett. **25**, 4117 (1984); S.G. Davies and C.L. Goodfellow. J. Chem. Soc. Perkin Trans. 1, 393 (1990); C. Baldoli, P. Buttero, E. Licandro, S. Maiorana, A. Papagni, and M. Torchino. Tetrahedron Lett. **34**, 7943 (1993); S.G. Davies and W.E. Hume. J. Chem. Soc. Chem. Commun. 251 (1995).
10. J. Brocard, M. Mahmoudi, L. Pelinski, and L. Maciejewski. Tetrahedron, **46**, 6995 (1990); C. Mukai and M. Hanoaka. Tetrahedron Lett. **34**, 6081 (1993); C. Mukai, W.J. Cho, and M. Hanoaka. Tetrahedron Lett. **30**, 7435 (1989); C. Mukai, W.J. Cho, I.J. Kim, M. Kido, and M. Hanoaka. Tetrahedron, **47**, 3007 (1991); C. Mukai, A. Mihira, and M. Hanoaka. Chem. Pharm. Bull. **39**, 2863 (1991); C. Mukai, M. Miyakawa, A. Mihira, and M. Hanoaka. J. Org. Chem. **57**, 2034 (1992).
11. A. Solladié-Cavallo, G. Lapitajs, P. Buchert, A. Klein, S. Colonna, and A. Manfredi. J. Organomet. Chem. **330**, 357 (1987); A. Solladié-Cavallo and M. Bencheqroun. J. Organomet. Chem. **403**, 159 (1991).
12. J. Brocard, L. Pelinski, and J. Lebibi. J. Organomet. Chem. **337**, C47 (1987).
13. C. Baldoli, P. Del Buttero, S. Maiorana, E. Licandro, S. Maiorana, and A. Papagni. J. Chem. Soc. Chem. Commun. 762 (1987); C. Baldoli, P. Del Buttero, and S. Maiorana. Tetrahedron, **46**, 7823 (1990).
14. A. Solladié-Cavallo, S. Quazzotti, S. Colonna, and A. Manfredi. Tetrahedron Lett. **30**, 2933 (1989); A. Solladié-Cavallo, S. Quazzotti, S. Colonna, A. Manfredi, J. Fischer, and A. DeCian. Tetrahedron: Asymmetry, **3**, 287 (1992); A. Solladié-Cavallo, S. Quazzotti, S. Colonna, and A. Manfredi. Tetrahedron Lett. **31**, 6185 (1990).
15. H. Koide and M. Uemura. Tetrahedron Lett. **40**, 3443 (1999).

[4] Copies of material on deposit may be purchased from the Depository of Unpublished Data, Document Delivery, CISTI, National Research Council of Canada, Ottawa, ON K1A 0S2, Canada (http://www.nrc.ca/cisti/irm/unpub_e.shtml for information on ordering electronically). Tables of data collection and refinement, atomic coordinates, and bond distances and angles reported in this paper have been deposited with the Cambridge Crystallographic Data Centre. Copies of the data can be obtained, free of charge, on application to the Director, CCDC, 12 Union Road, Cambridge CB2 1EZ, U.K. (Fax: 44-1223-336033 or e-mail: deposit@ccdc.cam.ac.uk).

© 2000 NRC Canada

16. A. Yanagisawa, K. Ishihara, and H. Yamamoto. Synlett. 411 (1997); T. Taniguchi and K. Ogasawara. Tetrahedron Lett. **38**, 6429 (1997); K. Ishihara, Y. Ishida, S. Nakamura, and H. Yamamoto. Synlett. 758 (1997).
17. K. Ishihara, H. Nakamura, S. Nakamura, and H. Yamamoto. J. Org. Chem. **63**, 6444 (1998).
18. Y.M.A. Yamada and M. Shibasaki. Tetrahedron Lett. **39**, 5561 (1998); Y.M.A. Yamada and S. Ikegami. Tetrahedron Lett. **41**, 2165 (2000).
19. D. Seebach, A. Pichota, A.K. Beck, A.B. Pinkerton, T. Litz, J. Karjalainen, and V. Gramlich. Org. Lett. **1**, 55 (1999); D.J. Macquarrie. Chem. Commun. 601 (1997).
20. M.K. McKay, M.J. Siwek, and J. R. Green. Synthesis, 1203 (1996).
21. K. Maruoka, T. Itoh, M. Sakurai, K. Nonoshita, and H. Yamamoto. J. Am. Chem. Soc. **110**, 3588 (1988); R.M. Kellogg. *In* Comprehensive organic synthesis. Vol. 8. *Edited by* B.M. Trost and I. Fleming. Pergamon, Oxford. 1991. Chap. 1.3.
22. M.T. Reetz. Organotitanium reagents in organic synthesis. Springer–Verlag, New York. 1986. pp. 84–85; M.T. Reetz. *In* Organometallics in synthesis. *Edited by* M. Schlosser. John Wiley and Sons, New York. 1994. Chap. 3, pp. 206–207.
23. R. Imwinkelried and D. Seebach. Org. Synth. **67**, 180 (1989).
24. V.M. Swamy, S.K. Mandal, and A. Sarkar. Tetrahedron Lett. **40**, 6061 (1999); S.K. Mandal and A. Sarkar. J. Org. Chem. **64**, 2454 (1999); S. Sur, S. Ganesh, V.G. Puranik, and A. Sarkar. J. Chem. Soc. Perkin Trans. 1, 977 (1998); S. Sur, S. Ganesh, D. Pal, V. G. Puranik, P. Chakrabarti, and A. Sarkar. J. Org. Chem. **61**, 8362 (1996).
25. M.R. Winkle, J.M. Lansinger, and R.C. Ronald. J. Chem. Soc. Chem. Commun. 87 (1980).
26. W.G. Kofron and L.M. Baclawski. J. Org. Chem. **41**, 1879 (1976).
27. M.T. Reetz, J. Westermann, R. Steinbach, B. Wenderoth, R. Peter, and S. Maus. Chem. Ber. **118**, 1421 (1985).
28. W.C. Still, M. Kahn, and A. Mitra. J. Org. Chem. **43**, 2923 (1978).
29. D.T. Cromer and J.T. Waber. International tables for X-ray crystallography. Vol. IV. Kynoch Press, Birmingham. 1974. Table 2.2 A.

© 2000 NRC Canada

Potentiometric study of cadmium(II) and lead(II) complexation by a cross-linked poly(acrylic acid). Comparison with the linear analogue

Catherine Morlay, Yolande Mouginot, Monique Cromer, Michelle Chatelut, and Olivier Vittori

Abstract: Cadmium(II) or lead(II) complex formation with an insoluble cross-linked poly(acrylic acid) was investigated in dilute aqueous solution ($NaNO_3$ 0.1 M, 25°C). Potentiometric titrations were carried out to determine the stability constants of the MA and MA_2 complex species formed. The Bjerrum's method, modified by Gregor et al. (1955), for the study of polymeric acids was used. The results obtained showed that lead(II) was more readily bound to the polymer. PbA_2 was the predominant species; the global stability constant log B_{102} was equal to 7.4. With cadmium(II), none of the complex species MA or MA_2 was predominant (log B_{102} = 6.0). Finally, the comparison of these results with those of our previous studies showed that the insoluble cross-linked poly(acrylic acid) and its hydrosoluble linear analogues present similar complexing properties towards cadmium(II), lead(II), copper(II), and nickel(II).

Key words: insoluble cross-linked poly(acrylic acid), cadmium(II), lead(II), complexation, potentiometry.

Résumé : La complexation du cadmium (II) et du plomb (II) par un acide polyacrylique réticulé insoluble a été étudiée en solution aqueuse diluée ($NaNO_3$ 0,1 M, 25°C). Les titrages potentiométriques réalisés ont permis de déterminer les constantes de stabilité des complexes de type MA et MA_2. La méthode de Bjerrum, modifiée par Gregor et al. (1955) pour l'étude des polyacides, a été utilisée. Les résultats obtenus montrent que le plomb (II) est mieux retenu par le polymère. L'espèce PbA_2 est prédominante ; sa constante globale de stabilité log B_{102} vaut 7,4. Avec le cadmium (II), aucune des formes MA ou MA_2 n'est prédominante (log B_{102} = 6,0). Enfin, la comparaison de ces résultats avec ceux de nos précédentes études montre que cet acide polyacrylique réticulé insoluble et ses analogues linéaires solubles présentent des propriétés complexantes similaires vis-à-vis des ions cadmium (II), plomb (II), cuivre (II) et nickel (II).

Mots clés : acide polyacrylique réticulé insoluble, cadmium (II), plomb (II), complexation, potentiométrie.

Introduction

Some insoluble cross-linked polymers, called superabsorbents, present many industrial applications which are linked to their important water-absorbing capacity (10 to several hundred times their dry weight) (1–3). Although the bulk of the research and development effort has been placed on disposable absorbent products, numerous other applications have been developed (water-retention of soils for agricultural applications, water-absorbing construction materials, electronics and cabling, food packaging, thickeners (2, 3)). Some interesting new applications of superabsorbents are emerging, for example in the cosmetic industry, to develop new sensors or for the controlled release of substances such as pharmaceuticals, pesticides, or fertilizers (3).

In our previous studies of metal complexation with linear hydrosoluble poly(acrylic acids) (HPAAs) of high molecular weight, we showed that HPAAs were able to trap different metal ions (4–7). There is some literature relative to this field of research but there is a complete lack of data for their insoluble cross-linked analogues, i.e., superabsorbents of a carboxylic nature.

The aim of this work was to study the metal complexation of an insoluble cross-linked PAA, Aquakeep® SAP X 50 R superabsorbent, under precise conditions of pH, ionic strength, and concentrations and to compare these results with those obtained with HPAAs, their hydrosoluble linear analogues. The metal ions considered, cadmium(II) and lead(II), are highly pollutant substances. This work was carried out in dilute aqueous solution using protometry as an investigation means. Observations of the polymer beads were also realized using scanning electron microscopy (SEM).

Theory

Molar concentration has little meaning for polymer compounds (4). Thus, we shall define for polycarboxylic acids the total content of titratable acid functions of the sample

Received July 16, 1999. Published on the NRC Research Press website on December 4, 2000.

C. Morlay[1], Y. Mouginot, M. Cromer, M. Chatelut, and O. Vittori. Laboratoire d'Electrochimie Analytique – LICAS, Université Claude Bernard Lyon 1, CPE, 43 Bvd du 11 novembre 1918, 69622 Villeurbanne CEDEX, France.

[1]Author to whom correspondence may be addressed. Telephone: (33) 4 72 44 82 63. Fax: (33) 4 72 44 84 79. e-mail: morlay@univ-lyon1.fr

© 2000 NRC Canada

Table 1. Main characteristics of Aquakeep® SAP X 50 R.

Particle size distribution	<100 μm	<1%
	100–500 μm	50–75%
	500–800 μm	20–40%
	>800 μm	<5%
Density	0.67 ± 0.05 g cm^{-3}	
Residual monomers	<100 ppm	
Residual humidity	5.5 ± 0.2%	
Water retention after 30 min.	31 ± 3 g g^{-1}	
Absorption capacity with 0.9% NaCl	57 g g^{-1}	
Gelling time	85 s	

under study (C_A) expressed in equiv. L^{-1}. C_A corresponds to the total reactive site (potentially complexing site) concentration of the polymer introduced in the analysis cell as used next for the complexation study.

Metal complexation by Aquakeep® was studied during the alkali titration of the protonated polyacid (HA) in the presence of metal ions (M). We chose to examine concentration ratios of complexing sites to metal ions ($R = C_A/C_M$, C_M: total metal ion concentration in the analysis cell) in aqueous solution higher than unity. The system under study could then be considered as a simple binary system and the formation of monomolecular complexes was only examined.

The Bjerrum (8) approach, modified by Gregor et al. (9) for the analysis of complexes formed with macromolecules, was used. The average coordination number ($\bar{r}$) can be calculated for every experimental point of the ligand titration curve in the presence of metal ions. The successive stability constants K_1 and K_2 as well as the global stability constants β_{102} and B_{102} for the formation of the MA_2 species were determined using the formation curves $\bar{r}$ vs. –log ([HA]/[H]) (or p([HA]/[H])); the values of p([HA]/[H]) were read for $\bar{r}$ = 0.5, 1.0, and 1.5. The mathematical treatment of the experimental data implies that the acid–base properties of the polymer (i.e., the variation of the apparent protonic dissociation constant K_A^H with pH) have been previously studied. All the definitions and assumptions needed for this work have been described in previous papers (4, 5, 10). We limited our investigations to the MA and MA_2 species. As explained earlier by Gregor et al. (9), it is not possible to estimate complexation constants of greater than second-order as the formation curves are subject to several uncertainties for $\bar{r} > 2.0$.

Experimental

Reagents

The poly(acrylic acid) used was Aquakeep® SAP X 50 R superabsorbent (Elf-Atochem Co. (Levallois-Perret, France)). All the experiments were carried out using the same batch of polymer which was stored in a polyethylene flask, at room temperature (20°C) and in the dark. It was used without any further treatment. Its main characteristics are presented in Table 1.

Metal ion stock solutions (2×10^{-2} M) were prepared from cadmium nitrate and lead nitrate (Fluka Chemika, Switzerland) and standardized using an EDTA disodium salt solution (Merck, Germany). For potentiometric titrations, a 0.1 M sodium hydroxide (Prolabo) solution was prepared and standardized with a 5×10^{-2} M (weighted amount) potassium monohydrogenophtalate (Fluka Chemika) solution. The standardized NaOH solution was kept free of carbonate using a carbon dioxide trap containing NaOH beads and fitted on the flask cap. A standardized 0.1 M solution was prepared from concentrated nitric acid (Prolabo). The stock solution of supporting electrolyte, $NaNO_3$ (Fluka Chemika), was 1 M. The other solutions prepared were described previously (10).

Table 2. Instrumental parameters used for the potentiometric study.

Instrumental parameter	
Response slope of the glass combination electrode	–57.7 ± 0.3 mV/decade
Volume increments (μL): Min	100
Max	200
Stability criterion or maximum increment delay	0.01 pH unit min^{-1} 300 s
Inflexion detection	Incremental

Apparatus and procedure

The apparatus description and use to perform the potentiometric analyses were presented earlier (10). The instrumental parameters chosen are shown in Table 2.

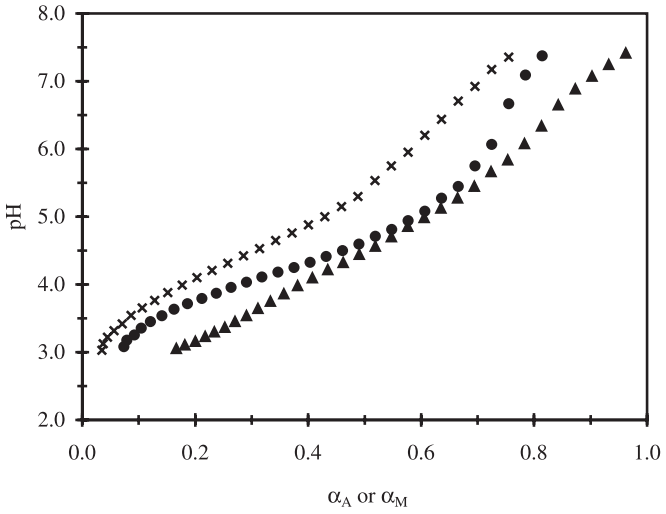
Aquakeep® (50.0 ± 0.1 mg) was introduced under a moderate agitation (vigorous enough to ensure a rapid homogenization and to avoid the settlement of the polymer beads, around 450 rpm) in the analysis cell containing a given volume of distilled water and 5 mL of a 1.0 M $NaNO_3$ solution. The polymer beads were left to swell for 20 min. An excess (5 mL) of the 0.1 M HNO_3 standardized solution was then added to allow the protonation of all the carboxylate groups. The reaction time was 20 min. Finally, a known volume of the metal ion stock solution was introduced in the analysis cell and a further 20 min. waiting time was respected. The sample total volume was 50 mL and metal ion final concentrations were $C_M = 2 \times 10^{-3}$ or 8×10^{-4} M for cadmium(II) and $C_M = 8 \times 10^{-4}$ or 4×10^{-4} M for lead(II).

The titration with the standardized carbonate-free 0.1 M NaOH solution was started after an initial nitrogen bubbling of 20 min. The pH of the sample was stable when the titration started. The measurements were performed at 25.0 ± 0.1°C, under a moderate agitation and under a nitrogen atmosphere. All the samples were treated in the same way. Each titration lasted nearly 5 h. The reproducibility of both cadmium(II) and lead(II) complexation was determined by carrying out the same experiment twice.

The Aquakeep® beads were observed using a scanning electron microscope (SEM) HITACHI model S 800. Aquakeep® (10.0 ± 0.1 mg) was introduced in a 100 mL 0.1 M $NaNO_3$ sample containing the studied metal ion at 8×10^{-4} M final concentration. An Aquakeep® blank was prepared without any metal ion. All samples were left 10 h under a moderate agitation and then filtrated. The Aquakeep® beads were dried at room temperature.

© 2000 NRC Canada

Fig. 1. Curves of pH vs. the dissociation coefficient of Aquakeep® in the absence (α_A, *x*) or in the presence (α_M) of metal ion for very close values of $R = C_A/C_M$ (● Cd(II), R = 8.4; ▲ Pb(II), R = 8.2; C_A = 6.7 mequiv. L^{-1}).



Results and discussion

The previous potentiometric study of the acid–base properties of Aquakeep® (10), showed that the polymer exhibits both a weak and a very weak acidity (specific values: 6.7 ± 0.1 and 2.1 ± 0.1 mequiv. g^{-1}, respectively). The weak acidity of Aquakeep® is characterized by a pK_m^H value of 5.40 ± 0.05. This study also showed that the carboxylic groups accounting for the very weak acidity of Aquakeep® dissociate at pH values above 7.5. As explained in the Theory section, the formation curves can be used only for $\bar{r} \leq 2.0$; consequently, in this study of metal complexation, we had to treat the experimental data contained in the 2.8–6.0 pH range. The very weak acidity of Aquakeep® was thus not considered. In the following, C_A represents the weak acidity content introduced in the analysis cell (C_A = 6.7 ± 0.1 mequiv. L^{-1} for 50.0 ± 0.1 mg of Aquakeep®).

Two ligand to metal ratios ($R = C_A/C_M$) were examined for each metal ion. R values were 3.4 and 8.4 for cadmium(II). Because of the shape of the formation curves obtained, we had to use a higher value of R for lead(II); the R values were 8.2 and 16.3. C_A was kept constant.

Calculations were made, using the formula proposed by Baes and Mesmer (11), to investigate the possible formation of metal hydroxides during the alkali titration of the weak acidity of Aquakeep®. Taking into account the value of C_M, we verified that neither soluble nor insoluble metal hydroxides were significantly formed up to a pH value of 7.5.

Qualitative study of complexation

Figure 1 shows the evolution of pH vs. the dissociation coefficient of Aquakeep® in the absence (α_A) or in the presence (α_M) of metal ions and for the same concentration ratio examined for cadmium(II) or lead(II) (R around 8.3). For any pH located in the pH range where complexation takes place, α_M is higher than the corresponding α_A. Moreover, by comparison with the curve obtained with the ligand alone, the "ligand + metal ion" titration curves show a supplementary release of protons (curves not shown) which is attributed to the formation of metal complexes. For R around 8.3, the complexation occurs significantly from pH = 4.0 for cadmium(II) and from pH = 3.0 for lead(II). Moreover, complexation appears to be more significant with lead(II) than with cadmium(II). These qualitative results are similar to those previously reported for the complexation study of HPAAs (5).

The SEM observation shows that, compared to the blank, the spherical structure of the Aquakeep® beads which have been in presence of metal ions has completely collapsed (Fig. 2). The cluster arrangement has also disappeared.

Quantitative study of complexation

Figure 3 shows the formation curves $\bar{r}$ vs. p([HA]/[H]) obtained in the presence of cadmium(II) or lead(II), respectively, and for the different C_A/C_M ratios considered. The maximum pH range investigated was 2.8–6.0. The formation curves obtained for lead(II)–Aquakeep® systems present a decrease of their slope for the average coordination number $\bar{r}$ in the 1.5–2.0 range (for R = 8.2, $\bar{r}$ = 2.0 corresponds to pH = 3.85 and α_M = 0.35). This plateau means that the corresponding PbA_2 complex species is thus the predominant species formed in that region compared to the PbA species. Concerning the cadmium(II)–Aquakeep® systems, the formation curve obtained for R = 8.4 do not present any plateau for $\bar{r}$ in the 0–2 range (for R = 8.4, $\bar{r}$ = 2.0 corresponds to pH = 4.60 and α_M = 0.48), which means that none of the two complex species CdA or CdA_2 becomes predominant in all that domain of $\bar{r}$.

Elsewhere, the formation curves obtained for both cadmium(II) or lead(II) – Aquakeep® systems present an important slope for $\bar{r}$ about 1 (for cadmium(II) and R = 8.4, $\bar{r}$ = 1.0 corresponds to pH = 3.97 and α_M = 0.27; for lead(II) and for R = 8.2, $\bar{r}$ = 1.0 corresponds to pH = 2.97 and α_M = 0.16). One may conclude that, for one metal ion, the stability constants of the MA and MA_2 species are quite close and that, as a consequence, both species exist with comparable concentrations in the corresponding pH domain.

Finally, the value of $\bar{r}$ still increases above $\bar{r}$ = 2.0. This suggests that in that region some other complexes may possibly be formed besides the MA_2 complex species but their precise nature cannot be found from the formation curves (9).

The same observations were formulated previously for the complexation of cadmium(II) or lead(II) with HPAAs (5) because the shapes of the formation curves were identical for each of the metal ions studied, respectively.

The values of log b_r were obtained by a graphical interpolation of the formation curves. The corresponding values of the complexation constants K_1, K_2, β_{102}, and B_{102} as well as the pH and pK_A^H values for which K_1, K_2, and B_{102} were determined are presented in Tables 3 and 4 for cadmium(II) and lead(II). The apparent dissociation constant of the ligand $K_A{}^H$, was determined from the curve pK_A^H vs. pH previously established (10). The experimental error on the values of log K (log K_1 or log K_2) was estimated at ±0.1. The experimental error on the values of log β_{102} or log B_{102} was estimated at ±0.2.

© 2000 NRC Canada

Fig. 2. Aquakeep® beads observed using SEM: (*a*) without any metal ion; (*b*) with Cd(II); or (*c*) with Pb(II).

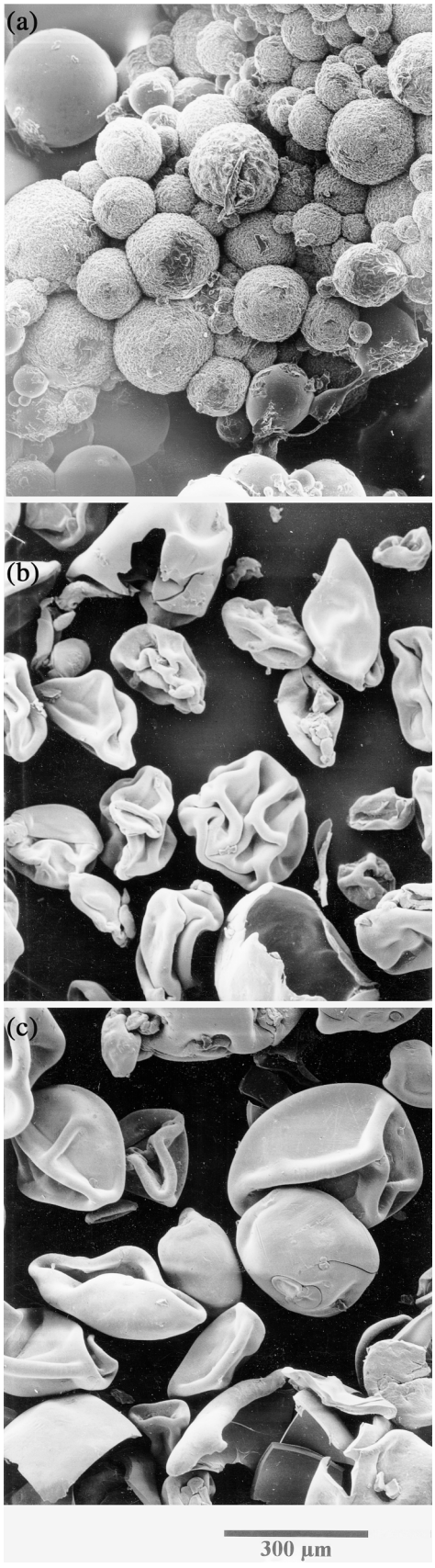


Fig. 3. Formation curves obtained for the Aquakeep®–Cd(II) systems (○ R = 3.4; ● R = 8.4; C_A = 6.7 mequiv. L^{-1}) and for the Aquakeep®–Pb(II) systems (△ R = 8.2; ▲ R = 16.3; C_A = 6.7 mequiv. L^{-1}).

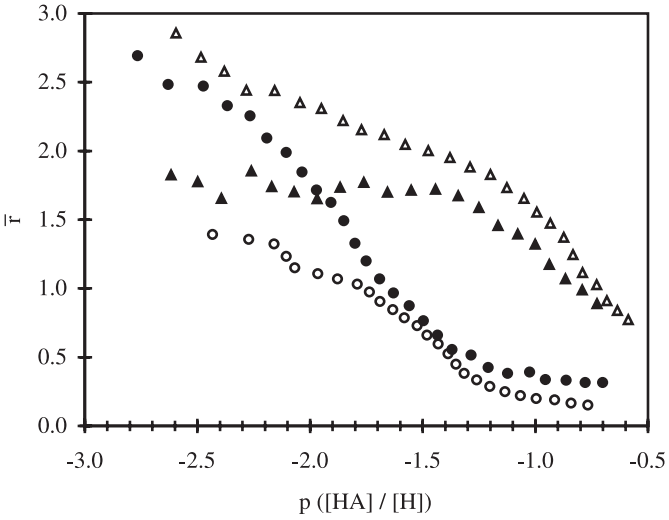


Table 3. Stability constants log K_1 and log K_2 and corresponding pH and pK_A^H values obtained for the Cd(II)–Aquakeep® and Pb(II)–Aquakeep® systems with different values of $R = C_A/C_M$ (C_A = 6.7 mequiv. L^{-1}).

	Cd(II)		Pb(II)	
R	3.4	8.4	8.2	16.3
log K_1[a] ($\bar{r}$ = 0.5)	3.2	3.3	(3.8)	(3.9)
pH	3.78	3.51	—	—
pK_A^H[b]	4.60	4.56	—	—
log K_2[a] ($\bar{r}$ = 1.5)	(2.8)	2.9	3.6	3.4
pH	—	4.25	3.25	3.45
pK_A^H[b]	—	4.75	4.55	4.55
log β_{102}[c]	—	6.2	—	—

[a]The error on log K_1 and log K_2 was estimated at ±0.1.
[b]The error on pK_A^H was estimated at ±0.01.
[c]The error on log β_{102} was estimated at ±0.2.

Because of the shape of the formation curves, it was not possible to determine the value of all the stability constants K_1, K_2, and thus β_{102}. In our previous work on HPAAs (5), we observed that the values of log β_{102} and log B_{102} were not significantly different. Making this assumption with Aquakeep®, we can estimate the missing values of the stability constants; these values are mentioned in brackets in Table 3. It appears that all the values of Table 3 are in very good agreement with those previously determined with HPAAs (5).

To more globally compare the complexing properties of HPAAs and Aquakeep®, Table 5 gives the log B_{102} values obtained with both types of polymer and with the four metal ions we studied, i.e., copper(II), nickel(II), cadmium(II), and lead(II) (5, 10). We can draw the following conclusions: (*i*) for a given metal ion, the values of log B_{102} are in very good agreement; and (*ii*) for both polymers the conditional stability constants of the complexes formed increase in the following order: Ni(II) < Cd(II) < Cu(II) < Pb(II).

© 2000 NRC Canada

Table 4. Values of B_2 and log B_{102} obtained for the Cd(II)–Aquakeep® and Pb(II)–Aquakeep® systems with different values of $R = C_A/C_M$ (C_A = 6.7 mequiv. L^{-1}).

	Cd(II)		Pb(II)	
R	3.4	8.4	8.2	16.3
B_2	3.2×10^{-4}	5.0×10^{-4}	3.5×10^{-2}	2.5×10^{-2}
pH	4.23	3.98	2.97	3.03
pK_A^H [a]	4.74	4.65	4.40	4.46
log B_{102} [b]	6.0	6.0	7.4	7.3

[a]The error on pK_A^H was estimated at ±0.01.

[b]The error on log B_{102} was estimated at ±0.2.

Table 5. Values of log B_{102} obtained with HPAA and Aquakeep®.

	Cu(II)	Ni(II)	Cd(II)	Pb(II)
HPAA[a]	6.6 (6.3)	5.4 (6.6)	6.1 (6.4)	7.1 (13.1)
	6.4 (12.6)	5.3 (13.2)	5.9 (12.9)	7.0 (26.1)
Aquakeep®	6.9 (3.3)[b]	5.3 (3.4)[b]	6.0 (3.4)[c]	7.4 (8.2)[c]
	6.5 (8.3)[b]	5.3 (8.6)[b]	6.0 (8.4)[c]	7.3 (16.3)[c]

Note: In both cases, the error on log B_{102} was estimated at ±0.2. The values of $R = C_A/C_M$ are given in brackets.

[a]Average mol wt = 2.5×10^5, C_A = 5.3 mequiv. L^{-1} (from ref. 5).

[b]C_A = 6.7 mequiv. L^{-1} (from ref. 10).

[c]This study.

We did not find any data in the literature relative to the complexation of cadmium(II) or lead(II) with a cross-linked poly(acrylic acid) or even with a resembling polymer (such as a cross-linked poly(methacrylic acid) for example). We did not consider studies relative to natural substances or natural waters as the complexing material in this case is not well defined and not comparable with our study.

Conclusion

The aims of this study were, first, to assess the binding properties of an insoluble cross-linked poly(acrylic acid) towards cadmium(II) and lead(II) in dilute aqueous solution and, secondly, to compare these results to those previously obtained in the same conditions with two linear hydrosoluble poly(acrylic acids) of high molecular weight (5).

The results obtained showed that both linear and cross-linked PAAs present very similar complexing properties towards the four metal ions we examined. Furthermore, the binding properties of both types of polymer increased, depending on the metal ion, in the following order: Ni(II) < Cd(II) < Cu(II) < Pb(II). Finally, as mentioned in a previous paper (5), compared to their monomer analogues (simple carboxylic acids such as glutaric or acetic acids), polymeric acids, cross-linked or linear, are better complexing agents.

Acknowledgments

We wish to thank the Elf-Atochem Co. who kindly provided the Aquakeep® SAP X 50 R superabsorbent.

References

1. P.M. Budd. *In* Industrial water soluble polymers. *Edited by* C.A. Finch. The Royal Society of Chemistry, Cambridge. 1996. Chap. 1.
2. K.S. Kazanskii and S.A. Dubrovskii. *In* Polyelectrolytes hydrogels chromatographic materials. *Edited by* S.A. Dubrovskii, A.E. Ivanov, K.S. Kazanskii, N.P. Kuznetsova, V.V. Saburov, G.V. Samsonov, and V.P. Zubov. Advances in polymer science 104, Springer–Verlag,. 1992. Chap. 3.
3. F.L. Buchholz. *In* Modern superabsorbent polymer technology. *Edited by* F.L. Buchholz and A.T. Graham. Wiley, New York. Chap. 5 and 7. 1998.
4. C. Morlay, M. Cromer, Y. Mouginot, and O. Vittori. Talanta, **45**, 1177 (1998).
5. C. Morlay, M. Cromer, Y. Mouginot, and O. Vittori. Talanta, **48**, 1159 (1999).
6. C. Morlay, M. Cromer, and O. Vittori. Water. Res. **34**, 455 (2000).
7. S. Perret, C. Morlay, M. Cromer, and O. Vittori. Water. Res. **34**, 3614 (2000).
8. J. Bjerrum. *In* Metal ammine formation in aqueous solution. Haase, Copenhagen. 1941.
9. H.P. Gregor, L.B. Luttinger, and E.M. Loebl. J. Phys. Chem. **59**, 34 (1955).
10. Y. Mouginot, C. Morlay, M. Cromer, and O. Vittori. Anal. Chim. Acta, **407**, 337 (2000).
11. C.F. Baes and R.E. Mesmer. The hydrolysis of cations. Wiley, New York. 1976. Chap. 13 and 15.

© 2000 NRC Canada

Bis(trimethylsilyl)methanesulfonyl and tris(trimethylsilyl)methanesulfonyl chlorides and their reactions by way of sulfenes[1,2]

James F. King, Kim M. Baines, Matthew R. Netherton, and Vinod Dave

Abstract: Bis(trimethylsilyl)methanesulfonyl and tris(trimethylsilyl)methanesulfonyl chlorides (**2c** and **2d**, respectively), have been prepared for the first time. Reactions of **2d** with nucleophiles give products evidently derived from bis(trimethylsilyl)sulfene (**1c**). Reaction of **2c** with piperidine gives the same piperidide as that from **2d**, presumably via **1c** formed by dehydrochlorination of **2c**, whereas water and fluoride ion yield products consistent with their formation via trimethylsilylsulfene (**1b**) formed from **2c** by attack at silicon with loss of the trimethylsilyl and chloro groups. No evidence for any enhanced stability in **1c** was found.

Key words: sulfonyl chlorides, sulfenes, silylsulfonyl chlorides, silylsulfenes, desilylation.

Résumé : Les chlorures de bis(triméthylsilyl)méthanesulfonyle et de tris(triméthylsilyl)méthanesulfonyle, respectivement **2c** et **2d**, ont été préparés pour la première fois. Les réactions de **2d** avec des nucléophiles conduisent à des produits qui, de toute évidence, dérivent du bis(triméthylsilyl)sulfène (**1c**). La réaction de **2c** avec la pyridine donne naissance au même pipéridure que celui obtenu à partir de **2c**, vraisemblablement par le biais de **1c** qui se formerait par déshydrochloration de **2c**; toutefois, les réactions avec l'eau et l'ion fluorure conduisent à des produits qui correspondraient à une formation via le triméthylsilylsulfène **1b** formé par une attaque au niveau du silicium avec perte des groupes triméthylsilyle et chloro. On n'a pas détecté de données suggérant que **1c** jouit d'une stabilité accrue.

Mots clés : chlorures de sulfonyle, sulfènes, chlorure de silylsulfonyle, silylsulfènes, désilylation.

[Traduit par la Rédaction]

Introduction

Over a number of years we have investigated the reactions of sulfonyl compounds, with a particular focus on those that lead to and from sulfenes (**1**) (2, 3). A significant component of this study in recent years has been the examination of the mechanisms of hydrolysis of alkanesulfonyl chlorides (**2**) and related compounds (4–8). Included in this latter work is a study of the hydrolysis of trimethylsilylmethanesulfonyl chloride (**2b**) (6), in which we observed that the only discernible mode of reaction of water or fluoride anion in an aqueous medium was by way of attack at the silicon atom with ultimate formation of products derived from sulfene (**1a**). The reaction in water was clearly following the pathway found by Block and Aslam (9) in the reaction of **2b** with cesium fluoride in acetonitrile. With aqueous hydroxide ion, silicophilic attack to form **1a** was the major pathway (65%), with proton removal leading to trimethylsilylsulfene (**1b**), a minor (35%) route (6). The trimethylsilyl group appeared to be mildly activating relative to an alkyl group in sulfene formation by dehydrohalogenation; k_{EOH} at 1°C for **2b** (reaction via **1b**) was found to be 6.0×10^2 M^{-1} s^{-1}, whereas the corresponding reactions of ethanesulfonyl, propanesulfonyl, and butanesulfonyl chlorides (by dehydrochlorination with hydroxide anion) have slightly lower rate constants (respectively, 5.47×10^2, 5.10×10^2, 4.47×10^2 M^{-1} s^{-1}) even at 25°C (4).

Within this context it was of interest to inquire about the corresponding chemistry of the unknown bis- and tris(trimethylsilyl)methanesulfonyl chlorides (**2c** and **2d**, respectively) and to determine by what means and how readily these materials might yield the sulfenes **1b** and **1c**. A potential bonus in the proposed study was the possibility that bis(trimethylsilyl)sulfene (**1c**) might be sufficiently stable or at least slow enough to react so that some kind of direct observation of sulfene **1c** at room temperature might be possible. Sulfenes as commonly generated are very short-lived species, and the parent sulfene itself (**1a**) has only been observed in matrices at low temperatures (e.g., 77 K); at the time this study began, all previous attempts to generate a

Received May 16, 2000. Published on the NRC Research Press website on December 5, 2000.

J.F. King,[3] K.M. Baines,[3] M.R. Netherton, and V. Dave. Department of Chemistry, The University of Western Ontario, London, ON N6A 5B7, Canada.

[1]Part 42 in the series Organic Sulfur Mechanisms. For part 41 see ref. 1.

[2]Taken in part from the Honors B.Sc. Thesis of M.R. Netherton, The University of Western Ontario, London ON. 1995.

[3]Authors to whom correspondence may be addressed. Telephone: (519) 661-2111, ext. 86348 (JFK), 86302 (KMB). e-mail: scijfk@julian.uwo.ca (JFK), kbaines2@julian.uwo.ca (KMB).

© 2000 NRC Canada

sulfene directly observable by NMR spectrometry, for example, had failed (see ref. 3 for details).[4] In support of the possibility that **1c** might be directly observable we recalled that trimethylsilylketene is evidently more stable than most simple ketenes (see ref. 14 and sources cited), and to the extent that sulfenes are analogues of ketenes, one may naively imagine similar behaviour with trimethylsilylsulfenes. Trimethylsilylsulfene itself (**1b**) had been found to react very rapidly under the conditions of its formation (6, 9), but the possibility remained that the doubly substituted sulfene (**1c**) might react more slowly.[5]

This paper reports the preparation of bis(trimethylsilyl)methanesulfonyl and tris(trimethylsilyl)methanesulfonyl chlorides (**2c** and **2d**), and a brief study of some of their reactions with nucleophiles and bases leading to products formed through intermediate sulfenes.

Results and discussion

The preparation of **2b** reported by Baukov et al. (16) involved reaction of the trimethylsilylmethyl Grignard reagent with sulfur dioxide followed by treatment with chlorine. Since preparations of both the bis- and tris(trimethylsilyl)methyllithium species had been described earlier (17, 18) they were, in our view, promising intermediates for the proposed syntheses. Zwanenburg and coworkers (19–21) had already reported that α-silylated organolithium species on treatment with sulfur dioxide at low temperature followed by warming to room temperature led to the corresponding sulfine, $R^1R^2C{=}SO$, postulated to arise from a Peterson elimination of Me_3SiO^- from the intermediate silylated sulfinate salt, $Me_3SiR^1R^2C\text{-}SO_2^-Li^+$. It seemed likely that sulfine formation could be avoided if the sulfinate salt were treated with chlorine prior to allowing the mixture to warm up. This was indeed found to be the case. As may be seen in Scheme 1, warming of the sulfinate gave the sulfine (**3**) whereas addition of chlorine to the cold sulfinate yielded the sulfonyl chloride (**2d**) in 71% yield. Similar treatment of bis(trimethylsilyl)methyllithium with sulfur dioxide followed by addition of chlorine at low temperature produced bis(trimethylsilyl)methanesulfonyl chloride (**2c**). The structures, **2c** and **2d**, follow from the mode of synthesis, full agreement of spectra and analyses with expectation, and the reactions summarized in Scheme 2.

Reaction of **2d** with cesium fluoride and neopentyl alcohol in acetonitrile following the procedure of Block and Aslam (9) for the generation of sulfene (**1a**) from **2b**, gave a product showing a ^1H NMR spectrum in full accord with the neopentyl ester (**4a**) (and which is very similar to that of the methyl ester prepared as indicated below). This product is, of course, that expected from silicophilic attack of fluoride

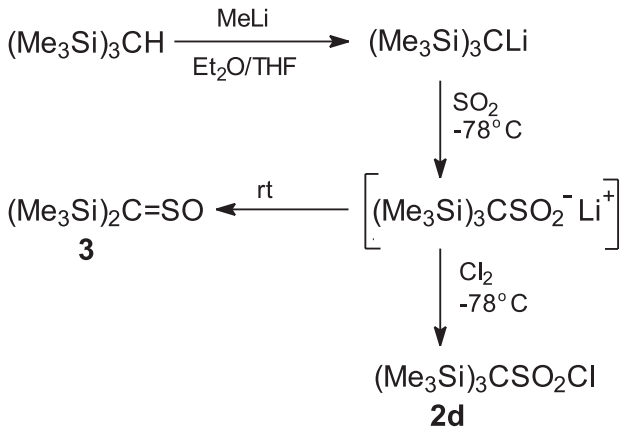
$R^1R^2C{=}SO_2$ — **1**

a) R^1, R^2 = H
b) R^1 = Me_3Si; R^2 = H
c) R^1, R^2 = Me_3Si

$R^1R^2R^3CSO_2Cl$ — **2**

a) R^1, R^2, R^3 = H
b) R^1 = Me_3Si; R^2, R^3 = H
c) R^1, R^2 = Me_3Si; R^3 = H
d) R^1, R^2, R^3 = Me_3Si

Scheme 1.



to yield bis(trimethylsilyl)sulfene (**1c**), followed by trapping of the sulfene with the alcohol. All attempts to observe **1c** by NMR spectrometry were unsuccessful; **2d** with CsF and CD_3CN in the absence of added sulfene traps showed in the ^{19}F NMR spectrum a decet appropriate to Me_3SiF, but neither ^1H nor ^{13}C NMR spectra showed any signals clearly assignable to **1c**.

With water, **2d** gave bis(trimethylsilyl)methanesulfonic acid (**5**), presumably also via **1c** which is trapped in the normal way by water. The structure (**5**) was confirmed by conversion with phosphorus pentachloride to the same sulfonyl chloride (**2c**) as that obtained above from bis(trimethylsilyl)methyllithium, sulfur dioxide, and chlorine. Esterification of **5** with trimethyl orthoformate by the method of Just and co-workers (22) gave methyl bis(trimethylsilyl)methanesulfonate (**4b**).

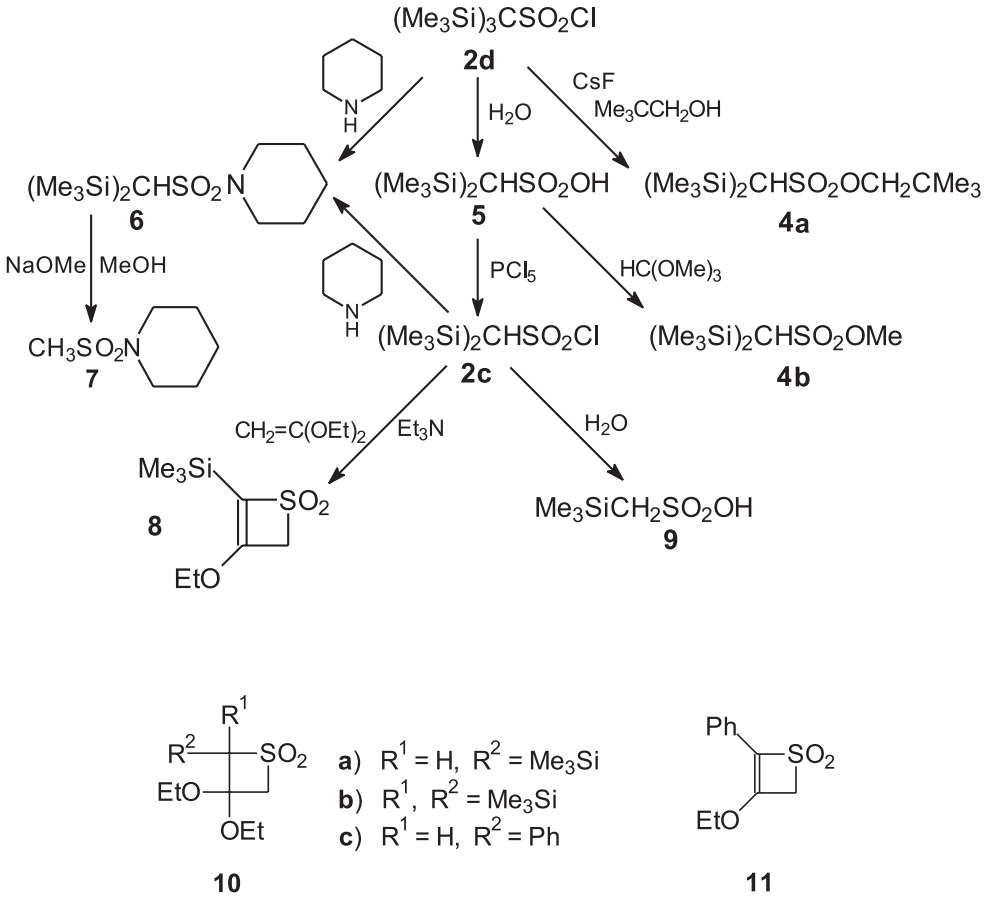
Further corroboration of this general picture was provided by the formation of the same sulfonpiperidide (**6**) by reaction of either **2d** or **2c** with piperidine. With **2d**, which lacks the α-hydrogen, piperidine reacts at one of the silicon atoms to form **1c**, but with **2c** the preferred mode of attack is

[4] After this work began we learned of the report by Skrypnik and Lyashchuk (10) that reaction of Arduengo's carbene (11) with sulfur dioxide gives a crystalline sulfene which is: (*i*) stable at low temperature; and (*ii*) at a "temperature above 25–30°C leads to a rapid decomposition … with SO_2 loss." Mention of this report requires a caveat concerning the reliability of work from this laboratory. Dixon and Arduengo and coworkers (12) re-examined a closely related report by Lyashchuk and Skrypnik (13) on the analogous formation of a ketene by reaction of the Arduengo carbene with carbon monoxide. The American authors: (*i*) were unable "to duplicate the experimental result reported by Lyashchuk and Skrypnik,"; and (*ii*) carried out extensive ab initio calculations, finally concluding that "no evidence is found for the existence of a stable ketene product [in this system]." (12). We had previously investigated two earlier reports by Skrypnik and co-workers of experimental results which appeared difficult to reconcile with previous experience, and found that the results reported by the Ukrainian workers were in both instances different from ours (ref. 3, pp. 708 and 710).

[5] It should be pointed out that the stabilization of trimethylsilylketene has been ascribed (14, 15) to hyperconjugation involving donation from the C—Si bond into the carbonyl system, and that no analogous hyperconjugation is possible with the sulfonyl analogues (**1b** or **1c**).

© 2000 NRC Canada

Scheme 2.



evidently at the α-proton with elimination of HCl to form the same sulfene (**1c**) which then yields **6**. With water, on the other hand, the normal reaction of **2c** (as had already been observed with **2b** (6, 23)), is silicophilic attack to yield the sulfonic acid with one fewer trimethylsilyl groups, i.e., **9**, presumably via **1b**; the acid was identical to that previously obtained as the minor product in the reaction of **2b** with hydroxide ion (6).[6] Further evidence for the formation of the sulfene by elimination of HCl with an amine was provided by the isolation (albeit in low yield) by treatment of **2c** with triethylamine and diethyl ketene acetal, of a product assigned structure **8** on the basis of its spectra and mode of synthesis. Formation of **8** may be readily imagined to take place by way of the initial bis(trimethylsilyl)sulfene – ketene acetal adduct (**10b**), formed in the same way as **10a** from the reaction of the triethylamine and the same ketene acetal with trimethylsilylmethanesulfonyl chloride, as reported by Shipov et al. (24). Loss of alkoxide in the formation and reactions of sulfene cycloadducts has been reported (25–27), with perhaps the closest analogue being Truce and Norell's conversion (25) of **10c** into **11** by the action of sodium ethoxide in dry ethanol. The formation of a carbanion from attack of a nucleophile on the trimethylsilyl group is well-known, and the ease of such cleavage with α-trimethylsilylsulfonyl compounds is strikingly shown by the reaction of **6** with 0.2 M sodium methoxide in methanol; 5 min at room temperature was sufficient to remove both trimethylsilyl groups to form methanesulfonpiperidide (**7**).

The present experiments taken with previous studies (6) reveal a consistent pattern in the reactions of these sulfonyl chlorides with nucleophiles. Water and fluoride anion are strongly silicophilic but not very basic, the result is that these reagents attack at silicon with formation of the sulfene lacking one trimethylsilyl group, and thence to derived products. With piperidine, which is a stronger base, attack at an α-hydrogen (where present) leads to the sulfene with the same number of trimethylsilyl groups, but where there is no α-hydrogen the silicophilic attack readily takes place. This behaviour is to be compared with that noted earlier for **1b** with: (*i*) triethylamine which led, in the presence of an enamine or a ketene acetal, to the enamine cycloadducts expected from **2b** (23); and (*ii*) hydroxide in which the major product is that of silicophilic attack (to give **2a**) and the minor product that of dehydrohalogenation (to give **2b**); the balance in favour of silicophilic attack of hydroxide is consistent with the stronger Si—O bond vs. Si—N.

[6] Note that a conceivable alternative route from **2c** to **9**, namely via a simple hydrolysis of **2c** to give **5** followed by desilylation of **5** to form **9**, is excluded by the observation that **5** is stable to these reaction conditions. The possibility that **2d** reacts by initial hydrolysis to $(Me_3Si)_3CSO_2OH$ followed by desilylation is not rigorously excluded by the present work but in view of the evidence in this and previous studies for sulfene formation by desilylation by the action of water or amines on **2b** and **2c**, it would seem perverse to propose a non-sulfene process from **2d**.

© 2000 NRC Canada

Experimental

Instruments and general procedures are as previously described (1); where not otherwise noted NMR spectra are of $CDCl_3$ solutions.

Tris(trimethylsilyl)methanesulfonyl chloride (2d)

Excess SO_2 (~10 mL) was condensed into dry THF (5 mL) at –78°C under an atmosphere of argon. A solution of $(Me_3Si)_3CLi$ (18) (10 mmol in THF) was added over 5 min; the solution became pale green. Immediately following the addition, a stream of dry Cl_2 was passed through the solution until it became colourless. The volatile material was removed at the rotary evaporator, and the residual solid taken up in petroleum ether (bp 35–60°C). The mixture was filtered through a sintered glass funnel, and the solvent evaporated leaving a white solid (2.34 g, 71%), mp 131°C (dec.). IR (film) ν_{max} (cm^{-1}): 1338 (vs), 1259 (vs), 1149 (vs), 834 (vs, br), 680 (s). ^1H NMR δ: 0.43. ^{13}C NMR δ: 63.7, 2.9. ^{29}Si NMR δ: 3.36. Exact mass calcd. for $C_{10}H_{27}ClO_2SSi_3$: 330.0728; found: 330.0723. Anal. calcd. C 36.36, H 8.18, Cl 10.60, S 9.69; found: C 36.33, H 8.23, Cl 10.69, S 9.27.

Bis(trimethylsilyl)sulfine (3)

To excess SO_2 (~5 mL) in dry THF (10 mL) at –78°C under argon was added $(Me_3Si)_3CLi$ (3 mmol in 7 mL of THF) over 2 min as above, and the solution allowed to come to room temperature, (turning from pale green to pale yellow). Saturated aq NH_4Cl (20 mL) was added and the mixture extracted with ether (3 × 20 mL). The solvent was removed yielding an orange oil (372 mg). Kugelrohr distillation (50°C, 1 torr (1 torr = 133.322 Pa)) yielded **3** as a colourless liquid (246 mg, 41% from $(Me_3Si)_3CH$). ^1H NMR δ: 0.31 (s, 9H), 0.25 (s, 9H). ^{13}C NMR δ: 194.7, 0.24, 0.20. ^{29}Si NMR δ: –3.48, –4.37. A sample of the sulfine was further purified by preparative thick layer chromatography on silica gel eluting with hexanes:benzene (1:1) yielding a colourless oil. Exact mass calcd. for $C_7H_{20}OSSi_2$ (M + 1): 207.0695; found (CI): 207.0687. Zwanenburg (21) refers to preparation of **3** in a table without further description.

Bis(trimethylsilyl)methanesulfonyl chloride (2c)

(i) From bis(trimethylsilyl)methyllithium

To stirred excess SO_2 (~25 mL) at –70°C was added a solution of $(Me_3Si)_2CHLi$ in ether (25 mL) (kindly supplied by F. Guérin and D.H. McConville) over 1 min, and the solution stirred for 15 min. To this solution, still at –70°C, Cl_2 gas was bubbled in and the solution allowed to stir at –70°C for 30 min. The volatile material was evaporated under reduced pressure and the residual oily solid taken up in petroleum ether (bp 35–60°C) and the mixture filtered through a sintered glass funnel. Removal of the solvent gave **2c** as a colourless solid, mp 71–73°C. IR ν_{max} (cm^{-1}): 1370 (s), 1198 (s). ^1H NMR δ: 3.26 (s, 1H), 0.34 (s, 18H). ^{13}C NMR δ: 63.4, 0.7. ^{29}Si NMR δ: 2.83. Anal. calcd. for $C_7H_{19}ClO_2SSi_2$: C 32.47, H 7.34, Cl 13.70, S 12.36; found: C 33.09, H 7.67, Cl 13.12, S 12.37.

(ii) From bis(trimethylsilyl)methanesulfonic acid (5)

A mixture of **5** (5 mg, 0.02 mmol) anhydrous ether (2 mL) and phosphorus pentachloride (15 mg, 0.07 mmol) was stirred at room temperature for 2 h. The volatile material was evaporated under reduced pressure, the residue taken up in petroleum ether, the mixture filtered, and the solvent evaporated as above, to yield a colourless solid showing the same ^1H and ^{13}C NMR spectra as those obtained from **2c** prepared as above.

Reaction of 2d with cesium fluoride and neopentyl alcohol

To a mixture of neopentyl alcohol (90 mg, 1 mmol) and cesium fluoride (71 mg, 0.5 mmol) in dry acetonitrile (7 mL) at 0°C under an atmosphere of dry argon was added **2d** (150 mg, 0.45 mmol) in acetonitrile (2 mL) in one portion. The mixture became pale brown in colour. After 2 h, the mixture was warmed to room temperature and stirred for an additional 1.5 h, whereupon the solvent was removed under reduced pressure and the residue taken up in CH_2Cl_2. Water was added and the mixture extracted with several small portions of CH_2Cl_2. The organic extracts were combined, dried over $MgSO_4$, and the solvent removed on the rotary evaporator yielding a pale brown waxy solid (92 mg). The ^1H NMR spectrum and mode of preparation are consistent with structure **4a**: δ: 3.80 (s, 2H), 2.39 (s, 1H), 0.97 (s, 9H), 0.27 (s, 18H).

Hydrolysis of tris(trimethylsilyl)methanesulfonyl chloride (2d)

$(Me_3Si)_3CSO_2Cl$ (**2d**) (160 mg, 0.485 mmol) was added to a solution of THF (1 mL) in water (5 mL). The solid dissolved quickly with evolution of heat. After 1 h, the solution was extracted with hexane (3 × 2 mL). The water was removed from the aqueous layer under reduced pressure (Rotovap) giving a brownish waxy solid. Hexane was added to the solid, giving a clear organic layer with dark coloured aqueous drops; the latter were discarded and the hexane removed under reduced pressure yielding **5** as white crystals (90 mg, 77%). ^1H NMR (D_2O) δ: 10.2 (br s), 2.46 (s, 1H), 0.26 (s, 18H). ^{13}C NMR δ: 45.5, 0.5. ^{29}Si NMR δ: 1.51.

Bis(trimethylsilyl)methanesulfonpiperidide (6)

(i) From tris(trimethylsilyl)methanesulfonyl chloride (2d)

Excess piperidine (1 mL, 10 mmol) was added dropwise to a solution of **2d** (200 mg, 0.61 mmol) in CH_2Cl_2 (5 mL), and the mixture stirred for 2 h. Water (10 mL) was added and the mixture extracted with ether (3 × 10 mL). The organic layers were combined, dried ($MgSO_4$), and the solvent removed on the rotary evaporator yielding an orange waxy solid. Column chromatography on silica gel (eluting with 35% ether in petroleum ether), followed by preparative thick layer chromatography gave the sulfonamide (**6**) (120 mg, 64%) as white needles, mp 72–73°C. IR ν_{max} (cm^{-1}): 1291 (s), 1277 (s); 1249 (s), 1128 (s), 851 (vs). ^1H NMR δ: 3.10 (m, 4H), 2.55 (s, 1H), 1.56 (m, 6H), 0.23 (s, 18H). ^{13}C NMR δ: 46.1, 44.3, 25.4, 23.9, 1.0. ^{29}Si NMR δ: 0.44. Exact mass calcd. for $C_{12}H_{29}NO_2SSi_2$: 307.1458; found: 307.1446.

(ii) From bis(trimethylsilyl)methanesulfonyl chloride (2c)

A solution of piperidine (100 mg, 1 mmol) in chloroform (0.5 mL) was added to a stirred solution of **2c** (32 mg, 0.1 mmol) in chloroform (1.0 mL) at 0°C and the mixture stirred at 0°C for 30 min and at room temperature for 1 h.

© 2000 NRC Canada

Chloroform was added and the mixture washed with water. The organic layer was dried and the solvent removed yielding **6** (30 mg) identical (mp, TLC, ^{1}H and ^{13}C NMR spectra) to the **6** prepared as above from **2d**.

Desilylation of bis(trimethylsilyl)methanesulfonpiperidide (6)

A solution of sodium methoxide (10 mL) (from Na, 50 mg, 2 mmol) was added to a solution of **6** (29 mg, 0.09 mmol) in methanol and the mixture stirred for 5 min. Water (5 mL) was added and the mixture extracted with small portions of ether. The ether extracts were combined, dried, and the solvent removed yielding methanesulfonpiperidide (**7**) (13 mg, 89%) as a white solid showing ^{1}H and ^{13}C NMR spectra identical to those of a sample of **7** prepared earlier from piperidine and **2a**, mp 48–49°C (28), lit. (29) mp 48.5–50°C. ^{1}H NMR δ: 3.16, (m, 4H), 2.74 (s, 3H), 1.66 (m, 4H), 1.54 (m, 2H). ^{13}C NMR δ: 46.8, 34.5, 25.4, 23.8.

Methyl bis(trimethylsilyl)methanesulfonate (4b)

A solution of **5** (10 mg, 0.04 mmol) in trimethyl orthoformate (0.5 mL) was heated for 18 h (22). Volatile materials were evaporated under reduced pressure leaving methyl bis(trimethylsilyl)methanesulfonate (**4b**) as a colourless solid, mp 52–53°C. IR ν_{max} (cm^{-1}): 1262 (s), 1297 (s), 1167 (s). ^{1}H NMR δ: 3.70 (s, 3H), 2.40 (s, 1H), 0.25 (s, 18H). ^{13}C NMR δ: 52.5, 43.5, 0.5. ^{29}Si NMR δ: 1.89. Exact mass calcd. for $C_8H_{23}O_3SSi_2$ (M + 1): 255.0906; found (CI): 255.0901.

Reaction of bis(trimethylsilyl)methanesulfonyl chloride (2c) with ketene diethyl acetal

Sulfonyl chloride (**2c**) (200 mg, 0.77 mmol) in ether (2 mL) was added with a positive pressure of argon over 2 min to a stirred solution of Et_3N (82 mg, 0.77 mmol) and ketene diethyl acetal (30) (95 mg, 0.8 mmol) in dry ether (3.0 mL) at 5°C. A white solid precipitated immediately; stirring was continued for 30 min at 5°C and then for 6 h at room temperature. The precipitate was removed by filtration through a sintered glass funnel and the solvent from the filtrate removed under reduced pressure leaving a viscous oil (214 mg). Preparative thick layer chromatography (twice, initially with hexanes:ethyl acetate (94:6) R_f = 0.35, then benzene:ether (95:5) developing twice, R_f = 0.38) gave a colourless oil (9 mg) showing the following spectra consistent with structure **8**: ^{1}H NMR δ: 4.55 (s, 2H), 4.04 (q, 2H), 1.38 (t, 3H), 0.28 m (s, 9H). ^{13}C NMR δ: 165.0, 132.9, 69.9, 69.3, 14.9, –0.7. Exact mass calcd. for $C_8H_{16}O_3SSi$: 220.0588; found: 220.0587.

Acknowledgements

We thank the Natural Sciences and Engineering Research Council of Canada (NSERC) for financial support in the form of an operating grant, and Drs. F. Guérin and D.H. McConville for the generous gift of a supply of bis(trimethylsilyl)methyllithium.

References

1. J.F. King, G. Yuyitung, M.S. Gill, J.C. Stewart, and N.C. Payne. Can. J. Chem. **76**, 164 (1998).
2. J.F. King. Acc. Chem. Res. **8**, 10 (1975).
3. J.F. King and R. Rathore. *In* The chemistry of sulphonic acids, esters, and their derivatives. *Edited by* S. Patai and Z. Rappoport. John Wiley and Sons, Chichester. Chap. 17. 1991.
4. J.F. King, J.Y.L. Lam, and S. Skonieczny. J. Am. Chem. Soc. **114**, 1743 (1992).
5. J.F. King, J.Y.L. Lam, and G. Ferrazzi. J. Org. Chem. **58**, 1128 (1993).
6. J.F. King and J.Y.L. Lam. J. Org. Chem. **58**, 3429 (1993).
7. J.F. King, J.Y.L. Lam, and V. Dave. J. Org. Chem. **60**, 2831 (1995).
8. J.F. King and M.S. Gill. J. Org. Chem. **63**, 808 (1998).
9. E. Block and M. Aslam. Tetrahedron Lett. **23**, 4203 (1982).
10. Y.G. Skrypnik and S.N. Lyashchuk. Sulfur Lett. **17**, 287 (1994).
11. A.J. Arduengo, III, R.L. Harlow, and M. Kline. J. Am. Chem. Soc. **113**, 361 (1991).
12. D.A. Dixon, A.J. Arduengo, III, K.D. Dobbs, and D.V. Khasnis. Tetrahedron Lett. **36**, 645 (1995).
13. S.N. Lyashchuk and Y.G. Skrypnik. Tetrahedron Lett. **35**, 5271 (1994).
14. T.T. Tidwell. *In* Ketenes. John Wiley and Sons, New York. 1995. pp. 348ff.
15. W.T. Brady and T.C. Cheng. J. Org. Chem. **42**, 732 (1977).
16. Y.I. Baukov, A.G. Shipov, L.V. Gorshkova, I.A. Savost'yanova, and A.V. Kisin. Zh. Obshch. Khim. **47**, 1677 (1977); (Eng. trans. 1538).
17. P.J. Davidson, D.H. Harris, and M.F. Lappert. J. Chem. Soc. Dalton Trans. 2268 (1976).
18. Z.H. Aiube and C. Eaborn. J. Organomet. Chem. **269**, 217 (1984).
19. M. van der Leij, P.A.T.W. Porskamp, B.H.M. Lammerlink, and B. Zwanenburg. Tetrahedron Lett. 811 (1978).
20. P.A.T.W. Porskamp, M. van der Leij, B.H.M. Lammerlink, and B. Zwanenburg. Rec. Trav. Chim. Pays-Bas, **102**, 400 (1983).
21. B. Zwanenburg. Rec. Trav. Chim. Pays-Bas, **101**, 1 (1982).
22. A.A. Padmapriya, G. Just, and N.G. Lewis. Synth. Commun. **15**, 1057 (1985).
23. G.D. Cooper, J. Org. Chem. **21**, 1214 (1956).
24. A.G. Shipov, A.V. Kisin, and Y.I. Baukov. Zh. Obshch. Khim. **49**, 1170 (1979); (Eng. trans. 1022).
25. W.E. Truce and J.R. Norell. J. Am. Chem. Soc. **85**, 3236 (1963).
26. R.H. Hasek, P.G. Gott, R.H. Meen, and J.C. Martin. J. Org. Chem. **28**, 2496 (1963).
27. Y. Shirota, T. Nagai, and N. Tokura. Tetrahedron Lett. 2343 (1968).
28. J.Y.L. Lam. Ph.D. Thesis, University of Western Ontario, London ON. 1993.
29. S. Ji, L.B. Gortler, A. Waring, A. Battisti, W.D. Closson, and P. Wriede. J. Am. Chem. Soc. **89**, 5311 (1967).
30. S.M. McElvain and D. Kundiger. Org. Syn. Coll. Vol. III, 506 (1955).

© 2000 NRC Canada

Synthesis and X-ray structure of 1,2,2,2-tetrakis(3-methoxyphenyl)ethanone

LeRoy H. Klemm and Timothy J.R. Weakley

Abstract: Photochemical reductive dimerization of 3,3′-dimethoxybenzophenone (**1b**) gave the symmetrical benzopinacol 1,1,2,2-tetrakis(3-methoxyphenyl)ethane-1,2-diol (**2b**), which was rearranged to the benzopinacolone 1,2,2,2-tetrakis(3-methoxyphenyl)ethanone (**3b**) by means of I_2 in boiling glacial HOAc. The structure of **3b** was indicated by ^{1}H NMR and determined definitively by X-ray crystallography. The crystals are monoclinic, space group $P2_1/c$, a = 12.250(2), b = 9.6997(12), c = 20.866(2) Å, β = 95.319(11)°, Z = 4, R = 0.053 for 4523 independent reflections. The structure establishes that the migrating 3-methoxyphenyl group retains bonding through its number 1′ carbon atom to the parent C_2-unit during the rearrangement process.

Key words: X-ray structure, pinacol–pinacolone rearrangement, chemical bonding.

Résumé : La réaction de dimérisation photochimique réductrice de la 3,3′-diméthoxybenzophénone (**1b**) fournit le benzpinacol symétrique 1,1,2,2-tétrakis(3-méthoxyphényl)éthane-1,2-diol (**2b**) qui se réarrange en benzopinacolone 1,2,2,2-tétrakis(3-méthoxyphényl)éthanone (**3b**) sous l'influence d'I_2 dans de l'acide acétique glacial bouillant. La structure du composé **3b** a été établie par RMN du ^{1}H et déterminé d'une façon définitive par diffraction des rayons-X. Les cristaux sont monocliniques, groupe d'espace $P2_1/c$ Å, β = 95,319°, Z = 4, R = 0,053 pour 4523 réflexions indépendantes. La structure permet de conclure que, durant le processus de réarrangement, le groupe 3-méthoxyphényle qui migre maintient sa liaison avec l'atome de carbone 1′ jusqu'à ce qu'il soit relié à l'unité C_2.

Mots clés : diffraction des rayons X, réarrangement pinacol–pinacolone, liaison chimique.

[Traduit par la Rédaction]

Introduction

The rearrangement of benzopinacol (**2a**) to benzopinacolone (**3a**) was described in 1877 (1). Convenient experimental procedures for the synthesis of **2a** from benzophenone (**1a**) and its conversion to **3a** were reported by Bachmann (2), who also investigated the relative migratory apititudes of various substituted phenyl groups (3–5). Comparison of the isolated yield of the isomeric ketones from rearrangement of diols **4a** and **4b** gave the order *p*-methoxyphenyl >>>phenyl > *m*-methoxyphenyl (3, 4, 6, 7) in migratory aptitude. A variety of Brönsted and Lewis acidic catalysts have been used for the pinacol rearrangement (1–3, 6, 8). For most symmetrical aromatic pinacols Bachmann and Ferguson (4) effected the transformation by refluxing 2–4 g of the diol, e.g., **4d**, with a mixture of AcCl, HOAc, and benzene for 2–4 days. However, this treatment was ineffective for rearranging the *m*-methoxyphenyl compounds **4a** and **4c**, which required "a more powerful reagent," viz. a solution of 0.05 g of I_2 in 15 mL of HOAc, plus refluxing for only 15–30 min. In contrast, compound **2d**, bearing the highly activating *p*-methoxy groups, is easily rearranged to **3d** under either of these reaction conditions, or even by heating in HOAc alone at 100°C for 10 min (7, 9). The less reactive parent benzopinacol (**2a**) undergoes rearrangement by heating with acid chlorides or aqueous acids, as well as by the I_2–HOAc method (2, 10). A solution of **2a** in HOAc alone required heating at 180–200°C in a sealed tube to accomplish rearrangement (1).

Consultation of the literature indicated that neither the benzopinacol **2b** nor the ketone **3b**, bearing four *m*-methoxyphenyl groups, had been reported. Since we had compound **1b** available from another project (11), we proceeded to ascertain: (*i*) if Scheme 1 could be completed by the Bachmann procedure; and, if so, (*ii*) if the aryl group on migrating from C-1 to C-2 would retain its bonding position to the molecule via carbon C-1′ i.e., if the *m*-methoxyphenyl group would undergo ipso-rearrangement exclusively (12).

Specifically, the known ketone **1b** was converted into diol **2b** (42% yield) and rearranged nearly quantitatively following closely the Bachmann procedures (2). Structural location of the methoxy groups in the resultant benzopinacolone was indicated by ^{1}H NMR and established definitively by X-ray crystallography of the isolable, purified product.[2]

Received June 22, 2000. Published on the NRC Research Press website on December 4, 2000.

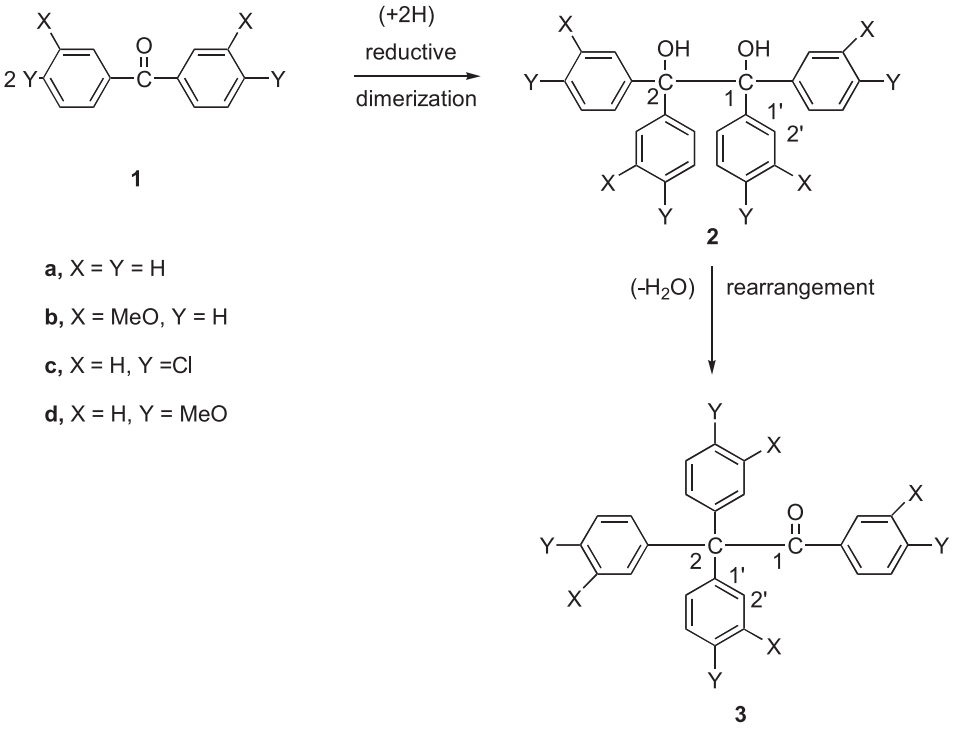
L.H. Klemm[1] and T.J.R. Weakley. Department of Chemistry, University of Oregon, Eugene, OR 97403-1253, U.S.A.

[1]Author to whom correspondence may be addressed. Telephone: (541) 346-1695. Fax: (541) 346-0487. e-mail: lklemm@oregon.uoregon.edu

[2]Supplementary material may be purchased from the Depository of Unpublished Data, Document Delivery, CISTI, National Research Council Canada, Ottawa, ON, Canada K1A 0S2 (http://www.nrc.ca/cisti/irm/unpub_e.shtml for information on ordering electronically). Some of the material has also been deposited with the Cambridge Crystallographic Data Centre. Copies of the data can be obtained, free of charge, on application to the Director, CCDC, 12 Union Road, Cambridge CB2 1EZ, U.K. (Fax: 44-1223-336033 or e-mail:deposit@ccdc.cam.ac.uk).

© 2000 NRC Canada

Scheme 1.



1

a, X = Y = H

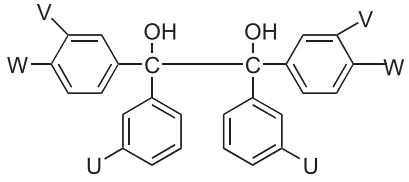
b, X = MeO, Y = H

c, X = H, Y =Cl

d, X = H, Y = MeO

2

3



4

a, U = W = H, V = MeO

b, U = V = H, W = MeO

c, U = Me, V = MeO, W = H

d, U = Me, V = H, W = MeO

Experimental

IR spectra were determined on KBr wafers by means of a Nicolet 5-DXB FTIR spectrophotometer. ^{1}H NMR spectra were recorded on a General Electric QE-300 instrument. Mass spectra were obtained at 70 eV by Dr. Richard Wielesek of this laboratory on a VG 12-250 instrument. Elemental analyses were conducted by Desert Analytics, Tucson, AZ.

Purification of 3,3′-dimethoxybenzophenone (1b)

This compound, available from a previous synthesis (11), was redistilled as a light yellow oil, bp 170–172°C (1.3 mm). EIMS *m*/*z* (%): 243 (18), 242 (M^+, 100), 211 (M^+ – MeO, 17), 135 ($MeOC_6H_4C{=}O^+$, 72), 107 ($MeOC_6H_4^+$, 15), 92 (27). ^{1}H NMR (in $CDCl_3$, δ): 7.45–7.3 (m, 6 aromatic H), 7.2–7.1 (m, 2 aromatic H), 3.87 (s, 6H, 2 MeO).

Preparation of 1,1,2,2-tetrakis(3-methoxyphenyl)ethane-1,2-diol (2b)

A solution of **1b** (7.08 g, 29.2 mmol), glacial HOAc (4 drops), and 2-propanol (100 mL) was exposed to midsummer sunlight in a tightly corked round-bottomed flask for 8 days. The colorless needles which formed were collected by filtration and rinsed with cold 2-propanol (2.97 g of **2b**, 42%), mp 153.5–156°C, raised to 157.5–158.5°C on recrystallizations from petroleum ether (30–60°C):acetone (1:1). EIMS *m*/*z* (%): 468 ($M^+ - H_2O$, <0.1), 242 ($(MeOC_6H_4)_2C{=}O^+$, 41), 135 ($MeOC_6H_4C{=}O^+$, 100), 109 (33), 107 ($MeOC_6H_4^+$, 35). FTIR (cm^{-1}): 3535 (OH), 1603, 1583, 1483, 1430, 1290, 1231 (OMe). ^{1}H NMR (in acetone-d_6, δ) 7.2–6.9 (m, 12 aromatic H), 6.67 (split d, J = 3.4 Hz, 4 aromatic H), 4.79 (s, 2 OH), 3.58 (s, 12H, 4 MeO). Anal. calcd. for $C_{30}H_{30}O_6$: C 74.06, H 6.21; found: C 74.26, H 6.11.

© 2000 NRC Canada

Table 1. Crystallographic data for compound **3b**.

Chemical formula	$C_{30}H_{28}O_5$
Refinement	F^2
Formula weight	468.55
Space group	$P2_1/c$
a, *b*, *c*, (Å)	12.250 (2), 9.6997 (12), 20.866 (2)
α, β, γ (°)	90, 95.319 (11), 90
V (Å^3)	2468.8 (9)
Z	4
d_{calc} (g/cm^3)	1.261
μ (cm^{-1})	0.85
Crystal size (mm)	0.15 × 0.23 × 0.37
Total reflections scanned	5117
R_{int} (for 0, *k*, ± ℓ)	0.026
Sec. extinction parameter (g)	6.9 (7) × 10^{-7}
No. rflns in refinement (*N*)	2658 [$I \geq \sigma(I)$]
	4523 (all independent data)
No. of parameters (*V*)	429
Weighting factor (*w*)	$4F_o^2/[\sigma^2(I) + (0.020I)^2]$
R(*F*), *wR*(*F*), *S* [$I \geq \sigma(I)$][a]	0.053, 0.049, 1.46
R(F^2), *wR*(F^2), *S* (all data)[a,b]	0.078, 0.105, 1.17
Max Δ/σ, last cycle	0.01
Residual electron density	0.40 to –0.41 e Å^{-3}

[a] $R(F) = \Sigma||F_o| - |F_c||/\Sigma|F_o|$; $S = [\Sigma w(|F_o| - |F_c|)^2/(N - V)]^{1/2}$; $I_o(\text{corr}) = I_o(1 + 2gI_c)$.
[b] $wR(F^2) = [\Sigma w(|F_o|^2 - |F_c|^2)^2/\Sigma w|F_o|^4]^{1/2}$.

Table 2. Some atomic bond lengths (Å) and angles (°) in **3b.**

Bond lengths	(Å)	Bond angles	(°)
O1—C1	1.213 (3)	O1-C1-C2	120.4 (2)
O4—C17	1.374 (3)	O1-C1-C21	119.0 (2)
O4—C29	1.431 (3)	O4-C17-C16	115.0 (2)
O5—C23	1.364 (3)	O4-C17-C18	124.2 (2)
O5—C30	1.419 (4)	O5-C23-C22	115.5 (2)
C1—C2	1.569 (3)	O5-C23-C24	124.7 (2)
C1—C21	1.496 (3)	C1-C2-C9	109.9 (2)
C2—C15	1.539 (3)	C1-C2-C15	110.8 (2)
C15—C16	1.381 (3)	C3-C2-C9	111.1 (2)
C15—C20	1.399 (3)	C3-C2-C15	114.7 (2)
C21—C22	1.382 (3)	C9-C2-C15	105.7 (2)
C21—C26	1.400 (4)	C17-O4-C29	117.4 (2)
		C23-O5-C30	118.2 (3)

Table 3. Some torsional angles (°) in **3b**.

Structure	Torsional angle (°)
O1-C1-C2-C3	–129.4 (2)
O1-C1-C2-C9	–10.0 (3)
O1-C1-C2-C15	106.4 (2)
O1-C1-C21-C22	–158.5 (2)
C1-C2-C3-C4	47.6 (3)
C2-C1-C21-C22	26.1 (3)
C2-C3-C4-C5	–177.9 (2)
C2-C9-C14-C13	178.0 (2)
C2-C15-C16-C17	–176.8 (2)
C4-C3-C2-C9	–71.0 (3)
C4-C3-C2-C15	169.3 (2)
C4-C5-O2-C27	–5.1 (4)
C12-C11-O3-C28	1.2 (5)
C18-C17-O4-C29	9.0 (4)
C24-C23-O5-C30	–1.5 (4)

Preparation of 1,2,2,2-tetrakis(3-methoxyphenyl)ethanone (3b)

A solution of **2b** (1.85 g, 3.81 mmol) and iodine (0.11 g, 0.41 mmol) in glacial HOAc (20 mL) was refluxed for 15 min and poured into a mixture of ice, water, and excess $NaHSO_3$. The cream-colored precipitate coagulated to a brittle solid on standing. The pulverized solid was washed with water and dried in air (1.8 g of **3b**, 100%), mp 100–104°C, converted to colorless prisms on recrystallization from Et_2O–petroleum ether and then from 95% ethanol, mp 108.5–109.5°C. FTIR (cm^{-1}): 1686 (C=O), 1597, 1292, 1256, 1236 (MeO). EIMS *m*/*z* (%): 468 (M^+, 0.4), 334 (31), 333 ($(MeOC_6H_4)_3C^+$, 100), 135 ($MeOC_6H_4C{=}O^+$, 33), 107 ($MeOC_6H_4^+$, 17). ^{1}H NMR (in $CDCl_3$, δ): 7.3–6.7 (m, 16 aromatic H), 3.68 (s, 9H, 3 MeO), 3.62 (s, 3H, MeO). Anal. calcd. for $C_{30}H_{28}O_5$: C 76.90, H 6.02; found: C 76.87, H 5.95.

X-ray analysis of 3b

A crystal suitable for X-ray analysis was obtained by recrystallization of the preceding **3b** from absolute ethanol. A colorless prism was mounted on a fiber. The orientation parameters and cell dimensions were obtained at 22°C from the setting angles of an Enraf–Nonius CAD-4 diffractometer (Mo Kα radiation, λ 0.71073 Å) for 25 centered reflections in the range of 11.6–13.7°θ. Data were collected by ω-2θ scans (ω width (0.85 + 0.35 tan θ)°, speed 4.1° per min) in the θ range 1.5–25.5°; *h* 0→14, *k* 0→11, ℓ –25→25. A SIR92 E-map (13) showed all of the non-hydrogen atoms. Hydrogen atoms were located and refined isotropically. The TeXsan program suite (14), incorporating complex atomic scattering factors, was used in all calculations.

Results and discussion

The ^{1}H NMR of **3b** shows a singlet for three equivalent MeO groups at δ 3.68 and for one MeO group at δ 3.62, consistent with the structure shown.

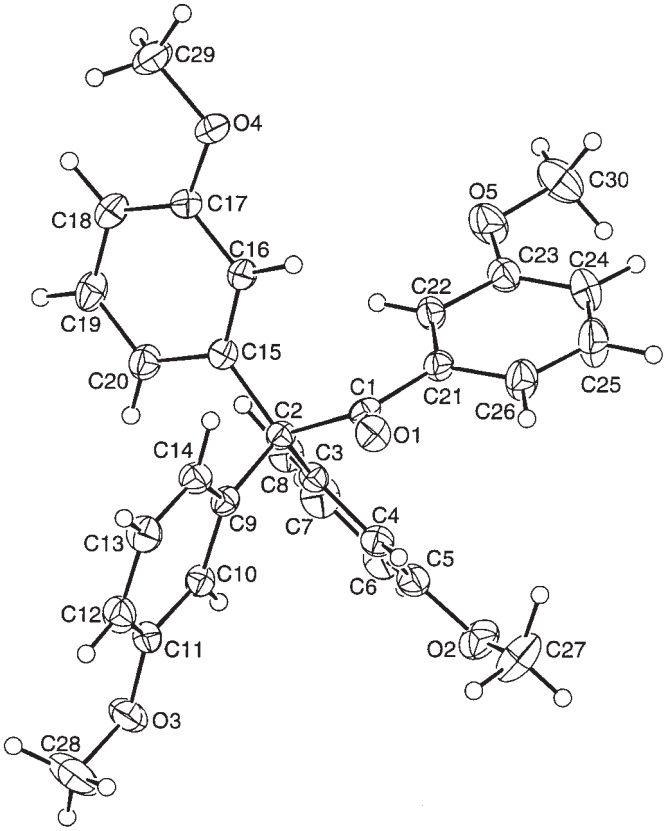
The crystallographic data for **3b** are given in Table 1; selected bond lengths and angles, in Table 2; and selected torsion angles, in Table 3. An ORTEP drawing is shown in Fig. 1.

It is apparent from Fig. 1 that the 3-methoxyphenyl group has undergone ipso-rearrangement during the benzopinacol →benzopinacolone transformation. The quantitative yield of crude **3b** from this reaction and a high recovery of analytically pure crystals of narrow melting range indicate that no more than a few percent (if any) of a structural isomer of **3b** could have formed.

The selected data in Table 2 illustrate limited variability in corresponding bond lengths in the aryl groups attached to C-1 and C-2. However, there is a 9° variation (from 105.7–114.7°) in the angles centered on C-2, perhaps due to crowding in the molecule around this tetra-substituted carbon.

© 2000 NRC Canada

Fig. 1. ORTEP (30% probability ellipsoids) plot for **3b.**



Notable in Table 3 is the fact that in every case the MeO group is only slightly twisted (1.2–9.0°) out of coplanarity with its benzene ring. However, in three of the cases the methyl portion of the MeO group is oriented toward the *para* carbon on the ring, while in the fourth case (C27) it is oriented toward the *ortho* carbon on its ring.

Acknowledgement

The assistance of Dawn Ring in some preliminary studies on this project is appreciated.

References

1. W. Thörner and T. Zincke. Ber. **10**, 1473 (1877).
2. W.E. Bachmann. *In* Organic syntheses. Coll. Vol. 2. *Edited by* A.H. Blatt. John Wiley, New York. 1943. pp. 71–74.
3. W.E. Bachmann and F.H. Moser. J. Am. Chem. Soc. **54**, 1124 (1932).
4. W.E. Bachmann and J.W. Ferguson. J. Am. Chem. Soc. **56**, 2081 (1934).
5. H. Adkins. *In* Organic chemistry. 2nd ed. Vol. 1. *Edited by* H. Gilman. John Wiley, New York. 1943. pp. 1067–1068.
6. Y. Pocker and B.P. Ronald. J. Org. Chem. **35**, 3362 (1970).
7. M. Migita. Bull. Chem. Soc. Jpn. **7**, 334 (1932).
8. M. Bartok and A. Molnar. *In* The Chemistry of ethers, crown ethers, hydroxyl groups and their sulphur analogues. Part 2. Suppl. E. *Edited by* S. Patai. John Wiley, New York. 1980. Chap. 16.
9. C.W. Shoppee. J. Chem. Soc. 506 (1936).
10. M. Gomberg and W.E. Bachmann. J. Am. Chem. Soc. **49**, 246 (1927).
11. L.H. Klemm, E.P. Antoniades, and C.D. Lind. J. Org. Chem. **27**, 519 (1962).
12. G.W. Wheland. Advanced organic chemistry. 2nd ed. John Wiley, New York. 1951. pp. 468–469; C.K. Ingold. Structure and mechanism in organic chemistry. 2nd ed. Cornell University Press, Ithaca, N.Y. 1969. p. 739.
13. A. Altomare, G. Cascarano, C. Giacovazzo, A. Guagliardi, M.C. Burla, G. Polidori, and N. Camalli. J. Appl. Crystallogr. **27**, 435 (1994).
14. TeXsan. Software for single-crystal structure analysis. Version 1.7. Molecular Structure Corporation, 3200A Research Forest Drive, The Woodlands, TX 77381, U.S.A. 1997.

© 2000 NRC Canada

Canadian Journal of Chemistry

Author Index
Volume 78, 2000

Revue canadienne de chimie

Index des auteurs
Volume 78, 2000

Abraham, M.H., 184
Abrams, S.R., 963
Acevedo, I.L., 1121
Acree, W.E., Jr., 184, 449, 459
Ahmed, A.R., 1178
Aicken, F.M., 415
Aknin, M., 986
Aliaga, C., 1052
Alibhai, N., 1345
Alper, H., 920
Alvarez-Toledano, C., 1299
Alvaro, G., 809
An, H., 884
Andraos, J., 508
Andreotti, D., 772
Andryukhova, N.P., 1285
Antipin, M.Y., 1511
Apeloig, Y., 1496
Arakawa, H., 291
Arango, J.O., 1421
Arca, M., 1147
Arslan, T., 884
Arya, P., 920
Atay, E., 84, 520
Aue, W.A., 95
Aumelas, A., 248
Auner, N., 1445
Back, M.H., 16
Bailey, M., 739
Baines, K.M., 1474, 1642
Baisch, G., 892
Ball, J.M., 464
Balsevich, J.J., 963
Balzarini, J., 1081
Baril, J., 490
Bassindale, A.R., 1479
Basso, E., 1441
Batchelor, R.J., 598
Batra, H., 1109
Becerra, R., 1428
Becht, J., 1380
Beck, E.J., 1060
Belzile, N., 51
Benn, M., 542
Bennet, A.J., 577
Berg, D.J., 255, 454
Bernard, G.M., 614
Bernardinelli, G., 280
Bertani, B., 809
Berthet, J.-C., 1305
Bezombes, J.-P., 1519
Bianchi, D.A., 1165
Biondi, S., 772
Birahda, K., 568
Blagoeva, I.B., 84, 520
Blais, P., 10
Blanco, S.T., 1587
Bodo, B., 487
Boeré, R.E., 1613
Boeré, R.T., 583, 1613
Boganov, S.E., 1428
Bonhoure, I., 1305
Bossard, A.R., 16
Botta, M., 925
Bottomley, F., 383
Boudjouk, P., 1396
Bourque, S.C., 920
Braekman, J.C., 1030
Bridges, C., 1289
Brook, M.A., 1357
Brossard, L., 307
Brown, M.A., 536
Brown, R.S., 1247
Brown, W., 800
Brun, P., 128
Buchanan, G.W., 316
Buncel, E., 474, 1251
Burschka, C., 1380
Cai, X., 1484
Camacho, A.G., 1121
Camerman, A., 26, 1045
Camerman, N., 26, 1045
Cameron, T.S., 118
Carballo, E., 1535
Cartier dit Moulin, C., 1305
Castan, P., 280
Castellan, A., 73
Cervantes, J., 1491
Cervantes-Lee, F., 1511
Chabot, C., 852
Chan, T.H., 776
Chang, J.-C., 224
Chapados, C., 64, 490, 1128
Chapleur, Y., 708
Charlton, J.L., 553
Chatelut, M., 1637
Chauhan, M., 1396
Chênevert, R., 275
Chiang, Y., 1627
Chiltz, F., 307
Chivers, T., 10
Chrusciel, J.J., 1405
Chubb, F.L., 84, 520
Chuca, I., 184
Chuit, C., 1519
Clarke, C.W., 1
Classon, B., 829
Clement, O., 474
Cobos, J.C., 1272
Collins, C., 151
Corelli, F., 925
Corey, J.Y., 1434
Corriu, R.J.P., 1519
Coumbarides, G.S., 935
Couture, P., 356
Couturier, D., 1242
Cow, C., 553
Crasto, C.F., 884
Crespo-Pinilla, M.S., 521
Cristobal-Telésforo, E., 248
Cromer, M., 1637
Csizmadia, I.G., 362, 395, 626
Cullen, J.M., 1575
Cunin, F., 1544
Curran, D.P., 791
Cyr, A., 307
D.Sa, R., 1178
Dag, Ö., 516
Daloze, D., 1030
Dapporto, P., 723
Das, S.K., 191, 838
Dass, G., 444
Dasser, M., 275
Dave, V., 1642
Dawes, R., 1035
De Backer, M., 1242
De Clercq, E., 1081
De Fina, K.M., 184, 449, 459
de Rossi, R.H., 233
De, A.K., 139
Dean, P.A.W., 590

© 2000 NRC Canada

Decken, A., 270
del Río, I., 1620
Demartin, F., 1147
Den Auwer, C., 1305
Denmark, S.E., 673
Devillanova, F.A., 1147
Dey, R., 1561
Dhawan, R., 784
Di Fabio, R., 809
Dogra, S.K., 191
Dominique, R., 838
Donati, D., 772
Donnadieu, B., 280
Downard, A., 10
Drake, J.E., 1214
Driega, A.B., 316
Drouin, M., 212
Dubey, K.K., 1561
Dubovik, I., 1511
Duceppe, J.-S., 739
Duff, S.J.B., 1553
Dufresne, C., 784
Duran, M., 328
Durst, T., 1345
Dwyer, J.R., 1035
Eames, J., 935
Edward, J.T., 84, 520
Egorov, M.P., 1428
Eichele, K., 118, 614
Einstein, F.W.B., 598
Ekelmans, D., 1030
Elguero, J., 1109
El-Hallag, I.S., 1170
El-Hefnawy, G.B., 1170
El-Saidi, M., 356
Enriz, R.D., 626
Ernst, B., 892
Fabre, P.-L., 280
Fattori, D., 925
Faure, R., 986
Faustov, V.I., 1428
Favier, F., 1544
Fisher, L., 409
Fletcher, K.A., 449
Foster, J., 1019
Foster, K., 800
Fradera, X., 328
Frank, S.A., 757
Franzén, R., 957
Fritz, G., 1388
Fryzuk, M.D., 1003
Fu, J.-m., 905
Fujita, K., 1089
Fusar-Bassini, D., 925
Futatsuki, K., 1089
Gable, K.P., 704
Galibert, A.M., 280
Gallant, R.T., 1295
Ganguly, T., 139
Garcia de la Fuente, I., 1272
Gauvin, A., 986
Gay, I.D., 598
Gaydou, E.M., 986
Gee, M., 118
Gehrhus, B., 1484
Gendron, R.A.L., 255, 454
Genêt, J.-P., 846
Gentile, G., 925
Ghoneim, E.M., 1170
Giacobbe, S., 809
Gibson, H.W., 347
Giesbrecht, G.R., 1003
Girard, C., 816
Glaser, R., 212
Glew, D.N., 1, 1204
Goesmann, H., 1388
González, J.A., 1272
Gossage, R.A., 1620
Gough, K.M., 1035
Grand-Maître, C., 739
Grasmann, M., 1445
Graziano, G., 1233
Greedan, J.E., 1289
Green, C.E., 184
Green, J.R., 1629
Grenier, L., 739
Gross, T., 1399
Grzegozek, M., 950
Gu, J.-H., 598
Guérin, B., 852
Guindon, Y., 852
Guthrie, J.P., 1295
Gutiérrez-Pérez, R., 1299
Guyon, F., 1570
Haaf, M., 1526
Hallberg, A., 829
Handerson, S., 527
Hannu, M.S., 1620
Haroon, S., 1561
Haynes, C.A., 1553
Hecht, S.M., 884
Heilporn, S., 1030
Hempel, A., 26, 1045
Hennigar, T.L., 568
Hernández-Ortega, S., 248
Herrschaft, B., 1445
Hijji, Y.M., 1421
Hinman, A.S., 1318
Hitchcock, P.B., 1484
Hou, X., 963
Hu, Y.-J., 838
Huang, X., 577
Hudrlik, A.M., 1421
Hudrlik, P.F., 1421
Hughes, D.W., 1474
Hughes, G., 868
Hum, G., 642
Hummer, M., 1445
Hursthouse, M.B., 1073
Hussein, S.M.I., 436
Iftime, G., 409
Igarashi, K., 657
Ikariya, T., 697
In, Y., 31
Infante, A.B., 521
Irvine, N., 963
Isaia, F., 1147
Ishitani, H., 666
Jankowski, C.K., 248
Jeanson, P., 307
Jefferson, G.R., 920
Jeffrey, K.R., 46
Jenkins, H.A., 590
Jiang, Z.-H., 322
Jiménez, R., 1491
Jiménez-Estrada, M., 248
Jobe, D.J., 464
Johnson, M., 133
Joly, H.A., 51
Jones, D.H., 1318
Jordan, R.W., 527
Jourdain, I.V., 1570
Jurkauskas, V., 800
Kabanyane, S., 270
Kagan, H.B., 816
Kagayama, A., 657
Karginov, V.A., 884
Kasahara, Y., 1553
Katampe, I., 1479
Katopodis, A., 892
Katz, M., 1121
Kaufman, T.S., 1165
Kelly, D.G., 1073
Keuthen, M., 1388
Kim, J.-H., 673
King, J.F., 1642
Kirby, C.W., 614
Kirschner, F., 1388
Klassen, V., 583
Klemm, L.H., 1647
Kliegel, W., 546, 1325
Knaus, E.E., 1081
Kobayashi, S., 666
Koerner, T., 1067
Koga, Y., 1553
Kresge, A.J., 508, 1627
Krishnamoorthy, G., 191
Kumar, D., 1109

© 2000 NRC Canada

Kumar, H., 427
Kvarnström, I., 829
Laikhter, A.L., 884
Lamarque, L., 128
Lamba, D., 925
Lambert, J.B., 1441
Laporte, F., 118
Lappert, M., 1484
Larsen, G., 206
Lautens, M., 868
Lavallée, P., 739
Leblanc, Y., 784
Leclercq, S., 1030
Lee, J., 642
Lee, S.-H., 347
Leigh, W.J., 1459
Lelj, F., 1147
Lessard, J., 307
Leung, C., 553
Lewars, E., 297
Leznoff, C.C., 167
Li, H., 51
Liao, D.-Z., 322
Light, M.E., 1073
Lin, A.C., 362
Lin, Y.-S., 224
Lin, Z.-P., 95
Lipari, F., 577
Lippolis, V., 1147
Lissi, E.A., 1052
Littke, A., 784
Liu, P., 133
Liu, X., 1143
Lociuro, S., 772
Lodder, M., 884
López, J.M., 1491
López-Cortés, J.G., 1299
Lubkowitz, G., 1325
Lutz, M., 1620
Machado, A.A.S.C., 1013
MacInnis, J.A., 1222
Mackintosh, N., 800, 852
Madic, C., 1305
MaGee, D.I., 1060
Majerus, S.L., 1345
Mak, M.L., 626
Malonga, H., 291
Manzer, L.E., 920
Marangoni, D.G., 1222
Martel, A.A., 307
Mastropaolo, D., 26, 1045
Masuda, J., 1613
Mata-Pérez, F., 521
Matern, E., 1388
Mathey, F., 118
Matsunaga, S., 31
Max, J.-J., 64, 490, 1128
McClelland, R.A., 1178, 1186
McKay, M.K., 1629
McKillop, A., 1158
Meiners, F., 1469
Ménard, H., 307
Ménichelli, C., 1128
Meou, A., 128
Merkley, N., 356, 942
Messanga, B.B., 487
Mestres, J., 328
Mislow, K., 41
Misra, K., 1561
Mogren, T., 800
Mohamed, M., 1357
Moharram, Y.I., 1170
Moisy, P., 1305
More O'Ferrall, R.A., 1594
Morlay, C., 1637
Mosquera, R.A., 1535
Mouginot, Y., 1637
Mukaiyama, T., 657
Murphy, D.G., 1594
Nagashima, T., 791
Naithani, R., 1109
Natansohn, A., 409
Neault, J.F., 291
Nefedov, O.M., 1428
Netherton, M.R., 1642
Neverov, A.A., 1247
Nickel, P., 26
Nikitin, K.V., 1285
Nikolova, P.V., 1553
Nishikawa, K., 1553
Nishino, H., 31
Norstrom, T., 963
Novetta-Delen, A., 291
Noyori, R., 697
O'Brien, D.M., 1594
Oehme, H., 1399
Ogilvie, W.W., 739, 852
Öhrlein, R., 892
Ohtsu, H., 31
Okanga, F.I., 338
Okoro, C.O., 1421
Ollerenshaw, J., 784
Onyido, I., 474
Ortega-Alfaro, M.C., 1299
Oscarsson, K., 829
Otín, S., 1587
Overman, L.E., 732
Owens, T.R., 1459
Ozturk, T., 1158
Padwa, A., 749
Pain, G., 772
Pal, A., 427, 444
Palepu, R., 151, 1222
Pandey, J.D., 1561
Pannell, K.H., 1511
Paoli, P., 723
Papkov, V., 1511
Paquette, L.A., 689
Paradise, B.J., 1526
Parvez, M., 10
Pascal, J.L., 1544
Pedras, M.S.C., 338
Pedrosa, G.C., 1121
Pena, C., 280
Penieres-Carrillo, G., 1299
Penner, G.H., 46
Pennington, L.D., 732
Perczel, A., 395
Peters, E.-M., 1388
Peters, K., 1388
Picard, J.-P., 1363
Pincock, A.L., 1019
Pincock, J.A., 1019
Pinto, B.M., 598
Plehiers, M., 1030
Poirier, R.A., 1067
Pojarlieff, I.G., 84, 520
Pokriefke, J.O., 546, 1325
Polborn, K., 1412
Popelier, P.L.A., 415
Postigo, M.A., 1121
Poupart, M.-A., 739
Qian, Y., 1143
Qiao, Z., 1143
Rajalingam, U., 590
Ratovelomanana-Vidal, V., 846
Rauzy, E., 1587
Reger, T.S., 749
Reinke, H., 1399
Ren, D., 1178
Rettig, S.J., 546, 1003, 1325
Rey, F., 1013
Reyé, C., 1519
Reyes-Chilpa, R., 248
Richter, I., 1380
Rifai, S., 1019
Rigo, B., 1242
Rivkin, A., 791
Roberts, E., 800
Rochon, P., 409
Roelens, S., 723
Roscoe, J.M., 16
Roush, W.R., 757
Roy, R., 838
Rozas, I., 1109
Ruffin, B., 73
Saak, W., 1469
Salpietro, S.J., 362, 626

© 2000 NRC Canada

Samuel, M.S., 1474
Samuelsson, B., 829
Sanchez, C., 1186
Sanchez, V., 383
Sangermano, M., 1030
Sanipelli, G.G., 464
Schmedake, T.A., 1526
Schmid, R., 265
Sham, S., 975
Shanmugham, M.S., 704
Shao, P., 255
Sharma, S., 427
Sharp, T.L., 184
Shaver, M.P., 568
Shawl, C.E., 1441
Shiftan, D., 212
Short, G.F., III, 884
Shvedov, D., 151
Sibi, M.P., 133
Sikorski, M., 963
Simoneau, B., 739
Singh, S.P., 1109
Sinha, H.K., 963
Sklenak, S., 1496
Smadja, J., 986
Smolik, M., 993
Snieckus, V.A., 905
Sondengam, B.L., 487
Sosa, C.P., 395
Soula, B., 280
Spek, A.L., 1620
Spurgin, M.A., 184
St-Denis, Y., 776
Steer, R.P., 963
Stephenson, C.R.J., 800
Stewart, A., 1380
Strunz, G.M., 270
Sumi, K., 697
Sun, B.-W., 322
Sung, K., 562
Surylo, P., 950
Şüzer, S., 516
Tacke, R., 1380
Tae, J., 689
Taillefumier, C., 708
Tajmir-Riahi, H.A., 291
Tam, W., 527
Tanaka, K.S.E., 577
Tanaka, R., 31
Taylor, P.G., 1479
Taylor, S.D., 642
Tee, O.S., 436, 1100
Thavonekham, B., 739
Thompson, K.A., 1019
Thompson, R.C., 383
Tobin, J., 151
Tokuda, H., 31
Tokuhisa, K., 238
Toner, A.J., 1073
Torres-Collín, L., 248
Toscano, R.A., 1299
Toteva, M.M., 84, 520
Tranmer, G.K., 527
Tremaine, P.R., 151
Trimble, L.A., 784
Tripathy, S., 1345
Trotter, J., 546, 1325
Tsou, N.N., 784
Tsuzuki, H., 238, 1089
Tuck, D.G., 536
Turner, I.E., 436
Upadhyaya, M., 1561
Van Calsteren, M.R., 248
van Koten, G., 1620
Van, T., 449, 459
Vank, J.C., 395
Vasisht, S.-K., 1412
Veglia, A.V., 233
Velasco, I., 1587
Venneri, P.C., 1194
Verani, G., 1147
Vila, A., 1535
Vittori, O., 1637
Vogels, C.M., 568
von Schnering, H.G., 1388
Vorontsov, I.I., 1511
Wachner, A.M., 46
Wagner, B., 892
Wagner, S., 1412
Wallbank, A.I., 568
Walsh, R., 1428
Wang, B.-C., 224
Wang, G.-L., 322
Wang, H.-G., 322
Wang, P.-Y., 224
Wang, Q., 1434
Wang, S., 975, 1289
Wang, Y., 1067
Wang, Z.-X., 1081
Warkentin, J., 356, 942, 1194
Wasylishen, R.E., 118, 614
Waterlot, C., 1242
Weakley, T.J.R., 1647
Weerassooriya, N., 935
Weidenbruch, M., 1469
West, R., 1526
Westaway, K.C., 1067
Westcott, S.A., 568
Westh, P., 1553
White, J.D., 704
Wiberg, N., 1412
Wiebe, L.I., 1081
Wienberg, N., 41
Williams, P., 542
Winkler, T., 892
Wolmershäuser, G., 583, 1613
Womiloju, O.O., 383
Wong, A., 975
Wooler, K., 642
Works, A.B., 757
Wozniak, M., 950
Wren, J.C., 464
Wu, G., 118, 614, 975
Xie, Y., 1143
Xu, J., 1143
Xu, Z., 383
Yadav, V.K., 542
Yamashita, Y., 666
Yamato, T., 238, 1089
Yan, S.-P., 322
Yang, H., 800
Yang, J., 1214
Yao, X.-K., 322
Yap, G.P.A., 316
Yazbeck, O.J., 436, 1100
Yip, C., 527
Yu, C.-M., 270
Zaworotko, M.J., 568
Zhang, Y., 1289
Zhao, Q.-H., 322
Zhou, X.-M., 598
Zhu, J., 577
Zhu, Y., 1143
Ziegler, T., 265
Zunic, V., 868

© 2000 NRC Canada

Canadian Journal of Chemistry

Contents
Volume 78, 2000

Revue canadienne de chimie

Sommaire
Volume 78, 2000

January / Janvier

ARTICLES

Colin W. Clarke and David N. Glew Aqueous nonelectrolyte solutions. Part XVI. Formula of deuterium sulfide D-hydrate and its dissociation thermodynamic functions **1**

Pierre Blais, Tristram Chivers, Andrew Downard, and Masood Parvez Synthesis and X-ray structures of amidinate, oxoamidate, and thioamidate complexes of boron **10**

John M. Roscoe, Alain R. Bossard, and Margaret H. Back A kinetic modeling study of ethylene pyrolysis **16**

Arthur Camerman, Donald Mastropaolo, Peter Nickel, Andrew Hempel, and Norman Camerman Structure of 8-[4′-(3″-nitrobenzamido)-benzamido]naphthalene-1,3,6-trisulfonate (NF-033), and molecular basis of its cellular toxicity **26**

Hironori Ohtsu, Reiko Tanaka, Yasuko In, Shunyo Matsunaga, Harukuni Tokuda, and Hoyoku Nishino New abietane diterpenoids from the cones of *Larix kaempferi* **31**

Noham Weinberg and Kurt Mislow On chirality measures and chirality properties **41**

Andrew M. Wachner, Kenneth R. Jeffrey, and Glenn H. Penner A 2D deuterium NMR study of molecular reorientation in $(CH_3)_3E^+X^-$ onium salts **46**

Helen A. Joly, Hongbo Li, and Nelson Belzile Pyrolysis gas chromatography – mass spectrometry of humic substances extracted from Canadian lake sediments **51**

Jean-Joseph Max and Camille Chapados Infrared titration of aqueous NaOH by aqueous HCl **64**

Brigitte Ruffin and Alain Castellan Photoyellowing of peroxide-bleached lignin-rich pulps: a photochemical study on stilbene–hydroquinone chromophores issued from β-5 units of lignin during refining and (or) bleaching **73**

Ergun Atay, Iva B. Blagoeva, Francis L. Chubb, John T. Edward, Ivan G. Pojarlieff, and Maria M. Toteva Assisted hydrolysis of *cis*-2-(3-phenylthioureido)cyclopentane-carbonitrile in alkaline solution. Solvent dependent switch from hydrolysis to rearrangement of the iminothiooxopyrimidine intermediate **84**

Zhong-Ping Lin and Walter A. Aue Gas-phase luminescence of aromatic carbonyl compounds in excited nitrogen at atmospheric pressure **95**

Myrlene Gee, Roderick E. Wasylishen, Klaus Eichele, Gang Wu, T. Stanley Cameron, F. Mathey, and F. Laporte Characterization of phosphorus chemical shielding tensors in a phosphole tetramer: a combined experimental and theoretical study **118**

Laurent Lamarque, Alain Méou, and Pierre Brun $Mn(OAc)_3$-promoted hydroxylation of α-carbomethoxy-γ-lactones by molecular oxygen **128**

Mukund P. Sibi, Pingrong Liu, and Michael D. Johnson A short synthesis of both enantiomers of enterolactone **133**

Avijit K. De and Tapan Ganguly Investigations on nonradiative transitions in different environments using excited (or ground state) 1,2,3,4-tetrahydroquinoline (THQ) as donor and ground state (or excited) 9-fluorenone (9FL) or 2-nitro-9-fluorenone (2N9FL) as acceptors A short synthesis of both enantiomers of enterolactone **139**

Christopher Collins, Joelle Tobin, Dmitri Shvedov, Rom Palepu, and Peter R. Tremaine Thermodynamic properties of aqueous diethanolamine (DEA), *N*,*N*-dimethylethanolamine (DMEA), and their chloride salts: apparent molar heat capacities and volumes at temperatures from 283.15 to 328.15 K **151**

IUPAC Recommendations / IUPAC recommendation **iii**

Instructions to Authors / Recommendations aux auteurs **I-1**

© 2000 NRC Canada

Notes for authors of papers presenting the results of X-ray crystal structure analyses / Recommandations aux auteurs d'articles décrivant a détermination de structures par diffraction des rayons Xcristallines **v**

Author Index / Index des auteurs **AI-1**

February / Février

ARTICLES

Clifford C. Leznoff 1999 Alfred Bader Award Lecture
From early developments in multi-step organic synthesis on solid phases to multi-nuclear phthalocyanines **167**

Karina M. De Fina, Tina L. Sharp, Michael A. Spurgin, Ivette Chuca, William E. Acree, Jr., Caroline E. Green, and Michael H. Abraham Solubility of the pesticide diuron in organic nonelectrolyte solvents. Comparison of observed vs. predicted values based upon Mobile Order theory **184**

Somes K. Das, G. Krishnamoorthy, and Sneh K. Dogra Excited state intramolecular proton transfer in 2-(2′-hydroxyphenyl)-1*H*-naphth-[2,3-*d*]-imidazole: effects of solvents and pH **191**

Gustavo Larsen A performance comparison between the CEP effective core potential/triple-split basis set approach and an all-electron computational method with emphasis on small Ti and V alkoxide complexes **206**

Robert Glaser, Dror Shiftan, and Marc Drouin The solid-state structures of (–)-scopolamine free base, (–)-scopolamine methobromide, (–)-scopolamine hydrobromide trihydrate, and of the pseudopolymorphic forms of (–)-scopolamine hydrochloride anhydrate and 1.66hydrate **212**

Bo-Cheng Wang, Yun-Shan Lin, Jian-Chuang Chang, and Pei-Yu Wang Theoretical studies of azulene and its derivatives **224**

Alicia Viviana Veglia and Rita Hoyos de Rossi Interaction of hydroxyphenyl alkyl ketones with β-cyclodextrin **233**

Takehiko Yamato, Kiwamu Tokuhisa, and Hirohisa Tsuzuki Medium-sized cyclophanes. part 51. Acylation of [2.2]metaparacyclophanes: through-space electronic interactions between two benzene rings **238**

M. Jiménez-Estrada, R. Reyes-Chilpa, S. Hernández-Ortega, E. Cristobal-Telésforo, L. Torres-Colín, C.K. Jankowski, A. Aumelas, and M.R. Van Calsteren Two novel Diels–Alder adducts from *Hippocratea celastroides* roots and their insecticidal activity **248**

Pengcheng Shao, Roland A.L. Gendron, and David J. Berg Synthesis and structural characterization of zirconium complexes containing aminodiolate ligands and their use as Lewis acid catalysts **255**

Rochus Schmid and Tom Ziegler Ethylene-polymerization by surface supported Cr(IV) species: possible reaction mechanisms revisited by theoretical calculations **265**

Sidima Kabanyane, Andreas Decken, Chao-Mei Yu, and George M. Strunz A new short synthetic approach to chlorocyclopentenones related to cryptosporiopsin via a ring expansion strategy: first synthesis of a fungitoxic metabolite from *Sporormia affinis* **270**

Robert Chênevert and Mohammed Dasser Enantioselective synthesis of syringolide 2 from D-arabinose **275**

Paul-Louis Fabre, Christophe Pena, Anne Marie Galibert, Brigitte Soula, Gérald Bernardinelli, Bruno Donnadieu, and Paule Castan Pseudo-oxocarbons complexes — complexation of 2,4-bis(dicyanomethylene)-cyclobutane-1,3-dione dianion with copper. X-ray identification and electrochemical properties of the dianion and copper(I) and (II) complexes **280**

J.F. Neault, A. Novetta-Delen, H. Arakawa, H. Malonga, and H.A. Tajmir-Riahi The effect of aspirin–HSA complexation on the protein secondary structure **291**

E. Lewars Benzooxirene, naphthooxirenes, and anthraceneoxirenes: the stabilization of the oxirene system by bond fixation in acenes. A comparison of ab initio and DFT in the investigation of annelated oxirenes **297**

Author Index / Index des auteurs **AI-1**

March / Mars

ARTICLES

André Cyr, Florence Chiltz, Paul Jeanson, Anna Martel, Louis Brossard, Jean Lessard, and Hugues Ménard Electrocatalytic hydrogenation of lignin models at Raney nickel and palladium-based electrodes **307**

© 2000 NRC Canada

G.W. Buchanan, A.B. Driega, and G.P.A. Yap Solid state stereochemistry of crown ethers: X-ray crystal structure and ^{13}C NMR studies of the LiNCS complex of 1,4,7,11-tetraoxacyclotetradecane **316**

Bai-Wang Sun, Qi-Hua Zhao, Dai-Zheng Liao, Zong-Hui Jiang, Shi-Ping Yan, Geng-Lin Wang, Xin-Kai Yao, and Hong-Gen Wang Crystal structure and ferromagnetic behavior of a *cis*-Co(II) complex with nitronyl nitroxide **322**

Xavier Fradera, Miquel Duran, and Jordi Mestres Comparative electronic analysis between hydrogen transfers in the CH_4/CH_3^+, $CH_4/CH_3^{\bullet}$, and CH_4/CH_3^- systems: on the electronic nature of the hydrogen (H^-, $H^{\bullet}$, H^+) being transferred. II. Analysis of electron-pair interactions from intracule and extracule densities **328**

M. Soledade C. Pedras and Francis I. Okanga Metabolism of analogs of the phytoalexin brassinin by plant pathogenic fungi **338**

Harry W. Gibson and Sang-Hun Lee 42-crown-14-based [2]catenane **347**

Nadine Merkley, Manal El-Saidi, and John Warkentin Radicals from fragmentation of benzyloxymethoxycarbenes in solution **356**

Alvin C. Lin, Salvatore J. Salpietro, Eugen Deretey, and Imre G. Csizmadia Multidimensional conformational analysis of allyl methyl disulfide: a key component of garlic **362**

Frank Bottomley, Victor Sanchez, Robert C. Thompson, Olusola O. Womiloju, and Zhiqiang Xu Organometallic oxides: preparation of the cluster $[(\eta\text{-}C_5Me_5)Mo]_4O_7$ by reduction of $[(\eta\text{-}C_5Me_5)MoCl(O)]_2(\mu\text{-}O)$ or $(\eta\text{-}C_5Me_5)MoCl_2(O)$ **383**

Judith C. Vank, Carlos P. Sosa, Andras Perczel, and Imre G. Csizmadia Peptide models XXVII. An exploratory ab initio study on the 21st amino acid side-chain conformations of *N*-formyl-L-selenocysteinamide (For-L-Sec-NH_2) and *N*-acetyl-L-selenocysteine-*N*-methylamide (Ac-L-Sec-NHMe) in their γ_L backbone conformation **395**

Author Index / Index des auteurs **AI-1**

April / Avril

ARTICLES

Gabriel Iftime, Lana Fisher, Almeria Natansohn, and Paul Rochon Photoinduced birefringence in copolymers containing Disperse Red 1 and styrene **409**

Fiona M. Aicken and Paul L.A. Popelier Atomic properties of selected biomolecules. Part 1. The interpretation of atomic integration errors **415**

Amalendu Pal, Sanjay Sharma, and Harsh Kumar Excess molar volumes and viscosities of binary mixtures of some *n*-alkoxyethanols with propylamine at 298.15 K **427**

Oswald S. Tee, Samer M. I. Hussein, Isabelle E. Turner, and Ogaritte J. Yazbeck Kinetics of acetal and orthobenzoate hydrolysis as probes of cyclodextrin–guest binding **436**

Amalendu Pal and Gurcharan Dass Excess molar volumes and viscosities of binary mixtures of triethylene glycol dimethyl ether (triglyme) with chloroalkanes at 298.15 K **444**

Karina M. De Fina, Tiffany T. Van, Kristin A. Fletcher, and William E. Acree, Jr. Solubility of diphenyl sulfone in organic nonelectrolyte solvents. Comparison of observed vs. predicted values based upon Mobile Order theory **449**

David J. Berg and Roland A.L. Gendron Synthesis, solid state structure, and solution behaviour of the lighter lanthanide bis(trimethylsilyl)amido chlorides, $[Ln\{N(SiMe_3)_2\}_2(THF)(\mu\text{-}Cl)]_2$ (Ln = Ce, Nd) **454**

Karina M. De Fina, Tiffany T. Van, and William E. Acree, Jr. Solubility of hexachlorobenzene in organic nonelectrolyte solvents. Comparison of observed vs. predicted values based upon Mobile Order model **459**

J.C. Wren, D.J. Jobe, G.G. Sanipelli, and J.M. Ball Dissolution of organic solvents from painted surfaces into water **464**

Omoshile Clement, Ikenna Onyido, and Erwin Buncel Metal ion–biomolecule interactions. Part 22. Cr(III)-catalyzed isotopic hydrogen exchange in methylimidazoles **474**

Bernard Blaise Messanga, Beibam Luc Sondengam, and Bernard Bodo Calodendroside A: a taxifolin diglucoside from the stem bark of *Ochna calodendron* **487**

Jocelyn Baril, Jean-Joseph Max et Camille Chapados Titrage infrarouge de l'acide phosphorique **490**

John Andraos and A. Jerry Kresge Correlation of rates of uncatalyzed and hydroxide-ion catalyzed ketene hydration. A mechanistic application and solvent isotope effects on the uncatalyzed reaction **508**

© 2000 NRC Canada

Şefik Süzer and Ömer Dag Reductive deposition of Au^{3+}(aq) on oxidized silicon surfaces **516**

ADDITIONS AND CORRECTIONS / AJOUTS ET CORRECTIONS

Ergun Atay, Iva B. Blagoeva, Francis L. Chubb, John T. Edward, Ivan G. Pojarlieff, and Maria M. Toteva **520**
Erratum: Assisted hydrolysis of *cis*-2-(3-phenylthioureido)cyclopentane-carbonitrile in alkaline solution. Solvent dependent switch from hydrolysis to rearrangement of the iminothiooxopyrimidine intermediate

IUPAC Recommendations / Recommandations de I'UICPA **iii**

Author Index / Index des auteurs **AI-1**

May / Mai

ARTICLES

M.S. Crespo-Pinilla, A.B. Infante, and F. Mata-Pérez Analysis of the electrode kinetics of Ni(II) reduction at the DME in the presence of nicotine **521**

Geoffrey K. Tranmer, Carol Yip, Sean Handerson, Robert W. Jordan, and William Tam Synthesis of 2,3-disubstituted norbornadienes **527**

M.A. Brown and D.G. Tuck Crystallographic and spectroscopic studies of adducts of indium (III) iodide with two cyclic ketones **536**

Veejendra K. Yadav, Philip Williams, and Michael Benn The synthesis of hydroxysmirnovine **542**

Wolfgang Kliegel, Jens O. Pokriefke, Steven J. Rettig, and James Trotter Diphenylboron complexes of the enol tautomers of arylpyruvic acids. Crystal and molecular structure of triethylammonium (2-nitrophenyl)pyruvato-diphenylboron(1-) **546**

Christopher Cow, Carmen Leung, and James L. Charlton Antiviral activity of arylnaphthalene and aryldihydronaphthalene lignans **553**

Kuangsen Sung Substituent effects on stability of oxiranes, oxirenes, and dioxiranes **562**

Michael P. Shaver, Christopher M. Vogels, Andrew I. Wallbank, Tracy L. Hennigar, Kumar Biradha, Michael J. Zaworotko, and Stephen A. Westcott Trans alkenylpyridine and alkenylamine complexes of platinum **568**

Kelly S. E. Tanaka, Jiang Zhu, Xicai Huang, Francesco Lipari, and Andrew J. Bennet Glycosidase-catalyzed hydrolysis of 2-deoxyglucopyranosyl pyridinium salts: effect of the 2-OH group on binding and catalysis **577**

René T. Boeré, Vicki Klassen, and Gotthelf Wolmershäuser Superamidines 2. Synthesis of the bulky ligand *N*,*N*′-bis-(2,6-diisopropylphenyl)-trifluoroacetamidine and its molybdenum carbonyl complex **583**

Umarani Rajalingam, Philip A.W. Dean, and Hilary A. Jenkins Solution multinuclear (^{31}P,^{111}Cd,^{77}Se) magnetic resonance studies of cadmium complexes of heterocyclic aromatic thiones and the structure of [tetrakis(2(1*H*)-pyridinethione)cadmium] nitrate, $[Cd(C_5H_5NS)_4](NO_3)_2$ **590**

Raymond J. Batchelor, Frederick W.B. Einstein, Ian D. Gay, Jian-Hua Gu, B. Mario Pinto, and Xue-Min Zhou Redox chemistry of the selenium coronand, 1,5,9,13-tetraselenacyclohexadecane, and a mechanistic study of the electron transfer reaction of its Cu(II) complex **598**

Guy M. Bernard, Klaus Eichele, Gang Wu, Christopher W. Kirby, and Roderick E. Wasylishen Nuclear magnetic shielding tensors for the carbon, nitrogen, and selenium nuclei of selenocyanates — a combined experimental and theoretical approach **614**

Melody L. Mak, Salvatore J. Salpietro, R. Daniel Enriz, and Imre G. Csizmadia An exploratory ab initio study on the conformations of ethylguanidine in its neutral [CH_3-CH_2-NH-C(=NH)NH_2] and protonated [CH_3-CH_2-NH-C$(NH_2)_2$] forms **626**

Gabriel Hum, Krista Wooler, Jeremy Lee, and Scott D. Taylor Cyclic five-membered phosphinate esters as transition state analogues for obtaining phosphohydrolase antibodies **642**

Author Index / Index des auteurs **AI-1**

© 2000 NRC Canada

June / Juin

This issue is dedicated to Professor S. Hanessian
Ce tirage est dédié au Professeur S. Hanessian

ARTICLES

Akifumi Kagayama, Koji Igarashi, and Teruaki Mukaiyama Efficient method for the preparation of pinacols derived from aromatic and aliphatic ketones by using low-valent titanium reagents in dichloromethane–pivalonitrile **657**

Yasuhiro Yamashita, Haruro Ishitani, and Shū Kobayashi Silver-catalyzed asymmetric amination of silyl enol ethers **666**

Scott E. Denmark and Jung-Ho Kim Diastereoselective alkylations of chiral, phosphorus-stabilized carbanions: *N*-alkyl substituent effects in *P*-alkyl-1,3,2-diazaphosphorinane 2-oxides **673**

Jinsung Tae and Leo A. Paquette Delineating the possibilities for intramolecular interception of the squarate ester cascade through the use of metalated enecarbamates **689**

Kenzo Sumi, Takao Ikariya, and Ryoji Noyori Efficient synthesis of optically active 2-amino-2′-diphenylphosphino-1,1′-binaphthyl and its derivatives **697**

Kevin P. Gable, M. Sundaram Shanmugham, and James D. White Preparation of homoallylic alcohols by reaction of aldehydes with η^3-allyl- and η^3-crotylmolybdenum complexes **704**

Claude Taillefumier and Yves Chapleur Enantiomerically pure decalinic structures from carbohydrates using intramolecular Diels–Alder and Ferrier carbocyclization **708**

Stefano Roelens, Paolo Dapporto, and Paola Paoli Hydrogen bonded supramolecular structures: a further insight into the diamine–diol recognition and self-assembly **723**

Larry E. Overman and Lewis D. Pennington A new strategy for synthesis of attached rings **732**

Bruno Simoneau, Pierre Lavallée, Murray Bailey, Jean-Simon Duceppe, Chantal Grand-Maître, Louis Grenier, William W. Ogilvie, Marc-André Poupart, and Bounkham Thavonekham Stereoselective synthesis of renin inhibitor BILA 2157 BS **739**

Albert Padwa and Thomas S. Reger Construction of bicyclic tetrahydroisoquinolinones by combination of an IMDAF-ring cleavage reaction of *N*-allyl-2-furan-2-yl-acetamides **749**

Scott A. Frank, Andrea B. Works, and William R. Roush Studies on the synthesis of the decahydro-*as*-indacene ring system of (–)-spinosyn A via transannular Diels–Alder reactions of substituted (*E,E,E*)-cyclododeca-1,6,8-trienes **757**

Daniele Andreotti, Stefano Biondi, Daniele Donati, Sergio Lociuro, and Gilles Pain Synthesis of novel pentacyclic β-lactam antibacterial agents **772**

Yves St-Denis and Tak Hang Chan Synthesis of 8-*epi*-castanospermine and 6,7,8-tri-*epi*-castanospermine **776**

Yves Leblanc, Claude Dufresne, Rajiv Dhawan, Jason Ollerenshaw, Adam Littke, Laird A. Trimble, and Nancy N. Tsou Dimerization of conjugated 1-indanones **784**

Tadamichi Nagashima, Alexey Rivkin, and Dennis P. Curran On the reduction of tertiary radicals by samarium diiodide (SmI_2) **791**

Hua Yang, Valdas Jurkauskas, Nicole Mackintosh, Tobias Mogren, Corey R. J. Stephenson, Katherine Foster, William Brown, and Edward Roberts Trifluoroacetic acid-mediated intramolecular formal N-H insertion reactions with amino-α-diazoketones: a facile and efficient synthesis of optically pure pyrrolidinones and piperidinones **806**

Romano Di Fabio, Giuseppe Alvaro, Barbara Bertani, and Simone Giacobbe Straightforward synthesis of new tetrahydroquinoline derivatives **809**

Christian Girard and Henri B. Kagan On diastereomeric perturbations **816**

Karin Oscarsson, Björn Classon, Ingemar Kvarnström, Anders Hallberg, and Bertil Samuelsson Solid phase assisted synthesis of HIV-1 protease inhibitors. Expedient entry to unsymmetrical substitution of a C_2 symmetric template **829**

Yun-Jin Hu, Romyr Dominique, Sanjoy Kumar Das, and René Roy A facile new procedure for the deprotection of allyl ethers under mild conditions **838**

© 2000 NRC Canada

Virginie Ratovelomanana-Vidal and Jean-Pierre Genêt Synthetic applications of the ruthenium-catalyzed hydrogenation via dynamic kinetic resolution **846**

B. Guérin, C. Chabot, N. Mackintosh, W.W. Ogilvie, and Y. Guindon Free radicals and Lewis acid. Chelation-controlled radical allylations of substituted α-halo- or α-phenylseleno-β-alkoxy esters. The endocyclic effect. **852**

Mark Lautens, Gregory Hughes, and Valentin Zunic Diastereoselective double ring closing metathesis reactions as an approach to symmetrical bicyclodienes **868**

Michiel Lodder, Curtis F. Crasto, Andrei L. Laikhter, Haoyun An, Tuncer Arslan, Vladimir A. Karginov, Glenn F. Short, III, and Sidney M. Hecht Synthesis of aspartic acid derivatives useful for the preparation of misacylated transfer RNAs **884**

Beat Ernst, Bea Wagner, Gabi Baisch, Andreas Katopodis, Tammo Winkler, and Reinhold Öhrlein Substrate specificity of fucosyl transferase III: An efficient synthesis of sialyl Lewis^x-, sialyl Lewis^a-derivatives and mimetics thereof **892**

Jian-min Fu and Victor Snieckus The directed *ortho* metalation – palladium catalyzed cross coupling connection. A general regiospecific route to 9-phenanthrols and phenanthrenes. Exploratory further metalation **905**

Howard Alper, Prabhat Arya, S. Christine Bourque, Gary. R. Jefferson, and Leo E. Manzer Heck reaction using palladium complexed to dendrimers on silica **920**

Gabriella Gentile, Daniela Fattori, Maurizio Botta, Federico Corelli, Domenico Fusar-Bassini, and Doriano Lamba Synthesis of dimeric and tetrameric macrolactams with cytotoxic activity **925**

Dedication / Dédicace **iii**

Author Index / Index des auteurs **AI-1**

July / Juillet

ARTICLES

Gregory S. Coumbarides, Jason Eames, and Neluka Weerasooriya Conformational effects in the diastereoselective protonation of chiral enolates derived from 2,4-dimethyl-1-tetralone using carbonyl chelating proton donors **935**

Nadine Merkley and John Warkentin Benzyloxy(4-substituted benzyloxy)carbenes. Generation from oxadiazolines and fragmentation to radical pairs in solution **942**

Marian Woźniak, Maria Grzegożek, and Piotr Suryło Methylamination of some 3,6-dinitro-1,8-naphthyridines with liquid methylamine – potassium permanganate **950**

Robert Franzén The Suzuki, the Heck, and the Stille reaction — three versatile methods for the introduction of new C—C bonds on solid support **957**

X. Hou, S.R. Abrams, J.J. Balsevich, N. Irvine, T. Norstrom, M. Sikorski, H.K. Sinha, and R.P. Steer Synthesis and photophysical properties of fluorophore-labeled abscisic acid **963**

Alan Wong, Simon Sham, Suning Wang, and Gang Wu A solid-state ^{133}Cs nuclear magnetic resonance and X-ray crystallographic study of cesium complexes with macrocyclic ligands **975**

Anne Gauvin, Jacqueline Smadja, Maurice Aknin, Robert Faure, and Emile-Marcel Gaydou Isolation of bioactive 5α,8α-epidioxy sterols from the marine sponge *Luffariella cf. variabilis* **986**

Marek Smolik Distribution of microamounts of some M^{2+} ions during $ZnSO_4 \cdot 7H_2O$ crystallization **993**

Michael D. Fryzuk, Garth R. Giesbrecht, and Steven J. Rettig Synthesis, characterization, and reactivity of scandium chloro, alkyl, aryl, and borohydride complexes, $Sc(\eta^5\text{-}C_5H_5)R[N(SiMe_2CH_2P^iPr_2)_2]$ (R = Cl, Me, Ph, and BH_4) **1003**

Francisco Rey and Adelio A.S.C. Machado Influence of the temperature on the viscosity measurements of solutions of a soil fulvic acid **1013**

J. Foster, A.L. Pincock, J.A. Pincock, S. Rifai, and K.A. Thompson The photoequilibration of the *ortho*-, *meta*-, and *para*-isomers of substituted benzenes in acetonitrile and the photoaddition of 2,2,2-trifluoroethanol (TFE) to the same isomers: a survey **1019**

© 2000 NRC Canada

M. Plehiers, S. Heilporn, D. Ekelmans, S. Leclercq, M. Sangermano, J.C. Braekman, and D. Daloze An expeditious synthesis of (±)-decahydro-5*H*-dipyrrolo [1,2-*a*:1′,2′-*c*]pyrimidine-5-carbonitrile: a formal synthesis of (±)-tetraponerines-1, -2, -5, and -6 **1030**

Kathleen M. Gough, Jason R. Dwyer, and Richard Dawes Ab initio analysis of C—H and C—C stretching intensities in Raman spectra of hydrocarbons **1035**

Author Index / Index des auteurs **AI-1**

August / Août

ARTICLES

Arthur Camerman, Donald Mastropaolo, Andrew Hempel, and Norman Camerman Hydrogen bonding interaction of diphenylbarbituric acid and 9-ethyladenine. Crystal structure of a 1:1 complex **1045**

C. Aliaga and E.A. Lissi Reactions of the radical cation derived from 2,2′-azinobis(3-ethylbenzothiazoline-6-sulfonic acid) ($ABTS^{\cdot+}$) with amino acids. Kinetics and mechanism **1052**

David I. MaGee and Ellen J. Beck The use of the Ramberg–Bäcklund rearrangement for the formation of aza-macrocycles: a total synthesis of manzamine C **1060**

Terry Koerner, Kenneth Charles Westaway, Raymond A. Poirier, and Y. Wang An unusually large secondary α-deuterium kinetic isotope effect in hydride ion S_N2 reactions **1067**

Michael B. Hursthouse, David G. Kelly, Mark E. Light, and Andrew J. Toner CP/MAS NMR and X-ray crystallographic characterization of *trans*-$PdX_2(PPh_2vinyl)_2$ (X = Cl, I); UV and $Et_2O{\cdot}BF_3$ reaction studies, including the formation of $[Pd(\mu\text{-}Cl)(PPh_2vinyl)_2]_2[BF_4]_2$ **1073**

Zhi-Xian Wang, Leonard I. Wiebe, Erik De Clercq, Jan Balzarini, and Edward E. Knaus Syntheses of 4-[1-(2-deoxy-β-D-ribofuranosyl)]-derivatives of 2-substituted-5-fluoroaniline: "cytosine replacement" analogs of deoxycytidine for evaluation as anticancer and antihuman immunodeficiency virus (anti-HIV) agents **1081**

Takehiko Yamato, Koji Fujita, Keigo Futatsuki, and Hirohisa Tsuzuki Medium-sized cyclophanes. Part 53. Synthesis and conformational studies, and photoinduced cyclization of *syn*-[n.2]metacyclophanenes **1089**

Oswald S. Tee and Ogaritte J. Yazbeck Transition state stabilization by micelles: thiolysis of *p*-nitrophenyl alkanoates in cetyltrimethylammonium bromide micelles **1100**

Shiv P. Singh, Dalip Kumar, Hitesh Batra, Rajesh Naithani, Isabel Rozas, and José Elguero The reaction between hydrazines and β-dicarbonyl compounds: proposal for a mechanism **1109**

Alberto G. Camacho, Miguel A. Postigo, Graciela C. Pedrosa, Inés L. Acevedo, and Miguel Katz Densities, refractive indices and excess properties of mixing of the *n*-octanol + 1,4-dioxane + 2-butanol ternary system at 298.15 K **1121**

Christophe Ménichelli, Jean-Joseph Max et Camille Chapados Coefficient d'activité de l'acide sulfurique déterminé par titrage infrarouge **1128**

IUPAC Recommendations / Recommandations de I'UICPA **iii**

Author Index / Index des auteurs **AI-1**

September / Septembre

ARTICLES

Zhengping Qiao, Yi Xie, Jianguang Xu, Xianming Liu, Yingjie Zhu, and Yitai Qian Synthesis of nanocrystalline $Cu_{2-x}Se$ at room temperature by γ-irradiation **1143**

Massimiliano Arca, Francesco Demartin, Francesco A. Devillanova, Francesco Isaia, Francesco Lelj, Vito Lippolis, and Gaetano Verani An experimental and theoretical approach to the study of the properties of parabanic acid and related compounds: synthesis and crystal structure of diethylimidazolidine-2-selone-4,5-dione **1147**

Turan Ozturk and Alexander McKillop The synthesis of pyrido(2,3,4-*kl*)acridine unit of some marine alkaloids **1158**

Darío A. Bianchi and Teodoro S. Kaufman A tosyliminium ion-based total synthesis of (±)-schefferine **1165**

© 2000 NRC Canada

Ibrahim S. El-Hallag, Gad B. El-Hefnawy, Youssef. I. Moharram, and Enass. M. Ghoneim Electrochemical studies of Schiff base compounds derived from antipyrine nucleus in ethanolic buffer solutions **1170**

Robert A. McClelland, Daniel Ren, Raechelle D'Sa, and Abid R. Ahmed Acidity constants and reactivities of the benzidine and *N*,*N*-dimethylbenzidine dications, the two electron oxidation intermediates of benzidine carcinogens **1178**

Cristina Sanchez and Robert A. McClelland The tamoxifen cation reacts to give indene products **1186**

Paul C. Venneri and John Warkentin Reaction of dimethoxycarbene with strained cyclic carbonyl compounds **1194**

David N. Glew **A**queous nonelectrolyte solutions. Part XVII. Formula of hydrogen sulfide hydrate and its dissociation thermodynamic functions **1204**

John E. Drake and Jincai Yang Synthesis, spectroscopic characterization and structural studies of organotin monothiocarbonates. Crystal structures of $Ph_3Sn[SCO_2Me]$ and $Ph_3Sn[SCO_2(i\text{-}Pr)]$ **1214**

Judith A. MacInnis, D. Gerrard Marangoni, and R. Palepu A study of micellization and the thermodynamic properties of a series of aqueous sodium cyclohexyl alkanoate surfactants **1222**

Giuseppe Graziano Solvation thermodynamics of cyclohexane **1233**

Christophe Waterlot, Daniel Couturier, Marc De Backer, and Benoît Rigo A study of hydrogenation of benzhydrols in the presence of catalytic amount of triflic acid **1242**

Communication

Alexei A. Neverov and R.S. Brown Catalysis of the methanolysis of acetylimidazole by lanthanum triflate **1247**

Author Index / Index des auteurs **AI-1**

October / Octobre

ARTICLES

Erwin Buncel 1999 R.U. Lemieux Award Lecture
Adventures with azo-, azoxy-, and hydrazoarenes: from the Wallach to the benzidine rearrangement. Molecular electronics **1251**

Juan Antonio González, Isaias Garcia de la Fuente, Jose Carlos Cobos Thermodynamics of mixtures with strongly negative deviations from Raoult's law. Part 3. Application of the DISQUAC model to mixtures of triethylamine with alkanols. Comparison with Dortmund UNIFAC and ERAS results **1272**

Kirill V. Nikitin and Nonna P. Andryukhova Synthesis of 5-alkyl- and 5-aryl-1,5-dihydro-2*H*-pyrrol-2-ones via coupling of *5*-chloro-1,5-dihydro-2*H*-pyrrol-2-ones with organometallic compounds **1285**

Yousheng Zhang, Suning Wang, Craig Bridges, and John E. Greedan Co(II) and Mn(II) complexes of 2,2′-thiodiethanol: $[Co^{II}(2,2'\text{-thiodiethanol})_2Cl_2]$ and $[Mn(2,2'\text{-thiodiethanol})Cl_2]_n$ **1289**

J. Peter Guthrie and Roger T. Gallant Thermodynamics of methanesulfonic acid revisited **1295**

J.G. López-Cortés, G. Penieres-Carrillo, M.C. Ortega-Alfaro, R. Gutiérrez-Pérez, R.A. Toscano, and C. Alvarez-Toledano Oxidative coupling-type mechanism of *N*,*N*-dialkylanilines in solvent-free conditions forming crystal violet derivatives. A clay-mediated and microwave-promoted approach **1299**

Isabelle Bonhoure, Christophe Den Auwer, Christophe Cartier dit Moulin, Philippe Moisy, Jean-Claude Berthet, and Charles Madic Molecular and electronic structure of $An^{IV}Fe^{II}(CN)_6{\cdot}xH_2O$ (An = Th, U, Np) compounds: an X-ray absorption spectroscopy investigation **1305**

David H. Jones and A. Scott Hinman The one-electron oxidation of hydroxy(tetramesitylporphyrinato)iron(III) **1318**

Wolfgang Kliegel, Gottfried Lubkowitz, Jens O. Pokriefke, Steven J. Rettig, and James Trotter Nitrones and oximes of bifunctional carbonyl compounds and their reaction products with diarylborinic acids. Crystal and molecular structure of examples of five-, six-, and seven-membered boron chelates **1325**

Sherry L. Majerus, Najma Alibhai, Sasmita Tripathy, and Tony Durst New syntheses of dillapiol [4,5-dimethoxy-6-(2-propenyl)-1,3-benzodioxole], its 4-methylthio and other analogs **1345**

IUPAC Recommendations / Recommandations de I'UICPA **iii**

Author Index / Index des auteurs **AI-1**

© 2000 NRC Canada

November / Novembre

This issue is dedicated to Professor Adrian G. Brook
Ce tirage est dédié au Professeur Adrian G. Brook

Mustafa Mohamed and Michael A. Brook Photolysis of tris(trimethylsilyl)silane: trapping of sisyl radicals **1357**

Jean-Paul Picard Bis(trimethylsilyl)methylamine (BSMA): tool or toy? **1363**

Reinhold Tacke, Alistair Stewart, Joachim Becht, Christian Burschka, and Ingo Richter Di[(hydroxyalkyl)dimethylammonium] tris[benzene-1,2-diolato(2–)]silicates and their germanium analogs: syntheses, crystal structure analyses, and NMR studies **1380**

G. Fritz, M. Keuthen, F. Kirschner, E. Matern, H. Goesmann, K. Peters, E.-M. Peters, and H.G. von Schnering Formation of organosilicon compounds 117: C-brominated 1,3,5-trisilacyclohexanes and their reactions with BuLi **1388**

Moni Chauhan and Philip Boudjouk Reduction of conjugate double bonds with trichlorosilane **1396**

Thoralf Gross, Helmut Reinke, and Hartmut Oehme Geminal bis(hypersilyl) compounds — the synthesis and structure of bis[tris(trimethylsilyl)silyl]silanes **1399**

Jerzy J. Chruściel A novel route to chlorodimethylsilane **1405**

Nils Wiberg, Susanne Wagner, Sham-Kumar Vasisht, and Kurt Polborn Adducts of sila-, germa-, and stannaethenes $Me_2E{=}C(SiMe_3)_2$ (E = Si, Ge, Sn) with anthracene: syntheses, structures, thermolyses **1412**

Paul F. Hudrlik, Jose O. Arango, Yousef M. Hijji, Cosmas O. Okoro, and Anne M. Hudrlik Alkoxides of *o*-silyl benzyl alcohols in cleavage reactions: approaches to benzyl and silyl anion equivalents **1421**

Rosa Becerra, Sergey E. Boganov, Mikhail P. Egorov, Valery I. Faustov, Oleg M. Nefedov, and Robin Walsh The insertion of germylene into the H—H bond; rate constant limits and thermochemistry. Ab initio and DFT calculations on the reactions of GeH_2 and SiH_2 with H_2 **1428**

Qingzheng Wang and Joyce Y. Corey Dehydrocoupling reactions of hydrosilanes with group 4 metallocenes Cp_2MY_2 (M = Ti, Zr, Hf; Y = F, OPh, NMe_2) **1434**

Joseph B. Lambert, Catherine E. Shawl, and Ernani Basso Neutral hyperconjugation and one-bond couplings between heavy atoms **1441**

N. Auner, M. Grasmann, B. Herrschaft, and M. Hummer Silaheterocycles 36 (1). Trichlorovinylsilane, lithium-*tert*-butyl, and 1,3-enynes: A versatile combination for the competitive formation of silacyclobutanes and silacyclobutenes **1445**

William J. Leigh and Thomas R. Owens The one- and two-photon photochemistry of benzylsilacyclobutanes, acyclic benzylsilanes, and 1,1,2-triphenylsilacyclobutane **1459**

Manfred Weidenbruch, Frank Meiners, and Wolfgang Saak Addition reactions of a dialkyl- and a diarylsilylene to cyanides RCN: Different pathways? (1) **1469**

Mini S. Samuel, Kim M. Baines, and Donald W. Hughes The photolysis of Si,Si-di-*tert*-butyltetramesitylsiladigermirane in the presence of methylmagnesium iodide **1474**

Alan R. Bassindale, Ibrahim Katampe, and Peter G. Taylor Improved simple synthesis of cyclic sulfates from trimethylsilyl chlorosulfonate **1479**

Xiaoping Cai, Barbara Gehrhus, Peter B. Hitchcock, and Michael F. Lappert Reactions of the stable bis(amino)silylene $Si[\{N(CH_2tBu)\}_2C_6H_4\text{-}1,2]$ with group 3 or lanthanide metal organic compounds. Crystal structures of $[Ln(\eta^5\text{-}C_5H_5)_3Si\{[N(CH_2tBu)]_2C_6H_4\text{-}1,2\}]\cdot C_7H_8$ (Ln = Y or Yb) **1484**

Rafael Jiménez, Juan Manuel López, and Jorge Cervantes Metal supported catalysts obtained by sol-gel in the hydrosilylation of phenylacetylene with R_3SiH organosilanes (R_3 = Ph_3, Ph_2Me, and $PhMe_2$) **1491**

Yitzhak Apeloig and Stepan Sklenak On the possible formation of Si=O, Si=S, and Si=Se double bonds via the reaction of silylenes with oxirane, thiirane, and selenirane, respectively. An ab initio theoretical study **1496**

Mikhail Yu Antipin, Ivan I. Vorontsov, Irene I. Dubovik, Vladimir Papkov, Francisco Cervantes-Lee, and Keith H. Pannell A low temperature reversible phase transition for 1,1′-bis(ferrocenyldimethylsilyl)ferrocenylene, $(\eta^5\text{-}FcSiMe_2C_5H_4)_2Fe$, an oligomeric model for silyleneferrocenylene polymers **1511**

Jean-Philippe Bezombes, Claude Chuit, Robert J.P. Corriu, and Catherine Reyé Preparation and characterization of organic-inorganic hybrid materials incorporating diphosphino moieties. Study of the accessibility of the phosphorus atoms included into the material **1519**

© 2000 NRC Canada

Michael Haaf, Thomas A. Schmedake, Bryan J. Paradise, and Robert West Synthesis and reactivity of the stable silylene *N*,*N*′-di-*tert*-butyl-1,3-diaza-2-sila-2-ylidene **1526**

Dedication / Dédicace **iii**

Author Index / Index des auteurs **AI-1**

December / Décembre

ARTICLES

Antonio Vila, Enrique Carballo, and Ricardo A. Mosquera AIM study on the transferability of the oxygen atom in linear ethers **1535**

Frédérique Cunin, Frédéric Favier, and Jean Louis Pascal Anhydrous perchlorato complexes of palladium(II): $Pd(ClO_4)_2$, $(ClO_2)_2Pd(ClO_4)_4$, and $(NO_2)_2Pd(ClO_4)_4$. Syntheses and structural analyses **1544**

Penka V. Nikolova, Sheldon J. B. Duff, Peter Westh, Charles A. Haynes, Yasutoshi Kasahara, Keiko Nishikawa, and Yoshikata Koga A thermodynamic study of aqueous acetonitrile: excess chemical potentials, partial molar enthalpies, entropies and volumes, and fluctuations **1553**

J.D. Pandey, S. Haroon, Krishna K. Dubey, Madhulika Upadhyaya, Ranjan Dey, and K. Misra Interactions of 6-aminopurine (adenine) in water and aqueous urea solutions **1561**

I.V. Jourdain and F. Guyon Syntheses and electrochemical characterization of heteroleptic cyclopentadienyl–bis(dithiolene) complexes of niobium and tantalum **1570**

John M. Cullen An approximate ab initio method based on the DIM model **1575**

Sofía T. Blanco, Inmaculada Velasco, Evelyne Rauzy, and Santos Otín Dew points of ternary methane + water + methanol. Measurement and correlation **1587**

R.A. More O'Ferrall, D.M. O'Brien, and D.G. Murphy Rate and equilibrium constants for formation and hydrolysis of 9-formylfluorene oxime: diffusion-controlled trapping of a protonated aldehyde by hydroxylamine **1594**

Robyn E. Boeré, René T. Boeré, Jason Masuda, and Gotthelf Wolmershäuser Preparation, X-ray structure, and dynamic solution behaviour of *N*,*N*′,*N*″-tris(2,6-diisopropylphenyl)- guanidine, and its reaction with molybdenum carbonyl **1613**

Ignacio del Río, Robert A. Gossage, Milja S. Hannu, Martin Lutz, Anthony L. Spek, and Gerard van Koten Synthesis and characterization of two new "pincer" complexes of zinc(II). The X-ray crystal structures of the five coordinate complexes $[ZnCl_2\{\eta^3\text{-}NN'N\text{-}2,6\text{-}(R_2NCH_2)_2C_5H_3N\}]$ (R = *n*-Bu or Me) **1620**

Y. Chiang and A.J. Kresge Determination of the acidity constant of isothiocyanic acid in aqueous solution **1627**

M. Kevin McKay and James R. Green Asymmetric synthesis based on chiral (arene)tricarbonylchromium acetal complexes. Addition reactions to the *ortho*-formyl complex **1629**

Catherine Morlay, Yolande Mouginot, Monique Cromer, Michelle Chatelut, and Olivier Vittori Potentiometric study of cadmium(II) and lead(II) complexation by a cross-linked poly(acrylic acid). Comparison with the linear analogue **1637**

James F. King, Kim M. Baines, Matthew R. Netherton, and Vinod Dave Bis(trimethylsilyl)methanesulfonyl and tris(trimethylsilyl)methanesulfonyl chlorides and their reactions by way of sulfenes **1642**

LeRoy H. Klemm and Timothy J. R. Weakley Synthesis and X-ray structure of 1,2,2,2-tetrakis(3-methoxyphenyl)ethanone **1647**

Note of appreciation **iii**

Author Index / Index des auteurs **AI-1**

Contents for volume 78 / Sommaire pour volume 78 **C-1**

© 2000 NRC Canada

Note of appreciation

The quality of the papers in this journal depends a great deal on the efforts of those who agree to act as critical readers of manuscripts. The editors gratefully acknowledge the following, who helped us between November 1, 1999 and October 31, 2000:

Abd-El-Aziz, A.S.
Abu Irhayem, E.
Acree, W.E.
Adam, W.
Adams, R.D.
Agosta B.
Agosta, W.C.
Albright, J.
Allara, D.L.
Allen, P.
Alper, H.
Alvarez-Cisneros, C.
Amyes, T.L.
Andersen, R.A.
Anderson, H.
Angelici, R.J.
Apeloig, Y.
ApSimon, J.W.
Armstrong, D.A.
Arndtsen, A.
Arnold. J.
Aroca, R.
Atherton, M.J.
Aube, J.
Bach, R.D.
Back, T.G.
Bader, R.F.W.
Bain, A.D.
Baird, M.C.
Baker, T.R.
Balch, A.L.
Bancroft, G.M.
Banoub. J.H.
Baranski, A.S.
Barrett, A.G.M.
Barriault, L.
Batey, R.A.
Beauchamp, A.
Belanger, D.
Beller, M.
Berg, D.J.
Bergens, S.H.
Bergman, R.G.
Berkowitz, D.B.
Bernasconi, C.F.
Bertrand, M.
Bin, S.
Bizzotto, D.
Blaser, H.U.
Blechert, S.
Block, E.
Bocarsly, A.B.
Bock, K.
Bodwell, G.J.
Boeré, R.T.
Bolton, J.R.
Boncella, J.M.
Bonneviot, L.
Boorman, P.M.
Börner, A.
Bosnich, B.
Botrel, A.
Boukouvalas, J.
Boulton, J.
Boyd, R.J.
Bradley, S.
Braunstein, P.
Breneman, C.M.
Breslow, R.C.D.
Brinker, B.
Brisard, G.M.
Brisse, F.
Brooker, M.H.
Brown, K.L.
Brown, R.S.
Buchanan, G.W.
Buchwald, S.
Buhro, W.E.
Bunce, N.J.
Buncel, E.
Burford, N.
Burger, K.
Buriak, J.
Bursten, B.
Butler, I.S.
Calhoun, L.A.
Cammi, R.
Campero, A.
Cantwell, F.
Caradonna, J.
Caravan, P.
Casey, C.P.
Caulton, K.G.
Cavell, R.
Chan, J.C.C.
Chan, T.H.
Chang, C.K.
Charette, A.B.
Che, C.M.
Chênevert, R.
Chin, J.
Chong, D.P.
Chong, J.M.
Choppin, G.R.
Chow, A.
Cioslowski, J.
Clark, P.
Clark, R.
Clark, W.C.
Collins, S.
Collman, J.P.
Comisarow, M.
Conte, V.
Cook. M.
Cooper, N.J.
Copp, B.R.
Cordell, G.A.
Corey, E.J.
Corey, J.Y.
Corma, A.
Corrigan, J.
Costes, J.P.
Cotton, F.A.
Cowie, M.
Cox, B.
Cox, R.A.
Crabtree, R.
Creager, S.E.
Crudden, C.
Crutchley, R.J.
Csizmadia, I.G.
Cullen, W.R.
da Silva, M.R.
Dakternieks, D.
Dannenberg, J.J.
Darensbourg, D.
de Dios, A.C.
Dean, P.A.W.
Decken, A.
Demerseman, B.
Detellier, C.
Deubel, D.
DeVries, R.A.
Dieter, K.
Dinnocenzo, J.P.
Dixneuf, P.H.
Dixon, K.R.
Dolphin, D.
Dory, Y.
Doucet, J.
Doyle, M.P.
Drago, R.S.
Drake, J.E.
Drent, E.
Dugas, H.
du Mont, W.W.
Dunbar, K.
Dunlap, R.A.
Durocher, G.

Note de reconnaissance

La qualité des articles publié dans notre revue dépend beaucoup de ceux qui acceptent de faire une lecture critique des manuscripts. Les directeurs scientifique expriment leur reconnaissance aux personne suivantes qui nous ont aidé, du 1er novembre 1999 au 31 octobre 2000 :

© 2000 NRC Canada

Durst, T.
Dyadin, Y.A.
Eaton, P.E.
Edwards, P.G.
Eguchi, S.Y.
Eisenstein, O.
Elzanowska, H.
Ercolani, C.
Estrin, D.A.
Fahidy, T.Z.
Fallis, A.G.
Falvey, D.E.
Farrar, D.
Figuears, F.
Finke, R.
Fish, R.H.
Fishbein, J.C.
Ford, P.C.
Fraenkel, G.
Francesconi, L.
Francisco, J.S.
Fraser-Reid, B.
Friesen, R.
Fryzuk, M.D.
Fu, G.
Fu, J.M.
Fyfe, C.A.
Fyles, T.M.
Gadosy, T.A.
Gajewski, J.J.
Gallop, M.A.
Gambarotta, S.
Gates, D.
Gatti, C.
Gawley, R.
Georghiou, P.E.
Gerwick, W.H.
Ghali E.
Giasson, R.
Gilchrist, T.
Giner, J.L.
Girolami, G.S.
Gladfelter, W.L.
Glass, R.S.
Goldman, A.
Goodgame, D.
Goodman, M.
Gough, K.M.
Grabner, G.
Gribble, G.W.
Griffith, W.P.
Grindley, T.B.
Grolier, J.P.
Guthrie, J.P.
Hadad, C.M.
Hahn, F.E.
Hakin, A.W.
Halterman, R.L.
Hanack, M.
Hanson, B.E.
Hanson, G.
Harman, W.D.
Harmata, M.
Harrington, D.
Harrod, J.F.
Hartman, S.J.
Hayward, G.
Heathcock, C.
Heinekey, M.
Herring, F.G.
Hidai, M.
Hill, C.L.
Hill, R.
Hindsgaul, O.
Hinman, A.S.
Hinz, H.J.
Hitchcock, A.P.
Hladyszowski, J.
Hoffman, R.V.
Holdcroft, S.
Holland, H.L.
Homborg. H.
Honig, B.
Hopf, H.
Horváth, I.
Houde, D.
Hoz, S.
Hsu, A.C.T.
Hughes, R.P.
Hunter, B.K.
Hutson, J.M.
Hynes, J.T.
Interrante, L.V.
Irish, D.E.
Izatt, R.M.
Jablonski, C.
Jackson, J.E.
Jäger, W.
James, B.R.
Janda, K.D.
Jardim, I.N.
Jaworski, J.
Jean-Claude, B.
Jensen, C.M.
Jerkiewicz, G.
Jessop, P.G.
Jia, G.
Johnston, L.
Jokisaari, J.
Jonah, C.D.
Jones, M.
Jones, P.G.
Jones, T.H.
Joó, F.
Jordan, R.B.
Jordan, R.F.
Joule, J.
Just, G.
Kadish, K.M.
Kamal, M.M.
Kapral, R.E.
Karelson, M.
Kaszynski, P.
Katritzky, A.R.
Katti, K.V.
Katzenelson, O.
Keay, B.
Keillor, J.
Kern, D.
Kerr, M.A.
King, F.
Kirby, A.J.
Klarner, K.
Kluger, R.
Knaus, E.E.
Koch, S.A.
Kollman, P.A.
Kool, E.
Koppenol, W.H.
Kotovych, G.
Kowalski, C.
Kozikowski, A.
Kresge, A.J.
Kroeker, S.
Kubas, G.J.
Kubiak, C.P.
Kwak, J.C.T.
Lajoie, G.
Lappert, M.
LaRock, R.
Lasia, A.
Lebel, H.
Leclerc, M.
Lee, D.G.
Lee, S.
Lee-Ruff, E.
Legzdins, P.
Lehn, J.M.
Leigh, W.J.
Leitner, W.
Lemieux, R.P.
Lessard, J.
Lessard, R.A.
Lever, A.B.P.
Lewis, L.N.
Lewis, N.G.
Leznoff, C.C.
Leznoff, D.B.
Li, P.K.
Liedl, K.R.
Lipkowitz, K.B.
Lipton, M.A.
Liu, G.
Loeb, S.J.
Lomozik, L.
Lubell, W.D.
Luche, J.
Lustyk, J.
Mabry, T.J.
Macartney, D.H.

© 2000 NRC Canada

Macgillivray, R.
Magnus, P.D.
Maitlis, P.M.
Majetich, G.
Majewski, M.
Maksic, Z.B.
Manakov. A.
Mann, K.R.
Manners, I.
Mansour, T.
Mar, A.
Marciniec, B.
Marder, T.B.
Margerum, R.H.
Marks, T.J.
Martell, A.E.
Martin, S.
Mather, A.
Mattes, R.
Mauk, G.
Mayer, J.M.
McAllister, M.A.
McAuley, A.
McClelland, R.A.
McCombie, S.W.
McCourt, F.R.W.
McDermott, M.
McGlinchey, M.J.
McMillin, D.R.
McMurry, J.E.
Menard, H.
Ménard, H.
Menzinger, M.
Meth-Cahn, O.
Mihichuk, L.
Mikkelsen, S.
Millero, F.J.
Mitchell, R.
Molina, J.M.
Molinski, T.F.
Molyneaux, R.
Moriarty, B.
Morris, R.H.
Mosquera, R.A.
Muchowski, J.M.
Münck, E.
Nelson, J.H.
Nguyen, M.T.
Nicholas, K.
Nickon, A.
Nigishi, E.I.
Niki, X.
Northey, R.
Novak, M.
Noyori, R.
Oakley, R.T.
O'Brien, P.
Öhman, L.O.
Olah, G.A.
Oro, L.
Ozin, G.A.
Pacey, P.D.
Padró, J.A.
Padwa, A.
Palepu, R.
Pan, G.X.
Panagiotopoulos, A.Z.
Paquette, L.A.
Parvez, M.
Passmore, J.
Patrick, B.O.
Pavlik, J.W.
Pearson, W.H.
Penner, G.H.
Peters, D.G.
Pettersson, L.
Picard, J.P.
Piers, E.
Piers, W.E.
Pietro, W.J.
Pignolet, L.
Pincock, J.A.
Pinto, B.M.
Poë, A.J.
Pojman, J.A.
Pomeroy, R.K.
Pope, M.T.
Porter, N.A.
Pregosin, P.S.
Protasiewica, J.
Quack, M.
Quail, J.W.
Quirke, J.
Ramondo, F.
Ratcliffe, C.
Rauchfuss, T.B.
Rauk, A.
Read, J.
Reber, C.
Rees, W.S.
Rehder, D.
Reid, B.F.
Reid, R.S.
Reinsborough, V.C.
Rempel, G.L.
Rempel, U.
Reynolds, W.F.
Richeson, D.S.
Richter-Addo, G.B.
Rigby, J.H.
Roberge, P.R.
Robertson, K.N.
Robins, M.J.
Robinson, B.H.
Rochon, F.D.
Roesky, H.
Rogers, R.D.
Rosenberg, L.
Rothwell, I.P.
Roy, R.
Royer, J.
Ruasse, M.F.
Rusling, J.F.
Sadlej, J.
Sadler, P.J.
Sage, M.L.
Sailor, M.J.
Salahub, D.
Sanger, A.
Saunders, G.
Saunders, W.H.
Savage, J.P.
Scheffer, J.R.
Scheidt, W.R.
Schepp, N.
Schiller, P.W.
Schleyer, P.V.R.
Schmidbaur, H.
Schneider, H.J.
Schramm, L.L.
Schrobilgen, G.
Schrock, R.R.
Schugar, H.
Schurko, R.
Schuster, G.
Schwan, A.
Scott, S.L.
Sebaibi, Y.
Secco, A.S.
Seddon, K.R.
Seebach, D.
Selegue, J.
Sen, A.
Sengupta, S.
Serpone, N.
Sessler, J.
Severson, M.W.
Sharp, P.
Sharpless, K.B.
Shaw, B.
Shaw, C.F.
Sherman, J.C.
Shine, H.J.
Shoesmith, D.
Siepmann, J.I.
Sigel, H.
Simándi, L.I.
Simoyi, R.H.
Skerlj, A.
Smith, F.E.
Smith, K.M.
Smith, M.B.
Smith, P.E.
Snyder, J.K.
Song, C.
Sorensen, T.S.
Spanget-Larsen, J.
Spector, T.I.
St. Jacques, M.
Stang, P.

© 2000 NRC Canada

Steer, R.P.
Steinbock, O.
Stephan, D.W.
Stillman, M.J.
Storer, R.
Storr, A.
Strauss, S.H.
Strekowkski, L.
Stryker, J.
Stynes, D.V.
Sureshan, C.A.
Swainson, I.P.
Sweigart, D.
Swofford, R.L.
Szarek, W.
Szillat, H.
Takats, J.
Tamm, M.
Taylor, N.J.
Tee, O.S.
Templeton, J.L.
Ternay, A.L.
Thakkar, A.J.
Thatcher, G.R.J.
Thompson, C.
Thompson, R.C.
Tidwell, T.T.
Tilley, D.T.
Tolman, W.
Toteva, M.
Townsend, C.A.
Townsend, L.
Travis, J.
Tremaine, P.R.
Trotter, J.
Trsic, M.
Tubergen, J.
Tuck, D.G.
Tully, J.
Turro, N.
Underhill, R.S.
Valentine, W.M.
van Koten, G.
van Leeuwen, P.W.N.M.
van Lier, J.E.
Vanysek, P.
Varma, V.
Vedejs, E.
Vera, J.H.
Verrall, R.E.
Vollhardt, K.P.C.
Voyer, N.
Wakselman, M.
Walton, J.
Wan, P.C.F.
Wang, S.
Wang, Z.Y.
Ward, M.
Ward, R.S.
Warkentin, J.
Warrener, R.N.
Wayland, B.B.
Waymouth, R.M.
Wayner, D.D.M.
Weil, J.A.
Weinberg, N.
Wenkert, E.
Werstiuk, N.H.
Westcott, S.A.
Whitcombe, T.
White, H.S.
White, M.A.
Whitney, R.A.
Wilhelm, E.
Wilsky, G.R.
Winkler, J.
Winnik, M.A.
Withers, S.G.
Wolf, M.
Wolfe, S.
Wong, C.H.
Woo, T.K.
Woods, R.
Woollins, J.D.
Wu, G.
Xia, S.
Zamboni, R.
Zaworotko, M.
Zhan, B.Z.
Ziegler, T.
Ziemlis, M.
Zubieta, J.
Zuman, P.

© 2000 NRC Canada